An Additional Formation of $CH_2{}^{80}BrBr$ *via* a Kinetic-energy-independent Process in the Highly Moderated ^{80m}Br-CH_4 Systems

Kenshi NUMAKURA,* Masakatsu SAEKI, and Enzo TACHIKAWA

Division of Chemistry, Japan Atomic Energy Research Institute, Tokai-Mura, Ibaraki

(Received July 21, 1971)

The moderator effect of Kr on the reaction of (I.T.)-activated ^{80}Br with CH_4 has been examined, keeping the ratio of Br_2/CH_4 at 0.02 or 0.05. The yield of $CH_2{}^{80}BrBr$ shows a slight decrease at the beginning of moderation and then tends to increase with further moderation. These facts suggest an additional formation of $CH_2{}^{80}BrBr$ *via* a thermal ionic process in highly-moderated systems. When the concentration of Br_2 is varied in the system containing 10 cmHg of CH_4 and from 40 to 36 cmHg of Kr, the yield of $CH_2{}^{80}BrBr$ first increases and then decreases, showing a broad maximum. This dependence not only partly explains the inconsistence of the present results with those previously reported, but also suggests the competition of two types of reaction in its formation. One must be the reaction of a radioactive radical with Br_2, leading to the formation of $CH_2{}^{80}BrBr$:

$$\cdot CH_2{}^{80}Br + Br_2 \longrightarrow CH_2{}^{80}BrBr.$$

The other type of reaction is a scavenging reaction of Br_2 for the reacting ^{80}Br atom.

The determination of the relative importance of the kinetic energy and the positive charge in reactions of the recoil Br atom is a current subject in the recoil Br chemistry. So far, many extensive investigations of the subject have been carried out, particularly on the reactions of ^{80}Br with CH_4.[1-4]

While the (n,γ)-activated ^{80}Br reacts with CH_4 to yield $CH_3{}^{80}Br$, mainly as a result of the recoil kinetic energy acquired by the ^{80}Br atom,[5] the (I.T.)-activated ^{80}Br reacts by two processes, one involving excess kinetic energy, and the other, a thermal process.

Following the determination of the total organic yield by Spicer and Gordus,[6] Tachikawa and Kahara[3] examined the molecular distribution of the products under a high concentration of bromine and reached the conclusion that $CH_2{}^{80}BrBr$ is formed principally *via* the kinetic energy-independent process, while $CH_3{}^{80}Br$ is formed *via* both kinetic-energy and kinetic energy-independent (thermal ionic) processes. Since the Br_2 additive is an efficient moderator of the ^{80}Br atom, it is rather desirable to use the smallest pressure of Br_2. Recently Yagi *et al.*[4] reexamined the above reactions in a Kr-moderated system, keeping $Br_2/CH_4=0.029$; they reached the different conclusions that $CH_3{}^{80}Br$ is principally formed *via* the kinetic-energy process and that $CH_2{}^{80}BrBr$ is formed *via* both processes.

These experiments were all carried out in the total pressure range from 50 cmHg to 76 cmHg. It has been reported that the yields of individual organic products increase with an increase in the total pressure, but tend to level off around 50 cmHg.[3] Thus, one of the possible factors which are responsible for the inconsistency among the results previously reported was the variation in the Br_2 added as a scavenger in the systems.

In the current set of experiments, we carefully studied the reactions, particularly in highly-moderated systems. The results obtained showed a characteristic in $CH_2{}^{80}BrBr$ with the Br_2 concentration. A qualitative explanation of the above contradiction has been attempted.

Experimental

The experimental procedure was the routine one for the study of ^{80}Br activated by the isomeric transition of ^{80m}Br; it involved the irradiation of Br_2 in a quartz ampoule, mixture with reactants and analysis of the products by means of radio-gas chromatography. The details can be found elsewhere.[3]

Materials. Bromine came from the Kanto Chemical Co., and was used after simple purification by vacuum distillation. Methane and krypton, the nominal purities of which were both 99.995%, were supplied by the Takachiho Chemical Co., and were used directly from the vessel.

Measurement of Br_2-pressure. In our previous experiments,[2,3] we used an oil manometer to measure the pressure of irradiated Br_2 added to reaction ampoules. However, it was rather difficult to measure a pressure of less than 1.0 cmHg by means of this apparatus. In the present set of experiments, therefore we used a digital precision pressure gauge, model 145 (Texas Instruments), which involves a quartz buldon gauge. This apparatus allows us to measure pressures down to 0.1 mmHg with precision of better than $\pm 5\%$.

Sample Processing. All relative products distributions were determined by radio-gas chromatography, employing a side window-type gas-flow counter. The inorganic bromides were isolated from the organic bromides by the insertion of a short glass column packed with potassium ferrocyanide into the gas stream ahead of the organic separation column. The separation column consisted of a celite base (60—80 mesh) coated with dioctyl sebacate (15% by weight) packed in a glass tube 4 mm in inside diameter and 5 m long. The major products observed were, in all cases, $CH_3{}^{80}Br$ and $CH_2{}^{80}BrBr$, although several minor products, such as $C_2H_5{}^{80}Br$ and $CH_2{}^{80}BrBr_2$, were also observed.

In the determination of the total organic yields, the products were frozen by dipping an ampoule into a liquid-nitrogen bath. The tip of the ampoule was cut in order to pour a mixture of 5 ml of 0.5M Na_2SO_3 and 3 ml of CCl_4. After sealing-off the tip, the ampoule was vigorously shaken. The organic phase was then separated from the inorganic one. Each phase contained in a vessel specially designed for count-

* On leave of absence from the Faculty of Engineering, Ibaraki University, Hitachi, Ibaraki.

1) J. B. Nicholas and E. P. Rack, *J. Chem. Phys.*, **48**, 4085 (1968).
2) E. Tachikawa, This Bulletin, **42**, 2404 (1969).
3) E. Tachikawa and T. Kahara, *ibid.*, **43**, 1293 (1970).
4) M. Yagi, K. Kondo, and T. Kobayashi, *ibid.*, **44**, 580 (1971).
5) E. P. Rack and A. A. Gordus, *J. Phys. Chem.*, **65**, 944 (1961).
6) L. D. Spicer and A. A. Gordus, "Chemical Effects of Nuclear Transformations," Vol. 1, IAEA, Vienna (1965), p. 185.

ing was measured by an end window-type gas-flow counter. The activity of ^{80}Br in each phase was corrected for ^{80m}Br and ^{82}Br using the decay curves of the activities. No correction for freezing, shaking, or separation was applied in the calculations of the total organic yield, since the decay correction based on the time spent for these processes was less than a few percent and could be disregarded. The percentage yields reported in this paper were the percentage of individual activities relative to the total organic activities observed, multiplied by the total organic yield.

Results

The effects of the moderator gas, Kr, on the individual product yields are graphically depicted in Fig. 1. The plots include all the results obtained from systems where the concentrations of Br_2 as a scavenger, relative to CH_4, were 0.02 and 0.05. In all cases, the total pressure was kept constant at 50±1 cmHg. At zero m.f. of Kr, the yields were 4.3±0.4% $CH_3{}^{80}Br$, 2.1±0.2% $CH_2{}^{80}BrBr$, and 6.4±0.6% total organic.

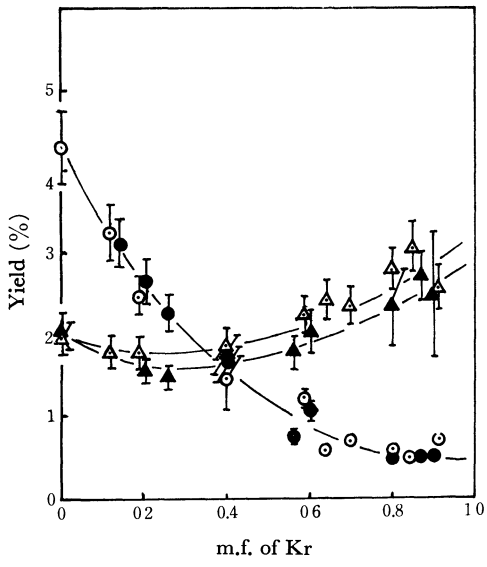

Fig. 1. The Kr-moderator effects on the individual products.
The ratio, Br_2/CH_4 was 0.02 and 0.05
Br_2/CH_4: 0.02 ●: $CH_3{}^{80}Br$ ▲: $CH_2{}^{80}BrBr$
Br_2/CH_4: 0.05 ⊙: $CH_3{}^{80}Br$ △: $CH_2{}^{80}BrBr$

As the dilution of the reaction system with Kr proceeded, the yield of $CH_3{}^{80}Br$ decreased and could be extrapolated to 0.6±0.1% at 1.0 m.f. of Kr in either case. However, the yield of $CH_2{}^{80}BrBr$ showed a slight decrease at the beginning of dilution, but it tended to increase when the m.f. of Kr exceeded 0.5. At 1.0 m.f. of Kr, the limiting yield of $CH_2{}^{80}BrBr$ was 2.9±0.3% or 3.2±0.3%; depending upon the value of Br_2/CH_4.

In order to examine the yield variation with the concentration of Br_2 in highly-moderated systems, the Br_2/CH_4 ratio was varied from 0.01 to 0.4, while keeping the pressure of CH_4 constant at 10 cmHg. Consequently, the pressure of Kr (40 to 36 cmHg) was adjusted to attain a total pressure of 50±1 cmHg. In view of the relative efficiency of Br_2 and Kr as kinetic-energy moderators for an energetic ^{80}Br, the change in moderator efficiency accompanied by the small variation in composition, cannot be important. The results obtained are plotted in Fig. 2. The variation in $CH_3{}^{80}Br$ did not exceed the experimental fluctuation from the value of 0.6±0.1% over the range studied. On the other hand, the yield of $CH_2{}^{80}BrBr$ increased with the increase in the ratio of Br_2/CH_4 at the beginning, and then decreased when the ratio exceeded around 0.15, showing a broad maximum in the range from 0.05 to 0.10 of Br_2/CH_4.

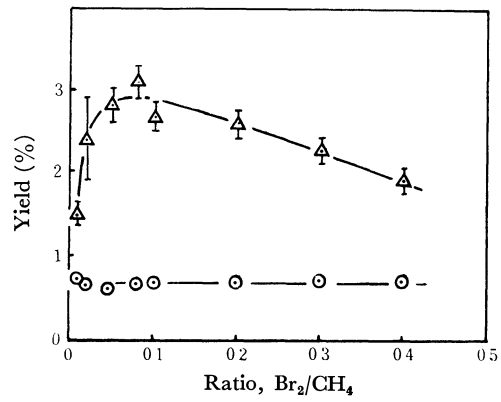

Fig. 2. The effects of the variation of the ratio, Br_2/CH_4 on the yields of $CH_3{}^{80}Br$ and $CH_2{}^{80}BrBr$ in the highly moderated systems (CH_4: 10 cmHg, Br_2: 0.1—4.0 cmHg, and the total pressure was kept constant at 50±1 cmHg by adjusting Kr-pressure).
⊙: $CH_3{}^{80}Br$ △: $CH_2{}^{80}BrBr$

Discussion

Comparisons with Reported Results. The total organic yield (6.4±0.6%) with no additive agreed reasonably well with those reported by Spicer and Gordus (6.8±0.8%)[6] and by Yagi *et al.* (7.0±0.3%).[4] However, when the limiting yields of the individual products at 1.0 m.f. of Kr are compared, a significant difference can be noticed between the present results and the Yagi *et al.* results. They reported the limiting yield of zero percent for $CH_3{}^{80}Br$ and 1.4% for $CH_2{}^{80}BrBr$. In their series of moderator experiments, the smallest m.f. of CH_4 reached was 0.25, and their extrapolation of the yields of products to 1.0 m.f. of Kr relied on results covering the range from zero to 0.75 m.f. of Kr. According to the present results, however, their extrapolated curves do not necessarily represent the real moderator curves under highly moderated conditions. For example, when the variations in $CH_3{}^{80}Br$ from zero to 0.7 m.f. of a moderator in the present results are taken into account, the extrapolation of $CH_3{}^{80}Br$ to zero percent at 1.0 m.f. of moderator is rather probable. Thus, their results can be understood to show the moderator effects of the products up to around 0.75 m.f. of moderator, but can not be extented to much further moderation.

The most significant difference between the present results and the reported ones, however, can be seen in the yield of $CH_2{}^{80}BrBr$ at a higher moderation, and consequently in its limiting yield at 1.0 m.f. of Kr. When the Br_2/CH_4 ratio was varied while keeping the pressure of CH_4 constant, at 5.0 cmHg (the pressure of Kr was also varied from 45 to 41 cmHg to attain

the total pressure of 51 cmHg), a dependence of the yield of $CH_2{}^{80}BrBr$ as the Br_2/CH_4 ratio similar to that shown in Fig. 2 was observed. This suggests that this kind of variation in the yield curve of $CH_2{}^{80}BrBr$ with the ratio can always be expected at high moderations and that a small variation in the ratio sometimes leads to a large difference in the yield of $CH_2{}^{80}BrBr$. Consequently, the limiting yields of $CH_2{}^{80}BrBr$ and of the total organic at 1.0 m.f. of Kr may vary considerably depending upon the amount of Br_2 added in highly moderated systems. Thus, if the Br_2/CH_4 ratio is varied little from 0.02 in such a high moderation, the difference in the yield of $CH_2{}^{80}BrBr$ between the two experiments, the present and the previous ones, can be easily accounted for.

In most of the moderator experiments previously reported,[7] the amount of Br_2 relative to that of the reactant was determined from scavenger curves in the unmoderated systems. Once it was determined, the Br_2/reactant ratio was kept constant or nearly constant throughout the m.f. of the moderator. With regard to this conventional selection of the Br_2/reactant ratio the present results are thus very suggestive. In conclusions, in order to identify the yields of the organic products as the kinetic-energy or kinetic-energy-independent yields, the present types of behavior of the products under highly moderated conditions, as well as the physical natures of the moderator[8] must be taken into account.

Kinetic-energy-independent Yields of Products. From the results shown in Fig. 1, it may be concluded that the kinetic-energy-independent yield of $CH_3{}^{80}Br$ was $0.6\pm0.1\%$, which corresponded to *ca.* 14% of the total $CH_3{}^{80}Br$ formed. This conclusion, however, includes the assumption that the moderator curve obtained reflects the true reaction processes involved in the formation of $CH_3{}^{80}Br$. Recent moderator experiments on ^{80m}Br–C_2H_6,[8] however, have indicated that when the reaction system is diluted with inert gases, the distribution of the charged ^{80}Br is modified so that an additional formation of $CH_3{}^{80}Br$ *via* the kinetic-energy-independent process occurs. Furthermore, in the present work the increase in the yield of $CH_2{}^{80}BrBr$ at a high moderation is an indication of the additional formation of the compound *via* the kinetic-energy-independent process. Thus, the present value of 0.6% for the kinetic-energy-independent yield of $CH_3{}^{80}Br$ should be understood to be a maximum value.

On the other hand, it is not possible to identify the observed yield of $CH_2{}^{80}BrBr$ with no additive as kinetic-energy and kinetic-energy-independent yields on the basis of the present results alone. Nevertheless, we preferred to conclude that it was mainly formed *via* the kinetic-energy-independent process and that the formation due to the kinetic-energy process was less important. This is qualitatively consistent with the conclusion reached in the early experiments using a rather high concentration of Br_2.[9] One support for the above prediction is given by the recent experiments in our laboratory.[10] When the $^{82}BrBr$ molecule is irradiated with the light of the wavelength of 2537 Å, an energetic ^{82}Br atom with 1.2 or 1.7 eV, but with no charge is formed. This atom reacts with CH_4 to give $CH_3{}^{80}Br$. The $CH_2{}^{80}BrBr$ was not detected within the limits of experimental uncertainty, and its yield, if it is also formed, must be less than a small percentage of that of $CH_3{}^{82}Br$. The results obtained with the reaction of ^{80}Br activated by the (n,γ) process with CH_4 were also consistent with the above prediction. The ^{80}Br thus activated has a higher energy and less charge than that from the (I.T.) activation, and it reacts with CH_4 to yield a total organic yield of 13.8%, principally *via* the kinetic energy process.[5,11] Spicer and Gordus reported that 89% of the total organic yield was $CH_3{}^{80}Br$, while 11% was $CH_2{}^{80}BrBr$. A further analysis of the results using the Estrup-Wolfgang kinetic theory showed that the yields due to the kinetic-energy processes were 12.3% for $CH_3{}^{80}Br$ and 1.0% for $CH_2{}^{80}BrBr$.[12] These values gave the ratio of 0.08 for $CH_2{}^{80}BrBr/CH_3{}^{80}Br$.

As a crude approximation, we attempt to evaluate the maximum yield of $CH_2{}^{80}BrBr$ due to the kinetic-energy process in the present reaction with the assumption that the value of 0.08 for the $CH_2{}^{80}BrBr/CH_3{}^{80}Br$ ratio also holds in the present reaction system. The maximum yield of the kinetic-energy process to form $CH_2{}^{80}BrBr$ was estimated to be $0.08\times3.9=0.3\%$, this, however, explains only 14% of the total yield of $CH_2{}^{80}BrBr$.

Effects of the Br_2 Concentration on $CH_2{}^{80}BrBr$ in Highly Moderated Systems. The appearance of the maximum in the yield of $CH_2{}^{80}BrBr$ in Fig. 2 can only be explained in terms of the competition between two types of reaction.[13] If at least a part of the yield is directly dependent on the presence of inactive bromine, the latter contributes to their formation. An example would be the reaction of a radioactive radical with Br_2, leading to the formation of $CH_2{}^{80}BrBr$:

$$\cdot CH_2{}^{80}Br + Br_2 \longrightarrow CH_2{}^{80}BrBr.$$

The other type of reaction involved is a scavenging reaction of Br_2 for the reacting ^{80}Br atom, since Br_2 is the reacting scavenger. At higher concentrations of inactive bromine, the collision of the reacting ^{80}Br with Br_2 becomes important and the yield is progressively

7) J.E. Willard, "Chemical Effects of Nuclear Transformations," Vol. 1, IAEA, Vienna (1965), p. 221.

8) E. Tachikawa and K. Yanai, *Radiochim. Acta*, **17**, 138 (1972).

9) E. Tachikawa and J. Okamoto, *Radiochim. Acta*, **13**, 159 (1970). In the series of previous experiments, the yield of $CH_2{}^{80}BrBr$ was constantly smaller than those expected from the present works. This is partly due to the experimental method used. In the previous works, the reaction mixture was once transferred into the injection loop for the radio-gas chromatographic analysis. Thus a constant fraction of $CH_2{}^{80}BrBr$ was lost due to the adsorption, mainly on the stopcock involved. Furthermore an addition of Xe or Ar as a moderator may lead to a different behavior of $CH_2{}^{80}BrBr$. However, this does not alter the conclusion previously reached that $CH_2{}^{80}BrBr$ was mainly formed *via* the kinetic-energy-independent process.

10) K. Hamanoue and E. Tachikawa, unpublished data.

11) M. Saeki, K. Numakura, and E. Tachikawa, This Bulletin, **45**, 1715 (1972).

12) M. Saeki and E. Tachikawa, presented at the 26th Annual Meeting of the Chemical Society of Japan, Hiratsuka, Kanagawa (April, 1972), to be appeared in this Bulletin.

13) Z. Abedinzadeh, R. Radicella, K. Tanaka, and M. Milman, *Radiochim. Acta*, **12**, 4 (1969).

reduced and the usual scavenger curve prevails.

The fact that a small concentration of Br_2 (6×10^{-2} m.f.) brings about such a sharp increase in the yield also means that the radical responsible for it must be reasonably stable and long-lived to be able to react with Br_2. Assuming the Maxwellian distribution of both $CH_2{}^{80}Br$ and Br_2, the life-time of the radical was calculated as $\geq10^{-7}$ sec.[14]

14) The calculation based on the equation,

$$Z = N_2\sigma_{12}^2\left(\frac{8kT}{\pi\mu}\right)^{1/2}$$

for the collision density (see S. W. Benson "The Foundations of Chemical Kinetics," MacGraw-Hill, New York, (1960) p. 153). The molecular diameter used are 4.27 Å for Br_2 and 4.0 Å for CH_2Br in analogy with CH_3Br (ref. J. O. Hirschfelder, C. F. Curtiss, and R. B. Bird, "The Molecular Theory of Gases and Liquid," John Wiley and Sons, Inc., New Yrok, (1960) p. 1110).

The formation of the $CH_2{}^{80}Br$ radical must involve the breaking of two C–H bonds. In an energetic reaction, the importance of the double-replacement reaction is already known.[15] However, the foramtion of the $CH_2{}^{80}Br$ radical in the present reaction system is probably initiated mostly *via* the kinetic-energy-independent process of ^{80}Br. The direct application of the double-replacement reaction to the present case, therefore cannot be made. As was suggested in a previous paper,[9] the formation of $(CH_4{}^{80}Br)^+$ is the most realistic primary step involved. However, the details of the reaction pass leading to $CH_2{}^{80}BrBr$ from $(CH_4{}^{80}Br)^+$ must await the carrying-out of further experiment.

15) R. Wolfgang, "Prog. Reaction Kinetics," Vol. 3 (1965) p. 97.

BULLETIN OF THE CHEMICAL SOCIETY OF JAPAN, VOL. 46, 4—8 (1973)

The Isomerization of Propylene Oxide on Metal Oxides and Silica-Magnesia Catalysts

Yasuaki OKAMOTO, Toshinobu IMANAKA, and Shiichiro TERANISHI

Department of Chemistry, Faculty of Engineering Science, Osaka University, Toyonaka

(Received December 6, 1971)

The isomerization of propylene oxide was carried out over silica-magnesia catalysts and metal oxides at 260—270°C using a pulse reactor. The main products of the reaction were propionaldehyde, acetone, allyl alcohol, 1-propanol, and acrolein. Propionaldehyde and acetone are produced on acidic and basic sites respectively. Allyl alcohol is formed over acid-base bifunctional catalysts. 1-Propanol and acrolein are mainly produced through hydrogen-transfer reactions between allyl alcohol and propionaldehyde and propylene oxide. As regards these reactions, acid-base bifunctional catalysts are favorable and the reaction rate depends on the electron-donating power of the hydrogen acceptor and the basic strength of the catalyst. The acid sites on silica-magnesia catalysts are attributed to the forsterite produced by the reaction of magnesium oxide and silica gel, and the basic sites, to the magnesium oxide remaining. The metal oxides, such as magnesium and calcium oxides, are considered to have very weak acid sites.

The activities and selectivities of a reaction on solid acids and bases are determined by studying their acidic and basic properties. It is important to clarify the relations between them. In our preceding papers,[1,2] it was found that the activities and selectivities of propylene oxide isomerization on zeolite catalysts and metal phosphates could be elucidated by the acidic and basic properties of catalysts.

According to Niiyama and his co-workers,[3] silica-magnesia catalysts prepared from magnesium hydroxide and silica gel by calcination at 600°C have acid and basic sites. In the present investigation, propylene oxide isomerization was carried out on silica-magnesia and metal oxide catalysts in order to confirm the proposed mechanisms of the reaction and the relationships between the selectivities and acidic and basic characters of the solid acids and bases. In the cases of zeolites[1] and metal phosphates,[2] the main products were acetone, propionaldehyde, and allyl alcohol. However, it was found that silica-magnesia and metal oxides produce considerable 1-propanol, the hydrogenated compounds of allyl alcohol, propionaldehyde, and propylene oxide. The reaction steps of 1-propanol formation are discussed. Moreover, the production mechanism of the acidic and basic properties of silica–magnesia catalysts was deduced from the results of X-ray diffraction.

Experimental

Materials. Silica-magnesia catalysts with different compositions were prepared as follows. Silica gel (Nakarai Chemicals, Ltd.; Silica gel No. III 200 mesh) and magnesium hydroxide (Wako Pure Chemical Industries, Ltd.) were mixed in water at 90°C for 12 hr, filtered, and calcined at 600°C for 6 hr in air. The compositions of the silica-magnesia catalysts used in our experiments were 0, 34, 51, 67, 76, and

1) T. Imanaka, Y. Okamoto, and S. Teranishi, This Bulletin, **45**, 3215 (1972).

2) T. Imanaka, Y. Okamoto, and S. Teranishi, *ibid.*, **45**, 1353 (1972).

3) H. Niiyama, S. Morii, and E. Echigoya, *Shokubai*, **13**, 57 (1971).

100 mol% of the magnesium oxide content. The surface areas of these catalysts were 405, 142, 307, 158, 145, and 68 m^2/g respectively. The metal oxides used were MgO, CaO, MnO, BaO, SrO, and ZnO. They were all commercial-grade except for MnO. MnO was prepared by the decomposition of $MnCO_3$ at 500°C under a vacuum for 48 hr. The reactants were commercial-grade.

Procedures. The isomerization of propylene oxide was carried out using a conventional pulse reactor in a helium carrier. The catalysts (20 mg) were treated at the reaction temperature in streaming helium for about 2 hr before reactions. The amount of reactant injected into the catalyst was 2 μl.

The acidic and basic properties of the catalysts, which were heated at 300°C for 2 hr in air, were measured by the conventional titrating method in benzene with a benzene solution of *n*-butylamine, and benzoic acid, using Hammett indicators.[4]

The structures of the calcined silica–magnesia catalysts were determined by X-ray analysis.

Results and Discussion

The surface areas, acidities, and basicities of the metal oxides are shown in Table 1. Figure 1 shows the dependencies of the acidity (measured at $H_0=+6.8$) and the basicity ($H_0=+7.2$) of the silica-magnesia catalyst on the magnesium-oxide content. Niiyama *et al.*[3] have reported almost the same behavior

Table 1. Properties of metal oxide catalysts

Catalyst	Surface area (m^2/g)	Acidity[a] (mmol/g)	Basicity[b] (mmol/g)
MgO	55.6	—	0.288
CaO	13.3	—	0.014
SrO	5.3	—	0.005
MnO	4.7	?[c]	?[c]
BaO	1.9	—	0.005
ZnO	7.4	0.046	—

a) measured at $H_0=+6.8$
b) measured at $H_0=+7.2$
c) cannot be measured due to its dark color

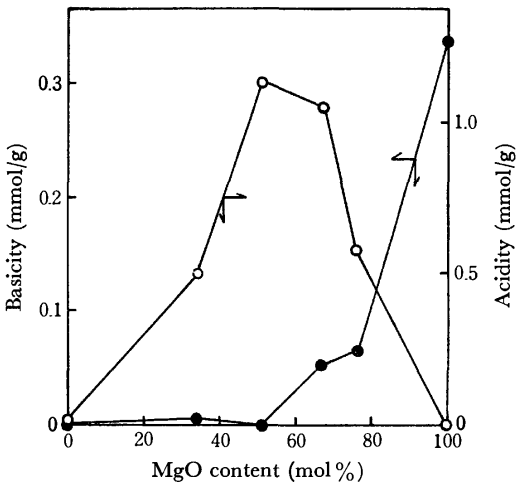

Fig. 1. Dependence of acidity and basicity of silica-magnesia catalysts on magnesium oxide content.
○: acidity, ●: basicity

of the acidic and basic properties of these catalysts. According to Fig. 1, the acidities of silica–magnesia catalysts increase and then decrease with an increase in the magnesium oxide content. An equimolar mixture of silica gel and magnesium oxide has the maximum acidity. The maximum acid strength of the silica–magnesia catalyst (measured for the 51% MgO-catalyst) is stronger than that of silica gel only; their H_0 values are +1.5 and +2.0 respectively. These facts indicate that new compound produced by a reaction of silica gel and magnesium oxide possesses stronger acid sites than does silica gel. According to Brewer and Steinberg,[5] silica–magnesia catalysts tempered at 400—700°C, and which have been prepared from an equimolar mixture of silica tetraethoxide and magnesium ethoxide, have a forsterite structure (Mg_2SiO_4) and strong Lewis acid sites. In the case of magnesia–boria catalysts, Tanaka and his co-workers[6] have reported that the unknown product formed is an active center for the aldol condensation of acetone. The X-ray analysis of our silica–magnesia catalysts indicates that silica gel has a structure of α-cristobalite, magnesium hydroxide disappears, magnesium oxide is formed, and forsterite is produced. According to Jander and Wuhrer,[7] the main product of the solid-state reaction of silica gel and magnesium oxide is forsterite and the amount of enstatite ($MgSiO_3$) is very small. Our results coincide with theirs. Figure 2 shows the dependence of the amounts of magnesium oxide, silica gel, and forsterite, as measured by X-ray analysis, on the magnesium oxide content. A comparison of Figs. 1 and 2 shows that the acidity correlates to the amount of forsterite and that the basicity correlates to that of the magnesium oxide remaining. Consequently, the strong acid sites on the silica–magnesia catalysts are

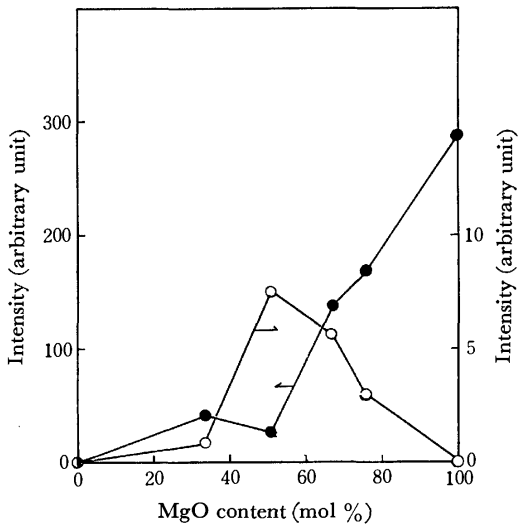

Fig. 2. Dependence of the amounts of magnesium oxide, and forsterite on the magnesium oxide content in silica-magnesia.
●: magnesium oxide, ○: forsterite

4) K. Tanabe "Solid Acids and Bases" Kodansha, Tokyo, Academic Press, New York, London (1970) pp. 6, 36.

5) H. Bremer and K. H. Steinberg, 4th Int. Congr. Cat. Moscow, Preprint of the paper No. 76 (1968).

6) A. Tanaka, I. Nozawa, and T. Shirasaki, *Shokubai*, **11**, 87 (1969).

7) W. Jander and J. Wuhrer, *Z. Anorg. Allg. Chem.*, **226**, 225 (1936).

Table 2. Product distributions of propylene oxide isomerization over silica–magnesia catalysts

Catalyst	R.T. (°C)	Conv[a] (%)	G.P. (%)	A (%)	PA (%)	AC (%)	ACR (%)	1-PrOH (%)	AA (%)	O.P. (%)
SM(0)	267	7.3	0.9	0.5	79.5	—	—	—	13.2	5.9
SM(34)	270	37.0	1.1	1.6	55.7	4.5	0.9	12.6	22.3	1.3
SM(51)	266	56.2	10.3	2.6	64.6	1.5	1.2	10.0	10.2	0
SM(67)	270	42.7	4.0	3.1	56.1	1.8	1.7	20.8	12.8	0
SM(76)	272	49.1	4.0	2.4	61.1	4.6	1.9	12.3	11.7	2.0
SM(100)	267	11.9	1.3	4.8	3.8	31.4	3.3	24.9	30.5	0

a) Conversion (%)/10 mg-Cat.
b) SM denotes silica-magnesia and the number in parenthesis indicates magnesium oxide content (mol %).
G.P.: Gaseous products, A: Acetaldehyde, PA: Propionaldehyde, AC: Acetone, ACR: Acrolein, 1-PrOH: 1-Propanol, AA: Allyl alcohol, O.P.: Other products.

Table 3. Product distributions of propylene oxide isomerization over metal oxide catalysts

Catalyst	R.T. (°C)	Conv[a] (%)	G.P.[a] (%)	A[a] (%)	PA[a] (%)	AC[a] (%)	ACR[a] (%)	1-PrOH[a] (%)	AA[a] (%)	O.P.[a] (%)
MgO	260	9.7	3.4	8.1	—	26.9	21.2	31.9	8.0	0.5
CaO	260	2.8	3.0	10.3	—	31.6	19.3	28.4	7.4	0
SrO	260	0.49	40.6	—	—	28.4	—	8.0	5.7	17.3
MnO	260	1.48	42.7	3.8	29.3	8.1	—	0.8	11.9	3.4

a) See Table 2.

deduced to be caused by the forsterite produced by the reaction of magnesium oxide and silica gel, and the basic sites, by the magnesium oxide. It is considered that the production of strong acid sites can be ascribed to the difference in electronegativity between silicon and magnesium, and that magnesium forms strong Lewis acid sites.

The isomerization of propylene oxide was carried out on silica–magnesia and metal oxide catalysts at 260°C. Tables 2 and 3 show the product distributions of this reaction on these catalysts. Barium oxide and zinc oxide have only a very low activity. The "other products" in these Tables contain condensed products. The gaseous products and acetaldehyde are decomposed products. Here, we will discuss the formation of propionaldehyde, acetone, allyl alcohol, *n*-propanol, and acrolein. In them, propionaldehyde, acetone, and allyl alcohol are the products of the propylene oxide isomerization. Figure 3 shows the dependence of the formations of propionaldehyde and acetone on the magnesium-oxide content of the silica–magnesia catalysts. When we compare Figs. 1 and 3, it is clear that propionaldehyde is formed on acid sites, and acetone on basic sites, as has been reported earlier.[2] Figure 4 shows the dependence of allyl alcohol and 1-propanol on the magnesium-oxide content. In the cases of zeolite catalysts and metal phosphates (except for calcium phosphate), the production of 1-propanol is very small, but silica–magnesia and metal oxide catalysts form very large amounts of 1-propanol. Taking into account the effects of pyridine and dichloroacetic acid on reactions over metal phosphates, 1-propanol has been assumed to be produced from hydrogen-transfer reactions of allyl alcohol.[2] In this paper, 1-propanol formation will be studied in detail.

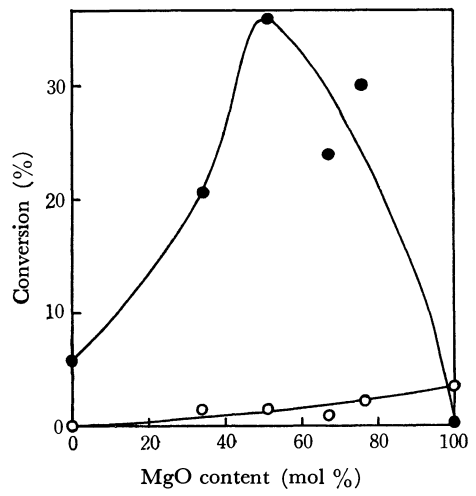

Fig. 3. Dependence of the conversion to propionaldehyde and acetone on the magnesium oxide content.
●: propionaldehyde, ○: acetone

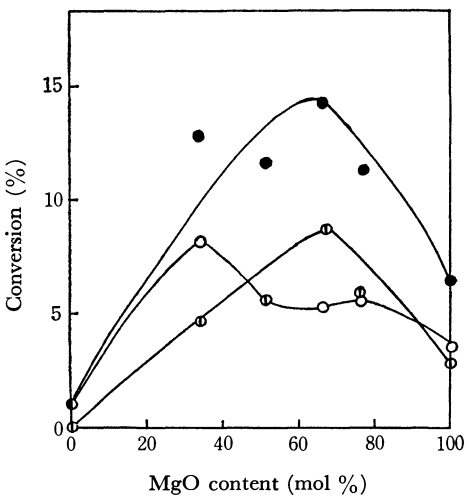

Fig. 4. Dependence of the conversion to allyl alcohol, 1-propanol, and original allyl alcohol on magnesium oxide content.
○: allyl alcohol, ◑: 1-propanol
●: original allyl alcohol

1-Propanol is considered to be a hydrogenated compound of allyl alcohol, propionaldehyde, and propylene oxide and to be formed by the following reaction processes (1)—(4):

$$CH_2=CH-CH_2OH + CH_2=CH-CH_2OH \longrightarrow CH_2=CHCHO + CH_3CH_2CH_2OH \quad (1)$$

$$CH_2=CH-CH_2OH + CH_3-CH-CH_2 \longrightarrow CH_2=CHCHO + CH_3CH_2CH_2OH \quad (2)$$

$$CH_2=CH-CH_2OH + CH_3CH_2CHO \longrightarrow CH_2=CHCHO + CH_3CH_2CH_2OH \quad (3)$$

$$CH_3CH_2CHO + CH_3-CH-CH_2 \longrightarrow CH_2=CHCHO + CH_3CH_2CH_2OH \quad (4)$$

Table 4. Hydrogen-transfer reactions over SM(67) at 260°C

Hydrogen donor	Hydrogen acceptor	Reactivity/g[a] (arbitrary unit)	$\Delta\nu_D$ (cm^{-1}) of hydrogen acceptor
AA	AA	1.3	~0[b]
AA	PO	30	59
AA	PA	61	85
PO or PA	PO or PA	0	59 or 85

a) calculated from the formation of 1-propanol.
b) estimated value.
AA: Allyl alcohol
PO: Propylene oxide
PA: Propionaldehyde

In Table 4, the reactivities for each reaction are given; here, in the case of propylene oxide, the formation of 1-propanol from Process (3) caused by the isomerization of propylene oxide is corrected. As is shown in Tables 2 and 3, considerable acrolein is produced over a series of catalysts. Though the amount of acrolein is smaller than that of 1-propanol, this fact is due to the high reactivity of the polymerization of acrolein; there is an approximate correlation between the amount of acrolein and that of 1-propanol. Therefore, Reactions (2) and (3) are found to be the main processes of 1-propanol formation. As alcohol is more easily dehydrogenated on basic sites than other reactants, it is deduced that allyl alcohol is the hydrogen donor and propionaldehyde and propylene oxide are acceptors. When one mole of 1-propanol is formed, one mole of allyl alcohol is consumed. Therefore, the sum of the formations of allyl alcohol and 1-propanol is considered to be the original amount of allyl alcohol formed. In Fig. 4, their sum is plotted against the magnesium-oxide content. The original formation of allyl alcohol has a maximum; this fact indicates that allyl alcohol is formed by an acid-base bifunctional catalyst, as was reported earlier.[2]

As regards the metal oxides, magnesium and calcium oxides have a high activity of allyl-alcohol formation. Malinowski *et al.*[8] deduced from ammonia adsorption studies that magnesium oxide has a very weak acid site. Taking into account the products of propylene-oxide isomerization, the other metal oxides can also be considered to have very weak acid sites, though the presence of acid sites cannot be detected by the indicator method. For allyl-alcohol production, even very weak acid sites are deduced to be favorable.

The acidic and basic properties of manganese monoxide cannot be measured because of its dark color. It is considered, on the basis of the product distribution of the propylene-oxide isomerization, that it has both acidic and basic properties.

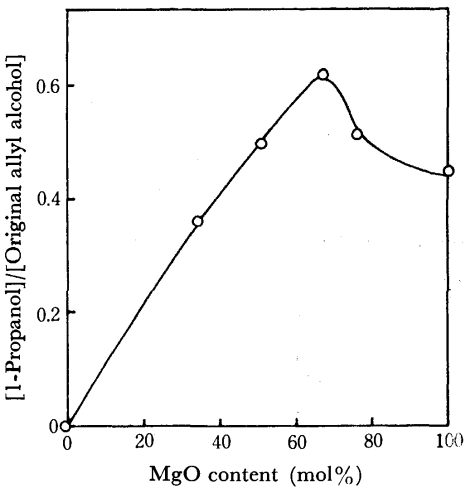

Fig. 5. Dependence of the ratio of 1-propanol to original allyl alcohol on magnesium oxide content.

Niiyama *et al.*[9] have reported that hydrogen-transfer reactions between alcohol and ketone are catalyzed by acid-base bifunctional catalysts. Figure 5 shows the relation between the ratio of the formation of 1-propanol and the original formation of allyl alcohol and magnesium oxide contents. The ratio has a maximum; this fact suggests the same conclusion. According to Table 4, magnesium and calcium oxides produce a very large amount of 1-propanol among all the metal oxides used. Magnesium oxide prepared from magnesium hydroxide gives a product distribution different from that of magnesium oxide supplied in the production of 1-propanol; that is, the selectivities for 1-propanol are 24.9 and 31.9% for prepared and supplied MgO respectively. According to the basic-strength measurements, the supplied MgO($H_0=+17.2$) has stronger basic sites than the prepared MgO($H_0=+15.0$). Therefore, as regards the basic properties favorable to the reaction, strong basic sites are effective.

The order of the activity of the hydrogen-transfer reaction between allyl alcohol and hydrogen acceptor is: propionaldehyde>propylene oxide>allyl alcohol; this order is that of the electron-donating power, $\Delta\nu_D$, of the hydrogen acceptor, which is given in Table 4. According to Kagiya,[10] the electron-donating power of a compound is defined as the relative difference (counted as wave numbers) of the OD adsorption band of methanol-*d* observed in the compound from

8) ST. Malinowski, S. Szczepanska, A. Bielanski, and J. Sloczynski, *J. Catal.*, **4**, 324 (1965).

9) H. Niiyama and E. Echigoya, 23rd Annual Meeting of the Chemical Society of Japan, No. 1 p. 51 (1970).

10) T. Kagiya, Y. Sumida, and T. Inoue, This Bulletin, **41**, 767 (1968).

that observed in benzene. The $\Delta\nu_D$ of allyl alcohol is estimated by taking into account the values of the electron-donating power of the C–C double bond in benzene ($\Delta\nu_D$; 0 cm^{-1}), styrene ($\Delta\nu_D$; 4 cm^{-1}), and so forth.

As regards the mechanism of the hydrogen-transfer reaction Niiyama *et al.*[9] have proposed a mechanism similar to that of Meerwein-Ponndorf reduction. Our results support their mechanism in the case of silica-magnesia catalysts. The following mechanism is plausible.

For process (2)

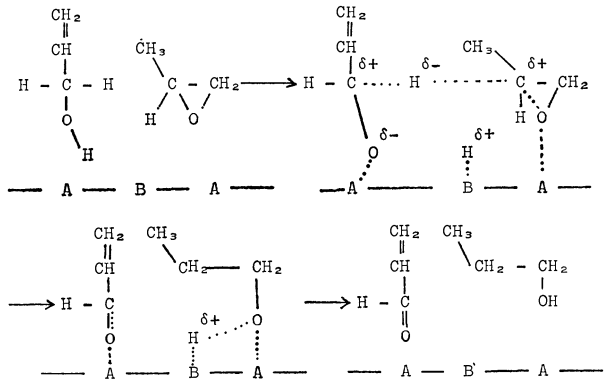

For process (3)

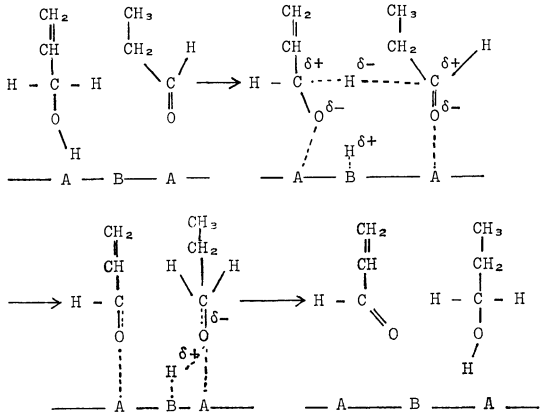

A: acid site B: basic site

That is, propionaldehyde or propylene oxide adsorbs on the acid site at the oxygen atom in them, and the electron density of the carbon atom adjacent to the oxygen atom becomes more positive. The larger the electron-donating power of the hydrogen acceptor, the more positive the carbon atom becomes. Allyl alcohol adsorbs on the basic site, dissociating the hydroxyl group, the electron density of the hydrogen atom at α-carbon becomes negative, and the hydride ion transfers to the positively-charged carbon atom of aldehyde or oxide. Therefore, a strong base is favorable. In the case of propylene oxide adsorbed on a weak acid site, 1-propanol is formed preferentially, as the electron density of α-carbon is smaller than that of β-carbon.[11]

However, in the cases of metal oxides which have only very weak acid sites, it may be considered that the interaction between the acid site and the oxygen atom of the hydrogen acceptor is negligible.

Conclusion

Propylene-oxide isomerization was carried out over silica-magnesia catalysts and metal oxides at 260—270°C using a pulse reactor. It has been concluded that propionaldehyde and acetone are produced on acidic and basic sites respectively. Considerable amounts of 1-propanol are formed on these catalysts, whereas it is not produced on metal phosphates and zeolites. Allyl alcohol is formed by acid-base bifunctional catalysts. It has been found that 1-propanol is mainly produced through the hydrogen-transfer reactions between allyl alcohol and propionaldehyde and propylene oxide. It has also been made clear that acid-base bifunctional catalysts are favorable for the hydrogen-transfer reactions and that the reaction rate depends on the electron-donating power of the hydrogen acceptor and also on the basic strength of the catalyst.

The production mechanisms of the acidic and basic properties of silica–magnesia catalysts were studied by X-ray analysis. The acid site is due to forsterite, while the basic site is due to the magnesium oxide remaining. In view of their reaction products, the metal oxides, such as magnesium and calcium oxides, are considered to have very weak acid sites.

11) K. Shimizu, K. Kato, and T. Yonezawa, 20th Annual Meeting of the Chemical Society of Japan (1967).

An Electron Spin Resonance Study of the Steroid Conformation — 6-Oxohelvolic Acid (Triketone) —

Takiko FUJISAWA, Shigenobu OKUDA,* and Yuzaburo FUJITA

Faculty of Pharmaceutical Sciences, The University of Tokyo, Hongo, Bunkyo-ku, Tokyo
**Institute of Microbiology, The University of Tokyo, Yayoi, Bunkyo-ku, Tokyo*

(Received March 30, 1972)

The triketone (6-oxohelvolic acid (IIa) or its tetrahydro-derivative (IIb)) was readily oxidized in air into the anhydride (IIIa or b) in an alkaline solution; it spontaneously turned red or deep green and then gradually lost its color. In this reaction process, the presence of a relatively stable intermediate radical was confirmed by the ESR measurement. As a result of an analysis of the well-resolved proton hyperfine structure of this radical, it was explained that the structure of helvolic acid is of the protostane type: that is, it is a distinctive structure of the *trans*-fusion of the A/B ring juncture and a boat form of the B-ring. A reasonable oxidation mechanism including this intermediate radical was presented.

In general, the physical methods of ORD or CD, NMR, and X-ray diffraction are widely used in conformational analyses of steroids; much valuable information has been thus obtained, as is illustrated in the textbook.[1]

However, although the most exact structural information can be derived from an X-ray analysis, provided that the steroid is obtained in a single crystal form, such an analysis can not tell us about delicate conformational changes in steroids in various solvents. Such information is, though, important for the study of stereochemical reaction processes.

On the other hand, ORD or CD is especially useful for the elucidation of the stereoconformations of steroids or terpenes in solutions. However, even in these cases, the determination has to be done in comparison with compounds of a close structure or of a known absolute configuration.

Apart from these methods, the proton NMR spectroscopy is a powerful method for use in the stereochemistry of steroids, and recent advances in this field, for example, the double-resonance method and high-field resonance method (100 MHz or higher frequency), provide valuable information on the absolute configurations of steroids.

The application of the ESR method to the study of the conformations of macromolecules is rather limited in the field of the stereochemistry of steroids because of necessity for an unpaired electron spin in the molecules. The "spin-labeling" method developed by McConnell *et al.*,[2] which involves attaching a stable simple radical (generally an *N*-oxide radical) on a macromolecule and detecting the subsequent delicate environmental conformational change around the labeled spin, has been proved to be a powerful tool for the study of biomolecules,[2] such as haemoglobin, DNA, and cell membranes. From a slightly different point of view, Russell *et al.*[3] have studied the conformations of various steroids, changing them into "semidione" radicals and treating them with *t*-BuOK in air; they have thus been able to classify the reactivities of $-CH_2$ groups neighboring a carbonyl or hydroxyl group. This method also informs us about the dynamic characters of ring inversion under various environmental conditions.

We are interested in the application of ESR to the stereoconformational studies of steroids, by making use of the extra-high sensitivity (10^{11} spins/gauss) of the ESR method and sensitive changes in hf splittings depending on the slight conformational change in the spin environment.

Helvolic acid (I), one of antibiotics first isolated from *Asperigillus fumigatus* by Waksman *et al.*,[4] has a growth-retarding effect on Gram-positive bacteria. Later, Okuda *et al.*[5] found that *Cephalosporium caerulenes* produced it in a much better yield than did *A. fumigatus*, and that this compound had a unique skeleton (protostane type)[6] of tetracyclic triterpenoid, in which the B-ring had a boat form. That is, this compound has a *trans*-syn-*trans* juncture in the A/B/C rings, unlike the *trans*-anti-*trans* juncture in usual steroids and triterpenoids. A revised absolute configuration has recently been presented based on extensive stereochemical and NMR studies of helvolic acid and its relatives.[7] In the course of this investigation, Inoue, Machida, and Okuda[8] have found that 6-oxohelvolic acid (IIa) or 1,2,24,25-tetrahydro-6-oxohelvolic acid (IIb) is very sensitive to oxygen in an alkaline solution, turning red or deep green respectively, gradually losing its color, and ultimately oxidizing into the anhydride (IIIa or b). These results, indicating a radical mechanism of the oxidation process, have prompted us to search for the presence of a relatively stable intermediate radical by making ESR measurements.

1) L. F. Fieser and M. Fieser, "Steroids," Reinhold Publishing Corp., New York, (1959); J. R. Hanson, "Introduction to Steroid Chemistry," Pergamon Press, London, (1967).

2) H. M. McConnell and B. G. McFarland, "Physics and Chemistry of Spin Labels," *Quart. Rev. Biophys.*, **3**, I (1970), pp. 91—136; O. H. Griffith and A. S. Waggoner, *Accounts Chem. Res.*, **2**, 17 (1969).

3) E. R. Talaty and G. A. Russell, *J. Amer. Chem. Soc.*, **87**, 4867 (1965); *J. Org. Chem.*, **31**, 3455 (1966).

4) S. A. Waksman, E. S. Horning, and E. L. Spencer, *J. Bacteriology*, **45**, 233 (1943).

5) S. Okuda, S. Iwasaki, M. I. Sair, Y. Machida, A. Inoue, and K. Tsuda, *Tetrahedron Lett.*, **1967**, 2295.

6) As this skeleton is considered to be that of the prototype of sterol, the name protostane was proposed for the skeleton. T. Hattori, H. Igarashi, S. Iwasaki, and S. Okuda, *Tetrahedron Lett.*, **1969**, 1023.

7) S. Iwasaki, M. I. Sair, H. Igarashi, and S. Okuda, *Chem. Commun.*, **1970**, 1119.

8) To be published in *Chem. Pharm. Bull.* (Tokyo).

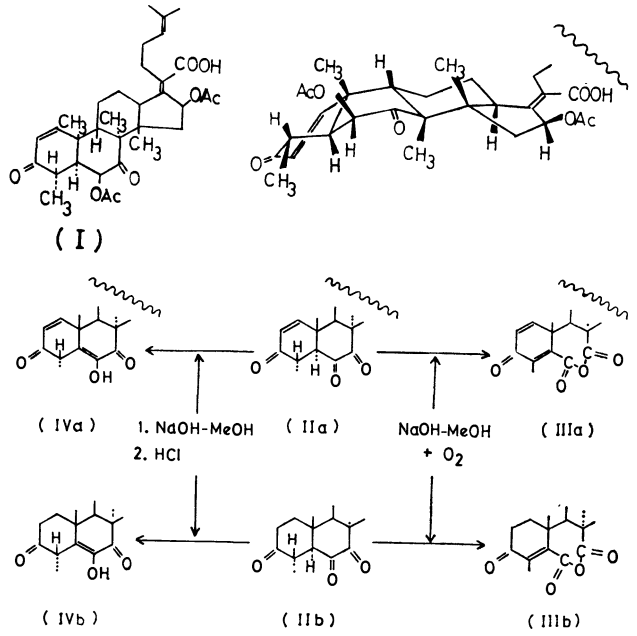

In this report, we will present some ESR results on the conformations of the triketone radicals—in other words, on that of helvolic acid.

Experimental

Materials. The triketones, IIa and IIb, were synthesized from helvolic acid in the laboratory of professor Okuda. The other reagents used were all of a G. R. grade.

Methods. ESR measurements were carried out at room temperature using a JEOL P-10 apparatus (Japan Electron Optics Laboratory Co., Ltd.) at the X-band and 100 KHz field modulation. The field calibration was made with reference to a standard sample of Mn^{2+}/MgO and a solution of Fremy's salt.

For the detection of an intermediate radical by the ESR method, an ESR sample tube with two compartments and a capillary tube was used in order to degas, introduce oxygen, mix the two solutions, and measure the ESR spectrum of the solution at room temperature.

Since an alkaline solution of the triketone is unstable toward oxygen, two separate solutions, one a neutral methanol solution of triketone and the other methanol containing KOH, were degassed thoroughly in each compartment attached to the sample tube by repeating the freeze-degas-thaw cycle; then the two solutions were mixed in one of the compartments at room temperature, followed by the introduction of an appropriate amount of oxygen. For the ESR measurements, a small amount of the colored solution was transferred into the capillary part of the sample tube, which was then inserted into the effective part of the microwave cavity.

The oxygen absorption kinetics were studied with a Warburg manometer.

Results and Discussion

It was confirmed that the two triketones, IIa and IIb, were very unstable toward oxygen in alkaline solutions, and were oxidized into the corresponding anhydrides, IIIa and IIIb. The molecular structures of the anhydrides were explained by the results of the UV, IR, and NMR measurements.[8] After a methanol solution of the triketone had been flushed with nitrogen and then made alkaline with 1 N NaOH, the color of the solution instantaneously changed from yellow to deep green or red in the case of IIb or IIa respectively. On the neutralization of this solution with HCl, the color of the solution returned again to yellow; enolized IIa (IVa) or its tetrahydro-derivative (IVb) was thus obtained in the yield of 100%.

It was found by Warburg's manometry that the amount of oxygen necessary to oxidize the triketone to its anhydride was one mole for one mole of triketone.

ESR experiments were carried out at room temperature, changing the concentration of the triketone in the range of 10^{-1}—10^{-3}M, and the concentration of alkali in the range of 1—1/100N.

According to the concentration of hydroxide relative to that of the triketone, various types of ESR spectra, A, B, C, D, and E (E'), with well-resolved hf structures and the *g*-factor of 2.004_3 were observed as is shown in Fig. 1. These spectra were fairly stable provided the amount of oxygen was not in excess, and they persisted even after one day.

With an increase in the hydroxide concentration relative to that of triketone, the ESR spectra were observed in the order of A, B, C, D, and E spectra for tetrahydro-triketone. For example, the mixed solution of 0.3 ml of 10^{-1}M tetrahydro-triketone in acetone, 0.05 ml of 2N NaOH, and 0.2 ml H_2O exhibited the D spectrum. After the observation of this spectrum, an appropriate amount of water was added, little by little, into the sample solution, and then the spectral type changed successively from D to C, to B, and finally to A. On the other hand, in the case of Δ^1-triketone, only the E' spectrum was observed in a low hydroxide concentration. A distinct difference between the E and E' spectra is that the latter has a well-resolved quartet hf structure in addition to that of the E spectrum.

Table 1. Hf splitting constants of triketone radicals (in gauss)

Signal	No. of Lines	a_1(1H)[a]	a_2(2H)[a]	a_3(3H)[a]	a_4(3H)[a]
A	15	6.1	3.7	1.2	—
B	16	6.0	3.8	1.2	—
C	18	5.8	4.0	1.1	—
D	14	5.5	4.0	1.3	—
E	13	4.1	4.0	1.3	—
E'[b]	43	4.0	4.0	1.2	0.4

a) Numbers of equivalent protons.
b) Observed only for Δ^1-triketone.

All the spectra were analyzed; the respective stick diagrams are shown below the spectra in Fig.1. The hyperfine constants of each spectrum are tabulated in Table 1. Some of the computer-simulated spectra are also shown in Fig. 2.

It is obvious that these hf structures are attributable to certain protons in these radical structures, since the proton is the only nuclear species to show the hf structure. As can easily be seen from the splitting constants in Table 1, the finding that the observed spectral patterns changed in a delicate manner with an increase

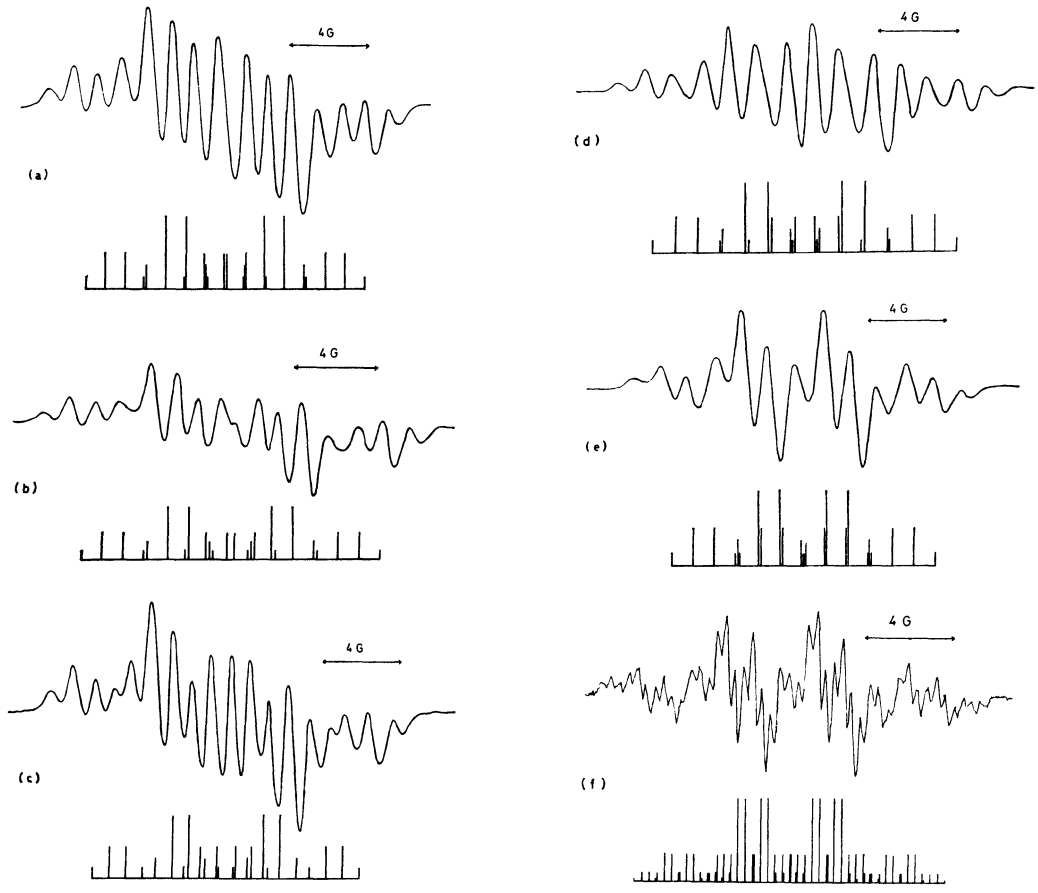

(a) A spectrum:
5 mg tetrahydro-triketone + 0.4 ml A solution

A solution		
	acetone	30 ml
	2N NaOH in H_2O	5 ml
	H_2O	20 ml

(b) B spectrum:
5 mg tetrahydro-triketone + 0.4 ml B solution

B solution		
	acetone	30 ml
	2N NaOH in H_2O	5 ml
	H_2O	13 ml

(c) C spectrum:
5 ml tetrahydro-triketone + 0.4 ml C solution

C solution		
	acetone	30 ml
	2N NaOH in H_2O	5 ml
	H_2O	6 ml

(d) D spectrum:
5 mg tetrahydro-triketone + 0.4 ml D solution

D solution		
	acetone	30 ml
	2N NaOH in H_2O	5 ml
	H_2O	0 ml

(e) E spectrum:
0.3 ml of 10^{-2}M tetrahydro-triketone in 99% methanol + 0.3 ml of 0.3N KOH in 99% methanol

(f) E′ spectrum:
0.3 ml of 10^{-2}M Δ^1-triketone in 99% methanol + 0.3 ml of 0.03—0.3N KOH in 99% methanol

All the spectra were recorded at room temperature under the following operation condition; microwave power 3 mW, modulation width 0.05—0.3 G.

Fig. 1. ESR spectra of the triketone radical.

in the hydroxide concentration is due to a gradual decrease in the largest hf constant, a_1, down to the value of the second hf constant, a_2, while the third hf constant, a_3, remains nearly constant throughout, from the A spectrum to the E spectrum. On the other hand, in the E′ spectrum of the Δ^1-triketone radical, the hf splitting constants, a_1 and a_2, are already equal in a rather low concentration of hydroxide ions compared with the case of tetrahydro-triketone, and it has the smallest quartet hf splitting, a_4=0.4 G.

These spectral patterns were observed not only with the oxidation by molecular oxygen, but also with that by H_2O_2 or $Fe(CN)_6^{3-}$, and no change in the spectral patterns was observed even in the H_2O (D_2O), MeOH (MeOD), acetone, and DMSO solvents. From these results, it can be considered that the radical may be an ion-type radical produced by the one-electron oxidation of the triketones.

It is reasonable to consider that the radical has a structure spin-localized in the B-ring rather than in the A-ring, because essentially similar spectral patterns, E and E′, were observed with both triketones. Accordingly, the protons at the 1- and 2-positions are not responsible for the observed hf structure.

The proton at the 5-position is so labile that it is easily detached by enolization in an alkaline solution, as is confirmed by the finding that IVa or IVb is obtained in a full yield by alkalization and subsequent neutralization in the absence of oxygen. With regard to this nature of the 5α-H and the finding that no apparent change in the spectral pattern was observed in a CH_3OD or D_2O containing solvent, it can rea-

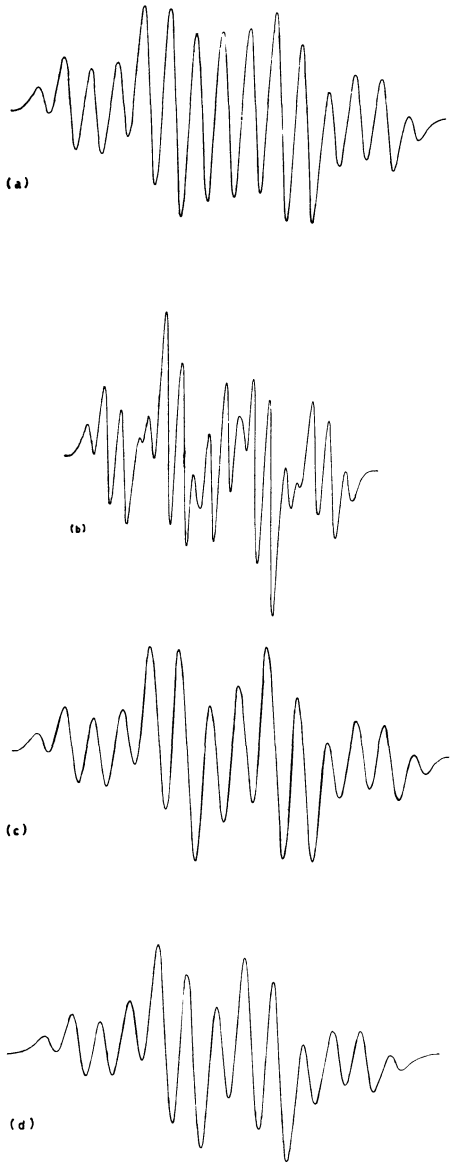

Fig. 2. Computer-simulated spectra of the triketone radical.
(a): A spectrum, (b): C spectrum, (c): D spectrum,
(d): E spectrum

sonably be concluded that this proton does not contribute to the hf structure either.

At first sight, it can easily be seen in Table 1 that each hf splitting constant makes two or three pairs of three equivalent protons, at least in the E and E′ spectra. This probably indicates that each hf splitting is due to a certain methyl group in the A- or B-ring.

Let us consider which methyl group causes the corresponding hf splitting.

The enolization processes for Δ^1- or tetrahydrotriketone with an increase in the hydroxide concentration may be ascribed to the group shown in Fig. 3, in view of the degrees of stabilization by π-conjugation, the relative enolizabilities of protons at various positions, and the structures of the final oxidation products.

Canonical structures of reliable radical species produced by one-electron oxidation at each step are shown in the brackets. The spin density in these radicals is thought to be mainly localized at the carbon atom of the 5-position. The fact that the observed g-factor,

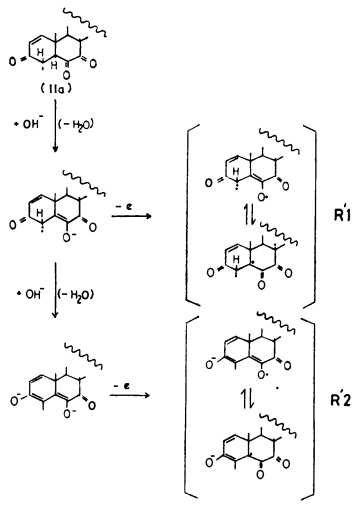

Fig. 3. Enolization processes for Δ^1-triketone and canonical structures of reliable radical species produced by one-electron oxidation.

$g=2.004_3$, is slightly larger than that of the free spin, $g_e=2.0023$, but much smaller than the empirical values of organic peroxy radicals,[9] $g_{av}=2.015$, is reasonably consistent with the envisaged radical structures.

It can easily be visualized, by means of the molecular models of the triketone radicals constructed on the basis of the confirmed *trans*-syn-*trans* juncture in

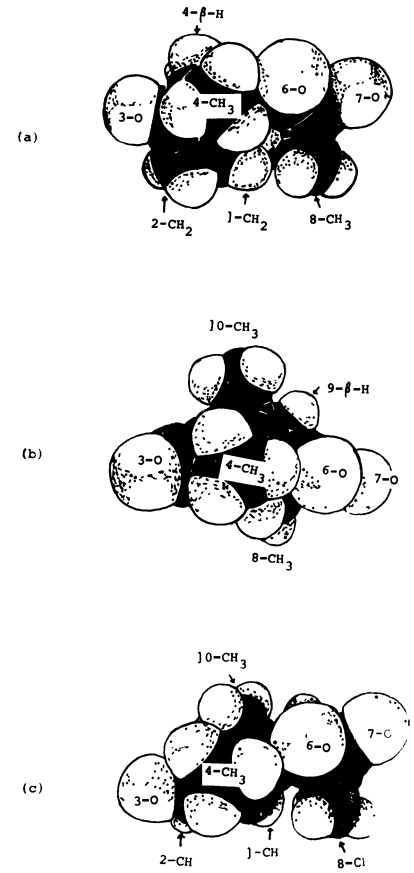

Fig. 4. Molecular models of the triketone radicals.
(a): R 1 radical, (b): R 2 radical, (c): R′ 2 radical

9) M. Bersohn and J. R. Thomas, *J. Amer. Chem. Soc.*, **86**, 959 (1964); K. U. Ingold and J. R. Morton, *ibid.*, **86**, 3400 (1964).

the A/B/C rings of helvolic acid (or triketone), that the rotational motion of a certain methyl group in the triketone radicals is significantly affected with the progress of the step-by-step enolization of the 5α-H and 4β-H. Let us denote the radicals as R1 and R2 for the tetrahydro-triketone radicals, and as R'1 and R'2 for the Δ^1-triketone radicals which are produced by the one-electron oxidation at each enolization step. Molecular models of the R1, R2, and R'2 are shown in Figs. 4a, b, and c respectively.

First, the structure of the tetrahydro-triketone radical is discussed. In the structure of the R1 radical, the free rotation of the 4-CH_3 group is partly hindered by the steric hindrance due to the bulky oxygen atom at the 6-position; that of the 8-CH_3 is also hindered by the 1-CH_2 as is shown in Fig. 4a. On the other hand, it can be seen that the 10-CH_3 group, floating above the molecular plane, rotates freely notwithstanding a degree of enolization (this is also the case with the Δ^1-triketone radical). In the R2 radical, the 4-CH_3 is able to rotate freely, since the proton at the 4-position is removed, extending the π-conjugation and increasing the planarity of the A-ring with the progress of enolization. This situation is clearly shown in Fig. 4b. However, the steric hindrance upon the 8-CH_3 due to the 1-CH_2 can not be removed in spite of further enolization. This is comprehensible from the fact that the 8-position, being apart from the π-conjugation around the 3, 4, and 5-positions, is buried in the rigid structure of the molecules. It goes without saying that the 10-CH_3 is free to rotate.

Next, let us proceed to the structure of the Δ^1-triketone radical. In this radical, the planarity of the A-ring is large compared with that of the tetrahydro-triketone radical because of the presence of a double bond between the 1-C and 2-C atoms. Moreover, in accordance with the methine group, =CH–, at the 1-position in place of the $-CH_2-$ group of the tetrahydro-triketone, there is no steric hindrance between the 8-CH_3 and the 1-CH before the enolization.

At the second step of the enolization, the free rotation of the 4-CH_3 group, which is partly hindered in the first step, becomes possible, as in the case of the tetrahydro-triketone radical.

It should be stressed here that a large spectral red-shift in an alkaline solution was observed for Δ^1-triketone compared with tetrahydro-triketone, and that only one ESR spectrum was observed in the former. This result may indicate that the former is further subjected to the second step of the enolization under similar conditions, as can easily be understood from the structure of its ready π-conjugation.

It may thus be considered that the observed E' spectrum corresponds to the R'2 radical, and that the smallest hf splitting constant of this radical can reasonably be assigned to the equivalent three protons of the 8-CH_3, since this hf splitting is observable only in the Δ^1-triketone radical. This is in accordance with the free rotation of this group; otherwise, such a small hf splitting might be obscured by the line-broadening due to hindered rotation, as is the case of the tetrahydro-triketone radical.

As to the third hf splitting constant, a_3=1.2 G, observed commonly throughout the spectra, A, B, C, D, E, and E', it is safe to assign this to the 10-CH_3 group.

The above two assignments are reasonable in view of configuration of the spin-localization in the radicals.

The remaining assignments for the hf splitting constants of a_1 and a_2 are not so simple, because the hf splitting constant, a_1, gradually decreases from the 6.1 G of the A spectrum to the 4.1 G of the E spectrum, while, on the other hand, the a_2 value increases slightly from the 3.7 G of the A spectrum to the 4.0 G of the E spectrum. Since the 4β-H and 4α-CH_3 are close to the 5-position, where an unpaired electron is localized, and are common for both triketones, these protons can be expected to exhibit rather large hf splittings.

At the first enolization step, the rotation of the 4α-CH_3 group is so restricted that the protons in this group are not magnetically equivalent because of the steric hindrance and also partly because of a weak interaction, probably a hydrogen-bond-like one between the oxygen atom at the 6-position and two of the three protons of the 4α-CH_3 group; such a configuration is also supported by the similar interaction between the oxygen atom at the 3-position and the remaining proton of the methyl group. In such a configuration, one of the three protons of the methyl group is nearly equatorial, while the others are axial, to the plane of the A-ring. Therefore, the latter two protons may contribute equivalently to a hf splitting, while the former does not.

One can expect a larger hf splitting due to the 4β-H than that due to the 4α-CH_3, since the 4β-H is axial to the plane and is located closer to the 5-position of spin-localization. The variation in the hf splitting constant, a_1, during the first enolization process may be explained by a delicate change in the angle between the $2p_z$ axis of the 5-carbon atom and the C–H axis of the 4β-H.

At the final step of the enolization process, the 4β-H is removed, leaving the 4-CH_3 at the 4-position; correspondingly, in their ESR spectral patterns, the observed hf splitting becomes the one due to three equivalent protons—that is, a_1 (one proton)=4.1 G≒ a_2 (two protons)=4.0 G. Thus, the three protons of the 4-CH_3 group can be attributed to the equivalent observed hf structure of the E or E' spectrum.

The above discussions are entirely based on the *trans*-syn-*trans* juncture in the A/B/C rings of helvolic acid; thereby, the hf splittings of the intermediate radicals are all reasonably explained. In other words, this result supports the conformation of helvolic acid, which has also been confirmed by other methods. The possibility of the epimerization of the A/B ring juncture during the oxidation reaction can reasonably be rejected on the basis of an analysis of the ESR spectra of the radicals; that is, such a conformational change obviously is not consistent with the observed hf splittings.

As has been described above, in the oxidation process of tetrahydro-triketone, the presence of an intermediate radical, R1 or R2, depending on the hydroxide

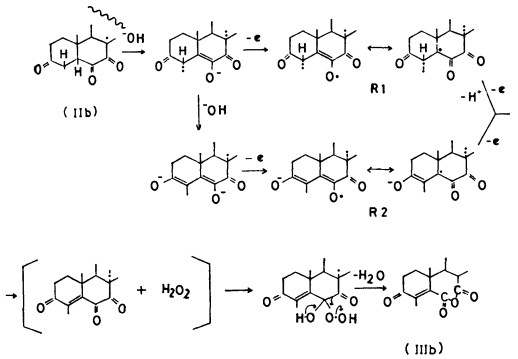

Fig. 5. The oxidation mechanism of the triketone to the anhydride.

concentration, has been confirmed by the ESR measurements, while, in the case of Δ^1-triketone, only the R'2 radical has been detected even in a rather low bydroxide concentration range. Therefore, the oxidation mechanism of the triketone to the corresponding anhydride *via* an intermediate radical may be shown as Fig. 5. In the case of tetrahydro-triketone, the reaction proceeds: IIb→R1→IIIb or IIb→R2→IIIb, depending on the hydroxide concentration. On the other hand, for Δ^1-triketone, only the way of IIa→R'2→IIIa is available independent of the hydroxide concentration, as can easily be understood from the above discussion.

Since the intermediate product, Int., has not been isolated in the present work, the rate-determining step is considered to be the one of its formation. The oxidation of the intermediate, thereafter, proceeds rapidly by the reaction with H_2O_2, which is formed in the preceding oxidation processes:

$$\left.\begin{array}{l}\text{the first one-electron oxidation step: } O_2+e=O_2^- \\ \text{the second one-electron oxidation step: } O_2+e=O_2^-\end{array}\right\} \xrightarrow{+2H^+} 2HO_2 \longrightarrow H_2O_2 + O_2$$

The oxidation of ketones with H_2O_2, leading to the insertion of an oxygen atom into a steroid nucleus, is well known in steroid chemistry.[10]

The above oxidation mechanism accords well with the experimental findings that one mole of oxygen was consumed in the oxidation of the triketone to the anhydride, and that a trace of hydrogen peroxide was detected in the final oxidation products.

10) C. Djerassi, "Steroid Reactions," Holden-Day, Inc., San Francisco, (1963), pp. 457—535.

BULLETIN OF THE CHEMICAL SOCIETY OF JAPAN, VOL. 46, 14—16 (1973)

Ion-Solvent Interaction of Tetraalkylammonium Ions in Solvents of High Dielectric Constant. III. Conductance and Walden Product of Some Partially Substituted Alkylammonium Ions in *N*-Methylacetamide and *N*-Methylpropionamide at Different Temperatures

Raj Deo SINGH

Department of Chemistry, Lucknow University, Lucknow, India

(Received March 8, 1972)

Ion-solvent interaction of some partially substituted alkylammonium ions in *N*-methylacetamide (NMA) and *N*-methylpropionamide (NMP) has been investigated from the point of view of electrical conductance and the derived Walden product. From the results, it seems that like tetraalkylammonium (R_4N^+) ions, Me_3NH^+ and $CeMe_3N^+$ ions are structure breakers in these solvents while Me_3PhN^+ ion is neither structure breaker nor structure maker.

In previous communications,[1,2] ion-solvent interaction of some symmetrically substituted tetraalkylammonium (R_4N^+) ions in NMF, NMA, and NMP has been investigated from the conductance data. It would be interesting to investigate how the partial and unsymmetrical substitution in the NH_4^+ ion will affect the nature of the ion-solvent interaction in these solvents. With this aim in view, the conductances of some available such salts namely, Me_3NHI, Me_3PhNI, and $CeMe_3NBr$ in NMA and NMP at different temperatures have been reported in the present communication and the data have been used to throw light on the mode of ion-solvent interaction.

Experimental

Trimethylammonium iodide (Me_3NHI), trimethylphenylammonium iodide (Me_3PhNI) and cetyltrimethylammonium bromide ($CeMe_3NBr$), obtained from B.D.H., were purified as follows:

Me_3NHI and Me_3PhNI were recrystallized twice from a mixture of methanol and ether (3:1). The salts were dried in a vacuum desiccator.

$CeMe_3NBr$ was dissolved in methanol and precipitated

1) R. D. Singh, P. P. Rastogi, and R. Gopal, *Can. J. Chem.*, **46**, 3525 (1968).

2) R. D. Singh and R. Gopal, This Bulletin, **45**, 2088 (1972).

with ether. The precipitated salt was dried in a vacuum desiccator.

NMA and NMP were purified in the manner given elsewhere.[1,2] The purified samples were stored in dark amber-coloured bottles in a dry nitrogen box and were used, as far as possible, the day after distillation. Although the solvents appeared to be quite stable, solvent correction was applied in determining the conductances of solutions. The rest of the experimental procedure and the degree of reliability of the apparatus were the same as those given in the previous communications on NMF, NMA, and NMP.

Results and discussion

Within the concentration (0.0005M to 0.02M) and temperature (30° to 55°) ranges studied here, the plots of equivalent conductance Λ and $\sqrt{c}$ were found to be almost straight lines for all the salts in NMA and NMP. It appears, therefore, that these salts are completely dissociated in NMA and NMP as has been reported by earlier workers.[3-7] Extrapolation of Λ *vs.* $\sqrt{c}$ curves to zero concentration leads to Λ_0-values given in Table 1. From these Λ_0-values, the ionic conductances λ_0^+ of the cations at different temperatures were obtained, using the appropriate transport number data already reported in literature;[8] these λ_0^+-values are given in Table 1.

Table 1. Limiting equivalent conductance in NMA and NMP at different temperatures

Salt and cation	Limiting equivalent conductance at					
	30°C	35°C	40°C	45°C	50°C	55°C
			NMA			
Me_3NHI	...	25.15	27.68	31.11	34.26	37.00
Me_3NH^+	...	11.73	13.01	14.92	16.52	17.80
Me_3PhNI	...	22.40	24.89	27.95	30.50	33.05
Me_3PhN^+	...	8.98	10.22	11.36	12.76	13.85
$CeMe_3NBr$	...	19.89	21.88	24.41	26.64	28.96
$CeMe_3N^+$	...	8.17	9.01	9.54	10.90	11.90
			NMP			
Me_3NHI	15.15	17.03	19.09	21.17	23.65	...
Me_3NH^+	6.81	7.68	8.64	9.62	10.71	...
Me_3PhNI	14.50	16.50	18.47	20.60	22.90	...
Me_3PhN^+	6.16	7.15	8.02	9.05	9.90	...
$CeMe_3NBr$	12.73	14.43	16.16	18.09	19.83	...
$CeMe_3N^+$	5.69	6.38	7.21	8.04	8.79	...

The applicability of limiting Debye-Hückel-Onsager conductance equation to solutions under study was examined. The conductance equation for 1:1 electrolyte can be written in the form

$$\Lambda = \Lambda_0 - \left[\frac{82.42}{(\epsilon T)^{1/2}\eta_0} + \frac{8.203\times 10^5}{(\epsilon T)^{3/2}}\Lambda_0\right]\sqrt{c}$$

which simplifies to

$$\Lambda = \Lambda_0 - (A + B\Lambda_0)\sqrt{c} = \Lambda_0 - S_T\sqrt{c}$$

for a constant temperature. The values of A and B are

$$A = \frac{82.42}{(\epsilon T)^{1/2}\eta_0},\quad B = \frac{8.203\times 10^5}{(\epsilon T)^{3/2}}$$

and the theoretical slope $S_T = (A + B\Lambda_0)$.

From Λ_0-values and other appopriate data on dielectric constant[7,9] and on viscosity η_0 (determined in this laboratory,[1,2]) the theoretical slopes S_T of the Λ *vs.* $\sqrt{c}$ curves have been obtained and are given in Table 2 at one temperature (40°C) only.

Table 2. Onsager slopes in NMA and NMP at 40°C

Salt	Theoretical slope (S_T)	Experimental slope (S_E)	% Deviation $\left(\frac{S_E - S_T}{S_T}\times 100\right)$
		NMA	
Me_3NHI	−13.9	−15.6	12
Me_3PhNI	−13.7	−15.8	15
$CeMe_3NBr$	−13.5	−15.4	14
		NMP	
Me_3NHI	−12.1	−13.2	9
Me_3PhNI	−12.1	−13.4	11
$CeMe_3NBr$	−11.0	−13.3	12

It may be noted from Table 2 that the experimental slopes S_E of the Onsager plots for these salts in the two solvents, are numerically greater than the theoretical slopes S_T. In view of the high dielectric constant of these solvents, incomplete dissociation of the salts in the usual sense is unthinkable, although Dawson and coworkers[3,5,6] have tried to explain the conductance results in NMA and NMP on this ground. As discussed in previous communication,[2] these deviations may be ascribed to the penetration[10-13] of cations by anions causing a sort of association[14] or to the greater resistance offered to the movement of the cations by solvent molecules, than that caused by viscosity of the solvent medium, so that the movement of the cations is more sluggish than expected from the theory.

The Walden products of the partially substituted alkylammonium ions at different temperatures have been calculated from the appropriate λ_0^+-values (given in Table 1) and viscosity data. From the cationic Walden product data, thus obtained, $\lambda_0^+\eta_0$ *vs.* temperature curves have been drawn and are given in Figs. 1 and 2.

It is obvious from the curves that like those of symmetrical tetraalkylammonium (R_4N^+) ions, the Walden product of Me_3NH^+ and $CeMe_3N^+$ ions in these amides decreases with the rise of temperature while for Me_3PhN^+ ion, it is approximately constant. The decrease in

3) L. R. Dawson, P. G. Sears, and E. D. Wilhoit, *J. Amer. Chem. Soc.*, **78**, 1569 (1956).
4) C. M. French and K. H. Glover, *Trans. Faraday Soc.*, **51**, 1428 (1955).
5) L. R. Dawson, E. D. Wilhoit, R. R. Holmes, and P. G. Sears, *J. Amer. Chem. Soc.*, **79**, 3004 (1957).
6) L. R. Dawson, R. H. Graves, and P. G. Sears, *ibid.*, **79**, 298 (1957).
7) T. B. Hoover, *J. Phys. Chem.*, **68**, 876 (1964).
8) R. Gopal and O. N. Bhatnagar, *ibid.*, **69**, 2382 (1965), **70**, 4070 (1966).
9) G. R. Leader and J. F. Gormley, *J. Amer. Chem. Soc.*, **73**, 5731 (1951).
10) W. Y. Wen and S. Saito, *J. Phys. Chem.*, **68**, 2639 (1964).
11) B. E. Conway, R. E. Verrall, and J. E. Desnoyers, *Trans. Faraday Soc.*, **62**, 2738 (1966).
12) R. Gopal and M. A. Siddiqui, *J. Phys. Chem.*, **72**, 1814 (1968), *ibid.*, **73**, 3390 (1969), *Z. Phys. Chem.*, **67**, 122 (1969).
13) R. Gopal and K. Singh, *ibid.*, **69**, 81 (1970).
14) S. R. C. Hughes and D. H. Price, *J. Chem. Soc., A*, **1967**, 1093.

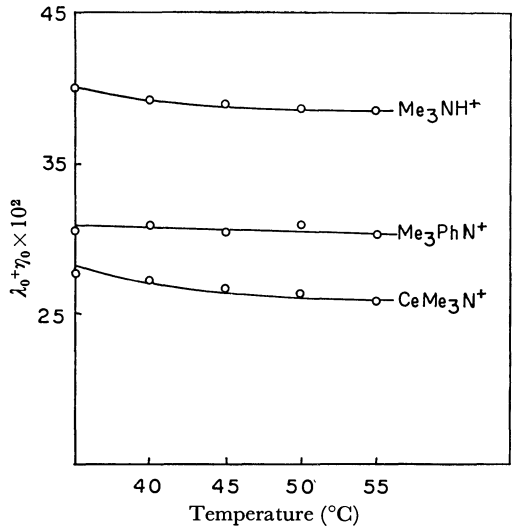

Fig. 1. Plot of $\lambda_0^+\eta_0$ *vs.* T in NMA

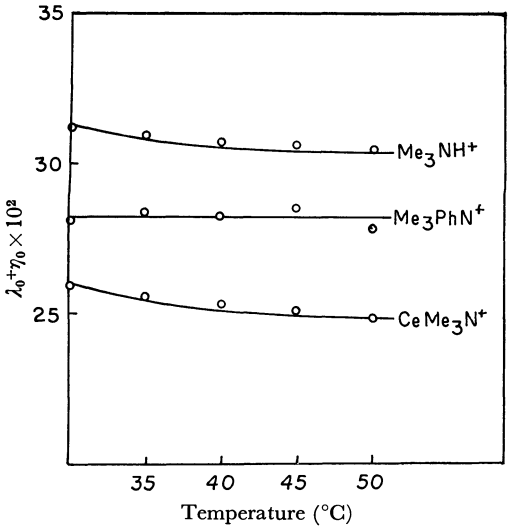

Fig. 2. Plot of $\lambda_0^+\eta_0$ *vs.* T in NMP

$\lambda_0^+\eta_0$ values of Me_3NH^+ and $CeMe_3N^+$ ions with the rise of temperature can be explained on the similar grounds as for R_4N^+ ions *i.e.*, electrostatic solvation and resultant breaking-up of the structure of the solvent medium occurs around the ions. The partially substituted alkylammonium ions, being similar to NMA and NMP in having the alkyl groups, do not promote the structure of the solvent[15] *i.e.*, "structure promotion" or "lyophobic solvation" is missing in these solvents in the presence of these ions. Further, although these ions are large which would reduce ion-solvent interaction, the large dipole moment[16] of the solvent molecule makes up for the large size of the ions so that an appreciable ion-solvent interaction would occur. Thus, there appears a net structure breaking[17] in the presence of the partially and mixed alkyl substituted ammonium ions because the electrostatic ion-solvent interaction would be stronger than the interaction between the solvent molecules themselves.

The approximate constancy of the Walden product of the Me_3PhN^+ ion indicates that this ion has, apparently no net effect on the structure of the solvents although it is rather unexpected since the $CeMe_3N^+$ ion which is quite large, appears to be a structure breaker. It may be that, due to the bulky phenyl group which may shield the positive charge on the nitrogen atom from the influence of the solvent dipole, the ion-solvent intraction is weak as is the case with the larger R_4N^+ ions in these solvents.[1,2]

Although it is rather unsafe to make any generalisation in view of the restricted number of salts studied, it appears that unsymmetrical and partially substituted ammonium ions, in general, behave similarly in NMA and NMP; also their behaviour is similar to that of R_4N^+ ions. The author feels the necessity of an extensive study, involving more ions of this type before a definite conclusion can be arrived at.

The author is grateful to Prof. Ram Gopal, Head, Department of Chemistry, Lucknow University, Lucknow, India for providing laboratory facilities and giving valuable suggestions during the course of this investigation. The financial assistance given by the Society of Sigma Xi and RESA of U.S.A., is gratefully acknowledged. The assistance given by C.S.I.R., India has also been valuable.

15) R. Gopal and O. N. Bhatnagar, *J. Indian Chem. Soc.*, **44**, 1082 (1967).
16) J. M. Notley and M. Spiro, *J. Phys. Chem.*, **70**, 1502 (1966).
17) O. D. Bonner, C. F. Jordon, and K. W. Bunzi, *ibid.*, **68**, 2450 (1964).

Dielectric Relaxation and Molecular Structure. III. Dielectric Relaxation Study of Some Anilines in Benzene Solutions at Different Temperatures

J. K. Vij,* Iqbal Krishan, and K. K. Srivastava
Physics Department, Panjab University, Chandigarh, India
(Received February 28, 1972)

Measurements of relative permittivity at 1 MHz and at 9.46 GHz, the refractive index for the Sodium D-line, have been made for (a) *N,N*-dimethylaniline, (b) *N,N*-diethylaniline, (c) *o*-chloroaniline, (d) *m*-chloroaniline and (e) *p*-chloroaniline at temperatures of 15, 25, 35, and 45°C in dilute solutions of benzene. Dielectric relaxation times $\tau(1)$ and $\tau(2)$ have been calculated by the method recently suggested by Higasi, Koga, and Nakamura in terms of the slopes a_0, a', a'', and a_D. It is remarked that $\tau(2)$ at the experimental frequency of 9.46 GHz leads to τ_1, the relaxation time for overall rotation, whereas $\tau(1)$ becomes an explicit function of τ_1 and τ_2. These determinations suggest the presence of both molecular and intramolecular rotations in the molecules. The results for $\tau(2)$ show a systematic decrease with increase in temperature whereas for $\tau(1)$ there seems to be no observable trend. The enthalpy and entropy of activation for molecular dielectric relaxation process has been determined. The enthalpy of activation for (a) and (b) is of the same order of magnitude (*i.e.*, 3 kcal/mol), and the same is true for the case of (d) and (e) (1.8 kcal/mol) but 6.8 kcal/mol for (c). It appears that in *o*-chloroaniline, there is a finite probability of H-Cl bond formation between one of the amino hydrogens and the neighbouring chlorine atom.

This work deals with the dielectric relaxation mechanism of systems with two Debye dispersions. A study on these molecules in different non-polar solvents at various temperatures has been reported.[1] On an examination of the values of $(a_\infty - a_D)$, the authors suggested the possibility of two Debye dispersions in these substances. Chitoku and Higasi[2] studied dimethylaniline in benzene and dioxane solutions at 20°C at three different frequencies in the main dispersion region. Besides giving useful information on the behaviour in two solvents, their results also suggested the presence of two Debye dispersions. Pure dimethylaniline has been studied by Grubb and Smyth,[3] Garg and Smyth[4] and, Srivastava.[5] Though the results differ to some extent, all agree that two dispersions exist in dimethylaniline. Pure diethylaniline was studied by Srivastava.[5] He reported the (Cole–Cole) distribution parameter value to be as high as 0.52/30°C. Recently Tucker and Walker[6] studied *m*- and *p*-chloroanilines at 25°C in dilute solutions of cyclohexane. They gave two dielectric relaxation time values, one for overall dielectric relaxation process and another for intramolecular process. Another remarkable result of their studies is the variation of the weight factor for intramolecular relaxation process with the concentration of the solute.

The present study has two objects. Firstly to get more insight into the nature of dielectric relaxation process, and secondly, since not many molecules of this type have been studied in a non-polar solvent at different temperatures, to get some clue as to their behaviour from the heats of activation for the dielectric relaxation process. For this, the validity of Eyring's equation[7–10] has been taken for granted although its validity is still a matter of debate.

The possibility of getting information on the presence of an intramolecular relaxation mechanism from the data at a single frequency in the dispersion region has been another controversial problem. But recent analysis by Higasi *et al.*,[12] shows that there definitely exists a possibility of estimating either of the two relaxation times. An attempt has therefore been made to use this method for an estimation of the dielectric relaxation time for the overall rotational process. It is pointed out that this method may become an alternative to Bergmann's[13] method for estimating both the dielectric relaxation times, under certain conditions.

Experimental

The liquids are of purity standards. The measurements for determining the relative permittivity at the temperatures of 15, 25, 35, and 45°C have been made by the same techniques. The values of the slopes are calculated from the experimental plots of the data *vs.* weight fraction.[1]

Calculations and Results

The Debye equation[14,15] in terms of a_0, a', a'', and a_∞ yields two independent equations

* Physics Department, Panjabi University, Patiala, India. Presently at Engineering School, Trinity College, Dublin, Ireland.

1) K. K. Srivastava and J. K. Vij, This Bulletin, **43**, 2307 (1970).
2) K. Chitoku and K. Higasi, *ibid.*, **39**, 2160 (1966).
3) E. L. Grubb and C. P. Smyth, *J. Amer. Chem. Soc.*, **83**, 4879 (1961).
4) S. K. Garg and C. P. Smyth, *J. Chem. Phys.*, **46**, 373 (1967).
5) K. K. Srivastava, *J. Phys. Chem.*, **74**, 52 (1970).
6) S. W. Tucker and S. Walker, *Can. J. Chem.*, **47**, 681 (1969).
7) J. G. Powles, *J. Chem. Phys.*, **21**, 633 (1953).
8) H. Eyring, *ibid.*, **4**, 283 (1936).
9) A. E. Stearn and H. Eyring, *ibid.*, **5**, 113 (1937).
10) S. Glasstone, K. J. Laidlar, and H. Eyring, "The Theory of Rate Processes," McGraw-Hill, New York, N. Y. (1941), pp. 544—551.
11) K. Higasi, "Dielectric Relaxation and Molecular Structure," Hokkaido University, Sapporo, Japan (1961) Ch. 11.
12) K. Higasi, Y. Koga, and M. Nakamura, This Bulletin, **44**, 988 (1971).
13) K. Bergmann, Doctoral Dissertation, Freiburg/Breisgav, West Germany, 1957.
14) P. Debye, *Z. Phys.*, **35**, 101 (1934).
15) K. Higasi, This Bulletin, **39**, 2157 (1966).

$$\tau(1)=\frac{a''}{\omega(a'-a_\infty)} \quad (1)$$

$$\tau(2)=\frac{a_0-a'}{\omega a''} \quad (2)$$

where a_0, a', a'', and a_∞ are defined in the linear range by the equations:

$$\epsilon=\epsilon_1+a_0\omega_2$$
$$\epsilon'=\epsilon'_1+a'\omega_2$$
$$\epsilon''=a''\omega_2$$
$$\epsilon_\infty=\epsilon_{1\infty}+a_\infty\omega_2$$

Subscript 1 refers to pure solvent, 2 to solute and ∞ to the values at infinite frequency. ω_2 may be taken as weight fraction of the solute. Having defined; $\tau(1)$ and $\tau(2)$ by Eqs. (1) and (2), Higasi, Koga, and Nakamura[12] have set up the following relations (3) and (4), between $\tau(1)$, $\tau(2)$; τ_1 and τ_2. τ_1 and τ_2 are the dielectric relaxation times for molecular and intramolecular rotations, respectively.

$$\tau(1)=A\tau_2$$

where $$A=\frac{[m-(m-1)C_2]+mx^2[1+(m-1)C_2]}{1+[1+(m^2-1)C_2]x^2} \quad (3)$$

$$m=\frac{\tau_1}{\tau_2},\quad x=\omega\tau_2$$

$$\tau(2)=B\tau_2$$

where $$B=\frac{m^2-(m^2-1)C_2+m^2x^2}{m-(m-1)C_2+mx^2[1+(m-1)C_2]} \quad (4)$$

At the experimental frequency of 9.46 GHz, the value of x (with the preknowledge of the approximate value of τ_2) is of the order of 10^{-1}. One can therefore safely neglect 1 in comparison to m without introducing much error.

Equation (4) is therefore reduced to

$$\tau(2)=\frac{\tau_1}{\tau_2}\cdot\tau_2=\tau_1 \quad (5)$$

Under similar circumstances, Eq. (3) yields

$$\tau(1)=\tau_1(1-C_2)+C_2\tau_2 \quad (6)$$

This shows that the results given by Eq. (2) in our case would correspond to the dielectric relaxation time for overall rotation and those given by Eq. (1) are the implicit functions of τ_1, τ_2, and C_2, the weight factor for intramolecular relaxation mechanism. It should be remarked that since the value given by $\tau(1)$ is a sort of average dielectric relaxation time, a_∞ should be the one corresponding to a_D after a due account for the infrared dispersion (Δa_D) has been made. In the present calculations, Δa_D has been neglected owing to its expected value between 5—10% of a_D which is within the range

Table 1. Values of a_0 (slope of ϵ *vs.* concn. curve), a' (slope of ϵ' *vs.* concn. curve), a'' (slope of ϵ'' *vs.* concn. curve) and a_D (slope of n_D^2 *vs.* concn. curve)

Temp. (°C)	a_0	a'	a''	a_D	Dielectric Relaxation (Time values in ps)		Literature values in ps		
					$\tau(1)$	$\tau(2)=\tau_1$	τ_0	τ_1	τ_2
					N,*N*-Dimethylaniline				
15	2.65	1.73	0.90	0.15	9.6	17.2	14.5[2]/20°C (B)[a]	28.0[4]/20°C (L)	1.5[4] (L)
25	2.54	1.88	0.87	0.17	8.6	12.8	13.7	13.4	—
35	2.41	1.74	0.93	0.18	10.0	12.1			
45	2.30	1.86	0.90	0.17	9.0	8.2			
					N,*N*-Diethylaniline				
15	2.70	1.07	0.84	0.11	14.4	33.7	33.2[2]/20°C		
25	2.48	1.00	0.82	0.12	15.7	30.5	—	32.9[1]	
35	2.27	1.16	0.76	0.13	12.4	24.6			
45	2.08	1.24	0.73	0.14	10.6	19.4			
					o-Chloroanoiline				
15	3.70	2.85	0.94	0.14	5.7	14.9			
25	3.43	2.80	0.90	0.19	5.7	11.5	—	6.5[1]/30°C	
35	3.12	2.77	0.77	0.20	4.9	7.5			
45	2.78	2.57	0.76	0.15	5.2	4.5			
					m-Chloroaniline				
15	6.75	4.20	2.67	0.16	10.9	15.7			
25	6.50	4.12	2.57	0.24	10.9	15.2	12.4[6] (C)	13.2[6] (C)	2[6] (C)
35	6.25	4.36	2.19	0.26	8.8	14.2		13.0[1]/30°C	
45	5.89	4.37	2.07	0.23	8.2	12.1			
					p-Chloroaniline				
15	8.70	5.68	2.81	0.16	8.5	17.6			
25	8.20	5.57	2.85	0.24	8.8	15.2	12.4[6] (C)	15.3[6] (C)	2[6] (C)
35	7.70	5.64	2.61	0.26	8.0	13.0		20.6[1]/30°C	
45	7.10	5.37	2.66	0.23	9.1	11.9			

a) The name of the solvent in which the measurements are made is given in brackets.
B=Benzene, L=Pure liquid and C=Cyclohexane, Benzene where not specified. Temperature: 25°C where not specified.

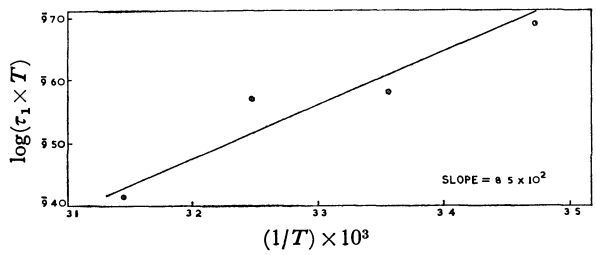

Fig. 1. Dimethylaniline

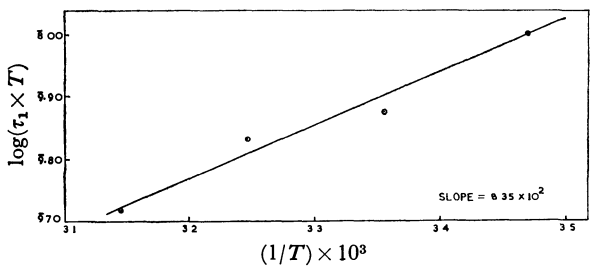

Fig. 2. Diethylaniline.

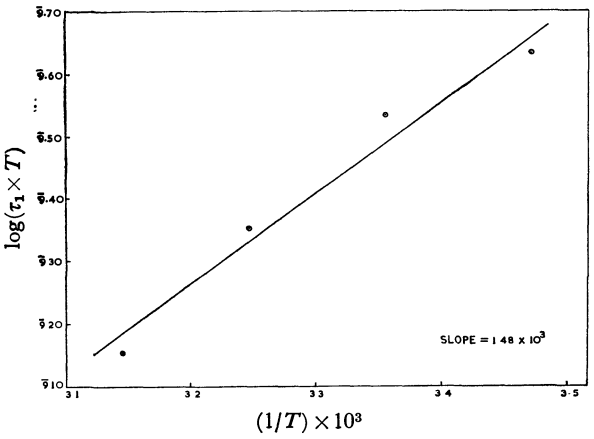

Fig. 3. *o*-Chloroaniline.

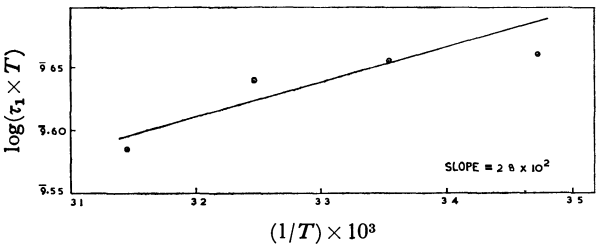

Fig. 4. *m*-Chloroaniline.

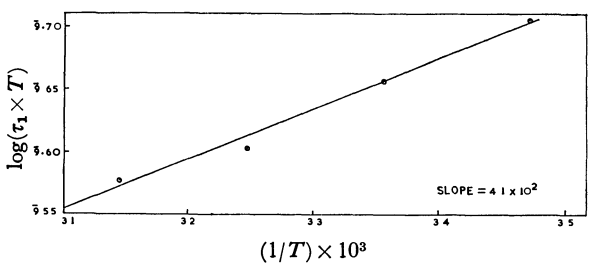

Fig. 5. *p*-Chloroaniline.

of the accuracies for a_0, a', a'', and a_D.

The determined values of a_0, a', a'', and a_D at temperatures of 15, 25, 35, and 45°C for the various molecules in benzene solutions are given in Table 1.

Free energy of activation (ΔF_ε), enthalpy of activation (ΔH_ε) and entropy of activation for the dielectric relaxation and viscous flow are calculated by using Eyring's equations.[10]

$$\tau = \frac{h}{kT} \exp \frac{\Delta F_\varepsilon}{kT}$$

$$\eta = \frac{hN}{V} \exp \frac{\Delta F_\eta}{kT} \tag{7}$$

where

$$\Delta F_\varepsilon = \Delta H_\varepsilon - T\Delta S_\varepsilon$$

and

$$\Delta F_\eta = \Delta H_\eta - T\Delta S_\eta \tag{8}$$

According to Eqs. (7) and (8), plots of $\log(\tau T)$ *vs.* $1/T$ and $\log(\eta T)$ *vs.* $1/T$ should be straight lines. Their slopes are equal to $\Delta H_\varepsilon/R$ and $\Delta H_\eta/R$, respectively. The plots of $\log(\tau_1 T)$ *vs.* $1/T$ for various substances are given in Figs. 1—5.

Table 2. Thermodynamic parameters

Temp. (°C)	Free energy of activation kcal/mol		Enthalpy of activation kcal/mol		Entropy of activation kcal/mol	
	ΔF_ε	ΔF_η	ΔH_ε	ΔH_η	ΔS_ε	ΔS_η
			N,N-Dimethylaniline			
15	2.66	2.89			4.3	−1.32
25	2.60	2.91	3.89	2.51	4.3	−1.34
35	2.67	2.93			4.0	−1.36
45	2.53	2.95			4.3	−1.38
			N,N-Diethylaniline			
15	3.04	2.89			0.59	−1.32
25	3.11	2.91	3.21	-do-	0.33	−1.34
35	3.10	2.93			0.37	−1.36
45	3.07	2.95			0.47	−1.38
			o-Chloroaniline			
15	2.58	2.89			14.4	−1.32
25	2.53	2.91	6.75	-do-	17.5	−1.34
35	2.37	2.93			14.2	−1.36
45	2.15	2.95			14.4	−1.38
			m-Chloroaniline			
15	2.60	2.89			−4.58	−1.32
25	2.70	2.91	1.28	-do-	−4.80	−1.34
35	2.77	2.93			−4.83	−1.36
45	2.63	2.95			−4.24	−1.38
			p-Chloroaniline			
15	2.67	2.89			−2.79	−1.32
25	2.70	2.91	1.87	-do-	−2.78	−1.34
35	2.71	2.93			−2.72	−1.36
45	2.76	2.95			−2.80	−1.38

Discussion

A perusal of dielectric relaxation time values for the molecules in Table 1 shows that $\tau(1)$ and $\tau(2)$ differ and the difference is beyond the theoretical and experimental errors involved in computing these with the help of Eqs. (1) and (2). An examination of $\tau(2)$ values for

all the molecules also shows a systematic decrease with an increase in temperature whereas $\tau(1)$ dose not seem to follow any trend. It might suggest the following:

i) The intra-molecular relaxation mechanism is such that the dielectric relaxation time associated with it does not change much with temperature. It might mean that the amino or substituted amino group relaxes by an inversion mechanism as postulated by Smyth.[16]

ii) The weight factor (C_2) for intramolecular relaxation mechanism increases with the increase in temperature such that at a higher temperature the total contribution to $\tau(1)$ according to Eq. (6) increases due to intramolecular rotation term and contribution to $\tau(1)$ decreases due to the remaining term for overall rotation both because of less $(1-C_2)$ value as well as lesser τ_1 value.

These suggestions perhaps can be verified if these types of measurements can be conducted at a few more frequencies particularly in the range of mm wavelength. However, the interpretation of the results might be difficult particularly for the substances like *o*, *m*, and *p*-chloroanilines, in view of the possibility for such molecules to have an intramolecular relaxation time associated with the rotation of the chloro group.[17-20]

N,N-*Dimethylaniline and* N,N-*Diethylaniline.* The values of dielectric relaxation time τ_1 or τ_2 for dimethylaniline and diethylaniline are 12.8 ps and 30.5 ps, respectively, at 25°C. These values show good agreement with those reported[1] from this laboratory *i.e.*, 13.4 ps and 32.9 ps at 25°C. These also show good agreement with even τ_0 values given by Chitoku and Higasi,[2] *i.e.*, 14.5 ps and 33.2 ps respectively at 20°C.

Enthalpy of activation for the two molecules is nearly the same which indicates that both have to overcome almost the same barrier height for overall rotation although the molecular size of diethylaniline might be more comparable to that of dimethylaniline. The entropy of activation for the two molecules is a small positive quantity indicating that the activated system is in a state of slight disorder in comparison to the initial system.

o-*Chloroaniline.* The dielectric relaxation time of overall rotation for *o*-chloroaniline at 25°C is 11.5 ps. This might seem to be small in comparison to the molecular size, but greater than that of the molecule formed by attaching any of the two groups. The reported[17] τ values for chlorobenzene are 7.4 ps to 9.6 ps. Recently $\tau(1)$ value of 3.9 ps has been reported[17] for this molecule at 20°C from observations at 100 GHz which might lead to some very interesting conclusion for the rigid molecules. For aniline in non-polar solvents, literature[6,17] τ values vary from 1.2—8.1 ps. The most remarkable observation appears to be the large enthalpy of activation in comparison to that of other molecules of this type. This suggests that at a particular temperature there exsits a finite probability of H–Cl bond formation between one of the amino hydrogens and the neighbouring chlorine atom and this possibility decreases with the increase in temperature. This conclusion supports that already given by Cumper and Singleton[21] from the dipole moment studies.

m- *and* p-*Chloroanilines.* The value of dielectric, relaxation time at 25°C incidentally is 15.2 ps for both the molecules. The value compares favourably well with 13.2 ps and 15.3 ps determined by Tucker and Walker in dilute solutions of cyclohexane for *m*- and *p*-chloroanilines respectively. The enthalpy of activation for both molecules is the same and the order of magnitude is quite less as compared to *o*-chloroaniline. This indicates that both molecules have the same potential barrier and H–Cl type of bond formation as stipulated for *o*-chloroaniline seems improbable. This appears quite acceptable due to the large distance between the amino hydrogens and chloro groups in these molecules.

The literature values of dielectric relaxation time of overall rotation are available only for *m*- and *p*-chloroanilines in dilute solutions of cyclohexane. An agreement with these values suggests that in future $\tau(1)$ and $\tau(2)$ method given by Higasi *et al.* might become a good alternative method for finding the dielectric relaxation times. Perhaps both τ_1 and τ_2 can be estimated with reasonable accuracy provided the measurements are made at two suitably selected frequencies depending upon the type and nature of the molecule.

One of us (JKV) is grateful to Prof. B. K. P. Scaife of Trinity College, Ireland, for his useful suggestions.

16) C. P. Smyth, "Molecular Relaxation Processes," Chemical Society Publication No. 20, Academic Press, London (1966), p. 8.
17) The dielectric relaxation time values have been tabulated in K. Chitoku, K. Higasi, M. Nakamura, Y. Koga, and H. Takahashi, This Bulletin, **44**, 992 (1971).
18) J. Ph. Poley, *J. Appl. Sci.*, **B4**, 337 (1955).
19) G. W. Chantry and H. A. Gebbie, *Nature*, **208**, 378 (1965).
20) M. Davies, G. W. F. Pardoe, J. Chamberlain, and H. A. Gebbie, *Trans. Fraday Soc.*, **66**, 273 (1970).
21) C. W. N. Cumper and A. Singleton, *J. Chem. Soc., B*, **1968**, 645.

A Study on the Kinetics and Mechanism of the Oxidation of Carbon Monoxide over Zinc Oxide

Jae Shi CHOI and Bo Won KIM

Department of Chemistry, Yonsei University, Seoul, Korea

(Received December 13, 1971)

A kinetic study on the oxidation reaction of carbon monoxide has been carried out between 260 and 350°C by means of the static method using *n*-type ZnO semiconductor as a catalyst under various oxygen and carbon monoxide pressure. The order of reaction between 260 and 320°C was found to be 1.5, with $dP_{CO_2}/dt=kP_{CO}\cdot P_{O_2}^{1/2}$. The Roginsky-Zeldovitsch equation,[1] $dP_{CO_2}/dt=ke^{-aP}$, fits well at 350°C. The mechanism of the reaction can be explained by the *n*-type character of ZnO.[2-4]

Hauffe,[5] Wagner,[6] and Schwab[7] studied the oxidation reaction of CO using metal oxide semiconductors. Several papers have affected on the activity and electronic configuration. Wagner and Schwab, who measured the conductivity on various metallic oxides, continued their researches on ZnO containing impurities such as Al_2O_3 and Li_2O. However, their theories did not agree with each other, or with those of many other investigators after them. Ambigues and Teichner[8] showed that a kinetic study combined with measurements of catalyst conductivity in the presence of reagents or products gives valuable information on the mechanism of the reaction. Chizhikova[9] studied the oxidation of CO over pure ZnO, ZnO (0.5 at % In), ZnO (0.5 at % Li) and ZnO (1.0 at % Li) *in vacuo* (10^{-2}–1 mmHg) from room temperature to 450°C. Their results and also those of the others did not agree with each other.

Ambigues and Teichner[8] showed that correlations between the electronic conductivity and catalytic activity could be investigated in two ways. First, a correlation exists between the conductivity and the rate constant of the reaction or the apparent activation energy of the reaction. The conductivity is usually modified by doping the catalyst with altervalent cations. Second, the electrical properties of the catalyst without doping can be studied during the course of reaction. From the change of the conductivity the state of the solid can be clarified.

Krause[10] conducted research on the oxidation of CO to CO_2 on oxide catalysts such as ZnO, NiO, and V_2O_5, and offered explanation in term of chemisorption of oxygen or carbon monoxide on the catalyst and desorption of the oxidized product. Otsuka[11] *et al.* studied the oxidation of CO over ZnO by measuring the adsorption of CO, O_2, and CO_2 on the catalyst in the temperature range 200—250°C under 50—300 mmHg. They concluded that the reaction rate was independent of the adsorption of CO and O_2. Matsuura *et al.*[12] also studied the oxidation of CO in the presence of ZnO as a catalyst at 200—500°C under 0.1—760 mmHg by both the flow and static methods. They concluded that the chemisorption of oxygen is the rate determining step.

We carried out research on the CO oxidation on pure ZnO prepared under various conditions by the static method. The kinetics and mechanism are discussed in this paper.

Experimental

Materials. Four samples A, B, C, and D of ZnO were prepared under different initial conditions (temperature and pressure).

ZnO: *Sample A*: Prepared by the thermal decomposition of c.p. $ZnCO_3$ in an electric furnace at 350°C in air for 1 hr.

After being cooled to room temperature, it was etched with $(NH_4)_2S_2O_8$ and dilute HNO_3, washed in distilled water and then dried in a vacuum desiccator.

Sample B: Prepared by the same method as for Sample A except for the decomposition temperature being 500°C, kept in a vacuum desiccator until used in experiment.

Sample C: Prepared by the same method as for Sample A except for the decomposition temperature being 650°C.

Sample D: Prepared by the same method as for Sample C except for the pressure of 10^{-3} mmHg.

Sample of ZnO prepared by the above methods were verified by X-ray diffraction. The yellow color was found to deepen in the order A<B<C<D.

The degree of nonstoichiometry (Zn excess) in Samples A, B, C, and D increased in the order A<B<C<D.[13]

Carbon Monoxide: The apparatus used for preparation of the CO gas is shown in Fig. 1.

Carbon monoxide was prepared by the reaction of formic acid with concentrated sulfuric acid. The reaction was carried out by passing formic acid through concentrated sulfuric acid in an evacuated Pyrex flask connected to a vacuum system. CO was purified with glass wool, KOH, $CaCl_2$, and P_2O_5, and stored in a container, which had been

1) S. Z. Roginsky and J. Zeldovitsch, *Acta Phys.*, **1**, 342, 554, 595, and 651 (1934).
2) N. S. Hannay, "Semiconductors," Reinhold Publishing. (1959), p. 580.
3) G. L. Clark and G. G. Howley, "The Encyclopedia of Chemistry," Reinhold Publishing Corporation, N. Y. (1958), p. 682.
4) W. E. Garner, "Chemistry of the Solid State," Academic Press Inc. Publishers, New York (1955), p. 133.
5) K. Hauffe and C. Wagner, *Z. Electrochem.*, **44**, 172 (1938).
6) C. Wagner *J. Chem. Phys.*, **18**, 69 (1950).
7) G. M. Schwab, *Z. Phys. Chem. (N. F.)*, **1**, 42 (1954).
8) P. Ambigues and S. J. Teichner, *Discuss. Faraday Soc.*, **41**, 362 (1966).
9) G. I. Chizhikova, *Kinet. Katal.*, **7**, 660 (1966).
10) A. Krause, *Oestar Chemiker-Ztig.*, **63**, 40 (1962).
11) K. Otsuka, K. Tanaka, and K. Tamaru, *Nippon Kagaku Zasshi*, **88**, 830 (1967).
12) I. Matsuura, T. Kubokawa, and O. Toyama, *ibid.*, **81**, 997 (1960).
13) L. V. Azároff, "Introduction to Solids," McGraw-Hill Book Company, New York (1960), p. 371.

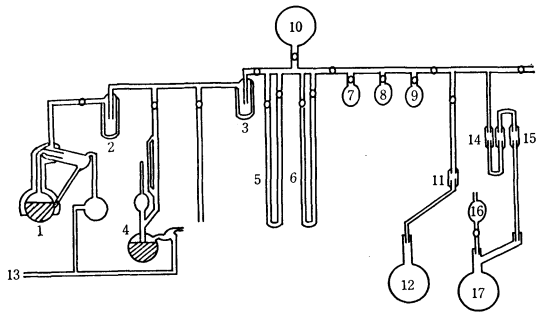

Fig. 1. Vacuum system.
1: Diffusion pump, 2,3: Dry ice trap, 4: McLeod gauge, 5,6: Manometer, 7,8,9: O_2 Storage tank, 10: CO Strorage tank, 11: $CaCl_2$ tube, 12: $KClO_3$ flask, 13: to Vacuum pump 14: $CaCl_2$ tube, 15: NaOH tube 16: HCOOH flask 17: H_2SO_4 flask.

evacuated to 10^{-5} mmHg.

Oxygen: The apparatus used for preparation of O_2 gas is shown in Fig. 1.

Oxygen obtained by heating potassium chlorate at about 600°C[14] was purified by passing over glass wool, P_2O_5 and $CaCl_2$. This was found to give a oxygen sufficiently free of catalytic poisons when used in catalytic reactions. The purity of the CO and O_2 gases was confirmed by gas chromatography.

Experimental Procedure. A half gram of ZnO (200 mesh) was distributed uniformly in the reaction chamber. After the pressure was reduced to 10^{-3}mmHg at room temperature, oxygen and carbon monoxide were added in a ratio of 70:140 (mmHg). The chamber was then placed in the electric furnace maintained at a constant temperature.

The change in pressure due to the progress of the reaction was monitored by a manometer connected to the reaction chamber at regular time intervals. To check separately the influence on this reaction of P_{O_2} and P_{CO} which are almost interdependent, the ratio of P_{O_2} and P_{CO} was varied, 70:70, 70:210, and 140:140 (mmHg), and the reaction rate measured in the same manner.

The resulting gas was confirmed to be carbon dioxide by gas chromatography after the reaction.

Results

The results from the reactions with Samples A, B, C, and D as catalysts at 260°C, 290°C, 320°C, and 350°C, respectively are given in Figs. 2—7.

The order of reaction is 1.5 for Samples A, B, C, and D at 260—320°C giving $dP_{CO_2}/dt=kP_{CO}P_{O_2}^{1/2}$. At 350°C, the Roginsky-Zeldovitsch equation,[1] $dP_{CO_2}/dt=ke^{-ap}$ (a; parameter, p; the amount of conversion, k; rate constant) holds; $\log(t+t_0)=ap-\log ka$ (Fig. 6). The rate constants from Figs. 2—6 are given in Tables 1 and 2. The activation energies calculated from Figs. 2—5 and Tables 1 and 2 are 16.04, 15.97, 14.86, and 13.69 kcal/mol, respectively. To check the influence of P_{O_2} and P_{CO} on these reactions separately, the ratio of P_{O_2} and P_{CO} was varied; 70:210, 70:140, 70:70, 140:70, and 140: 140 (mmHg) at 260°C on Sample C. The results can be seen in Fig. 6 and the rate constants in Table 2.

14) J. W. Moeller, "A Comprehensive Treatise on Inorganic and Theoretical Chemistry," Vol. 1, Longmans, Green and Co. Ltd., London (1946), p. 349.

Discussion

The rate equations on Samples A, B, C, and D can be classified into two types; one between 260 and 320°C and the other at 350°C. The 260 to 320°C readings do not agree with those of Ambigues and Teichner,[8] who showed that the rate is proportional to the square root of the oxygen pressure and independent of CO pressure, nor with those of Chizhikova,[9] who proposed that the kinetics of the oxidation of CO over pure ZnO is given by the equation $-dP_{CO}/dt=kP_{CO}^{0.5}$ and that over Li- and In-doped ZnO by the equation $-dP_{CO}/dt=kP_{CO}^{0.7}$. However, there is an agreement with the results

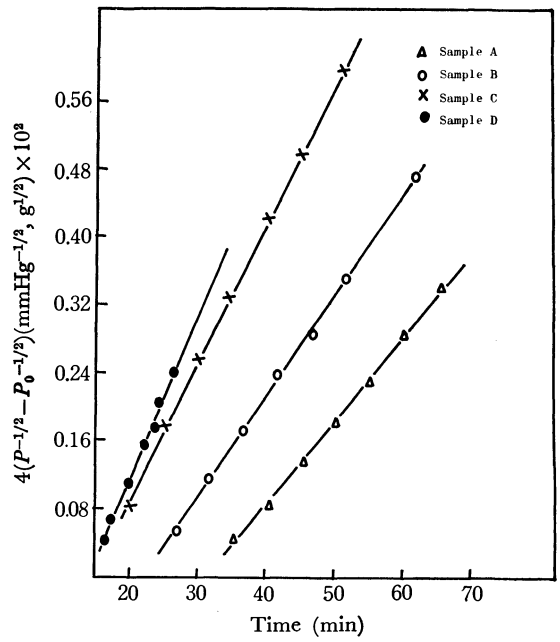

Fig. 2. The rates of oxidation reaction of carbon monoxide on ZnO at 260°C; P_{O_2}:P_{CO}=70:140; ZnO, 0.5 g (200 mesh).

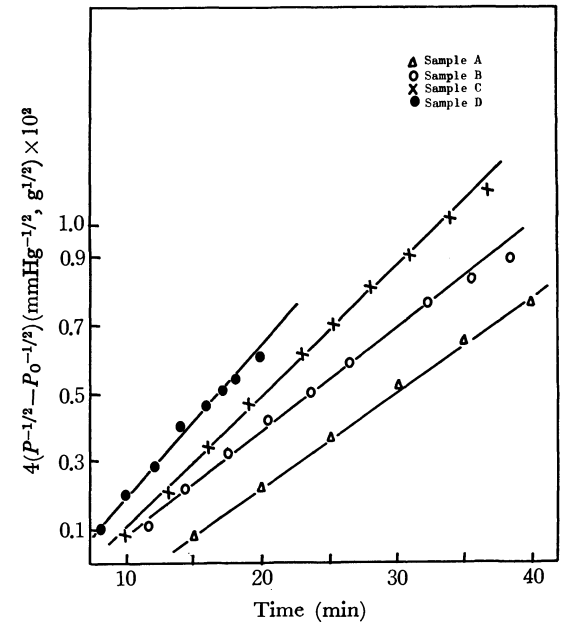

Fig. 3. The rates of oxidation reaction of carbon monoxide on ZnO at 290°C; P_{O_2}:P_{CO}=70:140; ZnO, 0.5 g (200 mesh).

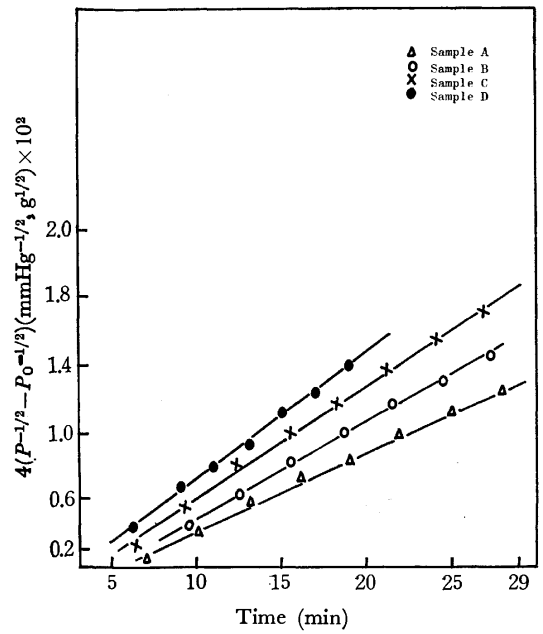

Fig. 4. The rates of oxidation reaction of carbon monoxide on ZnO at 320°C; P_{O_2}:P_{CO}=70:140; ZnO, 0.5 g (200 mesh).

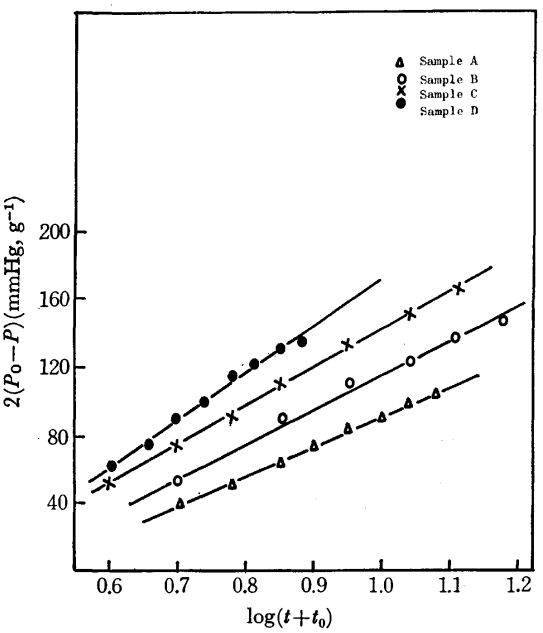

Fig. 5. The rates of oxidation reaction of carbon monoxide on ZnO at 350°C; P_{O_2}:P_{CO}=70:140; ZnO, 0.5 g (200 mesh).

TABLE 1. k VALUES AS A FUNCTION OF TEMPERATURE

k Sample	k(mmHg$^{-1/2}$ g$^{1/2}$ min^{-1})			k(g^{-1} min^{-1})
	260°C	290°C	320°C	350°C
A	1.00×10^{-4}	2.82×10^{-4}	4.63×10^{-4}	1.69×10^{-1}
B	1.20×10^{-4}	3.00×10^{-4}	5.52×10^{-4}	1.78×10^{-1}
C	1.62×10^{-4}	3.65×10^{-4}	6.70×10^{-4}	2.38×10^{-1}
D	1.95×10^{-4}	4.40×10^{-4}	7.21×10^{-4}	2.81×10^{-1}

of Otsuka *et al.*,[11] who showed that the over all reaction is $dP_{CO_2}/dt=kP_{CO}P_{O_2}^{1/2}$, and those of Matsuura *et al.*,[12] who explained that the initial rate of reaction as determined by the static method is $dP_{CO_2}/dt=kP_{CO}P_{O_2}^{1/2}$.

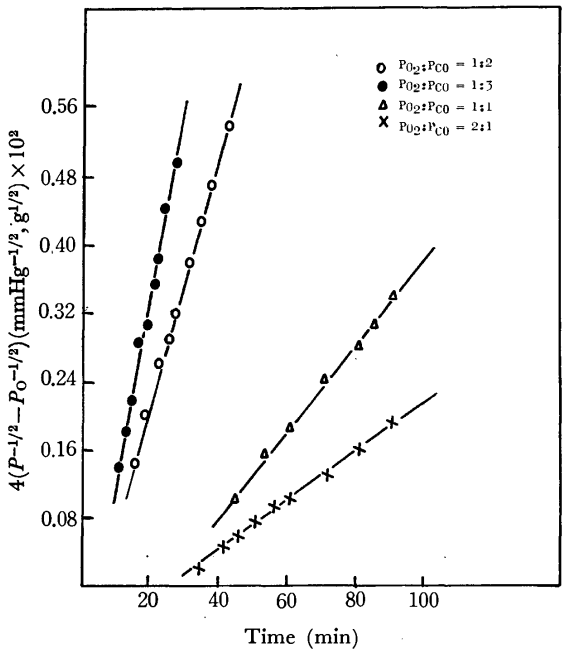

Fig. 6. The rates of oxidation reaction of carbon monoxide on ZnO (Sample C) under the various P_{CO} and P_{O_2} at 260°C; ZnO, 0.5 g (200 mesh).

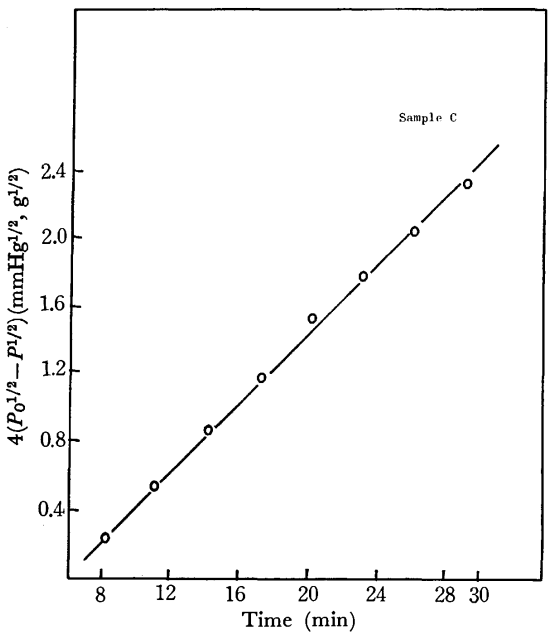

Fig. 7. The determination of the order of oxygen pressure in this kinetic equation at 260°C; P_{O_2}:P_{CO}=20:255; $dP_{CO_2}/dt=KP_{O_2}^{1/2}$

TABLE 2. k VALUES AS A FUNCTION OF P_{CO} AND P_{O_2} AT 260°C ON SAMPLE C

P_{O_2}	P_{CO}	k(mmHg$^{-1/2}$ g$^{1/2}$min^{-1})
70	210	2.24×10^{-4}
70	140	1.62×10^{-4}
70	70	0.52×10^{-4}
140	70	0.30×10^{-4}
140	140	0.96×10^{-4}

The 350°C reading does not correspond to any of the above research. We see from Fig. 3 that the catalytic activity of the ZnO Samples is in the order A<B<C <D. Thus the effect can be explained by the increase of *n*-type characteristic. Oxygen deficiency in ZnO can be due to the excess Zn dissolved in the interstitial sites of ZnO[15-19] when $ZnCO_3$ is decomposed thermally. The catalytic activity of ZnO dependent on the amount of excess Zn (or the amount of oxygen deficiency). The mechanism of the CO oxidation reaction is explained as follows; at first oxygen accepts electrons from the activated ZnO surface to be adsorbed on the active sites, O^-(ads) being thus formed.

$$\frac{1}{2}O_2(g) + e = O^-(ads)$$

Carbon monoxide reacts then with the O^-(ads) forming CO_2(ads). Carbon dioxide is then desorbed from the ZnO surface. This corresponds to Ambigues and Teichner's conclusions[8] that oxygen gas is adsorbed weakly while carbon monoxide gas is strongly adsorbed on the ZnO surface and carbon monoxide gas reacts on the O^-(ads) to form CO_2(g), *viz.*

$$\frac{1}{2}O_2(g) + e^- = O^-(ads)$$

$$O^-(ads) + CO(g) = CO_2(ads) + e^-$$

$$CO_2(ads) = CO_2(g)$$

where (g) is an abbreviation for the gas state and (ads) the adsorbed state. The mechanism is explained by means of the Rideal mechanism. For the same catalyst the reaction rate at high temperature is greater than that at a low temperature. At the same temperature the reaction rate for the catalyst prepared at high temperature is greater than that for the catalyst prepared at a lower temperature. The reaction rate for the case in which the catalyst prepared in a vacuum (the same temperature condition) is used is greater than that for the catalyst prepared in air (Table 1). At 260°C for Sample C the reaction rate is small when P_{O_2} is greater than P_{CO} and great when P_{O_2} is smaller than P_{CO} (Table 2). The results correspond to the deductions from the conductivity data obtained by Ambigues and Teichner[8] and also the degree of nonstoichiometry of ZnO (Zn excess). They correspond also to the result by Teichner. The conductivity at $P_{O_2}=3$ mmHg was greater than that at $P_{O_2}=160$ mmHg. After evacuation to 10^{-5} mmHg again, the conductivity at the initial oxygen pressure of $P_{O_2}=3$ mmHg became greater than that at $P_{O_2}=160$ mmHg.

	P_{O_2}	
log σ	3(mmHg)	160(mmHg)
log σ	$\bar{6}.80$	$\bar{7}.1$
log σ_0	$\bar{3}.50$	$\bar{4}.50$

Cited from *Discuss. Faraday Soc.*, **41**, 362 (1966).

These results show that if the oxygen pressure is increased, the amount of irreversibly adsorbed oxygen is increased, and if the oxygen pressure is decreased, the amount of irreversibly adsorbed oxygen is decreased. The mechanism for the CO oxidation reaction proposed here with is in line with the findings of Otsuka *et al.*[11] in that the adsorbed carbon monoxide did not influence this reaction either. The catalytic effect of ZnO depends on the sintering temperature and pressure, and the amount of excess Zn (or the amount of deficient oxygen) has an important effect on these reaction rates.

15) Hakze Chon and C. D. Prater, *Discuss. Faraday Soc.*, **41**, 380 (1966).
16) H. Krebs, "Fundamentals of Inorganic Crystal Chemistry," McGraw-Hill Publishing Company, London (1968), p. 162.
17) F. A. Kraeger, "Chemistry of Imperfect Crystals," North-Holland Publishing Company, Amsterdam (1964), p. 692.
18) J. H. Boer, "Reactivity of Solids," Elsevier Publishing Company, Amsterdam (1961), p. 381.
19) B. M. Arghiropoulos and S. J. Teichner, *J. Catal.*, **3**, 477 (1964).

Studies of the Molybdenum Catalysts. Part I. Changes in the State of the Hydrated Molybdenum Oxide Catalyst during a Reaction between Thiophene and Hydrogen

Noriyuki SOTANI and Masatomo HASEGAWA

College of Liberal Arts, Kobe University, Tsurukabuto, Nada, Kobe, 657

(Received March 31, 1972)

The reaction between thiophene and hydrogen on hydrated molybdenum oxide was studied. Structural and compositional changes in the catalyst were found during the hydrodesulfurization of thiophene. The main products of the reaction were *n*-butane, butenes, and hydrogen sulfide. The conversion of thiophene increased with the progress of the reaction and reached a steady value after passing through a maximum. This reaction process was distinguished into two stages. One is the "aging stage," and the other is the "stationary stage." At the aging stage, three reactions, that is: i) dehydration, ii) reduction, and iii) sulfurization occur. The catalyst reacts with the reactants and changes in structure and composition. Hydrated molybdenum oxide was converted to MoO_3 by liberating the structural water, and MoO_3 was reduced to MoO_2. A part of the MoO_3 was also sulfurized directly with thiophene to MoS_2 during the aging stage, but MoO_2 could not easily be sulfurized. At the stationary stage, no further change in the catalyst was found, and only the catalytic hydrodesulfurization of thiophene occurred. The conversion at the stationary stage, when the aging temperature was low, was larger than the conversion at a high temperature. The difference between the conversions at different reaction temperatures was assumed to result from the structural and compositional changes in the catalyst caused by the different temperatures of the aging processes. In this reaction, the dehydration at the aging stage controls the activity of the catalyst.

The mechanism of the hydrodesulfurization of thiophene has been studied by a number of workers, and the findings up to 1957 have been reviewed by McKinley.[1] Recently, because of the industrial importance of the desulfurization of petroleum, very many workers have studied the hydrodesulfurization of thiophene on cobalt molybdate supported on alumina[2-4] as a model reaction for the desulfurization of petroleum, and several mechanisms have been proposed for the reaction.

In most of these works, catalysts have been activated and stabilized by pretreatment with hydrogen,[5] hydrogen sulfide,[3] or thiophene[2] before the kinetic measurements. However, only a little attention has been given to the structural changes in the catalyst during the reaction and to the relation between such structural changes and the activities.[4]

The purpose of this work is to obtain basic information about such structural and compositional chagnes in the hydrated molybdenum oxide catalyst during the hydrodesulfurization of thiophene and the relation between such changes and the activity of the catalyst.

As a catalyst, we used hydrated molybdenum oxide powder, without any promoter and supporter, in order to avoid the complexity introduced by the addition of these substances.

In this investigation, the structural and compositional changes in hydrated molybdenum oxide during the hydrodesulfurization of thiophene were investigated by means of chemical, X-ray diffraction, and thermal analyses. We also tried to learn how the structural and compositional changes influence the activity of the catalyst.

Experimental

A usual flow method was used for the reaction. The reactants and products were analyzed by means of gas chromatograph directly connected to the flow line. Hydrogen purified by passing through the platinum catalyst and molecular sieves flowed at a rate accurately controlled to 0.1 mol/hr by means of a needle valve and an auxiliary regulator. The flow rate was measured by means of a rotor meter and a soap film meter. Thiophene was fed as a liquid to the evaporator by means of a calibrated hypodermic pump. The feed rate of the thiophene, 1.4×10^{-2} mol/hr, was so small compared with that of hydrogen that the partial pressure had no effect on the reaction. A small amount of benzene, 1×10^{-3} mol/hr, was used as a marker, because benzene did not decompose under the reaction conditions.

Catalyst. (A) Hydrated molybdenum trioxide, $MoO_3\cdot nH_2O$, was precipitated from a solution of ammonium molybdate by the addition of HNO_3. The precipitate was dried at 110°C for a day and was then calcined in air at 200°C for 6 hr. By differential thermal analysis (DTA) and thermogravimetric analysis (TGA), this oxide was found to be a hydrate of molybdenum trioxide. The water included in this oxide was kept at 400°C. This water was assumed to be a structural water. When this hydrated molybdenum oxide was left standing in a desicator, it absorbed about 0.26 mol of water, which was easily removed by heating at 200°C. This was physically-absorbed water.

(B) Anhydrous molybdenum trioxide, MoO_3, was prepared from hydrated molybdenum oxide by calcination in air at 600°C for 6 hr.

(C) Anhydrous molybdenum dioxide, MoO_2 was formed by reducing hydrated molybdenum oxide with hydrogen at 450°C for 5 hr.

(D) Molybdenum disulfide, MoS_2, was purchased from Wako Chemical Industries.

1) J. B. McKinley, "Catalysis," Vol 5, ed by P. H. Emmett, Reinhold Publishing Corporation, New York (1957), p. 405.
2) P. J. Owens and C. H. Amberg, Advances in Chemistry Ser., No. 33, p. 182 (1961).
3) Charles N. Satterfied and G. W. Roberts, *AIChE J.*, **14**, 159 (1968).
4) J. M. J. G. Lipsh and G. C. A. Shuit, *J. Catal.*, **15**, 179 (1969).
5) K. Toyoda and M. Kurita, *Shokubai*, **11**, 115P (1969).

The analysis of the sulfur content of the catalyst after the reaction was done gravimetrically by the $BaSO_4$ methods.[6]

Results

Conversion of Thiophene. Hydrated molybdenum oxide (1 gram) was used as the catalyst. To begin with, the catalyst was heated at a reaction temperature, of 350, 375, or 400°C. Then the reactants were introduced over the catalyst.

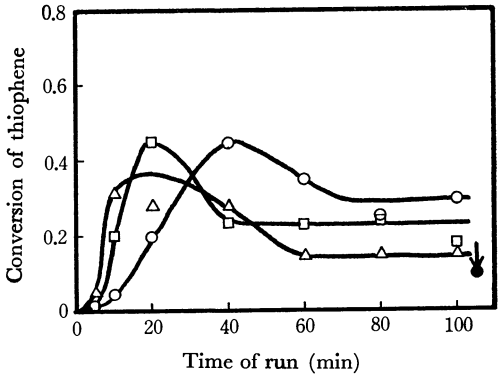

Fig. 1. The conversion of thiophene.
○: 350°C, □: 375°C, △: 400°C, ●: 350°C after 400°C

The conversion of thiophene, expressed in the ratio of the concentration decrease to the initial concentration, is shown in Fig. 1. The conversions at all the reaction temperatures have very similar curves with the reaction time. The conversion increased gradually and reached a steady value after reaching a maximum. We term the period when the conversion reached a steady value after the maximum, the "aging stage," and the period after the conversion reached the steady value, the "stationary stage."

The main products were *n*-butane, 1-butene, *cis*-2-butene, *trans*-2-butene, and hydrogen sulfide. Mercaptane, *tetra*-hydrothiophene and butadiene were not found, though they had been reported in previous works.[2,3] The products are also shown in Fig. 2a. The concentration of *n*-butane in the products was relatively large and reached a maximum when the conversion showed its maximum, at the aging stage. The ratio of C_4 products, calculated from the concentration of *cis*-2-butene as a standard, is shown in Fig. 2b. Only the ratio of *n*-butane shows its maximum at the aging stage, that of the butene shows a steady value. Hydrogen sulfide was not detected during the "aging stage." This suggests that most of the sulfur removed from thiophene by the reaction was consumed in the sulfurization of the catalyst. This shows that the reaction at the aging stage between thiophene and the catalyst is important in producing *n*-butane and molybdenum sulfide.

Reaction during the "Aging Stage." (1) Sulfurization of the Catalyst: sulfur content of the catalyst, determined by chemical analysis, is shown in Fig. 3 against the reaction time. This clearly shows that the catalyst was sulfurized by thiophene or by the hydrogen

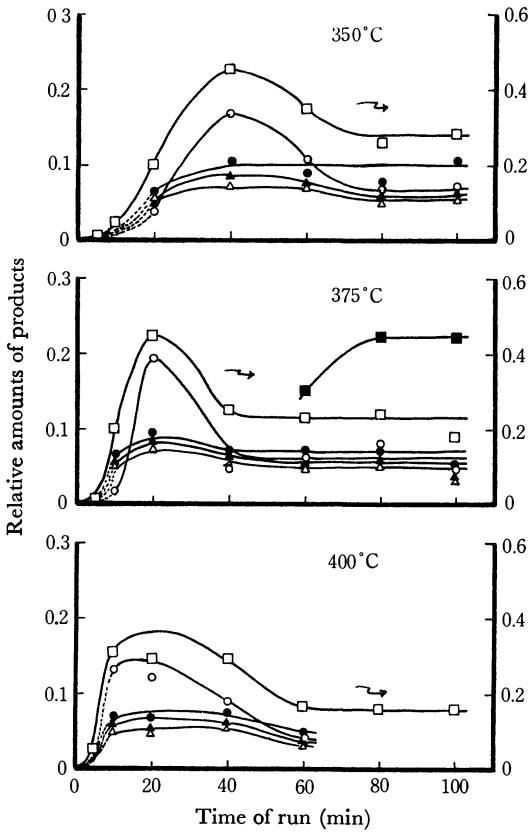

Fig. 2a. Reaction products.

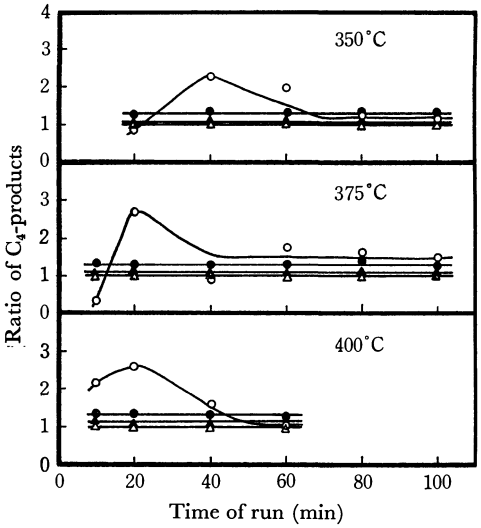

Fig. 2b. The ratio of reaction products.
□: Total conversion, ○: *n*-butane, ▲: 1-butene, ●: *trans*-2-butene, △: *cis*-2-butene, ■: hydrogen sulfide

sulfide produced by the hydrodesulfurization of thiophene. The sulfurization proceeded during the aging process and stopped when the aging process was over. Only the hydrodesulfurization of thiophene occurred at the stationary stage. The sulfur content of the catalyst at the stationary stage was large when the aging temperature was low. It is interesting that the catalyst is sulfurized more in the bulk when the temperature is low.

(2) Reduction of the Catalyst: besides the sulfuriza-

6) "Bunsekikagaku Binran," Maruzen, Tokyo (1961), p. 495.

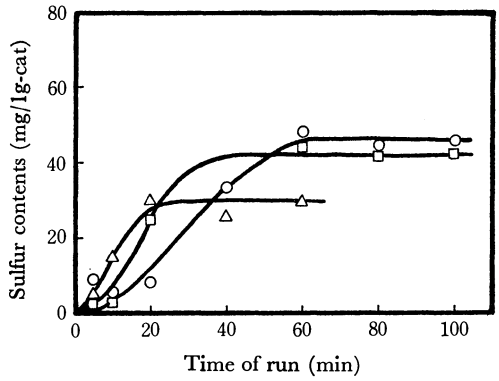

Fig. 3. Sulfur content of the catalyst.
○: 350°C, □: 375°C, △: 400°C

tion, the catalyst was reduced to MoO_2 during the aging stage. During the aging stage, the catalyst was transformed from $MoO_3 \cdot nH_2O$ to MoO_3 and then to MoO_2, as determined by the X-ray diffraction studies. The catalyst was found to be a mixture of these compounds in the course of the aging process. At the stationary stage, therefore, the catalyst was composed of MoO_2 and molybdenum sulfide.

Conversion during the "Stationary Stage." The lower the aging temperature, the larger the stationary value of the conversion at the stationary stage. The value of the conversion after the aging stage at 350°C was 0.3, about twice the value at 400°C.

The conversion was observed after the aging process at 400°C. The reaction temperature was subsequently lowered to 350°C, and then the conversion was determined. The conversion had decreased from 0.15 to 0.10, as is shown in Fig. 1 (the arrowed black point). We also observed the conversion at different reaction temperatures in order to obtain the temperature coefficient after the aging process at 350°C. The apparent activation energies calculated from these values were 3.2—4.4 kcal/mol. Therefore, the high stationary value of the conversion at a low temperature may be considered to be caused by chemical changes in the catalyst at the aging stage. Aging at low temperatures is more useful in obtaining a high activity for the hydrated molybdenum oxide catalyst.

Reactions on Other Samples. As has been described above, the catalyst in the course of the reaction consisted of a mixture of $MoO_3 \cdot nH_2O$, MoO_3, MoO_2, and MoS_2 at any reaction time and at any reaction temperature. Therefore, we also studied the conversion of thiophene, using each of these components as a catalyst. The results are shown in Fig. 4. In the case of MoO_3, the conversion changed in a manner similar to that in the case of $MoO_3 \cdot nH_2O$, but the stationary value of the conversion was somewhat smaller. In the case of MoO_2, the conversion was nearly constant throughout the reaction. On MoS_2, the conversion was not reproducible, so it was difficult to compare it with the conversion on other compounds. However, on MoS_2, the conversion was always high at first, rapidly decreased with the reaction time, and then reached a stationary value. We also studied partially-reduced MoO_3 at 350°C for 3 hr prior to the reaction. The conversion was very high at first, decreased, and then reached a stationary value.

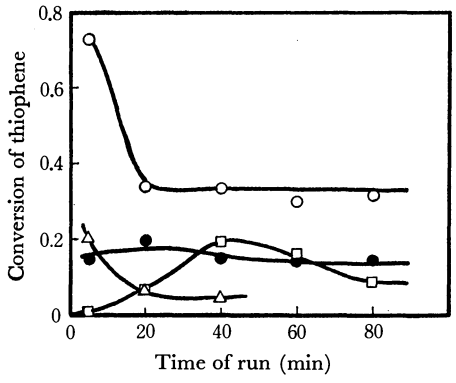

Fig. 4. The conversion of thiophene on various molybdenum compounds.
□: MoO_3, ●: MoO_2, ○: MoO_3+MoO_2, △: MoS_2

Discussion

As has been described above, the hydrated molybdenum oxide catalyst reacts with reactants at an early stage of the hydrodesulfurization of thiophene. The changes in the structure and composition caused by the reaction influence the final activity of the catalyst. That is, the aging temperatures dominate the activities of the hydrated molybdenum oxide catalyst.

Change in the Surface Area. The differences in the activities may be explained by the changes in the surface area of the catalyst. The BET surface area of hydrated molybdenum oxide before use was 3.4 m^2/g. The area increased to 8.6 m^2/g when the catalyst was used for 100 min at 350°C and to 8.0 m^2/g at 400°C. Thus, the difference in the surface area between the two reaction temperatures is not so large that we can not explain the difference in the conversion. That is, the activity does not depend on the surface area. Therefore, it is reasonable to conclude that the difference in the activity is attributable to the structural and compositional changes in the catalyst caused during the aging process.

Process of Structural Changes in the Catalyst. During the aging stage, three reactions occurred on the catalyst: i) dehydration, ii) reduction, and iii) sulfurization.

i) Dehydration: The catalyst removed the structural water during the aging process. The presence of the structural water seems to affect the reduction and the sulfurization. The process of the dehydration will be reported on in detail later.

ii) Reduction: The hydrated oxide was reduced to MoO_2 through an intermediate mixture of MoO_3 and MoO_2. At the stationary stage, a large portion of the catalyst consisted of MoO_2 at either reaction temperature.

iii) Sulfurization: At the same time, a small portion of the dehydrated MoO_3 was sulfurized. On the other hand, MoO_2 was not sulfurized easily.

To summarize the processes discussed above, we may conclude that the catalyst changes during the aging process as follows;

$$MoO_3 \cdot nH_2O \longrightarrow MoO_3 \begin{cases} \nearrow MoO_2 \\ \searrow MoS_2 \end{cases}$$

The catalyst is mainly composed of MoO_2 and MoS_2 at the stationary stage. The aging temperature has effects on the relative rate of the reduction and the sulfurization of MoO_3. In other words, the dehydration plays an important role in determining the rates of the reduction and the sulfurization.

Mechanism of the Sulfurization. The catalyst is considered to be sulfurized by two possible processes. One is direct sulfurization by thiophene (I). The other is sulfurized by hydrogen sulfide produced by the hydrodesulfurization of thiophene (II). That is:

(I) $MoO_3(MoO_2) + C_4H_4S + H_2 \longrightarrow MoS_2 + C_4\text{-Products} + H_2O$

(II) a) $C_4H_4S + H_2 \xrightarrow{\text{Catalyst}} H_2S + C_4\text{-Products}$

b) $H_2S + MoO_3(MoO_2) \longrightarrow MoS_2 + H_2O$

Biltz and Kochen proposed that MoS_3 is labilized at a high temperature.[7] Nanba and Aonuma[8] reported that the final state of molybdenum sulfide is MoS_2 in the hydrodesulfurization of thiophene. By a hydrogenation reaction, MoS_3 is easily reduced at a high temperature; $MoS_3+H_2 \rightleftharpoons MoS_2+H_2O$.[9] It is reasonable to suppose that MoS_2 is formed under these reaction conditions, even though the formation of MoS_2 has not been confirmed by X-ray diffraction analysis. It can be assumed that MoS_2 does not have a perfect hexagonal crystal structure, but an amorphous mosaic-like structure.

As is shown in Figs. 1 and 3, the sulfurization of the catalyst stops and only the (IIa) reaction proceeds at the stationary stage. During the aging stage, the sulfurization by two processes (I) and (IIb), is possible. However, for the following reasons, the (I) process may be concluded to be the main reaction process.

(1) When hydrated molybdenum oxide was sulfurized for 60 min at 350°C by a mixture of H_2+H_2S, there was only a trace of sulfur content of the catalyst. The catalyst was partially reduced to MoO_2, but a large portion of the hydrated molybdenum oxide was maintained unchanged. This shows that the sulfurization by thiophene (I) is easier than that by hydrogen sulfide (IIb). This is inconsistent with the results of Tarama *et al.*[10] on vanadium molybdate. They reported that molybdenum in vanadium molybdate supported on alumina was more easily sulfurized by hydrogen sulfide than by thiophene.

(2) Figure 2b shows the ratio of C_4 products. Only the ratio of *n*-butane shows a maximum, that of butenes shows a constant value from the beginning. This suggests that, at the aging stage, the (I) process occurs much more than the (IIa) process. The sulfurization by the I process occurs more than that by the (IIb) process.

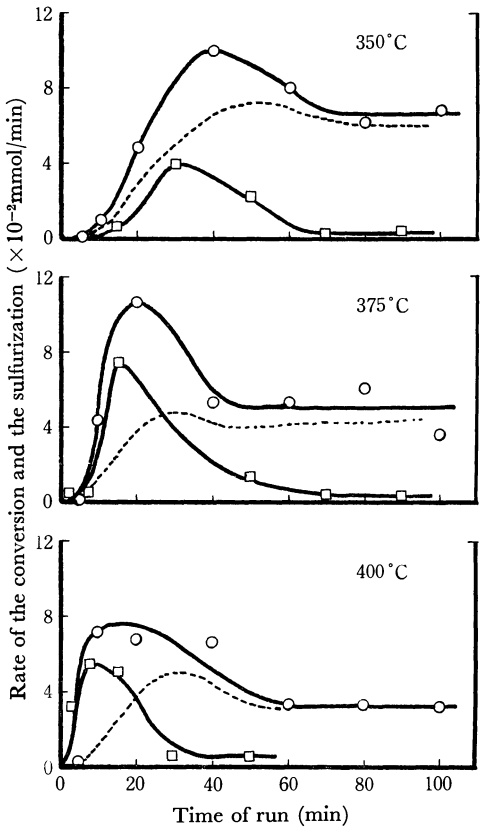

Fig. 5. The rate of the conversion of thiophene and the sulfurization of the catalyst.
○: conversion, □: sulfurization

(3) Figure 5 shows the rate of the sulfurization calculated from the sulfur analysis in Fig. 3 and the rate of the conversion of thiophene. A comparison of the two curves gives interesting information about the aging process. The rate of the conversion represents the rate of the total consumption of thiophene (I+IIa), which corresponds to the sum of the rate of the sulfurization of the catalyst (I+IIb) and the hydrodesulfurization (IIa). From these two reasons (I) and (2), the (IIb) process can be neglected more safely than the (I) process. Therefore, the difference between the rate of the conversion and the rate of the sulfurization represents the rate of hydrodesulfurization (IIa). The peaks of both curves agree at the aging stage. The dotted line in Fig. 5, which is the difference between the rate of the conversion and that of the sulfurization, shows the rate of net hydrodesulfurization (IIa). As it is relatively difficult for the (IIb) process to occur ,this suggests that the maximum of the conversion results from the overlapping of the sulfurization (I) with the hydrodesulfurization reaction (IIa).

When anhydrous MoO_2 was used as a catalyst, the sulfur content was 1.3 wt% after a reaction for 100 min at 350°C. This shows that MoO_2 is not easily sulfurized. On the other hand, the sulfur content of anhydrous MoO_3 after a reaction for 100 min at 350°C was 9.0 wt%. The conversion of neither anhydrous MoO_3 nor MoO_2 was very high compared with that

7) W. Biltz und A. Köchen, *Z. Anorg. Allgem. Chem.*, **248**, 172 (1941).
8) S. Nanba and T. Aonuma, *Kogyo Kagaku Zasshi*, **74**, 1324 (1971).
9) S. Shono, K. Itabashi, M. Yamada, and M. Kikuchi, *ibid*, **64**, 1357 (1961).
10) K. Tarama, S. Teranishi, Hattori, and Azuma, *Nenryo Kyokaishi*, **42**, 99 (1965).

of hydrated molybdenum oxide at the stationary stage. Richardson[11] has reported that MoO_2 itself has a mild activity in the hydrodesulfurization of thiophene.

From the results presented above, it may be concluded that the dehydration at the aging stage controls the rates of the reduction and the sulfurization and, consequently, influences the activity of the catalyst.

11) J. T. Richardson, *Ind. Eng. Chem. Fundamentals*, **3**, 154 (1964).

The nature of the structural water in hydrated molybdenum oxide and the process of the dehydration of the catalyst will be reported on later.

We are indebted to Dr. I. Motooka for measuring the DTA and TGA and to Mr. Y. Sasaki for measuring the BET surface area. We also wish to thank Dr. S. Kishimoto for his helpful discussions.

BULLETIN OF THE CHEMICAL SOCIETY OF JAPAN, VOL. 46, 29—34 (1973)

The Primary Process of the Photochemical Dimerization of Carbostyril (2-Quinolone) in an Aqueous Solution

Tetsu YAMAMURO, Norisuke HATA,* and Ikuzo TANAKA

Department of Chemistry, Tokyo Institute of Technology, Ohokayama, Meguro-ku, Tokyo
**Department of Chemistry, College of Science and Engineering, Aoyama Gakuin University, Chitosedai, Setagaya-ku, Tokyo*

(Received March 16, 1972)

Carbostyril dimerizes photochemically in an aqueous solution, in order to investigate the effect of a hydroxide ion on the primary process of the photochemical dimerization in an aqueous solution, both measurements of the quantum yields and flash spectroscopic experiments were carried out under various conditions. The experiments revealed that the photodimerization reaction proceeded through a bimolecular interaction between the triplet and the unexcited carbostyril molecules, although the triplet carbostyrilate ion was in equilibrium with the triplet carbostyril. The triplet carbostyrilate ion was proved not to be involved in the dimerization process.

As has been described in a previous paper,[1] the photochemical dimerization of carbostyril in deaerated ethanol proceeds through a bimolecular interaction of the triplet carbostyril with the unexcited one. Such a photodimerization has also been reported to take place in an aqueous solution.[2] Meanwhile, the acid-base equilibrium between the carbostyril (S_0) and the carbostyrilate ion (S_0^-) in their ground states has been shown spectrophotometrically in alkaline aqueous solutions as follows:[3]

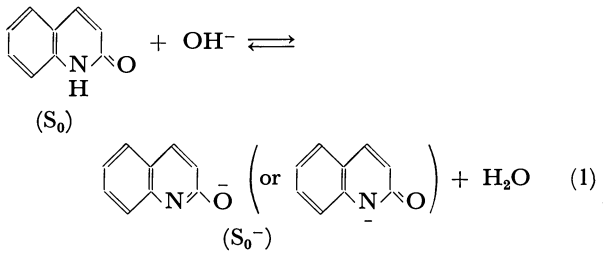

(S_0) (S_0^-) (1)

Therefore, in order to elucidate the primary process of the photochemical dimerization of carbostyril in such an alkaline solution, the present authors carried out investigations by means of measurements of the quantum yields and by means of flash spectroscopy.

Experimental

The carbostyril used in the experiment was prepared by treating quinoline *N*-oxide with tosyl chloride.[4] The product was purified by recrystallization from methanol several times. Standard specified solutions of sodium hydroxide (Yoneyama Yakuhin Co., Ltd.) were used as the solvents.

The light source employed in the steady-light experiments was a Toshiba high-pressure mercury lamp (H-400 P), while for the 313 nm irradiation a filter combination of a nickel sulfate solution with a UV-31 Toshiba filter was used. The measurements of the quantum yields were carried out by a procedure described previously.[1]

The flash photolysis apparatus was the same as was employed in the previous investigations.[1] The xenon flash lamp used for excitation was operated by discharging a bank of condensers of 1 μF charged to 14.75 kV, 109 joules of energy being dissipated; the duration time of the flash was 5 μsec.

Since the quantum yield of the disappearance of carbostyril was reduced to almost zero in the presence of oxygen in a solution, just as in the case of the ethanol solution,[1] all the experiments—both steady-light and flash spectroscopic—were performed on solutions deaerated by flushing nitrogen at room temperature.

Results

Figure 1 shows the absorption spectra of carbostyril in aqueous solutions containing different amounts of

1) T. Yamamuro, I. Tanaka, and N. Hata, This Bulletin, **44**, 667 (1971).
2) O. Buchardt, *Acta Chem. Scand.*, **17**, 1461 (1963).
3) G. W. Ewing and E. A. Steck, *J. Amer. Chem. Soc.*, **68**, 2181 (1946).
4) E. Ochiai and T. Yokogawa, *Yakugaku Zasshi*, **75**, 213 (1955).

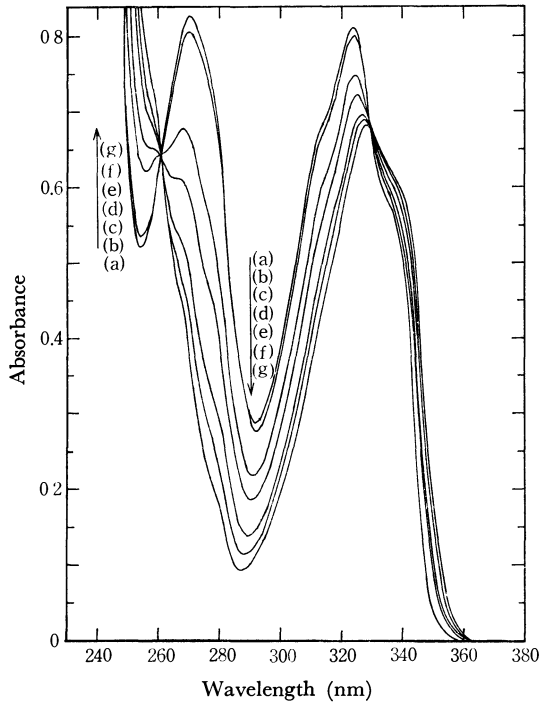

Fig. 1. Absorption spectra of carbostyril in aqueous solution containing different amounts of sodium hydroxide at room temperature (C: 1.23×10^{-4}M).
[OH$^-$]: (a) 0M, (b) 0.001M, (c) 0.01M, (d) 0.02M, (e) 0.05M, (f) 0.10M, (g) 1.0M

sodium hydroxide, where the isosbestic points were observed at 260.5 and 329.5 nm; that is, an acid-base equilibrium was indicated to exist between the carbostyril (S_0) and the carbostyrilate ion (S_0^-), as is represented by Eq. (1). In the present experiments, therefore, the concentrations of S_0 and S_0^- at equilibrium were evaluated by the following equations, respectively:

$$[S_0] = C/(1+K_G[OH^-])$$
$$[S_0^-] = CK_G[OH^-]/(1+K_G[OH^-]) \quad (2)$$

where K_G represents the equilibrium constant, and C, the sum of $[S_0]$ and $[S_0^-]$. The equilibrium constant (K_G) was calculated by means of Eq. (3), where ε_λ or ε'_λ is the molar extinction coefficient of S_0 or S_0^- at the λ wavelength and where D_λ is the absorbance of a solution containing S_0 and S_0^-. Thus, the slope of the straight-line obtained by:

$$\frac{(\varepsilon_\lambda-\varepsilon_\lambda')C}{D_\lambda-\varepsilon_\lambda'C} = 1 + K_G[OH^-] \quad (3)$$

plotting $(\varepsilon_\lambda-\varepsilon'_\lambda)C/(D_\lambda-\varepsilon'_\lambda C)$ against $[OH^-]$, gave the value of K_G as 62.3M^{-1}.

Steady-light Experiments. The quantum yields (Φ) of the carbostyril disappearance were determined as a function of the concentration of a hydroxide ion in an aqueous solution ($C=1.23\times10^{-4}$M) at room temperature. Figure 2 shows the results thus obtained where the plot of Φ against $[OH^-]$ was replaced by that of Φ *vs.* $[S_0]$. As may be seen from Fig. 2, the quantum yield increased very rapidly with an increase in the concentration of S_0 expect at very low concentrations of S_0, but at higher concentrations the quantum yield

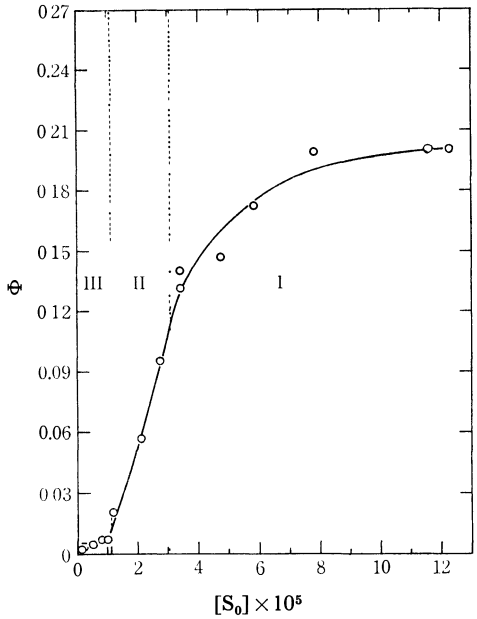

Fig. 2. Quantum yield of carbostyril disappearance *vs.* $[S_0]$ in alkaline aqueous solution at room temperature ($C=1.23\times10^{-4}$M).

gradually approached about 0.2. Because of such a characteristic dependence of Φ on $[S_0]$, it is convenient for the subsequent discussion to divide the concentration range of S_0 into three regions, I, II, and III, as is indicated in Fig. 2. On the other hand, the quantum yield in water was 0.21, regardless of the concentration of S_0 ($\approx C$).

Flash Spectroscopic Experiments. Figure 3 shows the T–T absorption of carbostyril in aqueous solutions con-

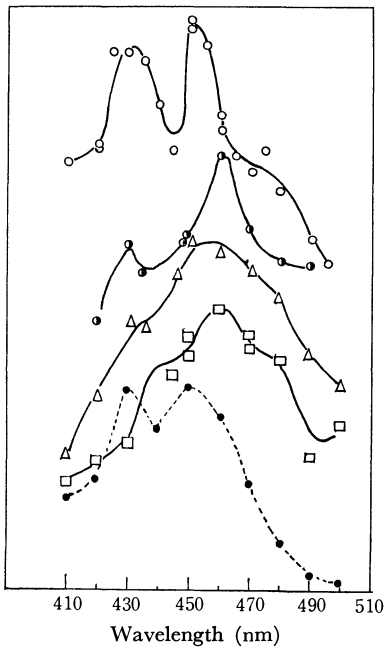

Fig. 3. Transient absorption of carbostyril at room temperature.
○: in water (C: 0.16×10^{-4}M)
◑: in 0.1M NaOH aqueous solution (C: 1.08×10^{-4}M)
△: in 0.5M NaOH aqueous solution (C: 1.13×10^{-4}M)
□: in 1.0M NaOH aqueous solution (C: 1.13×10^{-4}M)
●: in 70% ethanol aqueous solution (C: 0.30×10^{-4}M)

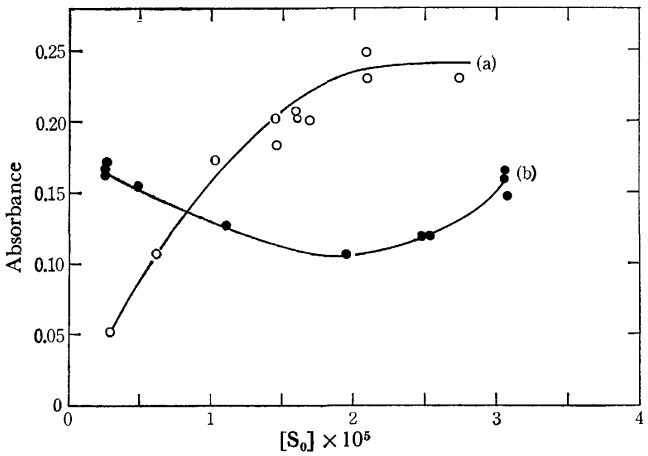

Fig. 4. Absorbance of transient absorption at 450 nm *vs.* $[S_0]$ at room temperature.
(a), ○: in water
(b), ●: in NaOH solution (C: 1.0×10^{-4}M)

taining different amounts of sodium hydroxide, and also in a 70% ethanol aqueous solution at room temperature. As can be seen from Fig. 3, the transient absorption was altered significantly when the solvent was changed from water to alkaline solutions. Figure 4 shows the plot of the absorbance of the transient absorption at 450 nm against $[S_0]$ in water (a) or a NaOH solution (b). It is clear from these figures that the transients observed in alkaline solutions consist of two kinds of species, the carbostyril (T_1) around 420—470 nm and the carbostyrilate ion (T_1^-) at about 440—490 nm, in their lowest triplet states. In addition, the transient absorption was confirmed to decay by means of first-order kinetics.

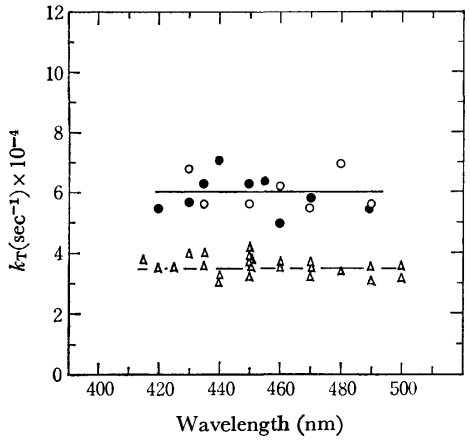

Fig. 5. Decay rate constant (k_T) of transient at various wavelengths at room temperature.
●: in water (C: 0.16×10^{-4}M)
○: in 0.1M NaOH aqueous solution (C: 1.08×10^{-4}M)
△: in 1.0M NaOH aqueous solution (C: 1.13×10^{-4}M)

Figure 5 shows first-order decay rate constants (k_T) determined at different wavelengths; the data indicate that the decay constant of the triplet carbostyril is nearly equal to that of the triplet carbostyrilate ion.

Next, the effect of the concentration of a hydroxide ion on the decay constant of the transients at 450 nm was examined at room temperature (Fig. 6). The (a)

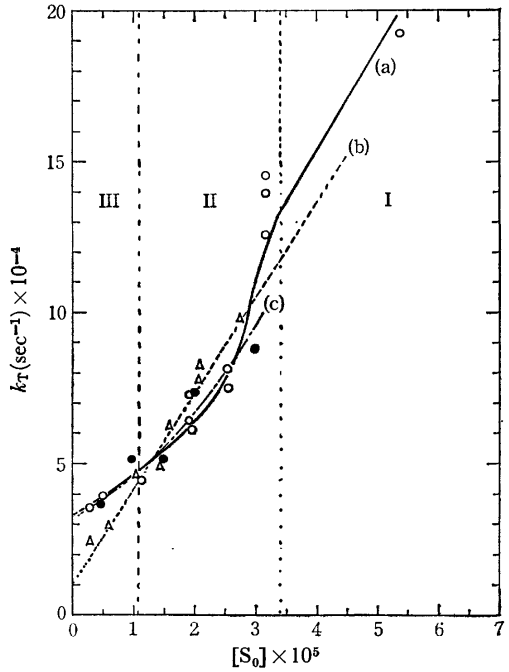

Fig. 6. Decay rate constant (k_T) of transients at 450 nm *vs.* $[S_0]$ at room temperature.
curve (a), ○: in alkaline aqueous solution (C: 1.13×10^{-4}M)
curve (b), △: in water
curve (c), ●: in alkaline aqueous solution ($[S_0^-]$: 1.0×10^{-4}M)

curve in Fig. 6 shows the plot of k_T against $[S_0]$ in the place of $[OH^-]$. The (b) curve illustrates the plot of k_T *vs.* $[S_0]$ in water, while the (c) curve is the plot of k_T *vs.* $[S_0]$ when $[S_0^-]$ was kept to 1.0×10^{-4}M. The slope (3.18×10^9 $sec^{-1}M^{-1}$) of the (a) curve in Region I was in good agreement with that (3.12×10^9 $sec^{-1}M^{-1}$) of the (b) curve, whereas the (a) curve in Region III coincided in slope with the (c) curve. It is obvious from these results that the dependence of $[S_0]$ of k_T is quite similar to that of the quantum yield shown in Fig. 2.

The decay constants of the transients at 450 nm were also measured as a function of the concentration of S_0^-, while the concentration of S_0 was kept constant at 0.15×10^{-4}M (Fig. 7). As a result, it was found to remain constant at 5.5×10^4 sec^{-1}, regardless of the concentration of S_0^-. Therefore, it seems reasonable to

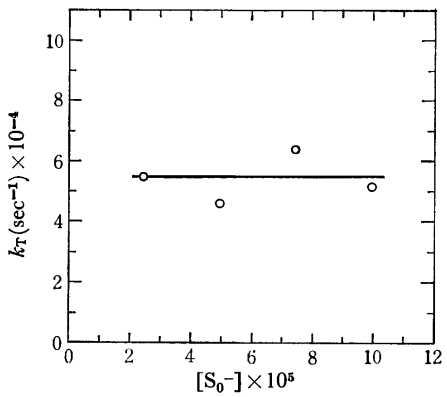

Fig. 7. Decay rate constant (k_T) of transients at 450 nm *vs.* $[S_0^-]$ in alkaline aqueous solution at room temperature ($[S_0]$: 0.15×10^{-4}M)

conclude that the decay rate constant is dependent on the concentration of only S_0, not S_0^-.

Discussion

The experimental results described in the preceding section suggest that the photochemical dimerization of carbostyril in an alkaline solution proceeds through a bimolecular interaction between the triplet and the ground-state carbostyrils, although the triplet carbostyrilate ion is considered to be in equilibrium with the triplet carbostyril. When we also assume an acid-base equilibrium between the carbostyril (S_1) and the carbostyrilate ion (S_1^-) in their excited singlet states, the following scheme, Scheme 1, can be generally postulated for the primary process of the photodimerization in an alkaline aqueous solution:

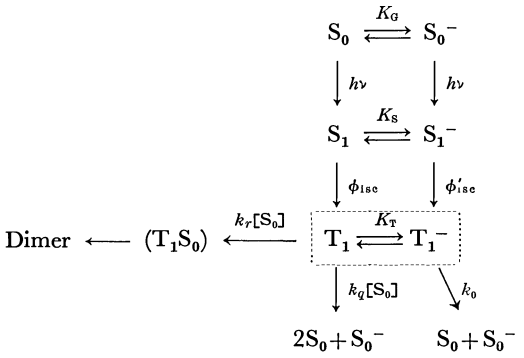

Scheme 1.

where K_G, K_S, and K_T represent the equilibrium constant in the ground, the excited singlet, and the lowest triplet states, and where ϕ_{isc} and ϕ'_{isc} are the efficiencies of the $S_1 \rightarrow T_1$ and, $S_1^- \rightarrow T_1^-$ intersystem crossing.[5]

Assuming photostationary state conditions, the quantum yield (Φ) of the carbostyril disappearance can be given by the following equation:

$$\Phi = \frac{k_r[S_0]}{k_T} \frac{\phi_{isc}+K_S[OH^-]\phi'_{isc}}{1+K_S[OH^-]} \quad (4)$$

where: $$k_T = (k_r+k_q)[S_0] + k_0 \quad (4')$$

and where k_r represents the apparent rate constant for the formation of the transient complex (T_1S_0), and k_q and k_0, the apparent quenching rate constants by S_0 or the apparent first-order decay rate constant of the transient species ($T_1+T_1^-$). We can then obtain Eq. (5) by substituting $[OH^-]=[S_0^-]/K_G[S_0]$ into Eq. (4):

$$\Phi = \frac{k_r[S_0]}{k_T} \frac{K_G[S_0]\phi_{isc}+K_S[S_0^-]\phi'_{isc}}{K_G[S_0]+K_S[S_0^-]} \quad (5)$$

On the basis of Eq. (5), a subsequent discussion of the primary process of the photochemical dimerization of carbostyril in an alkaline solution will be made in the concentration ranges of S_0 and OH^-, each divided into three regions, I, II, and III, as has been described before.

Region I ($[S_0] \gtrsim 3.40\times10^{-5}$M or $[OH^-] \lesssim 0.052$M).
In view of the results shown in Fig. 6 that the slope of the (a) curve in Region I is substantially equal to that of the (b) curve, the transient absorption observed may be regarded as being due mostly to the triplet carbostyril; hence, the triplet carbostyrilate ion is assumed not to exist appreciably in this region (Scheme 2).

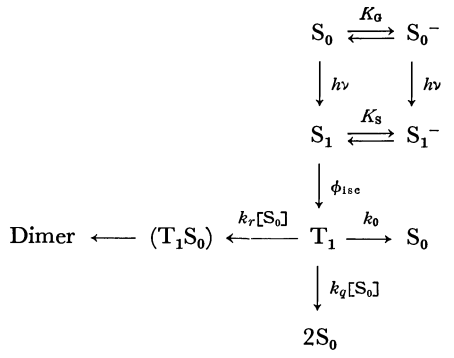

Scheme 2.

According to Scheme 2, Eq. (5) could be approximately expressed by Eq. (6).

$$\Phi = \frac{k_r[S_0]}{k_T} \frac{K_G[S_0]\phi_{isc}}{K_G[S_0]+K_S[S_0^-]} \quad (6)$$

On the other hand, k_r+k_q and k_0 were evaluated from the (b) curve in Fig. 6 to be 3.12×10^9 sec^{-1}M^{-1} and 1.12×10^4 sec^{-1} respectively, indicating that $(k_r+k_q)[S_0]/k_0$ is greater than 9.5. Consequently, Eq. (6) can be simplified to Eq. (7), if we assume that k_0 can be neglected compared with $(k_r+k_q)[S_0]$:

$$\Phi = \frac{k_r}{k_r+k_q} \frac{K_G[S_0]\phi_{isc}}{K_G[S_0]+K_S[S_0^-]} \quad (7)$$

By substituting for $[S_0^-]$ its equivalent, $C-[S_0]$, we obtain Eq. (8):

$$\frac{1}{\Phi} = \frac{1}{\phi_{isc}}\left(1+\frac{k_q}{k_r}\right)\left(\frac{K_SC}{K_G}\frac{1}{[S_0]}+\frac{K_G-K_S}{K_G}\right) \quad (8)$$

That is, $1/\Phi$ in Region I is expected to increase in proportion to $1/[S_0]$. It is shown in Fig. 8 that the plot of $1/\Phi$ against $1/[S_0]$ gives a straight-line relation; this is consistent with Eq. (8). From the slope (1.24×10^{-4}M) and the intercept (3.83) of the straight line, ϕ_{isc} and K_S were evaluated to be $0.21(1+k_q/k_r)$ and 13.0M^{-1} respectively.

Region III ($[S_0] \lesssim 1.11\times10^{-5}$ or $[OH^-] \gtrsim 0.23$M).
In Region III the concentration of carbostyril is extremely low compared with that of the carbostyrilate ion; thus, the latter is considered to be mainly concerned with a light absorption (Scheme 3).

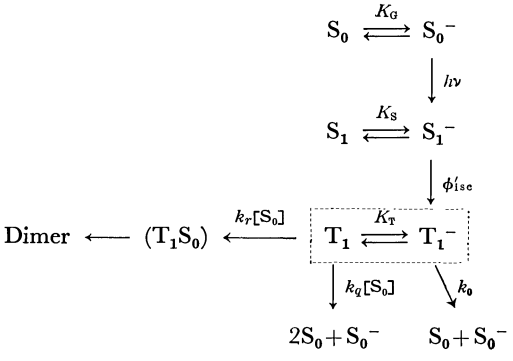

Scheme 3.

5) Although there exists quenching from the excited singlet states (S_1, S_1^-) to the ground states (S_0, S_0^-), there are not written in Scheme 1.

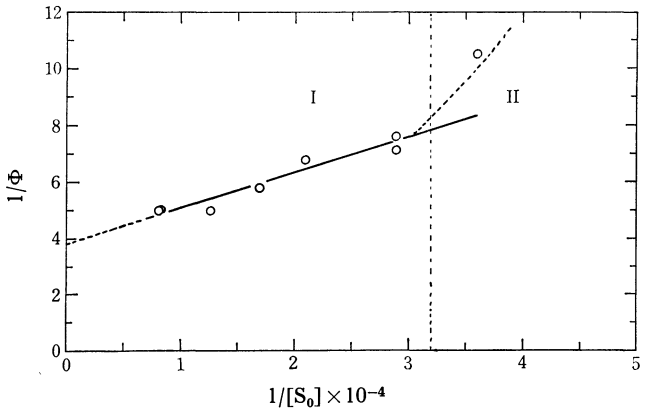

Fig. 8. $1/\Phi$ *vs.* $1/[S_0]$ in Regions I.

According to Scheme 3, Eq. (5) can be simplified as follows:

$$\frac{1}{\Phi} = \frac{1}{\phi'_{isc}}\left(1+\frac{k_q}{k_r}\right)\left\{\left(1+\frac{k_0}{k_r+k_q}\frac{1}{[S_0^-]}\frac{K_G}{K_S}+\frac{k_0}{k_r+k_q}\frac{1}{[S_0]}\right)+\frac{K_G[S_0]}{K_S[S_0^-]}\right\} \quad (9)$$

On the other hand, the values of k_r+k_q and k_0 were evaluated from the (a) curve in Fig. 6 to be 1.15×10^9 $sec^{-1}M^{-1}$ and 3.40×10^4 sec^{-1} respectively. In addition, the concentration of S_0^- in this region is around 11.8×10^{-5}M; hence:

$$1+\frac{k_0}{k_r+k_q}\frac{1}{[S_0^-]}\frac{K_G}{K_S}+\frac{k_0}{k_r+k_q}\frac{1}{[S_0]} \gtrsim 4.0$$

and $K_G[S_0]/K_S[S_0^-] \lesssim 0.48$; that is, $K_G[S_0]/K_S[S_0^-]$ is considered to be negligible compared with the other terms in Eq. (9). For this reason, we can further simplify Eqs. (9) to (10):

$$\frac{1}{\Phi} = \frac{1}{\phi'_{isc}}\left(1+\frac{k_q}{k_r}\right)\left(1+\frac{k_0}{k_r+k_q}\frac{1}{[S_0^-]}\frac{K_G}{K_S}+\frac{k_0}{k_r+k_q}\frac{1}{[S_0]}\right) \quad (10)$$

Accordingly, $1/\Phi$ in Region III is expected to vary linearly with $1/[S_0]$. In fact, it is shown in Fig. 9 that the plot of $1/\Phi$ against $1/[S_0]$ gives a linear relationship in accordance with Eq. (10); ϕ'_{isc} was estimated from the slope (9.91×10^{-4}M) of the straight line to be $3.0\times10^{-2}(1+k_q/k_r)$.

Region II ($1.11\times10^{-5}M \lesssim [S_0] \lesssim 3.40\times10^{-5}M$ or $0.23M \gtrsim [OH^-] \gtrsim 0.052M$). As can be seen from Fig. 6, both k_r+k_q and k_0 in Region II depend on the concentration of S_0. In Eq. (5) the ratio of $K_G[S_0]\phi_{isc}/(K_G[S_0]+K_S[S_0^-])$ to $K_S[S_0^-]\phi'_{isc}/(K_G[S_0]+K_S[S_0^-])$ corresponds to $[T_1]/[T_1^-]$, where T_1 and T_1^- are the triplet species produced by the intersystem crossing from S_1 and S_1^- respectively. Assuming that the triplet carbostyrilate ion is not quenched by S_0, k_q/k_r should be independent of $[S_0]$ and $[OH^-]$; thus, there could be $3.32 \lesssim [T_1]/[T_1^-] \lesssim 12.8$. Under these circumstances, the triplet carbostyrilate ion can be inferred to be mainly produced by the $S_1\rightarrow T_1\rightarrow T_1^-$ process, but not from S_1^- (Scheme 4).

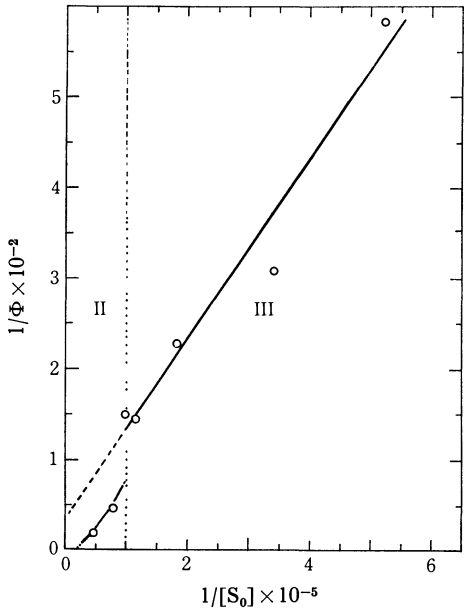

Fig. 9. $1/\Phi$ *vs.* $1/[S_0]$ in Region III.

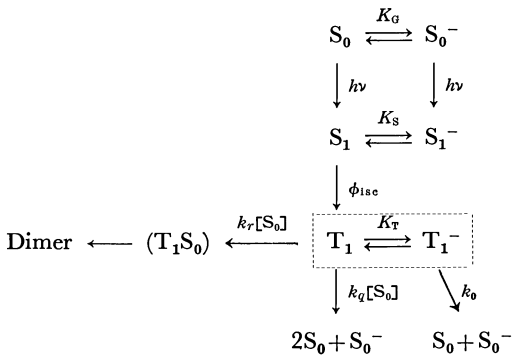

Scheme 4.

According to Scheme 4, Eq. (5) can be approximated as follows:

$$\frac{1}{\Phi} = \frac{1}{\phi_{isc}}\left(1+\frac{k_q}{k_r}\right)\left(\frac{k_0}{k_r+k_q}\frac{1}{[S_0]}+1\right)\times\left(\frac{K_S C}{K_G}\frac{1}{[S_0]}+\frac{K_G-K_S}{K_G}\right) \quad (11)$$

Figure 10 shows the plot of $1/\Phi$ against $1/[S_0]$, where a clear-cut straight-line relation was not observed in Region II as has been expected from Eq. (11). The decay rate (R) of the transient species ($T_1+T_1^-$) at equilibrium is given by the following equation:

$$R = \{(k_r+k_q)[S_0]+k_0\}[T_1+T_1^-]$$

Based on the fact that the photochemical dimerization proceeds through an interaction between T_1 (not T_1^-) and S_0, the decay rate (R) could also be given by the following relation:

$$R = (k_{ro}+k_{qo})[S_0][T_1] + k_0[T_1+T_1^-]$$

where k_{ro} and k_{qo} correspond to k_r and k_q respectively in water. Accordingly, Eq. (12) is obtained by a combination of the equations described above:

$$\frac{k_{ro}+k_{qo}}{k_r+k_q} = 1+\frac{[T_1^-]}{[T_1]} \quad (12)$$

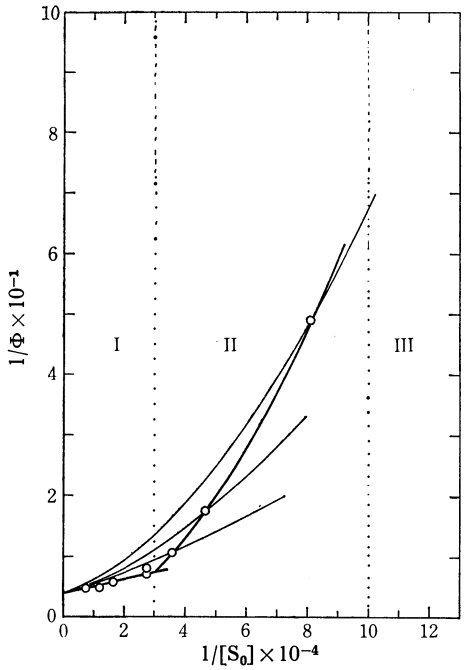

Fig. 10. $1/\Phi$ *vs.* $1/[S_0]$ in Regions I and II.

Since $[T_1^-]/[T_1]=K_T[OH^-]$, Eq. (12) can then be converted into Eq. (13).

$$\frac{k_{ro}+k_{qo}}{k_r+k_q} = 1 + K_T[OH^-] \qquad (13)$$

That is, if the assumptions that an acid-base equilibrium exists between the triplet carbostyril and the triplet carbostyrilate ion, and that the dimerization process involves only the triplet carbostyril, not the carbostyrilate ion, are reasonable, a linear relationship could be obtained between $(k_{ro}+k_{qo})/(k_r+k_q)$ and $[OH^-]$.

On the other hand, the values of $k_0/(k_r+k_q)$ at several concentrations of S_0, such as 2.77×10^{-5}M, 2.13×10^{-5}M, and 1.23×10^{-5}M, were calculated, by substituting the observed values of Φ (0.095, 0.057, and 0.021) respectively at these concentrations of S_0 into Eq. (11), to be 0.78×10^{-5}M, 1.79×10^{-5}M, and 3.21×10^{-5}M, respectively (Fig. 10). The value of $k_0/(k_r+k_q)$ in Region I or III was also estimated from the results in Fig. 6 to be 0.359×10^{-5}M or 2.96×10^{-5}M. From such estimations, $k_0/(k_r+k_q)$ in Region II was shown to exist between those in Regions I and III obtained from the flash experimental data; this is parallel to an increase in the concentration of the triplet carbostyrilate ion with a decrease in the S_0 value or an increase in the OH^- value.

The decay constant (k_T) of the transient species $(T_1+T_1^-)$ is derived from Eqs. (2) and (4') as follows:

$$k_T = (k_r+k_q)\left(\frac{C}{1+K_G[OH^-]}+\frac{k_0}{k_r+k_q}\right) \qquad (14)$$

Therefore, k_r+k_q and k_0 at various concentrations of OH^-, or S_0, were estimated by substituting the observed values of k_T into Eq. (14); the results are listed in Table 1. Both k_r+k_q and k_0 in Region II were observed to exist between the corresponding values in Regions I and III.

Table 1. Values of (k_r+k_q) and k_0 in Regions I, II, and III

Region	$[OH^-]$	$(k_r+k_q)\times10^{-9}$ ($sec^{-1}M^{-1}$)	$k_0\times10^{-4}$ ($sec^{-1}M^{-1}$)
I	0.0	3.12	1.12
	0.01	3.12	1.12
	0.02	3.12	1.12
	0.05	3.12	1.12
II	0.07	2.34	1.82
	0.1	1.68	3.01
	0.2	1.33	3.53
III	0.25	1.15	3.40
	0.3	1.15	3.40
	0.5	1.15	3.40
	1.0	1.15	3.40
	1.5	1.15	3.40

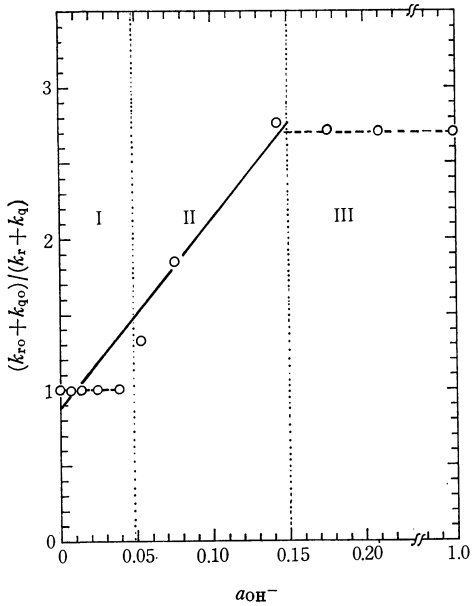

Fig. 11. $(k_{ro}+k_{qo})/(k_r+k_q)$ *vs.* a_{OH^-} in Regions I, II, and III.[6]

As can readily be seen from Fig. 11 using the values in Table 1, the plot between them gave a linear relationship, consistent with Eq. (13); the equilibrium constant (K_T) was then estimated from the slope to be $12.5M^{-1}$.

These facts also support the present idea about the primary process of photochemical dimerization in an alkaline aqueous solution.

The authors with to express their hearty thanks to Professor Yuji Mori of the Tokyo Institute of Technology for his kind discussion and to Professor Shiro Matsumoto of Aoyama Gakuin University for his permission to use the flash-photolysis apparatus.

6) The activities (a_{OH^-}) were estimated from the values of mean activity coefficients described in the following literatures; H. S. Harned and J. C. Heckel, *J. Amer. Chem. Soc.*, **55**, 4838 (1933) and G. Akerlof and G. Kegels, *ibid.*, **62**, 620 (1940).

Counterion Effect in the Electron-Transfer Reactions between a Tetracyanoethylene Radical Anion and Its Neutral Molecule

Masaaki OGASAWARA, Hidetoshi TAKAOKA, and Koichiro HAYASHI
Faculty of Engineering, Hokkaido University, Sapporo
(Received April 28, 1972)

The rates of homogeneous electron-transfer reactions between radical anions and neutral molecules were studied in a variety of tetracyanoethylenide systems in order to obtain information concerning the counterion effect on the electron-transfer reactions. The estimated values of the rate constants had the same order of magnitude at room temperature for all the systems, while the activation energies and the preexponential factors were markedly dependent on the natures of the counterions and the solvents. The obtained results are discussed in terms of the forms and structures of the radical anions.

The mechanism of an electron-transfer reaction between an organic radical anion and its neutral molecule is one of the most interesting problems concerning the relationship between the reactivities and the structures of radical ions in solution. Since Ward and Weissman[1] established the method for measuring the rapid rate of electron-transfer reaction by electron spin resonance (ESR), a number of electron-transfer reaction rates have been measured and it has been found that they are essentially dependent on the forms and structures of radical ions in solutions.[2-10]

In the systems where radical anions and their counterions exist in the form of an ion pair, any electron-transfer reaction is thought to be accompanied by a counterion-transfer through the formation of a sandwich structure at the transition state, as has been suggested by Adam *et al.*[2,11] Therefore, it can reasonably be expected that the natures of the counterions and solvent molecules coordinated to the ions profoundly affect the reaction behavior.

As for the radical ions of aromatic hydrocarbons, many authors[7,9,10] have reported in detail on the transfer rates in a number of different ion pairs with various alkali metal ions in various solvents. However, few studies have been made on the systems of *N*-containing radical anions.[5,8,12,16] In this article we will report the results obtained by the ESR technique on the electron-transfer reactions between the tetracyanoethylene radical anion ($TCNE^-$) and neutral tetracyanoethylene (TCNE) in 1,2-dimethoxyethane (DME) and tetrahydrofuran (THF). The effect of different counterions on the reaction rate was studied; the results will be discussed in terms of the ionic forms and structures of the radical ions in solution.

Experimental

Materials. TCNE of a guaranteed Reagent grade was purified by repeated sublimations *in vacuo*. The DME and THF were fractionally distilled over sodium metal, and the middle portions were stored over calcium hydride. They were rigorously dried with sodium mirror or sodium-potassium alloy *in vacuo* and degassed until 10^{-5} Torr before use. The alkali metal tetracyanoethylenides were prepared by reactions between alkali metals and TCNE dissolved in DME or THF. All the operations were carried out on the vacuum line.

The tetra-*n*-butylammonium salt was generated electrochemically in the solvent, using 0.1M tetra-*n*-butylammonium perchlorate as the supporting electrolyte. Alternatively, the crystalline tetra-*n*-butylammonium tetracyanoethylenide was prepared from tetra-*n*-butylammonium iodide and TCNE[13] and was dissolved in the solvent before use.

Measurements of Reaction Rates. Each radical anion solution for a rate experiment was sealed *in vacuo* into a ESR sample tube made of Pyrex, and then a known amount of TCNE was added through a break seal. The second-order rate constants were evaluated from the linewidth broadening in the ESR spectra produced by the addition of neutral TCNE. All the experiments were carried out at a slow exchange limit.[1] The ESR measurements were made with a JES-NE-2X spectrometer equipped with 100 kc field modulation. The temperature was kept constant within $\pm 1°$ with a JES-UCD-2X variable-temperature adaptor on the ESR cavity. The temperatures were determined by means of a copper-constantan thermocouple placed just under the sample tube in the cavity.

Results

The obtained ESR spectrum of a dilute solution of $TCNE^-$ was the same as that reported by Phillips *et al.*[12] No alkali metal splitting was observed in the various tetracyanoethylenide systems studied here. The increase in linewidth produced by the addition of neutral TCNE was linearly dependent on the concentration of added TCNE in the range from 1 to 6×10^{-2}M.

1) R. L. Ward, and S. I. Weissman, *J. Amer. Chem. Soc.*, **79**, 2086 (1957).
2) F. C. Adam, and S. I. Weissman, *ibid.*, **80**, 1518 (1959).
3) P. J. Zandstra, and S. I. Weissman, *ibid.*, **84**, 4408 (1962)
4) N. Hirota, and S. I. Weissman, *ibid.*, **86**, 2537 (1964).
5) J. M. Fritsch, T. Miller, and R. N. Adams, *Nature*, **205**, 382 (1965).
6) W. Bruning, and S. I. Weissman, *J. Amer. Chem. Soc.*, **88**, 373 (1966).
7) R. Chang, and C. S. Johnson, Jr., *ibid.*, **88**, 2338 (1966).
8) T. M. Miller, and R. N. Adams, *ibid.*, **88**, 5713 (1966).
9) N. Hirota, R. Carraway, and W. Schook, *ibid.*, **90**, 3611 (1968).
10) G. L. Malinoski, Jr., W. H. Bruning, and R. G. Griffin, *ibid.*, **92**, 2665 (1970).
11) A. C. Aten, J. Dieleman, and G. Hoijtink, *Discuss. Faraday Soc.*, **29**, 182 (1960).
12) W. D. Phillips, J. C. Rowell, and S. I. Weissman, *J. Chem. Phys.*, **33**, 626 (1960).
13) O. W. Webster, W. Mahler, and R. E. Benson, *J. Amer. Chem. Soc.*, **84**, 3678 (1962).

Table 1. Rate constants and activation energies for the electron-transfer reactions between tetracyanoethylene radical anions and their neutral molecules

Solvents	Counterions	Temp, °C	$k\times10^{-8}$ M^{-1} sec^{-1}	E_a[a] kcal mol^{-1}	Log A[a]
DME					
	Li^+	20	1.8	3.8±0.4	11
	Na^+	20	1.7	6.0±0.6	13
	K^+	20	1.5	7.6±0.6	14
	Bu_4N^+	10	1.3	6.5±0.6	14
THF					
	Li^+	20	1.5	2.2±0.4	10
	Na^+	20	1.3	3.6±0.5	11
	K^+	20	1.6	3.2±0.7	11
	Bu_4N^+[b]	20	1.9	4.7±0.6	12

a) Determined from the equation $k=A\exp(-E_a/RT)$.
b) Electrochemically prepared radical anion was used.

The estimated values of the rate constants were of the same order of magnitude at room temperature in all the systems, as is shown in Table 1.

The temperature dependence of the rates was investigated in the temperature range from −30° to 20°C. The plots of $\log k$ *vs.* $1/T$ gave almost straight lines, as is shown in Fig. 1. The apparent activation energies, calculated from the Arrhenius plots, are summarized in Table 1, together with the rate constants and the preexponential factors. The activation energies were markedly dependent on the natures of the counterions and the solvents. In DME it was found that the activation energies for alkali metal salts were in the order of $Li^+<Na^+<K^+$, and that of tetra-*n*-butylammonium salt gave a value intermediate between those of sodium and potassium salts. In THF, the evaluated activation energies were rather small in comparison with DME.

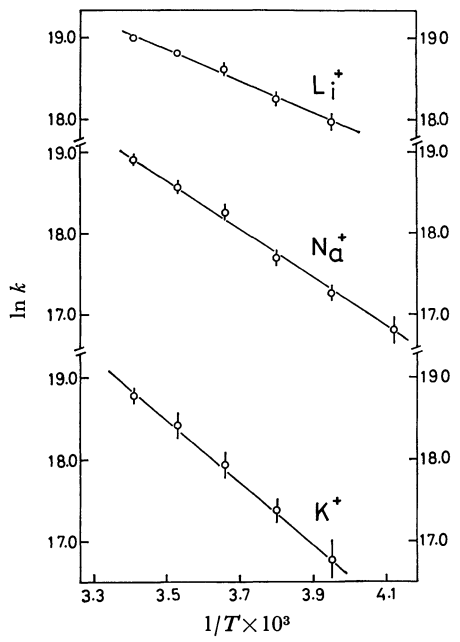

Fig. 1. Temperature dependence of the electron-transfer rates of various alkali metal tetracyanoethylenide systems in DME at the temperature range from −30° to 20°C; upper line: lithium salt; middle line: sodium salt; lower line: potassium salt.

The values for the alkali metal salts were found to be close to each other. Especially, almost the same value was obtained for the sodium and potassium salts, within the limits of experimental error. The system of tetra-*n*-butylammonium salt showed the largest activation energy in the solvent.

We also studied the cesium tetracyanoethylenide system, but the anomalously large ESR linewidth at higher concentrations of $TCNE^-$ prevented us from obtaining reliable data for this counterion.

Discussion

In order to understand the ionic forms and structures of the radical anions, it is profitable to compare the rate constants and activation energies obtained in this study with those of naphthalenide-naphthalene systems. Hirota *et al.*[9] clearly demonstrated the relationship between the structures of ion pairs and the kinetics of electron-transfer reactions in this system. The rate constants for solvent-separated ion pairs at 25°C were found to be of the order $10^9 M^{-1}sec^{-1}$, while those for contact ion pairs range from 5×10^6 to $10^8 M^{-1}sec^{-1}$. The activation energies were 2.9—3.6 kcal/mol for solvent-separated ion pairs and 4—6 kcal for contact ion pairs.

Although it is expected, on the basis of the information described above, that DME-alkali metal tetracyanoethylenide systems involve contact ion-pair structures, no metal splittings and spectral distortions characteristic to contact ion pairs were observed in the ESR spectra of these systems. Consequently, it may be supposed that these systems involve essentially solvent-separated ion pairs. This consideration is in accordance with the fact that small alkali metal ions are well solvated by DME and THF molecules.[14,15] Since normal straight lines are obtained in Arrhenius plots for these systems, we can conclude that essentially only one ionic form is present, at least in this temperature range.[9] This conclusion can be applied to all

14) D. N. Bhattacharyya, C. L. Lee, J. Smid, and M. Szwarc, *J. Phys. Chem.* **69**, 608 (1965).
15) C. Carvajal, K. J. Tölle, J. Smid, and M. Szwarc, *J. Amer. Chem. Soc.*, **87**, 5548 (1965).

the systems investigated, since similar straight lines are obtained in the remaining systems, also. Accepting the solvent-separated ion-pair model, the order of the activation energies in DME-alkali metal tetracyanoethylenide systems can easily be understood in the following manner. The thickness of the solvation shells around the metal ions is presumed to be in the order of $Li^+ > Na^+ > K^+$, therefore, the reverse order can be expected in the electrostatic interactions between metal ions and $TCNE^-$.[14] Accordingly, it seems reasonable that the activation energies estimated in this experiment are in the order of $Li^+ < Na^+ < K^+$, since a higher electrostatic interaction of the ion pair is thought to give a higher activation energy in the electron-transfer reactions.

In THF-alkali metal tetracyanoethylenide systems, the observed values of the rate constants suggest the contact-ion-pair model, whereas the values of the activation energy suggest the solvent-separated ion-pair model. However, the latter structure is more realistic in these systems, because no metal splittings and spectral distortions were observed in the ESR spectra, as in the case of DME. The activation energies for the alkali metal salts are rather small in comparison with those in the DME systems and are close to each other. These results suggest that alkali metal ions paired with $TCNE^-$ are well solvated in THF. In fact, it is reported that sodium ions have a larger solvated radius in THF as compared with DME.[15] A small but not negligible difference in the activation energies between lithium and the other metals can be attributed to the fact that the former ion is more highly solvated than the latter.[14]

In both solvents, tetra-*n*-butylammonium salt gives relatively large activation energies, indicating a strong electrostatic interaction between the alkylammonium ion and the radical anion in spite of its bulkiness. This is because bulky ammonium ions are not coordinated with either DME or THF molecules, as has been suggested by Szwarc *et al.*[15]

The magnitudes of the preexponential factors estimated increase with an increase in the activation energies. This is connected with the fact that nearly the same rate constant is obtained for all the systems. The preexponential factors for the THF systems range from 10^{10} to $10^{12} M^{-1} sec^{-1}$. These values are within the limits of those observed in usual liquid-phase reactions. However, rather unexpectedly large preexponential factors are evaluated in all the DME systems except for the lithium salt. It is likely that such large preexponential factors are characteristic of *N*-containing radical anions, because a similar phenomemon has been reported in the potassium 2,2′-bipyridinide system.[16] However, we cannot exclude another possibility that the activation energies are partly contributed by charge-transfer interaction between DME and neutral TCNE. In order to make a conclusive discussion of this problem, more detailed studies should be done in the future.

16) W. L. Reynolds, *J. Phys. Chem.* **67**, 2866 (1963).

Group Interactions in Polyelectrolytes. VI.[1] Amination Kinetics of Chloromethylated Polystyrene in *N,N*-Dimethylformamide and Dimethyl Sulfoxide

Hiroshi KAWABE and MASAYA YANAGITA

The Institute of Physical and Chemical Research, Wako-shi, Saitama

(Received May 2, 1972)

Although the apparent second-order rate constant of the amination of chloromethylated polystyrene with *n*-butylamine or with 2-aminobutanol decreased or increased, respectively, during the course of the amination in dioxane, as has been reported previously, both aminations as well as the aminations of benzyl chloride have been found to conform to the ordinary second-order kinetics in DMF and DMSO. The viscometric measurements have indicated that the viscosity of the reaction mixture decreased during the amination with *n*-butylamine and increased slightly during the amination with 2-aminobutanol, but no relation between the kinetic behavior and the viscometric changes in the reaction mixtures could be found. The magnitude of the rate constants was comparable to that of the amination of benzyl chloride, and it increased with an increase in the dielectric constant of the solvents in this order: dioxane$\ll$DMF$<$DMSO. The effects of the solvents on both the kinetic behavior in the aminations of the polymer and the magnitude of the rate constants have been discussed in terms of the interactions between the solvent and the solute molecules.

The quaternization of chloromethylated polystyrene (CMPS) with tertiary amines in various solvents was studied by Noda and Kagawa.[2] They reported that the initial rate of the quaternization with triethylamine increased with an increase in the dielectric constant of the solvents, like in ordinary Menschutkin reactions; they also reported that the rate in *N,N*-dimethylformamide (DMF) conformed completely to the ordinary second-order equation. Kawabe and Yanagita[3,4] investigated the aminations of CMPS with some primary and secondary amines in dioxane and found that the aminations apparently did not obey the second-order rate law. In the amination with *n*-butylamine or di-*n*-butylamine, the apparent second-order rate constant decreased as the amination proceeded, whereas it increased in the amination with 2-aminobutanol. In these cases, the amination kinetics could be expressed by rate equations which were derived by assuming that the reaction is subjected to the steric hindrance or "hydrophilic effect" of the already-aminated neighboring groups.

In the present study, the authors will deal with the amination of CMPS with *n*-butylamine in DMF and with that with 2-aminobutanol in DMF and dimethyl sulfoxide (DMSO); they will show that the rates conform to the second-order equation and that the rate constants in these solvents are markedly higher than those in dioxane. The effects of the solvents on the kinetic behavior in the aminations of CMPS, and also the dependence of the rate constants on the polarity of the solvents, will be discussed.

Experimental

Materials. The polystyrene and chloromethylated polystyrene (CMPS) were prepared and purified by the procedures described in previous papers.[3,4] The chlorine contents and the molecular weights of CMPS used in the present study are tabulated in Table 1. The 2-aminobutanol was prepared by the procedure described in a previous paper.[4] The other amines, benzyl chloride and the solvents, all of a reagent grade, were distilled before use; they were proved to be pure by their refractive indices. All the other chemicals were of a reagent grade, and de-ionized, de-carbonized water was used throughout the experiments.

Table 1. Chloromethylated polystyrene

Code	Content of Cl %	Degree of Chloromethylation	Molecular weight
SC-4	22.04	0.93	7.3×10^4
SC-5	21.15	0.87	10.3×10^4
SC-6	18.76	0.74	—

Kinetic Measurements. As has been described in the previous papers,[3,4] 150 m*l* of a solution containing one gram of CMPS or benzyl chloride and a large excess of amine (about twenty times as many moles as the chloromethyl group) was stirred at a constant temperature (within$\pm$0.1°). At appropriate intervals, aliquots were taken out, poured into dilute nitric acid, and titrated with 0.1N silver nitrate. The experimental conditions in the aminations of CMPS are listed in Table 2, where *a* denotes the initial concentration of an amine, and *b*, the initial concentration of the chloromethyl group of CMPS. In the amination of benzyl chloride, *a* was 1.06 mol/*l* and *b* was 0.053 mol/*l*. All the reaction except the amination of CMPS with di-*n*-butylamine, which was accompanied by the emulsification of the reaction mixture, were homogeneous and reached completion.

Viscometric Measurements. In the amination of CMPS, the viscosity change in the reaction mixture was also checked. After the reaction mixture had been prepared, a 10 m*l* portion of the solution was taken out and put into an Ostwald-type viscometer, while the temperature was kept constant (within $\pm$0.1°). At appropriate intervals, the flow times were measured, and the relative viscosity (η_{rel}) and the reduced viscosity (η_{sp}/c_p) were determined:

$$\eta_{rel} = \rho_p t/\rho_0 t_0, \quad \eta_{sp} = \eta_{rel} - 1$$

where c_p is the concentration of CMPS expressed by g/100 m*l* where ρ_0 and ρ_p are the densities of a pure solvent and a CMPS solution of the same concentration as the reaction mixture

1) Part V; H. Kawabe and M. Yanagita, This Bulletin, **44**, 896 (1971).
2) I. Noda and I. Kagawa, *Kogyo Kagaku Zasshi*, **66**, 857 (1963).
3) H. Kawabe and M. Yanagita, This Bulletin, **41**, 1518 (1968).
4) H. Kawabe and M. Yanagita, *ibid.*, **44**, 896 (1971).

Table 2. Amination of chloromethylated polystyrehe

Run	Amine[a)]	Solvent	Temp °C	CMPS	a[b)] mol/l	b[c)] mol/l	a/b
1	A	Dioxane	50	SC-4	0.8353	0.0415	20.1
2	A	Dioxane	55	SC-4	0.8480	0.0421	20.1
3	A	Dioxane	60	SC-4	0.8304	0.0414	20.1
4	A	Dioxane	65	SC-4	0.8346	0.0414	20.2
5	A	Dioxane	70	SC-4	0.8470	0.0416	20.9
6	A	DMF	18	SC-5	0.8211	0.0397	20.7
7	A	DMF	30	SC-5	0.7523	0.0375	20.1
8	A	DMF	40	SC-5	0.8205	0.0399	20.6
9	A	DMF	50	SC-5	0.8236	0.0400	20.6
10	B	DMF	30	SC-5	0.8046	0.0409	19.7
11	C	DMF	20	SC-4	0.8853	0.0422	21.0
12	C	DMF	30	SC-4	0.8862	0.0464	19.1
13	C	DMF	40	SC-4	0.8580	0.0409	21.0
14	C	DMF	50	SC-4	0.8852	0.0437	20.3
15	C	DMSO	20	SC-6	0.7123	0.0341	20.9
16	C	DMSO	25	SC-6	0.7005	0.0339	20.7
17	C	DMSO	30	SC-6	0.7070	0.0339	20.9
18	C	DMSO	35	SC-6	0.7077	0.0339	20.9
19	C	DMSO	40	SC-6	0.7100	0.0341	20.8
20	C	DMSO	20	SC-6	0.3557	0.0355	10.0
21	C	DMSO	20	SC-6	0.1800	0.0355	5.1
22	C	DMSO	20	SC-6	0.0362	0.0355	1.0

a) Amine A: *n*-butylamine; Amine B: di-*n*-butylamine;Amine C: 2-aminobutanol
b) a: Initial concentration of amine
c) b: Initial concentration of the polymer expressed in moles of chloromethyl group per litre

respectively, and where t_0 and t are the flow times of a pure solvent and the reaction mixture respectively. The values of c_p were 0.67—0.69, and those of ρ_p/ρ_0 were lower than 1.01 in the present experiments. The observed viscosity change in the reaction mixture was expressed in terms of the viscosity ratio (H), defined by the following equation:

$$H \equiv (\eta_{sp}/c_p)/(\eta_{sp}/c_p)_{\beta\to 0}$$

where β is the fractional conversion of the chloromethyl group. The numerical values of $(\eta_{sp}/c_p)_{\beta\to 0}$, which are the extraporated values of η_{sp}/c_p to $\beta=0$, are as follows:

n-butylamine: 0.5 (dioxane, 50°C), 0.46 (DMF, 50°C)
2-aminobutanol: 0.67 (dioxane, 40°C), 0.8 (DMF, 40°C), 0.51 (DMSO, 30°C)

Results

Amination with n-*Butylamine.* As has been reported previously,[3] the amination of benzyl chloride with *n*-butylamine in dioxane obeyed the second-order rate law, and the rate constant, k, was given by:

$$kt = \frac{1}{(a-b)} \ln \frac{b(a-x)}{a(b-x)} \equiv \overline{kt} \qquad (1)$$

where a and b are the initail concentrations of an amine and the chloromethyl group respectively, while x is the concentration of chloride ions after time t. The dependence of k on the temperature was expressed by:

$$k = A \exp(-E_a/RT) \qquad (2)$$

where A is the frequency factor and E_a, the activation energy.

In the amination of CMPS with *n*-butylamine in dioxane, the rate constant computed by Eq. (1) was not constant, but decreased as the amination proceeded, and the plot of $\overline{kt}$ against t could be expressed approximately by two lines which intersected near the half-amination.[3] This behavior can be explained by the assumption that the amination of the chloromethyl group situated between two already-aminated neighboring groups is sterically obstructed, and the over-all kinetics in the presence of a large excess of the amine ($a \gg b$) can be expressed by Eq. (3):

$$\beta = x/b = 1 - \frac{k_1-k_2}{2k_1-k_2} e^{-2k_1at} - \frac{k_1}{2k_1-k_2} e^{-k_1at} \qquad (3)$$

$$k_1 = \frac{1}{[(2-k_2/k_1)a-b]t} \ln \frac{1-\beta}{1-(2-k_2/k_1)\beta} \qquad (4)$$

$$k_2 = \frac{1}{(a-b)(t-\tau)} \left(\ln \frac{1-\alpha}{1-\beta} - \ln \frac{1-\chi/a}{1-\chi/b} \right) \qquad (5)$$

where k_1 and k_2 are the rate constants of the elementary reactions which are independent of the neighboring groups and under this influence respectively. In Eqs. (4) and (5), $\alpha=x/a$, τ and χ are the values of t and x respectively when $x_1 \simeq b/2$, and x_1 is the concentration of the group which is aminated independently of its neighbors.

Table 3. Amination of chloromethylated polystyrene with *n*-butylamine in dioxane

Temp °C	$k_1\times10^3$ l/mol·min	$k_2\times10^3$ l/mol·min	E_a kcal/mol	$A\times10^{-6}$ l/mol·min
50	6.59	3.84		
55	8.66	6.27	(k_1) 12.1±0.1	1.01
60	11.4	7.82		
65	15.0	9.44	(k_2) 12.1±0.9	0.601
70	19.8	12.2		

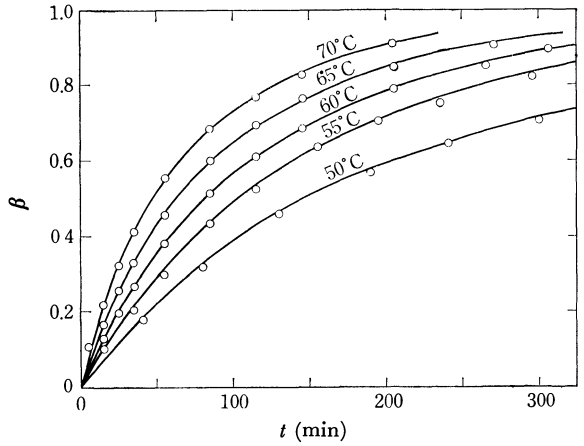

Fig. 1. Amination of chloromethylated polystyrene with *n*-butylamine in dioxane.
——: calculated values, ○: observed values

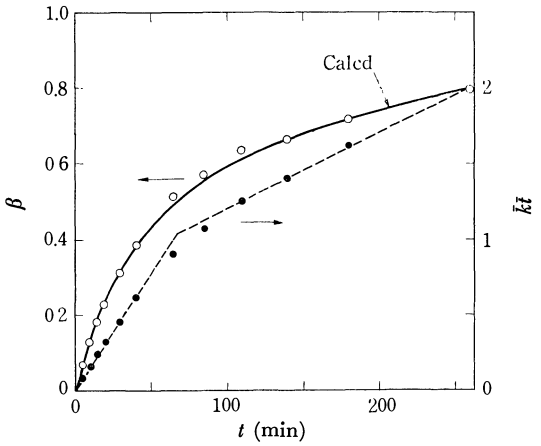

Fig. 2. Amination of chloromethylated polystyrene with di-*n*-butylamine in DMF.

The rate of the amination of CMPS with *n*-butylamine in dioxane has been re-mesaured in the present study in order to obtain a more accurate value for E_a; the results are shown in Fig. 1 and Table 3. The solid lines in Fig. 1, calculated on the basis of Eq. (3) by using the numerical values for k_1 and k_2 listed in Table 4, are in good agreement with the observed values of β, represented by the white circles. The values of E_a and A, computed by the least-squares method on the basis of Eq. (2), are also listed in Table 3.

TABLE 4. AMINATION OF CHLOROMETHYLATED POLYSTYRENE AND BENZYL CHLORIDE WITH *n*-BUTYLAMINE IN DMF

Temp °C	k_P[a] $\times 10^2$ *l*/mol·min	k_B[b] $\times 10^2$ *l*/mol·min	E_a kcal/mol	$A \times 10^{-6}$ *l*/mol·min
18	1.26	—		
20	—	1.61	(k_P) 11.4±0.1	4.89
30	2.78	3.21		
40	5.24	6.10	(k_B) 11.6±0.2	7.42
50	8.89	10.2		

a) k_P: Rate constant of chloromethylated polystyrene
b) k_B: Rate constant of benzyl chloride

In DMF, on the other hand, the aminations of both CMPS and benzyl chloride have turned out to obey the second-order law; their rate constants can be determined on the basis of Eq. (1). The rate constants are tabulated in Table 4. The figures of E_a and A are also listed in Table 4. The rate constants in DMF are much higher than those in dioxane.

In contrast to the amination of CMPS with *n*-butylamine, the amination of CMPS with di-*n*-butylamine in DMF showed a kinetic behavior similar to that in dioxane.[3] The results of the amination in DMF at 30°C are shown in Fig. 2. The $\overline{kt}$-t plot can be expressed approximately by two lines which intersect near $\beta=0.5$, and k_1 and k_2 are given by Eqs. (4) and (5) as follows:

$$k_1 = 1.83\times10^{-2},\ k_2 = 4.98\times10^{-3}\ l/\text{mol}\cdot\text{min}$$

In Fig. 2, the solid line was calculated on the basis of Eq. (3), and the observed values, represented by the white circles, fall substantially on the line.

The amination rates of CMPS with these amines could not be determined in DMSO, because the polymer was precipitated in the initial stage of the amination with *n*-butylamine and di-*n*-butylamine was not dissolved in DMSO.

Amination with 2-Aminobutanol. Although self-acceleration was observed during the amination of CMPS with 2-aminobutanol in dioxane,[4] in DMF or DMSO the amination of CMPS as well as that of benzyl chloride has been found to conform to the second-order rate equation. The rate constants computed by Eq. (1) are tabulated in Tables 5 and 6. The rate constants in DMF are much higher than those in dioxane,[4] and the rate constants in DMSO are even higher than those in DMF. The numerical values for E_a and A are also listed in Tables 5 and 6.

As has been mentioned above, the aminations of CMPS with *n*-butylamine and 2-aminobutanol, which show abnormal kinetic behavior in dioxane, are normal

TABLE 5. AMINATION OF CHLOROMETHYLATED POLYSTYRENE AND BENZYL CHLORIDE WITH 2-AMINOBUTANOL IN DMF

Temp °C	k_P[a] $\times 10^3$ *l*/mol·min	k_B[b] $\times 10^3$ *l*/mol·min	E_a kcal/mol	$A \times 10^{-7}$ *l*/mol·min
20	2.73	3.35		
30	6.18	7.20	(k_P) 13.1±0.2	1.53
40	11.6	14.7	(k_B) 13.3±0.1	2.93
50	22.3	28.1		

a) k_P: Rate constant of chloromethylated polystyrene
b) k_B: Rate constant of benzyl chloride

TABKE 6. AMINATION OF CHLOROMETHYLATED POLYSTYRENE AND BENZYL CHLORIDE WITH 2-AMINOBUTANOL IN DMSO

Temp °C	k_P[a] $\times 10^2$ *l*/mol·min	k_B[b] $\times 10^2$ *l*/mol·min	E_a kcal/mol	$A \times 10^{-7}$ *l*/mol·min
20	1.06	1.40		
25	1.55	1.97	(k_P) 12.2±0.2	1.24
30	2.06	2.75		
35	2.97	3.89	(k_B) 12.5±0.2	3.08
40	4.08	5.56		

a) k_P: Rate constant of chloromethylated polystyrene
b) k_B: Rate constant of benzyl chloride

in DMF and DMSO; that is, their rates, like those of benzyl chloride, are fully represented by the ordinary second-order equation. In these cases, therefore, even the amination of CMPS is considered to be controlled by the bimolecular reaction of chloromethyl groups and amine molecules, and the rate constants are considered to be independent of the initial concentrations of these amines. This has been confirmed in the amination of CMPS with 2-aminobutanol in DMSO. The rate constants computed by Eq. (1), which are shown in Table 7, are much the same over a wide range of amine concentrations.

Table 7. Dependence of rate constants on initial concentration of amine in the amination of chloromethylated polystyrene with 2-aminobutanol in DMSO (20°C)

a/b	21	10	5	1
a, mol/l	0.712	0.356	0.180	0.036
$k\times10^2$, l/mol·min	1.06	1.13	1.13	1.43 (1.46)[a]

a) The figure in parenthesis was computed by the equation, $kt=x/b(b-x)$.

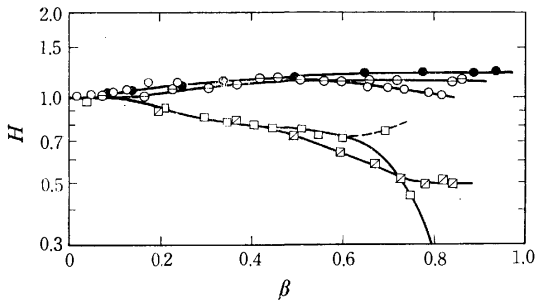

Fig. 3. Viscosity change of reaction mixture in the aminations of chloromethylated polystyrene.
□: *n*-butylamine in dioxane, ▨: *n*-butylamine in DMF
○: 2-aminobutanol in dioxane, ⊖: 2-aminobutanol in DMF, ●: 2-aminobutanol in DMSO

Viscosity Change in the Reaction Mixture During the Amination of Chloromethylated Polystyrene. The viscosity change in the reaction mixture in the amination of CMPS ($a/b=20$) is shown in Fig. 3, where the viscosity ratio, $H\equiv(\eta_{sp}/c_p)/(\eta_{sp}/c_p)_{\beta\to0}$, is plotted against β.

In the amination with *n*-butylamine, H decreases with an increase in β ($H<1$), whereas H increases slightly with an increase in β ($H>1$) in the amination with 2-aminobutanol. On the other hand, the influence of the solvent is less marked. These results show that there is no relation between the kinetic behavior in the amination of CMPS and the viscometric changes in the reaction mixtures.

Discussion

The apparent second-order rate constant of the amination of CMPS with *n*-butylamine in dioxane decreases as the amination proceeds, but the rate in DMF conforms to the ordinary second-order equation. This difference is considered to be related to the expansion and contraction of butylamine molecules in the two solvents, which are present as reagent molecules and also as substituents of the polymer. The Hildebrand solubility parameter, δ, is an index of cohesive interaction among molecules in a solution, and the calculated values of δ at 25°C are as follows: 9.15 (*n*-butylamine), 9.98 (dioxane), and 12.11 (DMF).[5] Since DMF is a poorer solvent for *n*-butylamine than dioxane, it may be possible that the relatively long molecule of *n*-butylamine contracts in DMF because of the attraction among segments of the molecule. On the other hand, in the amination of CMPS with di-*n*-butylamine ($\delta=8.42$[5]), a decrease in the rate constant with an increase in β has been observed even in DMF. In this case, however, di-*n*-butylamine is a secondary amine of a larger molecular weight than *n*-butylamine, and so the former is more bulky than the latter. The contraction of *n*-butylamine molecules in DMF may not be pronounced, but it seems to be sufficient to cancel a small steric obstruction of the neighboring groups, because no such steric effect has been observed in the amination of CMPS with *i*- or *s*-butylamine in dioxane.[7]

Although the rate of the amination of CMPS with 2-aminobutanol is self-accelerated in dioxane as a result of the "hydrophilic effect" of the neighboring hydroxyl group,[4] it conforms to the ordinary second-order kinetics in DMF and DMSO. The effect of the solvents on the kinetic behavior may be explained in terms of interactions between 2-aminobutanol molecules and solvent molecules. The additional solubility parameters of the related substances are: 16.17 (2-aminoethanol) and 13.31 (DMSO).[5] Dioxane must be a poorer solvent for 2-aminobutanol than DMF and DMSO. Not only are DMF and DMSO better solvents for aminoalcohol, but also these dipolar aprotic solvents are hydrogen-bond acceptors; therefore, they may interact with the hydroxyl groups to obstruct the accelerating effect of the neighboring hydroxyl group on the polymer.

The enthalpy of activation, ΔH^*, the entropy of activation, ΔS^*, and the free energy of activation, ΔG^*, are computed by these equations:

$$\begin{cases} \Delta H^* = E_a - RT \\ A/60 = e(kT/h)\exp(\Delta S^*/R) \\ \Delta G^* = \Delta H^* - T\Delta S^* \end{cases}$$

The numerical values for these thermodynamic quantities at 25°C, obtained on the basis of the E_a and A values, are summarized in Table 8.

The value of the rate constant of CMPS is about the same as that of benzyl chloride in any solvent; this is indicated by the ΔG^* values in Table 8. Provided that benzyl chloride is a proper model for DMPS, this fact suggests that the intrinsic reactivity of the functional group of CMPS may be essentially independent of its molecular weight.

The rate constant of the amination with 2-aminobutanol is lower than that of the amination with *n*-butyl-

5) The δ values are calculated at 25°C on the basis of the data given in Ref. 6.
6) J. A. Riddrick and W. B. Banger, "Organic Solvents," third edition, Wiley-Interscience (1970).
7) The present author's unpublished data.

TABLE 8. THERMODYNAMIC QUANTITIES AT 25°C IN THE AMINATION OF CHLOROMETHYLATED POLYSTYRENE AHD BENZYL CHLORIDE

Amine	Solvent	Chloride	$\Delta H^{\ddagger}$ kcal/mol	$\Delta S^{\ddagger}$ e. u.	$\Delta G^{\ddagger}$ kcal/mol
n-Butyl-amine	Dioxane	CMPS, k_1	11.5	−41.2	23.8
		k_2	11.5	−42.2	24.1
		Benzyl[a]	12.0	−41.5	24.3
	DMF	CMPS	10.8	−38.1	22.2
		Benzyl	11.0	−37.2	22.1
2-Aminobutanol	Dioxane[b]	CMPS, k_1	13.0	−40.3	25.0
		k_2	13.0	−38.2	24.4
		Benzyl	12.8	−40.3	24.8
	DMF	CMPS	12.5	−35.8	23.1
		Benzyl	12.7	−34.5	23.0
	DMSO	CMPS	11.6	−36.2	22.4
		Benzyl	11.9	−34.4	22.2

a) Calculated on the basis of the data given in Ref. 3.
b) Calculated on the basis of the data given in Ref. 4.

amine; *e.g.*, in DMF the former is about 20% of the latter, corresponding to a difference in $\Delta G^{\ddagger}$ of 0.9 kcal, and the $\Delta H^{\ddagger}$ of the former reaction is about 1.7 kcal higher than the latter. Accordingly, the lower rate in the amination with 2-aminobutanol seems to be related to the inductive effect of the hydroxyl group; however, it is necessary for a strict interpretation to compare 2-aminobutanol with 2-aminobutane.

On the other hand, the magnitude of the rate constants is greatly influenced by the solvents. The approximate values for the relative rate, expressed on the basis of the rate constant of benzyl chloride or CMPS in dioxane, are as follows:

n-butylamine (benzyl chloride): dioxane(1)<DMF(40)

2-aminobutanol (benzyl chloride and CMPS): dioxane(1) <DMF(20)<DMSO(80)

In the amination of both CMPS and benzyl chloride with 2-aminobutanol in dioxane, the rate constant is somewhat influenced by the initial concentration of the amine;[7] the relative rates, expressed on the basis of the rate constant extrapolated to a zero concentration of the amine, are:

2-aminobutanol (benzyl chloride and CMPS): dioxane(1) <DMF(40)<DMSO(160)

The order of the rate constants is in agreement with that of the dielectric constants of the solvents, D: dioxane (2.21)<DMF (36.71)<DMSO (46.68). It should be noted, however, that the plot of log k against $1/D$ is not linear.

In the amination with *n*-butylamine, the change of solvent from dioxane to DMF lowers the $\Delta H^{\ddagger}$ and increases the $\Delta S^{\ddagger}$. The lower $\Delta H^{\ddagger}$ in DMF may be explained principally in terms of the solvation of the transition state in this dipolar aprotic solvent. This solvation, however, is considered to be accompanied by a lowering of $\Delta S^{\ddagger}$. The observed enhancement of $\Delta S^{\ddagger}$ must be caused by some other factors, one of which may be the change in the configurational entropy of the solvent in the reaction mixture. The solubility parameter of benzyl chloride (δ=9.79[8]) is almost the same as that of dioxane, but the transition state is rather ionic and may have a considerably higher value for δ. The formation of the transition state may thus be accompanied by a decrease in the entropy of the solvent, dioxane. Since the δ value of DMF is much higher than that of dioxane, its entropy change may be relatively small.

In the amination with 2-aminobutanol, the lowering of the $\Delta G^{\ddagger}$ from dioxane to DMF is principally ascribable to the increase in the $\Delta S^{\ddagger}$, and the lowering of the $\Delta H^{\ddagger}$ is not so marked as in the case of *n*-butylamine. This discrepancy cannot be explained at the present time; further investigation is needed, especially in order to establish the dependence of the rate constant on the initial concentration of 2-aminobutanol in dioxane. On the other hand, the lowering of the $\Delta G^{\ddagger}$ from DMF to DMSO is substantially caused by the lowering of the $\Delta H^{\ddagger}$. This small entropy change can be understood if we assume that both DMF and DMSO are dipolar aprotic solvents and that their δ values are approximately the same. The lowering of the $\Delta H^{\ddagger}$ is brought about by the lowering of the potential energy of the activation complex, which may be more strongly solvated in DMSO than it is in DMF, for the former is more polar than the latter.

The authors wish to express their thanks to Mr. Masayuki Takahashi, Mr. Akihiro Kishi, and Mr. Sachio Fukushima for their helpful assistance in preparing the polymer and in carrying out the measurements.

8) The δ value is calculated on the basis of the data given in the book: Kirk-Othmer "Encyclopedia of Chemical Technology," second edition, Vol. 5, Interscience Publishers (1964), p. 282.

Kinetic Studies of the Dissociation and the Recombination Reaction in Aqueous Solutions of Monocarboxylic Acids by Means of Ultrasonic Absorption Measurements

Takayuki SANO, Tomohiro MIYAZAKI, Nobuhide TATSUMOTO, and Tatsuya YASUNAGA
Department of Chemistry, Faculty of Science, Hiroshima University, Higashisenda-machi, Hiroshima
(Received April 25, 1972)

The ultrasonic absorptions were measured in aqueous solutions of acetic, propionic, butyric, valeric, and chloroacetic acids as a function of the pH over the frequency range from 1.5 to 220 MHz at 25°C. From the dependences of μ'_{max} and f_r on pH, it was deduced that the perturbation of the ionization equilibrium of acids was the cause of the excess absorptions in dilute aqueous solutions. The kinetic parameters thus calculated were compared with those obtained by other methods.

It is well known that the ionization equilibrium exists in aqueous solutions of carboxylic acids. Their equilibrium constants have thus far been determined by means of static methods. However, the reaction is so rapid that the kinetic studies of this process could not be done until the appearance of the relaxation methods.

In 1964, Nürnberg and his co-workers[1] determined the dissociation and the recombination rate constants for a number of carboxylic acids by a kind of the relaxation method, the high-level faradaic rectification method. Eigen and his co-workers[2] have also determined the rate constants for some acids by the electric-field method.

On the other hand, the ultrasonic absorption measurements in liquid carboxylic acids have been carried out by many investigators.[3] As a result, it has been concluded that the absorption in pure carboxylic acid is due to the perturbation of the equilibrium between the cyclic dimer and the open dimer. However another type of absorption different from that in the liquid of pure acids has been observed in comparatively dilute aqueous solutions. The perturbation of the ionization equilibrium[4] has been expected to be a cause of this type of absorption, but no thorough consideration has been done of this absorption. Therefore, it seems that it would be very interesting to clarify the mechanism of the absorption and to compare the kinetic parameters obtained by the ultrasonic method with those obtained by other methods.

Experimental

In aqueous solutions of monocarboxylic acids, the ultrasonic absorption was measured by means of the pulse technique[5] over the frequency range from 1.5 to 220 MHz at various concentrations and pH's. The sing-around[6] method operated at 1.92 MHz was used to measure the sound velocity. The concentrations of the hydrogen ion were determined with a Hitachi-Horiba F-5 type pH meter. The densities were measured using a pycnometer. All the measurements were made at 25°C.

The monocarboxylic acids used were acetic, propionic, butyric, and valeric acids, in which the alkyl group consists of hydrocarbon only, and monochloro-, dichloro-, and trifluoro-acetic acids, which contain halogen atoms in the alkyl group. Guaranteed reagents were used throughout this study without further purification.

Results

The spectra of the ultrasonic absorption in the aqueous solutions of acetic acid are shown in Fig. 1. Double relaxations are observed in 3—6M solutions and are expressed by the following equation:

$$(\alpha\lambda)' = vf\left(\frac{\alpha}{f^2} - B\right) = vf\left[\frac{A_1}{1+(f/f_{r1})^2} + \frac{A_2}{1+(f/f_{r2})^2}\right], \quad (1)$$

where α is the ultrasonic absorption coefficient, λ is the wavelength of the acoustic wave, $(\alpha\lambda)'$ is the excess absorption per wavelength, v is the velocity of sound, f is the frequency of sound, A and B are the relaxational and classical absorptions respectively, and f_r is the relaxation frequency, and where the subscripts 1 and 2 refer to the absorption at the lower and higher fre-

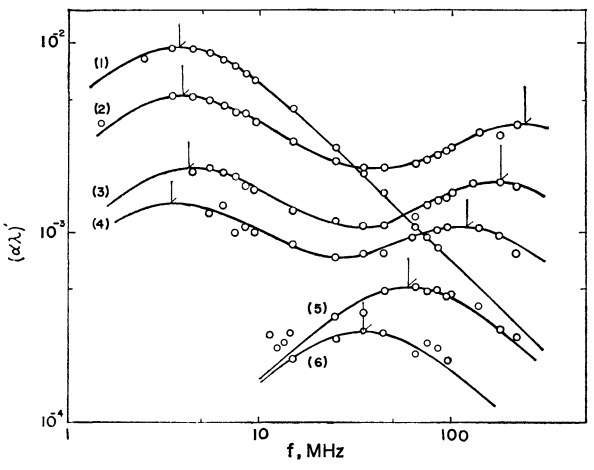

Fig. 1. Ultrasonic absorption spectra of acetic acid in aqueous solutions at 25°C. (1): 8.02M, (2): 6.01M, (3): 4.01M, (4): (4): 3.00M, (5): 1.45M, (6): 1.00M.

1) H. W. Nürnberg and H. W. Dürbeck, *Z. Anal. Chem.*, **205**, 217 (1964).
2) M. Eigen and J. Schoen, *Z. Elektrochem.*, **59**, 483 (1955), M. Eigen and K. Tamm, *ibid.*, **66**, 93 (1962).
3) B. Spakowski, *C. R. Acad. Sci. URSS.*, **18**, 169 (1938), J. Lamb and J. M. M. Pinkerton, *Proc. Roy. Soc., Ser. A*, **199**, 114 (1949), J. E. Piercy and J. Lamb, *Trans. Faraday Soc.*, **52**, 930 (1956).
4) L. G. Jackopin and E. Yeager. Technical Report No. 35 (1969).
5) N. Tatsumoto, *J. Chem. Phys.*, **47**, 4561 (1967).
6) T. Yasunaga, N. Tatsumoto, and M. Miura, This Bulletin, **37**, 1655 (1964).

quencies respectively.

In 1, 1.5, and 8M solutions single relaxations are observed; they may be represented as follows:

$$(\alpha\lambda)' = vf\left(\frac{\alpha}{f^2} - B\right) = vf\frac{A}{1+(f/f_r)^2} \qquad (2)$$

The solid lines in Fig. 1 are theoretical curves which are expressed by either Eq. (1) or (2). The values of the parameters, the relaxation frequency (f_r), and the maximum absorption per wavelength (μ'_{max}) are listed in Table 1, together with the velocity of sound (v), and the density (ρ).

Table 1. The acoustical characteristics of acetic acid at various concentrations at 25°C

M	f (MHz)	μ'_{max} (10^{-4})	pH	v (10^5 cm·sec^{-1})	ρ (g·cm^{-3})
8.02	3.8	95.0	1.43	1.4984	1.0494
6.02	4.0	51.9	1.67	1.5255	1.0392
	240	35.8			
4.01	4.3	21.3	1.85	1.5369	1.0270
	180	17.8			
3.00	3.5	13.9	1.93	1.5341	1.0147
	130	10.8			
1.45	60	5.2	2.23	1.5216	1.0066
1.00	35	3.1	2.26	1.5160	1.0047

As can be seen in Fig. 1, the excess absorption at the lower frequency decreases with a decrease in the concentration, and it entirely disappears in 1 and 1.5M solutions over the frequency range measured. This behavior of the spectra shows that the excess absorptions in 1 and 1.5M solutions correspond to those at the higher frequency in 3—6M solutions. On the other hand, the excess absorption in 8M, and that at the lower frequency in 3—6M solutions, seem to be identical with that in pure acetic acid. The mechanism of these absorptions has been discussed in detail by Atkinson and his co-workers.[7] Since our purpose in this paper is to investigate the mechanism of the absorption at higher frequencies, the measurements of the ultrasonic absorption were carried out in detail for a 1M solution, in which the absorption at lower frequencies disappears.

Now, assuming that the excess absorption is associated with the dissociation and the recombination reaction of the acetic acid, the best way to justify the above assumption is to measure the ultrasonic absorption at various pH's in the 1M solution, in which the excess absorption disappears at lower frequencies. Under these conditions, the results obtained are shown in Fig. 2, while the values of the ultrasonic parameters are listed in Table 2. It can be seen from Fig. 2 that both f_r and μ'_{max} are dependent on the pH. This fact may imply the validity of the above assumption.

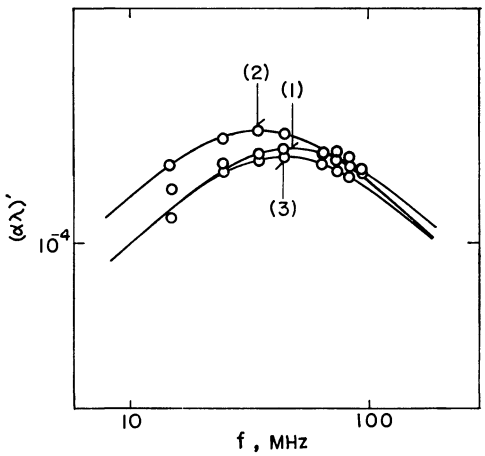

Fig. 2. Ultrasonic absorption spectra in 1.00M solution of acetic acid at 25°C. (1): pH 1.76, (2): pH 2.26, (3): pH 3.20.

In the dissociation and the recombination reaction of acid, which is generally represented by the following equation:

$$AH \underset{k_r}{\overset{k_d}{\rightleftarrows}} A^- + H^+$$

the relaxation time, τ, and μ'_{max} are given by the following equations:

$$\frac{1}{\tau} = 2\pi f_r = k_d + k_r(A^- + H^+) = k_r(K + A^- + H^+) \qquad (3)$$

Table 2. The acoustical characteristics of carboxylic acids at various pH's at 25°C

	M	pH	f_r (MHz)	μ'_{max} (10^{-4})	v (10^5 cm·sec^{-1})	ρ (g·cm^{-3})
Acetic acid	1.00	1.76	49±3	2.6	1.5156	1.0059
		2.26	35±2	3.1	1.5160	1.0047
		2.75	40±5	2.8	1.5169	1.0062
		3.20	45±5	2.4	1.5189	1.0070
Propionic acid	1.01	2.42	62±5	4.4	1.5275	1.0025
		3.16	40±5	1.9	1.5294	1.0030
		3.40	58±10	2.6	1.5307	1.0026
Butyric acid	0.507	1.90	50±3	1.5	1.5198	0.9992
		2.21	40±3	2.7	1.5197	0.9977
		2.55	45±2	3.1	1.5197	0.9966
		2.76	56±2	2.3	1.5199	0.9979
		3.00	65±5	1.8	1.5577	0.9982
Valeric acid	0.103	2.95	43±2	1.8	1.5034	0.9959
		2.67	28±2	1.4	1.5400	0.9958

7) R. D. Corsaso and G. Atkinson, *J. Chem. Phys.*, **55**, 1971 (1971).

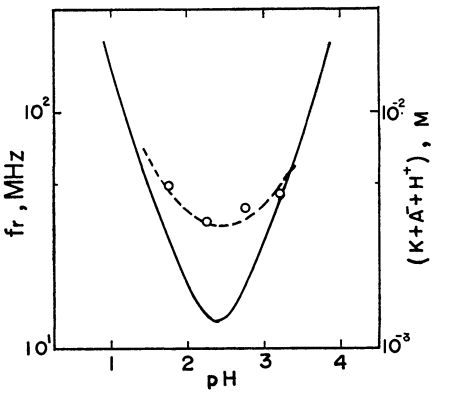

Fig. 3. Plot of the relaxation frequency *versus* pH; the experimental values of f_r are indicated by circles, and solid line shows the dependence of the calculated concentration term on pH.

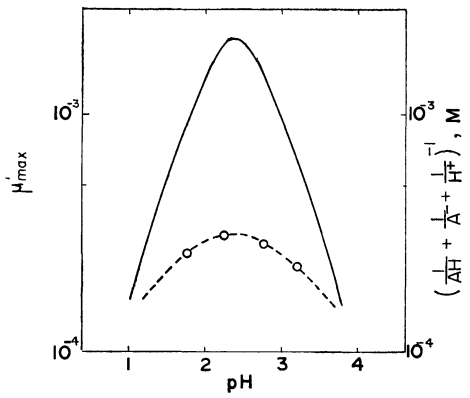

Fig. 4. Plot of maximum of the absorption per wavelength *versus* pH; the experimental values of μ'_{max} are indicated by circles, and the solid line shows the calculated concentration terms.

$$\mu'_{max} = \frac{(\Delta V)^2}{2\beta_0 RT}\left[\frac{1}{AH} + \frac{1}{A^-} + \frac{1}{H^+}\right]^{-1} \quad (4)$$

where k_d and k_r are the rate constants of the dissociation and the recombination respectively, K is the equilibrium constant, β_0 is the adiabatic compressibility, $\boldsymbol{R}$ is the gas constant, T is the absolute temperature, and ΔV is the volume change per mole for the reaction.

In Eqs. (3) and (4), k_r, k_d, and $\pi(\Delta V)^2/2\beta_0 \boldsymbol{R} T$ may be taken as constant, so both f_r, and μ'_{max} are directly proportional to the concentration. The concentration terms at various pH's can be calculated by using the equilibrium constant listed in the literature.[8] From the calculation of the terms in Eqs. (3) and (4), it is found that these terms have a maximum and a minimum at the corresponding pH. The results are presented in Figs. 3 and 4, together with the experimental values of f_r and μ'_{max} respectively. In view of the similarity of the behavior of the experimental values to that of the calculated terms against the pH, the assumption that the excess absorption in aqueous acetic acid is to be attributed to the perturbation of the ionization equilibrium of acid is strongly supported.

8) Landolt-Börnstein, "Physikalish-Chemische Tabellen," Springer (1936).

Table 3. The kinetic parameters for the dissociation and recombination reaction of carboxylic acids at 25°C

	k_d (10^5 sec^{-1})	k_r (10^{10} M^{-1}·sec^{-1})	$\Delta V^{a)}$ (cc·mol^{-1})
Acetic acid	3.1±1.3	1.8±0.8	12.9±2.9 (12.5)
Propionic acid	3.4±2.8	2.6±2.1	15.8±2.1 (13.7)
Butyric acid	6.4±2.6	4.3±1.7	12.3±1.1 (13.7)
Valeric acid	5.8±3.2	3.9±2.2	13.9±0.5
Monochloro-acetic acid	260±30	1.9±0.2	7.9±0.2 (9.2)

a) The values presented in parentheses have been repoted by Kauzman.[6]

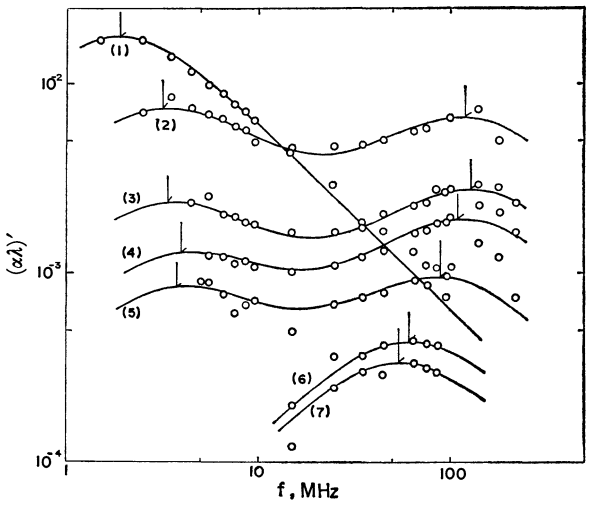

Fig. 5. Ultrasonic absorption spectra of propionic acid at 25°C. (1): 13.6M, (2): 4.98M, (3): 2.98M, (4): 2.49M, (5): 1.96M, (6): 1.01M, (7): 0.49M.

The k_d, k_r, and ΔV values were calculated by using Eqs. (3) and (4); they are listed in Table 3.

Secondly, in aqueous solutions of propionic, butyric, and valeric acids, the ultrasonic absorption were measured by the same procedure as was used in the acetic acid. The ultrasonic absorption spectra of the propionic acid at various concentrations are represented in Fig. 5. It may be seen from the figure that the excess

Table 4. The acoustical characteristics of propionic acid at various concentrations at 25°C

M	f_r (MHz)	μ'_{max} (10^{-4})	pH	v (10^5 cm·sec^{-1})	ρ (g·cm^{-3})
13.6	2.2	148	—	1.1524	0.9886
4.98	3.2	71.1	1.94	1.5142	1.0187
	120	6.4			
2.98	3.4	22.4	2.13	1.5453	1.0119
	130	2.7			
2.49	4.0	11.8	2.19	1.5463	1.0108
	110	1.6			
1.96	3.8	7.4	2.26	1.5434	1.0089
	90	8.8			
1.01	62	4.4	2.43	1.5275	1.0025
9.49	55	3.4	2.58	1.5139	0.9986

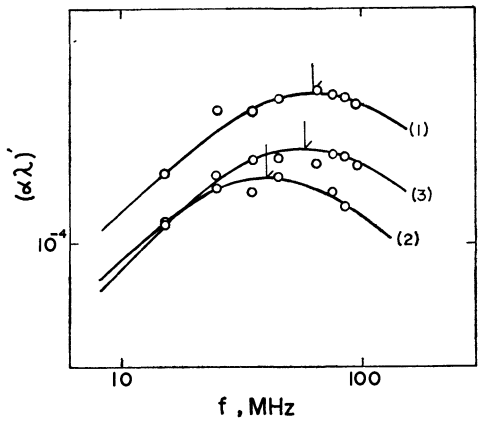

Fig. 6. Ultrasonic absorption apectra of 1.01M solution of propionic acid at 25°C. (1): pH 2.42, (2): pH 3.16, (3): pH 3.40.

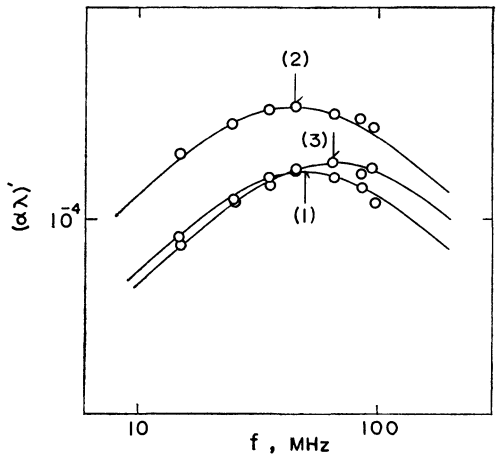

Fig. 7. Ultrasonic absorption spectra of 0.507M solution of butyric acid at 25°C. (1): pH 1.90, (2): pH 2.55, (3): pH 3.00.

absorptions at the lower frequency correspond to those in pure propionic acid, and that the absorptions in 0.5 and 1M solutions, represented by the single relaxation curves are identical with those at higher frequencies in solutions more concentrated than 2M. The relaxation parameters are listed in Table 4.

Next, Fig. 6 shows the ultrasonic absorption spectra in a 1M solution of the propionic acid at various pH's. Similarly, as is shown in Fig. 7, the ultrasonic absorptions were observed in 0.5M solutions of butyric acid at various pH's. In the butyric acid, however, the low solubility prevented the measurement of the dependence of the absorption on the concentration of the acid. Valeric acid is less soluble than butyric acid, so it is very difficult to investigate the dependence of the absorption not only on the acid concentration, but also on the pH. As the result of our great effort, however, the absorptions were measured in a 0.1M solution of the valeric acid at the values of pH, 2.69 and 2.75. The spectra are shown in Fig. 8. The relaxation parameters for propionic, butyric, and valeric acids are presented in Table 2.

As can be seen in Figs. 6—8, both f_r and μ'_{max} are dependent on the pH. The mechanism of these

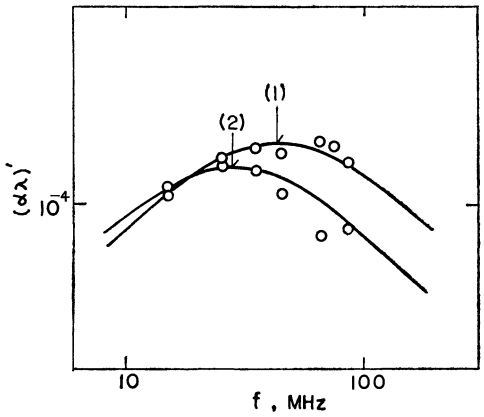

Fig. 8. Ultrasonic absorption spectra of 0.103M solution of valeric acid at 25°C. (1): pH 2.75, (2): pH 2.69.

acid. The kinetic parameters based on the reaction for each acid are calculated in a manner similar to the case of the acetic acid; they are listed in Table 3. The kinetic parameters for the acetic and propionic acids at various concentrations are presented in Table 5.

Table 5. The kinetic parameters for the dissociation and recombination reaction of acetic and propionic acids at various concentrations at 25°C

	M	k_d (10^5 sec^{-1})	k_r (10^{10} $M^{-1}\cdot sec^{-1}$)	ΔV ($cc\cdot mol^{-1}$)
Acetic acid	6.02	9.3	5.5	25.0
	4.01	10	5.9	17.9
	3.00	8.6	5.1	15.0
	1.45	6.3	3.7	11.9
	1.00	4.3	2.6	10.2
Propionic	4.98	5.7	4.4	33.8
acid	2.98	8.3	6.4	23.8
	2.49	7.8	6.0	19.1
	1.96	7.2	5.5	15.1
	1.01	7.0	5.4	12.7
	0.49	8.8	6.8	13.5

absorptions, therefore, may be due to the dissociation and recombination reaction of acid, as in the acetic

Thirdly, it is very interesting to study the variation in the kinetic parameters of monocarboxylic acids with the change in molecular structure. For this purpose, the ultrasonic absorptions were measured in aqueous solutions of halogeno carboxylic caids, which have quite different electronegativities from the above acids. The single relaxation curves obtained from the measurements of the absorption in 0.5 and 1M solutions of monochloro acetic acid are graphed in Fig. 9. The relaxation parameters are listed in Table 6. As the values of f_r, 180, and 220 MHz are near the end of the frequency range measured, it is thought that the experimental error may be larger than that of other acids. In this case, the kinetic parameters were also calculated on the basis of the expectation that the absorptions are associated with the perturbation of the ionization equilibrium of acid. The results are listed in Table 3. The ultrasonic absorptions were measured in 1M solutions of dichloro- and trifluoroacetic acids, but in both acids no excess absorption was observed in the fre-

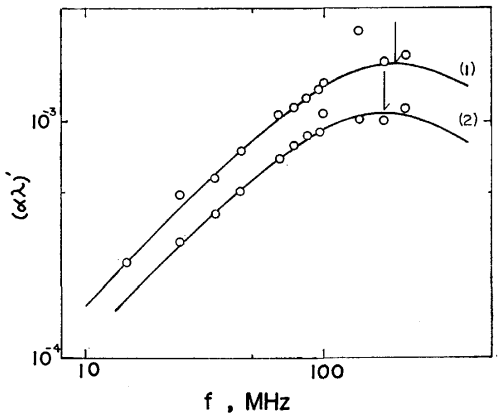

Fig. 9. Ultrasonic absorption spectra of 1.00M and 0.503M solutions of monochloroacetic acid at 25°C.

Table 6. The acoustical characteristics of chloroacetic acid at 25°C

M	pH	f_r (MHz)	μ'_{max} (10^{-4})	v (10^5 cm·sec^{-1})	ρ (g·cm^{-3})
0.50	1.56	180	10.9	1.5079	1.0131
1.00	1.36	200	17.5	1.5175	1.0299

quency range from 15 to 95 MHz. The values of α/f^2 are 31×10^{-17} and 36×10^{-17} cm^{-1}sec^2 in solutions of dichloro- and trifluoroacetic acids respectively, so the f_r values associated with the ionization equilibrium of acid can be expected to be higher than the frequency measured in this work.

Discussion

As can be seen in Table 3, the values of ΔV are in close agreement with those determined from the density measurements by Kauzman and his co-workers.[9] The values of the recombination rate constant, $\sim10^{10}$M^{-1}sec^{-1}, may be of an adequate order of magnitude as the rate of the diffusion-controlled reaction. As for the acetic acid, the values of the parameters may be comparable to those obtained from the ultrasonic absorption measurement by Yeager,[4] $k_r=5.5\times10^{10}$ M^{-1}sec^{-1}, $k_d=1.0\times10^6$ sec^{-1}, and $\Delta V=12.2$ cc·mol^{-1}.

Next, the Taft rule[10] can be applied to the relationship between the rate constants and the polar substituent constants. Taft's equation is given by:

$$\log k = \rho^*\sigma^*$$

where k is the rate constant, ρ^* is the constant characterized by only the type of the reaction, and σ^* is the polar substituent constant. In Fig. 10, the plots of $\log k_d$ and $\log k_r$ against σ^* are presented, together with the values for formic and benzoic acids obtained by Eigen and his co-workers.[2] $\log k_d$ is linearly correlated with σ^*, whereas $\log k_r$ is nearly constant within the experimental error. From the linear relationship between $\log k_d$ and σ^*, ρ^* was determined to be 1.7.

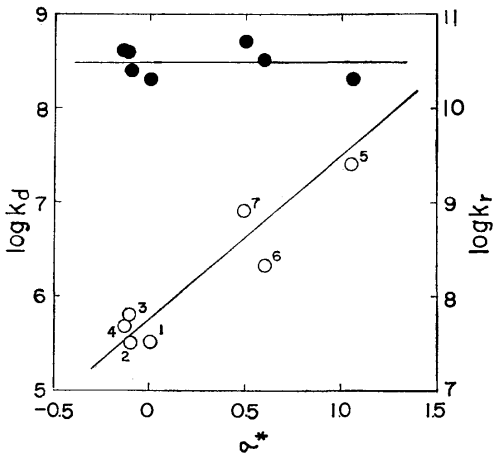

Fig. 10. Plot of $\log k_d$ (open circles) and $\log k_r$ (solid circles) *versus* polar substituent parameter σ^* for the various carboxylic acids. 1: acetic, 2: propionic, 3: butyric, 4: valeric, 5:monochloroacetic, 6: benzoic, 7: formic acids.

The value[11] of ρ^* found in the literature, estimated from the relationship between the ionization equilibrium constants of the carboxylic acids and σ^*, is 1.721 ± 0.025; this is in good agreement with that obtained for the recombination rate constants in the present work. This result suggests that the difference in the values of the equilibrium constants among the various carboxylic acids results not from the recombination rate constant, but from the dissociation rate constant. From these discussions, it can reasonably be concluded that the excess absorptions in dilute aqueous solutions of the carboxylic acids measured in the present work are associated with the perturbation of the ionization equilibrium of acids.

Finally, the kinetic parameters obtained from the ultrasonic absorption measurements of the acetic and propionic acids at various concentrations are listed in Table 5. As is shown in this Table, the rate constants for both the acids may be considered to be independent of the concentration, but the values of ΔV increase with an increase in the concentration of the solutions for each acid. For this result, the following three causes may be considered as the origin of the change in ΔV: 1) the experimental error, 2) the neglect of the activity coefficient, and 3) the change in the state of carboxylic acids in the solutions. The change in ΔV with the concentration, however, is far greater than the effects of 1) and 2). On the other hand, in the case of the ionization reaction of carboxylic acids it seems that the difference in the amount of hydration between the two species gives rise to the volume change, ΔV. The carboxylic acids form dimeric and polymeric molecules by intermolecular hydrogen bonding in concentrated solutions, and become electrically more neutral than the monomeric molecule. Therefore, the amount of hydrating water may decrease in the following order: ionic>monomeric>dimeric molecules, and the volume change between ionic and nonionic molecules may increase with an increase in the concentration. Consequently, the above feature in ΔV seems to result from the 3) effect, although this conclusion cannot be confirmed quantitatively at present.

9) W. Kauzman, A. Bodanszky, and J. Rasper, *J. Amer. Chem. Soc.*, **84**, 1777 (1962).
10) R. W. Taft, Jr., *ibid.*, **74**, 2729 (1952).
11) A. L. Henne and C. J. Fox, *ibid.*, **76**, 479 (1954).

Heat Capacity of Tetramethylsilane in the Region from 2 to 26 K and Premelting Range[1)]

Takako SHINODA, Hisae ENOKIDO, Yoji MAEDA,* Hiroshi TOMITA, and Yo-ichiro MASHIKO
National Chemical Laboratory for Industry, Shibuya-ku, Tokyo
(Received April 26, 1972)

The heat capacity of tetramethylsilane was measured at temperatures from 2 to 26 K and in the premelting temperature range for two crystalline forms. There are two crystalline forms in solid tetramethylsilane. The heat of fusion and triple point temperature of a stable form were found to be 1611.2±0.9 cal/mol and 174.049 K, while those of a metastable form to be 1396.0±0.8 cal/mol and 170.981 K. Tetramethylsilane was highly purified by preparative gas chromatography. The amount of impurity in the specimen of $Si(CH_3)_4$ was estimated to be 0.004_6 mol% from measurement of the melting point range for two crystalline forms. The Debye characteristic temperature at 0 K, $\theta_D(0)$, was derived from low temperature heat capacity data, and the $\theta_D(T)/\theta_D(0)$ curve was compared with those for $C(CH_3)_4$ and CF_4. Despite high purity, C_p values for two crystalline forms in the region below melting points increases abnormally with the rise of temperature. The phenomena were interpreted as due to effects of formation of vacancies in the crystals and of melting accompanied by molecular orientation transition; analysis of heat capacity curves for the two crystalline forms was made in the region befow the melting point.

In previous papers[2,3)] we reported on the thermodynamic properties of tetrahedral molecules, $C(CH_3)_4$ and CF_4, which undergo orientationally disordering transition below their melting point. In the present paper we treat tetramethylsilane $Si(CH_3)_4$ which does not undergo phase transition below its melting point.

Heat capacity data for $Si(CH_3)_4$ were given by Aston *et al.*[4)] In their work the sample used was of 99.88 mol% purity, and the heat capacity data were reported for temperatures 12 to 290 K. We have attempted to prepare $Si(CH_3)_4$ of higher purity, and provide more complete and accurate data on the heat capacity at lower temperatures and in the premelting range, supplementing the data for $T<12$ K.

The Debye characteristic temperature at 0 K, $\theta_D(0)$, is derived from the low temperature heat capacity data, and a comparison of the temperature dependence of $\theta_D(T)/\theta_D(0)$ is made with that for other tetrahedral molecules reported by the present authors taking into account the octupole interaction of molecules in the crystals.

A possible interpretation of premelting anomalies in two crystalline forms of $Si(CH_3)_4$ is offered by theories of lattice vacancies and simultaneous positional and orientational transitions, and the activation energies are estimated from the analysis of the heat capacity curves in the region below melting point.

Experimental

Materials. Tetramethylsilane was obtained from Matheson Coleman & Bell Co. In analytical experiments, a Shimadzu 4AT gas chromatograph was used with a thermal conductivity detector under the following conditions:

Column	3 mm×3 m, Silicone SE 30 (20%) on Shimalite W (80—100 mesh)
Temperature	30°C
Carrier gas	Helium at 40 ml/min.

A chromatogram of crude $Si(CH_3)_4$ is shown in Fig. 1. Retention times and percentage composition of crude $Si(CH_3)_4$ are shown in Table 1. The percentage composition was calculated by means of area under peaks.

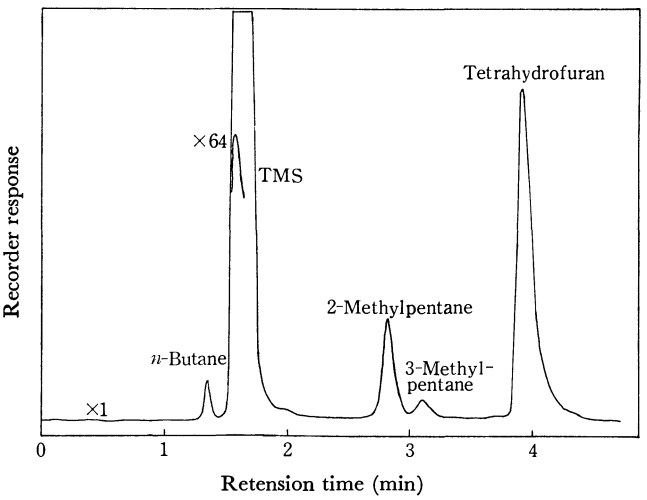

Fig. 1. Analytical gas chromatogram of crude $Si(CH_3)_4$.

TABLE 1. RETENTION TIMES AND PERCENTAGE COMPOSITION OF CRUDE $Si(CH_3)_4$

Components		Retention time	Calculated composition
Peak No.	Compound	(min)	(%)
1	*n*-Butane	1.3	0.02
2	Tetramethylsilane	1.6	98.12
3	2-Methylpentane	2.8	0.29
4	3-Methylpentane	3.1	0.03
5	Tetrahydrofuran	3.8	1.52

Attempts to remove impurities by a fractional distillation or zone refining were unsuccessful, but they were completely removed by preparative scale gas chromatography. A Varian Aerograph Autoprep 712 preparative instrument with a hydrogen flame ionization detector was used to prepare a

* Present address: Research Institute for Polymers & Textiles, Sawatari, Kanagawa-ku, Yokohama, Japan.

1) Presented at the 23rd Annual Meeting of the Chemical Society of Japan, Tokyo, April, 1970.

2) H. Enokido, T. Shinoda, and Y. Mashiko, This Bulletin, **42**, 84 (1969).

3)H. Enokido, T. Shinoda, and Y. Mashiko, *ibid.*, **42**, 3415 (1969).

4) J. G. Aston, R. M. Kennedy, and H. G. Messerly, *J. Am. Chem. Soc.*, **63**, 2343 (1941).

total of 100 ml of pure $Si(CH_3)_4$ under the following conditions:

Column	3/8 in (O.D.) × 50 ft Silicone SE 30 (10%) on Chromosorb A (60—80 mesh)
Temperature	80°C
Carrier gas	Nitrogen at 150 ml/min.
Sample size	2.0 ml injected manually

No impurities of the collected $Si(CH_3)_4$ were detected by analytical gas chromatography. However, the amount of solid-insoluble liquid-soluble impurity was determined by the measurement of melting point, the purity being found to be 99.995_4 mol%.

Apparatus. A new calorimeter was constructed to measure the heat capacity of substances which are solid or liquid at room temperature in the range from 2 K to 150°C. In basic design the cryostat is similar to the adiabatic calorimeter for condensed gases described previously.[5] The general assembly is illustrated in Fig. 2. About three liters of liquid helium can be held by a coolant container F (brass cylinder) which allows measurement to continue for a period longer than 12 hours at low temperature. A thermal station E (copper cylinder) has an internal volume of about 500 cc, and can contain liquid helium in the measurements at low temperature. A heater (#34 manganin) is wound around E, and a difference thermocouple is placed between the thermal station and the top of an adiabatic shield B. Thermocouple junctions (chromel p—constantan) are provided at the bottom of F and at E for their absolute temperature measurements. All electrical lead wires come from the top of the cryostat through a stainless steel pipe at the center. They wound round the cylinder at the bottom of F and also round E and B, entering inside the shield through 30 holes drilled at the bottom edge of the side of the adiabatic shield. In assembly, an inside jacket G is soldered to the bottom of F and an outside jacket H to the top plate both with Wood's alloy or solder.

A sectional view of the calorimeter vessel, made of silver-plated copper (0.2 mm thick) and with an internal volume of about 60 cc, is shown in Fig. 3. It is hung by means of nylon cords within the adiabatic shield. Eight vanes are soldered inside the vessel. The cap of the vessel is made of Kovar and attached to a Pyrex glass tube through which the vessel can be evacuated and sealed in a vacuum. A platinum thermometer with a heater (#34 manganin, 65 Ω) wound on it is cast into a re-entrant well with Wood's alloy. A germanium thermometer is attached to the bottom of the vessel by means of a sheath (copper). The platinum resistance thermometer used above 13.5 K had been calibrated at the National Bureau of Standards (J. L. Riddle, 1959). The temperature scale was re-calculated on the International Practical Temperature Scale of 1968 by using the tables of differences between the NBS-55 scale, the IPTS-48 and the IPTS-68 derived by Douglas[6] and Bedford *et al.*[7] The germanium resistance thermometer (Cryocal, Inc.) which had been calibrated on the thermodynamic scale at the NBS (Jacquelyn A. Wise, 1969) was used in the temperature range below 13.5 K. All measuring operations of the heat input and the resistances of the thermometers were manually carried out. The monitoring and control of adiabatic conditions were automatically made.[2]

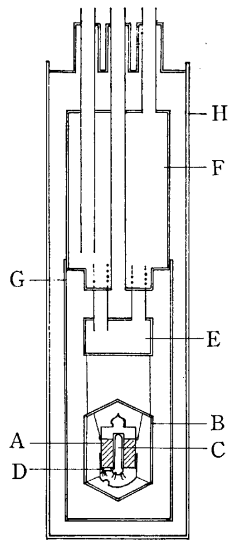

Fig. 2. Cross-section diagram of the cryostat.
A: calorimeter vessel, B: adiabatic shield, C: platinum thermometer, D: germanium thermometer, E: thermal station, F: coolant container, G: inside jacket, H: outside jacket.

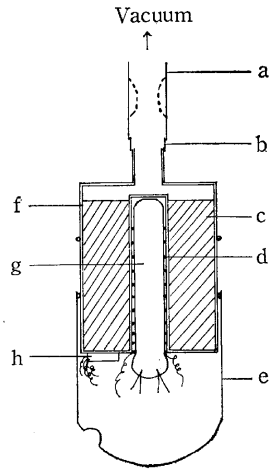

Fig. 3. Cross-section diagram of calorimeter vessel.
a: Pyrex glass tube, b: Kovar tube, c: vane, d: manganin heater, e: copper sheath, f: silver-plated copper vessel, g: platinum thermometer, h: germanium thermometer.

Results and Discussion

Heat Capacity of $Si(CH_3)_4$. The amount of sample in the calorimeter was determined to be 23.0475 g (=0.261233 mol, 35 cc) as liquid by measuring the filling weight. The measured values of heat capactiy in the region 2—26 K and in the premelting range are listed in Table 2. Corrections were made for curvature where necessary. At low temperature, temperature increments were about 0.3—1°. These increased to about 2° at higher temperature. The measurements of heat capacity below melting point were also made several times with various small temperature rise (0.1—0.8°) to determine detailed shapes of heat capacity curves for two crystalline forms in the premelting region. Equilibrium time after heating varied from less than one minute at low temperature to about 7—8 min at higher temperature. In the

5) T. Shinoda, T. Atake, H. Chihara, Y. Mashiko, and S. Seki, *Kogyo Kagaku Zasshi*, **69**, 1619 (1966).

6) T. B. Douglas, *J. Res. NBS*, **73A** 451 (1969).

7) R. E. Bedford, M. Durieux, R. Muijlwijk, and C. R. Barver, *Metrologia*, **5**, 47 (1969).

TABLE 2. HEAT CAPACITY OF $Si(CH_3)_4$
(Molecular weight 88.226; 1cal=4.1840 absolute joules; 0°C=273.15 K)

T(K)	C_p (cal/deg mol)	T(K)	C_p (cal/deg mol)	T(K)	C_p (cal/deg mol)	T(K)	C_p (cal/deg mol)
(Stable form)		12.568	1.095	129.930	26.95	167.726	32.94
2.178	0.004609	12.699	1.127	131.739	27.19	168.747	33.24
2.211	0.005407	13.235	1.269	131.891	27.23	169.761	33.70
2.378	0.005865	13.418	1.321	132.842	27.39	170.764	34.21
2.758	0.008470	14.007	1.474	133.834	27.53	171.581	35.02
3.104	0.01149	14.174	1.524	134.903	27.69	171.753	35.14
3.111	0.01112	15.037	1.793	135.909	27.86	172.441	36.93
3.462	0.01563	15.637	1.977	136.686	27.98	173.193	49.69
3.685	0.01862	15.900	2.056	136.946	28.06	(Metastable form)	
3.822	0.02022	16.520	2.259	137.964	28.20	136.092	28.44
4.104	0.02649	16.828	2.354	138.971	28.36	138.103	28.80
4.165	0.02739	17.371	2.532	140.000	28.51	140.117	29.13
4.478	0.03380	17.803	2.676	140.679	28.60	142.110	29.49
4.673	0.03953	18.288	2.837	140.978	28.64	144.155	29.78
4.804	0.04296	18.488	2.888	141.025	28.66	146.223	30.13
5.068	0.05152	19.243	3.154	142.730	28.91	148.252	30.46
5.121	0.05318	19.643	3.293	142.969	28.96	150.261	30.76
5.454	0.06620	20.146	3.451	144.714	29.22	152.249	31.11
5.470	0.06675	20.869	3.696	144.945	29.25	154.488	31.45
5.814	0.08241	21.019	3.755	146.747	29.53	156.501	31.76
5.880	0.08547	21.915	4.046	148.832	29.85	158.496	32.10
6.194	0.1025	22.196	4.144	150.345	30.08	160.474	32.45
6.292	0.1080	22.784	4.336	151.143	30.21	161.980	32.72
6.583	0.1269	23.491	4.566	152.388	30.39	163.025	32.93
6.700	0.1348	24.202	4.807	153.188	30.53	164.008	33.13
6.982	0.1558	24.666	4.950	155.045	30.81	164.938	33.35
7.111	0.1660	25.142	5.098	155.215	30.84	165.864	33.58
7.385	0.1901	25.749	5.289	157.049	31.13	166.584	33.89
7.522	0.2027	26.023	5.371	157.227	31.18	167.555	34.81
7.788	0.2283	105.995	23.29	159.058	31.42	168.506	36.07
7.939	0.2453	107.960	23.61	159.221	31.46	168.891	36.34
8.196	0.2732	109.905	23.92	159.803	31.52	169.420	39.11
8.364	0.2938	111.822	24.21	159.896	31.53	170.200	57.12
8.613	0.3243	113.764	24.51	161.200	31.71	170.294	89.21
8.792	0.3485	115.730	24.83	161.491	31.77	(Liquid)	
9.232	0.4117	117.756	25.14	162.238	31.90	172.372	38.95
9.665	0.4808	119.839	25.47	162.910	32.00	172.895	39.06
10.076	0.5528	121.898	25.78	163.269	32.06	173.939	39.07
10.333	0.6035	123.935	26.07	164.268	32.26	174.793	39.12
10.855	0.7014	125.952	26.36	165.320	32.46	175.985	39.23
11.832	0.9153	127.861	26.66	165.566	32.50	176.078	39.27
11.849	0.9205	127.951	26.67	166.702	32.74	177.448	39.33

vicinity of melting point and for the melting duration, it became about 14—30 min. We observed heat capacity anomaly to have a very large value (*i.e.* 49.69 cal/mol deg at 173.193 K for a stable form, and 135.4 and 308.7 cal/mol deg at 170.623 and 170.776 K for a metastable form). No hysteresis was observed.

Triple Points of Two Crystalline Forms of $Si(CH_3)_4$. When a sample of $Si(CH_3)_4$ is cooled from room temperature, it crystallizes in a metastable form and is then transforms into a stable form. The transition temperature is dependent upon the cooling rate.

The triple point of each form was obtained from a plot of equilibrium temperatures against reciprocals of the fraction melted. The result is summarized in Table 3. The triple point temperature for the sample of the stable form of $Si(CH_3)_4$ was found to be 174.049 K, and that of the metastable form 170.981 K. The values are also compared with those given by Aston *et al.* in Table 3.

Heats of Fusion of Two Crystalline Forms of $Si(CH_3)_4$. Data of the heat of fusion for the-two crystalline forms are summarized in Table 4 together with those obtained by Aston *et al.* The agreement is not very good, being beyond assigned uncertainties. This is probably due to the fact that it is difficult to estimate exactly a $\int C_p dT$ correction at temperatures slightly below melting point, because C_p value in the premelting range increases unusually with temperature, despite high purity of the

and unreasonable for the enthalpy of formation of vacancies as compared with the value of 3240±220 cal/mol obtained for neopentane. We attempted to interpret these values by assuming that $Si(CH_3)_4$ undergoes simultaneous positional and orientational transitions at melting point. According to a statistical treatment[8] of Ising lattice of three dimensions in terms of a series expansion method, the tail of heat capacity at sufficiently low temperature is given by the first term of low-temperature expansion:

$$C(\text{trans.}) \simeq (1/k)(E/T)^2 \exp(-E/(kT)), \quad (4)$$

where E corresponds to total (positional and orientational) energies of molecular interaction. It was also found by Aston *et al.*[3] that the height of potential barrier hindering internal rotation of methyl groups was considerably lower than that of neopentane. Thus, the values obtained may be regarded as the summation of the enthalpy of vacancy formation and the total energies of positional and orientational disordering of the molecules and internal rotation of methyl groups. However, it is very difficult to estimate each value from the summation without some information on crystal structure and molecular motions in the two forms of $Si(CH_3)_4$.

The calculation of the difference in entropy of metastable and stable forms at 170.981 K is summarized in Table 5. If the metastable form is cooled, it is transformed into the stable form with heat evolution. The entropy of transition is equal to the difference in the entropies of metastable and stable forms at transition temperature.

Table 5. Entropy difference between metastable and stable forms of Si $(CH_3)_4$

	ΔS (e.u.)
Liquid from 174.049 to 170.981 K	−0.693
Crystallization of Metastable Form	−8.165
	−8.858
Crystallization of Stable Form	−9.257
Stable Solid from 174.049 to 170.981 K	−0.663
	−9.920
$S_{\text{stable}} - S_{\text{metastable}}$ at 170.981 K	−1.062

Low Temperature Heat Capacity of $Si(CH_3)_4$. Figure 6 gives a graph of heat capacity measurement for solid $Si(CH_3)_4$ expressed in the form C_p/T^3 *versus* T^2. In the region $T^2<10$ (*i.e.*, $T<3.1$ K), the experimental value of C_p/T^3 increases sharply as T decreases. The situation resembles that of CD_4 crystal in the region $T<20$ K reported by Colwell *et al.*[9] The anomalous shape of the graph of C_p/T^3 *versus* T^2 may be accounted for by a certain amount of crystalline disorder, removal of the spatial degeneracy by crystalline field, isotope effects of partially deuterated methyl groups and some experimental errors. However, it does not seem worthwhile to do any analysis of heat capacity at this stage without further evidence.

If we are to describe the extra contribution to heat capacity as a Schottky-type anomaly, the heat capacity may be separated into a T^{-2} term and normal lattice terms. In a graph of $C_p \times T^2$ versus T^5, the intercept is the coefficient of extra contribution in T^{-2} to the heat capacity. The value 0.0051052 was used for the coefficient derived from the heat capacity data. The calculated $(C_p - 0.0051052)/T^3$ values are shown as a dashed curve in Fig. 6. This curve continues to decrease and approaches a constant value asymptotically, as shown in usual crystals. The constant value obtained corresponds to the Debye characteristic temperature of 136.8±2.0° at 0 K, $\theta_D(0)$. In order to compare the temperature dependence of $\theta_D(T)$ assuming $6N$ degrees of freedom for $Si(CH_3)_4$ with those for $C(CH_3)_4$ and CF_4, the values of $\theta_D(T)$ were plotted against temperature on a reduced scale using the $\theta_D(0)$, as shown in Fig. 7. Here the mean intramolecular rotational frequency of the methyl group in $Si(CH_3)_4$, 170.5 cm^{-1}, obtained by Durig *et al.*[10] from their far-infrared spectrum, was used and $C_p - C_v$ correction was neglected. In Fig. 7 the shape of the $\theta_D(T)/\theta_D(0)$ curve for $Si(CH_3)_4$ is rather similar to that for $C(CH_3)_4$ and CF_4, although there are differences in detail. This seems to demonstrate that the $Si(CH_3)_4$ crystal does not differ from a tetrahedral plastic crystal. Only its transition point of orientational disordering is very close to melting point as observed in the premelting phenomena in the heat capacity curve.

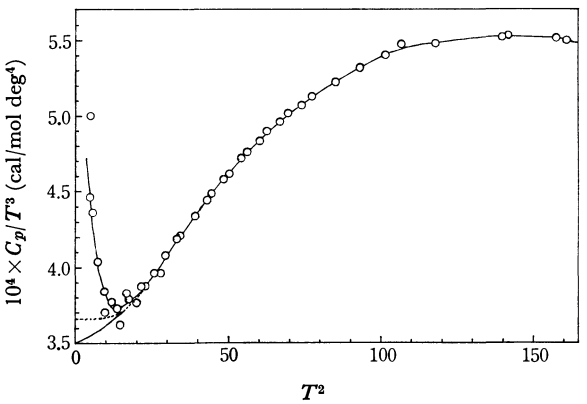

Fig. 6. Plot of C_p/T^3 *versus* T^2 for $Si(CH_3)_4$.

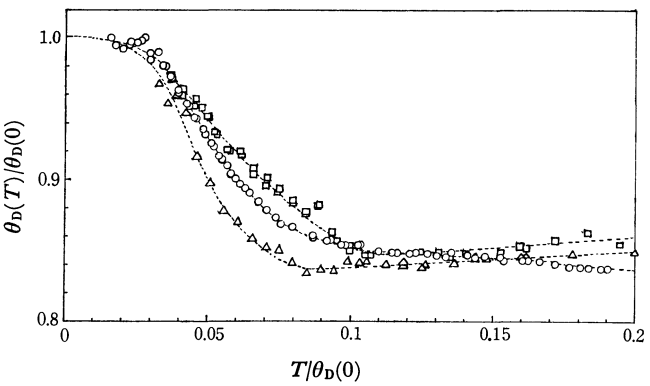

Fig. 7. $\theta_D(T)$ curve on a reduced basis of tetrahedral molecules
○: $Si(CH_3)_4$ ●: $C(CH_3)_4$ △: CF_4

8) C. Domb, *Advan. Phys.*, **9**, 289 (1960).

9) J. H. Colwell, E. K. Gill, and J. A. Morrison, *J. Chem. Phys.*, **39**, 635 (1963).

10) J. R. Durig, S. M. Craven, and J. Bragin, *J. Chem. Phys.*, **52**, 2046 (1970).

The Crystal Structures of Methyl Bromide and Methyl Iodide

Takemi KAWAGUCHI,* Masaya HIJIKIGAWA, Yoshinori HAYAFUJI, Masashi IKEDA, Reizo FUKUSHIMA, and Yujiro TOMIIE†

Faculty of Science, Kwansei Gakuin University, Nishinomiya

(Received May 6, 1972)

The crystal structures of methyl bromide and methyl iodide have been determined by the X-ray diffraction method at about −120°C and about −80°C respectively. Both the crystals are isomorphous, with orthorhombic space group D_{2h}^{16}—*Pnma*. Unit cells containing four molecules have the dimensions: $a=4.47_4(1)$, $b=6.42_0(2)$, and $c=9.15_0(1)$ Å for methyl bromide, and: $a=4.59_7(2)$, $b=6.98_7(1)$, and $c=10.11_7(1)$ Å for methyl iodide. These structures are quite different from that of methyl chloride, which has a symmetry of C_{2v}^{12}—$Cmc2_1$. In the three crystals, all the molecules are found on the mirror planes; the difference lies in the mutual orientations of the molecules.

As part of a series of investigations of various halogenated methanes, the crystal structures of methyl bromide and methyl iodide have been determined by the X-ray diffraction method. Since Burbank reported the crystal structure of methyl chloride,[1] several spectroscopists have discussed whether or not the crystal structures of methyl bromide and methyl iodide are isomorphous with that of methyl chloride.[2] The present authors will here report the crystal structures of these two compounds.

Experimental

Methyl bromide and methyl iodide, both from commercial sources (Tokyo Kasei Industries, Ltd. and Wako Pure Chemical Industries, Ltd., respectively), were purified repeatedly by recrystallization by cooling and by vacuum distillation, followed by sealing in thin-wall glass capillaries in vacuum (0.3 mm in internal diameter and 0.01 mm in wall thickness). The specimen was placed on an X-ray goniometer head and was crystallized by letting flow thereby a cold gas stream from liquid nitrogen. By means of careful temperature control, it was possible to grow a seed of a crystal very near to the size of the capillary at temperatures directly below the melting point (−93.7°C for methyl bromide and −66.5°C for methyl iodide); the crystal was then cooled gradually. It was found later that a single crystal of methyl bromide was grown with the [110] axis, and that a single crystal of methyl iodide was grown with the [100] axis, of the respective orthorhombic lattices nearly along the capillaries.

The cell dimensions of the two crystals were determined from oscillation and Weissenberg photographs around the axes mentioned above. These measurements were made at about −120°C for methyl bromide and at about −80°C for methyl iodide. From systematic extinctions ($0kl$ with $k+l$ odd and $hk0$ with h odd) and intensity distributions, both the crystals were found to belong to space group *Pnma* or $Pn2_1a$, with four molecules per cell. The crystal data for these two compounds are summarized in Table 1. The intensity data were collected by means of multiple-film oscillation photographs, using Ni-filtered Cu $K\alpha$ radiation; 212 independent reflections around the [110] axis for methyl bromide, and 177 such reflections around the [100] axis for methyl iodide, were used for the following analyses. The intensities measured visually were corrected for Lorentz-polarization and absorption effects by the cylindrical approximation, after which they were brought into respective common scales by considering different time exposures.

TABLE 1. CRYSTAL DATA

Methyl bromide, CH_3Br		Methyl iodide, CH_3I	
MW	94.94	MW	141.94
Mp	−93.7°C	Mp	−66.5°C
Tr. p.	−99.4		
Exp. temp.	−120	Exp. temp.	−80
Orthorhombic		Orthorhombic	
a	=4.474±0.012 Å	a	= 4.597±0.016 Å
b	=6.420±0.019	b	= 6.987±0.012
c	=9.150±0.013	c	=10.117±0.011
V	= 262.8 Å^3	V	= 324.9 Å^3
D_X	=2.399 g/cm^3	D_X	=2.901 g/cm^3
D_m[3]	=2.346 (at −195°C)	D_m[3]	=2.840 (at −79°C)
Z	= 4	Z	= 4
μ	=188.64 cm^{-1} (Cu $K\alpha$)	μ	=815.77 cm^{-1} (Cu $K\alpha$)
D_{2h}^{16}—*Pnma*		D_{2h}^{16}—*Pnma*	

Structure Determination and Results

Approximate co-ordinates of the halogen (bromine or iodine) and carbon atoms, deduced from the three-dimensional Patterson diagrams, indicated that these atoms lie on the mirror planes given by the space group *Pnma*. Least-squares refinement, omitting the hydrogen atoms, was applied by using isotropic temperature factors. No positive evidence was found that the space group should not be *Pnma*. The discrepancy indices, $R=\sum||F_o|-|F_c||/\sum|F_o|$, dropped to 0.11 for methyl bromide and to 0.12 for methyl iodide.

The observed and calculated structure factors are listed in Table 2, while the final sets of the positional and thermal parameters of the halogen and carbon atoms are listed in Table 3. The two crystal structures are isomorphous, having the symmetry D_{2h}^{16}-*Pnma*. There are four molecules in each unit cell. The halogen and carbon atoms lie on the mirror planes. Figure 1 shows a schematic drawing of the molecular

* To whom all correspondence should be addressed. Present address: Department of Research and Development, Nippon Crucible Co., Ltd., 925 Inada, Higashi-Osaka 577.

† Deceased on May 31st, 1967.

1) R. D. Burbank, *J. Am. Chem. Soc.*, **75**, 1211 (1953).

2) D. A. Dows, *J. Chem. Phys.*, **29**, 484 (1958); M. E. Jacox and R. M. Hexter, *ibid.*, **35**, 183 (1961); M. Ito, *ibid.*, **41**, 2842 (1964); R. Kopelman, *ibid.*, **44**, 3547 (1966).

3) W. Blitz and A. Sapper, *Z. Anorg. Allgem. Chem.*, **203**, 277 (1932).

TABLE 2. OBSERVED AND CALCULATED STRUCTURE FACTORS

(a) Methyl bromide

h	k	l	F_o	F_c	h	k	l	F_o	F_c	h	k	l	F_o	F_c	h	k	l	F_o	F_c	h	k	l	F_o	F_c	h	k	l	F_o	F_c
0	0	2	55.91	50.85	1	1	5	57.16	61.39	1	5	5	34.02	28.54	2	3	7	9.86	8.76	3	1	6	17.59	-16.55	4	0	2	9.93	-10.17
0	0	4	71.34	-75.26	1	1	6	19.86	15.93	1	5	6	8.62	7.64	2	3	8	3.63	4.18	3	1	8	21.49	-23.68	4	0	3	23.85	24.90
0	0	6	60.80	-60.50	1	1	7	20.23	19.38	1	5	7	9.29	9.55	2	3	9	4.07	3.95	3	1	9	2.85	-2.81	4	0	4	19.30	18.01
0	0	8	6.93	4,99	1	1	8	23,65	21.93	2	0	0	46,02	-37,70	2	4	0	19.59	-20.67	3	2	1	33.61	37,71	4	0	6	14.95	15.83
0	1	1	79.60	-62.08	1	1	9	16.76	-16.69	2	0	1	67,33	-51,49	2	4	1	30.41	-28.72	3	2	2	9.54	10.80	4	1	0	21.71	22.14
0	1	3	71.34	-84.70	1	2	1	49.64	-39.46	2	0	2	12,07	-12,49	2	4	2	7.92	-7,02	3	2	3	11.88	-11.04	4	1	1	14.33	14.77
0	1	5	7,22	-3.93	1	2	2	70.06	61,29	2	0	3	66,95	-74,82	2	4	3	46.15	-43.39	3	2	4	4.39	6,27	4	1	2	7.73	6.85
0	1	7	41,94	40.83	1	2	3	12.25	11.34	2	0	4	21,97	20.09	2	4	4	12.07	11.91	3	2	5	28.05	-31,96	4	1	3	19.92	21.99
0	2	0	106,63	-124.91	1	2	4	35.83	32.79	2	0	5	6.85	-7,18	2	4	5	4.01	-4.32	3	2	6	2.86	-3.46	4	1	4	13.59	-13.72
0	2	2	42,37	-40.03	1	2	5	30.01	31.51	2	0	6	16,77	17.31	2	4	6	12.62	10,70	3	2	7	9.81	-8,89	4	1	5	1.61	1.37
0	2	4	60.02	63,58	1	2	6	20.65	-19.92	2	0	7	37,13	34.81	2	4	7	23.78	21,74	3	2	8	3.52	-4.68	4	1	6	10.41	-11.05
0	2	6	61,64	52.83	1	2	7	8,34	8.75	2	0	9	18,89	18.42	2	5	0	32.62	-32.63	3	2	9	8,45	10.54	4	1	7	7.70	-11.60
0	2	8	5.92	-4,39	1	2	8	22.80	-24.55	2	1	0	84.62	-71.38	2	5	1	8,52	6.84	3	3	2	36,03	-43,01	4	2	0	28,69	27.03
0	3	1	41.15	43.22	1	2	9	9.86	-9.87	2	1	1	19.74	14.69	2	5	2	12.19	-10.25	3	3	4	25.78	-25.46	4	2	1	17.80	-14.52
0	3	3	56.70	62,39	1	2	10	2.19	-1.90	2	1	2	20.32	-21.99	2	5	3	12.28	10.09	3	3	5	6,92	-7.17	4	2	2	8.05	9.02
0	3	5	3,47	3,22	1	3	1	71.63	59.60	2	1	3	23.70	21.21	2	5	4	25.38	20.00	3	3	6	11,95	13.09	4	2	3	19.72	-22.14
0	3	7	36.38	-31.96	1	3	2	49.20	42,82	2	1	4	37.08	41.90	2	5	6	17,25	16.43	3	3	7	1.51	-2,21	4	2	4	15.69	-16.02
0	3	9	16,79	-14,83	1	3	3	14.51	-14.50	2	1	6	30.72	33,81	2	5	7	6.72	-5.45	3	3	8	16,36	18,89	4	2	6	12,45	-14,11
0	4	0	53,61	73.31	1	3	4	27.91	24.51	2	1	7	11.67	-11.13	2	6	0	9,81	11.31	3	4	1	24.69	-25.97	4	3	0	16.23	-17.43
0	4	2	24,84	24.31	1	3	5	45.11	-46.54	2	1	8	4,60	-5.26	2	6	1	18.71	15.66	3	4	2	10.85	-7,49	4	3	1	10.18	-11.64
0	4	4	49.22	-41.64	1	3	6	14.72	-12.37	2	1	9	5.90	-4.99	2	6	2	3.40	3.84	3	4	3	6,66	7,68	4	3	2	4.73	-5,38
0	4	6	45.06	-36.36	1	3	7	17.00	-15.19	2	1	10	14.32	15,33	2	6	3	23.50	23.89	3	4	4	4.02	-4,36	4	3	3	15.63	-17,26
0	4	8	2.80	3,06	1	3	8	21,48	-17.32	2	2	0	35,39	31.72	2	6	4	6,25	-6.61	3	4	5	20.19	22.39	4	3	4	9.12	10.84
1	0	1	46.83	47.39	1	3	9	12.70	13.24	2	2	1	51.36	43.66	3	0	1	40,37	-42,81	3	4	6	2.36	2,44	4	4	0	16.08	-19.04
1	0	2	63.01	-72,56	1	4	1	27,37	25.74	2	2	2	9.79	10.60	3	0	2	12,63	-12,28	3	4	7	5.59	6.24	4	4	1	9.02	10.24
1	0	3	12.48	-13.38	1	4	2	42.03	-40.34	2	2	3	61,30	64,23	3	0	3	12.49	12.58	3	4	8	4.85	3.33	4	4	2	6.03	-6.34
1	0	4	38.72	-37.60	1	4	4	27.06	-22.41	2	2	6	14,20	-15,30	3	0	4	5.60	-7,09	3	5	1	6.15	-5,25	4	4	3	13.45	15.61
1	0	5	35.17	-35.98	1	4	5	25.43	-21.57	2	2	7	28,08	-30,87	3	0	5	34.49	36.25	3	5	2	24.35	26.61	4	4	4	9.18	11.35
1	0	6	22.80	22,64	1	4	6	18,26	13.80	2	2	9	15.31	-16.43	3	0	6	4.01	3.89	3	5	4	15.29	15.99	4	4	5	1.48	1,70
1	0	7	9.79	-9.89	1	4	7	7.49	-6.07	2	3	0	59.04	53.73	3	0	7	11.44	10,02	3	5	5	4.83	4.48	4	5	0	7.95	10.83
1	0	8	29.56	27,66	1	4	8	20,43	17.13	2	3	1	13,95	-11,22	3	0	8	4.69	5.26	3	5	6	7.21	-8.24	4	5	1	4.89	7.27
1	0	9	10.89	11.15	1	5	1	36.48	-34.14	2	3	2	18.28	16,87	3	1	1	11.31	-10.92	3	6	1	14.59	14.32	4	5	2	2.76	3,36
1	1	2	64,84	-61.12	1	5	2	29.63	-25,04	2	3	3	18,28	-16,43	3	1	2	52.90	55.38	3	6	2	3.36	4.16	4	5	3	7.19	10.87
1	1	3	25.46	19.95	1	5	3	8,74	8.66	2	3	4	31,21	-32,44	3	1	4	29.68	32.48	3	6	3	3,47	-4.27	4	5	4	4,20	-6.79
1	1	4	34,11	-33.02	1	5	4	19.74	-14,75	2	3	6	25.17	-26.38	3	1	5	10.79	9.11	4	0	0	30.86	-30.48	5	2	1	1.35	-1.32
																				4	0	1	16.93	16.37	5	2	2	10.57	-16,02

(b) Methyl iodide

h	k	l	F_o	F_c	h	k	l	F_o	F_c	h	k	l	F_o	F_c	h	k	l	F_o	F_c	h	k	l	F_o	F_c	h	k	l	F_o	F_c
0	0	4	111,01	-114.32	0	6	0	56.02	-57.59	1	1	9	30.29	-24.74	1	4	6	15.43	16.41	2	0	5	15.10	-12.91	2	3	10	18.39	17.90
0	0	6	90.68	-95.79	0	6	2	19.90	-19.89	1	1	10	6.67	5.93	1	4	7	10.81	-12.86	2	0	6	33.09	28.43	2	4	0	29.01	-33.49
0	0	10	37.98	37.86	0	6	4	27.55	33.35	1	1	11	27.18	-21.45	1	4	8	28.74	28.24	2	0	7	61.08	49,56	2	4	1	35.83	-40.68
0	0	12	12.47	13,36	0	6	6	24.41	-30.80	1	1	12	9.04	-8.21	1	4	9	9.57	8.64	2	0	9	35.71	28.21	2	4	2	13.34	-11.28
0	1	3	138,88	-141.92	0	7	1	18.03	18.53	1	2	1	62.01	-63.74	1	4	10	7.23	6.47	2	0	10	11,76	-11,92	2	4	3	63.15	-62.30
0	1	5	21,79	-20,80	0	7	3	22.02	29.18	1	2	2	90.74	98,38	1	5	1	51.17	-51.71	2	1	2	22.24	-39.36	2	4	4	20.49	19.27
0	1	7	49.27	60,95	0	7	5	2.86	4.57	1	2	3	15.89	13.20	1	5	2	36.01	-35.86	2	1	3	33.18	36.98	2	4	6	19.57	17.23
0	1	9	35.86	37.22	0	7	7	12.92	-14.36	1	2	4	67.79	60,97	1	5	3	10.37	12.32	2	1	4	57.78	60,27	2	4	7	36.20	30.46
0	1	11	6.13	-5.31	0	8	0	25.68	25,36	1	2	5	57.74	49,39	1	5	4	23.89	-21.98	2	1	6	57.92	56,47	2	4	9	16,57	17.71
0	2	0	212.32	-185,70	0	8	2	6.92	8.79	1	2	6	31.88	-24,12	1	5	6	9.16	10.23	2	1	7	23.04	-16.60	2	5	0	46.49	-49.49
0	2	2	66.61	-61.46	0	8	4	11.90	-14.97	1	2	7	18.35	18.67	1	5	7	13.13	15.37	2	1	9	13.80	-10.77	2	5	1	8.00	10.77
0	2	4	90.96	96,53	1	0	2	97.74	-115.47	1	2	8	48.49	-40.64	1	5	8	15.71	16.06	2	1	10	32.76	-22,65	2	5	2	23.82	-17.67
0	2	6	70.18	83.48	1	0	3	20,13	-15,38	1	2	9	15,39	-12.34	1	5	9	12,08	-12.38	2	2	1	49.77	62.01	2	5	3	21.87	16.95
0	2	10	32.89	-33.63	1	0	4	79.37	-70.36	1	2	10	8.63	-9.12	1	6	1	19.75	-21.49	2	2	2	14.91	17.13	2	5	4	37.28	27,86
0	2	12	12.52	-11,97	1	0	5	67,66	-56.92	1	2	11	16,49	-11.94	1	6	2	30.57	33.76	2	2	3	77.89	93,40	2	5	6	30.46	26.99
0	3	1	69.14	68.07	1	0	6	33.74	27,42	1	3	1	98,73	91,19	1	6	4	23.40	21.63	2	2	4	27.28	-28.62	2	5	7	11,75	-7.99
0	3	3	87,18	104.55	1	0	7	22,61	-21,19	1	3	2	69.78	62,22	1	6	5	18.75	18.01	2	2	5	14.73	11.28	2	6	0	14.04	18.01
0	3	5	14,35	15.60	1	0	8	55.87	46.14	1	3	3	20.85	-21.32	1	6	6	8.82	-8.95	2	2	6	31,77	-24.94	2	6	1	25.53	21.78
0	3	7	44.43	-47,17	1	0	9	11.20	13.96	1	3	4	40.57	37,05	1	6	7	6.14	7.10	2	2	7	52.87	-43.69	2	6	2	6.80	6.10
0	3	9	29.73	-29.14	1	0	10	11,52	10.27	1	3	5	72,67	-71.70	1	6	8	13.29	-15.76	2	2	9	26,89	-25,04	2	6	3	34,45	33.73
0	3	11	4,21	4.19	1	0	11	18.80	13.42	1	3	6	20.00	-16.71	1	7	1	20.60	24.86	2	2	10	12.44	10.67	2	6	4	11.73	-10.62
0	4	0	104,11	111,89	1	0	12	13.81	-10.55	1	3	7	26.73	-24.83	1	7	2	15,15	17.31	2	3	0	61.14	83,72	2	6	5	5.03	4.23
0	4	2	38.95	38,20	1	1	1	133.31	-130,38	1	3	8	27.75	-25.76	1	7	3	4,82	-6.01	2	3	1	14.38	-18.02	2	6	6	9,93	-9.65
0	4	4	56.97	-62,75	1	1	2	92.93	-87.41	1	3	9	21.63	19,57	1	7	4	8.86	10.76	2	3	2	37.49	29,74	2	6	7	15,92	-17.20
0	4	6	49,03	-56,37	1	1	3	33.89	29.58	1	3	11	19.26	17.13	1	7	5	17.35	-21.42	2	3	3	33.85	-28.15	2	7	1	8.35	-5.19
0	4	10	18,58	23.84	1	1	4	48.74	-49.94	1	4	1	41,43	40.96	1	7	6	4.49	-5.13	2	3	4	53.86	-46.19	2	7	2	9.18	8.62
0	5	1	41.88	-39.09	1	1	5	111.80	95.00	1	4	2	60.98	-64.32	1	7	7	5.18	-7.73	2	3	6	54.02	-43.87	2	7	3	8,51	-8.24
0	5	3	56.15	-60.86	1	1	6	24.20	21.92	1	4	3	6.38	-8.73	1	8	1	9.07	9.37	2	3	7	16.71	12.98	2	7	4	13,37	-13,71
0	5	5	7.73	-9.28	1	1	7	39.55	32.15	1	4	4	42.16	-40.53	1	8	2	11.56	-14.78	2	3	9	11,87	8,52					
0	5	7	25.81	28,98	1	1	8	39.79	32.87	1	4	5	32.98	-33.20	2	0	4	25.39	33.12										

Table 3. Positional and thermal parameters of the halogen and carbon atoms, with their e.s.d.'s in parentheses

compound	atom	X	Y	Z	B (Å^2)
CH_3Br	Br	0.1544(9)	1/4(—)	0.0968(4)	3.51(7)
	C	0.3330(88)	1/4(—)	−0.0871(42)	3.35(73)
CH_3I	I	0.1571(15)	1/4(—)	0.0946(4)	4.60(9)
	C	0.3144(214)	1/4(—)	−0.1039(61)	4.00(128)

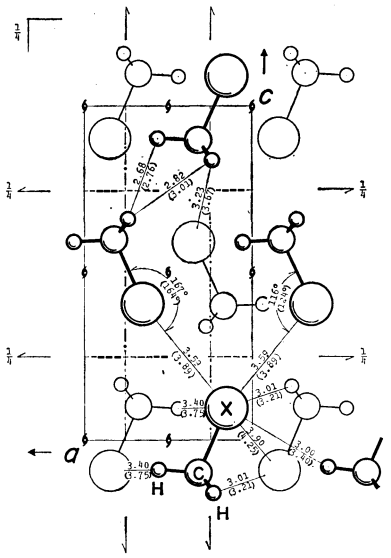

Fig. 1. Schematic drawing of the crystal structure of methyl bromide and methyl iodide, projected along the b axis. Interatomic distances and angles between neighboring molecules for methyl bromide and those for methyl iodide (in parentheses) are given.

arrangement of the two crystals, projected along the b axis. In this figure, an assumed orientation of the methyl group, as will be described later, is given, and the interatomic distances and angles between neighboring molecules for methyl bromide and those for methyl iodide (in parentheses) are given.

The bond distances between the halogen and carbon atoms are found to be $1.86_3\pm0.04$ for Br–C and $2.13_4\pm0.06$ Å for I–C. The corresponding values obtained by a microwave study[4] in the gaseous state are 1.9391 and 2.1392 Å. Because of the large e.s.d.'s of the carbon positions, it can not be said that these bond distances are different in their gaseous and crystalline states.

Each halogen atom is in contact with two halogen atoms of the neighboring molecules lying on the same mirror plane, with distances of 3.587 ± 0.008 for Br···Br and 3.895 ± 0.010 Å for I···I. These distances are much shorter than twice the conventional van der Waals radii, 3.90 for the bromine atom and 4.30 Å for the iodine atom. The juxtaposition of the molecules is such that:

	∠ C–X···X
Methyl bromide	116° and 167° ± 1°
Methyl iodide	124° and 164° ± 2°,

where X denotes the halogen atom. It should be noted that the smaller values, 116° and 124°, can be compared to the sp^3 tetrahedral angle, while the larger ones are not far from 180°.

Discussion

Egan and Kemp[5] have reported that there is a first-order phase transition in the crystal of methyl bromide, occurring at −99.4°C with a latent heat of 0.113 kcal/mol. Although the present structure determination was carried out for the crystal at about −120°C, much lower than the transition point, it might have been of a supercooled form of the high-temperature one (α). In order to clarify this question, the following experiment was carried out.

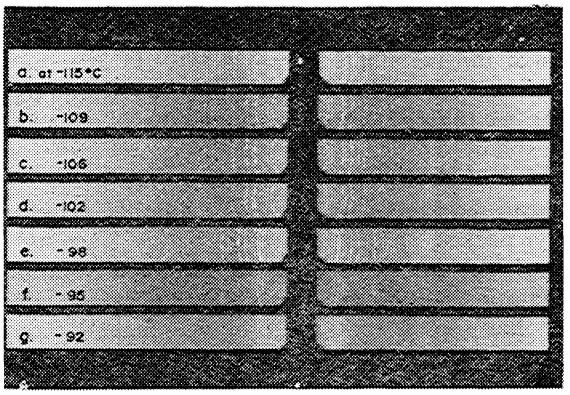

Fig. 2. Powder patterns for methyl bromide at various temperatures. a–d correspond to the low-temperature phase, e and f to the high-temperature phase, and g to the liquid phase.

A polycrystalline specimen of methyl bromide was heated to almost its melting point (−93.7°C), then cooled slowly, and subsequently repeatedly warmed-up and cooled-down. Powder patterns, given in Fig. 2, were taken at several temperatures, from −120° to −90°C. These patterns clearly show the existence of the phase transition between the temperatures of −102° and −98°C. The low-temperature phase (β) was identified as the crystal structure described in the previous section. The crystal structure of the high-temperature phase (α) must be of a form related to that of the low-temperature form, since the heat of transition is very small.

It is found that the crystal structure of methyl bromide (β) and methyl iodide are isomorphous and that they are quite different from that of methyl chloride. The crystal of methyl chloride is orthorhombic, with a tetramolecular cell with dimensions of a=6.495, b=5.139, and c=7.523 Å, and it belongs to space group C_{2v}^{12}—$Cmc2_1$.[1] However, if one replaces the methyl group by its counterpart halogen atom, the three

4) S. L. Miller, L. C. Aamodt, G. Dousmanis, C. H. Townes, and J. Kraitchman, *J. Chem. Phys.*, **20**, 1112 (1952).

5) C. J. Egan and J. D. Kemp, *J. Amer. Chem. Soc.*, **60**, 2097 (1938).

crystal structures will become almost the same as the structures of solid halogen crystals, Cl_2, Br_2, and I_2, which are known to be isomorphous.[6] The difference between the crystal structure of methyl chloride and those of methyl bromide and methyl iodide can be seen in the mutual orientation of the molecules. In the crystal of methyl chloride, the molecules lying on the mirror plane are aligned head to tail and are parallel with the molecules lying on the adjacent mirror planes. On the other hand, in the crystals of methyl bromide (β) and methyl iodide, the molecules lying on the mirror plane are aligned head to head and are antiparallel with the molecules lying on the adjacent mirror planes.

It was previously inferred by one of the present authors[7] that, in the crystals of Br_2 and, particularly, I_2, partial covelency, based upon the charge transfer from the $p\pi^*$- to the $p\sigma^*$-orbitals between the neighboring molecules lying on the mirror plane, plays a part in the intermolecular bonding. In the crystals of methyl bromide (β) and methyl iodide also, the mutual orientation of the molecules lying on the mirror planes seems to favor a covalent bonding between the halogen atoms of the neighboring molecules. It may be suggested that this intermolecular bonding is responsible for the exceedingly short distances for X···X; it can also explain why those crystal structures differ from that of methyl chloride.

As can be seen in Fig. 1, the methyl groups are loosely packed in the structures; this suggests that these groups are in a state of hindered rotation or reorientation. Indeed, an NMR study[8] of methyl iodide has shown that the observed second moment, ΔH_2^2, at -183°C is 8.4 gauss^2 and that the rotation sets in at about -150°C, where the line width, δH, decreases from 5 to 3 gauss. When an NMR study of powdered specimen of methyl bromide was carried out, it showed that an appreciable rotation of the methyl group occurred from its melting point down to the boiling point of liquid nitrogen. The line width, $\delta H \approx 4.7$ gauss, and the second moment, $\Delta H_2^2 \approx 7.5$ gauss^2, remain constant in this temperature range. Here, the theoretical values for the second moment are 27.6 and 5.0 gauss^2 for the stational and rotational states respectively. Figure 1 gives the most stable orientation of the methyl group, as suggested by the lattice-energy calculations.[9]

The actual alignment of molecules should correspond to the potential energy minimum. By keeping the unit-cell dimensions and the crystal symmetry, variations in the potential energies with the positional and orientational parameters of the respective molecules, which are X, Z, and θ for methyl bromide and methyl iodide and Y and θ for methyl chloride, were calculated by means of the lattice-energy calculations, as cited in the previous paper.[9] It was found that the potential minima based upon the rotational models of the methyl groups are in better agreement with the respcetive molecular arrangements than those based upon the stational models. Burbank assigned the crystal structure of methyl chloride the stational orientation of the methyl group by comparing the observed structure factors. However, it can be expected from the lattice-energy calculations that the rotation of the methyl group also occurs in the crystal of methyl chloride.

The authors wish to thank Professor Tokunosuké Watanabé for his helpful discussions during the preparation of this manuscript. They are also indebted to Dr. Akio Furusaki and Mr. Hiroyuki Utsumi for their assistance in these analyses, and to Dr. Asako Kawamori for her assistance in the NMR measurements.

6) L. W. G. Wyckoff, "Crystal Structures," Vol. 1, New York, London, Sydney: Wiley-Interscience (1964), p. 52.

7) Y. Tomiie, *Kwansei Gakuin Univ. Ann. Studies*, **10**, 208 (1961).

8) H. S. Gutowsky and G. E. Pake, *J. Chem. Phys.*, **18**, 162 (1949).

9) T. Kawaguchi, K. Takashina, T. Tanaka, and T. Watanabé, *Acta Crystallogr., B* **28**, 967 (1972).

The Crystal Structures of Methylene Dibromide and Methylene Diiodide

Takemi KAWAGUCHI,* Akira WAKABAYASHI, Mitsuhiro MATSUMOTO,
Toru TAKEUCHI, and Tokunosuké WATANABÉ
Faculty of Science, Kwansei Gakuin University, Nishinomiya

(Received May 6, 1972)

The crystal structures of methylene dibromide and methylene diiodide (Form II) have been determined by the X-ray diffraction method at about −90°C and about −20°C respectively. Both the crystals are isomorphous, with monoclinic space group C_{2h}^6-C2/c. Unit cells containing eight molecules have these dimensions: $a=12.239$ (12), $b=4.459(15)$, $c=15.212(16)$ Å, and $\beta=113.54(7)°$ for methylene dibromide, and $a=13.346(3)$, $b=4.720(90)$, $c=16.479(5)$ Å, and $\beta=114.48(8)°$ for methylene diiodide. The orientations of the methylene groups have been obtained by lattice-energy calculations.

As part of a series of investigations of molecular interactions on various halogenated methanes, the crystal structures of bromoform,[1] iodoform,[2] methyl bromide and methyl iodide[3] have already been reported. It has been found that bromoform and iodoform are isomorphous, and that methyl bromide and methyl iodide are also isomorphous, but their chlorine congeners have quite different structures. In this and succeeding papers, the crystal structure sof methylene diiodide, methylene dibromide, and methylene dichloride will be reported.

Marzocchi *et al.*[4] ascertained, by their spectroscopic studies, that methylene diiodide exists in two solid phases; one is a metastable form, I, melting at 5.54°C, while the other is a stable form, II, melting at 6.01°C; Form I is easily and irreversibly transformed to Form II at temperatures above 0°C. They also reported that methylene dibromide and methylene diiodide (II) are isomorphous and have a structure based on $P2_1/c$, while methylene dichloride has a structure based on *Pbcn*.

Experimental

Methylene dibromide and methylene diiodide from Nakarai Chemicals, Ltd., were purified by vacuum distillation and were sealed in thin-wall glass capillaries (0.3 mm in internal diamter and 0.01 mm in wall thickness). A single crystal was carefully produced in a way which has previously been described.[1,3] In all the experiments on these two crystals thus far carried out, it has been found that only one kind of zone axes grows nearly along the capillaries. This is the [010] axis of a monoclinic lattice. The single crystal obtained was gradually cooled to about −90°C for methylene dibromide and to about −20°C for methylene diiodide for the taking of oscillation and Weissenberg photographs.

The cell dimensions of both the crystals were determined from oscillation and Weissenberg photographs taken around the [010] axis, using Cu $K\alpha$ radiation. Intensity distributions and systematic extinctions ($h+k$ odd for hkl and l odd for $h0l$) showed that the crystals belong to space group Cc or $C2/c$, with eight molecules per cell. The crystal data are summarized in Table 1. The densities calculated are much larger than that for liquid, much as in the cases of bromoform, methyl bromide, and methyl iodide. These intensity distributions and the cell dimensions strongly suggest that the two crystals are isomorphous.

Table 1. CRYSTAL DATA

Methylene dibromide, CH_2Br_2	Methylene diiodide, CH_2I_2
MW 173.85	MW 267.84
Mp −52.8°C	Mp (II) 6.01°C
	(I) 5.54
Exp. temp. −90	Exp. temp. −20
Monoclinic; C_{2h}^6-C2/c	Monoclinic; C_{2h}^6-C2/c
$Z=$ 8	$Z=$ 8
$a=$ 12.239±0.012 Å	$a=$ 13.346±0.003 Å
$b=$ 4.459±0.015	$b=$ 4.72±0.09
$c=$ 15.212±0.016	$c=$ 16.479±0.005
$\beta=113.54\pm0.07°$	$\beta=114.48\pm0.07°$
$V=761.4$ Å^3	$V=944.7$ Å^3
$D_x=2.994$ g/cm^3	$D_x=3.765$ g/cm^3
$D_m=2.4953$ (at 20°C)	$D_m=3.3326$ (at 15°C)
2.999 (at −79°C)	4.013 (at −195°C)
$\mu=274.0$ cm^{-1} (Cu $K\alpha$)	$\mu=1121.2$ cm^{-1} (Cu $K\alpha$)
	139.2 (Mo $K\alpha$)

Integrated intensities were collected by means of the multiple-film method and the equi-inclination Weissenberg technique, using Ni-filtered Cu$K\alpha$ radiation for methylene dibromide and Zr-filtered Mo$K\alpha$ radiation for methylene diiodide. Here, the intensity data for methylene diiodide were recorded jointly by means of different time exposures. Reflections were observed up to the third layers around the [010] axes, though for methylene dibromide, 205, and for methylene diiodide, 244 independent reflections from the zero-th and first layers were used in order to determine the respective structures. The intensities were measured visually and corrected for Lorentz-polarization and absorption effects with the cylindrical approximation; then the intensities were brought into respective common scales by considering them at different time exposures.

Structure Determination

Approximate co-ordinates of the iodine atoms of methylene diiodide were found from the Patterson diagrams. With isotropic temperature factors, these

* To whom all correspondence should be addressed. Present address: Department of Research and Development, Nippon Crucible Co., Ltd., 925 Inada, Higashi-Osaka 577.

1) T. Kawaguchi, K. Takashina, T. Tanaka, and T. Watanabé, *Acta Crystallogr.*, **B28**, 967 (1972).
2) Y. Iwata, M. Oyama, T. Kawaguchi, and T. Watanabé, to be published.
3) T. Kawaguchi, M. Hijikigawa, Y. Hayafuji, M. Ikeda, R. Fukushima, and Y. Tomiie, This Bulletin, **46**, 53 (1973).
4) M. P. Marzocchi, V. Schettino, and S. Califano, *J. Chem. Phys.*, **45**, 1400 (1966); M. P. Marzocchi, P. Manzelli, V. Schettino, and S. Califano, *ibid.*, **49**, 5438 (1968); M. P. Marzocchi, and P. Maznelli, *ibid.*, **52**, 2630 (1970).

co-ordinates were refined by the least-squares method, based upon the centrosymmetric space group, $C2/c$. The reliability factor, $R=\Sigma||F_o|-|F_c||/\Sigma|F_o|$, dropped from 0.25 to 0.16. The difference Fourier synthesis gave merely a hint of the position of the carbon atom. Further refinement was applied in order to determine the positions of the iodine atoms with anisotropic temperature factors, where the anomalous dispersion effect was considered. The R values were finally indicated to be 0.12.

Another refinement based upon the non-centrosymmetric space group, Cc, was made in parallel. However, this gave no significant improvement. It was, therefore, concluded that the crystal structure of methylene diiodide belongs to the space group C_{2h}^6—$C2/c$.

The crystal structure determination of methylene dibromide was started using the least-squares method by substituting the final co-ordinates of the iodine atoms of methylene diiodide for those of the bromine atoms. The R value was about 0.3 at the begining and decreased to 0.25 with isotropic temperature factors of bromine atoms, where the anomalous dispersion effect was also considered. The difference synthesis gave merely a diffuse indication of the position of the carbon atom, much as for methylene diiodide. The least-squares refinement with anisotropic temperature factors for the bromine atoms reduced the R value to 0.21.

Results and Discussion

X-Ray Analysis. The observed and calculated structure factors are listed in Table 2, and the final sets of the positional and thermal parameters of the halogen atoms are summarized in Table 3. The two crystal structures are isomorphous, with the symmetry of $C2/c$. As has been mentioned in the previous section, Marzocchi *et al.* reported that the crystal of methylene diiodide has two forms, I and II, and that Form II is isomorphous with the crystal of methylene dibromide.[4] In view of our experimental procedure in obtaining the single crystal, the measurement for methylene diiodide must have been carried out on the stable form, II.

The interatomic distances for X···X in the molecules, where X denotes the halogen atom, are calculated to be 3.17 ± 0.02 Å for methylene dibromide and 3.56 ± 0.01 Å for methylene diiodide. These values are in excellent agreement with those given by electron dif-

Table 2. Observed and calculated structure factors

(a) Methylene dibromide

h	l	$\|F_o\|$	$\|F_c\|$
(k=0)			
0	6	104.02	54.83
0	8	292.76	279.05
0	10	86.21	52.23
0	12	149.10	145.80
0	14	53.78	40.54
0	16	53.45	60.70
2	0	24.20	19.45
4	0	248.16	275.51
6	0	90.82	46.79
8	0	55.01	50.02
10	0	44.86	22.00
12	0	89.29	80.11
14	0	8.82	7.31
2	2	14.40	12.80
6	2	34.45	32.33
8	2	206.58	202.21
10	2	28.41	34.92
12	2	29.26	84.21
2	-2	35.71	2.40
10	-2	32.82	40.72
12	-2	63.60	101.77
14	-2	39.44	29.89
2	4	25.69	12.72
4	4	166.13	217.93
6	4	58.42	33.39
8	4	59.91	51.27
10	4	31.01	19.80
12	4	49.43	52.41
2	-4	25.95	8.23
4	-4	302.52	256.37
6	-4	98.02	49.25
8	-4	16.90	30.70
10	-4	58.80	18.66
12	-4	111.64	101.59
14	-4	15.57	16.20
4	6	219.55	145.95
6	6	18.03	13.61
8	6	108.92	121.21
10	6	20.01	27.10
6	-6	22.77	57.72
8	-6	258.73	267.55
10	-6	26.69	39.83
12	-6	100.87	98.88
14	-6	54.04	40.09
2	8	24.94	5.72
6	8	32.95	19.74
8	8	43.33	39.22
10	8	11.45	14.81
6	-8	76.03	36.92
8	-8	29.84	3.57
10	-8	54.26	10.89
12	-8	92.93	103.26
14	-8	16.41	22.97
4	10	128.47	81.07
8	10	40.19	54.43
2	-10	12.00	13.87
4	-10	138.24	162.66
6	-10	18.33	48.78
8	-10	211.12	211.74
10	-10	19.82	31.09
12	-10	104.76	75.26
14	-10	53.71	42.29
2	12	21.47	1.76
4	12	15.11	76.62
6	12	13.20	9.34
4	-12	180.37	100.28
6	-12	50.37	21.35
8	-12	49.88	14.90
10	-12	49.43	2.21
12	-12	84.53	82.18
14	-12	12.55	25.26
4	14	50.05	41.76
2	-14	22.19	13.97
4	-14	53.00	89.10
6	-14	13.72	35.05
8	-14	124.97	135.52
10	-14	15.24	18.71
12	-14	90.17	43.20
14	-14	29.26	36.15
4	-16	101.16	50.26
8	-16	44.08	21.72
10	-16	33.38	5.70
12	-16	29.26	49.76
4	-18	12.07	37.69
8	-18	35.68	72.35
(k=1)			
3	0	94.41	114.95
5	0	84.90	81.82
7	0	137.99	135.98
9	0	78.02	63.87
11	0	79.94	67.03
3	1	209.39	227.79
5	1	148.89	161.00
7	1	161.09	149.83
9	1	63.98	49.88
11	1	45.77	39.73
3	-1	74.97	78.61
5	-1	53.44	43.61
7	-1	84.03	72.31
9	-1	79.24	81.20
11	-1	108.53	95.85
1	2	191.34	221.56
3	2	131.98	118.75
5	2	91.27	63.81
3	-2	147.06	125.42
5	-2	81.85	65.22
11	-2	55.88	56.28
1	3	157.78	123.90
3	3	100.25	73.26
7	3	50.73	49.28
9	3	40.19	56.74
11	3	72.53	66.40
1	-3	192.13	218.52
3	-3	263.87	243.05
5	-3	190.73	172.56
7	-3	143.75	171.05
9	-3	49.16	51.00
11	-3	47.25	46.58
3	4	73.57	85.71
5	4	45.59	62.33
7	4	90.57	89.26
9	4	48.64	39.06
11	4	48.47	52.19
1	-4	35.22	41.29
3	-4	102.16	109.75
5	-4	92.75	82.09
7	-4	205.90	158.41
9	-4	78.89	77.79
11	-4	66.16	70.96
1	5	159.09	160.63
3	5	144.18	157.74
5	5	109.23	116.83
7	5	109.49	103.90
9	5	53.44	37.94
11	5	28.94	27.26
1	-5	75.40	86.86
3	-5	42.80	58.35
5	-5	72.61	54.01
7	-5	12.90	82.02
9	-5	100.68	92.11
1	6	143.40	149.00
3	6	100.25	87.83
5	6	71.57	48.61
1	-6	121.43	157.52
3	-6	87.43	98.52
5	-6	43.15	51.26
11	-6	79.24	61.43
1	7	125.70	90.34
3	7	80.98	53.78
1	-7	144.79	152.95
3	-7	179.22	187.13
5	-7	125.18	137.43
7	-7	141.30	152.33
11	-7	66.60	43.18
1	8	34.96	28.13
3	8	40.62	53.05
7	8	51.69	43.63
1	-8	40.45	45.49
3	-8	95.63	79.35
5	-8	73.66	62.54
7	-8	84.21	141.62
9	-8	55.79	72.96
11	-8	79.76	59.42
1	9	94.15	94.35
3	9	102.95	90.50
5	9	73.31	69.15
7	9	70.09	58.55
1	-9	33.82	45.96
3	-9	36.79	32.35
5	-9	63.72	48.69
7	-9	92.40	72.11
9	-9	79.15	81.62
11	-9	128.14	103.12
1	10	88.74	84.20
3	10	59.10	53.56
5	10	38.36	29.76
1	-10	79.50	87.22
3	-10	51.69	62.61
5	-10	26.33	32.00
11	-10	69.74	52.69
1	11	79.33	55.31
3	11	41.49	32.65
1	-11	97.63	90.54
3	-11	120.38	117.35
5	-11	72.09	86.16
7	-11	79.15	106.86
1	12	42.89	27.55
1	-12	38.70	37.72
3	-12	69.48	45.62
5	-12	50.91	36.11
7	-12	75.84	101.15
9	-12	43.15	54.41
11	-12	48.03	38.08
1	13	27.98	47.02
5	-13	43.59	34.58
7	-13	66.95	50.07
9	-13	48.03	57.64
11	-13	88.39	76.62
11	-14	40.80	34.15
3	-15	68.26	61.80
5	-15	39.23	44.23
7	-15	43.50	60.81
3	-16	45.68	18.35
5	-16	30.68	14.24
7	-16	50.12	60.63
7	-17	43.50	28.52

(b) Methylene diiodide

h	l	$\|F_o\|$	$\|F_c\|$	h	l	$\|F_o\|$	$\|F_c\|$	h	l	$\|F_o\|$	$\|F_c\|$	h	k	$\|F_o\|$	$\|F_c\|$	h	l	$\|F_o\|$	$\|F_c\|$
(k=0)				-6	4	146.97	124.40	(k=1)				-5	6	134.81	96.58	-11	13	227.85	219.97
4	2	316.36	302.45	-6	6	217.83	172.76	1	5	261.40	244.85	-5	7	243.68	205.24	-11	15	73.74	82.63
4	4	432.69	451.28	-6	8	145.33	106.70	1	9	174.37	149.30	-5	8	112.66	82.36	-11	16	144.94	114.54
4	6	204.31	181.64	-6	10	171.36	163.46	1	10	170.57	158.71	-5	9	62.98	62.19	-11	17	133.55	170.59
4	8	369.74	332.05	-6	12	95.90	65.99	1	11	177.22	155.62	-5	10	74.69	64.69	-15	0	67.41	83.73
4	10	107.43	91.40	-6	14	134.12	132.19	1	12	83.86	58.11	-5	11	181.97	137.59	-15	1	123.74	150.60
4	12	213.87	218.07	-6	18	71.18	93.74	1	13	88.29	76.51	-5	12	81.65	56.73	-15	2	71.20	71.83
4	16	110.07	130.44	-8	2	407.97	429.61	1	14	82.60	94.67	-5	14	55.06	41.09	-15	4	80.38	96.69
6	0	138.41	98.57	-8	4	179.93	153.27	1	15	104.43	107.61	-5	15	83.86	81.17	-15	5	151.27	184.58
6	2	158.51	118.28	-8	6	446.20	457.11	3	7	158.55	128.12	-7	0	220.89	218.38	-15	6	86.71	94.21
6	6	117.65	89.74	-8	8	118.96	82.31	3	9	207.60	178.02	-7	1	100.00	89.41	-15	8	71.84	95.87
6	10	67.89	69.90	-8	10	390.50	395.72	3	10	125.95	113.02	-7	2	121.84	124.60	-15	9	154.75	197.23
8	0	220.79	192.55	-8	14	289.34	287.98	3	11	104.12	83.22	-7	3	367.41	364.57	-15	10	121.21	108.10
8	2	352.94	331.41	-8	18	147.63	163.84	3	12	57.28	43.63	-7	4	260.45	259.78	-15	12	93.36	79.67
8	4	205.96	186.46	-10	2	193.77	179.15	3	13	101.59	106.33	-7	5	160.13	124.07	-15	13	156.65	182.90
8	6	266.27	218.27	-10	6	231.34	203.52	3	14	83.23	69.89	-7	6	127.85	100.56	-15	14	95.00	106.64
8	8	119.95	151.56	-10	10	221.45	198.90	5	9	144.94	119.92	-7	7	380.07	344.26	1	3	190.51	221.20
8	10	140.38	126.35	-10	14	177.62	166.22	5	10	98.10	96.81	-7	8	273.11	253.06	1	5	208.23	244.85
8	12	75.14	106.96	-10	18	107.76	119.34	5	13	61.71	67.53	-7	9	186.08	139.90	1	6	215.51	238.63
10	2	170.70	140.02	-12	2	253.75	256.71	7	13	100.64	93.19	-7	10	82.60	57.01	1	7	211.08	199.74
10	6	107.10	101.88	-12	4	92.93	70.19	-1	5	180.38	135.23	-7	11	281.65	268.66	3	1	330.39	388.23
10	10	75.79	70.97	-12	6	259.68	264.81	-1	6	235.13	221.14	-7	12	198.11	205.09	3	2	197.16	220.30
12	2	238.59	212.39	-12	8	121.27	112.39	-1	7	288.30	246.12	-7	13	128.17	129.63	3	3	156.97	166.71
12	6	155.87	153.16	-12	10	237.60	230.04	-1	9	106.02	80.76	-7	15	172.16	179.40	3	4	68.99	107.62
12	10	125.23	98.67	-12	12	142.03	128.40	-1	10	130.70	138.11	-7	16	109.81	143.59	3	5	247.48	278.91
14	2	118.63	81.41	-12	14	181.25	170.00	-1	11	180.70	161.50	-7	17	80.70	103.01	3	6	153.49	168.93
14	4	93.59	73.55	-12	16	111.06	116.08	-1	13	54.75	47.07	-7	19	94.62	104.14	5	1	250.32	240.86
16	0	94.58	55.41	-12	18	85.35	107.51	-1	14	88.61	80.56	-9	0	84.81	74.44	5	2	132.60	138.30
16	2	104.13	104.00	-12	20	76.45	86.19	-1	15	109.50	95.02	-9	1	58.86	58.31	5	3	54.43	33.68
18	0	98.86	94.16	-14	0	89.31	90.37	-3	0	120.26	147.99	-9	3	96.84	84.68	5	4	67.72	58.15
0	6	163.45	110.02	-14	2	126.87	115.23	-3	1	159.18	170.25	-9	4	106.02	85.93	5	5	175.64	184.88
0	8	453.78	500.04	-14	4	112.37	105.91	-3	2	255.70	239.87	-9	5	96.21	85.10	5	6	110.13	125.17
0	10	148.62	114.63	-14	6	152.58	143.20	-3	3	407.92	434.09	-9	6	50.00	34.83	7	1	284.82	317.10
0	12	318.99	306.90	-14	8	131.49	118.44	-3	4	194.94	165.91	-9	7	86.39	55.55	7	2	87.66	116.72
0	14	105.78	92.93	-14	10	162.79	151.15	-3	5	150.95	116.90	-9	8	101.90	77.08	7	4	121.52	156.39
0	16	150.27	173.47	-14	12	110.40	122.62	-3	6	252.54	206.19	-9	9	101.27	88.58	7	5	185.45	234.08
-2	8	91.94	65.64	-14	14	144.67	133.50	-3	7	381.66	376.24	-9	12	77.53	54.10	7	6	54.43	88.67
-2	10	80.74	45.56	-14	16	106.12	114.55	-3	8	193.04	156.46	-9	13	68.36	69.17	7	8	84.81	101.02
-2	14	64.59	53.02	-14	18	93.26	98.49	-3	9	51.90	51.55	-11	0	142.73	164.49	7	9	129.43	153.72
-4	2	327.23	398.71	-16	2	136.10	115.43	-3	10	137.66	145.19	-11	1	160.76	186.13	9	1	126.27	97.09
-4	4	376.01	488.50	-16	4	111.38	92.05	-3	11	277.22	276.77	-11	3	173.74	174.09	9	2	65.82	75.27
-4	6	379.96	398.52	-16	6	115.01	108.34	-3	12	131.65	127.87	-11	4	183.87	189.72	9	5	70.26	88.65
-4	8	363.48	359.02	-16	8	143.02	121.89	-3	14	68.04	86.59	-11	5	238.93	230.90	11	1	146.52	152.47
-4	10	350.30	324.77	-16	10	94.25	82.67	-3	15	174.69	178.88	-11	6	92.72	51.41	11	3	130.70	131.65
-4	12	244.52	225.66	-16	12	133.46	132.69	-3	16	80.70	92.22	-11	7	188.30	166.39	11	4	88.93	125.15
-4	14	254.73	229.07	-16	16	94.25	119.72	-5	0	67.72	89.09	-11	8	171.84	187.53	11	5	95.57	115.17
-4	16	115.34	126.45	-18	4	96.56	117.32	-5	1	47.15	11.14	-11	9	259.50	243.95	11	7	71.20	84.57
-4	18	121.93	144.31	-18	8	134.12	135.51	-5	2	128.48	125.84	-11	10	68.36	64.91	15	3	109.50	110.04
-6	2	191.46	152.46	-18	12	135.44	142.32	-5	3	294.00	251.41	-11	11	142.09	129.88				
								-5	5	39.24	51.72	-11	12	160.45	158.11				

TABLE 3. POSITIONAL AND THERMAL PARAMETERS, WITH THEIR e.s.d.'s IN PARENTHESES

*The anisotropic thermal parameters for the halogen atoms are the form;

$\exp[-(\beta_{11}h^2+\beta_{22}k^2+\beta_{33}l^2+\beta_{12}hk+\beta_{23}kl+\beta_{31}lh)]$.

Parameter	Methylene dibromide		Methylene diiodide	
	Br (1)	Br (2)	I(1)	I(2)
X	0.0920 (7)	0.3499 (7)	0.0945 (4)	0.3591 (4)
Y	0.6639 (53)	0.6330 (54)	0.6650 (35)	0.6398 (32)
Z	0.1279 (7)	0.1270 (7)	0.1309 (4)	0.1276 (4)
β_{11}	0.0047 (6)	0.0050 (7)	0.0046 (3)	0.0022 (2)
β_{22}	−0.1232 (377)	−0.1070 (391)	0.0190 (235)	0.0550 (221)
β_{33}	0.0050 (5)	0.0055 (6)	0.0040 (3)	0.0025 (2)
β_{12}	−0.0009 (68)	−0.0075 (75)	−0.0018 (42)	0.0020 (38)
β_{23}	−0.0044 (60)	−0.0051 (64)	−0.0039 (36)	0.0001 (34)
β_{31}	0.0053 (10)	0.0050 (10)	0.0066 (5)	0.0015 (4)

fraction studies for the gaseous state—3.16_4[5] and 3.57_0 Å[6] (see Table 4). It may, therefore, be permissible to assume a rigid molecule in these crystals. Schematic drawings of the crystal structures of methylene dibromide and methylene diiodide are given in Figs. 1 and 2. Figure 1 is the projection of the structure on the (010) plane, and Fig. 2, the bounded projection on the (001) plane of the molecules lying in $Z\approx\pm0.13$. In these figures, the orientations of the methylene groups shown are those derived by the following lattice-energy calculations.

Lattice-energy Calculations. Though the carbon atoms of the two crystals were not located accurately on the basis of the X-ray intensity data, the most probable positions of these atoms could be derived by the following two methods. The first was to find the most plausible orientation of the methylene groups among their neighboring molecules. When the positions of the halogen atoms in the unit cell are accurately known, intermolecular atomic contacts can be obtained for various orientations by subjecting a rotation, θ, around the axis connecting the two halogen atoms,

5) H. A. Levy and L. O. Brockway, *J. Amer. Chem. Soc.*, **59**, 1662 (1937).

6) O. Bastiansen, *Tidsskr. Kjemi Bergv.*, **6**, 1 (1946).

TABLE 4. POSITIONAL PARAMETERS OF THE CARBON AND HYDROGEN ATOMS FOR THE MOST PROBABLE ORIENTATION, $\theta=190°$.
The molecular structures used are also listed.

	Methylene dibromide			Methylene diiodide		
	C	H(1)	H(2)	C	H(1)	H(2)
X	0.2105	0.2347	0.1740	0.2164	0.2405	0.1810
Y	0.4129	0.2398	0.3143	0.4124	0.2490	0.3190
Z	0.1120	0.1651	0.0420	0.1148	0.1642	0.0498
	Br–C	1.91 Å[5]		I–C	2.12 Å[6]	
	H–C	1.07 Å[a]		H–C	1.07 Å[a]	
	∠BrCBr	112°[5]		∠ICI	114.7°[6]	
	∠HCH	109.5°[a]		∠HCH	109.5°[a]	
	(Br...Br	3.16_4Å)[b]		(I...I	3.57_0Å)[b]	

a) Assumed.
b) Calculated by the present authors.

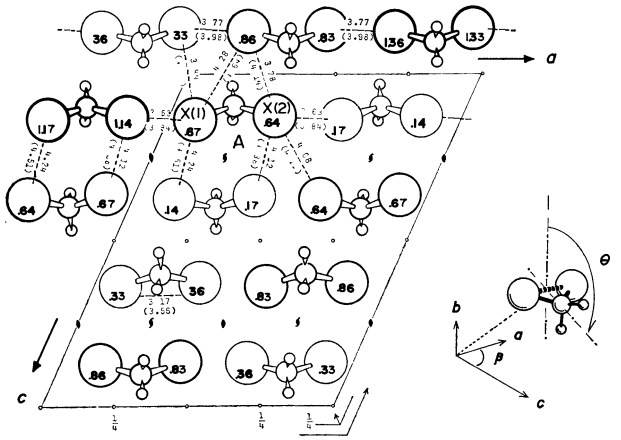

Fig. 1. Schematic drawing of the crystal structure of methylene dibromide and methylene diiodide, projected along the b axis. Numbers within circles indicate fractional co-ordinates, Y, of the iodine atoms. Interatomic distances for methylene bromide and those for methylene iodide (in parentheses) are also given.

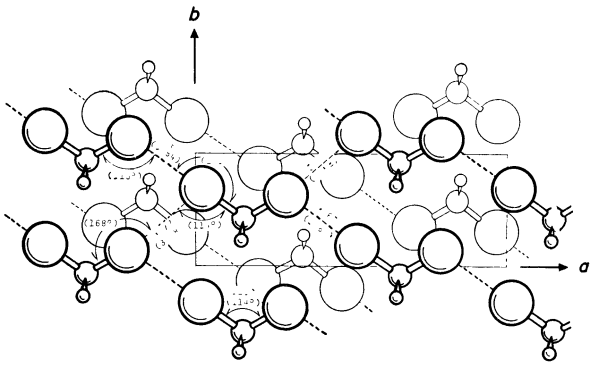

Fig. 2. Bounded projection of the crystal structure on the (001) plane. Molecules lying in $Z\simeq 0.13$ are drawn with thick lines and those lying in $Z\simeq -0.13$ with thin lines. Interatomic distances and angles for methylene dibromide and those for methylene diiodide (in parentheses) are also given.

X(1)···X(2), of a reference molecule, **A** (see Fig. 1), accompanied by the rotations of other molecules around their similar axes in accordance with the symmetry of the space group $C2/c$. The starting point of θ is taken as the orientation where the X–C–X plane of the **A** molecule is parallel to the b axis. Figure 3 shows the variations with θ of a number of contacts. (a) indicates methylene dibromide, and (b), methylene diiodide. Both of them indicates that the most plausible orientation located in the vicinity of $\theta\approx 190°$.

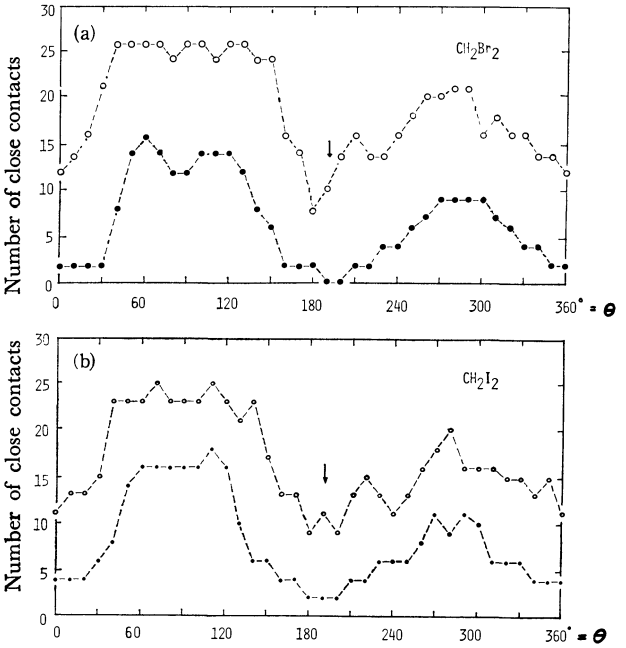

Fig. 3. Variation of number of contacts between neighboring molecules less than the van der Waals contacts, plotted by curve —○—. Curve—●— shows comparison with the van der Waals contacts multiplied by 0.9.
(a) for methylene dibromide and (b) for methylene diiodide.

The most reasonable orientation of the methylene group can also be found quantitatively by obtaining the potential energy minimum of the crystal, which can be calculated from the molecular interactions. Here, it is assumed that the potential energy can be described by the dispersion, the exchange repulsive, the dipole-dipole coupling, and the induced dipole interactions. Calculations were carried out by using Eq. (2) and the constants of A_{ij}, B_{ij}, and C_{ij}, which have been given in a previous paper,[1] together with the following constants:

Molecule	Dipole moment (debye)	Molecular polarizability (10^{-24} cm^3)
CH_2Br_2	1.39	8.30
CH_2I_2	1.10	11.84

The rotating scheme about the methylene group is the same as that described above.

In Fig. 4, (a) and (b) show the variations in the interaction energies for methylene dibromide and for methylene diiodide respectively. One can find results similar to those indicated in Fig. 3; the most probable orientation of the methylene group was found in the vicinity of $\theta\approx 190°$ for both the crystals. In Table 4 the positional parameters of the carbon and hydrogen atoms corresponding to the $\theta=190°$ orientation are given. As has been mentioned ealier, the X-ray intensity data were not sufficient to be used in the refinement

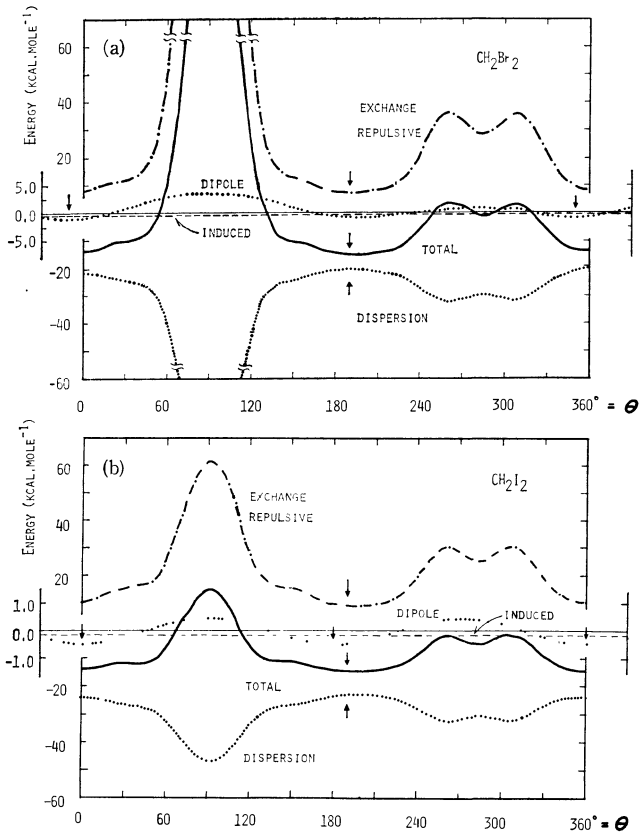

Fig. 4. Variations of the interaction energies with rotation θ. (a) for methylene dibromide, and (b) for methylene diiodide.

of the structures. In these orientations, the lattice energies arising from the four kinds of interaction amount to 14.4 for methylene dibromide and to 14.3 kcal/mol for methylene diiodide. The lattice energy of methylene diiodide can be compared with the sum of the experimental heats of vaporization, 10.2, and of fusion, 3.00 kcal/mol, for the stable form, II.[7] Most of the energies calculated came from the dispersion and the exchange repulsive interactions (see Table 5). As is shown in Fig. 4, the orientation of the methylene group is dominated by the repulsive term.

7) "Amercican Institute of Physics Handbook," McGraw-Hill Book Comp. Inc. (1957).

Table 5. Calculated lattice energies for the most probable orientation, $\theta=190°$, of the methylene group (in kcal/mol)

Compound	Dispersion	Exchange repulsive	Dipole dipole	Induced dipole	Total
CH_2Br_2	−20.57	7.24	−0.82	−0.26	−14.41
CH_2I_2	−23.06	9.35	−0.40	−0.15	−14.26

The crystal structure can be described as a sort of a layer structure parallel to the (001) plane. The X–C–X planes of all the molecules lie nearly on the layer planes. As can be seen in Fig. 1, the orientations of the molecular axes or the dipoles in the two immediate layers are almost parallel and almost antiparallel respectively.

Within the layer, the molecules are held together by noticeable short contacts. The interatomic distances between halogen atoms are 3.63 and 3.77 Å for Br···Br, and 3.84 and 3.98 Å for I···I; these are far less than twice the van der Waals radii, 3.90 for bromine and 4.30 Å for iodine. The two kinds of angles, C–X···X, between the neighboring molecules are not far from 90° (or the tetrahedral angle, 109.5°) and 180°. The quite close contacts and the characteristic geometries presented above with regard to the halogen atoms can be seen in other crystals, for example, solid bromine and iodine,[8] methyl bromide and methyl iodide,[3] and bromoform[1] and iodoform.[2] The partial intermolecular bonding effect between the bromine and, particularly, iodine atoms, which was suggested by Tomiie,[9] may contribute appreciably to the molecular arrangements of simple molecules with bromine or iodine atoms.

The authors wish to express their thankfulness to Dr. Akio Furusaki and Dr. Akio Takenaka for their help in these analyses.

8) L. W. G. Wyckoff, "Crystal Structures," Vol. 1, New York, London, Sydney: Wiley-Interscience (1964), p. 52.

9) Y. Tomiie, *Kwansei Gakuin Univ. Ann. Studies*, **10**, 208 (1961).

The Crystal Structure of Methylene Dichloride, CH_2Cl_2

Takemi KAWAGUCHI,* Kazuo TANAKA, Toru TAKEUCHI, and Tokunosuké WATANABÉ
Faculty of Science, Kwansei Gakuin University, Nishinomiya

(Received May 6, 1972)

The crystal structure of methylene dichloride has been determined by the X-ray diffraction method at about −120°C. The structure has a symmetry D_{2h}^{14}—*Pbcn*, and its orthorhombic tetramolecular cell has these dimensions: $a=4.249\pm0.001$, $b=8.138\pm0.020$, and $c=9.492\pm0.002$ Å. The positional parameters of the chlorine and carbon atoms are obtained by a three-dimensional Patterson function, followed by a least-squares refinement including the hydrogen atom. The structure thus obtained is in excellent agreement with the results of lattice-energy calculations. The crystal structure is quite different from that of methylene dibromide (and of methylene diiodide).

The crystal structures of various halogenated methanes have been reported on in previous papers in order to elucidate the molecular interactions in these molecular crystals. It has been shown that, in the crystals of mono- and tri-halogenated methanes, CH_3X and CHX_3, those of bromine- and iodine-substituted methanes are isomorphous, while those of chlorine-substituted methanes are quite different.[1-3]

Marzocchi *et al.* reported, based upon their spectroscopic measurements, that the crystals of methylene dibromide and the stable form of methylene diiodide, Form II, are isomorphous, but not with that of methylene dichloride.[4,5] In the preceding paper, it has been shown that the crystals of methylene dibromide and methylene diiodide (II) are isomorphous, with a symmetry C_{2h}^{6}—$C2/c$.[6]

In this paper the crystal structure of methylene dichloride, as determined by the X-ray diffraction method, will be reported. It will also be shown that the structure is in good agreement with that derived by means of lattice-energy calculations.

Experimental

Methylene dichloride from Wako Pure Chemical Industries, Ltd., was sealed in thin-wall glass capillaries (0.3 mm in internal diameter and 0.01 mm in wall thickness). A single crystal was carefully produced in the way described in previous papers.[1,3] The crystal used grew with the [010] zone axis of an orthorhombic lattice nearly along the capillary, and was then gradually cooled to about −120°C.

The unit-cell dimensions were determined from oscillation and Weissenberg photographs around the [010] axis taken by using Cu$K\alpha$ radiation. The intensity distributions and systematic extinctions (none for *hkl*, *0kl* with *k* odd, *hk0* with $h+k$ odd and *h0l* with *l* odd) indicated that the crystal belongs to the orthorhombic system, with a symmetry of space group D_{2h}^{14}—*Pbcn*. There are four molecules per cell and the X-ray density amounts to 1.718 g/cm³, where the observed densities, 1.327 at 20° and 1.761 g/cm³ at −194°C,[7] are referred to. The crystal data are summarized in Table 1.

Table 1. Crystal data

Compound	methylene dichloride, CH_2Cl_2
MW	84.83
Bp	39.95°C
Mp	−96.8°C
Exp. temp.	−120°C
Orthorhombic; D_{2h}^{14}—*Pbcn*	
Z	= 4
a	$=4.249\pm0.001$ Å
b	$=8.138\pm0.020$
c	$=9.492\pm0.002$
V	=328.21 Å³
D_x	=1.718 g/cm³
D_m	=1.327 (at 20°C)
	1.761 (at −194°C)
μ	=153.2 cm⁻¹ (for Cu$K\alpha$ radiation)

Integrated intensities of reflections, taken from six layers between the zeroth and the fifth layers around the [010] axis, were collected by means of the multiple-film method and the equi-inclination Weissenberg technique. The X-rays used were Ni-filtered Cu$K\alpha$ radiations. The intensities were measured visually and were corrected for Lorentz-polarization and absorption effects by cylindrical approximation, followed by bringing them into a common scale by considering with different time exposures. Inorder to determine the structure, 226 independent reflections were used.

Structure Determination

Since the crystal has the symmetry *Pbcn*, each molecule should be located on the C_2 site in the tetramolecular cell. Approximate co-ordinates of the chlorine and carbon atoms were immediately found with the aid of the three-dimensional Patterson function. A least-squares refinement was made for these co-ordinates with isotropic temperature factors. The reliability factors, $R=\sum||F_o|-|F_c||/\sum|F_o|$, decreased from 0.25 to 0.17.

Further refinement was made for the relative scales of the intensities from the six different layers, followed

* To whom all correspondence should be addressed. Present address: Department of Research and Development, Nippon Crucible Co., Ltd., 925 Inada, Higashi-Osaka, 577.

1) T. Kawaguchi, K. Takashina, T. Tanaka, and T. Watanabé, *Acta Crystallogr. B* **28**, 967 (1972).
2) Y. Iwata, M. Oyama, T. Kawaguchi, T. Watanabé, to be published.
3) T. Kawaguchi, M. Hijikigawa, Y. Hayafuji, M. Ikeda, R. Fukushima, and Y. Tomiie, This Bulletin, **46**, 53 (1973).
4) M. P. Marzocchi, V. Schettino, and S. Califano, *J. Chem. Phys.*, **45**, 1400 (1966); M. P. Marzocchi, P. Manzelli, V. Schettino, and S. Califano, *ibid.*, **49**, 5438 (1968).
5) M. P. Marzocchi and P. Manzelli, *ibid.*, **52**, 2630 (1970).
6) T. Kawaguchi, A. Wakabayashi, M. Matsumoto, T. Takeuchi, and T. Watanabé, This Bulletin, **46**, 57 (1973).
7) W. Blitz and A. Sapper, *Z. Anorg. Allgem. Chem.*, **203**, 277 (1932).

Table 2. (Cont.)

h	k	l	$\|F_o\|$	$\|F_c\|$	h	k	l	$\|F_o\|$	$\|F_c\|$
1	3	4	67.60	64.06	1	4	8	21.40	20.35
1	3	5	5.07	4.41	1	4	9	26.71	19.14
1	3	6	8.24	6.72	1	4	10	31.59	35.82
1	3	7	12.64	11.49	1	4	11	10.23	14.04
1	3	8	26.50	23.31	2	4	0	72.81	68.71
1	3	9	4.38	5.45	2	4	1	40.13	35.44
1	3	10	9.22	9.35	2	4	3	16.08	16.30
2	3	1	18.01	11.81	2	4	4	46.83	42.17
2	3	2	84.06	81.32	2	4	5	9.90	9.17
2	3	3	12.76	8.54	2	4	6	22.15	20.81
2	3	4	5.77	3.57	2	4	7	24.12	26.27
2	3	5	14.72	10.08	2	4	8	35.80	36.86
2	3	6	62.02	56.15	2	4	9	10.39	13.05
2	3	8	9.98	8.47	2	4	10	9.94	10.32
2	3	9	9.73	7.87	3	4	1	8.61	3.72
2	3	10	34.35	36.30	3	4	2	28.73	25.05
3	3	0	82.81	78.82	3	4	4	9.25	7.65
3	3	1	6.93	3.64	3	4	6	20.51	18.59
3	3	2	7.85	3.75	3	4	7	4.60	0.15
3	3	3	21.31	18.29	3	4	8	8.91	9.39
3	3	4	57.64	55.47	3	4	9	2.07	3.81
3	3	5	13.62	11.26	4	4	1	15.81	12.78
3	3	6	16.01	14.25	4	4	2	5.20	6.45
3	3	7	10.20	6.68	4	4	3	4.01	2.23
3	3	8	40.75	48.11	4	4	4	6.48	7.59
4	3	1	12.08	10.34	4	4	5	5.49	4.05
4	3	2	41.79	45.25	4	4	7	3.79	7.50
4	3	3	10.82	8.25	5	4	1	4.86	9.12
4	3	4	7.36	5.93	5	4	2	1.58	4.65
4	3	5	11.18	9.15	1	5	0	23.44	20.47
4	3	6	30.18	35.54	1	5	1	21.61	18.93
4	3	7	4.33	3.19	1	5	2	10.06	9.39
5	3	0	11.74	18.78	1	5	3	42.97	39.80
5	3	1	7.16	8.54	1	5	5	34.14	30.25
5	3	2	3.23	6.27	1	5	7	17.08	15.49
5	3	3	3.33	5.12	1	5	8	12.87	11.18
0	4	2	24.60	26.76	1	5	9	7.43	6.89
0	4	3	66.74	71.11	1	5	10	5.02	5.01
0	4	4	96.80	102.74	2	5	1	49.24	45.48
0	4	5	54.53	52.00	2	5	2	16.48	13.31
0	4	6	14.34	11.47	2	5	3	41.23	38.04
0	4	7	36.20	35.76	2	5	5	43.44	41.01
0	4	8	48.96	48.68	2	5	6	13.29	11.61
0	4	9	17.88	19.20	2	5	7	26.16	25.23
0	4	10	22.90	24.49	2	5	9	30.75	29.06
0	4	11	24.99	30.78	3	5	1	49.48	48.51
1	4	1	46.35	53.07	3	5	3	32.36	34.97
1	4	2	90.61	92.76	3	5	4	11.82	12.44
1	4	3	44.20	42.41	3	5	5	24.91	23.40
1	4	4	16.50	13.59	3	5	7	33.61	39.38
1	4	5	47.04	44.30	4	5	1	23.50	29.58
1	4	6	61.84	60.97	4	5	3	20.47	23.33
1	4	7	27.74	27.61	4	5	5	25.42	29.38

by the least-squares refinement, where the anomalous dispersion effect was taken into consideration for the chlorine atom. The difference Fourier synthesis indicated the probable coordinates of the hydrogen atoms. Successive refinement with anisotropic temperature factors for the chlorine and carbon atoms and with an isotropic temperature factor for hydrogen atom finally decreased the R value to 0.109.

Results

The observed and calculated structure factors are

Table 3. Positional and thermal parameters with their e.s.d.'s (in parentheses)

* The temperature factors are of the form $\exp[-B_{11}h^2+B_{22}k^2+B_{33}l^2+B_{12}hk+B_{23}kl+B_{31}lh)]$ for the chlorine and carbon atoms, and of the form $\exp[-B(\sin\theta/\lambda)^2]$ for the hydrogen atom.

Parameter	Cl	C	H
X	0.1846 (8)	0 (—)	0.1747 (266)
Y	0.1522 (6)	0.0307 (28)	−0.0369 (199)
Z	0.1195 (3)	1/4 (—)	0.2859 (109)
B_{11}	0.0529 (19)	0.0384 (97)	0.2 (27)
B_{22}	0.0095 (10)	0.0060 (50)	...
B_{33}	0.0053 (3)	0.0053 (15)	...
B_{12}	−0.0164 (21)	0 (—)	...
B_{23}	0.0034 (8)	0 (—)	...
B_{31}	−0.0077 (12)	0.0065 (65)	...

listed in Table 2, while the final set of the positional and thermal parameters of the atoms is summarized in Table 3. It is found that the bond distances and angles of the molecule calculated by using these coordinates are much closer to those of the gas molecule obtained by a microwave study.[8] A comparison between the two is shown in Table 4.

Table 4. Comparison of the molecular structures

	Microwave study[8]	Present work
C–H	1.068 ±0.005 Å	0.99 ±0.13 Å
C–Cl	1.7724±0.0005	1.768±0.013
Cl...Cl	2.935[a]	2.932±0.004
∠Cl–C–Cl	112.0±0.3°	112±1°
∠H–C–H	118.8 (C–H=C–D, ass.)	112±7

a) calculated by the authors.

The crystal structure is illustrated in Figs. 1 and 2. Figure 1 shows the projection along the b axis, and Fig. 2, the projection along the a axis. In these figures,

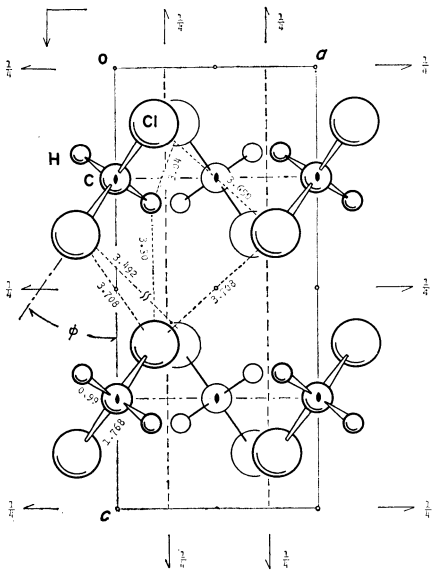

Fig. 1. Projection of the crystal structure along the b axis.

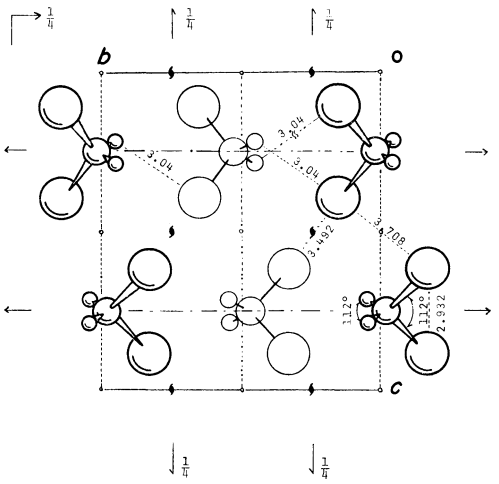

Fig. 2. Projection of the crystal structure along the a axis.

several interatomic distances between neighboring molecules are also shown. Here, the e.s.d.'s are about 0.005 for Cl···Cl and 0.1 Å for Cl···H. The intermolecular atomic distances were found to be close to the sums of the van der Waals radii.

Lattice-energy Calculations

In this section, it will be described how the same conclusion was obtained by means of lattice-energy calculations, given the unit-cell dimensions and the symmetry of the crystal.

If the molecular structure of methylene dichloride and the symmetry and dimensions of the crystal are

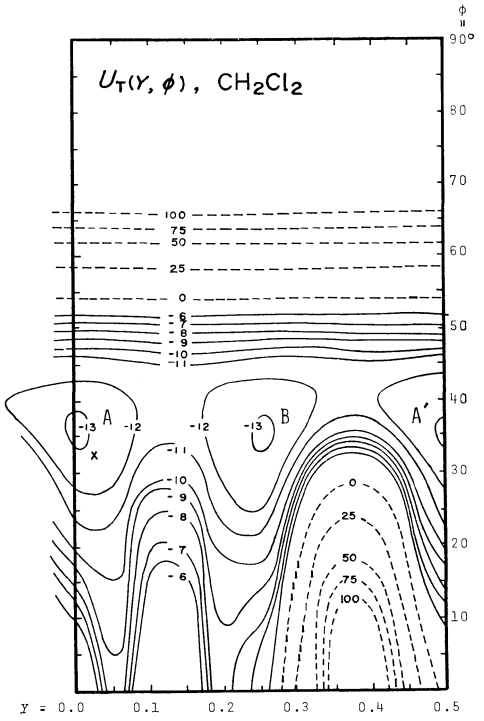

Fig. 3. Potential map, $U(Y,\phi)$. Contours with solid lines are at 1 kcal/mol intervals and contours with dashed lines show positive energy region, being at 25 kcal/mol intervals. Sign **X** indicates the crystal structure determined by the X-ray analysis.

8) R. J. Myers and W. D. Gwinn, *J. Chem. Phys.*, **20**, 1420 (1952).

TABLE 5. CALCULATED LATTICE ENERGIES FOR METHYLENE DICHLORIDE AND ITS RELATED COMPOUNDS, IN kcal/mol.

Compound	Note	Total	Dispersion	Exchange repulsion	Dipole-coupling	Induction
CH_2Cl_2	**A**[a)]	−13.07	−13.35	3.08	−2.51	−0.29
	B[a)]	−13.03	−13.23	2.95	−2.47	−0.29
	X-ray	−12.74	−13.22	3.04	−2.27	−0.29
CH_2Br_2	*C2/c*	−14.41	−20.57	7.24	−0.82	−0.26
CH_2I_2	*C2/c*	−14.26	−23.06	9.35	−0.40	−0.15

a) **A** and **B** denote the structures obtained by the lattice energy calculations.

given, one can describe the crystal structure, by using two structural parameters, Y and ϕ, where Y is the co-ordinate of the carbon atom, and ϕ, the angle of tilt of the reference molecule located on the two-fold axis, as is shown in Fig. 1. Lattice-energy calculations were made by using four kinds of molecular interactions; the dispersion, the exchange repulsion, the dipole-dipole coupling, and the induction effects, using the constants cited in the previous paper,[1)] together with a dipole moment of 1.62 Debye and a molecular polarizability of 6.48×10^{-24} cm^3. Calculations of the dipole-dipole interaction were carried out for every pair of molecules within a range of 40 Å, while those of the other three interactions were carried out for every pair of atoms within a range of 20 Å. The dipole-dipole interactions between eight nearest neighboring molecules were substituted for interactions between the divided bond moments (referred to 2.3 for $C^{(+)}-Cl^{(-)}$ bond and 0.4 debye for $C^{(+)}-H^{(-)}$ bond[9)]).

A potential map, $U(Y,\phi)$, was obtained; it is given in Fig. 3. Contours with solid lines are located at 1 kcal/mol intervals, while contours with dashed lines show the positive energy region, being at 25 kcal/mol intervals. Two stable structures were found as deep ravines, **A** and **B**, in the map, (Ravine **A'** is crystallographically equivalent to **A**): $U_A(Y=0.0,\ \phi=35°)=-13.08$ and $U_B(Y=0.25,\ \phi=35°)=-13.03$ kcal/mol. The present X-ray analysis gives a structure which is very close to Structure **A**, corresponding to $Y=0.030_7\pm0.003$ and $\phi=32.3\pm0.1°$, as is indicated by **X** in the map.

The lattice energy for the structure obtained by the X-ray analysis, together with those for Structures **A** and **B**, are given in Table 5. In this table, the lattice energies calculated for the crystals of methylene dibromide and methylene diiodide are also summarized for the sake of comparison.

Discussion

On the basis of an infrared spectroscopic study,[5)] Marzocchi and Manzelli reported that all the observed data on methylene dichloride are consistent with an orthorhombic *Pbcn* unit cell, in which four molecules are located on C_2 sites and tilt their symmetrical planes at $29\pm2°$ from one of the crystal axes. These spectroscopic conclusions, except for the mutual molecular arrangement, are in excellent agreement with those of the present work.

The potential map, $U(Y,\phi)$ in Fig. 3, suggests another probable crystal structure corresponding to the ravine, **B**. This structure can be derived from Structure **A** by a translation (0.25) of Y, while keeping ϕ constant. This structure can also be looked upon as being derived by orienting every molecule inversely along the *b* axis. It might be possible to obtain crystals with this structure by means of different procedures of crystallization.

The crystal structures of methylene dibromide and methylene diiodide, which are isomorphous with the symmetry *C2/c*, are quite different from that of methylene dichloride. The lattice energies calculated for the two crystals are added in Table 5. It is noticeable that the contribution of the dipole-dipole interactions in the crystal of methylene dichloride is much larger than those in the crystals of methylene dibromide and methylene diiodide. This suggests that the dipole-dipole interactions play an important role upon solidification, leading to a different crystal structure from those of methylene dibromide and methylene diiodide.

The authors are indebted to the Kwansei Gakuin University Computing Center for calculations.

9) R. Daudel, R. Lefebver, and C. Moser, "Quantum Chemistry, Methods and Applications," Interscience Publishers, Inc., New York (1959), p. 206.

The Vacuum Ultraviolet Photolysis of Liquid *n*-Hexane in the Presence of SF_6

Vadim I. PITCHOOZHKIN,* Hideo YAMAZAKI, and Shoji SHIDA

Laboratory of Physical Chemistry, Tokyo Institute of Technology, Meguro-ku, Tokyo

(Received May 10, 1972)

The photolysis of liquid *n*-hexane has been studied at room temperature and at −78°C by using the resonance lines of Xe and Kr. The main process is hydrogen detachment, giving the same amount of hydrogen and of hexenes; relatively small amounts of the decomposition and dimer products were also formed. Upon the addition of SF_6, the yield of the hydrogen detachment decreased strongly with an increase in the concentration of SF_6, and then approached a constant value of 0.65 relative to that in pure *n*-hexane. The total amount of fluorine-containing products detected in the presence of SF_6 was relatively small compared with the amount of the decrease in the hydrogen detachment. As another electron scavenger, $C_6H_{13}F$ was also tested; here, the decrease in the hydrogen detachment was quite small.

The ionic process in the radiolysis of hydrocarbons is one of the most important problems in radiation chemistry; as chemical approaches to this problem, various charge scavengers are used to elucidate the reaction mechanism.[1,2] By using this technique, a number of interesting results, such as the existence of ion-molecule reactions in liquid hydrocarbons,[3] have been obtained. However, the charge scavengers added may possibly react as radical scavengers or as deactivators of the excited states.[4] For quantitative experiments, the suitability of the charge scavenger should, therefore, be tested by using various methods. Along those lines, Holroyd[5,6] examined the energy-transfer process by using vacuum ultraviolet light in the system of liquid cyclohexane with N_2O; he observed a marked decrease in the photoproducts upon the deactivation of the solute. Lipsky and Hirayama[7-10] found that the donor fluorescence state in a hydrocarbon solution of the scintillator was deactivated by the addition of various electron scavengers, such as O_2, SF_6, N_2O, and CO_2. These experiments seem to indicate that the excited states of hydrocarbons can be quenched by electron scavengers. However, the details of this process are still unknown, so the present experiment was undertaken in order to clarify this process and to find ideal electron scavengers.

Experimental

The Xe and Kr lamps were constructed by the usual method.[11] The LiF window of the lamps was jointed with Araldite, and a Ba getter was used to obtain an intense resonance line by the removing impurity lines. The Xe and Kr lamps were operated with a microwave generator of 2450 MHz and 200 W made by the Ito Chotanpa Co. The intensities of the lamps were about $10^{15}-5\times10^{14}$ photon/sec, depending on the diameter of the lamps.

A sample of *n*-hexane (99.99% purity) was obtained from the Phillips Co.; it was purified by passing it through $Mg(ClO_4)_2$ and NaOH column to remove any CO_2 and H_2O and then led into the reaction vessel through a greaseless stopcock. SF_6 of a spectroscopic purity obtained from the Takachiho Co. and $C_6H_{13}F$ (purum) obtained from the Fluka A. G. Co. were used as electron scavengers without any further purification. The concentrations of SF_6 in the liquid *n*-hexane in the samples were determined by means of the partition ratios of SF_6 between the gas and liquid phases at room temperature and at −78°C, as measured by the use of a large amount of *n*-hexane.

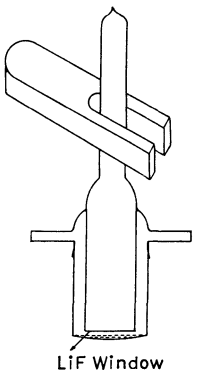

Fig. 1. Apparatus of photolysis in liquid phase.

The apparatus for the photolysis of liquid *n*-hexane is shown in Fig. 1. In the present experiment, the distance between the outer surface of the LiF window and the liquid surface was maintained at about 1 mm. Some experiments were also carried out by placing the LiF window in contact with the liquid surface. In the former case, the temperature of the reaction system was kept at −78°C to prevent direct photolysis in the gas phase. The intensity of light absorbed in the case of −78°C was fairly constant compared with that in the latter case.

After each run, the reactant and the products were condensed in a liquid-nitrogen trap. The noncondensable gases were gathered and measured by means of a Teopler-McLeod

* Present address: Laboratory of Radiation Chemistry, Department of Chemistry, Moscow Lomonosov State University, Moscow, USSR.

1) G. Scholes and M. Simic, *Nature*, **202**, 895 (1964).
2) F. Williams, *J. Amer. Chem. Soc.*, **86**, 3954 (1964).
3) A. A. Scala and P. Ausloos, *J. Chem. Phys.*, **47**, 5129 (1967).
4) M. B. Muratbekov and V. V. Saraeva, *Khim. Vys. Energ.*, **4**, 365 (1970).
5) H. A. Holroyd, *Adv. Chem. Ser.*, **82**, 488 (1968).
6) J. Y. Yang, F. M. Servedio, and H. A. Holroyd, *J. Chem. Phys.*, **48**, 1331 (1968).
7) F. Hirayama and S. Lipsky, International Conf. Scintillation Count. San-Francisco, p. 205 (1970).
8) S. Lipsky, *J. Chem. Phys.*, **38**, 2786 (1963).
9) C. W. Lawson, F. Hirayama, and S. Lipsky, *ibid.*, **51**, 1590 (1969).
10) F. Hirayama, and S. Lipsky, *ibid.*, **51**, 3616 (1969).
11) J. R. McNesby and H. Okabe, *Adv. Photochem.*, **3**, 157 (1964).

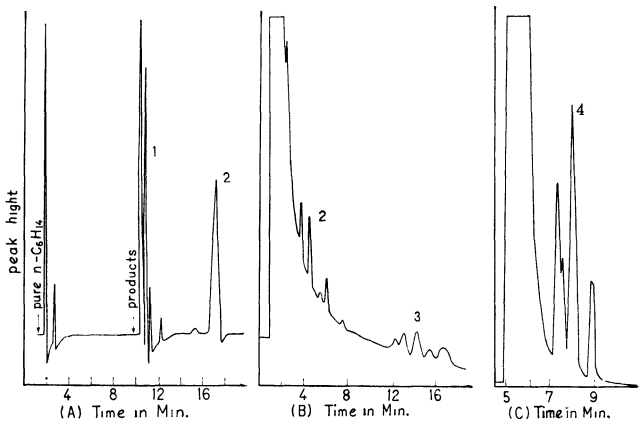

Fig. 2. Gas chromatogram of condensable products.

system. The noncondensable gases were mainly hydrogen. The condensable products, such as olefins and dimers, were analyzed by means of a Shimadzu gas chromatograph (Silicone D.C. 550, 5 m at 140°C and dimethyl sulpholane (10 m) at room temperature), equipped with a flame ionization detector. A Shimadzu electron-capture gas chromatograph was also used to detect the fluorine-containing products. The gas chromatograms of the condensable products are shown in Fig. 2, where (A) stands for the electron-capture detector, and where (B) and (C) indicate the flame-ionozation detector. The two peaks, Peak 1 and Peak 2, of the fluorine-containing products are magnified by the use of the electron-capture detector.

Results and Discussion

In the photolysis of liquid *n*-hexane, the main products were hydrogen and hexenes in almost identical amounts; small amounts of dimers and the decomposition products were also found. This means that the molecular detachment of hydrogen is the main process, unlike the radiolysis, where the hydrogen-atom splitting is the more important process. No difference was observed in the products between the Xe and Kr resonance lines. Holroyd[6] obtained almost the same results in his photolysis of liquid cyclohexane.

In the presence of SF_6, the relative yields of the major products, *i.e.* hydrogen and hexenes, decrease greatly, as is shown in Fig. 3. For sufficiently high

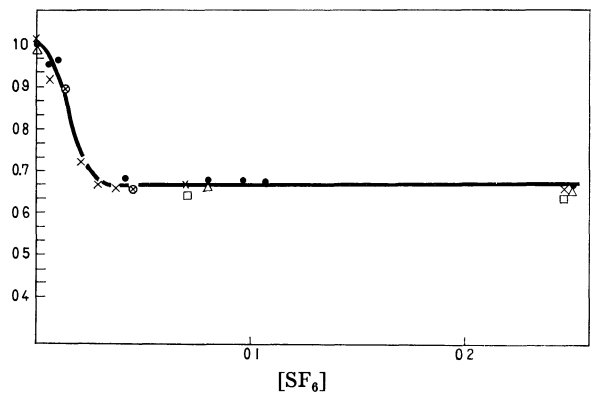

Fig. 3. The relative yields of hydrogen (●1470 Å, ×1236 Å) and hexenes (△1470 Å, □1236 Å) as a function of concentration of SF_6.

concentrations of SF_6, the yields of hydrogen and the total hexenes approach a constant value (*ca.* 0.65 relative to that of pure hexane), irrespective of the Kr and Xe resonance lines; a preliminary experiment with the Br resonance line showed the same tendency. The photolysis of *n*-hexane in the gas phase was also carried out, but no decrease in the relative yield was observed upon the addition of SF_6. As one possible mechanism, the energy transfer between *n*-hexane molecules may occur faster in the liquid phase than in the gas phase, and then the energy may be trapped by SF_6. The energies of the Kr (1236 Å), Xe (1470 Å), and Br (1634 Å) resonance lines are 0.4, 2.0, and 2.8 eV below the ionization potential of *n*-hexane. The Xe and Kr resonance lines may be able to excite the *n*-hexane molecule in the semi-ionized states or in locally-ionized states.[12]

The experimental results are quite similar for both the Xe and Kr resonance lines, indicating that the main process is the molecular detachment of hydrogen, which was often observed in the lower excitation of paraffins in the gas phase. As a general rule in the photolysis of paraffins, it was observed that the ratio of the atomic and molecular detachments of hydrogen increased with an increase in the photon energy.[14] Slightly below the ionization potential, the radius of the wave function of the excited electron is quite large; for example, the maximum of the radial-distribution function of the hydrogenic 2*s* orbital is five times larger than that of the 1*s* orbital. In liquid paraffin, the Onsager radius is several hundreds Ångstrom, so that within this radius the probability of geminate recombination is larger than that of free-ion formation. The states in which electrons reside between the Onsager radius and a radius several times larger than the radius of the ground state of a molecule may be called semi-ionized or locally ionized states, and a number of molecule may be present inside the orbital. When an electron approaches the positive ion, thus decreasing the radius of the orbital and the kinetic energy, the electron may enter into the lower excited state of the neutral molecule, where the molecular detachment of hydrogen, then takes place, as in the case of the photolysis of the gas phase.[14] Since the photolysis products in the liquid phase were quite similar to those in the gas phase, the same precursor of the reaction can be expected in both phases, as in the case of cyclohexane.[6] The preliminary experiment on the Br resonance line also shows the same dependence of the hydrogen-molecule splitting on the concentration of SF_6. The absorption coefficient of hexane is quite large at 1470 and 1236 Å, while that of SF_6 is relatively small.[15,16] Therefore,

12) The Br resonance line excites the *n*-hexane molecule to the first singlet excited state (8.2 eV (calcd), 8.3 eV (obsd)).[13]

13) J. W. Raymonda and W. T. Simpson, *J. Chem. Phys.*, **47**, 430 (1967).

14) K. Obi, H. Akimoto, Y. Ogata, and I. Tanaka, *ibid.*, **55**, 3822 (1971).

15) B. A. Lombos, P. Sauvageau, and C. Sandorfy, *J. Mol. Spectrosc.*, **24**, 253 (1967).

16) E. D. Nostrand and A. B. F. Duncan, *J. Amer. Chem. Soc.*, **76**, 3377 (1954).

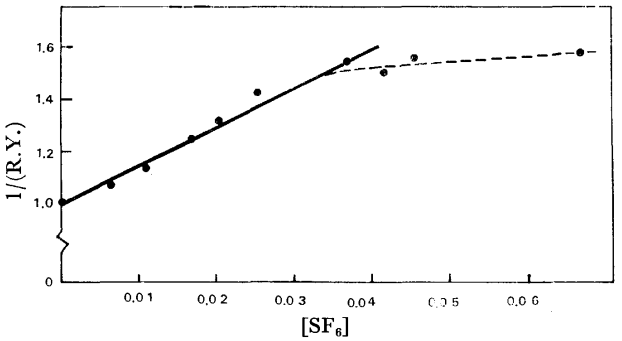

Fig. 4. The reciprocal plot of relative yields of hydrogen against concentration of SF_6.

the direct absorption of light by SF_6 is negligibly small.

In Fig. 4 the reciprocal relative yields (1/R.Y.) of the hydrogen detachment are plotted against the concentration of SF_6. A nearly straight line (solid line) is obtained for lower concentrations of SF_6. If the following reactions are postulated:

$$RH + h\nu \xrightarrow{k_1} RH^* \quad (1)$$

$$RH^* \xrightarrow{k_2} H_2 + R(-H) \quad (2)$$

$$RH^* + SF_6 \xrightarrow{k_3} \text{no hydrogen product} \quad (3)$$

$$RH^* + RH \longrightarrow RH + RH^* \quad (4)$$

where Eq. (4) shows the energy-transfer process to transport the excited state, RH*, to the vicinity of SF_6. Then, the steady-state treatment of the reaction yields the following relation:

$$1/\text{R.Y.} = 1 + k_3[SF_6]/k_2 \quad (5)$$

The k_3/k_2 ratio is obtained from the slope of the straight line extrapolated at the low concentration of SF_6. The value observed in this experiment is 15.0, while that of Holroyd was 4.5 in the photolysis of *n*-hexane in the presence of N_2O.[5] SF_6 is, thus, an acceptor stronger than N_2O in the energy-transfer process. This tendency is consistent with the measurement[7] of the fluorescence from the scintillator in a cyclohexane solution in the presence of various electron scavengers. The leveling-off at the higher concentrations of SF_6 (Fig. 3) was explained by the introduction of more than two excited states. Therefore, it may be considered that, in these excited states, only one excited state is responsible for discriminating the molecular detachment of hydrogen upon the addition of SF_6, as is shown in Eqs. (2) and (3), while the other excited states are not affected by the introduction of SF_6. The low-lying excited states of *n*-hexane were observed by the use of the electron reflection spectrum[17] and the emission spectrum.[18,19]

A prominent result is that the critical concentration of the scavenger is lower than that in the case of radiolysis. The reaction cross section calculated from the critical concentration of the scavenger is several hundred square Ångstrom. Such a large cross section was also observed in the energy-transfer process i n a propane isobutane mixture at a low temperature using EPR measurements[20] for isopropyl and isobutyl radicals; in this method, the effect of electron transfer is ruled out by the experimental condition that the ionization potential of the acceptor molecule is higher than that of the donor molecule. The large cross section may be explained by the fast movement of a pair of an electron and a positive ion. It is assumed that the excited state of hydrocarbon can react with SF_6 and form the state of charge separation[20,21]

$$RH^* + SF_6 \longrightarrow RH^+ + SF_6^- \quad (6)$$

The neutralization between RH^+ and SF_6^- is expected to form fluorine-containing products. The sharp decrease in the yield of hydrogen molecular detachment upon the addition of SF_6 can be explained by assuming a fast energy transfer or charge transfer to produce RH^+ and SF_6^-.

In a recent study of the radiolysis of benzene in presence of N_2O and COS, Sato *et al.*,[23] concluded that the energy transfer can take place neither through the superexcited state (20 eV) nor through the first excited state ($^1B_{2u}$), but must take place through some intermediate excited states between these states, although the details of energy transfer are not known.

Another possible explanation of the large reactive cross section is that a charge-transfer complex between *n*-hexane and SF_6 in either the ground or excited state may be formed and the detachment process may be perturbed by this complex formation. The weak interaction between the halogen molecule or halogen-containing compounds including SF_6 and paraffin was observed by the use of the spectroscopic method.[24,25] The gas chromatographic measurement with an iodine column showed the existence of a weak interaction between iodine and paraffins.[26] Therefore, the complex-formation mechanism appears to be a plausible explanation.

The quenching process by SF_6 may produce various fluorine-containing products. Several large peaks were detected in the electron-capture gas chromatogram (Fig. 1). One of the products was determined to be 1-fluorohexane (peak 1 in Fig. 2). These products increased with the increase in the concentration of SF_6. The total amount of these fluorine-containing products is smaller than that of the decrease in the hydrogen molecule.

To find an ideal electron scavenger without any deactivation by the energy-transfer process, 1-fluorohexane was tested. In the photolysis of liquid *n*-hexane,

17) L. M. Hunter, D. Lewis, and W. H. Hamill, *J. Chem. Phys.*, **52**, 1733 (1970).
18) P. B. Merkel and W. H. Hamill, *ibid.*, **54**, 1695 (1971).
19) F. Hirayama and S. Lipsky, *ibid.*, **51**, 3616 (1969).
20) M. Wakayama, Y. Hitotake, M. Fukaya, T. Miyazaki, K. Fueki, and Z. Kuri, the 14th Conf. Radiation Chem. Sapporo, 1971.
21) V. Cermak and Z. Herman, *Collect. Czech. Chem. Commun.*, **29**, 953 (1964).
22) H. Hottop and A. Niehaus, *J. Chem. Phys.*, **47**, 2506 (1967).
23) S. Sato, K. Hosoya, S. Shishido, and S. Hirokami, This Bulletin, **45**, 2308 (1972).
24) D. F. Evance, *J. Chem. Phys.*, **23**, 1424 (1955).
25) D. F. Evance, *J. Chem. Soc.*, 4229, (1957).
26) W. E. Falconer and R. J. Cvetanovic, *J. Chromatog.*, **27**, 20 (1967).

only a small decrease in the hydrogen yield was observed upon the addition of 1-fluorohexane.

The authors wish to thank Drs. Kinichi Obi and Masahiro Kawasaki for their help in making the various light sources. The authors also wish to thank Professor Ikuzo Tanaka and Dr. Yoshihiko Hatano for their helpful discussions. One of the authors (V. I. P.) is also indebted for financial support by the USSR-Japan Exchange Program of Scholars and Researchers.

BULLETIN OF THE CHEMICAL SOCIETY OF JAPAN, VOL. 46, 70—74 (1973)

Luminescence from 2,3-Dimethylbutane Containing Toluene in the Solid Phase at 77°K during γ-Irradiation

Tetsuo MIYAZAKI, Yoshiyuki SAITAKE, Zen-ichiro KURI, and Shigenori SAKAI
Department of Synthetic Chemistry, Faculty of Engineering, Nagoya University, Chikusa-ku, Nagoya
(Received May 12, 1972)

The luminescence from 2,3-dimethylbutane(2,3DMB) containing toluene in the solid phase has been measured at 77°K during γ-irradiation. The emission consists of fluorescence and phosphorescence from toluene. Since the emission becomes zero upon the removal of a γ-ray source, it cannot be due to a post-irradiation effect. It is concluded from the dependency of the intensity on the concentration of toluene that the luminescence is due to an intermolecular energy transfer from 2,3DMB to toluene during γ-irradiation. ESR studies of γ-irradiated 2,3DMB containing toluene have also been undertaken at 77°K in order to obtain some information on the intermolecular energy transfer. The toluene anion is formed in the γ-irradiated 2,3DMB containing toluene. The dimer cation of toluene is formed in the γ-irradiated 2,3DMB containing toluene and an electron scavenger. The luminescence from toluene in the 2,3DMB matrix decreases upon the pre-irradiation of the sample at 77°K. When the pre-irradiated sample is illuminated by the light from a tungsten lamp to photobleach the toluene anion, the luminescence during γ-irradiation is recovered. Since the intensity of the luminescence does not correspond at all to the amount of toluene anions, the luminescence from toluene in the 2,3DMB matrix during γ-irradiation must not be due to a neutralization reaction between a toluene anion and a migrating hole. It is suggested that the migration of energy from the irradiated 2,3DMB to toluene may occur *via* an excitation transfer reaction.

We have previously studied the radiolysis of hydrocarbons in the solid phase in order to elucidate the primary process and in order to obtain information about the reaction kinetics in the solid phase. In the previous studies, some phenomena peculiar to the solid-phase radiolysis have been reported.[1-3] On the basis of these results, we have proposed that two important problems must be solved in order to elucidate the mechanism of the solid-phase radiolysis. One is the species of the mobile entities produced in the solid-phase radiolysis. The other is how the condition of the solid-matrix, such as phase and defect, affects the chemical reactions.

It was found in the radiolysis of solid isobutane[1] that H_2 and C_4H_9 radicals are formed by the fragmentation of the excited isobutane molecule and that their yields decrease upon the addition of CCl_4 or toluene. These findings were interpreted as the assumption that the excitation transfer from the excited isobutane molecule to CCl_4 or toluene occurs in the solid state at 77°K.

If toluene is an efficient acceptor of excitation in the radiolysis of solid alkane, the luminescence from the excited toluene may be observed; the expected results were observed in the solid 2,3-dimethylbutane(2,3DMB) with the toluene additive during γ-irradiation at 77°K.

Those additives which are generally used as electron scavengers or charge scavengers in the liquid-phase radiolysis may react also with an excited molecule in solid-phase radiolysis.[4] Therefore, it is quite difficult to study the nature of the mobile entity in the radiolysis of solid alkane using the scavenger method. Since the ESR spectroscopy and the measurement of the luminescence reveal different aspects of the mobile entity, the radiolysis of an alkane-toluene mixture in the solid phase at 77°K was studied using both methods.

Experimental

2,3-Dimethylbutane(2,3DMB), supplied by the Tokyo Kagaku Seiki Co. with a purity of more than 99%, was passed through a 30 cm column packed with activated alumina and then distillated on a vacuum line before use. Gas-chromatographic analysis of 2,3DMB showed that the concentration of the other hydrocarbons with molecular weights smaller than 2,3DMB is less than 0.01%. The spectrograde toluene

1) a) T. Wakayama, T. Kimura, T. Miyazaki, K. Fueki, and Z. Kuri, This Bulletin, **43**, 1017 (1970). b) T. Miyazaki, T. Yamada, T. Wakayama, K. Fueki, and Z. Kuri, *ibid.* **44**, 934 (1971).

2) T. Wakayama, T. Miyazaki, K. Fueki, and Z. Kuri, *J. Phys. Chem.*, **74**, 3584 (1970).

3) T. Miyazaki, Y. Fujitani, T. Wakayama, K. Fueki, and, Z. Kuri, This Bulletin, **44**, 984 (1971).

4) a) T. Miyazaki, T. Wakayama, M. Fukaya, Y. Saitake, and Z. Kuri, 14th Japanese Conference of Radiation Chemistry, Sept., 1971, Sapporo, Japan. b) Y. Saitake, T. Miyazaki, T. Wakayama, M. Fukaya, and Z. Kuri, 26th Annual Meeting of the Chemical Society of Japan, April, 1972, Tokyo, Japan.

and phenylbromide were of a high purity and were used after distillation on a vacuum line. The nitrous oxide was also of a high purity and was used without further purification.

The samples were irradiated with γ-rays from a ^{60}Co source at 77°K, and in most cases at a dose rate of 3.84×10^{19} eV/g·hr, for the ESR studies and at one of 4.83×10^{17} eV/g·hr for the measurements of the luminescence.

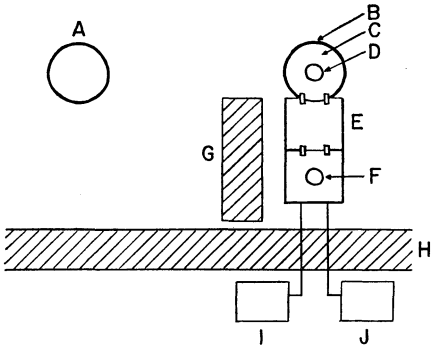

Fig. 1. Schematic diagram of the measurement of luminescence during γ-irradiation at 77°K.
A: ^{60}Co; B: Dewar flask; C: Liquid nitrogen; D: Sample; E: Monochrometer; F: Photomultiplier tube; G: Block of lead; H: Concrete wall; I: High voltage supplier; J: DC microvolt-ammeter.

The ESR spectra of irradiated samples were measured at 77°K on a JES-3BX ESR spectrometer. The luminescence was measured during γ-irradiation at 77°K. The apparatus for measuring the luminescence consisted of a high voltage supplier, a Shimadzu-Bausch-Lomb monochrometer, a photomultiplier tube (R-136) of the Hamamatsu TV Co. and a DC microvolt-ammeter. A schematic diagram of the apparatus is given in Fig. 1. When 2,3DMB containing toluene (2 mol%) was γ-irradiated at 77°K in the solid state, the photocurrent caused by the emission from toluene was about 1.2×10^{-6} ampere during γ-irradiation at a dose rate of 4.83×10^{17} eV/g·hr.

Results and Discussion

Luminescence from Toluene in the Solid 2,3DMB at 77°K during γ-Irradiation. Luminescence studies previously undertaken in radiation chemistry have mostly been concerned with the thermoluminescence or photo-induced luminescence of γ-irradiated samples, or with the luminescence in the liquid phase during γ-irradiation. There have been no studies of the limunescence from solid saturated hydrocarbons during γ-irradiation. The emission from a pure 2,3DMB is very weak during γ-irradiation at 77°K, but a small amount of toluene in 2,3DMB enhances the emission remarkably. The intensity of the luminescence is shown in Fig. 2 as a function of the concentration of toluene. The intensity increases sharply with an increase in the concentration of toluene and then gradually decreases beyond 2 mol% toluene. Since the intensity does not increase linearly with an increase in the concentration of toluene, the liminescence is not due to the direct absorption of the radiation energy by the solute toluene. The intensity of the emission from pure solid toluene during γ-irradiation is about three times stronger than that from 2,3DMB–toluene (1.3 mol%). With an electron fraction of toluene of 0.013 in the 2,3DMB–toluene,

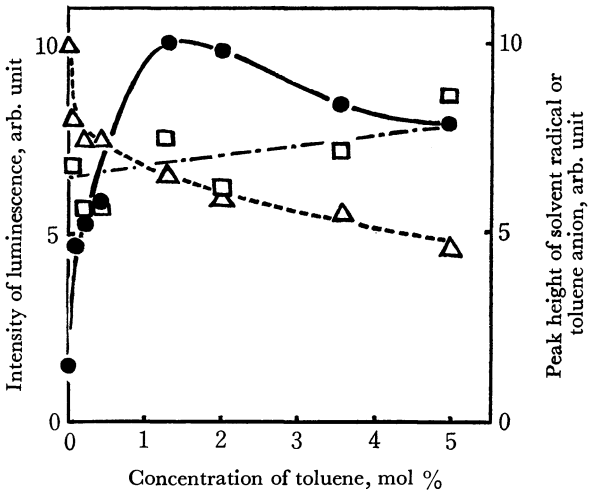

Fig. 2. Yilds of toluene anion, solvent radical, and luminescence in the γ-irradiation of 2,3 DMB at 77°K against concentration of toluene.
●—●: Intensity of luminescence during γ-irradiation.
△—△: Yields of solvent radical at the dose of 9.6×10^{18} eV/g.
□—□: Yields of toluene anion at the dose of 9.6×10^{18} eV/g.

the emission due to the direct absorption of the radiation energy by the toluene itself can be expected to amount at most to 4% of the total emission from 2,3DMB–toluene (1.3 mol%).

Since the emission from toluene in 2,3DMB becomes zero upon the removal of a γ-ray source, the emission cannot be due to a post-irradiation effect. The emission from toluene in the 2,3DMB matrix may be attributable to intermolecular energy transfer from 2,3DMB to toluene.

The emission spectrum from toluene in 2,3DMB is shown in Fig. 3. The spectrum consists of two peaks, with emission maxima near 280 and 390 nm. Since the fluorescence spectrum of toluene has a band with a maximum near 280 nm,[5] the emission band near 280 nm may be due to the fluorescence from the singlet-excited toluene. Since the phosphorescence spectrum

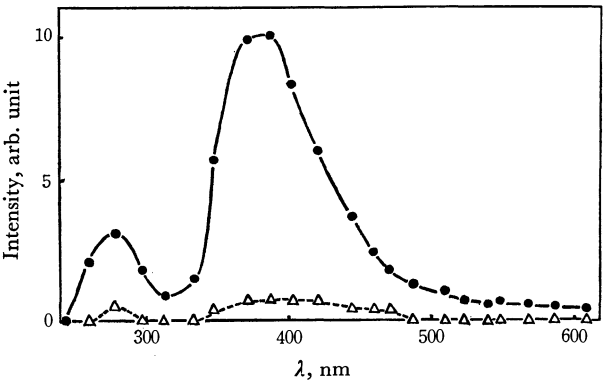

Fig. 3. Emission spectra of 2,3DMB–toluene during γ-irradiation at 77°K.
●—●: Emission from 2,3DMB–toluene (2 mol%).
△—△: Emission from 2,3DMB–toluene (2 mol%) after preirradiation of 4.73×10^{19} eV/g.

5) F. Hirayama and S. Lipsky, *J. Chem. Phys.*, **51**, 1939 (1969).

of toluene has a band with a maximum near 390 mn,[6] the emission band observed near 390 nm may be due to the phosphorescence from the triplet-excited toluene. The vibrational structure of the emission bands could not be measured with this instrument because of the noises caused by the γ-irradiation of photomultiplier, the bubbling of liquid nitrogen in the Dewar flask, and so on.

ESR Studies of γ-Irradiated 2,3DMB Containing Toluene in the Solid Phase at 77°K. The ESR spectrum of γ-irradiated 2,3DMB at 77°K is shown in Fig. 4A. It consists of five lines, with a splitting constant of 22 G. The spectrum may be assigned to the $\cdot CH_2CH(CH_3)$-$CH(CH_3)_2$ radical.[7]

The ESR spectrum of γ-irradiated 2,3DMB–toluene (2 mol%) is shown in Fig. 4B. The new spectrum, which is obtained by subtracting the spectrum of the solvent radicals, is shown with dotted lines. The spectrum consists of five lines, with a splitting constant of 3.8 G, and it is easily photo-bleached upon illumination with light from a tungsten lamp. It coincides well with that of the toluene anion produced by the γ-irradiation of i-C_4H_{10} containing toluene.[1a] The ESR spectrum of the toluene anion produced chemically consists mainly of five lines, with a splitting constant of 4.0 G.[7] The formation of the new spectrum is suppressed completely upon the addition of an electron scavenger, such as N_2O, C_6H_5Br, SF_6, or HBr, to the system. Therefore, the new spectrum may be assigned to the toluene anion.

The ESR spectra of γ-irradiated 2,3DMB–toluene (2 mol%) containing N_2O or C_6H_5Br are shown in Figs. 4C and D respectively. The new spectrum, which is obtained by subtracting the spectrum of the solvent radicals, is shown with dotted lines. Since the spectra have the splitting constants of 6.6 G and 7.0 G in Figs. 4C and D respectively, they cannot be assigned to the toluene anion. As the splitting constants of the monomer cation and the dimer cation of toluene are 14 G and 7.0 G respectively,[9] they may be assigned to the

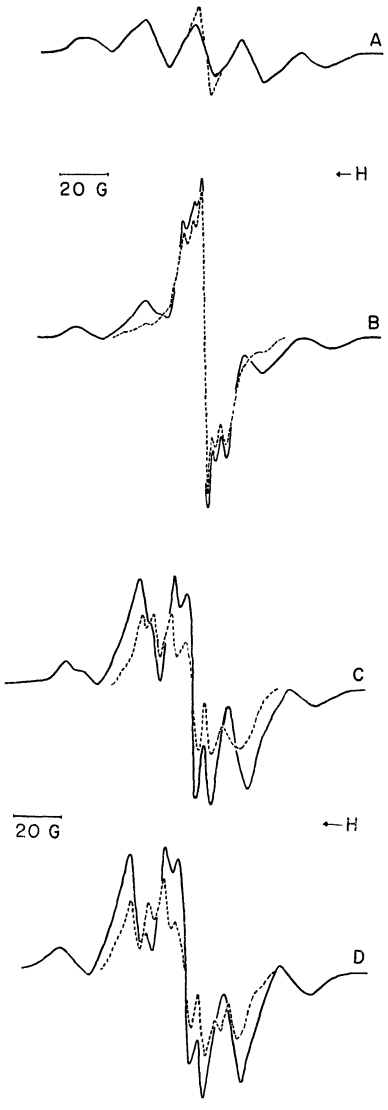

Fig. 4. A. ESR spectra of γ-irradiated 2,3DMB at 77°K. Dotted lines represent the spectrum of trapped electrons which are easily bleached by the illumination with a tungsten lamp.
B. ESR spectrum of γ-irradiated 2,3DMB–toluene (2 mol%) at 77°K. Dotted spectrum is obtained by subtracting the spectrum of solvent radical.
C. ESR spectrum of γ-irradiated 2,3DMB–toluene (2 mol%)–nitrous oxide (2 mol%) at 77°K. Dotted spectrum is obtained by subtracting the spectrum of solvent radical.
D. ESR spectrum of γ-irradiated 2,3DMB–toluene (2 mol%)–phenylbromide (2 mol%) at 77°K. Dotted spectrum is obtained by subtracting the spectrum of solvent radical.
Irradiation dose: 9.6×10^{18} eV/g. Spectrometer gain settings of A, B, C, and D are approximately the same.

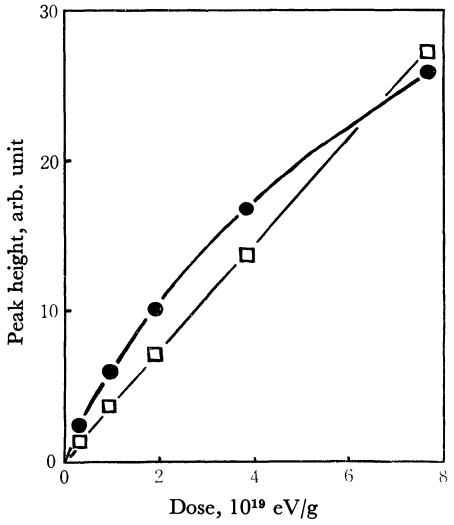

Fig. 5. Yields of toluene anion and solvent racical in the radiolysis of 2,3DMB–toluene (2 mol%) at 77°K against the total dose.
●: Toluene anion, □: Solvent radical.

6) Y. Kanda and H. Sponer, *J. Chem. Phys.*, **28**, 798 (1958).
7) M. Fukaya, T. Wakayama, T. Miyazaki, Y. Saitake, and Z. Kuri, 14th Japanese Conference of Radiation Chemistry, Sept., 1971, Sapporo, Japan.
8) S. P. Solodovnikov, *Zh. Strukt. Khim.*, **2**, 282 (1961).
9) S. Nagai, S. Ohnishi, and I. Nitta, This Bulletin, **44**, 1230 (1971).

dimer cation of toluene. These results suggest that the toluene is not always completely dissolved, but stands sometimes in the form of a cluster, depending upon the concentration.

The yields of the toluene anion and the solvent radical are shown in Fig. 2 as a function of the concentration of toluene.

The dose dependences of the yields of toluene anion and solvent radical are shown in Fig. 5. The rate of the production of the toluene anion decreases gradually with an increases in the dose, while the yields of solvent radical increase linearly.

Pre-irradiation Effect on the Luminescence from Toluene. A quite interesting effect is found on the luminescence from toluene in the 2,3DMB matrix. When the sample is pre-irradiated at 77°K with a certain dose, the intensity of the in-source luminescence becomes much lower than that from the sample without pre-irradiation. The emission spectra from the pre-irradiated sample are shown in Fig. 3 in comparison with the emission from the sample without pre-irradiation. The intensity of the luminescence at $\lambda=390$ nm is shown in Fig. 6 as a function of the dose of pre-irradiation. The liminescence is efficiently suppressed by the pre-irradiation of 3.84×10^{19} eV/g.

Since the toluene ions produced absorb the light of 390 nm, a part of the emission may be absorbed by the toluene ions. If the optical density of the toluene anion in γ-irradiated 2,3DMB–3-methylpentane(10 mol%)–toluene(2 mol%)[10] is measured at 77°K by means of UV–VL absorption spectroscopy, the intensity of the luminescence can be corrected by considering the optical density of the toluene ions at 390 nm. The pre-irradiation effect on the luminescence from 2,3DMB–3-methylpentane-toluene is approximately the same as that of 2,3DMB–toluene, which forms a cracked transparent plastic crystal (Fig. 6). Therefore, the optical density of the toluene anion in the γ-irradiated 2,3DMB–3-methylpentane–toluene may be used for the correction of the intensity of the luminescence from 2,3DMB–toluene. Thus, the corrected intensity is shown in Fig. 6 with a dotted line.

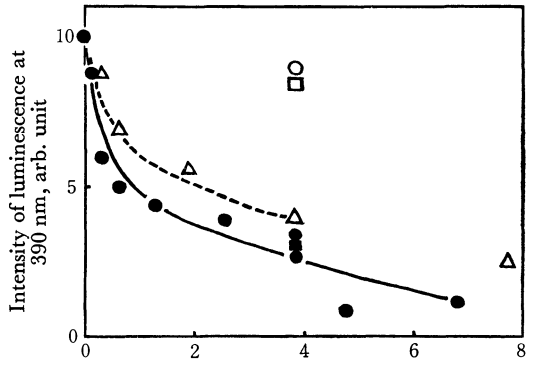

Fig. 6. Pre-irradiation effect on the luminescence from 2,3 DMB-toluene during γ-irradiation at 77°K.
●—●: Intensity of luminescence from 2,3DMB–toluene (2 mol%).
■: Intensity of luminescence from 2,3DMB–3-methylpentane (2 mol%)–toluene (2 mol%) which is pre-irradiated at the dose of 3.84×10^{19} eV/g.
--------: Corrected intensity of luminescence from 2,3-DMB–toluene (2 mol%).
△: The rate of formation of toluene anion in the γ-irradiation of 2,3DMB–toluene (2 mol%) at 77°K.
○: Intensity of luminescence from 2,3DMB–toluene (2 mol%) which is pre-irradiated at the dose of 3.84×10^{19} eV/g and then photobleached with light from a tungsten lamp for 10 min.
□: Intensity of luminescence from 2,3DMB–3-methylpentane (10 mol%)–toluene (2 mol%) which is pre-irradiated at the dose of 3.84×10^{19} eV/g and then photobleached with light from a tungsten lamp for 1 min.
The intensity of luminescence is measured at the wavelength of 390 nm. Initial rate of formation of toluene anion is nomalized to 10 for the comparison with the intensity of luminescence.

The results of Figs. 5 and 6 show that the intensity of the luminescence does not correspond at all to the yields of the toluene anions, but to their rates of formation. The luminescence diminished upon the pre-irradiation can be almost restored to the former value by the photobleaching of the toluene anion with the light from a tungsten lamp (Fig. 6). If the luminescence from toluene in the 2,3DMB matrix is due to a neutralization reaction between a toluene anion and a migrating hole, the intensity of the liminescence should be roughly proportional to the amount of the toluene anion (Reactions (1)—(4)). The experimental results, however, show that these mechanisms are not responsible for the luminescence of toluene:

$$2,3DMB \rightsquigarrow 2,3DMB^{+}_{m} + e^{-} \quad (1)$$

$$e^{-} + C_6H_5CH_3 \longrightarrow C_6H_5CH_3^{-} \quad (2)$$

$$2,3DMB^{+}_{m} + C_6H_5CH_3^{-} \longrightarrow 2,3DMB + C_6H_5CH_3^{*} \quad (3)$$

$$C_6H_5CH_3^{*} \longrightarrow C_6H_5CH_3 + h\nu \quad (4)$$

where $2,3DMB^{+}_{m}$ represents a migrating hole.

Therefore, the energy may be transferred from the matrix to the solute by non-ionic processes until the ionization occurs partly. One plausible mechanism may be represented as follows:

$$2,3DMB \rightsquigarrow 2,3DMB^{*} \quad (5)$$

$$2,3DMB^{*} + C_6H_5CH_3 \longrightarrow C_6H_5CH_3^{+} + e^{-} \quad (6)$$

$$\searrow\ C_6H_5CH_3^{*} \quad (7)$$

$$C_6H_5CH_3^{+} + e^{-} \longrightarrow C_6H_5CH_3^{*} \quad (8)$$

$$C_6H_5CH_3 + e^{-} \longrightarrow C_6H_5CH_3^{-} \quad (2)$$

$$C_6H_5CH_3^{*} \longrightarrow C_6H_5CH_3 + h\nu \quad (4)$$

where 2,3DMB* means an exciton. The absence of the migrating hole in the γ-irradiated 2,3DMB has also been suggested in the γ-irradiation of 2,3DMB containing carbon dioxide.[4b]

When the excited 2,3DMB is formed by the γ-irradiation at 77°K in the solid phase, the excitation of 2,3-DMB may migrate in the solid, probably as an exciton. The exciton may be trapped at the toluene molecule to form a toluene cation, an electron, or an excited

10) When 3-methylpentane is added in the 2,3 DMB matrix, the matrix becomes transparent without a cracking at 77°K and is suitable for the measurement of absorption spectra.

toluene molecule (Reactions (5), (6), and (7)). A part of the toluene cations and electrons may neutralize with each other (Reaction (8)) to form an excited toluene molecule. Then, the excited toluene molecule formed in Reactions (7) and/or (8) may emit light. The formation of a solute cation by excitation transfer was also pointed out in previous studies of the radiolysis of 2,3DMB in the solid phase[4b] and in polyethylene.[11]

The decreases in the intensity of the luminescence and in the rate of the formation of the toluene anion with dose may be due to the decrease in the amount of residual toluene with the dose. When the toluene ions formed by the pre-irradiation of 3.84×10^{19} eV/g are photobleached (Reaction (9)), the intensity of the luminescence recovered by the photobleaching is about 5 arb. unit, as is shown in Fig. 6.

$$C_6H_5CH_3^- \xrightarrow{h\nu} C_6H_5CH_3 + e^- \qquad (9)$$

The concentration of toluene anions before the photobleaching is about 3.3×10^{-3} mol%, if G(toluene anions)=0.6. The amount of toluene for the intensity of luminescence of 10 arb. unit in Fig. 6 is about $3.3\times10^{-3}\times2=6.6\times10^{-3}$ mol%.

We can, then, roughly estimate the distance of the exciton migration. The real concentration of toluene in the 2,3DMB crystalline lattice is about 6.6×10^{-3} mol%, *i.e.*, 6.6×10^{-5} mol fraction. Assume that the exciton migrates to the nearest neighboring molecules of toluene to give its energy to the toluene. Supposing that the number of molecules of the nearest neighbors of toluene is twelve; the number of 2,3DMB molecules, through which the exciton migrates before encountering a toluene, can then be estimated roughly as follows;

$$\frac{1}{6.6\times10^{-5}}\times\frac{1}{12} = 1.3\times10^{3} \text{ molecules}$$

This number of molecules is approximately equal to the calculated migration distance (10^3—10^4 molecules) of the exciton corresponding to the lowest singlet-excited state of alkane.[12]

However, the concentration of toluene anions 6.6×10^{-3} mol% is far below that of the solute, 2 mol%. This result can not yet be explained clearly, but the following assumption can be made temporarily: effective parts to receive the migrating energy are limited by the solubility or cluster formation of the additive, defect formation with the solute.

11) R. H. Partridge, *J. Chem. Phys.*, **52**, 2491 (1970).

12) T. Miyazaki, This Bulletin, **46**, 329 (1973).

BULLETIN OF THE CHEMICAL SOCIETY OF JAPAN, VOL. 46, 74—79 (1973)

Thermodynamic Properties of Some Isomeric Butyl Alcohol Mixtures[1]

Sachio MURAKAMI[2] and G. C. BENSON
Division of Chemistry, National Research Council of Canada, Ottawa, Canada, K1A OR6

(Received May 16, 1972)

Molar excess enthalpies and molar excess volumes are reported for binary mixtures of *n*-butyl alcohol with isobutyl alcohol, *sec*-butyl alcohol, and *t*-butyl alcohol. All of the measurements were carried out at 25°C except for the excess enthalpies of *n*-butyl alcohol–*t*-butyl alcohol which were determined at 26°C. Interpretation of the results in terms of a lattice model was investigated.

Measurements of the thermodynamic properties of binary mixtures of methanol with the four isomeric butyl alcohols were reported in previous publications.[3–5] Differences in the behaviour of these mixtures were attributed primarily to differences in hydrogen bonding. As an extension of our studies, we have measured the enthalpy and volume changes for the mixing of *n*-butyl alcohol with isobutyl alcohol (2-methyl-1-propanol), with *sec*-butyl alcohol (2-butanol) and with *t*-butyl alcohol (2-methyl-2-propanol).

Experimental

Details of the chromatographic purification of the isomeric butyl alcohols have been described.[5] Enthalpies and volumes of mixing were measured by successive dilution techniques, using a calorimeter[6] and dilatometer.[4] The uncertainties in the results for equimolar mixtures are estimated to be ± 0.5 J mol^{-1} for the molar excess enthalpies, and ± 0.0005 cm^3 mol^{-1} for the molar excess volumes.

Results

All of the measurements were carried out at 25.00 ± 0.01°C except for the determinations of the excess enthalpies of *n*-butyl alcohol–*t*-butyl alcohol mixtures. The latter were measured at 26.00 ± 0.01°C, since at 25°C

1) Issued as N.R.C.C. No. 12853.

2) N. R. C. C. Postdoctorate Fellow 1967-69. Present address: Department of Chemistry, Faculty of Science, Osaka City University, Sumiyoshi-ku, Osaka.

3) A. E. Pope, H. D. Pflug, B. Dacre, and G. C. Benson, *Can. J. Chem.*, **45**, 2665 (1967).

4) H. D. Pflug and G. C. Benson, *ibid.*, **46**, 287 (1968).

5) J. Polák, S. Murakami, V. T. Lam, H. D. Pflug, and G. C. Benson, *ibid.*, **48**, 2457 (1970).

6) S. Murakami, and G. C. Benson, *J. Chem. Thermodyn.*, **1**, 559 (1969).

operation of the calorimeter was upset by the tendency of the *t*-butyl alcohol to solidify in the hypodermic needle. Results for the molar excess enthalpy H^E and the molar excess volume V^E are listed in Tables 1 and 2, respectively. In all cases, x_1 indicates the mole fraction of *n*-butyl alcohol. Graphs of the results are shown in Figs. 1 and 2, where it should be noted that scales differing by a factor of 10 have been used in plotting the excess functions for some of the systems.

TABLE 1. EXPERIMENTAL VALUES OF THE MOLAR EXCESS ENTHALPY OF SOME BINARY ISOMERIC BUTYL ALCOHOL SYSTEMS

n-Butyl alcohol–isobutyl alcohol at 25°C		*n*-Butyl alcohol–*sec*-butyl alcohol at 25°C		*n*-Butyl alcohol–*t*-butyl alcohol at 26°C	
x_1	H^E J mol^{-1}	x_1	H^E J mol^{-1}	x_1	H^E J mol^{-1}
0.0376	1.7	0.0341	−14.8	0.0272	−59.9
0.0382	1.7	0.0774	−31.6	0.0343	−74.0
0.0951	4.0	0.1266	−48.3	0.0649	−133.9
0.1000	4.2	0.1756	−62.7	0.0677	−138.8
0.1412	5.6	0.2933	−87.4	0.1046	−202.3
0.1421	5.7	0.3519	−94.8	0.1144	−217.2
0.1859	7.0	0.4005	−98.7	0.1482	−266.5
0.1948	7.3	0.4185	−99.1	0.1585	−279.1
0.2353	8.2	0.4186	−99.2	0.1993	−328.0
0.2401	8.3	0.4573	−99.7	0.2065	−335.3
0.2886	9.2	0.4576	−100.6	0.2485	−375.0
0.2909	9.5	0.4711	−100.1	0.2527	−378.1
0.3435	10.0	0.4738	−100.2	0.3043	−413.2
0.3451	10.4	0.5057	−100.2	0.3085	−416.1
0.3940	10.7	0.5185	−99.3	0.3550	−437.0
0.3956	10.9	0.5186	−99.5	0.3570	−437.4
0.4141	11.1	0.5218	−99.0	0.4104	−450.5
0.4425	11.0	0.5494	−98.1	0.4109	−449.9
0.4478	11.3	0.5644	−96.9	0.4636	−451.4
0.4559	11.1	0.5702	−96.0	0.4784	−450.8
0.4781	11.0	0.5752	−95.3	0.5159	−442.7
0.4879	11.1	0.6016	−94.3	0.5375	−437.5
0.4988	11.4	0.6218	−91.5	0.5631	−427.2
0.5235	11.4	0.6237	−90.8	0.6077	−406.5
0.5354	11.1	0.6768	−84.2	0.6108	−405.6
0.5356	11.0	0.6863	−82.1	0.6137	−403.8
0.5449	10.9	0.7262	−75.8	0.6619	−372.1
0.5799	10.9	0.7278	−75.3	0.7095	−334.1
0.5806	10.9	0.7399	−72.5	0.7590	−288.8
0.5923	10.4	0.7761	−65.8	0.8125	−233.9
0.5952	10.3	0.8014	−59.2	0.8603	−182.7
0.6316	10.3	0.8055	−58.3	0.9022	−131.6
0.6344	9.7	0.8196	−55.6	0.9396	−83.5
0.6833	9.3	0.8606	−44.1	0.9747	−35.8
0.7362	7.8	0.8649	−43.7		
0.7425	8.1	0.8860	−36.7		
0.7868	6.6	0.9084	−30.9		
0.8027	6.7	0.9349	−22.1		
0.8302	5.5	0.9488	−17.8		
0.8509	5.3	0.9675	−11.3		
0.8682	4.3				
0.9085	3.2				
0.9162	3.0				
0.9598	1.5				
0.9685	1.1				

TABLE 2. EXPERIMENTAL VALUES OF THE MOLAR EXCESS VOLUME OF SOME BINARY ISOMERIC BUTYL ALCOHOL SYSTEMS AT 25°C

n-Butyl alcohol–isobutyl alcohol		*n*-Butyl alcohol–*sec*-butyl alcohol		*n*-Butyl alcohol–*t*-butyl alcohol	
x_1	V^E cm^3 mol^{-1}	x_1	V^E cm^3 mol^{-1}	x_1	V^E cm^3 mol^{-1}
0.0419	0.0003	0.0275	0.0017	0.0481	−0.0662
0.0785	0.0015	0.0652	0.0024	0.0963	−0.1176
0.1030	0.0026	0.0705	0.0033	0.1496	−0.1581
0.1649	0.0029	0.1123	0.0046	0.2050	−0.1868
0.1656	0.0034	0.1233	0.0044	0.2640	−0.2043
0.2315	0.0044	0.1632	0.0047	0.3195	−0.2115
0.2445	0.0033	0.1810	0.0051	0.3747	−0.2116
0.2935	0.0043	0.2150	0.0055	0.4273	−0.2066
0.3178	0.0038	0.2392	0.0055	0.4706	−0.1992
0.3492	0.0043	0.2702	0.0057	0.5720	−0.1726
0.3800	0.0036	0.3308	0.0055	0.6090	−0.1601
0.3987	0.0041	0.4285	0.0046	0.6652	−0.1408
0.4351	0.0038	0.4626	0.0044	0.7244	−0.1191
0.4447	0.0042	0.4822	0.0048	0.7825	−0.0959
0.4818	0.0039	0.5023	0.0041	0.8412	−0.0713
0.4883	0.0039	0.5249	0.0044	0.8940	−0.0484
0.5220	0.0038	0.5495	0.0039	0.9453	−0.0253
0.5235	0.0038	0.5735	0.0040		
0.5986	0.0035	0.6000	0.0035		
0.6523	0.0033	0.6312	0.0034		
0.7085	0.0029	0.6547	0.0030		
0.7676	0.0025	0.6877	0.0029		
0.8261	0.0021	0.7163	0.0024		
0.8838	0.0017	0.7493	0.0022		
0.9308	0.0013	0.7788	0.0021		
0.9696	0.0004	0.7846	0.0016		
		0.8159	0.0015		
		0.8403	0.0013		
		0.8449	0.0013		
		0.8786	0.0013		
		0.9015	0.0006		
		0.9047	0.0007		
		0.9373	0.0005		
		0.9568	−0.0001		
		0.9573	−0.0001		
		0.9738	0.0001		

The method of least squares was used to fit the results with equations of the type

$$X^E = x_1(1-x_1)\sum_{j=1}^{n} c_j(1-2x_1)^{j-1} \qquad (1)$$

where X^E is either H^E or V^E. The minimum number of coefficients required to represent the results adequately was determined by examining the statistical significance of the improvement in the fit with the increase in the number of coefficients. The values obtained for the coefficients c_j are summerized in Table 3, along with the standard error of estimate σ associated with each representation. The curves in Figs. 1 and 2 were calculated from Eq. (1) using these values for the coefficients.

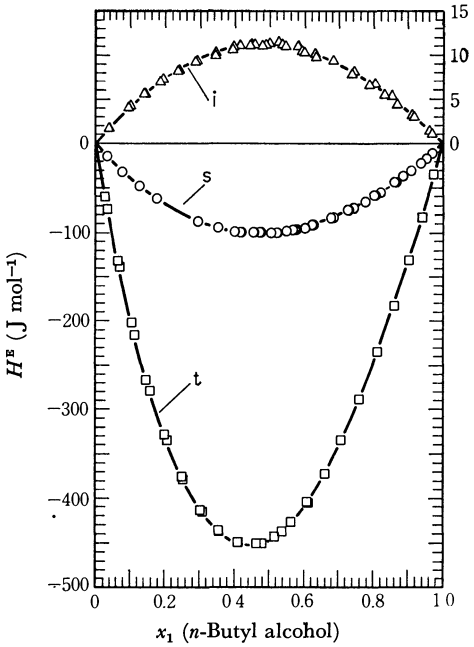

Fig. 1. Molar excess enthalpies of *n*-butyl alcohol–isomeric butyl alcohol mixtures. Experimental results; △: *n*-butyl alcohol–isobutyl alcohol at 25°C; ○: *n*-butyl alcohol–*sec*-butyl alcohol at 25°C; □: *n*-butyl alcohol–*t*-butyl alcohol at 26°C. Curves are least-squares representations of experimental results by Eq. (1). Labels *i*, *s*, and *t* indicate the three isomeric butyl alcohols used as second components. Ordinate scale at right is for mixtures containing isobutyl alcohol and ordinate scale at left is for those containing *s*-butyl alcohol or *t*-butyl alcohol.

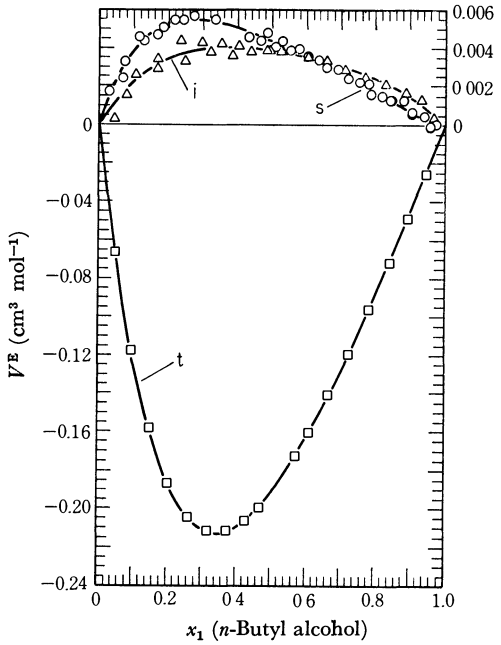

Fig. 2. Molar excess volumes of *n*-butyl alcohol–isomeric butyl alcohol mixtures at 25°C. Experimental results; △: *n*-butyl alcohol–isobutyl alcohol; ○: *n*-butyl alcohol–*sec*-butyl alcohol; □: *n*-butyl alcohol–*t*-butyl alcohol. Curves are least-squares representations of experimental results by Eq. (1). Labels *i*, *s*, and *t* indicate the three isomeric butanols used as second components. Ordinate scale at right is for mixtures containing isobutyl alcohol or *sec*-butyl alcohol, and ordinate scale at left is for those containing *t*-butyl alcohol.

TABLE 3. COEFFICIENTS FOR LEAST SQUARES FIT OF RESULTS BY EQ. (1)[a]

System	X^E	Coefficient				Std. error. σ
		c_1	c_2	c_3	c_4	
n-Butyl alcohol–isobutyl alcohol	H^E	44.68	4.44	−3.60		0.17
	V^E	0.01542	0.00574	0.00770		0.00032
n-Butyl alcohol–*sec*-butyl alcohol	H^E	−339.75	−47.06	−7.68		0.34
	V^E	0.01741	0.01448	0.01286	0.01251	0.00023
n-Butyl alcohol–*t*-butyl alcohol	H^E	−1787.28	−400.40	−52.46	−36.96	0.79
	V^E	−0.76783	−0.47710	−0.24097	−0.06597	0.00038

a) Units: H^E, J mol^{-1}; V^E, cm^3 mol^{-1}

Discussion

There is a fairly close similarity between Figs. 1 and 2, and graphs presented previously[5] for the excess enthalpies and volumes of methanol-isomeric butyl alcohol systems. In general the signs of the excess functions are the same for systems of the two sets with a common second component. However, the greater similarity in size of the component molecules in the present systems leads to smaller magnitudes for the excess functions than those observed for the methanol systems. Thus it appears that the qualitative discussion[5] of the role of hydrogen bonding in determining the excess properties of methanol–isomeric butyl alcohol mixtures is also valid for the present systems.

The generalized quasi-lattice theory of Barker[7,8] should be well suited for analysing the excess properties of mixtures in which association by hydrogen bonding occurs, since it deals explicitly with the specific interactions between different parts of the component molecules. It is customary to adjust the parameters characterizing these interactions to fit the theoretical values of the excess energy and/or free energy to the experimental results. In developing a Barker type of model for binary mixtures of butanol isomers, we found it useful also to consider the results reported earlier for methanol–isomeric butyl alcohol mixtures.[5]

The mixing process treated by Barker is one in which the volume for each molecule remains constant. However, it is useful to compare the theoretical values with experimental results measured essentially at constant pressure and corrected to constant total volume. In the case of the free energy, this correction is negligible and values of A_V^E, the molar excess Helmholtz free energy at constant volume are identified with values

7) J. A. Barker, *J. Chem. Phys.*, **20**, 1526 (1952).
8) J. A. Barker and F. Smith, *ibid.*, **22**, 375 (1954).

of G^E, the molar excess Gibbs free energy at constant pressure. The difference between U_V^E, the molar excess energy at constant volume, and H^E, the molar excess enthalpy at constant pressure, is more significant and can be estimated from the relation

$$H^E - U_V^E \approx TV^E(\alpha_1\phi_1+\alpha_2\phi_2)/(\kappa_1\phi_1+\kappa_2\phi_2) \quad (2)$$

where ϕ_i is the volume fraction of component i in the mixture, and α_i and κ_i are respectively the coefficients of expansion and isothermal compressibility for pure i. The curves for A_V^E and U_V^E at 25°C (Figs. 3—5) were obtained from the smoothed representations of the experimental results for G^E, H^E, and V^E. In calculating U_V^E, the values of α and κ listed in Table 4 were used. These values were derived previously[9] from density, velocity of sound, and heat capacity data. The one degree temperature deviation (from 25°C) of the *n*-butyl alcohol–*t*-butyl alcohol results for H^E was neglected.

Table 4. Values of the coefficient of thermal expansion α, and the isothermal compressibility κ for the component liquids at 25°C

Component	$10^3\alpha$ K^{-1}	$10^6\kappa$ atm^{-1}
Methanol	1.185	126.4
n-Butyl alcohol	0.937	94.5
Isobutyl alcohol	0.948	102.6
sec-Butyl alcohol	0.988	98.2
t-Butyl alcohol	1.344	126.1

Our model for binary alcohol mixtures assumes that an alcohol molecule of species i, containing m carbon atoms, occupies $r_i=m+1$ sites of a lattice with coordination number equal to four. Three different types of contact areas are recognized on the surface of the moledule: hydrocarbon denoted by I, hydroxyl oxygen by O, and hydroxyl hydrogen by H. A subscript (1) or (2) is added to these symbols when it is necessary to indicate that the contact is on a molecule of the first or second component in the mixture. The number of contact points of type a on a molecule of species i is denoted by Q_i^a. The values of Q_i^a were chosen to satisfy the condition

$$\sum_a Q_i^a = zr_i + z$$

Q^I was assigned values of 3 and 9 for methanol and the isomeric butyl alcohols respectively; values of $Q^O=2$ and $Q^H=1$ were adopted for all of the alcohols.

Table 5. Simplified scheme for interchange parameters U_{ij}^{ab} and A_{ij}^{ab}

Bond	U_{ij}^{ab}	A_{ij}^{ab}
$I_{(1)}$—$O_{(1)}$, $I_{(1)}$—$H_{(1)}$, $I_{(2)}$—$O_{(2)}$, $I_{(2)}$—$H_{(2)}$	0	0
$O_{(1)}$—$H_{(1)}$	U_1	A_1
$O_{(2)}$—$H_{(2)}$	U_2	A_1
$I_{(1)}$—$I_{(2)}$, $I_{(1)}$—$O_{(2)}$, $I_{(1)}$—$H_{(2)}$, $O_{(1)}$—$I_{(2)}$, $O_{(1)}$—$O_{(2)}$, $H_{(1)}$—$I_{(2)}$, $H_{(1)}$—$H_{(2)}$	U_3	A_3
$O_{(1)}$—$H_{(2)}$	U_1+U_3	A_1+A_3
$H_{(1)}$—$O_{(2)}$	U_2+U_3	A_2+A_3

Normally, 15 interchange energies U_{ij}^{ab} and 15 interchange free energies A_{ij}^{ab} would be needed to describe the interaction between all possible pairs of contacts of type a on species i and type b on species j. However, differences in the behaviour of the systems under consideration seem to be attributable primarily to differences in the proton accepting facility of the oxygen atoms attached to primary, secondary, and tertiary carbon atoms. We have therefore attempted to describe the interactions by three energy parameters and three free energy parameters according to the scheme shown in Table 5. This scheme singles out the four hydrogen bonds for special consideration, and divides them into two classes according to the host molecule of the oxygen atom involved. In addition it assumes that a nonspecific van der Waals interaction occurs between contacts on unlike molecules.

Detailed equations for the calculation of A_V^E and U_V^E can be found in Barker's original publications,[7,8] examples of their application to particular cases being also available.[8,10] The presentation here is limited to outlining the course of the calculations leading to the final selection of the interchange energies and free energies summarized in Table 6. The use of these parameters in the formulas of Barker leads to the results represented by the points in Figs. 3—5.

The methanol-isomeric butyl alcohol mixtures were considered first since experimental results for both A_V^E and U_V^E were available. In methanol–*n*-butyl alcohol and methanol–isobutyl alcohol mixtures, all of the oxygen atoms are attached to primary carbons. For these mixtures, A_1 and A_2 were set equal to -11420 J mol^{-1} and U_1 and U_2 to -28200 J mol^{-1}, where the numerical values are the same as those used by Barker and Smith[8]

Table 6. Values of interchange parameters for methanol–isomeric butyl alcohol mixtures and *n*-butyl alcohol–isomeric butyl alcohol mixtures

Component 1	Component 2	Interchange parameters J mol^{-1}					
		U_1	A_1	U_2	A_2	U_3	A_3
Methanol	*n*-Butyl alcohol	−28200	−11420	−28200	−11420	50	50
Methanol	Isobulyl alcohol						
Methanol	*sec*-Butyl alcohol	−28200	−11420	−30700	−14320	50	50
Methanol	*t*-Butyl alcohol	−28200	−11420	−32730	−15420	50	50
n-Butyl alcohol	Isobulyl allcoho	−28200	−11420	−28200	−11420	3.3	3.3
n-Butyl alcohol	*sec*-Butyl alcohol	−28200	−11420	−29180	−12800	3.3	3.3
n-Butyl alcohol	*t*-Butyl alcohol	−28200	−11420	−30960	−13650	3.3	3.3

9) G. C. Benson and V. T. Lam, *J. Colloid Interfac. Sci.*, **38**, 294 (1972).

10) G. C. Benson, S. Murakami, and D. E. G. Jones, *J. Chem. Thermodyn.*, **3**, 719 (1971).

for the hydrogen bonds in acetone–ethanol mixtures. The nonspecific interaction was assumed to be the same between methanol and any of the butyl alcohol molecules. It was further assumed that $U_3=A_3$; this also is in line with the findings for acetone–ethanol. Quite clearly these assumtions foregothe possibility of distinguishing theoretically between methanol–*n*-butyl alcohol and methanol–isobutyl alcohol mixtures. The experimental values of U_V^E for both sets of mixtures are very similar and a value of 50 J mol^{-1} for U_3 provides a fairly good representation of either. It can be seen from Fig. 3 that the points calculated for A_V^E reach a maximum falling between the peaks of the two experimental curves. Better individual fits of A_V^E were obtained by adjusting A_3 separately for each system, but even in that case it was not possible to reproduce the negative values of A_V^E observed experimentally. In both methanol–*sec*-butyl alcohol and methanol–*t*-butyl alcohol mixtures, A_2 and U_2 can be expected to differ from A_1 and U_1 since the configurations around the oxygen atoms are different. Values of A_2 and U_2 were obtained by successively adjusting them to make the theoretical results for A_V^E and U_V^E approximate the experimental observations.

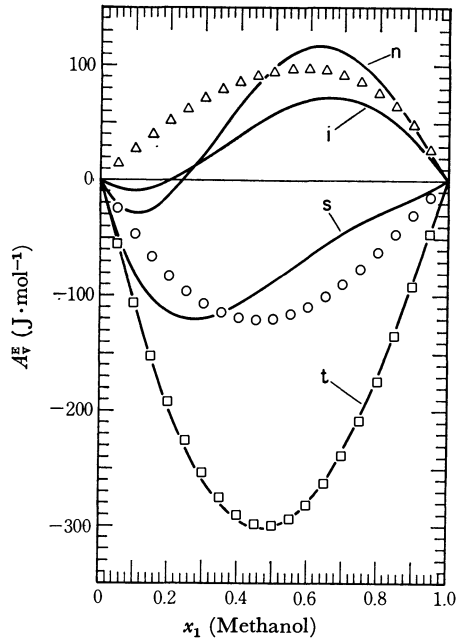

Fig. 3. Comparison of theoretical and experimental excess free energies at constant volume for methanol–isomeric butyl alcohol mixtures at 25°C. Points calculated from Barker theory; △: methanol–*n*-butyl alcohol and methanol–isobutyl alcohol; ○: methanol–*sec*-butyl alcohol; □: metanol–*t*-butyl alcohol. Curves represent the smoothed experimental results. Labels *n*, *i*, *s*, and *t* indicate the four isomeric butyl alcohols used as second components.

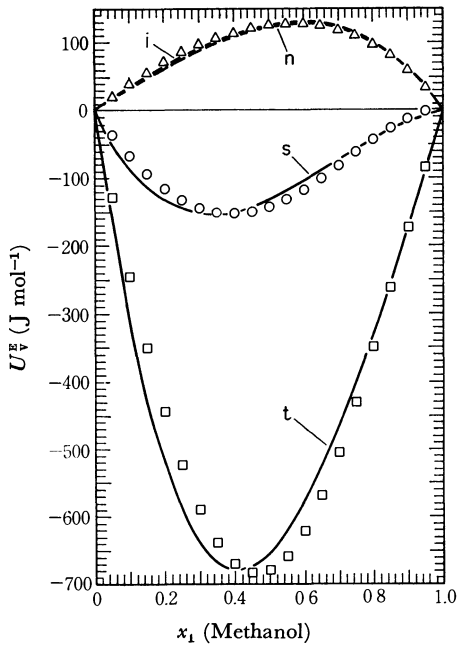

Fig. 4. Comparison of theoretical and experimental excess energies at constant volume for methanol–isomeric butyl alcohol mixtures at 25°C. Significances of points curves and labels are the same as in Fig. 3.

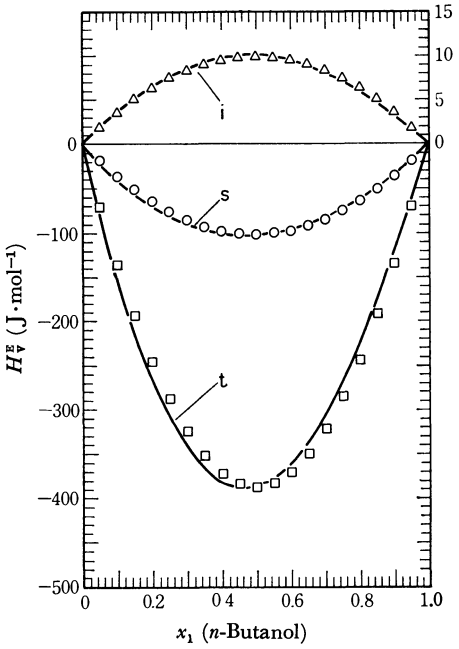

Fig. 5. Comparison of theoretical and experimental excess energies at constant volume for *n*-butyl alcohol–isomeric butyl alcohol mixtures at 25°C. Points calculated from Barker theory; △: *n*-butyl alcohol–isobutyl alcohol; ○: *n*-butyl alcohol–*s*-butyl alcohol; □: *n*-butyl alcohol–*t*-butyl alcohol. Curves represent the smoothed experimental results. Labels *i*, *s*, and *t* indicate the three isomeric butyl alcohols used as second components. Ordinate scale at right is for mixtures containing isobutyl alcohol, and ordinate scale at left is for those containing *sec*-butyl alcohol or *t*-butyl alcohol.

Calculations for *n*-butyl alcohol–isomeric butyl alcohol mixtures followed as closely as possible the treatment described for the methanol systems. However, since experimental results for A_V^E were not available it was further assumed that the bond interchange entropy terms

$$TS_{ij}^{ab} = U_{ij}^{ab} - A_{ij}^{ab} \qquad (4)$$

were the same as in the corresponding methanol systems. Fitting the U_V^E results for *n*-butyl alcohol–isobutyl alcohol led to a value of 3.3 J mol^{-1} for the nonspecific interchange energy between *n*-butyl alcohol and its isomers. Values of U_2 for the hydrogen bonds at secondary

and tertiary OH groups were then obtained by adjusting the calculations to fit U_V^E for mixtures of *n*-butyl alcohol with *sec*-butyl alcohol and *t*-butyl alcohol.

It should be noted that the calculations for methanol mixtures give values for the parameters characterizing the hydrogen bonds at secondary and tertiary OH groups which differ by five to ten percent from those resulting from the calculations for *n*-butyl alcohol mixtures. If the values of A_2 and U_2 obtained from the methanol mixtures are used to estimate U_V^E for mixtures of *n*-butyl alcohol with *sec*-butyl alcohol and *t*-butyl alcohol, the results have the correct sign but are three to five times larger in magnitude than observed experimentally. Thus it appears that estimates of U_V^E are fairly sensitive to the values of the interchange parameters used to describe the hydrogen bonds.

In summary, the Barker model described above reproduces the thermodynamic behavior of *n*-butyl alcohol–isomeric butyl alcohol mixtures fairly satisfactorily. Although it is doubtful that the absolute values of the bond interchange parameters are meaningful, the general features of these values are reasonable. In particular, the nonspecific interactions are very small compared to the hydrogen bonding, and furthermore the nonspecific interaction between the isomeric butyl alcohol is smaller than that between methanol and the butanols. Finally, the relative order of the values for the hydrogen bonds agrees with experimental evidence indicating that the proton accepting facility of the oxygen atoms in the present alcohols increases in the order primary<secondary<tertiary.[11]

The authors wish to express their thanks to Mr. P. J. D'Arcy and Mr. C. J. Halpin for their technical assistance throughout the course of this work.

11) W. Gerrard and E. D. Macklen, *Chem. Rev.*, **59**, 1105 (1959)

BULLETIN OF THE CHEMICAL SOCIETY OF JAPAN, VOL. 46, 79—82 (1973)

Mössbauer Study of the Thermal Decomposition Products of K_2FeO_4

Toshio ICHIDA*

Institute for Chemical Research, Kyoto University, Uji, Kyoto

(Received May 17, 1972)

The thermal decomposition process of a hexavalent iron compound, K_2FeO_4, was studied by means of the Mössbauer effect. The compound began to decompose in air at about 170°C, and an amorphous product was obtained by the decomposition below 200°C. The product showed a paramagnetic Mössbauer spectrum at 293°K, with an isomer shift and quadrupole splitting of $+0.40 \pm 0.02$ mm/sec and 0.64 ± 0.02 mm/sec respectively; it also showed a magnetically-split six-line spectrum at 4.2°K, with an internal magnetic field of 480 ± 5 kOe. These Mössbauer parameters are characteristic of the Fe^{3+} state. The intermediate valence states, Fe^{5+} or Fe^{4+}, were not observed during the decomposition process, and so it was concluded that the Fe^{6+} ions in K_2FeO_4 were reduced directly to Fe^{3+} ions. $KFeO_2$ was formed in air above 250°C, and the temperature dependence of the internal magnetic field showed the Néel temperature of $KFeO_2$ to be very high, 983 ± 10°K.

Previously, Scholder *et al.*[1,2] reported on the thermal decomposition process of a hexavalent iron compound, K_2FeO_4. According to their reports, the decomposition process below 700°C is represented as the following formula:

$$2K_2Fe^{6+}O_4 \longrightarrow K_3Fe^{5+}O_4 + KFe^{3+}O_2 + O_2,$$

and that above 700°C by:

$$K_3Fe^{5+}O_4 \longrightarrow KFe^{3+}O_2 + K_2O + (1/2)O_2.$$

Although Scholder[2] reported the existence of K_3FeO_4 and Na_3FeO_4 as examples of pentavalent iron compounds, there was no crystallographic justification of them. Indeed, the existence of no pentavalent iron compound has yet been established by physical means.

In recent years, it has been well known that the Mössbauer effect is very useful in the determination of iron valency in the solid state.[3-5] In the present study of the thermal decomposition products of a hexavalent iron compound, K_2FeO_4, the valence state of iron and the magnetic properties of the products were investigated by means of the Mössbauer effect.

Sample Preparation and Measurements

The sample-preparation method of K_2FeO_4 was similar to the procedure of Thompson *et al.*[6]

Into a sodium hypochlorite solution, granular sodium hydroxide was slowly stirred, while we permitted the

* On leave from Kawasaki Steel Corporation. Present address: Research Laboratories, Kawasaki Steel Corporation, 1, Kawasaki-cho, Chiba.

1) V. R. Scholder, H. V. Bunsen, F. Kindervater and W. Zeiss, *Z. Anorg. Allg. Chem.*, **282**, 268 (1955).

2) V. R. Scholder, Colloque International du C. N. R. S., 1112 (1964).

3) G. K. Wertheim and R. H. Herber, *J. Chem. Phys.*, **36**, 2497 (1962).

4) T. Shinjo, T. Ichida, and T. Takada, *J. Phys. Soc. Jap.*, **26**, 154 (1969).

5) T. Shinjo, T. Ichida, and T. Takada, *ibid.*, **29**, 111 (1970).

6) G. W. Thopson, L. T. Ockerman, and J. M. Schreyer, *J. Amer. Chem. Soc.*, **73**, 1379 (1951).

temperature to rise as high as 30°C; finally, the mixture was cooled to about 0°C. The precipitated sodium chloride was removed by filtration through a glass filter. To the alkaline hypochlorite solution at about 10°C, fine powder of ferric nitrate was slowly added. The solution was saturated with sodium hydroxide, and the temperature was maintained at about 30°C. The mixture was then filtered with suction through a coarse glass filter. By adding a saturated potassium hydroxide solution with stirring, precipitates of K_2FeO_4 were produced. The following cycle of purification was repeated more than three times: the precipitates of K_2FeO_4 were leached on a glass filter of a fine porosity with a 3M-KOH chilled solution. The liquid was drawn through the filter into a saturated potassium hydroxide solution, whose temperature was also kept at about 0°C. Because the solubility of K_2FeO_4 into a concentrated potassium hydroxide solution is much less than into a dilute solution, recrystallized K_2FeO_4 was thus obtained. The sample was purified by repeating this recrystallization.

The filtered precipitates of K_2FeO_4 were washed with benzene, 95% alcohol, and ether successively. The sample thus obtained was rapidly dried up and stored in a dry atmosphere. Particles of K_2FeO_4 showed a dark purple color and a needle shape (the longest axis was a few mm long).

By the X-ray diffraction technique, the sample was confirmed to be a single phase of K_2FeO_4. The measurements of the magnetization and the Mössbauer effect were carried out on the obtained samples at 80°K in order to confirm the absence of a ferromagnetic impurity and all iron ions except the hexavalent ones.[5]

Using the pure sample thus obtained, the thermal decomposition process of K_2FeO_4 was investigated. In the case of heating under high oxygen pressures, the K_2FeO_4 was held in a test tube of silica or gold. This test tube was placed in a cone-seal hydrothermal reaction vessel made of Stellite.

The decomposition products obtained were identified by using an X-ray diffractometer. Mössbauer effect measurements were carried out using an apparatus consisting of Elron's driving unit, AME-20, and Northern Scientific Co.'s 1024-channel pulse-height analyzer, NS-600. The temperature of the absorber was varied between 4.2 and 1023°K. The gamma ray source, ^{57}Co embedded in Cu metal, was always kept at room temperature. The calibration of the velocity scale was done by using pure Fe and α-Fe_2O_3 as the standard absorbers. The isomer shift is expressed relative to pure Fe.

Results and Discussion

Potassium ferrate, K_2FeO_4, gradually began to decompose in air at about 170°C. The X-ray diffraction pattern of the sample obtained by keeping K_2FeO_4 at 170°C in air for 10 days (Sample A) showed a slight trace of K_2FeO_4, but the sample kept for 90 days (Sample B) showed no diffraction peak. The Mössbauer spectra of the two samples measured at room temperature are shown in Fig. 1. As for Sample B, the Mössbauer spectrum measured at the temperature of liquid helium is shown in Fig. 2.

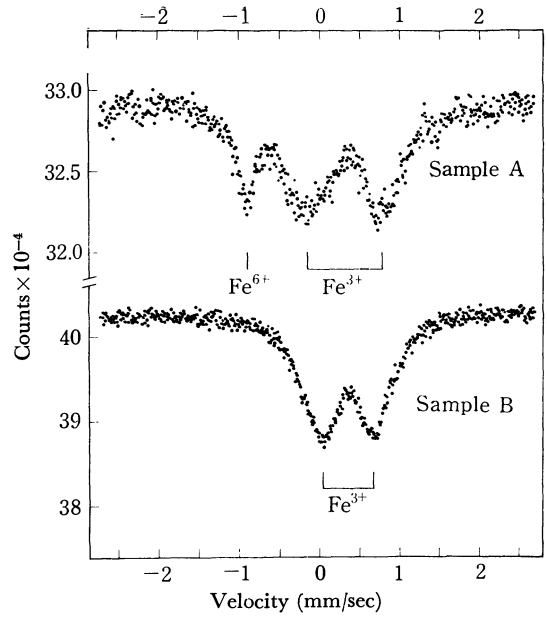

Fig. 1. Mössbauer absorption spectra at room temperature of ^{57}Fe in thermal decomposed products of K_2FeO_4 obtained at 170°C for 10 days (Sample A) and for 90 days (Sample B).

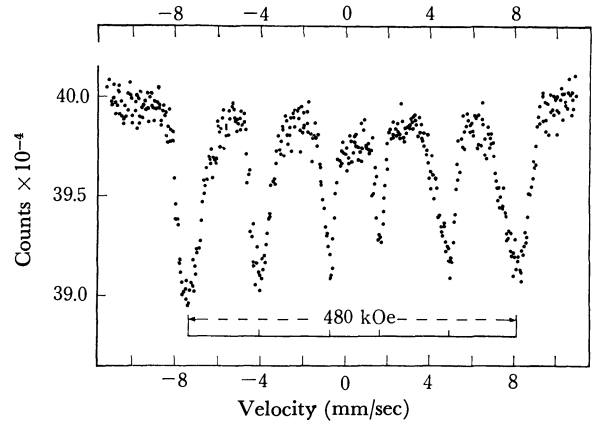

Fig. 2. Mössbauer absorption spectrum of ^{57}Fe in Sample B measured at 4.2°K.

As has previously been reported,[3-5] the Mössbauer absorption of K_2FeO_4 at room temperature is a sharp single line whose isomer shift is -0.89 ± 0.03 mm/sec; this is characteristic of the Fe^{6+} state. Below 5°K, magnetic hyperfine splitting appears. The internal magnetic field extrapolated to 0°K was 140 ± 7 kOe. The narrow single-line absorption at −0.90 mm/sec in Fig. 1 (Sample A) was due to the remaining Fe^{6+} ions. A broad quadrupole doublet was observed in the spectrum of Sample A; a similar broad symmetric absorption spectrum was also found in Sample B. As is shown in Fig. 2, the Mössbauer spectrum of Sample B measured at 4.2°K consisted of six broad absorption lines. The values of the internal magnetic field, 480 ± 5 kOe and the isomer shift, $+0.44\pm0.05$ mm/sec, show that the state of the iron was not Fe^{4+} or Fe^{5+} ions, but Fe^{3+} ions. The broad symmetric doublet in Fig. 1 was ascribed to the paramagnetic absorption of Fe^{3+}

in Fig. 4. Every iron atom occupies a crystallographically-equivalent site, tetrahedrally-surrounded by four oxygen atoms. The adjacent tetrahedrons of the oxygen atoms hold an apex in common, and the angle of Fe–O–Fe is 180°. The closest atomic approaches are O–O=2.72 Å, Fe–O=1.73 Å, and K–O=3.32 Å.

The Mössbauer spectrum of $KFeO_2$ at 293°K is shown in Fig. 5. The spectrum shows that iron is in trivalent state in $KFeO_2$ and that there is a magnetic ordering, even at room temperature, with an internal magnetic field of 505±5 kOe. The Mössbauer spectra obtained above 873°K are shown in Fig. 6. The internal magnetic field disappeared at 983±10°K. Therefore, the Néel temperature of $KFeO_2$ was estimated to be 983±10°K from the temperature variation in the internal magnetic field. Figure 7 shows the temperature dependence of the internal field. The Brillouin function for $S=5/2$ is also represented there for the sake of comparison. Previously, Kerler *et al.*[9,10]

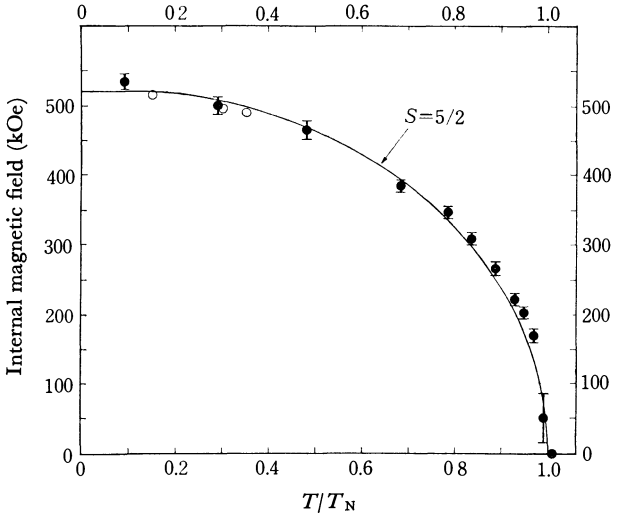

Fig. 7. The temperature dependence of the internal magnetic field in $KFeO_2$. Open circles are after Ref. 10. T_N is 983°K. Solid line represents the Brillouin function for $S=5/2$.

9) U. E. Fluck, W. Kerler, and W. Neuwirth, *Z. Anorg. Allg. Chem.*, **333**, 235 (1964).

10) W. Kerler, W. Neuwirth, E. Fluck, P. Kuhn, and B. Zimmerman, *Z. Phys.*, **173**, 321 (1963).

also measured the Mössbauer effect of $KFeO_2$ below 348°K. As is shown in Fig. 7, their data show a good agreement with the present data.

According to the results of the magnetic susceptibility measurements, $KFeO_2$ is a compensated antiferromagnet, but no anomaly was observed around the T_N value in the susceptibility-temperature curve. The present value, 983±10°K, is the highest among all the Néel temperatures of iron compounds thus far reported. Since the angle of Fe–O–Fe is 180° and the distance is very short (3.46 Å), the superexchange interaction must be very strong. Assuming that the spin directions of all the neighboring Fe^{3+} ions are antiparallel with each other, a completely compensated antiferromagnetic spin arrangement can be composed. This structure seems reasonable, although no experimental confirmation has yet been presented.

The decomposition temperature of K_2FeO_4 changed slightly with the oxygen pressure. Under the oxygen pressure of 500 atm, K_2FeO_4 began to decompose at about 250°C, while it began to decompose at 170°C in air. Independently of the oxygen pressure, it was confirmed by the Mössbauer-effect measurements that the Fe^{6+} ions in K_2FeO_4 were reduced directly to Fe^{3+} ions. There was no difference in the crystal structure and magnetic properties of the $KFeO_2$ samples obtained under various conditions. It was concluded that, in the low-temperature range, ultra-fine particles of a trivalent iron compound were formed and that, in the high-temperature range, K_2FeO_4 decomposed as follows:

$$K_2FeO_4 \longrightarrow KFeO_2 + KO_x + (2-x/2)O_2$$

The author would like to express his hearty thanks to Professor Toshio Takada, Professor Yoshichika Bando, Dr. Teruya Shinjo, Dr. Masao Kiyama, and Dr. Koji Kosuge for their prominent guidance and helpful discussions. Thanks are due to Dr. Mitsuo Imai and Dr. Koji Sanbongi of the Research Laboratories, Kawasaki Steel Corporation, for their warm encouragement. He also wishes to thank the Kawasaki Steel Corporation for giving him an opportunity to study at Kyoto University.

The Photolysis of Cyclopentanone

Shigeru TSUNASHIMA, Osamu OHSAWA, Chiharu TAKAHASHI, and Shin SATO
Department of Applied Physics, Tokyo Institute of Technology, Ookayama, Meguro-ku, Tokyo
(Received May 19, 1972)

The 326.1 nm direct photolysis and the cadmium-photosensitized reactions of cyclopentanone have been compared in order to clarify the role of the triplet state of cyclopentanone in the photolysis. The products observed in the both photolyses were carbon monoxide, ethylene, cyclobutane, and 4-pentenal. The results obtained in the direct photolysis were very similar to those obtained in the cadmium photosensitization. The ethylene/cyclobutane ratio was not affected by the pressure and temperature changes. The 4-pentenal/CO ratio increased with a decrease in the temperature. These similarities suggest that the decomposition of cyclopentanone takes place through the lowest triplet state in both the photolyses. The efficiency of cyclopentanone in quenching triplet cadmium was found to be about 0.8 times that of *cis*-2-butene.

The photochemistry of cyclopentanone has been the subject of active investigations for forty years.[1,2] It has been found that gaseous cyclopentanone decomposes to carbon monoxide and ethylene or cyclobutane, or rearranges to 4-pentenal, upon irradiation with 313.0 nm light, which corresponds to a weak n-π^* transition.[1,2] In the cases of aliphatic ketones, such as acetone, it is believed that the decomposition takes place through the triplet state. In spite of many investigations, however, there still remains considerable doubt about the role of the triplet state in the cyclopentanone photolysis.

Since Srinivasan could not observe the effects of oxygen, he proposed that the excited singlet states with various vibrational levels are responsible for the product formations.[3] Recently, Chup Yew Mok reinvestigated the system in detail and observed small effects of the addition of oxygen and 1,3-pentadiene. As he pointed out, the results could not be used either to prove or to disprove the role of the triplet state during the photolysis of cyclopentanone.[4] He explained his results in terms of the first excited singlet state.[4] On the other hand, Lee found that triplet benzene sensitized the 4-pentenal formation and suggested that the cyclopentanone triplet was important as a reaction intermadiate.[5] From their detailed studies of the fluorescence emission, they also suggested that the rate of intersystem crossing from the first excited singlet to the triplet is very fast.[6] Frey *et al.* examined the photolysis of *trans*-2,3-dimethylcyclopentanone and found that the products, such as cyclopentanone-, 4-pentenal-, and cyclobutane-derivatives, contained the *cis-trans* isomers.[7] They proposed that the reaction intermediate is a biradical form which can rotate freely. The biradical intermediate assumption had already been made by Benson and Kistiakowsky and by Blacet and Miller.[8,9]

Since a triplet cyclopentanone will be formed even in the triplet cadmium photosensitization, it is expected that a comparison with direct photolysis will give further information about the cyclopentanone photolysis. In the case of acetone photolysis, the method of cadmium photosensitization has been successfully applied to the investigation of the triplet state.[10]

Experimental

The cyclopentanone (Tokyo Kasei Ind.) was distilled bulb-to-bulb, with the middle third retained, after treating it with diphosphorus pentoxide. Gas-chromatographic analysis showed a trace amount of water as an impurity. Pure-grade *cis*-2-butene (Takachiho Shoji Co.,) was used as supplied. The cyclohexane (Tokyo Kagaku Seiki Co., pure-grade) was passed through a 2-m-silica gel column before use.

The quartz reaction cell used was 5.0 cm long and 4.8 cm in diameter, with a total volume, including access tubing, of about 90 m*l*; it was inserted in an electric furnace kept at the desired temperature within ± 1°C by means of an electric controller. A home-made cadmium discharge lamp, with argon (2 torr) as the buffer gas, was heated in a furnace kept at 270 ± 2°C by means of an electric controller. The 228.8 nm resonance line and visible lines were filtered out by means of a combination of a Toshiba UV-D25 filter and a Pyrex plate, so that the emerging light was mainly the 326.1 nm resonance line.

The reaction products obtained were analyzed by means of a gas chromatograph using a column of 5 m propylene glycol at 65°C, after removing the non-condensable gases at -196°C with a Toepler pump.

In the cadmium photosensitization, the light intensity absorbed by cadmium was measured by using the *cis-trans* isomerization of *cis*-2-butene as the actinometer. The quantum yield was assumed to be 0.5.[11]

Results and Discussion

Cadmium Photosensitization. In the case of the cadmium photosensitization, it is necessary to elevate the reaction temperature in order to increase the vapor

1) R. Srinivasan, *Advan. Photochem.*, **1**, 83 (1963).
2) R. B. Cundall and A. S. Davis, *Progr. Reaction Kinetics*, **4**, 149 (1967).
3) R. Srinivasan, *J. Amer. Chem. Soc.*, **81**, 1546, 1549 (1959); *ibid.*, **83**, 4344, 4348 (1961).
4) Chup Yew Mok, *J. Phys. Chem.*, **74**, 1432 (1970).
5) E. K. C. Lee, *ibid.*, **71**, 2804 (1967).
6) R. G. Shortridge, C. F. Rusbult, and E. K. C. Lee, *J. Amer. Chem. Soc.*, **93**, 1863 (1971); G. M. Breuer and E. K. C, Lee, *J. Phys. Chem.*, **75**, 989 (1971).
7) H. M. Frey, *Chem. Ind.*, **1966**, 947; H. M. Frey and D. H. Lister, *J. Chem. Soc. A*, **1970**, 627.
8) S. W. Benson and G. B. Kistiakowsky, *J. Amer. Chem. Soc.*, **64**, 80 (1942).
9) F. E. Blacet and A. Miller, *ibid.*, **79**, 4327 (1957).
10) S. Sato, C. Takahashi, and S. Tsunashima, This Bulletin, **43**, 1319 (1970).
11) S. Tsunashima and S. Sato, This Bulletin, **41**, 284 (1968); H. E. Hunziker, *J. Chem. Phys.*, **50**, 1288, 1294 (1969).

Table 1. Quantum Yields of Products in the Cadmium Photosensitization

Temp. °C	$P_{c\text{-}C_5H_8O}$ Torr	$P_{c\text{-}C_6H_{12}}$ Torr	Quantum Yields CO	C_2H_4	c-C_4H_8	C_4H_7CHO
273	1.89	0	0.15			
273	2.81	0	0.15	0.17		0.020
273	3.55	0	0.15	0.15	0.038	0.030
273	7.50	0	0.16	0.20	0.045	0.055
273	8.76	0	0.16	0.18	0.042	0.043
273	11.0	0	0.17	0.18		0.038
273	13.1	0	0.18	0.23	0.053	0.053
273	34.3	0	0.19	0.24	0.052	0.064
273	50.6	0	0.18	0.21		0.047
273	81.2	0	0.19	0.25	0.063	0.075
273	38.7	0	0.17	0.21	0.038	0.048
273	43.3	222	0.16	0.20	0.04	0.063
273	40.0	504	0.15	0.17	0.032	>0.062
295	41.8	0	0.21	0.25	0.048	0.052
315	45.3	0	0.25	0.30	0.055	0.051
333	44.5	0	0.28	0.34	0.061	0.039
352	47.2	0	0.29	0.36	0.068	0.032
352	41.4	0	0.30	0.36	0.065	0.029

pressure of cadmium metal. The thermal reactions of cyclopentanone at 273°C were found to be negligibly small. The products in the cadmium photosentitization were identified as carbon monoxide, ethylene, cyclobutane, and 4-pentenal, which were the same as those obtained in the 313.0 nm direct photolysis. The quantum yields of the product formations are listed in Table 1 as functions of the pressure and the temperature. The rate of carbon monoxide formation was almost constant at pressures higher than 10 Torr. A comparison with the case of the acetone photolysis[10] suggests that the effect of the light other than the 326.1 nm resonance line on the cyclopentanone photolysis is negligibly small in the present experiment. The quantum yield of carbon monoxide formation was 0.18 at 273°C. The relative yields of carbon monoxide, ethylene, cyclobutane, and 4-pentenal were almost constant at pressures above a few Torr; they were, respectively, 1.0, 1.2, 0.3, and 0.3 at 273°C.

Table 2. Quantum Yields of Products in the Cadmium Photosensitization in the Presence of *cis*-2-Butene at 270°C[a]

$P_{cis\text{-}2\text{-}C_4H_8}$ Torr	Quantum Yields CO	C_2H_4	c-C_4H_8	t-2-C_4H_8
0	0.19	0.24	0.064	0
1.0	0.17	0.22	0.057	0.021
1.7	0.19	0.25	0.054	0.044
2.2	0.17	0.22	0.057	0.049
3.0	0.16	0.20	0.036	0.089
4.1	0.17	0.21	0.051	0.087
5.2	0.12	0.15	0.035	0.13
6.8	0.16	0.22	0.048	0.17
7.7	0.17	0.20	0.048	0.17
9.5	0.13	0.15	0.041	0.14
11.0	0.13	0.16	0.039	0.18
12.3	0.13	0.16	0.040	0.20

a) $P_{c\text{-}C_5H_8O}$=22.6 Torr

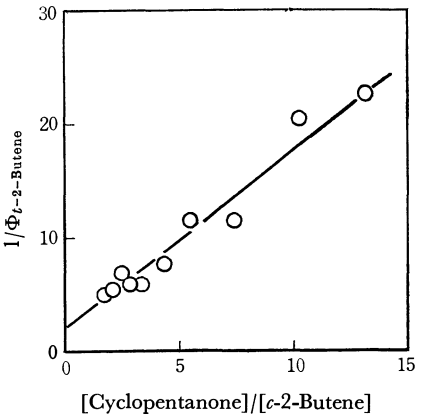

Fig. 1. Plots of the reciplocal of the quantum yield of *trans*-2-butene against the cyclopentanone/*cis*-2-butene pressure ratio.

When *cis*-2-butene was added to 22.6 Torr of cyclopentanone at 270°C, the quantum yields of the decomposition products (CO, ethylene, and cyclobutane) decreased with the increase in the quantum yield of *trans*-2-butene formation (Table 2). The reciprocal of the quantum yield of *trans*-2-butene is plotted against the cyclopentanone/*cis*-2-butene pressure ratio in Fig. 1. Obviously, a straight line was obtained. This result may be explained by the competitive quenching for triplet cadmium, as was discussed previously.[12] From the slope of the straight line in Fig. 1, the relative quenching efficiency of cyclopentanone against that of *cis*-2-butene was calculated to be 0.8 ± 0.2. The value is very large compared with that of paraffins and is close to that of olefins.[12] This suggests that the cyclopentanone molecule interacts with triplet cadmium strongly and is excited to the triplet state:

$$Cd + h\nu(326.1\text{ nm}) \longrightarrow Cd^* \quad (1)$$

$$Cd^* \longrightarrow Cd + h\nu \quad (2)$$

$$Cd^* + S_0 \longrightarrow Cd + T \quad (3)$$

where Cd*, S_0, and T represent, respectively, triplet cadmium, and the ground state and the triplet state of cyclopentanone.

In the presence of *cis*-2-butene, the observed decrease in the quantum yield of the decomposition product agreed with that calculated assuming the competitive quenching for triplet cadmium within the limits of experimental error. That is, the reaction of the excited cyclopentanone is not affected by the presence of *cis*-2-butene.

As is shown in Table 1, the quantum yields of the products formation at lower pressures were slightly smaller than those at higher pressures. This difference may be explained in terms of Reaction (2).

The total quantum yields of CO and 4-pentenal were less than unity, even at the highest pressure examined. This suggests that a part of the triplet cyclopentanone formed loses its excitation energy without forming any product.

12) S. Tsunashima and S. Sato, This Bulletin, **40**, 2987 (1967); S. Tsunashima, S. Satoh, and S. Sato, *ibid.*, **42**, 329 (1969).

In spite of the increase in the quantum yields of ethylene and cyclobutane formations with the increase in the temperature, the ethylene/cyclobutane ratio was independent of the temperature change. This suggests that the activation energy of the ethylene formation is slmost the same as that of the cyclobutane formation. It has been proposed that the tetramethylene diradical is an intermediate for the ethylene and cyclobutane formations:[7]

$$T \longrightarrow CO + \dot{C}H_2CH_2CH_2\dot{C}H_2 \quad (4)$$

$$\dot{C}H_2CH_2CH_2\dot{C}H_2 \longrightarrow 2C_2H_4 \quad (5a)$$

$$\longrightarrow c\text{-}C_4H_8 \quad (5b)$$

If the Process (4) occurs with a negligibly small activation energy, the Processes (5a) and (5b) should occur with an equal energy of activation.

The decomposition of cyclopentanone to carbon monoxide and ethylene is endothermic by 44.1 kcal/mol.[13] The excess energy for the decomposition is 43.6 kcal/mol in the cadmium photosensitization. If the total spin is conserved during the reaction, one of the ethylenes formed should be in the triplet and should be almost in the perpendicular form, since the excitation energy of the lowest triplet ethylene decreases with an increase in the twisting angle around the C–C bond from about 106 to 43 kcal/mol.[14]

In the presence of a large amount of cyclohexane, the quantum yield of the decomposition decreased, and that of 4-pentenal formation increased slightly; that is, the 4-pentenal/CO ratio increased. Since the products ratio of 4-pentenal/CO is independent of the competitive quenching of cyclohexane for triplet cadmium, the increase in the ratio suggests the presence of a collisional deactivation process for the 4-pentenal formation.

The results can, therefore, be explained in terms of the following simplified scheme:

$$T \longrightarrow CO + 2C_2H_4(\text{or } c\text{-}C_4H_8) \quad k_d \quad (6)$$

$$\longrightarrow C_4H_7CHO \quad k_i \quad (7)$$

$$\longrightarrow S_0 \quad k_s \quad (8)$$

$$T + M \longrightarrow C_4H_7CHO \quad k_{mi} \quad (9)$$

$$\longrightarrow S_0 + M \quad k_{ms} \quad (10)$$

The steady-state treatment of the above mechanism gives the following equation:

$$R(4\text{-pentenal})/R(CO) = k_i/k_d + (k_{mi}/k_d)[M] \quad (11)$$

Using the data in Table 1, k_i/k_d is estimated to be 0.3 at 273°C. The value of k_{mi}/k_d may be very small, so that the second term on the right-hand-side of Eq. (11) is negligibly small, even at the pressure of 80 torr.

With the increase in the reaction temperature, the quantum yield of the decomposition increased and that of the 4-pentenal formation decreased; however, the decrease in the 4-pentenal formation was less than the increase in the quantum yield of the decomposition. The apparent activation energy for the 4-pentenal/CO ratio was estimated to be 9 ± 3 kcal/mol. This may be explained by the difference in the activation energy between the Reactions (6) and (7) being 9 kcal/mol, on the assumption that the second term on the eight-hand-side of Eq. (11) is negligibly small. The second term is negligibly small at 273°C and at the pressures of cyclopentanone below 40 torr, as has been shown, and it is expected to decrease with an increase in the temperature, since the activation energy of Reaction (9) is probably smaller than that of Reaction (6).

326.1 nm Direct Photolysis. In the absence of cadmium vapor, carbon monoxide, ethylene, cyclobutane, and 4-pentenal were formed from cyclopentanone upon irradiation with the cadmium lamp. These products were the same as those obtained in the cadmium photosensitization, and also the same as those obtained in the 313.0 nm direct photolysis.[1,2] The experimental conditions were the same except for the absence of cadmium. The rates of the product formation were less than those obtained in the cadmium photosensitization. The relative yields of the products are listed in Table 3.

Table 3. Relative Yields of the Products in the 326.1 nm Direct Photolysis

Temp. °C	$P_{c\text{-}C_5H_8O}$ Torr	Relative Yields		
		$\frac{C_2H_4}{CO}$	$\frac{c\text{-}C_4H_8}{CO}$	$\frac{C_4H_7CHO}{CO}$
273	9.9	1.1	0.21	
273	37.9	1.5	0.21	
273	39.4	1.3	0.27	0.17
273	61.2	1.2	0.23	0.13
273	85.8	1.3	0.23	0.20
225	60.8	1.4	0.27	0.42
177	56.8	1.2	0.26	0.73

Assuming that the light intensity is the same as that in the cadmium photosensitization and that the value of ε is 4.7 l/mol cm,[15] the quantum yield of the carbon monoxide formation was estimated to be about 0.6 at 273°C. This value may be an upper limit, since the light intensity absorbed has been underestimated in the above treatment.[10]

The results obtained in the 326.1 nm direct photoolysis of cyclopentanone were very similar to those obtained in the cadmium photosensitization; *i.e.*, (1) the distributions of the products were almost the same at 273°C, (2) each product formation at 273°C was scarcely affected at all by the pressure change in either case, (3) the ethylene/cyclobutane ratios were constant whatever the pressure and temperature changes and were the same in both cases, and (4) the 4-pentenal/CO ratio decreased with the increase in the temperature, the apparent activation energy for the ratio in the direct photolysis being roughly 6 kcal/mol, slightly smaller than that obtained in the cadmium photosensitization. These similarities suggest that the precursor of the reaction products in the 326.1 nm direct photolysis is the same as that in the cadmium photosensitization.

13) S. W. Benson, "Thermochemical Kinetics," John Wiley and Sons, New York (1968).

14) T. Terao, S. Hirokami, S. Sato, and R. J. Cvetanović, *Can. J. Chem.*, **44**, 2173 (1966).

15) C. Takahashi, S. Tsunashima, and S. Sato, unpublished data.

By the absorption of 326.1 nm light, the lowest excited singlet cyclopentanone may be formed in the direct photolysis. The excited singlet cyclopentanone will cross over to the triplet state or converge to the ground state with or without fluorescence emission. The triplet cyclopentanone thus formed will disappear through Reactions (6)—(10), as was assumed in the case of the cadmium photosensitization.

The small pressure effect on the 4-pentenal/CO ratio may be explained by the small value of k_{mi}/k_d. The apparent activation energy in the ratio can also be explained as in the case of the cadmium photosensitization.

The 4-pentenal/CO ratio at 273°C and the apparent activation energy in the ratio obtained in the direct photolysis were slightly smaller than those obtained in the cadmium photosensitization. These differences may arise from the difference in the excess energy of the triplet cyclopentanone formed.[16] This difference in the excess energy may be small, however, because only small differences were observed between the two photolyses.

Comparison with 313.0 nm Direct Photolysis. In the case of the 313.0 nm direct photolysis of cyclopentanone, almost the same results were obtained as in the 326.1 nm photolyses, except for the pressure effect upon the 4-pentenal/CO ratio.

In the 313.0 nm photolysis, the 4-pentenal/CO ratio increased with the increase in the pressure at 123.8°C.[3] Chup Yew Mok has explained the pressure dependence of the ratio by a relation which is essentially the same as Eq. (11), although the assumed the singlet cyclopentanone to be the precursor of the reaction products; he found that the rate-constant ratio, which corresponds to k_{mi}/k_d in Eq. (11), decreased with an increase in the temperature.[4] A similar temperature dependence of the k_{mi}/k_d ratio was considered in the 326.1 nm photolyses. The differences in the reaction temperature and in the excitation energy may be enough to explain the difference in the 4-pentenal/CO ratio. It is not necessary to assume a different reaction mechanism for the 313.0 nm photolysis.

Srinivasan assumed that the reaction products were formed from the first excited singlet state, with various vibrational levels in the 313.0 nm photolysis.[3] His discussions were based on the fact that the effect of oxygen on the reaction was comparable to those of inert gasses.[3] Similar effects were obtained by Chup Ye Mok, using oxygen and 1,3-pentadiene.[4] These results cannot, however, conclusively exclude the presence of a triplet precursor for the reaction products, as was pointed out by Chup Yew Mok.[4] If oxygen and 1,3-pentadiene are inefficient in quenching the triplet cyclopentanone and/or if the lifetime of the triplet cyclopentanone is very short, the effect of oxygen or 1,3-pentadiene on the reaction can be expected to be small. If the excited singlet cyclopentanone is the precursor for the decomposition, the rate of the decomposition should be faster than that of the intersystem crossing. Lee *et al.* suggested that the rate of the intersystem crossing in cyclopentanone is very fast, as it is in acetone.[6] As was discussed in the previous sections, the assumption of the triplet precursor explains well the results of cyclopentanone photolyses.

Consequently, it may be said that the triplet state is responsible for the reaction products in the cyclopentanone photolysis, as is in the case of acetone.

16) D. C. Montague and F. S. Rowland, *J. Amer. Chem. Soc.*, **91**, 7230 (1969).

This research was supported by a grant from the Matsunaga Science Foundation.

Temperature Effect on Raman Intensity of Liquid Sample and Local Field Correction

Tsunetake FUJIYAMA

Department of Chemistry, Faculty of Science, The University of Tokyo, Hongo, Bunkyo-ku, Tokyo

(Received May 30, 1972)

The relative intensities of the 996 cm^{-1} line of liquid benzene and the 367 cm^{-1} line of liquid chloroform were observed at various temperatures with a high accuracy. The apparent intensity change due to the temperature was explained completely in terms of the local field effect, the density change, and the statistical distribution. The validity of Eckardt's correction factor was strongly supported. In the case of liquid chloroform, an intensity change due to intermolecular interaction was observed after the elimination of the above three factors. The reliability of the relative intensity measurements of Raman lines was discussed.

The reliability of relative intensity measurements of Raman spectra has been greatly increased in the past few years by improvements in laser Raman spectrophotometers. Raman intensity measurements observe light energy scattered from a sample; therefore, they have a great advantage, in principle, over intensity measurements of absorption spectra. They are free from the effects of a slit-function,[1] the effects related to anomalous dispersion,[2-6] the effects of multi-reflections inside sample layers,[7-10] the so-called baseline effects,[1,11] and so on, all of which are notorious difficulties in the intensity measurements of liquid samples by infrared absorption methods. Moreover, the handling of a sample is much easier in Raman than in infrared spectroscopy, especially when temperature-control is involved in the measurements. On the other hand, the reproducibility of successively-observed Raman intensities is often spoiled by casual changes in the experimental conditions; the setting of a sample cell, a slight deviation in optical alignment, the purity of the sample, the cleanness of the cell-window, and so on.

Paying careful attention to these factors, the intensities of the fundamental lines of liquid benzene and chloroform were measured. Liquid benzene was chosen because the intensity of the 996 cm^{-1} line is very strong and was expected to be observed with a high accuracy. Another reason for choosing that molecule was that the intensity change due to intermolecular interactions was expected to be very small in its system. In the case of liquid chloroform, strong intermolecular interaction was expected; therefore, the intensity change due to the temperature may exhibit different features from that of liquid benzene.

Experimental

The spectrometer used for the present work was designed and constructed by the authors.[12] The instrument is composed of a He-Ne gas laser source (NEC, GLG 108, 50 mW), a Spex 1401 double monochromator, a HTV R-376 photomultiplier (S-20 response), a handmade lock-in amplifier (375 cps), and a recorder.

The linearity of the whole system was carefully checked. First, the out-put current of the photomultiplier was plotted against the light energy. The linearity was perfect for the out-put from zero through 20 microampere, which was equivalent to an out-put voltage of 20 volts with $R_p = 1$ megaohm. Then, the linearity of the amplifier was tested using attenuator (0.1 − 120 db for each 0.1 db). Finally, the linearity of the whole system was checked by plotting the final recorder out-put voltage against the light-energy which passes through the entrance slit of the monochromator. The light-energy was attenuated by using neutral filters (Kenko, ND). From the standard errors estimated from the linear-fitting, the linearity of the whole system was ascertained to be less than 1 per cent of the full scale as long as the out-put voltage was less than 10 volts.

Special attention was paid to the temperature of the room so as to keep the out-put power of the laser source constant. The stability of the laser out-put during the individual spectral measurements was observed by monitoring the light energy

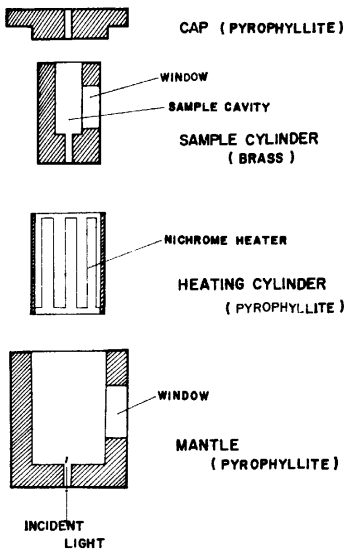

Fig. 1. Schematic Layout of High Temperature Cell.

1) K. S. Sehardi and R. N. Jones, *Spectrochim. Acta*, **19**, 1013 (1963).
2) P. N. Schatz, *ibid.*, **21**, 617 (1965).
3) S. R. Polo and M. K. Wilson, *J. Chem. Phys.*, **23**, 2376 (1955).
4) H. E. Hallam, "Infrared Spectra and Molecular Structure," Chapt. XII, Elsevier, N. Y. (1963).
5) A. A. Clifford and B. L. Crawford, Jr., *J. Phys. Chem.*, **70**, 1536 (1966).
6) T. Fujiyama and B. L. Crawford, Jr., *ibid.*, **72**, 2174 (1968).
7) M. Yasumi, This Bulletin, **28**, 489 (1955).
8) S. Maeda and P. N. Schatz, *J. Chem. Phys.*, **35**, 1617 (1961).
9) J. V. White and W. M. Ward, *Anal. Chem.*, **37**, 268 (1965).
10) T. Fujiyama, J. Herrin, and B. L. Crawford, Jr., *Appl. Spectry.*, **24**, 9 (1970).
11) W. J. Potts, Jr., "Chemical Infrared Spectroscopy," Vol. 1, John Wiley and Sons, Inc., N. Y. (1963).
12) T. Fujiyama and M. Tasumi, *Bunko Kenkyu*, **20**, 28 (1971).

which penetrated through the 100 per cent reflectance mirror of the laser cavity. When the power of the laser source drifted more than 1 per cent during the measurements, the data observed were completely discarded.

The high-temperature cell used for the measurements is illustrated in Fig. 1. It is mainly made of *pyrophyllite*, which is easy to shape and which is a good thermal insulator. Brass was used for the sample cylinder of Fig. 1 so as to obtain a homogeneous temperature atmosphere inside the cylinder, in which a sample cell (a $10\times10\times15$ mm cube) was placed. The temperature was controlled by changing the electric current supplied to the nichrome heater. The temperature was observed by means of a thermocouple directly inserted into the samples. The accuracy of the temperature measurements was believed to be within ±1°C.

The benzene and chloroform used for the measurements were commercial products and were used for the measurements just after fractional distillation. The purity of the samples was checked by the use of gas chromatography.

Results and Discussions

996 cm^{-1} Line of Benzene. The Raman intensity of the 996 cm^{-1} line of liquid benzene was observed in the temperature range from 24 through 70°C. The intensity was determined from the band area by the weight-method. The averaged value of the five intensity data was taken as the observed Raman intensity; it had a standard deviation of from 0.3 to 0.6 per cent. The observed relative intensity ratios are summarized in Table 1, where the relative intensity at 24°C is chosen as the standard. The relative error of the individual ratio is estimated to be ±1 per cent. Obviously, the relative intensity decreases more than 10 per cent as the temperature changes from 24 to 70°C. The results are also illustrated in Fig. 2.

TABLE 1. INTENSITY CHANGE OF THE 996 cm^{-1} LINE OF BENZENE

t(°C)	L/L_{24}	s/s_{24}	d/d_{24}	Lsd/Lsd_{24}	I/I_{24}
24	1.000	1.000	1.000	1.000	1.000
36	0.979	1.002	0.986	0.967	0.960
47	0.959	1.002	0.972	0.934	0.930
58	0.939	1.005	0.958	0.905	0.912
70	0.918	1.007	0.943	0.872	0.891

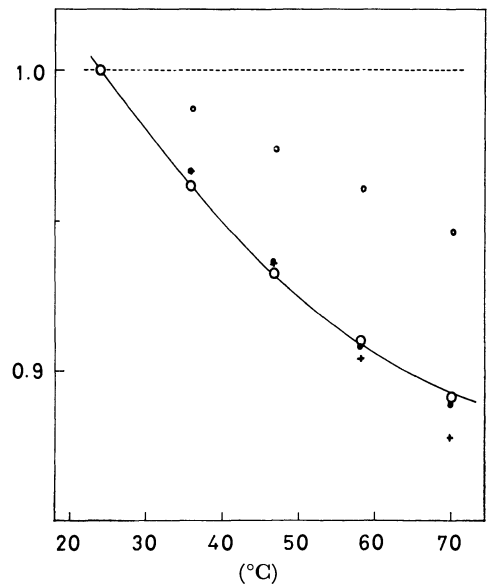

Fig. 2. Comparison of I/I_{24} and Lsd/Lsd_{24}
○: I/I_{24}, ○: d/d_{24}, +: Ld/Ld_{24}, ●: Lsd/Lsd_{24}

The apparent intensity change due to the temperature has been discussed by Person[13] for the infrared absorption case, where the importance of the local-field correction has been emphasized. For the case of Raman intensity, various authors have proposed correction factors to the local field that allow Placzek's intensity formula to be applied to liquids and/or solutions.[14-19] In addition to the local-field effect, the density change and the statistical distribution of molecules in relation to a vibrational state may contribute to the change in the apparent Raman intensity due to the temperature. These factors are all temperature-dependent and should be taken into account in interpreting the present results.

The density, d, as a function of the temperature may be found in the International Critical Tables.[20] The relative values of the density at various temperatures are summarized in Table 1, where the density at 24°C is chosen as a standard.

The statistical factor, s, may be expressed as:

$$s = \frac{1}{1-\exp(-hcv/kT)}$$

where v is the frequency displacement of a Raman line from that of the incident wave, T is the temperature, h is the Planck's constant, k is the Boltzmann constant, and c is the velocity of light. The calculated relative values of s are summarized in Table 1, where the s-value at 24°C is taken as a standard. The contribution of s to the change in the intensity is much smaller than the experimental error.

Eckardt[18] emphasized that the most appropriate factor for the local-field correction in Raman scattering, L, is:

$$L = (n_s/n_0)(n_s^2+2)^2(n_0^2+2)^2/81$$

where n_s is the refractive index at the Stokes frequency and where n_0 is the index at the frequency of the incident light. If the variation in the refractive index over the frequency range of the Raman shift is ignored, the equation reduces to:

$$L = \frac{(n^2+2)^4}{81}.$$

The calculated relative values of the local-field correction factor, L/L_{24}, are summarized in Table 1. Again, L at 24°C is taken as the standard. In the calculation, the refractive indices for different temperatures were

13) W. B. Person, *J. Chem. Phys.*, **28**, 319 (1958).
14) W. C. Mallard and J. W. Straley, *ibid.*, **27**, 877 (1957).
15) V. M. Pivovarov, *Opt. Spectrosc.*, **9**, 139 (1960).
16) G. Fini, P. Mirone, and P. Patella, *J. Mol. Spectrosc.*, **28**, 144 (1968).
17) P. Mirone, *Spectrochim. Acta*, **22**, 1897 (1966).
18) G. Eckhardt and W. G. Wagner, *J. Mol. Spectrosc.*, **19**, 407 (1966).
19) N. K. Sidorov, L. S. Stalmakhova, and N. V. Bogachyov, *Opt. Spectrosc.*, **30**, 375 (1971).
20) International Critical Tables, McGraw-Hill Book Company, Inc., N. Y., (1928), Vol. III, pp. 27ff.

estimated from the empirical Eykman equation:

$$\frac{n^2-1}{n+0.4} = \frac{d}{M} \times C,$$

where C is a constant characteristic for a molecule; M, the molecular weight, and d, the density.[21]

Finally, the products of L, s, and d were calculated; they are summarized in Table 1 (designated as (Lsd)). The relative values, $(Lsd)/(Lsd)_{24}$, are expected to agree with those of the relative intensity, I/I_{24}, if the factors considered here mainly contribute to the apparent intensity change due to the change in temperature. Actually, the agreement between these two sets of values is excellent. In Fig. 2, the observed relative intensities are compared with those corrected for these three factors, L, s, and d.

Table 2. Intensity change of the 367 cm^{-1} line of chloroform

t(°C)	L/L_{24}	s/s_{24}	d/d_{24}	Lsd/Lsd_{24}	I/I_{24}
24	1.000	1.000	1.000	1.000	1.000
35	0.981	1.002	0.986	0.970	0.866
40	0.957	1.003	0.980	0.941	0.815

367 cm^{-1} Line of Chloroform. Exactly the same procedures were applied to the 367 cm^{-1} line of liquid chloroform. The results are summarized in Table 2. It can be seen in the table that the relative intensity of the 367 cm^{-1} line decreases more than 20 per cent as the temperature changes from 24 to 40°C, while the calculated correction factor, $(Lsd)/(Lsd)_{24}$, decreases only 6 per cents. The discrepancy between the observed and the calculated intensity ratios corresponds to the real change in the intensity of the line on passing from 24 to 40°C; this can be explained with respect to the intermolecular interactions, such as the break-down of hydrogen bonding between chloroform molecules in the liquid phase on the elevating of the temperature. The details will be discussed elsewhere, together with the intensity change in the absorption spectra.

Local-field Correction and Conclusion. A few important conclusions can be drawn from the present results. The intensity change in the 992 cm^{-1} Raman line of liquid benzene can be completely explained by L, s, and d; that is, the Raman scattering cross section per molecule does not change when the temperature varies. Among the three factors, the local-field correction is the main factor changing the apparent intensity. Eckardt's formula is based upon these ideas: (1) the Lorentz-field consideration is applicable to the system, and (2) the scattering may be thought of as the absorption of a light quantum, followed by the emission of another quantum; therefore, the local-field correction for the scattering is the product of the local-field corrections for absorption and for spontaneous emission.[22,23] Therefore, the effect of the local field on the apparent intensity is much greater for the Raman than for the infrared absorption intensity. In the latter case, L is expressed as:

$$L = \frac{(n^2+2)^2}{9}$$

assuming the Lorentzfield.[3] It can easily be ascertained that the intensity change due to temperature variation cannot be explained by this formula, which means that the present results strongly support the assumption (2) of Eckardt and contradicts the propositions of the references.[14,15] It may also be concluded from the present results that the choice of the Lorentzfield for the liquid benzene is reasonable.

The other important conclusion drawn from the present result is that the L and d factors do not depend upon the frequency, ν; this means that the apparent intensity change due to the change in temperature is the same magnitude for all the Raman-shift region. Therefore, the factors do not contribute to the observed relative intensities of Raman lines with different frequencies. In the preceding discussions, the refractive index of a sample was assumed to take a constant value for all the frequency range under consideration. In a case where a sample is absorbing, *e.g.*, the case of a resonance Raman, the refractive index value changes considerably over the Raman-shift range. Therefore, the consideration of the local-field effect is extremely important.

Incidentally, it may be concluded that the measurements of the relative intensities of Raman lines are much easier and more reliable than those of the infrared absorption in the sense that the observed data are nearly free from any systematic errors which spoil the reliability of the relative intensities.

The author wishes to express his sincere thanks to Professor Takehiko Shimanouchi and all the members of his laboratory for giving the opportunity of completing this work.

21) Weissberger *et al.*, "Organic Solvents," Techinique of Organic Chemistry, Interscience Publishers, Inc., N. Y., 1955, Vol. VII.

22) J. A. Armstrong, N. Bloembergen, J. Ducuing, and P. S. Pershan, *Phys. Rev.*, **127**, 1918 (1962).

23) P. D. Maker and R. W. Terhune, *ibid.*, **137**, A801 (1965).

Catalytic Diacetoxylation of Dihaloethylenes in the Presence of Palladium Salts

Masahiro YAMAJI, Yuzo FUJIWARA, Ryuzo ASANO, and Shiichiro TERANISHI
Faculty of Engineering Science, Osaka University, Toyonaka, Osaka
(Received June 5, 1972)

The reaction of dihaloethylenes with acetate anions in the presence of palladium(II) salts gave *trans*-diacetoxyethylenes catalytically. It was found that the system, $PdCl_2$–NaOAc–CH_3CN is the best for the diacetoxylation of dihaloethylenes, and that palladium(II) salts catalyze the isomerization of *trans*-diacetoxyethylene to its 1,1-diacetoxy derivative. The mechanism was also discussed.

Palladium salts have been known to cause a wide variety of reaction.[1] It was generally thought that halide ion displacement of vinyl halides with nucleophiles was difficult because of their double bond character between carbon and halogen atoms.

Since Stern *et al.* explored the possibility of the nucleophilic substitution of vinyl chloride by an acetate anion in the presence of palladium(II) chloride to give vinyl acetate,[2] a few reports appeared concerning with the substitution.[3] However, examples are limited to only monohalides such as vinyl chloride or 2-chloropropylene. Interest in whether dihalides also undergo substitution reaction or not, prompted us to investigate the reaction of dihaloethylenes in detail. Interestingly enough we have found that in the presence of catalytic amounts of palladium(II) salts, various dihaloethylenes such as dichloro-, dibromo-, diiodo-, and bromochloroethylenes react readily with an acetate anion to produce diacetoxyethylenes,[4] and that they also react with various substituted acetate anions (XCH_2COO^-: X= C_2H_5, CH_3, Cl). In addition, in the course of this study, an isomerization of *trans*-diacetoxyethylene to 1,1-diacetate by palladium(II) salts was also found.

In this paper, we will describe the substitution reaction of dihaloethylenes with acetate anions, and the observation that *trans*-diacetoxyethylene isomerizes to its 1,1-diacetate derivatives in the presence of palladium(II) salts.

Results and Discussion

Reaction of cis-*Dichloroethylene with Acetate Anion.* In the substitution reaction of vinyl halide, the system, $PdCl_2$–Na_2HPO_4–isooctane-acetic acid was used,[2] but a dihaloethylene, *cis*-dichloroethylene, afforded no acetates under the similar reaction conditions. So, first, we investigated the reaction conditions under which the olefinic dihalides suffer the nucleophilic substitution reaction with an acetate anion.

Table 1 summarizes the results and shows that the system, $PdCl_2$–NaOAc can cause the diacetoxylation of *cis*-dichloroethylene catalytically, and that acetonitrile is the best solvent for the reaction. It seems that the solvent which has an appropriate ability of coordination to palladium(II) and can be easily displaced by the substrate dihalo-olefin, is suitable for the reaction. In typical, the reaction of *cis*-dichloroethylene with sodium acetate in the presence of a catalytic amount of $PdCl_2$ gave *trans*-diacetoxyethylene (123%[5]) and 1,1-diacetoxyethylene (39%) with a small amount of

Table 1. Diacetoxylation of *cis*-dichloroethylene by palladium(II) salts[a]

Palladium salt	Acetoxylating agent	Solvent	Yield, %[b] of *trans*-diacetoxyethylene
$Pd(OAc)_2$	AcOH	Isooctane	trace
$Pd(OAc)_2$	AcOH	—	trace
$Pd(OAc)_2$	—	Acetonitrile	7[c]
$PdCl_2$	NaOAc	Acetic acid	14[c]
$PdCl_2$	NaOAc	Acetonitrile	123[c]
$PdCl_2$	NaOAc	Dimethylformamide	42[c]
$PdCl_2$	NaOAc	Benzonitrile	8[c]
$PdCl_2$	NaOAc	Ethanol	trace
$PdCl_2$	NaOAc	Pyridine	—
$PdCl_2$[d]	AcOH	Isooctane	—

a) Reactions were carried out at 80°C for 8 hr unless otherwise stated.
b) Based on the Pd(II) catalyst.
c) 1,1-Diacetoxyethylene and *cis*-isomer were also formed in small amount.
d) Disodium hydrogen phosphate (Na_2HPO_4) was employed and the reaction was performed for 48 hr at room temperature.

Table 2. Reactivity of palladium(II) salts[a]

Palladium salt	Product and yield, %[b]	
	trans-diacetoxy-	1,1-diacetoxyethylene
$PdCl_2$	123	39[c]
$PdBr_2$	36	9
PdI_2	0.5	trace

a) Reactions were carried out at 80°C for 8 hr charging 0.09 mol of *cis*-dichloroethylene, 0.18 mol of NaOAc, 0.03 mol of palladium salt, and 200 ml of CH_3CN as a solvent.
b) Yields are based on palladium salt used.
c) *cis*-Isomer was also formed in a very small amount.

1) For example, P. M. Maitlis, "The Organic Chemistry of Palladium," Vol. I and II, Academic Press, New York, 1971.
2) E. W. Stern, M. L. Spector, and H. P. Lefti, *J. Catal.*, **6**, 152 (1966).
3) a) C. F. Kohll and R. van Helden, *Rec. Trav. Chim. Pays-Bas*, **87**, 481 (1968); b) H. C. Volger, *ibid.*, **87**, 501 (1968); c) M. Tamura and A. Yasui, *Kogyo Kagaku Zasshi*, **72**, 572 (1969); d) P. M. Henry, *J. Amer. Chem. Soc.*, **93**, 3853 (1971); **94**, 1527 (1972).
4) M. Yamaji, Y. Fujiwara, T. Imanaka, and S. Teranishi, This Bulletin, **43**, 2659 (1970).
5) Yields given in this paper are based on the amount of palladium salt used.

cis-diacetoxyethylene. And interestingly in this case, no monoacetate was produced.

In order to study the ligand effect on the reaction, the reactivities of $PdCl_2$, $PdBr_2$, and PdI_2 were compared (Table 2). The reactivity decreases in the order: Cl>Br>I. This may be explained in the following way: π-acceptor character increases with the order, Cl<Br<I,[6] so back donation from palladium to the substrate dihalo-olefin would be more restricted in the case of PdI_2. Thus the ease with which palladium(II) and the olefin form a stable π-complex, increases in the order, I<Br<Cl, then resulting in increase of the reactivity in this order. In addition, the bulkiness of the iodine atom would prevent the coordination of the substrate olefin to palladium(II). Consequently, $PdCl_2$–NaOAc–CH_3CN is the most effective system for the diacetoxylation of dihaloethylene.

The acetoxylation of *cis*-dichloroethylene gave 1,1- and *cis*-diacetoxyethylene as by-products. In order to study the reaction path of these products, isomerization of *trans*-diacetoxyethylene, a main product, was examined (Table 3).

Table 3. Isomerization of *trans*-diacetoxyethylene[a]

$PdCl_2$ mmol	NaOAc mmol	Reaction time, hr	Yield, %[b] diacetoxyethylenes	
			1,1-isomer	*cis*-isomer
0.06	None	6	31	trace
0.06	0.12	8	64	trace
None	0.12	8	—	30
0.06[c]	0.12	8	trace	98

a) Reactions were carried out at 80°C for 8 hr using CH_3CN as a solvent.
b) Based on *trans*-diacetoxyethylene.
c) The starting material was *cis*-diacetoxyethylene.

As is apparent from Table 3, *trans*-diacetoxyethylene isomerized to 1,1-diacetate (64% yield) in the presence of $PdCl_2$ and NaOAc. In addition, the table indicates that thermal isomerization of *trans*-diacetoxyethylene to its *cis* isomer takes place in the absence of $PdCl_2$. Therefore, it seems that both 1,1-diacetoxyethylene and its *cis* isomer[7] are derived from *trans*-diacetoxyethylene which is formed by diacetoxylation of the starting *cis*-dichloroethylene.

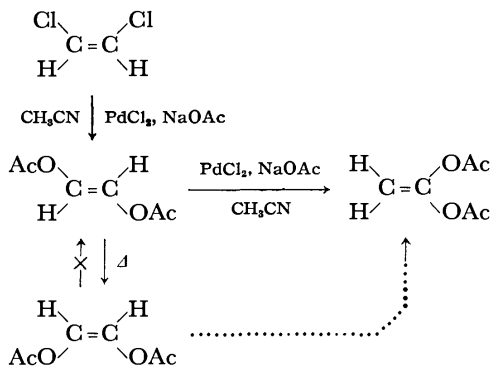

6) J. Chatt and B. L. Shaw, *J. Chem. Soc.*, **1962**, 5075.
7) *cis*-Diacetate produced in a small amount is not an initial product since it does not isomerize to *trans*-diacetate under the reaction conditions.

Table 4. Reaction of *cis*-dichloroethylene with substituted acetate anions[a]

Sodium salt	Yield, % of diacetate[b]	
	trans-isomer	1,1-isomer
C_2H_5–CH_2COONa	77	14[c]
CH_3–CH_2COONa	55	11[d]
Cl–CH_2COONa	trace[e]	—

a) Reactions were all carried out at 80°C for 8 hr, charging 0.02 mol of $PdCl_2$, 0.12 mol of sodium salt, 0.06 mol of *cis*-dichloroethylene, and 160 ml of CH_3CN.
b) Based on $PdCl_2$ used.
c) A trace amount of butyric anhydride was also formed.
d) A trace amount of propionic anhydride was also formed.
e) 1-Chloro-2-chloroacetoxyethylene was formed in a 0.4% yield.

Reaction of cis*-Dichloroethylene with Substituted Acetate Anions.* As it became apparent that $PdCl_2$–NaOAc causes diacetoxylation of *cis*-dichloroethylene, we further tried to extend this reaction. Examination was performed using the substituted acetate anions (XCH_2COO^-: X=C_2H_5, CH_3, Cl) as nucleophiles. The data listed in Table 4 show that the diacetoxylation could also occur in the cases of sodium butyrate, propionate, and chloroacetate other than sodium acetate, and that an electron donating group (CH_3, C_2H_5) increases the reactivity, indicating the nucleophilic nature of the reaction.

Reaction of trans*-Dichloroethylene, -Diiodoethylene, -Bromoiodoethylene, and-Dibromoethylene with Acetate Anion.* Since *cis*-dichloroethylene has been found to undergo diacetoxylation, other dihaloethylenes were investigated toward the reactivity in the presence of $PdCl_2$ and NaOAc (Table 5).

Table 5. Diacetoxylation of various dihaloethylenes[a]

Dihaloethylene	Yield, % of diacetoxyethylene[b]			
	trans-	1,1-	*cis*-	Total
trans-ClHC=CHCl	138	70	trace	208
cis-ClHC=CHCl	123	39	trace	162
BrHC=CHBr[c]	160	30	trace	190
trans-BrHC=CHI	33	23	5	61
trans-ICH=CHI	3	2	—	5

a) Reactions were carried out at 80°C for 8 hr using CH_3CN as a solvent.
b) Based on $PdCl_2$.
c) *cis* and *trans* Mixture (5:7).

It can be seen from Table 5, various dichloroethylenes can undergo diacetoxylation in the presence of $PdCl_2$ and NaOAc as *cis*-dichloroethylene does. The reactivity decreases in the order: Cl>Br>I.

1,2-Transfer of Acetoxy Group on Ethylenic Carbon Atoms. As mentioned above, it has been found that $PdCl_2$ catalyzes the isomerization of *trans*-diacetoxyethylene to 1,1-diacetoxyethylene. Palladium chloride without NaOAc can also affect the isomerization, but the yield decreases from 64% to 31%. This indicates that an acetate anion of NaOAc other than the starting *trans*-

diacetoxyethylene, is partly involved in the reaction.[8]

Palladium(II) catalyzed allylic isomerization of an acetate anion is well known,[9] but vinylic isomerization is the first example to our knowledge. Henry reported a palladium(II) catalyzed allylic isomerization of an acetate anion, and that two reactions actually take place involving an acetoxypalladation-deacetoxypalladation mechanism and 1,3-acetoxonium ion mechanism.[9]

$$MeCH{=}CHCH_2\overset{*}{O}Ac + -PdOAc \underset{AcOH}{\rightleftharpoons} MeCH(OAc)-CH{=}CH_2 + -Pd\overset{*}{O}Ac \quad (1)$$

In the present case, the isomerization reaction might proceed through a 1,2-acetoxonium intermediate (Eq. 2), and an acetoxypalladation-deacetoxypalladation might be operative in the exchange reaction of acetate anions (Eq. 3).

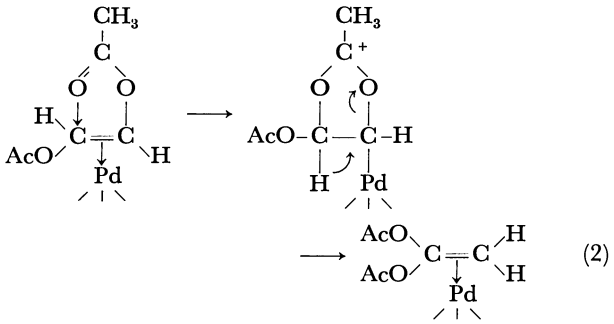

(2)

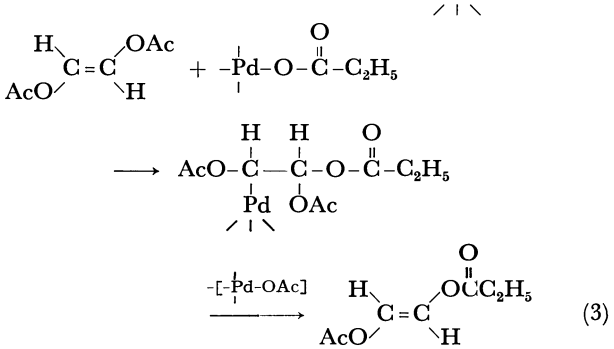

(3)

$PdBr_2$, PdI_2, $Pd(OAc)_2$, and $PdCl_2(CH_3CN)_2$ gave the isomerization but other metal salts, such as $RhCl_3$, $IrCl_3$, $NiCl_2$, $PtCl_2$, $FeCl_3$, or $CoCl_2$ gave no reaction.[10] Thus it can be said that this isomerization is characteristic for Pd(II) salts. This provides a very convenient synthetic method for preparing 1,1-diacetoxyethylene of which preparation was rather troublesome by other methods.

Mechanism of Acetoxylation. The Pd(II) catalyzed acetoxylation of dihaloethylenes gives a *trans*-diacetate as a main product. It seems that the acetoxylation takes place step by step[11] since the monoacetate was obtained from the reaction of *cis*-dichloroethylene and sodium chloroacetate.

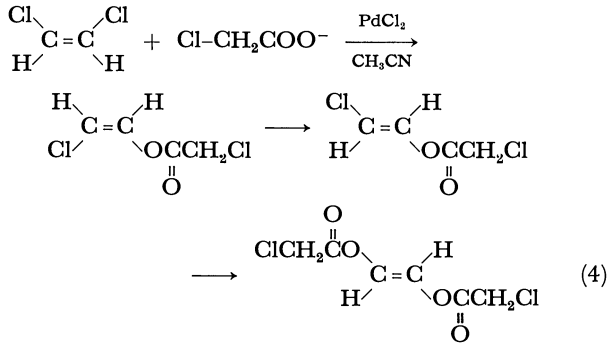

(4)

Finally, the diacetoxylation would proceed through the similar mechanism proposed to the acetoxylation of vinyl halides.[1,3a]

$$PdCl_2 + AcO^- \rightleftharpoons PdCl_2(OAc)^- \quad (5)$$

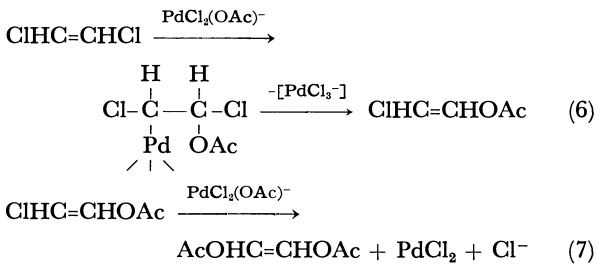

(6)

(7)

In conclusion, olefinic dihalides such as dihaloethylenes can also undergo acetoxylation by palladium(II) salt catalysts, to give *trans*-diacetates rather exclusively (Eq. 8). In addition, palladium(II) salts affect the isomerization of *trans*-diacetates to their 1,1-diacetate derivatives. These reactions provide a very convenient route to a wide variety of diacetate derivatives.

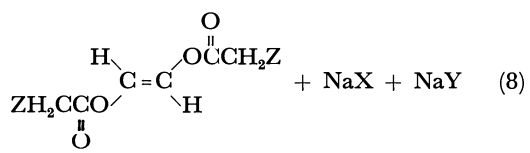

(8)

Experimental

All temperatures were uncorrected. The IR spectra were recorded on a JASCO IR-E spectrometer and the NMR spectra were measured on a Japan Electron Optics JNM-4H-100 spectrometer. Chemical shifts are given in τ units together with splitting patterns and relative integrated area.

Materials. *cis*- and *trans*-Dichloroethylene, and dibromoethylene (5: 7 *cis* and *trans* mixture) were commercial grade and distilled before use. *trans*-Diiodoethylene (mp 73—73.5°C)[12] and *trans*-bromoiodoethylene (bp 70—71°C/40-mmHg)[13] were prepared according to the methods reported.

8) This external acetate anion participation was confirmed by the fact that dipropionyloxyethylenes were obtained when *trans*-diacetoxyethylene was treated with sodium propionate and palladium chloride.[3d]

9) P. M. Henry, *Chem. Commun.*, **1971**, 328.

10) In the case of allylic isomerization, $PdCl_2$, $PtCl_2$, $RuCl_3$, $OsCl_3$, and $RhCl_3$ are reported to be effective catalysts.[9]

11) The reaction of the monoacetate to the diacetate may be very fast since no monoacetate was obtained in the reaction of dihaloethylenes with an acetate anion, and the *cis-trans* isomerization might take place in the stage of the monoacetate presumably due to its thermal stability.

12) A. Sabanejeff, *Ann. Chem.*, **178**, 109 (1875).

13) H. G. Viehe and E. Franchimont, *Ber.*, **96**, 3153 (1963).

Palladium(II) salts were commercial grade.

General Procedure for Diacetoxylation of Dihaloethylenes with Acetate Anion. Mixtures of the palladium salt, the dihaloethylene in three equiv amount, sodium acetate in six equiv amount, and the solvent were stirred for 8 hr at 80°C. The resulting mixture was filtered to remove $PdCl_2$ and small amounts of Pd metal formed. The filtate was poured into water and the organic material was treated with aqueous sodium carbonate solution, washed with water, and then dried over anhydrous $MgSO_4$. After evaporation of about half of the solvent, the residue was kept standing for several hours, and then *trans*-diacetoxyethylene crystallized, and mother liquid was subjected to preparative gas chromatography (Yanagimoto G-8, Apiezon L) to give 1,1-diacetate and/or *cis* diacetate. Specific examples of the reaction are given in detail below.

Reaction of cis-Dichloroethylene with Sodium Acetate. In a 250 ml, three necked, round-bottomed flask provided with a condenser with a calcium chloride tube at the top, and a stirrer, was placed a mixture of 0.09 mol of *cis*-dichloroethylene, 0.18 mol of sodium acetate, 0.03 mol of $PdCl_2$ and 200 ml of acetonitrile. The mixture was stirred for 8 hr at 80°C. After work-up as decsribed above, the residue crystallized partly. Recrystallization from ether-petroleum ether gave colorless crystals, mp 42—43.7°C. Purification was done by sublimation (4 mmHg) (5.31 g, 123% based on $PdCl_2$), mp 44—45°C which was assigned as *trans*-diacetoxyethylene by comparison of the IR spectra and mixture melting point with an authentic sample,[14] IR (neat) cm^{-1}: 976 (*trans* C-H), 1200 (C–O–C), 1380 (CH_3COO) and 1770 (C=O); NMR (CCl_4): 3.17 (s, 2H) and 7.83 (s, 6H). Found: C, 49.93; H, 5.60%. Calcd for $C_6H_8O_4$: C, 50.00; H, 5.60%.

From the mother liquor, two products were detected and these were separated by glpc. One (1.68 g, 39%) was assigned as 1,1-diacetoxyethylene and the other (trace amount) as *cis*-diacetoxyethylene by comparison with authentic samples,[14] 1,1-diacetoxyethylene; IR (neat) cm^{-1}: 877 (CH_2=), 1200 (C–O–C), 1380 (CH_3COO) and 1760 (C=O); NMR (CCl_4): 2.50 (s, 2H) and 7.80 (s, 6H). *cis*-Diacetoxyethylene; IR (neat) cm^{-1}: 1200 (C–O–C), 1380 (CH_3COO), 1620 (C=C) and 1760 (C=O); NMR (CCl_4): 5.40 (s, 2H) and 7.84 (s, 6H).

From the solvent evaporated, the starting *cis*-dichloroethylene was recovered without isomerization. Authentic *trans*- and *cis*-diacetoxyethylenes and 1,1-diacetate isomer were prepared by the modification of the method described by Shostakovskii *et al.*[14]

Reaction of cis-*Dichloroethylene with Sodium Propionate, Butyrate, and Chloroacetate.* The reaction of *cis*-dichloroethylene with sodium propionate was performed as described above. The products were *trans*-dipropionyloxyethylene (55%), 1,1-dipropionyloxyethylene (11%) and propionic anhydride (trace), *trans*-dipropionyloxyethylene; IR (neat) cm^{-1}: 935, 1150, 1343, 1460, and 1760; NMR (CCl_4): 3.27 (s, 2H), 7.56 (q, 4H, J=7 Hz), and 8.80 (t, 6H, J=7 Hz). 1,1-Dipropionyloxyethylene; IR (neat) cm^{-1}: 900, 1150, and 1750; NMR (CCl_4): 2.26 (s, 2H), 7.64 (q, 4H, J=7 Hz), and 8.84 (t, 6H, J=7 Hz).

Similarly the reaction with sodium butyrate gave *trans*-dibutyryloxyethylene (77%), IR (neat) cm^{-1}: 970, 1245, 1345, and 1760; NMR (CCl_4): 3.27 (s, 2H), 7.62 (t, 4H, J=7 Hz), 8.30 (m, 4H), and 9.00 (t, 6H, J=7 Hz), and 1,1-dibutyryloxyethylene (14%), IR (neat) cm^{-1}: 900, 1150, and 1750; NMR (CCl_4): 2.60 (s, 2H), 7.68 (t, 4H, J=6 Hz), 8.33 (m, 4H), and 9.02 (t, 6H, J=6 Hz), and butyric anhydride (trace).

The reaction with sodium monochloroacetate gave small amounts of 1,2-dichloroacetoxyethylene (probably *trans*), NMR (CCl_4): 3.60 (s, 2H) and 5.98 (s, 4H), and 1-chloro-2-chloroacetoxyethylene (0.4%), NMR (CCl_4): 2.58 (d, 1H, J=4.5 Hz), 4.40 (d, 1H, J=4.5 Hz), and 5.87 (s, 2H).

Isomerization of trans-*Diacetoxyethylene.* The reaction were carried out at 80°C for 8 hr with stirring, charging 0.18 mmol *trans*-diacetoxyethylene, 0.06 mmol of palladium chloride, 0.12 mmol of sodium acetate and 2 ml of acetonitrile. The reaction mixture was analyzed by glcg using tetralin as an internal standard. The results are shown in Table 3.

Isomerization of trans-*Diacetoxyethylene in the Presence of Sodium Propionate.* The reaction was performed at 80°C for 6 hr, charging 0.12 mmol of *trans*-diacetoxyethylene, 0.06 mmol of sodium propionate, 0.056 mmol of palladium chloride and 2.5 m*l* of acetonitrile. After work-up as usual, the reaction mixture was analyzed by glcg. There were obtained *trans*-1-acetoxy-2-propionyloxyethylene (28%), 1,1-diacetoxyethylene (14%) with small amounts of unidentified acetates. The starting *trans*-diacetoxyethylene was recovered in 42% yield. *trans*-1-Acetoxy-2-propionyloxyethylene, IR (neat) cm^{-1}: 945, 1105, 1150, and 1762; NMR (CCl_4): 3.22 (s, 2H), 7.55 (q, 2H, J=7 Hz), 7.80 (s, 3H) and 8.78 (t, 3H, J=7 Hz).

14) M. F. Shostakovskii, N. V. Kuznetsov, and Chemin Yang, *Izv. Akad. Nauk SSSR, Ser. Khim.*, **1962**, 710.

Phase Transition in the Ionic Modification of Phosphorus Pentachloride, $[PCl_4][PCl_6]$. Chlorine Nuclear Quadrupole Resonance Study

Hideaki CHIHARA and Nobuo NAKAMURA

Department of Chemistry, Faculty of Science, Osaka University, Toyonaka 560

(Received June 14, 1972)

Chlorine-35 nuclear quadrupole resonance frequencies in the ionic crystal $PCl_4^+ \cdot PCl_6^-$ were redetermined. Ten resonance lines were found and their temperature dependences were measured below the second order phase transition point at 102 K. The splitting $\Delta\nu_i$ in the resonance lines in the low temperature phase showed a similar temperature dependence as the order parameter. This was accounted for by a librational soft mode theory based on an anharmonic coupling between molecular or ionic librational modes in the crystal.

In 1967 we reported on the ^{35}Cl nuclear quadrupole resonance (NQR) and calorimetric studies of both ionic and molecular modifications of phosphorus pentachloride.[1] It was found that the ionic crystal $[PCl_4][PCl_6]$ undergoes a second order phase transition at 102 K, but the mechanism of the phase transition was not fully clarified because of insufficient accuracy in the heat capacity measurement as well as other experimental data concerning the phase transition.

Meanwhile, DiLorenzo and Schneider[2] measured the NQR frequencies in the same substance and observed some resonance lines at different frequencies from those reported by the present authors. Smith and Tong[3] pointed out later that there are altogether nine lines due to ^{35}Cl and that we missed a pair of doublets at 30.05 MHz and one of four lines at about 32.3 MHz. However, they did not report a broad line at 28.6 MHz which we had described previously.[1]

Now it has become evident from the three previous papers that there are ten NQR lines in Phase II (the low temperature phase) of $[PCl_4][PCl_6]$. This fact clearly indicates that all chlorine atoms in the chemical formula unit (P_2Cl_{10}) are at crystallographically non-equivalent sites in Phase II. Since our failure to observe three more resonance lines seems to be due to insufficient sensitivity of the spectrometer used, we attempted to re-examine all the ten resonance lines using a carefully constructed cryostat. In the present paper, we will discuss the NQR spectra in Phase II in relation to the crystal symmetry of both Phase I and II. It will be shown that the temperature dependence of the NQR frequencies can be explained by a librational soft-mode theory[4,5] which is based on an anharmonic coupling between the molecular or ionic librational modes.

Experimental

The NQR frequencies were measured on the same specimen as was used in the previous NQR study.[1] This had been stored in a sealed glass tube at room temperature for about three and half years after the original measurements of the temperature dependence of the NQR frequencies were carried out.

Some modifications were made of the experimental arrangement. The coaxial cable wire connecting the spectrometer and the sample coil was replaced by a thin-walled cupronickel tube running down the axis of a stainless-steel tube. Both tubes were silver-plated in order to improve spectral sensitivity.[6] The NQR frequencies were determined with a Takeda Riken Model TR-5578 digital frequency counter instead of the one used previously.

Results and Discussion

Spectra in Relation to Structure. The stable phase of phosphorus pentachloride contains two types of complex ion, PCl_4^+ and PCl_6^-, in a tetragonal unit cell of the space group P4/n at room temperature (Phase I).[7] The phosphorus atom and two of the six chlorine atoms in PCl_6^- lie on the four-fold axis and the phosphorus atom in PCl_4^+ is on the $\bar{4}$ axis. Other chlorine atoms are at general positions. All the four chlorine atoms in a PCl_4^+ cation are crystallographically equivalent and the four chlorine atoms in the PCl_6^- that lie in the *ac* plane are also equivalent.

Therefore, the number of resonance lines in Phase I observed in the previous work agrees with the number expected from the crystal structure. In Phase II, on the other hand, ten ^{35}Cl NQR lines were observed

TABLE 1. ^{35}Cl NUCLEAR QUADRUPOLE RESONANCE FREQUENCIES OF $[PCl_4][PCl_6]$ AT 20.9 K

	Frequency/MHz	Assignment
ν_1	28.5902±0.0004	
ν_2	29.7833±0.0009	
ν_3	30.0685±0.0008	PCl_6^-
ν_4	30.0772±0.0003	
ν_5	30.6029±0.0009	
ν_6	30.7569±0.0004	
ν_7	32.3827±0.0002	
ν_8	32.4898±0.0001	PCl_4^+
ν_9	32.5639±0.0001	
ν_{10}	32.7695±0.0003	

1) H. Chihara, N. Nakamura, and S. Seki, This Bulletin, **40**, 50 (1967).
2) J. V. DiLorenzo and R. F. Schneider, *Inorg. Chem.*, **6**, 766 (1967).
3) J. A. S. Smith and D. A. Tong, *J. Sci. Instr.*, Ser 2, **1**, (19868).
4) H. Chihara, N. Nakamura, and M. Tachiki, *J. Chem. Phys.*, **54**, 3640 (1971).
5) H. Chihara, N. Nakamura, and M. Tachiki, *ibid.*, to be published.
6) N. Nakamura and H. Chihara, *J. Phys. Soc. Japan*, **22**, 201 (1967).
7) D. Clark, H. M. Powell, and A. F. Wells, *J. Chem. Soc.*, **1942**, 642.

TABLE 2. ^{35}Cl NUCLEAR QUADRUPOLE RESONANCE FREQUENCIES (MHz) AT 78 AND 109 K COMPARED WITH PREVIOUS WORK

Temperature	Present work	Chihara, *et al.*[a]	DiLorenzo and Schneider[b]	
			unannealed	annealed
78 K	28.3951	28.424	—	—
(Phase II)	29.7111	29.720	29.65	29.61
	30.0272	—	—	—
	30.0602	—	30.08	30.07
	30.4574	30.478	30.47	30.45
	30.5719	—	—	30.62
	32.2791	32.288	32.30	32.28
	32.3843	32.396	—	—
	32.4198	—	32.42	—
	32.6023	32.620	32.63	32.61
109 K	28.0871	28.098		
(Phase I)	29.6377	29.647		
	30.1960	30.203		
	32.2808	32.28		

a) Ref. 1. b) Ref. 2

instead of the seven detected previously. The resonance frequencies at 20.9 K and their assignment are given in Table 1.

The present results are compared with the previous results[1,2] at 78 K (Phase II) and 109 K (Phase I) in Table 2. Our results in the two independent measurements differ slightly, which may be due to some error in the frequency and/or temperature measurements. DiLorenzo and Schneider[2] pointed out that the solid maintained at liquid nitrogen temperature for a period of four weeks gave a spectrum differing from that of a rapidly cooled sample both in the resonance frequency (see Table 2) and intensity. They attributed this aging phenomenon to the remedy of lattice strain by annealing. In an attempt to confirm such an effect of annealing we compared the spectrum of Phase II cooled rapidly down to liquid nitrogen temperature with that of the sample which had been stored at liquid nitrogen temperature for five weeks. No appreciable change in the spectrum due to aging was observed except for slight enhancement in the intensity of ν_5, ν_6, and ν_9.[8]

Temperature Dependence. The temperature dependence of all the resonance frequencies was measured again between 20 and 110 K. The result is shown in Fig. 1. Of the four resonance lines in Phase I, the two higher-frequency lines split into four when the crystal was cooled through the transition point ($T_{tr}=103\pm0.6$ K), whereas the other two lines (ν_1 and ν_2 in PCl_6^-) remained unsplit.

As was mentioned above two chlorine atoms in PCl_6^- are in special positions in Phase I (on the 4-fold axis). Therefore we can unambiguously assign ν_1 and ν_2 to these chlorines also in Phase II.

The four chlorine atoms in PCl_6^- (in the basal plane) as well as four in PCl_4^+ become non-equivalent in Phase II. This fact shows that both 4 and $\bar{4}$ symmetry axes are not conserved in Phase II. Thus, it is obvious that the transition is of the second order according to Landau's classification.[10] It is interesting to note that each set of four chlorine atoms in PCl_4^+ and PCl_6^- appears to split into quartets symmetrically separated on either side of the average frequency in Phase II. Moreover, ν_1 shows a discontinuous change in slope at T_{tr} whereas ν_2 shows barely discernible anomaly around T_{tr}. In Fig. 2 the splitting $\Delta\nu_i$ (i=3—6) is plotted against the reduced temperature T/T_{tr} for PCl_6^-. The magnitude of the splitting was measured from the averaged frequency of the four lines and reduced by $\Delta\nu_i(0)$, the splitting being extrapolated to 0 K. It can be seen from Fig. 2 that all $\Delta\nu_i$ depend

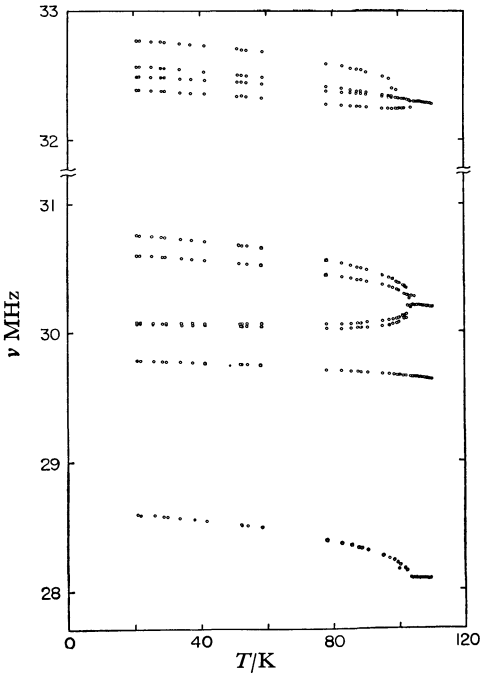

Fig. 1. Nuclear quadrupole resonance frequencies of $[PCl_4]$-$[PCl_6]$ between 20 and 110 K.

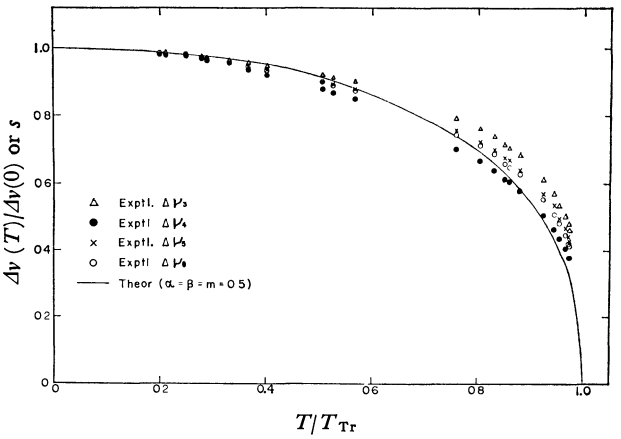

Fig. 2. Separation of lines ν_3 to ν_6 from their average, reduced by the separation at 0 K, as function of temperature (taken as the order parameter s).

8) The effect of the sample treatment on the heat capacity has been observed in the phase transition region.[9]

9) H. Chihara, M. Nakamura, and K. Masukane, This Bulletin, **46**, 97 (1973).

10) L. D. Landau and E. M. Lifshitz, "Statistical Physics," Pergamon Press, London, (1958).

similarly on temperature, suggesting that the splittings have a common cause.

Mechanism of the Transition. It is reasonable to consider that the phase transition is brought about by some reorientation of a PCl_6^- group about an axis perpendicular to its figure axis. Such a reorientation may be expressed by one parameter, *i.e.*, the angle of rotation θ from a fixed direction in the lattice. The magnitude of separation of the resonance line can be expanded in terms of θ as

$$\Delta\nu_i = A_i\theta + B_i\theta^2 + \cdots, \tag{1}$$

where θ can be measured from the original direction of the figure axis in Phase I. Here the tilt angle θ can be regarded as an order-parameter of the phase transition, and $\Delta\nu_i$ given in Fig. 2 can be taken as the same quantity if we neglect higher order terms of θ in Eq. (1).

In order to explain a similar type of phase transition in a chloranil crystal we have developed a librational soft mode theory which is based on an anharmonic coupling between molecular librational modes.[5,9,11] As the PCl_4^+ and PCl_6^- groups can be considered as rigid bodies, we can apply this theory to the phase transition of P_2Cl_{10}.

The Hamiltonian of the whole libration system is given by

$$H = \frac{P_\theta^2}{2I} + V(\theta) + \sum_i\left(\frac{P_i^2}{2I} + \frac{1}{2}I\omega^2\varphi_i^2\right) + \sum_i f(\theta)\varphi_i^2, \tag{2}$$

where $V(\theta)$ is the potential energy for a uniform mode, P_θ is its conjugate angular momentum, and the last term expresses the anharmonic coupling between the uniform mode and other librational modes φ_i treated as harmonic oscillators with frequency ω. We assume that $V(\theta)$ is of the form

$$V(\theta) = a(\theta^2 - p\theta^4 - q\theta^6), \tag{3}$$

which has a minimum at $\theta=\theta_0$ and satisfies the symmetry conditions in Phase I. The PCl_6^- ion is in the orientation of minimum potential energy θ_0 at 0 K. If the anharmonic coupling is taken into account in such a way as to make the librational frequencies $\Omega(\theta)$ of the Einstein mode to decrease with a decrease in θ, the Helmholtz energy is given by

$$A = V(\theta) + \boldsymbol{N}\boldsymbol{k}T\ln[1-\exp(-\hbar\Omega(\theta)/\boldsymbol{k}T)], \tag{4}$$

and the orientation giving the minimal A changes toward smaller θ as the temperature increases. The equilibrium orientation $\bar{\theta}$ can be determined from the condition $\partial A/\partial\theta=0$ at any temperature. The result is

$$\ln\left[\frac{\alpha}{\beta(1-s^2)\{1+(1-2m)s^2\}}+1\right] = (1+\alpha s^2)/t, \tag{5}$$

where $\alpha=If''(0)\theta_0^2/8\omega^2$, $\beta=a\theta_0^2/\hbar\omega$, $t=\boldsymbol{k}\boldsymbol{T}/\hbar\omega$, and $m=p\theta_0^2$ must be treated as adjustable parameters. The order parameter $s=\bar{\theta}/\theta_0$ was then calculated by using a NEAC-2200 electronic computer. The result is shown in Fig. 2 by a solid line, where α, β, and m were chosen so as to give the best fit to the experimental points. The adequacy of the set of parameters has been favorably examined by analyzing the excess heat capacity associated with the phase transition.[9]

On the other hand, the splitting of the resonance line due to PCl_4^+ ion shows no such regularity as is observed for PCl_6^- (Fig. 2) and the extent of the splitting is significantly small compared with the case of PCl_6^-. These facts suggest that the anharmonic coupling between the librational and the uniform modes of PCl_6^- plays a principal role in the cooperative ordering process and the splitting in the resonance line of PCl_4^+ is produced as a result of the second-order effect of ordering.

The authors wish to express their sincere gratitude to Professor M. Tachiki for his illuminating suggestions by which they have greatly benefitted.

11) H. Chihara and N. Nakamura, *J. Chem. Phys.*, to be published.

Heat Capacity of Solid Phosphorus Pentachloride between 4 and 150 K. Nature of the Transition at 102 K.

Hideaki CHIHARA, Minoru NAKAMURA,* and Kazuyuki MASUKANE**
Department of Chemistry, Faculty of Science, Osaka University, Toyonaka, 560
(Received June 14, 1972)

Molar heat capacity of solid P_2Cl_{10} was measured between 4 and 150 K with an adiabatic calorimeter, with particular attention to the phase transition at 102.0 ± 0.2 K. The heat and entropy of the transition were 148 ± 3 $Jmol^{-1}$ and 1.67 ± 0.03 $JK^{-1}mol^{-1}$. Shape and magnitude of the anomalous heat capacity depend on the method of preparation. Anomaly in the heat capacity begins at about 75 K, rises gradually to a maximum of 9.12 ± 0.08 $JK^{-1}mol^{-1}$ at 102.0 K and tails off at about 110 K. The shape of the excess heat capacity curve can be explained satisfactorily by the librational soft-mode theory which assumes that PCl_6 anions tend to change equilibrium orientation with temperature.

Stable ionic form (P_2Cl_{10}) of phosphorus pentachloride has a higher-order phase transition at about 102 K. A detailed study of nuclear quadrupole resonance in ionic and molecular forms of P_2Cl_{10} was reported together with a preliminary heat capacity measurement.[1] Reinvestigation of the nuclear quadrupole resonance and precision measurements of the solid heat capacities have now been carried out with particular attention to the phase transition. The present paper describes the heat capacity and its relation to the soft-mode theory of phase transition. The quadrupole resonance part has been revised and presented in the preceding paper.[2]

Experimental

Material. Solid phosphorus pentachloride (reagent grade, Yashima Chemicals Co.) was pulverized and subjected to fractional vacuum sublimation to remove phosphorus oxychloride $POCl_3$ which had contaminated the specimen through hydrolysis by humid air. Sublimation in a vacuum of 10^{-2}—10^{-3} Torr at 60°C onto a glass wall at room temperature gave about 100 g of Sample I out of 250 g of the original material. After the heat capacity measurements were concluded with Sample I in 1966, it was found that the results were not entirely consistent with the preliminary results. In view of the recent observations in the case of chloranil[3] that a broad phase transition is extremely sensitive to crystal imperfections, it was decided to prepare another specimen, Sample II, of well-developed crystallinity. Sample II differed from Sample I in that it was obtained by slow vacuum sublimation onto a glass wall maintained at liquid nitrogen temperature. This procedure gives rise to molecular modification, which upon warming to room temperature is transformed into the stable ionic modification.[1] In fact Sample II gave a sharp, intense quadrupole resonance spectrum both at room temperature and at liquid nitrogen temperature.[2] Unfortunately, Sample I was not examined by quadrupole spectroscopy when its heat capacity was determined, but it showed a perfectly normal quadrupole spectrum four years after its preparation.

The heat capacities of Sample I and II differed only in the transition region. Charging of the calorimeter with the specimen was done in a dry-box in nitrogen atmosphere and the calorimeter was sealed by use of Woods' alloy after about 2—3 Torr of He gas replaced the air in the calorimeter.

Heat Capacity Measurements. The calorimeter vessel is made of gold and has an inner volume of about 50 cm^3. A Leeds & Northrup platinum thermometer was inserted into the reentrant well at the center of the calorimeter using Wood's alloy to fill in the void space. Six radiant vanes inside the calorimeter improved thermal diffusivity in the specimen. Heater wires (#36 manganin) were wound both round the entire length of the platinum thermometer and round the lower quarter of the outside wall of the calorimeter. A carbon resistor (Allen-Bradley, 1/8W, 10 Ω at room temperature) was used for the temperature below 11K. Gold-plated, thin copper sheath which covered the lower part of the calorimeter and the head of the platinum thermometer was used to reduce the heat exchange due to radiation.

The temperature scale above 11K is based on the 1948 International Temperature Scales and the U.S. National Bureau of Standards Scale. The working scale below 11K has been described in a previous paper.[4] The measuring circuitry including control of the adiabatic mantles is the same as reported earlier.[5]

Results and Discussion

Measured Heat Capacities. The measured heat capacity values are given in Tables 1 and 2 for Samples I and II, respectively.[6] The measurements for Sample I extend between 4.6 and 134.2 K, whereas those for Sample II cover only the region between 55 and 150 K because the two separate measurements agreed quite satisfactorily (to within ±0.3%) below 85 K and above 107 K. The results for either sample were internally consistent with scatter of points within ±0.1% except for those of Sample I below 11 K where maximum scatter amounted to about 5%. Figure 1 gives a plot of the two measurements; In the transition region, Sample I gives smaller heat capacities than Sample II, the maximum difference being as large as about 5.23 $JK^{-1}mol^{-1}$ at 102 K. The most pronounced qualitative difference lies in the fact that the Sample I heat

* Present Address: Hitachi Laboratories, 4026, Omika, Kujicho, Hitachi, Ibaraki-ken.

** Present Address: Fuji Photo Film Co., Ltd., 26—30 Nishiazabu 2-chome, Minato-ku, Tokyo.

1) H. Chihara, N. Nakamura, and S. Seki, This Bulletin, **40**, 50 (1967).

2) H. Chihara and N. Nakamura, *ibid.*, **46**, 94 (1973).

3) H. Chihara and K. Masukane, *J. Chem. Phys.*, to be published.

4) H. Chihara and M. Nakamura, This Bulletin, **45**, 133 (1972).

5) T. Atake and H. Chihara, *J. Chem. Thermodynamics*, **3**, 51 (1971).

6) The values refer to one mole of P_2Cl_{10}.

TABLE 1. HEAT CAPACITY OF SOLID P_2Cl_{10} (Sample I).
(Weight of sample 54.241 g, Molecular weight 416.48)

T/K	C_p/J K^{-1} mol^{-1}	T/K	C_p/J K^{-1} mol^{-1}	T/K	C_p/J K^{-1} mol^{-1}	T/K	C_p/J K^{-1} mol^{-1}
Series I		45.392	88.39	96.505	164.01	99.500	166.72
12.257	13.44	47.368	91.48	97.527	165.22	100.110	168.23
13.420	16.46	49.311	94.75	98.542	166.48	100.716	169.22
14.282	18.71	51.297	97.95	99.551	167.60	101.321	169.29
14.661	20.19	53.229	101.30	100.556	168.78	101.924	170.03
15.468	22.42	55.271	104.69	101.554	169.62	102.526	170.37
16.261	24.76	Series III		102.563	170.40	103.126	170.96
16.980	26.73	56.959	106.85	103.585	170.99	103.725	170.98
17.803	28.96	59.016	110.52	104.610	171.43	104.310	171.21
18.718	31.76	61.006	113.55	Series V		104.906	171.71
19.663	34.42	62.995	116.09	103.980	171.06	105.509	171.77
20.708	37.21	64.988	119.27	104.992	171.57	106.118	172.81
21.770	40.07	66.987	122.04	106.001	172.48	106.726	172.71
22.825	42.88	68.982	124.89	107.005	172.89	107.333	172.91
Series II		70.976	127.63	108.006	173.70	107.946	173.26
21.561	39.67	72.958	130.50	109.003	174.34	108.556	174.44
22.669	42.58	74.959	133.40	110.489	175.91	Series VII	
23.599	44.97	77.035	136.51	112.457	177.43	4.590	0.649
24.602	47.73	79.194	139.69	114.408	179.70	5.379	0.910
25.511	49.77	Series IV		116.376	181.02	5.685	1.231
26.465	52.03	80.676	141.81	118.359	182.77	5.959	1.636
26.831	52.72	82.827	144.82	120.325	184.63	6.568	2.185
28.485	56.91	84.939	148.30	122.277	186.30	7.368	3.212
30.250	60.59	87.043	151.42	124.248	187.59	7.949	4.114
32.126	64.59	89.147	154.18	126.236	189.80	8.588	5.184
33.793	67.88	89.817	155.07	128.209	191.55	9.387	6.648
34.873	70.13	91.371	157.06	130.200	193.25	10.275	8.581
36.755	73.80	92.395	158.70	132.209	195.05	11.133	10.573
38.854	77.27	93.414	159.28	134.216	197.11	11.934	12.523
41.155	81.22	94.443	161.21	Series VI		12.895	15.067
43.327	84.87	95.478	162.60	99.023	166.16	14.017	18.553

TABLE 2. HEAT CAPACITY OF SOLID P_2Cl_{10} (Sample II).
(Weight of sample 40.053 g, Molecular weight 416.48)

T/K	C_p/J K^{-1} mol^{-1}	T/K	C_p/J K^{-1} mol^{-1}	T/K	C_p/J K^{-1} mol^{-1}	T/K	C_p/J K^{-1} mol^{-1}
Series I		84.060	148.05	106.546	172.88	147.729	208.05
55.067	103.87	85.098	149.44	Series III		149.821	209.56
56.212	105.70	86.129	151.20	105.783	172.66	Series IV	
57.337	107.50	87.150	152.75	106.675	172.51	94.595	163.40
58.507	109.27	88.162	154.48	107.608	173.24	95.556	165.12
59.725	111.22	89.168	155.68	108.525	173.61	96.510	167.08
60.988	113.29	90.166	157.22	109.516	174.21	97.458	167.92
62.293	115.35	91.158	158.60	110.532	175.08	98.400	169.73
63.579	117.27	92.143	160.10	111.543	176.27	99.149	171.16
64.844	119.37	93.122	161.41	112.701	177.07	99.713	172.24
66.089	120.91	94.046	162.49	113.954	178.32	100.270	172.96
67.317	123.02	94.867	164.02	115.329	179.60	100.827	173.82
68.528	124.66	95.636	165.22	116.826	180.95	101.334	174.51
69.607	126.40	96.403	166.81	118.315	182.18	101.793	174.94
70.614	127.78	97.163	167.89	119.796	183.69	102.252	175.33
71.611	129.33	97.921	169.10	121.437	185.37	102.665	175.53
72.540	130.44	98.674	170.14	123.237	186.94	103.031	175.34
73.464	131.68	99.424	171.53	125.027	188.00	103.444	174.89
74.440	133.28	100.170	172.92	126.806	190.10	103.951	173.73
75.460	134.71	100.912	173.92	128.574	191.62	104.505	172.86
Series II		101.652	174.79	130.567	193.32	105.057	172.91
75.398	134.19	102.297	175.52	132.775	195.29	105.608	172.87
76.520	136.51	102.849	175.49	134.962	197.32	106.251	172.89
77.630	137.81	103.402	174.66	137.132	199.16	106.995	173.02
78.728	139.56	103.957	173.93	139.283	201.11	107.750	173.37
79.816	141.20	104.511	173.20	141.421	203.05	108.493	173.59
80.893	142.86	105.111	172.77	143.548	205.00	109.223	174.13
81.959	144.55	105.806	172.77	145.643	206.13	109.942	174.28
83.015	146.28						

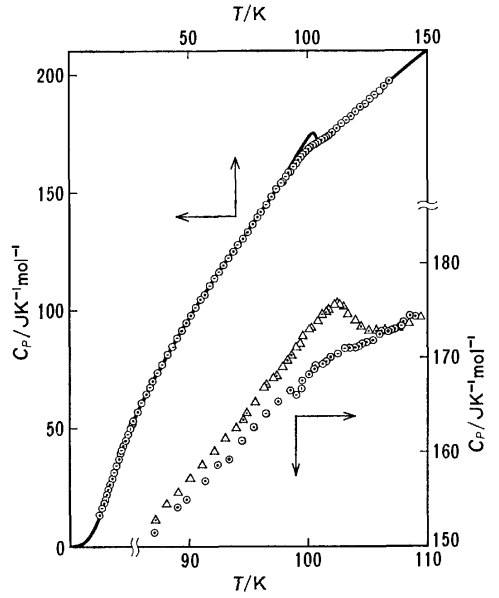

Fig. 1. Molar heat capacity of solid P_2Cl_{10}; ⊙ Sample I, △ Sample II; Solid curve above 50 K represents the result for Sample II.

capacity has nowhere a negative temperature coefficient, while the Sample II heat capacity shows a broad but distinct maximum at about 102 K. The behavior of the former is quite unlike the preliminary results obtained by use of a smaller calorimeter.[1] This is why we redetermined the heat capacities with the use of Sample II after about three years. In the following, we will use only the results of Sample II in discussing the effect of phase transition.

Table 3. Fundamental intra-ionic vibrations in P_2Cl_{10} (after Carlson).

Ion	Wave number/cm^{-1} (degeneracy)	Symmetry	Description
PCl_6^-	360 (1)	a_{1g}	P–Cl stretch
	281 (2)	e_g	P–Cl stretch
	449 (3)	f_{1u}	P–Cl stretch
	62 (3)	f_{1u}	Deformation
	150 (3)	f_{2g}	Deformation
	— (3)	f_{2u}	Deformation
PCl_4^+	459 (1)	a_1	P–Cl sym. stretch
	171 (2)	e	P–Cl sym. bend
	658 (3)	f_2	Degenerate stretch
	252 (3)	f_2	Degenerate bend

Separation of Anomalous Part of Heat Capacity. In order to amplify the extra heat capacity associated with the phase transition, contributions from the intra-ionic oscillations were calculated by the Einstein approximation and subtracted from the measured heat capacity values because all these contributions combined were expected to give a monotonous temperature dependence. Table 3 lists the relevant information on

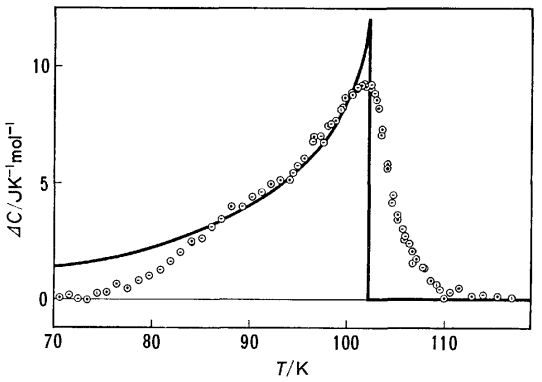

Fig. 2. Anomalous part of the heat capacity (Sample II). Solid curve represents Eq. (1) with α–β–m=0.5 as parameters determined by nuclear quadruplle resonance.

Table 4. Estimates of 'normal heat capacity' in the transition region

T/K	C_p/J K^{-1} mol^{-1}	T/K	C_p/J K^{-1} mol^{1}
70	126.9	100	163.5
76	135.2	106	170.2
82	143.0	112	176.1
88	150.6	118	181.0
94	157.4		

the vibrational spectra of PCl_4^+ cation having T_d symmetry and of PCl_6^- anion having O_h symmetry according to Carlson.[7] The wave numbers given in Table 3 are those at room temperature. We assumed that they do not change with temperature. Such contributions[8] having been subtracted, the residual heat capacity values were plotted on a large graph paper and a smooth 'normal' heat capacity curve was drawn to obtain the anomalous part, which is shown in Fig. 2. Estimates of the 'normal' heat capacity (including intra-ionic contributions) are given in Table 4. We see from Fig. 2 that the maximum extra heat capacity is 9.12 ± 0.08 J K^{-1} mol^{-1} at 102.0 ± 0.2 K,[9] the transition point being slightly lower than that determined from Fig. 1. The anomaly starts at about 75 K, gradually rises to maximum over a range of 27 K, and tails off at about 110 K. A shoulder centering at 90 K in Fig. 2 is not considered to be real but is probably due to some inadequacy in the tempreature scale. Since the temperature increments used in the measurements are about 0.6 K in the vicinity of the maximum, the transition is apparently of higher order than the second order transition in the Ehrenfest definition.[10] The heat of transition is 148 ± 3 Jmol^{-1} and the entropy of transition is 1.67 ± 0.03 J K^{-1} mol^{-1}.

Comparison with the Soft-mode Theory. As discussed

7) G. L. Carlson, *Spectrochim. Acta*, **19**, 1291 (1963).

8) The heat capacities corresponding to ν=62 cm^{-1} (f_{1u}) and to an unknown frequency (f_{2u}) were not taken into account for the reason discussed earlier.[1]

9) Extrapolation of the order parameter to zero gives 103~0.6 K as determined by quadrupole resonance but the difference is considered trivial.

10) From nuclear quadrupole resonance study,[2] symmetry elements appear abruptly at the transition and thus this is a second-order transition according to Landau's classification.[11]

11) L. Tisza, "On the General Theory of Phase Transitions" in "Phase Transformations in Solids" edited by R. Smoluchowski, *et al.*, John Wiley & Sons, Inc., New York, (1951).

in the preceding paper,[2] the transition in P_2Cl_{10} is related to a cooperative change in the orientation θ of the figure axis of PCl_6^- anions. The broad nature of the transition as well as the very small entropy of transition suggest that it is due to a kind of soft librational mode for which a simple theory has been developed.[12] By use of Eq. (4) of the preceding paper, we have

$$\Delta C = -Nk\frac{\alpha s x}{2\sinh^2(x/2)}\cdot\frac{ds}{dt},$$

where

$$x = (1+\alpha s^2)/t$$

and

$$\frac{ds}{dt} = \frac{\alpha x/2s}{\alpha^2 - 8\beta t\{m+(1-2m)s^2\}\sinh^2(x/2)}.$$

The significance of the parameters is the same as in Ref. 2. Numerical calculation of the excess heat capacity ΔC was made by using the parameter values

$$\alpha = \beta = m = 0.5$$

which give the best fit to the temperature dependence of the order parameter s as shown in Fig. 2 of Ref. 2. The result is shown in Fig. 2 by a solid curve. The theoretical curve, which was scaled down by a factor of 0.668, reproduces the important portion of the experimental ΔC. In view of the difficulty in estimating the 'normal' heat capacity values particularly below 90 K, the agreement between theory and experiment is considered excellent below the transition point. The scaling factor may be interpreted as indicating that only such librational modes that have small k, the wave vector, can couple with the uniform mode. Lack of agreement above the transition point is obviously due to inadequacy of the theory and may suggest the existence of some other lattice vibrational modes that play an important role in the transition phenomenon.

The authors would like to thank Mr. Tooru Atake for technical assistance during the course of this investigation.

12) H. Chihara, N. Nakamura, and M. Tachiki, *J. Chem. Phys.*, **54**, 3640 (1971).

BULLETIN OF THE CHEMICAL SOCIETY OF JAPAN, VOL. 46, 100—103 (1973)

The Second CMC of an Aqueous Solution of Sodium Dodecyl Sulfate. IV. Fluorescence Depolarization

Yukio KUBOTA, Michiko KODAMA,* and Masaji MIURA*

Department of Chemistry, Yamaguchi University, Yamaguchi

**Department of Chemistry, Faculty of Science, Hiroshima University, Higashisenda-machi, Hiroshima*

(Received June 20, 1972)

The depolarization of the fluorescence emitted from a dye solubilized in the micelle was measured over a wide concentration range of sodium dodecyl sulfate (SDS). The polarization of the fluorescence showed an abrupt increase at the 1st CMC and at about 70 mM of SDS; the latter agrees very closely with the 2nd CMC revealed by conductivity and viscosity measurements. This phenomenon implies that there is a certain change in the micelle structure at the 2nd CMC. The micellar size was calculated from the fluorescence depolarization data using Perrin's equation. The results showed that: (1) the micellar volume below the 2nd CMC is in good agreement with that determined by light-scattering, (2) the micellar volume gradually increases with an increase in the concentration of SDS, and (3) the micellar volume increases abruptly at the 2nd CMC.

In our previous papers, the micelle structure of aqueous solutions of sodium dodecyl sulfate (SDS) was investigated by systematic studies including measurements of the conductivity,[1] the density,[2] the viscosity,[2] and the light-scattering.[3] It was revealed by these measurements that, in addition to the 1st critical micelle concentration (CMC), there exists a 2nd CMC, where a change in the micelle structure takes place. Further, the viscosity and light-scattering measurements suggested that the size of the micelle increases at the 2nd CMC.

The micellar sizes of the surfactants in the neighborhood of the 1st CMC have been determined by such methods as light-scattering and osmotic pressures. However, little is known about the micellar size in the high-concentration region because some complications arise upon the application of the above methods to a concentrated solution.[4] Since the theoretical basis of the fluorescence depolarization method has been established by Perrin,[5,6] it has been used successfully in the study of the Brownian motion of a macromolecule in solution.[7-9] This method will provide a powerful tool for the determination of the size of a micelle if we obtain a suitable fluorescent molecule which can tightly

1) M. Miura and M. Kodama, This Bulletin, **45**, 428 (1972).
2) M. Kodama and M. Miura, *ibid.*, **45**, 2265 (1972).
3) M. Kodama, U. Kubota, and M. Miura. *ibid.*, **45**, 2953 (1972).
4) N. Sata and K. Tyuzyo, *ibid.*, **26**, 177 (1953).
5) F. Perrin, *J. Phys. Radium*, [VI], **7**, 390 (1926).
6) F. Perrin, *Ann. Phys.*, [X], **12**, 69 (1929).
7) G. Weber, *Biochem. J.*, **51**, 145, 155 (1952).
8) G. Weber, *Advan. Protein Chem.*, **8**, 447 (1953).
9) R. F. Steiner and H. Edelhoch, *Chem. Rev.*, **62**, 457 (1962).

combine with the micelle.[10-12] Very recently, we succeeded in preparing a derivative of acridine orange (AO) which possesses a dodecyl group; this dye can be expected to bind firmly to the SDS micelle, because the dye molecule has a long hydrocarbon chain and its charge is opposite to that of the micelle. The present paper will report some information about the size of the SDS micelle, particularly in the high-concentration region above the 2nd CMC.

Experimental

Materials. The SDS used in this study was the same as that described in a previous paper.[1] AO-10-dodecyl bromide (Fig. 1) was prepared by modifying the method of Miethke and Zanker;[13] a mixture of AO and 1-bromododecane (ten times the molar quantity of AO) was heated in an oil bath at 110—120°C for 12 hr. The dye thus produced was recrystallized from ethanol–ether and then subjected twice to chromatography on alumina, using ethanol as the eluent.

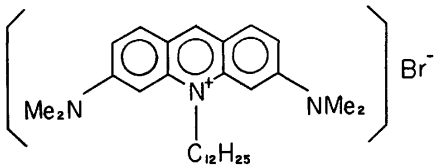

Fig. 1. AO-10-dodecyl bromide.

Methods. The absorption spectra were recorded with a Hitachi ESP-3T spectrophotometer.

The fluorescence spectra were measured with a Hitachi MPF-2A fluorescence spectrophotometer, using an R-106 photomultiplier. They were corrected for the spectral sensitivity of an optical system consisting of lenses, a monochromator, and a photomultiplier.

The degree of polarization of the fluorescence light (P) was measured with a Shimadzu light-scattering photometer equipped with a pair of polaroid dichroic filters to serve as the polarizer as well as the analyzer, and with suitable filters for the incident and fluorescence lights. A 436 nm mercury line was used as the exciting light; it was plane-polarized. The value of P was calculated by means of the following equation:

$$P = (I_{//} - I_{\perp})/(I_{//} + I_{\perp}) \quad (1)$$

where $I_{//}$ and $I_{\perp}$ are, respectively, the components of the fluorescence light parallel to and perpendicular to the direction of the polarization of the exciting light.

The fluorescence lifetimes were measured by means of a JASCO FL-10 phase fluorometer.[14]

All the measurements were carried out at temperatures from 17 to 40°C for SDS solutions containing constant amounts of the dye, (1—2.0)$\times 10^{-6}$M. In order to control the temperature of the solution, water from a thermostat was circulated through a water jacket surrounding the cell; the temperature was measured with a calibrated thermistor. One-centimeter quartz cells were used in all the measurements.

10) L. Arkin and C. R. Singleterry, *J. Amer. Chem. Soc.*, **70**, 3965 (1948).
11) C. R. Singleterry and L. A. Weinberger, *ibid.*, **73**, 4574 (1951).
12) S. Kaufman and C. R. Singleterry, *J. Colloid Sci.*, **7**, 453 (1952); **10**, 139 (1955); **12**, 465 (1957).
13) E. Miethke and V. Zanker, *Z. Physik. Chem. N. F.*, **18**, 375 (1958).
14) *Jasco Report*, **7**, 156, 187 (1970).

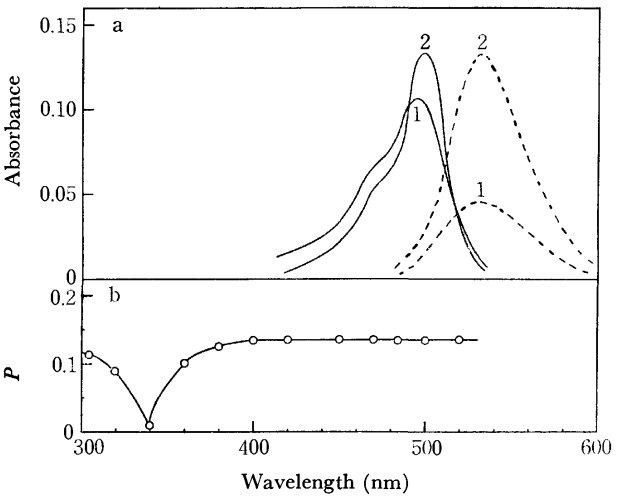

Fig. 2. Absorption (—), fluorescence (---), and fluorescence-polarization (-o-) spectra of the SDS-dye systems in aqueous solutions at 25°C. Fluorescence spectra were obtained with excitation at 460 nm. Fluorescence spectrum (1) is enlarged to a scale 10 times that of (2).
1: dye only (1.59×10^{-6} M), 2: SDS (0.1 M)

Results and Discussion

Figure 2 shows some typical findings on the absorption and fluorescence spectra of the SDS-dye systems. As may be noted from Fig. 2a, there occurred a many-fold enhancement in the fluorescence intensity of the dye above the 1st CMC. In addition, the dye fluorescence in the SDS solutions above the 1st CMC was markedly polarized (Fig. 2b), though that in water showed no polarization. The absorption spectra of the dye in SDS solutions had a peak at 500 nm corresponding to a monomeric species of the dye; this peak was shifted by a few nm towards longer wavelengths compared with that in water (Fig. 2a). The absorbance at 500 nm is plotted against the concentration of SDS in Fig. 3; the absorbance increases abruptly at about the 1st CMC, and then remains constant above that point. These spectral phenomena are rather common results in studies of the association of the dye with the micelle[10,11] and may imply that most of the dye molecules are tightly solubilized in the SDS micelles as a monomeric form. Hence, it is expected that the

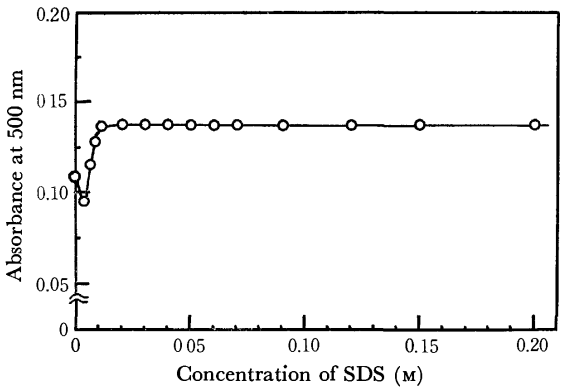

Fig. 3. Absorbance of the SDS-dye systems at 500 nm as a function of the concentration of SDS at 25°C.
Dye concn.: 20×10^{-6}M

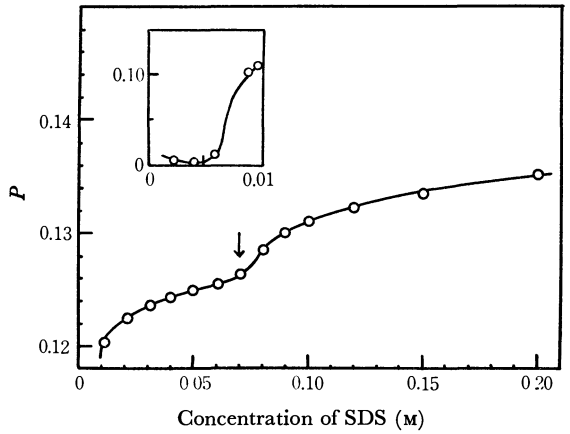

Fig. 4. A plot of the P value against the concentration of SDS at 25°C. The result in the neighborhood of the 1st CMC is shown under enlargement.

value of P reflects exactly the Brownian rotation of the SDS micelle in the solution.[10,11]

Figure 4 shows the relation between the P value and the concentration of SDS at 25°C. It may be seen in Fig. 4 that the P value increases abruptly at the 1st CMC and, in addition, at about 70 mM of SDS; the latter agrees very closely with the 2nd CMC revealed by other measurements.[1-3] This phenomenon may be attributed to a certain change in the micelle structure at the 2nd CMC.

According to Perrin,[5,6] the P value is related to the molar volume of the fluorescent molecule (V) by the following equation, on the assumption that the molecule undergoing rotation is spherical:

$$1/P - 1/3 = (1/P_0 - 1/3)(1+\tau RT/\eta V) \qquad (2)$$

where P_0 is the limiting value of P when $T/\eta=0$; R, the gas constant; T, the absolute temperature; τ, the lifetime of the fluorescence, and η, the viscosity of the solvent. The rotational relaxation time of this molecule (ρ) equals $3V\eta/RT$. In the micelle-dye systems, V in Eq. (2) is taken as the effective volume of the micelle in which the dye is solubilized.

The V value is dependent not only on the measured values of P, η, and T, but also on the values of τ and P_0. Singleterry *et al.*[10-12] developed an elegant technique for the determination of the effective micellar volume from the fluorescence-depolarization data. Their method, however, was incomplete because the fluorescence lifetimes had never been measured directly. In the present study, the values of τ in the SDS-dye systems were determined directly by means of a phase fluorometer.[14] The results at 25°C were as follows: (1) τ in water was 0.37 nsec and (2) τ in SDS solutions was constant (2.0 nsec) over a wide concentration range above the 1st CMC. According to Eq. (2), a straight line which cuts the $1/P$ axis at $1/P_0$ should be obtained when $1/P$ is plotted against T/η. Thus, the values of P_0 in the SDS-dye systems were determined experimentally by measuring the P value in the temperature range from 17 to 40°C and by then extrapolating the straight line to $T/\eta=0$. Some results are shown in Fig. 5, where the plots of $1/P$ *vs.* T/η at each concentration of SDS give the concordant value of $P_0=0.167$.

The effective micellar volumes of SDS at 25°C were calculated by introducing the quantities obtained above into Eq. (2), on the assumption that the micelle is spherical. In view of the findings on small-angle X-ray

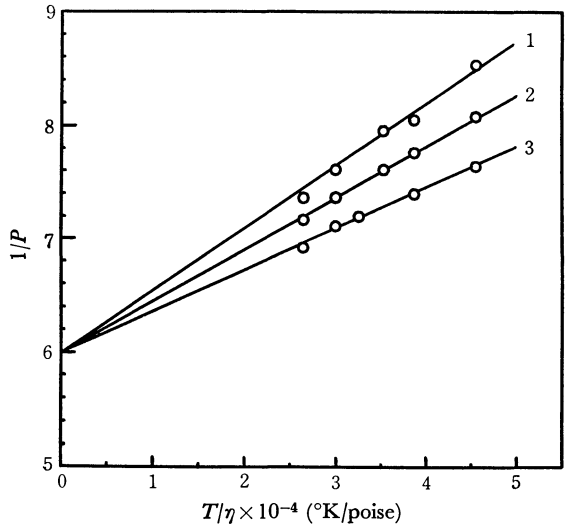

Fig. 5. Typical plots of $1/P$ *vs.* T/η for the SDS-dye systems at 25°C.
Dye concn.: 1.59×10^{-6}M
SDS concn.: 1: 0.05M, 2: 0.10M, 3: 0.20M

TABLE 1. DEPOLARIZATION RESULTS OF THE SDS–DYE SYSTEMS AT 25°C

SDS concn. (M)	P	ρ (nsec)	V (ml per gram micelle)
0.04	0.124_5	16.7	15400
0.05	0.125	17.0	15700
0.06	0.125_5	17.3	16000
0.07	0.126_5	17.8	16500
0.08	0.128	19.1	17700
0.09	0.130	19.9	18400
0.10	0.131	20.4	18800
0.12	0.132	21.4	19800
0.15	0.133	22.7	21000
0.20	0.135	23.9	22000

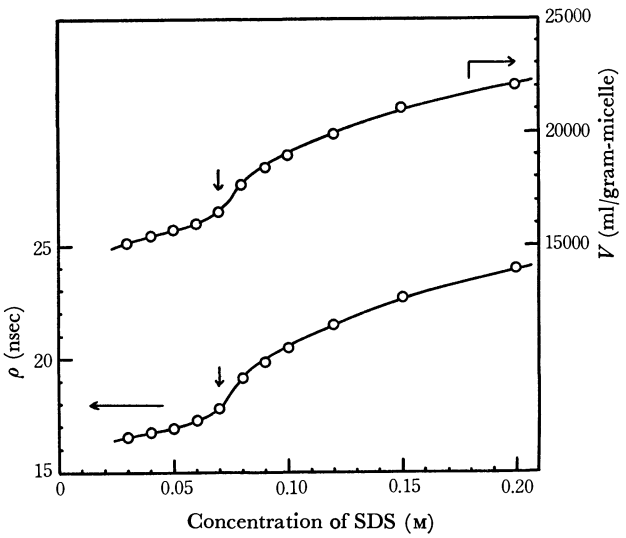

Fig. 6. Plots of ρ and V against the concentration of SDS at 25°C.

scattering,[15,16] this assumption seems reasonable in the concentration range investigated. The results are summarized in Table 1, where ρ and V represent, respectively, the rotational relaxation time of the micelle and the effective micellar volume. Figure 6 shows plots of ρ and V against the concentration of SDS. The depolarization results presented in Table 1 and Fig. 6 can be summarized as follows:

(1) The micellar volumes below the 2nd CMC range from 15500 to 16000 ml/gram-micelle.

(2) The micellar volume increases gradually with an increase in the concentration of SDS below the 2nd CMC.

(3) The micellar volume increases abruptly at the 2nd CMC, and then it increases again gradually with the comcentration.

The micellar density was estimated to be 1.09 g/ml by using the density data[2] obtained according to the method of Mukerjee.[17] Therefore, the micellar weight below the 2nd CMC becomes $(169—174)\times10^2$, which is in good agreement with the value (170×10^2) obtained by light-scattering measurements.[3] This agreement seems to confirm the assumption that the dye has no freedom of rotation with respect to the micelle in which the dye is solubilized. This may be caused by the firm binding of the dye to the SDS micelle, since the dye molecule has not only a charge opposite to the micelle, but also a long hydrocarbon chain. It can be concluded, therefore, that the depolarization of fluorescence observed reflects correctly the Brownian rotation of the SDS micelle and that the fluorescence depolarization method provides a direct means for the determination of the micellar size over a wide concentration range of SDS.

Evidence (2) is consistent with the studies of other investigators;[15,16,18-22] they showed that the micellar size increases with the concentration of the surfactant.

Evidence (3) is a fact which has newly observed in the case of SDS. This fact accounts well for the results of light-scattering, *i.e.*, the marked rise in the reduced intensities at the 2nd CMC. The reason why the micellar volume increases abruptly at the 2nd CMC is still not clear, however; this subject will be dealt with in the future.

15) F. Reiss-Husson and V. Luzzati, *J. Phys. Chem.*, **68**, 3504 (1964).
16) F. Reiss-Husson and V. Luzzati, *J. Colloid Interface Sci.*, **21**, 534 (1966).
17) P. Mukerjee, *J. Phys. Chem.*, **66**, 1733 (1962).
18) R. W. Matton, R. S. Stears, and W. D. Harkins, *J. Chem. Phys.*, **16**, 644 (1948).
19) H. A. Sheraga and J. K. Backus, *J. Amer. Chem. Soc.*, **73**, 5108 (1951).
20) K. Herrmann, *J. Phys. Chem.* **68**, 1540 (1964).
21) D. C. Robins and I. L. Thomas, *J. Colloid Interface Sci.*, **26**, 415 (1968).
22) P. Ekwall, L. Mandell, and P. Solyom, *ibid.*, **35**, 519 (1971).

BULLETIN OF THE CHEMICAL SOCIETY OF JAPAN, VOL. 46, 103—106 (1973)

Low-frequency Lattice Vibrations and Intermolecular Forces of the 9,10-Anthraquinone Crystal

Yoshio MIYAZAKI and Mitsuo ITO

Department of Chemistry, Faculty of Science, Tohoku University, Aramaki, Sendai

(Received July 4, 1972)

The low-frequency Raman active lattice vibrations of the 9,10-anthraquinone single crystal were measured at various temperatures from 26°C to −190°C, and the symmetry species of the observed Raman bands were determined by polarization measurements. From a comparison between the observed and calculated frequencies, it seems that Dashevsky's potential expresses well the intermolecular potential of the 9,10-anthraquinone crystal. It was also found that the temperature dependence of lattice vibrations can be explained reasonably with this potential.

The lattice vibrations of molecular crystals have attracted great attention because of their importance in the elucidation of the intermolecular potentials in crystals. One of the most important characteristics of the low-frequency lattice vibrations of molecular crystals is the great dependence of the frequencies upon the temperature. The frequency shifts due to changes in the temperature are generally different for different lattice vibrations; they often amount to 20—30% of the frequencies in the region from room temperature to the temperature of liquid nitrogen. These characteristics may be utilized in the study of the intermolecular potentials. Unfortunately, however, in molecular crystals it is very seldom that crystal structures at various temperatures over a wide range are well known in detail. For this reason, the highly useful experimental data of the effects of the temperature have been neglected.

One of the crystals whose structures have been determined at various temperatures over a wide range is the 9,10-anthraquinone crystal; Lonsdale *et al.* have reported the crystal structures at 20.5, −12.5, −72, −112, and −170°C.[1] It is, therefore, a good example

1) K. Lonsdale, H. J. Milledge, and K. El Sayed, *Acta, Crystallogr.*, **20**, 1 (1966).

Table 1. Observed lattice vibrations of 9,10-Anthraquinone (cm^{-1})

−190°C	−165°C	−145°C	−122°C	−88°C	−54°C	−27°C	0°C	26°C	Assign.
73	73	73	73	72	71	69	68	66	A_g
63	63	62	62	60	58	57	56	51	A_g
36	36	35	35	32	32	30	29	27	A_g
92	91	91	90	89	87	86	84	82	B_g
63	63	62	61	60	60	60	58	57	B_g

for use in testing the intermolecular potentials at various temperatures.

In the present experiment, the polarized Raman spectra of the low-frequency lattice vibrations of the single crystal of 9,10-anthraquinone were measured at various temperatures, and assignments of the observed Raman bands were given. The results obtained were then used to examine the intermolecular potentials proposed by various authors.

Experimental

9,10-Anthraquinone was purified by repeated zone refinements, and the single crystal was grown by Bridgman's method. The single crystal used in the Raman measurements was about $4\times5\times8$ mm, one of the edges of the crystal being parallel to the crystallographic b axis, which was determined by taking oscillation X-ray photographs.

The optical arrangement for the measurement of the polarized Raman spectra is almost the same as that reported previously.[2] A He-Ne gas laser of 6328 Å (Japan Electron Optics Laboratory Co., 50 mW) and a Nalumi model 750 Z-1200 double monochromator combined with a cooled head-on-type photomultiplier tube, followed by a photon-counting detector, were used for taking the Raman spectra.

The temperature of the single crystal was controlled in the region between room temperature and −190°C by regulating the flow speed of cooled nitrogen gas introduced into a cryostat. Even at the lowest temperature, no cracking of the crystal occurred, so the polarization experiments were carried out successively.

Results and Assignments

The crystal structure of 9,10-anthraquinone belongs to a monoclinic system, space group C_{2h}^5—$P2_1/a$, and it contains two molecules in a unit cell.[1] The optically-active lattice vibrations can therefore be divided into two parts; six librational modes ($3A_g+3B_g$) and three translational modes ($2A_u+B_u$). The vibrations of the g species are active only in the Raman spectrum, while those of the u species are active only in the infrared spectrum. The three A_g and three B_g Raman active lattice vibrations should be differentiated by means of a polarization experiment; that is, when the single crystal is excited by incident light polarized parallel to the b axis of the crystal, the Raman lines of the A_g and B_g vibrations should appear in the spectra of the $b_{//}$ and $b_{\perp}$ components of the scattered light respectively. Figure 1 shows typical spectra obtained in this way at 26 and −122°C. It may be seen that all the Raman lines except one of the B_g species are clearly identified.

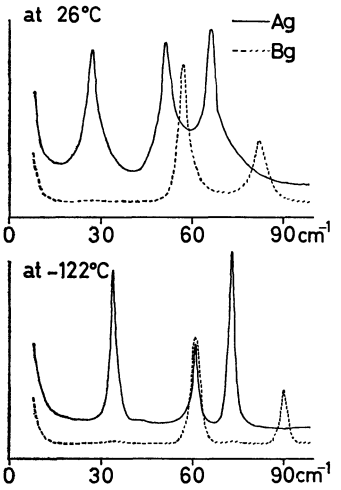

Fig. 1. Polarized Raman spectra of 9,10-anthraquinone single crystal.

The frequencies observed at various temperatures are summarized in Table 1, together with their assignments.

A Raman line of 115 cm^{-1} has been reported in the Raman measurement at room temperature by Singh *et al.*,[3] who assigned it to the lattice vibration. In our measurements, however, we were unable to find any Raman lines in the neighbourhood of 115 cm^{-1}. Instead, we found a weak Raman line at 148 cm^{-1}, which appears preferentially in the B_g spectrum. It is probably due to the combination band of 66 cm^{-1} (A_g) and 82 cm^{-1} (B_g).

Calculation of Lattice Vibrations

The calculation of lattice vibrations was performed in a rigid-body approximation according to the **GF** matrix method developed by Shimanouchi *et al.*[4,5] The intermolecular potential used was approximated by the sum of the atom-atom pair-by-pair potentials of the form:

$$V(r) = -Ar^{-6} + B\exp(-Cr),$$

where r is the interatomic distance and where A, B, and C are constants characteristic of the kind of atom pair. The potential of this type has often been used with great success in the calculation of many properties of molecular crystals, such as lattice vibrations, specific heat, and elastic constants.

We employed several sets of values of A, B, and C as proposed by different authors for the H···H and

2) M. Suzuki, T. Yokoyama, and M. Ito, *Spectrochim. Acta*, **24A**, 1091 (1968).

3) S. N. Singh and R. S. Singh, *ibid.*, **24A**, 1591 (1968).

4) T. Shimanouchi, M. Tsuboi, and T. Miyazawa, *J. Chem. Phys.*, **35**, 1597 (1961).

5) T. Shimanouchi and I. Harada, *ibid.*, **41**, 2651 (1964).

Table 2. Parameters in atom-atom potentials

		Ste I	Set II	Set III	Set IV
H···H	*A*	2.501	0.3960	0.3420	0.1487
	B	27.79	291.8	45.80	63.15
	C	3.740	4.860	4.082	4.640
C···C	*A*	3.717	2.487	2.390	3.293
	B	517.3	291.8	272.0	261.9
	C	3.600	3.580	3.546	3.520
O···O	*A*	2.459	2.459	2.459	2.459
	B	670.4	670.4	670.4	670.4
	C	4.330	4.330	4.330	4.330

A: units of mdyn. Å^7 *B*: mdyn. Å *C*: Å^{-1}

C···C atom pairs; they are the values proposed by Williams[6] (Set I), Kitaigorodsky[7] (Set II), Bartell-Crowell[8] (Set III), and Dashevsky *et al.*[9] (Set IV). For O···O, the values given by Dashevsky *et al.*[9] were always used. The values of *A*, *B*, and *C* used in the calculations are summarized in Table 2. The values for the heteroatom pairs were taken as follows;

$$A_{ab} = \sqrt{A_{aa} \times A_{bb}},$$
$$B_{ab} = \sqrt{B_{aa} \times B_{bb}},$$
$$C_{ab} = (C_{aa} + C_{bb})/2$$

for a···b.

The crystal structures of 9,10-anthraquinone at 20.5, −12.5, −72, −112, and −170°C have been reported by Lonsdale *et al.*[1] Therefore, the calculations were made for the structures at these temperatures by taking account of all the interactions of interatomic distances shorter than 3.2, 3.5, 3.5, 3.6, 4.0, and 4.1 Å for H···H, H···O, H···C, O···C, O···O, and C···C respectively. These limits were selected for the following reasons: (1) For the distances over these limits, the force constants are generally very small, (2) the numbers of the atom pairs to be included are almost the same over the range from 20.5°C to −170°C, and (3) when the limits of interactions are extended to 4.5 Å, the number of the atom pairs to be included increases about twice, but the calculated frequencies and eigen vectors change only a little.

Table 3. Observed and calculated frequencies at 20.5°C (cm^{-1})

	Set I	Set II	Set III	Set IV	Obsd[a]
A_g	124	117	102	73	66
	88	72	71	52	52
	53	38	40	30	28
B_g	133	123	109	77	73
	104	94	86	62	58
	83	71	68	50	—

a) Interpolated values to 20.5°C from Table 1.

The frequencies of lattice vibrations calculated under the above restrictions are given in Table 3. It may be seen that the calculated frequencies with the potentials of Set IV agree reasonably with the observed Raman frequencies, while the potentials of the other sets give higher frequencies. In Table 4, the frequencies obtained with the potentials of Set IV and the atomic coordinates at various temperatures are listed, together with the approximate vibration modes for 20.5°C.

Discussion

In the preceding section, we noted a great difference in the calculated frequencies between the potentials of Set I—III and Set IV. An inspection of the crystal structures shows that there exist interatomic pairs involving hydrogen atoms of short distances. Especially, we have a very short H···H distance of 2.2 Å, and found that the great difference in the calculated frequencies is mainly to be ascribed to the difference in the potentials of the H···H pair (and thereby of the H···C and H···O pairs) in the region of the short distances.

Beside the calculated lattice vibrational frequencies, their dependences upon the temperature provide a good check to see which potentials are more realistic. The observed and calculated frequency shifts of the indi-

Table 4. Calculated values with Set IV at various temperatures (cm^{-1})

	−170°C	−112°C	−72°C	−12.5°C	20.5°C	Approx. modes[a, b]		
A_g	85	81	81	78	73	61% R_x,	36% R_y,	3% R_z
	62	59	57	53	52	2% R_x,	21% R_y,	77% R_z
	36	34	33	31	30	37% R_x,	43% R_y,	20% R_z
B_g	90	86	85	82	77	39% R_x,	60% R_y,	1% R_z
	67	67	65	63	62	30% R_x,	11% R_y,	59% R_z
	54	54	52	50	50	31% R_x,	29% R_y,	40% R_z

a) R_x means rotational oscillation around x axis of molecule, and so on.
b) x, y, and z axes are chosen as follows;

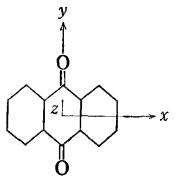

6) D. E. Williams, *J. Chem. Phys.*, **45**, 3770 (1966).
7) A. Kitaigorodsky, *J. Chim. Phys.*, **63**, 9 (1966).
8) Cited by D. A. Oliver and S. H. Walmsley, *Mol. Phys.*, **17**, 617 (1969).
9) V. G. Dashevsky, V. T. Struchykov, and Z. A. Akoppayan, *Zhr. Struk. Khim.*, **7**, 594 (1966).

TABLE 5. FREQUENCY SHIFTS BETWEEN 20.5°C AND −170°C (cm^{-1})

	Set I	Set II	Set III	Set IV	Obsd
A_g	17	19	15	12	8
	16	16	14	10	9
	7	6	6	6	8
B_g	19	20	16	13	8
	8	9	7	5	5
	7	7	6	4	—

vidual lattice vibrations between 20.5 and −170°C are given in Table 5. It may be seen that the calculated shifts with Set IV are of the same order of magnitude as the observed ones, while the calculated shifts with the other sets give larger shifts. This difference was found again to be ascribable mainly to the difference in H···H potentials in the region of short distances.

The fact that both the lattice vibrational frequencies and their shifts induced by the temperature change are well reproduced with the potentials of Set IV seems to indicate the preferability of the H···H potential of Set IV over those of the other sets, especially in the region of short interatomic distances.

BULLETIN OF THE CHEMICAL SOCIETY OF JAPAN, VOL. 46, 106—109 (1973)

Conductometric Determination of Ion-association Constants for Magnesium and Nickel Sulfates in Aqueous Solutions at Various Temperatures between 0°C and 45°C

Shunzo KATAYAMA

The Institute of Physical and Chemical Research, Hirosawa, Wako-shi, Saitama

(Received July 5, 1972)

Thermodynamic equilibrium constants for the ion-association in aqueous solutions of magnesium and nickel sulfates were determined by electrical conductivity measurements at various temperatures between 0°C and 45°C. The standard Gibbs energy and the enthalpy and entropy for the reaction $M^{2+}+SO_4^{2-} \rightleftharpoons M^{2+}\cdot SO_4^{2-}$ (M: Mg or Ni) were then calculated from the temperature-dependence of the ion-association constants. The values obtained are as follows: $\Delta G^\circ_{298} = -2.91$ kcal mol^{-1}, $\Delta H^\circ = 2.04$ kcal mol^{-1}, and $\Delta S^\circ_{298} = 16.6$ cal deg^{-1} mol^{-1} for $Mg^{2+}\cdot SO_4^{2-}$; and $\Delta G^\circ_{298} = -3.10$ kcal mol^{-1}, $\Delta H^\circ = 1.27$ kcal mol^{-1}, and $\Delta S^\circ_{298} = 14.7$ cal deg^{-1} mol^{-1} for $Ni^{2+}\cdot SO_4^{2-}$.

Different values are sometimes obtained for the formation constant of a given ion-pair when different experimental methods are used in its determination. For example, the formation constant of the ion-pair $[Co(NH_3)_6]^{3+}\cdot X^-$ (X: Cl, Br, I, NO_3) as determined by the spectroscopic method is significantly smaller than that determined by the conductometric method.[1,2] It is, thus, important to study whether such a discrepancy in the thermodynamic constant is attributable to the different working principles of various methods or simply to experimental errors.

This paper will deal with the conductometric determination of ion-association constants for magnesium and nickel sulfates in aqueous solutions at temperatures from 0 to 45°C. Except for a few investigations, the determination of ion-association constants has mostly been done at one particular temperature (say, 25°C). The temperature dependence of ion-association constants, however, is important because the standard enthalpies and entropies of ion-association will provide more useful information concerning the interaction between the ions than the formation constants at some fixed temperature.[3] The thermodynamic quantities determined by the present study are compared with the values obtained by Nair and Nancollas[4,5] by emf measurements, and also with the theoretical values based upon the electrostatic model of ion-pairs.

Experimental

Magnesium and nickel sulfates of an analytical reagent grade were recrystallized twice from conductivity water at a temperature between 10 and 20°C and then dried at room temperature. The purity of the samples was examined by a conventional chemical analysis of the components; the analysis gave results which were in good agreement with the theoretical values (Found: Mg^{2+}, 9.82; SO_4^{2-}, 38.93; H_2O, 51.20% for $MgSO_4\cdot 7H_2O$ and Ni^{2+}, 20.95; SO_4^{2-}, 34.39; H_2O, 44.73% for $NiSO_4\cdot 7H_2O$).

Solutions of different concentrations were carefully prepared by using conductivity water of a specific conductivity lower than 2.4×10^{-7} ohm^{-1} cm^{-1} at 25°C in an atmosphere of purified nitrogen gas.

The electrical conductivities at different temperatures were measured by the apparatus shown in Fig. 1. The apparatus consisted of the following two parts: (a) a deviation-linear-bridge operated at 1000 Hz which detected the difference in conductance between a conductivity cell and a given standard,

1) N. Tanaka, Y. Kobayashi, and M. Kamada, This Bulletin, **40**, 2839 (1967).
2) S. Katayama and R. Tamamushi, *ibid.*, **41**, 606 (1968).
3) J. E. Prue, *J. Chem. Educ.*, **46**, 12 (1969).
4) V. S. K. Nair and G. H. Nancollas, *J. Chem. Soc.*, **1958**, 3706.
5) V. S. K. Nair and G. H. Nancollas, *ibid.*, **1959**, 3934.

TABLE 1. EQUIVALENT CONDUCTIVITIES, Λ, OF $MgSO_4$ AND $NiSO_4$ IN AQUEOUS SOLUTIONS AT VARIOUS TEMPERATURES

Temp. (°C)	Concentration [mol/l]									
	0.0002	0.0003	0.0004	0.0005	0.0007	0.0010	0.0015	0.0020	0.0025	0.0030
					($MgSO_4$)					
0	63.40	62.20	61.15	60.25	58.70	56.84	54.55	52.75	51.23	50.04
5	74.12	72.68	71.44	70.37	68.55	66.41	63.66	61.53	59.75	58.33
10	85.55	83.85	82.38	81.09	78.97	76.50	73.31	70.83	68.80	67.11
15	97.49	95.53	93.84	92.33	89.90	87.05	83.37	80.42	78.15	76.24
20	110.10	107.81	105.89	104.18	101.32	98.15	93.93	90.58	87.95	85.76
25	123.29	120.65	118.49	116.58	113.35	109.69	104.93	101.23	98.14	95.69
30	137.34	134.24	131.63	129.50	125.95	121.85	116.32	112.12	108.67	105.90
35	151.32	148.05	145.22	142.68	138.71	134.12	127.93	123.23	119.38	116.30
40	166.62	162.95	159.55	156.73	152.00	146.77	139.87	134.65	130.37	126.94
45	181.83	177.70	173.94	170.82	165.60	159.80	152.09	146.28	141.50	137.79
					($NiSO_4$)					
0	63.22	61.78	60.63	59.59	57.89	55.85	53.23	51.20	49.58	48.19
5	73.85	72.15	70.80	69.59	67.57	65.18	62.10	59.71	57.82	56.18
10	85.20	83.21	81.64	80.21	77.86	75.07	71.50	68.72	66.52	64.62
15	97.06	94.72	92.90	91.27	88.57	85.36	81.25	78.07	75.55	73.35
20	109.50	106.90	104.78	102.91	99.80	96.14	91.46	87.83	84.96	82.47
25	122.56	119.60	117.20	115.07	111.54	107.38	102.08	97.97	94.74	91.92
30	136.11	132.78	130.08	127.69	123.73	119.03	113.06	108.39	104.79	101.64
35	150.06	146.34	143.28	140.62	136.20	130.93	124.24	119.04	115.01	111.50
40	164.51	160.34	156.98	153.96	149.06	143.18	135.75	129.92	125.43	121.55
45	179.55	174.92	171.12	167.69	162.28	155.72	147.59	140.93	136.03	131.71

(2) The starting approximation for γ is given by the classical Onsager equation:

$$\gamma_1 = \Lambda/[\Lambda_0 - S(c\cdot\Lambda/\Lambda_0)^{1/2}] \quad (8)$$

and higher approximations for the degree of dissociation, γ_i (i=2, 3, ···), are calculated by:

$$\gamma_i = \Lambda/[\Lambda_0 - S(c\gamma_{i-1})^{1/2} + Ec\gamma_{i-1}\log(c\gamma_{i-1}) + Jc\gamma_{i-1}] \quad (9)$$

(3) The mean activity coefficient, f, is estimated by means of the Debye-Hückel equation:

$$\log f = \frac{-Az^2\sqrt{I}}{1+Ba\sqrt{I}} \quad (10)$$

where z ($z=|z_+|=|z_-|$ for a symmetrical electrolyte) is the charge number; I, the ionic strength, and A and B, the theoretical coefficients.

All the calculations were performed on a FACOM 270-20/30 computer using a FORTRAN program.

Table 2 summarizes the values of Λ_0, K_A, and a thus determined for $MgSO_4$ and $NiSO_4$ at different temperatures. The K_A-values for $NiSO_4$ were larger than those for $MgSO_4$ at each temperature, while the temperature-coefficient of K_A for $NiSO_4$ was smaller than that for $MgSO_4$. The ion-size parameters for $NiSO_4$ and $MgSO_4$ were about 6 Å at temperatures ranging from 0 to 45°C. In Table 2, the present results are compared with the K_A values (shown in parentheses) obtained by Nair and Nancollas[4,5] using the emf method.

The standard enthalpy of association, $\Delta H°$, was determined from the linear plots of $\log K_A$ against T^{-1}, as is shown in Fig. 4, according to the relation:

$$d\ln K_A/d(1/T) = -\Delta H°/R \quad (11)$$

The standard Gibbs energy and the standard entropy of association, $\Delta G°$ and $\Delta S°$, were calculated by means of the well-known thermodynamic equations:

TABLE 2. LIMITING EQUIVALENT CONDUCTIVITIES, Λ_0, ION ASSOCIATION CONSTANTS, K_A, AND ION-SIZE PARAMETER, a, OF $MgSO_4$ AND $NiSO_4$ IN AQUEOUS SOLUTIONS AT VARIOUS TEMPERATURES

Temp. (°C)	Λ_0	K_A	a[Å]
		($MgSO_4$)	
0	68.15	103±1 (92±12)	5.59
5	79.75	108±1	5.71
10	92.15	116±2	5.87
15	105.15	121±2	5.95
20	118.90	129±2 (160±17)	6.09
25	133.30	135±2 (179±12)	6.18
30	148.70	147±5 (222±5)	6.29
35	164.15	151±3 (248±16)	6.30
40	181.20	167±4 (281±15)	6.33
45	198.05	175±3 (312±54)	6.33
		($NiSO_4$)	
0	68.40	156±3 (121±6)	5.86
5	80.00	162±3	6.06
10	92.40	168±3 (151±5)	6.14
15	105.40	176±4 (174±4)	6.33
20	119.10	183±3	6.38
25	133.45	187±3 (211±16)	6.28
30	148.40	191±3	6.22
35	163.90	201±3 (247±8)	6.30
40	180.00	209±4	6.31
45	196.85	217±3 (289±23)	6.27

(The values of K_A obtained by Nair and Nancollas from the emf measurement are shown in parentheses)

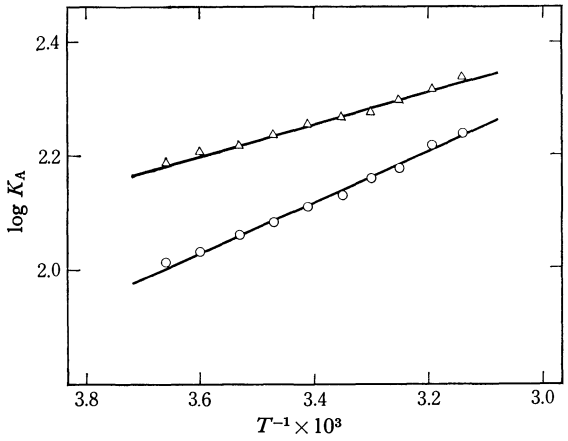

Fig. 4. Plots of log K_A against T^{-1} for magnesium sulfate (○) and nickel sulfate (△).

Table 3. Standard Gibbs energy, enthalpy, and entropy of ion-pair formation of $Mg^{2+} \cdot SO_4^{2-}$ and $Ni^{2+} \cdot SO_4^{2-}$

Ion-pair	ΔG°_{298} [kcal mol^{-1}]	ΔH° [kcal mol^{-1}]	ΔS°_{298} [cal deg^{-1} mol^{-1}]
$Mg^{2+} \cdot SO_4^{2-}$	−2.91	2.04	16.6
	(−3.07)	(4.84)	(26.2)
$Ni^{2+} \cdot SO_4^{2-}$	−3.10	1.27	14.7
	(−3.16)	(3.31)	(21.7)

(The values obtained by Nair and Nancollas from the emf measurement are shown in parentheses)

$$\Delta G^\circ = -RT \ln K_A \tag{12}$$

and:

$$\Delta G^\circ = \Delta H^\circ - T\Delta S^\circ \tag{13}$$

The values of ΔG°, ΔH°, and ΔS° for the association reaction (1) are given in Table 3, in which the values of Nair and Nancollas are also presented (in parentheses). Qualitatively, the present results show a tendency similar to those of Nair and Nancollas[4,5] obtained by the emf measurements. Quantitatively, however, the values of ΔH° and ΔS° obtained from the conductivity data are significantly smaller than those determined from the emf data.

It seems worthwhile to compare the experimental values of ΔH° and ΔS° with those theoretically predicted from the electrostatic model of ion-pairs. According to Fuoss' theory of electrostatic interaction, the ion-pair association constant, K_A, is given by this equation:[3,9]

$$K_A = \bar{v}e^b \tag{14}$$

with

$$\bar{v} = \frac{4\pi La^3}{3000}, \quad b = \frac{|z_+z_-|e^2}{\varepsilon akT}$$

where z_+ and z_- are the charge numbers of the cation and anion respectively, where ε is the dielectric constant, and where the other symbols have their usual meaning. Provided $\bar{v}$ is independent of the temperature, we obtain the following expressions for ΔH° and ΔS° from Eq. (14):[3]

$$\Delta H^\circ = -RTb\left(1 + \frac{d\ln\varepsilon}{d\ln T}\right) \tag{15}$$

and:

$$\Delta S^\circ = R\ln\bar{v} - Rb\left(\frac{d\ln\varepsilon}{d\ln T}\right) \tag{16}$$

With the values of $d\ln\varepsilon/d\ln T = -1.37$ for water at 25°C and $a = 6$ Å as determined from the conductivity data (see Table 2), Eqs. (15) and (16) give the theoretical values of $\Delta H^\circ = 1.05$ kcal mol^{-1} and $\Delta S^\circ = 14.4$ cal deg^{-1} mol^{-1} for the ion-pair formation of $M^{2+} \cdot SO_4^{2-}$ (M: Mg and Ni) at 25°C. These theoretical values are reasonably close to the experimental values we give in Table 3; this suggests that the electrostatic interaction exerts a dominant influence on the ion-pair formation of $Mg^{2+} \cdot SO_4^{2-}$ and $Ni^{2+} \cdot SO_4^{2-}$.

The author wishes to thank Dr. Reita Tamamushi for his many helpful discussions and suggestions during this work, and Dr. Katsuo Takahashi for the construction of the apparatus. He also wishes to thank Mrs. Kinuyo Takahashi and Miss Yoko Taguchi for the computer calculation.

9) R. M. Fuoss and F. Accascina, "Electrolytic Conductance," Interscience Publishers, Inc., New York, N. Y. (1959), Chap. XVI.

^{14}N Nuclear Quadrupole Resonances of 2-Aminopyrimidine

Hisao NEGITA, Kaoru SHIBATA, and Tsuneo KUBO
Department of Chemistry, Faculty of Science, Hiroshima University, Hiroshima
(Received July 28, 1972)

Four nuclear quadrupole resonance (NQR) lines due to ^{14}N nuclei of the ring nitrogens in 2-aminopyrimidine were paired for the powder sample by use of a frequency-modulated spectrometer and a Helmholtz coil for the Zeeman field (H). NQR parameters $e^2Qq=3707.2$ kHz and $\eta=0.0646$ were obtained for one nitrogen, and $e^2Qq=3759.6$ kHz and $\eta=0.0329$ for the other. Moreover, the frequency of the lower line of a pair of lines for the amino nitrogen was predicted from the shift of the higher line subjected to the Zeeman field in a single crystal. The region around the expected position was carefully swept and a very weak line was found at 2357.8 kHz. Thus $e^2Qq=3428.0$ kHz and $\eta=0.2488$ were deduced for the amino nitrogen. The quadrupole coupling constant for the amino nitrogen in 2-aminopyrimidine was smaller than that for the amino nitrogen in 2-aminopyridine. The asymmetry parameter for the amino nitrogen in 2-aminopyrimidine was smaller than that for the amino nitrogen in 2-aminopyridine and roughly equal to that for the amino nitrogen in aniline.

In the case of ^{14}N NQR, only one resonance line is found for the axially symmetric field gradient, and a pair of resonance lines are usually found for the asymmetric field gradient. However, when one of the pair, mostly the lower line, is too weak to detect, it may be difficult to determine whether the resonance is caused by a symmetric field gradient or not, as long as a frequency-modulated spectrometer is used. To overcome this difficulty, it is advantageous to inspect the line shift as well as the line broadening by applying the Zeeman field from a given direction. In the case of the axially symmetric field gradient, the line is flattened to both sides, whereas in the case of the non-axially symmetric one, the higher line shifts to the higher and *vice versa*, and the smaller the asymmetry parameter, the greater the line broadens.[1] In this way, two pairs of lines for the ring nitrogens in 2-aminopyrimidine were determined, the results being in good agreement with the assignment by Schempp.[2] As for the resonance due to the amino nitrogen in 2-aminopyrimidine, only the higher line of the pair was reported for the first time by Schempp. Thus the frequency of the lower line was calculated from its shift by the Zeeman field on a single crystal sample. A very weak line was found in the neighborhood of the calculated frequency. The resonance frequency differs from that reported recently by Schempp and Bray.[3] The derived quadrupole coupling constant and asymmetry parameter for the amino nitrogen in 2-aminopyrimidine were compared with those for the amino nitrogens in aniline and 2-aminopyridine.

Experimental

The ^{14}N NQR spectra of 2-aminopyrimidine were obtained by the frequency-modulated spectrometer described previously.[4] The resonance frequencies were measured by a heterodyne-type frequency meter BC-221 whose frequency was checked by a frequency counter TR-5578 of Takeda Riken Co. The Zeeman field was supplied by a Helmholtz coil, 40 cm in diameter and 20 cm in gap-width. The exact field strength of the coil was calibrated by measuring the Zeeman shifts of a given resonance line. The crystal was mounted in a rf coil so as to rotate independently about the horizontal and vertical axes. Thus, the Zeeman field could be applied to the crystal from any direction. All the measurements were carried out at liquid nitrogen temperature.

Commercial 2-aminopyrimidine was purified by recrystallization from a solution in organic solvent. About 10 g of the sample was used. The single crystal, 15 mm in diameter and 35 mm in length, was prepared by the Bridgman-Stockbarger method.

Results and Discussion

Since ^{14}N has a nuclear spin of unity, we can usually obtain a pair of resonance frequencies, ν_I and ν_{II}, as follows:

$$\nu_I = K(3-\eta), \quad (1)$$

$$\nu_{II} = K(3+\eta), \quad (2)$$

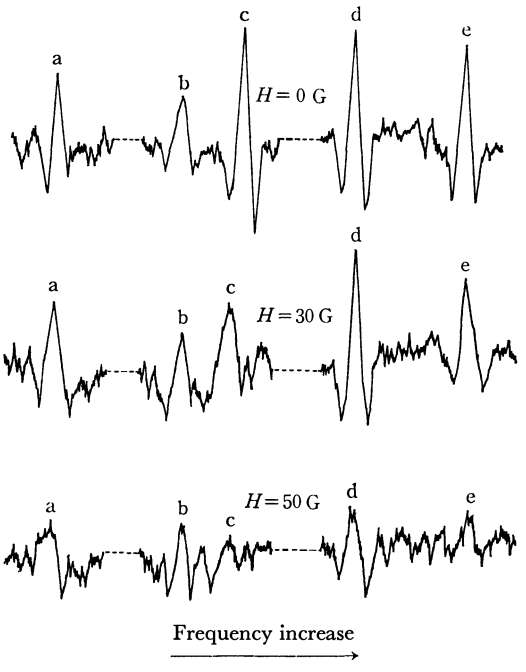

Fig. 1. Line shapes of ^{14}N NQR in the powder sample of 2-aminopyrimidine under the Zeeman field.

1) H. Negita, *J. Chem. Phys.*, **44**, 1734 (1966).
2) E. Schempp, Ph. D. Thesis, Brown University (1968).
3) E. Schempp and P. J. Bray, *J. Magn. Resonance*, **5**, 78 (1971).
4) H. Negita, M. Hayashi, and T. Okada, *J. Sci. Hiroshima Univ., Ser. A*, **35**, 85 (1971).

where $K=e^2Qq/4$, and e^2Qq and η are the quadrupole coupling constant and asymmetry parameter, respectively.

Determination of two Pairs of Resonance Lines for the Ring Nitrogens. Figure 1 shows how the shapes of five resonance lines of the powder sample, denoted by *a*, *b*, *c*, *d*, and *e* in the order of increasing frequency, change with the increase in strength of the Zeeman field. We see that resonance lines *c* and *e* become broader than *a* and *d*, with the increase in field strength. Therefore, *c* and *e* are paired together and they have a considerably smaller η value than *a* and *d*. From Eqs. (1) and (2), e^2Qq=3759.6 kHz and η=0.0329 were obtained for *c* and *e*, whereas the corresponding values for *a* and *d* are 3707.2 kHz and 0.0646, respectively. The results are consistent with those of Schempp[2] within experimental error.

On the other hand, as line *b* scarcely broadens even when H=50 G, it must have a large η value.

Detection of the Lower Line for the Amino Nitrogen.

The frequency of the higher resonance line for the amino nitrogen in 2-aminopyrimidine was reported by Schempp to be 2784.2 kHz.[2]

When $H \neq 0$ and η is small, the first-order perturbation method can be used, and the resonance frequencies are as follows:[5]

$$\nu_I' = 3K - (\eta^2K^2 + D^2\cdot\cos^2\theta)^{1/2}, \quad (3)$$

$$\nu_{II}' = 3K + (\eta^2K^2 + D^2\cdot\cos^2\theta)^{1/2}, \quad (4)$$

where $D=g\mu_0H$, and θ is the polar angle of the direction of the Zeeman field in the coordinates of the principal field gradients. The subscripts refer to the resonance lines corresponding to those in Eqs. (1) and (2) when D=0. When $H \neq 0$ and η is large, the second-order perturbation method has to be used. The resonance frequencies are as follows:[5]

$$\nu_I'' = K(3-\eta) + D^2(A+2B-C)/K, \quad (5)$$

$$\nu_{II}'' = K(3+\eta) + D^2(2A+B+C)/K, \quad (6)$$

where

$$A = \sin^2\theta\cdot\cos^2\varphi/(3+\eta), \quad (7)$$

$$B = \sin^2\theta\cdot\sin^2\varphi/(3-\eta), \quad (8)$$

$$C = \cos^2\theta/(2\eta), \quad (9)$$

and φ is the azimuthal angle of the direction of the Zeeman field in the coordinates of the principal field gradients.

The polar angle θ is related to the Eulerian angles ψ_1, ψ_2, and ψ_3 as shown in Fig. 2 by the equation:

$$\cos\theta = \sin\psi_2\cdot\sin\psi_3\cdot\sin\alpha\cdot\cos\beta + \cos\psi_2\cdot\sin\psi_3\cdot\sin\alpha\cdot\sin\beta + \cos\psi_3\cdot\cos\alpha, \quad (10)$$

where α and β are the polar and azimuthal angles of the direction of the Zeeman field in the coordinates fixed to the sample, respectively. The exact value of D is determined from the Zeeman shifts of line *c*, which has e^2Qq=3759.6 kHz and η=0.0329, in the single crystal. That is, Eqs. (3) and (10) can be used in order to obtain the value of D, since line *c* has a small η. From the Zeeman study of line *c* in the single crystal, it is found that ν_I' takes 2785.5, 2786.0, and 2783.1 kHz for the cases (α=0°, β=180°), (α=90°, β=180°), and (α=90°, β=200°), respectively. From these values, the value of D^2 was determined to be 807.8 kHz.[2]

5) P. A. Casabella and P. J. Bray, *J. Chem. Phys.*, **28**, 1182 (1958).

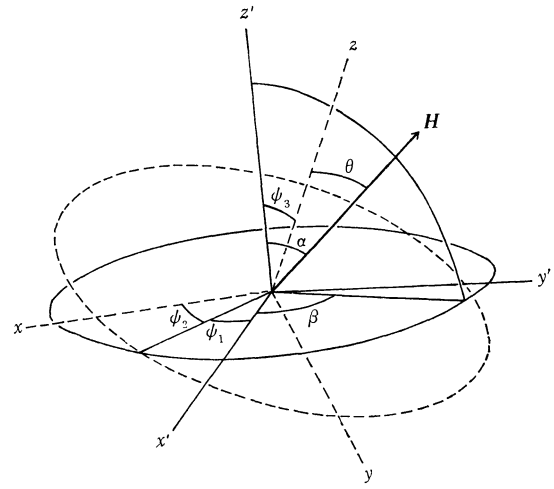

Fig. 2. Eulerian angles ψ_1, ψ_2, and ψ_3.
x, y, and z: the coordinates of the principal field gradients.
x', y', and z': the coordinates fixed to the sample.

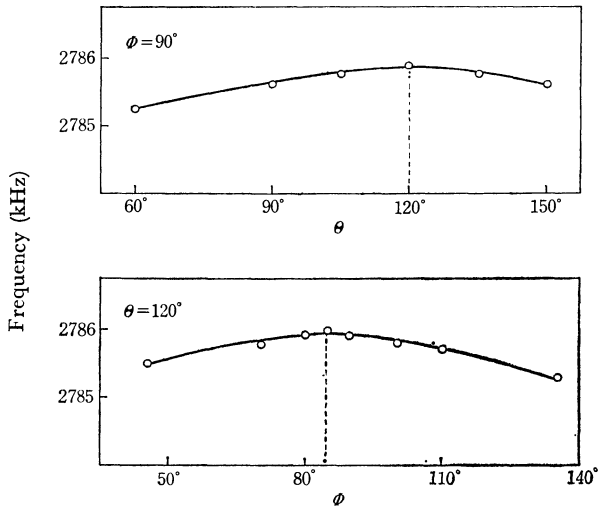

Fig. 3. The angular dependence of the Zeeman shifts of line *b*.

Figure 3 shows the anglar dependence of the Zeeman shifts of line *b* when the sample is rotated about a given axis. The Zeeman field was applied along the *Y*-axis of the laboratory frame as shown in Fig. 4, and the frequencies of line *b* were measured at various rotating angles (Θ) about the *X*-axis for a constant rotating angle (Φ=90°) about the *Z*-axis. The maximum frequency or shift was found for Θ=120°. Next, the frequencies were measured at various rotating angles (Φ) about the *Z*-axis for Θ=120°. The shift was maximum at Φ=85° and ν_{II}'' was estimated to be 2786.0 kHz. It is thus concluded that the principal *z*-axis of the field gradient lies in the *XY* plane when Θ=120° and Φ=90°, and coincides with the direction of the Zeeman field when

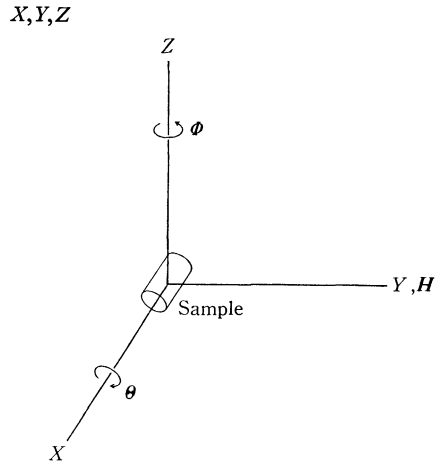

Fig. 4. The rotating angles Θ and Φ in the laboratory frame.

$\Theta=120°$ and $\Phi=85°$. Under the latter conditions, the relations $A=B=0$ and $C=1/(2\eta)$ are obtained from Eqs. (7), (8), and (9). Hence the following equation for ν_{II}'' is derived from Eq. (6): $2786.0=K(3+\eta)+807.8/(2\eta K)$. On the other hand, the higher line for the non-Zeeman field is expressed by $2784.2=K(3+\eta)$. Thus the NQR parameters for the amino nitrogen are calculated as $e^2Qq=3414.0\pm17.6$ kHz and $\eta=0.2630\pm0.0179$. Substituing these values into Eq. (1), the frequency of the lower line for the amino nitrogen is obtained to be 2335.4 ± 26.4 kHz for the non-Zeeman field. The neighborhood of this frequency was carefully swept again, and a very weak line was observed at 2357.8 kHz. These results are summarized in Table 1.

TABLE 1. ^{14}N NQR PARAMETERS IN 2-AMINOPYRIMIDINE

		ν_I (kHz)	ν_{II} (kHz)	$\lvert e^2Qq\rvert/h$ (kHz)	η (%)
Ring	N_1	2720.5	2840.3	3707.2	6.46
	N_2	2788.8	2850.7	3759.6	3.29
NH_2		2357.8	2784.2	3428.0	24.88

In general, we can not always attain the condition $\theta=0°$ by the consecutive procedures stated above. Accordingly, it is recommended to repeat the procedures until the self-consistent maximum shift is obtained, especially when the angle Φ for the maximum shift in the second procedure differs much from that fixed in the first procedure.

TABLE 2. ^{14}N NQR PARAMETERS FOR THE AMINO NITROGENS

Compound	$\lvert e^2Qq\rvert/h$ (kHz)	η (%)
Aniline[6]	3933	26.9
2-Aminopyridine[7]	3550.3	34.65
2-Aminopyrimidine	3428.0	24.88

Table 2 shows the quadrupole coupling constants and asymmetry parameters for the amino nitrogens in several similar compounds. The quadrupole coupling constant for the amino nitrogen in aniline is the largest,

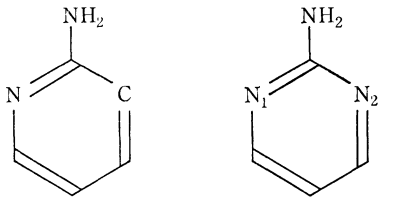

Fig. 5. The molecular frames of 2-aminopyridine and 2-aminopyrimidine.

while that for the amino nitrogen in 2-aminopyrimidine is the smallest. This suggests that the lone pair electrons of the amino nitrogen in aniline conjugate with π-electrons of the ring most weakly, while those of the amino nitrogen in 2-aminopyrimidine most strongly.

The asymmetry parameter of the amino nitrogen in 2-aminopyrimidine is nearly equal to that in aniline, but considerably smaller than that in 2-aminopyridine as shown in Table 2. This may be attributed to the molecular structure in which the nitrogen and carbon atoms in the ring are situated symmetrically or asymmetrically with respect to the C–N bond at the amino group.

Recently, π- and σ-electron densities for the ring nitrogen were derived from the following equations by Lucken:[8]

$$y - x = 2\eta e^2Qq/(3e^2Qq_p), \tag{11}$$

$$2 - y = (1-\eta/3)\cdot e^2Qq/[(1-\cot^2\gamma)\cdot e^2Qq_p], \tag{12}$$

where x and y are π- and σ-electron densities respectively, 2γ is the $\angle$CNC bond angle, and e^2Qq_p the quadrupole coupling constant due to one $2p$-electron of nitrogen atom. If it is assumed that $2\gamma=115.2°$ [9] and $e^2Qq_p=9$ MHz in Eqs. (11) and (12), both π- and σ-electron densities can be evaluated. Table 3 lists these values obtained for the ring nitrogens in pyrimidine[10] and 2-aminopyrimidine. We see that the amino group behaves like an electron-donor to the ring nitrogens. Simple LCAO MO calculations were carried out in order to make comparison with the results of NQR. The calculated values of π-electron densities for the ring nitrogens are qualitatively in good agreement with those predicted by NQR.

TABLE 3. π- AND σ-ELECTRON DENSITIES IN PYRIMIDINE AND 2-AMINOPYRIMIDINE

Compound		π		σ
		NQR	MO[a]	
Pyrimidine[9]		1.138	1.144	1.281
2-Aminopyrimidine	N_1	1.308	1.203	1.325
	N_2	1.299		1.308

a) The values of LCAO MO were calculated by the parameters such as $\alpha_N=\alpha+0.5\beta$, $\alpha_{C-N}=\alpha+0.1\beta$, $\alpha_{NH_2}=\alpha+0.4\beta$, $\alpha_{C-NH_2}=\alpha$, $\beta_{C-N}=\beta$, and $\beta_{C-NH_2}=0.6\beta$.

The total electron excess on the ring nitrogen can be computed from the values for the orbital occupation

6) C. T. Yim, M. A. Whitehead, and Donald H. Lo, *Can. J. Chem.*, **46**, 3595 (1968).
7) R. Ikeda, S. Onda, D. Nakamura, and M. Kubo, *J. Phys. Chem.*, **72**, 2501 (1968).
8) E. A. C. Lucken, "Nuclear Quadrupole Coupling Constants," Academic Press, London and New York (1969), p. 234.
9) P. J. Wheatley, *Acta Crystallogr.*, **13**, 80 (1960).
10) E. Schempp and P. J. Bray, *J. Chem. Phys.*, **46**, 1186 (1967).

numbers as follows:

$$z = x + 2y - 3 \quad (13)$$

From Table 3 and Eq. (13), the values of z are obtained to be 0.700 e^- for the ring nitrogens in pyrimidine and 0.958 e^- and 0.915 e^- for those in 2-aminopyrimidine. Thus, it is to be noted that the magnitudes of the electron transfer from the amino group to the ring nitrogens in 2-aminopyrimidine are larger by 0.258 e^- and 0.215 e^- respectively than that from the hydrogen atom in pyrimidine.

BULLETIN OF THE CHEMICAL SOCIETY OF JAPAN, VOL. 46, 113—115 (1973)

The Salting-out Adsorption of Isomeric Butyl Alcohols by Macroreticular Resin

Kie HISHINUMA, Hideo ŌKI, Yōichi KUROKAWA, and Norio YUI

Department of Applied Science, Faculty of Engineering, Tōhoku University, Aoba, Aramaki, Sendai

(Received October 14, 1971)

The salting-out adsorption of isomeric butyl alcohols on Amberlite (200) type designated as the macroreticular ion-exchange resin (MR type) was studied. On the basis of the difference in the salting-out effect of isomers, the separation of the isomer mixture in a dilute aqueous solution was attempted by using an aqueous ammonium sulfate solution as an eluent and the MR resin as a stationary phase. It seems that MR resin as the stationary phase is inadequate for the salting-out chromatography of isomeric butyl alcohols.

The salting-out effect in the two-phase system has been investigated on butyl alcohol in the aqueous and the butanol phases.[1] The present paper will report the salting-out adsorption of isomeric butyl alcohols on ion-exchange resin by determining the relative solubilities in an ammonium sulfate solution. The Amberlite (200) type of cation exchange resin was used. This resin, designated as macroreticular (MR) ion-exchange resin, is entirely different from the conventional homogeneous gels and has a rigid macroporous structure similar to those of the conventional absorbents.[2,3] Whereas the specific surface area for a conventional resin is very small (0.1 m^2/g), this resin has a surface area of 54.8 m^2/g.[2] On the basis of the difference in the salting-out effect on isomers, the separation of an isomer mixture in a dilute aqueous solution was attempted by using an aqueous ammonium sulfate solution as an eluent and the MR resin as the stationary phase. The designation "Salting-out Chromatography" has been proposed for such a method of separation.[4,5] The only convenient method known to the authors for the determination of each isomer in the above mixture is that of gas chromatography. However, in this case, such a method is not applicable because of the undesirable phenomena of water tailing.

Experimental

Procedure. All the chemicals were reagent-grade and were used without further purification. The Amberlite (200) type of cation exchange resin was converted to the ammonium form by the passage of 1 M ammonium sulfate solution and was then dried at 50°C overnight. This resin has the capacity of 4.3 meq/(g of dry resin), a water content of 44.8% and a pore size of 60—300 Å. The batch adsorption was made by adding 3—4 g of MR resin to 50 ml of a 0.5% butanol solution with a 0.5—3M ammonium sulfate solution. After this mixture had been allowed to stand at 25°C, overnight, the butyl alcohol in the aqueous solution was determined. In the case of column adsorption, the resin was packed into a column (ϕ 1.25 cm × 22.5 cm) water-jacketed and connected to a bath maintained at 25°C. Before elution, the resin was equilibrated with the eluent to be used. This was accomplished by allowing 300 ml of the eluent to pass through the column. A 0.5 mmol portion of the butyl alcohol was pipetted onto the bed. Then, the column was drained with a flow rate of 0.3 cm/min. The separation of isomers was attempted with the above-mentioned column and with a larger column of ϕ 1.7 × 70 cm. Both columns had an interstitial volume of 36%.

Analysis. The butyl alcohols were determined by oxidizing them in 50% sulfuric acid with dichromate and by measuring the reduced Cr(III) spectrophotometrically.[6] A 100 g portion of sodium dichromate was dissolved in water, and the mixture was diluted with water to 100 ml. A 5 ml portion of this solution was added to an 1000 ml solution of the concentrated sulfuric acid. At this time, the precipitate appeared, but it was redissolved on shaking. A 25 ml portion of a sample contanining 0.0025—0.01 mmol of butyl alcohol was pipetted into a 100 ml flask containing 25 ml of above oxidizing agent. Similarly, a flask was prepared by adding 25 ml of water to 25 ml of the oxidizing agent. The flask was heated in a boiling water bath for 15 min. After cooling to room temperature, the absorbance was measured at 610 mμ against the blank. Oxidizing anions such as nitrate and reducing ions such as halides interfered with this determination. Ammonium sulfate was the best eluent because of its large solubility in water and its great salting-out power.[4] Since the absorbance was slightly affected by ammonium sulfate,

1) Y. Kurokawa and N. Yui, *Nippon Kagaku Zasshi*, **88**, 276 (1967).

2) K. A. Kun and H. Hisayama, *Kagaku to Kogyo*, **21**, 1465 (1968).

3) R. Kunin, E. E. Meizner, J. A. Oline, S. A. Fisher, and N. Frisch, *Ind. Eng. Chem., Prod. Res. Develop.*, **1**, 140 (1962).

4) W. Rieman, *J. Chem. Educ.*, **38**, 338 (1961).

5) W. Funasaka, T. Kojima, K. Fujimura, and S. Kushida, *Bunseki Kagaku*. **15**, 835 (1966).

6) R. Sargent and W. Rieman, *Anal. Chim. Acta*, **14**, 381 (1956).

the plot of the absorbance *vs.* the concentration of butyl alcohol was made at each concentration of ammonium sulfate. Absorbance measurements were made with a HITACHI EPU-2A-type spectrophotometer.

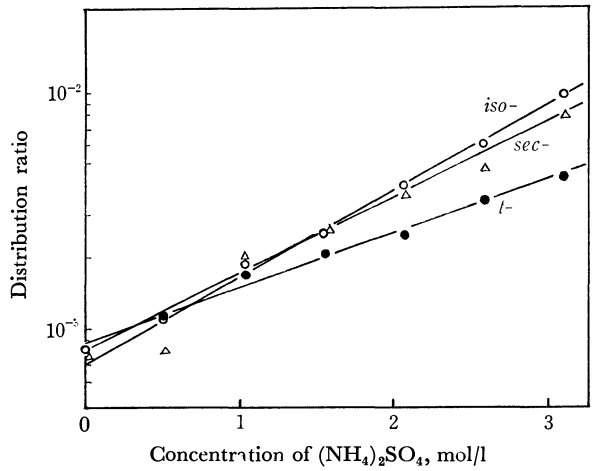

Fig. 1. Plots of log D *vs.* concentration of $(NH_4)_2SO_4$ for isomeric butanols with Amberlite 200.

Results and Discussion

The distribution ratio of butyl alcohol was defined as D=(the quantity of adsorption mmol/g-dry resin)/(concentration of aqueous solution mmol/l). Correction was made for the swelling and shrinking of the resin. The logarithms of these ratios are plotted against the concentration of ammonium sulfate in Fig. 1. These plots followed fairly closely this equation:

$$\log D = \log D^\circ + kM \qquad (1)$$

where D° is the distribution ratio in pure water, k is a salting-out coefficient, and M is the molarity of ammonium sulfate. Eq. (1) is very similar to Setshenow's equation.[1] The obtained values are represented in Table 1. D showed a rough tendency to decrease as the hydrophilic nature of the butyl alcohol increased. That is, the order of k was the same as that of the solubilities of butyl alcohols in water, (*tert*-butanol is completely miscible with water). The MR resin is observed to be much less sensitive to the nature of the solvent than conventional resin, but the results are not so much

Table 1. Distribution ratio and salting-out coefficinet

		Amberlite-200 batch	Amberlite-200 column	Dowex 1-X8 column	Dowex 50-X8 column
$\log D^\circ$	iso-	−0.145		0.330	0.130
	sec-	−0.073		0.150	0.039
	t-	−0.061		−0.125	−0.130
k	iso-	0.374		0.380	0.407
	sec-	0.322		0.422	0.419
	t-	0.238		0.414	0.408
$\log D$	iso-	0.613	0.645	1.00	0.944
	sec-	0.571	0.614	0.994	0.877
	t-	0.415	0.424	0.703	0.686

Eluent of 2M $(NH_4)_2SO_4$ was used.

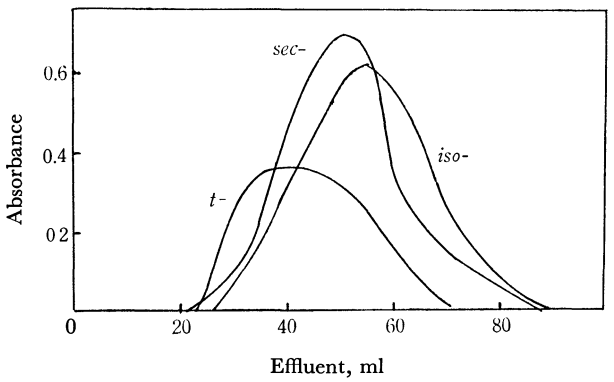

Fig. 2. Elution of isomeric butanol.
Column of ϕ 1.25×22.5 cm, 0.3 cm/min
Eluent of 2M $(NH_4)_2SO_4$

less sensitive in the literature.[3] The increase in the salt concentration of the eluent produced a greater affinity of the resin for butyl alcohol. The ionic groups on the resin would be solvated preferentially by water, and when salt was added, the resin would shrink because a part of the water was withdrawn to solvate the salt. Then, the solvated position around the ionic group on the resin could now be occupied by butyl alcohol.[7] Two kinds of solvent uptake by the resin might be considered. One might be a chemisorption as solvation around the ionic group on the resin, and the other, physisorption as fixing into the rigid macropores.[8] The adsorption of butyl alcohol on the MR resin was rather small, whereas the MR resin had a capacity as large as that of the conventional resin and had a much larger surface area. This suggests that water molecules are tightly bound to resin and may not be easily substituted by butyl alcohol molecules. Each isomeric butyl alcohol was eluted with a 3M ammonium sulfate solution. The elution graphs are shown in Fig. 2. They are very like each other. The ordinate is the absorbance of the Cr(III) formed by the reduction of dichromate by the butyl alcohol and is, therefore, proportional to the concentration of butyl alcohol in the eluent. Generally, a smaller mesh size of a resin produced a sharper elution curve, but no significant shift of the peak was observed. When the

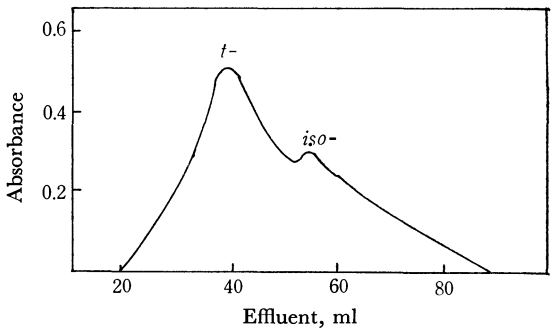

Fig. 3. Elution of isomers mixture.
Column of ϕ1.25×22.5 cm, 0.3 cm/min
Eluent of 2M $(NH_4)_2SO_4$

7) R. Sargent and W. Rieman, *J. Phys. Chem.*, **61**, 354 (1957).
8) T. Yamabe, K. Yamagata, and M. Seno, *Nippon Kagaku Zasshi*, **89**, 151 (1968).

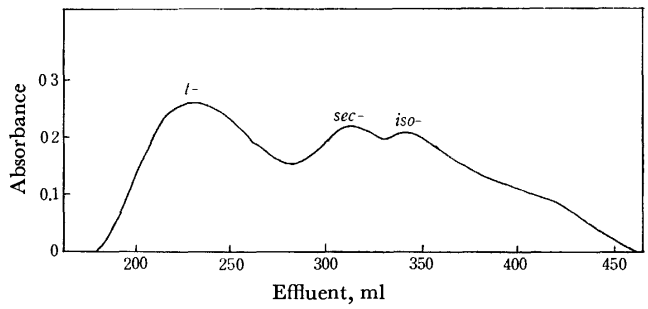

Fig. 4. Elution of isomers mixture.
Column of $\phi 1.75 \times 70.5$ cm, 0.26 cm/min
Eluent of 2M $(NH_4)_2SO_4$

quantity of butyl alcohol taken for elution was too large, the curve was wide and subject to tailing.

The distribution ratios in the column were obtained from the elution curves by using the following plate theory of chromatography:[9]

$$U = DV + V \quad (2)$$

U is the volume of the effluent collected by adding the sample to the peak. D is the distribution ratio, and V is the interstitial volume of the column. Table 1 represents a comparison of these values for the MR resin with those for the conventional resin. The separation of isomers was attempted with two columns. The elution of the first column for a mixture of *iso*- and *tert*-butanol is shown in Fig. 3. Another elution was performed by using a column much larger than the first (Fig. 4). The curves overlapped so badly that a satisfactory separation could not be achieved. The position of the peak was estimated from Eq. 2, and the value of D was obtained from the first column. The calculated values of U for *tert*-, *sec*-, and *iso*-butyl alcohol were 23.1, 29.5, and 31.2 ml respectively. The agreement between the calculated and observed values seems reasonable, though the peaks overlap (Fig. 4). The elution required 30 hr for the completion of a run. The separation might be made more completely with a column of a higher height. It seems that the MR resin as the stationary phase is inadequate for the salting-out chromatography of isomeric butyl alcohols.

The authors wish to express their thanks to Miss Shima Miura, who carried out part of the experimental work.

9) R. Sargent and W. Rieman, *J. Phys. Chem.*, **60**, 1370 (1956).

Properties of Water in Macromolecular Gels. V. Anomalous Temperature Dependence of the Nuclear Magnetic Resonance Line-width of Water in Macromolecular Gels

Masuo AIZAWA, Shuichi SUZUKI, Teruo SUZUKI,* and Hiroshi TOYAMA*

Research Laboratory of Resources Utilization, Tokyo Institute of Technology, Meguro-ku, Tokyo

**Japan Electron Optics Laboratory Co., Ltd., Akishima, Tokyo*

(Received March 22, 1972)

The line-width of the nuclear magnetic resonance (NMR) signal gets narrow, in general, with an increase in the temperature. In contrast, the NMR line-width of the water proton in agarose gels was found to increase with an increase in the temperature up to about 30°C. As for the other polysaccharide gels, such as curdlan-type polysaccharide, and κ- and λ-carrageenan gels, the NMR line-width of water increases with an increase in the temperature. The anomalous temperature dependence of the line-width was most marked in agarose gels than in other polysaccharide gels. The close relationship between the gel network, which consists of small cavities (microspace) of the micelle, and the magnitude of the anomality was revealed, this anomalous effect was named the "Micro-Space Effect."

The line-width of the nuclear magnetic resonance (NMR) signal is known to become narrow as a result of the activation of molecular movement with an increase in the temperature, namely, motional narrowing.[1] In contrast, the present authors have found that the NMR line-width of the water proton in agarose gels containing more than 30% of water became wide with an increase in the temperature. Thus, the molecular motion seems to get bounded with an elevation in the temperature.

It was shown in previous papers[2-3] that water in polysaccharide gels is markedly affected by the three-dimensional framework of the polymer. The thermal expansion of water, for example, was found to be extremely obstructed in gels. The double-helix model, in which the two chains of each pair are parallel and are twisted around each other, has been proposed for the possible structure of such polysaccharides as agarose and carrageenan. The proposed model[4-5] suggests a mechanism for the formation of gels when dilute aqueous solutions of these polysaccharides are cooled: chain segments associate in double helices to crosslink the chains in a three-dimensional framework which is then responsible for the shape and strength of the gel. Subsequently or simultaneously, the double helices could combine into larger aggregates. There is much evidence in support of such mechanism. Furthermore, the effect of structural variations on gel properties may be explained in terms of the model for junction zones. Therefore, the temperature effect on the properties of water may depend on the properties of the junction zones and the framework. The small cavities in the three-dimensional framework of polysaccharide gels can be called the micro-space. Water is included in this micro-space. Therefore, the three-dimensional framework in gels was presumed to be responsible for the anomalous temperature dependence mentioned above. In other words, the anomalous temperature effect was supposed to be related with the micro-space in gels.

Agarose gels are known to be quite different from other polysaccharide gels, such as κ-carrageenan, λ-carrageenan, and curdlan-type polysaccharide gels, in their gel properties. A different anomalous temperature dependence of the NMR linewidth can be expected for these polysaccharide gels. The NMR linewidth was measured for these polysaccharide gels compared with agarose gels in the temperature range from 0 to 60°C.

Experimental

Materials. The agarose, κ-carrageenan, λ-carrageenan and curdlan-type polysaccharide gels used in this study were prepared with distilled water treated with ion-exchanger resins, and were sealed in a standard NMR sample tube (5 mm O.D.). Curdlan-type polysaccharide,[6] a bacterial gel-forming β-1, 3-glucan, which was supplied by Takeda Chemical Industrials, Ltd., was obtained from a culture filtrate of a mutant strain (NTK-U, IFO 13140) of *Alcaligenes faecalis var. myxogenes strain* 10C 3K. These samples were assayed for their ash content by the atomic absorption method. The analytical results on the ash content are shown in Table 1. The water content of the sample was measured by drying it at 105°C for 24 hr and by that then weighing the dried matter after the NMR measurement.

NMR Spectra. The proton NMR spectra were obtained using a JNM-C-60HL high-resolution NMR spectrometer with an external-lock system. Since the signals were wider than those normally seen in high-resolution measurement, it

Table 1. Ash contents of the samples (mg/g dry matter)

	Mg	Ca	Na	K	Fe,Cu
Agarose	0.04	1.01	1.75	0.09	—
κ-Carrageenan	0.23	8.11	6.20	41.3	—
λ-Carrageenan	0.77	15.98	18.79	18.80	—
Curdlan type β-1,3-glucan	0.03	0.06	0.26	2.03	—

1) N. Bloembergen, E. M. Purcell, and P. V. Pound, *Phys. Rev.*, **73**, 706 (1948).

2) S. Suzuki, M. Aizawa, and M. Takahashi, *Kobunshi*, **20**, 674 (1971).

3) M. Aizawa and S. Suzuki, This Bulletin, **44**, 2967 (1971).

4) D. A. Rees, I. W. Steele, and F. B. Willismson, *J. Poly. Sci., Part C*, **28**, 261 (1969).

5) D. A. Rees, *Advan. Carbohydrate Chem.*, **24**, 267 (1969).

6) T. Harada, A. Misaki, and H. Saito, *Arch. Biochem. Biophys.*, **124**, 292 (1968).

was necessary to operate at the optimum rf power levels, just below signal saturation. The spectrometer was equipped with a variable-temperature controller which maintained the sample within ± 0.5°C of the desired temperature.

The temperature of a sample was calibrated by means of a copper-constantan thermo-couple placed inside the sample tube. The linewidth of the spectra is expressed in terms of half linewidth, *i.e.*, the linewidth at half of the maximum peak height.

Results

(1) Agarose Gels. The signal of the agarose proton is much wider than that of the water proton, as has been shown previously by broad-line NMR. Therefore, the proton signal in the high-resolution NMR spectra of agarose molecule can be distinguished from that of water.

The temperature dependence of the linewidth of the water proton in agarose gels was investigated in the range from 0 to 60°C at intervals of 5°C by high-resolution NMR. The spectra are illustrated for an agarose gel containing 92% of water at 10, 29, and 53°C in Fig. 1. The line shape remains evidently unchanged in the above temperature range, though the linewidth varies.

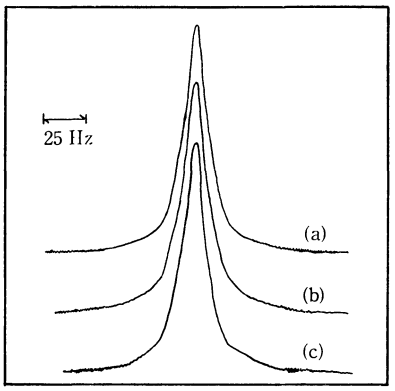

Fig. 1. NMR spectra of agarose gel containing 92% of water at (a) 53°C, (b) 29°C, and (c) 10°C.

The temperature dependence of the linewidth of the water proton in an agarose gel containing 92% of water is shown in Fig. 2. The linewidth was found to increase with an elevation of the temperature in the range from 0 to 35°C. In contrast, at temperatures higher than in the above range, the linewidth decreases as the temperature increases.

The linewidth temperature curves for agarose gels containing 79 and 72% of water are shown in Figs. 3 and 4. An anomalous temperature dependence was observed similar to that of the agarose gel containing 92% water.

(2) κ-Carrageenan and Curdlan-type Polysaccharide Gels. The gel properties of κ-carrageenan and curdlan-type polysaccharide gels are quite different from those of agarose gels. κ-Carrageenan and curdlan-type polysaccharide gels are very flexible, though the gel is weak in its gel strength. If the above anomalous temperature dependence of the line-width in agarose gels is related with the gel framework, different temperature dependences can be expected.

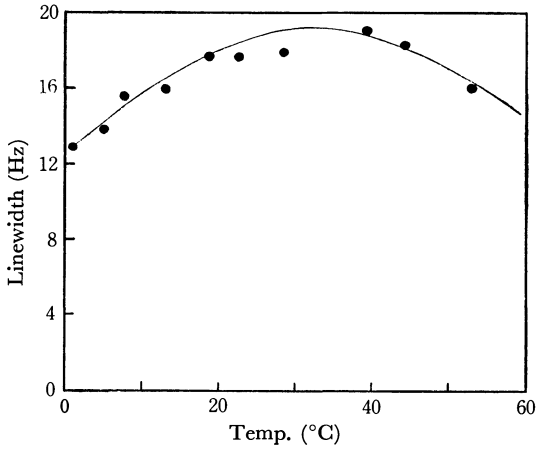

Fig. 2. Temperature dependence of the linewidth for agarose gel containing 92% of water.

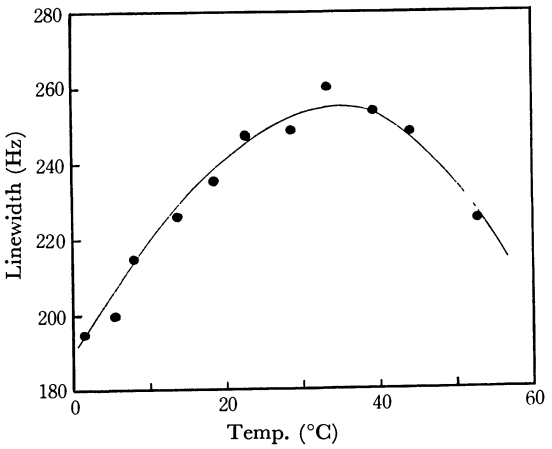

Fig. 3. Temperature dependence of the linewidth for agarose gel containing 79% of water.

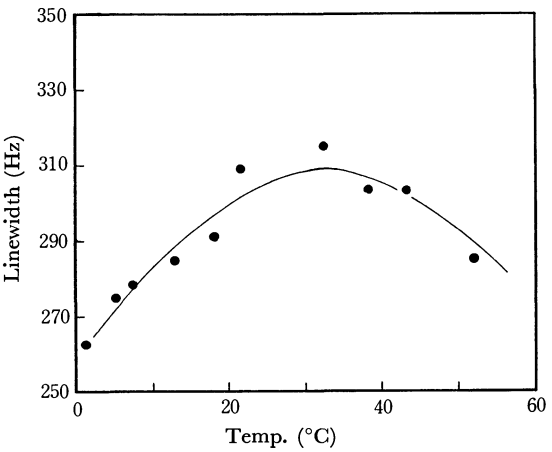

Fig. 4. Temperature dependence of the linewidth for agarose gel containing 72% of water.

The temperature dependence of the line-width for κ-carrageenan gels are illustrated in Fig. 5. For the gel containing 90.5% of water, the linewidth is not so dependent on the temperature as that of agarose gels. The linewidth, however, does not decrease with an increase in the temperature. Therefore, an anomalous temperature dependence was observed in such a

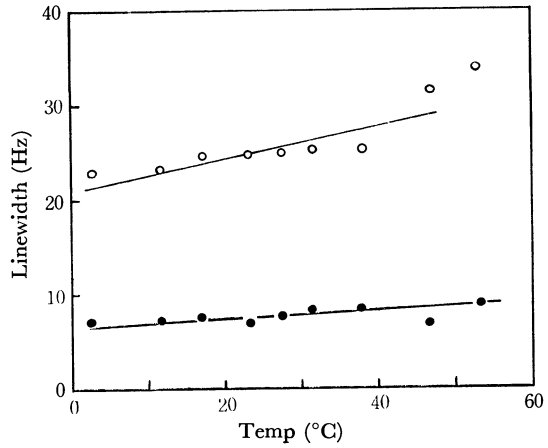

Fig. 5. Temperature effect on the linewidth of κ-carrageenan gel containing 85% of water (-○-) and 90.5% (-●-).

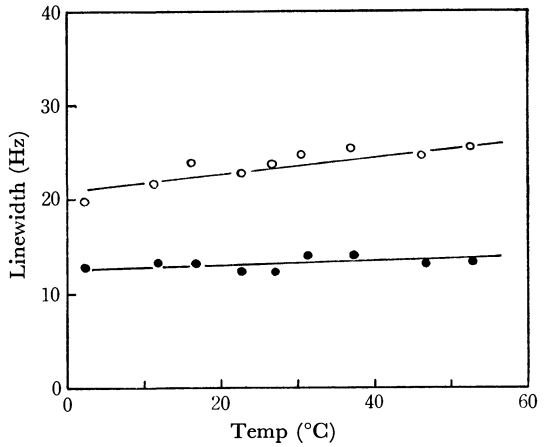

Fig. 6. Temperature effect on the linewidth of curdlan type polysaccharide gels containing 89.5% of water (-○-) and 91.8% (-●-).

gel. The κ-carrageenan gel containing 85% of water exhibited an evident anomalous temperature dependence of the linewidth, but it was, not so marked as in the agarose gels.

Figure 6 presents the temperature dependence of the NMR linewidth of the water proton in curdlan-type polysaccharide gels. The gels containing both 91.8 and 89% of water showed an anomalous temperature dependence similar to that of κ-carrageenan gels.

As was expected, the anomalous temperature dependence was confirmed in the κ-carrageenan gels and curdlan-type polysaccharide gels, though it was not so pronounced as in agarose gels. In addition, the maximum point in the linewidth *vs.* temperature curve, which was observed for agarose gels, was not detected for either κ-carrageenan gels or curdlan-type polysaccharide gels.

(3) λ-Carrageenan Gels. The gel strength of λ-carrgeenan gels is known to be not so strong as that of κ-carrageenan gels. The temperature dependence of the linewidth is postulated for the λ-carrageenan gels containing 93.5 and 88% of water in Fig. 7. These λ-carrageenan gels show a decrease rather than an increase in the linewidth with an elevation of the temperature. The anomalous temperature dependence

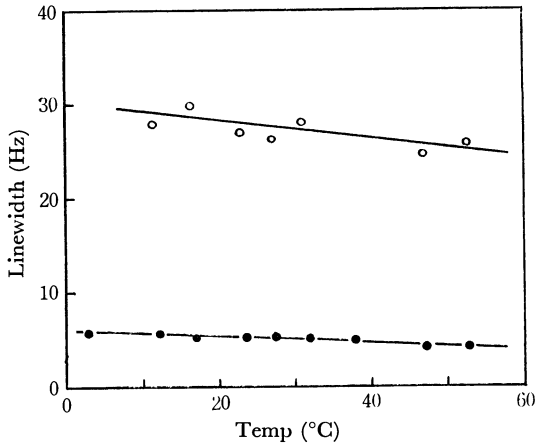

Fig. 7. Temperature effect on the linewidth of λ-carrageenan gel containing 88% of water (-○-) and 93.5% (-●-).

was not so enormous as that of the other gels.

Agarose, κ-carrageenan, curdlan-type polysaccharide, and λ-carrageenan gels exhibited an anomalous temperature dependence of the NMR linewidth of their water proton. The magnitudes of the anomalities were in the order; agarose>κ-carrageenan, curdlan type polysaccharide>λ-carrageenan gels. As was expected, this new finding regarding the anomalous temperature dependence of the line-width is closely related with the gel network. Agarose gels which have a strong network give the most marked anomality.

Discussion

Anomalous temperature effects on the nuclear magnetic resonance linewidth of the water proton in gels were found not only in agarose gels, but also in κ-carrageenan and curdlan-type polysaccharide, λ-carrageenan gels. The effect was the most prominent in the agarose gels.

The linewidth change depends not only on the motional state of the proton, but also on the so-called exchange association, the impurities, and so on. As is shown in Fig. 1, the line-shape of water in gels may be Lorentzian in the upper part and rather Gaussian in the lower part. The line shape remains unchanged in the temperature range surveyed. Proton exchange is estimated to be so rapid as to show no splitting in this system. Therefore, if the exchange association occurs, the linewidth can be expected to be narrowed. The impurities which influence the nuclear magnetic resonance are negligible, as is shown in Table 1. Therefore, the factors other than the motional state of the proton cannot explain those anomalous phenomena.

In view of the motional state of the proton, we assumed that this anomality can be explained by the relationship between the gel strength and the motional state of the water proton. Agarose gels are endowed with a high gel strength and elasticity, though κ-carrageenan and curdlan-type polysaccharide gels are flexible in texture. λ-carrageenan gels have a low gel strength. The magnitude of the anomality decreased with a decrease in the gel strength. The anomalous temperature effect was found to be related

with the strength of the gel network.

Gels, in general, are constructed of a macromolecular network consisting of a number of small cavities. Gels can enclose a large amount of water inside these cavities. Such cavities may be called "micro-space." The dimensions of the micro-space are estimated to be in the order from several Å to 10^2 Å. The properties of the micro-space, depend of course, on the steric properties of the network polymer. For instance, water inside the micro-space constructed of a rigid network may be markedly prevented from thermally expanding, because the expansion coefficient of the network polymer is much smaller than that of water, as was shown previously.[3] In other words, the motional state of water in a gel is closely related with the properties of the micro-space. Therefore, the above anomalous temperature effect on the linewidth of water can be explained in connection with the properties of the micro-space.

The important points regarding the behavior of water in gels are that the lower water contents of agarose gel containing less than 30% show no anomality in their temperature dependence, and that such an anomality is observed only above the transition points in the range from 0 to −20°C, as is shown in Fig. 8. At least three states of water, such as W_1, W_2, and W_3, can be considered for the behavior of water molecules in macromolecular gels, as was proposed previously, where W_1 and W_3 correspond to the so-called free water and bound water respectively.[2,3] The agarose gels containing less than 30% of water are dominated mainly by the specific state which corresponds to W_3. Therefore, most of the water in such gels may be stuck so tight by hydroxyl groups of agarose that it behaves just like the network polymer, even in thermal expansion. That is why no anomality was observed in such lower-water-content agarose gels.

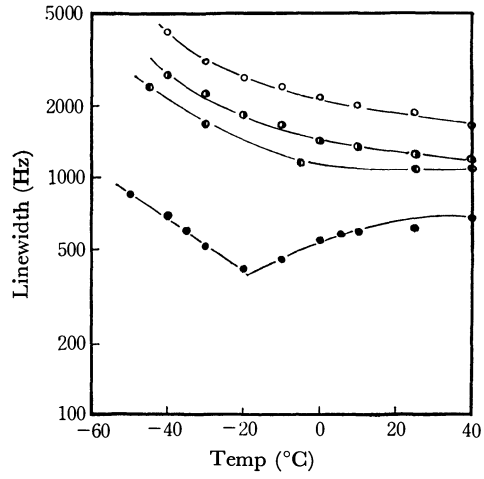

Fig. 8. NMR linewidth changes between −60°C and 40°C for varied water contents of agarose gel. -○- 10%, -◑- 19%, -◐-21.3%, -●- 43%.

Agarose gels containing a large amount of water gave an anomalous temperature dependence of the linewidth. The network polymer of the gel has not only hydrophylic sites, but also hydrophobic sites. Supposed that such hydrophobic sites expel water molecules in the micro-space, water molecules may lose their freedom.

Another important point is that the maxima were seen in the curve of the linewidth against the temperature for agarose gels, though the other gels gave no maxima. Though the gel-sol transition point of agarose gels is approximately 80°C, agarose gels soften around the above maxima. Such a softening is not so obvious in the other polysaccharide gels. In gels, a tremendous difference in thermal expansion coefficient can be supposed between the network polymer and entrapped water, as was indicated previously. The thermal expansion of enclosed water may be supposed on the basis of the network polymer. The thermal expansion of gels should be determined at the balance of the expansions of the network polymer and enclosed water. When the network polymer, however, cannot restrict the expansion of water, in other words, the nodes of the network polymer are relaxed with an increase in the temperature, the thermal expansion coefficient of the gels increases and the enclosed water becomes rather mobile. The maxima in the curve of the linewidth against the temperature for agarose gels can be attributed to such a point. Therefore, agarose gels should soften and the linewidth of water decreases with an increase in the temperature above this point.

On the basis of these results and discussion, the new finding regarding the anomalous temperature dependence can be explained by attributing it to the effect of the micro-space. The restriction of the motional state appears when the extreme difference between the framework of the micro-space, *i.e.*, the network polymer, and the enclosed molecules, *i.e.*, water, is in the physicochemical properties, such as the thermal expansion coefficient.

Brey[7] calculated the activation energy of water adsorbed on lysozyme through the temperature dependence of the NMR linewidth. As a lysozyme containing 488 mg/g of water showed a negative activation energy, he eliminated its activation energy from the other results without any discussion, though the temperature dependence was persented. These anomalous phenomena can be explained by the micro-space effect.

Summary

An anomalous temperature dependence of the NMR linewidth was found for water in macromolecular gels. In other words, the linewidth of the water proton increased with an elevation in the temperature.

The magnitude of this anomality was in the following order: agarose gels>κ-carrageenan, curdlan-type polysaccharide gels>λ-carrageenan gels. The gel with a rigid network gave an extinct anomality compared with the flexible network of the gel. This new-found anomality was explained by the "Micro-Space Effect."

7) W. S. Brey, Jr., T. E. Evans, L. H. Hitzrot, *J. Colliod Interface Sci.*, **26**, 306 (1968).

Effects of Pressure on the Chemical Properties of Solid Surface. VI. The Surface Acidity of the Compressed Zinc Sulfate

Takeshi KAWAKAMI, Akira USUI, and Yoshisada OGINO

Department of Chemical Engineering, Faculty of Engineering, Tohoku University, Aoba, Aramaki, Sendai

(Received June 24, 1971)

In order to clarify the mechanism of the acidity change due to compression, zinc sulfate was compressed under various pressures, ranging from 0 to 7000 kg/cm², and the surface acidity was measured and compared with the data of the structural change in the sample. According to the experimental results, the surface acidity varied on compression. At lower compacting pressures ($P\sim2500$ kg/cm²), the content of weak acid ($H_0=1.5$—3.3) was high and that of the strong acid was poor. These facts were explained by the higher content of anion-water, or heptahydrate, in the sample. In the pressure region of $P=2500<5500$ kg/cm², the acidity-pressure curve showed a maximum at 4500 kg/cm². Further, in this pressure range, the acidity-pressure curve paralleled well the respective curves of the X-ray peak width of hexahydrate pressure, the relative intensity of the IR $\nu_1(SO_4^{2-})$-pressure, and the half width of the IR $\nu_3(SO_4^{2-})$-pressure. It was considered that the acidity change in this pressure range is caused by the change in the content of the distorted structural unit of hexahydrate in the sample. In the highest pressure range, the content of weak acid was found to increase, whereas the content of strong acid was found to decrease. These results were discussed by considering the increased inclusion of tetrahydrate in the sample.

It has been revealed by the earlier works of the present authors[1-3] that the surface acidity of a solid varies on compression, and in the immediately preceding work[4] the authors have attemped to clarify the mechanism of the acidity change in aluminum sulfate. It has been demonstrated that the acidity change can be explained in terms of a microscopic structural change of the sample.

The purpose of the present work is to investigate whether or not the same mechanism as for the acidity change in aluminum sulfate is applicable to the acidity change in zinc sulfate. The details of the experimental results, including the acidity change, as well as the structural change in the sample will be described in this paper. Further, the validity of the previously-proposed mechanism of the acidity change will be demonstrated in the discussion.

Experimental

Material. The zinc sulfate heptahydrate was purified by means of recrystallization, and the resulting sulfate was used as the raw material for the sample.

Preparation of the Compressed Sample. The raw sulfate was compressed by the procedures described in the previous papers.[1-4] Briefly, the compression was carried out over a 10 min period under various pressures, ranging from 0 to 7000 kg/cm² and at a temperature of 20°C. The resulting cylindrical pellet, 6 mm in diameter and 2 mm in height, was pulverized in a mortar, and the powdered material was subjected to drying in a vacuum for 45 min at a temperature of 18°C. Then the powder served as a sample for the desired measurement. In order to minimize the effects of the change in ambient conditions, the following operations, *i.e.*, compressions, pulverizings, dryings, and weighings, were carried out in an air-conditioned room.

For the sake of convenience, the respective samples which were compressed under 0, 2500, 4500, 5500, and 7000 kg/cm² were defined as P_0, P_{2500}, P_{4500}, P_{5500}, and P_{7000}.

Surface Acidity. The surface acidity was determined by Benesi's method[5] with the following four indicators: dicinnamalacetone ($pK_a=-3.0$), crystal violet ($pK_a=0.8$), benzeneazodiphenylanmie ($pK_a=1.5$), and *p*-diphenylamino-azobenzene ($pK_a=3.3$). The acidity measurements were also carried out in an air-conditioned room.

Qualitative Tests for Lewis Acid. The identification of the Lewis acid center on the sample surface was carried out by the procedures used in a previous work.[4]

Surface Areas. The specific surface area of the sample evaluated by applying the BET thory to the adsorption data of nitrogen at −195°C.

Differential Thermal Analysis(DTA) and Thermogravimetric Analysis(TGA). DTA and TGA runs were carried out on a Rigaku Denki unit. The DTA curves and TGA curves were obtained at a temperature programming rate of 5°C/min.

X-Ray Diffraction. Powder X-ray diffraction patterns of the sample were obtained with a Shimadzu GX-1 X-ray Diffractometer. The Cu$K\alpha$ radiation (Ni filter) at 30 KV and 15 mA was used.

Infrared Spectroscopy. The infrared spectra for a 400~4000 cm^{-1} wave number range were obtained with a Perkin-Elmer Model 125 Infrared Spectrophotometer. In this work, a Nujol technique was employed.

Results

Surface Acidity. In Fig. 1, the acidity values of a given H_0 value are plotted against the compacting pressure. As can be seen in this figure, the acidity of $H_0=-3.0\sim0.8$ and the acidity of $H_0=0.8\sim1.5$ both increase with an increase in the compacting pressure and reach a maximum at a compacting pressure of 4500 kg/cm²; a further increase in the compacting pressure results in a decrease in the surface acidity. On the other hand, the pressure dependence of the content of weak acid ($H_0=1.5\sim3.3$) showed a com-

1) Y. Ogino and T. Kawakami, This Bulletin, **38**, 972 (1965).
2) Y. Ogino, T. Kawakami, and K. Tsurumi, *ibid.*, **39**, 639 (1966).
3) Y. Ogino, T. Kawakami, and T. Matsuoka, *ibid.*, **39**, 859 (1966).
4) T. Kawakami, A. Konno, and Y. Ogino, *ibid.*, **44**, 1772 (1971).
5) H. A. Benesi, *J. Phys. Chem.*, **61**, 970 (1957).

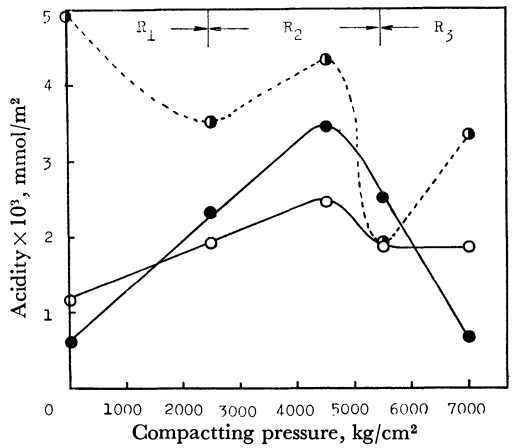

Fig. 1. Relations between the compacting pressure and the surface acidity: -○- H_0=−3.0~0.8, -●- H_0=0.8~1.5, -◑- H_0=1.5~3.3.

plicated behavior. Further, none of the samples showed any sign positive to the existence of Lewis acid.

Water Content. The water contents in samples compressed under various pressures are given in Table 1.

Table 1. Water Contents of the Samples compressed under Various Pressures

Compacting Pressure (kg/cm²)	0	2500	4500	5500	7000
Water Content (mol-H_2O/mol-$ZnSO_4$)	6.33	6.13	6.11	6.12	6.16

DTA and TGA. The DTA curves for various samples are given in Fig. 2. As can be seen in this figure, dehydration from the compressed sample occurred at 50, 98, and 240°C, while the dehydration from the uncompressed sample occurred at various temperatures. The TGA experiment and the chemical analysis

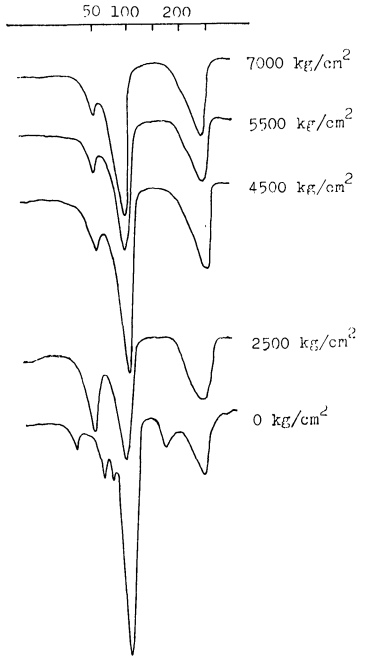

Fig. 2. D.T.A. curves for the samples compressed at various pressures.

Table 2. Amount of Dehydration at 50°C and 98°C

Samples	50°C	98°C
P_{2500}	1.7 mol-H_2O/mol-$ZnSO_4$	3.6 mol-H_2O/mol-$ZnSO_4$
P_{4500}	1.9 mol-H_2O/mol-$ZnSO_4$	3.2 mol-H_2O/mol-$ZnSO_4$
P_{5500}	1.9 mol-H_2O/mol-$ZnSO_4$	3.3 mol-H_2O/mol-$ZnSO_4$
P_{7000}	2.0 mol-H_2O/mol-$ZnSO_4$	3.3 mol-H_2O/mol-$ZnSO_4$

gave the corresponding amounts of dehydration at 50 and 98°C. The results are summarized in Table 2. The data given in this table show that the endothermic DTA peak appearing at 50°C for the compressed samples may be attributed to the dehydration;

$$ZnSO_4 \cdot 6H_2O \longrightarrow ZnSO_4 \cdot 4H_2O + 2H_2O$$

and that the peak appearing at 98°C may be attributed to the dehydration;

$$ZnSO_4 \cdot 4H_2O \longrightarrow ZnSO_4 \cdot H_2O + 3H_2O$$

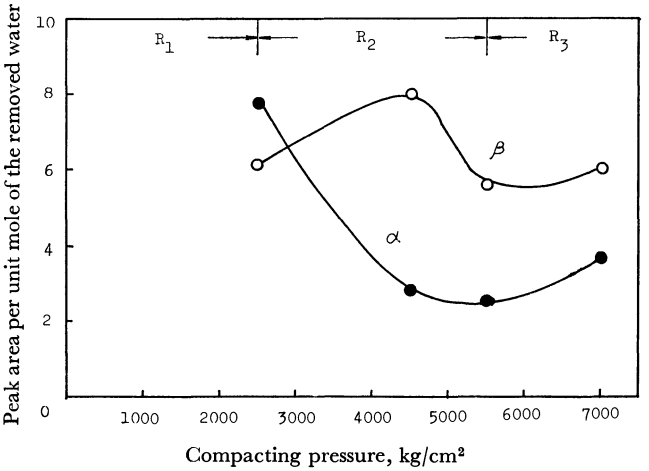

Fig. 3. Relations between the compacting pressure and the area of the endothermic peaks appaered at 50°C (-●-) and at 98°C (-○-).

The value of the endothermic DTA peak area per unit mole of removed water is given in Fig. 3. The area of the peak appearing at 50°C varied on compression and reached a minimum at a compacting pressure of 4500~5500 kg/cm². On the contrary, the area of the peak appearing at 98°C increased with an increase in the compacting pressure and reached a maximum at a compacting pressure of 4500 kg/cm². A further increase in the compacting pressure resulted in a decrease in this peak area.

As can be seen in Fig. 2, there is a marked difference between the DTA curve of the uncompressed sample and that of the compressed sample. The DTA curve for the former sample has many more endothermic peaks than the DTA curve for the latter sample. This means that the uncompressed sample contains many kinds of crystallization water. As can be seen in the next section, the compressed sample contains both zinc sulfate heptahydrate and zinc sulfate hexahydrate, whereas the compressed sample contains mainly hexahydrate. (The possibility of the coexistence of a small amount of heptahydrate can not be excluded. Further, the coexistence of tetrahydrate $ZnSO_4 \cdot 4H_2O$ is also seen at pressures higher than 5500 kg/cm²). Thus,

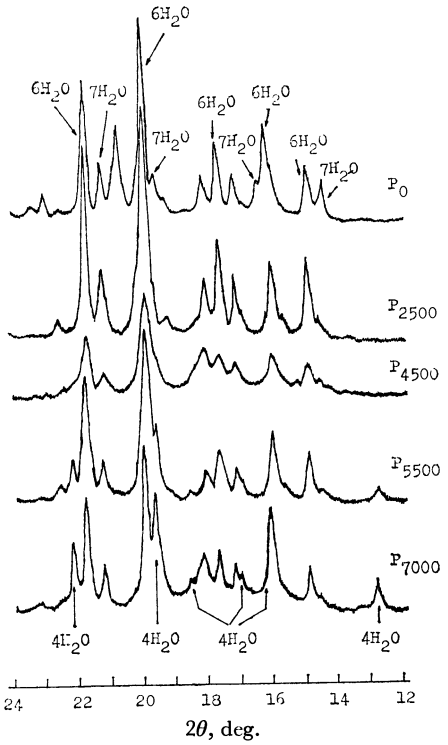

Fig. 4. X-ray diffraction patterns for various samples.

the complex DTA curve for the uncompressed sample may be attributed to the co-existence of hexahydrate and heptahydrate.

X-Ray Diffraction. Powder X-ray diffraction patterns for the various samples are igven in Fig. 4. From these patterns, it can be understood that the zinc sulfate used in this study consisted of crystals of heptahydrate[6] and hexahydrate.[7] Up to the compacting pressure of 4500 kg/cm^2, the line intensity of the heptahydrate decreased, and that of the hexahydrate increased, with an increase in the compacting pressure. However, this trend was reversed at compacting pressures higher than 4500 kg/cm^2.

Further, the degree of the broadening of the diffraction line for the hexahydrate increased with an increase in the compacting pressure from 0 to 4500 kg/cm^2, then it decreased at higher compacting pressures. In addition, diffraction peaks for tetrahydrate ($ZnSO_4 \cdot 4H_2O$) were found to appear (Fig. 4) in the diffraction pattern for the samples compressed at pressures higher than 5500 kg/cm^2.

Infrared Spectra. The infrared spectra for the sample compressed under various pressures are given in Fig. 5. Among the absorption bands in this figure, the bands assigned to ν_{OH} (3400 cm^{-1}), ν_{wag} (540 cm^{-1}),[8] and ν_{SO_2} (985 cm^{-1}) seemed to vary on compression. In view of the general difficulties in the comparison of the IR data for the polycrystalline hydrate, the following IR data are thought to include some ambiguities; they

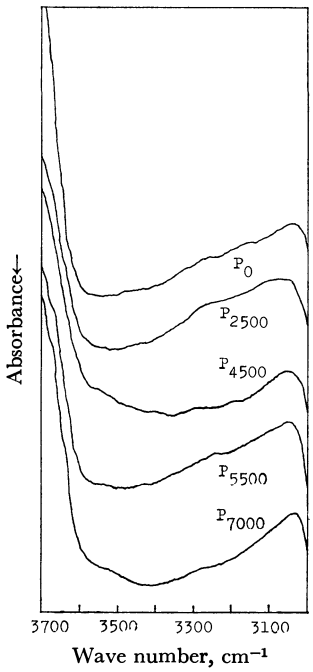

Fig. 5 A. Infrared spectra for various samples.

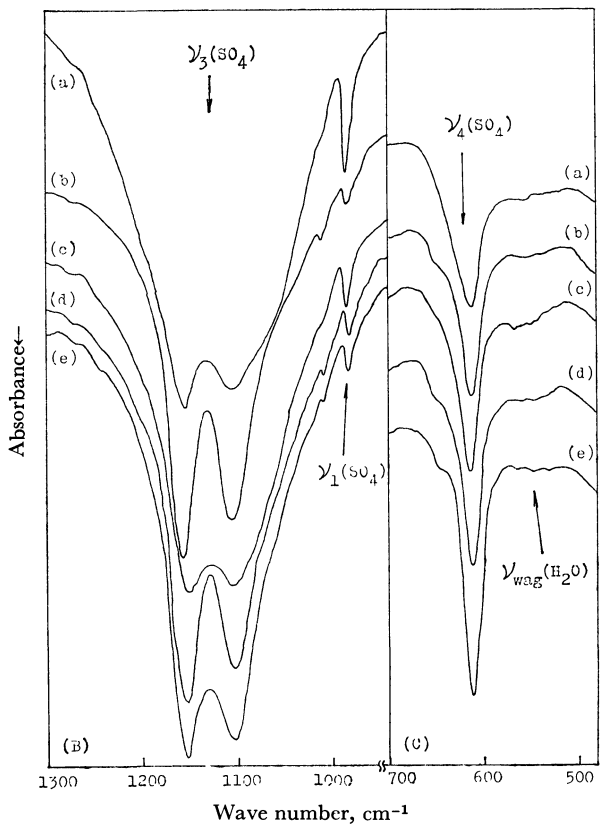

Fig. 5-B,C. Infrared spectra for the samples compressed at various pressures: (a) P_0; (b) P_{2500}; (c) P_{4500}; (d) P_{5500}; (e) P_{7000}.

must be regarded as qualitative data even if they are expressed by numerical values (*e.g.*, the intensity or the relative intensity):

i) The shape of the absorption band appearing at 2800~3600 cm^{-1}, which was assigned to the OH stretching vibration, seemed to vary on compression,

6) "Index to the Powder Diffraction Fill," ed. by J. V. Smith, ASTM Publications (1965), 9-395.

7) *Ibid*, 1-0352.

8) I. Nakagawa and T. Shimanouchi, *Spectrochimica Acta*, **20**, 429 (1964).

especially at 4500 kg/cm². From this fact, it was suspected that the absorption band for the P_{4500} sample shifted to somewhat lower wave numbers. However, this is only a suspicion. Because of the broad absorption band, the exact peak position could not be determined.

ii) The absorption appearing at 985 cm^{-1} was assigned to the ν_1 vibration of sulfate ions in the sample. The relative intensity[9] of this absorption against the intensity of the absorption for the ν_4 vibration of the sulfate ion (656 cm^{-1}) is given in Fig. 6. As can be seen in this figure, the relative intensity varied on compression.

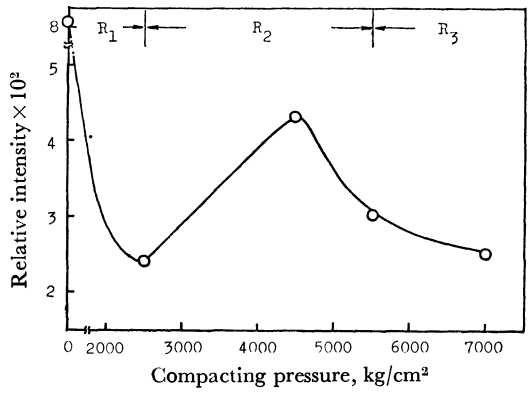

Fig. 6. Relations between the compacting pressure and the relative intensity of the ν_1 absorption against the ν_4 absorption for the sulfate ion.

iii) The absorption appearing at 540 cm^{-1} was assigned to the wagging vibration of the coordinated water in the sample. As can be seen in Fig. 5, the intensity[10] of this absorption seemed to increase with an increase in the compacting pressure, reaching a maximum at the compacting pressure of 4500 kg/cm², while it seemed to decrease at higher compacting pressures. Unfortunately, however, the reliability of this pressure-dependence for the H_2O wagging libration is not high enough because the absorption band at 540 cm^{-1} is broad and weak.

Discussion

Acidity Change on Compression and Related Data. Much as with the surface acidity of the other sulfates,[1-4] the surface acidity of zinc sulfate hydrate was found to vary on compression.

Generally speaking, the observed acidity change should be related to the structural change of the sample. However, as can be seen in Fig. 1, the surface acidity per unit surface area varied on compression. Therefore, the acidity change observed in the present study could not be attributed to the change in the surface area. Other factors must be related to the acidity change. It may be suspected that the dehydration from the sample might be directly causing the acidity change. However, efforts to correlate the acidity change with the degree of dehydration were not successful. It is difficult to derive any meaning from the small differences among the water contents of the various compressed samples (Table 1). In addition, approaches of this type seem to give little information about the microscopic cause of the acidity change.

In discussing the mechanism of the acidity change, the fact that the sample did not show any sign positive to Lewis acid must be taken into consideration. This fact and the experimental results given in Fig. 1 indicate that the acid which was found on the sample surface should be identified as Brönsted acid, which has a strength of $3.3 \geq H_0 \geq -3.0$. Therefore, the mechanism of the acidity change may be considered to include changes in the interaction among ions constituting the sample. From this point of view, the changes in the ionic arrangement in the sample must be compared with the acidity change.

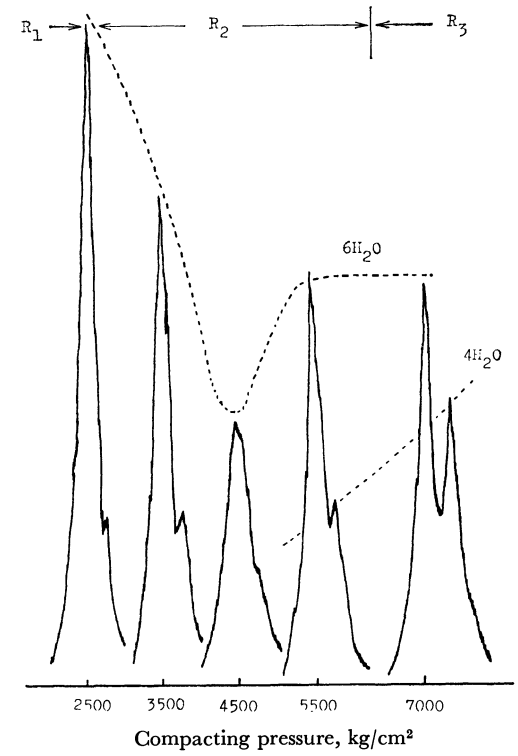

Fig. 7. Changes in the X-ray diffraction peak height (2θ= 20.2°).

On this point, information obtained from the X-ray diffraction study is useful. As can be seen in Fig. 7, the height of the X-ray diffraction peak at 2θ=20.2°, reached a minimum at the compacting pressure of 4500 kg/cm². Further, as can be seen in Fig. 8, the half-width of the diffraction peak reached its maximum at 4500 kg/cm². If these two figures are compared with Fig. 1, which shows the maximum acidity at 4500 kg/cm², an intimate relation between the acidity change and the change in the crystal structure becomes evident. However, the anomalously high acidities of H_0=1.5~3.3 for both samples of P=0 and P=7000 kg/cm² do not conform with the relation between the X-ray half-width (2θ=20.2°) and the compacting pressure (Fig. 8). These facts seem to indicate that factors other than the change in the X-ray peak at 2θ=20.2°

9) Defined by the ratio of the peak area.
10) Defined by the peak area.

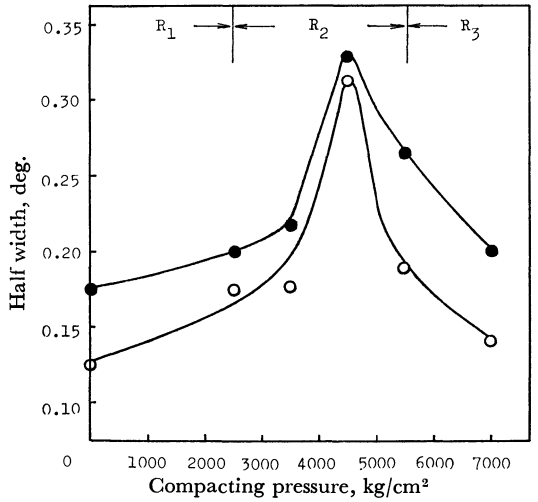

Fig. 8. Relations between the compacting pressure and the half-width of the X-ray diffraction peak for zinc sulfate hexahydrate: -●- $2\theta=20.2°$, -○- $2\theta=15.0°$.

(*i.e.*, the change in the crystal structure of hexahydrate) must be taken into consideration in order to discuss the acidities of the samples of $P=0$ and $P=7000$ kg/cm^2.

On the basis of the above discussion, the following discussion may be divided into three parts corresponding to three pressure regions-R_1, R_2, and R_3; R_1 ($P=0$ kg/cm^2) is a region where the anomalously high content of weak acid does not conform with the smaller half-width of the X-ray peak at $2\theta=20.2°$; R_2 ($P=2500\sim5500$ kg/cm^2) is a region where the acidity change conforms well with the change in the X-ray peak width, and R_3 ($P=5500$—7000 kg/cm^2) is a region where the existence of tetrahydrate becomes evident and the higher content of weak acid does not conform with the smaller X-ray half-width of hexahydrate ($2\theta=20.2°$).

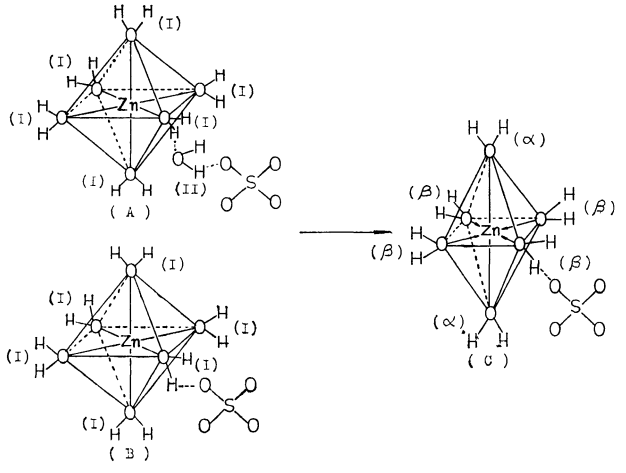

Fig. 9. Models of structural unit of zinc sulfate: (A) heptahydrate, (B) hexahydrate (not distorted), (C) hexahydrate (distorted).

Acidity Change and Structural Change in R_1. As can be seen in Fig. 1, the amount of weak acid ($H_0=1.5\sim3.3$) in the uncompressed sample was considerably great. On the other hand, the water content of this sample was also high compared with the other samples (Table 1). Further, the X-ray diffraction pattern for the uncompressed sample indicated rather strong peaks for heptahydrate. Therefore, it seems probable that the higher content of the weak acid in the uncompressed sample may be due to the higher content of anion-water (*cf.* Fig. 9-A) or to the presence of a heptahydrate.

In connection with the above discussion, it must be made clear that the relative intensity of the IR $\nu_1(SO_4^{2-})$ spectrum and the half-width of the $\nu_3(SO_4^{2-})$ spectrum were quite high for the uncompressed sample (Figs. 6, and 10). These facts may be ascribed to the higher content of anion-water. That is, it was considered that the anion-water may act to reduce the symmetry around sulfate ions in the sample.

The above view is rather crude, and more detailed discussions are desirable. Unfortunately, however, this is not possible at present. From a rather complicated feature appearing in the DTA chart for the uncompressed sample (Fig. 2), it is thought that the water molecules in this sample behave in a complex manner. Further, the easier dehydration observed at lower compacting pressures suggests that the uncompressed sample has an unstable structure. Thus, it is thought that the mechanism of the acidity change at compacting pressures lower than 2500 kg/cm^2 (in R_1) might be complex; more precise experimental work than the present experiments seem to be required to clarify the mechanism. For these reasons, detailed discussions of the acidity change in R_1 were not carried out in this paper.

One more point to be mentioned here is the low acidity for the strong acid ($H_0\leq1.5$) in this region (Fig. 1). Judging from the fact that the peak height for the X-ray diffraction of the uncompressed sample was generally high, both heptahydrate and hexahydrate seem to have their regular structural units. Therefore, there are few factors to strengthen the acid in the uncompressed sample. A higher content of anion-water may be an important factor in exhibiting the appearance of the strong acid. Thus, it may be possible to consider that the existence of heptahydrate is unfavorable for the appearance of strong acid.

Acidity Change and Structural Change in R_2.[11] As was mentioned in the previous section, the acidity change in this region was found to parallel well the change in the X-ray peak height or peak width for hexahydrate. Therefore, the acidity change in this region (R_2) may be related intimately to the change in the crystal structure of hexahydrate. Further, considering from the X-ray diffraction data (Fig. 4) and water content (Table 1), it may be estimated that the dominant species existing in the samples in the R_2 region are hexahydrate and that the existence of other species (heptahydrate and tetrahydrate) would have little effect on the acidity change because the contents of the latter species are considered to be small.

Under the provisions described above, the following discussions may be applicable to the acidity change in R_2. When changes in the crystal of hexahydrate occur, some changes in the structural unit constituting

11) It must be noted that all the figure referred to in this part should be confined to the pressure region of 2500—5500 kg/cm^2.

the crystallite of hexahydrate may be expected to occur. Therefore, the intimate relation between the acidity change in R_2 and the change in the X-ray diffraction peak for hexahydrate seems to mean that the acidity change may be caused by the change in the structural unit of hexahydrate. This view is in accord with the results obtained in the preceding work.[4] In order to aid the following discussions, models of the structural units of zinc sulfate hydrate,[8] including the model of hexahydrate, are given in Fig. 9.

The structural unit of $ZnSO_4 \cdot 6H_2O$ contains 6 moles of the coordinated water. However, the DTA data shown in Fig. 2 indicate that the coordinated water in the compressed sample is not equivalent. Further, the TGA data showed that 2 moles of the coordinated water were removed by the heating at ~50°C, and that the remaining coordinated water was removed by heating at higher temperatures. Therefore, it may be plausible to consider that the compressed sample contains two sorts of coordinated water. Thus, the 2 mol of coordinated water which were removed at 50°C were defined as α, and the other coordinated water was defined as β. The 4 mol of β may be considered to consist of 3 mol of β_1 and 1 mol of β_2. The respective dehydration temperatures of β_1 and β_2 are 98 and 240°C. Unfortunately, however, it is not possible to decide which one of the four coordinated water specimen is β_2.

There are many reasons to consider that the interactions between the central Zn^{2+} ion and the coordinated water vary on compression. As can be seen in Fig. 3, the DTA endothermic peak area per unit of mole of the removed water varied on compressing the sample. The peak area for the dehydration of α-water decreased on compression and reached its minimum at the compacting pressure of 4500~5500 kg/cm^2. On the contrary, the peak area for the dehydration of β_1-water reached its maximum at 4500 kg/cm^2. These facts indicate that the interaction between Zn^{2+} and β_1 reached its maximum at 4500 kg/cm^2, while the interaction between Zn^{2+} and α reached its minimum in the vicinity of this compacting pressure.

As has been mentioned in the experimental section, the interpretation of the IR data for such polycrystalline hydrates as are used in the present work involves many difficulties. Therefore, the following discussions of the IR data should be regarded as crude and approximate. The purpose of the present discussion is to show that the results of the IR experiments exhibit qualitative parallelisms with the other experimental data, *i.e.*, the surface acidity, the X-ray diffraction, and the DTA.

As has been mentioned in connection with the experimental results, the IR absorption band at 3400 cm^{-1} (OH stretching) for the P_{4500} sample was suspected to shift toward lower wave numbers (Fig. 5A, P=2000~5500 kg/cm^2). If this suspicion was not imaginary, the IR data in Fig. 5A (P=2000~5500 kg/cm^2) would support the theory that the strongest interaction of Zn^{2+} with β occurred at P=4500 kg/cm^2. Further, the IR absorption for the H_2O wagging libration (540 cm^{-1}) seemed to be most intensified at P=4500 kg/cm^2 (Fig. 5C). Although the reliability of this spectral change was not high enough, the strongest interaction of Zn^{2+} with β at P=4500 kg/cm^2 seems to be suggested.

In addition to the above-mentioned changes in the infrared spectra for water, Fig. 5 shows that the infrared spectra for the sulfate ion varied also on compression. The changes in the half-widths of the ν_3 vibration of the sulfate ion and the relative intensity of the ν_1 vibration of the sulfate ion are given in Fig. 10 (P=2500~5500 kg/cm^2). It can be seen that the largest change appeared at the compacting pressure of 4500 kg/cm^2. These facts seem to indicate that the interaction between the sulfate ion and its environments varied on compression. In view of the model of the structural unit, such changes as have been described above may be thought to occur easily. Presumably, the increased ν_1 absorption of SO_4^{2-}, which is originally inactive in the infrared absorption, may result from an increased interaction between the oxygen in the sulfate ion and the hydrogen in the coordinated water, β.

The acidity changes observed in the R_2 region seem to be explainable in terms of the structural unit of $ZnSO_4 \cdot 6H_2O$. The existence of two sorts of coordinated water, *i.e.*, α and β, means that the octahedron around the Zn^{2+} ion is distorted in the manner shown in Fig. 9-C (the distances between Zn^{2+} and H_2O (α) are extended and the distances between Zn^{2+} and H_2O (β) are shortened); moreover as has been mentioned in the previous section, the change in the interaction between the central Zn^{2+} and the coordinated water, β, may result from the change in the compacting pressure. The change in the interaction between Zn^{2+} and H_2O (β) may result in a change in the degree of the polarization of the H_2O (β) molecule in the following way:

$$Zn^{2+}\cdots O\begin{matrix}H\\ \\ H\end{matrix} \longrightarrow Zn^{2+}\cdots {}^{-\delta}O\begin{matrix}H^{\delta+}\\ \\ H\end{matrix}$$

Thus, the quantity of the protonic-acid center around the octahedral structural unit will vary. According to this mechanism, the acidity will become larger as the interaction between Zn^{2+} and H_2O (β) is increased.[12]

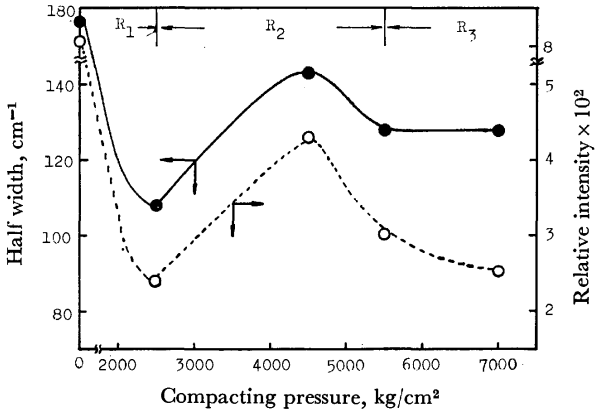

Fig. 10. Relations between the compacting pressure and the half width of the ν_3 absorption band of the sulfate ion (-○-), and the changes in the relative intensity of the ν_1 absorption against the ν_4 absorption for the sulfate ion (-●-).

12) G. Zundel, "Hydration and Intermolecular Interaction," Academic Press, New York (1969).

The parallelism between the acidity change (Fig.1) and the change in the dehydration peak area (Fig. 3) seems to indicate the validity of the above-mentioned mechanism for the acidity change. Further, the crude parallelism between the acidity change (Fig. 1) and the IR data for the OH stretching (Fig. 5A) and H_2O wagging libration (Fig. 5C) seems to be consistent with the proposed mechanism for the acidity change.

The interaction between the sulfate ion and the coordinated water (β) may also contribute to the acidity change. As has been mentioned in the previous section, the infrared spectra (Figs. 5 and 10) revealed that this interaction also varies on compression; the acidity change (Fig. 1) also paralleled the changes in the infrared spectra for the ν_1 and ν_3 vibrations of the sulfate ion (Fig. 10). Presumably, the compression resulted in a displacement of the sulfate ion nearer to the octahedral structural unit, and this promoted the polarization of the H_2O (β) molecule. Further support for this mechanism is given in Fig. 11. As can be seen in this figure, the relative intensity of the ν_1 absorption of SO_4^{2-} has a straight-line relationship to the acidity change.

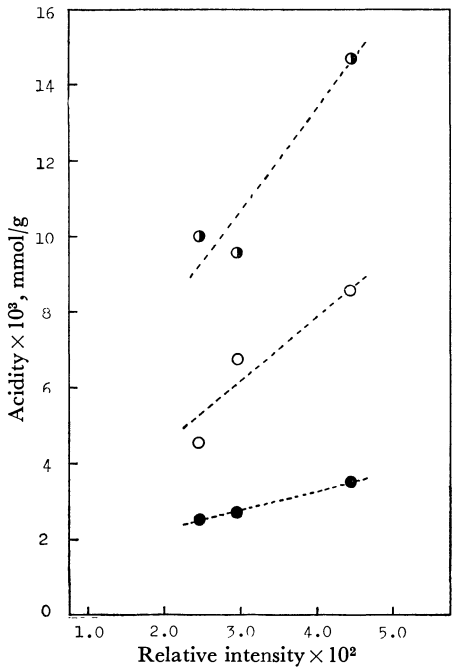

Fig. 11. Relations between surface acidity ($H_0=-3.0\sim 0.8$, -●-; $H^0=-3.0\sim 1.5$, -○-; $H^0=-3.0\sim 3.3$, -◑-) and the relative intensity of ν_1 absorption against the ν_4 absorption for the sulfate ion.

The pressure range of $P=4500\sim 5500$ kg/cm² seems to be a special region, though this pressure range was considered to belong to R_2. In this pressure range, the acidity was found to decrease despite the increasing pressure. As has been mentioned in the previous paragraphs, the decreasing acidity in R_2 is attributable to the decreasing distortion of the structural unit of hexahydrate. This decreasing distortion of the structural unit seems to be ascribable to the appearance of tetrahydrate. The X-ray diffraction data given in Fig. 4 show that the peak for tetrahydrate appears at 5500 kg/cm². It is probable that a part of the supplied energy of compression was consumed to produce tetrahydrate. Therefore, the energy to distort the structural unit may be reduced. Thus, the smaller content of the distorted structural unit and the smaller surface acidity may result. Of course, the formation of tetrahydrate would result in a decrease in the content of hexahydrate (probably accompanied by the formation of heptahydrate). However, judging from the rather weak diffraction peaks of tetrahydrate in R_2, other effects of tetrahydrate on the acidity change in R_2 may be considered to be small and negligible.

Acidity Change and Structural Change in R_3. As can be seen in Fig. 4, when the compacting pressure exceeds 5500 kg/cm² (especially at 7000 kg/cm²), the peaks for tetrahydrate ($ZnSO_4\cdot 4H_2O$) became evident. On the other hand, the content of weak acid ($H_0=1.5\sim 3.3$, R_3 in Fig. 1) and the DTA peak area (β_1, R_3 in Fig. 3) increased in this region, R_3. Therefore, it is not unlikely that these changes are related directly to the existence of tetrahydrate. Unfortunately, however, direct evidence for this view is lacking at present. Whether the higher content of weak acid ($H_0=1.5\sim 3.3$) in the sample compressed at 7000 kg/cm² is due directly to the existence of tetrahydrate, or to the somewhat increased content of heptahydrate, is not certain. (Considering from the fairly constant water content in the compressed sample of $P\geq 2500$ kg/cm², the formation of tetrahydrate may proceed through a disproportionation of hexahydrate. Thus, the formation of tetrahydrate may accompany the formation of heptahydrate. According to the discussion in Part I, the existence of heptahydrate may be a cause of the appearance of weak acids.)

The behavior of the strong acid ($H_0=-3.0\sim 1.5$) in this region (R_3) is also interesting. In spite of the increase in the X-ray diffraction peaks for tetrahydrate, the acidity of $H_0\leq 1.5$ tended to decrease beyond $P=5500$ kg/cm². Therefore, it may be said at least that the existence of tetrahydrate does not result in a marked increase in the content of strong acid. However, in view of the rather complicated structure and composition of the sample in this region (R_3), the possibility that the appearance of tetrahydrate might affect the acidity change (strong acid) in a complicated manner can not excluded.

One important role played by tetrahydrate in the acidity change (strong acid in R_3) seems to be the reduction of the compression energy which is available to distort the structural unit. In the pressure range where the appearance of tetrahydrate is more favorable, the energy of compression may be consumed mainly to form tetrahydrate; in that case, only a part of the energy would be consumed to distort the structural unit. Therefore, a great reduction in the content of strong acid may result. In addition, the formation of tetrahydrate would reduce the content of hexahydrate in the sample. That is, hexahydrate would be consumed and tetrahydrate and heptahydrate, both of which are considered to be ineffective for the appearance of strong acid, might be accumulated in the sample. These factors may also contribute to a reduction in the acidity of the lower H_0 values (strong acid).

Effects of Pressure on the Chemical Properties of Solid Surfaces. VII. Surface Basicities of Some Compressed Carbonates and Related Compounds

Shoe BABA and Yoshisada OGINO

Department of Chemical Engineering, Faculty of Engineering, Tohoku University, Aoba, Aramaki, Sendai

(Received June 28, 1971)

In order to investigate the effect of the compacting pressure on the surface basicities of solids, experiments were carried out by employing various carbonates, hydroxides, and oxides of alkali metals and alkaline earth metals as samples. That is, compacting pressures ranging from 0 to 15000 kg/cm^2 were applied to these samples, and the changes in the surface basicities were observed using an indicator method. It was observed that the surface basicities of various solid vary on compression. Further, the respective basicity change in cadmium carbonate, calcite, and aragonite could be explained by the change in the surface area of each of these samples. On the other hand, the basicity changes of both strontium carbonate and barium carbonate could be explained thus only with difficulty. From the results of the X-ray-diffraction study and the electron-diffraction study, the changes in the crystal structures of these samples were suspected of causing the basicity changes due to compressions. According to the results of infrared spectroscopic studies, changes in the symmetry around carbonate ions in the sample crystals were considered to be the cause of the basicity changes in strontium cabonate and barium carbonate.

It has been revealed by previous works[1-4] of this laboratory that the surface acidities of various solids including metal sulfates vary on compression. Considering from the conjugate characters of the acid and the base and from the findings in the previous works,[1-4] we can expect the surface basicity of a solid will also vary on compression.

The purpose of the present work is to confirm the above expectation. It will be demonstrated in this paper that the surface basicities of various solids vary on compression. Further, some additional experimental results which serve to explain the change will also be included in this paper.

Experimental

Materials. The following solids served as samples for the qualitative experimental works to disclose the pressure effect on the surface basicity:

Carbonates: $CaCO_3$(calcite), $SrCO_3$, $BaCO_3$, $KHCO_3$, K_2CO_3, $NaCO_3$, $NaCO_3 \cdot H_2O$, $(NH)_4CO_3$

Hydroxides: $Mg(OH)_2$, $Ca(OH)_2$, $Sr(OH)_2 \cdot 8H_2O$, $Ba(OH)_2 \cdot 8H_2O$

Oxides: BeO, MgO, CaO, ZnO, BaO

They were all obtained commercially as reagent-grade materials, except for the magnesium oxide, which was obtained by pyrolyzing a commercial magnesium hydroxide at 700°C. In addition, the following carbonates served as samples for the quantitative measurements of the basicity change as well as the structural change;

$CaCO_3$(calcite), $CdCO_3$: sodium nitrate structure

$CaCO_3$(aragonite), $SrCO_3$, $BaCO_3$: potassium nitrate structure

These materials were all obtained commercially as reagent-grade materials, except for the aragonite, which was prepared by drying precipitate obtained by mixing an aqueous calcium chloride solution with an aqueous sodium carbonate solution at 90～100°C.

Preparation of the Sample. The compression of the raw materials was carried out by essentially the same procedures as have been described in the preceding papers.[1-4] That is, the material was gently pulverized in an agate mortar, and then about 0.1 g of the powder was packed into the sample room of a piston-cylinder device. A desired pressure, ranging from 0 to 15000 kg/cm^2, was applied to the powder for 10 min at room temperature.[5] After compression, the resulting cylindrical pellet (1—2 mm in height and 6 mm in diameter) was pulverized in a mortar. The pulverized material was subjected to drying in a vacuum over a 1 hr period at room temperature. The resulting dry material served as a sample for a desired experiment.

Surface Basicity. The qualitative effect of pressure on the surface basicity was observed by the following procedures: by manipulation in a dry box, a given amount of the powder of the compressed sample was transferred to a 50 ml conical flask containing 10 ml of purified benzene. Then, several drops of a 0.1% phenolphtalein ($pK_a=9.3$) solution in benzene were added, and after 1 hr the surface color of the sample was observed. At the same time, a similar observation was carried out by using as uncompressed sample. The difference between the colors of the two samples was then recorded.

The quantitative determination of the surface basicity of the carbonate sample was carried out by employing the following method: by manipulation in a dry box, a given amount (0.05 g) of the sample powder was transferred to each of a a series (usually ten) of 50 ml conical flasks each containing 10 ml of purified benzene. Then enough 1/500 or 1/1000N benzoic acid in benzene was added to each of these ten samples so as to bracket the expected titer. After the samples had then stood for 20 hr. several drops of the indicator solution, *i.e.*, a 0.1% phenolphthalein solution in benzene, were added to each flask. The bracketed titer, *i.e.*, the titer of benzoic acid required to neutralize the surface base, could be determined easily by the observation of the surface color of each sample.

Surface Area. The specific surface area of the carbo-

1) Y. Ogino and T. Kawakami, This Bulletin, **38**, 972 (1965).
2) Y. Ogino, T. Kawakami, and K. Tsurumi, *ibid.*, **39**, 639 (1966).
3) Y. Ogino, T. Kawakami, and T. Matsuoka, *ibid.*, **39**, 859 (1966).
4) T. Kawakami, A. Konno, and Y. Ogino, *ibid.*, **44**, 1772 (1971).
5) Exceptionally, pressure was applied at a temperature of 100°C.

nate samples were evaluted by applying the BET theory to the absorption data of nitrogen at −195°C.

X-ray Diffraction. Powder X-ray diffraction patterns of carbonates which have a potassium nitrate structure were obtained with a Shimadzu GX-1 X-ray Diffractometer. The Cu$K\alpha$ radiation (Ni filter) at 30 KV and 20 mA was used.

Infrared Spectroscopy. The infrared spectra (600—1200 cm^{-1} wave number range) of carbonates which have a potassium nitrate structure were obtained with Perkin-Elmer Model 337 Infrared Spectrophotometer. A Nujol mull technique was employed in every case.

Electron Diffraction. Phtographs of the Debye-Scherrer rings of the strontium carbonate sample and the barium carbonate sample were obtained with an electron-diffraction apparatus (JEM-ADF) attached to a JEOLCO JEN-50 Electron Microscope. The operation was carried out at 50 KV and about 5 μA.

Results

Surface Basicity. The surface colors of the various samples are summarized in Table 1. As can be seen in this table, the compression at 4500 kg/cm² resulted in an increase in the surface color for about 2/3 of all the samples. In other words, the surface basicities of these samples increased on compression.

The results of the quantitative determination of the surface basicity are given in Fig. 1 (a, b), wherein the surface basicities of the samples with a sodium nitrate structure as well as the basicities of the samples with a potassium nitrate structure are both expressed as functions of the compacting pressure. As can be seen in this figure, the basicity of every carbonate increased considerably on compression, though the shape of the basicity-*vs.*-pressure curve was different from carbonate to carbonate. For example, the basicity of calcite, whose original basicity was nearly zero, increased monotonously with an increase in the compacting pressure and reached about 1.6×10^{-2} mmol/g at 15000 kg/cm². In contrast with this, the pressure-*vs.*-basicity curve for cadmium carbonate had a maximum at a pressure of about 7000 kg/cm², and the basicity at this pressure was about twice the original value.

Table 1. Effect of the compacting pressure on the surface basicities of various solids

Sample	Compacting Pressure		Change of Surface Color[a)]
	0 kg/cm²	4500 kg/cm₂	
Na_2CO_3	Slightly violet	violet	++
$Na_2CO_3\cdot H_2O$	Slightly violet	violet	++
$KHCO_3$	Very slightly pink	pink	++
K_2CO_3	Violet	violet	?
$(NH_4)_2CO_3$	Colorless	colorless	?
$CaCO_3$ (calcite)	Colorless	pink	++
$SrCO_3$	Slightly pink	slightly pink	+
$BaCO_3$	Slightly pink	slightly pink	+
$Mg(OH)_2$	Very slightly pink	slightly pink	++
$Ca(OH)_2$	Red violet	red violet	+
$Sr(OH)_2\cdot 8H_2O$	Violet	violet	+
$Ba(OH)_2\cdot 8H_2O$	Slightly violet	slightly violet	++
BeO	Slightly pink	slighly pink	+
MgO	Red violet	red violet	?
CaO	Red violet	red violet	?
ZnO	Slightly pink	slightly pink	?
BaO	Slightly violet	violet	+

(indicator; phenolphthalein (pK_a=9.3))
a) ++; increase, +; slightly increase, ?; uncertain

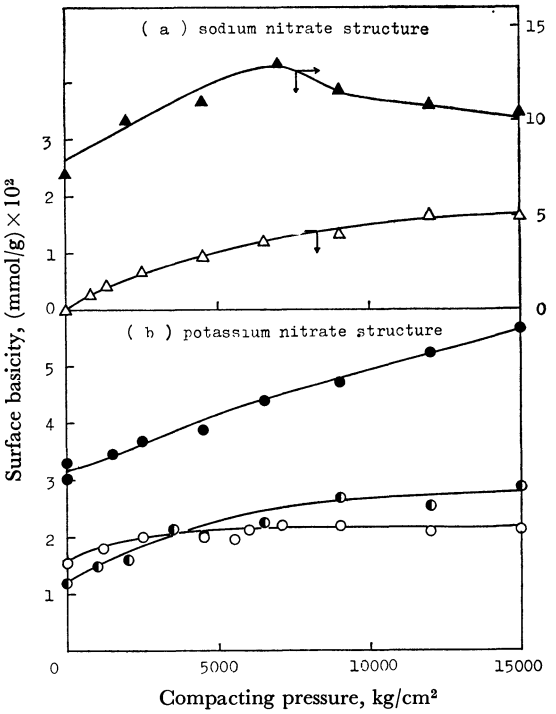

Fig. 1. Relations between the surface basicity and the compacting pressure.
△: $CaCO_3$ (calcite), ▲: $CdCO_3$, ◐: $CaCO_3$ (aragonite), ●: $SrCO_3$, ○: $BaCO_3$

Surface Area. As can be seen in Fig. 2 (a, b),

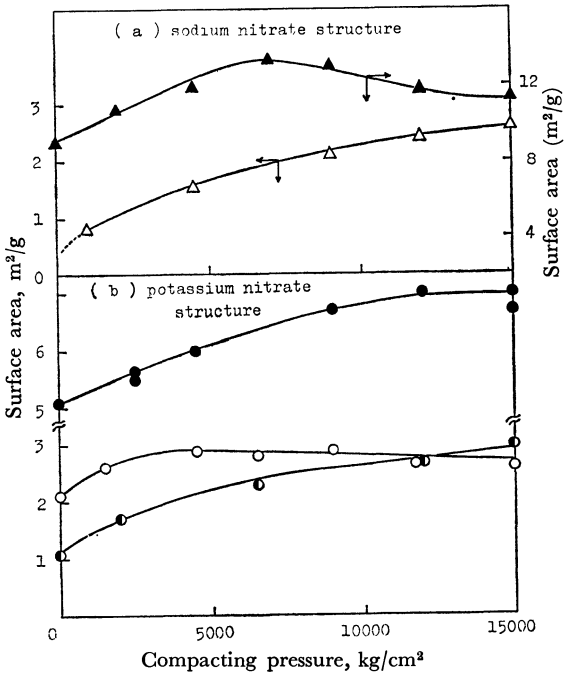

Fig. 2. Relations between the specific surface area and the compacting pressure.
△: $CaCO_3$ (calcite), ▲: $CdCO_3$, ◐: $CaCO_3$ (aragonite), ●: $SrCO_3$, ○: $BaCO_3$

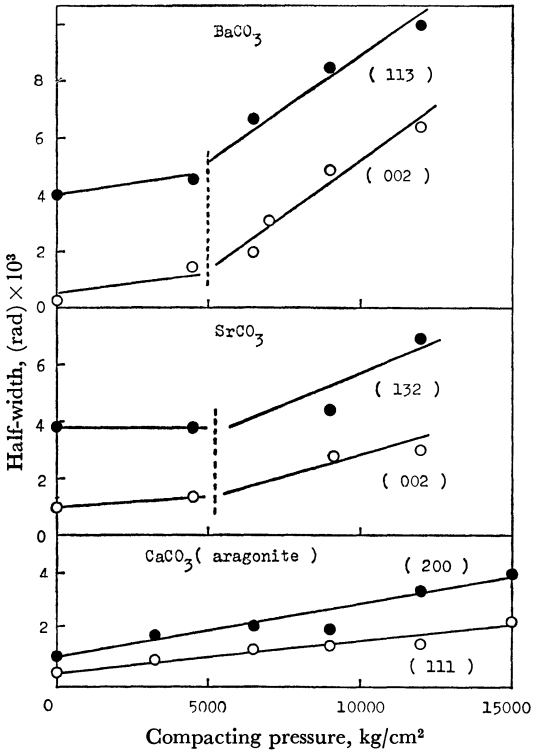

Fig. 3. Relations between the half-widths of the X-ray diffraction peaks and the compacting pressure.

the specific surface areas of every carbonate also varried on compression, though the shape of the surface area-*vs.*-pressure curve was different from carbonate to carbonate.

X-Ray Diffraction. Except for an increase in the halfwidth of the diffraction peak, no appreciable changes in their X-ray diffraction patterns resulted from the compressions of aragonite, strontium carbonate, and barium carbonate. The plots of the half-width against the compacting pressure are given in Fig. 3. Although the evaluation of the lattice distortion by applying Hall's method[6] to the broadening of the X-ray diffraction peaks was not possible, Fig. 3 reveals an interesting aspect of the pressure dependence of the half-width. The half-width of the diffraction peak for aragonite increased monotonously on an increase in the compacting pressure, whereas the half-width of both strontium carbonate and barium carbonate increased abruptly at a compacting pressure of about 5000 kg/cm².

Infrared Spectra. Examples of the infrared spectra for the samples with a potassium nitrate structure (aragonite, strontium carbonate, and barium carbonate) are given in Fig. 4. Two absorption bands, expressed as ν_1 and ν_2 in these spectra were assigned to the totally symmetric stretching vibration of the carbonate anion (CO_3^{2-}) and the out-of-plane deformation vibration of the same anion respectively. Further, the intensities[7] of the ν_1 absorptions of both strontium carbonate and barium carbonate were found to diminish at higher compacting pressures, while the intensities of the ν_2 absorptions of these samples varied little.[8] This behavior is depicted in Fig. 5. As can be seen in this figure, the $S\nu_1/S\nu_2$ ratio, where $S\nu_1$ is the intensity of the ν_1 absorption and $S\nu_2$ is the intensity of the ν_2 absorption, diminished pronouncedly at higher compacting pressures than 5000 kg/cm². In contrast with the pressure-dependent behaviors of the $S\nu_1/S\nu_2$ ratios

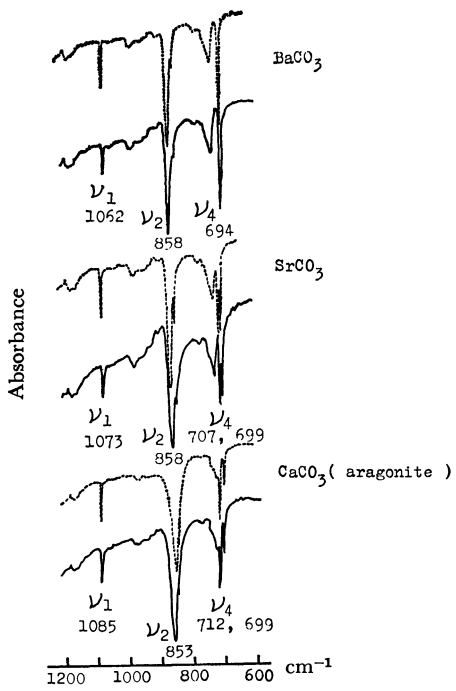

Fig. 4. Infrared spectra for the carbonates having potassium nitrate structure.
·····: uncompressed sample, ——: compressed sample (15000 kg/cm²)

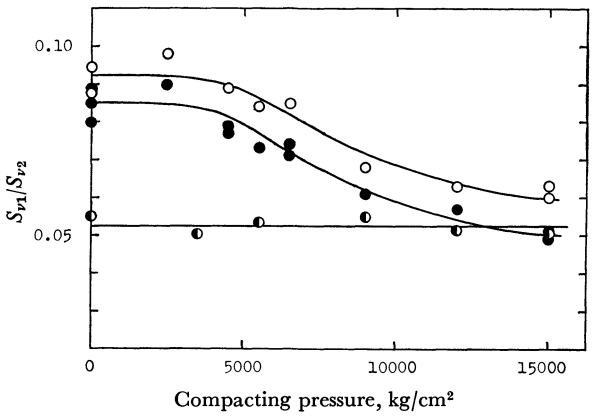

Fig. 5. Relations between $S\nu_1/S\nu_2$ ratios and the compacting pressure.
◐: $CaCO_3$ (aragonite), ●: $SrCO_3$, ○: $BaCO_3$

6) W. H. Hall, *Proc. Phys. Soc., Ser. A*, **62**, 741 (1949).
7) The absorption intensities were determined from the areas (half-width × peak height/2) of the absorption bands.
8) The intensity of the ν_3 absorption (1450 cm^{-1}), measured by a HCB mull technique, also varied little upon the compression, as is shwon in the next table:

TABLE. S_{ν_1}/S_{ν_2} FOR THE COMPRESSED CARBONATES

Pressure (kg/cm²)	0	7500	15000
$BaCO_3$	0.06	0.05	0.07
$SrCO_3$	0.05	0.05	0.06
$CaCO_3$ (aragonite)	0.04	0.05	0.04

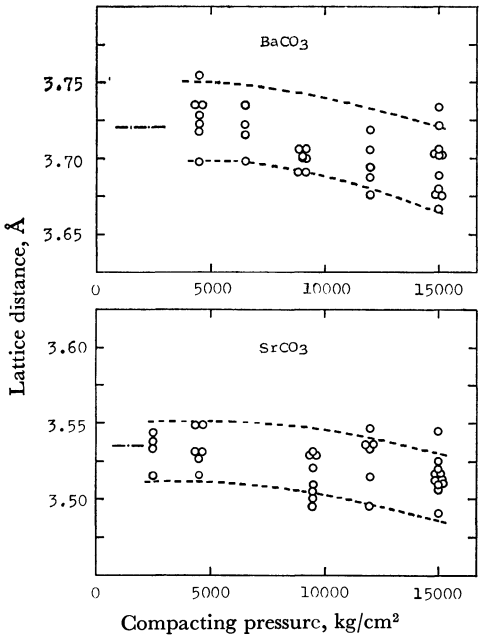

Fig. 6. Relations between the lattice distances for (111) planes of barium carbonate and strontium carbonate samples and the compacting pressure.
—·—: literature value for (111) plane

for strontium carbonate and barium carbonate, the Sv_1/Sv_2 ratio for aragonite was found to be independent of the compacting pressure (Fig. 5).

Electron Diffraction. On the basis of the photographs obtained from the electron-diffraction studies for strontium carbonate and barium carbonate, the lattice distances of the crystals of these samples were calculated. As is illustrated in Fig. 6, the lattice distances for the (111) planes of these samples diminished slightly with the increase in the compacting pressure. Considering the lager scattering of the experimental data shown in Fig. 6, a statistical treatment was applied on the data. The results are given in Table 2. It may be concluded from this table that the decrease in the lattice distance is appreciable.

TABLE 2. STATISTICAL TREATMENT OF THE DATA (THE ANALYSIS OF VARIANCE)

	f	$S\times10^6$	ϕ	$V\times10^6$	F_0	F (4.30; 0.05)
$BaCO_3$	pressures	4817	4	1204	3.97*	2.69
	errors	9102	30	303		
$SrCO_3$	pressures	2551	4	638	3.01*	2.69
	errors	6360	30	212		

(f; factor, S; sum of squares, ϕ; degrees of freedom, V; unbiased variance, F_0; observed F)

Discussion

Basicity Change on Compression. As can be seen in Table 1, the present work revealed that the surface basicities of many solid substances vary on compression. Generally speaking, the change in the surface basicity may be caused by the change in the structure of the sample. However, care must be taken to select suitable samples so as to obtain unambiguous structural data for the discussion of the basicity change. It was found by preliminary experiments that carbonates are suitable for this purpose. Thus, only discussions of the basicity changes in carbonates will be described in this paper.

For the sake of simplicity, the basicity changes in calcite and cadmium carbonate will be considered first. By comparing Fig. 1 (a) with Fig. 2 (a), it can easily be understood that the curves representing the basicity *vs.* pressure relations parallel the cruves representing the surface area-*vs.*-pressure relations. Therefore, the changes in the surface areas are supsected of causing the basicity changes in these samples. In fact, as can be seen in Fig. 7 (a), the surface basicity per unit of surface area for each of the two samples was independent of the compacting pressure. This verifies the validity of the suspicion.

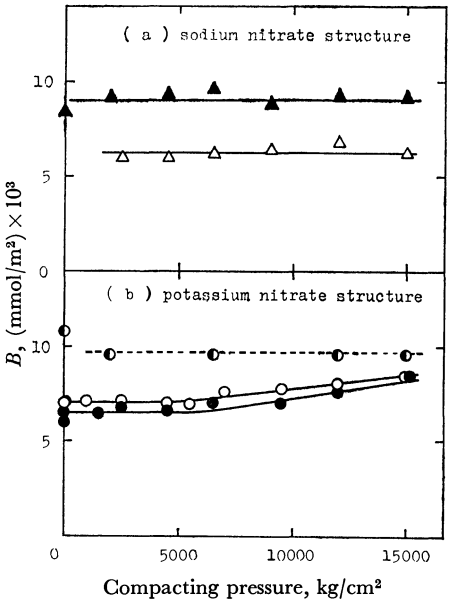

Fig. 7. Relations between B (the basicity per unit of surface area) and the compacting pressure.
△: $CaCO_3$ (calcite), ▲: $CdCO_3$, ◐: $CaCO_3$ (aragonite), ●: $SrCO_3$, ○: $BaCO_3$

In contrast with the above-mentioned simple behavior of the samples with the sodium nitrate structure, the samples with the potassium nitrate structure behaved somewhat complicatedly. That is, as can be seen in Fig. 7 (b), the basicity per unit of surface area of aragonite was found to be independent of the compacting pressure, whereas the surface basicity per unit of surface area of each of the other two samples (strontium carbonate and barium carbonate) showed a pressure dependence. This pressure dependence was small at pressures lower than 5000 kg/cm², but it tended to increase beyond this pressure. In the pressure range of 5000~15000 kg/cm², the pressure dependence was evaluated to be about 30%/1000 kg/cm².

Considering the facts described above, the basicity change in aragonite may be ascribed to the change in the surface area of this sample. That is, the reason for the basicity change in aragonite may be considered to be the same as for that in calcite or in cadmium

carbonate. However, the pressure dependences of the surface basicities of both strontium carbonate and barium carbonate can not be attributed to the cahnges in the surface areas. In order to explain the basicity changes in the strontium carbonate and barium carbonate samples, some other factors must be taken into consideration.

Crystal-structure Change upon Compression. The results of the X-ray diffraction study seem to give some information about the basicity changes in strontium carbonate and barium carbonate. As can be seen in Fig. 3, the half-width of the X-ray diffraction peak for each of these samples tended to increase at ~5000 kg/cm^2. The same tendency is observable in Fig. 7 (b), where the change in the basicity per unit of surface area for each of these two samples is depicted. These facts seem to suggest that the deformation of the crystallites resulted in the increases in the number of basic sites on the surfaces of the samples. Further, the electron-diffraction studies in the present work have revealed that the compression resulted in a decrease in the lattice distances ((111) plane) of strontium carbonate and barium carbonate. These facts also suggest the existence of an intimate relation between the respective basicity change of these samples and the deformation of the crystal structure in each of these samples. Unfortunately, however, because of the existence of larger scatterings in the X-ray diffraction data as well as in the electron-diffraction data, further discussions based on the changes in the crystal structure were not possible.

For the purposes of the present discussion, the infrared-absorption data appears to be more useful than the X-ray-diffraction data. That is, by comparing Fig. 5 with Fig. 7 (b), it can easily be seen that a close relation between the basicity change and the change in the Sv_1/Sv_2 ratio exists. Corresponding to the samll change in the basicity per unit of surface area of the aragonite sample, the Sv_1/Sv_2 ratio of this sample showed little pressure dependence. This fact supports the previous consideration that the observed basicity change (Fig. 1 (b)) of aragonite must result solely from the change in the surface area. On the other hand, the Sv_1/Sv_2 ratios of both strontium carbonate and barium carbonate varied considerably on compression, this tendency seems to correspond to the basicity changes in these samples (Fig. 7 (b)). Thus, in Fig. 8, the basicity changes, B/B_0[9] are plotted against the Sv_1/Sv_2 ratios. As can be seen in this figure, the B/B_0 *vs.* Sv_1/Sv_2 relations for both strontium carbonate and barium carbonate can be expressed by a single curve. This fact seems to indicate that the change in the ν_1 vibration of the carbonate ion in these samples is directly related to the basicity change.

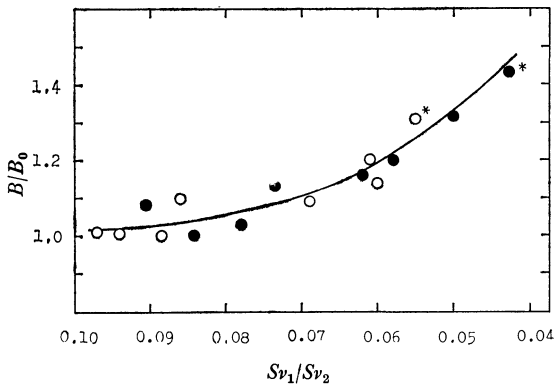

Fig. 8. The relation between the basicity change (B/B^0) and the change in the relative intensity of ν_1 vibration (Sv_1/Sv_2). ●: $SrCO_3$, ○: $BaCO_3$. (The mark * means the value obtained by using the sample compressed under the pressure of 15000 kg/cm^2 and at a temperature of 100°C.)

Analysis of IR Data. It is known that the ν_1 vibration of the carbonate ion becomes inactive for the infrared absorption when the ion is placed in site of D_{3h}, D_3, or C_{3h} symmetry.[10] However, when the site symmetry changes to C_{3v}, C_{2v}, C_3, C_2, or C_s, the ν_1 vibration becomes active for the infrared absorption. The crystal structures of calcium carbonate (aragonite), strontium carbonate, and barium carbonate are of the potassium-nitrate type and belong to the space group D_{16}^{2h}, and the site symmetry is C_s. Therefore, the ν_1 vibration of the carbonate ion becomes active for the infrared absorption. Thus, the observed invariance of the ν_1 absorption spectra of calcium carbonate means either that the original D_{2h} structure of this sample is preserved even in the compressed state or that the original site symmetry varied to C_{3v}, C_3, or C_2. However, few changes in the crystal structure (for example, a change to the calcite structure) were detected from the X-ray-diffraction data and the electron-diffraction data given above. Therefore, the possibility of change in the site symmetry in the calcium carbonate sample may be ignored. Thus, it seems probable to consider that the original crystal structure, D_{2h}, is preserved.

On the contrary, the pressure-dependent behavior of the infrared spectra of both strontium carbonate and

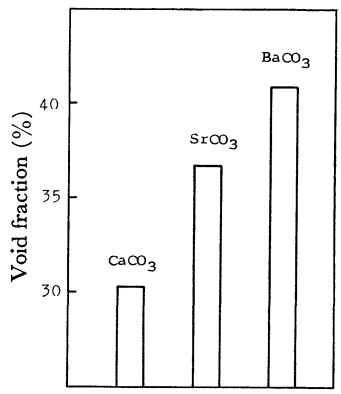

Fig. 9. The void fraction.
The void fractions were approximated by the following equation.
void fraction (%) $=(1-(v/V))\times 100$
v: sum of the volume of metal ions (4π(ionic radius)^3/3) and carbonate ions ($3\times 4\pi$(ionic radius of O^{2-})^3/3) in a unit cell
V: volume of a unit cell

9) B_0 was defined as the original basicity per unit of surface area, and B was defined as the basicity per unit of surface area of the compressed sample.

10) K. Nakamoto, "Infrared Spectra of Inorganic and Coordination Compounds," John Wiley & Sons. New York (1970), p. 61.

barium carbonate mean that the original D_{2h} structures of these samples varied on compression to direction where the symmetry of the crystal increases, *i.e.*, from C_s to D_{3h}, D_3, or C_{3h}.

Presumably, the structural changes being considered accompany contractions, for pressure acts to reduce the volume of a sample. As can be seen in Fig. 9, the void fraction of aragonite is considerably smaller than that of strontium carbonate or of barium carbonate. Therefore, it seems reasonable to consider that the smaller void fraction of aragonite hinders the contraction of this sample and that the original D_{2h} structure is preserved in the compressed state. On the contrary, the larger void fractions of strontium carbonate and barium carbonate may provide spaces to be contracted by the compression.[11]

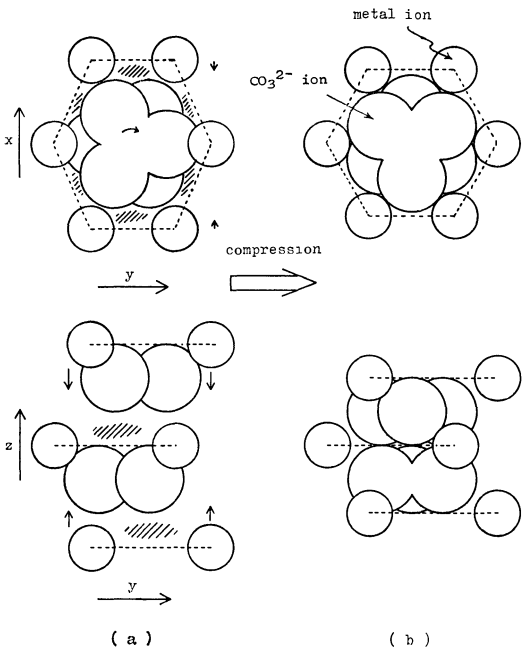

Fig. 10. The expected structural changes of strontium carbonate and barium carbonate due to compression.

The expected structural changes in strontium carbonate and barium carbonate are depicted in Fig. 10. The shaded areas in this figure are the spaces to be contracted by the compression. When these spaces are contracted, the following three changes may occur: (i) the original distorted hexagonal network, which is perpendicular to the z-axis constituted by metal ions, is transformed into a perfect hexagonal network; (ii) around the respective carbon atom, each carbonate ions rotates horizontally (parallel with the xy-plane), 30° from the original position, and (iii) each horizontal plane on which the center of the carbonate ion is located is brought to the hypothetical horizontal plane existing at the center of two nighboring hexagonal networks.

On the basis of the above mentioned discussion, a more precise model for the structural change was

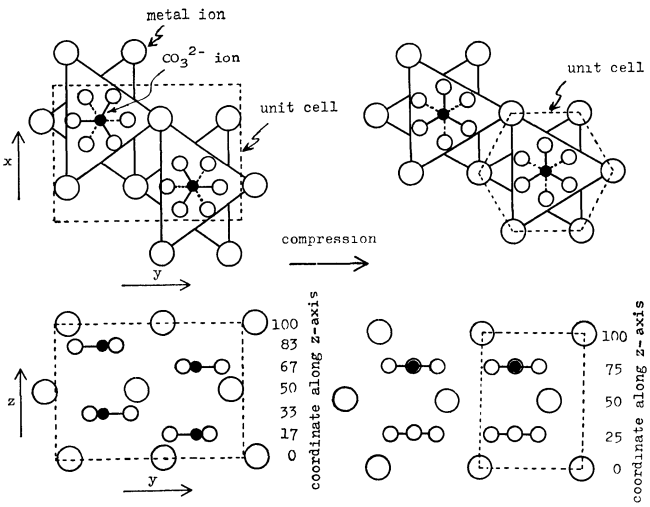

(a) D_2 symmetry (b) D_6 symmetry

Fig. 11. The expected structural change due to compression.

TABLE 3. FACTOR GROUP ANALYSIS OF THE CRYSTAL HAVING THE STRUCTURE DEPICTED IN Fig. 11 (b)

	Number of vibration					Selection rules	
	N	T	T'	R'	n	IR	Raman
A_1	1	0	0	0	1	inactive	active
A_2	4	1	1	1	1	active	inactive
B_1	2	0	1	0	1	inactive	inactive
B_2	3	0	1	1	1	inactive	inactive
E_1	5	1	1	1	2	active	active
E_2	5	0	2	1	2	inactive	active

	E	$2C_6$	$2C_3$	C_2	$3C_2'$	$3C_2''$
A_1	1	1	1	1	1	1
A_2	1	1	1	1	−1	−1
B_1	1	−1	1	−1	1	−1
B_2	1	−1	1	−1	−1	1
E_1	2	1	−1	−2	0	0
E_2	2	−1	−1	2	0	0
$U_R(p)$	10	0	2	0	4	2
$U_R(s)$	4	0	2	0	2	2
$U_R(s\text{-}v)$	2	0	2	0	2	0
$\pm 1+2\cos\phi_R$	3	2	0	−1	−1	−1
$\chi_R'(N)$	30	0	0	0	−4	−2
$\chi_R'(T)$	3	2	0	−1	−1	−1
$\chi_R'(T')$	9	−2	0	1	−1	−1
$1\pm 2\cos\phi_R$	3	2	0	−1	−1	−1
$\chi_R'(R')$	6	0	0	0	−2	0
$\chi_R'(n)$	12	0	0	0	0	0

a) The usual nomenclatures were used in this table.

11) If the compressibility of a solid is proportional to the void fraction, it may be expected that the change in the infrared spectra of barium carbonate will be larger than that of strontium carbonate because the former sample has a larger void fraction. However, the compressibility of a solid is affected by many factors, *i.e.*, the void fraction, the ionic radius, the crystal structure, *etc.*, and is not neceassarily propotional to the void fraction. Therefore, the fact the extents of the changes in the infrared spectra for both samples were nearly equal (Fig. 5) is not always in conflict with the different void fractions of the two carbonate samples. Although the details of the mechanisms of the compression are not clear, the more complete hexagonal structure of the barium carbonate crystal might reduce the degree of the contraction of void. Generally, a crystal of a higher symmetry, *i.e.*, regular cubic or hexagonal, is less compressible than a crystal of lower symmetry.

constructed to give Fig. 11. This figure was used as a basis for the factor group analysis designed to clarify selection rules for the infrared absorption. The results of the conventional-factor group analysis[12] are give in Table 3. This table indicates that both ν_1 vibration of the carbonate ions in the unit cell of the compressed sample (Fig. 11 (b)), which belong to the A_1 and B_1 or B_2 species, are inactive for the infrared absorption. Thus, it became clear that the intensity of the infrared ν_1 absorption diminishes as the symmetry of the sample crystal changes from the original D_{2h} type in the direction of the final D_6 type. The observed pressure-dependent spectral changes of strontium carbonate and barium carbonate may be considered to be examples of such cases as have been described above.

The authors wish to express their gratitude to Professor Koyo Aida, Faculty of Engineering, Tohoku University, for his permission to use the infrared spectrophotometer.

This paper is a part of a dissertation submitted by one of the authors (Shoe Baba) in partial fulfillment of the requirements for the degree of Doctor of Engineering in Tohoku University.

12) M. Tsuboi, "Kagaku no Ryoiki (an extra number)," Vol. 32, Nankodo, Tokyo (1961), p. 35.

BULLETIN OF THE CHEMICAL SOCIETY OF JAPAN, VOL. 46, 133—139 (1973)

Effects of Pressure on the Chemical Properties of Solid Surface. VIII. The Surface Acidity of the Compressed Magnesium Sulfate

Takeshi KAWAKAMI, Hiroyoshi BANBA, and Yoshisada OGINO

Department of Chemical Engineering, Faculty of Engineering, Tohoku University, Aoba, Aramaki, Sendai

(Received September 13, 1971)

In order to clarify the mechanism of the acidity change due to compression, magnesium sulfate was compressed under various pressures ranging from 0 to 12000 kg/cm^2, the surface acidities, the powder X-ray diffraction patterns, the DTA data, and infrared spectra of the compressed samples were thus obtained. According to the experimental results, the surface acidity of the sample did not vary upon the compression of low pressures (0—6000 kg/cm^2), and a further increase in the compacting pressure resulted in an increase in the surface acidity. From the results of the X-ray diffraction studies, infrared, and far infrared absorption studies and the DTA studies, the relations between the acidity change and the structural changes of the samples were discussed. As a result of this work, the observed acidity change was explained in terms of the distortion of the structural unit of magnesium sulfate.

In our previous studies[1-5] of the effects of pressure on the surface acidity of aluminum sulfate and zinc sulfate, explanations were given for the acidity change due to compression.

The present work has been undertaken to examine whether or not the same explanations are applicable to the acidity change of magnesium sulfate hydrate. The purpose of the present paper is to describe the details of the experimental results and to discuss the mechanism of the acidity change.

Experimental

Materials. Commercial magnesium sulfate heptahydrate was purified by means of recrystallization,[6] and the resulting sulfate was used as the raw material of the sample.

Preparation of the Compressed Sample. The raw sulfate was compressed by the procedures described in the previous papers.[1-5] The compression was carried out under various pressures ranging from 0 to 12000 kg/cm^2 and at a temperature of 20°C. Pressure was applied over a 10 min period. The resulting cylindrical pellet, 6 mm in diameter and 2 mm in height, was pulverized in an agate mortar, and the powdered material was subjected to drying in a vacuum over a 60 min period at a temperature of 18°C. Then, the powder served as a sample for the desired measurment. In order to minimize the effects from the change in ambient conditions, all the operations were carried out in an air-conditioned room.

For the sake of convenience, the respective samples which were compressed under 0, 2000, 4000, 6000, 8000, 10000, and 12000 kg/cm^2 were defined as P_0, P_{2000}, P_{4000}, P_{6000}, P_{8000}, P_{10000}, and P_{12000}.

Surface Acidity. The surface acidity was determined by Benesi's method[7] with the following two indicators: *p*-diphenylaminobenzene ($pK_a=3.3$) and phenylazonaphthylamine ($pK_a=4.0$). The acidity measurements were also carried out in an air-conditioned room.

Qualitative Tests for Lewis Acid. The Lewis-acid center on the sample surface was identified by the procedures used in a previous work[4] (color tests with phenolphthalein or trithylchloride).

1) Y. Ogino and T. Kawakami, This Bulletin, **38**, 972 (1965).
2) Y. Ogino, T. Kawakami, and K. Tsurumi, *ibid.*, **39**, 639 (1966).
3) Y. Ogino, T. Kawakami, and T. Matsuoka, *ibid.*, **39**, 859 (1966).
4) T. Kawakami, A. Konno, and Y. Ogino, *ibid.*, **44**, 1772 (1971).
5) T. Kawakami, A. Usui, and Y. Ogino, This Bulletin, to be published.
6) J. W. Mellor, "A Comprehensive Treaties on Inorganic and Theoretical Chemistry," IV, Longmans, Green and Co., 1923.
7) H. A. Benesi, *J. Phys. Chem.*, **61**, 970 (1957).

Surface Areas. The specific surface area of the sapmle was evaluated by applying the BET theory to the adsorption data of nitrogen at −195°C.

Differential Thermal Analysis (DTA) and Thermogravimetric Analysis (TGA). The DTA and TGA runs were carried out on a Rigaku Denki unit. The DTA curves and the TGA curves were obtained at a temperature-programming rate of 2°C/min.

X-Ray Diffraction. The powder X-ray diffraction patterns[8] of the sample were obtained with a Shimadzu GX-1 X-ray Diffractometer. The Cu-$K\alpha$ radiation (Ni filter) at 30 KV and 15 mA was used.

Infrared Spectroscopy. The infrared spectra (IR) for a 400—4000 cm^{-1} wave number range were obtained by means of Perkin-Elmer Model 125 Infrared Spectrophotometer. In these works, a Nujol technique was employed. To minimize the interferences from the air moisture, a sample which had been compressed and evacuated was kept in the vessel containing dry nitrogen. Then, immediately before the IR experiment, the sample was withdrawn from vessel and mixed with nujol as quickly as possible.

Results

Surface Acidity. The surface acidities (H_0=3.3—4.0) of samples compressed under various pressures are given in Fig. 1. The acidity values in this figure are given by *n*-butylamine titers per unit of the surface area. As can be seen in Fig. 1, the acidity did not vary of compressions of 2000—6000 kg/cm², but a further increase in the compacting pressure resulted in an increase in the surface acidity.

Further, additions of phenolphthalein or trithylchloride to the sample showed no sign positive to the existence of Lewis acid on the sample surface. Thus, the acid appearing on the sample could be identified as protonic acid.

Water Content. The water contents of the samples compressed under various pressures are given in Fig. 2. From this figure, it can be understood that the samples compressed at pressures higher than 6000 kg/cm² contain 6 mol of water per mole of $MgSO_4$.

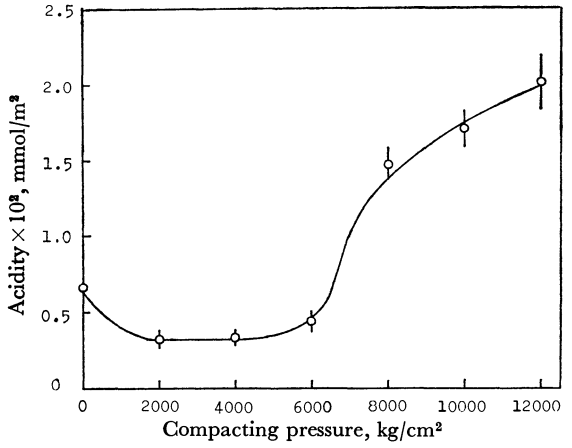

Fig. 1. Relations between the compacting pressure and the surface acidity (H_0=3.3—4.0).

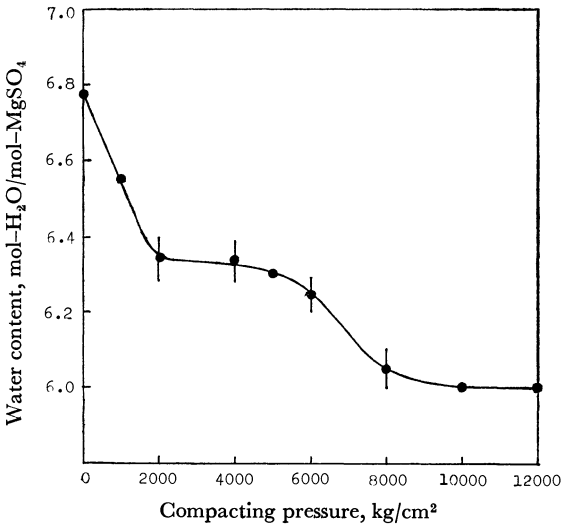

Fig. 2. Relations between the compacting pressure and the water contents.

X-Ray Diffraction. The powder X-ray diffraction patterns of the samples compressed under various pressures are given in Fig. 3. From these patterns, it can be understood that the sample consists of crystallites of magnesium heptahydrate[9] and hexahydrate.[10]

The half-widths of the diffraction peak for the heptahydrate (2θ=21.0°) and that of the hexahydrate

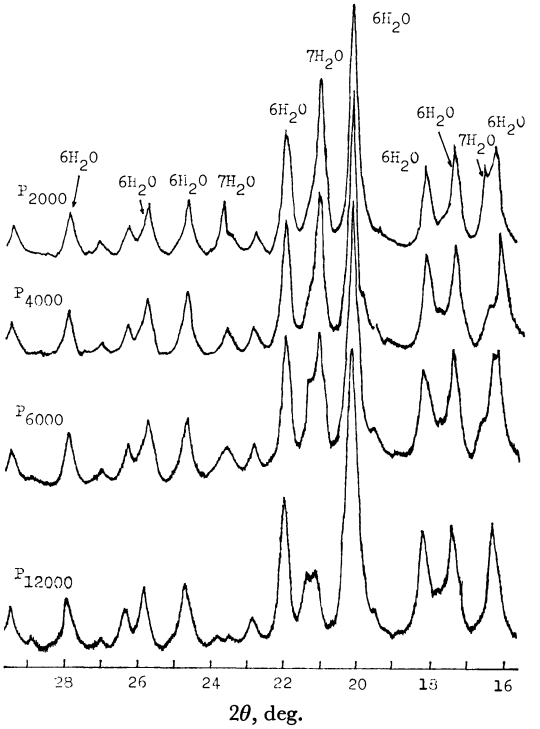

Fig. 3. X-ray diffraction patterns for various samples.

8) In the X-ray diffraction studies for some metal sulfates, e.g. $Al_2(SO_4)_3 \cdot 18H_2O$, it was found that the diffraction pattern varies from time to time. This phenomenon is due to the interference of air moisture, it was avoided by covering the compressed and evacuated sample with collodion. However, in the case of the samples used in the present study, the X-ray diffraction pattern did not vary with the time. Therefore, the collodion treatment was not carried out.

9) "Index to the Powder Diffraction File," ed. by J. V. Smith, ASTM Publication (1965), 8-467.

10) *Ibid.*, 1-0356.

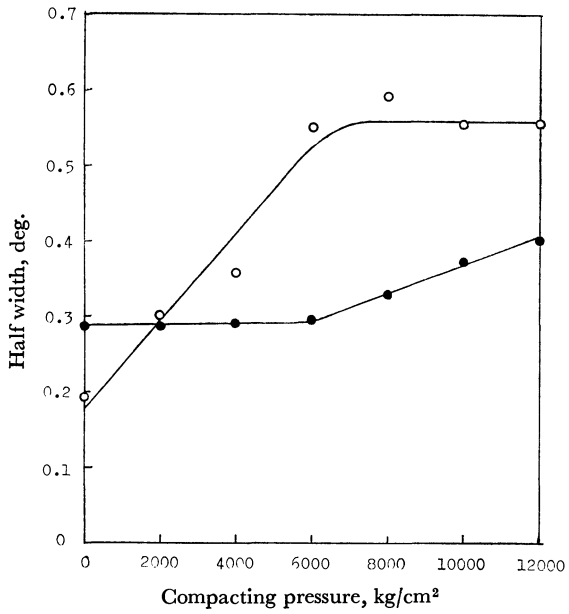

Fig. 4. Relations between the compacting pressure and the half widths of the X-ray diffraction peaks for magnesium sulfate heptahydrate (-○-, $2\theta=21.0°$) and for magnesium sulfate hexahydrate (-●-, $2\theta=20.2°$).

($2\theta=20.2°$) were found to vary on compression (Fig. 4). From this figure, it may be considered that the crystallites of heptahydrate were destroyed by the compression at pressures lower than 6000 kg/cm², while the crystallites of hexahydrate were little affected in this pressure range. The change in the half-width of the diffraction peak of hexahydrate was observed only at compacting pressures higher than 6000 kg/cm².

The relation between the compacting pressure and the relative intensity of the diffraction peak of heptahydrate ($2\theta=21.0°$) against the peak of hexahydrate ($2\theta=20.2°$) is given in Fig. 5. This seems to show that the relative content of heptahydrate to hexahydrate in the sample remained constant in the range of 2000—6000 kg/cm² and that the transition from heptahydrate to hexahydrate occurred somewhat above 6000 kg/cm². Such a discontinuous transition may be suggested by a rather discontinuous change in the water content in the sample (Fig. 2).

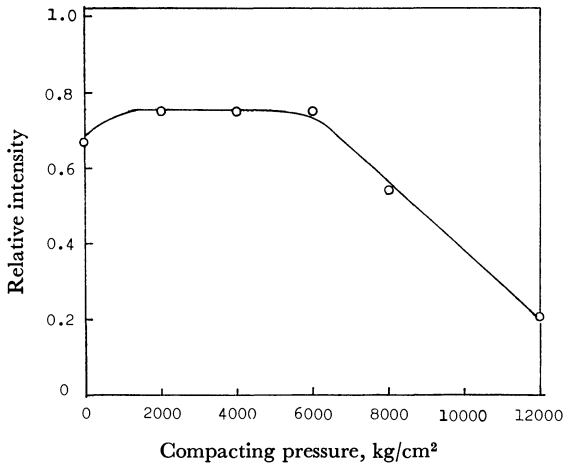

Fig. 5. Relations between the compacting pressure and the relative intensity of the X-ray diffraction peak of heptahydrate against the peak of hexahydrate.

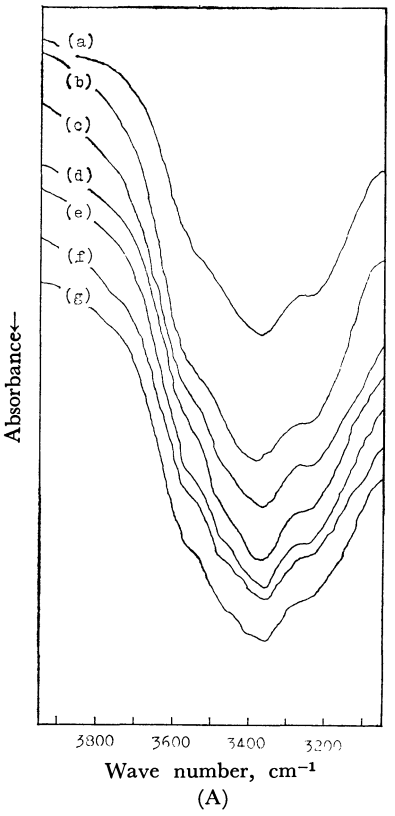

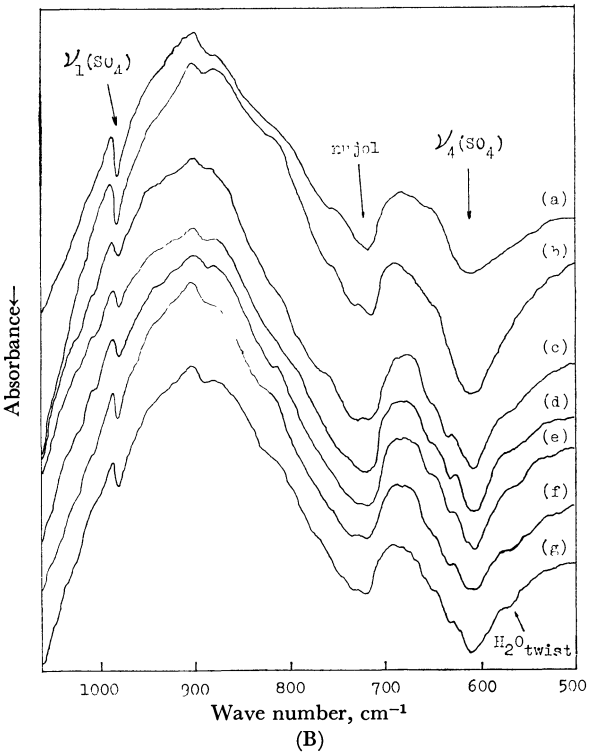

Fig. 6. Infrared spectra for the samples compressed at various pressures: (a) P_0; (b) P_{2000}; (c) P_{4000}; (d) P_{6000}; (e) P_{8000}; (f) P_{10000}; (g) P_{12000}.

Infrared Spectra. The infrared (IR) spectra of the samples compressed under various pressures are given in

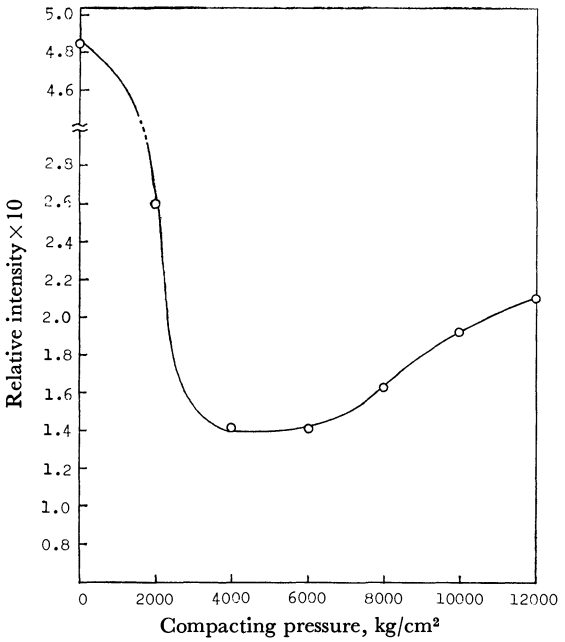

Fig. 7. Relations between the compacting pressure and the relative intensity of the ν_1 absorption against the ν_4 absorption for sulfate ion.

Fig. 6. The IR data may be summarized as follows;[11]

i) A broad band ranging from 3000 to 3600 cm^{-1} was assigned to the OH stretching vibration.[12] On compressing the sample at pressures higher than 6000 kg/cm^2, this band appeared to shift slightly toward lower wave numbers (Fig. 6-A). However, this is somewhat ambiguous because of the uncertainty of the exact peak position of the broad absorption band.

ii) An absorption band appearing at 985 cm^{-1} (Fig. 6-B) was assigned to the ν_1 vibration of the sulfate ion.[13] The relation between the compacting pressure and the relative intensity[14] of the ν_1 absorption against the ν_4 vibration for the sulfate ion (610 cm^{-1}) is given in Fig. 7. As can be seen in this figure, the relative intensity increased with an increase in the compacting pressure ranging from 6000—12000 kg/cm^2, while the relative intensity varied little at compacting pressures lower than 6000 kg/cm^2.

DTA and TGA. The DTA curves for various samples are given in Fig. 8. As can be seen in this figure, endothermic peaks appeared at various temperatures, and Peak I[15] can be attributed to the dehydration:[6]

$$MgSO_4 \cdot 7H_2O \longrightarrow MgSO_4 \cdot 6H_2O + H_2O$$

On the other hand, Peak II was attributed to the dehydration:

$$MgSO_4 \cdot 6H_2O \longrightarrow MgSO_4 \cdot 5H_2O + H_2O$$

According to the results of the TGA experiment, the

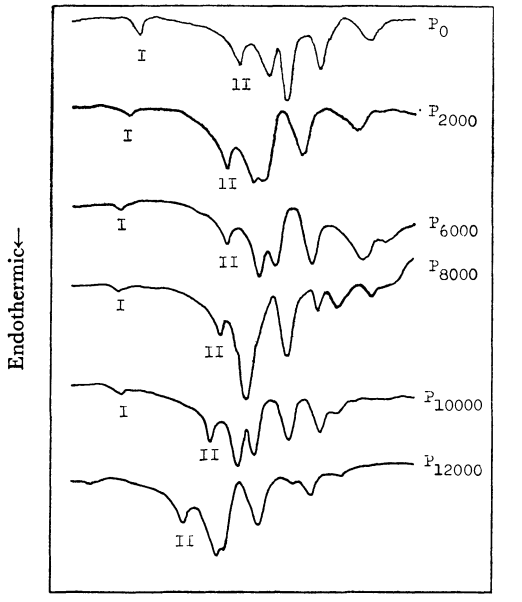

Fig. 8. DTA curves for the samples compressured at various pressures.

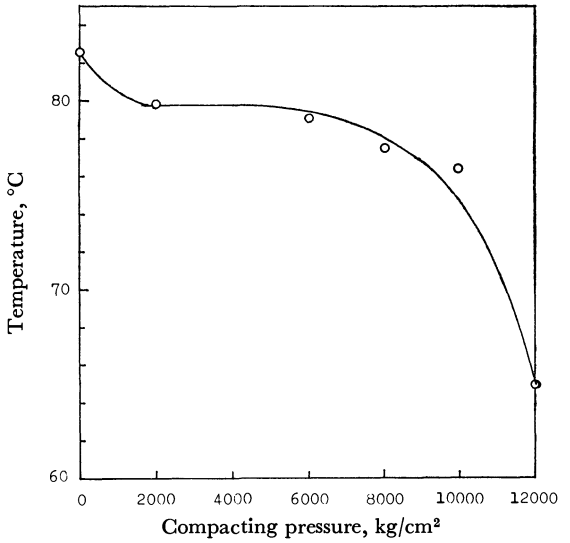

Fig. 9. Relations between the compacting pressure and the temperature of the DTA endothermic peak II.

11) The peak for H_2O_{rock} seemed to be overshadowed by a strong Nujol absorption and could not be detected on the IR chart. Further, the peak for H_2O_{twist} seemed to exist as a shoulder of the absorption peak of $\nu_4(SO_4)$. Since the shoulder peak was weak and broad, the existence of the peak is somewhat ambiguous and the effect of pressure on this peak could not be investigated. The peaks for ν(Mg-O) and for H_2O_{wag} could not be detected.

12) I. Gamo, This Bulletin, **34**, 760 (1961).

13) P. Krishnamurti, *Indian J. Phys.*, **5**, 183 (1930).

14) Approximated by the ratio of the peak height for ν_1 to that for ν_4. A precise determination of the peak area for the ν_4 was difficult because of the existence of a shoulder peak. Therefore, the ratio of the peak heights was used as a measured of the intensity ratio.

15) As can be seen in Fig. 8, the intensity of Peak I was very weak (especially for the compressed sample) compared with that of Peak II. This seems to mean that the phase change I requires far less energy than the phase change II. This view seems plausible because I is the dehydration of anion water and II is the dehydration of coordination water. Further, the compressed samples contain less anion water than 0.4 mol/mol-$MgSO_4$ (P=2000—12000 kg/cm^2). This would make the DTA peak I of the compressed sample smaller. Because of the instrumental limits, a quantitative comparison of the peak heights (I) of the different samples and the quantitative comparison of the peak height (I) with the water content (Fig. 2) were not possible.

amount of dehydration corresponding to the DTA endothermic peak II was found to be nearly one mole per unit mole of $MgSO_4$ for all of the samples.

Discussion

Acidity Change and X-Ray Diffraction Data. As can be seen in Fig. 1, the acidity values which varied upon compression were the values per unit of the surface area. Therefore, the acidity change can not be explained in terms of the change in the surface area. The acidity change due to compression must be attributed to structural changes other than that in the surface area.

A suggestion about the cause of the acidity change was derived from the information about the nature of the acid point. As was stated in the previous section, the acid point appearing on the surface of the compressed sample could be regarded as a protonic acid because the sample did not show any sign positive to the Lewis acid. Usually, the protonic-acid center and the water of crystallization are thought to be interrelated. Therefore, information about the change in the water of crystallization would be expected to throw some light on the cause of the acidity change.

X-Ray diffraction data revealed interesting aspects of the change in the crystallites of the sample hydrate. By a comparison of Fig. 4 with Fig. 1, it became evident that, in the pressure range of 2000—6000 kg/cm², where few changes in the surface acidity were observed, the half-width of the X-ray diffraction peak of hexahydrate was fairly constant, whereas the half-width of heptahydrate increased monotonously. Further, in the pressure range of 6000—12000 kg/cm², where the surface acidity was found to increase on compressing the sample, the half-width of the diffraction peak of hexahydrate increased, while that of the diffraction peak of heptahydrate varied little.[16] These facts strongly suggest that the disintegrations or distortions of hexahydrate crystallites play an important role in the acidity change, whereas the acidity change in the crystal of heptahydrate has little influence on the acidity change.

Probably, the change occurring in the hexahydrate crystallites is a distortion of the structural unit. Here, it must be pointed out that the X-ray diffraction data (Fig. 3) indicate the existence of heptahydrate even in the sample of P_{12000}, whereas the data on water content (Fig. 2) indicate 6 mol-H_2O/mol-$MgSO_4$ in this sample. Further, the DTA data (Fig. 8) indicate the existence of anion water in the P_{10000} sample, whose water content was also 6 mol-H_2O/mol-$MgSO_4$. A part of the cause of this discrepancy may be ascribed to the experimental error or to differences in the manner of sample handling in the different experiments. However, other factors must also be taken into consideration. For instance, the possibility that some lower hydrate may be contained in the sample could not be excluded. If the content of the lower hydrate is small or if the lower hydrate is in an amorphous state, its existence can not be detected by X-ray diffraction. Therefore, the water contents expected from the X-ray data would become larger than the true value. If the existence of the lower hydrate is true, posibilities that this hydrate may affect the acidity value arise. However, as can be seen in Fig. 2, the water content was fairly constant in the pressure range of 8000—12000 kg/cm². Therefore, it may be supposed that the content of the lower hydrate might also be constant in this pressure range. Thus, it is more plausible to consider that the acidity change in this pressure range is due to the distortion of the hexahydrate structure.

Structural Unit of Magnesium Sulfate Hydrate. As in the preceding works,[4,5] to serve for the discussion of the mechanism of the acidity change, models of the structural unit of magnesium sulfate hydrate[17] are given in Fig. 10. In this figure, A, B, and C are the models for heptahydrate, hexahydrate, and a distorted hexahydrate respectively. As can be seen in the figure, the central metal ion (Mg^{2+}) is coordinated by six water molecules, each of which is located on an apex of a hypothetical octahedron. In the structural unit of heptahydrate, one water molecule is located apart from the octahedron; this water may be regarded as anion water.

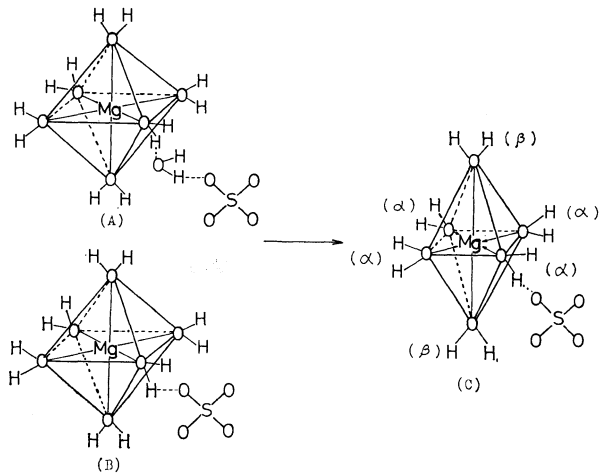

Fig. 10. Models of structural unit of magnesium sulfate: (A) heptahydrate, (B) hexahydrate (not distorted), (C) hexahydrate (distorted).

Changes in the Structural Unit of Heptahydrate. At pressures lower than 6000 kg/cm², only the changes in the structural unit of heptahydrate were taken into consideration, for the X-ray diffraction data (Fig. 4) indicated an invariance of hexahydrate structural unit in the samples compressed under low pressures.

Probably, the change occurring in the heptahydrate crystal is a liberation of the anion water (*cf.* Fig. 2). The coordinated water in heptahydrate would remain

16) At first sight, the X-ray data given in Fig. 3 (the decrease in the peak intensity and the splitting of the diffraction peak of heptahydrate at $2\theta=21°$) may give the impression that the distortion of the crystallites of heptahydrate occurred upon the compression of 6000—12000 kg/cm². However, this impression is erroneous; it is due to the abbreviation of the diffraction patterns of the P_{8000} and P_{10000} samples in the figure. It can be seen clearly in Fig. 4 that the half-width of the diffraction peak of heptahydrate is fairly constant in the pressure range of 6000—12000 kg/cm².

17) R. W. G. Wyckoff, "Crystal Structures," Interscience Publishers, Inc., New Yrok, (1960).

unaffected by the compression because those two elements are thought to be coordinated in the same manner as in the hexahydrate structural unit, which is considered not to vary at low pressures. Since anion water is not directly coordinated to the central Mg^{2+} ion, its liberation might have little effect on the ionization states of Mg^{2+} or of the coordinated water. Therefore, the observed invariance of the acidity of the sample compressed under low pressures is acceptable.

Changes in the Structural Unit of Hexahydrate. As has been stated in the previous sections, evidence that the change in the structural unit of hexahydrate occurred only at pressures higher than 6000 kg/cm^2 is presented by the X-ray peak broadenings (Fig. 4). Since the water content did not vary at pressures higher than ~6000 kg/cm^2, one possible change in the structural unit may be a distortion of the octahedron.

In the present research, a distorted octahedron structural unit, as is shown in Fig. 10-C, was considered. In this model, the distances between Mg^{2+} and H_2O (α) are shortend and the distances between Mg^{2+} and H_2O (β) are stretched. In such a distorted structural unit, interactions between Mg^{2+} and the coordinated water should differ in character from those in the normal structural unit (Fig. 10-B).

The results of the DTA experiments also support the idea that the octahedron structural unit is distorted at high pressures. As can be seen in Fig. 9, the dehydration temperature of the coordinated water decreases with an increase in the compacting pressure. This fact supports the idea that a part of the coordinated water, presumably H_2O (β), becomes unstable. In the distorted octahedral coordination, H_2O (β) may be weakly bound by the central Mg^{2+} ion because the distance between H_2O (β) and Mg^{2+} is stretched.

In connection with the change in the structural unit, the behavior of the sulfate ion against the compression should be taken into consideration. The IR spectra gave interesting information about the behavior of the sulfate ion. As can be seen in Fig. 7, the relative intensity of the IR ν_1 absorption against ν_4 absorption for the sulfate ion varied on compression. This fact seems to indicate that interaction between the sulfate ion and its environment varies on compression.

The decrease in the relative intensity of the $\nu_1(SO_4)$ absorption at lower compacting pressures (0—2000 kg/cm^2) may be related to the dehydration of anion water from the heptahydrate crystal (*cf.* Figs. 2 and 4). Presumably, the symmetry of the crystal field around the sulfate ion would be reduced by the existence of anion water and the ν_1 vibration (which is originally inactive for the infrared absorption) becomes active for the infrared absorption. As the releasing of anion water proceeds, the symmetry of the crystal field may recover and the peak of the ν_1 vibration may become weaker.

On the contrary, the increase in the relative intensity of the $\nu_1(SO_4)$ absorption at compacting pressures higher than 6000 kg/cm^2 may be related to the increased interaction between oxygen in the sulfate ion and hydrogen in the OH group of the coordinated water (α). Approaches of the sulfate ion to the octahedral structural unit become easier at higher compacting pressures. Further, at higher compacting pressures, anion water, which may hinder the approach of the sulfate ion to the octahedron, no longer exists.

Mechanism of the Acidity Change. The small influence of the change in the heptahydrate structure on the surface acidity is made obvious by a comparison of Fig. 1 with Figs. 2, 4, 5, and 7. Therefore, the following discussions will be confined to the acidity change as well as to the structural change at pressures higher than 6000 kg/cm^2.

The observed acidity change of magnesium sulfate hydrate seems to be explainable in terms of the change in the structural unit of $MgSO_4 \cdot 6H_2O$. That is, because of the distortion of the octahedral structure (Fig. 10-C), distances between the central Mg^{2+} ion and each coordinated water may vary; *i.e.*, the lengths of the four Mg^{2+}–H_2O (α) bonds are shortened and the lengths of the two Mg^{2+}–H_2O (β) bonds are stretched. Consequently, the degree of the interaction between Mg^{2+} and H_2O (α) may increase and the increased polarization of H_2O (α) may result. Thus, the polarized coordinated water can have a protonic acid property.

As has been discussed in the previous section, changes in the octahedral structural unit were considered to occur only at compacting pressures higher than 6000 kg/cm^2. Further, it was considered that the changes in the structural unit increase with an increase in the compacting pressure. Therefore, in the pressure range of 6000—12000 kg/cm^2, an increase in the compacting pressure may be considered to result in an increase in the content of polarized water (α). In other words, the compression at high pressures may result in an increase in the acidity of the sample.

The interaction between the sulfate ion and coordinated water (α) seems to contribute also to the acidity change. When the hydrogen-bridge donor property of the coordinated water (α) in the distorted structural unit increases, the hydrogen bond between the sulfate ion and the coordinated water (α) may be strengthened. Then, the distorted octahedral structural unit may be brought to a quasi-stable state by the aid of this strengthened hydrogen bond. Thus, the presence of the sulfate ion, which may be displaced nearer to the octahedron by the compression, seems to contribute to the acidity change. As has been discussed in the previous section, approaches of the sulfate ion to the octahedron were considered to be possible only at pressures higher than 6000 kg/cm^2, above which point the acidity change was observed.

The above-mentioned mechanism of the acidity change seems to be supported also by the linear relationship between the acidity change and the relative intensity of the IR ν_1 absorption for sulfate (Fig. 11).

Comparisons to the Acidity of Other Sulfates. The present mechanism for the acidity change in the compressed magnesium sulfate hydrate is almost identical with those proposed for the acidity changes in aluminum sulfate hydrate[4] and zinc sulfate hydrate.[5] In the acidity changes in these metal sulfates, including magnesium sulfate, interactions between the central cation and the octahedrally-coordinated water were thought

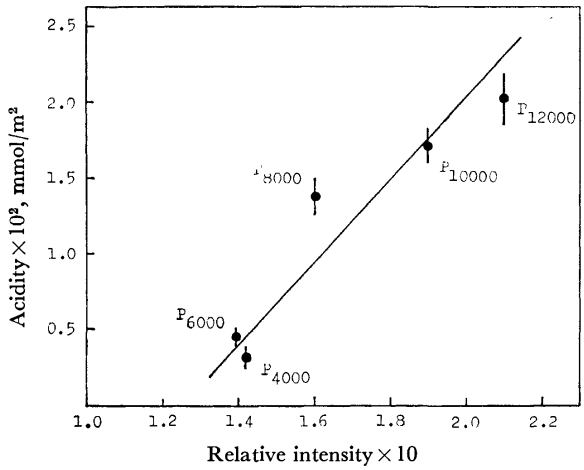

Fig. 11. Relations between surface acidity and the relative intensity of ν_1 absorption against ν_4 absorption for sulfate ion.

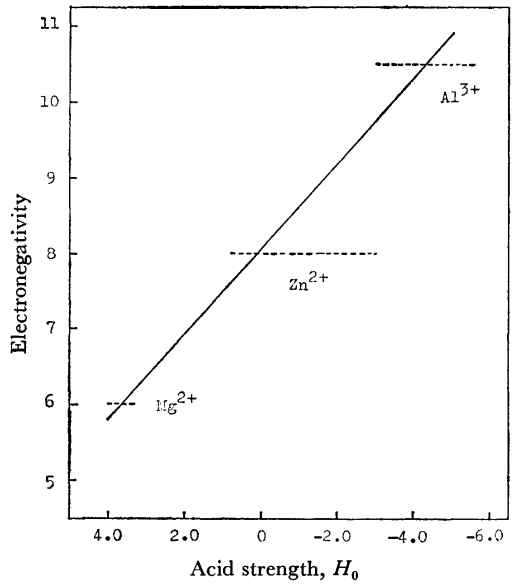

Fig. 12. Relations between electronegativities of some cations and the acid strength of the compressed sulfates containing the corresponding cations.

to play the most important roles. A question arises, therefore, if any differences among the acidic properties of these sulfates exist, for different cations (Al^{3+}, Zn^{2+}, Mg^{2+}) would yield differences in the strength of the cation field, which affects the degree of polarization in H_2O (α). Thus, the electronegativities of these cations[18] were compared with the observed values of the acid strength (H_0 values) of the corresponding sulfates (Fig. 12). As can be seen in this figure, an approximate linear relationship was obtained. The existence of such a simple relationship as above seems to support the validity of the common mechanism of the acidity changes for various metal sulfates.

In summarizing the published works of this series, the following point should be emphasized. The samples treated in these works were subjected to compression and evacuation. Further, it must be taken into consideration that the compacting pressure was released after the compression of the sample during a given period. Therefore, the observed pressure effects should be regarded as indirect ones. Some pressure effects might be relaxed by the release of the compacting pressure, and some other effects might be amplified or modified by the evacuation-dehydration. It must be remembered that the term "pressure effects" which is used in the works of this series means that the differences in the degree of compression induce diffrences in the effects of the other operations which follow the compression.

It seems to be important to study the details of the effects of evacuation as well as the effects of the pressure releasing. Measurements under pressure are also necessary in order to ascertain the direct effect of pressure. All of these works require special techniques and include many experimental difficulties, however, and so they were not included in the works of this series.

18) K. Tanaka, A. Ozaki, and K. Tamaru, *Shokubai*, **6**, 262 (1964).

ESR Studies of the Negative Ions of Biphenyl Derivatives. IV. Conformation of 4,4′-Polymethylenebiphenyl Anion Radicals

Kazuhiko ISHIZU, Fujito NEMOTO, Hideo HASEGAWA,* Koji YAMAMOTO,** and Masao NAKAZAKI**

Department of Chemistry, Faculty of Science, Ehime University Bunkyo-cho, Matsuyama
**Japan Electron Optics Laboratory, Akishima, Tokyo*
***Department of Chemistry, Faculty of Engineering Science, Osaka University, Toyonaka, Osaka*

(Received December 8, 1971)

The electron spin resonance has been observed for anion radicals of 4,4′-polymethylene bridged biphenyls which have various lengths of the polymethylene chain, from the carbon number of $n=11$ to that of $n=16$. The relation between the chain length of the methylene bridge and the ring-proton splitting were studied in order to see how the polymethylene span brings on a strain in the biphenyl ring. The geometrical structures of the sp^3-hybrid bond of the β-carbons were investigated on the basis of the observed values of the β-proton splitting in each derivative. In the cases of both pentadeca and hexadeca derivatives, the magnitude of both the *ortho*- and the *meta*-ring proton splitting are comparable with those of the 4,4′-diethylbiphenyl anion radical, the open-chain model of the present derivatives. A rotation of the β-methylene sp^3-bond is forbidden in this case, however, and the coupling constants of the β-methylene protons no longer exhibit an equivalent value; that is, two of these C–H bonds are placed on a coplanar biphenyl plane, but the others are twisted out by about 30° from the $2p_z$ axis of the ring-carbon atom. When the number of the methylene groups is reduced from thirteen to twelve, the magnitude of the *ortho*-ring proton coupling constant is greatly reduced. The HMO calculations of the spin density were carried out. The observed tendency of the ring-proton splitting can be qualitatively understood on the assumption that the coplanar biphenyl ring may be modified by twisting the phenyl groups about the central 1-1′ bond rather than by slanting them together against the original aromatic plane. A strong beam of the polymethylene chain also causes a modification of the geometrical structure of the β-methylene sp^3 bond and results in a reduction of the β-proton coupling constant to a large extent.

Polymethylenebiphenyls in which a suitable length of the polymethylene chain is bridged at the 2,4′-, 3,4′-, or 4,4′-positions have recently been synthesized, and their conformation have been studied by UV and NMR absorption spectroscopy.[1-3]

In the cases of the 4,4′-polymethylene derivatives, a molecular model suggests that at least thirteen methylene carbon atoms are necessary to set the bridge across the 4,4′-positions of the biphenyl ring without resulting in a strain in the molecule.

If the number of the methylene carbon atom is less than thirteen, the biphenyl ring is hard to held in the coplanar fashion. In this study, ESR observation has been carried out for the anion radicals of 4,4′-polymethylenebiphenyl, which have various numbers of polymethylene groups, from 11 to 16. The hyperfine coupling constants of either β-methylene or the ring proton are determined in order to elucidate the steric structure of these derivatives. The degree of the strain effected in the biphenyl ring could be estimated by a comparison of the values of the ring-proton splitting with those of 4,4′-diethyl biphenyl, an open-chain model of the present derivatives. The geometrical structure of the β-methylene carbons may be investigated on the basis of the measurement of the β-proton hyperfine coupling constant and its temperature dependence. The general structure of 4,4′-polymethylene biphenyl is given below;

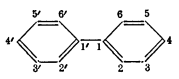

Experimental

The materials used in this studies were synthesized by a process previously established before. The physico-chemical indexes of the materials are listed in Table 1.

TABLE 1. PHYSICO-CHEMICAL INDEXES OF THE MATERIALS

Number of polymethylene carbon *n*	11	12	13	14	15	16
Mp(°C)	86—88	116—117	101—102.5	112.5—114.5	128—129	110—111

4,4′-Diethylbiphenyl (mp 82.5°C) was synthesized by an Ullman reaction on *p*-iodo-ethylbenzene. The anion radicals were prepared in dimethoxyethane (DME) by reduction with a potassium mirror kept in an acetone–dry ice bath.

The green-colored paramagnetic solution gave a strong ESR absorption, and the anion radicals were stable enough for the observation of the ESR spectra at room temperature. The ESR spectra were recorded by a JEOL ME-3X spectrometer operating with a 100 kHz magnetic field modulation. The magnetic field was calibrated by a perylene cation radical prepared in concentrated sulfuric acid.[4]

Results and Discussion

The Analysis of the ESR Spectra. The ESR spectrum of the 4,4′-hexadecabiphenyl anion radical recorded at −20°C is given in Fig. 1(a). One may easily determine the *ortho*- and the *meta*-proton hyperfine coupling constants (a^H_2 and a^H_3) by referring to those of the 4,4′-diethyl biphenyl anion radical, which have

1) M. Nakazaki and S. Isoe, *Chem. Ind.* (London), **1965**, 224.
2) M. Nakazaki and K. Yamamoro, *ibid.*, **1965**, 486.
3) K. Yamamoto, T. Horikawa, and M. Nakazaki *Tetrahedron Lett.* **1969**, 4597.
4) J. P. Colpa and J. R. Bolton, *Mol. Phys.*, **6**, 273 (1963).

already been reported.[5]

As for the β-proton splitting (a_4^H), however, neither the line intensity nor the total width of the spectrum were adequately explainable unless the non-equivalent values of the β-proton splitting were assumed; that is, a triplet splitting ($a_4^{H_A}$) arises out of the two methylene protons, but that of the others ($a_4^{H_B}$) vanishes to the order of the line width (200 m gauss).

The hyperfine coupling constants thus estimated are: $a_4^{H_A}=7.00$, $a_4^{H_B}<0.20$, $a_2^H=2.62$, and $a_3^H=0.46$ gauss. These values were confirmed by the computer calculation of the line intensity, as is shown in Fig. 1(b).[6] As the temperature is gradually elevated, the hyperfine structures began to change; the spectrum shown in Fig. 1(c) was recorded at room temperature. In this case, another triplet splitting, $a_4^{H_B}$ was recognized in addition to $a_4^{H_A}$, and the hyperfine structure could be understood well using the following hyperfine coupling components; $a_4^{H_A}=6.51$, $a_4^{H_B}=0.47$, $a_2^H=2.60$, and $a_3^H=0.47$ gauss. The computer-calculated spectrum shown in Fig. 1(d) also gives a good agreement with the observed spectrum. A similar temperature dependence of the β-proton splitting was observed for the 4,4′-pentadecamethylene derivative ($n=15$). When the number of the methylene group was reduced to $n=14$, the a_2^H value began to decrease, but the a_3^H value showed a slight increase. The triplet splitting of $a_4^{H_B}$ was hidden in the line-width, and it was not possible to observe the temperature dependence in this case for the temperature range of $-50\sim+50$°C. In the case of $n=13$, a further decrease in the $a_4^{H_A}$ value was noted, while either the a_2^H or the a_3^H values were almost comparable with those of tetradecamethylene biphenyl ($n=14$). Therefore, the critical length of the polymethylene chain for making a bridge between the 4,4′-position of the biphenyl without a strain resulting may be concluded to be $n=14$. The hyperfine coupling constants of both the *ortho*- or β-protons were strongly suppressed if the number of the methylene carbon atoms reduced to $n=12$, and further for the derivative of $n=11$.

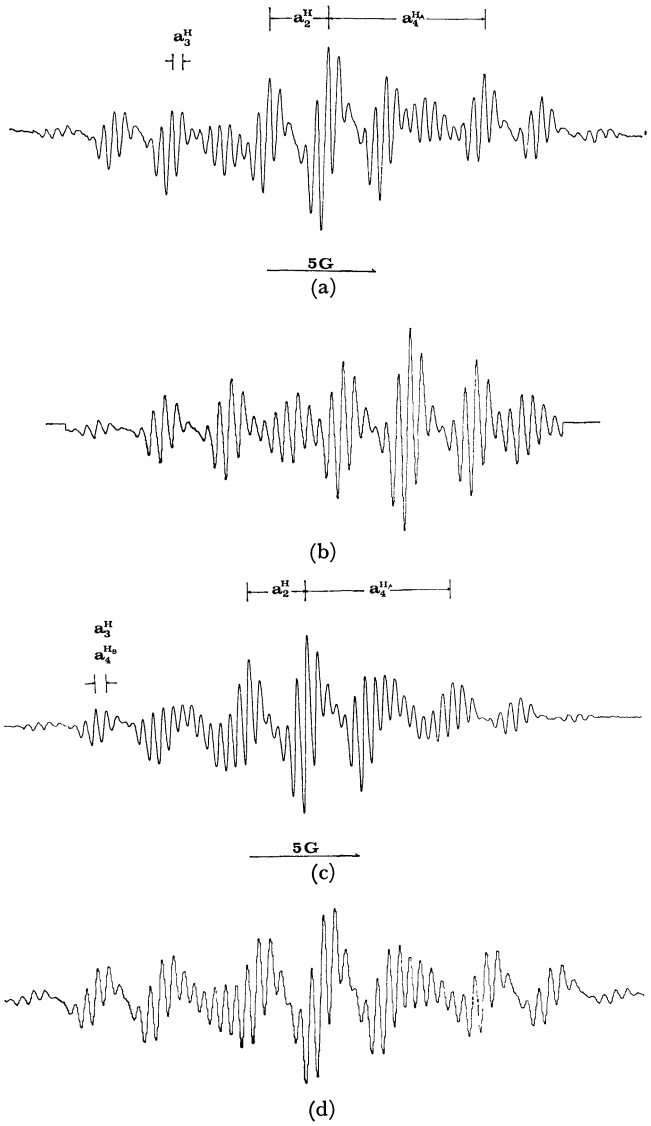

Fig. 1. 4,4′-Hexadecamethylenebiphenyl
a) ESR spectrum recorded at −20°C. b) computer simulated spectrum of (a). c) ESR spectrum recorded at room temperature. d) computer simulated spectrum of (c). A line shape is assumed to be as a Lorentzian with line width 0.2 gauss.

In Fig. 2(a), we show the ESR spectrum of 4,4′-dodecamethylenebiphenyl anion radical. The computer simulation of the spectrum again confirmed that the triplet splitting of $a_4^{H_B}$ came to have the same magnitude of the line-width, as is shown in Fig. 2(b). The hyperfine coupling constants of the 4,4′-polymethylene biphenyl anion radical thus determined are summarized in Table 2. The relations between the hyperfine coupling constants and the number of polymethylene carbon atoms are plotted in Fig. 3.

The Ring-proton Splitting. It can be seen from Table 2 and Fig. 3 that the polymethylene strain actually serves to reduce the a_2^H, accompanied by a

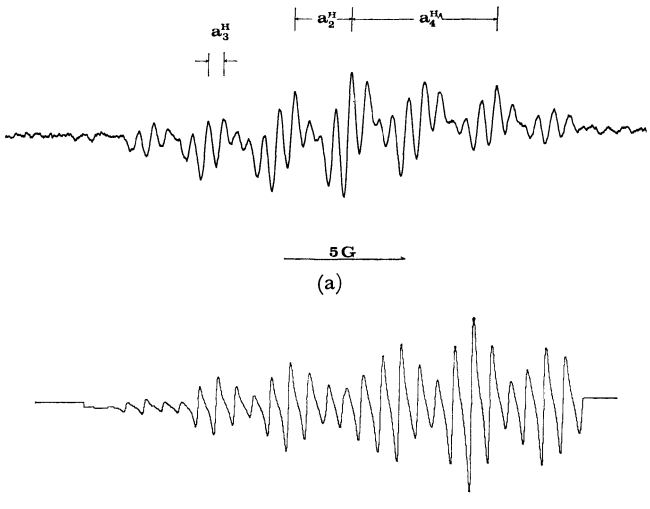

Fig. 2. 4,4′-Dodecamethylenebiphenyl
a) ESR spectrum recorded at +50°C. b) computer simulated spectrum of (a). A line shape is assumed to be as a Lorentzian with line width 0.3 gauss.

5) K. Ishizu, K. Mukai, H. Hasegawa, K. Kubo, H. Hishiguchi, and Y. Deguchi, This Bulletin, **42**, 2808 (1969).

6) The computer calculations of the spectra were carried out using a JEOL JEC-5 spectrum computer.

Table 2. Proton hyperfine coupling constants of 4,4′-polymethylenebiphenyl anion radicals (gauss)

	a_2^H	a_3^H	a_4^H	$a_4'^H$	Temp.(°C)
CH_3-	2.66	0.51	5.63	5.63	+25
C_2H_5-	2.68	0.51	3.99	3.99	0
n-C_3H_7-	2.68	0.48	3.62	3.15	−60
$-(CH_2)_{11}-$	2.18	0.63	5.49	—	0
$-(CH_2)_{12}-$	2.38	0.60	5.97	—	0
$-(CH_2)_{13}-$	2.58	0.52	6.16	—	0
$-(CH_2)_{14}-$	2.58	0.51	6.52	—	0
$-(CH_2)_{15}-$	2.67	0.45	6.54	0.45	0
	2.68	0.45	6.78	—	−20
$-(CH_2)_{16}-$	2.60	0.47	6.51	0.47	+25
	2.62	0.46	7.00	—	−20

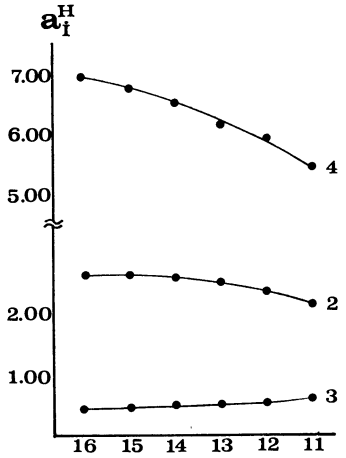

Fig. 3. The relation between the observed proton hyperfine coupling constant (a_i^H) and the number of the polymethylene groups (n), where the numeral represents the position (i) on the biphenyl ring.

slight increase in the a_3^H.

In order to explain the present results qualitatively, HMO calculations of the spin density were carried out on the assumptions that the polymethylene span modifies the structure of the coplanar biphenyl at the central 1-1′ bond and that the axis of the $2P_z$ AO of each 1,1′ ring carbon is either slanted (θ) or twisted (γ), as is shown in Fig. 4.

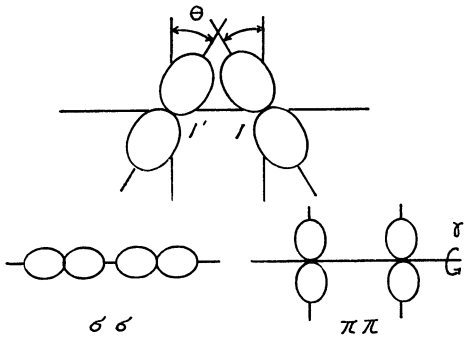

Fig. 4. $2P_z$ AO of the central 1, 1′ ring carbons slanted or twisted by the polymethylene bridge.

The resonance integral between the 1-1′ bond, $\beta_{11'}$, was calculated from the overlap integral, $S_{11'}$, as a function of both θ and γ; it may be expressed as follows.[7]

$$\beta_{11'} = \frac{S_{11'}/(1+S_{11'})}{S_{\pi\pi}/(1+S_{\pi\pi})}$$

$$\beta_{11'} = S_{\sigma\sigma}\sin^2\theta + S_{\pi\pi}\cos^2\theta\cos\gamma$$

The values of both the $S_{\sigma\sigma}$(0.3326) and $S_{\pi\pi}$(0.2186) integrals were used, referring to Kopineck's calculation,[8] where the bond distance of the C_1–C_1' bond was taken to be 1.539 Å.

For the sake of simplicity, the inductive parameter of the polymethylene group was rounded off to $\delta=-0.2$, taking into account that for methyl;[9] that is, the Coulomb integral of the *para*-position was estimated to be $\alpha_4=\alpha_4'=\alpha-0.2\beta$.

In Fig. 5, we show the relations between the theoretical spin density on the ring carbon atoms (ρ_i^π) and the twisting angle (γ), where the slanting angle (θ) is tentatively assumed to be 0, 15, and 30°.

As may be seen in Fig. 5, the spin density on the *ortho*-positions (ρ_2^π) shows a gradual increase, and that for the *meta*-positions (ρ_3^π), a decrease, with an increase in θ, contrary to the observed tendency of the spin density.

On the other hand, however, the HMO calculation gives an adequate explanation of the observed results, when the effect of the twisting of the phenyl rings (γ) is taken into account.

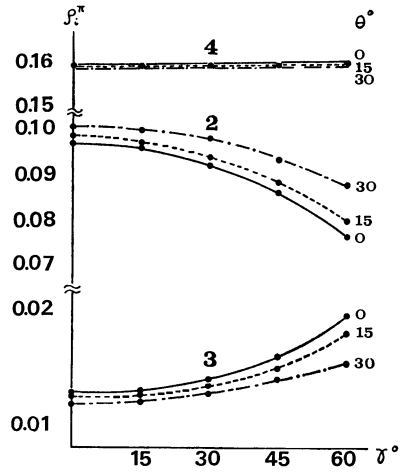

Fig. 5. Dependence of HMO spin density on the strain caused at the central 1-1′ bond of the biphenyl ring.

It is noteworthy here that the spin density on the *para*-positions is not affected everywhere. Based on the present calculation, one may speculate that the polymethylene bridge causes a strain in the molecule by twisting the phenyl rings rather than inclining them against the original aromatic plane.

The Methylene Proton Splitting. The β-proton coupling constant has been calculated by the following equation, expressed as a function of the angle between the carbon-hydrogen bond and the axis of the ring carbon $2P_z$ orbital:

7) John D. Roberts "Notes on molecular orbital calculations" W. A. Benjamin, Inc, New York (1962), p. 82.

8) H. J. Kopineck, *Z. Naturforsch.*, **5A**, 420 (1950).

9) A. Streitwieser, Jr. "Molecular orbital theory for organic chemists" John Wieley & Sons, Inc. New Yorkk (1961), p. 131.

$$a_i^H = \langle Q \rangle \rho_i^\pi,\ Q = B_0 + B\cos^2\varphi.^{10)}$$

In the case of the methyl derivative, the free rotation of the methyl group will average out the cosine term to $\langle\cos^2\phi\rangle = 1/2$, thus, the methyl-proton splitting is directly proportional, to the spin density, ρ_i^π, of the adjacent ring carbon atom, where the B_0 term is regarded as small in comparison with $B \approx 50$ gauss. According to this model, the ethyl proton splitting can also be well understood, assuming that $\langle Q \rangle$ is suppressed by about 25% by a restricted rotation of the ethyl group.

Recently, however, the fact of an exceptional hindered internal rotation of the alkyl group was demonstrated for the *n*-propyl derivative,[11] where it was recognized that a normal quintet splitting of the four β-protons fell into two sets of triplet splitting.

In the cases of the present derivatives, one may thus expect that a rotation of the β-methylene residue would be largely restricted not only by the large mass of the polymethylene chain, but also by its strong strain. This is indeed true, because the temperature dependence of the β-proton coupling constant has been found to be negligible for the derivatives of $n = 11$—13, and the lack of the two-methylene-proton splitting in the observed spectra suggests that one of the CH bond is tightly fixed on the aromatic plane.

When the length of the polymethylene chain increases, the biphenyl ring recovers its coplanar fashion and the β-proton coupling constants can be calculated in the same manner as was used for the open-chain derivative. McLachlan's calculation ($\lambda = 1.0$) of the spin density was carried out for the open-chain derivative; ρ_4^π was thus estimated to be 0.195, taking the Coulomb integral of the *para*-positions to be $\alpha_4 = \alpha_4' = \alpha - 0.2\beta$. The β-proton coulping constants, $a_4^{H_A}$ and $a_4^{H_B}$, were calculated to be 7.30 gauss and zero respectively, when the β-methylene residue takes the conformation ($\varphi = 30°$), as is illustrated in Fig. 6.

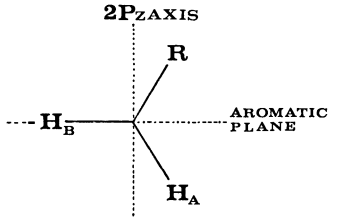

Fig. 6. The probable conformation of the β-methylene sp^3-bond in hexadecabiphenyl anion radical.

This must also be the case with the hexadecamethylenebiphenyl anion observed at −20°C. The occurrence of a small triplet splitting ($a_4^{H_B}$) observed at room temperature suggests that the torsional oscillation of the β-methyl residue is accelerated by thermal activation and that the sp^3-lobes of methylene group take a new equilibrium conformation.

Of interest is the magnitude of the β-proton splitting, which is lowered by the reduction of the chain length, for the MO calculation predicts that the spin density at the *para*-position will not be affected by a modification of the biphenyl ring.

The probably means that the polymethylene beam alters the conformation of the β-methylene sp^3 bond so as to reduce the orbital overlap between this hybrid orbital and $2P_z$ atomic orbital of the ring carbon atom. The beam is so strong that the freedom of the segment movement of the polymethylene is greatly suppressed, and the temperature dependence of the β-proton splitting is no longer observed in this case.

10) C. Heller and H. M. McConnell, *J. Chem. Phys.*, **32**, 1535 (1960).

11) F. Nemoto, K. Ishizu, and H. Hasegawa, *Chem. Lett.*, **1972**, 267.

Thermal Decomposition Reactions of Metal Oxalato Complexes in the Solid State. II.[1] Evolved Gas Analyses of Metal Oxalato Complexes

Kenzo NAGASE

Department of Chemistry, Tohoku University, Kawauchi, Sendai

(Received January 31, 1972)

The thermal decomposition reactions of a number of metal oxalato complexes in the solid state were studied by an EGA method in a helium atmosphere. As regards the decomposition stage of an anhydrous complex, the complexes investigated could be divided into three groups: the complexes of Mn(III), Fe(III), Co(III), Rh(III), Cu(II), Pd(II), and Pt(II), this first group giving only CO_2 as a gaseous product, decomposed by electron transfer from an oxalato ligand to a central metal ion; the complexes of Al(III) and Zn(II), this second group giving CO and CO_2 in the molar ratio of 1: 1, decomposed by C–O bond breaking to form a metal oxide with no change in the oxidation number of a central metal; and the complexes of V(III) and Cr(III), this third group giving CO_2 and a smaller amount of CO, decomposed through both the processes, electron transfer and C–O bond breaking. The subsequent decomposition reactions of the bivalent metal oxalato complexes formed upon heating the corresponding trivalent metal oxalato complexes were divided into two types: one is associated with further reduction of a central metal ion, while the other is associated with C–O bond breaking.

The thermal decomposition reactions of metal oxalato complexes have been studied by several techniques, and the stoichiometries for several complexes have been examined on the basis of their gaseous and solid products.

Broadbent *et al.*[2] have studied the thermal decomposition of $K_3[Fe(ox)_3]$ in a nitrogen atmosphere and found $K_2C_2O_4$ and a chalky yellow solid at 260°C, and, beyond 460°C, a mixture of K_2CO_3 and free iron, by a method of X-ray diffraction identification.

Wendlandt and Simmons[3,4] have suggested that the bivalent metal complexes formed upon heating $K_3[Mn(ox)_3]$ and $K_3[Co(ox)_3]$ below 200°C in a nitrogen atmosphere can be represented by the $K_2[Mn(ox)_2]$ and $K_2[Co(ox)_2]$ formulae on the basis of their reflectance spectra. Tanaka and Sato[5] have assigned the chalky yellow compound, which had been found by Broadbent,[1] to $K_2[Fe(ox)_2]$ on the basis of the infrared and reflectance spectra.

Bancroft *et al.*[6] have also examined the thermal decomposition of $K_3[Fe(ox)_3]$ and suggested the presence of $K_6[(C_2O_4)_2Fe(OX)Fe(C_2O_4)_2]$ (OX=quadridentate oxalato group) on the basis of the infrared spectrum; this differs from the conclusions reported by Broadbent[2] and Tanaka.[5]

Broadbent *et al.*[7] have reported that $K_3[Al(ox)_3]$ decomposes in two stages upon heating above 375°C and that the residue contains Al_2O_3, K_2CO_3, and K_2O, as determined by X-ray diffraction identification.

The studies mentioned above, however, are incomplete, particularly in gaseous products. In the present study, the thermal decomposition reactions of the metal oxalato complexes were studied by a method of EGA (evolved gas analysis) in the temperature range of 25—600°C, and on the basis of the gaseous products, the stoichiometries of the thermal reactions were reexamined; moreover, the stoichiometries for the other metal oxalato complexes will be newly presented.

Experimental

Materials. The complexes used in this study were prepared according to the literature. Analyses of the complexes have been reported in the preceding paper.[1]

Measurements of EG Curves. Evolved gas (EG) curves were obtained with an apparatus consisting of a Shimadzu GC-1C gas chromatograph and a Shimadzu PYR-1A pyrolyzer in a helium atomosphere, at a flowing rate of 50 ml/min. With the rearrangement, the exit line from a pyrolysis chamber is directly connected to a thermal conductivity detector, without passing through a column. The procedure is as follows: about a 3-milligram sample in a platinum boat is introduced into a pyrolysis chamber. After the air is swept out, the temperature of the sample is raised to 600°C at a heating rate of 5°C/min. Changes in the thermal conductivity by the evolved gas are recorded as a function of the temperature of the sample.

Analyses of Gaseous Products. Analyses of gaseous products were performed by the use of the above apparatus equipped with a column, composed of 2-meter-long and 3-millimeter-indiameter stainless steel tubing, packed with 60—80 mesh activated charcoal. The temperature of the detector and the column were maintained at 200°C and 150°C respectively. The procedure was as follows: the temperature at which a peak maximum is observed on a EG curve, and then a sample was introduced into the furnace and it was maintained at that temperature for about 5 min while helium carrier gas was routed through the bypass by means of a two-way valve. By changing the valve, carrier gas is routed through the pyrolysis chamber and gaseous products are carried into the chromatographic column. The retention times are 1.5 min for CO and 3.0 min for CO_2 under the conditions employed in this study.

Results and Discussion

The evolved gas (EG) curves of the metal oxalato

1) Paper I of this series: K. Nagase, This Bulletin, **45**, 2166 (1972).

2) D. Broadbent, D. Dollimore, and J. Dollimore, *J. Chem. Soc.*, **1967**, 451.

3) W. W. Wendlandt and E. L. Simmons, *J. Inorg. Nucl. Chem.*, **27**, 2317 (1965).

4) E. L. Simmons and W. W. Wendlandt, *ibid.*, **27**, 2325 (1965).

5) N. Tanaka and K. Sato, This Bulletin, **43**, 789 (1970).

6) G. M. Bancroft, K. G. Dhamawardhena, and A. G. Maddock, *Inorg. Nucl. Chem. Lett.*, **6**, 403 (1970).

7) D. Broadbent, D. Dollimore, and J. Dollimore, *Analyst*, **94**, 543 (1969).

Table 1. Analyses of gaseous products on each decomposition stage (%)

Complex	Stage I	Stage II	Stage III	Stage IV
$K_3[Al(ox)_3]\cdot 3H_2O$	H_2O	CO(50), CO_2(50)	—	CO(81), CO_2(19)
$K_3[V(ox)_3]\cdot 3H_2O$	H_2O	CO(27), CO_2(73)	—	CO(88), CO_2(12)
$K_3[Cr(ox)_3]\cdot 3H_2O$	H_2O	CO(32), CO_2(68)	CO(48), CO_2(52)	CO(77), CO_2(23)
$K_3[Mn(ox)_3]\cdot 3H_2O$	H_2O, CO_2		CO(45), CO_2(55)	CO(87), CO_2(13)
$K_3[Fe(ox)_3]\cdot 3H_2O$	H_2O	CO_2	CO(19), CO_2(81)	CO(23), CO_2(77)
$K_3[Co(ox)_3]\cdot 3H_2O$	H_2O	CO_2	CO_2	CO(45), CO_2(55)
$K_3[Rh(ox)_3]\cdot 4.5H_2O$	H_2O	CO_2	—	CO(82), CO_2(18)
$K_2[Cu(ox)_2]\cdot 2H_2O$	H_2O	CO_2	—	CO(89), CO_2(11)
$K_2[Zn(ox)_2]\cdot 2H_2O$	H_2O	CO(44), CO_2(56)	—	CO(87), CO_2(13)
$K_2[Pd(ox)_2]\cdot 3H_2O$	H_2O	CO_2	—	CO(91), CO_2(9)
$K_2[Pt(ox)_2]\cdot 2H_2O$	H_2O	CO_2	—	CO(70), CO_2(30)
$K_2C_2O_4\cdot H_2O$	H_2O	—	—	CO(87), CO_2(24)

complexes and potassium oxalate in the temperature range of 25—600°C are given in Figs. 1—3. These curves show that the complexes investigated decomposed in 3 or 4 stages. Gas analyses of each decomposition stage are sammarized in Table 1.

Dehydration (Stage I). All of the complexes immediately lost hydrated waters upon heating at about 100°C. Except for $K_3[Mn(ox)_3]\cdot 3H_2O$, the complexes showed the corresponding anhydrous plateaus on the EG curves. The dehydration of $K_3[Mn(ox)_3]\cdot 3H_2O$ took place with the decomposition of the anhydrous complex. For the complexes of Al(III), V(III), Cr(III), Fe(III), and Co(III), the peak corresponding to the dehydration splits into two or three, suggesting that water molecules are not held in the crystal lattice in an identical manner. On the other hand, the peaks of Rh(III), Pd(II), and Pt(II) are smooth, with no shoulder, water molecules being held equally in the crystal lattice.

Decomposition of Anhydrous Complexes (Stage II). In contrast to the dehydration, there are big variations in the temperatures at which the anhydrous complexes begin to decompose. Most of the complexes investigated decomposed in one step, but the complexes of Mn(III), Co(III), and Pd(II), which showed no anhydrous plateau, or only a short one, decomposed in two steps. The reason for this difference is not yet clear.

In Table 1, it should be noticed that the complexes can be divided into three groups: the complexes of Mn(III), Fe(III), Co(III), Rh(III), Cu(II), Pd(II), and Pt(II), giving only CO_2, belong to the first group; the complexes of Al(III) and Zn(II), giving CO and CO_2 in the molar ratio of 1: 1, belong to the second group; and the complexes of V(III) and Cr(III), giving CO_2 and a smaller amount of CO, belong to the third group.

The giving of only CO_2 suggests that electron transfer takes place from an oxalate to a central metal ion. The stoichiometries for the complexes in the first group may be represented by the following equations:

$$K_3[M^{III}(ox)_3] \longrightarrow K_2[M^{II}(ox)_2] + 1/2K_2C_2O_4 + CO_2 \quad (M=Mn, Fe, and Co)$$

$$K_3[M^{III}(ox)_3] \longrightarrow M + 3/2K_2C_2O_4 + 3CO_2 \quad (M=Rh)$$

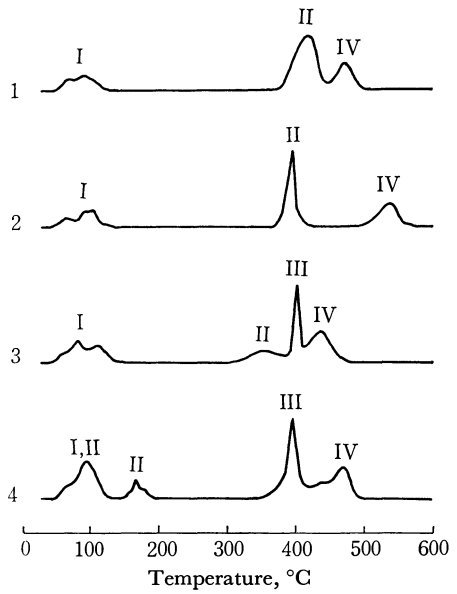

Fig. 1. EG curves of (1) $K_3[Al(ox)_3]\cdot 3H_2O$, (2) $K_3[V(ox)_3]\cdot 3H_2O$, (3) $K_3[Cr(ox)_3]\cdot 3H_2O$, and (4) $K_3[Mn(ox)_3]\cdot 3H_2O$ in a helium atmosphere.

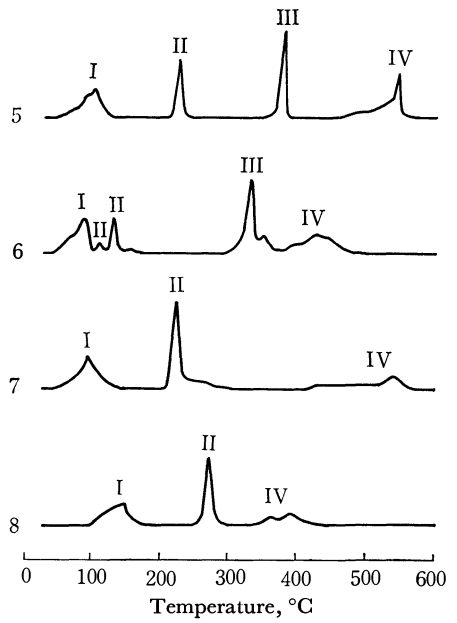

Fig. 2. EG curves of (5) $K_3[Fe(ox)_3]\cdot 3H_2O$, (6) $K_3[Co(ox)_3]\cdot 3H_2O$, (7) $K_3[Rh(ox)_3]\cdot 4.5H_2O$, and (8) $K_2[Cu(ox)_2]\cdot 2H_2O$ in a helium atmosphere.

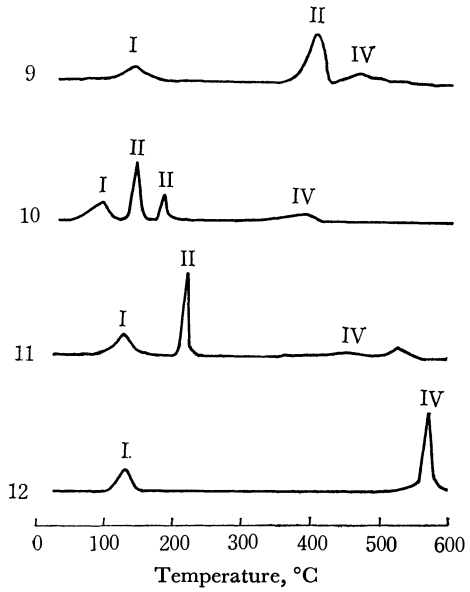

Fig. 3. EG curves of (9) $K_2[Zn(ox)_2]\cdot 2H_2O$, (10) $K_2[Pd(ox)_2]\cdot 3H_2O$, (11) $K_2[Pt(ox)_2]\cdot 2H_2O$, and (12) $K_2C_2O_4\cdot H_2O$ in a helium atmosphere.

$$K_2[M^{II}(ox)_2] \longrightarrow M + K_2C_2O_4 + 2CO_2$$
(M=Cu, Pd, and Pt)

The results from the TG and the DSC, which have been reported in the preceding paper, are consistent with these equations.

For the complexes in the second group, the following equations are possible:

$$K_3[Al(ox)_3] \longrightarrow 1/2Al_2O_3 + 3/2K_2C_2O_4 + 3/2CO + 3/2CO_2$$

$$K_2[Zn(ox)_2] \longrightarrow ZnO + K_2C_2O_4 + CO + CO_2$$

In this case, the decomposition of the complexes may be initiated by C–O bond breaking, thus forming a metal oxide with no change in the valency of the central metal. In fact, Dollimore *et al.* have confirmed the formation of Al_2O_3 upon the thermal decomposition of $K_3[Al(ox)_3]$. The results from the TG and the DSC, which have reported in the preceding paper, also support the above equations.

The decreasing order of the redox potentials of metal ions forming aquo ions is as follows:

Co(III)>Mn(III)>Pt(II)>Pd(II)>Rh(III)>Fe(III)
Cu(II)>V(III)>Cr(III)>Zn(II)>Al(III)

The complexes involving the metal ions listed on the left-hand side of Cu(II) in this series caused an electron transfer from an oxalate to a central metal upon heating, while the complexes of Al(III) and Zn(II), with the most negative potential, did not cause the electron transfer. The metal ions, V(III) and Cr(III) in reducibility, exist in the critical region. In view of the reducibility, in addition to the observation that the CO/CO_2 ratio was considerably smaller than 1, it may be supposed that the complexes of V(III) and Cr(III) in the third group decompose through both the processes, electron transfer and C–O bond breaking.

Subsequent Decomposition (Stage III). The decomposition of the bivalent metal oxalato complexes, probably $K_2[Cr(ox)_2]$, $K_2[Mn(ox)_2]$, $K_2[Fe(ox)_2]$, and $K_2[Co(ox)_2]$, which were formed by heating the corresponding trivalent complexes, can be divided into two types. One may be represented by the equation:

$$K_2[M^{II}(ox)_2] \longrightarrow M + K_2C_2O_4 + 2CO_2$$
(M=Fe and Co)

which involves electron transfer from an oxalate to a central metal ion, while the other may be represented by the equation:

$$K_2[M(ox)_2] \longrightarrow MO + K_2C_2O_4 + CO + CO_2$$
(M=Cr(II) and Mn(II))

which involves C–O bond breaking.

This division is supported by the reducibility of a bivalent metal ion as well as by the analyses of gaseous products. The decreasing order of the redox potentials of bivalent metal ions forming aquo ions is as follows:

Pt(II)>Pd(II)>Cu(II)>Co(II)>Fe(II)>
Zn(II)>Mn(II)

Subsequent Decomposition (Stage IV). The decomposition of the $K_2C_2O_4$ formed on the thermal decomposition of the complexes was the final decomposition stage in the temperature range of 25—600°C. From the EG curves, the peak maximum corresponding to the decomposition of $K_2C_2O_4$ appears at a lower temperature than that of pure $K_2C_2O_4$. This suggests that an included metal or a metal oxide may act as a catalyzer.

The analyses of the gaseous products in Table 1 show that the peak corresponding to the decomposition of $K_2C_2O_4$ involved CO and CO_2, which suggests that the decomposition of $K_2C_2O_4$ can be represented by the following equations:

$$K_2C_2O_4 \xrightarrow{I} K_2CO_3 + CO$$
$$K_2C_2O_4 \xrightarrow{II} K_2O + CO + CO_2$$
$$K_2C_2O_4 \xrightarrow{III} K_2O + 1/2C + CO_2$$

where Process I may be the main one for most of the complexes investigated, since CO is the main product for these complexes. The formations of K_2CO_3 and K_2O have been confirmed, by X-ray diffraction identification,[7] upon the thermal decomposition of $K_3[Al(ox)_3]$. The residue obtained by heating $K_3[Al(ox)_3]$ at 500°C was white, but the residue of pure $K_2C_2O_4$ at 600°C was gray. This difference suggests that Process III is possible for the decomposition of pure $K_2C_2O_4$, but impossible for the $K_2C_2O_4$ formed on the thermal decomposition of $K_3[Al(ox)_3]$. The $2CO \rightarrow CO_2+C$ reaction which has been suggested by several workers, may not occur under the conditions employed in this work, since carbon was not always formed upon heating the complexes at 600°C. The details of this stage will be reported later on the basis of analyses of solid products.

The author wishes to thank Professor Nobuyuki Tanaka, Tohoku University, for his valuable advice.

Polarographic Studies of the Anodic Oxidation of Mercury. I. Anodic Waves of Ammonia and Several Amines in *N,N*-Dimethylformamide

Yoshihisa MATSUI, Yukio KUROSAKI,* and Yoshio DATE
Department of Agricultural Chemistry, Shimane University, Nishikawazu, Matsue
(Received April 17, 1972)

The behavior of ammonia and several amines at the dropping mercury electrode was studied in *N,N*-dimethylformamide containing 0.10M Et_4NClO_4 by means of DC polarography and amperometric titration. Ammonia gave a diffusion-controlled anodic wave, which was attributed to the reversible oxidation of mercury to the 1:2 complex of mercury(II) with ammonia. A dilute solution of methylamine or dimethylamine gave a diffusion-controlled anodic wave similar to that of ammonia. A concentrated solution of each amine gave a prewave due to the adsorption of the electrolysis product, $Hg(am)_2^{2+}$, on the electrode surface. Trimethylamine also gave an anodic wave, but it was attributed to the oxidation of the amine itself to the corresponding cation radical. Ethylenediamine and 1,2-diaminopropane each gave a well-defined anodic wave over the concentration range examined. The wave was diffusion-controlled and was attributed to the reversible oxidation of mercury to the chelate compound of the $Hg(diam)_2^{2+}$ type. No adsorption phenomena were observed in this case. Aromatic amines such as aniline and β-naphthylamine gave no anodic waves. The overall stability constants of the 1:2 complexes of mercury(II) with ammonia, methylamine, dimethylamine, ethylenediamine, and 1,2-diaminopropane were evaluated by the analyses of the waves to be $10^{16.9}$, $10^{17.1}$, $10^{15.0}$, $10^{23.5}$, and $10^{24.0}M^{-1}$ respectively.

When the dropping mercury electrode is polarized anodically in a solution containing an ion or a compound which can form a stable complex with mercury(I) or mercury(II), an anodic diffusion current is observed at a potential less positive than the potential at which the anodic current due to the free dissolution of mercury flows. This is due to the electrolytic oxidation of mercury to the mercury complex; such polarographic behavior make it possible not only to determine the complexing agents quantitatively, but also to investigate the chemical and physicochemical properties of both complexing agents and their mercury complexes. Among them, the halide, cyanide, thiocyanate, sulfide, and thiosulfate ions, the compounds containing the thiol group, and their mercury complexes have often been studied in aqueous and nonaqueous solutions.[1,2] The compounds containing an amino group are also known to form considerably stable complexes with mercury.[3] Nevertheless, their electrochemical behavior on the dropping mercury electrode has rarely been examined,[4-6] probably because amines are in general such strong bases that, in a dilute aqueous solution, they react with water to form the corresponding ammonium and hydroxide ions. On the other hand, amines are in the free state in aprotic solvents; this must be favorable for a polarographic study of free amines. Thus, Coetzee and Kolthoff[6] have reported that some amines give well-defined anodic waves in acetonitrile. However, they gave no details of the electrode reactions.

The present investigation was undertaken in order to survey the anodic behavior of amines on the dropping mercury electrode in detail by means of DC polarography and amperometric titration. Among amines, ammonia (NH_3), methylamine ($MeNH_2$), dimethylamine (Me_2NH), trimethylamine (Me_3N), ethylenediamine, 1,2-diaminopropane, aniline, and β-naphthylamine were chosen for the present study. *N,N*-dimethylformamide (DMF) was used as a solvent, for it is aprotic and is frequently used in polarography.

Experimental

Materials. The DMF obtained commercially was dried over potassium carbonate for several days and then distilled under reduced pressure in the presence of a few lumps of calcium hydride. The tetraethylammonium perchlorate (Et_4NClO_4) used as a supporting electrolyte was prepared as has been described by Fujinaga *et al.*[7] The NH_3, $MeNH_2$, Me_2NH, and Me_3N were obtained commercially in aqueous solutions; their concentrations were 28, 30, 40, and 30% respectively. They were diluted with DMF in order to prepare cell solutions of the amines without the removal of water.[8] The concentration of each amine was determined by titration with an aqueous hydrochloric acid. The other amines studied were commercially obtained and were used without further purification. A solution of mercuric perchlorate in DMF was prepared as has been described previously.[9]

Apparatus. The DC polarography was carried out at 25°C with a Shimadzu polarograph, model RP-50. An H-type cell was used for the polarography. The bridged

* Present address: Matsue Technical High School, Matsue.

1) I. M. Kolthoff and J. J. Lingane, "Polarography," Interscience Publishers, New York (1952), pp. 511, 541, 561, 577, and 781.

2) C. K. Mann and K. K. Barnes, "Electrochemical Reactions in Nonaqueous Systems," Marcel Dekker, New York (1970), p. 476.

3) J. Bjerrum, *Chem. Rev.*, **46**, 381 (1950).

4) C. J. Nyman, D. K. Roe, and D. B. Masson, *J. Amer. Chem. Soc.*, **77**, 4191 (1955).

5) C. J. Nyman and R. A. Johnson, *Anal. Chem.*, **29**, 483 (1957).

6) J. F. Coetzee and I. M. Kolthoff, *J. Amer. Chem. Soc.*, **79**, 6110 (1957).

7) T. Fujinaga, K. Izutsu, K. Umemoto, T. Arai, and K. Takaoka, *Nippon Kagaku Zasshi*, **89**, 105 (1968).

8) The amount of water introduced into the cell solutions with the amines was thought to be too small (below 0.04%) to affect the polarographic behavior of the amines. In fact, it was found for $MeNH_2$ that the anodic waves measured in the presence of water up to 0.40% were essentially the same as that measured after the removal of water.

9) Y. Matsui and Y. Date, This Bulletin, **43**, 2052 (1970).

saturated calomel electrode proposed by Takaoka[10] was used throughout as a reference electrode. All the potentials were corrected automatically for the IR-drop across the electrolysis cell with a Shimadzu automatic potential corrector, model AIC-50. No cell solution was degassed, since some amines are so volatile that degassing would change the amine concentrations. The cathodic wave of oxygen appears at a potential too negative to influence the anodic wave of mercury. The current-time curves (*i-t* curves) were measured by means of the polarograph described above, with a minimum damping of amplitude and with a maximum chart speed of the recorder (160 mm/min). The response of the recorder was not very fast, but it was fast enough to observe qualitative features.

Results and Discussion

Anodic Waves of NH_3, $MeNH_2$, and Me_2NH. In polarographic behavior NH_3, $MeNH_2$, and Me_2NH are essentially similar to one another. Figures 1, 2, and 3 show their polarograms at various concentrations. Each of these depolarizers gave a single well-defined anodic wave at concentrations lower than 0.5 mM. At higher concentrations, $MeNH_2$ and Me_2NH gave

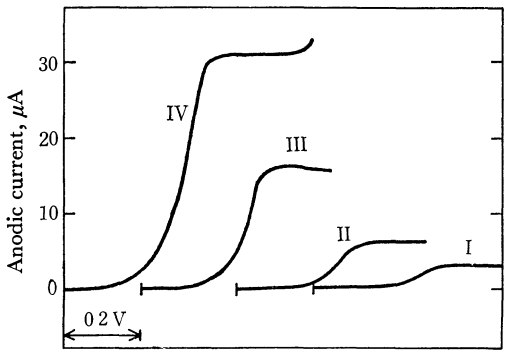

Fig. 1. DC polarograms of NH_3 in DMF at 25°C. Each polarogram was recorded from −0.10 V *vs.* SCE toward the positive potential.
I, 0.66 mM; II, 1.31 mM; III, 3.29 mM; IV, 6.57 mM

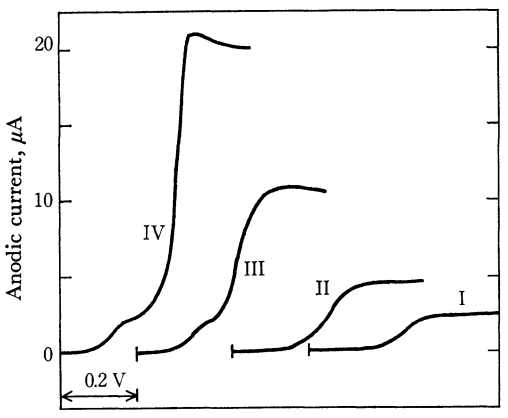

Fig. 2. DC polarograms of $MeNH_2$ in DMF at 25°C. Each polarogram was recorded from −0.10 V *vs.* SCE toward the positive potential.
I, 0.48 mM; II, 0.96 mM; III, 2.41 mM; IV, 4.82 mM

10) K. Takaoka, *Rev. Polarog.* (Kyoto), **14**, 63 (1966).

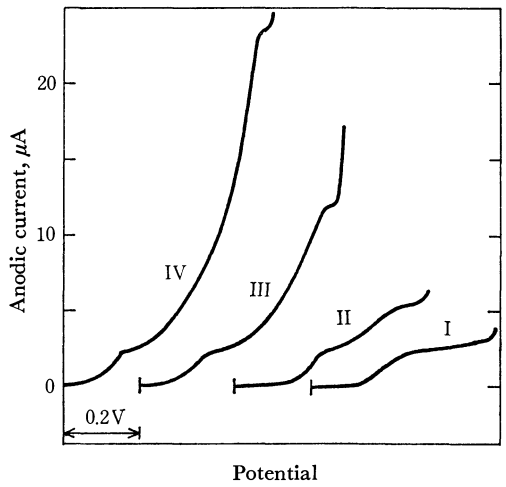

Fig. 3. DC polarograms of Me_2NH in DMF at 25°C. Each polarogram was recorded from 0.00 V *vs.* SCE toward the positive potential.
I, 0.53 mM; II, 1.06 mM; III, 2.65 mM; IV, 5.29 mM

prewaves, while NH_3 did not. For each depolarizer, as is shown, for example, in Tables 1 and 2 with respect to $MeNH_2$, the total limiting current (i_d) was virtually proportional to the bulk concentration of the depolarizer, and also to the square root of the effective pressure (h_{corr}) on the mercury drop; these facts indicate that the total limiting current is diffusion-controlled. On the other hand, the height (i_p) of each prewave of $MeNH_2$ and Me_2NH was virtually independent of the bulk concentration of the depolarizer and was proportional to h_{corr}; these facts indicate that the prewave

Table 1. Polarographic characteristics of methylamine at various concentrations at 25°C

Concn. (mM)	$E_{1/2}$, V *vs.* SCE		i_p (μA)[a]	I_d[b]
	prewave	total wave		
0.10	—	+0.157	—	2.88
0.24	—	+0.155	—	2.54
0.48	—	+0.151	—	2.60
0.96	—	+0.142	—	2.66
2.41	+0.017	+0.166	1.80	2.52
4.82	+0.032	+0.213	1.90	2.52

a) The height of the prewave.
b) Diffusion current constant, $I_d = i_d/C \cdot m^{2/3}t^{1/6}$ (μA·mM^{-1} mg$^{-2/3}$s$^{1/2}$).

Table 2. Relation between the limiting current of 1.26 mM methylamine and effective pressure on the dropping mercury electrode at 25°C

h_{corr} (cm)	i_p[a] (μA)	i_d[b] (μA)	i_p/h_{corr} (μA/cm)	$i_d/h_{corr}^{1/2}$ (μA/cm$^{1/2}$)
38.2	1.0	4.3	0.026	0.70
44.2	1.2	4.6	0.027	0.69
54.2	1.5	5.2	0.028	0.71
64.2	1.8	5.7	0.028	0.71
74.2	2.1	6.1	0.028	0.71
84.2	2.4	6.5	0.029	0.71

a) The limiting current of the prewave.
b) The limiting current of the total wave.

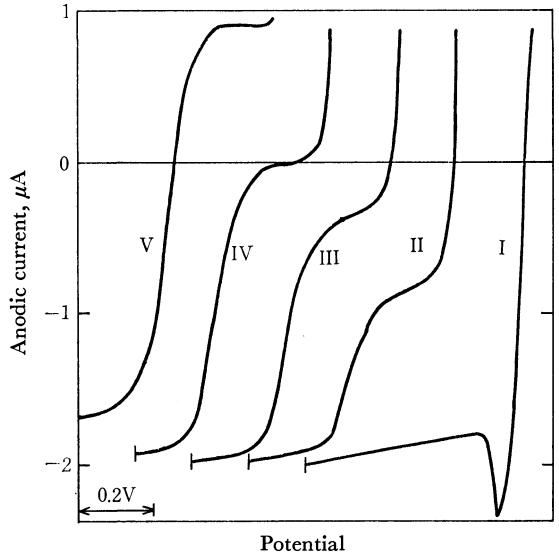

Fig. 4. The amperometric titration of 0.50 mM Hg(II) with $MeNH_2$ at 25°C. Each polarogram was recorded from −0.10 V *vs.* SCE toward the positive potential. The concentration of $MeNH_2$ added: I, 0.00 mM; II, 0.50 mM; III, 0.75 mM; IV, 1.00 mM; V, 1.25 mM

is characteristic of an adsorption current.

The composition of the mercury-amine complexes, which were considered to be formed during the electrode processes of the amines, was examined by the amperometric titration of the simple mercury(II) ion with each amine. The results for all three amines were virtually the same; as an example, the results of $MeNH_2$ are shown in Fig. 4. The simple mercury(II) ion gave a cathodic wave (accompanied by a maximum). The cathodic limiting current decreased with the amount of the amine added. At the same time, a second cathodic wave appeared at a less positive potential. The wave height increased in proportion to the amount of the amine added. When the quantity of the amine added was more than double that of mercury(II), the first cathodic wave disappeared, whereas an anodic limiting current appeared on the second wave. After that, the cathodic current of the second wave became virtually constant or decreased only slightly, while the anodic current increased in proportion to the excess amount of the amine. These results evidently show that the mercury(II) ion reacts with the amine (am) to form a complex of the $Hg(am)_2^{2+}$ type and that the complex is reduced at a potential corresponding to the second cathodic wave. The half-wave potential of this wave is approximately equal to that of the anodic wave of $MeNH_2$ shown in Fig. 2; this indicates that the electrode process is reversible. Thus, the electrode reaction can be expressed by the following equation:

$$Hg + 2am \rightleftarrows Hg(am)_2^{2+} + 2e \qquad (1)$$

Although Coetzee and Kolthoff[6] attributed the anodic waves of NH_3 and some amines in acetonitrile to the formation of salts of the $HgNH_2ClO_4$ type, this is implausible, at least in the case of the electrode process in DMF.

The diffusion coefficients of NH_3, $MeNH_2$, Me_2NH, and their mercury(II) complexes were evaluated by using the Ilkovic equation. The results are shown in Table 3, together with those for the other amines and their mercury(II) complexes. Compared with the data that the diffusion coefficient of NH_3 in water is 14.6×10^{-6} cm²/s (20°C)[11] and that of the simple mercury(II) ion in DMF is 3.92×10^{-6} cm²/s (25°C),[9] the values here obtained seem to be reasonable.

Table 3. Diffusion coefficients of amines and their complexes with mercury (II) in DMF at 25°C

Compound	$D_a\times10^{6}$ a) (cm²/s)	$D_c\times10^{6}$ b) (cm²/s)
NH_3	19.9	3.68
$MeNH_2$	18.8	4.01
Me_2NH	18.9	2.76
Ethylenediamine	15.0	5.59
1,2-Diaminopropane	12.9	4.83

a) Diffusion coefficient of amine.
b) Diffusion coefficinet of the 1:2 complex of mercury (II) with amine.

If the electrode process (1) is reversible, the equation of the wave should be expressed by:

$$E = E_0 - (RT/2F)\ln\beta_2 + (RT/2F)\ln k_0^2/k_2 + (RT/2F)\ln i/(i_d-i)^2 \qquad (2)$$

In this equation, E_0 represents the standard potential of the mercury-mercury(II) half-cell; β_2, the overall stability constant of the $Hg(am)_2^{2+}$ complex, and k_0 and k_2, the Ilkovic equation constants for the amine and $Hg(am)_2^{2+}$ respectively. Since the first three terms on the right-hand side of this equation are constant, a plot of $\log i/(i_d-i)^2$ *vs.* E should give a straight line, with a reciprocal slope of 0.030 V at 25°C. The results for the waves of 0.66 mM NH_3, 0.52 mM $MeNH_2$, and 0.24 mM Me_2NH are shown in Fig. 5. For each compound, a straight line with a reciprocal slope of about 0.030 V was obtained at the more positive potentials of the wave, whereas the plot deviated from the line at the less positive potentials of the wave. Similar plots were obtained for the waves of 0.33—1.32

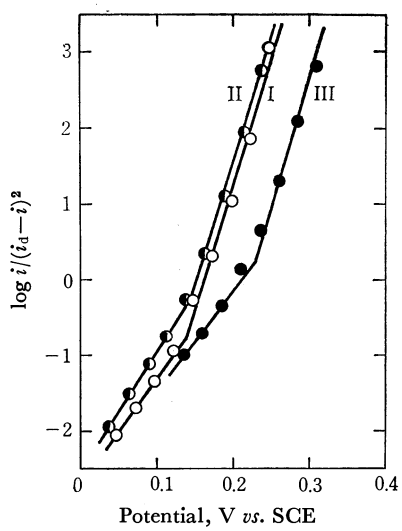

Fig. 5. The plots of $\log i/(i_d-i)^2$ *vs.* potential for the waves of 0.66 mM NH_3 (I), 0.52 mM $MeNH_2$ (II), and 0.24 mM Me_2NH (III).

11) D. M. Himmelblau, *Chem. Rev.*, **64**, 527 (1964).

mM NH_3, 0.10—0.66 mM $MeNH_2$, and 0.11—0.53 mM Me_2NH. The deviation of the plots can be attributed either to the partial formation of the higher amine complex, $Hg(am)_3^{2+}$, or to the adsorption of the electrolysis product, $Hg(am)_2^{2+}$, on the electrode surface. However, it was found that no equation derived by taking into account the formation of the higher complex[12] can explain the shape of the wave measured. Thus, at the less positive potentials of the wave a large part of the electrolysis product may be adsorbed on the electrode surface, and this may be responsible for the flowing of the extra anodic current. At the more positive potentials of the wave, the complex formed may cease to be adsorbed, and the polarographic curve may come to agree with that expressed by Eq. (2).

If Eq. (2) holds at the more positive potentials of each wave the value of β_2 can be estimated. For example, the potential at which the $\log i/(i_d-i)^2$ of the NH_3 wave equaled zero was graphically estimated to be 0.163 (average) V *vs.* SCE, E_0 is 0.557 V *vs.* SCE,[9] and the k_0 of NH_3 and the k_2 of $Hg(NH_3)_2^{2+}$ were 4.37×10^3 and 3.06×10^3 μA/M respectively. Consequently, β_2 was evaluated to be $10^{16.9}M^{-1}$. This value is comparable to that in water, that is, $10^{17.5}M^{-1}$.[13] The results of the other amines are listed in Table 4.

TABLE 4. OVERALL STABILITY CONSTANTS OF THE 1:2 COMPLEXES OF MERCURY (II) WITH AMINES IN DMF AT 25°C[a]

Compound	β_2, M^{-1}
NH_3	$10^{16.9}$
$MeNH_2$	$10^{17.1}$
Me_2NH	$10^{15.0}$
Ethylenediamine	$10^{23.5}$
1,2-Diaminopropane	$10^{24.0}$

a) Ionic strength: 0.10M

Furthermore, from Eq. (2) the following equation can easily be derived:

$$E_{1/2} = K - (RT/2F)\ln c_0 \qquad (3)$$

where $E_1/_2$ and c_0 are the half-wave potential and the bulk concentration of each amine respectively, and where K is a constant. The observed $E_1/_2$'s of the NH_3 waves are plotted in Fig. 6. When the concentration of NH_3 was less than 2 mM, the $E_1/_2$ was shifted, exactly in accordance with Eq. (3), to the less positive potential with an increase in the concentration. This indicates that Eq. (2) is valid in the low concentration range. However, when the concentration exceeded 2 mM, the $E_1/_2$ was shifted to the more positive potential with an increase in the concentration. Similar plots were obtained for $MeNH_2$ and Me_2NH, too. These may be well explained in terms of the inhibition of the anodic process by the electrolysis product adsorbed on the mercury electrode. That is, the concentration of each depolarizer may be so high that the surface

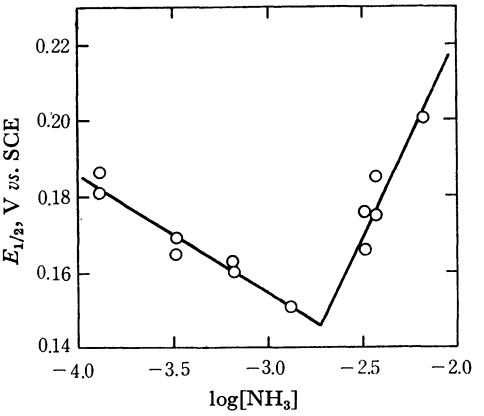

Fig. 6. Relation between the concentration of NH_3 and its half-wave potential.

of the mercury electrode may be completely covered by the film of the electrolysis product, which may then continue to inhibit the further diffusion of the depolarizer to the electrode until the complex is desorbed from the electrode at the more positive potential.

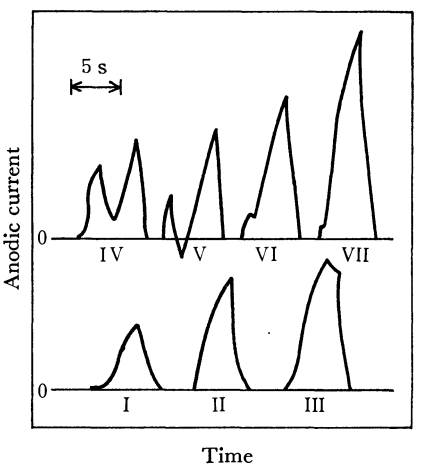

Fig. 7. The current-times curve of 1.5 mM Me_2NH at various potentials (25°C). Potential (V *vs.* SCE): I, 0.10; II, 0.15; III, 0.20; IV, 0.25; V, 0.30; VI, 0.40; VII, 0.50.

The inhibition of the electrode process by the adsorption was also observed by the measurement of the *i-t* curve during the growth of each mercury drop, especially in the case of Me_2NH (Fig. 7). In this case, the anodic current increased with the growth of a mercury drop at the potential of +0.15 V *vs.* SCE, corresponding to the mid-point of the Me_2NH prewave; this is characteristic of a diffusion-controlled process. On the other hand, at the potential of +0.20 V *vs.* SCE corresponding to the plateau of the prewave, the anodic current decreased somewhat before the dropping of mercury. At more positive potentials, the anodic current abruptly decreased in the course of the growth of a mercury drop. This is characteristic of an adsorption current and indicates that the electrode process is inhibited by the adsorbate layer. Similar results were observed in the case of $MeNH_2$, although that decrease in the current was not so great as in the case of Me_2NH.

If the adsorption of the mercury complexes obeys the

12) T. Murayama, T. Sawaki, and S. Sakuraba, This Bulletin, **43**, 2820 (1970).

13) L. G. Sillen and A. E. Martell, "Stability Constants of Metal-Ion Complexes," Special. Publ. **17**, Chem. Soc., London (1964), p. 155.

Langmuir isotherm, the maximum amount of the adsorbate per unit area (Z) can be evaluated by the following equation:[14]

$$Z = i_p/(knFm^{2/3}t^{-1/3}) \quad (4)$$

$$k = 0.85\ \mathrm{cm^2g^{-2/3}}\ \text{at } 25°\mathrm{C}$$

where n is the number of the electrons participating in the electrode process. For example, in the case of $MeNH_2$ n is equal to 2, and the mean value of i_p, measured when m and t are equal to 1.546 mg/s and 4.67 s respectively, is 1.85 μA. Therefore, Z is equal to 1.41×10^{-9} mol/cm^2, which indicates that one adsorbate molecule occupies an area of 11.8 Å^2 of the electrode surface. The value of Z for Me_2NH was 1.59×10^{-9} mol/cm^2 (10.4 Å^2/molecule).

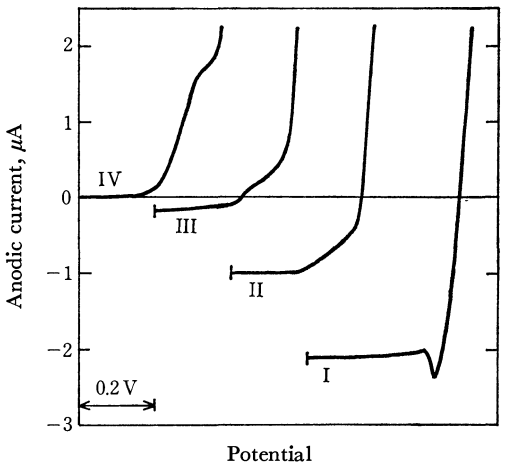

Fig. 8. The amperometric titration of 0.50 mM Hg(II) with Me_3N at 25°C. Each polarogram was recorded from +0.10 V *vs.* SCE toward the more positive potential. The concentration of Me_3N added: I, 0.00 mM; II, 0.50 mM; III, 1.00 mM; IV, 1.50 mM.

Anodic Wave of Me_3N. The polarogram of Me_3N was similar to that of $MeNH_2$. The wave height was virtually proportional to the bulk concentration of Me_3N and also to the square root of the effective pressure on the mercury drop; these facts indicate that the wave is diffusion-controlled (I_d=1.31 μA·mM^{-1} mg$^{-2/3}$s$^{1/2}$). However, the results of the amperometric titration of the simple mercury(II) ion with Me_3N were different from those with $MeNH_2$ and Me_2NH (Fig. 8). Although the height of the wave of the simple mercury(II) ion decreased with the increase in the amount of Me_3N, no reduction wave of the mercury complex appeared. The reduction wave of the simple mercury(II) ion almost disappeared when the concentration of the amine added exceeded twice that of the mercury(II) ion. It was also observed that the mercury(II) solution changed from colorless to a yellowish brown as the amine was added. These results indicate that the simple mercury(II) ion is chemically reduced by the amine to metallic mercury and the cation radical of the amine, which may then be liable to decompose to electro-inactive products. Thus, the anodic wave of Me_3N may not be due to the oxidation of mercury to its complex with the amine, but to the oxidation of the amine itself to the corresponding cation radical.

14) K. Hasebe and T. Kambara, *Rev. Polarog.* (Kyoto), **15**, 37 (1968).

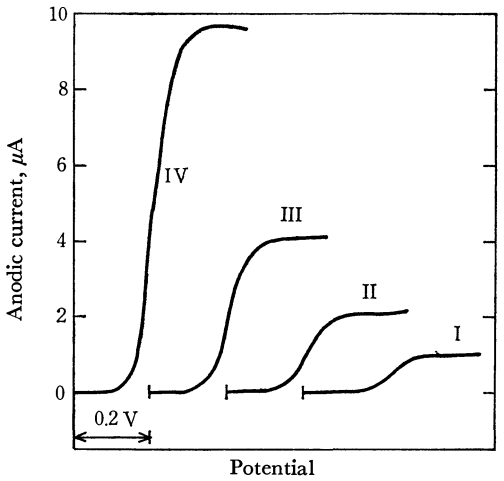

Fig. 9. DC polarograms of ethylenediamine in DMF at 25°C. Each polarogram was recorded from −0.25 V *vs.* SCE toward the positive potential. I, 0.25 mM; II, 0.51 mM; III, 1.01 mM; IV, 2.53 mM.

Anodic Waves of Ethylenediamine and 1,2-Diaminopropane. The polarographic behavior of ethylenediamine and that of 1,2-diaminopropane were similar to one another, but different from that of the monoamines examined above. Figure 9 shows the polarograms of ethylenediamine at various concentrations. Each diamine gave a well-defined anodic wave even in a concentrated solution. The height of the wave of each diamine was proportional to the bulk concentration of the diamine and also to the square root of the effective pressure on the mercury drop; these facts indicate that the wave is diffusion-controlled. The results of the amperometric titration of the simple mercury(II) ion with each diamine clearly indicated that the mercury(II) ion reacts with each diamine to form a complex of the $Hg(diam)_2^{2+}$ type.

If the anodic wave of each diamine is due to the formation of the 1:2 complex in a reversible process, Eq. (2) should hold. The plots of $\log i/(i_d-i)^2$ *vs.* potential were linear, in good accordance with Eq. (2), over the entire potential range of the anodic wave of each diamine. This is different from the results obtained for NH_3, $MeNH_2$, and Me_2NH and suggests that the mercury(II) complex with each diamine is not adsorbed on the electrode. This argument was supported by the measurements of the *i-t* curve and of the electrocapillary curve of each diamine. The absence of adsorption may be related to the formation of the chelate complex of mercury(II) with each diamine. A plot of $E_{1/2}$ *vs.* the logarithmic concentration of each diamine was virtually linear, in accordance with Eq. (3), over the whole range of concentration studied. The diffusion coefficients of each diamine and its mercury(II) complex, and the overall stability constants of the 1:2 complex, are listed in Tables 3 and 4 respectively.

It was found that the mercury(II) complexes of the diamines are more stable than those of the mono-

amines by a factor of about 10^7. It was also found that the values of β_2 in DMF are very close to those in water ($10^{23.42}M^{-1}$ for ethylenediamine and $10^{23.53}M^{-1}$ for 1,2-diaminopropane in 0.10N KNO_3 at 25°C[4]); this suggests that solvents have little effect on the stability of the complexes.

Anodic Behavior of Aromatic Amines. Although Coetzee and Kolthoff[6] have reported that aniline gives a well-defined anodic wave in acetonitrile, it gives no anodic wave in DMF. β-Naphthylamine also gives no anodic wave in DMF. These results are in clear contrast to those of the aliphatic amines. The complexing ability of the aromatic amines with mercury(II) may be lower than that of the aliphatic amines, just as the basicity of the former is lower than that of the latter.

BULLETIN OF THE CHEMICAL SOCIETY OF JAPAN, VOL. 46, 152—156 (1973)

The Synthesis of Crystalline Rare Earth Carbonates

Kozo Nagashima, Hisanobu Wakita,* and Akihiko Mochizuki

Department of Chemistry, Faculty of Science, Tokyo Kyoiku University, Bunkyo-ku, Tokyo 112

(Received April 20, 1972)

The factors which influence the crystallization of rare earth carbonates were studied. Crystalline rare earth carbonates were precipitated at various temperatures from aqueous solutions by using sodium carbonate, sodium bicarbonate, trichloroacetic acid, and urea as precipitants. The crystal parameters, compositions, and factors concerning the formations of various carbonates, such as lanthanite-type $Ln_2(CO_3)_3 \cdot 8H_2O$(Ln=La, Ce), tengerite-type $Ln_2(CO_3)_3 \cdot nH_2O$(Ln=Nd, Sm, Gd, Dy, Ho, Er, and Y, n=2—3), monoxocarbonate-type $Ln_2O(CO_3)_2 \cdot nH_2O$(Ln=La, Ce, Nd, and Sm, n=1—2) and a hydrated double carbonate of rare earth and sodium (rare earth= La, Ce, Nd, Sm, Gd, Dy, and Y) were determined by chemical analysis and X-ray powder diffractometry.

Rare earth carbonates of various compositions have been reported as a result of numerous syntheses and thermal analyses.[1-9] Many of the results reported and the accompanying discussions are, however, contradictory. The inconsistencies are due in part to preparatory difficulties and to a lack of structural data.

The carbonates of most metals are prepared by the following two common procedures: the precipitation of the compounds by alkali carbonates or bicarbonates from solutions containing the metal salt, and by passing carbon dioxide through an aqueous suspension of metal hydroxides. However, pure crystalline carbonates of the rare earth elements are difficult to prepare by these methods.

Crystalline rare earth carbonates are generally obtained by the hydrolysis of trichloroacetates of rare earth elements, but the precipitates of heavier lanthanoids prepared by other techniques usually appear amorphous when examined by X-ray powder diffractometry.[10]

Katsurai and Uda[11] prepared pure crystalline siderite, $FeCO_3$, by autoclaving a solution of ferrous ammonium sulfate in the presence of urea. The present authors have now successfully used this procedure in preparing the crystalline rare earth carbonates.

In general, the principal factors which influence the crystallization of scarcely-soluble compounds from aqueous solution are: (1) the nature of the precipitant, (2) the temperature and pressure, (3) the concentrations of the metal ion and the precipitant, and (4) the aging period. These factors have been repeated vaguely in almost all studies concerned with the synthesis of crystalline rare earth carbonates. To be considered in this investigation are the natures of the carbonates of lanthanum, cerium(III), neodymium, samarium, gadolinium, holmium, erbium, ytterbium(III), yttrium, and scandium, essentially even-atomic-numbered lanthanoids, as they are affected by the above conditions during the preparation.

Experimental and Results

Synthesis. *(1) Alkali Carbonate and Bicarbonate as Precipitant*: Similar results were obtained with sodium carbonate and sodium bicarbonate, but usually the bicarbonate gave a superior crystalline product. Crystalline carbonates of lanthanum, cerium(III), neody-

* Present address. Department of Chemistry, Faculty of Science, Fukuoka University, Fukuoka 814.

1) R. G. Charles. *J. Inorg. Nucl. Chem.*, **27**, 1498 (1965).

2) E. L. Head and C. E. Holley, Jr., "Rare Earth Research II," Gordon and Breach, New York, N. Y. (1964), p. 51.

3) E. L. Head and C. E. Holley, Jr., "Rare Earth Research IV," Gordon and Breach, New York, N. Y. (1965), p. 707.

4) R. L. N. Sastry, S. R. Yoganarisimhan, P. N. Mehrota, and C. N. R. Rao, *J. Inorg. Nucl. Chem.*, **28**, 1165 (1966).

5) M. Clarus Strouth, Ph. D. Thesis, Michigan State University, 1962.

6) G. Pannetier, J. Nataf, and A. Deireigne, *Bull. Soc. Chim. Fr.*, **5**, 318 (1965).

7) S. D. Ross and J. Goldsmith, *Spectrochim. Acta*, **20**, 781 (1964).

8) D. B. Shinn and H. A. Eick, *Inorg. Chem.*, **7**, 1340 (1968).

9) I. N. Tselik, V. Ya. Shvartsman, and V. D. Fedorenko, *Russ. J. Inorg. Chem.*, **13**, 53 (1968).

10) H. Wakita and K. Nagashima, This Bulletin, **45**, 2476 (1972).

11) T. Katsurai and M. Uda, *ibid.*, **43**, 3306 (1970).

Table 1. The influence of metal ion (Y^{3+}) concentration and aging period on the crystallization of rare earth carbonates[a)]

Temp. (°C)	50°C			70°C		
Concn of Y^{3+} (mol)	Aging period (day)			Aging period (day)		
	1	2	4	1	2	4
0.0002	No ppt	Large thin plate amor.	Large thin plate amor.	Large needle cryst.	Large needle cryst.	Large needle cryst.
0.0005	Thin plate amor.	Large thin plate amor.	Needle cryst.	Needle cryst.	Needle cryst.	Needle cryst.
0.0010	Thin plate amor.	Thin plate amor.	Needle cryst.	Needle cryst.	Needle cryst.	Needle cryst.
0.0020	Thin plate amor.	Needle cryst.	Needle cryst.	Small needle cryst.	Small needle cryst.	Small needle cryst.

a) All crystalline precipitates gave the tengerite type X-ray powder patterns.

mium, samarium, gadolinium, dysprosium, erbium, and ytterbium were produced by this method, whereas ytterbium and scandium gave only amorphous carbonates.

Procedure: To a constantly-stirred 10 ml portion of a 0.1M rare earth chloride solution contained in a beaker, we added a solution of twice the molar equivalent of sodium bicarbonate (or carbonate). The procedure was then repeated at various temperatures from 20 to 80°C. The total volume of the mixed solution was adjusted to 100 ml and was maintained at the desired temperature for one week. The precipitates were then filtered off, washed with water repeatedly, air-dried and subjected to microscopy, chemical analysis, X-ray powder diffractometry, and thermal analysis. The results for the precipitates obtained at higher temperatures agreed with those obtained by the other methods.

(2) Trichloroacetic Acid as the Precipitant: This is the most popular method for obtaining crystalline rare earth carbonates. Not only light lanthanoids, but also yttrium and heavy lanthanoids except for ytterbium, gave crystalline carbonates.[10)] Crystalline carbonates of the elements mentioned in (1) have been obtained in the temperature range from 40 to 120°C. Below 40°C, the rate of the hydrolysis of trichloroacetate was too slow for us to prepare sufficient amounts of carbonates.

Procedure: To a 10 ml portion of a 0.1M rare earth chloride solution contained in a beaker or flask, we added 5 ml of a 2.0 M trichloroacetic acid solution. The solution was adjusted with ammonia to pH 5—6, and the volume was adjusted to 100 ml. Beakers or flasks were placed in thermostatically-controlled baths at temperatures ranging from 40 to 120°C, at ten-degree intervals, for one week. For temperatures over 100°C, the flasks were equipped with reflux condensers, or sealed glass ampoules were used. The precipitates were then filtered off, washed with water, and air-dried.

(3) Urea as the Precipitant: A mixture of 10 ml of a 0.1M rare earth solution and 10 ml of a 0.2M urea solution was autoclaved for one week at various temperatures from 50 to 150°C. As has been mentioned by Head and Holley,[2)] the autoclaving of rare earth carbonates appears to produce good crystallization. The precipitates were filtered off, washed with water repeatedly, air-dried, and subjected to analysis.

In the case of yttrium, the formation reaction is expressed as:

$$3(NH_2)_2CO + 2YCl_3 + (6+n)H_2O \longrightarrow Y_2(CO_3)_3\cdot nH_2O + 6NH_4Cl.$$

(4) Factors Which Influence Crystallization: The following experiments were carried out for the purpose of studying the various factors which influence the crystallization of rare earth carbonates, such as the temperature, the concentration of metal ions and the aging period of the precipitates.

Experiment: 2-, 5-, 10-, and 20-ml portions of 0.1M rare earth chloride solutions were placed in beakers, and 1-, 2.5-, 5-, and 10-ml portions of a 2.0M trichloroacetic acid solution were added respectively. Then the pH values of mixed solutions were adjusted to 5—6 with ammonia and the volumes were adjusted to 100 ml. The beakers were placed in a thermostatically-controlled bath maintained in the temperature range of 50 to 70°C. After several days, the precipitates were filtered off, washed with water, air-dried, and subjected to microscopy and X-ray powder diffractometry. The results for the experiment using yttrium are summarized in Table 1.[12)] It can be seen that longer aging periods and lower concentrations of the metal ion produce larger crystals. It was also revealed that varying the concentration of metal ion does not change the structure of rare earth carbonates within the concentration range of the present work. In all cases, the tengerite structure was obtained.

Chemical Analyses and X-Ray Powder Diffractometry. Chemical analyses were carried out on the rare earth

Table 2. Chemical analysis of synthesized rare earth carbonates (quantities are molar ratios)

	M_2O_3 :	CO_2 :	H_2O
Monoxocarbonate type (La compound)	1.00	2.14	1.41
Lanthanite type (La compound)	1.00	2.97	8.04
Tengerite type (Y compound)	1.00	3.01	2.35
Yb compound[a)]	1.00	2.05	3.87
Sc compound[b)]	1.00	0.00	3.00

a) X-Ray amorphous. b) Hydroxide.

12) La, Ce, -and Nd gave good crystalline precipitates under the conditions of Table 1.

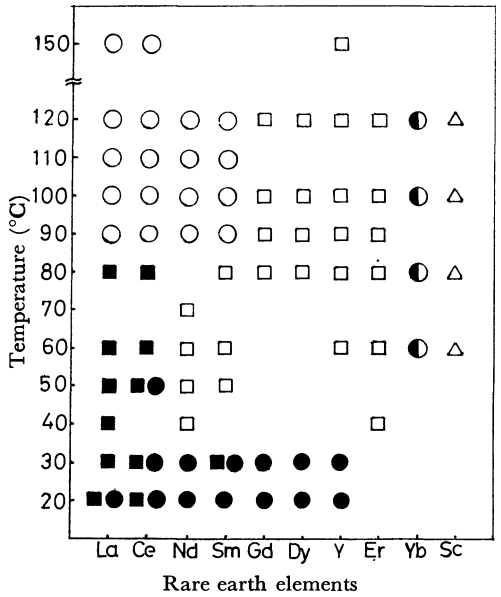

Fig. 1. Diagram showing the phases, formation temperature, and rare earth elements.
○: monoxocarbonate type, ●: double carbonate, ◐: amorphous, □: tengerite type, ■: lanthanite type, △: hydroxide

carbonates prepared by the prescribed methods. The carbonates were classified into five types according to their compositions. It was found that the compositions were affected by the temperature, but were not dependent on the method of preparation. The results of the chemical analyses of typical samples are shown in Table 2. The types of rare earth carbonates obtained at various temperatures are illustrated in Fig. 1. Rare earth elements on a horizontal axis are shown according to their ionic radii. The X-ray powder diffractions of the synthesized samples were recorded on a Rigaku Denki Geigerflex Diffractometer, applying Ni-filtered Cu$K\alpha$ radiation and employing metallic silicon as the internal standard.

By chemical and X-ray analyses, the natures of the following carbonates were determined.

(A) Monoxocarbonate Type (shown by open circles in Fig. 1). Experimental formula: $Ln_2O_3 \cdot 2CO_2 \cdot nH_2O$($n$=1—2)——Table 2. Carbonates of lanthanum, cerium(III), neodymium, and samarium prepared at 90°C and higher are of this type. The X-ray powder data for the lanthanum compound of this type are given in the third column of Table 3. So far as we can discover in the literature surveyed, this is the first report on the X-ray powder data for rare earth monoxocarbonate. Though a possibility still exists that the compound is a hydroxocarbonate, this type of carbonate was classified as monoxocarbonate $Ln_2O(CO_3)_2 \cdot nH_2O$ (n=1—2) through thermal analysis and a study of its infrared spectrum.

B) Lanthanite Type (shown by solid squares in Fig. 1). Lanthanum and cerium(III) ions, the largest two of the lanthanoid ions, form this type of carbonate in the temperature range from 20 to 80°C. This type of carbonate has the composition of $Ln_2(CO_3)_3 \cdot 8H_2O$ (Table 2) and gives an X-ray-powder-diffraction pattern (Table 3) identical with that of lanthanite,[8] a very rare, hydrated, rare earth carbonate mineral.

(C) Tengerite Type (shown by open squares in Fig. 1). Neodymium (40—70°C), samarium (30—80°C), gadolinium, dysprosium, yttrium, and erbium form this type of carbonate, with the formula of $Ln_2(CO_3)_3 \cdot nH_2O$(n=2—3)[10] (Table 2). Because of the experimental difficulty, the central area of Fig. 1 remains incomplete at present. It may be said, however, that the formation of the tengerite-type carbonate is characteristic of the heavier lanthanoids, excluding ytterbium. The X-ray diffraction data listed in Table

Table 3. X-Ray powder data for synthesized rare earth carbonates

Lanthanite type (La)			Tengerite type (Y)			Monoxocarbonate type (La)		Double carbonate (Gd)	
d (Å)	I	hkl	d (Å)	I	Probable hkl	d (Å)	I	d (Å)	I
8.61	100	002	7.589	90	001	5.65	60	13.23	100
4.79	15	020	5.673	70	020	5.00	20	6.56	45
4.50	10	200	4.604	100	200	4.37	60	4.35	35
4.27	50	113 004	3.890	70	201	4.32	50	3.254	1
4.18	15	022	3.782	30	030	3.74	100	2.602	12
3.98	10	202	3.573	50	220	3.42	90	2.167	7
3.89	10	014	3.046	5	300	2.986	70	1.856	1
3.85	10	104	2.967	40	310	2.812	15		
3.58	5	114	2.919	8	230	2.672	50		
3.29	15	213 220	2.696	15	320	2.457	20		
3.19	10	221 024	2.598	10	222	2.368	60		
3.07	20	204 222	2.537	30	321	2.146	20		
3.02	10	115				2.090	20		

a_0=9.00Å (calculated from 200)
b_0=9.58Å (calculated from 020)
c_0=17.22Å (calculated from 002)

a_0=9.21Å
b_0=11.35Å
c_0=7.59Å

3 coincide well with those of natural tengerite.[10] In the table, the indices and cell edges as well as the d values and intensities for the lanthanite-type lanthanum carbonate and those for the tengerite-type yttrium carbonate are listed.

(D) Double Carbonate (shown by the solid circle in Fig. 1). The double carbonate was obtained when sodium carbonate was used as the precipitant at lower temperatures. Lanthanum (20°C), cerium(III) (20—50°C), neodymium, samarium, gadolinium, dysprosium, and yttrium (20—30°C) form this double carbonate. In the cases of lanthanum and cerium(III), either the lanthanite type or the double carbonate forms, depending on minor variations in the preparation process. The composition of this double carbonate may be expressed as a hydrated double carbonate of rare earth and sodium. Further study is necessary, however, to determine the compositions of the compounds. The X-ray powder data for the double carbonate of gadolinium are listed in the last column of Table 3.

Table 4. X-Ray powder data for synthesized monoxocarbonates

La		Ce		Nd		Sm	
d (Å)	I	d (Å)	I	d (Å)	I	d (Å)	I
5.65	60	5.63	65	5.54	35	5.51	30
5.00	20						
4.37	60	4.34	100	4.29	80	4.26	75
4.32	50	4.30	75	4.25	100	4.24	70
3.74	100	3.72	95	3.68	80	3.66	70
3.42	90	3.39	80	3.33	40	3.30	100
2.986	70	2.974	80	2.953	30	2.937	20
2.955	25			2.932	40	2.894	60
2.812	15						
2.676	50	2.670	70	2.641	70	2.629	50
2.457	20	2.441	20	2.410	15	2.390	20
2.377	60			2.329	60	2.318	50
2.368	40			2.321	40	2.295	60
2.146	20	2.144	30	2.124	40	2.120	20
2.090	20	2.078	40	2.056	20	2.045	30
2.066	35	2.059	30	2.039	40	2.031	30
2.029	20	2.016	30	1.989	15	1.972	20
1.974	25	1.958	30	1.932	20	1.915	20
1.886	35						
1.873	60	1.869	40	1.835	35	1.822	35
1.855	15	1.833	15	1.806	15	1.789	20
1.745	10	1.738	20	1.717	15	1.703	15
1.706	15	1.690	20	1.664	10	1.648	10

With ytterbium, a crystalline carbonate was not formed by these procedures within the given temperature range; only an amorphous basic carbonate was obtained. Scandium, however, formed a crystalline hydroxide upon the hydrolysis of trichloroacetate or urea. The X-ray data of the respective monoxocarbonates (La, Ce, Nd, Sm) are listed in Table 4. In the table, it can clearly be seen that d values of carbonates of this type increase linearly with an increase in the ionic radii of rare earth elements.

Thermal Analysis of Monoxocarbonates. The thermal decomposition study of the monoxocarbonates was performed with a Choryo Keiki Thermobalance modified to record the thermogravimetric analysis (TGA), differential thermal analysis (DTA), and differential thermogravimetric analysis (DTG) curves simultaneously. The measurements were made in air at a heating rate of 5.4°C/min, using approximately 100 mg samples. The results of the TGA, DTA, and DTG analyses of lanthanum and neodymium monoxocarbonates are shown in Figs. 2 and 3. The decomposition processes of cerium and samarium monoxocarbonate were similar to that of neodymium. On the TGA curve for the lanthanum compound, there is initially a loss of water, leading to the plateau, which corresponds to the step of the anhydrous monoxocarbonate. The stability of this compound in one of the bases for assuming the formula of the initial compound to be hydrated monoxocarbonate. This plateau is prominent for the lanthanum compound. On the TGA curve for the neodymium compound, the temperature rise leads to dehydration and decarbonatation at the same time. The difference observed in the TGA curves was also observed in the DTA curves. The DTA curve in Fig. 2 shows that the exothermic effects in the 250—400°C range corresponds to the formation of the anhydrous monoxocarbonate. The continuous raising of the temperature leads to the formation of some intermediate phases, shown in the following processes, (1) and (2):

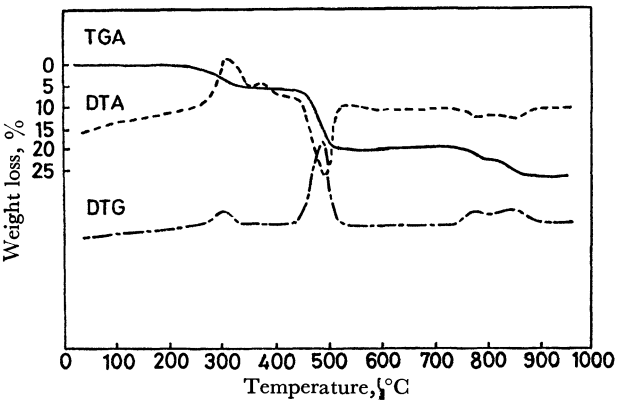

Fig. 2. TGA, DTA, and DTG curves of $La_2O(CO_3)_2 \cdot 1.4H_2O$

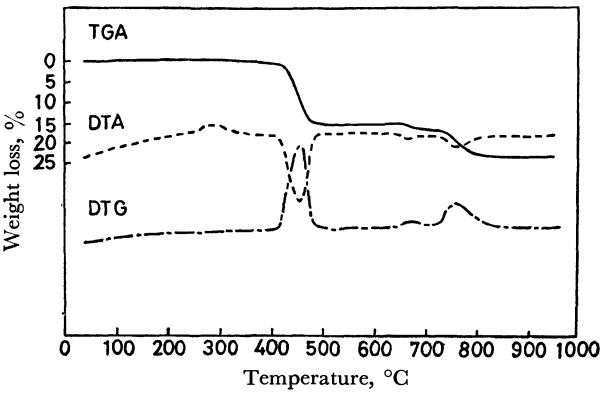

Fig. 3. TGA, DTA, and DTG curves of $Nd_2O(CO_3)_2 \cdot 1.5H_2O$

$$La_2O(CO_3)_2 \cdot 1.4H_2O \xrightarrow{ca.\ 300°C} La_2O(CO_3)_2 \xrightarrow{ca.\ 530°C} La_2O_3 \cdot 0.8CO_2 \xrightarrow{ca.\ 800°C} La_2O_3 \cdot 0.4CO_2 \xrightarrow{ca.\ 900°C} La_2O_3 \quad (1)$$

$$Nd_2O(CO_3)_2\cdot 1.5H_2O \xrightarrow{ca.\ 500^\circ C} Nd_2O_3\cdot 0.9CO_2 \xrightarrow{ca.\ 700^\circ C} Nd_2O_3\cdot 0.7CO_2 \xrightarrow{ca.\ 800^\circ C} Nd_2O_3 \quad (2)$$

Infrared Spectroscopy. Herzberg[13] gave the frequencies for the four modes of the free carbonate ion: ν_1, 1063 cm^{-1}; ν_2, 879 cm^{-1}; ν_3, 1415 cm^{-1}; and ν_4, 680 cm^{-1}, when the ν_3 and ν_4 modes degenerate. The ν_1 symmetrical streching mode is infrared-inactive for the free ion, but it may become active in the crystalline stage. Its presence and the splitting of degenerate modes indicate the presence of a dipole within the carbonate group. The D_{3h} symmetry of the free carbonate ion is thus lowered either to C_{2v} or to C_s symmetry. The splitting of the non-degenerate bands is generally an indication of nonequivalent carbonate groups in a given structure.[14]

The infrared spectra of the rare earth carbonates obtained in this work are shown in Fig. 4. The multiple splittings of all modes for the crystalline rare earth carbonates (lanthanite-type, tengerite-type, monoxocarbonate-type, and double carbonate) must be caused by several types of carbonate ions situated at crystallographically non-equivalent site.

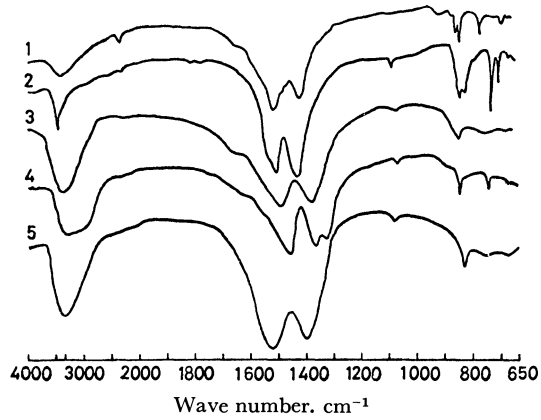

Fig. 4. Infrared absorption spectra of rare earth carbonates (in KBr disk).
1: tengerite type (Y), 2: monoxocarbonate type (Sm), 3: double carbonate (Sm), 4: lanthanite type (La), 5: amorphous carbonate (Yb).

The minerals —shortite, huntite, and parisite— which contain two nonequivalent CO_3^{2-} groups show similar spectra, with the splittings of all modes.[15]

Conclusion

It was found in this study that crystalline rare earth carbonates may be classified into several phases according to the ionic radii of rare earth elements and the preparation temperatures, and that the concentrations of the rare earth ion and the aging periods affect mainly the crystallization.

The preparation and the structure of lanthanite-type rare earth carbonates were previously studied by Shinn and Eick,[8] and the preparation and cell parameters of tengerite-type rare earth carbonates were described by Wakita and Nagashima.[10] The present investigation was clarified the formation temperature range for lanthanite-type and tengerite-type carbonates and the elements which form those carbonates.

The formation of rare earth monoxocarbonates through the decomposition of hydrated rare earth carbonates or oxalates has been reported by many investigators. The formation of crystalline substances in those cases is doubtful, however, because of the procedures used, and none of the investigators have referred to the formation of monoxocarbonate from an aqueous solution.

A rare earth double carbonate is indicated by the results of X-ray powder analyses, chemical analyses, infrared spectrometry, and thermal analyses. This appears to be the first time that such a rare-earth double-carbonate compound has been reported; further investigation of this class of rare earth carbonates is desirable.

13) G. Herzberg, "Molecular Spectra and Molecular Structure, II. Infrared and Raman Spectra of Polyatomic Molecules," D. Van Nostrand Co. Inc., New York, N. Y. (1945), p. 179.
14) R. P. Turcotte, J. O. Sawyer, and L. Eyring, *Inorg. Chem.*, **8**, 238 (1969).
15) H. H. Adler and P. F. Kerr, *Am. Mineral.*, **48**, 839 (1963).

The Viscosities of Aqueous Solutions Containing Metal Complexes. III. Iminodiacetato and Methyliminodiacetato Complexes[1]

Kiyoshi MIZUTANI and Motoo YASUDA

Department of General Education, Nagoya University, Chikusa-ku, Nagoya 464

(Received April 21, 1972)

The viscosities of aqueous solutions containing a metal chelate formed with iminodiacetic acid (H_2ida) or *N*-methyliminodiacetic acid (H_2mida) were measured with Cannon-Fenske capillary viscometers. Measurements were made in a Shibata viscosity bath maintained at 25±0.01°C. The Jones-Dole viscosity *B*-coefficient of each bis-ida chelate is lower than that of the corresponding bis-mida chelate, as may be expected. The *B*-coefficients for the mono-ida and mono-mida chelates were not determined accurately and will not be reported here. The *B*-value of *cis*(*N*)-[Co(ida)$_2$]$^-$ is higher than that of the *trans*-isomer. This is probably associated with the fact that the *cis*-isomer interacts with the solvent more strongly than the *trans*-isomer.

In the previous papers of this series, the viscosities of the luteo-type Co(III) and Co(II) complexes and the ethylenediaminetetraacetato (edta^{4-}) complexes[2a] and *trans*-1,2-cyclohexanediaminetetraacetato (cydta^{4-}) complexes were reported.[2b] The results showed, above all, that the *B*-coefficient of the Co(III) chelate formed with edta^{4-} or cydta^{4-} was much lower than those of the corresponding divalent metal chelates, and suggested that there might be a marked difference between the structures of [CoL]$^-$ and [ML]$^{2-}$ (L: edta^{4-} or cydta^{4-}; M: divalent metal ion). In order to study this problem in more detail, a viscosity study was made of aqueous solutions of metal chelates formed with iminodiacetic acid and *N*-methyliminodiacetic acid.

Experimental

Measurements. The viscosity *B*-coefficients of Co(III) and six divalent metal chelates were determined by means of Cannon-Fenske capillary viscometers with efflux times of ca. 520 and 600 sec respectively for distilled water. The viscosities and densities of the solutions were measured in a Shibata viscosity bath maintained at 25±0.01°C. The efflux times, measured with stopwatches to 0.1 sec, were easily reproducible to 0.2 sec.

Chelating Agents. Dotite H_2ida and Aldrich H_2mida were used. The analytical results for the C, H, and N contents showed these agents to be satisfactorily pure.

Complexes. The *cis*(*N*)- and *trans*(*N*)-potassium bis(iminodiacetato)cobaltates(III) were prepared following the method in the literature.[3] Divalent metal chelates of H_2ida and H_2mida were not isolated as crystals. Instead, solutions of these chelates were made up using metal nitrate (or chloride) and the K_2ida or K_2mida stock solutions.

Calculation. For each of the chelates studied, the relative viscosity, η/η_0, of aqueous solutions was expressed by the Jones-Dole equation:[4]

$$\frac{\eta}{\eta_0} = 1 + A\sqrt{c} + Bc \qquad (1)$$

where η and η_0 are the viscosities of the solution and of water respectively, and where c is the molar concentration of the solute. The coefficients, A and B, which are constants characteristic of the solute, were fully discussed by Gurney.[5] The *B*-coefficient was evaluated by a plot of $((\eta/\eta_0)-1)/\sqrt{c}$ *vs.* $\sqrt{c}$. A straight line was obtained for each case studied at concentrations below 0.06 mol/l. The slope of the resulting straight line gives the value of the *B*-coefficient for the solute. Because it has been shown to be true, for a wide variety of solutions, that B is composed additively of contributions from each of the solute species present in a solution, the *B*-value of the complex ion is obtained by subtracting a relatively small correction for the co-existing ionic species.

Results and Discussion

As both H_2ida and H_2mida are tridentate chelating agents, two kinds of chelates are formed following these equations:

$$M + L \rightleftarrows ML \qquad (2)$$

$$ML + L \rightleftarrows ML_2 \qquad (3)$$

where M is a metallic cation and where L is ida^{2-} or mida^{2-}. Accordingly, there are two kinds of viscosity *B*-coefficients, B_{ML} and B_{ML_2}, to be measured. Though we tried to obtain both of them, only the latter was determined accurately. Concerning the coefficient, B_{ML}, for the mono-chelate, only a rough value could be estimated because of several difficulties involved. For instance, in the lower pH range the dissociation of the chelate ML, that is, the reverse reaction of Eq. (2), occurs. This might tend to increase the viscosity of the solution. Next, in the higher pH range hydroxo-complexes, which might be formed by base hydrolysis, should be taken into account, and the chelate ML_2 must be considered to be present in the solution following Eq. (3), even though the solution contains stoichiometrical quantities of the metal ion and ligand. Furthermore, the B_{ML}-value is lower than the B_{ML_2}-value, and so more concentrated solutions should be used for the viscosity measurements of the mono-chelate. However, because of the low solubility of ML, which has no ionic charge, accurate measurements were impossible.

The *B*-coefficients of the bis-chelate ML_2 studied here are listed in Table 1. The pH value of each solution

1) Presented at the Symposium on Coordination Chemistry of the Chemical Society of Japan, Kyoto, Oct. 1968, and Tokyo, Nov. 1970.

2) a) M. Yasuda, This Bulletin, **41**, 139 (1968). b) *ibid.*, **42**, 2547 (1969).

3) J. Hidaka, Y. Shimura, and R. Tsuchida, *ibid.*, **35**, 567 (1962).

4) G. Jones and M. Dole, *J. Amer. Chem. Soc.* **51**, 2950 (1929).

5) R. W. Gurney, "Ionic Processes in Solution," McGraw-Hill Book Company, New Yrok (1953).

TABLE 1. VISCOSITY B-COEFFICIENTS OF IMINODIACETATO AND METHYLIMINODIACETATO COMPLEXES (25°C)

Metal	B(ida)	B(mida)
Cu^{2+}	0.72	0.83
Ni^{2+}	0.73	0.85
Co^{2+}	0.72	0.84
Zn^{2+}	0.80	0.88
Cd^{2+}	0.90	—
Pb^{+2+}	0.75	—
Co^{3+}	*cis* 0.49	—
	trans 0.42	—

used for viscosity measurement was between 7~9; the higher pH range was used for the chelate with a lower stability constant. Since the ida^{2-} and $mida^{2-}$ chelates have rather large stability constants, it may be assumed that there is no appreciable change in the viscosity of the solution due to the dissociation of the chelate in the pH range studied.

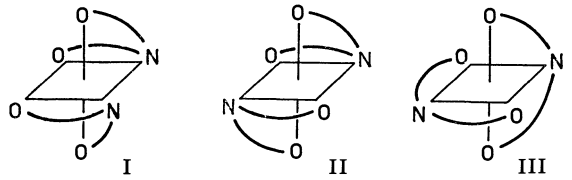

Fig. 1. The three possible geometric isomers of $[M(ida)_2]^{n-}$.

Three geometrical isomers are possible for the bis-chelate, $[M(ida)_2]^{n-}$ or $[M(mida)_2]^{n-}$, as is shown in Fig. 1. Two of them are *trans*(*N*)-forms, while the third is the *cis*(*N*)-form. However, only two isomers are isolated for Co(III)-ida chelates; one is *cis*(*N*) and the other is *trans*(*N*). The latter was assigned to Structure II by Hidaka *et al.* from the bond angles of a nitrogen atom of the ligand.[3] Later Cooke[6] tried several times to get the meridional *trans*-isomer (isomer III) by the elution of a mixture of the isomers from a Dowex 2-X8 anion-exchange resin in the chloride form, using NH_4Cl as the eluting agent. However, in no case was any evidence for a second *trans* isomer obtained. As he stated, the existence of this chelate can not be ruled out, and yet it is not considered that this chelate may be present appreciably. On the other hand, in the case of the bis-mida complexes of Co(III) the *trans*(*N*)-isomer alone is isolated.[6] The absence of the *cis*-isomer in this case and the dominance of the *trans*-isomer in the Co(III)-ida chelates were attributed to the presence of steric interactions between the amine groups in the *cis*-isomer. The values listed in Table 1 are, therefore, with the exception of Co(III) complexes, those for a mixture of *cis*- and *trans*-isomers which might be present in the solutions, although the values for the mida-chelates are considered to be practically those for the *trans*-isomers.

As may be seen from Table 1, the Jones-Dole viscosity *B*-coefficient of each ida-chelate is lower than that of the corresponding mida-chelate, as may be expected. The differences in *B*-values caused by the introduction of the methyl group on the amino nitrogen atom of ida^{2-} are 0.11~0.12 for Cu^{2+}, Ni^{2+}, and Co^{2+} complexes, and 0.08 for Zn^{2+}. That is, the differences are very much the same, except for the Zn^{2+} complex. However, as has been mentioned above, the differences may be caused by the *cis-trans* geometric effects as well as by the effect of the methyl group. Therefore, the lower value for the Zn^{2+} chelate can not be discussed easily. It is clear that there exists a definite difference between *cis*- and *trans*-$[Co(ida)_2]^-$. The higher value found for the *cis*-isomer is probably associated with the fact that this species interacts with the solvent more strongly than does the *trans*-isomer, evidently as a result of the permanent dipole moment associated with the *cis*-configuration.

The viscosity *B*-values for the edta- and cydta-chelates have been reported by Charles[7] and by one of the present authors[2] respectively. The order of the *B*-values for each divalent metal is as follows:

$$[M(ida)_2]^{2-} < [M(mida)_2]^{2-} \sim [Medta]^{2-} < [Mcydta]^{2-}$$

This meets our expectations. Now, it may be noted that the bis(mida)-chelates have very much the same values as the corresponding edta-chelates. While the edta-chelates have an enforced *cis*(*N*)-configuration about the metal, the mida-chelates probably have the *trans*-configuration. Therefore, it may be supposed that each mida-chelate has a lower *B*-coefficient than the corresponding edta-chelate, because the $edta^{4-}$ anion is practically equivalent to two anions of $mida^{2-}$ from the standpoint of molecular size. Therefore, the equality in *B*-values between the edta- and bis(mida)-chelates might be explained as follows; for the divalent metal chelates, which are much less stable than the corresponding Co(III)-chelate, there is not so large a difference in *B*-values between the *cis*- and *trans*-configurations, or the special stability of the edta-complex, compared with that of the mida-complex, plays a part, or some other factors, for example, the geometric configuration, are related to it. In connection with the second point mentioned above, metals with a greater affinity for the ligand generally form chelates with smaller *B*-values, as has been reported previously.[2] This applies also to the ida- and mida-chelates, as may be seen from Fig. 2; the ordinates are the *B*-values of

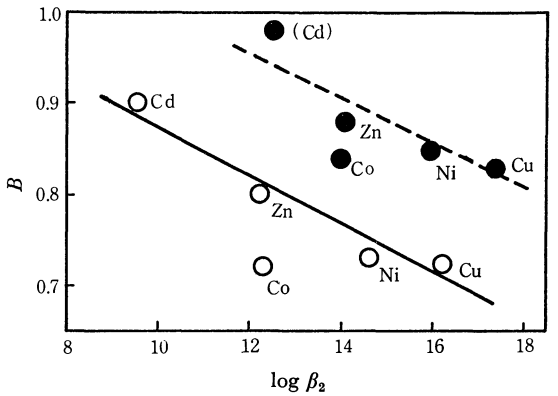

Fig. 2. Relation between the *B*-coefficient and the stability constant β_2: —○— ida-complex, —●— mida-complex.

6) D. W. Cooke, *Inorg. Chem.*, **5**, 1141 (1966).

7) R. G. Charles, *J. Amer. Chem. Soc.*, **78**, 3946 (1956).

the ida- or mida-chelates,[8] and the abscissas are the stability constants of these chelates.[9]

Finally, the *B*-coefficients of the Co(III) chelates will be discussed. The Co(III)-mida chelate, *trans*-K[Co(mida)$_2$], was prepared in a fashion analogous to that used for the *trans*-ida chelate, using an appropriate amount of H_2mida. However, its low solubility did not allow viscosity measurements. The *B*-values of the Co(III)-ida chelates are much lower than that of any of the divalent metal ida-chelates studied, as in the cases of the edta- and cydta-chelates. The solution of the *cis*-isomer showed no appreciable change in viscosity for at least 24 hr; thereafter the viscosity gradually decreased, probably because of the conversion of the *cis*- to the *trans*-configuration. It was unexpected that Co(III)-ida chelates have higher *B*-values than the Co(III)-edta chelate. This cannot be explained esaily, but we consider, at present, that the smaller *B*-value of the Co(III)-edta chelate might be caused by the extraordinary stability of the chelate, because chelates having higher stability constants have, in general, lower *B*-values, as has been mentioned above.

8) The *B*-value of the $[Cd(mida)_2]^{2-}$ anion (and also of $[Pb(mida)_2]^{2-}$) was not obtained because of its low solubility. Hence the value of $[Cdedta]^{2-}$ is plotted instead in Fig. 2, because $[M(mida)_2]^{2-}$ and $[Medta]^{2-}$ have very much the same *B*-coefficients for the divalent metal chelates studied.

9) a) S. Chaberek and A. E. Martell, *J. Amer. Chem. Soc.*, **74**, 5052 (1952). b) G. Schwarzenbach, G. Anderegg, W. Schneider, and H. Senn, *Helv. Chim. Acta*, **38**, 1147 (1955).

BULLETIN OF THE CHEMICAL SOCIETY OF JAPAN, VOL. 46, 159—162 (1973)

The Absolute Configuration of the $(-)_{589}$-Oxalatobis(ethylenediamine)-cobalt(III) Ion as Determined by X-Ray Structure Analysis

Tadashi AOKI, Keiji MATSUMOTO, Shun'ichiro OOI, and Hisao KUROYA

Department of Chemistry, Faculty of Science, Osaka City University, Sumiyoshi-ku, Osaka

(Received May 29, 1972)

The absolute configuration of $(-)_{589}$-[Co ox en_2]$^+$ has been determined by the X-ray diffraction method. The crystals of $(-)_{589}$-[Co ox en_2]Br·H_2O are orthorhombic, with the space group $P2_12_12_1$, and the unit cell dimensions are: $a=16.67(1)$Å, $b=12.40(1)$Å, $c=6.183(7)$Å, and $Z=4$. The crystal structure was solved by the conventional Patterson and Fourier methods, and refined by the least-squares procedure to an R factor of 9.97%. The cobalt atom has an octahedral coordination, being chelated by an oxalate anion and two ethylenediamine molecules which are of the *ob-lel* conformation. The absolute configuration of the complex cation can be denoted as $\Delta(\delta\lambda)$.

In previous papers, the crystal structures of $(+)_{589}$-[$CoCl_2en_2$]Cl·H_2O[1] and $(+)_{589}$-[$Co(CN)_2en_2$]Cl·H_2O[2] have been reported. The absolute configurations of the complex cations in these compounds are consistent with those assigned spectroscopically.[3-7] As a part of our X-ray studies of the absolute configurations of cobalt(III) complexes with C_2-symmetry, we have now determined the absolute crystal structure of $(-)_{589}$-[Co ox en_2]Br·H_2O (ox=oxalate anion).[8]

Experimental

The red plate-like crystals of $(-)_{589}$-[Co ox en_2]Br·H_2O were kindly provided by Dr. Jinsai Hidaka of Osaka University.

The unit cell dimensions were obtained by the least-squares refinement, using the θ values from zero-layer Weissenberg photographs on which powder lines of sodium chloride were super-imposed for calibration.

The crystal data are: FW=365.0; orthorhombic, $a=16.67(1)$Å, $b=12.40(1)$Å, $c=6.183(7)$Å; $Z=4$, $\mu=79.4$ cm^{-1} (for Ni$K\alpha$); space group $P2_12_12_1$ from systematic absences.

The intensities were estimated visually from the Weissenberg photographs of the $hk0$—$hk3$ and $h0l$—$h6l$ layers taken by means of the multiple-film and equi-inclination techniques. After they had been corrected for the Lp-factor, spot-shape,[9] and absorption, they were placed on a common arbitrary scale by internal correlation. A total of 1185 reflections were obtained; however, 91 of these were too weak to be observed and were assumed to be zero. The crystal specimens used for the data collection were cylinders 0.35 mm in diameter, the cylindrical axes being parallel to the b and c axes respectively.

Determination of the Crystal Structure

The initial coordinates for the cobalt and bromine atoms were deduced from a three-dimensional Patterson function. From the first Fourier synthesis phased on

1) K. Matsumoto, S. Ooi, and H. Kuroya, This Bulletin, **43**, 3801 (1970).
2) K. Matsumoto, S. Ooi, and H. Kuroya, *ibid.*, **44**, 2721 (1971).
3) T. E. McDermott and A. M. Sargeson, *Aust. J. Chem.*, **16**, 334 (1963).
4) R. D. Gillard and G. Wilkinson, *J. Chem. Soc.*, **1964**, 1368.
5) C. J. Hawkins and E. Larsen, *Acta Chem. Scand.*, **19**, 185 (1965).
6) T. Bürer, *Helv. Chim. Acta*, **46**, 242 (1963).
7) A. J. McCaffery, S. F. Mason, and B. J. Norman, *J. Chem. Soc.*, **1965**, 5094.
8) T. Aoki, K. Matsumoto, S. Ooi, and H. Kuroya, Proceedings of the 21st Annual Meeting of the Chemical Society of Japan (Osaka, 1968).
9) D. C. Philips, *Acta Crystallogr.*, **7**, 746 (1954).

Table 1. The final atomic coordinates, temperature factors, and their e.s.d.'s.[a] temperature factors are of the fofm: $\exp[-(h^2B_{11}+k^2B_{22}+l^2B_{33}+hkB_{12}+hlB_{13}+klB_{23})]$.

Atom	x	y	z	B_{11}	B_{22}	B_{33}	B_{12}	B_{13}	B_{23}
Br	0.6844(1)	0.2936(2)	0.8988(4)	0.0026(1)	0.0041(1)	0.0227(6)	0.0009(2)	−0.0005(4)	−0.0002(7)
Co	0.4904(2)	0.4080(2)	0.4283(6)	0.0025(1)	0.0034(1)	0.0183(9)	0.0004(2)	0.0004(6)	0.0002(10)
H_2O	0.223 (1)	0.753 (2)	0.091 (3)	0.0057(9)	0.0206(27)	0.0319(60)	−0.0107(26)	0.0029(48)	−0.0087(90)
O_1	0.452 (1)	0.362 (1)	0.710 (2)	0.0028(5)	0.0024(7)	0.0182(40)	0.0018(11)	0.0011(25)	−0.0009(36)
O_2	0.542 (1)	0.268 (1)	0.416 (2)	0.0033(5)	0.0027(8)	0.0151(34)	0.0015(10)	−0.0005(27)	−0.0013(39)
O_3	0.449 (1)	0.215 (1)	0.918 (2)	0.0044(6)	0.0041(9)	0.0171(37)	0.0004(13)	0.0034(30)	−0.0009(47)
O_4	0.541 (1)	0.112 (1)	0.596 (3)	0.0034(5)	0.0025(7)	0.0184(38)	0.0005(10)	−0.0015(29)	0.0036(42)
N_1	0.427 (1)	0.543 (1)	0.444 (3)	0.0016(5)	0.0023(9)	0.0279(59)	0.0009(11)	−0.0008(32)	−0.0048(50)
N_2	0.396 (1)	0.345 (1)	0.284 (3)	0.0018(5)	0.0033(10)	0.0196(49)	−0.0010(12)	−0.0008(29)	−0.0021(45)
N_3	0.542 (1)	0.446 (1)	0.151 (3)	0.0032(6)	0.0034(10)	0.0136(45)	0.0000(14)	0.0007(29)	0.0013(43)
N_4	0.585 (1)	0.476 (1)	0.569 (3)	0.0018(5)	0.0031(9)	0.0160(44)	−0.0015(11)	−0.0032(19)	0.0018(48)
C_1	0.341 (1)	0.514 (2)	0.404 (4)	0.0020(6)	0.0053(14)	0.0260(64)	0.0021(16)	0.0025(42)	−0.0008(74)
C_2	0.340 (1)	0.434 (2)	0.213 (4)	0.0030(8)	0.0031(12)	0.0302(75)	0.0007(16)	−0.0037(43)	−0.0061(61)
C_3	0.607 (1)	0.530 (2)	0.192 (4)	0.0032(8)	0.0037(13)	0.0248(68)	−0.0029(17)	−0.0019(42)	0.0051(59)
C_4	0.649 (1)	0.495 (2)	0.401 (4)	0.0024(7)	0.0066(16)	0.0272(69)	−0.0010(18)	0.0028(47)	0.0039(63)
C_5	0.524 (1)	0.208 (1)	0.575 (3)	0.0022(6)	0.0033(10)	0.0056(37)	−0.0011(14)	−0.0035(29)	−0.0015(54)
C_6	0.470 (1)	0.265 (1)	0.756 (4)	0.0023(7)	0.0031(12)	0.0207(57)	0.0013(15)	0.0002(38)	0.0041(56)

a) In order to represent the correct absolute configuration, the atomic coordinates in Table 1 should be set up in the left-handed system.

these two heavy atoms, all the non-hydrogen atoms were located. The structure was initially refined by four cycles of block-diagonal-matrix least-squares to an R factor of 12%, with an assumption of isotropic temperature factors, equal weights being employed for all reflections. The function minimized was $\sum w(|F_o|-|F_c|)^2$.

In the subsequent refinement, anisotropic thermal parameters were used. The weighting scheme employed was as follows:

$$w = 0.3 \quad \text{for } F_o < 6.1$$
$$w = 1.0 \quad \text{for } 30.6 \geq F_o \geq 6.1$$
$$w = 30.6/F_o \quad \text{for } F_o > 30.6$$

The atomic scattering factors were taken from the International Tables for X-ray Crystallography.[10] The real part of the dispersion correction was applied for the cobalt atom.[11] The three cycles of the least-squares calculation improved the R factor to 9.97%. In the last cycle, the shifts in the atomic coordinates were less than $(1/10)\sigma$ for heavy atoms and less than $(1/8)\sigma$ for light atoms. A difference synthesis of the electron density computed at this stage confirmed the crystal structure, though no peaks corresponding to any of the hydrogen atoms were yielded. The final atomic coordinates, the temperature factors, and their e.s.d.'s are given in Table 1. A complete list of the calculated and observed structure factors is preserved by the Chemical Society of Japan.[12]

In order to determine the absolute configuration of the complex cation, the oscillation photographs were taken with Cu$K\alpha$ radiation about the c axis. Some

Table 2. Calculated and observed intensities

h	k	l	$F_c^2(hkl)$	Obsd.	h	k	$\bar{l}$	$F_c^2(hk\bar{l})$
8	3	1	149	>	8	3	$\bar{1}$	903
13	3	1	223	<	13	3	$\bar{1}$	99
12	4	1	559	<	12	4	$\bar{1}$	168
3	5	1	652	<	3	5	$\bar{1}$	219
8	6	1	936	<	8	6	$\bar{1}$	342
12	6	1	682	>	12	6	$\bar{1}$	1634
1	7	1	677	>	1	7	$\bar{1}$	1556
10	7	1	2937	<	10	7	$\bar{1}$	1317
1	8	1	1361	<	1	8	$\bar{1}$	768
6	9	1	1074	<	6	9	$\bar{1}$	474
9	6	1	1986	>	9	6	$\bar{1}$	3251
9	1	1	3248	>	9	1	$\bar{1}$	5366
9	2	1	1001	>	9	2	$\bar{1}$	1587
4	3	1	3920	>	4	3	$\bar{1}$	6553

Bijvoet pairs, indicative of appreciable anomalous intensity differences, are listed in Table 2, together with the observed inequality relationships. The right-handed coordinate system for the reciprocal lattice was carefully used throughout the present work. The values of F_c^2 shown in Table 2 were calculated on the basis of the set of atomic coordinates given in Table 1. A comparison of the observed inequality relationships with the calculated ones indicates that the model used in the calculations is a mirror image of the absolute structure of the crystal.

Discussion

The crystal structure viewed along the c axis is shown in Fig. 1. The crystal is composed of $(-)_{589}$-[Co ox en_2]$^+$ complex cations, bromide anions, and water molecules, these being held together mainly by ionic forces. The hydrogen bonds are summarized in Table 3. One of the hydrogen atoms in the NH_2 groups involving N_1, N_2, and N_3, and both of the H atoms

10) "International Tables for X-ray Crystallography," Vol. III, Kynoch Press, Birmingham (1962), p. 202.

11) R. W. James, "The Optical Principles of the Diffraction of X-rays," G. Bell & Sons, London (1948), p. 608.

12) The complete data of the F_o–F_c table are kept as Document No. 7301 at the office of the Bulletin of the Chemical Society of Japan. A copy may be secured by citing the document number.

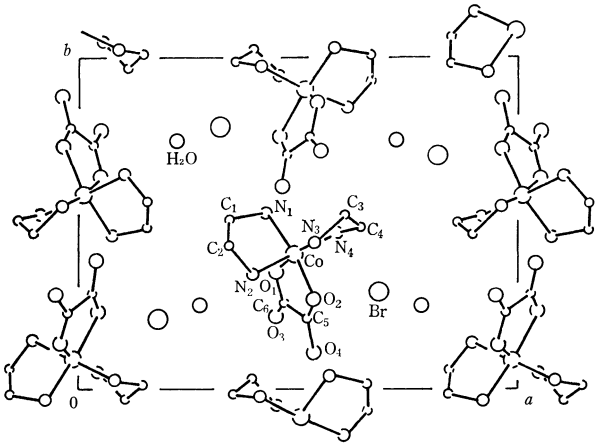

Fig. 1. The structure viewed along the *c* axis.

TABLE 3. POSSIBLE N-H···B HYDROGEN BONDS

The positions of the hydrogen atoms in the NH_2 groups were calculated on the assumption that the N-H bond length is 1.03Å.

N···B		N···B	H···B	∠N-H-B
N_1	$O(1-x, 1/2+y, 1/2-z)$	2.92Å	2.01Å	146°
N_2	$H_2O(1/2-x, 1-y, 1/2+z)$	3.01	2.02	160
N_3	Br	3.41	2.47	151
N_4	Br	3.47	2.46	167
N_4	$O_3(1-x,1/2+y, 1/2-z)$	3.02	2.11	146
Br	$H_2O(1-x, -1/2+y, 1/2-z)$	3.44		

linked to N_4, participate in the hydrogen bonding, in which the oxygen atom ($O_{(H_2O)}$) or $O_{(C=O)}$) or the bromide ion takes part as the base of the hydrogen bonds. Similarly, one of the water hydrogen atoms participates in the O-H—Br^- hydrogen bond, while the other appears to remain indifferent to any hydrogen bonding.

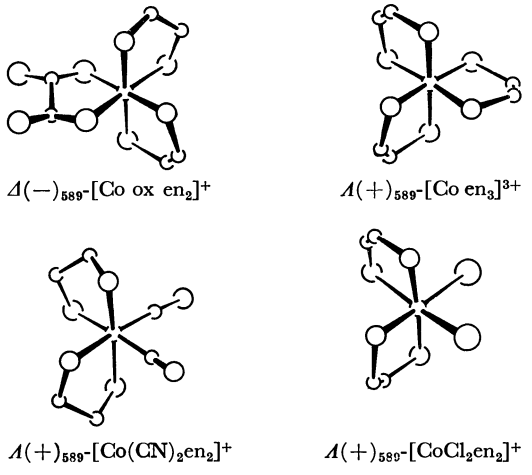

$\Delta(-)_{589}$-[Co ox en_2]$^+$ $\Delta(+)_{589}$-[Co en_3]$^{3+}$

$\Delta(+)_{589}$-[$Co(CN)_2en_2$]$^+$ $\Delta(+)_{589}$-[$CoCl_2en_2$]$^+$

Fig. 2. The absolute configurations of the complex ions.

The absolute configuration of the complex ion is depicted in Fig. 2. It is in accordance with that assigned before by several workers[3-7] and should be denoted as $\Delta(\delta\lambda)$. In the figure, the absolute configurations of $(+)_{589}$-[$Co(CN)_2en_2$]$^+$,[2] $(+)_{589}$-[$CoCl_2en_2$]$^+$,[1] and $(+)_{589}$-[Co en_3]$^{3+}$ [13] are also shown as references. The oxalate ion is planar, while the ethylenediamine molecules assume the "gauche" form and are disposed in the conformation of the *ob-lel* type.

By analogy with the trisethylenediamine complex,[14] the intramolecular potential energy of the bisethylenediamine complex increases in the order of *lel-lel*<*ob-lel*<*ob-ob*.[15] However, since the potential energy difference between the least stable and the most stable conformers may be about 0.2 kcal/mol in the case of [Co ox en_2]$^+$,[16] this complex could more readily assume less stable conformations than in the case of the trisethylenediamine complex. Although the hydrogen bonds in which the hydrogen atoms of NH_2 groups participate play an important role in stabilizing the

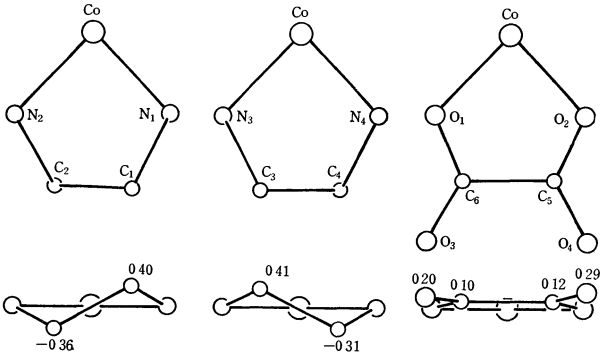

Fig. 3. The elevations and projections of the three chelate rings.

TABLE 4. THE BOND DISTANCES AND ANGLES IN THE COMPLEX ION

Co–N_1	1.99(2)Å	N_1–Co–N_2	86(1)°
Co–N_2	1.97(2)	N_3–Co–N_4	86(1)
Co–N_3	1.98(2)	O_1–Co–O_2	85(1)
Co–N_4	1.99(2)	Co–N_1–C_1	107(2)
Co–O_1	1.94(2)	Co–N_2–C_2	110(2)
Co–O_2	1.94(2)	Co–N_3–C_3	109(2)
N_1–C_1	1.50(3)	Co–N_4–C_4	109(2)
N_2–C_2	1.51(3)	Co–O_1–C_6	114(2)
N_3–C_3	1.51(3)	Co–O_2–C_5	112(2)
N_4–C_4	1.51(3)	N_1–C_1–C_2	107(2)
O_1–C_6	1.27(3)	N_2–C_2–C_1	104(2)
O_2–C_5	1.27(3)	N_3–C_3–C_4	106(2)
O_3–C_6	1.23(3)	N_4–C_4–C_3	107(2)
O_4–C_5	1.23(3)	O_1–C_6–C_5	113(2)
C_1–C_2	1.55(4)	O_2–C_5–C_6	115(2)
C_3–C_4	1.54(4)	O_3–C_6–C_5	120(2)
C_5–C_6	1.60(3)	O_4–C_5–C_6	119(2)
		O_1–C_6–O_3	127(2)
		O_2–C_5–O_4	126(2)

13) Y. Saito, K. Nakatsu, M. Shiro, and H. Kuroya, This Bulletin, **30**, 795 (1957).

14) E. J. Corey and J. C. Bailar, Jr., *J. Amer. Chem. Soc.*, **81**, 2620 (1959).

15) In this paper we have discussed the relative instability of the respective conformer of bisethylenediamine complex on the basis of the instability order *lel-lel-lel*<*ob-lel-lel*<*ob-ob-lel*<*ob-ob-ob*, for trisethylenediamine complex given by Corey and Bailar. However, Hawkins *et al.* have recently pointed out that this instability order should be revised to *lel-lel-lel*≃*ob-lel-lel*<*ob-ob-lel*<*ob-ob-ob* (*Inorg. Chem.*, **9**, 576 (1969)).

16) F. P. Dwyer, T. E. McDermott, and A. M. Sargeson, *J. Amer. Chem. Soc.*, **85**, 661 (1963).

less stable conformers of $[Cr\ en_3]^{3+}$,[17] this is not likely to be the case for the bisethylenediamine complex, as has been stated elsewhere.[1,2] Thus, the specific conformation of the bisethylenediamine complex might be mainly due to the crystal packing.

The projections and elevations of the three chelate rings are illustrated in Fig. 3. Although the oxalate chelate ring is nearly planar, the (O_1, C_6, O_3) plane is slant against the (O_2, C_5, O_4) plane by 4.3°, which is considerably less than the value (17°, on average) found in $K_2[Cu\ ox_2]\cdot 2H_2O$.[18] The plane of the oxalate ion is bent away from the (Co, O_1, O_2) plane by 6.4°. Probably this also comes from the crystal packing. The bond length of C_5–C_6 (1.60 Å) is considerably longer than that for the usual $C(sp^2)$–$C(sp^2)$ but it is comparable to that found in $K_2C_2O_4\cdot 2H_2O$ (1.573 Å).[19] In each of the two ethylenediamine chelate rings, one carbon atom is disposed above, and the other, below, the plane defined by the cobalt and two nitrogen atoms. The bond lengths and angles within the chelate rings are quite normal (Table 4).

The authors wish to express their thanks to Mr. Ken Hirotsu and Mr. Masayuki Hinamoto, who adapted the HBLS-4 and the RSSFR-3 computer programs to the FACOM 270-30 computer at Osaka City University. This research was aided in part by a Scientific Research Grant from the Ministry of Education, to which the authors' thanks are due.

17) K. N. Raymond, P. W. R. Corfield, and J. A. Ibers, *Inorg. Chem.*, **7**, 842 (1968).
18) M. A. Viswamitra, *Z. Kristallogr.*, **117**, 437 (1962).
19) D. J. Hodgson and J. A. Ibers, *Acta Crystallogr.*, **B25**, 469 (1969).

BULLETIN OF THE CHEMICAL SOCIETY OF JAPAN, VOL. 46, 162—165 (1973)

Studies on Actinoid Elements. V. The Determination of the Np(V)/Np(IV) Ratio in an Aqueous Solution by Means of the Partition Method

Akira OHYOSHI and Tsuneo KAWAMURA

Department of Industrial Chemistry, Faculty of Engineering, Kumamoto University, Kumamoto

(Received May 31, 1972)

The distribution study of neptunium ions in an aqueous solution containing Np(IV) and Np(V) was made using the metal chelate extraction system, TTA-benzene, or HDEHP-benzene at room temperature. The results obtained by this method were then compared with those obtained by spectrophotometry. In each system, a linear relationship was obtained between the fraction of the Np(V) ion and $1/(D+1)$, where D is the distribution ratio of neptunium. This analysis was performed with an accuracy of $\pm 5\%$ and was established within one minute in the case of the HDEHP-benzene system. The results obtained by this method were in good agreement with those obtained by spectrophotometry.

When a solution contains metal ions of different oxidation states, its composition is usually determined by spectrophotometry, potentiometry, *etc.* However, these methods, in which an appreciable concentration of the sample is required for measurement, appear not to be suitable for a nuclide like ^{239}Np, which is difficult to supply in so great a quantity which is difficult to handle because of its radioactivity.

In this experiment, we have attempted to use a radiochemical method, *i.e.*, a liquid-liquid partition of Np(IV) and Np(V) ions, to determine the oxidation state of neptunium.

Experimental

Reagents. Neptunium-237 oxide obtained from the Radiochemical Center, Amersham, was dissolved in nitric acid. The solution was then evaporated to dryness, and the residue was dissolved in 0.1M hydrochloric acid. This solution served as the stock solution of neptunium. The neptunium-239 was prepared from neutron-irradiated uranium dioxide by the thenoyltrifluoroacetone(TTA) extraction method.[1,2] The radiochemical purities of ^{237}Np and ^{239}Np were confirmed by studying the γ-ray spectra with a $2''\phi \times 2''$ NaI(Tl) detector connected to a TMC 400-channel pulse-height analyzer. The chemical purity of ^{237}Np was also checked by spectrophotometry. The tributyl phosphate (TBP) and di(ethylhexyl)phosphoric acid (HDEHP) were purified from commercial chemicals by the usual method.[3,4] The other reagents used were of a G.R. grade.

The sample solution of tetravalent neptunium-239 was prepared by a TTA-extraction method,[2,5,6] and by oxidizing this solution with a warm perchloric acid solution, the neptunium-239 was changed to the pentavalent state. Both sample solutions were freshly prepared before each experiment.

1) F. L. Moore, *Anal. Chem.*, **29**, 941 (1957).
2) F. L. Moore and J. E. Hudgens, *ibid.*, **29**, 1767 (1957).
3) D. F. Peppard, G. W. Mason, J. L. Maier, and W. J. Driscoll, *J. Inorg. Nucl. Chem.* **4**, 334 (1957).
4) D. F. Peppard, J.R. Ferraro, and G. W. Mason, *ibid.*, **7**, 231 (1958).
5) T. Ishimori and E. Nakamura, This Bulletin, **32**, 713 (1959).
6) J. O. Lilienzin and J. Stary, *J. Inorg. Nucl. Chem.*, **32**, 1357 (1957).

Apparatus. The γ-activity of the neptunium-239 was measured with a $5''\phi \times 5''$ well-type NaI(Tl) scintillation counter. A Hitachi EPS-2U spectrophotometer was used to determine the absorption spectra of the neptunium-237. The sample (about 1 ml) was transferred into a quartz cell with a 1 cm path length. A Hitachi-Horiba pH meter, model M-5, was used for the pH measurement.

Procedures. *Liquid-liquid Partition Study*: After 4 ml of 1.0M perchloric acid and a 0.5M TTA benzene solution (4 ml) or a 0.16M HDEHP benzene solution (4 ml) had been transferred into the centrifuge tubes, sample solutions (50 μl each) of different Np(V)/Np(IV) ratios were added to the mixture. The air in the tubes was displaced with nitrogen gas. Then the tubes were shaken mechanically for 10 min at room temperature because it was already known by preliminary experiments that this period was sufficient to equilibrate the partition of Np(IV) and Np(V) ions. In the case of the 0.16M HDEHP/benzene extraction system, since the pre-equilibration was made between the organic and aqueous phases, the partition was accomplished within 1 min. After the shaking and the centrifugation, an aliquot (2 ml) of each phase was transferred into a polyethylene tube and the γ-activity was measured in order to determine the distribution ratio, D. The hydrogen-ion concentration of the aqueous phase was determined by a titration method after the γ-activity measurements.

Spectrophotometry and Partition Study. In the course of the reduction reaction, the changes in the oxidation states were simultaneously measured by spectrophotometry and the partition method. Into a spectrophotometer cell containing a solution of citric acid and pentavalent neptunium, a pentavalent neptunium-239 solution was added. The mixture was then irradiated with the light of a tungsten lamp, and the cell was kept in a thermostat maintained at 20°C. The reactions were followed at the same time by spectrophotometry and by radiometry, with a partition between 0.16M HDEHP/benzene and the 1.0M perchloric acid solution.

Results and Discussion

Calculation of the Neptunium(V) Fraction from the Partition Data. As is already known, in a liquid-liquid partition system of neptunium species, the distribution ratio, D, is represented by Eq. (1):

$$D = [\mathrm{Np}]_{org}/[\mathrm{Np}]_{aq} = \frac{\gamma\text{-activity of } ^{239}\mathrm{Np/ml \text{ of organic phase}}}{\gamma\text{-activity of } ^{239}\mathrm{Np/ml \text{ of aqueous phase}}} \quad (1)$$

The fraction of pentavalent neptunium, X, is expressed as follows:

$$X = \frac{[\mathrm{Np(V)}]}{[\mathrm{Np(IV)}]+[\mathrm{Np(V)}]} \quad (2)$$

If we assume that there is no change in the oxidation states of neptunium in the extraction procedure, the net distribution ratio can be defined as follows:

$$D = \frac{[\mathrm{Np(IV)}]_{org}+[\mathrm{Np(V)}]_{org}}{[\mathrm{Np(IV)}]_{aq}+[\mathrm{Np(V)}]_{aq}} \quad (3)$$

The distribution ratios of the respective neptunium species are:

$$D^{IV} = [\mathrm{Np(IV)}]_{org}/[\mathrm{Np(IV)}]_{aq} \quad (4)$$

$$D^{V} = [\mathrm{Np(V)}]_{org}/[\mathrm{Np(V)}]_{aq} \quad (5)$$

A new function, Y, is defined by the following equation:

$$Y = 1/(1+D) \quad (6)$$

The material balance equation can be thus expressed concerning the pentavalent neptunium:

$$[\mathrm{Np(V)}]_{aq} + [\mathrm{Np(V)}]_{org} = [\mathrm{Np(V)}] \quad (7)$$

By introducing Eq. (5) into Eq. (7), Equation (8) is obtained:

$$[\mathrm{Np(V)}]_{aq} = 1/(1+D^{V})\cdot X/(1-X)\{[\mathrm{Np(IV)}]_{aq} + [\mathrm{Np(IV)}]_{org}\} \quad (8)$$

From Equations (3), (4), and (8), Eqs. (9) and (10) are obtained:

$$1/D = 1/D^{IV}\{1+(1+D^{IV})/(1+D^{V})\cdot X/(1-X)\} \quad (9)$$

$$1 + D = (1+D^{IV})\{(1+D^{V})-D^{V}X\}/\{(1+D^{V}) + (D^{IV}-D^{V})X\} \quad (10)$$

Since the $D^{V}X$ term is sufficiently small compared to unity, Equation (10) can be simplified and the Y function can be expressed as follows:

$$Y = 1/(1+D^{IV}) + [(D^{IV}-D^{V})/(1+D^{IV})(1+D^{V})]\cdot X \quad (11)$$

When the partition process is performed under constant experimental conditions, the distribution ratios, D^{IV} and D^{V}, are both constant; therefore, it can be expected that Y can be expressed as a linear function of X.

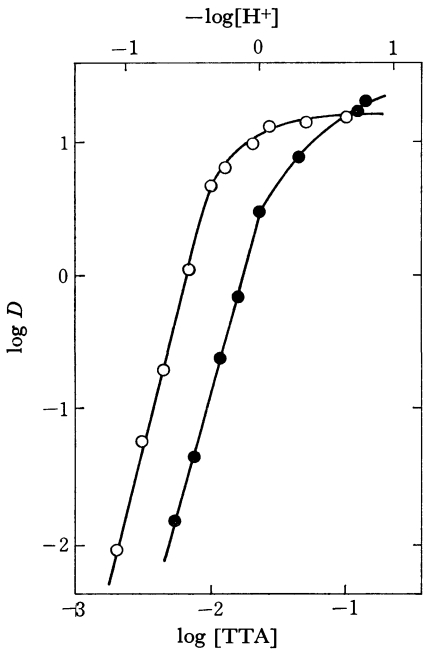

Fig. 1. Plots of log D *vs.* −log[H+] (●) and log D *vs.* log-[TTA] (○).

The Confirmation of the Valency State of the Neptunium Ion in the Sample Solution. The TTA extraction of the tetravalent neptunium ion was carried out in order to verify its valency state in a perchloric acid solution. The effect of the hydrogen ion concentration on the extraction was examined by using a 0.05M TTA benzene solution. As Fig. 1 shows, the relationship between log D and −log [H+] is linear, with a slope of 3.8, over the −log [H+] range from −0.6 to 0.0. The relationship between the TTA concentration and the distribution ratio was examined in 0.1M perchloric acid. As is shown in Fig. 1, the log-log plot of the distribution

Table 1. Distribution ratio of ^{239}Np for sample solution (D) and tetravalent state (D^{IV})

Partition system	Distribution ratio	
	D	D^{IV}
0.16M HDEHP -1M $HClO_4$	0.01±0.01	4.2±0.2
0.5M TTA -1M $HClO_4$	0.001±0.001	55 ±4

ratio and the TTA concentration shows a good linearity, with a slope of 4.0, over the TTA concentration range from 0.002 to 0.01M. These results indicate that the neptunium ion is tetravalent during the procedures.

The pentavalent neptunium ion was also confirmed by the partition method. The distribution ratio of ^{239}Np in the sample solution was measured with 0.16M HDEHP/benzene and 0.5M TTA/benzene *vs.* a 1M perchloric acid solution. The results obtained are given in Table 1, where the distribution ratios of Np(IV), D^{IV} are also shown as examples. These are mean values for three measurements. The differences between D^{IV} and D, 4×10^2 and 5×10^4, show that the neptunium exists in the form of an unextractable species. Since the hexavalent neptunium is extractable from the highly acidic solution,[1] the neptunium in the sample solution indicating such small D values may be considered to be in a pentavalent state, NpO_2^+.

The Rate of the Partition of Neptunium Ions. The partition rate of the neptunium ion between two phases may depend on various experimental conditions, such as the contact time, the way of shaking and the extracting reagent. Tests were made for tetra- and pentavalent neptunium ions using the two kinds of extractants, 0.50M TTA/benzene and 0.16M HDEHP/benzene, under constant shaking conditions and at a constant temperature. Same typical results are presented in Fig. 2. In the case of the TTA system, the partition was fairly rapid and gave reproducible data, while in the case of the HDEHP system, a pre-equilibration was necessary between an organic and an aqueous phase because the partition rate was appreciably small and the observed D value was not reproducible. As the contact time, 1 and 10 min were selected for the HDEHP and TTA systems respectively.

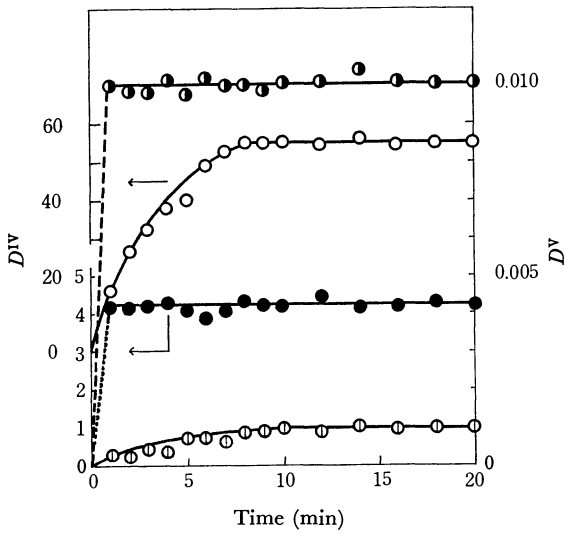

Fig. 2. The plot of D^{IV} or D^{V} *vs.* extraction time.
D^{IV}: ○ TTA, ● HDEHP, D^{V}: ◐ TTA, ◑ HDEHP

Determination of the Pentavalent Neptunium Fraction, X, from the Partition Data. The results are shown in Figs. 3 (TTA-benzene system) and 4 (HDEHP-benzene system) as plots of Y *versus* X. As has been expected, the plots indicate a good linear relationship between Y and X in both cases. However, it was found that the air on the extractant should be removed because the oxygen caused a transformation from Np(IV) to Np(V) during the shaking for 10 min, as is indicated by the closed circles in Fig. 3. On the other hand, since the shaking time is only one minute for the HDEHP system, the variation between the two oxidation states might be sufficiently small,

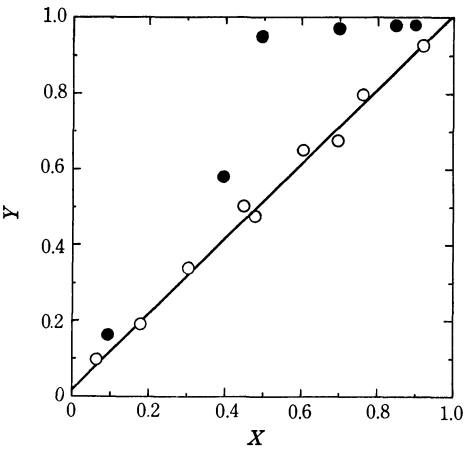

Fig. 3. The plot of $Y=1/1+D$ *vs.* X for TTA/benzene perchloric acid system.
○: Air replaced, ●: Unreplaced.

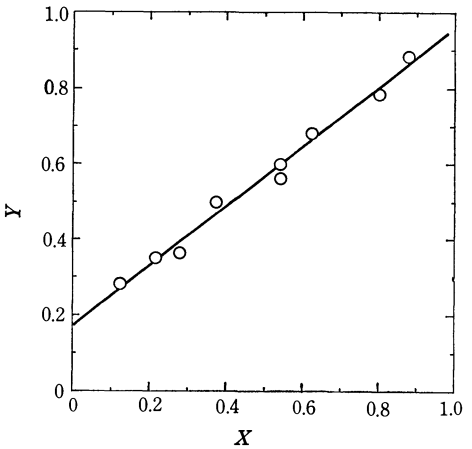

Fig. 4. The plot of $Y=1/1+D$ *vs.* X for HDEHP/benzene perchloric acid system.

The empirical equations were determined by a least-squares method as follows:

$Y=(0.015\pm0.003)+(0.983\pm0.001)\cdot X$; 0.50M TTA-benzene/1.0M $HClO_4$

$Y=(0.18\pm0.01)\pm(0.78\pm0.01)\cdot X$; 0.16M HDEHP-benzene/1.0M $HClO_4$.

Comparison of the Results from Two Different Analyses of Neptunium Ions. The spectrophotometry of neptu-

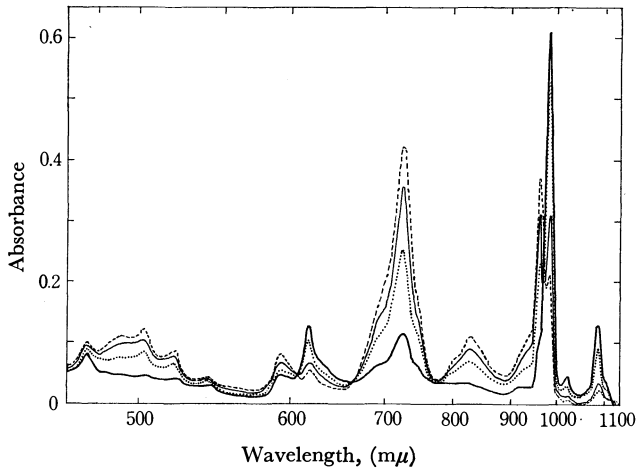

Fig. 5. Changes of absorption spectra of neptunium during the reduction with the reaction time.
Conditions; $[Np(V)]_0=1.52\times10^{-3}$M, [citric acid]$_0$=4.8×$10^{-2}$M, $[H^+]$=0.01M, at 20°C.
Reaction time: — 2 min, ··· 9 min, — 25 min, -- 35 min.
Irradiation; at 30 cm from 300 W tungsten light.

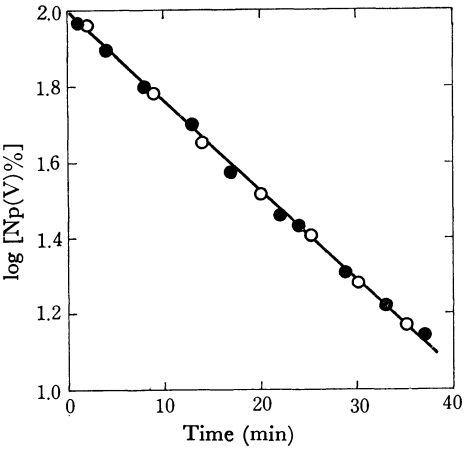

Fig. 6. Plots of the logarithm of neptunium (V) fraction *vs.* reaction time.
○: Spectrophotometry, ●: Partition method.

nium ions was carried out in order to compare the results with those from the partition method in the course of the kinetic run. A photochemical reduction of pentavalent neptunium ions was employed in this attempt. A mixture of $^{237}NpO_2^+$, $^{239}NpO_2^+$, and citrate ions was placed under the tungsten lamp and irradiated by visible light. The reduction of NpO_2^+ then proceeded *via* some photochemical processes. The details of this reaction will be reported elsewhere.

The changes in the absorbance due to the neptunium-237 and the changes in the distribution ratio of the neptunium-239 in the reacting solution were simultaneously measured at appropriate intervals.

Figure 5 shows the changes in the absorption spectra of neptunium with the reaction time during the course of reduction; the absorbances at 617 and 980 mμ corresponding to Np(V) decrease, while those at 723 and 960 mμ corresponding to Np(IV) simultaneously increase. The logarithmic plots of the Np(V) fraction *versus* the reaction time are shown in Fig. 6, using the data from spectrophotometry (○) and those from the partition method (●). This figure, where the open circles and the closed circles are observed on the same line, confirms that the results from these two methods are essentially the same. From the good linear relationship obtained, the reaction can be said to obey first-order kinetics.

Thus, the partition method can be used to determine the pentavalent neptunium fraction in a mixture of Np(V) and Np(IV) ions, especially when their concentrations are in a tracer scale. Furthermore, it may be used in studying the kinetics of a reaction between penta- and tetravalent neptunium ions.

The Ultraviolet Absorption Spectra and Hydrolysis of Bis(acetylacetonato)nickel(II) in Dichloromethane

Kiyoshi ISOBE, Yukio NAKAMURA, and Shinichi KAWAGUCHI

Department of Chemistry, Faculty of Science, Osaka City University, Sumiyoshi-ku, Osaka

(Received June 2, 1972)

The ultraviolet spectrum of $Ni(acac)_2$ in dichloromethane shows two maxima, at 265 and at 300 nm. The intensity ratio of these two bands is very sensitive to the water content of the solvent, the high-energy band decreasing and the low-energy band increasing with the water content. It is thus suggested that the trimeric $Ni(acac)_2$ might have only one absorption band, at 265 nm, in dichloromethane completely free from donor impurities. The UV spectrum of $Ni(acac)_2$ in dichloromethane changes with time due to the hydrolytic reaction. Even in the solvent containing 4.54×10^{-3}M water, acetylacetone was freed from the complex in the yield of 34.4% after 48 hours' standing. A minute amount of the residual complex was isolated; its tetrameric structure is suggested on the basis of its UV spectrum in methanol.

The ultraviolet spectra of thirty-one metal acetylacetonates were measured by Holm and Cotton[1] in chloroform and/or absolute ethanol in the 240—400 nm region, and were grouped into three classes. Bis(acetylacetonato)nickel(II) is present in ethanol entirely as the solvated species $Ni(acac)_2\cdot2EtOH$, and shows an absorption maximum at 294 nm ($\varepsilon=23700M^{-1}cm^{-1}$), accompanied by a shoulder on the longer-wavelength side. Similar absorption spectra were also observed for all other metal complexes except Cu(II), Fe(III), Co(III), Cr(III), and alkali metal acetylacetonates,[1] and are thought to be due to a π-π^* type transition.[2]

In chloroform, however, $Ni(acac)_2$ exhibits a very different spectrum than that in ethanol, having two maxima at 265 nm ($\varepsilon=15200$) and at 296 nm ($\varepsilon=12400$).[1] It is well established that $Ni(acac)_2$ exists as an octahedral trimer in crystals[3] and also in non-coordinating solvents.[4] The anomalous spectrum found in chloroform was explained by Cotton and Fackler[5] as due to the presence of both nonbridging and bridging chelate rings in the trimer. The former were presumed to give rise to the low-energy band at nearly the same wavelength as that of the absorption band observed in alcohol. On the other hand, the latter bridging rings were thought to cause the high-energy band, which disappears in donor solvents because of the depolymerization of the trimer.

In the course of our investigation of the reaction of $Ni(acac)_2$ with dry hydrogen bromide in dichloromethane,[6] the ultraviolet spectra of $Ni(acac)_2$ and other related compounds have been carefully examined. In this paper we will report the results we have obtained, which are different from those of Cotton and his co-workers.[1,5]

Experimental

Preparation of Complexes. *Anhydrous bis(acetyacetonato)-nikel(II), Ni(acac)$_2$*: Bis(acetylacetonato)diaquonickel(II) was prepared according to the Charles method,[7] recrystallized three times from methanol, and dehydrated by heating at 100°C *in vacuo* for 4 hr (Found: Ni, 22.82; C, 46.23; H, 5.54%).

Bis(acetylacetonato)dimethanolnickel(II), Ni(acac)$_2$(CH$_3$OH)$_2$: $Ni(acac)_2$ (2 g) was dissolved in 100 ml of light petroleum, and the mixture was refluxed for 30 min. To this solution we then added 30 ml of dry methanol and refluxed it for 30 min. The solution was then evaporated to about 40 ml and kept in a desiccator at room temperature. Sky-blue crystals were thus obtained. Found: Ni, 18.21; C, 44.43; H, 6.95%. Calcd for $C_{12}H_{22}O_6Ni$: Ni, 18.29; C, 44.90; H, 6.91%.

Bis(acetylacetonato)bis(pyridine)nickel(II), Ni(acac)$_2$py$_2$: Following the method of Hashagen and Fackler,[8] the direct reaction of $Ni(acac)_2$ with pyridine was conducted to obtain $Ni(acac)_2py_2$. Found: Ni, 14.46; C, 57.59; H, 5.87; N, 7.02%. Calcd for $C_{20}H_{24}N_2O_4Ni$: Ni, 14.14; C, 57.81; H, 5.78; N, 6.74%.

Tetrameric Complex [Ni(acac)(OCH$_3$)(CH$_3$OH)]$_4$: This compound was prepared according to the directions of Bertrand and Caine.[9] Found: Ni, 26.54; C, 37.53; H, 6.58%. Calcd for $C_7H_{14}O_4Ni$: Ni, 26.59; C, 38.58; H, 6.48%.

Presumably Tetrameric Complex Ni(acac)(OH)(H$_2$O)$_2$: $Ni(acac)_2(H_2O)_2$ (3 g, 1.02×10^{-2} mol) was dissolved in 300 ml of water, and to the mixture we added an aqueous solution (300 ml) of KOH (0.56 g, 1.00×10^{-2} mol); the resulting precipitate was separated and dried. Found: Ni, 28.35; C, 27.53; H, 5.61%. Calcd for $C_5H_{12}O_5Ni$: Ni, 27.84; C, 28.48; H, 5.74%.

Purification of Solvents. Dichloromethane and methanol were purified and dried by the standard methods.[10] The water contents of the dried solvents were determined by the Karl Fischer method to be 4.54×10^{-3} and 2.6×10^{-3}M respectively. Appropriate amounts of water was added to prepare solvents of various water contents up to 0.12M and 0.3M respectively.

Measurements. The ultraviolet absorption spectra were measured at room temperature on a Hitachi recording spectrophotometer, EPS-3T, using 1-cm quartz cells in the 210—

1) R. H. Holm and F. A. Cotton, *J. Amer. Chem. Soc.*, **80**, 5658 (1958).
2) D. W. Thompson, *Structure and Bonding*, **9**, 27 (1971).
3) G. J. Bullen, R. Mason, and P. Pauling, *Inorg. Chem.*, **4**, 456 (1965).
4) D. P. Graddon and E. C. Watton, *Nature*, **190**, 906 (1961).
5) F. A. Cotton and J. P. Fackler, Jr., *J. Amer. Chem. Soc.*, **83**, 2818 (1961).
6) K. Isobe, Y. Nakamura, and S. Kawaguchi, *Inorg. Nucl. Chem. Letters*, **7**, 927 (1971).
7) R. G. Charles and M. A. Pawlikowski, *J. Phys. Chem.*, **62**, 440 (1958).
8) J. T. Hashagen and J. P. Fackler, Jr., *J. Amer. Chem. Soc.*, **87**, 2821 (1965).
9) J. A. Bertrand and D. Caine, *ibid.*, **86**, 2298 (1964).
10) J. A. Riddick and W. B. Bunger, "Organic Solvents," 3rd ed., Volume 2 of "Techniques of Chemistry" ed. by A. Weissberger, Wiley-Interscience, New York (1970).

340 nm region. Freshly-distilled solvents were used to prepare $\sim 10^{-5}$ M solutions. The molar absorption coefficients of polymeric complexes are expressed on the basis of the gram-atom of nickel(II).

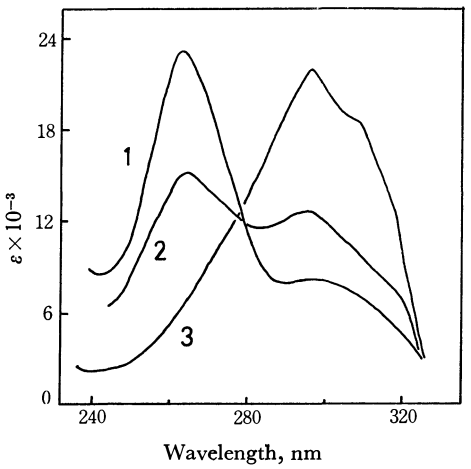

Fig. 1. Ultraviolet spectra of bis(acetylacetonato)nickel(II) in dichloromethane (curve 1), in chloroform (curve 2, ref. 5) and in methanol (curve 3).

Results and Discussion

Ultraviolet Spectra of $Ni(acac)_2$. Curve 1 in Fig. 1 represents the absorption spectrum of $Ni(acac)_2$, which was measured before 10 min after dissolution in dichloromethane containing 4.54×10^{-3}M water. The spectrum is very different from Curve 2 determined by Cotton and Fackler[5] in chloroform. The high-energy band at 265 nm is much larger (ε=23650), and the low-energy band at 300 nm is much smaller (ε=8450). This discrepancy is due not to the nature of the solvent employed, but to the difference in the water content. The peak-height ratio of the 265 and 300 nm bands decreases as the water content of dichloromethane is increased. The spectra of $Ni(acac)_2$ in dichloromethane containing 8.0×10^{-3}M water or 1.2×10^{-2}M methanol are quite similar to Curve 2 in Fig. 1. On the other hand, the peak-height ratio of the two absorption bands became even larger when dichloromethane was dried over calcium hydride for 2 days, and a $Ni(acac)_2$ solution was prepared in a vacuum system and measured in a sealed cell without exposure to air. It seems very probable that the low-energy band at 300 nm will not be observed for a dichloromethane solution containing no trace of water or other donor impurity. Thus, the 265 nm band may be concluded to be the only absorption by trimeric $Ni(acac)_2$ and the 300 nm band may be concluded to be caused by the donor impurity.

An aqueous solution of $Ni(acac)_2(H_2O)_2$ and a methanolic solution of $Ni(acac)_2(CH_3OH)_2$ both exhibit only one absorption maximum, at around 300 nm, with ε=21000 and 22000 respectively. In dry dichloromethane, however, both solvated complexes show the same spectra as that of the anhydrous trimer, indicating that the following trimerization equilibria are quickly attained and are favorable for the trimer under these conditions:

$$Ni(acac)_2L_2 \rightleftarrows \frac{1}{3}[Ni(acac)_2]_3 + 2L \quad (1)$$

The concentrations of the complexes, and hence of the coordinated solvents ($\sim10^{-5}$M), are nearly negligible compared to that of water ($\sim10^{-3}$M) contained *a priori* in dichloromethane. This situation seems to be the reason why $Ni(acac)_2(H_2O)_2$ and $Ni(acac)_2(CH_3OH)_2$ show no spectral difference from the anhydrous trimer. On the contrary, the spectrum of $Ni(acac)_2py_2$ in dichloromethane resembles that in methanol, showing an absorption band due to the acetylacetonate ligand only at 300 nm. It is thus certain that $Ni(acac)_2py_2$ is much more stable in dichloromethane and that Equilibrium (1) is favorable for the monomer adduct.

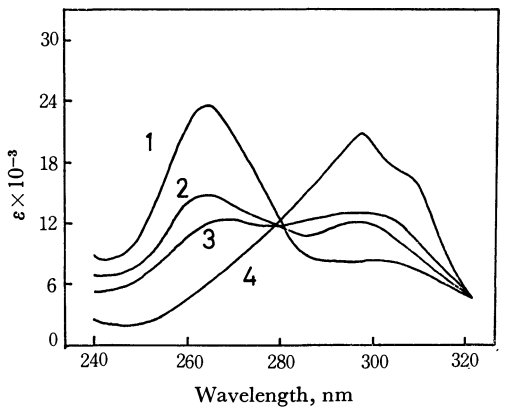

Fig. 2. Ultraviolet spectra of bis(acetylacetonato)nickel(II) in dichloromethane (curve 1), in dichloromethane containing methanol at the concentration of 1.2×10^{-2}M (curve 2) and 1.8×10^{-2}M (curve 3), and in methanol (curve 4). $[Ni(acac)_2]=1.776\times10^{-5}$M.

As is illustrated in Fig. 2, the peak-height ratio of the 265 and 300 nm bands decreases with an increase in methanol added to the dichloromethane solution of $Ni(acac)_2$, showing a gradual shift of Equilibrium (2)

$$Ni_3(acac)_6 + 6CH_3OH \rightleftarrows 3Ni(acac)_2(CH_3OH)_2 \quad (2)$$

$$K = \frac{[Ni(acac)_2(CH_3OH)_2]^3}{[Ni_3(acac)_6][CH_3OH]^6} \quad (3)$$

to the monomer side. Unfortunately, no absorption data in dichloromethane completely free from water are available, and so the determination of the equilibrium constant (3) is not possible. However, the concentrations of the trimer and the monomer are comparable, both lying in the region of 10^{-5}M when $\sim10^{-2}$M methanol is involved in dichloromethane. We can thus estimate K to be in the order of magnitude of 10^2M^{-4}.

Fackler[11] found that the reaction of bis(acetylacetonato)nickel(II) with pyridine in benzene proceeds *via* the intermediate $Ni_2(acac)_4py$, and estimated the equilibrium constants for the two steps by the spectrophotometric method:

$$2Ni_3(acac)_6 + 3py \rightleftarrows 3Ni_2(acac)_4py,$$

$$K_1 = \frac{[Ni_2(acac)_4py]^3}{[Ni_3(acac)_6]^2[py]^3} = ca.\ 10^{10}\ \text{M}^{-2}$$

11) J. P. Fackler, Jr., *J. Amer. Chem. Soc.*, **84**, 24 (1962).

$$Ni_2(acac)_4py + 3py \rightleftarrows 2Ni(acac)_2py_2,$$

$$K_2 = \frac{[Ni(acac)_2py_2]^2}{[Ni_2(acac)_4py][py]^3} = 2.7\times10^5\ M^{-2}$$

From these data, the equilibrium constant for the overall reaction (Eq. 4) is calculated to be $K=(K_1K_2^3)^{1/2}=ca.\ 10^{13}M^{-4}$:

$$Ni_3(acac)_6 + 6py \rightleftarrows 3Ni(acac)_2py_2 \qquad (4)$$

This value is very much larger than that (3) for the methanol adduct, conforming to the qualitative observation that $Ni(acac)_2py_2$ is quite stable and does not dissociate in dichloromethane.

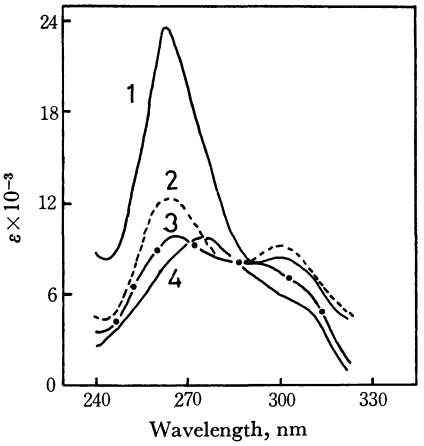

Fig. 3. Ultraviolet spectra of bis(acetylacetonato)nickel (II) in dichloromethane containing 4.54×10^{-3}M water at 10 min (curve 1), 1 hr (curve 2), 8 hr (curve 3) and 48 hr (curve 4) after dissolution.

The Hydrolysis Reaction of Ni(acac)$_2$ in Dichloromethane. Figure 3 represents the change with time of the ultraviolet spectra of $Ni(acac)_2$ in dichloromethane containing 4.54×10^{-3}M water. One hour after the dissolution, the high-energy peak was quite remarkably diminished, and it continued to decrease further with time. A new band gradually appeared in turn at 274 nm. Solutions of $Ni(acac)_2(H_2O)_2$ and $Ni(acac)_2(CH_3OH)_2$ in dry dichloromethane showed quite the same spectral change. When dichloromethane saturated with water (0.12M) was employed as the solvent, the 265 nm peak was not observed, but the 274 nm band appeared from the outset. The band position coincides with that of free acetylacetone, and suggests the occurrence of some hydrolytic reaction of $Ni(acac)_2$, thus liberating acetylacetone molecules. To confirm this possibility, a $Ni(acac)_2$ solution in dry dichloromethane was kept standing for 48 hr (Curve 4 in Fig. 3); the solvent was then distilled under reduced pressure. Acetylacetone in the distillate corresponded to 34.4% of the entire ligand.

In order to investigate the other hydrolysis product, a $Ni(acac)_2$ solution in water-saturated dichloromethane was kept standing for five days. A white, fuzzy precipitate resulted. The solvent was distilled under reduced pressure, and the residue was repeatedly washed with dichloromethane and then dried. This compound was soluble in methanol and exhibited the spectrum as shown by Curve 1 in Fig. 4. The yield of the compound was so minute that elemental analysis and other

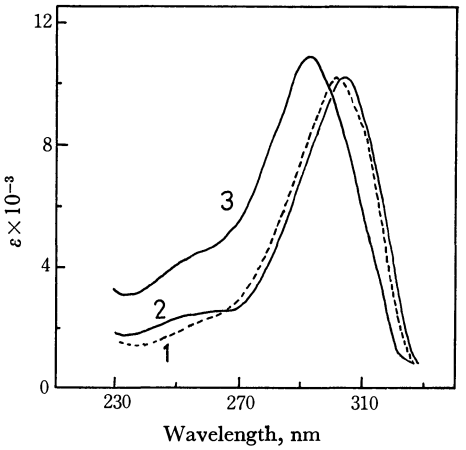

Fig. 4. Ultraviolet spectra in methanol of the hydrolysis product of bis(acetylacetonato)nickel(II) in dichloromethane (curve 1), $Ni(acac)(OH)(H_2O)_2$ (curve 2) and $[Ni(acac)(OCH_3)(CH_3OH)]_4$ (curve 3).

physical measurements were not possible, so a model compound was prepared for comparison.

Bertrand and his co-laborators synthesized a green compound $Ni(acac)(OCH_3)(CH_3OH)$ by the reaction of $Ni(acac)_2$ with equimolar potassium hydroxide in refluxing methanol.[9] The compound is tetrameric in chloroform and isostructural with $[Co(acac)(OCH_3)(CH_3OH)]_4$, which was shown by X-ray analysis to have a cubane-type structure.[12] The ultraviolet and infrared spectra of $[Ni(acac)(OCH_3)(CH_3OH)]_4$ were measured; they are shown in Figs. 4 and 5 respectively. As has been described in the Experimental section, an analogous hydroxo compound was prepared by the reaction of $Ni(acac)_2$ with potassium hydroxide in water. This compound, $Ni(acac)(OH)(H_2O)_2$, retains two molecules of solvent per nickel atom, and exhibits a very broad band in the O–H stretching region (Curve 1 in Fig. 5), a band which is sharpened by heating at

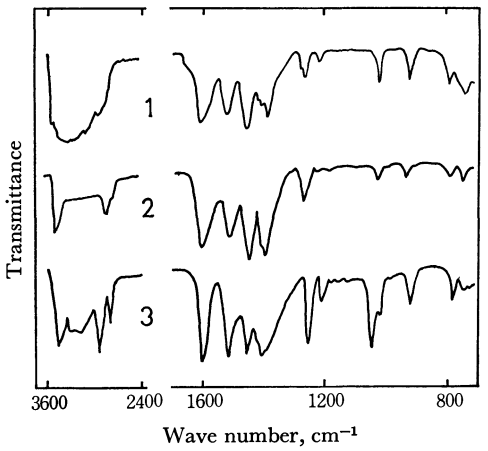

Fig. 5. Infrared spectra in Nujol (lower-frequency region) and in hexachlorobutadiene (higher-frequency region) of $Ni(acac)(OH)(H_2O)_2$ (curve 1), the same compound after heating at 100°C *in vacuo* (curve 2) and $[Ni(acac)(OCH_3)(CH_3OH)]_4$ (curve 3).

12) J. A. Bertrand, A. P. Ginsberg, R. I. Kaplan, C. E. Kirkwood, R. L. Martin, and R. C. Sherwood, *Inorg. Chem.*, **10**, 240 (1971).

100°C *in vacuo* (Curve 2 in Fig. 5). The infrared spectrum of $Ni(acac)(OH)(H_2O)_2$ bears a close resemblance to that of $[Ni(acac)(OCH_3)(CH_3OH)]_4$, and the former might also have a tetrameric structure similar to that of the latter, involving an excess H_2O molecule as the water of crystallization.

In Fig. 4 are reproduced the ultraviolet spectra of the tetrameric methoxo complex (Curve 2) and the presumably tetrameric hydroxo complex (Curve 3). They are very similar except that the latter is located in a little longer wavelength region than the former. It should be noted that the spectrum of the hydrolysis product of $Ni(acac)_2$ in dichloromethane (Curve 1) shows a striking resemblance to that of the synthesized hydroxo complex (Curve 2), suggesting an essential similarity between their structures.

If the hydrolysis of Ni $(acac)_2$ in dichloromethane proceeds according to Eq. (5), the yield of the freed acetylacetone will be 50% of the total acetylacetone contained in the starting complex. Cotton and

$$Ni_3(acac)_6 + 3nH_2O = \frac{3}{4}[Ni(acac)(OH)(H_2O)_{n-1}]_4 + 3acacH \quad (5)$$

Winquist[13] prepared a hexameric complex, $Ni_6(tfac)_{10}(OH)_2(H_2O)_2$ by drying a light green solid, presumably $Ni(tfac)_2(H_2O)_2$, at 108°C *in vacuo* for 24 hr; the solid had been obtained by a reaction between nickel(II) carbonate and trifluoroacetylacetone in refluxing benzene. If a similar hexameric complex is derived from $Ni(acac)_2$ in the present case, the yield of the freed acetylacetone will be 16.7%.

The observed yield of acetylacetone (34.4%) is higher than the value calculated for the above hexameric product (16.7%) and lower than that for the tetrameric product (50%). Although the tetrameric formulation seems preferable on the spectral basis, further detailed studies are desirable in order to establish the structure of the hydrolysis product of $Ni(acac)_2$ in dichloromethane.

The mechanism of the hydrolysis of bis(acetylacetonato)nickel(II) in dichloromethane containing more or less water is not certain as yet. However, it seems quite probable that the hydrolysis reaction of $Ni(acac)_2$ liberating an acetylacetone molecule does not proceed *via* $Ni(acac)_2(H_2O)_2$. If this is the case, the 300 nm band should rise with time at the expense of the 265 nm band. The observed results in Fig. 3 clearly obviate this possibility. Even when $Ni(acac)_2(H_2O)_2$ was dissolved in dichloromethane containing 4.54×10^{-3}M water, the spectrum was the same as that of a solution of anhydrous $Ni(acac)_2$, indicating a trimerization according to Eq. (1), and then it changed with time in the same fashion as shown in Fig. 3. Thus, the hydrolysis reaction of $Ni(acac)_2$ in question can be considered to start from the trimeric molecule.

The authors are grateful to the Ministry of Education for its financial assistance and also to the Daicel Co., Ltd. for the supply of acetylacetone.

13) F.A. Cotton and B.H.C. Winquist, *Inorg. Chem.*, **8**, 1304 (1969).

BULLETIN OF THE CHEMICAL SOCIETY OF JAPAN, VOL. 46, 169—175 (1973)

Derivatographic Studies on Transition Metal Complexes. IX.[1] Thermal CN-Bridging Reaction of Double Complex Salts in Solid Phase[2]

Ryokichi TSUCHIYA, Shigeo NAKAGAWA,* Akira UEHARA, and Eishin KYUNO

Department of Chemistry, Faculty of Science, Kanazawa University, Kanazawa

**Department of Chemical Engineering, Faculty of Technology, Kanazawa University, Kanazawa*

(Received June 3, 1972)

It was found by derivatography and spectral measurements that the double complex salts, $[Co(H_2O)_2N_4][Co(CN)_6]\cdot nH_2O$, where N_4 is $4NH_3$, two moles of ethylenediamine (en) or one mole of triethylenetetramine (trien), $[Co(NH_3)_2trien][Co(CN)_6]\cdot 2H_2O$, $[Co(NH_3)tepa][Co(CN)_6]\cdot 2H_2O$, where tepa is tetraethylenepentamine, and $[Co(H_2O)_2trien][Cr(CN)_6]\cdot 2H_2O$ underwent deaquation- or deammonation-CN-bridging formation reaction upon heating. The general tendency was observed to be as follows: the more stable the structural configuration of the coordination sphere, the higher the activation energy. In the case of the complex containing hexacyanochromate(III) as an anion, the activation energy for the bridging formation reaction is especially high as a result of possible flipping in CN bridging groups.

It is known that the hexaammine or aquopentaammine complexes of transition metals such as $[M(NH_3)_6]X_3$ or $[M(H_2O)(NH_3)_5]X_3$ liberate a part of ammonia or water by deammonation- or deaquation-anation upon heating, producing the corresponding acidopentaamine complexes as expressed by the fol-

1) Part VIII in this series: see R. Tsuchiya, M. Suzuki, and E. Kyuno, This Bulletin, **45**, 3105 (1972).

2) Presented at the 23rd Annual Meeting of the Chemical Society of Japan, Tokyo, April (1970).

lowing reactions:

$$[M(NH_3)_6]X_3(s) \xrightarrow{\Delta} [MX(NH_3)_5]X_2(s) + NH_3(g)$$

$$[M(H_2O)(NH_3)_5]X_3(s) \xrightarrow{\Delta} [MX(NH_3)_5]X_2(s) + H_2O(g),$$

where M is Co[3-6] or Cr[6,7] and X is halogens.

Thermal bridging reaction can be expected when X in the complexes of the above types is replaced by the relevant complex anions of the type $[M'X_6]^{3-}$ containing a ligand X which can form a bridge over two metals, *i.e.*, heating of some double complex salts will give the binuclear complexes as expressed by the following reactions:

$$[MA_nB_{6-n}][M'X_6] \xrightarrow{\Delta} [B_{6-n}M\text{-}X_n\text{-}M'X_{6-n}] + nA,$$

where M and M′ are central metal atoms, A is a volatile neutral ligand, B the ligand which can not be expelled by heating, X the ligand which can form the bridge between M and M′, and n the number of ligand A contained in the starting complexes.

It can be expected that the binuclear complexes produced have one, two or three bridges between two metals in the respective cases where n is 1, 2, or 3, the coordinated atoms forming two octahedrons holding a point, an edge or a face in common, respectively, as shown in Fig. 1.

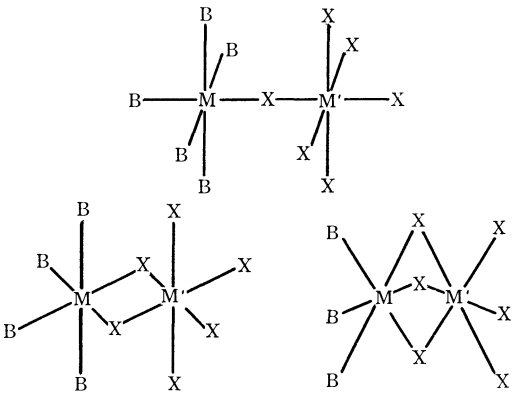

Fig. 1. Three possible types of bridged binuclear complexes.

No reports have been found on the above thermal reactions except for a study in which the complex $[(NH_3)_5Co\text{-}NC\text{-}Co(CN)_5]$ was prepared by isothermal heating and characterized by physical methods.[8]

We prepared a series of double complex salts containing water or ammonia as a volatile ligand A and CN^- as bridging group X, and examined the possibility of occurrence of these bridging formation reactions.

Experimental

Preparation of Double Complex Salts. *1)* cis-*Diaquotetraamminecobalt(III) Hexacyanocobaltate(III) Monohydrate,* cis-$[Co(H_2O)_2(NH_3)_4][Co(CN)_6]\cdot H_2O$ *(I).* To a 100 ml aqueous solution of 3.7 g of *cis*-diaquotetraamminecobalt(III) nitrate, *cis*-$[Co(H_2O)_2(NH_3)_4](NO_3)_3$,[9] a 100 ml of 3.3 g of potassium hexacyanocobaltate(III) $K_3[Co(CN)_6]$[10] was added. After a few minutes of stirring, red crystals were precipitated. After being filtered off, they were washed with water, ethanol and ether in turn and air dried.

Found: C, 18.16; H, 4.33; N, 35.89%. Calcd for $[Co(H_2O)_2(NH_3)_4][Co(CN)_6]\cdot H_2O$: C, 18.50; H, 4.66; N, 36.00%.

2) cis-*Diaquobis(ethylenediamine)cobalt(III) Hexacyanocobaltate(III) Trihydrate,* cis-$[Co(H_2O)_2en_2][Co(CN)_6]\cdot 3H_2O$ *(II).* When a solution of 4.9 g of *cis*-diaquobis(ethylenediamine)cobalt(III) bromide dihydrate, *cis*-$[Co(H_2O)_2en_2]Br_3\cdot 2H_2O$[11] in 20 ml of 1 N HNO_3 and a solution of 3.3 g of $K_3[Co(CN)_6]$ in 20 ml were mixed together and kept standing at room temperature for one day, fine red crystals were precipitated. They were treated and dried in a similar way to that described for 1).

Found: C, 24.77; H, 5.13; N, 29.13%. Calcd for $[Co(H_2O)_2en_2][Co(CN)_6]\cdot 3H_2O$: C, 24.80; H, 5.41; N, 28.91%.

3) cis-α-*Diaquotriethylenetetraminecobalt(III) Hexacyanocobaltate(III) Dihydrate,* cis-α-$[Co(H_2O)_2trien][Co(CN)_6]\cdot 2H_2O$ *(III).* The complex was obtained as pink crystals precipitated from a mixture of the two solutions, one containing 0.01 mol of *cis*-α-diaquotriethylenetetraminecobalt(III) salt, *cis*-α-$[Co(H_2O)_2trien]^{3+}$, and the other containing 3.3 g of $K_3[Co(CN)_6]$ in a similar manner to that for salt I, the former being prepared by the reaction of *cis*-α-carbonatotriethylenetetraminecobalt(III) perchlorate monohydrate, *cis*-α-$[CoCO_3trien]ClO_4\cdot H_2O$[12] (3.7 g) with 20% $HClO_4$ solution.

Found: C, 29.55; H, 5.25; N, 28.66%. Calcd for $[Co(H_2O)_2trien][Co(CN)_6]\cdot 2H_2O$: C, 29.28; H, 5.32; N, 28.45%.

4) cis-β-*Diaquotriethylenetetraminecobalt(III) Hexacyanocobaltate(III) Dihydrate,* cis-β-$[Co(H_2O)_2trien][Co(CN)_6]\cdot 2H_2O$ *(IV).* The double complex salt was prepared from 3.7 g of *cis*-β-$[CoCO_3trien]ClO_4$[12] as the starting complex cation in the same way as descrybed in 3). It was orange.

Found: C, 28.84; H, 5.13; N, 27.53%. Calcd for $[Co(H_2O)_2trien][Co(CN)_6]\cdot 2H_2O$: C, 29.28; H, 5.32; N, 28.45%

5) cis-β-*Diamminetriethylenetetraminecobalt(III) Hexacyanocobaltate(III) Dihydrate,* cis-β-$[Co(NH_3)_2trien][Co(CN)_6]\cdot 2H_2O$ *(V).* *cis*-β-diamminetriethylenetetraminecobalt(III) chloride, *cis*-β-$[Co(NH_3)_2trien]Cl_3$[13] and $K_3[Co(CN)_6]$ were used as starting materials for the preparation. The product was yellow crystals.

Found: C, 30.05; H, 5.68; N, 34.28%. Calcd for $[Co(NH_3)_2trien][Co(CN)_6]\cdot 2H_2O$: C, 29.37; H, 5.68; N, 34.28%.

6) *Amminetetraethylenepentaminecobalt(III) Hexacyanocobaltate(III) Dihydrate,*$[Co(NH_3)tepa][Co(CN)_6]\cdot 2H_2O$ *(VI).* One of the starting complexes, amminetetraethylenepentaminecobalt(III) bromide, $[Co(NH_3)tepa]Br_3$, was prepared from the corresponding bromo complex, $[CoBr\ tepa]Br_2$[14] in

3) M. Mori, R. Tsuchiya, and Y. Okano, This Bulletin, **32**, 1029 (1959).
4) N. Tanaka and M. Nanjo, *ibid.*, **37**, 1330 (1964).
5) M. Mori and R. Tsuchiya, *ibid.*, **33**, 841 (1960).
6) W. W. Wendlandt and J. L. Bear, *J. Inorg. Nucl. Chem.*, **22**, 77 (1961).
7) R. Tsuchiya, Y. Kaji, A. Uehara, and E. Kyuno, This Bulletin, **42**, 1881 (1969).
8) R. A. de Castelló, C. P. MacColl, N. B. Egen, and A. Haim, *Inorg. Chem.*, **8**, 699 (1969).
9) S. M. Jφrgensen, *Z. Anorg. Chem.*, **2**, 281 (1892).
10) A. Benedetti-Pichler, *Z. Anal. Chem.*, **70**, 258 (1927).
11) A. Werner and K. R. Lange, *Ann. Chem.*, **386**, 88 (1912).
12) A. M. Sargeson and G. H. Searle, *Inorg. Chem.*, **6**, 787 (1967).
13) E. Kyuno and J. C. Bailar, Jr., *J. Amer. Chem. Soc.*, **88**, 1125 (1966).
14) R. G. Pearson, C. R. Boston, and F. Basolo, *J. Phys. Chem.*, **59**, 304 (1955).

liquid ammonia. The aqueous solution containing 5.0 g of $[Co(NH_3)tepa]Br_3$ was mixed with a solution of 3.3 g of $K_3[Co(CN)_6]$ and cooled with ice in a similar manner to that described above. Yellow crystals were obtained and then treated as mentioned in 1).

Found: C, 32.18; H, 5.38; N, 31.75%. Calcd for $[Co(NH_3)tepa][Co(CN)_6]\cdot 2H_2O$: C, 32.54; H, 5.85; N, 32.53%.

7) cis-α-Diaquotriethylenetetraminecobalt(III) Hexacyanochromate(III) Dihydrate, cis-α-$[Co(H_2O)_2trien][Cr(CN)_6]\cdot 2H_2O$ *(VII).* The double complex salt was prepared from 3.7 g of *cis*-α-$[CoCO_3trien]ClO_4\cdot H_2O$[12] and 3.3 g of $K_3[Cr(CN)_6]$[15] in the same way as in the case of 3). The product was pink crystals.

Found: C, 30.72; H, 5.40; N, 28.98%. Calcd for $[Co(H_2O)_2trien][Cr(CN)_6]\cdot 2H_2O$: C, 29.70; H, 5.40; N, 28.86%.

8) μ-Cyanoaquobis(ethylenediamine)pentacyanodicobalt(III,III) Pentahydrate, $[(H_2O)en_2Co\text{-}NC\text{-}Co(CN)_5]\cdot 5H_2O$ *(VIII).* When one gram of *cis*-$[Co(H_2O)_2en_2][Co(CN)_6]\cdot 3H_2O$ was stirred in 400 ml of water, the compound gradually dissolved giving orange coloration. After being kept standing at room temperature for about a day, orange needle crystals appeared, which were dried after filtration.

Found: C, 23.86; H, 5.57; N, 27.87%. Calcd for $[Co_2en_2(H_2O)(CN)_6]\cdot 5H_2O$: C, 23.80; H, 5.60; N, 27.76%.

9) μ-Dicyanotriethylenetetraminetetracyanodicobalt(III,III) Pentahydrate, $[trien\ Co\text{-}(NC)_2\text{-}Co(CN)_4]\cdot 5H_2O$ *(IX).* When one gram of *cis*-α-$[Co(H_2O)_2trien][Co(CN)_6]\cdot 2H_2O$ was suspended in 200 ml of water and heated on a water bath, the double complex salt was completely dissolved with yellow color. The solution was concentrated to about half its volume on a water bath and kept standing at room tempetature, yellow crystals being precipitated. The complex was dried in a similar manner to that described above.

Found: C, 28.49; H, 5.46; N, 27.80%. Calcd for $[Co_2trien(CN)_6]\cdot 5H_2O$: C, 28.25; H, 5.53; N, 27.45%.

Derivatographic Measurements. The derivatograms were obtained with a MOM Derivatograph Typ-OD-102. All the measurements were carried out in a constant flow of nitrogen under the heating rate of 1°C/min. 0.4 or 0.5 g of sample was used in each run. The activation energies (E_a) and enthalpy changes (ΔH) were calculated by analysis of the DTA curves in the derivatograms.

Spectral Measurements. In order to examine the structural change during the course of the thermal reaction, the electronic spectra and IR spectra were measured with a Hitachi EPS and EPU-2A Spectrophotometers in both solution and powdered state and with a JASCO Model IR-E Spectrophotometer in mull state, respectively.

Isothermal Measurements. Isothermal determination of the deaquation or deammonation accompanied by bridging reaction was carried out by use of a Shimadzu TM-1A Thermobalance in static air at the desired temperature.

Results and Discussion

Derivatography. It was found that most of the salts do not show any distinct evidence for the bridging formation in the TG curve, except for some salts. As an example, the double complex salt, $[Co(H_2O)(NH_3)_5][Co(CN)_6]$, the simplest compound anticipated to give the binuclear complex, decomposed at 190°C without giving any plateau in the TG curve suggesting the bridging formation, as shown in Fig. 2.

15) J. H. Bigelow and J. C. Bailar, Jr., "Inorganic Syntheses," Vol. 2, (1946), p. 203.

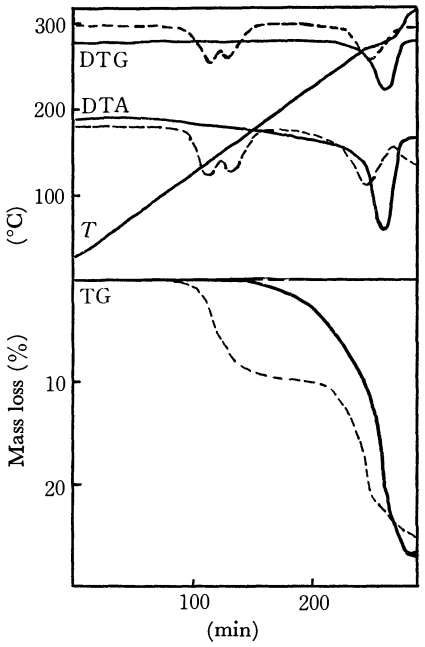

Fig. 2. Derivatograms of the double complex salts, $[Co(H_2O)(NH_3)_5][Co(CN)_6]$ (——) and I (----).

In several salts, however, distinct thermal reactions for the formation of the stable complexes containing CN bridges between two central metal atoms were found by the presence of one or two steady steps of the liberation of neutral ligands involved. The derivatograms of the diaquotetraammine-type double complex salt I, the diaquobis(ethylenediamine)-type one II. and the diaquotriethylenetetramine-type one III are shown in Figs. 2, 3, and 4, respectively.

In the double complex salt I, the DTA and DTG curves split into two peaks are observed in the temperature range 90—150°C, where the mass loss corresponding to two moles of water or to the sum of one mole of water and one mole of ammonia appears in

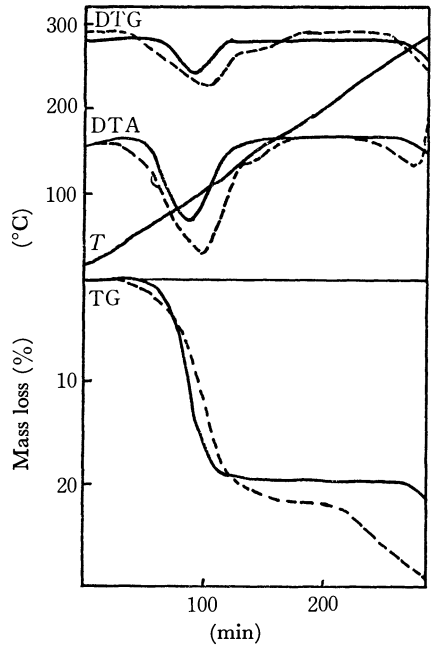

Fig. 3. Derivatograms of II (——) and VIII (----).

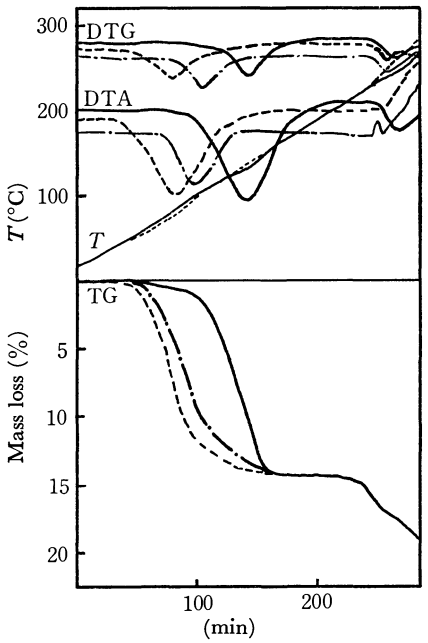

Fig. 4. Derivatograms of III (——), IV (----) and VII (---)

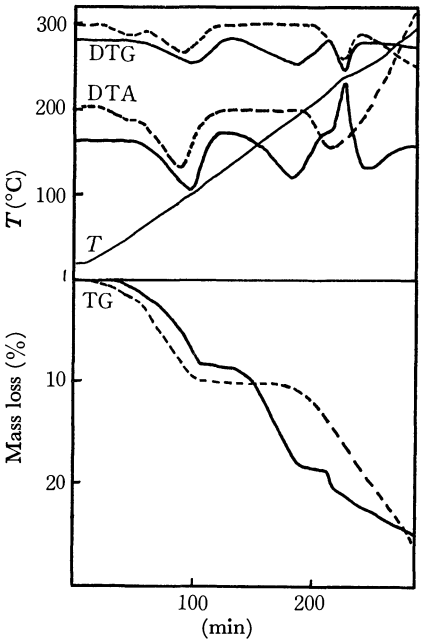

Fig. 5. Derivatograms of V (——) and VI (----).

the TG curve. However, since the ammonia evolution was not sufficient for detection in this step, the mass loss might be attributed to one mole of lattice water and one mole of coordinated water.

Salt II showed the mass loss corresponding to five moles of water in the region 50—120°C, and after that the weight of the sample remained constant till 260°C. The elemental analysis for the salt taken out from the furnace at 150°C was as follows: Found: C, 30.22; H, 4.90; N, 35.58%. Calcd for $[en_2Co_2(CN)_6]$: C, 30.47; H, 4.90; N, 35.53%. Thus, the thermal reaction product seems to be a binuclear complex containing two CN bridges as $[en_2Co(CN)_2Co(CN)_4]$.

The derivatogram of complex VIII which has one CN bridge is also included in Fig. 3. It is seen from the DTA and DTG curves that five moles of the lattice water are liberated from 60 to 120°C and then one mole of the coordinated water is continuously expelled to 160°C. Despite the loss of the coordinated water in complex VIII, the binuclear complex having the same two CN bridges as those obtained from complex II could not be found, the reason being not clear.

Salts III, IV, and VII give similar derivatograms to each other irrespective of the difference of the initiation dehydration temperatures, 90°C for III, 45°C for IV, and 75°C for VII, respectively, as seen in Fig. 4: two steps of the mass losses corresponding to two moles of the lattice water and to two moles of the coordinated water can not be distinguished from each other both in DTA and DTG curves. We also see that the *cis*-β-form double complex salt IV undergoes CN-bridging formation more easily than the corresponding *cis*-α-form one III and the complex containing $[Cr(CN)_6]^{3-}$ VII gives more readily the bridging formation than the corresponding cobaltate(III), III.

The derivatograms of the two double complex salts V and VI containing ammine as the labile ligand against heating are shown in Fig. 5.

Salt V shows two steps of mass losses at 50—120°C and 140—190°C, and then decomposes at 220°C. From the results of IR spectra and detection of ammonia, the first step is due to the liberation of two moles of the lattice water and the second to the deammonation reaction accompanied by the two CN-bridging formation.

Salt VI loses one mole of ammonia at 100—170°C, giving a complex containing one CN-bridge.

Electronic Spectra. On heating these double complex salts in the solid phase, the deaquation-bridging reaction accompanied by a distinct color change from red to yellow was observed, but scarcely in the deammonation-bridging reaction.

In the double complex salts, the first absorption bands of the complex cations $[Co(H_2O)_2N_4]^{3+}$ give a maximum in the neighborhood of 500 nm, whereas those of the complex anions $[Co(CN)_6]^{3-}$ and $[Cr(CN)_6]^{3-}$ give a maximum at 311 and 300 nm, respectively. Since the bands resulting from the hexacyanometallate anions are situated in the near-ultraviolet region, they scarcely affect the visible bands of the complex cations contained in the double complex salts. Therefore, the first absorption maxima of the cations constituting the double complex salts are considered to be those of the complexes themselves.

The numerical values for the first absorption bands of all the complexes prepared in the experimental section and those heated are listed in Table 1. The spectra of salts III and IV and those heated at 170°C, including VII heated at 170°C, are shown as representatives in Fig. 6, the spectra being measured by the diffuse reflectance method.

As seen in Table 1, the absorption bands of the double complex salts, when heated, are found to shift to the higher frequency region except for salts V and VI, *e.g.*, those of the complexes II, III, and IV are shifted to the neighborhood of 470 nm, which is almost similar

Table 1. Change of the absorption maxima upon heating of the double complex salts

Salts	λ_{max} (nm)	$\xrightarrow{\Delta}$	λ_{max} (nm)
I	510		485
II	504		467
III	505		472
IV	486		472
V	476		472
VI	476		474
VII	505		420
VIII	480		468
IX	462		

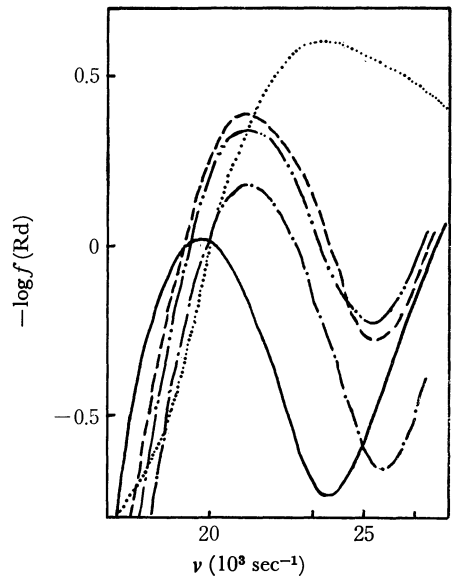

Fig. 6. Absorption spectra by the diffuse reflectance method of III at room temperature (——), III heated at 170°C (– – –), IV at room temperature (— · —), IV heated at 170°C (— · · —), and VII heated at 170°C (·····).

to that of hexaamminecobalt(III) complex, and above all, the wavenumber of the band of the thermal product from III is approximately close to that of IX. It is obvious that complex III undergoes the two-CN-bridging formation reaction upon heating to be converted into the binuclear complex IX.

Salt I liberates two moles of water upon heating, and the absorption band is shifted to 485 nm. Complex VIII has an absorption band at 480 nm, both bands coinciding with the band of aquopentaamminecobalt(III) complex. It seems that both the complex formed by heating I and complex VIII have one CN-bridge between two central metals and the cationic part has CoN_5O-type coordination. Complex VIII was found to give the absorption peak at 468 nm after the liberation of one mole of the coordinated water. The peak is close to that of the thermal bridging product of II. This suggests that complex VIII is converted into the two CN-bridging complex of CoN_6-type.

Only a slight shift of the band can be observed in V and VI (Table 1). It is obvious that in their thermal bridging reaction product, N atoms in CN^- bridges are coordinated to cobalt in the cationic part and C atoms participate in cobalt in anionic part; *i.e.*, the cationic part consists of CoN_6-type coordination, giving similar spectra to that of hexaamminecobalt(III) complex.

Complex VII heated at 170°C gives a broad absorption band in the wavelength region 430—390 nm in contrast to the case of Co–CN–Co type salts as shown in Fig. 6. It suggests that in contrast to the Co–CN–Co type salts which consist of CoN_6- and CoC_6-type coordination spheres combined with CN-bridges, the Co–CN–Cr type salt thermally obtained from VII consists of CoC_2N_4- and CrC_4N_2-type coordination spheres formed by the flipping of CN-bridges[8,16] and the overlap of their spectra appearing at 410 and 405 nm gives a broad band.

IR Spectra. IR spectra of the double complex salts we prepared except for those of VIII and IX show, in the frequency region of ν_{CN} stretching, one clear band at 2143—2149 or 2130 cm^{-1}, which is assigned to the terminal CN stretching vibration in $[Co(CN)_6]^{3-}$ or $[Cr(CN)_6]^{3-}$, respectively. With the progress of deaquation- or deammonation-anation, a new band whose extinction increases gradually appears at *ca.* 2190 cm^{-1} in addition to the original peak due to terminal-CN stretching. This is assigned to the stretching of CN bridging. The IR spectral data concerned with ν_{CN} for all the double complex salts and those heated are given in Table 2. As a typical example for the change of ν_{CN} bands, the spectra in the neighborhood of 2100—2200 cm^{-1} of salt IV at several steps of heating are shown in Fig. 7.

Table 2. Change of ν_{CN} in IR spectra of the double complex salts

Salts	ν_{CN}	$\xrightarrow{\Delta}$	ν_{CN}
I	2143		2143, 2190
II	2143		2143, 2190
III	2149		2149, 2196
IV	2149		2149, 2196
V	2143		2143, 2196
VI	2143		2143, 2190
VII	2130		2130, 2170
VIII	2143, 2220		
IX	2143, 2212		

The following three possible modes are considered for bridging structure:

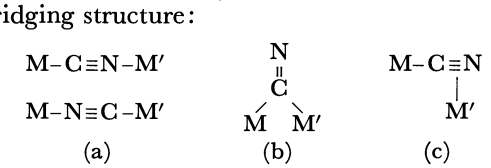

(a) would be the most possible mode, because the frequency of CN stretching vibration in both (b) and (c) should be lower than that of the terminal CN group in $[M(CN)_6]^{3-}$ and the possibility of the flipping reaction was observed as shown in the section of electronic spectra. However, if mode (a) is accepted, the complexes containing two CN-bridges in *cis* position

16) D. B. Brown and D. F. Shriver, *Inorg. Chem.*, **8**, 37 (1969).

Table 3. Enthalpy changes, ΔH, and activation energies, E_a, in the thermal bridging reactions of the double complex salts

Double complex salts	ΔH kcal/mol	E_a kcal/mol[a)]	E_a kcal/mol[b)]	E_a kcal/mol[c)]
I	9.6	59.0	57.7	(99.5)
	9.4	48.5	49.4	
II	12.5	23.9	23.7	
III	12.9	30.9	31.1	31.3
IV	11.2	18.8	19.2	
V	14.9	42.5	42.8	42.7
VI	3.1	20.9	39.0	
VII	6.7	44.9	43.5	45.7
VIII	8.4	32.0	32.0	

a) Estimated by analysis of the DTA curve.
b) Estimated by analysis of the DTG curve.
c) Calculated from the Arrhenius plots in the isothermal measurements.

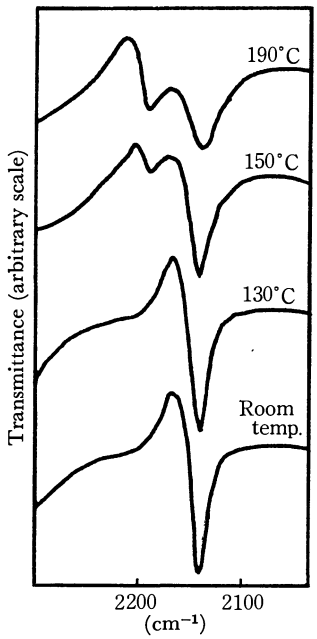

Fig. 7. Change of IR spectra in the frequency region of ν_{CN} of V at several steps of heating.

produced by the thermal reaction would not be binuclear but have the structure of either tetramer or polymer, since the bond M–C≡N–M′ or M–N≡C–M′ should be linear.

On the other hand, X-ray diffraction for the single crystal of $[(NH_3)_5Co\text{–}N{\equiv}C\text{–}Co(CN)_5]\cdot H_2O$[17] shows that the angle of Co–C–N is 172.4° and that of Co–N–C 159.8°. Thus, it is not unreasonable to consider the possibility of the presence of the binuclear complexes having structure (a) with bending M–C≡N–M′ or M–N≡C–M′ bonds in *cis* position, not (b) or (c). However, the presumption could not be verified, since the molecular weight determination could not be made because of the small solubility of the salts in many solvents.

Thermochemical Data. The data of the enthalpy changes ΔH and the activation energies E_a for the thermal reaction of the double complex salts are summarized in Table 3, the former being estimated from the analysis of DTA and the latter from the analysis of DTA or DTG curve in a similar manner to that described previously.[7]

The values of the enthalpy change for these thermal reactions of I through V are close to those for the general deaquation- or deammonation-anation reactions, but those for VI, VII, and VIII are remarkably small. This may be due to the large contribution of exothermic bridging formation throughout the reactions. It is found that the activation energies for the liberation of two neutral molecules increase in the order, IV<II<III<V<VII. This sequence can be explained as follows.

1. The α-trien chelate stabilizes the complex to a greater extent than ethylenediamine chelate, so that the coordinated water in salt III is not so easily liberated as in salt II.
2. Since β-trien chelate has a larger strain than α-trien chelate, the former expels the coordinated water more easily than the latter, making the activation energy in IV lower than in III.
3. The activation energy of V is larger than that of IV, which may be due to the greater difficulty of evolution of ammonia than water.
4. Salt VII has a larger activation energy than salt III. This might be due to the possibility of the flipping reaction in VII.

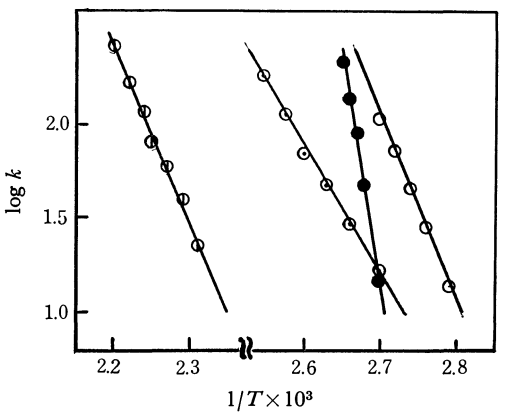

Fig. 8. Arrhenius plots for the bridging reaction of the double complex salts: I (●—●), III (⊙—⊙), V (◑—◑) and VII (○—○).

17) O. Hassel and J. R. Salvesen, *Z. Phys. Chem.*, **128**, 345 (1927).

Isothermal Measurements and Reaction Mechanism. The Arrhenius plots, $\log k$ *vs.* $1/T$, estimated by the isothermal measurements of the thermal bridging formation reactions of salts I, III, V, and VII are shown in Fig. 8, where k is the rate constant of the reaction calculated on the basis of the presumption of the first order. The activation energies obtained from the plots are also given in Table 3. They are in fairly good agreement with those obtained by derivatography except for I.

Taking into account the results from derivatography, isothermal measurements and the UV and IR absorption spectral measurements, it was concluded that, in the thermal bridging formation reaction of Co–Co double complex salts, the CN groups in the anionic part coordinate to cobalt in cationic part with *N*-atoms, but in that of Co–Cr salts, they coordinate to cobalt with C-atom as a result of CN flipping.

BULLETIN OF THE CHEMICAL SOCIETY OF JAPAN, VOL. 46, 175—178 (1973)

Polarographic Studies of Some Lanthanoids(III) in *N,N*-Dimethylacetamide

Makoto AIHARA and Seizo MISUMI
Inorganic Chemistry Laboratory, Faculty of Science, Kyushu University, Fukuoka
(Received June 6, 1972)

Polarographic behaviour of some lanthanoids(III) has been studied in *N,N*-dimethylacetamide. La(III), Pr(III), and Nd(III) showed irreversible, three-electron reduction wave and the other lanthanoids(III), Gd(III), Tb(III), Dy(III), Ho(III), Er(III), Tm(III), and Lu(III) except Sm(III), Eu(III), and Yb(III), gave irreversible, three-electron reduction wave with a pre-wave. The kinetic parameters for La(III), Pr(III), and Nd(III) were determined by means of Koutecky's method. Sm(III), Eu(III), and Yb(III) showed two-step reduction waves, the first wave being a reversible, one-electron reduction wave. These solvated lanthanoids(III) were investigated also by cyclic voltammetry.

The polarographic studies of Pb(II), Cd(II), *etc.*,[1] and alkali and alkaline earth metal[2] in *N,N*-dimethylacetamide (DMA) have been reported. However, lanthanoid(III) (Ln(III)) has not yet been investigated. It is interesting to compare the polarographic behaviour of each Ln(III), in particular the half-wave potential in DMA, with that in other non-aqueous solvents.

Important kinetic parameters for irreversible waves are transfer coefficient (α) and standard rate constant (k_s). There are few investigations of the rate constant of Ln(III) in non-aqueous solvents. Gaur and Zutshi[3] reported on the polarographic reduction of Eu(III) in formamide.

In this work polarographic and cyclic voltammetric studies and the kinetic parameters of some lanthanoids-(III) in DMA are presented.

Experimental

Materials. DMA was fractionally distilled three times from calcium hydride *in vacuo* (10 mmHg) under nitrogen and finally distilled in the absence of calcium hydride. Moisture in DMA was determined by Karl-Fischer titration to be 0.04%. Lanthanoid(III) perchlorates were prepared by dissolving the oxides in perchloric acid and drying at 60°C *in vacuo*. Tetraethylammonium perchlorate (TEAP) was used as the supporting electrolyte. All other reagents were of extra pure grade.

Apparatus. The electrolysis cell consists of three electrodes.[4] The reference electrode was an SCE with a salt bridge:

$$\left(\frac{0.5\text{M TEAP}}{\text{DMA}}\middle|\frac{1\text{M NaClO}_4}{\text{H}_2\text{O}}\middle|\frac{1\text{M NaCl}}{\text{H}_2\text{O}}\middle|\frac{1\text{M KCl}}{\text{H}_2\text{O}}\right).$$

DME was used for DC polarography ($m^{2/3}t^{1/6}=1.25$ mg$^{2/3}$/sec. in 0.1M TEAP-DMA medium at -2.4 V *vs.* SCE) and HDME (area of HDME; 0.051 cm^2) was used for cyclic voltammetry as thework ing electrode. Other apparatus were as described previously.[4]

Procedure. A sample solution of 0.1M TEAP-DMA containing 0.3~2.0 mM $Ln(ClO_4)_3$ of the final concentration was taken into a cell. After dried nitrogen gas was passed through it for 20 min., a polarogram was recorded. The junction potential was measured by using an SCE with a slowly flowing-type aqueous saturated KCl salt bridge and found to be 25 mV. All experiments were carried out at 25.0±0.1°C.

Results and Discussion

Polarograms of 0.3 mM Ln(III) except for Sm(III), Eu(III), and Yb(III) in DMA are shown in Fig. 1.

Each reduction wave of La(III), Pr(III), and Nd-(III) was single and irreversible in the concentration range 0.3~1.0 mM for Ln(III), whereas that of other lanthanoids(III) (Gd(III), Tb(III), Dy(III), Ho(III), Er(III), Tm(III), and Lu(III)) was single and irreversible with a pre-wave, the main wave becoming ill-defined with increasing concentration of Ln(III).

Polarographic data are shown in Table 1-1. The

1) S. Musha, T. Wasa, and K. Tani, *Rev. Polarog.* (Kyoto), **11**, 169 (1963).

2) V. Gutmann, M. Michlmayr, and G. Peychal-Heiling, *Anal. Chem.*, **40**, 619 (1968). *J. Electroanal. Chem.*, **17**, 153 (1968).

3) J. N. Gaur and K. Zutshi, *J. Electroanal. Chem.*, **11**, 390 (1966).

4) S. Misumi and M. Aihara, *Talanta*, **19**, 549 (1972).

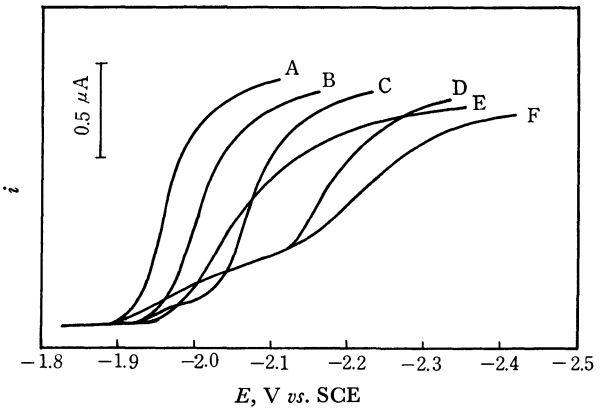

Fig. 1. Typical polarograms of 0.3 mM Ln(III) in DMA.
A: Pr(III), B: Nd(III), C: Gd(III), D: Er(III), E: La(III), F: Lu(III).

electrode reaction was found to be irreversible, of three-electron reduction and diffusion-controlled (Table 2-1). The diffusion current of the main wave decreased and the half-wave potential was shifted to a more negative value with decreasing ionic radius of Ln(III), the total wave height remaining nearly constant.

The effect of increasing concentration of water to DMA on the reduction wave was investigated. Typical polarograms of Pr(III) and Er(III) in water-DMA medium are shown in Fig. 2. The values of half-wave potential and wave-height for Pr(III) did not change with addition of water, but the reduction wave for Er(III) became a single wave even with 1% addition of water. It was observed that the half-wave potential of this wave was shifted toward a more positive value with increasing concentration of water.

TABLE 1. POLAROGRAPHIC DATA FOR Ln(III) IN 0.1 M TEAP IN DMA

1-1 [Ln(III)]=0.30mM

	$-E_{1/2}$ V vs. SCE	I_d	reciprocal slope mV	α
La (III)	2.04_0	2.26	78	0.25
Pr (III)	1.95_6	2.84	37	0.52
Nd (III)	2.00_8	2.56	40	0.49
Gd (III)	2.09_2	2.36	48	0.41
Tb (III)	2.11_3	1.74	40	0.46
Dy (III)	2.13_0	2.02	43	0.46
Ho (III)	2.16_3	1.51	45	0.44
Er (III)	2.18_7	1.67	47	0.42
Tm (III)	2.18_1	1.13	45	0.44
Lu (III)	2.22_9	1.18	52	0.35
1-2 [Ln(III)]=1.00mM				
Sm(III) (1st wave)	1.72_3	0.94	54	
(2nd wave)	2.10_6	0.77	38	
Eu(III) (1st wave)	0.53_8	0.89	59	
(2nd wave)	2.13_1	0.46	47	
Yb(III) (1st wave)	1.25_1	1.06	61	

TABLE 2. DEPENDENCE OF LIMITING CURRENTS ON THE HEIGHTS OF MERCURY COLUMN

2-1 [Ln(III)]=0.30mM

Metal ion	$i_l/\sqrt{h_{corr.}}$	Metal ion	$i_l/\sqrt{h_{corr.}}$
La (III)	0.121±0.007	Dy (III)	0.113±0.002
Pr (III)	0.160±0.001	Ho (III)	0.082±0.004
Nd (III)	0.140±0.006	Er (III)	0.088±0.006
Gd (III)	0.124±0.009	Tm(III)	0.065±0.001
Tb (III)	0.102±0.003	Lu (III)	0.064±0.003

2-2 [Ln(III)]=1.00mM

Metal ion	$i_l/\sqrt{h_{corr.}}$		$i_l/\sqrt{h_{corr.}}$
Sm (III) (1st wave)	0.181±0.001	(2nd)	0.169~0.148[a]
Eu (III) (1st wave)	0.166±0.003	(2nd)	0.073~0.060[b]
Yb (III) (1st wave)	0.186±0.002		

a) Temperature coefficient: 5.5~9.5%.
b) Temperature coefficient: 6.5~9.0%.

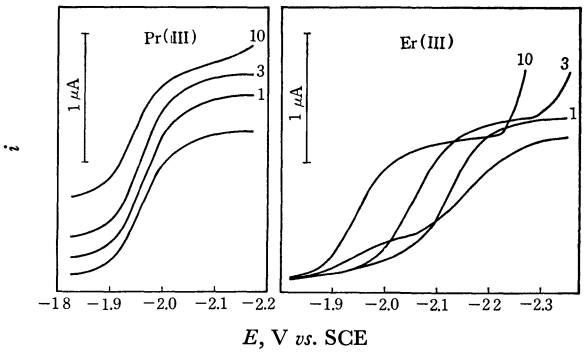

Fig. 2. Typical polarograms of 0.3 mM Pr(III) and Er(III) in water-DMA medium.
Numbers on curves refer to per-cent water added to the solution.

Cyclic voltammograms are shown in Fig. 3. No pre-wave was seen for La(III), Pr(III), and Nd(III) but one was observed for the other lanthanoids(III) such as Gd(III) and Tb(III). The height of the pre-wave also increased with decreasing radius of Ln(III). No anodic waves could be observed at this sweep rate because of the irreversibility of electrode reaction.

Polarograms for Sm(III), Eu(III), and Yb(III) are shown in Fig. 4. Sm(III) and Eu(III) showed two-step reduction waves but the second wave of Yb(III) was observed to overlap the residual current of the supporting electrolyte. Polarographic data are shown

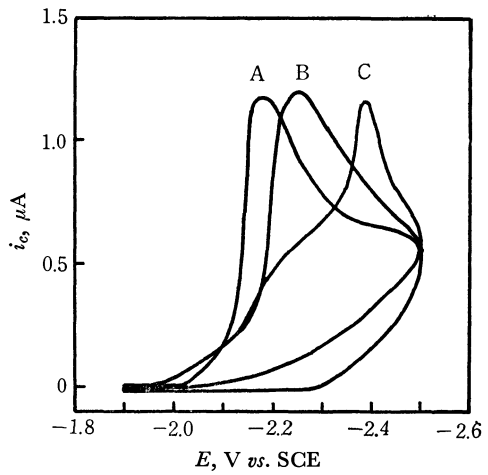

Fig. 3. Cyclic voltammograms of 0.3 mM Ln(III) in DMA.
A: Pr(III), B: Gd(III), C: Lu(III). Scan rate: 0.060 V/sec.

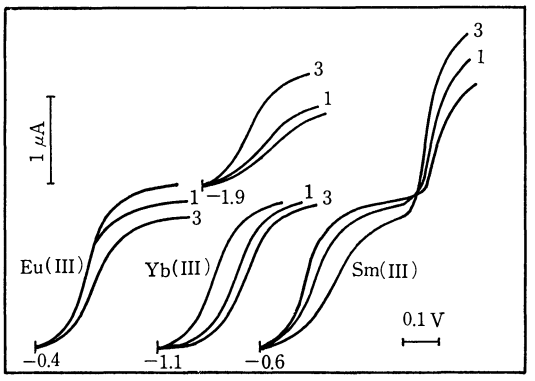

E, V *vs.* SCE

Fig. 4. Polarograms of 1.0 mM Sm(III), Eu(III) and Yb(III) in water-DMA medium.
Number on curves refer to per-cent water added to the solution.

in Table 1-2. The electrode reaction for the first wave is diffusion-controlled but the value of $i_l/\sqrt{h_{corr.}}$ for the second wave decreased with increasing mercury pressure (Table 2-2). The value of temperature coefficient was in the range 5~9%.

The value of reciprocal slope for the first wave is 54, 59, and 61 mV for Sm(III), Eu(III), and Yb(III), respectively. It was found that its electrode reaction is reversible and of one-electron reduction. The ratio of current for the first wave to that for the second wave is 0.84 for Sm(III) and 0.49 for Eu(III). The effect of water on the reduction wave is shown in Fig. 4. The half-wave potential for the first wave is shifted toward a more negative value and that for the second wave toward a more positive value with increasing concentration of water. The height of the second wave increases with the addition of water.

It is supposed that La(III), Pr(III), and Nd(III) would form a stable solvate species with DMA and these species would not be affected by the adidtion of water. The electrode reaction is assumed to be as follows.

$$[Ln(DMA)_x]^{3+} + yH_2O \rightleftarrows [Ln(DMA)_{x-y}(H_2O)_y]^{3+} + y(DMA)$$

$$[Ln(DMA)_x]^{3+} + 3e^- \longrightarrow Ln^0 + x\text{DMA} \quad (1)$$

$$[Ln(DMA)_{x-y}(H_2O)_y]^{3+} + 3e^- \longrightarrow Ln^0 + (x-y)\text{DMA} + yH_2O \quad (2)$$

Equations 1 and 2 correspond to the electrode reactions of the main wave and the pre-wave, respectively.

The half-wave potentials of the main waves corrected for the rubidium scale in three kinds of solvents (the donor numbers of DMA, *N,N*-dimethylformamide (DMF) and acetonitrile (AN) are 27.8, 26.6, and 14.1, respectively) are listed in Table 3. Values of the half-wave potentials are in the order AN[5]>DMF[6]>DMA. A comparison of these values shows that the half-wave potential is related to donor number and metal ion-solvent interaction depends on the polarographic overvoltage.

Table 3. Half-wave potential of Ln(III) in different solvents in volts *vs.* the half-wave potential of Rb^+

Ln(III)	Solvent		
	DMA	DMF	AN
La	−0.09	−0.05	0.45
Pr	0.00	−0.05	0.45
Nd	−0.05	−0.05	0.45
Gd	−0.14	−0.14	0.45
Tb	−0.16	−0.14	
Dy	−0.18	−0.16	
Ho	−0.21	−0.18	
Er	−0.23	−0.19	
Tm	−0.23		
Lu	−0.27		

The half-wave potential of the first wave for Sm(III) and for Eu(III) in water[5] was more negative than that in DMA. This explains the negative shift of half-wave potential caused by the addition of water. The electrode reaction of the first wave is reversible and of one electron reduction, but that of the second wave differs from that in other solvents (*e.g.* Eu(II)→Eu(0) in acetonitrile[5]).

The kinetic parameters for the reduction of La(III), Pr(III), and Nd(III) were calculated by means of Koutecky's method[7] and the values of E_s (standard electrode potential) were obtained by Hale and Parson's method.[8]

For the reaction where $k_s \leq 5 \times 10^{-4}$ cm/sec, there is a region near the top of the wave in which $\exp\{nF(E-E_s)/RT\} \ll 1$. Under these conditions Koutecky's equations can be simplified as follows.

$$i/i_d = F(\chi) \quad (3)$$

$$\chi = (12t/7D_0)^{1/2}k_f \quad (4)$$

where $F(\chi)$[9] is a power series in the variable (χ) and k_f is the rate constant for the forward reaction. k_f is related to the standard rate constant by the equation.

$$(k_s): k_f = k_s e^{-\alpha nF(E-E_s)/RT} \quad (5)$$

k_f and α can be determined from Eqs. (3), (4) ,and (5). When E equals E_s, $\exp\{nF(E-E_s)/RT\}$ becomes 1 and Koutecky's equations become

$$i/i_d = F(\chi)/2 \quad (6)$$

$$\chi = 2(12t/7D_0)^{1/2}k_f \quad (7)$$

By plotting $\log(F(\chi)/2)$ *vs.* $\log(\chi/2)$ and $\log(i/i_d)$ *vs.* $\log(12t/7D_0)^{1/2}k_f$, the intersection gives the point k_s.

$$k_f = k_s e^{-\alpha nF(E-E_s)/RT} = k_s$$

The values of α for La(III), Pr(III), and Nd(III) were determined also by plotting $\log \chi$ *vs.* E. The

5) I. M. Kolthoff and J. F. Coetzee, *J. Am. Chem. Soc.*, **79**, 1852 (1957).
6) G. Gritzner, V. Gutmann, and G. Schöber, *Mh. Chem.*, **96**, 1056 (1965).
7) J. Koutecký and J. Čižek, *Collection Czech. Chem. Commun.*, **21**, 836 (1956).
8) J. M. Hale and R. Parsons, *ibid.*, **27**, 2444 (1962).
9) J. Koutecký, *ibid.*, **18**, 597 (1953).

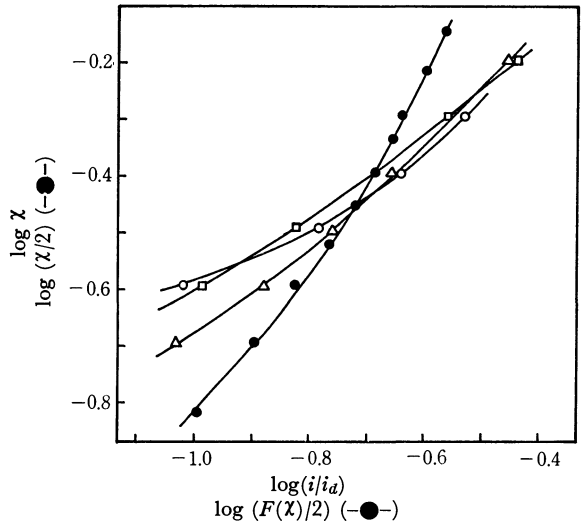

Fig. 5. Plot of log χ *vs.* log(i/i_d) and log($\chi/2$) *vs.* log($F(\chi)/2$). ○: La(III), △: Pr(III), □: Nd(III).

values were in agreement with those obtained by log-plot analysis. The results of the determination of $(k_s)_{ms}$ are given in Fig. 5 and kinetic parameters in Table 4, where $(\alpha_c)_{ms}$ and $(k_f)_{ms}$ mean the parameters determined directly from the experimental data without any theoretical correction.

Table 4. Data for parameters of reduction of La(III), Pr(III) and Nd(III) in DMA

	$(E_{1/2})_{irr}$ V *vs.* SCE	$(E_{1/2})_r$ V *vs.* SCE	$(\alpha_c)_{ms}$	$(k_s)_{ms}$ cm/sec
La	-2.04_0	-2.00_3	0.24	2.0×10^{-4}
Pr	-1.95_6	-1.93_7	0.49	2.2×10^{-4}
Nd	-2.00_8	-1.98_4	0.43	2.4×10^{-4}

On the other hand, the value of k_f^0 (the forward rate constant of the electron transfer at zero volt *vs.* NHE) was obtained by cyclic voltammetry. The value of k_f^0 (5.3×10^{-27} cm/sec) for La(III) is nearly identical with that (3.0×10^{-27} cm/sec) obtained by using k_s, but in the case of Pr(III) and Nd(III) the values of k_f^0 do not coincide with those obtained by using k_s, because of very small values of k_f^0.

The authors are grateful for financial support given by the Ministry of Education for this work. They are indebted to Miss E. Kamiunten for her help in the experiments.

BULLETIN OF THE CHEMICAL SOCIETY OF JAPAN, VOL. 46, 178—183 (1973)

Racemization Reactions of Cobalt(III) Complexes of Ethylenediaminetetraacetate and Trimethylenediaminetetraacetate

Hiroshi OGINO, Masatake TAKAHASHI, and Nobuyuki TANAKA
Department of Chemistry, Faculty of Science, Tohoku University, Aoba, Aramaki, Sendai

(Received June 6, 1972)

The kinetics of racemization reactions of ethylenediaminetetraacetatocobaltate(III), $Co^{III}edta^-$, and trimethylenediaminetetraacetatocobaltate(III), $Co^{III}trdta^-$, were investigated in acid solutions. The rate law for the racemization of $(+)_{546}Co^{III}edta^-$ is:

$$\frac{d[(+)_{546}Co^{III}edta^-]}{dt} = -2\frac{k_{r1}K_a + k_{r2}[H^+]}{K_a + [H^+]}[(+)_{546}Co^{III}edta^-]$$

where K_a is the equilibrium constant of the reaction:

$$(+)_{546}Co^{III}(H_2O)Hedta \rightleftarrows (+)_{546}Co^{III}edta^- + H^+$$

The values of k_{r1} and k_{r2} at 120°C and at an ionic strength of 0.53 are 2.0×10^{-5} sec^{-1} and 5.6×10^{-4} sec^{-1} respectively. The rate law for the racemization of $(+)_{589}Co^{III}trdta^-$ is:

$$\frac{d[(+)_{589}Co^{III}trdta^-]}{dt} = -2k'_{r2}[H^+][(+)_{589}Co^{III}trdta^-]$$

The value of k'_{r2} at 120°C and at an ionic strength of 0.53 is 1.9×10^{-5} l mol^{-1} sec^{-1}. It is known that the rate of the racemization reaction of optically-active $Co^{III}edta^-$ is accelerated by the presence of $Co^{II}edta^{2-}$ because of the electron-exchange reaction between these two species. In this paper, the electron-exchange reaction between $Co^{III}trdta^-$ and $Co^{II}trdta^{2-}$ is also investigated by the utilization of the optical activity. This reaction proceeds faster than the reaction between $Co^{III}edta^-$ and $Co^{II}edta^{2-}$.

Bailar[1] proposed a trigonal twist mechanism for the racemization reaction of the optically-active $Co^{III}edta^-$ complex. Cooke, Im, and Busch[2] investigated this reaction in the pH range from 2 to 4 and supported Bailar's proposal on the basis of the facts that this reaction gives a very large and positive entropy of activation and that the reaction rate is insensitive to the pH within the range studied. In this paper, the reaction of the racemization of $Co^{III}edta^-$ and $Co^{III}trdta^-$ will be investigated in solutions containing

1) J. C. Bailar, Jr., *J. Inorg. Nucl. Chem.*, **8**, 165 (1958).
2) D. W. Cooke, Y. A. Im, and D. H. Busch, *Inorg. Chem.*, **1**, 13 (1962).

hydrogen ions in concentrations of more than 0.05M, and the mechanisms will be discussed.

Im and Busch[3] investigated the kinetics of the electron-exchange reaction between $Co^{III}edta^-$ and $Co^{II}edta^{2-}$ by the utilization of optical activity. In this work, the kinetics of the electron-exchange reaction between $Co^{III}trdta^-$ and $Co^{II}trdta^{2-}$ was followed by a procedure similar to that of Im and Busch.[3] The results will also be presented in this paper.

Experimental

Optically-active $K[Co^{III}edta]\cdot 2H_2O$[4] and $K[Co^{III}trdta]\cdot 2H_2O$[5] were prepared by the procedures described in the literature. The ionic strength of the solutions was adjusted with potassium nitrate. The visible absorption spectra were recorded with a Hitachi EPS-3 pen-recording spectrophotometer. A JASCO model ORD/UV-5 spectrophotometer with a CD attachment was used for the kinetic studies of $Co^{III}edta^-$. In most cases, the rotations were measured at 550 nm. A JASCO model DIP-SL automatic polarimeter was used for the studies of $Co^{III}trdta^-$; the rotation was measured at the sodium D line unless otherwise stated.

The kinetics of the racemization reaction of $Co^{III}edta^-$ or $Co^{III}trdta^-$ was studied in potassium nitrate–nitric acid media. Sealed ampules filled with a solution containing an optically-active cobalt(III) complex, nitric acid, and potassium nitrate were placed in a thermostated oil-bath. The ampules were withdrawn at intervals from the oil-bath and cooled immediately. The solutions were then transferred to optical cells and submitted to measurements of the optical rotations. The kinetic stiudes of the electron-exchange reaction between $Co^{II}trdta^{2-}$ and optically-active $Co^{III}trdta^-$ were carried out at 90°C. To avoid the evaporation of the solution, the reaction vessel shown in Fig. 1 was employed.

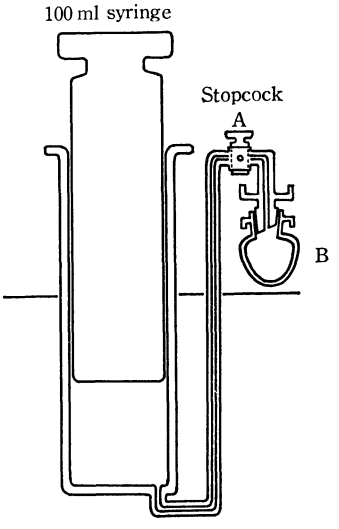

Fig. 1. Reaction vessel used for the kinetic study of the electron-exchange reaction between Co^{III} $trdta^-$ and Co^{II} $trdta^{2-}$.

3) Y. A. Im and D. H. Busch, *J. Amer. Chem. Soc.*, **83**, 3357 (1961).

4) F. P. Dwyer and F. L. Garvan, "Inorganic Syntheses," Vol. 6, (1960), p. 192.

5) H. Ogino, M. Takahashi, and N. Tanaka, This Bulletin, **43**, 424 (1970).

in an oil-bath of a given temperature. Portions of the solution were removed at intervals from the reaction vessel by opening the stopcock, A, and collected in a vessel, B. The solutions were then transferred to optical cells and submitted to measurements of the optical rotations. The pH of the solution was maintained with an acetate buffer. A Hitachi-Horiba F-5 pH meter was used for the measurement of the pH of the solution. It was found that $Co^{II}trdta^{2-}$ was slowly oxidized at 90°C. Therefore, air was expelled from the solution by passing through a stream of nitrogen gas before it was placed in a reaction vessel.

Results and Discussion

Racemization Kinetics of $Co^{III}edta^-$. The rate constants of the racemization reaction of $Co^{III}edta^-$ were determined by this equation:

$$-\log\left(\frac{\alpha_t}{\alpha_0}\right) = \frac{2}{2.303}k_r t \qquad (1)$$

where α_t and α_0 represent the optical rotations at time t and at time zero respectively. k_r denotes the observed rate constant of the racemization reaction. An example of the plots of $-\log(\alpha_t/\alpha_0)$ *vs.* time is shown in Fig. 2.

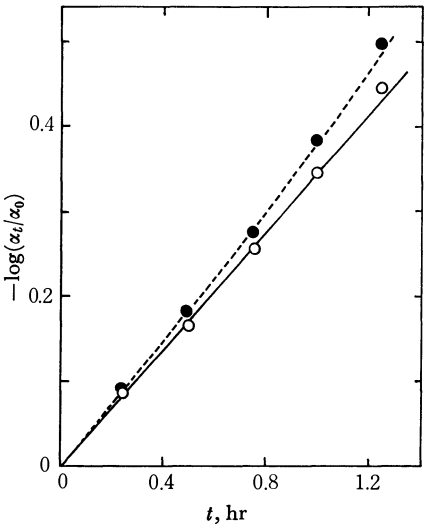

Fig. 2. Relation between $-\log(\alpha_t/\alpha_0)$ and t(solid circles). Open circles represent the values of $-\log(\alpha_t/\alpha_0)$ plotted after correction for the decreases in Co^{III} $edta^-$ by the decomposition reaction. Experimental condition: $[H^+]$= 0.421M, μ=0.53, 120°C.

It is apparent that the plots do not give a linear relation. The measurements of the visible spectra showed that the cobalt ions in $Co^{III}edta^-$ were gradually reduced to the divalent state with time. The decrease in the concentrations of $Co^{III}edta^-$ by this decomposition reaction was determined by the measurement of the visible absorption spectra, and the values of $-\log(\alpha_t/\alpha_0)$ were corrected. The values thus corrected were plotted against the time. The plots gave a straight line, as shown by the solid line in Fig. 2. The rate constant of the racemization, k_r, was calculated from the slope of this straight line. The values of k_r increased with the hydrogen ion concentrations.

It has been known that $Co^{III}edta^-$ is converted into

$Co^{III}(H_2O)Hedta$ in acid solutions.[6] Shimi and Higginson showed the formation of $Co^{III}(H_2O)Hedta$ by the measurement of the visible spectra of $Co^{III}edta^-$ in acid solutions.[7] The equilibrium constant of the reaction:

$$Co^{III}(H_2O)Hedta \rightleftarrows Co^{III}edta^- + H^+ \quad (2)$$

was determined to be 1.28 at 25°C and at an ionic strength of 1.0.[6,8] The formation of $Co^{III}(H_2O)Hedta$ is also shown on the circular dichroism curves (CD curves). In Fig. 3, a CD curve of $(+)_{546}Co^{III}edta^-$ measured in 4.21M HNO_3 (Curve A) is given and is compared with that of $(+)_{546}Co^{III}edta^-$ measured in a neutral solution (Curve B). Curve A is clearly different from Curve B.

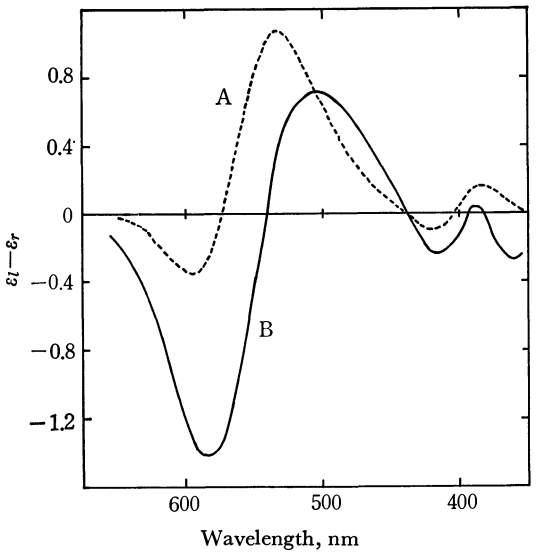

Fig. 3. CD curves of $(+)_{546}$ Co^{III} edta$^-$ in 4.21M HNO_3 (Curve A) and in water (Curve B).

The change in the k_r value with the hydrogen ion concentrations may be explained by considering the formation of $Co^{III}(H_2O)Hedta$ as follows:

$$(+)_{546}Co^{III}(H_2O)Hedta \rightleftarrows (+)_{546}Co^{III}edta^- + H^+ \quad (3)$$

$$(+)_{546}Co^{III}edta^- \xrightarrow{k_{r1}} (-)_{546}Co^{III}edta^- \quad (4)$$

$$(+)_{546}Co^{III}(H_2O)Hedta \xrightarrow{k_{r2}} (-)_{546}Co^{III}(H_2O)Hedta \quad (5)$$

In this reaction mechanism, k_r can be expressed as:

$$k_r = \frac{k_{r1}K_a + k_{r2}[H^+]}{K_a + [H^+]} \quad (6)$$

where K_a represents the equilibrium constant of Reaction (3). The plot of k_r $(K_a + [H^+])$ *vs.* $[H^+]$ is given in Fig. 4, which shows a linear relation. The values of k_{r1} and k_{r2} were determined from the intercept and the slope of the straight line respectively. The K_a values used here were calculated from the data reported by Dyke and Higginson.[6] The kinetic parameters are summarized in Table 1.

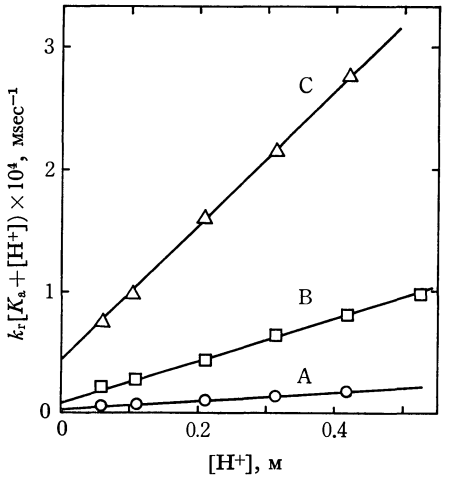

Fig. 4. Relation between $k_r(K_a+[H^+])$ and hydrogen ion concentration for $(+)_{546}$ Co^{III} edta$^-$. Temperature: 100°C (A), 110°C (B), and 120°C (C).

Table 1. Kinetic parameters of the racemization reaction of Co^{III} EDTA complex (μ=0.53 (KNO_3))

	k_{r1} sec^{-1}	k_{r2}, sec^{-1}
100°C	1.9×10^{-6}	3.9×10^{-5}
110°C	6.1×10^{-6}	1.6×10^{-4}
120°C	2.0×10^{-5}	5.6×10^{-4}
ΔH^*(kcal/mol)	32.9	38.5
ΔS^*(e.u.)	3.1	3.9

Cooke *et al.*[2] reported 3.9×10^{-6} sec^{-1} as the rate constant of the racemization reaction of $Co^{III}edta^-$ at 100°C, which corresponds to the k_{r1} in this work. They also reported that the activation energy and the entropy of activation were 40.6 kcal/mol (ΔH^*=39.9 kcal/mol) and 20.6 e.u. respectively. There is a significant discrepancy between the kinetic parameters determined in this work and those reported by Cooke *et al.* It should be recognized, however, that the gradual decomposition of $Co^{III}edta^-$ was not considered in the studies by Cooke *et al.*

Recently, it was found in this laboratory that the decomposition of $Mn^{III}edta^-$ in an aqueous solution led to the formation of $Mn^{II}edta^{2-}$, $Mn^{II}edtra^-$, Mn^{II}-edda, and some other products,[9] where edtra and edda denote $(^-O_2CH_2C)_2NCH_2CH_2NH(CH_2CO_2^-)$ and $(^-O_2CH_2C)NHCH_2CH_2NH(CH_2CO_2^-)$ respectively. It is not unreasonable that the decomposition products of $Co^{III}edta^-$ contain $Co^{II}edta^{2-}$, $Co^{II}edtra^-$, $Co^{II}edda$, and some other products similar to the decomposition products of $Mn^{III}edta^-$. In this work, the concentration of the hydrogen ion is kept higher than 0.05M. Under this experimental condition, divalent cobalt ions produced during the reaction are present in the form of aquo ions, Co^{2+}, so that the contribution of the electron-exchange reaction to the racemization reaction of $Co^{III}edta^-$ can be neglected. As Cooke *et al.* studied the racemization reaction in the pH range from 2 to 4,

6) R. Dyke and W. C. E. Higginson, *J. Chem. Soc.*, **1960**, 1998.
7) I. A. W. Shimi and W. C. E. Higginson, *ibid.*, **1958**, 260.
8) In this work, the determination of the equilibrium constant was repeated. The constant was found to the 1.31 at 25°C and at an ionic strength of 2.0 ($NaClO_4$), which is in good agreement with the value reported by Dyke and Higginson.[6]
9) H. Ogino, T. Shirakashi, and N. Tanaka, presented at the 24th Annual Meeting of the Chemical Soceity of Japan, Osaka (Apr. 1971).

the electron-exchange reaction between $Co^{III}edta^-$ and decomposition products might have accelerated the racemization reaction. Therefore, the kinetic parameters given in Table 1 seem to be more reliable than those reported by Cooke *et al.*

Although the entropy of activation for Reaction (4) is not a large positive value, this value may suggest that the acid-independent racemization of $Co^{III}edta^-$ proceeds through the trigonal twist mechanism, because it is expected that a dissociative mechanism will give a negative value for the entropy of activation.[2,7,10] Furthermore, it is unlikely that the acid-independent path is detectable in the range of hydrogen ion concentrations employed in this work (0.05—0.5M), because this mechanism requires the breaking of at least two Co–O bonds without protonation in an acid solution and rapid recombination after the inversion reaction. A similar situation exists even for the acid-dependent path. The entropy of activation of k_{r2} is a very large positive value. Therefore, it seems reasonable to say that the racemizations of $Co^{III}edta^-$ and $Co^{III}(H_2O)$-Hedta proceed through the trigonal twist mechanism. The values given in Table 1 indicate that $Co^{III}(H_2O)$-Hedta racemizes from 20 to 28 times faster than Co^{III}-$edta^-$. This implies that the decrease in the number of chelate rings in the EDTA complex makes the twist easier.

The Rây and Dutt mechanism[11] has been known to be an intramolecular racemization mechanism. It should be noted that, when the Rây and Dutt mechanism is applied to at least $Co^{III}edta^-$ and related complexes, this mechanism is identical with the mechanism proposed by Bailar.[1]

Racemization Kinetics of $Co^{III}trdta^-$. The reaction was followed by the procedure described for the Co^{III}-$edta^-$ complex. The plots of $-\log(\alpha_t/\alpha_0)$ *vs.* time after correction for the decomposition of $Co^{III}trdta^-$ with time gave a good linear relation. The plots of k_r *vs.* $[H^+]$ indicate linear dependencies, as shown in Fig. 5. The intercepts of the plots are essentially zero at all temperatures. Therefore, k_r can be expressed as:

$$k_r = k'_{r2}[H^+] \quad (7)$$

If $K_a \gg [H^+]$ is assumed, this relation can be formally derived from Eq. (6).

The visible spectra and CD cruves of $Co^{III}trdta^-$ did not show any changes with the increase in the hydrogen ion concentration up to 5M of nitric acid. This is quite different from the behavior of $Co^{III}edta^-$ in an acid solution. That is, the formation of $Co^{III}(H_2O)$-Htrdta is very unfavorable.

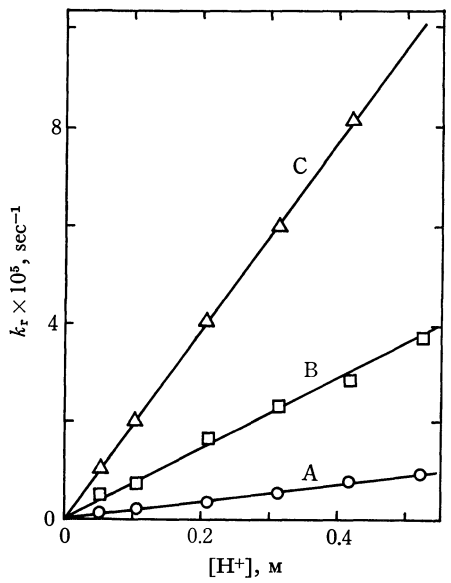

Fig. 5. Relation between k_r and hydrogen ion concentration for $(+)_{546}Co^{III}trdta^-$. Temperature: 120°C (A), 130°C (B), and 140°C (C).

Table 2. Kinetic parameters of the racemization reaction of Co^{III} TRDTA complex (μ=0.53 (KNO_3))

	k'_{r2}, 1 mol^{-1} sec^{-1}
120°C	1.9×10^{-5}
130°C	6.7×10^{-5}
140°C	2.0×10^{-4}
ΔH^*(kcal/mol)	37.5
ΔS^*(e.u.)	14.8

The values of k'_{r2}, the enthalpy of activation, and the entropy of activation are given in Table 2. The racemization reaction of $Co^{III}trdta^-$ is characterized by the facts that an acid-independent path is absent and that the over-all reaction rate is much smaller than that of $Co^{III}edta^-$. As the value of the acid dissociation constant of $Co^{III}(H_2O)Htrdta$ is not known, a comparison between the k'_{r2} value for $Co^{III}trdta^-$ and the k_{r2} value for $Co^{III}edta^-$ is not possible. Figure 5 shows that the acid-independent racemization reaction is extremely slow. One reason for this may be that, if $Co^{III}edta^-$ and $Co^{III}trdta^-$ racemize through the trigonal twist mechanism, the diamine chelate rings must be inverted, as shown in Fig. 6. The absolute configurations of $(-)_{546}Co^{III}edta^-$ [12] and $(-)_{546}Co^{III}$-

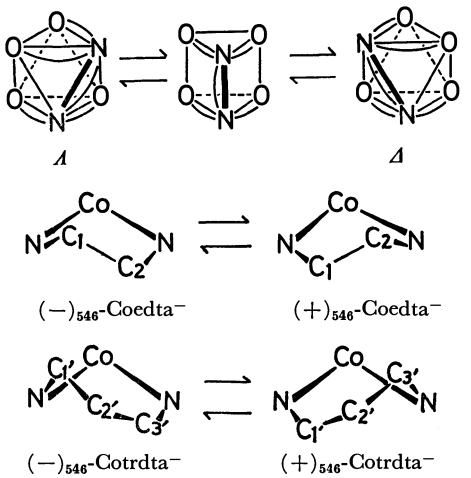

Fig. 6. Racemization processes of $Co^{III}edta^-$ and $Co^{III}trdta^-$ by the trigonal twist mechanism.

10) M. L. Morris and D. H. Busch, *J. Phys. Chem.*, **63**, 340 (1959).
11) P. Rây and N. K. Dutt, *J. Indian Chem. Soc.*, **20**, 81 (1943).
12) T. E. MacDermott and A. M. Sargeson, *Aust. J. Chem.*, **16**, 334 (1963).

trdta$^-$ [5] have been determined to be *A*. In a previous paper,[5] it was shown that the conformation of the trimethylenediamine chelate ring is a twist form. That is, the cobalt(III) ion, two nitrogen atoms, and one central carbon atom of trimethylenediamine ($C_{2'}$ in Fig. 6) lie on the same plane and there is a two-fold axis through the cobalt(III) ion and $C_{2'}$. In the racemization of $(-)_{546}Co^{III}edta^-$, the carbon atom, C_1, above the N–Co–N plane moves downward, while C_2, below the N–Co–N plane moves upward, as shown in Fig. 6. In the case of $(-)_{546}Co^{III}trdta^-$, the $C_{1'}$ above the N–Co–N plane moves downward and $C_{3'}$ below the N–Co–N plane, moves upward. In addition, the $C_{2'}$ atom must be fixed in the N–Co–N plane during the inversion process. Therefore, in the transition state, the cobalt(III) ion, two nitrogen atoms, $C_{1'}$, $C_{2'}$, and $C_{3'}$ must exist on the same plane. It is quite natural that this situation is sterically hindered and leads to the absence of an acid-independent path for $Co^{III}trdta^-$.

Electron-exchange Reaction between $Co^{II}trdta^{2-}$ and Co^{III}-trdta$^-$. The electron-exchange reaction between $Co^{II}trdta^{2-}$ and optically-active $Co^{III}trdta^-$ was followed by measurements of the decrease in optical rotation with the time. As the intramolecular racemization of optically-active $Co^{III}trdta^-$ is negligible under these experimental conditions, the reaction can be expressed as follows:

$$Co^{II}trdta^{2-} + \text{optically-active } Co^{III}trdta^- \xrightarrow{k_e} \text{racemic } Co^{III}trdta^- + Co^{II}trdta^{2-} \quad (8)$$

From Reaction (8), these relations:

$$-\log\left(\frac{\alpha_t}{\alpha_0}\right) = \frac{k_{obs}}{2.303}t \quad (9)$$

$$k_{obs} = k_e[Co^{II}trdta^{2-}] \quad (10)$$

can be derived. Figure 7 shows some examples of these plots, the slopes of which correspond to $k_{obs}/2.303$. The values of k_{obs} were found to be dependent

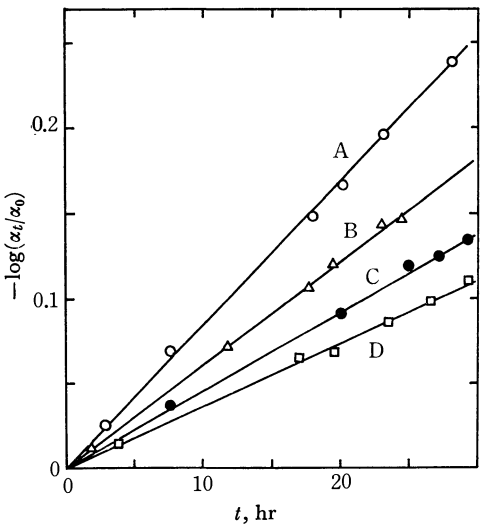

Fig. 7. Relation between $-\log(\alpha_t/\alpha_0)$ and t.
Experimental conditions: $[Co^{II}trdta^{2-}]$=13.45mM (A), 22.97 mM (B), 13.77 mM (C), and 13.80 mM (D); pH=3.04 (A), 3.58 (C), and 3.86 (B) and D)

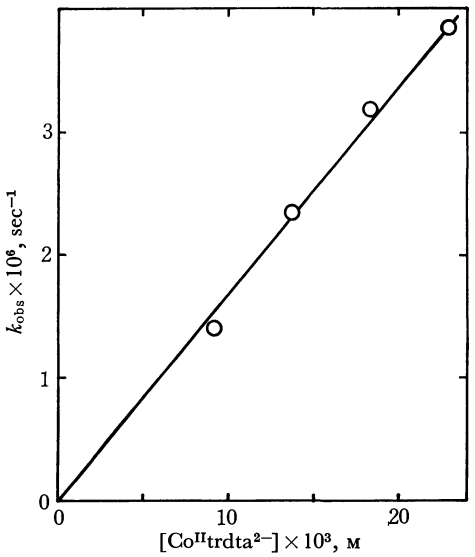

Fig. 8. Relation between k_{obs} and $[Co^{II}trdta^{2-}]$. pH=3.86

on both $[Co^{II}trdta^{2-}]$ and $[H^+]$. When the hydrogen ion concentration is kept constant, the k_{obs} values are proportional to $[Co^{II}trdta^{2-}]$, as shown in Fig. 8. The slope of the straight line which is shown in Fig. 8 corresponds to the rate of the electron-exchange reaction, k_e. The k_e values were determined at several pH values; the results are given in Table 3.

TABLE 3. RATE CONSTANTS OF THE ELECTRON-EXCHANGE REACTION OF Co-TRDTA SYSTEM AT μ=0.2 (KNO_3) AND 90°C

pH	k_e, 1 mol^{-1} sec^{-1}
3.86	1.55×10^{-4}
3.58	1.99×10^{-4}
3.04	3.74×10^{-4}

It is known that $Co^{II}trdta^{2-}$ is in equilibrium with $Co^{II}Htrdta^-$ as follows:[13]

$$Co^{II}Htrdta^- \rightleftharpoons Co^{II}trdta^{2-} + H^+ \quad (11)$$

Therefore, the electron-exchange reaction between Co^{II}-trdta^{2-} and $Co^{III}trdta^-$ can be expressed by this mechanism:

$$Co^{II}trdta^{2-} + \text{optically-active } Co^{III}trdta^- \xrightarrow{k_{e1}} \text{racemic } Co^{III}trdta^- + Co^{II}trdta^{2-} \quad (12)$$

$$Co^{II}Htrdta^- + \text{optically-active } Co^{III}trdta^- \xrightarrow{k_{e2}} \text{racemic } Co^{III}trdta^- + Co^{II}Htrdta^- \quad (13)$$

On the basis of this mechanism, the rate law can be derived as:

$$k_e = \frac{k_{e1}K^H + k_{e2}[H^+]}{K^H + [H^+]} \quad (14)$$

where K^H represents the equilibrium constant of Eq. (11). By use of the data given in Table 3 and Eq. (14), the values of k_{e1}, k_{e2}, and K^H were calculated. The results are given in Table 4, along with the data

13) G. Anderegg, *Helv. Chim. Acta*, **47**, 1801 (1964).

Table 4. Rate constants of electron-exchange reaction for Co-TRDTA and Co-EDTA systems (μ=0.2)

	Temp., °C	k_{e1}, l mol^{-1} sec^{-1}	k_{e2}, l mol^{-1} sec^{-1}	K^H, mol/l	Ref.
Co-TRDTA system	90	1.0×10^{-4}	1.1×10^{-3}	2.4×10^{-3}	This work
Co-EDTA system	90	8.1×10^{-5}	2.8×10^{-4}	1.1×10^{-3}	3

reported for the Co-EDTA system.[3]

The reactions proceed faster than the reaction between $Co^{II}edta^{2-}$ and $Co^{III}edta^{-}$ for both the acid-independent and the acid-dependent paths.

BULLETIN OF THE CHEMICAL SOCIETY OF JAPAN, VOL. 46, 183—186 (1973)

Studies on Nitrogen-Phosphorus Compounds. XXII.[1] The Synthesis and Properties of Phosphoric Aniline Diamide

Etsuro KOBAYASHI

National Chemical Laboratory for Industry, Honmachi, Shibuya-ku, Tokyo

(Received February 3, 1972)

In order to develop fireproof materials, a new compound, phosphoric aniline diamide, was prepared by employing phosphorus oxychloride, aniline, and ammonia as the starting materials. The conditions for the synthesis and the characteristics of the product have been investigated. Phosphoric aniline diamide can be prepared in the following way: 2 moles of aniline are added to 1 mole of phosphorus oxychloride diluted with chloroform, and the precipitate of aniline hydrochloride, a by-product, is separated from the solvent by filtration. A mixture of phosphoric amide and ammonium chloride is formed by the reaction between an excess of gaseous ammonia and the above filtrate at −10—20°C, and is then separated from the mother liquor. Crude phosphoric amide is extracted from the mixture with ethanol, and subsequent re-extraction with acetone yields the pure product with the formula $PONHC_6H_5(NH_2)_2$. The product thus obtained is composed of a white crystalline powder, soluble in water, ethanol and acetone but insoluble in various organic solvents. The compound shows its own characteristic X-ray diffraction pattern and IR absorption bands. Upon heating, the product melts at about 140°C; condensation occurs by de-ammoniation above 170°C, and conversion into insoluble condensed amidophosphates takes place.

Inorganic compounds with P–N bonds are of interest because of their covalency and the possibility of introducing different substituents into the phosphorus atom, and also because most of the compounds polymerize at moderate temperatures. As typical P–N compounds, phosphoric amides, the following types are known: $PO(OH)_2NH_2$, $POOH(NH_2)_2$, $PO(NH_2)_3$, $PONR_2(NH_2)_2$, $PO(OR)_2NH_2$, $POOR(NH_2)_2$, and $PONHR(NH_2)_2$. Some of these compounds have already been prepared by a reaction between the corresponding phosphoric chloride and ammonia at low temperatures.[2-4]

The author has also synthesized the phosphoric amides of $PONR_2(NH_2)_2$ type.[5] In this work, phosphoric aniline diamide, which is expected to have an excellent flame resistance because it contains an aromatic radical in its molecule, was initially formed by a reaction between phosphorus oxychloride, aniline, and ammonia in chloroform as the reaction medium. The pure product was then isolated from ammonium chloride by using ethanol and acetone as extractive solvents. In this paper an experimental study of the preparation and properties of this new compound is described.

Experimental

Synthesis. The flow sheet for the synthesis of phosphoric aniline diamide is shown in Fig. 1. The phosphoric amide can be prepared in the following way: 0.1 mole (15.3 g) of phosphoric oxychloride was placed in a three-necked flask and diluted with 100ml of chloroform. To this was added a solution containing 0.2 mol (18.6 g) of aniline in 80 ml of chloroform at room temperature. The precipitate of aniline hydrochloride (R·1) was separated by filtration from a solution containing phosphoric aniline dichloride. The above filtrate (SR1) was then added, drop by drop, into another three-necked fiask containing some ammoniacal chloroform at −15—20°C, simultaneously the reactant in the flask was vigorously stirred while a moderate basicity was maintained by passing gaseous ammonia into it. Thus, a mixture (R2) of phosphoric amide and ammonium chloride was precipitated. This was kept standing overnight and was then separated from the mother liquor (SR2). R2 was put into a stoppered Erlenmeyer flask containing 300 ml of ethanol and stirred. Thus, phosphoric amide and a portion of ammonium chloride contained in R2 were dissolved in ethanol, and the residue (R3) of ammonium chloride was isolated from the ethanol solution (SR3). Crude

1) a) The article was presented at the 26th Annual Meeting of the Chemical Society of Japan, Tokyo, April 4, 1972. b) Part XXI of this series: E. Kobayashi, *Nippon Kagaku Kaishi*, **1972**, 38.

2) H. N. Stockes, *J. Amer. Chem. Soc.*, **15**, 198 (1893); *ibid.*, **16**, 123; 140 (1894).

3) R. Klement and O. Koch, *Chem. Ber.*, **87**, 333 (1954).

4) M. Goehring and K. Niedenzu, *ibid.*, **89**, 1769 (1956).

5) E. Kobayashi, *Kogyo Kagaku Zasshi*, **74**, 1780 (1971).

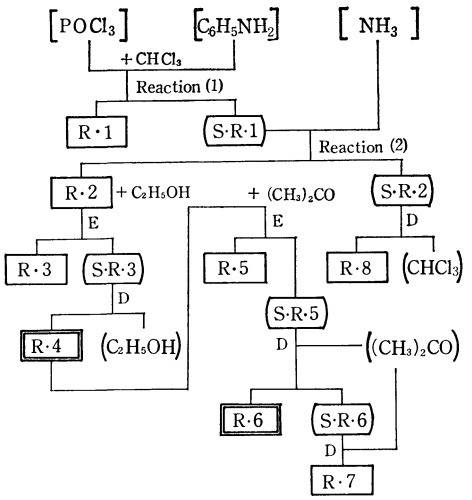

Fig. 1. Flow sheet for synthesis of phosphoric aniline diamides. R·1; $C_6H_5NH_2 \cdot HCl$, R·2; Mixture of phosphoric amide and NH_4Cl, R·3 and R·5; NH_4Cl, R·4; Crude phosphoric amide, R·6; Pure phosphoric amide, R·7 and R·8; Subproduct, D; Distillation, E; Extraction.

phosphoric amide (R4) including ammonium chloride as an impurity was obtained by the vacuum distillation of SR3. A large amount of acetone was poured into R4, and the mixture was stirred for several hours at 35°C. Thus, phosphoric aniline diamide alone was dissolved in acetone. The resulting residue (R5) of ammonium chloride was isolated from the acetone solution (SR5). When the above extractions was incomplete because of the low solubility of phosphoric aniline diamide in acetone, it was necessary to use acetone for the reextraction. Pure phosphoric aniline diamide (R6) was precipitated fron an acetone solution concentrated by vacuum distillation at 40°C: R6 was separated by filtration from the mother liquor (SR6) and finally vacuum-dried over phosphorus pentoxide.

Analysis. A sample solution for determining the phosphorus, total nitrogen, and chlorine was prepared as follows: 0.2—0.8 g of a solid sample was weighed exactly and dissolved in water, the volume of the solution being adjusted to 250 ml.

The phosphorus content was determined gravimetrically as magnesium pyrophosphate. The total nitrogen content was determined by Kjeldahl's method. The chlorine content was determined gravimetrically as silver chloride.

The molecular weight of the product was determined with a Mechrolab model 301A vapor-pressure osmometer. The powder diffraction pattern was obtained by using a Rigaku-Denki model 2001 diffractometer with Ni-filtered Cu$K\alpha$ radiation, with 20 KVP and 5 mA. The infrared absorption spectrum was measured with a Hitachi model EPI-S2 infrared spectrophotometer applying the method of KBr disks. The differential thermal analysis (DTA) and thermogravimetric measurements (TGA) were performed simultaneously in a nitrogen atmosphere and at a heating rate of 5°C/min with a Rigaku-Denki model DC-Cl-S thermal analyser.

Results and Discussion

Synthesis of $PONHC_6H_5(NH_2)_2$. The results of the synthesis and analysis of phosphoric amides are summarized in Table 1.

Reaction between Phosphorus Oxychloride and Aniline. Phosphoric aniline dichloride and aniline hydrochloride are formed by the reaction of 1 mol of phosphorus oxychloride with 2 mol of aniline as follows.

$$POCl_3 + 2C_6H_5NH_2 \longrightarrow PONHC_6H_5Cl_2 + C_6H_5NH_2 \cdot HCl \quad (1)$$

$$POCl_3 + 4C_6H_5NH_2 \longrightarrow PO(NHC_6H_5)_2Cl + 2C_6H_5NH_2 \cdot HCl \quad (1')$$

$$POCl_3 + 6C_6H_5NH_2 \longrightarrow PO(NHC_6H_5)_3 + 3C_6H_5NH_2 \cdot HCl \quad (1'')$$

Chloroform was chosen as the medium for the reaction because it does not react with phosphorus oxychloride. Further, chloroform dissolves phosphoric aniline dichloride, but aniline hydrochloride is insoluble in it. Carbon tetrachloride used for the previous synthesis of phosphoric amides[4,5] was not suitable, since phosphoric aniline dichloride is insoluble in carbon tetrachloride.

For a mole ratio of 2: 1 of $C_6H_5NH_2$ to $POCl_3$, 11.7—14.1 g of R–1 was obtained. These typical results approached the theoretical yield (12.9 g) of aniline hydrochloride. The analytical values of R–1 also agreed with the calculated values of each component in the $C_6H_5NH_2 \cdot HCl$, so that confirmation of Eq. (1) might be expected. However, in the experiments at mole ratios of 4: 1 and 6: 1, it was found that Eqs. (1)′ and (1)″ respectively are not invariably completed.

Reaction between SR1 and Ammonia. A mixture (R–2) of phosphoric amide and ammonium chloride was precipitated by a reaction between the filtrate SR1 containing phosphoric aniline dichloride and ammonia as shown by

$$PONHC_6H_5Cl_2 + 4NH_3 \longrightarrow PONHC_6H_5(NH_2)_2 + 2NH_4Cl \quad (2)$$

In this case, a large amount of R–2 was obtained with a mole ratio of 2: 1 of $C_6H_5NH_2$ to $POCl_3$. The high yield of crude phosphoric amide extracted from the above R2 with ethanol was expected as a matter of course. The yield of R2, however, decreased with an increase in the mole ratio of $C_6H_5NH_2$ to $POCl_3$, and the yield of R8 as a by-product increased. It is conceivable that the reaction product (R8) dissolves in chloroform because of non-polarity with the excess of combined aniline, since, on the synthesis of this phosphoric amide, the mole ratio of 2: 1 of $C_6H_5NH_2$ to $POCl_3$ was just what was expected. When the effects of the reaction temperatures on the yields of R2 and R8 were observed, no apparent difference was recognized at −15—20°C. However, it is evident that the polymerization by deammoniation of phosphoric amides is prevented when Reaction (2) takes place at low temperatures and when diffusion of the heat of reaction is kept smooth, and consequently, a high yield of orthophosphoric amide might be expected. At reaction temperatures above 20°C, there is a probability of the formation of condensed products. The resulting product is reddish-brown, a color which frequently appears in aniline salts.

TABLE 1. SYNTHESIS AND ANALYSIS OF PHOSPHORIC ANILINE DIAMIDES

No.	Reaction conditions					Yield					
	$POCl_3$ (g)	$C_6H_5NH_2$ (g)	N/P	Reaction[a] (1) (°C)	(2) (°C)	R·1 (g)	R·2 (g)	R·3 (g)	R·4 (g)	R·6 (g)	R·8 (g)
1	15.3	18.6	2.0	−10～−12	−10～−15	11.7	23.8	9.9	13.0	11.5	2.2
2	15.3	18.6	2.0	−10	−10	13.6	22.6	9.9	12.5	11.4	1.8
3	15.3	18.6	2.0	0	0	13.1	23.1	9.8	13.1	11.0	1.9
4	15.3	18.6	2.0	0±1	0±1	12.7	26.7	15.1	4.9	—	—
5	15.3	18.6	2.0	10	10	13.8	23.1	8.7	13.6	11.1	2.6
6	15.3	18.6	2.0	20	20	14.2	21.5	8.4	12.1	10.2	5.4
7	15.3	37.2	4.0	0±2	0	24.2	11.7	7.6	5.2	3.5	11.7
8	15.3	55.8	6.0	0	0	37.0	6.3	3.8	1.7	1.3	25.0

	Analysis of R·4					Analysis of R·6				
pH	P (%)	N (%)	Cl (%)	P:N:Cl (atomic ratio)	pH	P (%)	N (%)	P:N (atomic ratio)	Mp (°C)	MW
6.08	15.0	21.8	6.2	1.00:3.21:0.36	4.51	18.1	24.9	1.00:3.04	141—144	171
6.60	13.3	21.0	7.7	1.00:3.50:0.57	4.48	17.8	23.5	1.00:2.92	140—143	164
6.31	13.7	21.3	6.9	1.00:3.44:0.44	4.51	17.6	23.9	1.00:3.00	138—144	
5.90	14.1	19.6	3.1	1.00:3.08:0.02		17.8	24.5	1.00:3.04	142—146	168
						C; 41.1	H; 6.1			
6.40	13.1	21.7	7.0	1.00:3.67:0.46	4.59	17.9	23.9	1.00:2.95	143—146	
6.28	14.2	23.0	7.9	1.00:3.58:0.53	4.59	17.6	22.8	1.00:2.88	140—144	157
						C; 39.5	H; 6.0			
6.32	13.8	20.9	10.2	1.00:3.35:0.73	4.50	18.1	24.0	1.00:2.98	142—144	
5.90	10.2	20.0	15.6	1.00:4.35:1.34	4.55	18.0	24.1	1.00:2.96	139—150	169
						Cl; 0.1				
				(C; 42.11)[a] (H; 5.89)		(18.10)	(24.55)	(1.00:3.00)		(171)

a) (1): Reaction between $POCl_3$ and $C_6H_5NH_2$.
(2): Reaction between NH_3 and SR 1.
b) Numerals in parentheses indicate the calculated values of the composition of $PONHC_6H_5(NH_2)_2$.

Extraction of Crude Phosphoric Amide from R2. The R2 product consists of phosphoric amide and ammonium chloride. The two compounds cannot be easily separated because their reactions with various solvents resemble each other; that is, both materials are soluble in water and methanol, and insoluble in such organic solvents as chloroform, carbon tetrachloride, petroleum ether, and benzene. The author therefore chose ethanol and acetone as the solvents because they have a suitable polarity for the extraction of phosphoric amide from R2. Acetone does not dissolve ammonium chloride, but phosphoric amide is a little soluble in it, so that the direct extraction of phosphoric amide, by using acetone is not an efficient treatment. Thus, ethanol which also dissolves a small amount of ammonium chloride was used in the first extraction of phosphoric amide from R4. The residue R4 was a light yellowish-brown powder, containing 13—15% P, 20—23% N, and 3—8% Cl, as shown in Table 1. It is soluble in water, the solution being almost neutral. The P: N: Cl atomic ratios of the products were 1.0: 3.0—3.6: 0.0—0.6, in which the values of Cl correspond to the values of nitrogen which exceed 3.0. It might be understood that crude phosphoric amide R4 is contaminated with ammonium chloride.

Extraction of Phosphoric Aniline Diamide. In the preliminary experiments, it was confirmed that phosphoric aniline diamide is slightly soluble in acetone, but not ammonium chloride. Therefore, the pure phosphoric aniline diamide R6 was obtained from R4 by a previous method. However, because of the low solubility of phosphoric aniline diamide in acetone, a tendency for this compound to remain in the R5 residue was often observed in the chemical analysis of R5 and on the basis of X-ray diffraction data. An efficient extraction of phosphoric aniline diamide may also be expected by using a solvent in which 2—5 vol% of ethanol is added to acetone.

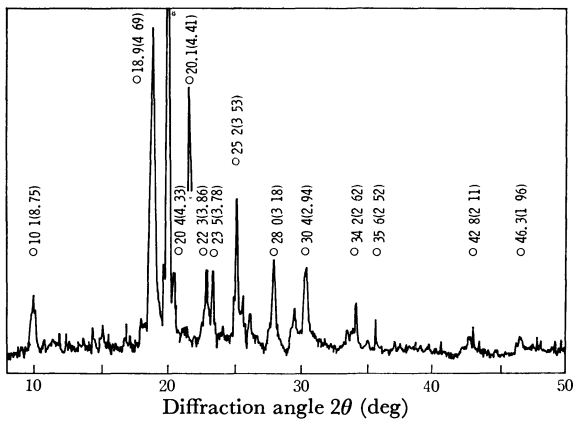

Fig. 2. X-ray diffraction spectrum of phosphoric aniline diamide. Numerals near peaks indicate distances (Å) between planes in crystals.

Properties of $PONHC_6H_5(NH_2)_2$. X-Ray Diffraction: Phosphoric aniline diamide is a white, crystalline powder. Each crystal is a tetragonal plate 5—30 μ in size, as determined by means of microphotography. The X-ray diffraction pattern is shown in Fig. 2. Three strong diffraction lines at 4.69, 4.41, and 3.53 Å can be used for identification. So far, single crystals of phosphoric aniline diamide of a suitable size have not been obtained, and an accurate interpretation of the X-ray data is not possible.

Solubility with Various Solvents. Compound $PONHC_6H_5 \cdot (NH_2)_2$ is soluble in water; its solubility is 3.49% at 0°C, and 5.66% at 25°C, and the pH of a 1% aqueous solution is 4.5. This compound is insoluble in such organic solvents as chloroform, carbon tetrachloride, petroleum ether, and benzene, but soluble in polar solvents such as methanol and ethanol, the solubility in the latter being 1.36% at 0°C and 2.39% at 25°C. The compound is slightly soluble also in acetone, the solubility being 0.23% at 0°C and 0.28% at 25°C. Therefore, on the complete extraction of R6 from R4, a large excess acetone is necessary for the treatment of R4.

Analysis of Purified Products. The percentage of each component in R6 agreed with that of the formula $PONHC_6H_5(NH_2)_2$. The P: N atomic ratios almost reached 1: 3, as shown in Table 1. The molecular weight of R6, as measured in the ethanol solution, was close to the calculated value (171.14) for this formula.

In the cases of Nos. 7 and 8, where the $C_6H_5NH_2/POCl_3$ mole ratios are 4: 1 and 6: 1, respectively, small amounts of R6 are obtained; the products can actually be denoted by $PONHC_6H_5(NH_2)_2$. The following process seems to take place: when 2 or 3 mol of aniline replace chlorine atoms in phosphorus oxychloride in Reactions (1) and (2), the part of which amount is greater than that of a connecting C_6H_5NH radical is replaced by NH_2 radical from ammonia giving rise to the formation of $PONHC_6H_5(NH_2)_2$.

Infrared Absorption Spectra. Previously, the infrared absorption spectra of $PO(NH_2)_3$ had been investigated by Stenger,[6] and those of $PON(C_2H_5)_2(NH_2)_2$ (crude) by the author,[5] but not the IR of $PONHC_6H_5(NH_2)_2$. The results are shown in Fig. 3.

In this spectrum, the absorption bands may be assigned as follows: There are N–H stretching vibrations at 3350 and 3220 cm^{-1}, the C–C stretching vibrations in aromatic compounds at 1600 and 1489 cm^{-1}, the C–N stretching vibrations in aromatic secondary amines at 1407 cm^{-1}, the N–H bending mode in secondary amines or the C–N stretching vibrations at 1291 and 1238 cm^{-1}, and the P–O stretching vibration at 1140 cm^{-1}, while the absorption bands in the range

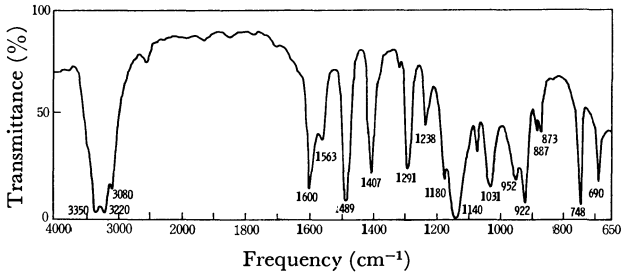

Fig. 3. Infrared spectrum of phosphoric aniline diamide.

of 1075 and 873 cm^{-1} are related to the NH_2 radicals. The assignment of the absorptions at 748 and 690 cm^{-1} is difficult. However, because though these peaks can be generally considered to represent the P–N stretching vibrations, the characteristic peaks of aniline as a raw material have also appeared at the same locations.

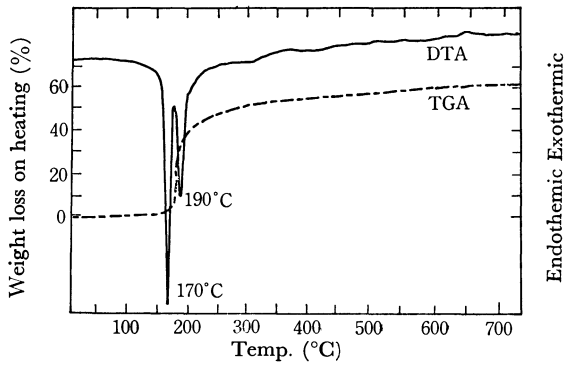

Fig. 4. DTA and TGA curves for phosphoric aniline diamide. Sample; 100 mg, Heating rate; 5°C/min, Current gas; Nitrogen 0.3l/min

Change in Product by Heating. When phosphoric aniline diamide is used in fireproof material its effect can be expected. In fact, both paper and fiber immersed in aqueous solutions of R4 or R6 exhibited a remarkable fireproof character. Both R4 and R6 reacted with formalin to form resinous products which are insoluble in water and fireproof. Upon heating, the $PONHC_6H_5(NH_2)_2$ melted at about 140°C and commenced condensation with deammoniation. The compound bubbled above 170°C after it formed a fire-resistant film.

The DTA and TGA curves for $PONHC_6H_5(NH_2)_2$ are shown in Fig. 4. Two endothermic peaks resulting from melting and condensation in the heated product appeared at 170 and 190°C, respectively. In this case condensation was recognized by the loss in weight shown by the TGA curve. Conversion of the phosphoric amide into the insoluble condensed phosphates was also confirmed by paper chromatography.

6) E. Stenger, *Z. Anorg. Allg. Chem.*, **310**, 114 (1961).

The Stability of Fused Rings in Metal Chelates. IX. Copper(II) and Nickel(II) Complexes of Schiff Bases Derived from Salicylaldehyde and Dipeptides Containing Glycine and/or β-Alanine

Yasuo NAKAO and Akitsugu NAKAHARA

Institute of Chemistry, College of General Education, Osaka University, Toyonaka, Osaka

(Received April 24, 1972)

Copper(II) and nickel(II) complexes of Schiff bases derived from salicylaldehyde(Sal) and dipeptides containing glycine and/or β-alanine have been prepared. It has been found that Schiff base ligands containing glycylglycine (Gly·Gly), glycyl-β-alanine (Gly·β-Ala) or β-alanylglycine (β-Ala·Gly) as the peptide moieties give rise to square-planar, quadridentate copper(II)- and nickel(II)-chelates, while the *N*-salicylidene-β-alanyl-β-alanine (Sal=β-Ala·β-Ala) does not form the same type of copper(II)- or nickel(II)-chelate. It is concluded on the basis of spectrophotometric, polarographic and other measurements that the stability decreases in the order 6-5-5-([Cu(Sal=Gly·Gly)])≧6-5-6-([Cu(Sal=Gly·β-Ala)])≧6-6-5-([Cu(Sal=β-Ala·Gly)])≫6-6-6-([Cu(Sal=β-Ala·β-Ala)])fused-ring system.

In a previous paper,[1] it was reported as the result of a comparative study on copper(II) complexes of Schiff bases derived from 2-acetylpyridine or 2-pyridinecarbaldehyde and some dipeptides that the stability of fused-ring systems in metal Schiff base chelates decreases in the order 5-5-6-≃5-6-5->5-5-5->5-6-6-membered ring system.[2] As an extension of our previous investigations we have studied the copper(II) and nickel(II) complexes of Schiff bases produced from salicylaldehyde and dipeptides such as glycylglycine, glycyl-β-alanine, β-alanylglycine, and β-alanyl-β-alanine. Structural formulas of these chelates are shown in Fig. 1, (Ia—V'). In this paper we describe the relationship between the structures of the chelates and their relative stabilities.

Copper(II) Complexes of the Schiff bases Derived from Salicylaldehyde and Glycylglycine, Glycyl-β-alanine, β-Alanylglycine or β-Alanyl-β-alanine (Ia—IVa). The sodium and potassium salts of *N*-salicylideneglycylglycinatocuprate(II) (Ia) were reported in detail.[3] In the present study we have newly prepared copper(II) chelates of Schiff bases obtained from salicylaldehyde and glycyl-β-alanine, β-alanylglycine, or β-alanyl-β-alanine (IIa, IIIa, and IVa, respectively). The chelates were prepared by reactions of each dipeptide with bis(salicylaldehydato)copper(II) in the pH range 9—11. Of these IIa and IIIa have been isolated as either potassium, calcium, or barium salts. The color of these salts is violet, and their IR spectra revealed that the structure of each complex is essentially the same as that in Ia regardless of the kind of cation. On the other hand, preparation of the copper(II) chelate of *N*-salicylidene-β-alanyl-β-alanine by the same method has resulted in the formation of a bright green complex. The decomposition temperature, absorption maximum for the *d-d* transition band and the half-wave

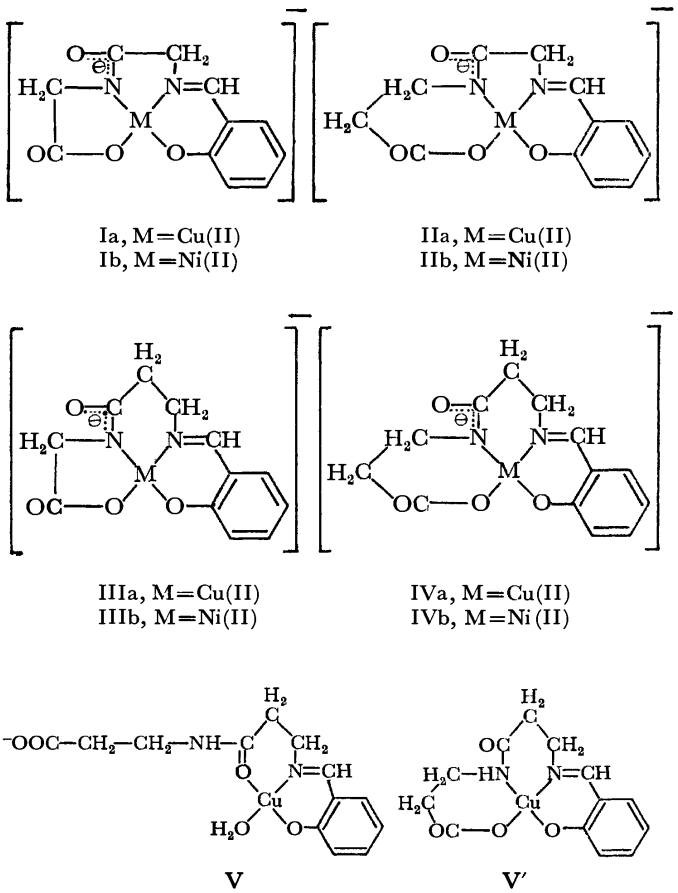

Ia, M=Cu(II)
Ib, M=Ni(II)

IIa, M=Cu(II)
IIb, M=Ni(II)

IIIa, M=Cu(II)
IIIb, M=Ni(II)

IVa, M=Cu(II)
IVb, M=Ni(II)

V

V'

Fig. 1. Structural formulae of copper(II) and nickel(II) chelates of Schiff bases derived from salicylaldehyde and dipeptides.

potentials for the reduction of copper(II) at the dropping mercury electrode of a green complex are given in Table 1, together with those of three violet complexes, Ia—IIIa. A comparison of some properties in Table 1 shows that the structure of the green complex may differ from that of the three violet complexes which have similar properties to each other. Since

1) Y. Nakao, H. Ishibashi, and A. Nakahara, This Bulletin, **43**, 3457 (1970).

2) The notations "5-5-6" etc. represent the skeletal structure of fused-chelate-rings in metal multidenate chelates in view of the numbers of ring members, starting from the metal chelate ring containing the carbonyl compound moiety.

3) A. Nakahara, This Bulletin, **32**, 1195 (1959).

TABLE 1. PROPERTIES OF COPPER(II) COMPLEXES Ia—IIIa, V (OR V')

	Complex	Decomp. temp.	Absorp. max. $\bar{\nu}_{max.}$ ($\times 10^3$) cm^{-1}	Half-wave potential *vs.* SCE, 25°C
Ia	Ba/2[Cu(Sal=Gly·Gly)]·$4H_2O$	263—275°C	17.7(log ε, 2.21)	−0.61 V
IIa	Ba/2[Cu(Sal=Gly·β-Ala)]·$4.5H_2O$	265—280	17.5(log ε, 2.24)	−0.59
IIIa	Ba/2[Cu(Sal=β-Ala·Gly)]·$3.5H_2O$	290—297	17.4(log ε, 1.93)	−0.55
V (or V')	[Cu(Sal=β-Ala·β-Ala)(OH_2)]	210—220	15.2(log ε, 1.75)[a]	b)

a) pH	$\bar{\nu}_{max}$($\times 10^3$)cm^{-1}	b) pH	$E_{1/2}^{(1)}$	$E_{1/2}^{(2)}$
6.5	15.2	6.3	−0.16V	−0.42V
8.4	16.4	7.9	−0.16	−0.42
10.3	16.8	8.7	−0.18	−0.43
11.2	16.8	9.4	−0.20	−0.43
		10.0	−0.21	−0.43
		11.4		−0.43

such properties as the color and decomposition temperature of the crystals and the absorption maximum for the *d-d* band in the 20% dimethyl sulfoxide aqueous solution are similar to those of *N*-salicylideneaminoacidatoaquocopper(II),[4] the green complex seems to be better explained by the structure V or V' rather than by IVa. The result of elemental analysis also supports the presumption. We have recently demonstrated from a pH-titration study that the deprotonation of amide >NH to CuL from $CuHL^+$ in the β-alanyl-β-alanine-Cu(II) chelate is more difficult than that in copper(II) chelate with glycylglycine, glycyl-β-alanine, or β-alanylglycine.[5] The difficulty in isolating copper(II) chelate of IVa-structure can be explained as due to the result described above and the increasing steric strain in 6-6-6-fused-ring system. Thus it can be concluded that the copper(II) complex IVa is less stable than complexes Ia—IIIa.

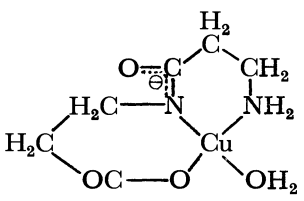

CuL

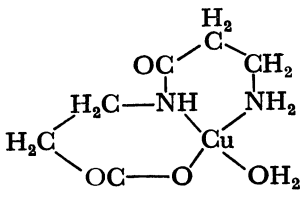

$CuHL^+$

From the decomposition temperatures, the absorption maxima of *d-d* transition bands and the polarographic half-wave potentials (nearly constant in the pH range 6—10) corresponding to the reduction of copper(II) in the chelates Ia—IIIa (Table 1), we see that the stability of the three copper(II) complexes differs only slightly. On the other hand, the polarographic behavior of the bright green complex is entirely different from that of the other violet complexes Ia—IIIa. The polarograms of the green complex corresponding to various pH values are given in Fig. 2. The reduction wave for the green complex consists of two steps, in which the ratio of the wave-height of the first and

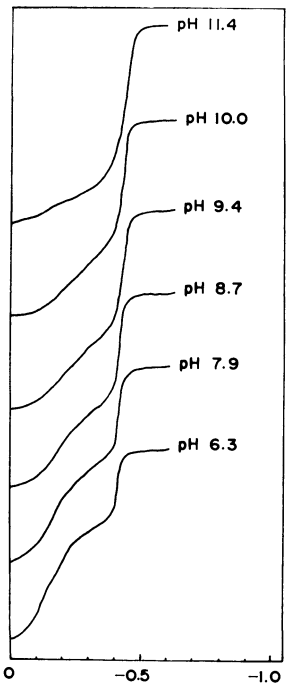

Fig. 2. Polarograms of salicylaldehyde-β-alanyl-β-alanine-copper(II) in various pH-values.

second reduction wave varies with pH values. The wave-height of the first reduction wave decreases but that of the second reduction wave increases with the rise in pH, the total wave-heights remaining unchanged. Thus, it is considered that two kinds of complexes exist in the pH range 6—11, and the ratio of their abundance changes with pH. The second wave on the polarogram can be estimated as the reduction wave due to the species IVa, as judged from the value of the half-wave potential and the increase of its wave-height with the rise in pH. On the other hand, the first wave is considered to be the reduction wave for the green complex V (or V'). The effect of pH on the *d-d* absorption band for the green complex was also examined. The results are shown in Table 1. We see that the *d-d* absorption band is hypsochromically shifted with increasing pH values. The absorption maximum at pH 6.5 is almost the same as those of *N*-salicylideneaminoacidatoaquocopper(II) complexes.[4]

4) Y. Nakao, K. Sakurai, and A. Nakahara, This Bulletin, **40**, 1536 (1967).

5) O. Yamauchi, Y. Hirano, Y. Nakao, and A. Nakahara, *Can. J. Chem.*, **47**, 3441 (1969).

In the pH region 10.3—11.2 the absorption maximum is observed at 16.8×10^3 cm^{-1}, showing the formation of a structure similar to that of copper(II) chelates Ia—IIIa. Thus, it can be considered that the most predominant structure of chelate in aqueous solution at around pH 11 should be the one represented by IVa. The reason why the species IVa cannot be isolated in the preparation of salicylaldehyde-β-alanyl-β-alanine-copper(II) chelate in aqueous solution in the pH range 9—11 was found to be as follows: V (or V') are preferentially separated from the solution because of its comparatively poor solubility when the equilibrium V (or V')⇋IVa takes place in an alkaline solution. From a comparison of the easiness of preparation and of the numerical data in Table 1, it may be concluded that the relative stability in the copper(II) chelates Ia—IVa decreases in the order: Ia(6-5-5)≧IIa-(6-5-6)≧IIIa(6-6-5)≫IVa(6-6-6). It is of interest to note that the chelate produced from copper(II), β-alanyl-β-alanine and 2-pyridinecarbaldehyde or 2-acetylpyridine (instead of salicylaldehyde) can easily be isolated as stable crystals,[1] but not IVa. This contrast is understood by taking the increasing strain in the 6-6-6-fused-ring system into consideration.

Nickel(II) Complexes of the Schiff Bases Derived from Salicylaldehyde and Glycylglycine, Glycyl-β-alanine, β-Alanylglycine or β-Alanyl-β-alanine (Ib—IVb). Nickel(II) complexes of Schiff bases derived from salicylaldehyde and dipeptides (Gly·Gly, Gly·β-ala, β-Ala·Gly, and β-Ala·β-Ala) were prepared. The nickel(II) complex Ib containing glycylglycine residue was isolated as potassium, calcium or barium salts. Their IR spectra showed no essential difference and were in good agreement with those for the corresponding salts of *N*-salicylideneglycylglycinatocuprate(II). From these IR-studies and the elemental analyses, it is evident that the structure of nickel(II) complex produced from salicylaldehyde, glycylglycine, and nickel(II) is of Ib. Similar findings were confirmed also for nickel(II) complexes of *N*-salicylidene-glycyl-β-alaninate and -β-alanylglycinate. Hence, the structures of those chelates are concluded to be of IIb and IIIb, respectively. The nickel(II) complex of Schiff base derived from salicylaldehyde and β-alanyl-β-alanine could not be isolated. During the course of preparation of nickel(II) complexes Ib—IIIb the original green solution turned orange with the rise in pH, giving orange crystals. The visible and ultraviolet absorption spectra for nickel(II) chelates Ib—IIIb in dimethyl sulfoxide-water (1: 1 by volume) are shown in Fig. 3. The absorption curves resemble those observed for nickel(II) complexes which are considered to have a square-planar structure.[6] In the case of salicylaldehyde-β-alanyl-β-alanine-nickel(II) complex, the color of reaction solution does not change during the course of preparation regardless of pH (5—11). Thus, all efforts to obtain the complex in crystal were unsuccessful. However, it may be considered from the absorption spectrum of the reaction solution diluted with water that the nickel(II) complex of *N*-salicylidene-β-alanyl-β-alaninate in solution have an octahedral structure.[6] This suggests that the complex is more stabilized in high-spin form (sp^3d^2) than in square-planar form. This is because of the rather weak ligand field of *N*-salicylidene-β-alanyl-β-alaninate, which contains a considerable strain in 6-6-6-fused-ring system IVb.

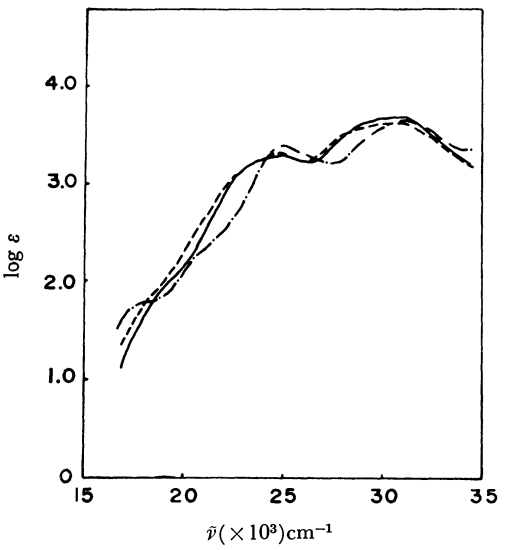

Fig. 3. VIS-UV spectra of Ba/2[Ni(Sal=Gly•Gly)]•H_2O (—), Ba/2[Ni(Sal=Gly•β-Ala)]•$3H_2O$ (--), and Ba/2[Ni (Sal=β-Ala•Gly)]•$2H_2O$ (——).

Experimental

Dipeptides[1] and Bis(salicylaldehydato)copper(II)[7] were prepared according to the directions described previously.

Bis(salicylaldehydato)nickel(II) was obtained by the same method as that for the corresponding copper(II) complex, using nickel acetate instead of copper acetate. *Potassium N-salicylideneglycylglycinatocuprate(II)* was prepared by the known method.[3] *Potassium* N-*salicylideneglycylglycinatonickelate-(II), Ib.* Into 15 ml of a water: ethanol mixture (2:1 by volume) were dissolved 0.34 g of glycylglycine and 0.78 g of bis(salicylaldehydato)nickel(II). The resulting mixture was adjusted to pH 9—10 by 1N-KOH solution and stirred at 25°C for an hour. The reaction product was deposited as orange powders and was recrystallized from water-ethanol. The results of elemental analyses are shown in Table 2.

Barium Salts of Copper(II) Chelates of Schiff Bases Derived from Salicylaldehyde and Dipeptides(Ia—IIIa), and Copper(II) Chelate Containing β-alanyl-β-alanine as Dipeptide Moiety (V or V'). *Method A*: To a mixture of 0.0025 mol of each dipeptide and 15 ml of water: ethanol (2: 1 by volume) was added 0.0025 mol of bis(salicylaldehydato)copper(II). The pH-values of each reaction solution were adjusted to 9—11 by using 1N-KOH solution. After it had been stirred at 25°C for an hour, the reaction mixture was filtered. The filtrate was passed through a column of the cation exchanger Amberlite IR-120B (Ba form). The column was washed with water, and the violet crystalline product adsorbed on the resin layer was extracted by hot water. The solution which had passed through the cation exchanger and the extracted aqueous solution were combined and concentrated *in vacuo* until violet crystals were considerably deposited. This was recrystallized from hot water (90°C). In the case of reaction system containing β-alanyl-β-alanine as dipeptide, the solution

6) S. Yamada and H. Nishikawa, This Bulletin, **36**, 755 (1963).

7) A. Nakahara, K. Hamada, I. Miyachi, and K. Sakurai, *ibid.*, **40**, 2826 (1967).

TABLE 2. ANALYTICAL DATA FOR THE POTASSIUM AND CALCIUM SALTS OF [M(Sal=dipeptide)]$^-$ (M=Cu(II), Ni(II))

Complex	C, %		H, %		N, %	
	Found	Calcd	Found	Calcd	Found	Calcd
K[Ni(Sal=Gly·Gly)]·H_2O	38.03	37.85	2.54	3.18	8.27	8.03
Ca/2[Cu(Sal=Gly·Gly)]·3.5H_2O	34.86	34.78	4.07	4.25	7.53	7.38
Ca/2[Cu(Sal=Gly·β-Ala)]·4.5H_2O	35.11	34.99	4.66	4.90	6.51	6.80
Ca/2[Ni(Sal=Gly·Gly)]·2H_2O	37.99	37.96	3.72	3.77	8.26	8.05
Ca/2[Ni(Sal=Gly·β-Ala)]·2.5H_2O	39.04	38.84	4.30	4.36	7.99	7.55

TABLE 3. ANALYTICAL DATA FOR Ba/2[M(Sal=dipeptide)] (M=Cu(II), Ni(II))

Complex	Cu or Ni, %		N, %	
	Found	Calcd	Found	Calcd
Ba/2[Cu(Sal=Gly·Gly)]·4H_2O	14.34	14.53	6.26	6.40
Ba/2[Cu(Sal=Gly·β-Ala)]·4.5H_2O	13.54	13.80	6.00	6.08
Ba/2[Cu(Sal=β-Ala·Gly)]·3.5H_2O	14.23	14.36	6.11	6.33
Ba/2[Ni(Sal=Gly·Gly)]·H_2O	15.26	15.50	7.29	7.40
Ba/2[Ni(Sal=Gly·β-Ala)]·3H_2O	13.75	13.69	6.68	6.54
Ba/2[Ni(Sal=β-Ala·Gly)]·2H_2O	14.24	14.29	7.20	6.82

which had passed through a column was evaporated to dryness *in vacuo*. The green products were recrystallized from water-acetone. Its aqueous solution gave no white precipitate by the addition of dilute sulfuric acid. Analytical data of the violet complexes are given in Table 3. Analytical data of the green complex are as follows: Found: C, 45.54; H, 4.70; N, 8.19%. Calcd for Cu($C_{13}H_{14}N_2O_4$)·H_2O: C, 45.41; H, 4.70; N, 8.15%.

Method B. Almost the same procedure as that in Method A was applied. After filtration of reaction mixture, the saturated solution of barium chloride (0.63 g) was added to the filtrate. Upon cooling the solution violet crystals were deposited, which were filtrated by suction and recrystallized from hot water (90°C).

Calcium Salts of Copper(II) Chelates of Schiff Bases Derived from Salicylaldehyde and Dipeptides (glycylglycine, glycyl-β-alanine) Ia—IIa. These complexes were obtained in a similar manner to method B using calcium chloride instead of barium chloride. Recrystallization from water or water-ethanol gave violet crystals, whose analytical data are given in Table 2.

Barium Salts and Calcium Salts of Nickel(II) Chelates of Schiff Bases Derived from Salicylaldehyde and Dipeptides (glycylglycine, glycyl-β-alanine, β-alanycine) Ib—IIIb. The same method of preparation as that for copper(II) complexes was employed. The results of elemental analyses are shown in Table 2 and 3.

Measurements. The VIS-UV absorption spectra were obtained with a Shimadzu spectrophotometer QR-50 at room temperature. The solvent used was 20% or 50% dimethyl sulfoxide aqueous solution. The IR spectra were recorded with a Hitachi EPI-2 infrared spectrophotometer. The measurements were carried out at room temperature using the pressed KBr disk technique in the wave number range 700—4000 cm^{-1} with a rock-salt prism. Polarographic measurements were carried out by the same method as already described.[1] Water was used as solvent. Concentration of the copper(II) chelates used was 5×10^{-4}M. The supporting electrolyte and the maximum suppressor used were 0.1M-KNO_3 and Triton X-100 (0.0018%), respectively. The pH-value of each solution was adjusted by KOH solution.

This work was supported in part by a grant from the Ministry of Education.

Sterically Controlled Syntheses of Optically Active Organic Compounds. XVII. Asymmetric Syntheses of Amino Acids by Addition of Benzoyl Cyanide to the Azomethine Compounds[1]

Kaoru HARADA and Tadashi OKAWARA

Institute for Molecular and Cellular Evolution and Department of Chemistry, University of Miami, Coral Gables, Florida, 33134 U.S.A.

(Received June 6, 1972)

The addition reactions of benzoyl cyanide to the Schiff's bases prepared from several aliphatic aldehydes with optically active benzylic amines were studied. The adioditn products were hydrolyzed and hydrogenolyzed to form optically active amino acids. The synthetic yields of optically active amino acids were in a range 15 to 57% and the optical purities were in a range 15—37%. When *S*-α-alkylbenzylamines were used, *S*-amino acids were obtained.

Addition reactions to the cabon-nitrogen double bonds have been studied.[2,3] Carbon-nitrogen double bonds react with hydrogen cyanide to form α-aminonitriles.[4-12] Hydrolysis of the aminonitriles yielded α-amino acids.

Partially optically active *N*-alkyl-α-aminopropionitrile (II) was prepared from optically active α-methylbenzylamine, acetaldehyde, and hydrogen cyanide[13] or from the same amine with lactnitrile.[14] *N*-α-Methylbenzyl aminoacetonitrile (II) was hydrolyzed and hydrogenolyzed to form optically active alanine. From the reaction mixture, highly optically active alanine (optical purity 85—98%) was isolated by crystallization in which fractionation of optical isomers would take place.[15]

Recently Patel and Worsley[16] reported an asymmetric synthesis of α-amino acids (mostly unnatural) by addition of hydrogen cyanide to the carbon-nitrogen double bond of the Schiff's base that was prepared from optically active α-methylbenzylamine and various aldehydes. The optical purities of amino acids they reported were very high (98—99%). The high optical purities have resulted from fractionation during the crystallization and washing procedures employed in the synthesis.[17]

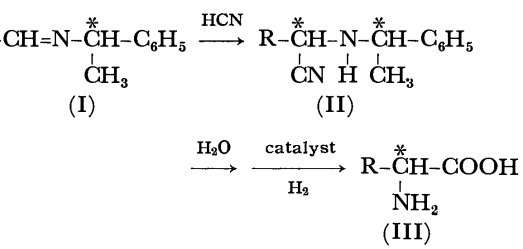

In this investigation, the addition reactions of benzoyl cyanide to azomethine compounds prepared from various optically active benzylic amines and aliphatic aldehydes were studied as shown in Scheme 1. The amines used were benzylamine, *S*-(−)-α-methylbenzylamine, *R*(+)-α-methylbenzylamine, *S*(−)-α-ethylbenzyl amine, and *S*(−)-α-(1-naphthyl)ethylamine. The aldehydes used were acetaldehyde, propionaldehyde, isobutyraldehyde, and isovaleraldehyde.

The addition reactions of benzoyl cyanide to the various azomethine compounds were carried out at room temperature in ether solution for 20—24 hrs. The

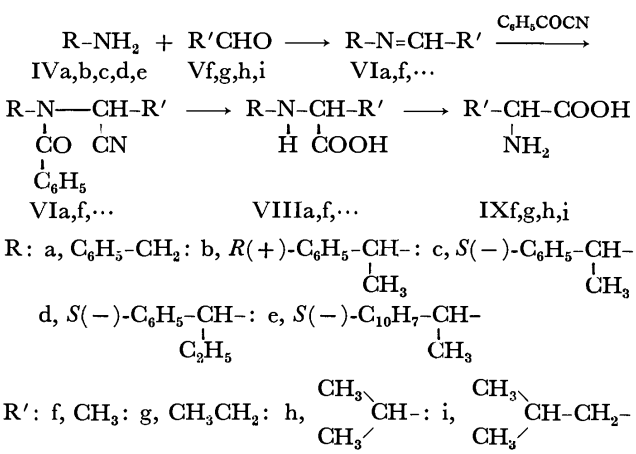

Scheme 1.

1) Contribution No. 224 of the Institute for Molecular and Cellular Evolution, University of Miami.

2) K. Harada, "Addition to the Azomethine Group," in "The Chemistry of the Carbon-Nitrogen Double Bond." ed. by S. Patai, Interscience Publishers, London (1970), p. 255.

3) J. P. Anselme, "Cycloaddition Reactions of Carbon-Nitrogen Double Bonds," in "The Chemistry of the Carbon-Nitrogen Double Bonds." ed. by S. Patai, Interscience Publishers, London (1970), p. 299.

4) G. E. P. Smith, Jr., and F. W. Bergstrom, *J. Amer. Chem. Soc.* **56**, 2095 (1934).

5) R. Tiollais, *Bull. Soc. Chim. Fr.*, **1947**, 959.

6) A. Dornow and S. Lupfert, *Chem. Ber.*, **89**, 2718 (1956).

7) G. H. Harris, B. R. Harriman, and K. W. Wheeler, *J. Amer. Chem. Soc.*, **68**, 846 (1946).

8) J. Collazos, *Chim. Ind.* (Paris), **86**, 47 (1961).

9) F. Adlickes, *J. Prakt. Chem.*, **161**, 271 (1943).

10) C. C. Porter and L. Hellerman, *J. Amer. Chem. Soc.*, **61**, 754 (1939).

11) H.A. Lillevik, R.L. Hossfeld, H.V. Lindstrom, R.T. Arnold, and R. A. Gortner, *J. Org. Chem.*, **7**, 164 (1942).

12) C. C. Porter and L. Hellerman, *J. Amer. Chem. Soc.*, **66**, 1652 (1944).

13) K. Harada, *Nature*, **200**, 1201 (1963).

14) K. Harada and S. W. Fox, *Naturwissenschaften*, **51**, 106 (1964).

15) K. Harada, T. Okawara, and K. Matsumoto, manuscript in preparation.

16) M. S. Patel and M. Worsley, *Can. J. Chem.*, **48**, 1881 (1970).

17) K. Harada and T. Okawara, manuscript in preparation.

TABLE 1. RACEMIC *N*-BENZYLAMINO ACIDS

N-Benzyl-(±)-amino aicd	Formula	Mp (°C)	Calcd C	Calcd H	Calcd N	Found C	Found H	Found N
$C_6H_5CH_2NHCH(CH_3)COOH$	$C_{10}H_{13}NO_2$	250—253	67.02	7.31	7.82	66.81	7.30	7.59
$C_6H_5CH_2NHCH(CH_3)CH_2COOH$	$C_{11}H_{15}NO_2$	245—246	68.37	7.82	7.25	68.27	7.82	7.25
$C_6H_5CH_2NHCH(CH(CH_3)_2)COOH$	$C_{12}H_{17}NO_2$	248—249	69.54	8.27	6.76	69.28	8.16	6.49
$C_6H_5CH_2NHCH(CH_2CH(CH_3)_2)COOH$	$C_{13}H_{19}NO_2$	224	70.56	8.65	6.33	70.37	8.51	6.15

resulting reaction products that contained *N*-benzoyl-*N*-alkylaminonitrile were hydrolyzed with 6N hydrochloric acid under reflux. The resulting *N*-alkylamino acids were separated by the use of a Dowex 50 ion exchange column. A part of the *N*-benzylamino acids was recrystallized from water and ethanol. The melting points and analytical data for the *N*-benzylamino acids are shown in Table 1. The *N*-alkylamino acids were then hydrogenolyzed with palladium on charcoal. The racemic amino acids prepared by the use of benzylamine were recrystallized for elemental analyses. The results are shown in Table 2.

The syntheses of optically active amino acids by addition reaction of benzoyl cyanide to Schiff's bases which are composed of optically acitve amines were carried out in a similar way. However, in order to remove the *N*-α-alkylbenzyl group, palladium hydroxide on charcoal instead of palladium on charcoal was used. A part of the resulting amino acids were converted to their corresponding DNP derivatives. The resulting DNP derivatives were then purified by the use of a Celite column,[18] without fractionation of optical isomers.[19] These DNP derivatives were used

TABLE 2. ELEMENTAL ANALYSES OF RACEMIC AMINO ACIDS PREPARED USING BENZYLAMINE

(±)-Amino acid	Formula	Calcd (Found) C	Calcd (Found) H	Calcd (Found) N
Alanine	$C_3H_7NO_2$	40.44 (39.91)	7.92 (7.84)	15.72 (15.49)
Butyrine	$C_6H_9NO_2$	46.59 (46.84)	8.86 (8.72)	13.58 (13.46)
Valine	$C_5H_{11}NO_2$	51.26 (50.98)	9.46 (9.64)	11.96 (11.87)
Leucine	$C_6H_{13}NO_2$	54.94 (55.10)	9.99 (9.77)	10.68 (10.62)

TABLE 3. SYNTHESES OF OPTICALLY ACTIVE AMINO ACIDS

R Group of amine	CH_3CHO (Alanine) $[\alpha]_D^{25a)}$	Optical purity[b] (%)	Yield (%)	CH_3CH_2CHO (Butyrine) $[\alpha]_D^{25a)}$	Optical purity (%)	Yield (%)	$CH_3CH(CH_3)CHO$ (Valine) $[\alpha]_D^{25a)}$	Optical purity (%)	Yield (%)	$CH_3CH(CH_3)CH_2CHO$ (Leucine) $[\alpha]_D^{25a)}$	Optical purity (%)	Yield (%)
Benzyl	—	—	57	—	—	40	—	—	38	—	—	41
R(+)-Me	−33.4	23.2	46	—	—	—	—	—	—	—	—	—
S(−)-Me	+36.4	25.2	49	+36.8	37.2	35	+21.4	19.7	22	+16.2	27.1	23
S(−)-Et	+29.4	20.3	52	+32.2	32.6	33	+18.5	17.0	26	+12.3	20.3	15
S(−)-Naph	+30.2	21.0	44	+30.6	31.0	30	+42.9	39.3	24	+15.0	25.1	21

Benzyl: benzylamine; *R*(+)-Me, *R*(+)-α-methylbenzylamine; *S*(−)-Me, *S*(−)-α-methylbenzylamine; *S*(−)-Et, *S*(−)-α-ethylbenzylamine; *S*(−)-Naph, *S*(−)-α-(1-naphthyl)ethylamine.

a) Specific rotations of DNP-amino acids measured in 1N NaOH.

b) Optical purity defined as $[\alpha]_D^{25}$ obsd/$[\alpha]_D^{25}$ of the compound × 100.
DNP-*S*(+)-alanine, $[\alpha]_D^{25}$ +143.9° (1N NaOH)
DNP-*S*(+)-butyrine, $[\alpha]_D^{25}$ +98.8° (1N NaOH)
DNP-*S*(+)-valine, $[\alpha]_D^{25}$ +109.1° (1N NaOH)
DNP-*S*(+)-leucine, $[\alpha]_D^{25}$ +59.5° (1N NaOH)

c) The yields are calculated from Schiff's bases.

18) J. C. Perrone, *Nature*, **167**, 513 (1951); A. Court, *Biochem. J.*, **58**, 70 (1954).

19) K. Harada and K. Matsumoto, *J. Org. Chem.*, **32**, 1790 (1967); K. Harada and T. Yoshida, This Bulletin, **43**, 921 (1970).

to measure the optical purities of resulting amino acids. The specific rotations, optical purities, and synthetic yields of amino acids are listed in Table 3. However, DNP-leucine is difficult to crystallize and the elimination of dinitrophenol from the DNPylated reaction mixture by sublimation before celite column chromatography is probably not complete. Therefore, the specific rotations and optical purities of leucine listed in Table 3 are thought to be lower than those of the actual values. The other part of amino acids were recrystallized from water and alcohol for elemental analyses. Some of the elemental analyses of optically active amino acids prepared from *S*(−)-α-methylbenzylamine are shown in Table 4.

Table 4. Elemental analyses of optically active amino acids using *S*(−)-α-methylbenzylamine

	Formula	Calcd (Found)		
		C	H	N
S-Alanine	$C_3H_7NO_2$	40.44 (40.33)	7.92 (7.87)	15.72 (15.69)
S-Butyrine	$C_4H_9NO_2$	46.59 (46.83)	8.86 (8.81)	13.58 (13.70)
S-Valine	$C_5H_{11}NO_2$	51.62 (50.87)	9.46 (9.34)	11.96 (11.68)
S-Leucine	$C_6H_{13}NO_2$	54.94 (55.10)	9.99 (9.89)	10.68 (10.43)

The overall yield of amino acid is in a range of 20—60%. The yield of alanine is the highest; however, the yields decrease as the size of the alkyl group of the aldehyde increases. In all cases the yields of racemic α-amino acids prepared from sterically least hindered benzylamine are the highest. When *S*(−)-amine and *R*(+)-amine were used, the configurations of the resulting amino acids were (*S*)- and (*R*)- respectively. The facts agree with the results obtained in the related Strecker type asymmetric synthesis.[13-17] The optical purities are in a range of 15—39%. The effect of optically active amines on the resulting amino acids is not clear, except in the case of valine synthesis. The optical purity of (*S*)-valine prepared by the use of *S*(−)-α-(1-naphthyl)ethylamine was 39% compared with less than 20% of optical purity prepared by α-methyl- or α-ethylbenzylamine.

Experimental

All hydrogenolysis reactions were carried out by the use of Paar 3910 shaker type hydrogenation apparatus. All optical activity measurements were carried out on a JASCO-ORD-UV 5 spectropolarimeter.

The specific rotations of optically active amines were:
R(+)-α-methylbenzylamine, $[\alpha]_D^{25}+41.5°$ (benzene)
S(−)-α-methylbenzylamine, $[\alpha]_D^{25}-42.3°$ (benzene)
S(−)-α-ethylbenzylamine, $[\alpha]_D^{25}-21.0°$ (benzene)
S(−)-α-(1-naphthyl)ethylamine, $[\alpha]_D^{25}-86.5°$ (benzene)

Preparation of the Schiff's Base (VI). To the solution of benzylic amine (0.01 mol) in 15 m*l* of anhydrous benzene was added a solution of an aldehyde (0.01 mol) in 15 m*l* of benzene under ice cooling. The solution was kept in ice water for five minutes under occasional shaking. Then the solution was kept at room temperature for twenty minutes. To the mixture, 5.0 g of anhydrous sulfate was added to remove precipitated water. The benzene solution was kept for another 12 hr at room temperature. The mixture was filtered to remove sodium sulfate and the filtrate was evaporated under reduced pressure at a temperature below 45°C using a water bath. The pale yellow syrup (Schiff's base) was used for addition without further purification.

Preparation of N-*Benzoyl*-N-*alkylaminoacetonitrile (VII).* Freshly distilled benzoyl cyanide (1.30 g, 0.01 mol) in anhydrous ether (15 m*l*) was added to a solution of the Schiff's base (0.01 mol) in 15 m*l* of anhydrous ether. The reaction mixture was allowed to stand for 20 hr at room temperature. Then the ether was evaporated and the residue was used for further hydrolysis.

N-*Alkylamino Acids (VIII).* The crude *N*-benzoyl-*N*-alkyl-aminoacetonitrile (VII) was refluxed with 6N HCl (30 m*l*) for 6 hr. After the hydrolysis was over, the hydrochloric acid was removed under reduced pressure. To the residue, water (20 m) was added and the evaporation procedures were repeated 3 times to minimize the residual hydrochloric acid. The residue was dissolved in a small amount of water and was applied to a Dowex 50 column (H^+ form, 19×2.3 cm). The column was washed with water and then the column was eluted with 1.5N aqueous ammonia. The fractions containing *N*-alkylamino acid were combined and were evaporated to dryness under reduced pressure. In the *N*-benzylamino acid preparation, the residue was divided into two portions. A part was recrystallized from water and ethanol for elemental analysis and the remaining part was used for further hydrogenolysis. The melting points and elemental analyses of racemic *N*-benzylamino acids prepared by the use of benzylamine are listed in Table 1.

Amino Acids (IX). The *N*-alkylamino acid was dissolved in a mixture (60 m*l*) of water and ethanol (1:1 in volume). The solution was mixed with 0.8 g of palladium hydroxide on charcoal (in the case of *N*-benzylamino acid, 5% palladium on charcoal was used), and was hydrogenolyzed for 12 hr. After hydrogenolysis was over, the catalyst was removed by filtration. Free amino acid was obtained by evaporation of the solvent. A part of the amino acid was recrystallized from water and ethanol for elemental analysis. The elemental analyses of racemic amino acid prepared by the use of benzylamine are listed in Table 2. The elemental analyses of optically active amino acid prepared from *S*(−)-α-methylbenzylamine are shown in Table 4. The optically active amino acids were converted to DNP-amino acids in the usual way,[20] and the resulting DNP-amino acids were purified by the use of a Celite column treated with pH 7 citrate–phosphate buffer.[18] The specific rotations, optical purities, and overall yields are shown in Table 3.

This work was supported by Grant NGR 10-007-052 from the National Aeronautics and Space Administration. The authors wish to express their thanks to Dr. Kazuo Matsumoto for valuable discussions. Thanks are extended also to Mr. Charles R. Windsor for amino acid analyses.

20) F. Sanger, *Biochem. J.*, **39**, 507 (1945); K. R. Rao and H. A. Sober, *J. Amer. Chem. Soc.*, **76**, 1328 (1954).

The Tautomeric Equilibria of 4-(Dialkylamino)azobenzene Derivatives

Shunzo YAMAMOTO, Norio NISHIMURA, and Shigeo HASEGAWA

Department of Chemistry, Faculty of Science, Okayama University, Tsushima, Okayama

(Received February 21, 1972)

The tautomeric equilibrium constants, K_t=[ammonium ion]/[azonium ion], of the first conjugate acids of 4-dialkylaminoazobenzene derivatives were estimated by the spectrophotometric method. The K_t values increase in this order: pyrrolidino- <dimethylamino- <diethylaminoazobenzenes. The effects of *N*-alkyl groups on the base strength of the amino and azo nitrogens were examined in order to explain the effects on the tautomeric equilibrium. The base strength of azo nitrogens is governed by the degree of the resonance interaction between the amino group and the rest of the molecule. For dimethylamino- and pyrrolidinoazobenzenes, the base strength of the amino nitrogen can also be explained in terms of the resonance effects, but the amino nitrogen of diethylaminoazobenzenes exhibits an anomalously high base strength, arising from the steric inhibition of the hydrogen bonding in the free base. The above order of K_t can be explained in terms of these cumulative resonance and steric effects.

The structures of the first conjugate acids of 4-aminoazobenzene derivatives have been the subject of much discussion.[1-4] Some authors[1,2] have identified the ammonium structure as the exclusive one of the conjugate acids of 4-dimethylaminoazobenzene. Others,[3,4] on the other hand, have concluded that the conjugate acid has the azonium structure.

Recently it has become clear, however, that there is a tautomeric equilibrium between the ammonium and the azonium forms.[5-8] The tautomeric equilibrium constants have been determined by several workers.[7-9] Jaffé *et al.*[7] determined the constants for a series of substituted derivatives of 4-dimethylaminoazobenzene by various methods, and found that the constants follow the Hammett equation.

A number of attempts[10-12] have been made to explain the structural effects on the basicities of alkylanilines. The base strength of *N,N*-dialkylaniline derivatives in 50% aqueous ethanol are in this order: *N*-phenylpyrrolidine< dimethylaniline< diethylaniline.[11] It has been proposed that solvation on the alkaline side of the ionization equilibrium lowers the free energy of *N*-phenylpyrrolidine and dimethylaniline, and that it is, therefore, base-weakening. The steric inhibition of solvation occurs with diethylaniline and is base-strengthening. It can be expected, therefore, that for 4-dialkylaminoazobenzenes the basicity of the amino nitrogen atom is similarly influenced by the alkyl groups, but the basicity of the azo nitrogen atoms is not so much influenced. As far as we know, there has been no study of the effect of *N*-substituents on the tautomeric equilibrium. The purpose of the present paper is to examine to what extent the tautomeric equilibrium of the first conjugate acids of 4-dialkylaminoazobenzene derivatives is influenced by a change in the alkyl groups.

Experimental

Compounds. The 4-dimethylamino- and 4-diethylaminoazobenzene derivatives were prepared by procedures described in a previous paper.[13] The 4-pyrrolidinoazobenzene derivatives were prepared by diazotizing aniline derivatives and by coupling the resulting diazonium salt with *N*-phenylpyrrolidine, which had been prepared by the methods given in the literature.[14] These azo compounds were purified by dissolving them into benzene, passing them through an alumina column, and then crystallizing them from benzene. The *N,N,N*-trimethyl-*p*-phenylazoanilinium chlorides were prepared by procedures described by Jaffé and Isaks.[7]

4-Dimethylaminoazobenzene: Mp 118—119°C (lit, 119—120°C.

4-Methyl-4'-dimethylaminoazobenzene: Mp 170—171°C (lit, 169.5—170°C).

4-Chloro-4'-dimethylaminoazobenzene: Mp 158—158.5°C (lit, 158—158.5°C).

4-Diethylaminoazobenzene: Mp 97—97.5°C (lit, 98°C).

4-Methyl-4'-diethylaminoazobenzene: Mp 112.5—113°C (lit, 113°C).

4-Chloro-4'-diethylaminoazobenzene: Mp 114°C. Found: C, 67.03; H, 6.42; N, 14.45%. Calcd: C, 66.77; H, 6.30; N, 14.60%.

4-Pyrrolidinoazobenzene: Mp 166—167°C. Found: C, 76.70; H, 6.68; N, 16.69%. Calcd: C, 76.46; H, 6.82; N, 16.72%.

4-Methyl-4'-pyrrolidinoazobenzene: Mp 187—188°C. Found: C, 77.07; H, 7.03; N, 15.79%. Calcd: C, 76.94; H, 7.22; N, 15.84%.

4-Chloro-4'-pyrrolidinoazobenzene: Mp 197—198°C. Found: C, 67.51; H, 5.72; N, 14.76%. Calcd: C, 67.24; H, 5.64; N, 14.70%).

N,N,N-*Trimethyl*-p-*phenylazoanilinium Chloride*: Mp 185.5—186°C (decomp.) (lit, 186—187°C).

N,N,N-*Trimethyl*-p-*(4-methylphenylazo)anilinium Chloride*: Mp

1) I. M. Klotz, H. A. Fiess, I. Y. Chen-Ho, and M. Mellody, *J. Amer. Chem. Soc.*, **76**, 5316 (1954).
2) H. H. Jaffé, *J. Chem. Phys.*, **23**, 415 (1953).
3) C. R. Bury, *J. Amer. Chem. Soc.*, **57**, 2115 (1935).
4) M. T. Rogers, T. W. Campbell, and R. W. Maatman, *ibid.*, **73**, 5122 (1951).
5) G. M. Badger, R. G. Buttery, and G. E. Lewis, *J. Chem. Soc.*, **1954**, 1888.
6) E. Sawicky, *J. Org. Chem.*, **21**, 605 (1956); **22**, 365, 621, 743 (1957).
7) Si-Jung Yeh and H. H. Jaffé, *J. Amer. Chem. Soc.*, **81**, 3283 (1959); M. Isaks and H. H. Jaffé, *ibid.*, **86**, 2209 (1964).
8) F. Gerson and E. Heilbronner, *Helv. Chim. Acta*, **45**, 42 (1962).
9) I. Ya. Bershtein and O. F. Ginzburg, *Zh. Org. Khim.*, **3**, 2032 (1967); *ibid.*, **4**, 1260 (1968).
10) H. C. Brown and A. Chan, *J. Amer. Chem. Soc.*, **72**, 2939 (1958).
11) A. T. Botini and C. P. Nash, *ibid.*, **84**, 734 (1962); C. P. Nash and G. E. Maciel, *J. Phys. Chem.*, **68**, 832 (1964).
12) J. W. Eastes and M. H. Aldridge, *J. Chem. Soc.*, **1969**, 922.
13) S. Yamamoto, N. Nishimura, and S. Hasegawa, This Bulletin, **44**, 2018 (1971).
14) J. V. Braun and G. Lemke, *Ber.*, **55**, 3556 (1922).

178.5—179°C (decomp.) (lit, 178—179°C).

N,N,N-*Trimethyl*-p-*(4-chlorophenylazo)anilinium Chloride*: Mp 183—184°C (decomp.) (lit, 184—185°C).

Measurements. The dipole moments and the absorption spectra of the bases were measured by the methods described in a previous paper.[13] The absorption spectra of unbuffered solutions were measured in *ca.* 50% aqueous ethanol (25 ml of the solution contained 12.5 ml of commercial 99% ethanol) with various concentrations of acids. The concentrations of all the azo compounds were about 3×10^{-5}M. The pH of the solutions was measured by means of a Hitachi-Horiba pH meter, Model M-5, calibrated with standard buffer solutions at 25±0.5°C. The dissociation constants, pK_a, were calculated by a standard method. The average deviations for all the compounds were within ±0.05 pH units.

Results

The spectra of some 4-dialkylaminoazobenzene derivatives in *ca.* 1N hydrochloric acid (50% aqueous ethanol), the acidity of which is necessary for the complete formation of the first conjugate acid, are given in Fig. 1. The A band at about 320 nm has been attributed to the conjugation band of the species of the ammonium form (II), while the C band at about 510 nm has been ascribed to that of the azonium form (III).[5-8] The spectra show that the first conjugate acids of 4-dialkylaminoazobenzene derivatives are equilibrium mixtures of II and III, as has been proposed by earlier workers.[5-8] It seems that the $\varepsilon_a/\varepsilon_c$ ratio gives a crude idea of the tautomeric equilibrium. The ε_a value is the apparent molar extinction coefficient at the wavelength maximum of the A band, and the ε_c value is that at the wavelength maximum of the C band. The $\varepsilon_a/\varepsilon_c$ ratio for various substituted

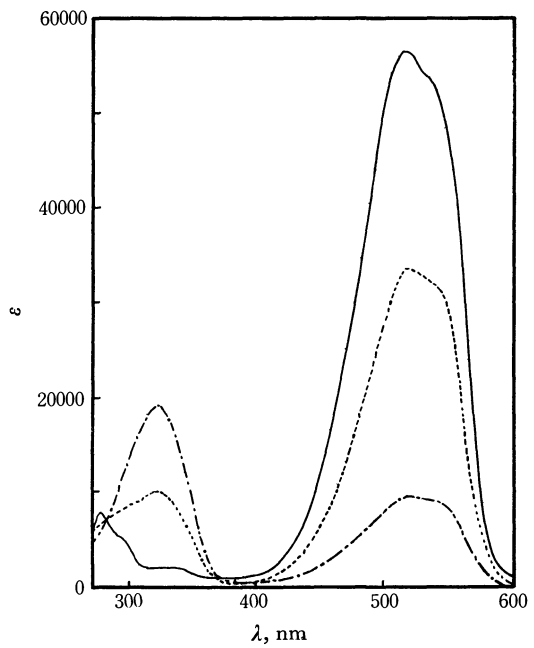

Fig. 1. Absorption spectra of 4-*N,N*-dialkylaminoazobenzene derivatives in *ca.* 1N hydrochloric acid in 50% aqueous ethanol.
------: 4-*N,N*-Dimethylaminoazobenzene
-·-·-: 4-*N,N*-Diethylaminoazobenzene
——: 4-Pyrrolidinoazobenzene

Table 1. Absorption spectra of 4-*N,N*-dialkylaminoazobenzene derivatives and their first conjugate acids

No	λ_{max} ($\varepsilon\times10^{-3}$)			$\varepsilon_a/\varepsilon_c$
	A band	B band[a]	C band	
1	320(10.1)	400(30.4)	516(33.6)	0.30
2	331(13.2)	400(31.8)	528(30.1)	0.44
3	325(12.9)	410(34.1)	520(33.0)	0.39
4	318(19.1)	407(32.3)	516(9.5)	2.03
5	332(21.8)	407(33.4)	528(6.7)	3.23
6	325(21.0)	416(34.0)	518(7.0)	2.98
7	324(3.0)	407(33.0)	516(57.7)	0.05
8	335(2.9)	407(32.8)	528(54.4)	0.05
9	329(3.0)	417(35.0)	520(58.1)	0.05

a) Conjugation band of base in cyclohexane

No.	Substituent
1	4-dimethylamino
2	4-methyl-4′-dimethylamino
3	4-chloro-4′-dimethylamino
4	4-diethylamino
5	4-methyl-4′-diethylamino
6	4-chloro-4′-diethylamino
7	4-pyrrolidino
8	4-methyl-4′-pyrrolidino
9	4-chloro-4′-pyrrolidino

4-dialkylaminoazobenzenes are shown in Table 1.

As is shown in Table 1, $\varepsilon_a/\varepsilon_c$ varies widely from compound to compound. This shows that the tautomeric equilibrium is sensitive to *N*-substituents; especially for 4-pyrrolidinoazobenzene derivatives the equilibrium greatly shifts to the azonium form.

It has been shown for 4-aminoazobenzene derivatives that ε_c increases, and that, simultaneously, ε_a decreases, with an increase in the sulfuric acid concentration.[9] In a very concentrated sulfuric acid (>12N), both bands, A and C, disappear, and at the same time a

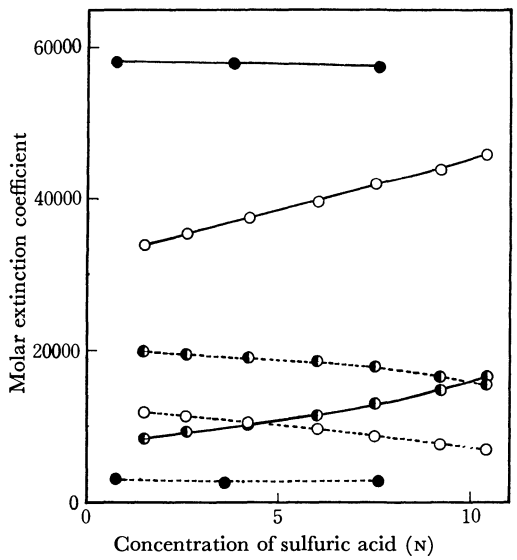

Fig. 2. Plots of molar extinction coefficients (ε_a and ε_c) against concentration of sulfuric acid.
------ ε_a —— ε_c
○: 4-chloro-4′-*N,N*-dimethylaminoazobenzene
◐: 4-chloro-4′-*N,N*-diethylaminoazobenzene
●: 4-chloro-4′-pyrrolidinoazobenzene

new band appears at about 410 nm; this latter band has been assigned to the diprotonated form.[7,8] Figure 2 shows a plot of ε_a and ε_c against the sulfuric acid concentration. As is shown in Fig. 2, for 4-dimethylamino- and 4-diethylaminoazobenzene derivatives ε_c increases and ε_a decreases with an increase in the sulfuric acid concentration. For 4-pyrrolidinoazobenzene, however, ε_a and ε_c are almost uninfluenced by the change in the acid concentration. This shows that, for dimethylamino- and diethylaminoazobenzenes, the tautomeric equilibrium shifts from the ammonium to the azonium form with an increase in the sulfuric acid concentration,[9] while for pyrrolidinoazobenzene the equilibrium does not change, since it has almost completely shifted to the azonium form even at lower concentrations of sulfuric acid. The molar extinction coefficient of the azonium form at *ca.* 510 nm (Band C) for dimethylamino- and diethylaminoazobenzenes cannot be obtained by direct photometric measurement, since they exist in both the azonium and ammonium forms. However, since pyrrolidinoazobenzenes exist exclusively in the azonium form, the ε_c values can be regarded as true molar extinction coefficients. If the molar extinction coefficients of the azonium forms (Band C) are the same for these three types of compounds with the same 4′-substituents, the tautomeric equilibrium constants can be estimated in the following way:

$$\text{Fraction of III} = \frac{\varepsilon_c}{\varepsilon_c^0}$$

$$\text{Fraction of II} = 1 - \frac{\varepsilon_c}{\varepsilon_c^0}$$

Therefore,
$$K_t = \frac{[\text{II}]}{[\text{III}]} = \frac{\varepsilon_c}{\varepsilon_c^0} - 1 \qquad (1)$$

where ε_c^0 is the ε_c value of 4-pyrrolidinoazobenzene derivatives.

According to Gerson and Heilbronner,[8] the equilibrium in question can be expressed as in the following chart:

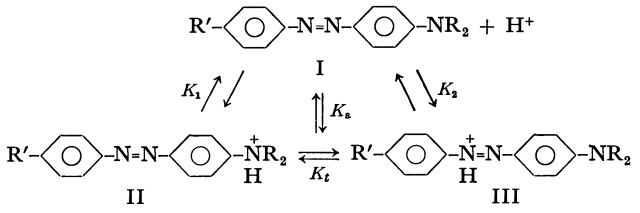

Chart 1.

In this case, the following equations may hold:

$$\begin{aligned} \varepsilon_a C &= \varepsilon_a^{\text{II}}[\text{II}] + \varepsilon_a^{\text{III}}[\text{III}] \\ \varepsilon_c C &= \varepsilon_c^{\text{II}}[\text{II}] + \varepsilon_c^{\text{III}}[\text{III}] \\ C &= [\text{II}] + [\text{III}] \end{aligned} \qquad (2)$$

where $\varepsilon_a^{\text{II}}$ and $\varepsilon_a^{\text{III}}$ are the molar extinction coefficients of II and III at the wavelength maximum of the A band, where $\varepsilon_c^{\text{II}}$ and $\varepsilon_c^{\text{III}}$ are those of II and III at the wavelength maximum of the C band, where [II] and [III] represent the concentrations of II and III respectively, and where C is the concentration of the free base added. Since $\varepsilon_a^{\text{III}}$ is small compared with $\varepsilon_a^{\text{II}}$, and since $\varepsilon_c^{\text{II}}$ is nearly zero, the tautomeric equilibrium constant, K_t, may be expressed as:

$$K_t = \frac{[\text{II}]}{[\text{III}]} = \frac{\varepsilon_c^{\text{III}}}{\varepsilon_a^{\text{II}}} \frac{\varepsilon_a}{\varepsilon_c} \qquad (3)$$

Gerson and Heilbronner[8] assumed that the value of the $\varepsilon_c^{\text{III}}/\varepsilon_a^{\text{II}}$ ratio for 4-dimethylaminoazobenzene is 3 on the basis of the data of Isaks and Jaffé, and that this value is valid for other 4-dimethylaminoazobenzene derivatives as well.

In the present case, however, $\varepsilon_c^{\text{III}}/\varepsilon_a^{\text{II}}$ was estimated in a different manner. From Eq. (2), it follows that

$$\varepsilon_c = \left(\frac{\varepsilon_c^{\text{II}} - \varepsilon_c^{\text{III}}}{\varepsilon_a^{\text{II}} - \varepsilon_a^{\text{III}}}\right)\varepsilon_a + \frac{\varepsilon_c^{\text{III}}\varepsilon_a^{\text{II}} - \varepsilon_c^{\text{II}}\varepsilon_a^{\text{III}}}{\varepsilon_a^{\text{II}} - \varepsilon_a^{\text{III}}}$$

Since $\varepsilon_a^{\text{II}} \gg \varepsilon_a^{\text{III}}$, and $\varepsilon_c^{\text{II}} \approx 0$,

$$\varepsilon_c = -\frac{\varepsilon_c^{\text{III}}}{\varepsilon_a^{\text{II}}}\varepsilon_a + \varepsilon_c^{\text{III}} \qquad (4)$$

According to Eq. (4), there should be a linear relationship between ε_c and ε_a. Various sets of ε_c and ε_a were obtained by changing the sulfuric acid concentrations; they were then plotted according to Eq. (4). A representative one is given in Fig. 3, which shows the validity of Eq. (4). The values of $\varepsilon_c^{\text{III}}/\varepsilon_a^{\text{II}}$ and $\varepsilon_c^{\text{III}}$ were obtained from the slope and the intercept of the line in Fig. 3. These values are given in Table 2. In Table 2, $\varepsilon_a^{\text{IV}}$ denotes the molar extinction coefficinet of *N,N,N*-trimethyl-*p*-phenylazoanilinium chlorides (IV) at the wavelength maximum of the band corresponding to that of the ammonium form (II).

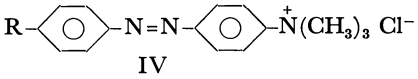

IV

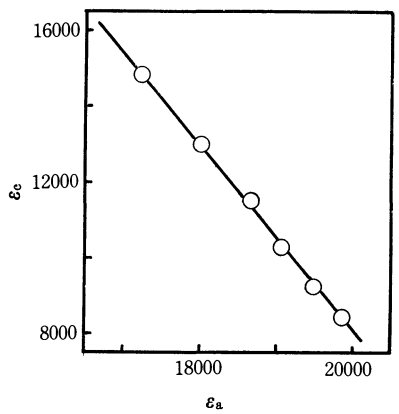

Fig. 3. Relationship between ε_a and ε_c for 4-chloro-4′-*N,N*-diethylaminoazobenzene

TABLE 2. MOLAR EXTINCTION COEFFICIENTS OF CONJUGATE ACIDS OF 4-*N,N*-DIALKYLAMINOAZOBENZENES

No[a)]	$\varepsilon_c^{\text{III}}/\varepsilon_a^{\text{II}}$	$\varepsilon_c^{\text{III}}$	$\varepsilon_a^{\text{II}}$	$\varepsilon_a^{\text{IV}}$
1	2.64	60400	22900	20400
2	2.54	61600	24200	22900
3	2.53	64000	25300	24100
4	2.67	59200	22200	—
5	2.43	58000	23900	—
6	2.43	56800	23400	—

a) Key is shown in Table 1.

Table 3. Tautomeric equilibrium constants of 4-*N*,*N*-dialkylaminoazobenzene derivatives

No[a)]	Tautomeric Equilibrium Constants			
	A	B	C	D
1	0.72	0.78	0.14	0.90
2	0.82	1.1	0.24	1.17
3	0.75	1.0	0.20	1.23
4	4.9	5.4	—	—
5	7.3	7.8	—	—
6	7.3	7.2	—	—
7	0.0	0.14	—	—
8	0.0	0.14	—	—
9	0.0	0.14	—	—

a) Key is shown in Table 1.
A : Obtained according to Eq (1).
B : Obtained according to Eq (3).
C : Ref. 7.
D : Ref. 8.

Since the electronic effect of the $-\overset{+}{N}(CH_3)_3$ group on the **A** band may be similar to that of the $-\overset{+}{N}H(CH_3)_2$ group, it should be $\varepsilon_a^{II} \approx \varepsilon_a^{IV}$. As expected, the agreement is quite satisfactory (Table 2), indicating again the validity of Eq. (4).

As is shown in Table 2, the $\varepsilon_c^{III}/\varepsilon_a^{II}$ ratio varies slightly from compound to compound. The tautomeric equilibrium constants calculated according to Eq. (3) are shown in Table 3. These values are in fair agreement with the corresponding values obtained according to Eq. (1). According to Jaffé and Yeh,[7] the molar extinction coefficient at *ca.* 320 nm of the azonium form is about 2000. In this case, therefore, ε_a is the sum of the contributions of both the ammonium and azonium forms. When ε_a is sufficiently large, as in the cases of dimethylamino- and diethylaminoazobenzenes, the contribution of the azonium form to ε_a can be neglected. However, as is shown in Table 1, ε_a is so small for pyrrolidinoazobenzenes as not to permit us to neglect the contribution of the azonium form. Therefore, the value (0.14) for pyrrolidinoazobenzenes obtained by Eq. (3) must be overestimated.

The values for 4-dimethylaminoazobenzene and the 4′-methyl and 4′-chloro derivatives are in good agreement with the values given by Gerson and Heilbronner,[8] but they differ from those obtained by Isaks and Jaffé,[7] as is shown in Table 3. This large discrepancy is due to the difference in the composition of the solvent. The present values were obtained in *ca.* 1N hydrochloric acid, whereas Isaks and Jaffé obtained theirs in much more acidic solutions. In their case, therefore, the equilibrium must have shifted to the azonium form, for the reason mentioned above.

Discussion

The tautomeric equilibrium constant, K_t, is a measure of the difference between the basicity of the amino nitrogen (pK_1) and that of the azo nitrogens (pK_2). Hence, an examination of the effects of *N*-alkyl groups on both pK_1 and pK_2 is necessary in order to interpret the effects on K_t. The values of K_1 and K_2 were calculated according to the following equations:

$$\frac{1}{K_2} = \frac{1}{K_a}\frac{1}{1+K_t}$$

$$\frac{1}{K_a} = \frac{1}{K_1} + \frac{1}{K_2} \qquad (5)$$

where K_1 and K_2 are the acid dissociation constants of the ammonium and the azonium ions respectively, and where K_a is the apparent acid dissociation constant of the first conjugate acid (Chart 1). All the pK_a values were determined by using a standard spectrophotometric method.[14] These values are listed in Table 4.

Table 4. Various equilibrium constants of 4-*N*,*N*-dialkylaminoazobenzene derivatives

Group[a)]	No[b)]	pK_a	K_t[c)]	pK_1[d)]	pK_2[d)]	K_t[e)]	pK_1[f)]	pK_2[f)]
1	1	2.00	0.72	1.62	1.76	0.78	1.64	1.75
	4	2.89	4.9	2.81	2.12	5.4	2.82	2.09
	7	2.38	0.0	—	2.38	0.14	1.46	2.38
2	2	2.17	0.82	1.83	1.91	1.1	1.89	1.85
	5	3.09	7.3	3.03	2.17	7.8	3.04	2.12
	8	2.43	0.0	—	2.43	0.14	1.57	2.43
3	3	1.88	0.75	1.52	1.63	1.0	1.58	1.58
	6	2.65	7.3	2.59	1.73	7.2	2.60	1.71
	9	2.15	0.0	—	2.15	0.14	1.23	2.15

a) Group 4′-Substituent
1 -H
2 $-CH_3$
3 -Cl
b) Key is shown in Table 1.
c) Obtained according to Eq. (1)
d) Obtained according to Eq. (5) using K_t values in the fourth column.
e) Obtained according to Eq. (3).
f) Obtained according to Eq. (5) using K_t values in the seventh column.

For all three groups in Table 4, pK_1 increases in this order: pyrrolidino-<dimethylamino-<diethylaminoazobenzenes. On the other hand, pK_2 increases in this order: dimethylamino-<diethylamino-<pyrrolidinoazobenzenes. The difference in pK_2 is rather smaller than that in pK_1.

The dipole moments of these compounds were measured in order to examine the electronic effect of the *N*-alkyl groups on both pK_1 and pK_2. As may be seen in Table 5, the dipole moments increase step-by-step in this order: dimethylamino-<diethylamino-<pyrrolidinoazobenzenes in each group. The increment is too large to ascribe to the inductive effect of these substituents.

Nash *et al.*[11] have shown, from comparisons of the ^{13}C chemical shifts, the ultraviolet spectra, and the molar refractions of *N*,*N*-dialkylaniline derivatives, that the degree of resonance interaction between the lone-pair electrons on nitrogen and the π-electrons of the

14) In order to obtain pK_a, the absorption spectra of the compounds were measured in various hydrochloric acid concentrations up to *ca.* 1N. For all of the compounds, three isosbestic points were observed in the range from 240 to 600 nm. This indicates that K_t is constant over these acid concentrations. Therefore, the standard method can be used for the determination of pK_a.

TABLE 5. DIPOLE MOMENTS OF 4-*N,N*-DIALKYLAMINOAZOBENZENE DERIVATIVES WITH RELEVANT DATA[a,b]

Group[c]	No[c]	*a*	*b*	R_M cc	*P* cc	μ D
1	1	5.27	0.19	71.9	281.6	3.17
	4	5.74	0.27	78.7	332.9	3.50
	7	6.60	0.29	76.6	369.4	3.76
2	2	3.50	0.15	76.5	225.2	2.66
	5	3.76	0.21	83.3	257.7	2.90
	8	4.80	0.22	81.2	306.5	3.20
3	3	9.20	0.22	76.7	516.3	4.61
	6	9.80	0.28	83.5	597.1	5.00
	9	10.40	0.30	81.4	623.0	5.13

a) Measured in benzene.
b) For notations used here see Ref. 13.
c) Key is shown in Tables 1 and 4.

benzene ring increases in this order: dimethylaniline< diethylaniline≈*N*-phenylpyrrolidine. In the case of dialkylaminoazobenzene derivatives, if it is assumed that the degree of resonance interaction between the amino group and the rest of the molecule increases in this order: dimethylamino-<diethylamino-<pyrrolidinoazobenzenes— if, that is to say, the degree of the contribution of the type

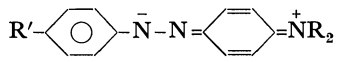

is the greatest for pyrrolidinoazobenzene and the smallest for dimethylaminoazobenzene— it can account for the order of the dipole moments. If the above proposal is reasonable, the transition energy of the conjugation band of these free bases should decrease and the molar extinction coefficient should increase in this order: dimethylamino-<diethylamino-<pyrrolidinoazobenzenes. An inspection of the data for B band in Table 1 supports this idea.

The order of pK_2 is the same as that of the dipole moments, as is shown in Tables 4 and 5. The basicity of azo nitrogens is hardly subject to inductive and steric effects of the alkyl groups, for the alkyl groups are apart from the azo group. Thus, the factor governing pK_2 must be the same as in the case of the dipole moments, since the greater the extent of the contribution of the above type, the greater the negative charge on one of the azo nitrogens.

An inhibition of the resonance decreases the potitive charge on the amino nitrogen and results in an increase in the base strength of the amino nitrogen, all other factors being equal. Therefore, pK_1 should increase in this order: pyrrolidino-<diethylamino-<dimethylaminoazobenzenes, but actually it increases in this order: pyrrolidino-<dimethylamino-<diethylaminoazobenzenes, as is shown in Table 4. This latter order is the same as that for *N,N*-dialkylaniline derivatives given by Nash and Maciel.[11] They have suggested that the alkyl groups in free diethylaniline produce so cluttered a situation in the vicinity of the nitrogen atom that the hydrogen bonding between hydroxylic solvent molecules and the nitrogen atom is inhibited. The resulting loss of solvation energy increases the free energy of the free base, reduces the energy gap between *N,N*-diethylaniline and its anilinium ion, and correspondingly increases the base strength of the former relative to dimethylaniline. Most of their discussion holds in our case as well, thus accounting for the anomalously high base strength of the amino nitrogen of diethylaminoazobenzenes.

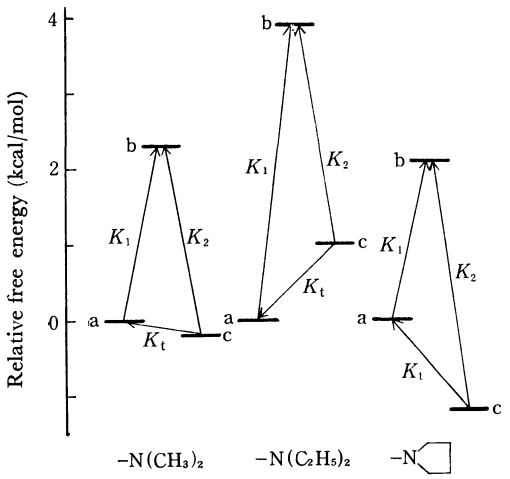

Fig. 4. The diagram of free energy.
a: ammonium ion, b: base + H^+, c: azonium ion.

On the basis of the data in Table 4, a diagram of the free energy was obtained by assuming that the ammonium ions of dimethylamino-, diethylamino-, and pyrrolidinoazobenzenes have equal free energies,[11] the energy of the ammonium ions being taken as the standard. As may be seen in Fig. 4, the free energy gaps between the ammonium ions and the azonium ions, $\Delta G = G(\text{ammonium ion}) - G(\text{azonium ion})$, increase in this order: diethylamino-<dimethylamino-< pyrrolidinoazobenzene; hence, the K_t values decrease in this same order.

The authors are deeply grateful to Miss Hiromi Ohtani for her elemental analysis.

Synthesis and Halochromism of 4- and 6-Styryl-2-aminotropones

Kimiaki IMAFUKU and Hisashi MATSUMURA

Department of Chemistry, Faculty of Science, Kumamoto University, Kurokami, Kumamoto

(Received March 2, 1972)

The methylation of 4-styryltropolones with diazomethane afforded two isomers, 2-methoxy-4-styryltropones and 2-methoxy-6-styryltropones. Their reactions with ammonia gave the corresponding 2-amino-4-styryltropones and 2-amino-6-styryltropones, respectively, by normal nucleophilic substitution. Infrared and ultraviolet absorption spectra were measured. The halochromism of 2-aminotropones was also examined, the halochromic shifts being found to be linearly correlated with the Hammett substituent constants.

Investigations have been carried out by Nozoe,[1,2] Haworth,[3] Tarbell,[4,5] and Kuraoka[6] on styryltropolones with particular interest in them as a potential intermediate in the synthesis of colchicine and its analogues.

The chemical reactivities of 4- and 6-styryl-substituted 2-methoxytropones,[7] 2-chlorotropones,[7] and 2-tosyloxytropones[8,9] towards nucleophilic reagents such as ammonia, amines, and hydroxide ion were studied by one of us (H. M.). More quantitative treatments of the reactivity of the styryltropolones[10,11] were made by measuring their dissociation constants and by correlating them to the Hammett substituent constants. Thus, it was established that the electronic effects of the substituents in the benzene ring can be transmitted through an ethylenic linkage to the tropolone nucleus. The dissociation constants of 4- and 6-styryl-2-aminotropones were measured and found to obey the Hammett equation.[12]

This communication deals with the synthesis of 4- and 6-styryl-2-aminotropones, which are used for the measurements of the dissociation constants of their conjugate acids.[12] The infrared and ultraviolet absorption spectra of 2-methoxytropones and 2-aminotropones were also measured, and the halochromism of 2-aminotropones is discussed quantitatively.

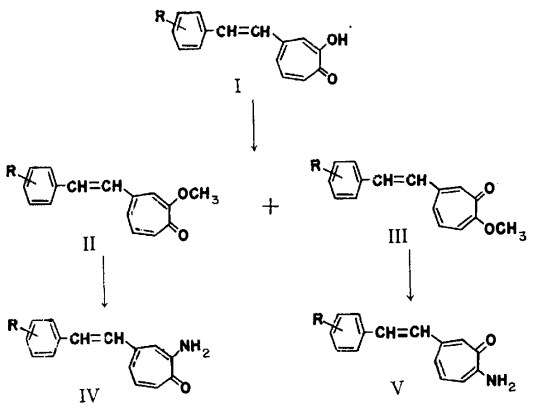

Fig. 1.

a R=H	e R=*m*-Cl
b R=*p*-OCH_3	f R=*p*-Br
c R=*p*-CH_3	g R=*p*-NO_2
d R=*p*-Cl	h R=*m*-NO_2

Results and Discussion

Synthesis. The starting materials, 4-styryltropolones (Ia—Ih) having substituent in the benzene ring, were prepared by the condensation of the corresponding benzaldehyde with 3-carboxy-4-carboxymethyltropolone[13] obtained from purpurogallin[14] and the decarboxylation of the condensation products.[15]

4-Styryltropolone (Ia) was methylated with diazomethane in ether to afford two isomers of methyl ether, 2-methoxy-4-styryltropone (IIa) and 2-methoxy-6-styryltropone (IIIa).[5,16] Similarly, seven 4-styryltropolone methyl ethers (IIb—IIh) and seven 6-styryltropolone methyl ethers (IIIb—IIIh) were obtained from seven 4-(substituted styryl)tropolones (Ib—Ih). These isomers could be readily and perfectly separated by means of preparative thin layer chromatography. The yields, melting points and analytical data are summarized in Table 1. The melting points of 6-isomers are higher than those of the corresponding 4-isomers.

Ammonolysis of 2-methoxy-4-styryltropone (IIa) and 2-methoxy-6-styryltropone (IIIa) with ammonia in absolute ethanol in a sealed tube afforded the corresponding 2-amino-4-styryltropone (IVa) and 2-amino-6-styryltropone (Va), respectively, by normal nucleophilic substitution.[7] 4-Styryl (IIb—IIh) and 6-styryl isomers (IIIb—IIIf) having substituent in the benzene ring were also aminated with ammonia to afford the corresponding seven 2-amino-4-styryltropones (IVb—IVh) and five 2-amino-6-styryltropones (Vb—Vf), re-

1) T. Nozoe, Y. Kitahara, K. Doi, and M. Endo, *Proc. Jap. Acad.*, **28**, 32 (1952).
2) T. Nozoe, Y. Kitahara, K. Doi, S. Masamune, M. Endo, M. Ishii, and J.-G. Shin, *Sci. Repts. Tohoku Univ., I*, **38**, 257 (1955).
3) W. D. Crow, R. D. Haworth, and P. R. Jefferies, *J. Chem. Soc.*, **1952**, 3705.
4) D. S. Tarbell, R. F. Smith, and V. Boeckelheide, *J. Amer. Chem. Soc.*, **76**, 2470 (1954).
5) D. S. Tarbell, K. I. H. Williams, and E. J. Sehm, *ibid.*, **81**, 3443 (1959).
6) T. Kuraoka, *Nippon Kagaku Zasshi*, **83**, 584, 587, 828, 831 (1962).
7) H. Matsumura, *ibid.*, **81**, 1763 (1960).
8) H. Matsumura, *ibid.*, **82**, 623 (1961).
9) H. Matsumura, *ibid.*, **82**, 774 (1961).
10) K. Imafuku, S. Nakama, and H. Matsumura, *Tetrahedron*, **26**, 1821 (1970).
11) K. Hamada, S. Nakama, K. Imafuku, K. Kurosawa, and H. Matsumura, *ibid.*, **27**, 337 (1971).
12) K. Imafuku and H. Matsumura, This Bulletin, in press.
13) R. D. Haworth and J. D. Hobson, *J. Chem. Soc.*, **1951**, 561.
14) J. D. Evans and M. M. Dehn, *J. Amer. Chem. Soc.*, **52**, 3647 (1930).
15) S. Nakama, K. Imafuku, and H. Matsumura, This Bulletin, **43**, 3265 (1970).
16) H. Matsumura, *Nippon Kagaku Zasshi*, **77**, 300 (1956).

TABLE 1. 4-AND 6-STYRYL-2-METHOXYTROPONES

Compound	R	Appearance[a]	Yield (%)	Mp (°C)	Formula	Found (%)			Calcd (%)		
						C	H	N	C	H	N
IIb	*p*-OCH_3	Y Nd	44.5	109—110	$C_{17}H_{16}O_3$	76.32	6.07		76.10	6.01	
IIc	*p*-CH_3	oil	35.9		$C_{23}H_{19}N_3O_9$[b]	57.56	4.08	8.38	57.38	3.98	8.73
IId	*p*-Cl	Y Pm	40.8	155—156	$C_{16}H_{13}ClO_3$	70.45	4.93		70.46	4.80	
IIe	*m*-Cl	Y Sc	45.5	146—148	$C_{16}H_{13}ClO_2$	70.36	4.84		70.46	4.80	
IIf	*p*-Br	Y Nd	48.8	141—142	$C_{16}H_{13}BrO_2$	60.88	4.39		60.59	4.13	
IIg	*p*-NO_2	Y Nd	22.8	224—225	$C_{16}H_{13}NO_4$	67.61	4.74	4.77	67.84	4.63	4.95
IIh	*m*-NO_2	Y Nd	22.8	175—176	$C_{16}H_{13}NO_4$	67.77	4.97	4.66	67.84	4.63	4.95
IIIb	*p*-OCH_3	Y Pl	30.3	146—148	$C_{17}H_{16}O_3$	75.91	6.12		76.10	6.01	
IIIc	*p*-CH_3	Y Pl	49.1	164—166	$C_{17}H_{16}O_2$	80.68	6.40		80.92	6.39	
IIId	*p*-Cl	Y Pl	39.8	160—161	$C_{16}H_{13}ClO_2$	70.39	4.88		70.46	4.80	
IIIe	*m*-Cl	L-Y Nd	42.7	160—161	$C_{16}H_{13}ClO_2$	70.57	4.74		70.46	4.80	
IIIf	*p*-Br	Y Sc	32.5	172—174	$C_{16}H_{13}BrO_2$	60.73	4.40		60.59	4.13	
IIIg	*p*-NO_2	L-Y Pd	13.3	253—255	$C_{16}H_{13}NO_4$			5.15			4.95
IIIh	*m*-NO_2	L-Y Pd	26.6	227—229	$C_{16}H_{13}NO_4$	68.00	4.44	4.84	67.84	4.63	4.95

a) Abbreviations: Y=yellow; L=light; Nd=needles; Pm=prisms; Sc=scales; Pl=plates; Pd=powder.
b) Picrate.

TABLE 2. 4- AND 6-STYRYL-2-AMINOTROPONES

Compound	R	Appearance[a]	Yield (%)	Mp (°C)	Formula	Found (%)			Calcd (%)		
						C	H	N	C	H	N
IVb	*p*-OCH_3	Y-O Pm	60.9	194—196	$C_{16}H_{15}NO_2$	75.61	5.98	5.58	75.87	5.97	5.53
IVc	*p*-CH_3	Y-B Ct	63.8	190—193	$C_{16}H_{15}NO$	81.09	6.41	5.95	80.98	6.37	5.90
IVd	*p*-Cl	Y-B Pm	58.2	211—213	$C_{15}H_{12}ClNO$	70.16	4.68	5.26	69.91	4.69	5.43
IVe	*m*-Cl	Y-O Pm	90.0	170—171	$C_{15}H_{12}ClNO$	69.82	4.77	5.71	69.91	4.69	5.43
IVf	*p*-Br	Y-O Ct	94.5	215—216	$C_{15}H_{12}BrNO$	59.52	4.10	4.62	59.62	4.00	4.64
IVg	*p*-NO_2	B Pd	63.4	265—267	$C_{15}H_{12}N_2O_3$	67.24	4.60	10.44	67.15	4.51	10.44
IVh	*m*-NO_2	B Ct	58.1	222—225	$C_{15}H_{12}N_2O_3$			10.29			10.44
Vb	*p*-OCH_3	Y-O Ct	90.0	151—153	$C_{16}H_{15}NO_2$			5.26			5.53
Vc	*p*-CH_3	Y-O Pm	95.7	175—176	$C_{16}H_{15}NO$	80.69	6.20	6.12	80.98	6.37	5.90
Vd	*p*-Cl	O Pl	68.8	183—184	$C_{15}H_{12}ClNO$	69.96	4.68	5.48	69.91	4.69	5.43
Ve	*m*-Cl	Y-O Pm	95.2	202—204	$C_{15}H_{12}ClNO$	69.63	4.66	5.35	69.91	4.69	5.43
Vf	*p*-Br	O Pl	99.7	199—201	$C_{15}H_{12}BrNO$	59.63	4.13	4.88	59.62	4.00	4.64

a) Abbreviations: Y=yellow; O=orange; B=brown; Pm=prisms; Ct=crystal; Pd=powder; Pl=plates.

spectively. However, the ammonolysis of both 2-methoxy-6-(*p*- and *m*-nitrostyryl)tropones (IIIg and IIIh) did not give the corresponding 2-aminotropones (Vg and Vh). The yields, melting points and analytical data are summarized in Table 2. In contrast to the case of methyl ethers, it was found that the melting points of 4-isomers are higher than those of the corresponding 6-isomers except for 2-aminotropones having *m*-chloro substituent.

These 2-aminotropones were hydrolyzed in alkali solution to give the corresponding original 4-styryltropolones.

Infrared Absorption Spectra. The infrared absorption spectra of the 2-methoxytropones (IIa—IIh and IIIa—IIIh) and 2-aminotropones (IVa—IVh and Va—Vf) were measured in chloroform. As characteristic bands, both of them have $\nu_{C=O}$ and δ_{CH} (in *trans* –CH=CH–) bands. 2-Aminotropones exhibit two ν_{NH} bands. These data are listed in Tables 3 and 4.

The geometry of the ethylenic linkage is *trans*, since the δ_{CH} bands are observed at 955—960 cm^{-1}. The carbonyl stretching bands of 6-isomers are observed in a lower wave number band than those of 4-isomers by *ca.* 10 cm^{-1}, if examined in detail. This might be due to the fact that the distance between the carbonyl group and the styryl group, which may conjugate with the former, is smaller in 6-isomers than in 4-isomers. It is found that, similar to 4-styryltropolones,[15] the $\nu_{C=O}$ bands of both 2-methoxytropones and 2-aminotropones are little affected by the substituents in the benzene ring.

Ultraviolet Absorption Spectra. The ultraviolet absorption spectra of 4- and 6-styryl-substituted 2-methoxytropones (IIa—IIh and IIIa—IIIh) and 2-aminotropones (IVa—IVh and Va—Vf) were measured in methanol, and are shown in Tables 3 and 4, respectively.

There is a remarkable difference between the spectra of 4-styryl- and 6-styryl-2-methoxytropones. On the other hand, the spectra of 4- and 6-styryl-2-aminotropones are very similar and hardly distinguishable, as shown in Fig. 2. However, when these 2-aminotropones are dissolved in acidic medium, they show different patterns. The spectra of 4- and 6-styryl-2-

Table 3. Spectral data for 4- and 6-styryl-2-methoxytropones

Compound	R	IR (cm^{-1})			UV: λ_{max} (log ε)			
		$\nu_{C=O}$	$\nu_{C=C}$	δ_{CH}				
IIa	H	1596	1576	958	242 (4.04)	310 (4.22)	355 (4.15)	
IIb	*p*-OCH_3	1588	1572	959	250 (4.20)	281 (4.10)	332 (4.09)	400 (4.39)
IIc	*p*-CH_3	1592	1572	959	248 (4.12)	280 (4.12)	318 (4.10)	386 (4.24)
IId	*p*-Cl	1586	1570	959	248 (4.15)	283 (4.28)	314 (4.27)	398 (4.36)
IIe	*m*-Cl	1596	1571	958	247 (4.16)	294 (4.31)	392 (4.30)	
IIf	*p*-Br	1594	1571	960	249 (4.15)	285 (4.27)	315 (4.27)	393 (4.36)
IIg	*p*-NO_2	1598	1578	954	261 (4.13)	322 (4.34)	400 (4.39)	
IIh	*m*-NO_2	1596	1577	959	277 (4.34)	294 (4.32)	359 (4.17)	391 (4.20)
IIIa	H	1584	1559	960	233 (4.04)	308 (4.51)		
IIIb	*p*-OCH_3	1583	1554	962	237 (4.24)	314 (4.55)	350 (4.48)	
IIIc	*p*-CH_3	1582	1553	962	251 (4.27)	317 (4.24)	363 (4.17)	
IIId	*p*-Cl	1582	1556	963	234 (4.17)	313 (4.52)		
IIIe	*m*-Cl	1583	1559	960	234 (4.17)	307 (4.55)		
IIIf	*p*-Br	1581	1554	961	233 (4.18)	314 (4.54)		
IIIg	*p*-NO_2	1584	1556	960	225 (4.17)	341 (4.54)		
IIIh	*m*-NO_2	1586	1560	961	231 (4.22)	303 (4.57)		

Table 4. Spectral data for 4- and 6-styryl-2-aminotropones

Compound	R	IR (cm^{-1})					UV: λ_{max} (log ε)			
		ν_{NH_1}	ν_{NH_2}	$\nu_{C=O}$	$\nu_{C=C}$	δ_{CH}				
IVa	H	3500	3360	1584	1559	960	233 (3.84)	323 (4.56)	425 (4.00)	
IVb	*p*-OCH_3	3500	3360	1586	1560	959	245 (4.11)	337 (4.57)	370 (4.32)	429 (4.11)
IVc	*p*-CH_3	3500	3360	1588	1560	960	239 (3.98)	327 (4.50)	430 (3.94)	
IVd	*p*-Cl	3500	3360	1590	1560	959	238 (4.06)	327 (4.63)	432 (4.03)	
IVe	*m*-Cl	3500	3360	1592	1562	955	236 (4.13)	320 (4.60)	432 (3.98)	
IVf	*p*-Br	3500	3360	1592	1562	959	238 (4.11)	327 (4.60)	432 (3.95)	
IVg	*p*-NO_2	3500	3360	1594	1560	960	222 (4.06)	282 (4.11)	337 (4.53)	444 (3.95)
IVh	*m*-NO_2	3500	3360	1588	1558	950	231 (4.14)	314 (4.59)	435 (3.95)	
Va	H	3510	3360	1582	1558	960	235 (4.02)	320 (4.66)	425 (4.00)	
Vb	*p*-OCH_3	3510	3360	1580	1558	958	249 (4.19)	331 (4.79)	428 (4.19)	
Vc	*p*-CH_3	3510	3360	1581	1559	960	245 (4.10)	328 (4.62)	430 (3.98)	
Vd	*p*-Cl	3510	3360	1581	1559	961	240 (4.15)	324 (4.67)	432 (4.01)	
Ve	*m*-Cl	3510	3360	1581	1559	959	240 (4.12)	320 (4.62)	431 (3.96)	
Vf	*p*-Br	3510	3360	1580	1559	960	246 (4.11)	326 (4.64)	432 (4.00)	

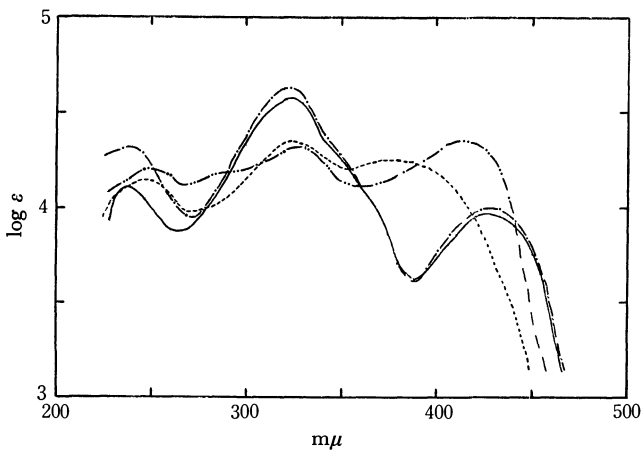

Fig. 2. The absorption spectra of 4- and 6-styryl-2-aminotropones.
——: IVa in neutral solution
------: IVa in acidic solution
——: Va in neutral solution
——: Va in acidic solution

aminotropones are shown in Fig. 2, as an example. Although their visible absorption bands show hypsochromic shifts, the 4-isomers show stronger shifts than the 6-isomers. The positions of the longest absorption bands in neutral and in acidic media are shown in Table 5, in terms of λ_B and λ_{BH^+} values, respectively.

The effects of the substituents in the benzene ring on the spectra can be seen from Tables 3 and 4. In general, the visible bands are shifted toward longer wavelength by *para* substituents, and the effect is roughly proportional to the Hammett substituent constants with the exception of electron-donating methoxy group. However, *meta* substituents cause little or none. A similar substituent effect is found in 4-aminostilbenes,[17] since the 2-aminotropone ring can be regarded as a non-benzenoid analogue of aniline and the spectroscopic properties of styryl-substituted 2-aminotropones can be directly compared with aminostilbenes. The longest absorption bands of the protonated ions are

17) H. Veschambre and A. Kergomard, *Bull. Soc. Chim. Fr.*, **1966**, 336.

TABLE 5. DISSOCIATION CONSTANTS AND VISIBLE SPECTRAL DATA FOR 4- AND 6-STYRYL-2-AMINOTROPONES

	No.[a]	R	σ	pK_a	λ_B	ν_B	λ_{BH^+}	ν_{BH^+}	$\Delta\nu$
4-Styryl	1	p-OCH_3	−0.268	2.71	428	23360	397	25190	1830
	2	p-CH_3	−0.170	2.64	428	23360	381	26250	2890
	3	H	0	2.54	428	23360	374	26740	3380
	4	p-Cl	0.227	2.39	430	23260	371	26950	3690
	5	p-Br	0.232	2.34	430	23260	374	26740	3480
	6	m-Cl	0.373	2.33	432	23150			
	7	m-NO_2	0.710	2.14	432	23150			
	8	p-NO_2	0.778	2.08	440	22730	364	27470	4740
6-Styryl	9	p-OCH_3	−0.268	2.69	429	23310	421	23750	440
	10	p-CH_3	−0.170	2.65	430	23260	420	23810	550
	11	H	0	2.57	429	23310	414	24150	840
	12	p-Cl	0.227	2.51	432	23150	415	24100	950
	13	p-Br	0.232	2.50	431	23200	415	24100	900
	14	m-Cl	0.373	2.42	430	23260	412	24270	1010

a) Numbers refer to those given in Figs. 3 and 4.

also sensitive to substituent effects in a manner parallel to the neutral species.

Halochromism and Substituent Effects. Rapoport *et al.*[18] measured the absorption spectra of 4-substituted 2-nitrophenols in neutral and in alkaline solutions, and showed theoretically that the difference between the longest absorption bands in two media are quantitatively related with the dissociation constants. These wavenumber shifts are also proportional to the Hammett substituent constants. This phenomenon is well-known in a number of azobenzene series such as 4-phenylazophenols[19] and 4-phenylazoanilines[20] as halochromism. It was found to hold in 5-phenylazotropolones which are non-benzenoid aromatic compounds.[21] The degree of halochromism of a compound can be defined as the frequency difference between the visible bands of the neutral and its conjugate acid or base.

We measured absorption spectra of 4- and 6-styryl-2-aminotropones in 50% aqueous methanol (pH *ca.* 6) and in 50% aqueous methanol containing hydrochloric acid (pH *ca.* 1). That only one species exists in each solution was checked by the pH changes of solution. The longest absorption spectra of both of these 2-aminotropones are shifted to shorter wavelength. The degree of shifts is larger in 4-styryl than in 6-styryl isomers as mentioned above. The wavelengths and wave numbers are listed in Table 5 as λ_B and ν_B for the neutral species and λ_{BH^+} and ν_{BH^+} for the protonated species, respectively. The $\Delta\nu$ values in the same Table give the difference between ν_B and ν_{BH^+} values. The dissociation constants (pK_a)[12] of these 2-aminotropones are also shown in Table 5.

When the $\Delta\nu$ values of 4- and 6-styryl-2-aminotropones are plotted against their pK_a values, the plots define the two lines for 4- and 6-isomers as shown in Fig. 3. The following equations are obtained by the least square method.

$$\text{(4-styryl)}\quad \Delta\nu = 12868 - 3891pK_a \quad (r=0.905)$$

$$\text{(6-styryl)}\quad \Delta\nu = 6434 - 2211pK_a \quad (r=0.961)$$

The magnitude of the pK_a values for suitable equilibria in phenyl derivatives is directly proportional to the Hammett substituent constants of substituent in the benzene ring. Thus, the $\Delta\nu$ values should be proportional to the substituent constants. Several examples of this type of correlation have been reported.[18-27]

When the $\Delta\nu$ values are plotted against the σ constants, two lines for 4- and 6-styryl-2-aminotropones are obtained as shown in Fig. 4. However, the $\Delta\nu$

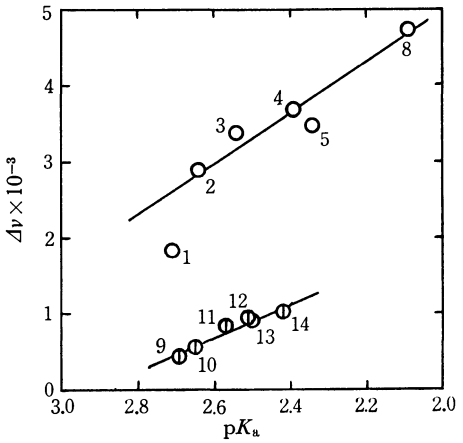

Fig. 3. The relationship between $\Delta\nu$ and pK_a.
○: 2-Amino-4-styryltropones
◑: 2-Amino-6-styryltropones

18) M. Rapoport, C. K. Hancock, and E. A. Meyers, *J. Amer. Chem. Soc.*, **83**, 3489 (1961).
19) W. R. Brode and V. E. Cheyney, *J. Org. Chem.*, **6**, 341 (1941).
20) L. M. Yagupol'skii and L. Z. Gandel'sman, *Zh. Obshch. Khim.*, **35**, 1252 (1965); **37**, 2101 (1967).
21) J. Griffins, *J. Chem. Soc., B*, **1971**, 801.
22) L. A. Jones and C. K. Hancock, *J. Org. Chem.*, **25**, 226 (1960).
23) C. K. Hancock and A. D. Clague, *J. Amer. Chem. Soc.*, **86**, 4942 (1964).
24) W. Bartok, P. J. Lucchesi, and N. S. Snider, *ibid.*, **84**, 1842 (1962).
25) H. H. Jaffé, D. L. Beveridge, and H. L. Jones, *ibid.*, **86**, 2932 (1964).
26) H. H. Jaffé, H. L. Jones, and M. Isaks, *ibid.*, **86**, 2934 (1964).
27) E. L. Wehring and L. B. Rogers, *ibid.*, **87**, 4234 (1965).

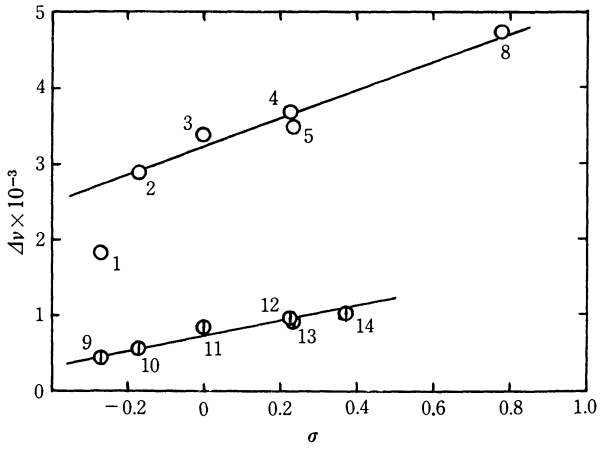

Fig. 4. The relationship between $\Delta\nu$ and σ.
○: 2-Amino-4-styryltropones
ⓘ: 2-Amino-6-styryltropones

value for 2-amino-4-(*p*-methoxystyryl)tropone having strongly electron-donating group considerably deviates from the regression line. The value is, therefore, not included in a calculation of the regression line. When an electrophilic substituent constants[28] ($\sigma^+ = -0.778$ for *p*-methoxy) is introduced, the plot of *p*-methoxy group is found to lie on the line. The regression equations are as follows.

$$\text{(4-styryl)}\quad \Delta\nu = 1879\sigma + 3235 \quad (r=0.984)$$

$$\text{(6-styryl)}\quad \Delta\nu = 882\sigma + 724 \quad (r=0.963)$$

The effect of substituents in the benzene ring on the electronic spectra is larger in 4-styryl than in 6-styryl isomers. This is consistent with the Hammett type analysis of both their dissociation constants.[12] Thus, it is found that the effect of resonance should not be neglected in the 4-isomers, since the effect in 4-isomers is about twice as much as in 6-isomers and σ^+ value fits better than the unmodified σ value for electron-donating *p*-methoxy group.

The excellent linear correlation between $\Delta\nu$ and pK_a or σ for 4- and 6-styryl-2-aminotropones suggests that similar relationships should hold for the other types of equilibria in troponoids having styryl group.

28) H. C. Brwon and Y. Okamoto, *ibid.*, **80**, 4980 (1958).

Experimental

All the melting points were measured on a Yanagimoto micro-melting point apparatus and uncorrected. The infrared and ultraviolet absorption spectra were taken on a JASCO IRA-1 and a Hitachi EPS-3T spectrophotometer, respectively.

4-Styryltropolones (Ia—Ih). The starting materials, 4-(substituted styryl) tropolones (Ia—Ih), were prepared according to a previous work.[15]

The corresponding benzaldehydes were treated with 3-carboxy-4-carboxymethyltropolone[13] obtained from purpurogallin[14] by sodium iodate oxidation, to give 3-carboxy-4-styryltropolones. The latter were sublimed at elevated temperature to afford 4-styryltropolones (Ia—Ih) with the elimination of carbon dioxide.

2-Methoxy-4-styryltropones (IIa—IIh) and 2-Methoxy-6-styryltropones (IIIa—IIIh). An excess of diazomethane in ether was added to a solution of 4-styryltropolones (Ia—Ih) (1 g, 3.3—4.2 mmole) in chloroform (20 ml), and the mixture was allowed to stand in a refrigerator (at *ca.* 5°C). After two days, the solvent was evaporated off under reduced pressure. The residue was dissolved in a small amount of chloroform and separated on silica gel plates (Wakogel B-10) with ethyl acetate as a developing solvent. Two bands of isomers of methyl ethers from 4-styryltropolones appeared. Each band was scraped out and extracted with chloroform. 2-Methoxy-4-styryltropones (IIa—IIh) and 2-methoxy-6-styryltropones (IIIa—IIIh) were obtained from the upper and the lower bands, respectively. Each methyl ether was recrystallized from benzene.

2-Amino-4-styryltropones (IVa—IVh) and 2-Amino-6-styryltropones (Va—Vf). A solution of 4- and 6-styryl-2-methoxytropones (IIa—IIh and IIIa—IIIh) (200 mg, 0.7—0.9 mmol) in absolute ethanol (10 ml), saturated with ammonia at ice-cooled temperature, was heated in a sealed tube for 3 hr at 100°C. The dark red solution was evaporated to give a reddish oil. The residue was crystallized by treating with a small amount of chloroform to afford 4- and 6-styryl-2-aminotropones (IVa—IVh and Va—Vf), respectively. These 2-aminotropones were recrystallized from either benzene or ethanol.

The Estimation of the Electronic Effects of Cyclopropyl and 2,2-Dichlorocyclopropyl Groups

Yoshiaki KUSUYAMA and Yoshitsugu IKEDA
Department of Chemistry, Wakayama University, Masagocho, Wakayama
(Received March 30, 1972)

The normal substituent constant, σ^0, and the resonance substituent constant, $\Delta\bar{\sigma}_R^+$, in the Yukawa and Tsuno treatment of cyclopropyl and 2,2-dichlorocyclopropyl were determined by the ionization of *m*-, *p*-substituted phenylacetic acids in 50% aqueous ethanol and by the solvolysis of α-(*m*-, *p*-substituted phenyl) ethyl chlorides in 80% aqueous acetone. For cyclopropyl, the obtained σ^0 value indicates an inductive electron-attracting behavior, while the $\Delta\bar{\sigma}_R^+$ value indicates a marked enhancement of the electron-releasing resonance effect on the electron deficient reaction center compared with alkyl groups. A minor resonance contribution was observed for the 2,2-dichlorocyclopropyl group.

It is well known that cyclopropane derivatives are remarkably different in their chemical properties compared with other cycloalkanes and alkanes. Of particular interest is the fact that the cyclopropane ring may enter into conjugated systems. Since Walsh[1] concluded, from his molecular orbital caluculations, that the cyclopropane ring posessed properties of a π bond character, numerous spectroscopic[2,3] and kinetic studies[4–11] have been carried out to examine the electronic properties of the cyclopropane ring. However, the influence of the cyclopropane ring is complicated by steric, inductive, and resonance effects. In order to attain a better understanding of the chemical behavior of the cyclopropane ring, it appeared to be of interest to estimate strictly the electronic contribution of the cyclopropyl group, using a system in which the steric factor is neglected.

The purpose of the present work has been to evaluate the electronic effect of the cyclopropyl group on the basis of a linear free-energy relationship. The σ^0-values[12–14] of cyclopropyl and 2,2-dichlorocyclopropyl have been determined from the dissociation of *m*-, *p*-substituted phenylacetic acids in 50% aqueous alcohol at 25°C, while the $\Delta\bar{\sigma}_R^+$ value in the Yukawa and Tsuno equation[14] has been determined from the solvolysis of α-(*m*-,*p*-substituted phenyl) ethyl chlorides in 80% aqueous acetone at 45°C.

Experimental

Materials. The materials were identified by means of spectroscopic and gas-chromatographic measurements and by elemental analyses. The NMR spectra were measured on a JEOL JMN-C-60HL (60MHz) spectrometer in CCl_4, with tetramethylsilane as the internal standard.

The unsubstituted and *p*-nitrophenylacetic acids were obtained commercially. The *m*-nitro derivative was obtained by the hydrolysis of the appropriate nitrile. The other phenylacetic acid derivatives were prepared by a modified Willgerodt reaction, using sulfur and morpholine, from the appropriate acetophenones. The acids were purified by recrystallization. The melting points are listed in Table 1. The syntheses of cyclopropylbenzene derivatives will be described below.

2,2-Dichlorocyclopropylbenzene. Sodium *t*-butoxide (145g) was vigorously stirred into a solution of styrene (73 g) and chloroform (167 g) in 500 ml of *n*-hexane cooled in water bath. The reaction mixture was then hydrolyzed by being added to 500 ml of ice-water. The hexane layer and hexane extracts were combined and dried with silica gel pellets, and the hexane was removed under reduced pressure. The product was distilled through a Widmer column fitted with a glass spiral core. Yield 92 g (70% from styrene). Bp 120°C/20 mmHg, NMR: δ 1.53—2.02 (2H, multiplet), 2.60—2.95 (1H, triplet), 7.15 (5H, singlet).

Cyclopropylbenzene. To a solution of 2,2-dichlorocyclo-

1) A. D. Walsh, *Nature*, **159**, 165, 712 (1947): *Trans. Faraday Soc.*, **45**, 179 (1949).

2) a) Selected references: R. Fuchs and J. J. Bloomfield, *J. Amer. Chem. Soc.*, **81**, 3158 (1959); M. Charton, *J. Chem. Soc.*, **1964**, 1205; W. G. Dauben and G. H. Berezine, *J. Amer. Chem. Soc.*, **89**, 3449 (1967); E. M. Kosower, and M. Ito, *Proc. Chem. Soc.*, **1962**, 25; J. A. Pete, *Bull. Soc. Chim. Fr.*, **1967**, 357; G. W. Cannon, A. A. Santilli, and P. Shenian, *J. Amer. Chem. Soc.*, **81**, 1660 (1959); A. L. Goodman and R. H. Eastman, *ibid.*, **86**, 908 (1964); L. A. Strait, D. Jambokar, R. Ketchaman, and M. Hrenoff, *J. Org. Chem.*, **31**, 3976 (1966); M. J. Jorgenson and T. Leung, *J. Amer. Chem. Soc.*, **90**, 3769 (1968); C. H. Heathcokck and S. R. Poulter, *ibid.*, **90**, 3766 (1968). b) R. J. Mohrbacher and N. H. Cromwell, *ibid.*, **79**, 401 (1957); R. Y. Levina, V. N. Kostin, P. A. Gembitekii, S. M. Shostakooskii, and E. S. Treschova, *Zh. Obsch. Khim.*, **31**, 1185 (1961). c) G. L. Closs and H. B. Klinger, *J. Amer. Chem. Soc.*, **87**, 3265 (1965).

3) a) R. G. Pews, *ibid.*, **89**, 5605 (1967). b) R. G. Pews and N. D. Ojha, *ibid.*, **91**, 5769 (1969).

4) a) Selected references: J. D. Roberts, and V. C. Chambers, *ibid.*, **73**, 5034 (1951); E. F. Cox, M. C. Carerio, M. S. Siluer, and J. D. Roberts, *ibid.*, **83**, 2719 (1961); C. G. Bergstrom and S. Siegel, *ibid.*, **74**, 145, 254 (1952). b) For recent reviews: H. G. Richey, Jr., "Carbonium Ions," Vol. 3, Ed. by G. Olah and P. v. R. Schleyer, Interscience Publishers, New York, N. Y. (1969); B. Wiberg, B. A. Andes, Jr., and A. J. Ashe, in "Carbonium Ions," Vol. 3, G. Olah and P. V. R. Schleyer, Interscience Publishers, New York, N. Y. (1969).

5) L. B. Jones and V. K. Jones, *Tetrahedron Lett.*, **1966**, 1493.

6) L. B. Jones and S. S. Eng, *ibid.*, **1968**, 1431.

7) H. C. Brown and J. D. Cleveland, *J. Amer. Chem. Soc.*, **88**, 2051 (1966).

8) R. C. Hahn, T. F. Corbin, and H. Schechter, *ibid.*, **90**, 3403 (1968).

9) Y. E. Rhodes and T. Takino, *ibid.*, **92**, 5270 (1970).

10) B. R. Ree and J. C. Martin, *ibid.*, **92**, 1660 (1970).

11) G. C. Robinson, *J. Org. Chem.*, **34**, 2517 (1969).

12) R. W. Taft, Jr., *J. Phys. Chem.*, **64**, 1805 (1960); R. W. Taft, Jr. and I. C. Lewis, *J. Amer. Chem. Soc.*, **80**, 2436 (1958); *ibid.*, **81**, 5343 (1959); R. W. Taft, Jr., S. Ehrenson, I. C. Lewis, and R. E. Glick, *ibid.*, **81**, 5354 (1959).

13) Y. Yukawa, Y. Tsuno, and M. Sawada, This Bulletin, **39**, 2274 (1966).

14) Y. Yukawa and Y. Tsuno, *Nippon Kagaku Zasshi*, **86**, 783 (1965).

Table 1. Melting points of phenylacetic acids

Substituent	Mp (°C)
H	78—79
p-CH_3	90—92 (92—93)[a,b,c]
p-C_2H_5	91 (91.5—92)[c]
p-*c*-C_3H_5	84.5
p-*c*-(2,2-Cl_2-C_3H_3)	110—111
p-C_6H_5O	161 (79.5)[c]
p-Br	114 (114—114.5)[c,d]
p-NO_2	154—155 (153)[c,f]
m-Br	101—102.5 (101—101.5)[e,f]
m-NO_2	117—118 (118.5—119)[a,g]

a) R. O. C. Norman, G. K. Radda, D. A. Brimacombe, P. D. Ralph, and E. M. Smith, *J. Chem. Soc.*, **1937**, 1430.
b) R. C. Elderfield and K. L. Burgess, *J. Amer. Chem. Soc.*, **82**, 1975 (1960).
c) Ref. 13.
d) E. Schwenk and D. Papa, *J. Org. Chem.*, **11**, 798 (1946).
e) J. G. Watkinson, W. Watkinson, and B. L. Yates, *J. Chem. Soc.*, **1963**, 5437.
f) C. D. Depuy and D. H. Froemsdorf, *J. Amer. Chem. Soc.*, **79**, 3710 (1957).
g) D. L. Yabroff and C. W. Porter, *ibid.*, **54**, 1199 (1932)

propylbenzene (50 g) in 2-propanol (100 g), sodium metal (23 g) was added. A vigorous exothermic reaction then occurred. The mixture was allowed to stand overnight and then hydrolyzed by the addition of ice water. Cyclopropylbenzene was obtained by the hexane extraction and distillation of the dried hexane extract. Yield, 18 g (67%). Bp 77°C/30 mmHg, NMR: δ 0.50—1.00 (4H, multiplet), 1.53—2.03 (1H, multiplet), 6.71—7.37 (5H, complicated).

p-*Cyclopropylacetophenone.* Cyclopropylbenzene was acetylated in accordance with the procedure given in the literature. Pure *p*-cyclopropylacetophenone (GLC analysis) was obtained by fractional distillation. Bp 130°C/7 mmHg (lit, bp 114—119°C/2.5—2.9 mmHg,[15] 142°C/12 mmHg,[16] 142—145°C/9 mmHg,[17] Mp 36°C (lit, 35—36°C,[15] 36°C[16,17]) NMR: δ 0.60—1.25 (4H, multiplet), 1.62—2.21 (1H, multiplet), 2.40 (3H, singlet), 6.86—7.73 (two 2H doublets, J= 8 Hz).

p-*Cyclopropylphenylacetic Acid.* *p*-Cyclopropylacetophenone (32 g), morpholine (30 g) and sulfur (11.2 g) were refluxed for 14 hr. Ethanol (99%, 130 ml) was then added. The mixture was heated to 80°C and filtered while hot. *p*-Cyclopropylphenylthioacetomorpholide was crystallized spontaneously on cooling in the filtrate. Yield, 44 g (85%). Mp 107—108°C.

The morpholide was refluxed with 300 ml of 15% potassium hydroxide for 12 hr. The alkaline solution was then acidified, and the precipitate was recrystallized from benzene. Yield, 24 g (83%). Mp 84—85°C, Found: C, 74.84; H, 6.86%. Calcd: C, 74.98; H, 6.86%.

Ethyl ester: Bp 145°C/10 mmHg, NMR: δ 0.50—0.95 (4H, multiplet), 1.17 (3H, triplet, J=8 Hz), 1.55—2.02 (1H, multiplet), 3.40 (2H, singlet), 4.02 (2H, quartet, J=7 Hz), 6.80—6.87 (4H, complicated).

p-*2,2-Dichlorocyclopropylacetophenone.* 2,2-Dichlorocyclopropylbenzene was converted to *p*-2,2-dichlorocyclopropylacetophenone in chloroform, using aluminum chloride and acetyl chloride at 10°C. Bp 153°C/23 mmHg, NMR: δ 1.93 (1H, doublet, J=9 Hz), 1.96 (1H, doublet, J=9 Hz), 2.50 (3H, singlet), 2.92 (1H, triplet, J=9 Hz), 7.19—7.93 (two 2H doublets, J=8 Hz).

p-*2,2-Dichlorocyclopropylphenylacetic Acid.* *p*-2,2-Dichlorocyclopropylacetophenone (48 g), morpholine (30 g), and sulfur (11.2 g) were refluxed gently for 20 hr. 99% Ethanol (40 ml) was then added, and the mixture was cooled with an ice bath. However, morpholide was not precipitated, but a pasty mass. To this, a 15% sodium hydroxide solution (400 ml) was added, and the mixture was refluxed for 7 hr. The mixture was filtered rapidly while hot with suction and acidified with diluted hydrochloric acid. Attempts to crystallize the resultant precipitate were unsuccessful. Methyl *p*-2,2-dichlorocyclopropylphenylacetate (9 g) was obtained by refluxing a mixture of the precipitate, methanol (50 ml), and concentrated sulfuric acid (5 ml) for 6 hr. Bp 122°C/2 mmHg. NMR: δ 1.68—2.05 (2H, multiplet), 2.62—2.98 (1H, triplet), 3.50—3.64 (2H, one doublet, 3H singlet), 7.20 (4H, singlet). The ester (6.5 g) was converted to the appropriate acid by alkaline hydrolysis. Yield, 4 g. Mp 110—111°C. Found: C, 54.05; H, 4.03; Cl, 29.14%. Calcd: C, 53.90; H, 4.11; Cl, 28.83%.

*α-(*p-*Cyclopropylphenyl)ethyl Alcohol.* *p*-Cyclopropylacetophenone (10 g) was converted to α-(*p*-cyclopropylphenyl)-ethyl alcohol (7 g) by $LiAlH_4$ (0.8 g) reduction according to the usual procedure. Bp 109°C/3.5 mmHg. Found: C, 81.53%; H, 8.70%. Calcd: C, 81.43%; H, 8.69%. NMR: δ 0.40—1.12 (4H, multiplet), 1.20—1.40 (3H, doublet, J= 6 Hz), 1.58—2.02 (1H, multiplet), 4.04—4.13 (1H, singlet), 4.38—4.78 (1H, quartet, J=8 Hz), 6.75—7.20 (4H, complicated).

*α-(*p-*Cyclopropylphenyl)ethyl Chloride.* Hydrogen chloride was passed over a solution of 7 g of α-(*p*-cyclopropylphenyl)-ethyl alcohol in 30 ml of dichloromethane for ten minutes. The mixture was then treated with anhydrous calcium chloride after which hydrogen chloride was again passed over for ten minutes. The reaction mixture was then filtered rapidly, and the dichloromethane and dissolved hydrogen chloride was removed under a reduced nitrogen pressure. The product was utilized for the rate measurement without further purification. Found: C, 72.88; H, 7.46; Cl, 19.44%. Calcd: C, 73.12; H, 7.24; Cl, 19.62%. NMR: δ 0.44—1.08 (4H, multiplet), 1.55—2.08 (1H, multiplet), 1.60—1.80 (3H, doublet, J=7 Hz), 4.72—5.13 (1H, quartet, J=7 Hz), 6.60—7.35 (4H, two doublets, J=8 Hz, further splits).

*α-(*m-*Cyclopropylphenyl)ethyl Alcohol.* The Grignard reagent from *m*-bromocyclopropyl benzene (15 g)[8] and magnesium (1.95 g) was treated with acetaldehyde (3.5 g). The mixture was then decomposed with a saturated ammonium chloride solution. Subsequent work-up by the usual method gave α-(*m*-cyclopropylphenyl) ethyl alcohol. Yield, 11 g. Bp 103°C/1 mmHg. NMR: δ 0.58—1.21 (4H, multiplet), 1.35—1.56 (3H, doublet, J=7 Hz), 1.70—2.20 (1H, multiplet) 2.96—3.20 (1H, singlet), 4.55—4.95 (1H, quartet, J=7 Hz), 6.80—7.35 (4H, complicated).

*α-(*m-*Cyclopropylphenyl)ethyl Chloride.* α-(*m*-Cyclopropylphenyl)ethyl alcohol (10 g) was converted to the appropriate chloride (7 g) by the method described above for the synthesis of α-(*p*-cyclopropylphenyl)ethyl chloride. Bp 78°C/3 mmHg. Found: C, 72.79; H, 7.20; Cl, 19.49%. Calcd: C, 73.13; H, 7.25; Cl, 19.62%. NMR: δ 0.45—1.16 (4H, multiplet), 1.47—2.13 (1H, multiplet), 1.71—1.80 (3H, doublet, J=6 Hz), 4.75—5.15 (1H, quartet, J=6 Hz), 6.70—7.30 (4H, multiplet).

*α-(*p-*2,2-Dichlorocyclopropylphenyl)ethyl Alcohol.* The treatment of *p*-2,2-dichlorocyclopropylacetophenone (10 g)

15) H. Hart and G. Levitt, *J. Org. Chem.*, **24**, 1261 (1959).
16) R. Y. Levina and P. A. Gembitskii, *Zh. Obsch. Khim.*, **31**, 3480 (1961).
17) R. Y. Levina, P. A. Gembitskii, V. N. Kostin, S. M. Shostakovskii, and E. G. Treshchova, *ibid.*, **33**, 359 (1963).

with $LiAlH_4$ in ether gave α-(*p*-2,2-dichlorocyclopropylphenyl)ethyl alcohol (7.5 g). Bp 145°C/2.5 mmHg. Mp *ca* 35°C. Found: C, 57.18; H, 5.09; Cl, 30.68%. Calcd: C, 57.16; H, 5.23; Cl, 30.68%. NMR: δ 1.18—1.40 (3H, doublet, J=6.5 Hz), 1.65—2.05 (2H, multiplet), 2.58—3.00 (1H, triplet, J=9.5 Hz), 3.75—3.88 (1H, singlet), 4.40—4.82 (1H, quartet, J=6.5 Hz), 6.76—7.40 (4H, multiplet).

α-(p-2,2-Dichlorocyclopropylphenyl)ethyl Chloride. α-(*p*-2,2-Dichlorocyclopropylphenyl)ethyl alcohol (7 g) was converted to α-(*p*-2,2-dichlorocyclopropyl) ethyl chloride (5 g) with hydrogen chloride in dichloromethane. The dichloromethane and dissolved hydrogen chloride were removed under reduced pressure. The product was then used directly for the rate measurement without any further treatment. Found: C, 54.02; H, 4.15; Cl, 42.83%. Calcd: C, 52.93; H, 4.40; Cl, 42.62%. NMR: δ 1.20—2.10 (2H, multiplet), 1.70—1.90 (3H, doublet, J=7 Hz), 2.63—3.02 (1H, triplet, J=9.5 Hz), 4.82—5.20 (1H, quartet, J=7 Hz), 7.00—7.53 (4H, complicated).

Measurements of pK_a. The pK_a values of the phenylacetic acids were determined by the potentiometric titration of the acid with sodium hydroxide in 50% (v/v) ethanol, using a pH meter (Hitachi Horiba F-5) with glass and with reference electrodes. The titration cell was a flat-bottomed, 100 ml beaker equipped with a water jacket maintained at 25.00±0.02°C. The base was added from the titration buret graduated to 0.01 ml. The sample was stirred magnetically. The pH meter and electrodes were standardized before each run against a pH 7 buffer (a neutral phosphate standard solution) and checked against a pH 4 buffer (a phthalate standard solution). Each new batch of commercial buffer was compared with previous sample before use. The electrodes were kept immersed in the solvent for a day before the measurements. The solvent was prepared in a large quantity. A sample of each acid was weighed and dissolved in the solvent (9.0×10^{-3}mol/l). A 25 ml portion of the solution was pipetted out and transferred into the titration, cell. After the cell had been equilibrated thermally, the acid solution was titrated with a 0.02N carbonate free sodium hydroxide solution in the same solvent. The pH was measured after each small addition of the base until pH 11. The measurements were repeated two or three times. The pK_a calculations were carried out by the method described in the literature.[8,18] Identical pK_a values were obtained from the pH at one-fourth and three-fourths neutralization. No correction was made for the liquid-junction potential.

Kinetic Measurements. The rates of the solvolysis of α-phenylethyl chlorides were determined in an 80% (v/v) aqueous acetone solution.[19] An accurately-weighed amount of chloride was made up to volume in a volumetric flask (150 ml, 0.02 mol/l). The mixture was then transferred to a reaction vessel immersed in a thermostated bath. Kinetic runs below 45°C were conducted in a 200 ml flask. When the solution had reached the temperature of the thermostat, a 10 ml portion was pipetted out, transferred into 50—100 ml of cold dry acetone (to stop the reaction) and free hydrogen chloride titrated with 0.02N sodium hydroxide, using bromocresol purple as the indicator. For the runs at 55°C and 65°C, the sealed-ampule technique was used. The reactions were continued until at least 70% completion. The rate constants were calculated from the integrated form of the first-order rate equation. The rate constants from different runs agreed within 1%.

18) R. Fuchs, C. A. Kaplan, J. J. Bloomfield, and L. F. Hatch, *J. Org. Chem.*, **27**, 733 (1962).

19) E. Berliner and N. Shieh, *J. Amer. Chem. Soc.*, **79**, 3849 (1957).

Results and Discussion

Normal Substituent Constants of Cyclopropyl and 2,2-Dichlorocyclopropyl Groups. It is desirable to determine the σ^0 from the dissociation of phenylacetic acids in water, as well as the σ from that of benzoic acid in water.[13] The substituent effect is, however, too small in these equilibria in water for us to obtain precise σ^0 values.[13,14] 50% ethanol was chosen as the medium, because in this solvent substituents influence the acid dissociation by a factor of 1.5 more than in water.[18,20] It was hoped that this solvent would result in a uniform deviation from the thermodynamic pK_a values and offer the advantage of the solubility of the acids. The ionization constants thus measured are given in Table 2. It is noteworthy that *p*-cyclopropylphenylacetic acid is measurably stronger than the *p*-alkyl derivatives.

Table 2. Apparent dissociation constants of phenylacetic acids in 50% ethanol at 25°C

Substituent	pK_a (±0.01)	Substituent	pK_a (±0.01)
H	5.63	*p*-C_6H_5O	5.60
p-C_2H_5	5.78	*p*-NO_2	5.01
p-CH_3	5.74	*m*-Br	5.40
p-*c*-C_3H_5	5.72	*p*-Br	5.38
p-*c*-(2,2-Cl_2-C_3H_3)	5.60	*m*-NO_2	5.11

The effects of substituents can be correlated linearly with those on the dissociation of phenylacetic acids in water,[21] as is illustrated in Fig. 1. As would be anticipated, a precisely linear correlation is observed for σ^0, with a ρ value of 0.775 (correlation coefficient,

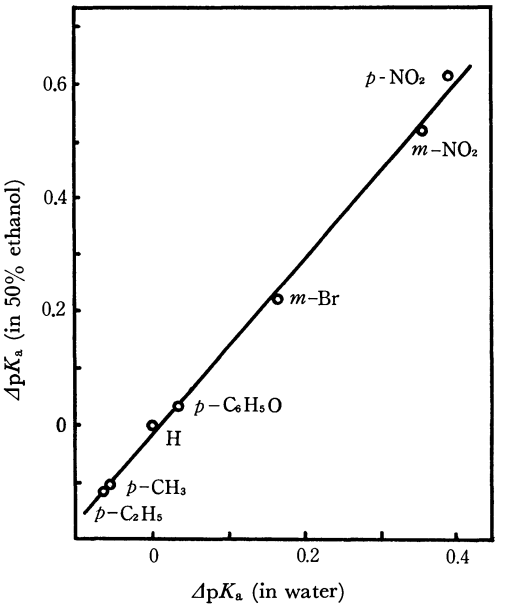

Fig. 1. Linear free energy relation for dissociation of phenylacetic acids at 25°C.

20) H. H. Jaffé, *Chem. Rev.*, **53**, 191 (1953).

21) J. F. J. Dippy and R. H. Lewis, *J. Chem. Soc.*, **1936**, 644; J. F. J. Dippy and F. R. Williams, *ibid.*, **1934**, 161; J. F. J. Dippy and J. E. Page, *ibid.*, **1938**, 357; A. Fisher, B. R. Mann, and J. Vaughan, *ibid.*, **1961**, 1093.

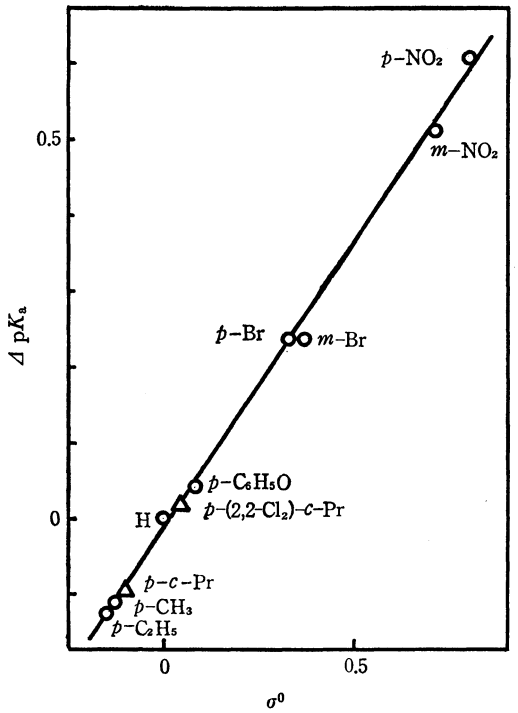

Fig. 2. Correlation of dissociation of phenylacetic acids in 50% ethanol with σ^0.

0.994, Fig. 2). It seemed reasonable to determine the σ^0 values for cyclopropyl and 2,2-dichlorocyclopropyl groups on the basis of this correlation.

Table 3. Substituent constants of alkyl groups

Substituent	σ^0	σ	σ^+	$\Delta\bar{\sigma}_R{}^+$
H	0.000	0.000	0.000	0.000
p-CH_3	−0.124[a]	−0.170[b]	−0.311[c]	−0.187[a]
p-i-C_3H_5	−0.156[a]	−0.15[b]	−0.280[c]	−0.124[a]
p-c-C_3H_5	−0.10± 0.01[d]	−0.22[d]	−0.45[d]	−0.35[d]
p-(2,2-Cl_2-c-C_3H_5	+0.05[d]		−0.02[d]	−0.07[d]
p-t-C_4H_9	−0.174[a]	−0.197[b]	−0.256[c]	−0.082[a]
p-C_6H_5	+0.062[a]	−0.01[b]	−0.156[c]	−0.218[a]
m-CH_3		−0.069[b]		
m-c-C_3H_6		−0.036[d]		

a) Ref. 13.
b) J. E. Leffler and E. Grunwald, "Rates and Equilibria of Organic Reaction," John Wiley & Sons, New York (1963), Chapt. 6, p. 128.
c) Ref. 23.
d) Present study.

The obtained σ^0 value for cyclopropyl (Table 3) shows more electron-withdrawing behavior than in other p-alkyl groups. This is inconsistent with Pews and Ojha's report, in which the σ^0 values for the cyclopropyl and ethyl groups, determined from the ^{19}F NMR chemical shift of fluorobenzenes,[3] are nearly identical. The tendency observed in present study, however, is in agreement with that of σ_m[8] and the kinetic results of the solvolysis, where the direct conjugative interaction between substituent and reaction site makes no contribution.[7,8,10] The relative electron-withdrawing effect of cyclopropyl is attributable to the inductive-electron attracting effect of the three-membered ring, which is constructed with a slightly increased electronegative carbon atom compared with the alkyl groups. This result is a proof of the proposed molecular orbital structures of cyclopropane,[1,22] in which the exo orbital of cyclopropane possesses considerably more s orbital character than sp^3. The σ^0 values of 2,2-dichlorocyclopropyl show a considerably strong inductive effect of the group caused by the highly electronegative chlorine atom. This is incompatible with the σ^* values[11] calculated from the pK_a of 2,2-dichlorocyclopropylacetic acid. The σ^0 values are useful for the estimation of the resonance effect of cyclopropyl and 2,2-dichlorocyclopropyl groups.

Resonance Effect of Cyclopropyl and 2,2-Dichlorocyclopropyl Groups. Considerable interest has been shown in the solvolysis of cyclopropyl carbinyl derivatives,[4] in which the cyclopropyl group exhibits large rate accelerations. In the cyclopropyl carbinyl system, however, the interpretation of the effect of the group is complicated by the immediate proximity of the positive reaction center. In order to estimate the electronic effects of cyclopropyl, the substituent constant,[23] σ^+, has been determined by several workers.[5,7,8,24] Each derived value, however, is more different than the general error in σ^+ values.

Thus, in order to probe the interaction mechanism of cyclopropyl with a cationic center more precisely, it was felt that substituent constants should be derived from the representative solvolysis reaction, in which experimental errors has been minimized. The solvolysis of α-phenylethyl chlorides[25] in 80% aqueous acetone was selected for this study because, in this reaction, the relative rates may be calculated from

Table 4. Rate constants and derived data for solvolysis of α-phenylethyl chloride in 80% aqueous acetone

Substituent	Temp (°C)	$k\times10^5$ (sec^{-1})	E_a (kcal)	log A
H	45	0.729 (1.00)[a]	22.3	10.1
p-c-C_3H_5	10	5.84	19.4	10.7
	20	18.9		
	30	56.6		
	45	258[b] (353)[a]		
p-2,2-Cl_2-	45	0.905 (1.24)[a]	22.4	10.4
c-C_3H_5	55	2.67		
	65	7.85		
m-c-C_3H_5	45	1.10 (1.50)[a]	24.3	11.7
	55	3.41		
	65	8.94		

a) Relative rate at 45°C.
b) Extrapolated from Arrhenius equation.

22) C. A. Coulson and W. Moffit, *J. Chem. Phys.*, **15**, 151 (1947).
23) H. C. Brown and Y. Okamoto, *J. Amer. Chem. Soc.*, **79**, 1913 (1957); *ibid.*, **80**, 4947 (1958); H. C. Brown, "Advances in Physical Organic Chemistry," Vol. 1, Academic Press, New York (1963), Chapt. 2, p. 34.
24) W. Hanstein, H. J. Berwin, and T. G. Traylor, *J. Amer. Chem. Soc.*, **82**, 829 (1970).
25) Ref. 13, 14, Y. Yukawa, Y. Tsuno, and Y. Kusuyama, To be published in detail.

Table 5. Relative rates of solvolysis of α-(*p*-alkylphenyl)ethyl chlorides in 80% aqueous acetone at 45°C.

H	1.00	*p*-*c*-C_3H_5[b]	353
p-CH_3[a]	41.5	*p*-2,2-Cl_2-*c*-C_3H_3[b]	1.24
p-C_2H_5[a]	34.0	*p*-C_6H_5[a]	11.1
p-*i*-C_3H_7[a]	34.1	*m*-CH_3[a]	2.11
p-*t*-C_4H_9[a]	19.3	*m*-*c*-C_3H_5[b]	1.51

a) Ref. 25.
b) Present work.

only Arrhenius equation and because the results previously obtained have been sufficient to elucidate the substituent effects.[13,14]

The observed rate constants are listed in Tables 4 and 5. The solvolysis of the *p*-cyclopropyl derivative is 353 times faster than that of the parent phenylethyl chloride and 234 times faster than the *m*-cyclopropyl derivatives (45°C). This marked exaltation of the *p*-cyclopropyl group is consistent with the results of other experimental studies of cyclopropyl systems[5,7,8] and indicates the strong contribution of the resonance effect to the transition state.

In the *para* position, some rate accelerations of *p*-alkyl groups have been observed, usually in electrophilic reactions; these accelerations have been attributed to hyperconjugation.[26] However, the exaltation of cyclopropyl in this study is remarkably larger than this effect. The *p*-cyclopropyl derivative is 10 times faster than the *p*-isopropyl homologue.

The solvolysis rate is depressed by a factor of 0.036 on 2,2-dichloro substitution on the *p*-cyclopropyl group. The relative rate of the *p*-2,2-dichlorocyclopropyl derivative for unsubstituted α-phenylethyl chloride is 1.24. No marked participation in the *gem*-dichlorocyclopropyl carbinyl chloride solvolysis has been observed in Robinson's work,[11] and it has been described as anomalous in comparison with other substituted cyclopropyl carbinyl solvolyses. The inductive effect of cyclopropyl increases upon the substitution of a more negative chlorine atom, and this decreases the solvolysis rate. However, the inductive effect may be decreased by the transmission of the cyclopropyl; if so, it will be impossible for it to affect the reaction center strongly. The observed results described above indicate the major importance of the resonance effect for the cyclopropyl and the depression of the effect for the 2,2-dichlorocyclopropane ring.

Product studies of α-(*p*-cyclopropylphenyl) and α-(*p*-2,2-dichlorocyclopropylphenyl)ethyl chloride solvolysis were conducted by means of an NMR examination. Only α-(*p*-cyclopropylphenyl) and α-(*p*-2,2-dichlorocyclopropylphenyl)ethyl alcohol respectively were detected.

The resonance effect of the substituents may be evaluated strictly in terms of the following linear free-energy relationship, presented by Yukawa and Tsuno:[13,14]

$$\log k/k_0 = \rho(\sigma^0 + r\Delta\bar{\sigma}_R^+) \quad (1)$$

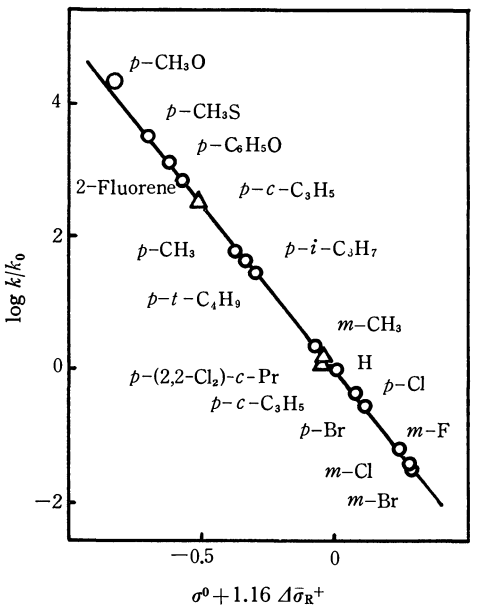

Fig. 3. Application of Eq. (1) to the solvolysis of α-phenylethyl chlorides.

where r is a constant depending on the resonance requirement of the reaction and where $\Delta\bar{\sigma}_R^+$ measures the capacities of the substituents to supply electrons by resonance. The application of the equation to the solvolysis of α-phenylethyl chlorides gave an excellent correlation,[25] with a correlation coefficient of 0.999, as is shown in Fig. 3.

$$\log k/k_0 = -4.95(\sigma^0 + 1.16\Delta\bar{\sigma}_R^+) \quad (2)$$

On the basis of this correlation, the resonance contributions of cyclopropyl and 2,2-dichlorocyclopropyl were estimated using σ^0 values obtained as has been described above (Table 3).

The $\Delta\bar{\sigma}_R^+$ for cyclopropyl indicates a marked contribution of the resonance effect. The magnitude relative to the alkyl groups is about twofold and shows the ability for a strong interaction with an electron-deficient center without ring opening. Thus, the striking exaltation in the cyclopropyl carbinyl systems is partly attributable to the behavior of the cyclopropane ring itself, although ring-opening products were generally produced. The perturbation of cyclopropyl over the hyperconjugative effect of alkyl groups may be evaluated by substructing the $\Delta\bar{\sigma}_{R\,i\text{-Pr}}^+$ from the $\Delta\bar{\sigma}_{R\,c\text{-Pr}}^+$. Thus, the value thus obtained (−0.226) indicates a remarkable ring-closure effect and an extra-delocalization of the intra-cyclic orbital of the cyclopropane ring. This situation is compatible with the two proposed molecular orbital models of cyclopropane.[1,22] The structure suggests that intra bonds possess considerable p orbital character and that they interact with the extra p orbitals of groups linked to the ring. Therefore, the mode of the contribution is different from the exalted hyperconjugation[27] and/or the σ-π vertical stabilization.[28]

26) J. W. Baker, "Hyperconjugation," Oxford Univesity Press, London (1952), p. 48.

27) J. D. Roberts and R. H. Mazur, *J. Amer. Chem. Soc.*, **73**, 2509 (1951).

28) T. G. Traylor, W. Hanstein, H. J. Berwin, N. A. Clinton, and R. S. Brown, *ibid.*, **93**, 5715 (1971).

The contribution of the resonance of 2,2-dichlorocyclopropyl is minor. The decrease in the contribution of the resonance ($\Delta\bar{\sigma}_{R\ p\text{-}c\text{-}Pr} - \Delta\bar{\sigma}_{R\ p\text{-}(2,2\text{-dichloro-}c\text{-}Pr)}$) is found to be two times that of the inductive effect ($\sigma^0_{p\text{-}c\text{-}Pr} - \sigma^0_{p\text{-}(2,2\text{-dichloro-}c\text{-}Pr)}$). The low reactivity of *p*-2,2-dichlorocyclopropyl is attributable mainly to the depression of the resonance effect by substitution with the chlorine atom. The decrease in the resonance is nearly identical with the ring-closure effect described above. It appears that, in the cyclopropyl, the developing charge was delocalized over the ring. However, in the 2,2-dichlorocyclopropyl, the chlorine atom interacts with the cyclopropane ring and the internal cyclopropane bond scarcely interacts at all with the reaction center. The exact interaction mechanism remains to be elucidated.

The solvolysis of the *m*-cyclopropyl derivative is slower than that of the *m*-methyl derivative. This fact fits previous evidence that cyclopropyl exhibits electron-attracting behavior in a system to which direct interaction with the reaction center cannot contribute as much as alkyl groups.[7,8,10,29]

The authors wish to thank Professor Yasuhide Yukawa and Yuho Tsuno for their many helpful discussions and suggestions during this work.

29) T. Sharpe and J. C. Martin, *J. Amer. Chem. Soc.*, **88**, 1815 (1966).

BULLETIN OF THE CHEMICAL SOCIETY OF JAPAN, VOL. 46, 209—212 (1973)

Polyether-amides from the Condensation of ω-(*p*-Carboxyphenoxy)-alkanoic Acids with Aliphatic Diamines

Taketoshi KITO, Tsutomu FUJIMOTO, Ryuzo MIKAMI, and Ichiro HIRAO*

Department of Chemical Engineering, Kyushu Institute of Technology, Tobata-ku, Kitakyushu
**Laboratory of Industrial Chemistry, Kyushu Institute of Technology, Tobata-ku, Kitakyushu*

(Received April 27, 1972)

Polyether-amides were prepared by the polycondensation of ω-(*p*-carboxyphenoxy)alkanoic acids (CPAA) and such aliphatic diamines as ethylenediamine, hexamethylenediamine, and piperazine. The polymers with higher intrinsic viscosities and moderate melting temperatures (200—240°C) were obtained from CPAA and hexamethylenediamine. The polymers from both CPAA and ethylenediamine or piperazine generally have low intrinsic viscosities; the former melted at higher temperatures than did the polyether-amides with hexamethylenediamine, while the latter melted at lower ones.

There are various types of polymers on the market in which polyamide, polyester, polyacrylonitrile, *etc.* are included. In addition, poly *p*-(2-hydroxyethoxy)benzoate, which can be classified as a type of polyether-ester, has been found to have some excellent characteristics as a fiber. Other polymers with an ether linkage in the main chain have been prepared from ω-(*p*-carboxyphenoxy)alkanoic acids by many authors. Izard[2] has prepared polyether-esters from ω-(*p*-carboxyphenoxy)alkanoic acids. Kawai and his co-worker[3] have prepared a polyether-ester from *p*-carboxyphenoxyacetic acid and ethylene glycol, and a polyanhydride from *p*-carboxyphenoxyacetic acid. The former melts at 90—93°C and has an intrinsic viscosity of 0.26 (in *m*-cresol at 30°C). Sofue and his co-worker[4] have reported resins prepared from ω,ω-bis(2-methoxy-4-carboxyphenoxy)alkanes and aliphatic diamines. They have inherent viscosities of more than 0.5 (0.5 g/100 ml of *m*-cresol, at 30°C) and melt at 160—230°C.

In connection with the synthesis of ω-(*p*-carboxyphenoxy)alkanoic acids, which we have already reported,[5] we attempted to prepare some polyether-amides by polycondensation from ω-(*p*-carboxyphenoxy)alkanoic acids and aliphatic diamines. They also have a phenyl nucleus and a phenyl-alkyl ether linkage and, in addition, have an amide linkage in the main chain in a repeating unit.

Results and Discussion

Nylon Salt. Nylon salts were prepared from ω-(*p*-carboxyphenoxy)alkanoic acids and aliphatic diamines, and the melting point of each salt was deter-

TABLE 1. MELTING POINT OF NYLON SALT

Type SEn: 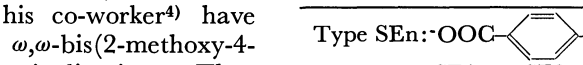						
	SE1	SE2	SE3	SE4	SE5	SE6
Mp(°C)	173	—	169.5	154.5	—	139
Type SHn: 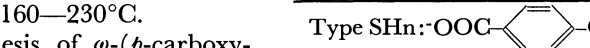						
	SH1	SH2	SH3	SH4	SH5	SH6
Mp(°C)	228	181	189	189	197	190
Type SPn: 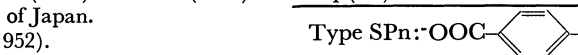						
	SP1	SP2	SP3	SP4	SP5	SP6
Mp(°C)	258.5	188	—	174	—	181
SK1: 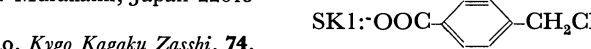						
Mp (°C), 199						

1) This paper was presented at the 24th (1971) and 26th (1972) Annual Meeting of the Chemical Society of Japan.
2) E. F. Izard, *J. Polym. Sci.*, **8**, 503 (1952).
3) W. Kawai and S. Tsutsumi, *Nippon Kagaku Zasshi*, **81**, 1167 (1960).
4) H. Sofue, K. Kaneshige, and K. Murakami, Japan 22613 (1964).
5) T. Kito, H. Minami, and I. Hirao, *Kygo Kagaku Zasshi*, **74**, 2313 (1971).

TABLE 2. POLYETHER-AMIDE

n	Polymer[a]	T_m(°C)	T_g(°C)	T_d(°C)	$[\eta]$[b]	Appearance
	Type En: Repeating unit -CO-C$_6$H$_4$-O(CH$_2$)$_n$CONH(CH$_2$)$_2$NH-					
1	E1	294	—	293	0.12	yellow, opaque
3	E3	319	76	295	0.16	white, opaque
4	E4	235	53	268	0.15	white, opaque
5	E5	273	44	279	0.49	white, opaque
6	E6	219	48	319	0.29	yellow, translucent
	Type Hn: Repeating unit -CO-C$_6$H$_4$-O(CH$_2$)$_n$CONH(CH$_2$)$_6$NH-					
1	H1	236	55	364	0.38	yellow, opaque
2	H2	—	—	—	—	rubberlike polymer, transparent
3	H3	193	53	365	0.12	white, opaque
4	H4–1	201	60	368	0.72	white, opaque
4	H4–2[c]	—	—	—	0.52	white, opaque
5	H5–1	217	58	409	0.70	pale yellow, opaque
5	H5–2[c]	—	—	—	0.98 1.05	white, opaque
6	H6–1	199	54	403	0.88	white, opaque
6	H6–2[c]	—	—	—	1.27	white, opaque
	Type Pn: Repeating unit -CO-C$_6$H$_4$-O(CH$_2$)$_n$ CON C$_4$H$_8$ N-					
1	P1	151	—	234	0.34	yellow, transparent
2	P2	—	—	—	—	yellow, viscous
3	P3	140	36	248	0.33	yellow, transparent
4	P4	130	40	296	0.31	yellow, transparent
5	P5	132	50	375	0.64	yellow, transparent
6	P6	113	41	328	0.46	yellow, transparent
	Type Kn: Repeating unit -CO-C$_6$H$_4$-CH$_2$(CH$_2$)$_n$ CONH(CH$_2$)$_6$NH-					
1	K1	263	—	393	0.49	white, opaque

a) Conditions of polymerization and of T_m, T_g, and T_d were described in the experimental.
b) In *m*-cresol at 25°C.
c) Polymerization was run in the absence of H_3PO_4.
d) Intrinsic viscosity of prepolymer.

mined by differential thermal analysis (DTA). The results are listed in Table 1. The melting point of 66-salt was determined by this method to be 198°C (lit,[6] 196—197°C). Of these salts, however, all attempts to prepare the nylon salts of SE2, SE5, SP3, and SP5 (for the symbols of SEn, SHn, and SPn, see Table 1) were unsuccessful because their analytical values of nitrogen deviated largely from the calculated values. SHn and SPn melted at higher temperatures than did SEn, and SEn and SPn melted with a loss of water, while the two endothermic peaks, that is, the melting and dehydration peaks, of SHn and 66-salt were distinguishable.

Polymerization. Seventeen polyether-amides were prepared by polycondensation. The physical properties and other characteristics are summarized in Tables 2 and 3. The polymerization consists of two steps. From the first step, the prepolymer is obtained by heating nylon salt in an autoclave for several hours, while raising the temperature gradually. From the second-step, a higher polymer is obtained by heating the prepolymer while stirring it under reduced pressure (0.1—0.5 mmHg). By this method, such ploymers as E6, H1, H3, H4, H5, H6, P4, and P6 (for the symbols of En, Hn, and Pn, see Table 2) were prepared, but E1, E3, E4, H2, P1, and P2 were prepared only by the first-step polymerization because H2 was a rubber-like polymer and we failed to raise the viscosities of E1, E3, E4, P1, and P2 by the second step polymerization. The prepolymers of E5, P3, and P5 were prepared by mixing equivalent amounts of diacid and diamine in a sealed glass-tube and by then heating it according to the procedure described in the first step polymerization.

TABLE 3. SOLUBILITY OF POLYMER IN ORGANIC SOLVENTS

Solvent	Solubility[a] (±)	Solubility[a] (−)
Acetic acid[b]	E1, E4, E6, H1, H4, P4—P6	E3, E5, H3, H5, H6, P1
Benzyl alcohol	E4, E6, H1, H3—H6, P3—P6	E1, E3, E5, P1
Dimethyl-formamide	E6, P3, P5	E1, E3—E5, P1, P4, P6

a) (±); soluble at 100°C. (−); insoluble even at 100°C
b) P3 was soluble in acetic acid at room temperature.

6) W. R. Sorenson and T. W. Campbell, "Kobunshi Gosei Zikkenho," Tokyo Kagakudozin, Tokyo (1963). p. 54.

(a) Melting Point (T_m): Although the Tm of Pn and Hn were evaluated by DTA as endothermic peaks, Pn showed no remarkable endothermic peak. Therefore, the Tm of Pn was determined as the point at which a sample reached a completely molten state.

The alternating character of the melting point associated with the methylene number was also observed in these polyether-amides, and it was found that the polymer containing an odd-numbered methylene group shows a higher melting point than that containing an even-numbered one. As is shown in Table 1, the melting points of nylon salt decreased in the order of SHn≒SPn>SEn, while, on the contrary, the melting points of polyether-amide decreased in the order of En>Hn>Pn. Especially, Pn melted at an appreciably lower temperature than did En and Hn, this being probably due to the structure of *N*-alkyl polyamide.

It is well known that the introduction of a phenyl nucleus into the main chain raises the melting point of the polymer, while the introduction of an ether linkage decreases it. For example, it has been reported that the polyamides from hexamethylenediamine and azelaic acid or sebacic acid melt at 205 and 209°C[7] respectively, while the polyamide from hexamethylenediamine and 1,4-bis(2-carboxyethyl)benzene, HOOC-CH_2CH_2- 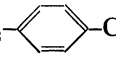 -CH_2CH_2COOH, melts at 295°C,[7] the difference being about 85°C. On the other hand, the polyamide from hexamethylenediamine and 3-(*p*-carboxymethoxyphenyl)propionic acid softens at 218°C (vicat penetrometer).[8] For the sake of comparison, a nylon salt (SK1) and polyamide (K1) analogous to SH1 and H1 respectively were prepared by us from hexamethylenediamine and 3-(*p*-carboxyphenyl)propionic acid, the latter being a diacid with an ether linkage of *p*-carboxyphenoxyacetic acid replaced by a methylene group. As a result, it was proved that K1 melted 27°C higher than H1 in spite of the fact that SK1 melted 29°C lower than SH1. The melting points of SK1 and K1 are also listed in Tables 1 and 2. The lower melting point of K1 compared with that of polyamide from 1,4-bis(2-carboxyethyl)benzene may be due to the fact that 3-(*p*-carboxyphenyl)propionic acid is an unsymmetrical diacid.

(b) Glass Transition Temperature (T_g): The glass transition temperatures of En and Hn were generally higher than that of nylon 66 or 6, but there was no such remarkable regularity between the Tg and the methylene number as was seen in Tm.

(c) Decomposition Temperature (T_d): The Td of Hn lay in the range from 360 to 410°C, while those of En and Pn were below 360°C except for P5. Under similar conditions, the weight loss of nylon 66 occurred at 361°C, which is nearly comparable to the value of H1—H4. The difference between Td and Tm was large for Hn and Pn, but small for En. The small difference for En may cause a lower intrinsic viscosity, because the polymerization was carried out in a molten state.

(d) Intrinsic Viscosity: The intrinsic viscosities of most polymers were less than 0.5; only H4, H5, H6, and P5 showed high values. In addition, it was proved that phosphoric acid was not an effective catalyst for these polymerizations. Thus, high polymers which have intrinsic viscosities of more than 1.0 were prepared in the absence of phosphoric acid.

(e) Fiber-forming Property: En did not have a fiber-forming property. Hn and Pn formed fibers when a glass rod was inserted into the molten polymer and then drawn up at a moderate rate, but only weak fibers were formed from En. H2 and P2 were rubber like and viscous materials respectively, both incapable of being formed into fibers.

Experimental

ω-(p-Carboxyphenoxy)alkanoic Acid. It was prepared according to a procedure described before.[5]

3-(p-Carboxyphenyl)propionic Acid. (a) 4-Carboxycinnamic Acid (I): A mixture of 104 g of pyridine, 2 g of piperidine, 25 g of malonic acid, and 19 g of methyl *p*-formylbenzoate was heated while being stirred for 2 hr on a water bath and was then refluxed for 30 min after 200 ml of water had been added. The reaction mixture was acidified with hydrochloric acid, and the resulting precipitate was collected on a filter and washed with water. Yield, 95%. Mp 207—208°C. Found: C, 63.90; H, 4.80%. Calcd for $C_{11}H_{11}O_4$: C, 64.06; H, 4.90%.

(b) Dimethyl Ester of (I): Twenty-six grams of (I) were esterified by refluxing for 8 hr with 200 ml of methanol and 4 ml of sulfuric acid. Yield 82%. Mp 124—124.5°C (AcOMe); lit,[9] 125.5—126.5°C. Found: C, 65.20; H, 5.48%. Calcd for $C_{12}H_{12}O_4$: C, 65.44; H, 5.50%.

(c) Methyl 3-(p-Methoxycarbonylphenyl)propionate (II): In 150 ml of methyl acetate, a 2.5 g portion of the methyl ester of (I) was dissolved. Palladium charcoal (containing 5% of palladium, 0.15 g) was added, and the mixture was hydrogenated between 50—60°C for 4 hr (the initial pressure of hydrogen was 20 kg/cm²). Yield 87%. Mp 27—28°C (aq. EtOH); lit,[10] 29—31°C (hexane). Found: C, 64.55; H, 6.21%. Calcd for $C_{12}H_{14}O_4$: C, 64.84; H, 6.36%. The IR absorption at 1644 cm^{-1} which was observed in the methyl ester of (I) disappered.

(d) 3-(p-Carboxyphenyl)propionic Acid: A mixture of 15 g of (II) and 540 ml of 5% aq. sodium hydroxide was refluxed for 2 hr. The mixture was then acidified with hydrochloric acid, and the precipitate was collected and washed with water. Yield 90%. Sublimes at about 280°C (water); lit,[10] melts at 286—289°C (AcOH). Found: C, 61.62; H, 5.16%. Calcd for $C_{10}H_{10}O_4$: C, 61.85; H, 5.19%.

Nylon Salt. (a) SE1, SH1, and SP1: Nylon salt was precipitated from an aqueous solution containing *p*-carboxyphenoxyacetic acid and an equivalent amount of diamine by dilution with methanol, and was then collected. Then, the salt was washed with ether and dried in a vacuum.

(b) SE3, SE4, SE6, SH2, SH3, SH4, SH6, SP2, SP6, and SK1: A solution of diamine in ethyl alcohol was added, drop by drop, to a boiling solution of an equivalent amount of diacid in ethyl alcohol. The salt was then filtered and recrystallized from aqueous methanol.

(c) SH5: This was prepared by the method (b), but the ethyl alcohol was replaced with *n*-propyl alcohol.

Polymerization. (a) First-step Polymerization: A mixture

7) Y. Iwakura, *Kobunshi*, **11**, 963 (1962).
8) P. R. Thomas and G. J. Tyler, Brit. 804225 (1956).
9) R. F. Heck, *J. Amer. Chem. Soc.*, **90**, 5518 (1968).
10) W. S. Emerson and R. A. Heimsch, *ibid.*, **72**, 5152 (1950).

of 10 g of nylon salt, 0.25 g of phosphoric acid, and 1.0 g of water was charged in a glass tube open at the top, and then the glass tube was placed in an autoclave. After the air had been replaced by nitrogen, the salt was heated to afford the prepolymer. The heating conditions were as follows: PE3; 150—200°C (8 hr), 200(12). PE4; ~150(3), ~180(3), ~200(2), 200(10), ~230(3). PE6; ~160(3), 160(3), ~250(2), 250(1). PH1; 150—200(2.5), ~250(5). PH2; ~150(2), ~180(1.5), ~200(2), 200(2). PH3; 150—180(2.5), ~200(4.5). PH4—1; 150—200(5), ~230(5). PH4—2(heated in the absence of phosphoric acid); ~180 (3), ~200(1.5), ~230(2), ~250(1), 250(2). PH5—1, PH5—2(see PH4—2) and PH6—1; 150—180(3), ~200(2), ~230(3.5). PH6—2(see PH4—2); 150—180(2.5), ~200 (1.5), ~250(1), 250(2). PP1; 180—200(4), ~230(6). PP2; 150—180(5). PP4; 150—180(2.5), ~200(5), PP6; 150—180(2), ~200(5.5). PK1; ~150(1), ~180(1.5), ~200(1.5), 200(1.5), ~230(3), ~250(1), 250(2). The first letter, P, in PEn, PHn, PPn, or PK1 indicates the "Prepolymer" of En, Hn, Pn, or K1.

(b) First-step Polymerization in a Sealed Tube: When nylon salt could not be prepared, a diamine and an equivalent amount of a diacid were sealed in a glass tube, and the polymerization was run according to the procedure described in (a). The heating conditions were as follows: PE5; 150—250°C (9hr), 250(10). PP3; 150—180(3.5), ~200(4.5). PP5; 150—180(2.5), ~200(3), ~250(5). However, the prepolymer of E1 was obtained by heating SE1 in a sealed tube as follows: 150—200(6), ~250(5), 250(12).

(c) Second-step Polymerization: The prepolymer was placed in a round-bottomed flask equipped with a side arm, which connected to a vacuum pump; the flask was then equipped with a mechanical air-tight stirrer and gradually brought to a high vacuum (0.5—0.1 mmHg) with heating and stirring. The heating conditions were as follows: E6; 250—265°C(6 hr). H1; 190—240(5.5). H3; 220—230(1.5). H4–1(prepared from PH4–1); 210—260(7). H4–2(from PH4–2); 220—250(5). H5–1(from PH5–1); 240—250(6). H5–2(from PH 5–2); 250—260(1). H6–1(from PH6–1); 220—270(2). H6–2 (from PH6–2); 220—270(2). P3; 200—240(5). P4; 200—230(6). P5; 210—280(6). P6; 200—260(6.5).

Melting Point (T_m) and Decomposition Temperature (T_d). The Tm was determined by observing the point at which the sample reached a completely molten state (for Pn) or by DTA (for En and Hn) (Rigaku Denki, cat. No. 8001MS; heating rate, 10°C/min). In the latter method, the Tm was defined as the intersecting point of a base line and a tangent line of the peak on the lower-temperature side. The Td was measured by TGA (Cho Keiryoki, TRDA$_1$-L; heating rate, 2.8°C/min in N_2) and was defined as the temperature at which the weight loss began to occur.

Glass Transition Temperature (T_g). The Tg was measured by means of a dilatometer.

Intrinsic Viscosity. The specific viscosity was measured in *m*-cresol at 25°C with an Ubbelohde viscometer, plotted *versus* the concentration, and extrapolated to zero.

Solubility in a Solvent. A mixture of 0.1 g of a sample and 3 ml of a solvent was allowed to stand for 24 hr at room temperature, with occasional shaking. If a clear solution was obtained by this treatment, the plus sign (+) was given. When some solid mass remained insoluble in a solution, the mixture was kept at about 100°C for 10 min with shaking; the plus-minus sign (±) was given when the solution became clear, and the minus sign (−), when some solid mass still remained insoluble.

BULLETIN OF THE CHEMICAL SOCIETY OF JAPAN, VOL. 46, 212—218 (1973)

Peptide Synthesis *via* *N*-Acylated Aziridinone. I. The Synthesis of 3-Substituted-1-benzyloxycarbonylaziridin-2-ones and Related Compounds[1)]

Muneji MIYOSHI

Department of Synthetic Chemistry, Research Laboratory of Applied Biochemistry, Tanabe Seiyaku Co., Ltd., Kashima-cho, Higashiyodogawa-ku, Osaka

(Received April 27, 1972)

Optically-active 3-substituted-1-benzyloxycarbonylaziridin-2-ones were synthesized from the corresponding benzyloxycarbonyl L-amino acids by the use of a dehydrating agent, such as phosgene, thionyl chloride, or phosphorus oxychloride. The reaction was carried out in THF at −20——30°C using triethylamine to neutralize the reaction solution exactly. Among the other *N*-protecting groups used in peptide chemistry, *p*-bromobenzyloxycarbonyl and *p*-chlorobenzyloxycarbonyl amino acids also gave the corresponding aziridinones quantitatively. Some of these *N*-acylated aziridinones were obtained in the crystalline form. A reaction mechanism was also described.

In 1908, Leuchs[2)] proposed aziridinone as a reactive intermediate when his *N*-carboxy-α-amino acid anhydride (NCA) rapidly lost carbon dioxide on heating to form polypeptide. Since then, aziridinone has been suggested as a possible reactive intermediate in peptide synthesis, though it has never been isolated from either amino acid or peptide derivatives.

In 1961, in the course of his studies of the Favorskii-

1) A part of this study has been reported in a preliminary communication. This Bulletin, **43**, 3321 (1970). Also presented at the 8th Symposium on Peptide Chemistry, Osaka, Nov. 1970, and at the 24th Annual Meeting of the Chemical Society of Japan, Osaka, April, 1971.

2) H. Leucks and W. Geiger, *Ber.*, **41**, 1721 (1908).

type rearrangement of *N*-*t*-butyl-*N*-chloroamide, Baumgarten[3] first detected an aziridinone as the intermediate; though it could not be isolated in a pure form, it showed a carbonyl band at 1847 cm^{-1} in IR spectra. One year later, he[4] succeeded in isolating *N*-*t*-butyl-3-phenyl-aziridinone.

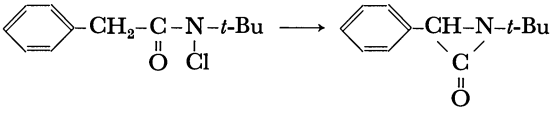

Recently, some of the aziridinones have been synthesized and their physical and chemical properties have also been clarified[5-9] to some extent. The typical synthetic routes reported so far are attributed to the dehydrohalogenation of either *N*-haloamides or α-haloamides, and it has been revealed that the *N*-substituent decisively influences the ease of ring formation and the stabilization of the corresponding aziridinone. All the aziridinones synthesized to date have the *N*-substituent, which is an electron-donating and sterically bulky alkyl group. Among them, *N*-*t*-butyl and *N*-adamantyl aziridinones have both been isolated in the pure form.

On the other hand, the reaction of an amino acid with phosgene ($COCl_2$) or thionyl chloride ($SOCl_2$) has been widely studied since Leuchs first obtained NCA. In 1950, Katchalski and Ben-Ishai[10] reported an improved route of synthesizing NCA by the use of benzyloxycarbonyl L-amino acid (Z-AA) and excess $SOCl_2$ at 40—60°C. One year later, Wieland and Bernhard[11] reported that Z-AA reacted with $COCl_2$ at 0°C in the presence of a *t*-amine to form Z-amino acid anhydride. The variety of products formed in each reaction depends upon both the reaction temperature and the presence or absence of the *t*-amine.

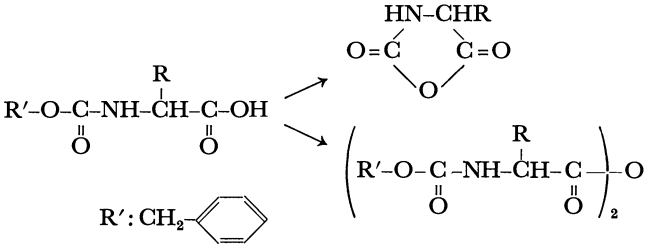

In the present paper, I wish to report a new synthesis of *N*-acylated aziridinones, which have an optically-active asymmetric carbon at *C*-3, from the corresponding L-acylamino acid. Some of them are isolated in the crystalline form.

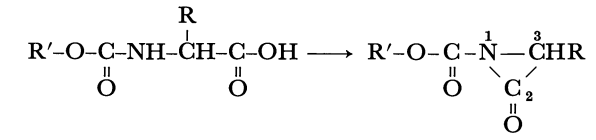

Results and Discussion

Synthesis of 3-Substituted-1-benzyloxycarbonylaziridin-2-ones. Z-AA dissolved in tetrahydrofuran (THF) did not react with an equivalent $COCl_2$ under stirring at −20——30°C during the first 30 minutes. As an equivalent triethylamine (TEA) in ether was added drop by drop, triethylamine hydrochloride (TEA–HCl) was formed, and a thin-layer chromatograph (tlc) developed in the buffer solution ($CHCl_3$: AcOEt: AcOH, 85: 15: 3) showed a new spot (R_f 0.4), which was detected by ninhydrin. When another equivalent TEA was added, drop by drop, to the mixture at the same temperature and the reaction solution was neutralized exactly, a different spot (R_f 0.9) appeared almost quantitatively. The IR spectra of the reaction solution at each reaction step are summarized in Table 1.

Table 1. IR of the reaction solution

Reaction solution	R_f	IR (cm^{-1})
Z-AA	0.5	$\nu_{C=O}$ 1715, 1690 ν_{NH} 3300
After adding an eq. TEA	0.4	$\nu_{C=O}$ 1790, 1720 ν_{NH} 3200
After adding two eq. TEA	0.9	$\nu_{C=O}$ 1840, 1690 ν_{NH} —

In order to isolate the final product of this reaction, ether was added to the reaction mixture at −20°C, the mixture was then quickly filtered to remove the TEA–HCl formed, and the filtrate was evaporated under reduced pressure on an ice-bath. Then to the residue were added ether and petroleum ether, and the mixture was kept in a refrigerator overnight. A small amount of the remaining Z-AA and the TEA–HCl precipitated was filtered off, and the filtrate was evaporated again. This procedure was repeated a few times, until the tlc of the solution showed a single spot at R_f 0.9. Attempts to crystallize the oil obtained after concentration did not succeed in most cases, though the oil in each case was rather stable at low temperatures.

Fortunately, when Z-L-phenylalanine (Z-Phe) was treated in the same manner, the product was obtained in the crystalline state in a refrigerator; it was subsequently recrystallized from ether and petroleum ether to afford colorless needles with mp of 73.0—73.5°C. $[\alpha]_D^{20}$ −36.0° (*c* 1, THF). IR: $\nu_{C=O}$; 1840, 1690 cm^{-1}. The results of elementary analysis agreed with the dehydration product of Z-Phe, and its structure was confirmed to the 3-benzyl-1-carbobenzoxyaziridin-2-one (I) from these results and other observations, which will be discussed later.

From a further study of this dehydration reaction, it was found that 3-substituted-1-benzyloxycarbonyl-

3) H. E. Baumgarten, R. L. Zey, and U. Krolls, *J. Amer. Chem. Soc.*, **83**, 4469 (1961).
4) H. E. Baumgarten, *ibid.*, **84**, 4975 (1962).
5) H. E. Baumgarten and J. F. Fuerholzer, *ibid.*, **85**, 3303 (1963).
6) J. C. Sheehan and I. Lengyel, *ibid.*, **86**, 1356 (1964); J. C. Sheehan and J. H. Beeson, *ibid.*, **89**, 362 (1967); J. C. Sheehan and M. M. Nafissi-V, *ibid.*, **91**, 1176 (1969); J. C. Sheehan and I. Lengyel, *Angew. Chem.*, **80**, 27 (1968).
7) I. Lengyel and D. B. Uliss, *Chem. Commun.*, **1968**, 1621.
8) K. Bott, *Tetrahedron Lett.*, **1968**, 3323.
9) E. R. Talaty and A. E. Dupuy, Jr., *Chem. Commun.*, **1968**, 790; E. R. Talaty and C. M. Utermoehlen, *ibid.*, **1970**, 473; E. R. Talaty, C. M. Utermoehlen, and L. H. Stekoll, *ibid.*, **1971**, 543.
10) E. Katchalski and D. Ben-Ishai, *J. Org. Chem.*, **15**, 1067 (1950).
11) T. Wieland and H. Bernhard, *Ann. Chem.*, **572**, 190 (1951).

Table 2. Analytical data of aziridinones

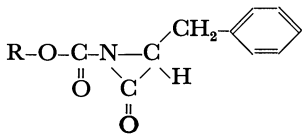

R	Mp (°C)	$[\alpha]_D^{20}$ in THF	Analysis (Calcd) C	H	N	
(I) $C_6H_5-CH_2-$	73—73.5	−36.0	(72.58) 72.60	(5.37) 5.33	(4.98) 5.11	
(II) Br-$C_6H_4-CH_2-$	86—87	−11.0	(56.68) 56.58	(3.92) 4.00	(3.89) 3.89	Br (22.19) 21.79
(III) Cl-$C_6H_4-CH_2-$	81—82	−26.5	(64.66) 64.40	(4.47) 4.46	(4.44) 4.45	Cl (11.23) 11.27

aziridin-2-ones were also synthesized by the same treatment using $SOCl_2$ or phosphorus oxychloride ($POCl_3$) instead of $COCl_2$. When Z-Phe was used as the starting material, the corresponding crystalline aziridinone was obtained; it was identified with the specimen afforded above.

When $SOCl_2$ was used as the dehydrating agent, one more equivalent TEA was required for the neutralization of the reaction solution to form a brown-colored SO_2–TEA complex.[12]

Synthesis of Other N-*Acylated Aziridinones.* Various *N*-protecting groups commonly used in peptide chemistry were examined by the treatment and reaction conditions used for Z–AA. A remarkable difference among them was observed.

Ring formation to the aziridinone proceeded when *p*-bromobenzyloxycarbonyl (Br–Z) and *p*-chlorobenzyloxycarbonyl (Cl–Z) amino acids were used. The dehydration of Br-Z-L-phenylalanine and Cl-Z-L-phenylalanine was carried out successfully, with the aid of equivalent $COCl_2$ in THF at −20°C, by the dropwise addition of two equivalent TEA in the way described above. Then the corresponding *N*-acylated aziridinones were obtained in the respective crystalline forms. The analytical data of these aziridinones are listed in Table 2.

When tosyl amino acid was used, considerable amounts of the corresponding *N*-acylated aziridinone were isolated, but it failed to crystallize.

On the contrary, in the case of the *p*-methoxybenzyloxycarbonyl group (PMZ), which is sterically very similar to the analogous carbobenzoxy groups mentioned above, the ring formation of PMZ amino acid proceeded with little detection.

In the cases of the *t*-butyloxycarbonyl (BOC) and *t*-amyloxycarbonyl (AOC) groups, which are widely used in solid-phase peptide synthesis, the corresponding expected aziridinones could not be detected.

When other acyl groups, such as benzoyl and acetyl, were used for the *N*-protection of amino acids, the ring compounds resulting from the treatment described above were found not to be aziridinone, but azlactone. From benzoyl-L-phenylalanine and acetyl-L-phenylalanine, the corresponding 2-substituted-4-benzyl-azlactones were obtained in good yields.

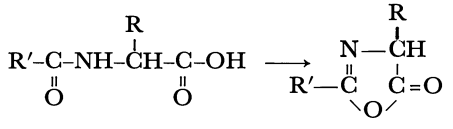

R′: CH_3, C_6H_5 (IV)

If *N*-benzyl L-amino acid was used as the starting material, optically-active benzylamino-*N*-carboxyanhydrides (*N*-Bzl-NCA) were synthesized under the same reaction condition; some of them were obtained in the crystalline form.

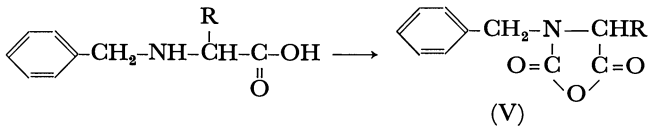

(V)

In any case, it is interesting to note that the *N*-substituents of amino acids leading to the formation of the corresponding *N*-acylated aziridinones are limited in some urethan-type groups (Z, Br–Z, Cl–Z) and the tosyl group investigated so far in this study.

Retention of Optical Activity. The aziridinones obtained to date have been synthesized by the dehydrohalogenation of *N*-haloamides or α-haloamides. Besides this type of reaction, the only optically-active aziridinone obtained *via* the optically-active α-haloamide was reported by Baumgarten[5] *et al.*

In the above route, a chance of partial racemization still remains during the abstraction of the chlorine atom on the asymmetric carbon at *C*-3.

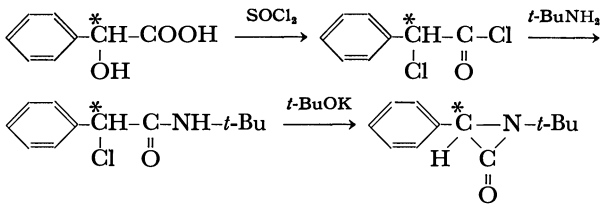

On the contrary, the new route to synthesize the *N*-acylated aziridinone reported here may be carried out by intramolecular dehydration between carboxyl and amino groups in L-acylamino acids. This new route involves no abstraction on the asymmetric carbon during the cyclization reaction, because the atomic sequence of the starting material in this study is in

12) L. C. Bateman, E. D. Hughes, and C. K. Ingold, *J. Chem. Soc.*, **1944**, 243.

striking contrast to that of haloamide.

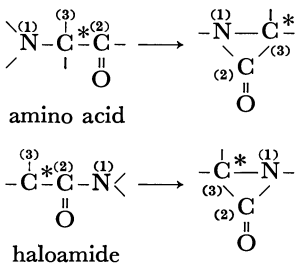

amino acid

haloamide

Accordingly, there is every possibility of retaining the whole optical activity in this new route. This fact is confirmed by deriving the aziridinones to the known optically-active amino acid derivatives.

Spectral Assay. Sheehan and Beeson[6] reported that *N*,3-di-*t*-butylaziridinone showed a carbonyl absorption band at 1835 cm^{-1} in the IR spectra. Later, the same band for *N*,3-di-adamantylaziridinone was observed at 1830 cm^{-1} by Talaty *et al.*[9]

All the *N*-acylated aziridinones obtained in this study show a carbonyl band due to the ring at 1840 cm^{-1} and the acyl carbonyl at 1690 cm^{-1}, and no amino band is detected in the range of 3100—3300 cm^{-1}. The IR spectra of II and III, which are typical examples of these aziridinones, are shown in Fig. 1.

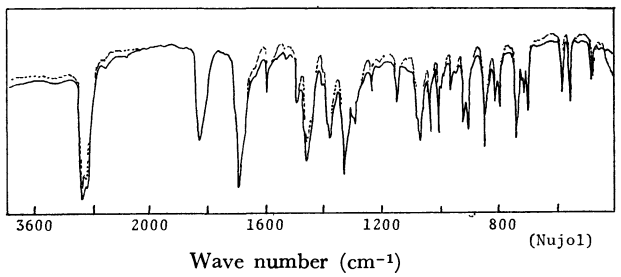

Fig. 1. IR spectra of aziridinones
—— II; ——III

The NMR data of the three crystalline aziridinones and Z-Phe which is the starting material of I, are shown in Table 3 and Fig. 2.

The triplet of the methine proton on the *C*-3 of I at 4.55 (δ) is caused only by the AB-type coupling with the methylene proton of the benzyl group. On the contrary, the methine proton of Z-Phe shows a quartet at 4.67 (δ) due to the adjacent amino proton.

The mass spectrum of the parent molecular ion of

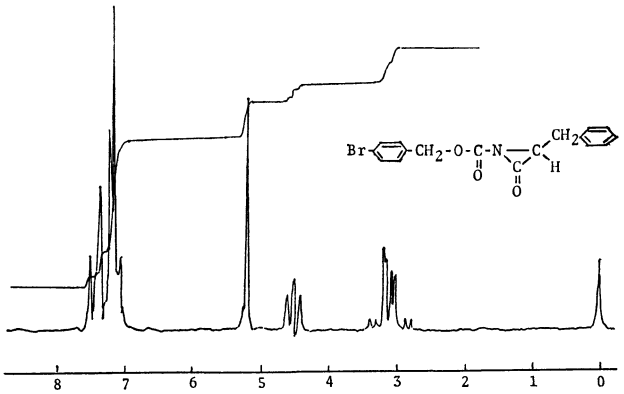

Fig. 2. NMR spectrum of II

I shows *m/e* 281 ($C_{17}H_{15}NO_3$). The *m/e* 253, which is derived from the fisson of the aziridinone ring, and *m/e* 238, 209, 192, 181, 162, 146, 128, 118, 117, and 91 ions are observed. Some of these assignments are shown in Scheme 1.

The mass spectra of II and III show M^+ 362 ($C_{17}H_{14}NO_3 \cdot Br$) and 315 ($C_{17}H_{14}NO_3 \cdot Cl$) respectively; the *m/e* ion values observed can also probably be identified with that of I mentioned above.

Isomeric Structures. The other possible isomeric structures, such as an epoxide (VI) and an azlactone must be taken into consideration with regard to the dehydration product from Z-Phe.

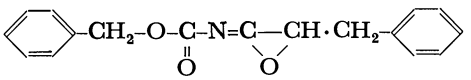

(VI)

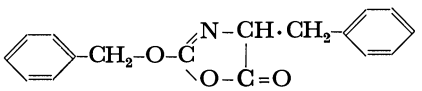

(VII)

With regard to VI, Sheehan and Beeson[6] reported the thermal decomposition of *N*,3-di-*t*-butylaziridinone at 175°C; they discussed the isomerization of the aziridinone to epoxide in order to explain the formation of pivalaldehyde and *t*-butyronitrile as the main products.

Azlactone would be another isomeric structure, though it has never yet been synthesized. Siemion

Table 3. NMR data of aziridinones
(δ, $CDCl_3$, 60 MHz)

Compound	NH	CH	CH_2- 	OCH_2- 	
I	—	4.55(*t*)	3.26(*dd*)	5.30(*s*)	7.21(*bs*)
			3.03(*dd*)		7.37(*bs*)
II	—	4.58(*t*)	3.22(*dd*)	5.26(*s*)	7.17(*bs*)
			2.95(*dd*)		7.40(*m*)
III	—	4.58(*t*)	3.23(*dd*)	5.27(*s*)	7.18(*bs*)
			2.96(*dd*)		7.38(*m*)
Z-Phe	5.45(*d*)	4.67(*q*)	3.10(*d*)	5.04(*s*)	7.18(*bs*)
					7.26(*bs*)

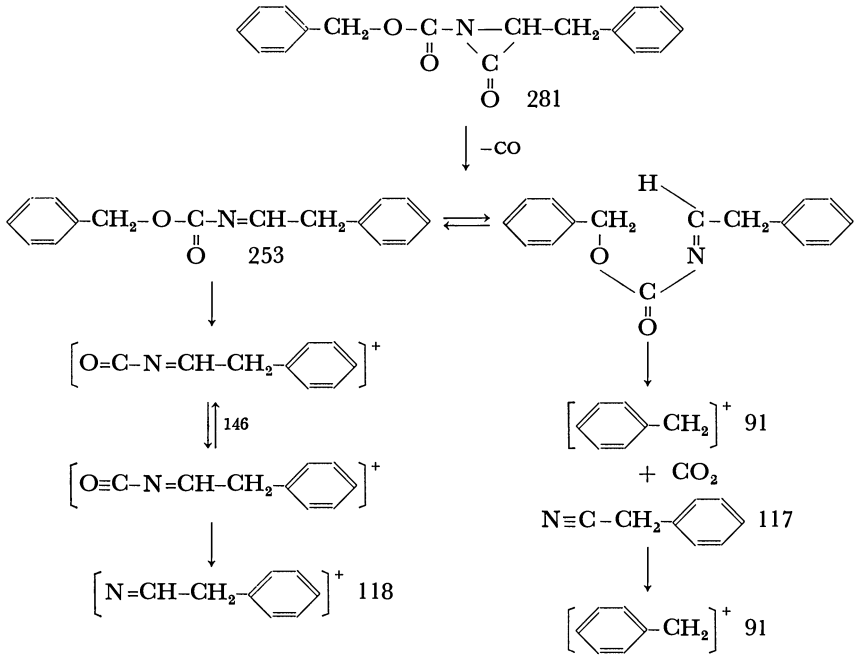

Scheme 1.

et al.[13] reported the only example of thiourethan-type azlactone (VIII), which was derived from benzyloxythiocarbonyl-L-phenylalanine; it was completely optically-inactive as had been expected. The IR spectra showed 1630 cm^{-1} ($\nu_{C=N}$) and 1720 cm^{-1} ($\nu_{C=O}$).

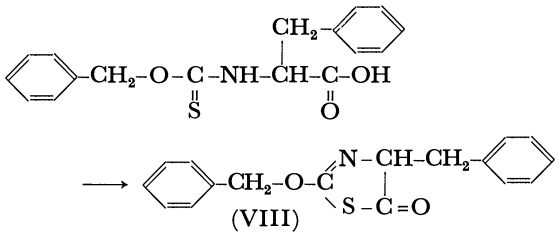

It has widely been accepted that the racemization during the peptide-coupling reaction must be caused by the formation of an azlactone.[14] Therefore, along with the results observed by the spectral assay, the retention of the whole optical activity in the dehydration product from Z–AA strongly supports that its structure should be the *N*-acylated aziridinone. To confirm the structure definitely, an X-ray analysis of Br-Z-aziridinone (II) is now in progress.

Reaction Mechanism. In the present study, dehydration of Z–AA to form 3-substituted-1-benzyloxycarbonylaziridinones took place by the use of $POCl_3$ as well as $COCl_2$ and $SOCl_2$, which contain two reactive halogen atoms in the molecule. Therefore, the pathway of this reaction may be partially similar to that of "the phosphorus oxychloride method" reported by Wieland and Heinke.[15]

A mechanistic approach was carried out using $SOCl_2$ as the dehydrating agent. In this case, three equivalent TEA are required to neutralize the reaction mixture exactly, because one more TEA is consumed for the neutralization of SO_2, as has been described earlier. The SO_2–TEA complex formed in the course of the reaction is brown and is insoluble in the THF–ether contained in the reaction system. Accordingly, by cutting off the reaction at each step when the addition of every equivalent TEA is over, the entire reaction may be divided into three steps. The TEA–HCl or SO_2–TEA complex precipitated at the end of each step of the reaction is collected by filtration.

It was found that an equivalent TEA–HCl was recovered almost quantitatively at the end of the first step, and that during this step the tlc of the reaction solution showed no aziridinone at R_f 0.9. At the end of the second step, when another equivalent TEA was added, the mass collected by filtration was rather small in amount and was still colorless, while tlc showed that the reaction proceeded about a half. A mixture of the rest of the TEA–HCl and an equivalent SO_2–TEA complex, which was brown in color, was obtained quantitatively in the last step of the reaction, when the reaction solution was neutralized exactly and the formation of the aziridinone was accomplished.

It is evident that $SOCl_2$ does not act as a chlorinating agent, but as a dehydrating one, at the lower temperatures treated in this study, and that the reaction proceeds *via* a mixed anhydride resulting from dehydrohalogenation between Z–Phe and $SOCl_2$ with the aid of TEA.

It should be noted that the use of ethylchloroformate or benzenesulfonyl chloride, commonly used as the mixed anhydride reagents in peptide chemistry, did not cause the ring closure under the above reaction conditions. Thus, another halogen atom containing in the intermediate mixed anhydride formed from Z–Phe and $SOCl_2$ must play an essential role as an effective leaving group in forming such a strained aziridinone. The abstraction of the hydrogen atom from the amino

13) I. S. Siemion, D. Konopinska, and Dzugaj, *Roczniki Chemii, Ann. Soc. Chim. Polonorum*, **43**, 989 (1969); I. Z. Siemion and D. Konopinska, *ibid.*, **44**, 785 (1970).

14) Optically active 2-phenyl-L-4-benzyl-azlactone was reported. M. Goodman and L. Levine, *J. Amer. Chem. Soc.*, **86**, 2918 (1964).

15) T. Wieland and B. Heinke, *Ann. Chem.*, **599**, 70 (1956).

nitrogen may take place by TEA, accompanied by the formation of TEA–HCl. Consequently, the nucleophilic attack of nitrogen to the carbonyl carbon would lead to the formation of an aziridinone ring.

The ease of abstraction of the hydrogen atom in the amino nitrogen may also be connected with the electronegativity of the nitrogen atom itself caused by the effect of *N*-substituents. The fact that PMZ–AA gave scarcely any of the corresponding aziridinone may be attributed to the relatively greater electronegative property of the urethan oxygen of the PMZ group in comparison with that of the Z group. The above electronegativity of the urethan oxygen of the PMZ group would affect the electron density of the amino nitrogen enough to prevent the abstraction of the hydrogen atom under the circumstances used in this study. It is well known that PMZ–AA is cleaved much more easily than Z–AA under mild acidic conditions. Similarly, in the cases of BOC–AA and AOC–AA, which are also easily cleaved under the same acidic conditions, the corresponding aziridinones were not obtained.

Experimental

The melting points are uncorrected. Thin-layer chromatography (tlc) was performed with silica gel G (Merck), and the spots were detected by ninhydrin on heating at 100°C after developing in a buffer solution ($CHCl_3$: AcOEt: AcOH, 85: 15: 3). The IR spectra were obtained using a Shimadzu IR-27G apparatus. The NMR spectra were recorded at 60 MHz in $CDCl_3$ with TMS as the internal standard using a Hitachi R-20A apparatus. The mass spectra were obtained by means of a Hitachi RMS-4 mass spectrometer. The optical rotations were measured with a Yanagimoto OR-100 apparatus.

The THF, ether and petroleum ether used throughout this experiment were dried over sodium metal wire after distillation. The $COCl_2$ gas was absorbed in dry ether to prepare the $COCl_2$–ether solution which was then stored in a refrigerator. The $SOCl_2$, $POCl_3$, and TEA were purified by distillation before use.

3-Benzyl-1-benzyloxycarbonylaziridin-2-one (I). (a) To a solution of Z-Phe (14.95 g, 0.05 mol) in 200 ml of THF was added $COCl_2$–ether solution (25 ml, containing 0.05 mol of $COCl_2$) at −20°C. TEA (7 ml, 0.05 mol) in 15 ml of ether was then added drop by drop to the solution over a period of 30 min, with stirring at −20°C. Tlc showed a spot at R_f 0.4. After 30 min, TEA (7 ml, 0.05 mol) in 15 ml of ether was added again to the reaction mixture under the same conditions as above. A spot appeared at R_f 0.9 on tlc. After an additional 30 min of stirring, 200 ml of ether was added to the reaction mixture. The TEA-HCl thus precipitated in a quantitative yield was removed by filtration, and the filtrate was evaporated under reduced pressure on an ice-bath. To the residue were added ether (200 ml) and petroleum ether (100 ml), then the mixture was stored in a refrigerator overnight. After the removal of a small amount of precipitate by filtration, the filtrate was evaporated again in the same manner as above. Then, ether (100 ml) and petroleum ether (300 ml) were added to the residue, which was then crystallized in a refrigerator for three days. The crude products thus formed were collected by filtration to afford 10.2 g (73%). For recrystallization, to the crude product was added 100 ml of ether at 0°C. After the removal of a small amount of undissolved material by filtration, petroleum ether (200 ml) was added to the filtrate, which was stored again in a refrigerator for several days to afford colorless needles (6.74 g, 48%). Recrystallization was then repeated once more in the same manner to give an analytical sample.

(b) Freshly distilled $SOCl_2$ (5.95 g, 0.05 mol) in 30 ml of ether was added to a solution of Z-Phe (14.95 g, 0.05 mol) in 200 ml of THF at −30°C. To the solution was added TEA (14 ml, 0.1 mol) in 30 ml of ether, drop by drop, over a period of 1 hr with stirring. Tlc showed two spots, at R_f 0.4 and 0.9. Then TEA (7 ml, 0.05 mol) in 15 ml of ether was added drop by drop to the reaction mixture at the same temperature. The reaction mixture gradually turned brown. After an additional 30 min, ether was added to the mixture; the mixture was subsequently filtered to romove quantitative yields of the TEA-HCl and SO_2-TEA complex thus precipitated; the yellowish filtrate, which showed a spot at R_f 0.9 on tlc, was then worked up in the manner described in (a). Subsequent recrystallization from ether and petroleum ether gave colorless needles (3.5 g, 25%), which were identified with those afforded by (a).

*3-Benzyl-1-*p*-bromobenzyloxycarbonylaziridin-2-one (II).* Br-Z-Phe[16] was prepared by a Schotten-Baumann reaction with L-phenylalanine and *p*-bromobenzyloxycarbonyl chloride. Mp 107—109°C. $[\alpha]_D^{20}$ −8.9° (*c* 1, MeOH). To a solution of Br-Z-Phe (7.56 g, 0.02 mol) in 50 ml of THF was added the $COCl_2$–ether solution (10 ml, containing 0.02 mol of $COCl_2$) at −20°C. TEA (5.6 ml, 0.04 mol) in 12 ml of ether was then added over a period of 1.5 hr to neutralize the reaction mixture at −20°C in the same manner as had been described above. Colorless prisms of II (3.2 g, 44%) were obtained after recrystallization.

*3-Benzyl-1-*p*-chlorobenzyloxycarbonylaziridine-2-one (III).* Cl-Z-Phe was synthesized with L-phenylalanine and *p*-chlorobenzyloxycarbonyl chloride in the same manner as Br-Z-Phe. Mp 80.5—82.0°C. $[\alpha]_D^{20}$ −7.5° (*c* 1, MeOH). To a solution of Cl-Z-Phe (6.66 g, 0.02 mol) in 50 ml of THF was added the $COCl_2$–ether solution (10 ml, containing 0.02 mol of $COCl_2$) at −20°C; TEA (5.6 g, 0.04 mol) in 12 ml of ether was subsequently added in the same manner as above to afford III as colorless needles (2.3 g, 37%) after recrystallization.

4-Benzyl-2-phenyl-5-oxazolone (IV). To a solution of benzoyl-L-phenylalanine (26.9 g, 0.1 mol) in 200 ml of THF was added the $COCl_2$–ether solution (50 ml, containing 0.1 mol of $COCl_2$) at −30°C. TEA (28 ml, 0.2 mol) in 80 ml of ether was then added dropwise over a period of 1.5 hr in order to completely neutralize the reaction mixture at the same temperature. A 200 ml portion of ether was then added to the reaction mixture, which was subsequently filtered to remove the TEA-HCl precipitated; the filtrate was evaporated *in vacuo* on an ice-bath. To the residue was added 300 ml of ether; the mixture was washed with an ice-cold 5% sodium bicarbonate aqueous solution and dried over magnesium sulfate. The organic layer was evaporated to about half its volume, and 150 ml of petroleum ether was added to the solution, which was then stored in a refrigerator overnight to afford 19.4 g of IV (73.3%). Recrystallization from ether and petroleum ether gave colorless needles (14.7 g, 58.6%). Mp 72—74°C. IR $\nu_{C=O}$ 1830, 1815 cm^{-1}. $\nu_{C=N}$ 1655 cm^{-1}. NMR (δ) 7.27 (bs, 5H), 7.69 (m, 4H), 4.68 (t, 1H), 3.42 (dd, 2H), 3.13 (dd, 2H). Found: C, 76.13; H, 5.18; N, 5.38%. Calcd for $C_{16}H_{13}NO_2$: C, 76.47; H, 5.22;

16) D. M. Channing, P. B. Turner, and G. T. Young, *Nature*, **167**, 487 (1951).

N, 5.57%. $[\alpha]_D^{20}$ 0° (*c* 1, THF).

3-Benzyl-4-phenyl-2,5-oxazolidinedione (V). A Schiff base from L-phenylglycine and benzaldehyde was reduced by catalytic hydrogenation to afford *N*-benzyl-L-phenylglycine. Mp 222—224°C. $[\alpha]_D^{20}$ +92.4° (*c* 1, AcOH). To a solution of *N*-benzyl-L-phenylglycine (4.8 g, 0.02 mol) in 15 ml of THF was added the $COCl_2$–ether solution (10 ml, containing 0.02 mol of $COCl_2$) at −30°C. TEA (5.6 ml, 0.04 mol) in 12 ml of ether was then added, drop by drop, in the manner described above. After the removal of the TEA–HCl precipitated by filtration, the filtrate was evaporated *in vacuo* on an ice-bath. To the residue was then added 300 ml of ether, and the mixture was washed with an ice-cold 5% sodium bicarbonate aqueous solution and dried over magnesium sulfate. Crystallization from ether and petroleum ether (1 : 2) gave 2.6 g of V. Mp 120—122°C. IR $\nu_{C=O}$ 1850, 1760 cm^{-1}. NMR (δ) 7.04—7.55 (m, 10H), 4.90 (s, 1H), 4.44 (q, 2H). Found: C, 71.79; H, 5.08; N, 5.28%. Calcd for $C_{16}H_{13}NO_3$: C, 71.90; H, 4.90; N, 5.24%. $[\alpha]_D^{20}$ +124.0° (*c* 1, THF).

The author wishes to express his hearty gratitude to Dr. S. Sakakibara for his guidance and to Professor I. Murata for his valuable advice on the spectral assay. Acknowledgement is made to Dr. T. Takayanagi and Dr. I. Chibata of Tanabe Seiyaku Co., Ltd., for their encouragement. Thanks are extended to Mr. H. Tamura for his assistance in the experimental work.

BULLETIN OF THE CHEMICAL SOCIETY OF JAPAN, VOL. 46, 218—221 (1973)

Syntheses of Isoprenoids by Telomerizations. VIII.[1,2] Anionic Telomerizations of Isoprene with Secondary Amines

Kunihiko TAKABE, Takao KATAGIRI, and Juntaro TANAKA

Department of Synthetic Chemistry, Faculty of Engineering, Shizuoka University, Hamamatsu

(Received January 11, 1972)

The anionic telomerizations of isoprene with secondary amines in the presence of alkali-metal catalysts were investigated under several conditions. The $n=2$ telomers were found to contain *N,N*-dialkyl(3,7-dimethyl-2,6-octadienyl)amine (**2A**) and *N,N*-dialkyl(2-isopropenyl-5-methyl-4-hexenyl)amine (**2B**) as the main components, $n=1$ and $n=3$ telomers were also identified. On the basis of these results, the mechanism of this anionic telomerization and the reactivity of the carbanions connected with this reaction were discussed.

It has been known that the naturally-occurring monoterpenes have 4,1-(geranyl-, neryl-, linalyl-, and terpinyl-) mainly and 4,3-(lavandulyl) coupled skeletons of isoprene. Many investigations have been made of the syntheses of these terpenes by means of the telomerizations of isoprene, but the C_{10} telomers obtained by cationic[3-5] or radical-initiated[6] telomerizations contain many products, and the yield of acyclic monoterpenes is low.

No studies of the synthesis of the terpenoids by anionic telomerization[7] have been carried out. Therefore, the anionic telomerizations[8] of isoprene with secondary amines were studied in detail. In this paper, we wish to report on the structures of the telomers, the reaction scheme, and the reactivity of the carbanions connected with this reaction.

Results and Discussion

The Structure of the Telomers. The structures of the telomers obtained were identified by means of IR, NMR, and the mass spectra; they are summarized in Tables 1 and 2.

Reaction Scheme. The yields of the telomers and the ratios of **1A/1B** obtained under various conditions are shown in Table 3. When the molar ratio of isoprene to diethylamine was 1/2, the $n=2$ telomers were not formed. The order of the catalytic activity was K>Na>Li, but the ratio of **1A/1B** was the reverse. Table 4 shows that the ratio of **1A/1B** was not influenced by the reaction time, and was nearly constant.

Therefore, the mechanism of this reaction is similar to that of alkali metal-catalyzed reactions of isoprene with alkylaromatics[9] and can be formulated as follows;

1) A part of this work was presented at the Annual Meeting of the Chemical Society of Japan, Osaka, April, 1971.

2) Part VII of this series: K. Takabe, T. Katagiri, and J. Tanaka, This Bulletin, **45**, 2662 (1972).

3) J. Tanaka, T. Katagiri, and T. Takeshita, *Nippon Kagaku Zasshi*, **89**, 65 (1968).

4) T. Asahara, M. Toyoda, and H. Kise, *Kogyo Kagaku Zasshi*, **72**, 1530 (1969).

5) K. Takabe, T. Katagiri, and J. Tanaka, *ibid.*, **74**, 1162 (1971).

6) T. Katagiri, K. Takabe, K. Ono, and J. Tanaka, *Nippon Kagaku Zasshi*, **91**, 393 (1970).

7) The anionic telomerizations of styrene with some *sec*-amines have been investigated in detail by Asahara *et al.* [T. Asahara, M. Seno, S. Tanaka, and N. Den, This Bulletin, **42**, 1996, 2337 (1969).]

8) The addition reactions of isoprene with some secondary amines have already been reported by Martirosyan *et al.* [G. T. Martirosyan, E. A. Grigoryan, and A. T. Bahayan, *Arm. Khim. Zh.*, **20**, 423 (1967); *Chem. Abstr.*, **68**, 48940 (1968).]

9) H. Pines and N. C. Shi, *J. Org. Chem.*, **30**, 280 (1965); W. M. Stalic and H. Pines, *ibid.*, **35**, 422 (1970).

Table 1. The structural formulas of the telomers

$n=1$	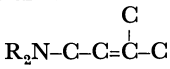	(**1A**) *N,N*-dialkyl(3-methyl-2-butenyl)amine
	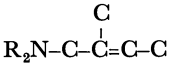	(**1B**) *N,N*-dialkyl(2-methyl-2-butenyl)amine
$n=2$	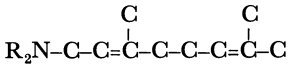	(**2A**) *N,N*-dialkyl(3,7-dimethyl-2,6-octadienyl)amine
	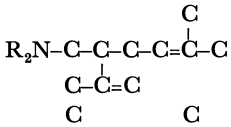	(**2B**) *N,N*-dialkyl(2-isopropenyl-5-methyl-4-hexenyl)-amine
	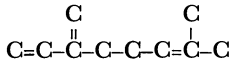	(**2H**) myrcene
$n=3$	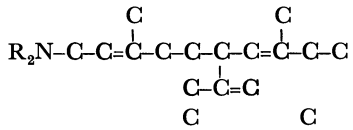	(**3B**) *N,N*-dialkyl(6-isopropenyl-3,9-dimethyl-2,8-decadienyl)amine
	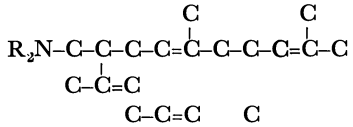	(**3C**) *N,N*-dialkyl(2-isopropenyl-5,9-dimethyl-4,8-decadienyl)amine
	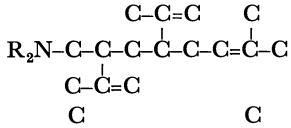	(**3D**) *N,N*-dialkyl(2,4-diisopropenyl-7-methyl-6-octenyl)amine
	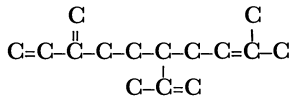	(**3H**) 6-isopropenyl-9-methyl-3-methylene-1,8-decadiene

Table 2. Characterization of the telomers

Telogen	Products (Mass; M^+)	IR (cm^{-1})	NMR (τ)
Me_2NH	**1A** (113)	1680, 817 (a trisubstituted double bond), 1020, 1040, (C–N), 2810, 2765, 2725 (R–NMe_2).	8.37(3H, s, –(CH_3)C=), 8.28 (3H, s, –(CH_3)C=), 7.90 (6H, s, CH_3–N⟨), 7.23(2H, d, J=7.2 Hz, =CH–CH_2–N⟨), 4.80 (1H, t, J=7.2 Hz, ⟩C=CH–).
	1B (113)	1680, 817 (a trisubstituted double bond), 1020, 1040 (C–N), 2810, 2765, 2725(R–NMe_2).	8.21—8.54 (6H, m, –(CH_3)C=), 7.96(6H, s, CH_3–N⟨), 7.36(2H, s, =C–CH_2–N⟨), 4.50—5.01 (1H, m, ⟩C=CH–).
	2A (181)	1665, 818 (trisubstituted double bonds), 1015, 1040 (C–N), 2815, 2760, 2720(R–NMe_2).	8.23—8.48(9H, m, –(CH_3)C=), 7.92(6H, s, CH_3–N⟨), 7.90—8.13(4H, m, =C–CH_2–CH_2–C=), 7.24 (2H, d, J=7.0 Hz, =CH–CH_2–N⟨), 4.70—5.15 (2H, m, ⟩C=CH–).
	2B (181)	1645, 883 (an end methylene group), 1670, 840 (a trisubstituted double bond), 1040 (C–N), 2815, 2760, 2720(R–NMe_2).	8.25—8.50(9H, bs, –(CH_3)C=), 7.91(6H, s, CH_3–N⟨), 7.69—8.08(5H, m, –CH_2–, ⟩CH–), 5.38 (2H, bs, ⟩C=CH_2), 5.03(1H, t, J=7.0 Hz, ⟩C=CH–).
	3B (249)	1645, 886 (an end methylene group), 1670, 830 (trisubstituted double bonds), 1040, 1015(C–N), 2815, 2760, 2725(R–NMe_2).	8.25—8.51(12H, m, –(CH_3)C=), 7.92(6H, s, CH_3–N⟨), 8.20—8.70(2H, m, –CH_2–), 7.75—8.12 (5H, m, =C–CH_2–, =C–CH⟨), 7.25(2H, d, J=7.0 Hz, =CH–CH_2–N⟨), 5.35(2H, bs, ⟩C=CH_2), 4.76—5.10 (2H, m, ⟩C=CH–).
	3C (249)	1645, 886 (an end methylene group), 1675, 840 (trisubstituted double bonds), 1040 (C–N), 2815, 2765, 2725(R–NMe_2).	8.20—8.53 (12H, bs, –(CH_3)C=), 7.90(6H, s, CH_3–N⟨), 7.70—8.18 (9H, m, –CH_2–N, =C–CH_2–, =C–CH⟨), 5.35(2H, bs, ⟩C=CH_2), 4.75—5.10(2H, m, ⟩C=CH–).
	3D (249)	1645, 885(end methylene groups), 1670, 843 (trisubstituted double bonds), 1040 (C–N), 2810. 2775, 2725(R–NMe_2).	8.25—8.52 (12H, bs, –(CH_3)C=), 7.92(6H, s, CH_3–N⟨), 8.50—8.80 (2H, m, –CH_2–), 7.80—8.12 (6H, m, –CH_2–N⟨, =C–CH_2–, =C–CH⟨), 5.38(4H, bs, ⟩C=CH_2), 4.90—5.10(1H, m, ⟩C=CH–).
Et_2NH	**1A** (141)	1670, 835 (a trisubstituted double bond), 1055, 1170, 1200 (C–N).	9.04(6H, t, J=7.1 Hz, CH_3–CH_2–N⟨), 8.39 (3H, s, –(CH_3)C=), 8.29(3H, s, –(CH_3)C=), 7.61 (4H, q, J=7.1 Hz, CH_3–CH_2–N⟨), 7.09 (2H, d, J=6.8Hz, =CH–CH_2–N⟨), 4.86(1H, t, J=6.8Hz, ⟩C=CH–).
	1B (141)	1670, 850 (a trisubstituted double bond), 1050, 1170, 1195(C–N).	9.03(6H, t, J=7.0 Hz, CH_3–CH_2–N⟨), 8.25—8.60 (6H, m, –(CH_3)C=), 7.61(4H, q, J=7.0 Hz, CH_3–CH_2–N⟨), 7.18(2H, s, =C–CH_2N⟨), 4.50—4.90 (1H, m, ⟩C=CH–).

TABLE 3. REACTIONS OF ISOPRENE WITH DIETHYLAMINES[a]

Cation	(g)	Temperature (°C)	Yield[b] of $n=1$ telomer (%)	Composition (%) (1A)	Composition (%) (1B)	(1A)/(1B)
Na	(0.2)	0—3	33	88	12	7.1
		40	64	84	16	5.4
		70	72	79	20	3.9
K	(0.3)	0—3	62	75	25	3.0
		40	80	71	18	3.9
Li	(0.1)	0—3	2	78	3	26
		40	12	95	5	20

a) Reaction condition; isoprene 6.8 g, isoprene/Et_2NH=1/2 (molar ratio), reaction time 1 hr.
b) Yields were calulated on the basis of isoprene added.

TABLE 4. REACTIONS OF ISOPRENE WITH DIETHYLAMINE[a]

Time (min)	Cat. Na Yield (%)[b]	Cat. Na (1A)/(1B)	Cat. K Yield (%)[b]	Cat. K (1A)/(1B)
15	2	6.5	51	2.7
30	43	6.8	85	2.8
60	59	6.5	89	2.9
120	82	6.4		
150	91	6.1	91	2.5

a) Reaction condition; isoprene 6.8 g, isoprene/Et_2NH=1/2 (molar ratio), cat. 0.2 g, reaction temperature 0—2°C.
b) Yields of $n=1$ telomers were calculated on the basis of isoprene.

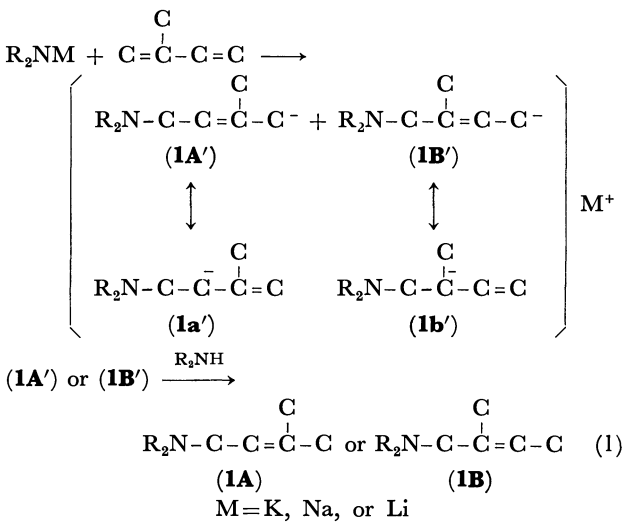

(1)

The preferential formation of **1A** over **1B** is likely to be due mainly to the difference in the stabilities of the carbanions **1A′** and **1B′** (*prim↔sec vs. prim↔tert*) and only a small extent to a steric interaction between the R group of R_2NM and the methyl group of isoprene on addition.

The effect of the molar ratio of isoprene to dimethylamine is shown in Table 5. The $n\geq 2$ telomers and a small amount of **2H** and **3H**[10] were formed as the reaction proceeded, as is shown in Table 6.

From these results, the schemes of the formation of the $n=2$ and 3 telomers are considered to be as is shown in Fig. 1.

Reactivity of Carbanions. It seems that such organosodium compounds (a) as **1A′**, **1a′**, **2A′**, **2a′**, **2B′**, **2b′**, **3A′**, **3B′**, **3C′**, and **3D′** react with isoprene or secondary amine; that is, propagation and transmetalation reactions occur competitively as follows:

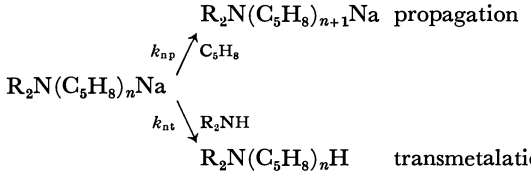

As is shown in Fig. 1 and Eq. (1), the telomers (**1A**, **1B**, **2A**, **2B**, **3A**, **3B**, **3C**, and **3D**) confirmed in this telomerization might be formed by the transmetalation of the primary carbanions (**1A′**, **1B′**, **2A′**, **2B′**, **3A′**, **3B′**, **3C′**, and **3D′**), the telomers formed by the transmetalation of the secondary carbanions (**1a′**, **2a′**, and **2b′**) were not confirmed, but it seems that these secondary carbanions react with isoprene to give the primary carbanions (**2B′**, **3B′**, and **3D′**) *i.e.*, propagation occurs.

From these results, the reactivity of the carbanions in this telomerization is considered to be as follows:

$k_{nt}[R_2NH] \approx k_{np}[C_5H_8]$ for the primary carbanions

$k'_{nt}[R_2NH] < k'_{np}[C_5H_8]$ for the secondary carbanions

TABLE 5. EFFECT OF MOLAR RATIO (ISOPRENE/Me_2NH) ON COMPOSITIONS OF TELOMERS

Molar ratio	$n=1$ telomer (g)	Composition (%) of $n=1$ telomer (1A)	Composition (%) of $n=1$ telomer (1B)	$n=2$ telomer (g)	Composition (%) of $n=2$ telomer (2A)	Composition (%) of $n=2$ telomer (2B)	Composition (%) of $n=2$ telomer (2H)	$n=3$ telomer (g)	Composition (%) of $n=3$ telomer (3B)	Composition (%) of $n=3$ telomer (3C)	Composition (%) of $n=3$ telomer (3D)	Composition (%) of $n=3$ telomer (3H)	$n\geq 4$ telomer (g)
1	2.0	76	24	t									0.2
2	2.0	54	46	2.1	12	87	t	0.3	18	18	50	t	0.6
3	1.5	16	84	2.6	14	84	2	1.6	24	26	40	t	1.0
5	0.3	6	94	3.0	32	62	4	3.0	22	34	31	2	4.7

a) Reaction condition; Me_2NH 1.8 g, Na 0.1 g, 40°C, 3 hr.

10) It is considered that these compounds have been formed by the anionic oligomerization of isoprene.[2]

Table 6. Effect of reaction time[a)]

Time (hr)	$n=1$ telomer (g)	Composition (%) of $n=1$ telomer (1A)	(1B)	$n=2$ telomer (g)	Composition (%) of $n=2$ telomer (2A)	(2B)	(2H)	$n=3$ telomer (g)	Composition (%) of $n=3$ telomer (3B)	(3C)	(3D)	(3H)	$n\geq 4$ telomer (g)
0.5	2.3	68	32	0.2	9	85	3	t					0.3
1	1.0	51	49	1.5	8	83	5	0.7	23	14	51	2	1.4
3	0.4	31	69	2.5	11	77	6	1.5	23	22	43	2	2.9
5	0.1	6	94	2.7	17	67	9	2.3	20	29	35	3	5.8

a) Reaction condition; isoprene 13.6 g, isoprene/Me_2NH=5(molar ratio), reaction temperature 15°C.

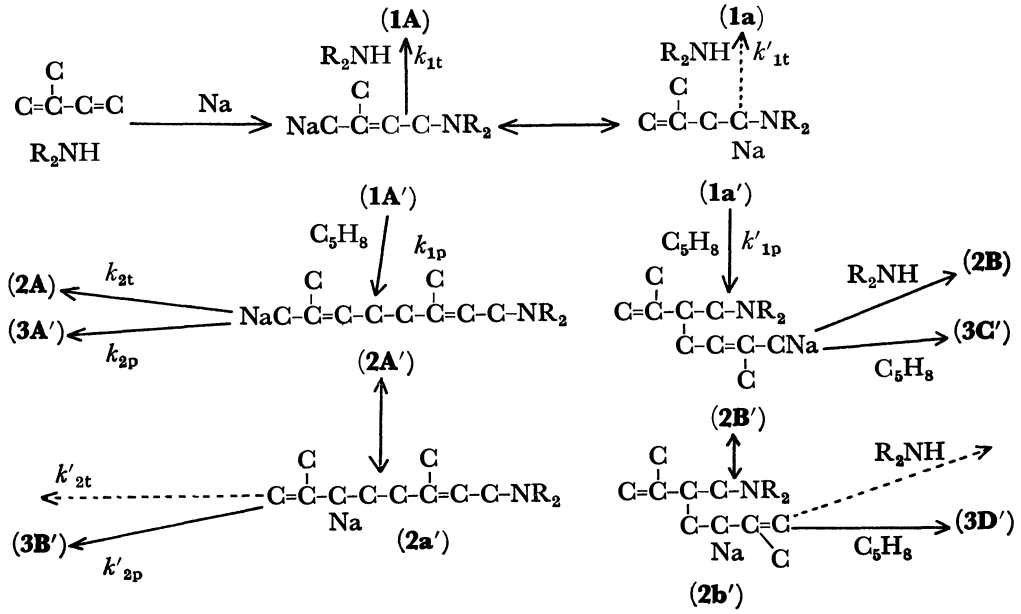

Fig. 1. Anionic telomerizations of isoprene with *sec*-amines.

Experimental

Materials. The secondary amines were commercial products of the purest grade, they were distilled and checked by glc. The isoprene was dried over anhydrous sodium sulfate and distilled in the presence of hydroquinone. The inorganic compounds were also commercial materials.

The Anionic Telomerization of Isoprene with Secondary Amine. For example, a mixture of dimethylamine (1.8 g) and isoprene (13.6 g) was placed in a pressure bottle. Then lumps of sodium (0.1 g) were added, and the mixture was allowed to react at 40°C for 3 hr while being stirring under a nitrogen atmosphere. After the reaction, the reaction mixture was cooled and treated with 10 ml of ethanol to decompose the sodium and organosodium compounds. Then the mixture was washed three times with a saturated sodium sulfate aqueous solution, and the organic layer was dried over anhydrous sodium sulfate. After the removal of the unreacted isoprene and dimethylamine under reduced pressure, the products were obtained (11.0 g). They included the $n=1$ telomer (0.3 g, bp 55—58°C/86 mmHg), and the $n=2$ telomer (3.0 g, bp 80—86°C/10 mmHg), the $n=3$ telomer (3.0 g, bp 80—90°C/1.5 mmHg), and the $n\geq 4$ telomers (4.7 g, residue), each telomer was analyzed by IR, NMR, and mass spectra after glc fractionation.

Measurements. All the products were analyzed after glc fractionation (15% Apiezone grease L/Celite 455, 4 mmϕ × 2.5 m, H_2: 50 ml/min). The IR spectra were recorded with a Perkin Elmer Model 337 spectrometer in a liquid film. The mass spectra were determined on a Hitachi RMU-7L spectrometer, and the NMR data, on a Hitachi-Perkin Elmer Model R-20 (60 MHz) spectrometer in carbon tetrachloride. The product ratios were determined by glc.

Syntheses of Isoprenoids by Telomerizations. IX.[1] Stereoselectivity of Telomers and the Effect of Telogens in Anionic Telomerizations Using Secondary Amines

Kunihiko TAKABE, Takao KATAGIRI, and Juntaro TANAKA
Department of Synthetic Chemistry, Faculty of Engineering, Shizuoka University, Hamamatsu
(Received January 20, 1972)

The stereoselectivity of the telomers and the effect of the telogens in the anionic telomerizations of isoprene with secondary amines were investigated. Dimethyl-, diethyl-, di-*n*-propy-l, diisopropyl-, and methylphenyl-amines, pyrrolidine, morpholine, and piperidine were used as the telogens. The ratio of *N,N*-dialkyl(3,7-dimethyl-2,6-octadienyl)amine(**2A**) to *N,N*-dialkyl(2-isopropenyl-5-methyl-4-hexenyl)amine(**2B**), which were obtained in these reactions, was varied with the sort of secondary amines, the yield of the telomers was found to be dependent on the acidity of the secondary amines. Moreover, **2A**, which was the main component of the $n=2$ telomers, was confirmed to have a *cis*-configuration—that is, *N,N*-dialkylnerylamine. However, the $n=1$ telomer of myrcene with secondary amine was *N,N*-dialkylgeranylamine. These results were interpreted in terms of the stability of the cyclic intermediate of the carbanions.

In the preceding paper,[1] it was reported that the anionic telomerizations of isoprene with secondary amines gave mainly *N,N*-dialkyl(3,7-dimethyl-2,6-octadienyl)amine(**2A**) and *N,N*-dialkyl(2-isopropenyl-5-methyl-4-hexenyl)amine (**2B**) as the $n=2$ telomers.

In this paper, the stereoselectivity of the telomers and the effect of the telogens in the telomerizations using several secondary amines will be discussed, and the intermediate carbanions will be presumed on the basis of these results.

Results and Discussion

Stereoselectivity of the Telomers. *N,N*-Diethyl(3,7-dimethyl-2,6-octadienyl)amine (**2A**) has two stereoisomers, *cis* and *trans*—that is, *N,N*-diethylnerylamine and *N,N*-diethylgeranylamine. The structure of the telomer (**2A**) was identified as *N,N*-diethylnerylamine from IR, mass,[2] NMR,[3] and glc analyses.[4]

On the other hand, *N,N*-diethylgeranylamine was obtained quantitatively by the anionic telomerization of myrcene (3-methylene-7-methyl-1,6-octadiene) with diethylamine.

These anionic telomerizations can be formulated by the equations shown in Figs. 1 and 2. The stereoselectivity of the telomers can be interpreted in terms of the intramolecular solvation[5,6] (coordinate metal-nitrogen bond[7]), as with **1a'** and **1Ms'** (the stability

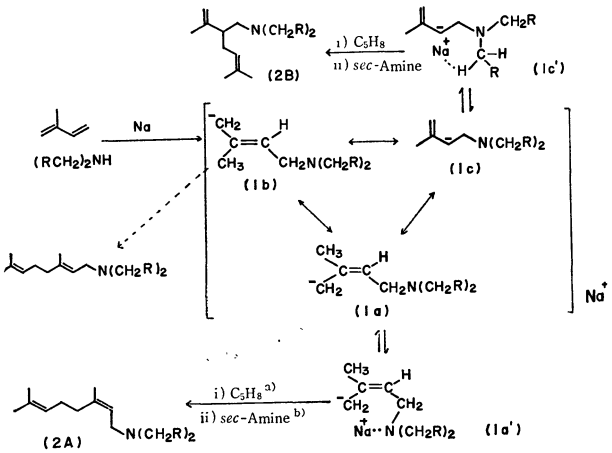

Fig. 1. Telomerization scheme of isoprene.
a) Propagation, b) Transmetalation

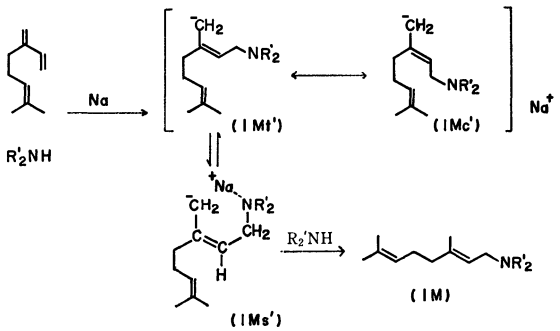

Fig. 2. Telomerization scheme of myrcene

of the carbanions: **1a'**>**1a**, **1b**, and **1Ms'**>**1Mt'**,**1Mc'**). Thus, it seems that the more stable carbanions (**1a'** and **1Ms'**) react with isoprene and the telomers (**2A** and **1M**) are formed stereoselectively.

The Effect of the Telogens. Dimethyl-, diethyl-, di-*n*-propyl-, and methylphenyl-amines were used as the telogens. The effects of these secondary amines on the yields and the compositions of the telomers are shown in Tables 1 and 2. The yields of the telomers varied with the sort of the secondary amines, they were in the following order: $Me_2NH > Et_2NH \approx (n\text{-propyl})_2NH > (\text{isopropyl})_2NH > C_6H_5NH(CH_3)$. It is possible

1) Part VIII of this series: K. Takabe, T. Katagiri, and J. Tanaka, This Bulletin, **46**, 218 (1973).

2) The data of the IR and mass spectra of **2A** agreed very closely with those of authentic *N,N*-diethylgeranylamine, which was synthesized from geranyl chloride and diethylamine.

3) Slight difference between the NMR spectrum of **2A** and that of *N,N*-diethylgeranylamine were observed in the shapes of the signals of τ 7.90—8.10(=CH-C**H**$_2$-C**H**$_2$-C=) and 8.25—8.46 (CH_3-C=).

4) The retention times of **2A** and *N,N*-diethylgeranylamine were 10.8 and 11.7 min respectively under the same glc conditions (15% Apiezon grease L/Celite 545, 2.5 m, 150°C, H_2: 50 ml/min).

5) S. Bank, *J. Amer. Chem. Soc.*, **87**, 3245 (1965).

6) Such a concept of a cyclic intermediate has also been reported in the case of *cis*-1,4-polymerization of isoprene [A. V. Tobolsky, and C. E. Rogers, *J. Polym. Sci.*, **40**, 73 (1959)].

7) D. W. Slocum and P. L. Gierer, *Chem. Commun.*, **1971**, 305.

Table 1. Effect of *sec*-amines on compositions of telomers (I)[a]

sec-Amine	Yield (g)	Composition of telomer (%)						2A/2B
		1A[b]	1B[c]	2A	2B	2H[c]	$n\geq 3$	
Me_2NH	10.2	t	2	7	23	1	66	0.3
Et_2NH	5.5	38	18	21	14	1	6	1.5
$(n\text{-Propyl})_2NH$	6.3	70	7	10	5	1	2	3.0
$(Isopropyl)_2NH$	2.8	92	—	t	t	6	—	—
$C_6H_5NH(CH_3)$	—							

a) Reaction condition; isoprene 13.6 g, isoprene/*sec*-amine=5(molar ratio), Na 0.1 g, reaction temperature 40°C, reaction time 3 hr.
b) *N,N*-Dialkyl(3-methyl-2-butenyl)amine.
c) *N,N*-Dialkyl(2-methyl-2-butenyl)amine.
d) Myrcene.

Table 2. Effect of *sec*-amines on compositions of telomers (II)[a]

sec-Amine	Yield (g)	Composition of telomer (%)						2A/2B
		1A	1B	2A	2B	2H	$n=3$	
Me_2NH[b]	8.5	2	13	6.5	39	1	37	0.2
Et_2NH	5.2	70	13	8.6	6.3	1	1	1.4
$(n\text{-Propyl})_2NH$	5.5	85	9	4.1	1.7	t	t	2.4
$(Isopropyl)_2NH$	3.8	93	—	—	—	3	t	—
$C_6H_5NH(CH_3)$	—							

a) Reaction condition; isoprene 10.2 g, isoprene/*sec*-amine=3(molar ratio), Na 0.1 g, reaction temperature 40°C, reaction time 3 hr.
b) Na 0.08 g.

Table 3. Effect of cyclic *sec*-amines on compositions of telomers

sec-Amine	Yield (g)	Composition of telomer (%)						2A/2B
		1A	1B	2A	2B	2H	$n=3$	
Pyrrolidine[b]	6.5	34	15	19	11	1.5	16	1.7
Piperidine[c]	6.3	46	19	8.0	4.5	1	19	1.8
Morpholine[d]	5.2	55	26	4.5	2.5	2	9	1.8

a) Reaction condition; isoprene 10.9 g, isoprene/*sec*-amine=4(molar ratio), benzene 15 ml, reaction temperature 50°C.
b) Na 0.2 g, reaction time 1.5 hr.
c) Na 0.1 g, reaction time 3.5 hr.
d) Na 0.1 g,reaction time 6 hr.

to explain these results by considering the acidity of the secondary amines[8] in the step of the transmetalation.

The ratios of **2A/2B**, which were obtained in these reactions, varied with the sort of the secondary amines as is shown in Tables 1 and 2. These ratios seems to correspond to the yields of the telomers. In the case of the cyclic secondary amines (pyrrolidine, piperidine, and morpholine), however, the ratios of **2A/2B** were nearly constant, as is shown in Table 3. This phenomenon may be interpreted by presuming the presence of the cyclic intermediate (**1c'**)[9] as is shown in Fig. 1.

The difference in the **2A/2B** ratio among these secondary amines—that is, the facility of the formation of **1c'**—seems to be dependent on the steric factor of the R group in **1c'**. For example, the formation of **1c'** may become more difficult in the case of di-*n*-propylamine than in the case of dimethylamine. The very preferential formation of **2B** over **2A** (**2A/2B**= 0.2) in the reaction using dimethylamine may be interpreted by considering the effect of the hyperconjugation of the methyl group. The result in the case of the cyclic secondary amines seems to be due to the lack of any steric difference in the formation of **1c'** among them.

Thus, the ratios of **2A/2B** are considered to be dependent on the degree of the formation of the stable carbanions, **1a'** and **1c'**.

Experimental

Materials. The secondary amines were commercial products of the purest grade, they were distilled and checked by glc. The isoprene and myrcene were dried over anhydrous sodium sulfate and distilled in the presence of hydroquinone. The inorganic compounds were also commercial materials.

Reaction Procedure. In a typical reaction, a mixture of isoprene (8.2 g) and morpholine (3.0 g) was allowed to

8) This has been reported in detail by Asahara *et al.* in relation to the acidity of the amines and reactivity in anionic telomerizations: T. Asahara, M. Senō, and S. Tanaka, *Seisan Kenkyu*, **23**, 304, 353, 356 (1971).

9) If so, the secondary carbanion (**1c**) should convert into a more stable carbanion (**1c'**), and **2B** should increase.

TABLE 4. CHARACTERIZATION OF TELOMERS DIALKYLAMINES

Telogen	Telomer	IR (cm^{-1})	NMR (τ)
Et_2NH	**2A**	1200, 1165, 1050(C–N), 1660, 830 (trisubstituted double bond).	4.65—5.18 (2H, m,–Ċ=C**H**–), 7.09 (2H,d, J=6.6 Hz, =CH–**CH_2**–N〈), 7.62(4H, q, J=7.0 Hz, 〉N–**CH_2**–CH_3), 7.89—8.09(4H, m, =CH–**CH_2CH_2**–C=), 8.24—8.47(6H, m, **CH_3**–Ċ=), 9.04(6H, t, J=7.0Hz, **CH_3CH_2**–).
	2B	1200, 1165, 1065(C–N), 1645, 890 (end methylene group), 1670, 835 (trisubstituted double bond).	4.76—5.16(1H, m, –Ċ=C**H**–), 5.39(2H, bs, –Ċ=**CH_2**), 7.31—8.17(5H,m, =C–**CH_2**–,=Ċ–Ċ**H**–), 7.57(4H, q, J=6.9 Hz, 〉N–**CH_2CH_3**), 8.26—8.48(9H, bs, **CH_3**–Ċ=), 9.08(6H, t, J=7.0 Hz, **CH_3CH_2**–).
$(n\text{-}C_3H_7)_2$ NH	**1A**	1028, 1065, 1160, 1180(C–N), 1675, 830 (trisubstituted double bond).	4.88 (1H, t, J=6.0 Hz, –Ċ=C**H**–), 7.14 (2H, d, J=6.0 Hz, =CH–**CH_2**–N〈), 7.74(4H, t, J=6.8 Hz, 〉N–**CH_2**–CH_2–), 8.30 (3H, s, **CH_3**–Ċ=), 8.40(3H, s, **CH_3**–Ċ=), 8.40—8.90(4H, m, –**CH_2**–), 9.15(6H, t, **CH_3CH_2**–).
	1B	1025, 1065, 1160, 1183(C–N), 1670, 820 (trisubstituted double bond).	4.53—5.03 (1H, m, –Ċ=C**H**–), 7.20(2H, s, =C–**CH_2**–N〈), 7.75 (4H, t, J=6.9 Hz,〉N–**CH_2**–CH_2–), 8.23—8.90(10H, m, **CH_3**–Ċ=, –**CH_2**–), 9.16(6H, t, J=7.1 Hz, **CH_3CH_2**–).
	2A	1030, 1065, 1090, 1165, 1185(C–N), 1670, 828 (trisubstituted double bond).	4.63—5.20 (2H, m, –Ċ=C**H**–), 7.06 (2H, d, J=6.8Hz, =CH–**CH_2**–N〈), 7.74 (4H, t, J=7.1 Hz, 〉N–**CH_2CH_2**–), 7.80—8.11(4H, m, =CH–**CH_2CH_2**–C=), 8.23—8.90 (13H, m, **CH_3**–Ċ=, –**CH_2**–), 9.15(6H, t, J=7.0 Hz, **CH_3**–CH_2–).
	2B	1020, 1075, 1190 (C–N), 1650, 885 (end methylene group), 1670, 840 (trisubstituted double bond).	4.90—5.14 (1H, m, –Ċ=C**H**–), 5.34 (2H, bs, –Ċ=**CH_2**), 7.74 (4H, t, J=7.0 Hz, 〉N–**CH_2**–CH_2–), 7.50—8.20 (9H, m, –**CH_2**–N〈, =C–**CH_2**–, =C–Ċ**H**–), 8.30—8.83(13H, m, **CH_3**–C=, –**CH_2**–), 9.14(6H, t, J=7.0 Hz, **CH_3**–CH_2–).
(*iso*-$C_3H_7)_2NH$	**1A**	1113, 1137, 1170, 1200(C–N), 1670, 830(trisubstituted double bond).	4.95 (1H, t, J=6.0 Hz, –Ċ=C**H**–), 6.80—7.37 (4H, m, =C–**CH_2**–N, –CH–N), 8.33(3H, s, **CH_3**–Ċ=), 8.40(3H, s, **CH_3**–C=), 9.09 (12H, d, J=6.3Hz, **CH_3**–ĊH–).

TABLE 5. CHARACTERIZATION OF TELOMERS (CYCLIC *sec*-AMINES)

Telogen	Telomer	IR (cm^{-1})	NMR (τ)
Pyrrolidine	**1A**	2770, 1200, 1140, 1030 (), 1665, 830 (trisubstituted double bond).	4.84(1H,t,J=6.1Hz,–Ċ=C**H**–), 7.09(2H, d, J=6.1 Hz, =CH–**CH_2**–N), 7.45—8.00(4H, m, –N–**CH_2**–), 8.16—8.65 (10H, m, **CH_3**–Ċ=, –**CH_2**–).
	1B	2780, 1198, 1138, 1082 (), 1670, 820 (trisubstituted double bond).	4.55—5.01(1H, m, –Ċ=C**H**–), 7.17(2H, s, =C–**CH_2**–N), 7.45—7.98 (4H, m, –N–**CH_2**–), 8.17—8.65 (10H, m, **CH_3**–Ċ=, –**CH_2**–).
	2A	2775, 1140, 1125, 1070, 1035, (), 1665, 830 (trisubstituted double bond).	4.65—5.10 (2H, m, –Ċ=C**H**–), 7.14 (2H, d, J=6.8 Hz, =CH–**CH_2**–N), 7.45—7.90 (4H, m, –N–**CH_2**–), 7.95—8.13 (4H, m, =CH–**CH_2**–**CH_2**–C=), 8.25—8.63(13H, m, **CH_3**–Ċ=, –**CH_2**–).
	2B	2780, 1150, 1130, 1070, 1035 (), 1650, 887(end methylene group), 1665, 838(trisubstituted double bond).	4.79—5.13(1H, m, –Ċ=C**H**–), 5.38(2H, bs, –Ċ=**CH_2**), 7.26—8.16 (9H, m, =C–**CH_2**–, =C–C**H**–, –N–**CH_2**–), 8.20—8.60 (13H, m, **CH_3**–C=, –**CH_2**–).
Piperidine	**1A**	2800, 2750, 1150, 1115, 1110, 1035, 990(), 1675, 840 (trisubstituted double bond).	4.88(1H, t, J=6.6 Hz, –Ċ=C**H**–), 7.26(2H, d, J=6.6 Hz, =CH–**CH_2**–N), 7.61—8.00 (4H, m, –N–**CH_2**–), 8.32(3H, s, **CH_3**–Ċ=), 8.43(3H, s, **CH_3**–Ċ=), 8.38—8.85(6H, m, –**CH_2**–).
	1B	2800, 2750, 1150, 1118, 1080, 1035, 990(), 1670, 828(trisubstituted double bond).	4.50—5.02(1H, m, –Ċ=C**H**–), 7.32(2H, s, =C–**CH_2**–N), 7.60—7.98 (4H, m, –N–**CH_2**–), 8.28—8.85 (12H, m, **CH_3**–Ċ=, –**CH_2**–).
	2A	2800, 2750, 1150, 1115, 1105, 1035, 990(), 1660, 830(trisubsti-	4.65—5.13 (2H, m, –Ċ=C**H**–), 7.24 (2H, d, J=6.6 Hz, =CH–**CH_2**–N), 7.50—7.95(4H, m, –N–**CH_2**–), 7.95—8.15

		tuted double bond).	(4H, m, =CH-CH_2-CH_2-C=), 8.20—8.80(15H, m, CH_3-Ċ=, -CH_2-).
	2B	2800, 2750, 1155, 1120, 1040, 990 (◯N-R), 1640, 887(end methylene group), 1660, 835 (trisubstituted double bond).	4.80—5.20(1H, m, -Ċ=C**H**-), 5.40(2H, bs, -Ċ=C**H**$_2$), 7.40—8.20(9H, m, =C-C**H**$_2$-, =C-C**H**-, -N-C**H**$_2$-), 8.25—8.80 (15H, m, C**H**$_3$-Ċ=), -C**H**$_2$-).
Morpholine	**1A**	2851, 2800, 1118, 1070, 1031, 1002, 868(O◯N-R), 1675, 842 (trisubstituted double bond).	4.87 (1H, t, J=7-1 Hz, -Ċ=C**H**-), 6.32—6.60 (4H, m, -C**H**$_2$-O), 7.19(2H, d, J=7.1 Hz, =CH-C**H**$_2$-N), 7.57—7.87 (4H, m, -C**H**$_2$-N), 8.30(3H, s, C**H**$_3$-Ċ=), 8.38(3H, s, C**H**$_3$-Ċ=).
	1B	2851, 2800, 1118, 1070, 1031, 1002, 868(O◯N-R), 1670, 832 (trisubstituted double bond).	4.53—5.01(1H, m, -Ċ=C**H**-), 6.60(4H, m, -C**H**$_2$-O), 7.28 (2H, s, =C-C**H**$_2$-N), 7.55—7.86(4H, m, -C**H**$_2$-N), 8.25—8.53(6H, m, C**H**$_3$-Ċ=).
	2A	2850, 2800, 1118, 1070, 1034, 1005, 868(O◯N-R), 1660, 830 (trisubstituted double bond).	4.60—5.12(2H, m, -Ċ=C**H**-), 6.33—6.60(4H, m, -C**H**$_2$-O), 7.18(2H, d, J=7.0 Hz, =CH-C**H**$_2$-N), 7.55—7.83 (4H, m, -C**H**$_2$-N), 7.85—8.12 (4H, m, =CH-C**H**$_2$-C**H**$_2$-C=), 8.22—8.47(9H, m, C**H**$_3$-Ċ=).
	2B	2850, 2800, 1140, 1118, 1070, 1034, 1010, 865(O◯N-R), 1640, 887 (end methylene group), 1660,830 (trisubstituted double bond).	4.80—5.15(1H, m, 5.15(1H, m, -Ċ=C**H**-), 5.24—5.47(2H, m, -Ċ=C**H**$_2$), 6.35—6.61(4H, m, -C**H**$_2$-O), 7.49—8.24 (9H, m, =C-C**H**$_2$-, =C-C**H**-, -C**H**$_2$-N), 8.37 (6H, s, C**H**$_3$-Ċ=), 8.42(3H, s, C**H**$_3$-Ċ=).

react in the presence of sodium (0.1 g) at 40°C for 3 hr while being stirred in a pressure bottle by the method described in the preceding paper.[1] The reaction products (5.9 g) included the n=1 telomer (bp 62.5—64.0°C/6 mmHg, 1.4 g), the n=2 telomer (bp 91.0—97.5°C/1.5 mmHg, 1.7 g), and the $n\geq 3$ telomer (residue, 2.6 g).

Reaction of Myrcene with Diethylamine. A mixture of myrcene (9.9 g) and diethylamine (3.6 g) was allowed to react in the presence of sodium (0.1 g) at 40°C for 3 hr, as has been described in the preceding paper.[1] The reaction products (8.0 g) included the n=1 telomer (bp 85—87°C/2 mmHg, 7.7 g) and the $n\geq 2$ telomers (residue, 0.2 g). The n=1 telomer was found by glc analyses to consist 90% of the compound **1M** (*N,N*-diethylgeranylamine).

Synthesis of N,N-*Diethylgeranylamine.* *N,N*-Diethylgeranylamine was prepared from geranyl chloride by a modification of Sandler's method.[10] Mass (*m/e*); 209(M^+), IR(cm^{-1}, liquid film); 1200, 1165, 1050(C-N), 1660, 830 (trisubstituted double bond). NMR (τ, CCl_4); 9.04 (6H, t, J=7.0 Hz, CH_3-CH_2-), 8.25—8.46 (9H, m, CH_3-C=), 7.89—8.09 (4H, m, =CH-CH_2-CH_2-C=), 7.62 (4H, q, J=7.0 Hz, CH_3-CH_2-N-), 7.09 (2H, d, J=6.6 Hz, =CH-CH_2-N◯), 4.69—5.18 (2H, m, -Ċ=C**H**-).

Identification of the Telomers. Glc (15% Apiezon grease L/Celite 545, 2.5 m, H_2) was used for the determination of the compositions of the telomers. The IR, NMR, and mass spectra were measured by the use of Perkin Elmer Model 337, Hitachi-Perkin Elmer Model R-20 (60 MHz), and Hitachi RMU-7L spectrometers respectively. The characterizations of the telomers which were obtained using secondary amines are shown in Tables 4 and 5.

The financial support for this work by the Ministry of Education, Japanese Government, is gratefully acknowledged.

10) S. R. Sandler and W. Karo, "Organic Functional Group Preparations," Academic Press, New York and London (1968), p. 324.

Synthesis and Biological Activity of Peptides Related to Eledoisin. I. Hexapeptide Amides Containing α-Hydroxy Acids[1,2]

Hiroshi SUGANO,[3] Ko HIGAKI, and Muneji MIYOSHI

Department of Synthetic Chemistry, Research Laboratory of Applied Biochemistry, Tanabe Seiyaku Co., Ltd. 962 Kashima-cho, Higashiyodogawa-ku, Osaka

(Received April 27, 1972)

A new series of eledoisin-like depsipeptides was synthesized in order to obtain some information about the relationship between the structure of the peptide backbone of eledoisin and the biological activity. Specific amino acids in the biologically-active hexapeptide analog of eledoisin, H-Lys-Phe-Ile-Gly-Leu-Met-NH_2 (**1**), were replaced by the corresponding α-hydroxy acids. The biological activities of these analogs were then compared with that of the standard one (**1**). On the blood pressure in rabbits, H-Lys-Phe-Ile-Glyc-Leu-Met-NH_2 (**4**) and H-Lys-Phlac-Ile-Gly-HyIc-Met-NH_2 (**6**) possessed a substantial activity, though lower than **1**, and H-Lys-Phlac-Ile-Gly-Leu-Met-NH_2 (**2**) and H-Lys-Phe-Ile-Gly-HyIc-Met-NH_2 (**5**) were almost as active as **1**. On the other hand, H-Lys-Phe-HyMeV-Gly-Leu-Met-NH_2 (**3**) exhibited much less activity. The results indicate that the amide bond between the phenylalanine residue and the isoleucine residue is essential for the hypotensive activity.

Eledoisin, Pyroglu-Pro-Ser-Lys-Asp-Ala-Phe-Ile-Gly-Leu-Met-NH_2, was isolated by Erspamer from extracts of salivary glands of *Eledone moshata* and *Aldrovandi*.[4] Its pharmacological action includes the induction of acute arterial hypotension and the stimulation of smooth muscles.[5]

Since the primary structure of eledoisin was elucidated and confirmed by synthesis,[6] a large number of analogs in which amino acids are replaced by other amino acids or in which the peptide chains are shortened have been synthesized.[7] These synthetic studies have given us much information about the sequence and specific amino acid residues required for pharmacological activity. That is, the *C*-terminal hexapeptide analog, H-Lys-Phe-Ile-Gly-Leu-Met-NH_2 (**1**), obtained by the replacement of alanine with lysine possesses a high biological activity.[8] The exchange of the phenylalanine residue and the isoleucine residue almost always leads to the formation of compounds with lower activity. It is, however, relatively harmless to exchange the glycine residue. The exchange of the methionine residue produces inactive compounds almost exclusively.[7]

However, there is no knowledge about the relationship between the structure of the peptide backbone and the specific biological activity of eledoisin. In order to obtain some information about the role of the peptide chain of eledoisin, especially about the necessity of the presence of an amide group for the compound to manifest its biological properties, the present authors synthesized several hexadepsipeptides in which phenylalanine, isoleucine, glycine, and leucine in the compound **1** were replaced with the corresponding α-hydroxy acids and assayed for eledoisin-like activity. The compound **1** was chosen as the model peptide of eledoisin in this study because it had been reported that the *C*-terminal pentapeptide, H-Phe-Ile-Gly-Leu-Met-NH_2, was needed in order to have an appreciable activity of eledoisin[7] and the compound **1** was almost as active as natural eledoisin.

Shemyakin *et al.* attempted to exchange the amide groups by ester groups in the biologically-active peptides, such as glutathione, opthalmic acid, and bradykinin.[9] However, no systematic studies of depsipeptide analogs of eledoisin have ever been performed.

We synthesized such depsipeptides as H-Lys-Phlac-Ile-Gly-Leu-Met-NH_2 (**2**), H-Lys-Phe-HyMeV-Gly-Leu-Met-NH_2 (**3**), H-Lys-Phe-Ile-Glyc-Leu-Met-NH_2 (**4**), H-Lys-Phe-Ile-Gly-HyIc-Met-NH_2 (**5**), and H-Lys-Phlac-Ile-Gly-HyIc-Met-NH_2 (**6**).

Optically active α-hydroxy acids were prepared from the corresponding amino acids by the method reported by Winitz *et al.*[10] The acids were converted into benzyl esters by refluxing them with benzyl alcohol in benzene in the presence of a catalytic amount of sulfuric acid or *p*-toluenesulfonic acid. In the synthesis of the depsipeptides, an ester bond was formed with the aid of benzenesulfonyl chloride in pyridine according to the method of Shemyakin *et al.*[11] All the

1) Presented in part at the 8th Symposium on Peptide Chemistry, Osaka, November, 1970.

2) The abbreviations recommended by the IUPAC-IUB commission on Biochemical Nomenclature (*J. Biol. Chem.*, **241**, 2491 (1966); **242**, 555 (1967)) have been used throught. In addition: Glyc=glycolic acid, HyMeV=α-hydroxy-β-methylvaleric acid, Phlac=β-phenyllactic acid and HyIc=α-hydroxyisocaproic acid. Amino acid and α-hydroxy acid symbols except Gly and Glyc denote the L-configuration.

3) To whom inquiries should be addressed.

4) V. Erspamer and A. Anastasi, *Experientia*, **18**, 58 (1962).

5) V. Erspamer and A. Glaesser, *Brit. J. Pharmacol.*, **20**, 516 (1963). V. Erspamer and G. F. Erspamer, *ibid.*, **19**, 337 (1962).

6) ED. Sandrin and R, A. Boissonnas. *Experientia*, **18**, 59 (1962).

7) E. Schröder and K. Lübke, "The Peptides", Academic press, New York and London (1966), p. 127.

8) L. Bernardi, G. Bosisio, F. Chillemi, G. De Caro, R. De Castiglione, V. Erspamer, A. Glaesser, and O. Goffredo, *Experientia*, **20**, 306 (1964).

9) M. M. Shemyakin, L. A. Shchukina, E. I. Vinogradova, G. A. Ravdel, and Yu. A. Ovchinnikov, *ibid.*, **22**, 353 (1966) and literatures cited therein. G. A. Ravdel, M. P. Filatova, L. A. Shchukina, T. S. Paskina, M. S. Surovikina, S. S. Trapeznikova, and T. P. Egorova, *J. Med. Chem.*, **10**, 242 (1967).

10) M. Winitz, L. Bloch-Frankenthal, N. Izumiya, S. M. Birnbaum, C. G. Baker, and J. P. Greenstein, *J. Amer. Chem. Soc.*, **78**, 2423 (1956).

11) M. M. Shemyakin, Yu. A. Ovchinnikov, V. T. Ivanov, and A. A. Kiryushkin, *Tetrahedron*, **19**, 581 (1963); M. M. Shemyakin, E. I. Vinogradova, M. Yu. Feigina, N. A. Aldanova, Yu. A. Ovchinnikov, and A. A. Kiryushkin, *J. Gen. Chem. USSR.*, **34**, 1796 (1964).

hexadepsipeptide amides obtained as dihydrochloride were found to be homogeneous by the criteria of paper chromatography, paper electrophoresis, thin-layer chromatography, and elemental analysis. The presence of the ester bond was confirmed by IR, which showed an ester carbonyl band near 1750 cm^{-1}.

The syntheis of H–Lys–Phlac–Ile–Gly–Leu–Met–NH_2 (**2**) was carried out according to Scheme 1:

di-BOC–Lys–OH + H–Phlac–OBzl (**7**)
↓ $C_6H_5SO_2Cl$/Pyridine
di-BOC–Lys–Phlac–OBzl (**8**)
↓ H_2/Pd
di-BOC–Lys–Phlac–OH (**9**) + H–Ile–Gly–Leu–Met–NH_2
↓ EtOCOCl/Et_3N
di-BOC–Lys–Phlac–Ile–Gly–Leu–Met–NH_2 (**10**)
↓ HCl in AcOH
H–Lys–Phlac–Ile–Gly–Leu–Met–NH_2·2HCl (**2**)

Scheme 1.

The di-*t*-butyloxycarbonyl(BOC)-didepsipeptide ester (**8**), obtained in a crystalline form, was converted to the acid (**9**) by hydrogenolysis. The di-BOC-hexapeptide amide (**10**), obtained by the mixed anhydride (MA) method, was treated with 2.5N hydrogen chloride in acetic acid to get the hygroscopic amorphous dihydrochloride (**2**).

Subsequently, H–Lys–Phe–HyMeV–Gly–Leu–Met–NH_2 (**3**) was synthesized as is shown in Scheme 2:

BOC–Phe–OH + H–HyMeV–OBzl (**11**)
↓ $C_6H_5SO_2Cl$/Pyridine
BOC–Phe–HyMeV–OBzl
↓ H_2/Pd
BOC–Phe–HyMeV–OH (**12**) + H–Gly–Leu–Met–NH_2
↓ EtOCOCl/Et_3N
BOC–Phe–HyMeV–Gly–Leu–Met–NH_2 (**13**)
↓ i) HCl in Dioxane ii) di-BOC-Lys-ONP (**14**)
di-BOC–Lys–Phe–HyMeV–Gly–Leu–Met–NH_2 (**15**)
↓ HCl in AcOH
H–Lys–Phe–HyMeV–Gly–Leu–Met–NH_2·2HCl (**3**)

Scheme 2.

The oily BOC-didepsipeptide benzyl ester, obtained through column chromatography on silica gel, was hydrogenolyzed with palladium on charcoal to yield the corresponding acid (**12**). **12** was coupled with glycyl-leucyl-methionine amide by the MA method to yield the amorphous BOC-pentapeptide amide (**13**) in a good yield. The protected hexapeptide amide (**15**) was prepared from the di-BOC-lysine *p*-nitrophenyl ester (**14**) and the pentapeptide amide which had been obtained after the removal of the protecting group of **13**.

H–Lys–Phe–Ile–Glyc–Leu–Met–NH_2 (**4**) was synthesized as is shown in Scheme 3:

BOC–Ile–OH + $ClCH_2COOBzl$
↓ Et_3N in AcOEt
BOC–Ile–Glyc–OBzl
↓ H_2/Pd
BOC–Ile–Glyc–OH (**16**) + H–Leu–Met–NH_2
↓ EtOCOCl/Et_3N
BOC–Ile–Glyc–Leu–Met–NH_2 (**17**)
↓ i) HCl in Dioxane ii) BOC-Phe-ONP (**18**)
BOC–Phe–Ile–Glyc–Leu–Met–NH_2 (**19**)
↓ i) HCl in Dioxane ii) di-BOC-Lys-ONP (**14**)
di-BOC–Lys–Phe–Ile–Glyc–Leu–Met–NH_2 (**20**)
↓ HCl in AcOH
H–Lys–Phe–Ile–Glyc–Leu–Met–NH_2·2HCl (**4**)

Scheme 3.

The benzyl ester of BOC-isoleucyl-glycolic acid was prepared by the reaction of BOC-isoleucine with benzyl chloroacetate in the presence of an equimolar amount of triethylamine. The ester was hydrogenolyzed to produce BOC-didepsipeptide acid (**16**). BOC-tetradepsipeptide amide (**17**) was synthesized by the MA method. Di-BOC-hexapeptide amide (**20**) was obtained by the stepwise elongation method.

H–Lys–Phe–Ile–Gly–HyIc–Met–NH_2 (**5**) was synthesized as follows (Scheme 4):

BOC–Gly–OH + H–HyIc–OBzl (**21**)
↓
BOC–Gly–HyIc–OBzl
↓ H_2/Pd
BOC–Gly–HyIc–OH (**22**) + H–Met–NH_2
↓ EtOCOCl/Et_3N
BOC–Gly–HyIc–Met–NH_2 (**23**)
↓ HCl in Dioxane
AOC–Phe–Ile–N_2H_3 (**24**) + H–Gly–HyIc–Met–NH_2·HCl (**25**)
↓ HNO_2
AOC–Phe–Ile–Gly–HyIc–Met–NH_2 (**26**)
↓ i) HCl in Dioxane ii) di-BOC-Lys-ONP (**14**)
di-BOC–Lys–Phe–Ile–Gly–HyIc–Met–NH_2 (**27**)
↓ HCl in AcOH
H–Lys–Phe–Ile–Gly–HyIc–Met–NH_2·2HCl (**5**)

Scheme 4.

The BOC-dipeptide benzyl ester was hydrogenolyzed to yield an acid (**22**), which was then coupled with methionine amide to afford the crystalline BOC-tripeptide amide (**23**). The condensation of the azide derived from AOC-dipeptide hydrazide (**24**) with tripeptide amide (**25**) gave an acylpentapeptide amide (**26**).

H-Lys-Phlac-Ile-Gly-HyIc-Met-NH_2 (**6**) was synthesized according to Scheme 5:

BOC-Ile-OH + H-Gly-HyIc-Met-NH_2 (**25**)
↓ EtOCOCl/Et_3N
BOC-Ile-Gly-HyIc-Met-NH_2 (**28**)
↓ HCl in Dioxane
di-BOC-Lys-Phlac-OH (**9**) + H-Ile-Gly-HyIc-Met-NH_2
↓ EtOCOCl/Et_3N
di-BOC-Lys-Phlac-Ile-Gly-HyIc-Met-NH_2 (**29**)
↓ HCl in AcOH
H-Lys-Phlac-Ile-Gly-HyIc-Met-$NH_2 \cdot 2HCl$ (**6**)

Scheme 5.

The BOC-tetradepsipeptide amide (**28**) was obtained by acylating tripeptide amide (**25**) by a mixed anhydride of BOC-isoleucine. The di-BOC-hexapeptide amide (**29**) was obtained from **9** and the tetradepsipeptide amide by the MA method. The removal of the BOC group lead to the desired depsipeptide amide dihydrochloride (**6**).

TABLE 1. PHARMACOLOGICAL RESULTS ON THE BLOOD PRESSURE IN RABBITS.

Compound	Relative activity[a)]
H-Lys-Phe-Ile-Gly-Leu-Met-NH_2 (**1**)	100
H-Lys-Phlac-Ile-Gly-Leu-Met-NH_2 (**2**)	90
H-Lys-Phe-HyMeV-Gly-Leu-Met-NH_2 (**3**)	10
H-Lys-Phe-Ile-Glyc-Leu-Met-NH_2 (**4**)	30
H-Lys-Phe-Ile-Gly-HyIc-Met-NH_2(**5**)	120
H-Lys-Phlac-Ile-Gly-HyIc-Met-NH_2(**6**)	30

a) Compared on the basis of the dose which caused fall of 20 mmHg of the blood pressure

A biological comparison of the five depsipeptide analogs to the standard compound (**1**) is given in Table 1. In the study of rabbit blood pressure, **2** and **5** were almost identical with **1**, and **4** and **6** possessed substantial activity, though it was lower than that of the parent hexapeptide, while **3** showed much less activity. These results show that the amide bond between the phenylalanine residue and the isoleucine residue play an important role in manifesting the hypotensive activity. Thus, it was found that, in the case of the replacement of the amide bond in the compound **1** by the ester bond, with no change in the amino acid side chain, the potency of the biological activity was strictly dependent upon the position replaced. To clarify this point, more precise investigations are required; such studies will be reported in the near future.

Experimental

All the melting points are uncorrected.

H-Phlac-OBzl (7). A solution of β-phenyllactic acid[10] (60 g, 360 mmol), *p*-toluenesulfonic acid monohydrate (5.5 g), and benzyl alcohol (180 ml) in benzene (360 ml) was refluxed in a Dean and Stark apparatus[12] for 30 min. The solution was washed with water, 4% sodium bicarbonate, and again water, dried over magnesium sulfate, and fractionated. A fraction boiling at 165—170°C/1 mmHg was collected; yield, 30 g (32.5%); $[\alpha]_D^{25}$ −13.0° (*c* 1, MeOH); $[\alpha]_D^{25}$ −10.9° (*c* 1.5, EtOH).

Di-BOC-Lys-Phlac-OBzl (8). To a solution of di-BOC-Lys-OH (34.6 g, 100 mmol) in a mixture of pyridine (100 ml) and tetrahydrofuran (100 ml), was added with stirring benzenesulfonyl chloride (19.5 g, 110 mmol) at −10°C over a period of 10 min. After 10 min, a solution of compound **7** (25.6 g, 100 mmol) in pyridine (40 ml) was added to the solution. The mixture was then allowed to stand at 0°C for 1 hr and at room temperature for 8 hr, and subsequently poured into water (1000 ml). The oil separated was extracted with ether. The extract was washed repeatedly with 2% hydrochloric acid, 4% sodium bicarbonate, and water, and dried over magnesium sulfate. The solvent was distilled off *in vacuo*, and crude product obtained as crystals was recrystallized from ether-*n*-hexane; yield, 57 g (85%); mp 60—62°C; $[\alpha]_D^{25}$ −28.1° (*c* 1, MeOH). Found: C, 65.73; H, 7.59; N, 4.48%. Calcd for $C_{32}H_{44}O_8N_2$: C, 65.73; H, 7.59; N, 4.79%.

Di-BOC-Lys-Phlac-OH (9). Compound **8** (5.84 g, 10 mmol) was dissolved in methanol (50 ml) and hydrogenolyzed in the presence of 10% palladium on charcoal. The filtrate from the catalyst was evaporated to dryness; yield of oil, 4.9% (100%).

Di-BOC-Lys-Phlac-Ile-Gly-Leu-Met-NH_2 (10). To a solution of **9** (4.5 g, 8 mmol) and triethylamine (1.2 ml) in chloroform (40 ml), was added ethyl chloroformate (880 mg, 8 mmol) at −15——10°C. After 15 min, there was added a solution of H-Ile-Gly-Leu-Met-$NH_2 \cdot HCl$[13] (4.3 g, 8 mmol) and triethylamine (1.2 ml) in dimethylformamide (100 ml) at −15——10°C, and this mixture was allowed to stand at room temperature overnight. The mixture was poured into cold water (1000 ml), and the resulting solid was extracted with ethyl acetate. The extract was washed successively with 1% hydrochloric acid, 4% sodium bicarbonate, and water. The solvent was then evaporated *in vacuo*, and the crude product was recrystallized from ethyl acetate-methanol-petroleum ether; yield, 4.6 g (62%); mp 190—192°C; $[\alpha]_D^{20}$ −35.6° (*c* 0.5, MeOH). Found: C, 57.43; H, 7.89; N, 10.53; S, 3.75%. Calcd for $C_{44}H_{73}O_{11}N_7S \cdot H_2O$: C, 57.08; H, 8.10; N, 10.59; S, 3.45%.

H-Lys-Phlac-Ile-Gly-Leu-Met-$NH_2 \cdot 2HCl$ (2). Compound **10** (200 mg) was dissolved in 2N hydrogen chloride in acetic acid (5 ml), and the solution was allowed to stand at room temperature for 20 min. The product was precipitated by adding dry ether, and the precipitate was collected by filtration, washed well with ether, and dried over sodium hydroxide *in vacuo*. It was dissolved in 60% methanol (4 ml), and an insoluble material was filtered off. The filtrate was con-

12) J. P. Greenstein and M. Winitz, "Chemistry of the Amino Acids," John Wiley & Sons, Inc., New York London (1961), p. 940.
13) E. Schröder, R. Schmiechen, and H. Gibian, *Ann. Chem.*, **679**, 195 (1964).

centrated to dryness over phosphorus pentoxide *in vacuo* to obtain the product; yield, 170 mg; mp 160—165°C $[\alpha]_D^{25}$ −48.1° (*c* 0.305, H_2O); R_f, 0.70.[14] Found: C, 50.83; H, 7.92; N, 12.36; S, 4.44; Cl, 8.84%. Calcd for $C_{34}H_{57}O_7N_7S \cdot 2HCl \cdot H_2O$: C, 51.12; H, 7.64; N, 12.28; S, 4.01; Cl, 8.89%. The amino acid ratios in the acid hydrolyzate were Lys 1.00, Ile 1.03, Gly 1.05, Leu 1.00, and Met 0.91.

H-HyMeV-OBzl (11). This was obtained from α-hydroxy-β-methylvaleric acid[10] (52.8 g, 400 mmol), benzyl alcohol (200 ml), and sulfuric acid (2 ml) as described for the preparation of **7**; yield of oil, 62 g (70%); bp 122—125°C /1 mmHg; $[\alpha]_D^{25}$ −12.7° (*c* 1.9, EtOH).

BOC-Phe-HyMeV-OH (12). BOC-Phe-OH (26.5 g, 100 mmol) was condensed with **11** (24.5 g, 110 mmol) by the benzenesulfonyl chloride method to yield an oil (33.8 g, 72%); this oil was then hydrogenolyzed in the presence of 10% palladium on charcoal; yield of oil, 24.6 g (64%).

BOC-Phe-HyMeV-Gly-Leu-Met-NH_2 (13). This compound was obtained from **12** (6.4 g, 16.8 mmol) and H-Gly-Leu-Met-$NH_2 \cdot HCl$[13] (6.9 g, 19 mmol) as described for the preparation of **10**; yield, 7.5 g (66%); mp 165—168°C; $[\alpha]_D^{25}$ −39.5° (*c* 1, MeOH). Found: C, 58.34; H, 7.89; N, 10.41; S, 4.81%. Calcd for $C_{33}H_{53}O_8N_5S$: C, 58.29; H, 7.85; N, 10.30; S, 4.71%.

Di-BOC-Lys-Phe-HyMeV-Gly-Leu-Met-NH_2 (15). Compound **13** (5.4 g, 8 mmol) was dissolved in 3N hydrogen chloride in dioxane (70 ml) at room temperature. After 20 min, the solution was evaporated to dryness in *vacuo*. The pentadepsipeptide amide hydrochloride thus obtained was dissolved in dimethylformamide (40 ml) and then neutralized with triethylamine (1.2 ml). Di-BOC-Lys-ONP (**14**)[15] (4.2 g, 9 mmol) was added to the solution, and the mixture was allowed to stand at room temperature for 20 hr. Water was added to the reaction mixture to precipitate the product, which was then collected by filtration, washed well with 2% hydrochloric acid, N ammonia, and water, and dried. Recrystallization from ethyl acetate-petroleum ether gave 4.4 g (60%) of a product; mp 192—195°C; $[\alpha]_D^{25}$ −37.8° (*c* 0.5, MeOH). Found: C, 58.13; H, 8.03; N, 10.57; S, 3.62%. Calcd for $C_{44}H_{73}N_7O_{11}S$: C, 58.19; H, 8.10; N, 10.79; S, 3.53%.

H-Lys-Phe-HyMeV-Gly-Leu-Met-$NH_2 \cdot 2HCl$ (3). This compound was obtained from **15** (200 mg) as described for the preparation of **2**; yield, 170 mg; mp 60—80°C; $[\alpha]_D^{25}$ −35.2° (*c* 0.25, H_2O); R_f, 0.72.[14] Found: C, 51.05;H, 7.83; N, 12.05; S, 4.25; Cl, 9.05%. Calcd for $C_{34}H_{57}O_7N_7S \cdot 2HCl \cdot H_2O$: C, 51.12; H, 7.64; N, 12.28; S, 4.01; Cl, 8.89%. The amino acid ratios in the acid hydrolyzate were Lys 0.98, Phe 0.96, Gly 1.00, Leu 1.00, and Met 0.76.

BOC-Ile-Glyc-OH (16). A solution of BOC-Ile-OH (15 g, 60 mmol), triethylamine (8 ml), and benzyl chloroacetate[16] (10.5 g, 60 mmol) in ethyl acetate (150 ml) was refluxed for 5 hr. The solution was washed with 2% hydrochloric acid, 4% sodium bicarbonate and water, dried over magnesium sulfate, and concentrated to dryness. The resulting oil (16 g) was dissolved in methanol (80 ml) and hydrogenolyzed in the presence of 5% palladium on charcoal. The solvent was distilled off *in vacuo*, and the crude acid was dissolved in 4% sodium bicarbonate, washed with ether, and acidified with 1% hydrochloric acid. The oil thus separated was extracted into ether. The ether was removed under reduced pressure; yield of oil, 7.7 g (60%).

BOC-Ile-Glyc-Leu-Met-NH_2 (17). This was obtained from **16** (7 g, 24.2 mmol) and H-Leu-Met-$NH_2 \cdot HCl$[13] (8.3 g, 25 mmol) as described for the preparation of **10**. The crude product was recrystallized from ethyl acetate-petroleum ether; yield, 8.7 g (68%); mp 171—177°C; $[\alpha]_D^{25}$ −39.0° (*c* 1, MeOH). Found: C, 54.01; H, 8.13; N, 10.82; S, 6.47%. Calcd for $C_{24}H_{44}N_4O_7S$: C, 54.13; H, 8.27; N, 10.52; S, 6.01%.

BOC-Phe-Glyc-Leu-Met-NH_2 (19). Compound **17** (4 g, 8 mmol) was dissolved in 3N hydrogen chloride in dioxane (60 ml) at room temperature. After 20 min, the solution was evaporated to dryness under reduced pressure. The tetradepsipeptide amide hydrochloride thus obtained was dissolved in dimethylformamide (30 ml), neutralized with triethylamine (1.1 ml), and then subjected to a reaction with BOC-Phe-ONP (**18**)[15] (3.1 g, 8 mmol). After standing overnight at roomt emperature, the solution was diluted with ethyl acetate (350 ml), washed with 2% hydrochloric acid, 4% sodium bicarbonate, and water, and dried over magnesium sulfate. The solvent was distilled off under reduced pressure, and the solid material was recrystallized from ethyl acetate-petroleum ether; yield, 4 g, (75%); mp 156—158°C; $[\alpha]_D^{25}$ −25.3° (*c* 1, MeOH). Found: C, 56.73; H, 7.97; N, 10.06; S, 4.84%. Calcd for $C_{33}H_{53}O_8N_5S \cdot H_2O$: C, 56.81; H, 7.89; N, 10.04; S, 4.59%.

Di-BOC-Lys-Phe-Ile-Glyc-Leu-Met-NH_2 (20). Compound **19** (1.3 g, 2 mmol) was treated with 3N hydrogen chloride in dioxane. The pentadepsipeptide amide hydrochloride thus obtained was dissolved in dimethylformamide (10 ml), neutralized with triethylamine (0.28 ml), and then subjected to a reaction with compound **14** (1 g, 2.1 mmol). The mixture was then treated as described for the preparation of **15**; yield, 1.5 g (80%); mp 146—149°C; $[\alpha]_D^{25}$ −36.0° (*c* 1, MeOH). Found: C, 57.39; H, 8.25; N, 10.29; S, 3.36%. Calcd for $C_{44}H_{93}O_{11}N_7S \cdot H_2O$: C, 57.08; H, 8.10; N, 10.59; S, 3.45%.

H-Lys-Phe-Ile-Glyc-Leu-Met-$NH_2 \cdot 2HCl$ (4). This compound was obtained from **20** (200 mg) as described for the preparation of **2**; yield, 170 mg, mp 65—80°C; $[\alpha]_D^{25}$ −26.7° (*c* 0.5, H_2O); R_f, 0.68.[14] Found: C, 51.05; H, 7.82; N, 12.13; S, 3.53; Cl, 9.13%. Calcd for $C_{34}H_{57}O_7N_7S \cdot 2HCl \cdot H_2O$: C, 51.12; H, 7.64; N, 12.28; S, 4.01; Cl, 8.89%. The amino acid ratios in the acid hydrolyzate were Lys 1.08, Phe 0.98, Ile 1.12, Leu 1.00, and Met 0.85.

H-HyIc-OBzl (21). This compound was obtained from α-hydroxyisocaproic acid[10] (25.4 g, 200 mmol), benzyl alcohol and sulfuric caid as described for the preparation of **7**; yield of oil, 26 g (60%); bp 113—115°C/1 mmHg; $[\alpha]_D^{25}$ −16.0° (*c* 2.1, EtOH).

BOC-Gly-HyIc-OH (22). Benzenesulfonyl chloride (17.7 g, 100 mmol) was added to a solution of BOC-Gly-OH (17.5 g, 100 mmol) in a mixture of tetrahydrofuran (200 ml) and pyridine (100 ml) at −10°C. Then compound **21** (22.2 g, 100 mmol) was added. The product was isolated and purified by column chromatography. The resulting oil (38 g) was hydrogenolyzed in the presence of 5% palladium on charcoal; yield of oil, 17 g (60%).

BOC-Gly-HyIc-Met-NH_2 (23). To a solution of **22** (18.86 g, 65 mmol) and triethylamine (9.2 ml) in chloroform (200 ml), was added ethyl chloroformate (7.6 g, 70 mmol) at −12——10°C. After 15 min, a solution of H-Met-$NH_2 \cdot HCl$[17] (12.8 g, 70 mmol) and triethylamine (9.8 ml) in dimethylformamide (50 ml) was added to the solution. The mixture was stirred at room temperature for 2 hr and then poured into water (500 ml), and the oil thus separated was

14) Paper chromatography was carried out on Toyo Roshi No.50 with *n*-butanol–acetic acid–water (4: 1: 1).

15) E. Sandrin and R. A. Boissonnas, *Helv. Chim. Acta*, **46**, 1637 (1963).

16) K. Seubert, *Chem. Ber.*, **21**, 281 (1888).

17) F. Chillemi, *Gazz. Chim. Ital.*, **93**, 1079 (1963).

extracted with chloroform. The extract was washed with 1% hydrochloric acid, 4% sodium bicarbonate, and water, and dried over magnesium sulfate. The solvent was distilled off under reduced pressure, and the product was recrystallized from ethyl acetate–petroleum ether; yield, 17 g (73%); mp 148—150°C; $[\alpha]_D^{25}$ −34.5° (*c* 1.25, MeOH). Found: C, 51.71; H, 8.04; N, 9.53; S, 7.66%. Calcd for $C_{18}H_{33}O_6N_3S$: C, 51.54; H, 7.93; N, 10.02; S, 7.63%.

AOC-Phe-Ile-NHNH$_2$ (24). A solution of AOC-Phe-Ile-OEt (8.4 g, 20 mmol) and hydrazine hydrate (10 g, 200 mmol) in methanol (20 ml) was refluxed for 48 hr. After ocoling, the crystal thus precipitated out was filtered, washed well with water, and recrystallized from methanol–water; yield, 6.4 g (78%); 171—172°C; $[\alpha]_D^{20}$ −45.9° (*c* 1, AcOH). Found: C, 62.16; H, 8.43; N, 13.53%. Calcd for $C_{21}H_{34}O_4N_4$: C, 62.04; H, 8.43; N, 13.78%.

AOC-Phe-Ile-Gly-HyIc-Met-NH$_2$ (26). Compound **23** (3 g, 7.1 mmol) was dissolved in 3N hydrogen chloride in dioxane (50 ml) at room temperature. After 30 min, the solvent was distilled off under reduced pressure, and the residue was triturated with ether. The product was dried *in vacuo* over sodium hydroxide; yield, 2.5 g (99%). This material (**25**) was used in the following reaction without further purification. To a solution of **24** (2.85 g, 7 mmol) in a mixture of 3N hydrochloric acid (11.2 ml) and dimethylformamide (280 ml), was added with stirring a chilled solution of sodium nitrite (483 mg, 7 mmol) in water (3 ml) at −18—−15°C. After 20 min, the solution was neutralized with triethylamine and there was added a solution of **25** (2.5 g, 7 mmol) obtained above and triethylamine (0.98 ml) in dimethylformamide (35 ml) at −15—−10°C. After the mixture had been stirred at room temperature for 3 hr, it was treated as described for the preparation of **10**; yield, 3.5 g (73%); mp 191—192°C; $[\alpha]_D^{25}$ −47.0° (*c* 1, MeOH). Found: C, 58.63; H, 8.14; N, 10.13; S, 4.40%. Calcd for $C_{34}H_{55}O_8N_5S$: C, 58.87; H, 7.93; N, 10.10; S, 4.61%.

Di-BOC-Lys-Phe-Ile-Gly-HyIc-Met-NH$_2$ (27). Compound **26** (1 g, 1.4 mmol) was treated with 3N hydrogen chloride in dioxane for 30 min at room temperature. The solvent was distilled off under reduced pressure. The product, which corresponded to H-Phe-Ile-Gly-HyIc-Met-NH_2·HCl, was added to a solution of **14** (700 mg, 1.5 mmol) in dimethylformamide (7 ml), together with triethylamine (0.2 ml); the mixture was then treated as described for the preparation of **15**; yield, 1 g, (77%); mp 199—201°C; $[\alpha]_D^{25}$ −44.4° (*c* 0.5, MeOH). Found: C, 57.48; H, 8.45; N, 10.36; S, 3.35%. Calcd for $C_{44}H_{73}O_{11}N_7S\cdot H_2O$: C, 57.08; H, 8.10; N, 10.59; S, 3.45%.

H-Lys-Phe-Ile-Gly-HyIc-Met-NH$_2$·2HCl (5). This compound was obtained from **27** (200 mg) as described for the preparation of **2**; yield, 180 mg; mp 230—233°C; $[\alpha]_D^{25}$ −28.8° (*c* 0.25, H_2O); R_f, 0.68.[14] Found: C, 50.84; H, 7.93; N, 12.59; S, 3.67; Cl, 9.25%. Calcd for $C_{34}H_{57}O_7N_7S\cdot 2HCl\cdot H_2O$; C, 51.12: H, 7.64; N, 12.28; S, 4.01; Cl, 8.89%. The amino acid ratios in the acid hydrolyzate were Lys 0.97, Phe 1.01, Ile 1.00, Gly 1.04, and Met 0.85.

BOC-Ile-Gly-HyIc-Met-NH$_2$ (28). To a solution of BOC-Ile-OH (1 g, 4 mmol) and triethylamine (0.56 ml, 4 mmol) in chloroform (50 ml), was added ethyl chloroformate (0.44 g, 4 mmol) at −12—−10°C. After 15 min, there was added a solution of H-Gly-HyIc-Met-NH_2·HCl (**25**) obtained from **23** (1.5 g, 3.6 mmol) and triethylamine (0.5 ml) in dimethylformamide (20 ml); the mixture was then stirred at room temperature for 3 hr. Then it was poured into water (100 ml), and the solid thus precipitated was extracted with ethyl acetate. The extract was washed with 1% hydrochloric acid, 4% sodium bicarbonate, and water, and dried over magnesium sulfate. The solvent was distilled off *in vacuo*, and the crude product was recrystallized from ethyl acetate–petroleum ether; yield, 1.25 g (59%); mp 140—142°C; $[\alpha]_D^{25}$ −46.0° (*c* 1, MeOH). Found: C, 53.68; H, 8.28; N, 10.78; S, 6.06%. Calcd for $C_{24}H_{44}O_7N_4S$: C, 54.12; H, 8.33; N, 10.52; S, 6.00%.

Di-BOC-Lys-Phlac-Ile-Gly-HyIc-Met-NH$_2$ (29). Compound **28** (1.7 g, 3.2 mmol) was dissolved in 3N hydrogen chloride in dioxane at room temperature. After 40 min, the solvent was distilled off *in vacuo*, and the residue, which corresponded to H-Ile-Gly-HyIc-Met-NH_2·HCl, was used in the following reaction without further purification. To a solution of compound **9** (2 g, 4 mmol) and triethylamine (0.56 ml) in chloroform (50 ml), was added ethyl chloroformate (440 mg, 4 mmol) at −10—−8°C. Then, a solution of the tetradepsipeptide amide hydrochloride obtained above in dimethylformamide (16 ml) was added and the mixture was treated as described for the preparation of **10**; yield, 1.9 g (52%); mp 148—150°C; $[\alpha]_D^{25}$ −50.0° (*c* 0.5, MeOH). Found: C, 57.26; H, 7.97; N, 9.25; S, 3.76%. Calcd for $C_{44}H_{72}O_{12}N_6S\cdot H_2O$: C, 57.01; H, 7.99; N, 9.07; S, 3.45%.

H-Lys-Phlac-Ile-Gly-HyIc-Met-NH$_2$·2HCl (6). This compound was obtained from **29** (200 mg) as described for the preparation of **2**; yield, 180 mg; mp 155—160°C; $[\alpha]_D^{25}$ −52.3° (*c* 0.285, H_2O): R_f, 0.75.[14] Found: C, 51.17; H, 7.70; N, 10.79; S, 4.23; Cl, 8.76%. Calcd for $C_{34}H_{56}O_8N_6S\cdot 2HCl\cdot H_2O$: C, 51.05; H, 7.56; N, 10.50; S, 4.00; Cl, 8.86%. The amino acid ratios in the acid hydrolyzate were Lys 0.93, Ile 1.00, Gly 1.05, and Met 0.83.

Pharmacological Assay. White male rabbits (2—3 kg) were anesthetized subcutaneously with 1.2 g/kg of urethane. Anesthesia was maintained with additional doses as needed. The arterial blood pressure was measured from a canulated carotid artery and recorded on a Kymograph by means of a mercury manometer. All the peptides were dissolved in physiological saline and injected into the femoral vein. Each dose was tested on five animals and always checked against the reference standard material, **1**. The activity of the peptides was compared on a weight basis. The data were obtained with five animals per group.

The authors wish to thank Professor N. Izumiya of Kyushu University and Director Dr. I. Chibata of Tanabe Seiyaku for their encouragement in the course of this study.

Synthesis and Biological Activity of Peptides Related to Eledoisin. II.[1] Hexapeptide Amides Containing *N*-Methylamino Acids[2,3]

Hiroshi SUGANO,[4] Ko HIGAKI, and Muneji MIYOSHI

Department of Synthetic Chemistry, Research Laboratory of Applied Biochemistry, Tanabe Seiyaku Co., Ltd. 962 Kashima-cho, Higashiyodogawa-ku, Osaka

(Received May 20, 1972)

Eledoisin-like hexapeptides were synthesized in order to obtain longer-lasting hypotensive analogs. A part of the amino acid of the standard peptide, H–Lys–Phe–Ile–Gly–Leu–Met–NH_2 (**1**), was replaced by *N*-methylamino acid. It was found, in these syntheses, that when the *C*-terminal amino acid of a carboxy component was an *N*-methylamino acid, a system of dicyclohexylcarbodiimide plus 1-hydroxybenzotriazole was a useful coupling agent. With regard to the hypotensive effect in rabbits, H–Lys–Phe–MeIle–Gly–Leu–Met–NH_2 (**2**) and H–Lys–Phe–Ile–Gly–MeIle–Met–NH_2 (**6**) show much less activity; H–Lys–MePhe–Ile–Gly–Leu–Met–NH_2 (**3**) and H–Lys–MePhe–Ile–Gly–MeLeu–Met–NH_2 (**7**) show a substantial activity, though weaker than the standard one. On the other hand, H–Lys–Phe–Ile–Gly–MeLeu–Met–NH_2 (**5**) and H–Lys–Phe–Ile–Sar–Leu–Met–NH_2 (**4**) show a higher activity than **1**. These results indicate that, in some cases, the replacement of an amide bond by an *N*-methylamide bond without any change in the side chain of amino acid would have an important influence on the activity. The duration of the action of *N*-methypeptildes synthesized was unexpectedly of the same order of magnitude as that of **1**.

In the preceding paper,[1] we described the synthesis and the biological activity of several hexadepsipeptide analogs of eledoisin, in which the amide bond was replaced with the ester bond in order to avoid cleavage by the proteolytic enzyme of the organism and, consequently, in order to obtain a longer-lasting compound. However, the duration of the depsipeptides synthesized was unexpectedly of the same order of magnitude as that of the standard peptide, H–Lys–Phe–Ile–Gly–Leu–Met–NH_2 (**1**). This shows that the ester bond would be hydrolyzed by the enzyme as readily as the original peptide bond and that, in order to produce a longer-lasting action, the peptide bond must be replaced by some other bond which can not be attacked by the enzyme.

Andreatta and Scheraga recently reported that a peptide involving *N*-methylamino acid was not attacked by the protease.[5] Thus, the His–MeAla bond in [Val[5], MeAla[7]]-angiotensin II is totally resistant to the aminopeptidase. Baldwin also showed that a peptide bond involving methylated arginine could not be hydrolyzed by trypsin.[6]

In the present investigation, from this point of view, the authors synthesized several hexapeptides, H–Lys–Phe–MeIle–Gly–Leu–Met–NH_2 (**2**), H–Lys–MePhe–Ile–Gly–Leu–Met–NH_2 (**3**), H–Lys–Phe–Ile–Sar–Leu–Met–NH_2 (**4**), H–Lys–Phe–Ile–Gly–MeLeu–Met–NH_2 (**5**), H–Lys–Phe–Ile–Gly–MeIle–Met–NH_2 (**6**), and H–Lys–MePhe–Ile–Gly–MeLeu–Met–NH_2 (**7**). In these peptides, a part of the amino acid of the standard peptide **1** was replaced with *N*-methylamino acid, and their biological activity was compared with that of **1**.

In compounds **2**, **3**, **4**, **5**, and **7**, none of the amino-acid side chains are altered, whereas the amino-acid side chain of compound **6** is different from the reference standard in the part of leucine.

Synthesis

Optically active *N*-methylamino acids were prepared by the method reported previously by Quitt *et al.*[7]

H–Lys–Phe–MeIle–Gly–Leu–Met–NH_2 (**2**) was synthesized according to Scheme 1. *t*-Amyloxycarbonyl (AOC)-phenylalanine was condensed with the *N*-methylisoleucine methyl ester (**8**) with dicyclohexylcarbodiimide (DCC) to yield the AOC-phenylalanyl-*N*-methylisoleucine methyl ester. The ester did not crystallize and was converted into AOC-dipeptide acid (**9**) by

AOC–Phe–OH + H–MeIle–OMe (**8**)
↓ DCC
AOC–Phe–MeIle–OMe
↓ NaOH
AOC–Phe–MeIle–OH (**9**) + H–Gly–Leu–Met–NH_2
7% ↓ EtOCOCl/Et_3N
AOC–Phe–MeIle–Gly–Leu–Met–NH_2 (**10**)
↓ i) HCl in Dioxane ii) di-BOC-Lys-ONP
di-BOC–Lys–Phe–MeIle–Gly–Leu–Met–NH_2 (**11**)
↓ HCl in AcOH
H–Lys–Phe–MeIle–Gly–Leu–Met–NH_2·2HCl (**2**)

Scheme 1.

1) Part I of this series; H. Sugano, K. Higaki, and M. Miyoshi, This Bulletin, **46**, 226 (1973).

2) Presented in part at the 91st Annual Meeting of the Pharmaceutical Society of Japan, Fukuoka, April, 1971.

3) The abbreviations recommended by the IUPAC-IUB commission on Biological Nomenclature (*J. Biol. Chem.*, **241**, 2491 (1966); **242**, 555 (1967)) have been used throughout. Amino acid and *N*-methylamino acid symbols except Gly and Sar denote the L-configuration.

4) To whom inquiries should be addressed.

5) R. H. Andreatta and H. A. Scheraga, *J. Med. Chem.*, **14**, 489 (1971).

6) G. S. Baldwin and P. R. Carnegie, *Science*, **171**, 579 (1971).

7) P. Quitt, J. Hellerbach, and K. Vogler, *Helv. Chim. Acta*, **46**, 327 (1963).

saponification, which did not proceed smoothly because of the bulkiness of the side chain and, in addition, that of the *N*-methyl group of *N*-methylisoleucine. The acid (**9**) was coupled with glycyl-leucyl-methionine amide to produce AOC-pentapeptide amide in a rather poor yield. This low yield may also be due to the bulky *C*-terminal amino acid in the carboxy component.

Di-*t*-butyloxycarbonyl (BOC)-hexapeptide amide (**11**) was prepared from the di-BOC-lysine *p*-nitrophenyl ester and the pentapeptide amide which had been obtained from AOC-pentapeptide amide (**10**) using 2N hydrogen chloride in dioxane. The BOC group was removed from compound **11** using 2N hydrogen chloride in acetic acid.

The route of synthesizing H–Lys–MePhe–Ile–Gly–Leu–Met–NH_2 (**3**) is shown in Scheme 2:

A)

di-BOC–Lys–OH + H–MePhe–OBzl (**12**)

↓ DCC

di-BOC–Lys–MePhe–OBzl

↓ H_2/Pd

di-BOC–Lys–MePhe–OH (**13**) + H–Ile–Gly–Leu–Met–NH_2

20% ↓ $EtOCOCl/Et_3N$

di-BOC–Lys–MePhe–Ile–Gly–Leu–Met–NH_2 (**15**)

B)

di-BOC–Lys–MePhe–OH (**13**) + H–Ile–Gly–Leu–Met–OMe

75% ↓ DCC/HOBt

di-BOC–Lys–MePhe–Ile–Gly–Leu–Met–OMe (**14**)

↓ NH_3 in MeOH

di-BOC–Lys–MePhe–Ile–Gly–Leu–Met–NH_2 (**15**)

↓ HCl in AcOH

H–Lys–MePhe–Ile–Gly–Leu–Met–$NH_2 \cdot 2HCl$ (**3**)

Scheme 2.

Compound **13**, obtained from the di-BOC-lysyl-*N*-methylphenylalanine benzyl ester by hydrogenolysis, was coupled with *C*-terminal tetrapeptide amide by the mixed anhydride method to afford the protected hexapeptide amide (**15**) in a low yield, accompanied by a considerable amount of ethoxycarbonyl-isoleucyl-glycyl-leucyl-methionine amide.

On the other hand, using DCC together with the 1-hydroxybenzotriazole (HOBt) developed by König and Geiger,[8] the di-BOC-hexapeptide ester (**14**) was obtained in a good yield from compound **13** and the tetrapeptide ester. No acylurea was detected on thin-layer chromatography.[9] Thus, the DCC–HOBt is recommendable for a coupling agent if the *C*-terminal amino acid of a carboxy component is a bulky *N*-methyl-amino acid.

Hexapeptide, H–Lys–Phe–Ile–Sar–Leu–Met–NH_2 (**4**), was synthesized in the following way (Scheme 3):

BOC–Ile–OH + H–Sar–OBzl (**16**)

↓ DCC

BOC–Ile–Sar–OBzl

↓ H_2/Pd

BOC–Ile–Sar–OH (**17**) + H–Leu–Met–OMe

↓ DCC/HOBt

BOC–Ile–Sar–Leu–Met–OMe (**18**)

↓ NH_3 in MeOH

BOC–Ile–Sar–Leu–Met–NH_2 (**19**)

↓ i) HCl in Dioxane
ii) BOC–Phe–ONP

BOC–Phe–Ile–Sar–Leu–Met–NH_2 (**20**)

↓ i) HCl in Dioxane
ii) di-BOC–Lys–ONP

di-BOC–Lys–Phe–Ile–Sar–Leu–Met–NH_2 (**21**)

↓ HCl in AcOH

H–Lys–Phe–Ile–Sar–Leu–Met–$NH_2 \cdot 2HCl$ (**4**)

Scheme 3.

BOC-isoleucyl-sarcosine, which was prepared by allowing BOC-isoleucine to react with the sarcosine benzyl ester by the DCC method, followed by hydrogenolysis over palladium on charcoal, was coupled with the leucyl-methionine ester by DCC–HOBt. Amidation followed by two successive stepwise elongations using the *p*-nitrophenyl ester and subsequent deprotection afforded the desired compound (**4**).

H–Lys–Phe–Ile–Gly–MeLeu–Met–NH_2 (**5**) and H–Lys–Phe–Ile–Gly–MeIle–Met–NH_2 (**6**) were synthesized according to Scheme 4:

BOC–Gly–OH + H–X–OMe (**22**) or (**8**)

↓ DCC

BOC–Gly–X–OMe

↓ NaOH

BOC–Gly–X–OH + H–Met–OMe
(**23a**) or (**23b**)

↓ DCC/HOBt

BOC–Gly–X–Met–OMe (**24a**) or (**24b**)

↓ NH_3 in MeOH

BOC–Gly–X–Met–NH_2 (**25a**) or (**25b**)

↓ HCl in Dioxane

AOC–Phe–Ile–N_2H_3 + H–Gly–X–Met–NH_2

↓ HONO

8) W. König and R. Geiger, *Chem. Ber.*, **103**, 788 (1970).

9) J. C. Sheehan and D. D. H. Young, *J. Amer. Chem. Soc.*, **80**, 1158 (1958); K. Hofmann, N. Yanaihara, S. Lande, and H. Yajima, *ibid.*, **84**, 4470 (1962); H. Schüssler and H. Zahn, *Chem. Ber.*, **95**, 1076 (1962).

AOC–Phe–Ile–Gly–X–Met–NH_2 (**26a**) or (**26b**)

↓ i) HCl in Dioxane ii) di-BOC-Lys-ONP

di-BOC–Lys–Phe–Ile–Gly–X–Met–NH_2 (**27a**) or (**27b**)

↓ HCl in AcOH

H–Lys–Phe–Ile–Gly–X–Met–NH_2·2HCl (**5**) or (**6**)

Scheme 4. X=MeLeu or MeIle

BOC-dipeptide acids (**23a** and **23b**) were obtained as crystals and were coupled with the methionine ester by the use of HObt and DCC. The BOC-tripeptide esters (**24a** and **24b**) thus obtained were amidated and deprotected to give tripeptide amide hydrochlorides. They were converted into AOC-pentapeptide amides (**26a** and **26b**) by the azide method. Deprotection and subsequent reaction with the di-BOC-lysine *p*-nitrophenyl ester afforded di-BOC-hexapeptide amides (**27a** and **27b**), which were then subjected to acidolysis to yield the desired compounds (**5** and **6**).

Further, H–Lys–MePhe–Ile–Gly–MeLeu–Met–NH_2 (**7**) was synthesized as follows:

BOC–Gly–MeLeu–Met–OMe (**23a**)

↓ i) HCl in MeOH ii) BOC-Ile-OH $EtOCOCl/Et_3N$

BOC–Ile–Gly–MeLeu–Met–OMe (**28**)

↓ i) HCl in MeOH ii) di-BOC-Lys-MePhe-OH (**13**) DCC/HObt

di-BOC–Lys–MePhe–Ile–Gly–MeLeu–Met–OMe (**29**)

↓ NH_3 in MeOH

di-BOC–Lys–MePhe–Ile–Gly–MeLeu–Met–NH_2 (**30**)

↓ HCl in AcOH

H–Lys–MePhe–Ile–Gly–MeLeu–Met–NH_2·2HCl (**7**)

Scheme 5.

Compound **23a** was used as the starting material (Scheme 5). Thus, **23a** was deprotected and was condensed with a mixed anhydride of BOC-isoleucine to afford the BOC-tetrapeptide ester (**28**). After the removal of the BOC group, compound **28** was coupled with di-BOC-dipeptide acid (**13**) with the aid of HObt and DCC. Amidation and deprotection gave the desired hexapeptide amide dihydrochloride (**7**).

None of the protected hexapeptide amides reported here, except di-BOC–Lys–Phe–Ile–Gly–MeIle–Met–NH_2 (**27b**), crystallized; they were purified by column chromatography on silica-gel. Compound **27b** was recrystallized from ethyl acetate. The hexapeptide amide dihydrochlorides were all amorphous and were shown to be homogeneous by paper chromatography, paper electrophoresis, and elemental analysis.

Results

The pharmacological results concerning rabbit blood pressure are summarized in Table 1.

The time of 50% recovery as well as that of 100% recovery shows that the duration of action of the *N*-methylpeptides synthesized here is of the same order of magnitude as that of the reference standard, **1**. These results suggest that the *N*-methylpeptide bond would be cleaved by the proteolytic enzyme of the organism as fast as the usual peptide bonds, or that other factors, as yet unknown, would participate in the deactivation of the peptides. As regards this point, a more precise study will be reported in a following paper.

Table 1 also shows that compound **2** and compound **6** have much less activity and that compounds **3** and **7** possess a substantial activity, though weaker than the standard one, **1**. On the other hand, compound **5** and compound **4** show a higher activity than **1**. It is reasonable that **6** exhibits a marked decrease in activity, because it has a different amino-acid side chain in the part of leucine which has been reported to be essential for activity.[10] Though the other compounds, **2**, **3**, **4**, **5**, and **7**, have the same side chains as **1**, they vary in the degree of biological activity. As may be seen in the case of depsipeptide analogs,[1] these results suggest that, in some cases, the replacement of an amide bond by an *N*-methylamide bond would have an important influence on the activity. To clarify this point, a more precise investigation is required; studies are currently in progress.

Experimental

All the melting points are uncorrected. Column chromatography was carried out on silica gel (Merck, 70—325 mech). The amino acid analysis was performed by the method reported by Kono *et al.*,[11] in which the acid hydrolysate was converted into the *t*-butyl ester of trifluoroacetylamino acid and the composition was determined by gas chromatography. The pharmacological assay was carried out as had been described previously.[1]

H–MeIle–OMe·HCl (8). Thionyl chloride (83 g, 0.7 mol) was stirred into methanol (120 ml) at −2—2°C. To this solution, *N*-methyl-L-isoleucine (18 g, 0.124 mol) prepared by the procedure developed by Quitt *et al.*[7] ($[\alpha]_D^{25}$ +29.0° (*c* 1, H_2O) was added; the solution was stirred at room temperature for 1 hr, and then refluxed for 3 hr. After evaporation, this procedure was repeated two times. The oily residue thus obtained was dissolved in water (50 ml), and the solution was basified with sodium bicarbonate and repeatedly extracted with ether. The ethereal solution was washed with a saturated sodium chloride solution and dried over magnesium sulfate. Into the filtered solution, dry hydrogen chloride was bubbled, and the white crystals thus obtained were collected and recrystallized from methanol–ether; yield, 15.7 g (65%); mp 156—157°C; $[\alpha]_D^{25}$ +40.1° (*c* 1, ethanol) [lit,[12] mp 154—155°C; $[\alpha]_D^{25}$ +39° (*c* 1, ethanol)]. (Found: C, 49.47; H, 9.30; N, 7.16; Cl, 17.95%).

AOC–Phe–MeIle–OH (9). Into a solution of *t*-amyloxycarbonyl-L-phenylalanine dicyclohexylammonium salt[13]

10) E. Schröder and K. Lübke, "The Peptides," Academic Press, New York and London (1966), p. 127.

11) Presented by T. Kono, M. Ishii, and K. Kotera at the 19th Annual Meeting of the Analytical Chemistry of Japan, Nagoya, November, 1970.

12) M. M. Shemyakin, Yu. A. Ovchinnikov, V. T. Ivanov, and A. A. Kiryushkin, *Tetrahedron*, **19**, 581 (1963).

13) S. Sakakibara, I. Honda, K. Takada, M. Miyoshi, T. Ohnishi, and K. Okumura, This Bulletin, **42**, 809 (1969).

TABLE 1. PHARMACOLOGICAL RESULTS ON THE BLOOD PRESSURE IN RABBITS

Compound	Dose μg/kg i.v.	Change mean arterial pressure mmHg	Change mean arterial pressure After sec	Average duration sec Recovery 50%	Average duration sec Recovery 100%
H-Lys-Phe-Ile-Gly-Leu-Met-NH_2 (**1**)	0.1	20± 4	17± 1	38± 7	74± 14
	1	45± 3	30± 5	60±15	140± 98
	5	58± 6	30± 5	121±29	323±148
H-Lys-Phe-MeIle-Gly-Leu-Met-NH_2 (**2**)	5	0	0	0	0
	10	4	15	29	10
	100	21± 3	26± 7	33± 6	88± 28
	500	26±24	33± 4	49±21	114± 58
H-Lys-MePhe-Ile-Gly-Leu-Met-NH_2 (**3**)	0.1	0	0	0	0
	0.5	16± 1	15± 2	20± 2	40± 12
	1	22± 3	25± 2	25± 4	63± 27
	5	27± 1	29± 2	32± 3	78± 12
	10	32± 4	36± 5	68±40	242±142
H-Lys-Phe-Ile-Sar-Leu-Met-NH_2 (**4**)	0.1	42± 4	24± 4	38± 5	175± 53
	0.5	50± 3	28± 3	69±11	299± 65
	1	52± 4	43± 8	99±10	372± 91
	5	57± 7	49±11	114±5	331± 53
H-Lys-Phe-Ile-Gly-MeLeu-Met-NH_2 (**5**)	0.1	24± 3	17± 2	17± 1	35± 7
	0.5	35± 2	20± 4	23± 2	95± 21
	1	36± 2	21± 3	32± 3	113± 20
	5	39±32	31± 5	57± 1	116± 22
	10	47± 4	33± 7	103±16	307±69
H-Lys-Phe-Ile-Gly-MeIle-Met-NH_2 (**6**)	1	0	0	0	0
	5	3± 2	5± 3	6± 4	8± 5
	10	5± 4	6± 4	6± 4	7± 5
	50	13	11	13	18
H-Lys-MePhe-Ile-Gly-MeLeu-Met-NH_2 (**7**)	0.1	1± 1	3± 3	2± 2	3± 3
	0.5	13± 2	13± 2	11± 1	46± 22
	1	21± 3	13± 2	14± 1	37± 7
	5	34± 3	19± 3	35±11	111± 28
	10	35± 1	19± 5	50±14	193± 38

(50 g, 0.11 mol) and **8** (20 g, 0.1 mol) in chloroform (300 ml), DCC[14] (22.7 g, 0.11 mol) was stirred at −5°C. After this mixture had been stirred overnight at room temperature, the dicyclohexylurea and dicyclohexylammonium chloride were filtered off. The filtrate was washed successively with 4% sodium bicarbonate, N hydrochloric acid, and water, and then dried over magnesium sulfate. The filtrate was evaporated *in vacuo* to yield an oil (31 g), which contained the acylurea[9] in some degree. This oil (30 g) was dissolved in a mixture of methanol (100 ml) and 4N sodium hydroxide (30 ml), and the solution was stirred for 20 hr at 0—5°C. After the dicyclohexylurea originating from the acylurea had been filtered off, the methanol was distilled off under reduced pressure below 40°C. The aqueous solution was washed with ether, acidified with N hydrochloric acid, and repeatedly extracted with ether. The combined ether extracts were washed with water and dried over magnesium sulfate. Evaporation gave crude crystals, which were recrystallized from ethyl acetate–petroleum ether; yield, 24 g (60%); mp 115—116°; $[\alpha]_D^{25}$ −61.9° (*c* 1, methanol). Found: C, 65.49; H, 8.47; N, 7.10%. Calcd for $C_{22}H_{34}O_5N_2$: C, 65.00; H, 8.43; N, 6.89%.

*AOC-Phe-MeIle-Gly-Leu-Met-NH_2 (**10**).* To a solution of **9** (8 g, 20 mmol) and triethylamine (3.1 ml) in chloroform (100 ml), ethyl chloroformate (2.4 g, 22 mmol) was added over a 15 min period at −12——10°C. After 15 min, a solution of glycyl-leucyl-methionine amide hydrochloride[15] (8 g, 22 mmol) and triethylamine (3.1 ml) in dimethylformamide (100 ml) was added, after which the solution was stirred overnight at room temperature. Then, it was poured into water (600 ml) and extracted with ethyl acetate. The ethyl acetate solution was washed successively with N hydrochloric acid, 4% sodium bicarbonate, and water, and then dried over magnesium sulfate. The filtrate was evaporated *in vacuo*, and the crude product was recrystallized from ethyl acetate–petroleum ether; yield, 1 g (7.05%); mp 204—206°C; $[\alpha]_D^{25}$ +22.1° (*c* 1, methanol). Found: C, 58.16; H, 8.41; N, 11.45; S, 4.65%. Calcd for $C_{35}H_{58}N_6O_7S\cdot H_2O$: C, 58.01; H, 8.28; N, 11.60; S, 4.42%.

*Di-BOC-Lys-Phe-MeIle-Gly-Leu-Met-NH_2 (**11**).* Compound **10** (400 mg, 0.6 mmol) was dissolved in 3N hydrogen chloride in dioxane (10 ml), and the solution was allowed to stand at room temperature for 30 min. The solvent was then distilled off *in vacuo*, and the residue was treated with ether. The pentapeptide amide hydrochloride thus obtained was dissolved in dimethylformamide (3 ml), neutralized with triethylamine (0.1 ml), and then subjected to a reaction with the di-BOC-lysine *p*-nitrophenyl ester[1] (400

14) J. C. Sheehan and G. P. Hess, *J. Amer. Chem. Soc.*, **77**, 1067 (1955).

15) K. Lübke, E. Schröder, R. Schmiechen, and H. Gibian, *Ann. Chem.*, **679**, 195 (1964).

mg, 0.85 mmol). After standing overnight at room tempetature, the solution was diluted with ethyl acetate (200 ml), washed successively with N hydrochloric acid, 4% sodium bicarbonate, and water, and dried over magnesium sulfate. The solvent was distilled off *in vacuo*, and the residue was precipitated as an amorphous powder from ethyl acetate–petroleum ether; yield, 420 mg (75%); mp 196—197°C; $[\alpha]_D^{25}$ −5.0° (*c* 0.5, methanol). Found: C, 57.98; H, 8.39; N, 11.73; S, 3.35%. Calcd for $C_{45}H_{76}O_{10}H_8S \cdot H_2O$: C, 57.50; H, 8.30; N, 11.92; S, 3.40%.

H–Lys–Phe–MeIle–Gly–Leu–Met–NH$_2$·2HCl (2) Compound **11** (200 mg) was dissolved in 2N hydrogen chloride in acetic acid (5 ml), and the solution was allowed to react at room temperature for 20 min. The product was precipitated by adding ice-cold dry ether (20 ml), and the precipitate was collected by filtration, washed well with ether, and dried over sodium hydroxide *in vacuo*. The product was dissolved in 60% methanol (4 ml), and an insoluble material was filtered off. The filtrate was concentrated to dryness over phosphorus pentoxide *in vacuo* to obtain the final product; yield, 170 mg; mp 159—164°C; $[\alpha]_D^{25}$ +27.3° (*c* 0.52, water); R_f, 0.79;[16] amino acid ratios in the acid hydrolyzate: Lys, 1.09; Phe, 1.01; Gly, 0.925; Leu, 1.00; Met, 0.99.[17] Found: C, 50.65; H, 7.99; N, 13.38; S, 3.48%. Calcd for $C_{35}H_{60}O_6N_8S \cdot 2HCl \cdot 2H_2O$: C, 50.66; H, 7.96; N, 13.51; S, 3.86%.

H–MePhe–OBzl–Tos–OH (12). A solution of *N*-methyl-L-phenylalanine[7] (18 g, 0.1 mol), *p*-toluenesulfonic acid monohydrate (21 g, 0.1 mol), and benzyl alcohol (100 ml) in benzene (100 ml) was refluxed in a Dean and Stark apparatus[18] for 48 hr. Ether (100 ml) was added to the solution, and it was kept at −20°C for 10 hr. The product, precipitated as crystals, was collected and recrystallized from methanol–ether; yield, 36 g (82%); mp 110—113°C; $[\alpha]_D^{25}$ +1.2° (*c* 1, ethanol). Found: C, 65.49; H, 6.09; N, 3.09; S, 7.21%. Calcd for $C_{24}H_{27}O_5NS$: C, 65.29; H, 6.16; N, 3.17; S, 7.25%.

Di-BOC–Lys–MePhe–OH (13). Into a solution of di-BOC-L-lysine dicyclohexylammonium salt[13] (28 g, 50 mmol) and **12** (22 g, 50 mmol) in chloroform (250 ml), DCC was stirred at −5°C. After it had been allowed to stand overnight, the dicyclohexylurea and dicyclohexylammonium chloride were filtered off. The filtrate was washed successively with 4% sodium bicarbonate, N hydrochloric acid, and water, and then dried over magnesium sulfate. The filtrate was evaporated *in vacuo* to yield an oil (25 g). This oil (25 g) was dissolved in methanol (300 ml) and was subjected to hydrogenolysis in the presence of 5% palladium on charcoal. After the filtration and evaporation of the solvent, the crude material was dissolved in 4% sodium bicarbonate, extracted with ether, acidified with N hydrochloric acid, and extracted into ether. The ether was then removed *in vacuo*, leaving a colorless, clear oil; yield, 20 g (80%); $[\alpha]_D^{25}$ −52.9° (*c* 1.55, methanol).

Di-BOC–Lys–MePhe–Ile–Gly–Leu–Met–OMe (14). Into a solution of **13** (5 g, 10 mmol) and HOBt[8] (1.4 g, 10 mmol) in tetrahydrofuran (50 ml), DCC was stirred (2.1 g, 10 mmol) at −5°C. After stirring for 1 hr at −5—5°C and then for 1 hr at room temperature, a solution of isoleucyl-glycyl-leucyl-methionine methyl ester hydrochloride[15] (4.8 g, 10 mmol) and triethylamine (1.4 ml) in tetrahydrofuran (20 ml) was added. After the mixture had then been allowed to stand overnight at room temperature, the dicyclohexylurea was filtered off. The filtrate was evaporated *in vacuo*, and the remaining oil was dissolved in ethyl acetate (200 ml). The ethyl acetate solution was washed successively with 1% hydrochloric acid, N sodium bicarbonate, and water, and dried over magnesium sulfate. The filtrate was evaporated to dryness under reduced pressure, and the crude product obtained was purified by column chromatography, being eluted with a mixture of ethyl acetate–benzene (1: 1); yield, 7.2 g (75%); $[\alpha]_D^{25}$ − 25.7°(*c* 1, methanol). Found: C, 58.29; H, 8.12; N, 10.25; S, 3.20%. Calcd for $C_{46}H_{77}O_{11}N_7S \cdot H_2O$: C, 57.89; H, 8.34; N, 10.27; S, 3.36%.

Di-BOC–Lys–MePhe–Ile–Gly–Leu–Met–NH$_2$ (15). a) To a solution of **13** (4 g, 8 mmol) and triethylamine (1.2 ml) in chloroform (100 ml), ethyl chloroformate (0.95 g, 8.8 mmol) was added over a 15 min period at −12—−10°C. After 15 min, a solution of isoleucyl-glycyl-leucyl-methionine amide hydrochloride[15] (3.8 g, 8 mmol) and triethylamine (1.2 ml) in dimethylformamide (20 ml) was added, and the solution was stirred overnight. Then, it was poured into water (200 ml) and extracted with chloroform. The chloroform extract was washed successively with 1% hydrochloric acid, 4% sodium bicarbonate, and water, dried over magnesium sulfate, and evaporated to dryness. The product was recrystallized from ethyl acetate–methanol–petroleum ether to yield ethoxycarbonyl-isoleucyl-glycyl-leucyl-methionine amide; yield, 2.3 g (58%); mp 247—249°C. Found: C, 52.10; H, 8.10; N, 13.65%. Calcd for $C_{22}H_{41}N_5O_6S$: C, 52.47; H, 8.21; N, 13.91%. From the mother liquor, the desired compound, **15**, was obtained; 1.5 g (20%); mp 180—182°C; $[\alpha]_D^{25}$ +14.6° (*c* 1, methanol). Found: C, 57.60; H, 8.28; N, 11.58; S, 3.18%. Calcd for $C_{45}H_{76}O_{10}N_8S \cdot H_2O$: C, 57.50; H, 8.30; N, 11.92; S, 3.40%.

b) A solution of **14** (4.7 g, 5 mmol) in methanol (100 ml) was saturated with dry ammonia gas at 0°C, and the solution was allowed to stand for 24 hr at room temperature. The reaction mixture was then concentrated to dryness under reduced pressure, and the residue was crystallized from ethyl acetate–methanol–petroleum ether; yield, 3.8 g (82%); mp 181—183°C; $[\alpha]_D^{25}$ +14.8° (*c* 1, methanol).

H–Lys–MePhe–Ile–Gly–Leu–Met–NH$_2$·2HCl (3). This was obtained from **15** (200 mg) by the method described for the preparation of **2**; yield, 180 mg; mp 103—105°C; $[\alpha]_D^{25}$ −19.1° (*c* 0.2, water), R_f, 0.77;[16] amino acid ratios in the acid hydrolyzate; Lys, 1.15; MePhe,1. 10; Ile, 1.08; Gly, 1.15; Leu, 1.00; Met, 0.85. Found: C, 51.06; H, 8.01; N, 13.60; S, 4.08%. Calcd for $C_{35}H_{60}O_6N_8S \cdot 2HCl \cdot 2H_2O$: C, 50.66; H, 7.96; N, 13.51; S, 3.86%.

H–Sar–OBzl·HCl (16). A solution of sarcosine (50 g, 0.6 mol), *p*-toluenesulfonic acid monohydrate (125 g, 0.66 mol) and benzyl alcohol (600 ml) in benzene (600 ml) was treated as described for the preparation of **12**. The crude product precipitated as *p*-toluenesulfonate was dissolved into water (100 ml), and the solution was basified with sodium bicarbonate and extracted with ethyl acetate. The extract was washed with a saturated sodium chloride solution and then dried over magnesium sulfate. To the filtered solution, 3N hydrogen chloride in dioxane (200 ml) was added, and the solution was evaporated *in vacuo* to dryness. The remaining crystal was recrystallized from methanol–ether; yield, 93 g (72%); mp 174—176°C. Found: C, 55.20; H, 6.58; N, 6.56; Cl, 16.46%. Calcd for $C_{10}H_{13}NO_2 \cdot HCl$: C, 55.68; H, 6.49; N, 6.49; Cl, 16.47%.

16) Paper chromatography was carried out on Toyo Roshi No.50 with *n*-butanol–acetic acid–water (4: 1: 1).

17) MeIle was present but not determined. Its presence was proved by paper chromatography of the acid hydrolysate [*n*-butanol–acetic acid–water (4: 1: 1) system] in which MeIle was perfectly separated from the other slower moving amino acids.

18) J. P. Greenstein and M. Winitz, "Chemistry of the Amino Acids," John Wiley & Sons, Inc., New York and London (1961), p. 940.

BOC-Ile-Sar-OH (17). This was obtained from BOC-isoleucine[13] and **16** (21 g, 100 mmol) as described for the preparation of **13**; yield of oil, 19.2 g (64%); $[\alpha]_D^{25}$ −31.0° (*c* 1.3, methanol).

BOC-Ile-Sar-Leu-Met-OMe (18). This was obtained from **17** (9.1 g, 30 mmol), HObt (4 g, 30 mmol), DCC (6.8 g, 33 mmol), and leucyl-methionine methyl ester hydrochloride[15] (9.5 g, 30 mmol) as described for the preparation of **14**. The crude product was purified by column chromatography on silica-gel, being eluted with ethyl acetate; yield of oil, 15.5 g (92%); $[\alpha]_D^{25}$ −51.3° (*c* 1.25, methanol).

BOC-Ile-Sar-Leu-Met-NH_2 (19). A solution of **18** (11.2 g, 20 mmol) in methanol (300 ml) was saturated with dry ammonia gas at 0°C, after which the solution was allowed to stand for 40 hr at room temperature. The reaction mixture was concentrated to dryness under reduced pressure, and the residual crystal was recrystallized from ethyl acetate-petroleum ether; yield, 9 g (80%); mp 188—191°C; $[\alpha]_D^{25}$ −55.0° (*c* 1, methanol). Found: C, 55.08; H, 8.44; N, 12.77; S, 6.06%. Calcd for $C_{25}H_{47}O_6N_5S$: C, 55.04; H, 8.62; N, 12.84; S, 5.87%.

BOC-Phe-Ile-Sar-Leu-Met-NH_2 (20). Compound **19** (5.5 g, 10 mmol) was dissolved in 3N hydrogen chloride in dioxane (100 ml), and the solution was allowed to stand at room temperature for 40 min. The solvent was then distilled off *in vacuo*, and the residue was triturated with ether. The tetrapeptide amide hydrochloride thus obtained was dissolved in dimethylformamide (40 ml), neutralized with triethylamine (1.6 ml), and then subjected to a reaction with the BOC-phenylalanine *p*-nitrophenyl ester (5.2 g, 13 mmol). The solution was treated as described for the preparation of **11**, and the crude product was recrystallized from ethyl acetate-methanol-petroleum ether; yield, 4.9 g (90%); mp 162—167°C; $[\alpha]_D^{25}$ −54.1° (*c* 1, methanol). Found: C, 58.47; H, 7.70; N, 11.85; S, 4.35%. Calcd for $C_{34}H_{56}O_7N_6S$: C, 58.95; H, 8.09; N, 12.13; S, 4.62%.

Di-BOC-Lys-Ile-Sar-Leu-Met-NH_2 (21). This was obtained from the di-BOC-lysine *p*-nitrophenyl ester (700 mg, 1.5 mmol) and the pentapeptide amide derived from compound **20** (1 g, 1.4 mmol) as described for the preparation of **11**; yield, 825 mg (63%); mp 154—160°C; $[\alpha]_D^{25}$ −57.3° (*c* 1, methanol). Found: C, 57.46; H, 8.30; N, 11.59; S, 3.26%. Calcd for $C_{45}H_{76}O_{10}N_8S\cdot H_2O$: C, 57.50; H, 8.30; N, 11.92; S, 3.40%.

H-Lys-Phe-Ile-Sar-Leu-Met-$NH_2\cdot 2HCl$ (4). This was obtained from **21** (200 mg) as described for the preparation of **2**; yield, 170 mg; mp 80—90°C; $[\alpha]_D^{25}$ −33.8° (*c* 0.5, water); R_f, 0.73;[16] amino acid ratios in the acid hydrolyzate; Lys, 1.07; Phe, 1.05; Ile, 1.05; Sar, 1.15; Leu, 1.00; Met, 0.94. Found: C, 51.64; H, 7.79; N, 13.62; S, 3.83%. Calcd for $C_{35}H_{60}O_6N_8S\cdot 2HCl\cdot H_2O$: C, 51.78; H, 7.89; N, 13.81; S, 3.94%.

H-MeLeu-OMe·HCl (22). This was obtained from *N*-methyl-L-leucine[7] as described for the preparation of **8**; yield (77%); mp 126.5—127°C; $[\alpha]_D^{25}$ +31.4° (*c* 1, ethanol) (lit,[12] mp 127—128°C; $[\alpha]_D^{25}$ +30° (ethanol)). (Found: C, 49.32; H, 9.21; N, 7.19; Cl, 18.17%).

BOC-Gly-MeLeu-OH (23a). Into a solution of BOC-glycine[13] (17.5 g, 100 mmol) **22** (20 g, 100 mmol), and triethylamine (14 ml) in chloroform (300 ml), DCC was stirred at −5°C. After the mixture had been allowed to stand overnight at room temperature, the dicyclohexylurea was filtered off and the filtrare was treated as described for the preparation of **9**. The crude product was recrystallized from ether-*n*-hexane; yield, 10.6 g (35%); mp 93—95°C; $[\alpha]_D^{25}$ −24.6° (*c* 1, methanol). Found: C, 55.46; H, 8.82; N, 9.18%. Calcd for $C_{14}H_{26}O_5N_2$: C, 55.61; H, 8.67; N, 9.27%.

BOC-Gly-MeIle-OH (23b). This was obtained from BOC-glycine (17.5 g, 100 mmol) and **8** (20 g, 100 mmol) as described above. The crude product was recrystallized from ethyl acetate-petroleum ether; yield, 10.2 g (33.8%); mp 139.5—140°C; $[\alpha]_D^{25}$ −1.1° (*c* 2, methanol). Found: C, 55.76; H, 8.53; N, 9.41%. Calcd for $C_{14}H_{26}O_5N_2$: C, 55.61; H, 8.67; N, 9.27%.

BOC-Gly-MeLeu-Met-OMe (24a). This compound was obtained from **23a** (20 g, 67 mmol), HObt (9.1 g, 67 mmol), DCC (16 g, 80 mmol), methionine methyl ester hydrochloride (14 g, 70 mmol), and triethylamine (9.8 ml, 70 mmol) as described for the preparation of **14**. The crude oil was purified by column chromatography on silica gel being eluted with a mixture of benzene and ethyl acetate (7: 3); yield of oil, 27 g (90%); $[\alpha]_D^{25}$ −9.2° (*c* 1, methanol).

BOC-Gly-MeIle-Met-OMe (24b). This was obtained from **23b** (9 g, 30 mmol), HObt (4 g, 30 mmol), DCC (6.6 g, 33 mmol), methionine methyl ester hydrochloride (6.6 g, 33 mmol), and triethylamine (4.6 ml, 33 mmol) as described above; yield of oil, 11.6 g, (87%); $[\alpha]_D^{25}$ +11.0° (*c* 1, methanol).

BOC-Gly-MeLeu-Met-NH_2 (25a). A solution of **24a** (16.5 g, 37 mmol) in methanol (300 ml) was saturated with dry ammonia gas at 0°C, and the solution was treated as described for the preparation of **19**; yield of oil, 13.2 g (84%); $[\alpha]_D^{25}$ −6.2° (*c* 1, methanol).

BOC-Gly-MeIle-Met-NH_2 (25b). This was obtained from **24b** (4.5 g, 10 mmol) as described for the preparation of **19**; yield of oil, 3.6 g (80%); $[\alpha]_D^{25}$ −17.8° (*c* 1, methanol).

AOC-Phe-Ile-Gly-MeLeu-Met-NH_2 (26a). Into a solution of *t*-amyloxycarbonyl-phenylalanyl-isoleucine hydrazide[1] (4 g, 10 mmol) in a mixture of 2N hydrochloric acid (20 ml, 40 mmol) and dimethylformamide (200 ml), a chilled solution of sodium nitrite (700 mg, 10 mmol) in water (1 ml) was stirred over a 15 min period at −15——13°C. After 20 min, the solution was neutralized with triethylamine; then a solution of triethylamine (1.4 ml) and the glycyl-*N*-methylleucyl-methionine amide hydrochloride obtained from **25a** (4.3 g, 10 mmol) in dimethylformamide (20 ml) was added at −10——5°C. After the reaction mixture had been stirred at room temperature for 3 hr, it was poured into water (1000 ml) and extracted with ethyl acetate. The extract was washed successively with N hydrochloric acid, 4% sodium bicarbonate, and water, dried over magnesium sulfate, and evaporated *in vacuo*. The oily residue (6.6 g) was purified by column chromatography on silica gel (Merck 0.2—0.5 mm) being eluted with a mixture of ethyl acetate and methanol (8: 2); yield of oil, 5.8 g (80%); $[\alpha]_D^{25}$ −23.9° (*c* 1, methanol). Found: C, 58.33; H, 8.14; N, 11.62; S, 4.24%. Calcd for $C_{35}H_{58}O_7N_6S\cdot H_2O$: C, 58.01; H, 8.28; N, 11.60; S, 4.42%.

AOC-Phe-Ile-Gly-MeIle-Met-NH_2 (26b). To a solution of the azide derived from *t*-amyloxycarbonyl-phenylalanyl-isoleucine hydrazide (4 g, 10 mmol) in dimethylformamide (200 ml), a solution of the glycyl-*N*-methylisoleucyl-methionine amide hydrochloride obtained from **25b** (4.3 g, 10 mmol) and triethylamine (1.4 ml) in dimethylformamide (20 ml) was added. The crude product was obtained as described above and was purified by column chromatography on silica-gel, being eluted with a mixture of ethyl acetate and methanol; yield of oil, 5.9 g (82%); $[\alpha]_D^{25}$ −15.8° (*c* 1, methanol). Found: C, 58.38; H, 8.25; N, 11.40; S, 4.23%. Calcd for $C_{35}H_{58}O_7N_6S\cdot H_2O$: C, 58.01; H, 8.28; N, 11.60; S, 4.42%.

Di-BOC-Lys-Phe-Ile-Gly-MeLeu-Met-NH_2 (27a). This was obtained from the di-BOC-lysine *p*-nitrophenyl ester (2.3 g, 5 mmol) and the pentapeptide amide derived from compound **26a** (3 g, 4.4 mmol) as described for the preparation of **11**. The crude product was purified by column chromatography on silica-gel, being eluted first with ethyl

acetate and then with a mixture of ethyl acetate and methanol (8: 2); yield of oil, 3 g (72%); $[\alpha]_D^{25}$ −26.5° (*c* 1, methanol). Found: C, 57.82; H, 8.18; N, 11.73; S, 3.18%. Calcd for $C_{45}H_{76}O_{10}N_8S \cdot H_2O$: C, 57.50; H, 8.30; N, 11.92; S, 3.40%.

Di-BOC-Lys-Phe-Ile-Gly-MeIle-Met-NH$_2$ (27b). This was obtained from the di-BOC-lysine *p*-nitrophenyl ester (1.9 g, 4 mmol) and the pentapeptide amide derived from compound **26b** (2.7 g, 3.8 mmol). The crude product was dissolved in ethyl acetate, and the product was precipitated gradually as crystals; yield, 2.1 g (61%); mp 212—213°C; $[\alpha]_D^{25}$ +8.3° (*c* 1, methanol). Found: C, 57.97; H, 8.18; N, 11.90; S, 3.36%. Calcd for $C_{45}H_{76}O_{10}N_8S \cdot H_2O$: C, 57.50; H, 8.30; N, 11.92; S, 3.40%.

H-Lys-Phe-Ile-Gly-MeLeu-Met-NH$_2$·2HCl (5). This was obtained from **27a** (200 mg) as described for the preparation of **2**; yield, 180 mg; mp 107—112°C; $[\alpha]_D^{25}$ −7.3° (*c* 0.3, water); R_f, 0.70;[16] amino acid ratios in the acid hydrolyzate: Lys, 1.14; Phe, 1.05; Ile, 1.00; Gly, 1.05; MeLeu, 1.02; Met, 0.99. Found: C, 50.42; H, 7.94; N, 13.65; S, 3.48%. Calcd for $C_{35}H_{60}O_6N_8S \cdot 2HCl \cdot 2H_2O$: C, 50.66; H, 7.96; N, 13.51; S, 3.86%.

H-Lys-Phe-Ile-Gly-MeIle-Met-NH$_2$·2HCl (6). This was obtained from **27b** (200 mg) as described for the preparation of **2**; yield, 170 mg, mp 85—100°C; $[\alpha]_D^{25}$ +34.0° (*c* 0.2, water); R_f, 0.70;[16] amino acid ratios in the acid hydrolyzate: Lys, 0.92; Phe, 0.99; Ile, 1.00; Gly, 0.97; Met, 0.98.[17] Found: C, 50.95; H, 8.11; N, 13.46; S, 3.93%. Calcd for $C_{35}H_{60}O_6N_8S \cdot 2HCl \cdot 2H_2O$: C, 50.66; H, 7.96; N, 13.51; S, 3.86%.

BOC-Ile-Gly-MeLeu-Met-OMe (28). Into a solution of BOC-isoleucine (2.3 g, 10 mmol) and triethylamine (1.4 ml) in chloroform (50 ml), ethyl chloroformate (1.1 g, 10 mmol) was stirred over a 15 min period at −11——10°C. After 15 min, there was added a solution of triethylamine (1.4 ml) and the glycyl-*N*-methylleucyl-methionine methyl ester hydrochloride derived from **23a** (4.5 g, 10 mmol) in chloroform (30 ml), the reaction mixture was then stirred at room temperature overnight. It was washed successively with N hydrochloride acid, 4% sodium bicarbonate, and water, and dried over magnesium sulfate. The filtered solution was evaporated to dryness under reduced pressure to yield the product; yield of oil, 4.9 g (88%); $[\alpha]_D^{25}$ −23.0° (*c* 1, methanol).

Di-BOC-Lys-MePhe-Ile-Gly-MeLeu-Met-OMe (29). This was obtained from **13** (7.6 g, 15 mmol), HOBt (2 g, 15 mmol), DCC (3.5 g, 17 mmol), and the isoleucyl-glycyl-*N*-methylleucyl-methionine methyl ester derived from **28** (8.2 g, 15 mmol) as described for the preparation of **14**. The crude oil was purified by column chromatography on silica-gel, being eluted with ethyl acetate; yield of oil, 10.6 g (77%); $[\alpha]_D^{25}$ −30.8° (*c* 1, methanol). Found: C, 58.01; H, 8.32; N, 10.33; S, 3.51%. Calcd for $C_{47}H_{79}O_{11}N_7S \cdot H_2O$: C, 58.32; H, 8.37; N, 10.13; S, 3.30%.

Di-BOC-Lys-MePhe-Ile-Gly-MeLeu-Met-NH$_2$ (30). A solution of compound **29** (9.7 g, 10 mmol) in methanol was saturated with ammonia gas at 0°C, after which the solution was allowed to stand for 24 hr at room temperature. The reaction mixture was then concentrated to dryness under reduced pressure, and the residue was dissolved in ethyl acetate and chromatographed on silica-gel, being eluted first with ethyl acetate and then with a mixture of ethyl acetate and methanol (8: 2); yield of oil, 7.7 g (81%); $[\alpha]_D^{25}$ −30.2° (*c* 1, methanol). Found: C, 57.56; H, 8.25; N, 11.28; S, 3.27%. Calcd for $C_{46}H_{78}O_{10}N_8S \cdot H_2O$: C, 57.98; H, 8.40; N, 11.76; S, 3.36%.

H-Lys-MePhe-Ile-Gly-MeLeu-Met-NH$_2$·2HCl (7). This was obtained from **30** (200 mg) as described for the preparation of **2**; yield, 180 mg; mp 109—115°C; $[\alpha]_D^{25}$ −22.7° (*c* 0.1, water); R_f, 0.74;[16] amino acid ratios in the acid hydrolyzate: Lys, 0.89; MePhe, 0.93; Ile, 1.00; Gly, 0.95; MeLeu, 1.06; Met, 0.92. Found: C, 51.02; H, 8.09; N, 13.26; S, 3.42%. Calcd for $C_{36}H_{62}O_6N_8S \cdot 2H_2O$: C, 51.24; H, 8.06; N, 13.28; S, 3.79%.

The authors wish to thank Professor N. Izumiya of Kyushu University, and Director Dr. I. Chibata of Tanabe Seiyaku for their encouragement in the course of this study.

Photochemical Reactions of Aromatic Compounds. XI[1] The Photochemical Cycloaddition of Vinyl Ethers to α-Naphthonitrile

Chyongjin PAC, Taizo SUGIOKA, Kazuhiko MIZUNO, and Hiroshi SAKURAI
The Institute of Scientific and Industrial Research, Osaka University, Suita-shi, Osaka
(Received April 28, 1972)

The photochemical reactions of α-naphthonitrile with vinyl ethers gave two stereo-isomeric (2+2) cycloadducts, *trans*-1-cyano-8-alkoxy-2,3-benzobicyclo[4.2.0]octa-2,4-diene **1** and the *cis* isomer, **2**, in 80—90% yields. From the results of fluorescence measurements and kinetic analysis, the photocycloaddition was established to occur from the lowest excited singlet state of α-naphthonitrile.

Recently much attention has been paid to the photocycloaddition of unsaturated bonds to aromatic rings. Although the photocycloaddition to the benzene ring has been well investigated,[2] the cycloaddition to the naphthalene ring has been less investigated; only a few examples have been studied, the (2+2) addition of acrylonitrile[3] or diarylacetylenes[4] to naphthalene, the (2+2+2) addition of dimethyl acetylenedicarboxylate to naphthalene,[5] the (4+4) addition of acyclic dienes to naphthalene,[6] and the (4+4) addition of furan to α-naphthonitrile.[7]

The present paper will describe the photochemical (2+2) cycloaddition of alkyl vinyl ethers to α-naphthonitrile (α-NN) and will suggest that the photocycloaddition takes place *via* an exciplex generated from the lowest excited singlet state of α-NN.

Results

Irradiation-results and Structural Assignment of Products. The irradiation of a mixture of α-NN and a large excess of methyl vinyl ether in methanol or benzene with a high-pressure mercury arc at room temperature through a Pyrex glass (>300 nm) and under a nitrogen atmosphere gave two isomeric 1:1-adducts, **1a** and **2a**, in 80—90% yields when 90—95% of α-NN was consumed. The formation-ratio of **1a** to **2a** was dependent on the solvent used; it was *ca.* 1 for a benzene solution and 2—3 for methanolic and acetonitrile solutions, though the total yields of the products did not change with the solvents used.

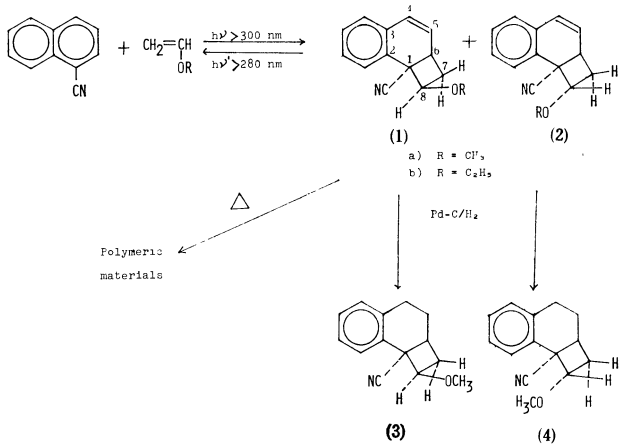

Chart 1.

The **1a** adduct, mp 86—87°C, was separated from **2a** by chromatography on the silica gel of the photolysate. On the other hand, **2a** could not be obtained in a pure form, since the chromatographic separation of **2a** from **1a** was incomplete and preparative vpc was not suitable because of the thermal instability of the adducts. Since **2a** was found to be thermally more stable than **1a** (*vide infra*), the photolysate from a benzene solution was subjected to thermolysis at 180—200°C; we thus obtained a mixture enriched with **2a**. The repeated chromatography of that mixture afforded **2a** containing only a small amount of **1a**.

The structure of the adducts was determined by IR, UV, and NMR analyses and by studying the mass spectroscopic data. The mass spectra of both adducts exhibit a weak parent peak at *m/e* 211, a strong peak at *m/e* 153 (α-NN), and a moderate peak at *m/e* 58 (C_3H_6O), along with other, far less important peaks. This fragmentation pattern strongly suggests the structure of 1:1-cycloadduct for the adducts. The two adducts have similar IR spectra, which show bands at 3040, 3020 (aromatic and olefinic C–H), 2990, 2930 (aliphatic C–H), 2210 (C≡N), 1640 (C=C), and 1140 cm^{-1} (C–O–C). The UV spectra, λ_{max}^{MeOH} (ε) 265 (7.6×10^3) and 300 nm (1.17×10^3) for **1a** and 265 (5.2×10^3) and 300 nm (sh) for **2a**, show that both adducts have a

1) Part X, C. Pac, T. Sugioka, and H. Sakurai, *Chem. Lett.*, **1972**, 39.

2) K. Okumura, S. Takamuku, and H. Sakurai, *Kogyo Kagaku Zasshi*, **72**, 200 (1969); J. G. Atkinson, D. E. Ayer, G. Buchi, and E. W. Robb, *J. Amer. Chem. Soc.*, **85**, 2257 (1963); B. E. Joband and J. D. Little-hailes, *J. Chem. Soc. C*, **1968**, 886; R. Srinivasan and K. A. Hill, *J. Amer. Chem. Soc.*, **87**, 4653 (1965); R. Srinivasan, *ibid.*, **93**, 3555 (1971); N. C. Perrins and J. P. Simons, *Chem. Comm.*, **1967**, 999; H. Morrison and W. I. Ferree, *ibid.*, **1969**, 268; G. Koltzenburg and K. Kraft, *Tetrahedron Lett.*, **1966**, 389; K. Kraft and G. Koltzenburg, *ibid.*, **1967**, 4357; K. E. Wilzbach and L. Kaplan, *J. Amer. Chem. Soc.*, **88**, 2067 (1966); **93**, 2073 (1971); D. Brce-Smith, *Pure Appl. Chem.*, **16**, 47 (1968); W. M. Hardham and G. S. Hammond, *J. Amer. Chem. Soc.*, **89**, 3200 (1967); J. D. Bradshaw, *Tetrahedron Lett.*, **1966**, 2033; D. Bryce-Smith, A. Gilbert, and J. Grzonka, *Chem. Commun.*, **1970**, 498; H.-D. Scharf and R. Klar, *Chem. Ber.*, **105** 575 (1972).

3) J. J. McCullough, *Chem. Commun.*, **1970**, 948; R. M. Bowman, T. R. Chamberlain, C. W. Huang, and J. J. McCullough, *J. Amer. Chem. Soc.*, **92**, 4106 (1970).

4) T. Teitei, P. J. Collin, and W. H. F. Sasse, *Aust. J. Chem.*, **25**, 171 (1972) and references cited therein.

5) E. Grovenstein, Jr., T. C. Campbell, and T. Shibata, *J. Org. Chem.*, **34**, 2418 (1969).

6) K. Kraft and G. Koltzenburg, *Tetrahedron Lett.*, **1967**, 4723.

7) Ref. 1.

Table 1. NMR data of **1a** and **2a**

Compounds	δ (Multiplicity)/Coupling constants (Hz)						
	C_4–H	C_5–H	C_6–H	$C_{7'}$–H	C_7–H	C_8–H	OCH_3
1a	6.32	5.86	3.02	1.95	2.51	4.40	3.35
	(d)	(q)	(oct)	(complex)		(q)	(s)
	$J_{4,5}=10$,	$J_{5,6}=6$,	$J_{6,7}=10$,	$J_{6,7'}=9$,	$J_{7,8}=8.5$,	$J_{7',8}=8$,	and $J_{7,7'}=10$
2a	6.33	5.75	3.14—3.5	234.	2.71	4.09	3.30
	(d)	(q)	(m)	(complex)		(t)	(s)
	$J_{4,5}=9$,	$J_{5,6}=4$,	$J_{6,7}=11$,	$J_{6,7'}=3$,	$J_{7,8}=J_{7',8}=8$, and	$J_{7,7'}=11$	

a) NMR spectra were taken for CCl_4 solutions using TMS as an internal standard and aromatic protons showed the signals at δ 6.9—7.5 as multiplets.

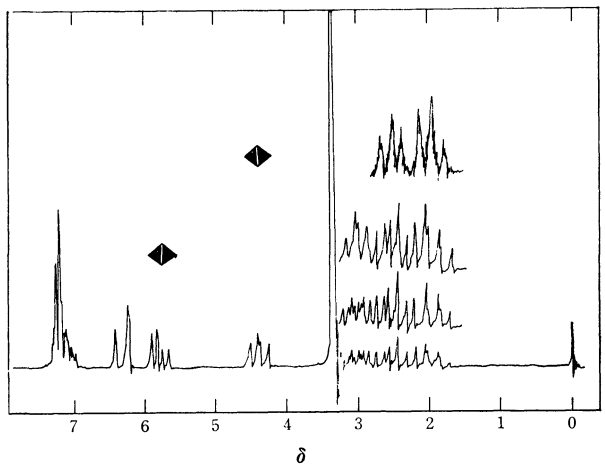

Fig. 1. NMR spectrum of **1a** in CCl_4.

1,2-dihydronaphthalene-chromophore.[8] From these spectral data, the structures of substituted napthhalene and the (2+4) cycloadduct can be safely eliminated.

The NMR spectra of the two adducts are similar (Table 1). The chemical shifts and the coupling constants are determined by first-order analysis of the spectra and a spin-decoupling method. The integral of signals shows that both **1a** and **2a** have four aromatic protons, two vinyl protons, two methine protons, two methylene protons, and three methoxy protons. Figure 1 shows the NMR spectrum of **1a** and the results of the spin-decoupling experiment. Irradiation at δ 5.77 changes the octet at δ 2.84—3.22 (C_6–H) into a quartet with the coupling constants of 9 and 10 Hz. Thus, it is confirmed that the two vinyl protons (C_4– and C_5–H) and the C_6-methine proton form an ABX-spin system ($J_{AX}\sim 0$ Hz) and that the X-part couples further with the adjacent unequivalent methylene protons (C_7– and $C_{7'}$–H). The quartet at δ 4.40 are clearly due to the C_8-proton. On irradiation at this position, the complex signal in the methylene region collapses into two triplets at δ 1.95 and 2.51, with a coupling constant of *ca.* 10 Hz. This result unambiguously shows, that the C_8-methine proton couples with the $C_{7,7'}$-methylene protons in an ABX type of coupling. Thus, these data establish the ring skeleton of **1a** to be 1-cyano-8-methoxy-2,3-benzobicyclo[4.2.0]octa-2,4-diene.

The similarity of the IR, UV, and NMR spectra between **1a** and **2a** strongly suggests that **2a** has the same ring skeleton as **1a**. Especially, the NMR data support the structure. The triplet at δ 4.09 and the ABX-type of signal pattern in the olefinic region cannot be resonably interpreted by the other possible structures of (2+2) cycloadducts. On irradiation at δ 4.09, the multiplet due to methylene protons collapses into a triplet with a coupling constant of 11 Hz at δ 2.71 and a quartet with coupling constants of 3 and 11 Hz at δ 2.34. These results unambiguously show that **2a** has the same spin system as **1a**, though the signal pattern of C_6–H of **2a** cannot be firmly established on account of the overlapping of the signal with that of the methoxy protons.

Therefore, the structural difference between **1a** and **2a** occurs from the stereochemical difference, the *cis* or *trans* configuration of the methoxy group to the cyano group, *i.e.*, the *endo*- or *exo*-location of the C_8-proton in relation to the benzene ring. In the case of benzo-polycyclic compounds, it is well known that an *endo*-proton is more shielded than an *exo*-proton.[9,10] Therefore, it is important to note that the signal of the C_8-proton of **2a** appears 0.31 ppm higher in field than that of the proton of **1a**. This fact requires the *endo*-location of the proton of **2a**. In the case of the dihydro isomers, **3** and **4** obtained by the catalytic hydrogenation of **1a** and **2a**, this type of anisotropic effect can be expected to be more evident for the C_8-proton, since the molecular models indicate that the C_8-proton of **4** is more closely located over the benzene ring than that of any other isomer. For the same reason, the methoxy protons of **3** must be most shielded. In fact, **4** shows the signal of the C_8-proton at a higher field (δ 3.67) than any other isomer, while the methoxy protons of **3** have the signal at the highest field (δ 3.21)

Table 2. Comparison of chemical shifts of C_8-proton and methoxy protons between **1a**, **2a**, **3**, and **4**

Protons	Compounds Chemical shift (δ)			
	1a	**2a**	**3**	**4**
C_8–H	4.40	4.09	4.27	3.67
OCH_3	3.35	3.30	3.21	3.35

8) W. Hückel, E. Ververa, and U. Wörfel, *Chem. Ber.*, **90**, 901 (1957); J. J. McCullough, *Can. J. Chem.*, **1969**, 757.

9) K. Tori, K. Aono, Y. Hata, R. Muneyuki, T. Tsuji, and H. Tanida, *Tetrahedron Lett.*, **1966**, 9.

10) H. E. Simmons, *J. Amer. Chem. Soc.*, **83**, 1657 (1961).

Table 3. NMR data of **1b** and **2b**[a)]

Compounds	δ(Multiplicity)/Coupling constants (Hz)					
	C_4–H	C_5–H	C_6–H	$C_{7'}$–H	C_7–H	C_8–H
1b	6.28	5.75	2.99	1.92	2.50	4.45
	(d)	(q)	(oct)	(complex)		(q)
	$J_{4,5}=10$,	$J_{5,6}=6$,	$J_{6,7}=10$,	$J_{6,7'}=8$,	$J_{7,8}=9$,	$J_{7',8}=8$, and $J_{7,7'}=10$
2b	6.3	5.75	3.1—3.3	2.32	2.55	4.16
	(d)	(q)	(m)	(complex)		(t)
	$J_{4,5}=10$,	$J_{5,6}=4$,	$J_{6,7}=9$,	$J_{6,7'}=3$,	$J_{7,8}=J_{7',8}=8$, and $J_{7,7'}=11$	

a) The adduct **1b** exhibited the signal of ethoxy group at δ 1.1 (t, CH_3, $J=7$ Hz) and 3.55 (q, OCH_2) and aromatic protons at δ 6.8—7.4 (m), and **2b** showed the signals at δ 1.18 (t, CH_3, $J=8$ Hz), 3.43 (q, OCH_2), and 6.8—7.5 (m, aromatic protons).

among the four isomers (see Table 2). Thus, these NMR data clearly establish that **1a** and **3** require the *exo*-location of the C_8-proton, *i.e.*, the *trans*-configuration between the cyano and methoxy groups, whlie **2a** and **4** have the *cis*-configuration.

Both **1a** and **2a** are thermally as well as photochemically unstable. When the adducts are subjected to vpc analyses by changing the temperature of the inlet-part, the peaks of **1a** and **2a** decrease over 180 and 230°C respectively. However, the peak of α-NN does not so increase, even upon the complete decomposition of **1a** and **2a**. When **1a** and **2a** are heated at 180°C and over 250°C respectively, brownish polymeric materials are mostly yielded, along with a small amount of α-NN. In contrast to the thermolysis, the irradiation of both adducts by a light longer than 280 nm affords α-NN in a quantitative yield. This result indicates that the photoaddition is competitive with the retro-reaction when both α-NN and the adducts absorb the incident light. However, the retro-reaction may be less important when methyl vinyl ether is present in an excess.

The photocycloaddition of ethyl vinyl ether to α-NN is also efficient in giving **1b** and **2b** in good yields. The relative ratio of **1b** to **2b** is again dependent on the solvent used and is similar to that of **1a** to **2a**. The structural determination of **1b** and **2b** was carried out by means of elemental analyses and spectroscopic data. The NMR data are listed in Table 3. On the other hand, vinyl acetate and isobutylene react only slowly with α-NN, and the products can not be isolated in a pure form. Although the photocycloaddition of acrylonitrile to naphthalene has been reported,[3)] the irradiation of α-NN in the presence of acrylonitrile affords no adducts, but only polymers. Moreover, the photoreaction of naphthalene with vinyl ethers results in the quantitative recovery of naphthalene upon irradiation for a longer time, though vpc analyses indicate the formation of at least four products in trace amounts.

Quantum Yield. On the irradiation of a dilute cyclohexane solution of α-NN containing ethyl vinyl ether at 313 nm, there appear an isosbestic point at 279 nm and new absorption maxima similar to those of **1b** and **2b** (Fig. 2). Therefore, the quantum yields for the disappearance of α-NN can be determined by monitoring the decrease in the absorbance at 307 nm, using a potassium ferroixalate actinometer. The reciprocals of the quantum yields are linearly changed

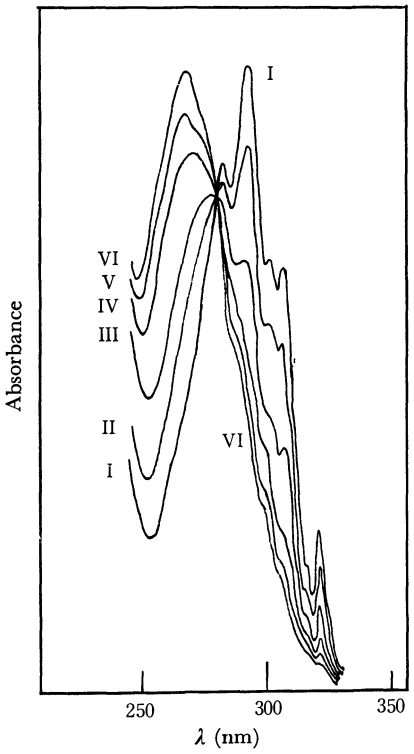

Fig. 2. Spectral change of a cyclohexane solution containing 1.5×10^{-4}M of α-NN and 0.93M of ethyl vinyl ether with time (min); I(0), II(1.5), III(5.0), IV(10.0), V(20.0), and VI(40.0). Absorbance is in an arbitary unit.

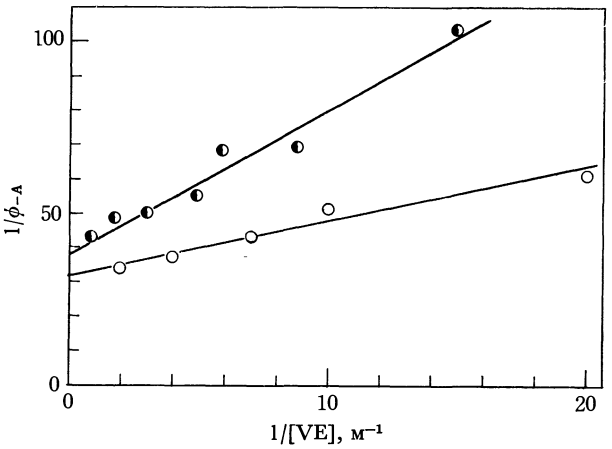

Fig. 3. The plots of $1/\phi_{-A}$ *vs.* 1/[VE] for degassed (-○-) and air saturated (-◐-) cyclohexane solutions, [α-NN]$=1.38\times10^{-4}$M.

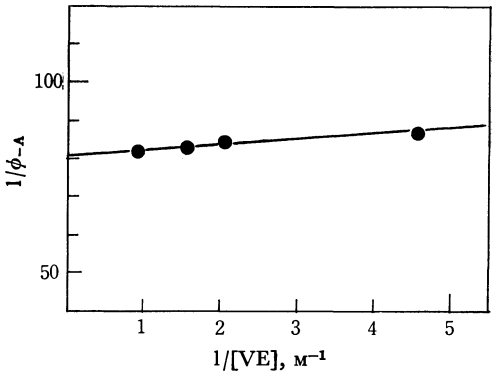

Fig. 4. The plots of $1/\phi_{-A}$ *vs.* 1/[VE] for air saturated methanolic solution, [α-NN]$=1.38\times10^{-4}$M.

with the reciprocals of the concentrations of ethyl viny ether; thus, the slopes and intercepts are determined to be 1.6M and 32 for degassed cyclohexane solutions, 4.1M and 39 for air-saturated cyclohexane solutions, and 1.5M and 82 for air-saturated methanolic solutions (Figs. 3 and 4).

Quenching of Fluorescence. A dilute cyclohexane or methanolic solution of α-NN emits a fluorescence with the maxima at 320—340 nm. The fluorescence is quenched by ethyl vinyl ether without any change in the shape of the spectra, and linear Stern-Volmer plots are obtained (Fig. 5). The slopes of the Stern-Volmer plots are determined to be 19M^{-1} for degassed cyclohexane solutions, 10.3M^{-1} for air-saturated cyclohexane solutions, and 51M^{-1} for air-saturated methanolic solutions.

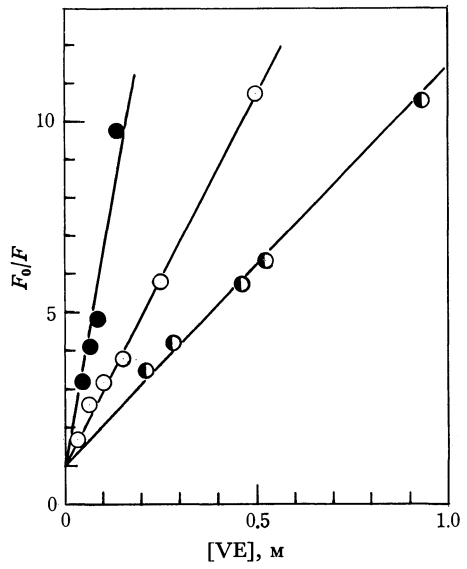

Fig. 5. The Stern-Volmer plots for the quenching of α-NN fluorescence with ethyl vinyl ether; degassed cyclohexane solutions (-○-), air saturated cyclohexane solutions (-◐-), and air saturated methanolic solutions (-●-). [α-NN]$=1.38\times10^{-4}$M.

On the other hand, acrylonitrile does not appreciably quench the fluorescence of α-NN. The fluorescence quenching with vinyl acetate is quite ineffective, as 0.8M of vinyl acetate causes only a *ca.* 10% decrease in the fluorescence.

Discussion

The effective fluorescence-quenching by ethyl vinyl ether indicates that the photochemical cycloaddition of ethyl vinyl ether to α-NN takes place from the lowest excited singlet state of α-NN (^{1}A). Moreover, benzophenone does not sensitize the photocycloaddition, though the photoreduction of benzophenone with benzhydrol is effectively quenched by α-NN. Therefore, a triplet mechanism can be safely eliminated.

$$A \xrightarrow{h\nu} {}^1A \quad (1)$$

$$^1A \xrightarrow{k_d} A \quad (2)$$

$$^1A + O_2 \xrightarrow{k_o} A + O_2 \quad (3)$$

$$^1A + VE \xrightarrow{k_r} \text{(intermediate)} \quad (4)$$

$$\text{(intermediate)} \xrightarrow{k_c} \mathbf{1} \text{ and } \mathbf{2} \quad (5)$$

$$\text{(intermediate)} \xrightarrow{k_n} \alpha\text{-NN} + VE \quad (6)$$

$$F_0/F = (1+k_r[VE])/(k_d+k_o[O_2]) \quad (7)$$

$$1/\phi_{-A} = \left(1+\frac{k_d+k_o[O_2]}{k_r[VE]}\right)\left(1+\frac{k_n}{k_c}\right) \quad (8)$$

Scheme 1.

In Scheme 1, therefore, a simplified singlet mechanism is described, from which the Stern-Volmer expression for fluorescence-quenching (7) and the rate equation (8) are derived. In the equations, let ϕ_{-A}, F_0, and F denote the quantum yield for the disappearance of α-NN and the fluorescence intensities in the absence and in the presence of ethyl vinyl ether (VE) respectively. The (2) process indicates all the unimolecular decay of ^{1}A involving radiative and nonradiative processes. In the case of air-saturated runs, the oxygen-quenching process (3) should be taken into account, whereas it can be neglected for degassed runs.

From the intercepts and the slopes in Figs. 3 and 4, the intercept-to-slope ratios can be calculated to be 20M^{-1} for degassed cyclohexane solutions, 9.5M^{-1} for air-saturated cyclohexane solutions, and 54.7M^{-1} for air-saturated methanolic solutions; these ratios are in good agreement with the slopes of the Stern-Volmer plots for the respective solutions in Fig. 5. This agreement, especially for the air-saturated runs, clearly shows that the photocycloaddition takes place in the lowest excited singlet state of α-NN, since both the intercept-to-slope ratio and the slope of the Stern-Volmer plots represent the same rate term, k_r/k_d for degassed runs or $k_r/(k_d+k_o[O_2])$ for air-saturated runs.

The fluorescence decay life of a degassed cyclohexane solution of α-NN was determined to be 17 nsec by the use of a TRW nsec flashspectrophotometer. The oxygen-quenching method,[11] using an L_0/L value ($=1+k_o[O_2]/k_d=1.77$), gave a similar decay life. From this value of the decay life, k_r can be calculated to be 1.1×10^9M^{-1}sec^{-1}, very close to the diffusion rate in-

11) I. B. Berlman, "Handbook of Fluorescence Spectra of Aromatic Molecules," Academic Press, New York and London (1965), p. 36.

cyclohexane (*ca.* 5×10^{9}M^{-1}sec^{-1}). Unfortunately, not many kinetic studies of the cycloaddition of π,π^*-singlet species to olefins have been reported,[3,12] and the rate constant, k_r, has not yet been given.

On the other hand, kinetic investigations of electronically-excited carbonyl compounds have been intensively carried out. In the n,π^*-triplet state, the oxetane-formation takes place through 1,4-biradicals, with rate constants of 5×10^{7}—10^{8}M^{-1}sec^{-1}.[13] In the present case, therefore, it is not suitable to suggest that a 1,4-biradical or 1,4-dipolar intermediate, **5**, is directly generated by the attack of ^{1}A on VE in a near diffusion rate, since ^{1}A might be considered to be less electrophilic than the n,π^*-triplet carbonyl compounds, which have been well established to have a high electrophilic character.

On the other hand, it has been reported that the photocycloaddition of acetone to dicyanoethylene[14] and that of propionaldehyde to cyclohexadiene[15] afford oxetanes by way of the exciplexes generated from the excited singlet state of the carbonyl compounds in a diffusion-controlled rate.[16] In many cases, the exciplex formation is well established to occur in a diffusion-controlled rate from the excited singlet state.[17] In the present case, therefore, the large value of k_r can be reasonably interpreted by assuming an exciplex intermediate. The inefficiency of acrylonitrile and the less effective nature of vinyl acetate in the fluorescence-quenching and the photoreaction may also suggest an exciplex intermediate with a charge-transfer character; ethyl vinyl ether is known to be an electron-rich olefin, whereas vinyl acetate has less of a donor-ability and acrylonitrile is an acceptor rather than a donor.

The rate constant for fluorescence-quenching, $k_r/(k_d+k_o[O_2])$, is about five times greater in methanol than in cyclohexane. This reflects the solvent-dependence of k_r, since the fluorescence intensity of α-NN was found to be similar both in air-saturated methanolic and cyclohexane solutions. In the exciplex-formation, polar solvents have been known to enhance the rate of fluorescence-quenching[7,18,19] and the reaction rate,[7,18] at least in some cases. Moreover, since an exciplex is a special case of well-known charge-transfer complexes, the solvation of exciplexes can occur and, in polar solvents, leads to species with configurations different from those of the exciplexes in non-polar solvents.[20] If this is the case, the solvent-dependent results of k_n/k_c and the product ratio are consistent with the exciplex mechanism. However, the solvent-dependence can possibly be explained as being caused by the solvation of the 1,4-biradical, **5**, generated from an exciplex, since solvent effects have been observed in the Norrish-type II photoelimination, which has been well established to proceed *via* a 1,4-biradical.[21] However, a discrete 1,4-dipolar intermediate is not a likely reaction intermediate, since the photoreaction in methanol gave neither a solvolytic nor an inserted product such as **6** or **7**, even under acidic and basic conditions.

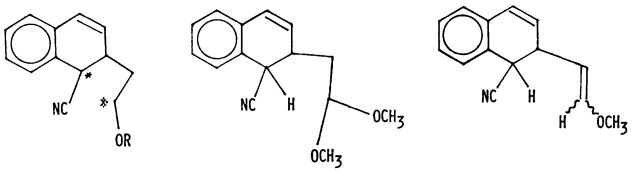

(5) (6) (7)

* = •or −
※ = •or +

Chart 2

Experimental

General. The spectroscopic analyses of the products were carried out as follows; the NMR spectra using a Hitachi Perkin-Elmer R-20 spectrophotometer, the IR spectra using a Hitachi EPI-S2 spectrophotometer, the UV spectra using Hitachi 124 spectrophotometer, the fluorescence spectra using a Hitachi MPF-2A spectrofluorometer, and the mass spectra using a Hitachi RMU-6E spectrometer. The yields and the product ratios were determined by vpc with a Shimadzu GC-3AF using a column of SE-30 (5% on Shimalite W, 1m) at 160°C. The thermal behavior of **1** and **2** was checked by vpc with a Shimadzu GC-2C equipped with a flame-ionization detector, by changing the temperature of the inlet-part. The solvents were purified as usual. The ethyl vinyl ether, vinyl acetate, and acrylonitrile were distilled over calcium chloride under a nitrogen stream before use. The methyl vinyl ether was distilled from a gas cylinder before use. The α-NN was purified by vacuum distillation.

Quantum Yields. The solutions were prepared by dissolving α-NN (1.38×10^{-4}M) and ethyl vinyl ether into cyclohexane or methanol. Monochromatic light at 313 nm was isolated through a Toshiba UV-D25 glass filter and a filter solution (0.2 g potassium chromate made up to 1 *l* with distilled water), with a path length of 10 mm from resomance lines of a high-pressure mercury arc. The light intensity (I^0) was determined by potassium ferrioxalate actinometry[22] to be 1.42×10^{-6} mol/cm^{2}min. Sample solutions placed in cuvettes (10 mm × 10 mm × 45 mm) were irradiated by the 313 nm light, and the decrease in the absorbance at 307 nm (κcd) was monitored in order to determine the quantum yields for the disappearance of α-NN (ϕ_{-A}). When natural logarithms of ($e^{\kappa cd}-1$) were plotted against the time (t, min), straight lines were obtained. The quantum yields (ϕ_{-A}) were obtained from the slopes of the lines by applying

12) O. L. Chapman and R. D. Lura, *J. Amer. Chem. Soc.*, **92**, 6352 (1970); J. Saltiel, J. T. D'Agostino, O. L. Chapman, and R. D. Lura, *ibid.*, **93**, 2805 (1971).
13) For examples, see, H. Sakurai, K. Shima, and S. Toki, *Nippon Kagaku Zasshi*, **89**, 537 (1968).
14) J. C. Dalton, D. M. Pond, and N. J. Turro, *J. Amer. Chem. Soc.*, **92**, 2173 (1970); J. C. Dalton, P. A. Wriede, and N. J. Turro, *ibid.* **92**, 1318 (1970).
15) T. Kubota, K. Shima, S. Toki, qnd H. Sakurai, *Chem. Commun.*, **1969**, 1462.
16) R. R. Hautala and N. J. Turro, *J. Amer. Chem. Soc.*, **93**, 5595 (1971).
17) For examples, see, A. Weller, *Pure Appl. Chem.*, **16**, 115 (1968); I. G. Lopp, R. W. Hendren, P. D. Wildes, and D. G. Whitten, *J. Amer. Chem. Soc.*, **92**, 6440 (1970).
18) C. Pac, T. Tosa, and H. Sakurai, This Bulletin, **45**, 1169 (1972).
19) K. Kaneta and M. Koizumi, *ibid.*, **40**, 2254 (1967).
20) N. Mataga, T. Okada, and N. Yamamoto, *Chem. Phys. Lett.*, **1**, 119 (1967); H. Yamashita and M. Koizumi, This Bulletin, **41**, 2313 (1968).
21) P. J. Wagner, *J. Amer. Chem. Soc.*, **89**, 5898 (1967).
22) C. G. Hatchard and C. A. Parker, *Proc. Roy. Soc., Ser. A*, **235**, 518 (1956).

Table 4. Elemental analyses of adudcts

Compounds	Bp (°C/mmHg) or Mp[°C]	Formula	Anal					
			Calcd			Found		
			C	H	N	C	H	N
1a	[86—87]	$C_{14}H_{14}NO$	79.59	6.20	6.63	79.83	6.24	6.51
2a	(113/0.01)	$C_{14}H_{13}NO$	79.59	6.20	6.63	79.43	5.94	6.45
1b	[58—58.5]	$C_{15}H_{15}NO$	79.97	6.71	6.22	80.33	6.47	5.84
2b	($102/10^{-3}$)	$C_{15}H_{15}NO$	79.97	6.71	6.22	79.86	6.74	6.11
3	($102/10^{-3}$)	$C_{14}H_{15}NO$	78.84	7.09	6.57	78.60	7.00	6.41
4	[65—65.5]	$C_{14}H_{15}NO$	78.84	7.09	6.57	78.72	7.12	6.54

this equation; $\ln(e^{\kappa cd}-1)=-1000\phi_{-A}I_0t+$ Constant, where κ is the molar extinction coefficient at 307 nm (5.39×10^3 l/mol cm).

Photochemical Reaction in Preparative Scale. a) The photochemical reaction of α-NN with methyl vinyl ether will be described as a typical run, since the procedures were identical in every case. The results of the elemental analyses of the adducts **1**—**4** are listed in Table 4. A methanolic solution (300 ml) containing 1 g of α-NN and 20 ml of methyl vinyl ether in a Pyrex doughnut-type vessel was irradiated for 20 hr with a high-pressure mercury arc at an ambient temperature. The unreacted vinyl ether and methanol were then distilled off *in vacuo*, and the residue was chromatographed on silica gel. After 0.1 g of α-NN had been eluted with a mixture of benzene (30%) in hexane, elution with 300 ml of benzene gave *ca.* 1 g of **1a** containing a small amount of **2a**, which solidified on standing overnight; it was recrystallized from methanol (mp 86—87°C). Further elution with benzene gave a mixture of **1a** and **2a** (0.1 g).

b) In a similar manner, a benzene solution containing 1 g of α-NN and 15 ml of methyl vinyl ether was irradiated for 15 hr. After the unchanged vinyl ether and benzene had been distilled off *in vacuo*, the residue was heated at 180—200°C for 20 min; the subsequent vacuum distillation of the pyrolysate gave an oil (bp 105—113°C/10^{-3}mmHg). The chromatographic treatment of the oil on silica gel gave 0.2 g of α-NN and 0.4 g of a mixture containing **2a** and a small amount of **1a**. The further chromatography of the latter fraction led to a decrease in the content of **1a** to a trace amount. The vacuum distillation of this fraction gave an oil (bp 102°C/10^{-3}mmHg), which did not solidify, even on storage in a refrigerator.

Hydrogenated Adducts, 3 and 4. An ethanolic solution containing 0.2 g of **1a** and **2a** was hydrogenated over Pd-charcoal (5%) at an ambient temperature for 2 hr. The complete hydrogenation was checked by vpc analyses. The filtration of the Pd-charcoal, followed by the evaporation of the ethanol, left an oil, which was then chromatographed on a short column of silica gel. In the case of **4**, it solidified on storage in a refrigerator overnight and was then recrystallized from methanol (mp 65—65.5°C). On the other hand, **3** did not solidify, even on storage in a refrigerator over several weeks.

Pyrolyses of 1a and 2a. The pyrolyses of crystalline **1a** (0.1 g) at 180—200°C for 1 hr gave a brownish glassy material, which was then chromatographed on silica gel. Elution with 500 ml of benzene gave less than 50 mg of α-NN; further elution with a mixture of ether and benzene (1: 9) afforded brownish glassy materials which could not be identified. Pyrolyses of **2a** at 250—260°C gave similar results, while heating at 180—200°C resulted in no appreciable change in the **2a**.

Photolyses of 1a and 2a. A methanolic or benzene solution of **1a** or **2a** (0.1 g/4 ml) in a Pyrex tube was irradiated with a high-pressure mercury are for 20 hr. During the course of the irradiation, vpc analyses of the photolysate were carried out at 1 hr intervals for the initial 5 hr; it was found that α-NN increased linearly with the disappearance of the adduct. Irradiation for about 10 hr resulted in the complete decomposition of the adduct, and further irradiation for 10 hr gave no additional change. After the irradiation, removal of a solvent left a solid, which was identified as α-NN by studing its IR, and mass spectra, and by a mixed-melting-point determination.

The authors wish to express their hearty thanks to Professor Masaharu Kawanishi and Dr. Naruhiro Owaki, The Institute of Scientific and Industrial Research, Osaka University, for their useful advice and kind guidance in determining the decay life of the fluorescence of α-NN with a TRW nsec spectrophotometer.

Studies of Organosulfur Compounds. IX. The Preparation of Organometal IVb Esters of Aromatic Thio Acid

Shinzi KATO, Wataru AKADA, Masateru MIZUTA, and Yoshio ISHII*

Faculty of Engineering, Gifu University, Kagamihara, Gifu

**Department of Synthetic Chemistry, Faculty of Engineering, Nagoya University, Chikusa, Nagoya*

(Received May 1, 1972)

It was found that the reactions of potassium salts of aromatic thio acid with chlorotrimethylsilane gave the corresponding thionoacyloxysilanes [$ArC(S)OSi(CH_3)_3$]. On the other hand, the reactions with chlorotrimethylgermanes or -stannane gave the corresponding thiol esters [$ArC(O)SM(CH_3)_3$, M: Ge, or Sn] containing the sulfur-metal (IVb) linkage in almost quantitative yields.

During the last decade, a number of reports[1-3] of organometallic sulfur compounds containing silicon, germanium, tin, and lead have been published. However, there have been very few reports[4-6] on any compounds containing the ≡M–S–CO–C≡ (M: IVb element) linkage except the tin compounds; further, many of the reported compounds (mainly tin compounds) have been described in patents [7g-r] without any characterization or description of their physical constants.

In this paper, the results of the reactions of potassium salts of aromatic thio acid with trimethylmetal IVb chlorides will be disclosed in the expectation that the corresponding thiolacyloxy-sialnes, -germanes, and -tins will be obtained.

Results and Discussion

When an equimolar amount of chlorotrimethylsilane was added to a suspension of potassium thiobenzoate in petroleum ether; the color of the reaction mixture changed from colorless to yellow, the subsequent vacuum distillation of the petroleum ether soluble parts gave orange yellow oil with a definite boiling point in almost quantitative yields. Surprisingly, the IR spectrum of this oil showed no absorption band of ν C=O; instead, the absorption bands at 1590 (ν C=C, aromatic), 1250 (δ CH_3, scissoring), 1238 (ν C=S), and 953 cm^{-1} (δ CH_3, rocking) were observed. The NMR peaks appeared at 9.54 τ ($SiCH_3$, s, 9H) and 1.90—3.20 τ (aromatic, m, 5H). In the visible spectrum, the maximum band at 437 mμ (ε 75) was observed. These results, together with the analytical results, indicate that the liquid is thionobenzoyloxylsilane with the Ic structure (Eq. (1)). By the similar treatment of other

$$C_6H_5\overset{O}{\overset{\|}{C}}S^-K^+ + (CH_3)_3SiCl \xrightarrow[-KCl]{rt} C_6H_5\overset{S}{\overset{\|}{C}}OSi(CH_3)_3 \quad (1)$$
Ic

substituted potassium thiobenzoates with chlorotrimethylsilane, the corresponding thionobenzoyloxysilanes were obtained in excellent yields, as is shown in Table 1. Gornowicz and Ryan[8] reported two methods for the preparation of thionoacyloxysilanes (Eqs. (2) and (3)).

$$[(CH_3)_3Si]_2NH + 3CH_3\overset{O}{\overset{\|}{C}}SH \longrightarrow 2(CH_3)_3SiO\overset{S}{\overset{\|}{C}}CH_3 + (NH_4)^+(AcS)^- \quad (2)$$

$$Ph_3SiCl + PhC(O)SH \xrightarrow{Et_3N} Ph_3SiO\overset{S}{\overset{\|}{C}}Ph + Et_3N\cdot HCl \quad (3)$$

However, the method reported in this paper is more useful than the method in the literature them because we could avoid using thio acids, which are generally unstable and unpleasant to work with.

The formation of the thion esters (I) might be derived from the strong affinity of silicon to the oxygen atom.

Contrary to the reactions with chlorotrimethylsilane, potassium thiobenzoate reacted readily with chlorotrimethylstannane at 45°C to give the expected (benzoylthio)trimethylstannane (IIIg) as a colorless oil in 98% yield (Eq. (4)). The IIIg structure could be

$$C_6H_5\overset{O}{\overset{\|}{C}}S^-K^+ + (CH_3)_3SnCl \xrightarrow[-KCl]{rt} C_6H_5\overset{O}{\overset{\|}{C}}SSnMe_3 \quad (4)$$
IIIg

1) E. W. Abel and D. A. Armitage, "Advances in Organometallic Chemistry," Vol. 5, ed. by G. A. Stone and R. West, Academic Press, New York (1967), p. 1.

2) A. Hass, "Sulfur in Organic and Inorganic Chemistry," Vol. 1, ed. by A. Senning, Marcell Dekker, INC, New York (1971), p. 3.

3) H. Schumann, I. Schumann-Ruidich, and M. Schmidt, "Organotin Compounds," Vol. 2, ed. by A. D. Sawyer, Meacel Dekker, INC, New York (1971), p. 297.

4) Silicon; H. Gilman and G. D. Lichtenwalter, *J. Org. Chem.*, **25**, 1064 (1960).

5) Germanium; a) M. C. Henry, and W. E. Davidson, *J. Org. Chem.*, **28**, 2252 (1962). b) H. Schumann, K. F. Thom, and M. Schmidt, *J. Organometal. Chem.*, **4**, 22 (1965). c) W. E. Davidson, K. Hills, and M. C. Henry, *ibid.*, **3**, 285 (1965).

6) Lead; a) R. Heap, B. S. Saunders, and G. Stacey, *J. Chem. Soc.*, **1951**, 658. b) M. C. Henry and A. W. Krebs, *J. Org. Chem.*, **28**, 225 (1962).

7) Tin; a) H. Schumann, K. F. Thom, and M. Schmidt, *Angew. Chem.*, **75**, 138 (1963). b) R. A. Cummins and P. Dunn, Australlia Common-wealth Department Supply Defence Standard Lab., **266**, 106 (1963); *Chem. Abstr.* **60**, 11503 (1964). c) H. Schumann, K. F. Thom, and M. Schmidt., *J. Organometal. Chem.*, **2**, 97 (1964). d) H. Schumann, K. F. Thom, and M. Schmidt, *ibid.*, **2**, 361 (1964). e) H. Schumann and M. Schmidt, *Angew. Chem.*, **77**, 1049 (1965). f) T. A. George and M. F. Lappert, *J. Organometal. Chem.*, **14**, 327 (1968). g) E. L. Weinberg and E. W. Johnson, U. S. 2648650 (1953). h) K. B. Kerr and A. W. Walda, U. S. 2702775–8 (1955). i) C. E. Best, U. S. 2713585 (1955), 2731440 (1955), 2731484 (1956). j) L. L. Baker, Brit. 855214 (1960). k) M. B. Bernbaum and E. R. Bertozzi, U. S. 3029267 (1962). l) R. J. Harper, Belg. 632271 (1964). m) A. M. Fernley, Brit. 1020791 (1961). n) V. Oakes, Brit. 1020612 (1966). o) M. Alicot and G. Mingasson, Fr. 1453490 (1966). p) H. Plum and A. Baker, Ger. 1234722 (1967). q) K. Sadataka, K. Itoh, K. Tami, and S. Suzuki, Neth. 169491 (1967). r) G. H. Reifenberg and W. J. Considine, Brit. 1173466 (1969).

8) G. A. Gornowicz and J. W. Ryan, *J. Org. Chem.*, **31**, 3439 (1966).

Table 1. Physical properties and elemental analyses of thionobenzoyloxysilanes [X-$C_6H_4C(S)OSi(CH_3)_3$]

Compd	Substituent X	Bp °C/3 mmHg	Yield %	Color[a]	Formula	Found (Calcd), % C	H	Cl	S
Ia	*p*-Cl	94.5	92	O (O)	$C_{10}H_{13}ClOSSi$	49.36 (49.04)	5.33 (5.35)	14.00 (13.94)	13.46 (13.10)
Ib	*m*-Cl	105	98	O (O)	$C_{10}H_{13}ClOSSi$	49.93	5.40	13.98	13.93
Ic	H	97	97	OY (O)	$C_{10}H_{14}OSSi$	57.36 (57.08)	6.88 (6.71)		15.21 (15.25)
Id	*p*-CH_3	117	98	OY (O)	$C_{11}H_{16}OSSi$	59.02 (58.86)	7.22 (7.19)		15.00 (14.30)
Ie	*m*-CH_3	113	98	OY (O)	$C_{11}H_{16}OSSi$	58.11	7.01		14.23
If	*o*-CH_3	108	96	OY (O)	$C_{11}H_{16}OSSi$	58.16	7.20		14.16
Ig	*p*-CH_3O	138	98	OY (O)	$C_{11}H_{16}O_2SSi$	54.79 (54.94)	6.69 (6.71)		13.33 (13.24)
Ih	*o*-CH_3O	77	95	OY (O)	$C_{11}H_{16}O_2SSi$	54.18	6.58		13.91

a) O: Orange, OY: Orange yellow, (O): Oil

Table 2. Physical properties and elemental analyses of substituted (benzoylthio)trimethylstannanes [X-$C_6H_4C(O)SSn(CH_3)_3$]

Compd	Substituent X	Mp °C	Yield %	Appearance[a]	Formula	Found (Calcd), % C	H	Cl	N	S
IIIa	*p*-NO_2	109 —111.0	97	Y (N)	$C_{10}H_{13}NO_3Sn$	34.77 (34.70)	3.77 (3.79)		4.11 (4.05)	9.33 (9.27)
IIIb	*m*-NO_2	79.5— 80.0	97	C (P)	$C_{10}H_{13}NO_3Sn$	34.83	3.71		4.16	9.46
IIIc	*o*-NO_2	73.0— 73.5	98	C (P)	$C_{10}H_{13}NO_3Sn$	34.65	3.84		4.23	9.22
IIId	*p*-Cl		96	C (O)	$C_{10}H_{13}ClOSSn$	35.81 (35.79)	4.01 (3.91)	10.93 (10.57)		9.83 (9.56)
IIIe	*m*-Cl		95	C (N)	$C_{10}H_{13}ClOSSn$	35.44	4.02	11.01		9.48
IIIf	*o*-Cl	64.5— 65.0	97	C (N)	$C_{10}H_{13}ClOSSn$	35.01	4.00	10.73		9.65
IIIg	H		99	C (O)	$C_{10}H_{14}OSSn$	40.01 (39.89)	4.79 (4.69)			10.68 (10.66)
IIIh	*p*-CH_3		98	C (O)	$C_{11}H_{16}OSSn$	42.33 (41.92)	5.23 (5.12)			10.28 (10.18)
IIIi	*m*-CH_3		96	C (O)	$C_{11}H_{16}OSSn$	42.01	5.21			10.33
IIIj	*o*-CH_3		97	C (O)	$C_{11}H_{16}OSSn$	41.91	5.16			10.00
IIIk	*p*-CH_3O	53.0— 54.0	98	C (P)	$C_{11}H_{16}O_2SSn$	39.83 (39.90)	4.79 (4.87)			9.46 (9.69)
IIIl	*o*-CH_3O	69.5— 70.0	94	C (N)	$C_{11}H_{16}O_2SSn$	39.88	4.83			9.58

a) Y: Yellow, C: Colorless, (N): Needles, (P): Plates, (O): Oil.

assigned by elemental analysis and spectral data: intensive absorption bands at 1631 (ν C=O) and 775 cm^{-1} (δ $SnCH_3$) in the IR spectrum, and at 9.43 τ (Sn–CH_3, s, 9H), 1.98—2.50 τ (aromatic, m, 5H), $J_{^{119}Sn-C-H}=59$ Hz, $J_{^{117}Sn-C-H}=56$ Hz in NMR spectrum. The analogous treatment of other potassium-substituted thiobenzoate with chlorotrimethylstannane gave the corresponding (benzoylthio)trimethylstannanes (IIIa—f and h—l) respectively in quantitative yields (Table 2). The formation of the stannyl esters, III, can be explained by the strong affinity of tin to sulfur atom.

The results obtained above encouraged us to investigate the reactions with chlorotrimethylgermane, bacause germanium is situated between silicon and tin in the peridical table. However, the analogous treatment of potassium thiobenzoate with chlorotrimethylgermane gave (benzoylthio)trimethylgermane (IIg)

$$C_6H_5\overset{\overset{O}{\|}}{C}SK + (CH_3)_3GeCl \xrightarrow[-KCl]{rt} C_6H_5\overset{\overset{O}{\|}}{C}SGe(CH_3)_3 \quad (5)$$
IIg

(Eq. 5). The IIg structure was established by elemental analysis and studies of the IR and NMR spectra. In the IR spectrum, intensive absorption bands at 1648 (ν C=O) and 829 cm^{-1} (δ $GeCH_3$) were observed. The NMR spectrum showed peaks at 9.33 τ ($GeCH_3$, s, 9H), and 1.00—2.78 τ (aromatic, m, 5H). By the analogous treatment of other potassium-substituted thiobenzoates with chlorotrimethylgermane, the corresponding (benzoylthio)trimethylgermanes (IIa—f and h—l) were obtained in excellent yields (Table 3). Germanium would be considered to have a higher affinity to the sulfur atom rather than the oxygen atom.

The silyl thion esters (I) thus obtained were readily hydrolyzed by moisture in air to give hexamethyldisiloxane and the corresponding thiobenzoic acid in almost quantitative yields. However, the germyl thiol esters (II) were fairly stable against moisture and were very slowly hydrolyzed to give hexamethyldigermoxane and the corresponding thiobenzoic acid. On the other hand, the trimethylstannyl thiol esters (III) were a very stable oil or crystals which could be recrystallized

TABLE 3. PHYSICAL PROPERTIES AND ELEMENTAL ANALYSES OF SUBSTITUTED (BENZOYLTHIO)TRIMETHYLGERMANES [(X-$C_6H_4C(O)SGe(CH_3)_3$]

Compd	Substituent X	Mp °C	Yield %	Appearance[a)]	Formula	Found (Calcd), % C	H	Cl	N	S
IIa	*p*-NO_2	61—62	96	Y (N)	$C_{10}H_{13}NO_3SGe$	40.44 (40.03)	4.26 (4.37)		4.59 (4.67)	10.46 (10.70)
IIb	*m*-NO_2	82—83	96	C (N)	$C_{10}H_{13}NO_3SGe$	39.94	4.33		4.71	10.58
IIc	*o*-NO_2		98	SY (O)	$C_{10}H_{13}NOS_3Ge$	39.99	4.36		4.66	11.00
IId	*p*-Cl		97	C (O)	$C_{10}H_{13}ClOSGe$	41.46 (41.53)	4.52 (4.52)	12.31 (12.25)		11.11 (11.09)
IIe	*m*-Cl		98	C (O)	$C_{10}H_{13}ClOSGe$	41.88	4.55	12.28		11.36
IIf	*o*-Cl		98	C (O)	$C_{10}H_{13}ClOSGe$	41.92	4.57	12.22		11.21
IIg	H		96	C (O)	$C_{10}H_{14}OSGe$	47.76 (47.10)	4.58 (5.54)			12.96 (12.59)
IIh	*p*-CH_3		98	C (O)	$C_{11}H_{16}OSGe$	49.99 (49.15)	6.07 (6.00)			11.42 (11.93)
IIi	*m*-CH_3		99	C (O)	$C_{11}H_{16}OSGe$	48.87	6.01			11.48
IIj	*o*-CH_3		98	C (O)	$C_{11}H_{16}OSGe$	49.11	6.11			12.00
IIk	*p*-CH_3O		97	C (O)	$C_{11}H_{16}O_2SGe$	46.43 (46.39)	5.70 (5.66)			11.58 (11.26)
III	*o*-CH_3O		98	C (O)	$C_{11}H_{16}O_2SGe$	46.40	5.62			11.68

a) Y: Yellow, C: Colorless, SY: Slight Yellow, (N): Needles, (O): Oil.

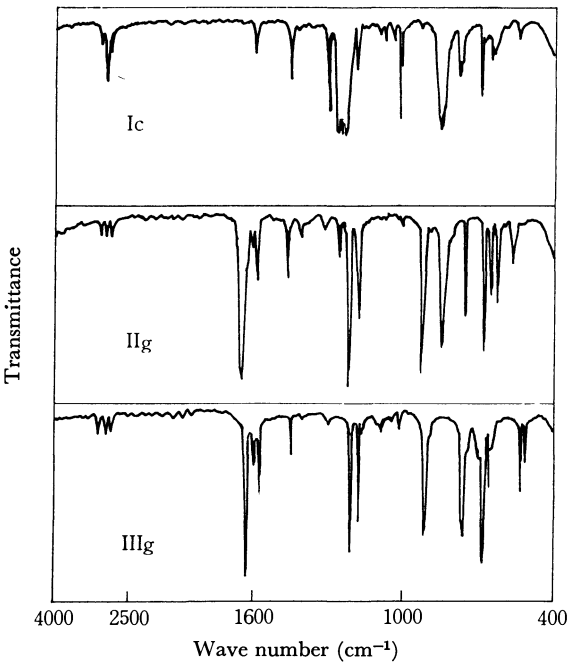

Fig. 1. IR spectra of thionobenzoyltrimethylsilane (Ic), (benzoylthio)trimethylgermane (IIg), and (benzoylthio)trimethyltin (IIIg) (Nujol mull).

from alcohols.

Spectral Data. *a) IR Spectra*: The IR spectra of thionobenzoyloxy trimethylsilane (Ic), (benzoylthio)-trimethylgermane (IIg), and -stannane (IIIg) are shown in Fig. 1 as typical examples. Bak *et al.*[9] reported that the two frequencies (*ν* C=S and C–S) obtained by a simplified force constant calculation must be looked for in the vicinity of 1200 (C=S) and 700 cm^{-1} (C=S), and that the absorption bands of the C=S band in a series of twenty-one carboxymethyl-dithio esters were observed between 1190—1225 cm^{-1}. Bellamy and Rogasch[10] have reported some results of dithio acid in a variety of solvents. The silyl esters (II) obtained showed necessarily two characteristic strong absorption bands near 1280 and 1240 cm^{-1} on both sides on the absorption band at 1250 cm^{-1} (δ $SiCH_3$). However, it is difficult to assign the former band to the *ν* C=S band because it is situated at a far higher frequency. Further, no the absorption band around 1240 cm^{-1} on (selenobenzoyloxy)trimethylsilane[11] was observed. For these reasons, the absorption band near 1240 cm^{-1} may be considered to be due to the

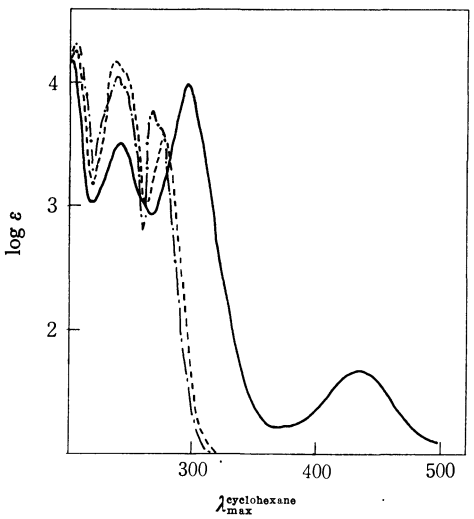

Fig. 2. The electronic spectra of thionobenzyltrimethylsilane (——), (benzoylthio)trimethylgermane (------), and (benzoylthio)trimethyltin (—·—).

9) B. Bak, L. Hansen-Nygarred, and C. Pedersen, *Acta Chem. Scand.*, **12**, 1451 (1958).

10) L. J. Bellamy and P. E. Rogasch, *J. Chem. Soc.*, **1960**, 2218.

11) S. Kato and H. Ishihara, *Tetrahedron Lett.*, **1972**, 3751.

12) All melting points are not corrected. The IR spectra were measured on a JASCO Grating Infrared spectrophotometer IR-G. The UV spectra were recorded on Hitachi 124 spectrophotometer. The NMR spectra were obtained by a JEOL H-60.

C=S stretching band on the silyl esters (I). This result also fits well with the assignment given by Bak *et al.*[9] and Bellamy.[10] In Table 4 the IR absorption bands at near 1240 cm^{-1} are shown.

Gilman and Lichtenwalter[4] reported that the ν C=O of (benzoylthio)triphenylsilanes appeared at 1690 cm^{-1}. The ν C=O values of the obtained trimethylgermyl (II) and -stannyl esters (III) were observed in the 1645—1677 and 1612—1645 cm^{-1} ranges respectively. These results indicate that the ν C=O on the esters with a ≡M–S–CO–C≡ linkage (M: Metal IVb) would have a lower frequency shift with an increase in the atomic number of the metal (IVb). These lower frequency shifts are probably caused by either the heavy atomic effect or the higher electron donating properties of IVb elements.

b) UV and Visible Spectra: The absorption spectra of (thionobenzoyloxy)trimethylsilane (Ic), (benzoylthio)trimethylgermane (IIg), and stannane (IIIg) are reproduced in Fig. 2, along with the absorption maxima (λ_{max}) in Table 4. As is shown in Fig. 2 and Table 4, (thionobenzoyloxy)trimethylsilanes have three cha-

Table 4. Spectral data of substituted thionobenzoyloxysilanes (I), (benzoylthio)trimethylgermanes (II) and stannanes (III).

Compd	IR, cm^{-1} (mull)			UV, mμ, cyclohexane λ_{max} (ε)			NMR, (CCl_4), τ			J(Hz)	
	νC=S	δ $SiCH_3$					$SiCH_3$	CH_3	CH_3O	Sn–C–H	Sn–C–H
Ia	1240	1250	845	255 (9600)	302 (12000)	439 (94)	9.54				
Ib	1240	1251	850	250 (6900)	292 (9600)	443 (85)	9.53				
Ic	1238	1251	853	247 (8000)	298 (9600)	437 (75)	9.54				
Id	1238	1250	852	253 (8200)	303 (13600)	436 (114)	9.54	7.62			
Ie	1237	1250	848	252 (7000)	300 (11500)	437 (97)	9.54	7.62			
If	1236	1250	850	242 (8900)	288 (7200)	427 (231)	9.54	7.67			
Ig	1236	1257	847	267 (7800)	321 (17700)	429 (150)	9.54		6.17		
Ih	1240	1250	851	246 (9100)	204 (5100)	426 (165)	9.56		6.17		
	ν C=O	δ $GeCH_3$					$GeCH_3$	CH_3	CH_3O		
IIa	1677[a]	1239	830	264 (13800)	287 (10000)		9.28				
IIb	1640[a]	1243	833	266 (22900)	257 (10500)		9.30				
IIc	1658	1240	832	237 (9400)			9.30				
IId	1655	1239	835	250 (17000)	269 (12400)		9.32				
IIe	1645	1238	831	240 (12000)	270 (8100)		9.31				
IIf	1622	1238	828	241 (8000)	260 (4500)		9.31				
IIg	1648	1238	829	240 (12900)	267 (8200)		9.33				
IIh	1645	1237	834	249 (14300)	267 (12400)		9.33	7.68			
IIi	1648	1245	835	243 (11500)	267 (8500)		9.33	7.68			
IIj	1649	1239	830	240 (11300)	267 (7500)		9.33	7.63			
IIk	1672	1240	839	222 (13200)	279 (19100)		9.34		6.16		
IIl	1659	1240	829	246 (9600)			9.37		6.16		
	ν C=O	δ $SnCH_3$					$SnCH_3$	CH_3	CH_3O		
IIIa	1622	1240	780	263 (12800)	291 (9300)		9.35			60.0	56.0
IIIb	1629	1202	782	226 (25100)			9.38			60.0	57.0
IIIc	1611[a]	1209	782				9.37			62.0	58.0
IIId	1625	1240	780	251 (16000)	278 (11700)		9.42			61.0	58.2

IIIe	1628		788	243 (9800)	274 (6800)	9.40			60.0	67.0
IIIf	1645[a)]	1210	787	243 (8400)	205 (5100)	9.40			60.0	56.4
IIIg	1631	1208	775	242 (11800)	271 (8100)	9.43			59.0	56.0
IIIh	1626	1217	782	250 (12700)	275 (11200)	9.43	7.68		59.5	55.5
IIIi	1632		783	245 (10900)	279 (8500)	9.43	7.68		58.0	56.2
IIIj	1633	1207	775	245 (9500)	270 (7000)	9.43	7.63		61.0	58.0
IIIk	1620[a)]	1215	777		283 (21000)	9.44		6.14	60.0	56.2
IIIl	1622[a)]	1204	782	248 (9000)	303 (5500)	9.48		6.16	56.2	53.0

a) KBr

racteristic maximum bands at 240—260 (ε 5000—10000), 288—305 (ε 7000—15000), and 426—443 mμ (ε 75—230). The former two bands may be ascribed to $\pi \rightarrow \pi^*$ with the latter are $n \rightarrow \pi^*$ transitions of the thiocarbonyl group. On the other hand, the (substituted-benzoylthiotrimethyl)germanes and -stannanes except for those with substituents in the *ortho* position and with a methoxy group in the *para* position, all showed two characteristic maximum absorption bands at 240—260 and 260—290 mμ with of molecular extinction coefficients over 8000.

Experimental[12)]

Materials. The potassium salts of substituted thiobenzoic acid were prepared by the method described by the literature;[13)] the chlorotrimethylsilane was distilled before use. Chlorotrimethylgermane[14)] and -tin[15)] were prepared similarly.

All the reactions were carried out under nitrogen. Some typical procedures are shown below, while the data are summarized in Tables 1—4.

Reaction of Potassium Thiobenzoate with Chlorotrimethylsilane. An equimolar amount of chlorotrimethylsilane was added to a suspension of 1.77 g (0.01 mol) of potassium thiobenzoate in petroleum ether (bp below 45°C), after which the mixture was stirred for 15 min at room temperature. After the removal of the insoluble parts by filtration, the evaporation of the solvent from the filtrate and the vacuum distillation of the residue gave 2.0 g of (benzoylthio)trimethylsilane (Ic).

Reaction of Potassium Thiobenzoate and Chlorotrimethylgermane. A solution of an equimolar amount of chlorotrimethylgermane (1.70 g, 0.011 mol) and potassium thiobenzoate in petroleum ether (bp below 45°C) (10 ml) was stirred for 1 hr at room temperature. After the insoluble parts were filtered, the vacuum removal of the solvent and the excess of chlorotrimethylgermane gave 2.37 g of chemically pure (benzoylthio)trimethylgermane (IIg).

Reaction of Potassium p-*Nitrothiobenzoate and Chlorotrimethyltin.* A solution of an equimolar amount of chlorotrimethyltin (2.08 g, 0.01 mol) and potassium *p*-nitrothiobenzoate (2.22 g, 0.01 mol) in petroleum ether (bp below 45°C) was refluxed for 1 hr. After the separation of the insoluble parts and the solvent, the recrystallization of the residue from ether–*n*-hexane gave 3.6 g of (*p*-nitrobenzoylthio)trimethyltin (IIIa) as colorless crystals.

13) S. Kato, T. Mitani, and M. Mizuta, submitted for publication in This Bulletin.

14) a) H. Sakurai, K. Tominaga, T. Watanabe, and M. Kumada, *Tetrahedron Lett.*, **1966**, 5493. b) F. H. Brooks and F. Glockling, "Inorganic Syntheses," Vol. XII, p. 58 (1970).

15) K. A. Kozeschkow, *Ber.*, **66**, 1661 (1933).

The Polymerization of Vinyl Monomers in the Presence of Surface Active Agents. III. The Rate of the Polymerization of Styrene

Teruzo ASAHARA, Manabu SENŌ, Shinsaku SHIRAISHI, and Yoshikazu ARITA

Institute of Industrial Science, University of Tokyo, Roppongi, Minato-ku, Tokyo

(Received May 1, 1972)

Styrene polymerized in the presence of sodium tetrapropylenebenzenesulfonate in an aqueous system without any ordinary initiators. The rate of the polymerization was dependent on the concentration of the surfactant and on the initial monomer concentration. The apparent activation energy of the polymerization was about 13.9 kcal/mol. The polymerization was inhibited by adding hydroquinone to the reaction system.

Imoto and Takemoto[1] have reported the homo- and graft polymerization of methyl methacrylate (MMA) onto fibers with hydroxylic pendant groups, especially onto cellulose. In their paper, they have also described that styrene (St) polymerized only with difficulty under the same reaction conditions. We ourselves have previously reported that the polymerization of MMA in the presence of anionic surface active agents, such as sodium tetrapropylenebenzenesulfonate and 2-dodecylbenzenesulfonate, in an aqueous system without any ordinary initiators gave a stable emulsion of poly(methyl methacrylate) (PMMA) with an unusually high molecular weight, and that the resultant polymer was recovered in a good yield.[2,3] During the course of the investigation, we found that styrene also polymerized in the presence of sodium tetrapropylenebenzenesulfonate about three times or more as much as in the case of MMA in an aqueous medium.

In this paper, we will describe the kinetic study of the polymerization of styrene; we will also consider the reaction in some detail.

Experimental

Materials. Styrene and acrylonitrile (AN) were purified by usual methods. Sodium tetrapropylenebenzenesulfonate (ABS) was purified according to the procedure described in our previous paper.[2]

Polymerization. In a four-necked, 100 ml, flat-bottomed flask equipped with a condenser, a dropping funnel, a nitrogen inlet tube, and a rubber stopper, given amounts of deionized water and ABS were placed; the mixture was then preheated to the reaction temperature (80°C except otherwise stated) for 40 min, during which period a slow stream of nitrogen was introduced into the mixture. A definite amount of a monomer was then added to the mixture through the dropping funnel and allowed to polymerize. For a kinetic experiment, 2 g portions of the reaction mixture were withdrawn by means of a syringe at definite time intervals, weighed accurately, and poured into 10 ml of methanol in order to precipitate the polymer formed. The polymer was collected by filtration, thoroughly washed with methanol, dried at 60°C under a vacuum, and weighed. The rate of polymerization was determined from the time-conversion curves. The molecular weight, $\overline{M}$, of the polystyrene thus obtained was determined from the intrinsic viscosity, $[\eta]$, by using this equation:[4]

$$[\eta] = 1.2\times10^{-5}\,\overline{M}^{0.71}.$$

The viscosity of the polymer solutions in toluene was measured according to an ordinary method at 30°C.

Determination of Number of Particles. For particle-size determination, a sample of about 1 g was taken from the reaction mixture and diluted 10 times by water containing 0.01% of hydroquinone to minimize any further change. It was deposited onto a collodion substrate in minute droplets approximately 2 microns in radius. The specimen was directly photographed by using a JEM-5Y electron microscope of 9800 magnification at 80 kV. A photograph was enlarged in length as much as 2 times. The diameter of the particles was measured by a Scale Lupe of 5 magnification on 50 to 100 particles on the enlarged photograph, and the average diameter was calculated. The number of particles in the reaction mixture was calculated from the average diameter and the density of the particles, which was approximated as 1.0.

Results and Discussion

As has been reported previously,[2] we have found that MMA polymerized in the presence of ABS in an aqueous system without any ordinary initiators. The initiation mechanism, however, has not yet been elucidated. Knowledge of whether or not this polymerization technique is applicable to other monomers may throw some light on the problem; thus, we attempted the polymerization of St in a manner similar to that used for MMA. It was found that St polymerized in an aqueous system in the presence of ABS as much three times or more as in the case of MMA. The polymerization reaction of St was inhibited by adding hydroquinone. This result shows that the polymerization reaction of St proceeds *via* a free radical mechanism.

The relationship between the rate of polymerization of St and the concentration of ABS was investigated. As is shown in Fig. 1, an approximately linear relation was found between the rate of polymerization, R_p, and the ABS concentration, [ABS], in the range studied.

$$R_p \propto [\mathrm{ABS}] \qquad (1)$$

Equation (1) did not agree with either the equation of the polymerization of MMA or that of the Smith-Ewart theory, but it was consistent with the equation

1) M. Imoto and K. Takemoto, *Kogyo Kagaku Zasshi*, **70**, 1851 (1967).

2) T. Asahara, M. Senō, S. Shiraishi, and Y. Arita, This Bulletin, **43**, 3895 (1970).

3) T. Asahara, M. Senō, S. Shiraishi, and Y. Arita, *ibid.*, **45**, 2862 (1972).

4) T. Oyama, K. Kawahara, and M. Ueda, *Nippon Kagaku Zasshi*, **79**, 727 (1958).

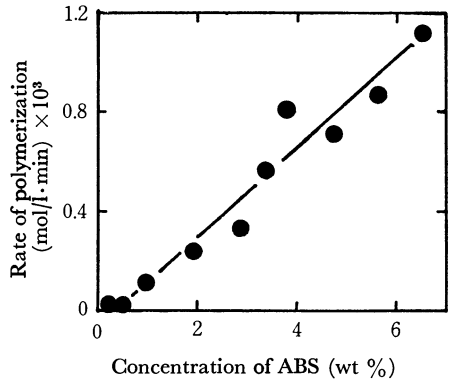

Fig. 1. Dependence of polymerization rate (mol/l·min) on ABS concentration (wt%).

of Medvedev,[5] as will be shown below.

Medvedev argued that the surface area was the most important parameter of the emulsion polymerization and developed a kinetic expression; in which R_P was proportional to the emulsifier concentration when primary radicals were formed in adsorbed emulsifier layers.

Therefore, the surface area may in a sense be one of the important parameters of the present polymerization system. Furthermore, the number of micelles may be considered to be another important parameter,because the number of micelles increases with an increase in the ABS concentration. Supposing that the radicals are generated only on the surface of the micelle, the number of radicals may increase with an increase in the number of micelles in our system.

In the case of AN, the polymerization did not occur even at higher concentration of ABS as is shown in Table 1. The solubility of AN in water, higher than that of St, is responsible for this behavior. This result, together with the fact reported before[2] that the polymerization of MMA did not occur in the medium of organic solvents, suggests that the formation of micelles may be essential for the polymerization in the present system.

Table 1. Polymerization of acrylonitrile

ABS (g)	AN (g)	Temp. (°C)	Time (hr)	Yield (%)
1.0	10.0	80	2	0
1.0	10.0	70	2	0
1.0	20.0	70	3	trace
2.0	10.0	75	3	trace[a]
3.0	10.0	75	2	0

water 100 g; under nitrogen atmosphere.
a) water 90 g and benzen 10 g under nitrogen atmosphere

The number of polymer molecues was calculated from the yields and the molecular weights of the polymers. The effects of the concentrations of ABS and St and of the reaction temperature on the number of polymer molecules are shown in Figs. 2 and 3 and in Table 2. It was noticeable that the number of polymer molecules increased with an increase in the concentration of ABS and a rise in the reaction temperature, but were nearly independent of the concentration of the monomer in the range above 1.5 mol%. This result suggests that the number of initiation species increased with an increase in the concentration of ABS and the reaction temperature.

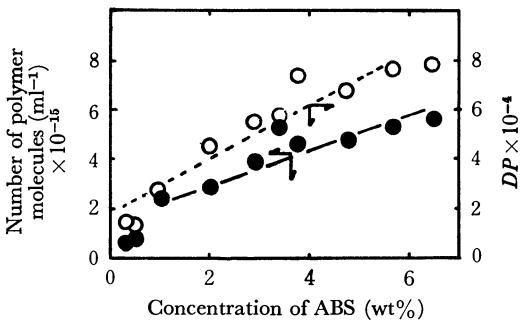

Fig. 2. Dependence of number of polymer molecules (ml^{-1}) and *DP* on ABS concentration (wt%).
St 10 g/aqueous phase 100 g, 2 hr, 80°C under nitrogen atmosphere.

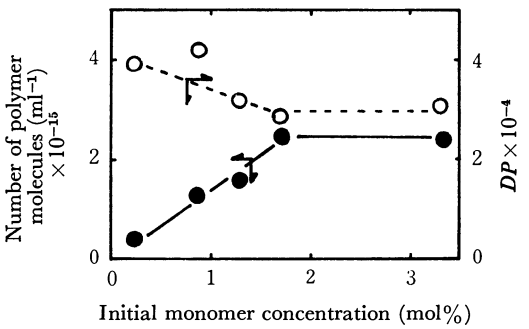

Fig. 3. Dependence of number of polymer molecules (ml^{-1}) and *DP* on initial monomer concentration (mol%). ABS 1 wt%, 80°C, 2 hr, under nitrogen atmosphere.

Table 2. Effect of reaction temperature on polymerization rate, *DP* and number of polymer molecules

Reaction temperature (°C)	Polymerization rate (mol/l·min) ×10³	*DP* ×10⁻⁴	Number of polymer molecules (ml^{-1}) ×10⁻¹⁵
70	0.74	4.22	1.04
80	1.14	2.82	2.43
85	1.14	2.44	2.76
90	2.30	2.61	5.16
100	3.50	2.20	11.3

St 10g/100g aqueous phase, ABS 1wt% under nitrogen atmosphere.

The reaction mixture was observed by means of an electron microscope, and the particle sizes were determined at reaction times of 30, 60, and 120 min at ABS concentrations of 1 and 3 wt%. The results are shown in Table 3. The particle sizes were nearly constant, most of them lying in the range from 300 to 400 Å, independent of the concentration of ABS and the reaction time. The maximum particles were from 1000 to 1200 Å in size, and new particles with smaller radii appeared at each reaction time, as is shown in Fig. 4. The number of polymer particles per unit of volume was about 1×10^{15}, which is of the same order as the number of polymer molecues esti-

5) G. E. Ham, "Vinyl Polymerization, Part II," Marcel Dekker, New York (1969), p. 19.

TABLE 3.

ABS (wt%)	Reaction time (min)	Average diameter (Å)	Number of polymer particles (ml^{-1})	Number of polymer molecules (ml^{-1})
1	30	345		
	60	407		
	120	384	0.52×10^{15}	3.3×10^{15}
3	30	427		
	60	410		
	120	414	0.94×10^{15}	3.8×10^{15}

St 10g/100g aqueous phase at 80°C under nitrogen atmosphere.

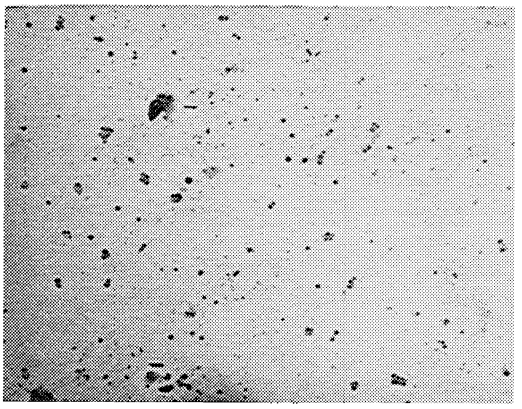

a

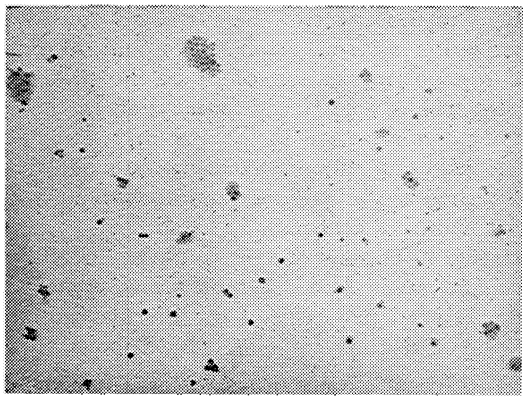

b

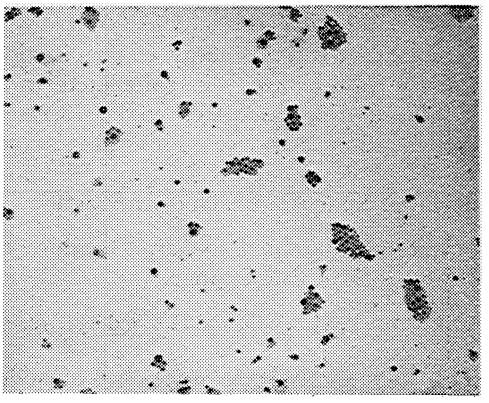

c

Fig. 4a, b, c. Electron micrographs of polystyrene latices. The samples are at reaction time; 30 min(a), 60 min(b), and 120 min(c).
ABS 3 wt%, St 10 g/aqueous phase 100 g (19600×).

mated previously. These results can be explained from the following considerations. The loci of the polymerization reaction are the interfaces between the micelles and the continuous medium; the radicals generated at the interface enter into the micelle, and hence the polymerization occurs.

By assuming that one polymer is formed in one micelle, the number of micelles can be calculated by:

$$N = (W/\bar{M}) \times 6 \times 10^{23},$$

where W is the yield of the polymer in grams and where $\bar{M}$ is the average molecular weight of the polymer.

The number of particles was about $(0.7 \text{ to } 4.0)\times 10^{15}$ ml^{-1} of the solution; this value was of the same order as in the general emulsion polymerization.[6]

From the above discussion, it can be concluded that the formation of micelles is an important factor in the generation of radicals and that the radicals do not enter into the particle from the water phase, but are generated only in the micelle. The ABS concentration was thought to be a factor in the production of radicals, and it was quantitatively understood that the relationship between the ABS concentration and the number of polymer particles was linear.

The rate of emulsion polymerization was usually independent of the initial monomer concentration and proportional to the monomer concentration in the polymer particles or micelles, but in our system the relationship between the rate of polymerization and the initial monomer concentration, $[M]_0$, defined in mol% calculated from the composition in the initial reaction mixture, was as is shown in Fig. 5. The dependence of R_p on $[M]_0$ was more remarkable than in the case of MMA. The apparent relationship can be written by:

$$R_p \propto [St]_0^{0.64}.$$

However, the dependence of R_p on the initial monomer concentration was small compared with that on the ABS concentration, as R_p may be considered to be almost independent of the initial monomer concentration in the range above 0.85 mol%, as is shown in Fig. 5.

These results may be well understood by suposing the following relation:

$$R_p \propto [M]_0[ABS]/([M]_0+[ABS]).$$

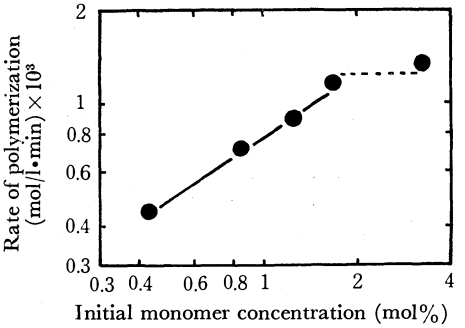

Fig. 5. Dependence of polymerization rate (mol/l•min) on initial monomer concentration (mol%).
ABS 1 wt%, 80°C under nitrogen atmosphere.

6) P. J. Flory, "Principles of Polymer Chemistry" Princeton Univ. Press (1953), p. 215.

When the experiment is conducted under the condition of $[M]_0 \gg [ABS]$, R_p is apparently expressed by $R_p \propto [ABS]$. On the other hand, when [ABS] is constant, R_p is almost constant in the range of $[M]_0 \gg [ABS]$, but R_p is slightly dependent on $[M]_0$ in the range where $[M]_0$ is not sufficiently larger than [ABS]. This explains the apparent relationship of $R_p \propto [St]_0^{0.64}$. The plot of R_p *vs.* $[ABS]/([M]_0+[ABS])$ also gave a straight line (Fig. 7); this shows a better linearity than the plot of R_p *vs.* [ABS].

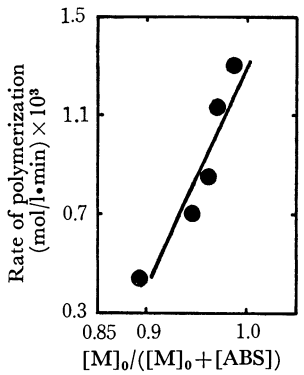

Fig. 6. Dependence of polymerization rate (mol/l•min) on $[M]_0/([M]_0+[ABS])$
ABS 1 wt%, 80°C under nitrogen atmosphere.

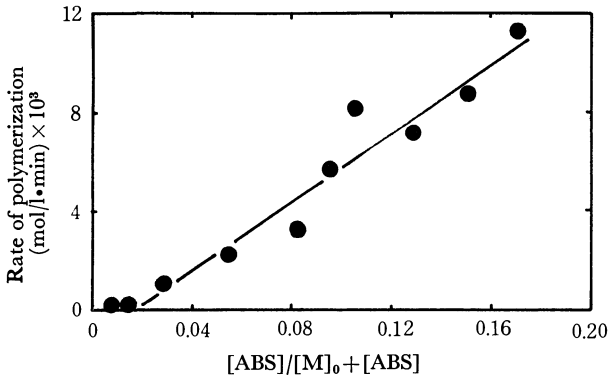

Fig. 7. Dependence of polymerization rate (mol/l•min) on $[ABS]/([M]_0+[ABS])$
St 10 g/aqueous phase 100 g, 80°C under nitrogen atmosphere.

From the relation between the polymerization rate and the reaction temperature shown in Table 2, the activation energy was calculated to be about 13.9 kcal/mol. This value is somewhat smaller than that of ordinary radical polymerization.

The average degree of polymerization, *DP*, calculated from the intrinsic viscosity was plotted against the ABS concentration, the initial monomer concentration, and the reaction temperature. As is shown in Figs. 2, 3, and 8, *DP* increases with an increase in the ABS concentration, and it is nearly independent of the concentration of the monomer, but decreases with the rise of the reaction temperature. *DP* is expressed by:

$$DP = R_p/(R_t+R_{tr}) = R_p/R_i$$

where R_p, R_t, R_{tr}, and R_i are the rates of the propagation reaction, the termination reaction, chain transfer to the monomer, and the initiation reaction respectively. Therefore, the activation energy derived from the temperature dependence of the *DP*, E_{DP}, is expressed as

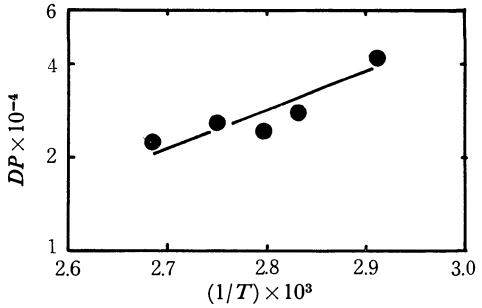

Fig. 8. Dependence of *DP* on $1/T$.
St 10 g/aqueous phase 100 g, ABS 1 wt%, 2 hr, under nitrogen atmosphere.

follows:

$$E_{DP} = E_p - E_i,$$

where E_p and E_i are the activation energies of propagation and initiation respectively. In general, E_i is larger than E_p, and therefore *DP* decreases with a rise in the reaction temperature, as is shown in Fig. 8. As is shown in Fig. 8, the activation energy of *DP* was calculated to be about −5.2 kcal/mol. On the other hand, the E_p of the emulsion polymerization of St was found by Morton[7] to be 7.4 kcal/mol. Using the values of E_{DP} and E_p mentioned above, E_i was calculated to be 12.6 kcal/mol, which is considerably smaller than those values found for the thermal polymerization or polymerization by radical initiators. The reason for the difference is not clear, but it may be attributed to the effect of the surfactant added to the polymerization system. Hohenstein and Mark investigated the polymerization of St in the presence and in the absence of soap; they found that, in the case of emulsion polymerization by potassium persulfate, E_i is about 17 kcal/mol, about 8 kcal/mol smaller than the value in the case of polymerization without soap.[8]

If this value, 8 kcal/mol, is applied to our system, the activation energy of the initiation of St in the absence of soap is 20.6 kcal/mol, which almost agrees with the activation energy of the thermal initiation of the St polymerization calculated by Tobolsky.[9]

It has been shown that, in the case of thermal and radical polymerization, the overall activation energy, *E*, can be calculated by the following equation:[10]

$$E = (1/2)E_i + [E_p - (1/2)E_t],$$

where E_t is the activation energy of termination. By this equation, $[E_p-(1/2)E_t]$ is calculated to be 7.6 kcal/mol because *E* is calculated to be 13.9 kcal/mol, as has been mentioned above. This value agrees with Tobolsky's value of about 6.3 kcal/mol,[11] which was found for the ordinary radical polymerization of St.

The authors are indebted to Mr. Toshihiro Shibata for his helpful technical assistance.

7) M. Morton, P. P. Salatiello, and H. Landfield, *J. Polym. Sci.*, **8**, 279 (1952).
8) W. P. Hohenstein and H. Mark, *ibid.*, **1**, 549 (1946).
9) K. E. Russel and A. V. Tobolsky, *J. Amer. Chem. Soc.*, **75**, 5052 (1953).
10) T. Otsu and K. Takemoto, "Experiments of Vinyl Polymerization," Kyoritsu Schuppan, Tokyo (1964), p. 256.
11) A. V. Tobolsky and B. Baysal, *J. Polym. Sci.*, **11**, 471 (1953).

The Reaction Mechanism of 2-Dimethoxymethyl-3-methoxypropiononitrile with Acetamidine. III.[1] The Reaction with Benzamidine[2]

Takenori NISHINO, Masumi KIYOKAWA, Yoshiyuki MIICHI, and Kanji TOKUYAMA

Shionogi Research Laboratory, Shionogi & Co., Ltd., Fukushima-ku, Osaka, 553

(Received May 16, 1972)

In order to elucidate the effect of basicities of amidines on their reactions with 2-dimethoxymethyl-3-methoxypropiononitrile (**1**), the reaction of **1** with benzamidine was studied. Products are similar to those from the reaction of **1** with acetamidine. The minor pathway in the reaction with acetamidine (Route B in Chart 1) was the major one in the reaction with benzamidine. This remarkable difference could be explained in terms of the electronic effect of 2-substituents of the intermediates (**4a** and **4b**) in both reactions and of basicities of acetamidine and benzamidine.

α-Formylpropiononitrile derivatives,[3] *e.g.*, 2-dimethoxymethyl-3-methoxypropiononitrile (**1**) and 2-dimethoxymethylacrylonitrile (**2**), are important building blocks for heterocyclic compounds.[4,5] When treated with acetamidine, **1** and **2** afford 2,7-dimethyl-5,6-dihydropyrimido[4,5-*d*]pyrimidine (**8a**), which is an important intermediate for thiamine since it is easily hydrolyzed to 2-methyl-4-amino-5-acetamidomethylpyrimidine (**9a**).[4] In previous papers we proposed a detailed pathway for the reactions as shown in Chart 1.[1,6] The pathway involves the major process **1**→**2**→**3a**→**4a**→**5a**→**6a**→**7a**→**8a** and minor ones **1**→**13**→**14a** and **6a**→**10a**→**11a** (=**8a**). Among the proposed intermediates, the key intermediate **4a** was successfully isolated in a fairly good yield but the others were not under usual reaction conditions.[1] To extend the scope of these reactions, the reaction of **1** with benzamidine was attempted. Since the basicities of reaction media were thought to play an important role for some steps of the reaction,[1] studies with less basic benzamidine[7] seemed necessary.

The reaction of **1** with benzamidine is expected to

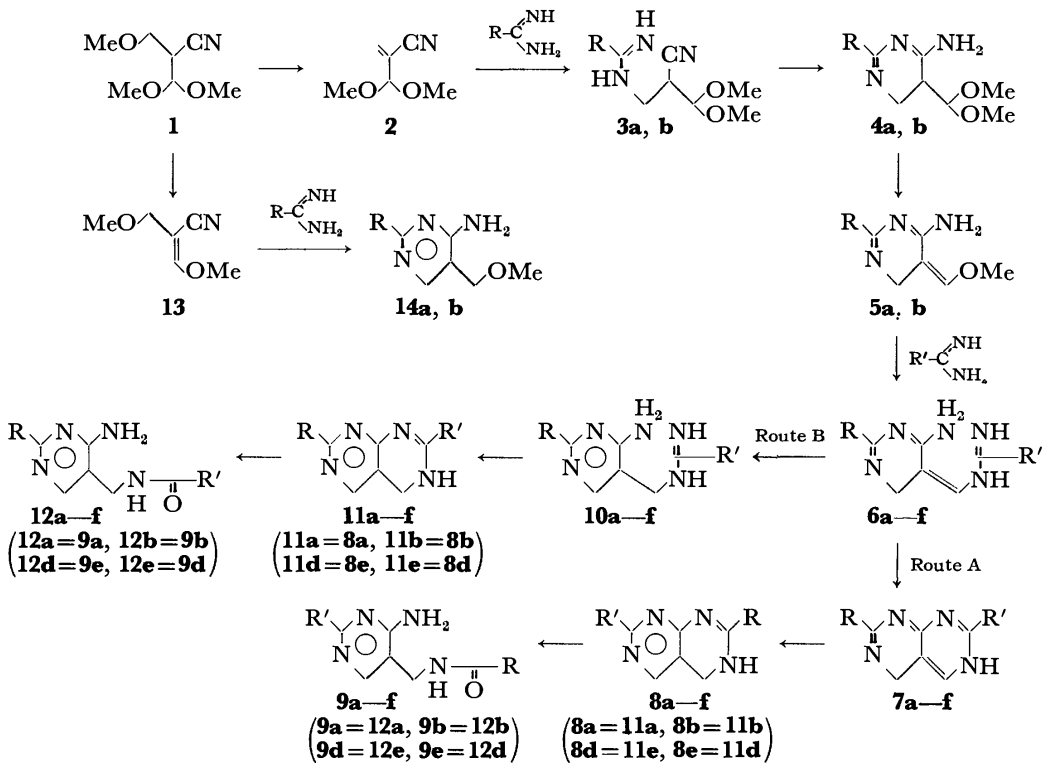

a: R=R′=Me b: R=R′=Ph c: R=Ph, R′=*p*-tolyl
d: R=Me, R′=Ph e: R=Ph, R′=Me f: R=Me, R′=Et

Chart 1.

1) For part 2, see T. Nishino, M. Kiyokawa, Y. Miichi, and K. Tokuyama, This Bulletin, **45**, 2010 (1972). A part of this paper was reported in a preliminary form; T. Nishino, M. Kiyokawa, and K. Tokuyama, *Tetrahedron Lett.*, **1968**, 4321.

2) Pyrimidines Part 11. For part 10, see Ref. 1.

3) G. A. Chelinstev, *Chem. Abstr.*, **40**, 4069 (1946).

4) A. Takamizawa, K. Tokuyama, and K. Tori, This Bulletin, **32**, 188 (1959), and references cited therein.

5) A. Takamizawa, K. Hirai, Y. Sato, and K. Tori, *J. Org. Chem.*, **29**, 1740 (1964).

6) T. Nishino, M. Kiyokawa, Y. Miichi, and K. Tokuyama This Bulletin, **45**, 1127 (1972).

7) P. A. S. Smith, "The Chemistry of Open-chain Organic Nitrogen Compounds," Vol. 1, Bengamin, New York (1965), p. 178.

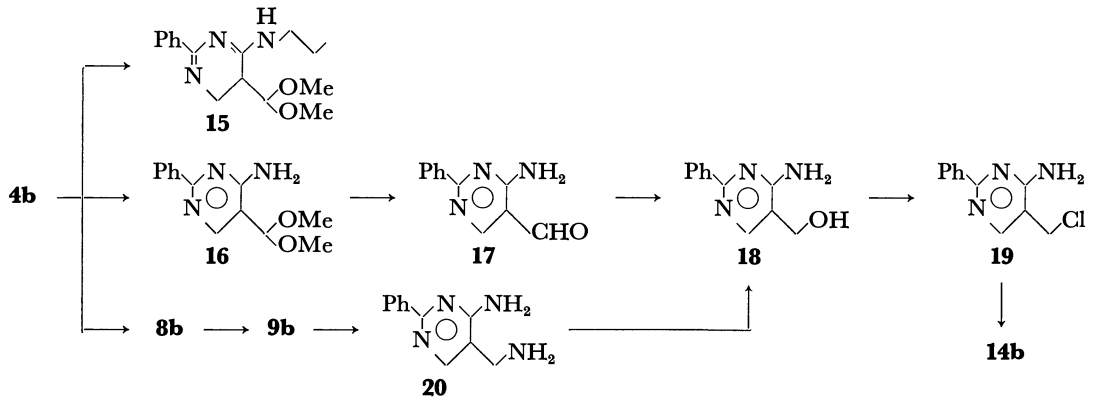

Chart 2.

proceed *via* the same pathway as that with acetamidine. When **1** with benzamidine was heated in methanol at 40°C for 6 hr, three products, **4b** (11%), **8b** (2.5%), and **10b** (6.8%), were obtained along with the recovery of 68% of **1**.

Compound **4b** showed an absorption band similar to that of 2-phenyl-4-amino-5,6-dihydropyrimidine in the UV spectrum.[6,8] **4b** was therefore tentatively characterized as 2-phenyl-4-amino-5-dimethoxymethyl-5,6-dihydropyrimidine, which corresponds to **4a**. The NMR spectrum supported the structure; *viz.*, it showed the signals of an ABXY system, in which H_6 and $H_{6'}$ constitute an AB part, H_5 an X part, and the methine proton of the acetal group a Y part, and of a 6-proton singlet due to two methoxy groups. When treated with *n*-propylamine, **4b** was easily converted into 4-*n*-propylamino analog of **4b** (**15**). This facile transamination suggested the existence of 4-aminodihydropyrimidine moiety.[1]

Unequivocal proof of the structure of **4b** was provided by its conversion into 2-phenyl-4-amino-5-methoxymethylpyrimidine (**14b**), an authentic sample of which was obtained from **13** and benzamidine in a way similar to the preparation of **14a** from **13** and acetamidine.[9] Treatment of **4b** with chloranil gave a pyrimidine (**16**), which was readily hydrolyzed to 5-formylpyrimidine (**17**). Reduction of **17** with sodium borohydride yielded 5-hydroxymethylpyrimidine(**18**), which was converted into **14b** *via* a 5-chloromethyl compound (**19**). The spectral and elementary analytical data supported the presence of the above intermediates **16**, **17**, and **18**.

The pathway **1**→**2**→**3b**→**4b**[1,6] was supported by the isolation of **4b**. When **2** was treated with benzamidine in 1,2-dimethoxyethane, the formation of **3b** was confirmed at the initial stages of the reaction. Although **3b** could not be isolated in a pure state because of its rapid cyclization to **4b**, its structure was supported by the IR and UV spectra which showed the presence of non-conjugate nitrile[1,6] and benzamidino groups.

Compound **8b**, $C_{18}H_{14}N_4$, showed the absorption maximum at 350 nm in the UV spectrum. It was also obtained by the further reaction of **4b** with benzamidine. Thus, **8b** should be the final product corresponding to **8a**. Hydrolysis of **8b** gave **9b**, which was further hydrolyzed to 2-phenyl-4-amino-5-aminomethylpyrimidine (**20**). Treatment of **20** with sodium nitrite gave the above-described 5-hydroxymethylpyrimidine **18**. These series of reactions and the NMR spectrum supported the structure of **8b**.

Compound **10b**, which gave a correct analysis for **8b** plus one mole of ammonia, was easily converted into **11b** (=**8b**) on heating and showed an absorption band similar to that of **9b** in the UV spectrum. Thus, **10b** was confirmed to be 2-phenyl-4-amino-5-benzamidinomethylpyrimidine corresponding to the intermediate of the minor pathway (Route B in Chart 1) in the reaction of **1** with acetamidine.

Formation of **8b** suggests that the second step of the reaction **4b**→**8b** also proceeded *via* the same pathway as that of the reaction with acetamidine **4a**→**8a**. However, it was somewhat surprising that the yield of **10b**, *viz.*, the contribution of Route B (see Chart 1), was much higher than in the case of the reaction of **1** with acetamidine.

To obtain the contribution ratio of Routes A (**6**→**7**→**8**) to B (**6**→**10**→**11**), the reaction of **4b** and *p*-toluamidine was examined. Treatment of **4b** with *p*-toluamidine in methanol followed by hydrolysis afforded a mixture of 2-phenyl-5-*p*-toluamidomethyl- (**12c**) and 2-*p*-tolyl-5-benzamidomethyl-4-aminopyrimidine (**9c**). The former pyrimidine **12c** was the product *via* Route B and the latter **9c** *via* Route A. Their structures were identified by comparison with those of authentic samples. The authentic **12c** was prepared by the reaction of **20** with *p*-toluchloride and **9c** by the reaction of **1** with *p*-toluamidine as outlined in Chart 3.

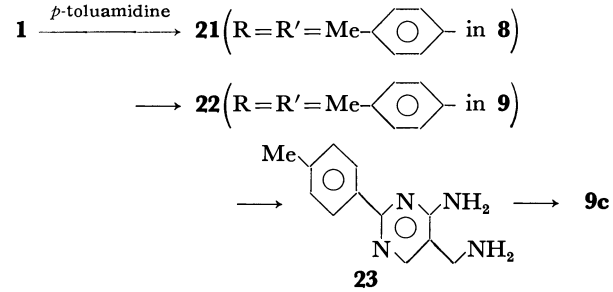

Chart 3.

8) S. Pietra, *Boll. Sci. Fac. Chim. Ind. Bologna*, **11**, 78 (1953).
9) A. Takamizawa and R. Maeda, *Yakugaku Zasshi*, **74**, 746 (1954).

Table 1. Yield of pyrimidines in the reactions of **4** and amidines

Starting material		Reaction time		Yield of pyrimidines (%) Molar ratio of amidine and amidine hydrochloride			
4	Amidine	hr		3:0[a)]	2:1	1:2	0:3
4b	*p*-Toluamidine	14	**9c**	(A) 30	75	67	48
			12c	(B) 46	12	6	trace
			9c+**12c**	70	87	73	48
4b	Acetamidine	5	**9e**	(A) 37	70	52	37.5
			12e	(B) 4	3	3	trace
			9e+**12e**	41	73	55	37.5
4a	Propioamidine	5	**9f**	(A) 44	87	—	28
			12f	(B) 6	8	—	6
			9f+**12f**	50	95	—	34
4a	Benzamidine	5.5	**9d**	(A) 22	65	36	trace
			12d	(B) 2	trace	trace	trace
			9d+**12d**	24	65	36	trace

A: Product *via* Route A. B: Product *via* Route B.

a) Containing a samll amount of sodium methoxide, since exact neutralization of the hydrochlorides of **4** and amidine was difficult.

The B/A ratio in the reaction of **4b** with *p*-toluamidine was determined by the integration of the respective singlets due to the methyl groups of *p*-tolyl moieties of **12c** and **9c** in the NMR spectrum of the product. The results are summarized in Table 1. The maximum yield of total pyrimidines was observed in the presence of some amount of benzamidine hydrochloride. On the other hand, the contribution of Route B increased with the decrease of the amidine hydrochloride; Route B became a major pathway in the absence of the hydrochloride. These interesting results prompted us to reinvestigate the reaction of **4a** with propioamidine under similar conditions. The ratio of two products, **12f** *via* Route B and **9f** *via* Route A, was determined by means of gas chromatography. The results are shown in Table 1. The maximum yield of total pyrimidines **12f** and **9f** was similarly observed in the presence of a similar amount of amidine hydrochloride, and the relative ratio of Route B increased with the decrease of the amidine hydrochloride. However, the contribution of Route B, *i.e.* the yield of **12f**, was always very low.

The remarkable contribution of Route B in the reaction of **4b** with benzamidines as compared with the reaction of **4a** with acetamidines can be explained in terms of the electronic effect of 2-substituents of possible intermediates **6a** and **6b**, and of the basicities of amidines.

The reactions of **4a** with benzamidine and of **4b** with acetamidine were carried out. Hydrolyzed products from the former reaction were **12d** (=**9e**) *via* Route B and **9d** (=**12e**) *via* Route A, and from the latter **12e** (=**9d**) *via* Route B and **9e** (=**12d**) *via* Route A. The structure of **9d** (=**12e**) was identified by its conversion into **9b** and that of **9e** (=**12d**) by comparison with an authentic sample prepared by the benzoylation of 2-methyl-4-amino-5-aminomethylpyrimidine (**24**).[10] The results were similar to those of the reaction of **4a** with propioamidine as shown in Table 1; Route B was always a minor pathway and the maximum yields of total pyrimidines were observed in the presence of suitable amounts of amidine hydrochlorides.

Table 1 shows that the relative ratio of Route B increases with the decrease of amidine hydrochloride. Route B proceeds by the abstraction of C_6 proton (H_6) of a possible intermediate **6** by an amidine base. Thus, it is reasonable that more basic conditions such as the absence of amidine hydrochlorides favors Route B.

For the abstraction of H_6 of **6**, the existence of an electron-attracting group such as the 2-phenyl group is more desirable. This is supported by the fact that the heating of a mixture of one mole each of **4a** and **4b** with sodium methoxide gave **14a** and **14b** in 1 : 10 ratio. The electronic effect can explain the fact that Route B was always minor in the reaction of **4a**. However, the yield of **12e** in the reaction of **4b** with acetamidine being lower than that of **12c** in the reaction of **4b** with *p*-toluamidine cannot be explained. Thus, Route B was expected to be favored in the former reaction since acetamidine is a stronger base than benzamidine.[7]

We considered the difference between the two reactions of **4b** to be caused by the faster cyclization of **6e**→**7e** than of **6c**→**7c**, and examined model reactions **10a**→**11a** (=**8a**) and **10b**→**11b** (=**8b**) for confirmation. Kinetic measurement for the reactions was carried out by following the increases of respective products. They showed first-order kinetics, the rate of **10a**→**11b** being higher than that of **10b**→**11b** at reflux temperature. By analogy, the cyclization of **6e**→**7e** would proceed faster than that of **6c**→**7c**. Therefore, two factors in **6c**, its slow cyclization to **7c** and the higher acidity of its C_6 position, favor Route B in the reaction of **4b** and *p*-toluamidine.

The appearance of maximum in the yields of total pyrimidines in the reaction of **4** and amidines (Table 1) may be accounted for as follows. As amidine hydrochloride catalyzes the elimination of methanol at the step **4**→**5**,[1] a higher concentration of amidine hydrochloride is desirable (see Chart 4). On th other

10) H. Andersag and K. Westphal, *Ber.*, **70**, 2035 (1937); R. Grewe, *Z. Phys. Chem.*, **242**, 89 (1936).

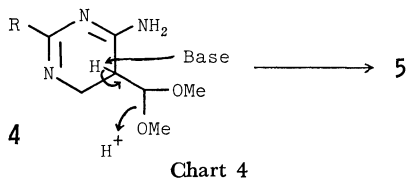

Chart 4

hand, a higher concentration of amidine is required for the step **5**→**6**. When the total amount of amidine and amidine hydrochloride is constant, both requirements can not be satisfied at the same time. Therefore, the maximum in yield appears at an appropriate ratio of amidine and amidine hydrochloride.

In conclusion, the reaction of **1** with benzamidine proceeds *via* the same pathway as that with acetamidine. The yields of the products depend on the amount of amidine hydrochlorides for both reactions. However, Route B, the minor pathway in the reaction with acetamidine, was observed as a major one in the reaction with benzamidine under the reaction conditions. The remarkable difference was essentially caused by the difference in electronic effect between phenyl and methyl groups.

Experimental

All the melting points were recorded on a Kofler block and have not been corrected. The NMR spectra were taken with a Varian A-60-A spectrometer, using tetramethylsilane as an internal reference. The chemical shifts were expressed in terms of δ values (s: singlet, d: doublet, t: triplet, q: quartet, m: multiplet). The molecular weights were determined by means of a vapor-pressure osmometer in acetone. The UV and IR spectra are shown in nm and cm^{-1}, respectively. The solvents used were removed under reduced pressure. The percentages of solutions of base and acid are given in w/w.

Reaction of 2-Dimethoxymethyl-3-methoxypropiononitrile (1) with Benzamidine. A solution of **1** (4.77 g) and benzamidine (3.87 g) in methanol (13 ml) was stirred at 40°C for 6 hr, and then evaporated to dryness. The residue was separated by alumina chromatography (Wakogel; 50 g). After removal of fraction 1 eluted with benzene (50 ml), fraction 2 was eluted with a mixture of benzene (25 ml) and ether (25 ml), and then the solvents were removed. A mixture of crystals, 2,7-diphenyl-5,6-dihydropyrimido[4,5-*d*]pyrimidine (**8b**), and an oil, **1**, was obtained. The crystals (199 mg; 2.5%) were collected by filtration, and **1** (3.8 g; 68%) was recovered from the filtrate. Recrystallization from acetonitrile gave columns of **8b** (35 mg). Fractions 3, eluted with ether (50 ml) and 4, eluted with a mixture of ether (96 ml) and ethanol (4 ml), gave 2-phenyl-4-amino-5-dimethoxymethyl-5,6-dihydropyrimidine (**4b**) (818 mg, 11%), which was purified by recrystallization from acetonitrile. The yield of pure **4b** was 198 mg (cubics). Fraction 5, further eluted with the above mixture (100 ml), gave 2-phenyl-4-amino-5-benzamidinomethylpyrimidine (**10b**) (570 mg, 6.8%), which was purified by recrystallization from acetonitrile. The yield of pure **10b** was 37 mg (cubics). **8b**: Mp 210.5—211.5°C. UV (CH_3CN) 254 (ε 72800), 312 (ε 13800), 350 (ε 9700). NMR (DMSO-d_6) 8.5—7.4 (m, 10H, phenyl), 8.35 (s 1H, H_4), 4.82 (s 2H, H_5). MS (*m/e*) 286 (M^+). Found: C, 75.50; H, 4.84; N, 19.35%. Calcd for $C_{18}H_{14}N_4$: C, 75.50; H, 4.93; N, 19.57%. **4b**: Mp 142°C (decomp.). UV (EtOH) 243 (ε 12900), 269 (ε 7000); (+HCl) 265, 286 (shoulder). IR(KBr) 1125, 1069 (acetal). NMR (pyridine-d_5) 7.3—7.5 (m 5H, phenyl), 4.13 (q, 1H, H_6, $J_{6,6'}$ 17.5 Hz, $J_{5,6}$ 6 Hz), 3.70 (q, 1H, $H_{6'}$, $J_{5,6'}$ 6 Hz), 2.80 (pair of triplet, 1H, H_5, J 8 Hz), 4.63 (d, 1H, C<u>H</u>$(OMe)_2$), 3.31 (s, 6H, CH$(O\underline{Me})_2$). MS (*m/e*) 247 (M^+), 215 (M^+-CH_3OH). Found: C, 63.27; H, 6.94; N, 16.78%. Calcd for $C_{13}H_{17}N_3O_2$: C, 63.14; H, 6.93; N, 16.99%. **10b**: Mp 156—158°C. UV (CH_3CN) 237 (ε 23000), 260 (shoulder), 284 (ε 8100), 297 (ε 7600); (+HCl) 254. NMR (DMSO-d_6) 7.3—8.0 (m, 10H, phenyl), 8.30 (s, 1H, H_6), 4.30 (s, 2H, $-CH_2-$). Found: C, 71.61; H, 5.51; N, 22.99%; mol wt, 293. Calcd for $C_{18}H_{17}N_5$: C, 71.26; H, 5.65; N, 23.09%; mol wt, 303.

Reaction of 2-Phenyl-4-amino-5-dimethoxymethyl-5,6-dihydropyrimidine (4b). (1) Reaction with n-*Propylamine*: A mixture of **4b** (0.7 g) and *n*-propylamine (7 g) in a sealed tube was heated at 100°C for 2 hr. After evaporation of *n*-propylamine, the residue was recrystallized from benzene. Columns of 2-phenyl-4-*n*-propylamino-5-dimethoxymethyl-5,6-dihydropyrimidine (**15**) were obtained (430 mg). Mp 116—117°C. UV (EtOH) 248 (ε 10800), 281 (ε 7100); (+HCl) 258. 290, 305 (shoulder). IR(KBr) 1110, 1065 (acetal). NMR ($CDCl_3$) 8.2—7.2 (m, 5H, phenyl), 3.43—3.77 (m, 3H, H_5, H_6), 4.35 (d, 1H, J 8 Hz, C<u>H</u>$(OMe)_2$), 3.37 (s, 3H) 3.38 (s, 3H) (CH$(O\underline{Me})_2$), 2.37 (q, 2H, $-HN-C\underline{H}_2-CH_2-$), 1.58 (m, 2H, $-CH_2-C\underline{H}_2-CH_3$), 1.00 (t, 3H, $-CH_2-C\underline{H}_3$), 5.9 (m, 1H, NH). Found: C, 66.53; H, 7.79; N, 14.43%; mol wt, 279.8. Calcd for $C_{16}H_{23}N_3O_2$: C, 66.41; H, 8.01; N, 14.52%; mol wt, 289.4.

(2) Reaction with Benzamidine: (a) A solution of **4b** (1.3 g) and benzamidine (0.7 g) in 1,2-dimethoxyethane (20 ml) was refluxed for 18 hr. The solvent was evaporated to dryness. The residue was recrystallized from methanol to give **8b** (1.14 g, 80%). (b) A solution of **4b** (2.47 g) and benzamidine (1.2 g) in methanol (7 ml) was heated at 50°C for 5 hr. The solution was evaporated to dryness and the residue was recrystallized from benzene to give crude **8b** (600 mg). The mother liquor was evaporated to dryness and the residue was separated by alumina chromatography (Wakogel; 50 g). Fractions 1, eluted with benzene (100 ml), and 2, eluted with a mixture of benzene (45 ml) and ether (5 ml), afforded a mixture of **8b** and **10b** (876 mg). Recrystallization of the mixture from acetonitrile gave **8b** (403 mg). The mother liquor was evaporated to dryness. Recrystallization of the residue gave **10b** (166 mg).

(3) Dehydrogenation: A mixture of **4b** (269 mg) and chloranil (270 mg) in benzene (40 ml) was refluxed for 3 hr and then separated by decantation from the precipitates. The benzene solution was washed with 4% sodium hydroxide solution (20 ml), dried over magnesium sulfate and evaporated to dryness. Recrystallization of the residue from benzene gave 2-phenyl-4-amino-5-dimethoxymethylpyrimidine (**16**) (needles; 35 mg). Mp 117—118°C. UV (CH_3CN) 240 (ε 29400), 260 (shoulder), 282 (ε 12000), 296 (ε 11000); (+HCl) 252. IR (Nujol) 3400, 3240 (NH_2), 1095, 1050 (acetal). NMR ($CDCl_3$) 8.54—7.31 (m, 5H, phenyl), 8.42 (s, 1H, H_6), 6.47 (s, 1H, C<u>H</u>$(OMe)_2$), 3.47 (s, 6H, CH$(O\underline{Me})_2$). Found: C, 63.43; H, 6.30; N, 17.02%; mol wt, 246. Calcd for $C_{13}H_{15}N_3O_2$: C, 63.66; N, 6.16; H, 17.13%; mol wt, 245.27.

2-Phenyl-4-amino-5-formylpyrimidine (17). A mixture of 2-phenyl-4-amino-5-dimethoxymethylpyrimidine (**16**; 485 mg), acetic acid (1.7 g), and water (2.7 ml) was heated at 100°C for 5 min. After cooling, crystals (342 mg) obtained were collected by filtration. Recrystallization of the crystals from methanol gave **17** (needles; 146 mg). Mp 180—180.5 °C. IR (Nujol) 2750, 1670 (CHO). NMR (DMSO-d_6) 7.4—8.5 (m, 5H, phenyl), 8.88 (s, 1H, H_6), 9.94 (s, 1H, CHO). Found: C, 66.20; H, 4.66; N, 20.88%. Calcd for $C_{11}H_9N_3O$: C, 66.32; H, 4.52; N, 21.10%.

2-Phenyl-4-amino-5-hydroxymethylpyrimidine (18). (i) Sodium borohydride (35 mg) was added to a methanol solution (10 ml) of **17** (200 mg), and the solution was stirred at room temperature for 30 min. After subsequent heating at 40—50°C for 30 min, the solvents was removed and the residue was extracted with acetone. The acetone extract was recrystallized from a mixture of acetone and benzene. Plates of **18** (107 mg) were obtained. Mp 134—135.5°C. IR (Nujol) 3440, 3300, 3200 (NH_2, OH). NMR ($CDCl_3$) 8.47—7.33 (m, 5H, phenyl), 8.07 (s, 1H, H_6), 4.60 (s, 2H, $-CH_2-$), 6.47 (2H, NH_2). Found: C, 65.65; H, 5.48; N, 20.71%. Calcd for $C_{11}H_{11}N_3O$: C, 65.67; H, 5.51; N, 20.88%.

(ii) A mixture of crude **20** (1.88 g), concd. hydrochloric acid (980 mg), and water (25 ml) was heated on a boiling-water bath, and sodium nitrite (650 mg) was added to the mixture. After heating for 2.5 hr, an additional amount of sodium nitrite (0.63 g) was added, and the solution was further heated for 2 hr on a boiling-water bath. Resinous substances which appeared were eliminated by decantation, the solution was neutralized with sodium carbonate, extracted with chloroform (150 ml), and then the chloroform was removed. Recrystallization of the residue from a mixture of benzene and acetone afforded **18** (456 mg).

2-Phenyl-4-amino-5-methoxymethylpyrimidine (14b). (i) Under cooling, **18** (402 mg) was added to phosphorous oxychloride (1.224 g) and the solution was heated at 85°C for 3 hr. After cooling, methanol (1 ml) was added to the solution which was left at room temperature overnight. Crystals (**19**) obtained were collected by filtration, and washed with methanol and then with benzene (1 ml). They were dissolved in methanol (3 ml) containing sodium methoxide, which had been prepared from sodium (150 mg) and methanol (5 ml). After being left standing at room temperature overnight, the solution was filtered from precipitated sodium chloride and then evaporated to dryness. Recrystallization of the residue from benzene gave **14b** (leaflets; 63 mg). Mp 130°C. UV (CH_3CN) 238 (ε 21600), 258 (shoulder, ε 14700), 281 (ε 8800), 286 (shoulder, ε 8600), 297 (ε 8300). IR (Nujol) 3480, 3300 (NH_2), 1085 (OMe). NMR ($CDCl_3$) 8.5—7.4 (m, 5H, phenyl), 8.23 (s, 1H, H_6), 4.43 (s, 2H, $-CH_2-$), 3.33 (s, 3H, OMe). Found: C, 66.95; H, 6.05; N, 19.38%; mol wt, 218. Calcd for $C_{12}H_{13}N_3O$: C, 66.95; H, 6.09; N, 19.52%; mol wt, 215.25.

(ii) To a solution of benzamidine (1.5 g) in 1,2-dimethoxyethane (50 ml), **13** (1.5 g)[11] was added in portions. After the solution was refluxed for 4.5 hr, the solvent was removed. Recrystallization of the residue from benzene gave **14b** (1.53g).

Reaction of 2-Dimethoxymethylacrylonitrile (2) with Benzamidine. To a stirred solution of benzamidine (18 g) in 1,2-dimethoxyethane (15 ml), **2** (22.7 g) was added at such a rate, as to keep the reaction temperature below 23°C within about 30 min. The solution was kept at room temperature. After 10 min a spot due to **3b** appeared in the tlc (a silica-gel plate; acetone, R_f 0.9—0.5). Isolation of **3b** in a pure state was unsuccessful. [**3b**: IR (Film) 2280 (non-conjugate CN). UV (CH_3CN) 225 (benzamidine moiety)]. After 1 day, crystals of 2-phenyl-4-amino-5-dimethoxymethyl-5,6-dihydropyrimidine (**4b**) appeared, which were collected by filtration. Recrystallization from acetonitrile yielded pure **4b** (15.4 g).

2-Phenyl-4-amino-5-benzamidomethylpyrimidine (9b). A mixture of 2,7-diphenyl-5,6-dihydropyrimido[4,5-*d*]pyrimidine (**8b**; 100 mg), potassium hydroxide (180 mg), ethanol (5 ml), and water (0.2 ml) was refluxed for 3 hr, and the solution was evaporated to dryness. The residue was recrystallized from a mixture of water and ethanol to give **9b** (leaflets; 64 mg). Mp 228—229.5°C. UV (CH_3CN) 210 (ε 11700), 298 (ε 12000); (+HCl) 254. IR (Nujol) 1613 (CONH). NMR (DMSO-d_6) 8.42—7.30 (m, 10H, phenyl), 8.17 (s, 1H,H_6), 4.35[s] (2H, $-CH_2-$). Found: C, 69.06; H, 5.21; N, 17.81%. Calcd for $C_{18}H_{16}N_4O \cdot \frac{1}{2}H_2O$: C, 68.93; H, 5.10; N, 17.87%.

2-Phenyl-4-amino-5-aminomethylpyrimidine (20). A mixture of **9b** (5.9 g), ethanol (35 ml), potassium hydroxide (12 g), ethanol (35 ml) and water (20 g) was refluxed for 30 hr and the solution was evaporated to dryness. Water (25 ml) was added to the residue. A brown oil appeared, which was extracted with chloroform (100 ml). The chloroform solution was dried over magnesium sulfate and then the solvent was removed. A brown oil (crude **20**; 4.03 g) was obtained. Concentrated hydroiodic acid was added to a part of the brown oil (187 mg), and crystals (**20**, hydroiodide) appeared. They were collected by filtration, washed with ethanol and recrystallized from methanol. The yield was 107 mg. Mp 268—272°C (decomp.). Found: C, 29.25; H, 3.14; N, 12.24%. Calcd for $C_{11}H_{12}N_4 \cdot 2HI$: C, 28.96; H, 3.09; N, 12.28%.

Cyclization of 2-Phenyl-4-amino-5-benzamidinomethylpyrimidine (10b). A solution of **10b** (40 mg) in methanol (4 ml) was refluxed for 6 hr and then evaporated to dryness. Recrystallization of the residue from acetonitrile gave 2,7-diphenyl-5,6-dihydropyrimido[4,5-*d*]pyrimidine (**8b**; 20 mg).

Reaction of 2-Phenyl-4-amino-5-dimethoxymethyl-5,6-dihydropyrimidine (4b) with p-*Toluamidine. General Procedure*: A mixture of **4b** (3 g), *p*-toluamidine and its hydrochloride in methanol (20 g) was refluxed for 14 hr. 48% Sodium hydroxide solution (10 g) and water (10 ml) were added to the solution and then refluxed for 3 hr. After cooling, the solution was diluted with water (50 ml). A powder appeared was collected by filtration. The filtrate was evaporated to dryness and water (60 ml) was added to the residue. An insoluble powder was collected by filtration. The two powders were combined (**9c**+**12c**). The relative ratio was determined by means of NMR spectroscopy using the integration of methyl singlets of **9c** (2.26 δ) and **12c** (2.18 δ) in pyridine-d_5. The data are shown in Table 1. (i) When the molar ratio of **4b**, *p*-toluamidine and *p*-toluamidine hydrochloride was 1:1:1, the combined powder was recrystallized from methanol. 2-Phenyl-4-amino-5-toluamidomethylpyrimidine (**12c**; 600 mg) was obtained as leaflets. The mother liquor was evaporated to dryness. Recrystallization of the residue from methanol gave 2-*p*-tolyl-4-amino-5-benzamidomethylpyrimidine (**9c**), but its purification was unsuccessful because a small amount of contaminated **12c** could not be eliminated. (ii) When the molar ratio of **4b** and *p*-toluamidine was 1:3, the combined powder was worked up in a procedure similar to that for (i). Pure **9c** was obtained (289 mg).

*2-*p*-Tolyl-4-amino-5-benzamidomethylpyrimidine (9c).* A mixture of 2-*p*-tolyl-4-amino-5-*p*-toluamidomethylpyrimidine (**22**; 120 mg), potassium hydroxide (12 g), ethanol (7 ml) and water (20 g) was refluxed for 34 hr. The solution was concentrated to 25 g and then water (50 ml) was added. By extraction with chloroform (50 ml), a syrup was obtained (crude **23**). Benzoyl chloride (100 mg) was added to a solution of the syrup (57 mg) in pyridine (700 mg) and left at room temperature. After 1 day, a mixture of water (10 ml), a 48% sodium hydroxide solution (500 mg) and methanol (5 ml) was added to the solution. The solution was heated at 100°C for 10 min, concentrated and poured into water (50 ml). Crystals obtained were collected by filtration and then recrystallized from methanol. Twenty miligrams of

11) Contained about 15% of **1** (determined by means of gas chromatography).

9c were obtained. Mp 236—237°C. UV (EtOH) 208 (ε 15300), 250 (ε 12500), 263 (shoulder), 282 (ε 6400), 297 (shoulder); (+HCl) 205, 258, 278 (shoulder). IR (KBr) 1613 (CONH). NMR (pyridine-d_5) 8.27 (s, 1H, H_6), 4.80, 4.67 (s, 1H+s, 1H, $-CH_2-$), 2.26 (s, 3H, Me). Found: C, 71.66; H, 5.45; N, 17.75%. Calcd for $C_{19}H_{18}N_4O$: C, 71.67; H, 5.70; N, 17.60%.

*2-Phenyl-4-amino-5-*p*-toluamidomethylpyrimidine (**12c**).* To a solution of 2-phenyl-4-amino-5-aminomethylpyrimidine (**20**; 400 mg) in pyridine (2 ml), *p*-toluchloride (400 mg) was added at 0°C and the solution was left at room temperature for 1 day. To the solution, a mixture of water (20 ml), 48% sodium hydroxide solution (1 g) and methanol (5 ml) was added. The solution was left at room temperature for 1 hr and then evaporated to dryness. Water (30 ml) was added to the residue. Crystals obtained were collected by filtration. Recrystallization from methanol gave **12c** (270 mg). Mp 235—236.5°C. UV (MeOH) 206 (ε 15600), 240 (ε 16400), 257 (shoulder), 281 (ε 5000), 295 (shoulder); (+HCl) 205, 252. NMR (pyridine-d_5) 8.27 (s, 1H, H_6), 4.77, 4.65 (s, 1H, s, 1H, $-CH_2$), 2.18 (s, 3H, CH_3-). Found: C, 71.91; H, 5.87; N, 17.86%. Calcd for $C_{19}H_{18}N_4O$: C, 71.67; H, 5.70; N, 17.60%.

*2-*p*-Tolyl-4-amino-5-*p*-toluamidomethylpyrimidine (**22**).* A solution of 2-dimethoxymethyl-3-methoxypropiononitrile (**1**; 500 mg), *p*-toluamidine (700 mg) in methanol (3 ml) was refluxed for 8 hr (formation of **21**), and 15% sodium hydroxide solution (2 g) was added. The solution was refluxed for 1 hr, poured into water (50 ml), and the precipitates (574 mg) were collected by filtration. Recrystallization of precipitates gave **22** (needles; 91 mg). Mp 235—239°C. UV (MeOH) 205 (ε 16600), 242 (ε 14700), 260 (shoulder), 282 (ε 6400), 296 (shoulder); (+HCl) 204, 256, 286 (shoulder). IR (KBr), 1614 (CONH). NMR (pyridine-d_5) 8.28 (s, 1H, H_6), 4.80, 4.67 (s, 1H + s, 1H, $-CH_2-$), 2.27 (s, 3H, Me), 2.20 (s, 3H, Me). Found: C, 72.45; H, 5.89; N, 17.50%. Calcd for $C_{20}H_{20}N_4O$: C, 72.27; H, 6.07; N, 16.86%.

*Reaction of 2-Methyl-4-amino-5-dimethoxymethyl-5,6-dihydropyrimidine (**4a**) with Propioamidine. General Procedure:*[1] Hydrochlorides of propioamidine (651 mg) and **4a** (443 mg) was added to methanolic sodium methoxide which had been prepared from an appropriate amount of sodium and methanol (6 ml). The solution was refluxed for 5 hr, filtered from precipitated sodium chloride and then evaporated to dryness. To the residue was added water (8 ml) and the aqueous solution was heated on a boiling-water bath for 1 hr. Removal of the water gave syrupy crystals. The total yield and relative ratio of **9f**[1] and **12f**[1] in the syrupy crystals were determined by means of UV spectroscopy and gas chromatography,[1] respectively. The data are shown in Table 1.

*Reaction of 2-Methyl-4-amino-5-dimethoxymethyl-5,6-dihydropyrimidine (**4a**) with Benzamidine. General Procedure:* Hydrochlorides of **4a** (443 mg) and benzamidine were added to methanolic sodium methoxide which had been prepared from an appropriate amount of sodium and methanol (6 ml). The solution was refluxed for 5.5 hr and then evaporated to dryness. The residue was dissolved in 40% acetic acid solution (5 ml) and then heated on a boiling-water bath for 7 hr. The solution was concentrated and the residue was neutralized with a saturated bicarbonate solution and then diluted with water (20 ml). Crystals of a mixture of **9d** and **12d** were collected by filtration. The relative ratio of **9d** and **12d** in the crystals was determined by means of NMR spectroscopy using the integration of the methyl singlets of **9d** (1.98 δ) and **12d** (2,40 δ) in methanol-d_4. Recrystallization of the above crystals from acetonitrile gave **9d** in a pure state. When molar ratio of **4a**, benzamidine and benzamidine hydrochloride was 1:2:1, the yield of isolated **9d** was 212 mg. Mp 199—200°C (leaflets). UV (MeOH) 242 (ε 21000), 290 (ε 7500); (+HCl) 255. IR (Nujol) 1655 (CONH). NMR (CD_3OD) 1.98 (s, 3H, MeCONH), 8.01 (s, 1H, H_6), 4.40 (s, 2H, $-CH_2-$), 7.3—8.3 (m, 5H, phenyl). Found: C, 64.19; H, 5.93; N, 22.36%. Calcd for $C_{13}H_{14}N_4O$: C, 64.44; H, 5.82; N, 23.13%.

*The Conversion of **9d** into **9b**.* A mixture of 2-phenyl-4-amino-5-amidomethylpyrimidine (**9d**, 430 mg), 48% sodium hydroxide (25 g) solution, and ethylene glycol (20 ml) was refluxed for 5 hr, and then evaporated to dryness. A yellow syrup (**20**) was obtained by extraction with chloroform (50ml). The syrup was dissolved in pyridine (4 ml) and then benzoyl chloride (320 mg) was added to the solution at 0°C. The solution was left in a refrigerator for 4 hr and then poured onto ice-water. Crystals obtained were collected by filtration and recrystallized from acetonitrile. The yield was 210 mg.

*2-Methyl-4-amino-5-benzamidomethylpyrimidine (**9e**=**12d**).* To a mixture of 2-methyl-4-amino-5-aminomethylpyrimidine (500 mg) and pyridine (4 g) was added benzoyl chloride (2 g) at 0°C. The solution was kept at room temperature overnight, and then evaporated to dryness. 10% Sodium hydroxide solution (50 ml) was added to the residue. The solution was evaporated to dryness and washed with cold water (10 ml). Recrystallization of the residue from methanol gave **9e** (225 mg). Mp 232—234°C (columns). UV (EtOH) 231 (ε 21700), 275 (ε 6700); (+HCl) 237. IR (KBr) 1675 (CONH). NMR (CD_3OD) 2.40[s] (3H, 2-Me), 7.98 (s, 1H, H_6), 4.42 (s, 2H, $-CH_2-$), 7.93—7.40[m] (5H, phenyl). Found: C, 64.35; H, 5.97; N, 23.30%. Calcd for $C_{13}H_{14}N_4O$: C, 64.44; H, 5.82; N, 23.13%.

*Reaction of 2-Phenyl-4-amino-5-dimethoxymethyl-5,6-dihydropyrimidine (**4b**) with Acetamidine. General procedure:* Hydrochlorides of **4b** (741 mg) and acetamidine (850 mg) were added to methanolic sodium methoxide which had been prepared from appropriate amounts of sodium and methanol (10 ml), and the solution was refluxed for 5 hr. 80% Acetic acid (5 ml) was added to the solution which was refluxed for 1.5 hr and then extracted with chloroform (100 ml). The chloroform layer was washed with a saturated sodium bicarbonate solution (10 ml) and then water (10 ml) and dried, and the chloroform was removed. Crystals of a mixture of **9e** and **12e** were obtained. The relative ratio of **9e** and **12e** in the crystals was determined by means of NMR spectroscopy using the integration of methyl singlets of **9e** (2.40 δ) and **12e** (1.98 δ) in methanol-d_4. The data are shown in Table 1. Recrystallization of the above crystals from methanol gave **9e**. When the molar ratio of **4b**, acetamidine, and acetamidine hydrochloride was 1:2:1, the yield of **9e** was 358 mg.

*Reaction of 2-Phenyl-4-amino-5-dimethoxymethyl-5,6-dihydropyrimidine (**4a**) with Sodium Methoxide.* To a mixture of **4a** hydrochloride (443 mg) and **4b** (493 mg) was added a sodium methoxide solution which had been prepared from sodium (138 mg) and methanol (15 ml). The solution was refluxed for 4 hr, filtered from precipitated sodium chloride and then evaporated to dryness. Extraction of the residue with chloroform gave a syrup (458 mg), which was a mixture of 2-phenyl-4-amino-5-methoxymethylpyrimidine (**14b**) and 2-methyl-4-amino-5-methoxymethylpyrimidine (**14a**). The ratio of **14b** and **14a** was determined to be 91.4:8.6 by means of gas chromatography (Apiezon grease L 30%, 1 m; column temperature, 234.5°C; carrier gas, He, flow rate, 90 ml/min; retention time, **14a**: 2.2 min, **14b**: 36.9 min). The syrup was chromatographed over alumina (Wakogel 10 g) with benzene (40 ml) and, subsequently, with a mixture of benzene

(30 ml) and ethyl acetate (30 ml). One hundred and sixty-three milligrams of **14b** was obtained.

*Cyclization Rates of 2-Methyl-4-amino-5-acetamidinomethylpyrimidine (**10a**) and 2-Phenyl-4-amino-5-benzamidinomethylpyrimidine (**10b**).* The rate constants for the two reactions were determined spectrophotometrically with a Perkin Elmer 139 spectrophotometer by following the increase of the absorbance at 310 nm due to **8a** in the reaction of **10a**, and that at 350 nm due to **8b** in the reaction of **10b** at reflux temperature (64.5°C).

*(1) The Decrease of **10a** (k_a)*: The hydrochloride of **10a** (6 mg) was dissolved in methanol in a 200 ml volumetric flask. The methanol solution was exactly neutralized with a dilute solution of potassium hydroxide in methanol and then the flask was filled to the mark with methanol at 26°C. $k_a = 7.3 \times 10^{-2} \mathrm{min}^{-1}$.

*(2) The Decrease of **10b** (k_b)*: Fourteen milligrams of **10b** was dissolved in methanol and then messed up to 200 ml at 26°C. $k_b = 4 \times 10^{-3} \mathrm{min}^{-1}$.

The authors express their deep gratitude to Professor Toshihiko Okamoto, the University of Tokyo, for his interest in this work.

BULLETIN OF THE CHEMICAL SOCIETY OF JAPAN, VOL. 46, 259—263 (1973)

Intramolecular Interaction between the Hydroxyl Group and the Oxirane Ring[1]

Michinori Ōki and Tetsuo Murayama

Department of Chemistry, Faculty of Science, The University of Tokyo, Hongo, Bunkyo-ku, Tokyo

(Received May 23, 1972)

The intramolecular interaction between the hydroxyl group and the oxirane ring has been detected by means of studying the infrared spectra in the 3μ region of various hydroxyalkyloxiranes. The O–H stretching absorptions of several compounds which have limiting structures in the sence of the conformational preference have been closely examined. The results indicate that the intramolecular interaction takes place between the hydroxyl group and the electron orbitals involved in the formation of the C–O bond, while that involving the electrons of the C–C bond can be neglected.

It has been established that the cyclopropane ring interacts with the hydroxyl group, the former acting as a proton acceptor.[2] This property of the cyclopropane ring is, of course, attributable to the strain of the bonds or to the low ionization potential of the electrons. Since the oxirane ring is an oxygen analog of the cyclopropane, it can naturally be expected that the oxirane ring will behave similarly; the study of the intramolecular interaction between the hydroxyl group and the oxirane ring is thus undertaken as an extension of the previous work.

Since the oxirane ring contains an oxygen atom, the three bent bonds of the ring, namely one C–C and two C–O bonds, are not equal. Because of the high electronegativity of the oxygen atom, oxirane has been reported to have a dipole moment (1.91 D)[3] which is slightly larger than those of tetrahydrofuran (1.63 D)[3] or dimethyl ether (1.29 D).[4] Thus, the electron densities of the bent bonds of the ring are clearly not equal, that of the C–C bond being tenuous.[5] It may be postulated, therefore, that the electron orbitals involved in the C–O bond formation, rather than the C–C bond of the oxirane ring, will interact with the hydroxyl group, if any O–H···oxirane interaction does exist.

This paper will deal with the detection of such an intramolecular interaction and with the dynamic stereochemistry which is necessary in establishing the interaction in detail. It will also seek to determine if the above expectation as to the site of the interaction is really correct.

Experimental

Spectral Measurements. The infrared absorption spectra in the 3μ region were measured on a Perkin-Elmer 112G single-beam grating spectrophotometer, the slit width being 0.8 cm^{-1} in this region. The apparent absorption curves were graphically separated into symmetrical curves.

Wako special-grade carbon tetrachloride was used in making up the solutions of alcohols. The concentrations of the solutions were *ca.* 0.003 mol/l. A quartz optical cell 2 cm thick was used.

The NMR spectra were taken on a JNM 3H-60 spectrometer.

Materials. All the alcohols except *erythro*-3,4-epoxy-4-methylpentan-2-ol (VIII) were prepared by the epoxidation of the appropriate unsaturated alcohols with perbenzoic acid. The acids were removed with calcium hydroxide during the reaction in order to avoid isomerization as much as possible.[6]

1) A preliminary report has been published: M. Ōki and T. Murayama, This Bulletin, **40**, 1997 (1967).

2) (a) L. Joris, P. von R. Schleyer, and R. Gleiter, *J. Amer. Chem. Soc.*, **90**, 327 (1968); (b) M. Ōki, H. Iwamura, T. Murayama, and I. Oka, This Bulletin, **42**, 1986 (1969); (c) Z. Yoshida, N. Ishiba, and H. Kusumoto, *J. Amer. Chem. Soc.*, **91**, 2279 (1969).

3) W. L. G. Gent, *J. Chem. Soc.*, **1957**, 58.

4) G. A. Barclay and R. J. W. Le Fèvre, *ibid.*, **1952**, 1643.

5) A. D. Walsh, *Trans. Faraday Soc.*, **45**, 179 (1949).

6) H. B. Hebest and B. Nicholls, *J. Chem. Soc.*, **1959**, 221.

The epoxidation of 4-methyl-3-penten-2-ol gave *threo*-3,4-epoxy-4-methylpentan-2-ol (VII); bp 67—68°C/15 mmHg, $n_D^{16.5}$ 1.4270. This compound was identical with the one obtained by the isomerization of *cis*-2-methyl-3,4-epoxypentan-2-ol.[7] (lit. bp 75—76°C/20 mmHg, n_D^{25} 1.4238). NMR (δ from TMS in CCl_4): 1.15 (3H, d, J=6 Hz), 1.26 (3H, s), 1.27 (3H, s), 3.20—2.80 (1H, m), 2.62 (1H, d, J=8 Hz), 4.10 (OH).

erythro-3,4-Epoxy-4-methylpentan-2-ol (VIII) (bp. 68.5—69°C/10 mmHg, $n_D^{16.5}$ 1.4271) was obtained by the isomerization of *trans*-2-methyl-3,4-epoxypentan-2-ol.[7] NMR (δ from TMS in CCl_4): 1.25 (3H, d, J=6 Hz), 1.30 (6H, s), 2.48 (1H, d, J=8.5 Hz), 3.48 (1H, m), 3.81 (OH).

Table 1. ν_{O-H} data of epoxy alcohols

Compound	ν_{max} (cm^{-1})	$A\times10^{-3}$[a] (mol·l·cm)	Relative intensity
2,3-Epoxypropan-1-ol (Glycidol) (I)	3638	0.21	1
	3611.8	2.9	14
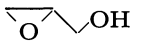	3590	3.1	15
2,3-Epoxy-3-methyl-butan-1-ol (II)	3638	1.6	1
	3612.4	4.0	2.5
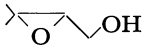			
trans-2,3-Epoxybutan-1-ol (III)	3638	0.62	1
	3610.0	2.8	4.5
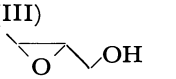	3583	4.0	6.4
2,3-Epoxy-2-methyl-propan-1-ol (IV)	3639	0.29	1
	3609	2.1	7.5
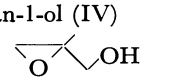	3578.1	4.2	15
trans-2,3-Epoxy-3-phenylpropan-1-ol (V)	3637	0.28	1
	3611.2	4.6	17
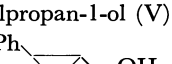	3590	3.1	11
3,4-Epoxybutan-2-ol (VI)	3607.0	2.6	1
	3573	2.7	1
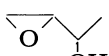			
threo-3,4-Epoxy-4-methylpentan-2-ol (VII)	3628	0.27	1
	3607.4	5.0	19
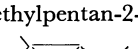			
erythro-3,4-Epoxy-4-methylpentan-2-ol (VIII)	3623.6	4.8	1
	3612	0.2	0.04
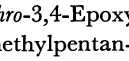	3567	1.7	0.37
trans-3,4-Epoxypentan-2-ol (IX)	3624	0.41	1
	3606.1	3.4	8.3
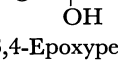	3569	3.3	7.9
3,4-Epoxy-2,4-dimethyl-pentan-2-ol (X)	3617	0.6	1
	3559.4	8.2	13.3
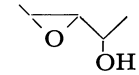			
trans-3,4-Epoxy-2-methyl-pentan-2-ol (XI)	3598	0.5	1
	3566.4	4.6	9.2
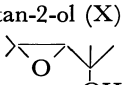			

a) "A" denotes the integrated intensity of the band.

7) C. B. Payne, *J. Org. Chem.*, **27**, 3819 (1962).

Results and Discussion

The spectral data of the O–H stretching absorptions (ν_{O-H}) of several 2,3-epoxypropan-1-ol derivatives are given in Table 1. Some representative curves are also given in Fig. 1.

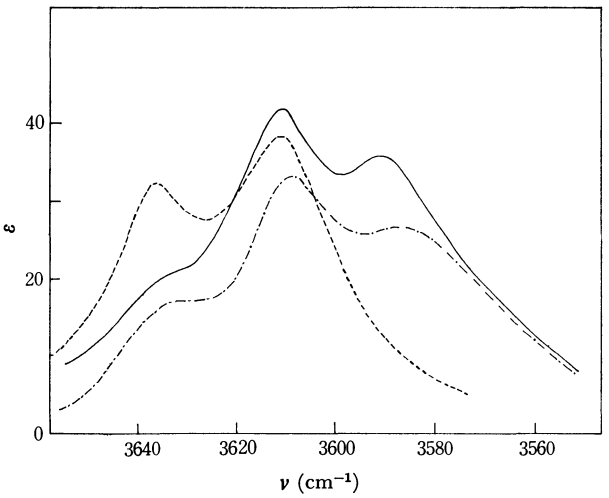

Fig. 1. ν_{O-H} absorption bands of 2,3-epoxypropan-1-ol (I: ——), 2,3-epoxy-3-methylbutan-1-ol (II: ------), and *trans*-2,3-epoxybutan-1-ol (III: —·—).

The ν_{O-H} curve of glycidol (I) apparently has three absorption peaks. One of the three maxima can certainly be assigned to the hydroxyl group which is hydrogen-bonded to the oxygen atom of the oxirane ring. In order to establish this assignment, the ν_{O-H} absorptions of several alcohols with a similar situation have been measured: tetrahydrofurfuryl alcohol and 2-hydroxymethyloxane[8] show their O–H···O bonded ν_{O-H} at 3602 and 3597 cm^{-1} respectively. It is then found that the band at the lowest frequency, 3590 cm^{-1}, is most probably the intramolecularly O–H···O-bonded band. The band at the highest wave number, 3638 cm^{-1}, can be assigned to the free OH group of the primary alcohol, because other primary alcohols are known to give rise to an absorption at *ca.* 3636 cm^{-1} [9]

Table 2. ν_{O-H} data of RCH_2OH

R	ν_{max} (cm^{-1})	$A\times10^{-3}$ (mol^{-1} l cm^{-2})	A_l/A_h[a]	Ref.
CH_3	3637.3	2.8	0.56	9
	3627	1.6		
$(CH_3)_2CH$	3641.5	3.6	0.50	9
	3628	1.8		
	3633.7	2.3	1.1	2b
	3619	2.6		

a) A_l and A_h denote integrated intensities of the bands at lower and higher frequencies, respectively.

8) S. A. Barker, J. S. Brimacombe, A. B. Foster, D. H. Whiffen, and G. Zweifel, *Tetrahedron*, **7**, 10 (1959).

9) M. Ōki and H. Iwamura, This Bulletin, **32**, 950 (1959).

(see Table 2). The third band, 3611.8 cm^{-1}, is located at too low a frequency to be assigned to a second rotamer of the primary alcohol, which usually gives the absorption near 3625 cm^{-1} and which is located at a lower frequency than the intramolecularly O–H··· cyclopropane interacting band (see Table 2). Thus, the last band is attributable to the O–H···oxirane interacting species.

2,3-Epoxy-3-methylbutan-1-ol (II), which carries two methyl groups at the C_3 of the ring, failed to show absorptions below 3600 cm^{-1}. However, when we removed the methyl group at C_3 which is *cis* to the hydroxymethyl group, the absorption band below 3600 cm^{-1} reappeared: the spectrum of *trans*-2,3-epoxybutan-1-ol (III) has a band at 3583 cm^{-1}, as is shown in Fig. 1 and Table 1.

These results may be interpreted as follows. In order to establish the intramolecular hydrogen bond between the hydroxyl group and the oxygen of the oxirane, the hydroxyl group must approach one of the lone-pair orbitals of the oxygen which are directed up and down in relation to the ring. However, if that conformation is taken in 2,3-epoxy-3-methylbutan-1-ol, the repulsive interaction between the *cis*-methyl and hydroxyl groups will be severe. Thus, the conformation is not favored in the case of compound II. Compound III, which lacks the *cis*-methyl group, has no severe interaction which would prevent the approach, and the O–H···O hydrogen bond is favored to show a band at 3583 cm^{-1}.

Although the band below 3600 cm^{-1} is lacking for compound II, a band is still observed at 3612.4 cm^{-1} which is attributable to the intramolecularly O–H··· oxirane interacting species. This fact offers support to the idea that the O–H···oxirane interaction takes place if the OH group approaches the ring within the plane of the ring, as was the case in O–H···cyclopropane interaction.[2] That is, edge-interaction is the favored process.

The absorption frequency (3590 cm^{-1}) of the intramolecularly O–H···O hydrogen-bonded species of glycidol (I) is higher by *ca.* 10 cm^{-1} than those of the glycidols (III, IV) which carry methyl groups. On the other hand, *trans*-2,3-epoxy-3-phenylpropan-1-ol (V), which is a phenyl-substituted glycidol, shows an absorption at almost the same frequency as glycidol itself. These results certainly reflect the electronic effect of the substituents.

The absorption frequencies (*ca.* 3610 cm^{-1}) due to the intramolecularly O–H···oxirane interacting species of glycidol and its homologs are apparently lower than those of the O–H···cyclopropane species.[2] This means that the electron density at the site in the acceptor is higher than that of cyclopropane, because the conformational situations are quite analogous. It can, then, be suggested that the interacting electron orbitals are not of the C–C bond, but of the C–O bond of the ring, because it is the C–O bond, not the C–C, which has a higher electron density than the C–C bond of the cyclopropane.

As to the substituent effect, there is another interesting phenomenon in connection with 3,4-epoxybutan-2-ol (VI), which is believed to be of steric origin. That is, this compound shows no band due to the free OH group. Instead, two bands are observed at 3573 and 3607.0 cm^{-1}; the former can be attributed to the O–H···O bonded species, and the latter, to the O–H··· oxirane interacting species. To understand why this compound does not show any free OH, the conformational consideration is very helpful. Since this alcohol contains two asymmetric carbons, there are a pair of racemates. The method of preparation, *i.e.*, the epoxidation of 3-buten-2-ol with perbenzoic acid, suggests that the alcohol which is under investigation is the *threo* isomer, since it is known that the application of the same procedure to 4-methyl-3-penten-2-ol gives rise to a *threo* isomer of 3,4-epoxy-4-methylpentan-2-ol (VII), as will be discussed later. Therefore, there are three conformations (VIa, VIb, and VIc) to be considered with respect to the rotation about the C_2–C_{OH} bond.

The H-inside conformation (VIa) has nothing unfavorable about it, because the repulsive interaction between hydrogens at C_3 and α to the hydroxyl group should be small. In addition, VIa can be stabilized because of the interaction between the hydroxyl group and the oxirane ring.

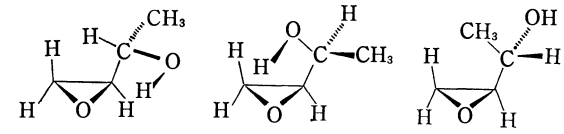

VIa VIb VIc

The OH-inside conformation (VIb) is unfavorable because of the steric interference between the hydrogen at C_3 and the OH group. However, this conformation can be stabilized due to the O–H···O bond formation.

On the other hand, the CH_3-inside conformation (VIc) is unfavorable because of the repulsion between the hydrogen at C_3 or the lone pair of the oxygen atom of the ring and the methyl group, and there is nothing to favor the conformation; it could be considered that the intramolecular interaction between the hydroxyl group and the electrons of the C–C bond in oxirane can take place, but this interaction would be of a very weak nature, if it existed at all, judging from a theoretical consideration of the electron density and the experimental evidence which will be given later.

Thus, the population of the VIc conformation must be small and O–H-free conformations within the skeletal frames of VIa and VIb must also be scarce, thus reducing the intensity of the free O–H band.

These results, together with the theoretical background, forced us to search for possible experimental evidence which clearly shows that the electron density at the C–C bond of the oxirane ring is really low. Thus, another approach has been undertaken: compounds which involve more severe steric requirements have been sythesized and their spectra examined.

The *threo* and the *erythro* isomers of 3,4-epoxy-4-methylpentan-2-ol (VII and VIII) have been selected as examples to study because the methyl group at C_3 exerts a severe steric effect and any conformational preference will thus be sharper than with compound

VI. The *threo* isomer (VII) has been obtained by the epoxidation of 4-methyl-3-penten-2-ol with perbenzoic acid. A consideration of the transition state of the epoxidation leads to the conclusion that the *threo* isomer is the main product, since it is a well-known fact that the peroxy acids attack the olefinic bond from the *cis* side of the hydroxyl group, probably because of the stabilization due to hydrogen-bond formation. This tentative conclusion is supported by the identity of the physical properties of the isolated product with those of the known *threo* isomer, which can be prepared by the isomerization of *cis*-3,4-epoxy-2-methylpentan-2-ol with the base.[7] The *erythro* isomer has been prepared by the isomerization of *trans*-3,4-epoxy-2-methylpentan-2-ol with the base.[7]

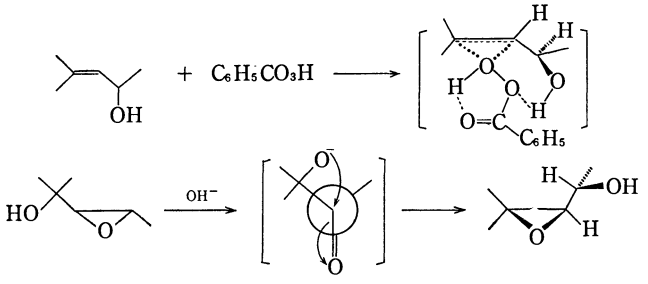

In the *threo* isomer VII, the H-inside conformation (VIIa) is the most stable, because the steric repulsion between the $CH_3CH(OH)$ group and the methyl group at C_3, which is *cis* to the $CH_3CH(OH)$ group, is the least. In addition, this conformation favors the intramolecular O–H···oxirane interaction. On the other hand, the O–H inside conformation (VIIb), which has the OH group above the ring, suffers from a severe steric interaction between the OH group and the methyl group at C_3, although this conformation may be stabilized due to the formation of the O–H···O bond. Thus, it can be concluded that the VIIb conformation is less stable than the VIIa conformation. The CH_3-inside conformation may be disregarded because its inner strain is high.

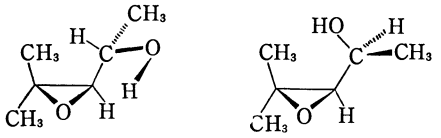

VIIa VIIb

The absence of any absorption below 3600 cm^{-1} and the presence of two ν_{O-H} bands at 3607.4 and 3628 cm^{-1} (Fig. 2 and Table 1) for Compound VII support the above discussion. The absorption at the higher frequency, which is assigned to the free OH group, is weak, and the band at the lower frequency is strong, also suggesting that the O–H···oxirane interaction is an exothermic process to a considerable extent.

In the *erythro* isomer VIII, if the hydroxyl group is to interact with the C–O of the oxirane ring, the methyl-inside conformation (VIIIa) must be taken. This conformation is, however, apparently unfavorable because of the severe interaction between the methyl group at C_3 and the $CH_3CH(OH)$ group. On the other hand, such a repulsive interaction will be less when H-inside conformation (VIIIb) is taken. In the VIIIb conformation, the O–H group may approach the C–C bond of the oxirane ring, but it is impossible for it to approach the C–O of the ring.

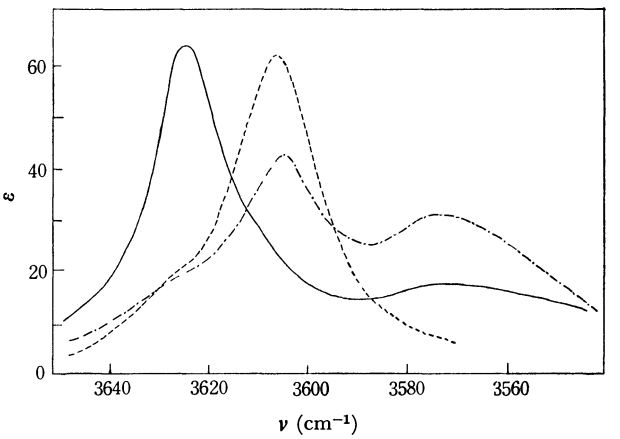

Fig. 2. ν_{O-H} absorption bands of *threo* (VII; ------) and *erythro* (VIII; ——) isomers of 3,4-epoxy-4-methylpentan-2-ol, and *trans*-3,4-epoxypentan-2-ol (IX; —·—).

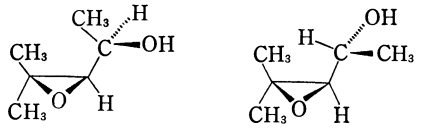

VIIIa VIIIb

In reality, the ν_{O-H} spectrum of VIII shows absorptions at 3623.6 and 3567 cm^{-1}, the former being by far the strongest band. Besides, the presence of a weak band at 3612 cm^{-1} is suggested by the separation of the observed band into symmetrical component bands. The results indicate that the intramolecular interaction between the OH group and the orbitals involved in the C–C bond is a very weak one, if there is any at all. If the C–C bond is really interacting, then Compound VIII should also have shown a strong band attributable to the O–H···oxirane interaction.

The discussions of the stable conformations of the diastereomers given above are also supported by the NMR spectra. The vicinal coupling constants (J_{vic}) of the ring proton with the α-protons of the *threo* and *erythro* isomers were 8.0 and 8.5 Hz respectively. The larger values of J_{vic} suggest that the average torsional angles made by the two $H-C_{methine}$ bonds are large;[10] that is, the populations of the H-inside conformers, VIIa and VIIIb, are large.

The steric effects of the *cis*-methyl group are clear from the spectrum of the *threo* isomer of *trans*-3,4-epoxypentan-2-ol (IX), which corresponds to a compound in which the *cis*-methyl group of the *threo*-3,4-epoxy-4-methylpentan-2-ol (VII) has been removed. IX shows a strong O–H···O-bonded band (Fig. 2), in contrast to the absence of the O–H···O bond in VII.

In view of the above discussions, it seemed that it would be interesting to examine the case where there were no small groups at the α-position of the alcoholic hydroxyl group. Thus, the ν_{OH} spectrum of 3,4-epoxy-

10) K. Tori, T. Kameno, and T. Nakagawa, *J. Org. Chem.*, **29**, 1136 (1964).

2,4-dimethylpentan-2-ol (X) was measured; it gave absorptions at 3617 and 3559.4 cm^{-1}. Apparently the band at the higher frequency can be assigned to the free hydroxyl group,[9] and that at the lower frequency, to the O–H···O bonded form. On the other hand, *trans*-3,4-epoxy-2-methylpentan-2-ol (XI), which lacks the methyl group *cis* to the $C(CH_3)_2OH$, showed absorptions at 3598 and 3566.4 cm^{-1}. Thus, compound X can be regarded as existing as both free and O–H···O interacting species, whereas compound XI exists as both the O–H···oxirane-interacting and the O–H···O-bonded species.

In addition to the fact that the OH-inside conformation of compounds X and XI can be stabilized by forming an O–H···O hydrogen bond, the CH_3-inside conformation (Xa and XIa) is the least stable, because the van der Waals radius of oxygen is smaller than that of the methyl. Thus, in both cases, the O–H···O bonded species exist as the major components.

The cause of the presence of the O–H···oxirane interacting species in XI may be the relative bulkiness

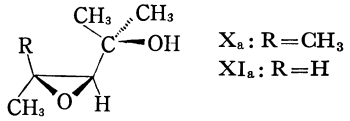

X_a: R=CH_3
XI_a: R=H

of the methyl group and hydrogen. Although the methyl-inside conformations (Xa and XIa) are more unstable than the OH-inside, such a confomration is not prohibitive if R is a hydrogen. If such a conformation is present, the O–H···oxirane interaction can be expected to occur to some extent. The Xa conformation is, however, almost prohibited because of the severe steric repulsion between the two methyl groups.

All the results presented above are explainable if the following two points are assumed: 1) the O–H···oxirane ring interaction takes place between the hydroxyl group and the C–O bond of the oxirane, but the interaction involving the C–C bond of the oxirane is negligible, and 2) the interaction takes place when the OH group approaches the oxirane ring within the plane of the ring.

BULLETIN OF THE CHEMICAL SOCIETY OF JAPAN, VOL. 46, 263—265 (1973)

Macro Rings. V.[1] Syntheses of Tetraoxaparacyclophanes Containing Two Biphenyl Nuclei

Joji NISHIKIDO,[2] Takahiko INAZU,* and Tamotsu YOSHINO

Department of Chemistry, Faculty of Science, Kyushu University, Hakozaki, Higashi-ku, Fukuoka

(Received May 25, 1972)

Three new tetraoxaparacyclophanes containing two biphenyl nuclei connected with oxypolymethyleneoxy bridges in the respective 4,4′-positions, such as 1,5,18,22-tetraoxa[5.0.5.0]paracyclophane I_3, 1,6,19,24-tetraoxa-[6.0.6.0]paracyclophane I_4, and 1,7,20,26-tetraoxa[7.0.7.0]paracyclophane I_5, were synthesized. The UV, IR, and NMR spectra of these paracyclophanes were compared with those of the corresponding open-chain compound, IV_3.

Three paracyclophanes, I_3, I_4, and I_5, in which the 4,4′-positions of two biphenyl molecules are connected with five-, six-, and seven-membered bridges respectively, were synthesized. The IR, UV, and NMR spectral properties of these compounds, I's, and of the corresponding open-chain compounds, IV_3, will be discussed.

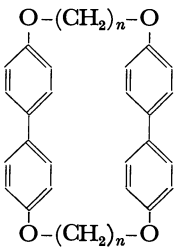

I_3: $n=3$, I_4: $n=4$, I_5: $n=5$.

Fig. 1. Tetraoxaparacyclophanes

The synthetic routes are shown in Schemes 1, 2, and 3. Three portions of a potassium salt of 4,4′-biphenyldiol were treated, respectively, with ethylene-, trimethylene-, and tetramethylene-chlorohydrins to give diols, II's, which were then treated with phosphorous tribromide to give dibromides, III's. The dibromides, III's, were also prepared in considerable yields by the condensation of 4,4′-biphenyldiol with polymethylene dibromides in the presence of potassium carbonate.[3] The dibromides, III's, were reduced with lithium aluminum hydride to IV′ compounds. These compounds were synthesized as reference compounds, which served as open-chain models of the cyclic compounds, I's, in a comparison of their spectra.

Most macrocyclic ethers, known as ansa compounds, are diethers which are generally prepared by the intramolecular condensation of compounds with a

1) Part IV of this series: Y. Urushigawa, T. Inazu, and T. Yoshino, This Bulletin, **44**, 2546 (1971).

2) Present address: KPA Laboratory, Asahi Chemical Industry Co., Ltd., Yokocho, Kawasaki.

* To whom reprint requests should be addressed.

3) R. Adams and L. N. Whitehill, *J. Amer. Chem. Soc.*, **63**, 2073 (1941).

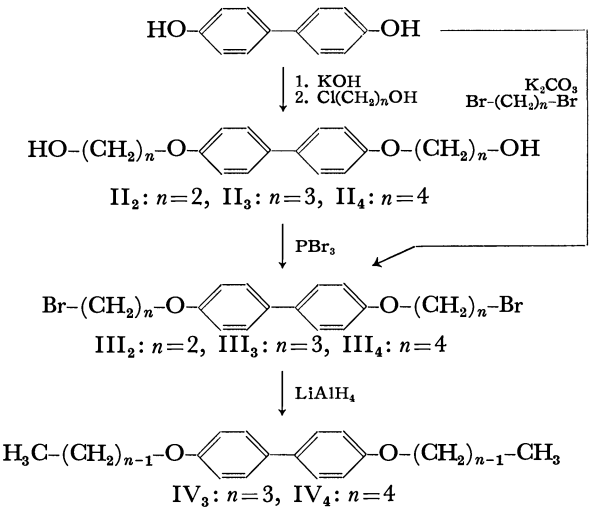

Scheme 1.

phenolic hydroxyl group and a long-chain ω-haloalkyloxy group.[3] Since the compounds to be synthesized in this investigation are tetraethers, though, it was difficult to use this method without alteration in the syntheses of tetraethers. Therefore, as is shown in Scheme 2, the intermolecular double condensation (Procedure A) and the one-step quadruple condensation (Procedure B) were adopted.

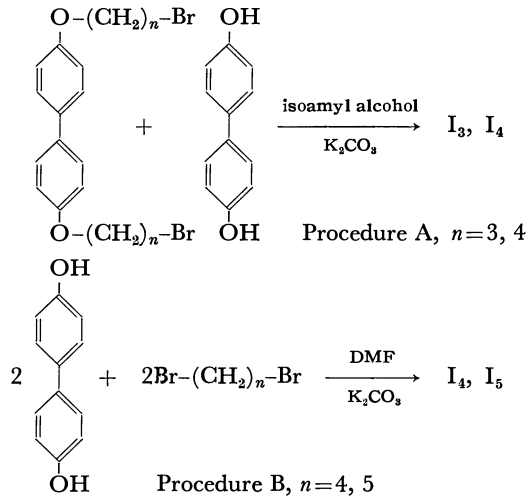

Scheme 2.

In Procedure A, paracyclophanes (I_3, I_4) were synthesized by allowing an equimolar mixture of 4,4′-biphenyldiol and 4,4′-bis(ω-bromoalkyloxy)biphenyl III's to react under high dilution condition. This reaction was carried out by dropping an isoamyl alcohol solution containing the respective reactant into a stirred suspension of anhydrous potassium carbonate in isoamyl alcohol[4] for over 80 hr.

In Procedure B, paracyclophanes (I_4, I_5) were synthesized by dropping, over a 30 hr period, a dimethylformamide solution containing 4,4′-biphenyldiol and polymethylene dibromide into a stirred mixture of anhydrous potassium carbonate in dimethylformamide; the products were thus obtained as crystalline solids. The yields of the cyclic compounds in both procedures were very low, but, unexpectedly, the yields of the products in the procedure B were appreciably higher than those in Procedure A.

In the hope of obtaining the tetraoxa[6.0.6.0]- and tetraoxa[8.0.8.0]paracyclophanes shown in Scheme 3, the intermolecular Wurtz reaction of 4,4′-bis(ω-bromoalkyloxy)biphenyl (III_3, III_4) was attempted under a nitrogen atmosphere both in the presence of a sodium adduct of tetraphenylethylene in tetrahydrofuran at room temperature and in the presence of molten sodium in boiling xylene, but no paracyclophane was obtained in either case.

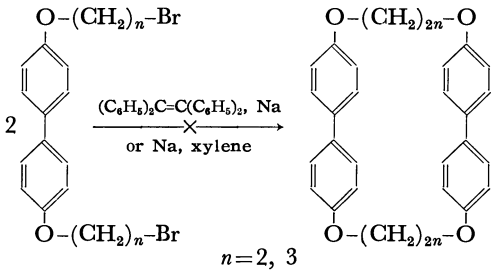

Scheme 3.

The cyclic structures of I_3, I_4, and I_5 were confirmed by their IR, UV, and NMR spectra, by elementary analyses, and by a molecular-weight determination. In the infrared spectra, the absorptions of the cyclic compounds, I's, were more complicated than that of the open-chain model, IV_3, in the 800—900 cm^{-1} region. These bands were used as a diagnosis[5] for the cyclic structure.

The NMR spectra suggest that the conformation of the two biphenyl nuclei in the macro ring may not be fixed rigidly, but may be flexible in a solution at room temperature. The peaks for benzene protons were found to shift upfield by 0.2—0.6 ppm from those of open-chain models, IV's. Among the paracyclophanes, I_3, I_4, and I_5, the peaks for benzene protons exhibited to shift to a higher field with a decrease in the methylene numbers in the oxypolymethyleneoxy bridges. These upfield shifts are due to the shielding by the biphenyl nuclei on the opposite side of the macro ring. The close resemblance of UV spectra of paracyclophanes, I's, to those of the corresponding open-chain models, IV's, reveals that the aromatic rings of I's are planar and that there is no strain in the macro rings.

The problem whether or not other small molecules are included in the empty space of the macrocyclic rings is also interesting; studies of these adducts are now in progress.

Experimental

All the melting points are uncorrected. The ultraviolet spectra were measured on a Hitachi ESP-3T spectrophotometer. The infrared spectra were measured on a Hitachi EPI-S2 spectrophotometer. The NMR spectra were recorded on Hitachi R-20 photometer, using tetramethyl silane as the internal standard and deuterochloroform as the solvent.

4) H. Stetter and E. E. Roos, *Chem. Ber.*, **87**, 566 (1954).

5) D. J. Cram and H. Steinberg, *J. Amer. Chem. Soc.*, **73**, 5961 (1951).

The molecular weights were measured by means of a Hitachi Perkin-Elmer 115 molecular weight apparatus, using benzene as the solvent.

4,4'-Bis(2-bromoethoxy)biphenyl, III_2. A mixture of 2 g (0.011 mol) of 4,4'-biphenyldiol, 8.27 g (0.044 mol) of ethylene bromide, 20 ml of acetone, 2 ml of water, and 5 g of potassium carbonate was refluxed with stirring on a steam-bath for 15 hr, after which an additional 1.75 g of potassium carbonate was added and stirring and refluxing was continued for 20 hr. The acetone was then distilled off with stirring to prevent bumping. The reaction mixture was then washed with water and recrystallized from a dioxane–ethanol mixture. White needles, mp 175—176°C; yield, 1.0 g (24%). Found: C, 48.22; H, 4.14%. Calcd for $C_{16}H_{16}Br_2O_2$: C, 48.03; H, 4.03%.

4,4'-Bis(3-bromopropoxy)biphenyl, III_3. A mixture of 10 g (0.054 mol) of 4,4'-biphenyldiol, 50 g (0.270 mol) of trimethylene dibromide, 40 ml of acetone, 6.7 ml of water, and 36 g of potassium carbonate was stirred and refluxed on a steam-bath for 40 hr. At the end of this period, the acetone was removed, and the reaction mixture was shaken with water. The product was recrystallized from a dioxane–ethanol mixture; white crystals, mp 127—128°C; yield, 13.8 g (60%). Found: C, 52.47; H, 4.94%. Calcd for $C_{18}H_{20}Br_2O_2$: C, 50.49; H, 4.67%.

4,4'-Bis(4-bromobutoxy)biphenyl, III_4. This was prepared in the same way as the corresponding 4,4'-bis(3-bromopropoxy)biphenyl, III_3. From 5 g (0.027 mol) of 4,4'-biphenyldiol, 25 g (0.107 mol) of tetramethylene dibromide, 15 ml of acetone, 3.4 ml of water, and 18 g of potassium carbonate, 8 g (65%) of a product was obtained; white crystals, mp 136°C. Found: C, 52.37; H, 5.26%. Calcd for $C_{20}H_{24}Br_2O_2$: C, 52.66; H, 5.30%.

4,4'-Dipropoxybiphenyl, IV_3. A suspension of 500 mg of the III_2 dibromide in 100 ml tetrahydrofuran was stirred, and then the solution was added, drop by drop, into a mixture of excess lithium aluminum hydride in 50 ml of tetrahydrofuran at room temperature; after stirring for an additional 1.5 hr, the mixture was refluxed for 6 hr. After cooling, the mixture was treated with water and extracted with benzene. The removal of the benzene under reduced pressure gave a white powder, which was recrystallized from an ethanol–benzene mixture to give 170 mg (55% yield) of a white crystalline powder; mp 156—158°C. NMR; 7.23 ppm (8H, quartet, aromatic), 3.955 (4H, triplet, O-**CH_2**), 1.85 (4H, quintet, O-CH_2-**CH_2**-CH_3), 1.05 (6H, triplet, O-CH_2-CH_2-**CH_3**). IR; 1609 cm^{-1} (m, ν_{ip} C=C), 1501 (s, ν_{ip} C=C), 1242 (s, ν_{as} C-O-C), 824 (s, δ_{op} H-C_{arom}). UV; λ_{max} 267 nm, $\varepsilon_{max}=5.9\times10^3$.

4,4'-Dibutoxybiphenyl, IV_4. This compound was prepared in exactly the same manner as the 4,4'-dipropoxybiphenyl, IV_3. The product was white crystals; mp 145—146°C. Yield, 60%.

1,5,18,22-Tetraoxa[5.0.5.0]paracyclophane, I_3. Into a 3 liter, four-necked reaction flask of the high-dilution apparatus, we placed 650 ml of dry isoamyl alcohol and 8 g of finely-powdered, anhydrous potassium carbonate which had been heated in an open dish over a free flame for 30 min. A solution of 2.997 g (0.007 mol) of 4,4'-bis(3-bromopropoxy)-biphenyl III_3 and 1.303 g (0.007 mol) of 4,4'-biphenyldiol in 850 ml of dry isoamyl alcohol was then introduced into a boiling alcohol–potassium carbonate mixture over an 85 hr period. A current of nitrogen was run through the circulatory system in order to minimize any oxidation of the 4,4'-biphenyldiol which might take place. After having been stirred and heated for an additional hour, the reaction mixture was allowed to cool, filtered to remove the inorganic salts present, and evaporated under diminished pressure on a water pump until only traces of the isoamyl alcohol remained. The dark, viscous material remaining was placed in a Soxhlet extractor and partially extracted with petroleum ether for 18 hr. A pale yellow mass remaining in the Soxhlet extractor was recrystallized form benzene to give white needles. Mp above 280°C; yield, 22 mg (0.7%). NMR; 6.80 ppm (16H, quartet, aromatic), 4.25 (8H, triplet, O-**CH_2**), 2.05 (4H, multiplet, O-CH_2-**CH_2**-CH_2-O). IR; 1609 cm^{-1} (m, ν_{ip} C=C), 1497 (s, ν_{ip} C=C), 1224 (s, ν_{as} C-O-C), 817 (s, δ_{op} H-C_{arom}). UV; λ_{max} 263 nm, $\varepsilon_{max}=1.1\times10^4$. Found: C, 79.76; H, 6.37%; mol wt, 452.1. Calcd for $C_{30}H_{28}O_4$: C, 79.62; H, 6.24%; mol wt, 452.5.

1,6,19,24-Tetraoxa[6.0.6.0]paracyclophane, I_4. *Method A*: This compound was prepared in the same way as the corresponding cyclic ether, I_3. In the reaction flask we placed 650 ml of dry isoamyl alcohol and 7 g of powdered potassium carbonate which had been heated to a red heat for 30 min. A solution of 3.194 g (0.007 mol) of 4,4'-bis(4-bromobutoxy)-biphenyl, III_4, and 1.303 g (0.007 mol) of 4,4'-biphenyldiol in 850 ml of dry isoamyl alcohol was then added to the boiling alcohol–potassium carbonate mixture over an 80 hr period. The product consisted of white prisms. Mp 235—236°C; yield, 13 mg (0.4%). NMR; 6.87 ppm (16H, quartet, aromatic), 4.16 (8H, multiplet, O-**CH_2**), 1.90 (8H, multiplet, O-CH_2-**CH_2**-**CH_2**-CH_2-O). IR; 1607 cm^{-1} (m, ν_{ip} C=C), 1496 (s, ν_{ip} C=C), 1245 (s, ν_{as} C-O-C), 820 (s, δ_{op} H-C_{arom}). UV; λ_{max} 264 nm, $\varepsilon_{max}=1.3\times10^4$. Found: C, 79.96; H, 6.74%; mol wt, 488.8. Calcd for $C_{32}H_{32}O_4$: C, 79.97; H, 6.71%; mol wt, 480.6.

Method B: A solution of 3.30 g (0.018 mol) of 4,4'-biphenyldiol and 3.82 g (0.018 mol) of tetramethylene dibromide in 800 ml of dimethylformamide was added, from a dropping funnel and over a 30 hr period, to a suspension of 30 g of potassium carbonate in 600 ml of dimethylformamide, the temperature being kept at 130°C. After stirring and heating for an additional hour, the reaction mixture was cooled, filtered to remove the inorganic salts, and then concentrated to about 400 ml. It was then placed in an ice box and allowed to stand overnight. Crystals were deposited. The material was crystallized from dimethylformamide to give white prisms. Yield, 320 mg (3.8%). The IR and NMR spectra of this compound were in accord with those of the cyclic compound, I_4, prepared by Method A.

1,7,20,26-Tetraoxa[7.0.7.0]paracyclophane, I_5. A solution of 4.66 g (0.0025 mol) of 4,4'-biphenyldiol and 5.75 g (0.025 mol) of pentamethylene dibromide in 800 ml of dimethylformamide was added, through a dropping funnel and over a 30 hr period, to a suspension of 30 g of potassium carbonate in 700 ml of dimethylformamide, the temperature being kept at 130°C. After stirring and heating for an additional hour, the reaction mixture was cooled, filtered to remove the inorganic salts, and concentrated to about 400 ml. It was then placed in the ice box and allowed to stand overnight. Crystals were deposited. The material was crystallized from dimethylformamide to give white needles. Mp 236°C; yield, 200 mg (3.1%). NMR: 6.98 ppm (16H, quartet, aromatic), 4.05 (8H, multiplet, O-**CH_2**), 1.75 (12H, multiplet, O-CH_2-**CH_2**-**CH_2**-**CH_2**-CH_2-O). IR; 1600 cm^{-1} (m, ν_{ip} C=C), 1495 (s, ν_{ip} C=C), 1227 (s, ν_{as} C-O-C), 812 (s, δ_{op} H-C_{arom}). UV; λ_{max} 265 nm, $\varepsilon_{max}=1.4\times10^4$. Found: C, 80.70; H, 7.30%; mol wt, 471.8. Calcd for $C_{34}H_{36}O_4$: C, 80.28; H, 7.13%; mol wt, 508.6.

This work was supported in part by a grant of the Ministry of Education and a grant of Takeda Science Foundation.

Syntheses of L-Threose and Methyl Di-*O*-acetyl-L-threuronate from *dextro*-Tartaric Acid

Gen NAKAMINAMI, Haruo EDO, and Masazumi NAKAGAWA

Department of Chemistry, Faculty of Science, Osaka University, Toyonaka, Osaka, 560

(Received June 2, 1972)

Reduction of methyl hydrogen di-*O*-acetyl-*dextro*-tartrate (I) with sodium borohydride in water afforded L-threono-γ-lactone (II). L-Threose (IV) was obtained on treatment of the γ-lactone (II) with an excess of disiamylborane. Reduction of ester chloride of di-*O*-acetyl-*dextro*-tartaric acid (VI) with tri-*n*-butyltin hydride yielded methyl di-*O*-acetyl-L-threuronate (VII). Attempts to reduce 2-deoxy-pentarate ester (X) derived from ester chloride (VI) *via* diazoketone (VIII) with sodium borohydride to give 2-deoxy-*threo*-pentono-γ-lactone (XI) gave unsatisfactory results. Formation of methyl L-*threo*-2,3-di-*O*-acetyl-5-chloro-5-deoxy-4-*C*-hydroxymethyl-4,4′-anhydropentonate (IX) in addition to diazoketone (VIII) was observed when ester chloride (VI) was treated with an excess of diazomethane. On the basis of the observed (—)-Cotton effect in the 290 nm region of ORD and CD spectra of L-threose (IV) and D-erythrose, possibility of the presence of an open chain non-hydrated *aldehyde*-form of aldotetrose in water was discussed.

dextro-Tartaric acid has been used widely as a starting material for syntheses of carbohydrates and their derivatives. L-Threuronate derivative (VII) was prepared by the Rosenmund reduction of ester chloride of *dextro*-tartaric acid derivative (VI).[1] Further reduction of VII with sodium amalgam afforded L-theritol *via* L-threonic acid.[1] Syntheses of L-threonolactone (II) and L-threuronate derivative (VII) have been achieved by the reduction of VI with tri-*tert*-butoxyaluminohydride.[2] The conversion of *dextro*-tartaric acid into L-apiose has been reported by Weygand and Scmiechen.[3]

We describe here some experiments to synthesize sugars and derivatives starting from *dextro*-tartaric acid carried out with the purpose of exploring the utility of complex hydride in carbohydrate chemistry.

It has been recognized that uronate esters could be reduced with sodium borohydride, in contrast to the failure of reduction of usual esters.[4] Treatment of monoethyl ester of *dextro*-tartaric acid with a large excess of sodium borohydride in anhydrous ethanol resulted in a partial recovery of the monoester accompanied by *dextro*-tartaric acid, hydrolysate of the ester. However, methyl hydrogen di-*O*-acetyl-*dextro*-tartrate (I) could be reduced to L-threono-γ-lactone (II) on treatment with sodium borohydride in water. The product obtained by the reaction of I (1 mol) with sodium borohydride (3.5 mol) in water was hydrolyzed without isolation with potassium hydroxide. Distillation of the hydrolysate *in vacuo* yielded crystalline L-threono-γ-lactone (II) in a 74% yield. Reduction of I could not be observed with the hydride in ethanol. The hydride in a mixture of ethanol and water afforded II in a low yield (47%). Facile reduction of I can reasonably be attributed to an enhanced electrophilicity of methoxycarbonyl funciton caused by the introduction

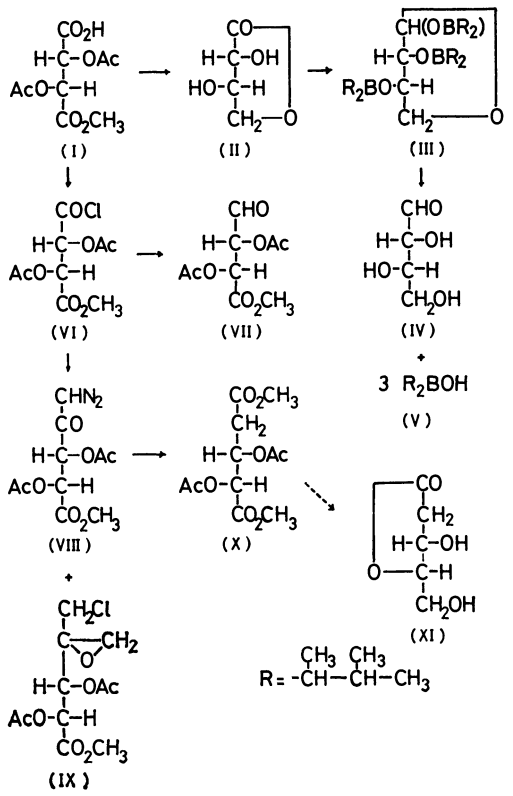

of electron withdrawing acetyl groups.[5] The present procedure of reduction of *dextro*-tartaric acid derivative (I) is more convenient and more practical than the older procedures[1,2] and L-threono-γ-lactone (II) can be obtained in a much higher yield.

Sodium borohydride reduction of aldono-γ-lactone to aldose proposed by Wolfrom and his co-workers[6] has been applied successfully to various aldonic acid lactones.[7] Usually, the reduction is performed in a weakly acidic buffer solution to avoid hydrolysis of the lactone ring. The reduction of II with an excess of

1) H. J. Lucas and W. Baumgarten, *J. Amer. Chem. Soc.*, **63**, 1653 (1941).

2) H. J. Bestmann and R. Schmiechen, *Chem. Ber.*, **94**, 751 (1961).

3) F. Weygand and R. Schmiechen, *ibid.*, **92**, 535 (1959).

4) For review, see "Neuere Methoden der Präparativen Organischen Chemie," Bd. IV, ed. by W. Foerst, Verlag Chemie, GmbH, Weinheim (1966), p. 200.

5) *Cf.*, J. A. Meschino and C. H. Bond, *J. Org. Chem.*, **28**, 3129 (1963).

6) M. L. Wolfrom and H. B. Wood, *J. Amer. Chem. Soc.*, **73**, 2933 (1951); M. L. Wolfrom and K. Anno, *ibid.*, **74**, 5583 (1952).

7) See, Ref. 4, p. 207.

sodium borohydride (2–12 equivalents) in the presence of boric acid or boric acid and Amberlite IR 120 (H^+)[8] gave unsatisfactory results. Although the formation of L-threose (IV) could only be detected by a weak spot on tlc, predominent formation of by-products was observed in the case of a large excess of the reducing agent and a large amount of II was recovered in the case a slight excess of the hydride. Bis(1,2-dimethylpropyl)borane (disiamylborane) has been used in the reduction of γ-lactones to γ-hydroxyaldehydes.[9] In view of the success of reduction of 2-deoxy-*erythro*-pentono-γ-lactone to 2-deoxy-*erythro*-pentose with the same borane,[10] the reaction of II with an excess of disiamylborane in tetrahydrofuran was performed at room temperature. After borinate ester (III) formed had been hydrolyzed on addition of water, disiamylborinic acid (V) was removed by extraction with ether. L-Threose (IV) was obtained from the aqueous layer as a syrup in a quantitative yield. No crystalline D- or L-threose has so far been obtained, and the crystalline D-threose reported by Freudenberg[11] which showed positive specific rotation appears to be in error.[12] The specific rotation of syrupy L-threose (IV) thus obtained and the melting point of its benzoylhydrazone agreed with the reported values (Table 1). The overall yield of L-threose (IV) from *dextro*-tartaric acid was found to be 46%. The present method seems to be superior to the reported methods in view of the simplicity of procedure and the high yield. The Wohl degradation of L-xylose derivative obtained from sorbitol to give L-threose (IV) requires several steps[16] and the glycol-cleavage of 1,3-benzylidene-L-arabitol derived from L-arabinose affords L-threose (IV) in a lower yield (36% based on L-arabinose).[15,17,18b]

Table 1. Specific rotations of IV and melting point of benzoylhydrazone of IV

	Found	Lit. values
$[\alpha]_D$ (in H_2O)	+12.2° (initial)→ +12.6° (after 3 days)	D-form: −12.3°[13]
		−11°[14]
		−11.6°[15]
		L-form: +12.5°[15]
		+13.1°[16]
Mp of benzoylhydrazone	167.5—169.0°C	L-form: 167—168°C (decomp.)[14]

Reduction of ester chloride (VI) with tri-*n*-butyltin hydride which proved to be an useful reagent in the conversion of acid chloride into aldehyde[19] afforded methyl di-*O*-acetyl-L-threuronate (VII) as a liquid. Although attempts to crystallize VII by means of vacuum distillation or chromatography on silica gel or alumina failed, liquid VII gave crystalline 2,4-dinitrophenylhydrazone in a 38% yield based on VI.

As stated previously, introduction of the acetoxyl group into a position adjacent to the alkoxycarbonyl group facilitates sodium borohydride reduction of the alkoxycarbonyl group to the hydroxymethyl group. Consequently, it was anticipated that 2-deoxy-pentarate ester (X) which could be derived from ester chloride (VI) *via* diazoketone (VIII) by a photochemical rearrangement[3] might afford 2-deoxy-*threo*-pentono-γ-lactone (XI) by a preferential reduction of the methoxycarbonyl group at 5-position. However, the reaction of X (1 mol) with various amounts of sodium borohydride (2.5—5.0 mol) in different solvents (water, methanol, tetrahydrofuran, or 2-propanol) gave unsatisfactory results. Only removal of acetyl groups was observed in the case of methanol solution. Treatment of X in tetrahydrofuran with the hydride resulted in a recovery of X. The reaction product obtained on treatment of X with the hydride in water or 2-propanol gave syrupy material after deacetylation by the ester-exchange reaction followed by hydrolysis of methyl ester groups. The syrup gave a weak spot corresponding to an authentic specimen of XI together with several spots of by-products. Since crystalline diazoketone (VIII), precursor of 2-deoxy-pentarate ester (X), could be scarcely obtained when the reaction of diazomethane with ester chloride (VI) had been carried out according to the reported method,[3] ester chloride (VI) was treated with an excess of diazomethane. The product was subjected to chromatography on silica gel which resulted in the separation of diazoketone (VIII) and another crystalline compound. The structure of epoxide ester (IX) could be assigned to the crystalline compound on the basis of elemental analysis and IR and NMR spectroscopic data. The NMR spectrum of IX in deuteriochloroform exhibited singlets at δ 2.91 (2H) and δ 3.73 (5H) which could be assinged to methylene protons of the epoxide ring, and protons of methyl in the ester and chloromethyl groups, respectively. The NMR spectrum of IX measured in benzene afforded more confirmative evidence, *i.e.*, methylene protons in the epoxide ring exhibited AB quartet [centered at δ 1.84 and 1.92 (J=10.2 Hz)], and protons of the chloromethyl group also split in AB quartet [centered at δ 2.88 and 2.93 (J=12.4 Hz)]. IX also gave a positive test for sodium thiosulfate-phenolphthalein reagent[20] indicating the presence of epoxide ring. The epoxy-ester (IX) may be formed by the reaction of diazoketone (VIII) with

8) H. L. Frush and H. S. Isbell, *J. Amer. Chem. Soc.*, **78**, 2844 (1956).
9) H. C. Brown and D. B. Bigley, *ibid.*, **83**, 486 (1961); H. C. Brown, D. B. Bigley, S. K. Arora, and M. M. Yoon, *ibid.*, **92**, 761 (1970).
10) G. Nakaminami, S. Shioi, Y. Sugiyama, S. Isemura, M. Shibuya, and M. Nakagawa, This Bulletin, **45**, 2624 (1972).
11) W. Freudenberg, *Ber.*, **65**, 168 (1932).
12) R. C. Hockett, *J. Amer. Chem. Soc.*, **57**, 2265 (1935).
13) R. C. Hockett, *ibid.*, **57**, 2260 (1935).
14) L. Hough and T. J. Taylor, *J. Chem. Soc.*, **1955**, 1212.
15) K. Gätzi and T. Reichstein, *Helv. Chim. Acta*, **21**, 195 (1938).
16) K. Iwadare, S. Fukunaga, and B. Kubota, This Bulletin, **12**, 116 (1937).
17) M. Steiger and T. Reichstein, *Helv. Chim. Acta*, **19**, 1016 (1936).
18) A. S. Perlin, "Methods in Carbohydrate Chemistry," Vol. 1, ed. by R. L. Whistler and M. L. Wolfrom, Academic Press, New York and London (1962), (a) p. 64; (b) p. 68.
19) L. F. Fieser and M. Fieser, "Reagents for Organic Synthesis," John Wiley & Sons, Inc., New York, London and Sydney (1967), p. 1193.
20) W. C. J. Ross, *J. Chem. Soc.*, **1950**, 2257; J. M. Ross, D. S. Tarbell, W. E. Lovett, and A. D. Cross, *J. Amer. Chem. Soc.*, **78**, 4675 (1956).

hydrogen chloride liberated[21] and another mole of diazomethane.[22]

Finally we wish to give some remarks on the optical rotatory properties of some compounds related to aldotetrose. L-Threono-γ-lactone (II) exhibited a negative Cotton effect in the ORD and CD spectra in agreement with the general rule proposed by Okuda, Harigaya, and Kiyomoto.[23] They concluded that the sign of the Cotton effect of aldonolactones is governed by the configuration of carbon atom at 2-position, *i.e.*, (*R*)- and (*S*)-configurations at 2-position gave negative and positive Cotton effects, respectively. The observed negative Cotton effect of L-threono-γ-lactone (II) is consistent with the (*R*)-configuration at 2-position.

An aqueous solution of L-threose (IV) obtained by the disiamylborane reduction of II showed a small negative Cotton effect at *ca.* 290 nm. Cantor and Peniston carried out polarographic studies on aqueous solution of carbohydrates and pointed out the presence of species reducible at dropping mercury cathode and estimated the amount of the reducible form.[24] They considered that the reducible species should be of *aldehydo*-form or its hydrated species of carbohydrates.[24] It was revealed later that the ORD spectra of aqueous solution of aldopentoses and aldohexoses usually exhibit a simple curve in a wavelength region longer than 210 nm and no Cotton effect can be observed in the region of $n\rightarrow\pi^*$ transition of carbonyl of aldehyde group.[25] In spite of the high content of the reducible form,[24] D-ribose also showed no Cotton effect in the region of carbonyl $n\rightarrow\pi^*$ transition. Thus, complete hydration of the free aldehyde group in open chain form of aldopentose or aldohexose was concluded.[26] L-Threose (IV) obtained by acid hydrolysis of an authentic 2,4-*O*-benzylidene-L-threose[18b] also showed a negative Cotton effect at *ca.* 290 nm. This indicates that the negative Cotton effect observed in L-threose (IV) derived from II can not be ascribed to the presence of any carbonyl containing impurity, but is an inherent property of IV (Fig. 1 and Table 2). The signal at δ 9.44 (singlet) in the NMR spectrum of L-threose (IV) in deuterium oxide can presumably be attributed to the proton of the free aldehyde group. Recently, the presence of a weak Cotton effect in the CD spectrum of D-erythrose in water was briefly reported.[27] This was confirmed by the present authors employing a syrupy D-erythrose obtained by the hydrolysis of crystalline 2,4-*O*-ethylidene-D-erythrose[18a] (Fig. 1 and Table 2). *glycero*-Tetrulose appears to be the most probable impurity of these aldotetroses. Rearrangement of L-threose or D-erythrose should result in L- or D-*glycero*-tetrulose, respectively. However, studies on *glycero*-tetrulose revealed that the L-isomer exhibits a positive and the D-isomer a negative Cotton effect in their ORD spectra.[28] Consequently, the negative Cotton effect of L-threose can not be attributed to the presence of L-*glycero*-tetrulose as an impurity. 2,4-*O*-Ethylidene-D-erythrose, starting material for the preparation of D-erythrose, shows a weak negative Cotton effect ($\Delta\varepsilon$ — 0.021) at 293 nm in water. Therefore, we can not hold the presence of a small amount of 2,4-*O*-ethylidene-D-erythrose as an impurity to be responsible for most of the observed negative Cotton effect of D-erythrose.

Tetrose may contain more of the open chain form than pentose and hexose in the ring-chain equilibrium, because furanose, the cyclic form of aldotetrose, is known to be less stable than pyranose. The observed Cotton effect in the region of $n\rightarrow\pi^*$ transition of the carbonyl group seems to indicate that some part of the open chain form of aldotetrose exists in non-hydrated *aldehydo*-form.

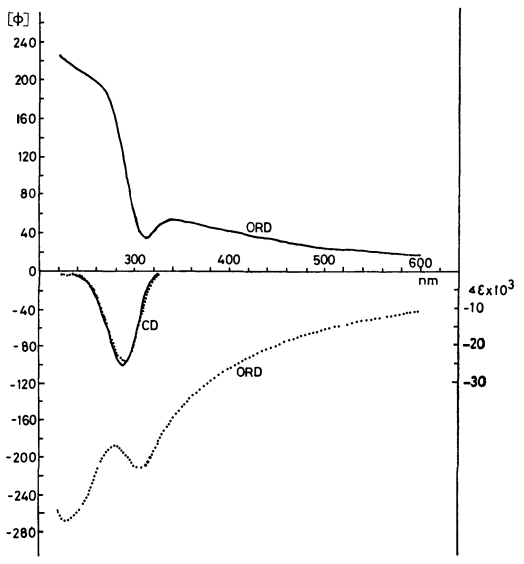

Fig. 1. ORD and CD spectra of L-threose (IV) (——) and D-erythrose (……) in water.

TABLE 2. ORD AND CD SPECTRA OF L-THREOSE (IV) AND D-ERYTHROSE

	ORD in H_2O[a]		CD in H_2O[b]
	$[\phi]_{min}$	$[\phi]_{max}$	$\Delta\varepsilon_{max}$
L-Threose	+ 35° (312 nm)	+188° (268 nm)[c]	−0.024 (288 nm)
D-Erythrose	−213° (304 nm)	−189° (278 nm)	−0.024 (290 nm)

a) L-Threose: after 3 days, measured at 20°C. D-Erythrose: after 24 hr, measured at 15°C.
b) L-Threose: after 30 hr. D-Erythrose: after a week.
c) Inflection.

21) *Cf.*, W. E. Bachmann and W. S. Struve, "Organic Reactions," Vol. 1, ed. by R. Adams, John Wiley & Sons, Inc., New York (1942), p. 38.
22) *Cf.*, C. D. Gutsche, "Organic Reactions," Vol. 8, ed. by R. Adams, John Wiley & Sons, Inc., New York (1954), p. 364.
23) T. Okuda, S. Harigaya, and A. Kiyomoto, *Chem. Pharm. Bull.* (Tokyo), **12**, 504 (1964).
24) S. M. Cantor and Q. P. Peniston, *J. Amer. Chem. Soc.*, **62**, 2113 (1940).
25) I. Listowsky, G. Avigad, and S. Englard, *ibid.*, **87**, 1765 (1965) and referances cited therein.
26) N. Pace, C. Tanford, and E. A. Davidson, *ibid.*, **86**, 3160 (1964).
27) T. M. Feeley, M. K. Hargreaves, and D. L. Marshall, *Tetrahedron Lett.*, **1968**, 4831.
28) T. Sticzay, C. Peciar, K. Babor, M. Fedoroňks, and K. Linek, *Carbohyd. Res.*, **6**, 418 (1968).

Experimental

The melting points were measured on a Mettler FP2 apparatus and uncorrected. The IR spectra were obtained on a Hitachi EPI-2 Spectrophotometer, the ORD and CD spectra on a Yanagimoto ORD-185, a JASCO ORD/UV-5 and a Roussel-Juan Dichrograph and the NMR spectra on a Varian A-60 or T-60 spectrometer using tetramethylsilane or sodium 2,2-dimethyl-2-silapentane-5-sulfonate as an internal standard, unless otherwise stated. Commercial silica gel (E. Merck, Darmstadt, Germany, 70—325 mesh) was immersed in 60% aqueous acetic acid and kept standing overnight. The gel was collected by suction filtration and washed thoroughly with water until the filtrate gave neutral test, and dried at 120°C for 15 hr. The silica gel thus treated was used in chromatography.

L-Threono-γ-lactone (II). To an ice-cooled and stirred solution of sodium borohydride (991 mg, 28.3 mmol) in water (15 ml) was added dropwise a solution of half-ester of di-*O*-acetyl-*dextro*-tartaric acid[1] (I, 2.0 g, 8.06 mmol) in water (23 ml). After the mixture had been stirred for 4 hr at room temperature, 2N hydrochloric acid (20 ml) was added and the water was removed under reduced pressure. Methanol was added to the residue and concentrated under reduced pressure. The procedure was repeated 3 times to complete the removal of boric acid as its methyl ester. Extraction of the residue with acetone gave an oily material (1.54 g), which was dissolved in methanol (15 ml) and mixed with potassium hydroxide (2.5 g, 45 mmol) in water (5 ml). The mixture was kept at room temperature for 15 min and then refluxed for 1 hr. 2N Hydrochloric acid (22 ml) was added to the cooled reaction mixture. The residue obtained by evaporating the water *in vacuo* was extracted with ethyl acetate. The oily material (998 mg) obtained from the extract was subjected to a vacuum distillation (0.088 mmHg). The fraction obtained from *ca.* 148°C (bath temp.) crystallized on standing. The crystals were washed with a small amount of ethyl acetate to yield fairly pure II (700 mg, 74%). Recrystallization from the same solvent afforded pure II, mp 67—69°C (lit. values: mp 65—68°C[29]; mp 61—64°C[2]), IR (Nujol mull): 3400 (O–H), 1770 (C=O) cm^{-1}, $[\alpha]_D^{17}=+46.7°$ (*c*, 1.54, CH_3OH) (lit. values: $[\alpha]_D^{21}=+47.0°$[29]; $[\alpha]_D^{19}=+51.2°$[30]), $[\phi]_{min}=-5210°$ (239.5 nm), $\Delta\varepsilon_{max}=-3.59$ (222.5 nm) (*c*, 2.11×10^{-3} mol/l, CH_3OH).

Found: C, 40.59; H, 5.14%. Calcd for $C_4H_6O_4$: C, 40.68; H, 5.12%.

Phenylhydrazide. Colorless plates, mp 153—157°C (lit. value: mp 161—161.5°C[29]).

Found: C, 52.98; H, 6.35; N, 12.16%. Calcd for $C_{10}H_{14}N_2O_4$: C, 53.09; H, 6.24; N, 12.38%.

L-Threose (IV). A solution of disiamylborane in tetrahydrofuran was prepared according to the usual method from a solution of 2-methyl-2-butene (4.275 g, 61.1 mmol) in the same solvent (15 ml) and a stock solution of diborane (34.2 ml, 0.445 mmol/ml, 15.2 mmol). To this was added dropwise under ice-cooling a solution of γ-lactone (II, 300 mg, 2.54 mmol) in the same solvent (12 ml) in nitrogen atmosphere. After the mixture had been kept at room temperature for 18 hr, water (1 ml) was added under stirring to the ice-cooled reaction mixture to decompose the excess of disiamylborane. It was then mixed with a further amount of water (60 ml) and stirred for 30 min at room temperature to hydrolyze borinate ester (III). The mixture was extracted with ether (25 ml×3) to remove disiamylborinic acid (V). The ethereal extract was washed with water (25 ml). The combined aqueous layer and washing were concentrated under reduced pressure. The residue was mixed with methanol and the solvent was removed *in vacuo*. After the procedure had been repeated 3 times, the residue was dried in an evacuated desiccator containing phosphorus pentoxide to give an almost colorless syrup (325 mg, $[\alpha]_D^{20}=+12.2°$ (initial)→ $+12.6°$ (after 3 days) (*c*, 2.55, H_2O)). The syrup was converted into crystalline benzoylhydrazone according to the reported method.[14] Syrupy L-threose (IV, 48 mg) gave 60 mg (63%) of benzoylhydrazone. Recrystallization from ethanol gave pure hydrazone as colorless fine needles, mp 167.5—169.0°C. IR (Nujol mull): 3500, 3360, 3240 (O–H, N–H); 1647 (amide-I): 1551 (amide-II) cm^{-1}.

Found: C, 55.44; H, 6.01; N, 11.74%. Calcd for $C_{11}H_{14}N_2O_4$: C, 55.45; H, 5.92; N, 11.76%.

Methyl Di-O-acetyl-L-threuronate (VII). A solution of acid chloride (VI,[3] 2.30 g, 8.63 mmol) in tetrahydrofuran (16 ml) was added to tri-*n*-butyltin hydride[31] (2.64 g, 9.07 mmol) over a period of 15 min. After stirring for 100 min, the solvent was removed under reduced pressure. The residue was mixed with petroleum benzine and water and the aqueous layer was washed twice with petroleum benzine. The combined benzine solution was washed with water. The combined aqueous layer was concentrated under reduced pressure to *ca.* 50 ml. The concentrated solution was treated with active charcoal–celite (1:1) and the filtrate was evaporated under reduced pressure. The residue was dried in an evacuated desiccator over phosphorus pentoxide to afford almost colorless syrup (1.57 g). A mixture of the syrup (116 mg), 2,4-dinitrophenylhydrazine (98 mg) and ethanol (3 ml) was refluxed for 3 hr. The crude crystals deposited were dissolved in benzene and the solution was passed through a short column of alumina. The crystals (99 mg, 38% based on acid chloride (VI)) were recrystallized from ethanol to give an analytical specimen, aggregate of yellow needles, mp 146.5—148.0°C (lit. value:[1] 148°C).

Found: C, 43.83; H, 3.94; N, 13.73%. Calcd for $C_{15}H_{16}N_4O_{10}$: C, 43.69; H, 3.91; N, 13.59%.

Methyl L-threo-*2,3-Di-O-acetyl-5-chloro-5-deoxy-4-C-hydroxymethyl-4,4'-anhydro-pentonate (IX).* Acid chloride (VI,[3] 0.0353 mol) was treated with diazomethane (0.107 mol) according to the reported method.[3] Crystalline diazoketone (VIII) obtained by evaporating the solvent under reduced pressure was filtered. Syrupy filtrate was dissolved in benzene–ethyl acetate (8: 2) and chromatographed on silica gel. Epoxy compound (IX) obtained from early fractions crystallized immediately (mp 63—79°C). Farther elution with the same mixed solvent afforded an additional diazoketone (VIII). Change of melting point of IX could not be observed after recrystallization from diisopropyl ether, ethyl acetate, or ether–petroleum benzine. IX gave immediate red coloration for cold sodium thiosulfate-phenolphthalein reagent[20] indicating the presence of the epoxide ring.

Found: C, 45.05; H, 5.08; Cl, 11.95%. Calcd for $C_{11}H_{15}O_7Cl$: C, 44.83; H, 5.13; Cl, 12.03%.

Financial support from Mr. Tokusuke Egawa, president of Kofuku-sogo Bank, is gratefully acknowledged.

29) K. Gätzi and T. Reichstein, *Helv. Chim. Acta*, **20**, 1298 (1937).
30) J. M. Perel and P. G. Dayton, *J. Org. Chem.*, **25**, 2044 (1960).
31) M. Ohara and R. Okawara, *J. Organometal. Chem.*, **3**, 484 (1965).

Hetera-*p*-carbophanes. I. Hetera-*p*-carbophanes Containing Two Amide Groups

Kazuhiko SAKAMOTO and Michinori ŌKI[1)]

Department of Chemistry, Faculty of Science, The University of Tokyo, Hongo, Tokyo

(Received June 9, 1972)

Several hetera-*p*-carbophanes containing two amide groups in the ansa chain were synthesized by the high-dilution method. Those which have shorter ansa chains than 15 atoms show no sign of the internal rotation of the benzene ring, even at higher temperatures, whereas that which has the ansa chain of 16 atoms shows no sign of the freezing of the motion, even at lower temperatures. The infrared spectra of these compounds suggest that the amide groups in these compounds exist as the *s-cis* conformation.

The restricted rotation of an aromatic ring in paracyclophanes was first demonstrated by the optical resolution of oxygen-containing hetera-*p*-carbophanes[2)] by Lüttringhaus.[3)] Later, Cram and his co-worker succeeded in resolving a [2.2]paracyclophane derivative,[4)] and Blomquist *et al.* reported the first resolution of carbo-*p*-carbophanes in 1961.[5)] A faster but still hindered rotation can, of course, be observed by the dynamic nuclear magnetic resonance technique. Thus, Cope *et al.* published a paper on the hindered rotation of an olefinic cyclophane (I) using the nonequivalence-collapse of the aromatic and aliphatic protons.[6)] On the other hand, Nakazaki *et al.* studied the nonequivalence of protons of an XCH_2 group which is attached to the benzene ring of a paracyclophane (II).[7)]

In general, paracyclophanes should have nonequivalent benzylic methylene protons, provided that the aromatic ring is unsymmetrically substituted and the rotation of the ring is slow enough on the NMR time scale. Actually, Cope *et al.* pointed out that the benzylic protons of I were nonequivalent.[6)] In the compounds of the type of II, the conformational distribution will, in principle, vary with the temperature because the stabilities of three rotamers concerned with the internal rotation about the C_{arom}–C_{CH_2X} bond are different. Thus, it is the authors' opinion that much more study is needed to clarify the various effects on the rate of the rotation of the aromatic ring in paracyclophanes and in order to discuss the effect of the variation in the population of the rotamers on the apparent barriers to the internal rotation.

This paper will deal with the syntheses and some spectroscopic properties of 10 hetera-*p*-carbophanes (III and IV) as the first probe of a series. The reason for the selection of these compounds is the simplicity of the analysis of the line shape. The rigidity and the mobility of these compounds as revealed by NMR spectroscopy will be reported.

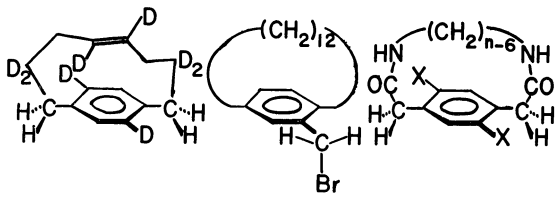

I II III_n X=H (n=12—16)
IV_n X=Me (n=12—16)

Experimental

Syntheses. The hetera-*p*-carbophanes, III_n and IV_n,[8)] were synthesized by the high-dilution method from the corresponding 1,4-phenylenediacetyl dichloride and α,ω-diamines. The routes of the syntheses of the former are depicted in Scheme 1, while the latter compounds were of commercial origin.

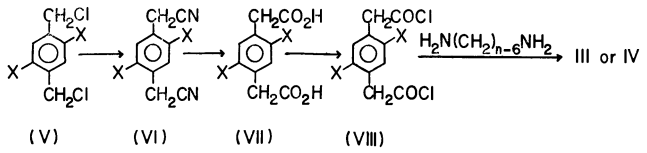

(V) (VI) (VII) (VIII)

Scheme 1.

All the melting points are uncorrected.

α^1,α^4-Dichlorodurene (V, X=Me). A mixture of 53 g (0.5 mol) of *p*-xylene, 106 g (1.3 mol) of 37% formaline, and 530 g of concentrated hydrochloric acid was heated at 60—70°C for 7—15 hr with stirring and while introducing dry hydrogen chloride. The resulting crystals were filtered, and the filtrate was extracted with ether. The crystals and the ether extract were combined and were thoroughly washed with a saturated aqueous solution of sodium bicarbonate and then with a sodium chloride solution. After drying over magnesium sulfate, the solvent and some α^2-chloro-1,2,4-trimethylbenzene were evaporated to yield the crude α^1,α^4-dichlorodurene. Recrystallization from ether gave 65 g of the pure compound; mp 128—129°C (lit, mp 133°C).[9)]

α^1,α^4-Dicyanodurene (VI, X=Me). A mixture of 50 g (0.25 mol) of the dichloride (V, X=Me), 37 g (0.75 mol) of powdered sodium cyanide, 800 ml of ethanol, and 150 ml of water was refluxed for 30 hr. The subsequent working-up of the reaction mixture in the usual manner gave 37 g (80%) of the crude dicyanide (mp 136—138°C), which was directly

1) To whom the correspondence should be addressed.
2) F. Vögtle and P. Neumann, *Tetrahedron*, **26**, 5847 (1970).
3) A. Lüttringhaus and H. Graler, *Ann. Chem.*, **550**, 67 (1940); **557**, 108, 112 (1945); A. Lüttringhaus and G. Eyring, *ibid.*, **604**, 111(1957).
4) D. J. Cram and N. L. Allinger, *J. Amer. Chem. Soc.*, **77**, 6289 (1955).
5) A. T. Blomquist, R. E. Stahl, Y. C. Meinwald, and B. H. Smith, *J. Org. Chem.*, **26**, 1687 (1961).
6) G. M. Whitesides, B. A. Pawson, and A. C. Cope, *J. Amer. Chem. Soc.*, **90**, 639 (1968).
7) M. Nakazaki, K. Yamamoto, and S. Okamoto, *Tetrahedron Lett.*, **1969**, 4597; This Bulletin, **45**, 1562 (1972).
8) The suffix denotes the number of atoms which constitute the ansa chain.
9) J. V. Braun and J. Nelles, *Ber.*, **67**, 1094 (1934).

Table 1. Hetera-*p*-carbophanes

Compound	Molecular formula	Mp (°C)	Analytical data C	H	N(%)	Mol wt (M^+)	Recrystallization solvent	Synthetic method (%)	IR (KBr) (cm^{-1}) ν_{NH}	Amide I	Amide II
III_{12}	$C_{16}H_{22}N_2O_2$	220.0—221.0	70.23	7.89	9.91[a]	274[a]	MeOH	A (<5)	3270	1640	1540
			70.04	8.08	10.21[a]	274[a]					
III_{13}	$C_{17}H_{24}N_2O_2$	290.5—291.5	70.22	8.71	9.42	288	MeOH	B (<5)	3300	1640	1560
			70.80	8.39	9.71	288					
III_{14}	$C_{18}H_{26}N_2O_2$	269.5—270.5	71.22	8.54	8.97	302	MeOH	B (<5)	3260	1640	1570
			71.49	8.67	9.26	302					
III_{15}	$C_{19}H_{28}N_2O_2$	269.0—270.0	72.08	9.07	8.71	316	MeOH	B (18)	3260	1635	1550
			72.12	8.92	8.85	316					
III_{16}	$C_{20}H_{30}N_2O_2$	289.0—290.0	72.60	9.00	8.23	330	MeOH	B (22)	3290	1640	1570
			72.69	9.15	8.48	330					
IV_{12}	$C_{18}H_{26}N_2O_2$	237.5—238.5	71.66	8.82	9.10	302	MeOH	A (13)	3320	1645	1545
			71.49	8.67	9.26	302					
IV_{13}	$C_{19}H_{28}N_2O_2$	226.0—227.5	71.98	8.65	8.63	316	MeOH	B (4.5)	3320	1645	1545
			72.12	8.92	8.85	316					
IV_{14}	$C_{20}H_{30}N_2O_2$	192.5—194.0	72.77	9.18	8.25	330	CH_2Cl_2–ether	B (5.7)	3320	1650	1555
			72.69	9.15	8.48	330					
IV_{15}	$C_{21}H_{32}N_2O_2$	200.0—201.0	73.00	9.51	7.84	344	CH_2Cl_2	B[b] (7.1)	3300	1640	1545
			73.22	9.36	8.13	344					
IV_{16}	$C_{22}H_{34}N_2O_2$	236.5—237.0	73.83	9.27	7.59	358	MeOH	B[b] (2.8)	3300	1640	1545
			73.70	9.56	7.81	358					

a) The numerical data in the upper column are those found and those in lower column are the calculated values.
b) The reaction was carried out at the boiling point of tetrahydrofuran without adding triethylamine.

used for the preparation of 2,5-dimethyl-1,4-phenylenediacetic acid. IR(KBr): 2240 cm^{-1} (ν_{CN}). NMR ($CDCl_3$, δ from internal TMS): 2.31 (6H, s); 3.62 (4H, s); 7.20 (2H, s).

α^1,α^4-Dicyano-p-*xylene (VI, X=H)* was obtained similarly in an 89% yield; mp 95.5—96.5°C (lit, mp 96°C).[10] IR (KBr); 2250 cm^{-1} (ν_{CN}). NMR ($CDCl_3$, δ from internal TMS): 3.76 (4H, s); 7.36 (4H, s).

2,5-Dimethyl-1,4-phenylenediacetic Acid (VII, X=Me). A mixture of 37 g (0.2 mol) of the dicyanide (VI, X=Me), 60 ml of concentrated sulfuric acid, and 80 ml of water was refluxed for 3 hr. The reaction mixture was then poured into ice–water after cooling to yield 20 g (39%) of the crude product. The sample, after purification, melted at 257—261°C with decomposition. IR(KBr); 1700 cm^{-1} (ν_{CO}).

1,4-Phenylenediacetic acid (VII, X=H) was prepared similarly in a 49% yield. Mp 227—230°C (decomposition) (lit, mp 240—241°C).[11] IR(KBr): 1710 cm^{-1} (ν_{CO}).

2,5-Dimethyl-1,4-phenylenediacetyl Dichloride (VIII, X=Me). A mixture of 10 g (38 mmol) of the dicarboxylic acid (VII, X=Me), 20 g (180 mmol) of thionyl chloride, and 120 ml of absolute ether was refluxed for 5 hr. The unreacted dicarboxylic acid was removed by filtration, and the exess thionyl chloride and the solvent were evaporated under reduced pressure to give 8 g (68%) of yellow crystals. The crude dichloride was used for the next reaction without further purification.

1,4-Phenylenediacetyl dichloride was obtained similarly in a 69% yield.

Syntheses of Hetera-p-*carbophanes (III and IV).* These compounds were prepared by two general methods. Method A was used for the compounds which were soluble in a benzene–toluene mixture. For the compounds which were sparingly soluble in a benzene–toluene mixture, the use of method B was preferable. The method of preparation, the melting points, the analytical data, and the solvents of recrystallization for each compound are summarizd in Table 1.

Method A. This method will be described by taking the case of 14,17-dimethyl-3,10-diaza-2,11-dioxo[12]paracyclophane (IV_{12}) as an example.

A solution of 3.4 g (13 mmol) of 2,5-dimethyl-1,4-phenylenediacetyl dichloride in 350 ml of a 1:1 (v/v) benzene–toluene mixture was slowly added to a vigorously-stirred mixture of 4.0 g (40 mmol) of triethylamine, 2.3 g (20 mmol) of hexamethylenediamine, and 500 ml of 1:1 (v/v) benzene–toluene over a period of 40 hr. The mixture was freed from any solid material by filtration and then evaporated *in vacuo* to give 0.5 g (13%) of pale yellow crystals. The recrystallization of the product from methanol afforded colorless, granular crystals; mp 237.5—238.5°C.

Method B. This method will be exemplified by the preparation of 3,13-diaza-2,14-dioxo[15]paracyclophane (III_{15}).

A solution of 1.65 g (7 mmol) of 1,4-phenylenediacetyl dichloride in 100—150 ml of tetrahydrofuran was slowly added to a vigorously-stirred and refluxing mixture of 1.5 g (15 mmol) of triethylamine and 1.1 g of nonamethylenediamine in 600—800 ml of tetrahydrofuran over a period of 25 hr, employing a high-dilution apparatus. After the solvent has then been removed, the residue was extracted with 100 —200 ml of dichloromethane. The extract was washed with dilute hydrochloric acid and then with saturated aqueous sodium chloride, and dried over magnesium sulfate. The evaporation of the solvent, after filtration, gave 0.5 g (18%) of pale yellow crystals which were recrystallized several times from methanol or dichloromethane. The pure compound consisted of colorless crystals; mp 269.0—270.0°C.

N,N'-Dipropyl-2,5-dimethyl-1,4-phenylenediacetamide (XV). To a solution of 3 g (31 mmol) of propylamine and 3 g of (30 mmol) of triethylamine in 50 ml of tetrahydrofuran, was added a solution of 2.6 g (10 mmol) of 2,5-dimethyl-1,4-phenylenediacetyl dichloride in 50 ml of tetrahydrofuran,

10) A. F. Titly, *J. Chem. Soc.*, **1926**, 515.
11) F. S. Kipping, *ibid.*, **56**, 21 (1888).

while the temperature was maintained below 5°C. The resulting solid was collected by filtration, washed with water, and recrystallized from methanol. The compound (mp 230.0—231.0°C), was thus obtained in a 1.5 g (50%) yield. IR (KBr): 3300 (ν_{NH}); 1640 (amide I); 1545 (amide II). Found: C, 71.23; H, 9.44; N, 8.96%; mol wt, 304 (M^+). Calcd for $C_{18}H_{28}N_2O_2$: C, 71.02; H, 9.27; N, 9.20%; mol wt, 304.

N,N'-Dipropyl-1,4-phenylenediacetamide (XIV) (mp 225.0—226.0°C) was similarly obtained in a 64% yield. IR(KBr): 3260 (ν_{NH}); 1635 (amide I); 1555 cm^{-1} (amide II). Found: C, 69.56; H, 8.86; N, 9.90%; mol wt, 276 (M^+). Calcd for $C_{16}H_{24}N_2O_2$: C, 69.53; H, 8.75; N, 10.14%; mol wt, 276.

1,8-Diaza-9,18-dioxocyclooctadecane (XVI). This compound was prepared in a manner similar to that described for the preparation of hetera-*p*-carbophanes (Method A) from decanedioyl dichloride and hexamethylenediamine. The compound melted at 216.0—218.0°C after recrystallization from dimethylformamide. IR (Nujol mull): 3300 (ν_{NH}); 1640 (amide I); 1545 (amide II). Found: C, 67.53; H, 10.59; N, 9.53%; mol wt, 282 (M^+). Calcd for $C_{16}H_{30}N_2O_2$: C, 68.04; H, 10.71; N, 9.92%; mol wt, 282.

Measurement of the Spectra. The infrared spectra were recorded on either a Hitachi EPI-G2 grating infrared spectrophotometer or a Perkin-Elmer 112G grating spectrophotometer. The NMR spectra were measured on a Hitachi R-20B spectrometer, and the mass spectra, on a Hitachi RMU-6L spectrometer.

Results and Discussion

Internal Rotation of the Aromatic Ring. The observed NMR spectra of III_{12} and IV_{12}—IV_{16} in a deuteriochloroform solution at 34°C are illustrated in Fig. 1. The high-resolution spectra of III_{13}—III_{16} could not be obtained because of their poor solubilities in the appropriate solvents.

It can be pointed out generally that the shapes of the signals of the bridge methylene protons in IV_n reflect the rigidity of the molecule: the compounds with the smaller ring give the complex spectra, while those of the larger ring, give the rather smooth spectra. The chemical shifts of the methylenes of the smaller ring are located in the high magnetic field, suggesting the anisotropy effect of the benzene ring.

The benzylic protons of III_{12} and IV_{16} gave signals of the A_2 type at 3.58 and 3.51 ppm respectively from the internal TMS, whereas those of IV_{12}, IV_{13}, IV_{14}, and IV_{15} gave signals of the AB type at *ca.* 3.54 ppm.

Considerations of the conformations of III_n and IV_n reveal that there are three conformations possible, the isomerism of which is caused by the rotation about the C_{CO}–C_{benzyl} bond: *syn*, *anti*, and *syn'* in Fig. 2.[12]

The Newman projections of these conformations, as separated forms for the two benzylic parts, are given in Fig. 3.

Since these molecules are rather rigid, the exchange among these conformations might be slow on the NMR time scale. However, looking at the data of III_{12}, the possibility that the slow exchange is the cause of the appearance of the AB signals can be rejected: if such were the case, III_{12} should also have

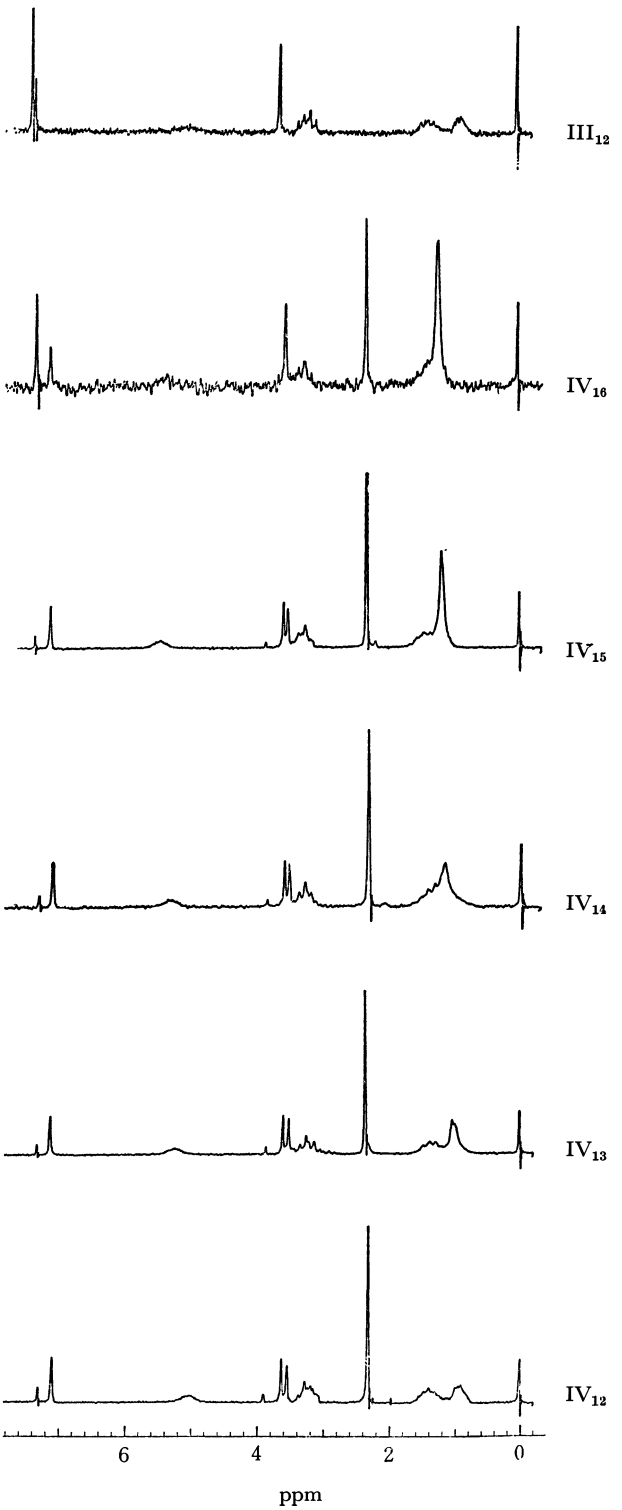

Fig. 1. NMR spectra III_{12} and IV_{12}—IV_{16} in $CDCl_3$ (δ from internal TMS).

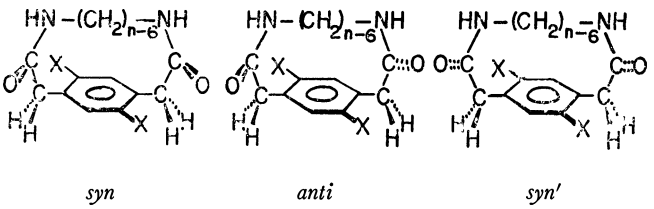

Fig. 2. Rotational isomerism about the C_{CO}–C_{benzyl} bond.

12) We are assuming that no isomerization is possible about the amide moiety. See the discussions below.

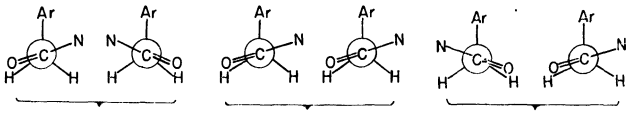

Fig. 3. Newman projections of rotational isomers about the C_{CO}–C_{benzyl} bond.

shown the AB signal for the benzylic protons. Thus, the slow internal rotation of the unsymmetrically-substituted benzene ring is the sole possible cause of the AB-type signals.

At least, at room temperature, the signals suggest that the internal rotation of the dimethylbenzene ring in IV_{15} is slow while that in IV_{16} is fast, on the NMR time scale. The temperature dependence of these spectra was thus studied in an attempt to obtain the kinetic data of the internal rotation: IV_{15} in 1,1,2,2-tetrachloroethane at higher temperatures (34—170°C) and IV_{16} in deuteriochloroform at lower temperatures (34—−50°C). To our suprise, however, the changes in signal shape according to the temperature change are so small that it is impossible to obtain the expected data.

The minimum and maximum free energies of activation may be obtained by applying this equation:[13]

$$\Delta G_c^* = 4.57 T_c\{9.97 + \log_{10}(T_c/\sqrt{\delta\nu^2 + 6J^2})\}$$

provided that the chemical shifts and the coupling constants are the same for both compounds when the internal rotation is slow enough and that the coalescence temperature (T_c) in the above equation is transferable to any temperature desired. Thus, since the AB quartet of the benzyl methylenes in IV_{15} did not colapse at 443°K, the minimum free energy of activation is obtained as 22.3 kcal/mol. Similarly, since the benzyl methylene signals of IV_{16} did not change in shape even at 223°K,[14] the free energy of activation for the internal rotation must be less than 10.8 kcal/mol. Therefore, the difference in barriers to the internal rotation of the benzene ring is at least 11.5 kcal/mol for these compounds. This large difference in the barriers by changing the number of bridge methylenes by only one is not without precedent. *trans*-Cyclodecene is known to have the barrier of 10.7 kcal/mol[15] by the dynamic NMR, and *trans*-cyclononene, one of 20 kcal/mol by the conventional kinetic technique.[16]

It is noteworthy that, although the coupling constants

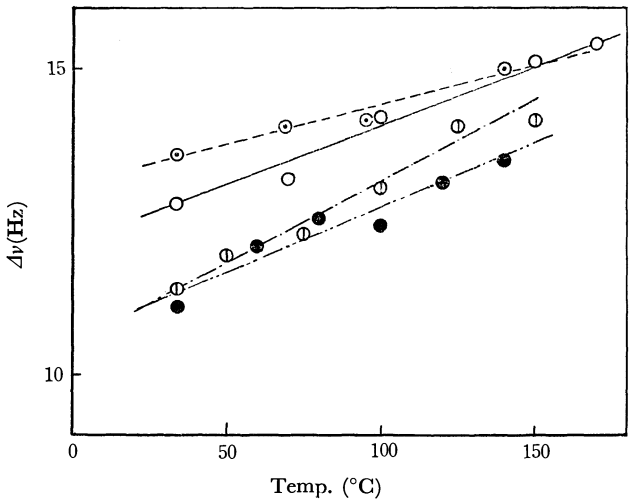

Fig. 4. Temperature dependence of the chemical shift difference between the benzylic methylene protons in IV_{12}—IV_{15}.
—○—; IV_{12}, ---⊙---; IV_{13}, —◑—; IV_{14}, ---●---; IV_{15}

did not change, even the benzylic methylene protons change their chemical shifts due to the temperature variation. This is a rather unexpected phenomenon, because no reason for the change can be deduced from the first approximation. The relation between the chemical shifts and the temperature are shown in Fig. 4. The chemical shifts show small but definite changes within the range of 1.5—3.0 Hz at the temperature of 34—*ca.* 150°C. The change in chemical shifts is linearly correlated with the temperature.

Such a temperature dependence may, in general, be attributed to solvation effects or the population effects. If the reasons for the temperature dependence of the spectra are attributed to the population effect, there will be two cases to be considered. The first is the isomeric conformations caused by the rotation about the C_α–C_{CO} bond, and the second is the change in the populations of the conformers (IX, X, and XI) formed by the rotation about the C_{ar}–C_α bond.

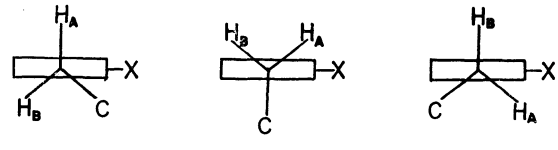

However, the change in population is not the likely cause of the change in chemical shifts. The change in population of the conformers on raising the temperature causes the averaging tendency of the signals, since the more unstable conformers increase in their populations. The data in Fig. 4 show, however, that the chemical shift differences between the A and B protons, rather, increase at higher temperatures.

Thus, the solvation effect becomes a more likely reason. Since, at lower temperatures, the solvated molecules reside close to the solute molecule for a longer time, the protons suffer from the anisotropy effects of various bonds and atoms. However, at higher temperatures, the effects will be more or less averaged out because of the faster motion of the molecules. These

13) J. A. Pople, W. G. Schneider, and H. J. Bernstein, "High-Resolution Nuclear Magnetic Resonance," McGraw-Hill Book Co., Inc., New York (1959); J. W. Emsley, J. Feeny, and C. H. Sutcliff, "High Resolution Nuclear Magnetic Resonance Spectroscopy", Pergamon Press (1965).

14) The apparent singlet signal may be the results of the accidental identity of the chemical shifts of the two benzylic protons in this solution system. Since the attempts to obtain spectra at low temperatures in other solvent systems have failed due to the poor solubility of the compound, we tentatively assume that the apparent singlet signal shows the fast exchange of the two ptorons. Incidentally, the corresponding diester compound has shown the splitting tendency of the singlet signal into a quartet at *ca.* −50°C in CH_2Cl_2–$CDCl_3$ (an unpublished work).

15) G. Binsch and J. D. Roberts, *J. Amer. Chem. Soc.*, **87**, 5157 (1965).

16) A. C. Cope, K. Banholzer, H. Keller, B. A. Pawson, J. J. Whang, and H. J. S. Winkler, *ibid.*, **87**, 3644 (1965).

differences should be able to cause the variation in chemical shifts to some extent.

The Conformations of the Amide Groups. It has been well documented that some amides exist as *s-cis* (XII) and *s-trans* (XIII) isomers. Lactams of the small rings cannot take the *s-trans* conformation due to the ring strain and exist solely as the *s-cis* conformation, whereas the open-chain amide is the most stable when the *s-trans* conformation is taken. In view of these facts, it will be interesting to study whether the amide groups in these hetera-*p*-carbophanes take the *s-cis* or the *s-trans* conformation. Thus, the N–H stretching absorption spectra, which have been extensively employed for the diagnosis of the conformation in question, have been examined in detail. The results obtained with dilute chloroform solutions are shown in Table 2, together with the data of the open-chain analogs (XIV and XV) and a simpler cyclic amide (XVI).

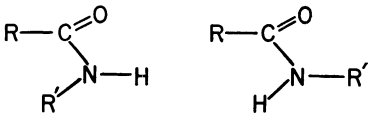

XII XIII

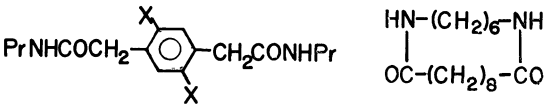

XIV (X = H)
XV (X = Me)

XVI

TABLE 2. ABSORPTION MAXIMA DUE TO N–H STERTCHING VIBRATION OF HETERA-*p*-CARBOPHANES AND RELATED COMPOUNDS IN $CHCl_3$ (cm^{-1})

Compound	*s-trans* (ε_{max})	*s-cis* or N–H···π interacting (ε_{max})
III_{12}		3436 (277)
IV_{12}		3433 (423)
III_{13}		3436 (171)
IV_{13}		3431 (259)
III_{14}		3437 (251)
IV_{14}		3433 (244)
III_{15}		3440 (267)
IV_{15}		3432 (188)
III_{16}		3439 (181)
IV_{16}		3431 (161)
XIV[a)]	3453 (133)	3437 (223)
XV[a)]	3449 (64)	3427 (192)
XVI	3453 (252)	

a) Graphically resolved.

As may be seen in the table, the hetera-*p*-carbophanes examined all show only one N–H stretching absorption, as does the dilactam (XVI), whereas the open-chain analogs (XIV and XV) show two ν_{NH} absorptions. The absorption of the dilactam (3453 cm^{-1}) corresponds to the frequencies of the well-documented *s-trans* conformation, and this compound is believed to exist as a bis-*s-trans* conformer.

The absorption frequencies of the hetera-*p*-carbophanes are rather low and are in the region of the *s-cis* conformation. However, the phenylacetamide derivatives are known to possess an internal N–H···π interaction[17] which causes a lowering of the absorption frequencies, even though the conformation is *s-trans*. Indeed, the N–H absorptions of the open-chain analogs at the lower frequencies must be attributed to the N–H···π interacting species, since the absorption coefficients of the lower band are too large to assign to the *s-cis* conformation.

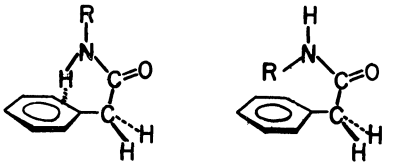

N–H···π intracting (*s-trans*) *s-cis*

Then a problem arises: why does the absorption appear at lower frequencies for the hetera-*p*-carbophanes? Is this a sign of an *s-cis* conformation or of N–H···π interaction? We would like to attribute the phenomena to the *s-cis* conformation of the amide groups for the following three reasons.

The first reason is the rigidity of the scale models. In the smaller ring compounds, although it is possible to make a model involving two *s-trans* conformations, this model tends to collapse when the support is removed, suggesting that this conformation has a high energy. It is also possible to make up a model involving *s-cis* and *s-trans* conformations. However, all the III_n and IV_n give only one absorption at about the same wave number, a number which is within the region attributable to the *s-cis* conformation. Therefore, a conformation involving the two *s-cis* amides is the more likely possibility.

The second reason is the consideration of the N–H···π interaction. The most favorable conformation for the interaction is the one in which the C_α–C_{CO} bond is perpendicular to the benzene ring (X); in this conformation, the N–H group approaches the π-lobe of the benzene ring from the top, and this gives the maximum overlap of the orbitals concerned. If the other conformations (*e.g.*, IX and XI) are taken and the overlap of the orbitals is decreased, the compound should show other N–H absorptions; these may be either free or interacting to a lesser extent. However, none of the hetera-*p*-carbophanes shows a second N–H band. Therefore, although this evidence is negative in nature, this can be taken as supporting the absence of the *s-trans* conformation.

The third reason is the evidence obtained by NMR spectroscopy. If there is an exchange between the *s-cis* and N–H···π interacting *s-trans* conformations, then there will be a change in the chemical shifts of the CH_2 protons, α to the nitrogen atom, since it is a well-

17) I. Suzuki, M. Tsuboi, and T. Shimanouchi, *Spectrochim. Acta*, **16**, 467 (1960).

known fact that the *s-cis* and *s-trans* amides give signals characteristic of their conformations and that, even though these conformations are not detected by NMR because of the fast rate of exchange, there should yet appear a change in the chemical shifts. However, in reality, no change in the chemical shifts of the CH_2N signals was observed.

The presence of the *s-cis* conformation only for III_n and IV_n, in contrast to the presence of *s-trans* for the dilactam XVI, is undoubtedly a reflection of the rigidity of the benzene ring in III and IV, which limits the conformation of the molecule.

BULLETIN OF THE CHEMICAL SOCIETY OF JAPAN, VOL. 46, 275—279 (1973)

The Peracid-oxidation of Tetraphenylallene: The Formation of Hydroxyindanone and Its Oxidative Transformation

Akira OKU, Kojiro SHIMADA, and Fujio MASHIO

Department of Chemistry, Kyoto Institute of Technology, Matsugasaki, Sakyo-ku, Kyoto, 606

(Received June 17, 1972)

The oxidation of tetraphenylallene (**1**) with *m*-chloroperbenzoic acid has been reported. Under acidic conditions, 1-hydroxy-1,3,3-triphenyl-2-indanone (**2**) was isolated in 45% yield, along with benzophenone (**3**) and the *m*-chlorobenzoate of **2** as minor products. In the presence of sodium carbonate, the oxidation products were 2,2,4,4-tetraphenyloxetanone (**6**), **3**, and 1,3,3-triphenyl-2,3-dihydro-5*H*-indene-2,5-dione (**5**). The prolonged oxidation of **2** with peracetic acid yielded α,α-diphenylphthalide (**9a**). The alkaline hydrolysis of **2** induced ring cleavage to give *o*-benzhydrylbenzilic acid (**15b**), whereas acid hydrolysis in ethanol or methanol gave the corresponding ethers, **16a** and **16b** respectively.

The intermediacy of allene oxides has attracted our attention in terms of olefin-epoxidation and valence tautomerism with cyclopropanone.[1] Vorlander[2] was the first to report the synthesis of tetraphenylallene dioxide by the cromic-acid oxidation of tetraphenylallene, but it was proved later[3] that the product was tetraphenyloxetanone instead of the dioxide. Recently Crandall and his co-workers[4] have reported extensive work on the isolation of allene dioxides, cyclopropanones, and oxetanones in the peracid oxidation of alkyl-substituted allenes. More significantly, Greene and Camp[5] have isolated 1,3-di-*tert*-butylallene oxide by using *m*-chloroperbenzoic acid as the effective reagent.

In the present study, we wish to report the peracid oxidation of tetraphenylallene (**1**), where the product formation is largely dependent on the pH of the oxidation mixture. Analogously to the earlier studies,[4] the intermediacy of tetraphenylallene oxide (**7**) and its corresponding spiro-dioxide (**8**), though not isolated, has been demonstrated. On the other hand, however, cationic alkylation on a benzene ring of substrates has taken place predominantly under acidic conditions to give 1-hydroxy-1,3,3-triphenyl-2-indanone (**2**),[6] while under the conditions buffered with sodium carbonate, 2,2,4,4-tetraphenyloxetanone (**6**) and 1,3,3-triphenyl-2,3-dihydro-5*H*-indene-2,5-dione (**5**) have been obtained instead of the indanone (**2**). It has also been found while examining the oxidative susceptibility of the indanone (**2**) to peracids that **2** undergoes a novel Baeyer-Villiger transformation involving the elimination of the benzoyloxy group.

Results and Discussion

Oxidation of Tetraphenylallene. The treatment of tetraphenylallene (**1**) with 2 equivalents of *m*-chloroperbenzoic acid in methylene chloride for 20 hr at 1—3°C (peracid consumption 60%) afforded a yellow

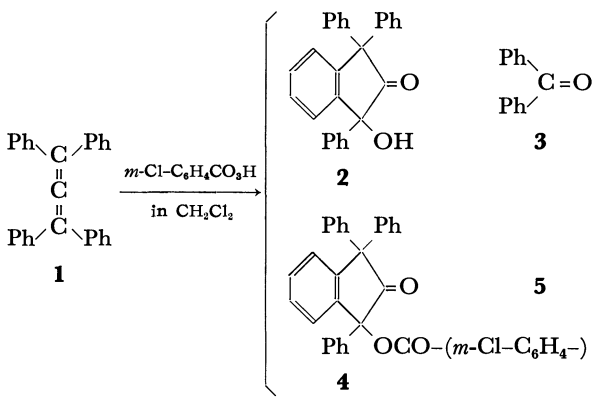

1) a) J. M. Pochan, J. E. Baldwin, and W. H. Flygare, *J. Amer. Chem. Soc.*, **90**, 1072 (1968); b) F. D. Greene, J. C. Stowell, and W. R. Bergmark, *J. Org. Chem.*, **34**, 2254 (1969).

2) D. Worlander and P. Winstein, *Ber.*, **56**, 1122 (1923).

3) G. B. Hoey, D. O. Dean, and C. T. Lester, *J. Amer. Chem. Soc.*, **77**, 391 (1955). See also **76**, 4988 (1954).

4) a) J. K. Crandall and W. H. Machleder, *ibid.*, **90**, 7292 (1968); b) J. K. Crandall, W. H. Machleder, and M. J. Thomas, *ibid.*, **90**, 7346 (1968); c) J. K. Crandall and W. H. Machleder, *ibid.*, **90**, 7347 (1968).

5) R. L. Camp and F. D. Greene, *ibid.*, **90**, 7349 (1968).

6) Acyclic hydroxyketones were the usual products of allene oxidation; *cf.* F. R. LaForge, and F. Acree, Jr., *J. Org. Chem.*, **6**, 208 (1941).

product mixture, which was then chromatographed to give four products: **2** (45%), **3** (3%), **4** (1%), and **5** (<1%), besides the unreacted allene (**1**) (25%).[7]

The structure of the main product (mp 160°C) was determined to be 1-hydroxy-1,3,3-triphenyl-2-indanone (**2**)[8] by the following analyses and by the chemical behavior to be described in the last section of the present paper. The infrared spectrum showed carbonyl (1760 cm^{-1}, indicative of a cyclic five-membered ketone) and hydroxyl (3560 cm^{-1}) absorptions. The NMR spectrum showed only a complex multiplet of aromatic protons. The elemental analysis ($C_{27}H_{20}O_2$) indicates that the allene ($C_{27}H_{20}$) was oxidized by two atoms of oxygen. Several possible structures other than **2** were also examined, but were ruled out. For example, tetraphenyloxetanone (**6**)[9] was the most expected product by analogy with Crandall's result, but it should show a much higher frequency of $\nu_{C=O}$ than that observed (for the oxetanone (**6**), see the next paragraph). The indanone (**2**) did not form hydrazone with 2,4-dinitrophenylhydrazine nor did it react with hydroxylamine.[10] A similar low reactivity has also been reported for 3-hydroxy-1,3-diphenyl-2-indanone.[11] The second product **3** was identified as benzophenone by comparison with authentic sample. The third product, **4** (mp 216°C), obtained in a low yield, turned out to be $C_{34}H_{23}O_3Cl$. An examination of its infrared spectrum, which shows two carbonyl absorptions at 1770 (strong) and 1730 cm^{-1} (stronger), indicates that a mixed structure with cyclic ketone and *m*-chlorobenzoate functions is preferable to other structures, such as acid anhydrides. The NMR spectrum showed only a complex multiplet of aromatic ring protons and no signal in the other regions. From these data, **4** is assumed to be the *m*-chlorobenzoate of **2**, as has been indicated above. In fact, the formation of **2** was confirmed in the acid hydrolysis of **4**. The minor product **5** was obtained in a trace; its structural determination will be described in the next paragraph.

In order to minimize the influence of *m*-chlorobenzoic acid in the reaction, an excess amount of finely-powdered sodium carbonate was added to the reacting mixture. In this buffered reaction, three products, **3** (10%), **5** (3%), and **6** (5%), were isolated, besides the unreacted allene (48%), after a reaction for 20 hr at 1—3°C (peracid consumption, 46%).

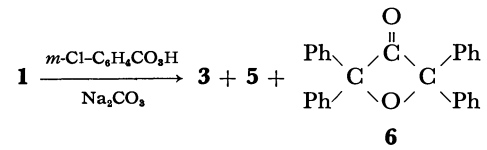

6

No appreciable formation of any other products was detected, although the isolated yields of the above products were low. It should be noted that the indanone (**2**) was not detected here, but that, instead, tetraphenyloxetanone (**6**) was formed. This implies that the formation of **2** occurred only under acidic conditions. The **6** product (mp 201°C) showed a carbonyl absorption at 1805 cm^{-1} (strained C=O) in its infrared spectrum, and the NMR spectrum showed only the existence of aromatic ring protons. The **5** product (mp 220°C), obtained as orange-yellow crystals, was found to be $C_{27}H_{18}O_2$ by the elemental analysis as well as a study of its mass spectrum (M^+ *m/e* 374). The infrared spectrum showed two carbonyl absorptions, at 1725 (s) and 1640 (vs) cm^{-1}. The ultraviolet spectrum showed two absorptions, at 367 nm (log ε 4.7) and 260 nm (log ε 4.5), characteristic of the multi-conjugated system involving carbonyl functions, such as *o*-quinone or fuchsone.[12] Its rather distinct NMR signals at τ 2.13 (1H, d, J=10 Hz), 3.41 (1H, a pair of doublet, J_1=10 Hz, J_2=1.5 Hz), and 3.68 (1H, d, J=1.5 Hz), in addition to the multiplets of aromatic hydrogens, are quite characteristic of the cyclic conjugating systems with a three-proton arrangement of $-CH_a=CH_b-C=CH_c-$ or $-CH_a=CH_b-CO-CH_c=$.[13] The structural elucidation of this product, based on an analysis of the above data, suggests a cross-conjugated diketone structure depicted below rather than any other available structures:

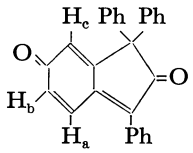

5

In this structure, *i.e.*, 1,3,3-triphenyl-2,3-dihydro-5*H*-indene-2,5-dione, the three protons on the quinone ring well account for the observed NMR spectrum, in which H_a is shifted downfield due to the diamagnetic anisotropy of the *peri*-phenyl group.

Scheme 1 illustrates the reaction route to accommodate these results. As has been proposed[4] the initial step in this sequence is the formation of allene

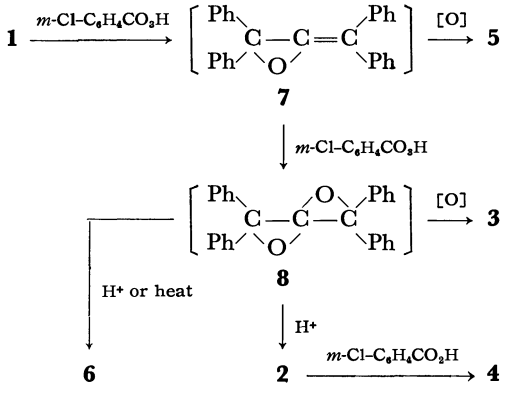

Scheme 1

7) Product yields indicated in this paper are those of the isolated and purified products unless otherwise mentioned.

8) Lit. mp 157—159°C by C.F. Koelsch, *J. Org. Chem.*, **3**, 456 (1938).

9) Other structures such as triphenylbenzoylethylene oxide, triphenylvinyl benzoate, phenyl triphenylacrylate, and 2-hydroxy-2,3,3-triphenyl-1-indanone were all ruled out by the analysis.

10) Graf, *Chem. Zentr.*, II, 3337, 3338 (1936).

11) S. Ecary, *C. R. Acad. Sci. Paris*, **224**, 1504 (1947).

12) L. C. Anderson and J. W. Steedly, Jr., *J. Amer. Chem. Soc.*, **76**, 5144 (1954).

13) L. M. Jackman and S. Sternhell, "Applications of Nuclear Magnetic Resonance Spectroscopy in Organic Chemistry," 2nd ed., Pergamon Press, Braunschweig, 1969, p. 340.

oxide (**7**), which is then further oxidized to form **8**. Both oxides are unisolated intermediates, but are likely sources of the isolated products. The failure to isolate the **7** and **8** intermediates can be attributed to the substituent effect of the phenyl group, which is in contrast to that of alkyl homologs.[4,5] Thus, tetraphenylallene is less reactive than the alkyl homologs toward the peracid, as may be seen in the imcomplete and slow conversion of the peracid and the allene (**1**). On the other hand, the **7** and **8** intermediates are much more susceptible to the acid-catalyzed (or thermal) transformation, probably because of the delocalization of cationic species by phenyl groups. The formation of the indanone (**2**) under acidic conditions clearly demonstrates the cationic alkylation of a phenyl ring *via* one of the few possible reaction paths. This route, however, is almost completely suppressed in a buffered reaction, and the oxetanone (**6**) is formed instead. This clear-cut distinction indicates an important role of pH in the product control, regardless of whether **6** is formed thermally or by acid catalysis. The formation of benzophenone, probably closely analogous to the formation of acetone from tetramethylallene,[4] cannot be interpreted well. The most likely precursor, however, seems to be the spirodioxide (**8**), which undergoes further oxidation to give **3** as was observed in the oxidation of **8** with cromic acid.[2] The formation of the *m*-chlorobenzoate (**4**) can be reasonably explained in terms of an acid-catalyzed esterification between **2** and *m*-chlorobenzoic acid. The formation of the diketone (**5**), observed more in the buffered reaction than in the acidic oxidation, reasonably rules out the possible intermediacy of the indanone (**2**) as a precursor of **5**. A plausible explanatory reaction sequence consists of an oxidative ring-hydroxylation of the allene oxide (**7**), followed by some cationic ring-formation and oxidation. However, sufficient evidence is not yet available to support this sequence.

Reaction of 1-Hydroxy-1,3,3-triphenyl-2-indanone (2). The stability of the indanone (**2**) in relation to *m*-chloroperbenzoic acid rules out the possibility that this material is the precursor of **3**, **5**, or **6**. The oxidation of **2** with peracetic acid after a prolonged reaction, however, afforded only one product. Its infrared spectrum showed a carbonyl absorption at 1775 cm^{-1}, and both its mass spectrum and elemental analysis ($C_{20}H_{14}O_2$, *m/e* 286) proved it to be either **9a** or **9b**.[14] Compound **9a** has been prepared from phthalic anhydride and phenyllithium,[15] whereas **9b** has been prepared from benzil and phenol.[16] As a result, it has been found that the product was α,α-diphenylphthalide (**9a**)

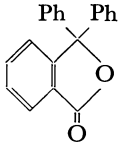

9a

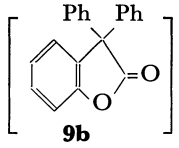

9b

14) Lit. mp of **9a** 116°C, see Ref. 15; lit. mp of **9b** 120°C, see Ref. 16.

15) J. M. Wilson, *J. Chem. Soc.*, 2297 (1951).

16) V. Liebig and P. Keim, *Ann. Chem.*, **360**, 200 (1908).

(15%); this presents us with a possible reaction scheme in which a novel Baeyer-Villiger-type transformation of α-hydroxyketone is involved (Scheme 2). Additionally, the fact that benzophenone was not formed in this reaction excludes any transformation in which the indanone (**2**) can be the precursor of benzophenone.

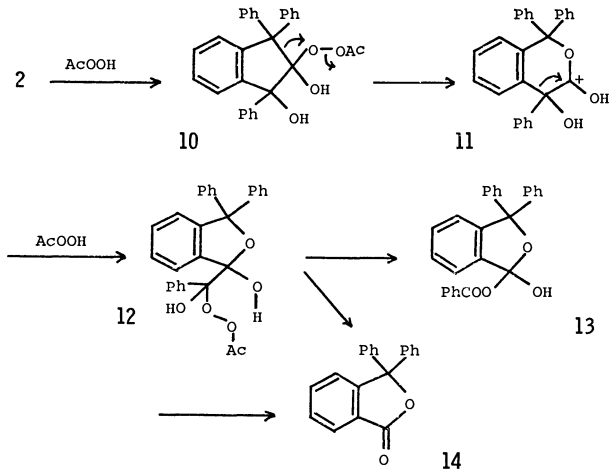

Scheme 2

Some supplemental reactions of the indanone (**2**) were carried out in order to determine the structure and reaction behavior of **2** in the oxidation system. The hydrolysis of **2** in aqueous potassium hydroxide gave a white solid of a potassium carboxylate (**15a**). This material was then acidified to yield its free acid (**15b**). The infrared spectrum and the NMR spectrum of **15b** are in good agreement with the structure of *o*-benzhydrylbenzilic acid,[8] and its formation can be interpreted in terms of a hydroxy-anion attack on the carbonyl function, followed by ring cleavage to form the trityl anion.

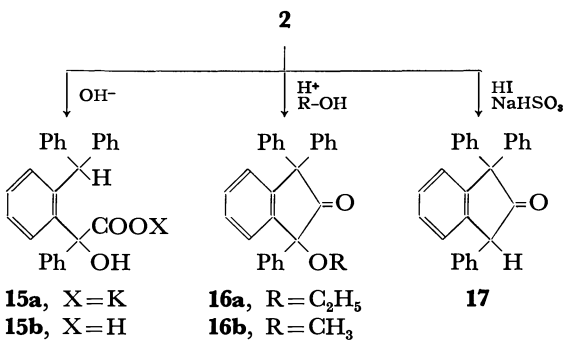

15a, X=K
15b, X=H

16a, R=C_2H_5
16b, R=CH_3

17

The treatment of **2** with ethanolic hydrochloric acid yielded 1-ethoxy-1,3,3-triphenyl-2-indanone (**16a**) in a good yield. The NMR spectrum of **16a**, however, showed a pair of quartets of the ethoxy methylene signal slightly split (by about 3 Hz), whereas the ethoxy methyl appeared unsplit. With the aid of a molecular model, this may be accounted for by a steric inhibition of the free rotation in this rather crowded molecule. Similarly, the methoxy derivative (**16b**) was obtained from a methanolic hydrochloric acid solution in a 73% yield. Somewhat related to the formation of the *m*-chlorobenzoate (**4**), the ether formation may be indicative of a possible nucleophilic displacement on

the position adjacent to the carbonyl. In addition, the tertiary hydroxy group of **2** was readily reduced by treating **2** with hydriodic acid and sodium bisulfite,[17] thus giving 1,1,3-triphenyl-2-indanone (**17**).

Experimental

Melting points are uncorrected. Infrared spectra were recorded on a JASCO IRA-1 grating spectrophotometer, NMR spectra were taken on a JEOL 4H-100 spectrometer (100 MHz) unless otherwise stated. Chemical shifts are relative to internal TMS and are given on τ scale. Mass spectra were obtained with a Shimadzu LKB-9000 mass spectrometer. Combustion analyses were performed by the Microanalytical Laboratory, Kyoto University.

m-Chloroperbenzoic Acid. The preparation of *m*-Cl-perbenzoic acid[18] on a laboratory scale was performed starting with *m*-toluidine according to the method indicated in the literatures.[19]

Tetraphenylallene (1).[20] Starting with diphenylmethyl bromide (120 g) and 1,1-diphenylethylene (88 g), and after several experimental procedures directed by the literature,[21] a pure solid of **1** (28.5 g, mp 165°C) was obtained.

Oxidation of 1 with m-Chloroperbenzoic Acid. To a solution of **1** (13.8 g, 0.04 mol) in methylene chloride (100 ml) was added a solution of 86% *m*-Cl-perbenzoic acid (16.6 g, 0.08 mol) in methylene chloride (250 ml) and the mixture was stirred for 20 hr at 1—3°C (peracid consumption 60%).[22] Then the mixture was washed three times with 10% aqueous sodium carbonate and two times with saturated aqueous sodium chloride. After the organic solution has been dried over anhyd magnesium sulfate, the solvent was removed by flash evaporation to give a yellow oil. Tlc showed two major spots, plus several (mainly three) minor spots. The crude oil was chromatographed on silica gel (Merck 70—325 mesh), first with carbon tetrachloride and then with chloroform. The first eluting fraction contained unreacted **1** (4.1 g, 25% recovery). The second fraction gave a colorless solid of 1,3,3-triphenyl-2-oxodihydro-1-indenyl *m*-Cl-benzoate (*4*), 0.2 g (1%); mp 216°C (ethanol); IR (CCl_4) 1770 (strong) and 1730 (stronger) cm^{-1} (both C=O); NMR (CCl_4) τ 2.7—3.2 (m).

Found: C, 79.54; H, 4.59%. Calcd for $C_{34}H_{23}O_3Cl$: C, 79.29; H, 4.50%.

The saponification of **4** with hot hydrochloric acid in dioxane, followed by the removal of the solvents, yielded a crude solid, which showed a tlc spot identical with that of indanone (**2**). The third fraction gave a viscous oil which gradually solidified on standing. The solid was recrystallized from diethyl ether to give 0.4 g (3%) of benzophenone (**3**). The fourth fraction was a viscous yellow oil, from which the diketone (**5**) was isolated (<1%). The physical data of **5** will be given in the next experimental paragraph. The fifth fraction consisted mainly of 1-hydroxy-1,3,3-triphenyl-2-indanone (**2**), which was purified by recrystallization from toluene to give 6.7 g (45%) of **2** as colorless needles; mp 161°C; IR 3560 (OH), 1760 cm^{-1} (C=O); UV $\lambda_{max}^{cyclohexane}$ 320 nm (log ε 2.5), 278 (3.56), 270 (3.34), 263 (3.31); NMR (CCl_4) τ 2.62—3.02 (m); *m/e* 376 (M^+).

Found: C, 86.34; H, 5.32%. Calcd for $C_{27}H_{20}O_2$: C, 86.15; H, 5.36%.

Oxidation of 1 with m-Chloroperbenzoic Acid in the Presence of Sodium Carbonate. To a solution of **1** (13.8 g, 0.04 mol) in methylene chloride (100 ml), we added 100 g of finely-pulverized sodium carbonate. To this suspension was then added 17.2 g (0.08 mol) of *m*-Cl-perbenzoic acid (assay 83%) dissolved in methylene chloride (250 ml), after which the mixture was stirred at 1—3°C for 20 hr (peracid consumption 45%). The inorganic salts were filtered out, and the filtrate was washed three times with 10% aqueous sodium carbonate and two times with saturated aqueous sodium chloride, and dried over anhyd. magnesium sulfate. The solvent was then removed by flash evaporation to give a yellow oil (4 tlc spots, but none of **2**, on a silica gel plate). The oil was chromatographed (silica gel, carbon tetrachloride and chloroform eluent). The first eluting fraction contained unreacted **1** (6.7 g, 48%). The second fraction consisted mainly of 2,2,4,4-tetraphenyloxetanone (**6**); 0.8 g (5%); mp 198—201°C (diethyl ether); IR (CCl_4) 1805 cm^{-1} (C=O); NMR (CCl_4) τ 2.77 (m).

Found: C, 86.05; H, 5.46%. Calcd for $C_{27}H_{20}O_2$: C, 86.14; H, 5.35%.

The third fraction was proved to consist mainly of **3**, as in the previous experimental paragraph. The fourth fraction was a deep yellow oil, the same component as the third chromatographed fraction obtained in the preceding experimental paragraph. This was purified by preparative tlc (silica gel), followed by recrystallization from ethanol, to give orange-yellow crystals of 1,3,3-triphenyl-2,3-dihydro-5*H*-indene-2,5-dione (**5**); 0.5 g (3%); mp 219 —220°C; IR (CCl_4) 1725 and 1640 cm^{-1} (C=O); NMR (THF) τ 2.13 (1H, d, J=10 Hz), 2.32 (2H, m), 2.50 (3H, m), 2.73 (10H, m), 3.41 (1H, q, J_1=10 Hz, J_2=1.5 Hz), 3.68 (1H, d, J=1.5 Hz); UV $\lambda_{max}^{cyclohexane}$ 367 nm (log ε 4.7), 260 (4.5); *m/e* 374 (M^+).

Found: C, 86.06; H, 4.81%. Calcd for $C_{27}H_{18}O_2$: C, 86.60; H, 4.85%.

Oxidation of 2 with Peracetic Acid. Peracetic acid was prepared by adding 90% hydrogen peroxide (10.8 ml, 0.40 mol) to a cold solution of acetic anhydride (44.9 g, 0.44 mol) in methylene chloride (100 ml); the mixture was then kept overnight in a refrigerator (peracid concentration 1.8×10^{-3} mol/g[22]). About 20 ml (40 mmol) of the above peracid solution and **2** (0.75 g, 2 mmol) dissolved in chloroform (30 ml) were mixed, and this mixture was stirred at 10—15°C for 11 days (peracid consumption 15%). The organic mixture was then washed three times with 10% aqueous sodium carbonate and two times with saturated aqueous sodium chloride, and then dried over anhyd. magnesium sulfate. The solvents were removed by flash evaporation to give a crude solid, which was chromatographed (silica gel, carbon tetrachloride eluent) to give **9a** (0.08 g, 15%) in addition to the unreacted **2** (0.5 g, 70% recovery). **9a**: colorless prismen crystal (diethyl ether); mp 117—118°C; mmp (with an authentic sample, see below) 117°C; IR (CCl_4) 1775 cm^{-1} (C=O); NMR (CCl_4) 2.46 (4H, m), 2.73 (10H, m).

α,α-Diphenylphthalide (9a). To a warm ethereal solution of phenyllithium prepared from lithium metal (9.36 g, 1.35 mol) and bromobenzene[14] (101 g, 0.64 mol), was added a solution of phthalic anhydride (20 g, 0.135 mol) in anhyd.

17) L. F. Fieser, "Organic Experiments," D. C. Heath and Co., Boston and Maruzen Co. Ltd., Tokyo, 1964, p. 93. See also Ref. 7 where the mp of **17** is reported 100—109°C.

18) Belg. 632—597, Oct. 21, 1963.

19) a) C. S. Marvel and S. M. McElvain, "Organic Syntheses," Coll. Vol. 1, p. 170. b) H. T. Clarke and E. R. Taylor, "Organic Syntheses," Coll. Vol. II, p. 135.

20) W. Tadros, A. B. Sakla, and A. A. A. Helmy, *J. Chem. Soc.*, 2687 (1961).

21) C. F. H. Allen and S. Converse, "Organic Syntheses," Coll. Vol. I, p. 226.

22) Determined by the method of; C. D. Wagner, R. H. Smith, and E. D. Peters, *Anal. Chem.*, **19**, 976 (1947).

dioxane (150 ml) over a 2 hr period. After the mixture has been heated for another hour, the mixture was hydrolyzed by 100 ml of water and the organic layer was dried over anhyd magnesium sulfate. The flash evaporation of the solvent then afforded a crude oil, which was distilled *in vacuo* to give a yellow oil; bp 200°C/4 mmHg. The treatment of the oil in hot ethanol separated **9a** (colorless crystals), 2 g (6%); mp 117°C; IR (CCl_4) 1775 cm^{-1} (C=O).

*Preparation of 3,3-Diphenylcoumaran-2-one (**9b**).* A mixture of benzil (50 g), phenol (50 g), and zinc chloride (50 g) was treated according to a procedure previously reported.[15] After following the work-up procedure, an oily material (*ca.* 1 g) was obtained. IR (liq. film) 1805 cm^{-1} (C=O).

*o-Benzhydrylbenzilic Acid (**15b**).* Compound **2** (1.1 g, 3 mmol), dissolved in ethanol (20 ml), was heated with 20% aq potassium hydroxide (2 ml) under a solvent reflux for 5 hr. On cooling, a white solid separated; this was recrystallized from ethanol to give potassium *o*-benzhydrylbenzilate (**15a**); 1.2 g (95%); mp 297°C; IR (nujol dispersion) 3570 and 3350 (OH), 1605 cm^{-1} (COOK).

Found: C, 70.66; H, 5.22%. Calcd for $C_{27}H_{21}O_3K$ (1.47 H_2O): C, 70.65; H, 5.25%.

An aqueous solution of **15a** was acidified with concd hydrochloric acid to give a precipitate of **15b**; 0.95 g (85%); mp 188°C (ethanol); IR (nujol dispersion) 3530 and 1695 cm^{-1} (COOH); NMR (acetone-d_6) τ 2.53 (2H, m), 2.90 (15H, m), 3.31 (2H, m), 3.86 (1H, s).

Found: C, 82.53; H, 5.52%. Calcd for $C_{27}H_{22}O_3$: C, 82.21; H, 5.62%.

*1-Ethoxy-1,3,3-triphenyl-2-indanone (**16a**).* A mixed solution of **2** (1.1 g, 3 mmol) and concd hydrochloric acid (5 ml) in ethanol (20 ml) was heated under reflux for 5 hr. After cooling, a white solid of **16a** separated from the solution; 0.9 g (73%); mp 166°C (cyclohexane); IR (CCl_4) 1760 (C=O) and 1085 cm^{-1} (C–O); NMR (CCl_4) τ 2.96 (19H, m), 6.74 and 6.76 (2H, a pair of q, $J=7$ Hz), 8.86 (3H, t).

Found: C, 86.70; H, 5.98%. Calcd for $C_{29}H_{24}O_2$: C, 86.11; H, 5.95%.

*1-Methoxy-1,3,3-triphenyl-2-indanone (**16b**).* A treatment of **2** (1.1 g, 3 mmol) with methanol similar to the above-described procedure used for **16a** gave **16b** (0.9 g, 78%); mp 168°C; IR (CCl_4) 1760 (C=O) and 1085 cm^{-1} (C–O); NMR ($CDCl_3$, 60 MHz) τ 2.90 (19H, m), 6.82 (3H, s).

Found: C, 86.41; H, 5.47%. Calcd for $C_{28}H_{22}O_2$: C, 86.13; H, 5.68%.

*1,3,3-Triphenyl-2-indanone (**17**).* A solution of **2** (1.1 g, 3 mmol) and 47% hydriodic acid (4 ml) in glacial acetic acid (15 ml) was heated for 1 min under solvent reflux.[16] After cooling, the solution was decolorized with 5% aq sodium bisulfite to give a colorless precipitate of **17**; 0.7 g (65%); mp 133—134°C (diethyl ether); IR (CCl_4) 1760 cm^{-1} (C=O); NMR (CCl_4, 60 MHz) τ 2.85 (19H, m), 5.33 (1H, s).

Found: C, 89.67; H, 5.69%. Calcd for $C_{20}H_{20}O$: C, 89.97; H, 5.59%.

The authors wish to thank Mr. Takeda of the Shimadzu Co. for his help in taking the mass spectra. Thanks are also due to Mr. Takayuki Kida for the NMR measurement.

BULLETIN OF THE CHEMICAL SOCIETY OF JAPAN, VOL. 46, 279—282 (1973)

Selective Homogeneous Hydrogenation of 3-Oxo-1,4-diene Steroids. II.[1] Effects of Basic Additives and of *para* Substituents on the Hydrogenation with Dichlorotris(triphenylphosphine)ruthenium

Shigeo NISHIMURA, Tomio ICHINO, Akira AKIMOTO, and Kiyoshi TSUNEDA*

Department of Industrial Chemistry, Tokyo University of Agriculture and Technology, Koganei, Tokyo
**Chemical Research Laboratory, Teikoku Hormone Manufacturing Co., Ltd., Shimosakunobe, Kawasaki*

(Received June 29, 1972)

The catalytic homogeneous hydrogenation of 1,4-androstadiene-3,17-dione (I) with dichlorotris(triphenylphosphine)ruthenium has been investigated in the presence of basic additives. The rate of hydrogenation increased with respect to added amines in the order pyridine<none<butylamine<aniline<diethylamine≅triethylamine. The hydrogenation was also promoted by the addition of calcium carbonate, but slightly retarded by that of sodium carbonate. The amount of triethylamine required for obtaining the maximum rate of hydrogenation has been determined. Addition of triethylamine also reduced the formation of 5α-androstane-3,17-dione produced by a different pathway from that for the formation of 4-androstene-3,17-dione (II), resulting in an increased selectivity for the formation of II. I was also hydrogenated with the ruthenium complexes having *p*-methoxy-, *p*-methyl-, and *p*-fluoro-substituted triphenylphosphines as ligands. The catalytic activity of the ruthenium complex was greatly enhanced by *p*-methoxyl and *p*-methyl groups and reduced by *p*-fluoro group when the catalyst was used in the presence of triethylamine.

In a previous paper[1] we showed that 3-oxo-1,4-diene steroids are selectively hydrogenated to the corresponding 3-oxo-4-enes with dichlorotris(triphenylphosphine)-ruthenium as a catalyst. Hydrogenation with the ruthenium complex also yielded small amounts of saturated 5α-ketones which were formed by a different pathway from that for the formation of 3-oxo-4-enes.

1) Part I: S. Nishimura and K. Tsuneda, This Bulletin, **42**, 852 (1969).

This was in contrast to the hydrogenation with chlorotris(triphenylphosphine)rhodium,[2,3] where saturated ketones were all formed consecutively *via* the intermediate 3-oxo-4-enes. It was also shown that the ratio of 3-oxo-4-ene to the saturated 5α-ketone formed increases with increasing hydrogen pressure and decreasing reaction temperature. Thus, with the ruthenium complex catalyst, high yields of 3-oxo-4-enes were obtained by hydrogenating the corresponding 3-oxo-1,4-dienes at a relatively low temperature and under a high hydrogen pressure.

In this study we have investigated the effects of added basic substances and of *para* substituents in the triphenylphosphine ligand on the hydrogenation of 1,4-androstadiene-3,17-dione (I) with the ruthenium complex as catalyst.

The Effects of Basic Additives. It is known that bases promote the formation of the hydrido complex of ruthenium, the active species in hydrogenation, according to the equation[4]

$$RuCl_2(PPh_3)_3 + H_2 + \text{base} = RuClH(PPh_3)_3 + \text{base}\cdot HCl \quad (1)$$

We have therefore studied the effect of the addition of various basic substances in the hydrogenation of I in benzene. We see from Table 1 that the rate of hydrogenation increased with respect to the added amines in the order pyridine<none<butylamine<aniline<diethylamine≅triethylamine. The hydrogenation was also effectively promoted by the addition of calcium carbonate, but retarded slightly by the addition of sodium carbonate. Figure 1 shows the effect of the varying amount of added triethylamine on the rate of hydrogenation of I. It is seen that the maximum rate is obtained when triethylamine is added in a slightly greater amount than that required by Eq. (1) and addition of the amine in further excess ureslts in the decrease in rate.

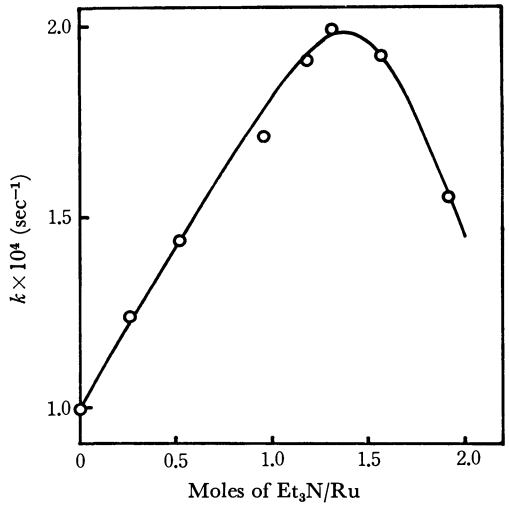

Fig. 1. Effect of the varying amount of added triethylamine on the rate of hydrogenation of I. I (500 mg) was hydrogenated with 50 mg of $RuCl_2(PPh_3)_3$ in 10 ml benzene at 50°C and 100 kg/cm² H_2.

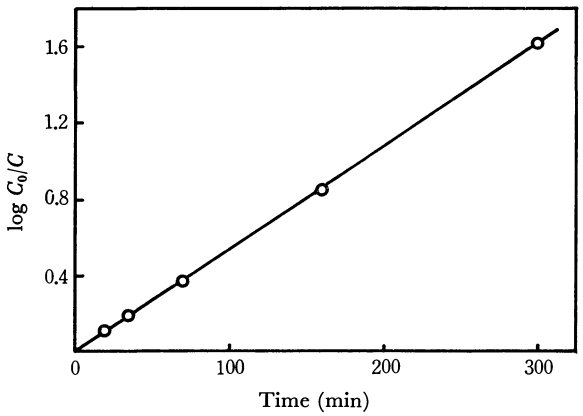

Fig. 2. First-order dependence of the rate of hydrogenation on the concentration of I. I (500 mg) was hydrogenated with 50 mg (0.052 mmol) of $RuCl_2(PPh_3)_3$ and 6.9 mg (0.068 mmol) of triethylamine in 10 ml benzene at 50°C and 100 kg/cm² H_2.

TABLE 1. EFFECT OF BASIC ADDITIVES ON THE HYDROGENATION OF 1,4-ANDROSTADIENE-3,17-DIONE (I) WITH DICHLOROTRIS-(TRIPHENYLPHOSPHINE)RUTHENIUM[a]

Additive[b]	Conversion of I, %
Triethylamine	95.4
Diethylamine	95.4
Butylamine	86.5
Aniline	88.1
Pyridine	62.7
Calcium carbonate	95.2
Sodium carbonate	73.0
None	76.0

a) I(500 mg) was hydrogenated with 50 mg of $RuCl_2(PPh_3)_3$ in 10 ml benzene at 40°C under a hydrogen pressure of 130—135 kg/cm² for 6 hr.

b) The amines were added in the stoichiometric amounts required by Eq. (1). Calcium and sodium carbonates were added in the amounts 21 and 22 mg (four times of the amounts required by Eq. (1)), respectively.

The rate of hydrogenation is strictly of first order in the concentration of I as shown in Fig. 2. This kinetic dependence of the rate on concentration is also in contrast to the hydrogenation of I with the rhodium complex where the rate obeys the Langmuir type equation in the same region of the concentration of I.[5]

Variations in the amounts of products during hydrogenation are shown in Fig. 3. Since the reaction pathways for the formation of saturated ketones (IIIα and IIIβ) are considered to be as shown in Scheme 1, the variation in concentration of 4-androstene-3,17-dione (II) can be expressed as a function of the concentration of I by the equation[6]

2) A. J. Birch and K. A. M. Walker, *J. Chem. Soc. C*, **1966**, 1894.

3) C. Djerassi and J. Gutzwiller, *J. Amer. Chem. Soc.*, **88**, 4537 (1966).

4) P. S. Hallman, D. Evans, J. A. Osborn, and G. Wilkinson, *Chem. Commun.*, **1967**, 305; P. S. Hallman, B. R. McGarvey, and G. Wilkinson, *J. Chem. Soc. A*, **1968**, 3143.

5) S. Nishimura and S. Kamihara, unpublished results.

6) J. H. de Boer and R. J. A. M. van der Borg, "Actes Congr. Intern. Catal.", 2e, Paris, 1960, p. 919 (Editions Technip, Paris, 1961).

Table 2. Hydrogenation of 1,4-androstadiene-3,17-dione (I) with dichlorotris(triarylphosphine)ruthenium[a]

Catalyst X in $RuCl_2[(p\text{-}XC_6H_4)_3P]_3$	Composition of reac. mixture (mol%) I	II	III	10^4k_X[b] (sec^{-1})	k_X/k_H[b]	k_X/k_H[b] with no added Et_3N	r_X/r_H[c] for $RhCl[(p\text{-}XC_6H_4)_3P]_2$
MeO	2.1	93.7	4.2	10.8	5.6	0.96	2.4
Me	3.9	93.3	2.8	9.0	4.6	1.8	2.1
H	49.8	48.4	1.8	1.9	1.0	1.0	1.0
F	91.5	8.5	trace	0.24	0.12	0.21	0.14

a) I (500 mg) was hydrogenated in the presence of 0.026 mmol of the ruthenium catalyst and 0.034 mmol of triethylamine in 10 ml benzene at 50°C under a hydrogen pressure of 100 kg/cm² for 1 hr.
b) k_X and k_H denote the first-order rate constants for the hydrogenation catalyzed by the ruthenium complex with *para* substituent X and not with substituent, respectively.
c) The ratio of rates of hydrogenation of cyclohexene catalyzed by the rhodium complex with *para* substituent X and with no substituent [Data from C. O'Connor and G. Wilkinson, *Tetrahedron Lett.*, **1969** 1375].

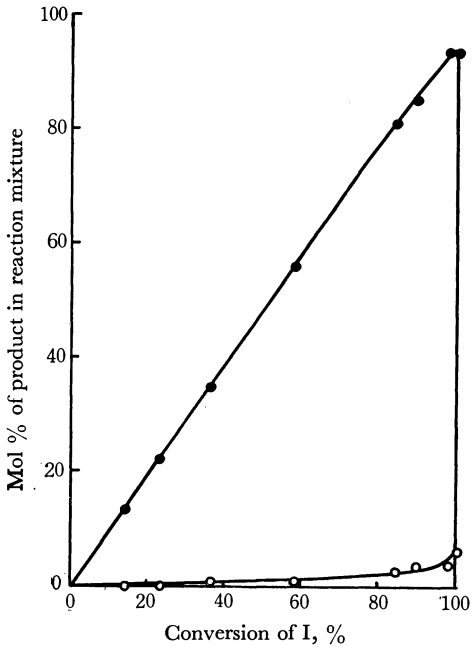

Fig. 3. Variations in the amounts of II (●) and III (○) in the reaction mixture as a function of the conversion of I. The points indicate individual experiments. Full lines give theoretical curves showing the variations in the amounts of II and III when f=0.983 and K=1/90 in Eq. (2). The reaction conditions are the same as in Fig. 2.

$$C_{II} = \frac{f}{K-1}(C_I - C_I^K) \qquad (2)$$

where $f=k_1/(k_1+k_3)$, $K=k_2/(k_1+k_3)$, and k_i's are the first-order rate constants for the corresponding reaction paths shown in Scheme 1. C_I and C_{II} are the concentrations of I and II, respectively, when the initial concentration of I is taken as unity. It follows from Eq. (2) that the variation in concentration of added IIIα and IIIβ is given by $1-C_I-f(C_I-C_I^K)/(K-1)$. By applying this relation to the observed change in the amount of IIIα and IIIβ, we obtain f=0.983 and K=1/90 as a most satisfactory set of values. This implies that the amount of IIIα formed by the reaction path (3) was depressed to the extent of only 1.7% in the presence of added triethylamine as compared with 10.5% for that in the absence of the amine.[1] On the other hand, the result indicates that hydroganetion of

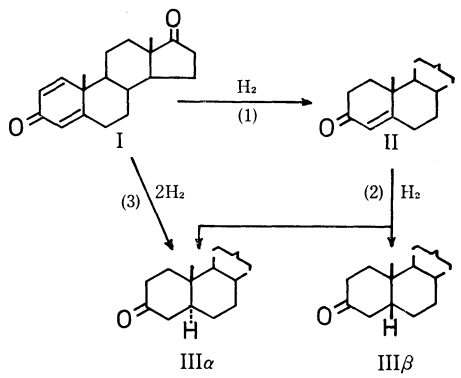

Scheme 1. Hydrogenation pathways of 1,4-androstadiene-3,17-dione.

II to IIIα and IIIβ, which practically did not take place in the absence of base,[1] occurs very slowly in the presence of triethylamine. The ratio of IIIα to IIIβ formed decreases toward the end of hydrogenation, indicating increasing contribution of the saturated ketones formed *via* II with the extent of hydrogenation.[7] The maximum yield of II is given by $f\times K^{K/(1-K)}$ and calculated to be 93.5% at 98.9% conversion of I from the obtained values of f and K.

The Effect of para *Substituents in the Triphenylphosphine Ligand.* It has been reported that the catalytic activity of chlorobis(triphenylphosphine)rhodium is enhanced by electron-releasing *para* substituents in the triphenylphosphine ligand, as observed in the hydrogenation of olefins.[8] As regards the ruthenium complex, the use of tri-*p*-tolyl- and tri-*p*-fluorophenylphosphines as ligands has recently been described in a patent.[9] We prepared the ruthenium complexes

7) Small amounts of IIIβ and an alcohol, possibly 3-hydroxy-5α-androstan-17-one, appear to be formed also by the reaction path (3). The ratio of IIIβ to IIIα, however, was much smaller than that in the products formed through II.

8) S. Montelatici, A. van der Ent, A. Osborn, and G. Wilkinson, *J. Chem. Soc. A*, **1968**, 1054; C. O'Connor and G. Wilkinson, *Tetrahedron Lett.*, **1969**, 1375.

9) J. P. Candlin, J. R. Jennings, and P. F. Todd, Brit. Pat. 1246123 (1971); *Chem. Abstr.*, **75**, 129935 m (1971).

9a) Note Added in Proof. After this manuscript was submitted to publication, preparations of *para*-substituted triphenylphosphineruthenium complexes and their use in an isomerization reaction have been described by Blum and Becker [*J. Chem. Soc. Perkin II*, **1972**, 982].

with tri-*p*-methoxyphenyl-, tri-*p*-tolyl-, and tri-*p*-fluorophenylphosphines as ligands and compared their catalytic activities in the hydrogenation of I.[9a] The results are summarized in Table 2. It is seen that the activity of the ruthenium complex is also enhanced by the electron-releasing *p*-methoxyl and *p*-methyl groups and decreased by the electron-withdrawing *p*-fluoro group. The effects of the *para* substituents seem to be more pronounced than in the case of the rhodium complex (see Table 2). It is to be noted that their electronic effects are observed in a proper order only in the presence of triethylamine.

The results show that the activity as well as the selectivity of dichlorotris(triphenylphosphine)ruthenium in the hydrogenation of I are greatly improved by the addition of an optimal amount of triethylamine. The activity of the ruthenium complex is further enhanced by the electron-releasing *p*-methoxyl and *p*-methyl groups in the triphenylphosphine ligand. Thus the hydrogenation of 3-oxo-1,4-diene steroids under these conditions might be useful for the preparation of the corresponding 3-oxo-4-enes. Typical examples of the preparation of II using the ruthenium complexes are given (see Experimental).

Experimental

Material. 1,4-Androstadiene-3,17-dione (I) was obtained from the Kikkoman Shoyu Co., Ltd., and used without further purification. Mp 142.5—143.5°C.[10]

Catalysts. Dichlorotris(triarylphosphine)ruthenium was prepared by refluxing ruthenium chloride trihydrate with six-fold excess of the triarylphosphine in ethanol for about 1 hr (for 2.5 hr in the case of tri-*p*-fluorophenylphosphine).

Dichlorotris(triphenylphosphine)ruthenium. Found: C, 66.93; H, 4.92%. Calcd for $C_{54}H_{45}Cl_2P_3Ru$: C, 67.64; H, 4.74%.

Dichlorotris(tri-*p*-methoxyphenylphosphine)ruthenium. Found: C, 60.92; H, 5.26%. Calcd for $C_{63}H_{63}Cl_2O_9P_3Ru$: C, 61.56; H, 5.18%.

Dichlorotris(tri-*p*-tolylphosphine)ruthenium. Found: C, 69.47; H, 5.38%. Calcd for $C_{63}H_{63}Cl_2P_3Ru$: C, 69.72; H, 5.86%.

Dichlorotris(tri-*p*-fluorophenylphosphine)ruthenium. Found: C, 57.94; H, 3.93%. Calcd for $C_{54}H_{36}Cl_2F_9P_3Ru$: C, 57.87; H, 3.24%.

Hydrogenation. The hydrogenation was performed in a 30 ml bomb equipped with a magnetic stirrer. The bomb was immersed in an oil bath maintained at a constant temperature.

Analysis of Product. The product was analyzed by gas chromatography (2% OV-17 at 250°C or 1.5% QF-1 at 220°C) after evaporation of the solvent followed by extraction with methylcyclohexane.

Examples of the Preparation of 4-Androstene-3,17-dione (II).

a) By Hydrogenation of I with Dichlorotris(triphenylphosphine)ruthenium. I (500 mg) was hydrogenated with 50 mg (0.052 mmol) of the ruthenium catalyst and 5.3 mg (0.052 mmol) of triethylamine in 10 ml benzene at 40°C under a hydrogen pressure of 130 kg/cm² for 8 hr. The benzene solution was passed through alumina followed by elution with benzene–ether. Evaporation of the solvent gave 498 mg of a solid residue. Recrystallization from acetone–hexane gave 447 mg of colorless needles (89% yield). Mp 169.5—171°C (98% purity by glpc analysis) (reported mp: 173—174°C[11]).

*b) By Hydrogenation of I with Dichlorotris(tri-*p*-tolylphosphine)ruthenium.* I (500 mg) was hydrogenated with 28 mg (0.026 mmol) of the ruthenium catalyst and 3.4 mg (0.034 mmol) of triethylamine in 10 ml benzene at 50°C under a hydrogen pressure of 100 kg/cm² for 2 hr. Treatment of the benzene solution in the same way as above gave 506 mg of a solid residue. Recrystallization from acetone–hexane gave 452 mg of light brown needles (90% yield). Mp 168.5—171°C (97.5% purity by glpc analysis).

*c) By Hydrogenation of I with Dichlorotris(tri-*p*-methoxyphenylphosphine)ruthenium.* I (2.0 g, recrystallized from ethanol–hexane, mp 144—145°C) was hydrogenated with 32 mg (0.026 mmol) of the ruthenium catalyst and 3.4 mg (0.034 mmol) of triethylamine in 10 ml benzene at 50°C under a hydrogen pressure of 100 kg/cm² for 2.5 hr. Treatment of the benzene solution in the same way as above gave 2.02 g of a solid residue. Recrystallization from acetone–hexane gave 1.82 g of colorless needles (90% yield). Mp 170—171°C (98.5% purity by glpc analysis).

The authors are grateful to Dr. Motohiko Kato of the Kikkoman Shoyu Co. and to Drs. Masanobu Sawai and Hiromu Mori of the Teikoku Hormorne Manufacturing Co. for their valuable suggestions.

10) All melting points were measured by an instrument for measurement of micromelting point, Mettler FP-2.

11) L. Ruzicka and A. Wettstein, *Helv. Chim. Acta*, **18**, 986 (1935).

Compounds Related to Acridine. X.[1] The Reaction of 9-Ethynylacridine with Active Methylene Compounds

Otohiko Tsuge[2] and Akiyoshi Torii*

Research Institute of Industrial Science, Kyushu University, Hakozaki, Higashi-ku, Fukuoka, 812
**Department of Industrial Chemistry, Kurume Technical College, Komorino, Kurume, 830*

(Received June 28, 1972)

In the presence of aqueous sodium hydroxide, 9-ethynylacridine (I) reacts with malononitrile and with ethyl cyanoacetate to yield the corresponding 1,1-disubstituted 3-(9-acridanylidene)propenes III. A similar reaction of I with diethyl malonate affords a 2:1 adduct VI and a 1:2 adduct VII. On the other hand, I reacts with acetylacetone to give 3-acetyl-5-(9-acridanylidene)-1-(9-acridinyl)pent-1,3-diene (IX). In this context, the reaction of 9-chloroacridine (XI) with active methylene compounds has been reinvestigated; XI reacts with malononitrile and with ethyl cyanoacetate to afford products XII with an acridane structure, while with diethyl malonate XI gives 9-di(ethoxycarbonyl)methylacridine (XIII), as has been reported previously.

Little is known about the reaction of heteroaromatics having an ethynyl group. Recently, we have reported[3] a convenient method of the preparation of 9-ethynylacridine (I) and some of its reactions.[3,4] Our previous studies[3,4] suggested that the acetylene I would react easily with active methylene compounds to form 2-substituted 1-(9-acridinyl)ethylenes. We will now report on the novel reaction of the acetylene I with active methylene compounds. In this connection, the present paper will also deal with the reaction of 9-chloroacridine with active methylene compounds.

Results and Discussion

The reaction of the acetylene I with malononitrile (IIa) in the presence of aqueous sodium hydroxide in ethanol at room temperature afforded a 1:1 adduct IIIa as violet prisms in an excellent yield. The spectral data of IIIa indicated that IIIa was not the expected 1-(9-acridinyl)-3,3-dicyanopropene (III'), but rather 3-(9-acridanylidene)-1,1-dicyanopropene (Scheme 1).

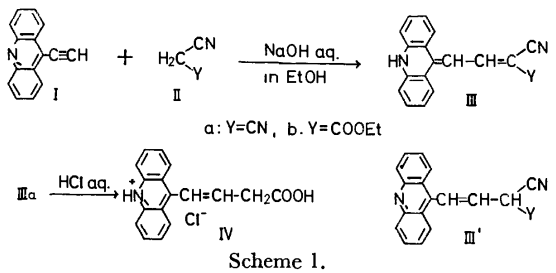

Scheme 1.

Similarly, the acetylene I reacted with ethyl cyanoacetate (IIb) to give the corresponding acridanylidene derivative IIIb. The hydrolysis of IIIa with hydrochloric acid afforded hydrochloride of 4-(9-acridinyl)-but-2-enoic acid (IV), whose structure was confirmed by the spectral data as well as by the results of microanalysis.

On the other hand, the reaction of acetylene I with diethyl malonate (V) under similar conditions afforded a 2:1 adduct VI and a 1:2 adduct VII of I and V, respectively, both as pale yellow prisms, in 36 and 4% yields respectively. On the basis of their spectral data, VI and VII were deduced to be 1,5-di(9-acridinyl)-3,3-di(ethoxycarbonyl)pent-1,4-diene, and either 1,1,3,3-tetra(ethoxycarbonyl)-2-(9-acridinylmethyl)propane (VII-1) or 1,1,4,4-tetra(ethoxycarbonyl)-2-(9-acridinyl)-butane (VII-2), respectively. The structures of VI and VII correspond to those of 1:1 Michael-type adducts of A to the acetylene I and to V respectively (Scheme 2).

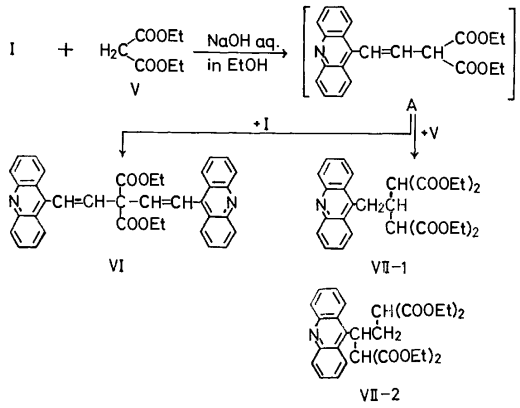

Scheme 2.

The reaction of the acetylene I with acetylacetone (VIII) yielded a product IX, whose molecular formula corresponded to that of the compound derived from a 2:1 adduct of I and VIII under the elimination of an acetyl group. From the inspection of its spectral data, IX was identified as 3-acetyl-5-(9-acridanylidene)-1-(9-acridinyl)pent-1,3-diene.

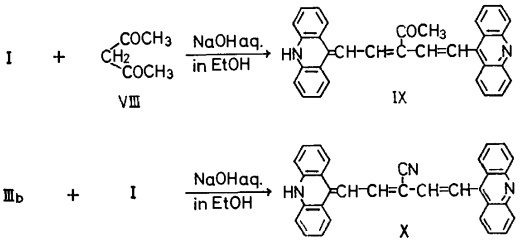

Scheme 3.

The two products VI and IX correspond to the compounds obtainable from two moles of the acetylene I and one mole of an active methylene compound.

1) Part IX of this series: O. Tsuge and A. Torii, *Org. Prep. Proced. Int.*, in press (1972).
2) To whom inquiries should be directed.
3) O. Tsuge and A. Torii, This Bulletin, **43**, 2920 (1970).
4) O. Tsuge and A. Torii, *Org. Prep. Proced. Int.*, in press (1972).

Therefore, the 1: 1 adduct would be expected to react with the acetylene I to give compounds of the VI or IX type.

Although IIIa did not react with the acetylene I, the reaction of IIIb with I afforded 5-(9-acridanylidene)-1-(9-acridinyl)-3-cyanopent-1,3-diene (X), whose structure corresponds to that of the compound derived from a 1: 1 adduct by decarbethoxylation. The structure of X was confirmed by the spectral data as well as by the results of microanalysis. The pathway for the formation of IX and X is not yet clear, however.

In view of the formation of the acridane-like compound III, it is conceivable that the products from the reaction of 9-chloroacridine (XI) with active methylene compounds have acridane-like structures. Investigations on the reaction of XI with active methylene compounds have been reported by several workers. Most of them[5-7] have reported the products to be derivatives of 9-methylacridine. Only Kröhnke and Honig[8] discussed the possibility of an equilibrium between acridine and acridane structures.

We investigated the reaction of XI with active methylene compounds in order to determine whether or not the products had the acridane structure. The reaction of XI with malononitrile (IIa) and with ethyl cyanoacetate (IIb) afforded products of the acridane type, XIIa and XIIb, while XI reacted with diethyl malonate (V) to give 9-di(ethoxycarbonyl)methylacridine (XIII), as has been reported in the literature.[5]

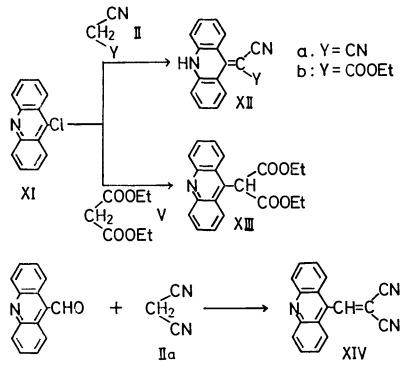

Scheme 4.

The UV spectra of the acridanylidene compounds, III, X, and XII, exhibited absorption bands in a longer-wavelength region. The UV spectrum of XIIa showed a strong band at 480 nm, while an absorption band appeared at 366 nm in the spectrum of 1-(9-acridinyl)-2,2-dicyanoethylene (XIV). This can be explained by the longer conjugation of the acridanylidene structures.

Experimental

All the melting points are uncorrected. The IR spectra were measured as KBr pellets, and the UV spectra were determined in ethanol solutions. The mass spectra were obtained on a Hitachi RMS-4 mass spectrometer with a direct inlet and an ionization energy of 70 eV, while the NMR spectra were determined at 60 MHz with a Hitach-R-20 NMR spectrometer, with TMS as the internal reference. The microanalyses were performed by Miss M. Akita of our laboratory.

Reaction of the Acetylene I with Malononitrile (IIa). A solution of 0.3 g of I, 0.1 g of IIa, and one drop of an aqueous saturated sodium hydroxide solution in 5 ml of ethanol was stirred at room temperature for 1 hr; during this time crystals were deposited. Filtration gave 0.36 g (91%) of violet crystals which, on recrystallization from ethanol, afforded 3-(9-acridanylidene)-1,1-dicyanopropene (IIIa), mp 280—281 °C, as violet prisms.

Found: C, 80.49; H, 3.95; N, 15.36%. Calcd for $C_{18}H_{11}N_3$: C, 80.28; H, 4.12; N, 15.61%.

IR cm^{-1}: ν_{NH} 3300, $\nu_{C\equiv N}$ 2240. NMR (DMSO-d_6) δ ppm: 6.85 (1H, doublet, =C**H**, 12 Hz), 7.15—8.1 (9H, complicated signal, =C**H** and aromatic protons (8H)), 12.1 (1H, singlet, N**H**, exchanged with D_2O). UV λ_{max} nm (log ε): 253 (4.65), 318 (4.0), 570 (4.5). Mass spectrum *m/e*: 269 (M^+).

Similarly, the acetylene I reacted with ethyl cyanoacetate (IIb) to give a 98% yield of the corresponding acridanylidene derivative IIIb, mp 246°C, as violet prisms (from ethanol).

Found: C, 76.20; H, 5.08; N, 8.67%. Calcd for $C_{20}H_{16}N_2O_2$: C, 75.93; H, 5.10; N, 8.86%.

IR cm^{-1}: ν_{NH} 3290, $\nu_{C\equiv N}$ 2245, $\nu_{C=O}$ 1675. NMR (DMSO-d_6) δ ppm: 1.28 (3H, triplet, C**H**$_3$), 4.19 (2H, quartet, C**H**$_2$), 6.8—8.5 (10H, complicated, olefinic (2H) and aromatic protons (8H)), 11.7 (1H, singlet, N**H**, exchanged with D_2O). UV λ_{max} nm (log ε): 252 (4.65), 316 (3.95), 550 (4.4). Mass spectrum *m/e*: 316 (M^+).

Hydrochloride of 4-(9-Acridinyl)but-2-enoic acid (IV). A suspension of 0.5 g of IIIa in 5 ml of concentrated hydrochloric acid was stirred at 95°C for 2 hr. Filtration gave 0.35 g (56%) of IV, mp 200—201°C, as yellow prisms.

Found: C, 68.14; H, 4.62; N, 4.85%. Calcd for $C_{17}H_{13}NO_2 \cdot HCl$: C, 68.11; H, 4.67; N, 4.67%.

IR cm^{-1}: ν_{NH} and ν_{OH} 3000—2300, $\nu_{C=O}$ 1730, Mass spectrum *m/e*: 263 ($C_{17}H_{13}NO_2^+$), 218 ($263^+ - COOH$, base peak), 204 ($218^+ - CH_2$), 178 ($204^+ - C_2H_2$).

Reaction of the Acetylene I with Diethyl Malonate (V). A solution of 0.3 g of I and 0.2 g of V in 5 ml of ethanol containing one drop of an aqueous saturated sodium hydroxide solution was stirred at room temperature for 1 hr. The reaction mixture was then concentrated *in vacuo* to leave a residue which, on recrystallization from petroleum ether (bp 40—65°C), gave 1,5-(9-acridinyl)-3,3-di(ethoxycarbonyl)-pent-1,4-diene (VI), mp 197—198°C, as pale yellow prisms. Yield, 0.15 g (36%).

Found: C, 76.28; H, 5.39; N, 4.84%. Calcd for $C_{37}H_{30}N_2O_4 \cdot H_2O$: C, 76.01; H, 5.52; N, 4.79%.

IR cm^{-1}: $\nu_{C=O}$ 1735. NMR ($CDCl_3$) δ ppm: 1.0 (6H, triplet, C**H**$_3$), 3.5 (4H, quartet, C**H**$_2$), 6.7—8.6 (20H, complicated, olefinic (4H) and aromatic protons (16H)). Mass spectrum *m/e*: 566 (M^+), 493 ($M^+ - COOEt$), 420 ($493^+ - COOEt$).

The mother liquor was evaporated *in vacuo* to leave a residue, which was then chromatographed on alumina, using benzene as the eluent, to give 30 mg (4%) of a 1: 2 adduct VII. Recrystallization from petroleum ether (bp 40—60°C) afforded pure VII, mp 102—103°C, as pale yellow prisms.

Found: C, 66.71; H, 6.33; N, 3.03%. Calcd for $C_{29}H_{33}NO_8$: C, 66.52; H, 6.35; N, 2.68%.

IR cm^{-1}: $\nu_{C=O}$ 1755, 1735. NMR ($CDCl_3$) δ ppm: 1.0

5) Y. Mizuno, K. Adachi, and K. Ikeda, *Chem. Pharm. Bull.* (Tokyo), **2**, 225 (1954).
6) A. A. Goldberg and Wm. Kelly, Brit. 600354 (1948).
7) E. N. Morgan and D. J. Tivey, Brit. 789696 (1958).
8) F. Kröhnke and H. L. Honig, *Ann. Chem.*, **624**, **97** (1959).

(12H, sextet, CH_3), 4.0 (13H, multiplet, CH_2 (10H) and CH (3H)), 8.0 (8H, multiplet, aromatic protons). Mass spectrum *m/e*: 523 (M^+), 450 ($M^+-COOEt$), 363 ($M^+-CH_2(COOEt)_2$), 204 ($363^+-CH(COOEt)_2$).

Reaction of the Acetylene I with Acetylacetone (VIII). To a solution of 0.5 g of I and 0.2 g of VIII in 10 ml of ethanol was added two drops of an aqueous sodium hydroxide solution; the reaction mixture was then stirred at room temperature for 15 hr. After it had been allowed to stand overnight, filtration gave 0.16 g (22%) of crystals. Recrystallization from dioxane afforded 3-acetyl-5-(9-acridanylidene)-1-(9-acridinyl)pent-1,3-diene (IX), mp 223—224°C, as violet prisms.

Found: C, 85.13; H, 5.38; N, 5.82%. Calcd for $C_{33}H_{24}N_2O$: C, 85.32; H, 5.21; N, 6.03%.

IR cm^{-1}: ν_{NH} 3280, $\nu_{C=O}$ 1620. UV λ_{max} nm (log ε): 249 (5.1), 346 (4.1), 525 (4.3). Mass spectrum *m/e*: 464 (M^+), 421 (M^+-COCH_3), 286 (M^+—acridinyl), 260 (M^+—9-ethynylacridine), 217 (260^+-COCH_3), 204 (9-ethynylacridine$^+$), 193 (base peak), 179 (acridine$^+$).

Reaction of the Acetylene I with the Acridanylidene Derivative IIIb. A solution of 0.15 g of I and 0.2 g of IIIb in 5 ml of ethanol was stirred at room temperature for 4.5 hr; during this time crystals were deposited. Filtration and recrystallization from dioxane gave 0.2 g (71%) of 5-(9-acridanylidene)-1-(9-acridinyl)-3-cyanopent-1,3-diene (X), mp 264—265°C, as violet prisms.

Found: C, 85.92; H, 4.56; N, 9.06%. Calcd for $C_{32}H_{21}N_3$: C, 85.88; H, 4.73; N, 9.39%.

IR cm^{-1}: ν_{NH} 3300, $\nu_{C\equiv N}$ 2220. UV λ_{max} nm (log ε): 250 (4.9), 318 (4.0), 570 (4.5). Mass spectrum *m/e*: 447 (M^+), 268 (M^+—acridine), 243 (M^+—9-ethynylacridine), 217 (243^+-CN), 204 (9-ethynylacridine$^+$), 193 (base peak), 179 (acridine$^+$).

Reaction of 9-Chloroacridine (XI) with Malononitrile (IIa). To a solution of 0.5 g of XI[9] and 0.5 g of IIa in 5 ml of ethanol was added four drops of an aqueous sodium hydroxide solution; the reaction mixture was then stirred at room temperature for 1.5 hr; during which time crystals were precipitated. Filtration gave 0.34 g (60%) of reddish orange crystals. Recrystallization from nitrobenzene afforded the 9-acridanylidene derivative XIIa, mp 339°C (lit,[7] mp 342°C), as reddish orange prisms.

IR cm^{-1}: ν_{NH} 3280, $\nu_{C\equiv N}$ 2215. UV λ_{max} nm (log ε): 240 (4.3), 294 (4.0), 480 (4.1). NMR (DMSO-d_6) δ ppm: 7.2—8.8 (8H, complicated, aromatic protons), 12.5 (1H, broad, NH, exchanged with D_2O).

Similarly, XI reacted with ethyl cyanoacetate (IIb) to give a 60% yield of the 9-acridanylidene derivative XIIb, mp 218°C (lit,[6] mp 222—224°C), as violet prisms.

IR cm^{-1}: ν_{NH} 3280, $\nu_{C\equiv N}$ 2210, $\nu_{C=O}$ 1660. UV λ_{max} nm (log ε): 247 (4.7), 293 (4.1), 480 (3.9). NMR (DMSO-d_6) δ ppm: 1.19 (3H, triplet, CH_3), 4.20 (2H, quartet, CH_2), 7.2—8.4 (8H, multiplet, aromatic protons), 12.40 (1H, broad, NH, exchanged with D_2O).

On the other hand, the reaction of XI with diethyl malonate (V) according to the reported method[5] gave the 9-methylacridine derivative XIII, mp 102—103°C (lit,[5] mp 100—102°C), as pale yellow prisms, as has been reported previously.

1-(9-Acridinyl)-2,2-dicyanoethylene (XIV). A solution of 1.0 g of acridine-9-carboxaldehyde[10] and 0.32 g of IIa in 10 ml of ethanol containing one drop of an aqueous sodium hydroxide solution was stirred at 60°C for 5 min. After the reaction mixture had been cooled, filtration gave 1.2 g (97%) of yellow crystals. Recrystallization from benzene afforded XIV, mp 181—182°C (decomp.), as yellow plates.

Found: C, 80.11; H, 3.65; N, 16.53%. Calcd for $C_{17}H_9N_3$: C, 79.98; H, 3.55; N, 16.46%. UV λ_{max} nm (log ε): 248 (4.9), 366 (3.8).

9) A. Albert and B. Ritchie, "Organic Syntheses," Coll. Vol. III, p. 53 (1955).

10) O. Tsuge, M. Nishinohara, and M. Tashiro, This Bulletin, **36**, 1477 (1963).

Studies of Enamines. II.[1] The Reaction of 4-(1-Piperidyl)- and 4-(1-Pyrrolidinyl)-3-penten-2-ones with Aryl Isocyanates

Otohiko TSUGE[2] and Akitaka INABA

Research Institute of Industrial Science, Kyushu University, Hakozaki, Higashi-ku, Fukuoka, 812

(Received July 1, 1972)

The reaction of aryl isocyanates with enamino ketones, derived from acetylacetone and secondary amines such as piperidine and pyrrolidine, has been investigated. At room temperature, enamino ketones react with phenyl, *p*-chlorophenyl and *p*-tolyl isocyanate to give 1:2 adducts, 3,5-diarylcarbamoyl derivative. In solution, these adducts exist in general as a mixture of two tautomers, 3-penten-2-one and 4-penten-2-one, the ratio depending on the solvent. Under reflux in benzene, the reaction of enamino ketones with phenyl isocyanate gives 4-amino-6-methyl-1-phenyl-5-phenylcarbamoylpyrid-2-one and its 3-phenylcarbamoyl derivative; the former is also obtained by heating the 1:2 adduct. On the other hand, 4-(1-pyrrolidinyl)-3-penten-2-one reacts with 1-naphthyl isocyanate to afford the 1:1 adduct, 5-(1-naphthylcarbamoyl)-4-penten-2-one.

Many investigations have been carried out on the reactions of enamines with isocyanates. Products of different types are formed depending on the structures of the enamines and on the reaction conditions. For example, the reaction of *β*-disubstituted enamines with phenyl isocyanate at low temperature gives *β*-amino-*β*-lactams,[3,4] while the reaction with two equivalents of the isocyanate at high temperature affords hydrouracils, the 1:2 cycloadducts.[5] On the other hand, enamines having *β*-hydrogen react with isocyanates to give the corresponding carboxamides.[6,7]

Although a few reports are available on the reactions of enamino ketones with electrophiles,[8-11] the reaction of enamino ketones with isocyanates has not been investigated. On the basis of previous studies,[8-11] the chemical behavior of enamino ketones can be understood in terms of the following mesomeric forms.

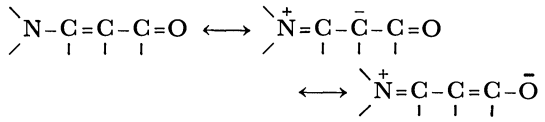

It thus appeared of interest to investigate the reaction of enamino ketones with isocyanates. We report on a new reaction of enamino ketones derived from acetylacetone with aryl isocyanates.

Results and Discussion

Reaction at Room Temperature. When 4-(1-piperidyl)-3-penten-2-one (Ia) was treated with two equivalents of phenyl isocyanate (IIa) in benzene at room temperature for 5 hr, a 1:2 adduct IIIa of Ia and IIa was obtained in 91% yield. Even when Ia was employed in excess, the 1:1 adduct was not formed and the 1:2 adduct IIIa was again obtained albeit in low yield.

The IR spectrum of IIIa showed bands ascribable to ν_{NH} and $\nu_{C=O}$ at 3390 and 1635 cm^{-1} respectively. The NMR spectrum in deuteriochloroform ($CDCl_3$) displayed signals at δ 2.0 (3H, CH_3), 4.08 (2H, CH_2), 11.58 and 11.96 ppm (each 1H, NH), besides piperidyl and aromatic protons. The 1:2 adduct was thus confirmed to be 3,5-di(phenylcarbamoyl)-4-(1-piperidyl)-3-penten-2-one (IIIa).

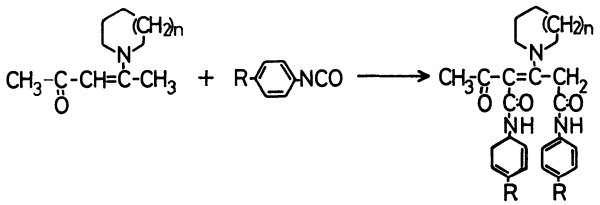

I
a: $n=1$
b: $n=0$

II
a: R=H
b: R=Cl
c: R=CH_3

III
a: $n=1$, R=H
b: $n=0$, R=H
c: $n=0$, R=Cl
d: $n=0$, R=CH_3

Scheme 1.

Similarly, the reaction of 4-(1-pyrrolidinyl)-3-penten-2-one (Ib) with phenyl (IIa), *p*-chlorophenyl (IIb), and *p*-tolyl isocyanate (IIc) in benzene gave the corresponding 1:2 adducts IIIb—IIId, respectively (Scheme 1).[12] The NMR spectra showed that the adducts III exist as a mixture of two tautomers, 3-penten-2-one and 4-penten-2-one.

Hydrolysis of both IIIa and IIIb with 18% hydrochloric acid gave IV. In view of the spectral data and identification with an authentic sample prepared from dimethyl *β*-ketoglutarate and aniline, IV was confirmed to be 1,3-di(phenylcarbamoyl)acetone; a singlet assignable to an olefinic proton at δ 5.88 ppm in its NMR spectrum suggests that IV exists in its

1) Part I of this series: O. Tsuge, M. Tashiro, and Y. Nishihara, *Nippon Kagaku Zasshi*, **92**, 72 (1971).
2) To whom inquiries should be directed.
3) M. Perelman and S. A. Mizsak, *J. Amer. Chem. Soc.*, **84**, 4988 (1962).
4) G. Opitz and J. Koch, *Angew. Chem.*, **75**, 167 (1963).
5) A. K. Bose and G. Mina, *J. Org. Chem.*, **30**, 812 (1965).
6) S. Hünig, K. Hübnev, and E. Benzig, *Chem. Ber.*, **95**, 926 (1962).
7) G. Berchtold, *J. Org. Chem.*, **26**, 3043 (1961).
8) C. A. Grob and H. J. Wilkens, *Helv. Chem. Acta*, **50**, 725 (1967).
9) J. Goerdeler and U. Keuser, *Chem. Ber.*, **97**, 2209 (1964).
10) G. H. Alt and A. J. Speziale, *J. Org. Chem.*, **29**, 794 (1964); *ibid.*, **30**, 1407 (1965).
11) M. Yoshimoto, T. Hiraoka, and Y. Kishida, *Chem. Pharm. Bull.* (Tokyo), **18**, 2469 (1970).
12) The product isolated from Ib and IIa was, however, a complex of IIIb and benzene, which on treatment with ethanol afforded pure IIIb.

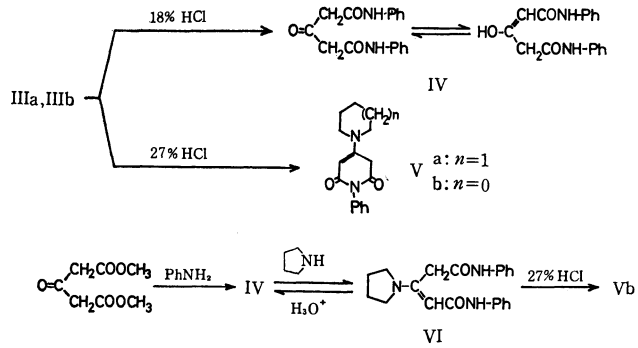

Scheme 2.

enol form in $CDCl_3$.

Treatment of IIIb with 27% hydrochloric acid afforded a new product Vb as reddish brown plates, whose molecular formula ($C_{15}H_{16}N_2O_2$) corresponded to that of a compound derived from IIIb by the elimination of both an acetyl and an anilino group. The IR spectrum of Vb displayed two crabonyl bands at 1645 and 1694 cm^{-1}. The NMR spectrum exhibited singlets at δ 3.60 (2H, C**H**$_2$) and 5.0 ppm (1H, =C**H**), besides pyrrolidinyl (8H) and phenyl protons (5H). These spectral data suggested V to be 1-phenyl-4-(1-pyrrolidinyl)-1,2,6-trihydropyridine-2,6(5H)-dione; Vb was indeed identical with an authentic sample prepared by the treatment of dianilide VI with 27% hydrochloric acid (Scheme 2).

A similar treatment of IIIa gave a mixture of IV and Va, identified by its spectral properties. However, Va could not be isolated in pure form.

Although the exact pathway for the hydrolysis of III is not clear, it can be considered to arise from the initial formation of dianilide VI, followed by hydrolysis or deanilination depending on the strength of hydrochloric acid.

The reaction of IIIa and IIIb with hydrazine hydrate afforded 3(5)-phenylcarbamoylmethyl-4-phenylcarbamoyl-5(3)-methylpyrazole (VII), whose structure was confirmed by its spectral data as well as by its elemental analysis.

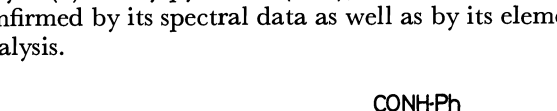

VII

Tautomerism of III. The NMR spectrum of IIIa indicated that it exists as the 3-penten-2-one of type A in $CDCl_3$. However, it has been clarified that all adducts of type III exist in general as a mixture of the 3-penten-2-one (type A) and 4-penten-2-one (type B) in solution, *e.g.*,

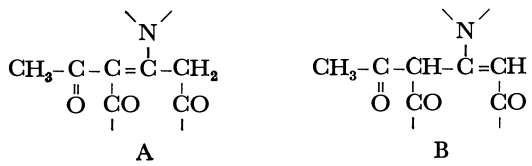

A B

As illustrated in Fig. 1 the NMR spectrum of IIIb in pyridine-d_5 can be understood as that of a 1:1 mixture of the corresponding A and B of IIIb.

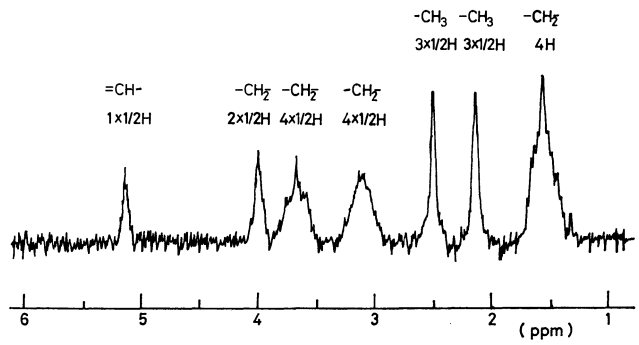

Fig. 1. NMR spectrum of IIIb in pyridine-d_5

The ratios of A to B in all III in solutions were similarly calculated; the results are summarized in Table 1.

Table 1. Ratio of A to B in III

III	A:B	Solvent
IIIa	1:0	$CDCl_3$
IIIa	2:3	DMSO-d_6
IIIa	1:1	Pyridine-d_5
IIIb	3:2	$CDCl_3$
IIIb	1:1	Pyridine-d_5
IIIb	1:2	DMSO-d_6
IIIc	1:2	$CDCl_3$
IIId	3:2	$CDCl_3$

On heating, IIIa and IIIb (but not IIIc) easily underwent elimination of water to give VIIIa and VIIIb.

Reaction under Reflux in Benzene. When Ia was treated with two equivalents of isocyanate IIa in refluxing benzene for 5 hr, two products VIIIa and IXa were obtained, but not IIIa.

The molecular formula of the major product VIIIa corresponded to that of the compound derived from a 1:2 adduct with loss of water. The IR spectrum of VIIIa exhibited bands assignable to ν_{NH} and $\nu_{C=O}$ at 3280 and 1645, 1663 cm^{-1}, and the NMR spectrum in $CDCl_3$ displayed singlets at δ 2.13 (3H, C**H**$_3$), 5.97 (1H, =C**H**), and 8.64 ppm (1H, N**H**), besides piperidyl (10H) and aromatic protons (10H). VIIIa was thus deduced to be 6-methyl-1-phenyl-5-phenylcarbamoyl-4-(1-piperidyl)pyrid-2-one. The mass spectrum supported the proposed structure for VIIIa.

The minor product IXa corresponded to a compound derived from a 1:3 adduct of Ia and IIa with loss of water. The IR spectrum of IXa was very similar to that of VIIIa showing bands ascribable to ν_{NH} and $\nu_{C=O}$ at 3300 and 1630, 1650 cm^{-1}. Its NMR spectrum in deuteriodimethylsulfoxide (DMSO-d_6) dis-

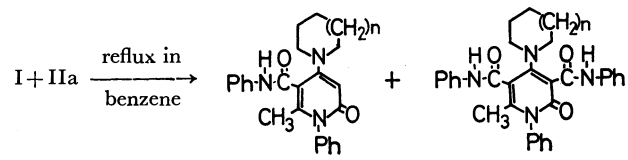

VIII IX

a: n=1, b: n=0

played singlets at δ 1.95 (3H, C**H**$_3$), 10.28 and 10.56 ppm (each 1H, N**H**), together with piperidyl (10H) and aromatic protons (15H). The results leave little doubt that IXa is 3,5-di(phenylcarbamoyl)-6-methyl-1-phenyl-4-(1-piperidyl)pyrid-2-one.

Under similar conditions, the reaction of Ib with IIa in refluxing benzene afforded 3,5-di(phenylcarbamoyl)-4-(1-pyrrolidinyl)pyrid-2-one IXb and a 2:1 complex of 5-phenylcarbamoyl-4-(1-pyrrolidinyl)pyrid-2-one VIIIb and *s*-diphenylurea. On heating with hydrochloric acid–acetic acid mixture, the 2:1 complex decomposed into its components VIIIb and *s*-diphenylurea.

As mentioned above, the structure of VIII corresponds to that of the compound obtainable from 1:2 adduct III with concurrent dehydration. When an ethanol solution of IIIa or IIIb was refluxed for 5 hr, the corresponding product VIIIa or VIIIb was obtained.[13] The formation of VIII under reflux in benzene can therefore be considered to proceed by the initial formation of 1:2 adduct III, followed by dehydration. On the other hand, VIII did not react with phenyl isocyanate (IIa); the pathway for the formation of IX has not yet been elucidated.

The reaction of enamino ketone Ib with 1-naphthyl isocyanate (X) at room temperature did not occur, but under reflux in benzene a 1:1 adduct XI was obtained in a small amount, together with *s*-di(1-naphthyl)urea and 1-(1-naphthyl)-2-(1-pyrrolidinyl)-urea; neither 1:2 adduct nor the product resulting from loss of water was formed.

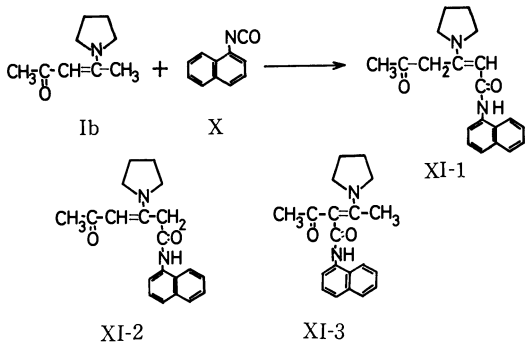

Scheme 3.

The IR spectrum of XI showed bands assignable to ν_{NH} and $\nu_{C=O}$ at 3000 and 1690 cm^{-1}. The NMR spectrum exhibited singlets at δ 2.21 (3H, C**H**$_3$), 4.20 (2H, C**H**$_2$), 5.15 (1H, =C**H**), and 10.96 ppm (1H, N**H**) besides pyrrolidinyl (8H) and aromatic protons (7H). Thus, it seems that XI is 4-(1-pyrrolidinyl)-5-(1-naphthylcarbamoyl)pent-4-en-2-one (XI-1) rather than XI-2 or XI-3 (Scheme 3).

Experimental

All melting points are uncorrected. The IR spectra were measured as KBr pellets on a Nippon Bunko IR-S spectrophotometer; the NMR spectra were determined at 60 MHz on a Hitachi R-20 NMR spectrometer with TMS as internal reference. The mass spectra were obtained on a Hitachi RMS-4 mass spectrometer with a direct inlet and an ionization energy of 70 eV. The elemental analyses were performed by Miss M. Akita.

Materials. *4-(1-Piperidyl)-3-penten-2-one (Ia)*: A solution of 5.0 g (0.05 mol) of acetylacetone and 8.5 g (0.1 mol) of piperidine in 700 ml of dry benzene was refluxed until a theoretical amount of water was distilled out (about 15 hr). The reaction mixture was concentrated to leave a residue. The distillation of the residue gave yellow viscous liquid (bp 122—123°C/7 mmHg), which on standing solidified. Recrystallization from petroleum ether (bp 30—45°C) afforded 6.5 g (78%) of Ia, mp 47—47.5°C (decomp.), colorless prisms.

Found: C, 71.76; H, 10.55; N, 8.43%. Calcd for $C_{10}H_{17}NO$: C, 71.86; H, 10.42; N, 8.38%.

4-(1-Pyrrolidinyl)-3-penten-2-one (Ib) was prepared according to the published procedure.[14] Mp 114—115°C (decomp.), (lit,[14] mp 115—116°C). Phenyl (IIa), *p*-chlorophenyl (IIb), *p*-tolyl (IIc) and 1-naphthyl isocyanate (X) were obtained commercially.

Reaction of 4-(1-Piperidyl)-3-penten-2-one (Ia) with Phenyl Isocyanate (IIa). *i) At Room Temperature*: A solution of 1.67 g (0.01 mol) of Ia and 2.38 g (0.02 mol) of IIa in 50 ml of benzene was stirred at room temperature for 5 hr, during which time crystals precipitated. Filtration gave crystals, which on recrystallization from ethanol below 50°C afforded 3.7 g (91%) of 3,5-di(phenylcarbamoyl)-4-(1-piperidyl)-3-penten-2-one (IIIa), mp 168.5—169°C (decomp.), as colorless needles.

Found: C, 71.17; H, 6.83; N, 10.42%. Calcd for $C_{24}H_{27}N_3O_3$: C, 71.09; H, 6.71; N, 10.36%.

NMR (in $CDCl_3$) δ ppm: 1.70 (6H, multiplet, C**H**$_2$), 2.0 (3H, singlet, C**H**$_3$), 3.87 (4H, multiplet, C**H**$_2$), 4.08 (2H, singlet, C**H**$_2$), 7.0—8.0 (10H, multiplet, aromatic protons), 11.58, 11.96 (each 1H, singlet, N**H**).

Similarly, the reaction of 4-(1-pyrrolidinyl)-3-pentene-2-one (Ib) with IIa, *p*-chlorophenyl (IIb) and *p*-tolyl isocyanate (IIc) gave the corresponding 1:2 adducts IIIb, IIIc, and IIId respectively. However, the product isolated from the reaction of Ib with IIa was a 2:1 complex of IIIb and benzene, which on treatment with ethanol afforded pure IIIb.

The 2:1 complex of IIIb and benzene: mp 131—132°C (decomp.), colorless needles.

Found: C, 72.91; H, 6.35; N, 9.68%. Calcd for $(C_{23}H_{25}N_3O_3)_2 \cdot C_6H_6$: C, 72.56; H, 6.51; N, 9.79%.

IR cm^{-1}: ν_{NH} 3280, 3230; $\nu_{C=O}$ 1706, 1640. Mass spectrum *m/e*: 373 (IIIb$^+$—H_2O), 78 ($C_6H_6^+$).

Recrystallization of the complex from ethanol below 50°C gave 1:2 adduct IIIb, mp 165—166°C (decomp.), as colorless needles. Yield, 65%.

Found: C, 70.29; H, 6.32; N, 10.72%. Calcd for $C_{23}H_{25}N_3O_3$: C, 70.57; H, 6.44; N, 10.74%.

IR cm^{-1}: ν_{NH} 3390, 3345; $\nu_{C=O}$ 1650. NMR (in $CDCl_3$) δ ppm: 1.89 (4H, multiplet, C**H**$_2$), 1.95 (3×2/5H, singlet, C**H**$_3$), 2.22 (3×3/5H, singlet, C**H**$_3$), 3.40 (4×2/5H, multiplet, C**H**$_2$), 3.57 (4×3/5H, multiplet, C**H**$_2$), 3.98 (2×3/5H, singlet, C**H**$_2$), 4.85 (1×2/5H, broad, =C**H**), 6.8—7.8 (10H, multiplet, aromatic protons), 9.80 (1H, broad, N**H**), 10.56 (1H, singlet, N**H**).

1:2 Adduct IIIc: mp 162—163°C, colorless needles. Yield, 40%.

13) When a solution of IIIa or IIIb in ethanol was gently heated below 50°C for a long time, their isomers IIIa′, mp 257—260°C (decomp.), and IIIb′, mp 179—180°C (decomp.), respectively, were formed. However, their structures have not yet been elucidated.

14) N. J. Leonard and J. A. Adamcik, *J. Amer. Chem. Soc.*, **81**, 595 (1959).

Found: C, 60.07; H, 5.13; N, 9.06%. Calcd for $C_{23}H_{23}N_3O_3Cl_2$: C, 60.00; H, 5.00; N, 9.13%.

IR cm^{-1}: ν_{NH} 3320; $\nu_{C=O}$ 1650, 1630. NMR (in $CDCl_3$) δ ppm: 1.90 (4H, multiplet, CH_2), 2.0 ($3\times2/3$H, singlet, CH_3), 2.18 ($3\times1/3$H, singlet, CH_3), 3.39 ($4\times1/3$H, multiplet, CH_2), 3.73 ($4\times1/3$H, multiplet, CH_2), 3.95 ($2\times1/3$H, singlet, CH_2), 5.41 ($1\times2/3$H, singlet, =CH), 6.9—7.7 (8H, multiplet, aromatic protons), 9.8 (1H, singlet, NH), 10.25 ($1\times1/3$H, singlet, NH), 10.70 ($1\times2/3$H, singlet, NH). Mass spectrum *m/e*: 463, 461, 459 (M^+).

1:2 Adduct IIId: mp 138—140°C, colorless crystals. Yield, 49%.

Found: 72.06; H, 7.10; N, 9.72%. Calcd for $C_{25}H_{29}N_3O_3$: C, 71.57; H, 6.97; N, 10.02%.

IR cm^{-1}: ν_{NH} 3245, 3180; $\nu_{C=O}$ 1695, 1630. NMR (in $CDCl_3$) δ ppm: 1.90 (4H, multiplet, CH_2), 1.99 ($3\times2/5$H, singlet, CH_3), 2.24 ($3\times3/5$H, singlet, CH_3), 2.30 (6H, singlet, CH_3), 3.40 ($4\times2/5$H, multiplet, CH_2), 3.68 ($4\times3/5$H, multiplet, CH_2), 3.96 ($2\times3/5$H, singlet, CH_2), 5.50 ($1\times2/5$H, singlet, =CH), 6.9—7.8 (8H, multiplet, aromatic protons), 9.37 ($1\times2/5$H, broad, NH), 9.6 (1H, broad, NH), 10.52 ($1\times3/5$H, broad, NH).

ii) Under Reflux in Benzene: A solution of 1.67 g (0.01 mol) of Ia and 2.38 g (0.02 mol) of IIa in 50 ml of benzene was refluxed for 5 hr. After cooling, filtration gave crystals, which on recrystallization from ethanol afforded 0.97 g (25%) of 6-methyl-1-phenyl-5-phenylcarbamoyl-4-(1-piperidyl)-pyrid-2-one (VIIIa), mp 266—268°C (decomp.), as colorless needles.

Found: C, 74.22; H, 6.78; N, 10.63%. Calcd for $C_{24}H_{25}N_3O_2$: C, 74.39; H, 6.50; N, 10.85%. Mass spectrum *m/e*: 387 (M^+).

The benzene filtrate was concentrated *in vacuo* to leave a residue. The residue was washed with ethanol to give crystals, which on recrystallization from benzene afforded 0.2 g (6%) of 3,5-di(phenylcarbamoyl)-6-methyl-1-phenyl-4-(1-piperidyl)-pyrid-2-one (IXa), mp 280—281°C, as colorless needles.

Found: C, 73.89; H, 6.00; N, 10.75%. Calcd for $C_{31}H_{30}N_4O_3$: C, 73.49; H, 5.97; N, 11.06%.

Similarly, the reaction of 1.53 g (0.01 mol) of Ib with 2.38 g (0.02 mol) of IIa gave 1.60 g (43%) of a 2:1 complex of VIIIb and *s*-diphenylurea, mp 228°C (decomp.), and 0.27 g of IXb, mp 272°C (decomp.), as both colorless prisms.

The complex; Found: C, 73.89; H, 5.72; N, 11.88%. Calcd for $(C_{23}H_{23}N_3O_2)_2\cdot C_{13}H_{12}N_2O$: C, 73.83; H, 6.04; N, 11.90%.

IR cm^{-1}: ν_{NH} 3290; $\nu_{C=O}$ 1700, 1674, 1636. NMR (in DMSO-d_6) δ ppm: 1.85 (4H, multiplet, CH_2), 1.88 (3H, singlet, CH_3), 3.40 (4H, multiplet, CH_2), 5.42 (1H, singlet, =CH), 7.0—8.0 (15H, multiplet, aromatic protons), 8.75, 10.75 (each 1H, singlet, NH). Mass spectrum *m/e*: 273 ($VIIIb^+$).

Compound IXb; Found: C, 73.34; H, 6.03; N, 11.19%. Calcd for $C_{30}H_{28}N_4O_3$: C, 73.15; H, 5.73; N, 11.38%.

IR cm^{-1}: ν_{NH} 3320; $\nu_{C=O}$ 1656, 1634. NMR (in DMSO-d_6) δ ppm: 1.75 (4H, multiplet, CH_2), 1.88 (3H, singlet, CH_3), 3.50 (4H, multiplet, CH_2), 6.9—7.8 (15H, multiplet, aromatic protons), 10.62, 10.82 (each 1H, singlet, NH). Mass spectrum *m/e*: 492 (M^+).

A solution of 1.0 g of the complex in 50 ml of concentrated hydrochloric acid–acetic acid mixture (1:1 vol/vol) was refluxed for 20 hr. After cooling, filtration gave 0.12 g of *s*-diphenylurea. The filtrate was concentrated *in vacuo* to leave a residue, which on several recrystallizations from ethanol afforded 0.25 g of pure VIIIb, mp 248—250°C (decomp.), as colorless prisms.

Found: C, 73.63; H, 6.50; N, 11.03%. Calcd for $C_{23}H_{23}N_3O_2$: C, 73.97; H, 6.21; N, 11.25%.

IR cm^{-1}: ν_{NH} 3265; $\nu_{C=O}$ 1660, 1645. NMR (in $CDCl_3$) δ ppm: 1.91 (4H, multiplet, CH_2), 2.08 (3H, singlet, CH_3), 3.47 (4H, multiplet, CH_2), 5.43 (1H, singlet, =CH), 7.0—7.7 (10H, multiplet, aromatic protons), 9.60 (1H, singlet, NH). Mass spectrum *m/e*: 273 (M^+).

Hydrolysis of 1:2 Adduct III. A solution of 1.0 g of IIIa in 10 ml of 18% hydrochloric acid was stirred at room temperature for 6 hr. Water was added to the reaction mixture and then the precipitated solid was filtered. Recrystallization from ethanol–petroleum ether mixture afforded 0.2 g (27%) of 1,3-di(phenylcarbamoyl)acetone (IV), mp 151—152°C (lit,[15] mp 155°C), as colorless plates.

Found: C, 68.98; H, 5.30; N, 9.30%. Calcd for $C_{17}H_{16}N_2O_3$: C, 68.90; H, 5.44; N, 9.46%.

IR cm^{-1}: ν_{NH} 3270; $\nu_{C=O}$ 1720, 1650. NMR (in pyridine-d_5) δ ppm: 3.8 (4H, broad, CH_2), 6.8—7.9 (19H, multiplet, aromatic protons), 10.8 (2H, broad, NH). Mass spectrum *m/e*: 296 (M^+).

Similarly, hydrolysis of IIIb gave IV in 30% yield. Compound IV was identical with an authentic sample prepared from dimethyl β-ketoglutarate and aniline.

1-Phenyl-4-(1-pyrrolidinyl)-1,2,6-trihydropyridine-2,6(5H)-dione (Vb). i) A solution of 1.0 g of IIIb in 15 ml of 27% hydrochloric acid was stirred at room temperature for 20 hr. The reaction mixture was poured into water and the precipitated solid was filtered. Recrystallization from ethanol–petroleum ether afforded 0.2 g (30%) of Vb, mp 214—216°C (decomp.), as reddish brown plates.

Found: C, 70.08; H, 6.26; N, 10.88%. Calcd for $C_{15}H_{16}N_2O_2$: C, 70.29; H, 6.29; N, 10.93%. Mass spectrum *m/e*: 256 (M^+).

ii) A solution of 5.92 g of IV and 10 ml of pyrrolidine in 50 ml of benzene was stirred at room temperature for 15 hr and then 30 ml of petroleum ether was added to the reaction mixture. Filtration afforded 6.50 g (93%) of dianilide VI, mp 174—175°C, as colorless needles.

Found: C, 72.29; H, 6.73; N, 12.15%. Calcd for $C_{21}H_{23}N_3O_2$: C, 72.18; H, 6.63; N, 12.03%.

IR cm^{-1}: ν_{NH} 3310; $\nu_{C=O}$ 1675. NMR (in $CDCl_3$) δ ppm: 1.79 (4H, multiplet, CH_2), 3.38 (4H, multiplet, CH_2), 4.54 (1H, singlet, =CH), 6.8—7.7 (11H, multiplet, aromatic protons and NH), 11.11 (1H, singlet, NH). Mass spectrum *m/e*: 349 (M^+).

Treatment of 1.0 g of VI with 10 ml of 27% hydrochloric acid gave 0.15 g of Vb. Hydrolysis of VI with 18% hydrochloric acid also afforded IV quantitatively.

Reaction of 1:2 Adduct IIIa with Hydrazine Hydrate. A solution of 1.0 g of IIIa and 5 ml of hydrazine hydrate in 20 ml of ethanol was stirred at room temperature for 5 hr. The reaction mixture was concentrated *in vacuo* to leave a residue, which on recrystallization from ethanol afforded 0.25 g (31%) of pyrazole derivative VII, mp 239—240°C, as colorless needles.

Found: C, 68.09; H, 5.27; N, 16.64%. Calcd for $C_{19}H_{18}N_4O_2$: C, 68.24; H, 5.42; N, 16.76%.

IR cm^{-1}: ν_{NH} 3240; $\nu_{C=O}$ 1650, 1630. NMR (in $CDCl_3$) δ ppm: 2.50 (3H, singlet, CH_3), 3.95 (2H, singlet, CH_2), 7.0—8.0 (11H, multiplet, aromatic protons and NH), 10.55, 11.07 (each 1H, singlet, NH). Mass spectrum *m/e*: 334 (M^+).

Reaction of Enamino Ketone Ib with 1-Naphthyl Isocyanate (X). A solution of 1.53 g (0.01 mol) of Ib and 1.69 g (0.01 mol) of X in 50 ml of benzene was refluxed for 16 hr. After cooling, filtration gave 0.34 g of a mixture of *s*-di(1-naphthyl)urea and 1-(1-naphthyl)-2-(1-pyrrolidinyl)urea. Fractional recrystal-

15) E. Besthorn and E. Garben, *Ber.*, **33**, 3443 (1900).

lization from ethanol afforded pure *s*-di(1-naphthyl)urea, mp 268—270°C (decomp.) (lit,[16] mp 270—314°C (decomp.)), and 1-(1-naphthyl)-2-(1-pyrrolidinyl)urea, mp 134—135°C. Both ureas were identical with authentic samples prepared from 1-naphthyl isocyanate and 1-naphthylamine or pyrrolidine, respectively.

16) J. W. Boehmer, *Rec. Trav. Chim. Pays-Bas*, **55**, 379 (1936).

The filtrate was concentrated *in vacuo* to leave a residue, which was washed with petroleum ether. Recrystallization of the insoluble solid from ethanol–petroleum ether afforded 0.32 g of 1: 1 adduct XI, mp 165—166°C (decomp.), as colorless needles.

Found: C, 74.39; H, 6.60; N, 8.60%. Calcd for $C_{20}H_{22}N_2O_2$: C, 74.51; H, 6.88; N, 8.69%. Mass spectrum *m/e*: 322 (M^+).

BULLETIN OF THE CHEMICAL SOCIETY OF JAPAN, VOL. 46, 290—291 (1973)

Preparation of *p*-Nitrophenyl 2-*O*-Acetyl-β-D-glucopyranoside and *N*-Acetyl-β-D-glucosaminidase Activity toward It. (Essential Requirement of 2-Acetamide Group of Substrate for *N*-Acetyl-β-D-glucosaminidase Hydrolysis)

Kazuhiko YAMAMOTO

Department of Chemistry, Faculty of Science, Osaka University, Toyonaka, Osaka

(Received April 11, 1972)

Paranitrophenyl 2-*O*-acetyl, and 2,3-di-*O*-acetyl-β-D-glucopyranoside (VI, VII) were synthesized in order to investigate the effect of the substitution of the amide-nitrogen of the substrate by oxygen on the *N*-acetyl-β-D-glucosaminidase hydrolysis. Paramethoxybenzylidene was used as an *O*-blocking group for the preparation, and it was found that this blocking group could be easilly removed without the destruction of *p*-nitrophenyl glycoside. The evidence that VI could not be hydrolysed with this enzyme indicated the essential requirement of the amide-nitrogen of the substrate for the enzyme action.

Several *p*-nitrophenyl 2-acylamino-2-deoxy-β-D-glucopyranosides containing several *N*-acyl substituents were synthesized recently in order to investigate the *N*-acyl specificity of *N*-acetyl-β-D-glucosaminidase [EC. 3. 1. 2. 30]. The *N*-acyl specificity of this enzyme was fairly well clarified in a previous study.[1] An attempt to investigate the effect of replacing the amide-nitrogen of the substrate with oxygen on the enzyme action led to the synthesis of 2-*O*-acetyl-β-D-glucopyranoside.

The present report will describe the preparation of *p*-nitrophenyl 2-*O*-acetyl-β-D-glucopyranoside (VI) and *p*-nitrophenyl 2,3-di-*O*-acetyl-β-D-glucopyranoside (VII) as the reference derivative, and the susceptibilty of VI toward the enzymic hydrolysis. *para*-Nitrophenyl glycoside was chosen as a consequence of the previous investigation. The greater reactivity of the 2-hydroxyl group as compared to the other secondary hydroxyl groups has been noted.[3] Therefore, it is most probable that the 2-*O*-acetyl derivative of II results in the reaction of II with a limited amount of acetic anhydride. The selective 2-*O*-acetylation of *p*-nitrophenyl 4,6-*O*-(*p*-methoxybenzylidene)-β-D-glucopyranoside (II) under limited conditions and the chromatographic purification of debenzylidenated products gave a pure *p*-nitrophenyl 2-*O*-acetyl-β-D-glucopyranoside (VI). The location of the acetyl group was confirmed by periodate-oxidation analysis. *para*-Methoxybenzylidene as the *O*-blocking group was used for the preparation because *p*-nitrophenyl glycoside was usually very acid-labile. This new blocking group, which has been reported to be smoothly cleaved under mild acidic conditions,[4] was removed more easily without the destruction of glycoside. The product III substituted with di-*O*-(*p*-methoxybenzylidene) was found in the case of the prolonged treatment.

The synthetic scheme and the compounds synthesized are shown in Fig. 1.

With regard to the enzymic hydrolysis, this sub-

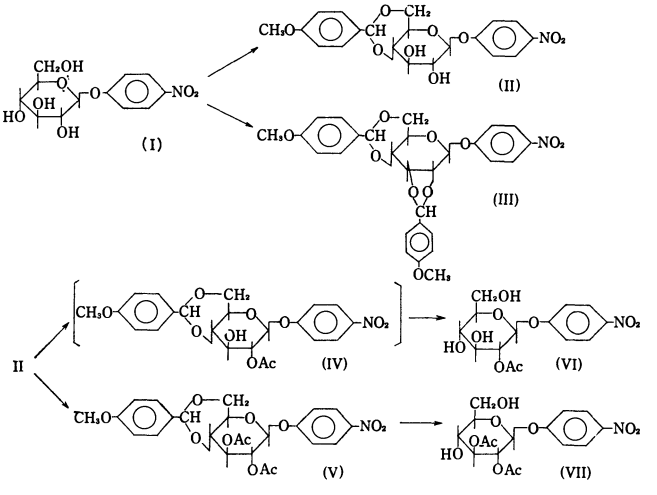

Fig. 1.

1) K. Yamamoto, *J. Biochem.*, **73**, (1973).
2) E. Glaser and W. Wulwek, *Biochem. Z.*, **145**, 514 (1924).
3) J. M. Sugihara, *Ad. Carbohyd. Chem.*, **8**, 1 (1953).
4) S. Chladek and J. Smrt, *Coll. Czech. Chem. Comm.*, **28**, 1301 (1963).

strate VI was not affected by *N*-acetyl-β-D-glucosaminidase. This evidence suggests that the –NH– group of the amide bond of 2-acetamide-2-deoxy-D-glucopyranoside is essential for the action of this enzyme.

Experimental

The melting points were determined by a micro-melting-point apparatus (Yanagimoto MFG.), and the optical rotations were measured by means of a recording spectropolarimeter (Yanagimoto MFG, ORD-185).

para-*Nitrophenyl 4,6-O-(p-methoxybenzylidene)-β-D-glucopyranoside (II).* To 50 ml of dimethylformamide solution of (I)[2] (1.0 g) we added 3 ml of anisaldehyde, 6 ml of ethylorthoformate, and 2 ml of trifluoroacetic acid.[4] After the reaction had continued for 8 hr at room temperature, the reaction mixture was evaporated *in vacuo* to dryness. The residue, suspended in a cold sodium bicarbonate solution, was collected by filtration. The crystallization of the dried raw product from toluene afforded a crystalline (II) (1.1 g, 79%); mp 190—192°C $[\alpha]_{589}^{20}=-21.7°$ (C, 0.773 in dimethylformamide) Found: C, 57.17; H, 5.08; N, 3.30%. Calcd for $C_{20}H_{21}O_9N$: C, 57.28; H, 5.05; N, 3.34%.

The same reaction mixture as above was kept for 20 hr. at room temperature and subsequently treated in the same manner. The first crystallization of the dried raw products from toluene and methanol gave 0.51 g (27%) of a crystalline product (III), and the mother liquor of III afforded 0.42 g of II upon further crystallization. Mp 288—289°C, $[\alpha]_{589}^{20}=+13.7°$ (*C*, 1.47 in dimethylformamide) Found: C, 62.68; H, 5.14; N, 2.61%. Calcd for $C_{28}H_{27}O_{10}N$: C, 62.56; H, 5.06; N, 2.61%.

para-*Nitrophenyl 2,3-di-O-Acetyl-4,6-O-(p-methoxybenzylidene)-β-D-glucopyranoside (V).* Five hundred and fifty mg of II were acetylated with 10 ml of acetic anhydride in 60 ml of pyridine. The evaporated residue of the reaction mixture was then crystallized from ethanol, thus giving 530 mg (88%) of V. Mp 252—253°C $[\alpha]_{589}^{20}=-5.82°$ (*C*, 0.923 in dimethylformamide). Found: C, 57.49; H, 5.05; N, 2.81%. Calcd for $C_{24}H_{25}O_{11}N$: C, 57.25; H, 5.01; N, 2.78%.

para-*Nitrophenyl 2,3-di-O-Acetyl-β-D-glucopyranoside (VII).* A 400 mg portion of V, dissolved in 45 ml of 66% acetic acid, was heated for 5 min in boiling water, and then the acetic acid solution was evaporated *in vacuo* to a heavy syrup. The crystallization of the heavy syrup from ethanol gave 190 mg (62%) of VII. Mp 183—185°C $[\alpha]_{589}^{20}=-24.9°$ (*C*, 0.553 in dimethylformamide). Found: C, 49.75; H, 5.04; N, 3.62%. Calcd for $C_{16}H_{19}O_{10}N$: C, 49.87; H, 4.97; N, 3.63%. The concentration of the mother liquors gave a further 90 mg (29%) of (VII). Mp 182—183°C.

Selective O-Acetylation of II and Preparation of (VI). A chloroform–pyridine solution (1: 1, 60 ml) of II (460 mg) was cooled to −10°C, and to this solution we added 230 mg of acetic anhydride in 10 ml of chloroform, drop by drop, over a 10 hr period. The residue, after the evaporation of the reaction mixture, showed three spots on a thin-layer chromatogram. As the fastest of them corresponded to V and the slowest to II, the middle spot was assumed to be the mono-*O*-acetylated product(IV). The residue was debenzylidenated in 66% acetic acid for 5 min at 100°C; the subsequent evaporation of the hydrolysate gave a heavy syrup. The chromatographic purification of VI from the contaminants was performed on a Bio-gel-P-2 column (2.0×200 cm). The heavy syrup, which had been washed three times with ether, was dissolved in 45 ml of water and then applied to a Bio-gel column (2.0×200 cm) and eluted with 0.01M acetic acid. The effluent was monitored by measuring the absorbance at 300 mu. The main peak, which was assumed to be VI from the thin-layer chromatographic identification, was collected and dried by lyophillization. It afforded 120 mg (33%) of the amorphous solid, which showed $[\alpha]_{589}$ and the following elemental analytical result; $[\alpha]_{589}^{20}=-36.9°$ (*C*, 0.430 in dimethylformamide). Found: C, 48.17; H, 4.99; N, 4.00%. Calcd for $C_{14}H_{17}O_9N$: C, 48.98; H, 4.99; N, 4.08%.

In the periodate oxidation, which was performed in 10 mM of sodium periodate (pH 5.5) at room temperature by measuring the amount of periodate consumed acording to Avigad's method.[5] VI Consumed 1 mole equivalent periodate; its analytical data are shown in Table 1. This evidence indicates that the specimen had the structure of VI.

Table 1. Periodate-oxidation analysis for VI

Compound	Amount for analysis (mol)	$NaIO_4$-Consumption: Moles of $NaIO_4$ consumed	Molar equivalent: observed	Molar equivalent: calculated
VI	2.15×10^{-6}	2.11×10^{-6}	0.98	1.00
	1.07×10^{-6}	1.18×10^{-6}	1.10	1.00
VII	2.08×10^{-6}	0.12×10^{-6}	0.058	0.00
	1.04×10^{-6}	0.00	0.00	0.00

N-Acetyl-β-D-glucosaminidase Activity toward VI. The enzyme specimen and the analytical procedure were the same as that of the previous report.[1]

Two mM of VI in a pH 4.5-citrate buffer were incubated with the enzyme (concentration from 0.5 ppm to 50 ppm) at 37°C for 24 hr. No *p*-nitrophenol liberated from VI could be detected.

The author wishes to thank Professor Y. Matsushima (Faculty of Science, Osaka University) for his continued interest and support during this work and Dr. K. Shingu (Faculty of Science, Osaka University) for his kind operation of recording spectropolarimeter.

5) G. Avigad, *Carbohyd. Res.*, **11**, 119 (1969).

Studies on Nitrile Salts. I. Dimerization of Nitriles Having α-Hydrogen in the Presence of Hydrogen Chloride

Shozo YANAGIDA, Tetsuo FUJITA, Masataka OHOKA, Ichiro KATAGIRI, and Saburo KOMORI

Department of Applied Chemistry, Faculty of Engineering, Osaka University, Yamadakami, Suita, Osaka

(Received February 9, 1972)

The compositions and structures of several stable nitrile-HCl salts previously reported were reinvestigated. Most of them have been found to have the composition of $2RC{\equiv}N\cdot 2HCl$ and have been identified as *N*-(α-chloroalkenyl)alkylamidine hydrochlorides (**3**) by mass and NMR spectra analyses. However, the 2:3 adduct from chloroacetonitrile was confirmed to be *N*-(α,α,β-trichloroethyl)chloroacetamidine hydrochloride. The scope and limitations of the dimerization reaction of nitriles having α-hydrogen with HCl were studied. Most nitriles having α-hydrogen react with HCl to give *N*-(α-chloroalkenyl)alkylamidine hydrochlorides (**3**). Their hydrolysis to diacylamines (**4**) was also investigated.

Since Gautier[1] first reported the reaction of propionitrile with hydrogen chloride in 1866, the reactions of nitriles with hydrogen halides have been well documented.[2-6]

It is now believed that nitriles react with HCl at a low temperature to form various salt-like species which are in equilibrium with each other, as is shown in Eq.1:

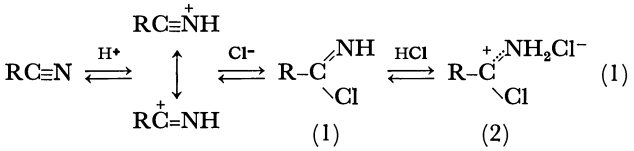

(1)

In addition, it has recently been ascertained,[7] on the basis of neutron-diffraction analysis, that the addition product prepared from acetonitrile and HCl at a low temperature has the structure of **2**($R=CH_3$), as was proposed by Allainstein and Schmidt.[8] On the other hand, there have been some reports concerning the addition products assigned to Structure **1**; Michael and Wing[9] assigned the nitrile salt prepared from propionitrile and HCl according to the method of Gautier[1] to propionimidoyl chloride (**1**, $R=C_2H_5-$) on the basis of the reaction with aniline. Similarly, a U. S. Patent[10] has claimed that 2-chloropropionitrile and 2-chlorobutyronitrile react with HCl in ether to give the corresponding imidoyl chloride (**1**, $R=CH_3CHCl-$, CH_3CH_2CHCl-).

In addition to the simple imidoyl chloride salts (**1** or **2**), some nitriles are known to form isolable dimeric hydrochlorides. Grudmann *et al.*[11] reported that some α-chloronitriles reacted with HCl in ether to give dimeric salts with the composition of $2RC{\equiv}N\cdot HCl$ and proposed the following structures on the basis of their salt-like properties:

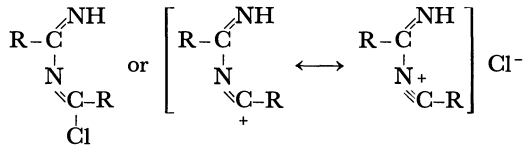

Zil'berman *et al.*,[12] however, reported that α-haloacetonitriles gave dimeric salts with the composition of $2RC{\equiv}N\cdot 3HCl$ under the same conditions and assumed the following dihydrochloride structure:

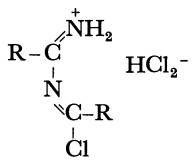

Recently we reported that the reaction of chloroacetonitrile with HCl gave the 2:2 adduct.[13] Hinkel and Treharne.[14] has also reported that, on standing, the unstable acetimidoyl chloride (**2**, $R=CH_3-$) changed slowly to *N*-(α-chloroethylidene)acetamidine hydrochloride, which has the composition of $2CH_3C{\equiv}N\cdot 2HCl$.

Similar dimeric salts of nitriles have also been postulated as intermediates in the reactions of nitriles in the presence of HCl.[2,4,13,15,16]

In view of the uncertainties surrounding the composition of stable nitrile-HCl salts, we have now undertaken a complete reinvestigation of the reactions of nitriles with HCl.

1) A. Gautier, *Compt. Rend.*, **63**, 920 (1866); see also *Ann. chem.*, **142**, 289 (1867).
2) E. N. Zil'berman, *Russian Chem. Rev.*, **31**, 615 (1962).
3) F. Johnson and R. Madronero, "Advances in Heterocyclic Chemistry," Vol. 6. A, R. Katritzky, Ed., Academic Press, New York, (1966), pp. 95—146.
4) W. Ruske, "Friedel-Crafts and Related Reactions," Vol. 3, part 1, G.A. Olah, Ed., Interscience, New York (1964), pp. 383—497.
5) R. Bonnett, "The Chemistry of the Carbon-nitrogen Double Bond," S. Patai, Ed., Interscience, New York (1970), pp. 597—662.
6) F. C. Schaefer, "The Chemistry of the Cyano Group," Z. Rapport, Ed., Interscience, New York (1970), pp. 239—306.
7) S. W. Peterson and J. M. Williams, *J. Amer. Chem. Soc.*, **88**, 2866 (1966).
8) E. Allenstein and A. Schmidt, *Spectrochim. Acta*, **20**, 1451 (1964).
9) A. Michael and J. F. Wing, *Am. Chem. J.*, **7**, 71 (1885).
10) E. W. Shand, U. S. 2411064 (1946).
11) C. Grundmann, G. Weisse, and S, Seide. *Ann. Chem.*, **577**, 77 (1952).
12) a) E. N. Zil'berman and A. Y. Lazaris, *J. Gen. Chem. USSR.*, **31**, 1224 (1961). b) A. Y. Lazaris, E. N. Zil'berman, and D. D. Strizhakov, *ibid.*, **32**, 890 (1962).
13) S. Yanagida, M. Ohoka, M. Okahara, and S. Komori, *J. Org. Chem.*, **34**, 2972 (1969).
14) L. E. Hinkel and G. J. Treharne, *J. Chem. Soc.*, **1945**, 866.
15) J. Houben, *Chem. Ber.*, **60**, 1759 (1927).
16) E. N. Zil'berman and P. S. Pyryalova, *J. Gen. Chem. USSR.*, **33**, 3348 (1963).

TABLE 1. MASS SPECTRA OF SOME DIMER SALTS (**3**)

3	Dimer Salts		Fragment ion peaks (relative intensity)[a]								
	R^1	R_2	$[M^+-HCl]$	$[M^+-HCl-Cl]$	$[R^1R^2CH-C{=}NH]$	$[R^1R^2CH-C{\equiv}N]$	Other peaks.				
3b	CH_3–	H	148(3)	111(11)	56(74)	55(26)	54(42)	38(26)	36(79)	29(29)	28(100)[b]
			146(8)								
3g	Cl–	H	190(5)	153(18)	78(25)	77(31)	51(8)	49(24)	42(58)	38(33)	36(100)
			188(15)	151(27)	76(77)	75(90)					
			186(15)								
3m	CH_3–	CH_3–	176(8)	139(32)	70(95)	69(100)	58(58)	56(34)	54(45)	43(98)	42(79)
			174(24)				41(66)	38(29)	36(84)		
3n	C_2H_5–	CH_3–	204(t)	167(3)	84(33)	83(40)	68(49)	57(52)	55(100)	54(46)	41(43)
			202(2)				38(22)	36(63)	29(59)	28(38)	27(35)
3t	Cl–	Cl–	260(8)	221(5)	114(4)	113(3)	185(10)	183(10)	175(32)	173(100)	171(100)
			258(18)	219(3)	112(23)	111(17)	78(18)	76(57)	38(9)	36(28)	
			256(25)		110(37)	109(25)					
			254(18)								
3u	CH_3–	Cl–	218(14)	181(46)	92(23)	91(39)	153(16)	151(24)	145(9)	143(27)	65(12)
			216(41)	179(68)	90(68)	89(92)	63(38)	56(54)	54(86)	38(35)	36(100)
			214(41)								
3v	$ClCH_2$–	Cl–		249(t)[c]	126(4)		213(t)	211(t)	209(t)	177(t)	151(8)
				247(t)	124(5)		149(13)	38(33)	36(100)		
				245(t)							
3w	*n*-C_4H_7–	Cl–	302(6)	267(5)	134(30)		259(16)	257(46)	255(46)	246(9)	244(24)
			300(19)	265(26)	132(90)		242(24)	209(65)	207(100)	96(40)	69(68)
			298(19)	263(40)			54(73)	38(17)	36(50)		
3x	C_6H_5–	Cl–				153(7)	116(100)	89(23)	38(28)	36(86)	
						151(21)					

a) 70 eV.
b) Molecular ion peaks corresponding 2,4,6-triethyl-*s*-triazine was also observed.
c) Ratio 8: 10: 5.

Results and Discussion

Reinvestigation of Stable Nitrile Salts Previously Reported. In order to clarify the discrepancies in the results of the reaction of chloroacetonitrile and HCl, we first undertook a careful reinvestigation of the addition product.

As was reported previously,[13] the melting point of the adduct varied in several repeated experiments. It has now been found, on the basis of analyses of the chlorine content and the IR spectra, that the adduct freshly prepared in ether below 0°C is quite different from that prepared by heating in a sealed tube using a solvent such as chlorobenzene, and that, on standing, the former gradually changes to the latter. The analysis of the chlorine content indicated that the former has the composition of $2ClCH_2C{\equiv}N\cdot 3HCl$, and the latter, the composition of $2ClCH_2C{\equiv}N\cdot 2HCl$. The hydrolysis of the both adducts gave bis(chloroacetyl)-amine (**4g**), indicating that both have a dimeric structure. The mass spectrum of the latter salt also supported the dimeric structure (Table 1). In their IR spectra (Nujol), the absorptions in the region of 1500 to 1700 cm^{-1} are quite similar, but only the former has the characteristic absorption at 1750 cm^{-1}.[17]

However, when the latter salt was left standing in drying pistol at 50°C under reduced pressure, the chlorine content decreased to 59.0%; this corresponds to the composition of $2ClCH_2C{\equiv}N\cdot HCl$, as was analyzed by Grundmann *et al.*[11] The mass spectrum showed not only the fragment ion peaks due to the dimer salt with the composition of $2ClCH_2C{\equiv}N\cdot 2HCl$, but also the molecular ion and fragment ion peaks due to 2,4,6-tris(chloromethyl)-*s*-triazine, suggesting that the salt suffered from degradation.[18]

In view of the above facts, we concluded that the initially-formed salt, $2ClCH_2C{\equiv}N\cdot 3HCl$ is gradually transformed to a more stable dimer salt, $2ClCH_2C{\equiv}N\cdot 2HCl$ (**3g**), which is then further transformed to 2,4,6-tris(chloromethyl)-*s*-triazine with a loss of HCl.[19]

The reinvestigation has now been extended to the addition products prepared by the reactions of dichloroacetonitrile, 2-chloropropionitrile, or propionitrile with HCl.

An analogous treatment of dichloroacetonitrile and 2-chloropropionitrile with HCl in ether readily gave the white addition products, as were previously reported.[10,11] The elemental analyses of these adducts (**3t** and **3u** in Table 2) indicated that they all had the empirical formula $R^1R^2CHC{\equiv}N\cdot HCl$. Their IR spectra in the region from 1500 to 1700 cm^{-1} were similar

17) We assumed that this absorption might be assigned to the cation $>C{=}N^+H-$, although the imminium bands were not observed clearly. B. Witkop, *Experientia.*, **10**, 420 (1954).

18) In its IR spectrum, the characteristic absorption was observed at 1760 cm^{-1}.

19) The formation of the *s*-triazines is under study in our group.

TABLE 2. PREPARATION AND ANALYSIS OF *N*-(α-CHLOROALKENYL)ALKYLAMIDINE HYDROCHLORIDES (DIMER SALTS) (**3**)

	Dimer salts (**3**)		Reaction conditions[a]		Yield[b] (%)	Mp (°C)	IR (Nujol) (cm^{-1})	Mass[c] (M^+-HCl)	Elemental analysis[d]		
	R^1	R^2	Molar ratio nitrile/HCl	Reaction time (hr)					C%	H%	N%
a)	H	H	1:1.12	136	67	—	1710	dec[e]			
b)	CH_3	H	1:1.72	136	86	125.0—127.5	1673 1588	146	38.88 (39.36)	6.63 (6.61)	15.05 (15.30)
c)	C_2H_5	H	1:1.38	114	63	102.0—104.0	1700 1600 1530	dec[e]	45.63 (45.51)	7.87 (7.64)	13.31 (13.27)
d)	*n*-C_4H_9	H	1:1.13	165	34	87.0—90.0	1695 1600 1540	dec[e]	54.05 (53.93)	9.30 (9.05)	10.50 (10.48)
e)	*n*-C_6H_{13}	H	1:1.33	171	37	115.0—116.5	1695 1600 1530	dec[e]	59.24 (59.43)	10.22 (9.98)	8.27 (8.66)
f)	Ph	H	1:1.23	46	53	135.0—138.0	1686 1606[f]	dec[e]	62.21 (62.55)	5.23 (5.25)	9.01 (9.12)
g)	Cl	H	g)	—	90	122.0—123.0	1695 1615	186	21.20 (21.45)	3.03 (2.70)	12.57 (12.51)
h)	$ClCH_2$	H	1:1.28	72	71 (90)[h]	93.0—95.0	1685 1600[f]	—	30.44 (28.06)	4.90 (4.00)	12.09 (11.12)
i)	$PhCH_2$	H	1:1.22	168	52 (81)[h]	178.0—180.0	1700 1670 1605	—	63.84 (64.48)	7.57 (6.01)	10.85 (8.36)
j)	CH_3O	H	1:1.49	2	i)						
k)	CH_3OCH_2	H	1:1.40	144	i)						
l)	$COOC_2H_5$	H	1:0.97	j)	i)						
m)	CH_3	CH_3	1:1.49 1:1.12[k]	48 72[k]	76 43[k]	193.0—194.0(dec)	1695 1585 1530	174	45.26 (45.21)	8.46 (7.64)	13.31 (13.27)
n)	C_2H_5	CH_3	1:1.93	288	75	162.5—164.0(dec)	1690 1585 1530	202	50.35 (50.21)	8.52 (8.42)	11.83 (11.71)
o)	*n*-C_3H_7	CH_3	1:1.43	260	48 (90)[h]	135.0—137.0	1693 1590	—	53.44 (53.93)	9.07 (9.05)	10.39 (10.48)
p)	*n*-C_4H_9	CH_3	1:1.82	600	57 (93)[h]	123.0—126.0	1690 1600	—	55.55 (56.94)	9.69 (9.56)	9.81 (9.49)
q)	Ph	CH_3	1:1.70	307	64	168.0—170.0	1693 1603	—	65.08 (64.48)	6.15 (6.01)	8.76 (8.36)
r)	$ClCH_2$	CH_3	1:1.40	240	82 (95)[h]	98.0—100.0	1690 1600 1530	dec[e]	35.28 (34.31)	5.36 (5.04)	10.40 (10.01)
s)	C_2H_5	C_2H_5	1:1.11	282	45 (75)[h]	147.0—148.0	1682 1592	—	53.73 (53.93)	8.94 (9.05)	10.51 (10.48)
t)	Cl	Cl	g)	g)	l)	119.0—121.0(dec)[m]	1698 1618 1520	254	16.15 (16.41)	1.43 (1.38)	9.59 (9.57)
u)	CH_3	Cl	n)	n)	l)	175.0—176.0(dec)[o]	1700 1615 1530	214	28.29 (28.60)	4.21 (4.00)	11.22 (11.12)
v)	$ClCH_2$	Cl	1:1.13	168[p]	97 (100)[l]	>110(dec)	1690 1615 1520[f]	q)	23.43 (22.46)	2.73 (2.51)	9.00 (8.73)
w)	*n*-C_4H_7	Cl	1:0.50	67	38[r]	145.0—148.0(dec)	1693 1610 1515	298	42.67 (42.88)	6.71 (6.60)	8.67 (8.34)
x)	Ph	Cl	1:0.57	70	46[r]	163.0(dec)	1650	q)	50.87 (51.09)	3.68 (3.75)	
y)	C_2H_5	Br	s)	76	51	130.0—133.0	1690 1605 1515	dec[e]	24.81 (26.04)	3.95 (3.83)	7.73 (7.59)
z)	Ph	Ph	1:4.63	432	t)						

a) Reaction temp., 60—65°C. b) Based on nitrile. c) 70 eV. d) Values in parentheses are calculated ones. e) The molecular ion and fragment ions probably due to the *s*-triazine having the composition of $(R^1R^2CHC{\equiv}N)_3$ were obserbed f) KBr disk. g) According to the method of Grundmann *et al.*,[11] ethyl ether was used as solvent. h) Based on reacted nitrile. i) See experimental section. j) For 20 days at room temp. k) Reaction temp., 100°C. l) Almost quantitatively. m) Lit,[11] 140°C. n) According to the method of U. S. Patent.[10] o) Lit,[10] 175°C. p) Reaction temp., room temp. q) See Table 1. r) Based on HCl used. s) Ethyl ether was used as solvent and heated to 60—65°C. t) Diphenylacetamide was formed in 20% yield.

enough for us to assume that they all had the same structure as the dimer salt, $2ClCH_2C{\equiv}N{\cdot}2HCl$ (**3g**), although sometimes their IR spectra showed a weak absorption around 1750 cm^{-1} as well as the precursor of **3g** described above.

On the other hand, the addition product from propionitrile was prepared by reacting propionitrile with excess HCl in a sealed glass tube at 60—65°C. The resulting addition product (**3b**) was found, on the basis of elemental analysis and the melting point, to be

Table 3. Preparation and analyses of 4[a], 5[b], and 6[c]

	Products R¹	R²	Yield (%)	Mp (°C)	IR(KBr) (cm^{-1})	Mass[d] (M^+)	Elemental analysis[e] C%	H%	N%
4b)	CH_3	H	55[f] (25)[g]	155.0—157.0[h]	3280 3180 1740				
4d)	n-C_4H_9	H	72	88.0— 90.0[i]	3280 3200 1740	213	66.11 (67.56)	10.23 (10.87)	6.29 (6.57)
4e)	n-C_6H_{13}	H	73	90.0— 91.0	3280 3190 1740	269	71.09 (71.32)	11.71 (11.60)	5.38 (5.20)
4f)	Ph	H	—	201.5—202.5	3280 3180 1730	253	76.39 (75.87)	5.93 (5.97)	5.62 (5.53)
4h)	$ClCH_2$	H	59	157.5—158.0	3285 3195[j] 1745	197	36.83 (36.39)	4.94 (4.58)	7.17 (7.07)
4i)	$PhCH_2$	H	81	108.0—109.0	3220 3140[j] 1740	281	77.05 (76.84)	6.99 (6.81)	5.18 (4.98)
4m)	CH_3	CH_3	50[g]	177.0—178.0[l]	3305 3215 1735	157	60.73 (61.12)	10.03 (9.62)	8.96 (8.91)
4o)	n-C_3H_7	CH_3	46	98.0— 99.0	3280 3195 1730	213	67.45 (67.56)	11.15 (10.87)	6.59 (6.57)
4p)	n-C_4H_9	CH_3	—	65.5— 67.0	3290 3200 1740	241	69.54 (69.67)	11.34 (11.27)	5.81 (5.80)
5)[b]	Cl	Cl	86	108.0—109.0	3222 2930 1704 1620 1524	255	18.80 (18.67)	0.76 (0.78)	5.11[n] (5.44)
4s)	C_2H_5	C_2H_5	30	84.5— 85.0	3280 3180 1732[j]	213	67.28 (67.56)	11.13 (10.87)	6.47 (6.57)
6)[c]	$ClCH_2$	CH_3	39	91.0— 91.5	3300 3180 1730 1690 1635 950	189	50.49 (50.67)	6.55 (6.38)	7.67[m] (7.39)
4u)	CH_3	Cl	65[g]	119.0—121.0	3330 3240[j] 1760	197	36.43 (36.38)	4.51 (4.58)	7.08 (7.07)
4v)	$ClCH_2$	Cl	27[k]	94.0— 96.0	3265 3190 1760	265	27.95 (27.00)	2.72 (2.64)	5.38 (5.25)
4y)	C_2H_5	Br	47	80.0— 83.0	3280 3200[j] 1750	313			4.97 (4.45)

a) 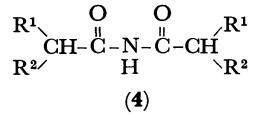 (**4**)

b) 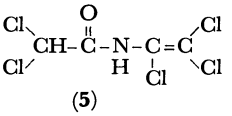 (**5**)

c) 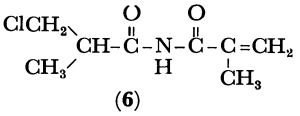 (**6**)

d) 70 eV. e) Values in parentheses are calculated ones. f) Hydrolysis using aq. Na_2CO_3. g) Yields in hydrolysis of the freshly prepared salts with water. h) Lit,[23] 153—154°C. i) Lit,[23] 174°C. j) Nujol. k) Acetone was used as solvent. l) Lit,[24] 92.5°C. m) NMR($CDCl_3$) (τ): 8.68(3H, doublet(J=6 Hz)), 7.98(3H, sharp singlet with fine structure), 6.0—6.5(3H, complex lines), 4.35(1H, complex lines), 4.10(1H, complex lines), 1.13(1H, broad line). n) NMR($CDCl_3$)(τ): 4.00(1H, singlet), 2.08(1H, broad line).

identical with a substance which had already been obtained by Gautier[1] and Michael.[9] Its IR spectrum did not show the absorption around 1750 cm^{-1} and indicated the same structure as the other adducts, **3g**, **3t**, and **3u**. Generally, the adducts obtained by heating in a sealed tube did not show the IR absorption around 1750 cm^{-1}.

As is shown in Table 1, their mass spectra exhibited the fragment ion peaks corresponding to M^+–HCl, M^+–HCl—Cl, $R^1R^2CHC{\equiv}\overset{+}{N}H$, and $R^1R^2CHC{\equiv}N$. Thus, all the addition products (**3b**, **3t**, and **3u**) have been confirmed to be dimer salts with the composition of $2R^1R^2CHC{\equiv}N\cdot 2HCl$. Further proof was obtained by the hydrolysis of the addition products to diacylamine **4** or **5**, as will be discussed below.

Dimerization of Other Nitriles Having α-Hydrogen with HCl. Nitriles were generally allowed to react with an excess of dry HCl in a sealed glass tube at 60—65°C until the reaction mixture became viscous enough (Table 2). In two cases, those of isobutyronitrile and 2,3-dichloropropionitrile, the whole reaction mixture solidified at the end of the reaction. In the other cases, when the viscous product was treated with dry ether or was left standing with ether in a refrigerator, the white or pale yellow product crystallized or solidified. Most of the adducts thus obtained were analytically pure, as is shown in Table 2. The addition product from acetonitrile was very hygroscopic, as was the dimeric product reported by Hinkel and Treharne.[14] On the basis of the data in Tables 1 and 2, and the hydrolysis to the corresponding diacylamines (**4**) (see next section), all of the addition products were identified as dimer salts with the composition of $2R^1R^2CHC{\equiv}N\cdot 2HCl$. It is worth pointing out that, in some of their mass

21) Shand[10] reported that water converted the salt from 2-chloropropionitrile to 2-chloropropionamide.

22) Grundmann *et al.*[2] reported that the treatment of the dimeric salt having the formula $(CHCl_2C{\equiv}N)_2HCl$, with water gave bis(dichloroacetyl)amine (**4t**).

23) K. Brunner, R. Grunner, and Z. Benes, *Monatsh.*, **48**, 123 (1927).

24) C. Norstedt and H. A. Wahlforss, *Chem. Ber.*, **25**, Ref. 637 (1892).

TABLE 4. NMR SPECTRA OF SOME DIMER SALTS (**3**)

Dimer salts (**3**)	Solvent	Temp.(°C)	Signal assignment (τ)					
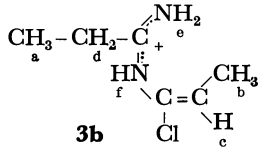 **3b**			(a) [3H]	(b) [3H]	(c) [1H]	(d) [2H]	(e) [2H]	(f) [1H]
	Liq. SO_2	20	8.67(t) (J=7.5Hz)	8.11(d) (J=6.7Hz) 8.08(d) (J=6.7Hz)	7.20(q)[a] (J=7.5Hz)	3.81(q) (J=6.7Hz) 3.79(q) (J=6.7Hz)	2.85(bs)[b] 1.75(bs)	−0.25(bs)[b]
	Liq. SO_2	0	8.60(t)	8.10(d) 8.07(d)	7.21(q)	3.80(q) 3.78(q)	2.84(bs) 1.84(bs)	−0.06(bs)
	Liq. SO_2	−35	8.60(t)	8.11(d) 8.08(d)	7.23(q)	3.79(q) 3.77(q)	2.80(bs) (2.44(bs)) 1.96(bs) (1.77(bs))	0.12(s)
	Liq. SO_2	−65	8.63(t)	8.12(d)	7.27(q)	3.82(q) 3.80(q)	2.81(s) (2.47(bs)) 2.12(s) (1.93(bs))	0.30(s)
	CF_3COOH	20	8.57(t) (J=7.5Hz)	8.08(d) (J=6.7Hz) 8.06(d) (J=6.7Hz)	7.21(q) (J=7.5Hz)	3.80(q) (J=6.7Hz) 3.78(q) (J=6.7Hz)	2.40(bs) 1.85(bs)	0.75(bs)
	d_6-DMSO	20	Decomposition					
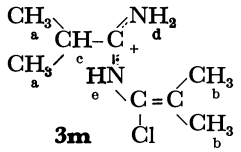 **3m**			(a) [6H]	(b) [6H]	(c) [1H]	(d) [2H]	(e) [1H]	
	Liq. SO_2	−28	8.59(d) (J=6.7Hz)	8.18(s) 8.05(s)	6.94(qui)[c] (J=6.7Hz)	2.95(b) 2.12(b)	0.50(b)	
	Liq. SO_2	−60	8.59(d)	8.17(s) 8.04(s)	6.98(qui)	2.92(b) 2.22(b)	0.64(b)	
	CF_3COOH	20	8.52(d) (J=6.7Hz)	8.14(s) 7.99(s)	6.94(qui)	2.44(b) 1.97(b)	1.04(b)	
	d_6-DMSO	20	8.72(d) (J=6.7Hz)	8.32(s) 8.14(s)	6.95(qui) (J=6.7Hz)	0.77(b) −0.11(b)	−1.71(b)	
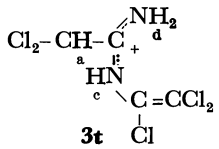 **3t**			(a) [1H]	(b) [2H]	(c)			
	CF_3COOH	20	3.06(s)	0.92(b) 0.73(b)	d)			
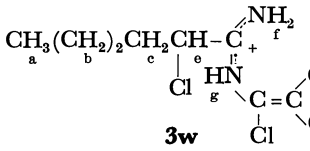 **3w**			(a) [3H]	(b) [8H]	(c) [2H]	(d) [2H]	(e) [1H]	(f) [2H]
	CF_3COOH	20	9.00[e]	*ca.* 8.46(m)	*ca.* 7.81(m)	7.27(t)	5.08[f]	1.10(bs) 0.48(bs)
			(g) [1H] −0.30(bs)					

a) (q)=quartet with fine line structure. b) (bs)=very broad. c) (qui)=quintet. d) The NH signal appears to be under the trifluoroacetic acid signal. e) Triplet with some distorted. f) Triplet with fine line structure.

spectra, the molecular-ion and degradation-ion peaks due to the *s*-triazine with the composition of $(R^1R^2CHC{\equiv}N)_3$ were observed instead of the degradation peaks due to the dimer salts (**3**).[19]

The reaction seems to proceed quantitatively. Especially, an excess of HCl and a prolonged reaction time seem to be beneficial for the reaction. Heating is not always necessary. Some α-chloronitriles quantitatively dimerize in ether under cooling, and isobutyronitrile reacts with a large excess of HCl at room temperature, although slowly, giving a quantitative yield of the salt (**3m**). A higher reaction temperature (100°C) did not favor the reaction (see **3m** in Table 2).

All attempts to prepare the solid dimer salts from methoxyacetonitrile, 3-alkoxypropionitriles, ethyl cyanoacetate, and diphenylacetonitrile were in vain (see Experimental Section).

Hydrolysis of the Dimer Salts (3) to Diacylamines (4). When most of the dimer salts (**3**) thus obtained were treated with water or with aqueous acetone or methanol, the corresponding diacylamines (**4**) were formed without being contaminated with other products (see Eq. 3). The yields and analytical data of the diacylamines (**4**) thus obtained are summarized in Table 3.[20]

It should be noted, however, that these dimer salts, **3b**, **3m**, and **3u**, were unreactive to water; they were recovered unchanged after the removal of water under reduced pressure. They were readily hydrolyzed by aqueous alkali to give these diacylamines, **4b**, **4m**, and **4u** respectively, as had been expected. However, the freshly-prepared ones were in part readily hydrolyzed by only cold water to give the corresponding diacylamines; this may be ascribed to the initial formation of unstable salts, such as 2: 3 adducts (see next section).

20) Diacylamines (**4**) were reported obtainable by the reaction of nitriles with carboxylic acids or acid chlorides. But the reaction conditions were very drastic (reaction temp. 100—250°C) and probably the yields may be low. (R. Otto and J. Troger, *Chem. Ber.*, **23**, 760 (1890)). This reaction provides a facile one-step synthesis of diacylamines (**4**).

As is shown in Table 3, the similar treatment of the dimer salts **3r** and **3t** with water gave anomalous products. The former afforded *N*-(3-chloro-2-methylpropionyl)-*N*-methacryloylamine (**6**), which must be formed by the further but partial dehydrochlorination of bis(3-chloro-2-methylpropionyl)amine (**4r**) during work-up, while the latter gave a partially-hydrolyzed product, *N*-(1, 2, 2-trichlorovinyl) dichloroacetamide (**5**).[25]

Structure of the Dimer Salts (3). The mass spectra of the dimer salts (**3**) indicated that one mole of HCl in the salts was intrinsically bonded and that another mole of HCl was present in the ionic form. The analysis of the ionic chlorine content also supported this fact.

The most interesting problem was to determine the structure of the protonated amidine function in these dimer salts (**3**). In view of the above interest, we undertook an NMR investigation of their structures.

The NMR spectra of **3b** measured in the range from −60 to 20°C using liquid SO_2 as the solvent show two sets of quartets for the vinyl proton at τ 3.79 and 3.81 in almost the same ratio, and two sets of doublets for the methyl protons attached to the vinyl group at τ 8.08 and 8.11 in the same ratio; both the quartets and the doublets are coupled to each other (J=6.7 Hz), suggesting the presence of a propenyl group as a mixture of *cis* and *trans* in almost equal proportions.

The NH protons give rise to three broad signals at 20°C. As the temperature is lowered, a narrowing of the signals and slight shift to higher magnetic fields are observed. Below −35°C, the two upfield peaks were split, giving new, small, broad signals at τ *ca.* 1.77—1.93 and *ca.* 2.44—2.47 respectively. The simplest interpretation of these data is that the upfield signals are due to $>C^1{=}N^2H_2$, with a hindered rotation about the C^1N^2 bond because of its partial double-bond character, and that the low-field signal is due to a highly acidic proton on the nitrogen, N^3. The behavior of the upfield N^2H_2 protons at low temperatures may unambiguously be ascribed to the internal rotation of the α-chloroalkenyl group about the C^1N^3 bond with the partial double-bond character, as is shown in Eq. (2):

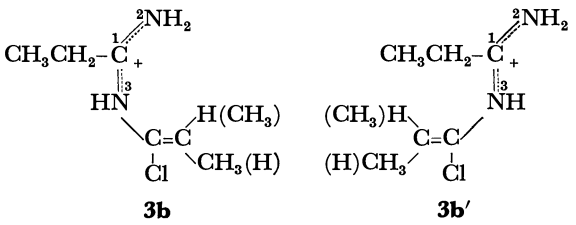

(2)

However, no splitting of the low-field N^3H signal was observed. The IR absorption patterns of **3b** in the region from 1500 to 1700 cm^{-1} are absolutely identical both in the solid state and in solution (in methanol).

The NMR spectrum of the 1: 1 adduct from chloroacetonitrile, however, was not reproducible in any solvent such as DMSO-d_6, CF_3COOH, and liquid SO_2. Taking into account its instability, the freshly-isolated adduct, $2ClCH_2C{\equiv}N\cdot 3HCl$, was analyzed instantly with a 100 MHz NMR spectrometer. The NMR spectrum (Fig. 1) suggests that the adduct has the following structure:

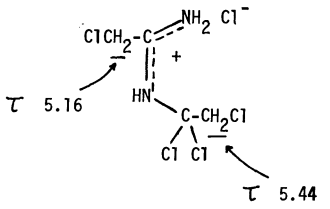

On the other hand, when the adduct was left standing under reduced pressure overnight, signals due to two pairs of methylene protons were deformed and signals attributable to the olefinic proton (*cis* and *trans*) appeared in its NMR spectrum (Fig. 2). These changes in the spectrum indicate the occurrence of partial dehydrochlorination, which may follow both A and B paths as follows:

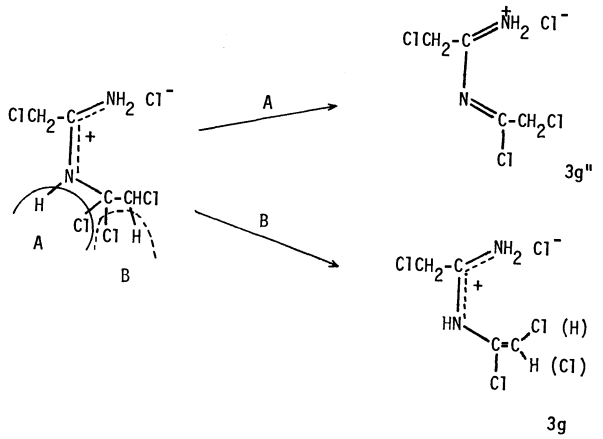

Accordingly, the lack of reproducibility of the NMR spectrum of the 2: 2 adduct from chloroacetonitrile was ascertained to be attributable to the indefinite contamination with **3g''** or the 2: 3 adduct.

Table 3 summarizes the NMR spectra of the 2: 2 adducts measured in this investigation. The data

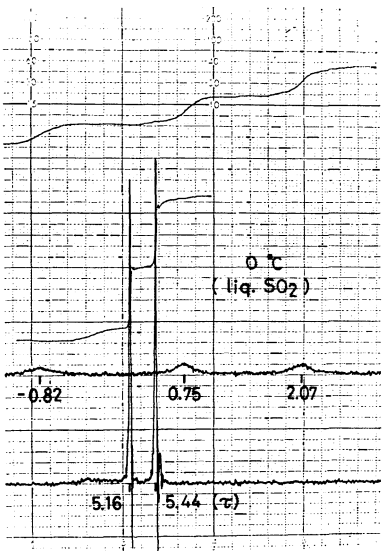

Fig. 1.

25) L. Hellerman, M. L. Cohn, and R. E. Hoen, *J. Amer. Chem. Soc.*, **50**, 1725 (1928).

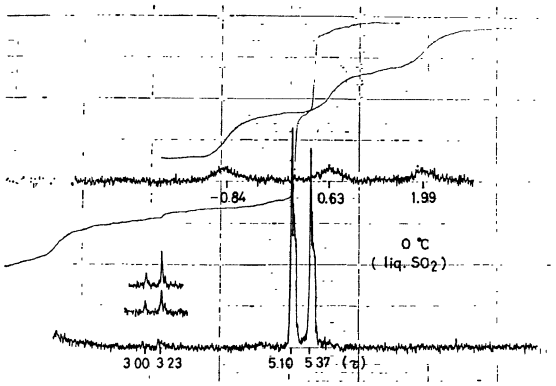

Fig. 2.

supported the general formula **3** as the structure of the dimer salts.

The reaction described above can now be presented as follows:

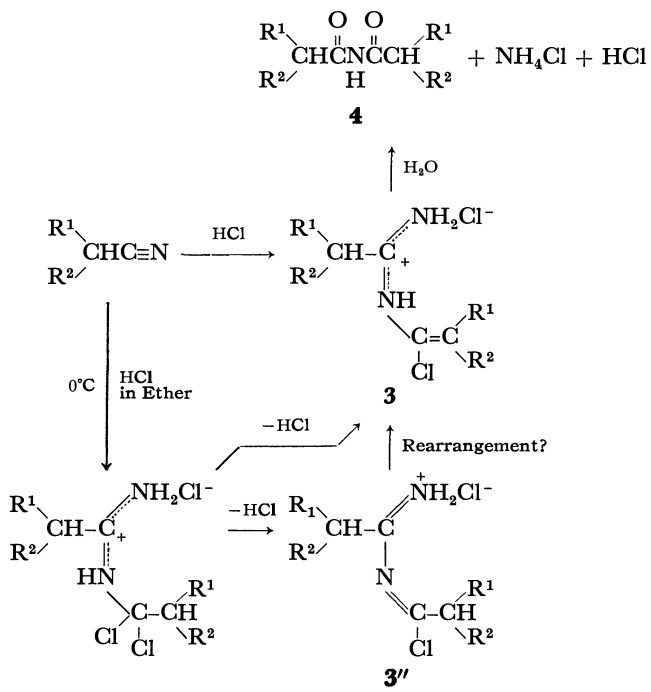

Extensive chemistry based on nitrile salts is now in progress in our group and will be described elsewhere.

Experimental

All the melting points were determined on a Yanagimoto micro-melting point apparatus and were corrected. The IR spectra were measured on a JASCO IR-E spectrometer; the NMR spectra, on JEOL JNM-G-60 and JNM-PS-100 spectrometers, with tetramethylsilane as the internal standard, and the mass spectra, on a Hitachi RMU-6E spectrometer.

General Procedure. In a 30 ml glass tube we placed 2—5 g of nitrile. The tube was then immersed in a mixture of ice and water, and dry HCl was allowed to be absorbed in it as much as possible. During that time, a white, crystalline solid, probably imidoyl chloride hydrochloride (**2**), was precipitated in some cases. The tube was stoppered, cooled in Dry Ice-acetone, sealed carefully, and heated to 60—65°C in a water bath until the reaction mixture was judged viscous enough. Table 2 lists the molar ratio of HCl to nitrile and the length of time. After the end of the reaction, the reaction tube was chilled in Dry Ice-acetone and opened carefully. After the removal of the HCl by warming, the stirring-in of dry ether caused the dimer salt to precipitate. When no solid precipitate appeared by this procedure, the mixture was then stored in a refrigerator for 24 hr or more, during which time the product was slowly crystallized and precipitated. Scratching the flask was sometimes beneficial for the solidification. The solid product was filtered, washed with dry ether, and dried under reduced pressure. In this manner, analytically-pure dimer salts were obtained and analyzed (Table 1). However, some salts (**3h, 3i, 3u,** and **3y**) required further purification. No attempt to find a good purification method was made.

Some reactions using ether as a solvent under cooling were carried out according to the methods previously reported.

The reaction of methoxyacetonitrile with HCl according to the general procedure, however, gave a black, hygroscopic substance. Ethyl cyanoacetate also gave a black, hygroscopic substance. The analogous treatment of 3-methoxypropionitrile or 3-butoxypropionitrile with HCl did not give the expected viscous reaction mixtures, and the starting nitriles were recovered. A small amount of the precipitated product consisted of ammonium chloride.

In the case of diphenylacetonitrile, di-*n*-butyl ether was employed as the solvent since the nitrile is solid. However, the resulting precipitate was identified as diphenylacetamide on the basis of following analytical results; mp 172—174°C (lit,[25] 167.5—168.5°C). Mass (M^+) 211. IR(KBr) 3380, 3180, 1650 cm^{-1}. Found: C, 79.59; H, 6.03; N, 6.67%. Calcd for $C_{14}H_{13}NO$: C, 79.59; H, 6.21; N, 6.63%. The formation of the amide is probably due to the degradation of di-*n*-butyl ether by HCl.

Preparation of the 2: 3 Adduct from Chloroacetonitrile. According to the method of Grundmann *et al.*,[11] chloroacetonitrile was allowed to react with HCl in ether under cooling. The resulting crystalline product was filtered by suction, left standing under reduced pressure for about 1 hr, and stored in a desiccator. Within 12 hr the white powder thus obtained was subjected to analysis. Found: Cl, 68.17%. Calcd for $C_4H_7N_2Cl_5$: Cl, 68.02%. Ionic chlorine content: Found: 40.56%. Calcd: 40.85%. The NMR tube containing the sample dissolved in liquid SO_2 was stored in a Dry Ice-acetone bath before measurement.

Hydrolysis of Dimer Salts (3). The dimer salt (**3**) (0.2—0.5 g) was dissolved in water (2—20 g). When the salt did not dissolve readily in cold water, the mixture was heated slightly, or methanol or acetone was added until the amidine salt dissolved. After a while, the diacylamine (**4**) was precipitated without being contaminated by other compounds, but in most cases several hours were required to observe the precipitation of diacylamines (**4**). Then, after the mixture had been allowed to stand overnight at room temperature, the diacylamine (**4**) formed was filtered with suction and dried. The diacylamines (**4**) thus obtained have a sufficient purity for synthetic use, but were further purified by sublimation and analyzed (Table 3).

When the amidines are resistant to hydrolysis in water, aqueous Na_2CO_3 was added until the mixture became alkali enough. Diacylamines **4** thus formed were treated in the same way.

In the hydrolysis of salt **3t**, after the filtration of **5**, the filtrate was extracted with ether. On evaporation, **5** was also obtained, but the further hydrolyzed product, bis(dichloroacetyl)amine (**4t**), was not isolated.

The authors wish to thank Mr. H. Moriguchi for

the mass spectra measurement, Mrs. M. Sakurai for the NMR measurement, and Miss J. Maenaka and Mr. and Mrs. Muneishi for elemental analyses. This work was supported in part by a grant-in-aid from Kokusan Gijutsu Shinkokai. We wish to express our thanks to the founder, the late Mr. Chikara Kurata.

BULLETIN OF THE CHEMICAL SOCIETY OF JAPAN, VOL. 46, 299—302 (1973)

Studies on Nitrile Salts. II.[1] A Facile One-step Synthesis of the Pyrimidine Nucleus

Shozo YANAGIDA, Tetsuo FUJITA, Masataka OHOKA, Reiji KUMAGAI, and Saburo KOMORI

Department of Applied Chemistry, Faculty of Engineering, Osaka University, Yamadakami, Suita, Osaka

(Received March 18, 1972)

The reaction of *N*-(α-chloroalkenyl)alkylamidine hydrochlorides (**1**) with phosgene was studied. The amidine hydrochlorides (**1a**—**h**) which were prepared from nitriles with more than two α-hydrogens reacted with phosgene at 100—105°C to give good yields of 4,6-dichloro-2,5-disubstituted-pyrimidines (**3a**—**h**). The amidine hydrochlorides (**1j**—**t**), which were obtained from nitriles with only one α-hydrogen, afforded 2-alkylidene-4,6-dichloro-5,5-disubstituted-2,5-dihydropyrimidines (**5j**—**t**) in good yields. The amidine hydrochloride **1i**, however, gave 2-dichloromethylidene-2,5-dihydro-5,5,6-trichloro-4(3*H*)-pyrimidinone (**4i**) under comparable conditions.

In our previous papers,[2-4] it was shown that the reaction of aliphatic nitriles or amides with phosgene and HCl gave good yields of 6-chloro-2,5-disubstituted-4(3*H*)-pyrimidinones (**2**), with traces of 4,6-dichloro-2,5-disubstituted-pyrimidines (**3**), and that arylacetonitriles gave 1,3-dichloroisoquinoline derivatives with the corresponding pyrimidinones (**2**) and pyrimidines (**3**). Further, we recently showed that most nitriles having α-hydrogen reacted with HCl to give *N*-(α-chloroalkenyl)alkylamidine hydrochlorides (**1**) almost quantitatively.[1]

On the basis of the reaction mechanism proposed for the formation of the pyrimidine derivatives (**2**) and (**3**),[2] the reaction of the amidine hydrochlorides (**1**) with phosgene may be expected to provide a convenient and facile one-step synthesis of the pyrimidine nucleus.

This paper will report the synthesis of pyrimidine derivatives, mainly **3** and **5**, based on this concept.

Results and Discussion

When *N*-(α-chloropropenyl)propioamidine hydrochloride (**1b**) was allowed to react with excess phosgene in chlorobenzene for 260 hr using a sealed glass tube at 60°C, 6-chloro-2-ethyl-5-methyl-4(3*H*)-pyrimidinone (**2b**) was obtained in a 60% yield, as had been expected (Scheme 1). However, the similar treatment of *N*-(α-chlorostyryl)phenylacetamidine hydrochloride (**1e**) with phosgene resulted in the recovery of the starting materials unchanged. Upon continued heating at 100—105°C for a period of 24 hr, 4,6-dichloro-2-benzyl-5-phenylpyrimidine (**3e**) was produced in a 75% yield. It is worth pointing out that 1,3-dichloroisoquinoline, which is the main product in the direct reaction of phenylacetonitrile with phosgene and HCl at 100°C,[4] was not formed. 6-Chloro-2-benzyl-5-phenyl-4(3*H*)-pyrimidinone hydrochloride, a precursor of **2e**,[2] first formed must be converted into **3e** by phosgene because of its strong electrophilicity at high temperatures (Scheme 1.).

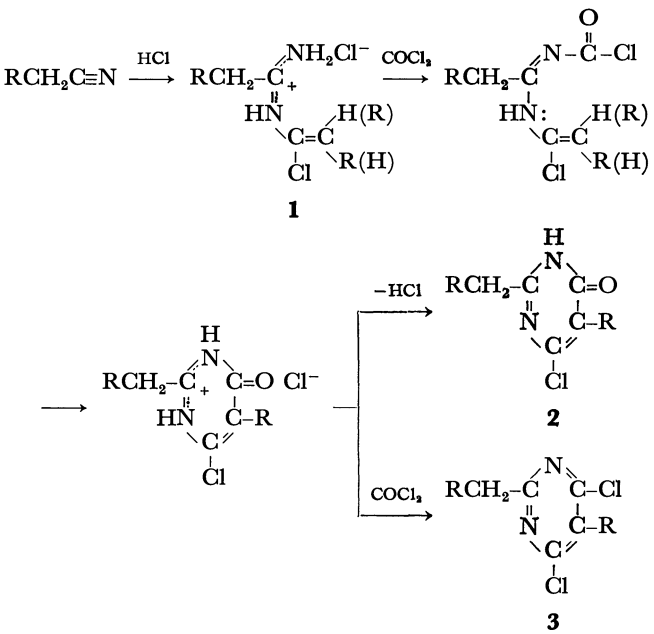

a) R=H; **b**) R=CH_3; **c**) R=CH_3CH_2; **d**) R=*n*-C_6H_{13}; **e**) R=Ph; **f**) R=$PhCH_2$; **g**) R=Cl; **h**) R=$ClCH_2$.

Scheme 1.

1) Part I: S. Yanagida, T. Fujita, M. Ohoka, I. Katagiri, and S. Komori, This Bulletin, **46**, 292 (1973).

2) S. Yanagida, M. Ohoka, M. Okahara, and S. Komori, *Tetrahedron Lett.*, No. 19, 2351 (1968), *J. Org. Chem.*, **34**, 2972 (1969).

3) S. Yanagida, H. Hayama, and S. Komori, *ibid.*, **34**, 4180 (1969).

4) S. Yanagida, M. Ohoka, and S. Komori, *ibid.*, **34**, 4127 (1969).

TABLE 1. PREPARATION AND ANALYSES OF 4,6-DICHLORO-2,5-DISUBSTITUTED-PYRIMIDINES (**3**)

3	R (R′=H)	Purification	Yield (%)	Bp (°C/mmHg) [Mp(°C)]	IR (neat) (cm^{-1})	Mass[a] (M^+)	NMR (CCl_4) (τ)	UV(C_6H_{12}) nm(ε_{max})	Elemental analysis[b] C%	H%	N%
3a[c]	H		>70[d]	—	1530[e]	—	—	—	—	—	—
3b	CH_3	Distillation	62	111.0—111.5/21	1565 1507	190	8.68(t, 3H) 7.59(s, 3H) 7.16(q, 2H)	260(4370)	43.98 (44.01)	4.10 (4.22)	14.57 (14.66)
3c	CH_3CH_2	Distillation	90 (crude)	84.0—85.0/3	1560 1506	218	9.02(t, 3H)[f] 8.78(t, 3H) 8.12(m, 2H) 7.15(t, 2H) 7.12(q, 2H)	—	50.07 (49.33)	5.42 (5.52)	12.40 (12.79)
3d	n-C_6H_{13}	Distillation	49	149.0—150.0/0.1	1560 1505	330	—	—	—	—	8.16 (8.46)
3e[c]	Ph	Recrystallized from ethanol	75	[136.0—[g] 138.0]	1550[h] 1495	—	—	234(11600) 265(6620)[i]	—	—	—
3f	$PhCH_2$	Recrystallized from ethanol	80	[69.5—70.0]	1550 1505	342	6.90(s, 4H)[j] 5.85(s, 2H) 2.88(s, 10H)	260(6150)	66.53 (66.48)	4.64 (4.70)	7.97 (8.16)
3g	Cl	Column chromatography	85	[28.0—30.0]	1530 1503	230	5.42(s)	232(13410) 268(7630) 275(6540)[i]	25.83 (25.90)	0.84 (0.87)	12.30 (12.08)
3h	$ClCH_2$	Column chromatography and distillation	79	113.0—116.0/3 [47.0—48.0]	1562 1510	258	6.66(t, 2H)[f] 6.03(t, 2H) 5.45(s, 2H)	225(7180)	32.31 (32.34)	2.24 (2.33)	10.54 (10.78)

a) 70 eV. b) Values in parentheses are calculated ones. c) Identified by comparison with authentic sample.[2,4] d) By glpc. e) Nujol. f) Measured in $CDCl_3$. g) Lit,[4] 136.0—138.0°C. h) KBr disk. i) Shoulder. j) 6.67(m, 4H), 5.63(s, 2H), 2.60—7.00(complex peaks, 10H) in CF_3COOH.

In view of the above facts, the reaction was extended to other amidines **1a**—**h**, employing 100°C as the reaction temperature. The expected dichloropyrimidines **3a**—**h** were obtained in good yields. (Scheme 1). It should be noted that the pyrimidine **3h** was obtained in a satisfactory yield by this reaction. As has been reported previously,[2] the direct reaction of 3-chloropropionitrile with phosgene in the presence of HCl gave a polymeric substance, and neither the pyrimidinone **2h** nor the pyrimidine **3h** was isolated.[5]

These pyrimidines **3** were confirmed on the basis of their physical properties and by elemental analysis, as is summarized in Table 1.

The NMR spectra of the pyrimidine **3f** are of particular interest. As is shown in Table 1, in CCl_4 the signals due to two pairs of methylene protons of the 2-phenethyl group were observed as a singlet, indicating that the phenyl ring of the 2-phenethyl group and the pyrimidine ring in **3f** are magnetically equivalent. A similar spectrum was also obtained in benzene. In CF_3COOH, however, this singlet signal was observed as an A_2B_2 pattern centered at τ 6.67, the signal due to methylene protons of the 5-benzyl group shifted to a lower field, and the signals of both phenyl ring protons, which were observed as a singlet in CCl_4, changed to a complex series of lines. The spectrum complexity is probably due to the protonation at the pyrimidine nitrogen.

We assumed that the driving forces of this cyclization reaction are the nucleophilicity of the β-carbon of a kind of enamino group [–NH–CCl=CHR] in the amidines **1** (Scheme 1)[6] and the prototropy of the hydrogen on the β-carbon. In view of these assumptions, the amidine hydrochlorides **1i**—**t** prepared from nitriles with only one α-hydrogen were expected to react with phosgene under comparable conditions to give a new type of pyrimidine derivative.

The treatment of the amidine hydrochloride **1i**, where both R and R′ are Cl, with phosgene under the same conditions as above led to a colorless compound, which was analyzed well for $C_5HON_2Cl_5$. The IR spectrum, taken in CCl_4, showed absorption bands at 3070, 2970, 2880 (NH), 1690 (C=O), 1590 (C=N), and 1530 (C=C) cm^{-1}. The series of absorption bands in the NH region were thought to be too low to assign to the NH stretching band. However, the NMR spectrum, measured in CCl_4, showed only a broad signal attributable to the NH proton at τ −2.85. In addition, the IR spectra in the region below 1700 cm^{-1} are quite identical both in the solid state and in solution (CCl_4). On the basis of these spectral analytic results, the compound was formulated as 2-dichloromethylidene-2,5-dihydro-5,5,6-trichloro-4(3*H*)-pyrimidinone (**4i**) rather than the following alternative structures:

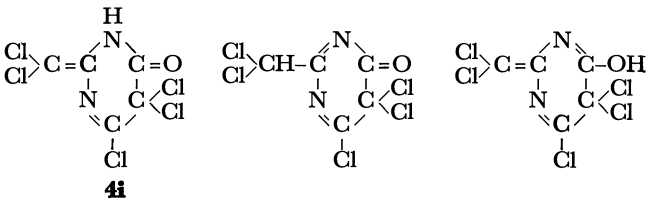

4i

5) It has been found in our laboratory that 3-chloropropionitrile reacts with phosgene and HCl in chlorobenzene at 100—105°C to give 1,3-dichloropropenyl isocyanate in a moderate yield, which fact will be reported eslewhere in the very near future.

6) G.H. Alt, "Enamines: Synthesis, Structure, and Reactions," Ch. 4, ed. by A.G. Cook, Marcel Dekker, New York, N. Y. (1969).

Table 2. Preparation and analyses of new type pyrimidine derivatives **4** and **5**

4 or 5	R	R′	Purification	Yield (%)	Mp (°C) [Bp(°C/mmHg)]	IR (neat) (cm^{-1})	Mass[a] (M^+)	NMR(CCl_4) (τ)	UV(C_6H_{12}) nm(ε_{max})	Elemental analysis[b] C%	H%	N%
4i	Cl	Cl	Recrystallized from petroleum ether–ether	97	130.0	1690[c] 1590 1530	280	−2.85(b)	295(3500) 275(3120)[d] 242(3990)	21.15 (21.27)	0.31 (0.36)	9.77 (9.92)
5j	CH_3	Cl	Sublimation	73	55.0—57.0	1553[e] 1518	258	7.48(s, 3H) 7.45(s, 3H)	226(5740) 260(3880)	32.14 (32.34)	2.09 (2.33)	10.81 (10.78)
5k	$ClCH_2$	Cl	Column chromatography	59	46.0—49.0	1552 1515	291[f]	5.44(s, 2H) 5.20(s, 2H)	232(8490) 258(3880)[d]	—	—	8.14 (8.52)
5l	n-C_4H_9	Cl	Distillation	93 (crude)	—	1550 1510	342	*ca.* 9.05(m, 6H) *ca.* 8.47(c, 8H) *ca.* 7.23(m, 4H)	—	—	—	8.01 (8.14)
5m	Ph	Cl	Sublimation	93	126.5—127.5	1540[e] 1500	386[g]	—	245(10560)	53.12 (53.16)	2.69 (2.62)	7.37 (7.29)
5n	Ph	CH_3	Recrystallized from petroleum ether	74	158.0—159.0	1645[e] 1605	342	7.97(s, 3H)[h] 7.49(s, 3H) 2.63(s, 10H)	296(22580)	66.39 (66.48)	4.47 (4.70)	8.32 (8.16)
5o	CH_3CH_2	CH_3CH_2	Column chromatography	56	[107.0—107.5/3]	1650 1610	274	9.13(t, 6H)[h] 8.95(t, 6H) 8.07(q, 4H) 7.48(q, 4H)	262(17600)	56.93 (56.73)	7.61 (7.32)	9.88 (10.18)

a) 70 eV. b) Values in parentheses are calculated ones. c) Both cases, KBr disk and in CCl_4(11 mg/*ca.* 1 ml). d) Shoulder. e) KBr disk. f) Corresponding to M^+-Cl. g) Molecular weight by vapor pressure osmometer (Mechrolab osmometer, Model 301A). h) Measured in $CDCl_3$.

On the other hand, other amidine hydrochlorides **1j—t** afforded further chlorinated pyrimidine derivatives formulated by the general formula **5** in good yields (Scheme 2):

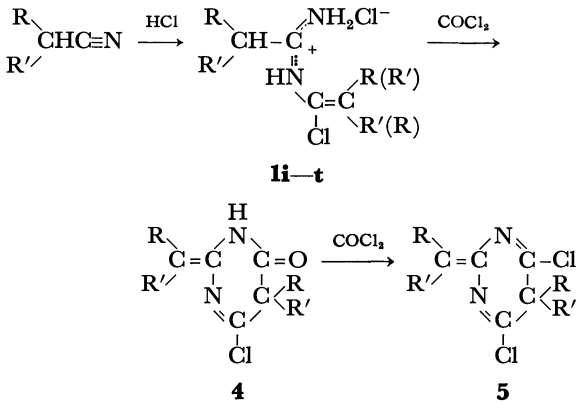

1i—t

4 **5**

i) R=Cl, R′=Cl; **j**) R=CH_3, R′=Cl;
k) R=$ClCH_2$, R′=Cl; **l**) R=n-C_4H_9, R′=Cl;
m) R=Ph, R′=Cl; **n**) R=Ph, R′=CH_3;
o) R=C_2H_5, R′=C_2H_5; **p**) R=CH_3, R′=CH_3;
q) R=CH_3CH_2, R′=CH_3; **r**) R=n-C_3H_7, R′=CH_3
s) R=n-C_4H_9, R′=CH_3; **t**) R=$ClCH_2$, R′=CH_3.

Scheme 2.

It is apparent that the pyrimidines **5** are formed through the chlorination of the initially-formed pyrimidinones **4** by phosgene, and that the pyrimidinone **4i** must be unreactive to phosgene under the reaction conditions employed.

The structures of **5j—o** were confirmed on the basis of their physical properties and by elemental analysis (Table 2). Attempts to isolate analytically-pure pyrimidines **5p—t** were unsuccessful. They were characterized by IR and mass spectra (see Experimental section).

It should be noted that, as is shown in Table 2, the IR absorptions attributable to the C=N and C=C stretching vibrations of **5j—m** are shifted to frequencies lower by about 100 cm^{-1} compared with those of the other pyrimidines **5o—t**. These large shifts may be explained by considering the following structures, based on the mesomeric effect:

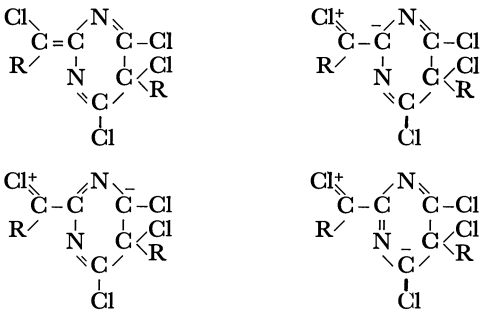

The IR spectra of the crude products from the amidines **1p—t** showed weak bands around 1750 cm^{-1} and medium bands attributable to the N=C=O stretching vibration around 2260 cm^{-1}, indicating the formation of by-products with a COCl group and/or an N=C=O group.[7] Accordingly, the crude products from **1p** and **1t** were treated with aniline, unexpectedly giving dimethylmalonoanilide and butylmethylmalonoanilide in 9 and 25% yields, respectively, based on the starting amidines. This fact suggests the formation

7) As noted in Ref. 6, some nitriles have been found to react with phosgene at high temperature to give α-chloroalkenyl isocyanates. In view of this fact, we assumed the compounds having N=C=O group to be corresponding isocyanates, which are probably produced through imidoyl chlorides formed by the degradation of the amidines **1** as follows;

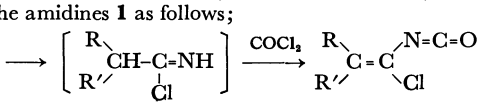

of disubstituted malonyl chlorides as by-products, we assumed that they were produced through the further reaction of the pyrimidines **5p—t** with phosgene.[8] However, no urea derivatives, which were thought to be derived from compounds with an N=C=O group, were isolated.[9]

Further studies of the reactivity of the pyrimidines **5** are now in progress in our laboratory.

Experimental

The melting points were determined on a Yanagimoto micro melting point apparatus and were corrected. The boiling points were uncorrected. The NMR spectra were obtained using a Model JNM-G-60 spectrometer (Japan Electronic Optics Laboratory Co.); the solvent was carbon tetrachloride, except where otherwise noted, with tetramethylsilane as the internal reference. The IR spectra were recorded with a Japan Electroscopic IR-E spectrophotometer, the mass spectra, with a Hitachi mass spectrometer, Model RMU-6E, and the UV spectra, with a Shimadzu double-beam spectrophotometer, UV-200.

Materials. *N*-(α-Chloroalkenyl)alkylamidine hydrochlorides (**1a—t**) were prepared according to the method reported previously.[1]

Reaction of the Amidine Hydrochlorides (1) with Phosgene. General Procedure: In a 150 ml glass tube we placed 1.6—3.0 g (*ca.* 20 mmol) of the amidine hydrochloride (**1**) and 20 ml of chlorobenzene. The tube was then immersed in a mixture of ice and water, and 6.2—7.4 g (*ca.* 75 mmol) of phosgene was bubbled into the mixture. The tube was stoppered, cooled in a Dry Ice–acetone mixture, sealed carefully, and heated to 100—105°C in an oil bath for 24 hr. The reaction tube was then chilled in the Dry Ice–acetone mixture and opened carefully. After the removal of the phosgene and chlorobenzene under reduced pressure, the resulting products were purified by recrystallization or distillation, if necessary, after column chromatographic separation, as is shown in Tables 1 and 2. The column chromatography was always done using silica gel, and all the products were eluted with petroleum ether.

In the cases of the pyrimidines **5p—t**, repeated distillations after column chromatography did not give the analytically-pure pyrimidines. They were all confirmed in the basis of their IR spectra. The mass spectra also supported the structure of **5**. The crude yields, boiling points, and IR absorption bands attributable to the C=N and C=O streching vibrations are as follows: **5p**: 1655 and 1620 cm^{-1}; **5q**: 58%, *ca.* 85.0—86.0°C/2 mmHg, 1655 and 1615 cm^{-1}; **5r** 52%, 130.0—130.5°C/2 mmHg, 1655 and 1610 cm^{-1}; **5s**: 45%, 1655 and 1610 cm^{-1}; **5t**: 63%, *ca.* 105°C/1 mmHg, 1660 and 1620 cm^{-1}.

Of particular interest is the fact that **5p** is very sensitive to moisture and that the purification of crude **5p** by column chromatography resulted in the unexpected isolation of 5,5-dimethylbarbituric acid (82% yield). An attempt to explain this formation is now under way.

Isolation of Disubstituted Malonoanilides. A typical procedure was as follows: a crude product (0.77 g) obtained from **1p** was mixed with aniline (1.5 g) in 1,2-dichloroethane (10 ml). The mixture was then allowed to stand overnight at room temperature. After the aniline hydrochloride precipitated had been filtered out with suction, the filtrate was concentrated under reduced pressure. The residue was chromatographed on silica gel; chloroform eluted 0.25 g of dimethylmalonoanilide (9% yield based on the amidine **1p**). It was recrystallized from dichloroethane–ether and analyzed as follows: mp 209.0—210.0°C (lit,[10] 205°C). IR (KBr disk) 3260, 3120, 1645, 1600 cm^{-1}. Mass spectrum (70eV) 282 (M^+). NMR ($CDCl_3$–CF_3COOH) (τ) 8.28 (s, 6H), 2.51—2.86 (m, 10H). Found: C, 72.23; H, 6.25; N, 9.78%. Calcd for $C_{17}H_{18}O_2N_2$: C, 72.32; H, 6.43; N, 9.92%.

Similarly, butylmethylmalonoanilide was isolated in a 25% yield based on the starting amidine **1s**, and was analyzed after recrystallization from ethanol as follows: mp 198.5—199.0°C, IR (KBr disk) 3340, 3240, 1660, 1600 cm^{-1}. Mass spectrum (70 eV) 324 (M^+). NMR (CF_3COOH) (τ) 8.95 (t, 3H), 8.46 (m, 4H), 8.02 (s, 3H), 7.67 (t, 2H), 2.57 (s, 10H), 0.15 (s, 2H). Found: C, 74.20; H, 7.29; N, 8.64%. Calcd for $C_{20}H_{24}O_2N_2$: C, 74.04; H, 7.46; N, 8.64%.

The authors wish to thank Mr. H. Moriguchi for the mass spectrum measurement, Mrs. M. Sakurai for the NMR measurement, and Miss J. Maenaka and Mr. and Mrs. Muneishi for elemental analysis. This work was supported in part by a grant-in-aid from Kokusan Gijutsu Shinkokai. We wish to express our thanks to the founder, the late Mr. Chikara Kurata.

8) In view of the formation of disubstituted malonyl chlorides, the following reaction can be considered;

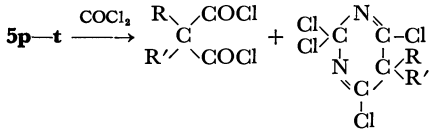

However, latter products have not been identified yet.

9) The following urea derivatives were expected;[4]

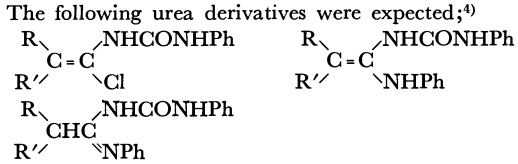

However, more polar solvent eluted only black tarry substance.

10) H. Staudinger, *Helv. Chim. Acta*, **8**, 312 (1922).

Studies on Nitrile Salts. III.[1] Dimerization of Nitriles Having No α-Hydrogen with Hydrogen Chloride

Shozo YANAGIDA, Tetsuo FUJITA, Masataka OHOKA, Ichiro KATAGIRI, Mikio MIYAKE, and Saburo KOMORI

Department of Applied Chemistry, Faculty of Engineering, Osaka University, Yamadakami, Suita, Osaka

(Received May 1, 1972)

The reaction of nitriles having no α-hydrogen, such as aromatic nitriles and thiocyanates, with hydrogen chloride was investigated. Benzonitrile, *p*-tolunitrile, *m*-tolunitrile and some thiocyanates gave analytically pure 2:2 adducts in their reactions with HCl in a sealed glass tube at 30—60°C. The structure of the adducts was elucidated on the basis of NMR analysis and the mechanism of the generalized dimerization of nitriles was discussed.

In this laboratory,[2] it was shown that nitriles having α-hydrogen reacted with HCl to give *N*-(α-chloroalkenyl)alkylamidine hydrochlorides (**1**), and that the amidines (**1**) are readily hydrolyzed in water giving diacylamines (**2**) as follows:

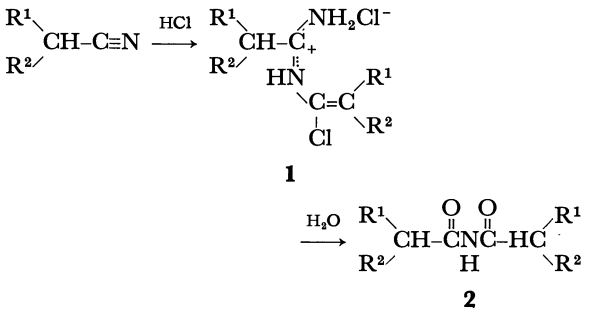

1

2

Our interest not only in extending this dimerization reaction to other cyano compounds but also in seeking an explanation for the reaction mechanism, prompted us to investigate the reaction of nitriles having no α-hydrogen with HCl.

Attempts to dimerize trichloroacetonitrile[3] or pivalonitrile with HCl have failed. However, it has now been found that some aromatic nitriles and thiocyanates undergo dimerization.

This paper reports their dimerization reaction, the structure of the resulting 2:2 adducts and the mechanism of the dimerization of nitriles.

Results and Discussion

Reaction of Aromatic Nitriles with HCl. It was so far believed[4] that some aromatic nitriles react with HCl at a low temperature (below 0°C) to give arylimidoyl chloride hydrochlorides, which are stable only in the atmosphere of HCl but decompose to the starting materials in the air. It has now been found that the treatment of benzonitrile with dry HCl in a sealed glass tube at a higher temperature (30—60°C) leads to the isolation of the white addition product having the empirical formula C_7H_6NCl, which is stable in the air. When this salt-like adduct was dissolved in water and allowed to stand overnight at room temperature, dibenzoylamine was formed in 44% yield. The hydrolysis of the adduct with aqueous alkali unexpectedly gave *N*-benzoylbenzamidine contaminated with a small amount of 2,4,6-triphenyl-*s*-triazine. These facts indicate that the product is a 2:2 adduct. However, the mass spectrum and melting point of the adduct were found essentially identical with those of 2,4,6-triphenyl-*s*-triazine, suggesting that pyrolysis of the adduct produces 2,4,6-triphenyl-*s*-triazine.

Similarly, *m*- and *p*-tolunitrile gave the corresponding adducts (Table 1). In the case of *o*-tolunitrile, *p*-nitrobenzonitrile, and *p*-chlorobenzonitrile, ethyl ether was employed as a solvent to increase the solubility of HCl, since the nitriles dissolve less amount of HCl or the nitriles are solid in some cases. However, the reaction resulted in the formation of the corresponding amides.[5]

Reaction of Thiocyanates with HCl. Allenstein and Quis[8] reported that methyl thiocyanate reacted with HCl at 0°C giving methyl thioimidoyl chloride hydrochloride. However, the reaction at a higher temperature was not studied. We have found that the reaction of ethyl thiocyanate with excess HCl in a sealed glass tube at 60°C affords a dimeric 2:2 adducts, the structure of which was supported by the IR and mass spectra, and hydrolysis to bis(ethylthioformyl)amine.

The reaction was extended to methyl, propyl, butyl, octyl, and benzyl thiocyanates. Their IR spectra indicate the formation of the corresponding 2:2 adducts, but their mass spectra showed molecular and fragment ion peaks due to the corresponding 2,4,6-tris(alkylthio)-*s*-triazines. Hydrolysis of these adducts did not give the expected bis(alkylthioformyl)amines but unidentified oily or tarry substances. In addition, the isolation of analytically pure adducts was unsuccessful except for the case of octyl thiocyanate.

1) Part II: S. Yanagida, T. Fujita, M. Ohoka, R. Kumagai, and S. Komori, This Bulletin, **46**, 299 (1973).

2) S. Yanagida, T. Fujita, M. Ohoka, I. Katagiri, and S. Komori, This Bulletin, **46**, 292 (1973).

3) Grundmann *et al.* reported the formation of the 2:1 adduct in the reaction of trichloroacetonitrile with HCl. C. Grundmann, G. Weisse, and S. Seide, *Ann. Chem.*, **577**, 77 (1952).

4) E. N. Zil'berman, *Russ. Chem. Rev.*, **31**, 615 (1962).

5) Especially *p*-chlorobenzamide was formed in 50% yield. The cleavage of ether linkage by hydrogen halides to an alcohol and a halide is well-known.[6] Thus the amide must be formed through imidates from nitriles, HCl and ethyl alcohol formed by the degradation of ethyl ether used as solvent.[7]

6) E. Stande and F. Patat, "The Chemistry of the Ether Linkage," S. Patai, Ed., Interscience Publishers, New York, N. Y. (1967), p. 21.

7) R. Roger and D. G. Neilson, *Chem. Rev.*, **61**, 179 (1961).

8) E. Allenstein and P. Quis, *Chem. Ber.*, **97**, 3162 (1964).

TABLE 1. PREPARATION AND ANALYSIS OF THE 2:2 ADDUCTS FROM AROMATIC NITRILES AND THIOCYANATES

Starting nitrile RC≡N	Mol Ratio HCl/RC≡N	Reaction temp. (°C)	Reaction time (hr)	Yield (%)	Mp (°C)	IR (KBr) (cm^{-1})	Elemental analysis[a] C%	H%	N%
$C_6H_5C{\equiv}N$	0.9	60	93	13	240—242[b]	1663 1635	60.29 (60.23)	4.08 (4.33)	10.03 (10.04)
$C_6H_5C{\equiv}N$	0.9	30	192	23					
$C_6H_5C{\equiv}N$	1.1	30	75 days	57					
p-$CH_3C_6H_4C{\equiv}N$	1.0	60	286	27	293[c]	1673 1635	63.12 (62.55)	5.38 (5.25)	9.32 (9.12)
p-$CH_3C_6H_4C{\equiv}N$	0.9	30	167	12					
m-$CH_3C_6H_4C{\equiv}N$	0.9	60	112	15	148—150[d]	1665 1645	62.66 (62.55)	5.28 (5.25)	9.20 (9.12)
$C_2H_5SC{\equiv}N$[e]	1.5	60	170	40	121.5—123.5	1617 1588	28.98 (29.15)	4.85 (4.89)	11.32 (11.33)
n-$C_8H_{17}SC{\equiv}N$	1.6	60	144	35	77—78	1620 1570	52.85 (52.03)	9.18 (8.73)	7.04 (6.74)

a) Values in parentheses are calculated ones. b) 2,4,6-triphenyl-s-triazine prepared melted at 242—243°C (lit,[22] 231—232°C). c) Melting point of 2,4,6-tirs(p-tolyl)-s-triazine: 278—279°C.[22] d) Melting point of 2,4,6-tris(m-tolyl)-s-tirazine: 152—153°C.[22] e) Mass spectrum shown in Experimental.

Structure of the 2:2 Adducts. Taking into account the basicity of nitrogen atoms of the conjugate base, the dimeric adducts from aromatic nitriles or thiocyanates were expected to have structure A rather than B. In addition, in view of the possible resonance structures of A, the structure may well be expressed by the delocalized structure A'. In fact, the NMR spectra support structure A' rather than A or B.

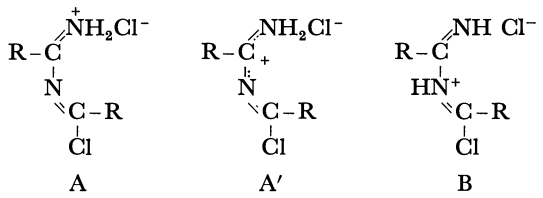

A A' B

In the NMR spectrum of the 2:2 adduct from benzonitrile measured at −33°C in liquid SO_2, two distinct signals attributable to NH protons were observed (Fig. 1a).

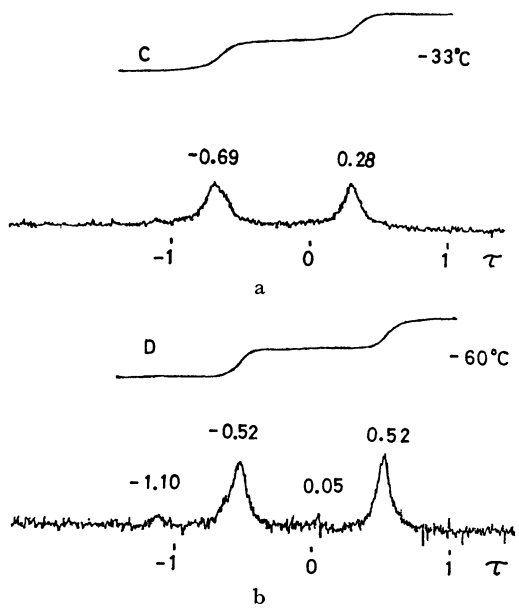

Fig. 1. NH_2 Signals in NMR Spectra of the 2:2 Adduct from Benzonitrile.

An increase in temperature led to broadening and coalescence of the signals. The adduct from ethyl thiocyanate also exhibited a similar spectral change (see Experimental). These observations indicate the presence of NH_2 group in the adducts. The nonequivalence of the two amino protons may be accounted for by the hindered rotation about the CN bond owing to its partial double bond character. In addition, two pairs of phenyl ring protons and two pairs of methylene protons of the ethylthio groups have almost the same chemical shift. If the adducts took either structure A or B, one pair of the protons should have been greatly deshielded by the localized positive charge. The appearance of new small signals in Fig. 1b is probably ascribed to the presence of the following geometrical isomer A'':

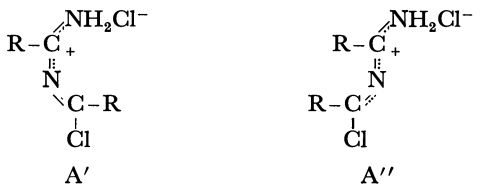

A' A''

Formation Mechanism of Dimeric Adducts. Some mechanisms for the dimerization of nitriles were proposed by several investigators[4,9,10] but they were still open to question.

von Braun *et al.*[11] and Prajsnar[12] reported that some N-substituted imidoyl chlorides having α-hydrogen, generated *in situ* from N-substituted amides, underwent dimerization, giving amidine derivatives as exemplified

9) W. Ruske, "Friedel-Crafts and Related Reactions," Vol. 3. Part 1. G. A. Olah, Ed., Interscience Publishers, New York, N. Y. (1964), p. 398.

10) F. Johnson and R. Madronero, "Advances in Heterocyclic Chemistry," Vol. 6, A. R. Katrizky, Ed., Academic Press, New York, N. Y. (1966), p. 95.

11) J. von Braun, F. Jostes, and H. Heymons, *Chem. Ber.*, **60**, 92 (1927).

12) B. Prajsnar, *Roczniki Chem.*, **36**, 1449 (1962); *Chem. Abstr.*, **59**, 5139 (1963).

by the following equation:[13]

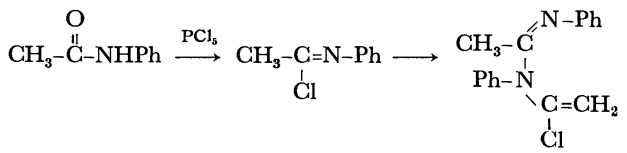

The reaction is quite comparable to the dimerization of nitriles in the presence of HCl.

In order to get spectral evidence of the dimeric products and to seek an explanation for the mechanism of the dimerization of imidoyl chlorides, we reinvestigated the reaction of acetanilide with PCl_5 or phosgene.

The reaction of acetanilide with PCl_5, followed by neutralization with aqueous ammonia, gave *N,N'*-diphenyl-*N*-(α-chlorovinyl)amidine as reported, which was confirmed on the basis of NMR analysis.[14] Phosgene also gave the identical amidine. These facts suggest that HCl formed during the reaction plays an important role in the dimerization.[15] Accordingly it may be concluded that imidoyl chlorides, especially having at least one α-hydrogen and free from steric hindrance around α-carbon atom, readily dimerize giving *N*-(α-chloroalkenyl)amidine derivatives.[16]

Recently Speziale and Freeman[17] showed that *N,N*-diethyl-1,2,2-trichlorovinylamine reacts with an amine giving a *N,N*-diethyl-*N'*-substituted dichloroacetamidine through the addition-elimination mechanism rather than the usual S_N2 mechanism.

In addition, it is claimed by a U. S. patent[18] that dimethyl cyanamide reacts with HCl to give *N,N*-dimethylaminoimidoyl chloride hydrochloride and that, on heating to 100°C, the hydrochloride dimerizes giving the 2: 2 adduct.

In view of these considerations and the facts gained through a series of these studies,[2] we propose the following sequence as a mechanism of the dimerization of nitriles with HCl:

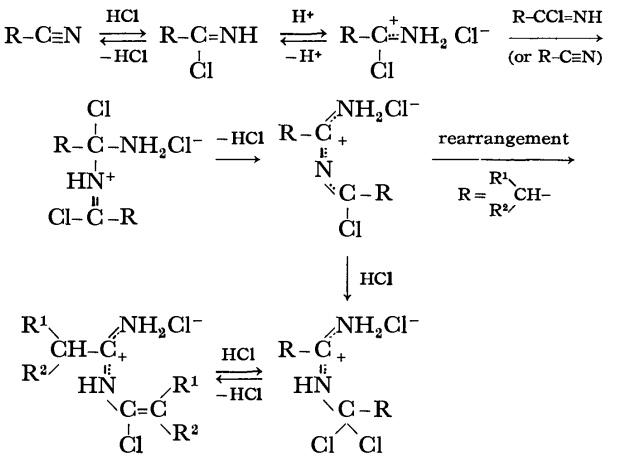

13) Braun proposed a mechanism involving a rearrangement to the enamine as follows:

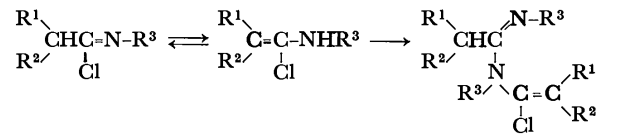

However, in view of the success in dimerization of nitriles which never undergo rearrangement to the enamine structure due to the absence of α-hydrogen, a similar mechanism for the dimerization of nitriles is unlikely.

The dimerization of *N*-substituted imidoyl chlorides,[11,12] the Pinner synthesis of imidates and the intramolecular amination of nitriles in the presence of HCl[19] may be interpreted in a similar manner, that is, displacement of chloride ion from imidoyl chloride hydrochloride by the nucleophilic imidoyl chloride, alcohol or amine.

Experimental

Melting points were determined on a Yanagimoto micro melting point apparatus and were corrected. The NMR spectra were obtained using a Model JNM-G-60 spectrometer (Japan Electronic Optics Laboratory Co.) with tetramethylsilane as an internal reference. The IR spectra were recorded with a Japan Electroscopic IR-E spectrophotometer, and the mass spectra with a Hitachi mass spectrometer Model RMU-6E.

Dimerization of Aromatic Nitriles or Thiocyanates with HCl. A typical procedure is as follows: Dry HCl was bubbled into benzonitrile (3 g, 29.1 mmol) in 30 ml glass tube under cooling in an ice bath (1.02 g, 28.0 mmol of HCl was absorbed). The glass tube, after being sealed, was placed in a water bath maintained at 60°C for 93 hr. As the reaction proceeded, the reaction mixture became viscous. The tube was opened carefully and excess HCl was removed. Addition of dry ether into the reaction mixture caused precipitation of the 2: 2 adduct, which was filtered with suction, dried and analyzed (Table 1) (1.0 g, 12.8% yield).

The reaction conditions and yields for the other cases are shown in Table 1. It should be noted that the longer the reaction time, the higher the yield.

The mass spectrum of the adduct from ethyl thiocyanate shows the following fragment ion peaks (70 eV): *m/e* (rel intensity) 181 (19) [$C_2H_5SC(=NH)N=CClS^+$], 175 (10) [$C_2H_5SC(=NH)N=C^+-SC_2H_5$], 149 (100) [$C_2H_5SC(=NH)N=C^+-Cl$]. NMR ($SO_2$) at −30°, τ 0.43 (bs, 1H), 0.86 (bs, 1H), 6.81 (q, 4H, J=7.5 Hz), 8.54 (t, 3H, J=7.5 Hz), and 8.59 (t, 3H, J=7.5 Hz); at −62°C, τ 0.55 (bs, 1H), 1.10 (bs, 1H), 6.82 (q, 4H, J=7.5 Hz), 8.55 (t, 3H, J=7.5 Hz), and 8.60 (t, 3H, J=7.5 Hz).

Hydrolysis of the 2: 2 Adduct from Benzonitrile or Ethyl Thiocyanate. According to the procedure reported previously,[2] 4 g of the adduct from benzonitrile was dissolved in 50 ml of water and left standing at room temperature overnight. The resulting precipitate was filtered with suction, dried and identified as dibenzoylamine on the basis of the following analysis (1.58 g, 44%): mp 149—152°C (lit,[20] 147—148°C).

Analogous treatment of the adduct from ethyl thiocyanate

14) Braun determined the structure on the basis of elemental analysis and hydrogenation to *N,N'*-diphenyl-*N*-ethylacetamidine.

15) S. Yanagida, M. Yokoe, I. Katagiri, M. Ohoka, and S. Komori, This Bulletin, **46**, 306 (1973).

16) R. Bonnet, "The Chemistry of the Carbon-nitrogen Double Bond," S. Patai, Ed., Interscience Publishers, New York, N. Y. (1970), p. 597.

17) A. J. Speziale and R. C. Freeman, *J. Amer. Chem. Soc.*, **82**, 909 (1969).

18) I. Hechanbleikner, U. S. 2768204 (1956).

19) F. F. Blicke, A. J. Zambite, and R. E. Stenseth, *J. Org. Chem.*, **26**, 1826 (1961).

20) K. Brunner, *Chem. Ber.*, **47**, 2679 (1914).

with water gave a pale yellow crystalline precipitate, which was purified by recrystallization from acetone–water and identified as bis(ethylthioformyl)amine (40%): mp 104—105.5°C. IR (KBr) 3236, 3150 (NH), 1710 (C=O) cm^{-1}. Mass spectrum (70 eV) *m/e* (rel intensity) 193 [M^+], 131 (20) [$C_2H_5SCONCO^+$], 103 [$C_2H_5SCON^+$], 89 (20) [$C_2H_5SCO^+$], 70 (100) [$HCONCO^+$], 62 (39) [$C_2H_5SH^+$], 29 (80) [$C_2H_5^+$], 27 (45) [$C_2H_3^+$]. Found: C, 37.40; H, 5.89; N, 7.40%. Calcd for $C_6H_{11}NS_2O_2$: C, 37.28; H, 5.74; N, 7.25%.

Isolation of N-*Benzoylbenzamidine.* The aqueous solution of the adduct from benzonitrile (1 g in 20 ml of water) was made basic to litmus with aqueous Na_2CO_3, causing rapid precipitation of a brown crystal. The IR spectrum indicated that it was a mixture of *N*-benzoylbenzamidine and a small amount of triphenyl-*s*-triazine. The product was recrystallized from petroleum ether giving pure *N*-benzoylbenzamidine: mp 98°C (lit,[21] 98°C). IR (KBr) 1603 (C=O) 1563 (C=N) cm^{-1}. Mass spectrum (70 eV) *m/e* (rel intensity) 224 (46) [M^+], 208 (t) [M^+-NH_2], 147 (46) [$M^+-C_6H_5$], 105 (100) [$C_6H_5CO^+$], 77 (86)[$C_6H_5^+$], 51 (34).

Reaction of Acetanilide with PCl_5. According to the same procedure as that of Braun *et al.*,[9] powdered acetanilide (27 g) was allowed to react with powdered PCl_5 (43.5 g), followed by neutralization with aqueous ammonia, giving crude *N,N'*-diphenyl-*N*-(α-chlorovinyl)acetamidine (16 g). Extraction with petroleum ether using a Soxhlet extractor, concentration and recrystallization from hexane gave an analytically pure amidine: mp 106—108°C (lit,[9] 119°C), IR (KBr) 1650, 1630, 1595 cm^{-1}. Mass spectrum (70 eV) *m/e* (rel intensity) 270 (15) [$M^+ + 1$], 269 (15) [M^+], 118 (100) [$CH_3C^+=N-C_6H_5$], 93 (44) [$C_6H_5NH_2^+$], 77 (59) [$C_6H_5^+$]. NMR ($CDCl_3$) τ 8.12 (s, 3H), 4.68 (d, 1H) (J=3 Hz), 4.61 (d, 1H) (J=3 Hz), *ca.* 2.5—3.4 (m, 10H).

The NMR signals at τ 4.68 and τ 4.61, which are attributable to olefinic protons, support the *N*-(α-chlorovinyl)structure.

Reaction of Acetanilide with Phosgene. In a 200 ml four necked flask fitted with a thermometer, a condenser, a mechanical stirrer and a gas inlet tube, 27 g of acetanilide and 100 ml of benzene were placed and heated to 60—70°C. With stirring, phosgene was bubbled into the mixture. At first a yellow precipitate was formed. Upon continued heating and bubbling phosgene, the precipitate dissolved, giving a red brown transparent mixture which was cooled and left standing overnight. After filtration, the filtrate was concentrated with rotary evaporator, giving 18.5 g of a red brown oily substance. 5.1 g of this was dissolved in 300 ml of water and insoluble substance was removed by filtration. The filtrate was made basic by adding 28% aqueous ammonia, affording 2.68 g of red-yellow viscous material which gradually solidified on standing. Extraction with petroleum ether and concentration gave 0.6 g of *N,N'*-diphenyl-*N*-(α-chlorovinyl)actamidine.

The authors wish to thank Mr. H. Moriguchi for the mass spectrum measurement, Mrs. M. Sakurai for the NMR measurement, and Miss J. Maenaka and Mr. and Mrs. Muneishi for elemental analysis. This work was supported in part by a grant-in-aid from Kokusan Gijutsu Shinkokai. We wish to express our thanks to the founder, the late Mr. Chikara Kurata.

21) E. Beckmann and K. Sandel, *Ann. Chem.*, **296**, 285 (1897).

22) A. Cook and D. Jones, *J. Chem. Soc.*, **1941**, 278.

BULLETIN OF THE CHEMICAL SOCIETY OF JAPAN, VOL. 46, 306—310 (1973)

Studies on Nitrile Salts. IV.[1] Trimerization of Nitriles to 1,3,5-Triazines by the Combined Catalyst PCl_5–HCl

Shozo YANAGIDA, Masaaki YOKOE, Ichiro KATAGIRI, Masataka OHOKA, and Saburo KOMORI

Department of Applied Chemistry, Faculty of Engineering, Osaka University, Yamadakami, Suita, Osaka

(Received June 8, 1972)

The combined catalyst PCl_5–HCl shows effective catalysis in the trimerization of some aromatic nitriles or trichloroacetonitrile to *s*-triazines (III). The scope and limitation of the trimerization, in comparison with other Lewis acids, and its mechanism were studied. It was confirmed that PCl_5 is effective both in the formation of an intermediate, nitrile–HCl 2:2 adduct, and in the reaction of the 2:2 adduct with another nitrile to *s*-triazine.

According to U.S. patents[2,3] aromatic nitriles can be trimerized to produce 2,4,6-triaryl-*s*-triazines (III) by heating at *ca.* 200—500°C in the presence of metal halides or the combined catalyst, $AlCl_3$–HCl. Wakabayashi *et al.* reported that 2-substituted-4,6-bis(trichloromethyl)-*s*-triazines are obtainable by the cotrimerization of trichloroacetonitrile with some nitriles in the presence of the combined catalyst, Lewis acids–HCl.[4] However, they did not study the combined catalyst PCl_5–HCl.

While reports have been made concerning the reactions of PCl_5 with some cyano compounds under various conditions, no reactions with aromatic nitriles have been studied yet.[5,6]

1) Part III: S. Yanagida, T. Fujita, M. Ohoka, I. Katagiri, M. Miyake, and S. Komori, This Bulletin, **46**, 303 (1972).

2) W. G. Toland, U. S. 360179 (1962).

3) J. Sandner and W. L. Fierce, U. S. 3071586 (1963).

4) K. Wakabayashi, M. Tsunoda, and Y. Suzuki, This Bulletin, **42**, 2924, 2931 (1969).

5) F. C. Schaefer, "The Chemistry of the Cyano Group," ed. by Z. Rapoport, Interscience Publishers, New York, N. Y. (1970), p. 253.

6) a) V. I. Schevchenko, N. K. Kulibaba, and A. V. Kirsanov, *J. Gen. Chem. USSR*, **38**, 328, 814 (1968); V. I. Shevchenko, N. K. Kulibaba, and A. V. Kirsanov, *ibid.*, **39**, 1656 (1969). b) H. P. Latscha, W. Weber, and M. Becke-Goehring, *Z. Anorg, Allg. Chem.*. **367**, 40 (1969).

In the course of our studies on the reactions of nitriles in the presence of HCl, it has been found that the combined catalyst PCl_5–HCl is quite effective in the trimerization of aromatic nitriles to *s*-triazines (III) under mild reaction conditions.

In the preceding paper[1] we reported that some aromatic nitriles (I) react with HCl in a sealed tube to afford the 2:2 adducts (II). Our desire to find an explanation for the trimerization of nitriles (I) prompted us to investigate the reaction of the 2:2 adducts (II) with aromatic nitriles (I) in the presence of PCl_5.

This paper reports the scope and limitation of catalysis of the PCl_5–HCl system in the trimerization of nitriles (I), in comparison with other Lewis acid–HCl systems, and a possible mechanism.

Results and Discussion

When benzonitrile (Ia) was allowed to react with PCl_5 in the presence of HCl in a sealed glass tube at 100—105°C, the reaction mixture solidified in 24 hr. The resulting solid product was identified as 2,4,6-triphenyl-*s*-triazine (IIIa) on the basis of its IR spectrum and elemental analysis. No product containing phosphorus atom was formed.

In order to know the role of PCl_5 in this reaction, we have studied the effect of varying the molar ratios of PCl_5 to benzonitrile from 0: 10 to 3: 10 on the yield under comparable conditions. An almost quantitative yield was obtained with a ratio 1: 10 or greater. A ratio 1: 50 was also effective, giving 60% yield of *s*-triazine (IIIa). In the absence of PCl_5, only a trace amount of IIIa was formed. When HCl was not used in the reaction,[7] 40% yield of IIIa was obtained after a period of 240 hr.

It is well-known that some Lewis acids catalyze the trimerization of aromatic nitriles.[2,3,8] However, the effectiveness of the combined catalyst Lewis acid–HCl has not been fully studied yet. From this point of view, some Lewis acid–HCl systems were examined.

Table 1. Catalysis of lewis acid–HCl in the trimerization of benzonitrile[a]

Catalyst[b]	Yield (%)
PCl_5–HCl	98
$SbCl_5$–HCl	62
PBr_3–HCl	20
$AlCl_3$–HCl	18
$SnCl_4$–HCl	21
$ZnCl_2$–HCl	13
$FeCl_3$–HCl	13

a) Reaction conditions: Procedure A (see Experimental), reaction temp. 24 hr.
b) Molar ratio of benzonitrile to Lewis acid, 10: 1.

We see from Table 1 that superior catalysis of PCl_5–HCl system was established. $SbCl_5$–HCl was also found effective, but the resulting *s*-triazine was contaminated with considerable amounts of further chlorinated *s*-triazines and required purification. Compared with the results of the U.S. patent using the combined catalyst $AlCl_3$–HCl,[3] the procedure using a closed vessel under milder reaction conditions is favorable for an increase in the yield.

The reaction using the combined catalyst PCl_5–HCl was extended to several other aromatic nitriles. When nitriles were solid, nitrobenzene was used as a solvent. Most nitriles trimerized to give the corresponding *s*-triazines (III) in satisfactory yields (Table 2). In the cases of *s*-triazines from *m*-tolunitrile and β-naphthonitrile, their mass spectra showed molecular ion peaks corresponding to *s*-triazines having one chlorine atom, indicating that the contamination with small amounts of monochlorinated *s*-triazines resulted from chlorination by PCl_5.

In the cases of *o*-tolunitrile, α-naphthonitrile and phthalonitrile, the expected triazines were not isolated; the former two were recovered unchanged, and when the reaction mixture from phthalonitrile was treated with water, only phthalimide was isolated.

The reaction was further extended to trichloroacetonitrile and 1,1,2-trichloropropionitrile, which have

Table 2. Synthesis of 2,4,6-triaryl-*s*-triazines (III) from aromatic nitriles (I)

III	Ar	Procedure[a]	Reaction time (hr)	Yield (%)	Mp (°C)	IR (KBr) (cm^{-1})	Mass[b] (M^+)
IIIa	C_6H_5–	A	24	98	242—243[c]	1527, 1372	309
IIIb	*p*-$CH_3C_6H_4$–	A	90	60	278—280[d]	1514, 1391	351
IIIc	*m*-$CH_3C_6H_4$–	A	120	63	142—147[e]	1530, 1370	351
IIId	*p*-$NO_2C_6H_4$–[f]	B	120	62(16)[g]	300[h]	1530, 1350	—
IIIe	*p*-CNC_6H_4–	B	120	34(26)[g]	350[i]	1515, 1370	—
IIIf	β-Naphthyl–	B	120	22	293—300[j]	1523, 1380	459
IIIg	*p*-$CH_3OC_6H_4$–	B	120	8	217—222[k]	1510	—
IIIh	CCl_3–	A[l]	240	82	92— 93	1540	—

a) See Experimental. b) 70 eV. c) Lit,[9] 231—232. d) Lit,[9] 278—279. e) Lit,[9] 152—153.
f) Anal: Found: C; 56.73, H; 2.52, N; 18.66%. Calcd: C; 56.76, H; 2.72, N; 18.91. g) The yield when $AlCl_3$ was used instead of PCl_5. h) Lit,[10] 360. i) Lit,[3] 504. j) Lit,[11] 290. k) Lit,[12] 224.
l) Reaction temp., room temp. m) Lit,[5] 93.

7) Strictly speaking, the presence of HCl can not be neglected since PCl_5 reacts with moisture giving HCl.
8) E. M. Smolin and L. Rapoport, "*s*-Triazins and Derivatives," Interscience Publishers, New York, N. Y. (1959), p. 147.
9) A. Cook and D. Jones, *J. Chem. Soc.*, **1941**, 278.
10) O. Davis, *ibid.*, **87**, 1831 (1905).
11) M. Kunz, K. Koeberle, and E. Berthold, U. S. 1989042 (1935).
12) P. Robin, *Ann. Chem.*, (Paris), (**9**), 16, 117 (1923).

no α-hydrogen susceptible to chlorination by PCl_5. Only trichloroacetonitrile gave 82% yield of 2,4,6-tris(trichloromethyl)-*s*-triazine by the reaction at room temperature for 240 hr.[13]

Mechanism. Some mechanisms for the trimerization of nitriles to *s*-triazines in the presence of acidic reagents have been proposed, but they still lack concrete evidences.[14]

Recently we found that some aromatic nitriles react with HCl, giving *N*-(α-chloroarylmethylidene)arylamidine hydrochlorides (II), and that their hydrolysis affords diaroylamines (IV) as follows;[1]

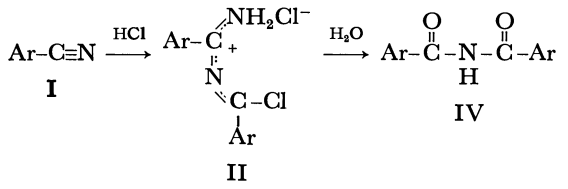

I II IV

On treatment of the reaction mixture obtained in the trimerization of benzonitrile using the combined catalyst PCl_5–HCl with water, dibenzoylamine (IVa) was formed. The yield of IVa was much greater than that in the absence of PCl_5 (Table 3). When $AlCl_3$ or $SnCl_4$ was used instead of PCl_5, dibenzoylamine (IVa) could also be isolated in the same way. The results indicate that the 2:2 adduct (II) is an intermediate to *s*-triazine (III) and that PCl_5 is effective in the dimerization of nitriles to II in the presence of HCl.

Table 3. Effect of lewis acids–HCl on the yields of dibenzoylamine (IVa) and the *s*-triazine IIIa[a]

Lewis acid	Yield of IVa (%)	Yield of IIIa (%)
None	12(18[b])	0
PCl_5	45	11
$AlCl_3$	24[c]	3
$SnCl_4$	11[c]	3

a) Reaction conditions: molar ratios, PhC≡N: HCl: PCl_5=1: 0.9: 0.1; reaction temp., 30°C; reaction time, 110 hr.
b) The yield of IIa.
c) Reaction time: 140 hr.

We observed that the pyrolysis of adducts (II) gives 2,4,6-triphenyl-*s*-triazines (III).[1] In order to estimate the sequence of this pyrolysis, differential thermal analysis of *N*-(α-chlorobenzylidene)benzamidine hydrochloride (IIa) was carried out (Fig. 1). On the basis of the decrease in weight and the analysis of the products, we estimated that two moles of amidine IIa reacts at 123°C, giving one mole of *s*-triazine IIIa, one mole of benzonitrile and four moles of HCl presumably through the following sequence;

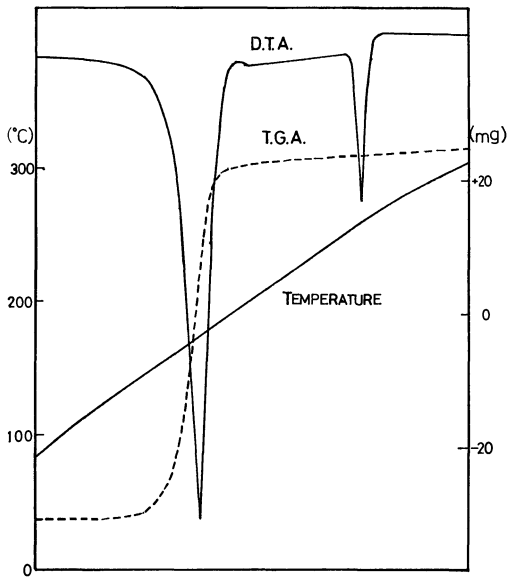

Fig. 1. Differential thermal and thermal gravimetrical analysis of *N*-(α-chlorobenzylidene)benzamidine hydrochloride (IIa).
Conditions for measurement: standard sample, α-Al_2O_3; amount of sample, 103.1 mg; sensitivity of gravimetry, ±50 mg; sensitivity of thermocouple, ±50 μV; heating rate, 2.5°C/min; circumstance, N_2: thermocouple, Pt–PtRh (13%); decrease of the weight (between 123—179°C), 52.0 mg (50.4%).

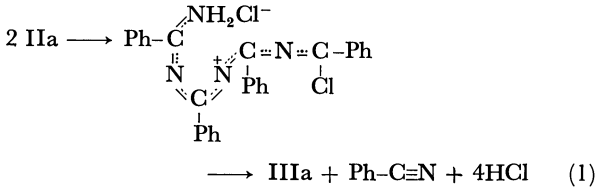

IIIa + Ph-C≡N + 4HCl (1)

For the purpose of obtaining further proof for the catalysis of PCl_5, the reaction of the 2:2 adducts (II) with other aromatic nitriles was effected under various conditions. In view of the pyrolysis of the adduct II, all the reactions were made at 30°C for 12 days.

The reaction of the 2:2 adduct IIa from benzonitrile with *p*-tolunitrile in the presence of PCl_5 and HCl gave, although in low conversion, a mixture of *s*-triazines consisting of 2,4-diphenyl-6-*p*-tolyl-*s*-triazine (IIIa′) and 2,4,6-tris(*p*-tolyl)-*s*-triazine (IIIb) as major products, and 2,4,6-triphenyl-*s*-triazine (IIIa) and 2-phenyl-4,6-bis(*p*-tolyl)-*s*-triazine (IIIb′) as minor products. Without PCl_5, however, only traces were obtained even at 60°C for 5 days. Analogous treatment of the 2:2 adduct IIb from *p*-tolunitrile with benzonitrile resulted in the major formation of IIIb′ and IIIa as expected.

Formation of IIIa and IIIb in these reactions apparently results from homotrimerization of benzonitrile and *p*-tolunitrile, respectively. In order to suppress the homotrimerization, the 2:2 adduct IIa was made to react with *p*-tolunitrile only in the presence of PCl_5, giving IIIa′ exclusively, although in a low conversion.

PCl_5 is believed to have an ionic character on the basis of X-ray analysis and its IR spectra in solution, no complexes of PCl_5 with nitriles being re-

13) Kornuta *et al.* reported that trichloroacetonitrile reacts with PCl_5 at 140—145°C giving pentachloroethylphosphorimidic trichloride. P. P. Kornuta, V. I. Schevchenko, and A. V. Kirsanov, *J. Gen. Chem. USSR.*, **37**, 2657 (1967).

14) a) M. Lora-tamayo and R. Madronero, "1,4-Cycloaddition Reactions", ed. by J. Hamer, Academic Press, New York, N. Y. (1967), p. 132. b) A. I. Meyers and J. G. Sircar, "The Chemistry of the Cyano Groups," ed. by Z. Rapoport, Interscience Publishers, New York, N. Y. (1970), p. 341.

cognized.[5,6,15,16] However, it was reported that its homologue $SbCl_5$ reacts with nitriles giving the 1:1 adduct R–C≡N·$SbCl_5$, which readily reacts with HCl or alkyl chlorides to give nitrilium salts.[17,18] Accordingly PCl_5 can be expected to act as a weak Lewis acid.[15] Lewis acids are known to polarize the cyano group and to increase not only the electrophilic character of carbon but also the nucleophilic character of nitrogen.[14a,19]

In view of these facts and the proposed mechanism for the dimerization of nitriles,[1] the trimerization can be explained as involving the following sequences.

$$\underset{\text{I}}{\text{Ar–C}\equiv\text{N}} + PCl_5 \rightleftarrows \underset{\text{I}'}{\text{Ar–C}\equiv\text{N}\ PCl_5} \qquad (2)$$

$$HCl + PCl_5 \rightleftarrows H^+PCl_6^- \qquad (3)$$

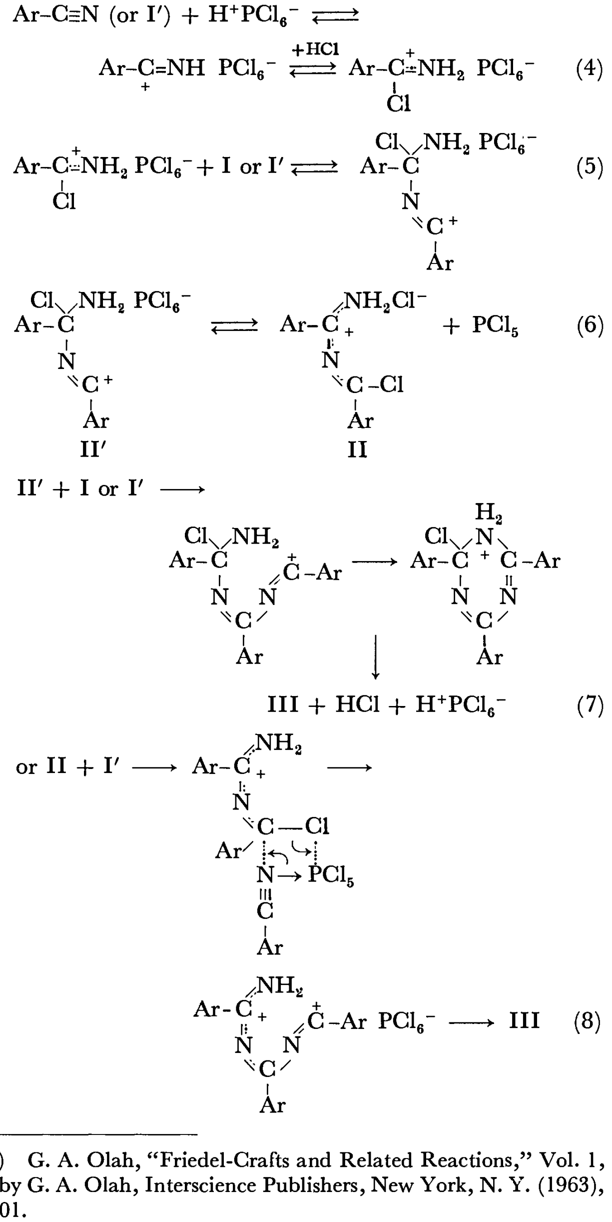

At a high reaction temperature, sequence 1 (pyrolysis of II) can not be neglected. The failure of *o*-tolunitrile, phthalonitrile and α-naphthonitrile to trimerize is probably due to the steric hindrance of *ortho* groups in the sequences 4 and 7 or 8. Formation of phthalimide implies the exclusive intramolecular dimerization of the two cyano groups induced by the combined catalyst PCl_5–HCl.[20]

To our knowledge, the trimerization reported here is the first example of the catalysis of PCl_5 as a Lewis acid.

Experimental

Melting points were determined on a Yanagimoto micro melting point apparatus and were corrected. The IR spectra were recorded with a Japan Electroscopic IR-E spectrophotometer, and the mass spectra with a Hitachi mass spectrometer Model RMU-6E. Thermal gravimetrical and differential analyses were carried out with a Rigaku Denki Thermoflex, and glpc analysis with a Yanagimoto G-8 apparatus.

General Procedure. *A. Without Solvent*: Aromatic nitrile (30—50 mmol) and Lewis acid (3—5 mmol) (molar ratio 10:1) were placed in a 30 ml glass tube. Dry HCl (15—25 mmol) was bubbled into the mixture under cooling. The tube was stoppered, cooled in Dry Ice–acetone, sealed carefully and heated to 100—105°C in an oil bath for an appropriate time. After the end of the reaction, the tube was chilled in Dry Ice–acetone and opened. The reaction mixture was poured into water and insoluble *s*-triazine was filtered with suction and dried. The *s*-triazine was recrystallized from a suitable solvent (acetone, nitrobenzene or acetic acid) when necessary for analysis.[8] The analytical results are summarized in Tables 1 and 2.

B. In Nitrobenzene: Into a mixture of aromatic nitrile (20—30 mmol), PCl_5 (3.3—3.8 mmol) (Molar ratio 10:1) and nitrobenzene (5—10 g), was bubbled dry HCl (12—18 mmol). The tube was sealed and heated to 100—105°C for an appropriate time. When the tube was opened and the reaction mixture was degassed on standing, a precipitate was formed except for the case of *p*-methoxybenzonitrile. The resulting precipitate was filtered with suction, washed with some appropriate solvents having low solubility for *s*-triazine (ether, alcohol and acetone), and dried. In the case of *p*-methoxybenzonitrile, the mixture was condensed under reduced pressure and the residue was treated with water and extracted with ether. The extract was evaporated, giving *s*-triazine IIIg.

Isolation of Phthalimide. The reaction mixture obtained from phthalonitrile according to procedure B was poured into aqueous acetone and allowed to stand at room temperature for 3 days. The mixture was then extracted with ether, and the extract was evaporated to give a small amount of precipitate, which was confirmed as phthalimide on the basis of the following analyses; mp 236—238°C (lit,[21] 238) IR (Nujol) 3230, 2775, 1745, 1312, 1055, and 715 cm^{-1}.

Isolation of Dibenzoylamine (IVa). The reaction mixture obtained from benzonitrile according to procedure A was poured into 50 ml of water. After filtration of the

15) G. A. Olah, "Friedel-Crafts and Related Reactions," Vol. 1, ed. by G. A. Olah, Interscience Publishers, New York, N. Y. (1963), p. 201.

16) I. R. Beattie and M. Webster, *J. Chem. Soc.*, **1963**, 38.

17) I. Klages and W. Grill, *Ann. Chem.*, **592**, 21 (1951).

18) E. Allenstein and A. Schmidt, *Spectrochim. Acta.*, **20**, 1451 (1964).

19) H. Hover, "Problems in Organic Reaction Mechanism," Wiley-Interscience, London, (1970), p. 119.

20) Some dicyano compounds can be cyclized intramolecularly in the presence of hydrogen halides, when the two cyano groups are situated close to each other at appropriate positions. However, the intramolecular cyclization of phthalonitrile in the presence of HCl has not been reported.

21) W. N. Hartley and E. P. Hedley, *J. Chem. Soc.*, **91**, 317 (1907).

s-triazine IIIa, the filtrate was extracted with ether to remove unreacted benzonitrile. The resulting aqueous phase was left standing at room temperature overnight. The needle-like crystal formed was filtered, washed with water and dried under reduced pressure. The product was confirmed by direct comparison with an authentic sample.[1)]

Reaction of II with Aromatic Nitriles in the Presence of PCl_5. A typical procedure is as follows. The 2:2 adduct IIa (1.02 g, 3.66 mmol), *p*-tolunitrile (4.10 g, 35 mmol) and PCl_5 (0.30 g, 1.44 mmol) were placed in a 30 ml glass tube. Dry HCl (0.68 g, 18.6 mmol) was bubbled into the mixture under cooling. The tube was sealed and placed in a thermostat at 30°C for 12 days. Ether was added to the reaction mixture, giving a crystalline product which was confirmed to be a mixture of IIa and IIb by IR spectrum analysis (1.78 g) The filtrate was mixed with water (30 ml) and extracted with 50 ml of ether. The extract was dried with $MgSO_4$ and evaporated, giving a precipitate. The viscous residue was triturated with methanol giving an additional precipitate. Both precipitates were combined together (0.2 g) and analyzed. IR and mass spectra indicated that the product is a mixture of 2,4-diphenyl-6-*p*-tolyl-*s*-triazine (IIIa′), 2,4,6-tris(*p*-tolyl)-*s*-triazine (IIIb), 2-phenyl-4,6-bis(*p*-tolyl)-*s*-triazine (IIIb′), and 2,4,6-triphenyl-*s*-triazine (IIIa). Their ratios were determined to be roughly 56:38:2:4 by glpc by assuming that the sensitivity is proportional to their weight percentages.

Glpc was performed with a column of silicon gum SE, 10% on Diasolid L (60—80 mesh, 3 mmϕ × 1 m column, 300°C, hydrogen carrier gas, 30 ml/min).

A similar reaction of the 2:2 adduct IIb from *p*-tolunitrile with benzonitrile in the presence of PCl_5–HCl gave a mixture of IIIb′, IIIa, IIIa′, and IIIb in an approximate ratio 22:74: trace: 4.

The reaction of IIa (1.05 g) with *p*-tolunitrile (4.30 g) only in the presence of PCl_5 (0.30 g) yielded a mixture (0.27 g) of IIIa′, IIIb, IIIb′, and IIIa in an approximate ratio 88:4:2:6.

BULLETIN OF THE CHEMICAL SOCIETY OF JAPAN, VOL. 46, 310—313 (1973)

The Alkylation of 3,5-Dimethylisoxazole

Choji KASHIMA, Shinji TOBE, Noboru SUGIYAMA, and Makoto YAMAMOTO
Department of Chemistry, Tokyo Kyoiku University, Otsuka, Tokyo

(Received June 26, 1972)

3,5-Dimethylisoxazole (**1**) was alkylated with sodium amide in liquid ammonia to give 3-methyl-5-alkylisoxazoles. By di- and tri-alkylation reactions using excess sodium amide, isoxazoles having secondary and tertiary alkyl groups at 5-position could be obtained. The hydrogenolysis and hydrolysis of these isoxazoles were also studied.

The reaction of β-diketones with hydroxylamine hydrochloride gives isoxazoles[1] which are regenerated to β-diketones by hydrogenolysis and hydrolysis,[2] showing that the formation and cleavage of isoxazoles is useful for the protection of β-diketones.

Few papers have reported on the alkylation of 3,5-dimethylisoxazoles. The 5-methylisoxazoles having the electron-withdrawing group at 4-position condense with benzaldehyde to give 4-substituted 5-styrylisoxazoles in the presence of amine or sodium methoxide as a catalyst.[3-5] Micetich reported[6] that the 5-methyl group of 3,5-dimethylisoxazole (**1**) is lithiated by butyl lithium in tetrahydrofuran. The lithio derivative reacts with benzyl chloride to give 3-methyl-5-phenylethylisoxazole (**5**). In both cases, the methyl group at 3-position of 3,5-dimethylisoxazoles does not react. Since it is well-known that the methyl group attached to such heterocyclic compounds as picoline[7] or quinaldine[8] is alkylated by sodium amide in liquid ammonia as a catalyst, alkylation on the methyl group at 5-position of **1** is expected.

We have studied the alkylation of 3,5-dimethylisoxazole (**1**) and obtained isomerically pure mono-, di-, and tri-alkylated isoxazoles by using an appropriate amount of sodium amide in liquid ammonia. Generation of β-diketones from these alkylated isoxazoles has also been carried out. The results are given in this paper.

Results and Discussion

3,5-Dimethylisoxazole (**1**) is expected to react at three reaction sites, 3-methyl, 5-methyl, and 4-position, in the electrophilic substitution reaction. For determination of the reaction site, **1** was treated with methyl iodide in the presence of equimolar sodium amide in liquid ammonia. The reaction product (yield, *ca.* 70%) showed methyl protons at δ 2.18, methine proton at δ 5.68 and ethyl protons at δ 2.68 and 1.26 in NMR.

1) W. Lampe and J. Smalinska, *Roczniki. Chem.*, **28**, 163 (1954)
2) S. D'Alcontres, *Gazz. Chim. Ital.*, **80**, 441 (1950).
3) A. Quilico and C. Musante, *ibid.*, **72**, 399 (1942).
4) N. K. Kochetkov, S. D. Sokolov, and V. M. Luboshnikova, *Zh. Obshch. Khim.*, **32**, 1788 (1962).
5) G. Renzi, V. Dal Piaz, and S. Pinzauti, *Gazz. Chim. Ital.*, **99**, 753 (1969).
6) R. G. Micetich, *Can. J. Chem.*, **48**, 2006 (1970).
7) D. Taub, R. D. Hoffsommer, C. H. Kuo, and N. L. Wendler, *J. Org. Chem.*, **30**, 3229 (1965).
8) F. W. Bergstrom and A. Moffat, *J. Amer. Chem. Soc.*, **59**, 1494 (1937).

From these data, the product was identified as 3-methyl-5-ethylisoxazole (**2**).[9] But neither 3-ethyl-5-methylisoxazole nor 3,4,5-trimethylisoxazole could be detected by NMR and vpc. Similarly, **1** was treated with ethyl bromide, *n*-propyl bromide, benzyl bromide and allyl bromide in the presence of sodium amide to give the corresponding products (**3**, **4**, **5**,[6] and **6**) alklated on 5-methyl position. Isopropyl bromide, one of the secondary alkyl halides, also gave 3-methyl-5-isobutylisoxazole (**7**). Similarly, **1** was reacted with 1,2-epoxybutane to give 3-methyl-5-(3-hydroxy)pentylisoxazole (**8**), which was easily oxidized to ketone (**9**) with chromic anhydride.

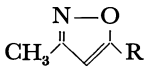

1: R=CH_3
2: R=CH_2CH_3
3: R=$CH_2CH_2CH_3$
4: R=$CH_2CH_2CH_2CH_3$
5: R=$CH_2CH_2C_6H_5$
6: R=$CH_2CH_2CH{=}CH_2$
7: R=$CH_2CH(CH_3)_2$
8: R=$CH_2CH_2CHOHCH_2CH_3$
9: R=$CH_2CH_2COCH_2CH_3$
12: R=$CH(CH_3)_2$
13: R=$C(CH_3)_3$
14: R=$CH(CH_2C_6H_5)_2$
17: R=$CH(CH_3)CH_2CH_3$

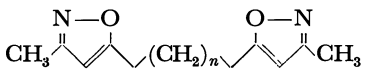

11: n=0, 3, 4, 5

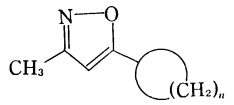

15: n=3, 4

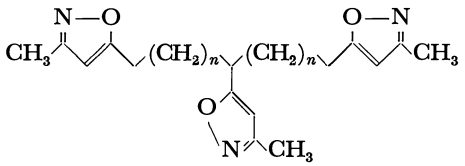

16: n=3, 4

Fig. 1.

When **1** was treated with a half molar α,ω-dibromoalkane (**10**, n=3, 4, 5), the corresponding α,ω-di(3-methyl-5-isoxazolyl)alkanes (**11**, n=3, 4, 5) were obtained. In the case of 1,2-dibromoethane (**10**, n=2), the anomalous reaction product 1,2-di(3-methyl-5-isoxazolyl)ethane (**11**, n=0) was obtained.[6] When **1** was treated with sodium amide in liquid ammonia in the absence of **10** (n=2) followed by hydrolysis with ammonium chloride, the starting material was recovered. Thus, 1,2-dibromoethane (**10**, n=2) apparently acted as an oxidative reagent in this anomalous reaction.

For di- and tri-alkylation of the 5-methyl group, we tried the reaction of **1** with excess amounts of sodium amide and methyl iodide. When 2 molar sodium amide and 2 molar methyl iodide were used, the products were 3-methyl-5-ethylisoxazole (**2**), 3-methyl-5-isopropylisoxazole (**12**) and 3-methyl-5-*t*-butylisoxazole (**13**). **2** was identified with the authentic sample by means of NMR and vpc. The structures of **12** and **13** were deduced from IR, NMR, and elemental analysis. When 3 molar sodium amide and 3 molar methyl iodide were used, **2**, **12**, and **13** were also obtained. When of 4 molar sodium amide and 4 molar methyl iodide were used, **13** was the sole product, and none of **2**, **12**, 3-ethyl-5-*t*-butylisoxazole and 3,4-dimethyl-5-*t*-butylisoxazole could be detected by NMR and vpc. The product ratios in these reactions are summarized in Table 1. Similarly, **1** was treated with 2 molar sodium amide and 2 molar benzyl bromide to give di-alkylation product, 3-methyl-5-(1,3-diphenyl-2-propyl)isoxazole (**14**). The reaction of **5** with benzyl bromide also gave **14**. The structure of **14** was confirmed by means of IR, NMR, and elemental analysis. In the NMR spectrum, the 3-methyl protons at δ 2.01 were deshielded by the sterically crowded phenyl groups.

Table 1. Product ratios in the reaction of **1** with methyl iodide

Molar ratio			Total yield	Product ratio		
1 :	CH_3I :	$NaNH_2$	(%)	2%	12%	13%
1	1	1	58	100	0	0
1	2	2	68	33	57	10
1	3	3	59	9	62	29
1	4	4	51	0	0	100

We see from these results that the di- and tri-alkylation reactions were accomplished in one step. They occurred on the same reaction site at 5-methyl group of **1**, and were controlled by the amount of sodium amide. Thus, 3-methyl-5-cycloalkylisoxazoles (**15**) were expected in the case of α,ω-dibromoalkane (**10**) and **1** in the presence of 2 molar sodium amide. When, 1,3-dibromopropane (**10**, n=3) was treated with equimolar **1** and 2 molar sodium amide, 1,5,9-tri(3-methyl-5-isoxazolyl)nonane (**16**, n=3) was obtained together with 1,5-di(3-methyl-5-isoxazolyl)pentane (**11**, n=3), but no 3-methyl-5-cyclobutylisoxazole (**15**, n=3). Similarly, 1,6,11-tri(3-methyl-5-isoxazolyl)undecane (**16**, n=4) and 1,6-di(3-methyl-5-isoxazolyl)hexane (**11**, n=4) were obtained from 1,4-dibromobutane (**10**, n=4), but no 3-methyl-5-cyclopentylisoxazole (**15**, n=4).

If two different alkyl halides are used in the presence of 2 molar sodium amide, 3-methyl-5-*sec*-alkylisoxazoles might be obtained. When **1** was treated with methyl iodide followed by ethyl bromide, 3-methyl-5-*sec*-butylisoxazole (**17**) was obtained as well as 5-ethyl- (**2**), 5-*n*-propyl- (**3**), and 5-isopropyl-3-methylisoxazole (**12**).

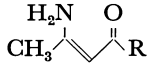

18

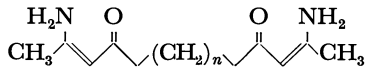

19

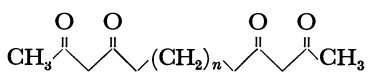

20

Fig. 2

9) H. Feuer and S. Markofsky, *J. Org. Chem.*, **29**, 935 (1964).

TABLE 2. PROPERTIES OF 3-METHYL-5-SUBSTITUTED-ISOXAZOLES

Compd.		Substituent	Bp (mp) °C/Torr	t_R[a] min	δ_{Me-3}[b] ppm	δ_{H-4}[b] ppm	Isoxazole[c] cm^{-1}
1		Me	49—50/29	3.0	2.15	5.77	1613
2		Et	83/45[d]	5.0	2.18	5.68	1612
3		*n*-Pr	60—64/16	8.3	2.16	5.64	1607
4		*n*-Bu	70—75/5	15.6	2.20	5.70	1608
5		$(CH_2)_2Ph$	135—136/3		2.09	5.59	1607
6		$(CH_2)_2CH=CH_2$	99—103/15	14.0	2.21	5.74	1609
7		*i*-Bu		11.3	2.19	5.70	1606
8		$(CH_2)_2CH(OH)Et$	170—190/15		2.19	5.77	1604
9		$(CH_2)_2COEt$	105—110/5		2.21	5.73	1609
11	$n=0$	$(CH_2)_2$Isox[e]	(92—94)		2.26	5.87	1602[f]
11	$n=3$	$(CH_2)_5$Isox[e]	183—187/3		2.17	5.87	1609
11	$n=4$	$(CH_2)_6$Isox[e]	(56)		2.25	5.78	1609[f]
11	$n=5$	$(CH_2)_7$Isox[e]	(<20)		2.18	5.68	1605
12		*i*-Pr	74—75/15	6.6	2.16	5.59	1602
13		*t*-Bu	53—54/2	7.7	2.17	5.63	1605
14		$CH(CH_2Ph)_2$			2.01	5.39	1605
16	$n=3$	$CH[(CH_2)_4Isox]_2$[e]	210—215/10^{-3}		2.19	5.71	1606
16	$n=4$	$CH[(CH_2)_5Isox]_2$[e]			2.19	5.65	1604
17		*sec*-Bu	58—60/5	11.3	2.22	5.72	1603

a) t_R is the retention time on Apiezon L at 130°C. b) Solvent is CCl_4. c) Liquid film. d) Ref. 11.
e) Isox is 3-methylisoxazolyl f) KBr.

These isomerically pure isoxazoles produced by alkylation on the 5-methyl group of **1** were hydrogenated by platinum oxide in ethanol. The structures of the hydrogenated products were confirmed to be 2-amino-2-alkene-4-one (**18**) by means of IR, NMR, and elemental analysis. Furthermore, 2,12-diaminotrideca-2,11-diene-4,10-dione (**19**, $n=3$), hydrogenated product from **11** ($n=3$), was hydrolyzed by dilute hydrochloric acid in ethanol to give the corresponding ketone, tridecane-2,4,10,12-tetraone (**20**, $n=3$).[10]

Thus, it is possible to alkylate the methyl group at the 5-position of isoxazole with sodium amide and alkyl halides in liquid ammonia. By di- and trialkylation reactions using excess sodium amide, the isoxazoles having secondary and tertiary alkyl groups at the 5-position can be obtained. Hydrogenolysis of these isoxazoles gave the 5-alkylated 2-amino-2-pentene-4-ones (**18**). By hydrolysis of **18**, the γ-alkylation products of β-diketones were obtained in good yields. These procedures enable the 1,1-di- and 1,1,1-trialkylation reactions to take place, it being much more difficult for them to do so by the direct γ-alkylation of 2,4-diketones.[11,12]

Experimental

3,5-Dimethylisoxazole (1). By the method of Lampe,[1] a mixture of acetylacetone (34.3 g), hydroxylamine hydrochloride (35.4 g) and potassium carbonate (34.5 g) was refluxed for 4 hr. After washing the mixture with water, the organic layer was distilled, bp 49—50°C/29 Torr. Yield 45%.

General Procedure for Mono-alkylation. A solution of sodium (1.15 g) in liquid ammonia (*ca.* 300 ml) was oxidized to sodium amide catalyzed with ferric chloride. To this sodium amide suspension was added **1** (5.00 g) in anhydrous ether (30 ml). After stirring for 1.5 hr under nitrogen stream, alkyl halide (0.05 mol) in anhydrous ether (30 ml) was added. Stirring was continued for another 3 hr. After the mixture was neutralized with ammonium chloride, ammonia was removed at room temperature. The residual ether solution was acidified with dilute hydrochloric acid. The ether extract was concentrated and purified by preparative vpc, fractional distillation and/or silica gel column chromatography.

3-Methyl-5-ethylisoxazole (2). Purified by the preparative vpc on polyethylene glycol succinate (1 m stainless steel column) at 103°C, yield 70%. The NMR spectrum was superimposable on that of the authentic sample.[9]

*3-Methyl-5-*n*-propylisoxazole (3).* Purified by fractional distillation, yield 45%.

Found: C, 67.27; H, 8.97; N, 11.00%. Calcd for $C_7H_{11}NO$: C, 67.17; H, 8.86; N, 11.19%.

*3-Methyl-5-*n*-butylisoxazole (4).* Purified by fractional distillation, yield 61%.

Found: C, 68.96; H, 9.44; N, 10.05%. Calcd for $C_8H_{13}NO$: C, 69.03; H, 9.41; N, 10.06%.

3-Methyl-5-phenylethylisoxazole (5). Purified by silica gel column chromatography with benzene–ethyl acetate mixture and fractional distillation, yield 70%. The NMR spectrum was superimposable on that of the authentic sample.[6]

3-Methyl-5-(3-butenyl)isoxazole (6). Purified by preparative vpc on polyethylene glycol succinate at 120°C, yield 44%.

Found: C, 69.27; H, 7.99; N, 10.05%. Calcd for $C_8H_{11}NO$: C, 70.04; H, 8.08; N, 10.21%.

3-Methyl-5-(3-hydroxypentyl)isoxazole (8). 1,2-Epoxybutane was used instead of alkyl halide and purified by fractional distillation and silica gel chromatography with benzene–ethyl acetate mixture, yield 15%.

Found: C, 63.63; H, 8.85; N, 8.30%. Calcd for $C_9H_{15}NO_2$: C, 63.88; H, 8.94; N, 8.28%.

10) K. G. Hampton, R. J. Light, and C. R. Hauser, *J. Org. Chem.*, **30**, 1431 (1965).
11) T. M. Harris and C. M. Harris, "Organic Reactions," Vol. 17, p. 155 (1969).
12) K. G. Hampton, T. M. Harris, and C. R. Hauser, *J. Org. Chem.*, **30**, 61 (1965).

1,5-Di(3-methyl-5-isoxazolyl)pentane (**11**, n=3). Purified by silica gel chromatography with benzene–ethyl acetate mixture, yield 84%.

Found: C, 66.35; H, 7.90; N, 11.86%. Calcd for $C_{13}H_{18}N_2O_2$: C, 66.64; H, 7.74; N, 11.96%.

1,6-Di(3-methyl-5-isoxazolyl)hexane (**11**, n=4). Purified by silica gel chromatography with benzene–ethyl acetate mixture and recrystallization from *n*-hexane, yield 77%.

Found: C, 67.81; H, 8.12; N, 11.09%. Calcd for $C_{14}H_{20}N_2O_2$: C, 67.71; H, 8.12; N, 11.28%.

1,7-Di(3-methyl-5-isoxazolyl)heptane (**11**, n=5). Purified by recrystallization from *n*-hexane, yield 70%.

Found: C, 68.31; H, 8.66; N, 10.57%. Calcd for $C_{15}H_{22}N_2O_2$: C, 68.67; H, 8.45; N, 10.68%.

1,2-Di(3-methyl-5-isoxazolyl)ethane (**11**, n=0). 1,2-Dibromoethane (**10**, *n*=2) used instead of alkyl halide and purified by recrystallization from *n*-hexane, yield 39%. The product was identified by the superimposable NMR and mp 92—94°C.[6]

General Procedure for Di-(tri-)alkylation. As described above, **1** (1.00 g) was treated with 0.02 mol (0.04 mol) of alkyl halide in the presence of 0.02 mol (0.04 mol) of sodium amide in liquid ammonia (*ca.* 50 ml).

3-Methyl-5-isopropylisoxazole (**12**). Purified by preparative vpc on Apiezon L (1 m stainless steel column) at 103°C and fractional distillation, yield 37%.

Found: C, 66.86; H, 9.04%. Calcd for $C_7H_{11}NO$: C, 67.17; H, 8.86%.

3-Methyl-5-t-butylisoxazole (**13**). Purified by fractional distillation, yield 51%.

Found: C, 68.93; H, 9.34; N, 10.14%. Calcd for $C_8H_{13}NO$: C, 69.03; H, 9.41; N, 10.06%.

3-Methyl-5-(1,3-diphenyl-2-propyl)isoxazole (**14**). Purified by silica gel chromatography with benzene–ethyl acetate mixture, yield 35%.

Found: C, 82.68; H, 6.85; N, 5.05%. Calcd for $C_{19}H_{19}NO$: C, 82.28; H, 6.91; N, 5.05%.

1,5,9-Tri(3-methyl-5-isoxazolyl)nonane (**16**, n=3). Purified by silica gel chromatography with *n*-hexane–ether mixture, yield of **16** (*n*=3) 12% and **11** (*n*=3) 25%.

Found: C, 67.07; H, 7.97; N, 10.95%; mol wt (mass), 371. Calcd for $C_{21}H_{29}N_3O_3$: C, 67.90; H, 7.87; N, 11.32%; mol wt, 371.47.

1,6,11-Tri(3-methyl-5-isoxazolyl)undecane (**16**, n=4). Purified by silica gel chromatography with *n*-hexane–ether mixture, yield of **16** (*n*=4) 15% and **11** (*n*=4) 19%. Found: C, 70.49; H, 8.43; N, 10.02%; mol wt (mass), 399. Calcd for $C_{23}H_{33}N_3O_3$: C, 69.14; H, 8.33; N, 10.52%; mol wt, 399.52.

3-Methyl-5-sec-butylisoxazole (**17**). To a mixture of sodium amide (790 mg) and 3,5-dimethylisoxazole (1.00 g) in liquid ammonia (*ca.* 50 ml) was added methyl iodide (1.43 g) in anhydrous ether (15 ml) with stirring. After 1.5 hr, ethyl bromide (1.11 g) in anhydrous ether (15 ml) was added to the reaction mixture. Stirring was continued for another 2.5 hr at −50°C. The products were purified by preparative vpc on Apiezon L at 130°C, yields **2**, 47%; **12**, 8%; **3**, 7%; **17**, 12%. Found: C, 68.91; H, 9.58; N, 9.86%. Calcd for $C_8H_{13}NO$: C, 69.03; H, 9.41; N, 10.06%.

Oxidation of **8**. A mixture of **8** (100 mg), chromic anhydride (600 mg) and pyridine (1.5 g) in dichloromethane (30 ml) was stirred for 30 min at 5°C. The dichloromethane extract from the reaction mixture was washed with aqueous sodium carbonate, dilute hydrochloric acid and water. Product (**9**) was purified by silica gel chromatography with benzene–ethyl acetate mixture, yield 50%. Found: C, 63.96; H, 7.96; N, 8.40%. Calcd for $C_9H_{13}NO_2$: C, 64.65; H, 7.84; N, 8.38%.

Hydrogenation of Isoxazoles. About one gram of isoxazoles was hydrogenated in ethanol (20 ml) catalyzed by platinum oxide (100 mg) at room temperature under ordinary pressure. After the catalyst was filtered off, the filtrate was concentrated and the corresponding products were recrystallized from *n*-hexane.

2-Amino-2-heptene-4-one (**18**, *R*=n-*Pr*). Yield 42%, mp 47.5°C. Found: C, 66.31; H, 10.32; N, 11.06%. Calcd for $C_7H_{13}NO$: C, 66.10; H, 10.30; N, 11.01%.

2-Amino-6-phenyl-2-hexene-4-one (**18**, *R*=$(CH_2)_2Ph$). Yield 95%, mp 103°C. Found: C, 76.09; H, 8.08; N, 7.06%. Calcd for $C_{12}H_{15}NO$: C, 76.15; H, 7.99; N, 7.40%.

2,12-Diaminotrideca-2,11-diene-4,10-dione (**19**, n=3). Yield 72%, mp 109°C. Found: C, 65.77; H, 9.36; N, 11.76%. Calcd for $C_{13}H_{22}N_2O_2$: C, 65.51; H, 9.31; N, 11.76%.

2,13-Diaminotetradeca-2,12-diene-4,11-dione (**19**, n=4). Yield 76%, mp 150°C. Found: C, 66.39; H, 9.67; N, 10.88%. Calcd for $C_{14}H_{24}N_2O_2$: C, 66.63; H, 9.59; N, 11.10%.

2,9-Diaminodeca-2,8-diene-4,7-dione (**19**, n=0). Yield 70%, mp 165°C. Found: C, 61.40; H, 8.39; N, 14.25%. Calcd for $C_{10}H_{16}N_2O_2$: C, 61.20; H, 8.22; N, 14.28%.

Hydrolysis of **19** (n=3). **19** (*n*=3) was dissolved in ethanol acidified to pH 4 with hydrochloric acid and the mixture was stirred for 10 hr at room temperature. After being neutralized with potassium carbonate, the mixture was extracted with ether. The residue from the extract was recrystallized from *n*-hexane, yield 52%, mp 67°C. The product was identified with the authentic sample[10] by IR and NMR spectra and mp.

Carbon Products Prepared from Variant Pitch Materials. VIII. The Preparation of Isotropic Pitch Carbon with a High Density

Sugio OTANI and Asao OYA

Faculty of Technology, Gunma University, Kiryu, Gunma

(Received June 7, 1972)

The present works were undertaken in order to prepare the isotropic Pitch Carbon with a high density and with a desired degree of graphitization. The tablets were prepared by pressing some kinds of variant pitch materials and were then heat-treated below 2600°C in N_2 gas. Isotropic Pitch Carbon with a high density and with a low degree of graphitization can be readily prepared by pressing the non-graphitizable variant pitch material under high pressure. On the other hand, for the purpose of preparating isotropic Pitch Carbon with a high density and with a high degree of graphitization, a graphitizable variant pitch material with a low softening point, —in other words, with a good ability of sintering— was pressed into tablets under low pressure. The typical properties of the Pitch Carbon thus obtained (H.T.T. 2600°C) were as follows: Bacon Anisotropic Factor: 1.01; Bulk density: 1.79 g/cc; d_{002}: 3.40 Å; Lc: 210 Å.

The high-temperature gas-cooled reactor (HTGR) has lately attracted considerable attention, simultaneously, the isotropic carbon products with a high density have been required as one of the most important materials for the reactor.[1,2]

It was previously reported by the present authors that carbon rods or tablets could be prepared from specific variant pitch materials instead of coke powder and pitch binder. The carbon articles prepared by this method were referred to as Pitch Carbon.[3] From the previous results, it was been found that the properties of Pitch Carbon can be changed greatly by choosing variant pitch materials and/or conditions of heat-treatment. These facts suggest the possibility of thus preparing a carbon product for the reactor use.

The present experiments were undertaken to prepare an isotropic Pitch Carbon with a high density and with various degrees of graphitization.

Experimental

In order to prepare the variant pitch materials, coal tar pitch was distilled at 500°C for 30 min by bubbling N_2 gas through it. The resulting variant pitch materials (to be referred to as variant pitch material-N) did not clearly exhibit its softening point (S.P.) by the penetration method[4] (heating rate: 30°C/min), but it was sintered to an appreciable extent after the measurement. This variant pitch material was crushed to under 100 mesh and was used in preparing the Pitch Carbon. This variant pitch material was then pressed into tablets 10 mm in diameter and about 10 mm thick. The tablets were pre-heated in air up to 300°C at about 1.5°C/min to prevent their deformation at the subsequent heating stage, and were then heat-treated in N_2 gas at a temperature below 2600°C for 10 min. In addition, four kinds of variant pitch materials (A,[5] C,[6] L,[7] Al[8]) were used in preparing Pitch Carbons with various degree of graphitizability. The details of their methods of preparation have been reported elsewhere. Unless otherwise noted, however, the variant pitch material used was variant pitch material-N.

As first, the relationships between the preferred orientation of graphite crystallite in Pitch Carbon and the following factors were examined: the graphitizability, the particle size of the variant pitch material, the heat-treatment temperature (H.T.T.), and the addition of natural graphite or needle cokes. Furthermore, the preferred orientation of Pitch Carbon was compared with those of the other carbon materials. For the representation of the preferred orientation of graphite crystallite, the Bacon Anisotropic Factor (BAF)[9] was measured from the orientation diagram which was obtained by using the X-ray transmission technique reported by Noda and Inagaki.[10] The value of BAF is 1.00 for the completely isotropic carbon product, and it increases with a lowering of its isotropy. Carbon sections about 0.5 mm thick were cut with their planes parallel to or vertical to the pressing direction of Pitch Carbon.

The interlayer spacing, d_{002}, and the crystallite thickness, Lc, of carbon specimens were calculated according to a method previously described.[4] Some carbon specimens gave composite (002) diffraction profiles. These profiles were separated into two symmetrical components, and the X-ray parameters of each component were calculated. Moreover, the properties such as the density and the porosity were measured, and the internal structure was observed according to a method previously described.[4]

Results and Discussion

1. The Preferred Orientation of the Graphite Crystallite in the Pitch Carbon. For all the carbon sections cut with their planes vertical to the pressing direction, the values of BAF were nearly 1.00. Therefore, the values for these sections will not be presented in this report; only the values for sections cut with their planes parallel to the pressing direction will be shown.

1.1. The Effect of the Graphitizability of Variant Pitch Materials (Table 1). Pitch Carbons were prepared from several kinds of variant pitch materials with various degree of graphitizability. As the degrees of

1) H. Suzuki, *Ceramics*, **4**, (4) 306 (1969).
2) T. Sasaki, *Tanso*, No. 64, 14 (1971).
3) S. Otani, A. Oya, and Y. Kitazume, *Nippon Kagaku Kaishi*, **1972**, 727.
4) S. Otani, A. Oya, and T. Fukabori, *Kogyo Kagaku Zasshi*, **72**, 317 (1969).
5) S. Otani, A. Oya, I. Nakagawa, and T. Fukabori, *ibid.*, **72**, 323 (1969).
6) S. Otani, A. Oya, and T. Nagashima, *ibid.*, **73**, 2095 (1970).
7) S. Otani and A. Oya, This Bulletin, **44**, 3181 (1971).
8) S. Otani and A. Oya, *Kogyo Kagaku Zasshi*, **73**, 1110 (1970).
9) G. E. Bacon, *J. Appl. Chem.* (London), **6**, 477 (1959).
10) T. Nada and M. Inagaki, *Kogyo Kagaku Zasshi*, **62**, 1300 (1959).

Table 1. The effect of the graphitizability of variant pitch materials

Variant pitch materials	Moulding pressure (kg/cm²)	HTT (°C)	d_{002} (Å)	Lc (Å)	BAF
Al[8]	400	2600	3.39	370	1.13
N	400	2600	3.41	270	1.11
A[5]	400	2600	3.41	220	1.06
C[6]	400	2600	3.41 3.45	200 43	1.05
L[7]	400	2600	3.42 3.45	150 30	1.00

graphitization of Pitch Carbon which were represented by d_{002} and Lc decreased, the values of BAF gradually decreased also. The Pitch Carbon which was prepared from the variant pitch material-L was completely isotropic; that is, the value of BAF was 1.00. From these results, it was found that the isotropic Pitch Carbon could easily be prepared from non-graphitizable variant pitch materials.

Table 2. The effect of the moulding pressure

Variant pitch materials	Moulding pressure (kg/cm²)	HTT (°C)	d_{002} (Å)	Lc (Å)	BAF
N	100	2600	3.41	270	1.07
N	400	2600	3.41	270	1.11
N	1600	2600	3.41	250	1.18

1.2. The Effect of the Moulding Pressure (Table 2). The values of BAF were remarkably increased with an increase in the moulding pressure. However, such a relation was not observed for the Pitch Carbon prepared from non-graphitizable variant pitch materials.

Table 3. The effect of the particle size of variant pitch material

Variant pitch materials	Moulding pressure (kg/cm²)	HTT (°C)	d_{002} (Å)	Lc (Å)	BAF
N	100	2600	3.41	270	1.07
N[a]	100	2600	3.39	270	1.05
N	400	2600	3.41	270	1.11
N[a]	400	2600	3.39	280	1.06

a) Crushed by ball mill for 8 hr.

1.3. The Effect of the Particle Size of Variant Pitch Materials (Table 3). The variant pitch material-N (under 100 mesh) was further crushed by the use of a ball mill for 8 hr and was then pressed into tablets. The tablets were then heat-treated in the way described above. It seems that the preferred orientation of Pitch Carbon generally falls off as the particle size of the variant pitch material decreases. However, the preferred orientation of the Pitch Carbon which was prepared from such fine pitch powder was scarcely affected by the moulding pressure.

1.4. The Effect of Heat-treatment Temperature (Table 4). The degree of the graphitization of Pitch Carbon was gradually increased by raising the temperature between 1400 and 2400°C. The values of BAF, on the whole, increased with the increase of H.T.T.

Table 4. The effect of heat-treatment temperature

Variant pitch materials	Moulding pressure (kg/cm²)	HTT (°C)	d_{002} (Å)	Lc (Å)	BAF
N	400	2600	3.41	270	1.11
N	400	2200	3.42	120	1.07
N	400	1800	3.43	77	1.09
N	400	1400	3.46	25	1.05
N	400	1000	3.42	25	1.05

Table 5. The effect of the addition of needle cokes or natural graphite

Additives	Moulding pressure (kg/cm²)	HTT (°C)	d_{002} (Å)	Lc (Å)	BAF
—	400	2600	3.41	270	1.11
25 wt% of needle cokes	400	2600	3.39	480	1.24
25 wt% of natural graphite	400	2600	3.35 3.40	1000 190	1.44
50 wt% of natural graphite	400	2600	3.35 3.40	1000 230	1.99

1.5. The Effect of the Addition of Needle Cokes or Natural Graphite (Table 5). The values of BAF were increased considerably by the addition of 25 wt% of natural graphite (under 100 mesh, Madacascar flaky graphite) or of needle cokes (under 100 mesh) which were very lamellar in shape. The further addition of natural graphite increased more remarkably the value of BAF for the resulting Pitch Carbon.

Table 6. The comparison with the other carbon materials

Carbon materials	Moulding pressure (kg/cm²)	HTT (°C)	d_{002} (Å)	Lc (Å)	BAF
Pitch carbon	400	2600	3.41	270	1.11
Carbon electrode	—	2600	3.38	480	1.18
Pyrolytic carbon	—		3.42	210	4.16
Vitro carbon	—	2600	3.45	27	1.02

1.6. The Comparison with Other Carbon Materials (Table 6). In order to evaluate the preferred orientation of the Pitch Carbon which was prepared from the variant pitch material-N, the values of BAF of the other carbon materials were measured. For the carbon electrode or Vitro Carbon,[11] the thin section was cut with its plane parallel to the pressing- or depositing-direction. Pyrolytic carbon exhibited an extremely remarkable preferred orientation, while, on the contrary, Vitro Carbon was almost isotropic. Pitch Carbon and the carbon electrode exhibited values of BAF intermediate between those of pyrolytic carbon and Vitro Carbon.

2. The Relationships between the Moulding Pressure and Some Properties of Pitch Carbon. Figure 1 shows microscopic photographs of Pitch Carbon which was

11) H. Honda, Y. Sanada, and T. Furuta, *Tanso*, No. 46, 2 (1966).

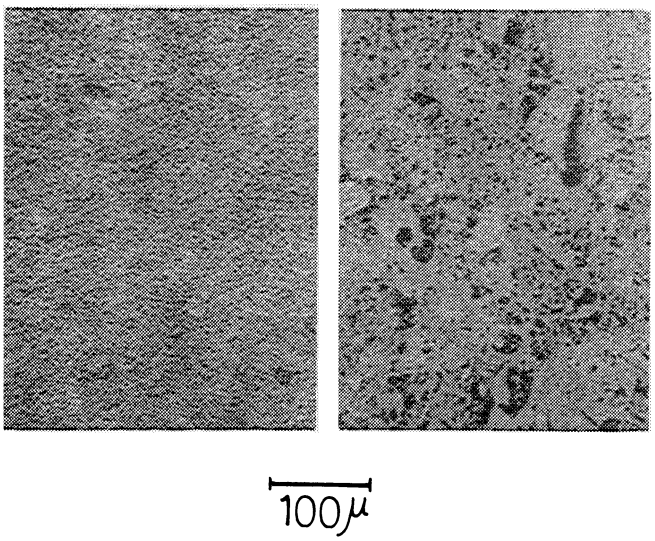

(a) Before heating (b) After heating

Fig. 1. Internal structures of pitch carbon pressed at 1600 kg/cm² (variant pitch material-N)

prepared from the variant pitch material-N by pressing at 1600 kg/cm². Large pores or grains were not observed in the tablet before the heat treatment. After the tablet had been heat-treated at 2600°C, on the other hand, large pores or grains were developed in it. From the above photographs, it is clear that these changes were caused by the coalescence and/or shrinkage of variant pitch particles at the heating stage.[6] This fact shows that the variant pitch material-N has a good ability of sintering. The internal structures of the other tablets (moulding pressure: 100 and 400 kg/cm²) before the heat treatment were similar to that shown in Fig. 1(a), and 2600°C-specimens gave less dense and less homogeneous structures than that shown in Fig. 1(b). Such differences are probably due to the difference in moulding pressure. The formation of cross-linkages among the molecules included in the pitch and the resulting elevation of the S.P. of pitch materials depended mainly on the progress of the oxidation reaction in the pre-heat treatment process in air. The oxygen is difficult to diffuse into closely-packed tablets. Therefore, these tablets tend to become semi-fused, thus having more mobility than in the solid state in this oxidation stage. As a result, a high moulding pressure accelerates sintering among particles of variant pitch materials.[6] A similar tendency of becoming semi-fused and accelerating the sintering can also be expected in the use of an oxidation temperature in the first stage lower than 300°C.[5]

The relationships between the bulk density of Pitch Carbons and the moulding pressure were as follows; 100 kg/cm²: 1.60 g/cm³, 400 kg/cm²: 1.64 g/cm³, 1600 kg/cm²: 1.83 g/cm³. For the Pitch Carbons pressed at 100 and 400 kg/cm², their bulk density were analogous in spite of the differences in the moulding pressure and in the values of BAF (r.f. 1.2).

3. Possibility of Isotropic Pitch Carbon with a High Density and with Various Degree of Graphitization.

According to the results described above, it seems that the preferred orientation of Pitch Carbon increases with a rise in the graphitizability of the variant pitch material used, but changes only slightly with an increase in the degree of graphitization upon heat treatment. These facts suggest that the preferred orientation of the final products is mainly determined at the moulding stage. In addition, the moulding pressure has scarcely no effect on the degree of graphitization of the resulting Pitch Carbon, but has a remarkable effect on the preferred orientation as well as the graphitizability of the variant pitch materials. The preferred orientation gradually became isotropic with a decrease in the moulding pressure. On the other hand, there were two methods for the preparation of Pitch Carbon with a high density. One is the use of the high moulding pressure described above, and the other is the acceleration of the sintering by using raw variant pitch materials with low S.P. and/or by applying a low oxidation temperature at the first stage.[6] The high-moulding-pressure-method is useful in the preparation of the isotropic Pitch Carbon with a low degree of graphitization which is prepared from non-graphitizable variant pitch materials such as chlorinated pitch.[6] It is clear that this method can not, however, be used for the preparation of isotropic Pitch Carbon with a high degree of graphitization, the other method would be better for this purpose. Since the degree of graphitization of Pitch Carbon is not affected by the moulding pressure, but is essentially affected by the graphitizability of the raw variant pitch, our purpose can be accomplished in the following manner. At first, graphitizable variant pitch materials with a low S.P. are moulded into tablets under a pressure lower than 100 kg/cm², and then the tablets are oxidized at as low temperature as possible within the limits required to prevent their deformation at the subsequent heating stage. By this treatment, the graphitizability of the product generally deteriorates to some extent. Therefore, even when this procedure is used, it is unavoidable that there is some limit to the improvement in the degree of graphitization of the resulting products.

4. Attempt to Make Isotropic Pitch Carbon with a High Density and with a High Degree of Graphitization.

When the tablet from material-N was heated under N_2 gas, it was deformed. From this fact, it seemed that the S.P. of the material-N was sufficiently low for this purpose. Therefore, the acceleration of the sintering was attempted by the control of the oxidation temperature in air. Moreover, for the improvement of the preferred orientation, a moulding pressure smaller than 100 kg/cm² was applied. The variant

TABLE 7. TYPICAL PROPERTIES OF ISOTROPIC PITCH CARBON WITH HIGH DENSITY

Pitch carbon	d_{002} (Å)	Lc (Å)	BAF
dia. 20 mm	3.39	210	1.02
dia. 40 mm	3.40	210	1.01

App. density (g/cm³)	Bulk density (g/cm³)	App. porosity (%)
2.12	1.75	17.3
2.12	1.79	15.4

pitch material-N (under 100 mesh) was pressed into tablets (diameter: 20 and 40 mm; thickness: about 10 mm) at 80 kg/cm^2. Then, the tablets were heated at the rate of 0.15°C/min up to 210°C in air, followed by heat-treatment at 2600°C in N_2 gas.

Some properties of the Pitch Carbon thus obtained are shown in Table 7. Both Pitch Carbons were almostly isotropic and were considerably improved in density in comparison with the other Pitch Carbons. In addition, their degrees of graphitization were considerably improved.

As a result, it seems reasonable to conclude that an isotropic carbon product with a high density, in addition to an improved degree of graphitization, can be prepared by the use of the method of preparing Pitch Carbon without any other techniques.

NOTES

BULLETIN OF THE CHEMICAL SOCIETY OF JAPAN, VOL. 46, 318—319 (1973)

The Determination of the Iodine Affinity of Poly(vinyl acetate)

Sadao HAYASHI, Masayuki KISHIBE, and Nobumasa HOJO
Faculty of Fiber Science and Technology, Shinshu University, Tokiiri, Ueda

(Received February 16, 1972)

In a previous paper, in which the complex between poly(vinyl acetate)(PVAc) and iodine in the presence of potassium iodide has been investigated, we have reported that the potentiometric titration curve for a PVAc suspension with iodine is of the same type as that for amylose.[1] However, it was found from the results of many experiments that the iodine affinity of PVAc (grams of iodine consumed by 100 g of PVAc) varies widely with the measurement conditions, because the reaction system between PVAc suspended in an aqueous solution and iodine is heterogeneous. Therefore, in the present paper, we wish to attempt a more accurate estimation of the iodine affinity of PVAc in an apparent homogeneous system.

Experimental

Materials. The PVAc samples used here were prepared by the solution polymerization of vinyl acetate in methanol and by the suspension polymerization of vinyl acetate, using benzoyl peroxide and potassium persulfate respectively. The degree of polymerization of the PVAc prepared by solution polymerization was about 500. The iodine, potassium iodide, and sodium thiosulfate were reagents of a guaranteed grade.

Measurements. A methanol solution (1 ml) containing PVAc (1.5×10^{-3}g) prepared by solution polymerization and iodine, the content of which was varied from 0.80×10^{-7} to 20.8×10^{-7} mol, was added to 40 ml of an aqueous solution of potassium iodide (6.42×10^{-3} mol), and the total volume was exactly adjusted 50 ml by adding water.[2] The mixture instantly showed a red-violet color. The colored solution was kept in a water bath thermostated at 15°C for an hour; then the absorbance and the potential values of the solution were measured by the use of a Hitachi-Horiba M-5 pH-meter and a Hitachi 101 spectrophotometer respectively.

The films of PVAc were prepared by casting a methanol solution of PVAc obtained by the solution polymerization and a PVAc suspension produced by the suspension polymerization on the polyethylene film. The films of PVAc thus obtained were dried in a vaccum, dipped in 100 ml of a 0.1N iodine solution (iodine/potassium iodide=1/4 by wt.) for 24 hr at 15°C, and then washed with water for two weeks. The amount of iodine reacted with PVAc was determined by the following method: the film reacted with iodine was dissolved by methanol (50 ml), and then it was titrated with a 0.1N sodium thiosulfate solution.

Results and Discussion

When the mixture of PVAc and iodine in methanol was added to an aqueous solution of potassium iodide, a red-violet complex was immediately formed. This complex was rapidly destroyed by adding sodium thiosulfate, and at that time the solution was transparent, after which it gradually became turbid because of the precipitation of PVAc. It is evident from this finding that, in the method used here, the reaction system of PVAc with iodine is apparently homogeneous.

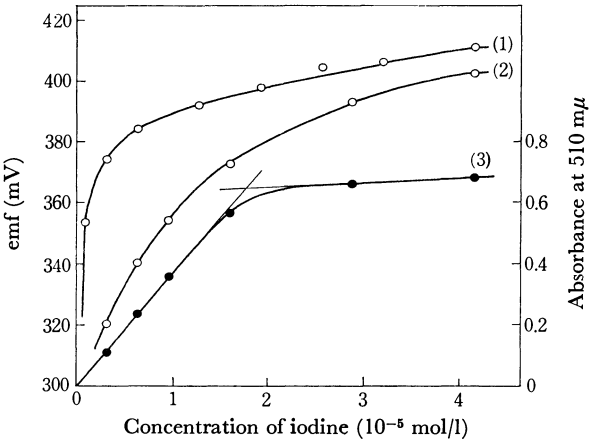

Fig. 1. Plots of emf (○) and absorbance (●) at 510 mμ versus concentration of iodine. PVAc concentration: 0.03 g/l.
(1) Curve of emf in the absence of PVAc,
(2) Curve of emf in the presence of PVAc,
(3) Curve of absorbance at 510 mμ in the presence of PVAc.

The potential values *versus* the concentration of iodine in the apparent homogeneous system are shown in Fig. 1, in which the potential values in solution increased with an increase in the concentration of iodine. This result has some similarity to that for the partially-saponified PVAc, which is easily soluble in water and which reacts with iodine to produce the red-violet complex.[1,3]

In a previous paper,[1] we could see a horizontal part in the potentiometric titration curve for the PVAc with iodine, where the potential values in solution remained constant upon the addition of iodine because the iodine added was consumed in the complex formation with PVAc suspended as particles in water.

Consequently, it is confirmed that the potentiometric titration curve for PVAc with iodine varies with the reaction conditions. On the basis of these data, we can explain the potentiometric titration curves for PVAc with iodine as follows: the fact that the titration curve for PVAc suspended in water is similar to that for

1) S. Hayashi, T. Nakabayashi, and K. Yoshida, This Bulletin, **43**, 3292 (1970).
2) S. Hayashi and C. Kawamura, *Kogyo Kagaku Zasshi*, **72**, 2491 (1969).
3) S. Hayashi, C. Nakano, and T. Motoyama, *Kobunshi Kagaku*, **20**, 303 (1963).

Table 1. Iodine affinities of PVAc in film

Samples			Results		
Area (cm^2)	Weight (g)	Thickness[a] (mm)	Degree of swelling in area[b]	Degree of swelling in weight[c]	Iodine affinity
PVAc obtainecd from solution polymerization					
3.15	0.4833	1.28	5.1	6.6	13.5
3.42	0.4562	1.10	3.8	6.2	13.4
4.01	0.4900	1.02	3.8	6.5	13.1
3.80	0.4554	0.99	4.0	6.3	13.2
3.96	0.4595	0.97	3.8	6.5	13.1
7.29	0.4135	0.47	4.0	6.9	10.6
8.12	0.4054	0.42	3.9	7.0	9.8
9.25	0.3154	0.28	4.4	7.3	8.2
PVAc obtained from suspension polymerization					
3.42	0.4935	1.44	1.8	4.8	12.6
4.14	0.4437	0.89	2.4	6.3	14.0
5.28	0.4797	0.76	2.0	6.7	15.7
6.60	0.4918	0.62	2.7	5.4	12.9
10.73	0.4914	0.38	2.9	4.4	10.7
11.22	0.3075	0.27	3.1	3.9	4.7

a) Thickness was calculated from area and weight by assuming that specific gravity of PVAc is 1.20.

b) Degree of swelling in area $= \frac{\text{Area of swelling film}}{\text{Area of original film}}$

c) Degree of swelling in weight $= \frac{\text{Weight of swelling film}}{\text{Weight of original film}}$

amylose indicates a heterogeneous reaction based on the diffusion of iodine into the PVAc particles suspended in water, without regard to the formation of a helical complex of a polymer with iodine postulated in the case of amylose.[4]

The relationship between the absorbance and the concentration of iodine in the apparent homogeneous system is shown in Fig. 1. When the amount of PVAc was kept constant, the maximum absorption was obtained by adding more than about 2.5×10^{-5} mol/l of iodine for 3.48×10^{-4} mol/l of monomer units in PVAc. This shows that PVAc has a stoichiometric relation with iodine. According to Bates *et al.*,[5] results of Fig. 1 show the iodine affinity of PVAc to be 12.2. This value is considerably larger than the value of 7.3 obtained in the heterogeneous system.[1] Furthermore, from Fig. 1, the molecular extinction coefficient of iodine in the complex was estimated to be 42200 l/mol·cm.

The iodine affinities of PVAc in film are summarized in Table 1. The swelling of a film began as soon as the film assumed a red-violet color; eventually it grew to several times the original film. When a thin film was used as a sample, it was observed that some of the polymers disperse into water from the film as the complex forms during a period of washing. On the other hand, when a thick film was used as a sample, no loss of polymers was observed, and the iodine affinities of PVAc were about the same. This indicates that, if the reaction conditions, such as the reaction time and the concentration of iodine, are given satisfactorily, the iodine affinities of PVAc are almost all the same, independent of the properties of the PVAc originating from the polymerization conditions. Consequently, the largest cause for the error in the iodine affinity of PVAc found by the potentiometric titration in the heterogeneous system[1] appears to be the insufficiency of the reaction conditions in its system. The average value of the iodine affinities of PVAc in film, except for the thin films, was 13.5. This value is in good agreement with that found from Fig. 1. Accordingly, the iodine affinity of PVAc obtained in the apparent homogeneous system is thought to be reasonable.

The stoichiometry indicates that one molecule of iodine reacts with about 24 vinyl acetate units in PVAc. However, in the absence of direct evidence, the arrangement of iodine molecules in the complex between PVAc and iodine can not be illustrated. Further work is now in progress.

4) R. E. Rundle, J. E. Foster, and R. A. Baldwin, *J. Amer. Chem. Soc.*, **66**, 2116 (1944).

5) F. L. Bates, D. French, and R. E. Rundle, *ibid.*, **65**, 142 (1943).

BULLETIN OF THE CHEMICAL SOCIETY OF JAPAN, VOL. 46, 320 (1973)

Phase Transition and Spin-exchange Interaction in Ion Radical Salts. Some Information Derived from ESR Measurements

Yôichi IIDA

Department of Chemistry, Faculty of Science, Hokkaido University, Sapporo

(Received March 14, 1972)

The prominent magnetic properties of solid ion radical salts have been the subject of many theoretical and experimental investigations over the past several years.[1-7] In certain ion radical salts, the extra electrons on the ion radical molecules appear to be paired by means of an exchange interaction.[1-7] In this case, the paramagnetic contribution to the susceptibility of these materials at any temperature, T, can be fitted approximately to the expression:

$$\chi_p = (2Ng^2\mu_B^2/3kT)\left(1+\frac{1}{3}e^{J/kT}\right)^{-1}, \quad (1)$$

which corresponds to an assembly of N quasimolecules with a singlet ground state and a triplet state lying an energy, J, above the ground state.

The intensity of the electron-spin-resonance (ESR) absorption, I, is known to be proportional to the value of χ_p. Therefore, since a plot of ln (IT) *versus* T^{-1} yields an approximately straight line, the singlet-triplet energy separation, J, can be estimated from the slope value of this straight line.[1,2,4]

If these ion radical salts undergo first-order phase transitions, an abrupt change in the singlet-triplet energy separation should be associated with the phase transition.[4-7] The J values in the low- and high-temperature phases have both been estimated by using this slope method. However, the slope method is not applicable when the intensity measurements cannot be made over a wide temperature range. In this case, the relative intensity ratio of the ESR absorptions at the transition temperature is useful for the determination of the J values below or above the transition temperature.

At the transition temperature, T_c, in the lower and higher temperature ranges, the singlet-triplet energy separations are represented by J and J', while the ESR absorption intensities are represented by I and I'. It is assumed, in Eq. (1), that only a change in the singlet-triplet energy separation is involved; that is, the value of N, g, or μ_B in the lower temperature range is assumed to be equal to the corresponding one in the higher temperature range. On this assumption, we obtain:

$$\frac{I'}{I} = \frac{3+\exp(J/kT_c)}{3+\exp(J'/kT_c)}. \quad (2)$$

Therefore, if the values of (I'/I), J, and T_c are known experimentally, the value of J' can be estimated by means of:

$$J' = kT_c \ln\left\{3\left(\frac{I'}{I}-1\right)+\frac{I'}{I}\exp(J/kT_c)\right\}. \quad (3)$$

We shall apply this method, for example, to the phase transition of $[(C_6H_5)_3PCH_3]^+$ $(TCNQ)_2^-$, one of the anion radical salts of 7,7,8,8-tetracyanoquinodimethane (TCNQ).

Several years ago, we examined the ESR spectra of $[(C_6H_5)_3PCH_3]^+$ $(TCNQ)_2^-$ and its variation with the temperature.[6] For this anion radical salt, the paramagnetism due to the excited triplet state has been established from the anisotropic zero-field splitting in the ESR absorption at low temperatures.[1] The phase transition takes place at T_c=315.7K,[8] where the intensity of the ESR absorption increases abruptly in the higher temperature range by a factor of (I'/I)= 1.9.[6] Although the singlet-triplet energy separation in the low-temperature phase, J, is known to be 0.065 eV by Kepler's susceptibility measurements,[5,9] there have been no experimental data on the value in the high-temperature phase. If J=0.065 eV in the low-temperature phase holds at the transition temperature, the singlet-triplet energy separation in the high-temperature phase, J', can be determined to be 0.039 eV by putting those values into Eq. (3). The appreciable reduction of the singlet-triplet energy separation in the high-temperature phase is found to be caused by the phase transition. On the other hand, the J' value estimated from the slope method is 0.03 eV or less, which is somewhat smaller than that estimated from the relative intensity-ratio method. However, since the observation of the ESR absorption intensities in the high-temperature phase was done over a limited temperature range,[6] the slope value for the singlet-triplet splitting in the high-temperature phase should be taken as only an indication.

The present intensity-ratio method in ESR absorption can be applied, in general, to the phase transitions of ion radical salts which possess a magnetic system composed of a singlet ground state and a triplet excited state. In some cases, this method gives more accurate information on the singlet-triplet energy separation than does the slope method.

1) D. B. Chesnut and W. D. Phillips, *J. Chem. Phys.*, **35**, 1002 (1961).
2) D. B. Chesnut and P. Arthur, Jr., *ibid.*, **36**, 2969 (1962).
3) M. T. Jones and D. B. Chesnut, *ibid.*, **39**, 1311 (1963).
4) D. D. Thomas, H. Keller, and H. M. McConnell, *ibid.*, **39**, 2321 (1963).
5) R. G. Kepler, *ibid.*, **39**, 3528 (1963).
6) Y. Iida, M. Kinoshita, M. Sano, and H. Akamatu, This Bulletin, **37**, 428 (1964).
7) Z. G. Soos and R. C. Hughes, *J. Chem. Phys.*, **46**, 253 (1967).
8) A. Kosaki, Y. Iida, M. Sorai, H. Suga, and S. Seki, This Bulletin, **43**, 2280 (1970).
9) Rigorously speaking, the J value was found to depend slightly on the temperature. However, the variation in J with the temperature is not observed in the ESR measurements, because one measures only the relative intensity. The ESR intensity, I, is proportional to $\exp(-J/kT)$, and if J varies as $J_0+\alpha T$, the linear term in T will appear only as a constant and, therefore, not show up in relative intensity measurements. By using the slope method of the ESR intensity, Chesnut and Phillips reported the J value to be 0.062 eV,[1] while Iida *et al.* reported it to be 0.08 eV.[6]

BULLETIN OF THE CHEMICAL SOCIETY OF JAPAN, VOL. 46, 321—322 (1973)

A Study of Catalytic Partial Oxidation of Hydrocarbons. XIII. The Effect of Bi_2O_3 Content in MoO_3-Bi_2O_3-P_2O_5 Catalysts on the Dehydration of Isopropyl Alcohol

Mamoru Ai and Sadao Suzuki

Research Laboratory of Resources Utilization, Tokyo Institute of Technology, Ookayama, Meguro-ku, Tokyo

(Received March 25, 1972)

The present authors have recently reported the effect of the Bi_2O_3 content in the MoO_3–Bi_2O_3–P_2O_5 ternary catalyst system on the oxidation of olefins, furan, and maleic anhydride.[1,2] It has been considered that, with an increase in the Bi_2O_3 content, the acidity of the catalysts changes; accordingly, the affinity, *i.e.*, the adsorptive action, of the catalysts for such basic compounds as olefins and furan, and that for such electron-acceptor-type compounds as carboxylic acid and oxygen, varies. We should measure directly the acidity of the catalyst system in order to cofirm those results. However, it is hard to measure the acidity by means of the conventional titration method, because both the acidity and the surface area are very small; moreover, the catalysts are dark—the low Bi_2O_3 content catalyst, for instance, is black. However, it is well known that there are good correlations between the acidic properties and activities of catalysts for many acid-catalyzed reactions,[3] so it seems appropriate to adopt the activity for the dehydration of alcohols as a measure reflecting the acidity of the catalyst.

In the present work, the dehydration of alcohols, especially that of isopropyl alcohol (IPA), was performed over a series of MoO_3–Bi_2O_3–P_2O_5 catalysts with various Bi/Mo ratios in order to study the dependency of the acidity on the Bi_2O_3 content and the relationship between the acidity and the activities for oxidation and isomerization reactions.

Experimental

The vapor-phase dehydration of alcohols, such as ethyl and isopropyl alcohols, was carried out over a series of MoO_3–Bi_2O_3–P_2O_5 catalysts with various Bi/Mo ratios (P/Mo=0.2 atomic ratio) in an ordinary continuous-flow-type reaction system.[4] The concentration of alcohol was about 2.2 mol% in nitrogen or air, and the flow rate was kept at 1.0 l/min (STP). The amount of the catalyst used was 20 ml (contact time=1.2 sec). The reaction temperature was varied from 160 to 300°C.

The reaction products were analyzed by gas chromatography; for propylene and ethylene: activated alumina and a 6 m column at 80°C; for alcohols and other oxygen-containing compounds: PEG20M and a 6 m column at 80°C. The other experimental procedures were similar to those employed in earlier works.[1-3]

The catalysts used in these experiments were the same as those used in previous works.[1,2] The surface area of these catalysts was 0.6 ± 0.3 m²/g, as determined by the BET method, using nitrogen at −195°C as the adsorbate, and their packing density was within the limits of 0.75—0.80 g/ml. Taking the experimental error into account, the dependence of these values upon the catalyst composition (Bi/Mo ratio) was obscure.

Results and Discussion

Dehydration of Ethyl Alcohol. Only a trace amount of ethylene was produced, even at about 300°C, over the entire range of Bi/Mo ratios. This shows that the acid strength of the catalyst is too weak to catalyze the dehydration of normal alcohol.[5]

Dehydration of Isopropyl Alconol. The effect of the reaction temperature on the conversion of isopropyl alcohol into propylene was studied over the MoO_3–Bi_2O_3–P_2O_5 catalysts in atmospheres both of nitrogen and of air. The results in nitrogen are shown in Fig. 1. Apart from propylene, only di-isopropyl ether and acetone were found in the product. The acetone formation, *i.e.*, the dehydrogenation, was very little in nitrogen—less than 1%. It was more appreciable in air, especially at high temperatures. Propylene was the main product in the dehydration above 180°C. The portion of propylene in the products decreased with a decrease in the temperature, and below 160°C, ether was predominant. The rate of propylene forma-

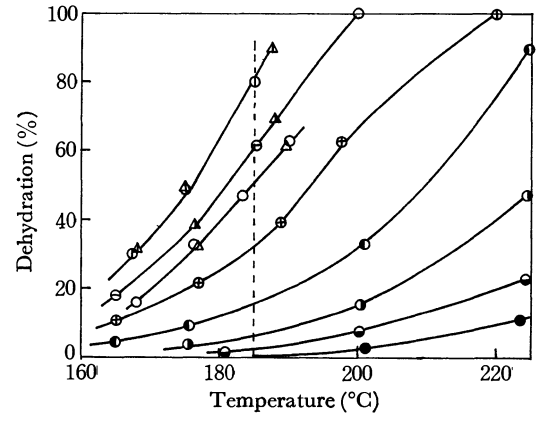

Fig. 1. Dependency of the isopropyl alcohol conversion to propylene on the reaction temperature over MoO_3–Bi_2O_3–P_2O_5 catalysts.
IPA=2.2% in N_2, contact time=1.2 sec,
○: Bi/Mo=0, △: 0.05, ◫: 0.1, ◬: 0.2, ⊖: 0.3, ▲: 0.4, ⊕: 0.7, ◐: 1.0, ◑: 2.0, ◒: 4, ●: ∞

1) M. Ai and S. Suzuki, *Nippon Kagaku Kaishi*, **1972**, 290.
2) M. Ai and S. Suzuki, *J. Catal.* **26**, 202 (1972).
3) K. Tanabe, "Solid Acids and Bases," Kodansha, Tokyo, and Academic Press, New York, London (1970), Chap. 5.
4) M. Ai, T. Niikuni, and S. Suzuki, *Kogyo Kagaku Zasshi*, **73**, 165 (1970).
5) Y. Murakami, S. Nishizawa, and H. Uchida, *Shokubai*, **13**, 108 (1971).

tion was almost of a zero order in isopropyl alcohol. No loss of activity was observed within 4—5 hr, even in the nitrogen atmosphere.

The value of the conversion to propylene at 185°C was adopted as a measure of the dehydration activity; the data are plotted as a function of the Bi_2O_3 content in Fig. 2. The value of the conversion to acetone in air at 185°C is also shown in Fig. 2. With an increase in the Bi_2O_3 content of the catalyst, the dehydration activity increases at first, passes through a maximum at the Bi/Mo atomic ratio of 0.1—0.2, and then decreases to the value of the pure Bi_2O_3 catalyst, which is extremely inactive. Although the shapes of the curves are almost the same, the activity in the air seems to be lower than that in nitrogen. Further investigation is necessary to clarify the effect of the atmosphere.

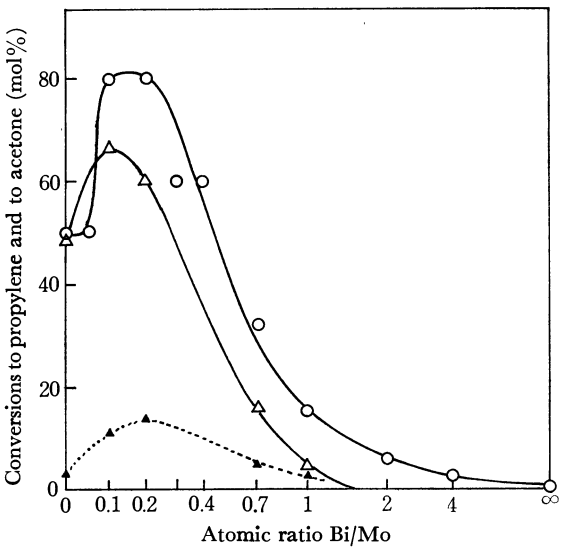

Fig. 2. Dehydration and dehydrogenation activities as a function of the Bi_2O_3 content.
temperature=185°C, IPA=2.2%, contact time=1.2 sec.
propylene---○: in nitrogen, △ : in air
acetone ---▲: in air (dotted line)

Discussion. If the dehydration activity really represents the acidity of a catalyst, it can be concluded from the results shown in Fig. 2 that a new acidic site is produced by adding Bi_2O_3 up to Bi/Mo= 0.1, that the acidity passes through a maximum at Bi/Mo=0.1—0.2, and that it then decreases sharply upon the further addition of Bi_2O_3.

If the acidity of the catalyst plays an important role in the oxidation and isomerization of olefin, a linear relation between the activities for these reactions and that for the dehydration must be obtained. The characters of the curves in Fig. 2 are quite similar to those of olefin oxidation.[1,2] Figure 3 shows the relationship between the dehydration activity for isopropyl alcohol and the oxidation and isomerization activities for butene. Both the oxidation and isomerization activities for butene increase steadily with an increase in the dehydration activity for IPA. Those results show that both the oxidation and isomerization activities are closely related to the acidities of the catalysts, which may support our explanation of the oxidation mechanism being based on the acid-base nature of the reactant and the catalyst.[1,2]

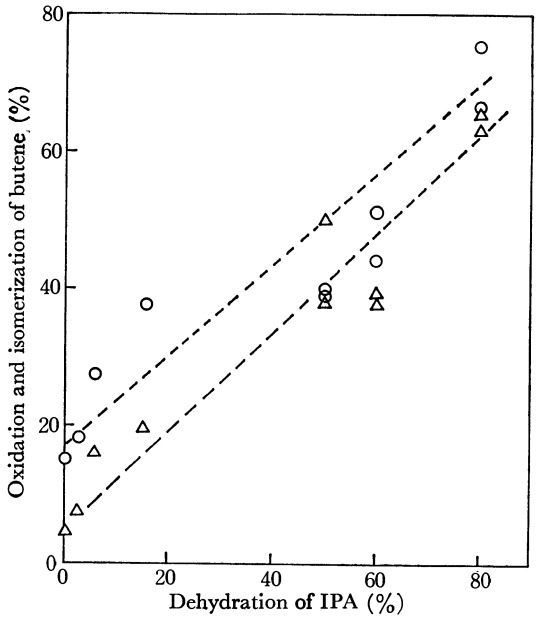

Fig. 3. Relation between the activity for IPA dehydration and the activities for oxidation and isomerization of butene.
IPA dehydration: 185°C, 2.2 mol% in nitrogen, contact time of 1.2 sec.
butene reactions: *cis*-2-C_4H_8=0.67% in air, contact time =1.6 sec.
○: over-all oxidation conversion of butene, 430°C
△: isomerization of *cis*-2-C_4H_8, 350°C:
[*trans*-2-C_4H_8+1-C_4H_8]/[*cis*-2-C_4H_8+*trans*-2-C_4H_8+ +1-C_4H_8]×100

BULLETIN OF THE CHEMICAL SOCIETY OF JAPAN, VOL. 46, 323—324 (1973)

The Effect of the Addition of γ-FeOOH Nuclei at the Initial Stage of Oxidation on the Formation of γ-FeOOH

Masao KIYAMA, Nariyasu JIKUHARA,* and Toshio TAKADA
Institute for Chemical Research, Kyoto University, Kyoto
(Received April 24, 1972)

The presence of green rusts has been considered to be indispensable for the formation of γ-FeOOH. Bernal *et al.* proposed, from a crystallochemical point of view, that γ-FeOOH was topotactically formed by the surface oxidation of the green rusts.[1] We recently reported that γ-FeOOH can be obtained not only from the green rusts in ferrous salt solutions, but also from acidic solutions containing ferrous ions, by selecting the oxidizing conditions.[2] It was found that, under the conditions where γ-FeOOH was formed together with α-FeOOH, the γ-FeOOH content in the oxidation product was affected by slight differences in the treatment before oxidation. The γ-FeOOH content may be determined by the ratio of the α-FeOOH nuclei to the γ-FeOOH nuclei formed at the initial stage of oxidation. In order to prove this assumption, an attempt has been made to change this ratio variously by adding very fine particles of α-FeOOH and γ-FeOOH to the solutions. The experimental results will be reported here.

Experimental and Results

The chemicals used in the present study were of a reagent grade. The fine particles of α-FeOOH used as nuclei were prepared by the hydrolysis of a ferric nitrate at 40°C for 50 hr, while those of γ-FeOOH were prepared *via* a green rust (I) by the oxidation of $Fe(OH)_2$ below 10°C in a ferrous chloride solution. The precipitates formed by hydrolysis and oxidation were filtered, washed with water, and then diluted with water to obtain turbid solutions containing 0.05 mol of the nuclei per liter. The particles of α-FeOOH were superfine (below 0.02 μ in size), while those of γ-FeOOH were flaky (about 0.3 μ in length).

Varying quantities of the turbid solutions were added to 3 l of a mixture of 0.21M-$FeCl_2$ and 1.44M-NaI solutions, and the resultant solutions were subjected to oxidation. The procedures of the oxidation and identification of the samples thus obtained were the same as have been described in a previous paper.[2] The contents of α-FeOOH, β-FeOOH, and γ-FeOOH were determined by comparing the relative intensities of the X-ray diffraction lines of α-FeOOH d(110) 4.18 Å, β-FeOOH d(110) 7.40 Å, and γ-FeOOH d(020) 6.3 Å.

Air was bubbled into the mixtures with and without 10 ml of the turbid solution of γ-FeOOH (containing 0.5 mmol of γ-FeOOH) at the rate of 300 l/hr for 20 hr at various temperatures for oxidation. The contents of three forms of FeOOH in the oxidation product thus obtained are plotted against the oxidizing temperature in Figs. 1 and 2. The γ-FeOOH content increases with the temperature and attains, at temperatures between 60 and 70°C, the maximum value, which is 40% when no turbid solution of γ-FeOOH has been added and 80% when it has been added.

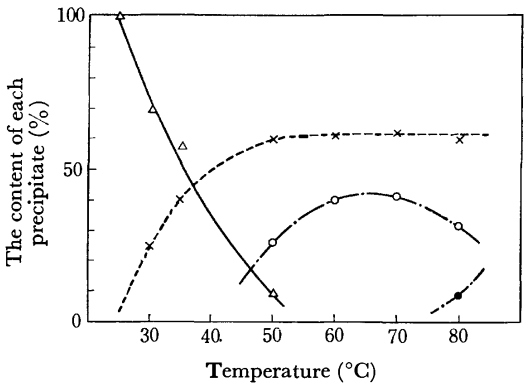

Fig. 1. The content of each precipitate in the oxidation products formed at various temperatures in a mixture of 0.21M-$FeCl_2$ and 1.44M-NaI solutions.
×: α-FeOOH, △: β-FeOOH, ○: γ-FeOOH, ●: α-Fe_2O_3

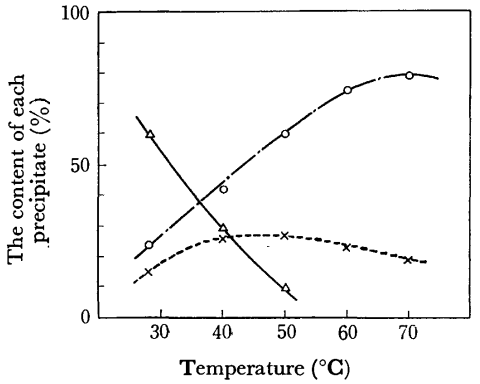

Fig. 2. The content of each precipitate in the oxidation products formed at various temperatures in the mixture containing 0.5 mmol of γ-FeOOH nuclei.
×: α-FeOOH, △: β-FeOOH, ○: γ-FeOOH

Varying quantities of the turbid solutions were added to 3 l portions of the mixture, and the resultant solutions were oxidized at 60°C for 20 hr. About 7 g (87 mmol) of an oxidation product was obtained from each solution, and the product consisted of only α-FeOOH, only γ-FeOOH, or their mixture. The γ-FeOOH content of the products is plotted against the amount of α-FeOOH or γ-FeOOH added in Fig. 3. When 2.5 mmol or more of γ-FeOOH was added to the mixture, only γ-FeOOH was formed, whereas when

* Present address: Toda Industrial Co., Ltd. 7–1, Yokogawa Shin-machi, Hiroshima.

1) J. D. Bernal, E. R. Dusgputa, and A. L. Mackay, *Clay Min. Bull.*, **4** (21), 15 (1959).
2) M. Kiyama and T. Takada, This Bulletin, **45**, 1923 (1972).

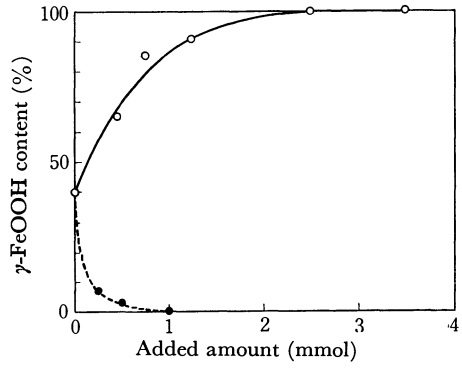

Fig. 3. The γ-FeOOH content of the oxidation products formed at 60°C in the mixtures containing different amounts of α-FeOOH and of γ-FeOOH nuclei.
●: α-FeOOH nuclei, ○: γ-FeOOH nuclei

1 mmol or more of α-FeOOH was added to it, only α-FeOOH was formed as the oxidation product. The effect of the addition of the nuclei on their formation may depend upon the particle size of the nuclei.

On oxidation, γ-FeOOH was not obtained from the $FeSO_4$ and $FeCl_2$ solutions, but other precipitates, such as α-FeOOH and β-FeOOH, were obtained. A turbid solution (100 ml) containing 5 mmol of γ-FeOOH was added to 3 l portions of these solutions containing 0.21 M-ferrous ions, and the resultant mixtures were oxidized at 60°C for 20 hr. The oxidation products thus obtained consisted of α-FeOOH only (when these solutions containing no γ-FeOOH nuclei were oxidized under the same conditions as above, too, only α-FeOOH was formed).

By oxidation, a hydroxo ferric complex which has H_2O and OH^- ligands may be formed together with other ferric complexes which have halogen ligands besides H_2O and OH^- ligands. The concentration of the hydroxo ferric complex depends on the conditions, such as the concentration of the halogen ions and the temperature. The precipitation of β-FeOOH may be due to the hydrolysis of the halo ferric complexes, while that of α-FeOOH and γ-FeOOH may be due to the hydrolysis of the hydroxo ferric complex. Which is formed, α-FeOOH or γ-FeOOH, presumably depends upon whether or not an epitaxial reaction occurs between the γ-FeOOH nucleus and the hydroxo ferric complex. The hydroxo ferric complexes may be epitaxially deposited on the γ-FeOOH nucleus to give a precipitate of γ-FeOOH. The formation of the γ-FeOOH nuclei and their growth on the nuclei may be influenced by the rate of formation of the hydroxo ferric complex.

BULLETIN OF THE CHEMICAL SOCIETY OF JAPAN, VOL. 46, 324—326 (1973)

The Kinetics of Proton-transfer Reaction in an Aqueous Solution of *n*-Butylamine by Means of Ultrasonic Absorption

Sadakatsu NISHIKAWA, Tetsuya NAKAMOTO, and Tatsuya YASUNAGA

Department of Chemistry, Faculty of Science, Hiroshima University, Higashisenda-machi, Hiroshima

(Received April 25, 1972)

Various mechanisms associated with the ultrasonic absorptions in aqueous solutions of amines have previously been proposed.[1-4] Some problems relating to the elucidation of the mechanisms seem, however, to be still in question. On the other hand, the clarification of the dynamic properties of aqueous solutions of amines may provide useful and fundamental information on the kinetics and mechanisms associated with the conformational changes of the protein molecules.

The purpose of the present investigation is to confirm the mechanism of the excess absorption in a dilute aqueous solution of *n*-butylamine in detail by measuring the ultrasonic absorption.

Experimental

The chemical used in the present experiment were of a guaranteed reagent grade. The *n*-butylamine was purified by distillation, and its purity was confirmed by the gas-chromatographic method to be higher than 99.9%. The pH of the solution was adjusted to the desired values using either NaOH or $HClO_4$. The ultrasonic absorptions were measured at the odd harmonic frequencies of 5 MHz and 20 MHz X-cut quartz crystals by the pulse technique.[5] The frequency range of the measurement was from 15 to 220 MHz. Since the aqueous solution of amine is highly basic, the cell was made air-tight, and nitrogen gas was passed over the solution to prevent the contamination of specimens by the oxidation with air. The sing-around method was employed at 1.92 MHz to measure the sound velocity. The pH values of the solutions were measured by a Hitachi-Horiba F-5 type pH meter. All the measurements were made at 20°C.

Results and Discussion

Figure 1 shows an example of the ultrasonic absorption spectra of aqueous solutions of *n*-butylamine. These

1) M. M. Emara, G. Atkinson, and E. Baumgartner, *J. Phys. Chem.*, **76**, 334 (1972).
2) J. F. Mckellar and J. H. Andreae, *Nature*, **195**, 865 (1962).
3) R. N. Baafield and W. G. Schneider, *J. Chem. Phys.*, **31**, 488 (1959).
4) M. Eigen and L. de Maeyer, Technique of Organic Chemistry, Vol. VIII, part 2, A. Weissberger, Jr., Ed., John Wiley and Sons, Inc., New York, N. Y., 1961.
5) N. Tatsumoto, *J. Chem. Phys.*, **47**, 4561 (1967).

Table 1. Ultrasonic parameters and densities for the solution of *n*-butylamine at 20°C

M	pH	ρ g cm^{-3}	c m sec^{-1}	A 10^{-16} dB	B sec^2 cm^{-1}	f_r MHz	$(\alpha\lambda)_{max}$ 10^{-3} neper
0.0322	11.39	0.9966	1484.0	44.5	21.0	36±10	1.3
0.0978	11.73	0.9953	1489.2	65.0	22.0	55±5	2.9
0.217	11.94	0.9936	1499.0	62.0	24.0	82±7	3.8
0.283	12.05	0.9928	1504.6	57.5	25.0	90±7	3.9
0.401	12.13	0.9917	1516.5	59.0	23.5	105±10	4.7
0.505	12.17	0.9909	1521.6	59.5	25.0	115±10	5.2
0.537	12.25	0.9901	1524.3	63.0	23.0	130±15	5.4

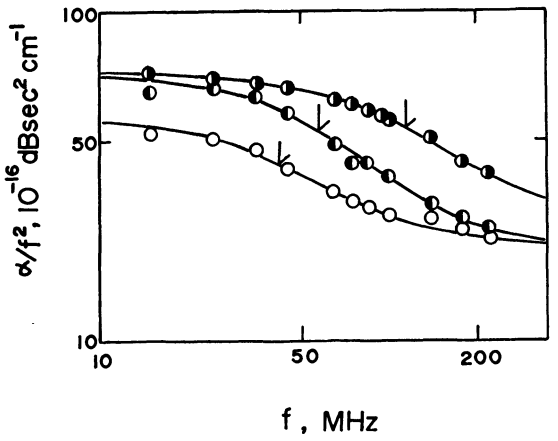

Fig. 1. Ultrasonic absorption spectra in aqueous solutions of *n*-butylamine at 20°C. The arrows show the relaxation frequencies:
◑: 0.505M, ◐: 0.0978M, ○: 0.0322M.

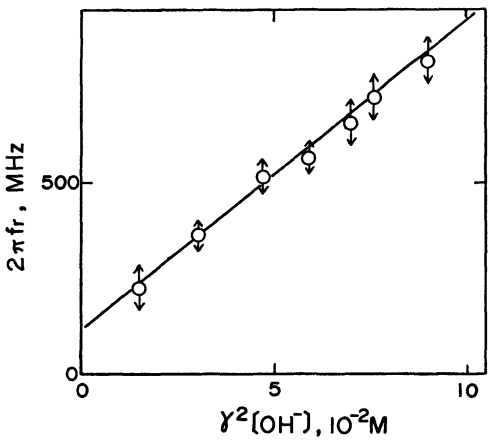

Fig. 2. The plots of $2\pi f_r$ *vs.* $\gamma^2[OH^-]$ for aqueous solutions of *n*-butylamine at 20°C.

spectra can be represented by the formula of a single relaxation as follows:

$$\alpha/f^2 = \frac{A}{1+(f/f_r)^2} + B \qquad (1)$$

where α is the absorption coefficient; f, the frequency; f_r, the relaxation frequency, and A and B, constants. The values of these constants were determined so as to obtain the best fit of the data to Eq. (1). The ultrasonic parameters and densities thus obtained are listed in Table 1. If these excess absorptions are due to hydrolysis, the reaction scheme is given by the following equation:

$$R\text{-}NH_3^+ + OH^- \underset{k_b}{\overset{k_f}{\rightleftharpoons}} R\text{-}NH_2 + H_2O. \qquad (2)$$

The reciprocal relaxation time is related to the rate constants and concentrations as follows:

$$1/\tau = 2\pi f_r = k_f[[R\text{-}NH_3^+]+[OH^-]]\Pi\gamma_i + k_b. \qquad (3)$$

where τ is the relaxation time, k_f and k_b are the forward and backward rate constants respectively, and γ_i is the activity coefficient. If the activity coefficients and concentrations of the $R\text{-}NH_3^+$ ion are equal to those of the OH^- ion at each concentration, Eq. (3) can be rewritten as:

$$1/\tau = 2\pi f_r = 2k_f\gamma^2[OH^-] + k_b \qquad (4)$$

The relationship between the ionic strengths and the activity coefficients of monoamine and OH^- ions has been given by almost the same curve.[6] Assuming that the relationship also holds for *n*-butylamine, the appropriate activity coefficients can be obtained graphically.

Figure 2 shows the plot of $2\pi f_r$ *vs.* $\gamma^2[OH^-]$. The linearity of the plot confirms that the mechanism of excess absorption is associated with hydrolysis. The forward and backward rate constants were calculated from the slope and intercept respectively of the plots. The standard volume change, ΔV, of the reaction can be determined in the following manner. The excess absorption per wavelength shows a maximum at the $f=f_r$ frequency and can be written as:

$$(\alpha\lambda)_{max} = \frac{1}{2}Af_rc \qquad (5)$$

where $(\alpha\lambda)_{max}$ is the maximum excess absorption per wavelength, and c, the velocity of sound. For a chemical process of the type represented by Eq. (2), the maximum excess absorption per wavelength can be represented by:

$$(\alpha\lambda)_{max} = \frac{1}{2}\pi\rho c^2\frac{(\Delta V)^2}{RT}\Gamma_c \qquad (6)$$

where ρ is the density and where $\Gamma_c=[1/[OH^-]+1/[R\text{-}NH_3^+]+1/[R\text{-}NH_2]]^{-1}$. In Table 2 the rate constants and the mean standard volume change associated with the hydrolysis of *n*-butylamine are tabulated, together with the results for other amines obtained by Eigen and his co-workers.[4,7,8]

6) J. Kielland, *J. Amer. Chem. Soc.*, **59**, 1675 (1937).

7) G. Maass, ph. D. Theses, Uni. of Gottingen (1962).

8) M. Eigen, G. Maass, and G. Schwarz, *Z. Phys. Chem.*, **74**, 319 (1971).

Table 2. Rate constants and standard volume change

System	k_f $M^{-1}sec^{-1}$	k_b sec^{-1}	ΔV $cm^3 mol^{-1}$
Ammonia	3.4×10^{10}	6.0×10^{5}	26.8
Methylamine	3.7×10^{10}	1.6×10^{7}	26.1
Ethylamine	3.2×10^{10}	1.4×10^{7}	24.3
n-Propylamine	3.0×10^{10}	1.2×10^{7}	24.0
n-Butylamine[a)]	$(4.1\pm0.7)\times10^{10}$	$(1.1\pm0.7)\times10^{8}$	32

a) This work

In addition, in order to confirm that the absorption mechanism is due to the perturbation of the equilibrium represented by Eq. (2), the ultrasonic absorptions at a constant concentration of *n*-butylamine were measured at various pH's. The theoretical dependences of $(\alpha\lambda)_{max}$ and f_r on pH can be calculated from Eqs. (3) and (6) respectively. In Fig. 3, the calculated variation of Γ_c with the pH is shown, together with the $(\alpha\lambda)_{max}$ obtained; the value of the equilibrium constant, $K=k_b/k_f$, in the literature[9)] was used to calculate the concentration terms in Eqs. (3) and (6) because large and serious errors usually occur in determining them from ultrasonic data. A reasonable dependence of f_r on pH was observed. This information also provides confirmation that the perturbation of the proton-transfer equilibrium is the origin of the excess absorption.

As a result, the value of the rate constant, k_f, for a diffusion-controlled reaction obtained in this study agrees very closely with the results obtained experimentally and theoretically for other compounds.[4,7,8,10,11)] The value of k_f obtained is, however, slightly different from those for other amines obtained by Eigen and his co-workers. This difference may be due to the fact that they have employed an equation, $1/\tau=2k_f\sqrt{KC_0}+k_b$, which is derived from Eq. (2) as an approximate form, where $C_0=[R\text{-}NH_2]+[R\text{-}NH_3^+]$.

9) M. C. Cox, D. H. Everett, D. A. Landsman, and R. J. Munn, *J. Chem. Soc., B*, **1968**, 1373.
10) H. Inoue, *J. Sci. Hiroshima Univ. Ser. A-II*, **34**, 17 (1970).
11) K. Applegate, L. J. Slutsky, and R. C. Parker, *J. Amer. Chem. Soc.*, **90**, 6909 (1970).

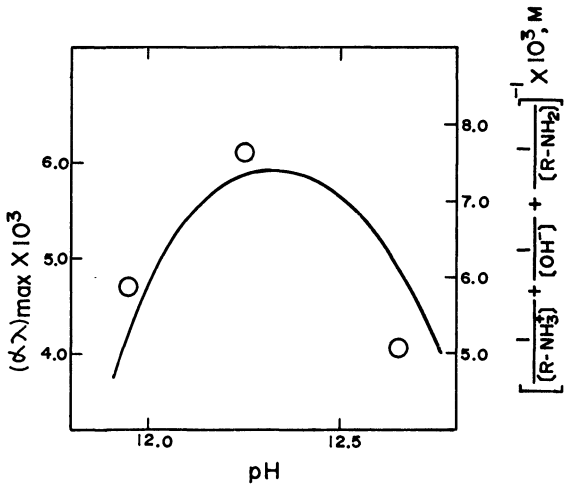

Fig. 3. The variation of $(\alpha\lambda)_{max}$ and Γ_c with pH in 0.537M *n*-butylamine. The solid line represents the predicted behavior of Γ_c. The circles are the experimental points of of $(\alpha\lambda)_{max}$.

As has been proposed by Eigen and his co-workers[8)] the recombination process of the OH^- ion with an acid in an aqueous solution might not be as simple as that described in Eq. (3). The process probably proceeds through the complex state expressed by next equations:

$$R\text{-}NH_3^+ + OH^- \underset{k_{21}}{\overset{k_{12}}{\rightleftharpoons}} R\text{-}NH_3^+ \cdots OH^- \underset{k_{23}}{\overset{k_{32}}{\rightleftharpoons}} R\text{-}NH_2 + H_2O \quad (8)$$

where the complex state is formed by the hydrogen bond. Therefore, the rate constants obtained should be given by:

$$k_f = k_{12}, \quad k_b = k_{21}\cdot\frac{k_{32}}{k_{23}} \quad (9)$$

Consequently, the value of k_f depends on the collision frequency of reactant partners, $R\text{-}NH_3^+$ and OH^-. In the case of relatively small molecules, as is shown in Table 2, the values of k_f are probably constant within the limits of experimental error.

BULLETIN OF THE CHEMICAL SOCIETY OF JAPAN, VOL. 46, 327—328 (1973)

Photochromism of *N*-3-Pyridylsydnone

Akio MITSUI* and Nozomu EBARA

Department of Chemistry, College of General Education, University of Tokyo, Komaba, Meguro-ku, Tokyo

(Received May 26, 1972)

Except for a few qualitative studies[1-4] the photochromism (PC) of *N*-3-pyridylsydnone (3PS) has been little investigated, the only mechanism proposed thus far being that of Mill *et al.*[3] who assumed the formation of a color center. However, the experiments described seem somewhat inexact and the mechanim has several drawbacks. The substance is very liable to decompose and available information is scanty. The present note attempts to contribute to the understanding of the PC of 3PS.

Radiolysis of 3PS. Mill's mechanism requires that the electron in the color center should be supplied from the molecule and leaves a $3PS^+$ cation radical. It is known that 3PS acts as an electron donor to form complexes with Cu^{2+}, Ni^{2+} or I_2.[5,6] This, however, does not necessarily mean that 3PS ionizes easily to form a cation radical. To clarify the mode of ionization of 3PS, γ-radiolysis was tried in a rigid matrix at 77°K.[7] It gave only $3PS^-$ (Fig. 1) and no cation radical was formed. This is against the color center mechanism.

Flash Photolysis of Solutions. Metz[2] has concluded from a solution experiment by steady irradiation that the PC of 3PS was restricted only to solid state. Solutions of 3PS (10^{-2} to 10^{-5} mol/l) in various solvents were subjected to flash photolysis (500 J, 5 μsec) in either the presence or absence of addenda (NaCl, KBr, O_2 or TCNE) which might affect the stability of 3PS ionic structures. In all cases no PC was observed down to the lifetime of 5 μsec. There were no effects of temperature, solvent polarity, solvent viscosity or presence of any electron acceptor. As the solution PC due to unimolecular reactions usually has a much longer lifetime under similar conditions, it is hard to regard PC of 3PS as an intramolecular process. Experiments in PVA or polystyrene also failed to show the PC.

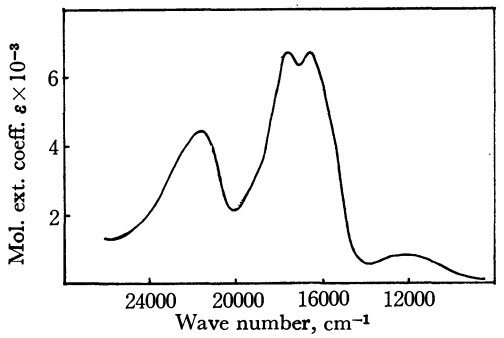

Fig. 1. Spectrum of $3PS^-$ in 2-methyltetrahydrofuran (Courtesy of Dr. T. Shida)

However, the effect of TMPD in an ethanol solution was remarkable. Although the solution showed no PC, 3PS seemed to stabilize in its stead the $TMPD^+$ radical. It was found that for a 4.0×10^{-4} mol/l TMPD solution, the presence of either 5.1×10^{-5} or 4.0×10^{-4} mol/l 3PS made 48.9 or 100%, respectively, of the recombination of $TMPD^+$ take place by way of electronated 3PS. Hence, the acceptor property of 3PS seemed to be manifest.

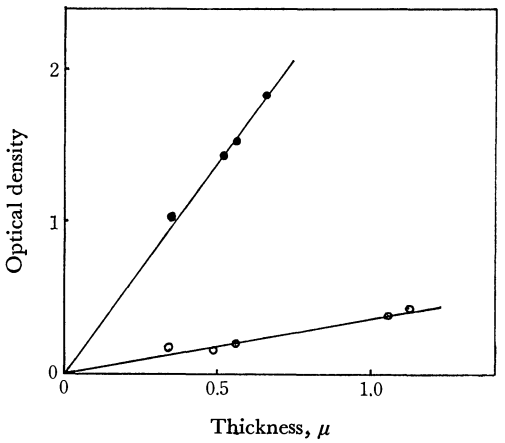

Fig. 2. Plots of OD against the thickness of the film (in μ): ○ at 605 nm, ● at 290 nm

PC in Crystal Films. Tien[1] could not decide whether the PC was confined to the surface of the crystals or it extended to within. We thus measured the maximum absorption intensity of the blue form obtained by constant irradiation of the oxygen-free evaporated crystal film. The thickness was determined from the interference pattern. The good linearity in Fig. 2 shows that the PC is distributed almost uniformly within the crystal entity. The plots were compared with those for the absorption by 3PS itself at 290 nm. Assuming tentatively that the extinction coefficient of the blue absorption was 10000 (double the value at 290 nm), the extent to which the PC took place amounted to 7.5%.

The dielectric constant of the crystal film was also measured. It did not change on irradiation until decomposition took place.

Polarization of Crystal Spectra. Spectra of two

* Present address: Fuji Photofilm Co., Ltd., Ashigara Factory, 210 Nakanuma, Minami-ashigara, Kanagawa, Japan.

1) J. M. Tien and I. M. Hunsberger, *J. Amer. Chem. Soc.*, **77**, 6604 (1955); **83**, 181 (1961).

2) F. I. Metz, W. C. Servoss, and F. E. Welsh, *J. Phys. Chem.*, **66**, 2246 (1962).

3) T. Mill, A. V. Roggen, and C. F. Wahlig, *ibid.*, **34**, 1139 (1961).

4) H. S. Gutowsky, R. L. Rutledge, and I. M. Hunsberger, *ibid.*, **29**, 1183 (1958).

5) S. M. Lee, U. S. 3549639 (1971).

6) H. Yamada and K. Kozima, *J. Amer. Chem. Soc.*, **82**, 1543 (1960).

7) We are very much indebted to Dr. T. Shida, the Institute of Physical and Chemical Research, for the experiment of γ-radiolysis.

kinds of sample film, one evaporated in a vacuum and the other precipitated from a nitromethane solution, are shown in Fig. 3. They differ considerably, which seems to be due to the preferred orientation in the crystal films rather than to polymorphism, since there is no indication of the latter. Assuming that the crystals mainly have their axes of growth (assigned later to the *b* axis) almost perpendicular to the quartz plate in an evaporated film, as is often the case, but parallel or at random in a precipitated film, the difference may be accounted for in terms of the factor group splitting. Comparison of the spectra of 3PS with the corresponding spectra of *N*-phenylsydnone (PhS), which is non-photochromic, shows that the splitting in the former is far more greater (1700 cm^{-1} compared with 750 cm^{-1} of PhS for the lowest band), and that the direction of the splitting is reversed (see arrows in Fig. 3).

The anisotropy in the blue band is astonishingly large. A single crystal was placed under a polarizing microscope and was observed visually. It was blue when the polarizer was perpendicular to the *b* axis, but pale yellow-green when the polarizer was parallel to the *ac* plane.

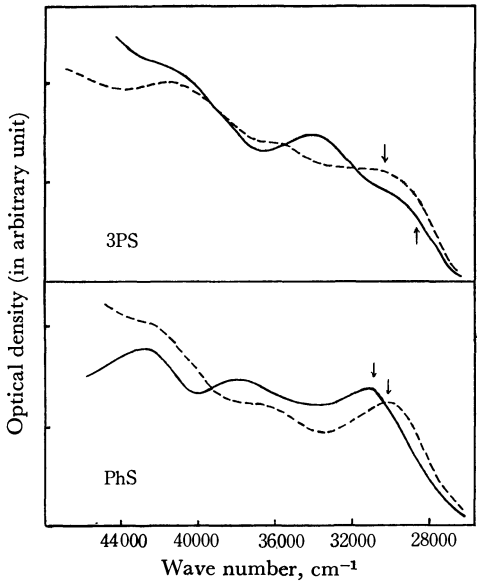

Fig. 3. Crystal spectra of 3PS and PhS.
——: evaporated film, ------: precipitated film.

Crystal Structure. In view of the large anisotropy in the crystal spectrum and the failure of observing solution PC, the crystal analysis of 3PS was carried out. The crystal of 3PS has orthorhombic structure with $a=22.9$, $b=7.0$, $c=8.6$ Å and $Z=8$. Three space groups conformed to the extinction rule, $P2_1ma$, Pm2a, and Pmma. Comparison with the crystal of PhS[8] ($P2_1/a$, $a=22.06$, $b=3.75$, $c=9.58$, $\beta=103°10'$, and $Z=4$) suggests that the space group of 3PS is possibly Pm2a (or Pmma) and that both structures do not differ greatly except that the crystal of 3PS consists of molecular layers stacked along the *b* axis, whereas in the crystal of PhS the molecules are stacked alternatively by a screw axis.

Discussion. Under suitable conditions every kind of organic PC except for that of 3PS was found to take place in solution. The absence of solution PC in 3PS suggests that it is not a unimolecular process such as ionization, isomerization or dissociation. Absence of an ESR signal in oxygen-free samples[4] shows that it does not involve radical formation. The marked polarization of the blue band in the *ac* plane suggests that the absorption is an intermolecular transition which is of CT type in nature, and that the interaction took place between the molecules in the same layer. The homoionic structure and the donor-acceptor property of sydnones seem to favor the complex formation. If this is the case, the formation of the complex may be invoked by some change in the molecular structure or in the molecular disposition in the crystal, which is induced photochemically. Metz[2] reported that the blue form was bleached by the application of e.m.f. Mill[3] observed that a surge of electric current occurred when the blue crystal was thermally bleached. Although the observations do not seem to be exact, they conform to the present mechanism.

8) G. M. J. Schmidt, *Bull. Res. Council, Israel*, **1**, 121 (1951).

BULLETIN OF THE CHEMICAL SOCIETY OF JAPAN, VOL. 46, 329—330 (1973)

The Migration of the Exciton in the Radiolysis of Alkanes

Tetsuo MIYAZAKI

Department of Synthetic Chemistry, Faculty of Engineering, Nagoya University, Chikusa-ku, Nagoya

(Received May 29, 1972)

A number of studies of the exciton migration in molecular crystals have been mostly concerned with aromatic crystals. Though the energy transfer in the γ-irradiated aromatic crystal has been interpreted in terms of the excitation transfer,[1] the possibility of the excitation transfer in the solid alkane has been ignored in radiation chemistry; only the energy transfer *via* an ionic process, such as a charge transfer, an ion-molecular reaction, or an electron capture, has been emphasized. Recently, however, Miyazaki *et al.* have found phenomena which suggest the migration of the exciton in the radiolysis of isobutane,[2] neopentane,[3] and 2,3-dimethylbutane.[4]

The theoretical treatment of the migration of the exciton in the alkanes has not been undertaken previously. In order to obtain some information on whether or not the electronic excitation transfer is possible in solid alkane, the theoretical treatment of irradiated aromatic materials[5] will be applied here to alkanes.

In order to occur at all, excitation transfer requires some interaction between excited and unexcited molecules. The interaction energy (u) can be approximated as the interaction between the transition dipoles of molecules. Since the transition dipoles can be represented by the experimentally-available oscillator strength (f), the interaction energy is given by:

$$u = -3f(ea_0)^2 \frac{R}{\Delta E} \frac{\Omega}{r} \qquad (1)$$

where a_0 is the first Bohr radius; R, the Rydberg energy; ΔE, the excitation energy; Ω, the geometric factor, depending upon the orientation of the transition dipole moments, and r, the distance between nearest neighboring molecules.

The oscillator strengths (f) of isobutane, neopentane, and 2,3-dimethylbutane were obtained by the integration of the absorption spectra;[6] they are shown in Table 1. The distances (r) between adjacent molecules of isobutane, neopentane, and 2,3-dimethylbutane were obtained from the densities at 77K; they are 5.3, 6.7, and 6.7 Å respectively. As for the geometric factor of transition dipole moments (Ω), the optimum condition is here considered to be that in which the transition dipoles are directed along the line joining the molecular centers. In this case, $\Omega=2$. The interaction energies calculated from Eq. (1) are shown in Table 1.

One can estimate roughly the migration distance of the exciton from the interaction energy by means of the following equation:[7]

$$u \simeq \frac{h\Delta n}{t}$$

where h denotes Planck's constant and Δn, the number of molecules through which the exciton migrates during its lifetime (t). The calculated distances of the exciton migration are shown in Table 1.

The interaction energies of isobutane, neopentane, and 2,3-dimethylbutane range from 0.01 to 0.1 eV (Table 1). These values are not small as compared with those of benzene calculated by Voltz.[5]

TABLE 1. CALCULATED VALUES OF THE TRANSITION DIPOLE-DIPOLE INTERACTION ENERGIES AND THE DISTANCES OF EXCITON MIGRATION IN IRRADIATED ALKANES

Compound	Excitation energy ΔE eV	Oscillator strength f	Interaction energy u, eV	Distance corresponding to different lifetimes, Δn[a]	
				10^{-8}—10^{-9} sec	10^{-11}—10^{-13} sec
Isobutane	(1st) 7.7	0.03			
	8.7	0.37	0.094	2.3×10^4—2.3×10^4	230—2
	9.4	0.13	0.031	7.5×10^4—7.5×10^3	75—1
Neopentane	(1st) 7.9	0.14	0.019	4.6×10^4—4.6×10^3	46—0
	8.4	0.04			
	9.0	0.47	0.075	1.4×10^4—1.4×10^3	140—1
2,3-Dimethylbutane	(1st) 7.9	0.08	0.011	2.7×10^4—2.7×10^3	27—0
	8.2	0.03			
	8.8	0.45	0.056	1.4×10^5—1.4×10^4	140—1

a) Unit is the number of molecules through which exciton migrates.

1) F. S. Dainton, I. Kosa-Somogyui, and G. A. Salmon, *Trans. Faraday Soc.*, **61**, 871 (1965).

2) a) T. Wakayama, T. Kimura, T. Miyazaki, K. Fueki, and Z. Kuri, This Bulletin, **43**, 1017 (1970). b) T. Miyazaki, T. Yamada, T. Wakayama, K. Fueki, and Z. Kuri, *ibid.*, **44**, 934 (1971).

3) T. Miyazaki, T. Wakayama, M. Fukaya, Y. Saitake, and Z. Kuri, 14th Japanese Conference of Radiation Chemistry, Sept. 1971, Sapporo, Japan; This Bulletin, in press.

4) T. Miyazaki, Y. Saitake, Z. Kuri, and S. Sakai, This Bulletin, **46**, 70 (1973).

5) R. Voltz, *Radiations Res. Rev.*, **1**, 301 (1968).

6) J. W. Raymonda and W. Simpson, *J. Chem. Phys.*, **47**, 430 (1967).

7) J. B. Birks, "Photophysics of Aromatic Molecules," John Wiley and Sons Ltd., (1970), p. 531.

8) F. Hirayama and S. Lipsky, *J. Chem. Phys.*, **51**, 3616 (1969).

Table 2. Experimental values of distances of exciton migration in irradiated alkanes

Host	Guest	Distance of exciton migration, Δn[a]	Reference
Isobutane	Carbontetrachloride	7	2), 3)
Isobutane	Propane	8	2), 3)
Neopentane	Cyclopentane	40	3), b)
Neopentane	Cyclohexane	85	3), b)
2,3-Dimethylbutane	Toluene	1.3×10^3	4)

a) Unit is the number of molecules through which exciton migrates.
b) M. Kato, T. Miyazaki, Y. Saitake, and Z. Kuri, to be presented at the 15th Japanese Conference of Radiation Chemistry, Oct. 1972, Osaka, Japan.

From the measurements of the fluorescence of liquid alkanes, the lifetimes of the lowest singlet-excited states were obtained: *n*-hexane (2×10^{-9} sec), cyclohexane (7×10^{-9} sec), *etc.*[8] Therefore, the lifetimes of the lowest singlet-excited state of neopentane and 2,3-dimethylbutane are probably 10^{-8}—10^{-9} sec. It is expected from the calculated values shown in Table 1 that the excitons of these alkanes in the lowest excited states can migrate through 10^4—10^3 molecules during their lifetimes. It is interesting to note that the distance obtained experimentally by the measurements of luminescence from solid 2,3-dimethylbutane containing toluene lies in the range expected from this calculation (Table 2).

In the solid-radiolysis of isobutane or neopentane containing other alkanes, it was suggested that the excitation transfer may occur *via* highly excited states.[3] Since the internal conversion from the highly excited states occurs very fast, the lifetime of the highly excited state may be extremely small as compared with that of the lowest singlet-excited state. An exact estimation of the lifetime of the highly excited state is currently impossible; from indirect theoretical and experimental evidence, however, it may be expected to lie between 10^{-11}—10^{-13} sec.[5,9] The calculated results in Table 1 show that the excitons in the highly-excited states of isobutane and neopentane migrate through 200—1 molecules during their lifetimes. It is interesting to note that the distances obtained experimentally in the radiolysis of isobutane and neopentane are 7—8 and 40—85 molecules respectively, which lie in the range expected from this calculation.

The author wishes to express his appreciation to Professor Noriaki Ito and Dr. Kenji Fueki of Nagoya University for their fruitful discussions and to Professor Zen-ichiro Kuri of Nagoya University for his encouragement.

9) C. L. Braun, S. Kato, and S. Lipsky, *J. Chem. Phys.*, **39**, 1645 (1963).

BULLETIN OF THE CHEMICAL SOCIETY OF JAPAN, VOL. 46, 331—332 (1973)

The d→d Absorption Spectra of Potassium Tris(8-quinolinolato)-nickelate(II) in Methanol-Chloroform Mixtures

Yoshinori YAMAMOTO

Department of Industrial Chemistry, Faculty of Engineering, Ibaraki University, Hitachi

(Received July 4, 1972)

The d→d absorption spectra of $K[NiQ_3]\cdot EtOH$,[1] which was prepared in our laboratory, in MeOH–$CHCl_3$ mixtures have been observed to vary greatly with the change in the ratio of the volume of $CHCl_3$ to that of MeOH. Such a large change in the spectrum cannot be attributed to normal solvent effects, in view of the fact that the absorption spectra of $Al(III)Q_3$ or $Fe(III)Q_3$ in various pure and mixed solvents are practically the same.[2]

In the present study, this spectral change was examined with the intention of exploring the basis for this change.

Results and Discussion

The spectra of $K[NiQ_3]\cdot EtOH$ in MeOH and MeOH–$CHCl_3$ mixtures are shown in Fig. 1.[3] The presence of the isosbestic points in Fig. 1 indicates that two species coexist at equilibrium and that normal solvent effects are negligibly small. The plot of the absorbance at 950 nm *vs.* the vol% of $CHCl_3$ shown in Fig. 2 indicates that the complex exists predominantly in one form (Species A) in MeOH, and in another form (B) in 80 vol% or more of $CHCl_3$. The absorption data summarized in Table 1, compared[4] with

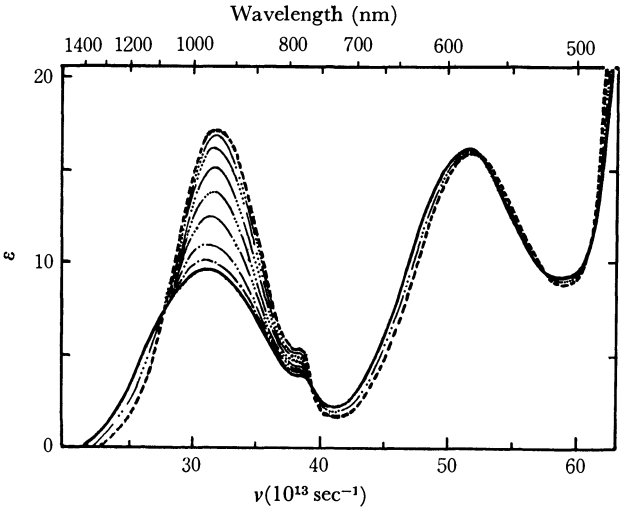

Fig. 1. Absorption spectra of $K[NiQ_3]\cdot EtOH$ in MeOH–$CHCl_3$ mixture. Concentration of the complex, $1.21_8\times 10^{-2}$M. Vol% of $CHCl_3$: ——, 0; —·—, 10; —··—, 20; —···—, 30; —····—, 40; —·····—, 50; —·····—, 60; —·····—, 70; ————, 80%.

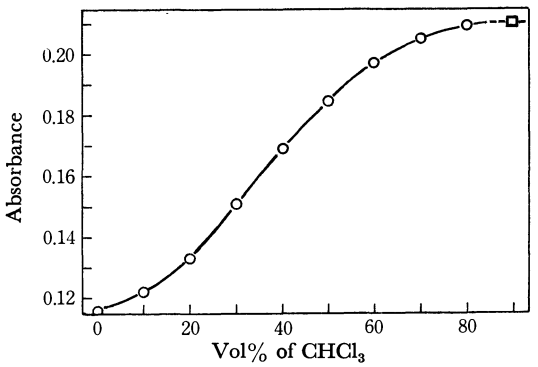

Fig. 2. Variation of absorbance at 950 nm with vol% of $CHCl_3$. Concentrations of the complex: ○: $1.21_8\times 10^{-2}$M (a 1 cm cell was used), □: 6.09×10^{-3}M (a 2 cm cell was used).

that[5] of $K[Ni(gly)_3]$, suggest that both species, A and B, are six-coordinated (3 O and 3 N atoms of three 8-quinolinolate ligands) complexes.

As is shown in Table 1, with the change from A to B the second band shows little change in either intensity or the position, while the first band shows a small blue shift and a significant increase in intensity. This trend of the spectral change shows a striking resemblance to that of the spectral changes attended by the steric changes from the *mer*-$[Co(O,N)_3]$ complexes to the *fac* isomers, which are described in the literature.[6] In DMSO the configuration of MQ_3, where M is Al(III), Co(III), or Rh(III), has been reported by Baker and Sawyer to be a *mer* structure.[7] The same configuration can be expected for the NiQ_3^- ion in MeOH. These facts suggest that the A species has a *mer* structure and that, accordingly, B has a *fac* structure.

The conversion to the *fac* form from the *mer* form may be explained in terms of the ion-pair formation. It is well known that, in the $[Co(en)_2Cl_2]^+$ system, in various dipolar solvents the ratio of the concentration of the *cis* and *trans* ions varies with the chloride-ion concentration, since the dipolar *cis* ion is stabilized by the ion-pair formation.[8] The *fac*-NiQ_3^-, whose three

1) In this paper, Q^- represents 8-quinolinol anion.

2) F. G. Zharovskii and V. L. Ryzhenko, *Vis. Kiiv. Univ., Ser. Fiz. Khim.*, **1968**, 56, 62; *Chem. Abstr.*, **71**, 107223t (1969); *ibid.*, **72**, 138055q (1970).

3) Potassium salts or certain solvents instead of $CHCl_3$ showed the same effect. See experimental section.

4) Matsuoka *et al.* drew the conclusion from the study of CoQ_3 and CrQ_3 that the position of 8-quinolinolate ligand in the spectrochemical series is almost same as that of glycinate ligand. (N. Matsuoka, Y. Shimura, and R. Tsuchida, *Nippon Kagaku Zasshi*, **82**, 1637 (1961).)

5) J. Hidaka and Y. Shimura, This Bulletin, **43**, 2999 (1970). (gly) represents glycinate ligand.

6) Data for glycinate, *dl*-alaninate and picolinic acidate ligands as (O, N) are available. J. Fujita and Y. Shimura, This Bulletin **36**, 1281 (1963).

7) B. C. Baker and D. T. Sawyer, *Anal. Chem.*, **40**, 1945 (1968).

8) W. R. Fitzgerald and D. W. Watts, *J. Amer. Chem. Soc.*, **89**, 821 (1967), and references therein.

Table 1. The d→d absorption data[a] of solutions of $K[NiQ_3]\cdot EtOH$ and $K[Ni(gly)_3]$

Complex	Solvent	Band I ν_{max} (log ε_{max})	Singlet Band ν_{max} (log ε_{max})	Band II ν_{max} (log ε_{max})	Band III ν_{max} (log ε_{max})	Ref.
$K[Ni(gly)_3]$	H_2O	30.5 (1.01)	39.7 (0.35)	50.2 (0.95)	83.0 (1.18)	5)
$K[NiQ_3]\cdot EtOH$	MeOH	30.9 (0.98)	38.5^{sh} (0.61)	51.5 (1.21)	b)	c)
	MeOH–$CHCl_3$ (20: 80 vol%)	31.9 (1.24)	38.5^{sh} (0.73)	51.9 (1.20)	b)	c)

a) The frequencies are given in 10^{13} sec^{-1}.
b) The third bands could not be observed owing to overlapping of the π–π^* transition bands.
c) This work.

anionic O atoms are concentrated around the c_3 axis, is expected to have a larger net dipole moment than the *mer* ion, and the formation of the ion pair K^+, NiQ_3^- in MeOH–$CHCl_3$ mixtures with dielectric constants lower than that of MeOH may not be negligible.

Experimental

Reagents and Solvents. All the chemicals used were of a guaranteed reagent quality. The solvents were from freshly-opened bottles of a G. R. quality.[9]

Preparation of Potassium Tris(8-quinolinolato)nickelate(II) Monoethanolate, $K[Ni(C_9H_6ON)_3]\cdot(C_2H_6O)$. A 10.0 g portion of KOH(86%) was suspended (almost dissolved) in 70 ml of EtOH, and the supernatant solution was added to 70 ml of EtOH containing 12.0 g of 8-quinolinol (0.083 mol),[10] after which the mixture was filtered out through a filter paper. To this filtrate, warmed about 70°C, a hot solution of 4.0 g of nickel(II) acetate tetrahydrate (0.016 mol) in 100 ml of EtOH was slowly added without stirring; the resultant clear, deep green, mixed solution was allowed to stand for two days. The fine, deep green crystals obtained were washed with EtOH several times, and dried at room temperature *in vacuo*. The yield, based on the nickel acetate, was 90% (8.3 g).

Found: C, 59.64; H, 4.06; N, 7.39; Q^-, 74.7%. Calcd: C, 60.44; H, 4.20; N, 7.29; Q^-, 75.0%.

The solvent of crystallization (EtOH) was released by heating at 175°C for 6 hr: the complex decomposed slightly. (Found: 8.07%. Calcd: 7.99%).

The complex was recrystallized from MeOH by adding ethanolic KOH, but it was sufficiently pure without recrystallization.

Measurement of Absorption Spectra. A 5.00 ml volume of the $6.09_1\times10^{-2}$M $K[NiQ_3]\cdot EtOH$ methanolic solution and an appropriate volume of $CHCl_3$ were placed in each of a series of 25 ml volumetric flasks, and then each solution was diluted to the mark with MeOH. Each reference solution, containing all the components except the complex, was prepared in a similar manner. After one hour's standing after the initial mixing, each solution was placed in a 1 cm quartz cell and its components determined by means of a Shimadzu MPS-50L spectrophotometer, the transmittance being read at room temperature. No spectral change with time was observed after one day's standing.

Other Systems. In a manner similar to that in the case of $CHCl_3$, the spectra of $K[NiQ_3]\cdot EtOH$–MeOH–S systems, where S is benzene, dioxane, diethyl ether, acetone, EtOH, KBr, KI, CH_3COOK, KOH, NaOH, *etc.*, were examined. In all cases, the shape of the maximum near 950 nm varied from a rounded hump for the complex–MeOH system to a sharp peak in the presence of S. In the present study, $CHCl_3$ as S was chosen for its greater ability to vary the spectra and for the higher solubility of the complex in this system, though the complex is scarcely soluble in pure $CHCl_3$.

The spectra of the complex–MeOH–KOH system are shown in Fig. 3.

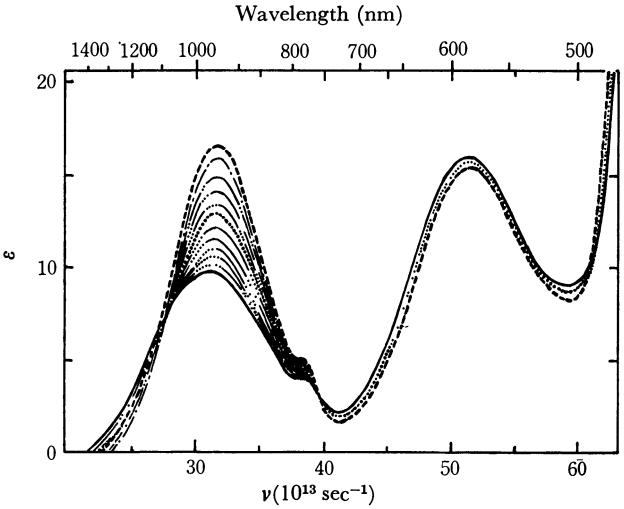

Fig. 3. Absorption spectra of $K[NiQ_3]\cdot EtOH$ in MeOH containing varying amounts of KOH. Concentration of the complex, $1.21_8\times10^{-2}$M. Concentrations of KOH: ——, 0; —·····—, 1.84×10^{-2}; —·····—, 3.68×10^{-2}; —·····—, 9.20×10^{-2}; —·····—, 1.47×10^{-1}; —·····——, 2.30×10^{-1}; ·····3.68×10^{-1}; —···—, 5.52×10^{-1}; —···—, 9.20×10^{-1}; —··—, 1.47; —·—, 2.30; ------, 3.68M.

The author is indebted to Professor Shinsuke Takei of Ibaraki University for his useful suggestions and encouragement.

9) $KNiQ_3$ in the commercially obtained dehydrated MeOH gave an identical spectrum with that of G. R. MeOH solution.
10) Experimentally, excess KOH and HQ gave fine crystals.

BULLETIN OF THE CHEMICAL SOCIETY OF JAPAN, VOL. 46, 333—334 (1973)

The Reductive Coupling Reactions of Some Chloromethylbenzene Derivatives with Iron(II) Complexes. II. Reduction by Anhydrous Iron(II) Chloride and Lithium Chloroferrate(II)

Kazuhiko ONUMA, Junzo YAMASHITA,* and Harukichi HASHIMOTO*

Department of Synthetic Chemistry, The University of Tokyo, Bunkyo-ku, Tokyo
**Department of Applied Chemistry, Faculty of Engineering, Tohoku University, Sendai*

(Received March 7, 1972)

Previously we reported[1] that ferrous chloride tetrahydrate reduces polyhalomethylbenzene derivatives to give coupling products.[2] Though some chelating ligands such as ethylenediamine can increase the yield of coupling products considerably,[1] hydrolysis by the water of crystallization or solvolysis by the ethanol solvent of the organic halides is unavoidable in these reactions, and this limits, in some cases, the synthetic usefulness of this reaction.[1,2]

To inhibit the side reactions, therefore, we prepared anhydrous ferrous chloride and lithium chloroferrate(II)—$LiFe^{II}Cl_3$—in acetonitrile as will be described in the Experimental Section[3] and investigated the reaction with organic halides.

TABLE 1. REDUCTIVE COUPLING OF BENZOTRICHLORIDE BY FERROUS CHLORIDE AND LITHIUM CHLOROFERRATE(II) IN ACETONITRILE

$FeCl_2$: 1.0×10^{-2} mol, $LiFeCl_3$: 2.0×10^{-2} mol, CH_3CN: 60 ml

Fe(II)	$PhCCl_3$: Fe	Temp. °C	Time hr	Product[a] (%) $PhCCl_2$-CCl_2Ph	Product[a] (%) $PhCCl$=$CClPh$
$FeCl_2$	1:1	80	5	51	—
	1:2	80	5	77	—
$LiFeCl_3$	1:1	50	5	74	—
	1:2	80	4	—	87[b]

a) Yield based on $PhCCl_3$ used.
b) Isomer ratio is *trans*: *cis*=33: 67.

TABLE 2. REDUCTIVE COUPLING OF DIPHENYLDICHLOROMETHANE BY FERROUS SALTS

$FeCl_2$: 1.0×10^{-2} mol, $LiFeCl_3$: 2.0×10^{-2} mol, CH_3CN: 60 ml

Fe(II)	Ph_2CCl_2: Fe	temp. °C	time hr	Product[a] (%) Ph_2CCl-$CClPh_2$	Product[a] (%) Ph_2C=CPh_2
$FeCl_2$	1:1	20	22	51[b]	—
	1:2	80	5	—	64[b]
$LiFeCl_3$	1:2	80	4	—	93

a) Yield based on Ph_2CCl_2 used.
b) Benzophenone and unreacted diphenyldichloromethane were recovered. The former is the product by hydrolysis of the latter during the after-treatment of the reaction mixture.

TABLE 3. REDUCTIVE COUPLING OF BENZAL CHLORIDE BY FERROUS SALTS

$FeCl_2$: 1.0×10^{-2} mol, $LiFeCl_3$: 2.0×10^{-2} mol, CH_3CN: 60 ml

Fe(II)	$PhCHCl_2$: Fe	Temp. °C	Time hr	product[a] (%) PhCHCl-CHClPh	product[a] (%) *trans*-PhCH=CHPh
$FeCl_2$	1:1	80	4	3[b]	6[c]
	1:2	80	24	—	28[c]
$LiFeCl_3$	1:1	30	24	5[b]	6[c]
	1:2	80	7	—	81

a) Yield based on $PhCHCl_2$ used.
b) *meso*-Isomer.
c) Benzaldehyde and unreacted benzal chloride were recovered. See the footnote b) in Table 2.

The results are tabulated in Tables 1—3. We wish to point out that reductive coupling products are obtainable in good yields without any competing side reactions. The use of the anhydrous salt is evidently superior to the use of the tetrahydrate; in the latter case, some additives are needed for good results.[1] In addition, anhydrous lithium chloroferrate(II) has been revealed to be the more powerful reductant. Thus, tolan tetrachloride is obtained from benzotrichloride by $FeCl_2$, but if $LiFeCl_3$ is employed (Fe(II)/$PhCCl_3\geq2$), benzotrichloride is further reduced to tolan dichloride, with a shorter reaction time than the $FeCl_2\cdot4H_2O$–DMSO system.[2]

Tetraphenylethylene is generally attained from diphenyldichloromethane by the use of ferrous salt under ordinary conditions (Table 2), and tetraphenyldichloroethane has been thought to be formed only intermediately. Reaction at a low temperature with $FeCl_2$, however, gave tetraphenyldichloroethane in a considerable yield.[4] Thus, it is seen that the highly selective reductive coupling of benzotrichloride and of diphenyldichloromethane is possible by the use of $FeCl_2$ or $LiFeCl_3$ in acetonitrile.

As may be seen in Table 3, the attempt to obtain stilbene dichloride from benzal chloride in a good yield failed (only 3% by $FeCl_2$ and 5% by $LiFeCl_3$). However, *trans*-stilbene was obtained in a high yield by employing $LiFeCl_3$ as the reductant. It should be

1) K. Onuma, J. Yamashita, and H. Hashimoto, This Bulletin, **43**, 836 (1970).
2) Similar results were reported in T. Shirafuji, Y. Yamamoto, and H. Nozaki, *ibid.*, **44**, 1994 (1971).
3) M. Asscher and D. Vofsi, *J. Chem. Soc., B*, **1968**, 947.
4) This attempt failed in previous studies because of the hydrolysis of the organic halide by the water of crystallization in $FeCl_2\cdot4H_2O$. The $FeCl_2\cdot4H_2O$–DMSO system gave also tetraphenyldichloroethane in a good yield at a low temperature with a smaller $FeCl_2\cdot4H_2O/Ph_2CCl_2$ mole ratio.[2]

noted that the $FeCl_2 \cdot 4H_2O$–CH_3CN[1] or –DMSO system[2] failed to obtain *trans*-stilbene from benzal chloride. All these reductions are thought to proceed step by step as follows;

$$Ph(R)CCl_2 \xrightarrow{2Fe(II)} Ph(R)CCl\text{–}CCl(R)Ph \xrightarrow{2Fe(II)} Ph(R)C{=}C(R)Ph$$

(R=Ph, Cl, H)

The reduction of benzyl chloride by $LiFeCl_3$ was also attempted, but only 4% of bibenzyl resulted. Benzyl bromide was converted to benzyl chloride under the same conditions.

As may be seen, the reactivity of lithium chloroferrate(II) is obviously superior to that of ferrous chloride. This may be partly due to the fact that $FeCl_4^-$ ion is very stable in acetonitrile.[5]

Experimental

Materials. The anhydrous ferric chloride and iron powder were used directly. The benzotrichloride, benzal chloride, benzyl chloride, and diphenyldichloromethane were distilled under reduced pressure and then used. The purification of acetonitrile was done in the following manner: it was distilled first from potassium permanganate and sodium carbonate, second from phosphorous pentoxide, and at last carefully under nitrogen from calcium hydride after reflux. The lithium chloride was dehydrated *in vacuo* at 150°C for several days.

Preparation of the Ferrous Solution. To a solution of anhydrous ferric chloride (2.6 g) and, if necessary, lithium chloride (1.02 g) in acetonitrile (70 ml), iron powder (1.8 g) was added under an atmosphere of nitrogen according to the Asscher and Vofsi method.[3] After standing for several hours, the solution was filtered and introduced into the reaction vessel. The concentration of the solution was determined by ceric titration just before the reaction. The concentration of chloride ions in the lithium chloroferrate solution was determined by Volhard's method. The $FeCl_2$ solution is almost colorless or slightly yellow, and the $LiFeCl_3$ solution is faintly violet. As these iron salts are very sensitive to air, they should be treated carefully in a nitrogen atmosphere.

Reaction Procedure. In a four-necked, 100 ml flask equipped with a nitrogen inlet, a thermometer, a magnetic stirrer, and a condenser, a 60 ml portion of a ferrous solution was introduced ($FeCl_2 = 1 \times 10^{-2}$: $LiFeCl_3 = 2 \times 10^{-2}$ mol/l): the reaction was then initiated by adding organic halide at the required temperature under nitrogen. After the completion to the reaction, 150 ml of water was poured in and then extracted with benzene. The benzene solution was then condensed, and the coupling products were isolated. The resinous by-products were removed through column chromatography (300 mesh alumina). All the products were recrystallized and identified by mp, IR NMR, and elemental analysis.[1]

Mixture of *cis*- and *trans*-tolan dichloride were separated by means of the difference in their solubility to alcohol, and the separated isomers were again recrystallized from alcohol. The melting point of the *trans* isomer is 145.0—146.0°C, while that of the *cis* isomer is 59.0—62.0°C. The melting point of tetraphenyldichloroethane is 161—167°C.

5) B. J. Hathaway and D. G. Holah, *J. Chem. Soc.*, **1964**, 2408.

BULLETIN OF THE CHEMICAL SOCIETY OF JAPAN, VOL. 46, 335—336 (1973)

A Fluorescence Study of a β-Structural 1-Dimethylamino-naphthalene-5-sulfonyl Poly-L-lysine Conjugate

Takayoshi Iio

Department of Physics, Faculty of Science, Nagoya University, Chikusa-ku, Nagoya

(Received May 31, 1972)

An α-helical poly-L-lysine (PLy) is irreversibly transformed in its conformation to a β-structure when the temperature of the solution is raised to 50°C.[1] It is agreed that the β-structure is stabilized by the hydrophobic bond between the side chains in addition to the hydrogen bond between the main-chain peptide groups. The intensity of the observed emission light of the 1-dimethylaminonaphthalene-5-sulfonate (DNS) bound to PLy is increased as the conformation of the DNS–PLy conjugate is changed from the α-helix to the β-structure (Fig. 1). On the other hand, the optical

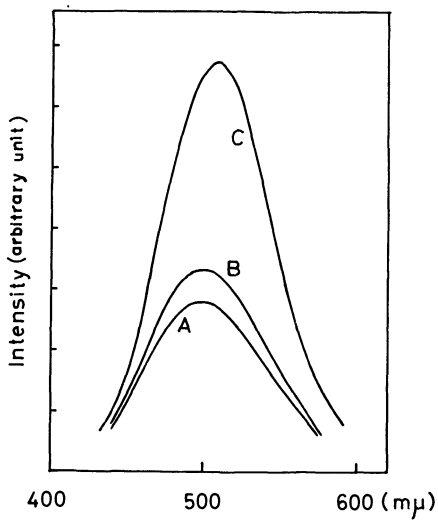

Fig. 1. Observed emission spectra of DNS-PLy conjugate in 0.01N KCl solutions at 20°C. Wavelength of excitation light was 350 mμ. A: Random coil (pH 5.8), B: α-Helix (pH 12.4), C: β-Structure (after heating the α-helical solution at 50°C for 30 min, then cooled to 20°C).

density of the conjugate at the wavelength of the excitation light scarcely changes during the conformational transition. The increase in the relative fluorescence intensity in the β-structural conjugate may be a reflection of the change in the environment around the DNS group. The DNS group may come in contact with the solvent molecules in the case of the α-helix; on the other hand, it may be incorporated in the hydrophobic region and surrounded by the hydrophobic residues when the conjugate takes the β-structure. As a support to this conclusion, we can offer the fact that the quantum yield of DNS is increased from 0.29 to 0.71 when the solvent is changed from water to *n*-butanol at 20°C.[2]

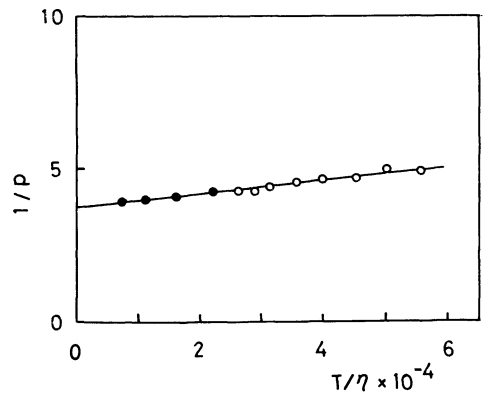

Fig. 2. Depolarization curve of β-structural DNS-PLy conjugate in 0.01N KCl (open circles) and in mixture of water and glycerine containing 0.01N KCl at 20°C (filled circles). Wavelength of excitation light and that of emission light were 350 mμ and 500 mμ, respectively.

We desire to obtain information on the rotational motion of the DNS group which is incorporated into the hydrophobic region. This information can be obtained from the depolarization curve[3,4] of the β-structural conjugate (Fig. 2). The isothermal plot (filled circle) and the heating plot (open circle) give the same straight line. From this plot, we can obtain the rotational relaxation time (ρ_h) at a particular temperature (T) of the DNS group bound to the β-structural PLy according to Eq. (1);

$$\rho_h = \left(\frac{1}{p_0} - \frac{1}{3}\right) \cdot \frac{3\tau}{\text{the slope}} \cdot \left(\frac{\eta}{T}\right)_T \qquad (1)$$

where p_0 is an intrinsic polarization, τ is the lifetime of the lowest excited state of the DNS group, and η is the viscosity of the solvent. The τ value is proportional to the relative fluorescence intensity,[5] so the τ value is obtained according to Eq. (2);

$$\tau_\beta = \tau_{coil} \cdot \frac{F_\beta}{F_{coil}} \cdot \frac{OD_{coil}}{OD_\beta} \qquad (2)$$

where F is the fluorescence intensity and OD is the optical density of the conjugate at the wavelength of the excitation light. The magnitude of F is calculated as follows: the corrected emission spectra which is obtained by calibrating the observed emission spectra (Fig. 1) for the detector system is plotted on graph paper, and the magnitude of F is determined by calculating the area beneath the curve. As the τ_{coil} value, we adopt 1.2×10^{-8} sec, this value is an average

1) B. Davidson and G.D. Fasman, *Biochemistry*, **6**, 1616, (1967).
2) E. J. Bowen and D. Seaman, "Luminescence in Organic and Inorganic Materials," ed. by H. Kallmann and G. Spruch, John Wiley, New York (1962), p. 153.
3) F. Perrin, *J. Phys. Radium.*, **7**, 390 (1926).
4) G. Weber, *Adv. Protein Chem.*, **8**, 415 (1953).
5) J. R. Laurence, "Physical Methods in Macromolecular Chemistry," ed. by B. Carroll, Marcel Dekker, New York (1969), p. 275.

of the measurements of three different DNS-protein conjugates in the neutral pH region.[6] The τ value for the β-structural conjugate is determined as 2.7×10^{-8} sec. Then we obtained $\rho_h=38.2\times10^{-8}$ sec for the β-structural conjugate at 20°C; this value is larger than that of the conjugate in the other conformations (see Ref. 7). The large value of ρ_h means that the rotational motion of the DNS group in the β-structural conjugate is extremely suppressed. The value of $\rho_h=38.2\times10^{-8}$ sec corresponds to the rotational relaxation time of a sphere with a radius of 50 Å, showing that the DNS group is incorporated in a very large β-structural region.

In the course of this experiment, we found a very interesting fact: the $1/p$ value of the β-structural conjugate do not depend on the wavelength of the excitation light (λ^{ex}). On the contrary, the $1/p$ values of the conjugate in the other conformations depend on the λ^{ex} value (Fig. 3). The DNS-protein conjugates show the same $1/p-\lambda^{ex}$ relationship as do the α-helical and random coiled conjugates.[8] The reason for these results is unknown at this stage; we wish to leave it for future investigation.

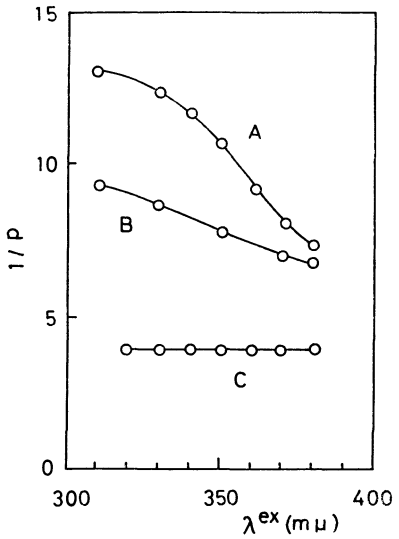

Fig. 3. Effect of wavelength of excitation light (λ^{ex}) on degree of polarization (p) of 500 mμ emission light in DNS-PLy conjugate. Measurements were performed in 0.01N KCl at 20°C. Slit width for excitation light was 6 mμ. Marks are the same as Fig. 1.

Experimental

DNS-Cl was bound to PLy (molecular weight, 30000) according to the method reported by Weber.[9] The molar ratio of the bound DNS to the L-lysyl residue was 1:48.5. All the fluorescence measurements were performed in a concentration of 3.5×10^{-6} mmol of DNS per ml. The fluorescence spectra and polarization of fluorescence were measured with a grating-type Hitachi Fluorescence Spectrophotometer MPF-2A. The degree of polarization (p) was calculated according to Eq. (3):

$$P=\frac{I_{vv}-GI_{hv}}{I_{vv}+GI_{hv}} \tag{3}$$

where I_{vv} and I_{hv} are, respectively the fluorescence intensity of vertically-polarized light and that of horizontally-polarized light when the solution is excited with vertically-polarized light, and where $G=I_{vh}/I_{hh}$ is a correction factor which is needed when the P value is measured using a grating-type fluorometer; here I_{vh} and I_{hh} are, respectively the fluorescence intensity of vertically-polarized light and that of horizontally-polarized light when the solution is excited with horizontally-polarized light. The depolarization curve was obtained by plotting the reciprocal of the polarization of the fluorescence ($1/p$) as a function of the temperature divided by viscosity (T/η in degree·poise^{-1}).

The author wishes to express very many thanks to Dr. K. Mihashi, and Dr. Y. Kawasaki (Nagoya University) and to Dr. S. Takahashi (Kyoto University) for their encouragement and discussions.

6) R. F. Steiner and A. J. McAlister, *J. Polym. Sci.*, **24**, 105, (1957).

7) T. Iio, Y. Iwashita, and H. Watanabe, This Bulletin, **45**, 2206 (1972).

8) J. K. Weltman and G. M. Edelman, *Biochemistry*, **6**, 1437 (1967).

9) G. Weber, *Biochem. J.*, **51**, 155 (1952).

10) R. F. Chen, H. Edelhoch, and R. F. Steiner, "Physical Principles and Techniques of Protein Chemistry," Part A, ed. by S. J. Leach, Academic Press, New York (1969), p. 171.

BULLETIN OF THE CHEMICAL SOCIETY OF JAPAN, VOL. 46, 337—338 (1973)

The Synthetic Reactions of Aliphatic Nitro Compounds. VII.[1] The Synthesis of α-Amino Acids from the Nitroacetic Ester[2]

Eisuke KAJI and Shonosuke ZEN

School of Pharmaceutical Sciences, Kitasato University, Shirokane, Minato-ku, Tokyo

(Received February 14, 1972)

As a short communication,[3] we previously reported the synthesis of DL-aspartic acid and DL-glutamic acid *via* the *C*-alkylation of nitroacetate[4] with halo esters. In this investigation, several neutral and basic amino acids were prepared by the same procedure.

Method (i), $R^1X + NaO_2N{=}CHCO_2Me$

Method (ii), $R^1X + O_2NCH_2CO_2Me + CHO_3Na$

$\xrightarrow{-NaX}$ $R^1{\cdot}CHR^2CO_2R^3$ **1**: $R^2{=}NO_2$; $R^3{=}CH_3$ **2**: $R^2{=}NH_2$; $R^3{=}CH_3$ **3**: $R^2{=}NH_2$; $R^3{=}H$

Chart 1.

This procedure is carried out by the reaction of the halides either with the sodium salt of nitroacetate (Method i) or with nitroacetate and sodium methylate (Method ii) in dipolar aprotic solvents, as is shown in Chart 1. When methyl bromoacetate, methyl β-bromopropionate, methyl iodide, isopropyl iodide, benzyl bromide, *N*-(β-iodoethyl)-phthalimide, *N*-(γ-iodopropyl)-phthalimide, and *N*-(δ-iodobutyl)-phthalimide were used as the halogeno compounds in the above reaction, dimethyl nitrosuccinate[3] (**1a**), dimethyl α-nitroglutarate[3] (**1b**), methyl α-nitropropionate[2] (**1c**), methyl α-nitroisovalerate[2,11] (**1d**), methyl α-nitro-β-phenylpropionate[2] (**1e**), methyl α-nitro-γ-phthalimidobutyrate (**1f**), methyl α-nitro-δ-phthalimidovalerate (**1g**), and methyl α-nitro-ε-phthalimidocaproate (**1h**) respectively resulted as the corresponding *C*-alkylated products. They could be obtained as crystalline diethylammonium or ammonium salts.

Furthermore, by the catalytic hydrogenation of the nitroesters (**1**) and the subsequent hydrolysis of the corresponding amino esters (**2**), DL-aspartic acid (**3a**), DL-glutamic acid (**3b**), DL-alanine (**3c**), DL-valine (**3d**), DL-phenylalanine (**3e**), DL-α,γ-diaminobutyric acid (**3f**), DL-ornithine (**3g**), and DL-lysine (**3h**) were obtained. These results are summarized in Tables 1 and 2.

Table 2. α-Nitroesters (**1**)

Compound	Bp, °C/mmHg (mp°C)	n_D^{20}
1a	70—72/0.05	1.4452
DS of **1a**	(103—104)	
1b	82—85/0.05[a]	1.4468
DS of **1b**	(62—65.5)	
1c	53—54/4[b]	1.4250[b]
DS of **1c**[12]	(110—114)	
1e	94—95/0.03~0.04[c]	1.5133
DS of **1e**	(116.5—119.5)	
1f	oily product	—
AS of **1f**	(135.5—140, dec.)	
1g	oily product	—
AS of **1g**	(163.5—165, dec.)	
1h	oily product	—
DS of **1h**	(119—123, dec.)	

DS: diethylammonium salt of **1**.
AS: ammonium salt of **1**.
a) Reported bp 116—118°C/2 mmHg.[10]
b) Reported bp 79°C/5 mmHg, n_D^{20} 1.4216[11]
c) Reported bp 110°C/0.01 mmHg, n_D^{20} 1.5100.[11]

Table 1. The yields of respective reaction steps

	Reaction condition	$R^1{\cdot}CH(NO_2){\cdot}CO_2CH_3$ (**1**) (%)		$R^1{\cdot}CH(NH_2)CO_2CH_3$ (**2**) (%)	$R^1{\cdot}CH(NH_2)CO_2H$ (HCl salt) (**3**) (%)
		Method i	Method ii		
a	Room temp, overnight	23	66	90	94
b	60±5°C, 2 hr.	88.5	57	92.4	90
c	Room temp, overnight	74.5	—	88	96
d	Room temp, overnight	20	—	80	84
e	Room temp, overnight	50	52	80	96
f	70±5°C, 6 hr.	10.6	—	38 (as HCl salt)	quantitative[b]
g	70±5°C, 6 hr.	29	—	85	76[b]
h	Room temp, 20 hr.	12.3[a]	—	98	99[b]

Method (i) employed Na salt of nitroacetate.
Method (ii) employed nitroacetate and sodium methylate.
a) Ag salt of nitroacetate was employed.
b) $R^1{=}H_2N{-}(CH_2)_n{-}$ (**3f**: $n{=}2$, **3g**: $n{=}3$, **3h**: $n{=}4$)

1) Part VI: S. Zen and M. Koyama, This Bulletin, **44**, 2882 (1971).
2) Presented at 24th Annual Meeting of Chemical Society of Japan, Osaka, April, 1971, Preprint Vol. III, p. 1530 (1971).
3) S. Zen and E. Kaji, This Bulletin, **43**, 2277 (1970).
4) S. Zen, M. Koyama, and S. Koto, *Kogyo Kagaku Zasshi*, **74**, 70 (1971).

Only when bromoacetate and sodium salt of nitroacetate were used was trimethyl β-nitrotricarballylate obtained as a by-product (in a 16.4% yield) in addition to the expected product, **1a**.

It has been found that the *C*-alkylation reaction of nitroacetate with the halides takes place only in dipolar aprotic solvents, as is shown in Table 3. As for the influence of the variation in halogen atoms, the reaction is found to be promoted in the order of I>Br>Cl.

All new compounds reported above (in Table 2) gave satisfactory results in C, H, and N analyses.

Table 3. Solvent effect on the yields of dimethyl α-nitrosuccinate (**1a**)

Solvent	Yield (%) of **1a**
Ethanol, methyl acetate, or dioxane	0
N-Methylacetamide	30
Dimethylformamide	57
Dimethylacetamide	66
Dimethyl Sulfoxide	55
Hexamethylphosphoramide	51

Experimental

Dimethyl α-Nitrosuccinate[5] *(**1a**) (A Typical Example of the General Procedure).* Method (i): Sodium salt of methyl nitroacetate (2.0 g, 14.2 mmol) was added to a solution of methyl bromoacetate (2.17 g, 14.2 mmol) in 50 ml of dimethylacetamide. This suspension was stirred overnight at room temperature. The reaction mixture was then added to 150 ml of water and extracted with benzene. The extract was concentrated, and the resultant syrup was subjected to fractional distillation under reduced pressure to give **1a** (0.63 g) in a 23% yield; IR (liquid film): 1745 (ester CO), 1565 and 1380 (C–NO_2) cm^{-1}, UV: λ_{max}^{MeOH} 275 mμ (ε 290). When the product was allowed to stand, a crystalline trimethyl β-nitrotricarballylate separated. Colorless prismatic crystals (0.30 g) were collected; 16.4% yield; mp 88.5—89.5°C (from ether–isopropyl ether); IR (KBr): 1730 (ester CO), 1560 and 1370 (C–NO_2) cm^{-1}; UV: λ_{max}^{MeOH} 283 mμ (ε 36). Found: C, 40.60; H, 4.68; N, 5.20%. Calcd for $C_9H_{13}NO_8$: C, 41.06; H, 4.94; N, 5.32%. An equimolar mixture of diethylamine and **1a** gave a diethylammonium salt of **1a** as a solid. Recrystallization from ethanol–ether gave needles; mp 103—104°C. Found: C, 44.90; H, 7.50; N, 10.11%.
Calcd for $C_{10}H_{20}N_2O_6$: C, 45.45; H, 7.58; N, 10.61%.

Method (ii): Sodium methylate (1.03N, 22.8 ml) in methanol was added to a solution of 3.1 g (26.1 mmol) of methyl nitroacetate and 4.0 g (26.1 mmol) of methyl bromoacetate in dimethylacetamide (100 ml). The mixture was stirred overnight at room temperature. The reaction mixture was then treated in a manner similar to that described in Method (i) to give a yellow syrup. After distillation, 3.3 g of **1a** were obtained. Yield, 66%.

*Amino Esters (A Typical Procedure for the Catalytic Reduction of α-Nitroesters, **1a**—**h**).* A solution of **1a** (1.0 g, 5.24 mmol) in methanol (50 ml) was hydrogenated for 1 hr with 2 ml of the Raney Nickel T-1[6] catalyst at room temperature under 40—50 *psi* of hydrogen in a Parr low-pressure hydrogenator.[7] The filtrate from the nickel was evaporated *in vacuo* to dryness to give the product (**2a**, 0.17 g) in a 90% yield. The amino esters, **2a**—**h**, were prepared by the same procedure, **1a**—**e** were thus proved to be identical with the authentic samples prepared by the esterification of the corresponding standard DL-amino acids.

α-Amino Acids (A Typical Procedure for the Hydrolysis of the Amino Esters). A mixture of 200 mg of **2a** and 6 ml of 6N hydrochloric acid was heated in a sealed tube at 110°C for about 16 hr (or under reflux for about 16 hr). The solution was then evaporated to dryness, and the residual syrup was washed with ether and acetone to obtain a colorless powder of the HCl salt of DL-aspartic acid (**3a**) in a 94% yield. This product was found to be identical with the authentic sample in its melting point, the result of elementary analysis, the IR, the R_f value, and in the corresponding *N*-2,4-dinitrophenyl derivative[8]. **3b**—**h** were prepared in the same way as **3a** from the corresponding aminoesters (**2b**—**h**).[9] The results are shown in Table 1.

The authors wish to thank Misses Keiko Yuhki and Kazuko Shibuya and Mr. Kotaro Uchida for their technical assistance.

5) Diethyl α-nitrosuccinate has been prepared from diethyl α-bromosuccinate and nitrite by R. Gelin and S. Gelin (*C.R. Acad. Sci., Paris*, **256**, 3705 (1963)).

6) X. A. Dominguez, I. C. Lopez, and P. Franco, *J. Org. Chem.*, **26**, 1625 (1961).

7) Parr Instruments (U.S.A.).

8) R. R. Porter and F. Sanger, *Biochem. J.*, **42**, 287 (1948); F. C. Green and C. M. Kay, *Anal. Chem.*, **24**, 726 (1952); H. M. Rice and F. J. Sowden, *Can. J. Chem.*, **30**, 575 (1952).

9) **3f**—**h** were obtained after the removal of the *o*-phthalic acid precipitated from an acid-hydrolysis mixture.

10) From the addition of magnesium complex of nitroacetic acid to methyl acrylate, yield of **1b** was 5.4% (V. M. Belikov and Yu. N. Belokon, *Izv. Akad, Nauk. SSSR. Ser. Khim.*, **1964** (6), 1134; *Chem. Abstr.*, **61**, 7094 (1964); N. J. Leonard and G. L. Shoemaker, *J. Amer. Chem. Soc.*, **71**, 1762 (1949).

11) H. L. Finkbeiner and G. W. Wagner, *J. Org. Chem.*, **28**, 215 (1963).

12) W. Steinkopf reported only the ammonium salt of **1c** in *Ann.*, **434**, 30 (1923).

BULLETIN OF THE CHEMICAL SOCIETY OF JAPAN, VOL. 46, 339—340 (1973)

Reaction of Troponoid with Ylide. IV.[1] A Conversion of Tropone into Cyclooctatrienone

Yukio SUGIMURA, Nobuo SOMA, and Yukichi KISHIDA
Central Research Laboratories, Sankyo Co., Ltd., Hiromachi, Shinagawa-ku, Tokyo

(Received March 13, 1972)

We have studied the reaction of tropone with various ylides and found a convenient one-step synthesis of 2,3-homotropones by the reaction of tropone with stable sulfonium ylide.[2] It has been reported that benzylsulfonium ylide is stable in solution at −70°C under a nitrogen atmosphere, but when treated with sodium hydroxide at 60°C, in an aqueous medium *p*-nitrobenzyldimethylsulfonium tosylate, it is converted quantitatively into a mixture of *cis* and *trans*-4,4′-dinitrostilbene.[3]

We attempted the reaction of tropone with *p*-nitrobenzyldimethylsulfonium bromide pretreated with sodium hydride at −40°C for five minutes, and obtained the products 2,3-di-*p*-nitrophenylpropiophenone (**3**, 44%), 2-*p*-nitrophenylcycloocta-2,4,6-trien-1-one (**4**, 6%), and 4,4′-dinitrodibenzyl[4] (**5**, 34%). The structural assignments of **3** and **4** were given by spectroscopic data. **3**: mp 110°C, $C_{21}H_{16}O_5N_2$ (elemental analysis and high resolution mass spectrum); IR: $\nu_{C=O}$ (Nujol) 1680 cm^{-1}; NMR (in $CDCl_3$, δ ppm): 3.20 (1H, d of d, J=14.0 and 7.5 Hz), 3.70 (1H, d of d, J=14.0 and 7.5 Hz), 5.02 (1H, t, J=7.5 Hz), 7.2—7.6 (7H, m), 7.8—8.2 (6H, m). **4**: pale yellow oil, $C_{14}H_{11}O_3N$ (elemental analysis and mass spectrum); IR: $\nu_{C=O}$ (liquid) 1660 cm^{-1}; NMR and NMDR (in $CDCl_3$, δ ppm, Fig. 1): 3.20 (2H, d, J=8.3 Hz, H-8). 5.87 (t of d, J=8.3 and 10 Hz, H-7), 6.46 (d of d of d, J=10, 4.5 and 2.0 Hz, H-6), 6.48 (d of d of d, J=12.0, 7.5 and 2.0 Hz, H-4), 6.71 (d of d, J=12.0 and 4.5 Hz, H-5), 7.03 (d of d, J=7.5 and 1.0 Hz, H-3), 7.45 (2H, A_2B_2), 8.13 (2H, A_2B_2).

A plausible mechanistic path for the formation of **3** and **4** is shown in Fig. 2. From the reaction of tropone with stable sulfur ylide[2] whose carbanion attacked the 2-position of tropone to give homotropone,

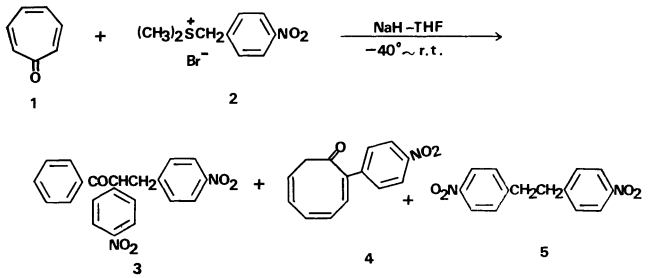

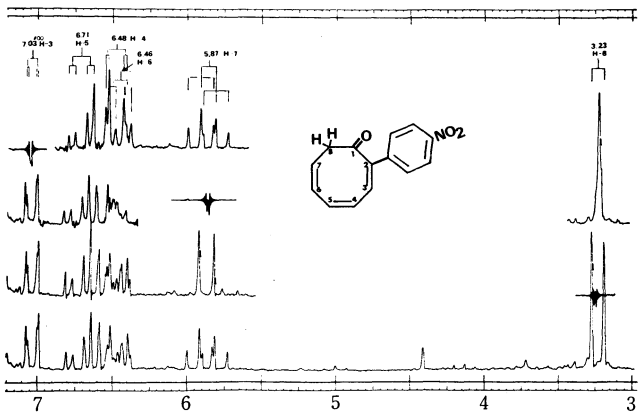

Fig. 1. NMR and NMDR of eight-membered ring protons of 2-*p*-Nitrophenylcycloocta-2,4,6-trien-1-one (**4**).

it is considered that the carbanion of the benzylsulfonium ylide attacked the 1-position of tropone. The ring enlargement of tropone to cyclooctatrienone in the reaction of tropone with diazoalkane has been reported by Franck-Neumann,[5] but the reaction proceeded *via* cycloaddition to the 2-, 3-positions of tropone (Δ^1-pyrazoline). For our present reaction, an intermediacy of carbene would be denied, because dinitrostilbene was not isolated and the isolation of the dibenzyl, **5**, suggests an intervention of radical mechanism.[6]

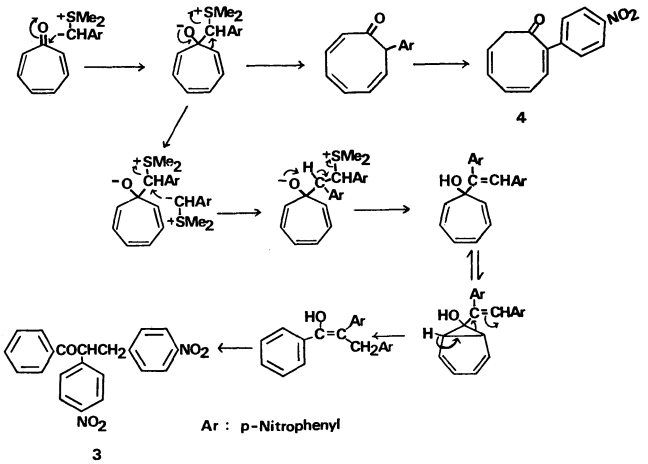

Fig. 2

Experimental[7]

Sodium hydride (50% oil dispersion, 2.4 g) was washed

1) Studies on Seven membered Ring Compounds XXXIX. Part III: Y. Sugimura, N. Soma, and Y. Kishida, This Bulletin, in press.

2) Y. Sugimura and N. Soma, *Tetrahedron Lett.*, **1970**, 1721.

3) C. G. Swain and E. R. Thornton, *J. Amer. Chem. Soc.*, **83**, 4033 (1961).

4) Sadtler Standard IR spectra, No. 20061. Sadtler Research Laboratories, Inc. (Philadelphia).

5) M. Franck-Neumann, *Tetrahedron Lett.*, **1970**, 2143.

6) J. E. Baldwin, W. F. Erickson, R. E. Hackler, and R. M. Scott, *Chem. Commun.*, **1970**, 576.

7) All mp are uncorrected. NMR spectra were taken with a Varian HA-100.

three times, each time with 30 ml of dry *n*-hexane, suspended in dry tetrahydrofuran and cooled to −40°C in aceton–dry ice bath. To the suspension, 13 g of *p*-nitrobenzyldimethylsulfonium bromide was added at the same temperature. After being stirred for five minutes, 5 g of freshly distilled tropone was added and the reaction mixture was stirred at −40°C for two hours, then warmed gradually to room temperature with stirring. The reaction mixture was poured onto ice–water and extracted with chloroform. The extract was dried over magnesium sulfate, condensed to give oily residue, and then subjected to silica gel (500 g) column chromatography. The first benzene eluate: 2.15 g (34%) of 4,4′-dinitro-dibenzyl (**5**), mp 180°C, which was identified with an authentic sample.[4] The second benzene eluate: 2.8 g (44%) of 2,3-di-*p*-nitrophenylpropiophenone (**3**), mp 111°C. Found: C, 66.93; H, 4.32; N, 7.39%. Calcd for $C_{21}H_{16}O_5N_2$: C, 67.01; H, 4.29; N, 7.44%. High resolution mass spectrum, M^+ (*m/e*) Found: 376.109. Calcd: 376.106. Benzene–chloroform (1: 1) eluate: 0.24 g (6%) of 2-*p*-nitrophenylcycloocta-2,4,6-trien-1-one (**4**). Found: C, 62.53; H, 5.92; N, 6.88%. Calcd for $C_{10}H_{11}O_3N$: C, 62.16; H, 5.74; N, 7.25%. Chloroform eluate: 3.16 g of the starting tropone.

We are grateful to Prof. T. Nozoe for his helpful discussion.

X-Ray Photoelectron Spectroscopic Study for the Reaction of Evaporated Iron with O_2 and H_2O

Kosaku KISHI and Shigero IKEDA

Department of Chemistry, Faculty of Science, Osaka University, Toyonaka, Osaka

(Received February 1, 1972)

Reactions of evaporated iron with O_2 and H_2O have been investigated by X-ray photoelectron spectroscopy. Binding energies of $Fe2p_{3/2}$ and Ols electrons were measured during the course of reactions and their variation was discussed in terms of the positive and negative charges of the iron and oxygen of the surface oxide formed, respectively, assuming a simple charge-chemical shift relation. They are compared with the binding energies of the Ols in SiO_2, Al_2O_3, Fe_2O_3, $Cd(OH)_2$, KOH, and $Ni(OH)_2$ and those of $Fe2p_{3/2}$ in various iron compounds. High reactivity of the surface oxide with H_2O and the resulting hydroxyl group formation were observed. A rough estimation of the Fe to O atomic ratio of the surface oxide was also carried out from the ratio of the Fe and O peak areas.

Dissolution and corrosive reactions of metals are largely influenced by the presence of oxygen. In our UV absorption study[1] for acetylacetone adsorption on oxygen-treated metals, two or more chemical states have been observed for the oxygen on the metal surfaces.

X-Ray photoelectron spectroscopy,[2] giving information on the surface and semisurface of solids, seems to be useful for studying the variation in the charge of the atom in question and in the valence band during the course of surface reaction. Application of the spectroscopy for catalysis research has been reviewed recently.[3]

Two kinds of oxygen were observed for the surface oxide of nickel by X-ray photoelectron spectroscopy.[4] We report here on variations in the $2p_{3/2}$ binding energy of iron and the ls of oxygen in an evaporated iron exposed to O_2 and H_2O. The core binding energy shifts were correlated to the charges of the atoms and compared with those of metal oxides, hydroxide and various iron compounds in order to investigate the chemical states and reactivity of the surface oxide.

Experimental

The apparatus for metal evaporation and reaction is illustrated in Fig. 1. Chamber (g) was evacuated for several hours at 10^{-6} Torr. The thin iron foil wound by tungsten filament (f) was then degassed by heating electrically and the metal was finally evaporated on copper plate (a). The iron sample was inserted (within 1 min) into chamber (c) for photoelectron measurement through a gate valve (d) without exposing the sample to air by use of rubber O-ring (e). The vacuum of (c) was 10^{-7} Torr. After recording the spectrum for the metal, the sample was pulled out to the reaction chamber and exposed to the gases to be studied. The sample plate was again inserted for spectral measurement on the surface species obtained.

Photoelectron spectra were measured with 0.1 eV step scan on a KEC-X2000 (Kokusai Electric Co.) electron

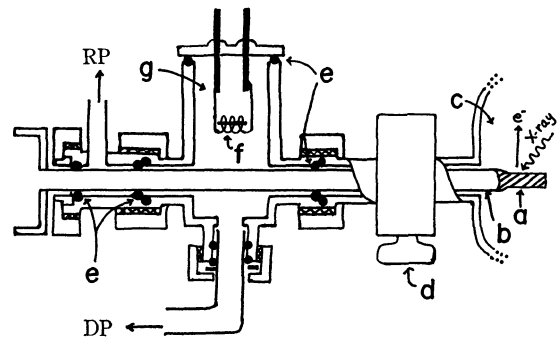

Fig. 1. Diagram of reaction chamber. (a): sample holder, (b): sample shaft, (c): photoemission chamber, (d): gate valve, (e): rubber O-ring, (f): tungsten filament, (g): reaction chamber.

spectrometer using $AlK\alpha_{1,2}$ X-ray line as an excitation source. The reproducibility of $Fe2p_{3/2}$ and Ols peak positions was within 0.2 eV.

Water was distilled and degassed in a vacuum. Commercial oxygen was led into a vacuum system and was dried with liquid nitrogen cooled trap. The purity of iron was 99.99%.

SiO_2(Mallinckrodt Chemical Works) and Al_2O_3(alumina activated for chromatography, Nakarai Pure Chemicals) were heated in a crucible at 600°C for 2 hr and after being left standing for 15 hr in the air, their photoelectron spectra were measured for the powder sample pressed on an adhesive aluminum tape. Fe_2O_3 was obtained in two ways, by heating ferric oxalate in a crucible at 500°C for 5 hr or at 700°C for 3 hr. $Ni(OH)_2$ and $Cd(OH)_2$ were produced by the reaction of $Ni(NO_3)_2$ and $CdCl_2$, respectively, with aq. KOH solution. Photoelectron spectra of $K_4Fe(CN)_6$, $K_3Fe(CN)_6$, $Fe_2(SO_4)_3(NH_4)_2SO_4 \cdot 24H_2O$, and KOH(Nakarai Pure Chemicals) were measured in powder without further purification.

Results

The $Fe2p_{3/2}$ and Ols photoelectron lines from the evaporated iron exposed to O_2 are shown in Fig. 2. Binding energies have been calculated using the value of 285.0 eV for Cls line of a contaminant observed in the background spectrum of evaporated fresh iron. For the fresh iron, the $Fe2p_{3/2}$ peak is located at 708.2 eV and the Ols at 532.4 and 530.6 eV (case a). The metal was then exposed to O_2 in succession (b, 0.01

1) K. Kishi, S. Ikeda, and K. Hirota, *J. Phys. Chem.*, **71**, 4384 (1967); K. Kishi and S. Ikeda. *ibid.*, **73**, 729 (1969).

2) K. Siegbahn, *et al.*, "ESCA; Atomic, Molecular and Solid State Structure Studied by Means of Electron Spectroscopy," Almqvist and Wiksells, Uppsala, 1967.

3) W. Delgass, T. R. Hughes, and C. S. Fadley, *Data Rev.*, **4**, 179 (1970).

4) K. Kishi and S. Ikeda, *Chem. Lett.*, **1972**, 245.

TABLE 1. BINDING ENERGIES AND INTENSITIES[a] OF $Fe2p_{3/2}$ AND Ols LINE FROM EVAPORATED IRON EXPOSED TO O_2

Oxidation condition	$Fe2p_{3/2}$		Ols	
	Binding energy (eV)	Intensity	Binding energy (eV)	Intensity
Fresh iron	708.2	100	530.7	4
		0	532.4	6
0.01 Torr O_2	708.2	42	530.7	19
1 min	711.4(3.2)[b]	34	532.7	10
0.5 Torr O_2	708.2	32	530.7	26
1 min	711.4(3.2)	35	532.7	11
10 Torr O_2	708.2	18	530.7	34
5 min	711.9(3.7)	36	532.7	12
100 Torr O_2	708.2	9	530.7	35
30 min	712.2(4.0)	37	532.7	13
$K_4Fe(CN)_6$	710.2(2.0)			
$K_3Fe(CN)_6$	711.6(3.4)			
Fe_2O_3	712.4(4.2)			
$Fe_2(C_2O_4)_3 \cdot 6H_2O$	713.8(5.6)			
$Fe_2(SO_4)_3(NH_4)_2SO_4 \cdot 24H_2O$	714.4(6.2)			
SiO_2			534.5	
Al_2O_3			532.5	
Fe_2O_3			530.4	
$Cd(OH)_2$			532.7	
KOH			531.9	
$Ni(OH)_2$			531.9	

a) The intensities are obtained from the respective peak areas and normalized with respect to the area of $Fe2p_{3/2}$ in fresh iron (100).
b) Chemical shifts from genuine Fe are given in parentheses.

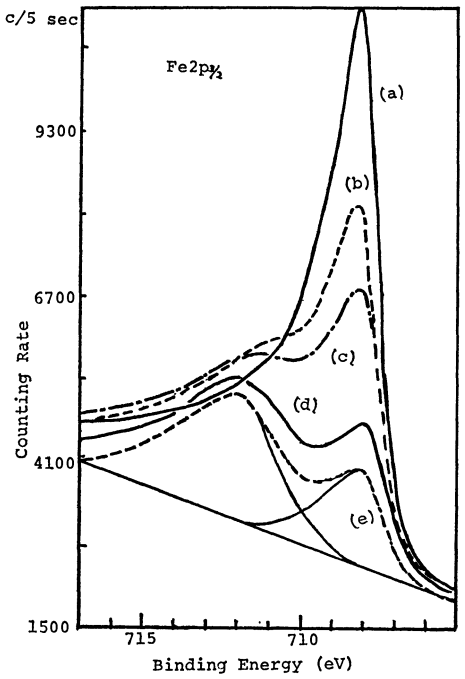

Fig. 2-(i). $Fe2p_{3/2}$ photoelectron lines from evaporated iron exposed to O_2 in succession. (a): fresh iron, (b): 0.01 Torr O_2; 1 min, (c): 0.5 Torr; 1 min, (d): 10 Torr; 5 min, (e): 100 Torr; 30 min.

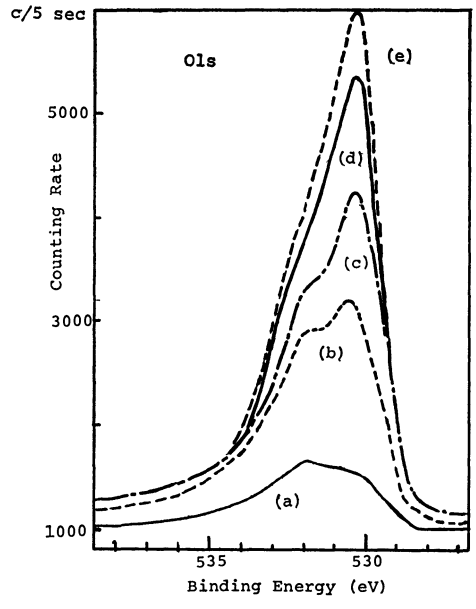

Fig. 2-(ii). Ols photoelectron lines from evaporated iron exposed to O_2 in succession.

Torr, 1 min; c, 0.5 Torr, 1 min; d, 10 Torr, 5 min; e, 100 Torr, 30 min). The genuine Fe peak was depressed and another peak appeared at high energy side. The chemical shift of this peak from the genuine one varied from +3.2 eV in case b to +4.0 eV in case e. With O peak, two peaks were observed and the low energy one increased mainly in intensity after oxidation, showing no shift in binding energy. These results of chemical shift and intensity are summarized in Table 1, with the corresponding chemical shifts

of various compounds for comparison. Each peak area was estimated by resolving roughly the two peaks graphically as exemplified by case e. In the case of $Fe2p_{3/2}$ peaks, the two peaks were resolved on considering the shape of fresh metal and bulk oxide peaks. However, the maximum peak positions and the peak area of the surface oxide could not be accurately determined, especially in the case of (b), because of their unsymmetrical profiles. Approximate values for Fe peaks are listed in Table 1.

Figure 3 shows the $Fe2p_{3/2}$ and the Ols peaks from the evaporated iron exposed to H_2O in succession (a, fresh iron; b, 1 Torr, 1 min; c, 15 Torr, 30 min; d, 15 Torr, 2 hr). As an example, the second Fe appeared at +3.2 eV from the genuine Fe in case d. With Ols, the high energy peak is larger in intensity than the other, unlike the cases for oxidation with O_2.

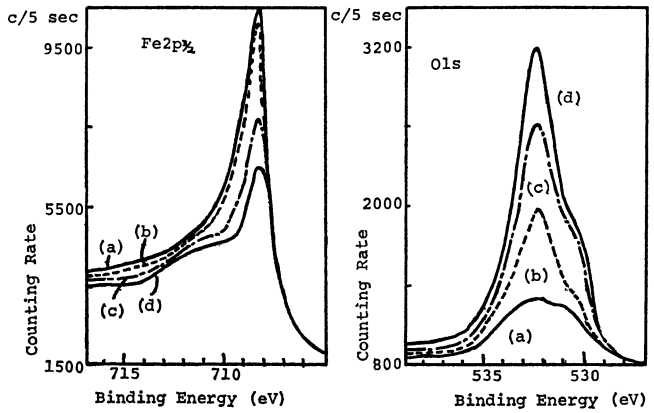

Fig. 3. $Fe2p_{3/2}$ and Ols photoelectron lines from evaporated iron exposed to H_2O in succession. (a): fresh iron, (b): 1 Torr H_2O; 1 min, (c): 15 Torr; 30 min, (d): 15 Torr; 2 hr.

Figure 4 shows the spectra of $Fe2p_{3/2}$, and Ols electrons. The $Fe2p_{3/2}$ for the surface oxide (case a, after exposing the metal to 200 Torr O_2 for 30 min) shifted 0.6 eV to low energy after the reaction with H_2O (15 Torr) for 1 hr (case b). The low energy Ols was depressed and the high energy one enhanced.

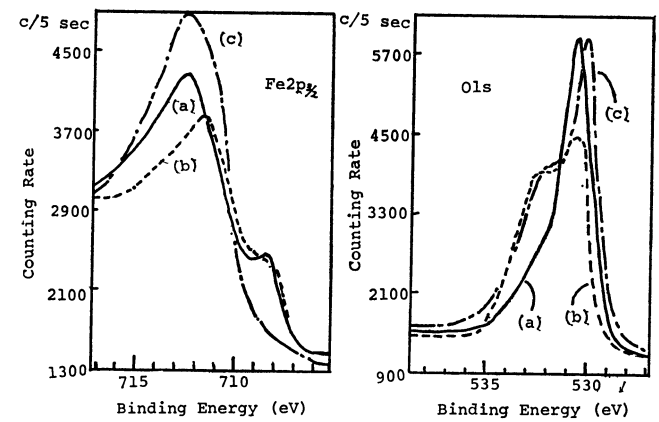

Fig. 4. Reaction of surface oxide with H_2O. $Fe2p_{3/2}$ and Ols photoelectron lines from, (a): iron metal exposed to 200 Torr O_2 for 30 min, (b): the surface oxide exposed to 15 Torr H_2O for 1 hr, (c): Fe_2O_3. (Counting rate unit for Fe_2O_3 is arbitrary.)

When Fe_2O_3 (case c, obtained by heating ferric oxalate at 700°C for 3 hr) was treated with H_2O for 2 hr, only a slight change was observed for the Ols peaks and none at all for the $Fe2p_{3/2}$.

Discussion

The high energy Ols peak for fresh iron is likely to be assigned to a contaminant or absorbed species except for the oxide since the low energy peak increased mainly in intensity (after exposing the metal to O_2). Measurable carbon and oxygen peaks due to a contaminant were also reported for prereduced Pt foil.[3] The peak area ratio of the high energy Ols to the Cls due to a contaminant, however, differs from that of fresh iron and gold, the ratio being larger considerably for iron. This suggests that on iron surface the active gases such as CO, CO_2, H_2O adsorbed with strong chemical force and hydrocarbons predominate on gold.

The low energy Ols for fresh iron can be assigned to the oxygen on the metal with a small amount of surface oxide under the pressure of 10^{-6}—10^{-7} Torr. The corresponding $Fe2p_{3/2}$ peak, however, could not be detected because of the broad tailing of the peak of high energy side. After reaction of the fresh iron with O_2, the second $Fe2p_{3/2}$ peak appeared, followed by the enhancement of the low energy Ols being shifted +3.2 eV (case b, c), +3.7 eV (d), and +4.0 eV (e) to high energy from the genuine Fe, as shown in Fig. 2. When the fresh iron was exposed immediately to 200 Torr O_2 for 30 min, the Fe shifted +4.2 eV, the same binding energy as for Fe_2O_3. The chemical shifts of Fe3p electrons of various iron compounds have been reported;[5] K_2FeO_4 (+5.3 eV from Fe metal), K_3FeF_6 (+5.3 eV), $K_3Fe(CN)_6$ (+2.6 eV) and Fe_2O_3 (+2.5 eV). If we assume that the localized positive charges on iron atoms are 3 and 0 in K_3FeF_6 and Fe metal, respectively, and that the Fe3p binding energies reflect only the charge of the metal and have a linear dependence on the charge, the positive charge of Fe in Fe_2O_3 is estimated to be 1.4.[6] In our results with $Fe2p_{3/2}$, the corresponding chemical shifts for all compounds measured are larger than those with the above 3p electrons (Table 1) and the shift of Fe_2O_3 is larger than that of $K_3Fe(CN)_6$. Assuming the positive charge of 1.5 for Fe_2O_3 giving the 4.2 eV shift of $Fe2p_{3/2}$, the iron atom in the surface oxide is considered to transfer, on the average, about 1.1 and 1.5 electrons to oxygen atoms when the chemical shift of the iron atom is +3.2 eV and +4.2 eV, respectively, after exposure to O_2. The localized charges

5) L. N. Kramer and M. P. Klein, *J. Chem. Phys.*, **51**, 3618 (1969).

6) In order to treat the relation of charge-chemical shift more strictly, a correction due to crystal potential effect should be included. However, there are several findings indicating that the expected differences in crystal potentials do not appear in the measured values. For example, the observed Nls binding energies are almost the same for the nitrates, $NaNO_3$ (407.4 eV), NH_4NO_3 (407.2 eV), and $[Rh(NH_3)_6](NO_3)_3$ (407.3 eV) (W. L. Jolly, *et al.*, *Inorg. Chem.* **8**, 2642 (1969). There are also no differences in the Al2p spectra for kaolinite (Al: 6-coordinate), microcline (4-coordinate), and sillimanite (half, 4-coordinate; half, 6-coordinate),[3]

on Fe in these oxides are not so large as in $Fe_2(C_2O_4)_3 \cdot 6H_2O$ (estimated charge, +2.0) and $Fe_2(SO_4)_3(NH_4)_2SO_4 \cdot 24H_2O$ (+2.2). In the latter, the number of H_2O is uncertain because of release of H_2O on evacuation. As an example, the dark green $[Cr(H_2O)_4Cl_2]Cl$ turned purple-red after photoelectron measurement, the coloration being immediately restored after exposure to air. This indicates that the H_2O is released from the complex on evacuation.

The Fe to O atomic ratio of the surface oxide was estimated roughly as follows. The peak area ratio of low energy Ols to $Fe2p_{3/2}$ and to Fe3p in Fe_2O_3 were approximately 1.3 and 1.9, respectively. These values, however, can not be used directly for the estimation of the Fe to O ratio of the surface oxide since electrons of low kinetic energy can only escape from near the surface, whereas electrons of high kinetic energy can escape from deeper inside the material, as illustrated in Figure 5. The kinetic

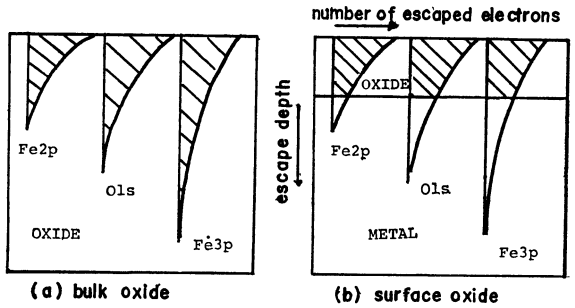

Fig. 5. Intensity-oxide depth relation for $Fe2p_{3/2}$, Ols, and Fe3p lines from surface oxide.

energy of electrons ejected from the Ols orbital (*ca.* 950 eV) is larger than that from the $Fe2p_{3/2}$ (*ca.* 770 eV), the escape depth thus being deeper for the former. Therefore, for the surface oxide where the genuine metal peak remains, the apparent peak area ratio ($Ols/Fe2p_{3/2}$) becomes smaller, as shown by the difference in the shaded parts of (a) and (b) in Fig. 5. This situation is reversed on the Ols to Fe3p (kinetic energy: *ca.* 1430 eV). In fact, the peak area ratio of metal-iron to oxide-iron was larger in the observation of the Fe3p electrons than in the $Fe2p_{3/2}$. For the surface oxide obtained after exposure to 200 Torr O_2 for 30 min, the observed peak area ratios of the Ols to the $Fe2p_{3/2}$ and to the Fe3p are about 1.0 and 1.9, respectively. This indicates that the Fe to O ratio is between about 1 : 1.2 and 1 : 1.5. On considering the differences in the kinetic energies (Ols–$Fe2p_{3/2}$: 180 eV, Fe3p–Ols: 480 eV), the Fe to O ratio is expected to be near 1 : 1.3. For the surface oxide $Fe_{1.0}O_{1.3}$, the negative charge of the oxygen is evaluated as about 1.1 using the positive charge of 1.5 for iron atom. The total area of the $Fe2p_{3/2}$ peaks decreased during the oxidation reaction. This might be due to the dilution of iron atoms with oxygen atoms (ionic radii: O^{2-}, 1.40 Å; Fe^{3+}, 0.64 Å) and the different mean escape depth between iron metal and oxide. For the surface oxide after exposure to 0.01 Torr O_2 for 1 min, the Fe to O ratio is approximately 1 : 0.7 and their estimated charges are +1.1 and −1.6 on Fe and O atoms, respectively. However, the binding energy difference was not observed for the oxygen atoms with the negative charges −1.1 and −1.6. This may be due to an inaccurate estimation of Fe to O peak area ratio in case b (Fig. 2).

The binding energy of Ols of the surface oxide is smaller than that of SiO_2 and Al_2O_3 by 3.7 and 1.7 eV, respectively, and larger than that of Fe_2O_3 by 0.3 eV. Although it is concluded from the chemical shift of $Fe2p_{3/2}$ that the surface oxide shows a larger covalent bonding than in other oxygen-coordinating compounds in the above discussion, of the metal oxides the surface oxide of iron exhibits larger ionicity than SiO_2 or Al_2O_3 as shown from the binding energy of Ols electrons. The linearity of the chemical shift-charge relation of the Ols peak is not so good as for the Nls or the Cls, but the negative charge of 0.5 corresponds roughly to the 3.5 eV shift.[7] The Ols binding energy of SO_4^{2-} is about 2.5 eV larger than that of Fe_2O_3 and the negative charge of oxygen in SO_4^{2-} was evaluated to be 0.83 from the positive charge of sulfur.[2] The 2.5 eV shift leads to the negative charge of about 1.18 for the oxygen in Fe_2O_3. The value is near that obtained from the positive charge of iron atom, 1.0, although the above relation could not be applied to the energy difference between the surface oxide and Fe_2O_3. In spite of larger negative charge the Ols binding energy of the surface oxide is larger by 0.4 eV than that of Fe_2O_3. We could not explain this although the Cls binding energy can not be taken as the same value for the two oxides as energy reference.

When the surface oxide was treated with H_2O, the low energy Ols was depressed followed by the enhancement of the high energy one (Fig. 4). The Ols main peak is also the high energy one when the fresh iron was exposed to H_2O (Fig. 3). The high energy Ols (532.6 eV) is located between the Ols binding energies of $Cd(OH)_2$ (532.7 eV) and KOH or $Ni(OH)_2$ (531.9 eV). This suggests that the hydroxyl group was formed on the reaction of the fresh iron or the surface oxide with H_2O. In the former, the reaction may be caused by a mixture of H_2O and O_2 remaining due to incomplete removal. When one oxide-oxygen was displaced by $2OH^-$, the total area of low and high energy Ols peaks should increase by the same amount with the decreased area of the low energy peak after reaction compared with the total area before reaction. In the spectrum the increase in the total area is actually indicated but the increased amount is somewhat smaller than expected. This is probably due to the depression of the Ols peaks caused by the increase of a contaminant hydrocarbon on the surface.

Fadley and Shirley[8] measured the photoelectron peaks of Fe foil heated in 10^{-2} Torr H_2 atmosphere and observed two oxygen peaks. The low energy Ols disappeared first at 360°C and was suggested to be assigned to more weakly adsorbed oxygen-containing

7) K. Siegbahn, *et al.*, "ESCA Applied to Free Molecules," North-Holland Pub. Co., Amsterdam (1969).

8) C. S. Fadley and D. A. Shirely, *Phys. Rev. Lett.*, **21**, 980 (1968).

gases. The high energy Ols, remaining even at 600°C, was assigned to the oxygen of the surface oxide. From the present study, the low energy one is more accurately assigned to the surface oxide-oxygen, and the disappearance of this peak after heating in the hydrogen stream can, therefore, be explained by the reduction of the oxide-oxygen with H_2 and consequent formation of hydroxyl group giving the high energy Ols peak. The hydroxyl group formation on iron surface will be also expected for the iron metal immersed in an aqueous solution. Experiments on the degree of depression of the low energy peak after reaction with H_2O suggested the hydroxyl group formation to be easier for the iron metal with fewer oxide layer. As an extreme case, Fe_2O_3 showed no such formation of hydroxyl group even after being exposed to H_2O for 2 hr although the high energy Ols peak may be due in part to the hydroxyl group formed already during the production of the Fe_2O_3. Such behavior was also observed for the acetylacetone adsorption on oxygen treated metal by UV absorption spectra.[1] Acetylacetone adsorption was accelerated after iron or manganese film was exposed to oxygen (1 Torr) for 1 min, but not detected on the metal oxide obtained by heating the metal film in the air at 200°C for 1.5 hr.

Hydrogen bonding is explained by the formation of molecular complex where partial electron transfer occurs from the proton-accepting species to the antibonding orbital of, for example, O–H bond of the proton donating species,[9] the O–H dissociation being an extreme case. The above hydroxyl group formation on the iron surface is also expected to occur followed by electron transfer from oxygen of the surface oxide to the antibonding orbital of H_2O. Thus, a higher reactivity to H_2O will be expected for the iron metal with a slight oxidation, where the oxygen atom has more localized orbital, donating electrons to H_2O, than for one in bulk oxide because of incomplete formation of the bulk oxide structure.

The $Fe2p_{3/2}$ chemical shift to low energy on reaction with H_2O suggests that the Fe–O bond became more covalent in the hydroxide.

Iron surface is easily oxidized to give approximately 20 Å of oxide under the conditions of 10^{-4} Torr oxygen and room temperature.[10] This oxide layer increased to about 25 Å at 760 Torr O_2. Under the present oxidation conditions of 100 Torr O_2, 30 min, and room temperature, the iron surface is expected to be oxidized approximately to the same depth. The peak area of low energy Ols for fresh iron has 1/9 area of the corresponding one obtained after oxidation with 100 Torr O_2 for 30 min. Assuming 25 Å thickness of the latter surface oxide, the oxide layer for fresh iron is estimated to be thinner than 3 Å. However, a relatively rapid formation of four oxide layers has been reported under the condition of 2×10^{-7} to 5×10^{-6} Torr and 24°C.[11] On the other hand, assuming the four oxide layers for the present fresh iron, a thickness larger than 100 Å is derived for the surface oxide after exposing to 100 Torr O_2. Further attempts are necessary for a quantitative discussion on the depth of the oxide layers. The escape depth of electrons for the above metal with the surface oxide is slightly larger than the thickness of the oxide layer obtained after reaction with 100 Torr O_2 for 30 min, since the genuine Fe peak still can be detected but with weak intensity. Estimated range of escape depth: 8 Å for 362 eV electrons in case of Ag[12] and *ca.* 100 Å for 860 eV electrons in that of iodostearic acid.[2] In the case of Au, an escape depth of 22 Å has been observed for 1200 eV electrons.[13] From these results and the dependence of the depth on the kinetic energy of electrons and on the atomic number of materials, the depth of the oxide for the fresh iron seems to be thinner than four oxide layers.

The above photoelectron data indicate the important role of oxygen in the dissolution reaction of metals into aqueous solution; in this case for iron, the formation of a transient oxide to bulk oxide with high reactivity to H_2O was revealed.

The authors wish to thank Dr. Y. Yokoyama and Mr. I. Watanabe, Osaka University, for assistance and suggestions in carrying out the experiment.

9) a) R. S. Mulliken and W. B. Person, "Molecular Complexes," Wiley-Interscience, New York, 1969. b) N. Mataga and T. Kubota, "Molecular Interactions and Electronic Spectra," Marcel Dekker, Inc., New York, 1970.

10) J. Kruger and H. T. Yolken, *Corosion*, **20**, 29 (1964).

11) S. Chang and W. H. Wade, *J. Phys. Chem.*, **74**, 2484 (1970).

12) P. W. Palmberg and T. N. Rhodin, *J. Appl. Phys.*, **39**, 2425 (1968).

13) Y. Baer, P. Heden, J. Hedman, M. Klasson, and C. Nordling, *Solid State Comm.*, **8**, 1479 (1970).

Energetic Reactions of ^{80}Br Activated by (I. T.) Process in C_3H_8–C_2H_6 and C_3H_8–CH_3Br Systems

Kenshi NUMAKURA* and Enzo TACHIKAWA

Division of Chemistry, Japan Atomic Energy Research Institute, Tokai-mura, Ibaraki

(Received February 21, 1972)

In order to examine the relative importance of the thermal ionic process in the reactions of ^{80}Br from the (I. T.) process with C_3H_8, we chose C_2H_6 or CH_3Br as diluents. Some assumptions have made in estimating the yield-variation of products from the diluents: 1) the rate of the reduction of the yields of the products from C_3H_8 caused by the addition of the diluent is the same for all of the products and 2) the ionic yield is zero over the whole range of concentrations of C_3H_8. With these assumptions, the analysis of the results shows that the contribution of the thermal ionic process in these binary systems has only minor importance; the products are, essentially, formed *via* energetic processes. It is also found that the ratio of n-$C_3H_7{}^{80}Br/i$-$C_3H_7{}^{80}Br$ per bond basis seems to decrease from 1.1 ± 0.1 on the addition of the diluent. This indicates that the formation of i-$C_3H_7{}^{80}Br$ is a lower energy process, relative to that of n-$C_3H_7{}^{80}Br$ in the present reaction system.

In recoil ^{80}Br chemistry, the method commonly used to distinguish excess kinetic energy processes from others consists of the addition to the reaction system of an inert gas as a kinetic-energy moderator.[1-6] However, when a reactant molecule is diluted with an inert gas having a higher ionization potential (IP) than that of Br, the charge distribution, and the energy distribution of ^{80}Br are both influenced. Thus, the moderator curve obtained must be carefully analyzed in order to ascertain the real nature of the reactions involved. For example, the limiting yield at 1.0 m. f. of a moderator simply means that the yield is due to the thermal processes in the moderactor atmosphere and does not necessarily indicate the thermal yield in the reactant atmosphere.

In the previous paper we examined the nature of the reacting ^{80}Br activated by the isomeric transition in ethane,[6] which has a lower IP than that of Br, and speculated about it principally as a kinetically-excited atom, probably with on charge, on the basis of the assumption that the isotopic variation in the products is significant only when the products are formed *via* energetic processes.

The present paper will deal with the reactions of ^{80}Br with C_3H_8 in the binary system; C_2H_6 and CH_3Br were chosen as counterparts. All of these molecules have lower IP values than that of Br. Thus we can expect that the thermal ionic processes of ^{80}Br are not important in these systems if the above speculations are generally true. The conclusion drawn from the present results is that ^{80}Br reacts principally *via* the energetic processes in these binary systems; this supports the assumptions that the relative IP of the atmosphere is a major controlling factor in determining the relative important of the thermal ionic processes of ^{80}Br.

An attempt has also been made to compare the reactivity of two kinds of C–H bonds in C_3H_8, since corrections for the ^{80}Br spectrum are not required except for the secondary decomposition of the primary products.

Experimental

The general experimental procedure is the standard one for recoil Br atom reactions,[4] involving the formation of ^{80}Br from the ^{80}Br(I. T.)^{80}Br nuclear reaction and the subsequent analysis of the radioactive products by radio gas chromatography. The total pressure was usually 700 ± 10 Torr except in the pressure-effect experiments. The ratio of Br_2 relative to the reactant was 0.02 ± 0.01 throughout the work.

Materials. The ethane and propane were supplied by the Takachiho Chemical Co. with nominal purities of 99.9% and 99.7%; they were used after washing with concentrated sulfuric acid and after purification by vacuum distillation. Methyl bromide from the Tokyo Kasei Co. was purified several times by vacuum distillation.

Addition of O_2. Initially many runs were made without the addition of O_2 to the reaction systems. The values of the yields of the products from the reaction of ^{80}Br with C_3H_8, particularly that for the yield of i-$C_3H_7{}^{80}Br$, were not reproducible. This was probably due to the reaction of the C_3H_6 present in C_3H_8 as an impurity with the irradiated Br_2. However, reproducible results were obtained when 65 Torr of O_2 was added to the reaction mixture at the beginning of the reactions.

Percent Yields. The propane used in the present work contains very little C_3H_6, but even this amount of propylene interferes with the measurement of the total organic yield from the systems containing C_3H_8 as a reactant. Thus the absolute yield has been measured only from the ^{80}Br-C_2H_6-$O_2(3.2\pm0.1\%)$ and ^{80}Br-CH_3Br-$O_2(2.5\pm0.1\%)$ systems by a solvent extraction method. Individual radioactivity yields have been obtained by dividing the activities in the radio gas chromatogram by the total ^{80}Br activity, as measured with a G–M counter 2 hr after sampling the gases. The relative yields have been normalized to the percentage yields using a correction factor determined from the sum of the relative yields and from the total organic yield found in the above systems. The radio gas chromatograms were analyzed on a FACOM 230—60 computor in order to obtain the relative yields of the products, using the BOB 7 series program[7] corrected for the background and for the radio-activity decay of nuclides.

1) R. Wolfgang, Progr. *Reaction Kinetics*, **3**, 97 (1965).
2) J. B. Nicholas and E. P. Rack, *J. Chem. Phys.*, **48**, 4085(1968).
3) J. Okamoto and E. Tachikawa, This Bulletin, **42**, 1504 (1969).
4) E. Tachikawa and T. Kahara, *ibid.*, **43**, 1293 (1970).
5) M. Yagi, K. Kondo, and T. Kobayashi, *ibid.*, **44**, 580 (1971).
6) E. Tachikawa and K. Yanai, *Radiochim. Acta*, **17**, 138 (1971).
7) H. Baba, H. Okashita, S. Baba, T. Suzuki, and H. Umezawa, *J. Nucl. Sci. Technol.*, **8**, 703 (1971).

Table 1. ^{80}Br stabilized in organic combination in Kr-moderated system

C_3H_8 (mmHg)	$\frac{C_3H_8}{C_3H_8+Kr}$	$CH_3{}^{80}Br$ (%)	$C_2H_5{}^{80}Br$ (%)	i-$C_3H_7{}^{80}Br$ (%)	n-$C_3H_7{}^{80}Br$ (%)	$CH_2{}^{80}BrBr$ (%)
594	0.945	1.0	0.53	0.21	0.64	0.40
551	0.869	1.0	0.54	0.26	0.60	0.36
448	0.695	0.84	0.45	0.22	0.46	0.37
399	0.592	0.86	0.36	0.15	0.39	0.31
349	0.529	0.74	0.35	0.08	0.25	0.21
307	0.467	0.85	0.29	0.11	0.28	0.20
300	0.449	0.75	0.31	0.12	0.28	0.19
200	0.310	0.59	0.15	0.10	0.13	0.16
118	0.167	0.66	0.11	0.05	0.09	0.12
100	0.150	0.63	0.11	0.09	0.07	0.05

Table 2. Percent ^{80}Br stabilized in organic combination in various binary mixtures

Press of C_3H_8	$\frac{C_3H_8}{C_3H_8+\text{additive}}$	$CH_3{}^{80}Br$ (%)	$C_2H_5{}^{80}Br$ (%)	i-$C_3H_7{}^{80}Br$ (%)	n-$C_3H_7{}^{80}Br$ (%)	$CH_2{}^{80}BrBr$ (%)
Additive: C_2H_6						
630	1.000	1.2	0.57	0.20	0.67	0.47
558	0.877	1.2	0.65	0.19	0.60	0.44
508	0.795	1.3	0.60	0.17	0.56	0.41
446	0.697	1.1	0.75	0.13	0.45	0.43
410	0.642	1.3	0.84	0.21	0.50	0.50
311	0.494	1.4	0.93	0.15	0.44	0.45
266	0.417	1.4	0.82	0.15	0.37	0.34
200	0.317	1.3	0.95	0.13	0.33	0.46
169	0.264	1.3	0.94	0.07	0.17	0.37
127	0.199	1.4	1.0	0.07	0.18	—
98	0.155	1.5	1.2	0.06	0.15	0.53
61	0.105	1.4	1.2	0.06	0.09	0.43
27	0.042	1.5	1.3	0.02	0.04	0.42
—	0.000	1.5	1.2	—	—	0.39
Additive: CH_3Br						
590	0.941	1.1	0.50	0.20	0.58	0.41
510	0.819	1.1	0.38	0.17	0.45	0.40
454	0.723	1.1	0.39	0.14	0.38	0.36
428	0.596	1.1	0.30	0.14	0.36	0.52
362	0.572	1.3	0.30	0.13	0.35	0.62
317	0.508	1.4	0.26	0.18	0.27	0.58
272	0.437	1.3	0.19	0.08	0.22	0.53
220	0.348	1.4	0.19	0.10	0.19	0.73
180	0.287	1.6	0.08	0.06	0.12	0.64
126	0.203	1.5	0.10	0.04	0.10	0.67
66	0.105	1.5	0.07	0.02	0.05	0.80
—	0.000	1.6	—	—	—	0.87

Results and Discussion

The five chief organic products observed from the reactions of (I. T.)-activated ^{80}Br with C_3H_8 were $CH_3{}^{80}Br$, n-$C_3H_7{}^{80}Br$, $C_2H_5{}^{80}Br$, i-$C_3H_7{}^{80}Br$, and $CH_2{}^{80}BrBr$. Table 1 summarizes the yields of the individual products obtained from the Kr-moderated systems. The yields of $C_2H_5{}^{80}Br$, n-$C_3H_7{}^{80}Br$, and $CH_2{}^{80}BrBr$ decreased with the increase in the m. f. of Kr, and could be extrapolated to zero at 1.0 m. f. of Kr. However, the $CH_3{}^{80}Br$ and i-$C_3H_7{}^{80}Br$ yields were extrapolated to 0.6±0.1% and 0.05±0.02% respectively. If one simply assigns these limiting yields at 1.0 m. f. of Kr as the thermal ionic yields, both $CH_3{}^{80}Br$ and i-$C_3H_7{}^{80}Br$ are found to be formed by two processes. One involves an excess kinetic energy, and the other, thermal ionic processes. The other products are principally formed *via* energetic processes of ^{80}Br. This simple assignment does not necessarily indicate the true reaction processes involved in the reactions of ^{80}Br in the C_3H_8 atmosphere, as has been discussed in our previous paper.[6] Since the IP of Kr is considerably higher than that of Br, the presence of the large amount

of Kr in the reaction system influences the charge neutralization as well as the energy degradation of ^{80}Br; thus, the charge and the kinetic energy distribution of ^{80}Br in the reaction energy range is different from those of a system with no additives. Thus, the results shown in Table 1 can firm that fractions of $CH_3{}^{80}Br$ and $i\text{-}C_3H_7{}^{80}Br$ are formed *via* thermal ionic processes in a highly Kr-moderated system.

As an alternative approach to the true reaction processes involved in the C_3H_8 atmosphere, one can study a binary system, using C_2H_6 or CH_3Br as a counterpart. The IP's of the constituents are 11.21 eV for C_3H_8, 11.65 eV for C_2H_6, and 10.6 eV for CH_3Br, compared to 11.84 eV for Br.[8] If the identity of the reacting ^{80}Br is primarily controlled by the IP of the constituents of the reaction systems, it is seems that the thermal ionic processes are of only minor importance in these binary systems. Thus, the yields of the products from one of the constituents will decrease with an increase in the m. f. of the other and can be extrapolated to zero at 1.0 m. f. of the latter. However, if this is not the case, the yields, as a function of the diluent, will reflect the thermal ionic processes.

Table 2 summarizes the yield-variation of products from various mixtures of C_3H_8 and C_2H_6, and from those of C_3H_8 and CH_3Br. *Iso-* and $n\text{-}C_3H_7{}^{80}Br$ were formed only from the reaction of ^{80}Br with C_3H_8, and their yields decreased smoothly from 0.20 ± 0.02 and 0.67 ± 0.07 respectively with the addition of the diluent to zero percent. However, in the C_3H_8–C_2H_6 mixtures, $CH_3{}^{80}Br$, $C_2H_5{}^{80}Br$, and $CH_2{}^{80}BrBr$ were formed from the reactions with either constituent and the sum of the yields was the same as the observed yields of these products. Similarly, in the C_3H_8–CH_3Br mixture, $CH_3{}^{80}Br$ and $CH_2{}^{80}BrBr$ were products from both constituents.

A separation of the observed yield at any m. f. of C_3H_8 into the yields originating from the individual constituents can be performed on two assumptions; one, that the thermal ionic yield is zero over the whole range of m. f. of C_3H_8, and the other, that the relative yield distribution among the products from the reactions with C_3H_8 is constant over the range of m. f. of C_3H_8. The first assumption is rather probable in view of the IP's of the constitutents involved. The second assumption, however, is a crude one, since the ratio of $n\text{-}C_3H_7{}^{80}Br/i\text{-}C_3H_7{}^{80}Br$ tends to vary slightly with the m. f. of the diluents(see below). However, the variation is only significant at a small m. f. of C_3H_8, where the yields of products from C_3H_8 are small. This amount of variation in the yield distribution, thus, will have only a minor influence on the subsequent discussion.

With these assumptions, the yields of these products at any m. f. of C_3H_8 can be calculated by multiplying the percentage yield of $n\text{-}C_3H_7{}^{80}Br$ by 1.8 for $CH_3{}^{80}Br$, by 0.85 for $C_2H_5{}^{80}Br$, and by 0.70 for $CH_2{}^{80}BrBr$. The solid curves in Figs. 1 and 2 indicate the calculated yields of these products from the reactions with C_3H_8.

8) F. H. Field and J. L. Franklin, "Electron Impact Phenomena and the Properties of Gaseous Ions," Academic Press, New York (1957), Appendix.

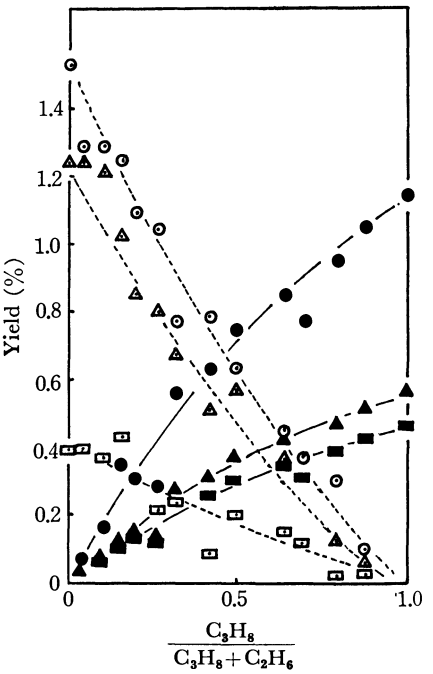

Fig. 1. Estimated yields from the reactions of ^{80}Br with C_3H_8 and C_2H_6 in the binary systems.
●: $CH_3{}^{80}Br$ from C_3H_8, ▲: $C_2H_5{}^{80}Br$ from C_3H_8,
■: $CH_2{}^{80}BrBr$ from C_3H_8, ⊙: $CH_3{}^{80}Br$ from C_2H_6,
△: $C_2H_5{}^{80}Br$ from C_2H_6, ⊡: $CH_2{}^{80}BrBr$ from C_2H_6.

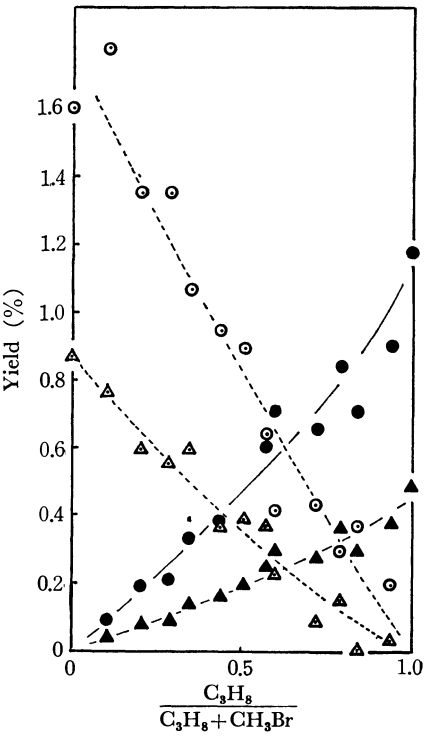

Fig. 2. Estimated yields from the reaction of ^{80}Br with C_3H_8 and CH_3Br in the binary systems.
●: $CH_3{}^{80}Br$ from C_3H_8, ▲: $CH_2{}^{80}BrBr$ from C_3H_8,
⊙: $CH_3{}^{80}Br$ from CH_3Br, △: $CH_2{}^{80}BrBr$ from CH_3Br

The dotted curves in the same figures are simply obtained from the difference between the calculated yields and the experimentally-determined yields at each measureing point and are assigned to the yield curves from the reactions with C_2H_6 or CH_3Br.

These results show that the yields of products which originated from either C_2H_6 or CH_3Br decreased zero upon the addition of C_3H_8, and that it is rather difficult to detect any interference of possible thermal ionic process in the yield variation. This implies that the thermal ionic process is not important in the present binary systems (see Appendix).

The oxygen added to suppress the radical formations of organic compounds amounts to roughly 9% of the reaction mixture. The IP of O_2 is intermediate between the first and the second IP of Br. Thus, its presence possibly influences the ^{80}Br spectrum towards preferring the formation of the thermal $^{80}Br^+$ ion. However, the influence will be smaller than that to be expected simply from its mole fraction judging from the point of the collision cross section for the ^{80}Br-O_2 and ^{80}Br-reactant molecule collisions. The analysis of the results (see Figs. 2 and 3) shows no positive evidence for the contribution of the thermal ionic process. Thus, it is conclusive that ^{80}Br reacts principally *via* the energetic processes to form organic compounds in the C_3H_8, C_2H_6, and CH_3Br atmospheres. However, when these reactants are diluted with a sufficiently large excess of Kr having a IP of 14.00 eV, the energy degradation and the charge neutralization of ^{80}Br are controlled through its collision with Kr. The thermal $^{80}Br^+$ was eventually obtained,[9] and its reaction became important. Those conclusions are consistent with the previous speculation[6] that the thermal ionic processes of ^{80}Br are almost negligible in a reaction system with a lower IP than that of Br.

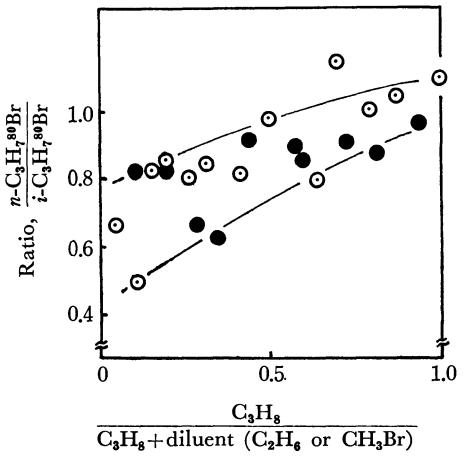

Fig. 3. Variation of n-$C_3H_7{}^{80}Br/i$-$C_3H_7{}^{80}Br$ per bond basis as a function of concentration of C_3H_8, relative to diluent.
⊙: C_3H_8-C_2H_6-O_2 system, ●: C_3H_8-CH_3Br-O_2 system

Reactivity of Primary and Secondary C–H Bonds in C_3H_8. In the recoil atom reactions, the chemical factors often play an important role in controlling the reactivity of various bonds. Two main difficulties have usually confronted such experiments: 1) the attainment of the "equivalent experimental conditions" for the comparison of the various chemical bonds, and 2) the failure of all of the molecules formed in the primary reactions to survive long enough to be measured.[10] The most important problem in trying to equalize conditions for an inter- or intra-comparison of different samples is in controlling the number and distribution *vs.* the energy of the hot collisions potentially available to an energetic atom prior to thermalization.[11–13] The cumulative absolute yield from a particular hot atom reaction is a function not only of the other hot reactions available to the energetic atom at all energies, but also of the rate of energy loss for the atom in nonreactive collisions. The measurement of the relative yields in an intramolecular system, however, ensures that each hot atom sums over the identical recoil atom spectrum and is free from the problem.

Propane includes both primary and secondary C–H bonds in a molecule, thus permitting a direct comparison of the reactivities of these C–H bonds toward the energetic ^{80}Br atom. The ^{80}Br *for H* reaction gives n- and i-$C_3H_7{}^{80}Br$, depending upon which kind of C–H bond is attacked. The bond dissociation energies are 4.23±0.04 eV for primary, and 4.1± 0.02 eV for secondary, C–H bonds.[14] If the chemical characteristics, including the bond strength, have some correlation with the reactivity toward the energetic ^{80}Br, it may appear in the relative yields of n- and i-$C_3H_7{}^{80}Br$.

Figure 3 shows the variation in the n-$C_3H_7{}^{80}Br/i$-$C_3H^{80}Br$ per bond basis as function of $C_3H_8/(C_3H_8+$ diluent) in the mixed system with C_2H_6 or CH_3Br. One can discuss the results without any correction for the ^{80}Br-spectrum, but they must be corrected for the decomposition reactions of the primary products. The most probable decomposition pathway both for n- and i-$C_3H_7{}^{80}Br$ is the elimination of $H^{80}Br$ to form

Table 3. Effects of the total pressure on the yields of n-$C_3H_7{}^{80}Br$ and i-$C_3H_7{}^{80}Br$ (Br_2/C_3H_8= 0.02 and O_2/C_3H_8=0.1)

Total pressure	i-$C_3H_7{}^{80}Br$ (%)	n-$C_3H_7{}^{80}Br$ (%)	$\frac{n\text{-}C_3H_7{}^{80}Br}{i\text{-}C_3H_7{}^{80}Br}$ (per bond basis)
55	0.12	0.17	0.47
211	0.17	0.43	0.84
337	0.17	0.43	0.84
558	0.19	0.55	0.96
698	0.21	0.66	1.1
710	0.20	0.67	1.1
773	0.20	0.69	1.2
1052	0.27	0.76	0.94
1600	0.27	0.83	1.0

9) F. Cacace and G. Stocklin, *J. Amer. Chem. Soc.*, **94**, 2518 (1972).

10) Y. N. Tang and F. S. Rowland, *ibid.*, **87**, 3304 (1965), **90**, 574 (1968).

11) Y. N. Tang, E. K. C. Lee, E. Tachikawa, and F. S. Rowland, *J. Phys. Chem.*, **75**, 1290 (1971).

12) E. K. C. Lee and F. S. Rowland, *J. Amer. Chem. Soc.*, **85**, 2907 (1963).

13) C. C. Chou and F. S. Rowland, *J. Phys. Chem.*, **75**, 1283 (1971).

14) E. Tachikawa, Ph, D. Thesis, Univ. of Calif., Irvine, (1967), p. 181.

C_3H_6. Such unimolecular reactions can be conveniently investigated through pressure variation experiments; the present pressure-dependent data are shown in Table 3. The yields of both *n*- and *i*-$C_3H_7{}^{80}Br$ increased with an increase in the pressure. The ratio between them also increased, with a preference toward *n*-$C_3H_7{}^{80}Br$, at the beginning, but tended to be constant at 1.1 ± 0.1 over a total pressure of 600 Torr. However, this value does not necessarily indicate the real yield ratio of the primary reactions, since the correct estimation must be based on measurements of their secondary decomposition products, measurements are not possible in this type of experiment. In the present semiquantitative consideration, no correction has been made for the secondary decompositions of the primary products, since no a priori basis for estimating a correction factor exists. Recent theoretical knowledge indicates that more than one chemical bond is involved in the substitution reaction of an energetic atom.[15] Furthermore, the intramolecular distribution of the excitation energy is attained within a few vibrations. Thus, even if the secondary decomposition of the primary products still occur at pressures higher than 600 Torr, the yield ratio of *n*-$C_3H_7{}^{80}Br$/*i*-$C_3H_7{}^{80}Br$ should be much less sensitive to the applied pressure.

With these allowances, one can notice a positive dependence of the ratio on the concentration of C_3H_8, although the points deviate considerably. The ratio is 1.1 ± 0.1 with no dilution, and seems to decrease with the diluent. This qualitatively implies that the difference in reactivities of two kinds of C–H bonds for ^{80}Br is not significant in the distribution spectrum of the ^{80}Br controlled by collisions, principally with C_3H_8, but that the reactivity of secondary C–H bonds relative to primary C–H bonds increases with the dilution. While the effects on energy moderation by an inert gas are relatively simple to evaluate, the effects of dilution by a second reagent are much more complex, since such a reagent influences the ^{80}Br-spectrum through both kinetic-energy moderation and reactive collisions. The total organic yields from systems variously diluted with a second reagent, however, are always very small, as may be seen in Table 2; this, the elimination of ^{80}Br through reactions with the diluent cannot be important in the present qualitative discussion. As dilution with the diluent proceeds, the kinetic energy spectrum of ^{80}Br available for the reactions with C_3H_8 tends to shift to the lower-energy end and the lower-energy process becomes preferred over the high-energy process. Thus, one can tentatively conclude that the formation of *i*-$C_3H_7{}^{80}Br$ is a lower energy process than the formation of *n*-$C_3H_7{}^{80}Br$.

The efficiency of the kinetic energy moderation varies depending upon the additive used in the binary systems. Thus, the rate of decrease in the *n*-$C_3H_7{}^{80}Br$/*i*-$C_3H_7{}^{80}Br$ ratio with dilution should be correlated with the additives used. Unfortunately, the scattering of the results exceeds the possible variation in the ratio due to the different moderating efficiency of the diluent.

The relative position of the energy range of the reactions with two kinds of C–H bonds is consistent with the pressure dependence of the yields of the reaction products. The failure of the billiard-ball type of approximation in the recoil atom reaction implies that the internal excitation energy of the primary substitution reaction products is a good guide for the average kinetic energy of the recoil atom at the time of reaction.[16–18] As the total pressure rises, the stabilization of the excited products become more probable. Thus, an increase in the *n*-$C_3H_7{}^{80}Br$/*i*-$C_3H_7{}^{80}Br$ ratio with the pressure will be reflected in the fact that *i*-$C_3H_7{}^{80}Br$ is less excited and has a longer life-time, than *n*-$C_3H_7{}^{80}Br$.

The present results thus furnish evidence that the secondary C–H bond is more subject to the *^{80}Br for H* reaction than is the primary C–H bond under kinetic-energy-moderated conditions. Although this is consistent with the C–H bond strength effect involving the higher reactivity of the weaker C–H bond than that of the stronger C–H bond, no definite impormation has been obtained here concerning the identity of the chemical nature affecting the reactivities of two kinds of C–H bonds.

The trend toward higher yields for reactions with less sterically obstructed C–H would favor a higher yield for *n*-$C_3H_7{}^{80}Br$ than that for *i*-$C_3H_7{}^{80}Br$, this is not supported by the experimental observations. If such a steric factor is also opperative in the present experiment, the assessment of the importance of the chemical nature must be increased by an equivalent counterbalancing factor.

Appendix

The kinetic theory for energetic atom reactions was developed by Wolfgang *et al.*[10,20] and has since been applied to various systems.[21] The assumptions involved in its application to the reaction systems of ^{80}Br have been discussed by Milman.[22] Success depends on the assumptions that neither S nor α is a function of the recoil atom energy, or that, if they are, the energy variations are slight and the function smooth. Another important assumption is that the initial energy of the recoil atom is sufficiently high for the atoms to have made a number of collisions in order to attain the statistical distribution of energies for the atoms in the reaction range. The average kinetic energy of the Br atom achieved from the molecular explosion of Br_2 can be estimated to be up to 100 eV, based upon the Coulombic interaction energy. Since our knowledge about the kinetic energy spectrum of Br is not yet complete, we assume this

15) D. L. Bunker and M. Pattengill, *Chem. Phys. Lett.*, **4**, 315 (1969), *J. Chem. Phys.*, **53**, 3041 (1970).

16) E. K. C. Lee and F. S. Rowland, *J. Amer. Chem. Soc.*, **85**, 897 (1963).

17) C. F. McKnight and J. W. Root, *J. Phys. Chem.*, **73**, 4430 (1969).

18) C. F. McKnight, N. J. Parks, and J. W. Root, *ibid.*, **74**, 217 (1970).

19) P. J. Estrup and R. Wolfgang, *J. Amer. Chem. Soc.*, **82**, 2665 (1960).

20) R. Wolfgang, *J. Chem. Phys.*, **39**, 2983 (1963).

21) E. P. Rack and A. A. Gordus, *J. Phys. Chem.*, **65**, 944 (1961).

22) M. Milman, *Radiochim. Acta*, **2**, 180 (1964).

to be reasonably justified in our case.

The developed equation for the yields of individual products from energetic reactions with a reactant in the moderated system, P_1, is:

$$P_1 = \frac{f_1}{\alpha} I_1 - \frac{f_1^2}{\alpha^2} K_1 + \frac{f_1^3}{\alpha^3} L_1 - \quad (1)$$

where f and α have their usual meanings.

Unless the total reactivity of the system is very high, the series will converge rapidly. In systems of a very low reactivity, as in the present case, only the first may be sufficient.

Table 4. Relative α-values in the ^{80m}Br-C_3H_8-C_2H_6 and ^{80m}Br-C_3H_8-CH_3Br systems

In C_3H_8-C_2H_6 system compound	intercept $\alpha(R)/I_1$	slope $\alpha(M)/I_1$	$\frac{\alpha(C_3H_8)}{\alpha(C_2H_6)}$
i-$C_3H_7{}^{80}Br$ from C_3H_8	4.0	4.0	1.0
n-$C_3H_7{}^{80}Br$ from C_3H_8	1.4	1.3	1.1
$CH_3{}^{80}Br$ from C_2H_6	0.66	0.68	1.0
$C_2H_5{}^{80}Br$ from C_2H_6	0.78	0.84	1.1
$CH_2{}^{80}BrBr$ from C_2H_6	2.4	3.7	1.5
			av. 1.1±0.2
In C_3H_8-CH_3Br system compound	intercept $\alpha(R)/I_1$	slope $\alpha(M)/I_1$	$\frac{\alpha(C_3H_8)}{\alpha(CH_3Br)}$
i-$C_3H_7{}^{80}Br$ from C_3H_8	4.8	6.3	0.76
n-$C_3H_7{}^{80}Br$ from C_3H_8	1.8	2.6	0.69
$C_2H_5{}^{80}Br$ from C_3H_8	2.1	2.6	0.81
$CH_3{}^{80}Br$ from CH_3Br	0.56	0.47	0.83
$CH_2{}^{80}BrBr$ from CH_3Br	1.2	0.88	0.74
			av. 0.77±0.06

Table 5. ^{80}Br recoil energies resulting from coulombic repulsion of $^{80m}BrBr$

Original charge on bromine	^{80}Br recoil energies (eV)
+2	3.2
+4	9.6, 12.9
+6	16.1, 25.8, 29.0
+8	22.4, 38.5, 48.2, 51.4
+10	29.0, 51.4, 68.0, 77.0, 80.4
+12	35.3, 64.3, 86.7, 102.7, 115.6

Thus, in a moderated system Eq. (1) may be modified to this equation:

$$\frac{1}{P_1} = \frac{\alpha(R)}{I_1} + \frac{\alpha(M)}{I_1}\left[\frac{f(M)+Af(O_2)}{f(R)}\right] \quad (2)$$

where $A=\alpha(O_2)/\alpha(M)$; when M is C_2H_6, $A=0.72$ was obtained using the results in Ref. 6). When we plot $1/P$ *vs.* $[f(M)+Af(O_2)]/f(R)$, the slope is $\alpha(M)/I_1$ and the intercept is $\alpha(R)/I_1$. The ratio of these gives $\alpha(M)/\alpha(R)$.

The results shown in Figs. 1 and 2 have been used for the kinetic treatment according to Eq. (2). Table 4 summarizes the $\alpha(M)/I_1$, $\alpha(R)/I_1$, and $\alpha(M)/\alpha(R)$ thus obtained. In the present kinetic analysis two important requirements are not fully satisfied. One of these is that, because the initial kinetic energy is relatively low (see Table 5) the equilibrium distribution of ^{80}Br can not be attained in the reaction energy range. The other is the exclusion of the energetic-$H^{80}Br$ yield from the considerations, which will introduce a serious error if we ignore the higher terms in Eq. (1). Despite these difficulties, reasonably consistent values are obtained for both $\alpha(M)/\alpha(R)$ values. These, in turn, indicate that the above assumptions are reasonably satisfied and that the present kinetic analysis is justified within our limits of experimental accuracy.

BULLETIN OF THE CHEMICAL SOCIETY OF JAPAN, VOL. 46, 351—354 (1973)

A New Catalyst for Ethylene Polymerization Containing Nickel Oxide

Ken-ichi MARUYA and Atsumu OZAKI

Research Laboratory of Resources Utilization, Tokyo Institute of Technology, Ohokayama, Meguro-ku, Tokyo

(Received February 23, 1972)

A new catalyst for ethylene polymerization $NiO–NiSO_4$, was found from a study of $NiO–SiO_2$, and $NiCl_2$ catalysts. The $Ni–NiSO_4$ catalyst prepared from mixtures of formate and sulfate is much less active than $NiO–NiSO_4$ prepared from mixtures of hydroxide and sulfate. Poisoning behavior of carbon monoxide and water is quite similar to $NiO–SiO_2$ catalyst. An equimolar mixture of $NiO–NiSO_4$ gives maximum activity. The active species is postulated to be hydroxy sulfate of nickel. The structure of the active site is discussed.

Nickel oxide-silica is known to be effective for the dimerization of ethylene at room temperature.[1] As an extention of the study on its active site various nickel salts were tested for their activity in dimerization. It was found that nickel chloride could be activated for dimerization, when it was evacuated at above 230°C after a preevacuation at 140°C.[2] Both catalysts have common features. (1) Isotopic mixing in ethylene [1,3] and isomerization of *n*-butene[4,5] simultaneously take place over these catalysts. (2) They are poisoned by a small amount of CO for dimerization but not for isomerization. (3) The rate

1) K. Kimura, H. A-I, and A. Ozaki, *J. Catal.*, **18**, 271 (1970).
2) K. Maruya, N. Ando, and A. Ozaki, *Nippon Kagaku Zasshi* **91**, 1125 (1970).
3) A. Ozaki, H. A-I, and K. Kimura, Int. Congr. Catal., 4th, Moscow, paper 40 (1968).
4) K. Maruya, N. Ando, and A. Ozaki, *Nippon Kagaku Zasshi* **92**, 699 (1971).
5) A. Ozaki, and K. Kimura, *J. Catal.*, **3**, 395 (1964).

of dimerization decreases with the increase in carbon number of olefin.[4,6] This similarity in catalytic properties suggests that an essentially identical active site is responsible for the dimerization over nickel oxide-silica and nickel chloride.

It has been suggested that the active site for dimerization is formed by an interaction of a nickel ion of low valency with an acid site.[1] The characteristic reaction on the low valent nickel is the chemisorption of CO and the isotopic mixing in ethylene. The acid site is characterized by butene isomerization.[5] It was shown that nickel oxide alone is activated for the isotopic mixing in ethylene by evacuation above 300°C, but it is inactive for the dimerization.[3] This is possibly due to the fact that no acid site can be developed on pure nickel oxide. An acid nature of nickel oxide silica has been shown.[1,5] Other catalyst systems for dimerization could thus be obtained by incorporating low valent nickel with acid component. This view was examined by combining nickel formate or hydroxide expected to give reduced nickel or nickel oxide after decomposition, with a number of sulfates which are known to be acidic.[7] In this way a new catalyst system of NiO–$NiSO_4$ was found for the polymerization of ethylene.

Experimental

Preparation. Catalysts containing nickel formate were prepared by evaporating mixed aqueous solutions of nickel formate and sulfate. Although nickel formate was deposited during the course of evaporation, the mixture was evaporated to dryness with stirring. The product thus obtained was green powder. The catalysts contianing nickel hydroxide were prepared by evaporating mixtures of nickel sulfate solution and the nickel hydroxide freshly prepared from nickel nitrate by precipitation with aqueous ammonia.

Procedure. The rate of polymerization of ethylene was determined at 30°C with an initial pressure of 45 cmHg, measuring pressure decrease in a constant volume static system, utilizing an oil manometer for less active catalysts. Reaction products were analyzed by gas chromatography using ODPN or pola-pack column. The rate of isomerization of 1-butene was estimated by conversion within 15 min at room temperature.

Results

Nickel Formate-based Catalyst (Catalyst I). Six sulfates (Mg^{2+}, Al^{3+}, Fe^{3+}, Co^{2+}, Ni^{2+}, and Cu^{2+}) were tested for their effectiveness as co-catalysts to nickel in the ethylene polymerization by combining each with nickel formate. It was found that only nickel sulfate was effective for the purpose.

Different mole ratios of nickel formate-nickel sulfate mixtures were evacuated at 300°C for 3 hr and tested for their activities. The rates of polymerization were so low that the pressure change was followed by an oil manometer. The pressure change with time is exemplified in Fig. 1. There is an induction period

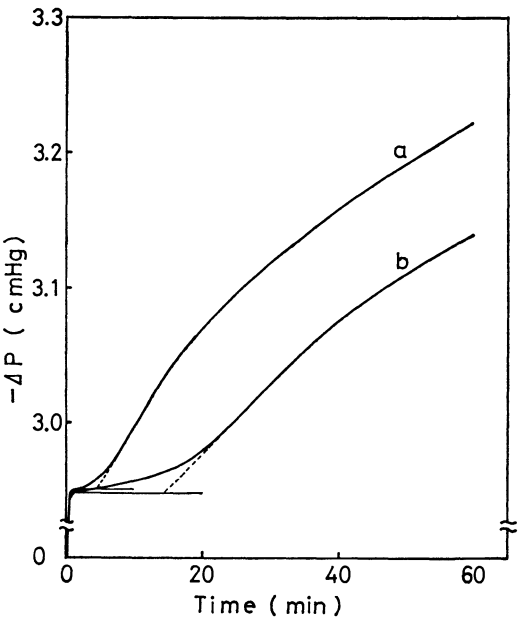

Fig. 1. Typical time course of ethylene polymerization over catalyst I.
$Ni(HCOO)_2/NiSO_4$=1 in a, 1/10 in b

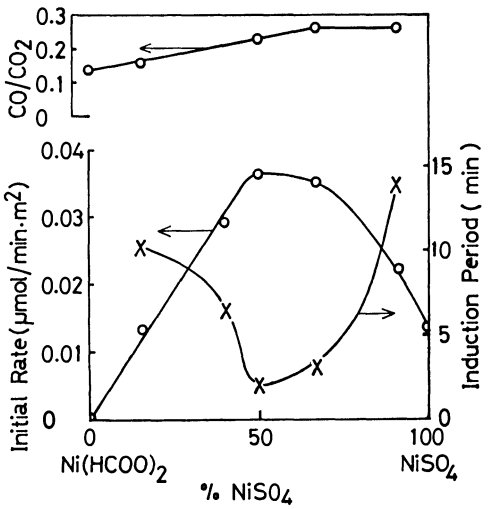

Fig. 2. Variations of induction period, initial rate of ethylene consumption and CO/CO_2 ratio in the decomposition product of $Ni(HCOO)_2$–$NiSO_4$ mixture with composition.

for the pressure change after a rapid initial change due to adsorption. The initial rates of ethylene consumption and the induction periods obtainable by the extrapolation shown in Fig. 1, are given in Fig. 2 as a function of catalyst composition. It can be seen that the maximum rate is obtained at around equimolar composition accompanied by minimum induction period, and that nickel sulfate itself has a small activity.

The product obtained from the gas phase was exclusively *n*-butenes.

The rate of ethylene consumption by the equimolar mixture was drastically reduced to about one seventh by 0.5 μmol/g of preadsorbed CO, or by 50 μmol/g of preadsorbed H_2O. However, in the case of pure nickel sulfate no effect of CO was observed.

6) M. Koizumi, *J. Institute Polytechnics, Osaka City Univ.*, **4**, No. 1, Series C (1953).
7) K. Tanabe and T. Takeshita, *Advan. Catal.*, **173**, 15 (1967).

The nature of decomposition product of nickel formate was examined by the reaction of C_2H_4 and D_2 on a catalyst rich in nickel sulfate ($Ni/NiSO_4=1/10$) at 30°C for 2 hr. Neither exchange nor hydrogenation was detected, suggesting that no metallic phase of nickel exists at least on the surface. The ratio of CO/CO_2 in the gaseous decomposition product from the catalyst mixtures is shown in Fig. 2 as a function of catalyst composition. It can be seen that the ratio increases with the concentration of nickel sulfate.

The decomposition of nickel formate has been described by several authors[8,11] in terms of the following two simultaneous reactions

$$Ni(HCOO)_2 \longrightarrow \begin{cases} Ni + H_2 + 2CO_2 & (a) \\ Ni + H_2O + CO + CO_2 & (b) \end{cases}$$

although the relative importance of each reaction seems to depend on reaction condition and particle size of the sample.[12] According to Kornienko,[13] however, about 10% of nickel is transformed into NiO in the absence of H_2 and CO. It was found in the present case that 3.4 (ml S. T. P.) of hydrogen was absorbed for 3 hr at 300°C by the decomposition product from 1 g of $Ni(HCOO)_2 \cdot 2H_2O$. It was suggested that the nickel formate was partly transformed into nickel oxide instead of metallic nickel. The presence of nickel sulfate appeared to enhance the formation of nickel oxide. Thus the question arose of whether the real catalyst might not be a composite of nickel oxide and nickel sulfate. This led to the following study of $NiO–NiSO_4$ system.

Nickel Hydroxide-based Catalyst (Catalyst II). An equimolar mixture of nickel hydroxide and nickel sulfate was evacuated at 300°C for 1 hr and tested for its activity in the ethylene polymerization at 30°C. The pressure change with time is shown in Fig. 3. It is obvious that ethylene is rapidly consumed with no induction period. The rate of consumption is about 30 times that by equimolar catalyst I. Figure 3 also shows another run in which 1 μmol/g of CO was preadsorbed. It is clear that the pressure change stops after the initial rapid decrease which should be due to adsorption process. This shows that carbon monoxide effectively poisons this catalyst also.

Since the initial decrease due to adsorption is nearly over within the first one minute, it is better to estimate the initial rate of ethylene consumption after this period. Thus the initial rates are obtained from the pressure change in the period 1—3 min and plotted against the temperature of evacuation (Fig. 4). It can be seen that the activity appears above 200°C reaching a maximum at 350°C. It is remarkable

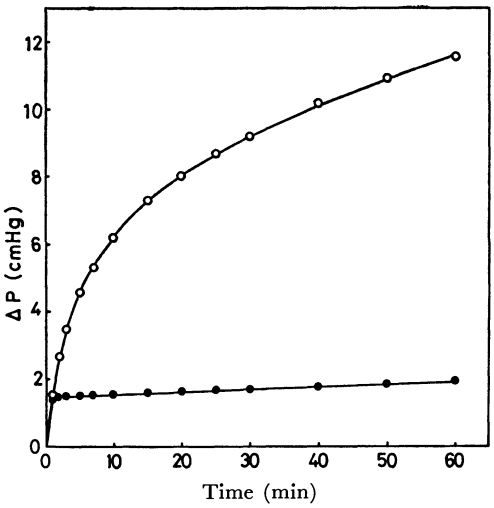

Fig. 3. Time course of ethylene polymerization at 30°C over $NiO–NiSO_4$ (1/1) catalyst evacuated at 300°C 1 hr. Solid circle shows the run with preadsorbed CO of 1 μmol/g.

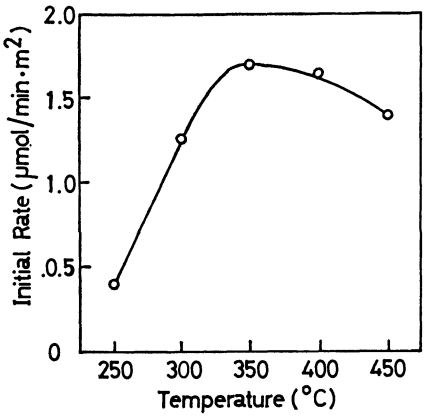

Fig. 4. Variation of initial rate with the evacuation temperature. $NiO/NiSO_4=1$.

that the acidity of nickel sulfate attains a maximum by the heat treatment at 350°C.[7]

The effect of composition on the initial rate per surface area was examined where the catalysts were evacuated at 250°C. As shown in Fig. 5, the maximum activity is obtained at equimolar composition. Another series of runs were made to study the effect of composition on isomerization of butene on this catalyst system. The result is also shown in Fig. 5. Since nickel sulfate is known to be acidic and to catalyze the isomerization of butene and since nickel oxide is known to be inactive, it can be expected that the activity of a mechanical mixture of the two components for the isomerization of butene increases with the content of nickel sulfate. In this respect the result shown in Fig. 5 is remarkable. The activity for isomerization also attains a maximum at the equimolar composition. This is not due to the change in surface area as shown in Fig. 5. The result, as well as that on the rate of polymerization, suggests that the mixture is not merely a mechanical mixture and the equimolar composition is significant as regards the active site.

The nature of the active site for isomerization was

8) A. A. Balandin, E. S. Grigoryan, and Z. S. Yanisheva, *Acta Physicochem. USSR*, **12**, 737 (1940); *J. Gen. Chem. USSR*, **10**, 1031 (1940).

9) L. L. Bitcumshaw, and J. Edwards, *J. Chem. Soc.*, **1950**, 1800.

10) T. Sasa, *Yuki Gosei Kagaku Kyokai Shi*, **11**, 463 (1953).

11) T. Yamanaka, Y. Takagi, and K. Taya, *Sci. Papers I. P. C. R.*, **5**, 78 (1959).

12) P. G. Fox, J. Ehretsmann, and C. E. Brown, *J. Catal.*, **20**, 67 (1971).

13) V. P. Kornienko, *Ukrain. Khim. Zhur.*, **18**, 579 (1952).

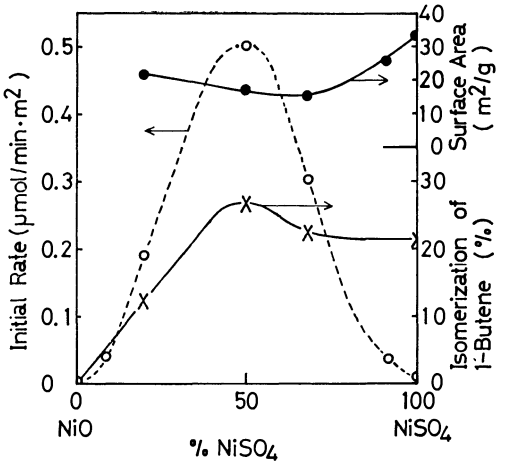

Fig. 5. Variations of initial rate of ethylene polymerization, extent of 1-butene isomerization and specific surface area with catalyst composition of NiO–$NiSO_4$ system.

examined by the effect of preadsorbed carbon monoxide. It was found that 1 μmol/g. cat. of carbon monixide gave no effect on the extent of isomerization, although the amount of carbon monixide was enough to inhibit the polymerization. The result is reasonable when the active site for isomerization is an acid one.

Discussion

The postulate for the active site could develop a new catalyst system formed by the interaction of nickel oxide with nickel sulfate. However, the postulate should be corrected on the basis of the present results. The term "low valent nickel" originated from the fact that the NiO–SiO_2 catalyst was drastically poisoned by carbon monoxide, since a low-valent nickel is favorable to chemisorb carbon monoxide.[1] Catalyst I of the present study was adopted to test the idea "low valent". That catalyst I was much less active than catalyst II shows that the metallic state of nickel is inadequate to form the active site. A slight activity observed in catalyst I can be ascribed to a small amount of nickel oxide formed in the decomposition of nickel formate. It is to be noted that the NiO–SiO_2 catalyst is remarkably deactivated by hydrogen reduction to Ni–SiO_2.[14] Even in Ni–SiO_2 catalyst we can assume unreduced nickel, because oxide reacted with silica gel is hardly reducible.[15]

An essential feature common to NiO–SiO_2 and NiO–$NiSO_4$ is the fact that both catalysts are activated by dehydration from the surface, forming a carbon monoxide-sensitive site. This is also observed with nickel oxide alone, although the dehydrated nickel oxide is not active for dimerization, but active for isotopic mixing in ethylene[3] and hydrogenation of ethylene.[16] The active site for dimerization has been postulated to be formed by an interaction of the carbon monoxide sensitive site of the nickel oxide with an acid site. In fact, the expected activity was obtained by incorporating nickel sulfate which is known to provide an acid site. However, it is to be noted that none of the other sulfates known to be acidic could give activity by incorporation with nickel formate. In view of this fact, it is interesting that the acidic component in NiO–SiO_2 is formed by the reaction between nickel hydroxide and silica gel, as observed in the SiO_2–Al_2O_3 system. It seems that nickel ion is involved in the acidic component to cause an effective interaction between the carbon monoxide sensitive site and the acid component.

We found that an equimolar mixture of $Ni(OH)_2$ and $NiSO_4$ gives a maximum activity. The equimolar mixture may be regarded as a hydroxy nickel sulfate $Ni_2(OH)_2SO_4$. Although the structure of hydroxy sulfate of nickel is unknown, there can be pairs of –Ni(OH) groups which are separated by sulfate ions as

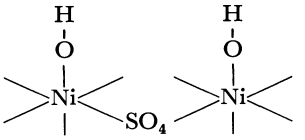

When the hydroxy sulfate is subjected to heat treatment, –Ni(OH) would be dehydrated forming two types of sites (A) and (B).

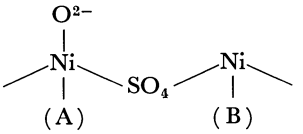

Since both (A) and (B) are coordinatively unsaturated, such pairs of nickel ion would disappear upon rearrangement at higher temperature. However, at intermediate temperature, pairs of (A) and (B) are likely to exist as an intermediate metastable state, being separated from each other by the sulfate ion. If this presumption is correct, site (A) may have a higher electron density than (B) owing to high electron density in the attached oxide anion. The observed poisoning by CO is reasonable on the type (A) site. It has been noted that CO poisons both the ethylene dimerization and the isotopic mixing in ethylene but not the isomerization of butene over the same catalyst.[1] This was confirmed with this catalyst system. The view is reasonably interpreted as selective occupation of type (A) site by CO, type (B) site being unoccupied. (B) is essentially an acid site and can act as a site for the butene isomerization.

The activation by heating in a vacuum followed by degradation at higher temperature is also reasonable as dehydration to form the pair of nickel ions followed by structural rearrangement. It is interesting that the activation of NiO–$NiSO_4$ reaches a maximum by heat treatment at 350°C at which the acidity of $NiSO_4$ reaches a maximum.[7] This coincidence would be reasonable if the basic structure is similar in both systems so that the maximum is determined by the temperature at which the structural rearrangment begins.

14) M. Koizumi, *Nippon Kagaku Kaishi*, **64**, 257 (1943).
15) J. J. B. van Eijk van Voorthuijsen, and P. Franzen, *Rec. Trav. Chim.* **70**, 793 (1951).
16) D. L. Harrison, D. Nicholls, and H. Steiner, *J. Catal.* **7**, 359 (1967).

Generalized Method for Calculating Löwdin Orbitals

Kazuya Suzuki, Shinsaku Maruyama, and Kunio Araki

Takasaki Radiation Chemistry Research Establishment, Japan Atomic Energy Research Institute, Takasaki

(Received March 9, 1972)

A generalized method for numerically calculating Löwdin orbitals is proposed, the method being an application of Frobenius' theorem in algebra. Löwdin transformation matrix $\mathbf{T}=\mathbf{S}^{-1/2}$ ($\mathbf{S}$ is overlap matrix) is calculated as $\mathbf{T}=\mathbf{U}\mathbf{S}_0^{-1/2}\mathbf{U}^t$, where $\mathbf{S}_0$ is a diagonal matrix whose diagonal elements are eigen values of $\mathbf{S}$, $\mathbf{U}$ is a matrix whose column vectors are eigen vectors of $\mathbf{S}$ and $\mathbf{U}^t$ is the transposed matrix of $\mathbf{U}$. It is proved that the eigen values of the overlap matrix of $\mathbf{S}$ are always positive for any choice of linearly independent atomic orbitals and that $\mathbf{S}^{-1/2}$, the inverse square-root of $\mathbf{S}$, exists within the range of real numbers. This method is useful for computer calculation by applying Jacobi's method.

Theoretical

Löwdin's method is used for orthonormalizing a given set of atomic orbitals and the transformed orbitals, Löwdin orbitals are useful for zero differential overlap approximation[1] (ZDO). However, for the numerical calculation of the Löwdin transformation matrix $\mathbf{T}=\mathbf{S}^{-1/2}$, only an expansion formula was shown[2,3] as

$$\mathbf{S}^{-1/2} = \mathbf{I} - 1/2\mathbf{D} + 3/8\mathbf{D}^2 - 5/16\mathbf{D}^3 + \cdots\cdots \quad (1)$$

where $\mathbf{S}$ is overlap matrix and an element of $\mathbf{S}$, s_{ij} is defined by

$$s_{ij} = \int x_i(v)x_j(v)\mathrm{d}v$$

x_i, x_j are atomic orbitals
$\mathbf{I}$; unit matrix
$\mathbf{D} = \mathbf{S} - \mathbf{I}$

If the value of the overlap integral s_{ij} is large, the convergence of Eq. (1) is not good. Generally, the value of overlap integral of pi orbitals is 0.20—0.30 and that of sigma orbitals 0.20—0.60. Thus, Eq. (1) is not considered to be sufficiently accurate for a detailed calculation on sigma orbitals. For other cases, in applying group theory, basic AO's are transformed into symmetry orbitals and the overlap integrals are inevitably large, if the orbitals belong to the same irreducible representation. Thus, a method for accurate calculation on the transformation matrix $\mathbf{T}=\mathbf{S}^{-1/2}$ is necessary.

In algebra, the regular matrix $\mathbf{S}$ is solved into the product of three factors:

$$\mathbf{S} = \mathbf{U}\mathbf{S}_0\mathbf{U}^t \quad (2)$$

where the matrices $\mathbf{U}$, $\mathbf{S}_0$, and $\mathbf{U}^t$ are as follows.

$$\mathbf{U} = \begin{pmatrix} u_{11} & u_{12} & \cdots\cdots & u_{1m} \\ u_{21} & u_{22} & \cdots\cdots & u_{2m} \\ \cdots & \cdots & \cdots\cdots & \cdots \\ \cdots & \cdots & \cdots\cdots & \cdots \\ u_{m1} & u_{m2} & \cdots\cdots & u_{mm} \end{pmatrix}$$

The column vector of $\mathbf{U}$, $\mathbf{u}_j(u_{1j},u_{2j},\cdots\cdots,u_{mj})$, is an eigen vector of $\mathbf{S}$. ($j=1,2,\cdots\cdots,m$)

$$\mathbf{S}_0 = \begin{pmatrix} s_1 & & 0 \\ & s_2 & \\ & & \ddots \\ 0 & & s_m \end{pmatrix}$$

The diagonal element of $\mathbf{S}_0$, s_j is an eigenvalue of $\mathbf{S}$ ($j=1,2,\cdots\cdots,m$).

$\mathbf{U}^t$; transposed matrix of $\mathbf{U}$

As the matrix $\mathbf{U}$ is unitary, $\mathbf{U}^t=\mathbf{U}^{-1}$, $\mathbf{U}\mathbf{U}^t=\mathbf{I}$ and $\mathbf{U}^t\mathbf{U}=\mathbf{I}$. By means of Eq. (2), we can calculate the matrix $\mathbf{D}$ of Eq. (1):

$$\mathbf{D} = \mathbf{S} - \mathbf{I} = \mathbf{U}(\mathbf{S}_0-\mathbf{I})\mathbf{U}^t$$
$$\mathbf{D}^2 = \mathbf{U}(\mathbf{S}_0-\mathbf{I})^2\mathbf{U}^t$$
$$\mathbf{D}^3 = \mathbf{U}(\mathbf{S}_0-\mathbf{I})^3\mathbf{U}^t$$
$$\cdots\cdots\cdots\cdots$$
$$\mathbf{D}^n = \mathbf{U}(\mathbf{S}_0-\mathbf{I})^n\mathbf{U}^t$$

Substituting these values for those of Eq. (1), we obtain the following equation.

$$\begin{aligned}\mathbf{S}^{-1/2} &= \mathbf{I} - 1/2\mathbf{U}(\mathbf{S}_0-\mathbf{I})\mathbf{U}^t + 3/8\mathbf{U}(\mathbf{S}_0-\mathbf{I})^2\mathbf{U}^t \\ &\quad - 5/16\mathbf{U}(\mathbf{S}_0-\mathbf{I})^3\mathbf{U}^t + \cdots\cdots \\ &= \mathbf{U}[\mathbf{I} - 1/2(\mathbf{S}_0-\mathbf{I}) + 3/8(\mathbf{S}_0-\mathbf{I})^2 \\ &\quad - 5/16(\mathbf{S}_0-\mathbf{I})^3 + \cdots\cdots]\mathbf{U}^t \\ &= \mathbf{U}[\mathbf{I} + (\mathbf{S}_0-\mathbf{I})]^{-1/2}\mathbf{U}^t \\ &= \mathbf{U}\mathbf{S}^{-1/2}\mathbf{U}^t\end{aligned}$$

The matrix $\mathbf{S}_0$ is diagonal, and we have

$$\mathbf{S}^{-1/2} = \mathbf{U} \cdot \begin{pmatrix} s_1^{-1/2} & & 0 \\ & s_2^{-1/2} & \\ & & \ddots \\ & & s_m^{-1/2} \end{pmatrix} \cdot \mathbf{U}^t \quad (3)$$

This is an exact and generalized expression for Löwdin transformation matrix $\mathbf{T}=\mathbf{S}^{-1/2}$, which is known in algebra as Frobenius' theorem;

Eigenvalues of matrix $F(\mathbf{A})$ are $F(\alpha_1),F(\alpha_2),\cdots\cdots,F(\alpha_m)$, where $\alpha_1,\alpha_2,\cdots\cdots,\alpha_m$ are eigenvalues of the matrix $\mathbf{A}$ and $F(x)=x^{-1/2}$.

It is proved that the eigenvalues $s_1,s_2,\cdots\cdots,s_m$ are always positive, not zero or negative. If one of the eigen values s_j is zero, the determinant of $\mathbf{S}$, Det $\mathbf{S}$ is zero (the matrix $\mathbf{S}$ is singular) and $\mathbf{S}^{-1}$, the inverse matrix of $\mathbf{S}$, does not exist. If the eigen value s_j is negative, the value of $s_j^{-1/2}$ is complex. It will be shown that no such cases exist.

1) J. A. Pople and G. A. Segal, *J. Chem. Phys.* **43**, S136, (1965)
2) P. O. Löwdin, *J. Chem. Phys*, **18**, 365, (1950).
3) P. O. Löwdin, *ibid.*, **21**, (1953).

The element of overlap matrix **S** is defined by

$$s_{ij} = \int x_i(v)x_j(v)\mathrm{d}v$$

and determinant of such a matrix is Gram's determinant (Gramian), which is transformed as follows.

$$\mathrm{Det}\,\mathbf{S} = 1/m\,!\iint\cdots\int \begin{Vmatrix} x_1(v_1) & x_2(v_1) & \cdots & x_m(v_1) \\ x_1(v_2) & x_2(v_2) & \cdots & x_m(v_2) \\ \cdots & \cdots & \cdots & \cdots \\ x_1(v_m) & x_2(v_m) & \cdots & x_m(v_m) \end{Vmatrix}^2 \mathrm{d}v_1\mathrm{d}v_2\cdots\mathrm{d}v_m$$

The atomic orbitals $x_1(v)$, $x_2(v)$, $\cdots$, $x_m(v)$ are linearly independent and then Det **S** is always positive.

$$\mathrm{Det}\,\mathbf{S} > 0$$

From Eq. (2), we have

$$\begin{aligned}\mathrm{Det}\,\mathbf{S} &= \mathrm{Det}\,(\mathbf{US_0U}^t) \\ &= \mathrm{Det}\,\mathbf{S}_0 \qquad (\mathbf{UU}^t=\mathbf{I}) \\ &= s_1s_2\cdots\cdots s_m\end{aligned}$$

then $s_1s_2\cdots\cdots s_m>0$

Thus it is proved that no one of the eigenvalues $s_1, s_2, \cdots\cdots s_m$ is zero and the matrix **S** is regular.

Next, it is shown all of them are positive. Considering the integral

$$Q = \int\left\{\sum_{j=1}^{m} p_jx_j(v)\right\}^2\mathrm{d}v$$

we find that Q is positive for arbitrary real numbers $p_1, p_2, \cdots\cdots, p_m$, except that the atomic orbitals $x_1(v)$, $x_2(v), \cdots\cdots, x_m(v)$ are linearly dependent (it is assumed that all the parameters p_j's are not zero). The integral Q is transformed into quadratic form:

$$\begin{aligned}Q &= \sum_{i,j=1}^{m}\int p_ip_jx_i(v)x_j(v)\mathrm{d}v \\ &= \sum_{i,j=1}^{m} p_ip_js_{ij} \\ &= (\mathbf{S}\boldsymbol{p}, \boldsymbol{p})\end{aligned}$$

where **S** is overlap matrix and $\boldsymbol{p}$ is non-zero vector $\boldsymbol{p}(p_1,p_2,\cdots\cdots p_m)$. Substituting **S** of Eq. (2), we obtain the following equation.

$$\begin{aligned}Q &= (\mathbf{US_0U}^t\boldsymbol{p}, \boldsymbol{p}) \\ &= (\mathbf{S}_0\mathbf{U}^t\boldsymbol{p}, \mathbf{U}^t\boldsymbol{p})\end{aligned}$$

here we introduce the parameter $\boldsymbol{q}(q_1,q_2,\cdots\cdots, q_m)$, which is transformed from the former parameter $\boldsymbol{p}(p_1, p_2 \cdots\cdots, p_m)$ as $\boldsymbol{q}=\mathbf{U}^t\boldsymbol{p}$.

$$\begin{aligned}Q &= (\mathbf{S}_0\boldsymbol{q}, \boldsymbol{q}) \\ &= s_1q_1^2 + s_2q_2^2 + \cdots\cdots + s_mq_m^2\end{aligned}$$

As the integral Q is also positive for real numbers $q_1, q_2, \cdots\cdots, q_m$, all the coefficients $s_1, s_2, \cdots\cdots, s_m$ are positive *i.e.* Q is positive definite quadratic form.

$$s_1 > 0,\ s_2 > 0, \cdots\cdots s_m > 0$$

Thus, Eq. (3) is always consistent for arbitrary functional systems $x_1(v)$, $x_2(v), \cdots\cdots, x_m(v)$, except for the case in which these functions are linearly dependent, in which case at least one of the eigenvalues of overlap matrix is zero and $\mathbf{S}^{-1/2}$, the inverse square-root matrix of **S**, does not exist.

Application of Eq. (3) to computer calculation is simple. In order to solve the secular equation of symmetric matrix **H** (Hamiltonian) or **F** (Hartree-Fock matrix), usually Jacobi's method is used. It is often preliminarily arranged as a subprogram. By using this, we can obtain the transformation matrix **T** as follows; eigen values and eigen vectors of **S** are calculated by Jacobi's method and then the diagonal elements $s_1, s_2, \cdots\cdots, s_m$ are substituted in Eq. (2) for the inverse square-root $s_1^{1/2}, s_2^{-1/2}\cdots\cdots, s_m^{-1/2}$. The process is easy programming. We might find the order of eigen values and eigen vectors, obtained by Jacobi's method, is indefinite and variable, depending on the diagonalizing operations. Nevertheless, the product of the matrices $\mathbf{S}=\mathbf{US_0U}^t$ and $\mathbf{S}^{-1/2}=\mathbf{US_0}^{-1/2}\,\mathbf{U}^t$ are uniquely determined. In other words, the matrices **S** and $\mathbf{S}^{-1/2}$ are invariable against the permutation of arbitrary eigenvalues and eigenvectors of **S**.

We have for an element of **S**, s_{pq}

$$\begin{aligned}s_{pq} &= \sum_{i,j=1}^{m} u_{pi}\delta_{ij}s_ju_{qj} \\ &= \sum_{j=1}^{m} u_{pj}s_ju_{qj}\end{aligned}$$

and similarly, for an element of $\mathbf{S}^{-1/2}$,

$$(\mathbf{S}^{-1/2})_{pq} = \sum_{j=1}^{m} u_{pj}s_j{}^{-1/2}u_{qj}$$

$$\mathbf{U} = \begin{array}{c} \\ \\ \\ p> \\ \\ q> \\ \\ \end{array}\begin{pmatrix} & & & \boldsymbol{u}_j & & \boldsymbol{u}_i & \\ u_{11} & u_{12} & \cdots & u_{1j} & \cdots & u_{1i} & \cdots \\ u_{21} & u_{22} & \cdots & u_{2j} & \cdots & u_{2i} & \cdots \\ \cdots & \cdots & \cdots & \cdots & \cdots & \cdots & \cdots \\ u_{p1} & u_{p2} & \cdots & u_{pj} & \cdots & u_{pi} & \cdots \\ \cdots & \cdots & \cdots & \cdots & \cdots & \cdots & \cdots \\ u_{q1} & u_{q2} & \cdots & u_{qj} & \cdots & u_{qi} & \cdots \\ \cdots & \cdots & \cdots & \cdots & \cdots & \cdots & \cdots \end{pmatrix}$$

As the summation is taken over all the elements of p-th row and q-th row, the total sum is invariant against permutation of arbitrary eigenvafues s_i, s_j and the corresponding column vectors u_i, u_j. Thus, the matrices **S** and $\mathbf{S}^{-1/2}$ are invariable against the change of the order of eigenvalues and eigenvectors.

Combination with group theory is also simple.[4] The basic AO's are at first transformed into symmetry orbitals and then ortho-normalized by the Löwdin transformation.

$$\begin{aligned}&\boldsymbol{x}_s = \mathbf{O}\boldsymbol{x}_a \quad (\boldsymbol{x}_s, \boldsymbol{x}_a, \text{ column vectors}) \\ \text{or}\quad &\boldsymbol{x}_s = \boldsymbol{x}_a\mathbf{O}^t \quad (\boldsymbol{x}_s, \boldsymbol{x}_a, \text{ row vectors}) \\ &\boldsymbol{x}_L = \boldsymbol{x}_s\mathbf{S}^{-1/2}\end{aligned}$$

where **O** is a unitary matrix determined from the symmetry of molecules. The vectors $\boldsymbol{x}_a$, $\boldsymbol{x}_s$, and $\boldsymbol{x}_L$ are the array of basic AO's, symmetry orbitals and ortho-normalized orbitals, respectively. The merit of these transformations lies in the invariability of the Hamiltonian and Hartree-Fock matrix.

4) J. A. Pople, D. P. Santry, and G. A. Segal, *J. Chem. Phys*, **43**, S 129, (1965).

Examples

Some examples of the Löwdin transformation matrix $\mathbf{T}=\mathbf{S}^{-1/2}$ are given as follows.

Ex. (1). *Pi Orbitals of Ethylene.*

C_1—C_2 the distance C_1—C_2; 1.34Å the value of overlap integral

$2p_{z1}$ $2p_{z2}$ $s_{12}=0.270$

The overlap matrix is as follows.

$$\mathbf{S}=\begin{bmatrix}1 & s\\ s & 1\end{bmatrix} \qquad s_{12}=s_{21}=s$$

By applying Eq. (2), the matrix **S** is transformed as

$$\mathbf{S}=\begin{bmatrix}1/\sqrt{2} & 1/\sqrt{2}\\ -1/\sqrt{2} & 1/\sqrt{2}\end{bmatrix}\begin{bmatrix}1+s & 0\\ 0 & 1-s\end{bmatrix}\begin{bmatrix}1/\sqrt{2} & -1/\sqrt{2}\\ 1/\sqrt{2} & 1/\sqrt{2}\end{bmatrix}$$

Then, by means of Eq. (3), we obtain

$$\mathbf{S}^{-1/2}=\begin{bmatrix}1/\sqrt{2} & 1/\sqrt{2}\\ -1/\sqrt{2} & 1/\sqrt{2}\end{bmatrix}\begin{bmatrix}1/\sqrt{1+s} & 0\\ 0 & 1/\sqrt{1-s}\end{bmatrix}\begin{bmatrix}1/\sqrt{2} & -1/\sqrt{2}\\ 1/\sqrt{2} & 1/\sqrt{2}\end{bmatrix}$$

Substituting s=0.270,

$$\mathbf{S}^{-1/2}=\begin{bmatrix}1.029 & -0.141\\ -0.141 & 1.029\end{bmatrix}$$

The same values are obtained also by Eq. (1).

Ex. (2). *Pi Orbitals of Allyl Radical.*

C_1 C_2 C_3 the distance C_1-C_2; 1.39Å
$<C_1C_2C_3=120°$

$2p_{z1}$ $2p_{z2}$ $2p_{z3}$ $s_{12}=0.246$
$s_{13}=0.035$

The overlap matrix **S** is as follows.

$$\mathbf{S}=\begin{bmatrix}1.000 & 0.246 & 0.035\\ 0.246 & 1.000 & 0.246\\ 0.035 & 0.246 & 1.000\end{bmatrix}$$

From C_{2v} symmetry of allyl radical the symmetry orbitals are obtained as $\Gamma=A_2+2B_1$

A_2; $1/\sqrt{2}\cdot 2p_{z1}-1/\sqrt{2}\cdot 2p_{z3}$

B_1; $2p_{z2}$, $1/\sqrt{2}\cdot 2p_{z1}+1/\sqrt{2}\cdot 2p_{z3}$

The overlap matrices of the symmetry orbitals are calculated to be

$$\mathbf{S}_{A2}=0.965$$

$$\mathbf{S}_{B1}=\begin{bmatrix}1.035 & 0.348\\ 0.348 & 1.035\end{bmatrix}$$

Then, the transformation matrices are obtained as follows.

$$\mathbf{S}_{A2}^{-1/2}=1.018$$

$$\mathbf{S}_{B1}^{-1/2}=\begin{bmatrix}1.030 & -0.183\\ -0.183 & 1.030\end{bmatrix}$$

The transformation matrix of AO basis is calculated by Eq. (3) as follows.

$$\mathbf{S}^{-1/2}=\begin{bmatrix}1.024 & -0.130 & 0.006\\ -0.130 & 1.048 & -0.130\\ 0.006 & -0.130 & 1.024\end{bmatrix}$$

Ex, (3) Sigma Orbitals of Methyl Radical.

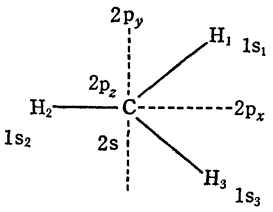

the distance C-H
1.08 Å
$<HCH=120°$

The radical $CH_3\cdot$ is assumed to be planar of C_{3v} symmetry.

The overlap matrix is as follows.

	$2p_z$	$2s$	$2p_x$	$2p_y$	$1s_1$	$1s_2$	$1s_3$
$2p_z$	1.000	0.000	0.000	0.000	0.000	0.000	0.000
$2s$	0.000	1.000	0.000	0.000	0.576	0.576	0.576
$2p_x$	0.000	0.000	1.000	0.000	0.233	−0.456	0.233
$2p_y$	0.000	0.000	0.000	1.000	0.403	0.000	−0.403
$1s_1$	0.000	0.576	0.233	0.403	1.000	0.256	0.256
$1s_2$	0.000	0.576	−0.465	0.000	0.256	1.000	0.256
$1s_3$	0.000	0.576	0.233	−0.403	0.256	0.256	1.000

The symmetry orbitals are determined to be $\Gamma=3A_1+2E$.

A_1; $2p_z$

$2s$

$1/\sqrt{3}\ (1s_1+1s_2+1s_3)$

E; $2p_x$

$1/\sqrt{6}\ (1s_1-2s_2+1s_3)$

$2p_y$

$1/\sqrt{2}\ (1s_1-1s_3)$

and their overlap matrices are calculated as

$$\mathbf{S}_{A1}=\begin{bmatrix}1.000 & 0.000 & 0.000\\ 0.000 & 1.000 & 0.998\\ 0.000 & 0.998 & 1.512\end{bmatrix}$$

$$\mathbf{S}_{E}=\begin{bmatrix}1.000 & 0.570 & 0.000 & 0.000\\ 0.570 & 0.744 & 0.000 & 0.000\\ 0.000 & 0.000 & 1.000 & 0.570\\ 0.000 & 0.000 & 0.570 & 0.744\end{bmatrix}$$

Using Eq. (3), we can obtain the following transformation matrices.

$$\mathbf{S}_{A_1}^{-1/2} = \begin{bmatrix} 1.000 & 0.000 & 0.000 \\ 0.000 & 1.563 & -0.699 \\ 0.000 & -0.699 & 1.204 \end{bmatrix}$$

$$\mathbf{S}_{E}^{-1/2} = \begin{bmatrix} 1.233 & -0.505 & 0.000 & 0.000 \\ -0.505 & 1.460 & 0.000 & 0.000 \\ 0.000 & 0.000 & 1.233 & -0.505 \\ 0.000 & 0.000 & 0.505 & 1.460 \end{bmatrix}$$

As for the transformation matrix of AO basis, the following result is obtained.

$$\mathbf{S}^{-1/2} = \begin{array}{c} \\ 2p_z \\ 2s \\ 2p_x \\ 2p_y \\ 1s_1 \\ 1s_2 \\ 1s_3 \end{array} \begin{array}{c} \begin{array}{ccccccc} 2p_z & 2s & 2p_x & 2p_y & 1s_1 & 1s_2 & 1s_3 \end{array} \\ \begin{bmatrix} 1.000 & 0.000 & 0.000 & 0.000 & 0.000 & 0.000 & 0.000 \\ 0.000 & 1.564 & 0.000 & 0.000 & -0.405 & -0.405 & -0.405 \\ 0.000 & 0.000 & 1.232 & 0.000 & -0.205 & 0.411 & -0.205 \\ 0.000 & 0.000 & 0.000 & 1.232 & -0.356 & 0.000 & 0.356 \\ 0.000 & -0.405 & -0.205 & -0.356 & 1.373 & -0.083 & -0.083 \\ 0.000 & -0.405 & 0.411 & 0.000 & -0.083 & 1.373 & -0.083 \\ 0.000 & -0.405 & -0.205 & 0.356 & -0.083 & -0.083 & 1.373 \end{bmatrix} \end{array}$$

From the three examples, we see that the transformation matrix deviates largely from unit matrix, especially in the case of sigma orbital (Ex. 3). Thus, it seems necessary to examine the parameters used in NDO method. As an example, Hartree-Fock matrix **F** and core Hamiltonian **H** are transformed as follows by the Löwdin transformation.

$$\mathbf{F}' = \mathbf{S}^{-1/2}\mathbf{F}\mathbf{S}^{-1/2}$$

$$\mathbf{H}' = \mathbf{S}^{-1/2}\mathbf{H}\mathbf{S}^{-1/2}$$

Usually, the symbol β_{ij} is used for i, j element of H'_{ij} which is determined from the spectroscopic data. By means of Eq. (3), one can calculate the value of β_{ij} and compare it with experimental one.

BULLETIN OF THE CHEMICAL SOCIETY OF JAPAN, VOL. 46, 358—363 (1973)

The Polymerization of α-Naphthylmethylvinylether and 3-Pyrenylmethylvinylether and Electrical Conductivity of Their Polymers

Shigeki Yoshimoto,* Kenichi Okamoto,** Hirotaka Hirata,*** Shigekazu Kusabayashi,** and Hiroshi Mikawa

Department of Applied Chemistry, Faculty of Engineering, Osaka University, Suita, Osaka

(Received March 17, 1972)

A new vinylmonomer with a large pendant π-electron group was synthesized. α-Naphthylmethylvinylether and 3-pyrenylmethylvinylether were polymerized in good yields, although their polymers have fairly low molecular weights. Both polymers have a fairly high isotacticity. Poly-3-pyrenylmethylvinylether showed a large photocurrent in its absorption region and a small photocurrent even above 500 to 1000 mμ. The doped TCNE significantly sensitized its photoconductivity.

Polycyclic aromatic hydrocarbons have been much studied as organic photoconductors.[1] The conductivity of polymers with a large aromatic ring as a side chain has also been studied because of the practical interest in their ability to form a photoconductive film. Poly-*N*-vinylcarbazole is one of the most photoconductive polymers which have ever been reported and used as material for electrophotography.[2] It has been suggested that the high photoconductive property of poly-*N*-vinylcarbazole is associated with the crystallinity.[3] Poly-3-vinylpyrene is the polymer with the largest aromatic ring as a side chain which has ever been synthesized.[4] Although the polymer is ordinarily poorly crystalline, spherulite is observed in the polarizing hot-stage after heat annealing, and it is also photoconductive.[4] The relationship between the conductivity and the crystallinity has also been found in other polymers.[5]

Many studies have been done on the stereoregular polymerization of vinylethers. As has been reported in connection with the polymerization of both tri-

* Present address: Central Research Laboratory, Sumitomo-denko Co., Ltd., Osaka.

** Present address: Department of Chemical Engineering, Faculty of Engineering, Yamaguchi University, Ube, Yamaguchi.

*** Present address: Pharmaceutical Department, Nagoya City University, Nagoya.

1) F. Gutmann, L. E. Lyons, "Organic Semiconductors", John Wiley & Sons, Inc., New York, (1967).

2) K. Morimoto, Y. Murakami and M. Ikeda, *National Technical Reports*, **15**, 125 (1969).

3) A. Kimura, Y. Yoshimoto, Y. Akana, H. Hirata, S. Kusabayashi, H. Mikawa, and N. Kasai, *J. Polym. Sci. A-2*, **8**, 643 (1970).

4) K. Tanikawa, S. Kusabayashi, and H. Mikawa, *Polym. Lett.*, **6**, 275 (1968); This Bulletin, **41**, 2719 (1968).

5) K. Okamoto, S. Kusabayashi and H. Mikawa, *Kogyo Kagaku Zasshi*, **73**, 1351 (1970).

methylsilylvinylether and benzylvinylether,[6] a vinylether with a large side-chain group is expected to give an isotactic polymer by cationic polymerization in nonpolar solvents.

In the present paper, the authors will report on the polymerization of α-naphthylmethylvinylether (NVE) and of 3-pyrenylmethylvinylether (PVE) as well as on the high isotacticities and the electrical conductivity of their polymers.

Experimental

Synthesis.

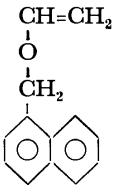

NVE

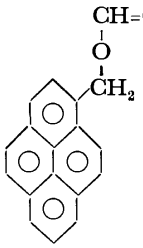

PVE

NVE. NVE was prepared according to the method reported by Watanabe and Conlon.[7] The crude material was purified by means of column chromatography (basic alumina, ligroin) and high vacuum distillation (bp 95°C/0.03 mmHg).

PVE. 3-Pyrenylaldehyde[4] was reduced to 3-pyrenylmethanol by the following procedures. A 25-g portion of 3-pyrenylaldehyde was dissolved in 800 cc of methanol with 4 g of $NaBH_4$, and the mixture was heated at about 40°C for 6 hr with stirring. After the excess $NaBH_4$ had then been decomposed by dilute acetic acid, most of the solvent was distilled away and the reaction product was extracted with benzene. The benzene solution was washed several times with water and dried over anhydrous potassium carbonate. The benzene was distilled away, and the resulting precipitate, 3-pyrenylmethanol, was washed several times with a benzene-ligroin mixture and recrystallized three times from ligroin. Yield, 15 g (60%); mp 126—127°C. Found: C, 88.27; H, 5.19%. Calcd for $C_{17}H_{12}O$: C, 87.90; H, 5.17%.

3-Pyrenylmethanol was transformed to 3-pyrenylmethylvinylether by the procedures similar to those used in the case of naphthylmethylvinylether.[7] The reaction mixture of 3-pyrenylmethanol (20 g), isobutylvinylether (500 cc), and $Hg(OCOCH_3)_2$ (1.8 g) was refluxed for a day; then another 1.0 g of $Hg(OCOCH_3)_2$ was added and reflux was continued for one more day. The reaction mixture was then washed with water, and the isobutylvinylether was removed by distillation. After being purified by column chromatography (basic alumina, ligroin), PVE was recrystallized three times from ligroin. Yield, 3.33 g (15%); mp 77—78°C. Found: C, 88.28; H, 5.46%. Calcd for $C_{19}H_{14}O$: C, 88.34; H, 5.17%. Its NMR signal consisted of a multiplet (ring protons) at 1.9—2.5 τ, a quartet (internal vinyl hydrogen) at 3.2—3.6 τ, a singlet (Py-CH_2-O-) at 4.8 τ, and a multiplet (terminal vinyl hydrogens) at 5.5—6.6 τ.

Polymerization. The polymerization conditions are summarized in Tables 1 and 2. The solvents were purified by ordinary methods. The initiators were distilled prior to use and were kept as a toluene solution under nitrogen. Polymerization was carried out in a vacuum sealed tube. Methanol was used as the precipitating agent.

Preparation of Poly-3-pyrenylmethylvinylether (PPVE) Doped with Tetracyanoethylene (TCNE). A certain amount of TCNE was added into a benzene solution of PPVE. After being stirred for an hour, the mixture was poured into a large amount of methanol or ligroin and the precipitate was washed with methanol or ligroin and dried *in vacuo*. The content of TCNE was estimated from the results of elementary analysis.

Measurement of the Electrical Conductivity. Both polymers were purified as much as possible by repeated precipitations before the measurement. As a thin film (10 μ thick) of poly-α-naphthylmethylvinylether (PNVE) could be formed on a nesa quartz plate by the cast method, its electrical conductivity was measured in an Au-PNVE-Nesa sandwich-type cell. As it was not possible to make thin films

Table 1. Polymerization of NVE.

No	Solvent[a]	Temp °C	Catalyst	Cat Concn mol%	Time hr	Yield %	Mol Wt[b]	Softening range °C
1	*n*-Heptane	25	$AlEtCl_2$	5	15	81	3760	90—100
2	*n*-Heptane	0	$AlEtCl_2$	5	10	71		
3	CH_2Cl_2	−78	$AlEtCl_2$	7	10	44	1400	
4	CH_2Cl_2	0	$AlEtCl_2$	7	10	59		
5	CH_2Cl_2	27	$AlEtCl_2$	7	10	43		
6	Toluene	−78	$AlEtCl_2$	7	0.5	50		
7	Toluene	−78	$AlEtCl_2$	7	1	67		
8	Toluene	−78	$AlEtCl_2$	7	2	61		
9	Toluene	−78	$AlEtCl_2$	1	2	79		
10	Toluene	−78	$AlEtCl_2$	2	2	72	4000	
11	Toluene	−78	$AlEtCl_2$	8	2	78		
12	Toluene	−78	$AlEt_3/TiCl_4$	2/2	2	73		
13	Toluene	−78	$AlEt_3/TiCl_4$	2/4	2	27		
14	Toluene	25	$BF_3(OEt_2)$	1	10	70		85—105

a) Monomer concentration; 0.1 mol/l.
b) Mol. Wt. was measured by a vapor pressure osmometer.

6) S. Murahashi, S. Nozakura, M. Sumi, S. Fujii, and K. Matsumura, *Kobunshi Kagaku*, **41**, 550 (1966). S. Murahashi, H. Yuki, T. Sano, U. Yonemura, H. Tadokoro, and Y. Chatani *J. Polym. Sci.*, **62**, S77 (1962).

7) W. H. Watanabe and L. E. Conlon, *J. Amer. Chem. Soc.*, **79**, 2828 (1957).

Table 2. Polymerization of PVE[a)]

No	Temp °C	Catalyst	Cat Concn mol%	Time hr	Yield %	Mol Wt[b)]	Softening range °C
1	−78	$AlEtCl_2$	4.7	22	52	1800	
2	−25	$BF_3(OEt_2)$	10	5	85		160—170
3	25	$BF_3(OEt_2)$	1	17	58	1570	170—200
4	25	$BF_3(OEt_2)$	2	17	63		
5	25	$BF_3(OEt_2)$	1.5	15	75	c)	c)
6	−78	$BF_3(OEt_2)$	1	20	50		150—170

a) Toluene was used as solvent. Monomer concentration was 0.1 mol/l. b) Mol. Wt. was measured by a vapor pressure osmometer. c) see Table 3.

Table 3. Fractionation of PPVE[a)]

Fraction	Solubility[b)]	Wt%	Mol Wt	Softening range °C
I	insoluble in tetrahydrofuran	3		250—280
II	soluble in tetrahydrofuran, insoluble in benzene	51	2900	220—230
III	soluble in both tetrahydrofuran and benzene	43	1400	185—195

a) The polymer of No 5 in Table 2 was used as a sample.
b) Each fraction was precipitated by methanol.

of both PPVE and PPVE doped with TCNE because of the low molecular weight of PPVE, the powder of the polymer was compressed into a disk under a pressure of 7000 kg/cm², upon which a pair of comb-type gold electrodes were evaporated under 10^{-5} mmHg. The surface-type cell thus obtained (distance between the electrodes, 0.02 cm; electrode length, 5 cm) was used for the electrical measurement of PPVE. Dark- and photocurrents were measured in a high vacuum (10^{-4}—10^{-5}mmHg) or in the air by the DC method with a Takedariken TR81 vibrating-reed electrometer. The monochromatized light from a 500 W xenon lamp was used, its intensity being controlled by neutral filters. The voltage was applied up to about 10000 V/cm. The measurements were carried out in the range from −10° to 70°C.

Results and Discussion

Polymerization. The polymerization results are shown in Tables 1 and 2. Both polymers, PNVE and PPVE, were obtained in good yields, although the molecular weight was fairly low. The difficulties in the chain growth of the monomers, especially in that of PVE, might be due to the steric effect of the large substituent groups under these catalytic conditions.

The polymerization of NVE proceeded rapidly within half an hour, but the polymer yield increased very slowly thereafter. The effect of both temperature and solvent on the polymer yield were very small.

PPVE was fractionated according to the solubility, as is shown in Table 3. Each fraction showed the same elementary composition. The main differences between fractions are found in the molecular weight, the melting point, and the IR absorption spectrum. The IR spectrum of each fraction is shown in Fig. 1. The most significant difference in the IR absorption observed at 1060 and 1135 cm^{-1}. The difference in the solubility must be due to the difference in the

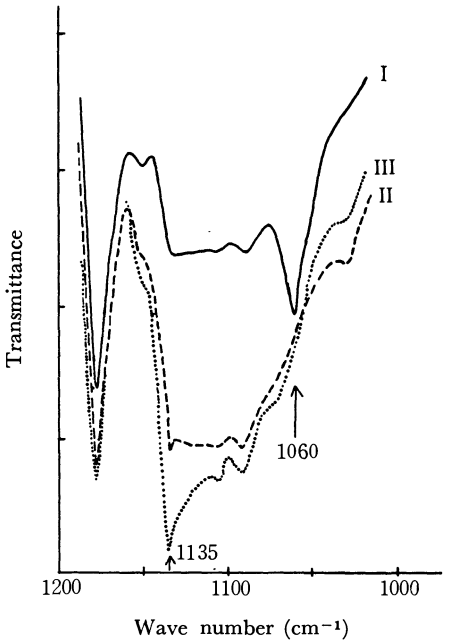

Fig. 1. IR spectra of each fraction of PPVE. Fractions I, II, and III.

molecular weight of the polymer. Fraction I, insoluble both in tetrahydrofuran and in benzene, has the highest melting temperature and probably the highest molecular weight. Fractions II and III have lower melting points and lower molecular weights. It is not clear whether these differences are due to the difference in crystallinity and/or to that in tacticity.

The tacticity of PNVE was studied by means of the IR spectrum of the polyvinylalcohol (PVA) led from the polymer. Dry HBr gas was bubbled into a toluene solution of PNVE with stirring at room temperature. The resulting precipitate, PVA, was washed with toluene and dried in a vacuum. The IR spectrum of

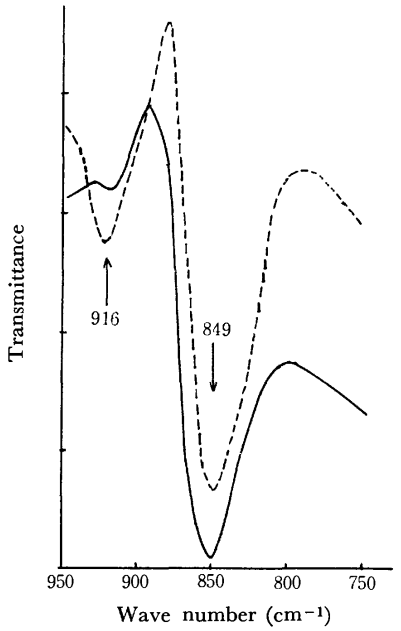

Fig. 2. IR spectrum of PVA.
solid line: PVA obtained from PNVE (No. 15 in Table 1), broken line: commercial atactic PVA.

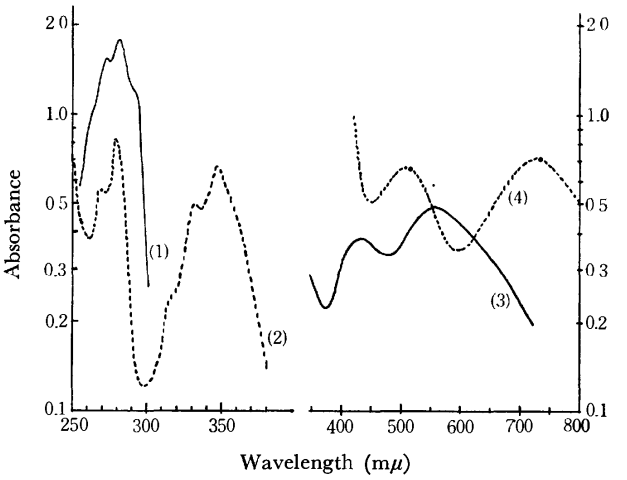

Fig. 3. UV absorption spectra of PNVE, PPVE and their CT complexes with TCNE in methylene chloride.
(1) PNVE (2.40×10^{-4} mol/l); (2) PPVE (8.8×10^{-4} mol/l); (3) PNVE (4.60×10^{-2} mol/l) and TCNE (8.2×10^{-3} mol/l); (4) PPVE (1.0×10^{-2} mol/l) and TCNE (7.0×10^{-2} mol/l).

PVA thus obtained was measured in a film; it is shown in Fig. 2. The absorbance ratio of 916 to 849 cm^{-1}, D_{916}/D_{849}, was reported to be a measure of the syndiotacticity of PVA.[8] The D_{916}/D_{849} ratio was found to be 0.03 for PVA from PNVE. This value corresponds to an isotacticity of 80—90%. The PNVE obtained by the above-mentioned procedure is, therefore, highly isotactic. The high isotacticity seems to result from the effect of the large substituent group on the polymerization.

PPVE was treated by a similar method, but the difficulty in cleaving this polymer to PVA hindered us from obtaining a clear answer as to the polymer tacticity. PPVE, however, might be safely said to have a fairly high isotacticity because of the effect of the bulky substituent group, which is larger than those of the polybenzyl- and polynaphthylmethyl-vinylethers.

PNVE is amorphous judging from the X-ray diffraction pattern, although it has a high isotacticity. An appropriate heat-treatment did not improve its crystallinity.

UV Absorption Spectra. Figure 3 shows the absorption spectra of the polymers and their charge-transfer complexes (CT complex) in methylene chloride. The CT complex of PNVE showed the same spectrum as did the CT complex of naphthylmethylethylether. The equilibrium constants for the CT complexes were calculated by means of the Benesi-Hildebrand equation. The equilibrium constant for the PNVE-TCNE complex was found to be 1.5 l/mol at 20°C in methylene chloride. This was much smaller than that for the naphthylmethylethylether-TCNE complex (4.5 l/mol at 20°C in methylene chloride). Similar results have been reported for the CT complexes of poly-*N*-vinylcarbazole and *N*-ethylcarbazole.[9] It may be noted that the steric effect on the equilibrium is considerable, even for the polymer such as PNVE, in which the side-chain group is separated from the main chain by the $-O-CH_2-$ bond.

Dark Conductivity. The dark current of PPVE was too small to be observed with a surface-type cell ($i_d \ll 10^{-15}$ A under 10000 V/cm). The sandwich-type cell of PNVE showed an ohmic dark current (specific conductivity at 50°C, $\sigma_{50}=10^{-18}\ \Omega^{-1}\ cm^{-1}$) whose activation energy was 1.9 eV in a high vacuum.

Photoconductivity. PNVE showed only a small photocurrent in the wavelengths shorter than 350 mμ.

Fractions II and III of PPVE in Table 3 were used for the measurements, no difference in electrical conductivity being observed between these fractions. The data to be presented below were obtained from Fraction III.

PPVE showed a large photoresponse, as is shown in Fig. 4. The photocurrent was proportional both to the applied voltage and to the light intensity at every wavelength, as is shown in Figs. 4 and 5. No appreciable photovoltaic current was observed. Figure 6 shows the spectral dependence of the photocurrent and the diffuse reflectance spectra. The diffuse reflectance spectra were measured using potassium bromide powder as a standard and are plotted using the Kubelka-Munk function, $f(R)=(1-R)/2R$, where R is the reflectance. The long-wavelength absorption peak was observed at 380 mμ in the solid state. This corresponds to the long-wavelength and low-intensity band of the pyrene ring, which has been observed at 376 mμ for 3-ethylpyrene and poly-3-vinylpyrene in a THF solution.[10] A maximum in the photocurrent

8) S. Murahashi, S. Nozakura, M. Sumi, H. Yuki, and K. Hatada, *J. Polym. Sci., B*, **4**, 65 (1966).

9) A. Rembaum, A. M. Hermann, and R. Haack, *J. Polym. Sci., A-1*, **6**, 1955 (1968).

10) K. Tanikawa, Thesis, Osaka University, 1970.

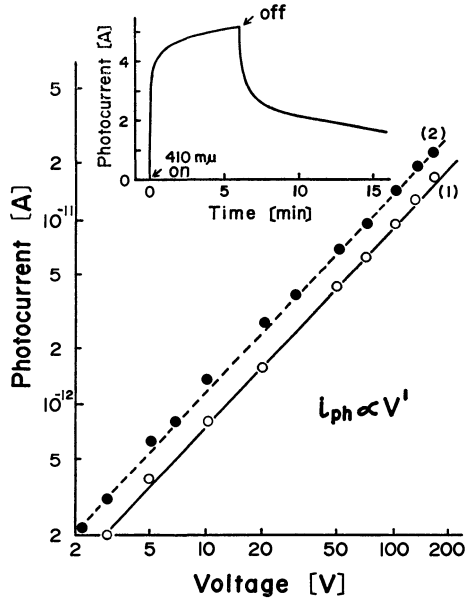

Fig. 4. Voltage dependence of photocurrent of PPVE.
(1) in high vacuum, (2) in air, under 410 mμ illumination. The photoresponse curve is also shown.

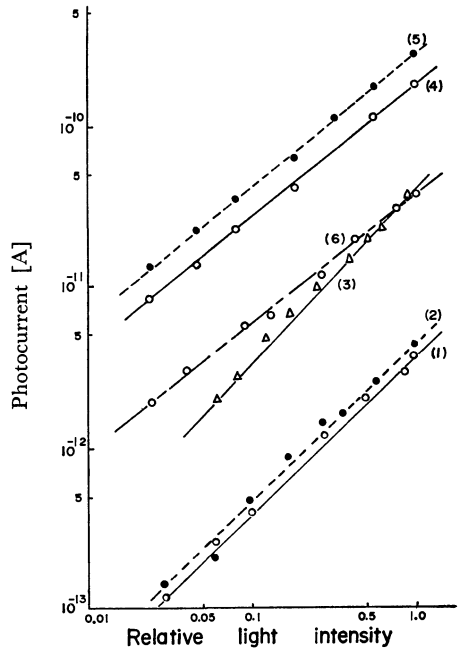

Fig. 5. Light intensity dependence of photocurrent of both PPVE and of PPVE doped with TCNE.
(1), (2), and (3); PPVE. (4), (5), and (6); PPVE doped with TCNE. (1) and (4) 420 mμ illumination in high vacuum, (2) and (5) 420 mμ illumination in air, (3) panchromatic light (from a 500 W xenon lamp) illumination in air, (6) 600 mμ illumination in high vacuum, under 2500 V/cm.

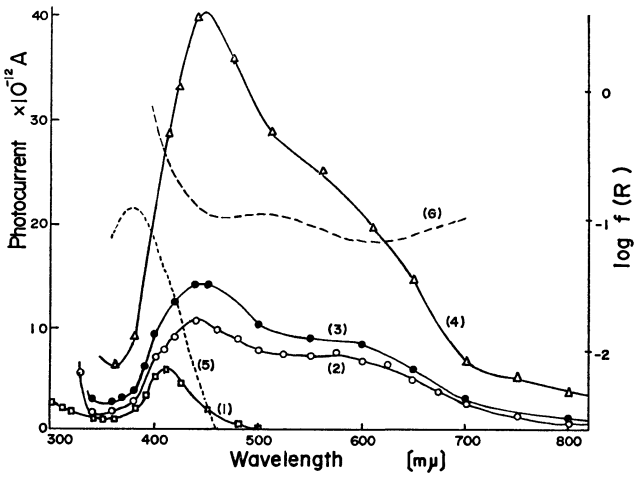

Fig. 6. Spectral response of photocurrent of PPVE sensitized with TCNE and diffuse reflectance spectra both of PPVE and of PPVE doped with TCNE.
Photocurrent was normalized for the light intensity of 1×10^{14} photons/cm² sec. (1) PPVE in high vacuum, (2) PPVE doped with TCNE (1 mol%) in high vacuum, (3) PPVE doped with TCNE (1 mol%) in air, (4) PPVE doped with TCNE (10 mol%) in high vacuum, under 2500 V/cm. The values in the curve (4) are 1/2 of the observed ones. (5) and (6) diffuse reflectance spectra of PPVE and PPVE doped with TCNE (1 mol%).

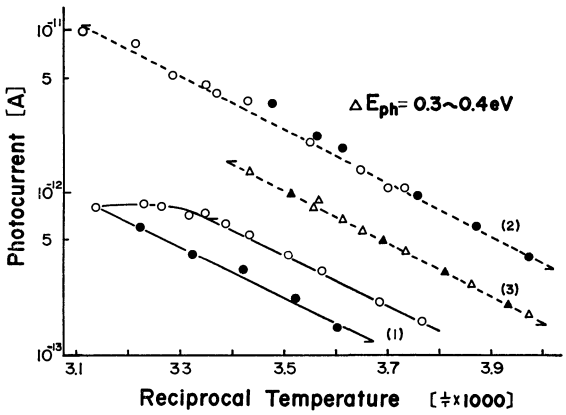

Fig. 7. Temperature dependence of photocurrent of PPVE.
(1) 420 mμ illumination in high vacuum, (2) 420 mμ illumination in air, (3) 600 mμ illumination in air, under 2500 V/cm. The values in the line (1) are 1/10 of the observed ones.

was observed at about 410 mμ, at a little longer wavelength than the absorption peak. A similar shift of the maximum in the photocurrent from the absorption peak has been also observed in poly-*N*-vinylcarbazole.[5] A small photocurrent was observed even above from 500 mμ to 1000 mμ, where PPVE has no absorption. The activation energy of the photocurrent, ΔE_a, in the equation; $i \propto \exp(-\Delta E_a/kT)$ was 0.3—0.4 eV at every wavelength in a vacuum or in air (Fig. 7). The magnitude of the photo-current was larger by two factors in air than in a high vacuum. This suggests that the majority carrier in PPVE is a hole rather than an electron. This sign of the carrier is the same as that in other polymers with large π-electron systems, such as poly-*N*-vinylcarbazole.[5]

Generally, polymers have many impurities which act as trapping centers. In many cases,[5,11] a re-excitation of the carriers trapped in the centers by

11) T. Tanaka, Y. Inuishi, *Japan. J. Appl. Phys.*, **6**, 1371 (1967).

Table 4. Sensitization factors of dark- and photoconductivities of PPVE by doped TCNE

TCNE Content mol%	Darkconductivity[a]	Photoconductivity[a]			
		700 mμ	550 mμ	450 mμ	410 mμ
1	larger than 10^2	36	35	5.3	1.3
10	larger than 5×10^3	186	250	40	5

a) The currents were measured under 2500 V/cm in a high vacuum at room temperature.

illumination creates the photocurrent which is sensitive to visible or IR light. PPVE showed this behavior; that is, even after the cell had been kept for many hours under no applied voltage in the dark at room temperature the photocurrent was observed for a while when the cell was illuminated with visible light under no applied voltage. This suggests that PPVE also has many deep traps, which may be the origin of the photocurrent in the visible and near IR regions.

Sensitization of the Conductivity of PPVE. The doping of TCNE sensitized both the dark- and photoconductivities of PPVE. The degree of sensitization increased with the doping amount, as is shown in Table 4. The sensitized dark- and photocurrents were ohmic. The sensitized photocurrent showed a sublinear dependence (0.8 power) on the light intensity, as is shown in Fig. 5.

Figure 8 shows the temperature dependence of the sensitized dark- and photocurrents. The activation energies for the dark- and photocurrents were 1.1 eV and 0.18—0.25 eV respectively, both *in vacuo* and in air. Doped TCNE decreased the activation energy for photocurrent of PPVE. A similar effect has been reported for other polymers.[13]

Its spectral dependence was not, however, consistent with the absorption spectrum of PPVE-TCNE system in the solid state, as is shown in Fig. 6. A maximum and a shoulder in the photocurrent were observed at about 450 mμ and in the 550—650 mμ region (the CT absorption region) respectively. Doped TCNE apparently caused the large increase in the photocurrent in the CT bands, especially in the shorter wavelength CT band. The CT excitation with a higher energy will generate the carriers more easily:

$$(D\cdots A) \xrightarrow{h\nu_{CT}} (D^+\cdots A^-)^* \longrightarrow D^+ + A^- \qquad (1)$$

In addition to the spectral sensitization mentioned above, the chemical sensitization was also observed. Doped TCNE enhanced the photocurrent in the absorption region of PPVE by a factor of 1.5—2.0 in the case of 1 mol% (doping amount) and by a factor of 5 in the case of 10 mol%. Similar behavior was observed in the photoconductivity of poly-*N*-vinylcarbazole; it can be explained in terms of both the field-assisted thermal dissociation of an excited CT complex and the excitation of the donor, A^-, by singlet excitons.[12] The same mechanism is applicable for the chemical sensitization of the photocurrent of PPVE by doped TCNE; that is,

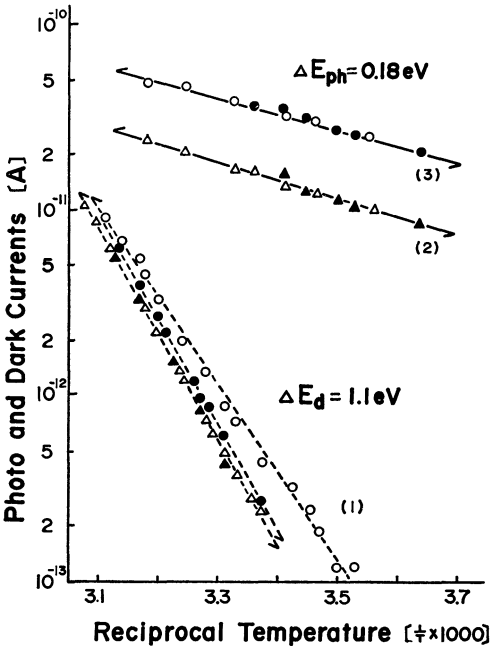

Fig. 8. Temperature dependence of photo- and dark- currents of PPVE sensitized with TCNE.
(1) dark current (○; 1-st heating, ●; 1-st cooling, △; 2-nd heating, ▲; 2-nd cooling), (2) photocurrent under 420 mμ illumination, (3) photocurrent under 600 mμ illumination, in high vacuum 2500 V/cm.

$$D \xrightarrow{h\nu} D^* \qquad (2),$$

$$D^* + A \longrightarrow (D^+\cdots A^-)^* \longrightarrow D^+ + A^- \qquad (3),$$

$$A^- + D^* \longrightarrow A + D^- \qquad (4),$$

where D is a donor molecule; D*, an excited singlet state of the donor; A, an acceptor molecule; $(D^+\cdots A^-)^*$, an excited CT complex; D^+ and D^-, ion radicals of the donor (mobile charge carriers), and A^- the anion radical of the acceptor (immobile). The gaseous electron affinity (EA_G) of TCNE and pyrene are 2.2 eV[14] and 0.58 eV[15] respectively. On the assumptions that the EA_G value of PPVE is equal to the value of pyrene, and that the polarization energy due to $PPVE^-$ is equal to that due to $TCNE^-$ in a pellet of PPVE doped with TCNE, the energy required for the excitation of an electron from $TCNE^-$ to the conduction level of PPVE is estimated to be 1.6 eV. As the energy of the singlet exciton (~3.2 eV) is larger than this value, Process (4) is probable.

12) K. Okamoto, S. Kusabayashi, and H. Mikawa, submitted to this Bulletin.

13) H. Meir, W. Albrecht, und U. Tshirwitz, *Ber. Bunsengesell. Physik. Chem.*, **73**, 795 (1969).

14) G. Briegleb, *Angew. Chem.*, **76**, 326 (1964).

15) W. E. Wentworth, E. Chem, and J. E. Lovelock, *J. Phys. Chem.*, **70**, 445 (1966).

The Viscosities of Aqueous Sodium Alkylsulfate and Alkyltrimethylammonium Bromide Solutions

Mitsuru TANAKA, Shoji KANESHINA,* Wataru NISHIMOTO,* and Hiroyuki TAKABATAKE*

Department of Chemistry, Faculty of Science, Fukuoka University, Nanakuma, Fukuoka

**Department of Chemical Engineering, Faculty of Engineering, Tokushima University, Minamijōsanjima-chō, Tokushima*

(Received April 21, 1972)

The viscosities of aqueous solutions of sodium alkylsulfate and alkyltrimethylammonium bromide have been measured at various temperatures from 5 to 55°C. The viscosity data have been interpreted in terms of the Jones-Dole equation, and the viscosity B coefficients for the alkylsulfate and alkyltrimethylammonium ions at various temperatures have been calculated. The B values for these ions are all positive; they decrease with an increase in the temperature and increase linearly with an increase in the alkyl-chain length. The increment of B is found to be 0.076/-CH_2- at 25°C. The energy and the entropy of activation for the viscous flow at 25°C have been calculated for these ions; they increase with an increase in the alkyl-chain length. This behavior of the B coefficient, and the energy and the entropy of activation for the viscous flow may be interpreted by saying that the longer-chain ions promote the hydrogen-bond structure of water around the hydrocarbon chain of these ions, while shorter-chain ions, *e.g.*, ethylsulfate and ethyltrimethylammonium ions, behave instead as structure breakers because of the predominance of the disordering effect on the water around the ionic head. The viscosities of micellar solutions have also been measured. The volume of micelles as a hydrodynamic moving unit in solution has been estimated.

The viscosities of aqueous surfactant solutions have been measured by many investigators in order to obtain information about the micelle-forming properties.[1]

Gurney,[2] Kaminsky,[3] and Nightingale[4] have emphasized that the B coefficients of the Jones-Dole equation of viscosity[5] provide significant informations about the nature of ion-solvent interaction. The division of the B value of electrolytes into individual ionic values has been attempted by Gurney.[2] Kaminsky has extended this treatment to a wide temperature range.[3] Further, Nightingale[4] has indicated that the influence of strong electrolytes upon the viscosity of the solvent can be interpreted as a rate process, and that the energy and entropy of activation for a viscous flow can be estimated for a number of ions; on the basis of such estimates, he has discussed the nature of the ion-solvent interaction.

Having a molecule composed of a hydrophilic ionic head and a hydrophobic long-chain tail is a characteristic of an ionic surfactant. With respect to the hydrophobic interaction between water and a hydrocarbon chain, there have been many experimental and theoretical studies, especially by Nemethy and Scheraga.[6]

In this paper, the interaction between long-chain ions and solvent water will be discussed on the basis of the ionic B coefficients and the energy and entropy of activation for the viscous flow of two homologues of surface-active substances, sodium alkylsulfates and alkyltrimethylammonium bromides.

Experimental

Materials. The homologous series of *n*-alkanols and *n*-alkylbromides used in the preparation of sodium *n*-alkylsulfates and *n*-alkyltrimethylammonium bromides with 2 to 12 carbon atoms were all found by gas chromatography to be pure. All the salts gave correct elemental analyses.

Sodium Alkylsulfates: The reaction mixture obtained by treating *n*-alkanols with chlorosulfonic acid was extracted with ether and then neutralized with sodium hydroxide. The longer-chain compounds were obtained from the ether layer, and the shorter compounds, from the water layer. The sodium alkylsulfates thus obtained were recrystallized from an acetone-methanol mixture.

Alkyltrimethylammonium Bromides: These compounds were prepared by the reaction of the corresponding *n*-alkylbromides with trimethylamine. They were purified by recrystallization from acetone.

The critical micelle concentrations (CMC) of surfactants with an alkyl chain from 8 to 12 carbon atoms were determined by means of surface-tension and electric-conductivity measurements; the CMC's obtained by both methods were in good agreement with those from other sources.[7] The surface tension *vs.* concentration curves did not exhibit a minimum in the vicinity of the CMC.

Measurement of Viscosity. All the measurements of viscosity were carried out at a constant temperature between 5 and 55°C (±0.01°C). All the solutions were prepared on a molal basis. Two Geist-Cannon type viscometers with a flow time of *ca.* 500 s for water at 25°C were employed. The viscometers were carefully cleaned, rinsed with distilled water and methanol, and dried before they were filled with a solution and immersed in a thermostat. The solutions were filtered before being introduced into the viscometers in order to remove dust, *etc.* The error in the flow time was 0.1 s. Two viscometers were calibrated with pure water and 20% and 30% sucrose solutions by means of Eq. (1):

1) L. M. Kushner, B. C. Duncan, and J. I. Hoffman, *J. Res. Natl. Bur. Stand.*, **49**, 85 (1952). N. Sata and K. Tyuzyo, This Bulletin, **26**, 177 (1953). P. Mukerjee, *J. Colloid Sci.*, **19**, 722 (1964). Y. Iwadare and T. Suzawa, *Nippon Kagaku Zasshi*, **90**, 1106 (1969).

2) R. W. Gurner, "Ionic Processes in Solution," McGraw-Hill Book Co., New York, N. Y., (1953).

3) M. Kaminsky, *Discuss. Faraday Soc.*, **24**, 171 (1957).

4) E. R. Nightingale, Jr., and R. F. Benck, *J. Phys. Chem.*, **63**, 1777 (1959).

5) G. Jones and M. Dole, *J. Amer. Chem. Soc.*, **51**, 2950 (1929).

6) G. Nemethy and H. A. Scheraga, *J. Chem. Phys.*, **36**, 3401 (1962).

7) K. Shinoda, T. Nakagawa, B. Tamamushi, and T. Isemura, "Colloidal Surfactants," Academic Press, New York, N. Y., (1963), p. 36.

$$\frac{\eta}{\rho} = Kt - \frac{L}{t} \quad (1)$$

where η is the absolute viscosity, ρ is the density, and t is the flow time. The characteristic constants of the viscometers, K and L, were 1.592×10^{-5} and 1.36×10^{-2} for one, and 1.613×10^{-5} and 0.75×10^{-2} for the other, respectively. For the absolute viscosities of water, and 20% and 30% sucrose solutions at 25°C, we used 0.008903, 0.01701, and 0.02741 poise[8] respectively. The densities are 0.99707, 1.07940, and 1.12512 g/ml[9] respectively. The densities of the solutions were measured at a given temperature with *ca.* 6-ml pycnometer; the error of measurement was within ±0.0001 g/ml.

Results and Discussion

The viscosities of the solutions were computed by means of Eq. (1). It was found that the $\rho=\rho_0(1+\alpha m)$ equation held for the densities of aqueous solutions of sodium alkylsulfate and alkyltrimethylammonium bromide over a wide range of concentrations and temperatures, where m is the molal concentration; ρ_0, the density of pure water, and α, a constant.

The viscosity data have been analyzed by means of the Jones-Dole equation[10]:

$$\eta_r = 1 + A\sqrt{m} + Bm \quad (2)$$

where $\eta_r(=\eta/\eta_0)$ is the relative viscosity of a solution and where A and B are constants characteristic of the solute electrolyte. Eq. (2) can, then, be rewritten as:

$$\frac{(\eta_r-1)}{\sqrt{m}} = A + B\sqrt{m} \quad (3)$$

The A coefficient represents the contribution from interionic electrostatic force.[11] The B coefficient is said to be a measure of the effective hydrodynamic volume of the solvated ions,[12] and to denote the order or disorder introduced by the ions into the solvent structure.

Plots of $(\eta_r-1)/\sqrt{m}$ *vs.* $\sqrt{m}$ for aqueous solutions of sodium alkylsulfate and alkyltrimethylammonium bromide at 25°C are given in Fig. 1. The A intercepts obtained were small in every case; at most they amounted to 0.01 in the aqueous solutions studied. The plots of Eq. (3) were found to be linear up to concentrations of 0.1 molality for solutions of salts with hydrocarbon chains shorter than the octyl compound, and up to the CMC for solutions of micelle-forming salts with a hydrocarbon chain of from 8 to 12 carbon atoms. The B coefficients obtained at various temperatures are presented in Table 1.

Viscosity B Coefficient. For a satisfactory discussion of the temperature dependence of the viscosity B coefficients, the individual B values of the component ions are needed. The division of the B coefficients into individual ionic values is a rather arbitrary process, because there is no quantity corresponding to the transport numbers used in ionic mobility assignments. Gurney[2] has computed the ionic B coefficients in aqueous solutions by equating the contributions of the K^+ and Cl^- ions to the B coefficient of KCl at 25°C. Kaminsky has extended this treatment to the temperature range from 15 to 45°C,[3] and obtained ionic values in good agreement with those reported by Cox and Walfenden[13] that were based on the mobility difference for the Li^+ and IO_3^- ions. We have followed Kaminsky's procedure and have used his data for the Na^+ and Br^- ions. The ionic B coefficients for the alkylsulfate and alkyltrimethylammonium ions thus obtained are given in Table 2.

B coefficients for the relatively small alkali and halide ions in an aqueous solution decrease with an

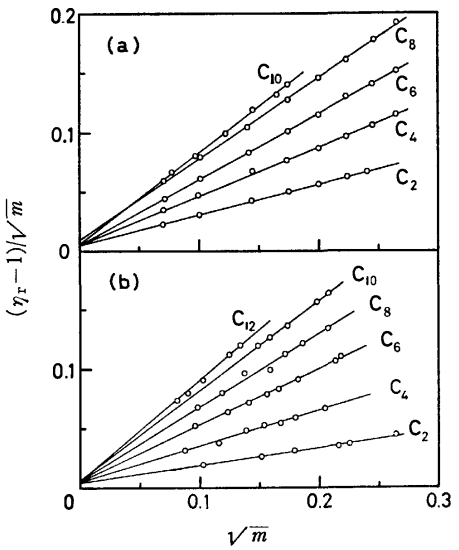

Fig. 1. Plots of $(\eta_r-1)/\sqrt{m}$ *vs.* $\sqrt{m}$ at 25°C. (a): sodium alkylsulfate, (b): alkyltrimethylammonium bromide.

Table 1. Viscosity B coefficients at various temperatures

Salt	Temperature, °C				
	5	15	25	35	55
C_2SO_4Na		0.26	0.25	0.24	0.23
C_4SO_4Na		0.43	0.41	0.39	0.37
C_6SO_4Na		0.61	0.56	0.52	0.49
C_8SO_4Na	0.85	0.77	0.71	0.65	0.56
$C_{10}SO_4Na$	0.90	0.83	0.77	0.71	
$C_{12}SO_4Na$	0.95	0.89			
		15	25	40	
C_2Me_3NBr		0.16	0.16	0.16	
C_4Me_3NBr		0.36	0.31	0.28	
C_6Me_3NBr		0.53	0.45	0.43	
C_8Me_3NBr		0.70	0.61	0.57	
$C_{10}Me_3NBr$		0.88	0.76	0.70	
$C_{12}Me_3NBr$		1.07	0.91	0.76	

8) J. R. Coe and T. B. Godfrey, *J. Appl. Phys.*, **15**, 625 (1944).
9) L. W. Tilton and K. Taylor, *J. Res. Natl. Bur. Stand.*, **18**, 205 (1937).
10) The molarity is used instead of the molality in the original Jones-Dole equation. But A and B obtained are almost the same in very dilute solution.
11) H. Falkenhagen and E. L. Vernon, *Physik. Z.*, **33**, 140 (1932).
12) E. R. Nightingale, Jr., *J. Phys. Chem.*, **63**, 1381 (1959).
13) W. M. Cox and J. H. Wolfenden, *Proc. Roy. Soc. Ser. A*, **145**, 475 (1934).

TABLE 2. IONIC B COEFFICIENTS AT VARIOUS TEMPERATURES

Ion	Temperature, °C				
	5	15	25	35	55
$C_2SO_4^-$		0.17	0.16	0.15	0.14
$C_4SO_4^-$		0.34	0.32	0.30	0.28
$C_6SO_4^-$		0.52	0.47	0.43	0.40
$C_8SO_4^-$	0.76	0.68	0.62	0.56	0.47
$C_{10}SO_4^-$	0.81	0.74	0.68	0.62	
$C_{12}SO_4^-$	0.86	0.80			
Na^+	0.09	0.09	0.09	0.09	0.09
		15	25	40	
$C_2Me_3N^+$		0.22	0.20	0.18	
$C_4Me_3N^+$		0.42	0.35	0.30	
$C_6Me_3N^+$		0.59	0.49	0.45	
$C_8Me_3N^+$		0.76	0.65	0.59	
$C_{10}Me_3N^+$		0.94	0.80	0.72	
$C_{12}Me_3N^+$		1.13	0.95	0.78	
Br^-		−0.06	−0.04	−0.02	

increase in the ionic size, often to negative values, and in such cases B increases with an increase in the temperature.[2] These ions are known as structure breakers. On the other hand, large molecular ions such as the tetraalkylammonium ions have large and positive B values.[14,15] Assuming that the viscosity of an electrolytic solution at a constant temperature can be interpreted by Einstein's equation[16]:

$$\eta_r = 1 + 2.5\phi \tag{4}$$

where ϕ is the volume fraction of the salts, and by combining with Eq. (2), Eq. (4) becomes:

$$2.5\phi = A\sqrt{m} + Bm \tag{5}$$

The $A\sqrt{m}$ term can safely be neglected in comparison with Bm in the present solution. Since also $\phi = C\overline{V}$ $(=C\sum\bar{v}_i)$, where C is the molarity, $\overline{V}$ and $\bar{v}_i$ are the partial molar volumes of the solute electrolyte and the i-th ions in solution respectively, and since $C \simeq m$, we obtain:

$$2.5\,\overline{V} = B \tag{6}$$

$$2.5\,\bar{v}_i = B_i \tag{7}$$

where: $$\sum B_i = B \tag{8}$$

Therefore, if the viscosity of an electrolytic solution can be explained by Einstein's equation, the viscosity B coefficient should be approximately linear with the partial molar volume of the solute, *i.e.*, the ionic size. A plot of B *vs.* $\overline{V}$ for sodium alkylsulfate and alkyltrimethylammonium bromide is found to be linear, as is shown in Fig. 2, where the partial molar volumes of the long-chain salts used are given in Table 3. The slopes of these straight lines, however, are not equal to 2.5, but are about two times it. The B coefficient decreases with the increase in the temperature, as will be mentioned later, whereas $\overline{V}$ slightly increases with

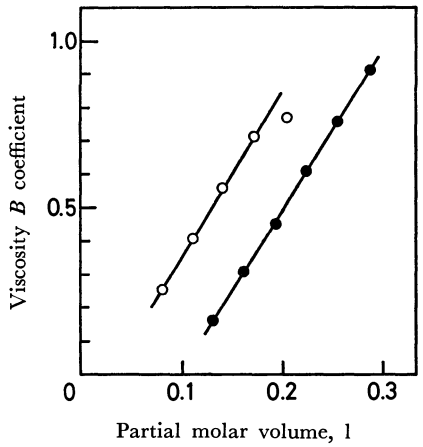

Fig. 2. Plots of viscosity B coefficients *vs.* partial molar volume of long chain salts at 25°C; sodium alkylsulfate (○), alkyltrimethylammonium bromide (●).

TABLE 3. PARTIAL MOLAR VOLUME OF LONG CHAIN SALTS AT 25°C

n	Partial molar volume, ml	
	C_nSO_4Na	C_nMe_3NBr
2	81.1	131.6
4	111.7	162.6
6	141.3	193.6
8	172.6	223.7[17]
10	204.1[17]	255.4[17]
12	234.4[17]	287.0[17]

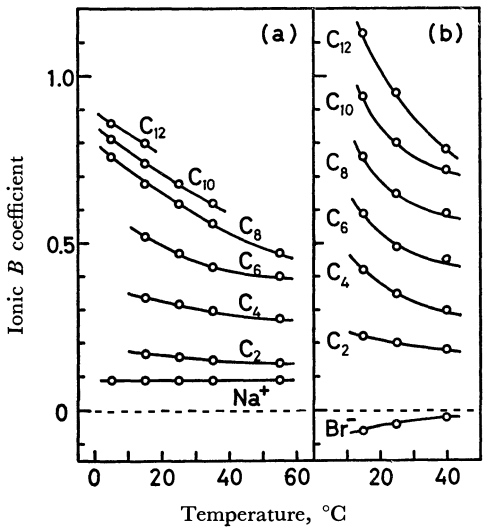

Fig. 3. Temperature dependence of ionic B values. (a): alkylsulfate and sodium ions, (b): alkyltrimethylammonium and bromide ions.

the increase in the temperature according to our unpublished data. Such behavior can not be accounted for only by the Einstein effect.

The B coefficients for alkylsulfate and alkyltrimethylammonium ions decrease with an increase in the tem-

14) E. R. Nightingale, Jr., *J. Phys. Chem.*, **66**, 894 (1962).
15) R. L. Key, T. Vituccio, C. Zawoyski, and D. F. Evans, *J. Phys. Chem.*, **70**, 2336 (1966).
16) A. Einstein, *Ann. Physik*, **19**, 289 (1906); **34**, 591 (1911).
17) J. M. Corkill, J. F. Goodman, and T. Walker, *Trans. Faraday Soc.*, **63**, 768 (1967).

perature, and the longer the alkyl chain length, the larger the negative temperature coefficient of B values, as is shown in Fig. 3. This tendency is similar to that for the tetraalkylammonium ions.[14,15] On the other hand, the B coefficient of a strong inorganic electrolyte increases with an increase in the temperature.[2] Therefore, the decrease in the B coefficient of these long-chain ions can be attributed to the interaction between the solvent water and the hydrocarbon part of the chain ions. The negative temperature coefficient of the B for the chain ion may be explained by the fact that these long-chain ions cause the water around the hydrocarbon part to become more ice-like than normal water,[18,19] and that this "ice-likeness" or "iceberg"[6] melts as the temperature is raised, causing the ionic B coefficient to be lowered.

The variation in the ionic B coefficient with the alkyl chain length is shown in Fig. 4. The ionic B

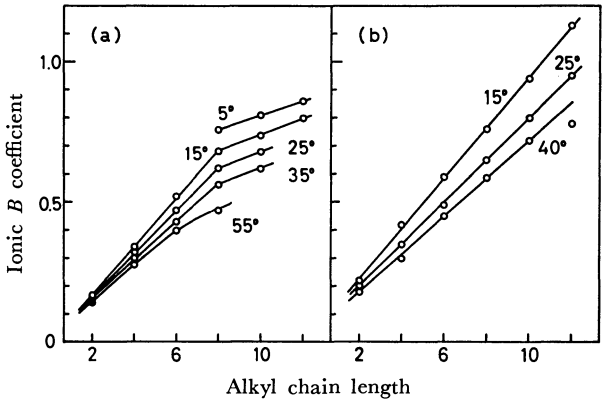

Fig. 4. Ionic B values at various temperature as a function of alkyl chain length. (a): alkylsulfate ions, (b): alkyltrimethylammonium ions.

coefficients of two homologous salts increase with an increase in the chain length at each temperature. This increase can be attributed to the Einstein effect of the additional methylene group and to the highly ordered "iceberg" structure around the hydrocarbon tail of the long-chain ions. The increase in the ionic B coefficient with the chain length is linear at 15 and 25°C except for alkylsulfate with carbon atoms larger than 8; the increments per methylene group are 0.076 for the alkylsulfate ion and 0.075 for the alkyltrimethylammonium ion at 25°C. At 15°C they are 0.085 and 0.091 respectively. Thus, these values are independent of the ionic heads of long-chain ions at a constant temperature. The plots of B values *vs.* the chain length for the alkylsulfate ion are found to be bent suddenly at the carbon number of 8, as is shown in Fig. 4, whereas this is not observed for the alkyltrimethylammonium ion.

Energy and Entropy of Activation for the Viscous Flow. The energy of activation for the viscous flow, $E^{\neq}$, according to the theory of absolute reaction rates presented by Eyring *et al.*,[20] is given by:

$$E^{\neq} = R\frac{\mathrm{d}\ln\eta}{\mathrm{d}(1/T)} \tag{9}$$

For an associated liquid such as water, the plot of ln η *vs.* $1/T$ is not linear; *i.e.*, $E^{\neq}$ varies with the temperature. By substituting Eq. (2) into Eq. (9), and by neglecting the $A\sqrt{m}$ term in Eq. (2), it follows that:

$$E^{\neq} = R\frac{\mathrm{d}\ln\eta_0}{\mathrm{d}(1/T)} + \frac{R}{1+Bm}\frac{\mathrm{d}(1+Bm)}{\mathrm{d}(1/T)} \tag{10}$$

where the first term of the right-hand side is identical with the energy of activation for the solvent water, $E_0^{\neq}$. Assuming that the difference between the activation energy of a solution and a solvent is equal to the activation energy for the flow of the solute, $\Delta E^{\neq}$, it follows that:

$$\Delta E^{\neq} = E^{\neq} - E_0^{\neq} = \frac{R}{1+Bm}\frac{\mathrm{d}(1+Bm)}{\mathrm{d}(1/T)} \tag{11}$$

The free energy of activation for the viscous flow is given by:

$$\Delta G^{\neq} = RT\ln\frac{\eta V}{hN} \tag{12}$$

where h is the Planck constant, N is the Avogadro number, and V is the molar volume of the moving unit. Subtracting the activation free energy for the solvent, $\Delta G_0^{\neq}$, from Eq. (12), the activation free energy for the flow of the solute is given by:

$$\Delta\Delta G^{\neq} = \Delta G^{\neq} - \Delta G_0^{\neq} = RT\ln\frac{\eta V}{\eta_0 V_0} \tag{13}$$

Since the activation enthalpy can safely be assumed not to differ appreciably from the activation energy, the entropy of activation of the solute, $\Delta\Delta S^{\neq}$, may also be calculated as:

$$\Delta\Delta S^{\neq} = \frac{\Delta E^{\neq} - \Delta\Delta G^{\neq}}{T} \tag{14}$$

Nightingale[4] has shown that the activation quantities of the solute can be represented by the following formulae:

$$\Delta E^{\neq} = \sum \nu_i \Delta E_i^{\neq},\ \Delta\Delta S^{\neq} = \sum \nu_i \Delta\Delta S_i^{\neq} \tag{15}$$

where $\Delta E_i^{\neq}$ and $\Delta\Delta S_i^{\neq}$ are the energy and the entropy of activation for the ionic components, and where ν_i is the number of ions per molecule of salt. He further assumed, in a manner similar to that in the evaluation of the ionic B coefficients, that the activation energy for the flow of the K^+ ion in solutions was approximately equal to that of the Cl^- ion. Following Nightingale's procedure, and using his data for the Na^+ and Br^- ions, the energies and entropies of activation for the flow of alkylsulfate and alkyltrimethylammonium ions were determined to be as is shown in Table 4.[21] It can be seen from Table 4 that the activation energies for the ions under consideration are all positive, that they in-

18) H. S. Frank and M. W. Evans, *J. Chem. Phys.*, **13**, 507 (1945).

19) H. S. Frank and W. Y. Wen, *Discuss. Faraday Soc.*, **24**, 133 (1957).

20) S. Glasstone, K. J. Laidler, and H. Eyring, "The Theory of Rate Processes," McGraw-Hill Book Co., New York, N. Y., (1941).

21) These values are based on the solution of 1 mol/kg in order to be compared with Nightingale's data, consequently that for the ions with alkyl chain longer than C_8 may be imaginary because of the micelles to be already formed at lower concentrations.

TABLE 4. IONIC ACTIVATION ENERGY AND ENTROPY FOR VISCOUS FLOW AT 25°C

Ion	$\Delta E_i^{\neq}$(cal)	$\Delta\Delta S_i^{\neq}$(e.u.)
$C_2SO_4^-$	120	−0.11
$C_4SO_4^-$	230	−0.03
$C_6SO_4^-$	440	0.44
$C_8SO_4^-$	610	0.77
$C_{10}SO_4^-$	580	0.56
Na^+	20	0.05
$C_2Me_3N^+$	240	0.40
$C_4Me_3N^+$	620	1.35
$C_6Me_3N^+$	720	1.45
$C_8Me_3N^+$	880	1.67
$C_{10}Me_3N^+$	1090	2.21
$C_{12}Me_3N^+$	1530	3.45
Br^-	−240	−0.85

crease with the increase in the chain length of ions, and that, unlike those for ethylsulfate and butylsulfate, the activation entropies for the other ions considered are positive. These results confirm the interpretation of the negative temperature coefficient of ionic B values. That is, those ions which have a positive activation energy and a positive viscosity B coefficient increase the viscosity of water by increasing the ice-like structure apo-surface.[22] However, the ethylsulfate ion, which has a negative activation entropy, is weakly peri-surface hydrated and scarcely increases the B value at all because of the order-destroying effect of the ionic head. These results, when considered along with the temperature dependence of the B values, indicate that the alkylsulfate and alkyltrimethylammonium ions with longer alkyl chains are structure makers and that ethylsulfate and ethyltrimethylammonium ions are structure breakers, while for the butylsulfate ion the two effects appear to cancel each other out.

Viscosity of Micelles Solutions. It seems likely that, in dilute aqueous solutions of association colloides, the micelles are reasonably spherical. The viscosity of these solutions may be represented by Einstein's equation. The concentration of micelles composed of n molecules, C_m(mol/l), is given by:

$$C_m = \frac{C-\mathrm{CMC}}{n} \tag{16}$$

The hydrodynamic volume of the micelle, V_m (l/mol), is given by:

$$V_m = \frac{n(\bar{v}_m + n_h v_h)}{1000} \tag{17}$$

where $\bar{v}_m$ (ml/mol) is the partial molar volume of the surfactant in the micellar state; v_h(ml/mol), the molar volume of water hydrated, and n_h, the number of moles of the hydrated water per mole of the surfactant.

22) Literally—away from the surface on the ion. While peri-surface means at and round-about the ionic surface. Ref. 10.

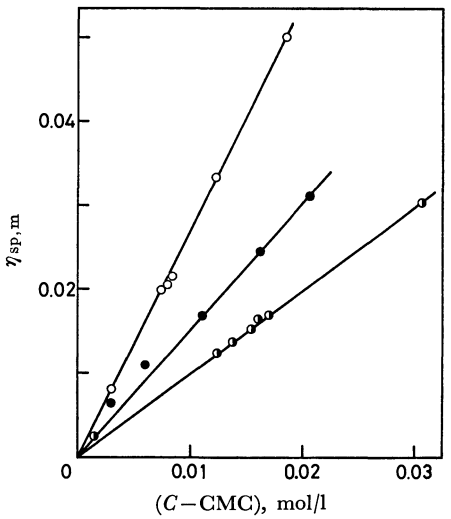

Fig. 5. Plots of $\eta_{sp,m}$ *vs.* (C−CMC) for the micellar solution at 25°C; sodium decylsulfate (●), sodium dodecylsulfate (○), decyltrimethylammonium bromide (◑).

TABLE 5. HYDRODYNAMIC VOLUME FOR MICELLES

Surfactant	$\bar{v}_m + n_h v_h$	$\bar{v}_m$[17]	n_h
$C_{10}Me_3NBr$	397	262.3	7—8
$C_{10}SO_4Na$	604	212.5	21—22
$C_{12}SO_4Na$	1108	246.2	47—48

In a micellar solution the viscosity of the solvent, η_0, should be replaced by the viscosity of the solution at the CMC η_m^0; then Eq. (4) becomes:

$$\eta_{sp,m} = \frac{\eta}{\eta_m^0} - 1 = \frac{\bar{v}_m + n_h v_h}{400}(C-\mathrm{CMC}) \tag{18}$$

A plot of $\eta_{sp,m}$ *vs.* (C-CMC) gives a straight line, as is shown in Fig. 5. The hydrodynamic volume of the micelle may be estimated from these slopes. The values of V_m thus obtained are presented in Table 5, together with the values of $\bar{v}_m$ and n_h. It can be seen from Table 5 that, in a homologous series, the longer the chain length, the larger the hydration number. However, n_h is larger than one would expect. Because the micelles of these ionic surfactants carry an electric charge in aqueous solutions, an electroviscous effect is always included as part of the measured intrinsic viscosity. Parker and Wasik[23] have shown that the intrinsic viscosities for sodium dodecylsulfate (SDS) in water and 0.2 M sodium chloride should differ by a factor of 2.3. Courchene,[24] with correction for the electroviscous effect, estimated 12 as the number of water for each surfactant molecule in the micelle. In this paper, the hydration number of SDS micelles in water is calculated to be about 13—14 from a similar correction for the electroviscous effect; this is in fair agreement with Courchene's value.

23) R. A. Parker and S. P. Wasik, *J. Phys. Chem.*, **62**, 967 (1958).
24) W. L. Courchene, *ibid.*, **68**, 1870 (1964).

Electrochemiluminescence of 9,10-Dichloroanthracene at Low Temperatures

Tamotsu MATSUMOTO, Masanori SATO, and Satoshi HIRAYAMA

Laboratory of Analytical Chemistry, Faculty of Textile Science, Kyoto Technical University, Matsugasaki, Sakyo-ku, Kyoto

(Received May 29, 1972)

The electrochemiluminescence (ECL) of 9,10-dichloroanthracene in methylene chloride was investigated at temperatures as low as −60°C. The cation was quite stable and the anion was unstable at room temperature. The anion, however, increased its stability as the temperature decreased and below *ca.* −40°C it was essentially stable. Temperature was also found to have great influence on the relative intensity of the two spectral components of the ECL of 9,10-dichloroanthracene. By lowering the temperature the components at the longer wavelength increased strongly compared with the other component. When the ECL was observed by applying a rectangular potential, the intensities of the two components decayed exponentially with the same decay constant. Therefore, it was concluded that the emission at the longer wavelength originated not from the products of electrolysis but from the excimer and that the primary process to produce these two emissions was the same.

It is well known that in aprotic solvents numerous aromatic compounds often show luminescence at the surface of an electrode to which an alternating potential is applied. This phenomenon, electrochemiluminescence (ECL), is mainly attributed to the annihilation of generated cations and anions. The first observation on ECL of many aromatic compounds was reported by Hercules.[1] Since then, detailed investigations on ECL have been carried out chiefly by Chandross *et al.*,[2,3] Zweig[4], Bard *et al.*[5,6] and Hercules *et al.*[7] and the various mechanisms of ECL have been postulated.

It is recognized that the observed ECL spectra sometimes contain longer wavelength emission which is not assignable to the corresponding fluorescence. The longer wavelength emission is often attributed to i) excimer fluorescence, ii) phosphorescence, or iii) fluorescence of the electrolytic products excited by energy transfer from excited molecules of the parent compound.

The following reaction scheme (A=aromatic) is considered to be appropriate to explain the phenomenon cited above, although a preannihilation mechanism[8] is not included.

$$\left.\begin{aligned} &A + e \longrightarrow A^-, \text{ cathodic process} \\ &A - e \longrightarrow A^+, \text{ anodic process} \end{aligned}\right\} \quad (1)$$

$$A^- + A^+ \rightleftharpoons {}^1(A\cdots A)^* \rightleftharpoons {}^1A^* + A, \quad (2)$$

$$A^- + A^+ \rightleftharpoons {}^3(A\cdots A) \longrightarrow {}^3A + A, \quad (3)$$

$${}^3A + {}^3A \rightleftharpoons {}^1(A\cdots A)^* \quad (4)$$

$${}^1A^* \longrightarrow A + h\nu_1, \text{ fluorescence} \quad (5)$$

$${}^1(A\cdots A)^* \longrightarrow 2A + h\nu_2, \text{ excimer fluorescence} \quad (6)$$

$${}^3A \longrightarrow A + h\nu_3, \text{ phosphorescence} \quad (7)$$

$${}^1A^* + B \longrightarrow A + {}^1B^*, \text{ B: electrolytic product} \quad (8)$$

$${}^1B^* \longrightarrow B + h\nu_4, \text{ fluorescence} \quad (9)$$

We consider here two mechanisms to produce an excimer, one of which is due to the triplet-triplet annihilation and the other involving direct formation through cation-anion annihilation. To reveal the emitting species of the observed ECL and to elucidate in detail the mechanism to produce them are of great value both in the study of emission spectroscopy and in the study of electron transfer reactions associated with a large change in enthalpy of reaction.

For the mechanism of ECL to be established, it is necessary to re-examine rigorously the electrochemical systems. For example, the character of the solvents has great influence on the electrochemical reactions. We have observed that dimethylformamide (DMF), frequently used for the study of ECL, is not suitable, because in this solvent most cations of aromatic molecules are not stable on account of DMF's strong nucleophilic property. For that reason the ECL processes (8) and (9) in which electrolytic products take part cannot be excluded from the plausible mechanisms of ECL. This has made the detailed discussion on the mechanism of ECL more complicated.

Therefore, it is essential to observe ECL spectra under the conditions where both anions and cations can exist stably. One of the best ways is to observe ECL spectra at low temperatures where undesirable reactions of ion radicals with solvent or impurities are greatly or completely retarded.

For rigorously quantitative treatment, electrochemical studies of aromatic compounds in aprotic solvents at low temperatures often involve difficulties in the choice of solvents, supporting electrolytes and a reference electrode, and through investigations have not been made until Van Duyne and Reilly's recent studies[9]. Only two investigations of ECL were done at low temperatures, one by Parker and Short[10] and the other by Weller and Zachariasse[11]. Although interest-

1) D. M. Hercules, *Science*, **145**, 808 (1964).
2) E. A. Chandross, J. W. Longworth, and R. E. Visco, *J. Amer. Chem. Soc.*, **87**, 3259 (1965).
3) E. A. Chandross and F. I. Sonntag, *ibid.*, **88**, 1089 (1966).
4) A. Zweig, "Advances in Photochemistry," Vol. 6, ed. by W. A. Noyes, Jr., G. S. Hammond, and J. N. Pitts, Interscience Publishers, New York, (1968) p. 425.
5) J. M. Malog, K. B. Prater, and A. J. Bard, *J. Phys. Chem.*, **72**, 4348 (1968).
6) L. R. Faulkner and A. J. Bard, *J. Amer. Chem. Soc.*, **90**, 6284 (1968).
7) T. C. Werner, J. Cheng, and D. M. Hercules, *ibid.*, **92**, 763, 5560 (1970).
8) D. L. Maricle and A. Maurer, *ibid.*, **89**, 188 (1967).
9) R. P. Van Duyne and C. N. Reilly, *Anal. Chem.*, **44**, 142, 153, 158 (1972).
10) C. A. Parker and G. D. Short, *Trans. Faraday Soc.*, **63**, 2618 (1967).
11) A. Weller and K. Zachariasse, *Chem. Phys. Lett.*, **10**, 197 (1971).

ing results were obtained by Parker and Short, they did not examine precisely their electrochemical system. On the other hand the latter authors' work concerned only with ECL spectra produced by the annihilation between the ion radicals of the two different molecules. By lowering the temperature not only the anion and the cation but also excimers will increase their stability, so that the observation of ECL spectra at low temperatures will become a useful means to study the mechanism of ECL involving excimer formation.

In order to elucidate the mechanism of the ECL of 9,10-dichloroanthracene (9,10-di-Cl-A), whose ECL spectrum had already been reported to be composed of the two components[12], electrochemical examinations of the ECL of this compound were performed at low temperatures. Large temperature effect was found not only on the ion radical stability but also on the ECL spectrum of 9,10-di-Cl-A. From the results obtained we will discuss the primary process of the observed ECL of 9,10-di-Cl-A.

Experimental

Materials. 9,10-di-Cl-A was synthesized by the method reported earlier[12] and purified by sublimation after recrystallization from carbon tetrachloride. Methylene chloride of guaranteed grade was further purified by distillation, dried over Molecular Sieve Linde 5A, and transferred to an electrolysis cell *in vacuo*. Dry tetrabutylammonium perchlorate (TBAP) or potassium perchlorate was used as a supporting electrolyte. Its concentration was *ca.* 0.05 M throughout the experiments.

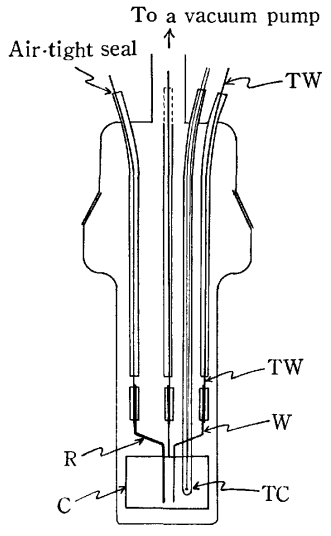

Fig. 1. Electrolysis cell.
W: working electrode, R: reference electrode, C: counter electrode, TC: thermocouple, TW: tungsten wire.

Apparatus. A Pyrex glass electrolysis cell is shown in in Fig. 1. The working electrode, W, is of Pt wire (0.05—0.08 cm diameter, 3 cm length); R is a reference electrode of Ag wire (0.1 cm diameter); and C is a counter electrode of Pt plate (1.5 cm×2.0 cm and 0.02 cm in thickness). These electrodes are connected to the outside leads through tungsten wires.

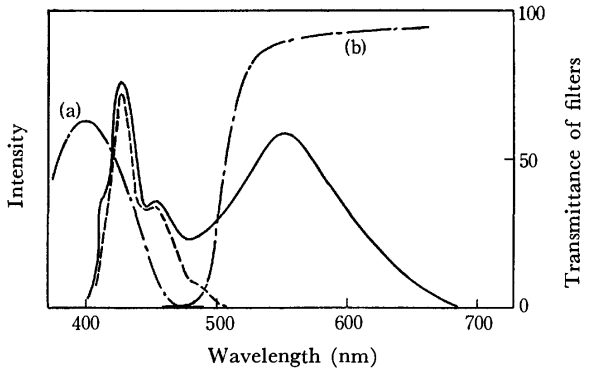

Fig. 2. Emission spectra of 9,10-di-Cl-A in DMF.
——: ECL (7×10^{-4} M), ----: fluorescence (7×10^{-4} M),
——: filters: (a) V-VIA, (b) V-051 (Similar ECL spectra were also observed in methylene chloride and acetonitrile.)

Aliquot amounts of 9,10-di-Cl-A and a supporting electrolyte were weighed into the electrolysis cell which was then evacuated by using an oil diffusion pump. The solvent was transferred into the cell *in vacuo* and the solution was degassed by repeating a freeze-pump-thaw cycle. The cell was then sealed off from the vacuum line and its cylindrical part was inserted into a transparent Dewar vessel made of Pyrex glass. By circulating cold nitrogen gas into the Dewar vessel, constant low-temperature was maintained. Temperatures were measured with a copper-constantan thermocouple.

Controlled potential electrolysis using a three-electrode configuration was performed by employing a potentiostat. Cyclic voltammograms were recorded on a Yokogawa *X–Y* Recorder Type 3077 at various temperatures. For the separate measurements of the intensities of two components of the ECL of 9,10-di-Cl-A (Fig. 2), Toshiba glass filters V-VIA and V-051 were used. Transmittance curves of these filters are also shown in Fig. 2. The light transmitted through each filter was measured with a Hamamatsu R136 photomultiplier and recorded on the *X–Y* recorder or on a Matsushita VP-541A oscilloscope. The observed light intensities should be proportional to the intensities of the corresponding emissions, so that the change in the ratio of these two intensities with temperature was thought to give us informations about the spectral change with temperature.

Results

Cyclic Voltammogram. The cyclic voltammograms of 9,10-di-Cl-A are presented in Figs. 3 and 4. In DMF both the anion and the cation are unstable at the room temperature. As the temperature decreases the re-oxidation current of the anion comes to be observed, corresponding to an increase of the stability of the anion radical. The cation, however, was still unstable at low temperature on account of the strong nucleophilic property of DMF.[9] In methylene chloride, known as a good solvent for cation radicals, the cation of 9,10-di-Cl-A was stable[14] but the anion was unstable. When the potential was reversed after producing the anion, near +0.9 V *vs.* Ag the oxidation current (probably due to secondary products

12) T. Matsumoto, M. Sato, S. Hirayama, and S. Uemura, This Bulletin, **44**, 1450 (1971).

14) The cation chemically produced in concentrated sulfuric acid also persists for several days without any change.

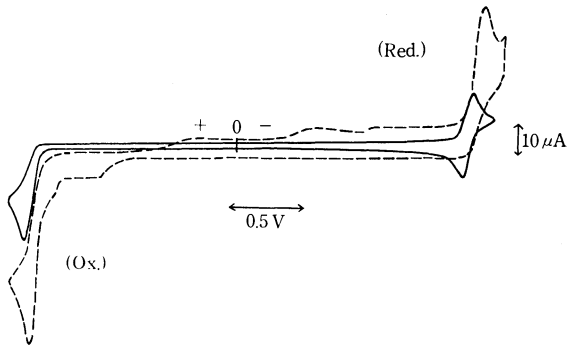

Fig. 3. Cyclic voltammogram of 9,10-di-Cl-A (10^{-3} M). Solvent: DMF, Supporting electrolyte: $KClO_4$, Potential sweep rate: 132 mV/s ——: −41°C, ----: room temperature

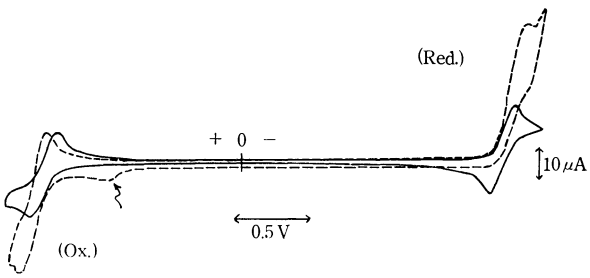

Fig. 4. Cyclic voltammogram of 9,10-di-Cl-A (10^{-3} M). Solvent: methylene chloride, Supporting electrolyte: TBAP Potential sweep rate: 144 mV/s
——: −56°C, ----: 7°C

of electrolysis) was observed (arrow in Fig. 4). Upon lowering the temperature this current finally disappears. In both cyclic voltammograms in Figs. 3 and 4 the difference between the anodic and cathodic peak potentials are larger than that of an ideal reversible wave. The peak current ratio for the anion radical couple was, however, close to unity even at a slow sweep rate of potential of 32 mV/s if the temperature was lower than *ca.* −40°C.[15] This shows almost complete stability of the anion at low temperatures. Similar results were obtained in acetonitrile.

In Fig. 5 the relationship between the applied potential and the observed emission intensity is shown. Light intensities were measured by using the photomultiplier without glass filters. This figure shows that as temperature decreases, the emission intensity becomes stronger and the emission lasts longer. Curiously the emission was observed only in the negative potential region even at low temperatures where both radical ions were considered to be stable. This phenomenon was independent of the direction of the potential sweep. From the results it is clear that the preannihilation mechanism is not suitable for the ECL of 9,10-di-Cl-A. In order to simulate the ECL-potential relationship, preliminary computer calculation was carried out by assuming that both ion radicals are completely stable and that the emission is observable only when the annihilation occurs be-

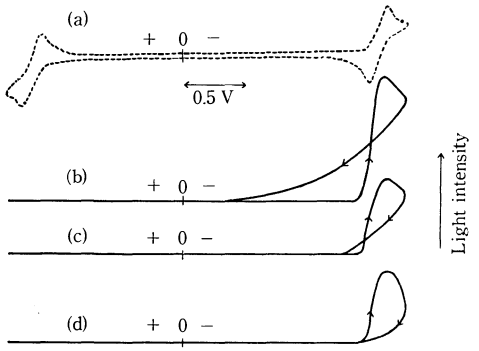

Fig. 5. Relationship between emission intensity and applied triangular potential.
[9,10-di-Cl-A] 10^{-3} M
Potential sweep rate: 580 mV/s
(a): Cyclic voltammogram (−48°C), (b): emission (−48°C), (c): emission (−5°C), (d): emission (+8°C)

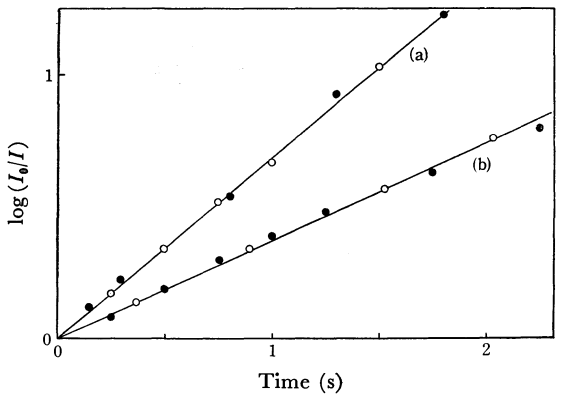

Fig. 6. $\log(I_0/I)$ *vs.* time plots for the two components of the ECL when a rectangular potential was applied.
I_0: maximum emission intensity
Curves: (a): 0°C, (b): −44°C
●: excimer, ○: fluorescence

tween an anion and a cation.[16] The theoretical emission-potential curve differs from the observed curves in that the emission is observable both in the negative and positive potential regions.

Temperature Effect on ECL. When a rectangular potential having an amplitude a little larger than the difference between the reduction and the oxidation potentials shown in Fig. 4 was applied to the working electrode, an emission, whose intensity decays with time, was observed every time when the sign of the potential changed. This differs from the situation found in the case of a triangular potential. For the decay curves observed when the potential changed from positive (cation) to negative (anion), a log I_0/I *vs.* time plot was carried out as illustrated in Fig. 6, where I_0 corresponds to the maximum light intensity and the time corresponding to this point was put equal to zero. The results were shown for the two cases, one for the decay observed through the glass filter V–VIA and the other through the glass filter V–051. Both decay curves are seen to follow approximately exponential decay. The apparent decay

15) T. Matsumoto, M. Sato and S. Hirayama, *Chem. Lett.*, **1972**, 603.

16) T. Matsumoto, M. Sato, S. Hirayama, and S. Uemura, unpublished results.

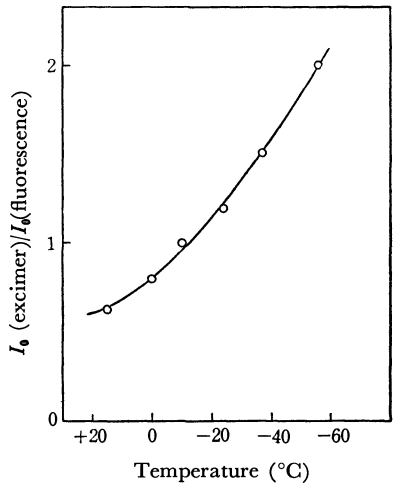

Fig. 7. Temperature dependence of the relative emission intensity of the two ECL components.
[9,10-di-Cl-A]10^{-3} M

constants for both curves are the same at the same temperature and diminish with a decrease in temperature. This is probably because the diffusion coefficients of molecules become smaller and stabilities of ion radicals increase as the temperature decreases.

The ratio of the peak heights of the two decay curves corresponding to the two emission components, designated by (I_0(excimer)/I_0(fluorescence)), is plotted against temperature in Fig. 7. The ratio continuously increases as the temperature decreases.

The emission from the excimer of 9,10-di-Cl-A by photo-excitation was observed by Chandross[17] in softened methylcyclohexane at low temperatures. In the same concentration region of 9,10-di-Cl-A, where its ECL was observed and at temperature as low as −60°C, no excimer emission was detected in either methylene chloride or DMF by photo-excitation.

In order to know the effect of concentration on the ECL spectra of 9,10-di-Cl-A, the ratio of the ECL intensity at 550 nm (excimer) to that at 450 nm (fluorescence) was measured in the concentration range of 10^{-3} to 10^{-4} M. As a measure of the fluorescence intensity, the light intensity at 450 nm was chosen in order to get rid of the effect of re-absorption of the fluorescent component at the shorter wavelength. The ratio showed a little increase as concentration increases, but its effect on ECL did not seem to have such a large effect as temperature had.

Discussion

Concerning the mechanism of the ECL of 9,10-di-Cl-A, it appears that the anion-cation annihilation process is indispensable and that this process occurs mostly in the bulk solution away from the working electrode. This is because we could not observe ECL when the electrolysis was carried out by applying triangular or rectangular potential in the region where only one type of ion was produced.

When we compare the emission *vs.* potential curve with the current *vs.* potential curve shown in Fig. 5, it is easily seen that the potential where ECL becomes observable almost coincides with the potential where the cathodic current begins to flow and that the potential where the ECL intensity reaches a maximum nearly corresponds with the cathodic peak potential. These results are compatible with the results of computer simulation.[16] ECL is still observable in the small negative potential region where a faradaic current is almost zero. This trend becomes more remarkable with the decrease of temperature as shown in Fig. 5. We can explain this in terms of the increased viscosity and stability of ion radicals at low temperatures. These facts indicate that ECL originates from the annihilation of ion radicals which have diffused away from the electrode.

There remains, however, an important question why the ECL could not be observed near the peak current potential where the cation was produced with a triagular potential. The results of computer simulation of the ECL based on the annihilation of the stable anion and cation radicals indicate that the ECL should be observed strongly in the two separate regions which correspond to the peak current potentials for reduction and oxidation. As far as the cyclic voltammetry concerns, both ion radicals are quite stable below −40°C,[15] so that we cannot find an pertinent explanation for the finding.

From the experiments at low temperatures it has also been assured that, of the two components of the ECL spectra of 9,10-di-Cl-A, the one at the longer wavelength corresponds to the emission from the excimer. The other possibility that the longer wavelength component is due to the secondary products of electrolysis is easily excluded,[6] because the emission intensity of this component increases as the anion increases its stability. The fact that an excimer is stabilized at low temperatures should also be noted. Combined with other experimental facts previously reported,[12] these new findings are thought to confirm our previous interpretation.

The primary process to produce two components of the ECL of 9,10-di-Cl-A is considered to be the same because the emission decay curves for the two components are the same at any temperature. However, it is not clear from the present work alone whether the mechanism to form the excimer is produced from reaction (2) or from reactions (3) and (4). The latter possibility, *i. e.*, the participation of the triplet state, has been pointed out by Weller and Zachariasse[11], and Freed and Faulkner[19] in an "energy deficient" ECL system. In our case, if we estimate roughly the enthalpy change in the anion-cation annihilation by the equation $\Delta H = E^{ox} - E^{red}$, where E^{ox} and E^{red} are the peak current potentials[20] for oxidation and reduction, respectively, the value of ΔH is of the same order as the energy of the lowest excited signlet state

17) E. A. Chandross and J. G. Ferguson, *J. Chem. Phys.*, **45**, 3554 (1966).

19) D. J. Freed and L. R. Faulkner, *J. Amer. Chem. Soc.*, **93**, 2097 (1971).

20) G. J. Hoytink, *Discuss. Faraday Soc.*, **45**, 14 (1968).

of 9,10-di-Cl-A[21]. In addition the energy required to form the excimer is smaller than that of the excited singlet state. Therefore, we cannot eliminate the the possibility of the direct excimer formation by the simple consideration of energy balance alone. The simplest and most reliable way to ascertain experimentally the participation of the triplet state in ECL would be to observe the T–T′ absorption of the molecule in the triplet state, using an optically transparent electrode (OTE) as a working electrode.[22] With the aid of OTE, the transient absorption due to the anion or the cation generated near OTE has been measured.[15] If the mechanism of ECL is primarily based on the reaction Schemes (3) and (4), the local concentration of the triplet state molecules is expected to be as high as that of the ion radicals, which will permit us to measure its absorption with OTE.

As has been discussed hitherto, no conclusion can be drawn as to the mechanism of ECL except that the primary process of the ECL of 9,10-di-Cl-A is the annihilation of the anion and cation. It should be noted, however, that the excimer emission observed in the ECL is much stronger than that observed by photo-excitation. In fact at a concentration as low as 5×10^{-4} M, no excimer emission was observed by photo-excitation even at *ca.* −60°C. Change in concentration did not have large effect on ECL. These results are considered to indicate either (i) the excimer is directly formed by the anion-cation annihilation, or (ii) the local concentration in the neighbourhood of the excited molecule (singlet or triplet) is quite high because the excited molecule which has been produced as a result of the electron transfer reaction between two ions — anion and cation — will always have its counterpart in its close vicinity. If the mechanism (i) is working in our case, it is quite interesting since it entails an efficient energy dissipation process in electron transfer reactions which are accompanied by a large change in reaction enthalpy.

21) I. B. Berlman "Handbook of Fluorescence Spectra of Aromatic Molecules," Academic Press, New York (1965), p. 127.

22) To ascertain the participation of a triplet molecule the effect of magnetic field on the intensity of ECL has been investigated by L. R. Faulkner and A. J. Bard (*J. Amer. Chem. Soc.*, **91**, 6495 (1969)) and K. S. V. Santhanam (*Can. J. Chem.*, **49**, 3577 (1971)).

BULLETIN OF THE CHEMICAL SOCIETY OF JAPAN VOL. 46, 373—380 (1973)

Photoelectron Spectra and Orbital Structures of Higher Alkyl Chlorides, Bromides, and Iodides

Katsumi KIMURA, Shunji KATSUMATA, Yohji ACHIBA, Hiroshi MATSUMOTO,* and Saburo NAGAKURA**

Physical Chemistry Laboratory, Institute of Applied Electricity, Hokkaido University, Sapporo

**Japan Spectroscopic Co., Ltd., Hachiohji, Tokyo*

***The Institute for Solid State Physics, The Universtiy of Tokyo, Roppongi, Minato-ku, Tokyo*

(Received June 19, 1972)

High-resolution photoelectron spectra of alkyl halides RX (R=ethyl, *n*-propyl, and *n*-butyl; X=Cl, Br, and I) were measured with the 584 Å line of helium. In the region below about 17 eV, six bands were observed for each of the ethyl halides, eight bands for each of the *n*-propyl halides, and ten bands for each of the *n*-butyl halides. All the observed vertical ionization energies were plotted against Pauling's electronegativity of the halogen atom, indicating that there are approximate linear relationships. Assuming Koopmans' theorem, total and partial sums of experimental orbital energies were calculated using the observed ionization energies for the individual alkyl halides and found to be well reproduced by calculating the sums of empirical orbital-energy values for several localized orbitals such as $n(X)$, $n'(X)$, $\sigma(C\text{–}X)$, $\sigma(C\text{–}C)$, $\pi(CH_3)$, $\pi'(CH_3)$, and $\pi(CH_2)$. From a comparison of the experimental and calculated partial orbital-energy sums, assignments of the photoelectron bands to the localized molecular orbitals were made for each of the alkyl halides.

It is known in photoelectron spectroscopy that removal of a lone-pair electron gives rise to the first ionization with a sharp band distinguishable from other types of electrons such as π and σ electrons. As a result, the ionization energies of the lone pair electrons can be accurately determined, thus attracting attention to the photoelectron spectra of various compounds containing halogen atoms.

With respect to alkyl halides, several photoelectron studies[1–6,8] have been carried out with high-resolution photoelectron technique during the last few years. Turner[1] first succeeded in measuring high-resolution photoelectron spectra for many compounds including some halogen-containing compounds. Ragle

1) D. W. Turner, "Molecular Photoelectron Spectroscopy," John Wiley & Sons, New York, N. Y. (1969).

2) J. L. Ragle, I. A. Stenhouse, D. C. Frost, and C. A. McDowell, *J. Chem. Phys.*, **53**, 178 (1970).

3) A. W. Potts, H. J. Lempka, D. G. Streets, and W. C. Price, *Phil. Trans. Roy. Soc. Lond.*, **A**, **268**, 58 (1970).

4) J. A. Hashmall and E. Heilbronner, *Angew. Chem. Internat. Edit.*, **9**, 305 (1970).

5) A. D. Baker, D. Betteridge, N. R. Kemp, and R. E. Kirby, *Anal. Chem.*, **43**, 375 (1971).

6) F. Brolgi and E. Heilbronner, *Helv. Chim. Acta*, **54**, 1424 (1971).

7) R. N. Dixon, J. N. Murrell, and B. Narayan, *Molecular Phys.*, **20**, 611 (1971).

8) A. D. Baker, D. Betteridge, N. R. Kemp, and R. E. Kirby, *Int. J. Mass Spectrum Ion Phys.*, **4**, 90 (1970).

et al.[2] reported on the photoelectron spectra of many halomethanes including methyl halides and interpreted each of the observed bands in terms of molecular orbital structure from a comparative study of the spectra. For a series of alkyl bromides, Hashmall and Heilbronner[4] reported an interesting comparison of their first ionization energies obtained from the high-resolution photoelectron spectra, and concluded that the first ionization energy is reduced by 0.2 eV by methyl substitution on the α-position and by 0.09 eV on the β-position.

Photoelectron spectra of methyl iodide and several alkyl iodides have been studied by Baker *et al.*[5] together with other halogen-containing compounds from an analytical point of view, indicating that there is a correlation between the first ionization energies and the Taft σ values of the alkyl groups.

The "lone pair" bands of the series of the alkyl iodides as well as alkyl bromides have been studied theoretically in detail by Brogli and Heilbronner[6] in terms of the spin-orbit coupling. The photoelectron bands associated with ionization from the formally non-bonding p orbitals of the halogen atoms in various halomethanes have been interpreted by Dixon *et al.*,[7] in terms of a pseudo one-electron hamiltonian.

Photoelectron data of *n*-butyl iodide except for the first-ionization band has not so far been found in literature. Several photoelectron studies of alkyl halides mentioned above are available, but no systematic and comparative photoelectron studies covering higher alkyl chlorides, bromides and iodides have been published yet.

We have carried out a systematic and comparative study of not only the first but also the higher ionization energies of ethyl, *n*-propyl and *n*-butyl halides by means of a high-resolution photoelectron technique, with the aim first to deduce some correlations of ionization energies of alkyl halides with carbon chain and electronegativity of the halogen atom, and secondly to clarify valence orbital structures of the series of normal alkyl halides up to the butyl halides.

Experimental

Commercial alkyl halides were used after purification. Measurements of photoelectron spectra were carried out with a JASCO PE-1 high-resolution photoelectron spectrometer, containing an electrostatic semispherical analyzer, using helium 584 Å (21.22 eV) resonance line. Detection of photoelectrons was made with an electron multiplier coupled to an amplifier, discriminater and rate meter. The typical working resolution of this spectrometer was 20—25 meV. Calibration of an ionization-energy scale from the analyzer voltage was carried out using known ionization energy values of Ar and Xe as standard substances.

Results and Discussion

Photoelectron Spectra and Ionization Energies. Observed photoelectron spectra for ethyl, *n*-propyl and *n*-butyl halides (X=Cl, Br, and I) are shown in Figs. 1—3. General aspects of these spectra differ from those of the corresponding methyl halides except for the first bands, the spectrum becoming successively complicated as the alkyl group is ascended.

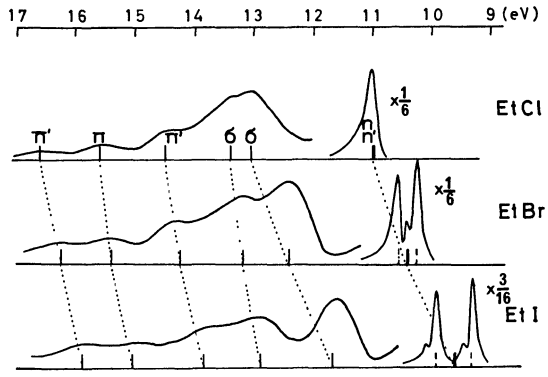

Fig. 1. Photoelectron spectra of ethyl halides.

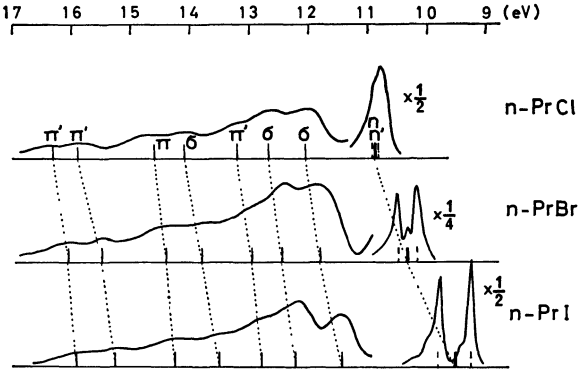

Fig. 2. Photoelectron spectra of *n*-propyl halides.

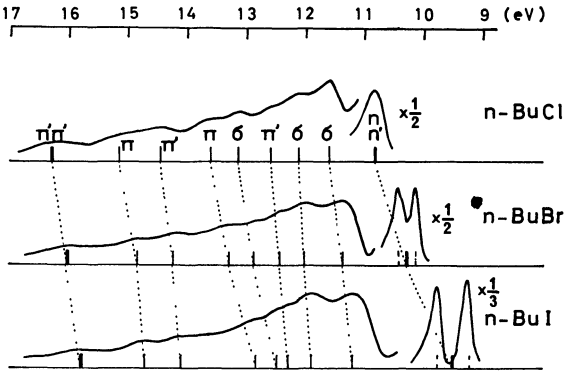

Fig. 3. Photoelectron spectra of *n*-butyl halides.

A comparative and systematic study is of merit for determining ionization energies from the photoelectron spectra.

First a brief review of the spectral features of methyl halides (CH_3X)[2,3] will provide a basis for interpreting electronic structures and photoelectron spectra of higher alkyl halides. In the methyl halides four photoelectron bands ascribed to different orbitals have been observed below *ca.* 22 eV. The first bands accompany spin-orbit splittings and vibrational structures are assigned to ionization of the non-bonding orbitals. The second bands ascribed to the C–X bonding orbitals show relatively broad maxima without any structure, and the third bands due to the pseudo

π orbitals of CH_3 are composed of double maxima due to the Jahn-Teller splitting. The fourth band appearing at *ca.* 20 eV has tentatively been assigned to the C 2s orbital.[3]

Spectral features observed for the higher alkyl halides are as follows.

Ethyl Halides. As seen from Fig. 1, a total of six bands appear for the individual ethyl halides, the first bands with structures very similar in spectral shape to those of the corresponding methyl halides. A slight shoulder appearing on high energy side of the second band of ethyl chloride is considered to be an independent band corresponding to the third inner orbital. Mean vertical ionization energies obtained from the maxima or shoulders of their photoelectron spectra are summarized in Table 1, the values obtained from the shoulders being shown in parentheses.

Table 1. Vertical ionization energies of ethyl halides (in eV)

	This work			Other works		
	EtCl	EtBr	EtI	EtBr[4]	EtI[5]	EtI[6]
$I_1(^2E_{3/2})$		10.28	9.34	10.30	9.37	9.35
$I_1(^2E_{1/2})$		10.60	9.93	10.61	9.93	9.93
$(I_1)_{av}$	11.01	10.44	9.63_5	10.45_5	9.65	9.64
I_2	13.07	12.44	11.66		11.68	
I_3	(13.4)	13.20	12.90		12.90	
I_4	14.50	14.25	13.85		13.80	
I_5	15.60	15.40	15.05		15.00	
I_6	16.60	16.25	15.90		15.90	

In order to find some correlation among the ethyl-halide data, we plotted the observed ionization energies against Pauling's electronegativities of the halogen atoms (Fig. 4) in which six kinds of observed ionization energies correspond well to each other. Such correlation diagrams are also drawn for other series of the alkyl halides in Fig. 4. In Fig. 5, the first and second ionization-energy plots of the ethyl halides are compared with those of the other higher halides.

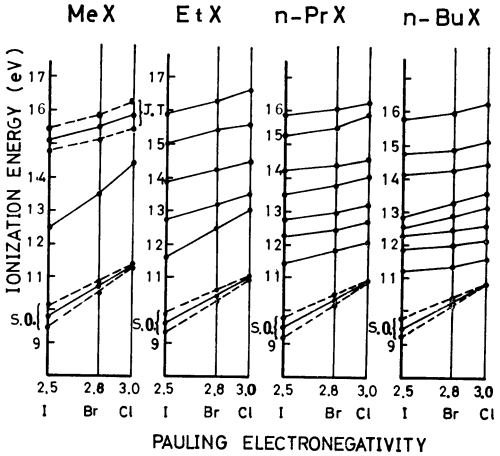

Fig. 4. Plots of ionization energies against Pauling's electronegativities of the halogen atoms. Corresponding points are connected by lines. (J. T. and S. O. denote the splittings of Jahn-Teller effect and spin-orbit coupling, respectively.)

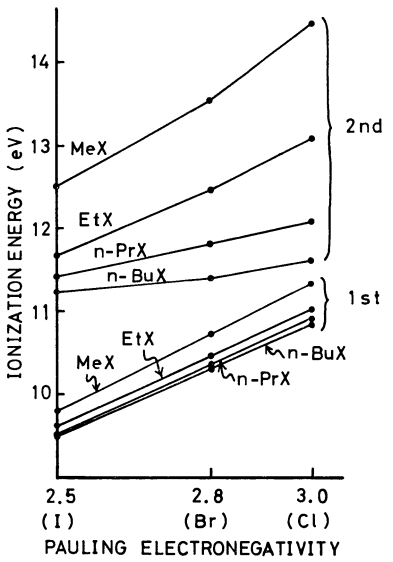

Fig. 5. Comparison of the first and second ionization-energy plots for the alkyl halides.

n-Propyl Halides. The photoelectron spectra of the series of the *n*-propyl halides are compared in Fig. 2. For these compounds a total of eight bands are distinguishable from the overall spectra. The resulting ionization energies are summarized in Table 2. Here also slight shoulders appear at *ca.* 13.2 eV for *n*-PrCl and *ca.* 12.9 and 13.8 eV for *n*-PrBr.

Table 2. Vertical ionization energies of *n*-propyl halides (in eV)

	This work			Other works		
	n-PrCl	*n*-PrBr	*n*-PrI	*n*-PrBr[4]	*n*-PrI[5]	*n*-PrI[6]
$I_1(^2E_{3/2})$		10.18	9.27	10.18	9.27	9.25
$I_1(^2E_{1/2})$		10.50	9.82	10.49	9.84	9.83
$(I_1)_{av}$	10.88	10.34	9.53_5	10.33_5	9.55_5	9.54
I_2	12.06	11.81	11.43		11.46	
I_3	12.68	12.45	12.22		12.25	
I_4	(13.2)	(12.9_5)	12.78		12.80	
I_5	14.10	(13.8)	(13.5)			
I_6	14.60	14.40	14.25		14.25	
I_7	15.90	15.50	15.25		15.30	
I_8	16.30	16.05	15.90		15.95	

Seven ionization energy values have already been reported for *n*-PrI by Baker *et al.*,[5] whereas we identified a total of eight bands including the 13.5 eV band which appears as only a slight shelf. Good correlations were obtained for the observed ionization energies among the *n*-propyl halides as in the case of the ethyl halide series.

n-Butyl Halides. In the *n*-butyl halides the situation is much more complicated with overlapping bands in the photoelectron spectra. However, we can identify a total of at least ten bands from the observed spectra of the *n*-butyl halides by the aid of the correlation diagram (Fig. 4). The resulting values are given in Table 3.

Some literature values, though incomplete, are available for comparison with the present data, as

TABLE 3. VERTICAL IONIZATION ENERGIES OF *n*-BUTYL HALIDES (IN eV)

	This work			Other works	
	n-BuCl	*n*-BuBr	*n*-BuI	*n*-BuBr[4]	*n*-BuI[6]
$I_1(^2E_{3/2})$		10.15	9.24	10.13	9.23
$I_1(^2E_{1/2})$		10.44	9.79	10.44	9.81
$(I_1)_{av}$	10.84	10.29_5	9.51_5	10.28_5	9.52
I_2	11.61	11.38	11.22		
I_3	12.13	12.03	11.90		
I_4	(12.6)	12.45	(12.3)		
I_5	13.14	(12.9)	12.50		
I_6	13.60	13.30	(12.8_5)		
I_7	14.45	14.25	(14.1)		
I_8	(15.1_5)	14.85	14.70		
I_9, I_{10}	16.25	16.00	15.75		

shown in Tables 1—3. For the alkyl chlorides except methyl chloride, no photoelectron data are available for comparison. For a series of alkyl bromides, no higher ionization energies have been reported previously. The first ionization energies including spin-orbit splittings reported by Hashmall and Heilbronner[4] were essentially in agreement with our corresponding data. Furthermore, in alkyl iodides, ethyl, *n*-propyl and *n*-pentyl iodides have been studied by photoelectron spectroscopy by Baker *et al.*,[5] but *n*-butyl iodide has not been included. As far as comparison is possible, excellent agreements were obtained.

Alkyl Substituent Effect on First Ionization. In Fig. 6, variations in the first mean ionization energies are shown for the alkyl halides from the methyl to *n*-butyl halides. Their higher normal homologues can be expected to tend to converge to nearly constant values.

It has been pointed out that the mean first ionization energies of the alkyl bromides are reduced by 0.2 eV per α-methyl substituent and by 0.09 eV per β-methyl substituent.[4] It is interesting to note that in the series of the alkyl chlorides, bromides and iodides, the ionization energy variation due to the methyl substitution on γ-position still amounts to as much as 0.02—0.05 eV.

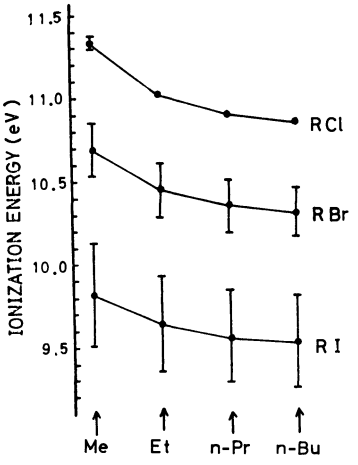

Fig. 6. The effect of carbon chain on the mean first ionization energies for the alkyl chlorides, bromides and iodides. Magnitudes of the spin-orbit splittings are also shown.

Correlation with Pauling's Electronegativity of Halogen Atom. It is interesting to examine how halogen atoms depend on ionization energies. The available ionization energies for the methyl halides are plotted for comparison (Figs. 4—6). As seen from Fig. 5, there are more or less linear relationships for many sets of ionization energy. Baker *et al.*[8] have pointed out that such a linear relationship is found for the first ionization energies of methyl halides. A similar correlation has now been found for the higher alkyl halides.

The gradient of the lines plotted in the correlation diagram is considered to express a measure of contribution from the halogen atoms. It is expected that the greater the contribution of the halogen atom, the steeper the line.

Let us consider the first ionization of the series of alkyl halides. The lowest straight lines corresponding to the first ionization show almost parallel relationships but become slightly less steep as the series ascends. The gradient of these lines may roughly be related to the magnitude of contribution of halogen p orbital by the following consideration. Assuming Koopmans' theorem, the lone-pair orbital ε_1 can be given by

$$\varepsilon_1 = c_x^2 F_{xx} + \sum_{\nu} c_{1x} c_{1\nu} F_{x\nu} + \cdots \quad (1)$$

where F_{xx} is a Hamiltonian element expressed in terms of the halogen p atomic orbitals. Since the molecular orbitals associated with the first ionization are expected to be largely contributed by the halogen p orbitals, coefficient c_x in the first term should be predominantly large. In the CNDO/2 approximation,[9] F_{xx} can be expressed by

$$F_{xx} = -\frac{1}{2}(I_x + A_x) + \cdots \quad (2)$$

It should be noticed that the first term in Eq. 2 is equivalent to Mulliken's electronegativity, which is in turn proportional to Pauling's electronegativity

$$\frac{1}{2}(I+A) = \chi\,(\text{Mulliken}) \propto \chi\,(\text{Pauling}) \quad (3)$$

Assuming that the rest of the terms in Eq. (1) be independent of the halogen atoms, the linearity and parallelism obtained for the lowest lines suggest that coefficients c_x have a nearly constant value for all the alkyl halides in spite of different kinds of halogen and alkyl group.

However, we see from Fig. 5 that the plots of the second ionization energies show no parallelism, the line slope becomes rapidly gentle as the series ascends. In *n*-propyl and *n*-butyl halides, in particular it is interesting to note that the second lines are considerably flat.

Total Orbital Energies. Since the total sum of eigenvalues of a secular equation is mathematically equal to its diagonal sum, total orbital energies should be unchanged before and after taking orbital interaction into account. Assuming Koopmans' theorem, this

9) J. A. Pople and G. A. Segal, *J. Chem. Phys.*, **44**, 3289 (1966).

Table 4. Comparison of experimental and calculated total orbital energies (in eV) for alkyl halides

		Exptl[a]	Calcd[b]	Difference
MeX	X=Cl	−68.83	−68.65	0.2
	Br	−65.89	−65.83	0.0
	I	−62.36	−62.57	−0.2
EtX	X=Cl	−95.19	−94.72	0.5
	Br	−92.42	−91.90	0.5
	I	−88.63	−88.64	0.0
n-PrX	X=Cl	−120.61	−120.79	−0.2
	Br	−117.64	−117.97	−0.4
	I	−114.40	−114.71	−0.3
n-BuX	X=Cl	−146.86	−146.86	0.0
	Br	−143.75	−144.03	−0.3
	I	−140.10	−140.77	−0.7

a) Obtained on the assumption of Koopmans' theorem using all the ionization energies observed for individual ethyl, *n*-propyl, and *n*-butyl halides (Tables 1—3). For the methyl halides, the ionization-energy values reported in Ref. 2 were used.
b) Calculated by substituting the orbital energies given in Table 5 into Eqs. (4)—(7).

sum rule may be applied to our ionization energy problem. For the individual alkyl halides we calculated total orbital energies using $-\{2(I_1)_{av}+I_2+I_3+\cdots\}$ in the energy range studied. The resulting total energies thus obtained are shown in Table 4.

In interpreting these experimental total orbital energies, we considered that the orbitals under study are composed of several localized orbitals such as n(X), σ(C–X), σ(C–C), $\pi(CH_3)$, $\pi(CH_2)$, schematically shown in Fig. 7, and found that empirical values given in Table 5 are very suitable for these assumed orbitals. Total orbital energies were calculated with these values using the following equations

$$E(\text{MeX}) = 2\varepsilon^0(n, \text{X}) + \varepsilon^0(\sigma, \text{C-X}) + 2\varepsilon^0(\pi, CH_3) \quad (4)$$

$$E(\text{EtX}) = E(\text{MeX}) + \varepsilon^0(\sigma, \text{C-C}) + \varepsilon^0(\pi, CH_2) \quad (5)$$

$$E(n\text{-PrX}) = E(\text{MeX}) + 2\varepsilon^0(\sigma, \text{C-C}) + 2\varepsilon^0(\pi, CH_2) \quad (6)$$

$$E(n\text{-BuX}) = E(\text{MeX}) + 3\varepsilon^0(\sigma, \text{C-C}) + 3\varepsilon^0(\pi, CH_2) \quad (7)$$

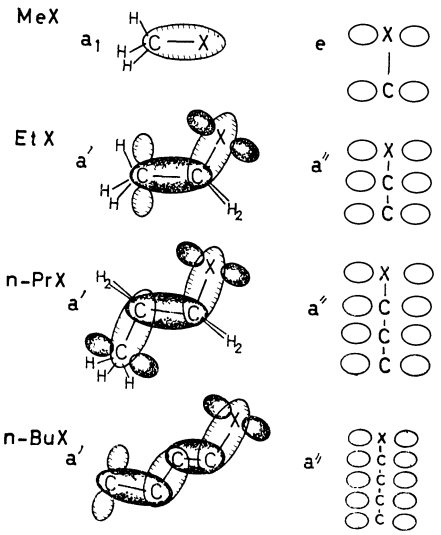

Fig. 7. Localized molecular orbitals used for the interpretation of the photoelectron data of the alkyl halides.

Table 5. Assumed orbital energies (in eV)

ε^0 (n, Cl) = −12.78[a]	ε^0 (σ, C-Cl) = −14.45[b]
ε^0 (n, Br) = -11.83_5[a]	ε^0 (σ, C-Br) = −13.52[b]
ε^0 (n, I) = -10.71_5[a]	ε^0 (σ, C-I) = −12.50[b]
ε^0 (σ, C-C) = −11.75	
ε^0 (π, CH_3) = ε^0 (π, CH_2) = −14.32	

a) Taken from the $(I_1)_{av}$ of the corresponding hydrogen halides reported in Ref. a) in Table 6.
b) Taken from the I_2 of the corresponding methyl halides reported in Ref. 2.

The calculated results are compared with the experimental ones in Table 4. It is interesting to see that the calculated total orbital energies are in good agreement with the experimental ones, strongly indicating that the molecular orbitals under consideration interact very slightly with inner orbitals such as C 2s and X *n*s orbitals.

The above agreements obtained for the total energy sums seem to support the existence of the concealed bands, whose ionization energy values are shown in parentheses in Tables 1—3.

As regards our estimation of the empirical energy values given in Table 5, the halogen non-bonding orbital energies were taken from the first mean ionization energies of molecules HX, shown in Table 6, since there is very little interaction between the non-bonding orbitals of these simplest halides and other valence orbitals. For C–X bands, their assumed unperturbed orbital energies were taken from orbital-energy values estimated from the second ionization energies of the methyl halides (Table 6), since the σ(C–X) orbitals belonging to a_1 symmetry do not interact with the n(X) and $\pi(CH_3)$ orbitals belonging to e symmetry and are considered to interact very slightly with inner orbitals of the same symmetry.

The $\pi(CH_3)$ orbital energy can not be determined directly from photoelectron spectra, since it always interacts with other orbitals to a considerable extent. However, from a comparison of the HX and MeX spectra, we can estimate the energy level of $\pi(CH_3)$

Table 6. Photoelectron data reported for hydrogen and methyl halides (in eV)[a]

	Lempka *et al.*[b]			Ragel *et al.*[2]		
	HCl	HBr	HI	MeCl	MeBr	MeI
$I_1(^2E_{3/2})$	12.74	11.67	10.38	11.29	10.53	9.50
$I_1(^2E_{1/2})$	12.82	12.00	11.05	11.37	10.85	10.13
$(I_1)_{av}$	12.78	11.83_5	10.71_5	11.33	10.69	9.81_5
I_2				14.45	13.52	12.50
I_3 (J. T.)				15.47	15.14	14.79
I_3' (J. T.)				16.25	15.85	15.44
$(I_3)_{av}$[c]				15.86	15.49_5	15.11_5

a) Essentially the same results have been reported for the hydrogen halides by D. C. Frost, C. A. McDowell, and D. A. Vroom [*J. Chem. Phys.*, **46**, 4255 (1967)], and for the methyl halides by Potts *et al.* (Ref. 3) who did not describe values for I_3' (J. T.).
b) H. J. Lempka, T. R. Passmore, and W. C. Price, *Proc. Roy. Soc. Ser. A*, **304**, 53 (1968).
c) Taken as the center of gravity of the Jahn-Teller splittings.

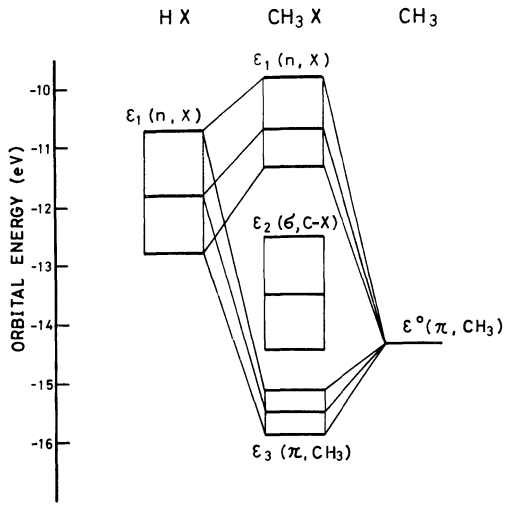

Fig. 8. Orbital energy levels of CH_3X (X=Cl, Br, and I), showing interactions of the n(X) and $\pi(CH_3)$ orbitals.

by considering that the first and third photoelectron bands result from an interaction of the halogen nonbonding and the CH_3 orbitals as shown in Fig. 8. Thus, assuming that

$$\{-I_1(CH_3X)\}_{av} + \{-I_3(CH_3X)\}_{av} = \{-I_1(HX)\}_{av} + \varepsilon^0(\pi, CH_3) \quad (8)$$

and using available data of ionization energy in the cases of X=Cl, Br, and I (see Table 6), we have $\varepsilon^0(\pi, CH_3) = -14.41$, -14.36 and -14.21 eV, respectively, with an average value of -14.32 eV.

The orbital energy of $\pi(CH_2)$ was assumed to be the same as that of $\pi(CH_3)$ for simplicity.

As shown in Fig. 9, the unperturbed C–C bonding

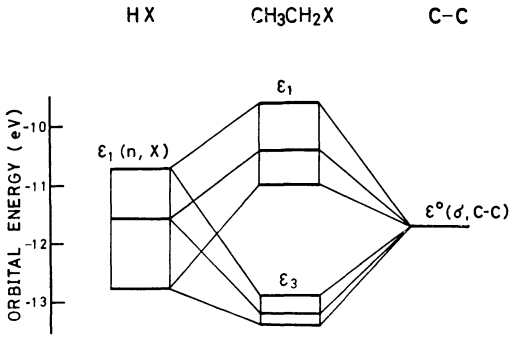

Fig. 9. Orbital energy levels ε_1 and ε_3 of C_2H_5X (X=Cl, Br, and I), showing interactions of the n(X) and σ(C–C) orbitals.

orbital energy $\varepsilon^0(\sigma, C–C)$ was estimated by taking the interaction between the C–C bonding and the halogen n'(X) orbitals of the ethyl halides into account. From the approximate equation

$$\{-I_1(EtX)\}_{av} + \{-I_3(EtX)\}_{av} = \{-I_1(HX)\}_{av} + \varepsilon^0(\sigma, C–C) \quad (9)$$

and with the available ionization energies, we obtained $\varepsilon^0(\sigma, C–C)$ values of -11.63, -11.80, and -11.82 eV in the cases of X=Cl, Br, and I, respectively, an average value of 11.75 eV being obtained.

From the agreements of the experimental and the calculated total orbital energies, we may conclude that our data of ionization energies shown in Tables 1—3 covers all the valence orbitals existing in the range higher than *ca.* -17 eV.

Assignments of Photoelectron Spectra. Orbital structures of the methyl halides are well understood and expressed approximately by[1-3]

$$\cdots e(\pi, CH_3)^4 a_1(\sigma, C–X)^2 e(np\pi, X)^4$$

in decreasing order of ionization energy. We found that the lower-energy shifts of the first bands of methyl halides compared with those of hydrogen halides can well be interpreted in terms of the interactions between the n(X) orbital and the $\pi(CH_3)$ orbital which is assumed to possess an orbital energy of about -14.3 eV (Fig. 8). Calculated and experimental sums for the methyl halides are shown in Table 7, indicating a validity of the selection of the $\pi(CH_3)$ energy values.

Ethyl halides are of symmetry C_s, so that molecular orbitals are divided into two species a′ and a″. As shown in Figs. 9 and 10, interactions in species a′ are considered to occur mainly between n(X) and σ(C–C) and between σ(C–X) and $\pi(CH_3)$, while in species a″ the n'(X), $\pi'(CH_3)$ and $\pi'(CH_2)$ orbitals considerably mix with one another (see also Fig. 6).

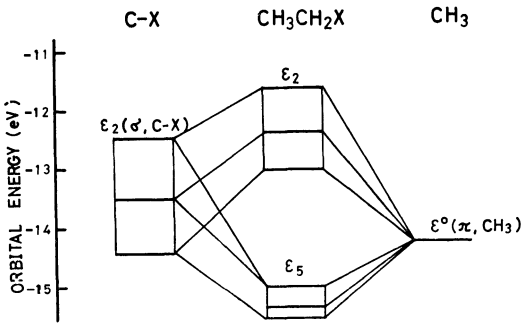

Fig. 10. Orbital energy levels ε_2 and ε_5 of C_2H_5X (X=Cl, Br, and I), showing interactions of the σ(C–X) and $\pi(CH_3)$ orbitals.

Using the sum rule mentioned before and the empirical energy values given in Table 5, it was found that the partial orbital-energy sums of $\{n$(X) and σ(C–C)$\}$, $\{\sigma$(C–X) and $\pi(CH_3)\}$ and $\{n'$(X), $\pi'(CH_3)$, and $\pi'(CH_2)\}$ are approximately equal to $-(I_1+I_3)$, $-(I_2+I_5)$ and $-(I'_1+I_4+I_6)$, respectively (Table 7). Good agreement of the partial sums of the calculated and experimental orbital energies makes it possible to assign the observed photoelectron bands of the ethyl halides. It might be concluded that I_2 and I_3 correspond to σ(C–X) and σ(C–C), respectively, with large contributions from $\pi(CH_3)$ and n(X), respectively. I_4, I_5, and I_6 can be assigned to $\pi'(CH_3)$, $\pi(CH_3)$ and $\pi'(CH_2)$, respectively. From the shapes of the first bands with spin-orbit splittings, it is not possible to distinguish the two bands corresponding to n(X) and n'(X) from each other which probably overlap closely.

For *n*-propyl halides, it is known that in gaseous phase there exist two types of rotational isomers, a *trans* form (symmetry C_s) and a *gauche* form (no symmetry).

TABLE 7. ASSIGNMENTS AND PARTIAL ORBITAL-ENERGY SUMS (IN eV)

Symmetry	Assignment		RCl	RBr	RI
	Methyl halides				
e	I_1, I_3	exptl[a]	−27.19	−26.18	−24.93
	n(X), π(CH_3)	calcd	−27.10	−26.15	−25.03
	Ethyl halides				
a'	I_1, I_3	exptl	−24.41	−23.64	−22.53
	n(X), σ(C-C)	calcd	−24.53	−23.58	−22.46
a'	I_2, I_5	exptl	−28.67	−27.84	−26.71
	σ(C-X), π(CH_3)	calcd	−28.77	−27.84	−26.82
a''	I_1', I_4, I_6	exptl	−42.11	−40.94	−39.38
	n'(X), π'(CH_3), π'(CH_2)	calcd	−41.42	−40.47	−39.35
	***n*-Propyl halides**				
a'	I_2, I_5	exptl	−26.16	−25.61	−24.93
	σ(C_2–C_3), σ(C-X)	calcd	−26.20	−25.27	−24.25
a'	I_1, I_3, I_6	exptl	−38.16	−37.19	−36.00
	n(X), σ(C_1–C_2), π(CH_3)	calcd	−38.85	−37.90	−36.78
a''	I_1', I_4, I_7, I_8	exptl	−56.28	−54.84	−53.46
	n'(X), π'(CH_3), $2\pi'$(CH_2)	calcd	−55.74	−54.79	−53.67
	***n*-Butyl halides**				
a'	I_1, I_3, I_5	exptl	−36.11	−35.22	−33.91
	n(X), σ(C_3–C_4), σ(C_1–C_2)	calcd	−36.28	−35.33	−34.21
a'	I_2, I_6, I_8	exptl	−40.36	−39.53	−38.77
	σ(C_2–C_3), σ(C-X), π(CH_3)	calcd	−40.52	−39.59	−38.57
a''	I_1', I_4, I_7, I_9, I_{10}	exptl	−70.39	−68.99	−67.41
	n'(X), π'(CH_3), $3\pi'$(CH_2)	calcd	−70.06	−69.11	−67.99

a) Used the values reported in Ref. 2.

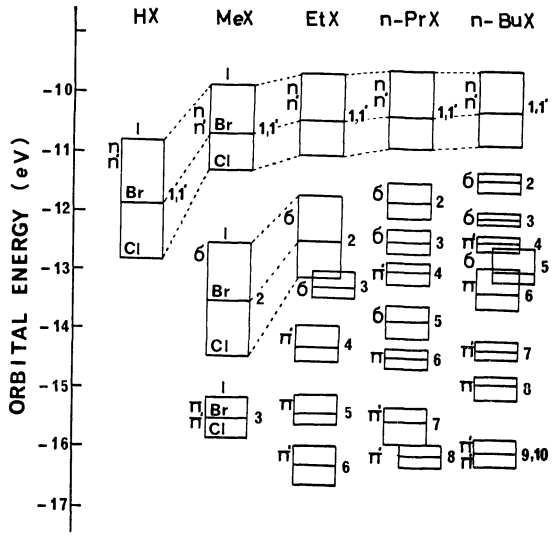

Fig. 11. Energy level diagram of the alkyl halides estimated from their photoelectron spectra, showing the effect of the successive methyl substitution.
In each block, the top line denotes RI, the middle line RBr and the bottom line RCl. Numbers 1,1',2,3,..... correspond to the orbitals starting from the highest occupied orbital to the inner orbitals successively. Letters n, n', σ, π, and π' indicate the assignments for the orbitals (see Table 7 for more details).

In the *trans* configuration, molecular orbitals of these compounds are divided into species a′ and a″, and those belonging to species a′ are expected to separate roughly into two minor groups, as shown in Table 7, one composed of σ(C_2–C_3) and σ(C–X), and the other of n(X), σ(C_1–C_2), and π(CH_3). The *gauche* form was neglected in the present discussion for simplicity. The a″ species includes the n'(X), π'(CH_3), and two π'(CH_2) orbitals (Fig. 7). The present ionization-energy data of the series of *n*-propyl halides were well interpreted in terms of the orbital interactions summarized in Table 7, good agreement being obtained for the partial sums of the calculated and experimental orbital energies.

We obtained results for the *n*-butyl halides from a similar analysis (Table 7). Here, a *trans* configuration was again assumed for these compounds, so that molecular orbitals are divided into two species a′ and a″. The orbitals belonging to a′ can be expected to separate further into two minor groups with little interaction, one composed of n(X), σ(C_3–C_4), and σ(C_1–C_2), and the other of σ(C_2–C_3), σ(C–X), and π(CH_3). Other orbitals, n'(X), π'(CH_3) and three π'(CH_2) are easily seen to belong to a″. Calculated partial sums for these groups are in good agreement with the corresponding experimental sums as shown in Table 7. From the investigation mentioned above, the following assignments were concluded.

EtX a′: $(I_1, I_3) \rightarrow \{n(\mathrm{X}), \sigma(\mathrm{C\text{-}C})\}$

$(I_2, I_5) \rightarrow \{\sigma(\mathrm{C\text{-}X}), \pi(\mathrm{CH_3})\}$

a″: $(I_1', I_4, I_6) \rightarrow \{n'(\mathrm{X}), \pi'(\mathrm{CH_3}), \pi'(\mathrm{CH_2})\}$

n-PrX a′: $(I_2, I_5) \rightarrow \{\sigma(\mathrm{C_2\text{-}C_3}), \sigma(\mathrm{C\text{-}X})\}$

$(I_1, I_3, I_6) \rightarrow \{n(\mathrm{X}), \sigma(\mathrm{C_1\text{-}C_2}), \pi(\mathrm{CH_3})\}$

a″: $(I_1', I_4, I_7, I_8) \rightarrow \{n'(\mathrm{X}), \pi'(\mathrm{CH_3}), 2\pi'(\mathrm{CH_2})\}$

n-BuX a': $(I_1, I_3, I_5) \rightarrow \{n(X), \sigma(C_3\text{-}C_4), \sigma(C_1\text{-}C_2)\}$

$(I_2, I_6, I_8) \rightarrow \{\sigma(C_2\text{-}C_3), \sigma(C\text{-}X), \pi(CH_3)\}$

a'': $(I_1', I_4, I_7, I_9, I_{10}) \rightarrow \{n'(X), \pi'(CH_3), 3\pi'(CH_2)\}$

All the experimentally determined levels are shown in Fig. 11.

From the present study the second ionization in the n-propyl and n-butyl halides can be assigned to the $\sigma(C_2\text{–}C_3)$ orbital rather than the σ(C–X) orbital, although these orbitals are mixed considerably. It should be pointed out that this fact is reflected on the slope of the second lines shown in the correlation diagram in Fig. 5, whereas the slope of the corresponding lines of the methyl and ethyl halides are much steeper, indicating large contributions from the σ(C–X) orbitals.

We are thus able to infer the possible assignments of all the observed photoelectron bands to orbitals which can be interpreted in terms of the localized molecular orbitals schematically shown in Fig. 7. We may say in general that the total or partial sum of appropriate ionization energies gives an important clue to spectral assignment in photoelectron studies.

BULLETIN OF THE CHEMICAL SOCIETY OF JAPAN, VOL. 46, 380—384 (1973)

The Polarized Absorption Spectra of Some β-Substituted Anthraquinones

Hiroyasu INOUE, Toshihiko HOSHI*, Junko YOSHINO*, and Yoshie TANIZAKI**

Department of Applied Chemistry, Faculty of Technology, Kanagawa University, Kanagawa-ku, Yokohama

**Department of Chemistry, College of Science and Engineering, Aoyama Gakuin University, Chitosedai, Setagaya-ku, Tokyo*

***Department of Chemistry, Faculty of Science, Tokyo Institute of Technology, Meguro-ku, Tokyo*

(Received June 24, 1972)

The polarized absorption spectra of 2-hydroxy-, 2-amino-, and 2,3-diaminoanthraquinones were measured in stretched PVA sheets below 47 kK, and semiempirical ASMO-SCF-CI calculations, including the variable β method, were carried out for these compounds. By a comparison of the observed and the calculated results, the π–π* bands of these compounds were assigned. Each of these compounds has six bands in the observed wave number region, four of which correspond to those of anthraquinone; the other two bands can be assigned to the intramolecular charge-transfer transitions.

In a previous paper,[1] we measured the polarized absorption spectra of the α-aminoanthraquinones and discussed the assignment of the electronic bands of these compounds. For instance, it has been found that 1-aminoanthraquinone has five absorption bands, at 20.4, 31.8, 35.5, 40.3, and 42.6 kK, in a PVA sheet. From the comparison of the observed and calculated results, the latter four bands have been found to correspond to those of anthraquinone,[2] and the band at 20.4 kK has been assigned to the intramolecular charge-transfer transition associated with a charge migration from the amino group to the carbonyl groups. The polarization direction of the charge-transfer transition was found to be along the C=O bond axis.

Also, in the case of β-substituted anthraquinone with a hydroxyl or amino group, the intramolecular charge-transfer transition is expected to occur. However, its polarization direction may be different from that of the corresponding α-substituted anthraquinone.

In the present paper, the electronic absorption spectra of 2-hydroxy-, 2-amino-, and 2,3-diaminoanthraquinones are studied by means of the polarized absorption spectra and theoretical calculations.

Experimental

Materials. The anthraquinone derivatives used here were kindly presented to us by Dr. Mitsuhiko Hida of The University of Tokyo. The PVA sheets were prepared from the commercially-available powder (mean degree of polymerization, 1500).

Measurements of the Polarized Absorption Spectra and Notations. The methods of the determination and analysis of the polarized absorption spectra were the same as have been described elsewhere.[3] The notations used in the figures are as follows:

$D_{\parallel}$ and $D_{\perp}$: Absorbances measured for incident light polarized parallel to and perpendicular to the stretched direction of the PVA sheet respectively.

R_d: Ratio between $D_{\parallel}$ and $D_{\perp}$, $D_{\parallel}/D_{\perp}$.

R_s: Degree of stretching of the PVA sheet.

θ: Orientation angle for a transition moment of a band, which can be calculated from the values of R_d and R_s; it indicates an angle between the transition moment and the orientation axis of a molecule.

Method of MO Calculation

We have used the semiempirical ASMO–SCF–CI method[4,5] with the variable β approximation.[6] The

1) H. Inoue, T. Hoshi, J. Yoshino, and Y. Tanizaki, This Bulletin, **45**, 1018 (1972).

2) H. Inoue, T. Hoshi, and Y. Tanizaki, *Nippon Kagaku Zasshi*, **92**, 501, (1971).

3) Y. Tanizaki and S. Kobudera, *J. Mol. Spectry.*, **24**, 1 (1967); Y. Tanizaki, This Bulletin, **38**, 1798 (1965); H. Inoue, T. Hoshi, T. Masamoto, J. Shiraishi, and Y. Tanizaki, *Ber. Bunsenges. Phys. Chem.*, **75**, 441 (1971); T. Hoshi, H. Inoue, J. Shiraishi, and Y. Tanizaki, This Bulletin, **44**, 1743 (1971).

4) R. Pariser and R. G. Parr, *J. Chem. Phys.*, **21**, 466, 767 (1953).

5) J. A. Pople, *Proc. Phys. Soc.* (London), **A68**, 81 (1955).

6) K. Nishimoto and L. S. Forster, *Theoret. Chem. Acta*, **3** 407 (1965).

resonance integrals, β_{rs}'s, were adjusted at every iteraction of the SCF calculations by using the following equations:

$$\beta_{CC} = -1.84 - 0.51\,P_{CC}$$
$$\beta_{CN} = -2.02 - 0.53\,P_{CN}$$
$$\beta_{CO} = -2.20 - 0.56\,P_{CO}$$

where P_{rs} is a π bond order between the r and s atoms. The one-center repulsion integrals were evaluated by use of the following valence-state ionization potentials (I_p(r)) and the electron affinities (E_a(r)):

I_p(C) = 11.42 eV, E_a(C) = 0.58 eV
I_p(N) = 25.00 eV, E_a(N) = 10.00 eV
I_p(O) = 17.32 eV, E_a(O) = 2.65 eV.

The two-center repulsion integrals were obtained from the Nishimoto-Mataga equation.[7] All singly-excited configurations associated with the transitions between each of the five highest occupied levels and each of the five lowest vacant levels were taken into account in the CI calculations.

Results and Discussion

Figure 1 shows the absorption spectra of 2-hydroxy-, 2-amino-, and 2,3-diaminoanthraquinones in ethanol solutions. The spectrum of anthraquinone is also shown for comparison. By comparing each spectrum of the β-substituted anthraquinones with that of anthraquinone, we can find an additional band in the visible region for the β-substituted anthraquinone. Moreover, an additional band may exist also in the near-ultraviolet region, because the absorption curve in this region is intricate in shape compared with the absorption curve of anthraquinone. In contrast with the present cases, α-aminoanthraquinones have one additional band in the visible region.[1]

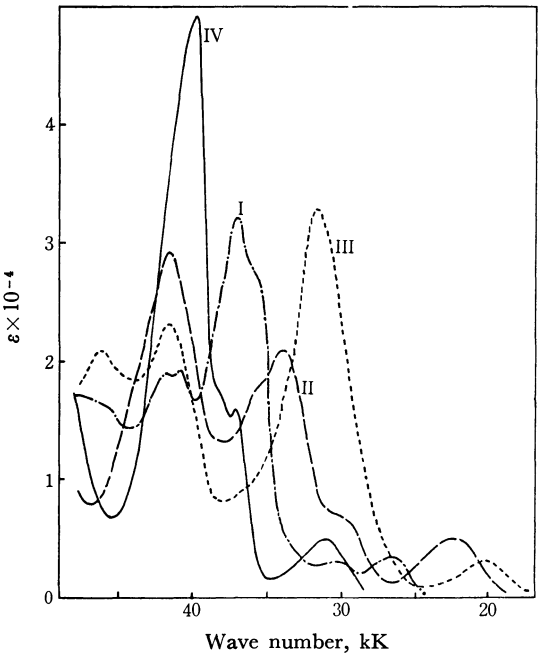

Fig. 1. Absorption spectra in ethanol solutions.
I: 2-Hydroxyanthraquinone, II: 2-Aminoanthraquinone, III: 2,3-Diaminoanthraquinone, IV: Anthraquinone

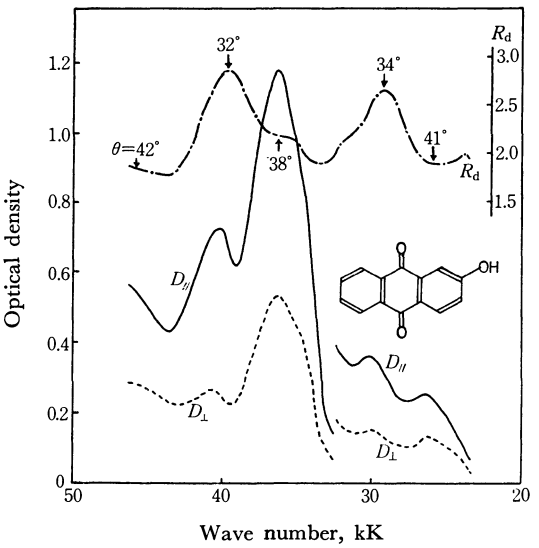

Fig. 2. The polarized absorption spectrum of 2-hydroxyanthraquinone. (R_s=5.8)

Figure 2 shows the polarized absorption spectrum of 2-hydroxyanthraquinone. From the features of the R_d and absorption curves, it is found that the compound has six absorption bands, at 26.3, 30.0, 34.5 (shoulder), 36.2, 40.3, and around 46 kK.

The observed results are compared with the calculated results in Table 1. A band corresponding to the calculated II transition is not found in the polarized absorption spectra. In the case of anthraquinone,[2] the corresponding band is observed around 32 kK. The calculated polarization directions of the III, V, and VI transitions are nearly along the X-axis of the molecule, and that of the IV transition is nearly along the Y-axis (Fig. 3). These results explain well the polarized absorption spectrum of this molecule. As in the cases of anthraquinonesulfonates and α-aminoanthraquinone,[1,2] a band polarized along the long axis of a molecule should have relatively large R_d values. Therefore, it is considered that the 30.0, 36.2, and 40.3 kK bands, with large R_d values, are polarized nearly along the X-(long) axis of the molecule, and that the 26.3, 34.5, and 46 kK bands, with small R_d values, are polarized along the Y-(short) axis.

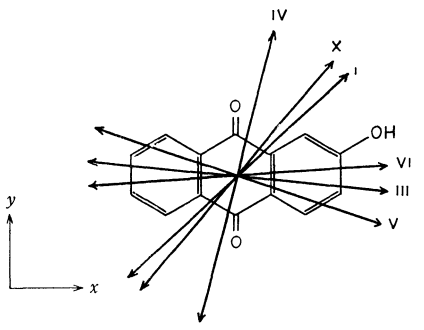

Fig. 3. The calculated polarization directions for 2-hydroxyanthraquinone.

7) N. Mataga and K. Nishimoto, *Z. Phys. Chem. N.F.*, **13**, 140 (1957).

TABLE 1. COMPARISON OF THE OBSERVED AND THE CALCULATED RESULTS FOR 2-HYDROXYANTHRAQUINONE

	Calcd			Obsd
	Transition energy (kK)	Oscillator strength	Polarization direction[a)]	Transition energy (kK)
I	28.3	0.1372	43°	26.3
II	31.2	0.0503	−11°	
III	31.6	0.0384	−6°	30.0
IV	35.0	0.4371	76°	34.5
V	38.0	0.6976	−19°	36.2
VI	40.6	0.3389	4°	40.3
VII	42.2	0.0187	22°	
VIII	44.9	0.0789	77°	
IX	45.2	0.0193	−60°	
X	46.1	0.2473	50°	~46

a) The angle against the X-axis.

TABLE 2. COMPARISON OF THE OBSERVED AND THE CALCULATED RESULTS FOR 2-AMINOANTHRAQUINONE

	Calcd			Obsd
	Transition energy (kK)	Oscillator strength	Polarization direction[a)]	Transition energy (kK)
I	26.5	0.1706	46°	21.7
II	30.8	0.0054	−40°	
III	31.6	0.0877	−6°	29.6
IV	34.7	0.3932	62°	34.6
V	36.9	0.7064	−26°	32.7
VI	40.1	0.2915	22°	40.6
VII	40.9	0.1542	−13°	
VIII	43.0	0.0321	4°	
IX	44.2	0.0199	54°	
X	45.0	0.1029	81°	~46
XI	46.8	0.4183	47°	

a) The angle against the X-axis.

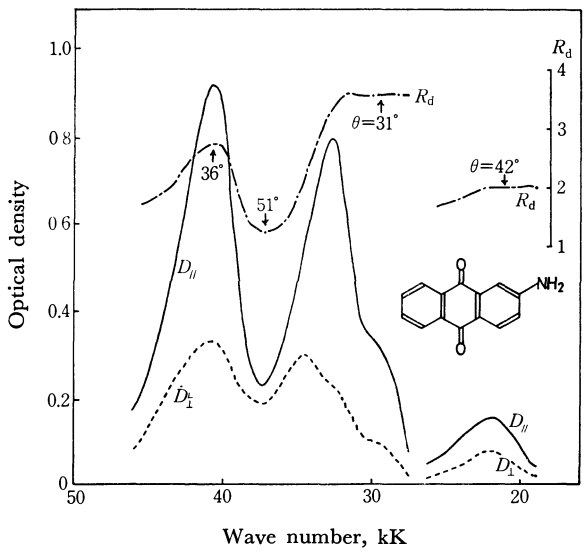

Fig. 4. The polarized absorption spectrum of 2-aminoanthraquinone. (R_s=9.0)

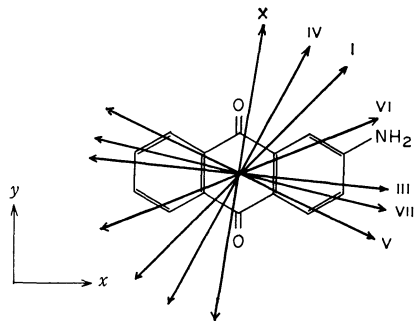

Fig. 5. The calculated polarization directions for 2-aminoanthraquinone.

Judging from the above-mentioned band positions, polarization directions, and relative intensities, the bands at 30.0, 34.5, 40.3, and 46 kK may correspond to the bands of anthraquinone at 30.8, 36.8, 39.7, and 43.4 kK respectively. The corresponding bands have also been found in each spectrum of the α-aminoanthraquinones.

Figure 4 shows the polarized absorption spectrum of 2-aminoanthraquinone. The bands corresponding to those of anthraquinone appear at 29.6, 34.6 (the absorption maximum appears only in the $D_\perp$ curve), 40.7, and around 46 kK (estimated from the R_d curve). The experimental results are summarized in Table 2 and compared with the results of the calculation. Figure 5 shows the calculated polarization directions. We can discuss the polarization directions of the two

Table 3. Comparison of the observed and the calculated results for 2,3-diaminoanthraquinone

	Calcd			Obsd
	Transition energy (kK)	Oscillator strength	Polarization direction	Transition energy (kK)
I	23.9	0.1390	Y	20.0
II	27.9	0.0140	X	
III	31.7	0.1534	X	
IV	34.2	0.7860	X	30.7
V	34.8	0.3320	Y	35.5
VI	37.7	0.0770	Y	
VII	39.9	0.0050	X	
VIII	40.9	0.4345	X	41.0
IX	40.9	0.0026	Y	
X	44.2	0.2574	Y	45.5
XI	45.4	0.2093	Y	

Table 4. The first and fourth excited state wave functions for 2,3-diaminoanthraquinone

$$\Psi_{\mathrm{I}} = 0.1137\,\phi_{6,11} - 0.1841\,\phi_{8,11} + 0.9632\,\phi_{10,11} + 0.1006\,\phi_{10,13}$$

$$\Psi_{\mathrm{IV}} = 0.1043\,\phi_{6,12} + 0.1079\,\phi_{7,11} - 0.1333\,\phi_{8,12} + 0.6239\,\phi_{9,11} - 0.1092\,\phi_{9,13} - 0.1185\,\phi_{9,15} + 0.6335\,\phi_{10,12} - 0.3669\,\phi_{10,14}$$

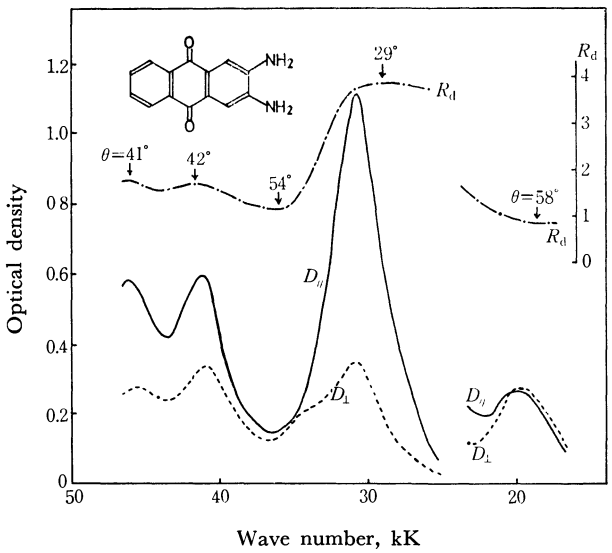

Fig. 6. The polarized absorption spectrum of 2,3-diaminoanthraquinone. (R_s=5.5)

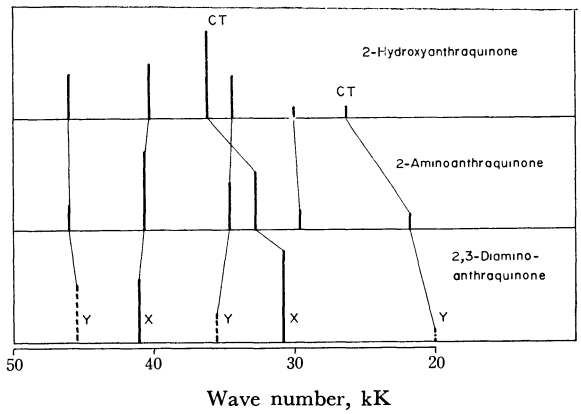

Fig. 7. Correlation diagram of the observed results.

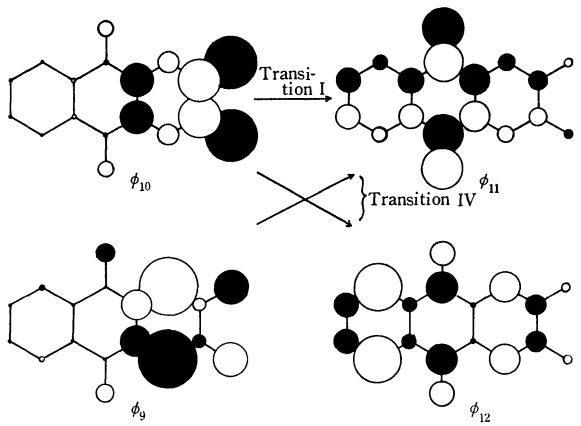

Fig. 8. Coefficients of the wave functions for 2,3-diaminoanthraquinone.

extra bands quantitatively, since the 21.7 kK band is isolated from the other bands and since the 32.7 kK band is not influenced in its polarization direction, because the intensities of the adjacent bands are very weak. The relative polarization direction of the 21.7 kK band with respect to that of the 32.7 kK band can be evaluated from the orientation angles as either 11° (=42°−31°) or 73° (=42°+31°). As has been shown above, the theoretical calculation shows the latter angle to be more reasanable.

The polarized absorption spectrum of 2,3-diaminoanthraquinone is shown in Fig. 6. The compound is assumed to belong to the C_{2v} point group; hence, the polarization direction of each band should be along the X- or Y-axis of the molecule. The extra bands of compound are found at 30.7 and 20.0 kK, and their orientation angles are 29° and 58° respectively. These bands are polarized perpendicularly to each other, because the sum of the orientation angles are approximately a right angle (29°+58°=87°). Since the

compound seems to orient in a manner similar to the cases of anthraquinonesulfonates and α-aminoanthraquinones,[1,2] that is, since the molecule orients its X-axis preferentially along the stretching direction of the sheet, the 30.7 kK band, with relatively large R_d values, is considered to be polarized along the X-axis, and 20.0 kK band, along the Y-axis. The experimental results obtained above are compared with the theoretical results in Table 3.

The results for the three compounds are compared in Fig. 7 as a correlation diagram. As may be seen from the figure, both of the two extra bands shift to the lower wave numbers with an increase in the electron-donating power of the substituent (OH→ NH_2) or with an increase in the number of the substituents. On the other hand, the positions of bands corresponding to the bands of anthraquinone are not significantly affected by the substitution. These tendencies can also be seen in the calculated results.

Table 4 presents the first and fourth excited state wave functions, which correspond to the two extra bands for 2,3-diaminoanthraquinone. The ψ_I is approximately represented by $\psi_{10,11}$ and the ψ_{IV}, by $\psi_{9,11}$ and $\psi_{10,12}$. The coefficients of the wave functions associated with the excitations are shown pictorially in Fig. 8. As may be seen from the figure, the charge migration from the amino to the carbonyl groups takes place in these excitations. Therefore, the I and IV transitions may be assigned to the intramolecular charge-transfer types. Similar results were obtained for 2-hydroxy- and 2-aminoanthraquinones.

BULLETIN OF THE CHEMICAL SOCIETY OF JAPAN, VOL. 46, 384—387 (1973)

Molecular Structure of *N*-Methylacetamide as Studied by Gas Electron Diffraction

Mitsuo KITANO, Tsutomu FUKUYAMA and Kozo KUCHITSU

Department of Chemistry, Faculty of Science, The University of Tokyo, Hongo, Bunkyo-ku, Tokyo

(Received June 29, 1972)

The bond distances (r_g) and angles (r_α) in *N*-methylacetamide have been determined by gas electron diffraction as follows: C–C=1.520±0.005 Å, N–C (methyl)=1.469±0.006 Å, N–C (carbonyl)=1.386±0.004 Å, C=O=1.225±0.003 Å, C–H (average)=1.107±0.005 Å, ∠N–C=O=121.8±0.4°, ∠C–N–C=119.7±0.8°, ∠C–C–N=114.1±1.5°, ∠H–C–H(average)=110.4±2° and ∠H–N–C(carbonyl)=110±5°. In comparison with the molecular structure in the crystal, the N–C(carbonyl) bond is about 0.10 Å longer, whereas the C–C and C=O bonds are about 0.02 and 0.01 Å shorter, respectively. The two methyl groups are in the *trans* conformation about the N–C (carbonyl) bond, no other conformer being observed.

N-Methylacetamide (Fig. 1) has frequently been taken as one of the simplest models of a polypeptide chain.[1] Previous studies of infrared, Raman and ultraviolet spectra,[2,3] the dipole moment,[2] and X-ray diffraction data[4] revealed the existence of the *trans* conformer in regard to the methyl groups about the C_2–N bond in all phases, whereas an infrared band (*ca.* 3429 cm^{-1}) observed by Russell and Thompson[5] in a dilute solution of carbon tetrachloride was tentatively assigned to the N–H stretching vibration of a *cis* conformer with an estimated abundance ratio of about 5%. The structure of this molecule in the gas phase was first investigated by the visual method of electron diffraction by Kimura and Aoki,[6] who estimated the N–C_3 distance and the C–N–C angle and also favored

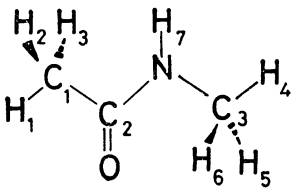

Fig. 1. *N*-methylacetamide.

the *trans* conformation. The rest of the structural parameters were transferred from those of acetamide determined by the same authors. In view of the importance of this molecule in chemistry and biochemistry, the present study was undertaken to determine its structure in the gas phase with higher accuracy.

Experimental

A commercial sample purified by vacuum distillation was heated to about 160°C by a high-temperature nozzle,[7] and diffraction photographs were taken with 40 kV electrons at camera distances of 111.80 mm (short) and 248.47 mm (long).[8] The scale factors of the diffraction patterns were

1) S. Mizushima, "Structure of Molecules and Internal Rotation," ed. by E. Hutchinson, Academic Press, New York (1954), p. 118.
2) S. Mizushima, T. Shimanouchi, S. Nagakura, K. Kuratani, M. Tsuboi, H. Baba, and O. Fujioka, *J. Amer. Chem. Soc.*, **72**, 3490 (1950).
3) T. Miyazawa, T. Shimanouchi and S. Mizushima, *J. Chem. Phys.*, **19**, 1479 (1951).
4) J. L. Katz and B. Post, *Acta Crystallogr.*, **13**, 624 (1960).
5) R. A. Russell and H. W. Thompson, *Spectrochim. Acta*, **8**, 138 (1956).
6) M. Kimura and M. Aoki, This Bulletin, **26**, 429 (1953).
7) A. Yokozeki and K. Kuchitsu, *ibid.*, **44**, 72 (1971).
8) Y. Murata, K. Kuchitsu and M. Kimura, *Jap. J. Appl. Phys.*, **7**, 591 (1970).

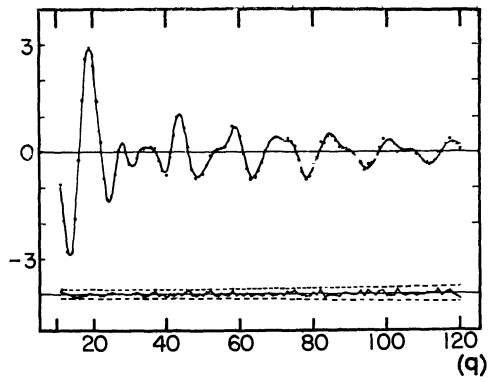

Fig. 2. Experimental and theoretical molecular intensities for *N*-methylacetamide. Typical observed $qM(q)$ values are shown in dots, and the best-fit theoretical is shown in the solid curve. The indices of resolution for long and short intensities are 0.950 and 0.763, respectively. The lower solid and broken curves represent the residuals and the error limits in the $qM(q)$ to a fractional error of 1×10^{-3} of the original photocurrent, respectively.

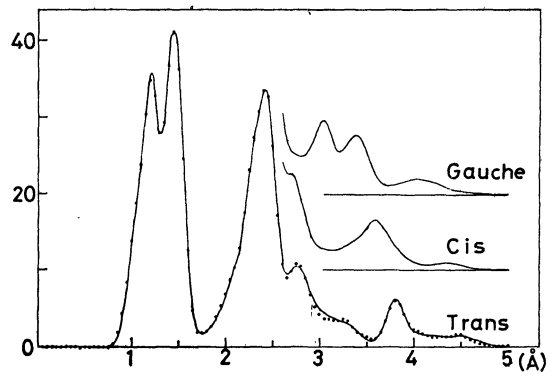

Fig. 3. Experimental (dots) and theoretical radial distribution curves. A damping factor, $\exp(1.599\times 10^{-4}q^2)$, is used.

calibrated to within 0.10% with reference to the r_a(C–O) distance of carbon dioxide (1.1646 Å)[8] for the short camera distance and to the r_a(N–N) distance of nitrogen (1.1007 Å)[9] for the long camera distance. The densities of four plates taken at each camera distance were measured by a digital microphotometer.[10]

Molecular intensities in the ranges $q=7$—50 and 30—120 Å^{-1} were obtained from the long and short distance data, respectively.[11] Since they agreed with each other in the overlapping region within experimental error (about 0.1 in the absolute $qM(q)$ scale), they were joined at 41 Å^{-1} (Fig. 2). The corresponding radial distribution curve shown in Fig. 3 has confirmed that the dominant conformer has *trans* methyl groups. Most of the calculations were carried out on a HITAC-5020E in the Computer Center of the University of Tokyo.

Analysis

The molecular intensity was analyzed under the following assumptions:

1) The molecule has a symmetry plane.
2) The two methyl carbon atoms are in the *trans* conformation about the C_2–N axis.
3) The *N*-methyl group is in the staggered conformation with the C_2–N bond.
4) One of the hydrogen atoms in the *C*-methyl group is in the eclipsed position with the C=O bond.
5) The methyl groups have local C_{3v} symmetry.
6) All the C–H distances are equal.
7) The r_α(N–H) distance is equal to the corresponding r_s(N–H) distance in formamide,[12] 1.002 Å.

The mean amplitudes of vibration and the vibrational corrections for the shrinkage effect[13] (r_a-r_α listed in Table 1) were calculated from a set of modified Urey-Bradley force constants determined by Itoh[14,15] from frequencies observed in the liquid phase. In the calculation of the vibrational corrections, contributions from the skeletal and methyl torsions, for which a conventional approximation of infinitesimal amplitudes breaks down,[16] were estimated by a high barrier

Table 1. Mean amplitudes and vibrational corrections for N-methylacetamide (in 10^{-4}Å)

	l	r_a-r_α		l	r_a-r_α
C_1–C_2	519	30	N···H_2	2165	187[b]
N–C_3	472	60	N···H_4	1007	83
C_2–N	439	16	C_3···H_1	1158	−264[b]
C_2=O	399	18	C_3···H_2	1867	112[b]
C_1–H_1	780	73	C_3···H_7	962	83
N–H_7	740	128	O···H_1	1395	376[b]
C_1···N	687	18	O···H_2	1755	−137[b]
C_1···C_3	697	−49[a]	O···H_4	1218	−249[b]
C_1···O	637	9	O···H_5	4404	339[b]
C_2···C_3	635	15	O···H_7	912	32
N···O	571	3	H_1···H_2	1262	30
C_3···O	1045	28[a]	H_1···H_4	1371	3
C_1···H_4	1201	−130[b]	H_1···H_5	2928	−31
C_1···H_5	1870	32[b]	H_1···H_7	1541	30
C_1···H_7	1426	5	H_2···H_4	2924	−33
C_2···H_1	1039	47	H_2···H_5	2194	−15
C_2···H_4	991	−156[b]	H_2···H_6	2070	−61
C_2···H_5	2432	86[b]	H_2···H_7	3707	−17
C_2···H_7	930	59	H_4···H_7	1579	60
N···H_1	1022	−349[b]	H_5···H_7	1541	92

a) The shrinkages due to the torsional motion around the C_2–N axis are included as mentioned in the text.
b) The shrinkage effects due to the two menthyl torsions are included.

9) K. Kuchitsu, This Bulletin, **40**, 498 (1967).
10) Y. Morino, K. Kuchitsu and T. Fukuyama, *ibid.*, **40**, 423 (1967).
11) Numerical experimental data of the leveled total intensity and the background have been deposited with the Chemical Society of Japan (Document No. 7302).
12) C. C. Costain and J. M. Dowling, *J. Chem. Phys.* **32**, 158 (1960).
13) K. Kuchitsu and S. J. Cyvin, "Molecular Structure and Vibrations," ed. by S. J. Cyvin, Chapter 12, Elsevier, Amsterdam (1972).
14) K. Itoh, Ph. D. Thesis, The University of Tokyo (1969).
15) K. Itoh and T. Shimanouchi, *Biopolymers*, **9**, 383 (1970).
16) T. Iijima and S. Tsuchiya, *J. Mol. Spectrosc.*, **44**, 88 (1972).
17) J. Karle and H. Hauptman, *J. Chem. Phys.*, **18**, 875 (1950).
18) D. A. Swick, I. L. Karle, and J. Karle, *ibid.*, **22**, 1242 (1954).
19) Y. Morino and E. Hirota, *ibid.*, **28**, 185 (1958).
20) L. S. Bartell and D. A. Kohl, *ibid.*, **39**, 3097 (1963).

approximation.[17-20] The skeletal torsion around the C_2–N axis was assumed to obey the potential function, $V=(1/2)V_2(1-\cos 2\phi)$, where V_2 is 20 kcal/mol as estimated by Warshel *et al.*[21] The contributions from this motion to the r_a-r_α for the skeletal atom pairs were −0.0040 Å for C_1–C_3 and 0.0053 Å for O–C_3. The contributions from the skeletal torsion to the corrections for other atom pairs involving hydrogen were ignored, since they are obscured by much larger contributions from the methyl torsions. The effects of the methyl torsions on the nonbonded pairs indicated as b) in Table 1 were estimated from threefold potential barriers of 1 and 2 kcal/mol for the *C*-methyl and *N*-methyl torsions,[22] respectively, whereas those on the bonded and next-to-bonded pairs were assumed to be independent of the torsional motion. Uncertainties equal to 100% of the values calculated above were included in the limits of error of the structural parameters. The uncertainties from this origin are practically negligible except for the H–C–H angle.

The asymmetry parameters κ for the bonded C–H and N–H distances were assumed to be[23] 1.8×10^{-5} Å^3, and the rest of the κ parameters were ignored.

The r_g distances and r_α angles[13,24] derived from least-squares analyses[25] are listed in Table 2 with their limits of error estimated from the internal consistency and reproducibility of the parameters with additional account of systematic errors.[25-27] The error matrix is given in Table 3. The theoretical molecular intensity and radial distribution curves based on this structure are compared in Figs. 2 and 3, respectively, with the corresponding observed curves.

The experimental radial distribution and molecular intensity curves were further examined in detail in order to corroborate the above-mentioned assumptions 2—4) concerning the skeletal and methyl conformations. As for the skeletal conformation, the observed molecular intensity curves (q=11 to 40) were analyzed by the least-squares method on the assumption that the system is composed of *trans* (with a dihedral angle of 180°), *cis* (0°) and *gauche* (60°) conformers. Their frame structures were assumed to be identical, and the abundance ratios were the only variable parameters. The analysis gave 98±5, 0±5, and 2±4%, respectively. Analyses of the radial distribution curve and the background functions[28-30] were

TABLE 2. STRUCTURAL PARAMETERS FOR *N*-METHYLACETAMIDE IN THE GAS AND CRYSTAL PHASES (IN Å AND DEGREES)

	Present study[a] Gas	K. A.[b] Gas	K. P.[c] Crystal
C_1-C_2	1.520_3 (5)	1.53	1.536 (16)
N-C_3	1.468_5 (6)	1.44 (40)	1.465
C_2-N	1.386_2 (4)	1.36	1.290 (13)
C_2=O	1.224_6 (3)	1.21	1.236 (12)
C-H (av)	1.106_7 (5)	1.09	—
∠N-C_2=O	121.8_3 (0.4)	125	123
∠C_2-N-C_3	119.6_7 (0.8)	117 (5)	120.5
∠C_1-C_2-N	114.1_2 (1.5)	113	116.5
∠H-C-H (av)	110.4 (2)	109.6	—
∠C_2-N-H	$110._4$ (5)	107	—

a) The r_g distances and r_α angles derived from the present analysis with estimated limits of error in parentheses. The limits of error of bond distances are in 10^{-3}Å units. b) Parameters estimated by visual method of gas electron diffraction by Kimura and Aoki.[6] c) Crystal structure determined by X-ray diffraction by Katz and Post[4] and estimated standard deviations.

TABLE 3. ERROR MATRIX FOR *N*-METHYLACETAMIDE[a]

	X_1	X_2	X_2	X_3	X_4	X_5	X_6	X_7	X_9	X_{10}	k_1	k_2
X_1	19	−4	−13	3	5	−8	−8	20	16	28	−9	35
X_2		15	8	8	−2	−28	−12	−8	−7	−32	13	−43
X_3			16	3	−5	−23	−8	−22	−11	−33	19	−35
X_4				19	7	−14	−9	−4	4	21	−23	−19
X_5					9	10	−4	14	1	19	−15	23
X_6						127	−42	36	−19	83	−46	93
X_7							44	4	14	39	19	31
X_8								71	22	87	−50	63
X_9									26	64	−21	33
X_{10}										315	−99	122
k_1											85	−57
k_2												184

a) X_1=C_1-C_2, X_2=C_2-N, X_3=N-C_3 X_4=C-H (average), X_5=C_2=O, X_6=∠C_1-C_2-N, X_7=∠C_2-N-C_3, X_8=∠H-C-H (average), X_9=∠N-C_2=O, X_{10}=∠C_2-N-H_7, k_1=index for long and k_2=index for short. Units ($\times10^{-4}$) for the distances are Å, those for the angles are rad., and those for the indices are dimensionless.

21) A. Warshel, M. Levitt, and S. Lifson, *J. Mol. Spectrosc.*, **33**, 84 (1970).
22) J. P. Lowe, *Progr. Phys. Org. Chem.*, **6**, 1 (1968).
23) K. Kuchitsu, This Bulletin, **40**, 505 (1967).
24) Y. Morino, K. Kuchitsu, and T. Oka, *J. Chem. Phys.*, **36**, 1108 (1962).
25) Y. Morino, K. Kuchitsu, and Y. Murata, *Acta Crystallogr.*, **18**, 549 (1965).
26) K. Kuchitsu, T. Fukuyama, and Y. Morino, *J. Mol. Struct.*, **1**, 463 (1968).
27) K. Kuchitsu, Ref. 13, Chapter 10.
28) Y. Morino and K. Kuchitsu, *J. Chem. Phys.*, **28**, 175 (1958).
29) M. Abe, K. Kuchitsu, and T. Shimanouchi, *J. Mol. Struct.*, **4**, 245 (1969).
30) A. Yokozeki and K. Kuchitsu, This Bulletin, **44**, 2926 (1971).

TABLE 4. COMPARISON OF SKELETAL STRUCTURES[a)]

	NMAA[b)]	Related compounds		Ref.
C-C	1.520 (5)	1.520 (3)	acetone	32, 33
N-C_{Me}	1.469 (6)	1.467 (2)	methylamine	31
		1.469 (4)	ethylenediamine	30
		1.455 (2)	dimethylamine[c)]	34
		1.466 (8)	dimethylamine[d)]	35
C=O	1.225 (3)	1.213 (4)	acetone	32, 33
∠C-C=O	124.1 (1.5)	122.0 (1)	acetone	32, 33
∠C-N-C	119.7 (0.8)	111.8 (0.6)	dimethylamine[c)]	34
		111.6 (0.6)	dimethylamine[d)]	35
∠C-C-N	114.1 (1.5)	110.2 (0.7)	ethylenediamine	30

a) The r_g distances in Å and r_α angles in degrees. The limits of error of bond distances are in 10^{-3} Å units. b) *N*-methylacetamide determined in the present study. c) r_a structure. d) r_s structure.

not more sensitive than the least-squares analysis and also limited the concentration of conformers other than *trans* to less than 5%. The staggered conformation of the *N*-methyl group with respect to the C_2–N bond resulted in significantly better agreement with experiment than the eclipsed conformation. On the other hand, the conformation about the *C*-methyl group is less definitive, because both the eclipsed and staggered models gave acceptable radial distribution curves within experimental error. The most probable parameters derived from a least-squares analysis based on the staggered model are essentially equal to those given in Table 2, except that the N–C_2=O angle is 121.5°.

Discussion

The present structure is compared in Table 2 with those determined in previous studies[4,6)] and in Table 4 with those for related molecules. The most remarkable difference in the structural parameters in the gas and solid phases is seen in the C_2–N bond distance (*ca.* 0.10 Å). The C_2=O and C_1–C_2 bonds are found to be slightly shorter in the gas phase (*ca.* 0.01 and 0.02 Å, respectively) than in the solid phase. The presence of intermolecular hydrogen bonds (N–H···O) in the crystal[4)] seems to be the principal origin of these differences. The C_3–N distance, on the other hand, is nearly equal to that in the crystal and is about 0.08 Å longer than the C_2–N distance. Since the C_3–N distance is also nearly equal to those in methylamine[31)] and ethylenediamine,[30)] this bond can be regarded as a normal C–N single bond.

In comparison with the structure of acetone,[32,33)] *N*-methylacetamide has a very similar C–C bond distance but a slightly (*ca.* 0.01 Å) longer C=O bond and a slightly (*ca.* 2°) larger C–C=O angle. The C–N–C angle in *N*-methylacetamide is larger than that in dimethylamine[34,35)] by more than 7°, and the C–C–N angle is larger than that in ethylenediamine[30)] by more than 3°.

The authors are indebted to Dr. Yasushi Koyama of Kwansei Gakuin University and to Professors Masao Kimura and Takao Iijima of Hokkaido University for helpful discussions.

31) H. K. Higginbotham and L. S. Bartell, *J. Chem. Phys.*, **42**, 1131 (1965).
32) T. Iijima, This Bulletin, **43**, 1049 (1970).
33) T. Iijima, *ibid.*, **45**, 3526 (1972).
34) B. Beagley and T. G. Hewitt, *Trans. Faraday Soc.*, **64**, 2561 (1968).
35) J. E. Wollrab and V. W. Laurie, *J. Chem. Phys.*, **48**, 5058 (1968).

The Distribution of 2-Thenoyltrifluoroacetone between Several Organic Solvents and an Aqueous Solution and Its Extraction of Sodium(I) into Methyl Isobutyl Ketone

Tatsuya SEKINE, Yoshihiro TAKAHASHI, and Naohiko IHARA

Department of Chemistry, Science University of Tokyo, Kagurazaka, Shinjuku-ku, Tokyo

(Received June 29, 1972)

Aqueous solutions containing sodium hydroxide and sodium perchlorate at various mixing ratios, 1 M Na(OH, ClO_4), were equilibrated with several organic solvents containing 2-thenoyltrifluoroacetone (TTA) at 25°C. From the measurements of the hydrogen-ion concentration of the aqueous phase, the $(K_D+1)K_a^{-1}$ values, where K_D is the distribution constant and K_a is the acid dissociation constant of TTA, were obtained; they were, $10^{7.17}$ (hexane), $10^{7.74}$ (CCl_4), $10^{8.01}$ (C_6H_6) and $10^{8.17}$ ($CHCl_3$). From the values of K_D obtained in another study, the value of K_a was determined to be $10^{-6.28}$. However, a much lower value than that expected was obtained for the MIBK system; this was due to the extraction of sodium(I) with TTA. The extraction was also confirmed by the distribution experiments of sodium(I). The extraction constant, $K_{ex}=[NaA]_{org}/[Na^+][A^-]$ (where A^- is the TTA anion), was found from these results to be $10^{0.86}$ in 1 M $NaClO_4$ and $10^{0.79}$ at an infinite dilution.

The solvent extraction of alkali metal ions with chelating extractants is usually poor except for that of lithium(I).[1-4] However, it was pointed out by Healy[3] that the extraction of alkali metal ions with 2-thenoyltrifluoroacetone (TTA)[3] and dibenzoylmethane[4] is very much enhanced by adduct formation (synergism); thus, even sodium(I) can be extracted to some extent with these chelating reagents if a neutral adduct-forming ligand, such as trioctylphosphine oxide, triphenylphosphine oxide, tributylphosphate, N,N-dibutylacetamide, ethylhexyl alcohol or nitromethane, is added.

The present authors have made a series of studies of the acid dissociation and two-phase distribution of several β-diketones. When the organic phase was nonpolar solvent, the chemical behavior of these reagents agreed with that statistically expected. However, when the solvent was methyl isobutyl ketone (MIBK), a deviation from the statistical expectation was found.

After an analysis, it was concluded that the above deviation is due to an extraction of the sodium(I) with TTA. This was also confirmed from the distribution ratio of sodium(I), measured by using a radioactive tracer.

Experimental

The sodium-24 tracer was obtained from the Japan Atomic Energy Research Institute as a sodium chloride solution. The TTA and MIBK were obtained from the Dojindo & Co. and the Tokyo Kasei Co., Ltd., respectively. The MIBK was washed several times with 0.1 M perchloric acid and with water, and then washed several times with 0.1 M sodium hydroxide and again with water. The sodium perchlorate was prepared from sodium carbonate and perchloric acid and was recrystallized three times from water. The other reagents were of an analytical grade. The sodium hydroxide solution was prepared by the dilution of its 50% aqueous solution with decarbonated water. A weighed portion of TTA was dissolved in an organic solvent, stored at least one day before the experiment, and then used as the stock solution.

All of the procedures were carried out in a thermostatted room at 25±0.3°C. Twenty-ml glass-stoppered tubes were used to equilibrate the two phases. A 5-ml portion of the TTA solution of an organic solvent, and a 5-ml portion of an aqueous solution which contained the 1 M sodium ion, and perchlorate and hydroxide ions at a certain molar ratio, 1 M Na(OH, ClO_4), were placed in the tubes. In the MIBK system, the two phases in the tube were placed on a rotating framework (20 rpm), agitated for three hr, and then centrifuged. In the other systems, the two phases were vigorously shaken for several minutes and then centrifuged. The hydrogen-ion concentration (in stoichiometric units) of the aqueous phase were determined potentiometrically with a glass electrode.

The experiment with the radioactive tracer was carried out as follows. The initial aqueous phase contained various amounts of sodium hydroxide and the sodium tracer. A 5-ml portion of this aqueous phase and a 5-ml portion of the MIBK solution, which contained an amount of TTA equivalent to the sodium hydroxide in the aqueous phase were placed in the tubes. The two phases were vigorously shaken for 3 min and then centrifuged. A 2-ml portion was pipetted from each phase and transferred into a small test tube. The γ-radioactivity of the sample was determined with a well-type scintillation counter (NaI). The distribution ratio was calculated as follows;

$$D = \frac{\gamma\text{-count-rate per ml of the org. phase}}{\gamma\text{-count-rate per ml of the aq. phase}}$$

Statistical

The acid dissociation constant and the two phase-distribution constants of a weak acid, HA, can be written as;

$$HA \rightleftharpoons H^+ + A^-$$

$$K_a = [H^+][A^-][HA]^{-1} \quad (1)$$

$$HA \rightleftharpoons HA_{(org)}$$

$$K_D = [HA]_{org}[HA]^{-1} \quad (2)$$

The ratio of these two values can be determined by a two-phase titration method[5] or by measurements of

1) G. A. Guter, G. S. Hammond, *J. Amer. Chem. Soc.*, **78**, 5166 (1956).
2) R. F. Apple, J. C. White, *Talanta*, **13**, 43 (1966).
3) T. V. Healy, *J. Inorg. Nucl. Chem.*, **30**, 1025 (1968).
4) T. V. Healy, *ibid.*, **31**, 499 (1969).
5) D. Dyrssen, *Svensk. Kem. Tidskr.*, **64**, 213 (1952),

the hydrogen-ion concentration of the aqueous phase, which initially contained various amounts of hydroxide ions and which were equilibrated with an organic phase containing an excess of the acid to the hydroxide ion.[6]

The statistical treatment for the latter method is as follows. In the following equations, the initial concentration of the acid in the organic phase will be denoted by $C_{HA(org)}$, and that of sodium hydroxide in the aqueous phase, by C_{OH}. The volumes of the two phases are always the same, and we assume no complex formation in the aqueous phase.

When no extraction of sodium salt occurs, the following equations can be obtained from Eqs. (1) and (2):

$$C_{HA(org)} = [A^-] + [HA] + [HA]_{org} = [A^-](1 + (K_D+1)K_a^{-1}[H^+]) \quad (3)$$

If $-\log [H^+]$ is not very high (*e.g.*, if $-\log [H^+]$ is below 11), it can be regarded that $C_{OH}=[A^-]+[OH^-]\simeq[A^-]$. Then, C_{OH} can be introduced into Eq. (3) instead of $[A^-]$ and we obtain:

$$C_{HA(org)}C_{OH}^{-1} - 1 = (K_D+1)K_a^{-1}[H^+] \quad (4)$$

On the other hand, when the sodium salts are extracted, the extraction equilibrium can be written as;

$$Na^+ + A^- \rightleftharpoons NaA_{(org)}$$

$$K_{ex} = [NaA]_{org}[Na^+]^{-1}[A^-]^{-1} \quad (5)$$

The initial concentration can then be written as (the other species in the organic phase, such as the dimer, are neglected):

$$C_{HA(org)} = [A^-] + [HA] + [HA]_{org} + [NaA]_{org} + [A^-]_{org} \quad (6)$$

When no dissociation in the organic phase is assumed, Eq. (6) can be rewritten as:

$$C_{HA(org)} = [A^-] + [NaA]_{org} + (K_D+1)K_a^{-1}[A^-][H^+] \quad (7)$$

Furthermore, when the concentration of the sodium ion can always be regarded as unity and when $-\log [H^+]$ is not very high (*e.g.*, when $[OH^-]<10^{-3}$, in other words, $[Na^+]_{initial}-[NaA]_{org}\simeq 1$ M):

$$C_{OH} = [A^-] + [NaA]_{org} = [A^-](1+K_{ex}) \quad (8)$$

From Eqs. (7) and (8), the following equation is obtained:

$$C_{HA(org)}C_{OH}^{-1} - 1 = (K_D+1)K_a^{-1}(K_{ex}+1)^{-1}[H^+] \quad (9)$$

Since the $C_{HA(org)}$ and C_{OH} values are known, and since the $[H^+]$ value can be determined by potentiometry, the $(K_D+1)K_a^{-1}(K_{ex}+1)^{-1}$ value can be determined from a set of experimental data, and when the values of K_D and K_a can be obtained by separate experiments, the K_{ex} value can be determined.

The distribution data of the second experiments, which were carried out by using a radioactive tracer, were treated as follows. Since the initial amount of sodium hydroxide is equivalent to that of the weak acid, TTA, in these systems, the $[Na(I)]_{org,total}=[TTA]_{org,total}$, and $[Na(I)]_{total}=[TTA]_{total}$ relations are always established. Provided that there is no dissociation of the species in the organic phase and no association of those in the aqueous phase, and furthermore, provided that the amount of the TTA in the HA form produced by the hydrolysis of A^- in the aqueous phase is much smaller than that of A^-, the following equations can be obtained:

$$[Na(I)]_{org,total} = [NaA]_{org} \quad (10)$$

$$[Na(I)]_{total} = [Na^+] = [A^-] \quad (11)$$

$$D = [NaA]_{org}[Na^+]^{-1} \quad (12)$$

From the above equations and Eq. (5):

$$K_{ex} = D[A^-]^{-1} = D[Na^+]^{-1} \quad (13)$$

When the distribution ratio is determined by radiometry, the value of $[Na^+]$ can be obtained as:

$$[Na^+] = C_{OH}(D+1)^{-1} \quad (14)$$

and from this value of $[Na^+]$, K_{ex} can be obtained by means of Eq. (13).

Results

Distribution Measurements. Table 1 gives the results of the distribution measurements. As may be seen from Eq. (13), the distribution ratio decreases with the decrease in $[Na^+]$ (and, at the same time, with that in C_{OH}). Since the ionic strength in the aqueous phase is not controlled in these systems, the extraction constants determined cannot be directly compared with each other. However, from these results, the following conclusions can be reached: (i) Part of the sodium (I) in the aqueous phase is extracted into MIBK with TTA. (ii) The value of K_{ex} increases with the decrease in the aqueous sodium-ion concentration and reaches a definite value. Thus, the K_{ex} at an infinite dilution can be estimated to be $10^{0.79}$.

Another series of distribution measurements were also carried out in systems where the electrolyte concentration in the aqueous phase was kept at 1 M by using sodium perchlorate. However, since sodium perchlorate is also to some extent extractable into the organic

Table 1. Distribution of sodium(I) between MIBK and aqueous phase containing sodium salt of TTA (no perchlorate) determined by radiometry[a]

$C_{OH}(=C_{HA(org)})$	log D	log $[Na^+]$	log K_{ex}[b]
2.0×10^{-1}	−0.45	−0.83	0.38
1.0×10^{-1}	−0.62	−1.09	0.47
5.0×10^{-2}	−0.77	−1.37	0.60
3.0×10^{-2}	−0.93	−1.57	0.64
2.0×10^{-2}	−1.07	−1.74	0.67
1.0×10^{-2}	−1.33	−2.02	0.69
8.0×10^{-3}	−1.36	−2.12	0.76
6.0×10^{-3}	−1.48	−2.24	0.76
4.0×10^{-3}	−1.62	−2.41	0.79
2.0×10^{-3}	−1.92	−2.70	0.78

a) The total amount of sodium ion is equivalent to TTA and the ionic strength in the aqueous phase is not controlled.
b) $\log D - \log [Na^+]$. Since the ionic strength in the aqueous phase changes, direct comparison of these data to each other is not suitable, especially in the higher $[Na^+]$ region.

6) T. Sekine and D. Dyrssen, *Anal. Chim. Acta*, **37**, 217 (1967).

TABLE 2. HYDROGEN ION CONCENTRATION IN THE AQUEOUS PHASE AS A FUNCTION OF INITIAL SODIUM HYDROXIDE CONCENTRATION

C_{OH}	Hexane		Carbon tetrachloride		Benzene		Chloroform		MIBK	
	a	b	a	b	a	b	a	b	a	b
6.98×10^{-2}	7.52	7.15	8.07	7.71	8.34	7.98	8.50	8.14	7.88	7.52
5.98×10^{-2}	7.33	7.16	7.89	7.72	8.17	7.99	8.32	8.15	7.77	7.60
4.98×10^{-2}	7.18	7.18	7.73	7.74	8.01	8.01	8.17	8.17	7.67	7.67
3.99×10^{-2}	6.99	7.17	7.58	7.76	7.84	8.02	8.02	8.19	7.56	7.74
2.99×10^{-2}	6.80	7.17	7.41	7.78	7.68	8.05	7.83	8.20	7.33	7.70
average		7.17		7.74		8.01		8.17		(7.65)

Volumes of the two phases are the same, the aqueous phase is 1 M $NaClO_4$.
The acid dissociation constant for TTA in 1 M $NaClO_4$ at 25°C is obtained to be $10^{-6.28}$ from the above constants and the values of K_D for each solvent.[8]
a $=-\log[H^+]$, b $=\log(K_D+1)/K_a$.

TABLE 3. HYDROGEN ION CONCENTRATION IN THE AQUEOUS PHASE IN MIBK-1 M $NaClO_4$ SYSTEM AS A FUNCTION OF INITIAL SODIUM HYDROXIDE CONCENTRATION, AND THE EQUILIBRIUM CONSTANTS CALCULATED[a]

C_{OH}	$C_{HA(org)}=0.05$ M		$C_{HA(org)}=0.1$ M		$C_{HA(org)}=0.2$ M	
	$-\log[H^+]$	$\log\frac{(K_D+1)}{K_a(K_{ex}+1)}$	$-\log[H^+]$	$\log\frac{(K_D+1)}{K_a(K_{ex}+1)}$	$-\log[H^+]$	$\log\frac{(K_D+1)}{K_a(K_{ex}+1)}$
4.99×10^{-2}	—	—	7.67	7.68	7.09	7.57
4.39×10^{-2}	8.14	7.28<	—	—	—	—
3.99×10^{-2}	8.00	7.40<	7.56	7.74	—	—
2.99×10^{-2}	7.79	7.62	7.33	7.70	6.88	7.63
2.39×10^{-2}	7.61	7.65	—	—	—	—
1.99×10^{-2}	7.47	7.65	7.09	7.69	—	—
1.40×10^{-2}	7.35	7.76	6.89	7.68	6.55	7.67
9.97×10^{-3}	7.09	7.69	6.75	7.71	—	—
8.97×10^{-3}	7.03	7.69	—	—	—	—
7.98×10^{-3}	—	—	6.68	7.74	6.25	7.63
6.98×10^{-3}	6.89	7.68	6.58	7.70	—	—
5.98×10^{-3}	—	—	6.58	7.78	6.15	7.66
4.99×10^{-3}	6.72	7.68	6.42	7.70	—	—
3.99×10^{-3}	6.60	7.66	6.32	7.70	5.95	7.64
2.99×10^{-3}	6.46	7.66	6.18	7.69	—	—
1.99×10^{-3}	6.34	7.72	5.97	7.66	5.65	7.65
average		7.68		7.71		7.64

$K_{ex}=[NaA]_{org}[Na^+]^{-1}[A^-]^{-1}$ $K_{ex_0}=[NaA]_{org}[H^+][Na^+]^{-1}[HA]_{org}^{-1}$
a) The equilibrium constant $\log(K_D+1)K_a^{-1}(K_{ex}+1)^{-1}$ is concluded to be 7.68.
From this value and the value of $(K_D+1)K_a^{-1}$ for this MIBK system determined in another study[8], the following extraction constants were obtained; $K_{ex}=10^{0.86}$, $K_{ex_0}=10^{-7.73}$.

phase,[7] a correction for this effect was necessary. In this case, as the accuracy of the experiments was not satisfactorily enough to make such a correction, no difinite value of K_{ex} could be obtained from these experiments.

Potentiometric Measurements. The value, $(K_D+1)K_a^{-1}$, obtained by introducing the values of $C_{HA(org)}$, C_{OH}, and $[H^+]$ into Eq. (4) agreed with the value computed by using the K_D and K_a^{-1} values experimentally obtained when the solvent was hexane, carbon tetrachloride, benzene, or chloroform. Thus we concluded that there was no extraction of sodium (I) with TTA into these solvents. Table 2 shows the values of $-\log[H^+]$ at equilibrium against the initial concentration of sodium hydroxide in the aqueous phase, C_{OH}, when the initial concentration of TTA in the organic phase, $C_{HA(org)}$, is 1.00×10^{-1} M. Table 2 also shows the $(K_D+1)K_a^{-1}$ values calculated by means of Eq. (4). Although a slight increase in $(K_D+1)\times K_a^{-1}$ with the decrease in C_{OH} is observed, it may be concluded that the values are nearly constant in each system.

The distribution constants of TTA in these systems were determined in another study in the authors' laboratory by the spectrophotometric method.[8] The values obtained were $10^{0.85}$, hexane; $10^{1.43}$, carbon tetrachloride; $10^{1.73}$, benzene; and $10^{1.89}$, chloroform With these distribution constants and the $(K_D+1)\times K_a^{-1}$ value obtained for each solvent in Table 2, the values of K_a were calculated to be $10^{-6.27}$, $10^{-6.30}$,

7) T. Sekine and T. Ishii, This Bulletin, **44**, 275 (1971).

8) Y. Hasegawa, *et al.*, unpublished work.

$10^{-6.28}$, and $10^{-6.27}$, from the results in the hexane, carbon tetrachloride, benzene, and chloroform systems, respectively. The acid dissociation constant of TTA in the 1 M sodium perchlorate solution at 25°C was thus estimated to be $10^{-6.28}$ as the average of these values.

The distribution constant of TTA between MIBK and 1 M sodium perchlorate had also been determined separately[8] to be $10^{2.31}$, and from the values of this K_D and the above K_a value, the log $(K_D+1)K_a^{-1}$ value in this system was expected to be $10^{8.59}$. However, as may be seen from Table 2, the value experimentally obtained, $10^{7.65}$ is about one-tenth of the expected value. The deviation may well be explained by the extraction of sodium with TTA which had already been demonstrated by the tracer experiments. Table 3 gives the values of $-\log [H^+]$ at equilibrium against the initial concentration of sodium hydroxide in the aqueous phase when the initial TTA concentrations in MIBK, $C_{HA(org)}$, are 0.05, 0.1, and 0.2 M and the values of the equilibrium constant, $(K_D+1)K_a^{-1}\times(K_{ex}+1)^{-1}$. The value of K_{ex} in Eq. (5) was calculated from this constant, and from the above $(K_D+1)\times K_a^{-1}$ value for the MIBK system, to be $10^{0.86}$.

The constant for metal extraction with chelating extractants is usually given by the following equation:

$$Na^+ + HA_{(org)} \rightleftharpoons NaA_{(org)} + H^+$$

$$K_{ex_0} = [NaA]_{org}[H^+][Na^+]^{-1}[HA]^{-1}{}_{org} \quad (15)$$

From Eqs. (5) and (15), the following relation can be obtained;

$$K_{ex_0} = K_{ex}\, K_a\, K_D^{-1} \quad (16)$$

Thus, K_{ex_0} in Eq. (15) can be calculated, from the constants cited above, to be $10^{-7.73}$.

Discussion

In order to make an analysis of the chemical equilibria in metal extraction system with a chelating extractant, the $(K_D+1)K_a^{-1}$ (when $K_D \gg 1$, $K_DK_a^{-1}$ can be used) is very important.[9] This value can be obtained naturally if the values of K_a and K_D can be found in the literature. However, these values are different when the ionic concentration in the aqueous phase is different, and the latter constant, K_D of course, is different in different solvents.

Although the two-phase titration method[5] seems to be applicable to such determinations of $(K_D+1)K_a^{-1}$, the simplified method demonstrated in this study also seems to be very useful for such a purpose, as has already been pointed out.[6] The usefulness of this method may be concluded from the fact that the values of K_a of TTA in 1 M sodium perchlorate calculated from the results of the four series of independent experiments using the different solvents shown in Table 2 are identical with each other.

It is well known that MIBK is a very good solvent for the TTA extraction of several metal ions, because the extraction is much enhanced by the use of this solvent over that using various non-polar solvents. For example, the extraction of alkaline earth ions with TTA is very effective when the solvent is MIBK, as was first reported by Kiba and Mizukami.[10] This enhancement has been quantitatively explained, in terms of adduct TTA chelate formation.[6]

The fact found in this study, that sodium(I) is extracted with TTA only when the solvent is MIBK, seems to indicate that the extraction of sodium with TTA due to an adduct formation of the chelate complex with MIBK, as in the case of the extraction of sodium(I) with TTA in benzene containing various neutral adduct-forming ligands.[3] Healy pointed out that two molecules of the adduct-forming ligand combine with one TTA sodium(I) chelate. In the present study, this solvation number could not be determined.

The value of the extraction constant, K_{ex_0}, in Eq. (5), $10^{-7.73}$, is not large, although it is much larger than that when the solvent is pure benzene, $10^{-11.16}$.[3] Thus, as has been described, the determination of K_{ex} from the distribution data when the aqueous phase is 1 M sodium perchlorate was not successful. On the other hand, it is very remarkable that the deviation of the hydrogen-ion-concentration data of the extraction experiments is quite large (one pH unit); thus, a reasonable extraction constant could be determined from the data.

The authors are very grateful to Dr. Yuko Hasegawa and Messrs. Yu Komatsu and Jun-ichi Yumikura of the present laboratory for their very helpful discussions. They are also grateful to Misses Etsuko Yamaguchi, Masumi Okamoto and Mr. Takaaki Shiokawa of the laboratory for their experimental aids.

9) T. Sekine and N. Ihara, This Bulletin, **44**, 2942 (1971).

10) T. Kiba and S. Mizukami, *ibid.*, **31**, 1007 (1958).

The Calculation of the π-Electron Orbital Energies of the Allyl Cation, Butadiene, and Cyclic Polyenes by Means of Green's Function Method

Katsumi SHIMADA, Sadao OKIDO, and Osamu TANIMOTO

Department of Applied Physics, Faculty of Engineering, Osaka City University, Sumiyoshi, Osaka

(Received June 29, 1972)

Green's function matrix method for the calculation of the orbital energies of π-electron systems, which has been discussed in previous papers, is applied to the allyl cation, butadiene, rectangular cyclobutadiene, and cyclic polyenes with various molecular lengths. The higher-order correction for the Hartree-Fock orbital energies are calculated, and in the case of butadiene the theoretical value of the ionization potential is discussed in comparison with the experimental data. The relation between the higher-order correction effect and the molecular length is illustrated in the cases of the cyclic polyenes. In particular, the breakdown of perturbation calculation based on the Hartree-Fock orbitals occurs in the case of the $C_{30}H_{30}$ molecule.

In our previous papers,[1,2] Green's function matrix method for π-electron system was discussed using several examples. These examples were of cases where the self-consistent-field (SCF) Green's function matrices can easily be calculated by the analytical method. In the present article, our method is applied to the allyl cation, butadiene, rectangular cyclobutadiene, and cyclic polyenes for the purpose of investigating the relation between the higher-order correction effect and the molecular length.

As is shown in References 1) [to be referred to as I] and 2), we are concerned with the calculation of the one-particle Green's function matrix $G(\omega)$, because the poles of $G(\omega)$ give the orbital energies. Using the perturbation method based on the Hartree-Fock orbitals, the one-particle Green's function matrix is given as follows:

$$G(\omega) = [g(\omega)^{-1} - \Sigma(\omega)]^{-1}, \tag{1}$$

where:

$$g(\omega) = [(\omega+\mu)I - (\alpha+\beta+\chi)]^{-1}. \tag{2}$$

The $g(\omega)$ matrix is Hartree-Fock Green's function matrix. (see Eq. (I.38)) The 'chemical potential', μ, is fixed at a certain value between the highest occupied level and the lowest unoccupied one. The α and β matrices are core integrals. In the following, we put:

$$\alpha_{ll} = -u - \sum_{l \neq m} \gamma_{lm}, \tag{3}$$

where u represents the ionization potential of a carbon atom in its valence state. Using the Pariser, Parr, and Pople's Hamiltonian, the elements of the Hartree-Fock field matrix, χ, are given by the following equations (from Eq. (I.31)):

$$\left.\begin{aligned} \chi_{ll} &= -i\int \frac{d\omega}{2\pi} e^{-i\omega(0^-)}\{\gamma_{ll}g_{ll}(\omega) + 2\sum_{p\neq l}\gamma_{lp}g_{pp}(\omega)\}, \\ \chi_{lm} &= i\gamma_{lm}\int \frac{d\omega}{2\pi} e^{-i\omega(0^-)}g_{lm}(\omega) \quad (l \neq m). \end{aligned}\right\} \tag{4}$$

The self-energy part, Σ, represents the correction of higher-order effects to the Hartree-Fock orbital energies:

$$\begin{aligned} \Sigma_{lm} = \sum_{pq}\gamma_{lp}\gamma_{mq}\int\frac{d\omega_1}{2\pi}\int\frac{d\omega_2}{2\pi} \\ \times\{2g_{pq}(\omega_1)g_{qp}(\omega_2)g_{lm}(\omega-\omega_1+\omega_2) \\ -g_{lq}(\omega_1)g_{qp}(\omega_2)g_{pm}(\omega-\omega_1+\omega_2)\}. \end{aligned} \tag{5}$$

(see Eq. (I.32))

The Allyl Cation

In the case of the allyl cation, the unperturbed Green's function matrix is given by:

$$g(\omega) = \begin{pmatrix} \omega+\mu-\alpha_{11}-\chi_{11} & -\beta_{12}-\chi_{12} & -\beta_{13}-\chi_{13} \\ -\beta_{12}-\chi_{12} & \omega+\mu-\alpha_{22}-\chi_{22} & -\beta_{12}-\chi_{12} \\ -\beta_{13}-\chi_{13} & -\beta_{12}-\chi_{12} & \omega+\mu-\alpha_{11}-\chi_{11} \end{pmatrix}^{-1}. \tag{6}$$

The residue of the (lm) element of the Green's function matrix is denoted as R_{lm}:

$$R_{lm} = \frac{1}{2\pi i}\int d\omega e^{-i\omega(0^-)}g_{lm}(\omega). \tag{7}$$

It can easily be seen that R_{lm} have the following relations:

$$\left.\begin{aligned} &2R_{11} + R_{22} = 1, \\ &R_{13} = R_{11}, \\ &R_{11}R_{22} = R_{12}^2 \end{aligned}\right\} \tag{8}$$

and

$$(\alpha_{11}-\alpha_{22}+\beta_{13}+\chi_{13})R_{12} = (\beta_{12}+\chi_{12})(1-2R_{22}).$$

The self-consistency conditions (4) are, then, written as:

$$\left.\begin{aligned} &(4\gamma_{12}-\gamma_{11}-2\gamma_{13})R_{22} = 2\chi_{11} - \gamma_{11} - 2\gamma_{13}, \\ &-\gamma_{12}R_{12} = \chi_{12}, \\ &(\gamma_{11}-2\gamma_{12})R_{22} = \chi_{22} - 2\gamma_{12}, \\ &\gamma_{13}R_{22} = 2\chi_{13} + \gamma_{13}. \end{aligned}\right\} \tag{9}$$

From these relations, the following algebraic equation is obtained:

$$\begin{aligned} A_1^2R_{22}^4 + A_1(2A_2-A_1)R_{22}^3 + \{A_2(A_2-2A_1)+8\beta_{12}^2\}R_{22}^2 \\ - (A_2^2+8\beta_{12}^2)R_{22} + 2\beta_{12}^2 = 0, \end{aligned} \tag{10}$$

where:

$$\left.\begin{aligned} A_1 &= -\frac{3}{2}\gamma_{11} + 2\gamma_{12} - \frac{1}{2}\gamma_{13}, \\ A_2 &= \alpha_{11} - \alpha_{22} + \frac{1}{2}\gamma_{11} - \gamma_{12} + \frac{1}{2}\gamma_{13} + \beta_{13}. \end{aligned}\right\} \tag{11}$$

Using the solution for R_{22} in the above equation (10), the Hartree-Fock field, χ, is obtained from Eq. (9). The orbital energies, ω_1, ω_2 and ω_3 ($\omega_1<\omega_2<\omega_3$), in the SCF approximation are easily obtained by the use of Eq. (2); they are listed in Table 1. The element of the SCF Green's function matrix is represented as;

1) O. Tanimoto and K. Shimada, *Mol. Phys.*, **23**, 745 (1972).
2) K. Shimada and O. Tanimoto, *ibid.*, **23** 765 (1972).

Table 1. The orbital energies of the allyl cation (in eV)

	Semi-empirical[3]	Löwdin orbitals(1)	Löwdin orbitals(2)
γ_{11}	10.84	17.62	
γ_{12}	7.52	8.92	
γ_{13}	5.63	5.57	
β_{12}	−2.85	−2.68	
β_{13}	−0.45	0	−0.45
u	11.42	11.54	
ω_3	−5.860 (−5.651)	−4.281 (−3.192)	−4.399 (−3.469)
ω_2	−9.761 (−9.659)	−8.933 (−8.519)	−8.493 (−8.080)
ω_1	−21.31 (−21.23)	−20.18 (−19.69)	−20.47 (−19.97)

The values in the bracket are the result of the SCF calculation. (1) As the values of the coulomb-integrals, those in the case of benzene[4] are adopted. (2) The value of β_{13} is used that of semi-empirical case.

Table 2.

(lm)	A_{lm}	B_{lm}	C_{lm}
11	A_{11}	0.5	$0.5-A_{11}$
22	$1-2A_{11}$	0	$2A_{11}$
12	A_{12}	0	$-A_{12}$
13	A_{11}	−0.5	$0.5-A_{11}$

$$g_{lm}(\omega)=\frac{A_{lm}}{\omega-\omega_1-i\delta}+\frac{B_{lm}}{\omega-\omega_2+i\delta}+\frac{C_{lm}}{\omega-\omega_3+i\delta}, \quad (12)$$

where A_{lm}, B_{lm}, and C_{lm} are certain constants simply related to one another, as is shown in Table 2. From the theorem of residues:

$$\begin{aligned}&\int\frac{d\omega_1}{2\pi}\frac{d\omega_2}{2\pi}g_{ij}(\omega_1)g_{kl}(\omega_2)g_{mn}(\omega-\omega_1+\omega_2)\\&=\frac{A_{ij}B_{kl}A_{mn}}{\omega-2\omega_1+\omega_2}+\frac{A_{ij}C_{kl}A_{mn}}{\omega-2\omega_1+\omega_3}+\frac{B_{ij}A_{kl}B_{mn}}{\omega+\omega_1-2\omega_2}\\&+\frac{B_{ij}A_{kl}C_{mn}+C_{ij}A_{kl}B_{mn}}{\omega+\omega_1-\omega_2-\omega_3}+\frac{C_{ij}A_{kl}C_{mn}}{\omega+\omega_1-2\omega_3}. \quad (13)\end{aligned}$$

$$g(\omega)=\begin{pmatrix}\omega+\mu-\alpha_{11}-\chi_{11} & -\beta_{12}-\chi_{12} & -\beta_{13}-\chi_{13} & -\beta_{14}-\chi_{14}\\ -\beta_{12}-\chi_{12} & \omega+\mu-\alpha_{22}-\chi_{22} & -\beta_{23}-\chi_{23} & -\beta_{13}-\chi_{13}\\ -\beta_{13}-\chi_{13} & -\beta_{23}-\chi_{23} & \omega+\mu-\alpha_{22}-\chi_{22} & -\beta_{12}-\chi_{12}\\ -\beta_{14}-\chi_{14} & -\beta_{13}-\chi_{13} & -\beta_{12}-\chi_{12} & \omega+\mu-\alpha_{11}-\chi_{11}\end{pmatrix}^{-1}. \quad (14)$$

For even alternant hydrocarbons, the theorem proved by Pople[6] states that:

$$P_{rr}=2\frac{1}{2\pi i}\int d\omega\, e^{-i\omega(0^-)}g_{rr}(\omega)=1. \quad (15)$$

From the above theorem, the following relation is obtained:

$$\alpha_{rr}+\chi_{rr}=\text{constant}\equiv\mu, \quad (16)$$

where the chemical potential, μ, is set at the center of the level scheme. The relation:

$$\beta_{13}+\chi_{13}=0 \quad (17)$$

is derived from the pairing theorem.[7] Using these relations, the elements of the SCF Green's function can be written thus:

$$\begin{aligned}g_{lm}(\omega)=&\frac{a_{lm}}{\omega-\beta_+-i\delta}+\frac{b_{lm}}{\omega+\beta_++i\delta}\\&+\frac{c_{lm}}{\omega-\beta_--i\delta}+\frac{d_{lm}}{\omega+\beta_-+i\delta}, \quad (18)\end{aligned}$$

where, assuming that $\beta_{12}=\beta_{13}\equiv\beta$ and $\beta_{14}=0$:

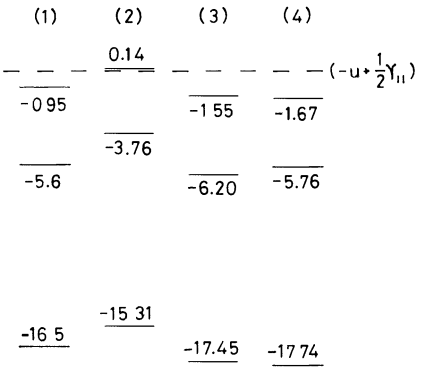

Fig. 1. The orbital energies of the allyl cation measured from the standard $-u+1/2\,\gamma_{11}$.
Case (1) is the result that is in the Salem's text and cases (2), (3) and (4) correspond to the first, second and third column in Table 1, respectively.

Using Eqs. (13) and (5), the orbital energies including the correlation effect were calculated from the secular equation (1); they are shown in Fig. 1, along with the results in Salem's text.[5] The orbital energies are measured from the standard $-u+\gamma_{11}/2$. In the case of the semi-empirical parameters, unlike the other cases, the highest energy level appears above the origin of the energy level. With regard to the electron-density distribution, we have the following relations:

$$q_{22}>2q_{11} \quad \text{(Case (2) in Fig. 1)}$$

and:

$$q_{22}<2q_{11} \quad \text{(Cases (1), (3) and (4) in Fig. 1)}$$

as q_{ii} is the electron-occupation number at the carbon atom, i. It shows the feature of the semi-empirical parameters that the correction for the Hartree-Fock orbital energies is smaller than that in other cases.

Butadiene

In the case of butadiene, the SCF Green's function matrix is given by:

3) H. O. Pritchard and H. A. Skinner, *Chem. Rev.*, **55**, 745 (1955) R. Pariser and R. G. Parr, *J. Chem. Phys.*, **21**, 466, 767 (1953).

4) R. G. Parr, "The Quantum Theory of Molecular Electronic Structure", Benjamin, New York (1963), p. 67.

5) L. Salem, "The Molecular Orbital Theory of Conjugated Systems", Benjamin, New York (1966), p. 68.

6) J. A. Pople, *Trans. Faraday Soc.*, **49**, 1375 (1953).

7) A. D. McLachlan, *Mol. Phys.*, **4**, 49 (1961).

TABLE 3.

(lm)	a_{lm}	b_{lm}	c_{lm}	d_{lm}
11	a_{11}	a_{11}	a_{22}	a_{22}
22	a_{22}	a_{22}	a_{11}	a_{11}
12	a_{12}	$-a_{12}$	a_{12}	$-a_{12}$
13	a_{12}	a_{12}	$-a_{12}$	$-a_{12}$
14	a_{11}	$-a_{11}$	$-a_{22}$	a_{22}
23	a_{22}	$-a_{22}$	$-a_{11}$	a_{11}

$$\left.\begin{aligned}\beta_+ &= -\frac{1}{2}[\{(\beta+\chi_{23}-\chi_{14})^2+4(\beta+\chi_{12})^2\}^{1/2} \\ &\quad -\beta-\chi_{14}-\chi_{23}], \\ \beta_- &= -\frac{1}{2}[\{(\beta+\chi_{23}-\chi_{14})^2+4(\beta+\chi_{12})^2\}^{1/2} \\ &\quad +\beta+\chi_{14}+\chi_{23}].\end{aligned}\right\} \quad (19)$$

The relations among the coefficients, a_{lm}, b_{lm}, c_{lm}, and d_{lm}, in Eq. (18) are given in Table 3, and

$$\left.\begin{aligned}a_{11} &= \frac{1}{4}[1+(\beta+\chi_{23}-\chi_{14})\{(\beta+\chi_{23}-\chi_{14})^2 \\ &\quad +4(\beta+\chi_{12})^2\}^{-1/2}], \\ a_{22} &= \frac{1}{2}-a_{11}, \\ a_{12} &= -\frac{1}{2}(\beta+\chi_{12})\{(\beta+\chi_{23}-\chi_{14})^2 \\ &\quad +4(\beta+\chi_{12})^2\}^{-1/2}=\sqrt{(a_{11}a_{22})}.\end{aligned}\right\} \quad (20)$$

From these equations and Eq. (4), the following equations can easily be obtained:

$$\left.\begin{aligned}\chi_{11} &= \frac{1}{2}\gamma_{11}+\gamma_{12}+\gamma_{13}+\gamma_{14}, \\ \chi_{22} &= \frac{1}{2}\gamma_{22}+\gamma_{12}+\gamma_{13}+\gamma_{23}, \\ \chi_{12} &= 2\beta\gamma_{12}\chi_{23}/(\beta\gamma_{23}-A\chi_{23}), \\ \chi_{14} &= -(\gamma_{14}/\gamma_{23})\chi_{23}\end{aligned}\right\} \quad (21)$$

and

$$4A^2\chi_{23}^4-8\beta\gamma_{23}A\chi_{23}^3+(20\beta^2-A^2)\gamma_{23}^2\chi_{23}^2 +2\beta\gamma_{23}^3A\chi_{23}-\beta^2\gamma_{23}^4=0, \quad (22)$$

where:

$$A=2\gamma_{12}-\gamma_{23}-\gamma_{14}. \quad (23)$$

Eq. (22) has two real solutions. We choose the solution which satisfies the condition:

$$\beta+\chi_{23}<0. \quad (24)$$

The orbital energies, including the correlation effect, are obtained and the numerical results are listed in Table 4, together with the SCF orbital energies. In other to compare the present results with the experimental results, the ionization potential is calculated. Using Slater orbitals, the ionization potential of *trans*-butadiene is calculated as below:

$$I_{\text{calc}}=u-\frac{1}{2}\gamma_{11}-\omega=9.01\text{ eV}\quad(8.80\text{ eV})$$

where ω is the energy of the higher occupied orbital given in Table 4 and where $u=11.54$ eV is used.

TABLE 4. NUMERICAL RESULTS OF π-ELECTRON ORBITAL ENERGIES IN BUTADIENE MOLECULE

	Slater orbitals[8]		Hall orbitals[9]
	cis-	*trans*-	*trans*-
γ_{11}	16.93		17.26
γ_{22}	16.93		17.56
γ_{12}	9.24		9.03
γ_{23}	8.69		8.63
γ_{13}	5.52		5.48
γ_{14}	4.68	3.83	3.78
β	−2.68		−2.68
χ_{12}	−4.37	−4.39	−4.28
χ_{23}	−1.42	−1.35	−1.37
χ_{14}	0.763	0.595	0.598
ω^{SCF}	±5.79 ±9.12	±5.72 ±9.16	±5.62 ±9.06
ω	±6.04 ±9.02	±5.93 ±8.99	±5.92 ±8.92
Δ	±0.25	±0.21	±0.30
$(\Delta=\omega-\omega^{\text{SCF}})$	∓0.10	∓0.17	∓0.14

The value in brackets is the result of the SCF calculation. The experimental value was given by Price and Walsh[10] as:

$$I_{\text{expt}}=9.07\text{ eV}.$$

Thus, our result is in good agreement with the experimental value. The effect of orbital reorganization during the ionization process was investigated by Devaquat and Salem.[11] Using the perturbation theory, they found only a small correction to the I_{SCF} value for the ionization potential in the SCF scheme; the correction is about 0.1 eV for closed-shell systems, such as the allyl cation or butadiene. On the other hand, the correlation energies obtained with our method are 0.2—0.5 eV, except for the semi-empirical parameters. Hence, the deviations in the orbital energies from the SCF values are determined by the correlation effect rather than by the orbital-distortion effect.

The Rectangular Cyclobutadiene

Here we will derive the equations for the orbital energies of the rectangular cyclobutadiene. From the SCF Green's function matrix:

$$g(\omega)=\begin{pmatrix}\omega & -\beta-\chi_{12} & 0 & -\beta'-\chi_{14} \\ -\beta-\chi_{12} & \omega & -\beta'-\chi_{14} & 0 \\ 0 & -\beta'-\chi_{14} & \omega & -\beta-\chi_{12} \\ -\beta'-\chi_{14} & 0 & -\beta-\chi_{12} & \omega\end{pmatrix}^{-1}. \quad (25)$$

we obtain the following self-consistency conditions:

$$\left.\begin{aligned}\chi_{11} &= \frac{1}{2}\gamma_{11}+\gamma_{12}+\gamma_{13}+\gamma_{14}, \\ \chi_{12} &= -\frac{1}{2}\gamma_{12}, \\ \chi_{13} &= \chi_{14}=0.\end{aligned}\right\} \quad (26)$$

We also obtain the orbital energies, $\omega_{\text{SCF}}=\pm\beta_\pm$,

8) R. G. Parr and R. S. Mulliken, *J. Chem. Phys.*, **18**, 1338 (1950).
9) G. G. Hall, *Trans. Faraday Soc.*, **50**, 773 (1954).
10) W. C. Price and A. D. W. Walsh, *Proc. Roy. Soc.*, Ser. A, **174**, 220 (1940).
11) A. Devaquet and L. Salem, *J. Chim. Phys.*, **62**, 1267 (1965).

where:

$$\beta_{\pm} = \beta \pm \beta' - \frac{1}{2}\gamma_{12}. \tag{27}$$

The matrix element of the self-energy part is given by:

$$\Sigma_{lm} = \frac{a}{4}\left(\frac{1}{\omega+3\beta_+} + \frac{(-1)^{l+m}}{\omega-3\beta_+} + \frac{\alpha_{lm}}{\omega+3\beta_-} + \frac{(-1)^{l+m}\alpha_{lm}}{\omega-3\beta_-}\right) + \frac{b}{4}\left(\frac{1}{\omega+\beta_++2\beta_-} + \frac{(-1)^{l+m}}{\omega-\beta_+-2\beta_-} + \frac{\alpha_{lm}}{\omega+2\beta_++\beta_-} + \frac{(-1)^{l+m}\alpha_{lm}}{\omega-2\beta_+-\beta_-}\right), \tag{28}$$

where:

$$\left.\begin{aligned} a &= \frac{1}{16}\{(\gamma_{11}-\gamma_{12})^2-(\gamma_{11}-\gamma_{13})^2+(\gamma_{11}-\gamma_{14})^2 \\ &\quad +(\gamma_{12}-\gamma_{13})^2+(\gamma_{13}-\gamma_{14})^2-(\gamma_{12}-\gamma_{14})^2\}, \\ b &= \frac{1}{16}\{3(\gamma_{11}-\gamma_{12})^2+(\gamma_{11}-\gamma_{13})^2-(\gamma_{11}-\gamma_{14})^2 \\ &\quad -(\gamma_{12}-\gamma_{13})^2+7(\gamma_{13}-\gamma_{14})^2+(\gamma_{12}-\gamma_{11})^2\} \end{aligned}\right\} \tag{29}$$

and

$$\alpha_{11} = \alpha_{12} = -\alpha_{13} = -\alpha_{14} = 1. \tag{30}$$

The orbital energies, $\omega=\pm\omega_{\pm}$, are given by the following equations:

$$\omega_+ = \beta_+ + \frac{a}{\omega_++3\beta_+} + \frac{b}{\omega_++\beta_++2\beta_-} \tag{31}$$

and

$$\omega_- = \beta_- + \frac{a}{\omega_-+3\beta_-} + \frac{b}{\omega_-+2\beta_++\beta_-}. \tag{32}$$

The Cyclic Polyenes

For the purpose of investigating the relation between the correlation energies and the molecular length, we will discuss the cyclic polyenes here. The systems of $4n+2$ π-electrons are considered in the following discussion. For the sake of simplicity, only the nearest-neighbour interactions are taken into account. The SCF Green's function, $g_{4n+2}(\omega)$, is given as below:

$$g_{4n+2}(\omega) = \begin{pmatrix} \omega & d & 0 & \cdots & d \\ d & \omega & d & \cdots & 0 \\ 0 & d & \omega & \cdots & 0 \\ \cdot & \cdot & \cdot & & \cdot \\ \cdot & \cdot & \cdot & & \cdot \\ d & 0 & 0 & \cdots & \omega \end{pmatrix}^{-1}, \tag{33}$$

where we put $\mu=\alpha+\chi_{ll}$ and $d=-\beta-\chi_{l,l\pm1}$. The poles of this Green's function matrix are given by:[12]

$$\det|g_{4n+2}(\omega)^{-1}| = -4d^{4n+2}\sin^2(2n+1)\theta = 0, \tag{34}$$

where:

$$\omega = -2d\cos\theta. \tag{35}$$

The solutions of the above equation are:

$$\theta_r = \frac{r}{2n+1}\pi, \tag{36}$$

where:

$$\left.\begin{aligned} &r = 0,\ 2n+1 \\ &r = 1, 2, \cdots, 2n \text{ (doubly degenerated levels).} \end{aligned}\right\} \tag{37}$$

12) C. Coulson, *Proc. Roy. Soc., Ser. A*, **164**, 383 (1938).

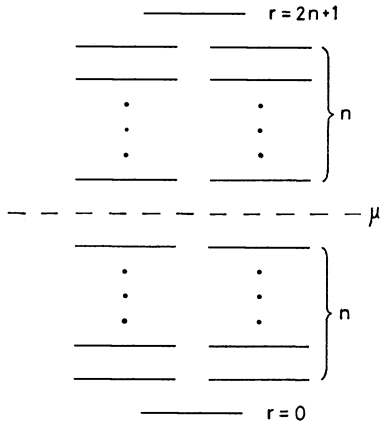

Fig. 2. The schematic orbital energies of the cyclic polyenes with $4n+2$ π-electrons.

The $4n+2$ suffix in $g_{4n+2}(\omega)$ will be disregarded hereafter for the sake of simplicity. The (lm) element of $g(\omega)$ is obtained thus:

$$g_{lm}(\omega) = \frac{\cos(2n+1+l-m)\theta}{2d\sin\theta\sin(2n+1)\theta}. \tag{38}$$

On the other hand, as is shown in Fig. 2, $g_{lm}(\omega)$ is written in the following form:

$$g_{lm}(\omega) = \sum_{r=0}^{n}\frac{a_{lm;r}}{\omega-\omega_r-i\delta} + \sum_{r=n+1}^{2n+1}\frac{b_{lm;r}}{\omega-\omega_r+i\delta}. \tag{39}$$

The transformation of the variables, ω to θ, is convenient for the following evaluation. Then, the contour on the complex plane is distorted to that shown in Fig. 3.

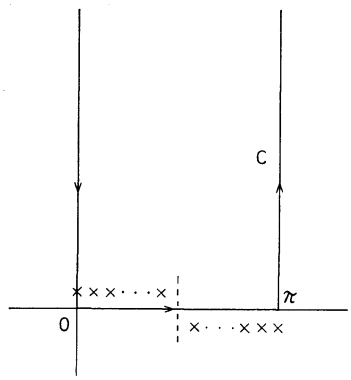

Fig. 3. The contour in the complex θ plane.
The mark × denotes the poles of the one-particle Green's function.

The residues are given by:

$$\begin{aligned} a_{lm;r} &= \lim_{\omega\to\omega_r}(\omega-\omega_r)\sum_j\frac{a_{lm;j}}{\omega-\omega_j} \\ &= \lim_{\theta\to\theta_r} w_r(\theta-\theta_r)\frac{\cos(2n+1+l-m)\theta}{\sin(2n+1)\theta} \\ &= \frac{w_r}{2n+1}\cos\frac{(l-m)r}{2n+1}\pi, \end{aligned} \tag{40}$$

$$b_{lm;r} = a_{lm;2n+1-r} = (-1)^{l-m}a_{lm;r}, \tag{41}$$

where, as the pole, $r=0$, exists on the contour, c, and as the other poles are included within c, we have:

$$w_0 = 1/2, \text{ and } w_r = 1 \text{ for } 1 \leqq r \leqq n. \tag{42}$$

Using Eq. (4) and the relations:

$$\left.\begin{aligned}&\sum_r \alpha_{ll;r} = \sum_{r=0}^{n} \frac{w_r}{2n+1} = \frac{1}{2n+1}\left(n+\frac{1}{2}\right) = \frac{1}{2}\\ &\text{and}\\ &\sum_r a_{l,l\pm1;r} = \frac{1}{2n+1}\left(\sum_{r=0}^{n} \cos\frac{r\pi}{2n+1} - \frac{1}{2}\right),\end{aligned}\right\} \quad (43)$$

we obtained the self-consistency conditions:

$$\left.\begin{aligned}&\chi_{ll} = \frac{1}{2}\gamma_0 + 2\gamma_1,\\ &\chi_{l,l\pm1;r} = -\frac{1}{2n+1}\frac{\cos\dfrac{n\pi}{2n+1}}{1-\cos\dfrac{\pi}{2n+1}}\end{aligned}\right\} \quad (44)$$

where $\gamma_0=\gamma_{ll}$ and $\gamma_1=\gamma_{l,l\pm1}$. Hence, we obtain the next relations:

$$\left.\begin{aligned}&\mu = \alpha + \chi_{ll} = \alpha + \frac{1}{2}\gamma_0 + 2\gamma_1 = -u + \frac{1}{2}\gamma_0,\\ &d = -\beta + \frac{\gamma_1}{2n+1}\frac{\cos\dfrac{n\pi}{2n+1}}{1-\cos\dfrac{\pi}{2n+1}}.\end{aligned}\right\} \quad (45)$$

The SCF orbital energies are obtained by using $\omega_r^{SCF}=-2d\cos\theta_r\equiv\beta_r$. The (lm) element of $\Sigma(\omega)$ can easily be obtained:

$$\Sigma_{lm}(\omega) = \sum_{rst} B_{rst}(lm)\left[\frac{1}{\omega+\beta_r+\beta_s+\beta_t} + \frac{(-1)^{l+m}}{\omega-\beta_r-\beta_s-\beta_t}\right], \quad (46)$$

where the coefficient, $B_{rst}(lm)$, is given by:

$$B_{rst}(lm) = \sum_{pq} \gamma_{lp}\gamma_{mq}(-1)^{p+q}[2a_{pq;r}a_{qp;s}a_{lm;t} - a_{lq;r}a_{qp;s}a_{pm;t}]. \quad (47)$$

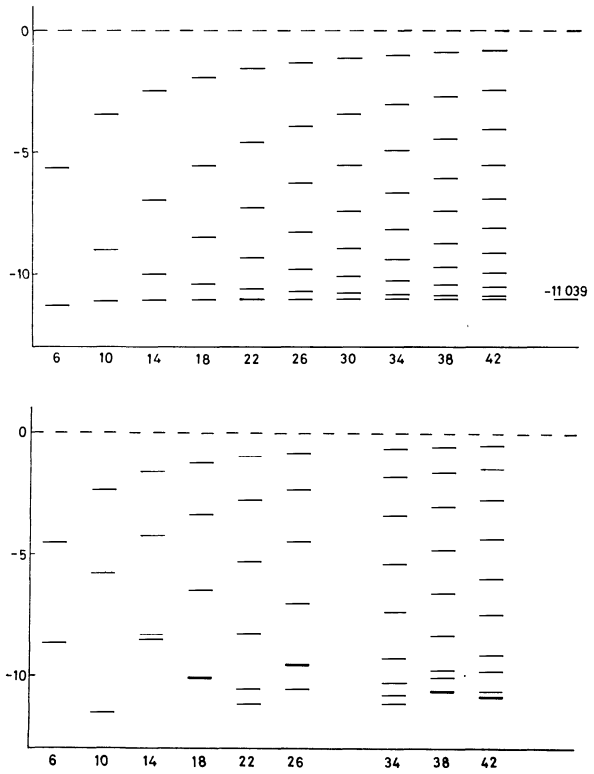

Fig. 4. The orbital energies of the cyclic polyenes of the SCF method and these including the correlation effect.

TABLE 5. THE ORBITAL ENERGIES OF THE CYCLIC POLYENES

	6	10	14	18	22	26	30	34	38	42
(1)	±5.653	±3.440	±2.467	±1.922	±1.574	±1.332	±1.155	±1.019	±0.912	±0.825
	±11.31	±9.007	±6.912	±5.534	±4.594	±3.919	±3.414	±3.023	±2.711	±2.458
		±11.13	±9.989	±8.478	±7.242	±6.279	±5.525	±4.924	±4.437	±4.035
			±11.09	±10.40	±9.303	±8.273	±7.393	±6.657	±6.041	±5.522
				±11.07	±10.61	±9.786	±8.939	±8.164	±7.481	±6.886
					±11.06	±10.73	±10.09	±9.392	±8.716	±8.096
						±11.05	±10.81	±10.30	±9.714	±9.125
							±11.05	±10.86	±10.45	±9.950
								±11.05	±10.90	±10.55
									±11.05	±10.92
										±11.04
(2)	±4.507	±2.360	±1.602	±1.214	±0.977	±0.818		±0.617	±0.550	±0.496
	±8.644	±5.781	±4.243	±3.340	±2.744	±2.328		±1.785	±1.598	±1.447
		±11.52	±8.304	±6.454	±5.262	±4.434		±3.362	±2.996	±2.701
			±8.495	±10.05	±8.265	±7.001		±5.341	±4.770	±4.307
				±10.10	±10.54	±9.520		±7.324	±6.558	±5.934
					±11.18	±9.571		±9.255	±8.309	±7.534
						±11.05		±10.27	±9.722	±9.097
								±10.78	±10.03	±9.787
								±11.12	±10.60	±10.61
									±10.60	±10.84
										±10.85

13) The Löwdin orbital parameters for benzene in Ref. 4 are used.

In the nearest-neighbour-interaction approximation, Eqs. (34) and (35) hold if ω and d are transformed to $\omega-\Sigma_{11}(\omega)$ and $d-\Sigma_{12}(\omega)$ respectively; that is,

$$-4[d-\Sigma_{12}(\omega)]^{4n+2}\sin^2(2n+1)\theta = 0. \quad (48)$$

Therefore,

$$\omega_r - \Sigma_{11}(\omega_r) = -2[d-\Sigma_{12}(\omega_r)]\cos\theta_r \quad (49)$$

is obtained, where θ_r is given by Eq. (36). Using these parameters[13];

$$\gamma_0 = 17.62\,\text{eV} \text{ and } \gamma_1 = 8.92\,\text{eV},$$

the numerical calculations are executed. The numerical results for $n=1-10$ are listed in Table 5 and are illustrated in Fig. 4.

In the case of the Hartree-Fock approximation, the energy of the $r=0$ level (the lowest occupied orbital), as measured from the center of the level scheme, monotonously increases as the π-electron number, $m=4n+2$, increases. At the limit, $m\to\infty$, the value of the lowest orbital energy approaches -11.039 eV in the case of the above-mentioned parameters. However, the orbital energies of occupied levels belonging to the other quantum number, r, monotonously decrease. By including the higher-order correction, these monotonous properties are broken down (see Fig. 4). The extremely close levels appear in the lower part of the level scheme. Furthermore, at $m=30$, the relation:

$$\omega_2 = \omega_5 + \omega_6 + \omega_7$$

is accidentally satisfied and the perturbation calculation is not adequate. The deviations from the Hartree-Fock orbital decrease as m increases, and the orbital energies approach the Hartree-Fock levels.

BULLETIN OF THE CHEMICAL SOCIETY OF JAPAN, VOL. 46, 397—400 (1973)

Solubility of Alkyl Bromides in Aqueous Polymer Solutions

Tsuneo Okubo, Shou-Xyng Chen, and Norio Ise
Department of Polymer Chemistry, Kyoto University, Kyoto

(Received July 4, 1972)

The solubility of alkyl bromides (alkyl : ethyl, *n*-propyl, *n*-butyl and *n*-amyl) in aqueous solutions of neutral polymers and polyelectrolytes was measured and discussed. The polymers used were polyacrylamide (PAAm), polyvinylalcohol(PVA), polyethyleneglycol(PEG), polyvinylpyrrolidone(PVP), polyethylenimine(PEI) and polyacrylic acid(PAA) and its salts. The solubility of alkyl bromide increased linearly with concentration of neutral polymer in the order PAAm>PVP~PEI>PEG>PVA~PAA. Sodium salt of PAA decreased the solubility of alkyl bromide, but organic salts of PAA such as tetraalkylammonium salts increased it. Using the equation $\ln (S_0/S)=km_2$, the limiting Setchénow constant k was obtained for these systems. The results were accounted for in terms of the hydrophobic structural modifications of water and the direct dipole and/or hydrophobic interactions between solute and cosolute.

In a previous paper,[1] the solubility of non-polar solutes, *i.e.*, naphthalene and biphenyl, in aqueous polymer solutions was reported. It was revealed that solvent-solute interactions, *viz.*, the structural effects of polymers on water, were most influential in determining the solubility. The cosolute-cosolute interactions or the solute-cosolute interactions except for those mediated by solvent water molecules were found to be negligible. In this paper we report on attempts to estimate the comparative strength of the solute-cosolute or cosolute-cosolute interactions and that of the solvent-solute interactions in polymer solution when cosolute is polar by measurements of the solubility of alkyl bromides. Studies on the solubility of the polar cosolute in polymer solutions have been carried out,[2] but the cosolutes were complicated compared with the alkyl bromids we used.

Experimental

Materials. Neutral polymers used as solutes were polyacrylamide (PAAm, degree of polymerization ($\overline{DP}$= 1800), polyvinylalcohol (PVA, $\overline{DP}$=1200, fractionated sample), polyethyleneglycol (PEG, $\overline{DP}$=140) and polyvinylpyrrolidone (PVP, $\overline{DP}$=220). Polyelectrolytes also used as solutes were sodium, tetramethylammonium (Me_4N–), tetraethylammonium (Et_4N–), tetra-*n*-propylammonium (Pr_4N–) and tetra-n-butylammonium (Bu_4N–) polyacrylates (PAA) obtained by neutralization of a polyacrylic acid(a product of Toa Gosei Chemicals Co., Nagoya, Japan, $\overline{DP}$= 640) with the corresponding hydroxide. Polyethylenimine (PEI, a product of Sumitomo Chemicals Co., Osaka, Japan, $\overline{DP}$=100) and unneutralized polyacrylic acid(PAA) were also used. Low molecular weight solutes were urea, tetramethylammonium bromide, tetraethylammonium bromide, tetra-*n*-propylammonium bromide and tetra-*n*-butylammonium bromide. Except for high molecular weight compounds, all the materials used were commercially available (Guaranteed reagent grade). Water was deionized by cation- and anion-exchange resins. Ethyl bromide (EtBr), *n*-propyl bromide (PrBr), *n*-butyl bromide (BuBr) and *n*-amyl bromide (AmBr) used as cosolute were further purified by distillation, and washed three times with water before use.

Solubility measurements. Excess cosolute was introduced into 20 ml test tubes containing 5 ml pure water or polymer solution with known concentration, wchich were sealed with stopper, shaken vigorously at first and placed for two to four days in a mechanical shaker in a thermostat at 25°C.

1) T. Okubo and N. Ise, *J. Phys. Chem.*, **73**, 1488 (1969).
2) Cf. e. g., J. Eliassaf, F. Eriksson, and F. R. Eirich, *J. Polymer Sci.*, **47**, 192 (1960).

After equilibration, a small portion of the homogeneous layer was taken out with a syringe and analyzed by gas chromatography. The apparatus used was GCG-550T with a thermal conductivity detector of Yanagimoto Mfg. Co., Kyoto. The column used was 2.2 m×3 mm ϕ. The stationary phase is Tide with carrier Neopak 1 A (mesh 60—80, products of Nishio Industry Co. Tokyo). The carrier gas was helium. The injection and detector temperatures were 125—135°C and 110°C, respectively. For ethyl bromide, *n*-pyropyl bromide, *n*-butyl bromide and *n*-amyl bromide, the column temperatures were 103, 100, 98 and 96°C, the helium flow rates 15, 20, 22.5 and 25 ml/min. and the bridge currents 100, 130, 150 and 200 mA, respectively. The solubilities of ethyl, n-propyl, n-butyl and n-amyl bromide are estimated to be 8.3×10^{-2}, 1.9×10^{-2}, 4.3×10^{-3} and 7.9×10^{-4} mol/l, respectively, at 25°C.

Rusults and Discussion

The solubilization[3] of *n*-butyl bromide in various neutral polymer solutions is shown in Fig. 1, in which

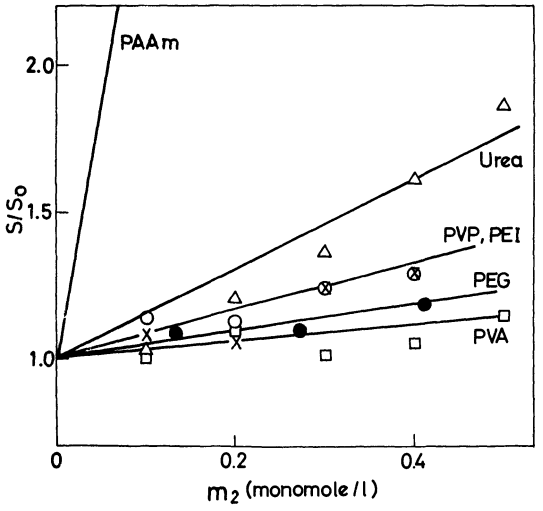

Fig. 1. Solubilization factor (S/S_0) of BuBr in various neutral polymer solutions at 25°C. ○: PVP, ×: PEI.

S_0 and S are the solubilities in pure water and in polymer solution, respectively, and m_2 is the polymer concentration. It is seen that S/S_0 becomes larger with increasing polymer concentration in the order:

$$\text{PVA} < \text{PEG} < \text{PVP} \sim \text{PEI} \ll \text{PAAm} \qquad (1)$$

On the other hand, the order for the non-polar hydrocarbons such as naphthalene and biphenyl was[1]

$$\text{PAAm} < \text{PVA} < \text{PEG} < \text{PEI} < \text{PVP} \qquad (2)$$

which was accounted for in terms of the iceberg enforcing effects. In other words, when an iceberg enhancing polymer is dissolved in water, a cage of water molecules is formed around the polymer solute, and the cosolute can then be incorporated within the same cage as the polymer. Thus, the solubility of the cosolute can be expected to be enhanced by the presence of iceberg enhancing polymers. The fact that

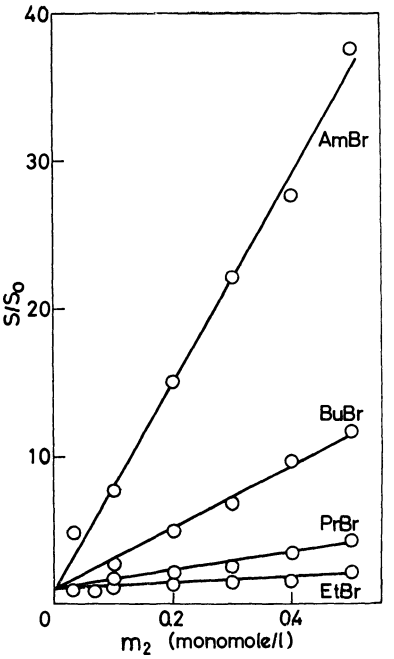

Fig. 2. Solubilization factor (S/S_0) of various alkyl bromides in polyacrylamide solution at 25°C.

the order (1) coincides with (2) except for PAAm indicates that the iceberg enforcing effect is still a main factor for the solubilization of polar cosolute as in the case of non-polar cosolute. Thus, the solute-solvent interactions are stronger than those between solute and cosolute or cosolute and cosolute. It should be recalled that PAAm solubilized most weakly non-polar cosolutes, whereas it solubilized most strongly polar cosolutes. This suggests that PAAm cannot greatly increase the solubility of polar cosolute by iceberg formation (carbamoyl groups of PAAm interfere with the formation) and some kind of complex formation of PAAm with alkyl bromide should exist. Solubilization of n-butyl bromide by urea is less strong than by PAAm, but fairly stronger than by other polymers. Thus, the carbamoyl groups contained both in PAAm and urea can be considered to interact strongly with butyl bromide by dipole-dipole interactions. The extent of the solubilization of butyl bromide by PVP, PEI, PEG and PVA is similar to that for naphthalene or biphenyl.

Figure 2 gives the solubilization of various alkyl bromides by PAAm. The solubility increases with the order:

$$\text{EtBr} < \text{PrBr} < \text{BuBr} < \text{AmBr} \qquad (3)$$

In other words, the larger the molecular weight of the cosolute, the more remarkable the solubilization. We see that the solubility increases linearly with the concentration of PAAm in the concentration region 0—0.5 monomol/l.

The solubilization effect by various water-soluble polymers is demonstrated in the following. Figures 3, 4 and 5 show the solubility of EtBr, PrBr, BuBr and AmBr in the presence of PVP PEI and PEG, respectively. The solubility increases in the order shown by the relation (3) but not that of EtBr by addition of

3) In this paper the term "solubilization" refers to the solubility increase by addition of the third substances. The correct term is "hydrotropy".[4]

4) F. A. Long and W. F. McDevit, *Chem. Revs.*, **51**, 119 (1952).

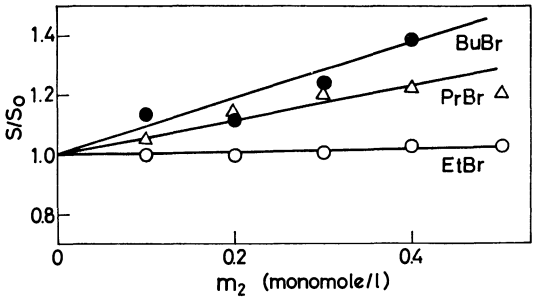

Fig. 3. Solubilization factor (S/S_0) of various alkyl bromides in polyvinylpyrrolidone solution at 25°C.

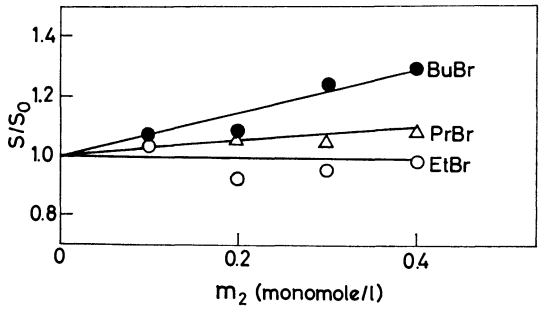

Fig. 4. Solubilization factor (S/S_0) of various alkyl bromides in polyethylenimine solution at 25°C,

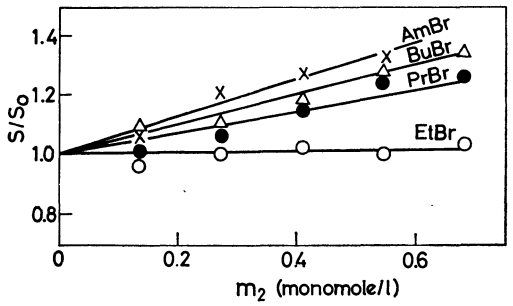

Fig. 5. Solubilization factor (S/S_0) of various alkyl bromides in polyethyleneglycol solution at 25°C.

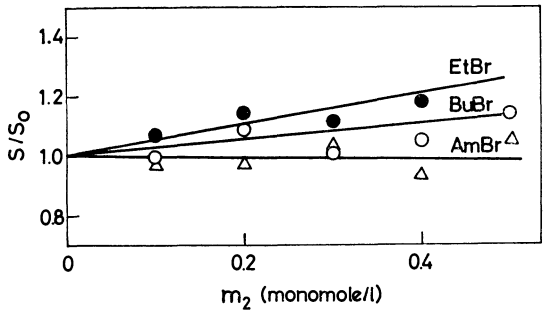

Fig. 6. Solubilization factor (S/S_0) of various alkyl bromides in polyvinylalcohol solution at 25°C.

these neutral polymers. Order (3) can be understood by the concept of the iceberg enforcing effect since it is known that the larger the volume of cosolute, the stronger the solubilizing effects.[1,4,5] Inequality (1) appears to hold also for PrBr. The specific interactions between polymer and cosolute such as dipole-dipole interactions do not seem to be significant in these polymers.

Figure 6 gives the experimental data for PVA. Solubilization is not so remarkable as in the case for naphthalene[1], and is in the order

$$\text{EtBr} > \text{BuBr} > \text{AmBr} \quad (4)$$

This indicates that the iceberg enforcing effect is unimportant on account of the interfering effect of OH groups with the iceberg formation,[1,6] and the interactions of the OH groups of PVA with polar cosolute (solute-cosolute interactions) certainly exist.

The Setchénow equation was reported to be valid for non-polar cosolute in various polymer solutions in dilute concentration regions, and the Setchénow constant, k, derived from the following equation was discussed in detail.[1]

$$\ln (S_0/S) = km_2 \quad (5)$$

For BuBr, $\ln(S_0/S)$ in various polymer solutions linearly decreased with increasing polymer concentration below 0.4 monomol/l except for PAAm solution. In the case of PAAm, deviation from linearity was found over 0.1 monomol/l, and the linearity between S/S_0 [not $\ln(S/S_0)$] and m_2 holds in the range 0—0.5 monomole/l (Fig. 2). The limiting Setchénow constants ($k/2.303$) derived for BrBu were −5.0, −0.31, −0.22, −0.21, −0.14 and −0.05 for PAAm, PVP, PEI, PEG, PAA and PVA, respectively.

Figure 7 shows the solubilization of BuBr in the presence of mixtures of PAAm and PVP. PAAm solubilized strongly BuBr whereas PVP did only weakly (Fig. 1). If no specific interaction exists between PAAm and PVP, the solubility should change as shown by the broken line. However, the solubility decreases at first with increasing PAAm and increases through a minimum. The decrease in solubilizing forces by mixing of PAAm and PVP may reflect that the polar carbamoyl groups of PAAm, which can solu-

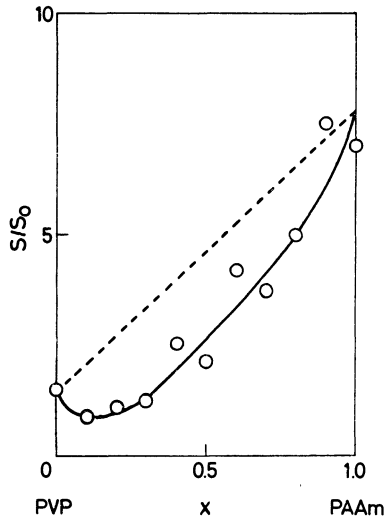

Fig. 7. Solubilization factor (S/S_0) of n-butyl bromide in mixture solution of polyvinylpyrrolidone and polyacrylamide at 25°C. m_2=0.3 monomol/l.

5) A. G. Leiga and J. N. Sarmousakis, *J. Phys. Chem.*, **70**, 3544 (1966).

6) W. Y. Wen and J. H. Hung. *ibid.*, **74**, 170 (1970).

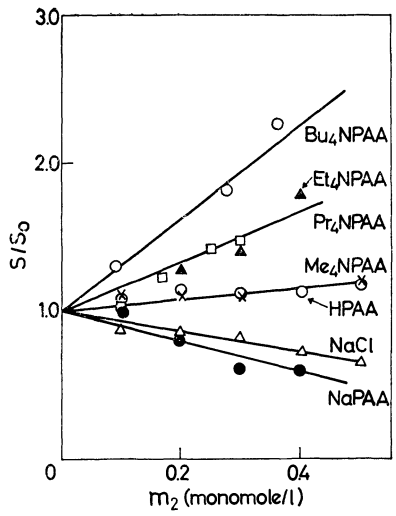

Fig. 8. Solubilization factor (S/S_0) of *n*-butyl bromide in various polyacrylate solutions at 25°C.

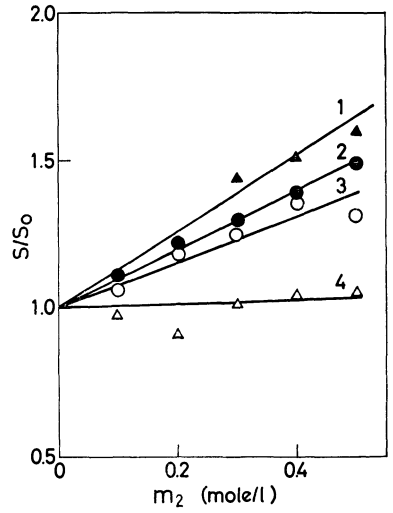

Fig. 9. Solubilization factor (S/S_0) of *n*-butyl bromide in various tetraalkylammonium bromide solutions at 25°C.
1 : Bu_4NBr, 2 : Pr_4NBr, 3 : Et_4NBr, 4 : Me_4NBr.

bilize alkyl bromide, combine with the polar side chain groups of PVP and the effective carbamoyl groups decrease. It is probable that complex formation takes place between PAAm and PVP. The behaviour of the desolubilization of the mixture of PVP and PAAm seems to be specific since the cosolute is more strongly solubilized by mixing of solutes than by individual solute.[7,8,9]

Figure 8 gives the solubility of BuBr in the presence of polyacrylic acid or its salts. The sodium polyacrylate and sodium chloride salt-out, whereas tetraalkylammonium salts show salting-in effects. It is seen that the solubility increases with increasing number of carbon atoms in organic gegenions, or with increasing hydrophobicity. The tendency has been observed for naphthalene and biphenyl.[1] The results indicate that the salting-in effect on the polar cosolute is also mainly determined by the hydrophobic interactions of solute with water molecules. The Setchénow constants ($k/2.303$) of BuBr were 0.54, −0.14, −0.49, −0.49, −0.88 for NaPPA, Me_4NPAA, Et_4NPAA, Pr_4NPAA and Bu_4NPAA, respectively.

Extensive study has been carried out on low molecular weight tetraalkylammonium salts.[6,10–14] We studied the solubilization effect for alkyl bromides by tetraalkylammonium bromide. Figure 9 shows the influence of the bromide on BuBr. The solubilization becomes stronger in the order

$$Me_4NBr < Et_4NBr < Pr_4NBr < Bu_4NBr \qquad (6)$$

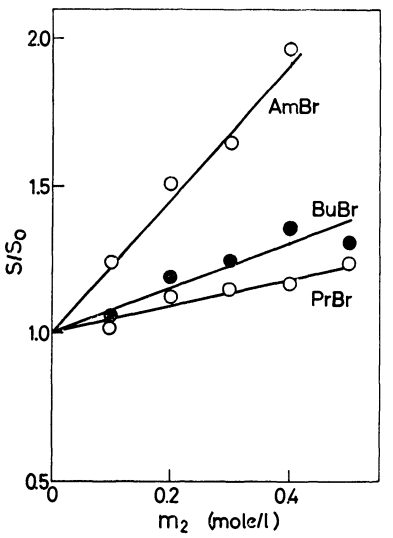

Fig. 10. Solubilization factor (S/S_0) of various alkyl bromides in tetraethylammonium bromide solution at 25°C.

This order was also found for tetraalkylammonium polyacrylates, but the strength of the solubilization is weaker by the bromide than by polyacrylate. Order (6) is the same as that found by Wen an Hung[6] for butane. This also indicates that hydrophobic interactions between the salts and water are the main factor determining the solubility of polar cosolutes (alkylbromide) as was the case for non-polar cosolute.

Figure 10 gives the solubilization data of n-propyl, n-butyl, and n-amyl bromides by tetraethylammonium bromide. The S/S_0 value is larger for larger alkyl groups. This is easily understood by the McDevit and Long equation,[15] which shows that the Setchénow coefficient is a linear function of the volume of the cosolute.

7) J. W. McBain and K. E. Johnson, *J. Amer. Chem. Soc.*, **66**, 9 (1944).
8) R. S. Stearns, H. Oppenheimer, E. Simon, and W. D. Harkins, *J. Chem. Phys.*, **15**, 496 (1947).
9) N. Ise and T. Okubo, unpublished results.
10) J. O'M Bockris, J. Bowler-Reed, and J. A. Kitchner, *Trans. Faraday Soc.*, **47**, 184 (1951).
11) R. L. Berger, Jr. and F. A. Long, *J. Phys. Chem.*, **60**, 1131 (1956).
12) N. C. Deno and C. H. Spink, *ibid.*, **67**, 1347 (1963).
13) A. Ben-Naim, *ibid.*, **71**, 1137 (1967).
14) H. E. Wirth and A. LoSurdo, *ibid.*, **72**, 751 (1968).
15) W. F. McDevit and F. A. Long, *J. Amer. Chem. Soc.*, **74**, 1773 (1952).

Diffusion Coefficients of Bolaform Electrolytes in Aqueous Solution

Hisashi UEDAIRA

Research Institute for Polymers and Textiles, Sawatari 4, Kanagawa-ku, Yokohama

(Received July 1, 1972)

The diffusion coefficients of sodium salts of *m*-benzene disulfonate, 1,5-naphthalenedisulfonate, 1,2-ethanedisulfonate, and 1,4-butanedisulfonate in aqueous solutions were measured at 25°. The concentration dependence of the diffusion coefficients for sulfonates decreased with increasing charge distance and was smaller than that of the corresponding ordinary 2 : 1 electrolytes. The concentration dependence of diffusion coefficient for sodium *m*-benzenedisulfonate was the largest. It is shown that bolaform electrolytes behave like normal 1 : 1 electrolytes in the concentration range where the ion atmosphere around each charged group is independent.

Bolaform electrolytes are a peculiar type of 2 : 1 electrolyte and the physico-chemical properties of their aqueous solutions are unusual. However, the cause of this peculiarity is not yet clarified. It was shown by Atkinson, Yokoi and Hallada[1] that the electrolytic conductances of bolaform electrolytes (*m*-benzenedisulfonate, 4,4′-biphenyl-disulfonate *etc.*) in aqueous solutions were interpreted by means of the Fuoss-Onsager equation. According to them, these behave as a spherical 2 : 1 strong electrolyte, irrespective of the position of sulfonic groups and the distance between them. Thomson, Rice and Nagasawa[2] found that the diffusion coefficients of potassium salts of *p*-benzene and 4,4′-biphenyldisulfonates in aqueous solutions show no concentration dependence. In contrast to their behavior in conductance, the diffusion coefficients of bolaform electrolytes are not explained by the theory of the ordinary strong electrolyte.

Bonner and Rogers,[3] and Bonner, Rushing and Torres[4] obtained the osmotic and activity coefficients for several bolaform electrolytes in which two sulfonic groups were separated by varying distance. They found that the thermodynamic properties of bolaform electrolytes markedly differed from those of normal electrolytes, especially in dilute solutions.

Thus, it is expected that the diffusion coefficients of bolaform electrolytes depend on the distance between the ionized groups and their positions. For the sake of confirmation, the diffusion coefficients were measured for sodium salts of *m*-benzenedisulfonate (*m*-Na_2BDS), 1,5-naphthalenedisulfonate (Na_3NDS). 1,2-ethanedisulfonate (Na_2EDS) and 1,4-buthanedisulfonate (Na_2BuDS) in aqueous solutions at 25°.

Experimental

The purification of sulfonates has been described elsewhere.[5]

The diffusion experiments were performed at 25±0.01° using a Spino Model-diffusion apparatus a Rayleigh interferometer. The standard 11 ml cell was used. For a typical run, nine photographic exposures were made at intervals ranging from 15 min. to 3 hr. Kodak type M glass photographic plates (4 in. by 5 in.) were used. The concentration difference in the solution on both sides of the diffusion boundary was so adjusted that the total number of Rayleigh fringe was 50 or 60. The procedure was the same as already reported.[6]

Deionized water was employed as the solvent for these systems. All the solutions were prepared by weight. Weighing was corrected to vacuum. The molar concentrations of solutions were calculated by means of the solution densities, which were mesurred with a 30 ml sprengel pycnometer at 25±0.01°.

To obtain the limiting diffusion coefficients, the conductances of the solutions were measured. The procedure was the same as that described.[5]

Results and Discussion

The mean concentration of each diffusion experiment and the corresponding value of diffusion coefficient are given in the Table. The diffusion coefficient for each salt at infinite dilution was calculated from the limiting mobility by the Nernst equation.

The values of the limiting equivalent conductances, λ°, of aqueous Na_2EDS and Na_2BuDS solutions determined from the plots of equivalent conductance against $(\text{normality})^{1/2}$, are 114.0 and 103.2 $cm^2\ ohm^{-1}\ equiv^{-1}$, respectively. It is not necessary to take into account the formation of ion-pair for the sulfonates. The values of λ° for *m*-Na_2BDS and Na_2NDS were taken from the works of Atkinson, Yokoi and Hallada,[1] and Eloworthy,[7] respectively.

The diffusion coefficient of 2 : 1 type electrolyte in an aqueous solution can be written in the form[8]

$$D = (D_0 + \Delta_1)\left(1 + c\frac{\mathrm{d}\ln y}{\mathrm{d}c}\right) \tag{1}$$

where D_0 is the Nernst limiting value of the diffusion coefficient, c the molarity, and y the activity coefficient in the molarity scale. Δ_1 is the first-order electrophoretic term and is expressed by the following equation for aqueous solutions at 25°

$$\Delta_1 = -8.07\times10^{-6}\frac{(z_1\lambda_2^0 + z_2\lambda_1^0)^2}{\lambda_0^2 z_1 z_2}\cdot\frac{\sqrt{I}}{1+0.3291\ a\sqrt{I}} \tag{2}$$

where I is the ionic strength, λ_1 and λ_2 are the limiting

1) G. Atkinson, M. Yokoi, and C. J. Hallada, *J. Amer. Chem. Soc.*, **83**, 1570 (1961).
2) G. Thomson, S. A. Rice, and M. Nagasawa, *ibid.*, **85**, 2537 (1963).
3) O. D. Bonner and O. C. Rogers, *J. Phys. Chem.*, **65**, 981 (1961).
4) O. D. Bonner, C. Rushing, and A. L. Torres, *ibid.*, **72**, 4290 (1968).
5) H. Uedaira and H. Uedaira, This Bulletin, **37**, 1885 (1964).
6) H. Uedaira and H. Uedaira, *ibid.*, **42**, 2140 (1969).
7) P. H. Eloworthy, *J. Chem. Soc.*, **1962**, 3718.
8) R. A. Robinson and R. H. Stokes, "Electrolyte Solutions," 2nd ed., Butterworths, London (1959).

TABLE. DIFFUSION COEFFICIENTS OF BOLAFORM ELECTROLYTES IN WATER AT 25°

Electrolytes	$c\times10^2$ (mol/l)	$D\times10^5$ (cm²/sec)
m-Na_2BDS	0	1.089
	0.7859	1.000_5
	2.3033	0.967_4
	3.8024	0.956_5
	5.4785	0.945_8
	9.4533	0.932_3
	14.8556	0.930_0
	19.3046	0.927_2
	21.9850	0.927_2
Na_2NDS	0	1.015
	0.8284	0.938_1
	2.3180	0.915_0
	3.5434	0.904_8
	4.9252	0.898_1
	6.0324	0.892_5
	9.8049	0.887_8
	11.4480	0.886_2
Na_2EDS	0	1.121
	1.0305	1.039_5
	2.4100	1.011_9
	5.7150	0.997_5
	12.0290	0.991_0
	15.1731	0.989_1
Na_2BuDS	0	1.029
	0.8123	0.967_9
	2.4649	0.941_3
	4.1902	0.931_2
	8.8209	0.917_2
	16.3539	0.911_1

mobilities of cation and anion, respectively, and z_1 and z_2 are the valencies of cation and anion, respectively. a is the parameter and its value is determined from the activity coefficient data.[8]

The values of the molal activity coefficients were obtained experimentally only for *m*-Na_2BDS and Na_2EDS.[3,4] In general, the activity coefficient of an electrolyte with a large ionic radius is not given by the Debye-Hückel formula. We used the following expression of the rational activity coefficient for 2 : 1 electrolyte solutions at 25°.[8]

$$\ln f = -\frac{4.08\sqrt{c}}{1+0.57\,a\sqrt{c}} + bc \qquad (3)$$

where a and b are the constants adjustable to fit the experimental curve.

Using the molal activity coefficient data,[3,4] and the densities, we obtain the following equation of the rational activity coefficients:

$$\ln f = -\frac{4.08\sqrt{c}}{1+3.899\sqrt{c}} + 0.0089\,c \quad (c<0.5\ \text{mol/l}) \qquad (4)$$

for *m*-Na_2BDS solution, and

$$\ln f = -\frac{4.08\sqrt{c}}{1+2.256\sqrt{c}} + 0.335\,c \quad (c<0.5\ \text{mol/l}) \qquad (5)$$

for Na_2EDS solution. An HITAC 8400 computer was used to apply the least square method to the data. The values of a in Eq. (3) for *m*-Na_2BDS and Na_2EDS are 6.84 and 3.96 A, respectively. Thus the theoretical equation for the diffusion coefficient of *m*-Na_2BDS in aqueous solution is

$$D\times10^5 = \left(1.089-\frac{1.480\sqrt{c}}{1+3.899\sqrt{c}}\right) \times\left[1+0.0089\,c-\frac{2.04\sqrt{c}}{(1+3.899\sqrt{c})^2}\right] \qquad (6)$$

Similarly, the equation for the diffusion coefficient of Na_2EDS in aqueous solution is

$$D\times10^5 = \left(1.121-\frac{1.448\sqrt{c}}{1+2.256\sqrt{c}}\right) \times\left[1+0.335\,c-\frac{2.04\sqrt{c}}{(1+2.256\sqrt{c})^2}\right] \qquad (7)$$

The theoretical curves of diffusion coefficients for *m*-Na_2BDS and Na_2EDS are given in Figs. 1 and 2. For the sake of comparison, the experimental curves of diffusion coefficients for *m*-Na_2BDS and Na_2EDS are included in the Figures. In both cases, the

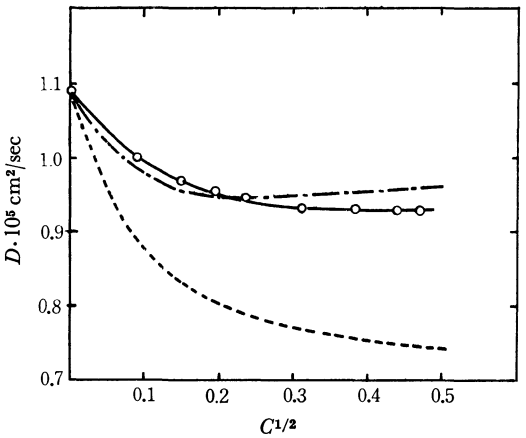

Fig. 1. Diffusion coefficients of *m*-Na_2BDS in aqueous solution.
—○—: in water, ——: Nernst-Hartley equation, ------: Eq. (6).

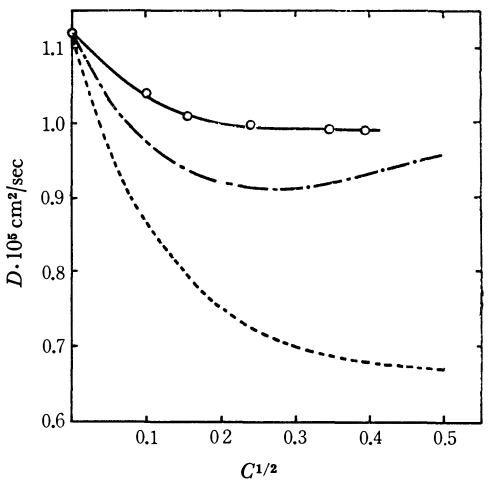

Fig. 2. Diffusion coefficients of Na_2EDS in aqueous solution.
—○—: in water, ——: Nernst-Hartley equation, ------: Eq. (7).

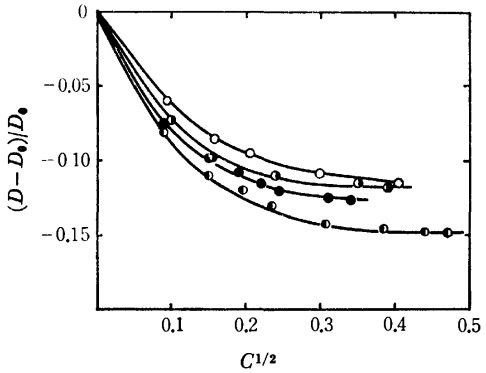

Fig. 3. Relative diffusion coefficients of sodium sulfonates in aqueous solution.
—○—: Na_2BuDS, —◑—: Na_2EDS, —●—: Na_2NDS, —◐—: *m*-Na_2BDS.

experimental values of diffusion coefficients are larger than the calculated values. That is, the concentration dependencies of the experimental values are remarkably smaller than those expected from Eqs. (6) and (7). A similar situation is expected also for Na_2NDS and Na_2BuDS.

From Eqs. (1), and (2), and (3), the concentration depedence of the diffusion coefficient decreases with increasing ionic radius, since parameter a is proportional to the ionic radius. Fig. 3 shows the relation $(D-D_0)/D_0$ against $c^{1/2}$ for various sulfonates in aqueous solutions. The ionic radius dependence of the diffusion coefficient holds for the aromatic and the aliphatic homologues, but the concentration dependence of the diffusion coefficient of Na_2EDS is smaller than that of Na_2NDS.

The experimental diffusion coefficients for these sulfonates show a tendency to approach constant values (Fig. 3), in contrast to normal electrolytes. The concentrations (c_t) at which the diffusion coefficints become constant are in the region 0.09~0.16 mol/l. The value of c_t for *m*-Na_2BDS is the largest.

As Eqs. (4) and (5) well reproduce the experimental values of activity coefficients, the chief discrepancy between the experimental and calculated values of the diffusion coefficients is caused by the overestimation of electrophoretic effect in Eq. (1).

On the assumption that the center of negative charge of a sulfonic group is located at the sulphur atom, the distance between two sulfonic groups are found to be 4.6 for Na_2EDS and *m*–Na_2BDS, and 7 A for Na_2BuDS and Na_2NDS. Only at an extreme dilution where $1/\kappa > R$, it is appropriate to assume that the bolaform ion is divalent and that the ion atmosphere is spherically symmetric. R is the charge distance of sulfonate ion and κ has the usual meaning. Atkinson, Yokoi and Hallada[1] explained the electrolytic conductances of *m*-Na_2BDS in aqueous solution by means of the Fuoss-Onsager equation for the spherical 2 : 1 strong electrolyte. The concentration range of their experiments was $0 \sim 45 \times 10^{-4}$ mol/l. At the concentration 45×10^{-4} mol/l, $1/\kappa$ is 26 A, thus $1/\kappa > R$. However, under experimental conditions of most diffusion measurements, we have $1/\kappa < R$, as the concentration range is 0,01~0,2 mol/l (the concentrations corresponding to 4.6 and 7 A are 0.145 and 0.0629 mol/l, respectively). Under these conditions, Eq. (1) does not hold. Thus, it is a reasonable to assume that the ion atmosphere about each charge is almost independent. Rice[9] showed that the electrophoretic effect for a bolaform ion was just twice that for an oridnary ion. The absolute value of this additional retarding effect increases with increasing concentration. However, Figs. 1 and 2 show that the effect of Δ_1 in Eq. (1) is overestimated. Thus Rice's theory not hold either, in which the retarding effect based on the asymmetry of the ion atmosphere is added to Δ_1 of Eq. (1).

In the diffusion of a single electrolyte, cation and anion should diffuse with the same final velocity. When the ion atmosphere about each ionized group is almost independent at the concentration $1/\kappa < R$, the motion of bolaform electrolyte approximates that of 1 : 1 electrolyte. Therefore, it is postulated that the electrophoretic effect on the bolaform electrolyte is the same as that on 1 : 1 electrolyte. For 1 : 1 electrolyte, this effect is expressed by the following relation.

$$\Delta_1 = -8.07 \times 10^{-6} \frac{(\lambda_1^0 - \lambda_2^0)^2}{\lambda_0^2} \cdot \frac{\sqrt{c}}{1+\kappa a} \qquad (8)$$

Thus, Δ_1 of the right hand side in Eq. (1) should be expressed by Eq. (8) under the condition $1/\kappa < R$.

Generally, the absolute value of Δ_1 for 1 : 1 electrolyte is small.[8] As an example, the value of λ_2^0 is 49.0 cm^2 ohm^{-1} $equiv^{-1}$ for methanesulfonate ion,[10] of which EDS ion consists, and the value of Δ_1 for sodium methanesulfonate (NaMS) is in the order of 10^{-10} from Eq. (8). Under the condition $1/\kappa < R$, the values of Δ_1 for the other sulfonates will be in the same order as that of NaMS, and can be neglected in comparison with D_0 in Eq. (1) (the value of D_0 is in the order of 10^{-5}). Thus Eq. (1) becomes the following Nernst-Hartley equilation.

$$D = D_0\left(1 + c\frac{\mathrm{d}\ln y}{\mathrm{d}c}\right) \qquad (9)$$

We see from Figs 1 and 2 that the values calculated from Eq. (9) lie nearer the experimental values than that of Eq. (1). The calculated value for *m*–Na_2BDS agrees with the experimental value. Thus it is clear that the concentration dependence of diffusion coefficient of bolaform electrolyte with long R is smaller than that of bolaform electrolyte with short R, as κ^2 is proportional to the concentration of electrolyte.

The frictional coefficient of non-spherical molecule depends on the size and shape. In the case of bolaform ion, the frictional coefficient is also affected by the ionic atmosphere. A rod like bolaform ion such as aliphatic sulfonate ion behaves like a monovalent ion, under the conditions where the ion atmosphere about each charge is almost independent. Therefore, the frictional coefficient of bolaform ion decreases, and the value of D_0 in Eq. (9) increases. Hence, the calculated value from Eq. (9) approaches

9) S. A. Rice, *J. Amer. Chem. Soc.*, **80**, 3207 (1958).
10) L. R. Dawson, M. Golben, G. R. Leader, and H. K. Zimmerman Jr., *J. Phys. Colloids Chem.*, **55**, 1499 (1951).

more closely the experimental value. Due to the bulkiness of molecule the frictional coefficient of aromatic sulfonate ion is little affected by the asymmetry of the ion atmosphere. The difference between Fig. 1 and 2 is thus accounted for.

The diffusion coefficient of a bolaform electrolyte will always be larger than the diffusion coefficient of a corresponding ordinary 2 : 1 electrolyte not in line with Rice's theory.

The author thanks Dr. Hatsuho Uedaira for helpful discussions, and Dr. S. Tomita, National Chemical Laboratory for Industry, for the use of a Spinco Model H.

BULLETIN OF THE CHEMICAL SOCIETY OF JAPAN, VOL. 46, 404—407 (1973)

The Molecular Structure of Antimony Trichloride as Determined by Gas-electron Diffraction[1)]

Shigehiro KONAKA and Masao KIMURA

Department of Chemistry, Faculty of Science, Hokkaido University, Sapporo

(Received July 11, 1972)

The molecular structure and mean amplitudes of $SbCl_3$ have been determined, by the sector-microphotometer method of gas-phase electron diffraction, to be as follows: r_g(Sb–Cl)=2.333±0.003 Å, r_g(Cl–Cl)=3.50±0.02 Å, θ_α=97.2°±0.9°, l(Sb–Cl)=0.063±0.004 Å, and l(Cl–Cl)=0.147±0.014 Å. The zero-point average structure derived from the diffraction results by the use of the estimated potential constants is consistent with the rotational constants, B_z, derived from the B_0 of microwave measurements. The joint use of the ED and MW data has given a value of 2.326±0.001 Å for r_z(Sb–Cl).

Some regularities exist among the molecular structures of trihalides of the Vb-group elements.[2–5)] That is, the experimental bond length is generally shorter than the sum of the covalent radii by an amont which can be related to the difference between the electronegativities of the central atom and the halogen. Valence angles increase with a decrease in the electronegativities of halogens relative to the Vb-group atom.

The molecular structure of antimony trichloride was previously investigated by the visual method of electron diffraction (ED)[6,7)] and by microwave spectroscopy (MW)[8)] (Table 1). The reported uncertainties in the MW structure are much smaller than those in the visual ED data. However, the bond angle given by MW seems to be too large by 2 or 3 degrees, whereas the bond length is reasonable, as judged from the trend found in the structures of many trihalides of the Vb-group atoms (see Figs. 3 and 4 of Ref. 4).

TABLE 1. PREVIOUS RESULTS ON THE MOLECULAR STRUCTURE OF $SbCl_3$

	r(Sb–Cl)	θ(ClSbCl)
ED(visual)[a)]	2.37 ±0.02 Å	104° ±2°
ED(visual)[b)]	2.37 ±0.02 Å	96° ±4°
MW[c)]	2.325±0.005 Å	99.5°±1.5°

a) Ref. 6 b) Ref. 7 c) Ref. 8

The present study was undertaken in order to determine the geometry of this molecule more accurately by the sector-microphotometer method of ED. At just the same time, Matsumura[9)] reinvestigated the microwave spectra and obtained the rotational constants, B_0, for $^{121}Sb^{35}Cl_3$ and $^{123}Sb^{35}Cl_3$, which were very close to the previous values, and also the B_0 values for $^{121}Sb^{37}Cl_3$ and $^{123}Sb^{37}Cl_3$, which had not been measured before. The structure determined from these rotational constants is: r_0(Sb–Cl)=2.323±0.005 Å and θ(ClSbCl)=96°50′±30′.[9)] The bond length is essentially equal to the previous MW value, but the angle is not. This structure is in fair agreement with the existing regularities in relation to the structures of related molecules.

In the present report, an electron-diffraction determination of the thermal average structure will be described. Furthermore, the consistency between the ED and MW data will be examined and the zero-point average structure will be derived by the joint use of both sets of data.

Experimental

A sample of antimony trichloride (over 99% pure) obtained from Wako Pure Chemical Industries, Inc., was used without further purification. Electron-diffraction photographs were

1) S. Konaka and M. Kimura, Presented at the Annual Meeting of the Chemical Society of Japan, Tokyo, April, 1970.
2) Y. Morino, K. Kuchitsu, and T. Moritani, *Inorg. Chem.*, **8**, 867 (1969).
3) F. B. Clippard, Jr., and L. S. Bartell, *ibid.*, **9**, 805 (1970).
4) S. Konaka and M. Kimura, This Bulletin, **43**, 1693 (1970).
5) K. Kuchitsu, "Gas Electron Diffraction, Combined Use of Electron-Diffraction and Spectroscopic Methods for Determining Molecular Geometry and Motions", MTP International Review of Science, A Biennal Series, G. Allen, Ed., 1972.
6) A. H. Gregg, G. C. Hampson, G. I. Jenkins, P. L. F. Jones, and L. E. Sutton, *Trans. Farad. Soc.*, **33**, 852 (1937).
7) S. M. Swingle, quoted by P. W. Allen and L. E. Sutton, *Acta Crystallogr.*, **3**, Pt. 1, 46 (1950).
8) P. Kisliuk and C. H. Townes, *Phys. Rev.*, **83**, 210 (1951).
9) C. Matsumura, Presented at the Annual Meeting of the Chemical Society of Japan, Tokyo, April, 1970.

taken with a diffraction unit employing an r^3-sector[10] and a high-temperature nozzle made of stainless steel[11] under the following conditions: camera length, 12.39 cm; accelerating voltage, about 42 kV; exposure time, 3—4 minutes; electron-beam current, about 0.24 μA and nozzle temperature, about 70°C. The pressure in the diffraction chamber during exposures was about 7×10^{-5} Torr. Diffraction patterns of CS_2 molecules were taken at the same nozzle temperature just after taking the sample patterns in order to measure the scale factor accurately.[12]

Photographs were recorded on Fuji process hard plates and were developed at 20°C for 5 min with a FD-131 developer diluted twice. The photographic densities were measured with a digital microphotometer at intervals of 1/3 mm.[4] The densities were converted to intensities by using the relation[4] $E=D(1+0.03D)$; they were also corrected for the imperfection of the sector opening from an ideal r^3-shape. Seven plates, four for $SbCl_3$ and three for CS_2, taken in the same sequence of exposures, were selected for structure analysis.

Analysis of Data

The intensities were leveled by the theoretical backgrounds calculated by the use of the elastic and inelastic scattering factors taken from the literature.[13-15] The experimental backgrounds and molecular intensities were determined by using the criterion that there should appear no ghost peak in the range of $r\leqq1.05$ Å in the radial distribution curve, which was itself calculated in a manner described elsewhere.[4]

The interatomic distances, r_a(Sb-Cl) and r_a(Cl-Cl), the mean amplitudes, l(Sb-Cl) and l(Cl-Cl), and the index of resolution, k, were determined by a least-squares fitting of the experimental molecular intensities to the following theoretical expression:

$$qM(q) = k\sum_{i\neq j} A_{ij}\mu_{ij}\cos\Delta\eta_{ij}\exp\left\{-\frac{1}{2}\left(\frac{\pi}{10}q\right)^2 l_{ij}^2\right\} \times\sin\left\{\frac{\pi}{10}q\left(r_{aij}-\left(\frac{\pi}{10}q\right)^2\kappa_{ij}\right)\right\} \quad (1)$$

Here, all the notations follow usual usage.[16] The asymmetry parameter, κ_{Sb-Cl}, was estimated to be 1.2×10^{-5} Å^3 by the diatomic approximation[17] and was fixed in the least-squares analysis. The κ_{Cl-Cl} was ignored. The thermal average distances, r_g, were obtained as sums of r_a and l^2/r_a.

The experimental molecular intensity and the theoretical one calculated from the best-fit parameters are shown in Fig. 1.[18] The least-squares results are listed in Table 2. An error matrix is given in Table 3.

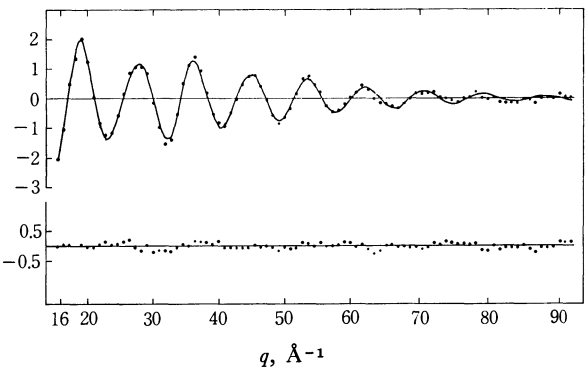

Fig. 1. Molecular intensity (dots for observed values and the solid curve for the best-fit theoretical intensity) and the residuals.

Table 2. Results of the least-squares analysis

	Average[a]	σ_1[b]	σ_2[b]
k	0.882	0.014	0.006
r_a(Sb-Cl)	2.3307	0.0010	0.0003
l(Sb-Cl)	0.0632	0.0017	0.0004
r_a(Cl-Cl)	3.4926	0.0072	0.0034
l(Cl-Cl)	0.1467	0.0054	0.0014

a) The averages of the results from four plates are listed.
b) The definitions of σ_1 and σ_2 are given in Ref. 19.

Table 3. Error matrix[a]

	k	r_a(Sb-Cl)	l(Sb-Cl)	r_a(Cl-Cl)	l(Cl-Cl)
k	231	9	72	66	71
r_a(Sb-Cl)		16	−1	2	7
l(Sb-Cl)			29	19	22
r_a(Cl-Cl)				118	9
l(Cl-Cl)					89

a) $\sigma_{ij}=\mathrm{sgn}[(\boldsymbol{B}^{-1})_{ij}][|(\boldsymbol{B}^{-1})_{ij}|\cdot\boldsymbol{V}^*\boldsymbol{P}\boldsymbol{V}/(n-m)]^{1/2}$, where the notations follow Ref. 19. Units for r_a and l are 10^{-4} Å and the index of resolution, k, is dimensionless.

Results and Discussion

The final results are summarized in Table 4, along with the limits of error estimated in the procedure described in a previous paper.[4] In order to derive a bond angle with a physically clear meaning,[20] the r_g distances were converted to the r_a distances by the following relation:[21,22]

$$r_a = r_g - \frac{\langle\Delta x^2\rangle+\langle\Delta y^2\rangle}{2r_e} - \delta r_{\mathrm{rot}} \quad (2)$$

10) Y. Murata, K. Kuchitsu, and M. Kimura, *Japan. J. Appl. Phys.*, **9**, 591 (1970).
11) M. Ogasawara and M. Kimura, unpublished.
12) The r_a(C-S) and r_a(S-S) distances at 70°C were estimated to be 1.5572 Å and 3.1080 Å, respectively, by the use of the spectroscopic constants taken from T. Ijima and Y. Morino, This Bulletin, **35**, 1661 (1962).
13) a) M. Kimura, S. Konaka, and M. Ogasawara, *J. Chem. Phys.*, **46**, 2599 (1967); b) M. Ogasawara, S. Konaka, and M. Kimura, *ibid.*, **50**, 1488 (1969).
14) C. Tavard, D. Nicolas, and M. Rouault, *J. Chim. Phys.*, **64**, 540 (1967).
15) R. F. Pohler and H. P. Hanson, *J. Chem. Phys.*, **42**, 2347 (1965).
16) S. Konaka, Y. Murata, K. Kuchitsu, and Y. Morino, This Bulletin, **39**, 1134 (1966).
17) K. Kuchitsu, *ibid.*, **40**, 505 (1967).
18) Numerical experimental data of the leveled total intensity have been deposited with the Chemical Society of Japan. A copy may be secured by citing the document number (Document No. 7303).
19) Y. Morino, K. Kuchitsu, and Y. Murata, *Acta Crystallogr.*, **18**, 549 (1965).
20) K. Kuchitsu, This Bulletin, **44**, 96 (1971).
21) K. Kuchitsu and S. Konaka, *J. Chem. Phys.*, **45**, 4342 (1966).
22) S. Konaka, This Bulletin, **43**, 3107 (1970).

TABLE 4. MOLECULAR PARAMETERS OF ANTIMONY TRICHLORIDE DETERMINED BY ED[a] (r AND l IN Å UNIT)

	Sb-Cl		Cl-Cl
r_g	$2.332_8 \pm 0.003_3$		3.499 ± 0.019
l	0.063 ± 0.004		0.147 ± 0.014
r_α	$2.328_7 \pm 0.003_3$		3.494 ± 0.019
θ_α(ClSbCl)		$97.2 \pm 0.9°$	
r_z	$2.324_8 \pm 0.004_2$		
θ_z(ClSbCl)		$97.2 \pm 1.0°$	

a) All parameters except for r_z and θ_z are given values at 343°K.

The stretchings due to the perpendicular thermal vibrations, $(\langle \Delta x^2 \rangle + \langle \Delta y^2 \rangle)/2r_e$, were calculated to be 0.0028 Å and 0.0020 Å for Sb–Cl and Cl–Cl respectively by using the harmonic potential constants estimated below.[22] The centrifugal stretchings, δr_{rot}, were evaluated to be 0.0013 Å and 0.0030 Å for Sb–Cl and Cl–Cl respectively.[23] The r_α-structure thus obtained is also given in Table 4.

The general quadratic potential field of a pyramidal XY_3-type molecule can be defined by using the following six potential constants associated with the internal symmetry coordinates, as has been described in a previous paper:[22]

$$\begin{aligned} F_{11} &= f_r + 2f_{rr}, \\ F_{12} &= f_{r\theta'} + 2f_{r\theta}, \\ F_{22} &= f_\theta + 2f_{\theta\theta}, \\ F_{33} &= f_r - f_{rr}, \\ F_{34} &= f_{r\theta'} - f_{r\theta}, \\ F_{44} &= f_\theta - f_{\theta\theta}. \end{aligned} \tag{3}$$

Since not all the potential constants can be determined uniquely from four vibrational frequencies, the experimental mean amplitudes were used as supplementary information. The fundamental frequencies measured in the liquid state[24] were used because those for the gas phase were not available. A sufficiently large number of sets of mean amplitudes were calculated from the potential fields compatible with the frequencies and compared with the observed mean amplitudes. The potential constants were then estimated to be as is shown in Table 5. The theoretical values of the mean amplitudes corresponding to the estimated potential constants were 0.062±0.006 Å and 0.134±0.008 Å for l(Sb–Cl) and l(Cl–Cl) respectively.

TABLE 5. POTENTIAL CONSTANTS OF $SbCl_3$ ESTIMATED FROM THE OBSERVED MEAN AMPLITUDES AND VIBRATIONAL FREQUENCIES (IN md/Å UNIT)

A_1 species		E species	
F_{11}	$2.0_6{}^{+0.2}_{-0.4}$[a]	F_{33}	$1.5_0{}^{-0.2}_{+0.1}$
F_{12}	-0.1 ± 0.2	F_{34}	0.2 ± 0.1
F_{22}	$0.22^{-0.02}_{+0.10}$	F_{44}	$0.20^{+0.07}_{-0.03}$

a) The uncertainties take the upper and lower signs in the same order.

The molecular structure given in Table 4 is very close to the r_0-structure determined by a recent microwave study.[9] However, this may not necessarily indicate that both the MW and the ED data are consistent, for different definitions of the molecular parameters were used. In order to see the consistency of the data, the r_α-structure measured by ED was converted to the zero-point average structure (r_z) and the rotational constants observed by MW were reduced to the rotational constants, B_z, corresponding to the r_z-structure. The observed ground-state rotational constants are given in Table 6.

TABLE 6. GROUND-STATE ROTATIONAL CONSTANTS AND ZERO-POINT AVERAGE ROTATIONAL CONSTANTS (IN MHz UNIT)

	$^{121}Sb^{35}Cl_3$	$^{123}Sb^{35}Cl_3$	$^{121}Sb^{37}Cl_3$	$^{123}Sb^{37}Cl_3$
B_0[a]	1753.6_0	1750.0_4	1670.3_5	1667.0_0
B_z	1751.4_3	1747.8_7	1668.3_2	1664.9_7

a) Determined by Matsumura.[9]

The following relations were used for deriving r_z(Sb–Cl) from r_α(Sb–Cl):[21]

$$r_z \simeq r_\alpha - (\langle \Delta z \rangle_T - \langle \Delta z \rangle_0) \tag{4}$$

$$\langle \Delta z \rangle \simeq \langle \Delta r \rangle - \frac{\langle \Delta x^2 \rangle + \langle \Delta y^2 \rangle}{2r_e} \simeq \frac{3}{2} a_3 \langle \Delta z^2 \rangle - \frac{\langle \Delta x^2 \rangle + \langle \Delta y^2 \rangle}{2r_e} \tag{5}$$

The Morse parameter, a_3, was assumed to be 2 Å^{-1}. The parallel and perpendicular mean amplitudes were computed from the estimated potential constants, and the correction term, $\langle \Delta z \rangle_T - \langle \Delta z \rangle_0$, was evaluated to be $0.003_9 \pm 0.002_5$ Å. On the other hand, the difference in bond angles, $(\theta_z - \theta_\alpha)$, was simply assumed to be $0 \pm 0.3°$.[25,26] The zero-point average structure thus estimated is also shown in Table 4.

The B_z values were derived from the B_0's as:[5]

$$B_z = B_0 - \delta B_{vib} - \delta B_{cent} \tag{6}$$

The sums of δB_{vib} and δB_{cent} were estimated, according to the theory of rotation-vibration interaction,[27,28] to be 2.17±0.11 MHz and 2.03±0.10 MHz for (^{121}Sb, ^{123}Sb)$^{35}Cl_3$ and (^{121}Sb, ^{123}Sb)$^{37}Cl_3$ respectively. The B_z values are also listed in Table 6.

In Fig. 2, the relation between r_z(Sb–Cl) and θ_z(ClSbCl), constrained by zero-point average rotational constants, are shown by four lines. The rectangle denotes the limits of the molecular structure determined by ED. The average structure corresponding to the crossing point of the MW lines is: $r_z = 2.324_8$ Å and $\theta_z = 96.2°$. This is slightly different from the r_0-structure,[9] $r_0 = 2.323 \pm 0.005$ Å and $\theta = 96°50' \pm 30'$. The MW bond angle appears to be about 1° smaller

23) M. Iwasaki and K. Hedberg, *J. Chem. Phys.*, **36**, 2961 (1962).
24) A. T. Kozulin and L. V. Biryulina, *Opt. Spectrosc.*, **28**, 135 (1970).
25) T. Moritani, K. Kuchitsu, and Y. Morino, *Inorg. Chem.*, **10**, 344 (1971).
26) K. Kuchitsu, T. Shibata, A. Yokozeki, and C. Matsumura, *ibid.*, **10**, 2584 (1971).
27) W. H. Shaffer, *J. Chem. Phys.*, **9**, 607 (1941).
28) H. H. Nielsen, *Rev. Mod. Phys.*, **23**, 90 (1951).

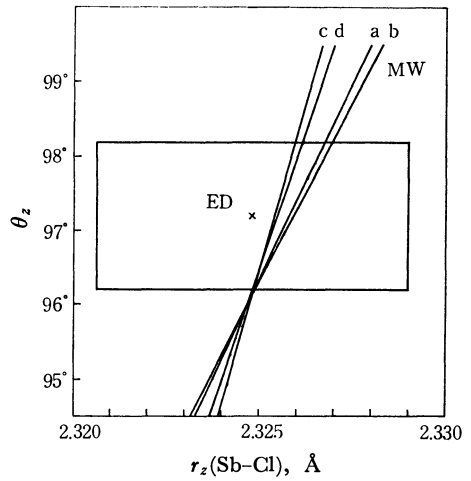

Fig. 2. The zero-point average structure obtained by ED and the relations given by the MW rotational constants (a): $^{121}Sb^{35}Cl_3$, (b): $^{123}Sb^{35}Cl_3$, (c): $^{121}Sb^{37}Cl_3$, (d): $^{123}Sb^{37}Cl_3$.

than the diffraction value, while the bond lengths from the two sets of data are in perfect agreement. However, it should be noted that the above MW structure is sensitive to a systematic error due to unknown isotopic shifts of the r_z-structure.[5] That is, the crossing point of the MW lines in Fig. 2 may shift remarkably even as a result of an isotope effect of r_z as small as 0.0003 Å. Since all the microwave lines pass near the center of the ED rectangle, we may conclude that the ED and MW data are consistent. By combining the ED valence angle with the MW lines, we can determine r_z(Sb–Cl) to be $2.325_9 \pm 0.001_1$ Å, which may be regarded as much more reliable and precise than the ED value. The corresponding r_g distance is 2.334± 0.003 Å.

The authors wish to thank Professor Takao Iijima for his helpful discussion and Mr. Makoto Ogasawara for his help in operating the high temperature nozzle. Numerical computations were performed on a FACOM 230—60 of the Hokkaido University Computing Center, to which the authors' thanks are also due.

BULLETIN OF THE CHEMICAL SOCIETY OF JAPAN, VOL. 46, 407—409 (1973)

Electron Diffraction Study of Dimethylmercury

Kuniaki KASHIWABARA,* Shigehiro KONAKA, Takao IIJIMA, and Masao KIMURA**

Department of Chemistry, Faculty of Science, Hokkaido University, Sapporo

(Received July 26, 1972)

Electron scattering by dimethylmercury has been studied for 42 keV electrons. The theoretical scattering factors currently used have shown satisfactory conformity to the observed scattering intensity, with the following distance parameters: r_g(Hg–C)=2.083±0.005 Å, r_g(Hg···H)=2.71±0.02 Å, and r_g(C–H)=1.106 Å (assumed). A comparison of the background functions has revealed that the scattering factors based on the relativistic Hartree-Fock-Slater potential are better than those based on the Thomas-Fermi-Dirac and Thomas-Fermi potentials. The zero-point average distance determined from the spectroscopic data has shown significant inconsistency with the diffraction result. The diffraction value is shorter than the spectroscopic one by 0.015 Å.

The phase-shift of complex atomic scattering factors in gas-phase electron diffraction has been a long-lasting topic in both theoretical and experimental studies.[1] For almost all the molecules investigated so far, theoretical predictions of the cut-off points have been in reasonable agreement with the experimental results, although the conclusions have sometimes been obscured by large experimental errors. However, a recent study of tetramethyllead has claimed that there was considerable inconsistency between the experimental results and the theory,[2] not only in the cut-off point but also in the background intensity. To prove or disprove the possibility that the inconsistency is inherent in the heaviest members of the atoms, dimethylmercury was chosen for the present study as a practically usable compound which showed closest kinship to tetramethyllead. The present study has disproved the possibility mentioned above, in accordance with the results of a similar study of mercuric chloride.[3]

The vibrational[4] and rotational spectra[5] indicate that the present molecule has a linear structure. As for the Hg–C bond length, Rao *et al.* have derived an r_0 value of 2.094±0.005 Å from the rotational constants,[5] whereas an earlier electron-diffraction study by Gregg *et al.* gave a value of 2.23±0.04 Å.[6] The present paper will, then, present a more accurate Hg–C distance determined by means of the current electron-diffraction technique.

* Present address: Chisso Polypropylene Fiber Industries, Ltd, Moriyama, Shiga.

** To whom correspondence should be addressed.

1) a) V. Schomaker and R. Glauber, *Nature*, **170**, 290 (1952); b) H. M. Seip, "Selected Topics in Structural Chemistry," Universitetsforlaget, Oslo (1967), pp. 26—68. c) M. Kimura, V. Schomaker, D. W. Smith, and B. Weinstock, *J. Chem. Phys.*, **48**, 4001 (1968).

2) T. Oyamada, T. Iijima, and M. Kimura, This Bulletin, **44**, 2638 (1971).

3) K. Kashiwabara, S. Konaka, and M. Kimura, *ibid.*, 46, 410 (1973).

4) H. S. Gutowsky, *J. Chem. Phys.*, **17**, 128 (1949).

5) K. S. Rao, B. P. Stoicheff, and R. Turner, *Can. J. Phys.*, **38**, 1516 (1960).

6) A. H. Gregg, G. C. Hampson, G. I. Jenkins, P. L. F. Jones, and L. E. Sutton, *Trans Faraday Soc.*, **33**, 852 (1937).

The rotational constants obtained by Raman spectroscopy[5] were corrected for the vibrational effect, and the zero-point structure was compared with the diffraction results. There was a disparity in the Hg–C distances, which, unfortunately, was left unsettled.

Diffraction Experiment and Analysis

The sample of dimethylmercury was purchased from the K&K Co., Inc., U. S. A., and was used without further purification. The diffraction experiment and the data analysis were carried out by our routine procedure of the sector-microphotometer method.[7] The experimental conditions were as follows: accelerating voltage,~42 kV; camera length, 244.3 mm; electron beam current, ~0.07 μA; sample pressure, 40 Torr, and exposure times, 20—30 sec. The photographs were taken at room temperature. Carbon disulfide was used as the reference substance to calibrate the scale factor. The data covered the range of q= 8—63.

Background Intensities. Two sets of scattering factors for mercury were used in the analysis:

a) The Thomas-Fermi-Dirac(TFD)-based elastic scattering factors[8] and the Thomas-Fermi(TF)-based inelastic scattering factors.[9]

b) The relativistic Hartree-Fock-Slater(RHFS)-based elastic and Hartree-Fock(HF)-based inelastic scattering factors.[10]

For carbon and hydrogen atoms, the HF-based elastic[8] and inelastic scattering factors[11] were used.

The total intensities leveled by the theoretical background function are shown in Fig. 1.[12] The overall consistency between the theoretical and observed background intensities may be regarded as satisfactory, irrespective of the scattering factors employed. However, a close examination in the smaller q region reveals that the discrepancy between the theoretical and observed intensities is much less for the set b than for the set a. This improvement due to the use of the set b was more markedly observed in the region of still smaller q, $q \leqq 8$, by means of a counting method. The small angle scattering by dimethylmercury and other molecules containing heavy atoms will be reported in a forthcoming paper.[13]

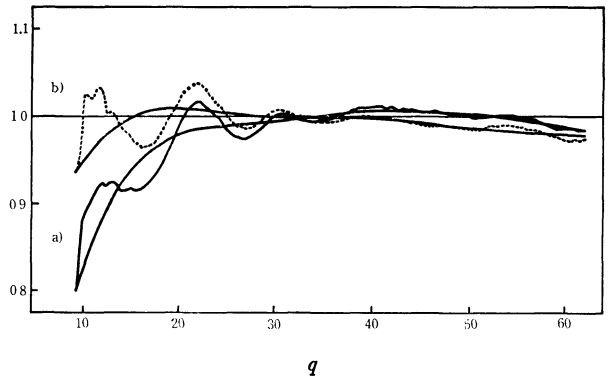

Fig. 1. The leveled total intensity. a): The set a of scattering factors was used, b): The set b was used. (see Text)

Molecular Structure. The bond distances were determined by a least-squares adjustment for the molecular intensity. Since the scattering power of the mercury atom is predominant, it is impracticable to determine the bond distances between light atoms. Thus, only the Hg–C and Hg···H distances were adjusted. The C–H distances were assumed to be 1.100 Å in r_a, and the other non-bonded distances, C···C, intramethyl H···H, and C···H, were constrained in r_α-parameters by assuming a linear structure. The intermethyl H···H distances were ignored, as the large mean amplitude caused by the nearly free rotation of the methyl tops[14] in addition to the small scattering power of hydrogen, makes the contribution from these terms less significant.

All the mean amplitudes were fixed at the values shown in Table 1, which were calculated by the use of the force constants determined by Miles *et al.*[15] The perpendicular amplitudes and the shrinkage corrections were also calculated as listed in Table 1. The calculated values of the parallel mean amplitudes are consistent with those given by Bribes and Gaufrès.[16] The torsional motion was neglected in these calculations. The r_α-values should, therefore, be interpreted as representing the average configuration where the torsional motion is frozen. The asymmetry parameters, κ, was estimated in the same way as in the previous paper.[2]

The results of the least-squares adjustment for the four best plates are summarized in Table 2. The indices of resolution were in the range of 0.86—1.05.

TABLE 1. MEAN AMPLITUDES AND SHRINKAGE CORRECTIONS OF DIMETHYLMERCURY AT 293 K (IN 10^{-4} Å UNITS)

	l_a	$r_a - r_\alpha$
Hg-C	551	34
Hg···H	1205	38
C···C	772	−13
C-H	785	102
C···H	1475	−27
H···H	1278	72

7) a) S. Konaka and M. Kimura, This Bulletin, **43**, 1693 (1970); b) H. Fujii and M. Kimura, *ibid.*, **43**, 1933 (1970).

8) a) M. Kimura, S. Konaka, and M. Ogasawara, *J. Chem. Phys.*, **46**, 2599 (1967); b) M. Ogasawara, S. Konaka, and M. Kimura, *ibid.*, **50**, 1488 (1969).

9) a) L. Bewilogua, *Phys. Z.*, **32**, 740 (1931); b) R. F. Pohler and H. P. Hanson, *J. Chem. Phys.*, **42**, 2347 (1965).

10) a) L. Schäfer, A. C. Yates, and R. A. Bonham, *ibid.*, **55**, 3055 (1971); b) D. T. Cromer, *ibid.*, **50**, 4857 (1969).

11) C. Tavard, D. Nicolas, and M. Rouault, *J. Chim. Phys.*, **64**, 540 (1967).

12) Numerical experimental data of the leveled total intensity by use of the set b scattering factors have been deposited with the Chemical Society of Japan. A copy may be secured upon request by citing the document number (Document No. 7304).

13) M. Kimura, S. Konaka, M. Nagashima and K. Kashiwabara, Proceedings of the 9th International Congress of Crystallography, Kyoto (September, 1972). *Chem. Phys. Lett.*, in press.

14) a) D. R. Boyd, H. W. Thompson and R. L. Williams, *Discuss. Faraday Soc.*, **9**, 154(1950); b) J. L. Bribes and R. Gaufrès, *Compt. Rend. Acad. Sci. Paris*, **C266**, 584 (1968).

15) M. G. Miles, J. H. Patterson, C. W. Hobbs, M. J. Hopper, J. Overed, and R. S. Tobias, *Inorg. Chem.*, **7**, 1721 (1968).

16) J. L. Bribes and R. Gaufrès, *J. Mol. Structure*, **9**, 423 (1971).

Table 2. Bond distances of dimethylmercury (in Å units)

	r_g	σ_1	σ_2	Limit of error
Hg–C	2.083	0.004	0.002	0.005
Hg···H	2.712	0.014	0.003	0.018
C–H	1.106	(assumed)		

The results shown in Table 2 were obtained by the use of the RHFS and HF scattering factors (set b), since they were considered to be better expressions of the true scattering factors, because of the better agreement of the experimental background with the theoretical one as well as the theoretical sophistication of the atomic potential itself. The best-fit theoretical molecular intensity is shown in Fig. 2, along with the observed values and the residuals. The agreement is satisfactory.

The use of the set a instead of the set b produced longer Hg–C and Hg···H distances by 0.005 Å and 0.009 Å respectively, with standard deviations similar to those for the set b. The indices of resolution were 0.94—1.13.

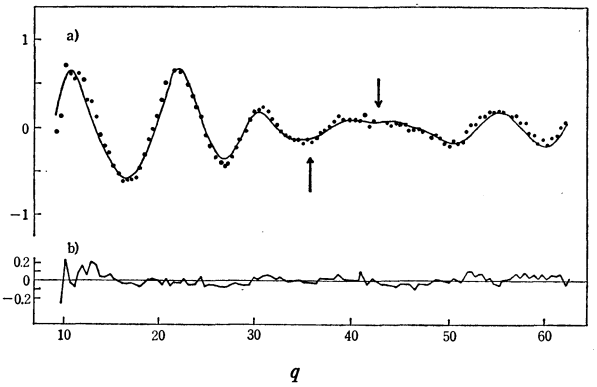

Fig. 2. a) The molecular intensity calculated by the best-fit model (solid curve). Dots are the observed values. The arrows indicate the theoretical cut-off points, $q^c_{Hg\cdots H}=35.8$ and $q^c_{Hg-C}=42.8$.

Zero-point Average Structure

The rotational constants of the normal and fully-deuterated species were observed by Rao *et al.*[5] The moments of inertia were corrected for the vibrational effect by the one-top formalism, which was reported elsewhere.[17] The effective and zero-point moments of inertia are listed in Table 3. The vibrational correction is relatively small for the *b*-constant of this molecule.

The zero-point average distance, r_z(Hg–C), was determined from the zero-point moments of inertia to be 2.095±0.006 Å. A relation between r_z(C–H) and ϕ_z(HCH) was also obtained, although neither of them can be determined separately. If, for instance, r_z(C–H) is assumed to be 1.096 Å, ϕ_z(HCH) can then be evaluated as 109°20′. The r_z(Hg–C) is insensitive to the possible isotope effect in the structure parameters of the methyl top as long as the effect is confined within reasonable limit.

17) T. Iijima and S. Tsuchiya, *J. Mol. Spectrosc.*, **44**, 88 (1972).

Table 3. Moments of inertia of dimethylmercury (in amu Å² units)

	I_b^{eff} a)	ΔI_b b)	$I_b^{(z)}$ c)
Normal	145.06±0.13	0.17	145.23
d_6-species	184.83±0.20	0.21	185.04

a) Observed by Rao *et al.* Ref. 5. b) Vibrational corrections. c) Zero-point moments of inertia.

The r_g distance obtained by the diffraction experiment was converted to the r_α^0 distance which can be compared with the r_z value.[18] The value of r_α^0 thus obtained was 2.080±0.005 Å, which shows a significant difference from the spectroscopic r_z value. This is equivalent to the fact that the B_0(ED) is larger than B_0(Raman) by about 1%. A similar amount of disparity in B_0 was observed by Tanimoto *et al.*[19] in the case of diacetylene and was elucidated by taking the bending-stretching interaction into account. Dimethylmercury also has a low-lying bending mode (~160 cm^{-1}). However, the same treatment applied to the present molecule would require a negative interaction constant, in contradiction to the cases of diacetylene and several linear molecules.[19]

It may be worth considering that the Raman B_0 value might be obscured by overlapping hot bands, as was pointed out by Maki in the case of cyanogen.[20] The effect of the overlapping of bending hot bands is, however, in the direction of increasing the disparity in the present results. Besides the effects of hot bands due to vibrationally-excited states, the effect of the rotation-torsion-vibration coupling seems to be important. At least, with regard to the infrared rotation-vibration bands, it was suggested by Kirtman that such a treatment would be promising in order to study some anomalous features of the spectra.[21]

Judging from the recorded readings of monitoring accelerating voltages there was no indication that the scale factor of the present experiment contained an exceptionally large error.

Numerical computations were carried out on a FACOM 230—60 of the Hokkaido University Computing Center and also on a FACOM 270—20 of the laboratory of Professor Kimio Ohno, whom the authors wish to thank for allowing them to use the facilities.

18) K. Kuchitsu, *J. Chem. Phys.*, **49**, 4456 (1968).
19) M. Tanimoto, K. Kuchitsu, and Y. Morino, This Bulletin, **44**, 386 (1971).
20) A. G. Maki, *J. Chem. Phys.*, **43**, 3193 (1965).
21) B. Kirtman, *ibid.*, **41**, 775 (1964).

Electron Diffraction Investigation of Gaseous Mercury(II) Chloride

Kuniaki KASHIWABARA*, Shigehiro KONAKA, and Masao KIMURA**

Department of Chemistry, Faculty of Science, Hokkaido University, Sapporo

(Received July 26, 1972)

The molecular structure of mercury(II) chloride has been determined by the sector-microphotometer method of gas-phase electron diffraction at accelerating voltages of 29 and 42 kV. The parameter values obtained are: r_g(Hg–Cl), 2.252±0.005 Å; l(Hg–Cl), 0.052±0.005 Å; r_g(Cl–Cl), 4.48±0.04 Å; and l(Cl–Cl), 0.09±0.04 Å. A linear structure has been confirmed within an error of 16°. The experimental mean amplitudes are consistent with the estimated values based on the spectroscopic data. No appreciable differences in the structure parameters have been found between the results of analysis carried out on the basis of the Thomas-Fermi-Dirac and the relativistic Hartree-Fock-Slater scattering factors.

Mercuric chloride has $D_{\infty h}$ symmetry in the normal state. The electronic[1] and vibrational spectra[2–4] measured in the gas phase and the result of mass-spectrometric observation[5] are all consistent with this symmetry. In earlier electron diffraction studies by means of the visual method,[6–8] the bond angle was not observed because of the relatively weak scattering power of the Cl–Cl atom pair. Later, Akishin *et al.* confirmed the linear structure within an error of 40°.[9] The bond lengths reported previously are 2.28,[6] 2.34±0.01,[7] 2.27±0.03,[8] and 2.29±0.02 Å,[9] all involving large uncertainties.

It has been known that the scattering theory based on the first Born approximation is insufficient for the interpretation of the diffraction patterns of about 40 keV electrons by molecules containing both heavy and light atoms. An improvement of the scattering theory has been made by replacing the Born-approximation atomic scattering factors by the complex scattering factors calculated by the partial-waves method.[10] The use of such complex scattering factors is essential for a precise structure analysis of such a molecule as $HgCl_2$, because phase factors have a large effect on the molecular scattering intensity. The complex scattering factors for heavy atoms have been calculated from the Thomas-Fermi-Dirac (TFD) potential[11] and also recently, from the relativistic Hartree-Fock-Slater (RHFS)[12] and the SCF Hartree-Fock (SCF HF)[13] wavefunctions. In a recent work on $Pb(CH_3)_4$, an appreciable discrepancy has been found between the theoretical and observed scattering intensities;[14] in connection with this, further investigations have been desired into the scattering factors for heavy atoms. An improvement of the scattering theory has also been made by adding intramolecular multiple scattering to the simple kinematical framework of the theory.[15] For linear molecules, however, the multiple scattering does not give interference terms dependent on the internuclear distances, at least, not in the first order approximation.[15]

The purposes of the present study are to determine the structure more accurately by the sector-microphotometer method of electron diffraction, to examine the adequacy of the reported scattering factors for mercury, and at the same time, to see whether or not the use of two sets of available scattering factors for mercury produces any difference in the results of analyses. Since the scattering factors are dependent on the accelerating voltage, diffraction photographs were taken at two different voltages, 29 and 42 kV.

Experimental

Research-grade mercuric chloride (about 99.5% pure) obtained from Wako Pure Chemical Industries, Inc., was used as the sample. A high-temperature nozzle[16] made of stainless steel was used to obtain a sufficient vapor pressure. Diffraction patterns were taken on Fuji process hard plates by using an r^3-sector with a diffraction unit which has been described elsewhere.[17] Three sets of experimental data were taken under the conditions shown in Table 1. The accelerating voltages were stabilized within 0.01%. Carbon disulfide was used as the reference material for the determination of the scale factors except for a set of plates taken at 29 kV and at a camera length of 25.89 cm. This set of data was scaled so that the molecular scattering intensities became

* Present address: Chisso Polypropylene Fiber Industries, Ltd., Moriyama, Shiga.

** To whom correspondence should be addressed.

1) a) M. Wherli, *Helv. Phys. Acta*, **11**, 339 (1938); **13**, 153 (1940); b) H. Sponer and E. Teller, *Rev. Mod. Phys.*, **13**, 75 (1941).

2) H. Braune and G. Engelbrecht, *Z. Phys. Chem.*, **B19**, 303 (1932).

3) W. Klemperer and L. Lindeman, *J. Chem. Phys.*, **25**, 397 (1956).

4) W. Klemperer, *J. Electrochem. Soc.*, **110**, 1023 (1963).

5) A. Büchler, J. L. Stauffer, and W. Klemperer, *J. Chem. Phys.*, **40**, 3471 (1964).

6) H. Braune and S. Knoke, *Z. Phys. Chem.*, **B23**, 163 (1932).

7) A. H. Gregg, G. C. Hampson, G. I. Jenkins, P. L. F. Jones, and L. E. Sutton, *Trans. Faraday Soc.*, **33**, 852 (1937).

8) L. R. Maxwell and V. M. Moseley, *Phys. Rev.*, **57**, 21 (1940).

9) P. A. Akishin, V. P. Spiridinov, and A. N. Khodchenkov, *Zhur. Fiz. Khim.*, **33**, 20 (1959).

10) a) J. A. Hoerni and J. A. Ibers, *Phys. Rev.*, **91**, 1182 (1952). b) J. A. Ibers and J. A. Hoerni, *Acta Crystallogr.*, **7**, 405 (1954).

11) a) M. Kimura, S. Konaka, and M. Ogasawara, *J. Chem. Phys.*, **46**, 2599 (1967); b) M. Ogasawara, S. Konaka, and M. Kimura, *ibid.*, **50**, 1488 (1969).

12) L. Schäfer, A. C. Yates, and R. A. Bonham, *ibid.*, **55**, 3055 (1971).

13) D. T. Cromer, *ibid.*, **50**, 4857 (1969).

14) T. Oyamada, T. Iijima, and M. Kimura, This Bulletin, **44**, 2638 (1971).

15) a) P. J. Bunyan, *Proc. Phys. Soc. London*, **82**, 1051 (1963); b) J. Gjønnes, *Acta Crystallogr.*, **17**, 1075 (1964); c) J. W. Liu and R. A. Bonham, *J. Mol. Structure*, **11**, 297 (1972). d) L. S. Bartell and T. C. Wong, *J. Chem. Phys.*, **56**, 2364 (1972).

16) M. Ogasawara and M. Kimura, Symposium on Molecular Structure, Chemical Society of Japan, October, 1967.

17) Y. Murata, K. Kuchitsu, and M. Kimura, *Jap. J. Appl. Phys.*, **9**, 591 (1970).

TABLE 1. EXPERIMENTAL CONDITIONS

Accelerating voltage (kV)	Camera length (cm)	Temperature (°C)	Beam current (μA)	Exposure time (min)	Observed range (q)	Number of plates
42	12.39	160—170	0.27	3—6	17—104	3
29	12.39	160—170	0.29	2—5	12—91	2
29	25.89	160—170	0.19	2—4	6—45	3

consistent with the interatomic distances determined by the other sets of data; it was used only for the examination of background intensities at small angles. The optical densities of the diffraction patterns, D, were measured with a digital microphotometer and were converted to the intensities, E, by assuming the relation, $E=D(1+0.03D)$, and the intensities were corrected for the imperfection of the sector shape.[18]

Analysis of Data

The elastic scattering factors for Hg and Cl used for the data analysis described in this section were those calculated by the partial-waves method based on the Thomas-Fermi-Dirac and the Hartree-Fock (HF) potentials respectively.[11] As for the inelastic scattering factors, the values based on the SCF HF wavefunction[13] and the HF potential[19] were used for Hg and Cl respectively. The 42 kV data were also analyzed using the RHFS elastic scattering factors for Hg, but no significant change was found in the result of analysis. This will be discussed in a later section.

The experimental scattered intensities were leveled by the theoretical background, to which the contribution from the elastic scattering factors for Hg is dominant. The experimental molecular intensities, $qM(q)$, were calculated as $q(I_T-I_B)/I_B$, where I_B is a smooth background drawn through the total intensity curve, I_T. The theoretical expression of $qM(q)$ is given by;

$$qM(q) = k\sum_{i\neq j} A_{ij}\mu_{ij}\cos(\Delta\eta_{ij})\exp\left\{-\frac{1}{2}\left(\frac{\pi}{10}q\right)^2 l_{ij}^2\right\} \times \sin\left\{\frac{\pi}{10}q\left(r_{aij}-\left(\frac{\pi}{10}q\right)^2\kappa_{ij}\right)\right\} \quad (1)$$

with the usual notations.[20]

The background curves were revised by the use of the non-negativity criterion for radial distribution curves. For this purpose, the following g_{ij} functions were chosen so as to fit theoretical $\mu_{ij}\cos(\Delta\eta_{ij})$.[18] For 42 kV:

$$g_{Hg-Cl} = 1.45\cos(0.0283q)$$

$$g_{Cl-Cl} = 2.2$$

and for 29 kV:

$$g_{Hg-Cl} = 1.45\cos(0.0326q)$$

$$g_{Cl-Cl} = 1.64\exp(-3.1\times10^{-4}q^2).$$

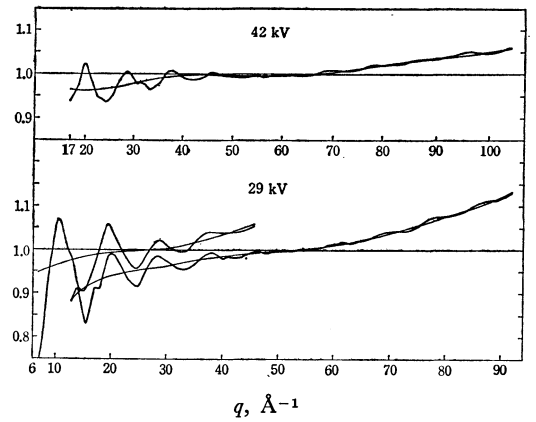

Fig. 1. Leveled total intensities and backgrounds.

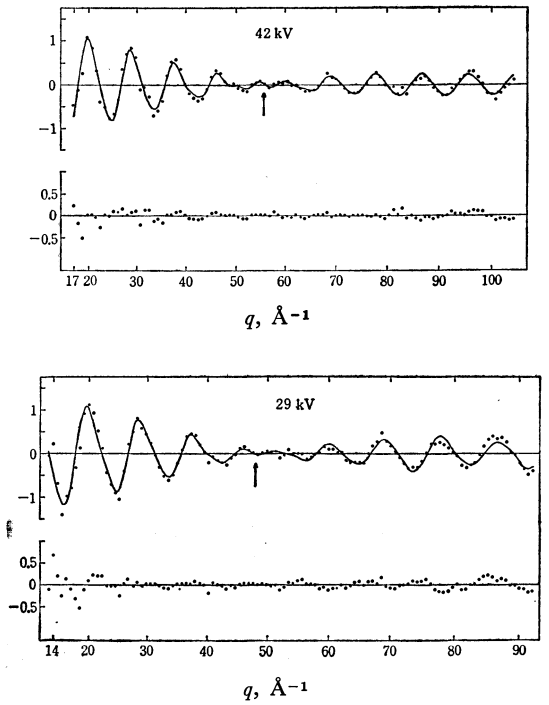

Fig. 2. Molecular intensities and the residuals.
Dots and solid curves show the observed values and the best-fit theoretical curves respectively. The arrows indicate the theoretical cut-off points based on the TFD scattering factors.

One of the leveled total intensities and its background thus obtained[21] are shown in Fig. 1 for each of the three combinations of accelerating voltage and camera length listed in Table 1.

The interatomic distances, r_a(Hg–Cl) and r_a(Cl–Cl), the mean amplitudes, l(Hg–Cl) and l(Cl–Cl), and the index of resolution, k, were determined by least-squares fittings of the experimental molecular intensities to

18) S. Konaka and M. Kimura, This Bulletin, **43**, 1693 (1970).
19) C. Tavard, D. Nicolas, and M. Rouault, *J. Chim. Phys.*, **64**, 540 (1967).
20) S. Konaka, Y. Murata, K. Kuchitsu, and Y. Morino, This Bulletin, **39**, 1134 (1966).
21) Numerical experimental data of the leveled total intensity have been deposited with the Chemical Society of Japan. (Document No. 7305).

TABLE 2. RESULTS OF THE LEAST-SQUARES ANALYSIS[a] (r_a AND l in Å UNITS)

		average	σ_1	σ_2
42 kV	k	0.852	0.023	0.028
	r_a(Hg-Cl)	2.2528	0.0018	0.0022
	r_a(Cl-Cl)	4.4720	0.0157	0.0192
	l(Hg-Cl)	0.0508	0.0019	0.0023
	l(Cl-Cl)	0.0777	0.0132	0.0162
29 kV	k	0.903	0.013	0.018
	r_a(Hg-Cl)	2.2501	0.0018	0.0026
	r_a(Cl-Cl)	4.4835	0.0200	0.0283
	l(Hg-Cl)	0.0540	0.0020	0.0024
	l(Cl-Cl)	0.0992	0.0166	0.0235

a) The weighted average of results from three plates for 42 kV and those from two plates for 29 kV are listed.

TABLE 3. Error matrix[a]

	r_a(Hg-Cl)	l(Cl-Cl)	r_a(Cl-Cl)	l(Cl-Cl)	k
r_a(Hg-Cl)	24	3	−3	−1	16
l(Hg-Cl)		26	10	18	69
r_a(Cl-Cl)			182	−17	37
l(Cl-Cl)				156	80
k					312

a) Elements of the matrix are given by $\sigma_{ij}=\mathrm{sgn}(B^{-1})_{ij}\{|(B^{-1})_{ij}|V'PV|/(N-m)\}^{1/2}$, where the notations follow Ref. 23. Units ($\times 10^{-4}$) for r_a and l are Å and the index of resolution, k, is dimensionless.

the theoretical expression with our conventional weighting scheme.[18] The asymmetry parameter, $\kappa_{\mathrm{Hg-Cl}}$, was fixed at an estimated value of 5.3×10^{-6} Å^3 in a diatomic approximation,[22] and the $\kappa_{\mathrm{Cl-Cl}}$ was assumed to be zero. The data analysis was made by using the computer program used for AsF_3.[18] The experimental molecular intensities, the theoretical curve calculated from the best-fit parameters, and the difference curves are shown in Fig. 2.

The results of the analyses are given in Table 2. An error matrix for a plate taken at 42 kV is given in Table 3. As may be seen in Table 2, the data at different accelerating voltages led to results consistent with each other. For the determination of the molecular parameters, the two results were averaged with weights inversely proportional to the squares of the limits of error, which were estimated from both random and systematic errors as follows. Since the standard deviations, σ_2, estimated from the fluctuations in the results are slightly larger than the standard errors, σ_1, as estimated by the least-squares treatment, $2.6\sigma_2$ was chosen as the random error corresponding to the 99% confidence interval.[18] The systematic error estimated for the interatomic distance includes the uncertainty in the scale factor and the errors associated with ambiguities in the κ values. For the means amplitudes, an error due to the uncertainty in the nozzle temperature was taken into account.

22) K. Kuchitsu, This Bulletin, **40**, 505 (1967).
23) K. Hedberg and M. Iwasaki, *Acta Crystallogr.*, **17**, 529 (1964).

TABLE 4. DISTANCES, MEAN AMPLITUDES AND SHRINKAGE (IN Å UNITS)

	r_g	l	δ_g
Hg-Cl	2.252±0.005	0.052±0.005	
			0.024±0.045
Cl-Cl	4.480±0.044	0.09±0.04	

Other systematic errors were ignored since they were estimated to be much smaller than the random error. The final results thus determined are listed in Table 4. The shrinkage, δ_g, given in this table was calculated as $2r_g$(Hg-Cl)$-r_g$(Cl-Cl).[24]

Discussion of the results

The mean amplitudes and shrinkage can be calculated from the vibrational frequencies according to an ordinary harmonic approximation.[24] The fundamental frequencies of $HgCl_2$ observed in the gas phase have been summarized by Klemperer *et al.* as follows[4,5]: ν_1, 360 cm^{-1} (the average of the frequencies from the Raman[2] and electronic spectra[1]); ν_2, 70 cm^{-1} (a value from the electronic spectra[1] which is close to the value of 71 cm^{-1} deduced by statistical thermodynamics[6]); and ν_3, 413 cm^{-1} (a value from the infrared spectra[3]). The values calculated from these frequencies at 165°C are as follows: l(Hg-Cl), 0.0506 Å; l(Cl-Cl), 0.0706 Å; and δ_g, 0.036 Å. They are consistent with the present experimental values. Since the bending frequency is very low, the above calculation might be insufficient for the l(Cl-Cl).[25] However, no further treatment was made because of the large experimental uncertainties in the mean amplitude and vibrational frequencies.

If we assume the shrinkage in this molecule to be 0.036 Å, then the bond angle in the r_a-structure[26] is found to equal 180°, within an uncertainty of 16°. The bond lengths obtained by the previous studies were too long, by from 0.02 to 0.09 Å.[6-9]

Figure 1 shows that the theoretical backgrounds based on the TFD scattering factor are in agreement with the experimental values within their uncertainties. Although the experimental backgrounds deviate by 10% or less from unity, the possibility of this amount of deviation being caused by extraneous scattering cannot ruled out judging from the shape of the leveled intensity and the observed indices of resolution. The agreement of the observed mean amplitude, l(Hg-Cl), with the theoretical one is another support for the adequacy of the scattering factors used. No significant deviations are seen between the observed and calculated molecular intensities as shown by the difference curves in Fig. 2; the agreement near the cut-off points, 55.8 Å^{-1} for 42 kV and 48.1 Å^{-1} for

24) S. J. Cyvin, "Molecular Vibrations and Mean Square Amplitudes," Universitetsforlaget, Oslo, and Elsevier Publishing Co., Amsterdam, 1968.
25) M. Tanimoto, K. Kuchitsu, and Y. Morino, This Bulletin, **43**, 2776 (1970).
26) Y. Morino, K. Kuchitsu, and T. Oka, *J. Chem. Phys.*, **36**, 1108 (1962).

29 kV in the q scale, is satisfactory for both accelerating voltages.

The data at 42 kV were also analyzed using the RHFS elastic scattering factor for Hg.[12] Since the calculated values are available only at 10, 40, 70 and 100 kV, the values for 42 kV were estimated by referring to the TFD values calculated at 40 and 42 kV. The theoretical cut-off point derived from the RHFS scattering factor is about 3 $Å^{-1}$ larger than that obtained from the TFD scattering factor.

The use of the RHFS scattering factor made the background curves in Fig. 1 closer to unity, and caused the index of resolution and mean amplitude, l(Hg–Cl), to decrease by 0.05 and 0.002 Å respectively. However, the magnitudes of the variations are within the experimental uncertainties or the limits of error. The other parameter values and their standard deviations were practically unchanged. In conclusion, both the TFD and the RHFS scattering factors are consistent with the results of the present experiment; they caused no significant difference in the results of the structure determination.

The authors wish to thank Professor Takao Iijima for his helpful discussions. The numerial computations were carried out on a FACOM 230—60 of the Hokkaido University Computing Center.

BULLETIN OF THE CHEMICAL SOCIETY OF JAPAN, VOL. 46, 413—416 (1973)

The Molecular Structure and Force Constants of Antimony Tribromide as Determined by Gas-phase Electron Diffraction

Shigehiro KONAKA and Masao KIMURA

Department of Chemistry, Faculty of Science, Hokkaido University, Sapporo

(Received July 28, 1972)

The molecular structure and mean amplitudes of $SbBr_3$ at 102°C have been determined by the sector-microphotometer method of gas-phase electron diffraction to be as follows: r_g(Sb–Br)=2.490±0.003 Å, r_g(Br–Br)=3.76±0.01 Å, θ_α=98.2°±0.6°, l(Sb–Br)=0.060±0.003 Å and l(Br–Br)=0.15±0.01 Å. General quadratic force constants have been determined from the observed mean amplitudes and vibrational frequencies. The molecular structure supports the validity of the empirical rules between a bond length and the covalent radii and electronegativities of its constituent atoms. An empirical equation, $\theta(YXY)=92+8x_X-3x_Y(+x_Z)$, has been proposed for the bond angles of Vb-group halides, $(Z)XY_3$, and the electronegativities, x.

Precise measurements of the molecular structures of simple inorganic compounds are essential to our understanding of chemical bonds. Recently, many of the molecular structure of trihalides of Vb-group atoms have been reinvestigated, and the regularity of the structures has been discussed in connection with the covalent radii and electronegativities.[1-4] However, we do have no up-to-date data on the molecular structures of several Vb-group trihalides.[3,4] The main purpose of the present study is to improve the structural data of antimony tribromide by the sector-microphotometer method of gas-phase electron diffraction. The structural parameters obtained by previous electron diffraction studies based on the visual method were: r(Sb–Br)=2.52±0.02 Å, θ(Br-SbBr)=96°±2°;[5] r(Sb–Br)=2.51±0.02 Å, and θ(Br-SbBr)=97°±2°.[6]

The general quadratic force field of antimony tribromide has not yet been reported. For its determination, some supplementary information in addition to the vibrational frequencies is required. Spectroscopic data, such as the Coriolis coupling or centrifugal distortion constants, are not available, but the vibrational mean amplitudes, as measured by electron diffraction, can be used for the force-field determination.[7-9] It is another purpose of the present study to determine the general force field of $SbBr_3$ by a combined use of the vibrational frequencies and the mean amplitudes.

Experimental

The sample of antimony tribromide was an extra-pure reagent obtained from Nakarai Chemicals, Inc. The sample was vaporized by using a high-temperature nozzle.[10] Diffraction photographs were taken on Fuji process hard plates with a diffraction unit equipped with an r^3-sector.[11] The experimental conditions were as follows: camera length, 12.39 cm; accelerating voltage, about 42 kV; exposure time,

1) Y. Morino, K. Kuchitsu, and T. Moritani, *Inorg. Chem.*, **8**, 867 (1969).
2) F. B. Clippard, Jr., and L. S. Bartell, *ibid.*, **9**, 805 (1970).
3) S. Konaka and M. Kimura, This Bulletin, **43**, 1693 (1970).
4) K. Kuchitsu, "Gas Electron Diffraction, Combined Use of Electron-Diffraction and Spectroscopic Methods for Determining Molecular Geometry and Motions," MTP International Review of Science, A Biennal Series, G. Allen, Ed., 1972.
5) A. H. Gregg, G. C. Hampson, G. I. Jenkins, P. L. F. Jones, and L. E. Sutton, *Trans. Farad. Soc.*, **33**, 852 (1937).
6) S. M. Swingle, quoted by P. W. Allen and L. E. Sutton, *Acta Crystallogr.*, **3**, Pt. 1, 46 (1950).
7) Y. Morino, Y. Nakamura, and T. Iijima, *J. Chem. Phys.*, **32**, 643 (1960).
8) M. Iwasaki and K. Hedberg, *ibid.*, **36**, 594 (1962).
9) S. Konaka, This Bulletin, **43**, 3107 (1970).
10) M. Ogasawara and M. Kimura, unpublished.
11) Y. Murata, K. Kuchitsu, and M. Kimura, *Japan. J. Appl. Phys.*, **9**, 591 (1970).

3—5 min; electron-beam current, about 0.28 μA; nozzle temperature, about 102°C. The pressure in the diffraction chamber during exposures was about 7×10^{-5} Torr. The diffraction patterns of CS_2 molecules were taken at the same nozzle temperature just after those of the sample in order to determine the scale factor accurately. The developing and photometric process were described in previous papers.[3,12] Eight plates, five for $SbBr_3$ and three for CS_2, taken in the same sequence of exposure, were selected for structure analysis.

Data Analysis

The intensities converted from the densities according to the $E=D(1+0.03\,D)$ relation were corrected for the imperfection of the sector shape and then leveled by means of the theoretical backgrounds.[13] The elastic and inelastic scattering factors were taken from the literature.[14-16] The experimental background and molecular intensities were determined according to our routine procedure.[3,12] The interatomic distances, r_a, the mean amplitudes, l, and the index of resolution, k, were determined by the least-squares fittings of experimental molecular intensities to the corresponding theoretical expression. The asymmetry parameter, κ_{Sb-Br}, was fixed at 1.1×10^{-5} Å^3, which was estimated by diatomic approximation,[17] and the κ_{Br-Br} was assumed to be zero.

The observed molecular intensity, $qM(q)$, and the theoretical one calculated by the use of best-fit parameters are shown in Fig. 1. The least-squares results are summarized in Table 1. An error matrix is given in Table 2. The thermal average distances, r_g, which were obtained as the sum of r_a and l^2/r_a, and the mean amplitudes are listed in Table 3, along with the estimated limits of error.

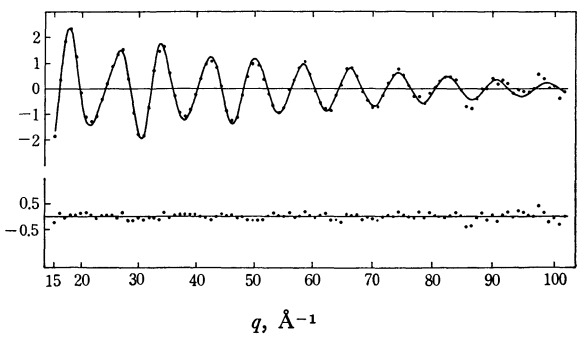

Fig. 1. Molecular intensity (dots for observed values and the solid curve for the best-fit theoretical intensity and the residuals.

Table 1. Results of the least-squares analysis (r and l in Å units)

	Average[a]	σ_1[b]	σ_2[b]
k	0.904	0.011	0.009
r_a(Sb-Br)	2.4882	0.0006	0.0004
l(Sb-Br)	0.0601	0.0008	0.0007
r_a(Br-Br)	3.7549	0.0044	0.0012
l(Br-Br)	0.1482	0.0033	0.0014

a) The averages of the results for five plates.
b) The definitions of σ_1 and σ_2 are given in Ref. 3.

Table 2. Error matrix[a]

	k	r_a(Sb-Br)	l(Sb-Br)	r_a(Br-Br)	l(Br-Br)
k	226	6	53	43	61
r_a(Sb-Br)		12	−1	3	3
l(Sb-Br)			17	10	14
r_a(Br-Br)				86	−5
l(Br-Br)					65

a) Units for r_a and l are 10^{-4} Å and that for the index of resolution k dimensionless.

Table 3. Molecular parameters of antimony tribromide at 375 K as determined by ED (r and l in Å units)

	Sb-Br	Br-Br
r_g	2.490±0.003	3.761±0.012
l	0.060±0.003	0.148±0.009
r_a	2.484±0.003	3.755±0.012
θ_a(BrSbBr)	98.2±0.6°	

Results and Discussion

Force Constants. In order to determine the quadratic force constants of antimony tribromide, the observed mean amplitudes were used together with the four fundamental frequencies measured in the liquid state.[18] The general quadratic force field can be expressed in terms of the symmetry coordinates as follows:[9]

$$2V = F_{11}S_1^2 + 2F_{12}S_1S_2 + F_{22}S_2^2 + F_{33}(S_{3a}^2+S_{3b}^2) + 2F_{34}(S_{3a}S_{4a}+S_{3b}S_{4b}) + F_{44}(S_{4a}^2+S_{4b}^2). \quad (1)$$

Here the symmetry coordinates are taken as:

$$S_1 = \frac{1}{\sqrt{3}}(\Delta r_1+\Delta r_2+\Delta r_3),$$

$$S_2 = \frac{1}{\sqrt{3}}r_e(\Delta\theta_{12}+\Delta\theta_{23}+\Delta\theta_{31}),$$

$$S_{3a} = \frac{1}{\sqrt{2}}(\Delta r_1-\Delta r_2),$$

$$S_{4a} = \frac{1}{\sqrt{2}}r_e(\Delta\theta_{23}-\Delta\theta_{31})$$

$$S_{3b} = \frac{1}{\sqrt{6}}(\Delta r_1+\Delta r_2-2\Delta r_3),$$

$$S_{4b} = \frac{1}{\sqrt{6}}r_e(\Delta\theta_{23}+\Delta\theta_{31}-2\Delta\theta_{12}),$$

12) S. Konaka and M. Kimura, This Bulletin, **46**, 404 (1973).
13) Numerical experimental data of the leveled total intensity has been deposited with the Chemical Society of Japan. A copy may be secured by citing the document number (Document No. 7306).
14) a) M. Kimura, S. Konaka, and M. Ogasawara, *J. Chem. Phys.*, **46**, 2599 (1967); b) M. Ogasawara, S. Konaka, and M. Kimura, *ibid.*, **50**, 1488 (1969).
15) C. Tavard, D. Nicolas, and M. Rouault, *J. Chim. Phys.*, **64**, 540 (1967).
16) R. F. Pohler and H. P. Hanson, *J. Chem. Phys.*, **42**, 2347 (1965).
17) K. Kuchitsu, This Bulletin, **40**, 505 (1967).
18) A. T. Kozulin and L. V. Biryulina, *Opt. Spectrosc.*, **28**, 135 (1970).

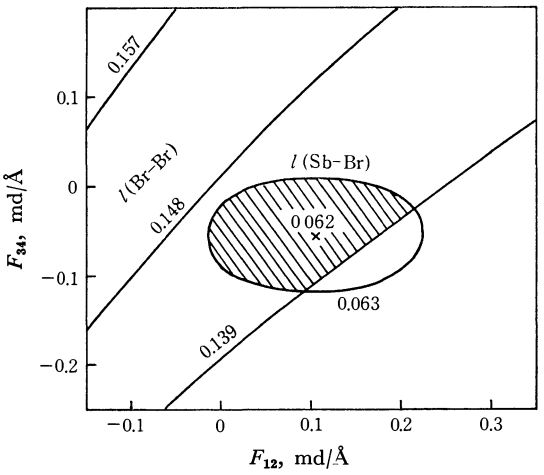

Fig. 2. Force constants of $SbBr_3$ allowed by the observed mean amplitudes at 375 K. An elliptical curve indicates the force constants giving the boundary of the observed value, 0.063 Å, for l(Sb-Br) and three parallel curves indicate those giving the observed value, 0.148 Å, and its boundary values, 0.157 Å and 0.139 Å, for l(Br-Br).

where Δr_i denotes the stretching of the i-th bond length; $\Delta\theta_{jk}$, the increase in the valence angle opposite to r_i, and r_e, the equilibrium bond length.

For given values of the off-diagonal force constants, F_{12} and F_{34}, the diagonal constants can be determined uniquely so as to reproduce the observed frequencies, under the condition that the stretching force constants, F_{11} and F_{33}, are larger than the bending ones, F_{22} and F_{44} respectively.[9] From the set of force constants, the corresponding mean amplitudes can be calculated. Figure 2 illustrates the force constants, F_{12} and F_{34}, allowed by the observed mean amplitudes. The shaded area denotes the force field compatible with all the experimental frequencies and mean amplitudes. The force constants thus determined are listed in Table 4.

Table 4. Force constants of $SbBr_3$ determined from the observed mean amplitudes and vibrational frequencies (in md/Å units)

	A_1 species		E species
F_{11}	1.72±0.17	F_{33}	1.33±0.07
F_{12}	0.10±0.11	F_{34}	−0.05±0.07
F_{22}	0.14±0.01	F_{44}	0.12±0.01

Structure. By using the above force constants, the r_g distances were converted to the r_α distances. The stretchings due to the perpendicular thermal vibrations were computed to be 0.0047 and 0.0021 Å for Sb–Br and Br–Br respectively. The calculated values for the centrifugal stretching were 0.0011 and 0.0034 Å for the bonded and non-bonded pairs respectively. The r_α distances and the corresponding bond angle are given in Table 3. Both the bond length (r_g) and the bond angle agree with the previous electron-diffraction values, obtained by the visual method, within their estimated limits of error.

The bond length of the trihalides of group-Vb elements, XY_3, can be given approximately by a modified Schomaker-Stevenson rule as:[4]

$$r_{X-Y} = r_X + r_Y - c|x_X - x_Y|.$$

Here, r_X and x_X are the covalent radius and the electronegativity of the X atom respectively, and c is an empirical constant which takes different values for the fluorides and the other halides.[4,19] In a previous paper,[3] the present authors proposed a slightly different empirical equation for the trihalides of group-Vb elements:

$$r_{X-Y} = r_X + r_Y - 0.06(x_X - x_Y)^2. \quad (4)$$

The Sb-Br distance estimated by Kuchitsu using Eq. (3) with c=0.04 Å is 2.51 Å,[4] while Eq. (4) gives a value of 2.49 Å for the covalent radii[20] and electronegativities[21] taken from the literature. Both are in agreement with the present observed value, 2.490 Å.

It has been found by recent experimental work[4] that the bond angles in the group-Vb-element trihalides generally decrease with an increase in the electronegativities of halogens relative to the central atoms, in accordance with the valence-shell electron-pair repulsion (VSEPR) theory proposed by Gillespie.[22] The observed bond angle in $SbBr_3$ confirms this finding, for it has a value between the angles in $SbCl_3$ and SbI_3, and smaller than those in PBr_3 and $AsBr_3$ (Table 5). The relationship between the bond angles and the electronegativities has been stated only qualitatively in previous studies. By examining the experimental data of the bond angles accumulated so

19) Equation (3) was originally proposed by Schomaker and Stevenson with c=0.09 Å as applicable to more general cases: V. Schomaker and D. P. Stevenson, *J. Amer. Chem. Soc.*, **63**, 37 (1941).

20) W. Gordy, W. V. Smith and R. F. Trambarulo, "Microwave Spectroscopy," John Wiley & Sons, Inc., New York (1953), p. 309.
21) W. Gordy and W. J. O. Thomas, *J. Chem. Phys.*, **24**, 439 (1956).
22) R. J. Gillespie, *J. Chem. Educ.*, **40**, 295 (1963); **47**, 18 (1970).
23) M. Otake, C. Matsumura, and Y. Morino, *J. Mol. Spectrosc.*, **28**, 316 (1968).
24) H. B. Bürgi, D. Stedman, and L. S. Bartell, *J. Mol. Structure*, **10**, 31 (1971).
25) K. Hedberg and M. Iwasaki, *J. Chem. Phys.*, **36**, 589 (1962).
26) P. Kisliuk and C. H. Townes, *ibid.*, **18**, 1109 (1960).
27) K. Kuchitsu, T. Shibata, A. Yokozeki, and C. Matsumura, *Inorg. Chem.*, **10**, 2584 (1971).
28) D. M. Barnhart, cited by K. Hedberg, *Trans. Amer. Crystallogr. Assoc.*, **2**, 79 (1966).
29) Y. Morino, T. Ukaji, and T. Ito, This Bulletin, **39**, 71 (1966).
30) T. Ukaji and H. Uchimura, presented at the 22nd Annual Meeting of the Chemical Society of Japan, Tokyo, March, 1969.
31) C. Matsumura and H. Takeo, "Symposium on Molecular Structure," Fukuoka, October, 1969.
32) C. Matsumura, presented at the Annual Meeting of the Chemical Society of Japan, Tokyo, April, 1970.
33) A. Almenningen and T. Bjorvatten, *Acta Chem. Scand.*, **17**, 2573 (1963).
34) K. Karakida, T. Fukuyama, and K. Kuchitsu, to be published.
35) T. Moritani, K. Kuchitsu, and Y. Morino, *Inorg. Chem.*, **10**, 344 (1971).
36) J. H. Secrist and L. O. Brockway, *J. Amer. Chem. Soc.*, **66**, 1941 (1944).
37) R. L. Kuczkowski and D. R. Lide, *J. Chem. Phys.*, **46**, 357 (1967).

TABLE 5. BOND ANGLES θ(YXY) OF GROUP-Vb HALIDES ZXY_3

	Obsd[a]	Calcd[b]		Obsd	Calcd
NF_3	102.37(3)[d]	104.2	SbF_3	94.0(25)[o]	94.6
NCl_3	107.1(5)[e]	107.0		95.0(8)[p]	
PF_3	97.8(2)[f]	97.0	$SbCl_3$	97.2(9)[q]	97.4
PCl_3	100.3(1)[g]	99.8		96.8(5)[r]	
	100.1(3)[h]		$SbBr_3$	98.2(6)[s]	98.0
PBr_3	101.0(4)[i]	100.4	SbI_3	99.1[t]	98.8
PI_3[c]	102(2)[j]	101.2	SPF_3	100.3(3)[u]	99.5
AsF_3	96.2(2)[k]	96.2	$SPCl_3$	101.8(2)[v]	102.3
	96.0(3)[l]		$SPBr_3$[c]	106(3)[w]	102.9
$AsCl_3$	98.6(4)[l]	99.0	OPF_3	101.3(2)[v]	100.5
$AsBr_3$	99.7(3)[m]	99.6	$OPCl_3$	103.3(2)[v]	103.3
AsI_3	100.2(4)[n]	100.4	$OPBr_3$[c]	108(3)[w]	103.9
			$H_3B \cdot PF_3$	99.8(1)[x]	99.0

a) Values in parentheses are uncertainties to be attached to the last significant digit of the θ-values. b) Calculated by Eq. (5). c) Determined by the visual method of electron diffraction. d) Ref. 23. e) Ref. 24. f) Ref. 1. g) Ref. 25. h) Ref. 26. i) Ref. 27. j) Ref. 6. k) Ref. 2. l) Ref. 9. m) Ref. 28. n) Ref. 29. o) Ref. 30. p) Ref. 31. q) Ref. 12. r) Ref. 32. s) present results. t) Ref. 33. u) Ref. 34. v) Ref. 35. w) Ref. 36. x) Ref. 37.

far, it has been found that there exists the following simple empirical relation:

$$\theta(^\circ) = 92 + 8x_X - 3x_Y. \quad (5a)$$

The bond angles calculated by means of Eq. (5a) using the electronegativities[21] are all close to the experimental values, as is shown in Table 5.

According to the VSEPR theory,[22] the YXY angle increases by the coordination of an atom to the lone-pair electrons of the central group-Vb atom. This has been confirmed by recent electron-diffraction work of phosphine compounds.[34,35] The YXY angles in ZXY_3 molecules may be approximated by the following equation, with an additional term, x_Z, to Eq. (5a):

$$\theta(^\circ) = 92 + 8x_X - 3x_Y + x_Z, \quad (5b)$$

where x_Z is the electronegativity of the coordinated Z atom. The calculated bond angles for the phosphine compounds are compared with the observed values in Table 5. Satisfactory agreements are seen except for the bromides. The elucidation of the origin of the discrepancy in $SPBr_3$ and $OPBr_3$ will be left for future investigations, as the data cited in Table 5 are those determined by the visual method.

The authors wish to thank Professor Takao Iijima for his helpful discussions. The numerical computations were performed on a FACOM 230—60 of the Hokkaido University Computing Center, to which the authors' thanks are also due.

The Electronic Absorption Spectra and Electronic Structures of Aromatic Azides, Nitrenes, and Diazonium Ions

Hiroshi KASHIWAGI, Suehiro IWATA,* Tsuguo YAMAOKA,** and Saburo NAGAKURA

The Institute for Solid State Physics, The University of Tokyo, Roppongi, Minato-ku, Tokyo

(Received July 26, 1972)

Electronic spectra were measured for azidobenzene, 1-azidopyrene, benzenediazonium ion, and 1-pyrenediazonium ion at room temperature, and also for nitrenobenzene and 1-nitrenopyrene at liquid nitrogen temperature. The π-electron structures of these compounds were calculated by the Pariser-Parr-Pople LCAO SCF MO CI method for the closed-shell systems and by the restricted open-shell SCF MO CI method for the open-shell systems. The calculated transition energies and oscillator strengths could satisfactorily explain the observed spectra. It was shown that the π-electron structures of azidobenzene and nitrenobenzene are similar to those of dimethylaniline and the benzyl or anilino radical, respectively.

Aromatic azides, nitrenes, and diazonium ions are interesting research subjects from both physicochemical and photochemical points of view. Reiser *et al.*[1] and also Tsunoda *et al.*[2] observed the electronic absorption spectra of azidobenzene and its derivatives. Theoretical studies of the electronic structure of azidobenzene have been made by several authors with the aid of the Hückel type MO method.[1-4] The more improved LCAO MO SCF CI calculation, however, has not yet been reported on azidobenzene.

The electronic absorption spectra of aromatic diazonium ions were measured by several authors.[5-11] The Hückel type MO studies of their electronic structures have been carried out by Evleth and Cox,[6] Schuster and Polansky,[9] Kikuchi *et al.*,[10] and Bochvar *et al.*[11] The more improved theoretical treatment based on the Pariser-Parr-Pople SCF MO method[12,13] has been made by Sukigara and Kikuchi[7] and also by Yoshida and Kobayashi.[14]

Reiser *et al.*[1,15,16] measured the electronic absorption spectra of several aromatic nitrenes at 77°K and interpreted the observed bands of nitrenobenzene from its similarity to that of the benzyl radical.[1] However, no detailed theoretical study with the aid of the MO method, was made on their electronic spectra.

We have measured the electronic absorption spectra of azidobenzene, nitrenobenzene, and benzenediazonium ion over a wider wavelength region than before and also measured the spectra of some new compounds; 1-azidopyrene, 1-nitrenopyrene, and 1-pyrenediazonium ion. In order to assign the observed spectra, we have theoretically studied the electronic structures of the compounds under consideration by the Pariser-Parr-Pople SCF MO CI method[12,13] and also by the restricted open-shell SCF MO CI method.[17]

Experimental

Materials. Azidobenzene and 1-azidopyrene were prepared by treating 10% hydrochloric acid solution of the corresponding amino-compounds with aqueous sodium nitrite solution and thereafter with aqueous sodium azide solution below 5°C. The precipitate of 1-azidopyrene separated by filtration of the solution was purified by means of column chromatography with active alumina. Azidobenzene was separated from the solution by centrifuging, washed with water, and finally distilled under reduced pressure.

Nitrenes were prepared by illuminating the rigid benzene and ethanol solutions of parent azides with a 500 W mercury lamp at 77 K.

Benzenediazonium fluoroborate and 1-pyrenediazonium fluoroborate were prepared by treating the corresponding amino-compounds with sodium nitrite in 10% hydrochloric acid below 5°C. The precipitates of benzenediazonium fluoroborate and 1-pyrenediazonium fluoroborate were obtained by adding excess 40% fluoroboric acid to the solutions and purified by repeated recrystallizations from methanol.

Ethanol and benzene used as solvents were purified by the methods described previously.[18,19]

Measurements. The electronic spectra of the ethanol solutions of azides and diazonium ions were measured at room temperature with a Cary spectrophotometer Model 14 R. Concerning the benzene and ethanol solutions of nitrenes, spectrophotometric measurements were made at

* Permanent address: The Institute of Physical and Chemical Research, Wako, Saitama.

** Permanent address: Department of Printing, Faculty of Engineering, Chiba University, Chiba.

1) A. Reiser, G. Bowes, and R. J. Horne, *Trans. Faraday Soc.*, **62**, 3162 (1966).

2) T. Tsunoda, T. Yamaoka, and K. Ikari, *Kogyo Kagaku Zasshi*, **72**, 156 (1969).

3) A. Reiser and R. Marley, *Trans. Faraday Soc.*, **64**, 1806 (1968).

4) G. Favini, *Gazz. Chim. Ital.*, **91**, 270 (1961).

5) T. Tsunoda and T. Yamaoka, *Nippon Shashin Gakkai-shi*, **29**, 197 (1966).

6) E. M. Evleth and R. J. Cox, *J. Phys. Chem.*, **71**, 4082 (1967).

7) M. Sukigara and S. Kikuchi, This Bulletin, **40**, 461 (1967).

8) L. A. Kazitsyna, N. B. Dzegilenko, A. V. Upadysheba, V. V. Mischenko, and O. A. Reutov, *Izv. Akad. Nauk SSSR, Ser. Khim.*, **1967**, 1925.

9) P. Schuster and O. E. Polansky, *Monatsh. Chem.*, **96**, 396 (1965).

10) S. Kikuchi, K. Honda, and M. Sukigara, *Seisan Kenkyu*, **19**, 161 (1967).

11) D. A. Bochvar, N. P. Gambaryan, V. V. Mischenko, and L. A. Kazitsyna, *Dokl. Akad. Nauk SSSR*, **175**, 839 (1967).

12) P. Pariser and R. G. Parr, *J. Chem. Phys.*, **21**, 466, 767 (1953).

13) J. A. Pople, *Trans. Faraday Soc.*, **49**, 1375 (1953).

14) Z. Yoshida and T. Kobayashi, This Bulletin, **45**, 742 (1972).

15) A. Reiser, H. M. Wagner, and G. Bowes, *Tetrahedron Lett.* **23**, 2635 (1966).

16) A. Reiser, H. M. Wagner, R. Marley, and G. Bowes, *Trans. Faraday Soc.*, **63**, 2403 (1967).

17) H. C. Longuet-Higgins and J. A. Pople, *Proc. Phys. Soc., Ser. A*, **68**, 591 (1955).

18) T. Yamaoka, H. Kashiwagi, and S. Nagakura, This Bulletin, **45**, 361 (1972).

19) H. Kashiwagi, T. Yamaoka, and S. Nagakura, *ibid.*, to be published.

77 K with a Shimadzu MPS type spectrophotometer at the Institute of Physical and Chemical Research.

The concentrations of the solutions used for the spectrophotometric measurements were in the range 10^{-4}—10^{-5} M.

Theoretical

For the calculation of the closed-shell systems, we adopted the Pariser-Parr-Pople SCF MO method.[12,13,20] The configuration interactions were considered by taking all the singly excited configurations for the benzene derivatives and by taking the lowest 40 singly excited configurations for each symmetry in the case of the pyrene derivatives. For the open-shell molecules, the restricted SCF MO CI procedure presented by Longuet-Higgins and Pople[17] was adopted. In this case the lowest 40 singly and doubly excited configurations were taken for each symmetry. The penetration integrals were neglected for both closed- and open-shell systems. The core reasonance integrals (β) were taken to be proportional to the corresponding overlap integrals, the value of β, −2.39 eV, for the C–C bond of the benzene ring being taken as the standard. Two-center Coulomb repulsion integrals were estimated by means of the Nishimoto-Mataga approximation.[21] One-center integrals were determined by taking the effect of charge densities according to the method presented by Iwata and Shida.[22]

The molecular structure of azidobenzene was first estimated on the basis of the well-known structures of benzene and CH_3N_3 determined by the electron diffraction experiment,[23] and finally taken by the standard bond order-bond length relation as shown in Fig. 1 (a).[24] The molecular structure of the benzenediazonium ion[25] shown in Fig. 1(b), was determined by the X-ray diffraction technique on the chloride crystal and was taken for calculation. The molecular structure of nitrenobenzene was taken by using the standard bond order-bond length relation as shown in Fig. 1(c). For the pyrene dirivatives, we adopted the results of the X-ray diffraction experiment of pyrene crystal[26] assuming all the angles to be 120° and the C–N and N–N bond lengths equal to those of the benzene derivatives.

The only out-of-plain (z axis) π-electron orbital on each atom taken in the calculation is shown in Figs. 1(a), (b), and (c) for azidobenzene, benzenediazonium ion, and nitrenobenzene, respectively. The ESR study[27,28] shows that the ground state of nitrenobenzene is the $n\pi$ type triplet in which one π-electron occupies the half filled orbital mostly localized on the nitrogen atom. Thus, the ground state of nitrenes under consideration may be regarded as odd π-electron systems.

The calculation was performed with a Facom 270—30 electronic computer at the Institute of Physical and Chemical Research.

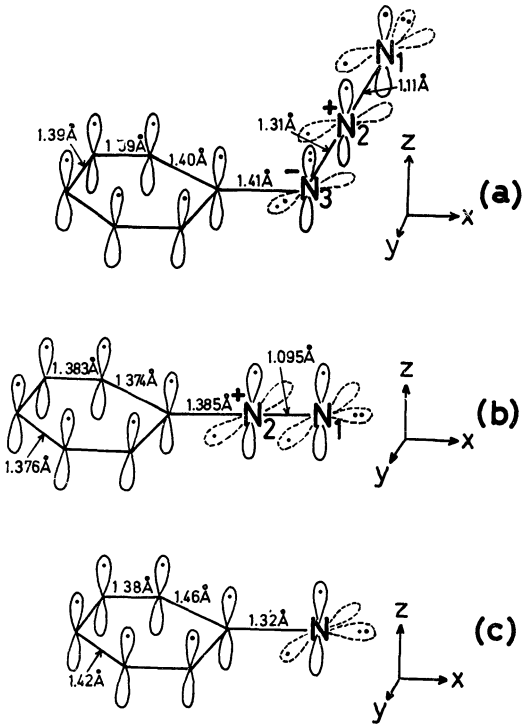

Fig. 1. π-Electron structures taken for a) azidobenzene, b) benzenediazonium ion, and c) nitrenobenzene.

Results and Discussion

Electronic Spectrum of Azidobenzene. Figure 2 shows the absorption spectrum of the ethanol solution of azidobenzene at room temperature. In addition to the bands below 45000 cm^{-1} reported by the previous

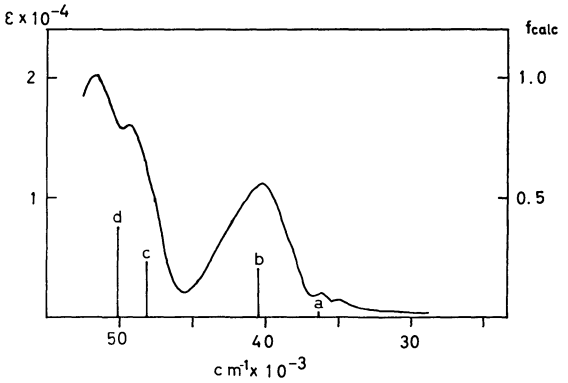

Fig. 2. The absorption spectrum of azidobenzene in ethanol at room temperature. The vertical lines represent the calculated transition energies and oscillator strengths (f_{calc}).

20) J. A. Pople, *Proc. Phys. Soc., Ser. A*, **68**, 81 (1955).
21) K. Nishimoto and N. Mataga, *Z. Phys. Chem. N. F.*, **12**, 335 (1957).
22) Details of the method will be published by S. Iwata and T. Shida.
23) C. N. R. Rao, *Dissertation Abstr.*, **19**, 968 (1959).
24) The following equations are used for the evaluation of the bond length from the bond order:
$l_{pq}=1.514-0.176\,P_{pq}$ for the C–C bond
$l_{pq}=1.472-0.207\,P_{pq}$ for the C–N bond
where l_{pq} and P_{pq} are bond length and bond order, respectively, between p and q atoms
25) C. Römming, *Acta Chem. Scand.*, **17**, 1444 (1963).
26) J. M. Robertson, *Proc. Roy. Soc., Ser. A*, **207**, 101 (1951).
27) J. A. R. Coope, J. B. Farmer, C. L. Gardner, C. A. McDowell, *J. Chem. Phys.*, **42**, 54 (1965).
28) E. Wasserman, L. C. Snyder, and W. A. Yager, *J. Chem. Phys.*, **41**, 1763 (1964).

TABLE 1. CALCULATED AND OBSERVED TRANSITION ENERGIES ΔE's (IN THE UNITS OF 10^3 cm^{-1}), AND OSCILLATOR STRENGTHS, f's, OF AZIDOBENZENE

	Calcd.					Obsd.	
	ΔE	Polarization[a]	f	Character[b]		ΔE	f
				1) Transitions concerning singlet excited states			
a	36.6	y>x	0.026	$0.70(5\rightarrow6)-0.49(4\rightarrow7)+0.51(3\rightarrow6)$	$CT_1+LE(B_{2u})$	35.0	0.018
b	40.3	x>y	0.205	$0.89(5\rightarrow7)+0.42(4\rightarrow6)$	CT_2	40.2	0.27
c	48.1	y	0.245	$0.67(5\rightarrow6)+0.62(4\rightarrow7)-0.41(3\rightarrow6)$	$CT_1+LE(B_{2u})+LE(B_{1u})$	49.3	0.22
d	50.2	x	0.379	$-0.38(5\rightarrow7)+0.31(3\rightarrow7)+0.84(4\rightarrow6)$	$LE(B_{1u})+LE(E'_{1u})$	51.7	0.39
e	55.3	y	0.681	$0.59(4\rightarrow7)+0.75(3\rightarrow6)$	$LE(E_{1u})+LE(B_{2u})$		
f	55.5	x	0.344	$0.92(3\rightarrow7)-0.33(4\rightarrow6)$	$LE(E'_{1u})+LE(B_{2u})$		
				2) Transitions concerning triplet excited states			
a'	23.7			$0.62(4\rightarrow6)+0.63(5\rightarrow7)+0.42(3\rightarrow7)$			
b'	30.9			$-0.34(4\rightarrow6)+0.77(5\rightarrow6)+0.38(3\rightarrow6)$			
c'	31.7			$0.68(4\rightarrow6)-0.53(5\rightarrow7)+0.33(5\rightarrow6)$			

a) Axes x and y are taken as shown in Fig. 1.

b) This column shows coefficients of main electron configurations the contribution of which exceeds 9%. $(i\rightarrow j)$ indicates the electron configuration corresponding to the one electron excitation from the i-th MO (φ_i) to the j-th MO (φ_j). The MO's used in the CI calculation are schematically shown in the following diagram.

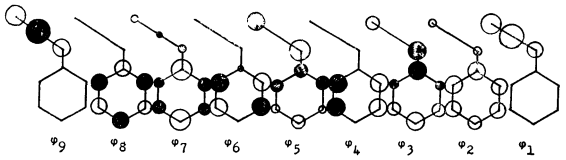

authors[1,2] new bands were newly observed at 49300 and 51700 cm^{-1}.

As is clearly seen in Table 1 in which the calculated transition energies and oscillator strengths are given together with the observed values, there is a good agreement between the calculated and observed ones. We show the nature of each transition by giving the coefficients of electron configurations mainly contributed to the corresponding excited state. The bands at 35000, 40200, 49300, and 51700 cm^{-1} can be interpreted as a shifted α band of benzene, an intramolecular charge-transfer (CT) band, a band with mixed characters of CT and local excitation (LE) corresponding to the α band of benzene, and a mixing band of the α and β bands of benzene, respectively. The shifted β bands of benzene may be expected to appear at higher frequencies than the observed wave number region. The present assignment of the absorption spectrum of azidobenzene is similar to that of dimethylaniline.[29] This means that the π-electrons of the azido group give an effect similar to those of the dimethylamino group to the absorption spectrum of benzene.

The π-electron densities and bond orders calculated for azidobenzene are listed in Table 2, which shows that the π-electron migrates from the azido group to the benzene ring by 0.05e. This means that the azido group is an electron donating one like the dimethylamino group.

Finally we found the $n\pi^*$ type transition at 30900 cm^{-1} ($\varepsilon\sim100$) for the concentrated solution of azidobenzene.

29) K. Kimura and S. Nagakura, *Mol. Phys.*, **9**, 117 (1965).

TABLE 2. CALCULATED π-ELECTRON DENSITIES AND BOND ORDERS OF AZIDOBENZENE AND BENZENEDIAZONIUM ION

1) Azidobenzene

π-Electron densities

Atoms[a]	Ground state	S_1 state	S_2 state	T_1 state
N_1	1.37	1.20	1.16	1.26
N_2	1.04	1.04	1.04	1.04
N_3	1.54	1.31	1.20	1.36

Bond orders

Bonds	Ground state	S_1 state	S_2 state	T_1 state
N_1-N_2	0.776	0.759	0.749	0.762
N_2-N_3	0.627	0.613	0.602	0.621
N_3-C	0.518	0.587	0.625	0.509

2) Benzenediazonium ion

π-Electron densities

Atoms[a]	Ground state	S_1 state	S_2 state	T_1 state
N_1	0.86	1.19	1.14	1.23
N_2	1.26	1.43	1.42	1.43

Bond orders

Bonds	Ground state	S_1 state	S_2 state	T_1 state
N_1-N_2	0.891	0.664	0.639	0.649
N_2-C	0.364	0.437	0.433	0.428

a) N_1, N_2, and N_3 are taken as shown in Fig. 1.

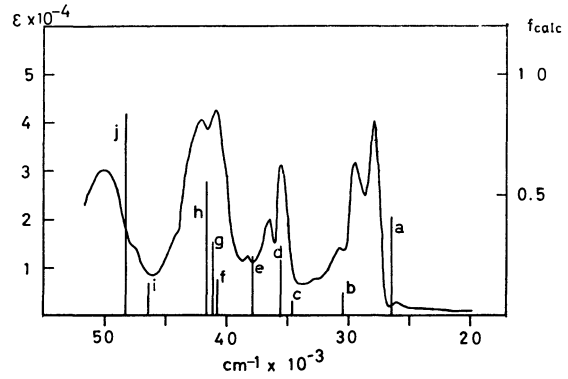

Fig. 3. The electronic absorption spectrum of 1-azidopyrene in ethanol at room temperature. The vertical lines represent the calculated transition energies and oscillator strengths (f_{calc}).

Electronic Spectrum of 1-Azidopyrene. Figure 3 shows the electronic absorption spectrum of 1-azidopyrene in the ethanol solution at room temperature. The calculated and observed peak wave numbers and oscillator strengths for various transitions with lower energies are given in Table 3. Although many transitions are expected in the region $(20\simeq50)\times10^3$ cm^{-1}, those with an oscillator strength greater than 0.05 are shown, except for the lowest energy transition at 26000 cm^{-1}. In the case of 1-azidopyrene, transitions cannot be characterized by three or four dominant electron configurations, except for the lowest two or three transitions. The characters of the transitions are therefore not shown in Table 3. The weak band at 26000 cm^{-1} may be regarded as a shifted α band of pyrene. Band a in Table 3 is assigned to LE (~50%)+CT (~50%), and bands b and d are characterized by CT. In spite of the existence of the CT bands, the spectral shape is similar to that of pyrene. This is because the absorption intensities of the main bands pertinent to the parent hydrocarbon are very strong and the CT bands are covered by them. Most of the observed peaks are attributed to the superposition of several transitions. The peak positions of the 1-azidopyrene spectrum are shifted toward longer wavelengths compared with those of the pyrene spectrum and are similar to those of the 1-aminopyrene spectrum.

TABLE 3. CALCULATED AND OBSERVED TRANSITION ENERGIES, ΔE's (IN THE UNITS OF 10^3 cm^{-1}) AND OSCILLATOR STRENGTHS (f) OF 1-AZIDOPYRENE[a]

	Calcd.			Obsd.	
	ΔE	Polarization[b]	f	ΔE	f
	24.8	x>y	0.0029	26.0	0.0042
a	26.4	y>x	0.41	27.9	0.52
b	30.4	y>x	0.09		
c	34.6	x~y	0.06		
d	35.6	x~y	0.23	35.5	0.31
e	37.9	x>y	0.25		
f	40.7	y	0.16		
g	41.1	y>x	0.31		
h	41.6	y	0.57	40.9	0.88
i	46.4	y>x	0.14		
j	48.2	y	0.84	50.0	0.47

a) We are concerned with only singlet excited states.
b) Axes x and y are taken to be parallel to the short and long molecular axes of pyrene, respectively.

Electronic Spectrum of the Benzenediazonium Ion.

TABLE 4. CALCULATED AND OBSERVED TRANSITION ENERGIES, ΔE's (IN THE UNITS OF 10^3 cm^{-1}) AND OSCILLATOR STRENGTHS, f's OF BENZENEDIAZONIUM ION

	Calcd.					Obsd.	
	ΔE	Polarization[a]	f	Character[b]		ΔE	f
				1) Transitions concerning singlet excited state			
a	33.4	y	0.078	0.63(4→5)+0.53(3→6)−0.52(4→7)	$CT_1+LE(B_{2u})$	33.9	0.085
b	38.8	x	0.32	0.91(3→5)+0.34(4→6)	CT_2	38.6	0.22
c	48.8	y	0.15	0.65(4→5)−0.63(3→6)+0.41(4→7)	$CT_1+LE(B_{2u})+LE(E_{1u})$	49.4	0.18
d	52.1	x	0.61	−0.34(3→5)+0.86(4→6)+0.32(3→7)	$LE(B_{1u})+LE(E'_{1u})$	51.9	0.32
e	60.1	y	0.78	0.35(4→5)+0.54(3→6)+0.73(4→7)	$CT_1+LE(E_{1u})+LE(B_{2u})$		
f	60.6	x	0.30	−0.33(4→6)+0.92(3→7)	$LE(E'_{1u})+LE(B_{1u})$		
				2) Transitions concerning triplet excited states			
a'	27.2			0.93(4→5)		20.7[7]	
b'	31.7			0.87(3→5)+0.34(4→6)			
c'	39.6			0.91(3→6)			

a) Axes x and y are taken as shown in Fig. 1.
b) See footnote b), Table 1.
The MO's used in the CI calculation are schematically shown in the following diagram.

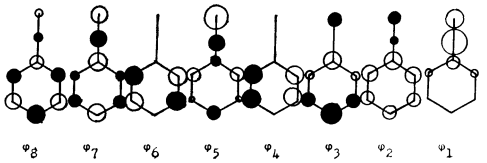

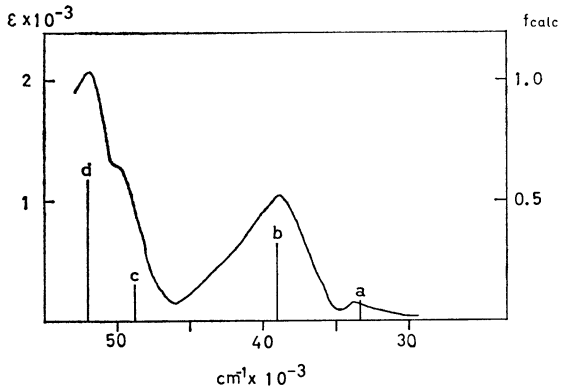

Fig. 4. The electronic absorption spectrum of benzenediazonium fluoroborate in ethanol at room temperature. The vertical lines represent the calculated transition energies and oscillator strengths (f_{calc}).

Figure 4 shows the electronic absorption spectrum of benzenediazonium fluoroborate in the ethanol solution. The bands below 40000 cm^{-1} are coincident in their positions and intensities with those given by Sukigara and Kikuchi.[7] The calculated transition energies and oscillator strengths are given in Table 4, together with the observed values. We can find a good agreement between the observed and calculated values both for the transition energies and for the oscillator strenghts. The nature of each transition is also shown in this table by giving the coefficient of the electron configuration mainly contributed to the corresponding excited state.

The observed absorption spectrum of the benzenediazonium ion is similar to that of azidobenzene. The characters of the bands are also similar to each other for both compounds. However, the directions of electron transfer between the substituent group and the benzene ring are reverse to each other for both compounds, *viz.*, in the case of the benzenediazonium ion, the substituent group acts as an electron acceptor. This is clear from the π-electron density given in Table 2.

The $n\pi^*$ type transition was observed at 30800 cm^{-1} ($\varepsilon \sim 120$) for the concentrated solution.

Electronic Spectrum of the 1-Pyrenediazonium Ion. Figure 5 shows the electronic absorption spectrum of

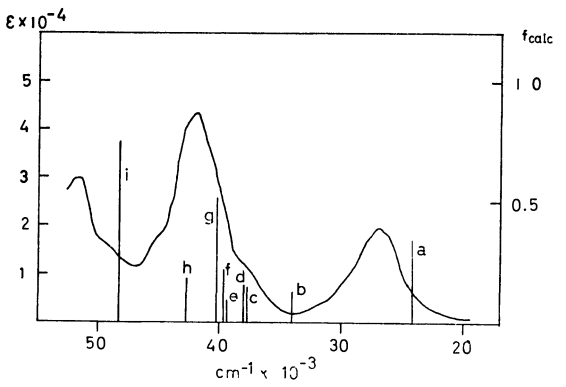

Fig. 5. The electronic absorption spectrum of 1-pyrenediazonium ion in ethanol at room temperature. The vertical line represent the calculated transition energies and oscillator strengths (f_{calc}).

Table 5. Calculated and observed transition energies, ΔE's (in the units of 10^3 cm^{-1}) and oscillator strengths, f's, of 1-pyrenediazonium ion[a]

	Calcd.			Obsd.	
	ΔE	Polarization[b]	f	ΔE	f
a	24.2	y>x	0.35	26.8	0.43
b	34.0	y∼x	0.14		
c	37.7	x∼y	0.15		
d	38.1	x>y	0.16		
e	39.2	y	0.10		
f	39.6	y>x	0.21		
g	40.2	y	0.52	41.9	0.82
h	42.7	y>x	0.19		
i	48.3	y	0.75	51.7	

a) We are concerned with only siglet excited states.
b) Axes x and y are taken to be parallel to the short and long molecular axes of pyrene, respectively.

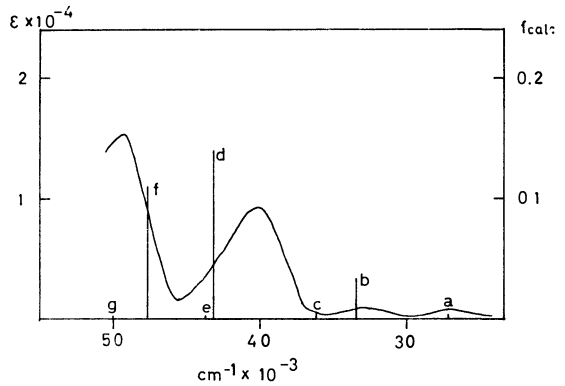

Fig. 6. The electronic absorption spectrum of nitrenobenzene in ethanol at 77°K. The vertical lines represent the calculated transition energies and oscillator strengths (f_{calc})

the 1-pyrenediazonium ion in the ethanol solution at room temperature. The transition energies and oscillator strengths are given in Table 5 for several transitions of lower energies and with oscillator strengths greater than 0.05. Band a in this table is assigned to LE (∼60%)+CT (∼40%), and band b to pure CT. Each of the observed peaks shown in Fig. 6 is the superposition of several bands.

Electronic Spectrum of Nitrenobenzene. Figure 6 shows the electronic absorption spectrum of nitrenobenzene in the ethanol solution. The bands at higher frequencies than 40000 cm^{-1} were newly found by the present authors. The observed transition energies and oscillator strengths are given in Fig. 6 together with the calculated values. There is a good agreement between the observed and calculated values both for transition energies and oscillator strengths. The nature of each transition is also shown in Table 6.

The electronic spectrum of nitrenobenzene resembles very much that of the benzyl, anilino, or phenoxyl radical. The two lower bands, a and b, can be assigned to the $\psi_0 \rightarrow \psi_+$ and $\psi_0 \rightarrow \psi_-$ transitions in the Dewar and Longuet-Higgins notation.[30] The strong bands

30) M. J. S. Dewar and H. C. Longuet-Higgins, *Proc. Phys. Soc., Ser. A*, **67**, 795 (1954).

TABLE 6. CALCULATED AND OBSERVED TRANSITION ENERGIES, ΔE's (IN THE UNITS OF $10^3\,cm^{-1}$) AND OSCILLALOR STRENGTH, f's, OF NITRENOBENZENE

	Calcd.					Obsd.	
	ΔE	Polarization[a]	f	Character[b]		ΔE	f
a	22.7	y	0.003	$0.77(3\rightarrow4)+0.43(4\rightarrow5)+0.30(2\rightarrow5)$	CT, B_1	27.2	0.0006
b	33.4	y	0.037	$0.45(3\rightarrow4)-0.73(4\rightarrow5)-0.33(2\rightarrow5)$	CT, B_1	33.0	0.01
c	36.2	x	0.005	$0.71(3\rightarrow5)-0.43(3\rightarrow5)'$	LE, A_1		
d	43.2	x	0.14	$0.42(2\rightarrow4)+0.42(4\rightarrow6)+0.48(1\rightarrow4)+0.30(4\rightarrow7)$	CT, A_1	41.5	0.18
e	43.8	y	0.003	$0.70(3\rightarrow6)+0.51(2\rightarrow5)+0.33(2\rightarrow5)'$	LE, B_1		
f	47.5	x	0.11	$0.39(2\rightarrow4)-0.49(4\rightarrow6)+0.41(1\rightarrow4)-0.35(4\rightarrow7)$	CT, A_1	48.9	0.14

a) Axes x and y are taken as shown in Fig. 1.
b) See footnote b), Table 1. $(k\rightarrow m)'$ is the abbreviated representation of an excited electron configuration: $(k\rightarrow m)'=1/\sqrt{6}\,[-2|\bar{k}\bar{l}m|+|\bar{k}lm|+|kl\bar{m}|]$. The MO's used in the CI calculation are schematically shown in the following diagram.

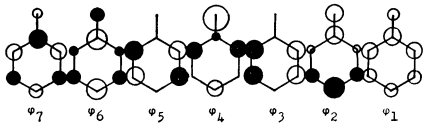

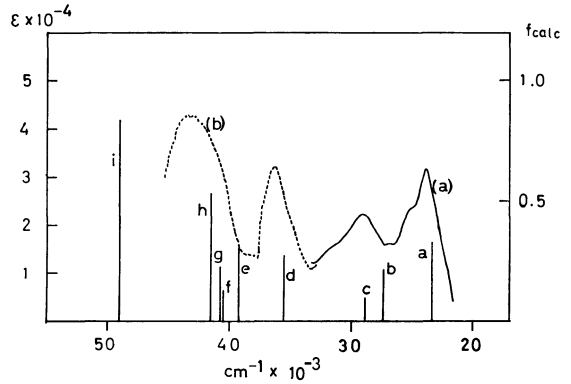

Fig. 7. The electronic absorption spectra of 1-nitrenopyrene in benzene and ethanol at 77 K. The vertical lines represent the calculated transition energies and oscillator strengths (f_{calc}).
a) in benzene, b) in ethanol.

TABLE 7. CALCULATED AND OBSERVED TRANSITION ENERGIES, ΔE's (IN THE UNITS OF $10^3\,cm^{-1}$) AND OSCILLATOR STRENGTHS, f's OF 1-NITRENOPYRENE

	Calcd.			Obsd.	
	ΔE	Polarization[a]	f	ΔE	f
a	23.3	y>x	0.33	23.8	0.58
b	27.4	y	0.21	29.0	0.48
c	28.9	x∼y	0.10		
d	35.5	y>x	0.28	36.4	0.39
e	39.2	x	0.32		
f	40.5	x>y	0.13		
g	40.8	x	0.23		
h	41.1	x	0.54	43.3	1.1
i	49.0	y	0.89		

a) Axes x and y are taken to be paralled to the short and long molecular axes, respectively.

of d and f are represented by the superposition of CT and back CT components, which are also transitions characteristic of open-shell systems. The weak bands of c and e are covered by the strong bands, d and f.

Electronic Spectrum of 1-Nitrenopyrene. Curves (a) and (b) in Fig. 7 show the electronic absorption spectra of 1-nitrenopyrene in the benzene and ethanol solutions at 77 K, respectively. The calculated and observed results for the transitions with higher oscillator strengths than 0.05 are given in Table 7.

In this case, the two lower absorption bands at 23800 and 29000 cm^{-1} represented by a and b, respectively, are assigned to $\psi_0\rightarrow\psi_+$ and $\psi_0\rightarrow\psi_-$ transitions in the Dewar and Longuet-Higgins notation.[30] Band c is assigned to the LE transition of pyrene. Since other transitions cannot be characterized by three or four dominant electron configurations, we do not show the characters of transitions in Table 7.

We should like to express our sincere thanks to Dr. Kazuo Shibata and Dr. Teruo Ogawa, The Institute of Physical and Chemical Research, for their kindness in permitting us to use the Shimadzu MPS spectrophotometer for measuring the absorption spectrum of the opaque solution at liquid nitrogen temperature.

The Electronic States of Tetracyanoethylene and Its Anion Radical as Studied by Their Infrared Spectra

Yôichi IIDA

Department of Chemistry, Faculty of Science, Hokkaido University, Sapporo

(Received August 3, 1972)

The infrared spectra of tetracyanoethylene (TCNE) and its anion radical in the rock-salt region were examined in order to observe any appreciable frequency differences between their corresponding bands. The vibrational assignments were made, and the basic Urey-Bradley force field was determined for the TCNE anion radical. By comparing them with those of the neutral TCNE, we discussed the difference in the electronic states between the neutral TCNE and its anion radical. The half-occupied molecular orbital of the TCNE anion radical was found to belong to the B_{2g} irreducible representation.

The infrared spectrum of an ion radical is known to be appreciably different from that of its neutral molecule.[1-11] The spectrum difference may be attributed to the difference in their intramolecular force fields. In a previous paper,[8] we examined the infrared spectra (650—4000 cm^{-1}) of *p*-chloranil and its anion radical. In order to explain the appreciable frequency differences between their corresponding bands, the fundamental frequencies were assigned, and the simple Urey-Bradley force fields were determined for both the neutral and anion radical molecules. It was found that the difference in the infrared spectra between these two molecules could be understood on the basis of the difference in their electronic structures caused by an extra electron on the *p*-chloranil anion radical.

The tetracyanoethylene (TCNE) molecule is known to be a strong electron acceptor, and its anion radical is stable.[12] The infrared and Raman spectra of the neutral TCNE were measured by Takenaka and Hayashi.[13] In order to make vibrational assignments and determine the force constants for this molecule, they carried out normal coordinate treatments for the in-plane vibrations by using the basic Urey-Bradley force field. On the other hand, Stanley *et al.* examined the infrared spectra of the sodium and potassium salts of the TCNE anion radical by using thin polycrystalline films.[5] Although they reported that the spectrum of the TCNE anion radical differs appreciably from that of the neutral TCNE, they did not assign the fundamental frequencies quantitatively or determine the force constants for the TCNE anion radical. Therefore, in the present paper, the fundamental frequencies were assigned and the basic Urey-Bradley force field was determined for the TCNE anion radical. The purpose of the present paper is to compare these data with those of the neutral TCNE and to investigate the difference in the electronic states between the neutral TCNE and its anion radical.

Calculations

First, let us consider the experimental and theoretical results on the neutral TCNE reported by Takenaka and Hayashi.[13] The observed fundamental frequencies in the infrared and Raman spectra of the neutral TCNE are given in Table 1. In order to assign the vibrational spectra, they used the ***GF*** matrix method developed by Wilson.[14] It was assumed that the vibrational spectra could be treated under the molecular point group V_h. A representative of each type of internal coordinate is shown in Fig. 1. The equilibrium bond lengths adopted are those determined from X-ray analysis by Bekoe and Trueblood:[15] $R_0=1.317$ Å, $r_0=1.449$ Å, and $l_0=1.15$ Å. For the

Table 1. The observed and calculated frequencies (cm^{-1}) for in-plane fundamental vibrations of the neutral TCNE and its anion radical

Species		The neutral TCNE		Its anion radical	
		Obsd[a]	Calcd[a]	Obsd[b],[c]	Calcd
A_g	ν_1	2250	2250		2193
	ν_2	1573	1573	(1371)	1365
	ν_3	679	647		650
	ν_4	536	525		523
	ν_5	—	122		121
B_{1g}	ν_6	2237	2232		2181
	ν_7	1284	1304		1331
	ν_8	508	503		505
	ν_9	251	251		251
B_{2u}	ν_{10}	2230	2239	2183	2191
	ν_{11}	1155	1152	1187	1181
	ν_{12}	429	433	—	434
	ν_{13}	—	111	—	111
B_{3u}	ν_{14}	2262	2257	2208	2202
	ν_{15}	959	980	970	996
	ν_{16}	579	591	—	593
	ν_{17}	—	157	—	156

a) Ref. 13. b) Ref. 5. c) Ref. 12.

1) Y. Matsunaga, *Can. J. Chem.*, **38**, 1172 (1960).
2) Y. Matsunaga, *Helv. Phys. Acta*, **36**, 800 (1963).
3) Y. Matsunaga, *J. Chem. Phys.*, **41**, 1609 (1963).
4) M. Kinoshita and H. Akamatu, *Nature*, **207**, 291 (1965).
5) J. Stanley, D. Smith, B. Latimer, and J. P. Devlin, *J. Phys. Chem.*, **70**, 2011 (1966).
6) Y. Matsunaga, *Nippon Kagaku Zasshi*, **89**, 905 (1968).
7) Y. Iida, *J. Phys. Soc. Jap.*, **27**, 1371 (1969).
8) Y. Iida, This Bulletin, **43**, 345 (1970).
9) Y. Iida, *ibid.*, **44**, 1271 (1971).
10) J. C. Moore, D. Smith, Y. Youhne, and J. P. Devlin, *J. Phys. Chem.*, **75**, 325 (1971).
11) I. N. Juchnovski and I. G. Binev, *Chem. Phys. Lett.*, **12**, 40 (1971).
12) O. W. Webster, W. Mahler, and R. E. Benson, *J. Amer. Chem. Soc.*, **84**, 3678 (1962).
13) T. Takenaka and S. Hayashi, This Bulletin, **37**, 1216 (1964).
14) E. B. Wilson, Jr., *J. Chem. Phys.*, **7**, 1047 (1939); **9**, 76 (1941).
15) D. A. Bekoe and K. N. Trueblood, *Z. Kristallogr.*, **113**, 1 (1960).

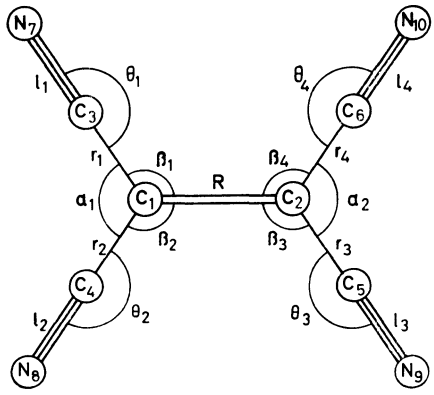

Fig. 1. The internal coordinates for the neutral TCNE or its anion radical.

bond angles, $\alpha_0=\beta_0=120°$ and $\theta_0=180°$ were assumed for the sake of simplicity. The normal vibrations of TCNE were reduced to the symmetry species:

$$\Gamma = 5A_g(R)+4B_{1g}(R)+4B_{2u}(IR)+4B_{3u}(IR) + 2A_u\,(\text{inactive})+2B_{1u}(IR)+2B_{2g}(R)+B_{3g}(R), \quad (1)$$

where the first four are the in-plane vibrations and the rest are the out-of-plane vibrations. (R) and (IR) indicate the Raman and infrared active modes respectively. In order to calculate the fundamental frequencies, the basic Urey-Bradley force field was used as the potential function for TCNE. For the in-plane vibrations, three bond-stretching (K(C=C), K(C-C), and K(C≡N)), three angle-bending (H(C–C–C), H(C–C=C), H(C–C≡N)), and four non-bonded repulsion force constants (F(C–C–C), F(C–C=C), F(C–C≡N), and C) were necessary. The constant, C, represents the repulsion between two carbon atoms in the *cis*-position.[16–18] Repetitions of the calculation with several sets of force constants were then carried out by the trial-and-error method by the use of the Jacobian matrix. For the in-plane vibrations, Takenaka and Hayashi obtained the final set of force constants shown in Table 2.[13] The fundamental frequencies calculated with these constants are compared in Table 1 with the observed values. The agreement is satisfactory except in the case of the 679 cm^{-1} frequency (ν_3) of the A_g species.

Table 2. The force constants estimated for the neutral TCNE and its anion radical (md/Å)[a]

Force constant	The neutral TCNE[b]	Its anion radical
K(C=C)	6.31	4.00
K(C-C)	4.80	5.23
K(C≡N)	16.84	15.70
H(C-C-C)	0.05	
H(C-C=C)	0.16	
H(C-C≡N)	0.13	
F(C-C-C)	1.11	
F(C-C=C)	1.04	
F(C-C≡N)	0.08	
C	0.11	

a) $F' = -0.1F$, $C' = -0.1C$. b) Ref. 13.

Next, let us consider the vibrational spectrum of the TCNE anion radical. The fundamental frequencies in the infrared spectrum of the potassium salt of the TCNE anion radical measured by Stanley *et al.* are also given in Table 1.[5,12] Since the counter cation of the salt is a simple alkali metal cation, the observed spectrum of the salt in the rock-salt region must be due solely to that of the TCNE anion radical itself. Its spectroscopic features are found to be appreciably dissimilar to those of the neutral TCNE. The most interesting new features in the TCNE anion radical spectrum are: (1) the very intense band at 1371 cm^{-1}, (2) the appreciable red-shifts of the doublet 2208 and 2183 cm^{-1} bands in the cyanide-stretching region compared to the 2262 and 2230 cm^{-1} bands in the neutral TCNE, and (3) the marked absence of absorption in the 600—1300 cm^{-1} region, where the strongest TCNE fundamental absorptions occur.[5] The C–C modes, which absorb strongly at 1155 and 959 cm^{-1} in the neutral TCNE, can be designated as the source of the very weak bands at 1187 and 970 cm^{-1} in the TCNE anion radical.

In order to explain these appreciable frequency differences, let us analyze the vibrational spectrum of the TCNE anion radical. Since the molecular and crystal structures of the potassium salt of the TCNE anion radical have not yet been ascertained, it was assumed that the molecular structure of the anion radical was almost identical with that of the neutral TCNE. This assumption means that the $\boldsymbol{G}$ matrix calculated for the neutral TCNE was also used for the anion radical (see below). Since only the intramolecular vibrations are expected to appear in the rock-salt region, the vibrational spectra of the crystalline compound can be approximately treated under the molecular point group V_h. In general, the effects of crystal fields on vibrational frequencies are small. Therefore, to a first approximation, its contribution to the spectrum of the TCNE anion radical was ignored in our treatment. Hence, twenty-four normal modes of vibrations for the TCNE anion radical were also reduced to the same symmetry species as in Eq. (1) of the neutral TCNE. (We calculated only the in-plane vibrations, because no out-of-plane vibration is expected to appear in the region now under consideration.) We have designated the very weak bands at 1187 and 970 cm^{-1} as the C–C modes in the TCNE anion radical. Since no other infrared-active fundamental modes occur between 600 and 2000 cm^{-1}, there is no apparent source for the intense 1371 cm^{-1} band in the anion radical. The assignment of this band is important in estimating the force constants of the TCNE anion radical. If a strong charge-transfer interaction takes place between the neighbouring TCNE anion radical species,[19] the

16) J. R. Scherer and J. Overend, *J. Chem. Phys.*, **33**, 1681 (1960).
17) D. E. Mann, T. Shimanouchi, J. H. Meal, and L. Fano, *ibid.*, **27**, 43 (1957).
18) D. E. Mann, L. Fano, J. H. Meal, and T. Shimanouchi, *ibid.*, **27**, 51 (1957).

19) The charge-transfer interaction between neighbouring ion radical molecules has been found with a number of crystalline ion radical salts. See, for example, Y. Iida and Y. Matsunaga, This Bulletin, **41**, 2615 (1968); Y. Iida, *ibid.*, **42**, 71, 637 (1969); Y. Iida, *ibid.*, **43**, 2772 (1970); Y. Iida, *ibid.*, **44**, 663, 1777 (1971); Y. Iida, *ibid.*, **45**, 105, 624 (1972).

Ferguson-Matsen theory of activation then applies and certain intense bands in the infrared spectrum can be assigned to totally symmetric modes.[20-22] By the use of this approach with the TCNE anion radical, the strong band at 1371 cm^{-1} can be assigned to the totally symmetric C=C stretching A_g mode,[5,10] which was observed at 1573 cm^{-1} in the Raman spectrum of the neutral TCNE.[13] The 202 cm^{-1} red shift seems to be consistent with the following discussion of the electronic states of TCNE and its anion radical (see below).

In order to calculate the fundamental frequencies, Wilson's ***GF*** matrix method was also applied to the TCNE anion radical; a representative of each type of internal coordinate for in-plane fundamental vibrations is given in Fig. 1. The basic Urey-Bradley force field was employed as the potential function. The notations for the three bond-stretching, three angle-bending, and four non-bonded repulsion force constants used are those for the neutral TCNE. At this time, it is assumed that the stretching force constants of the TCNE anion radical are different from those of the neutral TCNE, while the other force constants remain almost constant. Rigorously speaking, this treatment is not correct, but it is justified as long as the observed fundamental frequencies are mostly due to the bond stretching modes. Then, the trial force constant for the TCNE anion radical were taken by modifying the stretching force constants for the neutral TCNE determined by Takenaka and Hayashi.[13] Refinements of the force constants for the TCNE anion radical were then carried out by the trial-and-error method, making use of the Jacobian matrix. The final set of force constants thus obtained for the TCNE anion radical is given in Table 2, while in Table 1 the frequencies calculated with these constants are compared with the observed values. The calculated values of the fundamental vibrations were found to agree well with the observed values.

Discussion

Since a total of 10 force constants of the anion radical were evaluated from an experimental assignment of 5 frequencies, we suspect that these values of the force constants are not the best ones for the TCNE anion radical. However, the stretching force constants are still meaningful, because the observed fundamental frequencies are almost all due to the stretching modes. Therefore, below we will discuss only the difference in the stretching force constants between the neutral TCNE and its anion radical. As is shown in Table 2, K(C=C)=6.31 md/Å, K(C–C)=4.80, and K(C≡N)=16.84 for the neutral TCNE, while K(C=C)=4.00, K(C–C)=5.23, and K(C≡N)=15.70 for its anion radical. We can see that the extra electron on the TCNE anion radical causes the decrease in the K(C=C) and K(C≡N) values and the increase in the K(C–C) value.

It is well known that the stretching force constant, $K(12)$, of a bond (12) in a conjugated system is greatly affected by its bond order, $p(12)$. According to Coulson and Longuet-Higgins,[23] $K(12)$ can be expressed by:

$$K(12) = \{(1-p(12))K_s + p(12)K_d\} + \left\{\frac{K_s K_d(s-d)}{K_s(1-p(12)) + K_d p(12)}\right\}^2 \frac{\pi(1212)}{2}, \quad (2)$$

where K_s and K_d are the force constants associated with pure single and double bonds respectively, where π-(1212) is the self-polarizability of the bond (12), and where s and d are the bond lengths of pure single and double bonds respectively.

In a homopolar carbon-carbon bond, the second term involving the self-polarizability may be small.[24] In this case, the stretching force constant, $K(12)$, is predominantly determined by the bond order, $p(12)$. Therefore, the extra electron on the TCNE anion radical causes a decrease in the C=C bond order, p(C=C), and an increase in the C–C bond order, p(C–C), compared to those of the neutral TCNE. From the values of K(C=C) and K(C–C) in the infrared spectra, the decrease in p(C=C) was estimated to be 0.36, while the increase in p(C–C) was estimated to be 0.08, by using the empirical relationship between $K(12)$ and $p(12)$.[8]

On the other hand, in order to confirm these results, we further calculated the p(C=C) and p(C–C) values of the neutral TCNE and its anion radical by the use of the Hückel molecular orbital theory.[25] It was assumed that the extra electron on the TCNE anion radical enters in the lowest-vacant molecular orbital of the neutral TCNE. This orbital has the irreducible representation of B_{2g}, where the coefficients of the C_1, C_3, and N_7 atomic orbitals are given by 0.5305,

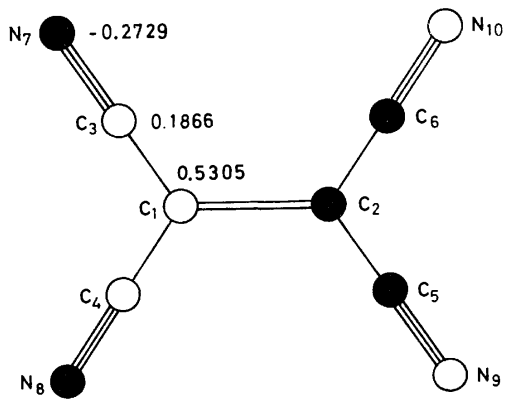

Fig. 2. Schematic representation of the half-occupied molecular orbital of the TCNE anion radical calculated from the Hückel molecular orbital method. The open and closed circles indicate that the coefficients of the atomic orbitals are positive and negative, respectively.

20) E. E. Ferguson and F. A. Matsen, *J. Chem. Phys.*, **29**, 105 (1958).
21) E. E. Ferguson and F. A. Matsen, *J. Amer. Chem. Soc.*, **82**, 3268 (1960).
22) E. E. Ferguson, *J. Chim. Phys.*, **61**, 257 (1964).
23) C. A. Coulson and H. C. Longuet-Higgins, *Proc. Roy. Soc. Ser. A*, **193**, 456 (1948).
24) A. Streitwieser, Jr., "Molecular Orbital Theory", John Wiley & Sons, New York and London (1961).
25) In calculating the Hückel molecular orbitals for the neutral TCNE, the Coulomb integrals of the C and N atoms are taken as α and $\alpha+\beta$, respectively, while the resonance integrals of the C=C, C–C and C≡N bonds, as β, 0.9β and 2.0β, respectively.

0.1866, and −0.2729 respectively (see Fig. 2). Therefore, the extra electron causes a decrease in p(C=C) by 0.28, and an increase in p(C–C) by 0.10, compared to the values of the neutral TCNE. These molecular orbital results are found to agree well with those evaluated from the infrared spectra.

In the heteropolar C≡N bond, although the expression of K(C≡N) *versus* p(C≡N) of the neutral TCNE or its anion radical is not so simple, the extra electron on the TCNE anion radical causes a decrease in K(C≡N); this decrease will definitely lead to a decrease of p(C≡N). In accordance with this view, the Hückel molecular orbital theory shows a decrease in p(C≡N) by 0.05 when an extra electron enters into the lowest-vacant orbital of the neutral TCNE.

Concluding Remarks

The present investigation clearly shows that the difference in the vibrational spectra between the neutral TCNE and its anion radical can be understood on the basis of the difference in their electronic structures. By using these differences, the half-occupied molecular orbital of the TCNE anion radical was found to belong to the B_{2g} irreducible representation. On the other hand, the crystal-field effect may make some contribution to the frequency shifts in these vibrational spectra. In fact, Moore *et al.* observed that certain vibrational frequencies of the TCNE anion radical salts are influenced by the species of the counter cations.[10] However, in a first approximation, this contribution can be neglected in comparison with that of the intramolecular force field.

Rigorously speaking, the $\boldsymbol{G}$ matrix for the anion radical is not identical with that for the neutral TCNE, since the molecular structure of the anion radical is slightly different from that of the neutral TCNE. The difference in their $\boldsymbol{G}$ matrices may make some contribution to the frequency difference. However, this contribution is negligibly small for the bands due to the bond-stretching modes.

The set of force constants obtained for the TCNE anion radical cannot be regarded as a unique solution, since the observation of the fundamental frequencies is limited to the infrared spectra. In this sense, it is also quite desirable to measure the Raman spectrum of the TCNE anion radical. We consider, however, that the set of force constants presented here is reliable enough for studying the difference in the stretching force constants between the neutral TCNE and its anion radical.

In conclusion, the application of the infrared spectra of a neutral molecule and its ion radical can provide valuable knowledge on their electronic structures as well as on their molecular structures. It is interesting to see that their frequency differences give some information concerning the nature of the half-occupied orbital in the ion radical molecular orbitals.

BULLETIN OF THE CHEMICAL SOCIETY OF JAPAN, VOL. 46, 426—430 (1973)

Comparison of the Conductance Equations of Fuoss-Onsager, Fuoss-Hsia and Pitts with the Data of Bis(2,9-dimethyl-1,10-phenanthroline)Cu(I) Perchlorate

Katsuhiko MIYOSHI

Department of Chemistry, Faculty of Science, Hiroshima University, Hiroshima

(Received August 14, 1972)

Conductance equations derived by Fuoss-Onsager (1965), Fuoss-Hsia (1967) and Pitts (1953) were compared using the conductance data of bis(2,9-dimethyl-1,10-phenanthroline)Cu(I) perchlorate in acetonitrile, nitrobenzene and nitromethane at 25°C, which have relatively high dielectric constant. The chelate salt was found to be completely dissociated in these solvents. Though the Pitts equation was found to reproduce the data more satisfactorily than the Fuoss-Onsager (F–O) and the Fuoss-Hsia (F–H) equations, the derived distance of the closest approach a from the Pitts equation was unrealistically small for the bulky complex salt. It was shown that the F–H equation is preferable for the analysis of conductance data for both associated and unassociated electrolytes.

Theoretical comparison of the conductance theories established by Fuoss and Onsager,[1,2] and Pitts[3] was made recently by Pitts *et al.*[4] They pointed out that though both theories were nominally based on the same model of "a charged sphere in a continuum" there were differences in formulation and procedure, and they criticised the boundary conditions used in the F–O theory. Fuoss and Onsager assumed that only the radial component of the vector velocity vanishes at contact and that the potential and field should be continuous when the distance between two ionic centers is equal to a. On the other hand, Pitts required the conditions that the asymmetric (perturbed) part of the potential must vanish at $r=a$ and the velocity vector vanish on the surface of the ion. They emphasized the superiority of the Pitts theory by comparing the extent of fitting of both theories to experimental data.

Stokes[5] was the first to compare these theories ex-

1) R. M. Fuoss and L. Onsager, *J. Phys. Chem.*, **61**, 668 (1957).
2) R. M. Fuoss, L. Onsager and J. F. Skinner, *ibid.*, **69**, 2581 (1965).
3) E. Pitts, *Proc. Roy. Soc. Ser. A*, **217**, 43 (1953).
4) E. Pitts, B. E. Tabor and J. Daly, *Trans. Faraday Soc.*, **65**, 849 (1969), *ibid.*, **66**, 693 (1970).
5) R. H. Stokes, *J. Phys. Chem.*, **65**, 1242 (1961).

perimentally and reported that the F–O equation reproduced the conductance data of hydrochloric acid in water at 25°C only up to 0.004 N, whereas the Pitts equation could be applied to 0.02 N. Fernandez-Prini and Prue[6] also compared these equations using high precision data of inorganic salts composed of monoatomic ions in water, methanol and dimethyl formamide all of which are hydrogen-bonded solvents and solvate strongly to ions, especially small ions. They found that the Pitts equation accounts satisfactorily for the experimental data and the derived parameters are reasonable except in methanol, in which the distance of the closest approach calculated by the Pitts equation was found to be smaller than that by the F–O equation by about 1 Å. However, it is ambiguous whether the derived a-value corresponds to the contact or the solvent-separated contact distance of an ion pair, since both types of ion pairs may exist in the hydrogen-bonded solvents such as water and methanol. A reasonable value of a can therefore have some arbitrariness.

Thus, measurements with bulky electrolytes in some aprotic organic solvents which do not seem to solvate ions strongly are expected to clarify whether a-values obtained are reasonable or not, since a-values in this case will correspond to the contact distances. Bis(2,9-dimethyl-1,10-phenanthroline)Cu(I) perchlorate was chosen because of its stability in solution and symmetry, thus being suitable as a model electrolyte for conductance measurement. Since the chelate cation is surrounded by bulky aromatic groups, the association constants are expected to be smaller than those of the hydrodynamically corresponding tetrabutylammonium salt in which the positive charge is located predominantly on the nitrogen atom.[7]

Experimental

Materials. Bis(2,9-dimethyl-1,10-phenanthroline)Cu(I) perchlorate (Dojin Chemicals Ltd.) was recrystallized from acetone solution. Its purity was checked by analysis. The analytical data were as follows. Found: C, 58.05; H, 4.11; N, 9.67%. Calcd for $C_{28}H_{24}N_4O_4ClCu$: C, 58.03; H, 4.17; N, 9.67%. The stability of the chelate cation in each solvent was confirmed by the absorption spectrum in the visible region. Nitrobenzene was washed three times with conductivity water, kept over anhydrous calcium chloride for several days and filtered off. The filtrate was passed through a molecular sieve and fractionated under reduced pressure (below 10 mmHg). The product was still slightly yellow, its specific conductance being negligibly small. Reagent grade acetonitrile was kept over potassium hydroxide pellets for 24 hr and distilled over phosphorus pentoxide, followed by fractionation. Its specific conductance was 3.3×10^{-8} ohm^{-1}cm^{-1}. Reagent grade nitromethane was dried with anhydrous calcium chloride and distilled over drierite under reduced pressure. A middle fraction was collected. Its specific conductance was 6.0×10^{-8} ohm^{-1}cm^{-1}. Purity of the solvents was checked by measuring their densities. Observed values were 1.1986 and 0.7766 for $PhNO_2$ and CH_3CN, respectively, which were in good agreement with the values in literature, viz., 1.1977[8] and 0.7767,[9] respectively. The density of CH_3NO_2 was 1.1298, slightly lower than the value 1.1312 reported by Kay *et al.*[10] They purified CH_3NO_2 by distillation at reduced pressure followed by fractional crystallization, which, however, was found to increase the water content. Water content of the solvents used was examined by titration with the Karl Fischer reagent and found to be less than 0.01 wt% in CH_3NO_2 and CH_3CN and 0.001wt% in $PhNO_2$. Other physical properties of the solvents were taken from literature.[8,9,10]

Apparatus and Procedure. Conductance measurements were carried out with a conductometer, type MY-7 (Yanagimoto Mfg. Co., Ltd.) with a Wheatstone bridge (800 c/s). All the resistances were calibrated with a resistance box (Yokogawa Electric Works Ltd.) standardized by Shinkawa Electric Co. Pyrex conductance cells were of Erlenmeyer type with lightly platinized electrodes, containing about 200 ml of solution, and were standardized with aqueous KCl solutions, using the Lind, Zwolenik and Fuoss constants.[11] Potassium chloride was recrystallized three times from conductivity water and dried at 500°C. Cells were washed with nitric acid and steam before each run. Cell solutions were thermostated to 25±0.01°C in a double water bath with a mercury-in-glass thermoregulator. In order to attain temperature equilibrium rapidly and avoid the polarization effect during measurements, the solution in the cell was stirred by a magnetic stirrer. All solutions were prepared gravimetrically since the molecular weight of the complex salt is very high (579.522). For each run, a sample of 100—110 mg was directly added to the solvent of known conductivity in the cell. After a constant value of resistance was attained, 30 ml of solution was siphoned out and an equal volume of the solvent was added to the cell. The procedure was continued until an appropriate concentration was attained. Concentration range was $\kappa a<0.2$ within which the approximations used to establish the conductance equations are valid. CH_3CN and CH_3NO_2 are so volatile and hygroscopic that a drybox was used for preparation of the solutions.

Results and Discussion

The measured equivalent conductance Λ and the corresponding concentration C in equivalents per liter are given in Table 1. These data were analyzed by means of the following three equations for unassociated electrolytes.

Fuoss-Onsager equation (1965)[2]:

$$\Lambda = \Lambda_0 - SC^{1/2} + E'C\ln(6E_1'C) + LC \qquad (1)$$

$$S = \alpha\Lambda_0 + \beta_0,\quad E' = E_1'\Lambda_0 - E_2',$$

$$E_1' = 2.942\times10^{12}/(DT)^3,$$

$$E_2' = 0.4333\times10^8/\eta(DT)^2,\quad L = L_1 + L_2(b),$$

$$ab = \beta = e^2/DkT$$

$$L_1 = 3.202E_1'\Lambda_0 - 3.420\,E_2' + \alpha\beta_0$$

$$L_2(b) = 2E_1'\Lambda_0 h(b) + 44E_2'/3b - 2E'\ln b$$

$$h(b) = (2b^2+2b-1)/b^3$$

6) R. Fernandez-Prini and J. E. Prue, *Z. Phys. Chem.* (Leipzig), **228**, 373 (1965).

7) K. Miyoshi, *J. Phys. Chem.*, **76**, 3029 (1972).

8) E. Hirsch and R. M. Fuoss, *J. Amer. Chem. Soc.*, **82**, 1018 (1960).

9) D. F. Evans, C. Zawoyski, and R. L. Kay, *J. Phys. Chem.* **69**, 3878 (1965).

10) R. L. Kay, S. C. Blum, and H. I. Schiff, *ibid.*, **67**, 1223 (1963).

11) J. Lind, J. Zwolenik, and R. M. Fuoss, *J. Amer. Chem. Soc.*, **81**, 1557 (1959).

Fuoss-Hsia equation (1967)[12] modified by Fernandez-Prini (1969)[13]:

$$\Lambda = \Lambda_0 - SC^{1/2} + EC\log C + J_1C - J_2C^{3/2} \quad (2)$$

$$E = E_1\Lambda_0 - E_2,\ E_1 = 2.3026(\kappa^2a^2b^2/24C),$$

$$E_2 = 2.3026(\kappa ab\beta_0/16C^{1/2}),\ J_1 = \delta_1\Lambda_0 + \delta_2$$

$$J_2 = \delta_3\Lambda_0 + \delta_4$$

$$\delta_1 = [(\kappa ab)^2/24C][1.8147+2\ln(ka/C^{1/2}) + 2h(b)]$$

$$\delta_2 = \alpha\beta_0 + \beta_0(\kappa a/C^{1/2}) - \beta_0[(\kappa ab)/16C^{1/2}] \times[1.5337+(4/3b)+2\ln(\kappa a/C^{1/2})]$$

$$\delta_3 = [b^2(\kappa a)^3/24C^{3/2}][0.6094+(4.4748/b)+(3.8284/b^2)]$$

$$\delta_4 = [\beta_0(\kappa ab)^2/24C][2h(b)-1.9384]+\alpha\beta_0(\kappa a/C^{1/2}) + [\beta_0(\kappa a)^2/C] - [\beta_0 b(\kappa a)^2/16C][1.5405+(2.2761/b)] - (\beta_0^2\kappa ab/16\Lambda_0C^{1/2})[(4/3b)-2.2194]$$

Pitts equation (1953)[3] modified by Fernandez-Prini and Prue (1965)[6,14]:

$$\Lambda = \Lambda_0 - SC^{1/2} + EC\log C + J_1C - J_2C^{3/2} \quad (3)$$

$$\delta_1 = (\kappa ab)^2[\ln(\kappa a/C^{1/2}) + 2/b + 1.7718]/12C$$

$$\delta_2 = \beta_0\kappa a/C^{1/2} + \beta_0\kappa ab[0.01387-\ln(\kappa a/C^{1/2})]/8C^{1\,2}$$

$$\delta_3 = (\kappa ab)^3[1.2929/b^2 + 1.5732/b]/6C^{3/2}$$

$$\delta_4 = \beta_0(\kappa a)^2/C + 0.23484\beta_0 b(\kappa a)^2/3C$$

All calculations were performed on a TOSBAC 3400 digital computer using the least squares method proposed by Kay.[15] The following equation was used.

$$\Delta\Lambda = \Lambda(\text{obsd}) - \Lambda(\text{calcd}) = \Delta\Lambda_0 + (C\partial J_1/\partial a - C^{3/2}\partial J_2/\partial a)\Delta a$$

(In Fernandez-Prini and Prue's paper, equation (8) is misprinted.) In order to bring the data into conformity with Fernandez-Prini's treatment, the data weighted by concentration were also analysed. No viscosity correction was made. Parameters obtained

Table 1.

CH_3CN		CH_3NO_2		$PhNO_2$	
$C\times10^4$	Λ	$C\times10^4$	Λ	$C\times10^4$	Λ
36.367	139.98	26.769	87.090	29.691	28.509
29.958	141.55	24.159	87.503	27.078	28.656
25.535	142.76	21.995	87.873	24.583	28.795
22.232	143.76	20.206	88.186	22.064	28.945
18.444	145.02	16.957	88.818	19.784	29.096
16.519	145.66	15.238	89.176	17.539	29.249
14.663	146.38	13.812	89.497	15.523	29.401
12.198	147.45	12.132	89.894	11.972	29.700
9.9121	148.52	10.875	90.206	9.3770	29.957
8.5128	149.27	9.4738	90.592	8.1487	30.085
				6.9359	30.224

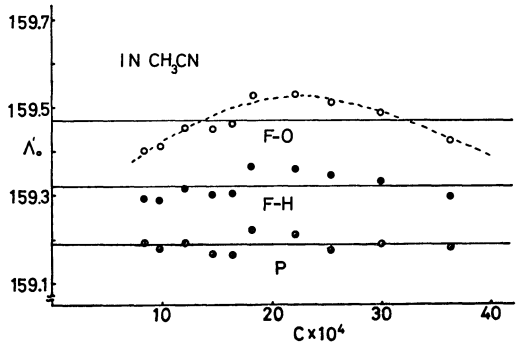

Fig. 1. Λ_0' plots in CH_3CN.

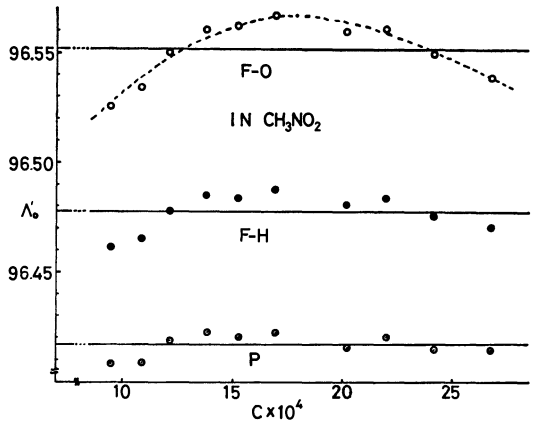

Fig. 2. Λ_0' plots in CH_3NO_2.

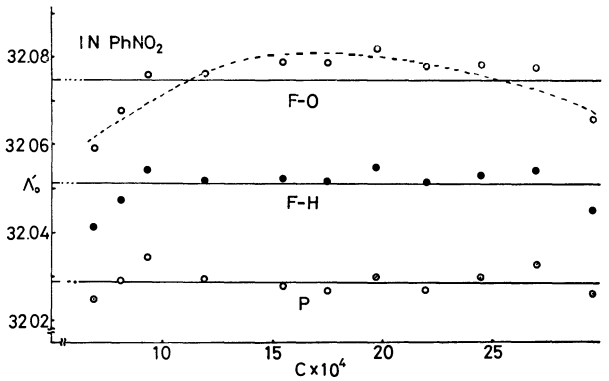

Fig. 3. Λ_0' plots in $PhNO_2$.

are given in Tables 2 and 3, where σ is a standard deviation. The complex salt was found to be completely dissociated in these solvents, since when the data were treated with a three-parameter equation involving the association constant K_A, a negative K_A with a larger standard deviation was derived. The magnitude of standard deviations in Tables 2 and 3 clearly indicates that the Pitts equation is preferable to the F–O and F–H equations.

As is suggested by Fernandez-Prini and Prue,[6] it is useful to introduce Λ_0' to examine the fitting,

$$\Lambda_0' = \Lambda(\text{obsd}) - \Lambda(\text{calcd}) + \Lambda_0$$

Λ_0' calculated from the observed conductance weighted by concentration is plotted against concentration in Figures 1, 2 and 3. We see that the Pitts equation

12) R. M. Fuoss and K-L. Hsia, *Proc. Nat. Acad. Sci.*, **57**, 1550 (1967).
13) R. Fernandez-Prini, *Trans. Faraday Soc.*, **65**, 3311 (1969).
14) According to the modification by Pitts in 1969, the numerical constant 0.23484 in δ_4 is reported to become 0.52772. E. Baumgartner, M. Busch, and R. Fernandez-Prini, *J. Phys. Chem.*, **74**, 1821 (1970).
15) R. L. Kay, *J. Amer. Chem. Soc.*, **82**, 2099 (1960).

Table 2. Derived parameters (unweighted)

		CH_3CN	CH_3NO_2	$PhNO_2$
Fuoss-Onsager	Λ_0	159.44	96.540	32.069
	a(Å)	4.22±0.04	4.54±0.04	4.35±0.03
	L	1247±16	777.3±7.8	266.4±2.7
	σ	0.046	0.014	0.007
Fuoss-Hsia	Λ_0	159.30	96.470	32.048
	a(Å)	4.64±0.02	5.01±0.40	4.73±0.01
	J_1	2169±8	1320±80	482.3±1.0
	J_2	3000±60	2000±1300	657.2±3.9
	σ	0.030	0.010	0.0046
Pitts	Λ_0	159.19	96.413	32.029
	a(Å)	3.46±0.02	3.85±0.24	3.47±0.01
	J_1	2347±5	1418±48	519.4±0.7
	J_2	5610±40	3600±800	1259±3
	σ	0.020	0.006	0.0032

Table 3. Derived parameters (weighted by concentration)

		CH_3CN	CH_3NO_2	$PhNO_2$
Fuoss-Onsager	Λ_0	159.47	96.552	32.075
	a(Å)	4.17±0.04	4.51±0.04	4.31±0.03
	L	1230±16	771.5±7.3	263.5±2.7
	σ	0.015	0.0042	0.0019
Fuoss-Hsia	Λ_0	159.32	96.478	32.051
	a(Å)	4.60±0.02	4.99±0.38	4.71±0.01
	J_1	2156±8	1320±80	480.4±0.8
	J_2	2950±50	2000±1200	649.5±2.3
	σ	0.010	0.0028	0.0013
Pitts	Λ_0	159.19	96.417	32.029
	a(Å)	3.45±0.01	3.84±0·22	3.47±0.01
	J_1	2344±5	1416±45	519.2±0.6
	J_2	5592±33	3600±700	1258±2
	σ	0.006	0.0016	0.0009

shows the best performance in every case. The plots of Λ_0' from the F–O equation have a curvature, meaning a deficiency of the concentration dependent terms in the equation. Similar results were obtained for hydrogen chloride in water and alkali metal halides in water, methanol and dimethyl formamide by Fernandez-Prini and Prue and for alkali metal halides in water by Pitts *et al.*[4] The plot from the F–H equation which contains $C^{3/2}$ term also seems to be curved, but the curvature is not so noticeable as that from the F–O equation. On the other hand, Tables 2 and 3 show that a-values obtained with the Pitts equation are considerably smaller than those with the F–O and F–H equations. This trend is also found by Fernandez-Prini and Prue.

Perchlorate ion is known to be one of the least solvated ions and it may be assumed that a large cation such as this chelate is not solvated, since the positive charge on the cation is screened by the bulky aromatic ligands. Thus a-values in this case will correspond to the contact distance between the cation and the anion.

It may thus be concluded that a-values from the Pitts equation are unrealistically small because the sum of the crystallographic radius of ClO_4^- and that of the chelate cation estimated from the bond lengths significantly exceeds 3.5 Å obtained with the Pitts equation. (The crystallographic radius of the chelate cation is not found in literature to the author's knowledge). It is also seen from Tables 2 and 3 that a-values derived with the F–O and F–H equations seem to be small for the bulky complex perchlorate. However, it should be noted that a-values generally show a considerable dependence upon the dielectric constant of the medium,[2,16] and that those obtained with tetraalkylammonium halides and picrates in CH_3NO_2, MeOH and CH_3CN are almost constant irrespective of a considerable variation in crystallographic radius and smaller than those expected from their ionic radii, viz., the derived a-values are 3.9± 0.3 Å,[10] 3.6±0.2 Å,[17] and 3.6±0.2 Å[9] for all the halides and picrates investigated in CH_3NO_2, MeOH and CH_3CN, respectively. Of course a viscosity correction affecting a-values to some extent[9] was made in

16) J. Lind and R. M. Fuoss, *J. Phys. Chem.*, **65**, 999, 1414 (1961), *ibid.*, **66**, 1727 (1962).
17) R. L. Kay, C. Zawoyski, and D. F. Evans, *ibid.*, **69**, 4208 (1965).

these cases. Evans and Gardam[18] found that when the F–H equation was applied to several tetraalkylammonium salts in alcohols, small but constant a-values were obtained which were independent of the dielectric constant. It is seen from Tables 2 and 3 that a-values from the F–H equation are slightly larger than those from the F–O equation. Though the continuum theory is adequate to describe the concentration dependence of the conductance, the size dependence in the F–O theory appears to need revision.[17]

The reason why the Pitts equation in general gives smaller values of a has been discussed by Fernandez-Prini and Prue[6,13] in outline and by Pitts[4] in detail. The main differences between these theories lie in the boundary conditions used to solve the equation of continuity. Pitts neglected the Brownian terms in the velocity of the ion from the viewpoint of the model his theory was based on. The Pitts equation does not allow for the kinetic (osmotic) term which contributes to the increase in the velocity of the ion in the F–O theory. Valleau[19] pointed out that this term should be regarded as completely unrealistic and should be dropped. Recently Carman[4,20] has stated from the consideration of the cancellation of terms in the F–O theory that the E value in the F–O theory should be $(E_1\Lambda_0-2E_2)$[21] but not $(E_1\Lambda_0-E_2)$. He emphasized that the F–O and Pitts theories are not mutually exclusive since they are based on the same model.

As Pitts *et al.*[4] pointed out, it is too complicated to discuss the two theories term by term and it is more useful to compare the resulting parameters. When the data of the complex salt in CH_3CN–CCl_4 and $PhNO_2$–CCl_4 mixtures with dielectric constants less than 15 were analyzed with the Pitts equation involving the association constant K_A term, no convergence was obtained whereas the F–O and the F–H equations gave reasonable parameters.[22]

From the present discussions, it is concluded that the F–H equation is recommended for the analysis of the conductance data of both unassociated and associated electrolytes also in these aprotic solvents.[13]

The author wishes to express his deep gratitude to Professor Yuroku Yamamoto, Hiroshima University, and to Mr. Toshihiro Tominaga for their valuable discussions and directions in the course of this study.

18) D. F. Evans and P. Gardam, *J. Phys. Chem.*, **72**, 3281 (1968).
19) J. P. Valleau, *ibid.*, **69**, 1745 (1965).
20) P. C. Carman, *ibid.*, **74**, 1653 (1970).
21) A. D'Aprano, *ibid.*, **75**, 3290 (1971).
22) K. Miyoshi and T. Tominaga, to be submitted in *J. Phys. Chem.*

BULLETIN OF THE CHEMICAL SOCIETY OF JAPAN, VOL. 46, 430—434 (1973)

Anodic Oxidation of Benzoic Acid in Nitriles

Yoshiharu MATSUDA,* Kazuo KIMURA, Chiaki IWAKURA, and Hideo TAMURA

Department of Applied Chemistry, Faculty of Engineering, Osaka University, Yamadakami, Suita, Osaka

(Received March 13, 1972)

The anodic oxidation of benzoic acid in acetonitrile and propionitrile was studied. Electrolysis was employed under a controlled potential or current. Benzoic acid was changed into an intermediate benzoyloxy radical through de-electronation in acetonitrile, and the resulting radical was reacted with acetonitrile to give *N*-acetylanthranilic acid in a 38% yield under constant potential electrolysis. In propionitrile, the anodic oxidation gave *N*-propionylanthranilic acid, *N*-propionylbenzamide, and dipropionylamine. No Kolbe-type reaction was observed.

Many works[1-3] have been reported on the anodic oxidation of aliphatic carboxylic acids, which is connected with the Kolbe reaction. On the other hand, the anodic oxidation of aromatic carboxylic acids has been investigated by only a few workers[4-8], and the mechanism has not yet been discussed. Therefore, it is of interest to investigate the anodic oxidation of aromatic carboxylic acids and discuss its mechanism. Fichter and Uhl[8] have reported that the anodic oxidation of benzoic acid in an aqueous solution gave hydroxybenzoic acid, hydroquinone, and catechol.

In an attempt at testing the solvent effect on the anodic oxidation of benzoic acid, we used acetonitrile and propionitrile instead of water. The electrolysis was employed under a controlled potential or current. Benzoic acid was changed into a benzoyloxy radical, the intermediate, through de-electronation in acetonitrile, and the resulting radical was reacted with the nitrile to give *N*-acetylanthranilic acid in a 38% yield under a constant potential electrolysis. In pro-

* Present address: Faculty of Engineering, Yamaguchi University, Tokimadai, Ube, Yamaguchi.

1) S. Glasstone and A. Hickling, *Trans. Electrochem. Soc.*, **75**, 333 (1939).

2) C. L. Wilson and W. J. Lippincott, *J. Amer. Chem. Soc.*, **78**, 4290 (1956).

3) K. Sugino, T. Sekine and N. Sato, *Electrochem. Technol.*, **1**, 112 (1963).

4) M. J. Allen, "Organic Electrode Process", Reinhold Publishing Corporation, New York, N. Y. (1958), p. 107.

5) S. Arita, N. Hirai, K. Yamamoto and K. Takeshita, *Kogyo Kagaku Zasshi*, **71**, 2018 (1968).

6) K. Koyama, K. Yoshida and S. Tsutsumi, Thi sBulletin, **39**, 516 (1966).

7) K. Sasaki and W. J. Newdy, *J. Electroanal. Chem.*, **20**, 162 (1969).

8) F. Fichter and E. Uhl, *Helv. Chim. Acta*, **3**, 22 (1920).

pionitrile, the anodic oxidation afforded *N*-propionylanthranilic acid, *N*-propionylbenzamide, and dipropionylamine. No Kolbe-type reaction was observed.

Experimental

Reagents. The benzoic acid, lithium perchlorate, acetonitrile, and propionitrile used were reagents guaranteed by JIS and the Wako Pure Chemical Ind. Co., Ltd. The nitriles were refluxed over phosphorus pentoxide and distilled.

Electrodes and Electrolytic Cells. A platinum wire sealed into a glass tube with the surface area of 0.289 cm^2 was used as the anode for the study of the mechanism. The volume of the H cell with a sintered glass disk diaphragm was 50 ml. In the electrolysis at a constant current or potential, a platinum plate with the effective surface area of 2×2 cm^2 was used as the anode, and the volume of the cell was 200 ml. The electrodes were polished with emery paper and then immersed in acetone for 10 min. Iron, nickel, lead, lead oxide, titanium, tantalum, and gold were also tested as anode materials. The base electrolyte solutions were nitriles containing lithium perchlorate, and benzoic acid was added to the anode compartment. The reference electrode was a saturated calomel electrode or a silver nitrate electrode (Ag/0.1 M $AgNO_3$ in CH_3CN), and a Luggin capillary and a salt bridge were used for the junction between a test electrode and a reference electrode. The cathode was a mercury-pool electrode. Triangular potential waves were generated by using a potentiostats and a function generator. The electrolysis was generally operated at a constant current or at a constant potential.

Measurement of Current-potential Curves. Argon gas was bubbled into the electrolyte for 10 min before the electrolysis. In the measurement by the stationary method, the anode potential was kept at each initial voltage in the range from 1.6 to 1.9 V (*vs.* SCE) for 5 min, and then the potential was anodically moved. In the case of single-sweep voltammetry, the anode potential was initially kept at 1.7 V (*vs.* Ag/0.1 N Ag^+) for 5 min, and then the potential was anodically swept at the rate of 16.2 mV/sec.

Anodic Oxidation of Benzoic Acid in Acetonitrile at a Constant Current. During the electrolysis, lithium perchlorate was sometimes added to the electrolyte to suppress the rise in the electric resistance of the electrolyte by the consumption of benzoic acid and lithium perchlorate. After the electrolysis, the solvent acetonitrile was removed from the anolyte by distillation and 100 ml of water was added to the residue. The aqueous solution was extracted with 100 ml of ether. After washing with 50 ml of water, the ether solution was dried over anhydrous sodium sulfate and concentrated. The residue (1.78 g) was chromatographed on Wakogel ($SiO_2 \cdot xH_2O$). Upon chromatography, the first fraction (eluent: n-hexane) gave 0.23 g of a yellow liquid (unidentified). The second fraction (eluent : benzene) afforded 0.37 g of benzoic acid. The third fraction gave 0.76 g of *N*-acetylanthranilic acid (mp 180—181°C (lit,[9] 186°C)); a mixed-mp determination with an authentic sample showed no depression. The structure was also identified by IR and mass spectra. The fourth fraction gave 0.40 g of a brown viscous liquid (unidentified). When the catholyte was treated by the same procedure, *N*-acetylanthranilic acid (0.13 g), benzoic acid (0.67 g), and an unidentified substance (0.95 g) were obtained.

9) A. Kaufmann, *Ber.*, **42**, 3480 (1909).

Anodic Oxidation of Benzoic Acid in Propionitrile at a Constant Current. After electrolysis, the anolyte and the catholyte were basified with aqueous sodium hydroxide and organic materials were extracted with 100 ml of ether, respectively. The organic layer was concentrated, and the residue (1.65 g) from the anolyte was chromatographed on Wakogel. The first fraction (eluent : hexane) gave 0.11 g of an unidentified liquid. The second fraction (eluent : benzene) afforded 0.48 g of *N*-propionylbenzamide (mp 97.0°C (lit,[10] 98°C)); the structure was identified as above. The third fraction (eluent : ether) afforded 0.39 g of dipropionylamine (mp 153—154°C (lit,[11] 153—154°C)); a mixed-mp determination with an authentic sample showed no depression; the structure was identified as above. The fourth fraction (eluent : ether and methanol) gave 0.63 g of a dark brown viscous liquid (unidentified). The aqueous layer was acidified with aqueous sulphuric acid, and then extracted with ether. After the removal of the ether, the residue (1.50 g) was similarly chlomatographed on Wakogel. The first fraction (eluent : hexane) gave 0.09 g of a brown viscous liquid (unidentified). The second fraction (eluent : benzene) gave 0.17 g of recovered benzoic acid, while the third fraction (eluent : benzene) gave 0.13 g of an unidentified yellow viscous liquid. The fourth fraction (eluent : ether) afforded 0.88 g of *N*-propionylanthranilic acid (mp 116—117°C (lit,[12] 117°C)); a mixed-mp determination with an authentic sample showed no depression; the structure was identified by means of the IR, mass, and NMR spectra. The fifth fraction (eluent : methanol) gave 0.21 g of a dark brown viscous liquid (unidentified). The catholyte was treated in the same way as above, giving *N*-propionylanthranilic acid (0.18 g), recovered benzoic acid (0.11 g), dipropionylamine (trace), and an unidentified substance (1.58 g).

Anodic Oxidation of Benzoic Acid in Acetonitrile at a Constant Potential. The anode potential was kept at 2.20 V against a silver nitrate electrode. The reaction products were treated in the same way as in the anodic oxidation of benzoic acid in acetonitrile at a constant current.

Results and Discussion

A typical potential-current curve of benzoic acid in acetonitrile obtained by the stationary method using a platinum-wire electrode is shown in Fig. 1. The anodic oxidation current was observed beyond 2.0 V against SCE. Similar potential-current curves were obtained in the anodic oxidation of benzoic acid in propionitrile. The single-sweep voltammetry was also applied. The shapes of the potential-current curves were similar to that obtained by the stationary method, and the oxidation current of benzoic acid was observed over 1.9 V against a Ag/0.1 N Ag^+ electrode.

By using single-sweep voltammetry, some materials were tested for the anode in acetonitrile containing lithium perchlorate in order to observe the effect of the base electrolyte. In the cases of platinum and gold electrodes, the current resulting from the anodic oxidation of the electrolyte was observed over approxi-

10) B. Prager, P. Jacobson, P. Schmidt and D. Stern, Beilsteins Handbuch der Organischen Chemie, Vierte Auflage, **9**, 213 (1926).

11) R. Otto and J. Tröger, *Ber.*, **23**, 759 (1890).

12) B. Prager, P. Jacobson, P. Schmidt and D. Stern, Beilsteins Handbuch der Organischen Chemie, Vierte Auflage, **14**, 340 (1931).

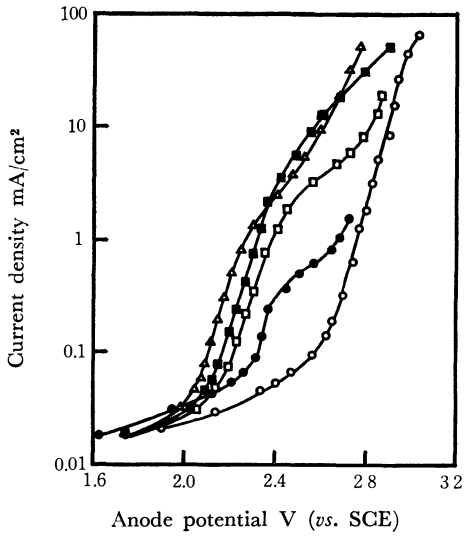

Fig. 1. Relation between anode potential and logarithm of current density on the anodic oxidation of benzoic acid in acetonitrile by stationary method. 30°C, Pt electrode.
—○—: acetonitrile+0.5 M $LiClO_4$
—●—: acetonitrile+5×10^{-4} M benzoic acid+0.5 M $LiClO_4$
—□—: acetonitrile+5×10^{-3} M benzoic acid+0.5 M $LiClO_4$
—■—: acetonitrile+5×10^{-2} M benzoic acid+0.5 M $LiClO_4$
—△—: acetonitrile+5×10^{-1} M benzoic acid+0.5 M $LiClO_4$

mately 2.3 V. Therefore, these electrodes were suitable for use as anodes in this study. In contrast, on the iron, nickel, lead, lead oxide, titanium, and tantalum anodes, the oxidation current of the electrolyte not containing benzoic acid appeared below 1.9 V. This result shows that these materials are not suitable as anodes.

The anodic oxidation of benzoic acid at a constant current gave mainly *N*-acetylanthranilic acid in a 20% yield,[13] together with unreacted benzoic acid and a small amount of unidentified products. The overall results of the electrolysis are shown in Table 1. The *N*-acetylanthranilic acid obtained in the catholyte must have migrated from the anolyte through the diaphragm.

During the electrolysis, a gas, which was confirmed by gas chromatography to be composed of nitrogen, oxygen, carbon dioxide, hydrogen, and methane, was evolved on both the anode and the cathode. The imbalance in the material balance in Table 1 must be due to the gas evolution.

Table 1. Results of anodic oxidation of benzoic acid in acetonitrile at a constant current

Anode: Pt, Cathode: Hg, Supporting electrolyte: 1.0 M $LiClO_4$, 30—36°C, 6 hr, Current: 0.4 A, Cell voltage: 18—45 V, Anode potential: 2.45—2.75 V *vs.* SCE, Initial content of benzoic acid: 4.00 g (32.8 mmol)

Product	*N*-Acetylanthranilic acid	Unidentified substance	Recovered benzoic acid
Anolyte	0.76 g (4.2 mmol)	0.63 g	0.37 g (3.0 mmol)
Catholyte	0.13 g (0.72 mmol)	0.95 g	0.67 g (5.5 mmol)

Evolved gas in anode compartment: $CO_2>H_2>CH_4$.

The anodic oxidation of benzoic acid in propionitrile at a constant current was done under conditions corresponding to those in acetonitrile. The overall experimental results are shown in Table 2. *N*-Propionylanthranilic acid, *N*-propionylbenzamide, and dipropionylamine were produced. During the electrolysis, the evolution of a gas composed of hydrogen, carbon dioxide, ethane, and ethylene was similarly observed.

The results of the anodic oxidation of benzoic acid at a constant potential are shown in Table 3. In this electrolysis, no gas evolution was observed, since the polarization on the anode was suppressed.

The comparison of the current efficiencies of the anodic oxidation of benzoic acid in acetonitrile between that at a constant current and that at a constant potential are shown in Table 4; we assumed that two electrons are consumed in the reaction process to produce *N*-acetylanthranilic acid. In the anodic oxidation at a constant potential, gas was not evolved and the side reactions was probably suppressed. Therefore, the material balance in Table 3 is explicable.

For the purpose of clearing the reaction mechanism, some electrochemical measurements were applied; the single-sweep voltammetry was introduced initially. A remarkable anodic oxidation current was measured over 2.0 V against the reference electrode. The Tafel relation was obtained in the potential range from 2.05 to 2.20 V, when the base current due to the anodic

Table 2 Results of anodic oxidation of benzoic acid in propionitrile at a constant current

Anode: Pt, Cathode: Hg, Supporting Electrolyte: 0.1 M $LiClO_4$, 30—37°C, 15 hr, Current: 0.2A, Cell voltage: 50—80 V, Anode potential: 2.20—2.24 V *vs.* SCE, Initial content of benzoic acid: 5.00 g (40.9 mmol).

Product	*N*-Propionyl-anthranilic acid	*N*-Propionyl-benzamide	Dipropionylamine	Unidentified substance	Recovered benzoic acid
Anolyte	0.88 g (4.6 mmol)	0.48 g (2.7 mmol)	0.39 g (3.0 mmol)	1.17 g	0.17 g (1.4 mmol)
Catholyte	0.18 g (0.93 mmol)	— —	trace trace	1.58 g	0.11 g (0.90 mmol)

Evolved gas in anode compartment: $H_2>CO_2\gg C_2H_6$, C_2H_4.

13) The yield was calculated as the ratio of the numbers of moles of the *N*-acetylanthranilic acid produced and the benzoic acid reacted.

Table 3. Results of anodic oxidation of benzoic acid in acetonitrile at a constant potential

Anode: Pt, Cathode: Hg, Supporting electrolyte: 0.5 M $LiClO_4$, 30°C, Anode potential: 2.20 V *vs.* Ag/Ag^+, 1690 coul., Initial content of benzoic acid: 2.00 g (16.4 mmol)

Product	*N*-Acetylanthranilic acid	Unidentified substance	Recoverd benzoic acid
Anolyte	0.25 g (1.4 mmol)	0.11 g	0.70 g (5.7 mmol)
Catholyte	0.18 g (1.0 mmol)	0.08 g	0.54 g (4.4 mmol)

Table 4. Current efficiencies of the electrolysis of benzoic acid at a constant current and a constant potential

	Yield of *N*-acetyl-anthranilic acid[a)]	Current efficiencies of the electrolysis based on the yield of *N*-acetylanthranilic acid
At a constant potential	38%	28%
At a constant current	20%	16%

a) The yield was calculated as the ratio of the numbers of the *N*-anthranilic acid produced and the benzoic acid reacted.

oxidation of the electrolyte not containing benzoic acid was deduced from each current value in order to estimate the net oxidation current of benzoic acid. These results are shown in Fig. 2. The linear relation between the logarithm of the concentration of benzoic acid and the current was obtained from the data shown in Fig. 3. Since the slope of the lines in Fig. 3 was 1, the reaction order for benzoic acid in the first electrochemical process should be first-order.

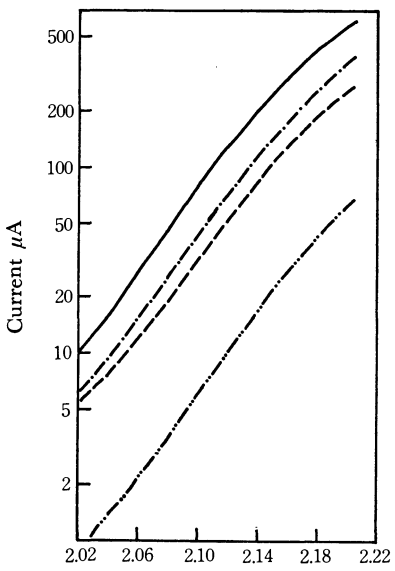

Fig. 2. Relation between anode potential and logarithm of current (deducted residual current) by single-sweep method. 0°C, sweep rate 16.2 mV/sec, Pt electrode (0.289 cm^2)
——: acetonitrile+10^{-3} M benzoic acid+sat. $LiClO_4$
——: acetonitrile+4×10^{-3} M benzoic acid+sat. $LiClO_4$
——: acetonitrile+6×10^{-3} M benzoic acid+sat. $LiClO_4$
——: acetonitrile+10^{-2} M benzoic acid+sat. $LiClO_4$

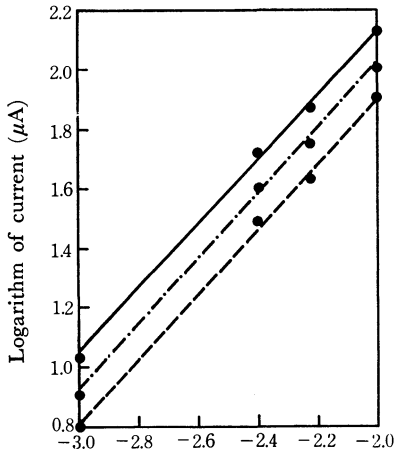

Fig. 3. Relation between logarithm of the concentration of benzoic acid and logarithm of the current by single-sweep method. 0°C, sweep rate 16.2 mV/sec, Pt electrode (0.289 cm^2)
Anode potential
——: 2.10 V (*vs.* Ag/0.1 N Ag^+)
——: 2.11 V (*vs.* Ag/0.1 N Ag^+)
——: 2.12 V (*vs.* Ag/0.1 N Ag^+)

On the basis of the results mentioned above, the rate determining process for the anodic oxidation of benzoic acid could be suggested to be a charge-transfer reaction and its reaction would be first-order for benzoic acid.

At the initial stage, the de-electronation of benzoic acid would produce the radical cation, $[PhCOOH]^+$, on the anode. This radical cation would easily release a proton to yield a benzoyloxy radical, as is shown in Scheme 1.

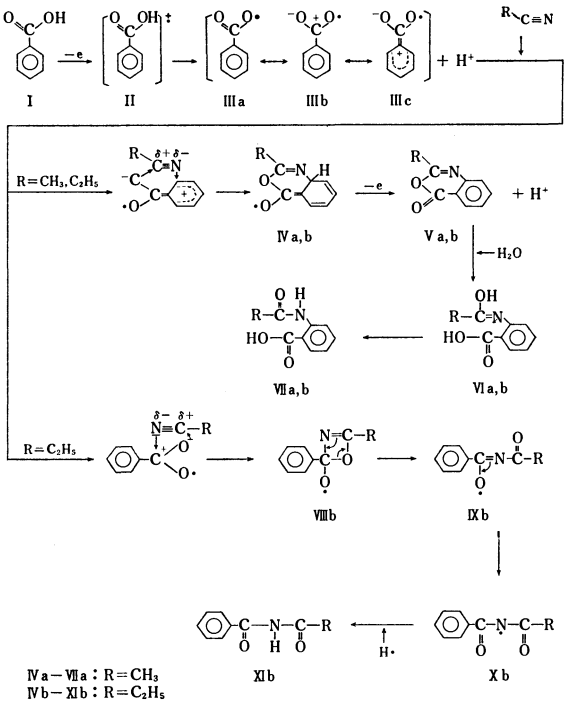

Scheme 1.

In general, the benzoyloxy radical generated by the pyrolysis of benzoyl peroxide in acetonitrile dose not react with acetonitrile to give *N*-acetylanthranilic acid. As acetonitrile is presumed to be inactive in this system, a considerable part of the benzoyloxy radical is expected to be decarbonated. In addition, some part of the benzoyloxy radical abstracts hydrogen from acetonitrile to form benzoic acid and the cyanomethyl radical, which then dimerizes to yield 1,2-dicyanoethane.

However, in this study, the benzoyloxy radical (III in Scheme 1) on the anode does not abstract hydrogen but reacts with acetonitrile, which would be rather active on the anode, to give a new radical (IVa). This radical (IVa) would be immediately oxidized and deprotonated on the anode to give an unstable product, 2-methyl-6*H*-1,3-benzoxazin-6-one (Va). During working-up, this unstable product (Va) would then be hydrolyzed to give *N*-acetylanthranilic acid (VIIa). The reaction mechanism of the anodic oxidation of benzoic acid in acetonitrile is outlined in Scheme 1. A similar reaction is considered for the formation of *N*-propionylanthranilic acid (VIIb) by the anodic oxidation of benzoic acid in propionitrile. Accordingly, on the anodic oxidation of benzoic acid in acetonitrile or propionitrile, the hydrogen at the ortho-position of benzoic acid is displaced by the acetamide or propionamide group in the main process.

On the anodic oxidation of benzoic acid in propionitrile, *N*-propionylbenzamide (XIb) and dipropionylamine were obtained, besides *N*-propionylanthranilic acid (VIIb), though the origin of these different reactivities between the solvent acetonitrile and the propionitrile has not yet been clarified. *N*-Propionylbenzamide (XIb) would be formed according to Scheme 1. Dipropionylamine might be obtained through the coupling of propionitrile and the following hydrolysis, or through the coupling of the propionyl and the *N*-propionyl radicals which arise from the successive electrolysis of the compound (XIb).

In conclusion, the anodic oxidation of benzoic acid in acetonitrile gave *N*-acetylanthranilic acid through the formation of a benzoyloxy radical, its reaction with acetonitrile to form 2-methyl-6*H*-1,3-benzoxazin-6-one, and the following hydrolysis. The anodic oxidation of benzoic acid in propionitrile gave *N*-propionylanthranilic acid, *N*-propionylbenzamide, and dipropionylamine.

The authors wish to express their thanks to Dr. Yoshiki Ohshiro for his helpful discussion and encouragement throughout the course of this work.

BULLETIN OF THE CHEMICAL SOCIETY OF JAPAN, VOL. 46, 434—441 (1973)

The Molecular and Crystal Structure of the *p*-Bromobenzoate of an Unusual Birch Reduction Product

Akio FURUSAKI, Nobuyuki HAMANAKA, and Takeshi MATSUMOTO
Department of Chemistry, Faculty of Science, Hokkaido University, Sapporo

(Received July 17, 1972)

It has already been found that the Birch reduction of 1,1,4aα-trimethyl-2α-hydroxy-8-methoxy-1,2,3,4,4a,9-hexahydrophenanthrene affords a tetrahydro derivative, contrary to expectations. The present paper will describe the details of the molecular structure of the unexpected reduction product, as revealed by an X-ray crystal analysis of its *p*-bromobenzoate (racemate). The crystals are triclinic, with two molecules in a unit cell of the dimensions: $a=11.155$, $b=18.123$, $c=5.912$ Å, $\alpha=94°39'$, $\beta=111°35'$, and $\gamma=90°42'$. The space group is $P\bar{1}$. The intensity measurement was made on an automatic four-circle diffractometer with Cu$K\alpha$ radiation. The structure was solved by the heavy-atom method, and was refined by the block-diagonal-matrix least-squares method, anisotropic thermal motions being assumed for all the non-hydrogen atoms. From a difference map, twenty-six of the thirty-one hydrogen atoms were also found. The final R factor was 6.5%. As a result of the present study, it has been found that the C ring of cyclohexene-type shows an unusual behavior. The length of the C–C single bond opposite to the double bond in this ring is found to be only about 1.34 Å. This remarkable shortening seems to be due to special vibrations of the two atoms concerned. The whole cyclohexene ring takes a considerably flattened, half-chair form.

It has recently been found that the reduction of I with *tert*-butyl alcohol and lithium in liquid ammonia produces a tetrahydro derivative, II (mp 162—164°C), and not the expected product, III or IV, and that the methoxyl group in the product obtained is much more reactive than those in usual allyl methyl ethers.[1] This enhanced reactivity of the methoxyl group seemed to be closely related with the conformation of the tricyclic system in the molecule. In order to obtain reliable information about the molecular conformation of II and to facilitate the understanding of the unusual chemical reactivity, an X-ray crystal analysis of its *p*-bromobenzoate (racemate) has been carried out.

Experimental

Colorless, single crystals of the racemic *p*-bromobenzoate, $C_{25}H_{31}O_3Br$, were obtained from an ether solution. Pre-

1) N. Hamanaka, T. Okuno, T. Nakajima, A. Furusaki, and T. Matsumoto, *Chem. Lett.*, in press.

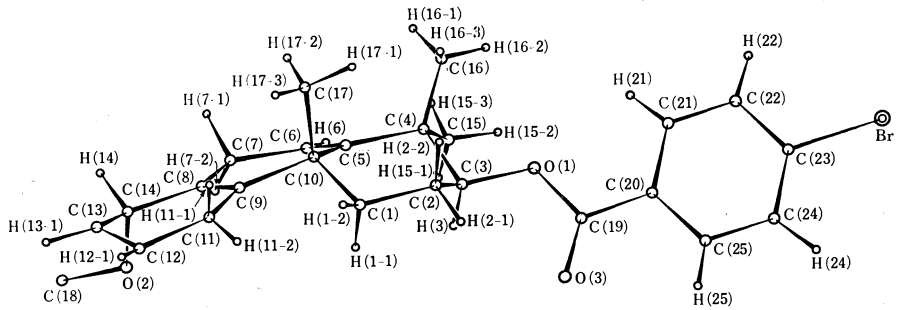

Fig. 1. The molecular framework and the numbering system of the atoms. The five hydrogen atoms which were not located in the difference map are not drawn. The absolute configuration in this picture is the inverse of those in Figs. 2, 3, and 4.

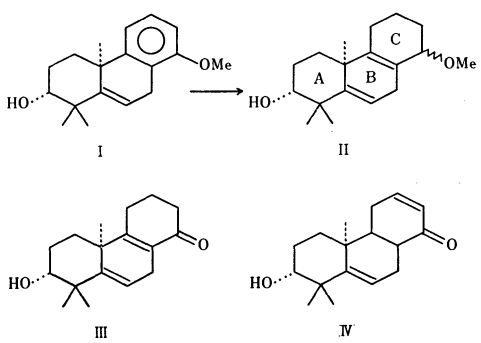

liminary photographic data and optical observations showed that the crystals were probably triclinic. The crystal data derived from diffractometer measurements are summarized in Table 1. A crystal with dimensions of about $0.1\times0.3\times0.5$ mm was sealed in a glass capillary tube and was used for the intensity measurement. The intensity data were collected with an automatic four-circle diffractometer at this University, using monochromatized Cu$K\alpha$ radiation. The intensities of the reflections with 2θ values up to 140° were measured by the ω–2θ scan technique; they were corrected for the Lorentz and polarization factors, but not for the absorption effect. In all, 3079 independent structure factors greater than $3\sigma(F)$ were obtained.

Table 1. The crystal data

Crystal system space group	Triclinic $P\bar{1}$
a	11.155±0.003 Å
b	18.123±0.003
c	5.912±0.002
α	94°39′±3′
β	111°35′±3′
γ	90°42′±3′
Z	2
D_x	1.378 g/cm³

Structure Determination

The space group was assumed to be $P\bar{1}$ throughout the present study. The position of the bromine atom was derived from a sharpened Patterson function. The first Fourier map, based on the heavy atom alone, yielded all the positions of the non-hydrogen atoms. The approximate coordinates thus obtained were first refined by the block-diagonal-matrix least-squares method, using isotropic temperature factors for all the atoms. Five cycles of the refinement reduced the value of the discrepancy factor, R, to 20.5%. Then, the least-squares refinement with anisotropic temperature factors for only the bromine atom was repeated. Consequently, it was found that the thermal parameters of the C(12) and C(13) atoms became very large (10.9 and 8.0 Å² respectively), although the R factor was decreased to 12.7%. In order to confirm the structure thus obtained, a difference synthesis was carried out, excluding five atoms: C(11), C(12), C(13), C(18), and O(2). The resulting map showed that the positions of the five atoms were all essentially correct, and that a single peak corresponded to each of these atoms. The structure thus confirmed was further refined by the least-squares method, anisotropic thermal motions being assumed for all the atoms; the R factor dropped to 8.7%. From a second difference Fourier map, twenty-six of the thirty-one hydrogen-atom positions were found. Further least-squares refinement including these hydrogen atoms reduced the R factor to 6.5%. The atomic parameters thus obtained are listed in Table 2.

All the calculations necessary for the present study were carried out on a FACOM 230—60 computer at the Computer Center of Hokkaido University.

Tables of the observed and calculated structure factors are preserved by the Chemical Society of Japan.

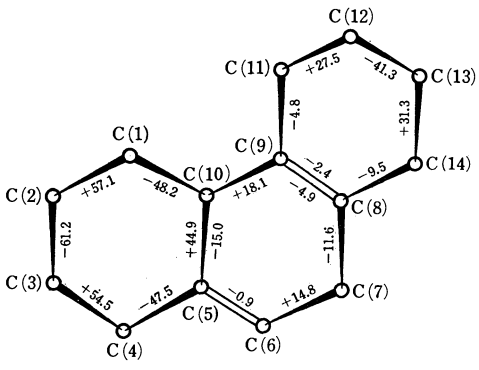

Fig. 2. The torsion angles for the tricyclic system (in degrees).

TABLE 2. THE FINAL ATOMIC PARAMETERS WITH THEIR STANDARD DEVIATIONS

(a) The non-hydrogen atoms

The parameters are multiplied by 10^4.

(1) The fractional coordinates

Atom	x/a	y/b	z/c	Atom	x/a	y/b	z/c
Br	1747.9(7)	8714.6(3)	2955.5(15)	C (12)	4766(7)	972(4)	7677(24)
O (1)	2749(4)	5094(1)	4763(6)	C (13)	3744(7)	492(4)	6884(22)
O (2)	2018(6)	851(2)	8332(9)	C (14)	2439(5)	802(2)	6347(10)
O (3)	3308(5)	5525(2)	8679(7)	C (15)	497(5)	4155(3)	3747(10)
C (1)	4313(4)	3269(2)	6110(9)	C (16)	1604(5)	3994(2)	839(8)
C (2)	4176(5)	4067(2)	5440(9)	C (17)	3420(6)	2562(3)	1916(10)
C (3)	2882(5)	4325(2)	5372(8)	C (18)	1553(8)	175(4)	8814(16)
C (4)	1725(4)	3874(2)	3473(8)	C (19)	2963(4)	5629(2)	6568(8)
C (5)	1922(4)	3049(2)	3982(7)	C (20)	2677(4)	6369(2)	5631(8)
C (6)	945(4)	2636(2)	4066(9)	C (21)	2116(5)	6455(2)	3157(9)
C (7)	1003(5)	1835(3)	4494(12)	C (22)	1819(5)	7153(2)	2375(10)
C (8)	2342(4)	1572(2)	5453(9)	C (23)	2121(4)	7761(2)	4083(10)
C (9)	3354(4)	1972(2)	5494(8)	C (24)	2683(5)	7690(2)	6530(10)
C (10)	3229(4)	2721(2)	4370(8)	C (25)	2954(5)	6987(2)	7297(9)
C (11)	4689(5)	1684(3)	6548(13)				

(2) The anisotropic temperature factors

These are expressed as

$$\exp\left[-(\beta_{11}h^2+\beta_{22}k^2+\beta_{33}l^2+\beta_{12}hk+\beta_{23}kl+\beta_{31}lh)\right].$$

Atom	β_{11}	β_{22}	β_{33}	β_{12}	β_{23}	β_{31}
Br	159.6(7)	24.1(1)	727.7(32)	22.4(4)	102.5(10)	305.0(24)
O (1)	150(4)	20(1)	249(11)	4(3)	28(5)	159(11)
O (2)	285(8)	30(1)	532(19)	−11(5)	71(7)	429(21)
O (3)	241(7)	29(1)	249(12)	12(4)	23(6)	105(15)
C (1)	86(4)	24(1)	353(18)	1(4)	45(7)	110(15)
C (2)	102(5)	25(1)	385(19)	−18(4)	28(8)	120(16)
C (3)	115(5)	20(1)	265(15)	2(3)	34(6)	138(14)
C (4)	96(4)	24(1)	219(14)	9(4)	35(6)	109(13)
C (5)	82(4)	23(1)	216(14)	4(3)	27(6)	100(13)
C (6)	80(4)	32(1)	381(19)	7(4)	83(8)	104(15)
C (7)	89(5)	33(1)	618(28)	−8(4)	125(11)	112(19)
C (8)	88(4)	21(1)	338(17)	7(3)	42(7)	99(14)
C (9)	87(4)	23(1)	295(16)	8(3)	25(7)	117(14)
C (10)	77(4)	22(1)	287(16)	4(3)	25(6)	133(13)
C (11)	101(5)	29(1)	705(31)	18(4)	88(11)	236(21)
C (12)	113(7)	44(2)	1819(86)	68(7)	345(24)	376(39)
C (13)	140(8)	38(2)	1561(73)	37(6)	330(21)	297(38)
C (14)	112(5)	24(1)	438(21)	−7(4)	61(8)	137(17)
C (15)	107(5)	31(1)	416(21)	25(4)	63(9)	193(17)
C (16)	126(6)	29(1)	235(15)	5(4)	47(7)	120(15)
C (17)	142(6)	34(2)	368(20)	14(5)	21(9)	271(19)
C (18)	220(10)	42(2)	759(38)	7(7)	181(15)	392(33)
C (19)	91(5)	25(1)	286(16)	−2(4)	17(7)	106(14)
C (20)	71(4)	22(1)	312(17)	−4(3)	9(7)	98(13)
C (21)	135(6)	23(1)	306(17)	−5(4)	9(7)	149(17)
C (22)	138(6)	27(1)	363(20)	10(4)	46(8)	159(18)
C (23)	85(4)	20(1)	535(23)	4(3)	65(8)	199(17)
C (24)	131(6)	24(1)	421(22)	−2(4)	−9(8)	159(18)
C (25)	98(5)	26(1)	322(18)	−4(4)	−18(8)	68(15)

(b) The hydrogen atoms

The positional and thermal parameters are multiplied by 10^3 and 10 respectively.

Atom	x/a	y/b	z/c	B
H(1-1)	424(4)	326(2)	763(8)	10(8)
H(1-2)	511(6)	309(3)	608(11)	31(12)
H(2-1)	482(5)	436(3)	670(10)	23(10)
H(2-2)	431(6)	405(3)	385(11)	34(12)
H(3)	280(6)	429(3)	687(11)	31(12)
H(6)	9(4)	284(2)	385(9)	13(9)
H(7-1)	52(6)	154(3)	288(11)	29(12)
H(7-2)	57(7)	172(4)	565(14)	50(16)
H(11-1)	501(7)	166(4)	543(13)	43(14)
H(11-2)	529(6)	201(3)	748(11)	29(11)
H(12-1)	554(5)	79(3)	798(11)	25(11)
H(13-1)	382(6)	−3(3)	743(12)	35(12)
H(14)	176(5)	47(3)	497(11)	26(11)
H(15-1)	41(7)	409(4)	512(13)	45(15)
H(15-2)	40(4)	467(2)	350(9)	12(9)
H(15-3)	−34(5)	391(3)	249(10)	20(10)
H(16-1)	100(6)	365(3)	−23(11)	30(12)
H(16-2)	133(5)	445(3)	49(10)	23(10)
H(16-3)	240(5)	397(3)	66(9)	17(9)
H(17-1)	343(5)	303(3)	119(10)	23(10)
H(17-2)	275(6)	233(3)	80(11)	32(12)
H(17-3)	415(8)	226(5)	217(16)	62(18)
H(21)	197(5)	602(3)	217(10)	19(9)
H(22)	139(6)	723(4)	74(13)	39(14)
H(24)	289(6)	816(3)	765(11)	31(12)
H(25)	338(5)	695(3)	899(11)	27(11)

Results and Discussion

The molecular framework thus obtained and the torsion angles for the A, B, and C rings are shown in Figs. 1 and 2 respectively. As will be seen in these figures, the C ring takes a considerably flattened half-chair form, with the methoxyl group, O(2)–C(18)H_3, placed in the axial position and on the opposite side of the mean plane of the molecule to the C(17) atom, while the A ring has a distorted chair form, with the O(1) atom in the equatorial position. On the other hand, the B ring containing two endocyclic double bonds exists in the boat conformation. The bond distances and angles, along with their estimated standard deviations, are given in Tables 3 and 4 respectively. The correction for the thermal motion was made on the assumption of a riding motion by means of the Busing-Levy method.[2] Considering their standard deviations, these values are all reasonable except for the C(12)–C(13) bond. The unusual behavior of this bond will be described in detail later.

The chair form of the A ring is somewhat distorted, as has been described above. This may be mainly due to the fusion of the B ring, but it may be partly due to the repulsion between the two axial methyl groups, C(16)H_3 and C(17)H_3. As will be seen in Fig. 2, the A ring is less puckered than the normal chair-shaped ring of cyclohexane. From the average valence angle in the ring, 112.2°, the average torsion angle is estimated to be 52.6° by using Altona's equation.[3] This value is in good agreement with the average of the six observed torsion angles, 52.2°. The conformations of the three methyl groups in the A ring are shown in Fig. 3. In order to avoid a closer approach of the H(16–3) and H(17–1) atoms, neither the C(16)-H_3 nor C(17)H_3 methyl group takes the ideal staggered conformation; the deviations are about 13° and 10° respectively. Thus, the H(16–3) and H(17–1) atoms maintain a distance of about 2.05 Å. On the other hand, the conformation of the equatorial C(15)H_3 group around the C(15)–C(4) bond also deviates by

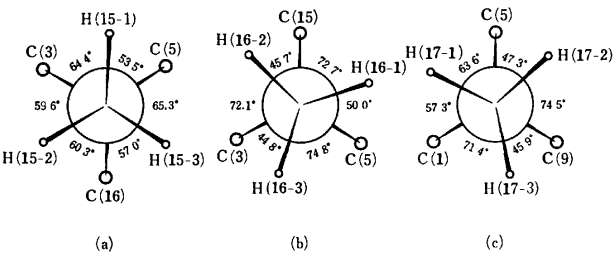

Fig. 3. The Newman projections along the bonds, (a) C(4)-C(15), (b) C(4)-C(16), and (c) C(10)-C(17).

2) W. R. Busing and H. A. Levy, *Acta Crystallogr.*, **17**, 142 (1964).

3) C. Altona, H. J. Geise, and C. Romers, *Rec. Trav. Chim.*, **85**, 1197 (1966).

Table 3. The bond distances with their standard deviations

(a) The bond distances between the non-hydrogen atoms
The distances corrected for the thermal motion are given in parentheses

Bond	Distance	σ	Bond	Distance	σ
C (1)-C (2)	1.526 (1.530)	0.006	C (10)-C (17)	1.548 (1.566)	0.008
C (1)-C (10)	1.548 (1.554)	0.005	C (11)-C (12)	1.490 (1.554)	0.011
C (2)-C (3)	1.510 (1.517)	0.007	C (12)-C (13)	1.340 (1.347)	0.010
C (3)-C (4)	1.535 (1.537)	0.005	C (13)-C (14)	1.498 (1.566)	0.009
C (3)-O (1)	1.462 (1.468)	0.005	C (14)-O (2)	1.413 (1.448)	0.009
C (4)-C (5)	1.550 (1.553)	0.005	C (18)-O (2)	1.414 (1.420)	0.009
C (4)-C (15)	1.526 (1.540)	0.008	C (19)-C (20)	1.486 (1.489)	0.006
C (4)-C (16)	1.547 (1.556)	0.007	C (19)-O (1)	1.332 (1.340)	0.005
C (5)-C (6)	1.333 (1.347)	0.007	C (19)-O (3)	1.195 (1.236)	0.006
C (5)-C (10)	1.527 (1.529)	0.006	C (20)-C (21)	1.386 (1.399)	0.007
C (6)-C (7)	1.491 (1.507)	0.007	C (20)-C (25)	1.382 (1.394)	0.006
C (7)-C (8)	1.490 (1.509)	0.007	C (21)-C (22)	1.383 (1.389)	0.006
C (8)-C (9)	1.325 (1.328)	0.007	C (22)-C (23)	1.382 (1.392)	0.006
C (8)-C (14)	1.523 (1.533)	0.006	C (23)-C (24)	1.367 (1.379)	0.008
C (9)-C (10)	1.545 (1.547)	0.006	C (23)-Br	1.898 (1.916)	0.004
C (9)-C (11)	1.506 (1.528)	0.007	C (24)-C (25)	1.386 (1.395)	0.006

(b) The bond distances involving the hydrogen atoms

Bond	D	σ	Bond	D	σ
C (1)-H (1-1)	0.93	0.05	C (15)-H (15-1)	0.87	0.09
C (1)-H (1-2)	0.96	0.07	C (15)-H (15-2)	0.97	0.05
C (2)-H (2-1)	0.94	0.05	C (15)-H (15-3)	1.02	0.05
C (2)-H (2-2)	1.00	0.07	C (16)-H (16-1)	0.93	0.05
C (3)-H (3)	0.93	0.07	C (16)-H (16-2)	0.90	0.05
C (6)-H (6)	1.00	0.05	C (16)-H (16-3)	0.93	0.06
C (7)-H (7-1)	1.01	0.06	C (17)-H (17-1)	0.99	0.06
C (7)-H (7-2)	1.01	0.10	C (17)-H (17-2)	0.87	0.05
C (11)-H (11-1)	0.86	0.09	C (17)-H (17-3)	0.96	0.09
C (11)-H (11-2)	0.88	0.05	C (21)-H (21)	0.91	0.05
C (12)-H (12-1)	0.88	0.06	C (22)-H (22)	0.93	0.07
C (13)-H (13-1)	1.01	0.06	C (24)-H (24)	1.00	0.06
C (14)-H (14)	1.03	0.05	C (25)-H (25)	0.95	0.06

about 3° from the ideal staggered conformation. The distance of the H(15-3) atom from the H(6) atom is about 2.14 Å.

The B ring contains two non-conjugated double bonds, C(5)=C(6) and C(8)=C(9). The latter double bond is somewhat twisted, although the former holds a good planarity. The deviations of the atoms from the least-squares best plane through the C(7), C(8), C(9), C(10), C(11), and C(14) atoms are given in Table 5. The angle of twisting around the C(8)=C(9) bond is estimated to be about 3.7° by averaging the torsion angles, C(7)-C(8)-C(9)-C(10) and C(14)-C(8)-C(9)-C(11). The angle between the above best plane and the least-squares plane through the C(4), C(5), C(6), C(7), and C(10) atoms is about 15.1°.

The C ring is the most interesting part of the present molecule, since it seems to have a close relation to the high reactivity of the methoxyl group. The conformation and dimensions of this ring are shown in Fig. 4. This figure includes three remarkable features. The first is that the length of the C(12)-C(13) bond, 1.340±0.010 Å, is too short for a C-C single bond, and that the C-C-C valence angles at the C(12) and C(13) atoms, 119.7±0.6° and 117.5±0.7°, are too large for tetrahedral valence angles. Judging from these dimensions alone, the C(12)-C(13) bond must be a C=C double bond. However, both elemental analysis and NMR spectrum demonstrate that the C(12) and C(13) atoms form a single bond.[1] The second is that the C(12) and C(13) atoms vibrate vigorously in a direction almost perpendicular to the mean plane of the C ring. The root-mean-square deviations and direction cosines in the principal axes of the thermal ellipsoids are given in Table 6. The largest root-mean-square deviations for the C(12) and C(13) atoms are no less than about 0.55 and 0.52 Å respectively. Even though the C(12)-C(13) bond distance is corrected for these large thermal motions, the correction is only about 0.007 Å as long as the riding motion is assumed. However, if the highly-correlated antiparallel motion is assumed for the two atoms, the corrected distance amounts to about 1.73 Å. Accordingly, the shortening of the C(12)-C(13) single bond might be explained by such a thermal motion effect, but it

TABLE 4. THE BOND ANGLES WITH THEIR STANDARD DEVIATIONS

	Angle	σ		Angle	σ
C (2) - C (1) - C (10)	114.3	0.3	C (1) - C (2) - H (2-1)	107	3
C (1) - C (2) - C (3)	108.9	0.4	C (1) - C (2) - H (2-2)	105	4
C (2) - C (3) - C (4)	114.0	0.4	C (3) - C (2) - H (2-1)	108	3
C (2) - C (3) - O (1)	109.3	0.4	C (3) - C (2) - H (2-2)	115	4
C (4) - C (3) - O (1)	106.9	0.3	H (2-1) - C (2) - H (2-2)	112	5
C (3) - C (4) - C (5)	107.0	0.3	C (2) - C (3) - H (3)	111	4
C (3) - C (4) - C (15)	108.2	0.4	C (4) - C (3) - H (3)	106	4
C (3) - C (4) - C (16)	111.4	0.4	O (1) - C (3) - H (3)	110	4
C (5) - C (4) - C (15)	112.2	0.4	C (5) - C (6) - H (6)	122	3
C (5) - C (4) - C (16)	111.5	0.4	C (7) - C (6) - H (6)	113	3
C (15) - C (4) - C (16)	106.5	0.4	C (6) - C (7) - H (7-1)	108	3
C (4) - C (5) - C (6)	119.5	0.4	C (6) - C (7) - H (7-2)	112	5
C (4) - C (5) - C (10)	119.6	0.3	C (8) - C (7) - H (7-1)	108	3
C (6) - C (5) - C (10)	120.9	0.4	C (8) - C (7) - H (7-2)	108	5
C (5) - C (6) - C (7)	124.7	0.5	H (7-1) - C (7) - H (7-2)	107	6
C (6) - C (7) - C (8)	113.4	0.4	C (9) - C (11) - H (11-1)	108	6
C (7) - C (8) - C (9)	122.7	0.4	C (9) - C (11) - H (11-2)	116	3
C (7) - C (8) - C (14)	114.1	0.4	C (12) - C (11) - H (11-1)	112	6
C (9) - C (8) - C (14)	123.2	0.4	C (12) - C (11) - H (11-2)	112	3
C (8) - C (9) - C (10)	122.7	0.4	H (11-1) - C 11) - H (11-2)	92	7
C (8) - C (9) - C (11)	120.2	0.4	C (11) - C (12) - H (12-1)	110	4
C (10) - C (9) - C (11)	117.0	0.3	C (13) - C (12) - H (12-1)	118	4
C (1) - C (10) - C (5)	109.2	0.3	C (12) - C (13) - H (13-1)	121	4
C (1) - C (10) - C (9)	108.7	0.3	C (14) - C (13) - H (13-1)	114	4
C (1) - C (10) - C (17)	109.9	0.4	C (8) - C (14) - H (14)	106	3
C (5) - C (10) - (9)	111.8	0.4	C (13) - C (14) - H (14)	109	3
C (5) - C (10) - C (17)	111.1	0.4	O (2) - C (14) - H (14)	106	3
C (9) - C (10) - C (17)	106.1	0.4	C (4) - C (15) - H (15-1)	116	6
C (9) - C (11) - C (12)	115.1	0.6	C (4) - C (15) - H (15-2)	112	3
C (11) - C (12) - C (13)	119.7	0.6	C (4) - C (15) - H (15-3)	114	3
C (12) - C (13) - C (14)	117.5	0.7	H (15-1) - C (15) - H (15-2)	107	6
C (8) - C (14) - C (13)	113.3	0.4	H (15-1) - C (15) - H (15-3)	102	6
C (8) - C (14) - O (2)	106.5	0.4	H (15-2) - C (15) - H (15-3)	104	4
C (13) - C (14) - O (2)	114.8	0.5	C (4) - C (16) - H (16-1)	109	3
C (20) - C (19) - O (1)	111.8	0.4	C (4) - C (16) - H (16-2)	110	3
C (20) - C (19) - O (3)	124.0	0.4	C (4) - C (16) - H (16-3)	112	4
O (1) - C (19) - O (3)	124.2	0.4	H (16-1) - C (16) - H (16-2)	108	5
C (19) - C (20) - C (21)	122.2	0.4	H (16-1) - C (16) - H (16-3)	113	5
C (19) - C (20) - C (25)	118.5	0.4	H (16-2) - C (16) - H (16-3)	106	5
C (21) - C (20) - C (25)	119.3	0.4	C (10) - C (17) - H (17-1)	110	3
C (20) - C (21) - C (22)	120.2	0.4	C (10) - C (17) - H (17-2)	112	4
C (21) - C (22) - C (23)	119.2	0.5	C (10) - C (17) - H (17-3)	109	5
C (22) - C (23) - C (24)	121.6	0.4	H (17-1) - C (17) - H (17-2)	101	5
C (22) - C (23) - Br	118.4	0.4	H (17-1) - C (17) - H (17-3)	117	6
C (24) - C (23) - Br	120.0	0.4	C (17-2) - C (17) - H (17-3)	109	6
C (23) - C (24) - C (25)	118.7	0.4	C (20) - C (21) - H (21)	114	3
C (20) - C (25) - C (24)	121.0	0.4	C (22) - C (21) - H (21)	126	3
C (3) - O (1) - C (19)	118.4	0.3	C (21) - C (22) - H (22)	123	4
C (14) - O (2) - C (18)	115.2	0.5	C (23) - C (22) - H (22)	118	4
C (2) - C (1) - H (1-1)	108	3	C (23) - C (24) - H (24)	117	3
C (2) - C (1) - H (1-2)	110	4	C (25) - C (24) - H (24)	124	3
C (10) - C (1) - H (1-1)	105	3	C (24) - C (25) - H (25)	117	3
C (10) - C (1) - H (1-2)	106	4	C (20) - C (25) - H (25)	122	3
H (1-1) - C (1)) H (1-2)	113	5			

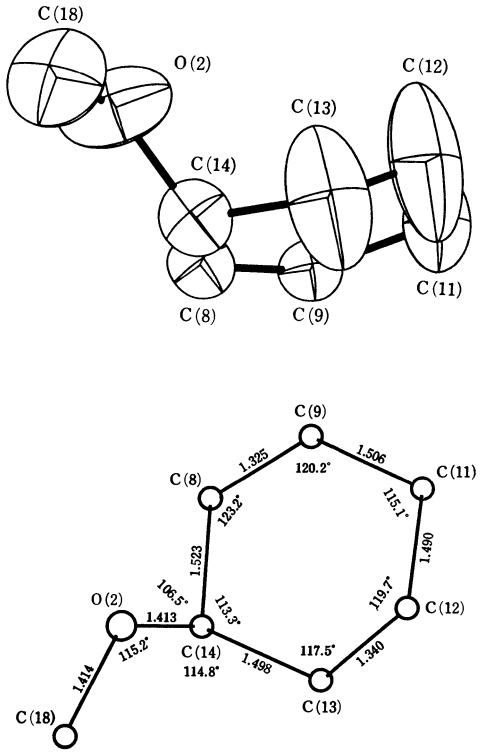

Fig. 4. The conformation and dimensions of the C ring. The thermal ellipsoids are scaled to enclose 50% probability.

seems to be difficult at the present stage to answer the question why these two atoms vibrate vigorously in a direction nearly antiparallel to each other. On the other hand, if this remarkable anisotropy of thermal motion were due to some disordering associated with the conformation of the C ring, the electron density distribution would afford double peaks for the C(12) and C(13) atoms, since the separation between two possible

Table 5. The deviations from the least-squares plane through the C(7), C(8), C(9), C(10), C(11), and C(14) atoms

Atom	Deviation	Atom	Deviation
C (7)	+0.035 Å	C (11)	+0.031 Å
C (8)	+0.010	C (14)	−0.048
C (9)	+0.021	C (5)	+0.311
C (10)	−0.049	C (6)	+0.348

positions is estimated to be about 0.76 Å from the observed distance for the C(12)–C(13) single bond. However, in fact, the difference map calculated excluding these atoms gave single peaks to them, as has been already mentioned in the section of Structure Determination. Hence, it seems to be unreasonable to think that the unusual behavior of the two atoms is to be explained by such a disordering. The third feature is that the methoxyl group is not in the equatorial position, but in the axial position, and that the half-chair form of the C ring is considerably more flattened than those in many other substances containing a cyclohexene ring.[4] The deviations from the least-squares best plane through the C(8), C(9), C(11), and C(14) atoms are no more than about 0.17 and 0.28 Å for the C(12) and C(13) atoms respectively; these values are considerably smaller than those found in cyclohexene, ±0.3673 Å.[5] One of the important factors which control the conformation of the C ring might be the H(1–2)···H(11–2) interaction, since the distance between the two hydrogen atoms, 2.17 Å, varies sensitively with the conformational change of the C ring. The methoxyl carbon atom, C(18), is placed at such a position that the O(2)–C(18) bond makes azimuthal angles of about 156.2° and 77.6° with the C(8)–C(14) and C(13)–C(14) bonds around the C(14)–O(2) bond respectively. It is interesting

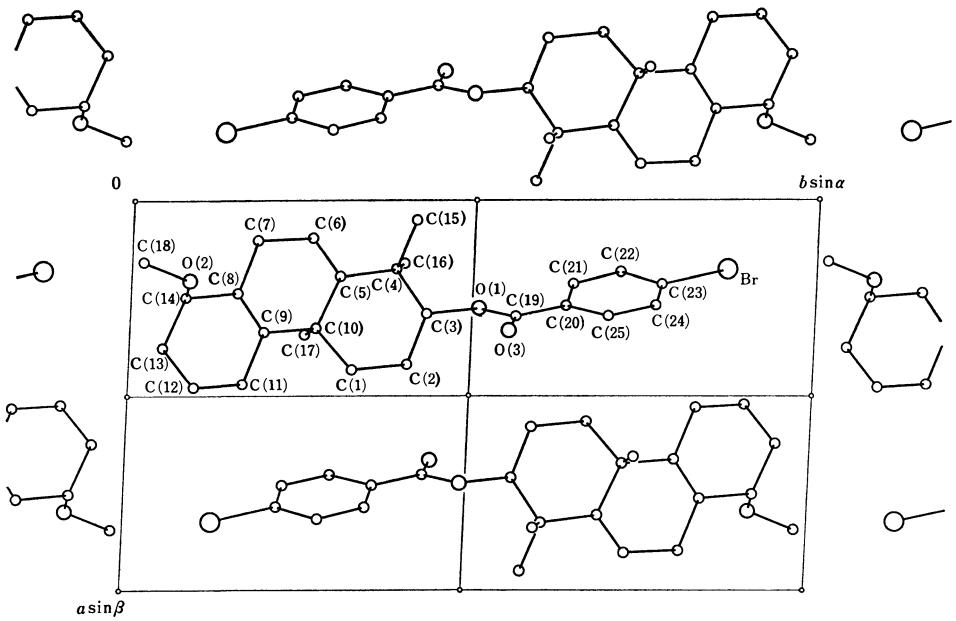

Fig. 5. The crystal structure viewed along the *c* axis.

4) B. Koch, *Acta Crystallogr.*, **B28**, 1151 (1972).

Table 6. The root-mean-square deviations and direction cosines in the principal axes of the thermal ellipsoids

$B_i=8\pi^2u_i^2$ where u_i is the root-mean-square deviation corresponding to the ith axis of the ellipsoid. C_{ia}, C_{ib}, and C_{ic} are the direction cosines of the i axis with respect to the orthogonal coordinate axes by $\boldsymbol{b}\times\boldsymbol{c}^*$, $\boldsymbol{b}$, and $\boldsymbol{c}^*$.

Atom	Axis i	B_i	u_i	C_{ia}	C_{ib}	C_{ic}
C (8)	1	2.55	0.180	0.050	−0.952	0.303
	2	3.71	0.217	0.771	0.229	0.594
	3	4.52	0.239	0.635	−0.204	−0.745
C (9)	1	2.91	0.192	0.073	−0.967	0.245
	2	3.57	0.213	−0.215	0.225	0.950
	3	3.74	0.218	−0.974	−0.122	−0.191
C (11)	1	3.33	0.205	0.169	−0.965	0.199
	2	4.02	0.226	0.981	0.185	0.066
	3	8.68	0.332	0.100	−0.184	−0.978
C (12)	1	2.55	0.180	−0.537	0.783	−0.313
	2	5.50	0.264	0.818	0.574	0.033
	3	23.91	0.550	0.206	−0.238	−0.949
C (13)	1	2.46	0.177	−0.082	0.949	−0.304
	2	5.98	0.275	0.961	0.156	0.229
	3	21.24	0.519	0.265	−0.273	−0.925
C (14)	1	2.57	0.180	−0.260	−0.941	0.217
	2	4.75	0.245	0.735	−0.047	0.676
	3	5.98	0.275	−0.626	0.335	0.704
O (2)	1	2.90	0.192	−0.284	−0.865	0.415
	2	5.88	0.273	−0.296	0.491	0.820
	3	12.38	0.396	−0.912	0.110	−0.395
C (18)	1	3.04	0.196	−0.302	−0.845	0.441
	2	8.99	0.338	0.917	−0.385	−0.109
	3	10.58	0.366	−0.262	−0.371	−0.891

Table 7. The principal intermolecular distances

(1)	I···II (III···I)		(4)	I···VIII (VIII···I)	
	Br···C (13)	3.94 Å		C (15)···C (15)	3.66 Å
(2)	I···IV (V···I)			C (15)···C (19)	3.82
	O (2)···C (17)	3.60 Å		C (15)···C (20)	3.81
	O (3)···C (21)	3.68	(5)	I···IX (IX···I)	
	C (8)···C (17)	3.84		Br···C (11)	3.96 Å
	C (9)···C (17)	3.83		C (1)···C (21)	3.87
	C (15)···C (16)	3.95		C (2)···C (2)	3.99
	C (25)···C (22)	3.66		C (2)···C (19)	3.84
(3)	I···VI (VII···I)			C (2)···C (20)	3.87
	Br···C (18)	3.70 Å		C (11)···C (23)	3.84

I: x/a, y/b, z/c (given in Table 2). II: x/a, $1+y/b$, z/c. III: x/a, $-1+y/b$, z/c. IV: x/a, y/b, $1+z/c$. V: x/a, y/b, $-1+z/c$. VI: x/a, $1+y/b$, $-1+z/c$. VII: x/a, $-1+y/b$, $1+z/c$. VIII: $-x/a$, $1-y/b$, $1-z/c$. IX: $1-x/a$, $1-y/b$, $1-z/c$.

to note in Fig. 4 that the O(2) atom as well as the C(13) atom vibrates rotationally with the C(8)–C(14) bond as an axis of rotation. It has already been mentioned that the five hydrogen atoms could not be found in the difference Fourier map. Three of them are methoxyl hydrogen atoms, and the remaining two are axial ones at the C(12) and C(13) atoms. It seems at first sight strange that only the equatorial hydrogen atoms at the C(12) and C(13) atoms can be located, notwithstanding the large thermal motions of these two carbon atoms. This may be explained by taking it into consideration that, since, in the cyclohexene molecule, the equatorial hydrogen atoms at the C(12) and C(13) atoms deviate by only about 0.10 Å from the double-bond plane,[5] there are always equatorial hydrogen atoms in the neighborhood of the double-bond plane even if the α and β hydrogen atoms exchange the axial and equatorial positions with each other by a flipping of the ring.

The *p*-bromobenzoate group is not planar as a whole, but the carboxylate group is twisted at an angle of about 7.1° from the benzene-ring plane. The C(3) and O(3) atoms also deviate by about 3.2° from the eclipsed conformation around the O(1)–C(19) bond. On the other hand, the benzoyl group takes roughly the *cis* conformation with the H(3) atom around the O(1)–C(3) bond; the deviation from the ideal *cis* conformation is about 21°. Consequently, the O(3) atom is situated at a very small distance (about 2.36 Å) from the H(3) atom. This suggests that these two atoms exert a stronger attractive force on each other than the usual van der Waals interaction.

The molecular arrangement viewed along the *c* axis is shown in Fig. 5. The principal intermolecular distances are listed in Table 7. The molecules are connected mainly by the usual van der Waals interactions.

The authors would like to express their thanks to Dr. Yoichi Shiozaki of this University for his advice on the intensity measurements.

5) J. F. Chiang and S. H. Bauer, *J. Amer. Chem. Soc.*, **91**, 1898 (1969).

The Coordination Bonding and Stability of the 1 : 1 Complexes of Copper(II) with Various Bidentate Ligands in Aqueous-methanolic Solutions

Hiroshi Yokoi, Masaki Otagiri, and Taro Isobe

Chemical Research Institute of Non-aqueous Solutions, Tohoku University, Katahira, Sendai

(Received December 23, 1971)

ESR and spectrophotometric studies have been made of a number of 1 : 1 complexes of copper(II) with ethylenediamine, its analogues, and amino acids in aqueous-methanolic solutions. It has been shown that the complexes in the solutions are characteristic of copper(II) ions with a normal tetragonal environment and that their metal-ligand bondings are intermediate in the degree of covalency between those of hydrated cupric ions and the corresponding 1 : 2 complexes. The disproportionation constants and their temperature dependences, determined for the 1 : 1 complexes by the ESR and spectrophotometric methods, have been discussed, with particular empahsis on the fact that those values are in fair agreement with those derived from the step-by-step formation constants and the thermodynamic data obtained in aqueous solutions in the literature.

It is a very interesting problem in coordination chemistry to study the bonding character and stability of the 1 : 1 complexes of copper(II) with various bidentate ligands in aqueous solutions, sinec the 1 : 1 complexes can be regarded as intermediates in the formation of the 1 : 2 complexes. This problem is also of importance in estimating the reaction mechanisms of various metal-ion-catalyzed-reactions in organic, inorganic, and biological chemistries.[1-4] There have been almost no other works on the physical properties of the 1 : 1 complexes in solution but the one reported by Lewis *et al.*; they interpreted the ^{17}O NMR and ESR results of aqueous solutions of cupric salts and of 1 : 1 and 1 : 2 complexes of copper(II) with ethylenediamine in terms of molecular orbitals.[5]

The purpose of the present paper is to investigate the metal-ligand bondings of the 1 : 1 complexes of copper(II) with ethylenediamine, its analogues, and amino acids in aqueous-methanolic solutions, to compare them with those of cupric ions and the 1 : 2 complexes using the ESR and spectrophotometric methods, and furthermore, to discuss the stability of the 1 : 1 complexes in solution.

Experimental

Materials. The 1 : 1 complexes of copper(II) with bidentate ligands were produced according to equilibrium by mixing cupric ions and the 1 : 2 complexes in solution, as will be described in detail later. $Cu(ClO_4)_2 \cdot 6H_2O$ was used as the source of the cupric ions. The 1 : 2 complexes employed here, which had been prepared and purified in a previous work,[6] were $[Cu(en)_2] \cdot (ClO_4)_2$, $[Cu(dmen)_2] \cdot (ClO_4)_2$, $[Cu(deen)_2] \cdot (ClO_4)_2$, $[Cu(tn)_2] \cdot (ClO_4)_2$, $[Cu(L\text{-ala})_2]$, $[Cu(L\text{-ser})_2]$, and $[Cu(\beta\text{-ala})_2] \cdot 6H_2O$, where en, dmen, deen, tn, L-ala, L-ser, and β-ala are ethylenediamine, *N,N*-dimethylethylenediamine, *N,N*-diethylethylenediamine, trimethylenediamine, the anions of L-alanine, L-serine, and β-alanine respectively. The $(0.970 \pm 0.005) \times 10^{-2}$ mol/l solution of the cupric ions and the 1.000×10^{-2} mol/l solutions of the 1 : 2 complexes were prepared using an equivolume mixture of water and methanol as the solvent; the concentration of cupric ions was checked by a usual colorimetric determination, using sodium diethyldithiocarbamate.[7]

Measurements. The sample solutions used for the ESR and spectrophotometric measurements were mixtures of the above-mentioned solution of cupric ion and any of the above-described solutions of the 1 : 2 complexes at various volume ratios. The ESR spectra were measured at the temperature of liquid nitrogen with a Hitachi 771 X-band ESR spectrometer. The measurements of the visible absorption spectra were carried out at room temperature with a Hitachi EPS-3T spectrophotometer, using 1-cm quartz cells.

Results and Discussion

When a cupric salt and a stable 1 : 2 complex of copper(II) with a bidentate ligand, A, are dissolved in an aqueous solvent, the following equilibrium is generally established in the solution (with charge and hydrated water molecules omitted):

$$Cu + CuA_2 \rightleftharpoons 2CuA \quad (1)$$

$$K = \frac{[CuA]^2}{[Cu][CuA_2]} \quad (2)$$

where CuA represents a 1 : 1 complex. The relative amounts of the three species in the solution, therefore, vary according to the K value.

The X-band ESR spectra for the systems containing the 1 : 1 complexes of copper(II) with ethylenediamine and L-alanine are shown in Figs, 1 and 2 as typical ESR spectra in this work; the other systems showed almost the same spectral behavior. The ESR line shapes observed for the randomly-oriented and magnetically-diluted samples of copper(II) complexes have been investigated in some detail.[8] Accordingly,

1) J. F. Speck, *J. Biol. Chem.*, **178**, 315 (1949); D. E. Metzler and E. E. Snell, *J. Amer. Chem. Soc.*, **74**, 979 (1952); M. Saito, K. Okawa, and S. Akabori, This Bulletin, **30**, 937 (1957); R. Hofstetter, Y. Murakami, G. Mont, and A. E. Martell, *J. Amer. Chem. Soc.*, **84**, 3041 (1962).

2) F. P. Dwyer, "Chelating Agents and Metal Chelates," ed. by F. P. Dwyer and D. P. Mellor, Academic Press, New York (1964), p. 335.

3) M. M. Jones, "Ligand Reactivity and Catalysis," Academic Press, New York (1968).

4) R. Breslow, "Bioinorganic Chemistry," ed. by R. F. Gould, Amer. Chem. Soc. Publ., Washington (1971), p. 21.

5) W. B. Lewis, M. Alei, Jr., and L. O. Morgan, *J. Chem. Phys.*, **44**, 2409 (1966); *ibid.*, **45**, 4003 (1966).

6) H. Yokoi, M. Otagiri, and T. Isobe, This Bulletin, **44**, 2395 (1971).

7) T. Callen and J. A. R. Henderson, *Analyst*, **54**, 650 (1929); Y. Tanaka and K. Ito, *Bunseki Kagaku*, **6**, 728 (1957).

8) R. H. Sands, *Phys. Rev.*, **99**, 1222 (1955); T. Vanngard and R. Aasa, Proc. 1st Intern. Congr. "Paramagnetic Resonance," Jerusalem, 1962, Academic Press, New York (1963), p. 509; R. Neiman and D. Kivelson, *J. Chem. Phys.*, **35**, 156 (1961).

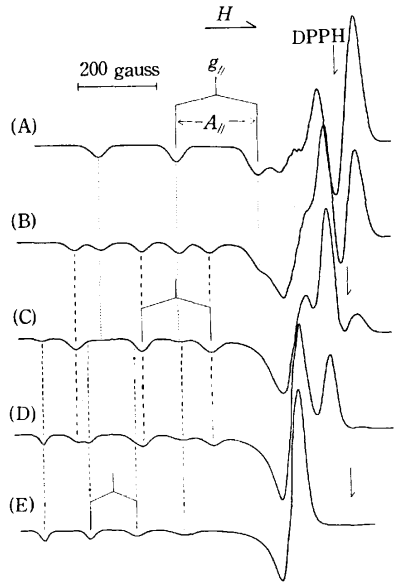

Fig. 1. The X-band ESR spectra of the mixtures of $Cu(ClO_4)_2 \cdot 6H_2O$ and $[Cu(en)_2] \cdot (ClO_4)_2$ in the following molar ratios (measured at 77K, total concentration of Cu(II) in each solution: 1×10^{-2} M, Solvent: an equivolume mixture of water and methanol).
(A) 0 : 1, (B) 1 : 3, (C) 1 : 1, (D) 3 : 1, (E) 1 : 0.

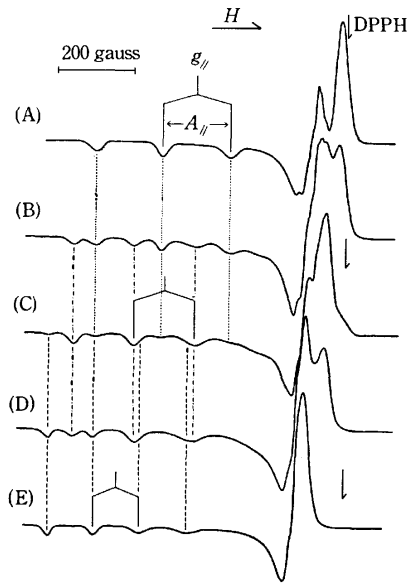

Fig. 2. The X-band ESR spectra of the mixtures of $Cu(ClO_4)_2 \cdot 6H_2O$ and $[Cu(L\text{-ala})_2]$ in the following molar ratios (measured at 77K, total concentration of Cu(II) in each solution: 1×10^{-2} M, Solvent: an equivolume mixture of water and methanol).
(A) 0 : 1, (B) 1 : 3, (C) 1 : 1, (D) 3 : 1, (E) 1 : 0.

it is clear that all the ESR spectra observed for the mixtures of the cupric salt solution and any of the 1 : 2 complex solutions are made up of the superposition of three different spectra, as Figs. 1 and 2 show. The several vertical dotted lines in these figures clearly point out that two of the three spectra are due to Cu and CuA_2, and the third spectrum, to CuA; there are not more than these three species in any sample solution, and the three species may coexist at equilibrium. It has also been shown that all the ESR spectra of the

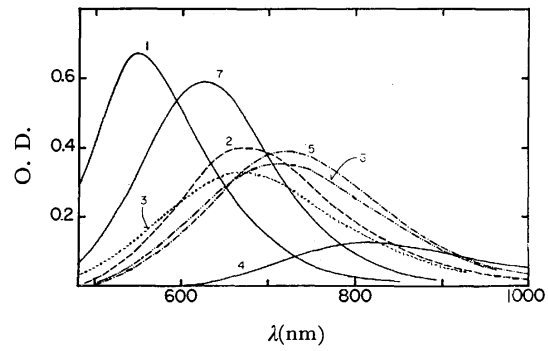

Fig. 3. The visible absorption spectra of the following complex species at room temperature (total concentration of Cu(II) in each solution: 1.00×10^{-2} M, Solvent: an equivolume mixture of water and methanol)
(1) $[Cu(en)_2] \cdot (ClO_4)_2$, (2) $[Cu(en)_2] \cdot (ClO_4)_2$, (2) $[Cu(en)_2] \cdot (ClO_4)_2 + Cu(ClO_4)_2$ (molar ratio of 1 : 1), (3) calculated spectrum of $[Cu(en)(OH_2)_2]^{2+}$, (4) $Cu(ClO_4)_2$, (5) $[Cu(L\text{-ala})_2] + Cu(ClO_4)_2$ (molar ratio of 1 : 1), (6) calculated spectrum of $[Cu(L\text{-ala})(OH_2)_2]^+$, (7) $[Cu(L\text{-ala})_2]$.

CuA_2 species employed in this work are of an axially-symmetrical type.[9,10] The computer simulation of ESR line shapes, furthermore, has revealed that any of the ESR spectra of Cu, CuA, and CuA_2 (A=en) in frozen aqueous solutions are characteristic of cupric ions with an axially-symmetric g tensor.[5] It can reasonably be concluded, from all the observed ESR line shapes in this work, that each of the CuA species also has a normal tetragonal copper(II) environment. The $g_{//}$ and $|A_{//}|$ values analyzed for all the species are listed in Table 1.

The visible absorption spectra of the same sample solutions as in Figs. 1 and 2 are shown in Fig. 3; they are typical of this work. The visible absorption spectrum of CuA can be obtained using the K value in Eq. (2) and the spectral data of Cu and CuA_2. A spectrophotometric method for determining the K value will be described later. Some of the analyzed data are listed in Table 1. It can be seen from this table the wavelength of the maximum absorption of CuA appears almost in the middle between those of Cu and CuA_2; this fact suggests that the ligand-field energies of CuA may be intermediate between those of Cu and CuA_2. Furthermore, concerning the dipole strength of the visible absorption transition, D, we found that CuA is intermediate in the D value between Cu and CuA_2. It has generally been accepted that the intensity of the visible absorption spectrum in a copper(II) complex always increases as the symmetry of its ligand field decreases.[11,12] Accordingly, it seems probable that CuA is not much lower in the symmetry of the ligand field than are Cu and CuA_2. From the fact of an axially-symmetric g tensor of CuA, and from

9) H. Yokoi and T. Isobe, This Bulletin, **41**, 2835 (1968); *ibid.*, **42**, 2187 (1969).
10) H. Yokoi, M. Sai, T. Isobe, and S. Ohsawa, *ibid.*, **45**, 2189 (1972).
11) C. J. Ballhausen, "Introduction to Ligand Field Theory," McGraw-Hill, New York (1962), p. 180.
12) C. R. Hare, "Spectroscopy and Structure of Metal Chelate Compounds," ed. by K. Nakamoto and P. J. McGrathy, John Wiley & Sons, New York (1968), p. 98, and the references therein.
13) H. Yokoi and T. Isobe, to be published.

Table 1. Experimental data of copper(II) complexes

Sample[a]	pH[b]	$g_{//}$	$\lvert A_{//}\rvert \times 10^4$ (cm^{-1})	Visible absorption maximum[c] λ(nm) ; ε	$D \times 10^3$ [d] ($Å^2$)	$k_{//}^2$ [e]
$Cu(OH_2)_4$	4.8	2.421	132	810 ; 13	2.2	0.78
$Cu(en)_2$	8.0	2.204	209	554 ; 66	8.5	0.54
$Cu(dmen)_2$	7.9	2.206	195	570 ; 146	18.6	0.53
$Cu(deen)_2$	8.0	2.210	185	594 ; 192	27.3	0.52
$Cu(tn)_2$	8.9	2.218	199	574 ; 110	15.0	0.56
Cu(L-ala)$_2$	7.9	2.262	181	622 ; 58	7.7	0.62
Cu(L-ser)$_2$	7.8	2.264	179	628 ; 52	7.1	0.63
Cu(β-ala)$_2$	8.7	2.282	141	630 ; 59	7.7	0.66
$Cu(en)(OH_2)_2$		2.281	185	682(666) ; 40(32)	5.6(5.4)	0.62
$Cu(dmen)(OH_2)_2$		2.286	179	693(680) ; 59(56)	8.7(8.9)	0.62
$Cu(dmen)(OH_2)_2$		2.268	177	692(690) ; 88(83)	13.9(14.2)	0.58
$Cu(tn)(OH_2)_2$		2.283	181	664(656) ; 48(47)	6.7(6.8)	0.64
Cu(L-ala)$(OH_2)_2$		2.320	167	718(705) ; 40(36)	5.9(5.6)	0.68
Cu(L-ser)$(OH_2)_2$		2.321	166	716(710) ; 38(33)	5.5(5.2)	0.68
Cu(β-ala)$(OH_2)_2$		2.322	160	728(726) ; 46(38)	6.3(5.9)	0.67

a) The samples represent the solutions of the complexes listed in this table, which are expressed with charge omitted, where an equivolume mixture of water and methanol was used as the solvent.
b) The pH at 25°C in a concentration of 0.01 M.
c) The values in parentheses are the data for the equimolar mixture of cupric ions and the 1 : 2 complexes in the above-mentioned solvent.
d) D represents the dipole strength of visible absorption transition;

$$D = 3.99 \times 10^{-20} \int \frac{\varepsilon_\sigma}{\sigma} d\sigma \quad (cm^2)$$

where σ expresses the wave number. The values in parentheses mean the same as given in the above footnote (b).
e) See the text.

the fact that CuA is intermediate in the values of D and of ligand field energies between Cu and CuA_2, it can be concluded that the ligand field of CuA is of an axial symmetry to almost the same degree as those of Cu and CuA_2. This conclusion, which is unexpected in view of the fact that the coordination symmetry of CuA is apparently less than tetragonal, agrees with the previously-reported suggestion that the symmetry of a ligand field is kept in as high a degree as possible for the copper(II) complexes in solution.[6]

The $g_{//}$ and $|A_{//}|$ values of CuA are intermediate between those of Cu and CuA_2, although CuA is somewhat closer to CuA_2 than to Cu in these values. The $g_{//}$ value is a good parameter for estimating the the degree of covalency of the metal-ligand bondings in planar copper(II) complexes; generally, the metal-ligand bondings become more covalent as the $g_{//}$ values increase.[13] The covalency of the metal-ligand bonding of CuA, therefore, is intermediate in degree between those of Cu and CuA_2. The same result can be derived from a consideration of the orbital reduction tion factors, one of which, $k_{//}^2$, is expressed in the following equation:

$$g_{//} - 2 = \frac{8\lambda_0 k_{//}^2}{\Delta E} \tag{3}$$

where λ_0 is the spin-orbit coupling constant for the free cupric ion and where $\Delta E = E_{x^2-y^2} - E_{xy}$. This $k_{//}^2$ value also has been considered to be an approximate parameter for expressing the degree of covalency of metal-ligand bondings for a series of square-planar copper(II) complexes structurally similar to each other.[14-16] The relative values of $k_{//}^2$ were calculated for all the copper(II) complexes dealt with here, using the energy value at the absorption peak as ΔE for convenience; they are listed in Table 1. It is clearly shown in this table that CuA is intermediate in the $k_{//}^2$ value between Cu and CuA_2. The findings that the metal-ligand bonding of CuA is intermediate in the degree of covalency between those of Cu and CuA_2, and that CuA is of a nearly tetragonal symmetry in the copper(II) ion environment, mean that the Cu-OH_2 bond in the molecular plane of CuA becomes stronger than that of Cu and the Cu–A bond of CuA, weaker than that of CuA_2, and, consequently, that, in CuA, the bond strength of in-plane Cu–OH_2 is almost equal to that of Cu–A.

When the step-by-step formation constants of K_1 and K_2 are expressed as follows (with charge and hydrated water molecules omitted):

$$Cu + A \rightleftarrows CuA \qquad K_1 = \frac{[CuA]}{[Cu][A]} \tag{4}$$

$$CuA + A \rightleftarrows CuA_2 \qquad K_2 = \frac{[CuA_2]}{[CuA][A]} \tag{5}$$

the following general equations can be set up, using K in Eq. (2):

$$\log K = \log K_1 - \log K_2 \tag{6}$$

14) K. W. H. Stevens, *Proc. Roy. Soc. Ser. A*, **219**, 542 (1953); J. Owen, *ibid.*, **227**, 184 (1955).
15) M. Gerloch and J. R. Miller, *Progr. Inorg. Chem.*, **10**, 1 (1968).
16) J. Hathaway and D. E. Billing, *Coord. Chem. Rev.*, **5**, 143 (1970).

TABLE 2. RESULTS OF THE OPTICAL ABSORPTION MEASURMENTS[a] FOR THE SYSTEM: $Cu+Cu(en)_2$[b]

			λ(nm)			
			500	510	520	530
		$Cu(en)_2$: Cu				
D'	(I)	1 : 0.97	0.072	0.090	0.108	0.127
	(II)	2 : 0.97	0.168	0.202	0.237	0.264
	(III)	3 : 0.97	0.228	0.273	0.315	0.349
ε_p			42.3	50.3	57.2	62.6
y	(I)		−28.8	−33.3	−36.7	−38.4
	(II)		−35.3	−41.2	−44.6	−47.4
	(III)		$-36._8$	−43.0	−47.0	−49.7
$\Delta\varepsilon$	(i)	from (I) and (II)	−39.4	−46.9	−49.2	−53.8
	(ii)	from (I) and (III)	$-39._1$	−46.0	−50.0	−53.3
	(iii)	from (II) and (III)	$-39._0$	−45.5	−50.6	−53.0
P	(i)		−1.17	-1.22_6	-1.15_0	-1.21_8
	(ii)		−1.17	-1.19_3	-1.17_3	-1.20_3
	(iii)		−1.16	-1.14_9	-1.21_9	-1.18_2
K	(i)		$26._5$	$21._7$	$30._7$	$22._4$
	(ii)		27	$24._7$	$27._1$	$23._7$
	(iii)		29	$30._9$	$22._3$	$26._0$
				Mean value: $K=26.1\pm0.7$		

a) At 25°C, Solvent: an equivolume mixture of water and methanol.
b) The system of $Cu+Cu(en)_2$ represents the mixture of $Cu(ClO_4)_2$ and $[Cu(en)_2]\cdot(ClO_4)_2$ in the above-described solvent.

TABLE 3. RESULTS OF THE OPTICAL ABSORPTION MEASUREMENTS[a] FOR THE SYSTEM: $Cu+Cu(L\text{-ala})_2$[b]

			λ(nm)			
			510	520	530	540
		$Cu(L\text{-ala})_2$: Cu				
D'	(I)	1 : 0.97	0.025	0.035	0.046	0.059
	(II)	2 : 0.97	0.063	0.083	0.105	0.130
	(III)	3 : 0.97	0.085	0.111	0.141	0.172
ε_p	(I)		15.5	21.1	25.2	30.6
y[c]			15.5	20.1	25.2	30.6
	(II)		−12.5	−15.8	−19.5	−22.3
	(III)		−12.9	−16.4	−19.8	−23.3
$\Delta\varepsilon$	(i)	from (I) and (II)	−13.0	−16.6	−20.7	−23.0
	(ii)	from (I) and (III)	−13.2	−17.0	−20.4	−23.9
	(iii)	from (II) and (III)	−13.4	−17.2	−20.2	−24.8
P	(i)		-1.05_0	-1.06_5	-1.08_2	−1.08
	(ii)		-1.06_2	-1.08_1	-1.06_9	-1.09_1
	(iii)		-1.10_5	-1.13_2	-1.04_1	-1.11_6
K	(i)		84	66	53	53
	(ii)		69	53	62	48
	(iii)		42	34	102	39
				Mean value: $K=59\pm5$		

a) At 25°C, Solvent: an equivolume mixture of water and methanol.
b) The system of $Cu+Cu(L\text{-ala})_2$ represents the mixture of $Cu(ClO_4)_2$ and $[Cu(L\text{-ala})_2]$ in the above-described solvent.
c) All the y values were calculated from Eq. (10), on the assumption that all the D' values have no error (the actual experimental error of D' is ±0.001).

Table 4. The values of log K

No.	System[a]	pH[b]	Solvent: water-methanol(1 : 1)[c]		Solvent: water	
			Spectrophotometric method (25°C)	ESR method (−50—−100°C)	Calcd[d] (25°C)	Temperature dependence[e] ($\log K_{25}-\log K_0$)
I	Cu+Cu(en)$_2$	5.7	1.42±0.02	1.61±0.05	1.43±0.03	−0.03±0.01
II	Cu+Cu(dmen)$_2$	5.6	2.10±0.03	2.72±0.10	2.04±0.39	(0.05)
III	Cu+Cu(deen)$_2$	5.9	1.99±0.05	2.86±0.12	2.62	
IV	Cu+Cu(tn)$_2$	6.3	2.26±0.05	2.66±0.10	2.65±0.04	−0.03±0.01
V	Cu+Cu(L-ala)	5.4	1.77±0.04	1.43±0.05	1.59±0.05	−0.06±0.01
VI	Cu+Cu(L-ser)$_2$	5.3	1.50±0.03	1.36±0.07	(1.60)[f]	(0.06)[f]
VII	Cu+Cu(β-ala)$_2$	5.8	1.36±0.04	1.40±0.07	1.76±0.06	0.13

a) The system means the mixtures of cupric ions and the 1 : 2 complexes (with charge and hydrated water molecules omitted). b) The pH at 25°C of the equivolume mixture of the 0.01 M aqueous-methanolic solutions of the two species in each system. c) An equivolume mixture of water and methanol. d) The values of log K in aqueous solution were calculated from Eq. (6) using the stepwise formation constants in the literature which determined in aqueous solution chiefly by the glass electrode method.[19,20] The values with errors express the means of two or more data. e) The value of ($\log K_{25}-\log K_0$) was used as a measure of the temperature dependence of log K in aqueous solution, where K_t represents K at t°C. The values with errors express the means of two or more data. f) Since the data for this system have not been reported, the values determined for the system Cu+Cu(L-thr)$_2$ were cited for reference, where L-thr represents the anion of L-threonine.

$$\log K = \frac{1}{2.30R}\left\{-\frac{(\Delta H_1-\Delta H_2)}{T}+(\Delta S_1-\Delta S_2)\right\} \quad (7)$$

where the symbols written in Eqs. (6) and (7) have their usual meanings. The values of log K were determined by the usual spectrophotometric method.[17]

When we represent the total concentrations of CuA_2 and Cu with xc and c respectively, and the concentration of CuA, with u, the equilibrium constant in Eq. (2) can be written by:

$$K = \frac{4u^2}{(xc-u)(c-u)} \quad (8)$$

On the other hand, the observed optical density, D', at a wavelength where the absorption of Cu is negligible is as follows:

$$D' = \varepsilon_p(xc-u) + 2\varepsilon_m u \quad (9)$$

where ε_p and ε_m mean the extinction coefficients of CuA_2 and CuA respectively. Furthermore, y and $\Delta\varepsilon$ were defined as follows:

$$y = \frac{D'-\varepsilon_p xc}{c} = (2\varepsilon_m-\varepsilon_p)\cdot\frac{c}{u} = \Delta\varepsilon\cdot\frac{u}{c} \quad (10)$$

From Eqs. (8) and (10), we obtain;

$$y^2 + P\cdot(1+x)\cdot y\cdot\Delta\varepsilon - P\cdot x\cdot\Delta\varepsilon^2 = 0 \quad (11)$$

where $P=K/(4-K)$. When two numerical sets of the x and y values at a certain wavelength are introduced into Eq. (11), we can find the values of $\Delta\varepsilon$ and P, from which the value of K can then be determined. The observed optical densities and the calculated values of y, $\Delta\varepsilon$, P, and K for the same systems as in Fig. 3 are listed in Tables 2 and 3. All the values of log K determined by this spectrophotometric method and by the previously-described ESR method[18] are listed in Table 4, together with the values of log K and their temperature dependences, which were calculated from Eqs. (6) and (7) using the step-by-step formation constants and the thermodynamic constants obtained in aqueous solutions by many investigators.[19,20]

It is clearly shown in Table 4 that the values of log K listed in the third, fourth, and fifth columns of the table are comparable to each other. All these values, moreover, are larger than the value of log K expected statistically, 0.60;[21] this means that there exist certain factors which promote the formation of the 1 : 1 complexes.[18,22-24] It seems likely that appreciably-accurate values of log K can be obtained by the ESR method, since all the magnetic parameters of CuA are intermediate in magnitude between those of Cu and CuA_2, since essential errors in estimating the concentrations of the three species are possibly cancelled out in Eq. (2).[18] However, the temperature at which the values of log K were determined by this ESR method is uncertain, although it is definitely a temperature between −50 and −100°C.[18] The temperature dependences of log K for all the systems in aqueous-methanolic solutions can be estimated by comparing the values of log K in the third and fourth columns of Table 4. In most systems, the temperature dependences in aqueous-methanolic solutions are in fair agreement with those in aqueous solutions. In System II, however, the temperature dependence of log K determined in this work is different

17) H. Yoneda, This Bulletin, **29**, 68 (1956).
18) H. Yokoi, M. Otagiri, and T. Isobe, This Bulletin, **44**, 2402 (1971).
19) L. G. Sillen and A. E. Martell, "Stability Constants of Metal-ion Complexes," (Special Publication No. 7), The Chemical Society, Burlington, London (1964).
20) J. J. Christensen and R. M. Izatt, "Handbook of Metal Ligand Heats and Related Thermodynamic Quantities," Marcel Dekker, New York (1970).
21) The value of 0.60 can be formally explained on the following scheme, assuming that there are $4n$ particles of Cu and A respectively in solution and A is bonded to either Cu or CuA with the same probability.
[$4n$ Cu+$4n$ A]→[($2n$ Cu, $2n$ CuA)+$2n$ A]→[n Cu, $2n$ CuA, n CuA_2]
Accordingly, $\log K=\log[Cu][CuA_2]=\log n\times n=\log 4=0.60$.
22) R. De Witt and J. I. Watters, *J. Amer. Chem. Soc.*, **76**, 3810 (1954); J. I. Watters, A. Aaron, and J. Mason, *ibid.*, **75**, 5212 (1953); J. I. Watters and E. D. Longham, *ibid.*, **75**, 4819 (1953).
23) S. Kida, This Bulletin, **29**, 805 (1956).
24) S. Kida, *ibid.*, **34**, 962 (1961).

in tendency from that obtained in aqueous solutions, although this result may not be accurate because of insufficient thermodynamic data on aqueous solutions for this system. The values of $\log K$ at 25°C listed in the third and fifth columns of Table 4 are somewhat different for the systems having relatively less stable 1 : 2 complexes. These differences may be due to the different solvent used, since the solvent effect on the complexes becomes more profound as they are less stable. Systems I—IV are those diamines, and Systems V—VII, those of amino acids. It is also shown in Table 4 that, in the former systems, the values of $\log K$ increase with a rise in the temperature, while in the latter systems the values decrease. The thermodynamic constants derived from these data are listed in Table 5. It is well known that, in complex formation, the nitrogen donors are softer than the oxygen donors and that both ΔH and ΔS are markedly lower for the formation of complexes by nitrogen than oxygen donors.[25] For both copper(II) complexes of ethylenediamine and L-alanine, the difference between ΔH_1 and ΔH_2 is quite small in magnitude, but the difference between ΔS_1 and ΔS_2 is markedly larger for the L-alanine complex than for the ethylenedimaine complexes; for the latter complex, $\Delta S_2=0$ and ΔS_1 is much smaller in magnitude than ΔS_1 and ΔS_2 for the former complex. Accordingly, the entropy term is more important in stabilizing the 1 : 1 complexes for amino acids than for diamines, as is clearly demonstrated in Table 5.

25) S. Ahrland, "Structure and Bonding," Vol. 5, ed. by C. K. Jørgensen, R. S. Nyholm, and R. J. P. Williams, Springer-Verlag, Berlin (1968), p. 118.

Table 5. Thermodynamic constants for $Cu + CuA_2 \rightleftarrows 2CuA$[a]

No.	System	(kcal/mol) ΔH	ΔS (e. u.)
I	$Cu+Cu(en)_2$	-0.51 ± 0.24 (-0.34 ± 0.10)	4.8 ± 0.7 (5.6 ± 0.3)
II	$Cu+Cu(dmen)_2$	-1.68 ± 0.43	4.0 ± 1.3
III	$Cu+Cu(deen)_2$	-2.35 ± 0.60	1.2 ± 1.7
IV	$Cu+Cu(tn)_2$	-1.08 ± 0.54	6.7 ± 1.6
V	$Cu+Cu(L\text{-ala})_2$	0.92 ± 1.27 (0.9)	11.2 ± 1.0 (9.9)
VI	$Cu+Cu(L\text{-ser})_2$	0.38 ± 0.35	8.1 ± 1.0
VII	$Cu+Cu(\beta\text{-ala})_2$	-0.11 ± 0.46	5.9 ± 1.3

a) The solvent used is an equivolume mixture of water and methanol. The temperature at which the K values are determined by the ESR method was assumed to be −75°C. The values in parentheses in the table are the ones derived from the data in aqueous solution in the literature.[19,20]

BULLETIN OF THE CHEMICAL SOCIETY OF JAPAN, VOL. 46, 447—451 (1973)

ESR Studies of Dimer Formation by the β-Diketone Chelate Complexes of Copper(II) in Toluene[1)]

Hiroshi Yokoi and Taro Isobe

Chemical Research Institute of Non-aqueous Solutions, Tohoku University, Katahira, Sendai

(Received January 6, 1972)

A study of the ESR spectra of several β-diketone chelate complexes of copper(II) in the frozen solution of toluene has revealed that triplet-state dimers are formed at high concentrations in the solution and that these dimers are in equilibrium with only the monomers. The approximate equilibrium constants have been determined by a careful analysis of the ESR spectra observed in various concentrations. Structures for the dimers have been suggested from magnetic parameters properly determined using a point dipole model.

In recent years, many ESR studies of the triplet state of binuclear copper(II) complexes have been carried out with especial interest being taken in the mechanisms of the magnetic interactions between the two copper atoms.[2-11)] There have, however, been only a few ESR investigations of the triplet state obtained by the dimerization of mononuclear stable copper(II) complexes.[12-14)] The ESR experiments described in this paper will establish the new fact that dimeric and

1) Preliminary report: H. Yokoi and T. Isobe, This Bulletin, **44**, 1446 (1971).

2) B. Bleaney and K. D. Bowers, *Proc. Roy. Soc. Ser. A*, **214**, 451 (1952).

3) H. Abe and J. Shimada, *J. Phys. Soc. Jap.*, **12**, 1255 (1957); H. Abe, *ibid.*, **13**, 987 (1958).

4) G. K. Kokoszka and G. Gordon, "Transition Metal Chemistry," ed. by R. L. Carlin, Vol. 5, Marcel Dekker, New York (1969), p. 181.

5) R. H. Dunhill, J. R. Pilbrow, and T. D. Smith, *J. Chem. Phys.*, **45**, 1474 (1966); J. F. Boas, R. H. Dunnhill, J. R. Pilbrow, R. C. Srivastava, and T. D. Smith, *J. Chem. Soc. A*, **1969**, 94.

6) J. H. Price, J. R. Pilbrow, K. S. Murray, and T. D. Smith, *J. Chem. Soc. A*, **1970**, 968; A. D. Toy, T. D. Smith, and J. R. Pilbrow, *ibid.*, **1970**, 2600.

7) J. F. Boas, J. R. Pilbrow, C. R. Hartzell, and T. D. Smith, *ibid.*, **1969**, 572; J. F. Boas, J. R. Pilbrow, and T. D. Smith, *ibid.*, **1969**, 723; J. F. Boas, J. R. Pilbrow, G. J. Troup, C. Moore, and T. D. Smith, *ibid.*, **1969**, 965; J. R. Pilbrow, S. G. Carr, and T. D. Smith, *ibid.*, **1970**, 723.

8) G. F. Kokoszka, M. Linzer, and G. Gordon, *Inorg. Chem.*, **7**, 1730 (1968).

9) R. L. Belford, N. D. Chasteen, H. So, and R. E. Tapscott, *J. Amer. Chem. Soc.*, **91**, 4675 (1969).

10) N. D. Chasteen and R. L. Belford, *Inorg. Chem.*, **9**, 169 (1970).

11) W. E. Hatfield, J. A. Barnes, D. Y. Jeter, R. Whyman, and E. R. Jones, Jr., *J. Amer. Chem. Soc.*, **92**, 4982 (1970).

12) J. F. Boas, J. R. Pilbrow, and T. D. Smith, *J. Chem. Soc. A*, **1969**, 721.

13) J. R. Pilbrow, A. D. Toy, and T. D. Smith, *ibid.*, **1969**, 1029.

14) G. O. Carlisle and W. E. Hatfield, *Inorg. Nucl. Chem. Lett.*, **6**, 633 (1970).

monomeric species coexist at equilibrium in the toluene solutions of some copper(II) β-diketonates. The purpose of this paper is to propose structures for the dimers and to determine the equilibrium constants through an analysis of the observed ESR spectra.

Experimental

Materials. The β-diketone chelate complexes of copper(II) employed in this work are $Cu(acac)_2$, $Cu(bzac)_2$, $Cu(Etacest)_2$, and $Cu(Meacest)_2$, where acac, bzac, Etacest, and Meacest are the anions of acetylacetone, benzoylacetone, ethyl acetoacetate, and methyl acetoacetate respectively. They were prepared and purified according to the usual method.[15] Commercial toluene was purified by successive shaking with sulfuric acid and sodium hydroxide, followed by drying over sodium and, finally, fractional distillation.

ESR Measurements. The ESR spectra of the above-mentioned complexes in toluene in various concentrations were measured at the temperature of liquid nitrogen over the field range of 0 to 6,000 gauss, using a Hitachi 771 X-band ESR spectrometer. The toluene solutions were transferred into quartz tubes 4 mm in internal diameter and then solidified with liquid nitrogen as quickly as possible. These frozen solutions were the actual samples for ESR measurements used in this work.

Results and Discussion

The observed ESR spectra of $Cu(Etacest)_2$ and $Cu(acac)_2$ in toluene at the temperature of liquid nitrogen are shown in Figs. 1 and 2 respectively. $Cu(Meacest)_2$ and $Cu(bzac)_2$ were similar to $Cu(Etacest)_2$ and $Cu(acac)_2$ respectively in the ESR line shape. These spectra are complicated, and all of them showed weak absorptions at the low-field of about 1,500 gauss. The ESR spectra in these figures which are constructed by excluding sharp absorption lines are similar in line shape to the spectra observed for various binuclear copper(II)

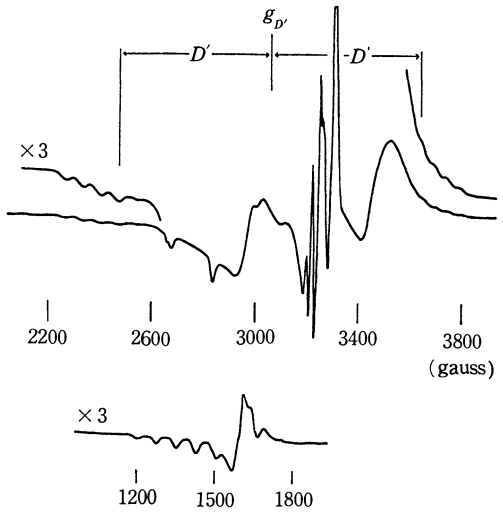

Fig. 1. The X-band first-derivative ESR spectrum of $Cu(Etacest)_2$ in toluene at 77K (c^0 : 1.03×10^{-2} M, the lower spectrum is the half-field spectrum of the $\Delta M=2$ transition).

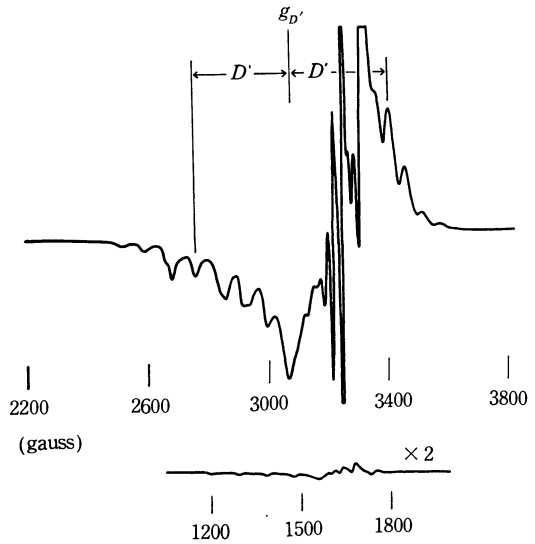

Fig. 2. The X-band first-derivative ESR spectrum of $Cu(acac)_2$ in toluene at 77K (c^0 : 2.22×10^{-3} M).

complexes with copper-copper spin interactions.[5-14] The ESR line shapes for randomly-oriented and magnetically-diluted copper(II) complexes have been studied in some detail by many investigators.[16] It can be clearly understood by a comparison of all these ESR line shapes that all the ESR spectra observed in this work are made up to the superposition of two types of spectra; one is due to triplet-state dimers, and the other, due to doublet-state monomers.

The spin Hamiltonian for triplet-state copper(II) dimers, on the assumption of axial symmetry, is written as follows:

$$H = \beta[g_{//}H_zS_z+g_\perp(H_xS_x+H_yS_y)] + D[S_z^2-S(S+1)/3] + A_{//}S_zI_z + A_\perp(S_xI_x+S_yI_y) \quad (1)$$

where all the symbols have their usual meanings. The zero-field splitting parameter, D, is composed of the following two terms:

$$D = D_{dd} + D_{pseudo} \quad (2)$$

In Eq. (2), D_{dd} expresses the magnetic dipole-dipole interaction term, and $D_{pseudo}=-J[(g_{//}-2)^2/4-(g_\perp-2)^2]/8$, where $-J$ is the energy separation between the singlet ground state and the first excited triplet state.[2] We wish now to estimate D_{dd}, from which the copper-copper atomic distance, R, can be estimated; then, the structures for the corresponding dimers can be proposed.[9,17] Since D only is a measurable value, D_{pseudo} must be estimated in order to determine D_{dd}. It has been considered that the structures for dimeric complexes in solution may be analogous to those in a crystal and that the $-J$ values in the two states may be almost the same.[14] The $-J$ value of $Cu(acac)_2$ in a crystal has been estimated to be less than 0.3 cm^{-1} from the value of θ in the

15) D. P. Graddon and E. C. Watton, *J. Inorg. Nucl. Chem.*, **21**, 49 (1961).

16) R. H. Sands, *Phys. Rev.*, **99**, 1222 (1955); T. Vanngard and R. Aasa, Proc. 1st Intern. Congr. "Paramagnetic Resonance," Jerusalem, 1962, Academic Press, New York (1963), p. 509; R. Neiman and D. Kivelson, *J. Chem. Phys.*, **35**, 156 (1961).

17) K. W. H. Stevens, *Proc. Roy. Soc. Ser. A*, **214**, 237 (1952).

Curie-Weiss formula[18,19] and from the unification phenomenon of two separate ESR absorption lines with different g values due to a spin-exchange interaction.[20] The value of D_{pseudo} for $Cu(acac)_2$ in a crystal, which can be calculated from the above-described equation of D_{pseudo} using the above-estimated $-J$ value, is no more than a small percentage of the experimentally-determined D values (about 0.05 cm^{-1}) in this work. Furthermore, a change in the $-J$ value does not sensitively contribute to the calculated R value.[10] The assumption of $D=D_{dd}$, therefore, holds approximately good for all the dimers in this work. The copper-copper atomic distance, R, can be approximately estimated by means of the following equation, derived by the use of a point dipole model:

$$R = (0.650\, g_{//}^2/D_{dd})^{1/3} \quad (3)$$

where $g_{//}$ and D_{dd} are the parameters defined in Eqs. (1) and (2).[9,17] It has been demonstrated that the agreement between the experimentally-determined R value and the R value estimated from Eq. (3) is fairly good.[10] A closer examination of the ESR spectra observed in this work shows that the hyperfine coupling constants observed at the two edges of the triplet spectra for $\Delta M=1$ are appreciably different from each other. Chikira and Isobe have revealed, through the computer simulation of these types of triplet ESR line shapes, that the above-mentioned differences in the hyperfine structure are due to the discrepancy between the principal axes of the D and A tensors in orientation.[21] They have also reported that, generally, the approximate R value can be obtained directly by substituting $g_{D'}$ and D' for $g_{//}$ and D_{dd} respectively in Eq. (3), regardless of the $-J$ value over a considerable wide range, where $g_{D'}$, and D' are defined in Figs. 1 and 2.[21] The analyzed results for all the complexes are listed in Table 1.

The first two complexes in Table 1 are quite similar to each other in ESR behavior; such is also the case with the other two complexes in the table. The molecular configuration of $Cu(acac)_2$ in a crystal is schematically shown in Fig. 3(A), where the R value

Table 1. Magnetic parameters and R[a] values

Copper(II) complex	Monomers			Dimers		
	$g_{//}$	$g_{\perp}$	$\lvert A_{//}\rvert$ $\times 10^4$ cm^{-1}	$g_{D'}$[b]	D'[b] $\times 10^4$ cm^{-1}	R (Å)
$Cu(Etacest)_2$	2.282	2.05	176	2.174	590	3.73
$Cu(Meacest)_2$	2.275	2.06	174	2.167	581	3.75
$Cu(acac)_2$	2.255	2.05	191	2.161	326	4.53
$Cu(bzac)_2$	2.255	2.05	192	2.157	331	4.50

a) R represents the copper-copper distance (Å).
b) The parameters are defined in Figs. 1 and 2.

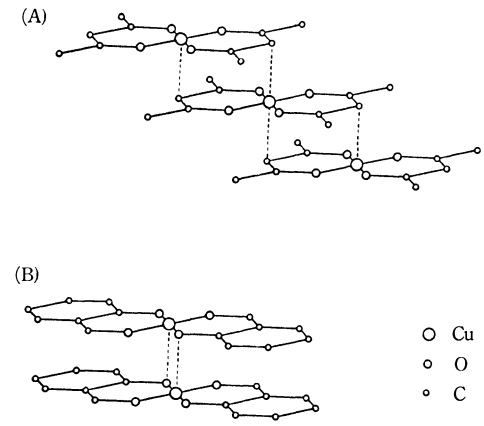

Fig. 3. The schematically represented crystal structures of (A): $Cu(acac)_2$ and (B): crystal form of bis-(salicylaldehydato)copper(II).

is 4.52 Å.[22] This R value surprisingly agrees with the R value calculated from D' value, as is shown in Table 1. Accordingly, it may be concluded that the dimeric structure of $Cu(acac)_2$ in toluene is the same as that in a crystal and that, furthermore, the dimers of $Cu(bzac)_2$ in toluene also have a similar structure. On the other hand, the crystal structure of Cu(Etacest)$_2$, whose R value is 4.53 Å,[23] is analogous to that of $Cu(acac)_2$; in their crystals, the carbon atoms of the –CH– groups of adjacent molecules occupy the apical positions of the copper atom. The R value calculated from D' for the dimers of Cu(Etacest)$_2$ in toluene is 3.75 Å, as is listed in Table 1. The large difference between the two R values for this complex clearly indicates that its dimeric structure in toluene is quite different from that in a crystal. Interestingly, (salicylaldehydato)copper(II), which is analogous in physical and chemical behavior to Cu(Etacest)$_2$,[26,27] has two different crystal structures[24,25]; one is similar to the crystal structure of $Cu(acac)_2$, and the other, to those of *N,N'*-disalicylidene ethylenediamine copper(II),[28] the γ-form of bis-(*N*-methyl-salicylaldiminato)copper(II),[29] and bis-(8-hydroxyquinolinato)copper(II).[30] The latter crystal structure is schematically shown in Fig. 3(B), where the directly-coordinating oxygen atoms of adjacent molecules occupy the apical positions of the copper atom. The R value is calculated to be 3.73 Å for this type of structure, assuming about 3.15 Å as a reasonable copper-apical oxygen distance. It seems likely, therefore, that the

18) J. H. Van Vleck, "The Theory of Electric and Magnetic Susceptibilities," Oxford Univ. Press (1932), p. 332.
19) J. J. Fritz and R. C. Taylor, *J. Amer. Chem. Soc.*, **80**, 4484 (1958).
20) G. Schoffa, O. Ristau, and B. E. Wahler, *Z. Physik. Chem.* (Leipzig), **215**, 203 (1960).
21) M. Chikira and T. Isobe, This Bulletin, **45**, 3006 (1972).
22) H. Koyama, Y. Saito, and H. Kuroya, *J. Inst. Polytech., Osaka City Univ.*, **4** C, 43 (1953).
23) G. A. Barclay and A. Cooper, *J. Chem. Soc.*, **1965**, 3746.
24) A. J. McKinnon, T. N. Waters, and D. Hall, *ibid.*, **1964**, 3290.
25) D. Hall, A. J. McKinnon, and T. N. Waters, *ibid.*, **1965**, 425.
26) A. E. Martell and M. Calvin, "Chemistry of the Metal Chelate Compounds," Prentice-Hall, New York (1952), p. 134.
27) H. Yokoi, M. Sai, and T. Isobe, *Chem. Lett.*, **1972**, 25.
28) D. Hall and T. N. Waters, *J. Chem. Soc.*, **1960**, 2644.
29) D. Hall, S. V. Sheat, and T. N. Waters, *Chem. Commun.*, **1966**, 436.
30) J. A. Bevan, D. P. Graddon, and J. F. McConnell, *Nature*, **199**, 373 (1963).

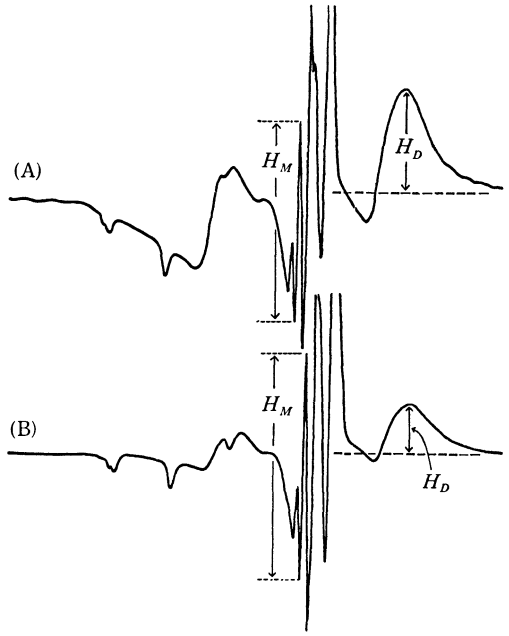

Fig. 4. The concentration dependence of the first-derivative ESR spectra of Cu(Etacest)$_2$ in toluene at 77K.
(A): $c^0=1.03\times10^{-2}$ M, (B): $c^0=0.23\times10^{-2}$ M.

dimers of Cu(Etacest)$_2$ in toluene have a structure analogous to the one shown in Fig. 3(B).

A large concentration dependece of the ESR spectra was observed for each of the complexes employed here, as is shown in Fig. 4. The Q value can now be defined as the intensity ratio of a certain absorption line of the dimers to a certain line of the monomers in a first-derivative ESR spectrum; for instance, $Q=H_D/H_M$ in the case of Fig. 4. It is clear that all the complexes in toluene regularly change in their Q values with their initial concentrations, as may be seen in Fig. 4. It seemed that it would be very interesting to see whether or not the following type of equilibrium is established in the solution:

$$2M \rightleftharpoons M_2 \tag{4}$$

$$K=\frac{[M_2]}{[M]^2} \tag{5}$$

where M and M_2 represent monomeric and dimeric molecules respectively. An attempt to establish the proof of the presence of such an equilibrium and to determine the K value will be described below.

When q is introduced as the proportional constant of the equation $Q=q\cdot([M_2]/[M])$, the following equation can be derived from Eq. (5):

$$2Q^2+qQ=Kq^2c^0 \tag{6}$$

where c^0 is the initial concentration of a complex in toluene. It was assumed that the $[M_2]/[M]$ ratio is equal to the ratio of one-half of the integrated intensity of the ESR spectral component due to the triplet-state dimers to the integrated intensity of the spectral component due to the monomers; the coefficient of one-half means that the transition of $\Delta M=1$ occurs twice within a whole-field sweep for each of the dimeric molecules, while it does so once for each of the monomeric molecules. The determination of the q value is troublesome and is responsible for the greatest error in evaluating the K value from Eq. (6). The q value was here determined by the following method.

There was a remarkable increase in the apparent intensity ratio of the ESR spectral component due to the monomers to the one due to the dimers as the c^0 value became smaller. For the monomers, accordingly, the approximate ratio of the totally-integrated spectral intensity to the height of a certain first-derivative ESR absorption line can be determined from an ESR spectrum observed in a very low concentration. Since the integrated intensity of the spectral component due to the monomers can be obtained for each of the observed ESR spectra using the above-determined ratio, the integrated intensity due to the dimers also can be determined by deducting the one due to the monomers from the totally-integrated intensity of the spectrum; the q value can then be straightforwardly evaluated from those intensity values.

The analyzed data for Cu(Etacest)$_2$, as an example, are listed in Table 2, where the q value was determined to be 0.14 ± 0.02 by using the absorption lines of H_D and H_M shown in Fig. 4. The plot of $2Q^2+qQ$ *vs.* c^0 for this complex is shown in Fig. 5. The data for

Table 2. Data on the plot of $2Q^2+qQ$ *vs.* c^0 for Cu(Etacest)$_2$ in toluene

$c^0\times10^2$ (mol/l)	H_M[a)]	H_D[a)]	$Q(=H_D/H_M)$	$2Q^2+qQ$[b)]
1.274	111.0	63.40	0.5712	0.7324
0.996	124.5	61.40	0.4932	0.5554
0.766	134.5	57.80	0.4297	0.4293
0.586	129.6	46.35	0.3576	0.3057
0.427	111.5	34.35	0.3081	0.2329
0.332	95.1	24.55	0.2581	0.1693
0.230	133.0	26.00	0.1954	0.1036
0.091	68.9	7.00	0.1016	0.0348

a) H_M and H_D (an arbitrary unit) are defined in Fig. 4.
b) The q value was assumed to be 0.14.

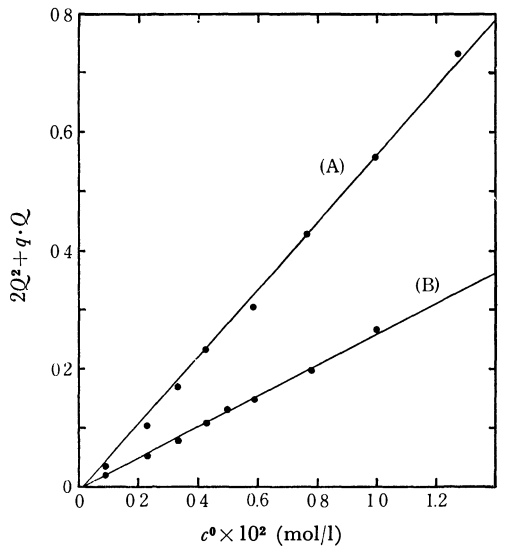

Fig. 5. The plots of $2Q^2+q\cdot Q$ vs. c^0 for (A): Cu(Etacest)$_2$ ($q=0.14$) and (B): Cu(Meacest)$_2$ ($q=0.12$).

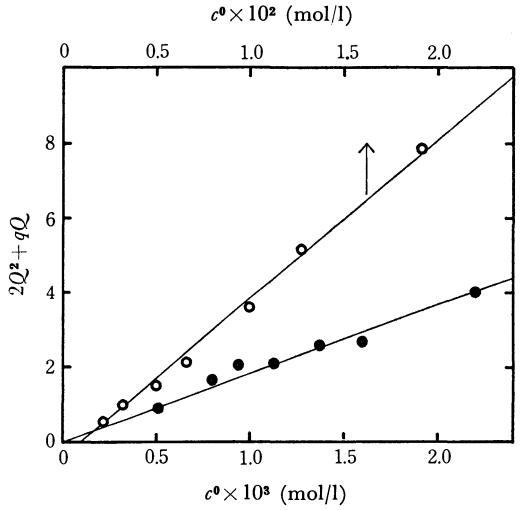

Fig. 6. The plot of $2Q^2+qQ$ *vs.* c^0.
●: $Cu(acac)_2$ ($q=0.090$)
○: $Cu(bzac)_2$ ($q=0.11$)

the other complexes are not listed here; only the plots are shown in Figs. 5 and 6. All these plots were clearly found to be linear; accordingly, the K values could be evaluated from the slopes of these linear plots. The K values thus obtained are listed in Table 3, together with the determined q values.

The fact that a plot of $2Q^2+qQ$ *vs.* c^0 gives a straight line for all the complexes in toluene indicates that both species of dimers and monomers are present in the equilibrium of Eq. (4) in the toluene solution of the complexes; the other species —for example, polymers— do not exist in the solution. The large K values determined for the first three complexes in Table 3 indicate that most molecules of the three complexes are dissolved into toluene as dimers. The linear plots above-described, furthermore, indicate that the reproducibility of this experimental method for estimating the equilibrium constants is not poor; the experimental method accompanying the solidification of the sample solutions in liquid nitrogen is applicable to various quantitative analyses, as in this case. The temperature at which the equilibrium constants are determined, however, is uncertain in this experiment, although it is undoubtedly near the freezing point of toluene (−95°C).[31,32] Such a dimer formation could not be observed in any of the various organic solvents ordinarily used other than toluene. Furthermore, bis-(dipivaloylmethanato)copper(II) and bis-(trifluoroacetylacetonato)copper(II), which are also β-diketone chelate complexes similar in various properties to $Cu(acac)_2$ and $Cu(Etacest)_2$ respectively, did not exhibit such a dimer formation in toluene; this experimental fact suggests the importance of the steric factors in the dimer formation. At any rate, the factors governing the dimer formation seem to be very complicated; a further investigation of this problem is now in progress.

Table 3. K and q[a] values

Copper(II) complex	q	$K \times 10^{-3}$
$Cu(Etacest)_2$	0.14 ±0.02	3.0 ±0.9
$Cu(Meacest)_2$	0.12 ±0.01	1.8 ±0.3
$Cu(acac)_2$	0.090±0.015	2.3 ±0.7
$Cu(bzac)_2$	0.11 ±0.01	0.35±0.05

a) See the text.

The authors wish to thank Mr. M. Chikira for many helpful discussions and suggestions during this work.

31) H. Yokoi, M. Otagiri, and T. Isobe, This Bulletin, **44**, 2402 (1971).
32) H. Yokoi, M. Otagiri, and T. Isobe, *ibid.*, **46**, 442 (1973).

Rocker-type DTA Apparatus for Fluid Samples

Satohiro TANAKA

National Chemical Laboratory for Industry, Hon-machi, Shibuya-ku, Tokyo

(Received February 15, 1972)

A Rocker-type DTA apparatus, with agitation by rocking, has been developed for use in the thermal analysis of various fluid mixture systems. The heater block, with its assembled cells, is continuously rocked at 20 r.p.m. with a rocking of 180° angle. The glass cell has a volume of about 8 ml and is sealed by means of a burner with a sample of about 5 ml. Distilled water is used as the inert reference in the reference holder. Two thermocouples are inserted in each cell, one to determine the temperature difference and the other for sample temperature measurements. The double thermocouple gives a constant transition temperature of the sample over a wide range of heating rates. The apparatus is applied to solid-liquid and starch-water systems. Variables affecting the DTA thermogram of the $K_2Cr_2O_7$–H_2O system are investigated, and a method is established to correlate the DTA curve with the solubility curve for the system.

It is sometimes necessary to perform the thermal analysis of heterogeneous fluid mixture systems such as solid-liquid and starch-water[1] systems. The most important conditions for the thermal analysis of such systems are to avoid the escape of the vapor of the samples and to avoid composition inhomogeneity in the sample cells. These conditions are usually obtained by the use of a sealed sample holder and by stirring the samples adequately.

Various stirring techniques are available; the final choice is dependent on the nature of the system to be investigated. Propellor-type stirrers driven by a shaft are sometimes used.[2,3] However they cease to operate when a fraction of the sample is solidified, and they allow the vapor of the sample to escape through the gland around the shaft of the stirrers and allow a considerable amount of heat to be conducted from or to the holder through the shaft. An alternative method is to use a sealed-in stirrer operated by means of a solenoid,[4] but in this case the stirrer stops when only a fraction of the sample is solidified and it is necessary to ensure that no electrical interference is produced in the temperature-measuring circuit in the solenoid. To ensure the adequate stirring of the sample inside a sealed holder, the rocking method[5–8] may be used. Here, the agitation of the sample continues until practically all the material has solidified, and at the same time the material is completely sealed in the holder. Gilpatrick *et al.*[8] have also described the use of a commercial rocker unit for phase studies of a molten salt system, NaF–KF–BF_3. In the apparatus to be described here, adequate stirring has also been obtained by applying the rocking method, and the DTA of solid-liquid and potato starch-water systems has been successfully performed.

Experimental

Apparatus. A whole diagram of the apparatus is shown schematically in Fig. 1. The center of gravity of the block assembly and the rack is adjusted to coincide with the shaft, the axle of rotation, so as to assure smooth rotation. The holder contents are then stirred by continuous rocking through an arc of 180° at a speed of 20 rpm achieved by means of a synchronous motor. The heater block is made of aluminum; a cross-section of heater block assembly is shown in Fig. 2. The holder used is made of glass; it is also shown in Fig. 2. The holder has a volume of about 8 ml and is sealed by means of a burner with a content of about 5 ml. The block is heated by a noninductively-wound nichrome wire insulated by a mica sheet against the surface of the block. The heater is controlled by a variable-voltage transformer to give the desired constant heating rates.

Chromel-Alumel thermocouples are used to measure the block, sample, and temperature differences. In the well of each holder, two junctions of the thermocouples are inserted to measure the temperature and temperature differences. This arrangement gives a constant transition temperature of sample over a wide range of heating rates. The electrical leads for the heater and thermocouples are hung in wide U-

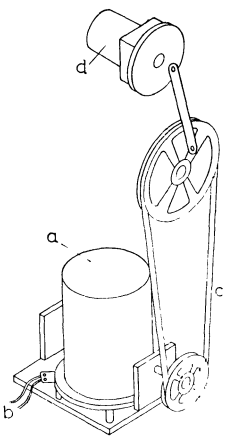

Fig. 1. Schematic diagram of rocker type DTA apparatus assembly. a: heater block with aluminum cover, b: electric lead wires, c: belt, d: synchronous motor.

1) S. Tomita, private request.

2) H. J. Borchardt and F. Daniels, *J. Amer. Chem. Soc.*, **79**, 41 (1957).

3) K. Tamura, K. Nakatsuka, and R. Fujishiro, This Bulletin, **39**, 20 (1966).

4) G. Takeya, T. Ishii, K. Makino, and S. Ueda, *Kogyo Kagaku Zasshi*, **69**, 1654 (1966).

5) G. Waddington, S. Sunner, and W. N. Hubbard, "Experimental Thermochemistry," Vol. 1, ed. by F. D. Rossini, Interscience Publishers, New York, N. Y. (1960), pp. 170, 191.

6) H. A. Skinner, J. M. Sturtevant, and S. Sunner, "Experimental Thermochemistry," Vol. 2, ed. by H. A. Skinner, Interscience Publishers, New York, N. Y. (1962), pp. 149, 186.

7) E. W. Comings, "High Pressure Technology," McGraw-Hill, New York, N. Y. (1956), p. 228.

8) L. O. Gilpatrick, S. Cantor, and C. J. Barton, "Thermal Analysis," Vol. 1, ed. by R. F. Schwenker, Jr., and P. D. Garn, Academic Press, New York, N. Y. (1969), p. 85.

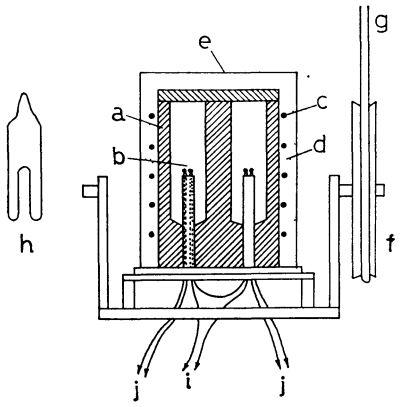

Fig. 2. Cross section of heater block and glass holder.
a: aluminum block, b: thermocouples, c: heater, d: thermal insulator, e: aluminum cover, f: wheel, g: belt, h: glass holder, i: temperature difference, j: temperature.

turns to prevent the breaking of the leads by the repeated bending introduced by the rocking of the assembly. The differential thermocouple emf is preamplified by Okura Model AM-1001 D. C. amplifier and fed to the input of a Rikadenki Model B-341 three-pen recorder. The block and sample temperatures emf are similarly fed to the inputs of the recorder without preamplification.

Materials. Benzoic acid, a standard sample for combustion calorimetry obtained from the Resource Research Institute, Japan, and Tokyo Kasei zone-refined naphthalene were used to calibrate the temperature thermocouple through their melting points. Kokusan Chemical Works extra-pure potassium dichromate, potassium nitrate, cobalt sulfate, and Wakō Junyaku potato starch were used without further purification. Distilled water was used as the reference material and as one component of the sample binary mixtures.

Results and Discussion

Some Examples. Figure 3 shows the effect of the heating rate on the peak temperatures.

Blank-run DTA curves of distilled water in both holders are shown in Fig. 4 and 5. The regular variation in the base line synchronous with the rocking cycle is increased with the increase in the sample temperature and the heating rate. The blank run in Fig. 4 is performed under a high heating rate in order to observe the irregularity of base line, while general runs with actual samples are performed under a mod-

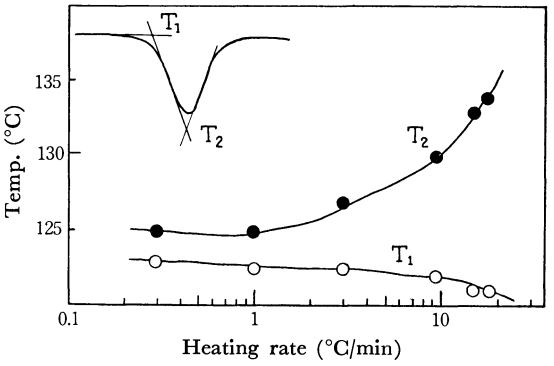

Fig. 3. Effect of heating rate on peak temperatures of benzoic acid melting.

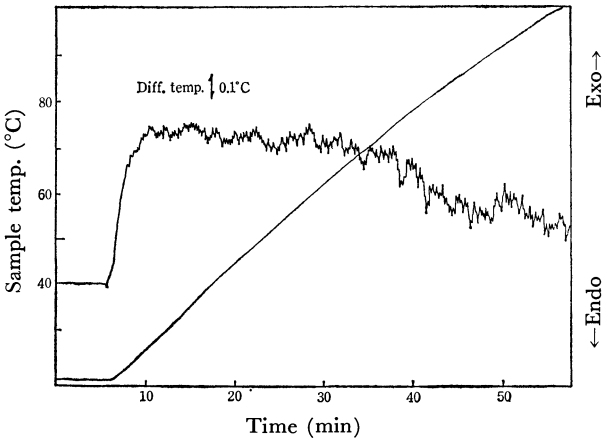

Fig. 4. Rocking DTA curve for H_2O in both holders.

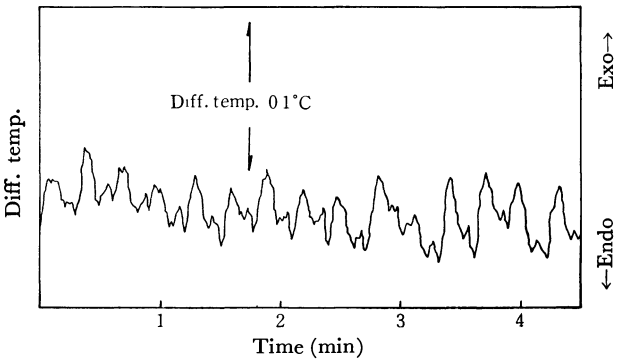

Fig. 5. Rocking DTA curve for H_2O in both holders at about 80°C.

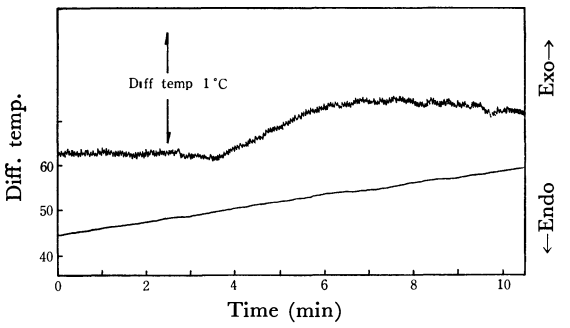

Fig. 6. Rocking DTA curve for $K_2Cr_2O_7$–H_2O ($K_2Cr_2O_7$/H_2O=0.354 wt. fraction).

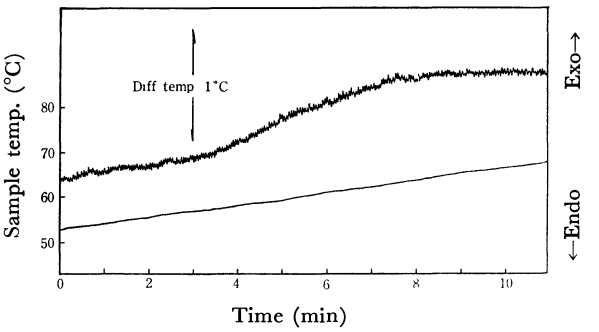

Fig. 7. Rocking DTA curve for KNO_3–H_2O (KNO_3/H_2O= 1.13 wt. fraction).

erate heating rate, nearly equal to or less than about 1°C/min., and have more smooth base lines than the run in Fig. 4.

DTA curves of various solid-liquid mixture systems of known compositions are shown in Figs. 6 to 8. A shift in the position of the base line to a new level is observed in Figs. 6 and 7. The temperature at which the shift occurs is nearly in agreement with the dissolution temperature in the literature.[9] The dissolution temperature, at which the solid phases in a mixture of the prepared compositions dissolve completely, are 50°C for $K_2Cr_2O_7/H_2O=0.354$ and 62°C for $CoSO_4/H_2O=1.13$,[9] while the shifts are found at about 50—63°C respectively. The two peaks at 53°C and 59°C are considered to be due to the dehydration reactions of $CoSO_4 \cdot 7H_2O$, but the peak temperatures cannot be identified with any one of the dehydration temperatures in the literature.[9]

The base-line shift is also found for the potato starch-water system, as is shown in Fig. 9. The shift temperature of about 60—62°C is in agreement with the gelatinization temperature of the starch in water.[10] The direction of the shift is from a lower heat capacity at a lower temperature to a higher capacity at a higher temperature. This display is graphically analogous to that shown in the DTA thermogram of a glass transition in a high polymer.

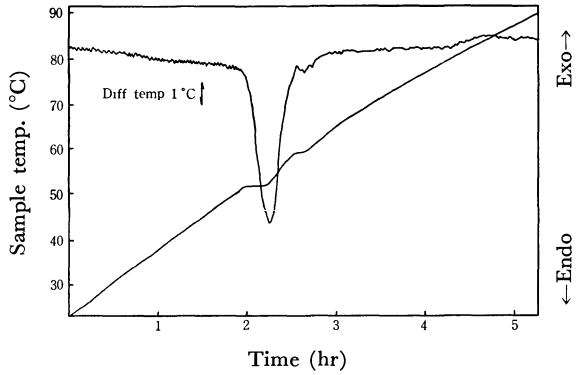

Fig. 8. Rocking DTA curve for $CoSO_4$-H_2O ($CoSO_4+H_2O$)=0.444 wt. fraction)

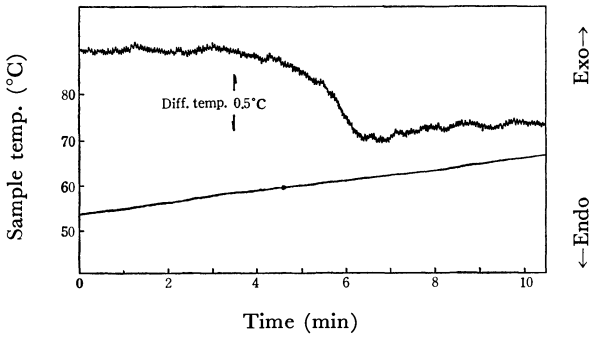

Fig. 9. Rocking DTA curve for gelatinization of potato starch in water. Potato starch 5.04 wt. % in solution.

9) The Chemical Society of Japan (ed.), "Kagaku-Benran," Maruzen, Tokyo (1958), p. 581.

10) J. Nikuni (ed.), "Denpun-Handbook," Asakura-Shoten, Tokyo (1961), p. 79.

DTA curves of a Solid-liquid System. The thermal analysis of a solid-liquid mixture system with this apparatus has been studied in some detail by investigating the thermal behavior of the $K_2Cr_2O_7$-H_2O system and the variables affecting the appearance of the DTA curve of the system. The requirements to achieve a reproducible DTA curve and a sharp shift (see Fig. 6) in the neighborhood of the dissolution temperature are as follows:

(1) the solid phase should be fine powder;
(2) the sample holder should be in good thermal contact with the wall of the DTA block and
(3) the proper heating rate should be chosen so as to give a precise solubility temperature from the shift of the DTA curve.

(1) and (3) are necessary to maintain the system under thermochemical equilibrium as much as possible during the course of the thermal analysis, while (2) is required to obtain a sharp shift of the curve.

The shift temperatures were selected from various portions of the DTA shift curve, as is illustrated in Fig. 10. Point A is the intersection of the extrapolated straight-line portion of the side of the shift with the base line at a lower temperature, while C is the extrapolated intersection with the base line at a higher temperature. Point B is the middle point of the AC line. The effect of the heating rate on the shift tem-

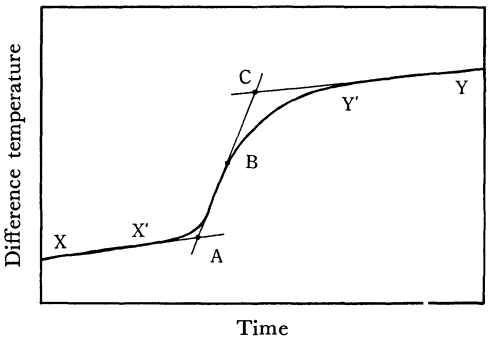

Fig. 10. A typical DTA curve for solid-liquid system.

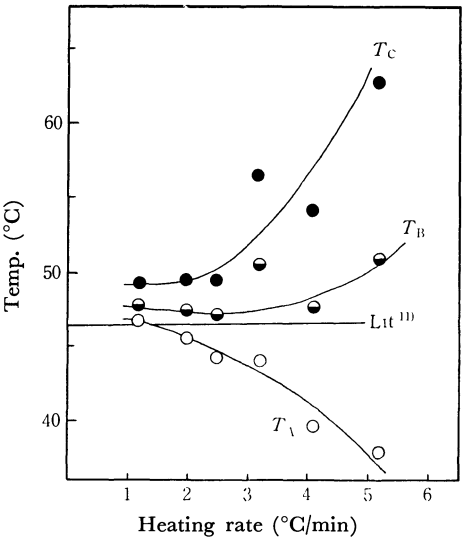

Fig. 11. Effect of heating rate on shift temperatures of DTA curve for $K_2Cr_2O_7$-H_2O.

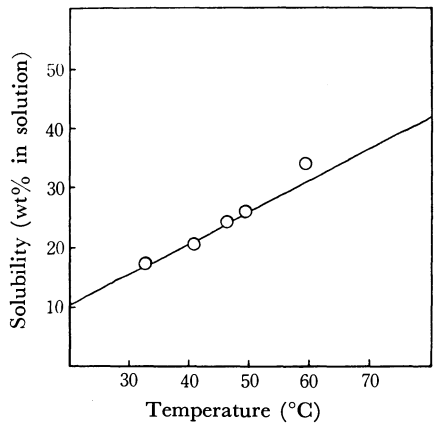

Fig. 12. Solubility curve of $K_2Cr_2O_7$ in water.
○: Experimental, ——: Literature.[11]

peratures at which the various points occurred during the dissolution process of the system is shown in Fig. 11. Temperature T_A, estimated at Point A, approaches the dissolution temperature[11] of the system in the prepared composition as the heating rate decreases and is approximately equal to the dissolution temperature at 1°C per minute. Since the best measure from T_A at 1°C per minute was thus obtained, this temperature was selected for other compositions of the systems. The temperatures, T_A, for the various compositions thus obtained are shown in Fig. 12; a comparison with the solubility curve from the literature[11] shows a satisfactory agreement between them.

Discussion of the DTA Shift Curve. In the DTA apparatus described here, adequate and continuous stirring is achieved by rocking; one can, therefore, assume a uniform temperature inside the holders and can set down equations describing the heat flow into the sample and reference holders as follows;

$$C_s \frac{dT_s}{dt} = h_s(T_b - T_s) + \frac{dQ}{dt} \quad (1)$$

$$C_r \frac{dT_r}{dt} = h_r(T_b - T_r). \quad (2)$$

Notations:
C=heat capacity of the holder
h= coefficient of heat transfer between the holder and the wall of the metal block
T=temperature
t=time
Q=heat evolved or absorbed in the sample holder
s, r, b=subscripts denote the quantity of the sample holder, the reference holder, and the metal block respectively

By subtracting (2) from (1), by rearranging, and by using the $y=T_s-T_r$ relation, one obtains;

$$C_s \frac{dy}{dt} + (C_s - C_r)\frac{dT_r}{dt} = -h_s y + (h_s - h_r)(T_b - T_r) + \frac{dQ}{dt}. \quad (3)$$

When the system under consideration is in a steady state, $dQ/dt=0$, the above equation becomes;

$$(C_s - C_r)\frac{dT_r}{dt} = -h_s y_0 + (h_s - h_r)(T_b - T_r), \quad (4)$$

where the subscript 0 denotes the quantity in the steady state. From (2) and (4), one obtains;

$$y_0 = \left(\frac{C_r}{h_r} - \frac{C_s}{h_s}\right)\frac{dT_r}{dt}. \quad (5)$$

The $y_0=(T_s-T_r)_0$ quantity is the height of the base line of the DTA curve in a steady state, and dT_r/dt is the heating or cooling rate of the system.

Let us consider the DTA curve shown in Fig. 10, which is a typical curve in the DTA of a solid-liquid system. Equation (5) becomes;

$$\left(\frac{C_r}{h_r} - \frac{C_{s,\,I}}{h_s}\right)\frac{dT_r}{dt} = y_{0,\,I} \quad (6)$$

for the lower temperature part of the XX' base line, and;

$$\left(\frac{C_r}{h_r} - \frac{C_{s,\,II}}{h_s}\right)\frac{dT_r}{dt} = y_{0,\,II} \quad (7)$$

for the higher temperature part of the Y'Y base line. Considering the relation:

$$y_{0,\,II} > y_{0,\,I} \quad (8)$$

$$dT_r/dt > 0 \quad (8')$$

for the curve, we obtain the following inequality relation from (6) and (7);

$$C_{s,\,I} > C_{s,\,II}. \quad (9)$$

Now let us consider a solid-liquid system in a closed vessel. We suppose that there are a pure solid state, a completely mixed liquid solution, and a negligible space of the vapor phase, and that the system is under a thermochemical equilibrium.

M=weight of the liquid phase
m=weight of the solid phase
C_{SL}=heat capacity per weight of the solid-liquid system in a closed vessel
C_L=heat capacity per weight of the liquid phase
C_S=heat capacity per weight of the solid phase
H_S=heat of solution per weight of the solid
$x=m/(M+m)$
T=temperature

During the heating of the system, the small quantity of heat input, dQ, has three components: two specific-heat components, $MC_L dT$ and $mC_S dT$, which raise the temperature of the system by dT, and heat-of-solution component, $H_S(-dm)$, where dm is the weight of the solid which dissolves when the temperature is raised by dT. Therefore, we obtain:

$$dQ = MC_L dT + mC_S dT + H_S(-dm),$$

and;

$$C_{SL} = \frac{1}{M+m}\frac{dQ}{dT} = C_L + x(C_S - C_L) - H_S\frac{dx}{dT} \quad (10)$$

for the heat capacity of the solid-liquid system.

Now we will confine our discussion to the $K_2Cr_2O_7$-H_2O system at the temperature range of about 10°C involving the dissolution temperature. As the temperature of the system rises, the C_{SL} quantity is approximately constant or varies linearly with T as may be

11) The Chemical Society of Japan (ed.), "Kagaku-Benran," Maruzen, Tokyo (1958), p. 634.

seen from a consideration of the variation of the three terms on the right-hand side of (10) in this system. At the dissolution temperature at which the solid phase completely dissolves into the liquid phase ($x=0$), the specific heat capacity becomes equal to C_L, and we have a discontinuous variation of the specific heat:

$$(C_{SL}-C_L)_{x=0} = -H_S \frac{dx}{dT}. \quad (11)$$

Since there are these experimental facts:

$H_S>0$ (the heat of solution is endothermic)

$dx/dT<0$ (the solid phase dissolves as the temperature rises)

for the $K_2Cr_2O_7$-H_2O system, we obtain this inequality relation;

$$C_{SL,\,x=0} > C_{L,\,x=0}. \quad (12)$$

(12) may be compared with (9). Since, in (9), the heat capacity, $C_{S,I}$, at lower temperature is that of the solid-liquid-mixture phase, and since $C_{S,II}$ at higher temperature is that of the liquid-solution phase, the relation (12) deduced from thermochemical consideration is in agreement with that (9) deduced from the analysis of the DTA shift curve.

The author wishes to acknowledge the contrbutions of Dr. Shigeru Tomita and Mr. Kazuki Terashima of this Institute for their suggestions and discussions, and of Mr. Eitaro Kitamura and Mr. Seiji Awano of this Institute toward the construction of the apparatus.

BULLETIN OF THE CHEMICAL SOCIETY OF JAPAN, VOL. 46, 456—459 (1973)

Kinetics of the Aquation of Iron(III) Monophenolate Complexes; Absence of the Acid-dependent Path

Koichi NAKAMURA, Toshihiko TSUCHIDA,* Akihiko YAMAGISHI, and Masatoshi FUJIMOTO

Department of Chemistry, Faculty of Science, Hokkaido University, Sapporo

(Received May 4, 1972)

The complex formation between Fe(III) and 10 kinds of phenols was investigated using a stopped-flow apparatus. It was confirmed that the reaction rate is acid-independent in the acid region 0.01—1.0 M. A mechanism for the aquation of the iron(III)-phenol complex is proposed in which a proton transfers intramolecularly from a co-ordinated water molecule to a phenolate ion, *viz.*, $Fe(OH_2)_5A^{2+} \rightarrow Fe(OH_2)_4(OH)\cdot AH^{2+}$. From the observed isotope effects it was concluded that the state of a proton of HA in $Fe(OH_2)_4(OH)\cdot AH^{2+}$ differs from that in a free phenol.

Extensive work has been made on the kinetics of the ligand substitutions of tervalent iron in aqueous solution.[1] Recently Cavasino and Di Dio obtained the substitution rate of Fe(III) for various monophenols using the temperature-jump method.[2] They concluded that in the acid region 0.01—0.09 M $HClO_4$, the complexes is formed through the reaction between $Fe(OH)^{2+}$ and a phenol molecule and that the rate of formation, 1.5×10^3 $M^{-1}sec^{-1}$, is almost independent of the kind of entering phenol.

The rate constants they obtained for the reaction of $Fe(OH)^{2+}$ and phenols are of the same order of magnitude as for the other ligands and in line with the proposal that the rate-determining step is the release of a co-ordinated water molecule from $Fe(OH)^{2+}$. However, the absence of the reaction path involving $Fe(OH_2)_6^{3+}$ and a phenol molecule means that the rate-determining step is no longer the release of a water molecule from $Fe(OH_2)_6^{3+}$. In other words, it is impossible to form the complex from the outer-sphere complex between $[Fe(OH_2)_6]^{3+}$ and a phenol molecule. This is an interesting result. However, the acid concentration chosen by Cavasino and Di Dio is not sufficiently high to conclude that there is no reaction path between $Fe(OH_2)_6^{3+}$ and a phenol molecule. We therefore performed the kinetic investigation of the reaction by pH-jump method at a higher acidity region (0.1—1.0 M $HClO_4$). It was confirmed that the reaction between $Fe(OH_2)_6^{3+}$ and a phenol does not lead to the complex in the acidity region studied. We conclude that during the course of the aquation reaction, proton transfer occurs intramolecularly from a co-ordinated water molecule to a phenolate ion. The isotope effect was also studied and discussed on the basis of the mechanism.

Experimental

Materials. Iron(III) perchlorate was prepared by heating the chloride with a small excess of perchloric acid and recrystallized *in vacuo*. The concentration of iron(III) was determined titrimetrically with EDTA. The perchloric acid content was determined by passing an aliquot of the solution through a column of cation-exchange resin in the hydrogen-form, and titrating the effluent with sodium hydroxide. The ionic strength was adjusted with the purified reagent grade sodium perchlorate.[3]

* Present address: Nihon Polyurethane Co. Ltd., Hodogaya-ku, Yokohama.

1) Recent results are summarized in F. P. Cavasino, *J. Phys. Chem.*, **72**, 1378 (1968).

2) F. P. Cavasino and E. Di Dio, *J. Chem. Soc., A*, **1970**, 1151.

3) Y. Kawai, T. Takahashi, K. Hayashi, T. Imamura, H. Nakayama, and M. Fujimoto, This Bulletin, **75**, 1417 (1972).

Phenols were purified according to Milburn.[4] The purity was confirmed by melting point and thin-layer chromatography.

Measurements. The optical densities were measured with a Hitachi recording spectrophotometer Model EPS-3T. pH was measured with a Radiometer equipped with G 200B glass electrode and K 100 reference calomel electrode. pD of the deuterium oxide solution was evaluated as 0.4 plus the pH-meter reading.[5] Kinetic measurements were performed using a Yanagimoto stopped-flow spectrophotometer Model SPS-1.

In the acid region, the equilibrium of the complex formation is written as

$$Fe^{3+} + HA \rightleftharpoons FeA^{2+} + H^+,$$

where HA denotes a phenol molecule. Since the equilibrium constant is in the order of 10^{-2} for monophenols, the concentration of the complex is greatly reduced in such a high acid region as 0.1—1.0 M. It is therefore difficult to obtain the rate constant at a high proton concentration by the ordinary mixing method. To overcome this difficulty, we rapidly mixed a solution of the complex in low acidic media with a solution containing a large amount of proton. The rapid pH-jump shifts the equilibrium towards dissociation. Since the proton transfer of aquo-iron(III) is generally much faster than the complex formation,[6] the observed decrease in the optical density corresponds to the aquation process of the complex in a high acid medium.

For the measurement of kinetic isotope effect a temperature-jump apparatus (Messanlagen Studiengesellschaft, Göttingen) was used.

Results

Static Measurements. Although the stability constants of complexes between iron(III) and various kinds of phenol were obtained by Milburn,[4] no consideration was given on the possibility of protolysis of a coordinated water in the complexes. We therefore tried to estimate the degree of the protolysis of the complex, spectrophotometrically, following scheme I.

$$\begin{array}{ccc} & (1) & (3) \\ & & \\ Fe^{3+} + HA & \overset{K_1}{\rightleftharpoons} & FeA^{2+} + H^+ \\ K_h \Big\| & & \Big\| K_G \\ H^+ + Fe(OH)^{2+} + HA & \overset{K_2}{\rightleftharpoons} & Fe(OH)A^+ + 2H^+ \\ & (2) & (4) \end{array}$$

Scheme I.

Under the conditions of $[Fe(III)]_t \ll [HA]_t$ ($[\ ]_t$ denotes the total concentration), the following relationship is derived from A, the optical density due to the complex, a, the total concentration of the phenol, and b, the total concentration of Fe(III).

$$\frac{1}{A} = \frac{1}{\varepsilon b}\left(1 + \frac{[H^+]+K_h}{aK}\right) \qquad (1)$$

where ε and K are defined as

$$\varepsilon = (\varepsilon_1 + \varepsilon_2 K_G/[H^+])/(1 + K_G/[H^+])$$

and

$$K = K_1(1 + K_G/[H^+]) .$$

ε_1 and ε_2 denote the extinction coefficients of FeA^{2+} and $Fe(OH)A^+$, respectively, and $K_G = K_2K_h/K_1$.

Figure 1 shows the plots of A^{-1} *vs.* a^{-1} for *p*-nitrophenol; the phenol forms a stable complex with Fe(III). The ratio $([H^+]+K_h)/(\text{slope})$ was found to be almost constant; they are 5.2×10^{-2} ($[H^+]=1.7\times10^{-2}$ M), 5.8×10^{-2} (8.8×10^{-3} M), 6.1×10^{-2} (5.6×10^{-3} M) and 5.7×10^{-2} (2.4×10^{-3} M). Since the ratio is equal to $\varepsilon_1 bK_1(1+\varepsilon_2/\varepsilon_1 \cdot K_G/[H^+])$, this result indicates that the value of $\varepsilon_2/\varepsilon_1 \cdot K_G/[H^+]$ is so small as to be within experimental error. The upper limit of K_G is estimated to be 10^{-4} M, assuming that $\varepsilon_2/\varepsilon_1$ is in the order of unity. The contribution of $Fe(OH)A^+$ to the optical density can also be neglected under the experimental conditions. In discussing the kinetic data, we used the stability constants obtained by Milburn.[4]

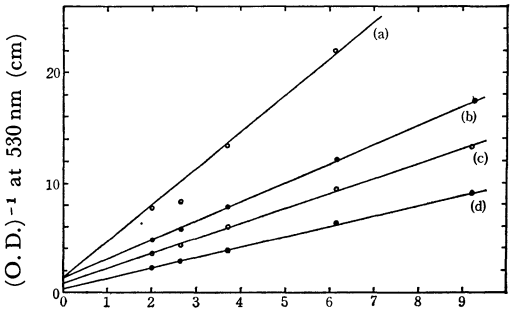

Fig. 1. Plots of equation (1) for *p*-nitrophenol.
$[Fe^{3+}]=1.03\times10^{-3}$ M, $[H^+]=$(a) $1.70)\times10^{-2}$ M, (b) 8.77×10^{-3} M, (c) 5.55×10^{-3} M, (d) 2.36×10^{-3} M, at 25.0°C.

Kinetics. The decrease in the optical density on the pH-jump measurements corresponds to the aquation of $Fe(OH_2)_5A^{2+}$ as elucidated above. Following a derivation similar to that of Cavasino and Di Dio,[2] the first-order rate constant is expressed in terms of the rate constants of individual paths in the above scheme as

$$k_{obs} = \frac{k_{13}[H^+]}{K_cK_H} + \frac{k_{24}K_h}{K_cK_H}, \qquad (2)$$

where k_{13} and k_{24} are the forward rate constants for the reaction between Fe^{3+} and HA, and between $Fe(OH)^{2+}$ and HA, respectively. The proton concentration at which the first term becomes predominant is expected to be above 0.3 M, since $K_h=3\times10^{-3}$ M and k_{13}/k_{24} is in the order of 10^{-2} for the reaction of Fe(III) with analogous ligands.[1] The proton concentration is higher than that chosen by Cavasino and Di Dio by one order of magnitude. For this very reason we performed the pH-jump experiment in such a high acidity region as 0.1—1 M.

Figure 2 shows the values of the first-order rate constant k_{obs} obtained for *p*-nitrophenol in the proton concentration range 0.01—0.9 M. The plots were found to be independent of proton concentration at

4) R. M. Milburn, *J. Am. Chem. Soc.*, **77**. 2064 (1955).
5) P. K. Glasoe and F. A. Long, *J. Phys. Chem.*, **64**, 188 (1960).
6) P. Hemmes, L. D. Rich, D. L. Cole, and E. M. Eyring, *ibid.*, **75**, 929 (1971).

TABLE 1. THE RATE CONSTANTS OF THE COMPLEX FORMATION AND AQUATION AT 25°C AND THE ACTIVATION PARAMETER FOR SUBSTITUTED PHENOLS. IONIC STRENGTH IS 0.1 M

HA	$10^{10}\times K_H$[a] (M)	$10^{-2}\times k_{obs}$ (sec^{-1})	$10^{-3}\times k_{24}$ (M^{-1} sec^{-1})	E_a (kcal)	$\Delta S^{\neq}$ (e. u.)
m-CH_3	1.32	2.6	0.9	10.3	−16.3
o-CH_3	0.63	1.7		13.0	−8.1
H	1.26	3.4	1.1	13.4	−5.4
p-Cl	7.94	2.2	1.2	13.1	−2.5
o-Cl	46.8	1.2	1.0	14.0	−4.0
p-Br	9.86	2.0	0.7	11.7	−10.8
o-Br	60.2	0.9	1.9	11.9	−13.1
p-NO_2	955	1.2	0.8	15.1	−0.4
m-NO_2	91.2	1.4	0.7	15.2	0.3

a) From Ref. 4.

TABLE 2. ISOTOPE EFFECTS OF THE EQUILIBRIUM CONSTANTS AND AQUATION RATES AT 25.0°C

Equilibrium	K_H	K_D	K_H/K_D
$Fe^{3+} \rightleftarrows Fe(OH)^{2+} + H^+$	3.45×10^{-3} M	2.40×10^{-3} M	1.44
$AH \rightleftarrows A^- + H^+$	9.67×10^{-8} M	2.22×10^{-8} M	4.36
$Fe^{3+} + A^- \rightleftarrows Fe(OH)^{2+} + AH$	3.57×10^4	10.8×10^4	0.331
Reaction	k_H sec^{-1}	k_D sec^{-1}	k_D/k_H
$FeA^{2+} \rightleftarrows Fe(OH)^{2+} + AH$	173	73	2.37

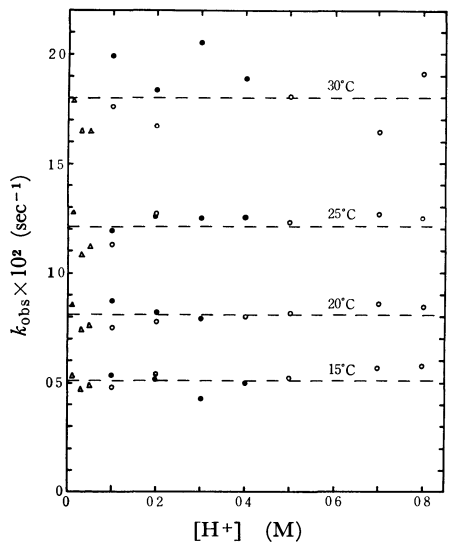

Fig. 2. Dependence of the first-order rate constant on the proton concentration for *p*-nitrophenol.
Ionic strength is (△) 0.10 M, (●) 0.65 M, (○) 1.00 M.

each temperature. The upper limit of k_{13} is estimated to be 1 M^{-1} sec^{-1}. The value is smaller than the rate constants obtained in the analogous reactions of $Fe(OH_2)_6^{3+}$ ($10-10^2$ M^{-1} sec^{-1}) by one or two order of magnitude. Figure 2 also shows that the rate of aquation is independent of the ionic strength.

Similar results were obtained for other phenols. In Table 1 are summarized the rate constants of the complex formation and aquation at an ionic strength 0.1 (M) and at 25.0°C together with the activation parameters from the data between 15 and 30°C.

Isotope effect on the rate constants was measured by the temperature-jump method. The rate, pH and optical densities were all measured at 95, 53 and 0% D_2O. The values were extrapolated to 100% D_2O by parabola. The results are given in Table 2 together with the isotope effects of the equilibrium constants of the protolysis of $Fe(OH_2)_6^{3+}$ and of the acid dissociation of *p*-nitrophenol.

Discussion

The results demonstrate that the rate constant is independent of the acid concentration. According to Eq. (2), this means that even in the acid concentrations 0.1—1.0 M, no reaction path is involved between Fe^{3+} and a phenol molecule in contrast to other ligands.[1] We attribute this anomalous fact to the proton transfer from an entering phenol molecule to OH^- in $Fe(OH)^{2+}$ in the course of the complex formation between $Fe(OH)^{2+}$ and AH, *viz.*,

$$Fe(OH_2)_4(OH)AH^{2+} \underset{K_1}{\rightleftharpoons} Fe(OH_2)_5A^{2+}, \qquad (3)$$

where K_1 is the equilibrium constant of the reaction. In the case of the reaction between $Fe(OH_2)_6^{3+}$ and a phenol molecule, the complex is not formed *via* a transient complex $Fe(OH_2)_5AH^{3+}$ as in (3), because $Fe(OH_2)_5AH^{3+}$ has no proton acceptor like OH^- in its ligands. Even 2,4-dinitrophenol, with an acid dissociation constant higher than that of acetic acid, follows this mechanism. The neutral species of acetic acid, CH_3COOH, reacts with $Fe(OH_2)_6^{3+}$ with the rate constant of 4.8 M^{-1} sec^{-1}.[7] Thus, the absence of the reaction path between $Fe(OH_2)_6^{3+}$ and a phenol molecule cannot be attributed only to the strong bonding of a proton to a phenolate ion. At the present stage it is not clear what factor in phenols brings about such an anomaly.

7) F. Accascina, F. P. Cavasino, and E, Di Dio, *Trans. Faraday Soc.* **65**, 489 (1969).

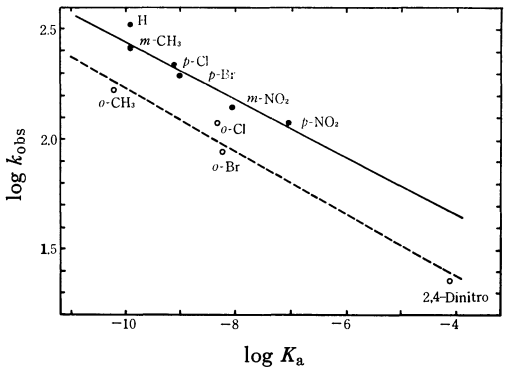

Fig. 3. Dependence of the first-order rate constants on the acid dissociation constants for substituted phenols.

In Fig. 3 is shown the dependence of the aquation rate on K_a of each phenol. Meta- and para-substituted phenols are on a straight line with a slope of 0.11. Ortho-substituted phenols are roughly on a line with a slope of the same magnitude but about 0.2 below the above groups. The linear dependence means that the stronger the bonding of a proton to a pnenolate ion, the lower the aquation rate. It is interpreted that K_i increases with decrease in K_a. The small slope, however, indicates that the change in K_a has a relatively small influence on K_i. This suggests that the proton of AH in $Fe(OH_2)_4(OH)$-AH^{2+} is in a different state from that in a free phenol molecule.

The isotope effects of kinetics and equilibrium lead us to a similar conclusion concerning the state of the proton in AH of $Fe(OH_2)_4(OH)AH^{2+}$. As shown in Table 2, the equilibrium constant of the following intermolecular proton transfer in D_2O, K_D is greater than that in H_2O, K_H,

$$Fe(OH_2)_5(OH)^{2+} + AH \underset{K_H}{\rightleftharpoons} Fe(OH_2)_6^{3+} + A^- \qquad (4)$$

Since a proton transfers from AH to OH coordinated to Fe^{3+} in both equilibria (3) and (4), we can expect the same isotope effect in equilibrium (3). Supposing that the isotope effect in the aquation reaction lies mainly in (3), we expect that the aquation rate is higher in D_2O than in H_2O. However, the observed aquation rate in H_2O is 2.37 times greater than in D_2O. The isotope effect was interpreted in terms of zero-point energy of the vibration of a proton.[8] Comparing the zero-point energy of the vibration of a proton of AH on the left-hand with that of OH_2 on the right-hand side of Eqs. (3) and (4), the observed isotope effects are expressed as

$$\frac{1}{2}h\nu_{OH} - \frac{1}{2}h\nu_{OD} > \frac{1}{2}h\nu_{AH} - \frac{1}{2}h\nu_{AD} \text{ in (3)}$$

and $$\frac{1}{2}h\nu'_{OH} - \frac{1}{2}h\nu'_{OD} < \frac{1}{2}h\nu'_{AH} - \frac{1}{2}h\nu'_{AD} \text{ in (4)}$$

where ν_{OH} and ν_{AH} are the frequencies of vibration of proton of OH_2 in $Fe(OH_2)_5A^{2+}$ and of AH in $Fe(OH_2)_4(OH)AH$, respectively, and ν'_{OH} and ν'_{AH} in $Fe(OH_2)_6^{3+}$ and in a free HA, respectively. If the proton in H_2O is not much affected in complexation,[9] or $\nu_{OH}=\nu'_{OH}$, we get

$$\frac{1}{2}h\nu_{AH} - \frac{1}{2}h\nu_{AD} < \frac{1}{2}h\nu'_{AH} - \frac{1}{2}h\nu'_{AD} \text{ or}$$

$$\nu_{AH} < \nu'_{AH}.$$

It then follows that a proton of AH in $Fe(OH_2)_4(OH)$-AH is more loosely bound to a phenolate than a proton of a free AH, and that this causes the depedence of an aquation rate on K_a to be small.

Another interesting feature is the composition of iron(III)-phenol complex. It is known that iron(III) forms only a 1 : 1 complex with phenols even in 500 time excess of phenol.[10] The above scheme predicts that 1 : 2 complexes would be formed *via* the reaction between $Fe(OH_2)_4(OH)A^+$ and HA. However, the hydrolysis is greatly depressed by the complexation. Thus, from the kinetic point of view, 1 : 2 complexes between iron(III) and a phenol molecule is very unlikely because of the above mechanism and the low hydrolysis of 1 : 1 complexes.

8) K. J. Laidler, "Chemical Kinetics," 2nd ed., McGraw-Hill, New York (1965), p. 90.

9) For example, the frequency of NH stretching vibration (3240 cm^{-1}) in $[Co(NH_3)_6]^{3+}$ differs only by 0.4% from that of NH stretching vibration (3252 cm^{-1}) in $[CoCl_2(NH_3)_4]^+$; see I. Nakagawa, T. Shimanouchi, and J. Hiraishi, Proceedings of the 8th International Conference on Coordination Chemistry, Vienna, Sept. 1964.

10) G. Ackermann and D. Hesse, *Z. Anorg. Allgem. Chem.* **367**, 243 (1969).

Polarographic Studies of the Anodic Oxidation of Mercury. II. The Anodic Adsorption Wave of Ethylamine in *N,N*-Dimethylformamide

Yoshihisa MATSUI and Yoshio DATE

Department of Agricultural Chemistry, Shimane University, Nishikawazu, Matsue

(Received June 3, 1972)

Ethylamine at concentrations lower than 0.5 mM in N,N-dimethylformamide gives a diffusion-controlled anodic wave due to the reversible oxidation of the mercury to a 1 : 2 complex of mercury(II) with the amine. At higher concentrations, another anodic wave appears at a potential less positive than the main wave; this has been attributed to the adsorption of the oxidation product on the mercury electrode. The adsorption prewave was analyzed on the basis of Brdička's theory, in which the Langmurian adsorption was assumed. It was shown that the nature of the prewave can be well interpreted on the additional assumption that the adsorption coefficient of the adsorbed complex decreases exponentially as the electrode potential becomes more positive.

In a previous paper,[1] it was shown that ammonia, methylamine, and dimethylamine anodically depolarize the dropping mercury electrode in N,N-dimethylformamide (DMF) to form 1 : 2 complexes of mercury (II) with the amines. Furthermore, it was suggested that the complexes are adsorbed on the electrode surface to cause the flowing of the extra anodic current. However, the nature of the anodic adsorption current has not yet been examined in detail.

The present study was undertaken not only in order to extend the previous study to ethylamine, but also in order to examine the characteristics of the anodic adsorption current in detail.

Experimental

The solvent, DMF, and the supporting electrolyte, tetraethylammonium perchlorate, were purified as had been described previously.[1] Ethylamine, which had been separated from a commercial 70% aqueous solution by the addition of a saturated NaOH solution, was dried and distilled over granular NaOH. The concentration of the amine in DMF was determined by titration against an aqueous hydrochloric acid. A solution of mercury(II) perchlorate in DMF was prepared as has been described elsewhere.[2]

Polarograms were obtained in a manner similar to that described before.[1] All the potentials reported in the present paper refer to an aqueous, saturated calomel electrode connected with a cell solution by means of a DMF-agar salt bridge.[3]

Results and Discussion

The polarographic behavior of ethylamine was examined with a dropping mercury electrode over a wide concentration range from 0.1 to 100 mM in DMF. The amine gave a single well-defined anodic wave at concentrations lower than 0.5 mM. At higher concentrations, another anodic wave appeared at a potential less positive than the main wave. The polarographic characteristics of these waves are summarized in Tables 1 and 2. The total limiting current (i_d) was virtually proportional to the bulk concentration of the amine, and also to the square root of the effective pressure (h_{corr}) on the mercury drop; these findings indicate that the total limiting current is diffusion-controlled. On the other hand, the limiting current (i_p) of the prewave was virtually independent of the bulk concentration of the amine when it was lower than 20 mM. It was also shown that the value of i_p increases in proportion to h_{corr}. These results indicate that the prewave has the nature of an adsorption current. At concentrations higher than 20 mM, the value of i_p gradually increased with an increase in the concentration. This may be at-

TABLE 1. POLAROGRAPHIC CHARACTERISTICS OF ETHYLAMINE AT VARIOUS CONCENTRATIONS[a]

Concn. (mM)	$E_{1/2}$ (V *vs.* SCE)		i_p[b] (μA)	I_d[c]
	prewave	total wave		
0.10	—	+0.184	—	2.22
0.26	—	+0.180	—	2.37
0.52	—	+0.160	—	2.42
1.02	+0.093	+0.176	1.62	2.35
2.18	+0.038	+0.176	1.80	2.55
5.50	−0.001	+0.167	1.80	2.52
10.9	−0.028	+0.166	1.85	2.67
21.8	−0.051	+0.179	1.97	2.55
54.4	−0.084	+0.272	3.10	2.42
100.0	−0.097	+0.333	4.85	2.35

a) $m=1.778$ mg/s, $t=3.79$ s.
b) The limiting current of the prewave.
c) Diffusion current constant: $I_d=i_d/C\cdot m^{2/3}t^{1/6}$ ($\mu A\cdot mM^{-1}\,mg^{-2/3}\,s^{1/2}$).

TABLE 2. RELATION BETWEEN THE LIMITING CURRENT OF 5.0 mM ETHYLAMINE AND EFFECTIVE PRESSURE ON THE DROPPING MERCURY ELECTRODE[a]

h_{corr}. (cm)	i_p[b] (μA)	i_d[c] (μA)	i_p/h_{corr} ($\mu A\cdot cm^{-1}$)	$i_d/h_{corr}^{1/2}$ ($\mu A\cdot cm^{-1/2}$)
38.7	0.87	17.2	0.022	2.76
44.7	0.97	18.6	0.022	2.79
54.7	1.20	20.4	0.022	2.75
64.7	1.40	23.2	0.022	2.88
74.7	1.51	23.6	0.020	2.73
80.3	1.63	24.9	0.020	2.78

a) $m=1.460$ mg/s, $t=4.44$ s.
b) The limiting current of the prewave.
c) The limiting current of the total wave.

1) Y. Matsui, Y. Kurosaki, and Y. Date, This Bulletin, **46**, 147 (1973).
2) Y. Matsui and Y. Date, *ibid.*, **43**, 2052 (1970).
3) K. Takaoka, *Rev. Polarog.* (Kyoto), **14**, 63 (1966).

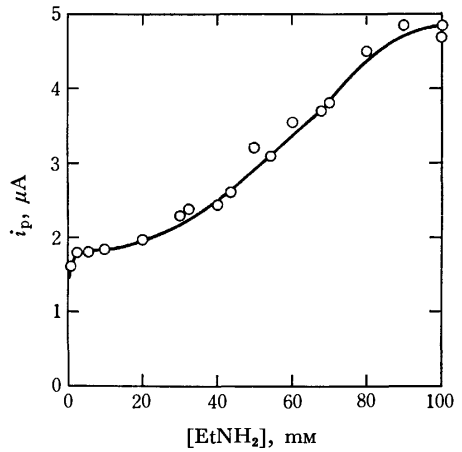

Fig. 1. Plot of the height of the prewave *vs.* the concentration of $EtNH_2$.

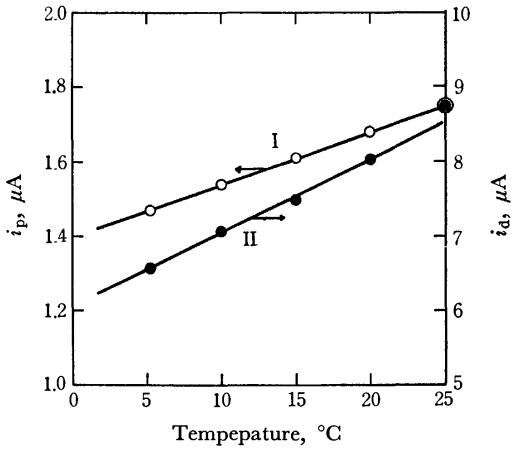

Fig. 2. Plot of the heights of the prewave (I) and the total wave (II) of $EtNH_2$ *vs.* temperature.
[$EtNH_2$] = 1.89 mM

tributed to the formation of additional superimposed layers of the adsorbate on the mercury surface, for the curve obtained by plotting i_p against the amine concentration resembles the B. E. T. isotherm (Fig. 1). The half-wave potential of the total anodic wave at high amine concentrations shifted toward the positive value as the concentration increased. The film of the adsorbate may inhibit the electrode process, thus causing the positive shift.

Figure 2 shows the effect of the temperature on the heights of the total wave and the prewave, which linearly increased with the temperature. The average rates of increase were 1.38% and 0.89% per degree respectively. These values also indicate that the former is controlled by diffusion, and the latter, by adsorption. The fact that the adsorption wave appeared at potentials less positive than the main wave suggests that the adsorbate is the oxidation product rather than the depolarizer.[4]

Figure 3 shows the effect of ethylamine on the electrocapillary curve in DMF containing 0.10 M tetraethylammonium perchlorate. A significant decrease in the surface tension of the mercury drop was

4) R. Guidelli, *J. Phys. Chem.*, **74**, 95 (1970).

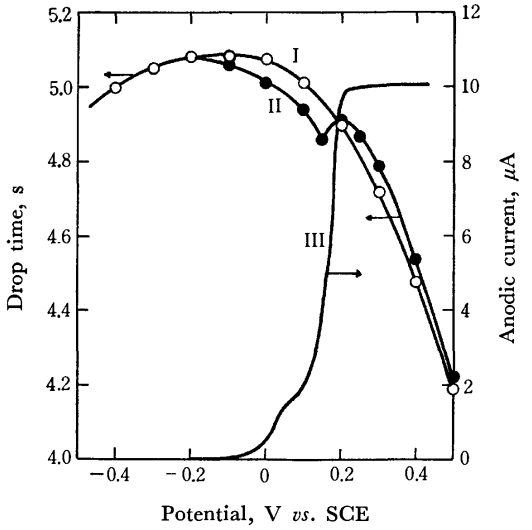

Fig. 3. Effect of $EtNH_2$ on the electrocapillary curve.
I, 0.10 M Et_4NClO_4; II, I+1.72 mM $EtNH_2$; III, Polarogram of 2.18 mM $EtNH_2$.

caused by the addition of a small amount of the amine. The decrease began at *ca.* 0.00 V *vs.* SCE, where the anodic prewave appeared, and finished at *ca.* +0.20 V *vs.* SCE, where the main wave just approached its plateau. It is obvious that the adsorption of the oxidation product on the electrode surface is responsible for the appearance of the prewave. It can also be presumed that the desorption of the product facilitates the electrolytic process.

Figure 4 shows the results of the amperometric titration of mercury(II) perchlorate against ethylamine. The limiting current of the mercury(II) ion decreased with the addition of ethylamine. At the same time, a second cathodic wave appeared at a more negative potential. The wave height increased in proportion to the ratio of the concentration of ethylamine to that of the mercury(II) ion, until the ratio exceeded 2.0. Thereafter, the wave of the mercury(II) ion disappeared, the height of the second cathodic wave reached a virtually constant value, and an anodic limiting current appeared and increased in proportion to the

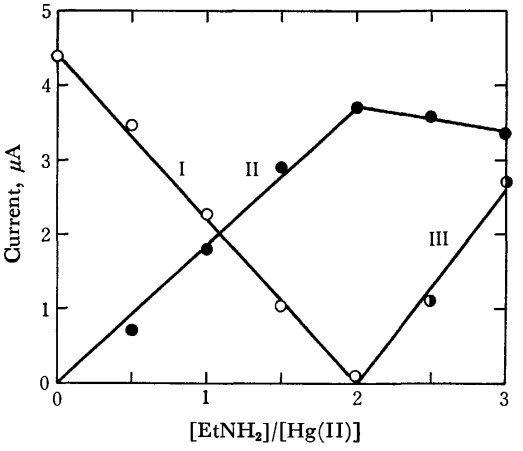

Fig. 4. Amperometric titration of Hg(II) with $EtNH_2$.
I : Wave height of the simple Hg(II) ion,
II : Wave height of the complex; $Hg(EtNH_2)_2^{2+}$,
III: Wave height of $EtNH_2$.

excess amount of the amine. These results are similar to those for methylamine reported in a previous paper;[1] it can likewise be thought that the mercury(II) ion reacts with ethylamine to form the 1 : 2 complex, $Hg(EtNH_2)_2^{2+}$, which then gives the second cathodic wave. It can also be considered that the anodic wave of the amine is due to the polarographically reversible oxidation of mercury to $Hg(EtNH_2)_2^{2+}$:

$$Hg + 2EtNH_2 \rightleftharpoons Hg(EtNH_2)_2^{2+} + 2e \quad (1)$$

Provided that the electrode process is simply expressed in terms of Eq. (1), the equation for the current-potential curve should be given by:[1]

$$E = E_0 - (RT/2F)\ln\beta_2 + (RT/2F)\ln k_0^2/k_2 + (RT/2F)\ln i/(i_d-i)^2 \quad (2)$$

In this equation, E_0 represents the ordinary standard potential of the mercury-mercury(II) half-cell; β_2, the overall stability constant of the complex of $Hg(EtNH_2)_2^{2+}$, and k_0 and k_2, the Ilkovič equation constants for the amine and the complex, respectively. The plot of log $i/(i_d-i)^2$ *vs.* E for the wave of 0.46 mM ethylamine is shown in Fig. 5. A straight line with the reciprocal slope of about 0.030 V was obtained at the more positive potentials of the wave, whereas the plot deviated from the line at the less positive potentials of the wave. In analogy with the case of methylamine,[1] the deviation may be due to the adsorption of the oxidation product, $Hg(EtNH_2)_2^{2+}$, on the electrode surface. On the assumption that Eq. (2) holds for the more positive potentials of the wave, the value of β_2 was estimated to be $10^{16.5}$. In this calculation, E_0 was taken to be 0.557 V *vs.* SCE.[2]

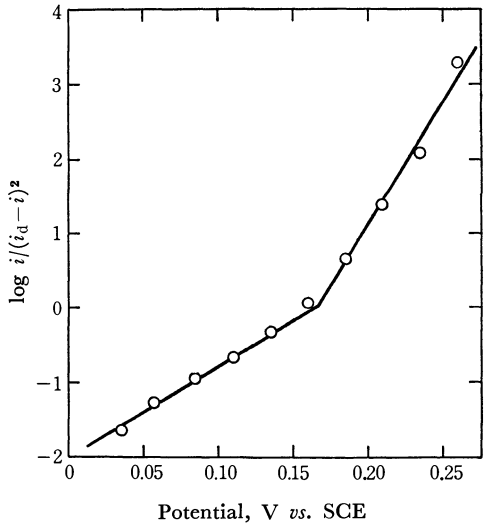

Fig. 5. Plot of log $i/(i_d-i)^2$ *vs.* potential for the wave of 0.46 mM $EtNH_2$.
Reciprocal slope: I; 0.030 V, II; 0.075 V.

The Analysis of the Adsorption Prewave. When the amine concentration was high enough, the adsorption prewave could be well resolved from the main wave. Furthermore, it seems, on the basis of the results shown in Fig. 1, that the adsorption obeys the Langmuir isotherm at amine concentrations lower than 20 mM. Therefore, we undertook to analyze the prewave on the basis of Brdička's theory of the adsorption wave. On assuming that the oxidation product, $Hg(EtNH_2)_2^{2+}$, is the only adsorbate, and that the adsorption obeys the Langmuir isotherm, the anodic current (i) can be related to the concentrations of the amine and the complex (a and x_2 respectively) on the electrode surface by the following equations:[5]

$$i_d - i = k_0 a \quad (3)$$

$$i = k_2 x_2 + (i_p w x_2/(1+wx_2)) \quad (4)$$

In this equation, w, is the adsorption coefficient of $Hg(EtNH_2)_2^{2+}$. The height of the prewave, i_p, is correlated with the maximum amount of substance adsorbed per unit area of the electrode (Z) by the following equation:

$$i_p = knFm^{2/3}t^{-1/3}Z \quad (5)$$

where

$$k = 0.85\ cm^2g^{-2/3} \text{ at } 25°C$$

and where n is the number of the electrons participating in the electrode process; m, the mass of mercury flowing out of the capillary per unit time, and t, the drop time. The value of Z for $Hg(EtNH_2)_2^{2+}$ at amine concentrations lower than 10 mM was calculated from this equation to be 1.17×10^{-9} mol/cm^2; this is slightly less than that for $Hg(MeNH_2)_2^{2+}$ (1.41×10^{-9} mol/cm^2 [1]).

When it is assumed that, at the potentials corresponding to the prewave, the amount of the oxidation product diffusing into the solution is negligibly small compared with that adsorbed on the electrode surface, Eq. (4) can be simplified as follows:

$$i = i_p w x_2/(1+wx_2) \quad (6)$$

Thus, a and x_2 are given by:

$$a = (i_d-i)/k_0 \quad (7)$$

$$x_2 = i/w(i_p-i) \quad (8)$$

On the other hand, the electrode potential is expressed by the equation:

$$E = E_0 - (RT/2F)\ln\beta_2 + (RT/2F)\ln x_2/a^2 \quad (9)$$

By introducing Eqs. (7) and (8) into Eq. (9), we obtain:

$$E = E_0 - (RT/2F)\ln\beta_2 + (RT/F)\ln k_0 - (RT/2F)\ln w + (RT/2F)\ln i/(i_p-i)(i_d-i)^2 \quad (10)$$

If the adsorption coefficient of $Hg(EtNH_2)_2^{2+}$ does not change with the potential, the first four terms on the right-hand side of Eq. (10) are constant. Then, the plot of log $i/(i_p-i)(i_d-i)^2$ *vs.* E should give a straight line with a reciprocal slope of 0.030 V at 25°C. The results for the prewaves given by 2.8—43.5 mM ethylamine are shown in Fig. 6. The plot gave a good straight line. However, the reciprocal slope (0.047 V) was significantly larger than the theoretical value. It might be considered that the increase in the reciprocal slope is due to the irreversibility of the electrode process. However, this can be ruled out in the present case, for the fact that the reciprocal slope of the log-plot was equal to 0.030 V for the wave

5) R. Brdička, *Z. Elektrochem.*, **48**, 278 (1942).

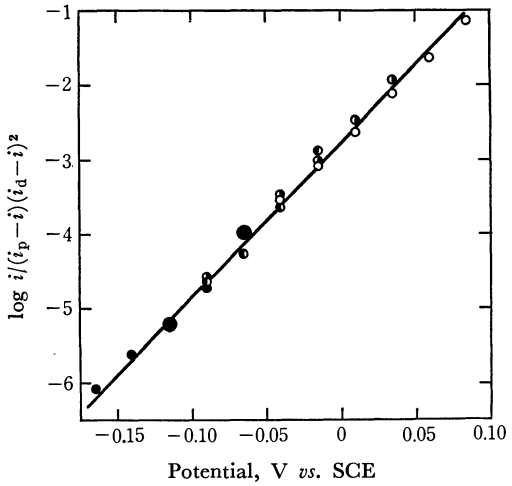

Fig. 6. Plot of log $i/(i_p-i)(i_d-i)^2$ *vs.* potential for the prewave of $EtNH_2$.
Concentration of $EtNH_2$: ○; 2.75 mM, ◑; 5.50 mM, ◐; 21.8 mM, ●; 43.5 mM.

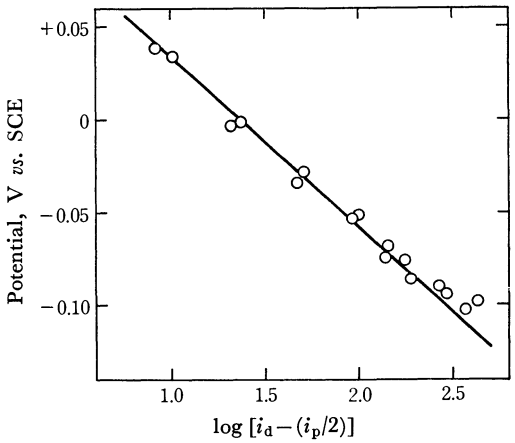

Fig. 7. Plot of the half-wave potential of the prewave of $EtNH_2$ *vs.* log $[i_d-(i_p/2)]$.
Slope: −0.092 V

of the amine at a low concentration, and the fact that the half-wave potential of the oxidation wave of the amine was approximately equal to that of the reduction wave of $Hg(EtNH_2)_2^{2+}$ obtained in the amperometric titration, show that the electrode process is reversible. According to Guidelli,[4] it is possible that the increase in the slope of the adsorption wave is caused by the change in the adsorption coefficient with the potential. Since the adsorbed complex, $Hg(EtNH_2)_2^{2+}$, has a positive charge, it seems natural to consider that the adsorption energy (φ) of the complex may be lowered, as the electrode potential becomes more positive, by an increase in the electronic repulsion between the adsorbed complex and the electrode. In fact, it was found that the polarographic behavior of the prewave can be well explained on the basis of the assumption that the energy of the electronic repulsion between the divalent positive ion and the electrode is in proportion to $2FE$. Then, φ may be written as:

$$\varphi_0 - \varphi = 2F\gamma E \tag{11}$$

where φ_0 is the adsorption energy at 0.00 V *vs.* SCE, and γ, the proportionality constant. On the other hand, w is generally proportional to exp (φ/RT),[5] so that:

$$w = w_0 \exp(-2F\gamma E/RT) \tag{12}$$

In this equation, w_0 corresponds to the adsorption coefficient at 0.00 V *vs.* SCE. By combining Eqs. (10) and (12), we obtain:

$$(1-\gamma)E = E_0 - (RT/2F)\ln\beta_2 + (RT/F)\ln k_0 - (RT/2F)\ln w_0 + (RT/2F)\ln i/(i_p-i)(i_d-i)^2 \tag{13}$$

This equation indicates that the reciprocal slope of the plot of log $i/(i_p-i)(i_d-i)^2$ *vs.* E is equal to $0.030/(1-\gamma)$ V at 25°C. By taking γ as 0.36, we obtain the slope of 0.047 V, which agrees with the observed value. From Eq. (13), Eq. (14) is readily derived:

$$E_{p,1/2} = C - (1/(1-\gamma))(RT/F)\ln(i_d-i_p/2) \tag{14}$$

where $E_{p,1/2}$ is the half-wave potential of the prewave, and C, the constant. This equation shows that $E_{p,1/2}$ should shift toward a more negative potential with an increase in the amine concentration. The relation between $E_{p,1/2}$ and log $(i_d-i_p/2)$ observed was virtually linear, with a slope of −0.092 V (Fig. 7); this is fairly well in agreement with the value, −0.094 V, calculated on the basis of Eq. (15), which γ is taken as 0.36. This is one evidence in support of the validity of Eq. (13). Since the numerical values of the constants and the variables in Eq. (13) are all either known or experimentally estimated except for w_0, it is possible to calculate the value of w_0. Thus, we obtained the value of w_0 as 4.6×10^6 l/mol for $Hg(EtNH_2)_2^{2+}$. This value is so large that it is consistent with the above assumption that the amount of the oxidation product diffusing into the solution is negligibly small compared with that adsorbed on the electrode surface at the potentials corresponding to the prewave of ethylamine.

Thus, it is obvious that the present method of treatment of an adsorption wave is plausible in this case. However, it is still uncertain whether or not it can generally be applied to the prewaves due to the adsorption of ionic compounds. This will be studied further in succeeding papers.

Polarographic Studies of the Anodic Oxidation of Mercury. III. The Adsorption of the Mercury(II) Complexes of Ammonia and Alkylamines on the Mercury Electrode Surface

Yoshihisa MATSUI, Hitoshi TAKAYA, and Yoshio DATE

Department of Agricultural Chemistry, Shimane University, Nishikawazu, Matsue

(Received June 3, 1972)

A solution of ammonia, methylamine, *n*-propylamine, isopropylamine, or *n*-butylamine in *N,N*-dimethylformamide gives an anodic prewave due to the adsorption of the oxidation product, $Hg(amine)_2^{2+}$, on the dropping mercury electrode. The shape of the prewave of each amine can be well interpreted by an equation derived on the basis of the assumptions that the adsorption follows the Langmuir isotherm and that the adsorption coefficient of the adsorbate complex decreases exponentially as the electrode potential becomes more positive. Some physicochemical properties of the mercury(II) complexes, such as the overall stability constants and the adsorption coefficients at 0.0 V *vs.* SCE, were determined by analyses of the polarographic waves.

In a previous paper,[1] it was shown that the shape of the anodic adsorption prewave given by ethylamine in *N,N*-dimethylformamide (DMF) can be well interpreted by an equation which is derived on the basis of the assumptions that the adsorption of the oxidation product, $Hg(EtNH_2)_2^{2+}$, follows the Langmuir isotherm and that the adsorption coefficient of the product decreases exponentially as the electrode potential becomes more positive. The change in the adsorption coefficient was attributed to the change in the energy of the electrostatic repulsion between the ionic adsorbate and the positively-charged electrode with a potential. However, it is still uncertain whether or not the treatment can be generally applied to the prewaves due to the adsorption of ionic species. The present study was undertaken in order to extend the previous study to the prewaves of ammonia and alkylamines other than ethylamine, *i.e.*, methyl-, *n*-propyl-, isopropyl-, and *n*-butylamine.

Experimental

The solvent (DMF) and the supporting electrolyte (tetraethylammonium perchlorate) were purified as had been described previously.[2] The *n*-propylamine, isopropylamine, and *n*-butylamine were commercially-obtained and were used after distillation. Aqueous solutions of ammonia and methylamine obtained commercially (28 and 30% respectively) were used for polarography without removing the water.

The DC polarography was carried out with a Yanagimoto polarograph, model P8-DP. A cadmium-cadmium chloride electrode proposed by Marple[3] was used as the reference electrode instead of the bridged saturated calomel electrode which had been used in the previous studies.[1,2] The cadmium electrode was connected with a cell solution by a DMF-methylcellulose bridge containing 0.5 M tetraethylammonium perchlorate. The reference electrode gave a stable and reproducible potential of −0.667 V *vs.* SEC. All the measurements were carried out at 25°C.

Results and Discussion

Electrode Reaction Mechanism. The polarographic behavior of *n*-propylamine, isopropylamine, and *n*-butylamine was examined over the wide concentration range from 0.1 to 100 mM. Similarly, the behavior of ammonia and methylamine, which had been examined previously,[2] was reinvestigated, since none of them had been examined at concentrations higher than 5 mM. The results for these depolarizers were very similar to one another and to that for ethylamine.[1] Thus, a dilute solution of each amine (below 0.5 mM) gave a single anodic wave. At concentrations higher than 1.0 mM, another anodic wave appeared in each amine, except ammonia, at a potential less positive than that of the main wave. In the case of ammonia, no prewave appeared until the concentration exceeded 5.0 mM. In every case, however, the prewave had the nature of an adsorption, whereas the total anodic wave was diffusion-controlled; this conclusion was confirmed by an examination of the dependence of the limiting currents on the amine concentrations and on the effective mercury pressure.

When mercury(II) perchlorate was added to each of the amine solutions, the polarographic wave of the resulting solution became partly cathodic. However, the half-wave potential of the total wave was scarcely influenced by the addition of the mercury(II) ion. When the concentration of the mercury(II) ion added becomes equal to half that of the amine, the total wave became completely cathodic. These results are similar to those for methyl- and ethylamine reported previously,[1,2] and it can likewise be considered that the anodic wave given by each amine in the present study is also due to the polarographically reversible oxidation of mercury to the 1 : 2 complex of mercury(II) with the amine (Eq. (1)):

$$Hg + 2am \rightleftharpoons Hg(am)_2^{2+} + 2e \qquad (1)$$

Figure 1 shows the results of log-plots ($\log i/(i_d - i)^2$ *vs.* potential) for the anodic waves given by dilute solutions of *n*-propylamine, isopropylamine, and *n*-butylamine. Similar plots have been reported in a previous paper[2] for the cases of ammonia and methylamine. A straight line with a reciprocal slope of 0.030 V was obtained at the more positive potentials of the wave in each amine, as had been expected from the current-potential equation derived from Eq. (1).[2] The deviation of the plot from the straight line at the less positive potentials of each wave may be caused by the adsorption of the oxidation product, $Hg(am)_2^{2+}$,

1) Y. Matsui and Y. Date, This Bulletin, **46**, 460 (1973).
2) Y. Matsui, Y. Kurosaki, and Y. Date, This Bulletin, **46**, 147 (1973).
3) L. W. Marple, *Anal. Chem.*, **39**, 844 (1967).

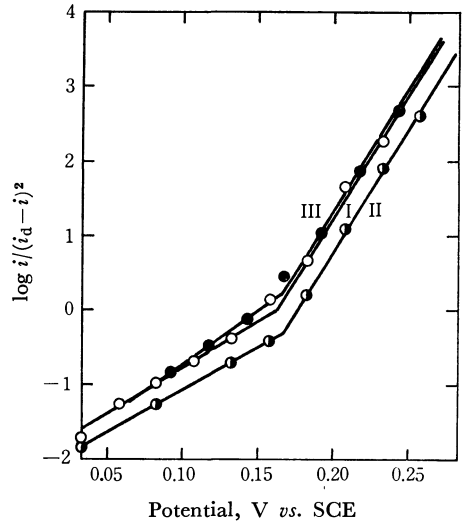

Fig. 1. Plots of $\log i/(i_d-i)^2$ *vs.* potential for the waves of 0.44 mM *n*-$PrNH_2$ (I), 0.82 mM *iso*-$PrNH_2$ (II), and 0.50 mM *n*-$BuNH_2$ (III).

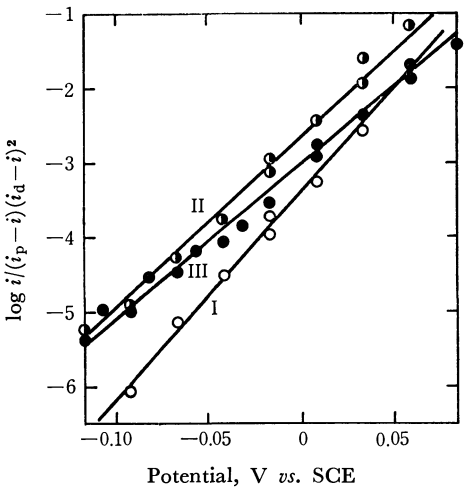

Fig. 2. Plots of $\log i/(i_p-i)(i_d-i)^2$ *vs.* potential for the prewawes of NH_3 (I), *n*-$PrNH_2$ (II), and *n*-$BuNH_2$ (III). Reciprocal slope: I; 0.036 V, II; 0.044 V, III; 0.047 V.

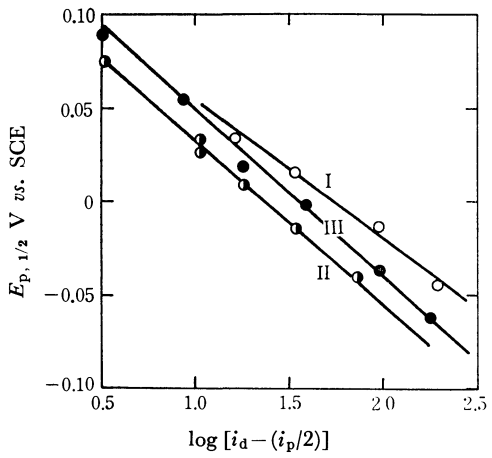

Fig. 3. Plots of the half-wave potentials of the prewaves of NH_3 (I), *n*-$PrNH_2$ (II), and *n*-$BuNH_2$ (III). *vs.* $\log [i_d-(i_p/2)]$. Slope: I; −0.072 V, II; −0.088 V, III; −0.090 V.

on the electrode surface.

Analyses of the Adsorption Prewaves. According to a previous paper,[1] if the adsorption of the oxidation product, $Hg(am)_2^{2+}$, follows the Langmuir isotherm, and if the adsorption coefficient of the complex exponentially decreases as the electrode potential becomes more positive, the plot of $\log i/(i_p-i)(i_d-i)^2$ *vs.* the potential for the adsorption prewave of each amine should give a straight line with a reciprocal slope of $0.030/(1-\gamma)$ V at 25°C, where γ is a proportionality constant in the equation relating the adsorption energy of the mercury(II) complex to the electrode potential,[1] and where i_p is the height of the prewave. Likewise, the plot of the half-wave potential ($E_{p,1/2}$) of the prewave *vs.* $\log[i_d-(i_p/2)]$ should be linear, with a slope of $-0.060/(1-\gamma)$ V at 25°C. These plots for ammonia, *n*-propylamine, and *n*-butylamine are shown in Figs. 2 and 3. In fact, the plot of $\log i/(i_p-i)(i_d-i)^2$ *vs.* the potential was virtually linear at any concentration of any amine. The plot of $E_{p,1/2}$ *vs.* $\log[i_d-(i_p/2)]$ was also virtually linear for each amine. Similar results were also obtained for methylamine and isopropylamine.

It is interesting that, in each amine, the absolute value of the slope in the plot of $E_{p,1/2}$ *vs.* $\log(i_d-(i_p/2))$ is virtually equal to double that of the reciprocal slope in the plot of $\log i/(i_p-i)(i_d-i)^2$ *vs.* the potential. This result agrees exactly with that expected theoretically. The values of γ evaluated from the slopes are listed in Table 1. Except for ammonia, all of them are virtually equal to one another. In ammonia, the value of γ is significantly smaller than those for alkylamines. This indicates that the mercury(II) complex of ammonia is more easily desorbed than those of alkylamines from the electrode surface as the electrode potential becomes more positive. In the adsorption of the mercury(II) complexes on the electrode, the electric repulsion between the positively-charged mercury (II) and the positively-charged electrode may be lowered by the shielding of the ligands present between them. In the complex of ammonia, however, the shielding effect may be small, probably because of the small size of the ligand. Therefore, the complex of ammonia may be more subject to the effect of the change in electric field in the vicinity of the electrode than the complexes of alkylamines. We will discuss this problem further later. In any event, all the results shown above clearly indicate that the present method of the analysis of an adsorption prewave is

Table 1. The proportionality constants, γ, for the complexes of mercury(II) with ammonia and alkylamines

Complexes	γ
$Hg(NH_3)_2^{2+}$	0.17
$Hg(MeNH_2)_2^{2+}$	0.32
$Hg(EtNH_2)_2^{2+}$	0.36[a]
$Hg(n\text{-}PrNH_2)_2^{2+}$	0.32
$Hg(iso\text{-}PrNH_2)_2^{2+}$	0.36
$Hg(n\text{-}BuNH_2)_2^{2+}$	0.36

a) Ref. 1.

applicable at least to the prewaves given by any alkylamines.

Some Physicochemical Properties of Alkylamines and Their Mercury(II) Complexes in DMF. Table 2 shows the diffusion coefficients (D_a) of several amines in DMF. They were evaluated from the total height of the anodič wave of each amine on the basis of the Ilkovič equation. The value of D_a decreases with an increase in the molecular weight of the amine. According to Kolthoff and Lingane,[4] the diffusion coefficient of uncharged substances is inversely proportional to the cube root of the molecular weight (M) of the substances. In fact, the plot of log D_a *vs.* log M for the amines studied was roughly linear, with a slope of −0.33 (Fig. 4). This shows that no alkylamines are essentially subject to solvation in DMF.

Table 3 shows the diffusion coefficients (D_c) of the mercury(II) complexes of ammonia and several alkylamines, as well as that of the mercury(II) ion. They were also evaluated from the height of the reduction wave of each mercury(II) complex or the mercury (II) ion on the basis of the Ilkovič equation. It is interesting that no values of D_c are so different from one another as the values of D_a are. It even seems that

Table 2. Diffusion coefficients of ammonia and alkylamines in DMF at 25°C

Compounds	Diffusion coefficients (cm^2/s)
NH_3	19.9×10^{-6} a)
$MeNH_2$	19.0×10^{-6}
	18.8×10^{-6} a)
$EtNH_2$	16.3×10^{-6}
n-$PrNH_2$	15.2×10^{-6}
isoPrNH_2	15.1×10^{-6}
n-$BuNH_2$	13.0×10^{-6}
Ethylenediamine	15.0×10^{-6} a)
1,2-Diaminopropane	12.9×10^{-6} a)

a) Ref. 2.

Table 3. Diffusion coefficients of the simple mercury(II) ion and the complexes of mercury(II) with ammonia and alkylamines in DMF at 25°C

Compounds	Diffusion coefficients (cm^2/s)
Hg^{2+}	3.9×10^{-6} a)
$Hg(NH_3)_2^{2+}$	3.7×10^{-6} b)
$Hg(MeNH_2)_2^{2+}$	4.0×10^{-6} b)
$Hg(EtNH_2)_2^{2+}$	3.6×10^{-6}
$Hg(n\text{-}PrNH_2)_2^{2+}$	4.4×10^{-6}
$Hg(iso\text{-}PrNH_2)_2^{2+}$	4.1×10^{-6}
$Hg(n\text{-}BuNH_2)_2^{2+}$	4.1×10^{-6}
$Hg(en)_2^{2+}$ c)	5.6×10^{-6} b)
$Hg(pn)_2^{2+}$ c)	4.8×10^{-6} b)

a) Y. Matsui and Y. Date, This Bulletin, **43**, 2052 (1970). b) Ref. 2. c) en: Ethylenediamine; pn: 1,2-Diaminopropane

4) I. M. Kolthoff and J. J. Lingane, "Polarography," Interscience Publishers, New York, N. Y. (1952), p. 57.

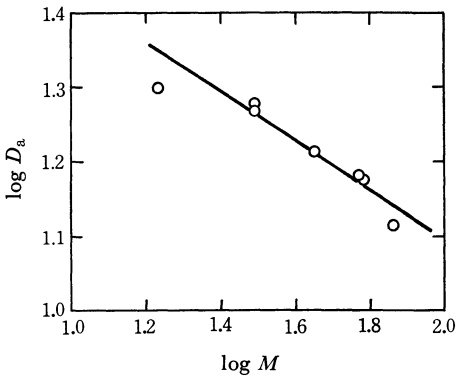

Fig. 4. Plot of log D_a *vs.* log M. Slope: −0.33

the values of D_c are virtually equal to one another. Since the mercury(II) ion usually forms a complex in which four ligands coordinate in the tetrahedral configuration, the "simple" mercury(II) ion may actually be coordinated by four molecules of the solvent, DMF. This idea is supported by the fact that the value of D_c is too small for the "simple" mercury (II) ion to be really simple. When the solvated mercury(II) ion forms a complex with ammonia or alkylamine, two of the four molecules of DMF coordinating to the mercury(II) ion are replaced by two molecules of the ammonia or the amine. In this case, however, it seems that the molecular weight or the size of the mercury(II) complex does not significantly change with the change in the kind of ligand. This may be the reason why the value of D_c is virtually invariant, irrespective of the kind of ligand in the mercury(II) complex.

Table 4 shows the overall stability constants (β_2) of the $Hg(am)_2^{2+}$ complex. They were evaluated from the results of the log-plots given in Fig. 1 in a manner which has been described previously.[2] All the values obtained are approximately equal to one another. There is no apparent tendency for the value of β_2 to increase or decrease with an increase in the size of the alkyl groups of the amines. According to Bjerrum,[5] the value of β_2 in an aqueous solution increases with an increase in the basic strength of

Table 4. Overall stability constants (β_2) of the complexes of mercury(II) with ammonia and alkylamines in DMF at 25°C

Complexes	β_2, $l\cdot mol^{-1}$
$Hg(NH_3)_2^{2+}$	$10^{17.0}$ ($10^{16.9}$ a))
$Hg(MeNH_2)_2^{2+}$	$10^{17.0}$ ($10^{17.1}$ a))
$Hg(EtNH_2)_2^{2+}$	$10^{16.5}$ b)
$Hg(n\text{-}PrNH_2)_2^{2+}$	$10^{16.7}$
$Hg(iso\text{-}PrNH_2)^{2+}$	$10^{16.3}$
$Hg(n\text{-}BuNH_2)_2^{2+}$	$10^{16.8}$
$Hg(en)_2^{2+}$ c)	$10^{23.5}$ a)
$Hg(pn)_2^{2+}$ c)	$10^{24.0}$ a)

a) Ref. 2. b) Ref. 1. c) en: Ethylenediamine; pn: 1,2-Diaminopropane

5) J. Bjerrum, *Chem. Rev.*, **46**, 381 (1950).

Table 5. Adsorption characteristics of the complexes of mercury(II) with ammonia and alkylamines on the mercury electrode in DMF at 25°C

Complexes	Z[a] mol/cm^2	a[b] Å^2/molecule	w_0[c] l/mol
$Hg(NH_3)_2^{2+}$	1.28×10^9	13.0	0.2×10^6
$Hg(MeNH_2)_2^{2+}$	1.24×10^9	13.4	0.8×10^6
	1.41×10^9 [d]	11.8[d]	
$Hg(EtNH_2)_2^{2+}$	1.17×10^9 [e]	14.2[e]	4.6×10^6
$Hg(n\text{-}PrNH_2)_2^{2+}$	0.79×10^9	21.0	2.5×10^6
$Hg(iso\text{-}PrNH_2)_2^{2+}$	0.87×10^9	19.1	1.6×10^6
$Hg(n\text{-}BuNH_2)_2^{2+}$	0.82×10^9	20.2	1.0×10^6

a) Z: The maximal amount of the adsorbate per unit area. b) a: The area of the electrode surface occupied by one adsorbate molecule. c) w_0: The adsorption coefficient of the adsorbate complex at 0.0 V *vs.* SCE. d) Ref. 2. e) Ref. 1.

amine. However, no such relation was observed in the present case. It is notable that the mercury(II) complexes of diamines are more stable than those of monoamines by a factor of about 10^7. This may be due to the chelate formation in the former complexes.

Table 5 shows the adsorption characteristics for the mercury(II) complexes of ammonia and alkylamines on the mercury electrode. The maximal amount of the adsorbate per unit of area (Z) and the area (a) of the electrode surface occupied by one adsorbate molecule were evaluated from the heights of the prewaves of ammonia and alkylamines by the use of an equation described previously.[2] The adsorption coefficients (w_0) of the adsorbates at 0.0 V *vs.* SCE were evaluated from the results of the log-plots in Fig. 2 in a manner which has previously been reported.[1] The values of a thus obtained are reasonable for the size of the mercury(II) complexes. They increase with an increase in the size of the alkyl groups of the amines. It is uncertain whether the alkyl groups in the mercury(II) complexes are oriented horizontally or vertically to the electrode surface. However, the values of a are large enough to suggest that the alkyl groups are horizontally oriented to the electrode surface.

An interesting result was obtained with regard to the value of w_0. Thus, the value for the complex of ammonia was the smallest of all, whereas that for the complex of ethylamine was the largest. With a further increase in the size of the alkyl groups of amines, the value of w_0 decreased. It seems that the value of w_0 is a measure of the adsorptivity of the mercury(II) complexes on the electrode surface. The larger the value of w_0, the stronger is the adsorptivity, and *vice versa*. In the adsorption of the mercury(II) complex on the mercury electrode immersed in a DMF solution, the hydrophobic interaction between the alkyl groups of the adsorbate complexes and the electrode may play no important role because of the high solubility of the aliphatic groups in the solution, although such an interaction is very important for the adsorption in an aqueous solution.[6] The interaction between the amino groups of the ligands and the electrode may also be negligible, for no alkylamines are significantly adsorbed on the electrode. Therefore, the adsorption of the mercury(II) complexes on the electrode may be caused by the attractive interaction between the mercury(II) ion and the electrode mercury. If so, the attractive force may decrease with an increase in the size of the ligand alkylamines present between the mercury(II) ion and the electrode. This may be responsible for the fact that the value of w_0 decreases in the order of the mercury(II) complexes of ethylamine, n-propylamine, isopropylamine, and n-butylamine. On the other hand, the w_0 values of the mercury(II) complexes of ammonia and methylamine are smaller than that of the ethylamine complex. In these cases, the ligands are so small that the mercury(II) ion in the complexes may be subject to the strong force of electrostatic repulsion from the electrode which is positively charged at 0.0 V *vs.* SCE. This presumption is in agreement with that derived above on the basis of the values of γ. Thus, the adsorptivity of each complex of mercury(II) with alkylamine may eventually be determined by the relative values of the two kinds of force, *i.e.*, the chemical attractive force and the electrostatic repulsive force of the electrode mercury acting on the mercury(II) ion.

In the present study, only ammonia and primary alkylamines have been examined. However, secondary alkylamines also give an anodic adsorption prewave, as has been reported previously.[2] This will be dealt with in a succeeding paper.

6) B. B. Damaskin and A. N. Frumkin, "Reactions of Molecules at Electrode," ed. by N. S. Hush, John Wiley & Sons, London (1971), p. 1.

NMR Study of Amino Acids and Their Derivatives. V. Structures and Formation Constants of Zinc–L-Aspartic Acid Complexes in Aqueous Solution

Hidehiro ISHIZUKA, Takeo YAMAMOTO, Yoji ARATA and Shizuo FUJIWARA

Department of Chemistry, Faculty of Science, The University of Tokyo, Hongo, Tokyo

(Received June 29, 1972)

NMR spectra of L-aspartic acid coordinated with Zn ions were measured in aqueous solution at various pH values. Three species of zinc–L-aspartic acid complexes were identified *i.e.*, 1 : 1 zinc–L-aspartic acid(zwitter ionic form) complex (MAH), and 1 : 1 and 1 : 2 zinc-aspartic acid(anionic form) complexes (designated as MA and MA_2, respectively). It is shown that, in MAH, the amino acid coordinates with Zn as a monodentate ligand, whereas in MA and MA_2, approximately 65% of the molecules of amino acid coordinate as a tridentate ligand. From the chemical shift data, the equilibrium constants for these complexes are determined as follows: pK_a-(MAH)$=5.3\pm0.2$ and $\log K_2=4.5\pm0.2$ where $K_a(MAH)=[MA][H^+]/[MAH]$ and $K_2=[MA_2]/[MA][A]$.

Nuclear magnetic resonance (NMR) has been successfully used in investigating the structure of amino acids in aqueous solution.[1] We have previously investigated the structure of L-cysteine,[2] L-phenylalanine[3] and L-serine[4]. The present paper reports an NMR study of L-aspartic acid–zinc ion system at various pH values. Structures of Zn–L-aspartic acid complexes which possibly exist in solution are presented together with their equilibrium constants.

Experimental

Reagent grade L-aspartic acid, zinc nitrate, tetramethylammonium chloride and sodium hydroxide were used to prepare solutions of zinc-free L-aspartic acid, 1 : 1 and 1 : 2 zinc-L-aspartic acid in water. The concentration of aspartic acid in each solution is 0.10 M. Five mM of tetramethylammonium chloride is added to each solution as an internal reference.

The pH of the solution was controlled by adding concentrated sodium hydroxide solution and measured with a Toa Dempa pH meter, Model HM-5A. NMR spectra were recorded with a JNM 4H-100 spectrometer operating at 100 MHz.

Results and Discussion

The α- and β-protons of L-aspartic acid are designated as follows:

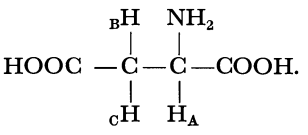

NMR spectra of this ABC three spin system were analyzed as described previously.[4]

Chemical Shift. Zinc-free Aspartic Acid Solution: Chemical shifts for zinc-free aspartic acid solutions are shown in Fig. 1, where stepwise shifts are observed in the pH range 4—5 and 9—11. These shifts are attributed to the dissociation of the β-COOH and NH_3^+ groups, respectively.[5] The three species and dissociation constants involved are designated as follows:

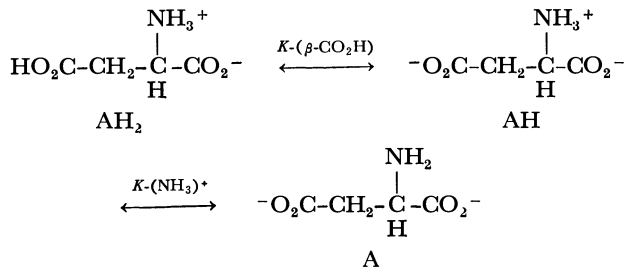

Chemical shifts of the three protons ν_A, ν_B and ν_C for AH and A forms are listed in Table 1. The $pK(NH_3^+)$ value estimated from the pH dependence of ν_A is in good agreement with values determined by the potentiometric titration method[6–8] (Table 2). The present result obtained above pH 7 agree well with those reported by Pachler[9] and Taddei and Pratt.[10]

Zn(II)–L-Aspartic Acid Solution: Figure 1 shows the chemical shift of the three protons in the 1 : 1 and 1 : 2 solutions, for the 1 : 1 solution the average values of ν_B and ν_C are obtained by analyzing the

TABLE 1. CHEMICAL SHIFTS OF α- AND β-PROTONS OF L-ASPARTIC ACID[a]

Form[b]	Zinc-free solution		1 : 1 Solution		1 : 2 Solution
	AH	A	MAH	MA	MA_2
pH	7.2	12.2	4.4	6.7	8.6
ν_A	71.8 Hz	37.4	72.1	50.2	50.9
ν_B	−36.9	−53.6	−37.7[c]	−39.9[c]	−41.4[c]
ν_C	−50.7	−90.1			

a) Chemical shift are in Hz unit from tetramethylammonium chloride. They are accurate to ±0.1 Hz. b) See text. c) The average value of ν_B and ν_C. The difference between ν_B and ν_C is smaller than 4Hz.

1) *Cf. e. g.*, J. J. M. Rowe, J. Hinton, and K. L. Rowe, *Chem. Rev.*, **70**, 1, (1970).
2) S. Fujiwara and Y. Arata, This Bulletin, **36**, 578, (1963).
3) S. Fujiwara and Y. Arata, *ibid.*, **37**, 344, (1964).
4) H. Ogura, Y. Arata, and S. Fujiwara, *J. Mol. Spectrosc.* **23**, 76, (1967).
5) The α-carboxyl group dissociates at a pH value which is outside the pH range covered in the present study.
6) H. Kroll, *J. Amer. Chem. Soc.*, **74**, 2034 (1952).
7) A. Albert, *Biochem. J.*, **50**, 690 (1952).
8) S. Chaberek, Jr. and A. E. Martell, *J. Amer. Chem. Soc.*, **74**, 6021 (1952).
9) K. G. R. Pachler, *Z. Anal. Chem.*, **224**, 211, (1967).
10) F. Taddei and L. Pratt, *J. Chem. Soc.*, **1964**, 1553.

TABLE 2. EQUILIBRIUM CONSTANTS OF ZINC ION-L-ASPARTIC ACID COMPLEX

	This work[a)]	Kroll[6)]	Albert[7)]	Martell[8)]
$pK(NH_3^+)$	9.8±0.1	9.60	9.98	9.46
$pK(MAH)$[b)]	5.3±0.2	—	—	—
$\log K_2$[c)]	4.5±0.2	—	—	4.31

a) The ionic strength is about 0.1.
b) $K(MAH) = \frac{[MA][H^+]}{[MAH]}$. c) $K_2 = \frac{[MA_2]}{[MA][A]}$.

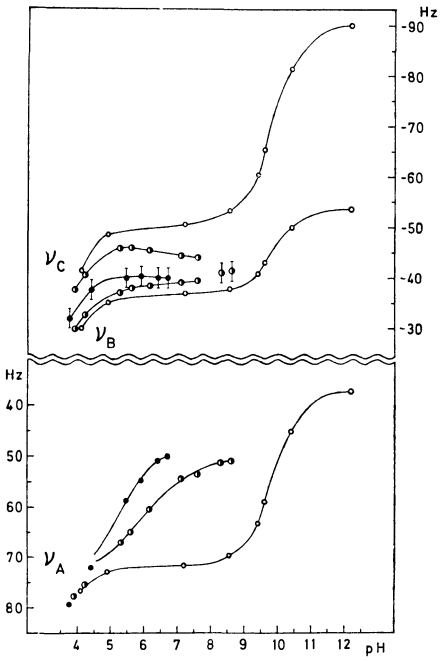

Fig. 1. The pH dependence of the chemical shifts for CH protons of L-aspartic acid.
● Zn(II)—Asp 1 : 1 solution
◑ Zn(II)—Asp 1 : 2 solution
○ Zn(II) free solution
The average values of ν_B and ν_C are plotted for the 1 : 1 solution, and pH≥8.3 for the 1 : 2 solution.

system as an AB_2 spin system and plotted, since $\Delta\nu_{BC}$, the difference between ν_B and ν_C, is too small (≲4 Hz) for the spectra to be analyzed as an ABC spin system.

In the titration curve for the A proton, high field shift due to dissociation of the NH_3^+ group occurs at a pH much lower than in the zinc-free aspartic acid solution, suggesting that the following complex formation takes place:

$$-NH_3^+ \rightarrow -NH_2\text{-}Zn^{2+}.$$

Figure 1 shows that the coordination of the amino group is complete at pH 6.7 and at pH 8.6 for the 1 : 1 and the 1 : 2 solutions, respectively.[11)] It should also be noted that the A-proton chemical shifts for these systems (columns 4 and 5, Table 1) are lower than that of zinc-free aspartic acid in A form. This low field shift may be due to participation of the amino group in the complex formation with zinc ion.

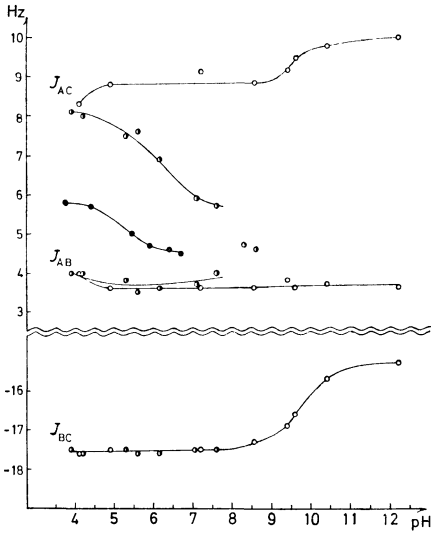

Fig. 2. The pH dependence of the spin coupling constant between CH protons of L-aspartic acid.
● Zn(II)—Asp 1 : 1 solution
◑ Zn(II)—Asp 1 : 2 solution
○ Zn(II) free solution
The average values of J_{AB} and J_{AC} are plotted for the 1 : 1 solution, and at pH≥8.3 for the 1 : 2 solution.

The difference $\Delta\nu_{BC}$ at pH 3.7—4.9 decreases in the following order: zinc-free, 1 : 2, 1 : 1 solutions. This suggests that at least one zinc–L-aspartic acid complex with a smaller $\Delta\nu_{BC}$ value exists in the pH range.[12)] It is assumed that the observed chemical shifts are the average of contributions from zinc-free and coordinated (1 : 1 and 1 : 2 complexes) aspartic acid as follows:

$$\Delta\nu_{BC(obs)} = f\Delta\nu_{BC(free)} + (c_1+c_2)\Delta\nu_{BC(coord)} \quad (1)$$

where

$$f + c_1 + c_2 = 1 \quad (2)$$

Here, f, c_1 and c_2 are the fractional population of zinc-free and coordinated (1 : 1 and 1 : 2 complexes) aspartic acid, respectively. The values of $\Delta\nu_{BC(free)}$ and $\Delta\nu_{BC(coord)}$ were obtained by the data for the zinc-free and 1 : 1 solutions respectively, as follows: $\Delta\nu_{BC(free)}$=11.4(pH 4.1)~13.4 Hz(pH 4.9) and $\Delta\nu_{BC(coord)}$≲4 Hz. Comparison of these values with $\Delta\nu_{BC(obs)}$ for the 1 : 2 and 1 : 1 solutions indicates that c_2 is negligibly small, $f \fallingdotseq c_1 \fallingdotseq 0.5$, $c_2 \fallingdotseq 0$ for the 1 : 2 solution and $f \fallingdotseq c_2 \fallingdotseq 0$, $c_1 \fallingdotseq 1$ for 1 : 1 solution (*cf.* Fig. 1). Thus, it may be concluded that a 1 : 1 complex (designated as MAH) is dominant in the pH range examined.

Spin Coupling Constant. The spin coupling constants for the 1 : 1, 1 : 2 and zinc-free aspartic acid solutions are shown in Fig. 2, where the average of J_{AB} and J_{AC} was plotted for the 1 : 1 solution throughout the pH range examined, and for the 1 : 2 solution at pH≳8.3.

The vicinal coupling constants, J_{AB} and J_{AC} obtained can be used to discuss possible conformations of L-

11) NMR spectra could not be measured at pH>6.7 and at pH>8.6 for the 1 : 1 and the 1 : 2 solutions, respectively, because of limited solubility of the samples.

12) $\Delta\nu_{BC(obs)}$ does not change by adding sodium nitrate to the zinc-free solution, indicating that $\Delta\nu_{BC}$ is independent of the ionic strength.

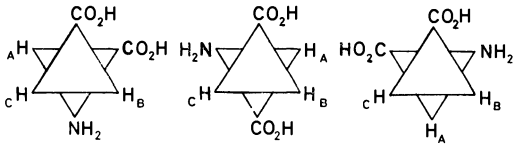

I II III

Fig. 3. The three rotational isomers of L-aspartic acid.

aspartic acid in the present systems. It is assumed that J_{AB} and J_{AC} are the statistical average of contributions from three rotational isomers I, II and III of staggered form, as shown in Fig. 3.

Thus

$$J_{AB} = p_I J_t + p_{II} J_g + p_{III} J_g \quad (3)$$

$$J_{AC} = p_I J_g + p_{II} J_t + p_{III} J_g, \quad (4)$$

where

$$p_I + p_{II} + p_{III} = 1. \quad (5)$$

Here, p_I, p_{II} and p_{III} are the fractional populations of the three rotational isomers, and J_t and J_g are the spin coupling constants between *trans* and *gauche* proton pairs, respectively. It is further assumed that J_t and J_g do not change when aspartic acid coordinates to zinc ion. This assumption may be confirmed by the following experiment. In L-alanine the spin coupling constant between alpha and beta protons was constant, *i. e.*, J=7.2 Hz, both at pH 4.2 and 6.7 in 1 : 2 zinc–L-alanine solution and at pH 2.5 and 6.0 in the absence of zinc ion. This result suggests that, since $p_I=p_{II}=p_{III}$ in L-alanine, J_t and J_g are not influenced by the coordination of the amino acid to zinc ion.

In the present study, J_t=13.6 Hz and J_g=2.6 Hz were used to obtain the fractional populations p_I, p_{II} and p_{III}.[4] Figure 4 shows the results for the 1 : 1, 1 : 2 and zinc-free aspartic acid solutions.[13]

In the pH region where MAH dominates, isomer I with the two carboxyl anions *gauche* to each other makes only a minor contribution in the 1 : 2 solution. This strongly suggests that in this pH region aspartic acid coordinates as a monodentate ligand using either one of the two carboxyl anions; aspartic acid as a bidentate ligand, coordinating with the α- and β-carboxyl groups, would result in a large populations the rotational isomer I. As Fig. 4 shows, p_{II} increases with pH and becomes constant and equal to about 65% at pH 6.7 and at pH 8.6 in the 1 : 1 and 1 : 2 solution, respectively; isomer III becomes dominant in the pH region where aspartic acid can coordinate with zinc ion in the A form (See Fig. 1). This result suggests that in this pH range L-aspartic acid behaves as a tridentate ligand, coordinating with the amino, α- and β-carboxyl groups to zinc ion. Although isomer III is dominant in these systems, p_I and p_{II} are also not negligibly small, suggesting that

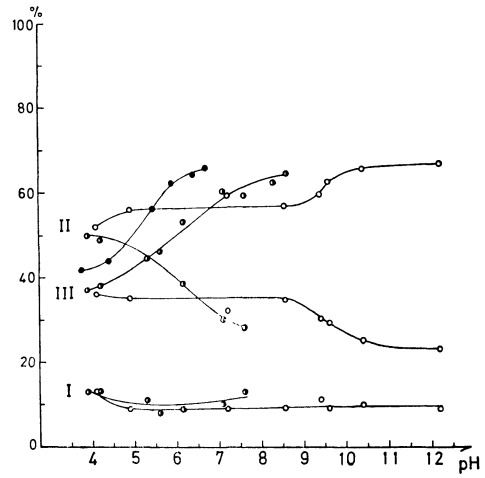

Fig. 4. pH dependence of the fractional populations of the fractional populations of the three rotational isomers.
● Zn(II)—Asp 1 : 1 solution
◑ Zn(II)—Asp 1 : 2 solution
○ Zn(II) free solution
Only the population of isomer III is plotted for the 1 : 1 solution and pH≥8.3 for the 1 : 2 solution.

bidentate species possibly exist as minor components; one of the possible species may be the isomer II coordinating with the amino and β-carboxyl groups, and another isomer I or II which coordinates with the amino and α-carboxyl groups.

In contrast to the above results, an x-ray diffraction study shows that only rotational isomer III is present in solid zinc aspartate trihydrate.[14] Martin and Mathur[15] suggested on the basis of their NMR study that in di(L-histidino)zinc complex a rotational isomer corresponding to the above mentioned isomer III is dominant in aqueous solutions. However, the pH of the solutions are not stated definitely, and the population of the rotational isomer is not given.

Equilibrium Constants among Zinc–L-Aspartic Acid Complexes. On the basis of the experimental results mentioned above, it is assumed that the following equilibria are dominant in the 1 : 1 and 1 : 2 zinc–aspartic acid solutions at pH≳4.5:

$$\mathrm{MAH} \overset{K(\mathrm{MAH})}{\longleftrightarrow} \mathrm{MA} + \mathrm{H^+}, \quad K(\mathrm{MAH}) = \frac{[\mathrm{MA}][\mathrm{H^+}]}{[\mathrm{MAH}]}, \quad (6)$$

$$\mathrm{MA} + \mathrm{AH} \overset{K(\mathrm{MA\text{-}AH})}{\longleftrightarrow} \mathrm{MA_2} + \mathrm{H^+},$$

$$K(\mathrm{MA\text{-}AH}) = \frac{[\mathrm{MA_2}][\mathrm{H^+}]}{[\mathrm{MA}][\mathrm{AH}]}. \quad (7)$$

Here, MAH denotes the 1 : 1 zinc–aspartic acid(AH form) complex, and MA and MA_2 the 1 : 1 and 1 : 2 zinc–aspartic acid(A form) complexes, respectively. The equilibrium constants were determined from the pH dependence of ν_A by curve fitting. It is assumed that ν_A of MAH is equal to that of AH. The pH dependence of ν_A for the 1 : 1 and 1 : 2 solutions cal-

13) The assignment of the curves to isomers I and II in Fig. 4 may be reversed. Considering steric hindrance, however, one would expect isomer II with two carboxyl anions *trans* to each other to be more stable than isomer I.

14) T. Doyne, R. Pepinsky, and T. Watanabe, *Acta Crystallogr.*, **10**, 438 (1957).

15) R. B. Martin and R. Mathur, *J. Amer. Chem. Soc.*, **87**, 1065, (1965).

culated using $pK(MAH)=5.3$ and $pK(MA\text{–}AH)=5.3$ is plotted in Fig. 1. These curves are in good agreement with the experimental data. The following stability constant for the 1 : 2 complex can be determined by using the values of $pK(MA\text{–}AH)$ and $pK(NH_3^+)$:

$$K_2 = \frac{[MA][A]}{[MA_2]}$$

The values of $pK(MAH)$ and $\log K_2$ are given in the second and third row, respectively, of Table 2, together with the reported $\log K_2$ value determined by the potentiometric titration method.[8]

Conclusion

Three zinc–L-aspartic acid complexes, MAH, MA and MA_2, were identified in the zinc ion–aspartic acid systems. The dominant($\sim$65%) species for MA and MA_2 is a tridentate complex with the amino acid coordinating with the amino, α- and β-carboxyl groups. As minor components, bidentate species are suggested to exist, where the ligand coordinates with the amino and α- or β-carboxyl groups. The dominant species for MAH is a monodentate complex coordinating with one of the two carboxyl groups. The equilibrium constants of these complexes, $pK(MAH)$ and $\log K_2$ were determined (Table 2).

BULLETIN OF THE CHEMICAL SOCIETY OF JAPAN, VOL. 46, 471—474 (1973)

Mechanisms and Kinetics of the Decomposition of Trioxalatocobaltate(III) in Aqueous Sulfuric Acid

Masaru KIMURA and Toshiro SATO

Department of Applied Chemistry, Yamagata University, Yonezawa

(Received July 5, 1972)

The kinetics of the thermal decomposition of the trioxalatocobaltate(III) complex were studied in a sulfuric acid solution in the absence and in the presence of oxygen from 25 to 40°C. The decomposition of trioxalatocobaltate(III) was described by the equation: $-d[Co(C_2O_4)_3^{3-}]/dt=(k_1+k_2[H^+])[Co(C_2O_4)_3^{3-}]$. The values of k_1 and k_2 were 6×10^{-6} sec^{-1} and 1.8×10^{-5} M^{-1} sec^{-1} respectively at 25°C. The values of the activation enthalpy change, $\Delta H_1^{\neq}$ and $\Delta H_2^{\neq}$, were 29.7 and 30.0 kcal mol^{-1} respectively. The values of the activation entropy change, $\Delta S_1^{\neq}$ and $\Delta S_2^{\neq}$, were 17.4 and 20.9 eu respectively at 40°C. Although hydrogen peroxide was formed in the presence of oxygen, and although a white precipitate of the polymerized products of acrylonitrile was found in the presence of acrylonitrile, neither oxygen nor acrylonitrile affected the kinetics of the decomposition of trioxalatocobaltate(III). The decomposition of peroxodisulfate was induced by the decompossition of trioxalatocobaltate(III). However, the rate of the decomposition of trioxalatocobaltate(III) was not affected by peroxodisulfate. On the other hand, both copper(II) and iron(III) ions were accelerators of the decompsition of trioxalatocobaltate(III). An anion radical of CO_2^- was predicted as an intermediate. The reaction mechanisms will be presented to account for these facts.

It has been known for many years[1] that trioxalatocobaltate(III) decomposes photochemically and thermochemically with internal redox to produce cobalt(II), carbon dioxide and oxalate. Recently, Kolthoff *et al.*[2] have found that hydrogen peroxide is formed upon the decomposition of trioxalatocobaltate(III) in the presence of oxygen in an acidic medium. The initial reaction is:

$$Co(C_2O_4)_3^{3-} \rightarrow Co(C_2O_4)_n^{(2-2n)} + (2-n)\,C_2O_4^{2-} + CO_2 + CO_2^- \quad (1)$$

The anion radical in Reaction (1) may be either $C_2O_4^-$ or CO_2^-. However, the two forms do not appear to be distinguishable on the basis of kinetic or spectroscopic evidence.[3] Following the consensus of previous workers, we will write CO_2 in the present paper.

It would be interesting to know if the CO_2^- radical would not reduce $Co(C_2O_4)_3^{3-}$, but the two would combine with each other to produce $C_2O_4^{2-}$. With the purpose of interpreting the reaction mechanisms, the rate of the decomposition of trioxalatocobaltate(III) was measured in the presence of oxygen, acrylonitrile, copper(II) ion, iron(III) ion, or peroxodisulfate, all of which may be able to react rapidly with the CO_2^-.

Experimental

Chemicals. The potassium trioxalatocobaltate(III) complex was synthesized following the directions of Sörensen.[4] A guaranteed-reagent-grade potassium peroxodisulfate of the Kanto Kagaku Co., Inc., was recrystallized twice from redistilled water and dried at 40°C in a vacuum desiccator. Extra pure acrylonitrile of the Kanto Chemical Co., Inc., was used without further purification. Cupric sulfate, ferric ammonium sulfate, sulfuric acid, oxalic acid and cobaltous sulfate, all of a guaranteed reagent grade were used without further purification. The water was purified by distillation from an alkaline permanganate solution. Pure

1) *a)* T. B. Copestake and N. Uri, *Proc. Roy. Soc., Ser. A*, **228**, 252 (1955); *b)* A. W. Adamson, H. Ogata, J. Grossman and R. Newbry, *J. Inorg. Nucl. Chem.*, **6**, 319 (1958).

2) I. M. Kolthoff, E. J. Meehan and M. Kimura, *J. Phys. Chem.*, **75**, 3343 (1971).

3) G. D. Cooper and B. A. de Graff, *ibid.*, **75**, 2897 (1971).

4) S. P. L. Sörensen, *Z. Anorg. Allg. Chem.*, **11**, 1 (1896).

nitrogen and oxygen were used for the experiments in the absence and in the presence of oxygen respectively.

Technique. A reaction was started by adding a given ammount of the trioxalatocobaltate(III) complex to the reaction mixture. The reaction mixture was saturated with either nitrogen or oxygen, which was bubbled through the reaction mixture. Aliquot samples were withdrawn at appropriate times and mixed with cold water to slow the decomposition of trioxalatocobaltate(III). The decomposition of trioxalatocobaltate(III) during under the analytical run at 20°C was practically negligible. The trioxalatocobaltate(III) concentration was measured at 600 nm in the visible spectrum in a solution of 0.05 M sulfuric acid at 20°C. The cobaltous(II) ion produced in the course of the decomposition of trioxalatocobaltate(III) does not interfere with the absorbance of trioxalatocobaltate(III) at 600 nm. In a few experiments in the presence of copper(II), the concentration of trioxalatocobaltate(III) was determined polarographically at +0.2 V *vs.* SCE. In an experiment in presence of peroxodisulfate, the sum of the concentrations of peroxodisulfate and trioxalatocobaltate(III) was determined by using the polarographic diffusion current at +0.2 V *vs.* SCE. Peroxodisulfate did not interfere with the visible spectrum of trioxalatocobaltate(III). The concentration of the cobaltous(II) ion was determined polarographically. The concentration of oxalic acid or the sum of oxalic acid and hydrogen peroxide was determined by titration with permanganate at 50°C.

Results and Discussion

Kinetics. As is shown in Figs. 1 and 2, the rate of the decomposition of trioxalatocobaltate(III) is of the first order with respect to trioxalatocobaltate-(III) in any given reaction mixture; i. e., the kinetics are described by the equation:

$$-\mathrm{d}[\mathrm{Co}(\mathrm{C_2O_4})_3{}^{3-}]/\mathrm{d}t = k_0[\mathrm{Co}(\mathrm{C_2O_4})_3{}^{3-}] \quad (2)$$

Figure 3 indicates that the overall rate constant (k_0) of the reaction is given by:

$$k_0 = k_1 + k_2[\mathrm{H^+}] \quad (3)$$

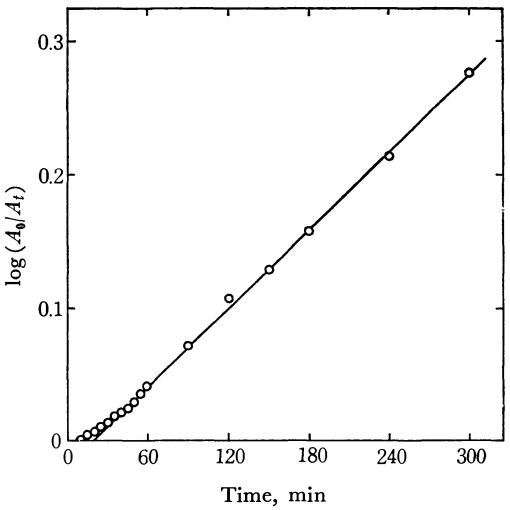

Fig. 1. First order plot for the decomposition of 4.0×10^{-3} M sulfuric acid at 25°C in dark and in nitrogen saturated.
Absorbances measured at 600 nm.
A indicates the optical absorbance, subscripts 0 and t refer, respectively, to zero-time and to any other time-t.

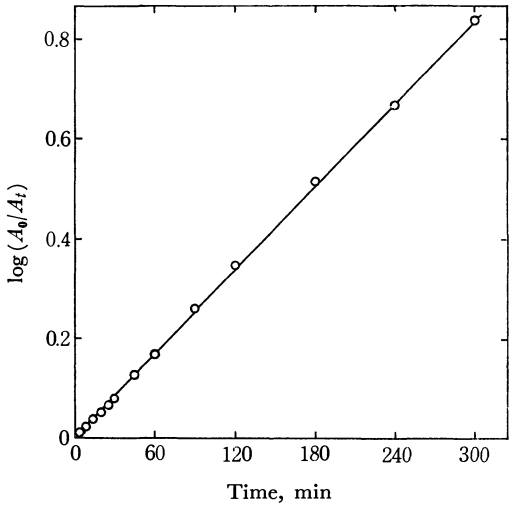

Fig. 2. First order plot for the decomposition of 4.0×10^{-3} M $K_3Co(C_2O_4)_3$ in nitrogen saturated 0.1 M sulfuric acid at 40°C.
Absorbances measured at 600 nm. A is the optical absorbance, subscripts 0 and t refer, respectively, to zero-time and to any other time-t.

where k_1 and k_2 are the rate constants of Reactions (8) and (8′) respectively.

Figure 1 indicates that there is an induction period in the initial stage of the reaction. However, the induction period disappears completely at 40°C, as can be seen in Figure 2. Recently Kruszyna and Milburn[5] have found a similar induction period at 25°C in a 1 M sulfuric acid solution. It will be necessary here to present a brief review from their discussion.[5] The existence of the induction period requires that there are two or more consecutive slow steps in a reaction sequence leading to cobalt(II); they predicted the following reaction mechanisms:

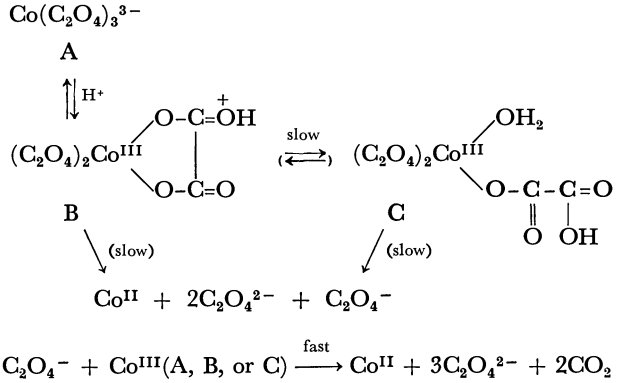

Their major points are that, during the very early stages of reaction, A and B will compete with C in the quenching of $C_2O_4^-$ radical, but for the middle and later stages of reaction, no significant amounts of A and B will remain, and $C_2O_4^-$ (or CO_2^-) will be quenched by C only.

The above assumption that the C_2O_4 radical reduces Co^{III} oxalato complex rapidly, is entirely inconsistent with our results. However, it appears that the induction

5) H. G. Kruszyna and R. M. Milburn, *Inorg. Chem.*, **10**, 1578 (1971).

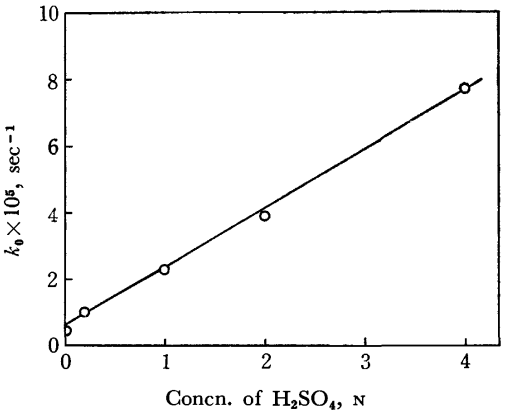

Fig. 3. Sulfuric acid dependence on the rate constant k_0. Condition: 4.0×10^{-3} M $K_3Co(C_2O_4)_3$; Dark; 25°C; N_2 sat. k_0 is the rate constant of the overall reaction (7).

period can be due to the slow steps, from A to C. Such slow steps would be accelerated by the elevated temperature, and the induction period must disappear under such conditions. This prediction is consistent with the fact that the induction period seems to disappear at 40°C.

Enthalpy and Entropy of Activation. The rate constants were determined at several temperatures. The logarithms of the rate constants were in a linear relation to $1/T$. The rate constants for the decomposition of trioxalatocobaltate(III) in 0.1 and 1.0 M sulfuric acid solutions, together with the enthalpy and entropy of activation, are given in Table 1.

Table 1. Temperature dependence on the rate of decomposition of trioxalatocobaltate(III). N_2 saturated; dark

Temp. °C	k_0 (sec^{-1}) in 0.1 M H_2SO_4	k_0 (sec^{-1}) in 1.0 M H_2SO_4	k_2 (sec^{-1} M^{-1})
25	1.0×10^{-5}	3.9×10^{-5}	1.8×10^{-5}
30	2.2×10^{-5}	8.8×10^{-5}	3.7×10^{-5}
35	5.2×10^{-5}	20.7×10^{-5}	9.6×10^{-5}
40	10.8×10^{-5}	46.5×10^{-5}	19.8×10^{-5}

$\Delta H_1^{\ddagger} = 29.7$ kcal; $\Delta H_2^{\ddagger} = 30.2$ kcal.

$\Delta S_1^{\ddagger} = 17.4$ eu; $\Delta S_2^{\ddagger} = 20.9$ eu at 40°C.

where $\Delta H_1^{\ddagger}$ and $\Delta S_2^{\ddagger}$ are the activation enthalpy and the entropy of Reaction (8), and where $\Delta H_2^{\ddagger}$ and $\Delta S_2^{\ddagger}$, those of Reaction (8′).

A number of workers[1,5-12] have proposed the monodentate oxalato species as an intermediate in the decomposition of the trioxalato metal complexes, $M(C_2O_4)_3^{3-}$; *e. g.*, in the case of trioxalatocobaltate(III), the following reactions are offered:

$$Co(C_2O_4)_3^{3-} + H_2O \rightarrow Co(C_2O_4)_2(OC_2O_3)(H_2O)^{3-} \quad (4)$$

$$Oo(C_2O_4)_3^{3-} + H_3O^+ \rightarrow Co(C_2O_4)_2(OC_2O_3H)(H_2O)^{2-} \quad (5)$$

In the present study, the enthalpy of the activation of the [H$^+$]-dependent reaction was almost equal to that of [H$^+$]-independent one. This may indicate that the decomposition of trioxalatocobaltate(III) occurs through two reactions (4) and (5). However, there have been many contradictory discussions: Kruszyna and Milburn[5] have emphasized that the protonated intermediate offers the major path for the decomposition and that the direct decomposition of $Co(C_2O_4)_3^{3-}$ occurs at a finite rate[13]. On the contrary, Aggett and Odell[9b] have suggested that the thermal decomposition of trioxalatocobaltate(III) proceeds through the unprotonated $Co(C_2O_4)_2(OC_2O_3)(H_2O)^{3-}$.

Partially-released monodentate oxalato intermediates may lead to a larger positive entropy change. This assumption is in agreement with the present results. Copestake and Uri[1a] have suggested that the hydrolysis reaction:

$$Co(C_2O_4)_3^{3-} + H_2O \rightarrow HCo(C_2O_4)_3^{2-} + OH^- \quad (6)$$

is improbable, since (a) solution of $K_3Co(C_2O_4)_3$ are neutral than alkaline, and (b) pH of a 10^{-2} M solution of $H_3Co(C_2O_4)_3$ is such that all the three hydrogen atoms are completely dissociated. That is, $H_3Co(C_2O_4)_3$ is a very strong acid. In view of these facts, the positive entropy change can hardly be expected to be due to the dehydration by the hydrogen ion.

Stoichiometry. To verify the stoichiometry of the reaction, 4.2×10^{-3} M trioxalatocobaltate(III) was kept in 0.1 M sulfuric acid solutions for 15 hr at 40°C. The solution was saturated with nitrogen or oxygen gas in a closed glass-stoppered vessel sealed with wax. Under these conditions, a green solution of trioxalatocobaltate(III) turns completely pink due to the formation of cobalt(II) ion. No trioxalatocobaltate(III) is left in the solution after 15 hours, and the cobalt(II) ion and oxalic acid are formed in the absence of oxygen as the decomposition products. Hydrogen peroxide is formed in the presence of oxygen. The amount of peroxide formed is equimolar to the amount of oxalic acid which disappears.[14] Therefore,

Table 2. Analysis of the decomposition products of 4.2×10^{-3} M $Co(C_2O_4)_3^{3-}$ in 0.1 M H_2SO_4

Cobaltous(II) ion M$\times10^3$	Oxalic acid M$\times10^3$	Conditions
4.24	10.2	N_2 sat. in Dark
4.17	10.3	N_2 sat. in Room light
4.20	10.1[a]	O_2 sat. in Room light

a) Sum of oxalic acid and hydrogen peroxide.

6) F. D. Graziano and G. M. Harris, *J. Phys. Chem.*, **63**, 330 (1959).

7) I. G. Murgulescu and T. Oncescu, *Z. Phys. Chem.* (Leipzig), **214**, 238 (1960).

8) W. Schneider, *Helv. Chim. Acta*, **46**, 1863 (1963).

9) (a) C. A. Bunton, J. H. Carter, D. R. Llewellyn, A. L. Odell and S. Y. Yih, *J. Chem. Soc.*, **1964**, 4622; (b) J. Aggett and A. L. Odell, *ibid., A*, **1968**, 1415.

10) L. Hin-Fat and W. C. E. Higginson, *ibid., A*, **1967**, 298.

11) a) D. Barton and G. M. Harris, *Inorg. Chem.*, **1**, 251 (1962); b) K. V. Krishnamury, *ibid.*, **1**, 422 (1962); c) H. Kelm and G. M. Harris, *ibid.*, **6**, 1743 (1967).

12) a) L. Damrauer and R. M. Milburn, *J. Amer. Chem. Soc.*, **90**, 3884 (1968); b) L. Damrauer and R. M. Milburn, Proc. Int. Conf. Coord. Chem., 12th, 1969, 38 (1969).

13) Only one experiment in a 1 M sulfuric acid solution at 25°C has been made in the work of Kruszyna and Milburn.[5]

14) The details were reported previously (see Ref. 2).

the sum of oxalic acid and hydrogen peroxide should be equal to the amount of oxalic acid formed in the absence of oxygen. The reaction products were analyzed. The results are listed in Table 2. Table 2 indicates that one mol/l of trioxalatocobaltate(III) produces 2.5 mol/l of oxalic acid in the absence of oxygen, or 2.5 mol/l of a total of oxalic acid and hydrogen peroxide in the presence of oxygen.

That is, in the case of the absence of oxygen the overall reaction is:

$$Co(C_2O_4)_3^{3-} \xrightarrow{k_0} Co(C_2O_4)_n^{(2-2n)} + (2.5-n)C_2O_4^{2-} \quad (7)$$

where n is 0, 1, and/or 2.

The Influence of Other Substances on the Decomposition Rate. Various substances were added to the reaction mixture of 4×10^{-3} M $K_3Co(C_2O_4)_3$ and 0.1 M H_2SO_4.

TABLE 3. INFLUENCE OF OTHER SUBSTANCES ON THE DECOMPOSITION RATE. SOLUTIONS OF 4.0×10^{-3} M $Co(C_2O_4)_3$, 0.1 M H_2SO_4, AND THE GIVEN SUBSTANCES. N_2-SATURATED UNLESS OTHERWISE STATED; IN THE DARK UNLESS OTHERWISE STATED; AT 40°C

Substances added[a)]	Rate constant, $k_0\times10^4$, sec^{-1}
None	1.1
None	1.0 (in O_2 sat.)
None	1.3 (in light[b)])
0.5% Acrylonitrile	1.0
1.0% Acrylonitrile	1.0
0.004 M $K_2S_2O_8$	1.0
0.002 M Fe(III)	1.1
0.01 M Fe(III)	2.2
0.002 M Cu(II)	1.1
0.015 M Cu(II)	1.7
0.01 M Co(II)	1.1
0.01 M $H_2C_2O_4$	1.0

a) The sulfate salts of Fe(III), Cu(II), and Co(II) were used.
b) A 100-watt tungsten lamp was placed at a distance of 15 cm from the reaction mixture.

(*a*) The decomposition rate in the solution in the presence of oxygen was almost equal to that in the absence of oxygen. In the presence of oxygen, hydrogen peroxide was formed in the course of the decomposition of trioxalatocobaltate(III).

(*b*) Though photochemistry is outside the scope of the present investigation, the decomposition rate in light exposed by a tungsten lamp was compared to that in the dark. As can be seen in Table 3, light accelerates the decomposition of trioxalatocobaltate(III). This appears reasonable, since trioxalatocobaltate(III) has been known to be photochemically active and to be used as a chemical actinometer.[1a)]

(*c*) Acrylonitrile did not affect the decomposition rate of trioxalatocobaltate(III), although its polymerized products were found in the reacting solution.

(*d*) The decomposition rate of trioxalatocobaltate(III) was not affected by the presence of peroxodisulfate. However, the decomposition of peroxodisulfate was induced by the decomposition of trioxalatocobaltate(III). This fact indicates that the CO_2^- radical formed by the decomposition of trioxalatocobaltate(III) reacts with peroxodisulfate as follows:

$$Co(C_2O_4)_3^{3-} \rightarrow Co(C_2O_4)_n^{(2-2n)} + (2-n)C_2O_4^{2-} + CO_2 + CO_2^- \quad (8)$$

$$Co(C_2O_4)_3^{3-} + H^+ \rightarrow Co(C_2O_4)_n^{(2-2n)} + (2-n)C_2O_4^{2-} + CO_2 + CO_2^- + H^+ \quad (8')$$

$$S_2O_8^{2-} + CO_2^- \rightarrow SO_4^- + SO_4^{2-} + CO_2 \quad (9)$$

(*e*) Both iron(III) and copper(II) ions accelerated the decomposition rate of trioxalatocobaltate(III). This can be accounted for by following reactions (8) and (8').

$$Fe(III) \text{ or } Cu(II) + CO_2^- \rightarrow CO_2 + Fe(II) \text{ or } Cu(I) \quad (10)$$

$$Co(C_2O_4)_3^{3-} + Fe(II) \text{ or } Cu(I) \xrightarrow{fast} Fe(III) \text{ or } Cu(II) + Co(C_2O_4)_n^{(2-2n)} + (3-n)C_2O_4^{2-} \quad (11)$$

Reactions (10) and (11) constitute a chain reaction.

Mechanisms. The radicals of CO_2^- and HO_2 are apt to be considered to be oxidized by trioxalatocobaltate(III), since both radicals are generally reductants; *e. g.*, in the present study, iron(III), copper (II), and peroxodisulfate were reduced by the radicals. However, none of our results supported the reaction between trioxalatocobaltate(III) and CO_2^- or HO_2 radical; rather, they supported the combination reaction of CO_2^- or HO_2 with each other to make the $C_2O_4^{2-}$ ion, or H_2O_2, respectively. Consequently, the following reaction mechanisms of the thermochemical decomposition of trioxalatocobaltate(III) are presented to account for these results:

$$Co(C_2O_4)_3^{3-} \xrightarrow{k_1} Co(C_2O_4)_n^{(2-2n)} + (2-n)C_2O_4^{2-} + CO_2^- + CO_2 \quad (8)$$

$$Co(C_2O_4)_3^{3-} + H^+ \xrightarrow{k_2} Co(C_2O_4)_n^{(2-2n)} + (2-n)C_2O_4^{2-} + CO_2 + CO_2^- + H^+ \quad (8')$$

$$2CO_2^- \xrightarrow{fast} C_2O_4^{2-} \text{ (in the absence of oxygen)} \quad (12)$$

$$CO_2^- + O_2 \xrightarrow{fast} O_2CO_2^- \text{ (in the presence of oxygen)} \quad (13)$$

$$O_2CO_2^- + H^+ \rightarrow HO_2 + CO_2 \quad (14)$$

$$2HO_2 \xrightarrow{fast} H_2O_2 + O_2 \quad (15)$$

The overall reaction corresponds to Reaction (7) and is consistent with the results of stoichiometry listed in Table 2.

The authors wish to thank the Ministry of Education for its financial support of this research.

Preparation and Characterization of Cobalt(III) Complexes with *N*-Carboxylate Derivatives of L-Prolinate

Ken-ichi OKAMOTO, Jinsai HIDAKA, and Yoichi SHIMURA

Department of Chemistry, Faculty of Science, Osaka University, Toyonaka, Osaka

(Received July 3, 1972)

Four cobalt(III) complex anions, bis(L-prolinate-*N*-monopropionato)-, (L-prolinate-*N*-monoacetato)(iminodiacetato)-, (L-prolinate-*N*-monopropionato)(iminodiacetato)- and (L-prolinate-*N*-monoacetato)(L-prolinate-*N*-monopropionato)cobaltate(III) were synthesized. They were isolated as sodium or potassium salts by ion-exchange column chromatography. These complexes were characterized on the basis of their absorption and circular dichroism spectra in the visible and near ultraviolet regions. All the complexes obtained in solid state have *trans(N)*-RR or *trans(N)*-R configuration. Two geometrical isomers were obtained for (L-prolinate-*N*-monopropionato)triamminecobalt(III) complexes.

L-prolinate is a unique aminocarboxylate bidentate ligand, since the secondary amine nitrogen of pyrrolidine ring coordinates stereospecifically to a metal ion with only S configuration. This has been recognized from circular dichroism (CD) studies[1] or X-ray crystal structure analyses[2,3] of several L-prolinato metal complexes. In the course of our study on stereochemistry of six isomers of bis(L-alaninate-*N*-monoacetato)cobaltate(III),[4] we found that an *N*-carboxylate derivative of L-prolinate, L-prolinate-*N*-monoacetate gave only two isomers of the bis(O,N,O-tridentato)cobalt(III) complex. This was explained from the viewpoint that the chiral nitrogen center of the coordinated L-prolinate-*N*-monoacetate takes only R configuration, and the ligand only a *facial* coordination. In the present paper, the stereochemistry of some cobalt(III) complexes of another L-prolinate derivative, L-prolinate-*N*-monopropionate is reported.

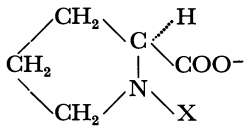

X=H : L-prolinate
X=CH_2COO^- : L-prolinate-*N*-monoacetate (abbreviated to L-proma^{2-})
X=$CH_2CH_2COO^-$: L-prolinate-*N*-monopropionate (abbreviated to L-promp^{2-})

The difference between L-proma^{2-} and L-promp^{2-} is that the former forms two five-membered chelate rings by coordination, whereas the latter forms a five- and a six-membered chelate ring by an α-aminocarboxylate part and an *N*-propionate foot, respectively.

Experimental

Preparation of Ligands. *(1)* *L-Proline-N-monoacetic Acid*: The preparation was reported previously.[4]

(2) *L-Proline-N-monopropionic Acid*: A solution of 25 g of L-proline in 54 ml of 4 N sodium hydroxide was mixed with a solution of 23.5 g of 3-chloropropionic acid in 54 ml of 2 N sodium hydroxide, and 80 ml of 4 N sodium hydroxide was added drop by drop to the mixture with vigorous stirring at 80—85°C on an oil bath. The pH of mixture was maintained in a 8—9 range during the reaction. After the sodium hydroxide solution had been added, the reaction mixture was heated at 85°C for about 20 min. This was cooled to 40°C and 36 ml of concentrated hydrochloric acid was added. The solution was concentrated in a vacuum evaporator at 40°C until white crystals appeared. The product was filtered off and the filtrate was concentrated again. After the operation was repeated six times (about 38 g of white crystals were obtained in total), a large amount of ethanol was added to the final filtrate. The white crystals separated were collected by filtration (26 g). The combined white crystals were contaminated with a small amount of sodium chloride. This was recrystallized from a warm (hydrochloric acid)-water (1 : 100) solution. The pure crystals were washed with ethanol and dried in a vacuum desiccator. $[\alpha]_D^{20}=-55.5°$ (c. 8.7, water). Found: C, 51.22; H, 6.98; N, 7.55%. Calcd for L-prompH$_2$=$C_8H_{13}NO_4$: C, 51.33; H, 7.00; N, 7.48%.

Preparation and Separation of Complexes. *(3)* trans(N)-*K*[*Co*(L-*proma*)$_2$]·3H_2O: The preparation of this complex was already reported.[4] One corresponding *cis(N)* isomer was obtained concurrently in solution, but it was not obtained in solid state because of poor stability.

(4) trans(N)-*Na*[*Co*(L-*promp*)$_2$]·3H_2O: A solution of 10 g (0.042 mol) of $CoCl_2\cdot 6H_2O$ in 10 ml of water was added to a solution of L-proline-*N*-monopropionic acid (0.084 mol) which was neutralized in advance by the addition of sodium hydroxide. To this was gradually added 10 g of lead dioxide and the resulting mixture was constantly stirred at about 50°C for an hr, whereupon the color of the solution turned from dark red to violet. After having been kept for 30 min at room temperature, the mixture was filtered to remove an excess of lead dioxide. A large amount of ethanol-acetone (1 : 1) mixture was added to the filtrate and a small amount of the resulting sodium chloride was filtered off. The filtrate was concentrated in a vacuum evaporator at about 30°C and poured into a column (25 mm×1500 mm) containing strong-base anion exchange resin (Dowex 1X8 200—400 mesh, chloride form). After the column had been swept with water, the adsorbed band was eluted with 0.075 N aqueous solution of sodium chloride at a rate of 2.5 ml per min. Only one violet band was eluted. The sodium chloride in the eluate was fractionally separated by adding an appropriate amount of ethanol to the concentrated solution. The desired complex was obtained by concentrating the filtrate almost to dryness. The product was washed with ethanol

1) T. Yasui, J. Hidaka and Y. Shimura, *J. Amer. Chem. Soc.*, **87**, 2762 (1965); T. Yasui, This Bulletin, **38**, 1746 (1965).
2) H. C. Freeman and I. E. Maxwell, *Inorg. Chem.*, **9**, 649 (1970); H. C. Freeman, L. G. Marzilli and I. E. Maxwell, *ibid.*, **9**, 2408 (1970).
3) T. Ito, F. Marumo and Y. Saito, *Acta Crystallogr.*, **B 27**, 1062 (1971).
4) K. Okamoto, J. Hidaka, and Y. Shimura, This Bulletin, **44**, 1601 (1971).

and then dried in a vacuum desiccator.

(5) trans(N)-*K*[*Co*(L-*proma*)(*ida*)]·2.5H_2O: A solution of 0.042 mol of iminodiacetic acid neutralized by sodium hydroxide was mixed with a neutralized solution of 0.042 mol of L-proline-*N*-monoacetic acid. To this was added gradually a solution of 10 g (0.042 mol) of $CoCl_2 \cdot 6H_2O$ in 10 ml of water and then 10 g of lead dioxide. After the mixture was constantly stirred at about 50°C for an hr, its pH was adjusted to 6.5 with 6 N hydrochloric acid. This was stirred again for an hr to complete the reaction. The solution turned violet. An excess of lead dioxide was filtered off. When a large amount of ethanol was added to the filtrate, a bluish violet deposit was obtained, which was filtered. It was confirmed from column chromatography and absorption measurements that the bluish violet deposit consisted of *trans(N)*- and *cis(N)*-Na[Co(ida)$_2$]. The concentrated filtrate was poured into a column (35 mm × 500 mm) containing the same resin as used in (4). Five colored bands *viz.*, a brownish red one (i) in a small amount, two red ones (ii) and (iii) and two violet ones (iv) and (v) in small amounts, were eluted in this order with 0.07 N aqueous solution of potassium chloride. The first spin-allowed d-d absorption band of each eluate showed that the first three, (i), (ii) and (iii), are of *trans(N)* type and the latter two (iv) and (v) of *cis(N)*. Of the three *trans(N)* eluates, (i) was confirmed to be *trans(N)*-[Co(ida)$_2$]$^-$[5] and (iii) *trans(N)*-[Co(L-proma)$_2$]$^-$[4]. Eluate (ii) was then concentrated in a vacuum evaporator. The coexisting potassium chloride was fractionally precipitated by adding ethanol to the concentrated solution and filtered off. Finally, a saturated solution of silver acetate was added drop by drop to the concentrated filtrate and the resulting silver chloride was filtered off. The desired complex was obtained by adding a large amount of ethanol to the filtrate and recrystallized from a small amount of water by adding ethanol. The pure complex was washed with ethanol and dried in a vacuum desiccator. Eluates (iv) and (v) were so unstable that they were not obtained in solid state.

(6) trans(N)-*K*[*Co*(L-*promp*)(*ida*)]·2H_2O: This complex was prepared and separated by a similar procedure to that for *trans(N)*-K[Co(L-proma)(ida)]. Four colored bands, a violet one (i), a reddish violet one (ii), a brownish red one (iii) in a small amount, and another violet one (iv) were eluted in this order. The absorption measurements of the eluates indicated that (i) contained *trans(N)*-[Co(L-promp)$_2$]$^-$, (iii) *trans(N)*-[Co(ida)$_2$]$^-$ and (iv) *cis(N)*-[Co(ida)$_2$]$^-$. Eluate (ii) was concentrated to dryness in a vacuum evaporator. The complex was extracted with a large amount of absolute ethanol and solidified by adding ether to the extract. After the resulting suspension was centrifuged, the complex was filtered and dried in a vacuum desiccator. The isolated potassium salt was hygroscopic.

(7) trans(N)-*K*[*Co*(L-*proma*)(L-*promp*)]·3H_2O: A solution of 10 g (0.042 mol) of $CoCl_2 \cdot 6H_2O$ in 10 ml of water was added to a neutralized equimolar mixture (0.042 mol) of L-proline-*N*-monoacetic acid and L-proline-*N*-monopropionic acid. To this was added 10 g of lead dioxide and the resulting mixture was mechanically stirred at about 40°C for an hr. The color of the solution turned from dark red to reddish purple. An excess of lead dioxide was filtered off and the filtrate was treated with a column as described in (4) and (5). Three colored bands, a violet one (i), a purple one (ii), and a red one (iii), were eluted in this order. It was confirmed from the absorption measurements that (i) contained *trans(N)*[Co(L-promp)$_2$]$^-$ and (iii) *trans(N)*-[Co(L-proma)$_2$]$^-$. Eluate (ii) was concentrated to dryness in a vacuum evaporator. Solidification was carried out by a similar procedure to that for *trans(N)*-K[Co(L-promp)(ida)]. The complex was obtained as hygroscopic potassium salt.

(8) trans(O)-[*Co*(L-*promp*)(NH_3)$_3$]ClO_4 *and* cis(O)-[*Co*(L-*promp*)(NH_3)$_3$]$ClO_4 \cdot 1/2H_2O \cdot 1/4C_2H_5OH$: A solution of 9 g (0.17 mol) of ammonium chloride and 10 ml of 28% aqueous ammonia (0.15 mol) in 15 ml of water was mixed with a neutral solution of 0.042 mol of L-proline-*N*-monopropionic acid. To this were added a solution of 10 g (0.042 mol) of $CoCl_2 \cdot 6H_2O$ in 10 ml of water and 10 g of lead dioxide. The reaction mixture was constantly stirred at about 40°C for an hr. The color of the solution turned from dark red to reddish yellow and finally to red. After having been allowed to stand at room temperature for 30 min, the mixture was filtered to remove an excess of lead dioxide, and the filtrate was kept in a refrigerator. A small amount of yellow depoint, $[Co(NH_3)_6]Cl_3$, was filtered off. The filtrate was poured into a column (35 mm × 500 mm) containing strong-acid cation exchange resin (Dowex 50WX8 200—400 mesh, sodium form). After the column had been swept with water, the adsorbed band was eluted with 0.1 N aqueous solution of sodium perchlorate at a rate of 2.5 ml per min. Two red bands, (i) in a small amount and (ii) in a large amount were eluted in this order. When eluate (i) was concentrated in a vacuum evaporator, red crystals appeared. Eluate (ii) was also concentrated in a vacuum evaporator; the desired complex was obtained in this case by adding a large amount of ethanol to the concentrated solution. This was recrystallized from a small amount of water by adding ethanol. Both the complexes were washed with ethanol and dried in a vacuum desiccator. On the basis of absorption measurements, isomers (i) and (ii) were confirmed to be *trans(O)* and *cis(O)* ones, respectively; the absorption maxima of isomer (i) are at 18.5 and 27.0×10^3 cm^{-1} with a shoulder at about 21.0×10^3 cm^{-1}, and of isomer (ii) 19.3 and 27.3×10^3 cm^{-1}.

The analytical results for the six new cobalt(III) complexes are given in Table 1.

Measurements. The electronic absorption spectra were measured by a Beckman DU spectrophotometer and Shimadzu spectrophotometer UV-200. The CD spectra were recorded with a Roussel-Jouan dichrograph. All the measurements were carried out in aqueous solutions at room temperature.

Results and Discussion

The *trans(N)* and *cis(N)* isomers of a [$Co^{III}(O)_4(N)_2$] type complex can be identified by the splitting pattern of their first spin-allowed d-d absorption bands.[6,7] All the [$Co^{III}(O)_4(N)_2$] type complexes show well-separated splitting components in their first absorption bands (Figs. 1 and 2, and Table 2); these are therefore assigned to the *trans(N)* structure. The corresponding *cis(N)* isomers are expected to be unstable because of a rather short contact (from molecular model considerations) of the pyrrolidine ring to another ligand coordinated.[4] No *cis(N)* isomers were detected in column chromatographic

5) J. Hidaka, Y. Shimura and R. Tsuchida, This Bulletin, **35**, 567 (1962); D. W. Cooke, *Inorg. Chem.*, **5**, 1141 (1966); B. B. Smith and D. T. Sawyer, *ibid.*, **7**, 922 (1968).

6) N. Matsuoka, J. Hidaka, and Y. Shimura, This Bulletin, **40**, 1868 (1967).

7) H. Yamatera, *ibid.*, **31**, 95 (1958); C. E. Schäffer and C. K. Jørgensen, *Mat. Fys. Medd. Dan. Vid. Selsk.*, **34**, No. 13 (1965).

TABLE 1. ANALYTICAL RESULTS (AMOUNTS IN %)

Complex salt	C		H		N	
	Found	Calcd	Found	Calcd	Found	Calcd
trans(*N*)-Na[Co(L-promp)$_2$]·3H$_2$O	37.67	37.95	5.53	5.57	5.56	5.53
trans(*N*)-K[Co(L-proma)(L-promp)]·3H$_2$O	35.10	35.44	5.03	5.15	5.57	5.51
trans(*N*)-K[Co(L-proma)(ida)]·2.5H$_2$O	29.57	29.67	4.32	4.30	6.34	6.29
trans(*N*)-K[Co(L-prmp)(ida)]·2H$_2$O	32.33	32.01	4.55	4.48	6.06	6.22
trans(*O*)-[Co(L-promp)(NH$_3$)$_3$]ClO$_4$	24.19	24.35	5.25	5.11	14.24	14.20
cis(*O*)-[Co(L-promp)(NH$_3$)$_3$]ClO$_4$·1/2H$_2$O·1/4C$_2$H$_5$OH	24.46	24.59	5.43	5.46	13.40	13.49

TABLE 2. ABSORPTION MAXIMA OF *trans*(*N*)-[Co(*O*,*N*,*O*-TRIDENTATO)$_2$]TYPE COMPLEXES

Complex ion	I Band		II Band		Ref.
	ν_{max}[a]	(log ε_{max})	ν_{max}[a]	(log ε_{max})	
[Co(L-proma)$_2$]$^-$	*ca.* 16.7 sh	(1.1)	27.1	(1.86)	(4)
	19.8	(1.79)			
[Co(L-promp)$_2$]$^-$	*ca.* 15.7 sh	(1.5)	25.1	(2.29)	
	18.2	(2.13)			
[Co(L-proma)(L-promp)]$^-$	*ca.* 16.0 sh	(1.2)	26.1	(2.08)	
	18.8	(1.95)			
[Co(L-proma)(ida)]$^-$	*ca.* 16.7 sh	(1.2$_5$)	27.6	(1.98)	
	19.8	(1.93)			
[Co(L-promp)(ida)]$^-$	*ca.* 16.0 sh	(1.2$_5$)	26.2	(2.06)	
	19.2	(1.94)			
[Co(ida)$_2$]$^-$	16.7	(1.06)	27.8	(1.75)	(5)
	20.4	(1.72)			

a) The wave numbers are given in 10^3 cm^{-1}.

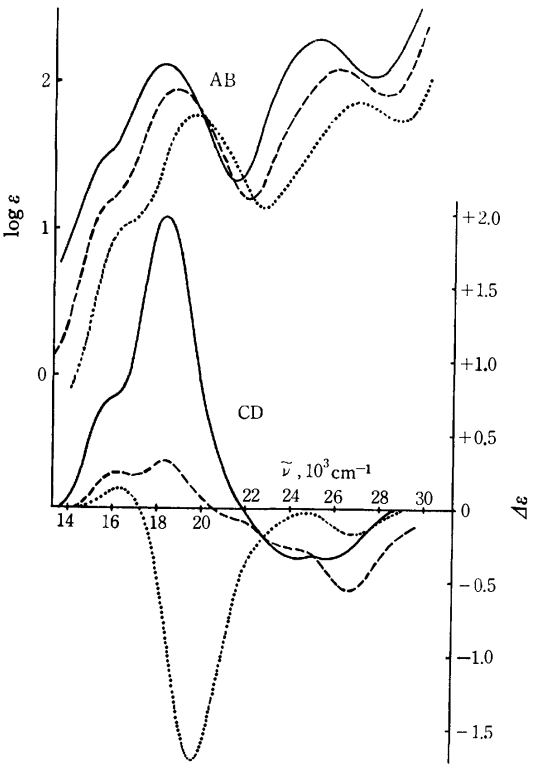

Fig. 1. Absorption and CD curves of *trans*(*N*)-RR-[Co(L-promp)$_2$]$^-$ (——), *trans*(*N*)-RR-[Co(L-proma)(L-promp)]$^-$ (— — —) and *trans*(*N*)-RR-[Co(L-proma)$_2$]$^-$ (----).

experiments of [Co(L-proma)(L-promp)]$^-$ and [Co(L-promp)$_2$]$^-$. Some indication of *cis*(*N*) isomers was obtained in the column chromatography of the ida-mixed complexes, but they were too unstable to isolate, except for the case of *cis*(*N*)-[Co(ida)$_2$]$^-$.

As is seen in Fig. 3, two isomers are possible for the *trans*(*N*) complex with two O,N,O-tridentate ligands. It is recognized[4,5,8] that the tridentate ligand such as ida^{2-} or L-proma^{2-} is hardly coordinated meridionally in Co(III) complexes, except for the case of *trans*(*O*)-[Co(ida)(dien)]$^{+}$[8]. L-promp^{2-} here employed forms a five- and a six-membered chelate ring by coordination. A molecular model examination reveals that the *N*-propionate moiety of L-promp^{2-} spans in a less strained circumstance than the *N*-acetate one of L-proma^{2-}. Thus it seems that a *meridional* coordination (Fig. 3a) is less improbable for L-promp^{2-} than for L-proma^{2-}. The preparation of [Co(L-promp)(NH$_3$)$_3$]$^+$ revealed the formation of the meridionally coordinated isomer, though the yield was very low. It was confirmed from the ion-exchange column chromatography and absorption measurements in the visible region that a major portion of the obtained triammine complex consists of the *cis*(*O*) isomer with *facial* coordination of L-promp^{2-} and that the *trans*(*O*) one with *meridional* coordination is formed in only a trace amount. Thus, it is assumed that the stable *trans*(*N*) complexes obtained in good yield take the

8) J. I. Legg and D. W. Cooke, *Inorg. Chem.*, **5**, 594 (1966).

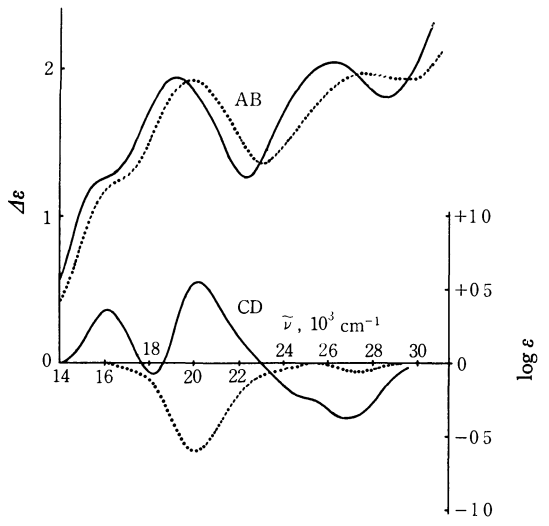

Fig. 2. Absorption and CD curves of *trans(N)*-R-[Co(L-promp)(ida)]$^-$ (——) and *trans(N)*-R-[Co(L-proma)(ida)]$^-$ (----).

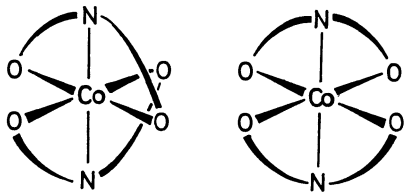

Fig. 3. Two possible isomers for a *trans(N)*-[Co(O,N,O-tridentato)$_2$] type complex: (a) *meridional-trans(N)*, and (b) *facial-trans(N)*.

facial coodinations (Fig. 3b) of L-promp^{2-}, L-proma^{2-} and ida^{2-} ligands.

The nitrogen atom of L-proma^{2-} or L-promp^{2-} is a chiral center in the present complexes. It can be considered that three isomers, RR, RS, and SS, with respect to the two coordinated nitrogen atoms, are possible for each bis(O,N,O-tridentato) complex. But it is well-established[1-4] that L-prolinate and its *N*-carboxylate derivatives cannot take configurations R and S, respectively, of the coordinated nitrogen atom. Consequently, only the RR type is possible for each of the *facial trans(N)* complexes. In fact, only one *trans(N)* isomer was obtained for each of the [Co(L-proma)$_2$]$^-$, [Co(L-proma)(L-promp)]$^-$ and [Co(L-promp)$_2$]$^-$ complexes. A quite similar consideration can be applied the mixed complexes with an ida^{2-} ligand, [Co(L-proma)(ida)]$^-$ and [Co(L-promp)(ida)]$^-$; thus each of them is assigned to *facial trans(N)*-R configuration.

Absorption and CD spectra. The five *facial trans(N)* complexes show reasonable correlation among their absorption spectra. The first and second spin-allowed d-d absorption bands of the bis type complexes are shifted to lower energy and intensified, in the order ida^{2-}→L-proma^{2-}→L-promp^{2-} (Figs. 1 and 2, and Table 2). A mixed complex, R-[Co(L-promp)(ida)]$^-$, shows its first band in a middle position between the first bands of parent complexes, RR-[Co(L-promp)$_2$]$^-$ and [Co(ida)$_2$]$^-$. Similar relationships are also substantiated for the other mixed complexes, R-[Co(L-proma)(ida)]$^-$ and RR-[Co(L-proma)(L-promp)]$^-$.

In contrast to these absorption behaviors, their CD spectra in the corresponding region differ significantly from each other (Figs. 1 and 2, and Table 3). In the first absorption band region, the lower energy CD bands commonly have a positive sign, though it seems that R-[Co(L-proma)(ida)]$^-$ lacks this CD band. Another common feature in the CD spectra of five *facial trans(N)*-R or -RR complexes is observed in the second absorption band region; namely all of them have negative CD. In contrast, the CD pattern in the region 17—22$\times 10^3$ cm^{-1} changes remarkably with substitution of ligands. That is, RR-[Co(L-proma)$_2$]$^-$ shows an intense negative CD band and RR-[Co(L-(promp)$_2$]$^-$ an intense positive one (Fig. 1 and Table 3). In the corresponding region, the mixed complex, RR-[Co(L-proma)(L-promp)]$^-$, shows two CD components, a positive one at 18.4$\times 10^3$ cm^{-1} and a negative one at about 27.1$\times 10^3$ cm^{-1}. R-[Co(L-proma)(ida)]$^-$ shows a negative major CD band which corresponds well to the major one of bis(L-proma) com-

Table 3. CD Data of *trans(N)*-[Co(*O,N,O*-tridentato)$_2$] type complexes

Complex ion	I Band region		II Band region		Ref.
	ν_{ext}[a]	($\Delta\varepsilon_{ext}$)	ν_{ext}[a]	($\Delta\varepsilon_{ext}$)	
RR-[Co(L-proma)$_2$]$^-$	16.2	(+0.14)	26.7	(−0.20)	4
	19.5	(−1.72)			
RR-[Co(L-promp)$_2$]$^-$	*ca.* 16.0 sh	(+0.75)	*ca.* 24.6 sh	(−0.34)	
	18.3	(+2.01)	*ca.* 25.7	(−0.34)	
RR-[Co(L-proma)(L-promp)]$^-$	16.2	(+0.23)	*ca.* 24.0 sh	(−0.28)	
	18.4	(+0.33)	26.7	(−0.56)	
	ca. 21.3 sh	(−0.06)			
R-[Co(L-proma)(ida)]$^-$	19.9	(−0.59)	27.5	(−0.05)	
R-[Co(L-promp)(ida)]$^-$	16.1	(+0.41)	*ca.* 25.0 sh	(−0.22)	
	18.2	(−0.08)	26.8	(−0.37)	
	20.2	(+0.57)			

a) The wave numbers are given in 10^3 cm^{-1}.

plex, while R-[Co(L-promp)(ida)]$^-$ shows two CD bands in the region 17—22 $\times 10^3$ cm^{-1} (Fig. 2 and Table 3). It seems that the sign reversal of the major CD band between RR-[Co(L-promp)$_2$]$^-$ and RR-[Co(L-proma)$_2$]$^-$ arises from the difference in the *N*-carboxylate moieties, since both the L-promp^{2-} and L-proma^{2-} ligands take the *facial* R(*N*) form by coordination and the resulting complexes take quite a similar configuration to each other. A similar sign reversal was reported[9] for the major CD bands in the visible region between copper(II) complexes of L-prolinate and its *N*-methyl derivative. Thus one should be surprised at the poor additivity of CD curves in the present complexes, rather than at the sign reversal between L-proma^{2-} and L-promp^{2-} complexes. The sum of CD curves of *trans(N)*-R-[Co(L-proma)-(ida)]$^-$ and -[Co(L-promp)(ida)]$^-$ poorly reproduces the observed curve of *trans(N)*-RR-[Co(L-proma)-(L-promp)]$^-$. A similar treatment for the CD curves of *trans(N)*-RR-[Co(L-proma)$_2$]$^-$ and -[Co(L-promp)$_2$]$^-$ also cannot reproduce the curve for the mixed complex *trans(N)*-RR-[Co(L-proma)(L-promp)]$^-$. These facts present a strange contrast to almost perfect additivity observed for several cobalt(III) complexes with some simple α-aminocarboxylates or their derivatives; for instance Koine *et al.*[10] showed that the CD curve of *trans(N)*-(L-alaninate-*N*,*N*-diacetato)(L-prolinato)-cobaltate(III) was clearly reproduced by summing up those of *trans(N)*-(L-alaninate-*N*,*N*-diacetato)(glycinato)cobaltate(III) and *trans(N)*-(ammoniatriacetato)(L-prolinato)cobaltate(III). Poor additivity of the present complexes would be related to less rigid conformations of the L-prolinate derivative tridentate ligands in a complicated sector spaces, which were produced by a rather low symmetry of the complexes, and which should have different space distributions of sector signs from one complex to another.

9) K. M. Wellman, S. Bogdansky, C. Piontek, C. R. Hare and M. Mathieson, *Inorg. Chem.*, **8**, 1025 (1969).

10) N. Koine, N. Sakota, J. Hidaka, and Y. Shimura, This Bulletin, **43**, 1737 (1970).

BULLETIN OF THE CHEMICAL SOCIETY OF JAPAN, VOL. 46, 479—483 (1973)

Kinetics and Mechanism of Formation of Monothiocyanato and Mononitrilotriacetato Complexes of Iron(III)

Shigenobu FUNAHASHI, Shoji ADACHI,* and Motoharu TANAKA**

Laboratory of Analytical Chemistry, Faculty of Science, Nagoya University, Chikusa-ku, Nagoya 464

(Received July 6, 1972)

Kinetics of the formation of monothiocyanato and mononitrilotriacetato complexes of iron(III) in aqueous solution have been studied by using a stopped-flow technique:

$$Fe^{3+} + SCN^- \underset{k_{-1}}{\overset{k_1}{\rightleftharpoons}} FeNCS^{2+}$$

$$FeOH^{2+} + SCN^- \underset{k_{-2}}{\overset{k_2}{\rightleftharpoons}} FeNCS^{2+} + OH^-$$

$$FeOH^{2+} + H_2nta^- \xrightarrow{k} Fe(nta) + H^+$$

Rate constants at 25°C and $\mu=0.5$ ($NaClO_4$) are as follows: $k_1=90\ M^{-1}\ sec^{-1}$, $k_{-1}=1.6\ sec^{-1}$, $k_2=5.1\times10^3\ M^{-1}\ sec^{-1}$, $k_{-2}=10\times10^{13}\ M^{-1}\ sec^{-1}$, $k=1.0\times10^5\ M^{-1}\ sec^{-1}$. Some discussions are made on the effect of hydroxide ion on the complex formation reactions.

The complex formation reactions of iron(III) have been extensively studied for various ligands: F^-[1], Cl^-[2-4], Br^-[4,5], azide[6-8], SCN^-[3,9], aliphatic acids[10-12], SO_4^{2-}[3,13,14], substituted phenols[15], acetylacetone[16], oxalic acid[17], substituted malonic acids[18], salicylic acid[19], sulfosalicylic acid[19], 8-hydroxyquinoline[19], salicylaldehyde[19].

According to the earlier kinetic studies, the reaction

* Present address: Hoya Glass-Work Ltd., Akishima, Tokyo.

** Responsible coauthor.

1) D. Pouli and W. MacF. Smith, *Can. J. Chem.*, **38**, 567 (1960).
2) R. E. Connick and C. P. Coppel, *J. Amer. Chem. Soc.*, **81**, 6389 (1959).
3) H. Wendt and H. Strehlow, *Z. Elektrochem.*, **66**, 228 (1962).
4) T. Yasunaga and S. Harada, This Bulletin, **42**, 2165 (1969).
5) P. Matthies and H. Wendt, *Z. Physik. Chem.* (Frankfurt), **30**, 137 (1961).
6) D. Seewald and N. Sutin, *Inorg. Chem.*, **2**, 643 (1963).
7) F. Accascina, F. P. Cavasino, and S. D'Alessandro, *J. Phys. Chem.*, **71**, 2474 (1967).
8) D. W. Carlyle and J. H. Espenson, *Inorg. Chem.*, **6**, 1370 (1967).
9) J. F. Below, Jr., R. E. Connick, and C. P. Coppel, *J. Amer. Chem. Soc.*, **80**, 2961 (1958).
10) F. P. Cavasino and E. Di Dio, "Progress in Coordination Chemistry", ed. M. Cais, Elsevier Publishing Company, New York, 1968, p. 174.
11) F. Accascina, F. P. Cavasino, and E. Di Dio, *Trans. Faraday Soc.*, **65**, 489 (1969).
12) R. N. Pandey and W. MacF. Smith, *Can. J. Chem.*, **50**, 194 (1972).
13) G. G. Davis and W. MacF. Smith, *ibid.*, **40**, 1836 (1962).
14) F. P. Cavasino, *J. Phys. Chem.*, **72**, 1378 (1968).
15) F. P. Cavasino and E. Di Dio, *J. Chem. Soc.*, **1970**, 1151.
16) W. K. Ong and R. H. Prince, *ibid.*, **1966**, 458.
17) E. G. Moorhead and N. Sutin, *Inorg. Chem.*, **5**, 1866 (1966).
18) F. P. Cavasino and E. Di Dio, *J. Chem. Soc., A*, **1971**, 3176.
19) P. G. T. Fogg and R. J. Hall, *ibid.*, **1971**, 1365.

rate constants for all the $Fe^{3+}+L$ reactions lie in the range $1—10^2\ M^{-1}\,sec^{-1}$, and those for the $FeOH^{2+}+L$ reactions in the range $10^2—10^5 M^{-1}sec^{-1}$ at 25°C. These results indicate that the substitution of a water molecule in the inner coordination sphere of the metal ion is the rate-determining process of the complex formation reaction.[20]

Since there is very little information on the kinetics of complex formation of iron(III) ion with multidentate ligands, we have studied the kinetics of iron(III) ion with nitrilotriacetate (tetradentate) to compare the results with the kinetic properties of monodentate ligands. Our primary intention was to determine whether the rate of the complex formation of iron(III) is controlled by the release of a water molecule in the inner coordination sphere or by the chelate ring closure (sterically controlled substitution) as found for some complexes,[21-23] and to elucidate the effect of hydroxide ion on the complex formation reactions.

Experimental

Reagents. *Iron(III) Perchlorate*: The reagent grade iron(III) chloride was dissolved in perchloric acid and chloride was expelled by evaporation. The absence of chloride ion was checked by silver nitrate. The iron(III) perchlorate was recrystallized twice from 60% perchloric acid solution. Its concentration was determined by a standard EDTA solution with Variamine Blue B as an indicator.[24]

Sodium Thiocyanate: The reagent grade sodium thiocyanate was recrystallized twice from distilled water. The thiocyanate solution was standardized by the method of Volhard.

Nitrilotriacetic Acid: The acid form of NTA obtained from Dojindo Co., Ltd., was recrystallized twice from distilled water. The purified NTA was dissolved in 1 equivalent of sodium hydroxide.

Methods of preparation of sodium perchlorate and sodium hydroxide have been described previously.[25]

Measurements. Supplementary spectra were taken on a JASCO Model ORD/UV-5 optical rotatory dispersion recorder and a Hitachi Perkin-Elmer 139 UV-VIS spectrophotometer.

Hydrogen ion concentration was determined by a Radiometer PHM-4d (Copenhagen) with a Type G202 B glass electrode and a Type K 401 calomel. A 1.00×10^{-2} M perchloric acid at an ionic strength of 0.5 M ($[HClO_4]+[NaClO_4]=0.5$ M) was used as a standard solution. The liquid junction potential was taken into consideration.

The acidities of solutions were adjusted by addition of a solution of sodium hydroxide prepared by electrolysis of a sodium perchlorate solution. Ionic strengths were adjusted by addition of sodium perchlorate.

The kinetics of formation of complexes of iron(III) was studied spectrophotometrically by means of a stopped-flow technique using a Rapid Scan Spectrophotometer Type RSP-2 (Hitachi, Ltd., Tokyo). The reactant syringes thermostated at 25±0.1°C were connected to the two-stage mixing chamber with eight jets, with which was aligned a quartz observation tube 10-mm long and 2-mm in diameter. The runs of reactions at a fixed wavelength (460 nm for $FeNCS^{2+}$ and 262.5 nm for Fe(nta)) in the absorption spectrum of the complex were memorized on an oscilloscope (Hitachi V-OL-Memoriscope). The screen of the oscilloscope was photographed. The traces of absorbance against reaction time were analyzed.

Results

Kinetics of Formation of the Monothiocyanato Complex of Iron(III).[26] The kinetic data are consistent with the assumption that the formation of $FeNCS^{2+}$ proceeds *via* two paths, one involving the reaction of Fe^{3+} with SCN^- and the other involving the reaction of $FeOH^{2+}$ with SCN^-, and that the equilibrium between Fe^{3+} and $FeOH^{2+}$ ($Fe^{3+}+H_2O\rightleftharpoons FeOH^{2+}+H^+$) is established throughout the course of the reaction. The rate of formation of $FeNCS^{2+}$ is then given by

$$\frac{d[FeNCS^{2+}]}{dt} = k_1[Fe^{3+}][SCN^-] + k_2[FeOH^{2+}][SCN^-] - k_{-1}[FeNCS^{2+}] - k_{-2}[FeNCS^{2+}][OH^-] \quad (1)$$

where the rate constants are defined by the following:

$$Fe^{3+} + SCN^- \underset{k_{-1}}{\overset{k_1}{\rightleftharpoons}} FeNCS^{2+} \quad (2)$$

$$FeOH^{2+} + SCN^- \underset{k_{-2}}{\overset{k_2}{\rightleftharpoons}} FeNCS^{2+} + OH^- \quad (3)$$

Since $C_{Fe} \gg C_{SCN}$, it follows that

$$[Fe^{3+}] = \frac{C_{Fe}}{1 + \frac{K^{-H}_{FeOH}}{[H^+]}}$$

where C_{Fe} is the total concentration of iron(III) and $K^{-H}_{FeOH}=[FeOH^{2+}][H^+]/[Fe^{3+}]=10^{-2.73}$.[14,27] Moreover, under the conditions used in this investigation $K^{-H}_{FeOH}/[H^+] \ll 1$.

Therefore

$$\frac{d[FeNCS^{2+}]}{dt} = \left(k_1 + \frac{k_2 K^{-H}_{FeOH}}{[H^+]}\right) C_{Fe}[SCN^-] - (k_{-1} + k_{-2}[OH^-])[FeNCS^{2+}] \quad (4)$$

Integrating Eq. (4) we get

$$\ln\left(1 - \frac{[FeNCS^{2+}]}{[FeNCS^{2+}]_{eq}}\right) = -\left(k_1 + k_{-1} + \frac{k_2 K^{-H}_{FeOH}}{[H^+]} + k_{-2}[OH^-]\right)t \quad (5)$$

where $[FeNCS^{2+}]_{eq}$ is the concentration of $FeNCS^{2+}$

20) D. J. Hewkin and R. H. Prince, *Coord. Chem. Rev.*, **5**, 45 (1970).
21) K. Kustin, R. F. Pasternack, and E. M. Weinstock, *J. Amer. Chem. Soc.*, **88**, 4610 (1966).
22) A. Kowalak, K. Kustin, R. F. Pasternack, and S. Petrucci, *ibid.*, **89**, 3126 (1967).
23) R. F. Pasternack and K. Kustin, *ibid.*, **90**, 2295 (1968).
24) N. Nakasuka and M. Tanaka, *Anal. Chim. Acta*, **36**, 422 (1966).
25) M. Tanaka, S. Funahashi, and K. Shirai, *Inorg. Chem.*, **7**, 573 (1968).
26) The iron(III) complex with thiocyanate appears to be $FeNCS^{2+}$ (monoisothiocyanatoiron(III)) as suggested by the following authors: S. Fronaeous and R. Larsson (*Acta Chem. Scand.*, **16**, 1447 (1962)), and A. Haim and N. Sutin (*J. Amer. Chem. Soc.*, **87**, 4210 (1965)).
27) L. G. Sillén and A. E. Martell, "Stability Constants of Metal Ion Complexes," Special Publication No. 17. The Chemical Society, London, 1964.

under equilibrium conditions. Then

$$\ln\left(1+\frac{A_t}{A_{eq}}\right) = -k_0 t \tag{6}$$

$$k_0 = k_1 C_{Fe} + k_{-1} + \frac{k_2 K_{FeOH}^{-H} C_{Fe}}{[H^+]} + \frac{k_{-2} K_w}{[H^+]} \tag{7}$$

where A_t and A_{eq} are the absorbances of the reaction system at t seconds after the start of the reaction and at equilibrium, respectively, k_0 a conditional rate constant obtained by experiments, and $K_w=[H^+][OH^-]$.

Some conditional rate constants under various experimental conditions are given in Table 1. These data indicate clearly a linear relationship between k_0 and the reciprocal concentration of hydrogen ion with a nonzero intercept (Fig. 1). Thus the conditional rate constant k_0 is expressed by

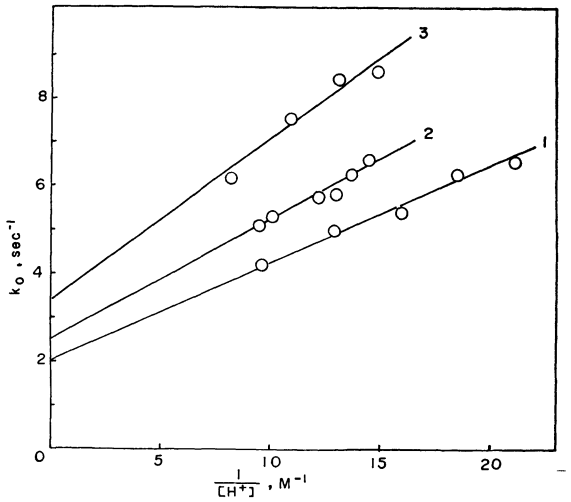

Fig. 1. k_0 as a function of the reciprocal concentration of hydrogen ion. $C_{SCN}=2.00\times10^{-4}$ M, 25°C, $\mu=0.5$ M ($NaClO_4$), 1: $C_{Fe}=3.98\times10^{-3}$ M; 2: $C_{Fe}=9.97\times10^{-3}$ M; 3: $C_{Fe}=2.00\times10^{-2}$ M.

$$k_0 = k_{0(1)} + k_{0(2)} \frac{1}{[H^+]} \tag{8}$$

Moreover, the values of intercepts ($k_{0(1)}$) are found proportional to the concentration of ferric ion (Fig. 2a). The values of slopes ($k_{0(2)}$) are also linearly related to the concentration of ferric ion (Fig. 2b). These results are consistent with the proposed reaction mechanism, *i.e.*,

$$k_{0(1)} = k_1 C_{Fe} + k_{-1} \tag{9}$$

$$k_{0(2)} = k_2 K_{FeOH}^{-H} C_{Fe} + k_{-2} K_w \tag{10}$$

The values of rate constants k_1, k_{-1}, $k_2K_{FeOH}^{-H}$, and $k_{-2}K_w$ were determined from the intercepts and the slopes of plots by the method of least squares: $k_1=90\pm5$ $M^{-1}sec^{-1}$, $k_{-1}=1.6\pm0.2$ sec^{-1}, $k_2K_{FeOH}^{-H}=9.5$ $M^{-2}sec^{-1}$, $k_{-2}K_w=0.19$ $M^{-1}sec^{-1}$. Using the values $K_{FeOH}^{-H}=1.87\times10^{-3}$ [14,27] and $\log K_w=-13.73$[28] at 25°C and $\mu=0.5$ M, we obtain $k_2=5.1\pm0.5\times10^3 M^{-1}sec^{-1}$ and $k_{-2}=1.0\pm0.1\times10^{13}$ $M^{-1}sec^{-1}$.

Kinetics of Formation of the Mononitrilotriacetato Complex of Iron(III). Under the present experimental conditions, the formation reaction of the mononitrilotriacetato complex of iron(III) is expressed as follows:

$$Fe' + nta' \xrightarrow{k_{0(H)}} Fe(nta) \tag{11}$$

where Fe′ and nta′ denote all the species of iron(III) not combined with NTA and those of NTA not combined with iron(III), respectively. The Fe(III)–NTA complex exists as Fe(nta).[29] The rate equation of the formation of the Fe(III)–NTA complex is given by[30]

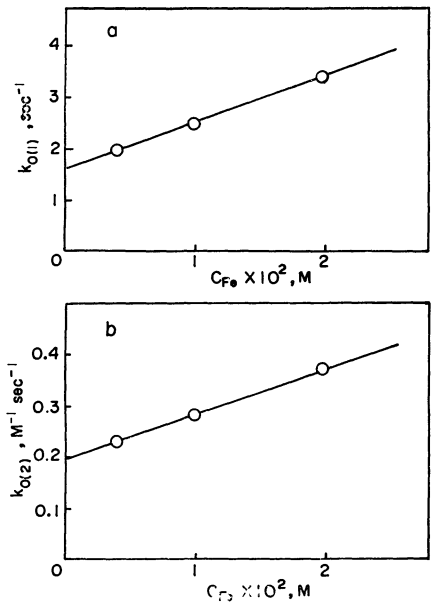

Fig. 2. Rate constants as a function of the total concentration of iron(III) ion.
a: Plot of $k_{0(1)}$ *vs.* C_{Fe}. b: Plot of $k_{0(2)}$ *vs.* C_{Fe}.

Table 1. Conditional rate constants k_0 of formation of the monothiocyanato complex of iron(III) at 25°C and $\mu=0.5$ ($NaClO_4$)

C_{Fe}, M	[H$^+$], M	k_0, sec^{-1}
3.98×10^{-3}	1.04×10^{-1}	4.20
	7.73×10^{-2}	5.00
	6.25×10^{-2}	5.40
	5.40×10^{-2}	6.25
	4.74×10^{-2}	6.55
9.97×10^{-3}	1.04×10^{-1}	5.10
	9.89×10^{-2}	5.30
	8.20×10^{-2}	5.75
	7.71×10^{-2}	5.80
	7.31×10^{-2}	6.25
	6.92×10^{-2}	6.60
2.00×10^{-2}	1.22×10^{-1}	6.15
	9.14×10^{-2}	7.55
	7.62×10^{-2}	8.45
	6.73×10^{-2}	8.60

$C_{SCN}=2.00\times10^{-4}$ M.

28) G. Lagerström, *Acta Chem. Scand.*, **13**, 722 (1959).

29) G. Schwarzenbach and J. Heller, *Helv. Chim. Acta*, **34**, 1889 (1951).

30) The protolytic reactions are sufficiently rapid for these steps to be assumed to be in equilibrium at all times.

$$\frac{d[Fe(nta)]}{dt} = k_{0(H)}[Fe'][nta'] \quad (12)$$

The linearity of the second-order plot for Eq. (12) is excellent. Thus we can estimate the conditional rate constant $k_{0(H)}$ from the slope of the second-order plot. Some conditional rate constants are given in Table 2.

The rate equation seems to be expressed as follows:

$$\frac{d[Fe(nta)]}{dt} = k_1[Fe^{3+}][H_2nta^-] + k_2[Fe^{3+}][H_3nta] + k_3[FeOH^{2+}][H_2nta^-] + k_4[FeOH^{2+}][H_3nta]$$
$$= \frac{\frac{k_1}{K_{H_3nta}[H^+]} + k_2 + \frac{k_3K^{-H}_{FeOH}}{K_{H_3nta}[H^+]^2} + \frac{k_4K^{-H}_{FeOH}}{[H^+]}}{\left(1+\frac{K^{-H}_{FeOH}}{[H^+]}\right)\left(1+\frac{1}{K_{H_3nta}[H^+]}\right)}[Fe'][nta'] \quad (13)$$

where

$$[Fe'] = [Fe^{3+}] + [FeOH^{2+}] = [Fe^{3+}]\left(1+\frac{K^{-H}_{FeOH}}{[H^+]}\right)$$

$$[nta'] = [H_3nta] + [H_2nta^-] = [H_3nta]\left(1+\frac{1}{K_{H_3nta}[H^+]}\right)$$

with $K_{H_3nta}=[H_3nta]/[H_2nta^-][H^+]=10^{1.9}$.[31] Therefore the conditional second-order rate constant $k_{0(H)}$ has the following relationship.

$$k_{0(H)}\left(1+\frac{K^{-H}_{FeOH}}{[H^+]}\right)\left(1+\frac{1}{K_{H_3nta}[H^+]}\right) = k_2 + \left(\frac{k_1}{K_{H_3nta}} + k_4K^{-H}_{FeOH}\right)\frac{1}{[H^+]} + \frac{k_3K^{-H}_{FeOH}}{K_{H_3nta}}\frac{1}{[H^+]^2} \quad (14)$$

Logarithm of the value of the left side of Eq. (14) is plotted against $-\log [H^+]$ in Fig. 3. The plot gives a straight line with a slope of two. This means that under the present experimental conditions the formation of the Fe(III)–NTA complex proceeds through the reaction of $FeOH^{2+}$ and H_2nta^-. We estimated the value of k_3 from the intercept of the straight line: $k_3=1.0\pm0.2\times10^5$ $M^{-1}sec^{-1}$ at 25°C and 0.5 M ionic strength.

Discussion

The kinetic behavior of the reactions in the present study is compared with the behavior predicted by the current general mechanism for metal-ligand complex formation as formulated by Eigen (Eigen mechanism),[32,33] which accounts for most kinetic data on the formation of complexes.

Values of k_1 and k_2 are given in Table 3 together with the corresponding values reported by other authors. The rate constants are in reasonable agreement with some previous kinetic results, the difference in conditions being taken into consideration.

31) G. Schwarzenbach and R. Gut, *Helv. Chim. Acta*, **34**, 1589 (1956).
32) M. Eigen and R. W. Wilkins in "Mechanisms of Inorganic Reactions," Advances in Chemistry Series, No. 49, Amercian Chemical Society, Washington, D. C., (1965).
33) M. Eigen and K. Tamm, *Z. Elektrochem.*, **64**, 115 (1960).

Table 2. Conditional rate constants $k_{0(H)}$ of formation of the mononitrilotriacetato complex of iron(III) at 25°C and $\mu=0.5$ ($NaClO_4$)

C_{Fe}, M	C_{NTA}, M	$-\log [H^+]$	$k_{0(H)}$, $M^{-1}sec^{-1}$
1.09×10^{-2}	5.00×10^{-3}	0.907	116
		0.940	123
		0.957	136
		0.994	148
	4.00×10^{-3}	0.796	64.5
		0.848	77.0
		0.891	103
		0·941	138
		0.995	187
	2.00×10^{-3}	0.909	101
		0.930	111
		0.948	120
		0.971	131
		0.993	146
5.00×10^{-3}	1.25×10^{-3}	0.820	98.5
		0.919	138
		1.006	206
		1.040	316
		1.228	396
		1.317	591
		1.408	815
		1.523	1.13×10^3
		1.600	1.67×10^3
		1.704	2.30×10^3
		1.801	2.86×10^3

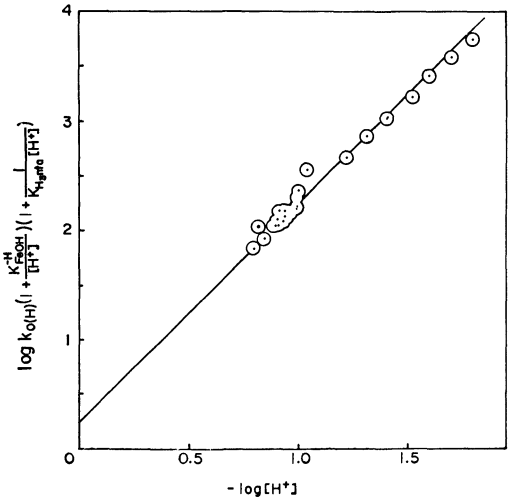

Fig. 3. Hydrogen ion dependence of the rate constants at 25°C and $\mu=0.5$ M ($NaClO_4$).
The straight line represents the theoretical straight line with a slope of two.

According to the Eigen mechanism, the complex formation reaction involves the fast formation of an outer-sphere complex followed by the substitution of a water molecule coordinated to the metal ion. Therefore the iron(III) complex formation can be depicted as follows:

$$Fe(H_2O)_6^{3+} + X^- \overset{K_{os}}{\rightleftharpoons} Fe(H_2O)_6^{3+}\cdots X^- \overset{k_w}{\longrightarrow} FeX(H_2O)_5^{2+} + H_2O \quad (15)$$

TABLE 3. VALUES OF RATE CONSTANTS AT 25°C FOR THE REACTIONS OF Fe^{3+} AND $Fe(OH)^{2+}$ WITH SCN^-

k_1, $M^{-1}sec^{-1}$	k_2, $M^{-1}sec^{-1}$	Reference
127±10	$1.0\pm0.1\times10^4$	Ref. 9[a]
150±50		Ref. 3
90± 5	$5.1\pm0.5\times10^3$	This work

a) $\mu=0.4$ M

$$FeOH(H_2O)_5^{2+} + X^- \overset{K_{OS(OH)}}{\rightleftharpoons} FeOH(H_2O)_5^{2+}\cdots X^- \overset{k_{w(OH)}}{\longrightarrow} FeX(H_2O)_5^{2+} + OH^- \quad (16)$$

where K_{OS} is the equilibrium constant for outer-sphere association and k_w is the first-order rate constant for the rate-determining water substitution. According to the above mechanism, the second-order rate constant obtained is equal to $K_{OS}k_w$. The rate for the reaction of $FeOH(H_2O)_5^{2+}$ is higher than that of $Fe(H_2O)_6^{3+}$. As pointed out in the formation of nickel(II) complexes,[34] it is understandable that the electron donation from hydroxide ion makes the dissociation of coordinated water molecules from $FeOH(H_2O)_5^{2+}$ faster than from the aquo ferric ion.

The combination of H^+ and OH^- is the fastest reaction possible in aqueous solution. The rate constant has been measured as 1.4×10^{11} $M^{-1}sec^{-1}$ at 25°C, a value corresponding to the theoretical limit for the rate of a chemical reaction (diffusion-controlled processes).[35] The value of the rate constant k_{-2} of the reaction of $FeNCS^{2+}$ with OH^- is 1.0×10^{13} $M^{-1}sec^{-1}$ which is greater by more than one order of magnitude than the rate constants for diffusion-controlled reactions.[36] This seems to suggest that the reaction proceeds through the mixed-ligand complex $Fe(OH)(NCS)^+$ involving OH^- and SCN^-, that is,

$$FeNCS(H_2O)_5^{2+} + H_2O \overset{K^{-H}_{Fe(OH)(NCS)}}{\longleftrightarrow} Fe(OH)(NCS)(H_2O)_4^+ + H_3O^+ \quad (17)$$

$$Fe(OH)(NCS)(H_2O)_4^+ \overset{k'_{-2}}{\longrightarrow} FeOH(H_2O)_5^{2+} + SCN^- \quad (18)$$

Thus we have the relationship

$$k_{-2} = K^{-H}_{Fe(OH)(NCS)}k'_{-2}/K_w \quad (19)$$

The hydrolysis constant of $FeNCS^{2+}$ was measured by Lister and Rivington: $[Fe(OH)(NCS)^+][H^+]/[FeNCS^{2+}]=6.5\pm1\times10^{-5}$ at 25°C and $\mu=1.2$.[37] Assuming that the value of $K^{-H}_{Fe(OH)(NCS)}$ is $10^{-4.2}$, we have estimated $k'_{-2}=10^{3.5}$, which is about 1000 times larger than the value of the rate constant k_{-1} for the dissociation of $FeNCS^{2+}$. The dissociation of SCN^- from $Fe(OH)(NCS)(H_2O)_4^+$ seems to be facilitated by the electron donation from OH^- to a greater extent than that from H_2O in $FeNCS(H_2O)_5^{2+}$. This is understood in the same way as in the complex formation where k_2 is greater than k_1.

From the results of the iron(III) complex formation (Eigen mechanism), it is expected that the rate constant for the reaction of $FeOH^{2+}$ with SCN^- is the same as for the reaction of $FeOH^{2+}$ with H_2nta^-, as the charge of reacting ligands is the same. In effect the value of the rate constant for H_2nta^- is 20 times greater than that for SCN^- which is approximately equal to the theoretical value expected from the Eigen mechanism. The enhanced rate for H_2nta^- can be accounted for in terms of the internal conjugate base mechanism proposed by Rorabacher.[38] To account for abnormality of the reaction of nickel ion with polyamines, he proposed a modification of the Eigen mechanism wherein a basic donor atom of a reacting multidentate ligand forms a hydrogen-bond to a coordinated water molecule, thereby stabilizing the outer-sphere complex and labilizing subsequent water loss.

Hydroxo group of $FeOH^{2+}$ is basic and H_2nta^- is acid. Thus the hydrogen-bond would be formed between $FeOH^{2+}$ and H_2nta^- thereby stabilizing more effectively the $FeOH^{2+}\cdots H_2nta^-$ outer-sphere complex than the $FeOH^{2+}\cdots SCN^-$ outer-sphere complex.

A similar enhancement of rate constants for the formation of iron(III) complexes has been observed in the formation of iron(III) complexes with some substituted malonic acids (HL). The rate constants for the reaction ($FeOH^{2+}+HL^-$) are 1.3×10^5, 1.2×10^5, 1.0×10^5, 1.0×10^5, 1.1×10^5 $M^{-1}sec^{-1}$ at 25°C and $\mu=0.5$ M for malonic, methylmalonic, *n*-butylmalonic, benzylmalonic, and cyclobutane-1,1-dicarboxylic acids, respectively.[18] It is understandable that larger values of rate constants in these reactions are due to the formation of hydrogen-bond between $FeOH^{2+}$ and HL^-.

34) S. Funahashi and M. Tanaka, *Inorg. Chem.*, **8**, 2159 (1969); **9**, 2092 (1970).
35) M. Eigen and L. De Maeyer, *Z. Elektrochem.*, **59**, 986 (1955).
36) M. Eigen, W. Kruse, G. Maass, L. DeMaeyer, *Progress in Reaction Kinetics*, **2**, 287 (1964).
37) M. W. Lister and D. E. Rivington, *Can. J. Chem.*, **33**, 1572 (1955).
38) D. B. Rorabacher, *Inorg. Chem.*, **5**, 1891 (1966).

Nickel(II), Cobalt(II), Palladium(II) and Beryllium(II) Chelates of 2,4,6-Heptanetrione[1]

Fumio SAGARA,* Hiroshi KOBAYASHI, and Keihei UENO

Department of Organic Synthesis, Faculty of Engineering, Kyushu University, Fukuoka 812

(Received July 6, 1972)

Divalent metal chelates of heptane-2,4,6-trione (H_2daa) were synthesized and their structures were discussed. Nickel(II), cobalt(II) and palladium(II) ions gave Ni(Hdaa)$_2\cdot 2H_2O$, Ni_2(daa)$_2\cdot 4H_2O$, Ni_2(daa)$_2\cdot$4Py, Co(Hdaa)$_2\cdot 2H_2O$, Co_2(daa)$_2\cdot 4H_2O$, Co_2(daa)$_2\cdot$4Py, Pd(Hdaa)$_2$ and Pd(Hdaa)$_2\cdot 2H_2O$ respectively, while beryllium(II) ion unexpectedly gave bis(2-amino-2-heptene-4,6-dionato)beryllium(II) which resulted from an amino-derivative of the original ligand. Spectroscopic results suggested that the coordination structure of nickel(II) and cobalt(II) ions was octahedral hexacoordinate, that of palladium(II) ion square planar tetracoordinate and that of beryllium(II) ion tetrahedral tetracoordinate. NMR study of the palladium(II) chelate suggested partial enolization of an uncoordinated carbonyl group. It was also found that nickel, cobalt and platinum ions promoted catalytically the bimolecular-condensation of heptane-2,4,6-trione.

In previous papers we have reported on the syntheses and keto-enol tautomerism of heptane-2,4,6-trione (H_2daa) and its methylated derivatives,[2] and also on the properties and structures of their copper(II) chelates.[3] The characteristic feature of this particular β,δ-triketone is that the planar ligand behaves as either monobasic bidentate ligand or dibasic terdentate ligand depending upon the conditions of reaction as well as the kind of metal ion involved. Thus it is of interest to see how heptane-2,4,6-trione reacts with divalent metal ions of various coordination structures. This paper reports on the syntheses, and on the structures of palladium(II), nickel(II), cobalt(II) and beryllium (II) chelates of heptane-2,4,6-trione.

Experimental

Apparatus and Procedure. All the melting points were not corrected. NMR spectra were recorded on a Varian A-60, using tetramethylsilane as an internal reference. Spectral measurements in infrared and visible regions, and thermogravimetric analyses were carried out as described previously.[3]

Synthesis of the Chelates. a) Palladium Chelates. Bis(heptane-2,4,6-trionato)palladium(II). [*Pd(Hdaa)$_2$*]: In 50 ml of methanol were dissolved 0.30 g (0.0017 mol) of palladium(II) chloride and 3.0 g (0.021 mol) of heptane-2,4,6-trione, and the mixture was kept standing overnight at room temperature. The resulting yellow powdery precipitates were collected by filtration, and the product was purified through a silica gel column (Wakogel *Q*-23) in the form of a chloroform solution. Yield 0.12 g (18% from palladium chloride).

Found: C, 42.81; H, 4.76%. Calcd for $C_{14}H_{18}O_6Pd$: C, 43.26; H, 4.67%.

Bis(heptane-2,4,6-trionato)palladium(II) Dihydrate. [*Pd(Hdaa)$_2\cdot 2H_2O$*]. To 300 ml of tetrahydrofuran was added 0.30 g (0.0017 mol) of palladium chloride and the mixture was stirred at room temperature for 3 days to give a clear solution. To this was added 3.0 g(0.021 mol) of heptane-2,4,6-trione, and the pH of the solution was adjusted to 4 (on pH indicator paper) with aqueous ammonia. After being refluxed for 4—5 hr, the solution was kept standing overnight at room temperature to give yellow powdery precipitates. The product was recrystallized from tetrahydrofuran. Yield 0.30 g (42% from palladium chloride).

Found: C, 40.08; H, 5.15%. Calcd for $C_{14}H_{18}O_6Pd\cdot 2H_2O$: C, 39.59; H, 5.22%.

b) Nickel Chelates. Bis(heptane-2,4,6-trionato)nickel(II) Dihydrate. [*Ni(Hdaa)$_2\cdot 2H_2O$*]. *Procedure A*: To 30 ml of an ether solution containing 2.80 g(0.0197 mol) of heptane-2,4,6-trione was added 0.30 g (0.0011 mol) of anhydrous bis(acetylacetonato)nickel(II), and the clear solution was left for 1 hr at room temperature to give blue powdery precipitates. The product was collected by filtration, washed with ether and air-dried. Yield 0.17 g (39% from the nickel acetylacetonate).

Found: C, 44.60; H, 6.01; Ni, 15.57%. Calcd for $C_{14}H_{18}O_6Ni\cdot 2H_2O$: C, 44.60; H, 5.88; Ni, 15.57%. $\bar{\nu}_{max}$ in 95% methanol (ε): 15.8 (6.3), 13.6 (shoulder) (2.9), and 9.3 kK (5.7). $\bar{\nu}_{min}$: 19.2 (0.9) and 12.2 kK (1.4).

Procedure B: A mixture of 0.98 g (0.0021 mol) of bis-(heptane-2,4,6-trionato)dinickel(II) tetrahydrate and 3.0 g (0.021 mol) of heptane-2,4,6-trione was carefully warmed at 55—60°C (slightly above the melting point of the ligand, mp 42.5—43.5°C). The green molten paste was kept at this temperature for 90 min with occasional stirring. After the reaction, 100 ml of ether was added portionwise to this reaction mixture to precipitate the pale green nickel chelate. Excess ligand was removed by filtration. The product was finally washed with ether and air-dried and was identified by IR spectral comparison with the nickel chelate obtained by procedure A. Yield 0.68 g (43% from the 2 : 2 nickel chelate)

Bis(heptane-2,4,6-trionato)dinickel(II) Tetrahydrate. [*Ni$_2$(daa)$_2\cdot 4H_2O$*]. *Procedure A*: To 50 ml of methanol was added 1.0 g (0.007 mol) of heptane-2,4,6-trione and 2.0 g (0.0069 mol) of nickel(II) nitrate hexahydrate, and pH of the solution was adjusted to about 7 with aqueous methanolic ammonia (1 : 1 by volume) to give bright green powdery precipitates. The product was collected by filtration, washed with water and dried under reduced pressure. Yield 1.5 g (93%).

The sample thus obtained is fairly soluble in various organic solvents such as methanol, chloroform and tetrahydrofuran. Recrystallization from methanol gave green crystallites. Thermogravimetric analysis on the recrystallized chelate showed 16% of weight decrease in the region between 100 and 160°C, which corresponded to the loss of four molecules of water (Calcd as a tetrahydrate: 15.3%).

Found: C, 35.10; H, 5.22; Ni, 25.03%. Calcd for C_{14}-

* Present address: Central Research Laboratories, Chisso Co., Ltd., Kamariya-machi, Kanazawa-ku, Yokohama 236

1) Contribution No. 254 from the Department of Organic Synthesis, Kyushu University.

2) F. Sagara, H. Kobayashi, and K. Ueno, This Bulletin, **45**, 900 (1972).

3) F. Sagara, H. Kobayashi, and K. Ueno, *ibid.*, **45**, 794 (1972).

$H_{16}O_6Ni_2 \cdot 4H_2O$: C, 35.80; H, 5.15; Ni, 25.00%.

$\bar{\nu}_{max}$ in 95% methanol (ε): 24.1 (shoulder) (530), 16.8 (16), 13.7 (shoulder) (11) and 10.0 kK (15). $\bar{\nu}_{min}(\varepsilon)$: 17.7 (13) and 12.2 kK (8.8).

Procedure B: A methanol solution (3 ml) containing 1.0 g (0.0027 mol) of bis(heptane-2,4,6-trionato)nickel(II) dihydrate was heated at 50°C for 30 min, to give blue powdery precipitates. The product was collected by filtration, washed with ether and air-dried. Yield 0.42 g (66%). The nickel chelate was found to be identical with the sample obtained by procedure A by infrared spectral comparison.

Pyridine Adduct of Bis(heptane-2,4,6-trionato)dinickel(II). [$Ni_2(daa)_2 \cdot 4Py$]. *Procedure A*: A mixture of 2.0 g (0.0043 mol) of bis-(heptane-2,4,6-trionato)dinickel(II) tetrahydrate and 50 ml of pyridine was stirred for several hours, and the resulting blue powdery precipitates were collected by filtration and air-dried. Yield 1.0 g (33%).

The pyridine adduct is fairly soluble in various organic solvents and can be recrystallized from methanol. Thermogravimetric analysis showed 44% weight decrease in the range 90—140°C, which indicated the loss of four pyridine molecules (Calcd: 44.2%).

Found: C, 57.12; H, 5.04; N, 8.16; Ni, 16.44%. Calcd for $C_{14}H_{16}O_6Ni_2 \cdot 4(C_5H_5N)$: C, 57.19; H, 5.08; N, 7.85; Ni, 16.44%.

Procedure B: To a hot solution of 490 mg (0.001mol) of bis(heptane-2,4,6-trionato)dinickel(II) tetrahydrate in 100 ml of methanol was added 100 ml of pyridine at 60°C. The green solution was kept at this temperature for 2 hr, when a small amount of glittering flaky precipitate was obtained. The solution was allowed to cool to room temperature for 3 hr. The resulting precipitate was collected by filtration and washed with a small amount of chilled methanol and air-dried. Yield 390 mg (52%). IR spectral comparison showed that the flaky product was identical with the powdery pyridine adduct from procedure A.

c) Cobalt Chelates. Bis(heptane-2,4,6-trionato)cobalt(II) Dihydrate. [$Co(Hdaa)_2 \cdot 2H_2O$]: A mixture of 0.67 g (0.0014 mol) of bis(heptane-2,4,6-trionato)dicobalt(II) tetrahydrate and 2.0 g (0.014 mol) of heptane-2,4,6-trione was treated at 52—54°C for an hour in a similar manner to that in procedure B for preparation of the 1 : 2 nickel chelate. The product was light pink powder. Yield 0.62 g (58% from the 2 : 2 cobalt chelate).

Found: C, 44.52; H, 6.09%. Cacld for $C_{14}H_{18}O_6Co \cdot 2H_2O$: C, 44.57; H, 5.88%.

When the dihydrate was dried at room temperature in a vacuum (0.3—0.4 mmHg) for a few hours, it turned from light pink to pink, affording a dehydrated product whose composition was found to be $C_{14}H_{18}O_6Co \cdot 1/4H_2O$ by elemental analysis.

Bis(heptane-2,4,6-trionato)dicobalt(II) Tetrahydrate. [$Co_2(daa)_2 \cdot 4H_2O$]. The 2 : 2 chelate was synthesized according to procedures essentially similar to those described for the 2 : 2 nickel chelate, either procedure A or B.

The 2 : 2 cobalt(II) chelate was obtained as brown powder from 2.5 g (0.018 mol) of heptane-2,4,6-trione and 5.13 g (0.018 mol) of cobalt(II) nitrate hexahydrate in methanol-water at 55—60°C with the final pH values 6—8. Yield 2.9 g (70%).

Thermogravimetric analysis on the tetrahydrate chelate revealed that a gradual weight loss due to four moles dehydration took place from room temperature to 180°C, leaving an anhydrous chelate $Co_2(daa)_2$ which decomposed spontaneously at 235°C.

Found: C, 35.94; H, 5.09; Co, 25.2%. Calcd for $C_{14}H_{16}O_6Co_2 \cdot 4H_2O$: C, 35.76; H, 5.15; Co, 25.07%.

The same 2 : 2 chelate was obtained by refluxing a methanol solution of bis(heptane-2,4,6-trionato)cobalt(II) dihydrate.

Pyridine Adduct of Bis(heptane-2,4,6-trionato)dicobalt(II). [$Co_2(daa)_2 \cdot 4Py$]. One gram of 2 : 2 cobalt chelate (tetrahydrate) was dissolved in a methanol-pyridine mixture, and the clear solution was concentrated by evaporation to give yellow brown crystalline precipitates. The product was collected by filtration and dried over phosphorus pentoxide and activated charcoal at room temperature under reduced pressure. Yield 1.2 g (80%).

Found: C, 56.46; H, 5.05; N, 7.76%. Calcd for $C_{14}H_{16}O_6Co_2 \cdot 4(C_5H_5N)$: C, 57.19; H, 5.08; N, 7.84%.

d) Beryllium Chelate. Bis(2-amino-2-heptene-4,6-dionato)beryllium(II). [$Be(aho)_2$]: Beryllium nitrate trihydrate (1.5 g, 0.008 mol) dissolved in ethanol (10 ml) was added to an ethanol solution (20 ml) of heptane-2,4,6-trione (2.31 g, 0.0163 mol) at 40°C. To the resulting pale pink solution was added 12 ml of a mixture of ethanol–aqueous ammonia (1 : 1 by volume) at 30—40°C and the solution was stirred for 10 min. After being left standing for an additional 40 min, the resulting pale yellow crystalline precipitates were collected by filtration and recrystallized from acetonitrile. Yield 1.73 g(75%). The product was found to be a 1 : 2 beryllium chelate of 2-amino-2-heptene-4,6-dione which resulted from the amination of terminal carbonyl oxygen of heptane-2,4,6-trione.

Found: C, 58.13; H, 6.97; N, 9.54%. Calcd for $C_{14}H_{20}O_4N_2Be$: C, 58.12; H, 6.97; N, 9.68%.

Results and Discussion

Synthetic Conditions of the Chelates. The 2 : 2 chelates of nickel(II) and cobalt(II) can be synthesized by procedures similar to those employed in the synthesis of bis(heptane-2,4,6-trionato)dicopper(II), either by subjecting the corresponding metal ion to the reaction with an equimolar amount of heptane-2,4,6-trione in methanol at pH about 7, or by heating a methanol solution of the corresponding 1 : 2 chelate.[3] The nickel(II) and cobalt(II) chelates were obtained as tetrahydrates.

On the other hand, the 2 : 2 chelate of palladium (II) could not be obtained despite our efforts to employ various reaction conditions including those mentioned above. The chelate obtained from the reaction mixtures was always 1 : 2 palladium(II) chelate, anhydrous or dihydrate, depending upon the reaction conditions. The main reason for the difficulty of forming a 2 : 2 palladium(II) chelate could be understood to be due to the larger ionic size of palladium(II) ion than that of copper(II), nickel(II) or cobalt(II) ion. Palladium(II) ion can hardly be accomodated in the binuclear centers of the 2 : 2 chelate.

It is interesting to note that the 1 : 2 palladium(II) chelate can be obtained in a dihydrate form as well as in an anhydrous form, while the chelates of copper(II), nickel(II) and cobalt(II) are obtained only in a dihydrate form. The dehydration of the latter chelates, even at reduced pressure and at lower temperature, always resulted in rearrangement into the corresponding 2 : 2 chelates. The relative stability of 1 : 2 palladium(II) chelate in an anhydrous form might be con-

TABLE 1. CATALYTIC CONDENSATION OF HEPTANE-2,4,6-TRIONE

Complex	Reaction conditions			Reaction product	
	Solvent	Temperature	Duration		Yield
$Ni_2(daa)_2 \cdot 4H_2O$	H_2daa	70°C	2 days	A[a)]	52%
$Co_2(daa)_2 \cdot 4H_2O$	H_2daa	70	1 hr	A	67
K_2PtCl_4	Water-methanol	Room temp.	1 hr	A	23
	Water-methanol	70	2 hr	B[a)]	34

a) Products A and B melted at 113 and 182°C, respectively. They were identified with the reported compounds by their melting points and elemental analyses. A. J. Birch, D. W. Cameron, and R. W. Rickards, *J. Chem. Soc.*, **1960**, 4395.

nected with the difficulty of forming 2 : 2 chelate as discussed above.

In the case of beryllium chelate, the use of ammonia to adjust the pH of reaction medium resulted in the amination of terminal carbonyl group in heptane-2,4,6-trione, so that only 1 : 2 chelate of the amino derivative was obtained. Attempts to obtain a 2 : 2 beryllium(II) chelate using various reaction conditions were unsuccessful.

In contrast to the relative easiness of obtaining 2 : 2 chelates with nickel(II) and cobalt(II), the corresponding 1 : 2 chelates could not be obtained by the standard procedures which were employed in the synthesis of 1 : 2 copper(II) chelate. During the course of an investigation on the synthesis of 1 : 2 chelates of nickel (II) and cobalt(II), it was found that the bimolecular condensation of heptane-2,4,6-trione was accelerated in the presence of 2 : 2 nickel or cobalt chelate according to the following reaction scheme.

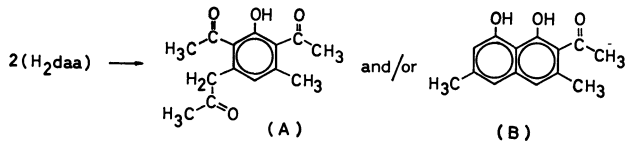

Scheme 1.

A similar effect was also observed with platinum(II) salt, but neither copper(II) ion nor copper(II) chelate was effective for promoting such condensation reactions. When pure heptane-2,4,6-trione was heated above its melting point, no cyclized condensation product has obtained. However, when an excess of the ligand was brought into contact with such metal chelates, especially at an elevated temperature, the cyclized product A or B was obtained in the reaction mixture depending upon the condition of reaction. Table 1 summarizes the result.

Thus, when nickel(II) or cobalt(II) ion was allowed to react with excess heptane-2,4,6-trione with the purpose of obtaining a 1 : 2 chelate, the reaction products were always a 2 : 2 chelate and cyclized by-products but no 1 : 2 chelate. Accordingly, the 1 : 2 chelates had to be prepared by the ligand exchange reaction between a bis(acetylacetonato)-metal chelate and heptane-2,4,6-trione in anhydrous ether, or by the reaction between 2 : 2 metal chelates and molten heptane-2,4,6-trione at a temperature slightly above its melting point.

Structures of Nickel(II)- and Cobalt(II) Chelates. The infrared spectra of 1 : 2 chelates of nickel(II) and cobalt(II), [$Ni(Hdaa)_2.2H_2O$ and $Co(Hdaa)_2.2H_2O$], show characteristic bands in 3000—3400 cm^{-1} and 1500—1700 cm^{-1} regions. A broad band with a maximum at 3280 cm^{-1} for the nickel- and 3400 cm^{-1} for the cobalt chelates can be assigned to the hydrated water. This makes a sharp contrast with those observed in the 1 : 2 copper(II)- and palladium(II) dihydrate chelates, where a sharp band at 3530 cm^{-1} and a multiplet weak band with maxima at about 3420, 3350 and 3260 cm^{-1} appear. The broad band of 1 : 2 nickel(II)- and cobalt(II) chelates suggests a rather strong coordination of water molecules to the central metal ion along the z axis, while the ligand molecules coordinate along the x—y plane. On the other hand, a multiplet band with fine structure of 1 : 2 copper(II) and palladium(II) chelates indicates the weaker interaction of hydrated water molecules with metal ion.

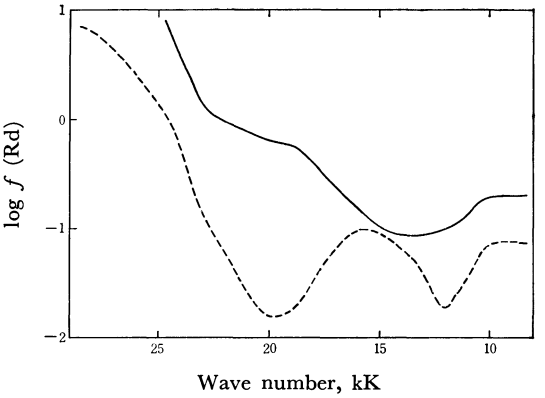

Fig. 1. Diffuse reflectance spectra of $Ni(Hdaa)_2 \cdot 2H_2O$ (-----) and $Co(Hdaa)_2 \cdot 2H_2O$ (——).

In the 1500—1700 cm^{-1} region, there are observed a sharp band at 1720 cm^{-1} for the nickel(II)- and 1695 cm^{-1} for the cobalt(II) chelates and a strong band with several shoulders at 1500—1600 cm^{-1} for the both chelates. These bands can be assigned to an uncoordinated carbonyl group and a coordinated carbonyl group in conjugated chelate ring system respectively as in the case of 1 : 2 copper(II) chelate.

The power reflectance spectra of the 1 : 2 chelates of nickel(II) and cobalt(II) are shown in Fig. 1. In the case of $Ni(Hdaa)_2.2H_2O$, two broad bands at 9300 and 15800 cm^{-1} with a shoulder at 25000 cm^{-1} were observed, and in the case of $Co(Hdaa)_2.2H_2O$, a band at 19000 cm^{-1} and a broad band at 9000—9500 cm^{-1} were observed. These spectra are found to be very much similar to those of bis(acetylacetonato)nickel-

(II) dihydrate[4] or -cobalt(II) dihydrate[5] respectively. These results strongly suggest the octahedral coordination structure around the central metal ion for both 1 : 2 chelates as proposed in structure I.

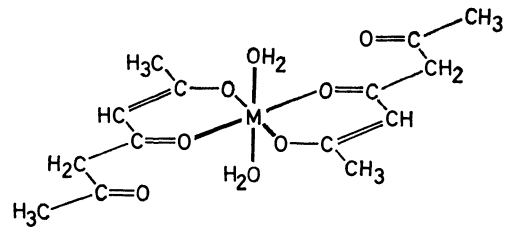

Structure I. M=Ni(II) or Co(II).

As to the 2 : 2 chelates of nickel(II) and cobalt(II), [$Ni_2(daa)_2.4H_2O$ and $Co_2(daa)_2.4H_2O$], infrared spectra were characterized with a broad band at 3200—3400 cm^{-1} and a band with shoulders at 1500—1600 cm^{-1}, which could be assigned to hydrated water and coordinated carbonyl groups in the conjugated chelate ring system, respectively. Absence of a band due to the uncoordinated carbonyl groups indicates that all carbonyl groups are involved in the coordination to the metal ions.

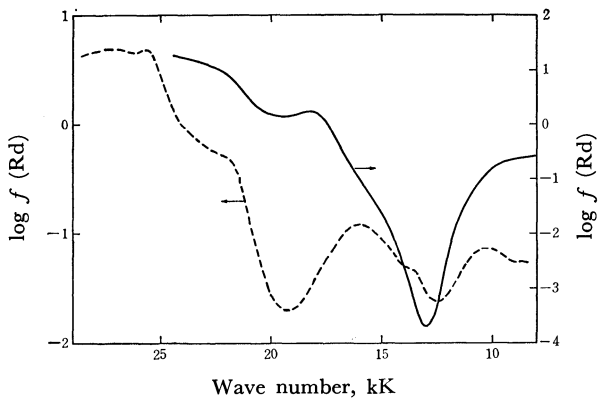

Fig. 2. Diffuse reflectance spectra of $Ni_2(daa)_2 \cdot 4H_2O$ (----) and $Co_2(daa)_2 \cdot 4H_2O$ (——).

The solid reflectance spectra of these hydrated chelates in visible region are shown in Fig. 2. They show two bands at 10400 and 16000 cm^{-1} with shoulders at 13500 and 22000 cm^{-1} for nickel(II) chelate, and a single band at 18200 cm^{-1} with shoulders at 9000 and 23000 cm^{-1} for cobalt(II) chelate. The results suggest that the coordination structure around nickel(II) or cobalt(II) ion is also octahedral.

The molecular weight of anhydrous 2 : 2 nickel(II) chelate in methanol, determined by the vapor pressure osmometer, was found to be 410 which is close to the calculated value of 397.7 for $Ni_2(daa)_2$. Consideation of these observations leads to the conclusion that the structures of $Ni_2(daa)_2.4H_2O$ and $Co_2(daa)_2.4H_2O$ can be assigned to structure II, in which four molecules of hydrated water coordinate to the central metal ions along the z axis.

4) G. Maki, *J. Chem. Phys.*, **29**, 162 (1958).
5) F. A. Cotton and R. H. Soderberg, *Inorg. Chem.*, **3**, 1 (1964).

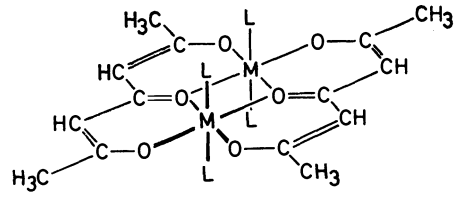

Structure II. M=Ni(II) or Co(II), L=H_2O or Pyridine.

Pyridine Adducts of 2 : 2 Chelates. Coordinated water in 2 : 2 nickel- and cobalt(II) chelates can easily be replaced by pyridine, affording the pyridine adducts having the formula $M_2(daa)_2.4Py$, where M denotes Ni(II) or Co(II).

The absence of infrared absorption band due to free carbonyl group at around 1700 cm^{-1} indicates that the coordination structure of heptane-2,4,6-trione remained intact and the addition of pyridine merely caused the replacement of coordinated water with pyridine.

The solid reflectance spectra of pyridine adducts in visible region shown in Fig. 3 are characterized by two

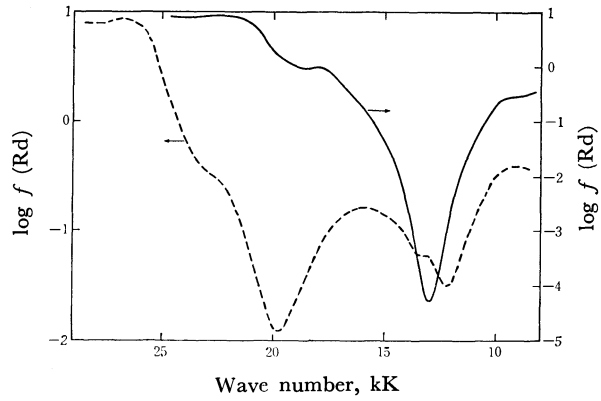

Fig. 3. Diffuse reflectance spectra of $Ni_2(daa)_2 \cdot 4Py$ (----) and $Co_2(daa)_2 \cdot 4Py$ (——).

broad bands at 9200 and 16000 cm^{-1} and shoulders at 13000 and 22500 cm^{-1} for nickel(II) chelate and at 9000, 18200 and 22000 cm^{-1} for cobalt(II) chelate, indicating the octahedral hexacoordinate structure around nickel(II) or cobalt(II) ion as shown in structure II.

Thermogravimetric analysis of the pyridine adducts as well as hydrates of 2 : 2 chelates revealed that pyridine or water dissociated above 90°C, leaving anhydrous 2 : 2 chelates.

Structure of Palladium(II) Chelate. The 1 : 2 palladium(II) chelate could be obtained either as dihydrate or anhydrous form. Infrared absorption spectrum of the anhydrous sample was characterized with a weak multiplet band at 3400 cm^{-1} region, a sharp strong band at 1730 cm^{-1} due to uncoordinated carbonyl groups, and complex bands in 1500—1600 cm^{-1} region due to coordinated carbonyl groups conjugated with olefinic chelate ring.

The NMR spectrum of the anhydrous chelate in $CDCl_3$ (1.0 M solution) is shown in Fig. 4. Peaks at δ=2.12, 2.24, 3.42 and 5.47 ppm can be assigned to methyl(a), methyl(b), methylene(c) and methine(d)

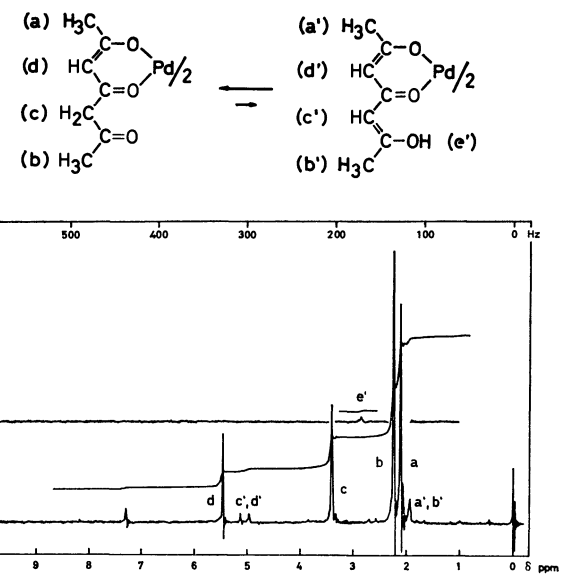

Fig. 4. NMR spectrum of the 1 : 2 palladium chelate and its tautomers. Assignments of the NMR peaks correspond to the protons indicated by alphabetical letters in the above structural formulae.

protons, respectively. However, weak peaks are also observed at $\delta=1.93$, 4.97, 5.13 and 11.85 ppm. If we consider the partial enolization of uncoordinated carbonyl groups, these weak peaks can be reasonably assigned to the protons of enolized chelate as indicated in Fig. 4.

Thus the weak multiplet infrared absorption band at 3400 cm^{-1} region can also be assigned to the enol hydroxyl group. The relatively weak intensity of the signals due to the enolic isomer, in the infrared and NMR spectra, indicates that the extent of enolization in the 1 : 2 palladium(II) chelate is rather small.

Thus, the anhydrous 1 : 2 palladium(II) chelate $Pd(Hdaa)_2$ can be assigned to structure I, but with no water. As to dihydrate chelate $Pd(Hdaa)_2 \cdot 2H_2O$, the most probable structure is I, with water molecules weakly coordinated to palladium(II) ion along z axis.

Structure of Beryllium(II) Chelate. Despite our effort to obtain a 1 : 2 beryllium(II) chelate of heptane-2,4,6-trione by the reaction of beryllium(II) ion with free ligand in an ethanol–ammonia medium, a 1 : 2 beryllium chelate of 2-amino-2-heptene-4,6-dione was obtained unexpectedly.

The result of elemental analysis indicates that it is a 1 : 2 chelate of monoamino derivative of heptane-2,4,6-trione. Two sharp infrared absorption bands at 3390 and 3300 cm^{-1}, which appeared at a relatively lower frequency region than usual primary amines, suggest that the primary amino group may coordinate to beryllium(II) ion.[6] Other characteristic bands at 1635 and 1525 cm^{-1} may be assigned to uncoordinated and coordinated carbonyl groups, respectively, though the frequency of the former band is slightly lower than that expected for α,β : γ,δ-unsaturated ketones.

Although there is no positive evidence, structure III is most likely to be assigned to bis(2-amino-2-heptene-4,6-dionato)beryllium(II) based on the following observations.

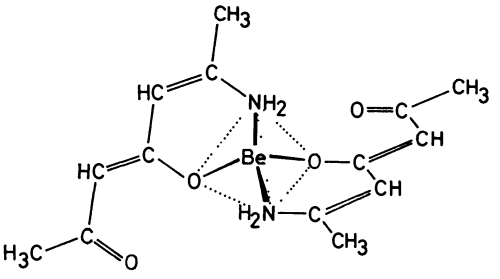

Structure III.

When acetylacetone was brought into reaction with beryllium(II) ion in the presence of ammonia, only bis(acetylacetonato)beryllium(II) was obtained. When 2-methoxy-2-heptene-4,6-dione[3] was brought into reaction with beryllium(II) ion in the presence of ammonia, the product was bis(2-methoxy-2-heptene-4,6-dionato)beryllium(II). Thus, the amination seems to be characteristic to β,δ-triketones. It does not proceed on β-diketones nor β,δ-triketones in which the terminal carbonyl group is fixed in the form of an enol ether. Thus, it is reasonable to assume that the chelation occurs between heptane-2,4,6-trione and beryllium(II) ion to give bis(heptane-2,4,6-trionato)-beryllium(II) as an intermediate product, which in turn reacts with ammonia to afford 2-amino-2-heptene-4,6-dionato chelate. When heptane-2,4,6-trione reacts with ammonia in the absence of metal ion, it is known that amination occurs on the terminal carbonyl group, affording 2,6-dimethyl-4-pyridone as a cyclization product.[7] Thus, it is likely that amination occurs on the chelated ligand but not on the free ligand, and that the position of amination may be on the terminal carbonyl group. As regards whether the 1 : 2 beryllium chelate is an O,O-coordinated structure with the amino group uncoordinated, or the rearrangement occurs after amination resulting in an O,N-coordinated structure with the carbonyl group uncoordinated, the latter seems probable. This is supported by the fact that 2-amino-2-heptene-4,6-dione is stable only in the form of beryllium chelate, and attempts to recover the free aminated ligand from the beryllium(II) chelate were unsuccessful, only giving the original heptane-2,4,6-trione. Therefore, the amino group might be protected by the coordination to the metal ion.

The authors are grateful to the Ministry of Education for financial support. They also thank Messrs. Isao Yoshida, Toshiaki Kozaki and Shizuhiko Honkawa for their assistance.

6) K. Nakamoto, "Infrared Spectra of Inorganic and Coordination Compounds", 2nd Ed., Wiley-Interscience, New York (1970), p. 151.

7) R. J. Light and C. R. Hauser, *J. Org. Chem.*, **25**, 158 (1960).

Calmagite:[1] The Formation Constants of Zinc(II) Chelates and Its Use as a Metal Indicator

Genkichi NAKAGAWA, Hiroko WADA, and Yoshio FUJITA

Nagoya Institute of Technology, Showa-ku, Nagoya

(Received July 12, 1972)

The acid dissociation constants of Calmagite [1-(2-hydroxy-5-methylphenylazo)-2-naphthol-4-sulfonic acid] and the formation constants of zinc(II) chelates have been determined spectrophotometrically at 25°C and at the ionic strengths of 0.1 and 1.0. In an ammoniacal medium zinc forms mixed-ligand complexes with Calmagite (I^{3-}) and ammonia (X); $ZnIX_n^-$. The formation constants of the zinc(II)-Calmagite chelates are $\log K_{ZnI}=11.75$, $\log K_{ZnI_2}=7.82$, $\log K^{X}_{ZnIX}=2.09$, and $\log K^{X}_{ZnIX_2}=1.70$ ($\mu=1.0$). Calmagite is recommended as an indicator for the titration of zinc(II) with EDTA. The color transition of Calmagite is clearer and sharper, and the aqueous solution of the indicator is more stable, than in the case of Eriochrome Black T.

Eriochrome Black T has been exclusively used as a metal indicator in the complexometric titration of magnesium, zinc, cadmium, lead, etc. Lindstrom and Diehl recommended Calmagite as the metal indicator for magnesium,[2] because the aqueous solution of Calmagite is more stable than that of Eriochrome Black T. However, Calmagite has not been so much used for a metal indicator as Eriochrome Black T. Kodama and Miyamoto[3] determined the stability constants of Calmagite chelates of copper(II), nickel(II), cobalt(II), zinc(II), cadmium(II), and lead(II) by the exchange reaction of Calmagite with the metalnitrilotriacetic acid chelates and proposed the use of Calmagite as an indicator for zinc, cadmium, and lead. Their value of the stability constant of zinc-Calmagite seems, however, to be too high in comparison with that of the zinc-Eriochrome Black T chelate.

The present paper will deal with the formation of mixed-ligand complexes of zinc-Calmagite chelates in an ammoniacal medium and with the behavior of Calmagite as a metal indicator for zinc in detail.

Experimental

Reagents. *Zinc Chloride*: Zinc metal (99.999%) was dissolved in hydrochloric acid to prepare a zinc chloride solution.

Calmagite: Calmagite from the Dōjindō Co., Ltd., was purified by a procedure described by Lindstrom and Diehl.[2] The Calmagite stock solution was prepared every week and was standardized with a copper standard solution by photometric titration.

EDTA: Reagent-grade EDTA·2Na obtained from the Dōjindō Co., Ltd., was dissolved in distilled water and standardized complexometrically against a standard zinc solution.

Ammonia Solution: A reagent-grade ammonia solution was distilled, and pure ammonia was collected in distilled water. The concentration of ammonia was determined with a standard hydrochloric acid solution.

Potassium Acetate and Potassium Nitrate: Reagent-grade chemicals were purified by recrystallization.

Acetic Acid, Boric Acid and Postassium Hydroxide: Reagent-grade chemicals were used without further purification.

Apparatus. A Hitachi Model 124 Double-beam Spectrophotometer, a Hitachi Model 356 Two-wavelength Double-beam Spectrophotometer, a Hitachi-Horiba pH Meter type F-5 equipped with Horiba glass and calomel electrodes, and a Hirama Automatic Recording Titrator were used.

Experimental Procedure. The ionic strength was maintained at 0.1 or 1.0 with potassium nitrate. The pH was adjusted by adding buffer solutions of potassium acetate-acetic acid, potassium hydroxide-boric acid, or ammonia-ammonium chloride. The absorbance of the solution was measured by the use of a silica cell with a light path of 1.0 cm. After measuring the absorbance, the accurate pH value was measured with a pH meter which had been calibrated with two standard buffer solutions. All the experiments were carried out at 25±1°C.

Results

The Acid Dissociation Constants of Calmagite. The dissociation of the free acid of Calmagite may be represented as follows:

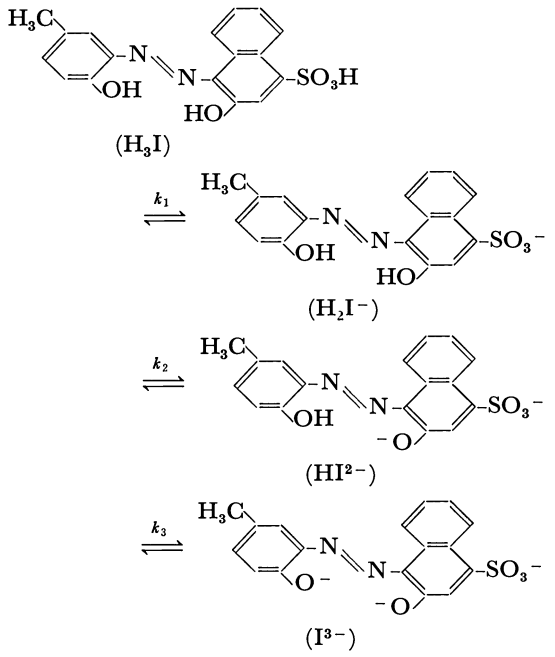

The predominant species of Calmagite in the solutions of pH 2—6, pH 9—10, and pH>13 are H_2I^-, HI^{2-}, and I^{3-} respectively. The acid dissociation constants (pk_2 and pk_3) were determined by the spectrophotometric method at an ionic strength of 0.1 or 1.0. Since

1) 1-(2-Hydroxy-5-methylphenylazo)-2-naphthol-4-sulfonic acid
2) F Lindstrom and H. Diehl, *Anal. Chem.*, **32**, 1123 (1960).
3) M. Kodama and K. Miyamoto, This Bulletin, **42**, 835 (1969).

the sulfonic acid group is a strong acid, the pk_1 could not be measured. The values of pk_2 and pk_3 given in Table 2 agree well with those of Lindstrom and Diehl.

The Formation Constants of Zinc(II)-Calmagite Chelates. Calmagite forms a 1 : 1 chelate with zinc when the concentration of zinc is in a sufficient excess compared with that of Calmagite. In the vicinity of pH 6, the predominant species of the free ligand being H_2I^-, the formation of ZnI^- is expressed as follows, and the equilibrium constant is given by Eq. (1) (The charge will be omitted in the equations for the sake of simplicity):

$$Zn^{2+} + H_2I^- \overset{K}{\rightleftharpoons} ZnI^- + 2H^+$$

$$K = \frac{[ZnI][H]^2}{[Zn][H_2I]} \quad (1)$$

The absorbance of the solutions containing Calmagite and about a hundredfold excess of zinc(II) were measured at 550 nm, where the difference in absorbance between ZnI^- and H_2I^- is sufficiently large. The variation in the absorbance with the pH is shown in Table 1. From these data, the value of the equilibrium constant, K, was evaluated by means of Hildebrand-Reilley's method[4] and the formation constant, K_{ZnI}, was calculated from K and the acid dissociation constants of Calmagite, k_2 and k_3:

$$K_{ZnI} = \frac{[ZnI]}{[Zn][I]} = \frac{K}{k_2 \times k_3} \quad (2)$$

Table 1. Absorbance of 1 : 1 zinc-calmagite chelate in solutions of various pH's[a)]

pH	Absorbance at 550 nm	pH	Absorbance at 550 nm
5.89	0.670	5.22	0.594
5.59	0.652	5.09	0.579
5.46	0.627	4.89	0.555
5.35	0.609		

a) $C_{Zn} = 2.00 \times 10^{-3}$ mol/l, $C_I = 2.86 \times 10^{-5}$ mol/l, Acetate buffer, $\mu = 1.0$ (KNO_3), 25°C, Cell length 1 cm.

Zinc(II) forms a 1 : 2 chelate with Calmagite at high pH values (pH>9) in the presence of a large excess of the ligand. The absorption spectra of the solutions containing 1.00×10^{-5} mol/l of zinc and 4.00×10^{-5} mol/l of Calmagite in the pH range from 9 to 10.5 (buffered with potassium hydroxide and boric acid) are shown in Fig. 1. Curves 1 and 5 are the absorption spectra of HI^{2-} and ZnI_2^{4-} respectively. From the absorbance at 640 nm, where the difference in absorbance between the ligand and the zinc chelate is large, the total concentration of the ligand combined with the zinc can be evaluated. The absorption spectra presented by Curves 2—4 show the successive formation of ZnI^- and ZnI_2^{4-} chelates. Under these experimental conditions, the concentration of the free zinc ion is negligible and the following stoichiometric relationships hold:

$$C_{Zn} = [ZnI] + [ZnI_2] \quad (3)$$

$$C_I = [ZnI] + 2[ZnI_2] + [HI] \quad (4)$$

where C_{Zn} and C_I are the analytical concentrations of zinc and Calmagite respectively and where [HI] is the total concentration of Calmagite not combined with the zinc ion.

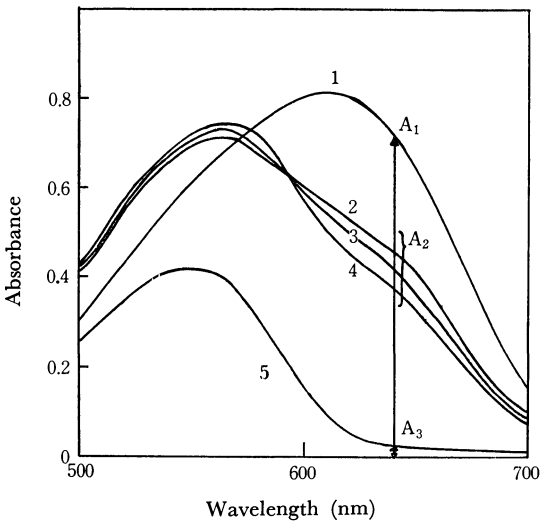

Fig. 1. Absorption spectra of zinc-Calmagite chelates.
$C_I = 4.01 \times 10^{-5}$ mol/l, $C_{Zn} = 1.00 \times 10^{-5}$ mol/l
1: Calmagite only, pH 10.10, 2: pH 9.42, 3: pH 10.02, 4: pH 10.64, 5: ZnI_2 (against reagent blank)

The [HI] values under the given conditions were calculated from the absorbances, A_1, A_2, and A_3, shown in Fig. 1. By representing the molar absorptivity of the ligand, HI^{2-}, and the chelates, ZnI^- and ZnI_2^{4-}, as ε_{HI}, ε_{ZnI}, and ε_{ZnI_2} respectively, we obtain:

$$A_1 = \varepsilon_{HI} C_I \quad (5)$$

$$A_2 = \varepsilon_{HI}[HI] + \varepsilon_{ZnI}[ZnI] + \varepsilon_{ZnI_2}[ZnI_2] \quad (6)$$

$$A_3 = \varepsilon_{ZnI_2} C_{Zn} \quad (7)$$

The absorption spectrum of the ZnI_2^{4-} chelate has same shape as that of the ZnI^- chelate, but the molar absorptivity of ZnI_2^{4-} is twice as much as that of ZnI^-:

$$2\varepsilon_{ZnI} = \varepsilon_{ZnI_2} \quad (8)$$

By combining Eqs. (4)—(8), and by disignating C_I/C_{Zn} as a, the total concentration of the free ligand is given by Eq. (9):

$$[HI] = \frac{(2A_2 - aA_3)C_I}{2A_1 - aA_3} \quad (9)$$

By substituting [HI] into Eqs. (3) and (4), we can obtain $[ZnI_2]$ and [ZnI] under the given conditions.

The successive formation constant of ZnI_2^{4-} is defined by Eq. (10):

$$K_{ZnI_2} = \frac{[ZnI_2]}{[ZnI][I]} \quad (10)$$

[I] can be calculated by means of Eq. (11):

$$[I] = [HI]k_3/[H] \quad (11)$$

A plot of $\log [ZnI_2]/[ZnI]$ *vs.* pI gave a straight line with a slope of -1, $\log K_{ZnI_2}$ was evaluated from the x-intercept.

4) G. P. Hildebrand and C. N. Reilley, *Anal. Chem.*, **29**, 258 (1957).

TABLE 2. ACID DISSOCIATION CONSTANTS AND COMPLEX FORMATION CONSTANTS OF ZINC-CALMAGITE AT 25°C

Acid dissociation constants		
pk_2	pk_3	Ionic strength
7.92	12.50	0.1 (KNO_3)
7.84	12.08	1.0 (KCl)

Complex formation constants				
$\log K_{ZnI}$	$\log K_{ZnI_2}$	$\log K^X_{ZnIX}$	$\log K^X_{ZnIX_2}$	Ionic strength
12.52	7.71			0.1 (KNO_3)
11.75	7.82			1.0 (KNO_3)
11.57		2.09	1.70	1.0 (KNO_3)

The successive formation constants, K_{ZnI} and K_{ZnI_2}, thus obtained are listed in Table 2.

The Formation of Mixed Ligand Complexes. The absorption spectra of 1 : 1 zinc-Calmagite chelates shift to longer wavelengths in an ammoniacal medium. Therefore, it is supposed that zinc may form the mixed ligand complexes, $ZnIX_n^-$, with Calmagite, I^{3-}, and with ammonia, X.

If the mixed ligand complexes are formed, the over-all formation constant of mixed ligand complexes can be defined by Eq. (12):

$$\beta_{ZnIX_n} = \frac{[ZnIX_n]}{[ZnI][X]^n} \tag{12}$$

and the total concentration of the zinc-Calmagite chelates [(ZnI)'] is given by Eq. (13):

$$[(ZnI)'] = [ZnI] + [ZnIX] + [ZnIX_2] + \cdots + [ZnIX_n] = [ZnI]\alpha_{ZnI(X)} \tag{13}$$

where:

$$\alpha_{ZnI(X)} = 1 + \sum_{n=1}^{n} \beta_{ZnIX_n}[X]^n \tag{14}$$

Since zinc ion forms ammine complexes in an ammoniacal medium, the total concentration of zinc not combined with Calmagite, [Zn'] is represented by Eq. (15):

$$[Zn'] = [Zn] + [ZnX] + [ZnX_2] + \cdots + [ZnX_m] = [Zn]\alpha_{Zn(X)} \tag{15}$$

$$\alpha_{Zn(X)} = 1 + \sum_{m=1}^{m} \beta_m[X]^m \tag{16}$$

where β_m is the over-all formation constant of zinc ammine complexes. Taking into account the protonation of Calmagite,

$$[I'] = [I]\alpha_{I(H)} \tag{17}$$

and:

$$\alpha_{I(H)} = 1 + \frac{[H]}{k_3} + \frac{[H]^2}{k_2k_3} \tag{18}$$

The conditional formation constant of the zinc-Calmagite chelate is given by Eq. (19)

$$K_{Zn'I'(ZnI)'} = \frac{[(ZnI)']}{[Zn'][I']} \tag{19}$$

The experiments were carried out under the conditions where $C_I=3.6\times10^{-5}$ mol/l, $C_{Zn}=6.5\times10^{-5}$ mol/l, $C_X=0.1$—1.0 mol/l in the pH range from 7 to 9, and $\mu=1.0$. Some typical absorption spectra are shown in Fig. 2. The absorbances, A_1, A_2, and A_3, in Fig. 2 are expressed as follows:

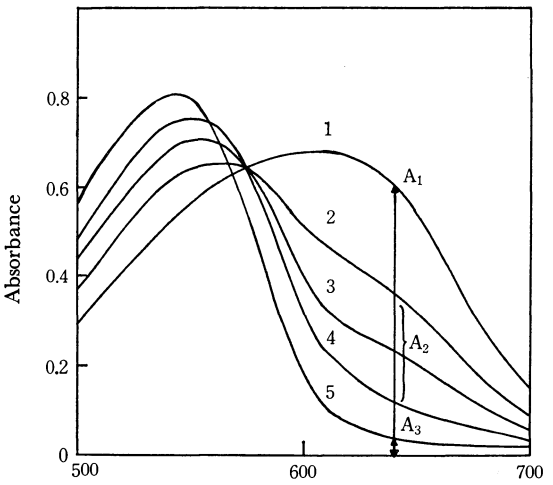

Fig. 2. Absorption spectra of mixed ligand complexes.
$C_I=3.59\times10^{-5}$ mol/l, $C_{Zn}=6.50\times10^{-5}$ mol/l
1: Calmagite only, pH 9.00, 2: pH 8.98, $[NH_3]=5.02\times10^{-1}$ mol/l, 3: pH 9.00, $[NH_3]=2.96\times10^{-1}$ mol/l, 4: pH 8.99, $[NH_3]=1.46\times10^{-1}$ mol/l, 5: pH 9.00, $[NH_3]=0$

$$A_1 = \varepsilon_I C_I \tag{20}$$

$$A_2 = \varepsilon_I[I'] + \varepsilon_{ZnI}[ZnI] + \sum_{n=1}^{n} \varepsilon_{ZnIX_n}[ZnIX_n] \tag{21}$$

$$A_3 = \varepsilon_{ZnI}C_I \tag{22}$$

where ε_I, ε_{ZnI}, and ε_{ZnIX_n} are the molar absorptivities of the free ligand, ZnI^-, and the mixed ligand complex, $ZnIX_n^-$, respectively. From the absorption spectra of ZnI^- and $ZnIX_n^-$, at 640 nm, ε_{ZnI} is found to be almost equal to ε_{ZnIX_n}. Therefore, [I'] can be calculated from the absorbances at 640 nm in a manner analogous to that used in the previous section:

$$[I'] = \frac{(A_2-A_3)C_I}{A_1-A_3} \tag{23}$$

Also, [(ZnI)'] and [Zn'] are given by Eqs. (24) and (25):

$$[(ZnI)'] = C_I - [I'] \tag{24}$$

$$[Zn'] = C_{Zn} - [(ZnI)'] \tag{25}$$

If we obtain the [I'] values from experiments, the conditional formation constant, $K_{Zn'I'(ZnI)'}$, under the given conditions can be calculated by means of Eqs. (19), (24) and (25).

By substituting Eqs. (13), (15), and (17) into Eq. (19), the conditional formation constant of mixed ligand complexes can be rewritten as follows:

$$K_{Zn'I'(ZnI)'} = \frac{K_{ZnI}\alpha_{ZnI(X)}}{\alpha_{Zn(X)}\alpha_{I(H)}} \tag{26}$$

Since [X] can be calculated from the total concentration of ammonia ($C_X=[NH_3]+[NH_4^+]$) and the pH value[5], $\alpha_{Zn(X)}$ in each experiment can be calculated by means of Eq. (16)[6] and $\alpha_{I(H)}$ can be obtained from the pHs of the solutions by means of Eq. (18). Using Eq. (26), $K_{ZnI}\alpha_{ZnI(X)}$ can be evaluated from $K_{Zn'I'(ZnI)'}$.

The relation of log $K_{ZnI}\alpha_{ZnI(X)}$ and pX[7] is shown in Fig. 3. log $K_{ZnI}\alpha_{ZnI(X)}$ is a function of pX and the curve approaches a straight line with a slope of 2 in the vicinity of pX=0. From these results, it is clear that zinc forms mixed ligand complexes with Calmagite and ammonia. $K_{ZnI}\alpha_{ZnI(X)}$ can be written as Eq. (27):

$$K_{ZnI}\alpha_{ZnI(X)} = K_{ZnI}(1+K^{X}_{ZnIX}[X] + K^{X}_{ZnXI}K^{X}_{ZnIX_2}[X]^2) \quad (27)$$

where:

$$K^{X}_{ZnIX} = \frac{[ZnIX]}{[ZnI][X]}, \quad K^{X}_{ZnIX_2} = \frac{[ZnIX_2]}{[ZnIX][X]}$$

From the data plotted in Fig. 3, the successive formation constants of the mixed ligand complexes were calculated by means of a HIPAC 103 computer using the least squares method; the following values were thus obtained: log K_{ZnI}=11.57, log K^{X}_{ZnIX}=2.09, and log $K^{X}_{ZnIX_2}$=1.70.

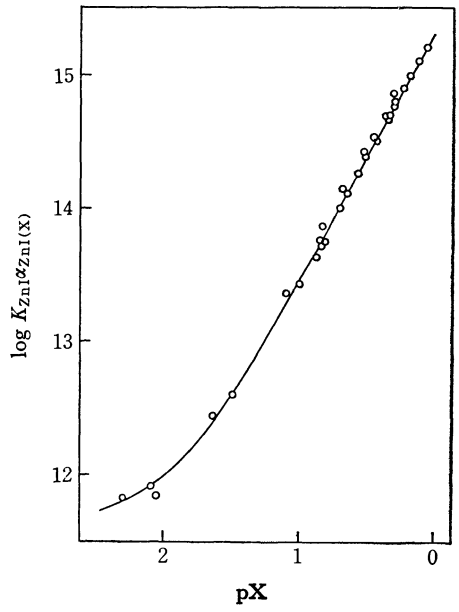

Fig. 3. log $K_{ZnI}\alpha_{ZnI(X)}$ *vs.* pX.

Use as a Metal Indicator for Zinc. In the chelatometric titration of metals, a sharp color change of the indicator is obtained at the equivalence point when the following relationships hold:[8]

$$pM_{\phi=0.5} - pM_{a=0} \gtrsim 3$$

$$pM_{a=2} - pM_{\phi=0.5} \gtrsim 3$$

where $pM_{a=0}$, $pM_{a=2}$, and $pM_{\phi=0.5}$ are pM's before titration, when titrated in a 100% excess and at a 50% color transition respectively.

$pM_{a=0}$, $pM_{a=2}$, and $pM_{\phi=0.5}$ were calculated under various conditions and plotted against the pH (Fig. 4). The optimum conditions for the titration of zinc with EDTA using Calmagite as an indicator can be predicted from the plots of pM *vs.* pH. Zinc forms hydroxide

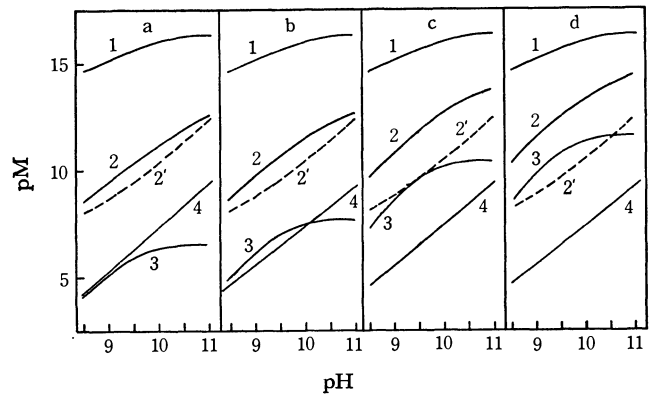

Fig. 4. Optimum conditions for titration of zinc.
$[NH_3]+[NH_4^+]$ (mol/l), a: 0.05, b: 0.1, c: 0.5, d: 1.0
1: $pM_{a=2}$, 2: $pM_{\phi=0.5}$, 3: $pM_{a=0}$, 4: $pM_{Zn(OH)_2}$, 2': $pM_{\phi=0.5}$ if mixed complexes do not form.

in the range of pH>8.5 when the total concentration of ammonia ($[NH_3]+[NH_4^+]$) is less than 0.1 mol/l. If the total concentration of ammonia is between 0.1 and 0.5 mol/l, it is expected that a sharp color transition of Calmagite can be observed at the equivalence point in the pH range from 8.5 to 10.5. When the concentration of ammonia is 1 mol/l or more, the indicator is considerably discolored before the equivalence point and the color transition after the equivalence point is sluggish.

These considerations were verified by photometric titration. In Fig. 5 the photometric titration curves are shown. The results of photometric titration are in close agreement with the theoretical results.

Discussion

In a previous paper[9] we reported that indium(III) forms mixed ligand complexes with 2-(2-pyridylazo)-4-methylphenol (PAC) and the acetate ion. It is of much interest now to have found that zinc(II) forms mixed ligand complexes with Calmagite and ammonia.

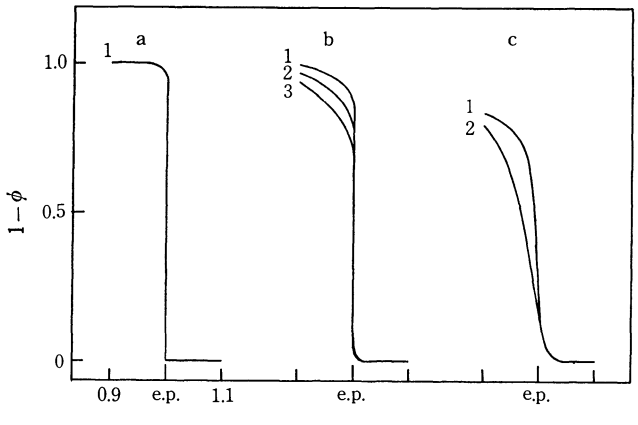

Fig. 5. Photometric titration curves.
$[NH_3]+[NH_4^+]$ (mol/), a: 0.1, b: 0.5, c: 1.0
pH, a: 1; 8.3—10.2, b: 1; 10.5, 2; 9.6, 3; 8.6, c: 1; 10.6, 2; 9.6

5) $k_{NH4}=10^{-9.25}$ was used.
6) $\beta_1=10^{2.59}$, $\beta_2=10^{4.91}$, $\beta_3=10^{6.92}$, and $\beta_4=10^{8.62}$ were used.
7) pX=−log[X]
8) M. Tanaka and G. Nakagawa, *Anal. Chim. Acta*, **32**, 123 (1965).
9) H. Wada and G. Nakagawa, *Nippon Kagaku Zasshi*, **89**, 499 (1968).

When the concetration of ammonia is less than 1 mol/l, it has been shown experimentally that less than two moles of ammonia coordinate with the zinc-Calmagite chelate. Since zinc may form octahedral complexes, three moles of ammonia might combine with the zinc-Calmagite chelate at an ammonia concentration of more than 1 mol/l. The successive formation constants of the mixed ligand complexes are smaller than those of corresponding zinc ammine complexes (log $K_{ZnX}=2.59$, log $K_{ZnX_2}=2.32$).

It has been recognized that the formation of mixed ligand complexes plays an important role in the complexometric titration of zinc. If zinc did not form mixed ligand Complexes with calmagite, the total concentration of ammonia should be kept near 0.1 mol/l. However, the titration can be carried out even in a solution containing a total of 0.5 mol/l of ammonia. The formation of the mixed ligand complexes makes the ammonia concentration in the solutions not critical. In the case of Eriochrome Black T, zinc also forms mixed ligand complexes with ammonia.

Calmagite has some advantageous properties as a metal indicator for the titration of zinc; *i. e.*, the aqueous solution of Calmagite is more stable and the color transition is clearer and sharper than in the case of Eriochrome Black T.

BULLETIN OF THE CHEMICAL SOCIETY OF JAPAN, VOL. 46, 493—495 (1973)

Polarographic Reductions of Alkaline Earth Metal Ions in Hexamethylphosphoramide. Effect of Cation of the Supporting Electrolyte*

Kosuke IZUTSU,** Sachiko SAKURA, and Taitiro FUJINAGA

Department of Chemistry, Faculty of Science, Kyoto University, Sakyo-ku, Kyoto

(Received July 17, 1972)

Polarographic reductions of barium, strontium and calcium ions in hexamethylphosphoramide (HMPA) have been investigated in the supporting electrolytes of various perchlorates. The reduction of these alkaline earth metal ions are strongly influenced by the cation of the supporting electrolyte. When the size of the cation of the supporting electrolyte is small and easily adsorbed on the negatively charged electrode surface as in the cases of Me_4N^+ and Et_4N^+ ions, the reduction of the metal ions does not occur until that of the supporting electrolyte. The reduction becomes easier with the increase of cationic size. Thus, in Hex_4NClO_4 or $LiClO_4$, these metal ions are reduced almost reversibly. These effects of the cation of the supporting electrolyte can be explained as electrode surface phenomena as in the reduction of alkali metal ions.

In a previous paper,[1] we reported on the polarographic reduction of alkali metal ions in hexamethylphosphoramide (HMPA). We observed a significant influence of the cation of the supporting electrolyte on reduction: Sodium ion in 0.05 M Et_4NClO_4, for example, is not reduced until the reduction of the supporting electrolyte takes place. In 0.05 M Pr_4NClO_4 and 0.05 M Bu_4NClO_4 solutions, however, it gives a small reduction wave, the limiting current of which is controlled by the rate of the preceding process. With 0.05 M $LiClO_4$ as a supporting electrolyte, a reversible, diffusion-controlled sodium wave is obtained at −2.47 V *vs.* Ag/0.1 M $AgClO_4$ (HMPA). We attributed these effects to the change of the double-layer properties with the species of the cation of the supporting electrolyte.

We have investigated the polarographic behavior of the calcium, strontium and barium ions in HMPA by use of various perchlorates as supporting electrolytes. A significant effect of the cation of the supporting electrolyte was also observed as in the reduction of alkali metal ions. The reduction of magnesium ion was not studied, because in the solution of magnesium perchlorate an unexpected wave was observed which might be due to some decomposition product of HMPA.

Apparatus and Reagents

Apparatus. The AC polarograms were recorded with a Yanagimoto polarograph, Type P8-AC. The dropping mercury electrode had the following characteristics in 0.05 M Et_4NClO_4-HMPA and at $h=62$ cm: $m=1.88$ mg/sec with the circuit open and $t=1.39$ sec at −2.6 V *vs.* Ag/0.1 M $AgClO_4$ (HMPA) electrode. Other apparatus were the same as described previously.[1]. All experiments were carried out at 25±0.1°C.

Reagents. Tetra-*n*-hexylammonium perchlorate (Hex_4NClO_4) was prepared from $AgClO_4$ and Hex_4NI (product of the Eastman Kodak Co.) in ethanol, and recrystallized three times from ethanol. It was air dried. Other tetraalkylammonium perchlorates and lithium perchlorate were prepared and dried following the previous procedures.[1] The calcium and strontium perchlorates were prepared by neutralizing the reagent grade calcium and strontium hydroxides, respectively, with perchloric acid. The barium perchlorate was obtained commercially. These alkaline earth perchlorates were dried in a vacuum at 200°C. HMPA was purified following the method in the previous report.[1]

Experimental

The polarographic behavior of the calcium, strontium and barium ions in HMPA was examined by use of Me_4NClO_4, Et_4NClO_4, Pr_4NClO_4, Bu_4NClO_4, Hex_4NClO_4, and

* Electrochemical Studies in Hexamethylphosphoramide. II. For Part 1, see Ref. 1).

** Present address: Department of Chemistry, Faculty of Science, Shinshu University, Matsumoto.

1) K. Izutsu, S. Sakura, and T. Fujinaga, This Bulletin, **45**, 445 (1972).

Table 1. Results of polarographic reductions of alkaline earth metal ions in HMPA[a)]

Supporting electrolyte	Ba^{2+}			Sr^{2+}			Ca^{2+}		
	$E_{1/2}$	i_l/C	$i_p/2i_l\tau^{1/2}$	$E_{1/2}$	i_l/C	$i_p/2i_l\tau^{1/2}$	$E_{1/2}$	i_l/C	$i_p/2i_l\tau^{1/2}$
Me_4NClO_4	not reduced			not reduced			not reduced		
Et_4NClO_4	not reduced			not reduced			not reduced		
Pr_4NClO_4	−2.42[b)]	0.1$_9$[b)]	—	not reduced			not reduced		
Bu_4NClO_4	−2.45[b)]	1.3$_0$[b)]	8.$_0$[b)]	−2.70[b)]	0.9$_4$[b)]	—	−2.82[b)]	0.9$_4$[b)]	6.$_1$[b)]
Hex_4NClO_4	(−2.41)[c)]	1.9$_4$[c)]	19.$_4$[c)]	(−2.61)[c)]	1.5$_8$[c)]	23.$_5$[c)]	(−2.76)[c)]	1.7$_4$[c)]	15.$_6$[c)]
$LiClO_4$	(−2.40)[c)]	2.4$_1$[c)]	13.$_6$[c)]	—	—	—	—	—	—

a) The concentration of the supporting electrolyte is 0.05 M in each case.
$E_{1/2}$: half-wave potential in V *vs.* Ag/0.1 M $AgClO_4$, i_l: limiting current in μA, i_p: AC peak height in μmho, C: concentration of the depolarizer in mM, and τ: drop time at the peak potential in sec.
b) Kinetic controlled, irreversible wave.
c) Diffusion controlled, reversible wave, but with a polarographic maximum.

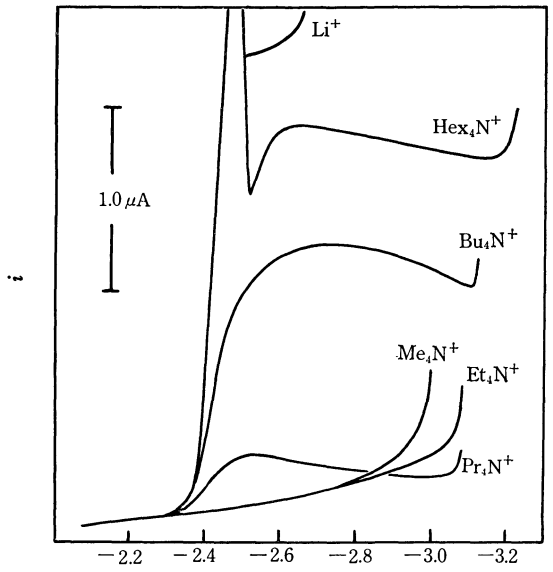

Fig. 1. Polarograms of 1.05 mM $Ba(ClO_4)_2$ in HMPA.
0.05 M solutions of various perchlorates are used as the supporting electrolytes. Cation of the supporting electrolyte is shown on each curve.

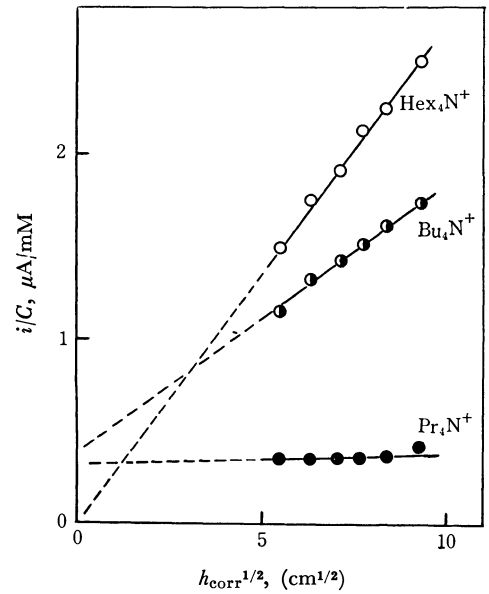

Fig. 2. Effect of the height of the mercury column on the limiting current of barium wave in HMPA.
Cations of the supporting electrolytes of 0.05 M perchlorates are shown on the curves.

$LiClO_4$ as supporting electrolytes. The results are summarized in Figs. 1, 4, and 5 and in Table 1.

Barium Ion. The barium ion in HMPA is irreducible when 0.05 M Me_4NClO_4 or 0.05 M Et_4NClO_4 is used as the supporting electrolyte (Fig. 1). In 0.05 M Pr_4NClO_4, however, a small wave appears at around −2.4 V and the limiting current is controlled by the rate of a preceding process, as judged from its dependence on the square root of the height of the mercury column (Fig. 2). In 0.05 M Br_4NClO_4, the barium wave is fairly well-defined but the i_l–$h^{1/2}$ relation in Fig. 2 shows that the limiting current is still not entirely diffusion-controlled. With 0.05 M Hex_4NClO_4 as the supporting electrolyte, a big maximum of the first kind is observed in the DC wave, but from the i_l–$h^{1/2}$ relation (Fig. 2) and from the high AC wave (Table 1) the reduction seems to be reversible and diffusion-controlled. The big limiting current observed in 0.05 M $LiClO_4$ is probably due to the maximum of the second kind.[1)]

Figure 3 shows the effect of Et_4NClO_4 on the barium wave in 0.05 M Hex_4NClO_4. It is noted that the addition of a very small amount of Et_4NClO_4 completely interferes with the reduction of the barium ion.

Strontium Ion. The strontium ion is irreducible in 0.05 M Me_4NClO_4, 0.05 M Et_4NClO_4, 0.05 M Pr_4NClO_4 (Fig. 4). With 0.05 M Bu_4NClO_4 as a supporting electrolyte, an irreversible wave is observed and the limiting current is controlled partly by diffusion and partly by the rate of a preceding process. In 0.05 M Hex_4NClO_4, a diffusion-controlled wave is obtained with the half-wave potential at about −2.61V, though the value is somewhat inaccurate due to the maximum of the first kind. The reduction in this supporting electrolyte seems to be reversible judging from the height of the AC polarographic wave (Table 1).

Calcium Ion. The calcium ion is irreducible in 0.05 M Me_4NClO_4, 0.05 M Et_4NClO_4, and 0.05 M Pr_4NClO_4 solutions (Fig. 5). In 0.05 M Bu_4NClO_4, an irreversible wave is observed, but the reduction is also controlled by the rate of a precedig process and then wave height is only half that of the diffusion wave. In 0.05 M Hex_4NClO_4 solution, the reduction of calcium ion preceeds reversibly, though an abnormal small maximum (or decrease of the base current) appears about 0.2V in advance to the main wave at $E_{1/2}=-2.76$ V, which also is accompanied by a small maximum (Fig. 5).

The calcium perchlorate salt is hygroscopic and the small amount of water from the salt makes the height of both

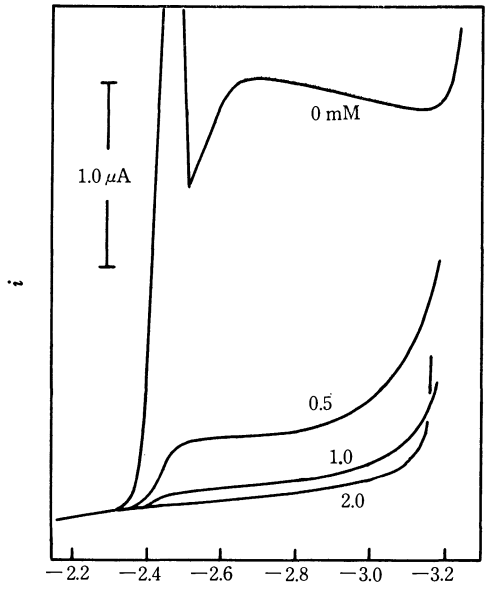

Fig. 3. Effect of the addition of the Et_4N^+ ion on the reduction wave of 1.07 mM barium ion in 0.05 M Hex_4NClO_4-HMPA.
Concentration of Et_4N^+ ion in mM is shown on each curve.

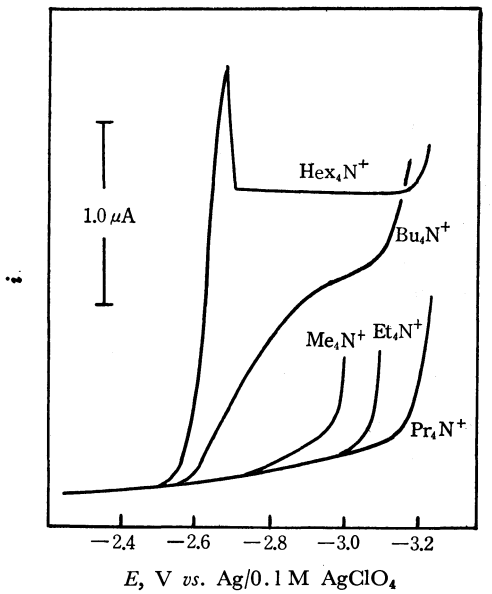

Fig. 4. Polarograms of 1.00 mM $Sr(ClO_4)_2$ in HMPA.
Cation of the supporting electrolyte is shown on each curve.

maxima increase. However, the reason for the appearance of the abnormal maximum, change of height and the shift of the potential of the abnormal maximum by the addition of water has not been elucidated yet.

Discussion

As in the case of alkali metal ions,[1] the reduction of alkaline earth metal ions in HMPA is strongly influenced by the cation of the supporting electrolyte. The effect is closely related to the size of the solvated cation of the supporting electrolyte. If the size of the solvated cation of the supporting electrolyte is small as in the cases of Et_4NClO_4 and Me_4NClO_4, the reduction

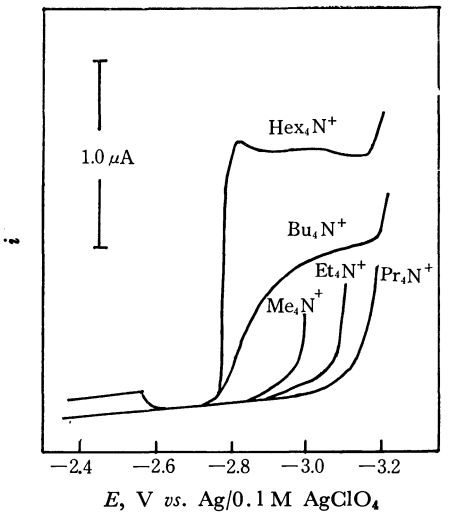

Fig. 5. Polarograms of 0.81 mM $Ca(ClO_4)_2$ in HMPA.
Cation of the supporting electrolyte is shown on each curve.

of all alkaline earth metal ions is made irreducible. The reduction becomes easier with the increase in size. In Hex_4NClO_4 solutions, the reduction of all alkaline earth metal ions proceeds reversibly and is diffusion-controlled. When the size is in between these two extremes, reduction is irreversible and the limiting current is kinetically controlled.

The adsorption of monovalent cation on the charged electrode surface at highly negative potential becomes easier with the decrease of the size of the solvated cation and, in the presence of two kinds of monovalent cations, a preferential adsorption of the smaller cation takes place.[1]

In the supporting electrolyte with small cation, the approach of heavily solvated alkali metal ions to the electrode surface is difficult and a preceding process is necessary in advance to the reduction of these ions. We considered this preceding process to be either a (partial) desolvation of the depolarizing cation or the penetration of the depolarizing ion through the adsorbed layer of the cation of the supporting electrolyte.

In HMPA, alkaline earth metal ions are heavily solvated and the Stokes law radii of the solvated ions 5.8—6.0Å for barium, strontium and calcium ions.[2] These values are much larger than 2.7Å for Et_4N^+, 3.2Å for MeN^+ and 3.7Å for Pr_4N^+, somewhat larger than 4.3Å for Bu_4N^+ and 4.9Å for Li^+, and approximately the same as 5.7Å for Hex_4N^+. Similar to the case of alkali metal ions, the reduction of alkaline earth metal ions in the supporting electrolyte with relatively small cation also seems to be difficult.

Gutmann *et al.*[3] reported that alkaline earth metal ions in dimethylacetoamide (DMA) are irreducible unless a small amount of water is introduced into the electrolytic solutions. They used Et_4NClO_4 as the supporting electrolyte. Alkaline earth metal ions in DMA also become reducible by using supporting electrolytes with larger cations.

2) T. Fujinaga, K. Izutsu, and S. Sakura, *Nippon Kagaku Kaishi*, submitted to publication.

3) V. Gutmann, M. Michlmayr and G. Peychal-Heiling, *J. Electroanal. Chem.*, **17**, 153 (1968).

Selective Activation of Methylene or Methine Groups in Coordinated Dipeptide Schiff Bases

Osamu UYAMA, Yasuo NAKAO, and Akitsugu NAKAHARA

Department of Chemistry, College of General Education, Osaka University, Toyonaka, Osaka

(Received July 18, 1972)

Nickel(II) and cobalt(III) chelates of the Schiff bases derived from salicylaldehyde and dipeptides such as glycylglycine, glycylalanine and alanylglycine have newly been prepared. The reactivity of methylene or methine groups in the dipeptide moieties of those Schiff base chelates has been investigated on the basis of their PMR spectra in D_2O. It has been confirmed that the methylene or methine protons of the *N*-terminal amino acid residue are more easily activated than those of the *C*-terminal amino acid residue.

It was demonstrated by Williams and Busch[1] that the methylene or methine protons of α-amino acids are activated on chelation with metal ions. Fore this, threonine had been synthesized from bis(glycinato)copper(II) and acetaldehyde in the presence of sodium carbonate.[2] It was reasoned that the amino group would be protected by coordination, and sufficient activation of the methylene group would result from the polarizing effect of the metal ion.[2-4]

Similar investigations have recently been extended to the case of coordinated dipeptides. For example, Noda *et al.*[5] reported that the main product out of the reaction between glycylglycine and formadehyde in the presence of copper(II) is serylglycine, not accompanied by glycylserine or serylserine at all. This suggests that the methylene group in the *N*-terminal amino acid residue is selectively activated on chelation with metal ion. On the other hand, Gillard *et al.*[6] reported that the methylene protons of the *C*-terminal amino acid residue in the cobalt(III) dipeptide chelates are replaced easily in alkaline solution by the deuterons of heavy water, but not those of the *N*-terminal amino acid residue.

In order to clarifying the two conflicting results, we have investigated the selective activation of methylene or methine groups in coordinated dipeptide Schiff bases.

This paper deals with the preparation of nickel(II) and cobalt(III) chelates of the Schiff bases derived from salicylaldehyde and dipeptides containing glycine and/or α-alanine, and the results of PMR study of those chelates in view of the selective activation of methylene or methine groups in coordinated dipeptide moieties. On the basis of our findings, the conclusions of Noda *et al.* and Gillard *et al.* have consistently been explained.

Experimental

Glycyl-α-alanine and *α-alanylglycine* were prepared according to the method of Hanson and Smith[7] and Miller *et al.*[8], respectively.

Na[Ni(Sal=Gly·Gly)]·H_2O was obtained in a similar way to that described in the preceding paper[9] employing 1 N sodium hydroxide solution. Found: C, 38.97; H, 3.29; N, 8.17%. Calcd for $Na[Ni(C_{11}H_9N_2O_4)]\cdot H_2O$: C, 39.67; H, 3.31; N, 8.42%.

K[Ni(Sal=L-Ala·Gly)]·H_2O: 1.5 g of L-alanylglycine and 3 g of bis(salicylaldehydato)nickel(II) were dissolved in 15 ml of water. The mixture was adjusted to pH 9—10 with 1 N potassium hydroxide solution, stirred at 25°C for an hour and filtered. To the filtrate was added 600 ml of a mixture of ether and ethanol (1 : 1 by volume) with constant stirring, orange crystals being deposited. These were dissolved in a small quantity of water, and then recrystallized by dropwise addition of a mixture of ethanol and ether (1 : 1 by volume). Found: C, 39.16; H, 3.22; N, 7.63%. Calcd for $K[Ni(C_{12}H_{11}N_2O_4)]\cdot H_2O$: C, 39.67; H, 3.58; N, 7.72%.

K[Ni(Sal=Gly-L-Ala)]·2H_2O was prepared by the same method as described above. Found: C, 37.73; H, 3.65; N, 7.42%. Calcd for $K[Ni(C_{12}H_{11}N_2O_4)]\cdot 2H_2O$: C, 37.82; H, 3.94; N, 7.35%.

Ba[Co(NO_2)$_2$(Sal=Gly·Gly)]·2H_2O: To a mixture of 4 g of $Na_3[Co(NO_2)_6]$ and 20 ml of water was added a solution of glycylglycine (1.3 g) and salicylaldehyde (1.2 g). The resulting mixture was adjusted to pH 9 with 2 N sodium hydroxide solution. After it had been stirred at 60°C for two hours, the reaction mixture was filtered. A hot saturated aqueous solution of $BaCl_2\cdot 2H_2O$(10 g) was then added to the filtrate. Upon cooling the solution, crystals were obtained and recrystallized from hot water. Found: C, 23.86; H, 2.36; N, 10.20%. Calcd for $Ba[Co(NO_2)_2(C_{11}H_9N_2O_4)]\cdot 2H_2O$: C, 23.68; H, 2.33; N, 10.05%.

Ba[Co(NO_2)$_2$(Sal=DL-Ala·Gly)]·3H_2O was obtained in the same way. Found: C, 24.22; H, 2.99; N, 9.69%. Calcd for $Ba[Co(NO_2)_2(C_{12}H_{11}N_2O_4)]\cdot 3H_2O$: C, 24.44; H, 2.89; N, 9.50%.

Ba[Co(NO_2)$_2$(Sal=Gly-L-Ala)]·2H_2O was obtained also in the same way. Found: C, 25.03; H, 2.65; N, 9.76%. Calcd for $Ba[Co(NO_2)_2(C_{12}H_{11}N_2O_4)]\cdot 2H_2O$: C, 25.21; H, 2.65; N, 9.80%.

PMR Measurement. The spectra were obtained by the use of a JEOL C-60HL Spectrometer for deuterium oxide solution containing about 200 mg of complex/0.8 ml D_2O. The chemical shift was measured relative to the sodium salt of trimethylsilylpropane sulfonic acid taken as an internal standard. The barium salts of the cobalt(III) complexes

1) D. H. Williams and D. H. Busch, *J. Amer. Chem. Soc.*, **87**, 4644 (1965).
2) M. Sato, K. Okawa, and S. Akabori, This Bulletin, **30**, 937 (1957).
3) Y. Ikutani, T. Okuda, and S. Akabori, *ibid.*, **33**, 582 (1960).
4) T. T. Otani and M. Winitz, *Arch. Biochem. Biophys.*, **90**, 254 (1960).
5) K. Noda, M. Bessho, T. Kato, and N. Izumiya, This Bulletin, **43**, 1834 (1970).
6) R. D. Gillard, P. R. Mitchell, and N. C. Payne, *Chem. Commun.*, **1968**, 1150.
7) H. T. Hanson and E. L. Smith, *J. Biol. Chem.*, **175**, 833 (1948).
8) A. Miller, A. Neidle, and H. Waelsh, *Arch. Biochem. Biophys.*, **56**, 11 (1955).
9) Y. Nakao and A. Nakahara, This Bulletin, **46**, 187 (1973).

were converted into lithium salts using lithium sulfate, with which the barium ion was precipitated as $BaSO_4$. The pD-adjustment was performed by the addition of 2 N NaOD-heady water solution. A Yanagimoto pH-66A pH meter equipped with a MGR-11A combined electrode was used after standardization with a Nakarai standard buffer solution (pH 6.86 and 9.18 at 25°C).

Results and Discussion

Proton NMR spectroscopy is a convenient method for studying the behavior of hydrogen atoms in metal Schiff base complexes. We prepared a series of diamagnetic nickel(II) and cobalt(III) complexes of the Schiff bases derived from salicylaldehyde and dipeptides (glycylglycine, glycyl-α-alanine and α-alanylglycine) and investigated their PMR spectra at various pD-values.

Nickel(II) Complexes. The structures of nickel(II) complexes are given in Fig. 1, in which the methylene or methine group of the *N*-terminal amino acid residue is denoted by (A), and that of the *C*-terminal amino acid residue by (B).

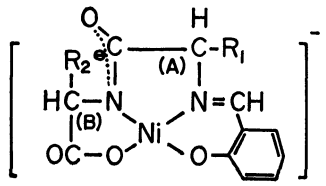

R_1, R_2=H or CH_3

Fig. 1. General structure of nickel(II)-dipeptide-Schiff base complexes.

The PMR spectra for $[Ni(Sal{=}Gly{\cdot}Gly)]^-$ are illustrated in Fig. 2; (a) is the spectrum recorded comparatively soon after the solution was prepared at room temperature and at pD 11.6. The resonance signals at 2.8 and 3.4 ppm are considered to be due to the methylene protons of (A) and (B), and those at 6.5—8 ppm the phenyl and the azomethine protons. Apparently the spectrum indicates that both the methylene protons of (A) and (B) are not replaced by deuterons. On the other hand, the spectrum shown in Fig. 2-(b), which was recorded after allowing the same solution to stand at 40°C for 27 days indicates that the signal at 3.4 ppm has decreased but not that at 2.8 ppm. This suggests that the only one methylene protons of either (A) or (B) are replaced by deuterons, but not those of the others. We see from Fig. 2-(c) that both the signals at 3.4 and 2.8 ppm decrease on allowing the solution to stand at 40°C and at pD 13.1 for 23 days. Under this condition the above trend is so remarkable as regards the signal at 3.4 ppm that even the mark of signal cannot be observed. It is considered that at this high pD-value both kinds of methylene protons are eventually activated, but the one is more easily activated than the other.

Figure 3 shows the spectra of $[Ni(Sal{=}L\text{-}Ala{\cdot}Gly)]^-$ under various conditions. Spectrum (a) recorded

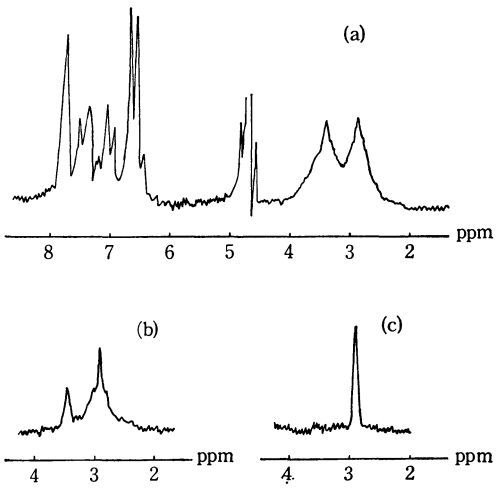

Fig. 2. PMR spectra of $[Ni(Sal{=}Gly{\cdot}Gly)]^-$: (a) pD 11.6, room temp., after 2 hr; (b) pD 11.6, 40°C, after 27 days; (c) pD 13.1, 40°C, after 23 days.

comparatively soon after preparing the solution (room temperature, pD 10.2) indicates that neither the protons of the methylene group (B)(R_2=H) or of the methine group (A)(R_1=CH_3) are replaced by deuterons. The resonance signal of a doublet at 1.2 ppm arises from the methyl protons, that at 2.8 ppm from the methylene protons of (B) and that of a quartet at 3.4 ppm from the methine proton of (A). As is seen in Fig. 3-(b), the methyl doublet at 1.2 ppm partly collapses on allowing the solution to stand at 40°C and at pD 11, producing a singlet on account of the deuterization of the methine proton of (A), but the signal at 2.8 ppm due to the methylene protons of (B) does not decrease.

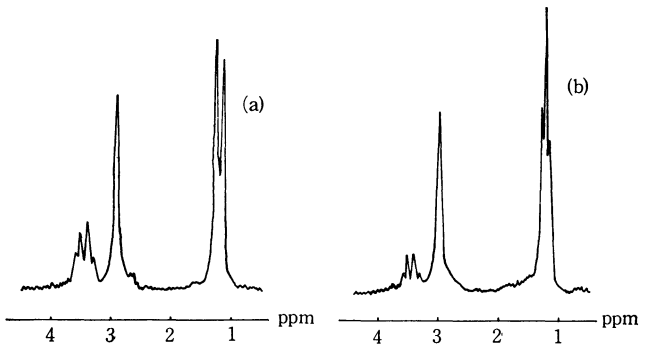

Fig. 3. PMR spectra of $[Ni(Sal{=}L\text{-}Ala{\cdot}Gly)]^-$: (a) pD 10.2, room temp, after 2 hr; (b) pD 11, 40°C, after 27 days.

The spectra of $[Ni(Sal{=}Gly{-}L\text{-}Ala)]^-$ under various conditions are illustrated in Fig. 4. (a) is the spectrum obtained comparatively soon after preparing the solution (room temperature, pD 10.6), indicating that the protons of both the methylene group (A) (R_1=H) and the methine group (B)(R_2=CH_3) are not replaced by deuterons. The resonance signal of a doublet[10] at 1.3 ppm arises from the methyl protons

10) Careful inspection of the signal shows that it is composed of a couple of doublets. This may be because of the coexistence of two isomers relative to the different conformation of the methyl group, namely, pseudo-equatorial and pseudo-axial.

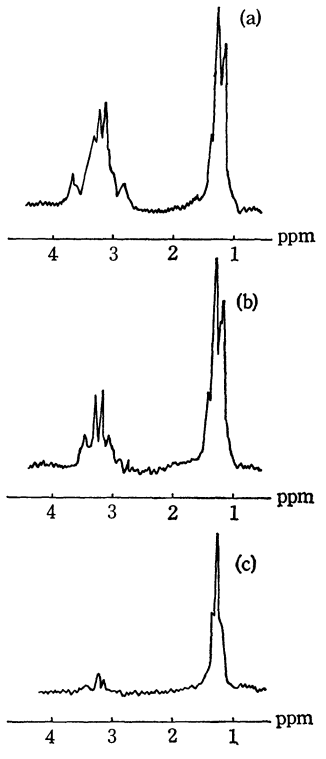

Fig. 4. PMR spectra of [Ni(Sal=Gly-L-Ala)]$^-$: (a) pD 10.6, room temp., after 2 hr; (b) pD 11, 40°C, after 27 days; (c) pD 14, 40°C, after 27 days.

(R_2=CH_3). The signals at 3—3.5 ppm arise from the methylene and the methine protons of (A) and (B), respectively. On allowing the solution to stand at 40°C and at pD 11 for 27 days, the signals at 3—3.5 ppm turn out to be a quartet on account of the deuterization of the *N*-terminal methylene protons, whereas the doublet at 1.3 ppm remains unchanged (Fig. 4-(b)). However, at pD 14 the signal at 3—3.5 ppm completely disappears and even the doublet at 1.3 ppm completely collapses to give a singlet on allowing the solution to stand at 40°C for 27 days. This indicates that i) only the *N*-terminal methylene or methine group is activated at around pD 11, and ii) the protons of both (A)- and (B)-methylene or methine group are activated at around pD 13—14, the former being activated more easily.

The preferential activation of the methylene or methine group at the *N*-terminal amino acid residue appears to be different from the conclusion of Gillard *et al.*[6] In order to clarify whether this arises from the formation of chelates of dipeptide Schiff bases instead of simple dipeptide chelates or from the difference in the kind of central metal ion, we have further investigated the pmr spectra of cobalt(III) complexes of similar dipeptide Schiff bases.

Cobalt(III) Complexes. Three new dinitro-cobalt(III) complexes of the Schiff bases derived from salicylaldehyde and dipeptides (glycylglycine, α-alanylglycine and glycyl-α-alanine) were synthesized. It was concluded that their structures are *trans* form, since their infrared spectra are quite similar to the corresponding planar nickel(II)-dipeptide-Schiff base complexes. The general structural formula of these complexes is shown in Fig. 5, in which the cobalt(III) chelate ring containing the *N*-terminal amino acid residue is denoted by (C) and that containing *C*-terminal amino acid residue by (D).

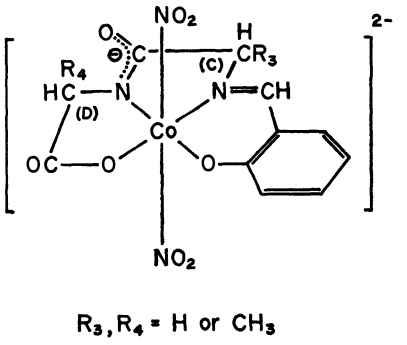

Fig. 5. General structure of cobalt(III)-dipeptide-Schiff base complexes.

The PMR spectra of $[Co(NO_2)_2(Sal{=}Gly{\cdot}Gly)]^{2-}$ in D_2O under various conditions are illustrated in Fig. 6. Spectrum (a), which was recorded comparatively soon after the preparation of the solution, shows that no protons of the methylene groups of (C) and (D) (R_3=R_4=H) are replaced by deuterons. The resonance signals at 4.1 and 4.5 ppm are due to the methylene protons of (C) and (D), and those at 6.5—8 ppm to the phenyl and the azomethine protons. After 3 days at 40°C (pD 10.6), the signal at 4.5 ppm decreased, but not that at 4.1 ppm (Fig. 6-(b)). This suggests that only one methylene group is activated at pD 10.6. Decomposition of the complex was observed in a stronger basic solution.

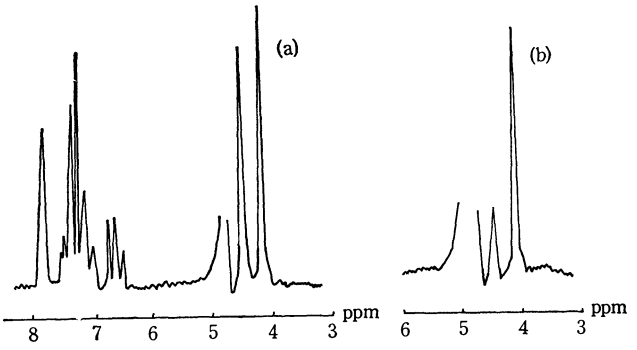

Fig. 6. PMR spectra of $[Co(NO_2)_2(Sal{=}Gly{\cdot}Gly)]^{2-}$: (a) pD 6.8, room temp., after 2 hr; (b) pD 10.6, 40°C, after 3 days.

Figure 7 shows the spectrum of $[Co(NO_2)_2(Sal{=}$DL-Ala·Gly$)]^{2-}$. It is obvious that the protons of methylene or methine groups are not replaced by deuterons within two hours at room temperature and at pD 7. The signal at 1.4 ppm arises from the methyl protons (R_3=CH_3), that at 4.2 ppm from the methylene protons (D) (R_4=H), and that of a quartet at 4.4 ppm from the methine proton (C). On allowing the solution to stand at 40°C and at pD 10.6 for a day, the doublet signal for the methyl group at 1.4 ppm slightly collapses to give a singlet on account of the deuterization of the methine proton (C), the signal

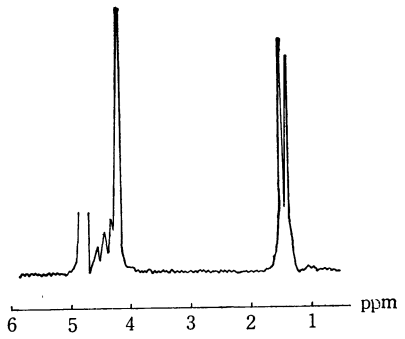

Fig. 7. PMR spectrum of $[Co(NO_2)_2(Sal=DL\text{-}Ala\cdot Gly)]^{2-}$: pD 7, room temp., after 2 hr.

for the methylene protons (D) remaining unchanged. Further deuterization expected to occur in the methylene group of (D) was not successfully observed on account of gradual decomposition of the complex. It can be said also for the cobalt(III)-dipeptide-Schiff base chelates that the methylene or methine group of (C) is activated more easily than that of (D). In other words, there is no essential difference between the nickel(II)- and cobalt(III)-chelates as far as the selective activation of the methylene or methine group in coordinated dipeptide Schiff bases is concerned.

Thus the confliction with the results of Gillard *et al.*,[6] who concluded the preferential activation of the methylene or methine group of (D), appears to arise from the difference in the structure of the terminal amino group (dipeptide Schiff base or simple dipeptide).

Reactions of Coordinated Dipeptide Schiff Bases with Formaldehyde. A preliminary experiment on the reactions of the above nickel(II) or cobalt(III) complexes with formaldehyde was carried out. In the case of the reaction of *N*-salicylideneglycylglycinatonickelate(II) in a slightly basic solution at 100°C the main products were serylglycine and α-hydroxymethylserylglycine. Apparently the result is consistent with the conclusion of the above described PMR-study and at the same time with the result reported by Noda *et al.*[5] Though the peptide they used was glycylglycine and not *N*-salicylideneglycylglycine, it might be considered that glycylglycine in the presence of copper(II) reacted with formaldehyde to form the Schiff base. If this is true, the selective activation of the methylene group at the *N*-terminal glycine moiety is understandable in the light of the above PMR-study. In the structure of the coordinated dipeptide Schiff bases, the electron-withdrawing effect of the metal ion can reach the α-carbon atom through azomethine nitrogen atom, whose electronic structure should differ entirely from that of the simple amino nitrogen in glycylglycine. This will probably enhance the reactivity of the *N*-terminal methylene group in glycylglycine moiety.

Thus, we proposed a reaction mechanism as illustrated in Scheme 1 for the reaction of Noda *et al.* The

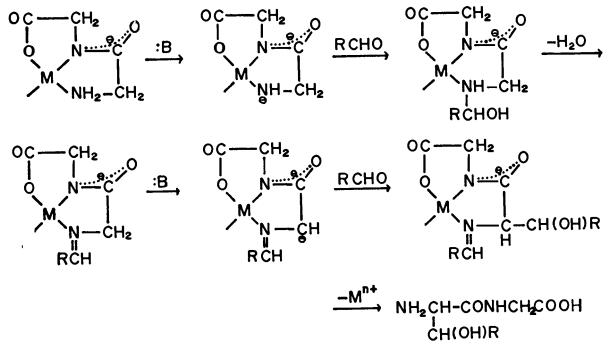

Scheme 1.

mechanism may explain why the main products of the reaction were serylglycine and α-hydroxymethylserylglycine. Further it is also consistent with the mechanism presented by Ichikawa *et al.*[11] for the reaction of the bis(glycinato)- or pyruvylideneglycinatocopper(II) with formaldehyde. It does not contradict the conclusion on the selective activation of the methylene or methine group at the *C*-terminal amino acid moiety only in simple dipeptide chelates.[6]

The authors are grateful to Mr. H. Okuda for PMR measurements. Expenses for this work were defrayed in part by a grant from the Ministry of Education.

11) T. Ichikawa, S. Maeda, T. Okamoto, Y. Araki, and Y. Ishido, This Bulletin, **44**, 2779 (1971).

Spectrophotometric Study on the Extraction of the Ternary Complex Composed of Vanadium(V), 8-Hydroxyquinoline-5-sulfonic Acid and Zephiramine

Tomihito KAMBARA and Masao SUGAWARA

Department of Chemistry, Faculty of Science, Hokkaido University, Sapporo

(Received July 28, 1972)

The ternary complex composed of vanadium(V),8-hydroxyquinoline-5-sulphonic acid (H_2QS), and zephiramine (Z^+Cl^-) was extracted into chloroform. The absorption maxima of the ternary complex in the organic layer were 375 and 580 nm at pH 2.8 and 375 nm at pH 4.8. The optimum pH range for the extraction was 4.5—5.4. Beer's law held for 1.29—35.6 μg of vanadium(V). The molar absorptivity of the complex was 0.99×10^4 cm^{-1} mol^{-1} l. The composition of the ternary complex was estimated to be $[VO_2^+Z^+(QS^{2-}Z^+)_2]_o$ and the extraction equilibrium was given by

$$VO_2^+ + 2[(HQS^-Z^+)]_o + Z^+ + 2OH^- \rightleftharpoons [VO_2^+Z^+(QS^{2-}Z^+)_2]_o + 2H_2O \quad (1)$$

The logarithm of the equilibrium constant K of this equation was found to be 32.57 ± 0.49.

Oxine, *N*-benzoylphenylhydroxylamine, hydrogen peroxide, and phosphotungstic acid have been used mainly for the determination of trace amounts of vanadium(V). 8-Hydroxyquinoline-5-sulphonic acid (H_2QS), a water-soluble oxine derivative, was also suggested as a chelating agent for vanadium(V).[1] However, details of analytical conditions are lacking. We have extracted ionic association complex of vanadium(V)-H_2QS chelate anion with zephiramine (tetradecyl-dimethyl-benzyl-ammonium chloride) into chloroform. Yellow coloration of the extract obtained from a weakly acidic medium was very stable and the intensity was proportional to the concentration of vanadium(V) in the aqueous layer. A dark green coloration was also obtained by extraction from an acidic medium. However, because of the low sensitivity and instability of coloration, the extraction from a weakly acidic medium is preferable for determination of vanadium(V).

Experimental

Reagent. *Vanadium(V) Standard Solution*: 0.1770 g of guaranteed ammonium metavanadate NH_4VO_3 (Kanto Chemicals Co.) was dissolved in 25 ml of 2 M H_2SO_4 and diluted to 1 liter with water. The solution was standardized by EDTA-titration using a Cu-PAN indicator. The solution was diluted as required.

H_2QS Solution: 1.00×10^{-3} M solution was prepared by dissolving H_2QS (Wako Chemicals Co.) into water.

Zephiramine Solution: 5.00×10^{-3} M solution was prepared by dissolving Dotite zephiramine in water.

Buffer Solutions: A sulphuric acid-acetate buffer solution was prepared by mixing 0.5 M solutions of sulphuric acid and sodium acetate. A borate buffer solution was prepared by mixing 0.1 M solutions of hydrochloric acid and borax.

Chloroform was purified by washing with sulphuric acid, diluted sodium hydroxide and water, followed by distillation.

The other reagents used were all of analytical reagent grade. Resin-deionized water was used.

Apparatus. A Shimadzu QV-50 spectrophotometer with 10-mm cells was used for measurements of absorbance. A Hatachi-Horiba, Model F-5, glass electrode pH meter was used for pH measurements. An Iwaki KM shaker was used.

Procedure. Vanadium(V) (25.5 μg) was dissolved with 6 ml H_2QS solution and 2.5 ml zephiramine solution in a 100 ml separatory funnel. The pH adjustment was performed with 15 ml of the sulphuric acid-acetate buffer solution in the range 4.7—4.9 and then filled up to 50 ml with water. The mixtures with 10 ml of chloroform were shaken for 10 min and left for 5 min to let the layers separate. The chloroform layer was transfered to a beaker containing anhydrous Na_2SO_4 and offered to a optical measurement. The absorbance of the extract at 375 nm was measured against the reagent blank obtained in the same way.

Results and Discussion

Absorption Spectra. Absorption spectra of the aqueous layer are presented in Fig. 1. The vanadium (V)-H_2QS chelate anion in water has an absorption maximum at 365 nm. The ternary complex formed by addition of zephiramine has different absorption maximum depending on pH value, *viz.*, 375 nm at pH 4.8, 395 and 580 nm at pH 2.8. The ionic association complex extracted into chloroform has a yellow coloration at pH 4.8 and dark green coloration at pH 2.8. The absorption maximum of the yellow extract is 375 nm and those of the dark green extract are 375 and 580 nm as shown in Fig. 2. The yellow

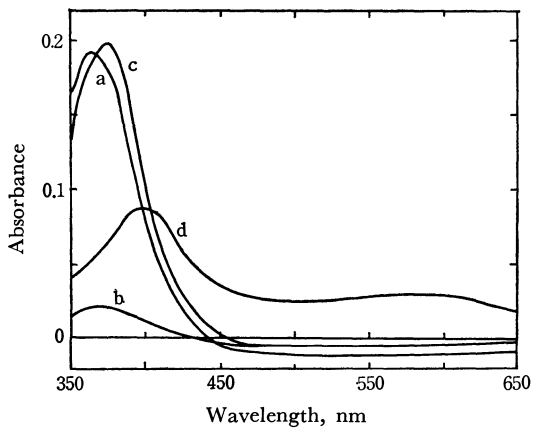

Fig. 1. Absorption spectra of V(V)-QS and V(V)-QS-Z complexes in aqueous layer.
Curve (a) $[V(V)]_w=2.0\times10^{-5}$ M, $[QS]_w=2.4\times10^{-4}$ M, pH 4.8, *vs.* reagent blank, (b) pH 2.8, Curve (c) $[V(V)]_w=2.0\times10^{-5}$ M, $[QS]_w=2.4\times10^{-4}$ M, $[Z]_w=5.0\times10^{-4}$ M, pH 4.8, *vs.* reagent blank, (d) pH 2.8.

1) F. D. Snell and C. T. Snell, "Colorimetric Methods of Analysis," vol. II, p. 453, 3rd Ed., (D. van Norstrand Co., Inc., New York).

TABLE 1. COMPARISON OF SENSITIVITY OF SOME COMMON SPECTROPHOTOMETRIC METHODS FOR VANADIUM(V)

Reagent	Chemical formula	Molar absorptivity (cm^{-1} mol^{-1} l)	Wavelength (nm)	Reference
Oxine	$VO(OH)Ox_2$	3220 ($CHCl_3$)	540	
		6200 ($CHCl_3$)	365	2
	$C_4H_9NH_3VO_2Ox_2$	7000 (benzene)	380	
N-Benzoylphenyl-hydroxylamine	$VO(OH)(BPA)_2$	4500 (benzene)	530	3
		4650 ($CHCl_3$)	510	4
4-(2-Pyridylazo)-resorcin and zephiramine		43000 ($CHCl_3$)	560	5
8-Hydroxyquinoline-5-sulphonic acid and zephiramine	VO_2+Z($QS^{2-}Z^+$)$_2$	9900 ($CHCl_3$)	375	

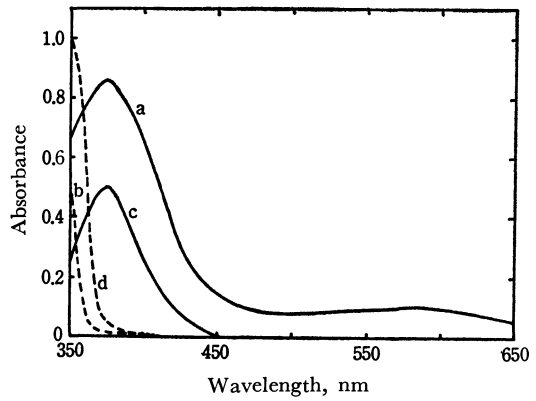

Fig. 2. Absorption spectra of the ternary complex V(V)-QS-Z in chloroform layer.
Curve (a) $[V(V)]_w = 2.0 \times 10^{-5}$ M, $[QS]_w = 2.4 \times 10^{-4}$ M, $[Z]_w = 5.0 \times 10^{-4}$ M, pH 2.8, *vs.* reagent blank, (b) reagent blank *vs.* $CHCl_3$, Curve (c) $[V(V)]_w = 1.0 \times 10^{-5}$ M, $[QS]_w = 1.2 \times 10^{-4}$ M, $[Z]_w = 5.0 \times 10^{-4}$ M, pH 4.8, *vs.* reagent blank, (d) reagent blank *vs.* $CHCl_3$, Volume of aqueous layer $V_w = 50$ ml, Volume of organic layer $V_o = 10$ ml.

extract was very stable and the absorbance at 375 nm was found to remain unchanged after being left standing for 6 hours, but that at 580 nm decreased in the dark green extract.

Effect of pH. The aqueous layer adjusted to various pH values was treated by the above procedure. It was found that optimum pH range for the extraction was 4.5—5.4; 2.4—2.8 for the dark green extract. In borate buffer solution, no stable and constant absorbance was obtained.

Effect of H_2QS and Zephiramine Concentrations. Concentrations of H_2QS and zephiramine were varied. Absorbance of the extract was found to be constant with concentration range higher than 10-fold of H_2QS and 20—40-fold of zephiramine to vanadium(V).

Effect of Shaking Time. Shaking time was varied from 3 min to 20 min in the above procedure. It was found that the quantitative extraction of vanadium(V) was attained for shaking longer than 5 minutes.

Extractability and Molar Absorptivity. A 50-ml portion of the aqueous layer containing 25.5 μg of vanadium(V) was shaken with 10 ml of chloroform, and the absorbance of the extract was measrued. 25 ml of the separated aqueous layer was then re-extracted with 5 ml of chloroform. Extractability was calculated from the sum of absorbances of the extracts and that of the first extract. It was found that 99.9% of vanadium(V) was extracted by a single extraction, the molar absorptivity of the ternary complex being 0.99×10^4 cm^{-1} mol^{-1} l. The molar absorptivity is larger than that of the corresponding oxine complex as shown in Table 1.

Calibration Curve. Extraction of varying amounts of vanadium(V) was carried out. Beer's law held in the concentration range 1.29—35.6 μg of vanadium(V). Sandell's sensitivity for the absorbance of 0.001 was 0.0051 μg cm^{-2}. The relative standard deviation obtained by 7 measurements was 0.74% for 25.5 μg of vanadium(V).

Composition of Vanadium(V)-H_2QS Complexes. A continuous variation method applied at pH 4.0 indicated that mole ratio of H_2QS to vanadium(V) was 2 : 1. The same result was obtained also by the mole ratio method.

Composition of the Ternary Complex. A continuous variation method of the three-component system[6-9] was applied to the determination of the composition of the ternary complex. The sum of concentrations of vanadium(V), H_2QS, and zephiramine in the aqueous layer was kept to 7.00×10^{-5} M and the extraction was carried out at pH 4.8. As shown in Fig. 3, maximum absorbance was obtained at the concentration ratio of vanadium(V): H_2QS: zephiramine = 1.2 : 2.5 : 3.5, namely 1 : 2 : 3. The above result was confirmed by using Affsprung's method.[10] It is known that the group V–OH in 8-hydroxyquinolate is acidic and reacts with amines.[11]

2) F. Umland, *Z. Anal. Chem.*, **190**, 186 (1962).
3) U. Priyadashi and S. G. Tandon, *Anal. Chem.*, **33**, 435 (1961).
4) H. Einaga and H. Ishii, *Bunseki Kagaku*, **17**, 839 (1968).
5) T. Yotsuyanagi, R. Yamashita, and K. Aomura, *ibid.*, **19**, 981 (1970).
6) T. Kambara, S. Matsumae, and K. Hasebe, *ibid.*, **19**, 462 (1970).
7) T. Kambara, M. Sugawara, and K. Hasebe, *ibid.*, **19**, 1239 (1970).
8) T. Kambara, M. Maeyama, and K. Hasebe, *ibid.*, **20**, 1249 (1971).
9) T. Kambara and M. Sugawara, This Bulletin, **45**, 1430, (1972).
10) H. E. Affsprung and T. W. Murphy, *Anal. Chim. Acta*, **32**, 381 (1965).
11) A. J. Blair, D. A. Pantory, and G. J. Minkoff, *J. Inorg. Nucl. Chem.*, **5**, 316 (1958).

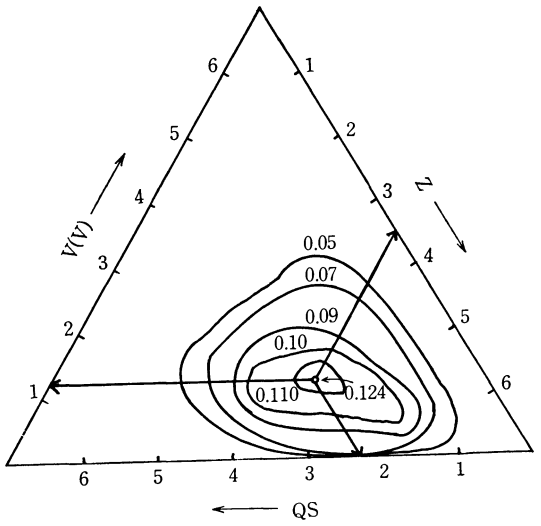

Fig. 3. Continuous variation method applied to three-component system of V(V)-QS-Z complex in organic layer. $V_w=50$ ml, $V_o=10$ ml, $[V(V)]_w+[QS]_w+[Z]_w=7.00\times10^{-5}$ M, pH 4.8, Wavelength: 375 nm, *vs.* $CHCl_3$.

The composition of the ternary complex was therefore estimated to be $[VO_2{}^+Z^+(QS^{2-}Z^+)_2]_o$.

Equilibrium Constant. Extraction of the ternary complex can be given by

$$VO_2{}^+ + 2[(HQS^-Z^+)]_o + Z^+ + 2OH^- \rightleftharpoons [VO_2{}^+Z^+(QS^{2-}Z^+)_2]_o + 2H_2O \quad (1)$$

with the equilibrium constant K

$$K=\frac{[VO_2{}^+Z^+(QS^{2-}Z^+)_2]_o}{[VO_2{}^+][(HQS^-Z^+)]_o{}^2[Z^+][OH^-]^2} \quad (2)$$

where subscript o denotes the organic layer. 50 ml of the aqueous layer, containig $*C$ mole of vanadium-(V), $2*C$ mole of H_2QS and $3*C$ mole of zephiramine was equilibrated with 10 ml of chloroform. By measurements of absorbance of the extract, concentration of the ternary complex C_T was calculated from the molar absorptivity. Equation (2) is then given by

$$K=\frac{[C_T]}{\left[*C-\frac{10}{50}C_T\right]\left[\frac{50}{10}\times2*C-2C_T\right]^2[*C][OH^-]^2} \quad (3)$$

The results obtained with various values of concentration of $*C$ are shown in Table 2. The logarithm of the equilibrium constant is 32.57 ± 0.49.

TABLE 2. EQUILIBRIUM CONSTANT OF V(V)-QS-Z TERNARY COMPLEX EXTRACTION SHOWN BY EQUATION (1)—(3)

*C (M)	Absorbance	C_T (M)	pH	log K
1.8×10^{-5}	0.251	2.53×10^{-5}	4.80	32.73
1.2×10^{-5}	0.111	1.12×10^{-5}	4.80	32.28
6.0×10^{-6}	0.025	2.52×10^{-6}	4.81	32.70

Ionic strength $\mu=0.456$, Molar absorptivity $\varepsilon=0.99\times10^4$ $cm^{-1}mol^{-1}$ l, Temp. 18.0°C,
$*C$=Initial amount of V(V) in 50-ml aqueous layer,
$2*C$=Initial amount of H_2QS in 50-ml layer,
$3*C$=Initial amount of Z^+ in 50-ml layer,
C_T=Final amount of the ternary complex in 10-ml $CHCl_3$-extract.

BULLETIN OF THE CHEMICAL SOCIETY OF JAPAN, VOL. 46, 502—506 (1973)

Kinetic Studies of the Nickel Maleate Complex Formation in Solution by the Pressure-jump Method

Shoji HARADA and Tatsuya YASUNAGA

Department of Chemistry, Faculty of Science, Hiroshima University, Higashisenda-machi, Hiroshima

(Received August 7, 1972)

Nickel maleate complex formation reaction in an aqueous solution, $Ni^{2+}+Mal^{2-} \underset{k_d}{\overset{k_f}{\rightleftharpoons}} NiMal$, where Mal^{2-} represents the maleate ion, was studied by the pressure-jump method. The rate constants and the stability constant were obtained; $k_f=8.4\times10^5\ M^{-1}\ s^{-1}$, $k_d=2.1\times10^3\ s^{-1}$, and $K=4\times10^2\ M^{-1}$ at 25°C and at $\mu\rightarrow0$. The thermodynamic parameters of this reaction were obtained from studies at various temperatures between 10 and 30°C. The results indicate that the nickel maleate is stable as a monodentated complex rather than as a chelate complex. Moreover, the nickel dicarboxylate complex formation reactions and the rate equations were discussed.

Static measurements of the stabilities of the chelate complexes[1-3] have revealed that the stabilities depend greatly on the carbon number or the structure of the ligands; *e. g.*, the five-membered ring complex is more stable than the six membered one. In the nickel dicarboxylate, the oxalate ion makes a more stable complex than that of the malonate.[4] The same ligand effects can also be observed in the kinetic measurements;[5,6] the difference in the stabilities has been attributed to that of the ligand-dissociation rate constants.

The nickel dicarboxylate complex formation reaction, which involves the replacement of the two coordinated water molecules, has usually been interpreted

1) F. Basolo and R. G. Pearson, "Mechanism of Inorganic Reactions," John Wiley and Sons, New York, N. Y., (1967).
2) F. A. Cotton and F. E. Harris, *J. Phys. Chem.*, **59**, 1203 (1955).
3) K. S. Rajan and A. E. Martell, *J. Inorg. Nucl. Chem.*, **29**, 523 (1967).
4) L. G. Sillen and A. E. Martell, "Stability Constants of Metal-ion Complexes," Special Publication No. 17, The Chemical Society, London, (1964).
5) G. H. Nancollas and N. Sutin, *Inorg. Chem.*, **3**, 360 (1964).
6) F. P. Cavasino, *J. Phys. Chem.*, **69**, 4380 (1965).

by the step-by-step mechanism proposed by Eigen *et. al.*[7] For the assignment of the relaxation effects, however, two different theories have been proposed. According to the first theory,[5,6,8,9] the rate-determining step is supposed to be the formation of the first bond between the metal ion and the ligand, whereas in the second theory[10,11] the ring closure of the chelate is assumed.

One of the two purposes of the present work is to discuss these two theories; the other was to ascertain the ligand effects on the stability constants, the rate constants, the reaction mechanisms, and the thermodynamic parameters of the nickel dicarboxylate complex formation reactions.

Experimental

All of the chemicals used were of a reagent grade. A stock solution of the nickel maleate was prepared by mixing a stoichiometric amount of $NiSO_4$ with maleic acid, and the sulfate ion was precipitated out as the insoluble $BaSO_4$. The solid $BaSO_4$ was removed by filtration. The concentration of the nickel maleate of the stock solution was determined by dimethylglyoxime titration. Each solution studied was prepared by diluting the stock solution to the desired concentration. The pH's of the solutions were 7.1—7.2, with most of the ligands in the dissociated form. No buffering or supporting electrolytes were added, and so the ionic strength of the solution was varied arbitrarily.

The pressure-jump apparatus used has been described in considerable detail elsewhere.[8] The only significant change made was that a single cell is now employed, rather than a double cell; *i. e.*, a valuable resistor was used in place of the reference cell. This improvement has resulted not only in making the experiments more easy, but also in increasing the signal-to-noise ratio. The time constant of the apparatus was 100 μs. The solution of either the nickel ion or the maleate ion in the absence of the other showed no relaxation effect in the present time range. This proved that the relaxation effect is due to the nickel maleate complex formation reaction.

The measurements were carried out at 10, 15, 20, 25, and 30°C in the concentration range from 5.06×10^{-4} to 5.06×10^{-2} M of the nickel maleate. The relaxation times quoted are the mean values of several runs.

Results

The experimental conditions and the observed relaxation times at 25°C are shown in Table 1. The concentration dependence of the relaxation time can be explained on the basis of this simple mechanism:

$$M^{2+} + L^{2-} \underset{k_d}{\overset{k_f}{\rightleftharpoons}} ML. \qquad (1)$$

where M^{2+} is the metal ion, L^{2-} is the ligand, and ML is the complex. For such a mechanism, $1/\tau$ is given by the expression:

$$1/\tau = k_f\gamma_\pm^2(C_M+C_L) + k_d \qquad (2)$$

where k_f, k_d are the rate constants of the complex formation and the dissociation at zero ionic strength respectively, where $\gamma_\pm$ is the mean activity coefficient of the free ions at a finite ionic strength, and where C_M, C_L are the concentrations of the metal and the ligand ions respectively.

Table 1. Relaxation times and experimental conditions for nickel maleate system at 25°C

C_o[a] (10^{-4} M)	C_{NiMal} (10^{-4} M)	$C_{Ni}=C_{Mal}$ (10^{-4} M)	μ (10^{-4})	$\gamma_\pm$	$1/\tau$ (10^3 s^{-1})
5.1	0.8	4.3	17.3	0.84	2.3
8.1	1.7	6.4	25.8	0.81	2.5
10.1	2.4	7.7	30.9	0.79	2.7
20.2	7.0	13.2	52.9	0.74	3.1
30.4	12.6	17.8	71.0	0.71	3.4
40.5	18.8	21.7	86.7	0.69	3.7
50.6	25.4	25.2	100.8	0.68	3.9
60.7	32.3	28.4	113.7	0.66	4.1
81.0	46.8	34.2	136.8	0.64	4.4
101.2	61.9	39.3	157.3	0.63	4.7
202.4	142.7	59.7	238.9	0.58	5.5
303.6	228.1	75.5	302.1	0.55	6.0
404.8	315.9	88.9	355.5	0.53	6.4
506.0	405.3	100.7	402.7	0.51	6.8

a) C_o refers to the total stoichiometric concentrations of the nickel maleate.

For the evaluation of the rate constants, $1/\tau$ is normally plotted against $\gamma_\pm^2(C_M+C_L)$. The intercept, corresponding to $\gamma_\pm^2(C_M+C_L)=0$, yields k_d, while k_f can be obtained from the slope. Such a plot requires a knowledge of the stability constant, K, in order to calculate the concentrations of the free ions. An appropriate literature value was not, however, available, and so the values were evaluated as follows. As the first approximation, a value of K which was roughly estimated from that of the succinate complex[9] was used to calculated the ionic concentrations. The mean activity coefficients were evaluated from the ionic strengths, which had themselves been calculated from the ionic concentration, using the Kielland equation.[12] Then, the $1/\tau$ values were plotted against $\gamma_\pm^2(C_M+C_L)$. The stability constant, which should coincide with the first estimated K value, was obtained from the ratio between k_f and k_d. Successive approximations were performed until a constant K value was obtained. The final results are shown in Fig. 1. The rate and the stability constants at various temperatures are given in Table 2.

The Arrhenius energies of activation, ΔE_f^* and ΔE_d^*, were obtained from the plot of $\log k_f$ and $\log k_d$ respectively against $1/T$, as is shown in Fig. 2. The other thermodynamic parameters of the complex formation, *i. e.*, the entropy of activation, ΔS_f^*, the enthalpy of activation, ΔH_f^*, and the free energy of activation, ΔG_f^*, were calculated from the following

7) M. Eigen and L. De Mayer, "Technique of Organic Chemistry," Vol. VIII, 2nd Ed., S. L. Friess, E. S. Lewis and A. Weissberger, Ed., Interscience Publishers, Inc., New York, N. Y., Part 2, (1963).

8) S. Harada, K. Amidaiji and T. Yasunaga, This Bulletin, **45**, 1752 (1972).

9) J. L. Bear and C. T. Lin, *J. Phys. Chem.*, **72**, 2026 (1968).

10) H. Hoffmann, *Ber. Bunsenges. Physik. Chem.*, **73**, 432 (1969).

11) U. Nickel, H. Hoffmann, and W. Jaenicke, *ibid.*, **72**, 526 (1968).

12) J. Kielland, *J. Amer. Chem. Soc.*, **59**, 1675 (1937).

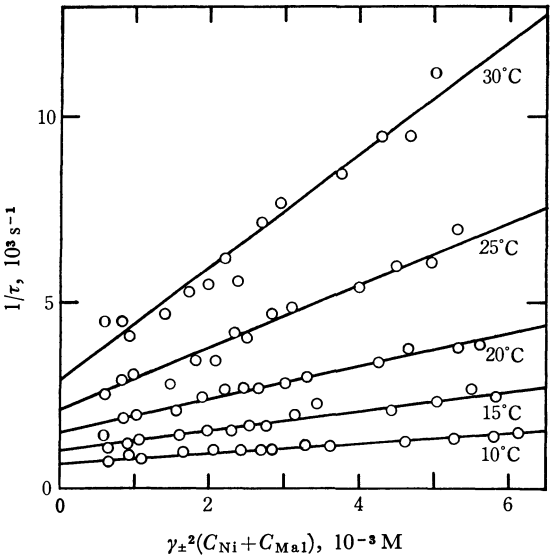

Fig. 1. $1/\tau$ *vs.* $\gamma_{\pm}^2(C_{Ni}+C_{Mal})$ plot at 10, 15, 20, 25, and 30°C.

TABLE 2. THE FORMATION AND DISSOCIATION RATE CONSTANTS AND THE STABILITY CONSTANTS OF NICKEL MALEATE ($\mu \to 0$)

t, °C	k_f, $M^{-1}s^{-1}$	k_d, s^{-1}	K, M^{-1}
10	1.4×10^5	0.7×10^3	2×10^2
15	2.6×10^5	1.1×10^3	2.5×10^2
20	4.5×10^5	1.5×10^3	3×10^2
25	8.4×10^5	2.1×10^3	4×10^2
30	14.6×10^5	2.9×10^3	5×10^2

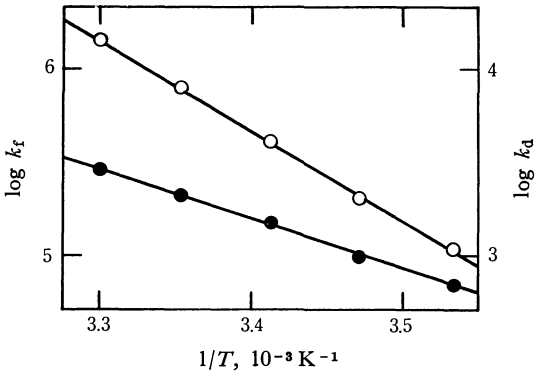

Fig. 2. Temperature dependency of k_f (○) and k_d (●).

TABLE 3. KINETIC DATA OF THE NICKEL MALEATE COMPLEX FORMATION AT 25°C ($\mu \to 0$)

K, M^{-1}	4×10^2
k_f, $M^{-1}s^{-1}$	8.4×10^5
k_d, s^{-1}	2.1×10^3
$E_f^{\neq}$, kcal mol^{-1}	20
$E_d^{\neq}$, kcal mol^{-1}	12
$\Delta G_f^{\neq}$, kcal mol^{-1}	9
$\Delta H_f^{\neq}$, kcal mol^{-1}	19
$\Delta S_f^{\neq}$, cal K^{-1} mol^{-1}	34
K_0, M^{-1}	25
k_1, s^{-1}	3.4×10^4

equations; they are listed in Table 3:

$$\log A = \log\frac{eRT}{Nh} + \frac{\Delta S_f^{\neq}}{2.3R} \tag{3}$$

$$\Delta H_f^{\neq} = \Delta E_f^{\neq} - RT \tag{4}$$

$$\Delta G_{f\neq} = \Delta H_f^{\neq} - T\Delta S_f^{\neq} \tag{5}$$

where A is the frequency factor.

Discussion

The complex formation reactions between a metal ion and a bidentate ligand have been usually represented by the following mechanism:

$$\underset{(I)}{M^{2+} + L^{2-}} \underset{k_{-0}}{\overset{k_0}{\rightleftharpoons}} \underset{(II)}{MO\overset{H}{\underset{H}{}}L} \underset{k_{-1}}{\overset{k_1}{\rightleftharpoons}} \underset{(III)}{M-L} \underset{k_{-2}}{\overset{k_2}{\rightleftharpoons}} \underset{(IV)}{ML}. \tag{6}$$

where (I) is the free ion, (II) is the outer-sphere complex, (III) is the monodentated complex, and (IV) is the bidentated chelate complex.

In the case of the nickel maleate, however, Eq. (6) cannot be applied directly. The stability constants of the nickel dicarboxylate in Table 4 show that the oxalate is a very stable five-membered chelate complex and that the malonate is a less stable six-membered chelate complex. The maleate and the succinate are much less stable, and their stability constants are nearly equivalent to that of the adipate. Moreover, the rate constants of the complex formation and the dissociation of the maleate and the succinate are quite similar to those of the adipate, as is shown in Table 4. Taking into account the fact that the adipate ion does not form a chelate complex,[13] these facts suggest that the maleate and the succinate ions do not form a chelate complex, either. Assuming that the concentration of the chelate complex is negligibly small in comparison with those of the other species, Eq. (6) can be simplified as follows:

$$\underset{(I)}{Ni^{2+} + Mal^{2-}} \underset{k_{-0}}{\overset{k_0}{\rightleftharpoons}} \underset{(II)}{NiO\overset{H}{\underset{H}{}}Mal} \underset{k_{-1}}{\overset{k_1}{\rightleftharpoons}} \underset{(III)}{Ni-Mal.} \tag{7}$$

In this reaction, the formation of the outer-sphere complex seems to be very fast, so the relaxation time of the rate-determining step of Eq. (7) is given by the equation:

$$1/\tau = \frac{k_1K_0\gamma_{\pm}^2(C_M+C_L)}{1+K_0\gamma_{\pm}^2(C_M+C_L)} + k_{-1} \tag{8}$$

where K_0 ($=k_0/k_{-0}$) is the outer-sphere complex formation constant. In the present experiments, $K_0\gamma_{\pm}^2(C_M+C_L)$ is much smaller than unity; therefore Eq. (8) can be simplified to:

$$1/\tau = k_1K_0\gamma_{\pm}^2(C_M+C_L) + k_{-1}. \tag{9}$$

Since the concentration of the outer-sphere complex is small, the overall stability constant is given as follows:

$$K = K_0\frac{k_1}{k_{-1}} = \frac{k_f}{k_d}. \tag{10}$$

13) H. Hoffmann and E. Yeager, *Ber. Bunsenges. Physik. Chem.*, **74**, 641 (1970).

Table 4. Rates and stability constants of the nickel dicarboxylate complexes at 25°C

Ligand	k_f ($M^{-1}s^{-1}$)	k_d (s^{-1})	K (M^{-1})	μ	Reference
Oxalate	7.4×10^4	3.6	2.1×10^4	0.1	5
	5.2×10^5	3.6	1.4×10^5	—	10
	—	—	2.0×10^5	0.1	4
Malonate	7.0×10^4	44	1.6×10^3	0.1	6
	4.2×10^5	35	1.2×10^4	→0	9a)
	—	—	1.6×10^3	0.1	17
Succinate	5.8×10^5	4×10^3	2.1×10^2	→0	9a)
	—	—	40	0.1	17
Adipate	8.5×10^3	4×10^3	2.1×10^2	—	10
	—	—	40	0.1	17
Maleate	8.4×10^5	2.1×10^3	4×10^2	→0	This work
	—	—	1.0×10^2	0.1	17
Malate	5.6×10^5	17	3×10^4	→0	8

a) The reported rate constant at 20°C was converted to the value at 25°C.

By comparing Eq. (9) with Eq. (2), the following equations were obtained:

$$k_f = k_1K_0 \tag{11}$$

$$k_d = k_{-1}. \tag{12}$$

The outer-sphere complex formation constant was calculated to be $K_0=25\ M^{-1}$ by the Fuoss equation.[14] Then, k_1 was calculated from k_f and Eq. (11) to be $3.4\times10^4\ s^{-1}$ at 25°C. The value is very close to the water-exchange rate constant on the nickel ion,[15] $k^*=2.7\times10^4\ s^{-1}$. This fact suggests that the rate-determining step of the nickel maleate complex formation is the loss of the water molecule from the inner coordination sphere of the nickel ion. Moreover, the value of k_d is in good agreement with the dissociation rate constant of the nickel maleate, $k_{-1}=2\times10^3\ s^{-1}$, reported by Hoffmann *et al.*[10,16] These coincidences of the data lead to the conclusion that the above procedures are valid.

The kinetic data of the nickel maleate complex formation in Table 3 can be compared with those of other complexes.[5,6,9] $\Delta E_f^{\neq}$, $\Delta H_f^{\neq}$, and $\Delta S_f^{\neq}$ are relatively larger than those of other, analogous nickel dicarboxylate complexes. These differences may be attributed to differences in the stabilities of the outer-sphere complexes. The stability constant can be referred to the literature value at $\mu=0.1$.[17] By dividing the value by $\gamma_\pm^2=0.154$, the stability constant at zero ionic strength was estimated to be $650\ M^{-1}$, which was almost the same, within the limits of experimental error, as our result.

The relaxation effects in the nickel dicarboxylate solution have been discussed by two different theories. In one theory,[5,6,8] the monodentated complex formation step, (II)⇌(III) in Eq. (6), is considered to be the rate-determining step. On the assumption that C_{II}, $C_{III}\ll C_I, C_{IV}$ and that $k_{-1}\ll k_2$, the rate constants in Eq. (2) were related to the parameters in Eq. (6) as follows:

$$k_f = K_0k_1\left(\frac{k_2}{k_2+k_{-1}}\right) \tag{13}$$

$$\simeq K_0k_1. \tag{14}$$

$$k_d = k_{-1}\left(\frac{k_{-2}}{k_2+k_{-1}}\right) \tag{15}$$

$$\simeq k_{-1}/K_2. \tag{16}$$

where $K_2=k_2/k_{-2}$. The values of k_1 obtained for many kinds of complexes by means of Eq. (14) are of the order of $\sim10^4\ s^{-1}$, which is very close to the water-exchange rate on the nickel ion;[15] hence, the loss of the water molecule from the inner-coordination sphere of the nickel ion may be considered to be the rate-determining step. The fact that the value of k_d reflects the stabilities of the chelate complexes can be interpreted in terms of Eq. (16), where K_2 shows the stabilities of the chelate. This theory may also be applied to the nickel dicarboxylate complex whose k_f is relatively large ($\gg10^5\ M^{-1}\ s^{-1}$), while at the same time, its k_d is very small. By this theory, Bear *et al.*[9] have assumed that the nickel succinate is a stable chelate complex, *i. e.*, $K_2\gg1$, and have obtained a large value for k_d. It can be seen from Eq. (16), however, that if $K_2\gg1$, k_{-1} will also become very large. The fact is in disagreement with the postulated condition, $k_{-1}\ll k_2$. If $K_2\simeq1$ is assumed, the rate equations become more complicated[18] than Eqs. (1) and (2). In the nickel succinate solution, the relaxation effect has been expressed by a single relaxation and the concentration dependency of τ can be expressed by Eq. (2). This means that the same interpretations should be applied to the succinate as to the maleate system. Moreover, the agreement of k_d with the dissociation rate constant of the succinate,[10,16] $k_{-1}\simeq3\times10^3\ s^{-1}$, indicates that Eq. (12) should be used rather

14) R. M. Fuoss, *J. Amer. Chem. Soc.*, **80**, 5059 (1958).
15) T. J. Swift and R. E. Connick, *J. Chem. Phys.*, **37**, 307 (1962).
16) H. Hoffmann and U. Nickel, *Ber. Bunsenges. Physik. Chem.*, **72**, 1096 (1968).
17) M. Yasuda, K. Yamasaki, and H. Ohtaki, This Bulletin, **33**, 1067 (1960).
18) G. H. Czerlinski, "Chemical Relaxation," Marcel Dekker Inc., New York, (1966).

than Eq. (16).

On the other hand, Hoffmann *et al.*[10,11] have considered that the rate-determining step of the complex formation is the chelate-ring closure, *i. e.*, (III)$\rightleftharpoons$(IV) in Eq. (6). They assumed that K_0k_1 is constant (8.5×10^5 M^{-1} s^{-1}) for all the nickel dicarboxylates and that the small difference in k_f can be attributed to the $k_2/(k_2+k_{-1})$ term. As can be seen from Eq. (15), however, when k_d becomes relatively large, the k_{-2}/k_2 term increases and C_{III} cannot be neglected in comparison with C_{IV}. This fact disagrees with the assumptions used in deriving Eqs. (13) and (15). Therefore, this procedure can be appropriately applied to a system where $k_f \ll 8.5\times 10^5$ M^{-1} s^{-1} and where at the same time, k_d is small.

In summary, when k_d becomes large, $k_d \gtrsim 10^3$ s^{-1}, C_{III} cannot be neglected and Eqs. (13) and (15) need to be re-evaluated. In some cases where C_{III} is much larger than C_{IV}, Eqs. (7) to (12) should be applied.

BULLETIN OF THE CHEMICAL SOCIETY OF JAPAN, VOL. 46, 506—509 (1973)

Study on Oxazolopyrimidines. VI. Formation of 3-Substituted Xanthines *via* 7(6*H*)-Iminooxazolopyrimidines

Yozo Ohtsuka

Sagami Chemical Research Center, Onuma, Sagamihara, Kanagawa

(Received August 8, 1972)

The condensation of several primary amines with 4-cyano-5-dialkoxymethylenaminooxazole gave 6-substituted 5-alkoxy-7(6*H*)-iminooxazolo[5,4-*d*]pyrimidines. These compounds were converted into 3-substituted xanthines by treatment with aqueous alkali or by heating in formamide. The present reaction was compared with an analogous reaction, formation of 9-substituted hypoxantines *via* 7-aminooxazolo[5,4-*d*]pyridimine derivatives, and the difference in the reaction course was discussed in terms of the effect of substituents on the stability of oxazolopyrimidine intermediates.

The reaction of 4-cyano-5-ethoxymethylenaminooxazole (I, R^2=H or alkyl, R^3=OEt) with amines giving 9-substituted hypoxanthines(V) *via* 7-alkyl-(aryl)aminooxazolopyrimidines(IV) has been reported previously.[1] This paper describes another mode of reaction in which the influence of the substituent in oxazolopyrimidine intermediates (II, R^2=alkoxy) leads to the formation of 3-substituted xanthines(III) under similar reaction conditions.

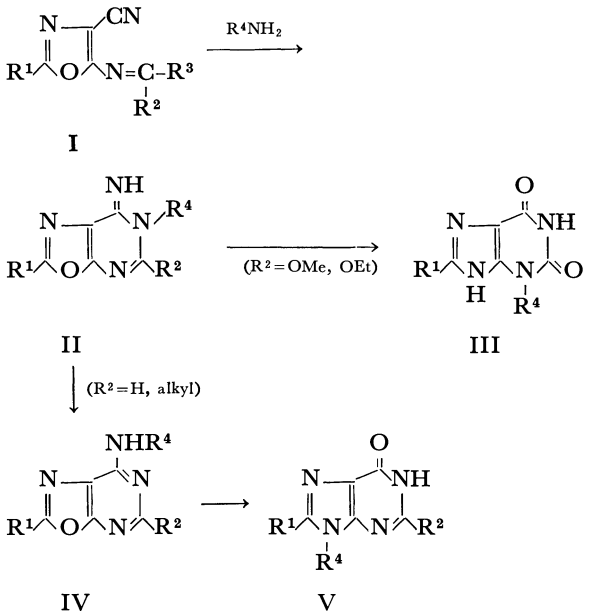

3-Substituted xanthines, important because of their biological properties[2] and of their usefulness as intermediates,[3] have been prepared previously from substituted ureas through pyrimidine derivatives.[3b,4-6] The present method provides a new route for the preparation of 3-substituted xanthines.

4-Cyano-5-diethoxymethylenaminooxazole(Ia, R^1=H, R^2=R^3=OEt) reacted with normal-alkylamines to give 6-alkyl-5-ethoxy-7(6*H*)-iminooxazolo[5,4-*d*]pyrimidines(IIa-e) as colorless crystals(Table 1). With several amines, such as isopropylamine, *t*-butylamine, aniline and benzylamine, isolation of products corresponding to compounds II has failed. The dimethoxymethylenamino compound(Ib, R^1=H, R^2=R^3=OMe), however, reacted with benzylamine to give the methoxy compound(IIf in Table 1). These products were relatively unstable and decomposed gradually on standing in moist air. The decomposition was greatly accelerated by the presence of a trace of alkali. The structure of these compounds was

1) Y. Ohtsuka, This Bulletin, **43**, 3909 (1970).

2) a) F. Bergamnn, A. Mahler, H. Burger-Rachamimov, and D. Diller, *Biochemistry*, **8**, 457 (1969). b) W. Stoll and E. Schmid, U. S. 2756229 (1956). c) H. T. Leidy and A. Sarko, Brit. 1157919 (1969).

3) a) V. M. Nesterov and I. E. Chubova, *Khim-Farm. Zh.*, **1**, 42 (1967).; *Chem. Abstr.*, **67**, 3071 (1967). b) Z. Neiman and F. Bergmann, *Israel J. Chem.*, **6**, 9 (1968).

4) M. Ishidate, M. Sekiya, Y. Ozaki and Y. Harada, *Yakugaku Zasshi*, **76**, 1107 (1956).

5) M. Sekiya and Y. Ozaki, *ibid.*, **86**, 854 (1966).

6) a) T. Kishikawa and H. Yuki, *Chem. Pharm. Bull.*, **14**, 1365 (1966). b) M. Ridi, G. Franchi, S. Mangiavacci and M. P. Lombardini, *Boll. Chim. Farm.*, **107**, 401 (1968); *Chem. Abstr.*, **69**, 96637 (1968).

Table 1. 5-R²-6-R⁴-7(6*H*)-Iminooxazolo[5,4-*d*]pyrimidines(II)

	R²	R⁴	Yield (%)	Mp (°C)	Empirical formula[a]	Calcd			Found		
						C(%)	H(%)	N(%)	C(%)	H(%)	N(%)
IIa	OEt	Me	50	122—124	$C_8H_{10}N_4O_2$	49.48	5.19	28.85	49.30	5.05	29.13
IIb	OEt	Et	57	113—114	$C_9H_{12}N_4O_2$	51.91	5.81	26.91	51.90	5.97	26.96
IIc	OEt	*n*-Pr	44	58—61[b]	$C_{10}H_{14}N_4O$	54.04	6.35	25.21	53.80	6.64	25.36
IId	OEt	*n*-Bu	42	171—172	$C_{11}H_{16}N_4O_2$	55.91	6.86	23.70	56.13	7.15	23.38
IIe	OEt	Phenethyl	53	212	$C_{15}H_{16}N_4O_2$	63.36	5.67	19.71	63.30	6.19	19.87
IIf	OMe	Benzyl	71	121—122	$C_{13}H_{12}N_4O$	60.93	4.72	21.87	60.65	4.53	21.99

a) Molecular weights were confirmed by MS spectra.
b) Attempt to isolate a more higher melting-point substance was failed.

Table 2. Spectroscopic properties of 5-R²-6-R⁴-7(6*H*)-iminooxazolopyrimidines(II)

	Compound		IR, ν_{max}^{KBr} (cm^{-1}) (Characteristic peaks)				NMR, δ (ppm)[a]		
	R²	R⁴					R²	R⁴	C_2-H
IIa	OEt	Me	3226	3115	1673	1603	1.38(t)	3.40(s)	8.26(s)
			1186	1000	763		4.43(q)		
							(5H)	(3H)	(1H)
IIb	OEt	Et	3278	3134	1684	1613	1.40(t)	1.70(t)	8.61(s)
			1180	1021	770		4.40(q)	4.77(q)	(1H)
							(5H)	(5H)	
IIc	OEt	*n*-Pr	3230	3120	1677	1600	1.36(t)	0.88, 1.5	8.29(s)
							4.44(q)	4.1 (7H)	(1H)
							(5H)		
IId	OEt	*n*-Bu	3450	3118	1657	(1638)	1.44(t)	0.97, 1.6	8.00(s)
			1608	1158	1072	784	4.62(q)	4.3 (9H)	(1H)
IIe	OEt	$Ph(CH_2)_2$		4045	1655	1602	1.22(t)	3.00, 4.33	8.01(s)
			1200	1070	781		4.21(q)	7.18(9H)	(1H)
							(5H)		
IIf	OMe	$PhCH_2$	3260	3120	1681	1610	4.02(s)	5.37, 7.3	7.67(s)
			1168	1062	764		(3H)	(7H)	(1H)

a) Determined in dimethylsulfoxide(DMSO)-d_6 solution except with IId ($CDCl_3$).

identified on the basis of their spectral properties (Table 2) and elementary analysis. It was supported by the structure of the products of the subsequent reaction (see later). The compound II and 7-alkylamino compound(IV) were distinguished by comparison of the following properties: i) The compound II's were generally less stable than the compound IV's especially when they were heated in polar solvents.[7] ii) The most intense IR band in the 1600 cm^{-1} region of II appears at a higher frequency region by about 40 cm^{-1} than that of IV. iii) In NMR spectra of IV, NH and α-CH of N-alkyl group were observed as broad peaks, whereas the spectra of II showed no distinct NH absorption and α-CH of N-alkyl group was observed as sharp lines, probably due to the rapid exchange of imino-proton with solvent.[8]

The oxazole-imidazole conversion in 7-aminooxazolopyrimidines[1,9] was applied to the compound II. Thus, by treatment with aqueous alkali(Method A) or by heating in formamide(Method B), compounds IIa–f were found to give 3-substituted xanthines(IIIa–f) as shown in Table 3. The structures of III's were confirmed by comparison with authentic samples or with the samples prepared from pyrimidine derivatives. Table 3 also showed an example of comparison between two methods of preparation. Better results were generally obtained with Method B, although all of II's gave III's by Method A. The formation of 9-sub-

Table 3. Preparation of 3-R⁴-xanthines from oxazolopyrimidine derivatives (II)

R⁴	Method	Yield (%)	Mp (°C)
Me	B	70	287—289
Et	A	41	310—311
	B	71	
n-Pr	B	95	287—289
n-Bu	B	65	279—280
$Ph(CH_2)_2$	B	80	315—316
$PhCH_2$	B	76	>310

7) The neutral molecules of some iminopyrimidines decomposed rapidly in aqueous solution: D. J. Brown, E. Hoerger and S. F. Mason, *J. Chem. Soc.*, **1955**, 4035.
8) W. R. Anderson and R. M. Silverstein, *Anal. Chem.*, **37**, 1417 (1965).
9) Y. Ohtsuka, This Bulletin, **43**, 954 (1970).

stituted xanthines or other rearranged products was not detected.

In previous studies on the conversion reaction of I into V, imino-intermediate(II) was not isolated. Careful re-examination of the reaction of 4-cyano-5-ethoxymethylenaminooxazole(Ic, $R^1=R^2=H$, $R^3=OEt$) and aqueous methylamine showed that the analogous imino-intermediate(IIg, $R^1=R^2=H$, $R^4=CH_3$) could be obtained in crude state (as shown by its IR and NMR spectrum), but further purification induced the Dimroth rearrangement into IVa($R^1=R^2=H$, $R^4=CH_3$). The rate of the rearrangement is known to decrease with an increase in electron density on the pyrimidine ring.[10] Therefore, in the present reaction, the electron-donating effect of the 5-alkoxy group may stabilize the structure II.

The preference of ring fission either at the oxazole or the pyrimidine ring of imino-intermediate(II) seemed to be determined by two factors. One is the electronic effect of the 5-substituent, and the other is the stability of the uracil-type intermediate, which is suggested by the following result. Under similar conditions to those in the change of II into III, 7-amino-5-ethoxyoxazolopyrimidine(IVb, $R^1=R^4=H$, $R^2=OEt$)[9] gave only 2-ethoxyhypoxanthine(Va, $R^1=R^4=H$, $R^2=OEt$). This compound, Va, was stable to hot aqueous alkali and hydrolysis to xanthine was only accomplished by refluxing in concentrated acid. Acid conditions are generally used for hydrolysis of an alkoxy group of pyrimidines or purines, and alkali seems to be effective only with compounds in which the alkoxy group is activated.[11] Thus, the easy conversion of II into III under alkaline condition seems to be assisted by the stability of the uracil-type intermediates(VI).

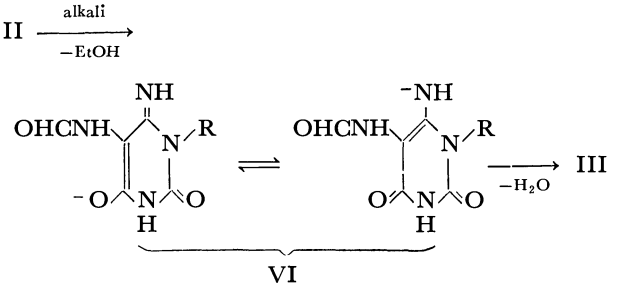

The easy hydrolysis of an ethoxy group probably initiates the reaction, but no experiment has been done to confirm the mechanism.

Degradation of purine derivatives generally occurs at the pyrimidine ring. With 7(6*H*)-iminooxazolopyrimidines, the two constituent rings have similar reactivity and the direction of ring rupture is determined by the character of the substituent. Other synthetic applications of the interesting properties of oxazolopyrimidine derivatives are being explored.

10) D. J. Brown, and B. T. England, *Aust. J. Chem.*, **21**, 2813 (1968).

11) a) D. J. Brown, "The Pyrimidines, Supplement I" (The Chemistry of Heterocyclic Compounds, Vol. 16), Wiley-Interscience, New York, N. Y., (1970), p. 170. b) J. H. Lister, "Purines" (The Chemistry of Heterocyclic Compounds, Vol. 24, Part II), Wiley-Interscience, New York, N. Y., (1971), p. 236.

Experimental

Melting points were measured on a hot-stage apparatus and uncorrected. The IR, NMR, and MS spectra were determined with a Perkin-Elmer 337, a Hitachi-Perkin-Elmer R-20B (60 MHz) and a Hitachi RMU-6E (70 eV) spectrometer, respectively.

Preparation of Starting Materials (I). Preparation of 4-cyano-5-diethoxymethylenaminooxazole (Ia) was described in a previous paper.[12] 4-Cyano-5-dimethoxymethylenaminooxazole (Ib) was prepared by the method analogous to that used for Ia. Thus, 5-amino-4-cyanooxazole (3.0 g), tetramethyl orthocarbonate (15 ml) and acetic anhydride (15 ml) were refluxed for 7 hr. The reaction mixture was distilled *in vacuo* and a fraction, bp 113—115°C/0.28 mmHg, was collected, which solidified on cooling. The product was recrystallized from methylcyclohexane to give colorless solid, mp 65.0—65.5°C (Yield; 47.8%). ν_{max}^{KBr}: 2208 cm^{-1} (C≡N). NMR ($CDCl_3$) δ: 7.52 (s, 1H, C_2-proton), 4.03 (s, 6H, methyl protons).

Found: C, 46.40; H, 3.68; N, 23.03%. Calcd for $C_7H_7N_3O_3$: C, 46.41; H, 3.68; N, 23.20%.

Preparation of Oxazolopyrimidine Derivatives (II). 5-Ethoxy-6-methyl-7(6H)-iminooxazolo[5,4-d]pyrimidine (IIa): To an ice-cooled aqueous solution of methylamine (30%, 1 ml), 4-cyano-5-diethoxymethylenaminooxazole (Ia, 2.0 g) was added in one portion. The mixture was stirred at room temperature until a solid was separated. On warming gradually to 40—50°C, the solid was melted and then a second solid started to precipitate. After 1 hr, the reaction mixture was cooled and resulting crystals (1.1 g) were collected by filtration. The compound IIb and IIc were prepared by this method.

5-Ethoxy-6-n-butyl-7(6H)-iminooxazolo[5,4-d]pyrimidine (IIId). An ethanol solution of *n*-butylamine (1.4 g in 15 ml) was mixed with Ia (1.5 g) under cooling. After stirring at room temperature for 15 min, the residual amine and ethanol were evaporated from the mixture under reduced pressure. Resulting crystals were dried *in vacuo* for 30 min and then refluxed in ethanol (20 ml) for 6 hr. Concentration of the mixture gave a light tan solid (1.0 g). This product was purified for analysis by re-precipitation from 4 N aqueous NaOH–HCl followed by recrystallization from water. The compound IIe was prepared by this method.

5-Methoxy-6-benzyl-7(6H)-iminooxazolo[5,4-d]pyrimidine (IIf). To a cold mixture of benzylamine (1.2 g) and Ib (2.0 g), a few drops of water added. Resuting semisolid was stirred at room temperature for 1 hr and then 50°C for 30 min. After cooling, the solid was collected and washed with water. Resulting crystals were dried *in vacuo* for 30 min and then refluxed in ethanol. The hot reaction mixture was filtered and the filtrate was concentrated to give a solid which was recrystallized from water-ethanol.

Reaction of 4-Cyano-5-ethoxymethylenaminooxazole (Ic) with methylamine. To an ice-cooled aqueous solution of methylamine (30%, 1 ml), Ic (1.65 g) was added in one portion. A solid started to precipitate immediately from solution, but on continued stirring it dissolved. After several minutes, a second solid precipitated. Immediate filtration and washing with a small quantity of cold water gave a crystalline solid (1.2 g). The second solid was identified as 5-ethoxy-7(6*H*)-imino-6-methyloxazolo[5,4-*d*]pyrimidine (IIg) from its IR (absence of nitrle group) and NMR spectrum (a broad NH-absorption at about 8.4 ppm and a

12) Y. Ohtsuka, This Bulletin, **43**, 187 (1970).

Table 4. Preparation of urea derivatives for 3-substituted xanthines

R	Yield (%)	Mp (°C)	Empirical formula	Calcd			Found		
				C (%)	H (%)	N (%)	C (%)	H (%)	N (%)
$RNHCONHCOCH_2CN$									
Et	51	172—173	$C_6H_9N_3O_2$	46.44	5.85	27.08	46.89	6.25	26.57
n-Pr	74	171—172	$O_7H_{11}N_3O_2$	49.69	6.55	24.84	49.69	6.67	25.00
n-Bu	85	153—154	$C_8H_{13}N_3O_2$	52.44	7.15	22.94	52.67	6.89	22.78
RNHCONHCOC(=NOH)CN									
Et	81	202—203	$C_6H_8N_4O_3$	39.13	4.38	30.43	39.17	4.23	30.58
n-Pr	92	194—195	$C_7H_{10}N_4O_3$	42.42	5.09	28.27	42.68	5.36	28.19
n-Bu	92	173—175	$C_8H_{12}N_4O_3$	45.28	5.70	26.40	45.22	5.76	26.53
RNHCONHCOCH(ON)NHCHO									
Et	53	166—167	$C_7H_{10}N_4O_3$	42.42	5.09	28.27	42.47	5.15	28.20
n-Pr	71	155—156	$C_8H_{12}N_4O_3$	45.28	5.70	26.40	45.43	5.62	26.48
n-Bu	45	158—159	$C_9H_{14}N_4O_3$	47.73	6.24	24.77	47.63	6.09	24.58

singlet at a about 7.9 ppm), but recrystallization from water or ethanol gave 7-methylaminooxazolo-pyrimidine (IVa).[1]

Preparation of 3-Substituted Xanthines from Oxazolopyrimidine Derivatives. Method A: A mixture of the compound II and a aqueous NaOH was warmed on a water bath until it became a homologous solution (5—30 min). After cooling, acidification of the reaction mixture by acetic acid gave the product.

Method B: The compound II was heated in formamide at 180°C for 5—15 min. Formamide was distilled off *in vacuo* and the residue was crystallized from water.

The structures of products were identified as 3-substituted xanthines from their elementary analysis and from the coinsidence of their spectroscopic properties (IR and NMR spectra) with those of authentic samples (IIIa and IIIf)[5,2b] or with those of samples prepared from pyrimidine derivatives by the method described below (IIIb—IIIe).

3-Phenethylxanthine (IIIe). This compound was obtained from IIe by Method B. Recrystallization from aqueous ethanol gave colorless needles, mp 315—316°C. ν_{max}^{KBr} cm^{-1}: 3122, 2820, 1700, 1561, 1427, 1218, 981, 830, 707. NMR (DMSO-d_6) δ: 8.00 (s, 1H, C_2-proton), 7.22 (s, 5H, phenyl protons), 4.20 and 2.96 (t, 2H, methylene protons, respectively).

Found: C, 60.68; H, 4.60; N, 22.08%. Calcd for $C_{13}H_{12}N_4O_2$: C, 60.93; H, 4.72; N, 21.87%.

Preparation of 3-Substituted Xanthines from Pyrimidine Derivatives. Cyanoacetylureas, $RNHCONHCOCH_2CN$, were prepared from substituted ureas and cyanoacetic acid by method of Traube.[13] These compounds were converted into isonitroso derivatives, RNHCONHCOC (=NOH)CN,[14] followed by reduction with zinc and formic acid to formylamine derivatives, RNHCONHCOCH(CN)NHCHO.[5] These compounds were treated with alkali[5] to give formylaminopyrimidines. Without further purification, these materials were heated under reflux in formic acid for 5 hr. 3-Substituted xanthines, thus obtained, were confirmed to be identical with the samples prepared from II's from their spectroscopic properties. Analytical data of these compounds were shown in Table 4.

The author wishes to thank Prof. S. Simamura for discussions and Mr. K. Sugimoto and Mr. T. Miyazaki for their technical assistance.

13) W. Traube, *Ber.*, **33**, 3047 (1900).
14) German 227390 (1910) (E. Merck).

The Reaction of Propargyl Compounds with Carbon Monoxide and Water in the Presence of Iron Carbonyl Catalyst

Fumio WADA and Tsutomu MATSUDA

Department of Organic Synthesis, Faculty of Engineering, Kyushu University, Hakozaki, Higashi-ku, Fukuoka-shi

(Received February 26, 1972)

The reaction of propargyl alcohol as well as its acetate and methyl ether with carbon monoxide and water in the presence of ironpentacarbonyl-amine catalyst under oxymethylation conditions proved to proceed at a much faster rate than that of 1-butyn-4-ol, 1-pentyn-5-ol and alkylacetylenes accompanied by elimination of the functional groups at C-3 to give dimethyl methylsuccinate. 3-Methyl-1-butyn-3-ol and 1-ethynylcyclohexanol reacted in a similar manner, but gave mixtures of unsaturated monoesters and diesters, saturated and unsaturated. The faster rate of reaction and the product obtained were interpreted by a scheme involving a concerted attack of hydroirontetracarbonyl anion, $HFe(CO)_4^-$, at the terminal position to split off the group at C-3. The mononuclear hydrido anion was assumed to be an active catalytic species in the reaction on the basis of both the infrared spectra of the catalyst system under the reaction conditions and the efficiency of potassium hydroxide as a base component.

In a series of investigations[1)] on the oxymethylation of unsaturated compounds by carbon monoxide and water (or hydrogen) in the presence of ironpentacarbonyl and a base, we found that this type of catalyst could bring about three kinds of reactions, oxymethylation, hydrogenation and carboxylation and that the principal course of the reaction depends on the structure of reactants as shown in the following reactions.

$$R\text{-}CH_2\text{-}CH{=}CH_2 \rightarrow R\text{-}CH_2\text{-}CH_2\text{-}CH_2(CH_2OH) + R\text{-}CH_2\text{-}CH(CH_2OH)\text{-}CH_3 \qquad (1)$$

$$\left.\begin{array}{l} CH_2{=}CH\text{-}CO_2CH_3 \rightarrow CH_3\text{-}CH_2\text{-}CO_2CH_3 \\ CH_2{=}CH\text{-}CH_2OH \rightarrow CH_3\text{-}CH_2\text{-}CH_2OH \end{array}\right\} \qquad (2)$$

$$CH_2{=}CH\text{-}(CH_2)_2\text{-}CO_2CH_3 \rightarrow CH_2(CH_2OH)\text{-}(CH_2)_3\text{-}CO_2CH_3 \text{ and isomers} + CH_3\text{-}(CH_2)_3\text{-}CO_2CH_3 \qquad (3)$$

$$C_2H_5\text{-}C{\equiv}CH \rightarrow C_2H_5\text{-}CH_2CH_2(CO_2CH_3) + C_2H_5\text{-}CH(CO_2CH_3)\text{-}CH_2(CO_2CH_3)$$

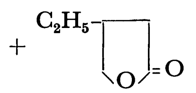
(4)

Simple olefins gave a mixture of oxymethylated products at 175°C, while α,β-unsaturated esters, nitriles and allylic alcohols were hydrogenated exclusively to the corresponding saturated compounds at a somewhat lower temperature. However, oxymethylation of the substituted compounds was found to occur when the double bond was separated from ester or hydroxyl group by more than one methylene group (Eq. (3)).[1d)] A similar effect of a neighboring double bond was observed by examining the time dependence of the products in the oxymethylation of isomeric hexadienes.[1b)] This paper deals with an extention of the neighboring substituent effect to acetylenic compounds, and presents both unusual behaviours of propargyl alcohol and its derivatives (I) and a probable structure of an active catalytic species in the reaction.

$$HC{\equiv}C\text{-}C(R_1)(R_2)\text{-}X$$

	Ia	Ib	Ic	Id	Ie
$R_1 =$	H	H	H	CH_3	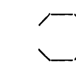
$R_2 =$	H	H	H	CH_3	
$X =$	OH	OAc	OCH_3	OH	OH

Results and Discussion

Products and their yields under vairous reaction conditions are summarized in Table 1. The reaction of propargyl alcohol proceeded rapidly at 175°C under concurrent formation of an unidentified by-product even in a short reaction time such as 40 min. The main product (II) formed as the sole product at 125°C was confirmed to be dimethyl methylsuccinate. Propargyl acetate and 3-methoxy-1-propyne showed similar reactivities and both afforded II in comparable yields. Formation of II from these compounds regardless of their functional groups can be explained by the route in which addition of methoxycarbonyl groups proceeded under elimination of the groups at C–3 *i. e.*, OH, OAc or OCH_3. Elimination accompanied by carboxylation also occurred in the reaction of the substituted propargyl alcohols, 3-methyl-1-butyn-3-ol (Id) and 1-ethynylcyclohexanol (Ie). However, these compounds afforded complex mixtures consisting of an unsaturated monoester and both saturated and unsaturated diesters. The structural features of these products suggest a reaction scheme in which the first carboxylation occurred exclusively at the terminal position and the subsequent step involving either the second carboxylation or hydrogenation led to the final products. The latter step seems to be considerably slower than the former for compounds which are sterically hindered by substitution at C–3. On the other hand, the reaction of 1-butyn-4-ol was found to proceed at a much slower rate as shown in Fig. 1.

---

1) a) T. Matsuda and T. Nakamura, *Kogyo Kagaku Zasshi*, **71**, 511 (1968), b) T. Matsuda and H. Honda, *ibid.*, **74**, 919 (1971), c) T. Matsuda, H. Kondo, and T. Nakamura, *ibid.*, **74**, 1135 (1971), d) T. Matsuda, H. Uchida, Y. Komori, and M. Nishikawa, *Nippon Kagaku Kaishi*, **1972**, 1103.

TABLE 1. PRODUCTS OBTAINED FROM PROPARGYL AND RELATED COMPOUNDS AND THEIR YIELDS

Material	Reaction conditions: No	Temp, °C	Time, hr	Products,[a] g
$HC{\equiv}C\text{-}CH_2OH$	1	175	6	II: 6.5, others: 2.0
	2	175	0.66	II: 6.7, others: 0.57
	3	125	8	II: 13.3
	4	150	5	II: 20.6, others: 1.79
	5[b]	150	5	II: 7.8, III: 1.7, IVa: 1.5, IVb: 1.4
	6[c]	125	6	II: 0.52, III: 0.7, IVa: 0.3, IVb: 0.12, others: 1.06
$HC{\equiv}C\text{-}CH_2OAc$	7	150	6	II: 10.8, others: 0.53
$HC{\equiv}C\text{-}CH_2OCH_3$	8	150	3	II: 7.16, others: 1.74
$HC{\equiv}C\text{-}C(CH_3)_2$	9	150	8	V: 0.96, VI: 3.22, VII: 3.14, VIII: 0.41, IX: 1.52, X: 4.95, XI: 0.48, others: 3.83
	10	70	144	V: 1.02, VI: 0.36, VII: 1.99, VIII: 3.07, IX: 2.87, X: 4.78, XI: 1.86, others: 1.2
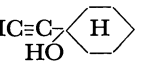	11	150	6	XII: 3.2, XIII: 1.4, XIV: 3.5, XV: 8.3
$HC{\equiv}C\text{-}(CH_2)_2OH$	12	150	25	XVI: 4.3, XVII: 1.7
$HC{\equiv}C\text{-}(CH_2)_3OH$	13	150	14	XVIII: 1.38, XIX: 1.49, XX: 2.46, others: 3.07

a)

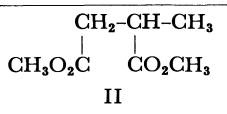

II

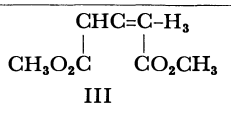

III

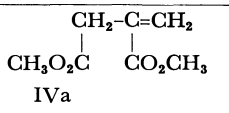

IVa

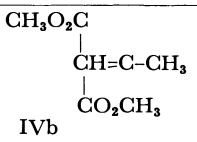

IVb

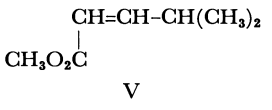

V

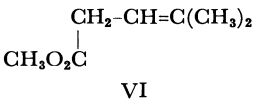

VI

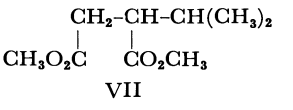

VII

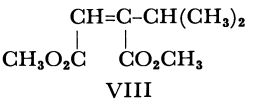

VIII

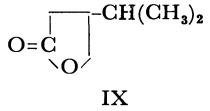

IX

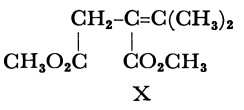

X

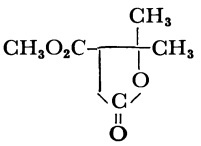

XI

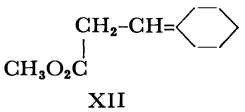

XII

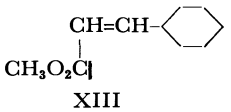

XIII

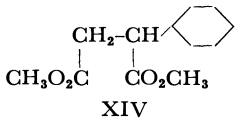

XIV

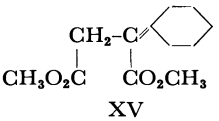

XV

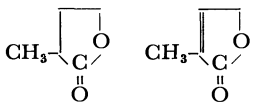

XVI XVII

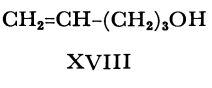

XVIII

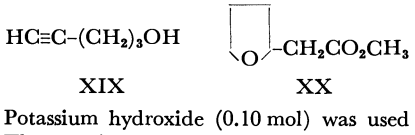

XIX XX

b) Potassium hydroxide (0.10 mol) was used in place of triethylamine.

c) The reaction was carried out under the initial carbon monoxide pressure, 3 kg/cm².

Formation of the product identified as α-methyl-γ-butyrolactone and α-methylcrotonolactone can be explained by a different pathway in which the addition of a methoxycarbonyl occurrs at β-carbon and then the hydroxyl group at C-3 takes part in the cyclization to give lactones. This means that the mechanism of formation of these lactones differs from that of the γ-lactones obtained from the reaction of alkylacetylenes (Eq. (4)). Although several compounds are left unidentified, the products from 1-pentyn-5-ol seem to be those which retained the original hydroxyl moiety. Thus, it is concluded that the elimination process plays an important role in the reaction of propargyl compounds, and gives rise to both the increased reaction rate and the characteristic feature of the products. A similar carbonylation under elimination of a functional group has been reported by Nogi and Tsuji[2] in the palladium catalyzed reactions of propargyl compounds in alcoholic solvents.

When we proceed to formulate a reaction course which includes the elimination of the electronegative group from the propargyl position, the formation of an intermediate of allenic structure would have to be considered as a possible pathway. However, the

2) T. Nogi and J. Tsuji, *Tetrahedron*, **25**, 4099 (1969).

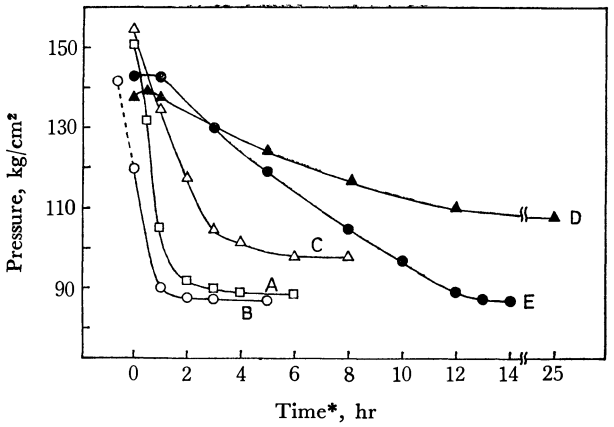

Fig. 1. Pressure changes in the reactions of typical acetylenic compounds at 150°C.
* Abscissa indicates the time elasped from the point reached at 150°C.
A: propargyl acetate.
B: propargyl alcohol with KOH, the pressure reached to a maximum at 125°C.
C: 3-methyl-butyn-3-ol.
D: 1-butyn-4-ol.
E: 1-pentyn-5-ol.

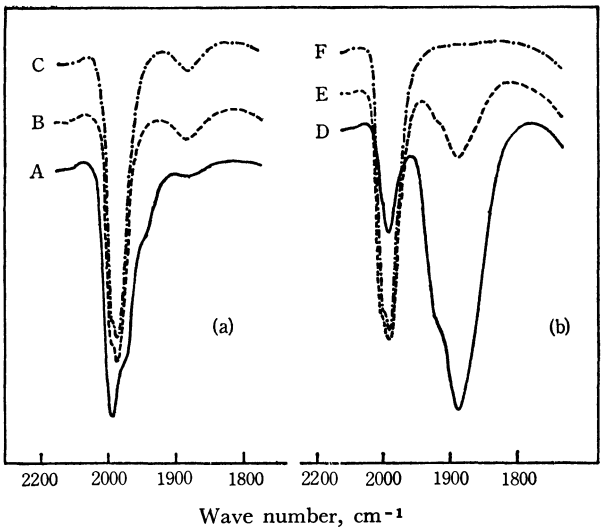

Fig. 2. Time dependence of catalyst mixtures at 150°C under carbon monoxide pressure in MeOH.
(a) $HFe_3(CO)_{11}^{-}H\overset{+}{N}Et_3$-$NEt_3$-$H_2O$; A: a starting mixture, B: after 1 hr, C: after 6.5 hr.
(b) $Fe(CO)_5$-KOH-H_2O; D: at the point reached at 125°C, E: after 0.5 hr, F: after 3 hr.

reaction of allene under the same conditions proved to be more sluggish than that of propargyl alcohol and led to a complex mixture in which neither methylsuccinate nor the corresponding unsaturated compounds was detected.

The reaction of propargyl alcohol utilizing potassium hydroxide in place of triethylamine was found to proceed in a similar way but at an increased rate, and provided an interesting difference from the oxymethylation of olefins, where potassium hydroxide proved to be a nearly ineffective base. Although the result suggests that the active species in the reaction of propargyl compounds is mononuclear hydroirontetracarbonyl anion, $HFe(CO)_4^-$, it is not clear why both triethylamine and potassium hydroxide act as an equally effective base, if we take into consideration the fact that the nature of the base is responsible for the formation of different kind of hydrido ironcarbonyls[3] according to the following reactions.

$$Fe(CO)_5 + 3KOH \rightarrow K^+HFe(CO)_4^- + K_2CO_3 + H_2O \quad (5)$$

$$3Fe(CO)_5 + NR_3 + 2H_2O \rightarrow HFe_3(CO)_{11}^{-}H\overset{+}{N}R_3 + 2CO_2 + 2CO + H_2 \quad (6)$$

A qualitative examination of these catalyst systems by infrared spectra revealed that the hydrido species formed under the present experimental conditions was not trinuclear but mononuclear anion, irrespective of the base utilized as shown in Fig. 2. This would imply that not only the nature of the base but also the presence of carbon monoxide under pressure is an important factor in determining the structure of hydrido ironcarbonyl species in solution. It is of interest that the absorption at 1880 cm^{-1} attributable to the mononuclear anion in methanol persisted unchanged for 6.5 hr at 150°C in the presence of triethylamine (Fig. 2a), but when potassium hydroxide was used, the anion initially formed in a larger quantity decreased rapidly and completely collapsed to ironpentacarbonyl after being heated for 3 hr at the same temperature (Fig. 2b), possibly by the consumption of potassium hydroxide due to repetition of reaction (5) and the following.

$$K^+HFe(CO)_4^- + H_2O \xrightarrow{CO} Fe(CO)_5 + H_2 + K_2CO_3 \quad (7)$$

We thus propose the scheme for the reactions of propargyl compounds as follows.

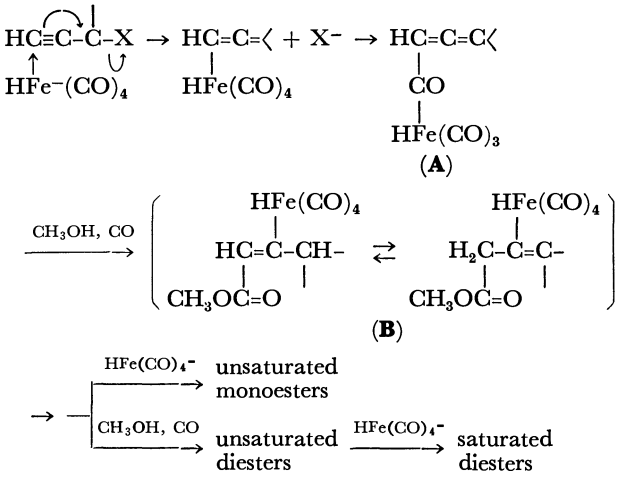

The essential step would be the concerted attack of mononuclear hydrido ironcarbonyl anion at the terminal carbon to split off the anion X^-, the following insertion of carbon monixide giving an acyl iron intermediate (**A**). Although the subsequent step leaves considerable ambiguity in the present stage of experiment, the reaction of methanol to **A** probably

3) R. B. King and F. C. A. Stone, "Inorganic Syntheses", Vol. VII, p. 193 (1963), W. McFarlane and G. Wilkinson, *ibid.*, Vol. VIII, p. 181 (1966).

affords another iron containing intermediate (**B**), which reacts in two ways: 1) hydrogenation by the hydrido anion to give unsaturated monoesters and 2) second carboxylation to unsaturated diesters. The facile formation of the hydrido anion from ironpentacarbonyl in the presence of potassium hydroxide would be resposible for the observation that pressure drop in experiment 5 started at a lower temperature (125°C) than 150°C (Fig. 1, curve B). However, potassium hydroxide essential for the regeneration of the hydrido anion from ironpentacarbonyl is consumed irreversibly to form potassium carbonate under the reaction conditions according to reactions (5) and and (7). The process constitutes a side reaction which inactivates the catalysis system and is presumably a principal factor distinguishing the function of potassium hydroxide from that of tertiary amines, and accounts for the formation of unsaturated diesters in experiment 5 as compared to nearly none in experiment 4 and also for the previous result[1a] where the catalysis system containing potassium hydroxide was nearly ineffective in the oxymethylation of olefins which required longer reaction time(20—30 hr) and higher reaction temperature (170—175°C).

Experimental

Materials. Commercial propargyl alcohol was purified by distillation. Propargyl acetate was prepared by acetylation propargyl alcohol. 3-Methoxy-1-propyne was obtained by debromination of 2,3-dibromo-1-methoxypropane.[4] 3-Methyl-1-butyn-3-ol, 1-ethynylcyclohexanol and 1-butyn-4-ol were synthesized by the reaction of sodium acetylide with acetone, cyclohexanone and ethylene oxide in liquid ammonia, respectively.[5] 1-Pentyn-5-ol was obtained by treatment of tetrahydrofurfuryl chloride with sodium amide in liquid ammonia.[6]

General reaction procedure. Acetylenic compound (0.25 mol), triethylamine (0.25 mol), water (0.40 mol), ironpentacarbonyl (0.05 mol) and 70 ml of methanol were placed in a 300 ml autoclave. After air was displaced with carbon monoxide, carbon monoxide was introduced until pressure became 90—100 kg/cm^2. The mixture was heated under stirring to the desired temperature ranging from 70 to 175°C in about one hour and held at the reaction temperature until the pressure drop substantially ceased. To a dark green reaction mixture was added 100—150 ml of saturated sodium chloride solution and the organic component was taken up by ether. After neutralizing the remaining amine, the ethereal solution was dried and concentrated. The product collected by distillation of the residue was analyzed by gas chromatography and the yeilds of each component were calculated by assuming a proportionality between peak area and weight. The main components of the product were separated by gas chromatography and determined by infrared spectra, NMR and elementary analysis.

Product Identification. The principal product (II) obtained from Ia, Ib and Ic was confirmed as dimethyl methylsuccinate by its infrared spectrum, NMR and elementary analysis (Found: C, 57.72%; H, 7.74%) and further substantiated by comparison with an authentic sample. The other three components found in the reaction of propargyl alcohol using potassium hydroxide as a base were separated analytically by gas chromatography. They gave the following results.

III: dimethyl methylmaleate, NMR: 2.25 (d, 3H), 3.72 (s, 3H), 3.73 (s, 3H) and 6.67 (quar, 1H). Found: C, 53.40; H, 6.53%. Calcd for $C_7H_{10}O_4$: C, 53.16; H, 6.37%.

IVa: dimethyl itaconate, NMR: 3.24 (d, 2H), 3.64 (s, 3H), 3.73 (s, 3H), 5.65 (m, 1H) and 6.22 (m, 1H).

IVb: dimethyl methylfumarate, NMR: 2.2 (d, 3H), 3.67 (s, 3H), 3.73 (s, 3H) and 5.75 (quar, 1H). Found: C, 53.20; H, 6.53%. Calcd for $C_7H_{10}O_4$: C, 53.16; H, 6.37%.

Their structure were further confirmed by hydrogenation to form dimethyl methylsuccinate.

Distillation of the reaction product from 3-methyl-1-butyn-3-ol gave two fractions. Two components V and VI in the lower fraction (64.0/85 —91.0°C/65 mmHg) and five components VII–XI in the higher fraction (105—147°C/4 mmHg were separated by gas chromatography and analyzed. No alcoholic component could be detected.

V: methyl β-isopropylacrylate (*cis* and *trans* mixture), NMR: 1.05 (d, 6H), 1.85—2.64 (m, 1H), 3.60 (s, 3H), 5.55 (quar, 1H) and 6.71 (quar, 1H). Found: C, 64.76; H, 9.16%. Calcd for $C_7H_{12}O_2$: C, 65.59; H, 9.44%.

VI: methyl 4-methyl-3-pentenoate, NMR: 1.59 (s, 3H), 1.70 (d, 3H), 2.87 (d, 2H), 3.55 (s, 3H) and 5.17 (m, 1H). Found: C, 65.89; H, 9.64%.

VII: dimethyl isopropylsuccinate, NMR: 0.91 (s, 6H), 1.90—2.75 (m, 4H), 3.56 (s, 3H) and 3.58 (s, 3H). Found: C, 57.48; H, 8.59%. Calcd for $C_9H_{16}O_4$: C, 57.43; H, 8.57%.

VIII: dimethyl isopropylmaleate or fumarate, NMR: 1.10(d, 6H), 2.50 (m, 1H), 3.50(s, 3H), 3.57 (s, 3H) and 5.58 (d, 1H). Found: C, 58.37; H, 7.76%. Calcd for $C_9H_{14}O_4$: C, 58.05; H, 7.85%.

IX: 3-isopropyl-γ-butyrolactone, $\nu_{C=O}$; 1780 cm^{-1}, NMR: 0.93 (d, 3H), 0.96 (d, 3H), 1.45 (m, 1H), 1.80—2.60 (m, 3H) and 3.50—4.40 (m, 2H). Found: C, 65.60; H, 9.24%. Calcd for $C_7H_{12}O_2$: C, 65.59; H, 9.44%

X: dimethyl isopropylidenesuccinate, NMR: 1.80 (s, 3H), 2.10 (s, 3H), 3.25 (s, 2H), 3.60 (s, 3H) and 3,65 (s, 3H). Found: C, 59.02; H, 7.77%.

XI: 4,4-dimethyl-3-methoxycarbonyl-γ-butyrolactone, $\nu_{C=O}$; 1780, 1740 cm^{-1}. NMR: 1.25 (s, 3H), 1.58 (s, 3H), 2.4—3.32 (m, 3H) and 3.73 (s, 3H). Found: C, 55.85; H, 7.26%. Calcd for $C_8H_{12}O_4$: C, 55.80; H, 7.03%.

Four compounds separated in a similar manner from the product of 1-ethynylcyclohexanol were identified as follows.

XII: methyl 3-cyclohexylidenepropionate, NMR: 1.53 (m, 6H), 2.10 (m, 4H), 2.94 (d, 2H), 3.62 (s, 3H) and 5.21 (t, 1H).

XIII: methyl trans-β-cyclohexylacrylate, NMR: 1.50 (m, 11H), 3.68 (s, 3H), 5.69 (quar, 1H) and 6.85 (quar, 1H).

XIV: dimethyl cyclohexylsuccinate, NMR: 1.61 (m, 6H), 1.95 (m, 4H), 2.48 (m, 4H), 3.62 (s, 3H) and 3.64 (s, 3H).

XV: dimethyl cyclohexylidenesuccinate, NMR: 1.63 (m, 6H), 2.22 (m, 2H), 2.65 (m, 2H), 3.28 (s, 2H), 3.62 (s, 3H) and 3.68 (s, 3H).

The gas chromatogram of the product from 1-butyn-4-ol indicated the presence of two principal components XVI and XVII, but no alcoholic component such as *n*-butanol and 3- or 2-butenol-1. Assignment of their lactone structures

4) I. M. Heilbron, E. R. H. Jones, and R. N. Lacey, *J. Chem. Soc.* **1946** 28.

5) A. L. Henne and K. W. Greenlee, *J. Amer. Chem. Soc.*, **67** 484 (1945).

6) E. R. H. Jones, G. Eglinton, and M. C. Whiting, "Organic Syntheses", Coll. Vol. IV, p. 755 (1963).

based on the higher carbonyl absorptions and the absence of methoxycarbonyl group were characterized by the NMR peak in 3.50 to 3.75 ppm region. The saturated lactone could be differentiated from an authentic β-methyl isomer by their γ-proton signals in the 3.5—4.5 ppm region.

XVI: α-methyl-γ-butyrolactone, $\nu_{C=O}$; 1770 cm^{-1}. NMR 1.22 (d, 3H), 1.67—2.17 (m, 1H), 2.17—2.82 (m, 2H) and 4.0—4.33 (m, 2H). Found: C, 59.94; H, 8.27%. Calcd for $C_5H_8O_2$: C, 59.98; H, 8.05%.

XVII: α-methyl-γ-crotonolactone, $\nu_{C=O}$; 1760 cm^{-1}, $\nu_{C=C}$; 1660 cm^{-1}. NMR: 1.9 (quar, 3H), 4.72 (m, 2H) and 7.18 (quar, 1H). Found: C, 60.50; H, 6.29%. Calcd for $C_5H_6O_2$: C, 61.21; H, 6.17%.

Distillation of the product from 1-pentyn-5-ol gave two fractions. Owing to the complex nature and less volatility, attempted separation of the components in the higher fraction by gas chromatography afforded no pure samples. The three principal components in the lower fraction were separated by gas chromatography, two of them being confirmed as 1-pentene-5-ol and the strating material by comparison of their infrared spectra and in accordance with the retention times. The other component was proved to be methyl tetrahydrofuryl acetate by comparison with an authentic compound.

XX: methyl tetrahydrofuryl acetate, $\nu_{C=O}$; 1742 cm^{-1}. Found: C, 57.89; H, 8.71%. Calcd for $C_7H_{12}O_3$: C, 58.31; H, 8.39%.

Infrared Examination of the Catalysis System. A catalyst mixture in methanol containing ironpentacarbonyl (or $HFe_3(CO)_{11}^-HN^+Et_3$), a base and water in the same ratio as that used in the above reactions under the initial carbon monoxide pressure of 100 kg/cm^2 was heated to 150°C under stirring. A small aliquot was withdrawn from the vessel to a glass pressure sampler at a suitable interval starting from the instant 150°C was reached (or from 125°C in the presence of potassium hydroxide). The change of the ironcarbonyl species was followed by infrared spectra immediately taken after sampling, using the absorptions at 1995 cm^{-1} for ironpentacarbonyl and 1880 cm^{-1} for mononuclear hydroirontetracarbonyl anion. Light brownish yellow color of each aliquot at the time of sampling was indicative of the absence (or disappearance) of trinuclear hydrido species, which is readily discernible by its strong deep red color with a quantity less than 0.1%. The color of the samples, however, gradually turned pink due to slow conversion of the mononuclear anion to trinuclear species under atmospheric pressure.

BULLETIN OF THE CHEMICAL SOCIETY OF JAPAN, VOL. 46, 514—517 (1973)

Asymmetric Hydrogenation of C=O Double Bond with Modified Raney Nickel Catalyst. XXV. Contributions of pH-Adjusting Reagents in the Asymmetric Hydrogenation

Tadashi TANABE*, Kazuo OKUDA, and Yoshiharu IZUMI

Division of Organic Chemistry, Institute for Protein Research, Osaka University, Suita, Osaka

(Received March 9, 1972)

In the asymmetric hydrogenation of methyl acetoacetate with modified Raney nickel catalysts, the effects of pH-adjusting reagents were studied using D-tartaric acid, L-2-hydroxyisovaleric acid, L-glutamic acid, and L-aspartic acid as the modifying reagents. The effects of various metal ions and ammonium ions were investigated at pH 5.0. The asymmetric activity of the catalyst modified with the 2-hydroxy monocarboxylic acid or 2-amino dicarboxylic acid was not affected by the pH-adjusting reagents. However, 2-hydroxy dicarboxylic acid was markedly influenced by the reagents. The univalent metal ion was more effective than divalent or ammonium ions. Sodium hydroxide was the best pH-adjusting reagent. The adsorption state of the modifying reagent was discussed on the basis of the effects of the pH-adjusting reagent.

In the asymmetric hydrogenation of methyl acetoacetate to methyl 3-hydroxybutyrate, the pH of a modifying solution has been found to affect the asymmetric activity of the catalyst.[1,2] All the modifying reagents which have been tested, except neutral amino acids,[3] can be classified into two groups according to the effects of the modifying pH, as is shown in Fig. 1.

Group A: The hydroxy dicarboxylic acids. The asymmetric activity of catalyst modified with an acid of this group is at its maximum at about pH 5 and decreases on both the acidic and alkaline sides.

Group B: The hydroxy monocarboxylic acids and most monoamino dicarboxylic acids. The asymmetric activity of a catalyst treated with this group of acids is not influenced by the modifying pH on the acidic side and decreases with an increase in the modifying pH.

It was suggested by Tatsumi[4] that the pH-dependency of the asymmetric activity of the catalyst modified with the 2-hydroxy carboxylic acid might be brought about by the neutralization of the carboxyl groups. However, the case of the pH-dependency and the factors producing the two different kinds of effects of the modifying pH was not clear. The in-

* Present address: Department of Medical Chemistry, Faculty of Medicine, Kyoto University, Sakyo-ku, Kyoto.

1) Y. Izumi, M. Imaida, H. Fukawa, and S. Akabori, This Bulletin, **36**, 21 (1963).

2) Y. Izumi, T. Harada, T. Tanabe, and K. Okuda, *ibid.*, **44**, 1418 (1971).

3) The effect of the modifying pH was not reported because of the lack of any investigation into the proper pH-adjusting reagent.

4) S. Tatsumi, This Bulletin, **41**, 408 (1968).

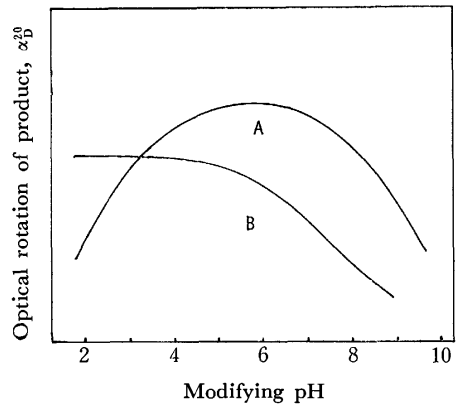

Fig. 1. Effect of modifying pH on modification at 0°C.

fluences of the various pH-adjusting ions were studied, and the adsorption state of the modifying reagent and the pH-dependency of the asymmetric activity are discussed.

Experimental

L-2-Hydroxyisovaleric Acid (HIV). The HIV was prepared by the method of Winitz *et al.*[5]

Divalent Metel D-Tartarates. Divalent metal D-tartarates were prepared from the metal chlorides and sodium tartarate.[6]

Preparation of Raney Nickel Catalyst. Raney nickel alloy (40% of nickel, 1.5 g) was developed with a 20% aqueous sodium hydroxide solution (20 ml) and the suspension was allowed to stand for 1 hr at 100°C. Then the catalyst was washed with total 500 ml of deionized water.

Preparation of the Modifying Solution and the Modification of the Catalyst. The pH of a 1—2% aqueous solution (100—200 ml) of a modifying reagent was adjusted to 5.0 with a diluted aqueous solution of the metal hydroxide or a solid metal oxide, except for the study of the effect of the divalent metal ion on the asymmetric activity of the catalyst modified with D-tartaric acid. As, with the divalent transition metal oxide or the hydroxide, the pH-adjustment of a D-tartaric acid solution was difficult, metal D-tartarate prepared from the corresponding metal chloride and sodium D-tartarate was saturated in 0.2—1 l of water and the resulting solution was adjusted to pH 5.0 with D-tartaric acid. The modifying solution thus prepared was brought to the specified temperature and poured onto the catalyst; the suspension was then kept, with occasional shaking, at the specified temperature for 1.5 hr. After the removal of the modifying solution by decantation, the catalyst was washed once with water and three times with methanol.

Hydrogenation of Methyl Acetoacetate and Measurement of the Optical Rotation of the Product. Methyl acetoacetate (17.5 ml) was hydrogenated with a modified catalyst obtained by the procedure described in the previous section, under an initial pressure of 90 kg/cm² at 60°C in a shaking autoclave. The catalyst was then removed by filtration and the filtrate was distilled under reduced pressure (bp 61—62°C/12 mmHg). The optical rotation of the methyl 3-hydroxybutyrate thus produced was measured without dilution in a 1-dm tube.

5) M. Winitz, L. Bloch Frankental, N. Izumiya, S. M. Birnbaum, C. G. Baker, and J. P. Greenstein, *J. Amer. Chem. Soc.*, **78**, 2423 (1956).

6) S. Hakomori, *Sci. Rep. Tohoku Univ.*, **16**, 841 (1927).

Results and Discussion

The Influence of the Remaining Developing Reagent. Though the Raney nickel catalyst was washed with a sufficient amount of water (500 ml of water/600 mg of catalyst) after development with a 20% sodium hydroxide solution, a small smount of the remaining sodium ion could interchange with the metal ions used for the pH-adjustment and influence the asymmetric activity of the catalyst. For the study of the effect of the metal ions remaining in the catalysts, the two kinds of catalysts, those developed with sodium hydroxide and with potassium hydroxide, were modified with D-tartaric acid, and the their asymmetric activities were compared each other. The results are shown in Table 1.

Table 1. Effect of residual developing reagent in Raney nickel catalyst

Mod. reagent	Develop. reagent	pH-Adjusting reageat	Optical rotation of product α_D^{40}
D-Tartaric acid	NaOH	NaOH	−7.73
D-Tartaric acid	KOH	NaOH	−7.32
D-Tartaric acid	NaOH	KOH	−3.70

The asymmetric activity of the catalyst developed with sodium hydroxide and modified with potassium tartarate is considerably lower than that of the catalyst modified with sodium tartarate. However, the asymmetric activity of the catalyst developed with potassium hydroxide and modified with sodium tartarate hardly differed from that of the catalyst developed with sodium hydroxide and modified with sodium tartarate. Accordingly, the exchange of the ions used for the pH-adjustment with the sodium ion remaining on the catalyst surface seems to be negligible, judging from the above results.

The Effect of the pH-Adjusting Reagents on the Asym-

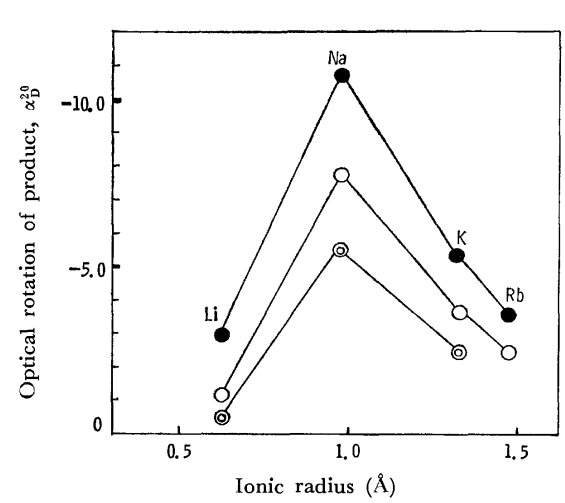

Fig. 2. Effect of pH-adjusting reagent. Catalysts were modified with D-tartaric acid, and D-malic acid at pH 5.0, 0°C and 100°C.
○: modified with D-tartaric acid at 0°C, ●: modified with D-tartaric acid at 100°C, ◎: modified with D-malic acid at 0°C.

metric Activity of the Catalyst Modified with the Hydroxy Dicarboxylic Acid. The Effect of the Univalent Alkaline Ion: On the modification with the acid belonging to Group A, the asymmetric activity of the catalyst increased with the elevation of the modifying pH in the acidic region and reached a maximum between pH 5 and 8. In the alkaline region, the asymmetric activity of the catalyst gently decreased with the elevation of the modifying pH. In the present investigation, the modifying solutions of D-tartaric acid and D-malic acid were adjusted to pH 5.0, and the effect the univalent metal ion was studied. The results are shown in Fig. 2.

An intimate relation between the asymmetric activities of the catalyst and the bulk of the ions used for the pH-adjustment of the modifying solutions was found in the cases of modifications with D-malic acid and D-tartaric acid at 0°C and 100°C. That is, bulkier or smaller ions than sodium decreased the asymmetric activity; an optimum value was observed with sodium. The facts suggest that metal ions contribute to the enantiotopic selection of the substrate and that at least one carboxyl group of the hydroxy dicarboxylic acid forms salt with the metal ion on the catalyst surface.

The Effect of the Mixed Univalent Ions: The modifying pH was adjusted with equal amounts of two kinds of cations and the asymmetric activities were compared with the calculated values, which were given as a mean of the values obtained with the catalysts treated with the solutions adjusted with the cations separately. As is shown in Table 2, the observed activities were not proportional to the concentrations of ions, and stronger bases predominantly controlled the asymmetric activity.

The Effect of the Divalent Metal Ions: The effect of the divalent metal ion was examined using divalent metal D-tartarate; the results are shown in Table 3. The calcium ion gave the catalyst a slightly higher symmetric activity than the zinc, cupric, ferrous, nickel, and cobaltous ions. These divalent ions gave much lower asymmetric activities than the monovalent ions. These facts suggest that the divalent cations, which can form intermolecular or intramolecular salts with the dicarboxylic acids, contribute to the adsorption of a modifying reagent in a different manner from the univalent cations.

The Effect of the Amines: The influence of the bulk of the alkyl substituent of ammonia was also studied; the results are shown in Table 4. The asymmetric activity of a catalyst was lower when modified with a solution adjusted with the amines than when modified with a solution adjusted with the sodium ion. No effect of the bulk of the alkyl substituents was observed.

The Effect of the Metal Ions on the Asymmetric Activity of the Catalyst Modified with Hydroxy Monocarboxylic Acid: As has already been reported in a previous paper,[7] the 2-hydroxy monocarboxylic acid differed

Table 2. Effect of mixed univalent metal ions on asymmetric activity of catalyst modified with D-tartaric acid

pH-Adjusting reagent	Optical rotation of product, α_D^{20}	Calcd.[a] Optical rotation, α_D^{20}
LiOH	−1.13	—
NaOH	−7.73	—
KOH	−3.70	—
NH_4OH	−0.62	—
NaOH+LiOH (1 : 1)	−6.09	−4.03
NaOH+KOH (1 : 1)	−4.40	−5.71
NaOH+NH_4OH (1 : 1)	−6.53	−3.18

a) The calcd. optical rotation: The average value of the two asymmetric activities of the catalysts pH-adjusted with NaOH and KOH separately.

Table 3. Effect of divalent metal ion on asymmetric activity of catalyst modified with D-tartaric acid

Modifying reagent	Optical rotation of product, α_D^{20}
Calcium D-tartarate·$4H_2O$	−1.71
Zinc D-tartarate	−0.63
Cupric D-tartarate[a]	−0.19
Ferrous D-tartarate·$2H_2O$	−0.37
Nickel D-tartarate·$2H_2O$	−0.40
Cobaltous D-tartarate	−0.66

a) The modifying pH was 4.8.

Table 4. Effect of amine on asymmetric activity of catalyst modified with D-tartaric acid

pH-Adjusting reagent	Optical rotation of product, α_D^{20}
NH_3	−0.62
NH_2CH_3	−0.88
$NH(CH_3)_2$	−0.59
$N(CH_3)_3$	−0.84
$N(C_2H_5)_4OH$	−0.45
Pyridine	+0.47
Piperidine	+0.19
Ethylenediamine	+0.11
α-Picolione	−0.07
Aniline[a]	−0.72
Imidazole	−0.22
Hydrazine	−0.96
Ethanolamine	−0.27

a) The modifying pH was 4.8.

Table 5. Effect of pH-adjusting reagent on asymmetric activity of catalyst modified with L-2-hydroxy-isovaleric acid

pH-Adjusting reagent	Optical rotation of product, α_D^{20}
LiOH	+0.32
NaOH	+0.31
KOH	+0.31
NH_4OH	+0.31

7) Y. Izumi, S. Tatsumi, and M. Imaida, This Bulletin, **39**, 2223 (1966).

from the 2-hydroxy dicarboxylic acid in that it gave the catalyst a constant asymmetric activity independently of the modifying pH in the acidic region.

The effects of univalent metal ions and ammonium ions were studied using a catalyst modified with L-2-hydroxyisovaleric acid (HIV). The results are shown in Table 5. The asymmetric activities of the catalysts modified with HIV were not affected by the pH-adjusting reagent and had values similar to that of the catalyst modified with a pH-adjusted solution containing the sodium ion. These results are quite different from the results obtained in the case of tartaric acid and show that the cation used for pH-adjustment does not take part in the adsorption of the hydroxy mono-carboxylic acid.

The Effect of Metal Ions and Ammonium Ions on the Asymmetric Activity of the Catalyst Modified with the Amino Acid: Most amino acids, except for α-alkyl substituted amino acids, are classified in Group A on the basis of their pH-dependency, and the asymmetric activities of the catalyst treated with those amino acids were not affected by the modifying pH in the acidic region.

The effects of metal and ammonium ions on the asymmetric activities of the catalysts treated with L-aspartic acid and L-glutamic acid were also studied; the results are shown in Tables 6 and 7.

The bulk of the univalent metal ions and ammonium ions, all except ethylenediamine and pyridine, did not affect the asymmetric activities; this is different from the results with D-malic acid and D-tartaric acid. Ethylenediamine and pyridine decreased the asymmetric activities of the catalysts. The divalent metal ions and the ammonium ions did not so decrease the asymmetric activities of the catalysts as was found on the modification with HIV, and the asymmetric activities of the catalysts were nearly the same when the pH of the modifying solution was adjusted, either with the amines or with the univalent cation, to that of the one modified with the solution pH-adjusted with the univalent cation.

Table 6. Effects of univalent and divalent metal ions on asymmetric activity of catalyst modified with amino acids

Modifying reagent	pH-Adjusting reagent	Optical rotation of product, α_D^{20}
L-Aspartic acid	LiOH	−1.28
	NaOH	−1.19
	KOH	−1.30
L-Glutamic acid	LiOH	−5.20
	NaOH	−5.03
	KOH	−5.21
	$Ca(OH)_2$	−3.51
	$Ba(OH)_2$	−3.44
	MgO	−4.13
$Ni(L\text{-}Glu)_2 \cdot 2H_2O$		−4.00[a]

a) Y. Izumi and T. Ninomiya, This Bulletin, **43**, 579 (1970).

Table 7. Effect of amines on asymmetric activity modified with amino acid

Modifying reagent	pH-Adjusting reagent	Optical rotation of product, α_D^{20}
L-Aspartic acid	NH_3	−1.14
	$N(CH_3)_3$	−1.12
	NaOH	−1.19
L-Glutamic acid	NH_3	−4.55
	NH_2CH_3	−4.76
	$NH(CH_3)_2$	−4.56
	$N(CH_3)_3$	−4.60
	Pyridine	−1.50
	Hydrazine	−4.13
	Ethylenediamine	−3.13
	Ethanolamine	−4.39
	NaOH	−5.03

Judging from these facts, the amino dicarboxylic acid seems to be adsorbed on the catalyst surface in a state which is not influenced by the ion used for the pH-adjustment, unlike the case of hydroxy dicarboxylic acid. That is, both the two carboxyl groups of the amino dicarboxylic acid may be used for the adsorption on the catalyst surface and may not form an ionic bond with the cation used for the pH-adjustment. Ethylenediamine and pyridine, which have a strong affinity for nickel, seem to be adsorbed competitively well onto the catalyst and inhibit the adsorption of the amino acid, thus decreasing the asymmetric activity of the catalyst.

The Adsorption State of the Modifying Reagent. It can be concluded, from the effects of the cations used for the pH-adjustment on the asymmetric activities of the catalysts modified with the hydroxy mono- and dicarboxylic acids at pH 5, that the α-carboxyl group of the hydroxy carboxylic acid contributes to the adsorption onto the catalyst surface and that the remaining ω-carboxyl group of the hydroxy dicarboxylic acid forms an ionic bond with the cation used for the pH-adjustment. The cation bound to the ω-carboxyl group takes part in the enantiotopic selection of the substrate as a substituent of the modifying reagent.

The α- and ω-carboxyl groups of an amino dicarboxylic acid chemically bind with the nickel catalyst, and the cations and amines used for the pH-adjustment of the modifying solution do not affect the asymmetric activities of the catalysts modified with amino acids. These facts are also supported by the findings by Ninomiya of our research group[8] that the absorption spectrum of the glutamic acid on the evaporated nickel film on quartz very similar to that of nickel chelate.

8) Part XXIII of this series: T. Ninomiya, This Bulletin, to be published.

Aldol Condensations of Aldehydes over Disodium Phthalocyanine[1,2]

Hiroo INOUE, Kenzo KUNIKAWA, and Eiji IMOTO

Department of Applied Chemistry, College of Engineering, University of Osaka Prefecture, Sakai, Osaka

(Received April 3, 1972)

Disodium phthalocyanine (Pc-Na_2) acts as a base for the aldol condensations of aldehydes, although it shows no effect upon those of ketones. In the aldol condensation of isobutyl aldehyde by Pc-Na_2 in *n*-hexane, 2,6-diisopropyl-5,5-dimethyl-1,3-dioxane-4-ol (III) is produced through two processes with different rates; the reaction proceeds first by the slower rate, and then by a more rapid rate after a certain reaction period. The process is different from that of the catalysis by sodium ethoxide. During the reaction, Pc-Na_2 is converted to sodium-free phthalocyanine (Pc-H_2) *via* an intermediate. The formation of the intermediate results in the retardation of the aldol condensation with the product and phthalocyanine anions. Furthermore, the adsorption of water on Pc-Na_2 brings about the retardation of the reaction.

In acid-base catalyses of organic compounds, the formation of a complex between catalyst and substrate brings about a rate enhancement and a specificity toward the catalyzed reaction. These catalyzed reactions are found in processes in frozen solutions,[3] in inclusion compounds,[4] in micellar solutions,[5] and in polymeric compounds[6] which have been studied as models for enzymic catalysis. Now we will attempt to study the dimerization of two substrates over a plate-like organic molecule with a character of an acid or a base. The present investigation will deal with the heterogeneous base-catalysis of Pc-Na_2 on the aldol condensations of aldehydes and ketones. The Pc-Na_2 contains ion pairs as an active site in a planar-macrocyclic π-system, and might have an affinity for aldehydes and ketones. Our purpose in this paper is to investigate the specific action of Pc-Na_2 as a base for the aldol condensation, and to find the correlation between the reactivity and the features of the chemical structure of Pc-Na_2.

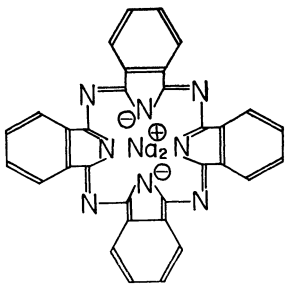

Pc-Na_2

Experimental

Materials. All of the aldehydes and ketones were purchased from commercial sources. These materials were distilled through a Vigreux column before use. The solvents were dried by the usual methods and were distilled twice before use. The Pc-Na_2 was prepared by heating sodium and *o*-phthalonitrile in *n*-amyl alcohol at 130—140°C according to the method reported by Barrett, Dent, and Linstead.[7] The purification was carried out by the following method: 10 g of Pc-Na_2 was dispersed in 20 ml of hot *n*-amyl alcohol, filtered off, washed several times with 20 ml of anhydrous ether, and dried over calcium chloride under the reduced pressure of 1 mmHg at 100°C for 3 hr, unless stated otherwise. The sodium content of the Pc-Na_2 used here was 7.99% (Calcd for Pc-Na_2: 8.24%). The IR spectrum of Pc-Na_2 had absorptions characteristic of the structure of the phthalocyanine dianion at 1640, 1040, and 790—770 cm^{-1}. On the other hand, the IR spectrum of Pc-H_2 agreed with that of α- and/or β-phthalocyanine, described in the literature.[8] The visible spectrum of Pc-Na_2 observed by means of a KBr plate showed broad absorptions at 620 (sh) and 720 mμ, while that of Pc-H_2 showed them at 650 and 740 (sh)mμ.

Procedures for Reactions. Similar procedures were used for all the reactions. In a typical experiment, a solution of 8.0 g of isobutyl aldehyde in 10 ml of *n*-hexane was placed in a 100-ml flask containing a Teflon stirring bar, and the flask was placed in a thermostat bath at 25±1°C. Immediately after nitrogen gas had passed into the system for 3 min, 0.1 g of Pc-Na_2 was added to the solution, the flask was capped with a stopper, and the solution was stirred vigorously by means of a magnetic stirrer. After a reaction period, 80 ml of *n*-hexane was added to the system to stop the reaction, the resulting solution was filtered off, and the precipitate was washed repeatedly with *n*-hexane. The combined *n*-hexane layer was then washed with a small amount of a 5—10 wt% hydrochloric acid solution and then water. *n*-Hexane and the volatile components were completely removed under reduced pressure. In the reaction time of 20 hr, 6.0 g of a residual oil was obtained; this oil was then submitted to an analysis of its product. On the other hand, the distillation of the oil (bp 90—91°C/2 mmHg) yielded 5.6 g (70%) of a mixture of 2,6-diisopropyl-5,5-dimethyl-1,3-dioxane-4-ol (III)[9] and the monoisobutyrate of 2,2,4-trimethyl-1,3-pentanediol (IV), which could be

1) Studies of organic catalysts. VI. Part V: H. Inoue, Y. Kida, and E. Imoto, This Bulletin, **41**, 692 (1968).

2) Presented at 24th Annual Meeting of the Chemical Society of Japan, Osaka, April, 1971.

3) a) R. E. Pincock and T. E. Kiovsky, *J. Amer. Chem. Soc.*, **88**, 51, 4455, 4704 (1966). b) R. E. Pincock, *Accounts Chem. Res.*, **2**, 97 (1969).

4) a) F. Cramer and W. Kampe, *J. Amer. Chem. Soc.*, **87**, 1115 (1965). b) N. Hennrich and F. Cramer, *ibid.*, 1121 (1965). c) M. L. Bender, R. L. Van Etten, G. A. Clowes, and J. F. Sebastian, *ibid.*, **88**, 2318, 2319 (1966); *ibid.*, **89**, 3242, 3253 (1967).

5) a) T. C. Bruice, J. Katzhendler, and L. R. Fedor, *ibid.*, **90**, 1333 (1968). b) C. Gitler and A. Ochoa-Solano, *ibid.*, **90**, 5004 (1968). c) E. H. Cordes and R. B. Dunlap, *Accounts Chem. Res.*, **2**, 329 (1969). d) G. J. Buist, C. A. Bunton, L. Robinson, L. Sepulveda, and M. Stam, *J. Amer. Chem. Soc.*, **92**, 4072 (1970).

6) a) C. C. Overberger and J. C. Salamone, *Accounts Chem. Res.*, **2**, 217 (1969). b) C. G. Overberger, M. Morimoto, I. Cho, and J. C. Salamone, *J. Amer. Chem. Soc.*, **93**, 3228 (1971). c) T. Kunitake and S. Shinkai, *ibid.*, **93**, 4247, 4256 (1971).

7) P. A. Barrett, C. E. Dent, and R. P. Linstead, *J. Chem. Soc.*, **1936**, 1719.

8) A. A. Ebert, Jr. and H. B. Gottlieb, *J. Amer. Chem. Soc.*, **74**, 2806 (1952).

separated by glc.

Analyses of Products. All of the products were identified by a comparison of their IR and NMR-spectra, the results of elementary analyses of their 2,4-dinitrophenylhydrazone, their retention times in glc, and their molecular weights with those of authentic specimens prepared by the methods described in the literature.[10] The identification of IV was based on the observation that the molecular weight was 218 (calcd for monoester, 216), and the alkaline hydrolysis of the ester gave, quantitatively, 2,2,4-trimethyl-1,3-pentanediol and isobutyric acid. However, IV was regarded as a mixture of two monoisobutyrates with an isobutyroyl group at the 1- or 3-hydroxyl group. The red-brown polymeric material (Va) prepared from acetaldehyde was converted to the 2,4-dinitrophenylhydrazone. Anal. Found: C, 57.46; H, 5.90; N, 11.06%. The avarage molecular weight of Va was 320. The IR spectrum of Va exhibited bands at 3400, 2950-2800, 1710, 1680, 1440, 1370, and 1100 cm^{-1}. The UV spectrum of Va in ethanol had absorptions at 233, 285, 324, and 360 mμ.

The amounts of all the products except for III and IV were determined by means of distillation. The amounts of III and IV were determined by the following method: after completely removing the reaction solvent, 0.1 g of the residue, containing III and IV, was dissolved in 2 ml of methanol, and then into the solution there was added a solution of 0.4 g of 2,4-dinitrophenylhydrazine in 100 ml of a 2 N hydrochloric acid solution. The resulting solution was kept standing overnight. The precipitate was then filtered off, dried over calcium chloride, and weighed. From the weight of the precipitate, the amount of III was determined within an error of ±3%. Furthermore, it was confirmed by glc that the mixture consists of only III and IV. The amount of IV was determined by substracting the amount of III from 0.1 g of the mixture. The value thus obtained agreed with that determined by the glc analysis within an error of ±2—3%.

Analysis of the Sodium Cation. A weighed amount (0.1—0.2 g) of a sample in a crucible was burned cautiously with a small flame, and then it was heated strongly for 3—5 hr to change it completely to ash. The ash was dissolved in 20 ml of distilled water and was then titrated with 1/10 N hydrochloric acid, using methyl orange as the indicator. The sodium content could be measured within an error of ±2% by this method.

Results and Discussion

Action of Pc–Na_2 as a Base. When Pc–Na_2 was dispersed in acetonitrile or ethyl acetate, no product was obtained, but the Pc–Na_2 was recovered unchanged. However, a dispersion of Pc–Na_2 in aldehydes resulted in the corresponding condensation products, such as I, II, III, IV, and V. The yields of these products changed depending on the structure of the starting aldehydes, as Table 1 shows. In the aldol condensation of acetaldehyde, the red-brown polymeric material (Va) was obtained in a 70% yield. The values of *m* and *n* of Va were 3—4 and 2—3 respectively. The IR spectrum of Va was similar to that of

$RCH_2CH(OH)CHRCHO$

I a: $R=CH_3$
b: $R=CH_3CH_2$

$RCH_2CH{=}CRCHO$

II a: $R=CH_3$
b: $R=CH_3CH_2$

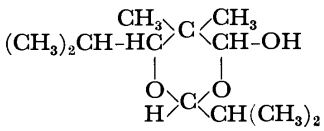

III

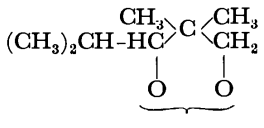

H-, $(CH_3)_2CHCO$-

IV

$RCH_2(-CH{=}CR-)_m(-CH(OH)CHR-)_nCHO$

V a: $R=H$
b: $R=CH_3$
c: $R=CH_3CH_2$

the polymer produced by using $(CH_3)_3N$[11] and Na–Hg[12] as the catalyst. The aldol condensation of propionaldehyde or *n*-butyraldehyde by Pc–Na_2 gave the corresponding aldols (Ia or Ib) and α,β-unsaturated aldehydes (IIa or IIb). Isobutyl aldehyde was converted to 2,6-diisopropyl-5,5-dimethyl-1,3-dioxane-4-ol (III) and the monoisobutyrate of 2,2,4-trimethyl-1,3-pentanediol (IV) in 21 and 50% yields respectively through a secondary reaction of the intermediate aldol. The sodium-cation content of the recovered phthalocyanine in all cases was in the range of 4.60—5.90%, which changed with the reaction conditions. The IR spectrum of the recovered phthalocyanine had the characteristic absorpions due to the phthalocyanine anion at 1642, 1040, and 790—770 cm^{-1}, and that due to the sodium-free phthalocyanine at 1000 cm^{-1}.

Table 1. Aldol condensations of aldehydes by Pc–Na_2 without solvent[a]

RR'CHCHO R	R'	Product	Yields, %[b]
H	H	Va	70[c]
CH_3	H	Ia, IIa, Vb	13, 15, 22[c]
CH_3CH_2	H	Ib, IIb, Vc	25, 23, 3[c]
CH_3	CH_3	III, IV	21, 50

a) The amount of Pc–Na_2 dispersed: 3.3 mol% in aldehydes. The reaction was carried out under a nitrogen atmosphere at room temperature for 20 hr.
b) The yields of I, II, III, and IV were based on aldehydes.
c) This was calculated by weight of polymer/weight of aldehyde × 100.

Ketones, such as acetone, methyl ethyl ketone, and acetophenone, could not undergo self-condensation by Pc–Na_2, not even at 100°C, although the sodium ethoxide-catalyzed condensation of acetone gave the polymeric material and phorone in 10 and 11% yields respectively. However, Pc–Na_2 acted as a base for the mixed condensation of isobutyl aldehyde and either acetone or methyl ethyl ketone (the molar ratio of isobutyl aldehyde to ketone; 2.4 or 2) under the same conditions as have been described above as giving

9) R. H. Saunders, M. J. Murray, and F. F. Cleveland, *ibid.*, **65**, 1714 (1943).
10) For a review, see A. T. Nielsen and W. J. Houlihan, "Organic Reactions," Vol. 16, p. 86 (1968).
11) a) ED. F. Degering and T. Stoudt, *J. Polym. Sci.*, **7**, 653 (1951). b) T. Imoto, T. Ota, and J. Kambara, *Nippon Kagaku Zasshi*, **82**, 492 (1961).
12) a) T. Imoto, K. Aotani, and T. Kojima, *ibid.*, **86**, 371 (1965). b) T. Imoto and T. Matsubara, *J. Polym. Sci.*, **56**, s4 (1962).

mainly the ketols (VIa and VIb) in 38 and 43% yields, and the α,β-unsaturated ketones (VIIa and VIIb) in 40 and 4% yields, respectively, based on the starting amounts of ketones. In addition to these products, a mixture of III and IV was obtained in a

$RCOCH_2CH(OH)CH(CH_3)_2$ $RCOCH{=}CHCH(CH_3)_2$

VI a: $R{=}CH_3$ VII a: $R{=}CH_3$

b: $R{=}C_2H_5$ b: $R{=}C_2H_5$

39% yield in the case of acetone, based on the starting amount of isobutyl aldehyde. Thus, it was found that Pc–Na_2 acts as a base for aldehydes and ketones, and that the action is specific for the aldol condensations of aldehydes.

Aldol Condensation of Isobutyl Aldehyde Catalyzed by Sodium Ethoxide. Sodium ethoxide was dispersed or dissolved in *n*-hexane, ethanol, and dimethyl sulfoxide, all containing isobutyl aldehyde. Sodium ethoxide, dispersed in *n*-hexane, changed from a solid to an emulsion state as the reaction proceeded, and III and IV were obtained as the products. In the case of the ethanol solvent, however, IV was converted further to 2,2,4-trimethyl-1,3-pentanediol and ethyl isobutyrate by the ester-exchange reaction. As Table 2 shows, it was observed in all cases that III is formed predominantly without an induction period. As the reaction time increased, however, the yield of III decreased and that of IV increased. The trends for the consecutive formation of IV were observed distinctly in the cases of the ethanol and dimethyl sulfoxide solvents. On the other hand, the heterogeneous catalysis in the *n*-hexane solvent tended to give a high yield of III, even in a prolonged reaction time. However, the increase in the amount of sodium ethoxide resulted in a rise in the yield of IV. IV would be produced by the intramolecular Cannizzaro reaction of the anion of III, derived from III with a base. Therefore, the effective concentration of the base must be of importance in the formation of IV.

The Condensation by Pc–Na_2. In *n*-hexane and acetonitrile solvents, III was first produced predominantly in the slow rate, as is shown in Fig. 1. After

Table 2. Aldol condensation of isobutyl aldehyde by sodium ethoxide[a)]

Solvent	C_2H_5ONa, mol/l	Reaction time, hr	Yield of Product, % III	IV[b)]
n-Hexane	3.0×10^{-1}	2	68	16
	3.0×10^{-1}	20	65	20
	1.8×10^{-3}	20	80	5
Ethanol	1.8×10^{-3}	2	19	1
	9×10^{-2}	2	51	(27)
	1.8×10^{-1}	2	6	(78)
	1.0×10^{-1}	20	0	20(31)
Dimethyl sulfoxide	9.0×10^{-3}	2	13	0
	4.5×10^{-2}	2	51	34
	9.0×10^{-2}	2	8	82
	9.0×10^{-2}	20	7	84

a) The concentration of isobutyl aldehyde: 5.5 mol/l. Reaction temperature: 25°C.

b) The brackets indicated the yield of diol.

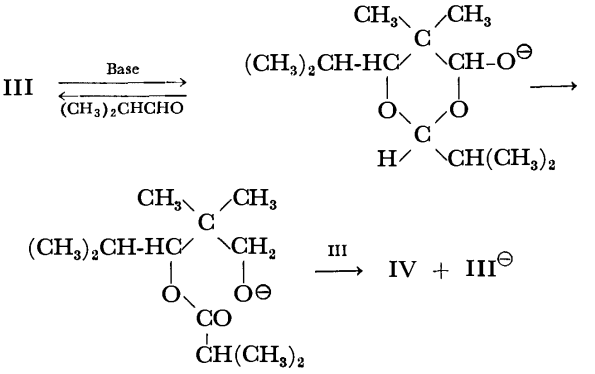

6 hr, the rate of the formation of III increased rapidly. When the yield of III reached about 60%, it was observed that III began to be converted to IV, as Table 3 shows. The fractional yield of IV in a longer reaction time became higher than in the case of sodium ethoxide. In the ethanol solvent, III and IV were first produced without the slow step; IV was converted further to 2,2,4-trimethyl-1,3-pentanediol and ethyl isobutyrate as the reaction time increased. These facts indicate that the dianion of Pc–Na_2 is transferred to ethanol, thus leading to the homogeneous catalysis by the ethoxide anion. Furthermore, the adsorption of two moles of water per mole of Pc–Na_2 resulted in a retardation of the condensation of isobutyl aldehyde by Pc–Na_2; that is, the yield of III in *n*-hexane was 30—40% after the reaction time of 9 hr. However, the presence of water resulted in the formation of III predominantly.

Table 3. Pc–Na_2 catalyzed aldol condensation of isobutyl aldehyde[a)]

Solvent	Reaction time, hr	Yield of Product, % III	IV[b)]
n-Hexane	6	11	2
n-Hexane	8	55	8
n-Hexane	15	34	41
Ethanol	20	0	22(55)

a) The concentration of isobutyl aldehyde: 5.5 mol/l. The amount of Pc–Na_2 dispersed: 9.0×10^{-2} mol/l. Reaction temperature: 25°C.

b) The brackets indicated the yield of diol.

Removal of the Sodium Cation from Pc–Na_2. After the aldol condensation of isobutyl aldehyde by the 100°C-dried Pc–Na_2 in *n*-hexane had been carried out for a reaction period under the conditions described above, the precipitate was collected by filtration and subsequently dried. The sodium content and the IR and visible spectra of the precipitate were measured. As is shown in Fig. 1, the curve of the change in the sodium content consisted of two steps. The flexion of the curve almost coincided with that of the formation curve of III. Furthermore, the formation of III was nearly parallel with the removal of the sodium cation during the period of the slow formation of III, the amount of III produced being 1.5—2 larger than that of the sodium cation removed.

On the other hand, the IR spectrum of the precipitate changed as the reaction proceeded. The ab-

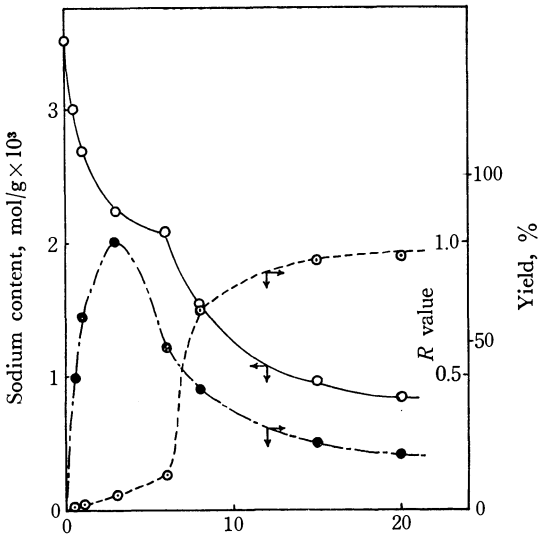

Fig. 1. The change of the sodium content (○) and the *R* value (●) of the recovered phthalocyanine, and the yield of the product (⊙) against the reaction time: the concentration of isobutyl aldehyde; 5.5 mol/l and the amount of Pc-Na_2 dispersed; 9×10^{-2} mol/l.

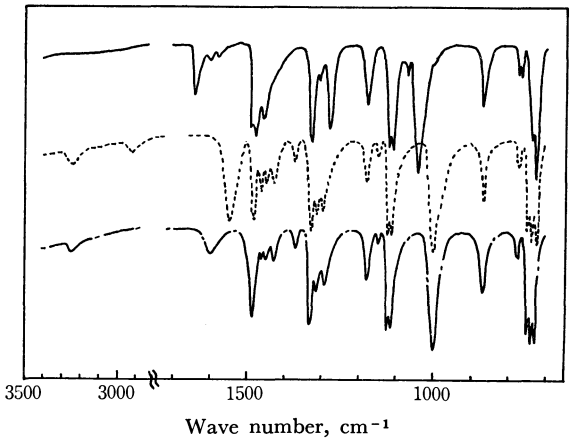

Fig. 2. The IR spectra of Pc-Na_2 (——), Pc-H_2 (— — —) and the intermediate (- - - -).

sorption peaks of the phthalocyanine anion and dianion at 1640 and 1040 cm^{-1} decreased, while that of the sodium-free phthalocyanine at 1000 cm^{-1} increased. In addition, a new band appeared at 1550 cm^{-1} (Fig. 2). The new band increased rapidly as the reaction proceeded, and then decreased. In Fig. 1, the ratio (R) of the intensity of the new band to that of a band at 870 or 1120 cm^{-1}, the intensity of which did not differ from Pc-Na_2 to Pc-H_2, is plotted against an interval of the reaction time. The maximum of the intensity ratio was observed in the reaction time of 3 hr,

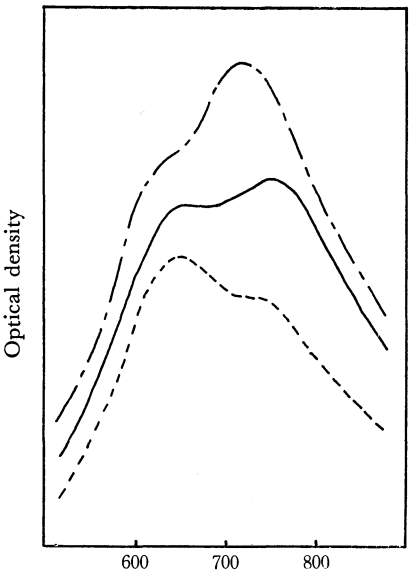

Fig. 3. The visible absorption spectra of Pc-Na_2 (— — —), Pc-H_2 (- - - -) and the intermediate (——) by KBr plate.

which lay in the slow step. When the reaction was carried out in 1/10 less Pc-Na_2 than that shown in Fig. 1, the intensity ratio was observed to reach a maximum sharply with a higher value in a shorter reaction time; then it decreased at a slower rate. These facts indicate that a stable intermediate exists in the reaction process. The sodium content of the intermediate with the maximum value of R at 1550 cm^{-1} was 3.86%. This value means that the intermediate is a monosodium phthalocyanine derivative. Its visible absorption spectrum, as observed by means of a KBr plate, showed two absorptions, at 650 and 750 mμ, although that of Pc-H_2 had absorptions at 650 and 740 (sh) mμ, as is shown in Fig. 3. The new band at 1550 cm^{-1} did not change even when the intermediate was heated at 100°C under a reduced pressure of 1 mmHg for 2 hr, but it disappeared when it was dispersed in ethanol, and the resulting IR spectrum agreed with that of Pc-H_2. Thus, the intermediate was a monosodium derivative with IR and visible spectra which differed from those of Pc-Na_2, Pc-NaH, and Pc-H_2, and with the departing sodium cation with a slow rate. However, the structure of the intermediate is not yet clear. When the intermediate was converted to Pc-H_2, the reaction proceeded rapidly by means of a catalysis similar to that in the case of sodium ethoxide. However, the consecutive formation of IV occurred more easily in the presence of the phthalocyanine molecule than in the case of sodium ethoxide. This may be caused by the fact that the product anion is concentrated over the phthalocyanine molecule.

The Reactions of Stannic Halides with Some Triphenylphosphine, -arsine and -stibine-substituted Iron Carbonyls

Tetsuo TAKANO

Department of Chemisjry, Faculty of Science, The University of Tokyo, Hongo, Tokyo

(Received April 6, 1972)

The reactions of stannic chloride and bromide with triphenylphosphine, -arsine and -stibine tetracarbonyl iron(0) undergo oxidative-elimination reactions to afford new binuclear organometallic compounds in good yields; $Fe(CO)_4EPh_3+SnX_4 \rightarrow Fe(CO)_3EPh_3SnX_4+CO$ (E=P, As, Sb; X=Cl, Br; Ph=C_6H_5), where one molecule of carbon monoxide is discharged. The complexes are characterized by elemental analysis, by infrared and Mössbauer spectroscopies, and by conductivity measurements; these data are used to predict their possible formulation as nonionic, hexa-co-ordinate iron derivatives of the $Fe(CO)_3(X)(EPh_3)(SnX_3)$ type containing a tin-to-iron metal-metal bond.

A number of Lewis acid-base adducts containing hetero metal-metal bonds have previously been prepared by treating zerovalent transition-metal carbonyl complexes with main-group metal halides.[1),2)] These reaction may, for convenience, be devided into two classes: (a) oxidative-addition reactions and (b) oxidative-elimination reactions, according to whether or not the elimination of carbon monoxide occurs during the reaction.[3)] Examples of Reaction (a) are found among numerous mercury-to-transition-metal-bonded compounds.[4-6)] By Reaction (b) Graham and Kummer have synthesized a series of tin-molybdenum- and tin-tungsten-bonded compounds.[7)] It is also hoped that, with a good choice of ligands, iron carbonyl derivatives will undergo a reaction of either the (a) or (b) type with appropriate main-group halides to yield new hetero binuclear compounds.

In this paper syntheses of tin-iron-bonded compounds will be described, and the structure and the nature of the isolated products will be discussed on the basis of the spectroscopic data.

Experimental

All the preparative procedures were carried out under nitrogen, and the solvents available were purified by distillation prior to use. The stannic chloride and stannic bromide were commercially obtained. The substituted-iron carbonyls were prepared according to the methods in the literature, and their purities were checked by both elemental analysis and by studying their infrared spectra.[8-10)]

Preparation of $Fe(CO)_3PPh_3SnCl_4$. A solution of stannic chloride (10 mM) dissolved in 50 ml of dichloromethane was stirred, by drop, into triphenylphosphine tetracarbonyliron (10 mM) in the same solvent. As the reaction proceeded, the solution gradually changed from yellow into red; at the same time a vigorous evolution of carbon monoxide was observed. After the solution had been stirred for an hour, the solvent was removed under reduced pressure. The red residue was then extracted in 20 ml of nitromethane; the solution was subsequently allowed to stand in a refrigerator until yellow crystals separated.

Procedures similar to this were used to prepare other tin-iron-bonded compounds.

The molecular weights were measured osmometrically in methyl ethyl ketone. The magnetic susceptibilities were determined by the Gouy method at room temperature. The electric conductivities in nitromethane solutions were determined at 25°C using a Radiometer type CDM 2d-Conductivitymeter. The infrared spectra were obtained as Nujol mull on a Hitachi EPI-G2 Grating Spectrometer. The Mössbauer spectra were recorded with a Hitachi 505 Mössbauer Spectrometer equipped with a cryostat maintaining a γ-ray emitter (^{57}Co diffused onto platinum foil) and an absorber at the temperature of liquid nitrogen.

Results and Discussion

Results of the elemental analyses and the physical properties for the isolated Sn-Fe complexes are summarized in Tables 1 and 2 respectively. These products can be described by the general formula $Fe(CO)_3EPh_3SnX_4$, where E is P, As, or Sb, where X is Cl or Br, and where Ph is C_6H_5. They are diamagnetic, yellow-to-orange crystals and are sufficiently stable in air for various physicochemical experiments. They are readily soluble in chloroform, benzene, nitromethane, alcohols, and many other polar organic solvents. The obtained molecular weights correspond to a monomer structure. The electric conductivities in nitromethane and the infrared frequencies in the carbonyl stretching region are given in Table 3. The conductivities of the products suggest their essentially nonionic character, in spite of the observed small conductance, which is presumably due to partial dissociation in nitromethane. The observed low molecular weights in methyl ethyl ketone reflect it.

Each complex exhibits three carbonyl stretching bands. It is interesting to note that the averaged stretching frequencies of each product undergo a high shift of about 100 cm^{-1} compared to the starting iron carbonyl complexes, $Fe(CO)_4EPh_3$.

Figure 1 shows the ^{57}Fe Mössbauer spectra of $Fe(CO)_4PPh_3$ and $Fe(CO)_3PPh_3SnCl_4$. The isomer shift and the quadrupole splitting values of the products are presented in Table 4, along with the values of the related iron carbonyl complexes. In triphenylarsine

1) J. C. Kotz and D. G. Pedrotty, *Organometal. Chem. Rev.*, *A*, **4**, 479 (1969).
2) D. F. Shriver, *Accounts Chem. Res.*, **3**, 231 (1970).
3) J. Lewis and S. B. Wild, *J. Chem. Soc.*, *A*, **1966**, 69.
4) D. M. Adams, D. J. Cook, and R. D. W. Kemmitt, *ibid.*, **1968**, 1067.
(5 J. L. Dawes and R. D. W. Kemmitt, *ibid.*, **1968**, 1072.
6) K. Edgar, B. F. G. Johnson, J. Lewis, and S. B. Wild, *ibid.*, **1968**, 2851.
7) R. Kummer and W. A. G. Graham, *Inorg. Chem.*, **7**, 310 (1968).
8) J. Lewis, R. S. Nyholm, S. S. Sandhu, and M. H. B. Stiddard, *J. Chem. Soc.*, **1964**, 2825.
9) A. F. Clifford and A. K. Mukherjee, *Inorg. Chem.*, **2**, 151 (1963).
10) M. H. Stiddard, *J. Chem. Soc.*, **1962**, 4712.

Table 1. Elemental anylyses

Compound	C	H	X	Fe	Mol. wt.
$C_{21}H_{11}O_3Cl_4SnPFe$	38.03 (38.06)	2.24 (2.28)	20.89 (21.40)	7.1_3 (8.43)	550 (663)
$C_{21}H_{11}O_3Br_4SnPFe$	30.11 (30.01)	1.73 (1.80)	38.17 (38.03)	5.1_3 (6.64)	780 (841)
$C_{21}H_{11}O_3Cl_4SnAsFe$	34.99 (35.69)	2.03 (2.14)	20.28 (20.07)	7.6_9 (7.90)	570 (707)
$C_{21}H_{11}O_3Br_4SnAsFe$	28.80 (28.52)	1.69 (1.71)	36.41 (36.14)	5.0_4 (6.31)	810 (884)
$C_{21}H_{11}O_3Cl_4SnSbFe$	33.26 (33.48)	1.94 (2.01)	18.92 (18.82)	5.2_8 (7.41)	690 (753)
$C_{21}H_{11}O_3Br_4SnSbFe$	26.89 (27.08)	1.46 (1.62)	34.76 (34.32)	4.7_5 (6.00)	860 (931)

Table 2. Physical properties and yields

Compound	Melting point (°C)	Color	Yield %	Conductivity (μ cm^2 ohm^{-1} mol^{-1})
$Fe(CO)_3(Cl)PPh_3SnCl_3$	111—111.5 (dec)	Yellow	90	14.0
$Fe(CO)_3(Br)PPh_3SnBr_3$	120.5—121 (dec)	Orange yellow	93	22.1
$Fe(CO)_3(Cl)AsPh_3SnCl_3$	113—113.5 (dec)	Yellow	83	12.5
$Fe(CO)_3(Br)AsPh_3SnBr_3$	124 (dec)	Orange	91	35.2
$Fe(CO)_3(Cl)SbPh_3SnCl_3$	125—126 (dec)	Orange	75	20.0
$Fe(CO)_3(Br)SbPh_3SnBr_3$	124 (dec)	Orange yellow	78	28.3

Table 3. Infrared spectroscopic data ($CHCl_3$ solution)

Compound	C-O Stretching frequencies (cm^{-1})		
$Fe(CO)_3(Cl)PPh_3SnCl_3$	2110 (w)	2062 (s)	2044 (s)
$Fe(CO)_3(Br)PPh_3SnBr_3$	2102 (w)	2053 (s)	2044 (s)
$Fe(CO)_3(Cl)AsPh_3SnCl_3$	2111 (w)	2063 (s)	2043 (s)
$Fe(CO)_3(Br)AsPh_3SnBr_3$	2104 (w)	2056 (s)	2042 (s)
$Fe(CO)_3(Cl)SbPh_3SnCl_3$	2102 (w)	2055 (s)	2036 (s)
$Fe(CO)_3(Br)SbPh_3SnBr_3$	2100 (w)	2052 (s)	2037 (s)

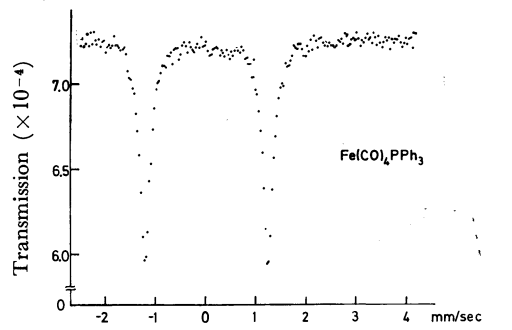

a) Doppler velocity *vs.* $Na_2[Fe(CN)_5NO]\cdot 2H_2O$

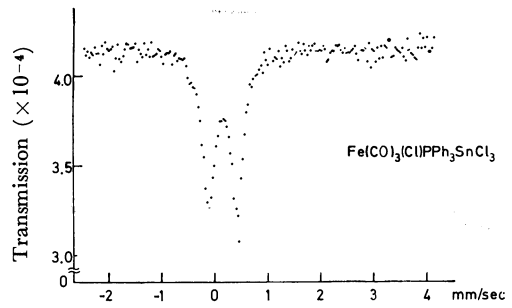

b) Doppler velocity *vs.* $Na_2[Fe(CN)_5NO]\cdot 2H_2O$

Fig. 1. The Mössbauer specra of a) $Fe(CO)_4PPh_3$ and b) $Fe(CO)_3(Cl)PPh_3SnCl_3$.

derivatives, the Mössbauer effect could not be measured because of the large non-reasonant absorption of arsenic nuclides. It can readily be seen that each product shows a more positive isomer shift and

Table 4. ^{57}Fe Mössbauer data (78 K)

Compound	I. S.	Q. S.
$Fe(CO)_3(Cl)PPh_3SnCl_4$	0.19	0.64
$Fe(CO)_3(Cl)SbPh_3SnCl_4$	0.14	0.48
$Fe(CO)_4SbPh_3$	−0.11	3.22
$Fe(CO)_4PPh_3$	−0.04	2.92
$Fe(CO)_3(PPh_3)_2$	−0.03	3.12
$Fe(CO)_5$	0.05	2.52

I. S. Isomer shift *vs.* $Na_2[Fe(CN)_5NO]\cdot 2H_2O$ (mm/sec).
Q. S. Quadrupole splitting (mm/sec).

quadrupole splitting smaller than the starting iron carbonyl complex. The small quadrupole splitting suggests that the products have a more symmetrical environment around the iron atom, probably a hexa-co-ordinate octahedral structure containing a tin-iron metal-metal bond. The determination of the precise structure of $Fe(CO)_3AsSnBr_4$ by single-crystal X-ray analysis is currently in progress in this laboratory.

It can be concluded that the iron derivatives obtained here should be formulated as $Fe(CO)_3(X)EPh_3(SnX_3)$ and that an ionic formulation such as $[Fe(CO_3)EPh_3\text{-}SnX_3]X$ or $[Fe(CO)_3EPh_3X]SnX_3$ should be ruled out. The above reactions may proceed as follows:

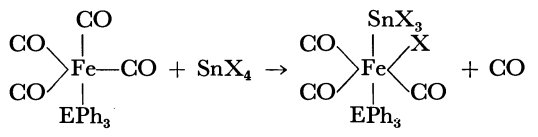

(1)

The elimination of one molecule of carbon monoxide was confirmed by gas-burette measurements. Thus, the reaction may reasonably be classified as an oxidative-elimination reaction and the products may be regarded as Lewis acid-base adducts.

Under the same preparative conditions as in the above experiments, no reaction occurred between iron carbonyl derivatives, $Fe(CO)_4EPh_3$, $Fe(CO)_3\text{-}(EPh_3)_2$, and tetramethyltin, trimethyltin chloride, dimethyltin dibromide, and tin tetraiodide. Probably these failures are due to the low Lewis acidity of the metal-halide reactants.

The Cobalt Carbonyl-catalyzed Hydroesterification of Butadiene with Carbon Monoxide and Methanol

Akio MATSUDA

National Chemical Laboratory for Industry (Tokyo Kogyo Shikensho), Mita, Meguro-ku, Tokyo

(Received April 12, 1972)

The cobalt carbonyl-catalyzed hydromethoxycarbonylation of butadiene is studied. The reaction proceeds in the presence of a pyridine base to give methyl 3-pentenoate. Isoquinoline is found to be a better solvent for the production of methyl 3-pentenoate than pyridine, not only because the yield of the ester is somewhat higher in the presence of isoquinoline than in the presence of pyridine, but also because it is far less volatile than pyridine, so that the product can be easily separated from the solvent and the catalyst by distillation. Also, the hydromethoxycarbonylation of methyl 3-pentenoate under somewhat different conditions is found to give a good yield of dimethyl adipate. The hydroformylation of methyl 3-pentenoate is studied as well. The effect of such a solvent as THF, benzene, and acetonitrile in increasing the selectivity to methyl 5-formylpentanoate is found to increase in this order: acetonitrile < benzene < THF.

In the first paper of this series it was reported that the initial rate of the cobalt carbonyl-catalyzed hydroesterification of propylene was remarkably promoted by the presence of a small amount of hydrogen and an excess of pyridine.[1] In a following paper concerning the hydroesterification of acrylonitrile, the reaction mechanism was discussed on the bases of the kinetic results and the IR study of the reaction intermediates.[2]

The present investigation will deal with the hydroesterification of butadiene. The results varied in some respects from those of previous studies which dealt only with mono-olefins.[1,2] For example, in the hydroesterification of mono-olefins, hydrogen added in the synthesis gas played a significant role in accelerating the reaction.[1,2] However, in the present hydroesterification of butadiene, hydrogen exerted essentially no effect on the reaction rate. On the other hand, the effect of pyridine on the hydroesterification of butadiene was remarkable in that both the reaction rate and the selectivity to methyl 3-pentenoate steadily increased with an increase in the concentration of pyridine. The inhibition by a large excess of pyridine which is usually observed in the case of mono-olefins[1,2] did not appear at all in this experiment. The reaction proceeded in pyridine at a relatively low temperature (100—140°C), and methyl 3-pentenoate was selectively produced.

It has already been found by Imyanitov et al. that the hydrocarboxylation of butadiene also proceeded in the presence of pyridine to give 3-pentenoic acid.[3] They also reported the results of their hydroesterification of butadiene in the presence of pyridine;[4] they carried out the reaction at a higher temperature (210 °C), and obtained a mixture of unsaturated and saturated mono esters and saturated diesters. On the other hand, in the present investigation a better method for the selective production of methyl 3-pentenoate by the hydroesterification of butadiene was explored. As a result, it was found that isoquinoline was a better solvent than pyridine for this purpose, not only because the yield of methyl 3-pentenoate was somewhat improved when the reaction was carried out in the presence of isoquinoline instead of pyridine, but also because isoquinoline (bp 240°C) is less volatile than pyridine (bp 115°C), so methyl 3-pentenoate can be easily removed from the reaction mixture by vacuum distillation at a low temperature, the catalyst and isoquinoline being left as a residue.

The hydroesterification and the hydroformylation of the resulting methyl 3-pentenoate to give the corresponding diesters and formyl esters were also examined.

Experimental

Such reagents as butadiene, carbon monoxide, methanol, and pyridine were obtained commercially. The butadiene was 99% pure. The carbon monoxide was 99.5% pure, containing 0.018% hydrogen. The amount of butadiene remaining in the gas phase after the reaction was analyzed by passing the gas through methanol cooled by dry ice, followed by the gas-chromatographical analysis of the methanol solution. The amount of the dissolved butadiene and that of each product in the liquid product were also gas-chromatographically analyzed. The gas-chromatographical analyses were performed with a 9-m column of propyleneglycol-adipic acid polyester at the column temperature of 150°C (2-ethylhexyl acetate was added as an internal standard when necessary). Standard samples for the gas-chromatographical analyses were prepared as follows. Dimethyl adipate, methyl *n*-pentanoate, and methyl 4-pentenoate were prepared by the esterification of commercially-obtained adipic acid, *n*-pentanoic acid, and 4-pentenoic acid with methanol. The others were prepared by the distillation of the reaction products with a rectifier of the spinning-band type, followed by separation with a preparative gas-chromatograph (Perkin-Elmer F-21). These samples were identified by means of their IR and NMR spectra.

Methyl 3-Pentenoate: IR spectrum: C=O (ester) 1744 cm^{-1}, NMR spectrum: CH_3 τ 8.33, CH_2 τ 7.05, OCH_3 τ 6.40 (singlet), CH τ 4.50 (the NMR spectrum was complex because the sample was a mixture of *cis*- and *trans*-forms)

Methyl 2-Pentenoate: IR spectrum: C=O (ester) 1730 cm^{-1}, C=C (conjugated with C=O) 1662 cm^{-1}. NMR spectrum: CH_3 τ 8.88 (triplet), CH_2 τ 7.76 (quintet), OCH_3 τ 6.34 (singlet), $CH(-COOCH_3)$ τ 4.27 (sextet), $CH(-CH_2)$ τ 3.07 (sextet)

1) A. Matsuda and H. Uchida, This Bulletin, **38**, 710 (1965)
2) A. Matsuda, *ibid.*, **40**, 135 (1967).
3) N. S. Imyanitov and D. M. Rudkovskii, *J. Applied Chemistry of USSR* (English translation), **41**, 157 (1968).
4) N. S. Imyanitov and D. M. Rudkovskii, *Zh. Prikl. Khim.*, **39**, 2335 (1966).

Dimethyl α-Methylglutarate: IR spectrum: C=O (ester) 1742 cm^{-1}. NMR spectrum: CH_3 τ 8.83 (doublet), CH_2-(-CH) τ 8.19 (quintet), CH_2 (-$COOCH_3$) τ 7.73 (triplet), CH τ 7.45—7.8 (multiplet), OCH_3 τ 6.38, 6.40.

Dimethyl Ethylsuccinate: IR spectrum: C=O (ester) 1740 cm^{-1}. NMR spectrum: CH_3 τ 9.06 (triplet), CH_2(-CH_3) τ 8.39 (quintet), CH(-$COOCH_3$) τ 7.35—7.75 (multiplet), CH_2(-$COOCH_3$) τ 7.35 (doublet), OCH_3 τ 6.36, 6.38.

Methyl 5-Formylpentanoate: IR spectrum: C=O (ester and aldehyde) 1720—1740 cm^{-1}. NMR spectrum: CH_2CH_2 (-CH_2COOCH_3) τ 8.2—8.4 (overlapped multiplet), CH_2-(-$COOCH_3$), CH_2(-CHO) τ 7.4—7.8 (overlapped multiplet), OCH_3 τ 6.37 (singlet), CHO τ 0.23 (triplet). The structure of this compound was further confirmed by its oxidation with air, followed by esterification with methanol into dimethyl adipate.

Methyl 4-Formylpentanoate: IR spectrum: C=O (ester and aldehyde) 1740, 1710 cm^{-1}. NMR spectrum: CH_3(-CH-CHO) τ 8.88 (doublet), CH_2(-CH_2COOCH_3) τ 7.9—8.5 (multiplet), CH_2(-$COOCH_3$) τ 7.67 (triplet), CH(-CHO) τ 7.5—7.9 (overlapped multiplet), OCH_3 τ 6.39 (singlet), CHO τ 0.39 (doublet). The structure of this compound was further confirmed by its oxidation with air and by its subsequent esterification with methanol into dimethyl α-methylglutarate.

Methyl 3-Formylpentanoate: IR spectrum: C=O (ester and aldehyde) 1740, 1710 cm^{-1}. NMR spectrum: CH_3(-CH_2) τ 9.02 (triplet), CH_2(-CH_3) τ 8.1—8.6 (multiplet), $CHCH_2$-(-$COOCH_3$) τ 7.2—7.8 (multiplet), OCH_3 τ 6.40 (singlet). CHO τ 0.35. The structure of this compound was further confirmed by its oxidation with air and by its subsequent esterification with methanol into dimethyl ethylsuccinate.

The reactions were carried out with a 300-ml (or a 100-ml) stainless steel autoclave. The catalyst, $Co_2(CO)_8$, was put into a small Teflon cup and placed on a wing of the stirrer so that the reaction would not start until the stirring (an up-and-down motion) began. For the measurement of the initial rate, a small portion of the reaction mixture was withdrawn a short, definite time after the stirring began; this portion was gas chromatographically analyzed with the aid of an internal standard (methyl benzoate or benzonitrile) which had been added to the reaction mixture before the reaction.[5]

The effect of bases was examined by carrying out the reaction in the presence of various bases. In control experiments carried out in the absence of a base (in toluene or acetonitrile), the reaction products were confirmed, by the measurement of the IR spectra, not to contain any carbonylated product (there was an absence of absorption at 1700—1800 cm^{-1}). The effect of the pyridine concentration was examined by varying the concentration of pyridine in a solvent mixture (acetonitrile plus pyridine) from zero to 100%.

The methyl 3-pentenoate for the hydroesterification and hydroformylation experiments was continuously produced by the hydroesterification of butadiene, using isoquinoline as the solvent. A solution consisting of 5.4 g of $Co_2(CO)_8$, 8.6 g of methanol, and 34 g of isoquinoline was pumped into a 100 ml stainless steel autoclave, and the autoclave brought to the condition of 130°C and 300 kg/cm^2 by heating and by introducing carbon monoxide from a pressure reservoir; the stirrer was started, and then butadiene was continuously fed from the bottom of the autoclave at a rate of 0.05 mol/hr, the carbon monoxide being supplied from the pressure reservoir to keep the pressure constant. Three hours after the start of the reaction, the reaction was interrupted and reaction mixture was totally withdrawn from the bottom of the autoclave through a cooling tube. The volatile components including methyl 3-pentenoate were then separated from the reaction mixture by vacuum distillation at a low temperature (below 50°C), while an isoquinoline solution of cobalt carbonyl was recovered as a residue. This recovered isoquinoline solution of cobalt carbonyl was catalytically active, and was used again in the next run. The effect of recycling the catalyst solution is illustrated in Table 1.

5) The use of 2-ethylhexyl acetate as an internal standard was avoided, since it can undergo transesterification with methanol under the reaction condition. The effect of the addition of a small amount of methylbenzoate (or benzonitrile) on the results of the reaction was negligible.

Table 1. The effect of recycling the catalyst solution

Exp. No.	Conversion of butadiene (%)	Selectivity (%)[a]	
		M3P	VC
1	92	87	8.7
2	94	89	11
3	85	88	12
4	90	89	11
5	81	86	8.2

a) *cf.* Table 3.

Results

The Addition of Bases. The effectiveness of bases in increasing the yield of methyl 3-pentenoate decreased in this order: γ-picoline>isoquinoline>pyridine>3,4-lutidine>β-picoline>4-vinylpyridine>α-picoline, quinoline, 4-cyanopyridine>triethylamine (Table 2). Triethylamine was almost ineffective. In the absence of pyridine bases, methyl 3-pentenoate was not produced, while only the conversion of bu-

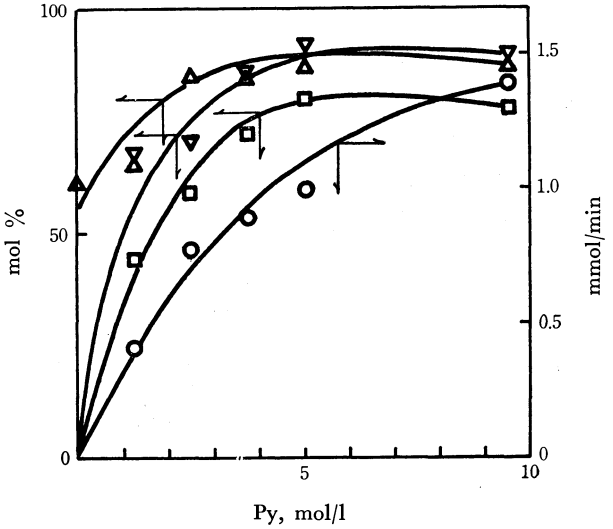

Fig. 1. The effect of the pyridine concentration.
—○—: Initial rate (mmol/min)
—△—: Conversion of butadiene (%)
—□—: Yield of methyl 3-pentenoate (%)
—▽—: Selectivity to methyl 3-pentenoate (%)
The abscissa is expressed in terms of the concentration at room temperature in 50 ml solution containing methanol (8 g), methyl benzoate (1 g), pyridine and acetonitrile. Experimental methods are same as described in Table 2.

TABLE 2. THE EFFECT OF THE ADDED BASES ON THE HYDROESTERIFICATION OF BUTADIENE
methanol (8 g), methyl benzoate (1 g), base (10 g), diluted with acetonitrile to 50 ml (room temp.); 0.1 mol butadiene, 4 mmol $Co_2(CO)_8$; reaction temp. 140°C, pressure (constant) 300 kg/cm², reaction time 3 hr

%	Initial rate[a] (mmol/min)	Conversion (%)	methyl 3-pentenoate	
			Yield (%)	Selectivity (%)
None	0	61	0	0
Pyridine	0.77	85	59	70
γ-Picoline	0.67	90	77	86
Isoquinoline	0.60	89	65	73
3,4-Lutidine	0.44	76	56	74
β-Picoline	0.34	83	45	54
4-Vinylpyridine	0.20	74	37	50
α-Picoline	0.13	53	4.7	8.9
Quinoline	0.075	56	4.6	8.2
4-Cyanopyridine	0.035	—	5.0	5.0
Triethylamine	—	31	0.3	1.0

a) The initial rate was calculated from the analysis of a sample withdrawn 10 min after the reaction started.

TABLE 3. THE EFFECT OF PRESSURE (I)
0.25 mol methanol, 1 g benzonitrile, 0.48 mol pyridine, 0.1 mol butadiene, 4 mmol $Co_2(CO)_8$; reaction temp. 100°C, reaction time 18 hr; in 300 ml autoclave.

Pressure (constant)	Initial rate[a] (mmol/min)	Conversion (%)	Selectivity (%)[b]	
			M3P	VC
100	0.029	33	87	13
150	0.065	63	94	4.4
200	0.12	66	95	5.0
300	0.12	63	92	7.5

a) The initial rate was calculated from the analysis of a sample withdrawn 60 min after the reaction started.
b) Abbreviations M3P and VC stand for methyl 3-pentenoate and 4-vinyl 1-cyclohexene.

TABLE 4. THE EFFECT OF PRESSURE (II)
0.25 mol methanol, 0.15 mol pyridine, 0.1 mol butadiene, 1 mmol $Co_2(CO)_8$; reaction temp. 140°C, reaction time 1.5 hr; in 100 ml autoclave.

Initial pressure (kg/cm²)	Conversion (%)	Selectivity (%)[a]	
		M3P	VC
150	20	46	30
300	44	63	22
600	87	87	7.2

a) *cf.* Table 3.

tadiene increased. This increase in the conversion is due to the polymerization, not to the hydroesterification of butadiene (cf. Experimental section).

The Effect of the Pyridine Conecntration. The initial rate increased with the increase in the concentration of pyridine (Fig. 1). The conversion of butadiene, and the yield of, and the selectivity, to methyl 3-pentenoate all increased with the increase in the concentration of pyridine; however, they reached a maximum at the concentration of 5 mol/l and remained essentially unchanged thereafter.

The Effect of the Carbon Monoxide Partial Pressure. The effect of the pressure was examined at two different temperatures (100 and 140°C). The results are shown in Tables 3 and 4. The initial rate at 100°C increased with the increase in the pressure; it reached a maximum at 200 kg/cm² and leveled off thereafter. The conversion of butadiene and the selectivity to methyl 3-pentenoate both increased with the increase in the pressure, reached a maximum at 200 kg/cm², and declined thereafter. The selectivity to 4-vinyl 1-cyclohexene decreased as the pressure was increased. from 100 to 150 kg/cm², reached a minimum at 150—200 kg/cm², and then increased.

At 140°C, on the other hand, the conversion of butadiene and the selectivity to methyl 3-pentenoate both increased, while the selectivity to 4-vinyl 1-cyclohexene decreased with the increase in the pressure in the range from 150 to 600 kg/cm².

The Effect of the Hydrogen Partial Pressure. Two hydroesterification runs of butadiene were carried out, with and without hydrogen, and the results were compared. Of the two experiments (listed in Table 5), one was carried out in the absence of hydrogen, while the other one was carried out with an initial hydrogen pressure of 137 kg/cm² under identical conditions; these experiments were carried out with the same carbon monoxide partial pressure, the initial pressure in the former experiment being 380 kg/cm², while that in the latter experiment was 517 kg/cm² (380+137). In the presence of hydrogen, the resulting methyl 3-pentenoate was partly hydrogenated into methyl *n*-pentanoate. Also, the dimerization of butadiene into 4-vinyl 1-cyclohexene and the polymerization of butadiene into unidentified polymers were accelerated and the selectivity to methyl 3-pentenoate decreased. Clearly hydrogen has no accelerating effect on the hydroesterification of butadiene, since the yield of methyl 3-pentenoate plus its hydrogenation product, methyl *n*-pentanoate, did not increase with the presence of hydrogen.

The Hydroesterification of Methyl 3-Pentenoate. The cobalt carbonyl-catalyzed hydroesterification of methyl

Table 5. The effect of hydrogen

0.25 mol methanol, 0.15 mol pyridine, 0.1 mol butadiene, 1 mmol $Co_2(CO)_8$, reaction temp. 140°C, reaction time 2.5 hr

Initial pressure (kg/cm²)		Conversion (%)	Selectivity (%)[a]			
Pressure,	P_{H_2}		M3P	MP	VC	Residue
380	0	71	79	—	5.8	15
517	137	78	55	6.3	20	19

a) Abbreviation MP stands for methyl *n*-pentanoate. For others *cf.* Table 3.

Table 6. The hydroesterification of methyl 3-pentenoate

0.05 mol methyl 3-pentenoate, 0.125 mol methanol

Diluent(g)	$Co_2(CO)_8$ (mmol)	Py (mmol)	Temp. (°C)	Initial press. (kg/cm²)	Time (hr)	Conv. (%)	Selectivity (%)[a]					
							MP	M2P	M4P	E1	E2	E3
Toluene 15	2	16	160	130	4	87	1.7	—	—	81	13	3.0
Toluene 10	2	127	200	300	1	100	15	—	—	68	12	3.3
Benzene 10	1	127	180	200	2	90	13	—	—	69	9.1	1.7
n-Heptane 10	1	127	180	200	2	94	14	—	—	68	10	2.1
Benzene 10	1	0	180	200	2	64	12	56	9.4	5.3	3.9	2.6
None	1	127	180	200	2	21	—	—	—	3.7	—	—

a) Abbreviations M2P, M4P, E1, E2, and E3 stand for methyl 2-pentenoate, methyl 4-pentenoate, dimethyl adipate, dimethyl α-methylglutarate, and dimethyl ethylsuccinate. For another *cf.* Table 5.

Table 7. The effect of the reaction temperature of the first stage on the direct syntheses of diesters

0.25 mol methanol, 0.15 mol pyridine, 0.1 mol butadine, 4 mmol $Co_2(CO)_8$; Initial pressure of the first stage 500 kg/cm²; Temperature of the second stage 200°C; Reaction time 3 hr (first stage), 1 hr (second stage)

Temperature (first stage) (°C)	Initial press. (second stage) (kg/cm²)	Conv. (%)	Selectivity (%)[a]					
			MP	M2P	M3P	E1	E2	E3
130	520	94	12	1.4	7.4	47	9.5	2.5
120	526	93	9.9	1.0	5.7	49	9.9	2.5
110	530	95	11	1.1	5.8	51	12	3.1

a) *cf.* Table 6.

3-pentenoate proceeded at 160—200°C in the presence of pyridine and such a solvent as benzene, toluene, or *n*-heptane; dimethyl adipate was produced in a good yield, while dimethyl α-methylglutarate and dimethyl ethylsuccinate were produced in minor amounts. The results are summarized in Table 6. Methyl 3-pentenoate was partly hydrogenated to methyl *n*-pentanoate in spite of the fact that the reaction was carried out in the absence of hydrogen. Hydrogen can be formed from methanol and carbon monoxide in the presence of cobalt carbonyl.[6] In fact, it was confirmed that hydrogen was produced from methanol and carbon monoxide under the conditions of Table 6, and that carbon dioxide and methyl acetate were produced, together with hydrogen, without the formation of dimethylether:

$$2CH_3OH+2CO \longrightarrow CH_3COOCH_3+CO_2+H_2$$

In the presence of a small excess of pyridine(Py/$Co_2(CO_8)$=8), the reaction proceeded at 160°C. In the presence of a large excess of pyridine (Py/$Co_2(CO)_8$=127), however, a higher temperature (180—200°C) and the use of such a solvent as has been mentioned above were necessary for the reaction to proceed. In the absence of pyridine, on the other hand, only the isomerization of methyl 3-pentenoate into methyl 2-pentenoate and methyl 4-pentenoate took place, with the hydroesterification occurring very sparingly.

The Direct Synthesis of Dimethyl Adipate from Butadiene, Carbon Monoxide, and Methanol. It has been found that the hydroesterification of butadiene proceeded in the presence of pyridine at 100—140°C to give methyl 3-pentenoate, but the further hydroesterification of methyl 3-pentenoate did not occur at these temperatures. On the other hand, in the experiments cited in Table 6, it has also been found that the hydroesterification of methyl 3-pentenoate proceeded in the presence of pyridine at 160—200°C to give diesters. Therefore, it should be possible, by the combination of the above two results, to synthesize diesters directly from butadiene, i. e., by merely carrying out the reaction in two steps, at two different temperatures. For example, the hydroesterification of butadiene was carried out at 110—130°C as the first-stage reaction, and then the temperature was raised to 200°C to carry out the reaction of the second stage(Table 7). The selectivity to each diester increased as the temperature of the first stage decreased; this is probably because

6) G. Natta, P. Pino, and R. Ercoli, *J. Amer. Chem. Soc.*, **74**, 4496 (1952).

TABLE 8. THE RESULTS OF THE HYDROFORMYLATION OF METHYL 3-PENTENOATE
methyl 3-pentenoate (0.1 mol) diluted with the solvent to 100 ml (room temp.), $Co_2(CO)_8$ 2 mmol (No. 1) 0.02 mmol (No. 2—11)

No.	Solvent	Temp. (°C)	Press. (kg/cm²)	Reaction time (min)	Conv. (%)	Selectivity (%)[a]					5F/(4F+3F)
						M2P	MP	5F	4F	3F	
1	Benzene	140	100	60	100	0	8.2	25	8.6	4.3	1.9
2	Benzene	200	250	60	99.6	0.09	19	34	16	8.6	1.4
3	Benzene[b]	200	250	60	99.3	0.23	18	32	16	7.5	1.4
4	Benzene[c]	200	250	30	90.0	6.5	17	41	23	10	1.2
5	Benzene[d]	200	250	30	95.7	5.8	18	40	27	10	1.1
6	Acetonitrile	200	250	60	92.7	9.1	20	33	25	9.3	0.96
7	THF	200	250	60	98.1	1.0	17	48	23	9.5	1.5
8	THF	170	150	210	98.9	1.2	15	48	20	8.7	1.7
9	THF[c]	170	150	90	84.0	21	11	40	23	9.0	1.3
10	Dioxane	200	250	60	100	0	21	41	20	10	1.4
11	Methyl acetate	200	250	60	96.2	2.6	18	40	21	8.7	1.3

a) Abbreviations 5F, 4F, and 3F stand for methyl 5-formylpentanate, methyl 4-formylpentanoate and methyl 3-formylpentanoate. For others *cf.* Table 6.
b) Carried out in the presence of 0.2 mmol of triphenyl phosphine.
c) Carried out in the presence of 20 mmol of pyridine.
d) Carried out in the presence of 200 mmol of pyridine.

the selectivity to methyl 3-pentenoate in the first stage increased as the temperature of that stage decreased.

The addition of a small amount of water (up to 10 mmol) had almost no effect on a similar reaction carried out in two stages (1st stage, 140°C, 600 kg/cm²: 2nd stage, 200°C, 600—610 kg/cm²), although the yield of dimethyl adipate decreased somewhat in the presence of 20 mmol of water.

The Hydroformylation of Methyl 3-Pentenoate. The hydroformylation of methyl 3-pentenoate was carried out in the presence of $Co_2(CO)_8$ at 140—200°C, under the synthesis gas ($Co/H_2=1$) pressure of 100—250 kg/cm². The effect of the solvent and such a ligand as pyridine or triphenylphosphine is shown in Table 8. In the presence of 2 mmol of $Co_2(CO)_8$, the reaction proceeded at 140°C (100 kg/cm²) and formylesters were produced, but the selectivity to formylesters was only 38 per cent, presumably because the formylesters easily polymerized under such a high concentration of $Co_2(CO)_8$.

When the amount of $Co_2(CO)_8$ was reduced to to 0.02 mmol, the reaction did not occur at 140°C; however, it proceeded at 200°C(250 kg/cm²) and the selectivity to formylesters increased to 59 per cent (No. 2). The addition of triphenylphosphine had almost no effect on the reaction(No. 3). The addition of pyridine increased the selectivity to formylesters to 74—77 per cent(No. 4,5); however, the selectivity to methyl 5-formylpentanoate did not increase so much(40—41%), as it worked to decrease the 5F/(4F+3F) ratio. On the other hand, when acetonitrile was used as a solvent(No. 6), the total selectivity to formylesters increased to 67 per cent while the 5F/(4F+3F) ratio decreased remarkably(0.69). When tetrahydrofuran(THF) was used as the solvent(No. 7,8), on the other hand, the selectivity to the total formylester increased(77—81%), together with the 5F/(4F+3F) ratio (1.5—1.7). When pyridine was added to the THF solvent(No. 9), the 5F/(4F+3F) ratio decreased to 1.3, the selectivity to methyl 5-formyl-pentanoate declining to 40 per cent as a result.

TABLE 9. THE EFFECT OF SOLVENTS ON THE INITIAL RATE OF THE ISOMERIZATION OF METHYL 3-PENTENOATE

Solvent	Initial rate of formation (mmol/min)	
	Methyl 2-pentenoate	Methyl 4-pentenoate
Benzene	2.0	0.42
Acetonitrile	1.4	0.07
THF	2.4	0.49

The fact that the selectivity to total formylesters increased by the use of such a solvent as THF, dioxane, methyl acetate, and acetonitrile instead of benzene, or by the addition of pyridine to the benzene solvent, suggests that the polymerization of formylester slows down in the presence of those above-mentioned solvents or pyridine. The fact that the 5F/(4F+3F) ratio increased in the order of acetonitrile<methyl acetate<benzene, dioxane<THF may have a bearing upon the ease of the isomerization of methyl 3-pentenoate in these solvents.

The Initial Rate of the Isomerization of Methyl 3-Pentenoate. For the measurement of the initial rate of the isomerization of methyl 3-pentenoate, the reactions were carried out in a 100-ml autoclave with 0.02 mol of methyl 3-pentenoate diluted with a solvent to 50 ml(room temp.) and with 0.2 mmol of $Co_2(CO)_8$, at 140°C under a constant pressure (70 kg/cm²) of carbon monoxide containing 2% hydrogen; under these conditions (a very low hydrogen partial pressure), only the isomerization of methyl 3-pentenoate occurred measurably without the hydroformylation. A small portion of the reaction mixture was withdrawn from the autoclave 10 minutes after the stirring began; this portion was analyzed. The results are summarized in Table 9. Clearly, the isomerization of methyl

3-pentenoate into methyl 2-pentenoate and methyl 4-pentenoate proceeds more rapidly in THF than in benzene, and this isomerization proceeds most slowly in acetonitrile.

Discussion

The cobalt carbonyl-catalyzed oxo reaction of butadiene is known to yield a mixture of mono aldehydes and ketones, without any formation of dialdehydes. It is believed that butadiene is hydrogenated by $HCo(CO)_4$ into butenes, which then undergo hydroformylation to give monoaldehydes.[7]

In the case of the present hydroesterification of butadiene, however, the reaction was carried out with carbon monoxide containing almost no hydrogen, and it was observed that the reaction started in the presence of $Co_2(CO)_8$ without any induction time, and that the reaction rate did not increase upon the addition of hydrogen (Table 5). Presumably, $HCo(CO)_4$, the active intermediate of the oxo reaction, does not take part in the present reaction. As a matter of fact, the inhibition by pyridine observed in the usual oxo reaction (as a result of salt formation between $HCo(CO)_4$ and pyridine)[8] was not observed here, and the reaction was successfully carried out in pyridine. Dicobalt octacarbonyl undergoes disproportionation in the presence of pyridine (Eq. (1)), as has been stated by Wender *et al.*[9]; that this also occurs during the reaction is evident form the fact that the strong absorption of $Co(CO)_4^-$ at 1890 cm^{-1} and the weak bands at 1960—2100 cm^{-1} (probably the absorption of $Co^+(CO)_4Py$) appeared on the IR spectrum of the pyridine solution of $Co_2(CO)_8$ when it was treated under the present reaction conditions.

$$Co_2(CO)_8 + Py \longrightarrow Co^+(CO)_4Py(+Co(CO)_4^-) \quad (1)$$

Therefore, the present reaction probably involves the ion-pair, $Co^+(CO)_4Py(+Co(CO)_4^-)$, as the active intermediate; however, the mechanism is still not clear, nor will it be until more detailed studies of the reaction intermediate are performed.

The hydroesterification of methyl 3-penteonate, on the other hand, evidently involves $HCo(CO)_4$ as the active intermediate, since the reaction was retarded by a high concentration of pyridine and since the hydrogenation took place simultaneously(Table 6). The isomerization of olefins can proceed by the cycle of the addition and elimination of $HCo(CO)_4$.[10] Thus, four types of alkylcobalt tetracarbonyls can be produced from methyl 3-pentenoate in the following equilibrium:

$$CH_3CH_2CH{=}CHCOOCH_3 + HCo(CO)_4 \rightleftharpoons CH_3CH_2CH_2CH(Co(CO)_4)COOCH_3 \quad (\alpha)$$

$$CH_3CH{=}CHCH_2COOCH_3 + HCo(CO)_4 \rightleftharpoons CH_3CH_2CH(Co(CO)_4)CH_2COOCH_3 \quad (\beta)$$

$$CH_2{=}CHCH_2CH_2COOCH_3 + HCo(CO)_4 \rightleftharpoons CH_3CH(Co(CO)_4)CH_2CH_2COOCH_3 \quad (\gamma)$$

$$CH_2CH_2CH_2CH_2COOCH_3 \quad | \quad Co(CO)_4 \quad (\delta)$$

The mechanism of the formation of ester in the presence of pyridine *via* an alkylcobalt tetracarbonyl intermediate have already been discussed in a previous paper;[2] dimethyl adipate should result *via* δ, dimethyl α-methylglutarate from γ, dimethyl ethylsuccinate from β, and dimethyl propylmalonate from α. The facts that the selectivity to esters decreased in the order of dimethyl adipate>dimethyl α-methylglutarate>dimethyl ethylsuccinate, and that dimethyl propylmalonate was not detected in the products, suggest that the hydroesterification rates *via* these intermediates decrease in the order of $\delta>\gamma>\beta$, and that the α-intermediate is extraordinarily unreactive in this reaction.

The hydroformylation of methyl 3-pentenoate may also proceed *via* these intermediates, *i. e.*, by the formation of acylcobalt tricarbonyls from these intermediates, followed by its hydrogenation to give formylesters according to the mechanism proposed by Heck;[11] 5-formyl-(5F), 4-formyl-(4F), 3-formyl-(3F), and 2-formyl-(2F) esters should result from the δ, γ, β, and α intermediates respectively. The fact that the effectiveness of solvents in increasing the 5F/(4F+3F) ratio decreased in the order of THF>benzene, dioxane>methyl acetate>acetonitrile may be explained in connection with the fact that the effect of solvents in increasing the rate of the isomerization of methyl 3-pentenoate decreased in a similar order; THF>benzene>acetonitrile (Table 8), since the 5F/(4F+3F) ratio will increase as the rate of the isomerization of γ into the δ intermediate increases. However, another possibility exists that the equilibrium toward the straight-chain acylcobalt carbonyl may be particularly favored in THF, as has been mentioned by Takegami *et al.*,[12] who studied the isomerization of acyl-

7) W. Rupilius and M. Orchin, *J. Org. Chem.*, **36**, 3604 (1971).
8) I. Wender, H. W. Sternberg, M. Orchin, "Catalysis," **V**, p. 109 (1957), Reinhold Publ. Corp., New York.
9) I. Wender, H. W. Sternberg, and M. Orchin, *J. Amer. Chem. Soc.*, **74**, 1216 (1952).
10) P. Taylor and M. Orchin, *ibid.*, **93**, 6504 (1971).
11) R. F. Heck, "Advances in Organometallic Chemistry," Vol. 4, 255 (1966), Academic Press, New York-London.
12) Y. Takegami, Y. Watanabe, H. Masada, Y. Okuda, K. Kubo, and C. Yokokawa, This Bulletin, **39**, 1495 (1966).

cobalt carbonyls in various solvents. In a previous paper concerning the intramolecular hydroesterification of allylalcohol,[13] it has already been mentioned that the double-bond isomerization of allylalcohol is reduced by the use of acetonitrile as a solvent.

In conclusion, it can be said that THF is effective in increasing the ratio of the straight-chain formylester, because it accelerates the isomerization of γ- into the δ-intermediate, or because the equilibrium toward the straight-chain acylcobalt carbonyl is particularly favored in THF, or because of a combination of the above two factors. Also, it may be said that acetonitrile decreases the ratio of the straight-chain formylester because it retards the isomerization of γ- into the δ-intermediate.

13) A. Matsuda, This Bulletin, **41**, 1876 (1968).

The author wishes to thank Dr. Ken-ichiro Bando for his valuable suggestions and discussions. The authors also wishes to thank Mr. Kazuhiko Endo and Mr. Tsutomu Tsuruoka for their assistance in the experimental work.

BULLETIN OF THE CHEMICAL SOCIETY OF JAPAN, VOL. 46, 530—534 (1973)

The Reaction of β-Amino α,β-Unsaturated Esters with Amines

Yasukazu YOKOYAMA and Akira TAI

Research Center of Tekkosha Co., Ltd., Yahata-cho, Musashino-shi, Tokyo

(Received April 13, 1972)

The reactions between amines and 1,4-bis(ethoxycarbonyl)-2,5-bis(alkyl- or arylamino)-1,4-cyclohexadiene(I) and its analogs are studied. The main products are *N,N'*-disubstituted urea(II) and 1,4-bis(alkyl- or arylamino)-1,4-cyclohexadiene(V) instead of the expected carboxamide. The presence of small amounts of ethyl *N*-substituted carbamate (III) in the products leads to the conclusion that the reaction proceeds through two successive steps: the nucleophilic attack by an amine upon a carbonyl carbon atom of the ethoxycarbonyl group, with a cleavage of a carbon-carbon bond to give III and V, and the amidation of III *in situ*, giving II. The rate of the second step is much faster than that of the first step. The formation of II occurs in the compounds with a β-amino α,β-unsaturated carbonyl group.

The treatment of carboxylic esters with amines is known to be a convenient method for the preparation of carboxamides. However, the reactions between 1,4-bis(ethoxycarbonyl)-2,5-bis(alkyl- or arylamino)-1,4-cyclohexadiene(I) and amines give *N,N'*-disubstituted urea(II), but none of the expected carbxamide.

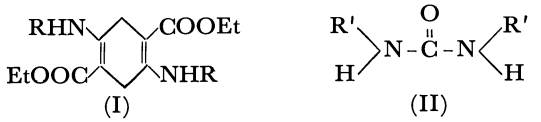

(I) (II)

a: R=R'=$CH_3(CH_2)_4$-
b: R=R'=C_6H_5-

Similar results have been reported by Roberts and Edwards[1] in the reaction of ethyl β-anilinocrotonate (VI) with aniline. While this type of the reaction is expected to occur generally in compounds with a β-amino α,β-unsaturated carbonyl group, no details of the reaction mechanism have been reported. In this paper, the reaction pathway will be elucidated and the reaction mechanism will be explained.

Results and Discussion

When Ia was heated with pentylamine at temperatures above 230°C in toluene, the reaction proceeded to a certain extent, thus giving *N,N'*-dipentylurea(IIa). The same reaction product was obtained in a good yield by the treatment of Ib with pentylamine. The absence of *N*-pentyl-*N'*-phenylurea and/or *N,N'*-diphenylurea in the products of the latter case excluded the possibility of the transfer of the RNH- group in I to the product during the reaction.

The formation of II might result from the transfer of the carbonyl group from I to the amine used in the reaction. There are two possible pathways, depending on whether the cleavage of the C–C or that of the C–O bond takes place first, as is represented in Scheme 1.

Roberts and Edwards[1] assumed that the cleavage of ethyl β-anilinocrotonate(VI) with aniline took place through the route shown in (1B), but the presence of an intermediate (IV) has not yet been confirmed. The analyses of the reaction products obtained by keeping a mixture of Ib and aniline for 1 hr at 230°C in toluene revealed the presence of small amounts of ethyl *N*-phenylcarbamate(III), but an absence of the carboxamide(VI). The same analytical results were obtained for the reaction products of VI with aniline. In both reactions, the formation of decarboxylated products was detected. The formation of IIb by the treatment of III with aniline was also confirmed. The reactions, therefore, must proceed along the route shown in (1A).

The overall rate of this reaction was mostly controlled at the steps from I to III, since the yield of II from III was four times that from I under the same reaction conditions.

1) R. M. Roberts and E. B. Edwards, *J. Amer. Chem. Soc.*, **72**, 5537 (1950).

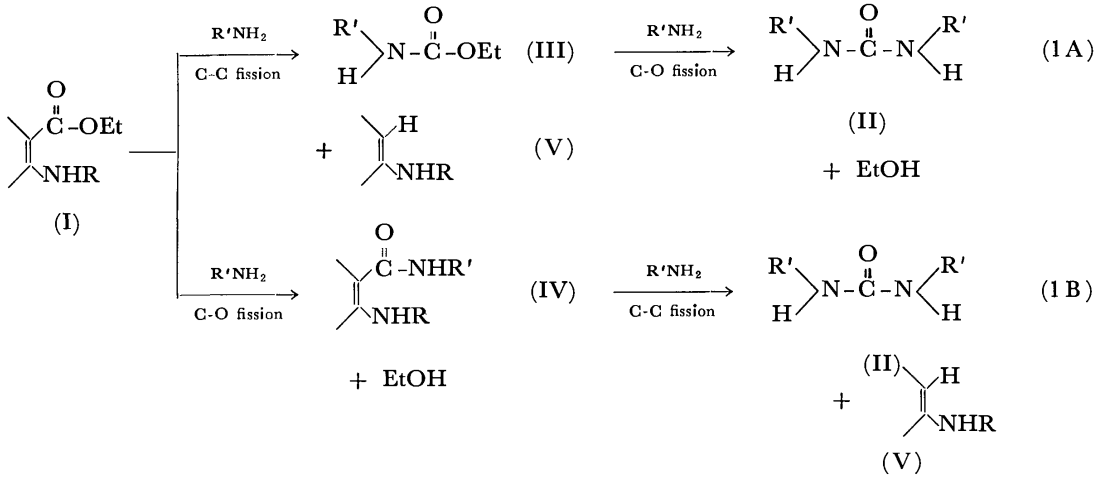

Scheme 1.

Table 1. Effects of the pK_a values of amines on the yield of *N,N'*-disubstituted urea[a)]

Amines; RNH_2 R	pK_a [b)]	Product	Mp (°C)	Yield (%)	$k_2 \times 10^4$ [c)] (sec^{-1})
$CH_3(CH_2)_4$-	10.63	*N,N'*-dipentylurea	97—100	31.7	12.9
p-$CH_3OC_6H_4$-	5.34	*N,N'*-bis(4-methoxyphenyl)urea	229—230	15.0	5.17
p-$CH_3C_6H_4$-	5.10	*N,N'*-di-*p*-tolylurea	257—258	10.9	3.48
C_6H_5-	4.60	*N,N'*-diphenylurea	242	8.85	2.98
p-ClC_6H_4-	3.98	*N,N'*-bis(4-Chlorophenyl)urea	278—279	8.48	2.87
m-$CH_3C_6H_4$-	4.72	*N,N'*-di-*m*-tolylurea	215—217	6.20	2.06
m-ClC_6H_4-	3.50	*N,N'*-bis(3-chlorophenyl)urea	242—244	3.26	0.90

a) Reaction conditions: A solution of 1.00×10^{-2} mol of amine and 2.46×10^{-3} mol of Ib in 10 ml of toluene was heated at 230±1°C for 1 hr.

b) Taken from: S. Patai, "The chemistry of the amino group", Interscience Publishers, New York, N. Y. (1968), p. 174, 182.

c) Calculated from an integrated form of bimolecular rate equation as below;

$$k_2 = 1/[C_0t(M-2)]\times\ln(M-2Y)/M(1-Y)$$

Y: Yield of II in a period of first 1 hr, M: Initial molar ratio of reactants; [amine]/[(I)], C_0: Initial molar concentration of I, t: reaction time; 3.6×10^3 sec.

The effects of the pK_a values of amines on the reaction rate were investigated in the reactions of Ib with various amines. The yields and rate constants roughly evaluated by fitting the integrated form of the bimolecular rate equation to the yields are listed in Table 1. The reactivity of the amines examined increased with the increase in their basicity, and the logarithm of the rate constants fell near a line when plotted against the pK_a values of the corresponding amines (Fig. 1). The reaction appeared to be a nucleophilic substitution at the carbonyl carbon atom involving slow C–N bond formation, followed by a relatively fast C–C bond fission proceeding through a tetrahedral intermediate.

The rate of the reaction was also affected by the nature of the substituent(R) on the nitrogen atom of I. The yields of IIb in reactions between aniline and various *N*-substituted I are shown in Table 2. The yields increased in the order of: R=alkyl, H, aryl; this order was the reverse of that of the basicity of amines, RNH_2. The electron density on the carbonyl carbon atom in I increases with the increase in the electron-donating effect of the RNH– group exerted through the double bond, inhibiting the nucleophilic attack of $R'NH_2$.

To gain insight into the factors which govern the

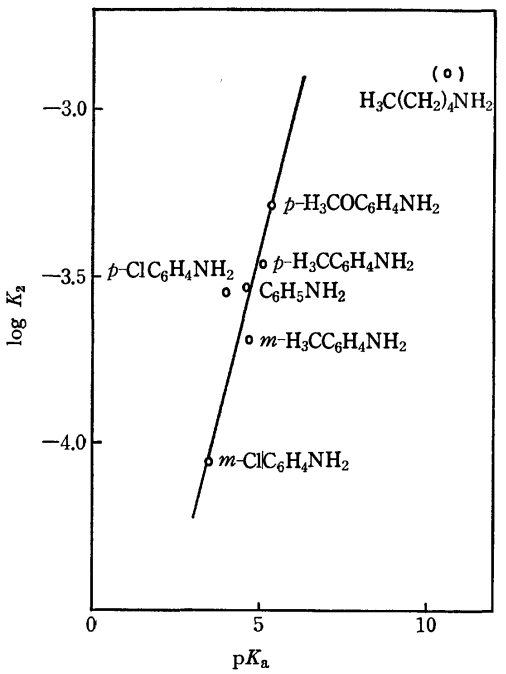

Fig. 1. The relation between the apparent second-order rate constant (k_2) and the pK_a values of amines.

TABLE 2. THE YIELD OF *N,N'*-DIPHENYLUREA BY THE REACTION BETWEEN ANILINE AND I[a]

R	RHN, COOEt / EtOOC, NHR	pK_a value of RNH_2[b]	Yield of *N,N'*-diphenylurea (%)
$CH_3(CH_2)_4$-	(Ia)	10.63	2.0
C_6H_5-	(Ib)	4.60	27.4
p-$CH_3C_6H_4$-	(Ic)	5.10	27.2
p-ClC_6H_4-	(Id)	3.98	28.1
p-$CH_3OC_6H_4$-	(Ie)	5.34	26.0
H-	(If)	9.24	5.9

a) Reaction conditions: A solution of 8.0×10^{-2} mol of aniline and 1.0×10^{-2} mol of I in 40 ml of toluene was heated at 230±2°C for 1 hr.
b) Taken from: S. Patai, "The chemistry of the amino group", Interscience Publishers, New York, N. Y. (1968), pp. 174, 182.

facile C–C bond cleavage, various types of β-anilino α,β-unsaturated carbonyl compounds were subjected to reactions with aniline. The results are summarized in Table 3. The C–C bond cleavage occurred not only in β-anilino α,β-unsaturated carboxylic esters, but also in the β-anilino α,β-unsaturated ketone. On the other hand, the compounds in which the α,β-double bond is incorporated with an aromatic system gave neither II nor amide.

Aliphatic β-amino α,β-unsasurated carbonyl compounds exist exclusively in the enamine form[2] and are capable of reaction with an electrophile on nitrogen or on an α-carbon atom, as is shown by the mesomeric forms, (1) and (2):

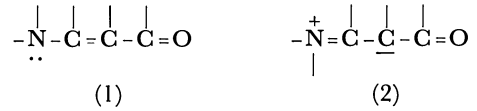

(1) (2)

The electron-donating sites in enamines may take part in the proton-transfer step in the reaction pathway, directing the reaction to the fission of the C–C bond instead of the C–O bond.

The proposed reaction mechanism is shown in Scheme 2.

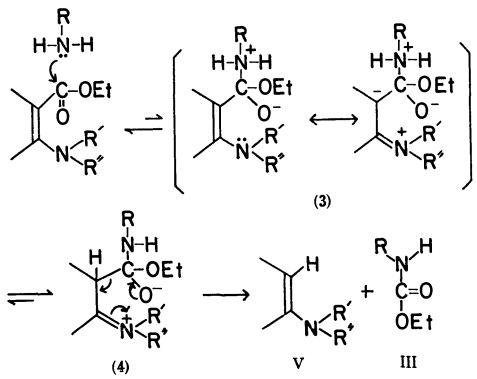

Scheme 2.

The ammonium hydrogen in (3) transfers either to the carbon atom or to the nitrogen atom, instead of to the ethoxyl oxygen atom, as is the case with an ordinary amidation.

TABLE 3. REACTIONS BETWEEN ANILINE AND β-ANILINO α,β-UNSATURATED CARBONYL COMPOUNDS

Compounds		mol	Aniline mol	Solvent toluene (ml)	Reaction conditions Temp(°C)	Time(min)	Product	Yield (%)
CH_3-C(NHPh)=CH-COOEt	(VI)	9.3×10^{-3}	4.3×10^{-3}	10	230±2	60	*N,N'*-diphenylurea	27.0
CH_3-C(N(Me)Ph)=CH-COOEt	(VII)	4.3×10^{-3}	2.2×10^{-2}	10	230±2	60	*N,N'*-diphenylurea	23.0
CH_3-C(NHPh)=C(CH_2CH_3)-COOEt	(VIII)	4.6×10^{-3}	2.2×10^{-2}	10	235±2	60	*N,N'*-diphenylurea	45.0
CH_3-C(NHPh)=CH-CO-CH_3	(IX)	4.6×10^{-3}	2.2×10^{-2}	10	230±2	120	acetanilide	27.8
EtOOC, NHPh / PhHN, COOEt	(X)	2.5×10^{-3}	1.1×10^{-1}	—	217±2	120	2,5-dianilinoterephthalic acid, ethyl hydrogen 2,5-dianilinoterephthalate, *N*-ethylaniline	17.4, 37.7, 36.5[a]
COOEt / NHPh	(XI)	1.8×10^{-3}	1.1×10^{-1}	—	230±2	120	2-anilinobenzoic acid	trace

a) Estimated by the area of the peak in glc.

2) G. O. Dudek and R. H. Holm, *J. Amer. Chem. Soc.*, **83**, 2099 (1961).

In the case of enamines, protonation takes place rapidly on nitrogen and is followed by a transfer of the proton to the carbon.[3] Therefore, the final product of the proton-transfer step is presumably a C-protonated step (4), which gives III and V through the C–C bond cleavage. The resulting III was then considerably quickly converted to II by the reaction with the excess amine presented.

Experimental

The infrared spectra were recorded on a Hitachi EPI-G3 spectrometer. The analyses of the volatile substances were carried out by means of a Hitachi Model 063 gas chromatograph equipped with a thermal conductivity cell. A 100× 0.5 cm packed column of Apiezon L (25%) on Chromosorb-W was used at a flow rate of 40 ml/min of He gas. For thin-layer chromotagraphy (tlc), a plate of Silica-gel HF (E. Merk Co.) was used. Plates were developed with Solvent 1 (ether/hexane=20/30) or Solvent 2 (benzene/tetrahydrofuran/acetic acid=25/25/1). For column chromatography, a column of 20×1.8 cm was prepared by slurrying silica gel (Wako Gel C-200, Wako Chemical Co.) in benzene for packing. The melting points and boiling points were not corrected.

Materials. All the reagents except those listed below were obtained from commercial sources and were used without further purification. The aniline, pentylamine, and toluene were dried over synthetic zeorite (Zeorum A-4, Tekkosha Co.) and distilled before use. The solid amines listed in Table 1 were purified by recrystallization. The ethyl *o*-anilinobenzoate(XI) was purified by silica gel column chromatography before use. The 1,4-bis(ethoxycarbonyl)-2,5-bis(alkyl- or arylamino)-1,4-cyclohexadiene(Ia: mp 76—77°C, Ib: mp 164—165°C, Ic: mp 218—220°C, Id: mp 240—243°C, Ie: mp 187—188°C, If: mp 117—119°C)[4], the ethyl β-anilinocrotonate(VI)[1] (bp 116—122°C/3×10^{-2} mmHg), the ethyl β-(*N*-methylanilino)-crotonate(VII)[5] (bp 110—120°C/4×10^{-3} mmHg), the ethyl α-ethyl β-anilinocrotonate(VIII)[1] (bp 105—107°C/5×10^{-3} mmHg), the 4-anilino-3-penten-2-one(IX)[6] (mp 47—48°C), the diethyl 2,5-dianilinoterephthalate(X)[7] (mp 142—143°C), and the 1,4-cyclohexanedione[8] (mp 71—73°C) were prepared by published procedures.

Reactions. *a) Ia with Pentylamine*: In a glass ampoule, 1.0 g (2.5 mmol) of Ia, 0.78 g (10 mmol) of pentylamine, and 10 ml of toluene were placed. The free space was filled up with nitrogen before the ampoule was sealed. The ampoule was then heated at 230°C for 1 hr in an oil bath. The contents of the ampoule were subsequently transferred to a flask and were concentrated to half of their original volume. The crystals which appeared were collected by filtration, washed with cold ethanol, and dried in a vacuum to give 0.017 g of IIa, which was confirmed by a comparison of its IR spectrum with that of an authentic sample prepared from urea and pentylamine.[9] Recrystallization from ethanol gave an analytically pure sample: mp 98—100°C, Found: C, 66.01; H, 12.07; N, 13.92%. IR(cm^{-1}): 3345(–NH–), 2960(–CH_3), 2925(–CH_2–), 1625, 1580, and 1276 (amide).

b) Ib with Pentylamine: From 1.00 g (2.46 mmol) of Ib, 0.87 g (10 mmol) of pentylamine, and 10 ml of toluene, 0.226 g of white crystals was obtained by the procedure described in *a)*. The product was determined to be IIa by a mixed-melting-point determination with an authentic sample.

c) Ib with Aniline. A mixture of 1.00 g (2.46 mmol) of Ib, 0.93 g (10.0 mmol) of aniline, and 10 ml of toluene was heated at 230°C in a way similar to that described in *a)*. A white precipitate which separated when the reaction mixture was brought to room temperature was collected by filtration, washed with 10 ml of cold toluene, and dried in a vacuum to give 0.09 g of IIb, which was confirmed by a comparison of its IR spectrum with that of an authentic sample. Recrystallization from toluene gave an analytical sample: mp 242°C, Found: C, 73.64; H, 5.75; N, 13.12%. IR (cm^{-1}): 3325 and 3280(–NH–), 1652, 1557, and 1319 (amide), 755 and 695(phenyl).

A small portion of the filtrate was freed from aniline and toluene under reduced pressure. The residue was dissolved in 1 ml of benzene and was then placed at the top of the column. Elution was achieved with 100 ml portions of each of the following series of solvents: benzene, benzene/ether=80/20, benzene/ether=50/50, ether, and methanol. About 90 fractions of 5 g each were collected. The constituents of each fraction was determined by tlc. Fractions 1—4 gave nothing. Fractions 5—8 gave a mixture of two substances, which appeared at the R_f value of 0.61 (Compound A) and 0.58 (Compound B) in tlc (Solvent 1). The isolation of each compound was achieved by preparative tlc. Compound A (red crystals, mp 141—142°C) was found to be completely identical with X by IR spectroscopic analysis and by a mixed-melting-point determination with an authentic sample. Compound B [brown oil, IR(cm^{-1}): 3390 and 3350(–NH–), 1690, 1256, and 1216(ester), 1602 and 1500(C=C, aromatics), 1317(C–N), 745 and 700(phenyl)] was assumed to be ethyl 2,5-dianilinobenzoate(XII) on the basis of its IR spectrum, which was almost the same as that of *N,N'*-diphenyl-*p*-phenylenediamine(XIII) except for additional absorptions suggesting the presence of an ester group in the molecule. Fractions 9—14 showed a single spot on tlc (Solvent 1). The removal of the solvent from it gave a light yellow oil. The compound changed spontaneously to brown solids upon contact with air. Recrystallization from benzene gave pale gray crystals: mp 146—150°C. IR(cm^{-1}): 3390(–NH–), 1602 and 1500(C=C, aromatics), 1317(C–N), 822(*p*-disubstituted benzene), 745 and 700(phenyl). Its IR spectrum and the R_f value of tlc completely matched those of an authentic sample of *N,N'*-diphenyl-*p*-phenylenediamine. Since compounds with a cyclohexadiene ring are easily converted to aromatic compounds when they are brought into contact with air in the presence of the solvent, X, XII, and XIII were supposed to have been derived from Ib, 1-ethoxycarbonyl-2,5-dianilino-1,4-cyclohexadiene(XIV), and 1,4-dianilino-1,4-cyclohexadiene(Va) respectively, all of which existed in the original reaction products. The formation of XIII by the treatment of air with the Schiff's base obtained from 1,4-cyclohexanedione and aniline was confirmed by a separate experiment. Thus, the decarboxylation of Ib resulting in a Schiff's base (Va) was indirectly confirmed. Fractions 15—26 gave practically nothing. Fractions 27—32 showed a single spot on tlc (Solvent 1). The removal of the solvent from any one of them gave a thick oil which solidified on standing in a refrigerator. Recrystallization from ethanol gave white crystals: mp 51—53°C, IR(cm^{-1}):

3) E. J. Stamhuis and W. Mass, *J. Org. Chem.*, **30**, 2156 (1965).
4) F. Higashi, A. Tai, and K. Adachi, *J. Polym. Sci. Part A*-1, **8**, 2563 (1970).
5) A. Risaliti and P. Bruni, *Ann. Chem.*, (Rome), **53**, 595 (1963).
6) E. Roberts and E. E. Turner, *J. Chem. Soc.*, **1929**, 1832.
7) A. Tai, F. Higashi, and S. Yokomizo, *J. Polym. Sci. Part A*-1, **9**, 2481 (1971).
8) W. G. Dauben, "Organic Syntheses," **45**, p. 25, (1965).
9) T. L. Davis and K. Blanchard, *J. Amer. Chem. Soc.*, **45**, 1817 (1923).

3315(-NH-), 3050(aromatics), 2975(aliphatics), 1722, 1240, and 1060(ester), 1705, 1540, and 1320(amid), 750 and 695 (phenyl). With respect to the IR spectrum, the R_f value of tlc, and the mixed-melting-point determination, the compound was identical with an authentic sample of ethyl *N*-phenylcarbamate(III). Fractions 33—36 gave a mixture of aniline, III, and IIb. Fractions 37—39 gave IIb. Fractions 40—62 gave nothing. Fractions 63—70 gave deep red crystals, which were identical with ethyl hydrogen 2,5-dianilinoterephthalate in IR spectrum and in the R_f value of tlc. This compound was expected to have been converted X, which existed in Ib as an impurity. The details of the reaction products between aniline and X are described in *j*). Fractions 71—90 gave practically nothing.

d) Ib with Various Amines. The amounts of reagents in each run were adjusted to 2.46 mmol of Ib, 10 mmol of amines, and 10 ml of toluene. The reaction were carried out at 230°C for 1 hr. The resulting *N,N'*-disubstituted urea was isolated from the reaction products by the process described in *a*). The yields and products of each run are listed in Table 1.

e) Various I Substances with Aniline. The reactions were carried out in the way described in *a*). The yield of IIb in each run is listed in Table 2.

f) VI with Aniline. A mixture of 1.9 g of VI, 4.0 g of aniline, and 10 ml of toluene was heated in a way similar to that described in *a*). IIb(0.53 g) was separated from the reaction products. The distillation of the filtrate gave three fractions; bp 35—40°C/50 mmHg(toluene), bp 78—82°C/13 mmHg, and nonvolatile substances. The gas chromatogram(at 150°C) of the fraction at bp 78—82°C/13 mmHg showed two peaks, at R_t=2.2 min and 4.1 min. The former peak was identical with that of aniline, while the latter peak was matched that of the anil of acetone prepared by the method of Kuhn and Schretzmann.[10] The tlc(Solvent 1) of the nonvolatile substance showed a big spot at R_f=0.55. The isolation of this substance by preparative tlc gave light yellow crystals. The IR spectrum, mp, and R_f value of this compound were identical with those of an authentic sample of III.

g) Other β-Anilino α,β-unsaturated Carboxylic Acid Esters with Aniline. In a way similar to that described in *a*), VII and VIII were subjected to a reaction with aniline. The results are listed in Table 3.

h) IX with Aniline. The reaction was carried out in a manner similar to that in the case of I. The tlc(Solvent 1) of the products showed a big spot (R_f=0.04). The compound corresponding to this spot was isolated by preparative tlc and was determined to be acetanilide by an IR spectroscopic analysis and by a mixed-melting-point determination with an authentic sample. From one-twentieth of the product, 10.7 mg of acetanilide were obtained as crystals; mp 112—114°C.

i) III with Aniline. A mixture of 1.0 g of III, 2.2 g of aniline, and 10 ml of toluene was subjected to a reaction under the same conditions as in *a*). IIb was thus obtained in a yield of 0.50 g. (39%).

j) X with Aniline. Since the reaction between X and aniline in the presence of the solvent (toluene) was slow, the reaction was carried out in the absence of the solvent. Thus, a mixture of 1.0 g of X and 19 ml of aniline was heated for 2.0 hr at 220°C in a sealed tube. The product was then roughly divided into a nonvolatile solid and a volatile liquid by vacuum distillation. The solid was composed of three substances, which appeared at R_f values of 0.66 (Compound A), 0.46 (Compound B), and 0.37 (Compound C) in tlc(Solvent 2). Each compound was isolated by preparative tlc and its structure was determined by IR spectroscopic and elemental analysis to be as follows: Compound A: unchanged X; Compound B: ethyl hydrogen 2,5-dianilinoterephthalate, Found: C, 68.67; H, 5.43; N, 7.39%. Calcd for $C_{22}H_{20}N_2O_4$: C, 70.20; H, 5.36; N, 7.44%. IR(cm^{-1}), 3360(-NH-), 1698, 1264, and 1160 (ester), 1668 and 1540 (-COOH), 750 and 694(phenyl); Compound C: 2,5-dianilinoterephthalic acid, Found: C, 66.01; H, 4.72; N, 7.63%. The IR spectrum of this compound was identical with that of a saponification product of X. The gas chromatogram of the volatile liquid obtained at 120°C showed two peaks, corresponding to aniline (R_t=1.5 min) and *N*-ethylaniline (R_t=2.7 min) respectively.[11] The structure of the latter compound was confirmed by a study of its IR spectrum.

k) XI with Aniline. Acid-freed XI (1.0 g) and aniline (10 m*l*) were heated for 2 hr at 230°C in a sealed tube. The tlc (Solvent 2) of the product showed two prominent spots, at R_f 0.62 (aniline) and 0.78(XI), and one weak spot, at R_f 0.64(2-anilinobenzoic acid). No further treatment of the product was undertaken.

10) R. Kuhn and H. Schretzmann, *Chem. Ber.*, **90**, 557 (1957).

11) It has been reported that alkyl-oxygen fission in the hydrolysis of esters might occur if the carbonium ion to be formed is sufficiently stable[12] or if the rate of the $B_{AC}2$ reaction of the ester is remarkably diminished by steric hindrance.[13] In this reaction, it may be considered that the nucleophilic attack of aniline molecules occurred hardly at all at the carbonyl carbon atom, but more at the alkyl carbon atom. Therefore, alkyl-oxygen fission occurred to form acid and *N*-ethylaniline. The further details of this reaction will be reported separately.

12) G. S. Hammond and J. T. Rudesill, *J. Amer. Chem. Soc.*, **72**, 2769 (1950).

13) L. R. C. Barclay, N. D. Hall, and G. A. Cooke, *Can. J. Chem.*, **40**, 1981 (1962).

Reaction of *O,O*-Dialkyl Dithiophosphoric Acid. III.[1] Reductive Cleavage Reactions of Nitrogen-Nitrogen Bond by *O,O*-Diethyl Dithiophosphoric Acid

Shigeru Oae, Nobuko Tsujimoto,[2] and Akira Nakanishi

Department of Applied Chemistry, Faculty of Engineering, Osaka City University, Sumiyoshi-ku, Osaka

(Received May, 6, 1972)

o-Nitroaniline was obtained when tri(*o*-nitrophenyl) triaziridine(I) was allowed to react with excess *O,O*-diethyl dithiophosphoric acid. It was found that azobenzene derivatives(IIa-e) are converted into the corresponding reduction products aniline derivatives(IVa-e) in the reaction with excess *O,O*-diethyl dithiophosphoric acid. Similarly, arylhydrazines (IIIa-c) were converted into the corresponding aniline derivatives (IVa,d,e) by the action of *O,O*-diethyl dithiophosphoric acid.

In a previous paper,[1] we reported on the reactions between *O,O*-dialkyl dithiophosphoric acid and various compounds having a semipolar linkage. Meanwhile, we have found that compounds having a less polarized nitrogen-nitrogen linkage or none at all, such as tri-(*o*-nitrophenyl)triaziridine(I), azobenzene(IIa—e), and arylhydrazine(IIIa—c), also readily react with *O,O*-diethyl dithiophosphoric acid to afford the corresponding reduction products. The reduction of tri(*o*-nitrophenyl)triaziridine(I) to *o*-nitroaniline, and the formation of *o*-nitroaniline from I appear to support the structure of I to be of triaziridine ring. The reduction of IIa—e to anilines and benzidine in the reaction with *O,O*-diethyl dithiophosphoric acid is also interesting, since there has been no report that azobenzene is reduced by organic reducing agents. Meanwhile in the N–N bond cleavage reaction of IIIa—c with *O,O*-diethyl dithiophosphoric acid, nucleophilic substitution on the nitrogen atom (Chart 3) appears to take place to afford anilines (IVa,d,e). This is one of only a few known examples of nucleophilic substitution on the nitrogen atom. This paper gives a detailed account of the N–N bond cleavage reaction with an acidic mercaptan, *O,O*-diethyl dithiophosphoric acid ($pK_a=1.62$[3]).

Results and Discussion

Reaction of Tri(o-nitrophenyl)triaziridine(I) with $(EtO)_2PS_2H$. Recently, tri(*o*-nitrophenyl)triaziridine(I), a remarkably stable derivative of the triaziridine ring system,[4,5] has been prepared by the thermolysis of *o*-nitrophenyliminopyridinium betaine.[6] However, catalytic hydrogenation of I over PtO_2 or the reduction of I with Zn/AcOH afforded *o*-phenylenediamine,[6] *viz.*, both the nitro group and triaziridine ring were similtaneously reduced. The reaction of I with a large excess of $(EtO)_2PS_2H$ at 80°C for 24 hr[7] gave *o*-nitroaniline in a 12% yield and unreacted I (70%) as shown by Eq. (1). Thus $(EtO)_2PS_2H$ is the first selective reducing agent which cleaves the N–N bond of aziridine ring without reducing *o*-nitro group. This strongly suggests the structure of I to be of a three-membered triaziridine ring. Although we could neither detect nor isolate any such intermediate as

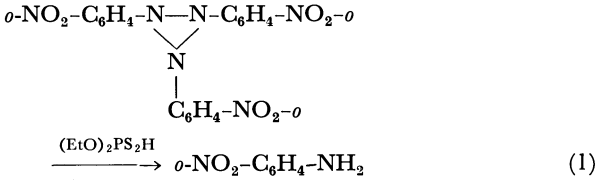

(1)

2,2′-dinitroazobenzene, the reduction pathway undoubtedly involves the cleavage of azo (–N=N–) and/or hydrazo (–NH–NH–) linkages. We therefore allowed azobenzene derivatives to react with $(EtO)_2PS_2H$ and found the reaction to proceed more easily than I. The conversion of I into *o*-nitroaniline is considered to follow the scheme shown in Chart 1. The initial step of the reaction between I and $(EtO)_2PS_2H$

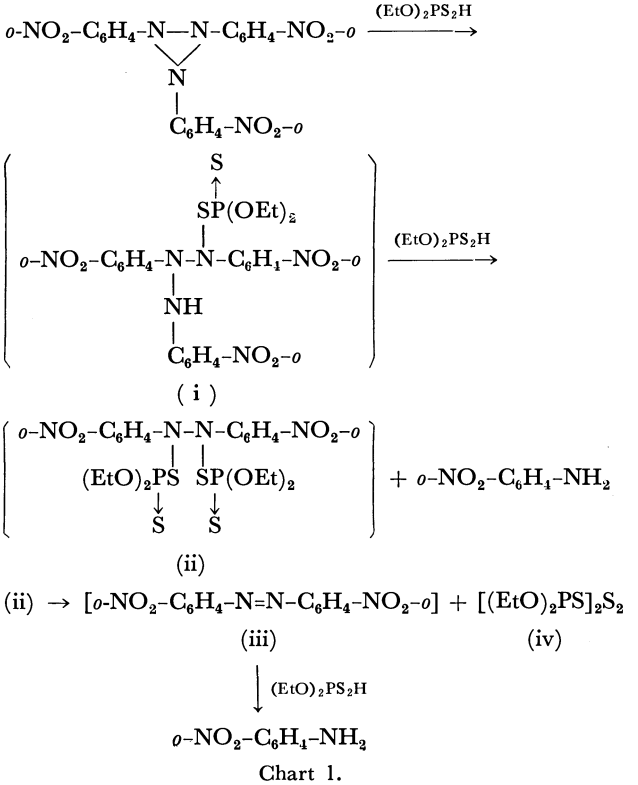

Chart 1.

1) Part II; S. Oae, A. Nakanishi, and N. Tsujimoto, *Tetrahedron*, **28**, 2981 (1972).

2) Present Address: Faculty of Pharmaceutical Sciences, Osaka University, Toneyama, Toyonaka, Osaka.

3) M. I. Kabachnik, S. T. Ioffe, and T. A. Mastryukova, *J. Gen. Chem. U.S.S.R.*, **25**, 653 (1955); *Chem. Abstr.*, **50**, 3850i (1956).

4) M. Colonna and A. Risalti, *Gazz. Chim. Ital.*, **41**, 204 (1961).

5) M. S. Gibson, *Tetrahedron*, **18**, 1377 (1962).

6) Y. Tamura, N. Tsujimoto, M. Ikeda, and K. Tomita, Abstracts of the Third International Congress of Heterocyclic Chemistry, Tohoku University, Sendai, Japan, 1971, p. 252.

7) I did not react with conc. H_2SO_4 or thiophenol and was then recovered.

would be the formation of an intermediate(i), which reacts further with another mole of $(EtO)_2PS_2H$ to afford an intermediate(ii) and *o*-nitroaniline. (ii) then immediately changes to azobenzene(iii) and bis-[*O,O*-diethyl thiophosphoryl]disulfide(iv). (iii) is readily reduced to *o*-nitroaniline by $(EtO)_2PS_2H$ under the reaction conditions.

Reaction of Azobenzene(IIa—e) with $(EtO)_2PS_2H$. As anticipated 2,2′-dinitroazobenzene(iii) can be reduced smoothly with $(EtO)_2PS_2H$ to *o*-nitroaniline. It is well-known that azobenzene is reduced to the corresponding reduction product by treatment with such inorganic reducing agents as $Na_2S_2O_4$,[8] NH_2-$NH_2 \cdot H_2O$/Cu,[9] or HCl/Zn.[10] However, it is not known that azobenzene is reduced to aniline in the reaction with any organic reducing agent, such as acidic mercaptans. Actually the reaction between azobenzene(IIa) (1 mol) and $(EtO)_2PS_2H$ (10 mol) at 70°C for 24 hr gave benzidine and aniline (IVa) in the yields of 27% and 40%, respectively [Eq. (2)]. Since no reaction takes place when azobenzene is treated with a large excess of thiophenol either in the presence or absence of *p*-Tol-SO_3H, the reduction of azobenzene with $(EtO)_2PS_2H$ is caused by the inherently-built-in high acidity and nucleophilicity of the dithiophosphoric acid.

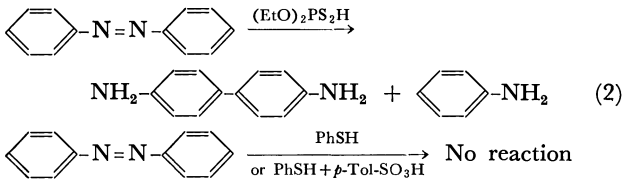

(2)

The reaction with $(EtO)_2PS_2H$ was successfully applied to the reduction of a few substituted azobenzene derivatives (IIb—e) [Eq. (3)]. The results are listed in Table 1. In an attempt to trap an intermediate of this reaction an equimolar mixture of IIa and *O,O*-diethyl dithiophosphoric acid was kept at 0°C for 24 hr, and then 10% benzidine and 38% recovered IIa were obtained. Thus, neither intermediate nor aniline (IVa), a reduction product of azobenzene, could be obtained. However, benzidine and IVa are presumed to be formed *via* an initial formation of hydrazobenzene(Va) or its derivative. We therefore allowed Va to react with *O,O*-diethyl dithiophosphoric acid. The results are summarized in Table 2.

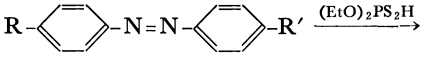

IIb: R=H, R′=Cl
c: R=Me, R′=Cl
d: R=R′=Me
e: R=R′=Cl

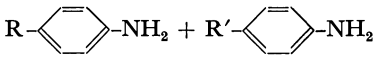

(3)

IVb: R=H, R′=Cl
c: R=Me, R′=Cl
d: R=R′=Me
e: R=R′=Cl

A mixture of hydrazobenzene(Va) (1 mol) and excess *O,O*-diethyl dithiophosphoric acid was heated at 70°C for 24 hr. As in the case of IIa, benzidine and IVa were obtained in the 50% and 32% yields, respectively. IIa was obtained when less than two moles of $(EtO)_2PS_2H$ was used. In order to understand the process of formation of IIa, 4,4′-dichlorohydrazobenzene(Vb) (1 mol) was treated with $(EtO)_2PS_2H$ (1 mol); 4,4′-dichloroazobenzene(IIe) (50%) and 4-chloroaniline(IVe) (50%) were obtained. When $(EtO)_2PS_2H$ was used as an acid catalyst, the same reaction occurred (Table 3). This is in line with the observation[10] that in acid catalysis one molecule of hydrazo compound becomes oxidized to the azo compound, while another is reduced to two molecules of amine.

As regards the reaction mechanism for the conversion of IIa into benzidine and IVa, the sequence of reactions shown in Chart 2 is conceivable. The initial step of the reaction between II and *O,O*-diethyl dithiophosphoric acid would be the formation of an intermediate(v) similar to that[11] between azobenzene and an arenesulfinic acid which has also a similar pK_a

TABLE 1. YIELD OF ANILINE DERIVATIVES (IVb-e) BY TREATMENT OF AZOBENZENE DERIVATIVES (IIb-e) WITH EXCESS *O,O*-DIETHYL DITHIOPHOSPHORIC ACID AT 70°C

Aniline deriv.	Yield (%)
IVb	23[a]
IVc	50[b]
IVd	63
IVe	93

a) Yield was a mixture of aniline and 4-chloroaniline.
b) Yield was a mixture of 4-methylaniline and 4-chloroaniline.

TABLE 2. REACTION OF HYDRAZOBENZENE(Va) WITH *O,O*-DIETHYL DITHIOPHOSPHORIC ACID AT 70°C

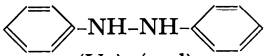 (Va) (mol)	$(EtO)_2PS_2H$ (mol)	Yield of product (%) 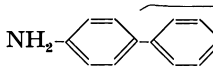 (IVa)	(IIa)	Recov. (Va)
1	10	50	32	—	—
1	1	17	10	30	—
1[a]	1	10	9	37	7

a) The reaction mixture was kept at room temperature.

8) L. F. Fieser, "Organic Syntheses," Coll. Vol. II, p. 39 (1950).
9) H. Kubota, T. Akita, and T. Yokojima, *Yakugaku Zasshi*, **78**, 1194 (1958).
10) H. J. Shine, "Mechanism of Molecular Migrations," ed. by B. S. Thyagarajan, Vol. 2, p. 191, Interscience, New York (1969).
11) W. Bradley and J. D. Haunon, *J. Chem. Soc.*, **1962**, 2713.

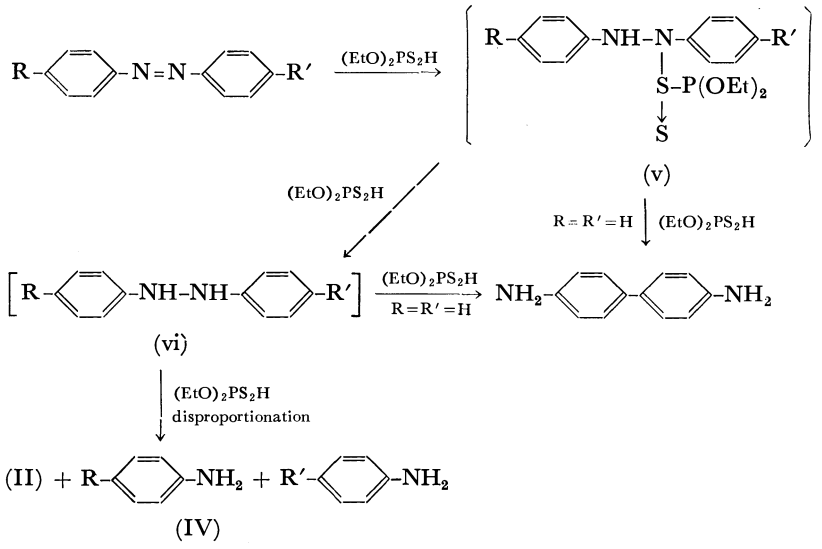

Chart 2.

Table 3. Reaction of 4,4'-dichlorohydrazobenzene(Vb) with *O,O*-diethyl dithiophosphosphoric acid at room temperature[a)]

$(EtO)_2PS_2H$ (mol)	(Vb) (mol)	Reaction time	Yield (%) of product (IIe)	(IVe)
1	1	24 hr	50	50
0.2	1	7 day	50	50

a) An equimolar mixture of 4-chloro-4'-methylhydrazobenzene(Vc) and *O,O*-diethyl dithiophosphoric acid gave IIc(50%), IVc(25%), and IVe(25%). There was no cross-over of amine group between 4-chloroaniline and 4-methylaniline during the course of reaction.

value 1—1.5.[12)] Then the intermediate(v), upon reaction with another mole of $(EtO)_2PS_2H$, gives benzidine or hydrazobenzene derivatives(vi), which, however, could not be isolated. Hydrazobenzene (vi) would either be reduced with $(EtO)_2PS_2H$ to aniline or rearrange to benzidine or undergo acid catalyzed disproportionation[10)] to give II and IV.

Reaction of Arylhydrazine (IIIa—c) with $(EtO)_2PS_2H$. Since hydrazobenzene was found to be cleaved readily by $(EtO)_2PS_2H$, we applied this procedure for the N–N bond cleavage of arylhydrazine(IIIa—c). When a mixture of phenylhydrazine(IIIa) (1 mol) and $(EtO)_2PS_2H$ (10 mol) was heated at 70°C for 24 hr, aniline (IVa) was obtained in a 51% yield. In an alternative procedure to prepare IVa, an equimolar mixture of IIIa and $(EtO)_2PS_2H$ in ether was kept at room temperature to give hygroscopic phenylhydrazinium *O,O*-diethyl dithiophosphate (viia). The structure of viia was identified by NMR and IR spectra (Tables 5,6). The salt (VIIa) was then heated under refluxing in benzene to yield IVa. Similarly, other arylhydrazines (IIIb, c) were also reduced to the corresponding aniline derivatives (IVd, e), as listed in Table 4. These reactions are assumed to proceed *via* the formation of an intermediate salt (vii) prior to the formation of the

12) P. Rumph and J. Sadet, *Bull. Soc. Chim. Fr.*, **1958**, 450.

Table 4. Reaction of arylhydrazine(IIIc) with *O,O*-diethyl dithiophosphoric acid

Hydrazine deriv.	Yield (%) of an-line deriv.
IIIa	51
IIIb	65
IIIc	60

reduction product VI and *S*-amino-*O,O*-diethyl dithiophosphate (VIII). Compound (VIII) is so unstable that, upon being kept standing, it is converted into bis[*O,O*-diethyl thiophosphoryl]disulfide (VI).[1)]

These reduction reactions of azobenzenes (IIa—e) and arylhydrazines (IIIa—c) with *O,O*-diethyl dithiophosphoric acid are interesting examples of nucleophilic substitution on the nitrogen atom.

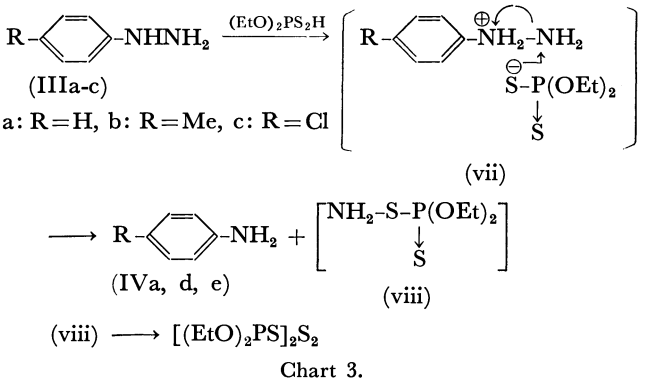

Chart 3.

Experimental

The NMR spectra were measured on a Hitachi-Perkin Elmer R-20 Spectrometer (60 Mc) and the IR spectra on a Japan Spectroscopic Co., Ltd. IR-G spectrometer. Boiling and melting points were uncorrected.

O,O-*Diethyl Dithiophosphoric Acid.* Prepared from phosphorus pentasulfide and absolute ethanol according to the procedure of Kabachnik and Mastryukova,[13)] bp 64—66°C/

13) M. I. Kabachnik and T. A. Mastryukova, *Izvest. Akad. Nauk S.S.S.R., Otdel. Khim. Nauk*, 121 (1953); *Chem. Abstr.*, **48**, 3244e (1954).

2 mmHg(lit,[13] bp 81.5—82.5°C/5 mmHg).

Tri(o-nitrophenyl)triaziridine. Prepared from the thermolysis of *N-o*-nitrophenyliminopyridinium betaine at 140—150°C,[6] mp 132—133°C(lit,[6] mp 132—133°C).

Azobenzene(IIa). Prepared by the usual method,[14] mp 66—67°C (lit,[14] mp 66—67.5°C from ethanol).

4-Chloroazobenzene(IIb). Prepared from azoxybenzene and phosphorus trichloride according to the procedure of Vozza,[15] mp 89°C from ethanol (lit,[15] mp 87—88°C).

4,4'-Disubstituted Azobenzene(IIc-e). Prepared from the reaction between zinc chloride double salt of *p*-substituted benzene diazonium chloride and the corresponding Grignard reagent according to the procedure of Nomura.[16]

4-Chloro-4'-methylazobenzene(IIc), mp 152—153°C (lit,[17] mp 153°C)

4,4'-Dimethylazobenzene(IId), mp 140—141°C (lit,[18] 140—141°C)

4,4'-Dichloroazobenzene(IIe), mp 177—178°C (lit,[18] mp 177—178°C)

Hydrazobenzene(Va-c). Prepared from the corresponding azobenzene using 80% hydrazine hydrate and copper powder according to the procedure of Kubota, *et al.*[9]

Hydrazobenzene(Va), mp 124—126°C(lit,[19] mp 126°C)
4,4'-Dichlorohydrazobenzene(Vb), mp 123—124°C(lit,[19] mp 124°C)

4-Chloro-4'-methylhydrazobenzene(Vc), mp 123—124°C (lit,[17] mp 124°C)

Aryhydrazine(IIIa-c). Pure arylhydrazines were obtained by either distillation or recrystallization of commercial compounds.

Phenylhydrazine(IIIa), bp 140°C/20 mmHg(lit,[20] bp 137—138°C/18 mmHg)

4-Methylphenylhydrazine(IIIb), mp 64—66°C(lit,[21] mp 65—66°C)

4-Chlorophenylhydrazine(IIIc), mp 88—89°C(lit,[22] mp 88°C)

Reaction of Tri(o-nitrophenyl)triaziridine with $(EtO_2)PS_2H$. Tri(*o*-nitrophenyl)triaziridine(500 mg) was reacted with 5 g of $(EtO)_2PS_2H$ at 80°C. After 24 hr aqueous Na_2CO_3 was added to this reaction mixture of remove excess $(EtO)_2PS_2H$. The reaction products were extracted with $CHCl_3$ from *aq.* Na_2CO_3 solution, and then chromatographed(silica gel column) with benzene-hexane(1 : 1) to give bis[*O,O*-diethyl thiophosphoryl] disulfide, 90 mg of *o*-nitroaniline(12%), and 560 mg of recovered tri(*o*-nitrophenyl)triaziridine(70%).

Reaction of Azobenzene(IIa) with Excess $(EtO)_2PS_2H$. A mixture of IIa(1.82 g, 0.01 mol) and $(EtO)_2PS_2H$(18.6 g, 0.1 mol) was heated at 70°C for 24 hr. Excess Na_2CO_3 was added to the reaction mixture and the product was extracted with benzene. After removal of benzene at atmospheric pressure, the residue was chromatographed through a silica gel column with $CHCl_3$ as an eluent to give benzidine, 0.40 g, 27%, mp 113—115°C (lit,[23] mp 115—120°C) and aniline(IVa), 0.74 g, 40%. These compounds were identified by comparing their IR spectra and melting points with those of the corresponding authentic samples. In this reaction small amounts of three other unidentified liquids were also obtained.

Reaction of Azobenzene Derivatives(IIb-c) with excess $(EtO)_2PS_2H$. A mixture of IIb-e(0.01 mol) and $(EtO)_2PS_2H$-(0.1 mol) was heated at 70°C until the reaction mixture changed in to a clear solution. The mixture was treated with excess Na_2CO_3 and extracted with benzene. The benzene solution was extracted with 10% aqueous HCl and the aqueous layer was concentrated under reduced pressure to obtain HCl salts of aniline derivatives (IVb-e). A small amount of water was added to the crude salts of IVb-e and neutralized with Na_2CO_3 and then extracted with benzene. The benzene layer was dried over $MgSO_4$ and concentrated under atmospheric pressure to give aniline derivatives(IVb-e), which were found to be identical with the authentic samples in melting points and IR spectra. The amounts of IVb and IVc were estimated by comparison with the mixture of authentic samples. The yields are summarized in Table 1.

Reaction of an Equimolar Mixture of Azobenzene(IIa) and $(EtO)_2PS_2H$. To a solution of IIa(1.82 g, 0.01 mol) in ether(5 ml) was added dropwise a solution of $(EtO)_2PS_2H$ (1.86 g, 0.01 mol). The mixture was allowed to stand at 0°C overnight. The white precipitates were collected and washed thoroughly with ether to give crude *O,O*-diethyl dithiophosphate of benzidine. The crude salt of benzidine was neutralized with aqueous Na_2CO_3 and then extracted with benzene. The benzene solution was dried over $MgSO_4$ and upon removal of the benzene benzidine, 0.19 g, 10%, mp 113—116°C(lit,[23] mp 115—120°C), was obtained. The ether filtrate was concentrated to give orange crystals, which were recrystallized from ethanol to give recovered azobenzene, 0.7 g, 38%, mp 64—66°C(lit,[14] mp 66—67.5°C).

Reaction of Hydrazobenzene(Va) with Excess $(EtO)_2PS_2H$. A mixture of Va(1.84 g, 0.01 mol) and $(EtO_2)PS_2H$(18.6 g, 0.1 mol) was heated at 70°C for 24 hr. Excess Na_2CO_3 was added to the reaction mixture and the mixture was extracted with benzene. After removal of the benzene at atmospheric pressure, the residue was chromatographed through a silica gel column with $CHCl_3$ as an eluent to give benzidine, 0.92 g, 50%, mp 113—116°C(lit,[23] mp 115—120°C) and aniline(IVa)(0.60 g, 31%), which were found to be identical with the corresponding compounds.

Reaction of an Equimolar Mixture of Hydrazobenzene (Va) and $(EtO)_2PS_2H$ at 70°C. To a solution of Va(1.84 g, 0.01 mol) in ether (5 ml) was added dropwise a solution of $(EtO)_2PS_2H$ (1.86 g, 0.01 mol). The mixture was heated at 70°C overnight. The white mass was collected and washed thoroughly with ether to give crude *O,O*-diethyl dithiophosphate of benzidine. The crude salt of benzidine was neutralized with aqueous Na_2CO_3 and then extracted with benzene. The benzene solution was dried with $MgSO_4$ and the benzene was removed to give benzidine, 0.32 g, 17%, mp 112—116°C(lit,[23] 115—120°C). The ether filtrate was concentrated to give an orange residue. The residue was chromatographed through a silica gel column with $CHCl_3$ as an eluent to give aniline(0.19 g, 10%) and azobenzene (IIa), 0.55 g, 30%, mp 65°C(lit,[14] mp 66—67.5°C).

Reaction of an Equimolar mixture of Hydrazobenzene(Va) and $(EtO)_2PS_2H$ at 0°C. To a solution of Va(1.84 g, 0.01 mole) in ether (5 ml) was added dropwise a solution of $(EtO)_2PS_2H$ (1.86 g, 0.01 mol). The mixture was allowed to stand at 0°C overnight. Treatment of the reaction mixture in a manner similar to that described above gave benzidine (0.18 g, 10%), mp 112—116°C(lit,[23] mp 115—120°C),

14) H. E. Bigelow and D. B. Robinson, "Organic Syntheses," Coll. Vol. III, p. 103 (1955).
15) J. F. Vozza, *J. Org. Chem.*, **34**, 3219 (1969).
16) Y. Nomura, This Bulletin, **34**, 1648 (1961).
17) H. Wieland, *Ber.*, 48, 1110 (1915).
18) K. Nakagawa and T. Tsuji, *Chem. Pharm. Bull.*, **11**, 296 (1963).
19) P. Grammatcakis, *Bull. Soc. Chem. Fr.*, 951 (1951).
20) G. H. Goleman, "Organic Syntheses," Coll. Vol. 1, p. 442 (1941).
21) E. Fisher, *Ber.*, **9**, 890 (1876).
22) H. Voswinckel, *ibid.*, **34**, 2351 (1901).
23) N. Zinin, *Ann.*, **137**, 376 (1866).

TABLE 5. NMR SPECTRA OF ARYLHYDRAZINIUM O,O-DIETHYL DITHIOPHOSPHATE

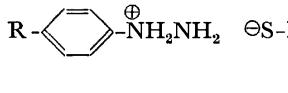

Comp.	Chemical shift (in $CDCl_3$ from ext. TMS, ppm)				Coupling constant (Hz)		
	Ethyl group		Amine-H	Aromatic-H	Methyl group	$J_{CH_3-CH_2-}$	J_{CH_2-O-P}
IIIa	1.15 (6H, t)	4.00 (4H, q, d)	8.15 (4H, s)	7.20—7.40 (5H, m)	—	7	11
IIIb	1.31 (6H, t)	4.12 (4H, q, d)	8.36 (4H, m)	7.20—7.25 (4H, m)	2.41	7	11
IIIc	1.20 (6H, t)	3.98 (4H, q, d)	8.60 (4H, s)	7.18—7.40 (4H, m)	—	7	11

aniline(IVa) (0.18 g, 9%), and azobenzene(IIa), 0.67 g, 37%, mp 65°C(lit.[14] mp 66—67.5°C) while recovering hydrazobenzene(Va), 0.13 g, 7%, mp 123—126°C(lit,[19] mp 126°C).

Reaction of an Equilimolar Mixture of 4,4'-Dichlorohydrazobenzene (Vb) and $(EtO)_2PS_2H$. To a solution of Vb (2.52 g, 0.01 mole) in ether (10 ml) was added dropwise a solution of $(EtO)_2PS_2H$(1.86 g, 0.01 mol). The mixture was allowed to stand at room temperature for 24 hr, and the ether was removed to give crystals which were then washed with ethanol to give 4,4'-dichloroazobenzene(IIe), 1.25 g, 50% mp 176—177.5°C (lit,[18] mp 177—178°C). The ethanol filtrate was condensed and neutralized with aqueous Na_2CO_3 and then extracted with benzene. After removal of the benzene at atmospheric pressure, the residue was recrystallized from ether to give 4-chloroaniline(IVe), 1.27 g, 50%, 71—72°C (lit,[24] mp 72.5°C).

Reaction of 4,4'-Dichlorohydrazobenzene(Vb) with $(EtO)_2PS_2H$ as Acid Catalysis. To a solution of Vb(2.52 g, 0.01 mol) in ether(10 ml) was added dropwise a solution of $(EtO)_2PS_2H$(0.37 g, 0.002 mol). The reaction mixture was allowed to stand at room temperature for 7 days. Treatment of the reaction mixture in a manner similar to that described above gave 4,4'-dichloroazobenzene(IIe) (1.25 g, 50%) and 4-chloroaniline(IVe) (1.27 g, 50%), which were identical with the corresponding authentic samples.

Equimolar Reactions between 4-Chloro-4'-methylhydrazobenzene (Vc) and $(EtO)_2PS_2H$. To a solution of Vc (2.32 g, 0.01 mol) in ether(10 ml) was added dropwise an etheral solution of $(EtO)_2PS_2H$(1.86 g, 0.01 mol). The mixture was allowed to stand at room temperature for 24 hr. Ether was removed to give orange crystals. The crystals were washed with ethanol to give 4-chloro-4'-methylazobenzene (IIc) (1.15 g, 50%), mp 152—153°C(lit,[17] mp 153°C). There is no crossover of aniline group between 4-chloroaniline and 4-methylaniline during the course of reaction. The ethanol filtrate was condensed and neutralized with aquoeus Na_2CO_3 and then extracted with benzene. After removal of the benzene at atmospheric pressure, the residue containing 4-chloroaniline and 4-methylaniline was determined spectrometrically.

TABLE 6. IR SPECTRA OF ARYLHYDRAZINIUM O,O-DIETHYL DITHIOPHOSPHATE

Comp.	ν_{max}^{KBr} (cm^{-1})					
IIIa	3250,	1025,	1010,	940,	920,	680
IIIb	3220,	1030,	1015,	940,	680,	660
IIIc	3250,	1020,	1005,	940,	900,	660

General Procedure for the Reaction of Arylhydrazine(IIIa-c) with Excess $(EtO)_2PS_2H$. A mixture of IIIa–c(0.01 mol) and $(EtO)_2PS_2H$(0.01 mol) was heated at 70°C until the reaction mixture changed into a clear solution. The mixture was treated with excess Na_2CO_3 and extracted with benzene. The benzene solution was extracted with 10% aqueous HCl and dried over $MgSO_4$ and then condensed to give a colorless oil(1.5—2.0 g), which was identical with the authentic sample, bis[O,O-diethyl thiophosphory]disulfide.[25] Aqueous HCl solution (10%) was concentrated under reduced pressure to give HCl salt of aniline derivatives (IVa, d, e). A small amount of water was added to the crude salts of IVa,d,e and neutralized with Na_2CO_3 and then extracted with benzene. The benzene solution was dried over $MgSO_4$. Removal of benzene gave aniline derivatives (IVa,d,e). The yields of IVa,d,e are given in Table 4.

Reaction of an Equimolar of Arylhydrazine(IIIa–c) and $(EtO)_2PS_2H$. To a solution of IIIa–c(0.01 mol) in ether(10—50 ml) was added dropwise an ether solution of $(EtO)_2PS_2H$(0.01 mol). The mixture was allowed to stand at room temperature for several hours. The precipitates were collected and recrystallized from ether to give arylhydrazinium O,O-diethyl dithiophosphate quantitatively. These products were hygroscopic white needles and identified by their NMR and IR spectra listed in Table 5 and 6. A solution of arylhydrazinium O,O-diethyl dithiophosphates in benzene was heated under refluxing for 1—2 days. After removal of the benzene at atmospheric pressure, the residue was distilled or recrystallized to give aniline derivatives (IVa,d,e) (50—70% yield).

24) C. R. Noller and P. Liang, *J. Amer. Chem. Soc.*, **54**, 670 (1932).

25) A. E. Lippman, *J. Org. Chem.*, **31**, 471 (1966).

Chemistry of Cyanoacetylenes. Part XIV.[1] One-step Synthesis of Some Ethynyl Heterocycles and Their Reactions with Diazomethane

Tadashi SASAKI, Shoji EGUCHI, and Michio SUGIMOTO

Institute of Applied Organic Chemistry, Faculty of Engineering, Nagoya University, Furo-cho, Chikusa-ku, Nagoya 464

(Received May 9, 1972)

The Ritter reaction of cyano- and chlorocyanoacetylene with appropriate substrates provided a facile one step synthesis of 4,4-dimethyl-2-ethynyloxazoline (**5**), 4,4,6-trimethyl-2-ethynyl (**7**) and -2-chloroethynyl-5,6-dihydro-1,3-oxazine (**8**), 5,5-dimethyl-3-isopropylidene-2-ethynyl- (**10**) and -2-chloroethynyl-1-pyrroline (**11**). On treatment with diazomethane, **7** gave 4,4,6-trimethyl-2-(4-1*H*-pyrazolyl)- (**13**) and -2-(3-1*H*-pyrazolyl)-5,6-dihydro-1,3-oxazine (**14**) in 42 and 40% yields respectively, while **8** afforded only 4,4,6-trimethyl-2-[3-(4-chloro-1-methyl)-pyrazolyl]-5,6-dihydro-1,3-oxazine (**15**) in 52% yield. On the other hand, **10** gave 5,5-dimethyl-3-isopropylidene-2-(3-1*H*-pyrazolyl)-1-pyrroline (**16**) in 64% yield and **11**, 5,5-dimethyl-3-isopropylidene-2-[3-(4-chloro-1-methyl)-pyrazolyl]-1-pyrroline (**17**) in 16% yield.

We reported that cyano- and chlorocyanoacetylene undergo the Ritter reaction with some olefins and alcohols to give the corresponding propiolamide derivatives.[2,3] As an extension of this study, we have applied the Ritter reaction[4] of the cyanoacetylenes to the synthesis of some ethynylheterocycles by using appropriate substrates.

We employed 2-methylallyl alcohol (**4**), hexylene glycol (**6**) and 2,5-dimethyl-2,5-hexanediol (**9**) with the hope of synthesizing 2-ethynyl- and 2-chloroethynyl derivatives of 4,4-dimethyloxazoline, 4,4,6-trimethyl-5,6-dihydro-1,3-oxazine, and 5,5-dimethyl-3-isopropylidene-1-pyrroline from our interest in their pharmacological activity[5] and utility as synthetic intermediates.[6]

Results and Discussion

The Ritter Reactions. The reaction of 2-methylallyl alcohol (**4**) with cyanoacetylene in sulfuric acid (95%) at 0°C for 1 hr afforded a complex mixture of products, from which an oily basic product **5** was obtained in 4.9% yield by distillation under reduced pressure. The structure of **5** was determined as 4,4-dimethyl-2-ethynyloxazoline from analytical and spectral data. The IR absorptions at 3300, 2160, and 1620 cm^{-1} demonstrated the presence of C≡CH and C=N functions, and NMR ($CDCl_3$) spectrum manifested signals at τ 6.05 (s, 2H, $C\underline{H}_2$), 7.05 (s, 1H, C≡C$\underline{H}$) and 8.70 (s, 6H, $C(C\underline{H}_3)_2$), supporting the above assignment. The Ritter reaction of 2-methylallylchloride (**1**) with cyanoacetylene is known to afford *N*-(chloro-*t*-butyl)propiolamide **2** in a good yield,[2] and the cyclization of **2** with ethanolic potassium hydroxide gives the corresponding 2-vinyloxazoline derivatives **3**.[2] We examined the direct cyclization of **2** with potassium hydroxide in tetrahydrofuran and proved that **2** gave also 2-ethynyloxazoline **5** in 24% yield (Scheme 1). Attempts to improve the yield of **5** in the Ritter reaction of **4** with cyanoacetylene were unsuccessful because of the formation of large amounts of intractable polymeric materials, and therefore, the cyclization method of **2** was concluded to be superior to the Ritter reaction of **4** in this case.

Treatment of hexylene glycol **6** with an equimolar amount of cyanoacetylene in sulfuric acid afforded the desired 2-ethynyl-5,6-dihydro-1,3-oxazine derivative **7** (Scheme 2). The best yield of **7** was 26.5% which

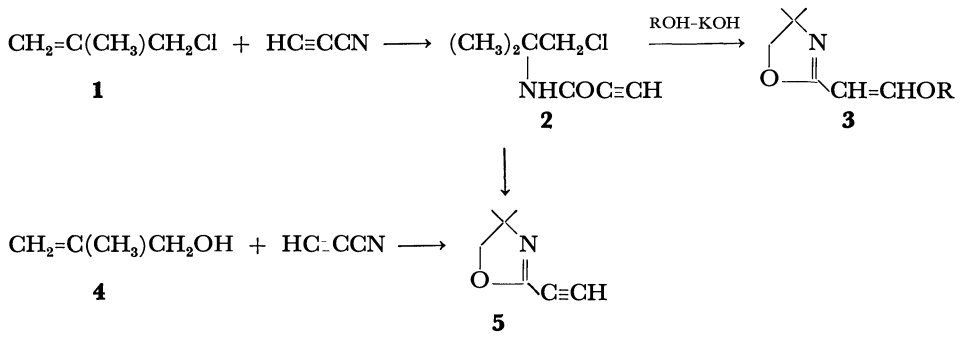

Scheme 1.

1) Part XIII: T. Sasaki and A. Kojima, *Tetrahedron Lett.*, **1971**, 4593.

2) T. Sasaki, S. Eguchi, and K. Shoji, *J. Chem. Soc. C*, **1969**, 406.

3) T. Sasaki, S. Eguchi, and T. Oyobe, This Bulletin, **43**, 1252 (1970).

4) For recent reviews, see (a) L. I. Krimen and D. J. Cota, "Organic Reactions," Vol. 17, p.p. 213—325 (1969); (b) F. Johnson, "Advances in Heterocyclic Chemistry," Vol. 6, p.p. 95—146, ed. by A. R. Katritzky and A. J. Boulton, Academic Press, New York and London (1966).

5) For example, see Z. Eckstein and T. Urbânski, "Advances in Heterocyclic Chemistry," Vol. 2, p. 311, ed. by A. B. Katritzky and A. J. Boulton, Academic Press, New York and London (1963).

6) For example, see (a) A. I. Meyers and E. W. Collington, *J. Amer. Chem. Soc.*, **92**, 1176 (1970); (b) A. I. Meyers, E. M. Smith, and A. F. Jurjevich, *ibid.*, **93**, 2314 (1971), and preceding papers.

was obtained under drastic conditions at 50°C. Only a trace amount of **7** was produced under milder conditions at room temperature. The structural elucidation of the product was based on the analytical and spectral data: **7** showed a molecular ion peak at *m/e* 151 (M^+) in the mass spectrum, and strong IR (KBr) absorptions at 3200 and 2130 (C≡CH) and 1625 (C=N) cm^{-1}. The NMR ($CDCl_3$) signals at τ 5.5—6.1 (broad m, 1H, 6-H), 7.38 (s, 1H, C≡CH), 8.0—8.5 (m of AB portion of an ABX pattern, 2H, CH_2), 8.65 (d, J=6.1 Hz, 3H, 6-CH_3) and 8.78 (s, 6H, 4,4-$(CH_3)_2$) were in line with the assigned structure.

$(CH_3)_2C(OH)CH_2CH(OH)CH_3$ + HC≡CCN ⟶

6

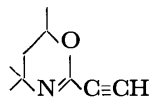

7

$(CH_3)_2C(OH)CH_2CH(OH)CH_3$ + ClC≡CCN ⟶

6

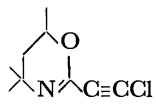

8

Scheme 2.

The Ritter reaction of **6** with chlorocyanoacetylene under the same conditions at 50°C gave 2-chloroethynyl-4,6,6-trimethyl-5,6-dihydro-1,3-oxazine (**8**) in 21.6% yield. The assigned structure was evidenced by analytical and spectral data.

The reaction of 2,5-dimethyl-2,5-hexanediol (**9**) with cyanoacetylene afforded 2-ethynyl-5,5-dimethyl-3-isopropylidene-1-pyrroline (**10**) as a colorless oil. A molecular formula $C_{11}H_{15}N$ was evidenced by analysis and mass spectral molecular weight, *m/e* 161 (M^+). The assigned structure was compatible with the NMR spectrum which revealed signals at τ 6.83 (s, 1H, C≡CH), 7.63 (q, J=2.3 Hz, 2H, CH_2), 7.78 (t, J=2.3 Hz, 3H, C^aH_3), 8.22 (s, 3H, C^bH_3) and 8.75 (s, 6H, 5,5-$(CH_3)_2$). The yield of **10** varied 46—60% depending on the addition method (see Experimental) (Scheme 3).

$(CH_3)_2C(OH)CH_2CH_2C(CH_3)_2OH$ + HC≡CCN ⟶

9

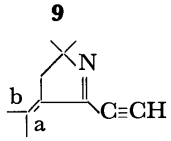

10

$(CH_3)C(OH)CH_2CH_2C(CH_3)_2OH$ + ClC≡CCN ⟶

9

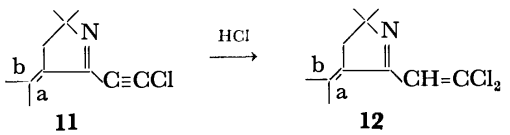

11 **12**

Scheme 3.

The same reaction of **9** with chlorocyanoacetylene gave 2-chloroethynyl-5,5-dimethyl-3-isopropylidene-1-pyrroline (**11**), purification of which was difficult because of facile decomposition; **11** was characterized by the spectral data: *m/e* 196 (M^+) and 198 (M+2) in 3 : 1 ratio; ν_{max}^{film} 2260, 1655, and 1540 cm^{-1}; τ (CD-Cl_3) 7.65 (q, J=2.3 Hz, 2H, CH_2), 7.83 (t, J=2.3 Hz, 3H, C^aH_3), 8.25 (s, 3H, C^bH_3), and 8.79 (s, 6H, 5,5-$(CH_3)_2$). The assigned structure of **11** was also supported by the reaction with diazomethane as described below. On distillation of crude **11** under reduced pressure, a crystalline product **12** was obtained in a low yield, which gave *m/e* 232 (M^+) and 234 (M+2) with a ratio of 3 : 2; ν_{max}^{KBr} 1650, 1620, 1565, and 750 cm^{-1}; τ ($CDCl_3$) 3.38 (s, 1H, C=CH), 7.60 (q, J=2.3 Hz, 2H, CH_2), 8.05 (t, J=2.3 Hz, 3H, C^aH_3), and 8.71 (s, 6H, 5,5-$(CH_3)_2$). The structure of **12** was assigned as 2-β,β-dichlorovinyl-5,5-dimethyl 3-isopropylidene-1-pyrroline. The formation of **12** is rationalyzed by the Markownikov addition[7,8] of hydrogen chloride to **11** (Scheme 3). It is uncertain whether the origin of hydrogen chloride is **11** itself or some other chloroethynyl side-products in the Ritter reaction.

Reaction of **7**,**8**,**10**, *and* **11** *with Diazomethane.* The formation of pyrazole derivatives by 1,3-dipolar cycloaddition reactions of diazomethane to acetylenic bonds is well-known.[9] However, only a few studies have been made on unsymmetrically substituted acetylenes with a bulky heterocyclic rings.[10,11]

On treatment with a large excess of diazomethane in ether at room temperature, **7** afforded two crystalline products **13** and **14** in 42 and 40% yields, respectively. Both products were 1 : 1 adducts on the basis of their mass spectra, *m/e* 193. Compound **13** was assigned as 4,4,6-trimethyl-2-(4-1*H*-pyrazolyl)-5,6-dihydro-1,3-oxazine by appearance of a singlet signal at τ 2.15 for two protons, and **14** as 4,4,6-trimethyl-2-(3-1*H*-pyrazolyl)-5,6-dihydro-1,3-oxazine by the NMR signals at τ 2.48 and 3.38 (both d, J=1.9 Hz, each 1H) (Scheme 4). On the other hand, the reaction of **8** with diazomethane afforded only one product **15** in 52% yield, which was characterized as 4,4,6-trimethyl-2-[3-(4-chloro-1-methyl)pyrazolyl]-5,6-dihydro-1,3-oxazine by analysis and spectral data: *m/e* 241 (M^+) and 243 (M+2) with a 3 : 1 ratio; τ ($CDCl_3$) 2.68 (s, 1H, 5-H of the pyrazole), 5.70 (m, 1H, 6-H), 6.01 (s, 3H, NCH_3), 8.10 (m, 2H, CH_2), 8.62 (d, J=6.0 Hz, 3H, 6-CH_3) and 8.70 (s, 6H, 4,4-$(CH_3)_2$). The fact that

7) S. W. Benson and G. R. Haugen, *J. Phys. Chem.*, **70**, 3336 (1966).

8) R. C. Fahey, "Topics in Stereochemistry," Vol. 3, p. 237, ed. by E. L. Eliel and N. L. Allinger, John Willey and Sons, Inc. (1968).

9) For reviews, see R. Huisgen, R. Grashey, and J. Sauer, "Cycloaddition Reactions of Alkenes," in "The Chemistry of Alkenes," p.p. 806—878, ed. by S. Patai, Interscience, New York (1964); (b) H. G. Viehe, "Chemistry of Acetylenes," p. 462, Marcel Dekker, New York (1969).

10) For the reaction of ethynyldiazomethane with acctylene, see H. Reimlinger, *Ann. Chem.*, **713**, 112 (1968).

11) For 1,3-dipolar cycloaddition reactions of 5-nitro-2-furyldiazomethane, see T. Sasaki, S. Eguchi, and A. Kojima, *J. Heterocyclic Chem.*, **5**, 243 (1968).

7 affords an isomeric mixture of **13** and **14** in *ca.* 1 : 1 ratio and that **8** gave only **15** suggests that the orientation of the cycloaddition was controlled by the electronic factor rather than the steric one.[12]

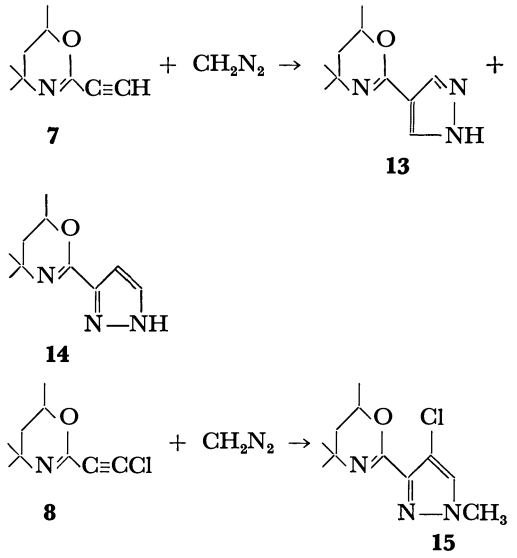

Scheme 4.

The reaction of **10** and **11** with diazomethane afforded only one adduct each **16** and **17** in 64 and 16 (from **11**)% yields, respectively (Scheme 5). The structural assignments were based on analytical and spectral data: **16** showed characteristic vinyl proton signals at τ 2.52 (d, J=1.9 Hz, 1H, 5-H of the pyrazole), and 3.55 (d, J=1.9 Hz, 1H, 4-H of the pyrazole). **17** showed one vinyl proton signal at τ 2.63 (s) and *N*-methyl protons signal at τ 6.12 (s), supporting the assigned structures.

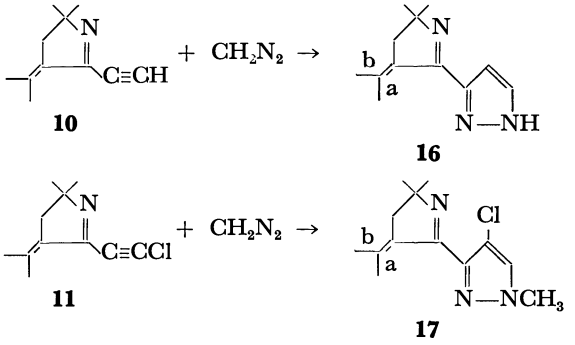

Scheme 5.

The formation of each single product in the above reactions indicates that 1-pyrroline ring in **10** and **11** is more electron-withdrawing than 1,3-oxazine ring in **7** and **8**. Simultaneous *N*-methylation of the pyrazole rings from the chloroethynyl derivatives is apparently ascribable to lower basicity of the pyrazole ring by the presence of an electronegative chloro-substituent.[13]

12) For the reaction of diazomethane with cyanoacetylenes, see T. Sasaki and K. Kanematsu, *J. Chem. Soc. C*, **1971**, 2147.

13) For a review, see R. Gompper, "Advances in Heterocyclic Chemistry," Vol. 2, p.p. 245—286, ed. by A. R. Katritzky, A. J. Boulton, and J. M. Lagowski, Academic Press, New York and London (1963).

Experimental

All mp and bp are uncorrected. NMR spectra were recorded on a JEOL-C-60HL spectrometer at 60 MHz with TMS as the internal standard, and mass spectra on a JEOL-OISG mass spectrometer at 75 eV. IR spectra were obtained with a JASCO IR-S spectrometer. Microanalyses were carried out with a Perkin-Elmer 240 Elemental Analyzer.

*Reaction of Cyanoacetylene with 2-Methylallyl Alcohol (**4**).* To a stirred sulfuric acid (95%, 15 ml) was added slowly a mixture of **4** (3.60 g, 0.050 mol) and cyanoacetylene[14] (2.55 g, 0.050 mol) under ice-cooling over a period of 10 min. After stirring was continued for further 1 hr, the mixture was poured onto ice-water (ca. 300 ml) and washed with chloroform (30 ml×5). The water layer was basified with 20% aqueous sodium hydroxide under ice-cooling and extracted with chloroform (30 ml×5). The dried (Na_2SO_4) extracts were evaporated to give 2.4 g of crude basic products. Flask distillation at 0.11 mmHg gave a distillate trapped at liquid nitrogen temperature, which was further purified by passing through a neutral alumina column using benzene as an eluent to give 0.301 g (4.9%) of analytically pure *2-ethynyl-4,4-dimethyloxazoline* **5**: n_D^{18} 1.4905; *m/e* 123 (M^+); λ_{max}^{MeOH} 219 nm (ε 4000).

Found: C, 68.53; H, 7.32; N, 11.27%. Calcd for C_7H_9NO: C, 68.27; H, 7.37; N, 11.37%.

*Cyclization of N-(Chloro-t-butyl)propiolamide **2** to **5**.* A mixture of **2** (0.22 g, 1.4 mmol) and potassium hydroxide (0.13 g) in dry THF (10 ml) was refluxed under nitrogen atmosphere for 4 hr. The cooled mixture was treated with water and extracted with chloroform (10 ml×5). The work-up afforded **5** in 23.8% yield.

*Reaction of Cyanoacetylene with Hexylene Glycol (**6**).* A mixture of cyanoacetylene (1.3 g, 0.025 mol) and **6** (2.95 g, 0.025 mol) was added to stirred sulfuric acid (20 ml) over a period of ca. 10 min at room temperature; the temperature was raised up to *ca.* 50°C and stirring was continued for 1 day at room temperature. The mixture was poured onto ice-water and extracted with chloroform (80 ml×5) after being basified with 20% aqueous sodium hydroxide. The combined extracts were dried (Na_2SO_4) and evaporated to give a dark brownish residue which was distilled to afford *2-ethynyl-4,4,6-trimethylethyl-5,6-dihydro-1,3-oxazine* **7**) (1.0 g, 26.5%); an analytical sample was obtained after recrystallization of the solidified distillate from *n*-hexane: bp 54—56°C (0.6 mmHg); mp 75—77°C; λ_{max}^{EtOH} 208 nm (ε 9250).

Found: C, 71.25; H, 8.80; N, 9.37%. Calcd for $C_9H_{13}NO$: C, 71.49; H, 8.67; N, 9.26%.

*Reaction of Chlorocyanoacetylene with **6**.* The reaction of chlorocyanoacetylene[15] with **6** under similar conditions to those described above gave *2-chloroethynyl-4,4,6-trimethyl-5,6-dihydro-1,3-oxazine* (**8**) (21.6%): bp 67—68°C (0.4 mmHg); n_D^{20} 1.5035; ν_{max}^{film} 2260 and 1638 cm^{-1}; λ_{max}^{EtOH} 222 nm (ε 10000); τ ($CDCl_3$) 5.80 (m, 1H, 6-H), 8.20 (m, 2H, CH_2), 8.68 (d, J=6.1 Hz, 3H, 6-CH_3), 8.78 (s, 6H, 4,4-$(CH_3)_2$); *m/e* 185 (M^+) and 187 (M+2) in 3 : 1 ratio.

Found: C, 58.01; H, 6.84; N, 7.31%. Calcd for $C_9H_{12}NOCl$: C, 58.21; H, 6.51; N, 7.54%.

*Reaction of Cyanoacetylene with 2,5-Dimethyl-2,5-hexanediol (**9**).* To a stirred sulfuric acid (20 ml) was added **9** (3.65 g, 0.025 mol) slowly below 5°C over a 1-hour period,

14) S. Murahashi, T. Takisawa, S. Kuroda, and S. Maikawa, *Nippon Kagaku Zasshi*, **77**, 1689 (1956); *Chem. Abstr.*, **53**, 5163f (1959).

15) E. Kloster-Jensen, *Acta Chem. Scand.*, **18**, 1629 (1964).

followed by addition of cyanoacetylene (1.3 g, 0.025 mol) over a period of 20 min under ice-cooling. After stirring was continued for 1 day at room temperature, the work-up and distillation afforded *2-ethynyl-5,5-dimethyl-3-isopropylidene-1-pyrroline* (**10**) (2.42 g, 60%) as an oil: bp 61—62°C (0.5 mmHg); n_D^{18} 1.5231; ν_{max}^{film} 3300, 3200, 2140, 1655, and 1640 cm^{-1}; λ_{max}^{MeOH} 267 nm (ε 11000), 223 (6900), and 208 (6100).

Found: C, 81.84; H, 9.65; N, 8.51%. Calcd for $C_{11}H_{15}N$: C, 81.93; H, 9.38; N, 8.69%.

Addition of cyanoacetylene to sulfuric acid, followed by that of **9** lowered the yield of **10** to 46%.

Reaction of Chlorocyanoacetylene with ***9***. A similar reaction of chlorocyanoacetylene (2.2 g, 0.025 mol) with **9** (3.65 g, 0.025 mol) afforded crude *2-chloroethynyl-5,5-dimethyl-3-isopropylidene-1-pyrroline* (**11**) (5.0 g, quantitative) as a brownish oil which was characterized by spectral data (see Text) but it decomposed gradually on standing. Distillation under reduced pressure gave *2-(β,β-dichlorovinyl)-5,5-dimethyl-3-isopropylidene-1-pyrroline* (**12**) (7% from **9**) as an oil which solidified on standing. Recrystallization from *n*-hexane gave an analytically pure sample of **12**: bp 72—75°C (0.5 mmHg); mp 53—55°C; λ_{max}^{MeOH} 252 nm (ε 9000), infl. 231 and 223 nm.

Found: C, 57.12; H, 6.47; N, 5.85%. Calcd for $C_{11}H_{15}NCl_2$: C, 56.91; H, 6.51; N, 6.03%.

Reaction of ***7*** *with Diazomethane.* Treatment of **7** (151 mg, 1.00 mmol) with a large excess of ethereal diazomethane at room temperature for 1 day, followed by removal of excess diazomethane and the solvent afforded a solid residue (153 mg) which was recrystallized from *n*-hexane–dichloromethane to give *4,4,6-trimethyl-2-(4-*H*-pyrazolyl)-2,6-dihydro-1,3-oxazine* (***13***) (81 mg, 42%) as colorless crystals: mp 169—172°C; ν_{max}^{KBr} 3160, 1660, 1640, and 1580 cm^{-1}; λ_{max}^{EtOH} 220 (ε 13200); τ ($CDCl_3$) −1.75 (s, 1H, NH), 2.15 (s, 2H, 3′-H and 5′-H in the pyrazole ring), 5.75 (m, 1H, 6-H), 8.05 (m, 2H, CH_2), 8.65 (d, J=6.0 Hz, 3H, 6-CH_3), and 8.72 (s, 6H, 4,4-$(CH_3)_2$); *m/e* 193 (M^+).

Found: C, 62.32; H, 7.85; N, 21.88%. Calcd for $C_{10}H_{15}N_3C$: C, 62.15; H, 7.82; N, 21.75%.

Purification of the mother liquor on a silica gel column eluting with $CHCl_3$–MeOH afforded *4,4,6-trimethyl-2-(3-*1H*-pyrazolyl)-5,6-dihydro-1,3-oxazine* (***14***) (72 mg, 40%) as a semi-solid material: ν_{max}^{film} 3160, 1660, 1640, and 1560 cm^{-1}; λ_{max}^{MeOH} 224 nm (ε 12000); τ ($CDCl_3$) −0.92 (s, 1H, NH), 2.48 and 3.38 (each d, J=1.9 Hz, each 1H, CH=CH), 5.70 (m, 1H, 6-H), 8.05 (m, 2H, CH_2), 8.57 (d, J=6.01 Hz, 3H, 6-CH_3), and 8.67 (s, 6H, 4,4-$(CH_3)_2$); *m/e* 193 (M^+).

Found: C, 62.26; H, 7.63; N, 21.83%. Calcd for $C_{10}H_{15}N_3O$: C, 62.15; H, 7.82; N, 21.75%.

Reaction of ***8*** *with Diazomethane.* Treatment of **8** (186 mg, 1.00 mmol) with excess diazomethane in ether at room temperature for 1 day gave a solid product after removal of the solvent, which on recrystallization from *n*-hexane–dichloromethane afforded *4,4,6-trimethyl-2-[3-(4-chloro-1-methyl)pyrazolyl]-5,6-dihydro-1,3-oxazine* (***15***) (126 mg, 52.1 %) as colorless crystals: mp 78—80°C; ν_{max}^{KBr} 1660 and 1650 cm^{-1}; λ_{max}^{EtOH} 224 nm (ε 10200).

Found: C, 55.10; H, 6.79; N, 17.09%. Calcd for $C_{11}H_{16}N_3OCl$: C, 54.65; H, 6.67; N, 17.38%.

Reaction of 10 *with Diazomethane.* A similar treatment of **10** (161 mg, 1.00 mmol) with excess diazomethane for 1 day afforded *5,5-dimethyl-2-(3-1*H*-pyrazolyl)-3-isopropylidene-1-pyrroline* (***16***) (130 mg, 63.9%) as crystals after recrystallization from ether–*n*-hexane: mp 133—135°C; ν_{max}^{KBr} 3160, 1655, 1585, and 1545 cm^{-1}; λ_{max}^{MeOH} 252 nm (ε 10000); τ ($CDCl_3$) 0.02 (s, 1H, NH), 2.52 and 3.55 (each d, J=1.9 Hz, each 1H, CH=CH), 7.45 (q, J=1.65 Hz, 2H, CH_2), 8.28 (s, 3H, C^bH_3), 8.32 (t, J=1.65 Hz, 3H, C^aH_3), and 8.68 (s, 6H, 5,5-$(CH_3)_2$(; *m/e* 203 (M^+).

Found: C, 70.96; H, 8.38; N, 20.67%. Calcd for $C_{12}H_{17}N_3$: C, 70.90; H, 8.43; N, 20.67%.

Reaction of ***11*** *with Diazomethane.* A similar treatment of crude **11** with excess diazomethane in ether followed by purification on a neutral alumina column eluting with $CHCl_3$–MeOH afforded *5,5-dimethyl-2-[3-(4-chloro-1-methyl)pyrazolyl]-3-isopropylidene-1-pyrroline* (***17***) (16% from **9**) as a semi-solid: ν_{max}^{film} 1650, 1590, and 1540 cm^{-1}; λ_{max}^{MeOH} 250 nm (ε 6800); τ ($CDCl_3$) 2.63 (s, 1H, C=CH), 6.12 (s, 3H, NCH_3), 7.45 (q, J=1.7 Hz, 2H, CH_2), 8.19 (s, 3H, C^bH_3), 8.45 (t, J=1.7 Hz, 3H, C^aH_3), and 8.65 (s, 6H, 5,5-$(CH_3)_2$); *m/e* 252 (M^+) and 254 (M+2) in 3 : 1 ratio.

Found: C, 62.32; H, 6.92; N, 16.68%. Calcd for $C_{13}H_{18}N_3Cl$: C, 62.02; H, 6.92; N, 16.68%.

Substituent Effects on Dissociation Constants of 4- and 6-Styryl-2-aminotropones

Kimiaki IMAFUKU and Hisashi MATSUMURA

Department of Chemistry, Faculty of Science, Kumamoto University, Kurokami, Kumamoto

(Received May 18, 1972)

The dissociation constants of two series of 4- and 6-styryl-2-aminotropones were measured spectrophotometrically in 50% aqueous methanol at 20°C. It was found that Hammett's free energy relationship is applied to the analysis of substituent effects, with $\rho=0.59$ and 0.40, respectively, and that there is a difference between the electronic effects of the two isomers.

The transmission of electronic effects from one aromatic ring to another through the linkage between them has recently aroused considerable interest. For stilbenes which have an ethylene linkage between two benzene rings, the dissociation constants of various 4-aminostilbenes[1] and 4-hydroxystilbenes[2] and the chemical shifts of 4-fluorostilbenes[3] were measured. It was found that the electronic effect of the substituent in one ring is transmitted through the ethylene linkage to the *p*-substituent in another ring and is correlated by the Hammett equation.

One of the authors (H. M.) investigated the reactions of 4-styryltropolone and its derivatives, which have a similar ethylene linkage, with various nucleophilic reagents.[4] In order to examine the reactivities quantitatively, we measured the dissociation constants of some 4-[5] and 5-styryltropolones[6] (Fig. 1). We found that the electronic effects of substituents in the benzene ring are transmitted through the ethylene linkage to tropolone nucleus, though the effects are small as in the case of stilbenes.[1,2]

In 4-styryltropolone, there are two tautomeric forms, *viz.*, 2-hydroxy-4-styryltropone and 2-hydroxy-6-styryltropone. The dissociation constants of 4-styryltropolones are, therefore, a combination of two non-equivalent tautomeric forms evidenced by the different ultraviolet absorption spectra of 4- and 6-styryl-2-hydroxytropones[7] and the substituent effects in these two forms should differ.

In order to determine the difference of substituent effects between the 4- and 6-(substituted styryl)tropones, the dissociation constants of 4- and 6-styryl-2-aminotropones (Fig. 1) were measured spectrophotometrically. It was shown that a difference in the electronic effect between the two forms actually exists.

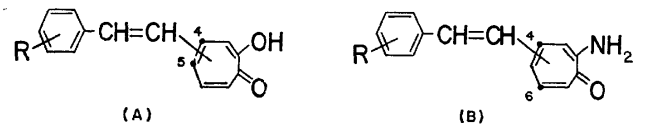

Fig. 1. (A) 4- and 5-Styryltropolones.
(B) 4- and 6-Styryl-2-aminotropones.

Results and Discussion

Dissociation Constants. The dissociation constants of two series of 2-aminotropones, *viz.*, 2-amino-4-styryltropones and 2-amino-6-styryltropones with substituent in the benzene ring, were determined spectrophotometrically in 50% aqueous methanol at 20°. The results expressed in terms of pK_a values are summarized in Table 1. Since activity coefficients were not introduced into the calculations, the dissociation constants do not represent thermodynamic terms, giving only a relative measure of base strength.

Table 1. Dissociation constants of 2-amino-4- and 6-styryltropones

No.	R	pK_a	
		4-Styryl	6-Styryl
1	*p*-OCH_3	2.71	2.69
2	*p*-CH_3	2.64	2.65
3	H	2.54	2.57
4	*p*-Cl	2.39	2.51
5	*p*-Br	2.34	2.50
6	*m*-Cl	2.33	2.42
7	*m*-NO_2	2.14	—
8	*p*-NO_2	2.08	—

Numbering of substituents refers to that given in Figs. 2 and 3.

The dissociation constants are comparable to the pK_a value (2.17) of 2-aminotropone.[8] Further, the 4- and 6-styryl-2-aminotropones show the pK_a values between 2.08 [4-(*p*-nitrostyryl)] and 2.71 [4-(*p*-methoxystyryl)], and are less basic than *p*-(substituted styryl)-anilines (*i.e.* 3'- and 4'-substituted 4-aminostilbenes [pK_a 3.43 (*p*-nitro) to 3.86 (*p*-methoxy)]).[1] This is attributed to the electron-withdrawing effect of the carbonyl group adjacent to the amino group in tropone nucleus.

Substituent Effects. When the pK_a values of 2-amino-4-styryltropones are plotted against the Hammett

1) H. Veschambre and A. Kergomard, *Bull. Soc. Chim. Fr.*, **1966**, 336.
2) H. Veschambre, G. Dauphin, and A. Kergomard, *ibid.*, **1967**, 2846.
3) R. G. Pews and N. D. Ojha, *J. Amer. Chem. Soc.*, **91**, 5769 (1969).
4) H. Matsumura, *Nippon Kagaku Zasshi*, **77**, 300 (1956); **78**, 669 (1957); **81**, 1763 (1960); **82**, 623, 775 (1961); H. Matsumura and S. Nagamura, *ibid.*, **85**, 901 (1964).
5) K. Imafuku, S. Nakama, and H. Matsumura, *Tetrahedron*, **26**, 1821 (1970).
6) K. Hamada, S. Nakama, K. Imafuku, K. Kurosawa, and H. Matsumura, *ibid.*, **27**, 337 (1971).
7) H. Matsumura, Ph. D. Thesis, Tohoku University (1961).
8) T. Hiratsuka and S. Seto, presented at 1 st Symposium on Nonbenzenoid Aromatic Chemistry, Sendai (1966).

substituent constants, σ,[9] of the substituent in the benzene ring, the plot gives the line shown in Fig. 2, and the following equation is obtained by the least square method.

$$pK_a = 2.53 - 0.59\sigma \quad (r=0.993)$$

For the 2-amino-6-styryltropones, a similar Hammett plot is given (Fig. 3) and the following equation is obtained.

$$pK_a = 2.58 - 0.40\sigma \quad (r=0.992)$$

Thus, it was found that the electronic effects of the substituents in the benzene ring are transmitted through the ethylene linkage to the amino group in the tropone nucleus and are correlated by the Hammett equation. However, the effects are small and considered to be

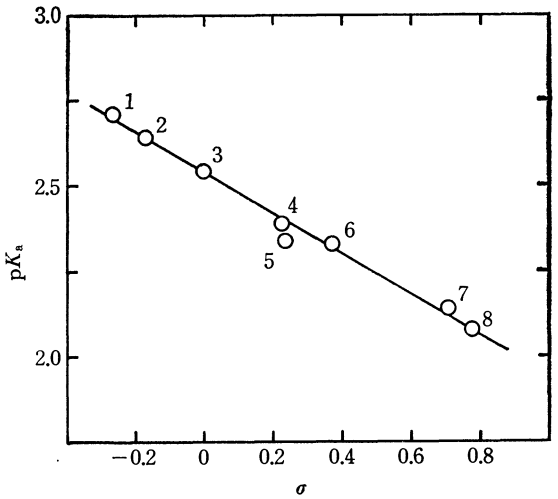

Fig. 2. The Hammett plot of pK_a's of 2-amino-4-styryltropones.

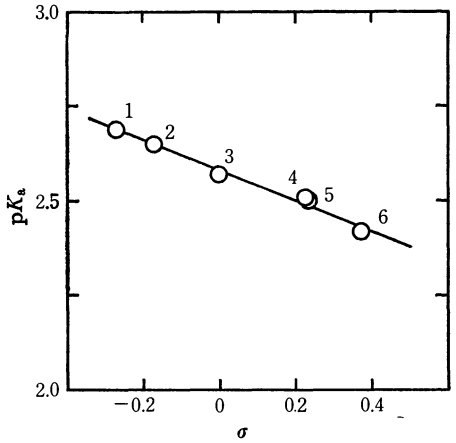

Fig. 3. The Hammett plot of pK_a's of 2-amino-6-styryltropones.

inductive, since the styryl group in these 4- and 6-styryl-2-aminotropones is located at such a position that the resonance interaction between the styryl group and the reaction centre of tropone nucleus is inhibited.

When the 4-styryl and 6-styryl derivatives are compared with each other, the reaction constant (0.59) of 4-styryl isomers is larger than that of 6-styryl isomers (0.40) because of the difference in distance between the styryl group and the amino group. However, both of them are comparable to the ρ value of the dissociation of 4-aminostilbenes (0.42 in 50% aqueous ethanol at 20°).[1]

Experimental

Materials. The 2-amino-4-styryltropones and 2-amino-6-styryltropones were prepared by the method des-

Table 2. 2-Amino-4-styryltropones and 2-amino-6-styryltropones

Styryl group	Substituent	Mp (°C)	Analysis (%) Found C	Found H	Found N	Calcd C	Calcd H	Calcd N
4-Styryl	H	194—195[a]						
	p-OCH_3	194—196	75.61	5.98	5.58	75.87	5.97	5.53
	p-CH_3	190—193	81.09	6.41	5.95	80.98	6.37	5.90
	p-Cl	211—213	70.16	4.68	5.26	69.91	4.69	5.43
	m-Cl	170—171	69.82	4.77	5.71	69.91	4.69	5.43
	p-Br	215—216	59.52	4.10	4.62	59.62	4.00	4.64
	p-NO_2	265—267	67.24	4.60	10.44	67.15	4.51	10.44
	m-NO_2	222—225			10.29			10.44
6-Styryl	H	137—138[b]						
	p-OCH_3	151—153			5.26			5.53
	p-CH_3	175—176	80.69	6.20	6.12	80.98	6.37	5.90
	p-Cl	183—184	69.96	4.68	5.48	69.91	4.69	5.43
	m-Cl	202—204	69.63	4.66	5.35	69.91	4.69	5.43
	p-Br	199—201	59.63	4.13	4.88	59.62	4.00	4.64

a) Mp. 194.5—195°C (Ref. 10).
b) Mp. 137—138°C (Refs. 10 and 11).

9) H. H. Jaffé, *Chem. Revs.*, **53**, 191 (1953).
10) H. Matsumura, *Nippon Kagaku Zasshi*, **81**, 1763 (1960).
11) D. S. Tarbell, K. I. H. Williams, and E. J. Sehm, *J. Amer. Chem. Soc.*, **81**, 3443 (1959).

cribed elsewhere.[12]

4-Styryltropones[13] were treated with an excess of diazomethane in chloroform to give two isomers, *viz.*, 2-methoxy-4-styryltropones and 2-methoxy-6-styryltropones. The two isomers were separated by preparative thin layer chromatography.

Each methyl ether was ammonolyzed with ammonia in absolute ethanol in a sealed tube to give the desired 2-amino-4-styryltropones or 2-amino-6-styryltropones. They were purified by recrystallization from ethanol or benzene.

Their melting points and analytical data are listed in Table 2.

Measurements of the Dissociation Constants. The dissociation constants of the 2-amino-4-styryltropones and 2-amino-6-styryltropones were measured spectrophotometrically in 50% aqueous methnol at 20° by the method of Flexer *et al.*[14]

These constants were obtained by using the equation

$$pK_a = pH - \log \frac{\varepsilon_{BH^+} - \varepsilon}{\varepsilon - \varepsilon_B}$$

where ε_B and ε_{BH^+} are the molar extinction coefficients of the base and conjugate acid, respectively. As an example, the spectral change of 2-amino-4-styryltropone upon pH change of medium is shown in Fig. 4.

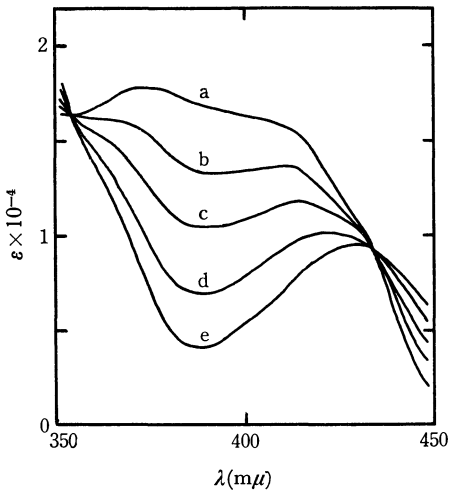

Fig. 4. Electronic Spectra of 2-Amino-4-styryltropone in 50% aqueous methanol.
a: pH 1.03 (conjugate acid), b: pH 2.15, c: pH 2.52, d: pH 3.09, e: pH 6.34 (free base)

The absorption spectra were taken on a Hitachi EPS-3T spectrophotometer, and the pH values were measured by a Hitachi-Horiba F-5 pH meter.

12) K. Imafuku and H. Matsumura, This Bulletin, **46**, 199 (1973).
13) S. Nakama, K. Imafuku, and H. Matsumura, *ibid.*, **43**, 3265 (1970).
14) L. A. Flexer, L. P. Hammett, and A. Dingwall, *J. Amer. Chem. Soc.*, **57**, 2103 (1935).

BULLETIN OF THE CHEMICAL SOCIETY OF JAPAN, VOL. 46, 546—550 (1973)

Solvent Effect on the Free Radical Phenylation with Phenylazotriphenylmethane

Michio KOBAYASHI, Hiroshi MINATO, and Nobuko WATANABE

Department of Chemistry, Faculty of Science, Tokyo Metropolitan University, Fukazawa, Setagaya, Tokyo

(Received June 1, 1972)

The effect of solvent on free radical phenylation of arenes was studied by using phenylazotriphenylmethane as the source of phenyl radical. Mixtures of two arenes were phenylated in a solvent (CCl_4, CH_3CN, DMSO, or cyclohexane), and isomer distributions of diaryls produced were determined. The effect of salts ($NaNO_2$, KNO_2, $NaClO_4$) was also studied in DMSO. Both the solvent effect and salt effect suggest the contribution of polar structure in the transition states for the formation of phenylcyclohexadienyl radicals.

Decomposition of phenylazotriphenylmethane (PAT) yields phenyl radical and triphenylmethyl radical.[1] An investigation on the effect of solvents on the rate of the homolysis of PAT showed that the solvent effect is not too great, and an isokinetic relationship holds.[2] The isomer distributions and partial rate factors in phenylations of arenes with PAT were reported in a previous paper.[3]

Although phenylations of arenes have been investigated with various phenyl radical sources (benzoyl peroxide, *N*-nitrosoacetanilide, the Gomberg reaction, *etc.*),[4] their experimental conditions vary considerably and little evidence has been given which warrants the arguments based on the comparison of these data. It has recently been established that free radical phenylation with phenylazo *p*-tolyl sulfone is very little affected by changes in temperature.[5] The effect of solvents on free radical phenylation has not been reported in the literature. Although solvent effects on free radical reactions are believed to be small, a considerable solvent effect was reported on photo-chlorination of

1) W. A. Pryor, J. T. Echols, Jr., and K. Smith, *J. Amer. Chem. Soc.*, **88**, 1189 (1966); M. Harada, R. Ito, T. Migita, and O. Simamura, *Kogyo Kagaku Zasshi*, **69**, 962 (1966).

2) W. G. Bentrude and A. K. McKnight, *Tetrahedron Lett.*, 3147 (1966).

3) M. Kobayashi, H. Minato, N. Watanabe, and N. Kobori, This Bulletin, **43**, 258 (1970).

4) G. H. Williams, "Homolytic Aromatic Substitutions," Pergamon Press, Oxford (1960).

5) M. Kobayashi, H. Minato, M. Kojima, and N. Kamigata, This Bulletin, **44**, 2501 (1971).

substituted toluenes by Russell and Williamson, Jr.[6]

When isomer distributions and partial rate factors in phenylation of arenes are determined, usually a phenyl-radical generator is dissolved in an equimolar mixture of benzene and an arene, and thermally or photochemically decomposed; the amounts of diaryls produced are determined by use of glc, IR, or the isotope dilution method. In these methods, the reacting substrates themselves are the solvents. Thus, what is really determined is the results of reactions of different substrates in different media (solvents). These methods are based on an assumption that solvent effect is negligible in these free radical reactions. However, no one can say *a priori* that the stability of a substituted cyclohexadienyl radical in nitrobenzene is the same as that in anisole. For accurate comparison, aromatic substrates should be phenylated in a large amount of a common inert solvent.

PAT is an effective phenyl radical generator, and its rate of decomposition is very little affected by solvent. In order to investigate the effect of solvent on the free radical phenylation of arenes, arenes have been phenylated with PAT in a large amount of a solvent (CCl_4, CH_3CN, DMSO, or cyclohexane). The effect of added salts ($NaNO_2$, KNO_2, or $NaClO_4$) has also been investigated in DMSO. Results of these investigations are given in this paper.

Experimental

Materials. Solvents and aromatic substrates were purified according to the methods described in "Organic Solvents."[7]

Analyses of Phenylation Products. *(a) In DMSO*: Nitrogen was bubbled through a mixture of PAT (5 mmol), two arenes (0.125 mol each) and DMSO (0.50 mol) for one hr for removal of oxygen, and then the mixture was heated at 60°C till evolution of nitrogen ceased. After an internal standard for glc determination was added, the mixture was washed with water in order to remove DMSO, and concentrated under reduced pressure. The residual oil was analyzed by glc (10% Apiezon L-Chromosorb column, 2 m or 5 m; a Hitachi K53 Gas Chromatograph).

(b) In CH_3CN: A mixture of PAT (5 mmol), two arenes (0.125 mmol each) and CH_3CN (1.0 mol) was treated in a manner similar to that described above for the experiment with DMSO.

(c) In CCl_4: A mixture of PAT (5 mmol), two arenes (0.125 mol each) and CCl_4 (1.0 mol) was also similarly treated. Because of the occurrence of reactions with CCl_4, yields of diphenyls were less, and much 1,1,1-triphenyl-2,2,2-trichloroethane and some benzophenone were found.

(d) In Cyclohexane: Because of smaller solubility of PAT in this solvent, 5 mmol of PAT was dissolved in 1.25 mol of cyclohexane and 0.125 mol each of two arenes. In this solvent, much cyclohexylation of arenes by cyclohexyl radical took place, and glc determination of diaryls and cyclohexylarenes was possible only in a few cases. Thus, the data in cyclohexane should be evaluated with some reservation.

Calculation of Partial Rate Factors. Partial rate factors for PhCN, PhCl, and PhEt were obtained from the isomer distributions of diaryls produced by the decomposition of PAT in mixtures of benzene, an arene and a solvent. In the experiments with PhOMe and $PhNO_2$, removal of these high-boiling arenes requires high temperature, and some nonsubstituted diphenyl is lost during concentration. The partial rate factors for PhOMe and $PhNO_2$ were therefore calculated from the partial rate factors of chlorobenzene and the isomer distributions of diaryls produced by the decomposition of PAT in mixtures of chlorobenzene, an arene, and a solvent.

Rates of Decomposition of PAT. Rates of decomposition of PAT were determined by measureing the rates of evolution of nitrogen.

Results and Discussion

The rates of decomposition of PAT were found to be of first order. As shown in Table 1, the rate constants vary to some extent in different media, but not too greatly.

Table 1. First order rate constants of decomposition of PAT in various media at 60°C[a]

Solvent	PhH	$(CH_2)_6$	MeCN	DMSO	CCl_4
$10^4k_1(sec^{-1})$	4.66	4.62	3.80	3.10	2.60
Solvent	PhH–PhEt	PhCl–$PhNO_2$	PhCl–PhOMe	PhH–PhCl	
$10^4k_1(sec^{-1})$	4.67	4.36	3.97	3.64	
Solvent	DMSO–PhMe–PhCl	DMSO–PhCl–$PhNO_2$	DMSO–PhCl–PhOMe		
$10^4k_1(sec^{-1})$	4.42	3.58	3.40		
Solvent	DMSO–PhH–PhEt	DMSO–PhCl–PhH	DMSO–PhCl–PhEt		
$10^4k_1(sec^{-1})$	2.96	2.74	2.33		
Solvent	CCl_4–PhCl–PhOMe	CCl_4–PhCl–$PhNO_2$	CCl_4–PhH–PhEt		
$10^4k_1(sec^{-1})$	3.00	2.90	2.50		
Solvent	CCl_4–PhH–PhCN	CCl_4–PhH–PhCl	$(CH_2)_6$–PhH–PhCl		
$10^4k_1(sec^{-1})$	2.40	2.30	3.72		
Solvent	DMSO–KNO_2–PhCl–$PhNO_2$	DMSO–KNO_2–PhCl–PhOMe			
$10^4k_1(sec^{-1})$	3.93	3.64			
Solvent	DMSO–$NaNO_2$–PhCl–PhOMe	DMSO–$NaNO_2$–PhCl–$PhNO_2$			
$10^4k_1(sec^{-1})$	3.11	3.00			

a) Error range was usually ±3%.

6) G. A. Russell and R. C. Williamson, Jr., *J. Amer. Chem. Soc.*, **86**, 2357 (1964).

7) J. A. Riddick and E. E. Toops, Jr., "Organic Solvents," 2nd Edition, Interscience Publishers, New York (1955).

Phenylation of several arenes was carried out in various media using PAT as the phenyl radical source. Atkinson, Perkins, and Ward recently reported that when PAT was decomposed in chlorobenzene the *ortho*-phenylated cyclohexadienyl radical was trapped by trityl radical, and 2-chloro-1,4-dihydro-4-tritylbiphenyl was formed.[8] In our experiments, the residual oil obtained by concentration of the reaction mixture was fed directly to the injection port of the gas chromatograph, and any coupling products formed must have been thermolyzed to diaryl and triphenylmethane; therefore the normal diaryl distribution was observed.

TABLE 2. ISOMER DISTRIBUTIONS OF DIARYLS FORMED FROM PAT AT 60°C[a]

Arene		Solvents				
		None	CCl_4	MeCN	DMSO	$(CH_2)_6$
PhOMe	*o*-	67.0	55.7	63.7	75.2	59.7%
	m-	22.5	24.8	21.9	17.6	28.3
	p-	10.5	19.5	14.4	7.2	12.0
PhEt	*o*-	50.1	62.5	48.1	58.4	(b)
	m-	34.1	24.5	35.8	26.2	(b)
	p-	15.8	13.0	16.1	15.5	(b)
PhCl	*o*-	59.9	(b)	61.3	74.5	83.9
	m-	22.6	(b)	22.1	15.6	9.7
	p-	17.5	(b)	16.6	9.9	6.5
PhCN	*o*-	67.6	(b)	68.1	63.6	(b)
	m-	10.1	(b)	10.2	12.3	(b)
	p-	22.4	(b)	21.6	24.1	(b)
$PhNO_2$	*o*-	78.4	66.4	61.4	76.2	(b)
	m-	9.2	8.9	10.6	7.9	(b)
	p-	12.4	24.7	28.0	16.9	(b)

a) Experimental error was ±5%.
b) Determination by glc was not possible due to the presence of by-products.

TABLE 3. PARTIAL RATE FACTORS IN PHENYLATION OF ARENES WITH PAT IN VARIOUS MEDIA AT 60°C

Arene		None	Solvents			
			CCl	MeCN	DMSO	$(CH_2)_6$
PhOMe	*o*-	4.16	1.57	3.38	3.27	2.03
	m-	1.44	0.69	1.14	0.87	1.22
	p-	1.32[a]	1.07	1.56	0.70	1.29
PhEt	*o*-	1.98	2.96	1.72	1.62	—
	m-	1.50	1.16	1.29	0.73	—
	p-	1.28	1.23	1.16	0.86	—
PhCl	*o*-	3.83	4.23	3.51	3.80	(2.16)
	m-	1.45	1.26	1.24	0.82	—
	p-	2.32	—	1.86	0.93	—
PhCN	*o*-	6.83	—	8.94	8.86	—
	m-	1.03	0.84	1.35	1.72	—
	p-	4.55	4.98	5.69	6.71	—
$PhNO_2$	*o*-	9.58	9.69	7.26	10.99	—
	m-	1.14	1.29	1.26	0.95	—
	p-	3.04	7.18	6.63	4.62	—

a) The value 1.32 should replace the value 2.6 given in our previous paper by mistake.[3] The correct ρ value for the left half of the V-shaped line for phenylation in aromatic solvents is, therefore, −0.460 instead of −1.51.

8) D. J. Atkinson, M. J. Perkins, and P. Ward, *J. Chem. Soc. C*, **1971**, 3240.

Isomer distributions and partial rate factors are shown in Tables 1 and 3. It is clear that variations in isomer distribution and partial rate factors are greater than experimental error. The variations in isomer distributions in particular are fairly great. In general, when the amount of an *o*-isomer increases, the amount of the corresponding *p*-isomer decreases.

When the logarithms of *meta* and *para* partial rate factors are plotted against σ values, *meta* partial rate factors do not vary much with σ values, whereas the plots for *para* partial rate factors usually form V-shaped lines. The ρ value in the right half region is +1.06 in acetonitrile and +0.93 in DMSO; these values differ from the corresponding value for benzoyl peroxide in aromatic solvents (+1.15), that for *N*-nitrosoacetanilide in aromatic solvents (+1.27), and that for phenylazo *p*-tolyl sulfone in aromatic solvents (1.38). The data indicate that the reactivities of arenes with phenyl radical depend on the type of phenyl radical source and also of the solvents used.

The partial rate factors for anisole and benzonitrile are greater in the solvents of greater polarity. This can be rationalized in terms of the stabilization of the transition states by solvation with polar solvents; there must be contribution of a polar structure to the transition states for formation of cyclohexadienyl radicals (a substituted cyclohexadienyl radical form is shown below for the sake of convenience).

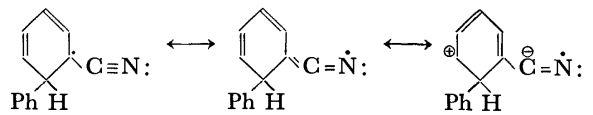

When anisole is used as a substrate, the partial rate factors in anisole alone are greater than those in CCl_4 or cyclohexane. This can be ascribed to the fact that anisole itself is a polar solvent.

With ethylbenzene the partial rate factors in polar solvents are smaller than those in CCl_4. This is probably because the contribution of polar structure to transition state is very little when an ethyl group is a substituent.

Since the partial rate factors are the ratios of the reactivities of arenes with that of benzene (or chlorobenzene), the solvent effects observed on partial rate factors should be understood as the difference between the solvent effects on the reactivities of arenes and those on benzene (or chlorobenzene). The solvent effects on the partial rate factor for the *ortho* position of chlorobenzene are very small as shown in Table 3, and we can assume that the solvent effects on partial rate factors represent the solvent effects on the reactivities of arenes. In fact, when phenylation of an equimolar mixture of anisole and benzene was compared with that of an equimolar mixture of anisole and chlorobenzene, the results were the same within experimental error.

The solvent effects on the partial rate factors of nitrobenzene are fairly large, but it is difficult to give an adequate explanation. It might have something to do with the fact that nitrobenzene itself is a polar solvent.

Effect of Temperature on Partial Rate Factors and Isomer

Table 4. Isomer distributions and partial rate factors in phenylations at different temperatures

Arene		Isomer distribution		Partial rate factor	
		60°C	80°C	60°C	80°C
PhOMe	*o*-	75.2	68.7	3.27	2.40
	m-	17.6	19.7	0.87	0.69
	p-	7.2	10.0	0.70	0.72
PhCl	*o*-	74.5	78.5	3.80	2.33
	m-	15.6	13.5	0.82	0.41
	p-	9.9	8.0	0.93	0.49
PhNO	*o*-	76.3	76.9	10.99	9.57
	m-	7.9	7.7	0.95	0.96
	p-	16.9	15.3	4.62	3.82

Table 5. Effect of salts on isomer distributions at 60°C[a)]

Arene		No Salt	$[NaClO_4]=0.70$	$[NaNO_2]=0.45$	$[NaNO_2]=0.84$	$[NaNO_2]=0.66$
PhOMe	*o*-	75.2	73.1	70.8	71.6	
	m-	17.6	19.3	18.4	18.4	
	p-	7.2	7.7	10.9	9.9	
PhEt	*o*-	58.4	54.2			
	m-	26.2	32.6			
	p-	15.5	13.2			
PhCl	*o*-	74.5	64.4			62.6
	m-	15.6	20.6			19.5
	p-	9.9	15.0			17.4
PhCN	*o*-	63.6	63.5			
	m-	12.3	11.4			
	p-	24.1	25.2			
$PhNO_2$	*o*-	76.2	55.1		68.0	
	m-	7.9	11.0		6.5	
	p-	33.9	33.9		25.6	

a) In DMSO. [PAT]=0.12 M.

Table 6. Effect of salts on partial rate factors at 60°C[a)]

Arene		No Salt	$[NaClO_4]=0.70$	$[NaNO_2]=0.45$	$[NaNO_2]=0.66$	$[NaNO_2]=0.84$
PhOMe	*o*-	3.27	4.10	3.03		3.00
	m-	0.87	1.08	0.80		0.77
	p-	0.70	0.86	0.95		0.84
PhEt	*o*-	1.62	2.62			
	m-	0.73	1.58			
	p-	0.86	1.28			
PhCl	*o*-	3.80	4.23		3.51	
	m-	0.82	1.35		1.11	
	p-	0.93	1.97		2.06	
PhCN	*o*-	8.86	11.85			
	m-	1.72	2.10			
	p-	6.71	9.35			
$PhNO_2$	*o*-	10.99	6.67			6.95
	m-	0.95	1.33			0.66
	p-	4.62	8.24			5.23

a) In DMSO. [PAT]=0.12M.

Distribuitons. The partial rate factors in phenylation of arenes with phenylazo *p*-tolyl sulfone change very little with temperature.[5)] Table 4 compares the isomer distributions and the partial rate factors in phenylation with PAT at 60 and 80°C. It is clear that they change very little with temperature in this case too. Since partial rate factors are always smaller at higher temperatures, the activation energy for phenylation of benzene must be a little greater than those for phenylation of substituted benzenes.

Effect of Salts on Partial Rate Factors and Isomer Distributions. If the solvent effect is due to the contribution of polar structures to transition state, addition of salts to the medium is expected to result in change

in partial rate factors and isomer distributions. Arenes were phenylated in the media containing sodium perchlorate and sodium nitrite. The results are summarized in Tables 5 and 6. The effect of added salts is fairly great in chlorobenzene and nitrobenzene; in both cases the amount of the *ortho* isomer decreases and that of the *para* isomer increases upon addition of salt. In the case of nitrobenzene, the presence of $NaClO_4$ and $NaNO_2$ in about the same concentration results in different isomer distributions. Thus, not only the ionic strength but also the kind of anion probably influence the stabilization of transition state. Since DMSO solvates cations strongly but solvates anions very little, the anions added are more free than the counter cations, thus directly contributing to the stabilization of transition state.

Decrease in the amount of *ortho* isomers and increase in that of *para* isomers could arise either from the decrease of *ortho* partial rate factors or from the increase of *para* partial rate factors. Table 6 shows that, in general, partial rate factors increase upon addition of salts and the increase of *para* partial rate factors are especially great. Only one exception is the case of nitrobenzene, in which the *ortho* partial rate factor decreased upon addition of salts. Thus both the solvent effect and the salt effect are irregular in the case of nitrobenzene.

Although more detailed investigations are required for understanding the salt effect in phenylation, the fact that all the partial rate factors (except for that of the *ortho* position of nitrobenzene) increase upon addition of salts suggests that the contribution of polar structure in the transition state is greater for the addition of phenyl radical to substituted benzenes than that of phenyl radical to benzene itself; increase in ionic strength should stabilize the transition state for the addition of phenyl radical to substituted benzenes.

In conclusion, both the solvent effect and salt effect suggest the contribution of polar structure in the transition state for the addition of phenyl radical to arenes.

BULLETIN OF THE CHEMICAL SOCIETY OF JAPAN, VOL. 46, 550—553 (1973)

Synthetic Studies by the Use of Carbonates. II.[1] An Easy Method of Preparing Cyclic Carbonates of Polyhydroxy Compounds by Transesterification with Ethylene Carbonate

Hajime KOMURA, Teruo YOSHINO, and Yoshiharu ISHIDO

Department of Chemistry, Faculty of Science, Tokyo Institute of Technology, O-okayama, Meguro-ku, Tokyo

(Received June 14, 1972)

Transesterification reactions of polyhydroxy compounds, such as 1-*O*-*p*-nitrobenzoyl-, 1-*O*-benzylglycerols, 1,2;3,4-di-*O*-, 3,4-*O*-isopropylidene-D-mannitols, 1,2-*O*-isopropylidene-α-D-glucofuranose, uridine, 1,2;5,6-di-*O*-isopropylidene-D-mannitol, and D-mannitol, by ethylene carbonate were attempted; the corresponding products were obtained in good yields except in the case of uridine, which gave 2,2′-anhydro-1-β-D-arabinofuranosyluracil.

Since the synthesis of α-D-glucofuranose 1,2;5,6-dicarbonate from D-glucose and phosgene, although in a considerably low yield, was reported,[2] a number of sugar carbonates have been prepared for the purpose of investigating the partial blocking of hydroxy groups of carbohydrates by the use of phosgene, alkyl or aryl chloroformates, diphenyl carbonate under basic conditions, by the use of carbonyl diimidazole, or by changing the *O*-methylene group into carbonate through oxidation with permanganate.[3] In contrast with such blocking groups as alkylidene and arylidene groups, the carbonate group can easily be removed under basic conditions, and it has been widely used in the field of carbohydrate chemistry with due regard to its properties.

Results and Discussion

In view of the glycidol[4] and glycerol 1,2-carbonate[5] syntheses involving the reaction of ethylene carbonate (**1**) with glycerol, the present authors investigated the preparation of cyclic carbonates of polyhydroxy compounds, taking the stability and wieldiness of **1** into consideration. The starting materials were selected on the basis of the following categories: i) 1-*O*-*p*-nitrobenzoyl-(**2**), 1-*O*-benzylglycerols(**3**), 1,2;3,4-di-*O*-(**4**), 3,4-*O*-isopropylidene-D-mannitols(**5**), and 1,2-*O*-isopro-

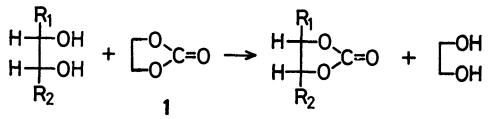

Scheme I.

1) T. Yoshino, S. Inaba, H. Komura, and Y. Ishido, This Bulletin, in contribution.

2) C. F. Allpress and W. N. Haworth, *J. Chem. Soc.*, **1924**, 1223.

3) W. N. Haworth and W. Maw, *ibid.*, **1926**, 1751; L. Hough and J. E. Priddle, *ibid.*, **1961**, 581; W. Schroeder, U. S. 3284438; O. T. Schmidt, A. Distelmaier, und H. Reinhard, *Chem. Ber.*, **86**, 741 (1953).

4) H. A. Bruson and T. W. Reiner, *J. Amer. Chem. Soc.*, **74**, 2100 (1952).

5) J. B. Bell, V. A. Currier, and J. D. Malkemus, U. S. 2915529; *Chem. Abstr.*, **54**, 6552 (1960).

Table 1. Preparations of carbonates by transesterification reaction with ethylene carbonate (**1**)

Starting Material	Reaction Conditions		Product	
			Yield	IR Absorption[a]
1-*O*-*p*-Nitrobenzoylglycerol (**2**)	130—140°C/20—30 mmHg	2 hr	30%[b]	1785 cm^{-1}
1-*O*-Benzylglycerol (**3**)	150/15	1[c]	80	1790
1,2;3,4-Di-*O*-isopropylidene-D-mannitol (**4**)	160/40	1	90	1790
3,4-*O*-Isopropylidene-D-mannitol (**5**)	150—160/30	1	65	1785, 1800
1,2-*O*-Isopropylidene-α-D-glucofuranose (**6**)	140—145/40	1	71	1785, 1800
Uridine (**7**)	140—145/15	1.5	71[d]	—
1,2;5,6-Di-*O*-isopropylidene-D-mannitol (**8**)	160/40	1	76	1785
D-Mannitol (**9**)	150/20	6	65	1790, 1820

a) The absorption bands stand for those of five-membered cyclic carbonate. b) In this reaction, ethylene glycol di-*O*-*p*-nitrobenzoate(**16**) was obtained in 16% yield as a by-product. c) A catalytic amount of sodium bicarbonate was applied in this case. d) This product was identified with 2,2′-anhydro-1-β-D-arabinofuranosyluracil(**18**).

pylidene-α-D-glucofuranose(**6**) as involving vicinal primary and secondary hydroxyl groups, and ii) uridine (**7**) and 1,2;5,6-di-*O*-isopropylidene-D-mannitol(**8**) as involving vicinal secondary hydroxyl groups. iii) D-Mannitol was, in addition, used because it involved both types of vicinal hydroxyl groups. These compounds were heated with 3—4 mol of **1** under reduced pressure to remove the ethylene glycol co-produced in the course of the reactions. Moreover, the reactions were carried out in a Pyrex-glass flask to avoid the decomposition of the carbonate once formed, in view of the results reported by Reist *et al.*,[6] and by Hall and Hough.[7] The results are demonstrated in Table 1. In the cases of **4**, **5**, **6**, **8**, and **9**, the corresponding cyclic carbonates, *i.e.*, 1,2;3,4-di-*O*-isopropylidene-D-mannitol 5,6-carbonate(**10**), 3,4-*O*-isopropylidene-D-mannitol 1,2;5,6-dicarbonate(**11**), 1,2-*O*-isopropylidene-α-D-glucofuranose 5,6-carbonate(**12**),[8] 1,2;5,6-di-*O*-isopropylidene-D-mannitol 3,4-carbonate(**13**), and D-mannitol 1,2;3,4;5,6-tricarbonate(**14**), were obtained in 90, 65, 71, 76, and 65% yields respectively. On the other hand, different results were obtained in the cases of **2**, **3**, and **7**. The reaction with **2** gave a mixture of the corresponding 1,2-carbonate(**15**) and di-*p*-nitrobenzoate of ethylene glycol(**16**) in 30 and 16% yields respectively. These results may be explained in terms of the susceptibility of the carbonyl carbon of the *p*-nitrobenzoyl group to the nucleophilic attack of the hydroxyl group of ethylene glycol. Since the reaction with **3** was confirmed by means of tlc to leave a small amount of **3** in the reaction mixture, even after 2 hr, the reaction was carried out in the presence of sodium bicarbonate as a catalyst to afford 1-*O*-benzylglycerol

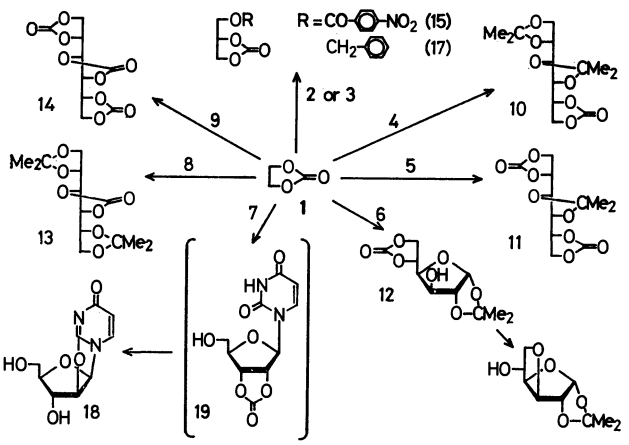

Scheme II.

2,3-carbonate(**17**) in an 80% yield. Moreover, contrary to expectations, **7** afforded 2,2′-anhydro-1-β-D-arabinofuranosyluracil(**18**) selectively. **18** was considered to be produced *via* the 2′,3′-carbonate of **7** (**19**); *i.e.*, the 2′-carbon of **19** was subjected to the intramolecular nucleophilic substitution reaction by the carbonyl group of the 2-position to produce **18**; this result may be ascribed to the nucleophilicity of the carbonyl group being larger than that of the hydroxyl group of ethylene glycol. The structures of the products obtained here were confirmed by elemental analyses, and by a study of the IR, NMR, and UV spectra.

On the basis of these results, it can be concluded that **1** can also be used in the preparation of the five-membered cyclic carbonate of polyhydroxy compounds.

Experimental

All the melting points are uncorrected. The IR spectra were taken with a Hitachi EPI-2S apparatus. The UV spectrum was measured on a Hitachi EPS-3T in distilled water. The NMR spectra were taken with a Varian XL-100 apparatus.

1-O-p-Nitrobenzoylglycerol (2). According to the method of Hennis,[9] glycerol α-monochlorohydrin (11 g,

6) E. J. Reist, R. R. Spencer, and B. R. Baker, *J. Org. Chem.*, **23**, 1958 (1958) [Mp 231—233°C (dec.) (**12**); Mp 52—54°C, $[\alpha]_D^{28}$ +30.5° (1%, H_2O) (3,6-anhydro derivative of **6**)].

7) L. D. Hall and L. Hough, *J. Chem. Soc.*, **1963**, 5301 [Mp 224—225°C (sublimation: 210°C), $[\alpha]_D$ −31.8° (*c* 0.5, Me_2CO) (**12**); Mp 53.2—54.6°C, $[\alpha]_D$ +28.7° (*c* 1.6, H_2O) (3,6-anhydro derivative of **6**)].

8) W. N. Haworth and C. R. Porter, *ibid.*, **1929**, 2796 [Mp 223—224°C (dec.), $[\alpha]_{5780}^{20}$ −36°]; A preparation of this compound by the same procedure was recently reported in a paper (P. A. Gent, R. Gigg, and R. Conant, *J. Chem. Soc. Perkin Trans. I.*, **1972**, 248) as a part of an investigation on phenyloxazoline derivative of amino-sugars.

9) H. E. Hennis, J. P. Easterly, Jr., L. R. Collins, and L. R. Thompson, *Ind. Eng. Chem.*, **6**, 193 (1967); H. E. Hennis, L. R. Thompson, and J. P. Long, *ibid.*, **7**, 96 (1968).

100 mmol) and sodium *p*-nitrobenzoate (19 g, 100 mmol) were suspended in dimethylformamide (150 ml), together with tetraethylammonium iodide (TEAI) (13 g, 50 mmol); the mixture was then heated at 130—140°C for 2 hr with stirring. After cooling, acetone (100 ml) was added to the resultant mixture, and the solvents were evaporated *in vacuo* to give a sirup after the filtration of the unchanged TEAI. After the sirup had been dissolved in hot ethyl acetate (50 ml) and left to stand overnight in a refrigerator, pale yellow crystals of **2** (12.7 g, 52.7%) were obtained. Mp 107—107.5°C. IR(KBr): 1720 cm^{-1} (ester C=O). Found: C, 49.31; H, 4.72; N, 5.72%. Calcd for $C_{10}H_{11}O_6N$: C, 49.79; H, 4.60; N, 5.81%.

3-O-p-Nitrobenzoylglycerol 1,2-Carbonate (15). *1-O-p-*Nitrobenzoylglycerol (**2**) (7.2 g, 30 mmol) was heated, together with ethylene carbonate (**1**) (9.0 g, 105 mmol), at 130—140°C/20—30 mmHg for 2 hr, and finally again at 140°C/10 mmHg, until the distillation of **1** stopped. The residue was chromatographed on a column (diameter: 5 cm) of silica gel (100 g), with chloroform–ethyl acetate (99:1) used for the elution, after which the effluent was fractionated into a volume of 10 ml. The concentration of Fractions No. 41—75 *in vacuo*, followed by recrystallization from ethyl acetate, gave ethylene glycol di-*p*-nitrobenzoate (**16**) (1.7 g, 16%). Mp 142—143.5°C. Found: C, 53.08; H, 3.08; N, 7.89%. Calcd for $C_{16}H_{12}O_8N_2$: C, 53.34; H, 3.36; N, 7.78%. The concentration of Fractions No. 88—214 *in vacuo*, followed by recrystallization from ethyl acetate, gave **15** (2.4 g, 30%). Mp 149.5—150°C. Found: C, 49.30; H, 3.16; N, 5.31%. Calcd for $C_{11}H_9O_7N$: C, 49.44; H, 3.40; N, 5.24%. IR(KBr): 1785 (five-membered cyclic carbonate), 1720 (ester C=O), 1270, 1170 (ester C–O–C), 1520, and 1345 (NO_2) cm^{-1}.

1-O-Benzylglycerol 2,3-Carbonate (17). The transesterification reaction was carried out by the same procedure as above, using 1-*O*-benzylglycerol (**3**) (5.4 g, 30 mmol) and **1** (9.0 g, 105 mmol) together with a catalytic amount of sodium bicarbonate (0.1 g), at 150°C/15 mmHg for 1 hr. After the filtration of the precipitated crystals and the washing of the crystals with ethyl acetate (5 ml), the filtrate and washings were combined; the mixture was then concentrated *in vacuo* to give a heavy liquid. The residue was distilled to give **17** (5.6 g, 80%) boiling at 146—147°C/0.17 mmHg (Found: C, 63.53; H, 5.53%).[10] IR(NaCl): 1790 cm^{-1} (five-membered cyclic carbonate). Without sodium bicarbonate, it was necessary to prolong the reaction to 2.5 hr in order to afford an almost equal yield of the product.

1,2-O-Isopropylidene-α-D-glucofuranose 5,6-Carbonate (12). 1,2-*O*-Isopropylidene-α-D-glucofuranose (**6**)[11] (22 g, 100-mmol) and **1** (30 g, 350 mmol) were fused at 140—145°C/40 mmHg for 1 hr, and the **1** was finally removed by reducing the pressure to 17 mmHg. The residual crystals were recrystallized from ethanol to give **12** (17 g, 71%).[6,7,8] Mp 219—220°C (dec.); 223—224°C (measured in a capillary tube of Hario-glass: decomposed after fusion without coloration). $[\alpha]_D^{22}$ −29° (*c* 1.0, Me_2CO). IR(KBr): 1785 and 1800 cm^{-1} (five-membered cyclic carbonate). NMR (acetone-d_6, TMS): δ 5.94 (H-1, d, $J_{1,2}$=3.3 Hz), 4.50 (H-2, d, $J_{2,3}$=0 Hz), 4.29 (H-3, q, $J_{3,4}$=3.5 Hz), 4.46 (H-4, sex., $J_{4,5}$=3.2 Hz), 5.05 (H-5, octet, $J_{5,6}$=8.7 Hz and $J_{5,6'}$=6.4 Hz), 4.46 (H-6, t, $J_{6,6'}$=8.7 Hz), 4.53 (H-6', q), 4.71 (HO-3, q, $J_{3,OH}$=4.5 Hz and $J_{4,OH}$=1.0 Hz), 1.25 and 1.40 (Me, two s, unassignable). On the use of a usual commercial flask in the above reaction, 3,6-anhydro-1,2-*O*-isopropylidene-α-D-glucofuranose was obtained in an 80% yield by treating the resultant reaction mixture with distilled water (300 ml), by the subsequent extraction of the aqueous solution with ether (200 ml ×4), followed by washing with water (200 ml), by the evaporation of the solvent *in vacuo* to a semicrystalline sirup after drying with anhydrous sodium sulfate, and by the recrystallization of the residue from light petroleum ether. Mp 44—46°C.[6,7,12,13]

2,2'-Anhydro-1-β-D-arabinofuranosyluracil (18). A transesterification reaction was similarly carried out in this case by treating uridine (**7**) (2.5 g, 10 mmol) and **1** (3.0 g, 35 mmol) at 140—145°C/15 mmHg for 1.5 hr. After about 1 hr, the crystallization of the product occurred; the crystals were, after cooling, treated with methanol (5 ml). They were filtered and recrystallized from 25% aqueous methanol to give **18** (1.6 g, 71%). Mp 238—244°C (dec.). $[\alpha]_D^{22}$ −22.2° (*c* 1.0, H_2O). $\lambda_{max}^{H_2O}$ 224 (ε 7860) and 251 nm (ε 7600). $\lambda_{min}^{H_2O}$ 236 nm (ε 5940). A slight shoulder was observed at about 270 nm.[14]

1,2;3,4-Di-O-isopropylidene-D-mannitol 5,6-Carbonate (10). The transesterification was carried out by treating 1,2;3,4-di-*O*-isopropylidne-D-mannitol (**4**)[15] (1.3 g, 5 mmol) and **1** (1.5 g, 17.5 mmol) at 160°C/40 mmHg for 1 hr; the residual crystals were then recrystallized from ethanol to give colorless crystals of **10** (1.3 g, 90%). Mp 111—112°C. $[\alpha]_D^{22}$ −50° (*c* 0.97, Me_2CO). IR (KBr): 1790 cm^{-1} (five-membered cyclic carbonate). Found: C, 54.08; H, 6.88%. Calcd for $C_{13}H_{20}O_7$: C, 54.16; H, 6.99%. Without recrystallization, the product was already analytically pure enough.

3,4-O-Isopropylidene-D-mannitol 1,2;5,6-Dicarbonate (11). 3,4-*O*-Isopropylidene-D-mannitol (**5**)[15] (1.1 g, 5 mmol) and **1** (1.5 g, 17.5 mmol) were heated together at 150—160°C/30 mmHg for 1 hr, and the residue was, after cooling, dissolved in ethanol (*ca.* 10 ml). After the solution had then been allowed to stand at room temperature, colorless needles of **11** (0.9 g, 65%) were obtained. This product was analytically pure enough without recrystallization (Found: C, 48.15; H, 5.19%). Mp 205—207°C. $[\alpha]_D^{22}$ −16.3° (*c* 1.0, Me_2CO).[16]

1,2;5,6-Di-O-isopropylidene-D-mannitol 3,4-Carbonate (13). 1,2;5,6-Di-*O*-isopropylidene-D-mannitol (**8**)[17] (1.3 g, 5 mmol) and **1** (1.5 g, 17.5 mmol) were heated at 160°C/40 mmHg for 1 hr. The raw crystals, obtained in the same manner as above, were recrystallized from ethanol to give colorless crystals of **13** (1.1 g, 76%). Mp 144—145°C.[18] $[\alpha]_D^{22}$ −111° (*c* 0.97, Me_2CO). IR (KBr): 1785 cm^{-1} with a shoulder at

10) J. Cunningham and R. Gigg, *J. Chem. Soc.*, **1965**, 1553 [Bp 150°C/0.08 mmHg (**17**)].

11) O. T. Schmidt, "Methods in Carbohydrate Chemistry," Vol. II, ed. by R. L. Whistler, M. L. Wolfrom, and J. N. BeMiller, Academic Press Inc., New York (1963), pp. 321—322.

12) NMR data of this compound is completely agreed with those reported by Abraham *et al.* (R. J. Abraham, L. D. Hall, L. Hough, and K. A. McLanchlan, *J. Chem. Soc.*, **1962**, 3699.).

13) H. Ohle, C. Vargha, und H. Erlbach, *Ber.*, **61**, 1211 (1928), [Mp 56—57°C, $[\alpha]_D^{20}$ +29.3° (*c* 3.1, H_2O)].

14) J. J. Fox and I. Wempen, *Tetrahedron Lett.*, **1965**, 643 ($\lambda_{max}^{H_2O}$ 223 and 249 nm with a slight shoulder at 270 nm, Mp 246—248°C); A. Hampton and A. W. Nichol, *Biochemistry*, **5**, 2076 (1966) (Mp 238—244°C).

15) L. F. Wiggins, *J. Chem. Soc.*, **1946**, 13.

16) G. Hannisch und G. Henseki, *Chem. Ber.*, **100**, 3225 (1967), [Mp 214°C, $[\alpha]_D$ −21° (*c* 1, Me_2CO)].

17) E. Baer, *J. Amer. Chem. Soc.*, **67**, 338 (1945).

18) B. R. Baker and H. S. Sachder, *J. Org. Chem.*, **28**, 2135 (1963), [Mp 147°C, $[\alpha]_D^{25}$ +8.0° (0.9%) (**13**)]; L. Hough, J. E. Priddle, and R. S. Theobald, *J. Chem. Soc.*, **1961**, 1934 [Mp 146.5—147°C, $[\alpha]_D^{20}$ +14.9° (*c* 1.8, Me_2CO) (**13**); Mp 233—234°C (dec.), $[\alpha]_D^{20}$ +31.9° (*c* 2.1, Me_2CO) (**14**)].

* A part of this paper was presented at the 26th Annual Meeting of the Chemical Society of Japan (April, 1972; Hiratsuka).

1810 cm^{-1} (five-membered cyclic carbonate).

D-*Mannitol 1,2;3,4;5,6-Tricarbonate (**14**).* D-Mannitol (**9**) (1.8 g, 10 mmol) and **1** (9.0 g, 105 mmol) were heated together at 150°C/20 mmHg for 6 hr. The residue was dissolved in ethanol (*ca.* 10 ml), and the resultant crystals, obtained on standing at room temperature, were recrystallized from glacial acetic acid to give **14** (1.7 g, 65%) (colorless needles). Mp 228—229°C. $[\alpha]_D^{22}$ +33.2° (*c* 1.0, Me_2CO).[18] IR (KBr): 1790 and 1820 cm^{-1} (five-membered cyclic carbonate).

The authors are grateful to the Ministry of Education, Japanese Government, for a Scientific Research Grant-in-Aid, and to the Kurata Foundation for a grant. Moreover, they also wish to thank Dr. Masatsune Kainosho, Central Research Lab., Ajinomoto Co., Inc., for the assignment of the NMR spectra, and the members of the Laboratory of Organic Analysis, Department of Chemistry, Tokyo Institute of Technology.

BULLETIN OF THE CHEMICAL SOCIETY OF JAPAN, VOL. 46, 553—556 (1973)

Synthetic Studies by the Use of Carbonates. III.[1] The Condensation Reactions of Ethylene Carbonate with a Variety of Phenols Catalyzed by Lithium Hydride or Tetraethylammonium Halides

Teruo Yoshino, Shigeru Inaba, and Yoshiharu Ishido

Department of Chemistry, Faculty of Science, Tokyo Institute of Technology, O-okayama, Meguro-ku, Tokyo

(Received June 14, 1972)

The condensation reactions of ethylene carbonate with a variety of phenols in the presence of tetraethylammonium halides were examined; they were found to give the corresponding aryl β-hydroxyethyl ethers in good yields. The reactions in the presence of lithium hydride in place of the tetraethylammonium halides were also examined for the sake of comparison, and these results were discussed.

The first paper of this series[2] described the condensation reactions of ethylene carbonate(**1**) with hydrohalides of various amines, which resulted in the formation of β-hydroxyethylated ammonium salts in good yields. Although the condensation reaction of **1** with phenols in the presence of potassium carbonate or sodium hydride had previously been reported,[3] the present authors investigated the reaction in the presence of lithium hydride or tetraethylammonium halides in place of the above inorganic salt or hydride because of their greater wieldiness; we also investigated the possibility that the reaction might be carried out under completely neutral conditions by the use of the ammonium halides.

Results and Discussion

Reactions Catalyzed by Lithium Hydride. Phenols were subjected to a condensation reaction with an equimolar amount of **1** in the presence of the corresponding phenoxide ion, which had been generated by treating the phenols with a catalytic amount of lithium hydride, as is shown in Scheme 1; the results are shown in Table 1. Phenol, *p*-nitrophenol, salicylanilide, and

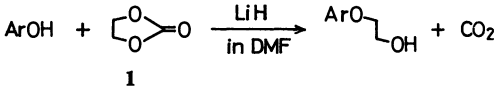

1

Scheme I.

Table 1. Reactions of ethylene carbonate (**1**) with some phenols catalyzed by lithium hydride[a]

Phenols	Reaction conditions		Products	
	Temp, °C	Period, hr	Mp (Bp), °C	Yield, %
Phenol	145—150	7	(89—92/0.4 mmHg)	88.5
p-Nitrophenol	150	6	83—85	90
2,4-Dinitrophenol	150—160	3	—	—[b]
Salicylanilide	145	2.5	109—112	86
β-Naphthol	145	2	72—74	74

a) All the reactions were carried out by the use of 10 mmol of **1** and 11 mmol of phenols in dimethylformamide (5 ml) and a catalytic amount of lithium hydride was applied as catalyst.
b) This phenol was quantitatively recovered.

1) H. Komura, T. Yoshino, and Y. Ishido, This Bulletin, **46**, 550 (1973).
2) T. Yoshino, S. Inaba, H. Komura, and Y. Ishido, *ibid.*, in contribution.
3) a) W. W. Carlson and L. H. Cretcher, *J. Amer. Chem. Soc.*, **69**, 1952 (1947). b) W. W. Carlson, U. S. Pat. 2448767 (1948). c) S. Fumasoni, *Ann. Chem.* (Rome), **54**, 73 (1964).

β-naphthol gave the corresponding aryl β-hydroxyethyl ethers in 88.5, 90, 86, and 74% yields respectively. However, 2,4-dinitrophenol gave none of the expected ether and was recovered quantitatively in spite of the almost quantitative evolution of carbon dioxide gas. Even the use of an equimolar amount of sodium hydride resulted in a quantitative recovery of 2,4-dinitrophenol. The difference observed between the case of the phenol and those of the other phenols can be explained by supposing that the β-2,4-dinitrophenoxyethoxide ion formed in the course of the reaction might be subject to a subsequent intramolecular substitution reaction to give ethylene oxide and the 2,4-dinitrophenoxide ion because of the lowered electron density on the β-methylene carbon arising from the strong electron-withdrawing effect of the 2,4-dinitrophenyl group (Scheme II).

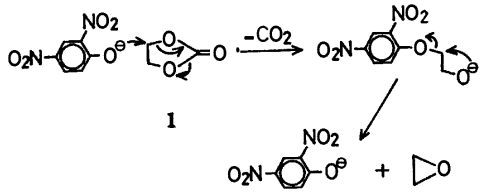

Scheme II.

Reactions Catalyzed by Tetraethylammonium Halides. The decomposition reaction of **1** in the presence of metal halides[4] or tetraalkylammonium halides[5] has been shown to give ethylene oxide *via* the β-haloethoxide ion, accompanied by the evolution of carbon dioxide gas. In view of the reaction mechanism (Scheme III),

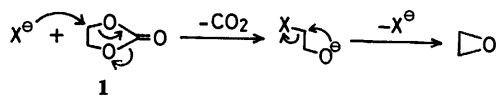

Scheme III.

the addition of phenols to the reaction system was assumed to bring about the formation of the corresponding aryl β-hydroxyethyl ethers, as is depicted in Scheme IV; *i.e.*, the resultant β-haloethoxide ion may

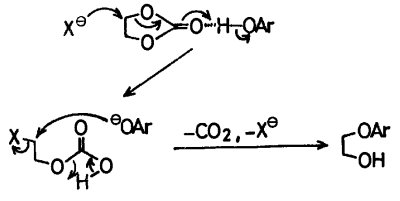

Scheme IV

abstract a proton from the phenols to afford ethylene halohydrin and the phenoxide ion, and the halohydrin may then be subject to the nucleophilic attack by the anion to afford the corresponding aryl β-hydroxyethyl ethers. On the basis of this assumption, a variety of phenols were heated with **1** at 140°C in the presence of tetraethylammonium halides as the catalyst until the evolution of carbon dioxide gas ceased. The series of phenols shown in Table 2 gave the corresponding aryl β-hydroxyethyl ethers in high yields. In contrast with the above case, in which lithium hydride was used as the catalyst, 2,4-dinitrophenol gave the corresponding ether in a 73% yield.

The reaction may be explained as proceeding *via* a concerted mechanism (Scheme IV)[6] in view of the facts that the reaction of **1** with tetraethylammonium halides giving ethylene oxide requires a reaction temperature above 160°C at least,[2] that no reaction of **1** with phenols takes place even at 180°C, and that the reactions described here can easily take place even at 130—140°C, *i.e.*, the reaction may be induced by the nucleophilic attack of the halide ion as well as by the electron-withdrawing effect of the carbonyl group of **1** enhanced by the hydrogen bonding with phenols. The reaction is apparently different from that catalyzed by lithium hydride, since no basic species are involved in the final reaction mixture.

The procedure is, furthermore, characterized by the following points: 1) Aryl β-hydroxyethyl ethers are obtainable in high yields under completely neutral conditions. 2) The end-point of the reaction can be noticed by measuring the volume of carbon dioxide

Table 2. Reactions of ethylene carbonate (**1**) with a variety of phenols catalyzed by tetraethylammonium halides[a]

Phenols	Reaction conditions		Products	
	Temp, °C	Period, hr	Mp (Bp), °C	Yield, %
Phenol[b]	140	4.0	(116/12.5 mmHg)	95
p-Nitrophenol[b]	150	4.0	83—85	91
o-Nitrophenol[b]	135	10.0	(170—180/10—15)	78
m-Nitrophenol[c]	170	0.5	86—87.5	93
2,4-Dinitrophenol[b]	140	2.3	110.5—111	73
p-Methoxyphenol[c]	155—160	2.5	63—65	81
p-Cresol	170	1.3	(84—95/0.4)	80
β-Naphthol	130	4.0	72—73	98
p,p'-Isopropylidenediphenol[b]	130	6.0	100.5—101.5	77

a) All the reactions were carried out by the use of 10 mmol of **1** and 11 mmol of phenols. b) These reactions were carried out in the presence of tetraethylammonium iodide (3.6 mmol) as catalyst. c) These reactions were carried out in the presence of tetraethylammonium bromide as catalyst in dimethylformamide (5 ml).

4) a) A. Hilt, J. Trived, und K. Hamann, *Makromol. Chem.*, **89**, 177 (1965). b) K. Gulbins, G. Benzing, R. Maysenhölden, und K. Hamann, *Chem. Ber.*, **93**, 1975 (1960).

5) A. L. Shapiro, *Zh. Org. Khim.*, **4**, 2065 (1968): *ibid.*, **5**, 1207 (1967).

6) A kinetic study is now in progress in our laboratory, and will be reported elsewhere.

gas evolved. 3) The easy separation of the catalysts from the resultant reaction mixture is possible by distributing them between the organic solvent and water, and the catalysts can be recovered in almost quantitative yields by the concentration of the aqueous layer.

Experimental

All the melting points are uncorrected. The IR spectra were taken with a Hitachi EPI-2S apparatus, while the NMR spectra were measured with a Varian T-60 spectrometer, using tetramethylsilane (TMS) or sodium 2,2-dimethylsilapentanesulfonate (DSS) as the internal standard.

Preparation of Aryl β-Hydroxyethyl Ethers by the Use of Lithium Hydride as a Catalyst. *β-Hydroxyethyl Phenyl Ether*: A solution of phenol (2.8 g, 30 mmol) in dimethylformamide (DMF, 5 ml) was treated with lithium hydride (10 mg) at 100°C until no evolution of hydrogen gas was noticed. Ethylene carbonate (**1**) (2.8 g, 33 mmol) was then added to the solution, and the mixture was heated at 145—155°C until the evolution of carbon dioxide gas ceased (about 7 hr). The DMF was then evaporated *in vacuo*, the resultant sirup was extracted with chloroform (100 ml), and the extract was washed with water (30 ml×2). The organic layer was concentrated and distilled. Yield, 2.4 g; 89%. Bp 89—92°C/0.04 mmHg (lit.[3] 118°C/10 mmHg). IR (NaCl): 3355, 1080 (OH), and 1246 (Ph–O–C) cm^{-1}. NMR ($CDCl_3$, TMS): δ 3.97 (m, –C**H**$_2$–).

β-Hydroxyethyl p-*Nitrophenyl Ether*: The reaction of *p*-nitrophenol (7.0 g, 50 mmol) with **1** (4.4 g, 50 mmol) catalyzed by lithium hydride (10 mg) in DMF (5 ml) was carried out at 150°C for 6 hr; raw crystals similarly obtained were recrystallized from ethanol to give the product. Yield, 6.4 g; 90%. Mp 83—85°C. IR (KBr): 3230, 1076 (OH), 1273 (Ar–O–C), 1508, and 1344 (NO_2) cm^{-1}. NMR ($CDCl_3$, TMS): δ 4.00 (2H, A_2B_2 type J=4 Hz, –C**H**$_2$OH) and 4.20 (2H, Ar–O–C**H**$_2$–).

Found: C, 52.39; H, 5.01; N, 7.70%. Calcd for $C_8H_9O_4N$: C, 52.40; H, 4.95; N, 7.65%.

β-Hydroxyethyl o-*Phenylcarbamoylphenoxy Ether*: The reaction of salicylanilide (2.1 g, 10 mmol) with **1** (1.0 g, 11 mmol) in DMF (10 ml) catalyzed by lithium hydride (5 mg) was carried out at 145°C for 2.5 hr. Yield, 2.2 g; 86%. Mp 109—112°C (from methanol). IR (KBr): 3310, 1075 (OH), 1240 (Ar–O–C), and 1642 (–CO–NH–) cm^{-1}. NMR (DMSO-d_6, DSS): δ 4.20 (2H, A_2B_2 type J=5 Hz, –C**H**$_2$–OH) and 4.60 (2H, Ar–O–C**H**$_2$).

Found: C, 70.24; H, 5.70; N, 5.36%. Calcd for $C_{15}H_{15}O_3N$: C, 70.02; H, 5.88; N, 5.44%.

β-Hydroxyethyl β-Naphthyl Ether: The reaction of β-naphthol (2.9 g, 20 mmol) with **1** (2.0 g, 22 mmol) in DMF (5 ml) catalyzed by lithium hydride (5 mg) was carried out at 145°C for 2 hr. Mp 72—74°C {from benzene–petroleum ether (1: 1); lit.[3] 76.7°C}. IR (KBr): 3325, 1085 (OH), and 1253 (Ar–O–C) cm^{-1}. NMR ($CDCl_3$, TMS): δ 4.02 (2H, A_2B_2 type J=4 Hz, –C**H**$_2$OH) and 4.20 (2H, Ar–O–C**H**$_2$–).

Reaction of 1 with 2,4-Dinitrophenol. a) The reaction of **1** (2.7 g, 30 mmol) with 2,4-dinitrophenol (5.4 g, 30 mmol) was carried out at 150°C by the use of lithium hydride (10 mg). The evolution of gases ceased after about 3 hr. The resultant mixture was dissolved in chloroform (100 ml), and the extract was successively washed with 1M aqueous hydrochloric acid (40 ml) and water (40 ml×2). The concentration of the organic layer *in vacuo* after drying with anhydrous calcium chloride recovered 2,4-dinitrophenol (5.0 g, 93%). b) When sodium hydride (50% in oil) (0.5 g, 10 mmol) was used in place of lithium hydride in the above reaction, 2,4-dinitrophenol (5.1 g, 94%) was recovered. c) When sodium hydride (50% in oil) (1.4 g, 30 mmol) was used in the above reaction, the phenol (5.0 g, 93%) was also recovered.

Preparation of Aryl β-Hydroxyethyl Ethers Catalyzed by Tetraethylammonium Halides. *β-Hydroxyethyl Phenyl Ether*: A mixture of phenol (1.88 g, 22 mmol), **1** (1.94 g, 22 mmol), and tetraethylammonium iodide (1.0 g, 0.36 mmol) was heated at 145°C. The evolution of carbon dioxide gas ceased after about 4 hr. The resultant mixture was dissolved in chloroform (100 ml) and then washed with water (20 ml). The concentration of the organic layer after drying with anhydrous calcium chloride and subsequent distillation gave the product (2.62 g, 95%). Bp 116°C/12.5 mmHg.

β-Hydroxyethyl p-*Nitrophenyl Ether*: A mixture of *p*-nitrophenol (2.8 g, 20 mmol), **1** (2.0 g, 22 mmol), and tetraethylammonium iodide (1.0 g, 0.36 mmol) was heated at 150°C for 4 hr. The resultant mixture was dissolved in benzene (50 ml), and then the precipitated tetraethylammonium iodide was removed by filtration. The filtrate was evaporated *in vacuo* to dryness to give crude, pale yellow crystals, which were subsequently recrystallized from ethanol. Yield, 3.26 g; 91%. Mp 83—85°C.

β-Hydroxyethyl o-*Nitrophenyl Ether*: A mixture of *o*-nitrophenol (2.8 g, 20 mmol), **1** (1.94 g, 22 mmol), and tetraethylammonium iodide (1.0 g, 0.36 mmol) was heated at 130°C for 1 hr; the resultant mixture was treated in the same way as above and then distilled. Yield, 2.85 g; 78%. Bp 170—180°C/10—15 mmHg. IR (KBr): 3425, 1090 (OH), 1250 (Ar–O–C), 1522, and 1360 (NO_2) cm^{-1}. NMR ($CDCl_3$, TMS): δ 3.97 (2H, A_2B_2 type J=5 Hz, –C**H**$_2$OH) and 4.25 (2H, Ar–O–C**H**$_2$–).

Found: C, 52.50; H, 5.01; N, 7.56%. Calcd for $C_{15}H_{15}O_3N$: C, 52.46; H, 4.95; N, 7.65%.

β-Hydroxyethyl m-*Nitrophenyl Ether*: The reaction of *m*-nitrophenol (1.40 g, 10 mmol) with **1** (0.88 g, 10 mmol) was carried out in the presence of tetraethylammonium bromide (2.1 g, 10 mmol) in DMF (5 ml) at 170°C for 30 min. Raw crystals obtained in the same manner as above were recrystallized from methanol. Yield, 1.70 g; 93%. IR (KBr): 3250, 1050 (OH), 1240 (Ar–O–C), 1520, and 1345 (NO_2) cm^{-1}. NMR ($CDCl_3$, TMS): δ 4.03 (2H, A_2B_2 type J=4 Hz, –C**H**$_2$OH) and 4.71 (2H, Ar–O–C**H**$_2$–).

Found: C, 52.22; H, 5.16; N, 7.56%. Calcd for $C_{15}H_{15}O_3N$: C, 52.46; H, 4.95; N, 7.65%.

β-Hydroxyethyl 2,4-Dinitrophenyl Ether: A mixture of 2,4-dinitrophenol (2.68 g, 20 mmol), **1** (1.94 g, 22 mmol), and tetraethylammonium iodide (1.78 g, 5 mmol) was heated at 140°C for 2.25 hr; the resultant mixture was treated in the same way as above to give raw crystals, which were then recrystallized from ethanol. Yield, 3.30 g; 73%. Mp 110.5—111°C. IR (KBr): 3200, 1070 (OH), 1280 (Ar–O–C), 1520, and 1350 (NO_2) cm^{-1}. NMR ($CDCl_3$, TMS): δ 3.85 (2H, A_2B_2 type J=5 Hz, –C**H**$_2$OH), and 4.46 (2H, Ar–O–C**H**$_2$–).

Found: C, 42.29; H, 3.77; N, 12.56%. Calcd for $C_{15}H_{14}O_5N_2$: C, 42.11; H, 3.53; N, 12.28%.

β-Hydroxyethyl p-*Methoxyphenyl Ether*: A mixture of *p*-methoxyphenol (3.7 g, 30 mmol) and **1** (2.7 g, 33 mmol) was heated together with tetraethylammonium bromide (2.1 g, 10 mmol) at 155—160°C for 2.5 hr; raw crystals obtained in the same way as above were then recrystallized from ethanol. Yield, 3.34 g; 88%. Mp 63—65°C. IR (KBr): 3300, 1070 (OH), and 1230 (Ar–O–C) cm^{-1}.

Found: C, 64.23; H, 7.19%. Calcd for $C_9H_{12}O_3$: C, 64.27; H, 7.19%.

β-Hydroxyethyl p-*Methylphenyl Ether*: A mixture of *p*-cresol (1.08 g, 10 mmol) and **1** (0.88 g, 10 mmol) in DMF (5 ml) was heated together with tetraethylammonium bromide (2.10 g, 10 mmol) at 170°C for 1.3 hr, and the resultant mixture was treated as above. The raw liquid thus obtained was distilled. Yield, 1.22 g; 80%. Bp 84—95°C/0.4 mmHg. IR (NaCl): 3300, 1070 (OH), and 1240 (Ar–O–C) cm^{-1}. NMR ($CDCl_3$, TMS): δ 3.90 (4H, Ar–O–C**H**$_2$–C**H**$_2$–OH).

Found: C, 71.24; H, 7.94%. Calcd for $C_9H_{12}O_2$: C, 71.01; H, 7.95%.

β-Hydroxyethyl β-Naphthyl Ether: The reaction of β-naphthol (2.88 g, 20 mmol) with **1** (1.94 g, 22 mmol) catalyzed by tetraethylammonium iodide (1.0 g, 0.36 mmol) was carried out at 130°C for 4 hr; the resultant mixture was treated as above to give raw crystals, which were then recrystallized from ethanol. Yield, 3.71 g; 98%. Mp 72—73°C.

2,2-Di-[p-*(β-hydroxyethyloxy)-phenyl*]-*propane.* A mixture of 2,2-di-(*p*-hydroxyphenyl)propane (2.3 g, 20 mmol) and **1** (1.94 g, 22 mmol) was heated together with tetraethylammonium iodide (1.28 g, 5 mmol) at 130°C for 6 hr; raw crystals obtained in the same way as above were then recrystallized from ethanol. Yield, 2.38 g; 77%. Mp 109—111°C (lit.[7] 110.5°C). IR (KBr): 3460, 1090 (OH), and 1250 (Ar–O–C) cm^{-1}. NMR ($CDCl_3$, TMS): δ 3.93 (2H, A_2B_2 type J=6 Hz, –C**H**$_2$OH), and 4.03 (2H, Ar–O–C**H**$_2$–).

The authors are grateful to the Ministry of Education, Japanese Government, for a Scientific Research Grant-in-Aid, and to the members of the Laboratory of Organic Elemental Analysis.

7) E. Dyer and H. Scott, *J. Amer. Chem. Soc.*, **79**. 672 (1956).

BULLETIN OF THE CHEMICAL SOCIETY OF JAPAN, VOL. 46, 556—561 (1973)

On the Mechanism of the Acid Catalysis and New Activating Agents in the Fusion Reaction of an Acylated Sugar with a Purine Derivative*

Masao SEKIYA, Teruo YOSHINO, Hisayuki TANAKA, and Yoshiharu ISHIDO

Department of Chemistry, Faculty of Science, Tokyo Institute of Technology, O-okayama, Meguro-ku, Tokyo

(Received June 19, 1972)

An examination of the site where the acidic catalysts might strongly interact in the fusion reaction of a purine derivative with a fully-acylated sugar led to the conclusion that a purine derivative was activated by the interaction with the catalysts, and, moreover, resulted in the discovery of a new type of activating agent other than the acidic catalysts which had previously been known in the fusion method. In the presence of an excess amount of activating agents, *e.g.*, *p*-nitrophenol, the condensation reaction of theophylline with 1,2,3,4,6-penta-*O*-acetyl-*β*-D-glucopyranose proceeded, even in the absence of *p*-toluenesulfonic acid, to give the corresponding nucleoside. Some of the activating agents were found to form molecular compounds with theophylline, and a few of the latter to afford the corresponding nucleoside similarly. A possible mechanism for the activation process of theophylline by the above agents was discussed.

In a previous paper[1] concerned with the fusion reaction of a purine derivative with an acylated sugar, an assumption concerning such a mechanism of acid catalysis was made involving two possibilities (Scheme I): A) The acidic catalyst might interact with an acylated sugar molecule to afford the C-1 carbonium ion (**1**), and **1** might then successivly be subject to the attack of a purine (**2**) to give the corresponding nucleoside (**3**). B) Alternatively, the catalyst might interact with an electron-sufficient nitrogen atom in the purine nucleus to form an activated complex (**4**), and **4** might then be subject to the reaction with an acylated sugar, accompanied by the elimination of acetic acid, thus affording **3**. In order to solve this problem, a competitive reaction of a purine derivative with a phenol for condensation with a fully-acetylated sugar in the presence of an acidic catalyst was examined; the results thus obtained will be described in the present article.

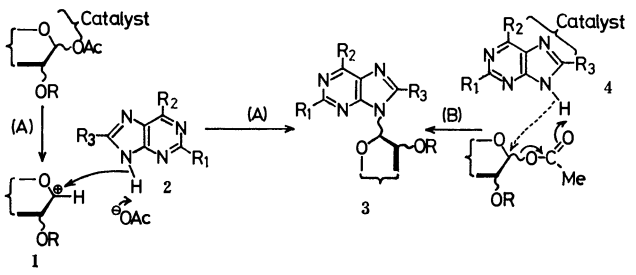

Scheme I.

Results and Discussion

To confirm the above proposed mechanism of the acid catalysis, a condensation reaction of 1,2,3,4,6-penta-*O*-acetyl-*β*-D-glucopyranose (**5a**) with theophyl-

* A part of this paper was presented at the Symposium on the Charge Transfer Complexes, June 10, 1969 (Nagoya).

1) Y. Ishido, A. Hosono, K. Fujii, Y. Kikuchi, and T. Sato, *Nippon Kagaku Zasshi*, **87**, 752 (1966).

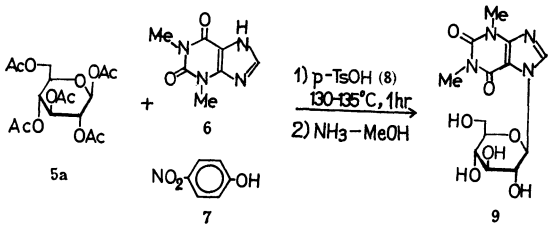

Scheme II.

line (**6**) in competition with *p*-nitrophenol (**7**), in the presence of *p*-toluenesulfonic acid (**8**) as a catalyst, was carried out as a model experiment (Scheme II). After the addition of **5a** (10 mmol) to a homogeneously prefused mixture of **6** (10 mmol), **7** (30 mmol), and **8** (0.05 mmol), the mixture was stirred at 130—135°C under atmospheric pressure and then treated as usual. 7-β-D-Glucopyranosyltheophylline (**9**) was selectively obtained in a 67% yield after the deacetylation of the corresponding tetra-*O*-acetate. This result is of much interest in view of the molar ratio of **6** to **7** and the considerably lowered reaction temperature in comparison with that (160°C) applied in an equimolar fusion reaction of **5a** with **6**.[2] No by-product other than a small amount of *p*-nitrophenyl acetate was observed by tlc or by a column chromatographic separation test on the mixture prior to the deacetylation. The reaction which proceeds *via* the mechanism A may be expected to give a mixture of acetates of *p*-nitrophenyl D-glucopyranosides (**10**) and **9**. On the other hand, the reaction *via* the mechanism B may be expected to give **9** selectively, since **8** should strongly interact with the most basic **6**. Moreover, tetra-*O*-acetate of the β-anomer of **10** (**10a**) was examined by using it in the reaction in place of **5a** in the same way as above, based on the assumption of a possible course of the formation of **9** *via* **10**; however, this examination resulted in the quantitative recovery of **10a**. Accordingly, it was concluded that the acid catalysis takes place *via* the mechanism B.

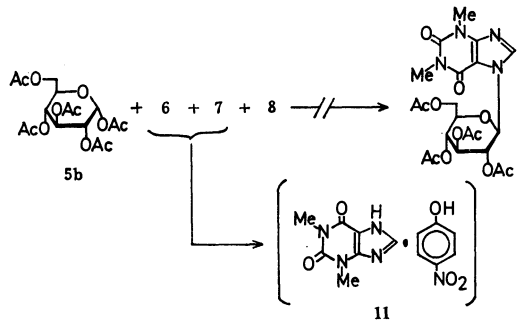

Scheme III.

The application of 1,2,3,4,6-penta-*O*-acetyl-α-D-glucopyranose (**5b**) (the α-anomer of **5a**) to the above competitive reaction, on the other hand, resulted in the formation of a molecular compound (**11**), composed of equimolar **6** and **7**, in a quantitative yield, and **5b** was recovered almost quantitatively (Scheme III). The recovery of **5b** in this case may be explained by considering that the difference in the stability of the 1-*O*-acetyl group between **5a** and **5b** arises from the anomeric effect.[3] The formation of **11** was remarkably interesting in view of the nature of the molecular compounds, whose components are generally accepted to be linked with each other by an intermolecular interaction such as polarization bonding;[4] hence, its properties were examined. Since **11** separated out on the dissolution of the resultant reaction mixture in benzene, the preparation of **11** from **6** and **7** was attempted by dissolving them in hot chloroform, benzene, and toluene respectively; the solution gave **11** in a fairly good yield in each case after having been allowed to cool at room temperature. However, the use of water, ethanol, or nitromethane as a solvent furnished no molecular compound. Moreover, considerable differences were observed in the IR spectral comparison of **11** with each component, as may be seen in Fig. 1. These differences suggest that a certain intermolecular interaction might exist between **6** and **7**, and that **6** might be activated by an intermolecular interaction such as polarization bonding. On the basis of this assumption, an equimolar fusion reaction of 1,2,3,5-tetra-*O*-acetyl-β-D-ribofuranose (**12**) (mp 82°C) with **11** (mp 148—150°C) was attempted at 130 and at 150°C respectively for 3 hr without the acidic catalyst, followed by deacetylation; this gave 7-β-D-ribofuranosyltheophylline (**13**) in 30 and 59% yields respectively (Scheme IV). The activation of **6** by **7** was thus con-

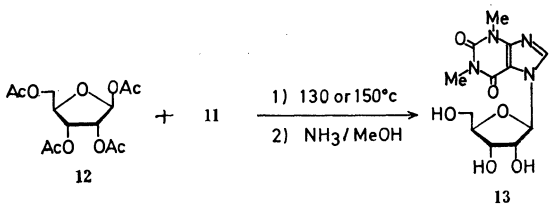

Scheme IV.

firmed, and the corresponding fusion reaction of **5a** with **6** in the presence of an excess amount of **7** was carried out. The acetate of **9** was also obtained in a good yield, although this reaction required a longer period than that in the presence of **8**. These results are of much interest in view of the fact that **7** exerts no catalytic effect on the fusion reaction when a catalytic amount is used, although it is acidic ($pKa=7.14$). Thus, the possibility of the activation of a purine by a compound other than the acidic catalysts, which have been known to be active in the fusion method,[1] was established.

In view of the above results, an extensive search for compounds which might behave as activating agents for a purine in the fusion reaction with a fully-acylated sugar was carried out by means of the reaction of **5a**

2) T. Shimadate, *ibid.*, **83**, 212 (1962): According to this paper, the equimolar fusion reaction of **5a** with **6** takes place at 160°C in the presence of **8** or zinc chloride, respectively, and gave the equimolar compound of **9** with **6** in 7% and 3% yield, respectively.

3) R. U. Lemieux and N. J. Chu, 133rd Meeting Amer. Chem. Soc., Abstracts of Papers, 31N (1958); R. U. Lemieux, 135th Meeting Amer. Chem. Soc., Abstracts of Papers, 5E (1959).

4) S. C. Wallwork, *J. Chem. Soc.*, **1961**, 494.

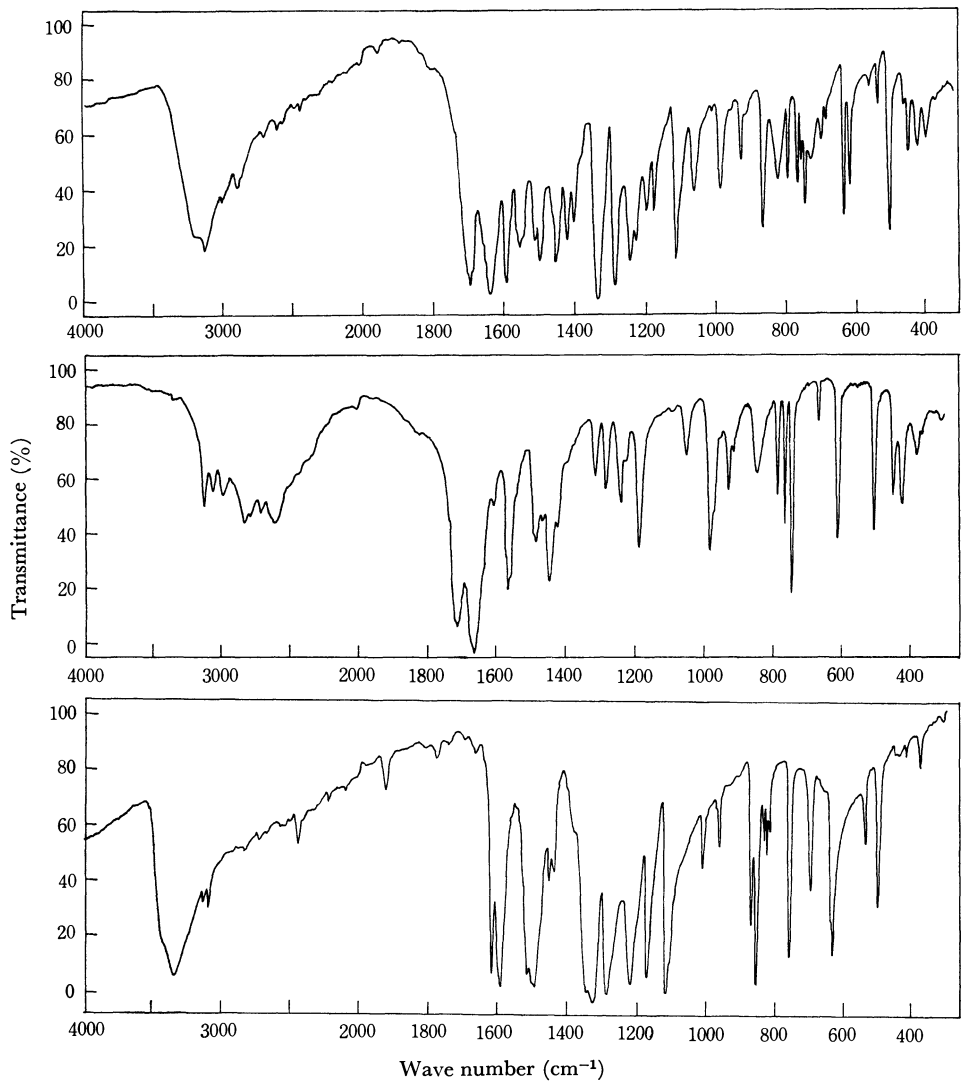

Fig. 1. The IR absorption spectra of theophylline: *p*-nitrophenol (**11**), theophylline (**6**), and *p*-nitrophenol (**7**) in turn from up to down.

with **6** in the absence of **8**. In the light of the properties of **7**, the potential activating agents were chosen as below:

I) Compounds with a nitro group as an electron-attracting group,
nitrobenzene, *p*-chloronitrobenzene, and methyl *p*-nitrophenyl ether (*p*-nitroanisole).

II) Phenols,
a) *o*-, *m*-nitrophenols (**14**), 2,4-dinitrophenol, and 2,4,6-trinitrophenol (picric acid)
b) phenol, *o*-, *m*-, *p*-chlorophenols, and *p*-methoxyphenol.

III) Carboxylic acids and their derivatives,
a) aromatic carboxylic acids,
benzoic acid, *o*- (**15**), *m*-nitrobenzoic acid (**16**), *o*-, *m*-chlorobenzoic acids, and salicylic acid (**17**)
b) aliphatic carboxylic acids,
acetic acid, propionic acid, and maleic acid
c) acid anhydrides and esters,
succinic anhydride, phthalic anhydride, and methyl *o*-, *m*-nitrobenzoates.

IV) Acceptor in EDA complexes,
p-benzoquinone.

V) Amides,
a) aromatic sulfonamides,
p-toluenesulfonamide (**18**), *N*-methyl- (**19**), *N*,*N*-dimethyl-*p*-toluenesulfonamides (**20**), *p*-chlorobenzenesulfonamide (**21**), *N*-acetyl- (**22**), and *N*-phenyl-*p*-toluenesulfonamides (*p*-toluenesulfonanilide) (**23**).
b) carboxyamides,
benzamide, benzanilide, and salicylamide.

Using the order of these categories, we made a general survey of the factors affecting the activation process of **6** in the condensation reaction. No activating agent was found among the compounds in Category I; this fact suggested that acidic as well as electron-attracting substituents might be required for the activation of **6**. To confirm this view, the compounds in Categories II and III were examined; the results supported the theory, although only **14**, **15**, **16**, and **17** were found to be effective. This fact, moreover, suggested that the activation process of **6** might be delicately connected with the correlation in the mutual

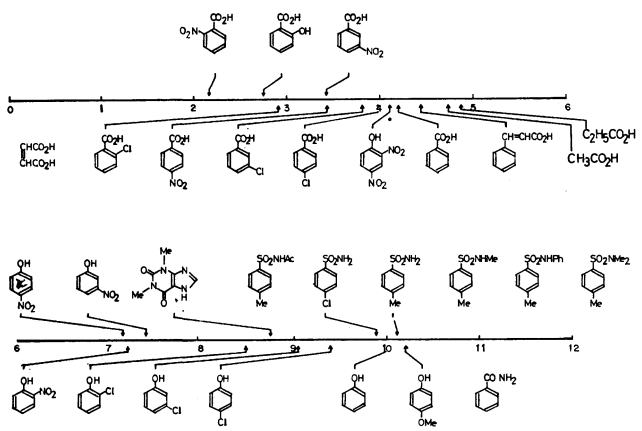

Fig. 2.

position of substituents on the aromatic nuclei, and that aromatic nuclei might be required, at least for the activation. Subsequently, an examination of *p*-benzoquinone (Category IV), which is well known as a typical acceptor in the field of electron-donor-acceptor (EDA) complexes,[4] was carried out; it was found to be ineffective. Moreover, all the sulfonamides in Category Va (**18**—**23**) were found to be effective, in contrast with the carboxyamides in Category Vb. In view of these results, a consideration was made of the factors affecting the activation of **6**: (1) The activation process is conceivably independent from the homogeneity of the reaction system, since all the attempted reactions were carried out in a completely homogeneous state. (2) The possibility of the participation of such a potential active intermediate as **10** was also denied for such compounds as 2,3,4,6-tetra-*O*-acetyl-1-*O*-*o*-nitrobenzoyl-*β*-D-glucopyranose gave no nucleoside even when treated with **6** in the presence of *o*-nitrobenzoic acid in the same way as has been described in the examination reaction of **10a** with **6**, although the formation of a transesterification product had been confirmed in the fusion reaction of **5a** with various carboxylic acids.[5] (3) In considering the possibility that the activation effect of these compounds in Categories II—V might depend on their acidity, they were arranged in the order of their p*Ka* values, as is shown in Fig. 2, and the effective and ineffective ones were placed above and under the line graduating in p*Ka* value. It was thus proved that the effectiveness of the activating agents is independent of their acidity. (4) Consequently, the activation of **6** was deduced to be brought about by such a certain intermolecular interaction as was noticed between **6** and **7**. Incidentally, an intermolecular interaction of such species of heterocyclic compounds has recently been discussed by Shefter[6] in his X-ray crystal structure analysis of the molecular compounds of *p*-chlorosalicylic acid with caffeine[6a] and with theobromine.[6b]

The nature of the intermolecular interaction in these cases was described as the polarization bonding which was proposed by Wallwork.[4] Moreover, it has been shown that **6** and caffeine are both capable of forming EDA complexes with *p*-benzoquinone in water,[7] and that the rate of the alkaline hydrolysis of methyl *trans*-cinnamate is reduced by the addition of such imidazole homologues as **6** because of the formation of EDA complexes.[8] Although the preparations of molecular compounds of all the applied agents with **6** were attempted on the basis of the above facts by dissolving equimolar amounts of them in hot chloroform, no molecular compound such as **11** was isolated except in the cases of **14**, **15**, **16**, **17**, *m*-chlorobenzoic acid, and salicylamide. In addition, *p*-nitro- and 3,5-dinitrobenzoic acid, which can not be used in the reaction because of their high melting points, also gave the corresponding molecular compounds. These results are summarized in Table 2. The IR spectra of these molecular compounds were considerably different from those of each component; the difference was especially remarkable in the specific absorption band of the N–H stretching of **6**. The absorption band was significantly simplified or sharpened by forming the corresponding

Table 1. Condensation reaction of 1,2,3,4,6-penta-*O*-acetyl-*β*-D-glucopyranose (**5a**) with theophylline (**6**) in the presence of activating agents[a]

Activating agent	Reaction temp. (°C)	Period (hr)	Yield of 7-*β*-D-glucopyranosyltheophylline tetra-*O*-acetate (%)
p-O_2N–C_6H_4–OH	130—135	5	35 (90[b] 67[c])
m-O_2N–C_6H_4–OH	130—135	11	15 (94[b])
o-O_2N–C_6H_4–CO_2H	150—155	3	70
o-HO–C_6H_4–CO_2H	160—165	3	30
p-Me–C_6H_4–SO_2NH_2	160	3	71
p-Cl–C_6H_4–SO_2NH_2	150—155	3	58
p-Me–C_6H_4–SO_2NHMe	155—160	4	41
p-Me–C_6H_4–SO_2–NMe_2	160—165	9	58
p-Me–C_6H_4–SO_2NHPh	170	3	50

a) All the reaction were carried out by the use of **5a**(10 mmol), **6**(10 mmol) and activating agents (30—50 mmol).
b) These reactions were carried out for 1 hr in the presence of *p*-TsOH(0.5 mmol).
c) The yield stands for that of 7-*β*-D-glucopyranosyltheophylline(**9**) obtained by deacetylation of the tetra-*O*-acetate described in footnote b with methanolic ammonia.

5) Y. Ishido, H. Tanaka, K. Iwabuchi, and T. Sato, *Nippon Kagaku Zasshi*, **87**, 1113 (1966).
6) a) E. Shefter, *J. Pharm. Sci.*, **57**, 350 (1968); b) E. Shefter, T. E. Brennan, and P. Sackman, *Chem. Pharm. Bull.*, **19**, 746 (1971).
7) T. Okano and K. Aida, *Yakugaku Zasshi*, **87**, 1243 (1967).
8) J. A. Mollica, Jr., and K. A. Connors, *J. Amer. Chem. Soc.*, **89**, 308 (1967).

Table 2. Molecular compounds of theophylline (**6**) with some compounds[a)]

Countercomponent	Mp (°C)		Molecular compounds					
			Calcd			Found		
			C	H	N(%)	C	H	N(%)
p-O_2N-C_6H_4-OH	148—150	$C_{13}H_{13}O_5N_5$:	48.90	4.10	21.94	48.89	3.80	21.87
m-O_2N-C_6H_4-OH	150—160	$C_{13}H_{13}O_5N_5$:	48.90	4.10	21.94	49.19	3.69	22.03
o-O_2N-C_6H_4-CO_2H	160—168	$C_{14}H_{12}O_6N_5$:	48.42	3.77	20.17	48.64	3.55	20.42
m-O_2N-C_6H_4-CO_2H	200—202	$C_{14}H_{12}O_6N_5$:	48.42	3.77	20.17	48.71	3.52	20.20
p-O_2N-C_6H_4-CO_2H[b)]	191—195	$C_{14}H_{12}O_6N_5$:	48.42	3.77	20.17	48.68	3.69	20.15
o-HO-C_6H_4-CO_2H	183—184	$C_{13}H_{13}O_5N_4$:	52.83	4.43	17.60	52.70	4.13	17.84
3,5-$(O_2N)_2C_6H_3$-CO_2H[b)]	190—191	$C_{14}H_{12}O_8N_6$:	42.87	3.08	21.43	42.87	3.19	21.53
m-Cl-C_6H_4-CO_2H[c)]	182—185	$C_{14}H_{12}O_4N_5Cl$:	49.93	3.89	16.64	49.83	3.81	16.84
o-HO-C_6H_4-$CONH_2$[c)]	187—210	$C_{14}H_{14}O_4N_5$:	52.99	4.77	22.07	53.22	4.72	22.40

a) All the preparations were carried out by the use of **6**(10 mmol) and countercomponents (11 mmol), respectively, in chloroform (30—50 ml) under reflux.
b) The condensation reaction of **5a** with **6** was not attempted on account of their high melting point.
c) The corresponding molecular compounds could not affect the reaction of **5a** with **6**.

molecular compounds. Moreover, the IR spectroscopic behavior of the phenolic hydroxyl group of **7** was easily detected by examining the spectrum of the molecular compound of **7** with caffeine, which is the $N_{(7)}$-methyl derivative of **6**, in a similar manner. The shift of the O–H stretching absorption band to a lower frequency from the original band of **7** was estimated to be about 180 cm^{-1}. Although various individual variations were observed, similar tendencies were recognized in the specific IR absorption bands of all the countercomponents other than **7**. The magnitude of the activation by such intermolecular interaction is considered to be delicately affected by the correlative position on the aromatic nuclei and by the chemical properties of each functional group in view of the facts that all the homologues are not necessarily effective for the reaction in each category, and that **16** is not effective for the reaction of **6** with **5a**, but is effective for that of **6** with 2,3,4,6-tetra-*O*-acetyl-1-*O*-trichloroacetyl-β-D-glucopyranose.[9] Moreover, there may be no correlation between the formation of a crystalline molecular compound and the activation of **6** in view of the facts that all the sulfonamides are effective for the reaction, although they gave no crystalline molecular compound, and that *m*-chlorobenzoic acid and salicylamide, which are ineffective for the reaction, afforded the corresponding molecular compounds. Furthermore, the intermolecular interaction observed among these molcular compounds was assumed to be not so strong on the basis of the facts that no formation of crystalline molecular compounds took place in such polar solvents as water, ethanol, and nitromethane, and that their UV absorption spectra could not be determined because of the dissociation into their components in the concentration of 10^{-4} mole per liter in chloroform. On the basis of these facts, **6** was deduced to be activated by the polarization bonding with the activating agents described above.

It may be concluded from these experiments that a new type of fusion method for the synthesis of purine nucleosides involving an intermolecular interaction between a purine and an activating agent was established.[10]

Experimental

All the melting points are uncorrected. The IR absorption spectra were taken with a Hitachi-225 in a pellet of potassium bromide, while the NMR spectra were taken with a Varian T-60 in deuteriochloroform ($CDCl_3$) by the use of tetramethylsilane (TMS) as the internal standard.

Competitive Reaction of Theophylline (6) with p-*Nitrophenol (7) for the Condensation with 1,2,3,4,6-Penta-*O*-acetyl-β-*D*-glucopyranose (5a).* Theophylline (**6**) (1.8 g, 10 mmol), *p*-nitrophenol (**7**) (4.2 g, 30 mmol), and *p*-toluenesulfonic acid (**8**) (100 mg, 0.5 mmol) were heated in an oil-bath (130—135°C) to fuse them homogeneously under stirring, and then 1,2,3,4,6-penta-*O*-acetyl-β-D-glucopyranose (**5a**) (3.9 g, 10 mmol)[11] was added to the prefused mixture. After the addition, the mixture was stirred for 1 hr at that temperature under atmospheric pressure, and then it was allowed to cool at room temperature. The resultant mixture was dissolved in benzene (300 ml), and the solution was successively washed with a 1M aqueous sodium hydroxide solution to remove the co-produced acetic acid, unchanged **6**, and **7**, and with water, and then dried over anhydrous calcium chloride. After removing the desiccant by filtration, the organic layer was concentrated *in vacuo* to a pale yellow half-glassy sirup. The sirup was dissolved in methanol (200 ml) and was mixed with methanolic ammonia (200 ml) which had been prepared by saturating methanol with ammonia gas at 0°C. After standing in a round-bottomed flask (500 ml) with a tight stopper at room temperature overnight, the mixture was cooled in an ice-bath and then concentrated *in vacuo* to about a quarter of the original volume. The crystals thus precipitated were filtered by suction and were dissolved in water (10 ml) by warming. The solution was mixed with acetone (100—150 ml) after decoloration with active charcoal. After the solution had been stored in a refrigerator overnight, the resultant crystals were filtered and dried over phosphorus

9) M. Sekiya, T. Yoshino, H. Tanaka, and Y. Ishido, unpublished data: The tetra-*O*-acetate of **9** was obtained in 55% yield.

10) The reaction is found to be also applicable to the other purine derivatives such as $N_{(6)}$-benzyladenine *etc.*, to which the usual fusion reaction has been inapplicable, and the results will be published elsewhere.

11) E. Fischer, *Ber.*, **49**, 584 (1916).

pentoxide at 110°C *in vacuo* to give 7-β-D-glucopyranosyltheophylline (**9**)[12] (2.3 g, 67% yield). Mp 265—267°C. $[\alpha]_{578}^{21}$ −3° (*c* 1.0, H_2O). $\lambda_{max}^{H_2O}$ 275 nm (ε 7200). The NMR spectra of the above sirup was taken prior to deacetylation; it was found to be almost as pure as 7-(2′,3′,4′,6′-tetra-*O*-acetyl-β-D-glucopyranosyl)theophylline: δ ($CDCl_3$) 1.92 (3H; AcO-2′), 2.04, 2.07 (9H; AcO-3′, 4′, and 6′), 3.43, 3.60 (6H; MeN-1 and 3), 3.95—4.30 (3H; H-5′, $6'_a$, and $6'_b$), 5.2—5.7 (3H; H-2′, 3′, and 4′), 6.21 (1H; H-1′, $J_{1',2'}=10$ Hz), and 7.90 (1H; H-8) ppm.

*The Molecular Compound of Theophylline (**6**) with* p-*Nitrophenol (**7**): Theophylline—*p-*Nitrophenol (**11**).* a) On the use of 1,2,3,4,6-penta-*O*-acetyl-α-D-glucopyranose (**5b**)[13] in the competitive reaction in place of **5a**, white scaly crystals were separated when the resultant reaction mixture was dissolved in benzene. The crystals were filtered and dried over phosphorus pentoxide at 110°C *in vacuo*, and a molecular compound composed of equimolar **6** and **7** (**11**) (3.1 g, 97% yield) was obtained. Mp 148—150°C. The IR spectrum of **11** is shown in Fig. 1. However, no new absorption band was found in either its UV or visible region spectrum. After the removal of the residual **7** as described in the previous experiment, the organic layer was concentrated *in vacuo* to give **5b** (3.5 g, 90% recovery). b) **11** was also obtained quantitatively by dissolving an equimolar amount of **6** (1.8 g, 10 mmol) and **7** (1.6 g, 11.4 mmol) in hot chloroform (30—50 ml), and by then allowing the solution to cool at room temperature.

*An Equimolar Fusion Reaction of the Molecular Compound (**11**) with 1,2,3,5-Tetra-*O*-acetyl-β-D-ribofuranose (**12**).* To 1,2,3,5-tetra-*O*-acetyl-β-D-ribofuranose (**12**)[14] (3.2 g, 10 mmol) prefused at 130°C, was added finely-powdered **11** (3.2 g, 10 mmol), after which the mixture was stirred at 130°C for 3 hr under atmospheric pressure. The resultant reaction mixture was dissolved in chloroform (150—200 ml), successively washed with a 1M aqueous sodium hydroxide solution and water in the same way as has been described in the first example of this section, and dried over anhydrous calcium chloride. The solution was, after the desiccant had been removed by filtration, concentrated *in vacuo* to a sirup; the sirup was then dissolved in methanol (100 ml) and mixed with methanolic ammonia, as has been described above. After standing in a refrigerator overnight, the solution was evaporated *in vacuo* to dryness and the residue was triturated with ethanol (10 ml). The resultant crystals were filtered and recrystallized from ethanol (*ca.* 200 ml) with the use of active charcoal to give 7-β-D-ribofuranosyltheophylline (**13**) (1.2 g, 39% yield). Mp 189.5—191°C. $[\alpha]_D^{25}$ +27.1° (*c* 1.02, H_2O). $\lambda_{max}^{H_2O}$ 274 nm (ε 8400). This product was identified with an authentic specimen.[1] **13** was also obtained in a 59% yield by carrying out this reaction at 150°C for 3 hr.

*Examination for the Potential Activating Agents by Means of the Condensation Reaction of **6** with **5a**.* The reactions of the examination were carried out with each potential compound under the conditions summarized in Table 1 or by managing to make the reaction system homogeneous; the resultant reaction mixtures were treated in the same way as has been described in the first example of this section. On the basis of the properties of the potential agents applied, the procedures for their removal from the resultant mixtures were varied as below. a) Phenols, *p*-toluene-, and *p*-chlorobenzenesulfonamide: The washing procedure of the organic solution of each resultant mixture was carried out with a 1M aqueous sodium hydroxide solution. b) Carboxylic acids: The procedure was carried out with an aqueous sodium carbonate or bicarbonate solution. c) *p*-Chloro- and *p*-methoxynitrobenzene: These compounds were removed by steam distillation. d) The other amides and acid anhydrides: These were separated by the column chromatography of the resultant reaction mixtures; that is, the mixtures were treated on a short column (d: 3 cm) packed with Mallinckrodt silicic acid (100 mesh, 45 g); the column was first eluted with chloroform to give the potential activating agents as the first, and **5a** as the second fraction. Successive elution with benzene–methanol (9: 1) gave the tetra-*O*-acetate of **9** as the third fraction; unchanged **6** was obtained by the following elution with ethanol. The third fraction thus obtained was evaporated at 30—40°C, and then again at 100°C, finally to a half-glassy sirup, and weighed. The purity of each of the above products can be checked NMR spectroscopically by a comparison of the ratio of 2′-*O*-acetyl (δ 1.92 ppm) to other *O*-acetyl (*ca.* δ 2.06 ppm) signals in the integration curve. The yields demonstrated in Table 1 were calculated from the weight and this ratio in the NMR spectra of each product. To make sure of the composition of each product, the products were examined by tlc (eluting solvent: benzene–methanol=9: 1 v/v). In the case of *p*-nitrophenol (**7**), *p*-nitrophenyl acetate (*ca.* 100 mg) was obtained as a fraction before that of **7**.

Preparation of Molecular Compounds. As has been described in the second example of this section, the potential activating agents were each dissolved in hot chloroform together with an equimolar amount of **6**, after which the solution was allowed to cool at room temperature for crystallization. The precipitated crystals were subsequently filtered and dried at 110°C *in vacuo* over phosphorus pentoxide. The IR spectra of the molecular compounds of **6** with *m*-nitrophenol (**14**), with *o*-(**15**), *m*-nitrobenzoic acid (**16**), and with salicylic acid (**17**) showed the same tendency as has been described in the case of **11**. The experimental results are summarized in Table 2. No new absorption band was, on the other hand, observed in either the UV or the visible region spectrum similar to those of **11**. Almost the same results were obtained by the use of benzene, toluene, or xylene as the solvent for the preparation.

Preparation of the Molecular Compound of Caffeine with p-*Nitrophenol (**7**).* As has been described in the previous experiment, equimolar amounts of caffeine (1.95 g, 10 mmol) and **7** (1.60 g, 11 mmol) were dissolved in xylene (50 ml) under reflux, and the resultant solution was allowed to cool at room temperature for crystallization. The needles thus precipitated were filtered and dried at 110°C over phosphorus pentoxide *in vacuo* to give the molecular compound (3.20 g, 95% yield). Mp 154.5—156°C. Found: C, 50.36; H, 4.61; N, 20.64%. Calcd for $C_{14}H_{15}N_5O_5$: C, 50.45; H, 4.54; N, 21.00%. IR (KBr): 3170 cm^{-1} (phenolic OH).

The authors are grateful to the Ministry of Education, Japanese Government, for a Scientific Research Grant-in-Aid, and to the Kurata Foundation for a grant. They also wish to thank Professor Takeshi Nakajima, Tohoku University, for his valuable suggestion as to the structure of the molecular compounds, and Mr. Masaru Koezuka for his help with elemental analysis.

12) E. Fischer und B. Helferich, *ibid.*, **47**, 210 (1914).
13) C. S. Hudson and J. K. Dale, *J. Amer. Chem. Soc.*, **37**, 1264 (1915).
14) H. Zinner, *Chem. Ber.*, **83**, 517 (1950).

The Reversible Acylation of β-Diketone with Acyl Chloride in the Presence of Aluminum Chloride

Kiyotada MATSUI, Masatoshi MOTOI, and Tetsuro NOJIRI*

Department of Industrial Chemistry, Faculty of Technology, Kanazawa University, Kodatsuno, Kanazawa
**Fuji Chemical Industry Co., Kamiichi, Toyama*

(Received June 21, 1972)

The treatment of acetylacetone (I) with *n*-butyryl chloride in the presence of aluminum chloride in nitrobenzene gave *n*-butyrylacetone and di-*n*-butyrylmethane at 45°C. The same products were obtained, along with *n*-butyric acid, when *n*-butyrylacetone or di-*n*-butyrylmethane was treated with acetyl chloride under analogous conditions. The reactions between I and benzoyl chloride and between benzoylacetone or dibenzoylmethane and acetyl chloride gave products consisting of I, benzoylacetone, dibenzoyl-, diacetylbenzoyl-, acetyldibenzoyl-, tribenzoyl-methane, and benzoic acid. These findings show that β-diketone can reversibly react with acyl chloride to form new β-diketones by way of the mixed triacylmethanes. The acylation mechanism is discussed.

In our previous papers[1] it was shown that the aluminum chloride-catalyzed acylation of ethyl acetoacetate with aroyl chloride, accompanied by deacylation, involves the following sequence of four-step equilibria among the substrate and products in the presence of aroyl and acetyl chlorides:

$$(CH_3CO)_2CHCOOC_2H_5 \rightleftarrows CH_3COCH_2COOC_2H_5 \rightleftarrows$$
$$CH_3\overset{\overset{ArCO}{|}}{C}HCOOC_2H_5 \rightleftarrows ArCOCH_2COOC_2H_5 \rightleftarrows$$
$$(ArCO)_2CHCOOC_2H_5$$

The similar acylation[2] of acetylacetone (I) with *n*-butyryl chloride was established to proceed by the coordination of the acyl chloride with the metal atom of the β-diketone complex. The purpose of this paper is to give more information on the reaction of β-diketones with acid chlorides other than the *n*-butyryl chloride.

As is shown in Table 1, the butyrylation of I with *n*-butyryl chloride and the acetylation of *n*-butyrylacetone or di-*n*-butyrylmethane with acetyl chloride in the presence of aluminum chloride in nitrobenzene all gave the same products—I, *n*-butyrylacetone, di-*n*-butyrylmethane, and *n*-butyric acid—at 45°C. The latter acid obviously results from the hydrolysis of the *n*-butyryl chloride derived from the starting butyrylated ketones except when *n*-butyryl chloride is used. The products resulting from either the benzoylation of I or the acetylation of benzoylacetone or dibenzoylmethane consisted of I, benzoylacetone, dibenzoylmethane, and benzoic acid; also, triacylmethanes and aluminum chelate of dibenzoylmethane, $[(C_6H_5CO)_2CH]_3Al$, were obtained under certain conditions. Tribenzoylmethane was isolated in every case, while acetyldibenzoyl- and diacetylbenzoyl-methane were not always isolated. The latter was obtained particularly, along with the former in small amounts, when I was benzoylated in a stream of dry nitrogen gas for a shorter reaction time in order to avoid the effect of the hydrogen chloride formed. Both mixed triacylmethanes were also obtained from aluminum trisacetylacetonate, which could undergo benzoylation without liberating a large amount of hydrogen chloride because of its enolate structure. From these facts, it appears that the mixed triacylmethanes tend to decompose more easily into β-diketones and acyl chlorides as the amount of hydrogen chloride formed is increased. The acid chlorides thus formed can react with any β-diketones present in the reacting mixture to yield the triacylmethanes. Among these, the mixed triacylmethanes act as intermediates for the formation of the new β-diketones. Apparently, there is the following equilibrium in the presence of the acyl chlorides and aluminum chloride:

$$CH_3COCH_2COR \rightleftarrows CH_3\overset{\overset{ArCO}{|}}{C}HCOR \rightleftarrows$$
$$RCOCH_2COAr \rightleftarrows \overset{\overset{COR}{|}}{C}H(COAr)_2$$
$$R = CH_3 \text{ or } Ar$$

Triacetylmethane, though not isolated, seems to take part in this equilibrium, because it is known to be synthesized by the aluminum chloride-catalyzed reaction of I with acetyl chloride.[3]

In the presence of various amounts of aluminum chloride, I was benzoylated with 2 equivalents of benzoyl chloride under comparable conditions. The use of a 0.3 equivalent of the condensing agent afforded the benzoylated ketones (including tribenzoylmethane) and the aluminum chelate of dibenzoylmethane in a relatively low and a high yield respectively, but the former were obtained in high yields at the expense of the latter on the increase of the condensing agent to a 0.5 or 0.7 equivalent. Accordingly, it seems that the increase in the condensing agent allows the benzoylation to proceed with a high yield by hindering the formation of the stable aluminum chelate. The control of the chelate-ring formation by aluminum chloride has also been visualized as spectral evidence for the action of aluminum chloride on I[2] or aluminum trisacetylacetonate.[4] The above variation in yield with the amount of aluminum chloride was also observed with the butyrylation reaction.[2] In this case,

1) K. Matsui and T. Nojiri, *Nippon Kagaku Zasshi*, **86**, 531 (1965); T. Nojiri and K. Matsui, *ibid.*, **87**, 880 (1966).

2) T. Nojiri, I. Hashimoto, M. Motoi, and K. Matsui, This Bulletin, **42**, 3359 (1969).

3) L. Birkenbach, K. Kellermann, and W. Stein, *Ber.*, **65**, 1075 (1932).

4) T. Nojiri, M. Motoi, and I. Hashimoto, This Bulletin, **44**, 850 (1971).

Table 1. Reaction of β-diketone with acyl chloride

Substrate (15 mmol)	Reactant RCOCl (mol ratio)	$AlCl_3$ (mol ratio)	Reaction time (hr)	I	$BtCH_2Ac$	Bt_2CH_2		BtOH
I	BtCl 2	0.5	1	(34)	22	0		
I	BtCl 1	1	1	(25)	33	5		
$BtCH_2Ac$	AcCl 1	1	1	25	(34)	6		21
Bt_2CH_2	AcCl 1	1	1	7	36	(29)		20
					$BzCH_2Ac$	Bz_2CH_2	Bz_3CH	BzOH
I	BzCl 2	2	3	(4)	23	33 0	4	
I	BzCl 2	1.2	3	(4)	32	34 [1]	5	
I	BzCl 2	0.7	3	(5)	40	36 [1]	8[c]	
I	BzCl 2	0.5	3	(4)	46	36 [2]	6[c]	
I	BzCl 2	0.3	3	(5)	47	20 [9]	3[c]	
I	BzCl 2	0.5	1	(5)	50	29 [1]	4	
I	BzCl 1	0.5	1.5, N_2	(8)	43	7 [4]	tr[d]	
I	BzCl 1	0.5	3	(13)	29	6 0	tr	
$BzCH_2Ac$	BzCl 1	0.5	3	tr	(23)	43 [29]	3	
$BzCH_2Ac$	AcCl 1.2	0.5	3	12	(39)	10 [tr]	tr[c]	5
Bz_2CH_2	AcCl 1.2	0.5	3	tr	24	(53) [36]	tr	21
$(Ac_2CH)_3Al$ (5 mmol)	BzCl 6	1.5	3	3	27	41 [11]	4[e]	
Ac_2CHBz	BzCl 1	0.5	3	tr	35	35 [12]	2[f]	
I	BzCl 2	2	5[b]		12	37 [6]	1	
					p-NO_2Bz-CH_2Ac	(*p*-$NO_2Bz)_2CH_2$		
I	*p*-NO_2BzCl 2	0.5	3		29	44 [35]		
I	*p*-NO_2BzCl 2	2	5[b]		5	67 [40]		
I	*p*-NO_2BzCl 3	3	5[b]		2	85 [40]		
						$(ClAc)_2CH_2$		
I	ClAcCl 2	1[a]	3[b]			41		

Solvent: $C_6H_5NO_2$ 10 ml, a) $(ClCH_2)_2$ 5 ml; reaction temp.: 45°C, b) 55°C; N_2: The reaction was carried out in a stream of nitrogen gas. ( ): The yield of recovered material. [ ]: The yield of Al chelate of β-diketone (included in the yield of β-diketone). c) less than 1% yield of acetyldibenzoylmethane. d) both 1.7%, yields of diacetylbenzoyl- and acetyldibenzoyl-methane; e) 2.2, 0.2%. f) 2.3, 0.7% yields respectively.

however, relatively large amounts of aluminum chloride were required to give the products in a maximum yield, but no aluminum chelate was obtained, even when a small amount of aluminum chloride was used. On the other hand, the fact that the yields of the benzoylated ketones were decreased on the use of more than 1.2 equivalents of aluminum chloride suggests that the liberation of aluminum chloride causes the condensation to proceed, and that an excess of aluminum chloride tends to coordinate with the acyl chloride resulting from the coordination complex between acyl chloride and dichloroaluminum β-diketonate complex as was pointed out in a previous paper.[2] Such a coordination complex is in the forms of II and III (Scheme 1), which should be in a rapid mobile equilibrium because of the abilities of chlorine and carbonyl oxygen in the acyl chloride to coordinate with the metal atom of enolate. Complex II must be more favorable for the intramolecular condensation to form triacylmethane, which is then deacylated easily to give β-diketone as shown in Scheme I.

However, there is no denying an acyl exchange through Complex III. Moreover, when an ester was used as the acylating agent, a coordination complex corresponding to III proved to lead directly to a new

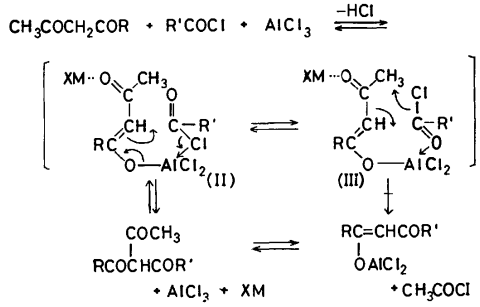

MX=$AlCl_3$ or HCl; R=CH_3 or C_3H_7, where R'=C_3H_7; R=CH_3 or C_6H_5 where R'=C_6H_5

Scheme I.

β-diketonate. Such a transacylation will be reported in our next paper.[5]

In the reaction of benzoylacetone with benzoyl chloride or in that of dibenzoylmethane with acetyl chloride, the yields of dibenzoylmethane and especially of its aluminum chelate were far higher than those from the reaction of I with benzoyl chloride. The high yield of the aluminum chelate can be explained as being due mainly to high concentrations of dibenzoylmethane

5) K. Matsui and M. Motoi, This Bulletin, **46**, 565 (1973).

compared with those of aluminum chloride in the reacting mixture. However, in the reaction of I with *p*-nitrobenzoyl chloride the high yields of di-*p*-nitrobenzoylmethane and its aluminum chelate seem to be ascribable to the susceptibility of certain intermediates to acylation or deacetylation, as well as to the high stabilities of the final products.

From the standpoint of synthetic chemistry, this acylation of I is useful for preparing β-diketones, such as di-*p*-nitrobenzoylmethane and di-chloroacetylmethane, sensible to alkali. Their yields are shown in Table 1.

Experimental

Materials. The benzoylacetone[6] (mp 59°C) and the dibenzoylmethane[7] (mp 79—80°C) were prepared according to the literature. Commercial acetyl chloride was used after distillation; bp 51—52°C. The chloroacetyl[8] (bp 104—105°C), benzoyl[9] (bp 192°C) and *p*-nitrobenzoyl chlorides[9] (bp 160°C/26 mmHg), were prepared from the corresponding carboxylic acids, commercially obtained, according to the literature. The diacetylbenzoyl- and acetyldibenzoyl-methane were prepared by the benzoylation of acetyl- and benzoylacetone respectively, according to the Schotten-Baumann method; the former has mp of 30—31°C and bp of 107—108°C/2 mmHg, its copper chelate, mp 247—249°C (benzene), (lit,[10] mp 35°C, bp 167°C/22 mmHg, copper chelate mp 228°C), while the latter has mp of 106.5—107.5°C, (lit,[11] 99—101°C). The other materials were described previously.[2]

Acylation Method and Separation Procedure for Product. Both were the same as in the previous paper,[2] except for the following:

a) Butyrylated Product: For the estimation of *n*-butyric acid, the sodium bicarbonate extract was acidified with sulfuric acid and then extracted with ether. The ether extract was dried, evaporated carefully, and then analyzed, using acetophenone as the internal standard, by gas-liquid chromatography at 130°C.

b) Benzoylated Product: The reaction mixture, quenched with crushed ice and hydrochloric acid, was shaken with ether to separate it into 2 layers. The lower layer was extracted with ether 2 days later; then, after 5 or more days, the dibenzoylmethane which gradually crystallized out was collected by filtration. The upper layer, freed from aluminum chloride, was occasionally shaken with an aqueous sodium bicarbonate solution until the Beilstein test for benzoyl chloride became negligible. The partial distillation of the aqueous extract gave a distillate containing a slight amount of acetophenone (obtained as its 2,4-dinitrophenylhydrazone). The pot residue was acidified to give benzoic acid. The above organic layers were combined and separated successively into a crude copper chelate of each, diacetylbenzoylmethane, acetylacetone, acetyldibenzoylmethane, and benzoylacetone, according to our usual fractionation method,[12] which consists of fractional extraction (the step-by-step extraction of an acid with small, successive portions of alkali, followed by thin-layer chromatographic test of the acidified extracts) and subsequent treatment with a copper acetate solution. The remaining organic layer was steam-distilled *in vacuo* to remove the nitrobenzene. The residual solid was triturated with ether, and then an aluminum chelate of dibenzoylmethane was filtered off.[13] The ethereal filtrate was shaken with a copper acetate solution to give a copper chelate of dibenzoylmethane. This chelate is insoluble in ether after drying.

The copper chelates suspended in their ether solution, when consisting mainly of the copper chelates of the first three substances above, were freed from the chelate of acetylacetone by washing them with aqueous acetic acids (3%); then the ether was replaced with a small amount of benzene to crystallize a chelate of acetyldibenzoylmethane, which was collected by filtration. The solvent of the filtrate was replaced with a small amount of ether to crystallize the chelate of diacetylbenzoylmethane. The ethereal mother liquor gave a slight amount of the chelate of benzoylacetone on concentration. The above aqueous acetic acid washings and the copper acetate solution used for the chelate preparation were shaken with methylene chloride in order to obtain the chelate of acetylacetone.

Acetyldibenzoylmethane: Its copper chelate was shaken with ether and hydrochloric acid; the ether layer was then evaporated to leave colorless crystals; mp 106—107°C (ligroin).

Diacetylbenzoylmethane: Its copper chelate, slightly soluble in ether, was recrystallized from benzene to give cobalt-blue crystals (mp 246—248°C), which were decomposed as above to give an oil.

Tribenzoylmethane: This substance, present in both free and copper chelate forms, was present mainly in the crude copper chelates of benzoylacetone and of dibenzoylmethane. Each crude chelate (weighed) was decomposed as above to give a solid, which was dissolved in acetone–ethyl acetate; then, after 24 hr, the solvent was replaced with ether to give tribenzoylmethane in an ether-insoluble form (mp 235—237°C (acetone)). This tribenzoylmethane does not form its copper chelate directly.

Acetylacetone: Its copper chelate was decomposed to give a liquid. Its 2,4-dinitrophenylhydrazone has mp of 125—126°C (lit,[14] 122°C).

Benzoylacetone: The recrystallization of the copper chelate from methanol gave greenish-blue needles; mp 200—202°C (lit,[15] 195—196°C). This chelate was decomposed as above to give colorless needles; mp 60—61°C (petroleum ether).

Dibenzoylmethane: The decomposition of its copper or aluminum chelate gave light yellow needles; mp 80—81°C (methanol).

All the above substances were identified by the mixed-melting point method and/or by means of their similarity in thin-layer chromatographic behavior with authentic samples, except for impossible cases. Each yield other than that of tribenzoylmethane was calculated from the weight of the copper chelate.

c) p-Nitrobenzoylated Product: The reaction mixture quenched was shaken with a small amount of ether; then

6) G. T. Morgan and R. W. Thomason, *J. Chem. Soc.*, **125**, 754 (1924).

7) A. Magnani and S. M. McElvain, "Organic Syntheses," Coll. Vol. III. p. 251 (1955).

8) W. J. Hickinbottom, "Reactions of Organic Compounds," Longmans, Green and Co. Inc., New York (1957), p. 292.

9) R. Adams and R. L. Jenkins, "Organic Syntheses," Coll. Vol. I. p. 394 (1956).

10) J. U. Nef, *Ann. Chem.*, **277**, 59 (1894).

11) L. Claisen, *ibid.*, **291**, 25 (1896).

12) K. Matsui, T. Nojiri, M. Motoi, and R. Takatsuka, *Yuki Gosei Kagaku Kyokai Shi*, **28**, 943 (1970).

13) H. Kaneyuki, This Bulletin, **35**, 523 (1962).

14) R. L. Shriner, R. C. Fuson, and D. Y. Curtin, "Systematic Identification of Organic Compounds," 4th ed. John Wiley & Sons, Inc., New York (1956), p. 316.

15) W. Wislicenus and W. Stoebner, *Ber.*, **35**, 539 (1902).

it was separated into two layers with a centrifuge. From the organic layer a solid was filtered off and then washed with ether. The solid was dissolved in tetrahydrofuran and acidified with hydrochloric acid to give di-*p*-nitrobenzoylmethane; mp 248°C (tetrahydrofuran). The combined organic solution was freed from *p*-nitrobenzoic acid with a sodium bicarbonate solution; then it was steam-distilled *in vacuo*. The pot residue was triturated with ether, and then di-*p*-nitrobenzoylmethane was filtered off. The ethereal filtrate, after it had been shaken with a copper acetate solution, was evaporated to dryness and triturated with methanol; then a copper chelate was filtered off. This, when decomposed, gave *p*-nitrobenzoylacetone; mp 115—116°C (methanol). (lit,[16] 112—113.5°C), (Found: N, 7.1%). The concentration of the methanolic filtrate gave a small amount of *p*-nitroacetophenone; mp 80—81°C (ethanol). These substances were identified by the mixed-melting-point method with authentic samples.[13]

16) H. Burgess, *J. Chem. Soc.*, **1927**, 2017.

d) Dichloroacetylmethane: The reaction mixture, quenched, was shaken with ether. After washing with water, the ether layer was shaken with a copper acetate solution; then it was filtered and washed with ether to give a crystalline copper chelate. The upper layer of the filtrate was washed with dilute acetic acid and subsequently concentrated to give the same chelate as above. Dilute sulfuric acid (10%) was added in portions to the mixture of the copper chelates and fresh ether with stirring until the ether layer became colorless. The ether layer was then dried over sodium sulfate, concentrated, and cooled to give colorless needles; mp 41.5—42.5°C (ether–petroleum ether), (lit,[17] solid at 0°C). Found: C, 35.84; H, 3.56; Cl, 41.66%; mol wt (benzene), 168. Calcd for $C_5H_6Cl_2O_2$: C, 35.50; H, 3.55; Cl, 41.95%; mol wt, 169.

The authors are grateful to Mr. Yoshitaka Itatani of the Faculty of Pharmacy, Kanazawa University, for his elemental analyses.

17) A. Stieglits and O. Horn, *Chem. Ber.*, **84**, 607 (1951).

BULLETIN OF THE CHEMICAL SOCIETY OF JAPAN, VOL. 46, 565—569 (1973)

The Transacylation between β-Diketone and Ester in the Presence of Aluminum Chloride

Kiyotada MATSUI and Masatoshi MOTOI

Department of Industrial Chemistry, Faculty of Technology, Kanazawa University, Kodatsuno, Kanazawa

(Received June 21, 1972)

The reaction of acetylacetone with an equivalent of phenyl benzoate in the presence of 2 equivalents of aluminum chloride in nitrobenzene afforded benzoylacetone (26% yield), dibenzoylmethane (4%), and phenyl acetate (37%), together with small amounts of phenolic ketones at 45°C. The total yield, based on the acyl groups introduced into the β-diketones, is similar to the yield of the ester newly formed. Such a similarity, suggestive of a transacylation, was also observed both on the use of *p*-nitrophenyl benzoate and on the treatment of benzoylacetone with phenyl benzoate or on that of dibenzoylmethane with *p*-nitrophenyl acetate. The non-formation of triacylmethanes is a strong evidence for the transacylation reaction, in which β-diketones and some esters exchange acyl groups directly. The analogous treatment of acetylacetone with α-naphthyl benzoate produced phenolic ketones, such as 2-acetyl- and 4-acetyl-1-naphthol, and the same benzoylated ketones as above in yields of 30 and 32% respectively. The considerably higher ratio of the 2-acetyl to the 4-acetyl isomer than that from the Fries rearrangement of α-naphthyl acetate indicates that another transacylation is accompanied by a rearrangement proceeding through complexes different from those in the Fries rearrangement.

In the course of studies[1] of the aluminum chloride-catalyzed acylation reaction of active methylene compounds with acid chlorides, the use of *p*-nitrophenyl benzoate, which is known to react only as an acylating agent for the Friedel-Crafts reaction,[2] was tried in the acylation of acetylacetone (I) in order to obtain insight into the mechanism of this acylation reaction. Thus, benzoylated ketones, such as benzoylacetone (II) and dibenzoylmethane (III), and *p*-nitrophenyl acetate were both obtained in about the same yields:

$$(CH_3CO)_2CH_2 + p\text{-}O_2NC_6H_4OOCC_6H_5 \longrightarrow CH_3CO\text{-}CH_2COC_6H_5 + (C_6H_5CO)_2CH_2 + p\text{-}O_2NC_6H_4OOCCH_3$$

This seems to imply that a transacylation between the reactants is involved in this unusual acylation reaction. The purpose of this paper is to report on such reactions between β-diketones and some esters.

The reaction of I with an equivalent of phenyl benzoate in the presence of an equivalent of aluminum chloride in nitrobenzene at 45°C for 3 hr gave II and phenyl acetate in low yields, as is shown in Table 1. The increase in the condensing agent to 2 equivalents afforded III in addition to the foregoing products, all in noticeably high yields, together with small amounts of phenolic ketones, such as *o*-hydroxy-, *p*-hydroxyacetophenone, and *p*-hydroxybenzophenone. The formation of III can be explained as being due to the benzoylation of the II formed, because the similar benzoylation of II gave III and phenyl acetate in about the same yields. The yields of the main prod-

1) a) T. Nojiri, I. Hashimoto, M. Motoi, and K. Matsui, This Bulletin, **42**, 3359 (1969); b) T. Nojiri, M. Motoi, and I. Hashimoto, *ibid.*, **44**, 850 (1971); c) K. Matsui, M. Motoi, and T. Nojiri, *ibid.*, **46**, 562 (1973).

2) E. H. Man and C. R. Hauser, *J. Org. Chem.*, **17**, 397 (1952).

TABLE 1. REACTIONS OF β-DIKETONE WITH ESTER AND OF DIACETYLBENZOYLMETHANE WITH PHENOL

Reactant		Reaction time (hr)	Product (%)						
Substrate (10 mmol)	Acylating agent mol ratio		II	III	PhOAc	1-HO-2-Ac-C_6H_4	1-HO-4-Ac-C_6H_4	1-HO-4-Bz-C_6H_4	PhOBz
I	PhOBz 1[a)]	3	7	—	13				(81)
I	PhOBz 1	3	26	4	37	0.3	1.2	2.1	(55)
I	PhOBz 1[a')]	3	28	4	37	0.7	4.0	2.2	(57)
I	PhOBz 1	1	15	—	23	tr	tr	tr	(76)
I	PhOBz 1	20	40	15	57	2.7	11.7	5.8	(19)
I	PhOBz 1	3[c)]	32	7	47	1.0	4.2	2.3	(44)
I	PhOBz 2	3	31[d)]	5[d)]	47[d)]	0.7	0.6	1.2	(75)
II	PhOBz 1	3	(45)	30	33	0.4	1.2	1.5	(64)
I	PhOBz 1[b)]	3	9	tr	12	tr	tr	tr	(85)
I	PhOBz 1[b)]	20	19	1	29	0.4	0.7	0.6	(67)
$(Ac_2CH)_3Al$ (10/3 mmol)	PhOBz 3	3	3	—	4	tr	tr	tr	(93)
PhOH	Ac_2CHBz 1	3	57	—	64		2.4		[e)]
III	PhOAc 1	3	0	(97)	(79)	0.8	4.7	0	0
					p-NO_2-C_6H_4OAc				*p*-NO_2-C_6H_4OBz
I	*p*-NO_2-C_6H_4OBz 1[a)]	3	tr	0	0				(99)
I	*p*-NO_2-C_6H_4OBz 1	3	39	20	76				(5)
III	*p*-NO_2-C_6H_4OAc 1	3	14	(86)	(43)				14
					p-Me-C_6H_4OAc				*p*-Me-C_6H_4OBz
I	*p*-MeC_6H_4OBz 1	3	21	1	33		[f)]		(67)
					o-Me-C_6H_4OAc				*o*-Me-C_6H_4OBz
I	*o*-MeC_6H_4OBz 1	3	17	1	23		[f)]		(70)
			p-$NO_2C_6H_4CO$-CH_2Ac		PhOAc				$PhOCOC_6H_4$-NO_2-*p*
I	$PhOCOC_6H_4NO_2$-*p* 1	3	3	—	4				(98)

$AlCl_3$: mol ratio 2, a) 1, a') 3; solvent: $C_6H_5NO_2$ 7 ml, b) $(ClCH_2)_2$ 7 ml; reaction temp.: 45°C, c) 55°C; d) The yields based on I, the others based on phenylbenzoate; ( ): the yields of recovered materials; e) 8 and 30% yields of diacetylbenzoylmethane and of phenol respectively; f) Identification of the phenolic ketones could not be effected because of small amounts.

ucts were not increased adequately by the increase either in the condensing agent to 3 equivalents or in the acylating agent to 2 equivalents. The rise in the reaction temperature to 55°C led to some increase in yields, and the extension of the reaction time to 20 hr, giving relatively higher yields of the benzoylated ketones, resulted in an increase in the phenolic ketones at the expense of both phenyl acetate and recovered benzoate. The other products isolated were phenol, benzoic acid (both in 1—8% yields), and the unchanged I and phenyl benzoate; no triacylmethane was isolated, in contrast with the results of a similar acylation with acid chlorides.[1c)] However, there is one common feature—the acylation with either the ester or the *n*-butyryl chloride[1a)] requires 2 equivalents of aluminum chloride in order to obtain a satisfactory yield. Such a requirement for the condensing agent was also observed, more markedly, in the reaction of I with *p*-nitrophenyl benzoate. On the other hand, the similarity of the total yield based on the benzoyl groups introduced into the β-diketones (*e.g.*, the yield of III obtained from I, noted in Table 1, should be doubled) to the yield of phenyl acetate is suggestive of a transacylation during the reaction.

TABLE 2. FRIES REARRANGEMENT OF ESTER AND REACTION BETWEEN PHENOL AND ACYL CHLORIDE AT 45°C

Reactant (10 mmol)	Product (%)				
	1-HO-2-Ac-C_6H_4	1-HO-4-Ac-C_6H_4	1-HO-4-Bz-C_6H_4	PhOAc	PhOBz
PhOAc	7	9		(75)	
PhOH+AcCl	14	50		30	
PhOBz			4		(89)
PhOH+BzCl			22		72

$AlCl_3$: 10 mmol; solvent: $C_6H_5NO_2$ 7 ml; reaction time: 3 hr; ( ): the yield of recovered material.

The esters present in the reacting mixture are subject to some extent to the rearrangement to yield phenolic ketones, but it is a question whether or not the formation of these products is due to acyl chlorides, which may be generated as intermediates because of the similarity of the conditions to those for the acylation with acyl chloride.[1c)] Therefore, the reaction of phenol

with acid chloride and the Fries rearrangement of the phenyl ester were carried out under conditions similar to those used for the present reaction. In consequence, in the reaction between I and phenyl benzoate, the slight yields of hydroxyacetophenones, contrasting with the moderate yield of the phenyl acetate, are due to the Fries rearrangement of the phenyl acetate formed, not to the reaction of phenol with acetyl chloride (Table 2). Similarly, as compared with the moderate yield of the benzoylated ketones or of the unaltered benzoic ester, the low yield of *p*-hydroxybenzophenone is ascribable to the Fries rearrangement of the phenyl benzoate used, not to the reaction of phenol with benzoyl chloride. Judging from these facts, not only the phenolic ketones, but also the acetic ester and β-ketones obtained, do not seem to be formed by the action of the acyl chlorides suspected of being intermediates.

With the benzoylation of aluminum trisacetylacetonate, the use of benzoyl chloride gave II, III, and tribenzoylmethane in considerably high yields, similar to those from the analogous benzoylation of I,[1c] whereas the use of phenyl benzoate gave only II in a 3% yield (Table 1). The use of *p*-nitrobenzoyl chloride for the acylation of I afforded di-*p*-nitrobenzoylmethane in a high yield, while a similar acylation with phenyl *p*-nitrobenzoate gave a less acylated product, *p*-nitrobenzoylacetone, in a low yield. The ester as acylating agent seems to follow a course differing substantially from that of acid chloride.

In the aluminum chloride-catalyzed reaction between synthesized diacetylbenzoylmethane and phenol (Scheme 1, Path c, R=CH_3), II and phenyl acetate were obtained in relatively high yields (Table 1), but the triacylmethane, which has not been isolated, was recovered and the phenol remained unchanged in a considerably higher yield than that from the present acylation reaction. This suggests that the triacylmethane capable of behaving as an acylating agent, if formed as an intermediate, can survive the reaction of I with phenyl benzoate. However, not even the isolation of stable tribenzoylmethane was accomplished. The above findings indicate that the present acylation, predominating over the Fries rearrangement, proceeds by transacylation between I (or II) and phenyl benzoate (Path a), without forming triacylmethane (Path b). The transacylation can be explained in terms of an intramolecular condensation of a complex which is generated by the ability of the carbonyl oxygen of the ester to coordinate with the metal atom of the dichloroaluminum β-diketonate complex proposed previously.[1a] The reaction mechanism is illustrated in Scheme 1.

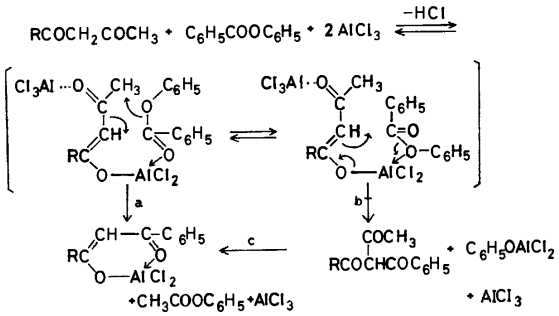

R=CH_3 or C_6H_5

Scheme 1.

This mechanism is also supported by the idea that the acylation of I with an ester, giving higher yields of β-diketones in nitrobenzene than those in ethylene chloride, seems to proceed by some charge separation in the transition state.

The acylation of I with different benzoic esters showed that, except for ethyl benzoate which failed to react, the substituted phenyl benzoates gave decreasing yields of β-diketones in this order: *p*-nitrophenyl>phenyl>*p*-cresyl>*o*-cresyl benzoate. With acetic esters, phenyl acetate failed to react with III, whereas *p*-nitrophenyl acetate did react to give equimolar amounts of II and *p*-nitrophenyl benzoate.

Table 3. Reaction of acetylacetone with naphthyl benzoate, Fries rearrangement of naphthyl ester, and reaction of naphthol with acyl chloride at 45°C

Reactant (10 mmol)	Product (%)						
	II	III		1-HO-2-Ac-$C_{10}H_6$	1-HO-4-Ac-$C_{10}H_6$	1-HO-4-Bz-$C_{10}H_6$	α-$C_{10}H_7$-OBz
I+α-$C_{10}H_7OBz$[a]	26	3		21	9	21	(30)
α-$C_{10}H_7OAc$				50	41		
α-$C_{10}H_7OH$+AcCl				33	44		
α-$C_{10}H_7OBz$						46	
α-$C_{10}H_7OH$+BzCl						66	
			β-$C_{10}H_7$-OAc			2-HO-1-Bz-$C_{10}H_6$	β-$C_{10}H_7OBz$
I+β-$C_{10}H_7OBz$[a]	22	2	16			13	(47)
β-$C_{10}H_7OAc$			(79)				
β-$C_{10}H_7OH$+AcCl			90				
β-$C_{10}H_7OBz$						37	(55)
β-$C_{10}H_7OH$+BzCl						72	21

$AlCl_3$: mol ratio 1, a) .2; solvent: $C_6H_5NO_2$ 7 ml; reaction time: 3 hr; ( ): the yield of recovered material.

These facts indicate that the transacylation is facilitated by electron-attracting groups in the phenol portion of the ester and rendered somewhat difficult by electron-donating groups. With substituted benzoic esters other than that described above, phenyl *p*- and *o*-toluate also gave slight amounts of copper complexes from the β-diketone fraction separated from the reaction mixture; therefore, further studies were not undertaken.

α-Naphthyl benzoate and its β-isomer, when used, were subjected to the Fries rearrangement to form relatively large amounts of 4-benzoyl-1- and 1-benzoyl-2-naphthol respectively, giving both the foregoing β-diketones. Simultaneously, the latter ester gave β-naphthyl acetate, whereas the former gave 2-acetyl- and 4-acetyl-1-naphthol, instead of the acetic ester (Table 3). Here again, the two yields of the benzoylated ketones and of acetyl-1-naphthols are similar to each other. The Fries rearrangement of α-naphthyl acetate and the acylation of α-naphthol with acetyl chloride, when carried out under conditions comparable to those of the present reaction, gave isomeric mixtures of acetyl-1-naphthols in the 2-acetyl/4-acetyl ratios of 1.2 and 0.8 respectively. The higher isomer ratio of 2.3 obtained from the reaction of I with α-naphthyl benzoate suggests that, independently of the intermediate α-naphthyl acetate as well as of acetyl chloride, the acetyl-1-naphthols form by way of complexes different from those in the Fries rearrangement.[3] It can be deduced that an acetylium ion to be formed from a coordination complex as is illustrated in Scheme 1, concurrent with the closure of the chelate ring of the new β-diketonate, can uniquely complex with a leaving α-naphthoxide ion without becoming free; then it can migrate more easily to the 2 position in the nucleus to give the isomeric mixture.

Experimental

Materials. The following benzoic esters were prepared from the corresponding phenols and benzoyl chloride according to the Schotten-Baumann method: phenyl (mp 70—71°C (lit,[4] 70°C)), α-naphthyl (mp 57.5—58.5°C (lit,[5] 56°C)), β-naphthyl (mp 109—109.5°C (lit,[6] 106°C)), and *o*-cresyl benzoate (bp 301°C (lit,[7] 307—308°C/728 mmHg)). *p*-Nitrophenyl (mp 147.5—148.5°C (lit,[8] 142.5°C)), *p*-cresyl benzoate (mp 73°C (lit,[9] 71.5°C)), phenyl *p*-nitrobenzoate (mp 131—132°C (lit,[10] 129°C)), and *p*-nitrophenyl acetate (mp 77.5—78°C (lit,[11] 81—82°C)) were prepared from the corresponding phenols and acid chlorides. α-Naphthyl and β-naphthyl acetate were prepared from the corresponding naphthols and acetic anhydride in the presence of a catalytic amount of concentrated sulfuric acid, which melted at 45.5—46°C (lit,[12] 46°C) and 70—70.5°C (lit,[13] 70°C) respectively.

Reaction Method and Separation Procedure. Both were the same as in our previous paper[1c] except for the use of esters as acylating agents and the following points.

a) Product from the Reaction with Phenyl Benzoate: The reaction mixture, quenched, was shaken with cold hydrochloric acid and ether, and then separated into two layers. The upper layer was freed from benzoic acid with a sodium bicarbonate solution, dried over sodium sulfate, concentrated, and then distilled under reduced pressures (16—20 mmHg). At a later stage of the distillation, a small amount of nitrobenzene was supplied in order to remove the volatile substances completely. From the distillate phenol, phenyl acetate and *o*-hydroxyacetophenone (sometimes a slight amount of acetophenone also) were determined by glpc analysis on a column (0.3×200 cm) packed with polyethylene succinate (30%) on celite (hydrogen flow, 40 ml/min), using dimethyl azelate as the internal standard at 200°C. From the remaining distillate, acetyl- and benzoyl-acetone were obtained as their respective copper chelates according to our fractionation method.[1c,14] This method was also applied to the pot residue to obtain three extracts. The first extract, in ether, was shaken with a copper acetate solution; then the solvent was replaced with a small amount of ether–petroleum ether (1:2) to crystallize a copper chelate of benzoylacetone. The mother liquor was evaporated to leave a crude *p*-hydroxyacetophenone. The same treatment of the second extract gave the same chelate, along with a crude *p*-hydroxybenzophenone. The third extract and extracted residue were combined, evaporated, and then steam distilled *in vacuo* to remove the nitrobenzene. The trituration of the residue with ether gave an ether-insoluble aluminum chelate[1c] of dibenzoylmethane. The resulting ether solution was freed from dibenzoylmethane with a copper acetate solution; it was then evaporated to give phenyl benzoate, which was recrystallized from ethanol. The crude *p*-hydroxy-acetophenone and -benzophenone were treated individually with a dilute sodium hydroxide solution to remove slight amounts of the copper chelates; then they were purified according to the fractional extraction method described in a previous paper.[14] The former melts at 110—111°C, the latter, at 135—136°C. Both melting points were undepressed on admixture with authentic samples.

b) Product from the Reaction with p-*Nitrophenyl Benzoate*: The separation procedure was the same as above except for the following. From the pot residue, much of the *p*-nitrophenyl acetate was removed by crystallizing it from benzene–petroleum ether. The mother liquor was concentrated and then chromatographed on a column packed with silica gel. The eluents used, benzene–petroleum ether (1:1), the same (2:3), benzene, and benzene–ether (3:1), eluted successively dibenzoylmethane, *p*-nitrophenyl benzoate, a mixture, and *p*-nitrophenol respectively. The mixture (weighed) in ether was extracted with successive, small portions of a 0.1N sodium hydroxide solution to obtain benzoylacetone; then it was concentrated to crystallize *p*-nitrophenyl acetate; mp 78—79°C, undepressed on admixture with an authentic sample.

c) Product from the Reaction with o- *or* p-*Cresyl Benzoate*: The mixture distilled with nitrobenzene, after glpc analysis for determining cresyl acetates and cresols, was separated into acetyl– and benzoyl–acetone according to the fractionation method. The pot residue was treated with benzene–

3) M. J. S. Dewar and L. S. Hart, *Tetrahedron*, **26**, 973 (1970).
4) W. J. Wohlleben, *Ber.*, **42**, 4370 (1909).
5) W. Authenrich and P. Mühlinghaus, *ibid*, **40**, 748 (1907).
6) W. Koenigs and R. W. Carl, *ibid.*, **24**, 3900 (1891).
7) A. L. Bernoulli and A. St. Goar, *Helv. Chim. Acta*, **9**, 762 (1926).
8) G. Neumann, *Ber.*, **19**, 2019 (1886).
9) G. Heller, *ibid.*, **46**, 1503 (1913).
10) L. C. Reiford, R. Taft, and H. P. Lankelma, *J. Amer. Chem. Soc.*, **46**, 2054 (1924).
11) A. Kaufmann, *Ber.*, **42**, 3482 (1909).
12) O. Miller, *Ann. Chem*, **208**, 247 (1881).
13) O. Miller, *Ber.*, **14**, 1602 (1881).
14) K. Matsui, T. Nojiri, M. Motoi, and R. Takatsuka, *Yuki Gosei Kagaku Kyokai Shi*, **28**, 943 (1970).

petroleum ether (1: 3) to crystallize *p*-cresyl benzoate. The mother liquor was concentrated and chromatographed using benzene–petroleum ether (1: 1) and benzene–ether (1: 1), which gave *p*-cresyl benzoate and benzoylacetone respectively. *o*-Cresyl benzoate, when used, was determined by a glpc analysis of the pot residue. From the remainder, benzoylacetone was separated by alkaline extraction.

d) Product from the Reaction with α-Naphthyl Benzoate: The pot residue was chromatographed similarly using benzene–petroleum ether (2: 3), the same (1: 1), and benzene–ether (1: 1), which gave three effluents successively. The evaporation of the first effluent gave α-naphthyl benzoate, which was then recrystallized from ether–petroleum ether; mp 58—59°C. The solvent of the second effluent was replaced with ether, freed from dibenzoylmethane as described above, and then extracted fractionally with the 0.1N sodium hydroxide solution to separate 2-acetyl-1-naphthol, which was then recrystallized from petroleum ether–ether; mp 100—101°C (lit,[15] 100—101°C). The concentration of the remaining ether solution gave α-naphthyl benzoate; mp 57—58°C. The third effluent was made up to about 100 ml by the addition of ether; then it was treated as above with the 0.1N sodium hydroxide solution to separate 4-acetyl-1-naphthol, which was subsequently recrystallized from benzene–ethanol; mp 204—206°C (lit,[15] 200—201°C). The solvent of the remaining solution was replaced with benzene to crystallize 4-benzoyl-1-naphthol; mp 165—166°C, (lit,[15] 163—164°C). The mother liquor was separated into 4-acetyl-, 4-benzoyl-1-naphthol, and benzoylacetone according to the fractional extraction method. The melting points of the three acylated naphthols were undepressed on admixture with authentic samples.

e) Product from the Reaction with β-Naphthyl Benzoate: The pot residue was chromatographed using as eluents benzene–petroleum ether (1: 1), the same (3: 1), benzene, and ether; this gave β-naphthyl benzoate, a mixture, β-naphthol, and benzoylacetone respectively. The ether solution of the mixture was freed from dibenzoylmethane as above and then evaporated to leave a solid. This solid in a small amount of benzene was chromatographed using benzene–petroleum ether (3: 2); this gave β-naphthyl acetate (mp 69.5—70°C (ether–petroleum ether)) and 1-benzoyl-2-naphthol (mp 144—145°C (benzene), (lit,[15] 140—141°C)). Both were undepressed on admixture with authentic samples.

f) Product from the Reaction with Phenyl p-*Nitrobenzoate*: The separation procedures were the same as in the case of *a*). The alkaline extract from the ether solution of the pot residue and the ether extract from the aqueous solution containing aluminum chloride both gave *p*-nitrobenzoylacetone. This was then recrystallized from methanol; it melts at 113—114°C, undepressed on admixture with an authentic sample.

g) Product from the Reaction between Diacetylbenzoylmethane and Phenol: The mixture distilled with nitrobenzene, the ethereal extract from the aqueous layer containing aluminum chloride, and the pot residue were separated individually by the usual fractionation method into copper chelates of diacetylbenzoylmethane and of benzoylacetone. However, the former chelate from the pot residue was contaminated with *p*-hydroxyacetophenone, which was isolated by alkaline extraction.

Acylation of Phenol with Acid Chlorides and the Fries Rearrangement of Esters. For the former reaction, phenol was dissolved in a solution of aluminum chloride in nitrobenzene; then acid chloride was added. For the Fries rearrangement, the ester was added to the nitrobenzene solution of aluminum chloride. Each product obtained was treated according to the appropriate separation procedure described above.

15) G. G. Joshi and N. M. Shah, *J. Indian Chem. Soc.*, **29**, 225 (1952).

BULLETIN OF THE CHEMICAL SOCIETY OF JAPAN, VOL. 46, 569—572 (1973)

Putranjic Acid. Synthesis and Stereostructure

Reiko AOYAGI, Yoshihiko MORIYAMA, Takahiko TSUYUKI, and Takeyoshi TAKAHASHI
Department of Chemistry, Faculty of Science, The University of Tokyo, Hongo, Bunkyo-ku, Tokyo
(Received July 6, 1972)

Putranjic acid, isolated from *Putranjiva roxburghii* has been synthesized from friedelane-2,3-dione and has been shown to be (2S)-2-hydroxy-3,4-seco-friedelan-3-oic acid.

Several friedelin derivatives have been isolated from stem-bark, leaves and seeds of *Putranjiva roxburghii* (Euphorbiacea).[1-10] From the acidic fraction of the stem-bark of the plant, Garg and Mitra[1,5] and Seshadri *et al.*[6,8] independently isolated putranjic acid[11] and putric acid, respectively, which were found to be the same triterpene monohydroxy-acid, 2-hydroxy-3,4-seco-friedelan-3-oic acid (I).

1) H. S. Garg and C. R. Mitra, *Phytochemistry*, **7**, 2053 (1968).
2) a) G. R. Chopra, A. C. Jain, and T. R. Seshadri, *Curr. Sci.*, **37**, 301 (1968); *Chem. Abstr.*, **69**, 93685q (1968). b) G. R. Chopra, A. C. Jain, T. R. Seshadri, and G. R. Sood, *Indian J. Chem.*, **8**, 776 (1970); *Chem. Abstr.*, **74**, 1024a (1971).
3) P. Sengupta, A. K. Chakraborty, A. M. Duffield, L. J. Durham, and C. Djerassi, *Tetrahedron*, **24**, 1205 (1968).
4) P. Sengupta and J. Mukherjee, *ibid.*, **24**, 6259 (1968).
5) H. S. Garg and C. R. Mitra, *Tetrahedron Lett.*, **1969** 231.
6) G. R. Chopra, A. C. Jain, and T. R. Seshadri, *Curr. Sci.*, **38**, 101 (1969); *Chem. Abstr.*, **70**, 106704t (1969).
7) G. R. Chopra, A. C. Jain, and T. R. Seshadri, *Indian J. Chem.*, **7**, 1179 (1969); *Chem. Abstr.*, **72**, 67139g (1970).
8) G. R. Chopra, A. C. Jain, and T. R. Seshadri, *Indian J. Chem.*, **8**, 401 (1970); *Chem. Abstr.*, **73**, 45626g (1970).
9) H. S. Garg and C. R. Mitra, *Planta Med.*, **19**, 352 (1971); *Chem. Abstr.*, **75**, 20688g (1971).
10) H. S. Garg and C. R. Mitra, *Phytochemistry*, **10**, 865 (1971).
11) In this paper, we use the name putranjic acid, which was first given by Garg and Mitra to the acid.

The structure of putranjic acid[5,8] has been deduced from spectral and chemical data, although no direct comparison with friedelin derivatives has been made. Thus, the configuration of any asymmetric center in this acid has been left undetermined. In a preliminary communication,[12] we have reported the synthesis of putranjic acid from friedelane-2,3-dione (II). The complete stereostructure of putranjic acid has been shown to be (2S)-2-hydroxy-3,4-seco-friedelan-3-oic acid (III). Detailed experimental data are given below.[13]

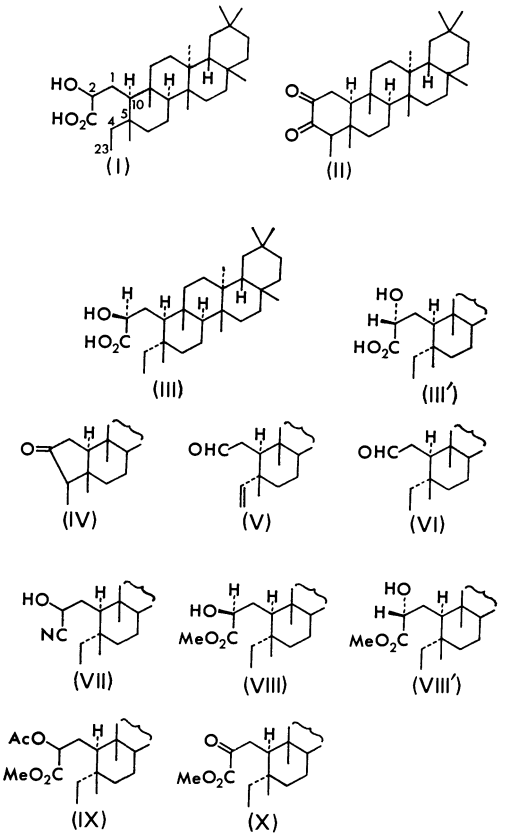

Friedelane-2,3-dione (II)[14] was subjected to benzylic acid rearrangement by refluxing with potassium hydroxide in diethylene glycol. The resulting hydroxy-acid was treated with lead tetraacetate in acetic acid to give norfriedelin (IV),[15] which was shown to contain its epimer by glc examination. On treatment with base, the mixture afforded pure norfriedelin (IV). Thus the alkaline unstable component would probably be 4α-methyl epimer of IV.

Norfriedelin (IV) was irradiated with a high pressure mercury lamp in *n*-hexane and converted into 5α-vinyl-10β-formylmethyl-des-A-friedelane (V),[16] which on catalytic hydrogenation gave 5α-ethyl-10β-formylmethyl-des-A-friedelane (VI).[8] The saturated aldehyde (VI) was identical with a product which had been obtained by photoreaction of friedelin.[17]

The saturated seco-aldehyde (VI) was converted into its cyanohydrin derivative (VII), which was further hydrolyzed with hydrochloric acid and acetic acid. On treatment with diazomethane, the reaction products gave two hydroxy-esters (VIII and VIII') and an acetoxy-ester (IX). The hydroxy-esters (VIII and VIII') were separated by silica gel column chromatography into VIII [mp 176.5—177.0°C, $[\alpha]_D^{25}$ −2.0° ($CHCl_3$)] and VIII' [mp 133—134°C, $[\alpha]_D^{25}$ +2.5° ($CHCl_3$)]. The hydroxy-ester (VIII) was identical with methyl putrate (methyl putranjate,[1] mp 176°C, $[\alpha]_D$ −23.5°; methyl putrate,[8] mp 175—176°C, $[\alpha]_D$ −8.3°) with respect to mp, IR, NMR, MS, and tlc. There are some discrepancies between our optical rotation values and those reported by two Indian groups. The disagreements depend on the purity of the samples and on the accuracy of measurement.

The acetoxy-ester (IX) was hydrolyzed with potassium hydroxide and treated with diazomethane to give a mixture of VIII and VIII'. This shows that the acetoxy-ester (IX) consists of an epimeric mixture. The total yields of VIII and VIII' were 23.9 and 21.0%, respectively, from the saturated seco-aldehyde (VI).

Oxidation of VIII and VIII' with the Jones reagent gave the same keto-ester (X) [mp 153°C]; the spectral data were identical with those of methyl oxoputranjate[5] (methyl oxoputrate[8]).

The hydroxy-esters (VIII and VIII') were hydrolyzed with potassium hydroxide in ethanol to give hydroxy-acids, (III) [mp 227.0—227.5°C, $[\alpha]_D^{35}$ +19° ($CHCl_3$)] and (III') [mp 240.0—241.5°C, $[\alpha]_D^{35}$ −1.0° ($CHCl_3$)], respectively. The hydroxy-acid (III) was identical

Table

Acid		$[\alpha]_{Acid}$	$[\alpha]_{Me\text{-}ester}$	$[\alpha]_{Acid} - [\alpha]_{Me\text{-}ester}$
Lactic[18]	S	+ 3.82°	− 8.25°	+12.07°
	R	− 2.26°	+ 7.46°	− 9.72°
Leucic[19,20]	S	+19.4°	−12.5°	+31.9°
	R	−19.4°	+19.2°	−38.6°
I	S	+19° (III)	− 2.0° (VIII)	+21°
	R	− 1.0° (III')	+ 2.5° (VIII')	− 3.5°
Putranjic[1]	S	+ 1°	−23.5°	+24.5°
Putric[8]	S	+21.3°	− 8.3°	+29.6°

12) R. Aoyagi, E. Furukori, Y. Moriyama, T. Tsuyuki, and T. Takahashi, *Chem. Lett.*, **1972**, 451.

13) Sengupta *et al.* recently established the configurations of all asymmetric centers in putranjivic acid (3,4-seco-friedel-4(23)-en-3-oic acid) by synthesis of methyl putranjivate from friedel-3-ene through a lengthy pathway [P. Sengupta and A. K. Dey, *Tetrahedron*, **28**, 1307 (1972)]. The synthesis indicates the establishment of configurations of putranjic acid except C-2 position. The configuration at C-2 of putranjic acid was determined as S by CD measurement of its xanthate; This result is in line with our conclusion.

14) V. V. Kane and R. Stevenson, *J. Org. Chem.*, **25**, 1394 (1960).

15) L. Ruzicka, O. Jeger, and P. Ringnes, *Helv. Chim. Acta*, **27**, 972 (1944).

16) R. Aoyagi, T. Tsuyuki, and T. Takahashi, This Bulletin, **43**, 3967 (1967).

17) F. Kohen, A. S. Samson, and R. Stevenson, *J. Org. Chem.*, **34**, 1355 (1969); R. Stevenson, T. Tsuyuki, R. Aoyagi, and T. Takahashi, This Bulletin, **44**, 2567 (1971).

18) I. Heilbron ed., "Dictionary of Organic Compounds," Vol. 4, 1994 (1965), Maruzen, Tokyo.

19) C. G. Baker and A. Meister, *J. Amer. Chem. Soc.*, **73**, 1336 (1951).

20) C. Fuganti and D. Ghirngheli, *Gazz. Chim. Ital.*, **99**, 316 (1969).

with natural putranjic acid with respect to mp, IR and optical rotation (putranjic acid,[1] mp 218—220°C, $[\alpha]_D$ +1°; putric acid,[8] mp 220—222°C, $[\alpha]_D$ +21.3°). The mixture with an authentic sample showed no melting point depression. While the optical rotation values of these two natural products did not coincide, our value was almost the same as that of Seshadri's group.

Optical rotations of some α-hydroxy carboxylic acids bearing methylene group in β-position and those of their methyl esters are listed in the Table. As a rule, the differences ($\Delta=[\alpha]_{Acid}-[\alpha]_{Me\text{-}ester}$) are positive in *S*-configuration and negative in *R*-configuration. The configuration at C-2 of putranjic acid should therefore be of *S*-configuration. Consequently putranjic acid is shown to be (2*S*)-2-hydroxy-3,4-seco-friedelan-3-oic acid; that is 10β-[(2*S*)-2-carboxy-2-hydroxy]ethyl-5α-ethyl-des-A-friedelane (III).

Experimental[21]

Isolation of Friedelane-2,3-dione (II). The "cork smoker wash solid"[22] was washed with acetone to remove the dark colored impurities and extracted with benzene below 15°C. Evaporation of the benzene gave a dark brown solid, to which hot acetone was added and heated for a while under reflux. The hot suspension was filtered. On cooling the filtrate gave a crude crystal, a 1:1 mixture of friedelin and friedelane-2,3-dione, which was dissolved in benzene and passed through a column of alumina. Friedelane-2,3-dione (II),[14] eluted with ethyl acetate, was crystallized from the same solvent, and showed mp 271—272°C. The content of II was about 30% based on the starting material.

Norfriedelin (IV) from II. A suspension of II (10 g) in diethylene glycol (250 ml) was heated under reflux with potassium hydroxide (10 g) for 4.5 hr under a nitrogen atmosphere. After cooling, water (1 l) was added. Precipitates were collected on a filter paper and washed with water. The dried precipitates were dissolved in acetic acid (1.5 l) and lead tetraacetate (24 g) was added to the solution, which was stirred for two days at room temperature. After destroying the excess lead tetraacetate with ethylene glycol (20 ml), the acetic acid was evaporated to give crude norfriedelin. The product gave one spot on tlc, but was shown to contain a small amount of its C-4 methyl epimer by glc examination (column; Diasolid H-523, 250°C, retention time 31.4 and 28.8 min, respectively). The epimeric mixture was treated with alkali to afford pure norfriedelin with a longer retention time. Recrystallization from acetone gave 6.0 g of norfriedelin (IV),[15] mp 240.5—241.5°C, ν_{max} (Nujol) 1735 cm^{-1}, M^+ 412.

5α-Vinyl-10β-formylmethyl-des-A-friedelane (V) from IV. Norfriedelin (IV, 997 mg) was irradiated with a high pressure mercury lamp in *n*-hexane (700 ml) for 45 hr under an argon atmosphere at room temperature. The reaction products were separated by silica gel column chromatography and an aldehyde fraction was collected and crystallized from acetone to afford 236 mg of 5α-vinyl-10β-formylmethyl-des-A-friedelane (V),[16] mp 162.5—163.5°C, ν_{max} (Nujol) 2700, 1713, 1660, 1000, and 903 cm^{-1}, M^+ 412, NMR ($CDCl_3$) δ 9.70 (t, J=2—3 Hz, -CHO).

5α-Ethyl-10β-formylmethyl-des-A-friedelane (VI) from V. The unsaturated seco-aldehyde (V, 600 mg) was dissolved in ethanol (60 ml) and hydrogenated in the presence of 10% Pd-C (14 mg) for 1 hr at room temperature. The usual treatment and recrystallization from ether gave 5α-ethyl-10β-formylmethyl-des-A-friedelane (VI,[8] 57.4 mg) as needles, mp 181.0—181.5°C, ν_{max} (Nujol) 2720 and 1708 cm^{-1}, no absorption of double bond, M^+ 414, NMR ($CDCl_3$) δ 9.70 (t, J=2—3 Hz, -CHO).

Methyl Putranjate (VIII) and Its Epimer (VIII') from VI. Saturated aldehyde (VI, 50 mg) was dissolved in ethanol (50 ml) and acetic acid (5 ml), and a solution of potassium cyanide (300 mg) in water (1 ml) was added dropwise under stirring at room temperature. The reaction mixture was further stirred for 12 hr and extracted with ether, and the ethereal extract was washed with water. Cyanohydrin (VII) was separated from the starting material (VI) by silica gel column chromatography. Without further purification, it was dissolved in a mixture of acetic acid (30 ml) and concentrated hydrochloric acid (3 ml). This was heated under reflux for 1 hr and after the usual work-up the reaction product was treated with diazomethane in ether and chromatographed on silica gel (50 g) to give three compounds. Fractions, first eluted with benzene, gave 13.6 mg of *O*-acetyl-ester (IX), ν_{max} (Nujol) 1750, 1225, 1078, and 1058 cm^{-1}, M^+ 516, NMR (CCl_4) δ 3.76 (s, $-COOCH_3$), 2.11 (s, $-OCOCH_3$). This fraction gave one spot on tlc.

A second product was collected by further elution of the same solvent. On recrystallization from methanol–water, 3.3 mg of VIII' was obtained, mp 133—134°C, $[\alpha]_D^{25}$ +2.5° (*c* 1.0, $CHCl_3$), ν_{max} (Nujol) 3520, 1708, 1065, and 1025 cm^{-1}, Found: C, 78.16; H, 11.22%. Calcd for $C_{31}H_{54}O_3$: C, 78.42; H, 11.47%. M^+ 474 (the fragmentation pattern was the same as that of VIII), NMR (CCl_4) δ 3.78 (s, $-COOCH_3$).

Further elution with the same solvent gave methyl putranjate (VIII). Recrystallization from methanol–water gave 6.0 mg of VIII, mp 176.5—177.0°C, $[\alpha]_D^{25}$ −2.0° (*c* 0.80, $CHCl_3$), ν_{max} (Nujol) 3530, 1730, and 1100 cm^{-1}, Found: C, 78.21; H, 11.48%. Calcd for $C_{31}H_{54}O_3$: C, 78.42; H, 11.47%. M^+ 474, NMR (CCl_4) δ 3.78 (s, $-COOCH_3$), 3.95 (t, J=5.5 Hz, -CHOH).

Acetoxy-ester (IX, 13.6 mg) was hydrolyzed with potassium hydroxide (20 mg) in ethanol (30 ml) at 40°C for 4 hr. The hydrolysate was treated with diazomethane in ether and separated by silica gel chromatography to give VIII (5.9 mg) and VIII' (7.2 mg) after recrystallization. Thus, the total yields of methyl putranjate (11.9 mg) and its epimer (10.9 mg) were 23.9 and 21.1%, respectively, based on the saturated aldehyde (VI).

Putranjic Acid (III) and Its Epimer (III') from VIII and VIII'. Methyl putranjate (VIII, 50 mg) and potassium hydroxide (10 mg) in ethanol (30 ml) were warmed at 40°C for 4 hr. The acid, after being acidified with hydrochloric acid, was extracted with ether and recrystallized from methanol–water, giving 47.5 mg of putranjic acid (III), mp 227.0—227.5°C, $[\alpha]_D^{35}$ +19° (*c* 0.38, $CHCl_3$) ν_{max} (Nujol) 3520 and 1720 cm^{-1}.

The epimeric acid (III', 35 mg) was obtained from VIII' (40 mg) by the same procedure, mp 240.0—241.5°C, $[\alpha]_D^{35}$ −1.0° (*c* 0.38, $CHCl_3$), ν_{max} (Nujol) 3430 and 1703 cm^{-1}.

Methyl Putranjate (VIII) from Putranjic Acid (III). To putranjic acid (18 mg) in ether (10 ml) was added diazomethane in ether. After evaporation the residue was chromatographed and recrystallized from methanol–water to

21) All melting points were determined on a hot block and uncorrected. IR and mass spectra were measured using Hitachi EPI-G2 and Hitachi RMU-6 spectrometers. NMR spectra were taken on a Hitachi Model R-24 NMR spectrometer at 60 MHz, using TMS as an internal standard. Tlc was carried out on silica gel G (E. Merck).

22) R. Stevenson, *J. Org. Chem.*, **26**, 2142 (1961).

yield methyl putranjate (VIII, 16 mg). Mp, IR, and tlc were identical with those of the authentic sample.

By the same procedure the epimeric acid (III′) was converted into the ester (VIII′).

Methyl Oxoputranjate (X) from VIII and VIII′. Methyl putranjate (VIII, 11.0 mg) was dissolved in acetone at 0—5°C and the Jones reagent (7 ml) was added dropwise with stirring for 1.5 hr. The reaction mixture was extracted with ether and the ethereal extract was washed with water. Distillation of the solvent and recrystallization from methanol gave methyl oxoputranjate (X, 10.0 mg) as white needles, mp 153°C, ν_{max} (Nujol) 1750, 1730, and 1083 cm^{-1}, Found: C, 78.52; H, 10.83%. Calcd for $C_{31}H_{52}O_3$: C, 78.76; H, 11.09%. NMR (CCl_4) δ 3.80 (s, $-COOCH_3$), 2.65 (q, $-CO-CH_2-$), 1.88 (t, J=6 Hz, C-10 H).[23]

The epimeric hydroxy-ester (VIII′) gave the same oxidation product (X) by the same reaction procedure.

The authors wish to thank Professor T. R. Seshadri for the generous gift of the authentic sample of methyl putrate, and Professor C. R. Mitra for the authentic sample of putranjic acid. The authors are also grateful to the Ministry of Education for a grant-in-aid.

23) Lit. methyl oxoputranjate,[5] mp 148—149°C, NMR δ 1.9 (t, J=5.5 Hz, 1H), 2.75 (q, J=5.5 and 4.5 Hz, 2H: methyl oxoputrate, mp 152—154°C, $[\alpha]_D$ +24.0°, ν_{max} (KBr) 1760 cm^{-1}, NMR (CCl_4) δ 3.82, 2·67 (q), 1.9 (t, J=5 Hz).

BULLETIN OF THE CHEMICAL SOCIETY OF JAPAN, VOL. 46, 572—576 (1973)

Syntheses of New Arginine Derivatives as a Substrate for Trypsin or Papain[1]

Norio NISHI and Junzo NOGUCHI

Department of Polymer Science, Faculty of Science, Hokkaido University, Sapporo

(Received July 13, 1972)

Two new enzymic substrates, tosyl-L(D or DL)-arginine-*p*-nitroanilide (L-TAPA, D-TAPA, and DL-TAPA) and acetyl-L(D or DL)-arginine-*p*-nitroanilide (L-AAPA, D-AAPA, and DL-AAPA) were synthesized by the route for benzoyl-L-arginine-*p*-nitroanilide (L-BAPA) reported previously. The previous method for synthesis of L-BAPA was then improved by the direct benzoylation of L-arginine-*p*-nitroanilide dihydrochloride (L-APA), into which N^{α}-benzyloxycarbonyl-N^{ω}-nitro-L-arginine-*p*-nitroanilide was converted by the simultaneous removal of benzyloxycarbonyl and nitro groups with hydrogen fluoride. This route has the advantages of shorter reaction steps and a better over-all yield than in the case of the previous method. The method is also applicable to the synthesis of L(D or DL)-AAPA, but it is hard to prepare L(D or DL)-TAPA by the method.

L-Arginine derivatives of amide,[2-5] the methyl or ethyl ester[6-10] and α- or β-naphthylamide[11,12] have been useful as substrates for trypsin or papain. However, it has been very difficult to synthesize the derivatives of L-arginine-*p*-nitroanilide because of the racemization during the synthetic process, although these materials seem to be useful in measuring photometrically the accurate activity of enzyme.[13] Recently, we prepared benzoyl-L-arginine-*p*-nitroanilide (L-BAPA) without any racemization.[14] Using L- and D-BAPA against papain, it was revealed that D-antipode acts as a competitive inhibitor against L-antipode. These materials were also utilized to study the reaction rate using DL-BAPA as a substrate.[15] In this paper, an improved method for the preparation of L-BAPA and the preparation of tosyl-L (D or DL)-arginine-*p*-nitroanilide hydrochloride (L-TAPA, D-TAPA, and DL-TAPA), acetyl-L (D or DL)-arginine-*p*-nitroanilide hydrochloride (L-AAPA, D-AAPA, and DL-AAPA), L-arginine-*p*-nitroanilide dihydrochloride (L-APA), and benzoyl-D-arginine-*p*-nitroanilide hydrochloride (D-BAPA)[13] will be described. These derivatives will be useful in giving some interesting information about the variation in the reaction mechanism of the enzyme according to the effect of the *N*-protecting groups and the inhibition by D-antipode.

Experimental

The ultraviolet and visible absorption spectra were measured with a Hitachi 124 spectrophotometer. The optical rotations

1) This work was presented at the 8th Symposium on Peptide Chemistry, Osaka, Nov. 26—27, 1970.

2) M. Bergmann, J. S. Fruton, and H. Pollok, *J. Biol. Chem.*, **127**, 643 (1939).

3) K. Hofman and M. Bergmann, *ibid.*, **130**, 81 (1939).

4) M. Bergmann and J. S. Fruton, *Advan. Enzymol.*, **1**, 63 (1941).

5) G. W. Schwert, H. Neurath, S. Kaufman, and J. E. Snoke, *J. Biol. Chem.*, **172**, 221 (1948).

6) G. W. Schwert and Y. Takenaka, *Biochem. Biophis. Acta*, **16**, 570 (1955).

7) B. C. W. Hummel, *Can. J. Biochem. Physiol.*, **37**, 1393 (1959).

8) M. E. Brown, *New Eng. J. Med.*, **260**, 331 (1959).

9) E. Ronwin, *J. Biochem. Physiol.*, **40**, 1725 (1962).

10) A. M. Siegelman, A. S. Carlson, and T. Robertson, *Arch. Biochem. Biophys.*, **97**, 159 (1962).

11) R. E. Plapinger, M. M. Nachlas, M. L. Seligman, and A. M. Seligman, *J. Org. Chem.*, **30**, 1781 (1965).

12) M. M. Nachlas, R. E. Plapinger, and A. M. Seligman, *Arch. Biochem. Biophis.*, **108**, 266 (1964).

13) B. F. Erlanger, N. Kokowsky, and W. Cohen, *ibid.*, **95**, 271 (1961).

14) N. Nishi, S. Tokura, and J. Noguchi, This Bulletin, **43**, 2900 (1970).

15) S. Tokura, N. Nishi, and J. Noguchi, *J. Biochem.* (Tokyo), **69**, 599 (1971).

were measured with a Yanagimoto Direct-reading Polarimeter, Model OR-10, and an Automatic Recording Polarimeter, Model OR-1. The elemental analysis was carried out by means of a Yanagimoto C.H.N. Corder, Model MT-2, and a Coleman Nitrogen Analyser, Model 29. The melting points for the samples over 220°C were determined with a Mitamura hot-stage apparatus.

N^{α}-Benzyloxycarbonyl-N^{ω}-nitro-L-arginine-p-nitroanilide (I). This was prepared by a method previously described.[14]

N^{α}-Benzyloxycarbonyl-N^{ω}-nitro-DL-arginine-p-nitroanilide (DL-I). This was prepared from N^{α}-benzyloxycarbonyl-N^{ω}-nitro-DL-arginine (50.0 g, 142 mmol) and *p*-nitrophenyl isocyanate (47.0 g, 286 mmol) by the same method as I. Yield, 44 g (65.7%); mp 191°C. Found: C, 50.7; H, 4.78; N, 20.7%. Calcd for $C_{20}H_{23}N_7O_7$: C, 50.7; H, 4.90; N, 20.7%.

N^{α}-Benzyloxycarbonyl-N^{ω}-nitro-D-arginine-p-nitroanilide (D-I). This was prepared from N^{α}-benzyloxycarbonyl-N^{ω}-nitro-D-arginine[16] (3.0 g, 8.4 mmol) and *p*-nitrophenyl isocyanate (2.8 g, 17.0 mmol) by the same method as I. Yield, 3.1 g (77.5%); mp 178°C; $[\alpha]_D^{29}$ −53.0° (*c* 1.05, HMPA[17]).

N^{ω}-Nitro-L-arginine-p-nitroanilide Hydrobromide (II). This was prepared by the method previously described.[14]

N^{ω}-Nitro-DL-arginine-p-nitroanilide Hydrobromide (DL-II). This was prepared by the same method as II from N^{α}-benzyloxycarbonyl-N^{ω}-nitro-DL-arginine-*p*-nitroanilide (DL-I) (40.0 g, 84.5 mmol), using hydrogen bromide. Yield, 32.0 g (90.1%); mp 155°C. Found: C, 34.5; H, 4.58; N, 22.9; Br, 18.8%. Calcd for $C_{12}H_{18}N_7O_5Br$: C, 34.3; H, 4.32; N, 23.3; Br, 19.0%.

N^{ω}-Nitro-D-arginine-p-nitroanilide Hydrobromide (D-II). This was prepared by the same method as (II) from N^{α}-benzyloxycarbonyl-N^{ω}-nitro-D-arginine-*p*-nitroanilide (D-I) (6.6 g, 13.9 mmol), using hydrogen bromide. Yield, 4.2 g (71.7%); mp 175°C; $[\alpha]_D^{25}$ −43.1° (*c* 1.0, DMF[18]). Found: C, 34.9; H, 4.41; N, 23.0; Br, 18.7%. Calcd for $C_{12}H_{18}N_7O_5Br$: C, 34.3; H, 4.32; N, 23.3; Br, 19.0%.

L-Arginine-p-nitroanilide Dihydrochloride (L-APA. III). N^{α}-Benzyloxycarbonyl-N^{ω}-nitro-L-arginine-*p*-nitroanilide (I, 15.0 g, 31.7 mmol) was treated with hydrogen fluoride at 0°C for 3 hr to remove the nitro and the benzyloxycarbonyl groups; the procedure was the same as that used for N^{α}-tosyl-N^{ω}-nitro-L-arginine-*p*-nitroanilide (V). After the evaporation of hydrogen fluoride, the residue was dissolved in 400 ml of water, then, the solution was extracted with ether to remove the anisole. To the aqueous solution, treated with charcoal, 12M hydrochloric acid (5.2 ml, 62.4 mmol) was added; the solution was then evaporated to dryness in order to convert the hydrofluoride into the hydrochloride. In order to replace the hydrofluoride completely with hydrochloride, the residue was dissolved again in 1M hydrochloric acid (60 ml, 60 mmol) and the solution was evaporated to dryness. The crystalline hydrochloride was collected with ethanol and then dried. 9.7 g (83.3%); mp 242°C. It was recrystallized from water and ethanol. Yield, 9.4 g (80.8%); mp 245°C; $[\alpha]_D^{23}$ +81.7° (*c* 1, water). Found: C, 39.5; H, 5.72; N, 22.7; Cl, 19.1%. Calcd for $C_{12}H_{20}N_6O_3Cl_2$: C, 39.2; H, 5.49; N, 22.9; Cl, 19.3%.

N^{α}-Tosyl-N^{ω}-nitro-L-arginine-p-nitroanilide (V). N^{ω}-Nitro-L-arginine-*p*-nitroanilide hydrobromide (II, 5.0 g, 11.9 mmol) was dissolved in a mixture of tetrahydrofuran and water (9:1, 50 ml) and then cooled to −3°C. After the addition of triethylamine (3.8 ml, 27.4 mmol) to the solution, tosyl chloride (2.95 g, 15.5 mmol) in 9 ml of tetrahydrofuran was dropped with stirring over 5 min. After reaction for 2 hr, it was kept for another 3 hr at room temperature. Then the solution was evaporated to dryness at room temperature. The residue was crystallized by washing it with ether, water, 1M hydrochloric acid, water, and 5% sodium bicarbonate successively. The crystals were collected by filtration, washed with water and ether, and then dried. Yield, 5.8 g (98.8%); mp 155°C. It was recrystallized from tetrahydrofuran and water. Yield, 5.3 g (90.3%); mp 161°C; $[\alpha]_D^{20}$ −3.6° (*c* 1.0, HMPA). Found: C, 46.2; H, 4.67; N, 19.6%. Calcd for $C_{19}H_{23}N_7O_7S$: C, 46.2; H, 4.70; N, 19.9%.

N^{α}-Tosyl-N^{ω}-nitro-DL-agrinine-p-nitroanilide (DL-V). This was prepared by a method similar to that used for V from N^{ω}-nitro-DL-arginine-*p*-nitroanilide hydrobromide (DL-II) (5.0 g, 11.9 mmol) and tosyl chloride (2.94 g, 15.4 mmol). Yield, 5.2 g (88.6%); mp 214°C. Found: C, 46.1; H, 4.82; N, 19.6%. Calcd for $C_{19}H_{23}N_7O_7S$: C, 46.2; H, 4.70; N, 19.9%.

N^{α}-Tosyl-N^{ω}-nitro-D-arginine-p-nitroanilide (D-V). This was prepared from N^{ω}-nitro-D-arginine-*p*-nitroanilide hydrobromide (D-II) (1.0 g, 2.38 mmol) and tosyl chloride (0.59 g, 3.10 mmol) by the same method as was used for V. Yield, 1.0 g (85.2%); mp 161°C; $[\alpha]_D^{20}$ +3.6° (*c* 1.0, HMPA).

N^{α}-Tosyl-L-arginine-p-nitroanilide Hydrochloride (L-TAPA, VIII). N^{α}-Tosyl-N^{ω}-nitro-L-arginine-*p*-nitroanilide (V, 5 g, 10.1 mmol) was mixed with anisole (5 ml, 46.2 mmol) in a HF-reaction cylinder. Forty milliliters of hydrogen fluoride dried with CoF_3 were collected in the cylinder under cooling with liquid nitrogen; the mixture was then allowed to react at 0°C for 40 min with stirring. The excess HF was removed under reduced pressure, and the residue was kept *in vacuo* for another 2 hr. The residue was crystallized by trituration with ether. The crystallized hydrofluoride was suspended in 200 ml of 3M hydrochloric acid and then stirred for one hour at room temperature to convert it into the hydrochloride. After cooling, the crystalline hydrochloride was filtered, washed with 3M hydrochloric acid and a small amount of ice cold water, and then dried. In order to complete the replacement of hydrochloride, a 75 ml portion of 3M hydrochloric acid was added to the hydrofluoride salt in glacial acetic acid and the solution was evaporated *in vacuo* to dryness at room temperature. The residue was again dissolved in a mixed solvent of acetic and hydrochloric acid, and the solvent was removed, repeatedly; then it was recrystallized from ethanol. Yield, 3.7 g (75.3%); mp 245°C; $[\alpha]_D^{23}$ −32.0° (*c* 1.0, DMF). Found: C, 47.2; H, 5.13; N, 17.0; Cl, 7.10%. Calcd for $C_{19}H_{25}N_6O_5ClS$: C, 47.1; H, 5.20; N, 17.3; Cl, 7.31%.

N^{α}-Tosyl-L-arginine-p-nitroanilide p-Toluenesulfonate (L-TAPA·CH_3·C_6H_4·SO_3H, X). L-Arginine-*p*-nitroanilide dihydrochloride (III, 1.4 g, 3.81 mmol) was dissolved in water (56 ml), and then the mixture was cooled to 0°C. After adding an ether solution (56 ml) of tosyl chloride (0.94 g, 4.95 mmol), an aqueous solution (5 ml) of sodium hydroxide (0.50 g, 12.5 mmol) was dropped in over a thirty-minute period with vigorous stirring. The reaction was continued for one hour at 0°C and for 2 hr at room temperature. Carbon dioxide was bubbled into it for a few minutes to precipitate crystals. This material was dissolved in a mixture of 1M hydrochloric acid and glacial acetic acid, and then the solution was evaporated to dryness. The product was collected with water and recrystallized from water. Yield, 0.30 g (12.7%); mp 206°C. Found: C, 50.0; H, 5.16; N, 13.4%. Calcd for $C_{26}H_{32}N_6O_8S_2$: C, 50.3; H, 5.20; N, 13.5%.

N^{α}-Tosyl-DL-arginine-p-nitroanilide Hydrochloride (DL-TAPA, DL-VIII). This was prepared by the same method as

16) H. Yajima and K. Kubo, *J. Amer. Chem. Soc.*, **87**, 2039 (1965).
17) HMPA: hexamethylphosphoramide.
18) DMF: dimethylformamide.

was used for VIII from N^{α}-tosyl-N^{ω}-nitro-DL-arginine-*p*-nitroanilide (DL-V) (4.0 g, 8.11 mmol), using hydrogen fluoride. Yield, 3.1 g (78.9%); mp 224°C. Found: C, 46.7; H, 5.11; N, 17.3; Cl, 7.20%. Calcd for $C_{19}H_{25}N_6O_5ClS$: C, 47.1; H, 5.20; N, 17.3; Cl, 7.31%.

N^{α}-*Tosyl-*D*-arginine-*p*-nitroanilide Hydrochloride (*D*-TAPA. *D*-VIII).* This was prepared by the same method as was used for VIII from N^{α}-tosyl-N^{ω}-nitro-D-arginine-*p*-nitroanilide (D-V) (0.9 g, 1.83 mmol), using hydrogen fluoride. Yield, 0.7 g (79.1%); mp 245°C; $[\alpha]_D^{23}$ +32.3° (*c* 1.0, DMF). Found: C, 47.2; H, 47.2; H, 5.18; N, 17.1; Cl, 7.10%. Calcd for $C_{19}H_{25}N_6O_5ClS$: C, 47.1; H, 5.20; N, 17.3; Cl, 7.31%.

N^{α}-*Acetyl-*N^{ω}*-nitro-*L*-arginine-*p*-nitroanilide (VI).* N^{α}-Nitro-L-arginine-*p*-nitroanilide hydrobromide (II, 10 g, 23.8 mmol) was dissolved in a mixture of tetrahydrofuran and water (9: 1, 100 ml), and then the mixture was cooled to −3°C. After the addition of triethylamine (7.7 ml, 55.6 mmol) to the solution, acetic anhydride (3.2 ml, 31.7 mmol) was dropped into it with stirring in 5 min. After 4 hr, the pH was adjusted to 4 by the addition of 1M hydrochloric acid, and then the solution was evaporated to dryness at room temperature. The residue was crystallized by treatment with 1M hydrochloric acid, filtered, washed with water, and then dried. Yield, 7.8 g (86.0%); mp 185°C. It was then recrystallized from DMF and water. Yield, 7.5 g (82.7%); mp 193°C; $[\alpha]_D^{29}$ +61.7° (*c* 1.0, HMPA). Found: C, 44.5; H, 4.70; N, 25.4%. Calcd for $C_{14}H_{19}N_7O_6$: C, 44.1; H, 5.02; N, 25.7%.

N^{α}-*Acetyl-*N^{ω}*-nitro-*DL*-arginine-*p*-nitroanilide (DL-VI).* This was prepared by the same method as was used for VI from N^{ω}-nitro-DL-arginine-*p*-nitroanilide hydrobromide (DL-II) (5.0 g, 11.9 mmol) and acetic anhydride (1.8 ml, 17.8 mmol). Yield, 3.5 g (77.2%); mp 215°C. Found: C, 44.2; H, 4.93; N, 25.4%. Calcd for $C_{14}H_{19}N_7O_6$: C, 44.1; H, 5.02; N, 25.7%.

N^{α}-*Acetyl-*N^{ω}*-nitro-*D*-arginine-*p*-nitroanilide (D-VI).* This was prepared by the same method as was used for VI from N^{ω}-nitro-D-arginine-*p*-nitroanilide hydrobromide (D-II) (1.0 g, 2.38 mmol) and acetic anhydride (0.36 ml, 3.56 mmol). Yield, 0.6 g (66.2%); mp 193°C, $[\alpha]_D^{29}$ −61.9° (*c* 1.0, HMPA).

N^{α}-*Acetyl-*L*-arginine-*p*-nitroanilide Hydrochloride (*L*-AAPA. IX).* (Method A). N^{α}-Acetyl-N^{ω}-nitro-L-arginine-*p*-nitroanilide (VI, 5.0 g, 13.1 mmol) was treated with hydrogen fluoride to remove the nitro group by the same procedure as was used for N^{α}-tosyl-N^{ω}-nitro-L-arginine-*p*-nitroanilide (V). After treatment with ether, the dried residue of hydrofluoride was dissolved in a mixture of 1M hydrochloric acid (70 ml) and glacial acetic acid (30 ml): then the solution was evaporated to dryness *in vacuo* at room temperature to convert it into its hydrochloride. The residue was crystallized with acetone, filtered, washed with acetone, and then dried. Yield, 4.6 g (85.5%); mp 135—136°C. This crude material was then dissolved in a small amount of 1M hydrochloric acid, and acetone was added to the mixture until the solution was faintly clouded. N^{α}-Acetyl-L-arginine-*p*-nitroanilide hydrochloride was crystallized out on standing at 0°C with trituration by repeating the gradual addition of acetone and cooling. The crystals were filtered out, washed with acetone, and then dried. Yield, 3.9 g (72.8%); mp 139°C; $[\alpha]_D^{20}$ −19.0° (*c* 1.0, water). Found: C, 41.0; H, 6.00; N, 20.4; Cl, 9.00%. Calcd for $C_{14}H_{21}O_4N_6Cl \cdot 2H_2O$: C, 41.1; H, 6.16; N, 20.6; Cl, 8.67%.

(Method B). L-Arginine-*p*-nitroanilide dihydrochloride (III, 0.3 g, 0.82 mmol) was dissolved in water (12 ml), the solution was cooled to 0°C after ether (12 ml) had then been added. Acetic anhydride (0.09 ml) and then an aqueous solution (1.4 ml) of sodium carbonate (0.14 g, 1.27 mmol) were added into it with vigorous stirring. The reaction mixture was kept for 1 hr at 0°C and then for another hour at room temperature. The solution was evaporated to dryness after being acidified to pH 3 with concentrated hydrochloric acid. The residue was dissolved in a mixture of 1M hydrochloric acid and glacial acetic acid (1:1 v/v, 20 ml) and the solution was evaporated to dryness. After this procedure had been repeated once more, the residue was dissolved in ethanol to remove the sodium chloride and the solution was evaporated. The crude product was recrystallized from 1M hydrochloric acid and acetone by the same procedure as that of Method A. Yield, 0.25 g (74.8%); mp 139°C; $[\alpha]_D^{20}$ −19.0° (*c* 1.0, water).

N^{α}-*Acetyl-*DL*-arginine-*p*-nitroanilide Hydrochloride (*DL*-AAPA, DL-IX).* This was prepared by the same method as was used for IX from N^{α}-acetyl-N^{ω}-nitro-DL-arginine-*p*-nitroanilide (DL-VI) (3.0 g, 7.87 mmol), using hydrogen fluoride. Yield, 2.8 g (91.1%); mp 230°C. Found: C, 42.9; H, 5.60; N, 21.2; Cl, 9.00%. Calcd for $C_{14}H_{21}O_4N_6Cl \cdot H_2O$: C, 43.0; H, 5.93; N, 21.5; Cl, 9.07%.

N^{α}-*Acetyl-*D*-arginine-*p*-nitroanilide Hydrochloride (*D*-AAPA, D-IX).* This was prepared by the same method as was used for IX from N^{α}-acetyl-N^{ω}-nitro-D-arginine-*p*-nitroanilide (D-VI) (0.5 g, 1.31 mmol), using hydrogen fluoride. Yield, 0.3 g (56.0%); mp 139°C; $[\alpha]_D^{20}$ +19.0° (*c* 1.0, water). This product was lyophilized and stored in a dark place. Found: C, 41.3; H, 5.93; N, 20.1; Cl, 9.0%. Calcd for $C_{14}H_{21}O_4N_6Cl \cdot 2H_2O$: C, 41.1; H, 6.16; N, 20.6; Cl, 8.67%.

N^{α}-*Benzoyl-*L*-arginine-*p*-nitroanilide Hydrochloride (*L*-BAPA, VII).* (Method A). L-Arginine-*p*-nitroanilide dihydrochloride (III, 5.0 g, 13.6 mmol) was dissolved in water (200 ml) and then cooled to 0°C. After the addition of benzoyl chloride (1.75 ml, 15.2 mmol) and ether (200 ml) to the solution, an aqueous solution (23 ml) of sodium carbonate (2.25 g, 21.2 mmol) was dropped into it with vigorous stirring in 15 min. The reaction mixture was kept for 1 hr at 0°C and for 3 hr at 20°C. The precipitate was then collected by filtration and washed with a small amount of water. To a hot solution of this material in 50% acetic acid (100 ml), 1M hydrochloric acid (50 ml) was added and nitrogen was bubbled in for a few minutes. After it had then been cooled to room temperature, the solution was evaporated to dryness and the residue was treated with ethanol and evaporated repeatedly to remove the acetic acid completely. It was then recrystallized from ethanol. Yield, 4.6 g (77.7%); mp 225°C; $[\alpha]_D^{25}$ +14.2° (*c* 1.0, water). Found: C, 52.2; H, 5.35; N, 19.2; Cl, 8.00%. Calcd for $C_{19}H_{23}N_6O_4Cl$: C, 52.2; H, 5.33; N, 19.3; Cl, 8.15%.

(Method B). N^{α}-Benzyloxycarbonyl-N^{ω}-nitro-L-arginine-*p*-nitroanilide (I, 5 g, 10.5 mmol) was treated with hydrogen fluoride as has been described in the case of L-arginine-*p*-nitroanilide dihydrochloride (L-APA, III). After the evaporation of the hydrogen fluoride, the residue was dissolved in water (150 ml) and the solution was extracted with ether to remove the anisole. The aqueous solution was then cooled to 0°C, and the pH was adjusted to 9 by the addition of sodium carbonate. Benzoyl chloride (1.25 ml, 10.8 mmol) and ether (10 ml) were vigorously stirred into it, and the reaction was continued for 2 hr. The precipitate in a syrup was crystallized by acidification to pH 1—2 with concentrated hydrochloric acid and then kept overnight in an ice box. The crystalline product was filtered, washed successively with dilute hydrochloric acid, a small amount of ice water, and ether, and then dried. It was subsequently recrystallized from ethanol. Yield, 2.5 g (53.8%); mp 224°C. The product was dissolved in hot water (50 ml) and treated with charcoal; the solution was concentrated to about 15 ml and then crystallized with

trituration. To the mixture, 1M hydrochloric acid (15 ml) was added, after which the mixture was cooled for one hour at 0°C. The crystalline N^{α}-benzoyl-L-arginine-*p*-nitroanilide hydrochloride was filtered, washed with a small amount of water, and then dried. Yield, 2.4 g (52.3%); mp 225°C; $[\alpha]_D^{25}$ +14.2° (*c* 1.0, water). Found: C, 52.7; H, 5.47; N, 19.4; Cl, 8.1%. Calcd for $C_{19}H_{23}N_6O_4Cl$: C, 52.5; H, 5.33; N, 19.3; Cl, 8.15%.

N^{α}-*Benzoyl*-N^{ω}-*nitro*-D-*arginine*-p-*nitroanilide (*D-*IV)*. This was prepared by the same method as was used for IV[14] from N^{ω}-nitro-D-arginine-*p*-nitroanilide hydrobromide (D-II) (1.0 g, 2.38 mmol) and benzoyl chloride (0.31 ml, 2.62 mmol). Yield, 0.7 g (66.4%); mp 246°C; $[\alpha]_D^{26}$ −61.0° (*c* 1.12, HMPA).

N^{α}-*Benzoyl*-D-*arginine*-p-*nitroanilide Hydrochloride (*D-*BAPA,* D-*VII)*. This compound was prepared by the same method as was used for VII[14] from N^{α}-benzoyl-N^{ω}-nitro-D-arginine-*p*-nitroanilide (D-IV) (0.65 g, 1.47 mmol), using hydrogen fluoride. It has no crystalline water and is sparingly soluble in water. Yield, 0.4 g (62.7%); mp 225°C; $[\alpha]_D^{25}$ −14.2° (*c* 1.0, water). Found: C, 52.7; H, 5.47; N, 19.0; Cl, 8.0%. Calcd for $C_{19}H_{23}N_6O_4Cl$: C, 52.5: H, 5.33; N, 19.3; Cl, 8.15%.

To make it easily soluble in water, it was redissolved in water and lyophilized. The crystals contain crystalline water and were stored in a brown sample bottle. Found: C, 47.9; H, 5.94; N, 17.5; Cl, 7.20%. Calcd for $C_{19}H_{23}N_6O_4Cl \cdot 2.5H_2O$: C, 47.6; H, 5.88; N, 17.5; Cl, 7.39%, mp 100—150° (broad).

The Ultraviolet and Visible Absorption Spectra of L-*TAPA,* L-*AAPA, and* L-*APA*. The ultraviolet and visible absorption spectra of L-TAPA, L-AAPA, and L-APA in an aqueous sodium chloride solution are shown in Fig. 1. The absorption spectra of L-BAPA[14] and *p*-nitroaniline[13] are also shown in Fig. 1. The values of the molar extinction coefficients, ε, at the optimum absorptions are as follows:

L-TAPA: 317 mμ, $\varepsilon = 1.10 \times 10^4$
L-AAPA: 316 mμ, $\varepsilon = 1.14 \times 10^4$
L-APA: 304 mμ, $\varepsilon = 1.14 \times 10^4$

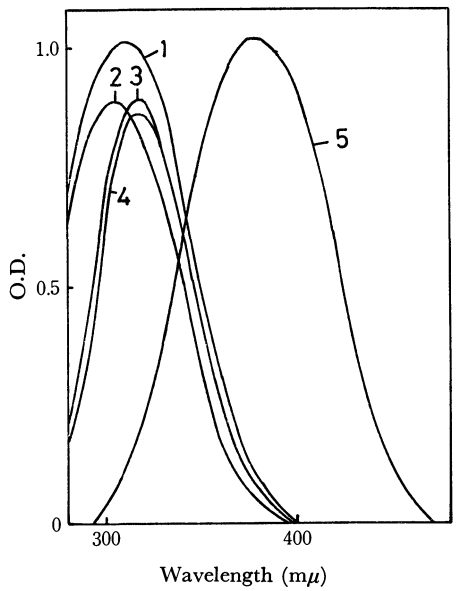

Fig. 1. Absorption spectra of L-AAPA, L-TAPA, and L-APA, all at concentration of 7.8×10^{-5}M in 0.05M NaCl solution, pH 6.2 and 22°C. 1: L-BAPA[12,1)], 2: L-APA, 3: L-AAPA, 4: L-TAPA, 5: *p*-nitroaniline.[12)]

Results and Discussion

The synthetic routes shown in this paper are summarized in Scheme 1.

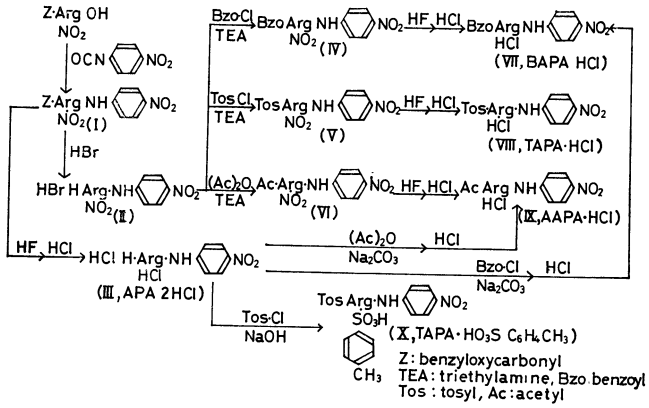

Scheme 1.

The Syntheses of L(D *or* DL)-*TAPA,* L(D *or* DL)-*AAPA, and* D-*BAPA*. The synthetic route of optically active L-BAPA described previously[14] was followed in order to avoid the racemization through the formation of oxazolone in the reaction. N^{α}-Benzyloxycarbonyl-N^{ω}-nitro-L-agrinine-*p*-nitroanilide was prepared by a reaction between N^{α}-benzyloxycarbonyl-N^{ω}-nitro-L-arginine and *p*-nitrophenyl isocyanate, because the α-carboxyl group of N^{α}-benzyloxycarbonyl-N^{ω}-nitro-arginine can easily be cyclized into its δ-lactam, also, the amino group of *p*-nitroaniline is too inactive to form an amide bond in the ordinary way. The benzyloxycarbonyl group was removed with hydrogen bromide, and then the product was benzoylated by benzoyl chloride; finally, the nitro group was removed with hydrogen fluoride[19] into L-BAPA. This route was also applicable to the synthesis of L-AAPA (IX) and L-TAPA (VIII) by acetylation or tosylation. The nitro group with hydrogen fluoride could be sufficiently removed in 40 min at 0°C, as was L-BAPA. The hydrofluoride of L-TAPA formed by denitration with hydrogen fluoride is convertible into its hydrochloride up to about 90% by stirring the suspension of the salt in 3M hydrochloric acid for 1 hr at room temperature. Then, the product was dissolved in a mixture of glacial acetic acid and 3M hydrochloric acid (1: 1 v/v) at room temperature and the solvent was evaporated *in vacuo*. Since L-AAPA is soluble in hydrochloric acid, L-AAPA hydrofluoride can be converted into its hydrochloride by the repeated concentration of the solution in a mixture of glacial acetic acid and 1M hydrochloric acid (1: 1 v/v) at room temperature. The calcium nitrate test of hydrogen fluoride showed negative in the L-TAPA hydrochloride and L-AAPA hydrochloride produced. DL-TAPA, and DL-AAPA, and D-TAPA, D-AAPA, and D-BAPA, were also prepared from DL-arginine hydrochloride and D-arginine hydro-

19) S. Sakakibara, Y. Shimonishi, Y. Kishida, M. Okada, and H. Sugihara, This Bulletin, **40**, 2164 (1967); S. Sakakibara, Y. Kishida, R. Nishizawa, and Y. Shimonishi, *ibid.*, **41**, 438 (1968); S. Sakakibara, N. Nakamizo, Y. Kishida, and S. Yoshimura, *ibid.*, **41**, 1477 (1968).

chloride respectively by the same method. These properties are summarized below:

Compound	Mp (°C)	$[\alpha]_D$ (°)	ε at optimum absorption
L-TAPA·HCl	245	−32.0 (*c* 1.0, DMF)	1.10×10^4 (317 mμ)
D-TAPA·HCl	245	+32.3 (*c* 1.0, DMF)	
DL-TAPA·HCl	224	0	
L-AAPA·HCl·$2H_2O$	139	−19.0 (*c* 1.0, water)	1.14×10^4 (316 mμ)
D-AAPA·HCl·$2H_2O$	139	+19.0 (*c* 1.0, water)	
DL-AAPA·HCl·H_2O	230	0	
L-APA·2HCl	245	+81.7 (*c* 1.0, water)	1.14×10^4 (304 mμ)
D-BAPA·HCl	225	−14.2 (*c* 1.0, water)	

The Improved Synthetic Method of L-*BAPA and* L-*AAPA.* The method of synthesizing L-BAPA through the (I)—L-APA(III)—L-BAPA(VII) route had shorter reaction steps and a better overall yield than the previous method.[14] L-Arginine-*p*-nitroanilide dihydrochloride (L-APA, III) was derived from N^{α}-benzyloxycarbonyl-N^{ω}-nitro-L-arginine-*p*-nitroanilide (I) by the simultaneous removal of the benzyloxycarbonyl group and the nitro group with hydrogen fluoride, after which the hydrofluoride was converted into its hydrochloride by a method similar to that described above. In this case, the protecting groups were removed with hydrogen fluoride for 3 hr at 0°C, because the complete reaction had hardly proceeded at all in 40 min at 0°C. L-BAPA(VII) was obtainable from L-APA (III) by the benzoylation of the α-amino group with sodium carbonate as a base. The reaction was carried out homogeneously in emulsion by vigorous stirring in a mixture of water and ether (1: 1 v/v). By this route, L-BAPA can be prepared in one step from I without isolating L-APA. The yield of L-BAPA in the method is 52—63%. Moreover, the experimental treatment was simplified exceedingly. L-AAPA was also prepared by the same method, but the expected results were not obtained in the preparation of L-TAPA by the direct tosylation of L-APA. L-APA does not react with tosyl chloride in sodium carbonate, but forms *p*-toluenesulfonate of L-TAPA in sodium hydroxide; the yield was very low and it was very difficult to convert it into its hydrochloride. Therefore, this method seems to be unsuitable for the preparation of L-TAPA.

The Attempts at the Preparations of D-*TAPA and* D-*AAPA by Enzymic Digestion.* Erlanger *et al.* prepared D-BAPA by the enzymic digestion of DL-BAPA.[13] We have now used the method in the preparation of D-TAPA and D-AAPA from DL-TAPA and DL-AAPA, but we found it to be almost entirely unsuitable in both cases. In DL-TAPA, the reaction proceeds very slowly and, a large amount of enzymes and a long reaction time were necessary to complete the reaction; moreover, it was necessary to use a lot of solution for the reaction, because DL-TAPA was more sparingly soluble in water than DL-BAPA. In the case of DL-AAPA, the self-decomposition of DL-AAPA was assumed in a phosphate buffer and the D-AAPA produced was easily soluble in water and was very difficult to separate from the sub-products, such as acetyl-L-arginine or *p*-nitroaniline, and enzymes. Although D-BAPA was prepared from DL-BAPA by the biochemical method, the direct synthesis seems to be more easier than the enzymic preparation. The absorption spectra of TAPA, AAPA, and APA have their bases at about 400 mμ much like BAPA, and the enzymic activity can be measured by means of the amount of *p*-nitroaniline formed at 410 mμ, the same as with BAPA. When TAPA is used as a substrate, DMF or DMSO should be used to increase the solubility in water. AAPA and APA are easily soluble in water and may be used as substrate or inhibitor, although AAPA tends to self-decompose into the deacetylation or cleavage of the amide bond in a phosphate buffer. When L(D)-BAPA was stocked in a crystalline form, a part of it sometimes became sparingly soluble in water, although no changes were assumed in the chromatography or absorption spectrum. The lyophilized crystal contains crystalline water and is more easily soluble in water than the crystal without water. Therefore, it is desirable to use the lyophilize method in the preparation of L(D)-BAPA as a substrate. The details of the substrates will be published elsewhere.

The authors are very much indebted to Dr. Seiichi Tokura for the measurement of the enzymic activity.

New Syntheses of Maculosidine and Pteleine

Tetsuya SEKIBA

Faculty of Chemical Engineering, Toyama Technical College, Hongo, Toyama

(Received July 14, 1972)

2,3-Dihydromaculosidine and 2,3-dihydropteleine were obtained from 2,4-dimethoxy- and 4-methoxy-aniline by condensation with diethyl β-benzyloxyethylmalonate, followed by methylation and subsequent cyclodebenzylation with polyphosphoric acid. The dehydrogenation of the dihydro compounds with 2,3-dichloro-5,6-dicyanobenzoquinone gave maculosidine (4,6,8-trimethoxyfuro[2,3-*b*]quinoline) and pteleine (4,6-dimethoxyfuro[2,3-*b*]quinoline) in relatively high yields. Similarly, evolitrine (4,7-dimethoxyfuro[2,3-*b*]quinoline) and γ-fagarine (4,8-dimethoxyfuro[2,3-*b*]quinoline) were also prepared.

Maculosidine, together with kokusaginine, was isolated from the leaves of *Flindersia maculosa* Lindl.[1] Its structure can be represented as 4,6,8-trimethoxyfuro[2,3-*b*]quinoline (Ia), as has been shown by spectral and degradative studies.[2] Pteleine (4,6-dimethoxyfuro[2,3-*b*]quinoline (Ib)) was found in the roots of *Platydesma campanulata* Mann[3] and *Ptelea trifoliata* L.[4] The syntheses of Ia[5] and Ib[6] from 2,4-dimethoxyaniline (IIa) and 4-methoxyaniline (IIb) were reported by Govindachari and his co-workers, and by Pai *et al.*, according to the method of Tuppy and Böhm.[7] This procedure, however, was troublesome and did not give satisfactory results.

This paper will describe convenient syntheses of Ia, b from IIa, b by a modification of Ohta and Mori's method.[8] In a similar manner, improved syntheses of evolitrine (Ic, 4,7-dimethoxyfuro[2,3-*b*]quinoline) and γ-fagarine (Id, 4,8-dimethoxyfuro[2,3-*b*]quinoline) can also be realized.

With the removal of ethanol (two moles), the condensation of aniline derivatives (IIa—d) and diethyl β-benzyloxyethylmalonate in diphenyl ether gave the 4-hydroxy-2-quinolone derivatives (IIIa—d), which were then easily methylated with diazomethane into the 4-methoxy compounds (IVa—d). While the IR spectra of IVa—d indicated the absence of the hydroxyl group, which was present in those of IIIa—d (*ca.* 3200—3500 cm^{-1}) (Table 1), the NMR spectra[9] of

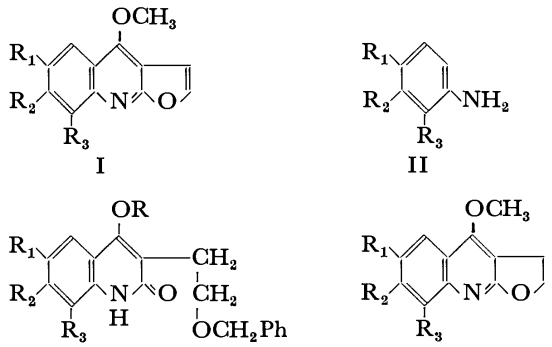

I II III R=H IV R=CH$_3$ V

a) $R_1=R_3=OCH_3$, $R_2=H$ c) $R_2=OCH_3$, $R_1=R_3=H$
b) $R_1=OCH_3$, $R_2=R_3=H$ d) $R_3=OCH_3$, $R_1=R_2=H$

TABLE 1. IR SPECTRAL DATA OF THE COMPOUNDS (I, III, IV, AND V)

	III[a] (cm^{-1})	IV[a] (cm^{-1})	V[a] (cm^{-1})	I[b] (cm^{-1})
a	3360, 1655	1605	1615, 1520	1625, 1520
b	3200, 1670	1660	1630, 1526	1630, 1510
c	3500, 1640	1650	1630, 1520	1620, 1530
d	3360, 1640	1640	1630, 1520	1625, 1520

a) Nujol b) KBr

IVa—d exhibited signals for three protons (δ *ca.* 3.93s ppm) (Table 2) of the methoxy group. IVa—d gave positive color reactions with ferric chloride in ethanol (*e.g.*, IVa (reddish brown)), suggesting the presence of a keto-enol tautomerism of the amide group. The cyclodebenzylation of IVa—d with polyphosphoric acid yielded 2,3-dihydrofuro[2,3-*b*]quinoline derivatives (Va—d). The structures of Va—d were assigned on the basis of the NMR spectra, which showed signals at δ *ca.* 3.5t and 4.5t attributable to two methylene protons of a dihydrofuran ring system (Table 3). Difficulty had been experienced in the dehydrogenation of the dihydro derivatives of furoquinoline alkaloids (*e.g.*, dihydroacronycidine[10] and dihydrokokusaginine[11,12]) by treatment with *N*-bromosuccinimide, followed by dehydrobromination. The dehydrogenation of Va—d with 2,3-dichloro-5,6-dicyanobenzoquinone (DDQ), however, gave furo[2,3-*b*]quinoline derivatives (maculosidine (Ia),[1] pteleine (Ib),[3,4] evolitrine (Ic),[13]

1) R. F. Brown, P. T. Gilham, G. K. Hughes, and E. Ritchie, *Aust. J. Chem.*, **7**, 181 (1954).
2) R. H. Prager, E. Ritchie, and W. C. Taylor, *ibid.*, **13**, 380 (1960).
3) F. Werny and P. J. Sheuer, *Tetrahedron*, **19**, 1293 (1963).
4) V. I. Frolova, A. D. Kuzovkov, and P. N. Kibal'chich, *Zh. Obshch. Khim.*, **34**, 3499 (1964); *Chem. Abstr.*, **62**, 2800 (1965).
5) T. R. Govindachari and S. Prabhakar, *Indian J. Chem.*, **1**, 17 (1963).
6) B. R. Pai, S. Prabhakar, P. S. Santhanam, M. Seetha, and V. Sudarsanam, *ibid.*, **2**, 491 (1964).
7) H. Tuppy and F. Böhm, *Monatsh. Chem.*, **87**, 720 (1956).
8) T. Ohta and Y. Mori, *Tokyo Yakka Daigaku Kenkyu Nempo*, **10**, 100 (1960); *Chem. Abstr.*, **56**, 4806 (1962).
9) The NMR spectra in this paper were measured with a Hitachi R-20 spectrometer (60 MHz), using tetramethylsilane as the internal standard (δ value in $CDCl_3$); s singlet; bs broad singlet; d doublet; t triplet; m multiplet.
10) T. R. Govindachari, B. R. Pai, S. Prabhakar, P. S. Santhanam, and V. Sudarsanam, *Indian J. Chem.*, **3**, 71 (1965).
11) T. Ohta and Y. Mori, *Yakugaku Zasshi*, **82**, 549 (1962).
12) Y. Kuwayama, *ibid.*, **82**, 703 (1962).
13) R. G. Cooke and H. F. Haynes, *Aust. J. Chem.*, **7**, 273 (1954), **11**, 225 (1958); T. Sato and T. Ohta, This Bulletin, **31**, 161 (1958); T. Ohta and Y. Mori, *Yakugaku Zasshi*, **78**, 446 (1958).

TABLE 2. NMR SPECTRAL DATA OF 3-(2-BENZYLOXYETHYL)-4-METHOXY-2-QUINOLONES (IVa—d)[9]

	IVa	IVb	IVc	IVd
CH_3–O	3.85s	3.83s	3.88s	
	3.93s (6H)	3.94s	3.98s	3.92s (6H)
β-CH_2–CH_2	3.05t (J=7.2 Hz)	3.08t (J=7.2 Hz)	3.17t (J=7.2 Hz)	3.01t (J=7.2 Hz)
α-CH_2–O	3.80t (J=7.2 Hz)	3.83t (J=7.2 Hz)	3.86t (J=7.2 Hz)	3.77t (J=7.2 Hz)
$C_6H_5CH_2$	4.54s	4.55s	4.61s	4.52s
NH	9.12bs	12.50bs	12.40bs	9.20bs

TABLE 3. NMR SPECTRAL DATA OF 2,3-DIHYDROFURO[2,3-*b*]QUINOLINES (Va—d) AND FURO[2,3-*b*]QUINOLINES (Ia—d)[9]

	Va	Vb	Vc	Vd
β-CH_2–CH_2	3.53t (J=7.8 Hz)	3.55t (J=7.8 Hz)	3.82t (J=7.8 Hz)	3.57t (J=7.8 Hz)
α-CH_2–O	4.53t (J=7.8 Hz)	4.56t (J=7.8 Hz)	4.64t (J=7.8 Hz)	4.56t (J=7.8 Hz)
CH_3–O	3.83s 3.93s 4.12s	3.86s 4.15s	3.92s 4.24s	3.94s 4.13s
Arom. H	6.61d(J=2.5 Hz)	7.1—7.75m (3H)	6.86—7.60m (3H)	6.85—7.65m (3H)
	6.86d (J=2.5 Hz)			
	Ia	Ib	Ic	Id
CH_3–O	3.88s 4.02s 4.36s	3.90s 4.38s	3.90s 4.33s	4.07s 4.40s
Arom. H	6.68d (J=2.5 Hz)	7.0—8.0m (5H)	6.94—7.20m (5H)	7.0—7.9m (5H)
	6.97d (J=2.5 Hz)			
	7.03d (J=2.5 Hz)			
	7.56d (J=2.5 Hz)			

TABLE 4. 3-(2-BENZYLOXYETHYL)-4-HYDROXY-2-QUINOLONES (IIIa—d)

Compounds	Mp (°C)	Cryst. form	Yield (%)	Formula	Analysis (%) Found / Calcd	UV λ_{max} mμ(log ε)
IIIa	235.5—237.5	Colorless[a] needles	90	$C_{20}H_{21}O_5N$	C 67.66 / 67.59 H 5.94 / 5.96 N 3.98 / 3.94	228sh (4.43) 290 (3.97) 251 (4.50) 338 (3.77) 280 (4.00) 353sh (3.70)
IIIb	172—174	Pale yellow[b] needles	39	$C_{19}H_{19}O_4N$	C 69.98 / 70.14 H 5.94 / 5.89 N 4.18 / 4.31	231.5 (4.62) 324sh (3.79) 275.5 (3.96) 336 (3.90) 285.5 (3.89) 353sh (3.81)
IIIc	156.5—158	Colorless[a] plates	57	$C_{19}H_{19}O_4N$	C 70.18 / 70.14 H 5.89 / 5.89 N 4.40 / 4.31	222 (4.78) 282 (3.94) 242sh (4.17) 301.5 (4.01) 249 (4.08) 314 (4.22) 272sh (3.91) 328 (4.22)
IIId	148—149.5	Colorless[b] plates	66	$C_{19}H_{19}O_4N$	C 70.05 / 70.14 H 6.06 / 5.89 N 4.56 / 4.31	244 (4.46) 289.5 (3.95) 251 (4.44) 320 (3.59) 270sh (3.89) 334sh (3.44) 279 (3.96)

a) from ethanol b) from ethyl acetate sh shoulder

and γ-fagarine (Id)[14]) in *ca.* 50% yields. The properties of synthetic samples of Ia—d were identical with those recorded for natural specimens.[1,3,4,13,14]

Experimental[15]

3-(2-Benzyloxyethyl)-4-hydroxy-2-quinolones (IIIa—d).—A mixture of 2,4-dimethoxyaniline (IIa (6.4 g)) or monomethoxy derivatives (IIb—d (5.4 g)) and diethyl β-benzyloxyethylmalonate (14.5 g)[16] in diphenyl ether (30 ml) was heated under stirring at 250°C for about 30 min, by which time 5 ml (2 mol equivalent) of ethanol had been distilled

14) B. Berinzaghi, A. Muruyabal, and V. Deulofeu, *J. Org. Chem.*, **10**, 181 (1945).

15) All the melting points are uncorrected; the UV spectra of the compounds were measured in ethanol.

16) G. M. Bennett and A. L. Hock, *J. Chem. Soc.*, **1927**, 472: W. R. Kirner and G. H. Richter, *J. Amer. Chem. Soc.*, **51**, 2503 (1929).

TABLE 5. 3-(2-BENZYLOXYETHYL)-4-METHOXY-2-QUINOLONES (IVa—d)

Compounds	Mp (°C)	Cryst. form	Yield (%)	Formula	Analysis (%) Found C H N	Analysis (%) Calcd C H N	UV λ_{max} mμ (log ε)			
IVa	105—106	Pale yellow[a] leaves	quant.	$C_{21}H_{23}O_5N$	68.44 6.37 3.80	68.28 6.28 3.79	232 255 279	(4.34) (4.37) (3.91)	290sh 347 363sh	(3.80) (3.75) (3.66)
IVb	157—158	Pale yellow[a] needles	68	$C_{20}H_{21}O_4N$	70.62 6.36 4.08	70.78 6.24 4.13	234 261.5 271.5 282sh	(4.62) (3.89) (3.91) (3.82)	329sh 343.5 360.5sh	(3.71) (3.89) (3.78)
IVc	132.5—134	Colorless[b] needles	82	$C_{20}H_{21}O_4N$	70.78 6.09 4.31	70.78 6.24 4.13	238sh 255 283	(4.55) (3.84) (3.82)	309 323	(4.01) (4.24)
IVd	68.5—69.5	Colorless needles	96	$C_{20}H_{21}O_4N$	70.95 6.38 4.11	70.78 6.24 4.13	235.5 252 279	(4.34) (4.45) (3.95)	329 343sh	(3.55) (3.37)

a) from ethanol b) from dilute ethanol.

TABLE 6. 2,3-DIHYDROFURO[2,3-*b*]QUINOLINES (Va—d)

Compounds	Mp (°C) Found/Lit.	Cryst. form	Yield (%)	Formula	Analysis (%) Found C H N	Analysis (%) Calcd C H N	UV λ_{max} mμ(log ε)			
Va	188—191	Colorless[a] plates	83	$C_{14}H_{15}O_4N$	64.24 5.86 5.34	64.36 5.79 5.36	220 247 266	(4.44) (4.56) (3.80)	276 326 342	(3.40) (3.63) (3.64)
Vb	169.5—160.5	Colorless[a] plates	35	$C_{13}H_{13}O_3N$	67.33 5.67 5.87	67.52 5.67 6.06	230 260.5 268.5 279sh	(4.66) (3.77) (3.77) (3.62)	311sh 325 339	(3.42) (3.71) (3.72)
Vc	135—136 136—137[12]	Colorless[a] needles	39	$C_{13}H_{13}O_3N$	67.32 5.88 6.04	67.52 5.67 6.06	225.5 243sh 251sh 276 287	(4.72) (4.20) (3.88) (3.64) (3.71)	300sh 306sh 313.5 319.5 327	(3.78) (3.92) (4.05) (4.05) (4.02)
Vd	171—172 168—170[17]	Colorless[a or b] plates	46	$C_{13}H_{13}O_3N$	67.32 5.96 6.03	67.52 5.67 6.06	248 268sh 279	(4.60) (3.73) (3.79)	290 314 326	(3.70) (3.42) (3.43)

a) from ethanol b) from methanol

off. The solution was then poured into 300 ml of petroleum benzine, and the mixture was allowed to stand overnight. The solvent was decanted, and the residual oily precipitate was dissolved in chloroform. The chloroform solution was extracted with five 100 ml portions of a 5% sodium hydroxide solution. Washed with chloroform, the alkaline solution was acidified with an aqueous acetic acid solution (1: 1). The acidic solution was extracted with chloroform. After the solvent had been evaporated, the residue was triturated with ether and recrystallized to give IIIa—d (Tables 1, 4).

3-(2-Benzyloxyethyl)-4-methoxy-2-quinolones (IVa—d). A solution of IIIa—d (5.0 g) in chloroform (70 ml) was treated with an ethereal diazomethane solution, and then the mixture was allowed to stand overnight. After a usual work-up, the product was recrystallized to give IVa—d (Tables 1,2,5), which gave a light brown or a reddish brown color with ferric chloride in ethanol.

2,3-Dihydrofuro[2,3-b]quinolines (Va—d). A mixture of IVa—d (0.7 g) and polyphosphoric acid (13 g) was heated at 120—130°C for 1.5—3 hr. The cooled mixture was poured into water, and the insoluble materials were filtered off. The aqueous solution was neutralized with diluted aqueous ammonia. The precipitate was collected, washed with water, and recrystallized to give Va—d (Tables 1,3,6).

Furo[2,3-b]quinolines (Ia—d). To a solution of Va—d (1.0 g) in dry benzene (150 ml), DDQ (1.0 g) was added, the mixture was then stirred under reflux for 8 hr in an atmosphere of nitrogen. The reaction mixture was filtered, and the solvent was evaporated *in vacuo*. The residue was dis-

17) M. F. Grundon and N. J. McCorkindale, *J. Chem. Soc.*, **1957**, 2177.

TABLE 7. FURO[2,3-*b*]QUINOLINES (Ia—d)

Compounds	Mp (°C) Found/Lit.	Cryst. form	Yield (%)	Formula	Analysis (%) Found C H N	Calcd C H N	UV λ_{max} mμ(log ε)
Ia	183—185	Pale yellow[a,b]	55	$C_{14}H_{13}O_4N$	65.01	64.86	247 (4.76) 305 (3.72)
	182—184[1]	plates			5.13	5.05	283sh (3.78) 337 (3.43)
					5.30	5.40	293 (3.83) 353 (3.42)
Ib	134—136	Pale yellow[a]	60	$C_{13}H_{11}O_3N$	68.11	68.11	236.5 (4.69) 294 (3.97)
	134—135[3,4]	needles			4.90	4.84	249 (4.59) 307 (4.02)
					5.96	6.11	268 (3.70) 332 (3.75)
							285sh (3.83) 347.5 (3.72)
Ic	110—112	Pale yellow[a]	49	$C_{13}H_{11}O_3N$	68.30	68.11	245.5 (4.79) 307 (3.98)
	114—115[13]	needles			4.88	4.84	255sh (4.29) 318 (3.96)
					5.94	6.11	289sh (3.76) 332 (3.88)
							299sh (3.89)
Id	137—139	Colorless[a]	53	$C_{13}H_{11}O_3N$	68.11	68.11	223 (4.21) 270sh (3.87)
	138—140[14]	needles			4.83	4.84	240sh (4.53) 310 (3.26)
					6.01	6.11	246 (4.64) 323 (3.22)
							253sh (4.54)

a) from petroleum benzine b) from benzene

solved in chloroform, and the solution was extracted with dilute hydrochloric acid. After the aqueous solution had been neutralized with dilute aqueous ammonia, the resulting precipitate was collected and recrystallized to give Ia—d (Tables 1,3,7). The product was purified by means of chromatography on alumina (300 mesh, chloroform–2% ethanol).

The author wishes to express his deep gratitude to Professor Kenji Fukui, Hiroshima University, for his encouragement through the course of this work.

BULLETIN OF THE CHEMICAL SOCIETY OF JAPAN, VOL. 46, 580—583 (1973)

The Reaction of Methyl 2-Dimethoxymethyl-3-methoxypropionate with Amidines[1,2]

Takenori NISHINO, Yoshiyuki MIICHI, and Kanji TOKUYAMA
Shionogi Research Laboratory, Shionogi & Co., Ltd., Fukushima-ku, Osaka 553

(Received July 21, 1972)

The reaction of methyl 2-dialkoxymethyl-3-methoxypropionate with acetamidine has been reported to afford 2-methyl-4-hydroxy-5-methoxymethylpyrimidine (**13a**) by a different mode than the reaction of 2-dimethoxymethyl-3-methoxypropionitrile (**1**), which affords dihydropyrimidopyrimidine (**4**). As the presence of this difference seemed to be somewhat curious from the viewpoint of the reaction mechanism, the reaction of methyl 2-dimethoxymethyl-3-methoxypropionate (**7**) with acetamidine was reinvestigated. The reaction products were **13a** and acetamidinomethylpyrimidine (**17a**). Similar results were obtained by the reaction of **7** with benzamidine. As the compound **17** corresponds to **4**, the reaction of **7** was concluded to proceed in a manner similar to that of **1**; that is, no essential difference exists between the reactions of **1** and **7** with amidines.

In previous papers,[2-5] we have presented the pathway of the reaction of 2-dimethoxymethyl-3-methoxypropionitrile (**1**) with amidines. The reaction proceeds mainly *via* the pathway of **1** → 2-dimethoxymethylacrylonitrile (**2**) → dihydropyrimidines (**3**) → dihydropyrimidopyrimidines (**4**). The existence of the minor pathway of **1** → 2-methoxymethylene-3-methoxy-

1) Pyrimidines, 12, for Part 11, see Ref. 2. A part of this paper was reported in a preliminary form: T. Nishino, Y. Miichi, and K. Tokuyama, *Tetrahedron Lett.*, **1970**, 4335.

2) T. Nishino, M. Kiyokawa, Y. Miichi, and K. Tokuyama, This Bulletin, **46**, 253 (1973).

3) T. Nishino, M. Kiyokawa, Y. Miichi, and K. Tokuyama, *ibid.*, **45**, 1127 (1972).

4) T. Nishino, M. Kiyokawa, Y. Miichi, and K. Tokuyama, *ibid.*, **45**, 2010 (1972).

5) M. Tanaka and K. Tokuyama, paper read at the 92nd annual meeting of The Pharmaceutical Society of Japan, Kinki University, Higashiosaka, Osaka, April, 1972, Abstract 6M4-3.

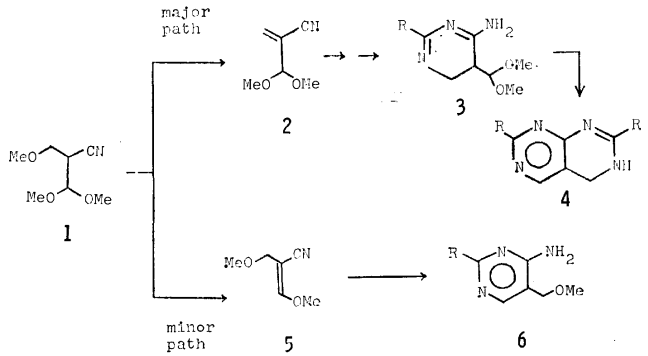

Chart 1.

propionitrile (**5**) → 5-methoxymethylpyrimidines (**6**) was also established.

Similar results can naturally be expected in the reaction of the ester analog of **1**. However, the reaction of the ester analog with acetamidine did not yield products corresponding to **3** and **4**, but only the product corresponding to **6**.[6] Although an explanation of this remarkable difference between the two reactions had been proposed, it seems to be somewhat in conflict with the revised mechanism of the reaction of **1** with acetamidine. Therefore, we attempted to reinvestigate the reaction of the ester analog.

Methyl 2-dimethoxymethyl-3-methoxypropionate (**7**), 2-dimethoxymethylacrylate (**9**), and 2-methoxymethylene-3-methoxypropionate (**10**) were prepared by the usual methods[6] and were used as the starting materials. Their structures were identified by a comparison of their spectra with the spectra of the corresponding propionitriles.[6-8]

At the outset, the possibility of the conversion of **7** into **9** was examined. When a mixture of **7** and sodium methoxide was left at room temperature overnight, the spot of **7** disappeared in the tlc. Without purification, the product was treated with acetamidine to give a pyrimidine (**12**), $C_{14}H_{22}N_2O_6$, which showed the bands due to ester and acetal groups in the IR spectrum and a behavior similar to that of 2-methyl-4-hydroxy-5-methoxymethylpyrimidine (**13a**)[9] in the UV. Therefore, its structure was identified as 2-methyl-4-hydroxy-5-(2′-carbomethoxy-2′-dimethoxymethyl-3′-methoxy)-propylpyrimidine. The NMR spectrum also supported this structure.

By analogy with the base-catalyzed reaction of **1**,[3] a dimeric substance of **7** (**11**) should exist in the product. The possible intermediate, **11**, suggested the presence of the equilibrium, **7** ⇌ the anion of **7** (**8**) ⇌ **9** under basic conditions, since **11** would be formed by the reaction of **8** with **9**, as shown in Chart 2. Consequently, the formation of the reaction products with **9**, corresponding to the product from the major pathway

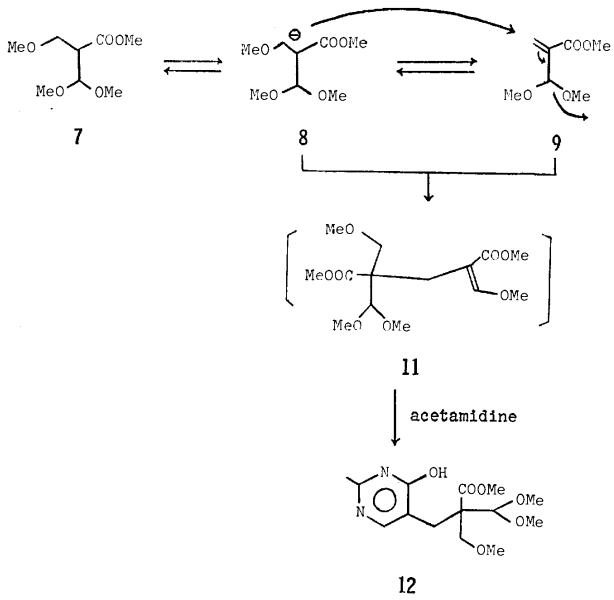

Chart 2.

of the reaction of **1**, was anticipated in the reaction of **7** with acetamidine.

When a mixture of **7** and acetamidine was refluxed in methanol, **13a** and another product (**17a**) were obtained as expected. The structure of **17a** was identified as 2-methyl-4-hydroxy-5-acetamidinomethylpyrimidine by a comparison of the spectral data with those of an authentic sample.[4] The relative ratio of the yields of **13a** and **17a** was about 3: 2, as determined by NMR spectroscopy.

It is quite natural to consider that **17a** was formed *via* a pathway corresponding to that of the reaction of **1**. Chart 3 shows a possible pathway *via* **9** and a dihydropyrimidine (**14**) as key intermediates.

The step **14**→**17a** was proved in a previous paper.[4] The treatment of **9** with acetamidine in 1,2-dimethoxy-

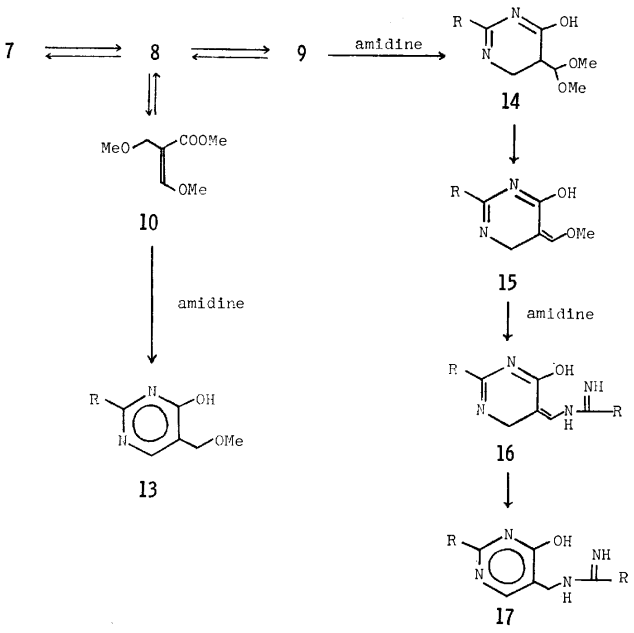

Chart 3.

6) A. Takamizawa, K. Tokuyama, and H. Satoh, *Yakugaku Zasshi*, **79**, 664 (1959).
7) A. Takamizawa, K. Ikawa, and M. Narisada, *ibid.*, **78**, 632, 637 (1958).
8) A. Takamizawa, K. Hirai, and S. Sumimoto, *Chem. Pharm. Bull.* (Tokyo), **14**, 238 (1966).
9) A. Takamizawa, *Yakugaku Zasshi*, **74**, 756 (1954).

ethane at a low temperature did not afford **13a**, but **14a** as the major product, along with a limited amount of **17a**. On the other hand, that of **10** in 1,2-dimethoxyethane instantly yielded only **13a** in a high yield. These results support the above pathway.

Similar results were obtained in the reaction of **7** with benzamidine. When a mixture of **7** and benzamidine was refluxed in methanol for a long time, crystals appeared which had a correct analysis for $C_{18}H_{16}N_4O$. Therefore, the structure of the crystals was identified as that of the phenyl analog of **17a** (**17b**). The structure was also confirmed by the spectral data. From the mother liquor, the phenyl analog of **13a** (**13b**) was isolated, its structure was confirmed from the combined data of elemental and spectral analyses.

The above results support the idea that the reaction with benzamidine proceeded in a manner similar to that with acetamidine. The relative ratio of the yields of **13b** and **17b** was about 2: 1.

As has been described above, the pathway of the reaction of **1** with amidines can be applied to the reaction of **7**. It can be concluded that there is no essential difference between the two reactions.

Experimental

All the melting points were recorded on a Kofler block and have not been corrected. The NMR spectra were taken with a Varian A-60-A spectrometer, using tetramethylsilane as the internal reference, and the chemical shifts were expressed in δ values (s: singlet, d: doublet, t: triplet, q: quartet, m: multiplet, bs: broad singlet). The UV spectra were observed in methanol and are reported in nm. The molecular weights were determined by means of a vapor-pressure osmometer in benzene. The solvents used were removed under reduced pressure.

Methyl 2-Dimethoxymethyl-3-methoxypropionate (**7**) was prepared by the usual method.[6] Bp 62°C/2 mmHg. $N_D^{26.2}$ 1.4211. IR_{film} 1744 cm^{-1} (ester), 1100, 1070 (acetal). NMR (CCl_4) 3.42—3.58 (m, 2H, H_3, AB part), 2.86 (m, 1H, H_2, M part; J_{AM} 4.5 Hz, $J_{BM}=J_{MX}$ 8 Hz), 4.43 (d, 1H, C<u>H</u>$(OMe)_2$, X part), 3.65 (s, 3H, COOMe), 3.23 (s, 3H), 3.25 (s, 3H, CH$(O\underline{Me})_2$), 3.28 (s, 3H, 3-MeO). Found: C, 50.06; H, 8.42%; mol wt, 200. Calcd for $C_8H_{16}O_5$: C, 49.99; H,8.39%; mol wt, 192.

Methyl 2-Dimethoxymethylacrylate (**9**) *and Methyl 2-Methoxymethylene-3-methoxypropionate* (**10**) were prepared by the usual methods.[6] **9**: Bp 42—44°C/3.5 mmHg. $N_D^{26.2}$ 1.4295. IR_{film} 1730 cm^{-1} (ester), 1630 (C=C), 1100, 1075, 1055 (acetal, C–O–C). NMR (CCl_4) 6.23 (d, 1H, H_3, $J_{3,3'}$ 2 Hz), 5.90 (q, 1H, $H_{3'}$, $J_{3',A}$ 1 Hz), 5.10 (d, 1H, H_A, C<u>H</u>$(OMe)_2$), 3.27 (s, 6H, CH$(O\underline{Me})_2$), 3.72 (s, 3H, COOMe). Found: C, 52.49; H, 7.70%; mol wt, 191. Calcd for $C_7H_{12}O_4$: C, 52.94; H, 7.55%; mol wt, 160. **10**: purified by gas chromatography (Column, PEG 20 M 20%, 176±2°; flow rate, helium 25.0 ml/min). $N_D^{26.5}$ 1.4644. IR_{film} 1712 (ester), 1642 cm^{-1} (C=C). UV 237 (ε 15200). NMR (CCl_4), 3.98 (s, 2H, H_3), 7.33 (s, 1H, =C<u>H</u>OMe), 3.18 (s, 3H, 3-MeO), 3.85 (s, 3H, =CHO<u>Me</u>), 3.65 (s, 3H, COOMe). Found: C, 52.69; H, 7.73%, mol wt, 162. Calcd for $C_7H_{12}O_4$: C, 52.49; H, 7.55%; mol wt 160.

Reaction of Methyl 2-Dimethoxymethyl-3-methoxypropionate (**7**) *with Sodium Methoxide.* A mixture of **7** (2 g) and sodium methoxide (265 mg) was left at room temperature overnight. The spot due to **7** disappeared in the tlc. A solution of acetamidine, which has been prepared from acetamidine hydrochloride (1.32 g), sodium (200 mg), and methanol (13 ml), was then added to the mixture. The solution was refluxed for 5 hr, and then the solvent was removed. The residue was extracted with ether. The ether-extracted syrup was fractionated by column chromatography (alumina, 40 g,; benzene 7: methanol 1: ethyl acetate 2, v/v). From the initial fractions, crystals were obtained. The recrystallization of the crystals from ethyl acetate gave acetamide. From the mother liquor, needles of **12** were obtained; this substance was then recrystalized from ether. The yield was 30 mg. Mp 132.4—133°C. IR_{KBr} 1740 cm^{-1} (ester), 1650 (C=N), 1100 (C–O–C). UV 278 (ε 6000), +HCl 265. +NaOH 276. MS 314 (M^+). NMR (CD_3OD) 7.73 (s, 1H, H_6), 4.58 (s, 1H, C<u>H</u>$(OMe)_2$), 3.58 (s, 2H, –C<u>H</u>$_2$–OMe), 3.65 (s, 3H, COOMe), 3.47 (s, 6H, CH$(O\underline{Me})_2$), 3.20 (s, 3H, $CH_2O\underline{Me}$), 2.88 (s, 2H, C_5-CH_2), 2.33 (s, 3H, C_2-Me). Found: C, 53.69; H, 7.15; N, 9.07%. Calcd for $C_{14}H_{22}N_2O_6$: C, 53.49; H, 7.05; N, 8.91%.

Reaction of Methyl 2-Dimethoxymethyl-3-methoxypropionate (**7**) *with Amidines.* *(1) Reaction with Acetamidine*: (i) Acetamidine hydrochloride (2.25 g) was dissolved in a solution of sodium (0.505 g) in methanol (15 ml) and then the sodium chloride thus precipitated was filtered out. To the filtrate, **7** (2 g) was added, after which the solution (18.65 g) was refluxed for 6 hr. One gram of the solution was used for the determination of the relative ratio of **13a** and **17a** by NMR spectroscopy, using methanol-d_4 as the solvent. Singlets due to the methylene group of **13a** at 4.30 δ and that of **17a** at 4.20 δ were integrated. The ratio (**13a** : **17a**) was 3: 2. The remainder of the solution was evaporated to dryness, and the residue was fractionated by column chromatography [silica gel (40 g), ethanol]. From the initial fractions, **13a** (720 mg, 45%) was obtained.[9] (ii) Five grams of **7** were treated in methanol (20 ml) with acetamidine hydrochloride (5.4 g), and sodium (1.2 g). The solvent was then removed, and the residue was washed with dioxane (100 ml) and subsequently recrystallized from ethanol. Plates of **17a** (132 mg) were obtained; they were purified as the dihydrochlorides [mp 237—240°C (dec)].[4]

(2) Reaction with Benzamidine: A solution of **7** (1.5 g) and benzamidine (2.1 g) in methanol (10 ml) was refluxed for 15 hr. After cooling, there appeared crystals (**17b**, 345 mg) which were collected by filtration. The filtrate was evaporated to dryness and then washed with petroleum ether. The petroleum ether contained **7**. The residue was chromatographed over silica gel (30 g). The first fraction, eluted with ether (150 ml) afforded a mixture of **13b** and **17b** (37 mg). The second fraction, eluted with a mixture (150 ml) of ether (10 parts) and ethanol (1 parts) and the third one, eluted with a mixture (120 ml) of ether (1 part) and ethanol (1 part) gave needles of **13b** (565 mg). **13b**: mp 188.5—191.2°C (dec), (recryst. from ethanol). UV 242 (ε 15200), 296 (ε 1100), +HCl 242, 281, +NaOH 237, 282, 295. IR_{KBr} 1663 cm^{-1} (C=C, C=N). NMR ($CDCl_3$) 8.18 (bs, 1H, H_6), 4.44 (d, 2H, –CH_2–, J=1 Hz), 3.32 (s, 3H, MeO–). Found: C, 66.62; H, 5.48; N, 12.88%. Calcd for $C_{12}H_{12}N_2O_2$: C, 66.65; H, 5.59; N, 12.96%. **17b**: leaflets, mp 255.5—257°C (dec) (recryst. from methanol). UV 235 (ε 28300), 295 (ε 10000), +HCl 235, 285, +NaOH 234, 285, 294. IR_{KBr} 1695, 1625 cm^{-1} (C=C, C=N). MS 304 (M^+), 287 (M^+–NH_3), 200 (M^+–C(=NH)–Ph), 185 (M^+–HN–C(=NH)–Ph). Found: C, 71.27; H, 5.28; N, 18.59%. Calcd for $C_{18}H_{16}N_4O$: C, 71.03; H, 5.30; N, 18.41%.

Reaction of Methyl 2-Dimethoxymethylacrylate (**9**) *with Aceta-*

midine. Acetamidine hydrochloride (5.3 g) was added to a methanolic sodium methoxide, prepared from methanol (20 ml) and sodium (1.2 g), after which the solution was filtered to remove precipitates. The filtrate was evaporated to dryness, and to the residue 1,2-dimethoxyethane (7 ml) was added. Under stirring, a solution of **9** (3 g) in 1,2-dimethoxyethane (7 ml) was added to the solution in portions at below 5°C. The solution was left in a refrigerator for 2 days and then neutralized with methanolic hydrogen chloride. The crystals of the dihydrochloride of **17a** (2.3 g)[4] were collected by filtration.

*Reaction of Methyl 2-Methoxymethylene-3-methoxypropionate (**10**) with Acetamidine.* Acetamidine hydrochloride (1.2 g) was added to methanolic sodium methoxide, which had been prepared from methanol (6 ml) and sodium (302 mg). The solution was filtered from precipitated sodium chloride and then evaporated to dryness. A solution of **10** (700 mg) in 1,2-dimethoxyethane (2 ml) was added to a mixture of the residue and 1,2-dimethoxyethane (3 ml). Crystals appeared instantly; they were collected by filtration and then extracted with chloroform. The evaporation of the chloroform gave **13a** (635 mg).[9]

The authors express their deep gratitude to Professor Toshihiko Okamoto, the University of Tokyo, for his discussion.

BULLETIN OF THE CHEMICAL SOCIETY OF JAPAN, VOL. 46, 583—586 (1973)

The Structure of Shikokianidin, a Minor Component of *Isodon shikokianus* Hara

Takahiko Isobe, Tadao Kamikawa, Isao Kubo, and Takashi Kubota
Faculty of Science, Osaka City University, Sugimoto-cho, Sumiyoshi-ku, Osaka

(Received July 24, 1972)

Shikokianidin from *Isodon shikokianus* Hara is formulated as structure (**3**) on the basis of chemical and spectroscopic evidence.

The isolation of two bitter principles, oridonin (**1**) and shikokianin (**2**) from the extract of *Isodon shikokianus* Hara has already been reported.[1] From the less polar fractions of the extract we have obtained a new, non-bitter diterpene, designated shikokianidin (**3**), $C_{26}H_{34}O_9$, mp 218—219°C, $[\alpha]_D$ −109°. Shikokianidin showed hydroxylic, acetoxy and 6-membered ketonic absorptions in the infrared spectrum (ν_{max} 3450, 1745, 1725, 1260, and 1230 cm^{-1}). Its NMR spectrum (Fig. 1) showed signals attributable to two tertiary C-methyl groups (δ 1.10 and 1.41), three acetyl groups (δ 1.95, 2.02, and 2.12), and a hydroxyl group (δ 4.33, s, exchangeable with D_2O). These spectroscopic data account for eight oxygen atoms out of nine of those of shikokianidin. In addition, there is a three-proton multiplet at *ca.* δ 4.9 which could be assigned to three –CH(OAc)–protons. The lack of a signal for –CH(OH)– in the NMR spectrum confirmed the tertiary nature of the free hydroxyl group. Other significant features of the NMR spectrum of (**3**) include signals arising from ≡C–CH_2–O– (δ 4.23, dd, J=2 and 10 Hz; δ 4.84, dd, J=1.5 and 10 Hz) and a terminal methylene group (δ 5.07, dd, J=1.5 and 3 Hz; δ 5.43, t, J=3 Hz). From analogy with congeners the former group probably constitutes a hemiacetal system and the latter is involved in the D ring.

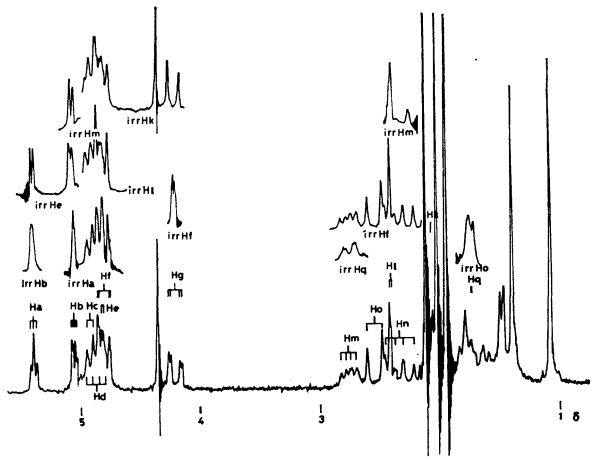

Fig. 1. The NMR spectrum of shikokianidin (**3**).

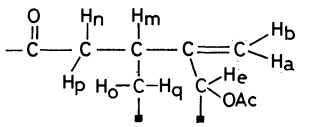

(4)

Spin decoupling (NMDR) experiments performed on shikokianidin demonstrated the presence of structural unit (**4**). On irradiation of the H_e proton located at δ 4.85 (d, J=1.5 Hz), the triplet at δ 5.43 (H_a) collapsed to a doublet (J=3 Hz), showing the removal of allylic coupling and the retention of geminal coupling (J_{gem}=3 Hz). When the H_a proton was irradiated the H_e proton appeared as a singlet with a small splitting (J<1 Hz), indicative of a neighbouring quaternary centre, and the H_b proton (δ 5.07) collapsed to a doublet ($J\simeq$1 Hz). On the other hand, when the H_m proton located at δ 2.77 (q, J=5 and 9 Hz) was irradiated, the H_b proton collapsed to a sharp doublet ($J_{a,b}$=3 Hz) and the H_n proton at δ 2.36 (q, J=9 and 16 Hz) to a doublet ($J_{n,p}$=16 Hz). Conversely,

1) T. Kubota and I. Kubo, This Bulletin, **42**, 1778 (1969).

irradiation at δ 1.75 (H_q) resulted in the collapse of the H_m proton signal to a broad double doublet ($J_{m,n}$= 9, $J_{b,m}$=2 Hz), and irradiation of the H_o proton at δ 2.56 (d, $J_{o,q}$=13 Hz) resulted in the collapse of the multiplet at δ 1.75 to a doublet ($J_{m,q}$=5 Hz). The results suggest that the H_m proton is coupled to H_b, H_n, and H_q and the latter two protons to H_p and H_o, respectively, and the dihedral angles between H_m and H_p, H_m and H_o are both close to 90°. The magnitude of the geminal coupling constant between H_n and H_p (J=16 Hz) suggests that these two protons are adjacent to a carbonyl group.[2] Furthermore, NMDR experiments of **3** afforded evidence for the presence of structural unit (**5**).

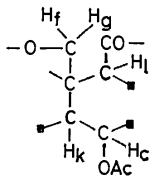

(5)

On irradiation of the H_l proton at δ 2.42 (d, J= 1.5 Hz), the double doublet pattern for H_f proton (δ 4.84, J=1.5 and 10 Hz) was reduced to a doublet (J=10 Hz) showing the removal of long-range coupling through a W-configuration and the retention of geminal coupling. Irradiation at the centre of the double doublet for H_f proton resulted in the collapse of the H_l proton signal to a singlet and the H_g proton signal to a doublet (J=2 Hz). The chemical shift of the H_l proton is indicative of the presence of a neighbouring carbonyl group.[3] On irradiation at δ 2.06 (H_k proton), the double doublet pattern for H_g proton (δ 4.23, J=2 and 10 Hz) was reduced to a doublet (J=10 Hz) and the double doublet pattern for H_c proton (δ 4.93, J=5 Hz) was reduced to a singlet, showing the removal of both long-range coupling through a W-configuration and vicinal coupling. Thus expansion of the part structures **4** and **5** to **6** would be admissible if we assume that shikokianidin has ent-kaurane skeleton with a hemiacetal ring. Further evidence to support this part structure was provided by acid treatment of shikokianidin.

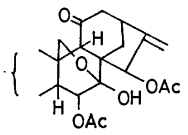

(6)

Treatment of **3** with 2N hydrochloric acid gave a seco-aldehyde **7**, $C_{24}H_{32}O_8$. The NMR spectrum of the seco-aldehyde showed the presence of two tertiary C-methyl groups (δ 1.07 and 1.33), two acetyl groups (δ 1.90 and 2.09), a hydroxyl group (δ 4.56, exchangeable with D_2O), two olefinic protons conjugated with an aldehyde (δ 6.00, s; δ 6.33, d, J=1.5 Hz) and an aldehyde proton (δ 9.51, s). (see Fig. 2, where the lower part of the spectrum is omitted).

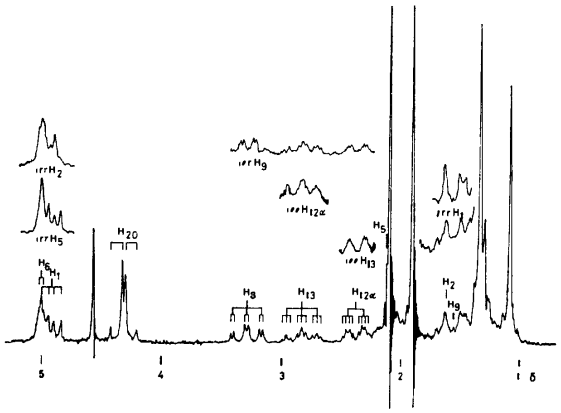

Fig. 2. The NMR spectrum of seco-aldehyde (**7**).

NMDR experiments demonstrated the presence of the part structure (**8**).

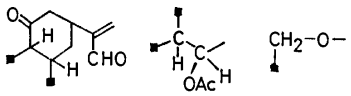

(8)

The results lead to assignment of structure **7** to the seco-aldehyde except for the position of one secondary acetoxy group in ring **A**. From biogenetic grounds, it is most reasonable to place this acetoxy group at position C_1 or C_3. The NMR spectrum of **7** showed a one proton quartet at δ 4.91 (J=6 and 10 Hz) and a one proton doublet at δ 4.99 (J=4 Hz), the latter being assigned to H_7 (on irradiation at δ 2.14 this collapsed to a singlet), and the former to $H_{1\beta}$ or $H_{3\beta}$ (on irradiation at δ 1.63 this collapsed to a doublet J=10 Hz). The axial nature of this proton was evident from the large axial-axial coupling (J=10 Hz) and small axial-equatorial coupling (J=6 Hz). The splitting pattern of this proton is quite similar to that of the C_1 proton of shikokianin (**2**).[4] A possible mechanism for this transformation would be a hydrolysis of the allylic acetate with concomitant opening of the hemiacetal as demonstrated in trichokaurin,[5] followed by reverse aldol reaction and re-cyclization to hemiacetal.

Catalytic reduction of shikokianidin gave dihydro-

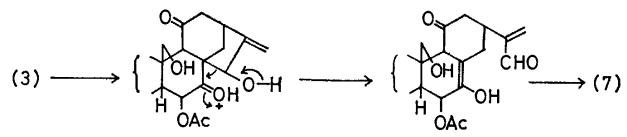

2) T. Takahashi, *Tetrahedron Lett.*, **1964**, 565.
3) S. Forsen and T. Norin, *ibid.*, **1964**, 2845.
4) The original assignment of the NMR spectrum of **2** was incomplete and some conflicting results were reported.[1] The correct assignment is as follows; two tertiary *C*-methyl protons (δ 1.16 and 1.18), two acetyl protons (δ 1.91 and 2.11), two hydroxyl protons (δ *ca.* 4.7, C_7-**OH** and δ 5.93, d, J=12 Hz, C_6-OH; both exchangeable with D_2O), $H_{12\beta}$ (δ 2.82, q, J=4 and 15 Hz), $H_{12\alpha}$ (δ 2.40, q, J=9 and 15 Hz), $H_{14\alpha}$ (δ 2.84, d, J=13 Hz), H_{13} (δ 3.07, q, J=4 and 9 Hz), H_6 (δ 4.01, q, J=10 and 12 Hz), ≡C-CH_2-O- (δ 4.11, d, J=10 Hz with small splitting; δ 4.44, q, J=2 and 10 Hz), H_1 (δ 4.74, q, J=5 and 10 Hz), H_{11} (δ 4.86, t, J=4 Hz) and two olefinic protons (δ 5.50 and 6.00).
5) E. Fujita, T. Fujita, M. Shibuya, and T. Shingu, *Tetrahedron*, **25**, 2517 (1969).

shikokianidin (**9**), $C_{26}H_{36}O_9$. The NMR spectrum of **9** showed the presence of a secondary methyl group (δ 0.71, d, J=7 Hz) and a –CH(OAc)– proton (δ 4.86, d, J=10 Hz). NMDR experiments demonstrated that the proton attached to the secondary methyl group and the proton of the type –CH(OAc)– are vicinal (on irradiation at δ 2.51, both the secondary methyl and the –CH(OAc)– proton signals collapsed to singlets). Since the hydrogenation of the C_{15} double bond is assumed to occur from the less hindered side of the molecule, the newly introduced secondary methyl is presumably β. The dihedral angle between the protons H_{15} and H_{16} is assumed to be 0° from the coupling constant (J=10 Hz). Thus the acetoxy group at C_{15} can be assigned as β.

Treatment of **9** with methanolic ammonia gave trisdeacetyldihydroshikokianidin (**10**), $C_{20}H_{30}O_6$, with an IR frequency (1710 cm^{-1}) compatible with a cyclohexanone. The NMR spectrum (in $CDCl_3$–C_5D_5N) showed signals for one secondary (δ 0.96, d, J=7 Hz) and two tertiary (δ 1.07 and 1.11) *C*-methyl groups, three –CH(OH)– protons (δ 3.90, q, J=7 and 9 Hz, H_1; δ 4.57, d, J=11 Hz, H_{15}; δ 4.78, q, J=3 and 8 Hz, H_6) and ≡C–CH_2–O– protons (δ 4.60, q, J= 1 and 12 Hz; δ 5.95, d, J=12 Hz).

From analogy with the congeners a tentative assignment of stereochemistry as shown in **3** can now be extended to shikokianidin. On examination of a molecular model, the proton H_5 and the proton H_9 are in close proximity (both axial). When the proton at C_5 was irradiated, NOE enhancement was observed in the integrated area of H_9 signal (15%). Another relative stereochemistry may now be deduced from a consideration on the NMR data of shikokianidin. As already discussed, the acetoxy groups at C_1 and C_{15} can be assigned as α and β, respectively. The C_6 proton gives rise to a doublet (J=4 Hz). This suggests an equatorial disposition with coupling to an adjacent axial C_5 proton (the ring B takes a boat conformation). The C_{13} proton showed a spectrum assumed to be the X part of an ABX system ($J_{12\alpha,13}$= 9 Hz, $J_{14\beta,13}$=5 Hz, with small allylic coupling). This suggests that the C_{13} proton is equatorial and the dihedral angles between H_{13} and $H_{12\beta}$, and H_{13} and $H_{14\alpha}$ are both 90°. The stereochemistry of the seco-aldehyde produced by an acid-treatment of **3** can now be formulated as **7**. It is anticipated that ring C takes a strain-free chair form and that the ring junctures take the most stable *trans-anti-trans* configuration. The C_8 proton (δ 3.28) showed a six-line spectrum with coupling constants $J_{8,9}=J_{8,14\beta}$=12 Hz, $J_{8,14\alpha}$=3 Hz. The low-field shift of this signal is attributable to the proximity of the hemiacetal oxygen atom.[6] The C_{13} proton (δ 2.82) showed a nine-line spectrum with coupling constants $J_{12\beta,13}=J_{13,14\beta}$=13 Hz, $J_{12\alpha,13}=J_{13,14\alpha}$= 4 Hz.

Shikokianidin shows a positive CD. However, no similar compounds are available for a comparative study.

Finally, we have confirmed the proposed structure by relating **3** to shikokianin (**2**), which in turn relates to nodosin.[7] Lithium aluminum hydride reduction of **3** gave a mixture of three reduction products. One of the reduction products was deacetylshikokianidin. The other two products were isomeric pentaols (**11**) and (**12**). On the other hand, the reduction of shikokianin (**2**) with lithium aluminum hydride gave pentaol (**11**), the latter proving to be identical with one of the pentaols derived from **3**. Thus the structure of shikokianidin including the absolute configuration has been established.

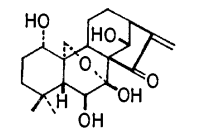
(1)

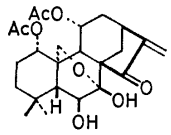
(2)

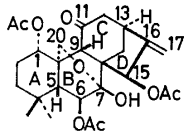
(3)

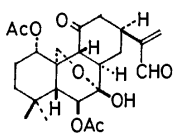
(7)

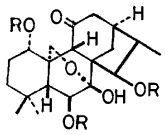
(9) R=Ac
(10) R=H

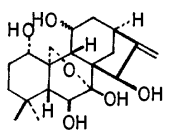
(11) 11α-OH
(12) 11β-OH

Experimental

NMR spectra were determined on a JEOL PS-100 (100 MHz) spectrometer in deuterochloroform solutions, unless otherwise stated. IR spectra were recorded on Nujol mull with a Japan Spectroscopic IR-S spectrophotometer. CD data were obtained in chloroform solution with a Jasco ORD/UV-5 (equipped with CD attachment). Column chromatography was performed with Mallinckrodt silicic acid.

Isolation. The dried leaves of *Isodon shikokianus* Hara were extracted with ether. The crude extract was treated with activated charcoal, concentrated and chromatographed in ether over silicic acid. Elution with the same solvent gave shikokianidin, shikokianin, and oridonin in this order. The less polar fractions were collected and recrystallised from ethanol to give pure shikokianidin (**3**), mp 218—219°C, $[\alpha]_D$ −109° (pyridine). Found: C, 63.79; H, 7.14%. Calcd for $C_{26}H_{34}O_9$: C, 63.66; H, 6.99%, ν_{max} 3450, 1745, 1725, 1260 and 1230 cm^{-1}, λ_{max}^{EtOH} 301 nm (ε 77).

Acid-treatment of Shikokianidin (3). Shikokianidin (320 mg) was heated in refluxing methanol (15 ml) containing 2N hydrochloric acid (15 ml) for 3 hr. On cooling, crystals were separated and recrystallised from ethanol to give the seco-aldehyde (**7**), mp 268—269°C. Found: C, 64.24; H, 7.31%. Calcd for $C_{24}H_{32}O_8$: C, 63.98; H, 7.61%, ν_{max} 3400, 1730, 1700 and 1240 cm^{-1}.

6) L. M. Jackman and S. Sternhell, "Applications of Nuclear Magnetic Resonance Spectroscopy in Organic Chemistry," Pergamon Press, London (1969), p. 80.

7) E. Fujita, T. Fujita, and M. Shibuya, *Tetrahedron Lett.*, **1966**, 3153; E. Fujita, T. Fujita, and M. Shibuya, *Chem. Pharm. Bull.* (Tokyo), **16**, 506 (1968).

Dihydroshikokianidin (9). Shikokianidin was hydrogenated in ethanol over 10% palladium-charcoal. The crude product was recrystallised from dilute ethanol to give dihydroshikokianidin (**9**) as colorless prisms, mp 178—180°C, Found: C, 63.33; H, 7.43%. Calcd for $C_{26}H_{36}O_9$: C, 63.40; H, 7.37%, ν_{max} 3480, 1730, 1260, and 1230 cm^{-1}, δ 0.71 (3H, d, J=7 Hz, *sec* CMe), 1.09 and 1.39 (each 3H, *tert* CMe), 1.98, 2.00, and 2.14 (each 3H, OAc), 2.34 (1H, d, J=1 Hz, H_9), 4.22 (1H, dd, J=2 and 10 Hz, H_{20}), 4.34 (1H, s, OH), 4.83 (1H, dd, J=1 and 10 Hz, H_{20}), 4.87 (1H, d, J=10 Hz, H_{15}), *ca.* 4.9 (1H, m, H_1).

Trisdeacetyldihydroshikokianidin (10). Dihydroshikokianidin (100 mg) was dissolved in ammonia saturated methanol (20 ml). After the mixture had been left standing for 23 days at room temperature, it was concentrated to dryness under reduced pressure. The residue was chromatographed over preparative plates to give trisdeacetyldihydroshikokianidin (**10**), (29 mg), mp 268—271°C (dec) (from acetone–light petroleum). Found: C, 65.50; H, 8.30%. Calcd for $C_{20}H_{30}O_6$: C, 65.55; H, 8.25%, ν_{max} 3360, 1710, and 1180 cm^{-1}, δ ($CDCl_3$-C_5D_5N) 0.96 (3H, d, J=7 Hz, *sec* CMe), 1.07 and 1.11 (each 3H, *tert* CMe), 2.25 (1H, s, H_9), 2.72 (1H, dd, J=1 and 6.5 Hz, H_5), 3.90 (1H, q, J=7 and 9 Hz), 4.57 (1H, d, J=11 Hz, H_{15}), 4.60 (1H, dd, J=1 and 12 Hz, H_{20}), 4.78 (1H, dd, J=3 and 8 Hz, H_6), 5.47 (broad OH), 5.95 (1H, d, J=12 Hz, H_{20}).

Reduction of Shikokianidin with LAH. Shikokianidin (50 mg) was refluxed with lithium aluminum hydride (100 mg) in ether (20 ml) for 3 hr. The excess of the reagent was decomposed with ethyl acetate and the resulting emulsion was washed with dilute hydrochloric acid and then with water. Drying and evaporation of the solution gave a residue which was purified by tlc ($CHCl_3$–MeOH, 9:1) to yield deacetylshikokianidin and the mixture of pentaols (A) and (B). Pentaol (A) was identified as ent-5β,20-epoxykaur-16-ene-1β,6α,7α,11β,15α-pentaol (**11**) by tlc (solvent system: $CHCl_3$–MeOH, 9: 1; AcOEt–CH_2Cl_2, 7: 3; CH_2Cl_2–Me_2CO, 1: 1).

Reduction of Shikokianin with LAH. Similarly, shikokianin (300 mg) was reduced with lithium aluminum hydride to give pentaol (**11**), mp 253—255°C (dec) (from methanol–chloroform), Found: C, 64.18; H, 8.28%. Calcd for $C_{20}H_{30}O_6 \cdot 1/2H_2O$: C, 63.98; H, 8.32%, ν_{max} 3300, 1650, and 1565 cm^{-1}.

We are grateful to Dr. K. Kuriyama, Shionogi Research Laboratory, for the CD measurements.

BULLETIN OF THE CHEMICAL SOCIETY OF JAPAN, VOL. 46, 586—588 (1973)

The Jacobsen Reaction of Iodopseudocumenes and Related Compounds. Orientation in the Iodination of Halopseudocumenes[1]

Hitomi SUZUKI and Takashi SUGIYAMA*

Department of Chemistry, Faculty of Science, Hiroshima University, Higashi-sendamachi, Hiroshima

**Institute for Chemical Research, Kyoto University, Gokasho, Uji, Kyoto*

(Received July 18, 1972)

The Jacobsen reaction of iodopseudocumenes and related compounds was investigated. Both 3- and 5-iodopseudocumenes gave essentially the same product which consisted of 3,5-diiodopseudocumene (VI, 53%), 3,6-diiodopseudocumene (VII, 44%) and 5,6-diiodopseudocumene (VIII, 3%). The unexpected result was interpreted in terms of a mechanism involving a prior interconversion of the 3- and 5-iodo isomers followed by the ordinary process of aromatic disproportionation. 6-Iodopseudocumene gave VII as the major product. By prolonged contact with concentrated sulfuric acid, VI and VIII were found to undergo partial isomerization to give VII. Early structural assignment by Smith and Moyle for two diiodopseudocumenes was revised. Reactions of 4- and 5-iodohemimellitenes with sulfuric acid gave 4,6-diiodohemimellitene (XII) as the major product. A diiodohemimellitene melting at 114°C was found to be a mixture of XII and 4,5-diiodohemimellitene (XI), the former being predominant. Isomeric chloro-, bromo-, and iodopseudocumenes were iodinated with iodine-periodic acid dihydrate and the orientation in the products was determined.

5-Chloropseudocumene (I, X=Cl) reacts with concentrated sulfuric acid to give 3-chloropseudocumene-5-sulfonic acid (II, X=Cl).[4] 5-Bromopseudocumene (I, X=Br) behaves similarly, giving 3-bromopseudocumene-5-sulfonic acid (II, X=Br) along with small amounts of 3,5,6-tribromopseudocumene.[5] The reaction is known as the Jacobsen reaction.

5-Iodopseudocumene (III) was reported to afford

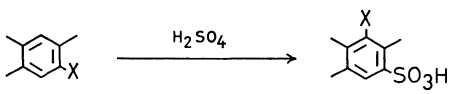

I II

two diiodopseudocumenes and two sulfonic acids derived from an iodopseudocumene and pseudocumene, respectively.[6] Although Kürzel did not designate specific structures for these products, Smith and Moyle formulated them as 3,6-diiodopseudocumene (VII), 5,6-diiodopseudocumene (VIII), 3-iodopseudocumene-5-sulfonic acid (II, X=I), and pseudocumene-5-sulfonic

1) The Reaction of Polysubstituted Aromatics. XXX. Part XXIX: H. Suzuki and K. Nakamura, *Synthesis*, **1972**, 606.

2) C. L. Moyle and L. I. Smith, *J. Org. Chem.*, **2**, 112 (1937).

3) H. Suzuki and R. Goto, This Bulletin, **36**, 389 (1963).

4) O. Jacobson, *Ber.*, **22**, 1580 (1889).

3) L. I. Smith and C. L. Moyle, *J. Amer. Chem. Soc.*, **58**, 1 (1936).

6) C. Kürzel, *Ber.*, **22**, 1586 (1889).

acid (II, X=H), respectively.[2] The assignment has since been cited.[7] However, the 3,6-orientation of iodine atoms in the disproportionation product of III is rather unexpected because the Jacobsen reaction of aromatic iodo compounds is usually known to proceed like a progressive iodination of the starting compound.[8] Thus the reaction of III and related compounds with sulfuric acid was re-examined in some detail.

Kürzel reported that III dissolved in sulfuric acid and left to stand at room temperature gave an oily mass which, by vacuum distillation and subsequent cooling, could be separated into colorless plates melting at 73°C and an oily substance freezing below 0°C.[6] We repeated the experiment and examined the oily product by gas chromatography as well as by direct comparison with the infrared and ^{1}H-NMR spectra of authentic specimens. The product was found to be a mixture of all three isomeric diiodopseudocumenes consisting of 3,5-diiodopseudocumene (VI; mp 8—9°C; bp 202—204°C/21 mmHg; 53%), VII (mp 75—76°C; 44%), and VIII (mp 51—52°C; bp 197—199°C/18 mmHg; 3%).[9] Some 3,5,6-triiodopseudocumene (mp 193—195°C) was also formed, whose amount steadily increased on prolonged treatment with sulfuric acid. It was therefore concluded that the Kürzel diiodopseudocumenes were most likely to be VI and VII, the former being possibly accompanied by some other isomers.

The idea that the unusual 3,6-orientation of iodine atoms in the product might arise from a rearrangement of the initially formed VI and VIII does not seem likely, since diiodopseudocumenes were found to be quite slow to isomerize under the same conditions. Thus the only other possibility is that III in contact with sulfuric acid partly isomerized to 3-iodopseudocumene (IV), which was then iodinated to give VI and VII. In order to confirm this, IV and 6-iodopseudocumene (V) were prepared and treated in a similar manner. The 3-iodo isomer gave essentially the same product as that obtained from III, whereas the 6-iodo isomer gave VII along with a very small amount of VIII.

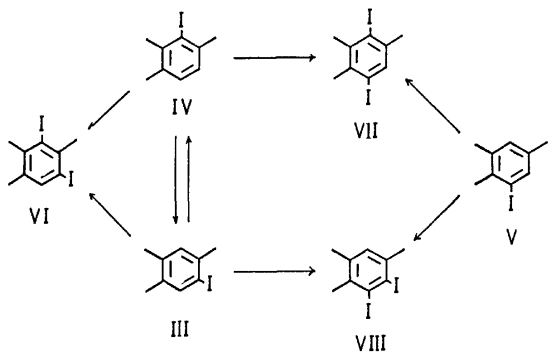

When a dilute solution of III or IV in dichloromethane was stirred with a small amount of sulfuric acid at room temperature, both isomers were found to undergo mutual interconversion, giving a mixture of III (87—92%) and IV (8—13%). In contrast, V showed little tendency to isomerize but underwent slow disproportionation.

The composition and constitution of sulfonated products were not further investigated, but the only major sulfonic acid obtained from either one of the reaction mixtures was identified as pseudocumene-5-sulfonic acid (II, X=H). An iodopseudocumenesulfonic acid (amide; mp 193—194°C) isolated in small amounts from the reaction mixture of V was probably 6-iodopseudocumene-3-sulfonic acid.

The other isomeric iodotrimethylbenzenes similarly underwent facile disproportionation. Both 4- and 5-iodohemimellitene (IX and X) reacted with sulfuric acid to give 4,6-diiodohemimellitene (XII) as the major product which was usually accompanied by an appreciable amount of 4,5-diiodohemimellitene (XI) and some 4,5,6-triiodohemimellitene (XIII). A diiodohemimellitene melting at 114°C, obtained from the Jacobsen reaction of 5-iodohemimellitene,[3] was found to be an intimate mixture of XI and XII, the latter being predominant. Iodomesitylene gave either diiodomesitylene or triiodomesitylene depending on the conditions employed.[10]

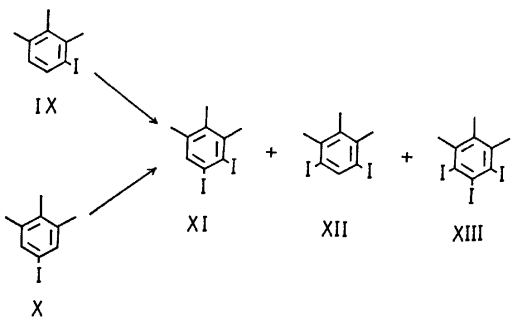

So far no quantitative data have been found in literature on the electrophilic reaction of halopseudocumenes. Accordingly, it seemed of interest to extend our work to the ordinary iodination of various isomeric halopseudocumenes, in order to see how they behave towards electrophilic iodine under the condition in which no migration of substituent groups was allowed. The iodination with iodine-periodic acid dihydrate was clean and smooth, and the products were determined by means of gas chromatography and ^{1}H-NMR spectroscopy. The results are summarized in Table 1. Combined directing effects of substituent groups agreed fairly well with the ones predicted from the additivity principle. For 3-chloropseudocumene some discrepancy was observed, which probably arose from the underestimation by the additivity principle of the rate of substitution at the position *para* to chlorine atom.

In sharp contrast to the product from the Jacobsen reaction, the above iodination products from III and V contained a substantial amount of VIII. Although

7) For example, L.I. Smith, "Organic Reactions," Vol. 1, John Wiley & Sons, Inc., New York (1944); H. J. Shine, "Aromatic Rearrangement," Elsevier, London (1967); H. Cerfountain, "Mechanistic Aspects in Aromatic Sulfonation and Desulfonation," Interscience, London (1968).

8) H. Suzuki, This Bulletin, **36**, 1643 (1963); H. Suzuki and R. Goto, *Nippon Kagaku Zasshi*, **84**, 167 (1963).

9) The structures of all these compounds were determined by independent synthesis.[16]

10) A. Tohl and R. Eckel, *Ber.*, **26**, 1099 (1893).

Table 1. Products from the iodination of halopseudocumenes with iodine-periodic acid dihydrate

Halopseudocumene		Product composition (%)[a]	
3-Halo series		5-Iodo	6-Iodo
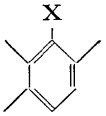	X=Cl	40.5	59.5
	=Br	57.8	42.2
	=I	69.3	30.7
5-Halo series		3-Iodo	6-Iodo
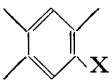	X=Cl	61.8	38.2
	=Br	74.6	25.4
	=I	79.9	20.1
6-Halo series		3-Iodo	5-Iodo
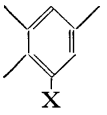	X=Br	62.8	37.2
	=I	63.3	36.7

a) Determined gas chromatographically. Dihalopseudocumenes appeared in the order; 3,6- >3,5- >5,6-.

VI and VIII could be partly converted into VII on prolonged contact with sulfuric acid, such isomerization was not so rapid and complete as to rationalize the marked difference in the composition. The result can be reasonably explained in terms of a mechanism involving partial isomerization of III to IV which, even in a small concentration, would undergo preferential iodination due to favorable electronic and steric reasons. The predominance of VII in the product mixture probably resulted from its greater stability towards the deiodination-reiodination process.

The present result represents the second clearly observed deviation from the established rule for the Jacobsen reaction of aromatic iodo compounds. The first example was observed in the reaction of 2-iodo-*m*-xylene, which underwent rapid isomerization into the 4-iodo isomer followed by disproportionation, giving 4,6-diiodo-*m*-xylene as the final product.[11]

Experimental

All melting and boiling points are uncorrected. Infrared spectra were measured on Nujol mulls with a Jasco DS-402 G spectrophotometer. ^{1}H-NMR spectra were obtained for carbon tetrachloride solutions on a JEOL PS-100 spectrometer using TMS as an internal reference. Gas chromatographic data were obtained on a Hitachi Model F6-D gas chromatograph using a capillary column (0.5 ϕ, 45 m) coated with Apiezon Grease L at column temperature of 165°C.

5-Iodopseudocumene (*III*; mp 36—37°C[6]; bp 135—136°C/21 mmHg) was prepared from a commercial pseudocumidine (2,4,5-trimethylaniline). IR: 868, 946, and 1145 cm^{-1}; NMR; 7.90 (2 Me), 7.72 (Me), 3.14 (aromatic H), and 2.55 τ (aromatic H).

3-Iodopseudocumene (IV). 2,3,6-Trimethylphenylmagnesium bromide was prepared in the usual manner from 3-bromopseudocumene (bp 112—114°C/18 mmHg; 15 g)[12], magnesium (1.9 g), and dried tetrahydrofuran (70 ml). Iodine (*ca.* 20 g) was slowly added to the Grignard solution. The mixture was heated under gentle reflux for 30 min and hydrolyzed with excess dilute hydrochloric acid. The organic layer was separated, dried and concentrated, and the residue was distilled to give product (16.2 g, 87%) boiling at 140—141°C/25 mmHg. IR: 778, 802, 984, 1131, and 1169 cm^{-1}; NMR: 7.75 (Me), 7.64 (2 Me), and 3.18 τ (2 aromatic H).

Found: C, 44.21; H, 4.49%. Calcd for $C_9H_{11}I$: C, 43.92; H, 4.51%.

6-Iodopseudocumene (*V*; bp 138—139°C/24 mmHg) was prepared from 6-bromopseudocumene (bp 120—121°C/22 mmHg)[5] in a similar manner. IR: 785, 848, 1005, 1124, and 1256 cm^{-1}; NMR: 7.84 (Me), 7.77 (Me), 7.71 (Me), 3.22 and 2.60 τ (aromatic H).

Found: C, 44.19; H, 4.52%. Calcd for $C_9H_{11}I$: C, 43.92; H, 4.51%.

4-Iodohemimellitene (*IX*; bp 144—145°C/22 mmHg) and *5-iodohemimellitene* (*X*; mp 34—36°C)[13] were prepared from the corresponding trimethylanilines.[14,15] Synthesis of diiodo and triiodo derivatives of pseudocumene and hemimellitene used as authentic specimens will be described in the accompanying paper.[16]

General Procedure for the Jacobsen Reaction. i) A solution of iodotrimethylbenzene (4.9 g, 0.02 mol) in dichloromethane (20 ml) was stirred vigorously with concentrated sulfuric acid (4.9 g, 0.05 mol) at room temperature. After 15 hr the reaction was quenched by the addition of water, and the organic layer was separated, washed with dilute aqueous sodium sulfite and dried over anhydrous magnesium sulfate. The oily substance (3.3—3.8 g) obtained after removal of the solvent was directly examined by infrared and ^{1}H-NMR spectroscopy as well as by thin-layer and gas-chromatography.

ii) Iodotrimethylbenzene (4.9 g, 0.02 mol) was stirred with concentrated sulfuric acid (15 g, 0.15 mol) overnight at room temperature. The dark mixture was poured on crushed ice and a pasty solid was extracted with a mixture of dichloromethane and light petroluem. The extract was washed with dilute aqueous sodium sulfite and then passed over a short alumina column to remove some polymeric substance formed during the course of reaction. The eluate was evaporated and the residual oil or semi-solid (1.5—2.0 g) were directly subjected to gas chromatographic and spectral inspection.

Procedure for the Iodination of Halopseudocumenes.[17] A mixture of halopseudocumene (0.05 mol), iodine (5.1 g), periodic acid dihydrate (2.28 g), and 80% acetic acid (40 ml) containing catalytic amount of sulfuric acid was heated with stirring at 70—75°C for several hours until the color of iodine disappeared. After cooling, water was added and an oily precipitate or a semisolid mass was extracted with ether; the ethereal extract was dried over calcium chloride and distilled. A mixture of iodinated halopseudocumenes (90—97%) was obtained mostly distilling over in the range shown below;

Iodinated chloropseudocumenes, bp 167—170°C/16 mmHg
Iodinated bromopseudocumenes, bp 173—177°C/16 mmHg
Diiodopseudocumenes, bp 197—200°C/20 mmHg

11) H. Suzuki and R. Goto, *Nippon Kagaku Zasshi*, **84**, 284 (1963); H. Suzuki, K. Maruyama, and R. Goto, This Bulletin, **38**, 1474, 1590 (1965).

12) L. I. Smith and M. A. Kiess, *J. Amer. Chem. Soc.*, **61**, 284 (1939).

13) C. Liebermann and M. Kardos, *Ber.*, **46**, 198 (1913).

14) M. G. Barclay, A. Burawoy, and G. H. Thomson, *J. Chem. Soc.*, **1944**, 109.

15) F. M. Beringer and I. Ugelow, *J. Amer. Chem. Soc.*, **75**, 2635 (1953).

16) H. Suzuki and Y. Haruta, This Bulletin, **46**, 589 (1973).

17) H. Suzuki, K. Nakamura, and R. Goto, *ibid.*, **39**, 128 (1966); H. Suzuki, "Organic Syntheses," Vol. 51, p. 94 (1971).

Syntheses of Diiodo and Triiodo Derivatives of 1,2,3-Trimethylbenzene *(Hemimellitene)* and 1,2,4-Trimethylbenzene *(Pseudocumene)*. A Convenient Use of Polyiodo Derivatives for the Characterization of Polyalkylbenzenes and Their Derivatives[1]

Hitomi SUZUKI and Yasuhiro HARUTA*

Department of Chemistry, Faculty of Science, Hiroshima University, Higashi-sendamachi, Hiroshima
**Department of Chemistry, Faculty of Science, Kyoto University, Sakyo-ku, Kyoto*

(Received July 18, 1972)

A complete set of diiodo and triiodo derivatives of 1,2,3-trimethylbenzene and 1,2,4-trimethylbenzene has been prepared and their physical properties are recorded. Use of polyiodo derivatives as a means for characterizing polyalkylbenzenes and their derivatives has been proposed.

In a reinvestigation of the Jacobsen reaction of 5-iodo-1,2,4-trimethylbenzene,[2] some diiodo and triiodotrimethylbenzenes were required as reference compounds. A survey of literature revealed that only one[3] of the six diiodotrimethylbenzenes and one triiodotrimethylbenzene[3] have so far been characterized. The present paper describes the synthesis of a complete set of diiodo and triiodo derivatives of the trimethylbenzenes given in the title.

Diiodotrimethylbenzenes. In a previous paper,[5] the Jacobsen reaction of 5-iodo-1,2,3-trimethylbenzene was reported to give diiodo-1,2,3-trimethylbenzene melting at 114°C. Reinvestigation of the product revealed that it was in fact an intimate mixture of two diiodo-1,2,3-trimethylbenzenes. The major component was identified as 4,6-diiodo-1,2,3-trimethylbenzene (IV; mp 129—130°C) through the synthesis *via* two routes from 1,2,3-trimethylbenzene (Scheme 1). The minor component was identical with the authentic 4,5-diiodo-1,2,3-trimethylbenzene (mp 67—69°C) obtained from the iodination of 5-iodo-1,2,3-trimethylbenzene.

Direct iodination of 1,2,3-trimethylbenzene with two equivalent amounts of iodinating agent (iodine–periodic acid dihydrate)[6] gave a mixture of the 4,5- and 4,6-diiodo isomers in the ratio 1 : 1.95. Less soluble IV

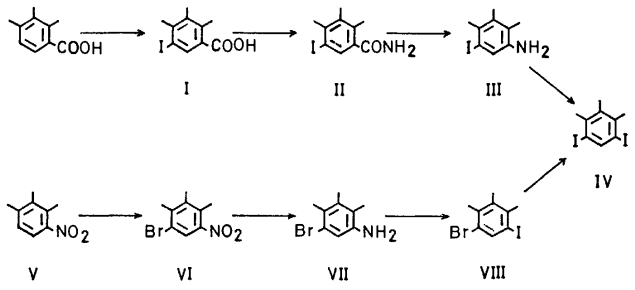

Scheme 1.

was readily obtained as beautiful needles, but a small amount of isomeric impurity tenaciously clinging to the product was difficult to remove.

Two diiodo-1,2,4-trimethylbenzenes of unidentified structures were reported to be formed from the Jacobsen reaction of 5-iodo-1,2,4-trimethylbenzene.[7] Direct iodination of 1,2,4-trimethylbenzene with two equivalents of the iodinating agent was found to give 3,5-diiodo-1,2,4-trimethylbenzene (XIII) as the major product (*ca.* 80%).[8] However, separation of this product from the accompanying isomers was difficult due to a slight difference in boiling point. Pure XIII was obtained from 2,4,5-trimethylbenzoic acid (IX; durylic acid) according to the sequence shown in Scheme 2.

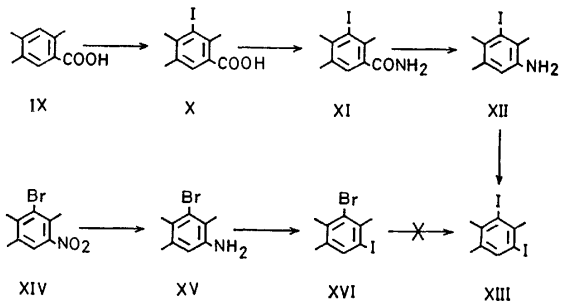

Scheme 2.

Fractional distillation of the product from nitration of 1,2,4-trimethylbenzene gave the 3-nitro compound as an early distillate, which was reduced to 2,3,6-trimethylaniline (XVII) and treated with iodine under alkaline conditions to give 4-iodo-2,3,6-trimethylaniline (XVIII). Diazotization and the subsequent treatment with aqueous potassium iodide gave 3,6-diiodo-1,2,4-trimethylbenzene (XIX).

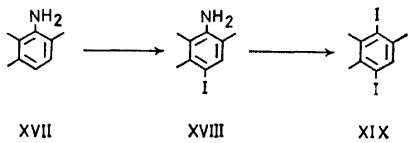

Scheme 3.

1) The Reaction of Polysubstituted Aromatics. XXXI. Part XXX: This Bulletin, **46**, 586 (1973).
2) H. Suzuki and T. Sugiyama, *ibid.*, **46**, 586 (1973).
3) 2,4-Diiodo-1,3,5-trimethylbenzene and 2,4,6-triiodo-1,3,5-trimethylbenzene; both were first obtained by the Jacobsen reaction of 2-iodo-1,3,5-trimethylbenzene.[4]
4) A. Töhl and R. Eckel, *Ber.*, **26**, 1099 (1893).
5) H. Suzuki and R. Goto, This Bulletin, **36**, 389 (1963).
6) H. Suzuki, K. Nakamura, and R. Goto, *ibid.*, **39**, 128 (1966); H. Suzuki, "Organic Syntheses," Vol. 51, p. 94 (1971).
7) C. Kürzel, *Ber.*, **22**, 1586 (1889).
8) The product was found to be a mixture of 3,5-diiodo-1,2,4-trimethylbenzene (79%), 5,6-diiodo-1,2,4-trimethylbenzene (17%), and 3,6-diiodo-1,2,4-trimethylbenzene (4%).

5,6-Diiodo-1,2,4-trimethylbenzene (XXIII) required a lengthy synthetic route. Attempts to introduce an iodine atom directly at the 6-position of 2,4,5-trimethylaniline failed due to the inevitable formation of tarry substance. *N*-Acetyl derivative could be iodinated at the 6-position but removal of the acetyl group was not possible under alkaline conditions. Under forced acidic conditions, elementary iodine was liberated instead.

Triiodotrimethylbenzenes. Literature contains only 2,4,6-triiodo-1,3,5-trimethylbenzene (triiodomesitylene).[4] Iodine-periodic acid as iodinating agent readily converted 1,2,3- and 1,2,4-trimethylbenzenes into the corresponding triiodo derivatives, both of which were high-melting crystals poorly soluble in cold organic solvents. On storage under diffused light, 4,5,6-triiodo-1,2,3-trimethylbenzene gradually turned yellow.

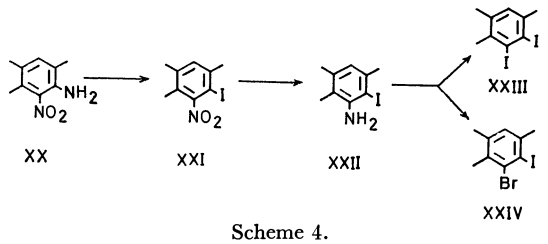

Scheme 4.

Use of Polyiodo Derivatives for Characterization Purpose. Iodine–periodic acid as an iodinating agent provides a simple direct route to polyiodopolyalkylbenzenes. Ease

Table 1. Physical properties of some polyiodo and haloiodo derivatives of polyalkylbenzenes

Compound		Mp (°C)	^{1}H NMR[a] (τ)	IR (cm^{-1})
1,2,3,4-Tetramethylbenzene series				
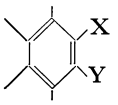	X=Cl, Y=I	168—169	7.84(1), 7.78(1) 7.61(1), 7.50(1)	776, 891, 956, 1195
	X=Br, Y=I	190—191	7.82(1), 7.79(1) 7.54(1), 7.47(1)	758, 880, 945, 1189
	X=I, Y=I	190—191	7.80(2), 7.40(2)	745, 876, 940, 1184
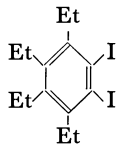		84—85	8.86(2), 8.84(2) 7.31 (2 CH_2) 6.92 (2 CH_2)	786, 983, 1005, 1053, 1062, 1071, 1172, 1314
1,2,3,5-Tetramethylbenzene series				
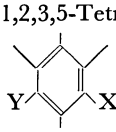	X=Cl, Y=I	166—168	7.76(1), 7.72(1) 7.56(1), 7.38(1)	919, 982, 1159
	X=Br, Y=I	177—178	7.71(1), 7.64(1) 7.54(1), 7.27(1)	915, 968, 1152
	X=I, Y=I	150—151	7.68(1), 7.54(2) 7.11(1)	911, 957, 1145
1,2,4,5-Tetramethylbenzene series				
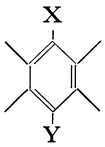	X=Cl, Y=I	171—172	7.62(2), 7.52(2)	692, 989, 1076
	X=Br, Y=I	175—176	7.53(2), 7.47(2)	681, 981, 1068
	X=I, Y=I	140—141	7.46(4)	675, 976, 1063
1,2,3-Trimethylbenzene series				
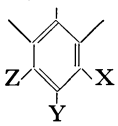	X=I, Y=Et Z=I	98—99	8.87(1), 7.64(1) 7.49(2), 6.66 (CH_2)	777, 916, 981, 1058, 1144
	X=Br, Y=I Z=I	232—234	7.68(1), 7.47(1) 7.32(1)	920, 1001, 1207, 1335
1,2,4-Trimethylbenzene series				
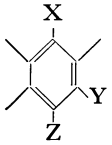	X=I, Y=Et Z=I	51—53	8.89(1), 7.42(2) 7.41(1), 6.95 (CH_2)	984, 1162
	X=Cl, Y=I Z=I	194—196	7.55(1), 7.31(1) 7.10(1)	846, 953, 1006, 1142, 1342
1,3,5-Trimethylbenzene series				
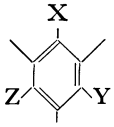	X=Et, Y=I Z=I	63—64	8.92(1), 7.51(2) 7.19 (CH_2), 7.08 (1)	791, 927, 946, 971
	X=Cl, Y=I Z=I	174—175	7.31(2), 7.04(1)	944, 1347

a) Numerals in parentheses refer to the number of methyl groups.

of access makes polyiodo derivatives useful for the characterization of polyalkylbenzenes and their derivatives. They are especially so when the given sample is a liquid available only in a small amount, since the introduction of iodine atoms multiplies molecular weight and converts a liquid hydrocarbon into a well-crystallized solid with moderate melting range. Polyiodo derivatives are preferred to polynitro and polybromo derivatives, because the latters are often accompanied by side-chain substituted products and their mixture melting test is sometimes deceptive due to a slight depression of melting point. Physical properties of some polyiodo and mixed haloiodo derivatives of polyalkylbenzenes, most of which are new, are summarized in Table 1.

Experimental

All melting and boiling points are uncorrected. Infrared spectra were recorded in Nujol on a Jasco DS-402G spectrophotometer. ^1H NMR spectra were measured in carbon tetrachloride solutions on a JEOL PS-100 spectrometer against internal TMS.

5-Iodo-2,3,4-trimethylbenzamide (II). A mixture of 5-iodo-2,3,4-trimethylbenzoic acid (I, 14.0 g)[9] and thionyl chloride (10 g) was warmed until there was no more evolution of gaseous product. After removal of excess thionyl chloride under reduced pressure, the residual solid was dissolved in benzene, and dry ammonia gas was bubbled through the solution. The precipitate was filtered off and recrystallized from hot dioxane to give amide as white needles (13.1 g, 94%), mp 275—276°C. IR: 687, 716, 765, 884, 1041, 1113, 1187, 1542, 1624, 1649, 3160, and 3330 cm^{-1}.

Found: C, 41.60; H, 4.21%. Calcd for $C_{10}H_{12}NIO$: C, 41.54; H, 4.19%.

3-Iodo-2,4,5-trimethylbenzamide (*XI*; mp 236—237°C) was prepared in a similar manner from 3-iodo-2,4,5-trimethylbenzoic acid (X).[9] IR: 702, 827, 889, 990, 1125, 1405, 1624, 1649, 3150, and 3320 cm^{-1}.

Found: C, 41.52; H, 4.07%. Calcd for $C_{10}H_{12}NIO$: C, 41.54; H, 4.19%.

5-Iodo-2,3,4-trimethylaniline (III). A solution of potassium hydroxide (11.2 g) and bromine (12 g) in water (100 ml) was poured on II (9.6 g) suspended in ethanol (100 ml). The mixture was stirred at room temperature for 5 hr and then a solution of potassium hydroxide (15 g) in water (50 ml) was added. The temperature was maintained at 50—60°C for 3 hr and then at 60—70°C for 3 hr. Finally the reaction mixture was steam-distilled to give amine as white solid, which was recrystallized from light petroleum to yield pure product (1.6 g, 18%), mp 79—80°C. IR: 754, 844, 866, 947, 1115, 1206, 1273, 1288, 1573, 1618, 3320, and 3410 cm^{-1}; NMR; 8.03 (Me), 7.81 (Me), 7.70 (Me), 6.75 (NH_2), and 3.04 τ (aromatic H).

Found: C, 41.53; H, 4.74%. Calcd for $C_9H_{12}NI$: C, 41.40; H, 4.63%.

3-Iodo-2,4,5-trimethylaniline (*XII*; mp 57—58°C) was obtained in a similar manner from XI. IR: 784, 855, 979, 1231, 1275, 1285, 1548, 1598, 1630, 3190, 3290, and 3380 cm^{-1}; NMR: 7.80 (Me), 7.73 (Me), 7.70 (Me), 6.65 (NH_2), and 3.70 τ (aromatic H).

Found: C, 41.67; H, 4.72%. Calcd for $C_9H_{12}NI$: C, 41.40; H, 4.63%.

4-Iodo-2,3,6-trimethylaniline (XVIII). To a suspension of sodium hydrogen carbonate (17 g) in water (150 ml), 2,3,6-trimethylaniline (XVII; bp 125—127°C/18 mmHg; 9.0 g) dissolved in ether (80 ml) was added. Stirring was continued for an hour, after which the solvent was removed and a black residual solid was steam-distilled. The amine separated as white needles in the distillate was collected by filtration and recrystallized from light petroleum, mp 100—101°C. Yield, 8.2 g (47%). IR: 754, 839, 854, 869, 972, 1080, 1167, 1311, 1560, 1621, 3270, and 3360 cm^{-1}; NMR: 7.96 (Me), 7.86 (Me), 7.71 (Me), 6.08 (NH_2), and 3.58 τ (aromatic H).

Found: C, 41.58; H, 4.56%. Calcd for $C_9H_{12}NI$: C, 41.40; H, 4.63%.

6-Bromo-4-nitro-1,2,3-trimethylbenzene (VI). A mixture of 4-nitro-1,2,3-trimethylbenzene (V; bp 147—149°C/18 mmHg; 7.0 g) and bromine (10 g) was allowed to stand overnight at room temperature. Hydrogen bromide evolved gently and a solid product was obtained, which was crystallized from hot ethanol to give pale yellow needles (9.1 g, 88%), mp 82—83°C. IR: 664, 711, 755, 819, 868, 943, 1038, 1188, 1353, and 1520 cm^{-1}; NMR: 7.69 (Me), 7.67 (Me), 7.55 (Me), and 2.22 τ (aromatic H).

Found: C, 44.46; H, 4.37%. Calcd for $C_9H_{10}NBrO_2$: C, 44.28; H, 4.13%.

5-Nitro-1,2,4-trimethylbenzene (mp 70—71°C; bp 127—129°C/22 mmHg) treated with bromine in a similar manner to that above gave *3-bromo-5-nitro-1,2,4-trimethylbenzene* (*XIV*; mp 89—90°C). NMR: 7.61 (Me), 7.56 (Me), 7.48 (Me), and 2.52 τ (aromatic H).

Found: C, 44.37; H, 2.48%. Calcd for $C_9H_{10}NBrO_2$: C, 44.28; H, 4.13%.

5-Iodo-6-nitro-1,2,4-trimethylbenzene (XXI). To a solution of 6-nitro-2,4,5-trimethylaniline (XX, 9 g)[10] in sulfuric acid (20 ml) was added finely powdered sodium nitrite (3.6 g) with stirring. The mixture was stirred for 30 min and then poured onto crushed ice. The resulting solution of diazonium salt was filtered and the filtrate was added to a solution of potassium iodide (10 g) in a small amount of water. After the mixture was left to stand overnight, the precipitated tan solid was filtered off and passed over a short alumina column with a mixture of benzene and ligroin. From the eluate the iodo compound was obtained as prisms (11.2 g, 77%), mp 130—131°C. IR: 759, 871, 905, 969, 1152, 1255, and 1523 cm^{-1}; NMR: 7.84 (Me), 7.73 (Me), 7.55 (Me), and 2.88τ (aromatic H).

Found: C, 37.29; H, 3.44%. Calcd for $C_9H_{10}NIO_2$: C, 37.13; H, 3.46%.

4-Bromo-6-iodo-1,2,3-trimethylbenzene (VIII), 3-bromo-5-iodo-1,2,4-trimethylbenzene (XVI), and 6-bromo-5-iodo-1,2,4-trimethylbenzene (XXIV) were prepared from the corresponding bromoanilines by a similar procedure. The products were purified through distillation followed by recrystallization from light petroleum.

VIII: mp 97—99°C. IR: 844, 856, 906, 1007, and 1155 cm^{-1}; NMR: 7.69 (Me), 7.68 (Me), 7.62 (Me), and 2.13 τ (aromatic H).

Found: C, 33.22; H, 3.05%. Calcd for $C_9H_{10}BrI$: C, 33.26; H, 3.10%.

XVI: bp 174—177°C/16 mmHg. IR: 734, 805, 866, 948, 993, 1151, and 1350 cm^{-1}; NMR: 7.80 (Me), 7.74 (Me), 7.40 (Me), and 2.48 τ (aromatic H).

Found: C, 33.80; H, 3.11%. Calcd for $C_9H_{10}BrI$: C, 33.26; H, 3.10%.

XXIV: mp 45—46°C; bp 173—176°C/14 mmHg. IR: 758, 804, 864, 961, 993, 1013, 1032, 1138, and 1355 cm^{-1};

9) H. Suzuki, This Bulletin, **44**, 2871 (1971).

10) M. H. Huender, *Rec. Trav. Chim. Pays-Bas*, **34**, 1 (1913).

NMR: 7.79 (Me), 7.59 (Me), and 3.09 τ (aromatic H).

Found: C, 33.26; H, 3.16%. Calcd for $C_9H_{10}BrI$: C, 33.26; H, 3.10%.

6-Iodo-2,3,5-trimethylaniline (XXII). Stannous chloride dihydrate (30 g) was dissolved in a mixture of hydrochloric acid (d=1.18, 35 ml) and ethanol (35 ml). To this solution was added XXI (9.7 g) with stirring. After the end of reaction, sodium hydroxide solution was added until the precipitated stannic hydroxide redissolved, and the solution was steam-distilled. Amine was separated from the distillate by ether-extraction and recrystallized from light petroleum. Colorless needles (6.5 g, 75%), mp 81—82°C. IR: 838, 973, 1017, 1106, 1282, 1318, 1552, 1622, 3290, and 3370 cm^{-1}; NMR: 7.95 (Me), 7.85 (Me), 7.71 (Me), 6.03 (NH_2), and 3.57 τ (aromatic H).

Found: C, 41.40; H, 4.58%. Calcd for $C_9H_{12}NI$: C, 41.40; H, 4.63%.

5-Bromo-2,3,4-trimethylaniline (VII; mp 86—87°C) and *3-bromo-2,4,5-trimethylaniline (XV*; mp 57—59°C) were prepared in a similar manner from VI and XIV, respectively.

VII: IR: 766, 845, 874, 954, 1116, 1206, 1217, 1279, 1295, 1586, 1619, 3340, and 3430 cm^{-1}; NMR: 8.05 (Me), 7.85 (Me), 7.77 (Me), 6.73 (NH_2), and 3.36 τ (aromatic H).

Found: C, 50.59; H, 5.72%. Calcd for $C_9H_{12}NBr$: C, 50.48; H, 5.65%.

XV: IR: 800, 857, 986, 1232, 1278, 1290, 1554, 1607, 1635, 3190, 3290, and 3390 cm^{-1}; NMR: 7.83 (Me), 7.81 (Me), 7.76 (Me), 6.66 (NH_2), and 3.72 τ (aromatic H).

Found: C, 50.42; H, 5.91%. Calcd for $C_9H_{12}NBr$: C, 50.48; H, 5.65%.

4,6-Diiodo-1,2,3-trimethylbenzene (IV). Method 1: Sodium nitrite (0.5 g) was added below 10°C to a solution of III (1.4 g) in sulfuric acid (8 ml). After stirring for 30 min, the mixture was poured onto crushed ice, and the resulting solution was filtered and added to a solution of potassium iodide (1.5 g) in a small amount of water. The mixture was allowed to stand overnight, and the black precipitate was collected by filtration and passed over a short alumina column with light petroleum. From the eluate IV was obtained as colorless plates (0.8 g, 40%), mp 129—130°C. IR: 834, 856, 899, 999, and 1148 cm^{-1}; NMR: 7.68 (Me), 7.62 (2 Me), and 1.88 τ (aromatic H).

Found: C, 29.20; H, 2.78%. Calcd for $C_9H_{10}I_2$: C, 29.06; H, 2.71%.

Other diiodotrimethylbenzenes were prepared in a similar manner from the corresponding iodotrimethylanilines.

3,6-Diiodo-1,2,4-trimethylbenzene (XIX): mp 75—76°C. IR: 739, 852, 992, 1129, and 1248 cm^{-1}; NMR: 7.67 (Me), 7.53 (Me), 7.47 (Me), and 2.47 τ (aromatic H).

Found: C, 29.13; H, 2.66%. Calcd for $C_9H_{10}I_2$: C, 29.06; H, 2.71%.

3,5-Diiodo-1,2,4-trimethylbenzene (XIII): Mp 8—9°C; bp 202—204°C/21 mmHg. IR: 732, 791, 866, 942, 983, 1142, and 1342 cm^{-1}; NMR: 7.76 (Me), 7.66 (Me), 7.27 (Me), and 2.46 τ (aromatic H).

Found: C, 29.21; H, 2.62%. Calcd for $C_9H_{10}I_2$: C, 29.06; H, 2.71%.

5,6-Diiodo-1,2,4-trimethylbenzene (XXIII): Mp 51—52°C; bp 197—199°C/18 mmHg. IR: 746, 788, 865, 955, 990, 1013, 1031, 1131, and 1351 cm^{-1}; NMR: 7.76 (Me), 7.52 (Me), 7.47 (Me), and 3.07 τ (aromatic H).

Found: C, 29.19; H, 2.68%. Calcd for $C_9H_{10}I_2$: C, 29.06; H, 2.71%.

Method 2: The Grignard reagent was prepared in the usual manner from VIII (5.2 g), magnesium (0.4 g), and tetrahydrofuran (40 ml). To the reagent was added at one time dried magnesium iodide (4.5 g) and an additional amount of magnesium (0.6 g), and the mixture was stirred overnight under reflux. After being cooled the mixture was rapidly stirred and iodine (*ca.* 11—12 g) was added in small portions until the brown color began to persist. Excess dilute hydrochloric acid was added, and the organic layer was separated, dried, and evaporated to leave a light brown solid. It was fractionally distilled under reduced pressure and the fraction boiling at 190—200°C/17 mmHg was collected and crystallized from light petroleum. Colorless plates (0.8 g, 14%), mp 124—128°C, were spectroscopically identical with the compound obtained by method 1.

The above procedure applied to 3-bromo-5-iodo-1,2,4-trimethylbenzene (XVI) gave unsatisfactory results, since the bromine atom at the 3-position was found to be slow to react.

4,5-Diiodo-1,2,3-trimethylbenzene and triiodo derivatives of 1,2,3- and 1,2,4-trimethylbenzenes were prepared by the direct iodination of 5-iodo-1,2,3-trimethylbenzene and two corresponding hydrocarbons, respectively, with iodine–periodic acid dihydrare.[6]

4,5-Diiodo-1,2,3-trimethylbenzene: Mp 67—69°C. IR: 835, 858, 902, 997, and 1193 cm^{-1}; NMR: 7.86 (Me), 7.82 (Me), 7.42 (Me), and 2.47 τ (aromatic H).

4,5,6-Triiodo-1,2,3-trimethylbenzene: Mp 232—235°C. IR: 916, 999, 1198, and 1328 cm^{-1}; NMR: 7.65 (Me), and 7.31 τ (2 Me).

Found: C, 21.62; H, 1.70%. Calcd for $C_9H_9I_3$: C, 21.71; H, 1.82%.

3,5,6-Triiodo-1,2,4-trimethylbenzene: Mp 193—195°C. IR: 751, 814, 946, 984, 1128, 1225, and 1325 cm^{-1}; NMR: 7.46 (Me), 7.27 (Me), and 6.93 τ (Me).

Found: C, 21.58; H, 1.76%. Calcd for $C_9H_9I_3$: C, 21.71; H, 1.82%.

General Procedure for the Preparation of Polyiodo Derivatives from Polyalkylbenzenes. A polyalkylbenzene (*ca.* 0.1—0.3 g) dissolved in 80% acetic acid (5 ml) containing a catalytic amount of sulfuric acid was rapidly stirred and heated with iodine (1.0 g) and periodic acid dihydrate (0.45 g) at 70—80°C for 30 min—1 hr. The mixture was then poured into aqueous sodium hydrogen sulfite to remove excess reagent. The white precipitate was collected by filtration and crystallized from ethanol.

Studies on Amino-hexoses. XVII. Identification of the Deamination Products from D-Glucosaminitol

Tomoyuki BANDO and Yoshio MATSUSHIMA

Department of Chemistry, Osaka University College of Science, Toyonaka

(Received July 26, 1972)

The nitrous deamination products of D-glucosaminitol were fractionated with a Dowex-1 free base column after the reaction mixture had been reduced with sodium borohydride. The chromatography gave discrete five peaks, four of which were identified as 2-deoxy-D-*arabino*-hexitol, 2-deoxy-D-*ribo*-hexitol, 2-hydroxymethyl-2-deoxy-D-*arabino*(or *ribo*)-pentitol and D-mannitol in a total yield over 90%. The nitrous deamination products fractionated with a Dowex-1 borate column were identified as 2-deoxy-D-*arabino*-hexose, 2-deoxy-D-*erythro*-3-hexulose, 2-hydroxymethyl-2-deoxy-D-*arabino*(or *ribo*)-pentose and D-mannitol. The formation of products other than D-mannitol was interpreted in terms of intramolecular rearrangement accompanying nitrous deamination.

The nitrous deamination reaction of amino-sugars was once of an unclarified nature in sugar chemistry.[1] However, owing to the progress in the theory of reactivity and molecular conformation,[2] it is now well understood that glucosamine and galactosamine give 2,5-anhydro-mannose and 2,5-anhydro-talose respectively by nitrous deamination, while mannosamine gives glucose, all of these amino-sugars having more or less rigid molecular conformation due to the ring structure.

One of the present authors demonstrated that nitrous deamination of glucosaminitol, which can take various conformations due to the chain structure, gave 2-deoxy-*arabino*-hexose(2-deoxy-glucose) in about 30% yield.[1] The remainder of the reaction products was not identified because of difficulty of analysis. In the present paper are described the results obtained using various chromatographic techniques in the analysis of the reaction products which, as expected, comprise various compounds. These compounds were identified in the following way: A mixture of nitrous deamination products which was highly reducing to Park-Johnson reagent[8] was reduced with sodium borohydride, the reducing groups of the products thus being converted into alcoholic groups. The mixture of the polyhydric alcohols obtained was then fractionated with a column of Dowex-1 free base[3-6] and each fraction was compared with the authentic samples by means of mixed melting point measurement, gas-liquid chromatography, or periodate oxidation.[7,8] On the other hand, the nitrous deamination mixture was directly fractionated with a Dowex-1 borate column,[9] each fraction separated being reduced with sodium borohydride, and the products were compared with the authentic samples by means of gas-liquid chromatography. A probable mechanism of the deamination reactions and the pro-

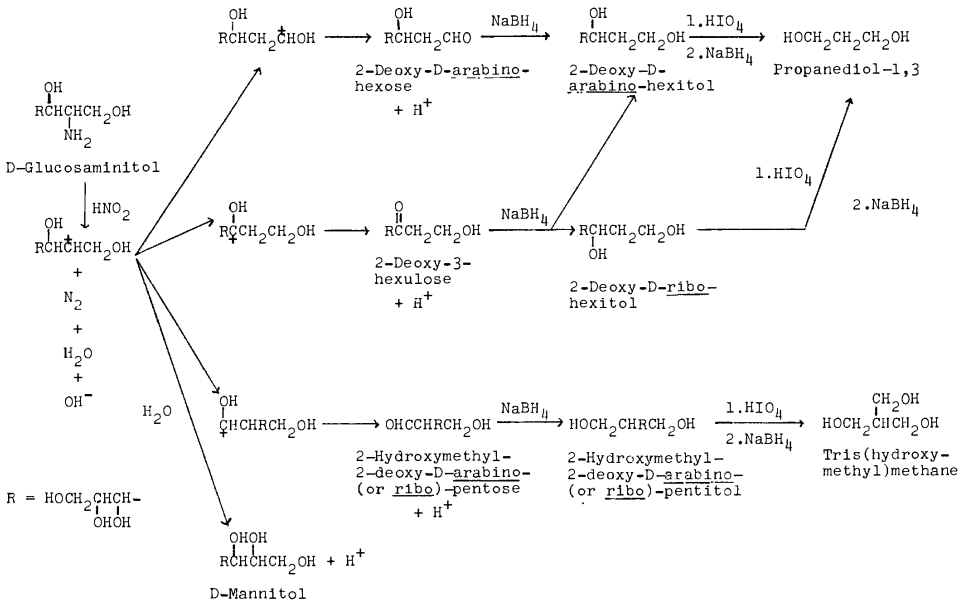

Scheme 1.

1) Y. Matsushima, This Bulletin, **24**, 144 (1951).
2) S. Hase and Y. Matsushima, *J. Biochem.*, **66**, 57 (1969).
3) Y. Matsushima, T. Miyazaki, and J.T. Park, *ibid.*, **54**, 109 (1963).
4) P.W. Austin, F.E. Hardy, J.G. Buchanan, and J. Baddiley, *J. Chem. Soc.*, **1963**, 5350.
5) Y. Matsushima and T. Miyazaki, *J. Biochem.*, **55**, 464 (1964).
6) F. Yaku and Y. Matsushima, *Nippon Kagaku Zasshi*, **87**, 969 (1966).
7) T. Ikenaka, *J. Biochem.*, **54**, 328 (1963).
8) S. A. Barker and P. J. Somers, *Carbohyd. Res.*, **3**, 220 (1966).
9) J. X. Khym and L. P. Zill, *J. Amer. Chem. Soc.*, **73**, 2399 (1951).
10) J.T. Park and M.J. Johnson, *J. Biol. Chem.*, **181**, 149 (1949).

cedure of the analyses are summarized in Scheme 1.

Experimental

Deamination Reaction. To a solution of 2.0 g of D-glucosaminitol free base (mp 132—134°C)[1] in 40 ml of water was added 1.5 g sodium nitrite, and to this mixture was added dropwise 2.0 ml of acetic acid under mechanical stirring at room temperature. After being left to stand overnight, the reaction mixture showed strong reducing action to Park-Johnson reagent[10], ninhydrin reaction becoming negative.

Reduction of the Deamination Products. The pH of the deamination mixture was adjusted to 7—8 by adding potassium borate and to this solution was added 1.5 g of sodium borohydride. The whole mixture was allowed to stand overnight at 4°C. Excess borohydride was decomposed by treating with Dowex-50 free acid, and the filtrate from the resin was evaporated *in vacuo*. The residue was co-distilled three times with methanol to remove boric acid, and was used for the following column chromatography.

Separation of the Reduced Products. The reduced products corresponding to 2.0 g of glucosaminitol were dissolved in a small amount of water, and the solution was placed on a Dowex-1X4 (OH^- form, 100—200 mesh, 3×110 cm) column. Elution was carried out at the velocity of 1 ml per minute using water free from carbon dioxide as an eluent, each 10 ml fraction being collected. The chromatographic pattern as detected by a color reaction of formaldehyde[11] which had been produced by periodate oxidation of the substances is shown in Fig. 1.

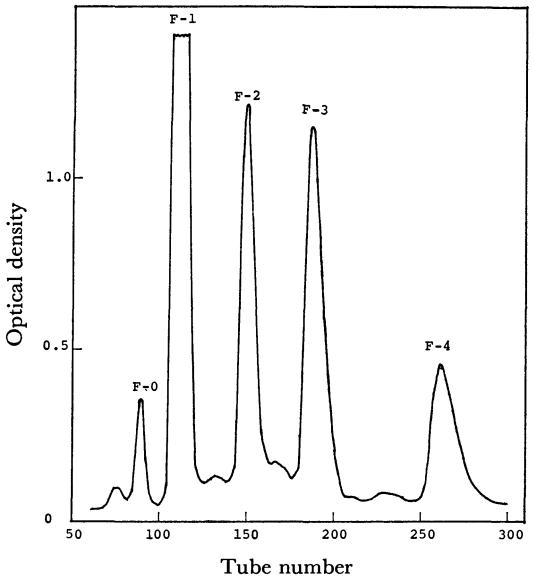

Fig. 1. Dowex-1X4 free base column chromatography of the reduced deamination products.

The results of gas-liquid chromatography of each fraction are shown in Table 1. We see that the fraction F-0 in the Dowex-1 chromatography seemed to be heterogenous and the yield was too low for further study. Crystallization occurred upon evaporation of the solvent *in vacuo* except for the cases of F-0 and F-3.

The yield of each fraction is given in Table 1. Physical constants, elemental analyses, and molecular formulae of each fraction are summarized in Table 2.

11) T. Nash, *Biochem. J.*, **55**, 416 (1953).

Table 1. Recovery, theoretical yield, and retention ratio (R_s) to the internal standard (pentaerythritol) in gas-liquid chromatography

The retention time of the internal standard is 5.6 min. The conditions of gas-liquid chromatography are identical with those described under Fig. 3.

Fraction	Recovery (mg)	Yield (%)	R_s of each fraction	R of authentic samples
F-0	25	1.67	0.535 1.83 2.0	—
F-1	827	55.14	3.22	3.23
F-2	213	14.21	3.34	3.36
F-3	249	16.60	2.74	—
F-4	73	4.44	5.11	5.12

Table 2. Melting point, specific rotation, elemental analysis, and molecular formula according to elemental analysis of the fractions F-1—4

	Mp (°C)	$[\alpha]_D^{20}$ in H_2O	Elemental analysis C%	Elemental analysis H%	Molecular formula
F-1	105—108	+16.2	43.09	8.45	$C_6H_{14}O_5$
F-2	88— 90	−13.1	42.79	8.41	$C_6H_{14}O_5$
F-3	sirup	−3.2	42.89	8.88	$C_6H_{14}O_5$
F-4	165—167.5	0	39.53	7.77	$C_6H_{14}O_6$

Calcd for $C_6H_{14}O_5$: C, 43.36%; H, 8.49%.
Calcd for $C_6H_{14}O_6$; C, 39.56%; H, 7.75%.

Periodate Oxidation of F-1—4. The oxidation products were reduced with sodium borohydride and analyzed by gas-liquid chromatography. The results are summarized in Table 3. As judged from the various evidence mentioned above, the fractions F-1—4 should be 2-deoxy-D-*arabino*-hexitol, 2-deoxy-D-*ribo*-hexitol, 2-hydroxymethyl-2-deoxy-D-*arabino* (or *ribo*)-pentitol, and D-mannitol respectively, the structural formulae of which are shown in Scheme 1.

Table 3. The periodate oxidation products of the fractions F-1—4 successively reduced with sodium borohydride

	HIO_4[7] (mol)	HCHO[11] (mol)	HCOOH[8] (mol)	Product
F-1	2.95	1.05	2.26	1,3-Propanediol
F-2	2.70	1.04	2.18	1,3-Propanediol
F-3	1.85	1.00	1.29	Tris(hydroxymethyl)methane
F-4	4.95	2.00	4.00	—

Direct Separation of the Deamination Products. The chromatographic pattern of the separation of the deamination products using a Dowex-1 borate column is shown in Fig. 2. Of the four peaks observed the peak F-4′ showed no reducing power. The patterns of gas-liquid chromatography of F-1′—4′ are shown in Fig. 3 (a—d). The yield of each fraction was calculated on the basis of the gas-liquid chromatogram of the deamination mixture shown in Fig. 4, and the data are summarized in Table 4. The borohydride-reduced fractions F-1′—3′ were also analyzed by gas-liquid chromatography, and the results are shown in Fig. 3(a—c) as broken lines. F-1′ gave 2-deoxy-D-*arabino*-hexitol, F-2′ 2-hydroxymethyl-2-deoxy-D-*arabino*(or *ribo*)-pentitol, and F-3′ 2-deoxy-D-*ribo*- and *arabino*-hexitol, F-4′ was a non-reducing substance which

was identified as D-mannitol. In conclusion, D-glucosaminitol gave the following four compounds by nitrous deamination, the structural formulae of which are also shown in Scheme 1: 2-deoxy-D-*arabino*-hexose, 2-hydroxymethyl-2-deoxy-D-*arabino*-(or *ribo*)-pentose, 2-deoxy-D-*erythro*-3-hexulose, and D-mannitol. A very small amount (0.6%) of a substance which showed retention time identical with 2,5-anhydro-D-mannitol[12] was observed in gas-liquid chromatography. However, the substance was not studied in detail due to the lack of material.

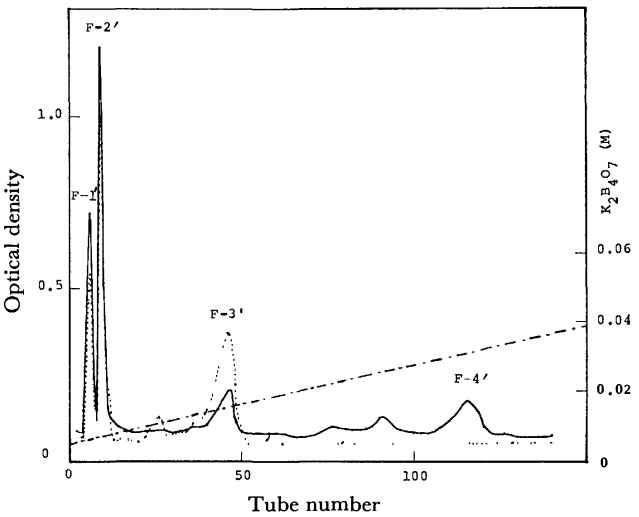

Fig. 2. Dowex-1X10 borate column (200—400 mesh, 0.9×17 cm) chromatography of the deamination mixture.
---- Concentration of potassium borate (eluent).
—— Formaldehyde determined by acetylacetone method[11] after the specimen had been oxidized with periodate.
—— Reducing power determined by Park-Johnson method.[10]

Table 4. Yields of the deamination products determined by means of gas-liquid chromatography

	Yield (%)
F-1′	45.8
F-2′	17.2
F-3′	22.8
F-4′	4.6

Preparation of the Reference Compounds. (a) 2-Deoxy-D-*arabino*-hexitol was prepared by reducing 250 mg of commercial 2-deoxy-D-*arabino*-hexose with sodium borohydride. Crystals appeared in ethanol solution giving 125 mg of the specimen which melted at 105—108.5°C, and had $[\alpha]_D^{20}$ +18.2 (*c*, 4.06 in H_2O). Found: C, 43.70; H, 8.50%. Calcd for $C_6H_{14}O_5$: C, 43.36; H, 8.49%. Bergmann *et al.*[13] gave mp 104—106°C, and $[\alpha]_D$ +17.5 (*c*, 10.0 in H_2O). (b) 2-Deoxy D-*ribo*-hexitol was prepared by reducing 2-deoxy-D-*ribo*-hexose which was synthesized by the known procedures.[14-17] Two hundred and ninety milligrams of the hexose was reduced

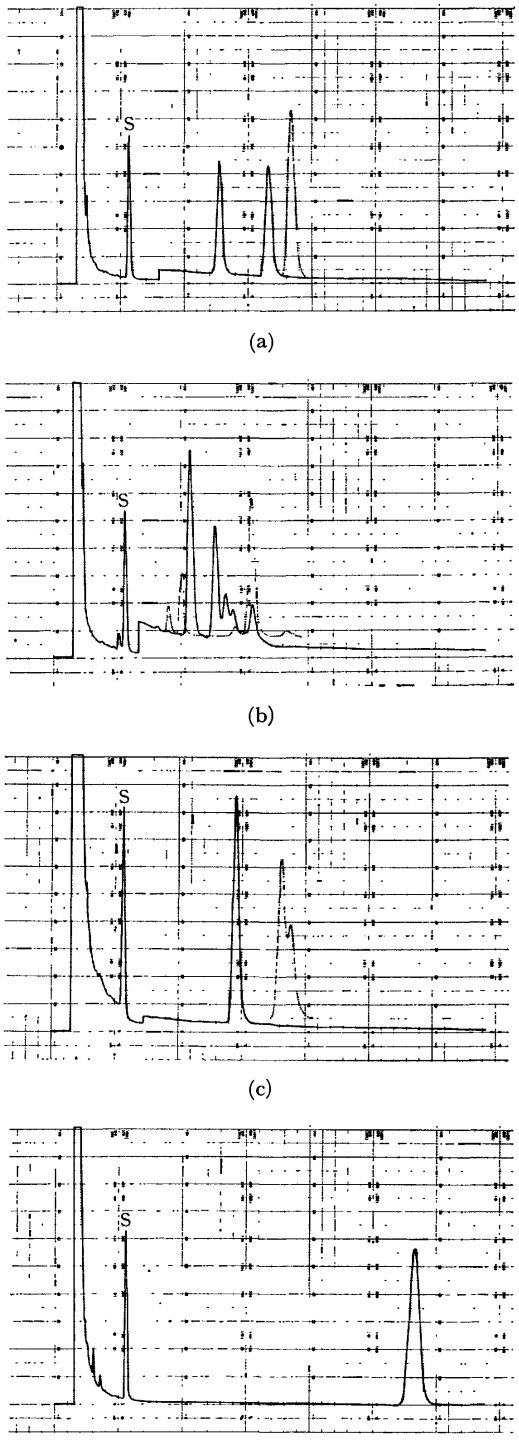

Fig. 3(a—d). Gas-liquid chromatography of the fractions F-1′—4′. A glass column (0.3×300 cm) was packed with 3% SE 52 on 90—100 mesh Chromosorb W which had been treated with dimethyldichlorosilane. The flow rate of the carrier nitrogen was 22 ml per minute, and the column temperature was 180°C. The internal standard(S) was pentaerythritol. Fig. 3(a) shows the anomers of 2-deoxy-D-*arabino*-hexose, the reduction product of which shows retention time identical with 2-deoxy-D-*arabino*-hexitol (broken line). Fig. 3(b) shows heterogeneity of the fraction F-2′. However, the main peak of the reduced F-2′ had retention time identical with that of F-3. The fraction F-3′[Fig. 3(c)] gave upon reduction two hexitols, 2-deoxy-D-*arabino*- and *ribo*-hexitols. Fig. 3(d) shows D-mannitol.

12) L. F. Wiggins, *Nature*, **165**, 566 (1950).
13) M. Bergmann, H. Shotte, and W. Leschinsky, *Ber.*, **56**, 1052 (1923).
14) N. K. Richtmyer and C. S. Hudson, *J. Amer. Chem. Soc.*, **63**, 1727 (1941).
15) D. A. Prins, *ibid.*, **70**, 3955 (1948).
16) L. Vargha and J. Kuszmann, *Chem. Ber.*, **96**, 411 (1963).
17) W. W. Zorbach and A. P. Ollapally, *J. Org. Chem.*, **29**, 1790 (1964).

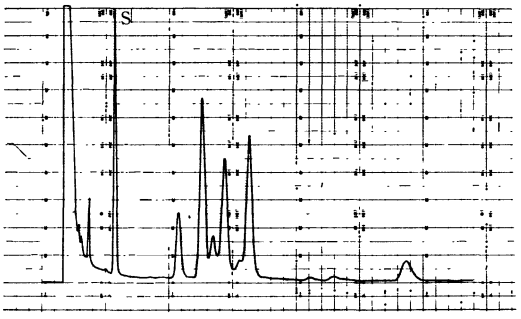

Fig. 4. Gas-liquid chromatography of the deamination mixture before fractionation. All the conditions of the chromatography were identical with those described under Fig. 3.

with sodium borohydride, giving 225 mg of the hexitol which crystallized from ethanol–ether mixture. mp 89—91°C, $[\alpha]_D^{20}$ −9.8° (*c* 7.1, H_2O); Found: C, 43.15; H, 8.48%. Calcd for $C_6H_{14}O_5$: C, 43.36; H, 8.49%. (c) 2.5-Anhydro-D-mannitol was prepared by the known method. mp 100—102°C, $[\alpha]_D^{20}$ +53 (*c* 1.17, H_2O). Bera *et al.*[18] gave mp 100—101°C, $[\alpha]_D^{20}$ +58.2. Found: C, 44.00; H, 7.34%. Calcd for $C_6H_{12}O_5$: C, 43.90; H, 7.37%. (d) D-Mannitol was prepared by reducing commercial D-mannose with sodium borohydride. mp 167—168°C. Braham[19] gave mp 166—168°C. Found: C, 39.46; H, 7.73%. Calcd for $C_6H_{14}O_6$: C, 39.56; H, 7.75%. (e) Tris(hydroxymethyl)methane was prepared by lithium aluminum hydride reduction of the reaction mixture of ethyl malonate and formaldehyde[20]. To 16 ml of ethyl malonate was added 1.0 g of potassium bicarbonate, and to this mixture was added dropwise 7.0 ml of commercial formaldehyde solution under stirring. The mixture was extracted with ether after 2 hours, and the extract was washed with saturated ammonium sulfate and then with water. The ether solution was dried over anhydrous magnesium sulfate. Eight grams of lithium aluminum hydride was added to about 100 ml of the ether solution, and the solution was refluxed overnight. Excess lithium aluminum hydride was decomposed by treatment with ethyl acetate, and the reaction mixture was evaporated *in vacuo*. The residue was acetylated with acetic anhydride–sodium acetate, and the reaction mixture was extracted with chloroform. The chloroform extract was evaporated *in vacuo* and the residue was treated with sodium methoxide in methanol. The mixture of polyhydric alcohols thus obtained was analyzed first by gas-liquid chromatography using the standard trimethylsilylation method. The chromatogram showed three distinct peaks, two of which were identified as propanediol-1,3 and pentaerythritol. The remaining peak was expected to be tris(hydroxymethyl)methane. A preparative chromatography using Dowex-1 free base[4-6] was successful in fractionating three substances, one of which was identified as tris(hydroxymethyl)methane by elemental analyses of itself and its tri-3,5-dinitrobenzoyl derivative. mp 87—89°C. Found: C, 46.47; H, 9.70%. Calcd for $C_4H_{10}O_3$: C, 45.27; H, 9.50%. Tri-3,5-dinitrobenzoyl derivative gave mp 155.5—156°C. Found: C, 43.54; H, 2.60; N, 11.89%. Calcd for $C_{25}H_{16}O_{18}N_6$: C, 43.62; H, 2.34; N, 12.21%.

18) B. C. Bera, A. B. Foster, and M. Stacey, *J. Chem. Soc.*, **1956**, 4531.

19) J. M. Braham, *J. Amer. Chem. Soc.*, **41**, 1707 (1919).

20) P. Block, Jr., "Organic Syntheses," Vol. 40, p. 27 (1960).

BULLETIN OF THE CHEMICAL SOCIETY OF JAPAN, VOL. 46, 596—599 (1973)

The Photo-induced Addition of Acetic Acid to Cyclohexene Derivatives[1)]

Ta-Yan LEONG, Takeshi IMAGAWA, Koichi KIMOTO, and Mituyosi KAWANISI

Department of Industrial Chemistry, Faculty of Engineering, Kyoto University, Yoshida, Sakyo-ku, Kyoto 606

(Received August 1, 1972)

The irradiation of methyl 3-cyclohexene-1-carboxylate in acetic acid in the presence of benzene as a sensitizer yields methyl *trans*-4-acetoxycyclohexanecarboxylate predominantly, together with a small amount of methyl *trans*-3-acetoxycyclohexane-1-carboxylate; the corresponding *cis*-isomers are not detected. Under the same conditions, on the irradiation of dimethyl esters of *cis*- and *trans*-4-cyclohexene-1,2-dicarboxylic acids, the two possible isomers of acetic-acid adducts with respect to each starting substance are obtained. The irradiation of *trans*-8-oxabicyclo[4.3.0]non-3-ene gives the two possible acetic-acid adducts, whereas in the case of the irradiation of the *cis*-isomer, only two equatorially-substituted acetic-acid adducts are obtained. The structural elucidation and the mechanism of the formation of these compounds are discussed.

The incorporation of protic solvents in excited cycloalkenes by sensitization has proved a fertile field for mechanistic as well as synthetic olefin photochemistry.[2-8)] We have been engaged in studies aimed at

1) Partly presented at the 25th Annual Meeting of the Chemical Society of Japan, Tokyo, October, 1971.

2) a) P. J. Kropp and H. J. Krauss, *J. Amer. Chem. Soc.*, **91**, 7466 (1969) and references cited therein. b) P. J. Kropp, *Pure Appl. Chem.*, **24**, 585 (1970).

3) a) J. A. Marshall, *Accounts Chem. Res.*, **2**, 33 (1969). b) J. A. Marshall, *Science*, **170**, 137 (1970). c) For recent related paper, J. A. Marshall and J. P. Arrington, *J. Org. Chem.*, **36**, 214 (1971).

4) a) H. Compaignon de Marcheville and R. Beugelmans, *Tetrahedron Lett.*, **1968**, 6331. b) R. Beugelmans and H. Compaignon de Marcheville, *Chem. Commun.*, **1969**, 241. c) D. Guénard and R. Beugelmans, *Tetrahedron Lett.*, **1970**, 1705.

5) J. A. Waters and B. Witkop, *J. Org. Chem.*, **34**, 3774 (1969).

6) M. Tada and H. Shinozaki, This Bulletin, **43**, 1270 (1970).

7) S. Fujita, Y. Hayashi, T. Nômi, and H. Nozaki, *Tetrahedron*, **27**, 1607 (1971).

8) H. Prinzbach and W. Eberbach, *Chem. Ber.*, **101**, 4083 (1968).

the application of this reaction;[9] we have found that cyclohexenes and cycloheptenes containing an acyloxy group at the allylic and homoallylic positions gave products resulting from the regiospecific addition of polar solvents,[9b] and have assumed the participation of the oxygen functions in the orientation of the reaction pathways.[9d,e] As an extension of this research, as well as a comparison with the results obtained previously, we have now studied the stereochemistry of the polar addition of acetic acid to methyl 3-cyclohexene-1-carboxylate (I) together with cyclohexenes with two substituents, VIII and XI, and bicyclic compounds, XIV and XVII.

Results and Discussion

When methyl 3-cyclohexene-1-carboxylate (I) was irradiated in acetic acid in the presence of benzene as a sensitizer, methyl *trans*-4-acetoxycyclohexane-1-carboxylate (II) was obtained predominantly, together with a small amount of methyl *trans*-3-acetoxycyclohexane-1-carboxylate (III) in a 60% yield (II: III= 97: 3). Authentic specimens of II and III were obtained by using the previously-reported method.[10] The identity of the photoproducts with the authentic specimens was satisfactory. We had already observed that, in the case of cyclohex-3-en-1-yl acetate under similar conditions, only a *cis-trans* mixture (*ca.* 1: 1) of 1,4-diacetoxycyclohexane was obtained regiospecifically; here the contribution of the oxygen functions to the transition state and/or to the intermediate at the protonation stage had been assumed.[9d] In the present case, a possible mechanism for the formation of II and III is depicted in Scheme 1, which indicates that the formation of II and III is due to the intermediacy of oxonium ions. The protonation of photo-excited six-membered cyclic olefin in protic media giving carbonium-ion species appears to be established.[2,3] Therefore, the formation of a carbonium ion (IV) is not exceptional; this in turn collapses into oxonium ions (V) and (VII). The incorporation of the 1,4- or 1,3-bridged ions, such as (V) or (VII), was advanced by Noyce in speaking of the reaction of methoxycyclohexanecarboxylic acids with acetic anhydride.[11] If we assume an equilibrium between these oxonium ions (V) and (VII), in which the doubly-bridged ion (VI) represents the transition state, the exclusive formation of *trans*-products (1,4- and 1,3-) can be understood. It should be noted that this mechanism can also explain the predominant formation of the thermodynamically more stable 1,4-isomer (II). Thus, in the present case, the participation of the oxygen function presumably plays an important role in directing the reaction pathways as well. We will return to the discussion of the mechanistic aspects of the protonation stage after more experimental facts are known.

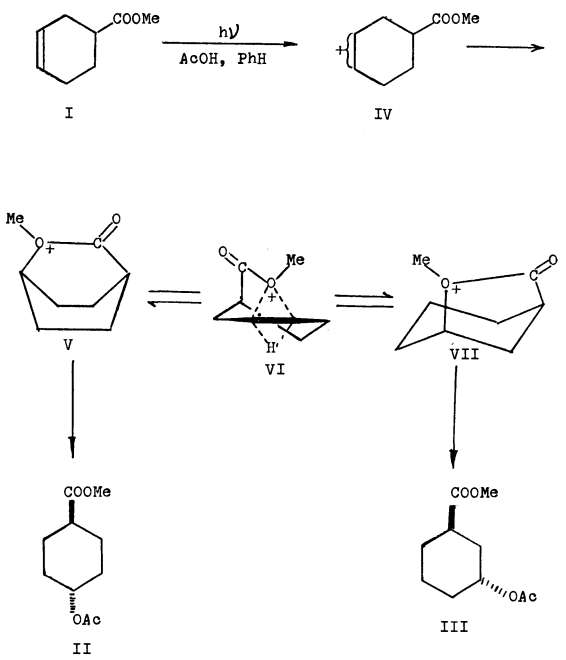

Scheme 1.

When dimethyl 4-cyclohexene-*cis*-1,2-dicarboxylate (VIII) was irradiated in acetic acid under the same conditions, dimethyl *c*-4-acetoxycyclohexane-*r*-1,*c*-2-dicarboxylate (IX) and dimethyl *t*-4-acetoxycyclohexane-*r*-1,*c*-2-dicarboxylate (X)[12] were obtained in a 25% yield (IX: X=71: 29).

The photoreaction of dimethyl 4-cyclohexene-*trans*-1,2-dicarboxylate (XI) was effected similarly; dimethyl *c*-4-acetoxycyclohexane-*r*-1,*t*-2-dicarboxylate (XII) and dimethyl *t*-4-acetoxycyclohexane-*r*-1,*t*-2-dicarboxylate (XIII) were obtained in a 25% yield (XII: XIII= 34: 66). The structures of IX, X, XII, and XIII were deduced from the respective IR and NMR spectra and were further elucidated by comparison with the authentic specimens prepared by the acetylation of the corresponding known alcohols.[13,14]

Judging from the products of these photoreactions, it can be deduced that, in the cases of VIII and XI, the role of the participation of the oxygen functions is unimportant.

The irradiation of *trans*-8-oxabicyclo[4.3.0]non-3-ene (XIV) yielded the two possible acetic-acid adducts, *t*-3-acetoxy-*r*-1-*trans*-8-oxabicyclo[4.3.0]nonane (XV) and *c*-3-acetoxy-*r*-1-*trans*-8-oxabicyclo[4.3.0]nonane (XVI), in a ratio of XV: XVI=80: 20 (yield=6%). The NMR spectra of XV and XVI showed half-band widths, W_H, of 14 and 8 Hz respectively for the –C**H**–OAc protons; thus, the structures of XV and XVI were unambiguously proved to have the structures shown in Scheme 2, since the fused systems have a *trans*-configuration and an inversion of the structure

9) a) M. Kawanisi and H. Kato, *Tetrahedron Lett.*, **1970**, 721. b) T. Okada, K. Shibata, M. Kawanisi, and H. Nozaki, *Tetrahedron Lett.*, **1970**, 859. c) H. Kato and M. Kawanisi, *Tetrahedron Lett.*, **1970**, 865. d) M. Kawanisi, Symposium on Photochemistry 1970, Kyoto, p. 122. e) K. Shibata, T. Okada, and M. Kawanisi, *Nippon Kagaku Kaishi*, *in* press.

10) E. Hardegger, Pl. A. Plattner, and F. Blank, *Helv. Chim. Acta*, **27**, 793 (1944).

11) D. S. Noyce and H. I. Weingarten, *J. Amer. Chem. Soc.*, **79**, 3098 (1957).

12) To designate the relative configuration the IUPAC 1968 Tentative Rules, Section E, have been adopted throughout this work. See *J. Org. Chem.*, **35**, 2849 (1970).

13) J. Klein and E. Dunkelblum, *Tetrahedron*, **23**, 205 (1966).

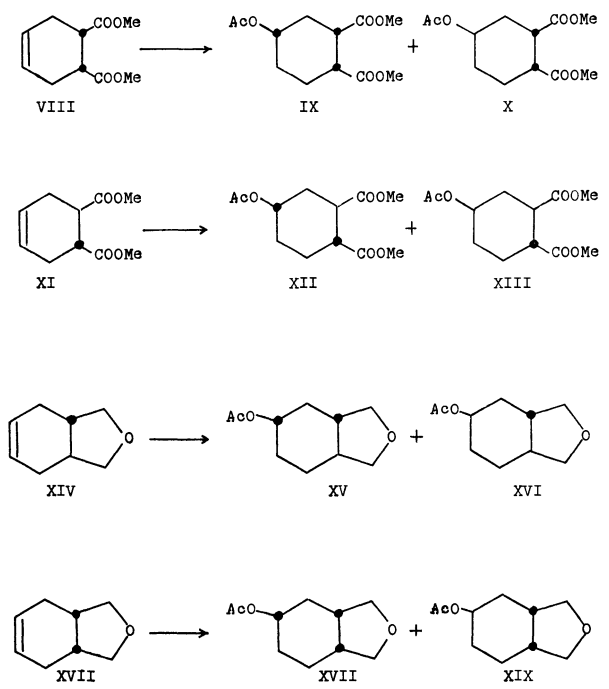

Scheme 2.

is impossible. An independent synthesis of XV and XVI was possible by means of the hydroboration of XIV, followed by alkaline oxidation and acetylation.[14]

On the other hand, when the photochemical reaction of *cis*-8-oxabicyclo[4.3.0]non-3-ene (XVII) was effected under the same conditions, two isomeric adducts were obtained, *t*-3-acetoxy-*r*-1-*cis*-8-oxabicyclo[4.3.0]nonane (XVIII) and *c*-3-acetoxy-*r*-1-*cis*-8-oxabicyclo[4.3.0]-nonane (XIX) in a ratio of 67: 33 (yield=5%); both had broad signals of W_H=14—17 Hz for the methine protons of –C**H**–OAc in their NMR spectra, indicating that the protons are situated axially. The adducts were assumed to have the structures indicated as XVIII and XIX, with equatorial acetoxy groups, which are thermodynamically more stable. A detailed description of the conformations of the alcoholic analogs of XVIII and XIX will appear in a separate paper.[15]

The small yield in the reaction of these bicyclic olefins can be ascribed to the inefficiency of the conversion into the distorted transoid olefins[2,3] *via* their triplet state because of the rigidity of the ring system. Bicyclic olefins such as bicyclo[3.3.1]non-3-ene were found to be fairly reactive toward the photoreaction in protic media, presumably because their structure has some flexibility.[9a]

Although Mundy succeeded in demonstrating the possibility of the long-range nonbonded electronic participation of the oxygen atom in XVII in ground-state chemistry,[16,17] the small yield in the present case restrains us from further discussion of the possible existence of such interaction in excited-state chemistry.

Experimental

All the temperature are uncorrected. Microanalyses were performed by Mrs. Kiyoko Fujimoto of our laboratory. The IR spectra were obtained in neat liquid film on a Shimadzu IR-27-G spectrophotometer. The NMR spectra were taken in 10% CCl_4 solutions on a JEOL C-60-H spectrometer, and the chemical shifts (δ) are reported relative to TMS as an internal standard. The glc analysis and separations were performed with a Shimadzu GC-4APT using a 3 m×3 mm column with 15% polyethylene glycol on 60/80 Chromosorb W operating at 180°C with a He flow rate of 40 ml/min. The MS spectra were taken using a Hitachi RMS-4 mass-spectrometer operated at 70 eV.

Starting Materials. Compounds I, VIII, and XI were prepared in the manner described in the literature.[14] The method of preparing XIV followed the one proposed by Eliel and Pillar;[18] XVII was obtained in asimilar manner and had properties identical with those reported by Christol *et al.*[19]

Photoreaction of Methyl 3-Cyclohexene-1-carboxylate (I) in Acetic Acid. A solution of I (3.27 g; 0.023 mol) and benzene (3 ml) in acetic acid (80 ml) was irradiated for 48 hr by means of a medium-pressure mercury arc in a quartz vessel. The photolysate was diluted with water (100 ml), neutralized (Na_2CO_3), extracted (ether), washed (water), and dried (Na_2SO_4). The adducts, II and III, were separated from the unreacted I by column chromatography (Al_2O_3) and isolated by preparative glc. II and III were obtained in a 60% yield in a ratio of 97: 3. They were identical in all respects with the authentic samples synthesized by the reported methods.[14]

*Photoreaction of Dimethyl 4-Cyclohexene-*cis*-1,2-dicarboxylate (VIII).* A mixture of VIII (5 g; 0.025 mol), benzene (3 ml), and acetic acid (85 ml) was irradiated for 48 hr and then treated in the manner described above. The adducts were obtained as a mixture by column chromatography and were purified by distillation. The mixture of IX and X (IX: X=71: 29) boiled at 114°C/4 mmHg (Yield: 25%). Found: C, 55.70; H, 6.52%. Calcd for $C_{12}H_{18}O_6$: C, 55.80; H, 7.03%. IX and X were separated by glc. The structure of IX was characterized by the following spectral data: IR: 2943(s), 1765(s), 1755(s), 1255(s), 1210(s), 1135(m), 1115(w), 1091(m), 1055(s), 1032(m), 1015(m), 923(w), 902(w), 855(w), 830(w), and 774(w) cm^{-1}. NMR: δ 4.91—4.41(m, 1H), 3.67(s, 6H), 3.08—2.31(m, 2H), 1.95(s, 3H), 2.31—1.30(m, 6H). MS: *m/e* 258(M^+ small), 227(M^+ −31, 4%), 198(M^+ −60, 20%), 185(43%), 166(80%), 138(100%). The structure of X was characterized similarly: IR: 2950(s), 1755(s), 1740(s), 1250(s), 1202(s), 1120(m), 1072(m), 1041(m), 1035(m), 999(m), 958-(w), 832(w), 776(w), cm^{-1}. NMR: δ 5.06—4.73(m, 1H), 3.65(s, 6H), 3.03—2.09(m, 2H), 1.98(s, 3H), 2.27—1.35(m, 6H). MS: *m/e* 258(M^+ samll), 227(M^+ −31, 32%), 198(M^+ −60, 21%), 166(79%), 138(80%), 79(100%).

Dimethyl *c*-4-acetoxycyclohexane-*r*-1,*c*-2-dicarboxylate (IX) was synthesized by the acetylation of the dimethyl *c*-4-hydroxycyclohexane-*r*-1,*c*-2-dicarboxylate obtained by the reduction of dimethyl 4-oxocyclohexane-*cis*-1,2-dicarboxylate as has been described by Klein *et al.*[14] Dimethyl *t*-4-acetoxycyclohexane-*r*-1,*c*-2-dicarboxylate (X) was obtained independently by the acetylation of the dimethyl *t*-4-hydroxycyclohexane-*r*-1,*c*-2-dicarboxylate prepared by the hydro-

14) J. Klein, E. Dunkelblum, and D. Avrahami, *J. Org. Chem.*, **32**, 935 (1967).
15) K. Kimoto, T-Y. Leong, T. Imagawa, and M. Kawanisi, *Can. J. Chem.*, **50**, 3805 (1972).
16) B. P. Mundy, A. R. DeBernardis, and R. D. Otzenberger, *J. Org. Chem.*, **36**, 3830 (1971).
17) *Cf.* B. Rickborn and S-Y, Low. *ibid.*, **30**, 2212 (1965).
18) E. L. Eliel and C. Pillar, *J. Amer. Chem. Soc.*, **77**, 3600 (1955).
19) H. Christol, A. Donche, and M. F. Plenar, *Bull. Soc. Chim. Fr.*, **1966**, 1315.

boration of dimethyl 4-cyclohexene-*cis*-1,2-dicarboxylate.[13] The IR and NMR of IX and X synthesized in the above manner were identical in all respects with those of the photochemical products.

Photoreaction of Dimethyl 4-Cyclohexene-trans-*1,2-dicarboxylate (XI).* The irradiation of XI was similarly carried out using 6 g (0.03 mol) of XI in 100 ml of acetic acid, with 3.6 ml of benzene as a sensitizer. The isomeric mixture (bp 114°C/4 mmHg) of the photoproducts, XII and XIII in a ratio of 34: 66, was obtained in a 25% yield. Found: C, 55.70; H, 7.07%. Calcd for $C_{12}H_{18}O_6$: C, 55.80; H, 7.03%. The adducts, XII and XIII, were isolated in the manner described before. The structure of XII was assigned according to the following data: IR: 2950(m), 1742(s), 1244(s), 1072(w), 1040(s), 1018(s), 978(w), 941(w), 901(w), 853(w), 754(w) cm^{-1}. NMR: δ 4.91—4.19(m, 1H), 3.66(s, 6H), 2.89—1.81(m, 8H), 1.98(s, 3H). MS: *m/e* 258(M^+ small), 227(M^+ −31, 4%), 198(M^+ −60, 12%), 185(20%), 166(100%), 138(88%).

The structure of XIII was deduced similarly from the following spectral data: IR: 2970(m), 1741(s), 1240(s), 1039(s), 1019(s), 990(m), 958(w), 895(w), 857(w), 761(w) cm^{-1}. NMR: δ 5.15—4.96(m, 1H), 3.64(s, 6H), 2.85—1.30(m, 8H), 2.02(s, 3H). MS: *m/e* 258(M^+ small), 227(M^+ −31, 9%), 198(M^+ −60, 16%), 185(36%), 167(45%), 166(96%), 138(100%).

XII and XIII were independently obtained by the acetylation of the mixture of dimethyl *c*-4- and *t*-4-hydroxycyclohexane-*r*-1,*t*-2-dicarboxylates prepared from the hydroboration of XI, as has been previously reported.[14] The products synthesized in this manner were identical with the photochemical products.

Photoreaction of trans-*8-Oxabicyclo[4.3.0]non-3-ene (XIV).* A mixture of XIV (1.245 g; 0.1 mol), benzene (2 ml), and acetic acid (50 ml) was irradiated in the way previously described. A mixture of the photoproducts, *t*-3-acetoxy-*r*-1-*trans*-8-oxabicyclo[4.3.0]nonane (XV) and *c*-3-acetoxy-*r*-1-*trans*-8-oxabicyclo[4.3.0]nonane (XVI), was obtained in a 6% yield (XV: XVI=80: 20). The adducts were separated by glc. The structures of XV and XVI were supported by the following data. For XV: IR: 2932(s), 2890(s), 1736(s), 1242(s), 1090(w), 1060(w), 1018(s), 980(w), 955(w), 890(m) cm^{-1}. NMR: δ 5.11—4.40(m, 1H, W_H=14 Hz), 4.06—3.5(m, 2H), 3.51—2.81(m, 2H), 1.96(s, 3H), 2.31—1.01(m, 8H). MS: *m/e* 184(M^+ small), 141(M^+ −43, 13%), 124(M^+ −60, 66%), 79(100%). For XVI: IR: 2960(s), 2890(s), 1748(s), 1218(m), 1121(w), 1018(s), 974(w), 895(m) cm^{-1}. NMR: δ 5.30—5.03(m, 1H, W_H=8 Hz), 4.11—3.65(m, 2H), 3.48—2.98(m, 2H), 1.99(s, 3H), 2.35—1.24(m, 8H). MS: *m/e* 184(M^+ 3%), 141(M^+ −43, 40%), 124(M^+ −60, 14%), 43(100%).

Microanalyses were performed on the respective alcohols obtained by the LAH reduction of XV and XVI. For the alcohol from XV: Found: C, 67.57; H, 9.93%. For the alcohol from XVI: Found: C, 67.36; H, 10.19%. Calcd for $C_8H_{14}O_2$: C, 67.57; H, 9.93%.

Independent Synthesis of XV and XVI. A solution of XIV (1 g) in 5 ml of tetrahydrofuran was subjected to hydroboration, followed by alkaline oxidation, as has been described by Klein *et al.*[14] The alcohols thus obtained were converted into the corresponding acetates with a mixture of acetic anhydride and boron trifluoride etherate. The acetates obtained in this way were shown to have an isomeric ratio of XV: XVI=54: 46. The mixture of the acetates was separated into XV and XVI by glc; they were shown to be identical in all respects with those obtained photochemically.

Photoreaction of cis-*8-Oxabicyclo[4.3.0]non-3-ene (XVII).* The procedure was essentially the same as that for XIV; the adducts obtained in a 5% yield. Found: C, 65.01; H, 8.76%. Calcd for $C_{10}H_{16}O_3$: C, 65.19; H, 8.75%. This mixture was separated into *t*-3-acetoxy-*r*-1-*cis*-8-oxabicyclo-[4.3.0]nonane (XVIII) and *c*-3-acetoxy-*r*-1-*cis*-8-oxabicyclo-[4.3.0]nonane (XIX) by preparative glc (XVIII: XIX=67: 33); the isomers had the following properties. For XVIII: IR: 2950(s), 2900(s), 1742(s), 1460(w), 1370(m), 1255(s), 1236(s), 1083(s), 1050(s), 1034(s), 1016(s), 995(w), 960(w), 900(m), 720(w) cm^{-1}. NMR: δ 5.01—4.52(m, 1H, W_H=17 Hz), 3.91—3.40(m, 4H), 2.51—1.09(m, 11H). MS: *m/e* 184(M^+ 2%), 141(M^+ −43, 24%), 124(M^+ −60, 28%), 43(100%). For XIX: IR: 2950(s), 2900(s), 1741(s), 1370(m), 1240(s), 1060(w), 1020(s), 895 cm^{-1}. NMR: δ 5.12—4.66(m, 1H, W_H=14 Hz), 4.04—3.33(m, 4H), 2.64—1.14(m, 11H). MS: *m/e* 184(M^+ 2%), 141(M^+ −43, 30%), 124(M^+ −60, 30%), 43(100%).

The elemental analysis of each isomer was performed upon the corresponding alcohol derived from the LAH reduction of XVIII and XIX. For the alcohol from XVIII; Found: C, 67.57; H, 10.17%. For the alcohol from XIX; Found: C, 67.35; H, 9.65%. Calcd for $C_8H_{15}O_2$: C, 67.57; H, 9.93%.

Professor Hitosi Nozaki is thanked for his interest in this work.

Dimerization of Isoprene by Palladium-Diphosphine Complex Catalyst

Kuniyuki TAKAHASHI,* Go HATA, and Akihisa MIYAKE

Basic Research Laboratories, Toray Industries, Inc., Tebiro, Kamakura

(Received August 7, 1972)

Oligomerization of isoprene catalyzed by the $PdBr_2(Ph_2PCH_2CH_2PPh_2)_2$–PhONa catalyst was studied. The catalyst activity was greatly enhanced by the addition of phenol. Five linear dimers were identified. Distribution of the isomeric dimers was remarkably affected by the molar ratio of phenol to isoprene. The reaction in the presence of a small amount of phenol (phenol/isoprene=1/30) gave 2,7-dimethyl-1,*trans*-3,7-octatriene derived from a tail-to-tail dimerization almost selectively, while the addition of a large amount of phenol (phenol/isoprene=1/1.5) afforded head-to-head dimers (2-vinyl-5-methyl-1,6-heptadiene and 3,6-dimethyl-1,*cis*-3,7-octatriene) as main dimers (more than 40% of all the dimers). In a 1:3 ratio of phenol to isoprene the dimers consisted of mainly 2,6-dimethyl-1,*trans*-3,7-octatriene derived from a head-to-tail dimerization.

It is well-known that oligomerization of 1,3-butadiene to cyclic or linear products is catalyzed by some transition metal complexes. A new type of linear dimerization of 1,3-butadiene catalyzed by transition metal compounds of group VIII of the periodic table, completed by addition of a compound having at least one active hydrogen atom to give 2,7-octadienyl derivatives as main products, has recently been found.[1-6] In this reaction palladium complexes, especially palladium-triphenylphosphine complexes, are the most effective.

In connection with the above reaction, we have found[7] that the reaction of 1,3-butadiene with active methylene compounds or amines catalyzed by palladium-diphosphine complexes gives 1:1 adducts of 1,3-butadiene to the active methylene compounds or the amines. This type of reaction was not applicable to other active hydrogen compounds such as phenol, alcohols and carboxylic acids, but the reaction in phenol was found to give a linear dimer 1,3,7-octatriene in a good yield. Further research has led us to find that a palladium-diphosphine complex catalyst shows a high catalytic activity in the linear dimerization of 1,3-butadiene and isoprene by addition of a catalytic amount of phenol.

The present paper deals with the dimerization of isoprene in the presence of $PdBr_2$ $(Ph_2PCH_2CH_2PPh_2)_2$, PhONa and PhOH as a catalyst system. Some catalysts containing chromium,[8] titanium,[9] hafnium,[10] and zirconium[11] have been reported to give linear dimers along with other oligomers. Zerovalent palladium-triphenylphosphine complexes have been also reported[12] to catalyze the reaction in 2-propanol to afford 2,7-dimethyl-1,3,7-octatriene almost selectively.

The reaction of isoprene catalyzed by a combination of $PdBr_2(Ph_2PCH_2CH_2PPh_2)_2$, PhONa and a small amount of phenol also gave 2,7-dimethyl-1,3,7-octatriene almost selectively, but it was found that by adding a large amount of phenol the reaction afforded 2,6-dimethyl-1,3,7-octatriene as the main product and other linear isomers as minor products.

The results given below deal with our work to determine the structure of the isomeric dimers of isoprene and to investigate the effect of phenol on the distribution of the isomers.

Experimental

Reagent. Isoprene was dried on calcium chloride and distilled under an argon atmosphere. Phenols were purified by distillation. Dibromobis(ethylenebisdiphenylphosphine) palladium (II) was prepared according to the procedure given by Chatt *et al.*[13]

Analysis. Gas-chromatography was used for identification and quantitative analysis. A squalane-on-Celite column and a Silicone DC 550 capillary column (a length: 90 feet, a diameter: 0.02 inch) were used. 4-Vinyl-cyclohexene was used as an internal standard. A preparative gas-chromatography apparatus equipped with a squalane-on-Celite column was used to isolate the products. IR, NMR, UV and mass spectra were also used to identify the products. Samples for the measurement of mass spectra were introduced directly to the mass spectrophotometer from gas-chromatography apparatus equipped with a capirally column.

General Procedure for the Dimerization of Isoprene. To a 100 ml stainless steel autoclave, $PdBr_2(Ph_2PCH_2CH_2PPh_2)_2$, PhONa, PhOH, isoprene and benzene were charged under an argon atmosphere. The autoclave was heated at 150°C with stirring.

Results and Discussion

The dimerization of isoprene catalyzed by a combination of $PdBr_2(Ph_2PCH_2CH_2PPh_2)_2$, PhONa and a small amount of PhOH gave a linear dimer almost

* Present address: Pioneering Research & Development Labs., Toray Industries, Inc., Sonoyama, Otsu, Shiga.

1) S. Takahashi, T. Shibano, and N. Hagihara, *Tetrahedron Lett.*, **1967**, 2451.
2) S. Takahashi, T. Shibano, and N. Hagihara, This Bulletin, **41**, 454 (1968).
3) E. J. Smutny, *J. Amer. Chem. Soc.*, **89**, 6793 (1968).
4) E. J. Smutny, H. Chung, K. C. Dewhirst, W. Keim, T. M. Shryne ,and H. E. Thyret, Preprints of Symposium on Homogeneous Catalytic Reactions Involving Palladium, B100 (1969).
5) G. Hata, K. Takahashi, and A. Miyake, *Chem. Ind.* (London), **1969**, 1836.
6) G. Hata, K. Takahashi, and A. Miyake, *J. Org. Chem.*, **36**, 2116 (1971).
7) K. Takahashi, A. Miyake, and G. Hata, This Bulletin, **45**, 1183 (1972).
8) G. Wilke, *J. Polym. Sci.*, **38**, 45 (1959).
9) J. Itakura and H. Tanaka, *Makromol. Chem.*, **123**, 274 (1969).
10) A. Misono, Y. Uchida, K. Furuhata, and S. Yoshida, This Bulletin, **42**, 1383 (1969).
11) A. Misono, Y. Uchida, K. Furuhata, and S. Yoshida, *ibid.*, **42**, 2303 (1969).
12) S. Takahashi, T. Shibano, and N. Hagihara, Preprints of 24th Symposium on Catalysts, p. 4 (1969).
13) J. Chatt, F. A. Hart, and H. R. Watson, *J. Chem. Soc.*, **1962** 2537.

Table 1. Spectral and physical properties of the products

Product[a]	NMR[b] (τ)	IR (cm^{-1})	UV[c] ($m\mu$)	bp (°C)	n_D^{25}
A	9.03(3H, d, J=6.0 Hz), 8.58(2H, m), 8.2—7.7(3H, m), 5.20(2H, m), 5.12(2H, s), 5.03(1H, m), 4.78(1H, m), 4.40(1H, m), 3.72(1H,q, J=18.5 Hz, 11.0 Hz).	1644, 1612, 992, 908, 891	225(ε 18000)	161	1.4570
B	9.06(3H, d, J=6.0 Hz), 8.28(3H, s), 7.9(3H, m), 4.1—5.3(6H, m), 3.96(1H,d, J=16.0 Hz)	1644, 1612, 991, 962, 910, 881	230(ε 24000)	167	1.4704
E	8.30(3H, s), 8.22(3H, s), 7.9(4H, m), 5.36(2H, s), 5.22(2H, s), 4.5(1H, m), 3.94(1H, d, J=17.0 Hz)	1650, 1613, 963, 883	230(ε 25000)	176	1.4721

a) A: 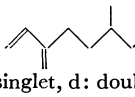 , B: 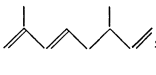 , E: 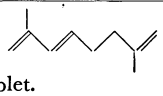

b) s: singlet, d: doublet, q: quartet, m: multiplet.

c) Measured in ethanol.

selectively. On the other hand, the reaction in the presence of a large amount of PhOH afforded various linear dimers. It was also found that the distribution of linear dimers was remarkably affected by the amount of phenol added. The gas chromatography of the dimers carried out with a 90 feet Silicone DC 550 capirally column is shown in Fig. 1.

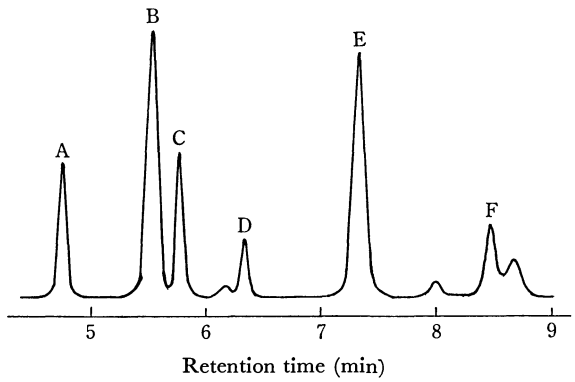

Fig. 1. Gas-chromatograph of isoprene dimers
column: Silicone DC 550 (90 ft, 0.02 in)
temperature: 110°C

Products A, B, and E (Fig. 1) were isolated purely and identified by spectroscopic methods. The spectroscopic data are shown in Tables 1 and 2. Products A, B, and E were apparently derived from head-to-head, head-to-tail, and tail-to-tail dimerization of isoprene, respectively.

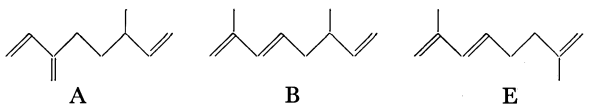

A B E

Product C was separated as a mixture with product D. Hydrogenation of the mixture gave only one product, 3,6-dimethyloctane, which was confirmed by the vpc equipped with a capillary column. The NMR spectrum of the mixture showed characteristic signals at τ 3.30 and 3.70 (two quartets, 1H), and τ 8.19 and 8.30 (two singlets, 3H). The intensity ratio of the lower chemical shift to the higher in each pair coincided with the weight ratio of C to D involved in the sample for the measurement of the NMR spectrum. This indicates that the signals at τ 3.30 and 8.19 are due to C and other signals to D. The chemical shifts due to

Table 2. Mass spectral data (relative intensities)

m/e	% of base peak				
	A	B	C	D	E
41	78	21	27	25	39
53	36	23	27	24	36
55	31	30	20	17	14
67	46	6	4	5	7
68	100	4	3	3	6
79	10	21	25	23	36
81	15	100	100	100	100
93	26	6	4	4	11
107	22	8	5	4	11
121	10	9	5	4	17
136	2	3	3	4	3

H* and H** of *cis* form in the following general fomula are lower (H*: 20—40 Hz,[14] H**: 0.07 Hz[15]) than those of the *trans* form. On the other hand, the mass spectra of C and D were equal (Table 2). Thus, the

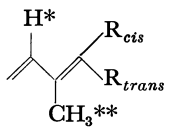

structures of C and D were presumed as 3,6-dimethyl-1, *cis*-3,7-octatriene and 3,6-dimethyl-1, *trans*-3,6-octratriene, respectively.

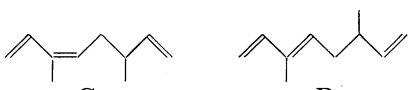

C D

Product F was identified as a mixture of 1-methyl-4-(2-propenyl)cyclohexene and 1-methyl-3-(2-propenyl)-cyclohexene, which were derived from the Diels-Alder reaction of isoprene by spectroscopic measurements. Other products were not identified.

The effect of phenol on the distribution of the isomeric dimers was investigated and the results are summarized in Table 3. The reaction in the absence

14) C. G. Cardenas, *Tetrahedron Lett.*, **1969**, 4013.

15) R. B. Bates and D. M. Gales, *J. Amer. Chem. Soc.*, **82**, 5749 (1960).

TABLE 3. REACTIONS IN PHENOL[a]

Phenol mol	Isoprene mol	Conv.[b] %	Dimers[c] %	Distribution of isomeric dimers[d] A	B	C	D	E	F	Others	Trimers[e] %
0.0	0.3	19	43	—	—	17	trace	26	57	trace	20
0.01	0.3	90	86	—	6	—	—	89	1	1	12
0.05	0.3	96	72	trace	37	1	trace	55	1	6	22
0.1	0.3	95	57	1	60	8	2	28	—	1	24
0.1	0.2	94	58	2	57	15	3	21	trace	2	28
0.2	0.3	75	32	19	34	22	1	9	11	4	34

a) Reaction conditions: $PdBr_2(Ph_2PCH_2CH_2PPh_2)_2$ 0.25 mmol, PhONa 2.5 mmol, benzene 15 ml, 150°C, 1 hr.
b) Conversion of isoprene.
c) Based on the conversion of isoprene.
d) A: 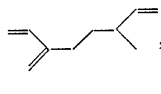 , B: 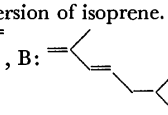 , C: 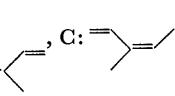 , D: 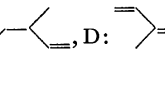 , E: 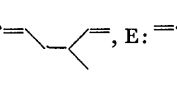 ,
F: Methylpropenylcyclohexens.
e) Based on the conversion of isoprene.

TABLE 4. EFFECT OF SUBSTITUTED PHENOL ON THE DISTRIBUTION OF DIMERS[a]

Substituted phenol	Conv.[b] %	Dimers[c] %	Distribution of isomeric dimers[d] A	B	C	D	E	F	Others	Trimers[e] %
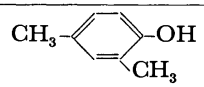	94	82	trace	26	trace	trace	64	trace	10	12
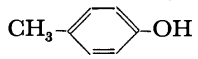	93	74	1	46	3	2	38	2	8	24
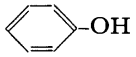	95	57	1	60	8	2	27	—	2	24
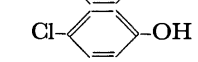	13	46	2	1	22	trace	1	71	3	trace

a) Reaction conditions: $PdBr_2(Ph_2PCH_2CH_2PPh_2)_2$ 0.25 mmol, PhONa 2.5 mmol, benzene 15 ml, isoprene 0.3 mol, substituted phenol 0.1 mol, 150°C, 1 hr.
For b), c), d), and e), refer to Table 3

of phenol gave only a small amount of dimers.[16] However, by adding phenol the catalytic activity was greatly enhanced and linear dimers were afforded in a fairly good yield. With the increase of the amount of phenol, the yield of the dimers decreased while that of the trimers, whose structure was not investigated, increased. It is interesting that the distribution of 2,6-dimethyl-1, *trans*-3,7-octatriene (B), which was derived from the head-to-tail dimerization of isoprene, went up to 60% when 0.1 mol of phenol (to 0.3 mol of isoprene) was added. Further increase of the amount of phenol yielded a considerable amount of the head-to-head dimers (A) and (C) as main products (about 40% in dimers) although the head-to-head addition seems difficult to occur because of repulsion between methyl groups or for some such steric reason. The tail-to-tail isomer 2,7-dimethyl-1, *trans*-3,7-octatriene (E) was given almost selectively in the presence of only a small amount of phenol, but the yield decreased considerably with the increase of phenol. It was confirmed that the variation of the distribution of the isomeric dimers was influenced mostly by the molar ratio of phenol to isoprene.

The results of the investigation on the effect of substituted phenol are shown in Table 4. It is obvious that the effect of substituted groups on the distribution of isomeric dimers and the yield of the dimers is very large. The reaction in the presence of 2,4-xylenol gave linear dimers, mainly 2,7-dimethyl-1, *trans*-3,7-octatriene in a 82% yield. On the other hand, the reaction in *p*-chlorophenol yielded only a small amount of linear dimers, mainly 3,6-dimethyl-1, *cis*-3,7-octatriene, in a 14% yield, the reactivity being much smaller than that in 2,4-xylenol.

16) The diphosphine complex $PdBr_2(Ph_2CH_2CH_2PPh_2)_2$ had no catalytic activity. A zero-valent complex $Pd(Ph_2CH_2CH_2PPh_2)_2$ showed low catalytic activity. The catalytic activity of Pd(0) complexes, which is presumed to be similar to that of Pd(II) complexes,[7] was not studied in detail.

The Syntheses of Trimethyl *dl*-3-(Methoxycarbonylmethyl)-1,2,4-cyclopentanetricarboxylates[1]

Shosuke Ito and Yoshimasa Hirata

Department of Chemistry, Faculty of Science, Nagoya University, Chikusa-ku, Nagoya

(Received August 21, 1972)

The five trimethyl *dl*-3-methoxycarbonylmethyl-1,2,4-cyclopentanetricarboxylates have been synthesized and their configurations determined. A comparison of their spectral properties with those of the corresponding ester obtained from ikarugamycin indicates that the latter has a *cis*, *trans*, *trans* configuration.

In the course of structural studies of a new antibiotic, ikarugamycin, a monocyclic tetramethyl ester, I ($C_{14}H_{20}O_8$) was obtained as one of the chromic acid oxidation products of ikarugamycin and has played an important role in the determination of the structure and the stereochemistry of ikarugamycin.[2]

The structure of I was assumed to be trimethyl 3-methoxycarbonylmethyl-1,2,4-cyclopentanetricarboxylate on the basis of the concomitant formations of tetramethyl 1,2,3,4-butanetetracarboxylate and tetramethyl 1,2,3,4-cyclopentanetetracarboxylate[2a] and of the following spectral data: δ 2.1—3.4 (8H, m), 3.58 (3H, s), 3.60 (6H, s), 3.63 (3H, s); *m/e* 316.1160. In order to determine the structure and stereochemistry of I, five stereoisomers of trimethyl *dl*-3-methoxycarbonylmethyl-1,2,4-cyclopentanetricarboxylates (Ia—Ie) were synthesized and their stereochemistry was unambiguously established.

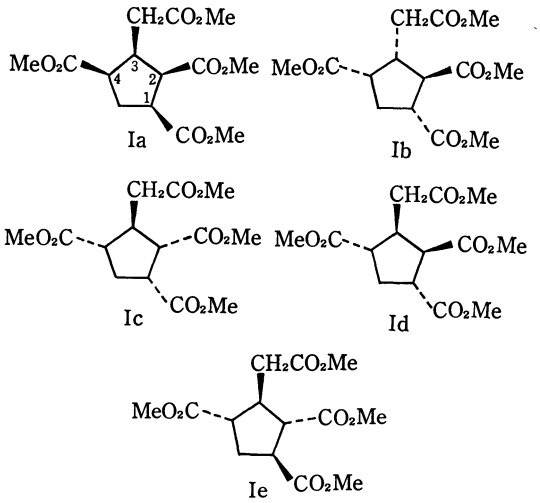

The syntheses of two the stereoisomers, Ia[3] and Id,[4] had already been reported. The *cis*, *cis*, *cis*-isomer (Ia) had been prepared by the oxidation of *endo*-dicyclopentadiene with ozone and then with performic acid. Three stereoisomers (the *trans*, *trans*, *cis*-isomer (Ib), the *cis*, *trans*, *trans*-isomer (Ic), and the *trans*, *cis*, *trans*-isomer (Id)) were obtained by the oxidative fission of the double bond of each of three stereoisomeric 2-methoxycarbonyl-3-methoxycarbonylmethylbicyclo[2.2.1]hept-5-enes (IIa, IIb, and IIc respectively). The two *trans*-dimethyl esters (IIa and IIb) were prepared by the Diels-Alder reaction of cyclopentadiene with dimethyl *trans*-glutaconate and were separated by preparative glc. The stereochemistry of those stereoisomers was determined as follows. The dimethyl ester (IIb) was hydrolysed to the corresponding dicarboxylic acid (IIe), which was then easily converted into an iodolactone, IIIa, when treated with iodine and potassium iodide in the presence of sodium bicarbonate.[5] The IR spectrum of IIIa shows two absorption bands for a γ-lactone (1805 cm^{-1}) and a carboxylic acid (1739 cm^{-1}). The NMR spectrum of IIIa exhibits close similarities with that of IIIb[6] with respect to the chemical shifts and the coupling constants of three protons (H-1, 5-*endo*, and 6-*exo*). In addition, the iodolactone (IIIa) was reconverted into the carboxylic acid (IIe) when treated with zinc in acetic acid.[5] The above facts indicate that the iodolactone has the structure IIIa. Accordingly, the configuration of IIb was established. The *exo*, *cis*-dimethyl ester (IIc) was prepared, although in a low yield, by the Arndt-Eistert reaction of the half methyl ester derived from *exo*, *cis*-bicyclo[2.2.1]hept-5-ene-2,3-dicarboxylic anhydride.[7] By heating under reflux with methanolic sodium methoxide, the dimethyl ester, Ia, was completely isomerized to the fifth isomer (Ie) as the main product, together with Ic as a minor product.

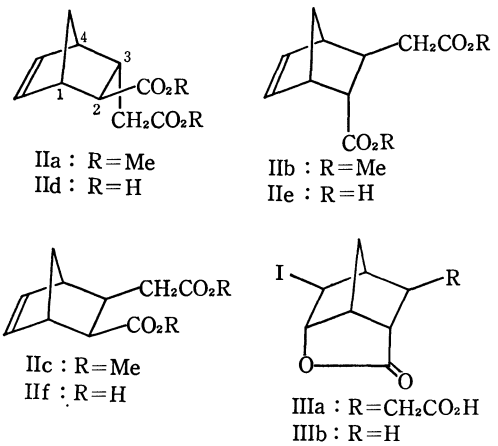

1) A part of this work was preliminarily reported in Ref. 2b.

2) a) S. Ito and Y. Hirata, *Tetrahedron Lett.*, **1972**, 1185. b) S. Ito and Y. Hirata, *ibid.*, 2557 (1972).

3) M. I. Fremery and E. K. Frieds, *J. Org. Chem.*, **28**, 2537 (1963).

4) R. H. Sullivan, Ger. 1078120 (1960).

5) For example, J. Meinwald, S. S. Labana, and M. S. Chadha, *J. Amer. Chem. Soc.*, **85**, 582 (1963).

6) R. M. Moriarty, H. Gopal, H. G. Walsh, K. C. Ramey, and D. C. Lini, *Tetrahedron Lett.*, **1966**, 4555.

7) D. Craig, *J. Amer. Chem. Soc.*, **73**, 4889 (1951).

The IR and NMR spectra and the behavior upon glc of the naturally derived ester (I) were identical with those of the synthetic *cis, trans, trans*-ester (Ic). On the other hand, the other isomers (Ia, Ib, Id, and Ie) were different from I in many respects.

Experimental

All melting points were uncorrected. The IR spectra were recorded on a JASCO IR-S spectrometer. The NMR spectra were recorded on a Nihondenshi JNM-C60H spectrometer, using CCl_4 as the solvent, unless otherwise stated. The chemical shifts are given in ppm relative to the internal TMS, and the coupling constants are given in Hz. The mass spectra were obtained on a Hitachi RMU-6D mass spectrometer operating with an ionization energy of 70 eV. The glc were carried out on a Varian Aerograph 1828-4 instrument. All the microanalytical samples of oily materials were obtained by the preparative glc.

Trimethyl cis, cis, cis-*3-Methoxycarbonylmethyl-1,2,4-cyclopentanetricarboxylate (Ia).* A solution of *endo*-dicyclopentadiene (300 mg) in methanol (60 ml) was ozonized at −70°C until the solution turned blue. The excess ozone was removed with a nitrogen stream, and then the solvent was evaporated under reduced pressure. After adding 98% formic acid (30 ml) and 53% hydrogen peroxide (4.5 ml), the mixture was stirred at 0°C for 1 hr and then at room temperature overnight. After the excess oxidizing reagents had been destroyed with sodium bisulfite, the mixture was concentrated under reduced pressure. The residue was digested in methanol and then filtered. The filtrates were concentrated under reduced pressure. The treatment of the residue with diazomethane gave a crude methyl ester (910 mg), which was chromatographed on silica gel (15 g) and eluted with *n*-hexane–ether (2: 1) to give 210 mg (29%) of Ia as a colorless oil; δ 2.0—3.3 (8H, m), 3.60 (6H, s), 3.62 (6H, s); *m/e* 316 (M^+). Found: C, 52.77; H, 6.85%. Calcd for $C_{14}H_{20}O_8$: C, 53.16; H, 6.37%.

trans-*2-Methoxycarbonyl-3-methoxycarbonylmethylbicyclo[2.2.1]-hept-5-enes (IIa and IIb).* A solution of dimethyl *trans*-glutaconate (2.88 g) and cyclopentadiene (6.6 g) in toluene (10 ml) was heated at 150°C for 22 hr. The subsequent distilation of the mixture gave 2.05 g (61%) of a mixture of IIa and IIb (bp 143—152°C/18 mmHg), which was then chromatographed on silica gel (70 g) and eluted with *n*-hexane–ether (6: 1) to give the following three fractions: Fraction 1 (1.20 g); IIa: IIb=4: 1, Fraction 2 (0.27 g); IIa: IIb= 1: 1, and Fraction 3 (0.45 g); IIa: IIb=1: 19. The pure samples of IIa and IIb were obtained by preparative glc (5% OV-17 column at 200°C) from Fractions 1 and 3 respectively. 2-*exo*-3-*endo*-isomer (IIa): δ 3.57 (3H, s), 3.62 (3H, s), 6.15 (2H, m); *m/e* 224 (M^+), 164, 159, 151, 66. 2-*endo*-3-*exo*-isomer (IIb): δ 3.55 (3H, s), 3.59 (3H, s), 5.96 (1H, dd, 5.6, 3.0), 6.19 (1H, dd, 5.6, 3.0); *m/e* 224 (M^+), 164, 159, 151, 66.

exo,cis-*2-Methoxycarbonyl-3-methoxycarbonylmethylbicyclo[2.2.1]-hept-5-ene (IIc).* A solution of[7] *exo,cis*-bicyclo[2.2.1]hept-5-ene-2,3-dicarboxylic anhydride[7] (2.5 g) in methanol (25 ml) was refluxed for 2 hr. The subsequent removal of the solvent under reduced pressure gave a half methyl ester ($\nu_{max}^{CHCl_3}$ 1741, 1711 cm^{-1}), which was then dissolved in benzene (20 ml). To the stirred solution, oxalyl chloride (4 ml) was added at 0°C; the mixture was kept at 0°C for 0.5 hr and then at room temperature for 2 hr. The solvent and the excess reagent were removed under reduced pressure to afford a crude acid chloride, which was then dissolved in benzene (10 ml). To a stirred, ethereal diazomethane (120 ml), the benzene solution was added, drop by drop at −10——5°C over a period of 0.5 hr; the mixture was then stirred at 0°C for 0.5 hr and subsequently at room temperature overnight. The removal of the solvent gave a crude diazoketone ($\nu_{max}^{CHCl_3}$ 2150, 1746, 1643 cm^{-1}), which was then dissolved in methanol (100 ml). A mixture of the methanol solution and silver oxide (freshly prepared from 1 g of silver nitrate) was refluxed for 2 hr with stirring. The mixture was then treated with charcoal, filtered through celite, and washed methanol. The filtrates were concentrated under reduced pressure to give a reddish oil (3.1 g), which was chromatographed on silica gel (35 g). Elution with *n*-hexane–ether (2: 1) afforded a mixture (0.63 g) containing IIc, which was purified by preparative glc (5% SE-30 column at 230°C) to give 0.21 g (7%) of IIc as a colorless oil; δ 3.64 (6H, s), 6.20 (2H, m); *m/e* 224 (M^+), 164, 159, 151, 66.

Alkaline Hydrolyses of IIa, IIb, and IIc. (a) 2-*endo*-3-*exo*-dicarboxylic acid (IIe): A solution of IIb (255 mg) in methanol (3 ml) and 10% aqueous potassium hydroxide (3 ml) was heated at 50°C for 2 hr. Working-up usual gave 155 mg (70%) of IIe as plates; mp 158—159°C (from chloroform). Found: C, 61.19; H, 6.08%. Calcd for $C_{10}H_{12}O_4$: C, 61.21; H, 6.17%. (b) 2-*exo*-3-*endo*-dicarboxylic acid (IId): The hydrolysis of IIa (21 mg) as described in (a) afforded 10 mg (55%) of IId as plates; mp 115—117°C (from benzene-*n*-hexane). Found: C, 61.29; H, 6.21%. Calcd for $C_{10}H_{12}O_4$: C, 61.21; H, 6.17%. (c) *exo,cis*-dicarboxylic acid (IIf): The hydrolysis of IIc (43 mg) as described in (a) afforded 32 mg (85%) of IIf as plates; mp 144—146°C (from benzene-*n*-hexane). Found: C, 61.63; H, 6.12%. Calcd for $C_{10}H_{12}O_4$: C, 61.21; H, 6.17%.

Trimethyl trans, trans, cis-*3-Methoxycarbonylmethyl-1,2,4-cyclopentanetricarboxylate (Ib).* Into a solution of IIa (102 mg) in methanol (20 ml), ozone was passed at −70°C until the solution turned blue. The excess ozone was removed with a nitrogen stream, and then the solvent was evaporated under reduced pressure. To the residue, 98% formic acid (10 ml) and 35% hydrogen peroxide (1 ml) were added; the solution was subsequently stirred at 0°C for 3 hr, and then at room temperature overnight. After destroying the excess oxidizing reagents with sodium bisulfite, the mixture was concentrated under reduced pressure to leave a residue, which was digested in methanol and then filtered. The filtrates were concentrated under reduced pressure to leave an oily residue. Further treatment with diazomethane gave a crude methyl ester, which was purified by preparative tlc with *n*-hexane–ether (1: 1) as a mobile phase to give 104 mg (73%) of Ib as a colorless oil; δ 2.1—3.4 (8H, m), 3.62 (6H, s), 3.68 (6H, s): *m/e* 316 (M^+). Found: C, 53.90; H, 6.67%. Calcd for $C_{14}H_{20}O_8$: C, 53.16; H, 6.37%.

Trimethyl cis, trans, trans-*3-Methoxycarbonylmethyl-1,2,4-cyclopentanetricarboxylate (Ic).* The dimethyl ester, IIb (101 mg), was oxidized as in the case of IIa to give 91 mg (64%) of Ic as a colorless oil; δ 2.1—3.5 (8H, m), 3.58 (3H, s), 3.60 (6H, s), 3.64 (3H, s); *m/e* 316 (M^+). Found: C, 53.36; H, 6.76%. Calcd for $C_{14}H_{20}O_8$: C, 53.16; H, 6.37%.

Trimethyl trans, cis, trans-*3-Methoxycarbonylmethyl-1,2,4-cyclopentanetricarboxylate (Id).* The dimethyl ester, IIc (32 mg), was oxidized as in the case of IIa to give 45 mg (100%) of Id as a colorless oil; δ 2.0—3.5 (8H, m), 3.61 (3H, s), 3.63 (3H, s), 3.67 (3H, s); *m/e* 316 (M^+). Found: C, 52.64; H, 6.46%. Calcd for $C_{14}H_{20}O_8$: C, 53.16; H, 6.37%.

Base-catalysed Equilibration of Ia: The Formation of Trimethyl trans, trans, trans-*3-Methoxycarbonylmethyl-1,2,4-cyclopentanetricarboxylate (Ie).* A solution of Ia (540 mg) and sodium methoxide in methanol (prepared from 200 mg of sodium and 10 ml of methanol) was refluxed for 1 hr. After having

been acidified with diluted hydrochloric acid, the reaction a mixture was concentrated under reduced pressure and then extracted with ether. The ethereal extracts were washed with water and a saturated sodium chloride solution, and then dried over anhydrous magnesium sulfate. The subsequent removal of the solvent gave a brown residue, which was chromatographed on silica gel (10 g) and eluted with *n*-hexane–ether (2:1) to give 345 mg (64%) of pure Ie as a colorless oil. Further elution with *n*-hexane–ether (1:1) gave a mixture (70 mg) of Ie and Ic. The latter was purified by preparative glc to give 15 mg of pure Ic. Ie: δ 1.9—3.5 (8H, m), 3.60 (3H, s), 3.64 (3H, s), 3.66 (6H, s); *m/e* 316 (M^+). Found: C, 52.90; H, 6.39%. Calcd for $C_{14}H_{20}O_8$: C, 53.16; H, 6.37%.

The Formation of Iodolactone IIIa. To a solution of the dicarboxylic acid, IIb (98 mg), and sodium bicarbonate (168 mg) in water (30 ml), a solution of iodine (254 mg) and potassium iodide (0.5 g) in water (1.5 ml) was added; the mixture was then stirred at room temperature for 20 hr in the dark. After extraction with ether, the aqueous layer was acidified with 6N hydrochloric acid, treated with sodium bisulfite until it became a clear, colorless solution, and then extracted with ether. The ethereal extracts were succesively washed with water and a saturated sodium chloride solution, and then dried over anhydrous magnesium sulfate. The evaporation of the solvent afforded crude crystals, which were recrystallized from chloroform to give 124 mg (76%) of IIIa as plates; mp 138—141°C; $\nu_{max}^{CHCl_3}$ 1800, 1786, 1725 (shoulder), 1716 cm^{-1}; ν_{max}^{THF} 1805, 1739 cm^{-1}; δ^{CDCl_3} 1.7—2.7 (7H, m), 3.18 (1H, m, H-1), 3.91 (1H, broad d, 2.4, H-5-*endo*), 5.11 (1H, broad d, 5.1, H-6-*exo*), 9.3 (1H, broad s, disappeared on addition of D_2O). Found: C, 37.29; H, 3.43%. Calcd for $C_{10}H_{11}O_4I$: C, 37.29; H, 3.44%.

Conversion of IIIa into IIb. A mixture of IIIa (31 mg) and zinc powder (100 mg) in acetic acid (10 ml) was stirred at room temperature for 0.5 hr, and then filtered through celite. The filtrate was concentrated to leave a residue, which was subsequently dissolved in diluted hydrochloric acid and extracted with ether. The extracts were washed with water and dried over anhydrous magnesium sulfate. The evaporation of the solvent afforded an oil, which was crystallized from chloroform to give 8 mg of plates; mp 155—157°C. The IR spectrum (KBr) of this material was completely identical with that of IIb.

BULLETIN OF THE CHEMICAL SOCIETY OF JAPAN, VOL. 46, 605—610 (1973)

Optically Active Triptycenes. V.* Synthesis, Optical Resolution and Absolute Configuration of 2,7-Disubstituted Triptycenes.

Masaaki KURITANI Yoshiteru SAKATA, Fumio OGURA and Masazumi NAKAGAWA
Department of Chemistry, Faculty of Science, Osaka University, Toyonaka, Osaka 560

(Received June 29, 1972)

2,7-Dicarboxytriptycene retaining C_2-axis of symmetry was synthesized from 1,5-dichloroanthraquinone. Optical resolution of the triptycene afforded (+)- and (−)-enantiomers. The absolute configuration of (+)-2,7-dicarboxytriptycene was determined as 1R,6R by chemical correlation with (+)-2-methoxy-7-methoxycarbonyltriptycene which has 1R,6S configuration as confirmed by chemical transformation and X-ray structure analysis using the Bijvoet method. Starting from (+)-2,7-dicarboxytriptycene, a series of 2,7-disubstituted triptycenes having 1R,6R configuration has been prepared.

As pointed out in previous papers of this series,[1,2] optically active triptycenes can be regarded as most suitable compounds for the study of rotatory properties in view of their definite molecular geometry and the well-marked electronic transition of benzenoid chromophores.

It is desirable to synthesize simpler and well-defined dissymmetrical systems to facilitate theoretical approaches, since the X-ray analysis of (+)-2,5-dimethoxy-7-dimethylaminotriptycene hydrobromide (XVIII) by the Bijvoet method gave an antipodal absolute configuration[3] to that deduced by the rigorous analysis of CD spectra of this series of trisubstituted triptycenes.[4] If we take into account the effect of substitution on the direction of polarization of the transition of benzenoid chromophore,[5,6] C_2-symmetrical triptycenes having the same substituents at 2,7-positions seem to be favorable model compounds for the present purpose.

The present paper deals with the synthesis, optical resolution and determination of absolute configuration of 2,7-dicarboxytriptycene (VII) and the transformation of VII into various kinds of C_2-symmetrical 2,7-disubstituted triptycenes. The route of synthesis of VII is outlined in Scheme 1. 1,5-Dicarboxyanthraquinone (III) was prepared by acid hydrolysis of dicyano derivative (II) derived from 1,5-dichloroanthraquinone (I). III was reduced to 1,5-dicarboxyanthracene (IV).

* For preliminary report, see, J. Tanaka, F. Ogura, M. Kuritani, and M. Nakagawa, *Chimia*, **26**, 471 (1972); M. Kuritani, Y. Sakata, F. Ogura, and M. Nakagawa, *ibid.*, **26**, 470 (1972). For Part IV of this series, see Ref. 9.

1) A. Sonoda, F. Ogura, and M. Nakagawa, This Bulletin, **35**, 853 (1962).

2) F. Ogura, Y. Sakata, and M. Nakagawa, *ibid*, **45**, 3646 (1972).

3) N. Sakabe, K. Sakabe, K. Ozeki-Minakata, and J. Tanaka, presented at the 9th International Congress of Crystallography (1972); *Acta Crystallogr.*, **B 28**, 3441 (1972).

4) J. Tanaka, K. Ozeki-Minakata, F. Ogura, and M. Nakagawa, *Nature, Phys. Sci.*, **241**, 22 (1973).

5) J. R. Platt, *J. Chem. Phys.*, **19**, 263 (1951); J. Petruska, *ibid.*, **34**, 1111 (1961).

6) A. C. Albrecht and W. T. Simpson, *ibid.*, **23**, 1480 (1955); J. Tanaka, This Bulletin, **36**, 833 (1963).

Treatment of the sodium salt of IV with dimethyl sulfate afforded dimethyl ester (V). 2,7-Dimethoxycarbonyltriptycene (VI) was obtained by the addition of benzyne generated from diazotized anthranilic acid[7] with V.

Isomeric 5,7-dimethoxycarbonyltriptycene (VIII) having a plane of symmetry was prepared as a reference compound by a similar sequence of reaction starting from 1,8-dichloroanthraquinone[8] (Scheme 2).

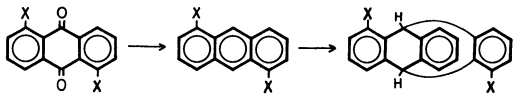

I, X=Cl
II, X=CN
III, X=COOH
IV, X=COOH
V, X=$COOCH_3$
VI, X=$COOCH_3$
VII, X=COOH

Scheme 1.

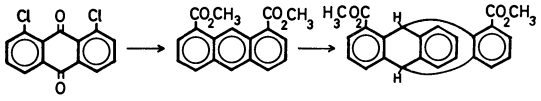

VIII

Scheme 2.

After several experiments, the optical resolution of VII obtained from VI was attained with equimolar cinchonidine and cinchonine. Optically pure (+)-dicarboxylic acid (VII) was obtained from the cinchonidine salt by decomposition with acetic acid. On the other hand, the cinchonine salt afforded (−)-VII.

(+)-Dicarboxylic acid (VII) was converted into acid sodium salt by the action of equimolar methanolic sodium methoxide (Scheme 3). The reaction of excess dimethyl sulfate with the acid salt afforded (+)-half ester (IX). (+)-Half ester was converted into (+)-2-amino-7-carboxytriptycene (X) by the Curtius reaction *via* acid chloride, acid azide and isocyanate. The diazonium salt derived from (+)-amino derivative (X) was hydrolyzed to yield (+)-2-hydroxy-7-carboxy triptycene (XII). The reaction of dimethyl sulfate with (+)-XII afforded (+)-2-methoxy-7-methoxycarbonyltriptycene (XIV). The methoxy-methyl ester (XIV) was found to be identical with the authentic (+)-2-methoxy-7-methoxycarbonyltriptycene (XVI) prepared by a different route and proved to have 1R, 6R absolute configuration by chemical correlation with (+)-2,5-dimethoxy-7-substituted-triptycenes (XVIII and XVII).[2,9] (+)-XIV and (+)-XVI showed identical IR, NMR, UV, and CD spectra, and the mixed melting point showed no depression. Consequently, the absolute configuration of (+)-2,7-dicarboxytriptycene (VII) was demonstrated to be 1R,6R. The UV and CD spectra of (+)-XIV and (+)-XVI are given in Fig. 1.

The reaction sequence of transformation of (+)- or (−)-VII into C_2-symmetrical 2,7-disubstituted triptycenes is outlined in Scheme 4. (+)-Diaminotriptycene (XIX) was prepared from (+)-VII by the Curtius reaction *via* acid chloride, acid azide and isocyanate. Methylation of (+)-XII with trimethyl phosphate afforded (+)-dimethylamino derivative (XX). (−)-Dinitrotriptycene (XXI) could be prepared by the pertrifluoroacetic acid oxidation of (−)-diamine (XIX). The reaction of nitrosobenzene with (−)-XIX in acetic acid gave bis-phenylazo derivative (XXII). (+)-Difluoro derivative (XXIII) was prepared by the Schiemann reaction of (+)-XIX. Hydrolysis of diazonium salt derived from (+)-XIX yielded (+)-dihydroxytriptycene (XXIV) which was converted into (+)-diacetate (XXV) and (+)-dimethoxy derivative (XXVI). Diacid amide prepared from (+)-dicarboxylic acid (VII) was dehydrated with thionyl chloride in dimethylformamide to give (+)-dicyanotriptycene (XXVII). (+)-Dimethoxycarbonyltriptycene (VI) obtained from (+)-VII was reduced with lithium aluminum hydride to yield (+)-bis(hydroxymethyl)-triptycene (XXVIII) which could be oxidized to (+)-diformyl derivative (XXIX) with chromium trioxide-pyridine complex. The reaction of thionyl chloride with (+)-glycol (XXVIII) afforded bis-chloromethyl derivative which gave (+)-dimethyltriptycene

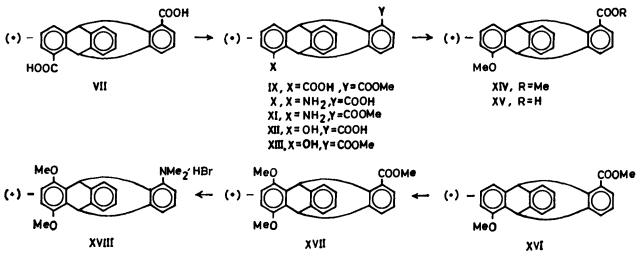

VII
IX, X=COOH, Y=COOMe
X, X=NH_2, Y=COOH
XI, X=NH_2, Y=COOMe
XII, X=OH, Y=COOH
XIII, X=OH, Y=COOMe
XIV, R=Me
XV, R=H
XVI
XVII
XVIII

Scheme 3.

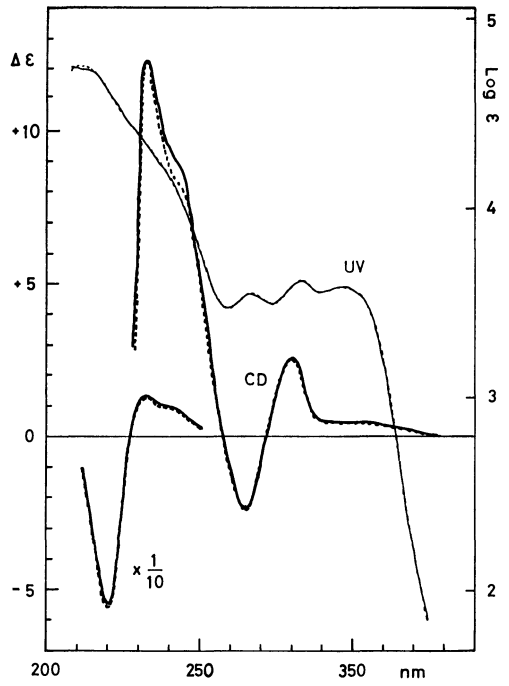

Fig. 1. UV and CD spectra of (+)-XIV (——) and (+)-XVI (------) in dioxane.

7) L. Friedman and F. M. Logullo, *J. Amer. Chem. Soc.*, **85**, 1549 (1963).

8) S. Akiyama, S. Misumi, and M. Nakagawa, This Bulletin, **35**, 1829 (1962).

9) Y. Sakata, F. Ogura, and M. Nakagawa, *ibid.*, **36**, 611 (1973).

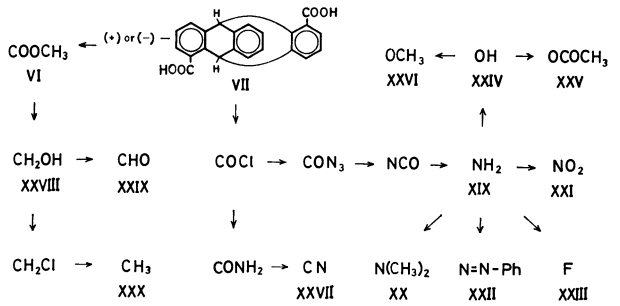

Scheme 4.

(XXX) on treatment with lithium aluminum hydride in boiling tetrahydrofuran.

In view of the method of preparation and the stable cage structure of triptycene skeleton, it is evident that (+)-series of 2,7-disubstituted triptycenes thus prepared has the same absolute configuration as (+)-VII (1R,6R) and (−)-series has an antipodal configuration.

Experimental

All the melting points are not corrected. Purified anhydrous solvents were used unless otherwise stated. Ligroin with bp 60—80°C was used. The IR spectra were measured with Hitachi EPI-2 and JASCO DS-301 spectrophotometers. The NMR spectra were obtained on a Varian A-60 spectrometer using TMS as an internal standard. Chemical shifts are recorded in τ unit. The UV spectra were measured with a Hitachi EPS-3T spectrophotometer. The optical rotations were measured with Rudolf 200S-80 and Yanagimoto ORD-185 spectropolarimeters at 15°C unless otherwise stated. The CD spectra were obtained on a Roussel-Jouan Dichrograph B, II-CD-185 and JASCO J-20 spectropolarimeter with CD attachments. The inflections and shoulders are indicated with an asterisk. The measurements of UV and CD spectra in an acidic medium were performed in methanol containing 10 vol% of 0.1M hydrochloric acid (abbreviated as MeOH–HCl). The experimental procedures referred to the optically active substances unless otherwise stated.

1,5-Dicyanoanthraquinone (II).[10] A mixture of I (50 g, 0.18 mol), cuprous cyanide (40 g, 0.45 mol) and phenylacetonitrile (460 ml) was refluxed for 70 min. The insoluble material was washed with benzene and digested with boiling 4M nitric acid to give II (44.5 g, 95.5%), mp >360°C, IR (Nujol mull): 2200 ($\nu_{C\equiv N}$) cm^{-1}.

1,5-Dicarboxyanthraquinone (III).[10] Water (200 ml) was added to a solution of II (86.0 g, 0.333 mol) in concentrated sulfuric acid (1000 ml) under ice-cooling. After being heated to 160°C for 1.5 hr, the mixture was poured onto water (1500 ml) to give dark brown crystals of III (80.5 g, 85.1%), mp >360°C, IR (Nujol mull): 1690 ($\nu_{C=O}$) cm^{-1}.

1,5-Dicarboxyanthracene (IV). A solution of III (27.16g, 0.0955 mol) in 15% aqueous ammonia (1200 ml) was treated with zinc dust (52 g) under stirring at 85—95°C. Stirring was continued for 5 hr at the same temperature under occasional addition of zinc dust and ammonia. The filtrate was treated with charcoal and acidified with 12M hydrochloric acid to afford IV as yellow crystals, mp >360°C, IR (Nujol mull): 1690 ($\nu_{C=O}$) cm^{-1}.

1,5-Dimethoxycarbonylanthracene (V). Thoroughly dried acid (IV, 99.8 g, 0.775 mol) was mixed with a methanolic sodium methoxide (from sodium, 23 g and methanol, 1400 ml) and the mixture was refluxed for 2 hr. Freshly distilled dimethyl sulfate (130 g, 1.031 mol) was added dropwise to the solution. After refluxing for 22 hr, the reaction mixture was concentrated under reduced pressure. Yellow crystals (107.1 g, 97.1%) obtained on addition of water (100 ml) to the concentrated mixture were recrystallized from methyl acetate and from benzene to yield pure V, yellow rods, mp 200—201°C, IR (KBr-disk): 1702 ($\nu_{C=O}$) cm^{-1}, NMR ($CDCl_3$): 0.28 (s, 2H, $C^{9,10}$-H), 1.58—2.58 (m, 6H, C^{2-4}-H and C^{6-8}-H), 5.91 (s, 6H, $-CO_2CH_3$), UV: $\lambda_{max}^{dioxane}$ (ε) 406 (8360), 385 (9820), 365 (7730), 348* (4060), 260.5 (12100), 224.4* (19400), 221.5 (19800) nm.

Found: C, 73.46; H, 4.80%. Calcd for $C_{18}H_{14}O_4$: C, 73.78; H, 4.80%.

When IV was treated with phosphorus pentachloride at 150—160°C and the product was mixed with methanol, V was obtained in a 35% yield along with 1,5-dimethoxycarbonyl-9-methoxyanthracene, greenish yellow rods, mp 135°C (8.5%).[11]

2,5-Dimethoxycarbonyltriptycene (VI) and the Adduct of Maleic Anhydride with 1,5-Dimethoxycarbonylanthracene (V). To a stirred solution of V (24.7 g, 0.084 mol) under gentle reflux was added dropwise a solution of anthranilic acid (12.4 g, 0.091 mol) in tetrahydrofuran (300 ml) over a period of 8 hr. Isoamyl nitrite (5.0 g, 0.038 mol) and anthranilic acid (5.0 g, 0.036 mol) were then added and the mixture was refluxed for further 2 hr. Brownish yellow solid (57.0 g) obtained by concentration of the reaction mixture was mixed with xylene (320 ml) and maleic anhydride (15.0 g) and refluxed for 1 hr. Water and dichloromethane (each 200 ml) were added to the reaction mixture and the organic layer was washed successively with 5% aqueous potassium hydroxide and water and dried. The brown residue obtained from the organic layer was dissolved in benzene and chromatographed on alumina. Crystalline solid (26.67 g, 85.8%) obtained from the benzene eluate was recrystallized from methanol and then sublimed *in vacuo* to afford pure VI, mp 209—209.5°C, IR (KBr-disk): 1717 ($\nu_{C=O}$) cm^{-1}, NMR (CCl_4): 2.21—3.11 (m, 12H, aromatic and bridgehead), 3.94 (s, 6H, $-CO_2CH_3$), UV: $\lambda_{max}^{dioxane}$ (ε) 298 (7270), 288* (6590), 222 (39200) nm.

Found: C, 77.61; H, 4.89%. Calcd for $C_{24}H_{18}O_4$: C, 77.82; H, 4.90%.

The adduct was isolated on acidification of the alkaline washings. The adduct, after recrystallization from acetone, was sublimed *in vacuo* to yield pure material, mp 258°C, IR (KBr-disk): 1862,1782($\nu_{C=O}$, anhydride), 1718($\nu_{C=O}$, $-CO_2CH_3$) cm^{-1}, UV: $\lambda_{max}^{dioxane}$ (ε) 222.5 (broad, 24000), 289 (4140) nm.

Found: C, 66.58; H, 4.08%. Calcd for $C_{22}H_{16}O_7$: C, 67.34; H, 4.11%.

2,7-Dicarboxytriptycene (VII). A solution of VI (18.09 g) in acetic acid (300 ml) containing 3M sulfuric acid (4 ml) was refluxed for 21 hr to precipitate fairly pure VII (16.6 g) in a quantitative yield. Recrystallization of VII from acetic acid yielded pure crystals containing 1 mol of acetic acid, mp 325°C (decomp.) (sublimed at 260°C).

Found: C, 71.71; H, 4.51%. Calcd for $C_{22}H_{14}O_4 \cdot C_2H_4O_2$: C, 71.63; H, 4.51%.

Crystals of VII free from acetic acid could be obtained on heating at 80°C for 6 hr *in vacuo*, mp 332—335°C (decomp.) (sublimed at 260°C), IR (KBr-disk): 1685 ($\nu_{C=O}$) cm^{-1}, NMR (DMSO-d_6): 2.23—3.18 (m, aromatic and bridgehead), UV: λ_{max}^{EtOH} (ε) 211 (44400), 287.5 (5600), 299 (6180) nn.

Found: C, 76.81; H, 4.21%. Calcd for $C_{22}H_{14}O_4$: 77.18; H, 4.12%.

10) *Cf.*, W. Waldmann and A. Oblath, *Ber.*, **71**, 366 (1938).

11) *Cf.*, S. Akiyama, F. Ogura, and M. Nakagawa, This Bulletin, **44**, 3443 (1971).

Optical Resolution of dl-*2,7-Dicarboxytriptycene (VII).* To a hot solution of *dl*-VII (10.058 g, 0.0294 mol) in ethanol (350 ml) was added cinchonidine (8.649 g, 0.0294 mol) and the mixture was refluxed for 1 hr. Colorless solid (mp 188—195°C) obtained by concentration of the mixture was refluxed in methyl acetate (2350 ml) for 6.5 hr.[12] The mixture, on standing overnight in a refrigerator, gave crystals containing 1 mol of methyl acetate, mp 187—194°C, 8.305 g, $[\alpha]_{350}$ −261.0° (*c* 0.528, methanol). The salt was recrystallized 4 times from methyl acetate to give optically pure material, mp 186—189°C, $[\alpha]_{350}$ −146.3° (*c* 0.436, methanol).

Found: C, 74.62; H, 5.96; N, 4.19%. Calcd for $C_{41}H_{36}N_2O_5 \cdot C_3H_6O_2$: C, 74.35; H, 5.96; N, 3.94%.

Decomposition of the optically pure salt with acetic acid (150 ml) yielded (+)-VII (1.053 g) as colorless crystals, mp 342.5—350.0°C (decomp.) (sublimed at 260°C), ORD: $[\alpha]_{600}$ +33.33°, $[\alpha]_D$ +33.3°, $[\alpha]_{500}$ +54.81°, $[\alpha]_{400}$ +140.7°, $[\alpha]_{350}$ +328.1° (*c* 0.540, methanol), CD: λ_{max}^{MeOH} ($\Delta\varepsilon$) 304 (+1.6), 282 (+5.3), 259 (−1.7), 244 (−4.0), 233 (+6.0), 219 (−49.7) nm.

Found: C, 76.81; H, 4.21%. Calcd for $C_{22}H_{14}O_4$: C, 77.18; H, 4.12%.

The initial mother liquor was mixed with acetic acid to afford (−)-VII with a low optical purity, mp 321—328°C (decomp.) (sublimed at 275°C), $[\alpha]_{350}$ −129.4° (*c* 0.4325, methanol).

Starting from *dl*-VII (11.338 g, 0.033 mol), ethanol (350 ml) and cinchonine (9.749 g, 0.033 mol), crude cinchonine salt was prepared by an essentially similar procedure with (+)-enantiomer. A suspension of the salt in methyl acetate (2000 ml) was refluxed for 3 hr, and then concentrated to 800 ml. Crystals deposited on standing the solution in a refrigerator overnight were recrystallized 4 times from the same solvent to yield optically pure salt, $[\alpha]_{500}^{12}$ +112.1° (*c* 0.5925, methanol). The crystals obtained on treatment of the optically pure salt with acetic acid were recrystallized from acetic acid to afford pure (−)-VII, 1.227 g, mp 342—350°C (decomp.) (sublimed at 260°C), ORD: $[\alpha]_{600}$ −33.2°, $[\alpha]_D$ −33.9°, $[\alpha]_{500}$ −56.8°, $[\alpha]_{400}$ −141.9°, $[\alpha]_{350}$ −332.9° (*c* 0.5425, methanol).

Found: C, 77.04; H, 4.15%. Calcd for $C_{22}H_{14}O_4$: C, 77.18; H, 4.12%.

5,7-Dimethoxycarbonyltriptycene (VIII). According to the method used for VI, a solution of anthranilic acid (1.74 g, 0.0127 mol) in tetrahydrofuran was added dropwise to a mixture of 1,8-dimethoxycarbonylanthracene[8] (3.6 g, 0.012 mol), isoamyl nitrite (1.62 g, 0.0138 mol) and dichloromethane (58 ml). Crude crystals obtained after treatment of the reaction mixture with maleic anhydride were recrystallized from methanol to yield fairly pure VIII (2.84 g, 62.7%) which was recrystallized from the same solvent to give pure VIII, mp 176—177°C, IR (KBr-disk): 1720 ($\nu_{C=O}$) cm^{-1}, NMR (CCl_4): 2.04—3.13 (m, 11H, aromatic and C^6-H), 4.62 (s, 1H, C^1-H), 5.99 (s, 6H, $-CO_2CH_3$). The signal of the bridgehead proton at a proximate position to both ester groups (C^1-H) was shifted to the aromatic region by anisotropy of the ester carbonyl groups. UV: $\lambda_{max}^{dioxane}$ (ε) 222 (39600), 286 (5520), 298 (6010) nm.

Found: C, 77.58; H, 4.74%. Calcd for $C_{24}H_{18}O_4$: C, 77.82; H, 4.90%.

(+)-2-Carboxy-7-methoxycarbonyltriptycene (IX). (+)-VII (2.009 g, 5.868 mmol) was mixed with equimolar sodium methoxide in methanol (39 ml) prepared from sodium (0.35 g) and methanol (100 ml). The mixture, after being refluxed for 1 hr, was evaporated under reduced pressure to give monosodium salt. Thoroughly dried acid salt suspended in benzene (70 ml) was mixed with freshly distilled dimethyl sulfate (0.740 g, 5.868 mmol) and the mixture was refluxed. After 4.5 hr, an additional amount of dimethyl sulfate (0.740 g) in benzene (20 ml) was added and refluxing was continued for further 16.5 hr. The reaction mixture was worked up to give a mixture of (+)-VII and (+)-IX as crystalline solid. The mixture was extracted with benzene. (+)-IX (1.604 g, 76.7%) was obtained from the benzene extract and recrystallized from benzene–ligroin, mp 252°C (sublimed at 200°C), [racemate, mp 246—249°C (decomp.) (sublimed at 200°C)], NMR ($CDCl_3$): −0.80 (broad, s, 1H, -COOH), 2.10—3.03 (m, 12H, aromatic and bridgehead), 6.00 (s, 3H, $-CO_2CH_3$), UV: λ_{max}^{MeOH} (ε) 298 (6600), 287 (5900), 240* (10500), 207 (62900) nm, CD: λ_{max}^{MeOH} ($\Delta\varepsilon$) 306 (+1.64), 283 (+4.90), 258 (−1.04), 242 (−2.08), 234 (+2.0) nm.

Found: C, 77.58; H, 4.52%. Calcd for $C_{23}H_{16}O_4$: C, 77.51; H, 4.53%.

The benzene insoluble residue was recovered (+)-VII which was also obtained by acidification of the aqueous layer of the initial extraction (total 26.9% recovery).

(+)-2-Amino-7-carboxytriptycene (X). (+)-IX (4.00 g, 11.2 mmol) in tetrahydrofuran (60 ml) was refluxed with excess thionyl chloride (10 ml) for 2 hr, and the volatile material was removed under reduced pressure to give crude acid chloride [IR (Nujol mull): 1760 ($\nu_{C=O}$, -COCl), 1720 ($\nu_{C=O}$, $-CO_2CH_3$) cm^{-1}]. A solution of sodium azide (0.900 g in 10 ml of water) was added to an ice-cooled and stirred solution of acid chloride in tetrahydrofuran (40 ml), After being stirred for 3 hr at the same temperature, the reaction mixture was worked up to give acid azide [IR (Nujol moll): 2140 ($\nu_{N=\overset{+}{N}=\overset{-}{N}}$), 1720 ($\nu_{C=O}$, $-CO_2CH_3$), 1685 ($\nu_{C=O}$, $-CON_3$) cm^{-1}]. The azide gave isocyanate [IR (Nujol mull): 2250 ($\nu_{N=C=O}$), 1720 ($\nu_{C=O}$, $-CO_2CH_3$) cm^{-1}] upon heating to 135°C for 6 hr. A mixture of isocyanate, ethanol (150 ml), potassium hydroxide (20 g) and water (50 ml) was refluxed for 25 hr to give crude amino carboxylic acid (X, 2.109 g, 60.1%). Recrystallization of crude X from methyl acetate–petroleum ether (bp 35—45°C) yielded pure X containing 1 mol of methyl acetate. The crystals melted once at 170°C and immediately crystallized again and re-melted with decomposition at 234—235°C [racemate, mp 167—169°C(decomp.)], IR (KBr-disk): 3380 (ν_{N-H}), 1690 ($\nu_{C=O}$, $-CO_2CH_3$) cm^{-1}.

Found: C, 74.30; H, 5.42; N, 3.62%. Calcd for $C_{21}H_{15}NO_2 \cdot C_3H_6O_2$: C, 74.40; H, 5.46; N, 3.59%.

The methyl acetate could be removed by heating the crystals *in vacuo*.

(+)-2-Amino-7-methoxycarbonyltriptycene (XI). A mixture of X (0.500 g), methanol (10 ml) and concentrated sulfuric acid (1 ml) was refluxed to yield (+)-XI in a quantitative yield, mp 161—162°C (from methyl acetate–petroleum ether and then from ligroin) [racemate, mp 194—195°C (decomp.)], UV: λ_{max}^{MeOH} (ε) 293.5 (5760), 269 (3380), 240* (19000), 217 (36700), 207.5 (45200); $\lambda_{max}^{MeOH\text{-}HCl}$ (ε) 293 (3900), 276 (2980), 270* (2140), 240* (12600), 208.5 (52200) nm, CD: λ_{max}^{MeOH} ($\Delta\varepsilon$) 285 (+5.10), 265 (−3.23), 238 (+3.11); $\lambda_{max}^{MeOH\text{-}HCl}$ ($\Delta\varepsilon$) 302 (+0.19), 290 (−0.12), 273 (+3.48), 269 (+3.33), 252 (+0.75), 238 (−5.60), 226 (+2.90) nm.

Found: C, 80.89; H, 5.20; N, 4.23%. Calcd for $C_{22}H_{17}O_2N$: C, 80.71; H, 5.23; N, 4.28%.

(+)-2-Hydroxy-7-carboxytriptycene (XII). (+)-XI (1.736 g) in acetic acid (20.5 ml) was added to an ice-cooled and stirred solution of sodium nitrite (0.421 g) in concentrated sulfuric acid (3 ml). After 2 hr, the resulting solution of diazonium

12) This procedure is essential for effective resolution. Initially formed salt seems to rearrange in boiling methyl acetate to a stable form which has larger difference in solubility between the diastereomers.

salt was added dropwise to boiling 3M sulfuric acid (300 ml), yielding crude (+)-XII (1.135 g, 65.2%). Recrystallization of the crude material from methyl acetate–petroleum ether and from methyl acetate–benzene afforded pure (+)-XII, mp 269—271°C (decomp.) [racemate, mp 263—264°C (decomp.)].

Found: C, 78.69; H, 4.45%. Calcd for $C_{21}H_{14}O_3$: C, 80.24; H, 4.49%.

(+)-2-Hydroxy-7-methoxycarbonyltriptycene (XIII). Treatment of (+)-XII with methanol and sulfuric acid afforded (+)-XIII, mp 217—225°C (from ligroin) [racemate, mp 231—234°C], IR (KBr-disk): 3400 (ν_{O-H}), 1697 ($\nu_{C=O}$) cm^{-1}.

Found: C, 80.29; H, 5.02%. Calcd for $C_{22}H_{16}O_3$: C, 80.47; H, 4.91%.

(+)-2-Methoxy-7-methoxycarbonyltriptycene (XIV). A mixture of (+)-XIII (0.5188 g), dimethyl sulfate (0.66 g), anhydrous potassium carbonate (3 g) and acetone (70 ml) was refluxed for 8 hr under stirring to give crude (+)-XIII in a quantitative yield, mp 240—241°C (from methanol) [racemate, 219—222°C], IR (KBr-disk): 2850 (ν_{C-H}, $-OCH_3$), 1715 ($\nu_{C=O}$) cm^{-1}, NMR ($CDCl_3$): 2.33—3.17 (m, 11H, aromatic and C^6-H), 4.07 (s, 1H, C^1-H), 6.05 (s, 3H, $-CO_2CH_3$) 6.18 (s, 3H, $-OCH_3$), UV: $\lambda_{max}^{dioxane}$ (ε) 209.5 (53300), 215 (51100), 267 (3550), 283.5 (4130), 296 (3880); λ_{max}^{MeOH} (ε) 208.5 (67700), 215* (54300), 240* (13900), 266.5 (3430), 283 (4030), 296 (3750) nm, CD: $\lambda_{max}^{dioxane}$ ($\Delta\varepsilon$) 220 (−55.8), 232 (+12.7), 242* (+9.23), 265 (−2.31), 280 (+2.65), 325—290 (very broad peak, +0.41); λ_{max}^{MeOH} ($\Delta\varepsilon$) 232 (+12.6), 262 (−2.05), 276 (+2.51), 320—290 (very broad peak, +0.40) nm.

Found: C, 80.44; H, 5.24%. Calcd for $C_{23}H_{18}O_3$: C, 80.68; H, 5.30%.

The melting point showed no depression on admixture with an authentic specimen of (+)-XVI (mp 240—241°C).[9]

(+)-2-Methoxy-7-carboxytriptycene (XV). A mixture of (+)-XIV (0.200 g), acetic acid (20 ml) and 3M sulfuric acid (10 ml) was refluxed for 19 hr to yield (+)-XV, mp 267°C (decomp.) (from aqueous acetic acid) [racemate, mp 299—300°C (decomp.)], NMR (DMSO-d_6): 2.20—3.18 (m, 11H, aromatic and C^6-H), 3.93 (s, 1H, C^1-H), 6.13 (s, 3H, $-OCH_3$).

Found: C, 80.28; H, 4.91%. Calcd for $C_{22}H_{16}O_3$: C, 80.47; H, 4.91%.

(+)-2,7-Diaminotriptycene (XIX). (+)-Dicarboxytriptycene (VII, 432.5 mg) in tetrahydrofuran was refluxed for 2 hr with excess thionyl chloride, crude acid chloride (450.8 mg) being obtained by evaporating volatile material under reduced pressure. To an ice-cooled solution of the acid chloride in tetrahydrofuran was added a solution of sodium azide (155 mg) in water (2 ml). After 3 hr, the reaction mixture was poured onto water to give acid azide [386.8 mg, IR (Nujol mull): 2120 ($\nu_{N=\overset{+}{N}=\overset{-}{N}}$), 1685 ($\nu_{C=O}$) cm^{-1}]. A solution of thoroughly dried azide in benzene (100 ml) was refluxed for 4 hr. Isocyanate [388.2 mg, IR (Nujol mull): 2210 ($\nu_{C=O}$) cm^{-1}] obtained by evaporating the solvent *in vacuo* was mixed with water (10 ml), 99% ethanol (50 ml) and potassium hydroxide (4.0 g) and the mixture was refluxed for 6 hr. The reaction mixture was poured onto ice-water to yield crude (+)-XIX (319.6 mg) which was recrystallized from benzene and dried *in vacuo* at 110°C for 5 hr to give pure (+)-XIX, mp 266—267°C (sublimed at *ca.* 230°C) [racemate, mp 279—283°C (decomp.), sublimed at *ca.* 210°C], NMR ($CDCl_3$): 2.55—3.72 (m, 10H, aromatic), 4.62 (s, 2H, bridgehead), 6.45 (broad s, 4H, $-NH_2$), UV: λ_{max}^{MeOH} (ε) 194 (56900), 219.5 (56500), 240* (20900), 269 (4040), 275 (3320), 295 (3660); $\lambda_{max}^{MeOH\text{-}HCl}$ (ε) 212.5 (64400), 262* (1330), 269 (2230), 276.5 (2910) nm, CD: λ_{max}^{EtOH} ($\Delta\varepsilon$) 214 (−61.2), 227.5 (+55.3), 258* (−11.7), 268 (−17.1), 283* (+1.53), 297 (+6.37); $\lambda_{max}^{EtOH\text{-}HCl}$ ($\Delta\varepsilon$) 250.5 (+0.95), 262 (−2.22), 274 (−0.41), 277.5 (+0.31) nm.

Found: C, 84.45; H, 5.69; N, 9.90%. Calcd for $C_{20}H_{16}N_2$: C, 84.48; H, 5.67; N, 9.85%.

(+)-2,7-Bis(dimethylamino)triptycene (XX). After a mixture of (+)-XIX (197 mg) and trimethyl phosphate (200 mg) had been refluxed for 3 hr, a solution of sodium hydroxide (1.7 g) in water (2 ml) was added and the mixture was refluxed for 30 min. Water (30 ml) was added to the reaction mixture. Crude (+)-XX (0.226 g) deposited after being left to stand overnight was recrystallized from 99% ethanol and then sublimed *in vacuo* to give pure (+)-XX, mp 215—215.5°C (sublimed at 170°C) [racemate, mp 209—210°C, (sublimed at 160°C)], NMR ($CDCl_3$): 2.45—3.33 (m, 10H, aromatic), 4.07 (s, 2H, bridgehead), 7.22 (s, 12H, $N-CH_3$), UV: λ_{max}^{MeOH} (ε) 225 (42000), 240* (25200), 260* (15400), 275* (5000), 295* (1500) nm, CD: λ_{max}^{MeOH} ($\Delta\varepsilon$) 220 (−37.72), 236 (+24.33), 271 (−7.06), 292 (+1.11) nm.

Found: C, 84.86; H, 6.96; N, 8.26%. Calcd for $C_{24}H_{24}N_2$: C, 84.66; H, 7.11; N, 8.23%.

(−)-2,7-Dinitrotriptycene (XXI). To an ice-cooled and stirred mixture of dichloromethane (4.5 ml) and 90% hydrogen peroxide (0.24 ml) was added trifluoroacetic anhydride (1.5 ml). After 5 min, a solution of (−)-diamine (XIX, 297 mg) in the same solvent (10 ml) was added and the mixture was refluxed for 1 hr. After washing (aqueous sodium carbonate and water) and drying, the solvent was removed to yield yellow solid which was recrystallized from benzene–ligroin to afford pure (−)-XXI, mp 320—326°C (sublimed at 160°C) [racemate, mp 325—331°C (decomp.), (sublimed at 200°C)], UV: λ_{max}^{MeOH} (ε) 207* (61500), 254 (11200), 315 (4350) nm, CD: λ_{max}^{MeOH} ($\Delta\varepsilon$) 242 (+12.12), 282 (−2.15), 306 (+1.21), 328 (−0.91) nm.

Found: C, 69.31; H, 4.22; N, 7.08%. Calcd for $C_{20}H_{12}O_4N_2$: C, 69.76; H, 3.51; N, 8.14%.

(−)-2,7-Bis(phenylazo)triptycene (XXII). A mixture of (−)-diamine (XIX, 489.1 mg), nitrosobenzene (400 mg) and acetic acid (6 ml) was heated in a sealed tube at 200°C for 2 hr. The solvent was removed *in vacuo* and the residue dissolved in benzene was passed through a column of alumina (50 g). Crude crystals (600 mg) obtained from benzene eluate was recrystallized from benzene–ethanol to give pure (−)-XXII, mp 216—217°C [racemate, mp 272—273.1°C], NMR (CS_2): 1.82—3.02 (m, 20H, aromatic), 3.30 (s, 2H, bridgehead), UV: λ_{max}^{MeOH} (ε) 212 (53300), 232 (28000), 240* (23800), 242* (19000), 253* (12600), 258* (10800), 325 (33500), 440 (1600) nm, CD: λ_{max}^{MeOH} ($\Delta\varepsilon$) 216 (+11.3), 236 (+15.1), 248 (−6.40), 272 (−1.8), 320 (+9.56), 355 (−10.82), 438—432 (−1.38) nm.

Found: C, 82.69; H, 4.84; N, 11.88%. Calcd for $C_{32}H_{22}N_4$: C, 83.09; H, 4.79; N, 12.11%.

(+)-2,7-Difluorotriptycene (XXIII). A solution of (+)-XIX (500 mg) in hot concentrated hydrochloric acid (6 ml) was chilled to −15—−20°C and a solution of sodium nitrite (270 mg) in water (2 ml) was added under stirring. Sodium fluoroborate (500 mg) in a small amount of water was added to the mixture. After being stirred for 1 hr at the same temperature, diazonium fluoroborate deposited was filtered and washed successively with cold water, methanol and ether. Diazonium salt (550 mg) thus obtained was gradually heated to 150°C and maintained at the same temperature for 3 hr, resulting in a purple solid. The product dissolved in benzene was treated with active charcoal and recrystallized from aqueous ethanol to afford pure (+)-XXIII, mp 224—226°C [racemate, mp 236—139°C (decomp.)], NMR ($CDCl_3$): 2.30—3.20 (m, 10H, aromatic), 3.99 (s, 2H, bridgehead), UV: λ_{max}^{MeOH} (ε) 212.5 (60300), 235* (7920), 255* (2140), 260*

(2070), 268 (1700), 276 (1320) nm, CD: λ_{max}^{MeOH} ($\Delta\varepsilon$) 225 (+1.18), 255 (−2.40), 268 (+1.48), 278 (+2.83) nm.

Found: C, 82.68; H, 4.19%. Calcd for $C_{20}H_{12}F_2$: C, 82.74; H, 4.17%.

(+)-2,7-Dihydroxytriptycene (XXIV). To a solution of (+)-XIX (3.90 g) in acetic acid (80 ml) was added a solution of sodium nitrite (1.485 g) in water (4 ml) at 14—17°C. After being stirred for 3 hr at the same temperature, the mixture was added to boiling 3M sulfuric acid (240 ml) over a 30 min-period and boiling was continued for 1 hr. Brown solid (2.60 g) isolated from the reaction mixture was converted into acetate (XXV) and the purified (+)-XXV was reduced by lithium aluminum hydride to give pure (+)-XXIV, mp 280°C (from ethanol), UV: λ_{max}^{MeOH} (ε) 216.5 (51,800), 234 (12900), 240* (10000), 262* (3150), 267.5 (4070), 276.5 (3780), 286 (3510); $\lambda_{max}^{MeOH\text{-}NaOH}$ (ε) 217 (49,400), 245* (22500), 270 (4590), 277.5 (4530), 330 (5590) nm, CD: λ_{max}^{MeOH} ($\Delta\varepsilon$) 219 (+31.33), 232 (−5.53), 250 (−6.70), 264* (−4.75), 280 (+4.29), 285 (+4.58); $\lambda_{max}^{MeOH\text{-}NaOH}$ ($\Delta\varepsilon$) 215 (−38.8), 232 (+36.5), 268 (−11.6), 300 (+3.22), 303 (+3.24) nm.

Found: C, 83.59; H, 4.97%. Calcd for $C_{20}H_{14}O_2$: C, 83.90; H, 4.93%.

(+)-2,7-Diacetoxytriptycene (XXV). Crude crystals of (+)-XXV (1.05 g) obtained by heating a mixture of (+)-XXIV (800 mg), acetic anhydride (50 ml) and sodium acetate (2.0 g) at 100°C for 20 hr were dissolved in benzene and passed through a column of silica gel (30 g). Concentration of the filtrate afforded (+)-XXV, mp 209.8—213.7°C (from benzene–ligroin and from ethanol), NMR ($CDCl_3$): 2.45—3.23 (m, 10H, aromatic), 4.42 (s, 2H, bridgehead), 7.50 (s, 6H, CH_3CO_2-), UV: λ_{max}^{MeOH} (ε) 214 (59800), 240* (4200), 255* (1290), 262 (1220), 269 (1710), 276.5 (1990) nm, CD: λ_{max}^{MeOH} ($\Delta\varepsilon$) 235 (−0.38), 257 (−1.69), 269 (+0.75), 276 (+1.38) nm.

Found: C, 77.62; H, 4.90%. Calcd for $C_{24}H_{18}O_4$: C, 77.82; H, 4.90%.

(+)-2,7-Dimethoxytriptycene (XXVI). A mixture of (+)-2,7-dihydroxytriptycene (XXIV, 200 mg), dimethyl sulfate (300 mg) and acetone (50 ml) was refluxed for 19 hr in the presence of anhydrous potassium carbonate (3.0 g) to afford crude crystals of (+)-XXVI (200 mg). The crude material was recrystallized from ethanol–benzene to yield pure (+)-XXVI, mp 277.8°C, NMR ($CDCl_3$): 2.20—3.38 (m, 10H, aromatic), 4.00 (s, 2H, bridgehead), 6.08 (s, 6H, CH_3O-), UV: $\lambda_{max}^{dioxane}$ (ε) 218.5 (46800), 240* (9300), 263* (3380), 268 (4110), 276.5 (3560), 285 (3100) nm, CD: $\lambda_{max}^{dioxane}$ ($\Delta\varepsilon$) 225 (+44.16), 250 (−12.39), 271* (+2.09), 278 (+3.09), 284 (+2.93) nm.

Found: C, 84.33; H, 5.80%. Calcd for $C_{22}H_{18}O_2$: C, 84.05; H, 5.77%.

(+)-2,7-Dicyanotriptycene (XXVII). Thionyl chloride (1.27 g) was added to a solution of (+)-VII (300 mg) in tetrahydrofuran (30 ml) and the mixture was refluxed for 2 hr. Crude acid chloride (326.2 mg) was obtained by removing volatile material under reduced pressure. The reaction of 28% aqueous ammonia (7.5 ml) with acid chloride (288.9 mg) in tetrahydrofuran (15 ml) at room temperature afforded acid amide [292.7 mg, IR (Nujol mull): 3100 (ν_{N-H}), 1660 ($\nu_{C=O}$) cm^{-1}]. A mixture of acid amide (282.8 mg), dimethylformamide (40 ml) and thionyl chloride (4 ml) was heated to 70—80°C for 8 hr. The reaction mixture was filtered to remove sulfur deposited and the filtrate was passed through a short column of alumina (10 g). Colorless solid (108 mg) obtained from the eluate was recrystallized from methanol to yield pure (+)-XXVII, mp 261—262°C (sublimed at 210°C) [racemate, mp 247—250.5°C], IR (KBr-disk): 2230 ($\nu_{C\equiv N}$) cm^{-1}, NMR ($CDCl_3$): 2.18—2.92 (m, 10H, aromatic), 4.03 (s, 2H, bridgehead), UV: λ_{max}^{EtOH} (ε) 212* (37900), 222* (38600), 235* (20500), 280* (4750), 288.5 (6330), 298 (8090) nm, CD: λ_{max}^{EtOH} ($\Delta\varepsilon$) 220 (−28.6), 231 (+10.8), 240 (−2.86), 251 (+1.91), 280 (+6.34), 303 (+1.04) nm.

Found: C, 86.45; H, 4.12; N, 9.18%. Calcd for $C_{22}H_{12}N_2$: C, 86.82; H, 3.97; N, 9.21%.

(+)-2,7-Dimethoxycarbonyltriptycene (VI). (+)-Dicarboxylic acid (VII) was treated with methanol containing concentrated sulfuric acid to give (+)-VI, mp 170—171°C (from methanol), CD: $\lambda_{max}^{dioxane}$ ($\Delta\varepsilon$) 222 (−37.6), 235 (+6.71), 244 (−2.58), 257 (−0.97), 282 (+5.90), 305 (+1.83) nm.

Found: C, 77.56; H, 5.02%. Calcd for $C_{24}H_{18}O_4$: C, 77.82; H, 4.90%.

(+)-2,7-Bis(hydroxymethyl)triptycene (XXVIII). Reduction of (+)-VI with lithium aluminum hydride afforded (+)-XXVIII in a quantitative yield, mp 220—221°C (from carbon tetrachloride followed by vacuum sublimation) (sublimed at 190°C) [racemate, 203.5—205°C (sublimed at 170°C)], IR (KBr-disk): 3390 (ν_{O-H}) cm^{-1}, NMR ($CDCl_3$): 2.50—3.01 (m, 10H, aromatic), 4.01 (s, 2H, bridgehead), 5.17 (s, 4H, methylene), 8.03 (s, 2H, OH), UV: λ_{max}^{MeOH} (ε) 215 (60700), 240* (4800), 264* (1570), 272.5 (2640), 276.5* (2820), 280.5 (3720) nm, CD: λ_{max}^{MeOH} ($\Delta\varepsilon$) 238 (−1.54), 250(+0.62), 258 (−0.89), 270 (+2.16), 277 (+1.33), 282 (−0.89) nm.

Found: C, 84.02; H, 5.74%. Calcd for $C_{22}H_{18}O_2$: C, 84.05; H, 5.77%.

(+)-2,7-Diformyltriptycene (XXIX). A solution of (+)-XXVIII (180.4 mg) in pyridine (2 ml) was added to an ice-cooled and stirred suspension of chromium trioxide-pyridine complex (from the trioxide, 150 mg and pyridine, 2 ml) and the mixture was kept in a refrigerator overnight. Crude crystals (123.9 mg) were sublimed twice under reduced pressure to give pure (+)-XXIX, mp 244—247°C (decomp.) (sublimed at 175°C) [racemate, mp 249—253°C (decomp.) (sublimed at 195°C)], IR (KBr-disk): 1690 ($\nu_{C=O}$) cm^{-1}, NMR ($CDCl_3$): −0.18 (s, 2H, CHO), 2.30—3.05 (m, 12H, aromatic and bridgehead), UV: λ_{max}^{MeOH} (ε) 209 (54800), 215* (47300), 238* (18700), 251 (20500), 260* (16000), 278 (2290), 305* (4810), 318 (5470) nm, CD: λ_{max}^{MeOH} ($\Delta\varepsilon$) 228 (−23.3), 246 (+2.8), 260 (−4.7), 276 (+2.6), 296 (+3.2), 324 (+1.5) nm.

Found: C, 84.92; H, 4.57%. Calcd for $C_{22}H_{14}O_2$: C, 85.14; H, 4.55%.

(+)-2,7-Dimethyltriptycene (XXX). A solution of (+)-XVIII (239 mg) in benzene (25 ml) was refluxed with thionyl chloride (5 ml). Crude bis-chloromethyl derivative dissolved in tetrahydrofuran (15 ml) was added to a mixture of lithium aluminum hydride (772 mg) and the same solvent (75 ml). After being refluxed for 16 hr, a benzene solution of the product was passed through a column of alumina (20 g). The crystals obtained from the filtrate were recrystallized from aqueous methanol to give pure (+)-XXX, mp 133—137°C (decomp.) [racemate, mp 154.5—157°C (sublimed at 130°C)], NMR ($CDCl_3$): 2.53—3.18 (m, 10H, aromatic), 4.36 (s, 2H, bridgehead), 7.50 (s, 6H, CH_3), UV: λ_{max}^{MeOH} (ε) 198 (63900), 214* (70500), 217.5 (72300), 240* (5980), 257* (1400), 263 (1370), 270.5 (1910), 274.5* (1460), 278.5 (2340) nm, CD: λ_{max}^{MeOH} ($\Delta\varepsilon$) 259 (−3.5), 270.5 (+1.3), 278 (+1.8) nm.

Found: C, 93.06; H, 6.51%. Calcd for $C_{22}H_{18}$: C, 93.57; H, 6.43%.

Optically Active Triptycenes. IV.[1] Synthesis of Optically Active 2- or 5-Substituted 7-Carboxytriptycenes

Yoshiteru SAKATA, Fumio OGURA, and Masazumi NAKAGAWA

Department of Chemistry, Faculty of Science, Osaka University, Toyonaka, Osaka 560

(Received August 11, 1972)

Starting from anthraquinone-1-carboxylic acid (I), 2-methoxy- and 5-methoxy-7-carboxytriptycenes (VIIa and VIIb) have been synthesized. Optical resolution of the triptycenecarboxylic acids with brucine afforded (+)-VIIa and (+)-VIIb. The absolute configuration of (+)-VIIa was determined to be 1R,6R by the chemical correlation with (+)-2,5-dimethoxy-7-methoxycarbonyltriptycene. From a comparison of the CD spectrum of (+)-5-methoxy-7-carboxytriptycene (VIIb) with that of (+)-2-acetoxy-5-methoxy-7-methoxycarbonyltriptycene (XIIIb), 1R,6R absolute configuration was assigned to (+)-VIIb. (+)-2-Hydroxy-5-phenylazo-7-carboxytriptycene (XIIa) was derived from (+)-VIIa. (+)-2-Chloro- and (+)-5-chloro-7-carboxytriptycenes (XVIIIa and XVIIIb) have been prepared from 5-chloro- and 8-chloro-1-carboxyanthraquinones (XIVa and XIVb). The absolute configuration of (+)-XVIIIa was determined to be 1R,6R by the chemical correlation with (−)-VIIa *via* (+)-2-chloro-5-methoxytriptycene (XIX).

The synthesis and optical resolution of 2,5,7-trisubstituted triptycenes have been reported in previous papers of this series,[2-4] and studies on C_2-symmetrical 2,7-disubstituted derivatives will be reported in the following paper.[5]

The present paper deals with the synthesis, optical resolution of 2- and 5-substituted 7-carboxytriptycenes and the determination of their absolute configuration by chemical correlation.

Anthraquinone-1-carboxylic acid (I) obtained by chromium trioxide oxidation of benzanthrone[6] was nitrated by the reported method[7] to yield 1-carboxy-5-nitro-anthraquinone (IIa) and 1-carboxy-8-nitro-anthraquinone (IIb). Treatment of the nitro compounds (IIa and IIb) with potassium hydroxide in methanol afforded methyl ether derivative (IIIa or IIIb). Carboxymethoxyanthracene (IVa or IVb) obtained by reduction of IIIa or IIIb with zinc dust and aqueous ammonia was converted into methyl ester (Va or Vb) by the usual method. Reaction of benzyne generated by the decomposition of benzenediazonium carboxylate[8] with Va or Vb gave 2-methoxy-7-methoxycarbonyl or 5-methoxy-7-methoxycarbonyltriptycene (VI or VIb). 2-Methoxy-7-carboxytriptycene (VIIa) obtained by the hydrolysis of VIa was treated with 0.5 equivalent of brucine dihydrate in ethanol. Recrystallization of the brucine salt from ethanol yielded (+)-VIIa with positive rotation in the visible region. The triptycene derivatives derived from (+)-VIIa will be referred to the (+)-series. The brucine salt of VIIb was recrystallized from acetone to afford (+)-VIIb. (+)-Hydroxycarboxylic acid (VIIIa) obtained on treatment of (+)-VIIa with a mixture of hydrobromic acid and hydriodic acids in acetic acid was converted into methyl ester (+)-IXa. Acetylation of (+)-IXa gave (+)-acetoxy methyl ester (+)-XIa, and coupling of benzenediazonium salt with (+)-VIIIa afforded (+)-azocarboxylic acid (+)-XIIa.

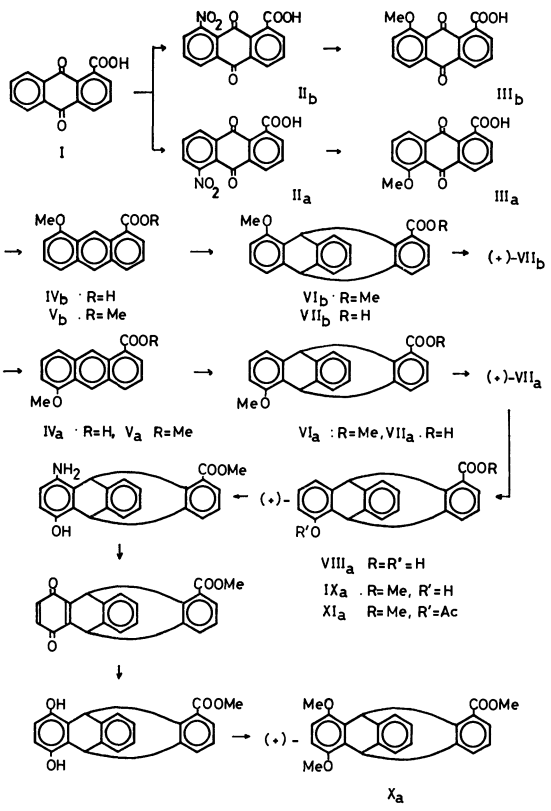

Scheme 1.

Coupling of diazotized sulfanilic acid with (+)-IXa followed by reduction afforded *p*-aminophenol derivative which was oxidized to yield *p*-benzoquinone derivative. Hydroquinone derivative obtained from the quinone was converted into dimethyl ether(+)-Xa. The dimethyl ether derivative (+)-Xa thus prepared was found to be identical with (+)-2,5-dimethoxy-7-meth-

1) For Part III of this series, see Ref. 4.
2) A. Sonoda, F. Ogura, and M. Nakagawa, This Bulletin, **35**, 853 (1962).
3) F. Ogura, Y. Sakata, and M. Nakagawa, *ibid.*, **45**, 3646 (1972).
4) F. Ogura and M. Nakagawa, This Bulletin, **46**, 651 (1973).
5) M. Kuritani, Y. Sakata, F. Ogura, and M. Nakagawa, *ibid.*, **46**, 605 (1973).
6) E. B. Barnett, J. W. Cook, and H. H. Grainger, *Ber.*, **57**, 1775 (1924).
7) F. Ullmann and W. van der Schalk, *Ann. Chem.*, **388**, 199 (1912).
8) L. Friedman and F. M. Logullo, *J. Amer. Chem. Soc.*, **85**, 1549 (1963).

oxycarbonyltriptycene (+)-X, derived from 1-methoxycarbonylanthracene and *p*-benzoquinone.[3] Since the absolute configuration of (+)-2,5-dimethoxy-7-dimethylaminotriptycene hydrobromide prepared from (+)-2,5-dimethoxy-7-methoxycarbonyltriptycene (+)-X has been proved to be 1R,6S using the Bijvoet method,[9] the absolute configuration of (+)-Xa now prepared can be determined as 1R,6S. Consequently, the 2,7-disubstituted triptycenes of (+)-series derived from (+)-VIIa should have the same 1R,6R absolute configuration.

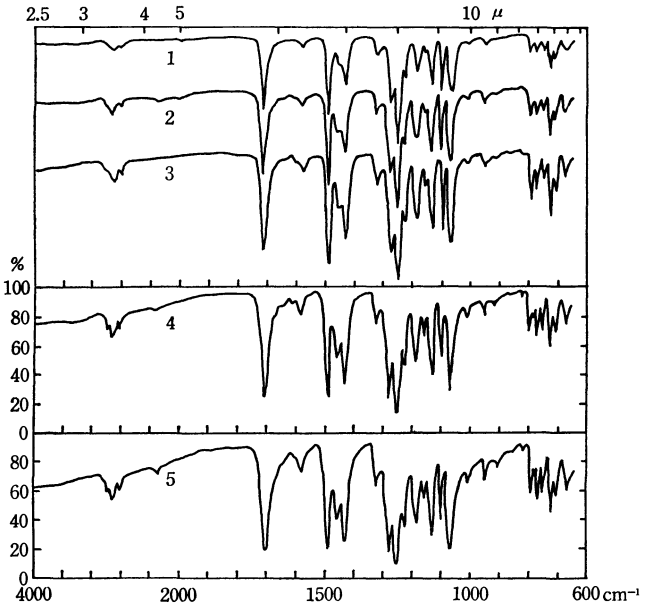

Fig. 1. IR spectra (KBr-disk) of (+)- and (—)-2,5-dimethoxy-7-methoxycarbonyltriptycene prepared by different process.
1: *dl*-Xa, 2: *dl*-Xb, 3:*dl*-X, 4: (+)-X, 5: (+)-Xa

dl-2-Methoxy-7-methoxycarbonyltriptycene (VIa) and *dl*-5-methoxy-7-methoxycarbonyltriptycene (VIb) could be transformed into *dl*-2,5-dimethoxy-7-methoxycarbonyltriptycene (*dl*-Xa and *dl*-Xb) according to the same reaction sequence used in the preparation of (+)-Xa from (+)-VIa. *dl*-2,5-Dimethoxy-7-methoxycarbonyltriptycene (*dl*-Xa, *dl*-Xb, and *dl*-X[3]) showed identical melting point (mp 227.0—228.5°C) and the mixed melting points showed no depression. As illustrated in Fig. 1, their IR spectra were found to be superimposable.

(+)-VIIb showed a negative Cotton effect in the longest wavelength region of the CD spectrum in contrast with the positive Cotton effect of (+)-VIIa in the same wavelength region. However, (+)-2-methoxy-5-acetoxy- and (+)-2-acetoxy-5-methoxy-7-methoxycarbonyltriptycenes (XIIIa and XIIIb) showed UV and CD spectra closely related with those of (+)-VIa and (+)-VIIb, respectively (Figs. 2 and 3). Since the absolute configuration of (+)-XIII has been established to be 1R,6S in relation to (+)-X,[4] 1R,6R absolute configuration may reasonably be assigned to

9) N. Sakabe, K. Sakabe, K. Ozeki-Minakata, and J. Tanaka, presented at the 9th International Congress of Crystallography (1972) and *Acta Crystallogr.*, **B 82**, 3441 (1972).

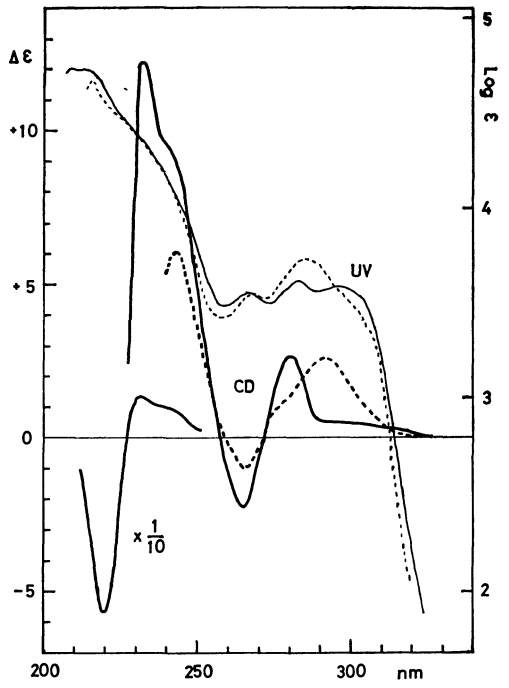

Fig. 2. UV and CD spectra of (+)-VIa (——) and (+)-XIIIa (····) in dioxane

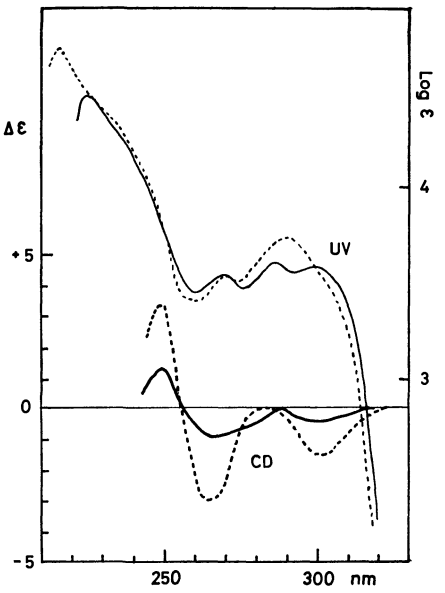

Fig. 3. UV and CD spectra of (+)-VIIb (——) and (+)-XIIIa (····) in dioxane

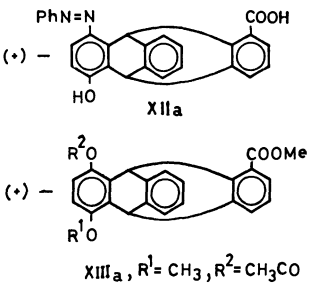

XIIIa, $R^1 = CH_3$, $R^2 = CH_3CO$
XIIIb, $R^1 = CH_3CO$, $R^2 = CH_3$

Formulae 1.

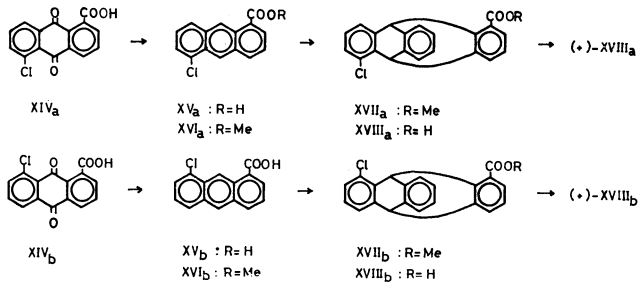

Scheme 2.

(+)-VIIb. The CD spectrum of (+)-XIa also showed a negative Cotton effect in the longest wavelength region.

In order to get information on the effect of magnitude of electric transition moment on the rotatory properties, replacement of the methoxyl group (spectroscopic moment 30)[10] in VIIa and VIIb with chlorine atom (spectroscopic moment 6)[10] was undertaken. 5-Chloroanthraquinone-1-carboxylic acid (XIVa) and 8-chloroanthraquinone-1-carboxylic acid (XIVb) prepared from anthraquinone-1-sulfonic acid by the reported method[11] were reduced to anthracene derivatives (XVa and XVb) by the procedure used in the preparation of IVa and IVb. The reaction of its methyl ester (XVIa or XVIb) with benzyne afforded chlorotriptycenecarboxylate (XVIIa or XVIIb). Chlorotriptycenecarboxylic acid (XVIIIa or XVIIIb) derived from XVIIa or XVIIb were resolved by means of brucine to yield optically pure (+)-5-chlorotriptycene-1-carboxylic acid, (+)-XVIIIa or 7-chlorotriptycene-1-carboxylic acid, (+)-XVIIIb.

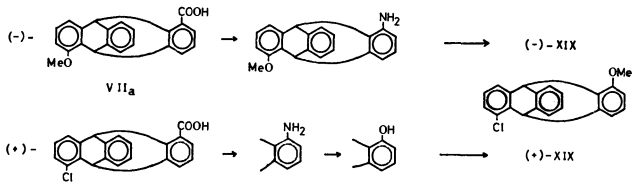

Scheme 3.

(+)-2-Chloro-7-carboxytriptycene (XVIIIa) was converted by the Curtius reaction into 2-chloro-7-hydroxytriptycene *via* 2-chloro-7-amino derivative. Methylation of the phenolic derivative afforded (+)-2-chloro-5-methoxytriptycene (XIX). On the other hand, the Curtius reaction of (−)-2-methoxy-7-carboxytriptycene (VIIa) obtained from the mother liquor of the optical resolution of *dl*-VIIa by means of brucine in *ca.* 60% optical purity, yielded 2-methoxy-7-aminotriptycene which could be converted into (−)-2-chloro-5-methoxytriptycene (XIX) by the Sandmeyer reaction. The IR spectra of (+)-XIX and (−)-XIX thus prepared were found to be superimposable and their CD spectra showed antipodal curves. The absolute configuration of (−)-VIIa has been estimated to be 1S,6S on the bases of X-ray structure analysis by the

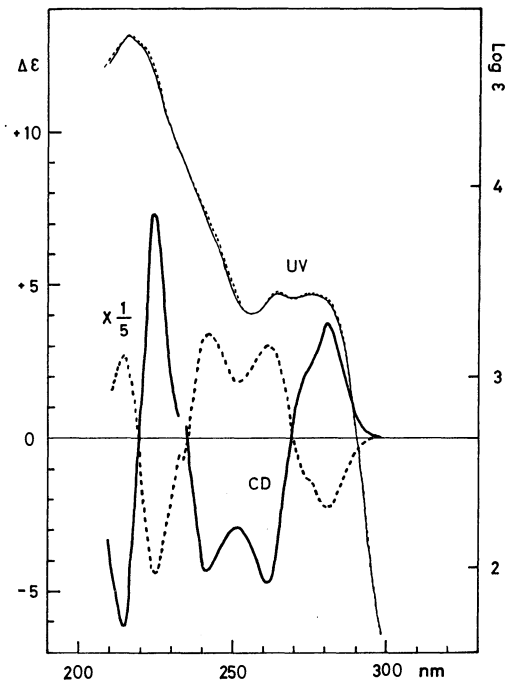

Fig. 4. UV and CD spectra of (+)-XIX (——) and (−)-XIX (····, optical purity 60%) in dioxane

Bijvoet method and the chemical correlation. Consequently, the absolute configuration of (+)-2-chloro-7-carboxytriptycene (XVIIIa) could be concluded to be 1R,6R on the same ground.

The bridgehead proton (C^1–H) proximate to carbomethoxy group and chlorine atom in XVIIb exhibited NMR signal at τ 2.57, whereas the signal of bridgehead proton (C^6–H) proximate to carbomethoxy group in XVIIa appeared at τ 3.00. The down-field shift of signal of the former compound could be attributed to magnetic anisotropy, van der Waals effect and electric field effect of the substituent groups.[12] The down-field shift of signal of bridgehead proton proximate to methoxycarbonyl group in VIb (τ 2.55) as compared with that of VIa (τ 3.00) indicates that the methoxyl group in VIb should occupy the 10-position. Consequently, the structure of IIb was firmly established to be 8-nitroanthraquinone-1-carboxylic acid.[13] The same effect of substituent groups on NMR spectrum was observed in the anthracene derivatives (Va and Vb) (see Experimental).

Experimental

All the melting points are not corrected. The IR (KBr-disk method) and UV spectra were measured with JASCO-402 and Hitachi EPS-3T spectrophotometers, respectively. The NMR spectra in deuteriochloroform were obtained on a Varian A-60 spectrometer using TMS as an internal standard. The CD spectra were measured with a Roussel-Jouan Dichrograph B and II CD-185.

5-Nitroanthraquinone-1-carboxylic Acid (IIa) and 8-Nitroanthra-

10) J. R. Platt, *J. Chem. Phys.*, **19**, 263 (1951).

11) F. Ullmann and P. Kerteoz, *Ber.*, **52**, 545 (1919); R. S. Cahn, W. O. Jones, and J. L. Simonsen, *J. Chem. Soc.*, **1933**, 444; T. Maki and Y. Nagai, *Kogyo Kagaku Zasshi*, **33**, 1310 (1930).

12) I. Mori, T. Kadosaka, Y. Sakata, and S. Misumi, This Bulletin, **44**, 1649 (1971).

13) The position of nitro group in IIb was presumed to be the 8-position without firm experimental evidence.[7]

quinone-1-carboxylic Acid (IIb). Anthraquinone-1-carboxylic acid obtained from benzanthrone[5] was nitrated by the reported method.[12] IIa was obtained from the fraction less soluble in ethanol. The residue obtained on evaporating the ethanolic mother liquor was recrystallized from water to yield yellow crystals, mp 288—295°C. The IR spectrum of this substance showed absorptions characteristic of 1,8-disubstituted anthraquinone[14] at 810 and 755 cm^{-1}. The yellow crystals (IIb) were converted into methyl ester in the usual way, mp 147.0—148.4°C (from methanol), IR: 1723 ($\nu_{C=O}$, $-COOCH_3$), 1678 ($\nu_{C=O}$, quinone), 1540, 1328 ($C-NO_2$) 802, 743 (1,8-disubstituted anthraquinone) cm^{-1}.

Found: C, 62.53; H, 3.08; N, 4.26%. Calcd for $C_{16}H_9O_6N$: C, 61.74; H, 2.91; N, 4.50%.

5-Methoxyanthraquinone-1-carboxylic Acid (IIIa) and the Methyl Ester. A mixture of crude IIa (10 g), sodium hydroxide (15 g) and methanol (300 ml) was refluxed for 8 hr. The residue obtained by concentration of the dark red reaction mixture was mixed with water (300 ml). The insoluble material was removed by filtration. The filtrate was acidified with concentrated hydrochloric acid to yield crude IIIa as yellow solid, mp 270—280°C (decomp), 9.2 g (97%). Treatment of crude IIIa with methanol containing sulfuric acid afforded methyl ester, yellow needles, mp 184.5—186.0°C (from methanol), IR (KBr-disk): 2840 (ν_{C-H}, $-OCH_3$), 1727 ($\nu_{C=O}$, $-COOCH_3$), 1664 ($\nu_{C=O}$, quinone), 815, 707 (1,5-disubstituted anthraquinone) cm^{-1}.

Found: C, 68.60; H, 4.06%. Calcd for $C_{17}H_{12}O_5$: C, 68.91; H, 4.08%.

8-Methoxyanthraquinone-1-carboxylic Acid (IIIb) and the Methyl Ester. According to the procedure used for IIIa, crude IIb (69.4 g) was converted into crude IIIb (49.6 g, 75.3%) which was recrystallized from acetic acid, mp 270—285°C (decomp). Methyl ester, yellow needles, mp 228.5—229.5°C (from methanol) was obtained by the usual method, IR: 2840 (ν_{C-H}, $-OCH_3$), 1720, 1664 ($\nu_{C=O}$, $-COOCH_3$, quinone), 800, 745 (1,8-disubstituted anthraquinone) cm^{-1}.

Found: C, 69.05; H, 3.85%. Calcd for $C_{17}H_{12}O_5$: C, 68.91; H, 4.08%.

5-Methoxyanthracene-1-carboxylic Acid (IVa). A mixture of crude IIIa (33 g), 15% aqueous ammonia (1.1 liter) and zinc dust (55 g) was heated with stirring on a boiling water-bath for 8 hr. At 2 hr intervals, zinc dust (4 g) and concentrated aqueous ammonia (30 ml) were added to the reaction mixture. Excess zinc dust was removed by filtration and washed with aquous ammonia. The combined filtrate and washings were treated twice with active charcoal. The hot filtrate was made acid to Congo red with concentrated hydrochloric acid, yielding crude IVa as yellow precipitate, 26.0 g (88.1%), mp *ca.* 215°C (decomp.).

5-Methoxy-1-methoxycarbonylanthracene (Va). A mixture of crude IVa (25.0 g), anhydrous methanol (880 ml) and concentrated sulfuric acid (14 ml) was refluxed for 8 hr. After the solvent had been removed, the residue was mixed with water and extracted with benzene. The concentrated extract was subjected to a chromatography on alumina (700 g). Elution with benzene afforded crude methyl ester (Va, 17.9 g, 67.8%). The crude material was recrystallized from methanol to yield pure Va, yellow needles, mp 130.5—131.5°C, IR: 2830 (ν_{C-H}, $-OCH_3$), 1700 ($\nu_{C=O}$, $-COOCH_3$) cm^{-1}, NMR: τ 0.48 (C^9-H), 1.15 (C^{10}-H), 5.97 ($-COOCH_3$ and $-OCH_3$).

Found: C, 76.65; H, 5.22%. Calcd for $C_{17}H_{14}O_3$: C, 76.67; H, 5.30%.

8-Methoxyanthracene-1-carboxylic Acid (IVb). Reduction of crude IIIb (49.0 g) by the method used for IVa afforded crude IVb (39.3 g, 81.7%), mp *ca.* 180°C (decomp.). The crude material was used in the following reaction.

8-Methoxy-1-methoxycarbonylanthracene (Vb). Esterification of crude IVb (38 g) according to the method used for IVa followed by chromatography on alumina afforded crude Vb (17.0 g, 42.5%). The crude material was recrystallized from methanol to yield pure Vb, yellow leaflets, mp 132—132.5°C, IR: 2835 (ν_{C-H}, $-OCH_3$) 1705 ($\nu_{C=O}$, $-COOCH_3$), cm^{-1}. NMR: τ 0.05 (C^9-H), 1.63 (C^{10}-H), 5.93 ($-COOCH_3$ and $-OCH_3$).

Found: C, 76.76; H, 5.33%. Calcd for $C_{17}H_{14}O_3$: C, 76.67; H, 5.30%.

2-Methoxy-7-methoxycarbonyltriptycene (VIa). To a mixture of Va (3.0 g, 11 mmol), isoamyl nitrite (2 ml, 15 mmol) and 1,2-dimethoxyethane (20 ml), stirred under gentle reflux, was added over 20 min period a solution of anthranilic acid (2.6 g, 19 mmol) in the same solvent (10 ml), and then an additional amount of isoamyl nitrite (2 ml). A solution of anthranilic acid (2.6 g) in the same solvent (10 ml) was again added to the mixture over a period of 20 min. The mixture was stirred for further 10 min under reflux. Crystals deposited on cooling the mixture on an ice-salt bath were collected by filtration and washed 4 times with cold methanol–water (4: 1, 10 ml), yielding crystalline material (1.6 g). The material in xylene (20 ml) was refluxed for 5 min with maleic anhydride (1.0 g, 10 mmol) to remove the unreacted anthracene derivative. After the solvent had been removed under reduced pressure, the residue was dissolved in benzene and chromatographed on alumina (100 g) to afford VIa as colorless crystals, mp 232—232.5°C, IR: 2836 (ν_{C-H}, $-OCH_3$), 1713 ($\nu_{C=O}$, $-COOCH_3$) cm^{-1}, UV: $\lambda_{max}^{dioxane}$ (ε) 209.5 (53400), 215 (51000), 267 (3550), 283.5 (4100), 296 (3810) nm, NMR: τ 2.33—3.17 (m, 11H, aromatic and C^1-H), 4.07 (s, 1H, C^6-H), 6.05 (s, 3H, $-COOCH_3$).

Found: C, 80.72; H, 5.33%. Calcd for $C_{23}H_{18}O_3$: C, 80.68; H, 5.30%.

5-Methoxy-7-methoxycarbonyltriptycene (VIb). To a solution of Vb (4.286 g, 16.1 mmol) and isoamyl nitrite (1.9 g, 16 mmol) in dichloromethane (20 ml), stirred under reflux, was added a solution of anthranilic acid (2.3 g, 16.8 mmol) in tetrahydrofuran (60 ml) over a period of 5 hr. Pale yellow residue obtained on evaporation of the solvent was mixed with xylene (50 ml) and maleic anhydride (3.5 g, 36 mmol). After refluxing for 1 hr, water (70 ml) and dichloromethane (70 ml) were added to the reaction mixture. The organic layer was washed successively with cold 5% aqueous potassium hydroxide (20 ml × 5) and water, and dried (sodium sulfate). The residue obtained on evaporating the solvent was dissolved in benzene and chromatographed on alumina (120 g), yielding VIb (1.843 g, 33.4%) which was recrystallized from ethyl acetate to give pure VIb, colorless crystals, mp 220—221.5°C, IR: 2835 (ν_{C-H}, $-OCH_3$), 1708 ($\nu_{C=O}$, $-COOCH_3$) cm^{-1}, UV: $\lambda_{max}^{dioxane}$ (ε) 220 (44600), 268 (3740), 285 (4680), 295 (4260) nm, NMR: τ 2.55 (C^1-H), 4.55 (C^6-H), 6.00 ($-COOCH_3$).

Found: C, 80.52; H, 4.72%. Calcd for $C_{23}H_{18}O_3$: C, 80.68; H, 5.30%.

2-Methoxy-7-carboxytriptycene (VIIa). A mixture of VIa (1.231 g), acetic acid (30 ml) and 10% aqueous sulfuric acid (45 ml) was refluxed for 25 hr. VIIa (1.067 g) was obtained on cooling the reaction mixture. The filtrate gave a second crop of VIIa (94 mg) (total yield, quantitative). Pure VIIa, mp 299.0—300°C was obtained on recrystallization from acetic acid, IR: 2830 (ν_{C-H}, $-OCH_3$), 1677 ($\nu_{C=O}$, $-COOH$) cm^{-1}, UV: $\lambda_{max}^{dioxane}$ (ε) 298 (3810), 285 (4010), 269 (3460), 224 (31100) nm.

Found: C, 80.27; H, 4.83%. Calcd for $C_{22}H_{16}O_3$: C,

14) N. Oi, *Chem. Pharm. Bull.* (Tokyo), **5**, 153 (1957).

80.47; H, 4.91%.

5-Methoxy-7-carboxytriptycene (VIIb). Hydrolysis of VIb (790 mg) according to the above method afforded VIIb (660 mg, 95%) which was recrystallized from aqueous acetic acid, yielding pure VIIb, mp 305—308°C, IR: 2830 (ν_{C-H}, -OCH_3), 1680 ($\nu_{C=O}$, -COOH) cm^{-1}.

Found: C, 80.20; H, 4.61%. Calcd for $C_{22}H_{16}O_3$: C, 80.47; H, 4.91%.

Optical Resolution of 2-Methoxy-7-carboxytriptycene (VIIa).

To a hot solution of VIIa (4.70 g, 14.3 mmol) in 99% ethanol (270 ml) was added brucine dihydrate (3.08 g, 7.80 mmol) in one portion. After refluxing for 15 min, the mixture was allowed to stand overnight to deposit brucine salt (5.1 g). The salt was recrystallized twice from 99% ethanol to yield pure material, mp 196.0—198.0°C, IR: 3510 (ν_{N-H}), 1655 ($\nu_{C=O}$, -COO^-) cm^{-1}, $[\alpha]_{350}^{20}$ −268° (*c* 0.117, dioxane).

The pure salt (1.125 g) was dissolved in acetic acid (10 ml) on warming up to 90—95°C for 5 min. White precipitate (478 mg) obtained on addition of water (30 ml) to the acetic acid solution was recrystallized from acetic acid to give pure (+)-VIIa mp 267°C (decomp.), IR: 2830 (ν_{C-H}, -OCH_3), 1673 ($\nu_{C=O}$, -COOH) cm^{-1}, $[\alpha]_D^{20}$ +15.4°, $[\alpha]_{405}^{20}$ −74.4° (*c* 0.187, dioxane).

Found: C, 80.26; H, 4.76%. Calcd for $C_{22}H_{16}O_3$: C, 80.47; H, 4.91%.

(+)-2-Methoxy-7-methoxycarbonyltriptycene (VIa). A mixture of (+)-VIIa (35 mg), methanol (5 ml) and concentrated sulfuric acid (0.2 ml) was refluxed for 5 hr. Crystals (33 mg) deposited on cooling the reaction mixture were washed with a small amount of methanol and recrystallized from the same solvent to yield pure ester, (+)-VIa as colorless, rods, mp 240—241°C, IR: 2830 (ν_{C-H}, -OCH_3), 1714 ($\nu_{C=O}$, -$COOCH_3$) cm^{-1}, CD: $\lambda_{max}^{dioxane}$ ($\Delta\varepsilon$) 325—288 (+0.4), 280 (+2.6), 265 (−2.5), 242* (+8.3), 232 (+12.2), 220 (−56.8) nm.

Found: C, 80.81; H, 5.34%. Calcd for $C_{23}H_{18}O_3$: C, 80.68; H, 5.30%.

Optical Resolution of 5-Methoxy-7-carboxytriptycene (VIIb).

To a hot solution of VIIb (170 mg, 0.518 mmol) in acetone (5 ml) was added brucine dihydrate (111 mg, 0.258 mmol). After refluxing for 15 min, crystals deposited (84 mg) were recrystallized from acetone (6 ml) to give brucine salt, 31 mg, $[\alpha]_{350}^{15}$ −206° (*c* 0.34, chloroform). (+)-VIIb obtained from an acetic acid solution of the brucine salt on dilution with water was sublimed *in vacuo* to give pure (+)-VIIb, mp 310—313°C, $[\alpha]_{600}$ +21.1°, $[\alpha]_D$ +23.7°, $[\alpha]_{400}$ +55.3°.

Found: C, 80.00; H, 4.85%. Calcd for $C_{22}H_{16}O_3$: C, 80.47; H, 4.91%.

The residue obtained on concentrating the mother liquor of recrystallization of brucine salt was decomposed to yield (−)-VIIb with unknown optical purity (negative rotation in the visible wavelength region).

The experiments were repeated under the same and different conditions, but no optical resolution could be achieved except for the above described run. The cause of the poor reproducibility is not clear.

(+)-2-Hydroxy-7-carboxytriptycene (VIIIa). A mixture of (+)-VIIa (467 mg), acetic acid (10 ml), 48% hydrobromic acid (10 ml) and 52% hydriodic acid (1 ml) was refluxed for 15 hr. The resulting red reaction mixture was poured onto water (80 ml) containing sodium hydrogen sulfite, and extracted with chloroform (20 ml×4). The extract was washed with water and dried (sodium sulfate). The residue (426 mg, 95.3%) obtained by evaporation of the solvent was recrystallized from petroleum ether–methyl acetate to yield pure (+)-VIIIa, mp 269—271°C (*dl*-VIIIa, mp 263.0—264.0°C), IR: 3020, 3200 (ν_{C-H}), 1683 ($\nu_{C=O}$, -COOH) cm^{-1}, UV: $\lambda_{max}^{95\%EtOH}$ (ε) 300* (3400), 286 (4350), 269 (3410), 214* (46200) nm.

Found: C, 80.05; H, 4.36%. Calcd for $C_{21}H_{14}O_3$: C, 80.24; H, 4.39%.

(+)-2-Hydroxy-7-methoxycarbonyltriptycene (IXa). The reaction mixture obtained on refluxing a mixture of (+)-VIIIa (393 mg), anhydrous methanol (7 ml) and concentrated sulfuric acid (0.4 ml) for 8 hr was poured onto water (40 ml). The crude ester (404 mg, 98.5%) obtained as a white precipitate was recrystallized from cyclohexane–methyl acetate to give pure (+)-IXa, mp 217—225°C (*dl*-IXa, mp 231—234°C), IR: 3400 (ν_{O-H}), 1697 ($\nu_{C=O}$) cm^{-1}.

Found: C, 80.20; H, 4.76%. Calcd for $C_{22}H_{16}O_3$: C, 80.47; H, 4.91%.

(+)-2,5-Dimethoxy-7-methoxycarbonyltriptycene (Xa). A mixture of concentrated hydrochloric acid (0.14 ml) and ice-water (5 ml) was added to an ice-cooled solution of sulfanilic acid (185 mg, 0.97 mmol), sodium carbonate (57 mg) and sodium nitrite (82 mg) in water (5 ml), and the mixture was stirred for 30 min at 0°C. To the resulting solution of diazotized sulfanilic acid was added a solution of (+)-IXa (219 mg, 0.667 mmol) in methanol (20 ml) and water (4 ml) containing sodium hydroxide (147 mg). After being stirred for 1 hr at room temperature, the deep red reaction mixture was poured onto water (40 ml). Sodium hydrosulfite was added in small portions at 40—50°C until the color of the mixture turned light yellow, and then extracted with ethyl acetate (20 ml×4). The extract was washed with a saturated sodium chloride solution (20 ml×2) and dried (sodium sulfate). Aminophenol derivative (195 mg) obtained by evaporating the solvent was mixed with 2N sulfuric acid (35 ml). Ethanol was then added to result in a homogeneous solution. Ferric sulfate (3.3 g) was added to the solution and the mixture was kept for 2 hr on a boiling water-bath. After cooling, the reaction mixture containing yellow precipitate was extracted with chloroform (20 ml×4). The extract was worked up in the usual way to yield crude quinone derivative. The crude quinone in ethanol (10 ml) was reduced with a saturated aqueous solution of sodium hydrosulfite. Water was added to the resulting pale yellow mixture and extracted with ether. The dried extract was concentrated to yield crude hydroquinone derivative (116 mg). A mixture of the hydroquinone, acetone (5 ml), anhydrous potassium carbonate (1.0 g) and dimethyl sulfate (0.4 ml) was refluxed for 5 hr. The reaction mixture was mixed with water (50 ml) and extracted with benzene (20 ml×4). After washing and drying, the extract was concentrated to *ca.* 20 ml and chromatographed on alumina (5 g) to yield (+)-Xa (83 mg). Pure (+)-Xa was obtained by recrystallization from benzene, mp 261.5—262.5°C. (+)-Xa thus obtained showed no depression of melting point [mixed mp 261.5—262.3°C] on admixture with (+)-2,5-dimethoxy-7-methoxycarbonyltriptycene [(+)-X, mp 261.5—262.5°C] prepared by a different route.[3] Both compounds showed identical IR spectra. The optical purity of (+)-Xa was confirmed by comparison of $\Delta\varepsilon$ value at 267 nm in dioxane [(+)-Xa: $\Delta\varepsilon$=−3.15, (+)-X: $\Delta\varepsilon$=−3.06[3]].

Found: C, 77.55; H, 5.46%. Calcd for $C_{24}H_{20}O_4$: C, 77.40; H, 5.41%.

(+)-2-Acetoxy-7-methoxycarbonyltriptycene (XIa). A mixture of (+)-IXa (70 mg), acetic anhydride (3 ml) and a small amount of anhydrous sodium acetate was heated on a boiling water-bath for 3 hr. After cooling, water was added to the reaction mixture. Crystals deposited were recrystallized from methanol to yield (+)-XIa, colorless rods, mp 175.5—176.5°C, IR: 1767 ($\nu_{C=O}$, -$OCOCH_3$), 1723 ($\nu_{C=O}$, -$COOCH_3$) cm^{-1}, UV: $\lambda_{max}^{dioxane}$ (ε) 294 (3830), 276.5 (2170),

215 (53300) nm, CD: $\lambda_{max}^{dioxane}$ ($\Delta\varepsilon$) 285 (−0.6), 272.5 (+1.5), 260 (−1.16) nm.

Found: C, 78.43; H, 4.77%. Calcd for $C_{24}H_{18}O_4$: C, 77.82; H, 4.90%.

dl-XIa: mp 189.0—191.5°C, IR: 1755 ($\nu_{C=O}$, -$OCOCH_3$), 1708 ($\nu_{C=O}$, -$COOCH_3$) cm^{-1}.

(+)-2-Hydroxy-5-phenylazo-7-carboxytriptycene (XIIa). To a solution of (+)-VIIIa (93 mg, 0.30 mmol) in methanol (5 ml) and 10% aqueous potassium hydroxide solution (1.5 ml) was added a solution of benzenediazonium chloride prepared from aniline (46 mg, 0.49 mmol), concentrated hydrochloric acid (0.15 ml), water (0.5 ml) and sodium nitrite (36 ml). After the mixture had been stirred for 10 min at 0°C, water (20 ml) was added to the resulting red solution and extracted with dichloromethane. The residue obtained by working up the extract was dissolved in ether–benzene (1: 1) and chromatographed on silica gel. Pure (+)-XIIa, red crystals, mp 279—280°C, was obtained by recrystallization from benzene–cyclohexane (1: 1), IR: 3100—3600 (broad), 3040, 1685 ($\nu_{C=O}$, -COOH) cm^{-1}, UV: $\lambda_{max}^{95\%EtOH}$ (ε) 466 (3700), 359 (17700), 269 (10200) nm, CD: $\lambda_{max}^{dioxane}$ ($\Delta\varepsilon$) 450 (−2.9), 319 (−0.9), 277 (+6.1) nm.

The azotriptycene (XIIa) gave no satisfactory elemental analysis presumably owing to its incomplete combustion.

Found: C, 78.11; H, 4.73; N, 5.91%. Calcd for $C_{27}H_{18}O_3N_2$: C, 77.50; H, 4.34; N, 6.69%.

5-Chloroanthraquinone-1-carboxylic Acid (XIVa) and 8-Chloroanthraquinone-1-carboxylic Acid (XIVb). Anthraquinone-1-sulfonic acid was converted into XIVa and XIVb according to the reported method.[11]

5-Chloroanthracene-1-carboxylic Acid (XVa). A mixture of crude XIVa (6 g), 14% aqueous ammonia (350 ml) and zinc dust (10.5 g) was stirred on a water-bath at 90°C. Zinc dust and aqueous ammonia were further added in small portions during the course of reaction until the deep red color of the reaction mixture turned greenish grey. Excess zinc dust was removed by filtration. The filtrate was treated with active charcoal and the hot filtrate was made acidic to Congo red with concentrated hydrochloric acid to precipitate crude XVa as yellowish brown solid, 4.5 g, mp >300°C.

8-Chloroanthracene-1-carboxylic Acid (XVb). Crude XIVb (9.9 g) was converted into XVb (6.9 g, 78%) according to the procedure given above.

Methyl 5-Chloroanthracene-1-carboxylate (XVIa). A mixture of crude XVa (21.7 g), anhydrous methanol (680 ml) and concentrated sulfuric acid (10.8 ml) was refluxed. The reaction mixture was worked up in the usual way and extracted with benzene. The benzene solution was chromatographed on alumina to yield XVIa (11.0 g, 48%) which was recrystallized from methanol to give pure XVIa, light yellow needles, mp 131.5—132.5°C, IR: 1690 ($\nu_{C=O}$, -CO_2CH_3) cm^{-1}, NMR: τ 0.40 (C^9-H), 1.70 (C^{10}-H), 5.95 (-CO_2CH_3).

Found: C, 71.24; H, 4.16; Cl, 13.26%. Calcd for $C_{16}H_{11}O_2Cl$: C, 70.99; H, 4.10; Cl, 13.10%.

Methyl 8-Chloroanthracene-1-carboxylate (XVIb). Crude XVb was converted into XVIb according to the method used for the 5-chloro isomer. Pure XVIb was obtained by repeated recrystallization from methanol and petroleum ether–methyl acetate, light yellow leaflets, mp 126.0—126.8°C, IR: 1700 ($\nu_{C=O}$, -CO_2CH_3) cm^{-1}, NMR: τ 0.00 (C^9-H), 1.58 (C^{10}-H), 5.93 (-CO_2CH_3).

Found: C, 70.75; H, 4.07; Cl, 13.23%. Calcd for $C_{16}H_{11}O_2Cl$: C, 70.99; H, 4.10; Cl, 13.10%.

2-Chloro-7-methoxycarbonyltriptycene (XVIIa). To a mixture of XVIa (4.7 g, 17 mmol), dichloromethane (94 ml) and isoamyl nitrite (2.9 ml, 22 mmol), stirred vigorously under gentle reflux, was added a solution of anthranilic acid (2.72 g, 20 mmol) in tetrahydrofuran (62 ml) over a period of 5 hr. After being refluxed for further 1 hr, the solvent was removed under reduced pressure. Maleic anhydride (3.6 g, 37 mmol) and xylene (55 ml) were added to the residue and refluxed for 3.5 hr. The reaction mixture was mixed with dichloromethane (100 ml) and water (100 ml). The organic layer was washed with 5% aqueous potassium hydroxide solution (30 ml × 5) and water, successively, and dried. The dichloromethane was removed by distillation and the residue was chromatographed on alumina. Slightly crude XVIIa (1.75 g, 29.1%) obtained from benzene eluate was recrystallized from cyclohexane to yield pure XVIIa, mp 164—165°C, IR: 1710 ($\nu_{C=O}$, -$COOCH_3$) cm^{-1}, UV: λ_{max}^{EtOH} (ε) 216 (56600), 263 (1550), 280* (2710), 295 (3990) nm, NMR: τ 3.00 (C^6-H), 4.04 (C^1-H), 6.03 (-$COOCH_3$).

Found: C, 76.30; H, 4.30; Cl, 10.02%. Calcd for $C_{22}H_{15}O_2Cl$: C, 76.19; H, 4.36; Cl, 10.22%.

5-Chloro-7-methoxycarbonyltriptycene (XVIIb). The product obtained by the reaction of XVIb (3.0 g) with benzyne generated by the above method was chromatographed on alumina, yielding slightly crude XVIIb (1.2 g, 31.2%). Pure XVIIb was obtained by recrystallization from cyclohexane, mp 248—249°C, IR: 1710 ($\nu_{C=O}$, -$COOCH_3$) cm^{-1}, UV: λ_{max}^{EtOH} (ε) 216 (55000), 263 (1550), 280* (2590), 295 (3740) nm, NMR: τ 2.57 (C^6-H), 4.57 (C^1-H), 6.00 (-$COOCH_3$).

Found: C, 76.16: H, 4.12; Cl, 10.54%. Calcd for $C_{22}H_{15}O_2Cl$: C, 76.19; H, 4.36; Cl, 10.22%.

2-Chloro-7-carboxytriptycene (XVIIIa). A mixture of XVIIa (979 mg), acetic acid (100 ml) and 10% aqueous sulfuric acid (30 ml) was refluxed for 10 hr. The crystals deposited on cooling the reaction mixture were combined with the second crop obtained from the concentrated filtrate. The combined crystals (quantitative yield) were recrystallized from benzene–cyclohexane to give pure XVIIIa, mp 295—296°C, IR: 1680 ($\nu_{C=O}$, -COOH) cm^{-1}.

Found: C, 75.80; H, 3.79; Cl, 10.39%. Calcd for $C_{21}H_{13}O_2Cl$: C, 75.79; H, 3.94; Cl, 10.66%.

5-Chloro-7-carboxytriptycene (XVIIIb). XVIIb was converted into XVIIIb according to the method given above, mp 217°C (from methanol), IR: 1680 ($\nu_{C=O}$, -CO_2CH_3) cm^{-1}.

Found: C, 75.76; H, 4.24; Cl, 10.86%. Calcd for $C_{21}H_{13}O_2Cl$: C, 75.79; H, 3.94; Cl, 10.66%.

Optical Resolution of 2-Chloro-7-carboxytriptycene (XVIIIa). Brucine dihydrate (1034 mg, 2.40 mmol) was added to a solution of XVIIIa (796 mg, 2.40 mmol) in 99% ethanol (30 ml). After the mixture had been refluxed for 10 min, the solvent was removed under reduced pressure. The residue was recrystallized twice from acetone to yield pure brucine salt, mp 195—199°C, $[\alpha]_{350}$ −154°, $[\alpha]_{400}$ −54.0°, $[\alpha]_{500}$ −6.00°, $[\alpha]_D$ +4.00° (*c* 0.50, $CHCl_3$).

Found: C, 72.76; H, 5.32; N, 3.85; Cl, 4.62%. Calcd for $C_{44}H_{39}O_6N_2Cl$: C, 72.66; H, 5.41; N, 3.85; Cl, 4.88%.

The brucine salt was dissolved in hot acetic acid and diluted with water to precipitate (+)-XVIIIa, mp 289—291°C (decomp.), $[\alpha]_{350}^{15}$ +103°, $[\alpha]_D^{15}$ +19.4° (*c* 0.515, dioxane), CD: $\lambda_{max}^{dioxane}$ ($\Delta\varepsilon$) 287 (−1.2), 275 (+3.2), 259 (−1.3) nm.

Found: C, 75.30; H, 3.75%. Calcd for $C_{21}H_{13}O_2Cl$: C, 75.79; H, 3.94%.

Optical Resolution of 5-Chloro-7-carboxytriptycene (XVIIIb). To a solution of XVIIIb (128 mg, 0.4 mmol) in ethanol (6 ml) was added brucine dihydrate (172 mg, 0.4 mmol) and the mixture was refluxed for 30 min. The mixture was allowed to stand overnight. The crystals deposited were recrystallized from methyl acetate to afford pure brucine salt, mp 225—231°C.

Found: C, 72.56; H, 5.43; N, 3.83; Cl, 4.62%. Calcd for $C_{44}H_{39}O_6N_2Cl$: C, 72.66; H, 5.41; N, 3.85; Cl, 4.88%.

A hot acetic acid solution of the brucine salt was diluted with water to result in the precipitation of (+)-XVIIIb, mp 285—277°C, CD: $\lambda_{max}^{dioxane}$ ($\Delta\varepsilon$) 285 (−0.8), 275 (+1.3) nm.

Found: C, 75.64; H, 3.75%. Calcd for $C_{21}H_{13}O_2Cl$: C, 75.79; H, 3.94%.

(+)-2-Chloro-7-methoxytriptycene (XIX). A mixture of (+)-2-chloro-7-carboxytriptycene (XVIIIa, 0.330 g), thionyl chloride (0.4 ml) and tetrahydrofuran (10 ml) was refluxed for 2 hr. The volatile material was removed under reduced pressure to give crude acid chloride (0.350 g). To an ice-cooled solution of the crude acid chloride in tetrahydrofuran (15 ml) was added a solution of sodium azide (130 mg, 2.0 mmol) in water (1 ml). After the mixture had been stirred for 2 hr, the reaction mixture was poured onto water (100 ml). The solid deposited was washed thoroughly with water and dried *in vacuo*. The well-dried acid azide (0.304 g) was spread on the bottom of a 100 ml Erlenmeyer flask in a thin layer and gradually heated to 120°C avoiding the atmospheric moisture. After being kept at the same temperature for 2 hr, 99% ethanol (30 ml) containing potassium hydroxide (2.0 g) was added to the resulting isocyanate. After being refluxed for 6 hr, the ethanol was removed under reduced pressure. The residue was mixed with water (100 ml) and extracted with benzene. The extract, after being washed with a saturated sodium chloride solution and dried, was concentrated under reduced pressure to give amino derivative (0.250 g). The chloro-aminotriptycene thus obtained was dissolved in acetic acid (10 ml) and a solution of sodium nitrite (0.058 g) in water (2 ml) was added to the solution in small portions over 20 min period under stirring at 10—15°C. After being stirred for further 30 min, the resulting red solution of diazonium salt was added dropwise to boiling 6N sulfuric acid (30 ml). After further boiling for 10 min, water was added to the reaction mixture to make 100 ml of mixture and extracted with benzene. After being washed and dried, the extract was concentrated under reduced pressure to give phenolic derivative (0.263 g). A mixture of the crude phenol, acetone (15 ml), anhydrous potassium carbonate (1.2 g) and dimethyl sulfate (0.3 ml) was refluxed for 8 hr under stirring. The residue obtained by evaporation of the solvent under reduced pressure was mixed with water (40 ml) and extracted with benzene. The extract was worked up in the usual way. A benzene solution of the crude methyl ether was passed through a column of alumina (10 g). The crystals (186 mg) obtained from the initial filtrate (110 ml) were chromatographed on alumina (30 g). Elution with ligroin–benzene (2: 3) afforded colorless crystals (58 mg) which were recrystallized from methanol and then sublimed *in vacuo* to give pure (+)-XIX, mp 235—236.0°C, UV: $\lambda_{max}^{dioxane}$ (ε) 280 (2500), 276 (2620), 273* (2600), 268* (2580), 264 (2600), 217 (60500) nm, CD: $\lambda_{max}^{dioxane}$ ($\Delta\varepsilon$) 280 (+3.74), 275* (+2.28), 262 (−4.71), 242 (−4.31), 224 (+36.8), 216 (−31.0) nm.

Found: C, 78.93; H, 4.74; Cl, 11.00%. Calcd for $C_{21}H_{15}OCl$: C, 79.12; H, 4.74; Cl, 11.12%.

(+)-XIX thus prepared was admixed with approximately the same amount of (−)-XIX. The mixed melting point was found to be 240.5—241.4°C indicating the formation of a racemic compound.

(−)-2-Chloro-7-methoxytriptycene (XIX). Thionyl chloride (0.8 ml) was added to a solution of (−)-2-methoxy-7-carboxytriptycene (VIIa, 604 mg) with *ca.* 60% optical purity, obtained from the mother liquor of optical resolution of *dl*-VIIa with brucine, in tetrahydrofuran (20 ml). After the mixture had been refluxed for 2 hr, the volatile material was removed under reduced pressure to give crude acid chloride [659 mg, IR: 1750 ($\nu_{C=O}$, -COCl) cm^{-1}]. To an ice-cooled solution of the acid chloride in tetrahydrofuran (30 ml) was added a solution of sodium azide (254 mg) in water (2 ml). After being stirred for further 2 hr at the same temperature, the reaction mixture was poured onto ice-water (200 ml). Thoroughly dried acid azide [88 mg, IR: 2130 ($\nu_{N=N^+=N^-}$), 1680 ($\nu_{C=O}$) cm^{-1}] was heated to 180°C as previously to give isocyanate [66 mg, IR: 2250 ($\nu_{N=C=O}$) cm^{-1}]. A mixture of the crude isocyanate (343 mg), potassium hydroxide (2.0 g), water (10 ml) and 99% ethanol (50 ml) was refluxed for 6 hr. After the solvent had been removed under reduced pressure, the residue was mixed with water (200 ml) and extracted with benzene. Concentration of the extract, after washing and drying, under reduced pressure afforded amino derivative [338 mg, IR: 3480, 3390 (ν_{N-H}) cm^{-1}]. A solution of sodium nitrite (925 mg) in water (2 ml) was added to an ice-cooled mixture of the amine (402 mg) in concentrated hydrochloric acid (5 ml). Freshly prepared cuprous salt [from cupric sulfate pentahydrate (500 mg), sodium chloride (130 mg), sodium hydrogen sulfite (106 mg), sodium hydroxide (70 mg) and water (24 ml)] was dissolved in concentrated hydrochloric acid (5 ml). To the solution of cuprous chloride in hydrochloric acid was added the diazotized amine in the same acid, and the mixture was kept at 80°C for 1 hr. Crude crystals (377 mg) obtained by diluting the reaction mixture with water were dissolved in *n*-hexane–benzene (1: 1) and percolated through a column of alumina. Crystals (260 mg) obtained from the initial filtrate (100 ml) were recrystallized from methanol and then sublimed *in vacuo* (bath temp. 200°C/2 mmHg) to give (−)-XIX, mp 234.0—235.0°C, UV: $\lambda_{max}^{dioxane}$ (ε) 280 (2530), 276 (2770), 273* (2670), 268* (2570), 264 (2750), 217 (60000) nm, CD: $\lambda_{max}^{dioxane}$ ($\Delta\varepsilon$) 281 (−2.23), 275* (−1.39), 269 (+3.00), 242 (+3.42), 225 (−22.0), 215 (+13.0) nm.

The optical purity of (−)-XIX thus obtained was found to be 60%.

Found: C, 78.99; H, 4.59; Cl, 11.10%. Calcd for $C_{21}H_{15}OCl$: C, 79.12; H, 4.74; Cl, 11.12%.

Tubercidin. Its Conversion into 5′-Deoxytubercidin

Kentaro ANZAI and Masanao MATSUI

The Institute of Physical and Chemical Research, Wako-shi, Saitama

(Received January 24, 1972)

Tubercidin (I) was converted into 5′-deoxytubercidin (IV). Mesylation of 2′,3′-*O*-isopropylidenetubercidin (IX) afforded-2′,3′-*O*-isopropylidene-5′-*O*-mesyltubercidin (XVIII), which *in situ* was treated with benzoyl chloride. The product, N^6,N^6-dibenzoyl-2′,3′-*O*-isopropylidene-5′-*O*-mesyltubercidin (XXII), was converted into N^6,N^6-dibenzoyl-5′-deoxy-5′-iodo-2′,3′-*O*-isopropylidenetubercidin (XXIV). Catalytic hydrogenation of XXIV afforded N^6-benzoyl-5′-deoxy-2′,3′-*O*-isopropylidenetubercidin (XXVII). 5′-Deoxytubercidin (IV) was obtained on debenzoylation and deacetonation of XXVII.

Tubercidin (4-amino-7-(D-ribofuranosyl)-7*H*-pyrrolo-[2,3-*d*]pyrimidine)[1,2] (I)[3] was first isolated by Anzai *et al.*[4] from the fermentation broth of *Streptomyces tubercidicus*[5] in 1957. It has selective bactericidal activities against *Mycobacterium tuberculosis* of human and bovine types[4] as well as high activities against NF mouse sarcoma[4] and some experimental tumors.[6] Its clinical use was examined for cancer patients, and was shown to be highly toxic.

Several works[7] were directed to the total synthesis of I and related antibiotics including toyocamycin (II)[8] and sangivamycin (III),[9] both of which were also reported to have high activities against experimental tumors.

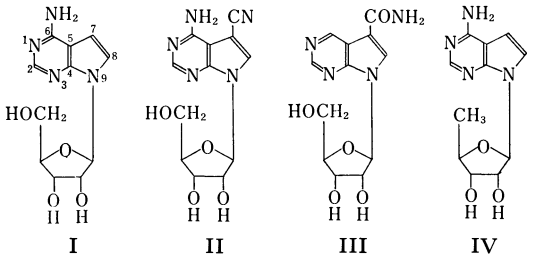

I II III IV

In 1969 Tolman *et al.* succeeded in the synthesis of these three compounds.[10] They as well as others synthesized derivatives of tubercidin whose pyrro[2,3-*d*]-pyrimidine moiety was subjected to various substitution.[11] Phosphorylated derivatives of tubercidin, *i.e.* tubercidin-5′-phosphate,[12,15] dan tubercidin-3′,5′-cyclophosphate,[13] and the oligonucleotide analogues[14] were also synthesized, and their biological activities were investigated.[15] However, the modification of the ribose moiety has never been reported, and our investigation has been undertaken along this line. In this paper the conversion of I to 5′-deoxytubercidin (IV) will be described.

5′-Deoxyadenosine has been synthesized from adenosine[16] through a route involving catalytic reduction of N^6-acetyl-5′-deoxy-5′-iodo-2′,3′-*O*-isopropylidene-adenosine (V) which was synthesized from 2′,3′-*O*-isopropylidene-5′-*O*-tosyladenosine (VI)[17] by treatment with sodium iodide in acetic anhydride.

We followed this experiment and found that the yield of V was moderate (58%), but that of VI was good (90%). The iodide substitution reaction of VI yielding V is likely to compete with the formation of the cyclonucleoside VII.

Synthesis of the tubercidin analogue of V was attempted. Under the same conditions as applied to

1) S. Suzuki and S. Marumo, *J. Antibiot.* (Tokyo), *Ser. A*, **13**, 360 (1960); *ibid.*, **14**, 34 (1961).

2) Y. Mizuno, M. Ikehara, K. A. Watanabe, S. Suzaki, and T. Itoh, *J. Org. Chem.*, **28**, 3329 (1963).

3) 7-Deazaadenosine is a synonym of tubercidin. Various derivatives of tubercidin have been named in general from the numbering of adenosine, which is also adopted in this paper.

4) K. Anzai, G. Nakamura, and S. Suzuki, *J. Antibiot.* (Tokyo), *Ser. A*, **10**, 201 (1957).

5) G. Nakamura, *ibid.*, **14**, 90 (1961).

6) L. R. Duvall, *Cancer Chemotherapy Rept.*, **30**, 61 (1963); S. P. Owen, and C. G. Smith, *ibid.*, **36**, 19 (1964); M. Saneyoshi, R. Tokuzen, and F. Fukuoka, *Gann*, **56**, 219 (1965); C. G. Smith, W. L. Lummis, and J.E. Grady, *Cancer Res.*, **19**, 847 (1959); G. Acs, E. Reich, and M. Mori, *Proc. Natl. Acad. Sci. U.S.*, **52**, 493 (1964); L.L. Bennett, Jr., and D. Smithers, *Biochem. Pharmacol.*, **13**, 1331 (1964); L. L. Bennett, Jr., M. H. Vail, S. Chumley, and J. A. Montgomery, *ibid.*, **15**, 1719 (1966); L. L. Benett, Jr., Schnebli, M. H. Vail, P. W. Allan, and J. A. Montgomery, *Mol. Pharmacol.*, **2**, 432 (1966); L. L. Bennett, P. W. Allan, D. Smithers, and M. H. Vail, *Biochem. Pharmacol.*, **18**, 725 (1969); W. H. Wolberg, *ibid.*, **14**, 1921 (1965).

7) Y. Mizuno, M. Ikehara, K. A. Watanabe, and S. Suzaki, *Chem. Pharm. Bull.* (Tokyo), **11**, 1091 (1963); E. C. Taylor, and R.W. Hendess, *J. Amer. Chem. Soc.*, **87**, 1995 (1965); R. L. Tolman, R. K. Robins, and L. B. Townsend, *J. Heterocycl. Chem.*, **4**, 230 (1967); H. Iwamura, and T. Hashizume, *Agr. Biol. Chem.* (Tokyo), **32**, 1010 (1968); R.L. Tolman, and L.B. Townsend, *Tetrahedron Lett.*, **1968**, 4815. B. C. Hinshaw, J. F. Gerster, R. K. Robins, and L. B. Townsend, *J. Heterocycl. Chem.*, **6**, 215 (1969).

8) H. Nishimura, K. Katagiri, K. Sato, M. Mayama, and N. Shimaoka, *J. Antibiot.* (Tokyo), *Ses. A*, **9**, 60 (1956); K. Ohkuma, *ibid.*, **14**, 343 (1961).

9) K. V. Rao and D. W. Renn, *Antimicrobial Agents Chemotherapy*, **1963**, 77; K. V. Rao, *J. Med. Chem.*, **11**, 939 (1968).

10) R. L. Tolman, R. K. Robins, and L. B. Townsend, *J. Amer. Chem. Soc.*, **91**, 2102 (1969).

11) J. F. Gerster, B. Carpenter, R. K. Robins, and L. B. Townsend, *J. Med. Chem.*, **10**, 326 (1967); J. A. Montgomery and K. Hewson, *ibid.*, **10**, 665 (1967).

12) J. E. Pike, L. Slechta, and P. F. Wiley, *J. Heterocycl. Chem.*, **1**, 159 (1964); A. R. Bloch, R. J. Leonard, and C. A. Nichol, *Biochem. Biophys. Acta*, **138**, 10 (1967); S. C. Uretsky, G. Acs, E. Reich, M. Mori, and L. Altwerger, *J. Biol. Chem.*, **243**, 306 (1968).

13) A.R. Hanze, U.S. 3300479 (1967).

14) A.R. Hanze, U.S. 3309358 (1967); A.R. Hanze, *Biochemistry*, **7**, 932 (1968); M. Ikehara, and T. Fukui, *J. Mol. Biol.*, **38**, 437 (1968); M. Ikehara, and E. Ohtsuka, *Biochem. Biophys. Commun.*, **21**, 257 (1965); M. Nirenberg, P. Leder, M. Bernfield, R. Brimacombe, J. Trupin, F. Rottman, and C. O'Neal, *Proc. Nat. Acad. Sci. U.S.*, **53**, 1161 (1965).

15) C.G. Smith, G.D. Gray, R.G. Carlson, and A.R. Hanze, *Advan. Enzyme Regul.*, **5**, 121 (1967).

16) W. Jahn, *Chem. Ber.*, **98**, 1706 (1965); J. R. McCarthy, Jr., R.K. Robins, and M.J. Robins, *J. Amer. Chem. Soc.*, **90**, 4993 (1968).

17) R. Kuhn and W. Jahn, *Ber. Chem*, **98**, 1699 (1965).

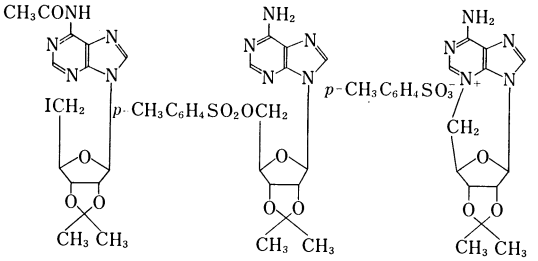

V VI VII

the synthesis of VI 2',3'-*O*-isopropylidenetubercidin (IX)[18] was converted into 2',3'-*O*-isopropylidene-5'-*O*-tosyltubercidin (VIII) in a 76% yield.[20] However, contrary to expectation, the following treatment of VIII with sodium iodide and acetic anhydride afforded cyclonucleoside X[21] as the main product and the tosyl iodo compound XVII as a minor one. None of the acetyl iodo compound corresponding to V was obtained.

With excess tosyl chloride and at a higher temperature, cyclonucleoside XI, N^6-tosylate XII and N^6,5'-*O*-ditosylate XIII were obtained in low yields, X being still the predominant product.

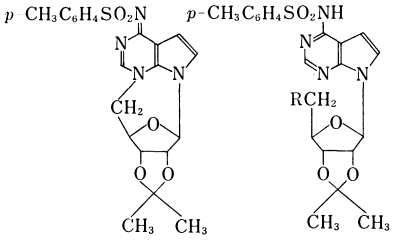

XI XII R=OH
XIII R=*p*-$CH_3C_6H_4SO_3$

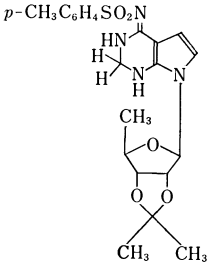

XV

Facile transformation of VIII into X was confirmed by storing VIII in a desiccator at room temperature for 2 days to give a mixture of VIII and X (28: 72), *i.e.*, VIII is transformed easily into X even in the solid state. This is in contrast with the fact that 38% of VI is transformed into VII under the same conditions.

18) W. J. Wechter and A. R. Hanze, U. S. 3336289 (1967).
19) J. Zemlicka and A. Holy, *Collect. Czech. Chem. Commun.*, **32**, 3159 (1967).
20) Tosylation was carried out at −15°C to −20°C as reported[17] for the synthesis of VI, though Mizuno *et al.* obtained VIII at a higher temperature (0°C) in a 30% yield.
21) Though the reported UV spectrum, λ_{max}^{EtOH} 281 mμ (ε 11.7×10³), and that measured by the authors, λ_{max}^{EtOH} 293 (ε 11.2×10³), 275 (shoulder, ε 10.0×10³) and 214 mμ (ε 22.7×10³) differ, analytical data and other properties show that both samples are the same.

Thus, another route to IV should be explored on account of the lability of VIII.

Tosylate XIII was reduced with lithium aluminium hydride in tetrahydrofuran, XIV being expected to be produced in one step. However, the main product was a deoxydihydro derivative XV, XIV being obtained only as a minor one.

The dihydro compound XV lacks a NMR signal corresponding to the hydrogen at C-2 of tubercidin and shows a doublet at δ 1.30 assignable to the methyl group.

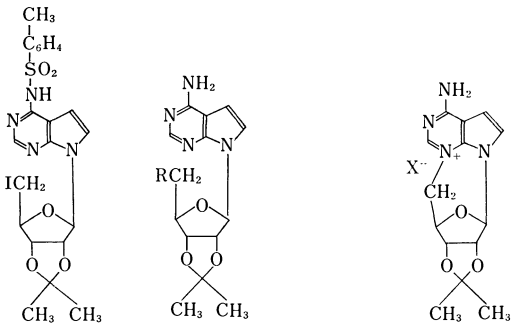

XVII VIII R=*p*-$CH_3C_6H_4SO_3$ X X=*p*-$CH_3C_6H_4SO_3$
IX R=OH XIX X=CH_3SO_3
XIV R=H
XVI R=CH_3CO_2
XVIII R=CH_3SO_3

In the mass spectrum the molecular ion was observed at *m/e* 446 and the base peak at M^+-2. Further fragmentations schematically shown in Chart 1 are also consistent in structure with that proposed for XV.

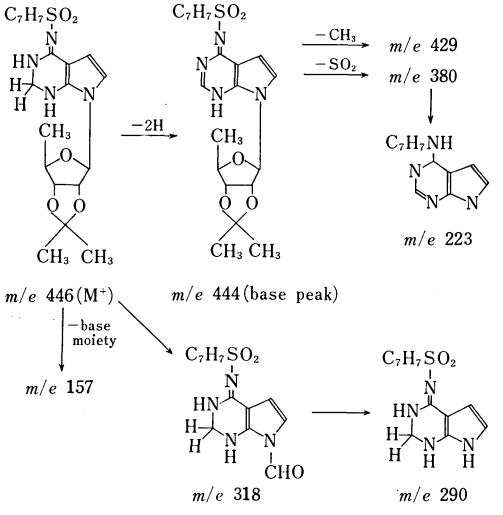

Treatment of XIV with dilute hydrochloric acid afforded IV, the NMR spectrum of which exhibited a three proton doublet at δ 1.28 assignable to the methyl group. The low yield of IV (1% from IX) in this procedure is, as mentioned above, attributable to the susceptibility of VIII to form X.

To prevent cyclonucleoside formation an attempt was made to protect the amino group of IX prior to *O*-tosylation. Ketal IX was treated with acetic anhydride in methanol. The reaction could not be brought to completion, and the product which was, unexpectedly, 5'-*O*-acetyl-2',3'-*O*-isopropylidenetubercidin (XVI) was obtained in a low yield.

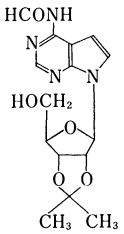

XXVIII

An attempt to prepare the N^6-dimethylaminomethylene derivative[19] using dimethylformamide dimethyl acetal as a reagent was also unsuccessful, and N^6-formyl-2′,3′-*O*-isopropylidenetubercidin (XXVIII) was obtained in a low yield.

2′,3′-*O*-Isopropylidene-5′-*O*-mesyltubercidin (XVIII) was treated with sodium iodide and acetic anhydride. Here again the formation of the cyclonucleoside XIX was predominant and XVIII was also converted into XIX easily on being left in a desiccator. Excess mesyl chloride afforded no N^6-mesyl compound.

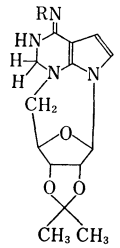

XX R=CH_3SO_2
XXI R=*p*-$CH_3C_6H_4SO_2$

Reduction of XIX with sodium borohydride in an aqueous solution was investigated, the nucleophilic attack at C-5′ of hydride anion being expected to afford the deoxy compound XIV. However, the product was intractable gummy material, and the dihydro cyclonucleoside XX was isolated from the reaction mixture in a low yield. The NMR spectrum of XX shows that two protons at C-5′ as well as those at C-2 are unequivalent. The mass spectrum is also consistent with the proposed structure, and the fragmentations are characterized by the cleavage of 2H, CH_3, CHO, $-NH-CH_2-$, $-CH_2CHO-$, and CH_3SO_2 from the molecular ion.

Similarly, X was reduced with sodium borohydride to give N^6-tosyl cyclonucleoside XXI. The close similarity of the UV spectrum of XXI to that of XV also supports the structural assignment.

Finally the conversion of tubercidin into 5′-deoxytubercidin was accomplished in the following manner. After mesylation of IX was carried out in pyridine at 0°C, excess benzoyl chloride was added to the reaction mixture without isolation of XVIII. N^6,N^6-Dibenzoyl-2′,3′-*O*-isopropylidene-5′-*O*-methanesulfonyltubercidin (XXII) was obtained along with a small amount of the tribenzoyl compound XXIII.

Compound XXII was treated with sodium iodide in methyl ethyl ketone to give three products. The main product was N^6,N^6-dibenzoyl-5′-deoxy-5′-iodo-2′,3′-*O*-isopropylidenetubercidin (XXIV), the monobenzoyl iodo compound XXV being obtained as a minor

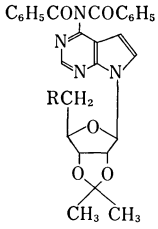

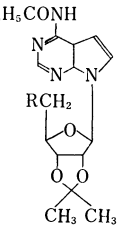

XXII R=CH_3SO
XXIII R=$C_6H_5CO_2$
XXIV R=I
XXVI R=H

XXV R=I
XXVII R=H

one. Another crystalline product was proved to have the molecular formula $C_{21}H_{21}N_3O_6$.[22]

Catalytic hydrogenation of XXIV afforded N^6,N^6-dibenzoyl-5′-deoxy-2′,3′-*O*-isopropylidenetubercidin (XXVI) and N^6-benzoyl-5′-deoxy-2′,3′-*O*-isopropylidenetubercidin (XXVII), the latter being the predominant product. Treatment of XXVII with dilute sodium hydroxide afforded 5′-deoxy-2′,3′-*O*-isopropylidenetubercidin (XIV), and the isopropylidene group of XIV was removed by heating in 80% aqueous acetic acid. Thus, tubercidin was converted into 5′-deoxytubercidin.

Experimental

2′,3′-O-Isopropylidene-5′-O-p-toluenesulfonyltubercidin (VIII) and its Cyclonucleoside Formation. The reaction was carried out under the same conditions as reported by Kuhn and Jahn.[17] Tosyl chloride (500 mg) was added at once to a solution of 2′,3′-*O*-isopropylidenetubercidin (IX) (500 mg) in pyridine (3 ml) cooled at −20°C. The solution was stirred for 2 hrs and was allowed to stand overnight at −15°C to −20°C. Ice-cooled water was added to the solution and the product was extracted with chloroform. The organic layer was washed with cold 2N H_2SO_4 and then with water. The solvent was evaporated to dryness below 30°C, affording 598 mg of the residue (yield, 76%). Though the maximum of the UV absorption was initially found at 270 mμ which is characteristic for the pyrrolo[2,3-*d*]pyrimidine chromophore of tubercidin, it gradually shifted to a higher wavelength on prolonged standing.

The residue was kept in a desiccator for 2 days at room temperature (15—25°C) and was distributed again between chloroform and water. The organic layer was evaporated to dryness below 30°C yielding 157 mg of syrup. Evaporation of the aqueous layer to dryness afforded 433 mg of crystalline solid, which was identical with a sample of the cyclonucleoside X obtained by the method reported by Mizuno *et al.*[2]

These results show that 72% of VIII was converted into X under the above-mentioned conditions.

For comparison 2′,3′-*O*-isopropylideneadenosine (500 mg) was tosylated under the same conditions affording 706 mg of a crude sample of 2′,3′-*O*-isopropylidene-5′-*O*-*p*-toluenesulfonyladenosine (VI) (yield, 90%). The product was kept in a desiccator at room temperature for 2 days and was distributed between chloroform and water. Evaporation of the organic layer as well as the aqueous layer to dryness afforded 430 mg and 266 mg of the residue, respectively, showing that

22) The loss of one nitrogen atom seems to be unusual. The NMR spectrum suggests that it is a cyclonucleoside showing characteristic signals of ABX type corresponding to two unequivalent methylene protons at C-5′.

38% of VI was converted into VII.

N^6-p-*Toluenesulfonyl-5'-deoxy-5'-iodo-2',3'-O-isopropylidenetubercidin (XVII).* A crude sample of VIII obtained from 2 g of IX was heated at 100°C in acetic anhydride (60 ml) in which sodium iodide (4 g) had been dissolved. After evaporation of acetic anhydride the residue was distributed between chloroform and an aqueous solution of sodium sulfite, and the organic layer was washed repeatedly with water. Column chromatography on silicic acid (benzene: ethyl acetate=1: 1) afforded 41 mg of XVII which was crystallized from ethyl acetate and ligroin. It decomposed gradually at 100—115°C; $\lambda_{max}^{methanol}$ 290 mμ (ε 19400).

Found: C, 44.77; H, 4.18; N, 9.83, S, 5.62%. Calcd for $C_{21}H_{23}N_4O_5SI$: C, 44.21; H, 4.06; N, 9.62; S, 5.71%.

Tosylation of 2',3'-O-Isopropylidenetubercidin (IX) at Room Temperature. Isolation of N-Tosylated Products. Tosyl chloride (4.9 g) was added at once to a solution of IX (2.2 g, 0.75 mmol) in pyridine (20 ml). After the solution was left standing at room temperature for 3 days, the products were distributed between an ice-cooled aqueous solution of sodium bicarbonate and ethyl acetate. The organic layer was concentrated to dryness, and the residue was extracted with hot methanol. The methanol insoluble substance was crystallized from dimethylformamide and methanol, and was assigned as 3,5'-cyclonucleoside (XI) of N^6-*p*-toluenesulfonyl-2',3'-*O*-isopropylidenetubercidin; yield, 110 mg; mp >300°C; $\lambda_{max}^{methanol}$ (ε) 313 (13800) and 220 mμ (33500); NMR (100 MHz, DMSO-*d*): 1.17, 1.42 (two isopropylidene methyls), 2.32 (s-3H, C<u>H</u>$_3$C$_6$H$_4$SO$_2$-), 4.13, 4.83 (a pair of doublet, 2H, H-2' and H-3', $J_{2',3'}$=6 Hz), 4.32 (broad d, 1H, H_a-5', J_{gem}=15 Hz), 4.6—5.0 (complex, 2H, H-4' and H_b-5'), 6.33 (s, 1H, H-1'), 6.62, 7.34 (a pair of doublet, 2H, -C<u>H</u>=C<u>H</u>-N<, $J_{7,8}$=4 Hz), 7.26, 7.80 (a pair of doublet, 4H, CH$_3$C$_6$<u>H</u>$_4$SO$_2$-, J_{orth}=8 Hz) and 8.24 ppm (s, 1H, -N=C<u>H</u>-N=).

Found: C, 56.95; H, 4.99; N, 12.77; S, 7.17%. Calcd for $C_{21}H_{22}N_4O_5S$: C, 57.00; H, 5.01; N, 12.67; S, 7.25%.

The methanol extract was fractionated with column chromatography on silicic acid, developed with a mixture of benzene and ethyl acetate (1: 1). Two compounds were obtained. One, moving faster and assigned as N^6-*p*-toluenesulfonyl-2',3'-*O*-isopropylidenetubercidin (XII), was crystallized from benzene; yield, 275 mg; mp 106—109°C: $\lambda_{max}^{methanol}$ (ε) 291 (16200) and 220 mμ (18600); $[\alpha]_D^{23}$ −77.5 (*c* 0.48, chloroform).

Found: C, 52.84; H, 5.45; N, 11.72; S, 7.55%. Calcd for $C_{21}H_{24}N_4O_6S\cdot H_2O$: C, 52.70; H, 5.48; N, 11.71; S, 6.70%.

The other compound, assigned as N^6,5'-*O*-di-*p*-toluenesulfonyl-2',3'-*O*-isopropylidenetubercidin (XIII), could hardly be separated from XII, and to obtain an analytical sample chromatography was repeated. It crystallized from benzene; yield, 300 mg; mp 106—109°C; $\lambda_{max}^{methanol}$ (ε) 291 (19600) and 223 mμ (35900).

Found: C, 54.73; H, 4.92; N, 9.30; S, 9.72%. Calcd for $C_{28}H_{30}N_4O_8S_2$: C, 54.71; H, 4.92; N, 9.12; S, 10.43%.

Similarity of the UV spectrum of XII with that of XIII shows that XIII is not a *N,N*-ditosyl compound.

Reduction of N^6,5'-O-*di*-p-*toluenesulfonyl-2',3'-O-isopropylidenetubercidin (XIII) with $LiAlH_4$.* A solution of XIII (300 mg) in tetrahydrofuran (20 ml) was refluxed with $LiAlH_4$ (300 mg) for 20 hr, and excess of the reagent was decomposed in the usual manner. The products were extracted with ethyl acetate and developed on a column of silicic acid. Two compounds were obtained. The less polar one assigned as 1,2-dihydro-N^6-*p*-toluenesulfonyl-5'-*O*-deoxy-2',3'-*O*-isopropylidenetubercidin (XV) was eluted from the column with a mixture of benzene and ethyl acetate (1: 1) and was obtained as a glass melting at 75—85°C; yield, 90 mg; $\lambda_{max}^{methanol}$ (ε) 308 (6900), 252 (14200) and 222 mμ (19800); NMR (60 MHz, $CDCl_3$): 1.30 ppm (d, 3H, $J_{4',5'}$=6 MHz).

Found: C, 56.81; H, 5.74; N, 12.29; S, 6.90%. Calcd for $C_{21}H_{26}N_4O_5S$: C, 56.48; H, 5.87; N, 12.25; S, 7.18%.

The other compound, assigned as 5'-deoxy-2',3'-*O*-isopropylidenetubercidin (XIV), was eluted from the column with a mixture of ethyl acetate and methanol (19: 1). The spectral data were identical with those of a sample obtained by alkaline hydrolysis of N^6-benzoyl-2',3'-*O*-isopropylidenetubercidin (XXVII).

Acetylation of 2',3'-O-Isopropylidenetubercidin (IX) in Methanol. Acetic anhydride was added (2 ml, each time) at 8 hr intervals (three times) at room temperature to a methanolic solution of IX (1 g/10 ml). After 24 hr the solution was poured on an ice-cooled aqueous solution of sodium bicarbonate. The product was extracted with ethyl acetate and separated from the starting material by silicic acid chromatography using a solvent system of ethyl acetate and methanol gradually increasing the content of the latter.

It was assigned as 5'-*O*-acetyl-2',3'-*O*-isopropylidenetubercidin (XVI), the UV spectrum being similar to that of tubercidin; $\lambda_{max}^{methanol}$ 270 mμ (ε 11000); M^+ 348 ($C_{16}H_{20}N_4O_5$); ν_{max}^{KBr} 1745 cm^{-1} (ester).

Found: C, 55.15; H, 5.93; N, 15.55%. Calcd for $C_{16}H_{20}N_4O_5$: C, 55.16; H, 5.93; N, 16.08%.

Reaction of 2',3'-O-Isopropylidenetubercidin (IX) with Dimethylformamide Dimethylacetal. Dimethylformamide dimethyl acetal (0.5 ml) was added at once to a solution of IX (200 mg) in dimethylformamide (5 ml). The solution was heated at 70°C for 60 hr and then left standing at room temperature for 14 hr. After the solvent was removed, the residue, which showed two distinct spots on tlc, was applied to column chromatography on silicic acid. The less polar compound, assigned as N^6-formyl-2',3'-*O*-isopropylidenetubercidin (XXVIII), was eluted from the column with ethyl acetate and obtained as a syrup; yield, 40 mg: Mass: M^+ 334.1292 (Calcd for $C_{15}H_{18}N_4O_5$ 334.1278), M^+ +CO 362.1196 (Calcd for $C_{16}H_{18}N_4O_6$ 362.1226).

To obtain an analytical sample, fractional precipitation from ethyl acetate and ligroin was effective.

Found: C, 53.54; H, 5.23; N, 15.92%. Calcd for $C_{15}H_{18}N_4O_5$: C, 53.88; H, 5.43; N, 16.76%.

The other compound, eluted with a mixture of ethyl acetate and methanol (9: 1), was found to be the starting material.

3,5'-Cyclonucleoside Methanesulfonate (XIX) of 2',3'-O-Isopropylidenetubercidin. Mesyl chloride (1.432 g, 13.2 mmol) was added dropwise to an ice-cooled and stirred solution of IX (1.224 g, 4 mmol) in pyridine (30 ml). After the solution was kept at 0°C overnight, it was poured on an ice-cooled aqueous solution of sodium bicarbonate. The product, 2',3'-*O*-isopropylidene-5'-*O*-methanesulfonyltubercidin (XVIII), was extracted with ice-cooled chloroform and the organic layer was heated under reflux for 1 hr. The product XIX was hardly soluble in solvents and could be easily separated from XVIII by extraction with water; yield, 1.2 g. To prepare an analytical sample, fractional precipitation from methanol and benzene was effective: mp 188°C; $\lambda_{max}^{methanol}$ (ε) 293 (11200), 275 (10000) and 214 mμ (22700).

Found: C, 45.97; H, 5.23; N, 14.24; S, 8.27%. Calcd for $C_{15}H_{20}N_4O_6S\cdot 1/2H_2O$: C, 45.79; H, 5.38; N, 14.24; S, 8.15%.

Reduction of the Cyclonucleoside XIX with Sodium Borohydride. $NaBH_4$ (800 mg) was added at once to an aqueous solution of XIX (800 mg/10 ml), and the solution was stirred at room temperature for 6 hr. Extraction with chloroform and evaporation of the solvent afforded 400 mg of the residue, which was then purified with silicic acid chromatography. A compound showing a distinct spot on tlc was obtained. It was

assigned as 3,5′-cyclonucleoside (XX) of N^6-methanesulfonyl-1,2-dihydro-2′,3′-*O*-isopropylidenetubercidin; syrup; yield, 35 mg; $\lambda_{max}^{methanol}$ (ε) 308 (7000), 240 (15600) and 222 mμ (18200); Mass: M$^+$ 368 ($C_{15}H_{20}N_4O_5S$), M$^+$ −2H 366, M$^+$ −CH_2NH 260; NMR (100 MHz, $CDCl_3$): 1.34, 1.52 (two isopropylidene methyls), 3.02 (s, 3H, CH_3SO_2N=), 3.29 (q, 1H, H_a-5′, J_{gem}=24 Hz, $J_{5'a,4'}$=3 Hz), 4.70, 4.96 (a pair of doublet, 2H, –NH–CH_2–N=, J_{gem}=6 Hz), 5.62 (s, 1H, H-1′), 6.36 and 6.44 ppm (a pair of doublet, 2H, –CH=CH–N=, $J_{7,8}$=4 Hz).

With increase of methanol content in the developing solvent, gummy materials which tailed on tlc were eluted, and an attempt to obtain another compound failed.

Reaction of the Cyclonucleoside X with Sodium Borohydride. $NaBH_4$ (10 mg) was added to an aqueous solution of X (10 mg/ml), and the solution was stirred at room temperature for 1 hr. The product, 3,5′-cyclonucleoside (XXI) of 1,2-dihydro-N^6-*p*-toluenesulfonyl-2′,3′-*O*-isopropylidenetubercidin, was extracted with ethyl acetate, and was fractionally precipitated with ethyl acetate and ligroin to give a syrup; yield, 3 mg; $\lambda_{max}^{methanol}$ (ε) 312 (5700), 245 (shoulder, 8400) and 220 mμ (17500); Mass: M$^+$ 444.1455 (Calcd for $C_{21}H_{24}N_4O_5S$ 444.1468), M$^+$−H−SO_2 379.1724 ($C_{21}H_{23}N_4O_3$ 379.1770), M$^+$−$C_7H_7SO_2$ 289.1289 ($C_{14}H_{17}N_4O_3$ 289.1301), M$^+$−$C_7H_7SO_2$−CH_2N 261.1126 ($C_{13}H_{15}N_3O_3$ 261.1113).

N^6,N^6-Dibenzoyl-2′,3′-O-isopropylidene-5′-O-methanesulfonyltubercidin (XXII). Mesyl chloride (1.37 g, 12 mmol) was added dropwise to a stirred and ice-cooled solution of IX (3.06 g, 10 mmol) in pyridine (10 ml), and the solution was kept at 0°C overnight. Benzoyl chloride (4.2 g, 30 mmol) was added, and after the solution was left overnight in a refrigerator it was poured on an ice-cooled aqueous solution of sodium bicarbonate. The products were extracted with chloroform and separated with column chromatography on silicic acid. The less polar product, eluted with a mixture of benzene and ethyl acetate (4: 1), was crystallized from ethyl acetate and ligroin, and was assigned as N^6,N^6,5′-*O*-tribenzoyl-2′,3′-*O*-isopropylidenetubercidin (XXIII); yield, 170 mg; mp 110—113°C; $\lambda_{max}^{methanol}$ (ε) 281 (11600), 273 (12000) and 226 mμ (43000); $[\alpha]_D^{25}$ −38.1° (*c* 17.0, chloroform).

Found: C, 67.37; H, 4.87; N, 8.99%. Calcd for $C_{35}N_{30}N_4O_7$: C, 67.95; H, 4.89; N, 9.06%.

The main product, N^6,N^6-dibenzoyl-2′,3′-*O*-isopropylidene-5′-*O*-methanesulfonyltubercidin (XXII), was eluted from the column with a mixture of benzene and ethyl acetate (1: 1). After being crystallized from ethyl acetate and ligroin, the yield was 3.38 g; mp 110—113°C; $\lambda_{max}^{methanol}$ (ε) 280 (shoulder, 11100), 240 (shoulder, 27200) and 222 mμ (33400); NMR (60 MHz, $CDCl_3$): 1.38, 1.63 (two isopropylidene methyls), 2.86 (s, 3H, $C\underline{H}_3SO_2$-) and 7.3—7.9 ppm (complex, 10H, $C_6\underline{H}_5CONCOC_6\underline{H}_5$); $[\alpha]_D^{25}$ −13.4° (*c* 1.61, chloroform).

Found: C, 58.66; H, 4.69; N, 9.33; S, 5.39%. Calcd for $C_{29}H_{28}N_4O_8S$: C, 58.77; H, 4.76; N, 9.46; S, 5.41%.

Reaction of N^6,N^6-Dibenzoyl-2′,3′-O-isopropylidene-5′-O-methanesulfonyltubercidin (XXII) with Sodium Iodide. A solution of XXII (1.284 g, 2 mmol) and sodium iodide (1.3 g, 8 mmol) in methyl ethyl ketone (20 ml) was refluxed for 30 min. After sodium mesylate which rapidly precipitated was removed by filtration, the products were distributed between an aqueous solution of sodium sulfite and chloroform. The organic layer was taken, washed with water and concentrated to dryness. The residue (1.18 g) was applied to column chromatography on silicic acid, developed with a mixture of benzene and ethyl acetate increasing ethyl acetate content gradually. The main product, N^6,N^6-dibenzoyl-5′-deoxy-5′-iodo-2′,3′-*O*-isopropylidenetubercidin (XXIV), was eluted first and was crystallized from ethyl acetate and ligroin; yield, 784 mg; mp 105—112°C; $\lambda_{max}^{methanol}$ (ε) 280 (12000) and 223 mμ (21000); $[\alpha]_D^{23}$ −51.2° (*c* 0.91, chloroform).

Found: C, 53.90; H, 3.99; N, 8.83; I, 20.42%. Calcd for $C_{28}H_{25}N_4O_5I$: C, 53.85; H, 4.04; N, 8.97; I, 20.32%.

N^6-Benzoyl-5′-deoxy-5′-iodo-2′,3′-*O*-isopropylidenetubercidin (XXV) was eluted next, and was purified with fractional precipitation from ethyl acetate and ligroin; syrup; yield, 77 mg; $\lambda_{max}^{methanol}$ (ε) 299 (9800), 235 (shoulder, 22000) and 223 mμ (27000); M$^+$ 520.0583 (Calcd for $C_{21}H_{21}N_4O_4I$ 520.0607).

The starting material, which moved slightly more slowly than XXV, was also isolated; yield, 48 mg. It was also found by other experiments that attempts to complete the reaction by prolonged reaction time resulted in the decrease of the yield of XXIV.

The most polar substance, eluted from the column with a mixture of benzene and ethyl acetate (1: 1) was obtained as crystals; yield, 100 mg; mp 191—193°C. The structure is still undetermined.

N^6,N^6-Dibenzoyl-5′-deoxy-2′,3′-O-isopropylidenetubercidin (XXVI) and N^6-Benzoyl-5′-deoxy-2′,3′-O-isopropylidenetubercidin (XXVII). The iodo compound XXIV (784 mg) was catalytically hydrogenated at room temperature for 3 hr in 95% ethanol (20 ml) containing sodium acetate (1 g) in the presence of 10% Pd-C (200 mg). Ethanol was removed by evaporation and the residue was extracted with chloroform. Tlc showed the presence of two compounds which were separated with column chromatography on silicic acid developed with a mixture of benzene and ethyl acetate (2: 1). The less polar compound, assigned as N^6,N^6-dibenzoyl-5′-deoxy-2′,3′-*O*-isopropylidenetubercidin (XXVI), was crystallized from ethyl acetate and ligroin; yield, 58 mg; mp 192—194.5°C; $\lambda_{max}^{methanol}$ (ε) 280 (shoulder, 11500) and 223 mμ (33500); $[\alpha]_D^{23}$ −60.8° (*c* 0.45, chloroform); M$^+$ 498.1882 ($C_{28}H_{26}N_4O_5$ 498.1903); NMR (60 MHz, $CDCl_3$): 1.37, 1.62 (two isopropylidene methyls) and 1.39 ppm (d, 3H, $C\underline{H}_3$-ÇH–, $J_{4',5'}$=7 Hz).

Found: C, 66.93; H, 5.05; N, 11.16%. Calcd for $C_{28}H_{26}N_4O_5$: C, 67.46; H, 5.26; N, 11.24%.

The main product, N^6-benzoyl-5′-deoxy-2′,3′-*O*-isopropylidenetubercidin (XXVII), was eluted later and crystallized from ethyl acetate and ligroin; yield, 430 mg; mp 128.5—129.0°C; $\lambda_{max}^{methanol}$ (ε) 300 (9400) and 224 mμ (26400); $[\alpha]_D^{23}$ −43.2° (*c* 0.84, chloroform); M$^+$ 394.1675 (Calcd for $C_{21}H_{22}N_4O_4$ 394.1641); NMR (60 MHz, $CDCl_3$): 1.37, 1.63 (two isopropylidene methyls) and 1.38 ppm (d, 3H, $C\underline{H}_3$–ÇH–, $J_{4',5'}$=6 Hz).

Found: C, 63.98; H, 5.48; N, 14.88%. Calcd for $C_{21}H_{22}N_4O_4$: C, 63.94; H, 5.62; N, 14.21%.

5′-Deoxy-2′,3′-O-isopropylidenetubercidin (XIV). A solution of XXVII (100 mg) in 50% ethanol (10 ml) containing 0.05N NaOH was refluxed. Tlc monitoring showed that the reaction was complete after 1 hr, and the product was homogeneous. Extraction with chloroform and concentration to dryness afforded 70 mg of syrup: $\lambda_{max}^{methanol}$ 268 mμ (ε 11900); M$^+$ 290.1422 (Calcd for $C_{14}H_{18}N_4O_3$ 290.1379).

5′-Deoxytubercidin (IV). A solution of XIV (150 mg) in 80% acetic acid (20 ml) was refluxed for 5 hr and concentrated to dryness. The residue, which was homogeneous on tlc, was crystallized from ethanol and benzene, and assigned as 5′-deoxytubercidin (IV) containing one mole of acetic acid; yield, 110 mg; mp 203—207°C; $\lambda_{max}^{methanol}$ 270 mμ (ε 12700); NMR (100 MHz, DMSO-*d*): 1.28 (d, 3H, $C\underline{H}_3$–ÇH–, $J_{4',5'}$=6 Hz), 1.92 (s, 3H, $C\underline{H}_3COOH$), 6.03 (s, H-1′, $J_{1',2'}$=5 Hz), 6.63, 7.27 (a pair of doublet, 2H, –C$\underline{H}$=C$\underline{H}$–N=, $J_{7,8}$=3 Hz) and 8.04 ppm (s, 1H, –N=C$\underline{H}$–N=).

Found: C, 50.03; H, 5.70; N, 18.19%. Calcd for $C_{13}H_{18}$-

N_4O_5: C, 50.31; H, 5.85; N, 18.06%. $[\alpha]_D^{23}$ −70.3° (*c* 0.48, DMSO).

Acetic acid was lost on heating at 100°C for 4 hr *in vacuo*. M^+ 250.1078 ($C_{11}H_{14}N_4O_3$ 250.1066).

Found: C, 52.28; H, 5.54; N, 22.29%. Calcd for $C_{11}H_{14}N_4O_3$: C, 52.79; H, 5.64; N, 22.39%.

The authors express their hearty thanks to Kaken Kagaku Co. Ltd. for the supply of tubercidin.

BULLETIN OF THE CHEMICAL SOCIETY OF JAPAN, VOL. 46, 623—626 (1973)

Structural Effects on the Properties of Nonionic Surfactants. II. Acetal Type Homogeneous Nonionics Having Polyoxyethylene Chains Terminated with Methoxyl Group[1]

Hideo TAKAHASHI and Tsunehiko KUWAMURA

Department of Synthetic Chemistry, Faculty of Engineering, Gunma University, Tenjincho, Kiryu

(Received July 8, 1972)

A series of homogeneous acetal nonionics (AGM types) with the general formula $RCH[O(C_2H_4O)_mCH_3]_2$ were prepared from higher alkanals (C_8–C_{14}) and several pure polyoxyethylene (POE) glycol monomethylethers (m: 3—6), and purified by repeated distillation *in vacuo*. Cloud point, critical micelle concentration (CMC) and molecular area on adsorbed film were determined for AGM types. The results were compared with data on homogeneous acetals (AG types) having terminal hydroxyl in POE chains. The result confirms the suggestion that two POE chains in AG strongly interact with each other owing to intramolecular hydrogen-bonding and intertwisting. AGM are extremely low foaming nonionics although their ability to lower surface tension is comparable to that of the usual nonionics.

The object of this study is to clarify the effect of multi-chain hydrophile in polyether type nonionics on surfactant properties. It is well-known that molecular area (A) of polyether type nonionics is determined by the chain length of POE. Van Voorst Vader[2] theoretically interpreted the fact that $A/m^{1/2}$, where m is a unit number of POE chain, is constant, on the basis of a random coil configuration of POE chain. However, A of AG types with the general formula $RCH[O(C_2H_4O)_mH]_2$ is only slightly greater than that of simple type nonionics $RCH_2O(C_2H_4O)_mH$ (S types).[3] Thus, we have assumed that two POE chains are closely situated by acetal linkage and by mutual interaction owing to hydrogen-bonding of terminal hydroxyl groups, holding an intertwisted configuration rather than random coil. We have also suggested that the configurational characteristics of AG types should be related to the fact that their cloud point is unexpectedly low and CMC decreases with increasing m.

We measured cloud point, surface tension and foaming power for a series of AGM having terminal methoxyl in place of hydroxyl in POE chains in order to confirm the interaction between two geminal POE chains. Discussion is given on surface film state and the configuration of acetal type nonionics in aqueous solution.

Experimental

Materials. Straight alkanals purified as described previously were used.[3] POE monomethylethers were obtained by the fractional distillation of polyaddition products of ethylene oxide to methyl cellosolve. They were determined to be 99% pure by glc on Carbowax 20 W. Unit number m was evaluated from integrated NMR spectra, where signals of terminal methyl and methylene protons of POE chains appeared at 3.30 and 3.55 ppm, respectively.

Preparation of AGM Acetals. In a reaction flask, were placed 0.75 mol of POE monomethylether, a catalytic amount of concentrated hydrochloric acid and 0.15 mol of alkanal which were heated at 60°C for 4 hr. The reaction mixture was then treated in the same way as described in the preparation of AG[3] and finally distilled under reduced pressure in a stream of nitrogen to give a colorless AGM acetal. Purity and structure of the products were confirmed by elementary analysis, thin layer chromatography, IR and NMR spectra.

Measurements. Cloud point was measured on a 1.0% aqueous solution. Equilibrium surface tension γ at 20 ± 1°C and foaming power at 25 ± 1°C were measured by the methods described previously.[3] In addition to the surface tension method, iodine solubilization method[4] was used for the determination of CMC. In the latter the minimum transmittance at 390 mμ (T_{390}) referring to iodine-surfactant micelle complex was measured with a Hitachi spectrophotometer ES-20 and plotted against concentration.

Results and Discussion

Preparation of pure acetal nonionics was insured by use of pure starting materials and careful final purification. Physical constants, properties and analytical data to assess the purity of POE monomethylethers and AGM products are shown in Tables 1 and 2.

1) Presented in part at the 9th Annual Meeting of the Oil Chemists' Society of Japan, Sendai, 8th. October 1970.

2) F. van Voorst Vader, *Trans. Faraday Soc.*, **56**, 1078 (1960).

3) T. Kuwamura and H. Takahashi, This Bulletin, **45**, 617 (1972).

4) S. Ross and J. P. Olivier, *J. Phys. Chem.*, **63**, 1671 (1959).

Table 1. Properties and hydroxyl content of polyoxyethylene glycol monomethylethers $CH_3O(C_2H_4O)_mH$

m	Bp, °C/mmHg	n_D^{25}	OH%	
			Found	Calcd
3	86— 89/1	1.4355	10.7	10.4
4	123—125/1	1.4439	8.3	8.2
5	145—147/1	1.4489	6.5	6.7
6	160—167/1	1.4513	5.6	5.7

The IR spectra of AGM showed no carbonyl and hydroxyl absorption but a strong absorption at 1000—1100 cm^{-1}. In the NMR spectra (in CCl_4), five signals at δ=0.88, 1.27, 3.30, 3.55, and 4.50 ppm due to the protons of methyl, methylene in the alkyl chain, methoxyl, methylene in POE chains and methine in acetal linkage respectively, were observed with reasonable intensity (Fig. 1). Plotting of refractive index of AGM against m gave a smooth curve suggesting no contamination with impurity (Fig. 2). In all cases of preparation, purity rather than yield was emphasized. The yields given in Table 2, however, represent practical values as compared with those in the conventional method which consists of several steps to build up a homogeneous nonionics containing such a large number of m.

Cloud point was plotted against m giving characteristic smooth curve (Fig. 2). In order to clarify the structural effect of hydrophile on hydration, cloud point is represented as a function of Davies's HLB value in Fig. 3. If the "group numbers" proposed by Davies[5]

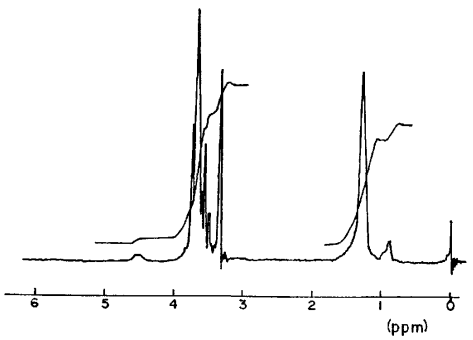

Fig. 1. NMR spectrum of AGM-12(6).

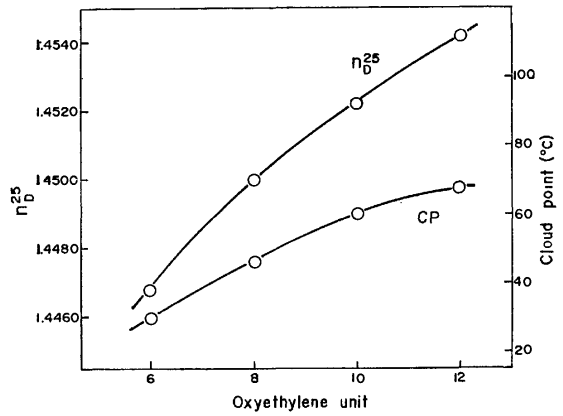

Fig. 2. Plots of refractive index and cloud point *vs.* oxyethylene unit number (m).

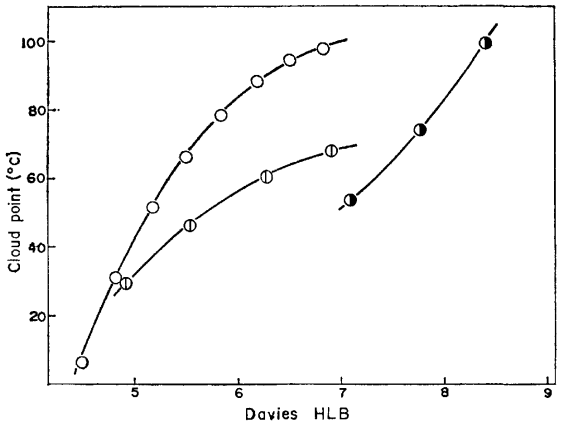

Fig. 3. Plots of cloud point *vs.* Davies HLB. ◐; AGM-12, ◑; AG-12, ○; S-12 (Data in Ref. 6 for the homogeneous polyoxyethylene n-dodecanol).

have a universality for various types of nonionics, the curve of AGM would be superimposable on those of S and AG types.[3] However, they are situated separately in the following order: S, AGM, and AG from left to right in Fig. 3. The result suggests a discount of Davies "group number" for acetal type nonionics. Such a hindrance to hydration for AG could be discussed on the basis of the following three structural factors. (1) The interaction between two POE chains

Table 2. Properties, analytical data and yields of AGM types

Nonionics	R	$2m$	Bp, °C/mmHg	n_D^{25}	Cloud point, °C	Anal (Calcd)		Yield %
						C%	H%	
AGM-8(6)	C_7	6	189/1.5	1.4440	34.0	60.01(60.25)	10.49(10.57)	35
AGM-10(6)	C_9	6	190—192/1.0	1.4453	33.0	61.52(61.77)	10.66(10.80)	30
AGM-12(6)	C_{11}	6	213—216/1.0	1.4468	30.0	63.03(63.13)	10.97(11.00)	45
AGM-12(8)	C_{11}	8	238—240/1.0	1.4500	46.0	61.77(61.83)	10.70(10.72)	45
AGM-12(10)	C_{11}	10	266—270/1.0	1.4522	60.5	60.82(60.87)	10.53(10.52)	40
AGM-12(12)	C_{11}	12	300—304/0.5	1.4542	67.0	60.09(60.13)	10.31(10.36)	20
AGM-14(6)	C_{13}	6	220—222/0.2	1.4484	28.5	64.26(64.33)	11.10(11.18)	40
AGM-14(8)	C_{13}	8	266—271/0.9	1.4509	45.0	62.84(62.92)	10.85(10.89)	40
AGM-14(10)	C_{13}	10	300—306/0.9	1.4532	59.0	61.79(61.86)	10.63(10.67)	20

5) J. T. Davies, Proc. Intern. Congr. Surface Active Substances, 2nd, London, Vol. I, p. 426 (1957).

6) S. Schüring and W. Ziegenbein, *Tenside*, **6**, 161 (1967).

in a molecule due to hydrogen-bonding of terminal hydroxyl groups. (2) Very close situation of two POE chains by acetal linkage. (3) The presence of two oxyethylene units adjacent to the hydrophobe. The hindrance related to (2) and (3) can be observed in some multi-chain type nonionics derived from α,α'-glyceryl diethers[7] and alkyl ethers of pentaerythritol.[8] On the basis of (1), the fact that the replacement of two terminal hydroxyl with methoxyl causes the shift of the cloud point-HLB curve to the left side can be explained (Fig. 3), but the curve for AGM cannot be superimposed on that for S type. We see that, in the region of cloud point 50—60°C, 40—60% of the hindrance for AG is due to (1) and the rest to (2) and (3). In the region of high cloud point, however, the interaction in (1) may be significantly released and the cloud point markedly rises up by regaining of hydration capacity, so that the curve for AG is somewhat concave in contrast to the typical convex curves for AGM and S types.

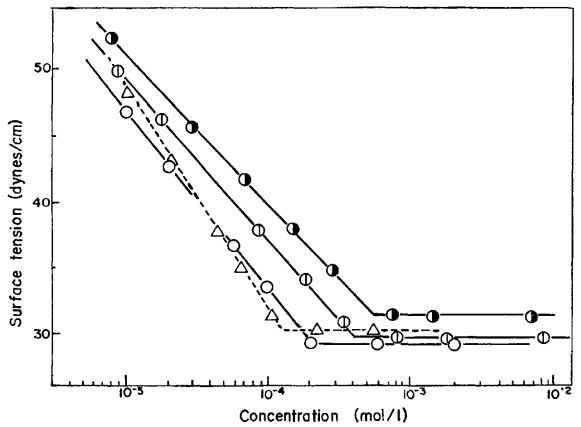

Fig. 4. Plots of γ *vs.* concentration. ○; AGM-12(6), ◐; AGM-12(8), ◑; AGM-12(10), △; AG-12(6).

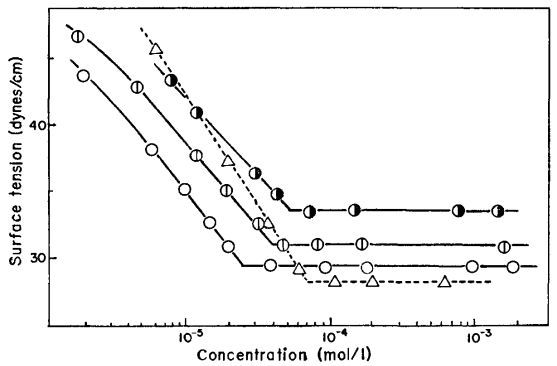

Fig. 5. Plots of γ *vs.* concentration. ○; AGM-14(6), ◐; AGM-14(8), ◑; AGM-14(10), △; AG-14(6).

On the measurement of aqueous surface tension, considerably long periods of ageing (2—4 hr) were observed for AGM as well as AG. Plots of the obtained γ *vs.* logarithm of the concentration for AGM are shown in Figs. 4 and 5. From the slope of the curves, surface excess Γ and molecular area A at CMC were determined by applying the simple form of Gibbs' adsorption equation. They are listed together with the related data for AG and S in Table 3.

The magnitude of A apparently increases in the order S<AG<AGM. However, A of AGM does not yet attain twice as large as that of the corresponding S[9,10] (*e.g.*, it is appropriate to compare among AGM-12(10), AG-12(10), and S-12(5)). Plots of $A/m^{1/2}$ for S and of $A/(2m^{1/2})$ for AG and AGM against m gave three straight lines which increase the negative slope in the order S<AGM<AG (Fig. 6). This indicates that A of S expectedly increases in proportion to $m^{1/2}$ and that the increment of A per one POE chain for AGM with increasing m is smaller than that for S and greater than that for AG.

Table 3. Surface active properties of AGM, AG, and S types at 20°C

Nonionics	γ_{CMC} (dynes/cm)	CMC × 10^4 (mol/l) I[c]	CMC × 10^4 (mol/l) II[d]	$\Gamma \times 10^{10}$ (mol/cm²)	A (Å²)	$A/m^{1/2}$
AG-12(6)	30.2	1.23	—	3.05	54.5	31.5
AG-12(10)	33.8	0.206	—	2.83	58.6	26.2
AGM-12(6)	29.2	2.11	1.72	2.42	68.5	39.5
AGM-12(8)	29.7	4.05	3.40	2.17	76.3	38.2
AGM-12(10)	31.3	5.78	5.00	1.99	83.2	37.2
AG-14(6)	28.2	0.650	—	3.19	52.0	30.0
AG-14(10)	36.2	0.170	—	3.05	54.5	24.4
AGM-14(6)	29.5	0.250	0.320	2.51	66.1	38.2
AGM-14(8)	31.0	0.403	0.430	2.28	72.8	36.4
AGM-14(10)	33.6	0.552	0.605	2.05	81.0	36.2
S-12(5)[a]	29.7	6.8	—	3.88	43	19.2
S-12(5)[b]	—	—	—	—	56.0	25.0

a) Data in Ref. 10 for the homogeneous polyoxyethylene *n*-dodecanol, the number of oxyethylene unit is shown in parentheses.
b) Data in Ref. 9.
c) Determined by surface tension method.
d) Determined by iodine solubilization method.

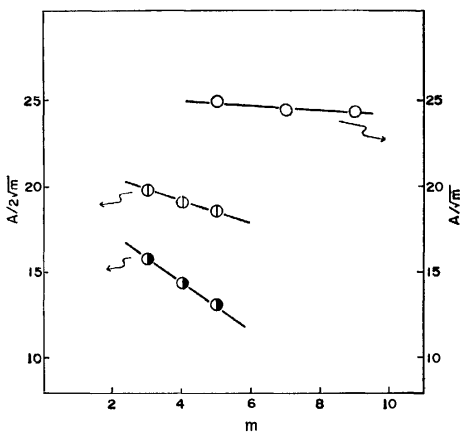

Fig. 6. Plots of $A/m^{1/2}$ and $A/(2\ m^{1/2})$ *vs.* m. ◐; AGM-12, ◑; AG-12, ○; S-12 (Data in Ref. 9 for the homogeneous polyoxyethylene *n*-dodecanol).

7) T. Kuwamura and E. Kameyama, *Kogyo Kagaku Zasshi*, **65**, 1266 (1962).
8) T. Kuwamura and H. Fukutomi, Proc. Intern. Congr. Surface Active Substances, 5th, Barcelona, Vol. I, p. 71 (1968).
9) H. Lange, *Kolloid-Z.*, **201**, 131 (1965).
10) N. Ohba and A. Takahashi, Proc. Intern. Congr. Surface Active Substances, 5th, Barcelona, Vol. II, p. 481 (1968).

The results could be discussed on the basis of structural factors as regards the hindrance of hydration for acetal nonionics. For AG containing factors (1) and (2), the interaction between two POE chains in a molecule is so pronounced that POE chains in surface film might take a significantly stretched and intertwisted configuration. Although the interaction is considerably released for AGM lacking factor (1), the POE chains still do not take such free random coils as those of S but undergo a sort of configurational restriction. All acetal nonionics we studied contain the shorter POE chains ($m<6$), for which van Voorst Vader's theory might virtually not be applicable. Thus, the characteristic film state of acetal nonionics might be due to shortness of POE chains attached. As for homogeneous S types ranging in m 1—10, however, the data obtained by Lange[11] with the use of film balance method gave no evidence for configurational transformation in surface film with variation in m.

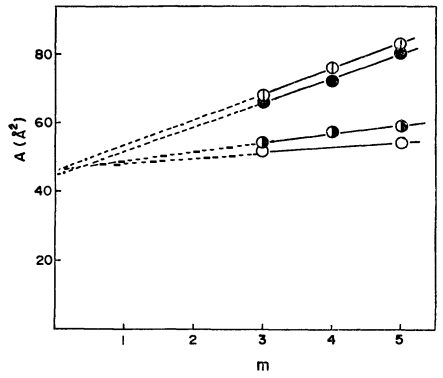

Fig. 7. Plots of A *vs.* *m*. ⦶; AGM-12, ●; AGM-14, ◑; AG-12, ○; AG-14.

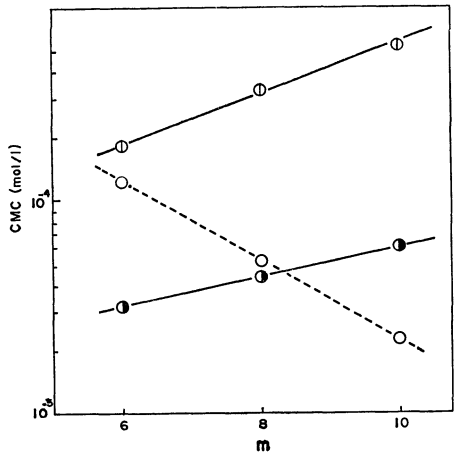

Fig. 8. Plots of CMC *vs.* *m*. ⦶; AGM-12, ◑; AGM-14, ○; AG-12.

11) H. Lange, *Kolloid-Z.*, **182**, 123 (1962).

Table 4. Foam volume (ml) of AGM, AG, and S types at 25°C

Nonionics	Concentration of solution (wt%) 0.1			0.5		
	Standing time (min) 0	1	5	0	1	5
AGM-12(6)	60	0	—	70	0	—
AGM-12(8)	50	0	—	50	0	—
AGM-12(10)	60	0	—	70	0	—
AGM-12(12)	70	0	—	80	0	—
AGM-14(8)	70	0	—	90	0	—
AG-12(6)	130	10	0	170	20	0
S-12($\overline{6.1}$)[a]	250	200	100	260	260	160

a) Ethylene oxide condensate of *n*-dodecanol prepared by the base-catalyzed method. The average number of ethylene oxide added is shown in parentheses.

Interesting information was obtained from plots of *A vs. m* for acetal nonionics. In Fig. 7, is shown the extrapolation of the linear *A vs. m* plots for AG and AGM varying in hydrophobe chain length. All the extrapolations converge at $m=0$ and give a limiting area, 45—47 Å², which seems to be equivalent to molecular area of hydrated higher alkanal, $RCH(OH)_2$, in a closely packed film.

The CMC values determined by two methods are listed in Table 3. We found that[3] CMC of AG decreases with an increase in m contrary to m dependence of CMC for the conventional nonionics[12] and suggested that this phenomenon is closely related to a configurational feature of hydrophile in AG. Plots of logarithm of CMC *vs.* *m* gave a straight line with positive slope for AGM in contrast to negative one for AG (Fig. 8). We also see that CMC of acetal nonionics increases by the replacement of terminal hydroxyl groups with more hydrophobic methoxyl groups.

It is concluded that the relatively low CMC and the abnormal trend on micellization of AG is caused by factor (1), which significantly affects hydration and configuration of POE chains.

The foaming property of AGM is markedly low as compared with those of S and AG (Table 4). It is likely that the greater cross section of the hydrophile and the hydrophobic terminal groups in AGM are unfavorable to closely packed alignment as regards the strength of foam film.

The authors wish to thank Miss Y. Umezu and the late Mr. M. Gotoh for their assistance in the experiment, and Givaudan Co. Ltd. for the supply of alkanal. Acknowledgement is made to the Ministry of Education for financial aid.

12) P. Becher, "Nonionic Surfactant," ed. by M. J. Schick, Marcel Dekker Inc., New York, (1967), p. 478.

NOTES

BULLETIN OF THE CHEMICAL SOCIETY OF JAPAN, VOL. 46, 627—628 (1973)

Topochemical Studies. II. The Crystal and Molecular Structure of the Second Polymorph of Chalcone, Ph-CH=CH-CO-Ph

Kenji OHKURA,* Setsuo KASHINO, and Masao HAISA

Department of Chemistry, Faculty of Science, Okayama University, Tsushima, Okayama

(Received June 13, 1972)

Crystals of chalcone are polymorphic and exist in many forms with different melting points.[1] Photochemistry of chalcone in solid state is of interest from a topochemical point of view because polymorphic modifications of this compound show significant differences in chemical behavior against ultraviolet light. Crystal structure of form I (mp 59°C) has been determined by Rabinovich,[2] the molecules are arranged in alternating layers related by the two-fold screw-axis along [001] and the shortest contact between C=C group is 5.2 Å so that crystals of this modification are light-stable. We have obtained crystals of form II and determined the crystal and molecular structure of this modification.

Experimental

The material was prepared by the condensation of benzaldehyde and acetophenone in alcoholic sodium hydroxide.[3] Crystals obtained by slow evaporation from ether solution were orthorhombic parallelepipeds elongated along the *b*-axis.

Crystal data: $C_{15}H_{12}O$; $M=208.2$; mp=56°C, orthorhombic, $a=10.90(2)$, $b=11.90(1)$, $c=17.93(1)$ Å, $V=2324.6$ Å^3, $Dm=1.179$, $Dc=1.178$ g·cm^{-3}, $Z=8$. Absorption coefficient for Cu $K\alpha$; $\mu=6.88$ cm^{-1}. $F(000)=880$.

Systematically absent spectra: $h0l$ when l odd, $0kl$ when k odd, $hk0$ when $h+k$ odd. Space group *Pbcn*.

Reflections were recorded with Cu$K\alpha$ radiation for the layers $h0l$ to $h8l$ and $0kl$ to $1kl$ by means of the equi-inclination Weissenberg technique. A total of 726 independent non-zero reflections were measured visually. Corrections for the Lorentz and polarization factors and for the spot-shape were applied.

Structure Determination and Refinement

Approximate positional parameters y and z of all the non-hydrogen atoms were obtained from a Harker section for the two-fold screw-axis along the *a*-axis. Approximate positional parameters x were estimated from a three-dimensional sharpened Patterson map.

Refinement was carried out by means of the block-diagonal least-squares method,[4] with anisotropic temperature factor for all the non-hydrogen atoms. The R index became 0.143 for all the observed reflections. A difference Fourier synthesis at this stage revealed all the hydrogen atoms. Further refinement including the hydrogen atoms with isotropic temperature factors reduced the R index to 0.110 for 726 observed reflections. The following weight system was adopted:

TABLE 1. ATOMIC PARAMETERS AND THEIR E.S.D.'S ($\times 10^4$) FOR NON-HYDROGEN ATOMS

Anisotropic thermal parameters are expressed as $\exp(-B_{11}h^2-B_{22}k^2-B_{33}l^2-B_{12}hk-B_{13}hl-B_{23}kl)$.

Atom	x/a	y/b	z/c	B_{11}	B_{22}	B_{33}	B_{12}	B_{13}	B_{23}
C(1)	1048(7)	5176(7)	−884(4)	111(8)	114(8)	53(3)	−32(12)	5(8)	−35(8)
C(2)	531(8)	5963(7)	−1343(4)	187(12)	96(9)	60(3)	43(15)	3(11)	−10(10)
C(3)	1248(9)	6835(7)	−1655(4)	184(11)	136(9)	44(3)	19(16)	−12(10)	5(9)
C(4)	2470(9)	6886(7)	−1489(4)	184(11)	137(9)	48(3)	−19(18)	−3(11)	−17(8)
C(5)	3024(8)	6091(6)	−1012(4)	173(10)	93(8)	53(3)	−40(14)	18(10)	−22(9)
C(6)	2314(7)	5224(6)	−727(4)	155(9)	87(7)	38(2)	−3(13)	12(9)	−34(7)
C(7)	2949(7)	4411(6)	−231(4)	140(8)	97(8)	55(3)	−25(13)	−20(9)	−14(8)
C(8)	2445(7)	3543(6)	116(4)	104(8)	120(7)	44(3)	12(13)	−5(9)	−19(8)
C(9)	3224(6)	2763(7)	583(4)	105(8)	123(9)	56(3)	15(13)	3(9)	−23(9)
C(10)	2612(7)	1942(6)	1084(3)	116(8)	126(8)	31(2)	59(13)	−4(8)	−24(7)
C(11)	3350(8)	1449(8)	1633(5)	151(11)	179(11)	51(3)	82(17)	−4(10)	−16(10)
C(12)	2818(10)	678(8)	2114(4)	247(15)	179(11)	47(3)	182(21)	9(12)	29(10)
C(13)	1618(9)	337(8)	2030(5)	220(14)	145(11)	57(4)	107(19)	49(13)	18(10)
C(14)	939(9)	818(8)	1493(5)	193(12)	118(9)	60(3)	31(18)	12(11)	51(10)
C(15)	1403(7)	1605(7)	1003(4)	123(8)	134(8)	48(3)	40(14)	12(9)	1(9)
O(16)	4328(5)	2825(5)	547(4)	103(5)	178(8)	102(3)	−12(10)	−35(8)	48(9)

* Present address: Kyowa Carbon Co. Ltd., Ushimado, Okayama.

1) C. Weygand, *Ann. Chem.*, **472**, 154, 174 (1929).
2) D. Rabinovich, *J. Chem. Soc., B*, **1970**, 11.
3) E. P. Kohler and H. M. Chadwell, "Organic Syntheses," Coll. Vol. I, p. 78 (1956).
4) Y. Okaya and T. Ashida, HBLS IV. The Universal Crystallographic Computing System (I), p. 65, The Crystallographic Society of Japan (1967).

Table 2. Atomic parameters and their e.s.d.'s for hydrogen atoms

Atom	x/a	y/b	z/c	B(Å^2)
H(17)	0.053(7)	0.442(6)	−0.073(4)	7.2
H(18)	−0.046(6)	0.587(5)	−0.146(3)	3.7
H(19)	0.082(6)	0.740(6)	−0.202(4)	2.7
H(20)	0.311(7)	0.748(7)	−0.174(4)	6.8
H(21)	0.399(7)	0.612(6)	−0.088(4)	4.1
H(22)	0.397(7)	0.437(6)	−0.018(4)	4.4
H(23)	0.158(7)	0.357(6)	0.008(4)	5.7
H(24)	0.416(8)	0.178(7)	0.175(4)	7.6
H(25)	0.334(7)	0.046(6)	0.247(5)	7.4
H(26)	0.140(9)	−0.035(8)	0.245(5)	10.2
H(27)	−0.008(9)	0.074(7)	0.153(5)	9.0
H(28)	0.081(7)	0.202(6)	0.058(4)	6.5

$\sqrt{w} = 14.0/F_o$ when $F_o > 14.0$,
$\sqrt{w} = 1.0$ when $14.0 \geq F_o \geq 2.0$
and
$\sqrt{w} = 0.0$ when $2.0 > F_o$.

The final atomic parameters for non-hydrogen atoms and their estimated standard deviations are given in Table 1 and those for hydrogen atoms in Table 2.

The atomic scattering factors used were those of Hanson, Herman, Lea, and Skillman.[5] Computations were performed on the HITAC 5020E computer of the Computer Center of the University of Tokyo.

Results and Discussion

The average bond length of the C–C bonds in the two benzene rings is 1.386 Å. The bond lengths of the C–C single bonds between trigonal carbon atoms are 1.486, 1.511, and 1.486 Å for the C(6)–C(7), C(8)–C(9), and C(9)–C(10) bonds, respectively. They are slightly larger than the expected value 1.466 Å[6] for sp^2-sp^2 single bond. The C=C and C=O bond lengths are 1.325 and 1.208 Å respectively, which are comparable to the corresponding values, 1.319 and 1.206 Å, in form I of chalcone.[2] The average length of the C–H bonds is 1.07 Å.

The C(6)–C(7)–C(8) angle, 126.5°, is significantly greater than 120°. Similar results have been reported for several disubstituted ethylenes:[7] 127.6° for form I of chalcone[2] and 127.2° for *p*-methoxychalcone.[8] The C(1)–C(6)–C(5) angle, 120.1°, seems to be normal, although it has been pointed out[7] that a decrease in the corresponding angle is observed in the benzene ring with the -CH=CHR substituent: 118.2° in the form I of chalcone,[2] 117° in *p*-methoxychalcone[8] and 117.7° in 2,5-distyrylpyrazine.[7] In Table 3 the pertinent conformational details of form II are compared with those of form I[2] of chalcone.

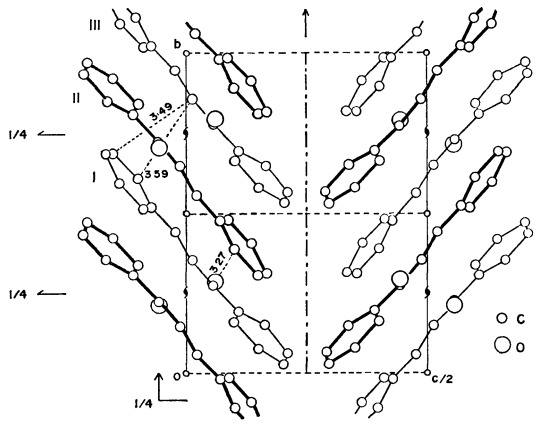

Fig. 1. Projection of the crystal structure along the *a*-axis. Short intermolecular contacts are shown by broken lines. Key for molecules I: x, y, z II: $1-x, 1-y, 1-z$ III: $1/2-x, 1/2+y, z$.

The projection of the crystal structure along the *a*-axis is shown in Fig. 1 together with short intermolecular contacts. The long axis of the molecule declines by about 50° from the *a*-*c* plane and is nearly parallel to [021]. The pairs of molecules related by the *b*-glide plane are stacked along the *b*-axis. This mode of packing allows loose intermolecular contacts around the atoms C(6), C(9), and C(10); for which the C–H distances are 3.4, 3.4, and 3.6 Å, respectively. This is consistent with the fact that the density of the crystals of form II is smaller than that of form I.

The distances between neighboring ethylenic double-bonds are greater than 4.76 Å; thus the crystals of the second polymorph of chalcone might be light-stable.

Table 3. Comparison of the conformational details of the two forms of chalcone

	Form II[a]	Form I[b]
Maximum deviations of the non-hydrogen atoms	+0.375 Å (C(12))	+0.25 Å (C(8))
from the mean molecular plane	−0.354 Å (O(16))	−0.20 Å (C(3))
Dihedral angle between two benzene rings	13.7°	11.1°
Rotation of the benzene ring		
C(1)—C(6) about C(6)—C(7) bond	0.6°	9.3°
C(10)—C(15) about C(9)—C(10) bond	21.6°	4.1°
Twist about C(8)—C(9) bond	9.7°	16.9°

a) This work. b) Ref. 2.

5) H. P. Hanson, F. Herman, J. D. Lea, and S. Skillman, *Acta Crystallogr.*, **17**, 1040 (1964).
6) M. G. Brown, *Trans. Faraday Soc.*, **55**, 694 (1959).
7) Y. Sasada, H. Shimanouchi, H. Nakanishi, and M. Hasegawa, This Bulletin, **44**, 1262 (1971).
8) D. Rabinovich and G. M. J. Schmidt, *J. Chem. Soc., B*, **1970**, 6.

BULLETIN OF THE CHEMICAL SOCIETY OF JAPAN, VOL. 46, 629—630 (1973)

The Charge-transfer Complexes of Metal Chelates of 8-Quinolinol with 7,7,8,8-Tetracyanoquinodimethane

Shigeo KOIZUMI and Yôichi IIDA

Department of Chemistry, Faculty of Science, Hokkaido University, Sapporo

(Received June 15, 1972)

Although there have been a large number of charge-transfer complexes made of electron donors and acceptors,[1] there are few donor molecules that are known to be composed of organic metal chelates. In 1962 Melby *et al.* prepared an unusual (1 : 1) complex between the copper chelate of 8-quinolinol, Cu(Ox)$_2$, and 7,7,8,8-tetracyanoquinodimethane, TCNQ.[2] Williams and Wallwork investigated the crystal and molecular structure of this complex in order to see whether or not the predominant factor influencing the orientation and packing of the molecules was the charge-transfer interaction between the donor of Cu(Ox)$_2$ and the acceptor of TCNQ.[3]

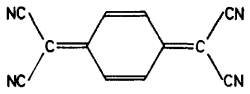

Fig. 1. 7,7,8,8-Tetracyanoquinodimethane (TCNQ).

The present paper will describe the (1 : 1) complexes of the copper and palladium metal chelates of 8-quinolinol with TCNQ.[4] The measurements of the diffuse reflection spectra of these solid complexes were attempted in order to ascertain the charge-transfer transitions in the solid-state spectra. We will show that these complexes are essentially charge-transfer complexes, in which the metal chelates of 8-quinolinol act as electron donors, and TCNQ, as an acceptor. On the other hand, we reported earlier on the charge-transfer complexes of Cu(Ox)$_2$ and Pd(Ox)$_2$ with various halogen-substituted *p*-benzoquinones.[5,6] Therefore, the complexes of Cu(Ox)$_2$–TCNQ and Pd(Ox)$_2$–TCNQ are interesting in comparison with these charge-transfer complexes.

Experimental

The crystals of Cu(Ox)$_2$–TCNQ were prepared according to the method of Melby *et al.*[2] They were deposited when boiling solutions of the components in chloroform were mixed and allowed to cool very slowly. The Pd(Ox)$_2$–TCNQ complex was prepared in a way similar to that used for Cu(Ox)$_2$–TCNQ.

These complexes were pulverized and diluted with potassium bromide. The diffuse reflection spectra of the solid complexes were recorded as the difference in the reflectance between the mixture and pure potassium bromide by means of a Beckman DK-2A spectroreflectometer. The solid-state spectra were then obtained by plotting the diffuse reflection spectra using the Kubelka-Munk equation, $f(R)=(1-R)^2/2R$, in which R is the reflectance.

The Cu(Ox)$_2$-TCNQ Complex

According to Williams and Wallwork,[3] this complex crystallizes as black triclinic crystals (space group $P\bar{1}$), with one molecule of the complex in the unit cell. The component molecules are stacked in a plane-to-plane manner, so that the double bond adjacent to one dicyanomethylene group of TCNQ lies over the 5 : 8 positions of one donor molecule, while the other double bond is similarly oriented with respect to the benzenoid ring of the centrosymmetrically-related donor molecule. The perpendicular separation of the molecules, in the region of overlap, is approximately 3.2 Å. These crystallographic features, although there appears to be a specific interaction between the dicyanomethylene group of TCNQ and the benzenoid group of the oxinate, are common in structures of the π-π charge-transfer type.

The solid-state spectrum of this complex (Fig. 2, Curve (a)) shows intense band peaks at 12.1 kK and 23.9 kK and a shoulder around 29.6 kK. The high-energy band at 23.9 kK and the shoulder around 29.6 kK arise mostly from the absorptions due to the component molecules, while the broad band at 12.1 kK appears in the low-energy region, where neither of the component molecules absorb. This low-energy band at 12.1 kK seems to be attributable to the charge-transfer transition from the donor of Cu(Ox)$_2$ to the acceptor of TCNQ for the following reasons. In the Cu(Ox)$_2$–*p*-chloranil charge-transfer complex, the corresponding band is located at 15.9 kK.[6,7] The electron

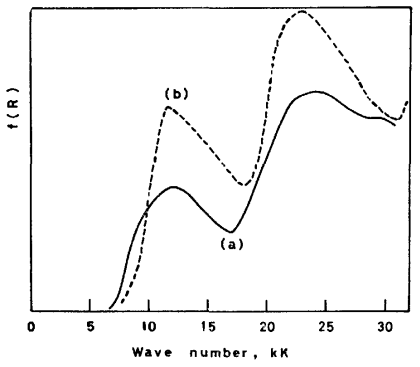

Fig. 2. The solid-state spectra of (a) Cu(Ox)$_2$-TCNQ and (b) Pd(Ox)$_2$–TCNQ.

1) G. Briegleb, "Elektronen-Donator-Acceptor Komplexe," Springer-Verlag, Berlin-Göttingen-Heidelberg (1961).

2) L. R. Melby, R. J. Harder, W. R. Hertler, W. Mahler, R. E. Benson, and W. E. Mochel, *J. Amer. Chem. Soc.*, **84**, 3374 (1962).

3) R. M. Williams and S. C. Wallwork, *Acta Crystallogr.*, **23**, 448 (1967).

4) The palladium chelate of 8-quinolinol is abbreviated as Pd(Ox)$_2$.

5) S. Koizumi and Y. Iida, This Bulletin, **44**, 1436 (1971).

6) Y. Iida, *ibid.*, **44**, 2564 (1971).

7) A. S. Bailey, R. J. P. Williams, and J. D. Wright, *J. Chem. Soc.*, **1965**, 2579.

affinities of TCNQ and *p*-chloranil have been reported to be $E_A(\text{TCNQ})=1.7$ eV and $E_A(p\text{-chloranil})=1.3_7$ eV respectively.[8] If one assigns the band at 12.1 kK of the $Cu(Ox)_2$–TCNQ complex to the charge-transfer transition, the difference in the charge-transfer energies between these two complexes, $h\nu_{CT}(Cu(Ox)_2\text{–}p\text{-chloranil})-h\nu_{CT}(Cu(Ox)_2\text{–TCNQ})$, should be caused mostly by the difference in the electron affinities between TCNQ and *p*-chloranil. In accordance with this view, the observed value of $h\nu_{CT}(Cu(Ox)_2\text{–}p\text{-chloranil})-h\nu_{CT}(Cu(Ox)_2\text{–TCNQ})=0.47$ eV was found to agree almost exactly with $E_A(\text{TCNQ})-E_A(p\text{-chloranil})=0.3_3$ eV.

The $Pd(Ox)_2$-TCNQ Complex

The assignment of the band at 12.1 kK of the $Cu(Ox)_2$–TCNQ complex to the charge-transfer transition was confirmed by replacing the donor of $Cu(Ox)_2$ by $Pd(Ox)_2$. The ionization potential of $Pd(Ox)_2$ has been reported to be lower than that of $Cu(Ox)_2$ by 0.16 eV.[6,7] For the common acceptor of TCNQ, the difference in the ionization potentials of the donor molecules mainly causes the variation in the charge-transfer energies. Therefore, one can expect that the charge-transfer energy of $Pd(Ox)_2$–TCNQ will be lower than that of $Cu(Ox)_2$–TCNQ by that amount.

Figure 2, Curve (b), shows the observed solid-state spectrum of the $Pd(Ox)_2$–TCNQ complex. It has strong absorption band peaks at 11.6 kK and 22.8 kK and a slight shoulder around 32.0 kK. The high-energy band at 22.8 kK and the shoulder around 32.0 kK are attributable to the absorptions due to the component molecules. The energy value of the low-energy band at 11.6 kK of $Pd(Ox)_2$–TCNQ was found to be lower than that of $Cu(Ox)_2$–TCNQ by 0.06 eV. Therefore, although this energy difference is not sufficient, as is to be expected from the ionization potential difference between $Cu(Ox)_2$ and $Pd(Ox)_2$, one can also assign the low-energy band at 11.6 kK of the $Pd(Ox)_2$–TCNQ complex to the charge-transfer transition from the donor of $Pd(Ox)_2$ to the acceptor of TCNQ. On the other hand, the charge-transfer band of the $Pd(Ox)_2$–*p*-chloranil complex has been reported to be located at 14.8 kK.[6,7] Thus, the difference in the charge-transfer energies, $h\nu_{CT}(Pd(Ox)_2\text{–}p\text{-chloranil})-h\nu_{CT}(Pd(Ox)_2\text{–TCNQ})=0.40$ eV, was again found to agree well with $E_A(\text{TCNQ})-E_A(p\text{-chloranil})=0.3_3$ eV.

Discussion

The crystallographic features and also the marked appearance of the strong charge-transfer absorptions clearly show that the $Cu(Ox)_2$–TCNQ and $Pd(Ox)_2$–TCNQ complexes behave as usual π-π charge-transfer-type complexes. Bailey *et al.* have reported the virtual ionization potentials of the donors of $Cu(Ox)_2$ and $Pd(Ox)_2$ to be 7.3 eV and 7.1 eV respectively.[7] Their electron-donor strengths are of the order of pyrene or perylene in the series of aromatic hydrocarbons.[9] It is interesting to note that the electron-donor strengths of these metal chelates of 8-quinolinol are much influenced by the species of the central metal ions.

8) G. Briegleb, *Angew. Chem.*, **76**, 326 (1964).
9) H. Kuroda, *Nature*, **201**, 1214 (1964).

BULLETIN OF THE CHEMICAL SOCIETY OF JAPAN, VOL. 46, 631—632 (1973)

Ionization of Aromatic Molecules *via* σ-Complex with Aluminum Chloride in Solid Phase

Hiroyasu SATO and Yoshifumi AOYAMA
College of Liberal Arts, Kagoshima University, Kagoshima
(Received July 19, 1972)

While Perkampus and Kranz[1] observed the formation of σ-complex of aromatic molecules on an evaporated film of aluminum chloride, Terenin *et al.*[2] observed that of aromatic cation radical on it. The condition of formation of these two species does not seem to have been clarified. We would like to show that the formation of tetracene cation radical takes place by way of a σ-copmlex. For anthracene, an additional intermediate was found between the σ-complex and the cation radical.

Procedure. Aluminum chloride was prepared from aluminum and silver chloride by the procedure described in an earlier report.[3] The cell assembly used in this study was similar to that shown in it. A break-off seal containing aluminum chloride was fused to the cell assembly. After evacuation (10^{-3} mmHg), the sublimed film of aromatic molecule was prepared on the inside wall of the cell. The break-off seal was then broken and aluminum chloride vapor was brought into contact with the sublimed film of aromatics.

Primary Step: σ-Complex Formation. The absorption spectra of colored products given by the contact of aromatics and aluminum chloride vapor were essentially in accordance with those of Perkampus and Kranz,[1] and can be interpreted in terms of σ-complex formation, as discussed by them (π-v complex in their notation).

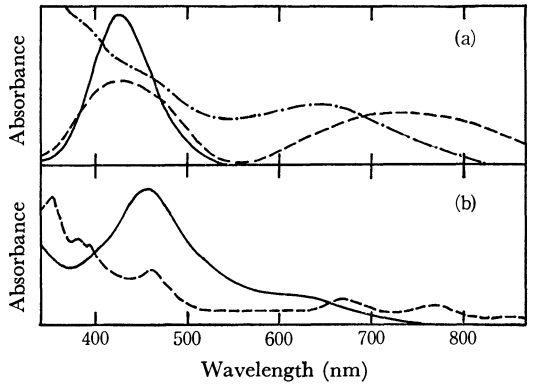

Fig. 1. Absorption spectra of anthracene- and tetracene-aluminum chloride system.
(a): anthracene–aluminum chloride
—— aluminum chloride in excess
– – – anthracene in excess (before heating)
– – – – anthracene in excess (after heating)
(b): tetracene–aluminum chloride
—— before heating, – – – – after heating.

Table 1. Absorption spectra of tetracene- and anthracene–aluminum chloride system
(Positions of Bands, nm)

Aromatic Molecule	Before Heating	After Heating
Tetracene	354	355, 385
	450	395, 670
	650	760, 850
Anthracene		
Aluminum chloride in excess	420	420
Anthracene in excess	420	730
	665	

Cation Radical Formation on Heating. The colored σ-complex was heated over a free flame. In the cases of anthracene and tetracene, the spectra changed into those which have the characteristics of cation radical. These spectra are shown in Fig. 1. The positions of bands are shown in Table 1. The spectra of cation radicals of these molecules are well-established.[4,5] Anthracene cation has absorption maximum at 735 nm, and tetracene cation at 348, 397, 667, 752, 833 nm.[5] The spectra of the heated products are quite similar to those of the cation radical. The samples gave ESR signals which were structureless and broad. The values of ΔH_{msl} were 7.2 G for anthracene, 5.6 G for tetracene. These findings seem to support the formation of aromatic cation radical in these systems.

In producing tetracene cation radical, no excess aromatics was necessary (in contrast with anthracene, *vide infra*). An approximate isosbestic point was obtained in its reaction from σ-complex into cation. Thus, this cation seems to arise from the σ-complex. In the case of anthracene the reaction was more complex.

Cation Radical Formation in Anthracene. The yellow σ-complex of anthracene did not change into its cation radical on heating, without the presence of an excess of anthracene. When the σ-complex was brought into contact with an excess of anthracene (supplied from another break-off seal), the yellow color changed into deep green. No heating was necessary, but a little warming accelerated the reaction. The deep green material (hereafter called species 665) showed an absorption maximum at 665 nm, and when it was heated over a free flame the color changed to

1) H. H. Perkampus and Th. Kranz, *Z. Phys. Chem., N. F.*, **34**, 213 (1962); *ibid.*, **38**, 295 (1963).
2) a) A. N. Terenin, V. A. Barachevsky, E. I. Kotov, and V. A. Holmogorov, *Spectrochim. Acta*, **19**, 1797 (1963). b) A. N. Terenin, *Advan. Catal.*, **15**, 227 (1964).
3) H. Sato, K. Hirota, and S. Nagakura, This Bulletin, **38**, 962 (1965).
4) W. I. Aalversberg, G. J. Hoijtink, E. L. Makor, and W. P. Weijland, *J. Chem. Soc.*, **1959**, 3049, 3055.
5) D. Distler and G. Hohlneicher, *Ber. Bunzenges. Phys. Chem.*, **74**, 960 (1970). Numerals are read from the figure.

dark brown. This dark brown material has an absorption maximum at 730 nm, and gave the ESR signal mentioned above. 9,10-Dimethylanthracene and 9,10-diphenylanthracene gave corresponding σ-complexes (λ_{max} at 425 and 430 nm, respectively). However, addition of excess aromatics did not give any species corresponding to species 665, and no cation radical was given on heating. When an excess of 9,10-disubstituted anthracene was added to anthracene σ-complex (with $AlCl_3$ in excess), neither species 665 nor cation formation was observed. When an excess of anthracene was added to 9,10-disubstituted anthracene σ-complex (with $AlCl_3$ in excess), species 665 was formed and anthracene cation was obtained on heating. These findings seem to show that cation radical is formed only *via* species 665, the latter not being obtained for 9,10-disubstituted anthracene. Thus, cation radical is not derived directly from a σ-complex, but from an additional intermediate, species 665. The presence of this species is reported. Actually it almost always appears when ionization of anthracene is found on solid Lewis acid.[2,6] However, its true nature has not been assigned, neither has its relation to ionization been noted. Hall[6] once assigned it tentatively to the dication but without any reasoning at all. On the other hand, Aalversberg *et al.*[4] remarked that anthracene is peculiar in the point that it is more liable than expected from its ionization potential to form cation radical on contact with Lewis acid in solution. The presence of species 665 as an ionizing intermediate may clarify these points.

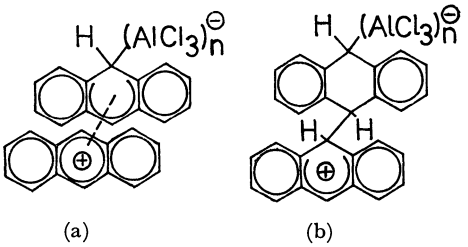

(a) (b)

Fig. 2. Expected structures for the "665 species."
(a): a π-complex, (b): a σ-complex.

In order to determine the structure of species 665, an attempt was made to measure its NMR spectrum in solution. However, the attempt failed, because it decomposed on contact with the solvent used (dry chloroform, dimethyl sulfoxide, benzene, *etc.*). Thus we cannot give any definite molecular structure to this species, but we might say that it is either a π-complex or a σ-complex as shown in Fig. 2, considering that anthracene can dimerize at 9,10-position and that steric hindrance of 9,10-substituents prevents its formation.

6) W. K. Hall, *J. Catal.*, **1**, 53 (1962).

BULLETIN OF THE CHEMICAL SOCIETY OF JAPAN, VOL. 46, 632—634 (1973)

Effect of Substituents on the Keto-Enol Equilibrium of Alkyl-substituted β-Diketones

Hideo KOSHIMURA, Jun SAITO,* and Teiji OKUBO**

Tokyo Metropolitan Industrial Technology Center, Kita-ku, Tokyo
**Mitsui Toatsu Chemicals, Inc., Totsuka-ku, Yokohama*
***National Chemical Laboratory for Industry, Shibuya-ku, Tokyo*

(Received January 26, 1972)

β-Diketones are commonly used as extractants in the solvent extraction of many metals. In the elucidation of the mechanism of the extraction process, it is necessary to know the nature of the extractant. It is well known that β-diketones possess keto-enol tautomerism. Burdett and Rogers[1] have determined the percentages of enol tautomers for acetylacetone and several β-diketones containing the trifluoromethyl group.

In a previous paper of this series,[2] the separation of various metals with the alkyl-substituted β-diketones was reported. In the present investigation, twenty-six alkyl-substituted β-diketones were used in order to establish the effects of substituents on the keto-enol equilibria.

Experimental

Materials. The alkyl-substituted β-diketones used in the present study were synthesized by the method of Hauser and Adams.[3] The compositions were confirmed by elemental analysis. Acetylacetone, trifluoroacetylacetone, and hexafluoroacetylacetone were purchased from the Dojindo Co. and were redistilled before use.

Nuclear Magnetic Resonance Measurements. All the spectra of NMR were recorded at 60MHz with a Japan Electron Optics Model JNM C-60 spectrometer. During the measurements, the temperature was held at 24°C. The chemical shifts of the signal were measured with respect to the tetramethylsilane used as the internal standard, the peak positions are given in parts per million downfield from the internal TMS (δ). The accuracy of the measurement was within

1) J. L. Burdett and M. T. Rogers, *J. Amer. Chem. Soc.*, **86**, 2105 (1964).

2) H. Koshimura and T. Okubo, *Anal. Chim. Acta*, **49**, 67 (1970); **55**, 163 (1971).

3) C. R. Hauser and J. T. Adams, *J. Amer. Chem. Soc.*, **66**, 1220 (1944).

about ±0.03 ppm. Equilibrium constants were obtained by the integration of the keto and enol resonance peaks. At least six integrations were performed; the percentage of the enol tautomer was accurate to within ±2%. The spectra of these β-diketones were measured in the pure liquid state.

Results and Discussion

The identification of the resonance signal for the proton of the α-position in the enol and keto forms in β-diketone from the chemical shift has been possible. The percentages of the enol and keto tautomers have been determined by the integration of the relative intensities of these resonances for a given compound. While two possible enol structures can be postulated for unsymmetrically-substituted β-diketones, as, for example, by thenoyltrifluoroacetylacetone,[4] these peaks for two enol forms can not be observed independently within the limits of this experiment.

The proton chemical shifts of the α-proton in the enol and keto tautomers, their percentages, and the corresponding equilibrium constants are summarized in Table 1 for each of the β-diketones.

From Table 1, it can be seen that the enolic content of these β-diketones increases considerably with an increase in the branching of the alkyl chain near the donating oxygen atom. The enolic content of the alkyl group increases, to a certain extent, with the increase in chain length. However, the enolic contents of β-diketones containing methyl groups are slightly higher than those of β-diketones containing ethyl groups. The enolic contents of β-diketones containing a two-ethyl-group system are lower than would be expected from the effect of the ethyl group in this series. No explanation for the difference will be offered. However, a similar relation was observed with β-diketones containing the alkoxy group. Ness and McElvain[5] have pointed out that the enolic content of β-diketones containing the ethoxy group was lower than that for methoxy and other alkoxy-group systems. In the presence of phenyl groups there is a greater tendency for an increase in enolization. Burdett and Rogers[1] have pointed out that the substitution of electron-withdrawing groups, such as the trifluoromethyl groups, and the aromatic ring in β-diketones results in an increase in enolization. Park *et al.*[6] have

Table 1. The chemical shift of the α-proton of keto and enol and keto-enol equilibrium constant of alkyl-substituted β-diketones

Substitution group R	R′	Chemical shift δ, ppm $-CH_2-$	$-CH=$	Enol %	Equilibrium constant log K ([enol]/[keto])
CH_3	CH_3	3.62	5.56	81.2	0.636
C_2H_5	C_2H_5	3.55	5.52	80.0	0.602
n-C_4H_9	n-C_4H_9	3.50	5.49	91.7	1.045
n-C_5H_{11}	n-C_5H_{11}	3.47	5.45	91.7	1.045
i-C_3H_7	i-C_3H_7	3.61	5.51	95.8	1.358
i-C_4H_9	i-C_4H_9	3.41	5.43	95.3	1.308
t-C_4H_9	t-C_4H_9	3.68	5.72	98.0	1.690
CH_3	C_2H_5	3.57	5.53	82.1	0.662
CH_3	i-C_5H_{11}	3.50	5.46	91.6	1.037
CH_3	s-C_4H_9	3.58	5.52	93.4	1.151
CH_3	i-C_3H_7	3.60	5.53	91.6	1.037
CH_3	t-C_4H_9	3.58	5.40	93.7	1.173
C_2H_5	n-C_3H_7	3.53	5.50	85.2	0.760
C_2H_5	i-C_5H_{11}	3.52	5.49	88.5	0.887
C_2H_5	i-C_4H_9	3.49	5.48	89.2	0.917
C_2H_5	i-C_3H_7	3.56	5.50	90.8	0.994
C_2H_5	t-C_4H_9	3.58	5.60	93.4	1.152
n-C_3H_7	i-C_4H_9	3.54	5.48	93.7	1.173
n-C_5H_{11}	i-C_4H_9	3.54	5.50	94.6	1.243
C_6H_5	C_2H_5	3.93	6.06	93.9	1.188
C_6H_5	n-C_3H_7	3.93	6.10	95.9	1.369
C_6H_5	n-C_4H_9	3.92	6.10	95.6	1.337
C_6H_5	i-C_3H_7	3.99	6.12	97.0	1.509
C_6H_5	i-C_4H_9	3.88	6.05	97.4	1.574
C_6H_5	i-C_5H_{11}	3.93	6.10	96.8	1.481
C_6H_5	t-C_4H_9	4.00	6.25	98.1	1.713

Table 2. The chemical shift of the enol OH proton and the acid dissociation constant of β-diketones

No.	Substitution R	R′	pK_a	Chemical shift δ, ppm
1	CF_3	CF_3	4.35[a]	12.94
2	CF_3	CH_3	6.30[b]	14.43
3	CH_3	CH_3	8.84[c]	15.58
4	C_2H_5	C_2H_5	9.55[c]	15.86
5	i-C_3H_7	i-C_3H_7	9.82[c]	16.15
6	CH_3	t-C_4H_9	10.00[c]	16.30
7	t-C_4H_9	t-C_4H_9	11.57[c]	16.76

a) Ref. 7. b) Ref. 8. c) Ref. 2.

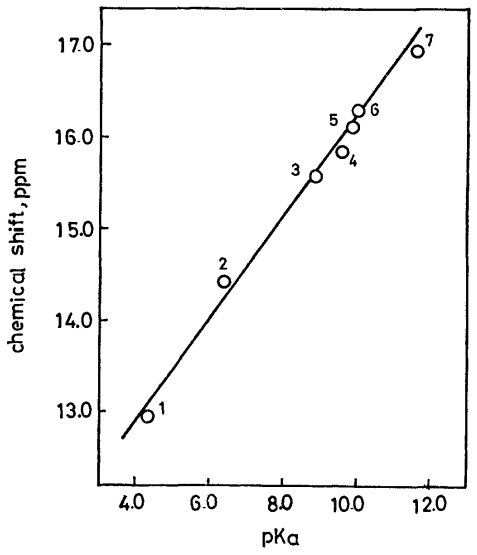

Fig. 1. Relative chemical shift of the enol OH proton *vs.* p*K*a of β-diketones.
Numbers correspond to entries in Table 2.

4) G. Pukanic, N. C. Li, W. S. Brey, Jr., and G. B. Savisky, *J. Phys. Chem.*, **70**, 2899 (1966).

5) A. B. Ness and S. M. McElvain, *J. Amer. Chem. Soc.*, **60**, 2213 (1938).

6) J. D. Park, H. A. Brown, and J. R. Lacher, *ibid.*, **75**, 4753 (1953).

also suggested the stabilization of the enol tautomer in trifluoroacetylacetone by an F–HO intermolecular bond.

It would appear that the high enol content for a given compound is a result of electron release in the region of the oxygen atom in the carbonyl group. The correlation between the substitution group and the enolic contents of the β-diketones in this study suggests that the keto-enol ratio is probably dependent on the difference in the electron density of the alkyl groups.

It is known that the enol OH protons show a considerable variation in chemical shift, particularly among the β-diketones. Lintvedt and Holtzclaw[7] have pointed out that the chemical shift of the enol OH proton is shifted downfield on an increase in the basicity of the substituent with the β-diketones. The chemical shifts of the OH proton are given in Table 2 for β-diketones whose acid-dissociation constant is known from the literature.[2,8,9] The results from the present study are plotted in Fig. 1; a linear relationship exists between the chemical shift of the enol OH proton and the acid-dissociation constant. A higher acid-dissociation constant corresponds to a lower chemical shift of the enol OH proton and, presumably, to a stronger intermolecular hydrogen bond. A similar relation was observed with thiazolylazophenol derivatives.[10]

The authors are deeply indebted to Mr. Kenzo Fujii and Mr. Tamotsu Minami of Mitsui Toatsu Chemicals, Inc., for their considerable assistance with the NMR spectra. They also gratefully acknowledge the valuable help of Dr. Totaro Goto in discussions relating to this work.

7) R. L. Lintvedt and H. F. Holtzclaw, Jr., *Inorg. Chem.*, **5**, 239 (1966).

8) L. G. Van Uitert, W. C. Fernelius, and B. F. Douglas, *J. Amer. Chem. Soc.*, **75**, 457 (1953).

9) J. C. Reid and M. Calvin, *ibid.*, **72**, 2948 (1950).

10) S. Kamata, S. Toda, and S. Nagata, *Nippon Kagaku Zasshi*, **88**, 24 (1967).

BULLETIN OF THE CHEMICAL SOCIETY OF JAPAN, VOL. 46, 634—635 (1973)

Infrared Analysis of Copolymers. II. The Sequence Distribution of Methyl Acrylate Units in Methyl Acrylate–Styrene Copolymers

Naobumi Ōi, Koichi Moriguchi, Hiro-o Shimada, and Fusako Hashimoto
Central Research Laboratory, Sumitomo Chemical Co., Ltd., Tsukahara, Takatsuki, Osaka

(Received July 6, 1972)

In the infrared spectra of copolymers, the characteristic stretching vibrations such as the C=O stretching mode in acrylate copolymers, have generally been considered to be independent of the sequence environment. In fact, in methylacrylate (MA)–styrene(ST) copolymers Kamiyama *et al.* noted that no shift of the peak position of the carbonyl absorption band is observed with changes in the composition, although the half-band width decreases regularly with a decrease in the MA content.[1)]

However, we recently found that the C≡N stretching mode in acrylonitrile(AN)–styrene(ST) copolymers is sensitive to sequence environment and, hence, useful in determining the sequence distribution in AN–ST copolymers.[2)] In order to ascertain whether this is a phenomenon characteristic of all copolymers with polar groups, the infrared spectra of MA–ST copolymers were studied.

Experimental

The random copolymers were prepared by copolymerizing MA and ST monomers, with benzoyl peroxide as the initiator, at 60°C. The low-conversion copolymers thus obtained were used for the infrared measurement. The MA–ST copolymer prepared with ethylalminum sesquichloride[3)] was also used. These samples are listed in Table 1. The MA contents of copolymers were determined by NMR spectrometry.

The infrared spectra were recorded in a benzene solution with a Hitachi-Perkin Elmer 125 grating infrared spectro-

Table 1. Sequence distribution in methyl acrylate–styrene copolymers

Mole % of MA		Conversion (%)	νC=O (cm^{-1})	P_{MM} (obsd)	P_{MM} (calcd)	P_{MMM} (calcd)
Feed Mixture	Copolymer					
100	100	—	1739.6	—	1.0	1.0
98.1	89.3	8.1	1739.1	0.89	0.91	0.83
97.0	85.0	4.5	1738.8	0.83	0.82	0.67
94.9	80.1	3.7	1738.4	0.75	0.78	0.61
90.0	68.7	3.6	1737.6	0.57	0.62	0.39
76.5	54.6	2.8	1736.6	0.36	0.36	0.13
66.9	49.4	1.8	1736.0	0.23	0.27	0.07
12.3	13.0	2.5	1734.9	0	0	0
9.9	11.0	2.5	1735.0	0.02	0	0
6.5	7.3	2.4	1734.9	0	0	0
—[a)]	50.4	—	1735.0	0.02	—	—

a) The copolymer prepared with $AlEt_{1.5}Cl_{1.5}$.[3)]

1) F. Kamiyama, H. Matsuda, and H. Inagaki, *J. Phys. Chem.*, **71**, 4153 (1967).

2) N. Ōi, K. Miyazaki, K. Moriguchi, and H. Shimada, *Kobunshi Kagaku*, **29**, 388 (1972).

3) M. Hirooka, H. Yabuuchi, J. Iseki, and Y. Nakai, *J. Polym. Sci., Part A-1*, **6**, 1381 (1968).

meter which was calibrated against the absorption bands of atmospheric H_2O in 1800—1700 cm^{-1}.

Results and Discussion

The observed $\nu_{C=O}$ frequencies are summarized in Table 1. It is apparent that the C=O stretching mode of MA units regularly shifts to lower frequencies as the MA content decreases, and attains to a constant frequency in copolymers with low MA contents. This fact suggests that the peak positions of the carbonyl absorption bands are correlated to the sequence distributions of MA units in copolymers. Thus, the $\nu_{C=O}$ frequencies were plotted against P_{MM} and P_{MMM}, which are the probabilities for finding the MA–MA and MA–MA–MA linkages respectively in a chain. These probabilities were calculated for low-conversion copolymers from the feed compositions and the reactivity ratios for MA and ST, $r_{MA}=0.20$ and $r_{ST}=0.75$,[4] according to the equations in Ref. 5.

Figure 1 shows that $\nu_{C=O}$ is linearly proportional to P_{MM}. Thus, the following equation was used to calculate P_{MM} values in copolymers:

$$\nu C{=}O = aP_{MM} + bP_{MS}$$

In this equation, P_{MS} is the probability of finding the MA–ST linkage in a copolymer chain and the coefficients, a and b, represent the frequencies of the carbonyl bands for MA units in the MA–MA and MA–ST diads respectively. The a coefficient was evaluated from the spectrum of the MA homopolymer, and b, from the spectra of the copolymers with low MA contents, because the MA units are essentially isolated. As $P_{MM}+P_{MS}=1$, $a=1739.6$, and $b=1734.9$ in a benzene solution, the P_{MM} values of random copolymers can be

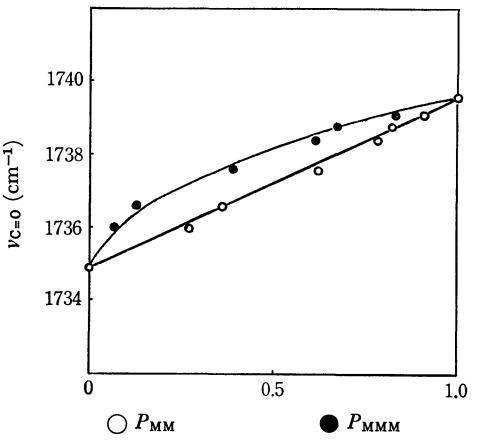

Fig. 1. The C=O stretching frequencies related to the probabilities of MA–MA and MA–MA–MA linkages in methyl acrylate(MA)–styrene copolymers.

determined by measuring the $\nu_{C=O}$ frequencies in a benzene solution and by using the following equation:

$$P_{MM}=(\nu C{=}O-b)/(a-b)=(\nu C{=}O-1734.9)/4.7$$

The measured P_{MM} values are in reasonably good agreement with the calculated values, as is shown in Table 1. Moreover, noteworthy that the measured P_{MM} value of the copolymer prepared with ethylaluminum sesquichloride is nearly zero; this fact supports the idea that such a copolymer has a highly alternating sequence.[3]

In conclusion, the carbonyl stretching mode in MA–ST copolymers is sensitive to the sequence environment and is, hence, useful for determining the sequence distribution of MA units.

The authors are grateful to Dr. Masaaki Hirooka and Mr. Yoshiki Komiyama for providing samples of the copolymers.

4) T. Alfrey, Jr., E. Mers, and H. Mark, *J. Polym. Sci.*, **1**, 37 (1946).

5) H. J. Harwood and W. M. Ritchey, *J. Polym. Sci., Part B*, **2**, 601 (1964).

BULLETIN OF THE CHEMICAL SOCIETY OF JAPAN, VOL. 46, 636—637 (1973)

Magnetic Circular Dichroism of $Cu(acac)_2$, $Fe(acac)_3$, and $Co(acac)_3$

Hajime KATÔ and Junichi GOHDA
Department of Chemistry, Faculty of Science, Kobe University, Nada-ku, Kobe

(Received May 9, 1972)

The magnetic circular dichroism (MCD) spectra of $Cu(acac)_2$, $Fe(acac)_3$, and $Co(acac)_3$ have been measured; they are shown in Fig. 1.

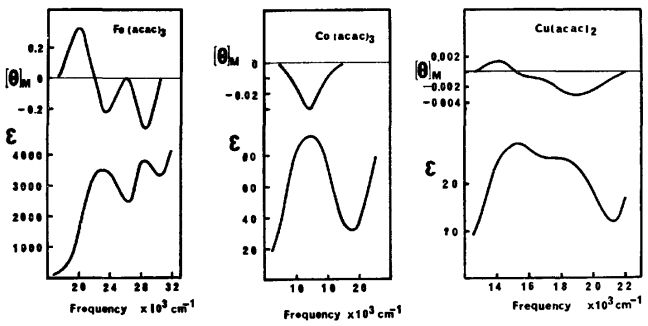

Fig. 1. The experimental MCD and absorption spectra of $Fe(acac)_3$, $Co(acac)_3$, and $Cu(acac)_2$. $[\theta]_M$ is the molar ellipticity per unit magnetic field. ε is the molar extinction coefficient. MCD has been measured by the techniques described in detail in an earlier paper.[5,8]

There has been considerable discussion concerning the assignment of bands appearing in the visible region of the spectrum of bis(acetylacetonato)copper(II), $Cu(acac)_2$, but no final solution to the problem has yet appeared.[1-4] One of the present authors (H.K) has studied the MCD of some Cu^{2+} complexes and found that the B-term of the MCD parameters is dominant in the MCD of the Cu^{2+} complexes at room temperature.[5] According to the analysis, the MCD line shape of $Cu(acac)_2$ suggests two possible assignments: the order of the energy levels is $|xz, yz \gg |x^2\text{-}y^2 \gg |z^2 \gg |xy>$ or $|z^2 \gg |x^2\text{-}y^2 \gg |xz, yz \gg |xy>$, where the locations of the x and y axes are in the plane and along the C_2 axes. However, in order to understand the high-frequency shift of the peak with a large negative MCD band from the maximum point of the absorption band, it is reasonable to assume a positive MCD band in the 16500 cm^{-1} region. Therefore, we propose this order of energy levels; $|xz, yz \gg |x^2\text{-}y^2 \gg |z^2 \gg |xy>$ on the basis of the MCD analysis.[5] Assuming the transition energies to be 14500, 16500, and 18500 cm^{-1} for the $^2B_{1g} \rightarrow {}^2A_{1g}$, $^2B_{1g} \rightarrow {}^2B_{2g}$, and $^2B_{1g} \rightarrow {}^2E_g$ transitions respectively, we have calculated the oscillator strengths and the Faraday parameter B (Table 1). The zeroth moment of the MCD satisfies the relation:[6]

$$\int_{band}([\theta]_M/\nu)d\nu = -33.53(B + C/kT)$$

The values of $(B+C/kT)$ are extracted by simple numerical integrations of the experimental data. By estimating the line shape, we have obtained the experimental values shown in Table 1. The estimated values of B for the lower two bands depend on the estimation of the line shape. However, the order of magnitude is in very good agreement with the calculated ones; these results support the present assignment.

The MCD spectra of $Co(en)_3^{3+}$ and $Co(ox)_3^{3+}$, which are of a D_3 symmetry, were studied by McCaffery and his co-workers.[7] The MCD of $Co(acac)_3$ (Fig. 1) is very similar in appearance to the MCD of the 17000 cm^{-1} band of $Co(ox)_3^{3+}$. $[\theta]_{M_{max}}/\varepsilon_{max}$ is 2×10^{-4}, which is of the same order of magnitude as the value for the $^1A_1 \rightarrow {}^1E_a$ band of $Co(ox)_3^{3+}$. The resemblance to $Co(ox)_3^{3+}$ shows that the static distortion is the major factor governing the d-d intensities. Since the ground state, $^1A_1$, is nondegenerate, the MCD of the 16800 cm^{-1} band of $Co(acac)_3$ shows that the Faraday B-term is absolutely dominant. However, the maximum contribution of an A-term to MCD, $[\theta^A]_{M_{max}}$, is given by $3\sqrt{3}\omega_{ja}{}^{(0)}A/4\Gamma_{ja}{}^2\hbar$. The magnitude of A/D for the $^1A_1 \rightarrow {}^1E$ transition in a D_3 symmetry in solution is theoretically given as $1/2\beta k$, where $k(>0)$ is the orbital angular momentum reduction factor. The value of D is obtained from $\int \varepsilon d\nu$. Then, $A(^1A_1 \rightarrow {}^1E_a)$ is $0.098\beta k$ (in Debye^2 unit). Using the experimental values of $\omega_{ja} \simeq 16800$ cm^{-1} and $\Gamma_{ja} \simeq 4000$ cm^{-1}, we obtain $[\theta^A]_{M_{max}} = 0.0028k$. This value is about 10% of $[\theta]_{M_{max}}$. Therefore, we cannot estimate the magnitude of the quenching of the excited-state angular momentum.

The ground state of $Fe(acac)_3$ is $^6A_1$. In such a case, where the ground state is spin-degenerate and orbitally nondegenerate, the spin-orbit splitting of the orbitally degenerate excited state causes the C terms of the split components of the transition no longer to cancel and gives rise to a MCD changing in sign

Table 1. Oscillater strengths and faraday parameter B for $Cu(acac)_2$

f^{Obs}	B^{Obs} a)	Energy (cm^{-1})	Assignment	f^{Cal}	B^{Cal} a)
3×10^{-4}	-0.6×10^{-5}	14500	$^2B_{1g} \rightarrow {}^2A_{1g}$	5×10^{-4}	-0.4×10^{-5}
1×10^{-4}	-0.2×10^{-5}	16500	$^2B_{1g} \rightarrow {}^2B_{2g}$	1×10^{-4}	-0.2×10^{-6}
3×10^{-4}	1.9×10^{-5}	18500	$^2B_{1g} \rightarrow {}^2E_g$	5×10^{-4}	0.8×10^{-5}

a) In units of $\beta \times$ Debye^2/cm^{-1}.

1) T. S. Piper and R. L. Belford, *Mol. Phys.*, **5**, 169 (1962).
2) J. P. Fackler, F. A. Cotton, and D. W. Barnum, *Inorg. Chem.*, **2**, 97 (1963).
3) C. Dijkgraaf, *Theor. Chim. Acta*, **3**, 38 (1965).
4) H. C. Allen, *J. Chem. Phys.*, **45**, 553 (1966).
5) H. Katô, *Mol. Phys.*, **24**, 81 (1972).
6) P. N. Schatz and A. J. McCaffery, *Quart. Rev.*, **23**, 552 (1969).
7) A. J. McCaffery, P. J. Stephens, and P. N. Schatz, *Inorg. Chem.*, **6**, 1614 (1967).

through the band.[7,8] However, the bands of moderate intensity at about 23000 and 29000 cm^{-1} can plausibly be assigned to allowed charge-transfer transitions, $^6A_{1g} \rightarrow {}^6T_{1u}$ ($^6A_1 \rightarrow {}^6E + {}^6A_2$). The magnitude of spin-orbit spliting is determined by $\langle {}^6A_{1g}|H_{so}|{}^6T_{1u}\rangle$, which is reduced to one-electron matrix elements, $\langle d|H_{so}|L\rangle$ for the $d^5L^2 \rightarrow d^6L$ transition and $\langle L'|H_{so}|d\rangle$ for the $d^5 \rightarrow L'd^4$ transition. These two-center integrals are small; therefore, the C-term must be negligible. The magnitude of A/D for the $^1A_1 \rightarrow {}^1E$ transition in a D_3 solution is given by $\langle E||\mu||E\rangle i/\sqrt{6} \propto \beta$. Therefore, the expected MCD is of the β-type (which is defined in Ref. 9); this contradicts the observed one. Therefore, the observed MCD must be the B-term; it shows the existence of three bands, at 20000, 24000, and 28500 cm^{-1}. Hanazaki and his co-workers[10] predicted the existence of three bands, a transition to $V_1(E)$, $V_1(A_2)$ at 17000 cm^{-1} with $f=0.007$, a transition to $V_6(E)$ at 24000 cm^{-1} with $f=0.095$, and a transition to $V_8(E)$, $V_4(A_2)$ at 26500 cm^{-1} with $f=0.039$. The present MCD analysis supports their assignments. A much more detailed analysis of the B-term would confirm our assignments. MCD studies of the solvent effects of some copper β-diketonates are now in progress in our laboratory.

8) H. Katô, *J. Chem. Phys.*, in press.

9) H. Katô, This Bulletin, **45**, 1281 (1972).

10) I. Hanazaki, F. Hanazaki, and S. Nagakura, *J. Chem. Phys.*, **50**, 265, 276 (1969).

BULLETIN OF THE CHEMICAL SOCIETY OF JAPAN, VOL. 46, 637—639 (1973)

The Design and Performance of a Long-path "Multi-flame" Burner for Atomic Absorption Spectrophotometry

Taketoshi NAKAHARA, Haruyuki DATE, Makoto MUNEMORI, and Sôichirô MUSHA

Department of Applied Chemistry, College of Engineering, University of Osaka Prefecture, Mozu-umemachi, Sakai

(Received June 26, 1972)

In atomic absorption spectrophotometry, different kinds of burners must be used depending on the nature of the flames employed. For example, a 10-cm slot burner is used for an air-acetylene flame, a 5-cm slot burner for a nitrous oxide-acetylene flame, and a nebulizer-burner of the total-consumption type for air-hydrogen and inert gas-hydrogen flames. Several elements require a specific flame; for example, refractory elements require a nitrous oxide-acetylene flame, and some others prefer low-temperature inert gas-hydrogen flames. Therefore, at least the three kinds of burner mentioned above must be provided when a good number of elements are to be determined under the best conditions.

In this experiment, a long-path slot burner of a new type, one which permits various flames to burn, was designed and constructed. Its performance and use in atomic absorption spectrophotometry will be described below. The authors call this new burner a "multi-flame" burner.

Design and Construction

The production of a stationary flame requires that the stream velocity of the fuel-oxidant mixture through the burner slot is at least equal to the burning velocity. If this condition is not met, the flame is liable to flash back down the burner and cause an explosion in the nebulizer chamber. The problems of designing burners for relatively high-temperature flames particularly arise principally from the fact that gas mixtures with high flame temperatures usually have high burning velocities. This requires a limitation of the size of burner slot, with the attendant disadvantage of easier blockage by deposits of salt or carbon particles. It may be noted also that, for some gas mixtures, the burning velocity increases with the temperature of preheating,[1] so the burner head should be kept sufficiently cool; it must

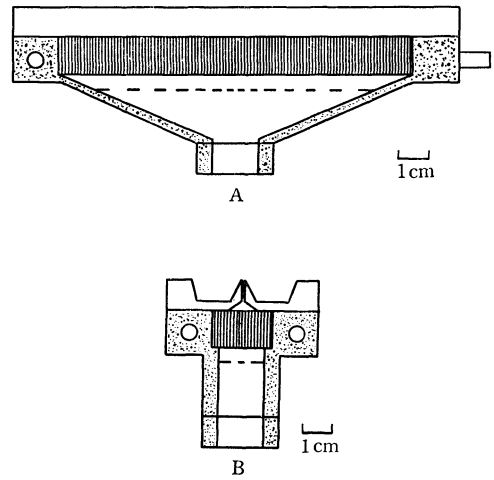

Fig. 1. Diagram of a "multi-flame" burner designed and constructed for atomic absorption spectrophotometry.
A: front view, B: side view. ▥ porous ceramic plate, ▦ brass casting, ▭ brass, ---- baffle, ○ duct for water-cooling.

1) A. G. Gaydon and H. G. Wolhard, "Flames, Their Structure, Radiation and Temperature," Chapman and Hall, London (1960), p. 80.

in any case be kept well below the ignition temperature of the gas mixture.

In view of these requirements, a new-type burner head which can be adapted to any premixed-type burner was designed. The burner head is shown schematically in Fig. 1. It consists of a burner top and a top holder, both of which are made of brass because of its facility of construction, though stainless steel would be preferred. The burner top consists of two pieces of surface-ground plate of the same features; these pieces form a slot and grooves. The slot serves as a nozzle. An outlet area of the nozzle is 1/23 that of the inlet. The length and width of the slot are 11.5 and 0.045 cm respectively. The height of the nozzle is 1.0 cm. To ensure an adequate entrainment of secondary air, the outer surfaces of the nozzle are tapered toward the groove, which is 1.7 cm wide and 0.7 cm deep. The rapid build-up of carbon particles and salt deposition, and the production of water when hydrogen is used as a fuel, were thereby minimized. To maintain the stability of hydrogen flames, which are liable to flash back down the burner and cause an explosion in the nebulizer chamber because of their higher burning velocity, a porous ceramic plate which contains about 50 holes (0.5 mm in diameter) per cm^2 and which is 1.25 cm thick, commonly used for a gas-infrared stove, is placed inside the top holder. Two ducts are provided in the top holder for cooling the burner top with water. The purpose of these ducts is to increase the effectiveness of the quenching action at the burner slot.[2)]

Experimental

In this study the "multi-flame" burner was fitted to a Techtron nebulizer chamber, and its utility was examined on acetylene or hydrogen with air, nitrous oxide, or inert gas (argon or nitrogen) entrained air. The placement of the burner relative to the optical axis of the spectrophotometer (a Nippon Jarrell-Ash Model AA-1 atomic absorption/flame emission spectrophotometer) was effected by means of a compound slide assembly mounted on an optical bench. The single beam-single pass system was arranged in the usual manner. The light beam was modulated at a frequency of 90 Hz by means of a mechanical light-chopper. The flow rates and pressures of the fuels and nebulizing gases were controlled by means of needle valves and were measured by means of calibrated flow meters.

The premixed acetylene or hydrogen flames were formed and extinguished on the burner in much the same manner as that on a welding torch. An acetylene diffusion flame or a hydrogen diffusion flame was first formed at the necessary flow rate (1.0—1.2 l/min for acetylene and 7.2—9.0 l/min for hydrogen). The nebulizing gas (air, nitrous oxide, argon or nitrogen) was then slowly introduced into the nebulizer chamber until the pressure of a nebulizing gas attained 1.5 kg/cm^2, at which point the flow rates of the nebulizing gases were 4.9, 3.8, 4.5, and 5.0 l/min for air, nitrous oxide, argon, and nitrogen respectively. The sample aspiration rates were 8.85, 9.35, 8.90, and 8.95 ml/min with air, nitrous oxide, argon, and nitrogen respectively at the same pressure of 1.5 kg/cm^2. Slight variations in the flow rates and pressures of the nebulizing gases caused only a negligible change in the sample aspiration rates. The flame was extinguished by first terminating the nebulizing gas flow. In particular, a violent flash-back may occur if the acetylene flow is stopped before the nitrous oxide flow. The burner was employed under water-cooling for all the flames. Although the cooling of the burner head promoted salt deposition at the burner slot, the lower temperature of the burner slot markedly reduced the possibility of flash-back.

Performance and Characteristics of a "Multi-flame" Burner

Winefordner *et al.* have used the argon(entrained air)-hydrogen flame[3,4)] and the nitrogen(entrained air)-hydrogen flame[5)] in atomic fluorescence spectrophotometry and in flame emission spectrophotometry[6)] with satisfactory results. On the other hand, Menis and Rains[7)] have described that the argon(entrained air)-hydrogen flame with a premixed-type burner system was unstable and that unsuccessful results were obtained for the atomic absorption spectrophotometry of arsenic. In this study, however, not only an argon (entrained air)-hydrogen flame, but also a nitrogen (entrained air)-hydrogen flame, when used with the "multi-flame" burner, was found to be remarkably stable and useful for atomic absorption spectrophotometry.

With this burner, atomic absorptions were measured for various elements. The elements studied were aluminum, bismuth, cadmium, calcium, copper, iron, lead, magnesium, mercury, strontium, tin, and zinc. These elements were chosen for a variety of reasons: efficiency of atomization, background absorption at the wavelength of atomic absorption measurement, susceptibility to chemical interferences, refractory oxide formation, *etc.* The atomic absorptions were measured for each element at various flame compositions and flame heights. Linear analytical calibration graphs were obtained for all the elements and for all the flames. A comparison of the sensitivities for 1% absorption of the elements studied under the optimum experimental conditions for each flame is shown in Table 1.

Salt deposition occurred along the burner slot after a very long period (about five hours) of operation and resulted in flame distortion. The burner clogging depends on the total concentration of solutes in the solutions sprayed into the flame. To minimize this burner clogging, a pure solvent was sprayed into the flame between each measurement. Any remaining particles on the burner slot could easily be cleaned off by passing a thin board through the slot a few times. Air was run out through the burner during the cleaning of the burner slot.

It may be seen from the results shown in Table 1

2) R. Friedman and W. C. Johnson, *J. Appl. Phys.*, **21**, 791 (1950).

3) C. Veillon, J. M. Mansfield, M. L. Parsons, and J. D. Winefordner, *Anal. Chem.*, **38**, 204 (1966).

4) M. P. Bratzel, R. M. Dagnall, and J. D. Winefordner, *ibid.*, **41**, 713 (1969).

5) M. P. Bratzel, R. M. Dagnall, and J. D. Winefordner, *ibid.*, **41**, 1527 (1969).

6) K. Zacha and J. D. Winefordner, *ibid.*, **38**, 1537 (1966).

7) O. Menis and T. C. Rains, *ibid.*, **41**, 952 (1969).

Table 1. Comparison of the sensitivities for 1% absorption of some elements in the flames with a "multi-flame" burner

Element	Wavelength of measurement (nm)	Sensitivity for 1% absorption (ppm)						
		A	B	C	D	E	F	G
Aluminum	309.2	—	2.2	—	—	—	—	1.1
Bismuth	223.1	0.14	0.8	0.18	1.0	0.10	0.11	0.7
Cadmium	228.8	0.009	0.04	0.02	0.05	0.005	0.006	0.03
Calcium	422.7	0.09	0.03	0.2	0.3	0.2	0.7	0.03
Copper	324.7	0.04	0.2	0.04	0.1	0.04	0.05	0.1
Iron	248.3	0.05	0.1	0.09	0.2	0.1	0.2	0.15
Lead	283.3	0.3	0.9	0.4	1.0	0.3	0.2	0.5
Magnesium	285.2	0.003	0.01	0.01	0.01	0.03	0.02	0.008
Mercury	253.7	1.0	6.0	0.9	3.6	1.1	1.3	15.0
Strontium	406.7	0.07	0.1	0.05	0.6	0.8	2.9	0.2
Tin	224.6	2.6	2.0	0.28	13.8	0.27	0.32	1.2
Zinc	213.9	0.007	0.03	0.008	0.02	0.006	0.009	0.04

A: Air-acetylene flame. B: Nitrous oxide-acetylene flame. C: Air-hydrogen flame. D: Nitrous oxide-hydrogen flame. E: Argon(entrained air)-hydrogen flame. F: Nitrogen (entrained air)-hydrogen flame. G: Results obtained by Slavin.[8]

that the new "multi-flame" burner can be satisfactorily used with several gas mixtures and that it gives some increase in sensitivity for some elements, compared with those values obtained using a commercial burner.[8] Furthermore, the hydrogen flame using argon or nitrogen as a nebulizing gas gives significantly better sensitivities for some elements, but severe chemical interferences are likely to occur, because the flame temperature is much lower. The "multi-flame" burner is completely silent in operation, even when using hydrogen as a fuel.

Hydrogen flames with argon(entrained air) and nitrogen(entrained air) would be useful for the atomic absorption spectrophotometric study of some elements which are easily atomized in a low-temperature flame, such as arsenic, bismuth, cadmium, tin, selenium, and zinc.

8) W. Slavin, "Atomic Absorption Spectroscopy," Interscience Publishers, New York, N. Y. (1968), p. 60.

BULLETIN OF THE CHEMICAL SOCIETY OF JAPAN, VOL. 46, 639—641 (1973)

The Atomic Absorption Spectrophotometric Determination of Zinc in Premixed Inert Gas(Entrained Air)-Hydrogen Flames and the Measurement of the Flame Temperature

Taketoshi NAKAHARA, Makoto MUNEMORI, and Sôichirô MUSHA

Department of Applied Chemistry, College of Engineering, University of Osaka Prefecture, Mozu-umemachi, Sakai

(Received June 26, 1972)

Previous studies have indicated that the premixed inert gas(entrained air)-hydrogen flame produced with a "multi-flame" burner[1] can be used as a suitable atom reservoir for the determination of bismuth[2] and tin[3] by atomic absorption spectrophotometry. This paper will describe the application of this flame to the atomic absorption spectrophotometric determination of zinc and, in addition, the measurement of its temperatures using a thermocouple probe.

Whereas the temperatures of most flames can only be measured satisfactorily by such spectroscopic techniques as the Ornstein iron two-line method[4-6] and the sodium line-reversal method,[5,7] the cool inert gas-(entrained air)-hydrogen flame gives a temperature of only a few hundred degrees centigrade,[8] and it can be measured fairly reliably by inserting a thermocouple probe into the flame.[9]

1) T. Nakahara, H. Date, M. Munemori, and S. Musha, This Bulletin, **46**, 637 (1973).

2) T. Nakahara, M. Munemori, and S. Musha, *ibid.*, in press.

3) T. Nakahara, M. Munemori, and S. Musha, *Anal. Chim. Acta*, **62**, 267 (1972).

4) J. D. Winefordner, J. M. Mansfield, and T. J. Vickers, *Anal. Chem.*, **35**, 1611 (1963).

5) L. de Galan and J. D. Winefordner, *J. Quant. Spectrosc. Radiat. Transfer.*, **7**, 703 (1967).

6) G. F. Kirkbright, M. K. Peters, M. Sargent, and T. S. West, *Talanta*, **15**, 663 (1968).

7) J. H. Gibson, W. E. L. Grossman, and W. D. Cooke, *Anal. Chem.*, **35**, 266 (1963).

8) R. M. Dagnall, K. C. Thompson, and T. S. West, *Analyst* (London), **92**, 506 (1967).

9) R. Smith, C. M. Stafford, and J. D. Winefordner, *Anal. Chem.*, **41**, 946 (1969).

Experimental

Apparatus. All the atomic absorption measurements were made using a Nippon Jarrell-Ash Model AA-1 atomic absorption/flame emission spectrophotometer. A long-path "multi-flame" burner[1] constructed in the authors' laboratory was mounted on a Techtron nebulizer chamber, and a single pass system was used. The height in the flame was taken as zero when the light beam from the hollow-cathode lamp just touched the top of the burner head. The analytical wavelength was 213.9 nm, and the light source was a multi-element (Cu–Fe–Mn–Zn) hollow-cathode lamp (Westinghouse, Type No. 45492), operated at 10 mA. The gas-flow rates were carefull regulated by means of needle valves and were monitored on calibrated flow meters.

Reagents. A standard zinc solution containing 1000 ppm of zinc was prepared by dissolving 1.000 g of high-purity zinc metal in 10 ml of hydrochloric acid and by then diluting this mixture to 1000 ml with distilled water. Various concentrations were made by diluting the stock solution.

Results and Discussion

Flame Parameters. The flames employed in this study produced 5 and 8% absorptions respectively when nitrogen and argon were used as the nebulizing gases. The absorbance values cited in this study were corrected for this background absorption.

The optimum flame parameters for zinc atomic absorption are summarized below. Argon(entrained air)-hydrogen flame: hydrogen flow rate, 3.6 l/min; argon flow rate, 4.5 l/min; argon pressure, 1.5 kg/cm^2; height of the flame, 4 mm above the top of the burner head. Nitrogen(entrained air)-hydrogen flame: hydrogen flow rate, 5.4 l/min; nitrogen flow rate, 5.0 l/min; nitrogen pressure, 1.5 kg/cm^2; height of the flame, 6 mm above the top of the burner head. Under these flame conditions, the hydrogen flames are almost invisible and are very quiet. The sample aspiration rates were 8.90 and 8.95 ml/min with argon and nitrogen respectively.

Calibration Graph for Zinc. Under the optimum conditions outlined above, the straight calibration graphs were obtained over the range of 0—0.5 ppm of zinc in argon(entrained air)-hydrogen and nitrogen-(entrained air)-hydrogen flames. The sensitivities for 1% absorption for zinc were 0.005 and 0.007 ppm in argon(entrained air)-hydrogen and nitrogen(entrained air)-hydrogen flames respectively.

Effects of Acids. The interference effect of acids on the determination of zinc was studied. The concentration of zinc was 0.5 ppm, and the concentration range of acids was from 0.5 to 2.0M. The acids examined were hydrochloric, nitric, perchloric, and sulfuric acids. The results obtained in both inert gas(entrained air)-hydrogen flames are shown in Fig. 1. It can be seen from Fig. 1 that the interference from the acids is greater in the nitrogen(entrained air)-hydrogen flame than in the argon(entrained air)-hydrogen flame. Hydrochloric and nitric acids caused little or no interference with the determination of zinc, but perchloric and sulfuric acids, particularly in the nitrogen(entrained air)-hydrogen flame, had a depressing effect on the zinc atomic absorption. Furthermore, the depressing interference from perchloric and sulfuric acids was considerably dependent upon the flame composition, becoming greater as the flames became reducible.

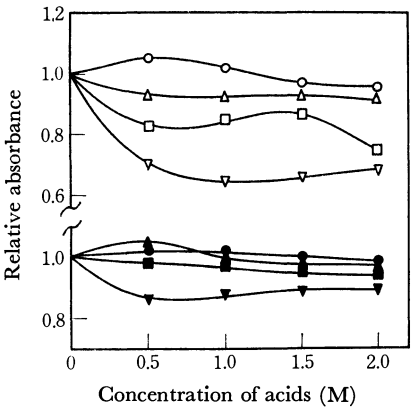

Fig. 1. Effect of acids on zinc atomic absorption. Concentration of zinc: 0.5 ppm. In an argon(entrained air)-hydrogen flame: (●) hydrochloric acid; (▲) nitric acid; (■) sulfuric acid; (▼) perchloric acid. In a nitrogen(entrained air)-hydrogen flame: (○) hydrochloric acid; (△) nitric acid; (□) sulfuric acid; (▽) perchloric acid.

Effects of Various Other Elements. The effects of the presence of 10- and 100-fold weight excesses of various diverse elements on the determination of zinc were studied at the 0.5 ppm level. Some severe chemical interferences were observed to depress the zinc atomic absorption. The refractory compound-formers, such as aluminum, beryllium, boron, silicon, and vanadium, exhibited a greater depressing interference with the zinc atomic absorption.

Because flame composition and flame height have been found to be important parameters in the study of interference,[10] the hydrogen-flow rate and the flame height in the inert gas(entrained air)-hydrogen flames were varied to see what effect, if any, would be produced on the depressing interference; it was found that the depressing interference was dependent on these parameters.

Effect of Lanthanum on the Depressing Interference. In an attempt to eliminate the depressing interference due to aluminum, beryllium, boron, *etc.*, the effects of third elements on the depressing interference were studied. The elements examined were barium, iron, mercury, lanthanum, lithium, magnesium, sodium, lead, antimony, tin, and yttrium. Some elements were found to eliminate the depressing interferences. Lanthanum was the most effective of the elements examined. When solutions were prepared so as to contain 2000 ppm of lanthanum(as chloride) as an interference-releasing agent, all the chemical interferences were completely removed. This phenomenon would be applicable to the determination of zinc in various practical samples.

Measurement of the Flame Temperatures. Dagnall

10) J. A. Dean and T. C. Rains, "Flame Emission and Atomic Absorption Spectrometry," Vol. 1, Marcel Dekker, New York, N. Y. (1969).

et al.[8] have reported that the hydrogen-nitrogen diffusion flame and the shielded air-hydrogen flame give temperatures of only a few hundred degrees centigrade, and that they can be measured fairly reliably by inserting a calibrated thermocouple probe into the flame. Furthermore, Smith *et al.*[9] have described the temperature profiles of turbulent hydrogen diffusion flames, the temperatures of which were measured with the aid of an iridium/60% iridium-40% rhodium thermocouple.

The temperatures of the inert gas(entrained air)-hydrogen flames were measured in this study by inserting a platinum/90% platinum-10% rhodium thermocouple probe into the flames. The thermocouple was made of 0.2 mm diameter platinum and platinum-rhodium (90—10%) wires which were welded to give a bead junction *ca.* 0.4 mm in diameter. The joined wires were mounted in two-bore, ceramic insulators of high-purity alumina. The thermocouple was mounted on a manually-operated horizontal/vertical traverse mechanism. The thermoelectric emf was measured on a millivoltmeter calibrated in units of 0.05 mV, and the temperature was determined by referring to a calibration table.[11]

The variation in the flame temperature with the flame height and the hydrogen-flow rate, at the flame center only, was measured for the argon(entrained air)-hydrogen flame and for the nitrogen(entrained air)-hydrogen flame with the aspiration of distilled water. The results obtained are shown in Fig. 2. For both the flames, the temperatures could be reproduced to $\pm$10 K at any point on the central axis of the flame. As the hydrogen flow rate was increased, the flame became larger and the flame temperature increased, as is shown in Fig. 2. Furthermore, the maximum

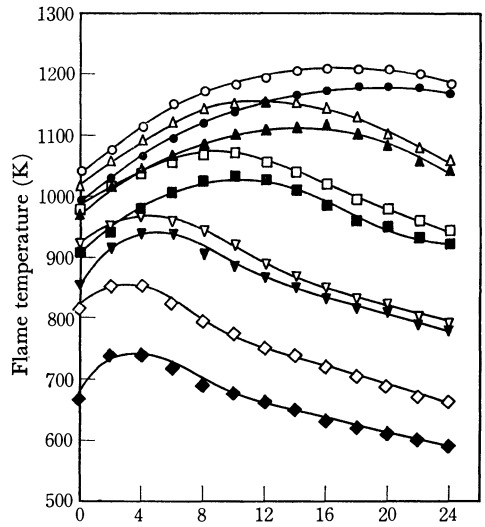

Fig. 2. Flame-temperature variation along central, vertical axis of the inert gas(entrained air)-hydrogen flames.
Hydrogen flow rate in an argon(entrained air)-hydrogen flame: (◇) 3.6 l/min; (▽) 5.4 l/min; (□) 7.2 l/min; (△) 9.0 l/min; (○) 10.8 l/min. Hydrogen flow rate in a nitrogen (entrained air)-hydrogen flame: (◆) 3.6 l/min; (▼) 5.4 l/min; (■) 7.2 l/min; (▲) 9.0 l/min; (●) 10.8 l/min.

temperature shifted toward the higher part in the flame with the increase in the hydrogen flow rate. When distilled water is not sprayed into the flame, the flame temperatures about 4 mm above the top of the burner head increase by only 20 K. It may be noticed in Fig. 2 that the temperature in the argon-(entrained air)-hydrogen flame was higher at any point than that in the nitrogen(entrained air)-hydrogen flame. This is presumably due partially to the differences in interference effects on the zinc atomic absorption described above.

11) The Chemical Society of Japan Ed., "Kagaku Binran," (Kisohen), Maruzen, Tokyo (1966), p. 1096.

BULLETIN OF THE CHEMICAL SOCIETY OF JAPAN, VOL. 46, 641—642 (1973)

Sesquiterpenoids of *Parabenzoin praecox*

Keiko OHARA, Yoshimoto OHTA, and Yoshio HIROSE
The Institute of Food Chemistry, Dojimanaka, Kita-ku, Osaka

(Received March 13, 1972)

The essential oil of *Parabenzoin praecox* (Sieb. et Zucc.) Nakai, distributed in the southern part of Japan, has been reported to be composed mainly of several monoterpenoids, with *cis*-ocimene the major one, together with a few sesquiterpenoids, such as caryophyllene.[1] In this paper, we wish to report the analysis of the sesquiterpenoid fraction of this oil and the structural determination of two new sesquiterpenoids, α-copaene-11-ol (I) and 8-acetoxy-elemol (III), isolated from this source. In our experiments, unlike as in the previous results,[1] camphor was isolated as the main component of the oil and the following known sesquiterpenoids were isolated, α-copaene, β-elemene, β-caryophyllene, elemophyllene, α-muurolene, β-selinene, δ-cadinene, γ-cadinene, nerolidol, elemol, ledol, epicubenol, spathulenol, γ-eudesmol, T-cadinol, T-muurolol, δ-cadinol, α-eudesmol, β-eudesmol, and α-cadinol.

α-Copaene-11-ol, Compound (I) ($C_{15}H_{24}O$ (M^+ *m/e* 220), needle crystals, mp 99.5—100.5°C, $[\alpha]_D$ +9.2° in $CHCl_3$) was shown to have the following groupings, $-C(CH_3)_2OH$ (ν_{max} 3350 cm^{-1} (hydroxyl group), $\delta^{CCl_4}_{ppm}$

1) H. Shinozaki, *Kogyo Kagaku Zasshi*, **24**, 444 (1921); H. Komae, N. Hayashi, S. Kosela, and T. Aratani, *Flavour Industry*, **2**, 427 (1971).

1.04 (6H s.), *m/e* 59 ($C_3H_7O^+$, 100%)), $>CCH_3$ (δ 0.77 (3H s.)), and $-HC=C(CH_3)-$ (δ 1.62 (3H br.s.), 5.13 (1H br.s.)). The dihydro-derivative of I obtained by catalytic reduction (PtO_2/EtOH) was further hydrogenolyzed with PtO_2 in acetic acid to yield two hydrocarbons (both M^+ *m/e* 206) in a ratio of 3: 1, they were identical with copane and ylangane respectively. The dehydration of I with thionyl chloride in pyridine and the subsequent selective hydrogenation of the resulting terminal double bond with tris(triphenylphosphine) chlororhodium in benzene afforded α-copaene as the main product. From these results, Compound (I) was concluded to have α-copaene skeleton and a hydroxy group at C-11, as is shown by Formula (I). Although the absolute configuration of this compound was not determined, it is presumed that I has the same stereostructure as (−)-α-copaene on the basis of the coexistence of this and α-copaene($[\alpha]_D$ −4.9°) in the same oil. The isomerization of this alcohol, catalyzed by 0.1N hydrochloric acid in 80% aqueous dioxane, yielded a new bicyclic compound (II) ($C_{15}H_{24}O$ (M^+ *m/e* 220) $[\alpha]_D$ +52°). The spectral data of this compound showed the presence of $-C(CH_3)_2OH$ (ν_{max} 3400 cm^{-1}, δ 1.14 and 1.19 (each 3H s.) and *m/e* 59 (100%)), tri- and tetrasubstituted double bonds (δ 1.58 (6H s.) and 5.63 (1H br.s.)). This compound was presumed to be δ-cadinene-11-ol, since the mother hydrocarbon, α-copaene, yields δ-cadinene and α-murolene on acid treatment.[2)]

In another experiment, α-copaene-11-ol was isolated from the wood oil of *Litseae japonica* (Thumb.) Juss. as the major component of the sesquiterpene alcohol fraction.

8-Acetoxyelemol, Compound III ($C_{17}H_{28}O_3$ (M^+ *m/e* 280)), a minor component of the oil, showed the following spectral data, ν_{max} 3350, 1730, 1240, 910, and 890 cm^{-1}, δ 1.08 (3H s.), 1.15 (6H br.s.), 1.69 (3H br.s.), 2.00 (3H s.), 4.60—5.00 (5H m.), and 5.75 (1H d.d.). These spectra are identical with those of elemol except for the additional signals due to an acetoxy group (ν_{max} 1730 and 1240 cm^{-1}, and δ 2.00 (3H s.)). On heating in a sealed tube or on glc separation at 200°C, this compound afforded a dehydrated derivative (IV) ($C_{17}H_{26}O_2$). The NMR spectrum of IV showed the presence of an isopropenyl group instead of a $-C(CH_3)_2OH$ group in III. The NMR spectrum of the hexahydro-derivative (V), obtained by the hydrogenation of IV, exhibited the presence of a proton at δ 4.75, this confirmed the secondary nature of the acetoxy group. The position of this acetoxy group was decided to be at C-8 on the basis of the following experiments. β-Elemenone (VI) was hydrogenated with PtO_2 in acetic acid to yield a saturated ketone (VII). The subsequent lithium aluminium hydride reduction of VII afforded two secondary alcohols, VIII and IX, the minor product (VIII), carrying an equatorial hydroxyl group (H-8 at δ 3.40, $W_1/_2$ 24 Hz), was acetylated with Ac_2O in pyridine to yield an acetate which was identical with V in all respects. From these results, the structure of Compound III can be represented by Formura (III). The coexistence of III and elemol ($[\alpha]_D$ −3.5°) in the same oil also suggests the stereochemistry.

At present, there have been found only a few cadalene-type compounds carrying a hydroxyl group at C-11 as our alcohol (I) does, and since, in the genesis of cadalene-type alcohols a S_N1-like attack of a water molecule on the C-10 carbonium ion from the mediate germacrenoid cation is generally accepted, the hydroxylation at C-11 probably occurs after the cadalene skeleton has been formed. Such *de novo* hydroxylation is quite rare in sesquiterpenoids, and further study of the biogenesis of the compounds of this type should be undertaken.

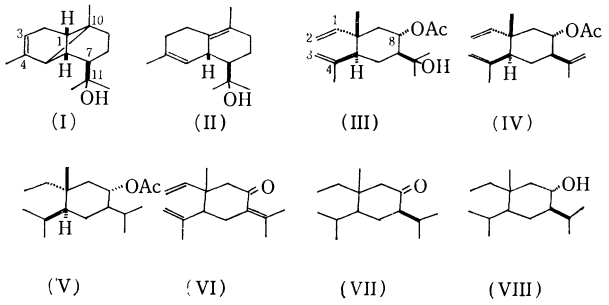

Experimental

Stems (16.5 kg) and leaves (15.0 kg) of *Parabenzoin praecox* were collected in Osaka Prefecture. Each was extracted with acetone, and the extract, after the evaporation of the solvent, was steam-distilled. After the removal of acidic components from the distillate, neutral oils were obtained in the amounts of 12.9 g and 20.8 g from the stems and the leaves respectively. No significant difference in their constituents could be detected by analytical gas chromatography using a capillary column (HB-2000, 45 m × 0.25 mm), therefore, the two oils were combined for analysis. The combined oil was separated into a hydrocarbon fraction (18.8 g) and a fraction of oxygenated compounds (14.1 g) by column chromatography on neutral alumina. Each component of the hydrocarbon fraction was purified by column chromatography on silica gel, followed by preparative glc (Varian, model 90-P, 20 ft. × 3/8 in. aluminium column packed with 10%-Carbowax 20M on Diasolid L at 180—200°C, using helium as the carrier gas). The oxygenated compound fraction was distilled under reduced pressure (3 mmHg) to separate sesquiterpenoids from monoterpenoids roughly. Each sesquiterpenoid, as well as α-copaene-11-ol (I) and 8-acetoxyelemol (III), was purified by column chromatography on silica gel, this was followed by preparative glc under the same condition as those for used for hydrocarbons except in the case of III. 8-Acetoxyelemol (III) was isolated using a 5ft. × 3/8 in. column of Carbowax 20 M at 175°C. The compounds thus isolated were identified with authentic samples by comparing their RT on glc, and thier IR, NMR, and MS spectra.

α-Copaene-11-ol (I); *m/e* 220 (rel. int. 2%, M^+), 202 (7.5%, M^+-H_2O), 187 (11%, $M^+-H_2O-CH_3^+$), 162 (52%, $M^+-C_3H_6O^+$), 159 (41%), 147 (30%), 132 (38%), 119 (47%), 105 (55%), 91 (43%), 59 (100%, $C_3H_7O^+$).

8-Acetoxyelemol (III); *m/e* 280 (0.05%, M^+), 220 (0.3%, $M^+-CH_3CO_2H$), 202 (0.9%, $M^+-CH_3CO_2H-H_2O$), 162 (22%), 147 (23%), 119 (69%), 117 (71%), 108 (47%), 59 (42%, $C_3H_7O^+$), 43% (100%, $C_3H_7^+$).

2) Y. Ohta, K. Ohara, and Y. Hirose, *Tetrahedron Lett.*, **1968**, 4181.

BULLETIN OF THE CHEMICAL SOCIETY OF JAPAN, VOL. 46, 643 (1973)

The Pyrolysis of Dialkyl α-Acyloxyphosphonates

Yoshiki OKAMOTO and Hiroshi SAKURAI

The Institute of Scientific and Industrial Research, Osaka University, Yamada-kami, Suita-shi, Osaka

(Received March 27, 1972)

Several dialkyl α-acyloxyalkyl (aralkyl) phosphonates (I) were prepared,[1] and their behavior in pyrolysis was investigated.

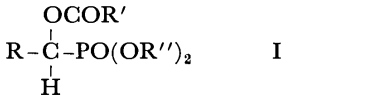

I

I-a,	$R=C_6H_5$,	$R'=CH_3$,	$R''=C_2H_5$
I-b,	C_6H_5,	CH_3,	C_3H_7
I-c,	C_6H_5,	C_3H_7,	C_2H_5
I-d,	C_3H_7,	C_6H_5,	C_2H_5
I-e,	C_3H_7,	CH_3,	C_2H_5
I-f,	C_6H_5,	CH_3,	CH_3
I-g,	C_2H_5,	CH_3,	CH_3
I-h,	C_6H_5,	CH_3,	$CH(CH_3)_2$

In every run, 0.1 mol of I was pyrolyzed in a distillation flask heated by means of a metal bath. I-a, I-b, I-c, I-d, and I-e decomposed rapidly in the range from about 260 to 280°C, and alkyl carboxylates (R'COOR'') were quantitatively obtained as the sole distillable product (>97% pure by glc).

The pyrolysis was over in a few minutes. However, I-f and I-g were stable at this temperature. I-f and I-g began to decompose at 320°C and gave a mixture of methyl acetate, acetic acid, methyl alcohol, and benzaldehyde or propionaldehyde. In the presence of a catalytic amount of phosphoric acid, the temperature of the beginning of decomposition of I-f fell to 260°C and only methyl acetate was obtained. I-h decomposed at 190°C, and propylene, benzaldehyde, and acetic acid were obtained. When the pyrolysis of an equimolar mixture of I-b and I-c was performed, propyl acetate, ethyl acetate, ethyl butyrate, and propyl butyrate were obtained in the mole ratio 1.1: 1.0: 1.2: 1.1, as was determined by glc analysis. When a mixture of propyl acetate and ethyl butyrate was refluxed for 10 min in the presence of a small amount of phosphoric acid, interesterification did not occur. These results indicate that the formation of alkyl carboxylate from I is catalyzed by acid and proceeds by means of an intermolecular mechanism:

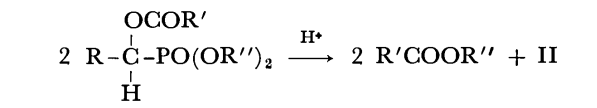

The structure of the undistillable product (II-a) obtained by the pyrolysis of I-a was identified from the following findings. II-a was a resin-like and hygroscopic solid, softening at 140—150°C. It was dissolved in water, and a small amount of an insoluble, oily matter was removed. When the solution was acidified with hydrochloric acid, a viscous matter was precipitated; this matter was separated and dried in a vacuum (yield, 98%), (II-a') mp 135—140°C. Found: C, 54.21; H, 5.54; P, 15.52%. Calcd for $C_{18}H_{22}O_6P_2$: C, 53.92; H, 5.59; P, 15.63%. UV λ_{max} 260 mμ, 11400 (in water). II-a' was refluxed with 6N hydrochloric acid for 24 hr. The hydrolyzed product: mp 142—145°C. Found: C, 47.06; H, 5.18; P, 18.08%. Calcd for $C_{14}H_{14}O_6P_2$: C, 49.42; H, 4.18; P, 18.20%. Acid value, 549 (Calcd for $C_{14}H_{14}O_6P_2$, tetrabasic acid 564). When treated with bromine water, II-a' gave a quantitative yield of the bromide, which was then recrystallized from ether; mp 159—160°C. Found: C, 39.75; H, 4.33; Br, 30.82%. Calcd for $C_{18}H_{22}O_6Br_2P_2$: C, 38.87; H, 4.28; Br, 29.93%. The methyl ester of II-a', esterified with diazomethane, MW: 435.5 (Cryscopic in benzene). Calcd for $C_{20}H_{26}O_6P_2$: 424.4. NMR $\tau(CCl_4)$ 8.8 (6H, t), 6.2—6.6 (10H, m), 2.72 (10H, s).

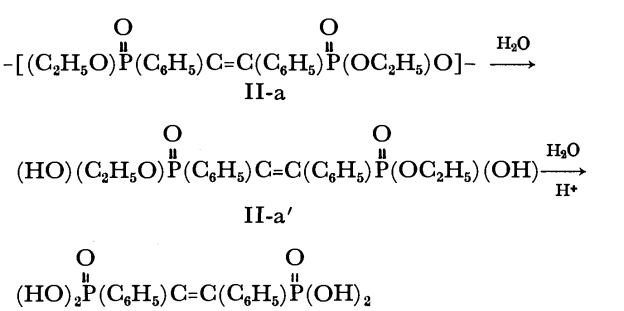

II-a

II-a'

1) M. S. Kharasch, R. A. Mosher, and I. S. Bengelsdorf, *J. Org. Chem.*, **25**, 1000 (1960).

BULLETIN OF THE CHEMICAL SOCIETY OF JAPAN, VOL. 46, 644—646 (1973)

The Synthesis of the Derivatives of Silacyclopentanol and Silacyclopentylamine

Tsunao ARAKI, Daiyo TERUNUMA, Fumio KATO, Hiroshi KANEDA, and Akira IINO

Department of Applied Chemistry, Faculty of Science and Engineering, Saitama University, Urawa

(Received April 22, 1972)

Recently, several papers have been reported on the synthesis and reactions of carbofunctional derivatives of silaheterocyclic compounds.[1] The present authors previously reported the synthesis[2] and polymerization[3] of silacyclo-pentene and -pentane derivatives. In this paper, we wish to report the synthesis of several new derivatives of silacyclopentanol and silacyclopentylamine 3,3,5-trimethyl-3-silacyclopentylphenylurethane (**3**), 1,1,3-trimethyl-4-acetoxy-1-silacyclopentane(**4**), 1,1,3-trimethyl-4-acryloxy-1-silacyclopentane(**5**), 1,1,3-trimethyl-4-methacryloxy-1-silacyclopentane(**6**), 1,1,3-trimethyl-4-amino-1-silacyclopentane(**7**), 1,1,3-trimethyl-4-acetylamino-1-silacyclopentane(**8**), 1,1,3-trimethyl-4-acryloylamino-1-silacyclopentane(**9**), and 1,1,3-trimethyl-4-methacryloylamino-1-silacyclopentane(**10**). The starting material, 1,1,3-trimethyl-1-silacyclopent-3-ene(**1**), was prepared in a 38% yield[2] by a modification of the method of Weyenberg *et al.*[4] The hydroboration and oxidation[5] of **1** with diborane and alkaline hydrogen peroxide gave 1,1,3-trimethyl-1-silacyclopentan-4-ol(**2**).[1b] **2** was reacted readily with phenyl isocyanate, acetyl chloride, acryloyl chloride, and methacryloyl chloride to afford **3**, **4**, **5**, and **6** respectively (Scheme 1).

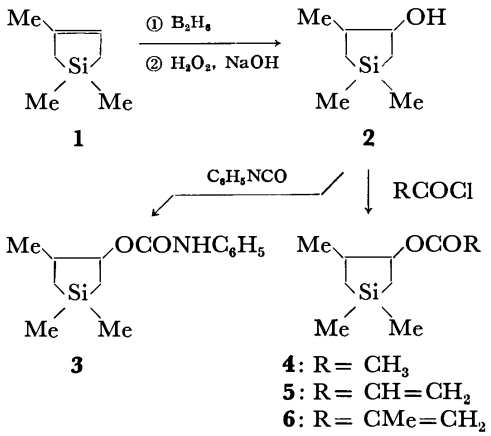

Scheme 1.

3 was a highly viscous liquid soluble in common organic solvents, such as CCl_4, Et_2O, and EtOH. The esters of silacyclopentanol, **4**, **5**, and **6**, were liquid and stable under ordinary conditions. In the case of compounds **5** and **6**, the addition of a small amount of hydroquinone as a polymerization inhibitor was necessary for obtaining them in better yields. Other new silacyclopentane derivatives were synthesized according to Scheme 2. The amination of chloroalkylsilane with ammonia has been successfully employed in the preparation of aminoalkylsilane.[6] This method, however, cannot be used in the synthesis of silacyclopentylamine because of the instability of the chloro-derivatives of silacyclopentane. *Via* hydroboration in diglyme, Brown and Zweifel[7] succeeded in preparing amines from hidered olefines, such as 1-methylcyclohexene, 1-methylcyclopentene, and α-pinene. By applying this method, hydroboration followed by treatment with NH_2OSO_3H in glyme (bp 82°C) in place of diglyme (bp 160°C), **7** was obtained in a 16.9% yield (Scheme 2). When tetrahydrofuran was used as the solvent, the yield of **7** was decreased to about 5%.

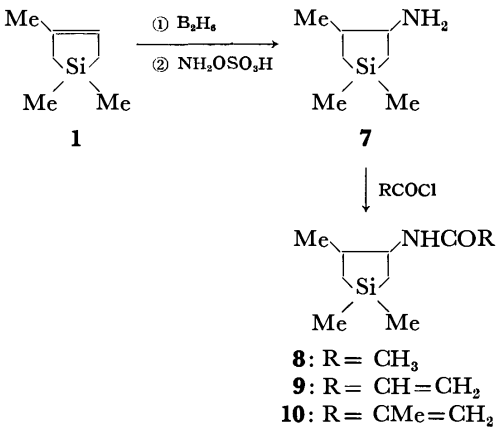

Scheme 2.

7 was a liquid miscible in common organic solvents and was stable under ordinary conditions. **7** was identified by an analysis of the IR and NMR spectra. (IR spectrum: silicon containing a five-membered ring,[8] 1080, 1030, and 1020 cm^{-1}; NMR spectrum: the two singlets at τ=9.91 and 9.88 for Si-$(CH_3)_2$ show that the silacyclopentane ring remains intact.) **7** was found to undergo reaction with acyl chlorides, such as acetyl chloride, acryloyl chloride, and meth-

1) a) A. G. Brook and J. B. Pierce, *J. Org. Chem.*, **30**, 2566 (1965). b) G. Manuel, P. Mazerolles, and J. G. Florrence, *J. Organometal. Chem.*, **30**, 5—19 (1971). c) D. Seyferth, R. Damraure, S. B. Andrews, and S. S. Washburne, *J. Amer. Chem. Soc.*, **93**, 3709 (1971).

2) T. Araki, D. Terunuma, and T. Fuse, This Bulletin, **45**, 293 (1972).

3) T. Araki, D. Terunuma, T. Sato, N. Nagai, M. Furuichi, and S. Nakamura, *ibid.*, **44**, 2725 (1971).

4) D. R. Weyenberg, L. H. Toporcer, and L. E. Nelson, *J. Org. Chem.*, **33**, 1975 (1968).

5) H. C. Brown and G. Zweifel, *J. Amer. Chem. Soc.*, **81**, 247 (1959).

6) L. H. Sommer and J. Rockett, *ibid.*, **73**, 5130 (1951).

7) H. C. Brown and G. Zweifel, *ibid.*, **82**, 4708 (1960).

8) V. M. Vdovin, K. S. Pushchevaya, N. A. Belikova, and R. Syltanov, *Dokl. Akad. Nauk SSSR.*, **136**, 96 (1961).

acryloyl chloride, to yield **8**, **9**, and **10** respectively. Compounds **8**, **9**, and **10** were colorless crystals. Their structural assignment was done by the analysis of the IR and NMR spectra. The acryloyl and methacryloyl derivatives, **5**, **6**, **9**, and **10**, could be polymerized easily by a radical initiator, such as BPO or AIBN. More detailed studies of the polymerization of these compounds are in progress.

Experimental

The NMR spectra were measured by means of a Varian A-60 spectrometer, using tetramethylsilane as the internal standard. The infrared spectra were obtained on a Shimadzu IR-27C spectrophotometer.

Preparation of ***2***. To a tetrahydrofuran (30 ml) solution of 12.6 g (0.1 mol) of **1** cooled at 0°C, we added gaseous diborane generated from 1.9 g of sodium borohydride in diglyme and boron trifluoride etherate over a period of 2 hr. After this mixture had stood for 2 hr at room temperature, small chips of ice were added to hydrolyze the excess diborane. The solution was immersed in an ice bath, and 11 ml of 3M sodium hydroxide was added, followed by 11 ml of 30% hydrogen peroxide over a period of 1 hr. One hour later the organic layer was separated and the aqueous layer was extracted with ether. The combined organic layer was dried over anhydrous sodium sulfate and distilled to yield 9.8 g (68%) of **2**. Bp 82—86°C/30 mmHg, n_D^{20} 1.4553.

Preparation of ***3***. Phenyl isocyanate (0.03 mol) was added to 3.6 g (0.025 mol) of **2** at room temperature. After 15 min at 75°C, a small amount of water was added to the mixture to hydrolyze the excess phenyl isocyanate. The mixture was then diluted with 20 ml of carbon tetrachloride. Filtration and distillation gave 4.0 g (75.3%) of **3**. NMR: τ 9.87 (s, 6H, CH_3–Si), 8.98 (d, 3H, C–CH_3), 8.40—9.50 (m, 4H, CH_2–Si), 7.80—8.30 (m, 1H, CH–Me), 5.41 (sextet, 1H, CH–O), 2.50—3.25 (m, 6H, –NH–Ph). IR: 3400(m), 2950 (m), 1720 (s), 1601 (m), 1550 (m), 1240 (s), 1075 (m), 1050 (m), 1030 (m), 850 (m). Bp 145—147°C/0.15 mmHg n_{20}^D 1.5303. Found: N, 5.47; Si, 10.53%. Calcd for $C_{14}H_{21}O_2NSi$: N, 5.32; Si, 10.62%.

Preparation of ***4***. To a mixture of 4.8 g (0.033 mol) of **2** and 4 g (0.04 mol) of triethylamine in 30 ml of dry ether was added 3.1 g (0.04 mol) of acetyl chloride in 10 ml of dry ether at 0°C with stirring. Then the mixture was refluxed for 1.5 hr. The ether layer was separated from precipitates of triethylamine hydrochloride. The ether layer was washed with five 20 ml portions of water, and then dried over anhydrous sodium sulfate. Distillation gave 3.14 g (68.4%) of **4**. NMR: τ 9.80, 9.83 (two singlets, 6H, CH_3–Si), 9.01 (d, 3H, C–CH_3), 8.50—9.75 (m, 4H, CH_2–Si), 8.05 (s, 3H, CO–CH_3), 5.40 (sextet, 1H, CH–O). IR: 2935 (m), 1740 (s), 1250 (s), 1080 (m), 1050 (s), 1025 (m), 850 (s). Bp 100—104°C/70 mmHg, n_D^{20} 1.4438. Found: Si, 14.34%. Calcd for $C_9H_{18}O_2Si$: Si, 15.08%.

Preparation of ***5***. The synthesis procedure was similar to that described above. To a solution of 4.8 g of **2** and 4 g of triethylamine in 30 ml of dry ether, we added 3.62 g (0.04 mol) of acryloyl chloride in 10 ml of dry ether in the presence of a small amount of hydroquinone as a polymerization inhibitor. NMR: τ 9.82, 9.85 (two singlets, 6H, CH_3–Si), 9.01 (d, 3H, C–CH_3), 8.40—9.70 (m, 4H, CH_2–Si), 7.70—8.30 (m, 1H, CH–Me), 5.35 (sextet, 1H, CH–O), 3.50—4.40 (m, 3H, CH=CH_2). IR: 2950 (m), 1735 (s), 1610 (s), 1210 (m), 1070 (m), 1050 (w), 1020 (w), 850 (m). Yield, 2.24 g (34.1%); Bp 58—61°C/3.5 mmHg, n_D^{20} 1.4580. Found: Si, 13.24%. Calcd for $C_{10}H_{18}O_2Si$: Si, 14.30%.

Preparation of ***6***. The procedure was similar to that used for **4**. To a solution of 4.8 g of **2** and 4 g of triethylamine in 30 ml of dry ether, we added 4.17 g (0.04 mol) of methacryloyl chloride in 10 ml of dry ether in the presence of a small amount of hydroquinone. NMR: τ 9.82, 9.86 (two singlets, 6H, CH_3–Si), 9.05 (d, 3H, C–CH_3), 7.40—8.30 (m, 1H, CH–Me), 5.40 (sextet, 1H, CH–O), 4.56 (m, 1H, C=CH), 4.00 (m, 1H, C=CH). IR: 2980 (m), 1725 (s), 1640 (m), 1300 (m), 1250 (m), 1180 (s), 1070 (m), 1050 (m), 1020 (m), 840 (s). Yield, 1.96 g (37.1%); Bp 77—79°C/2.5 mmHg, n_D^{20} 1.4590. Found: Si, 12.83%. Calcd for $C_{11}H_{20}O_2Si$: Si, 13.36%.

Preparation of ***7***. To a flask containing 12.6 g (0.1 mol) of **1** in 30 ml of glyme at 0°C, we added gaseous diborane generated from 1.9 g of sodium borohydride in diglyme and boron trifluoride etherate over a period of 2 hr. After this mixture had stood 2 hr at room temperature, a solution of 13.6 g (0.12 mol) of hydroxylamine-*O*-sulfonic acid in 25 ml of glyme was added; the solution was then refluxed for 4 hr. The reaction mixture was cooled, treated with 20 ml of concentrated hydrochloric acid, and poured into 200 ml of water. The acidic phase was extracted with ether to remove glyme and the residual boronic acid. The aqueous solution was then made strongly alkaline with sodium hydroxide, and the amine was extracted with ether. The ether extract was dried over potassium hydroxide and distilled. NMR: τ 9.00—9.70 (m, 4H, Si–CH_2), 9.04 (d, 3H, C–CH_3), 8.80 (m, 2H, –NH_2), 7.38 (octet, 1H, CH–N). IR: 3350 (w), 3250 (w), 2940 (s), 1580 (m), 1450 (m), 1400 (m), 1360 (m), 1250 (s), 990 (w), 830 (s). Yield, 2.40 g (16.9%); Bp 74—75°C/42 mmHg, n_D^{20} 1.4535. Found: N, 9.50; Si,18.22%. Calcd for $C_7H_{17}NSi$: N, 9.77; Si, 19.53%.

Preparation of ***8***. Into a mixture of 1.43 g (0.01 mol) of **7** and 1.2 g (0.012 mol) of triethylamine in 20 ml of dry ether, we stirred 0.94 g (0.012 mol) of acetyl chloride in 10 ml of dry ether at 0°C. After the addition was completed, the mixture was stirred at room temperature for 3 hr. The ether layer was separated from precipitates of triethylamine hydrochloride, and then washed with five 15 ml portions of water. The ether solution was dried over anhydrous sodium sulfate. On the evaporation of the solvent, we obtained 1.43 g (77.5%) of a colorless solid product. This product was recrystallized from petroleum ether. NMR: τ 9.86 (s, 6H, CH_3–Si), 9.02 (d, 3H, C–CH_3), 8.50—9.60 (m, 4H, CH_2–Si), 8.07 (s, 3H, O=C–CH_3), 7.40—8.30 (m, 1H, CH–Me), 2.31 (d, 1H, NH). IR: 3300 (m), 3150 (w), 2950 (m), 1650 (s), 1560 (m), 1300 (m), 1250 (m), 1085 (w), 1070 (m), 1040 (w), 850 (s). Yield, 1.04 g (56.3%); Mp 99.5—100°C. Found: N, 7.40; Si, 14.76%. Calcd for $C_9H_{19}OSi$: N, 7.56; Si, 15.10%.

Preparation of ***9***. The synthesis procedure was similar to that described above. Into a mixture of 1.43 g (0.01 mol) of **7** and 1.2 g (0.012 mol) of triethylamine in 20 ml of dry ether, we stirred 1.09 g (0.012 mol) of acryloyl chloride in 10 ml of dry ether at 0°C in the presence of a small amount of hydroquinone. NMR: τ 9.88, 9.91 (two singlets, 6H, CH_3–Si), 9.00 (d, 3H, C–CH_3), 8.40—9.50 (m, 4H, CH_2–Si), 7.80—8.50 (m, 1H, CH–Me), 6.32 (m, 1H, CH–N), 4.50 (q, 1H, CH=C), 3.70 (t, 2H, C=CH_2), 2.32 (d, 1H, CH–N). IR: 3330 (m), 3130 (w), 3080 (m), 1660 (s), 1610 (m), 1550 (m), 1250 (m), 1160 (m), 1070 (m), 1000 (w), 980 (m), 840 (m). Yield, 1.20 g (61.3%); Mp 114—115°C. Found: N, 6.95; Si, 13.01%. Calcd for $C_{10}H_{19}OSi$: N, 7.90; Si, 14.18%.

Prepatation of ***10***. The procedure was similar to that described above. To a solution of 1.43 g (0.01 mol) of **7**

and 1.2 g (0.012 mol) of triethylamine in 20 ml of dry ether, we added 1.25 g (0.012 mol) of methacryloyl chloride in 10 ml of dry ether in the presence of hydroquinone. NMR: τ 9.89, 9.92 (two singlets, 6H, CH_3–Si), 9.00 (d, 3H, C–CH_3), 8.40—9.50 (m, 4H, CH_2–Si), 8.13 (s, 3H, O=C–CH_3), 7.80—8.60 (m, 1H, CH–Me), 6.33 (m, 1H, CH–N), 4.78 (m, 1H, C=CH), 4.40 (m, 1H, C–CH), 3.40 (d, 1H, NH). IR: 3300 (m), 2940 (m), 1660 (m), 1620 (s), 1540 (s), 1250 (m), 1160 (m), 1070 (m), 1005 (m), 980 (w), 840 (s). Yield, 1.37 g (64.8%); Mp 102—103°C. Found: N, 6.49; Si, 12.82%. Calcd for $C_{11}H_{21}NOSi$: N, 6.63; Si, 13.24%.

The authors wish to thank Dr. H. Nohira for his many helpful discussions and the Shinetsu Kagaku Co. for providing the dimethyldichlorosilane.

Table 1. Competitive nitration of toluene and benzene with nitric acid in various organic solvents

Solvent	Temp. °C	k_T/k_B	Isomer ratio			Partial rate factor			S_f	o/p
			o-	*m*-	*p*-	o_f^T	m_f^T	p_f^T		
CCl_4	30	2.31	58.9	4.4	36.7	4.08	0.30	5.08	1.228	1.60
	40	2.23	59.1	4.7	36.2	3.95	0.31	4.84	1.193	1.63
	50	2.15	58.2	4.9	36.9	3.75	0.31	4.76	1.186	1.57
n-C_6H_{14}	20	2.82	57.4	4.2	38.4	4.85	0.35	6.49	1.268	1.49
	30	2.50	56.7	4.7	38.6	4.25	0.35	5.79	1.218	1.46
	40	2.45	56.4	5.0	38.6	4.14	0.36	5.67	1.197	1.46
cyclo-C_6H_{12}	20	2.56	56.2	4.6	39.2	4.31	0.35	6.02	1.235	1.43
	30	2.44	57.3	4.6	38.1	4.19	0.33	5.57	1.227	1.50
	40	2.20	55.9	4.9	39.2	3.68	0.32	5.17	1.208	1.42
CH_2Cl_2	20	17.3	56.6	3.1	40.3	29.3	1.60	41.8	1.416	1.40
	30	15.8	56.3	3.8	39.9	26.6	1.80	37.8	1.322	1.41
CH_3NO_2	30	19.7	59.3	4.2	36.5	35.0	2.48	43.1	1.240	1.62
	40	17.7	58.3	4.8	36.9	30.9	2.54	39.2	1.188	1.57
	50	16.3	59.0	5.1	35.9	28.8	2.49	35.1	1.149	1.64
CH_3CN	50	13.8	59.1	5.0	35.9	24.4	2.07	29.7	1.156	1.64

Table 2. Summary of nitration of toluene and benzene

Reaction condition		k_T/k_B	Isomer ratio			Partial rate factor			S_f	o/p
			o-	*m*-	*p*-	o_f^T	m_f^T	p_f^F		
HNO_3[12] $HOAc-H_2O$	45°C	24.5	56.5	3.5	40.0	42	2.5	58	1.366	1.41
HNO_3[4b] CH_3NO_2	30°C	21	58.5	4.4	37.1	37	2.8	47	1.225	1.57
HNO_3[5] CH_3NO_2	25°C	21	61.7	1.9	36.4	38.9	1.3	45.8	1.547	1.69
$AcONO_2$[4b] Ac_2O	30°C	23	58.4	4.4	37.2	40	3.0	51	1.230	1.56
$AcONO_2$[5] Ac_2O	25°C	23	63.3	2.8	33.9	46.5	2.1	48.5	1.364	1.86
$AcONO_2$[12] Ac_2O	0°C	27	61.4	1.6	37.0	49.7	1.3	60.0	1.664	1.65
NO_2BF_4[3] $C_4H_8SO_2$	25°C	1.67	65.4	2.8	31.8	3.2	0.14	3.2	1.354	2.05
HNO_3[6] CCl_4	25°C	17.2	—	—	—	—	—	—	—	—
HNO_3[7] CCl_4	25°C	1.2	—	—	—	—	—	—	—	—

Results and Discussion

The results of the competitive nitration of toluene and benzene in non-polar or polar solvents are shown in Table 1. The results of previous works mainly related to the nitration in organic solvents are given in Table 2 for comparison. We see that the rate ratios (k_T/k_B) of nitration in the organic solvents studied have a value of about 20 in all cases except for the case of Olah *et al.*[3] and Bonner *et al.*[7] However, the result of the latter differs from that of Coombes,[6] although Coombes suggests that the discrepancy is due to heterogeneity. According to our results in carbon tetrachloride, *n*-hexane, and cyclohexane, the lower values of k_T/k_B were obtained. In the nitration of toluene involving an ideally strong electrophile, in which the π-complex formation is rate-determining, an *ortho* to *para* ratio of 2: 1 and a lower value of k_T/k_B would be obtained.[3] The *ortho*/*para* ratios in the above three solvents are not so high as expected on the basis of the lower values of k_T/k_B in Table 1. All the partial rate factors of the *meta* position (m_f^T) in the above three solvents are below 1. The results are in line with those of Olah *et al.*[3]

Hughes *et al.*[4a] indicated by conductivity measurements that the self-dissociation of nitric acid is represented as follows:

$$2HNO_3 \rightleftharpoons NO_2^+ + NO_3^- + H_2O$$

They showed that according to Raman spectroscopic observations, anhydrous nitric acid contains approximately 1% of nitronium ion and solutions of nitric acid in organic solvents such as nitromethane contain no detectable amount of nitronium ion. On the other hand, in the nitration of aromatics with nitric acid in carbon tetrachloride, the rate dependence on nitric acid concentration was indicated by Coombes,[6] and Bonner *et al.*[7] to be an order of 5 or 6. Thus nitronium ion may not exist as free ion but as aggregate

Table 3. Relationship between dielectric constants and rate ratios

Solvent	ε (20°C)	k_T/k_B
Carbon tetrachloride	2.23	2.15— 2.31
n-Hexane	1.89	2.45— 2.82
Cyclohexane	2.02	1.75— 2.56
Methylene dichloride	9.08	15.8 —17.3
Nitromethane	35[a)]	16.3 —19.7
Acetonitrile	37.5	13.8

a) The value at 30°C.

such as $NO_2^+\cdots NO_3^-$ or $NO_2^+\cdots NO_3^-\cdot HNO_3$. This aggregation might partly correspond to the smaller value of the *ortho*/*para* ratios.

The relationships between dielectric constants and rate ratios are summarized in Table 3. This indicates that the more polar the solvent, the higher the substrate selectivity (k_T/k_B). The activation parameters are shown in Table 4. We see from Tables 1 and 4 that the values of k_T and ΔE_B are larger than those of k_B and ΔE_T, respectively. On the other hand, the values of $\Delta S_B^{\neq}$ are larger than those of $\Delta S_T^{\neq}$. Thus, toluene is nitrated faster with nitric acid than benzene ($k_T > k_B$), primarily depending upon the differences in activation energies with the compensating effects in the entropies of activation. It is concluded that in the competitive nitration of toluene and benzene with nitric acid in organic solvents, the polarity of solvents affects the relative rate constant (k_T/k_B) considerably.

Table 4. Activation parameter

Solvent	$\Delta E_B - \Delta E_T$ (kcal·mol^{-1})	$\Delta S_T^{\neq} - \Delta S_B^{\neq}$ (cal·mol^{-1}·deg^{-1})
Carbon tetrachloride	0.67	−0.56
n-Hexane	1.26	−2.3
Cyclohexane	1.35	−2.68
Nitromethane	1.83	−0.11

BULLETIN OF THE CHEMICAL SOCIETY OF JAPAN, VOL. 46, 648—649 (1973)

The Reaction of Elemental Sulfur with Organic Compounds. V. Reactions of Optically Active Sulfoximine with Elemental Sulfur and with Diphenyl Disulfide[1]

Shigeru OAE, Yoshiyuki TSUCHIDA, and Naomichi FURUKAWA

Department of Applied Chemistry, Faculty of Engineering, Osaka City University, Sumiyoshi-ku, Osaka

(Received June 5, 1972)

The stereochemistry of sulfur compounds having S–N bonds such as sulfilimine and sulfoximine has recently drawn considerable attention.[2-7] Cram and his coworkers reported a stereospecific cleavage of S–N bond of sulfoximine with $NOPF_6$ or HNO_2 to afford the corresponding sulfoxide having the same configuration as that of the original sulfoximine.[2,3]

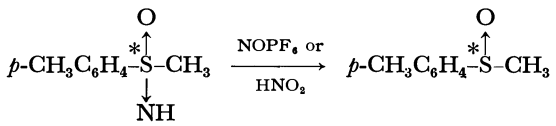

We reported a convenient method of deimination of sulfoximine by treatment with elemental sulfur or diphenyl disulfide to the corresponding sulfoxide in nearly quantitative yield.[1] In this paper we report on a stereochemical course and plausible mechanism of the reaction.

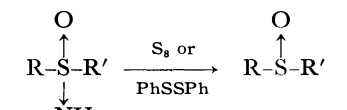

1: R=*p*-$CH_3C_6H_4$–, R′=CH_3–
2: R=Ph–, R′=CH_3–

The results of the reaction with optically active methyl *p*-tolyl sulfoximine are shown in the table. We see that the reaction proceeds stereospecifically retaining nearly completely the original configuration around the sulfur atom. The reaction with optically active methyl phenyl sulfoximine was found to give a similar result. These stereochemical observations suggest that the hybridization at sulfur atom of sulfoximine is left undisturbed in the course of the reaction.[8] A conceivable mechanistic pathway is shown below.

In view of the basic nature of the imino group of sulfoximine,[9] the initial step of the reaction is considered to involve a nucleophilic attack of the nitrogen atom of sulfoximine on the sulfur atom of S–S bond forming a dipolar intermediate (**3**). In the following step, **3** would decompose through the attack of thiolate anion on the nitrogen atom eventually cleaving off

1) Paper IV; S. Oae, Y. Tsuchida, K. Tsujihara, and N. Furukawa, This Bulletin, **45**, 2856 (1972).
2) D. J. Cram, J. Day, D. R. Rayer, D. M. von Schriltz, D. J. Duchamp, and D. C. Garwood, *J. Amer. Chem. Soc.*, **92**, 7369 (1970).
3) T. R. Williams, R. E. Booms, and D. J. Cram, *ibid.*, **93**, 7338 (1971).
4) C. R. Johnson and C. W. Schroeck, *ibid.*, **93**, 5303 (1971).
5) C. W. Schroeck and C. R. Johnson, *ibid.*, **93**, 5305 (1971).
6) E. U. Jonsson, C. C. Bacon, and C. R. Johnson, *ibid.*, **93**, 5306 (1971).
7) E. U. Jonsson and C. R. Johnson, *ibid.*, **93**, 5308 (1971).
8) For detailed accounts of substitution on sulfur atom; a) S. Oae, *Quart. Reports on Sulfur Chem.*, **5**, 53 (1970); b) see Ref. 2).
9) S. Oae, K. Tsujihara, and N. Furukawa, *Chem. Ind.* (London) **1968**, 1596.

Table 1. Reaction of optically active sulfoximine

Reaction	$[\alpha]_D$ (optical purity)	Condition	Product	$[\alpha]_D$ (Optical purity)
(−)-(*R*)-**1**+S_8	−33.4° (100%)	neat 160°C 10 min	(+)-(*R*)-*p*-TolS(O)CH_3	+147° (98%)
(−)-(*R*)-**1**+PhSSPh	−33.4° (100%)	*o*-$C_6H_4Cl_2$ reflux 18 hr	(+)-(*R*)-*p*-TolS(O)CH_3	+148° (99%)
(+)-(*S*)-**2**+S_8	+33.8°	neat 160°C 10 min	(−)-(*S*)-PhS(O)CH_3	−141° (95%)

p-Tol=*p*-$CH_3C_6H_4$-

sulfoxide.[10] Thus the sulfoxide formed can maintain the same configuration as that of sulfoximine.

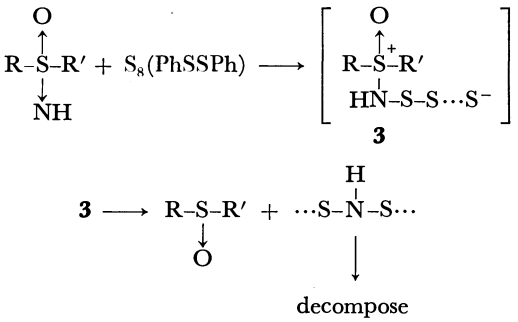

Experimental

Materials. Optically pure (−)-(*R*)-methyl *p*-tolyl sulfoximine ((−)-(*R*)-**1**) was prepared from optically pure (+)-(*R*)-methyl *p*-tolyl sulfoxide ($[\alpha]_D$=+150°, *c* 0.67, acetone) according to the method used by Cram *et al.*[2] $[\alpha]_D$=−33.4° (*c* 1.86, acetone); lit, $[\alpha]_D$=−33.4° (*c* 2.275, acetone).

(+)-(*S*)-Methyl phenyl sulfoximine ((+)-(*S*)-**2**) was prepared through resolution of sulfoximine according to the method used by Fusco and Tenconi.[11] To a solution of *d*-camphor-10-sulfonic acid (15 g) in ethanol was added methyl phenyl sulfoximine (6.5 g) and the mixture was refluxed for an hour. Acetone (50 ml) was then added to the reaction mixture and cooled in a refrigerator overnight. The crystals deposited were collected by filtration and recrystallized several times from a mixture of acetone–ethanol: mp 176°C, $[\alpha]_D$=+45.3° (methanol). The salt of sulfoximine-*d*-camphor-10-sulfonic acid was dissolved in a cold dilute sodium hydroxide solution and extracted with chloroform, washed with water and dried over anhydrous magnesium sulfate. After the solvent was evaporated, oily (+)-(*S*)-**2** was obtained and used for the reaction without further purification. $[\alpha]_D$=−33.8° (*c* 3.62, acetone).

Elemental sulfur was purified by recrystallization of commercial sulfur from benzene: mp 114°C.

Diphenyl disulfide was prepared from thiophenol by iodine oxidation in water: mp 61°C.

Reaction of (−)-(R)-1 with Sulfur. A mixture of 0.153 g (1 mmol) of (−)-(*R*)-**1** and 0.032 g (1 mg-atom) of sulfur was placed in a glass tube and heated in an oil bath maintained at *ca.* 160°C for 10 min. The red colored product was chromatographed on silica gel with chloroform as an eluent. Methyl *p*-tolyl sulfoxide was obtained as the main product in an almost quantitative yield. After recrystallization several times from ether–hexane, the optical rotation was measured; $[\alpha]_D$=+147° (*c* 0.54, acetone). The sulfoxide was 98% optically pure. Since the starting sulfoximine was nearly optically pure, the reaction is 98% stereospecific.

Reaction of (−)-(R)-1 with Diphenyl Disulfide. Diphenyl disulfide, 0.218 g (1 mmol), and (−)-(*R*)-**1**, 0.153 g (1 mmol) were dissolved in 5 ml of *o*-dichlorobenzene and refluxed for about 18 hr. The product was treated in a similar manner to that described above and the sulfoxide was obtained in 99% optical purity. $[\alpha]_D$=+148° (*c* 0.63, acetone).

Reaction of (+)-(S)-2 with Sulfur. This reaction was carried out in a similar manner to that described. After chromatography oily sulfoxide was obtained and the optical rotation was measured without further purification. $[\alpha]_D$=141° (*c* 19.3, ethanol) 95% optically pure (optically pure methyl phenyl sulfoxide, $[\alpha]_D$=149°[12]).

10) There is the possibility of substitution on the sulfur atom. If the nucleophilic attack of thiolate anion on the sulfur atom of **3** should occur to form a hypothetical pentacoordinated sulfur intermediate (**4**), the configuration of the resulting sulfoxide would be either retained, inverted or racemized depending on the mode of displacement on the sulfur atom. However, such a valence expanded sulfur intermediate is not necessary for interpreting the results of the stereochemistry of the reaction of optically active sulfoximine with sulfur or diphenyl disulfide.

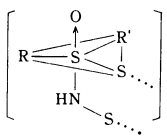

4

11) R. Fusco and F. Tenconi, *Chim. Ind.*, (Milan), **47**, 61 (1965); *Chem. Abstr.*, **62**, 10357h (1965).

12) J. Jacobus and K. Mislow, *J. Amer. Chem. Soc.*, **89**, 5228 (1967).

BULLETIN OF THE CHEMICAL SOCIETY OF JAPAN, VOL. 46, 650—651 (1973)

The Reaction of Elemental Sulfur with Organic Compounds. VI.[1] ^{35}S-Tracer Study of Aromatic Displacement Reaction of Thianthrene, Phenoxathiin, Dibenzothiophene and Their Oxidation Compounds by Sulfur

Shigeru OAE, Shigeo MAKINO, and Yoshiyuki TSUCHIDA

Department of Applied Chemistry, Faculty of Engineering, Osaka City University, Sumiyoshi-ku, Osaka

(Received June 6, 1972)

We reported on aromatic displacement reactions which take place when diphenyl sulfide, diphenyl sulfone,[2] and halobenzenes[3] are heated with elemental sulfur at elevated temperature as follows.

$$Ph^{35}SPh + S \longrightarrow Ph^{35/2}SPh + {}^{35/2}S \quad (1)$$

$$Ph^{35}SO_2Ph + S \longrightarrow PhSPh + {}^{35}SO_2 \quad (2)$$

$$PhX + S \longrightarrow PhS_xPh + S_xX_2 \quad (3)$$

It is of interest that these three reactions essentially involve displacement of aromatic substituents (sulfonyl, sulfide groups and halogen) by a sulfur atom of elemental sulfur without any rearrangement or migration.[4] We have extended the investigation to reactions of elemental sulfur with a few polycyclic aromatic sulfur compounds, *i.e.*, thianthrene (**1**), phenoxathiin (**4**), dibenzothiophene (**7**), and their oxidation compounds (sulfones **2**, **5**, **8** and sulfoxides **3**, **6**, **9**). This paper will describe the reactions in detail.

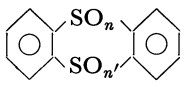

1: $n=0$, $n'=0$
2: $n=2$, $n'=2$
3: $n=0$, $n'=1$

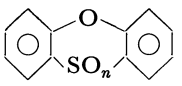

4: $n=0$
5: $n=2$
6: $n=1$

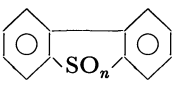

7: $n=0$
8: $n=2$
9: $n=1$

Sulfur Exchange Reaction of 1, 4, and 7 with Elemental Sulfur. The results of the tracer experiments using ^{35}S-labeled compounds are shown in the table. The sulfur exchange reaction was found to take place when **1**-^{35}S or **4**-^{35}S was heated with elemental sulfur at above 300°C. Under similar reaction condition **7** did not undergo such reaction, while prolonged heating of the reactant resulted in the formation of a polymer-like substance with evolution of H_2S. This is reasonable since the strength of C–S bond of **7** is increased by the intraresonance stabilization of the thiophene ring to retard the cleavage of C–S bond.

Reactions of 2, 5, and 8 with Sulfur. The reduction of **2** by elemental sulfur to **1** was reported earlier.[5] The reactions of **5** and **8** with elemental sulfur were found to proceed under the usual conditions giving the corresponding reduction compounds **4** and **7** respectively. The results of the tracer experiments of these reactions are also shown in the table. We see that

TABLE 1. ^{35}S-TRACER EXPERIMENT

Reactant ($\times 10^5$ cpm/mmol)	Product ($\times 10^5$ cpm/mmol)	Displacement of sulfur (%)	Reaction condition	Yield of product (%)
1 (5.23)[a]	**1** (4.44)	85.2	320°C 2 hr	69
4 (9.72)[a]	**4** (3.51)	72.0	330°C 2 hr	93
7 (8.87)[a]	**7** (0.015)	0.17	330°C 2.5 hr	14
2 (1.76)	**1** (0.34)	80.7	345°C 2.5 hr	66
5 (1.97)	**4** (0.21)	89.2	335°C 3 hr	18
8 (7.69)[a]	**7** (6.63)	87.0	320°C 2 hr	38
3 (8.97)	**1** (8.16)	9.0	250°C 30 min	75
6 (1.92)	**4** (1.90)	1.0	250°C 30 min	80
9 (7.67)[a]	**7** (0.012)	0.2	250°C 30 min	51

a) Radioactivity of elemental sulfur-35. In these reactions nonactive reactants (**1**, **4**, **7**, **8**, and **9**) were reacted with radio active elemental sulfur.

the sulfonyl group in all the sulfones **2**, **5**, and **8** was replaced by sulfur atom of elemental sulfur in the main path of the reaction. The fact that these three reactions do not proceed *via* a simple reduction, namely the S–O bond cleavage of the sulfonyl group, can be attributed to the large bond strength of S–O bond in these sulfones.[6]

Reactions of 3, 6, and 9 with Sulfur. We carried out the reduction of the sulfoxides **3**, **6**, and **9** which have a weaker S–O bond than that of sulfone.[6] These sulfoxides were found to be reduced to the corresponding sulfides at somewhat lower temperatures than for the sulfones. The tracer experiments (Table) clearly suggest the reaction to be a simple reduction (S–O bond cleavage).

Mechanism of the Reaction. Sulfur is known to undergo homolytic cleavage of S–S bond at an elevated temperature and to exist as a mixture of many allotropes S_2, S_3, S_4, *etc.*[7] In these aromatic displacement reactions these allotropes of sulfur, which are expected to be active radical species, seem to be actually involved in the initial attack on the aromatic carbon atom bearing sulfur atom, although the subsequent steps are still unclarified. A plausible mechanistic pathway is as follows.

1) Paper V. S. Oae, Y. Tsuchida, and N. Furukawa, This Bulletin, **46**, 648 (1973).
2) S. Oae and S. Kawamura, *ibid.*, **36**, 163 (1963).
3) S. Oae and Y. Tsuchida, *Tetrahedron Lett.*, **1972**, 1283.
4) S. Oae, M. Nakai, Y. Tsuchida, and N. Furukawa, This Bulletin, **44**, 445 (1971).
5) B. F. Krafft and R. E. Lyons, *Ber.*, **29**, 435 (1896).
6) It is known that the force constant of S–O bond in sulfone 9.5×10^5 dyn/cm, is appreciably higher than that of sulfoxide (7.5×10^5 dyn/cm); C. C. Price and S. Oae, "Sulfur Bonding," Ronald Press, Inc., New York (1962), p. 66.
7) a) B. Meyer, "Elemental Sulfur," ed. by B. Meyer, Interscience, New York, 1964. b) B. Meyer, T. V. Dommen, and D. Jenson, *J. Phys. Chem.*, **75**, 912 (1971).

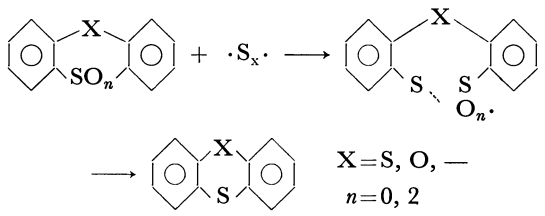

Experimental

Materials. Compounds **1**, **4**, and **7** were prepared by the usual method. **1**, mp 155°C (lit,[8] 159°C); **4**, mp 56.5°C (lit,[9] 57.5—58°C); **7**, mp 96°C (lit,[10] 99°C).

Radioactive **1**, **4**, and **7**. A mixture of **1** (3.04 g) and radioactive sulfur (0.90 g) was heated for 2 hr at *ca.* 330°C. The resulting mixture was poured into 10% aqueous NaOH solution and refluxed for 3 hr to remove elemental sulfur. The water insoluble **1**-^{35}S was filtered and recrystallized from methanol. Compound **4**-^{35}S was prepared similarly by the sulfur exchange reaction of **4** with radioactive elemental sulfur.

Radioactive **2**, **3**, **5**, and **6** were prepared by oxidation of **1**-^{35}S or **4**-^{35}S with a required amount of 30% H_2O_2 in acetic acid. **2**-^{35}S, mp above 300°C (lit,[11] 324°C); **3**-^{35}S, mp 137.5°C (lit,[12] 143°C); **5**-^{35}S, mp 143°C (lit,[13] 147—148°C); **6**-^{35}S, mp 150.5—151°C (lit,[13] 158—159°C).

Compounds **8** and **9** were similarly prepared from **7**. **8**, mp 227.5—228°C (lit,[14] 230°C); **9**, mp 185.5°C (lit,[15] 188°C).

Reactions of 1—9 with Elemental Sulfur. The reactions were carried out by the following general procedure. A mixture of 1 mmol of aromatic sulfur compound and 1 matom of sulfur (2 matom in the case of the reactions of **1** and **2**) was placed in a glass tube and heated in a metal bath. The resulting mixture was poured into 10% aqueous NaOH solution and refluxed for several hours. After cooling, the water insoluble precipitate was filtered and passed through a column elution chromatography (silica gel, hexane) and then recrystallized from alcohol for counting of activity.

Counting of Radioactivities. The activities of all the compounds were counted by TEN liquid scintillation counter in toluene solution using POPOP as a scintillator.

8) G. Dongherty and P. D. Hammond, *J. Amer. Chem. Soc.*, **57**, 117 (1935).
9) C. M. Suter and C. E. Maxwell, "Organic Syntheses," Coll. Vol. II, p. 485 (1943).
10) H. Golmen and A. L. Jacoby, *J. Org. Chem.*, **3**, 108 (1938).
11) C. Graebe, *Ann.*, **179**, 182 (1875).
12) K. Fries and W. Vogt, *ibid.*, **381**, 321 (1911).
13) H. D. K. Drew, *J. Chem. Soc.*, **1928**, 520.
14) J. Stenhouse, *Ann.*, **156**, 333 (1870).
15) C. Courtot and C. Pomonis, *C. R. Acid. Sci. Paris*, **182**, 893 (1926).

BULLETIN OF THE CHEMICAL SOCIETY OF JAPAN, VOL. 46, 651—653 (1973)

Optically Active Triptycenes. III.* Synthesis of Optically Active 2-Methoxy-5-acyloxy- and 2-Acyloxy-5-methoxy-7-methoxycarbonyltriptycenes

Fumio OGURA and Masazumi NAKAGAWA

Department of Chemistry, Faculty of Science, Osaka University Toyonaka, Osaka 560

(Received June 12, 1972)

A report was given on the synthesis and optical resolution of 2,5-diacetoxy-7-carboxytriptycene (I).[1] The present paper deals with the transformation of (+)-I into the title compounds. As outlined in Scheme 1, (+)-2,5-dihydroxy-7-carboxytriptycene (II) obtained by the hydrolysis of (+)-I was converted into (+)-methyl ester (III). Monomethylation of (+)-III by the Robinson method[2] with some modification afforded (+)-2-methoxy-5-hydroxy-7-methoxycarbonyltriptycene (IV) and 2-hydroxy-5-methoxy-7-methoxycarbonyltriptycene (V) together with a small amount of 2,5-dimethoxy-7-methoxycarbonyltriptycene and 7-methoxycarbonyltriptycene-2,5-quinone. Formation of the quinone seems to be attributable to the presence of a small amount of peroxide in tetrahydrofuran used as a solvent. The isomeric (+)-IV and (+)-V could be separated on column chromatography on alumina. Treatment of (+)-IV and (+)-V with dimethyl sulfate afforded an identical dimethyl ether, 2,5-dimethoxy-7-methoxycarbonyltriptycene. The structures of IV and V could be confirmed by IR spectroscopy, *i.e.*, the IR spectrum in chloroform of

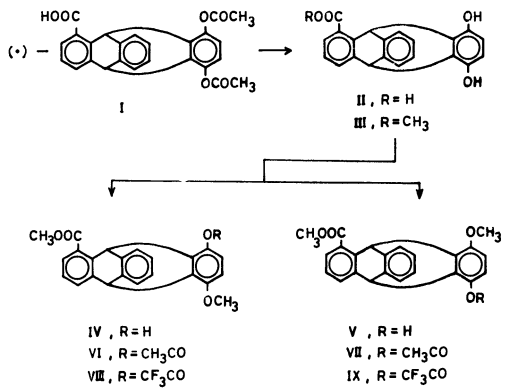

Scheme 1.

* For a preliminary report, see Ref. 6. For part II of this series, see Ref. 7.

1) A. Sonoda, F. Ogura, and M. Nakagawa, This Bulletin, **35**, 853 (1962).

2) R. Robinson and J. C. Smith, *J. Chem. Soc.*, **1926**, 393.

IV exhibits a broad absorption due to hydrogen bonded hydroxyl group even in a dilute solution indicating the proximate spatial positions of hydroxyl and methoxycarbonyl groups. On the other hand, the absorption of associated hydroxyl group observed in the spectrum of V disappeared on dilution indicating the absence of intramolecular hydrogen bonding. The fact that the carbonyl stretching vibration ($\nu_{C=O}$) of IV in chloroform is observed at a lower wave number (1710 cm^{-1}) than that of V (1720 cm^{-1}) is also consistent with the assigned structures.

Acylation of (+)-IV and (+)-V with acetic and trifluoroacetic anhydrides gave two sets of optically active isomers, VI, VII and VIII, IX. The structures of VI and VII were also supported by the measurement of dipole moment using 2-acetoxy-5-methoxytriptycene as a reference substance[3] which was prepared by a similar procedure from 2,5-dihydroxytriptycene.[4]

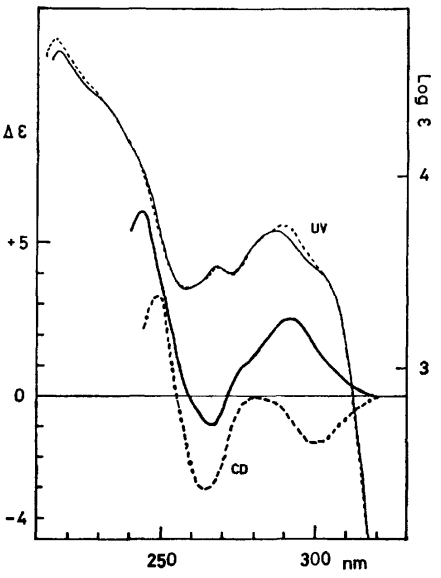

Fig. 1. UV and CD spectra of VI (——) and VII (----) in dioxane.

The absolute configurations of optically active triptycenes described above are evident in relation to I, *i.e.*, all of them have 1*R*,6*S* configuration since the absolute configuration of (+)-2,5-dimethoxy-7-methoxycarbonyltriptycene derived from (+)-I was proved to be 1*R*,6*S* on the basis of X-ray structure analysis by the Bijvoet method.[5] The UV and CD spectra of (+)-VI and (+)-VII are shown in Fig. 1. The sign of the longest wavelength Cotton effect is reversed as suggested by the ORD data.[6] This indicates that the center of transition dipole of $^1B_{2u}$ state in the hydroquinone ring is displaced in opposite direction according to the inversion of the position of electron attractive substituent. However, the CD spectral pattern at shorter wavelength region suggests that the effect is restricted to the $^1B_{2u}$ state.

Experimental

The experimental procedures refer to optically active substances unless otherwise stated. The IR and UV spectra were obtained on Hitachi EPI-2 and Hitachi EPS-2 spectrophotometers, respectively. The optical rotations and CD spectra were measured with a Rudolf Model 200S-80 spectropolarimeter and a Roussel-Jouan Dichrograph B, respectively. The inflections and shoulders are indicated by an asterisk.

2,5-Dihydroxy-7-methoxycarbonyltriptycene (III). A mixture of II[6] (1.0 g), methanol (5 ml) and concentrated sulfuric acid (0.3 ml) was refluxed for 8 hr. After being left standing overnight, the crystals deposited were washed successively with methanol and water to yield pure III, mp 294—297°C [racemate, mp 285—290°C].

Found: C, 76.59; H, 4.74%. Calcd for $C_{22}H_{16}O_4$: C, 76.73; H, 4.68%.

IR (KBr-disk): 3600—3100 (ν_{O-H}), 1680 ($\nu_{C=O}$) [racemate, 1683] cm^{-1}. UV: $\lambda_{max}^{dioxane}$ (ε) 298 (8610), 269.5 (2940), 261.5 (2370), 214.5 (45400) nm. ORD (15°C): $[M]_{5791}$ +95.0°, $[M]_{5461}$ +115.7°, $[M]_{4358}$ +230.4°, $[M]_{4047}$ +318.9°, $[M]_{3650}$ +547.5° (*c* 0.420, dioxane).

2-Methoxy-5-hydroxy-7-methoxycarbonyltriptycene (IV), 2-Hydroxy-5-methoxy-7-methoxycarbonyltriptycene (V), 2-Methoxy-5-acetoxy-7-methoxycarbonyltriptycene (VI), and 2-Acetoxy-5-methoxy-7-methoxycarbonyltriptycene (VII). A solution of III (4.50 g) in tetrahydrofuran (90 ml) was mixed with sodium methoxide in methanol (from sodium, 0.6 g and methanol, 75 ml). To the resulting suspension of sodium salt was added a solution of dimethyl sulfate (1.6 g) in tetrahydrofuran (15 ml) in an atmosphere of nitrogen. After being stirred overnight and left to stand overnight, the product dissolved in benzene–tetrahydrofuran (5: 1) was chromatographed on alumina (130 g) and eluted successively with benzene–tetrahydrofuran (5: 1 and 1: 1), tetrahydrofuran, and tetrahydrofuran–methanol (100: 1 and 10: 1). Dimethyl ether and quinone derivatives were obtained from benzene–tetrahydrofuran eluate and could be separated on re-chromatography on alumina. Tetrahydrofuran and tetrahydrofuran–methanol (100: 1) eluates afforded a mixture of IV and V, the former in abundance. A mixture of the same isomers rich in V was obtained from tetrahydrofuran–methanol (10: 1) eluate.

Acetylation: A mixture containing a larger amount of IV (0.5 g) in tetrahydrofuran (10 ml) was refluxed with acetic anhydride (1.5 g) for 1.5 hr to yield VI, mp 270—271°C (from methyl acetate) [racemate, mp 279—280°C], IR (KBr-disk): 2855 (ν_{C-H}, $-OCH_3$), 1765 ($\nu_{C=O}$, CH_3COO-), 1716 ($\nu_{C=O}$, $-COOCH_3$) cm^{-1}.

Similarly, a mixture rich in V afforded VII, mp 278—279°C (from methanol–methyl acetate) [racemate, mp 269—270°C, from methyl acetate], IR (KBr-disk): 2845 (ν_{C-H}, $-OCH_3$), 1750 ($\nu_{C=O}$, CH_3COO-), 1722 ($\nu_{C=O}$, $-COOCH_3$) cm^{-1}.

Found: VI, C, 74.48; H, 5.01%. VII, C, 74.69; H, 5.06%. Calcd for $C_{25}H_{20}O_5$: C, 74.99; H, 5.03%.

UV: $\lambda_{max}^{dioxane}$ (ε) VI, 217 (45700), 268 (3470), 288 (5290); VII, 216 (52700), 268.5 (3410), 290 (5660) nm. ORD: VI (15°C), $[M]_{5791}$ +402.4°, $[M]_{5461}$ +466.5°, $[M]_{5000}$ +583.0°, $[M]_{4358}$ +873.5°, $[M]_{4047}$ +1104°, $[M]_{3650}$ +1312° (*c* 0.8975, dioxane); VII (16.5°C), $[M]_{5791}$ +3.0°, $[M]_{5000}$ +3.0°, $[M]_{4358}$ −23.6°, $[M]_{4047}$ −51.3°, $[M]_{3650}$ −152.2°

3) F. Ogura, Y. Toshiyasu, K. Kimura, R. Fujishiro, and M. Nakagawa, This Bulletin, **37**, 757 (1964).

4) P. D. Bartlett, M. J. Ryan, and S. G. Cohen, *J. Amer. Chem. Soc.*, **62**, 2649 (1942).

5) N. Sakabe, K. Sakabe, K. Ozeki-Minakata, and J. Tanaka, presented at the 9th International Congress of Crystallography (1972), *Acta Crystallogr.*, **B24**, 3441 (1972).

6) F. Ogura and M. Nakagawa, This Bulletin, **38**, 155 (1965).

(c 0.7990, dioxane). CD: $\lambda_{max}^{dioxane}$ ($\Delta\varepsilon$) VI, 291 (+2.6), 266.5 (−1.07), 244 (+6.12); VII, 300 (−1.51), 266 (−3.07), 262.5 (−2.92), 249 (+3.31) nm.

Hydrolysis and Esterification: A mixture of *dl*-VI (0.50 g), acetic acid (35 ml) and 3N sulfuric acid (15 ml) was refluxed for 8 hr to yield 2-methoxy-5-hydroxy-7-carboxytriptycene (0.4 g, mp 280—287°C). The crude material in acetone–methanol was treated with an ethereal solution of diazomethane to afford *dl*-IV, mp 279—280°C (from benzene).[7] The same treatment of *dl*-VII gave 2-hydroxy-5-methoxy-7-carboxytriptycene, mp 290—302°C which gave *dl*-V, mp 255—258°C (from benzene) on treatment with diazomethane. Optically active VI and VII were converted into IV, mp 249—251°C and V, mp 256—258°C by the same method.

Found: IV, C, 76.91; H, 5.01%. V, C, 77.73; H, 5.06%. Calcd for $C_{23}H_{18}O_4$: C, 77.08; H, 5.06%.

IR (KBr-disk): IV, 3700—3200 (ν_{O-H}), 2840 (ν_{C-H}, $-OCH_3$), 1707 ($\nu_{C=O}$, $-CO_2CH_3$); V, 3700—3100 (ν_{O-H}), 2840 (ν_{C-H}, $-OCH_3$), 1715, 1695 ($\nu_{C=O}$, $-CO_2CH_3$) cm^{-1}. ORD: IV (14—16°C), $[M]_{5791}$ −120.4°, $[M]_{5461}$ −121.5°, $[M]_{5000}$ −144.1°, $[M]_{4358}$ −210.4°, $[M]_{4047}$ −273.1°, $[M]_{3650}$ −482.4° (c 0.286, dioxane); V (12.5—16°C), $[M]_{5791}$ −76.7°, $[M]_{5461}$ −85.7°, $[M]_{5000}$ −113.2°, $[M]_{4358}$ −179.2°, $[M]_{4047}$ −236.9°, $[M]_{3650}$ −382.0° (c 0.472, dioxane).

2-Methoxy-5-trifluoroacetoxy-7-methoxycarbonyltriptycene (VIII) and 2-Trifluoroacetoxy-5-methoxy-7-methoxycarbonyltriptycene (IX). Trifluoroacetylation of mixtures of IV and V followed by chromatography on silica gel according to the method used for VI and VII afforded VIII, mp 262—263°C (from benzene–benzine) and IX, mp 241—243°C (from benzene–benzine).

Found: VIII, C, 66.30; H, 4.10%. IX, C, 66.50; H, 3.87%. Calcd for $C_{25}H_{17}O_5F_3$: C, 66.08; H, 3.77%.

IR (Nujol mull): VIII, 1805 ($\nu_{C=O}$, CF_3CO_2-), 1722 ($\nu_{C=O}$, $-CO_2CH_3$); IX, 1802 ($\nu_{C=O}$, CF_3CO_2-), 1716 ($\nu_{C=O}$, $-CO_2CH_3$) cm^{-1}. UV: $\lambda_{max}^{dioxane}$ (ε) VIII, 215.5 (48500), 267 (3910), 285 (4910); IX, 215 (49300), 261 (3580), 267.5 (4010), 288 (5420) nm. ORD: VIII (12—14°C), $[M]_{5791}$ +379.1°, $[M]_{5461}$ +441.2°, $[M]_{5000}$ +565.7°, $[M]_{4358}$ +842.0°, $[M]_{4047}$ +1059°, $[M]_{3650}$ +1558° (c 0.2780, dioxane); IX (11—14°C), $[M]_{5791}$ −3.8°, $[M]_{5461}$ −9.1°, $[M]_{4358}$ −42.3°, $[M]_{4047}$ −85.4°, $[M]_{3650}$ −191.3° (c 0.3990, dioxane).

2-Acetoxy-5-methoxytriptycene and 2,5-Dimethoxytriptycene. According to a previously described method, 2,5-dihydroxytriptycene[4] was methylated and the product was chromatographed on alumina. The benzene–tetrahydrofuran (10: 1) eluate afforded the dimethyl derivative, mp 241—243°C (from acetic acid).

Found: C, 84.21; H, 5.80%. Calcd for $C_{22}H_{18}O_2$: C, 84.05; H, 5.77%.

IR (KBr-disk): 2850 (ν_{C-H}, $-OCH_3$) cm^{-1}. UV: $\lambda_{max}^{dioxane}$ (ε) 217 (57300), 262 (2720), 271 (3030), 277.5 (4430), 294 (4,050) nm.

Acetylation of the monomethylated product obtained from the tetrahydrofuran–methanol (100: 1) eluate yielded 2-acetoxy-5-methoxytriptycene, mp 274—275.5°C (from acetic acid).

Found: C, 80.77; H, 5.29%. Calcd for $C_{23}H_{18}O_3$: C, 80.68; H, 5.30%.

IR (KBr-disk): 2850 (ν_{C-H}, $-OCH_3$), 1745 ($\nu_{C=O}$, CH_3CO_2-) cm^{-1}. UV: $\lambda_{max}^{dioxane}$ (ε) 217 (58500), 261 (2990), 270 (3140), 277.5 (3880), 288 (2040) nm.

7) F. Ogura, Y. Sakata, and M. Nakagawa, This Bulletin, **45**, 3646 (1972).

BULLETIN OF THE CHEMICAL SOCIETY OF JAPAN, VOL. 46, 653—655 (1973)

The Synthesis of [6.0.6.0]Paracyclophane

Riichiro NAGANO, Joji NISHIKIDO, Takahiko INAZU,* and Tamotsu YOSHINO

Department of Chemistry, Faculty of Science, Kyushu University, Hakozaki, Higashi-ku, Fukuoka 812

(Received June 14, 1972)

It has been reported that 1,6,19,24-tetraaza[6.0.6.0]- and 1,6,19,24-tetraoxa[6.0.6.0]paracyclophane form an inclusion compound with benzene or dioxane.[1,2] These cyclophanes have nitrogen or oxygen atoms attached to biphenyl nuclei. To see if the presence of such hetero atoms had any effect on the inclusion of a guest molecule in an empty space of the macro cyclic compounds, [6.0.6.0]paracyclophane, I, constructed with two biphenyl nuclei and two hexamethylene bridges, was synthesized as a reference compound free from hetero atoms. No addition compound of the I cyclophane with benzene has been isolated under similar conditions. [6.0.6.0]Paracyclophane, I, and its open-chain model compound, XI, were synthesized as is shown in Figs. 1 and 2. We adopted the acyloin condensation of the diester, V, in the ring-closing step. In the NMR spectrum of I, the signals for aromatic protons showed an A_2B_2 pattern, and the peaks of I, centered at 7.15 ppm, were found to shift toward an upper field by 0.18 ppm compared with those of the open-chain model, XI.

The electronic spectrum of I (λ_{max} 255 nm, ε_{max} 2.9×10^4 in *n*-hexane) showed a slight blue shift and a hypochromic effect compared with that of the open-chain compound, XI, (λ_{max} 258 nm, ε_{max} 4.46×10^4 in *n*-hexane), the shapes of the curves being virtually the same. The shapes of the electronic spectra of 1:1 electron-donor-acceptor complexes of I and XI with tetracyanoethylene (TCNE) in dichloromethane were virtually the same. However, the λ_{max} at the longest wavelength in the spectra (λ_{max} 398, 418, 578 nm) of the I-TCNE complex showed a blue shift by 10 nm compared with that in the spectra (λ_{max} 400, 417, 588 nm; ε 588 nm 770) of the XI–TCNE complex. Accordingly, the I–TCNE complex appears, unexpect-

* To whom all correspondences should be addressed.

1) H. Stetter and E. E. Roos, *Chem. Ber.*, **87**, 566 (1954).

2) J. Nishikido, T. Inazu, and T. Yoshino, This Bulletin, to be published.

Table 1.

Compd	Cryst. form[a]	Cryst. solv.[a]	Mp, bp °C	Prd.	Formula	Analyses, % Found C	Found H	Calcd C	Calcd H	Yield %
I[b]	w.n	Hx–Bz	157 —157.5		$C_{36}H_{40}$	91.22	8.51	91.47	8.52	70.0
II			bp 149.5—150/0.23							93.3
III	w.p	Bz	191 —192	A	$C_{40}H_{42}O_6$	77.85	7.03	77.64	6.84	78.9
V	w.pl	Bz	160	B	$C_{40}H_{46}O_4$	81.35	7.92	81.32	7.85	34.4[c]
VI	w.p	Hx–Bz	198 —201[d]		$C_{36}H_{38}O_2$	86.04	7.69	86.01	7.62	30.1
VIII	w.pl	Bz	220 —221	A	$C_{30}H_{26}O_2$	86.02	6.43	86.09	6.26	79.8
IX	w.n	$CHCl_3$	142	B	$C_{30}H_{30}$	92.34	7.82	92.26	7.74	91.0
X	cw.p	Hx–Bz	220[e]	A	$C_{36}H_{38}O_2$	86.05	7.63	86.01	7.62	62.5
XI	cw.n	Bz–Et	157 —158	B	$C_{36}H_{42}$	91.10	8.79	91.08	8.92	86.3

a) cw=creamy white. n=needles. p=powder. pl=plates. w=white. Bz=benzene. Et=ethanol. Hx=*n*-hexane.
b) Found; mol wt, 457.8 in benzene (Hitachi Perkin-Elmer 115 model). Calcd; mol wt,. 472.7.
c) from the keto ester III.
d) turned yellow at 189—192°C.
e) began to sinter at 178°C.

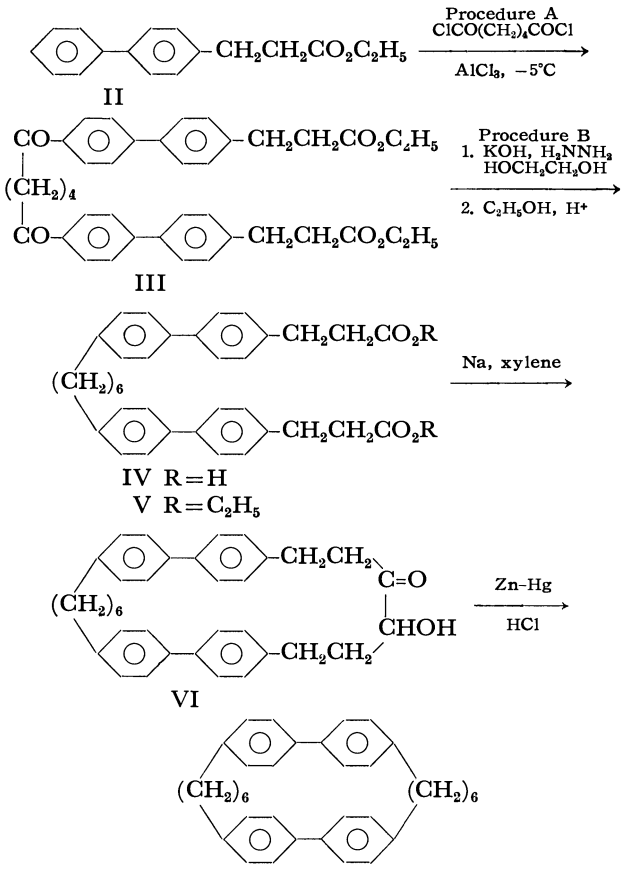

Fig. 1.

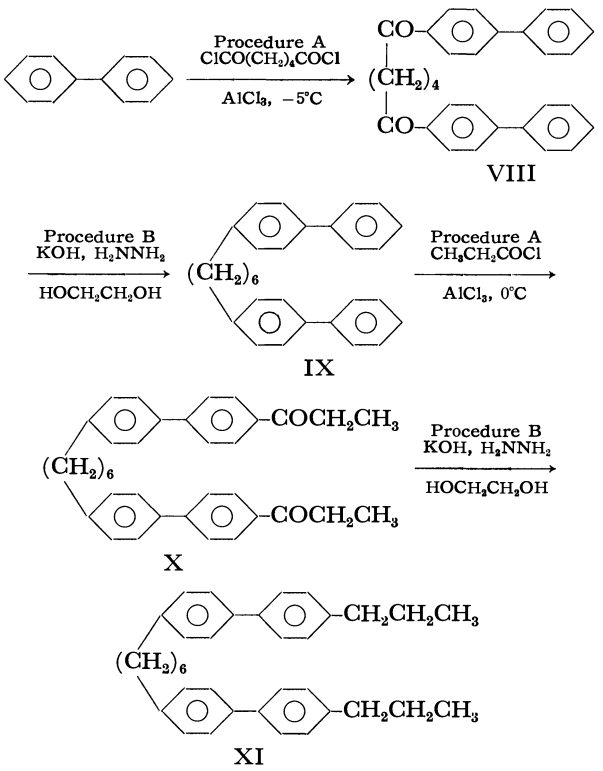

Fig. 2.

edly, to be less stabilized than the XI–TCNE complex; this is in contrast to the reports[3] that the well-known [*m.n*]paracyclophane-TCNE complexes are generally more stabilized than their corresponding open-chain compound-TCNE complexes, where *m* and *n* range from 2 to 6.

3) D. J. Cram and R. H. Bauer, *J. Amer. Chem. Soc.*, **81**, 5971 (1959); D. J. Cram and L. A. Singer, *ibid.*, **85**, 1080 (1963); D. J. Cram and M. Sheehan, *ibid.*, **91**, 3553 (1969).

Experimental

All the melting and boiling points are uncorrected. The electronic spectra were measured on a Hitachi EPS-3T spectrophotometer. The NMR spectra were recorded on a Hitachi R-20 model at 60 MHz, using tetramethylsilane as the internal standard and $CDCl_3$ as the solvent.

1,6-Bis[4'-(2-ethoxycarbonylethyl)-4-biphenylyl]-1,6-hexanedione, III. Procedure A: Ethyl biphenyl-4-acrylate[4] was reduced to ethyl biphenyl-4-propionate, II, by catalytic hydrogenation with palladium-on-carbon in ethanol at room temperature. Into a mixture of 80.5 g of the ester, II, and 28.9 g of adipyl chloride in 500 ml of tetrachloroethane, we stirred

4) D. H. Hey, *J. Chem. Soc.*, **1931**, 2478.

150 g of anhydrous aluminum chloride, portion by portion, at −10°C. The dark green reaction mixture was kept below 0°C for 7 hr and was then allowed to come to room temperature. The mixture was poured onto crushed ice. The organic layer was separated, and the solvent was removed by steam distillation. A light brown solid was thus obtained.

1,6-Bis[4'-(2-ethoxycarbonylethyl)-4-biphenylyl]hexane, V. Procedure B: A mixture of 6.2 g of the keto ester, III, and 70 g of 80% hydrazine hydrate in 400 ml of ethylene glycol was refluxed for an hour. Then potassium hydroxide was slowly added in small portions. The yellowish-gray mixture was refluxed for 24 hr, while two 50 ml portions of 80% hydrazine hydrate and 100 ml portions of ethylene glycol were added at 10 hr intervals. After the usual treatment, a crude reduction product, IV, was obtained. This reduction product, IV, was esterified by the usual method.

3-Hydroxy-4-oxo[6.0.6.0]paracyclophane, VI. A solution of 4.43 g of the diethyl ester, V, in 1 l of xylene was stirred into 2.90 g of dispersed sodium in 1 l of xylene over 41 hr under a nitrogen atmosphere. The usual work-up of the reaction mixture[5] then gave crude acyloin, 1.136 g (30.1%). A small sample was chromatographed on silica gel with benzene.

[6.0.6.0]Paracyclophane, I. Activated zinc was prepared by swirling 12 g of zinc with a solution of 1.5 g of $HgCl_2$ and 1.5 ml of concentrated HCl in 28.5 ml of water. To the zinc we then added 20 ml of glacial acetic acid, 40 ml of toluene, 20 ml of concentrated HCl, and 251 mg of the acyloin.

The mixture was refluxed for 10 hr, during which time two 30 ml portions of concentrated HCl were added. After the usual treatment, 165 mg of the crude I was obtained (70%). The crude cyclophane, I, was chromatographed on silica gel with benzene; the subsequent evaporation of the column filtrates gave solid residues. In the mass spectrum, the molecular ion peak was found as the base peak at *m/e* 472 (Hitachi RMS-4 model).

The equilibrium constant of the XI–TCNE complex was determined to be $K=1.53$ l/mol by a modified Benesi-Hildebrand plot.[6]

5) D. J. Cram and H. Steinberg, *J. Amer. Chem. Soc.*, **73**, 5691 (1951).

6) R. P. Lang, *ibid.*, **84**, 1185 (1962).

BULLETIN OF THE CHEMICAL SOCIETY OF JAPAN, VOL. 46, 655—656 (1973)

Organic Syntheses by Means of Noble Metal Compounds. XLIX.[1] Oxidation of 3-Hexenedioate to 2,4-Hexadienedioate Catalyzed by Palladium Chloride and Copper(II) Chloride

Tosaku SUSUKI and Jiro TSUJI

Basic Research Laboratories, Toray Industries Inc., Kamakura

(Received June 21, 1972)

Divalent palladium is a unique oxidizing agent and it can abstract hydrogen from various organic compounds.[2] This is exemplified in the nucleophilic substitution of olefins and coupling of aromatic compounds in its presence. This led us to investigate the possibility of liquid phase oxidative dehydrogenation of carbonyl compounds to α,β-unsaturated compounds as shown below.

$$-\overset{\overset{\displaystyle O}{\|}}{C}-CH_2CH_2- \longrightarrow -\overset{\overset{\displaystyle O}{\|}}{C}-CH=CH-$$

An attempted oxidation of cyclohexanone with palladium chloride in acetic acid gave phenol, probably formed through cyclohexenone, but it was impossible to stop the reaction at the stage of cyclohexenone formation.[3] The oxidation of diethyl 3-hexenedioate (I) was then attempted in acetic acid in the presence of sodium acetate. As expected, the ester was dehydrogenated smoothly to give 2,4-hexadienedioate(II) (diethyl *trans,trans*-muconate) in 78% yield.

$$EtO_2C-CH_2CH=CHCH_2-CO_2Et \quad (I)$$

$$\longrightarrow EtO_2C-CH=CH-CH=CH-CO_2Et \quad (II)$$

As is often the case in the oxidation reaction with divalent palladium, addition of cupric chloride made the reaction catalytic with regard to palladium chloride.

The reaction can be explained in the following way. At first, the acidic α hydrogen of I is abstracted with the base to give anion, which attacks palladium chloride to form μ-dichlorobis(1-carbethoxy-3-carbethoxymethyl-π-allyl)dipalladium(III). The formation of π-allylic complexes from β,γ-unsaturated esters is a known reaction.[5] The acidic hydrogen α to the ester group in the complex III is then abstracted, followed by reductive elimination of palladium to give rise to II. Reoxidation of the reduced palladium with cupric

1) Part XLVIII. J. Tsuji, M. Hara, and Y. Mori,, *Tetrahedron*, **28**, 3721 (1972).

2) J. Tsuji, *Accounts Chem. Res.*, **2**, 144 (1969).

3) Selective oxidation of cyclohexanone and other ketones to α,β-unsaturated ketones using bis(triphenylphosphine)dichloropalladium was recently reported.[4]

4) R. J. Theissen, *J. Org. Chem.*, **36**, 752 (1971).

5) J. Tsuji and S. Imamura, This Bulletin, **40**, 197 (1967).

chloride makes the reaction a catalytic cycle with palladium. As an evidence of this mechanism, complex III was isolated when a part of the reaction mixture was taken out during the course of reaction.

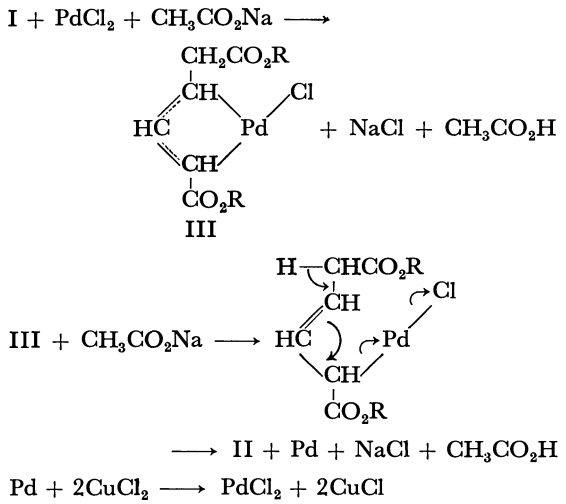

The reaction is another example of the unique oxidation catalyzed by palladium chloride. It is feasible because of two properties of divalent palladium, π-allylic complex formation from β,γ-unsaturated esters and abstraction of active hydrogens.

Experimental

A mixture of palladium chloride (3.6 g, 0.02 mol), sodium acetate (6.0 g), ethyl 3-hexenedioate (8.0 g, 0.04 mol) in acetic acid (60 ml) was stirred at 70° for 50 min, during which period metallic palladium precipitated gradually. After filtration, the solution was diluted with water and extracted with ether. Distillation of the ethereal solution gave an oily mixture (7.0 g, 125—130°C/6 mm) which partly crystal lized on cooling. Filtration and recrystallization from *n*-hexane gave crystals (3.1 g, 78%) which proved to be diethyl *trans*, *trans*-muconate, and were identified by their IR and NMR spectra and mixed mp determination (60—61°C) with an authentic sample.

Catalytic process was carried out in the following way. Diethyl 3-hexenedioate (10 g) was heated with a mixture of palladium chloride (1.8 g), cupric chloride (13 g) and sodium acetate (6 g) in acetic acid (60 ml) at 80° for 7 hr stirring. After the usual work-up, an oily distillate was isolated (8.5 g, 110—120°C/6 mm). Gas chromatographic analysis showed that the distillate contained 6.4 g of ethyl muconate.

BULLETIN OF THE CHEMICAL SOCIETY OF JAPAN, VOL. 46, 656—657 (1973)

Convenient Preparation of Methyl 2-Acetamido-4,6-*O*-benzylidene-2-deoxy-α-D-glucopyranoside

Kazuhiko YAMAMOTO and Taku HAYASHI

Department of Chemistry, Osaka University College of Science, Toyonaka, Osaka

(Received June 22, 1972)

The *O*-benzylidene group is a good protective group for preparing several sugar derivatives, but some difficulties in its preparation and the lower yield of product have sometimes been encountered in reactions of sugar with benzaldehyde and a catalyst. The use of freshly-distilled benzaldehyde and anhydrous zinc chloride seems to give a higher yield.[1] In order to eliminate some tedious treatments, the preparation of the *O*-benzylidene group by an acetal exchange reaction was attempted. Its use in the preparation of methyl 2-acetamido-4,6-*O*-benzylidene-2-deoxy-α-D-glucopyranoside (II) led to an almost quantitative yield. When methyl 2-acetamido-2-deoxy-α-D-glucopyranoside (I) was treated with benzaldehyde dimethyl acetal and a catalytic amount of *p*-toluenesulfonic acid in dimethylformamide (DMF), the reaction was shown to be completed within 1 hr, judging from the thin-layer chromatogram of the reaction mixture. Moreover, benzaldehyde dimethylacetal was also found to be more suitable for *O*-benzylidenation because the reagent, stored for several months, gave the same yield of the *O*-benzylidenated product.

When the same reaction was performed under reduced pressure, methyl 2-acetamido-3-*O*-(α-methoxybenzyl)-4,6-*O*-benzylidene-2-deoxy-α-D-glucopyranoside (III) was found to be produced in the reaction mixture, but it was not produced under atmospheric conditions. The structure of (III) was confirmed by elemental analysis and NMR spectroscopy, and was also supported by the experimental evidence that (III) was formed by the reaction of (II) with benzaldehyde dimethylacetal under reduced pressure.

No 3-*O*-substitution with the α-methoxybenzyl group in 4,6-*O*-benzylidene sugar has been found so far; therefore, this seems to be the first example of a mixed acetal of benzaldehyde between the hydroxyl of sugar and simple alcohol. The 3-*O*-(α-methoxybenzyl) group was found to be more acid-labile than the 4,6-*O*-benzylidene group, as had been expected; it was removed selectively by treatment with 90% acetic acid at 0°C. The thin-layer chromatographic analysis of 90% acetic acid hydrolysis for (III) is shown in Fig. 1.

Recently, during the preparation of our manuscript, Evans[2] reported the preparation of methyl 4,6-*O*-benzylidene-α- and β-D-glucopyranosides by a similar

1) K. Freudenberg, H. Toepffer, and C. C. Andersen, *Ber.*, **61**, 1758 (1928).

2) M. E. Evans, *Carbohyd. Res.*, **21**, 473 (1972).

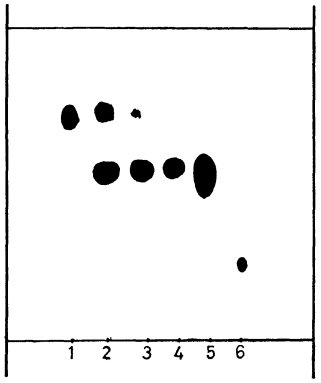

Fig. 1. Thin layer chromatogram of hydrolysates of (III).
1: Compound (III), 2: Hydrolysate of (III), sampling after 1 min, 3: Hydrolysate of (III), sampling after 1 min, 4: Hydrolysate of (III), sampling after 6 min, 5: Compound (II), 6: Compound (I).

manner and noted that the preparation of the *O*-benzylidene group with benzaldehyde dimethyl acetal and *p*-toluenesulfonic acid was a better procedure.

Experimental

The melting points were determined with a micro melting point apparatus (Yanagimoto, MFG) and uncorrected. The optical rotations were measured with a Jasco DIP-SL photoelectric automatic polarimeter at 25.0°C. The NMR spectra were recorded with a Varian T-60 NMR spectrometer. Thin-layer chromatography was performed on Silica gel H (Merck) developed with the solvent (toluene: acetone: pyridine= 2: 1: 1), and spots were detected by spraying with 5% methanol–sulfuric acid.

Benzaldehyde dimethyl acetal was prepared by the method of Claisen,[3] using methyl orthoformate instead of the ethyl derivative, and showed bp 215—218°C/760 mmHg (lit,[4] 207°C).

Reaction of I with Benzaldehyde Dimethyl Acetal under Atmospheric Pressure. To a solution of I[5] (5.0 g) in 50 ml of dimethylformamide, we added 14 ml of benzaldehyde dimethyl acetal and 0.5 g of *p*-toluenesulfonic acid; the reaction was then performed at 40°C for 1 hr. After determining the completion of the reaction by thin-layer chromatography, which indicated a spot (R_f 0.54) corresponding to authentic (II)[6] and the disappearance of (I), the reaction mixture was evaporated *in vacuo* to dryness. The white residue was suspended in a dilute sodium bicarbonate solution and collected by filtration. The crystallization of dried raw product from methanol gave a pure (II) (6.3 g, 91%); mp 255—259°C (lit,[6] 255°C), $[\alpha]_D^{25}$ +75.5° (*c*, 1.04, dimethylformamide), (lit, +19° chloroform,[6] +70° chloroform[7]). Found: C, 56.77; H, 6.68; N, 4.12%. Calcd for $C_{16}H_{21}O_6 \cdot H_2O$: C, 56.29; H, 6.79; N, 4.10%.

The $[\alpha]_D$ value observed by Kasai was referred to because his value was comparable to our value and because he used the α-glycoside purified by column chromatography. (The $[\alpha]_D$ values reported for I were +105° by Neuberger and +131° by Kasai.[7])

Reaction under Reduced Pressure. a): The same reaction mixture as above was kept at 40°C under reduced pressure (15 mmHg) for 8 hr. A similar treatment of the reaction mixture afforded 7.3 g (78%) of a crystalline (III), which showed a mp of 193—196°C and $[\alpha]_D^{25}$ +52.5° (*c*, 1.22, dimethylformamide); NMR spectrum (in deuteriochloroform, with tetramethylsilane as the internal standard). δ 7.43 m; (aromatic, 10H), 5.60 s; (CH of acetal, 2H), 4.80 d; (anomeric, 1H) 3.44 s; (OMe of acetal, 3H), 2.04 s; (OMe of glycoside, 3H) 1.15 s; (NAc, 3H). Found: C, 65.17; H, 6.85; N, 3.18%. Calcd for $C_{24}H_{29}O_7N$: C, 65.00; H, 6.59; N, 3.16%.

b): A solution of 5.0 g of (II), 14 ml of benzaldehyde dimethyl acetal, and 0.5 g of *p*-toluenesulfonic acid in 50 ml of dimethylformamide was allowed to react under reduced pressure (15 mmHg) at 40°C for 8 hr; then, the mixture was treated as has been mentioned above. The crystallization of the crude product gave 6.0 g (92%) of a crystalline III. Mp 192—196°C, $[\alpha]_D^{25}$ +51.7° (*c*, 1.02, dimethylformamide) Found: C, 64.87; H, 6.82; N, 3.16%. Calcd for $C_{24}H_{29}O_7N$: C, 65.00; H, 6.59; N, 3.16%.

The melting point was not depressed by admixture of the specimen prepared in a).

Acid Hydrolysis of III. A 10 mg portion of (III) dissolved in 1 ml of 90% acetic acid (v/v), was kept in an ice bath (0°C). Aliquots of 0.3 ml were removed at 1-, 3- and 6- min intervals and neutralized with 0.5 ml of pyridine. Each sample removed at each interval was applied to a tlc plate, and developed with toluene: acetone: pyridine (2: 1: 1). The thin-layer chromatogram of the hydrolysates is shown in Fig. 1. It can be concluded from the thin-layer chromatogram that the 3-*O*-(α-methoxybenzyl) group of III is completely hydrolysed by 90% acetic acid over 6 min at 0°C, while, on the contrary, the 4,6-*O*-benzylidene group was not affected under these conditions.

The authors are most grateful to Professor Y. Matsushima (Faculty of Science, Osaka University) for his continued interest and support during this work.

3) L. Claisen, *Ber.*, **40**, 3903 (1907).
4) E. W. Adames and H. Adkins, *J. Amer. Chem. Soc.*, **47**, 1358 (1925).
5) Z. Zilliken, C. S. Rose, G. A. Braun, and P. Gyorgy, *Arch. Biochem. Biophys.*, **54**, 392 (1955).
6) A. Neuberger, *J. Chem. Soc.*, **1941**, 550.
7) S. Kasai, The thesis for Master of Science (Osaka University), 1967.

BULLETIN OF THE CHEMICAL SOCIETY OF JAPAN, VOL. 46, 658—659 (1973)

The Preparation of *p*-Nitrophenyl 2-Acetamido-3-*O*-methyl-2-deoxy-β-D-glucopyranoside

Kazuhiko YAMAMOTO

Department of Chemistry, Osaka University College of Science, Toyonaka, Osaka

(Received June 30, 1972)

The title compound is required for a mechanistic study on the *N*-acetyl-β-D-glucosaminidase [EC. 3.2.1. 30] hydrolysis. The 3-*O*-substitution of 2-acetamido-2-deoxy-D-glucose is usually achieved by a reaction on the 4,6-*O*-benzylidene derivative as an intermediate.[1] However, in the case of *p*-nitrophenyl glycoside which is very acid-labile, the destruction of glycoside occurs when the 4,6-*O*-benzylidene group is removed. The cleavage of *p*-nitrophenyl glycoside under the conditions which had been used for debenzylidenation (in 66% acetic acid at 100°C for 30 min) was determined. The results (Table 1) indicate that *ca.* 30% of the *p*-nitrophenyl 2-acetamido-2-deoxy-β-D-glucopyranoside is damaged under those conditions. A more easily removable group than *O*-benzylidene was desirable, and *p*-methoxybenzylidene group was selected because it was found to be cleaved by the milder treatment.[2] Moreover, a further application of *O*-(*p*-methoxybenzylidene)-blocking and an improved procedure for *O*-benzylidenation was attempted in connection with the previous studies.[2,3] *O*-Benzylidene formation by acetal exchange reaction was recently reported as a convenient method.[3,4] Although *p*-methoxybenzaldehyde was less reactive than benzaldehyde, the preparation of 4,6-*O*-(*p*-methoxybenzylidene) derivative in good yield by the acetal exchange reaction of *p*-methoxybenzaldehyde dimethyl acetal was also successful.

TABLE 1. DESTRUCTION OF *p*-NITROPHENYL GLYCOSIDES UNDER THE CONDITIONS USED FOR DEBENZYLIDENATIONS

	p-Nitrophenyl 2-acetamide 2-deoxy-β-D-glucopyranoside	*p*-Nitrophenyl-β-D-glucopyranoside
10 min	12%	1.3%
20 min	22%	1.7%
30 min	29%	2.1%

The treatment of I with *p*-methoxybenzaldehyde dimethyl acetal and a catalytic amount of *p*-toluenesulfonic acid under reduced pressure afforded an almost quantitative yield of II, which was then methylated by Kuhn's method. Then, the removal of 4,6-*O*-(*p*-methoxybenzylidene) group led to the title compound (IV). The conditions for the removal of the blocking group were successfully achieved by the treatment with 90% acetic acid at 100°C for 1 min.

The synthetic scheme and compounds prepared are shown in Fig. 1.

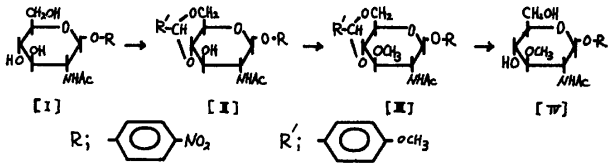

Fig. 1.

Experimental

The melting points were determined by means of the Yanagimoto-micro melting point apparatus and uncorrected. Optical rotations were measured by means of a recording spectropolarimeter (Yanagimoto ORD-185). Thin-layer chromatography was performed on Silica Gel H (Merck), and spots were detected with 5% sulfuric acid in methanol.

p-Methoxybenzaldehyde dimethyl acetal was prepared by the method of Claisen.[5] Methyl orthoformate was used in place of ethyl orthoformate. Bp 95—96°C/1.0 mmHg (lit,[6] bp 261—263°C/760 mmHg). (Found: C, 65.96; H, 7.76%. Calcd for $C_{10}H_{14}O_3$: C, 65.91; H, 7.74%).

p-Nitrophenyl 2-Acetamido-4,6-O-(p-methoxybenzylidene)-2-deoxy, β-D-glucopyranoside (II). *p*-Nitrophenyl 2-acetamido-2-deoxy-β-D-glucopyranoside (I)[7] (3.5 g) dissolved in 150 ml of dimethylformamide (DMF), was treated with 15 ml of *p*-methoxybenzaldehyde dimethyl acetal and 0.50 g of *p*-toluenesulfonic acid at 40°C for 8 hr under reduced pressure (15 mmHg). The reaction mixture was evaporated *in vacuo* to dryness, and then the residue, suspended in a cold saturated sodium bicarbonate solution, was collected by filtration. The precipitate dried *in vacuo* was crystallized from toluene and acetone; 4.5 g (96%) of (II) were thus obtained. Mp 239—240°C (dec.), $[\alpha]_{589}^{25}$ −14.5° (*c*, 0.813, DMF). Found: C, 57.25; H, 5.41; N, 5.93%. Calcd for $C_{22}H_{24}O_9N_2$: C, 57.39; H, 5.25; N, 6.08%.

Unlike as in the case of benzaldehyde dimethyl acetal,[3] the formation of mixed acetal at 3-hydroxyl could not be observed when the experiment was conducted under reduced pressure.

p-Nitrophenyl 2-Acetamido-3-O-methyl-4,6-O-(p-methoxybenzylidene)-2-deoxy-β-D-glucopyranoside (III). To a solution of II (0.50 g) in 20 ml of DMF, we added 30 ml of methyl iodide and 5.0 g of barium oxide. The reaction mixture was then allowed to stand at room temperature for 20 hr. The filtrate, freed from insoluble materials, was evaporated *in vacuo* to dryness. The subsequent crystallization of the residue form toluene and chloroform afforded 0.32 g (62%) of III. Mp 250—251°C (dec), $[\alpha]_{589}^{25}$ −5.59° (*c*, 0.760, DMF). Found C, 58.12; H, 5.51; N, 5.90%. Calcd for $C_{23}H_{26}O_9N_2$: C, 58.22; H, 5.52; N, 5.90%.

A second crop of crystalline III (0.12 g, 23%) was obtained from the evaporation of the mother liquor. Mp 249—251°C (dec.).

1) *Cf.* for example; A. Neuberger, *J. Chem. Soc.*, **1941**, 50.
2) K. Yamamoto, This Bulletin, **46**, 290 (1973).
3) K. Yamamoto and Taku Hayashi, *ibid.*, **46**, 656 (1973).
4) M. E. Evans, *Carbohyd. Res.*, **21**, 473 (1972).
5) L. Claisen, *Ber.*, **40**, 3903 (1907).
6) L. Claisen, *ibid.*, **31**, 1010 (1898).
7) D. H. Leaback, "Biochemical Preparation," **10**, 118 (1963).

p-*Nitrophenyl 2-Acetamido-3-*O*-methyl-2-deoxy-β-*D*-glucopyranoside (IV).* Two hundred mg of (III) in 20 ml of 90% acetic acid (v/v) were heated to 100°C for 1 min, and then the acetic acid solution was evaporated *in vacuo* to dryness. The subsequent crystallization of the residue from ethanol gave 60 mg (40%) of a crystalline IV. Mp 186—187°C (dec.), $[\alpha]_{589}^{25}$ −34.8° (*c*, 0.467, DMF). Found: C, 50.32; H, 5.70; N, 7.71%; Calcd for $C_{15}H_{20}O_8N_2$: C, 50.56; H, 5.56; N, 7.86%.

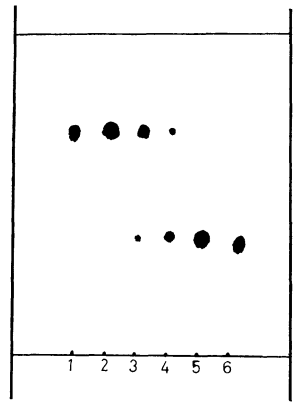

Fig. 2. Thin layer chromatogram of (III) treated with 90% acetic acid at 50°C.
1: Compound (III), 2: Reaction mixture of III, Sampling at 0 min, 3: Reaction mixture of III, Sampling after 2 min, 4: Reaction mixture of III, Sampling after 5 min, 5: Reaction mixture of III, Sampling after 10 min, 6: Compound (IV).

The further crystallization of the mother liquor from ethanol and ether afforded a second crop of IV (70 mg, 47%). Mp 184—187°C (dec.).

Treatment of III with 90% Acetic Acid. The reaction of III (1.0 mg) in 1.0 ml of 90% acetic acid (v/v) was followed by sampling the aliquots of 0.2 ml at 2, 5, and 10 min intervals. Each sample, after it had been neutralized with 0.5 ml of pyridine, was applied to a tlc plate and developed in toluene: pyridine: acetone (2: 1: 1). A thin-layer chromatogram of the reaction mixture is shown in Fig. 2.

The removal of the *O*-(*p*-methoxybenzylidene) group was completed within 10 min at 50°C. Then, the conditions (at 100°C for 1 min) were good enough for the removal because the reaction rate was about 32 (2^5) times faster at 100°C than at 50°C.

Acid Hydrolysis of p-*Nitrophenyl-β-*D*-glucopyranoside and* p-*Nitrophenyl-2-acetamido-2-deoxy-β-*D*-glucopyranoside.* A solution of each *p*-nitrophenyl glycoside (1 mg) in 1.0 ml of 66% acetic acid was heated at 100°C, and 0.2 ml aliquots were removed at 10, 20, and 30 min intervals. Three ml of 0.5M-sodium cabonate were then added to it, and the absorbance was measured at 400 nm. The destruction of glycosides was estimated from the amount of *p*-nitrophenol which was liberated from the glycosides by acid hydrolysis. The results are shown in Table 1.

The author wishes to thank Professor Yoshio Matsushima, Faculty of Science, Osaka University for his continued interest and support during this work and Mrs. Hiroko Kuritani for her kind operation of ORD instrument.

BULLETIN OF THE CHEMICAL SOCIETY OF JAPAN, VOL. 46, 659—660 (1973)

Preparation of Hydroquinone Derivatives

Susumu IWABUCHI, Minoru KOBAYASHI, Kazuo SUZUKI, and Kuniharu KOJIMA
Department of Applied Chemistry, Faculty of Engineering, Chiba University, Yayoi-cho, Chiba

(Received July 6, 1972)

Nakabayashi and Cassidy prepared hydroquinone-bis-δ-lactone (Ia) by heating 2,5-bis(2′-carbethoxy)-hydroquinone.[1] We previously reported on the preparation of 2,5-dimethylhydroquinone-bis-δ-lactone

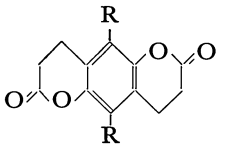

Ia: R=H
Ib: R=CH_3

I

(Ib).[2] In the course of our studies on redox polymers containing hydroquinone or benzoquinone units in polymer chains,[3,4] we prepared some hydroquinone derivatives including 2,3,5-trimethylhydroquinone-δ-lactone (II). In this paper, we describe the preparation of the lactone (II), 2-(3′-hydroxypropyl)-3,5,6-trimethylhydroquinone (III), and 2-(3′-hydroxypropyl)-3,5,6-trimethylbenzoquinone (IV).

We attempted to synthesize hydroquinone alcohol (III) from the malonic ester (V) *via* the carboxylic acid (VI) and its ester (VII). When V was heated in hydrobromic acid at 140—160°C for 15 hr, the lactone (II), 6-hydroxy-5,7,8-trimethyl-3*H*,4*H*-dihydrocoumarin, was obtained in a good yield instead of VI. The IR spectrum (KBr disk) of II showed characteristic absorption bands at 3482 and 1740 cm^{-1}, assignable to hydroxyl and lactone carbonyl groups, respectively. The NMR spectrum in acetone-d_6 gave signals at δ (ppm) 2.20 (s, 9H, CH_3) and 2.73 (m, 4H, CH_2). These spectral data and elemental analysis verify the formation of II.

When the bis-malonic ester (VIII) was subjected to the same treatment, the carboxylic acid IXa was formed from VIIIa after 3 hr,[1] while the bis-lactone (Ib) was obtained from VIIIb as in the case of V.

1) N. Nakabayashi and H. G. Cassidy, *J. Polym. Sci., A-1*, **7**, 1275 (1969).
2) S. Iwabuchi, M. Ueda, and K. Kojima, *ibid., A-1*, **9**, 3405 (1971).
3) M. Ueda, S. Iwabuchi, and K. Kojima, *ibid., B*, **9**, 367 (1971).
4) S. Iwabuchi, M. Ueda, T. Shioda, H. Suda, and K. Kojima, *Kobunshi Kagaku*, in press.

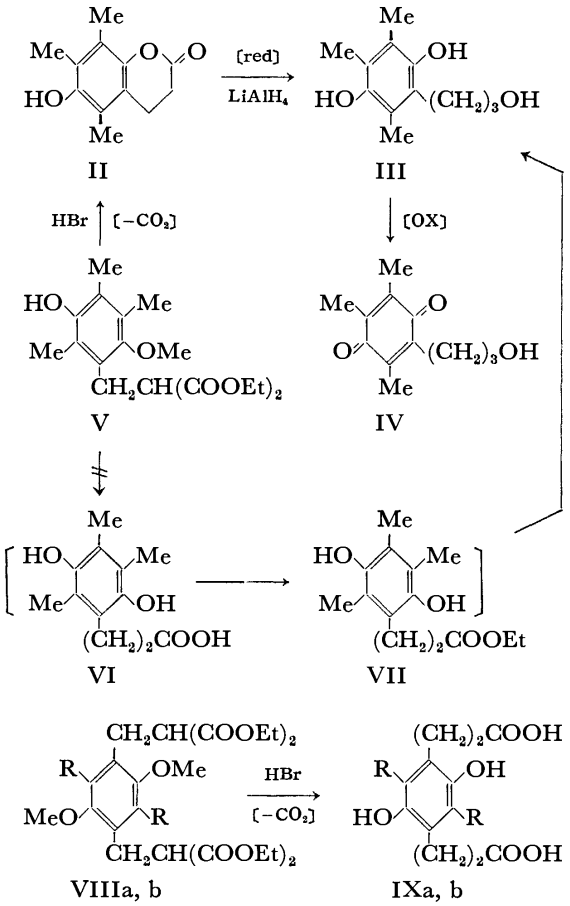

(Suffixes denote a: R=H and b: R=CH_3)

Reduction of II with lithium aluminum hydride yielded 2-(3′-hydroxypropyl)-3,5,6-trimethylhydroquinone (III). The IR spectrum (KBr) showed characteristic bands at 3420 and 3150 cm^{-1}, assignable to hydroxyl groups, but not to carbonyl or ester groups. The NMR spectrum in acetone-d_6 showed signals at δ(ppm) 1.37 (qui, 2H, CH_2), 1.75 (s, 9H, CH_3), 2.40 (tr, 2H, CH_2), 3.16 (tr, 2H, CH_2O), 5.95 (s, 1H, OH), and 6.75 (s, 1H, OH).

Hydroquinone alcohol (III) was oxidized with lead tetracetate to yield 0.95 g (53%) of benzoquinone alcohol (IV); mp 42—43°C. The IR spectrum showed characteristic bands at 3210 cm^{-1} (OH) and 1645 cm^{-1} (quinone C=O). The NMR spectrum in $CDCl_3$ showed signals at δ(ppm) 1.73 (m, 2H, CH_2), 2.05 (s, 9H, CH_3), 2.50 (s, 1H, OH), 2.63 (tr, 2H, CH_2), and 3.63 (tr, 2H, CH_2O).

5) N. Nakabayashi, G. Wegner, and H. G. Cassidy, *J. Org. Chem.*, **33**, 2539 (1968).

Experimental

Preparation of II. 22 g (0.063 mol) of V[5] was heated in 440 ml of 48% HBr solution up to 120°C (bath temp.) and for 2 hr to remove ethyl bromide. The tempetature was then raised to 140°C (3 hr) and finally to 160°C (15 hr). The raw product crystallized from the solution upon cooling in an ice bath. It was filtered, washed with water and dried. Recrystallization from *p*-xylene gave 8.7 g of II as pale yellow needles (yield: 68%); mp 172—173°C (lit,[6] 173—174°C). Found: C, 69.73; H, 6.79%. Calcd for $C_{12}H_{14}O_3$: C, 69.88; H, 6.84%.

Preparation of III. The method of Karret and Banerjed for the reduction of coumarin[7] was applied to II with the following modification. To a stirred suspension of 3.0 g (0.08 mol) of $LiAlH_4$ in 150 ml dry THF cooled with ice was added dropwise 100 ml THF containing 10.3 g (0.05 mol) of II. After the vigorous reaction had subsided, the mixture was refluxed for 2 hr. Excess hydride was decomposed by careful addition of water, and the mixture was neutralized with acetic acid. To this was added 50 ml of saturated aq. NH_4Cl soln. The upper, organic layer was decanted and the lower extracted with four 150 ml portions of THF. The combined THF layers were dried over magnesium sulfate. After the solvent was removed by evaporation from the dried mixture, the residue was recrystallized from chloroform to give 6.58 g (64%) of III as white crystals; mp 135—136°C. Found: C, 68.35; H, 8.62%. Calcd for $C_{12}H_{18}O_3$: C, 68.54; H, 8.63%.

Preparation of IV. To a solution of 1.82 g (8.7 mmol) of III in 70 ml THF were added 70 ml of water under stirring and then 4.43 g (10 mmol) of lead tetracetate. The mixture was refluxed for 30 min. After addition of aqueous NaOH, the mixture was extracted with ether. Red-yellow oil obtained on removal of ether was recrystallized from THF–*n*-heptane to yield 0.95 g (53%) of IV as yellow crystals; mp 42—43°C. Found: C, 69.19; H, 7.80%. Calcd for $C_{12}H_{16}O_3$: C, 69.20; H, 7.74%.

Solvents and Reagents. Solvents were purified in the usual way just before use. Commercial $LiAlH_4$ and lead tetracetate were used without further treatment.

Spectral Measurements. IR data were obtained with a Perkin-Elmer Model 421 spectrophotometer and NMR data with a Varian Associates Model A-60 spectrometer.

We wish to thank Professor H. G. Cassidy for his continuous encouragement throughout this research. One of us (S.I.) is indebted to The United States Public Health Service for postdoctoral support at Yale University. Thanks are also due to Dr. Akira Terahara for the measurement and interpretation of the spectral data.

6) L. I. Smith and R. O. Deneyes, *J. Amer. Chem. Soc.*, **58**, 306 (1936).

7) P. Karret and P. Banerjed, *Helv. Chim. Acta*, **32**, 1692 (1942).

BULLETIN OF THE CHEMICAL SOCIETY OF JAPAN, VOL. 46, 661—662 (1973)

Studies of Saturated Heterocyclic Compounds. Preparations and PMR Spectra of *cis* and *trans* 2,5-Disubstituted 1,3-Dioxolan-4-ones[1]

Yoshihiro ASABE, Shoji TAKITANI, and Yojiro TSUZUKI*

Faculty of Pharmaceutical Sciences, Science University of Tokyo, Ichigayafunagawara-machi, Shinjuku-ku, Tokyo
**Department of Chemistry, Science University of Tokyo, Kagurazaka, Shinjuku-ku, Tokyo*

(Received July 11, 1972)

Although a number of investigations have been made into the chemistry of 1,3-dioxolan-4-ones,[2-5] studies of their geometrical isomers have been left undeveloped, presumably because of the difficulty in the isolation and identification of each isomer. The present work aims at isolating the *cis* and *trans* isomers of some 2,5-disubstituted homologues by means of preparative thin-layer chromatography (tlc) and at assigning these isomers by means of PMR spectroscopy. The product of 2-trichloromethyl-5-phenyl-1,3-dioxolan-4-one(I) was found by PMR spectral studies to be a mixture of *cis* and *trans* isomers. The integrated signal intensities really showed the mixture to be in a ratio of about 1: 1.3(=b: a). Each isomer (a: mp 67—68°C, in the upper band; b: mp 88—89.5°C, in the lower band) was isolated from the mixture by means of tlc; the identification of the 1,3-dioxolan-4-one ring of each isomer was made by studying the stretching vibrations ($\nu_{C=O}$) in their IR spectra.[5,6] In Fig. 1, the PMR spectra of the a-isomer are shown; signals due to 5-H and 2-H appear at τ 4.43 and τ 4.03 respectively, and signals due to the phenyl-ring protons are observed as an almost single peak at τ *ca.* 2.63. On the other hand, as is shown in Fig. 2, the b-isomer gives signals arising from 5-H and 2-H at τ 4.56 and τ 4.13 respectively, and shows signals due to the phenyl-ring protons as complicated multiplets at τ *ca.* 2.56. No detectable change in the spectral pattern was observed at elevated temperatures (to *ca.* 100°C, in $CCl_2=CCl_2$). In the *trans* form, it is expected that the phenyl-ring protons give a spectral pattern similar to those of the 5- or 2-phenyl derivatives. On the other hand, it may be expected for the *cis* form that the phenyl-ring protons will give a complicated spectral pattern because of larger chemical-shift differences among the ring protons due to the predominant anisotropic effect of the Cl atoms in the trichloromethyl group,[5] which is located on the same side as the phenyl group in the five-membered ring. In this regard, the isomer in the lower band (b-isomer) on the tlc, which shows the phenyl-ring proton signals as a complicated spectrum, should be *cis*, and the isomer in the upper band (a-isomer) on the tlc, which gives the phenyl-ring proton signals as a simple pattern, much like those of the 5- and 2-phenyl-1,3-dioxolan-4-ones (III and IV respectively), should be assigned as the *trans* form. Although the spectra of the phenyl-ring protons in $CCl_2=CCl_2$ as well as in $(CD_3)_2CO$ and $CDCl_3$ differ from those in CCl_4 because of the solvent effect, the same conclusion was derived for the same reasons.[7] As is shown in Fig. 1,

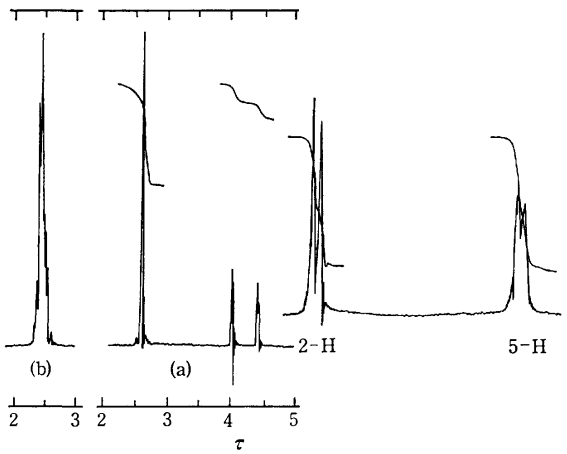

Fig. 1. 100 MHz PMR spectra of the isomer in the upper band (a-isomer, *trans*) (a): in CCl_4 (b): in $(CD_3)_2CO$.

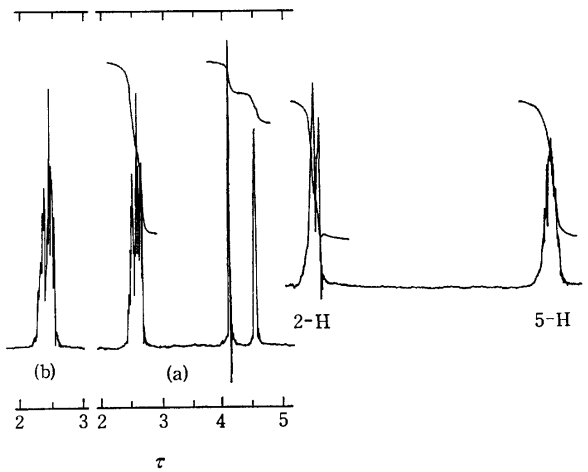

Fig. 2. 100 MHz PMR spectra of the isomer in the lower band (b-isomer, *cis*) (a): in CCl_4 (b): in $(CD_3)_2CO$.

1) Presented at the Annual Meeting of the Pharmaceutical Society of Japan, April, 9, 1971 (Fukuoka).

2) R. C. Elderfield and F. W. Short, "Heterocyclic Compounds," Vol. 5, ed. by R. C. Elderfield, John Wiley & Sons, New York (1957), Chap. 1.

3) E. L. Salmi and A. Pohjolaninen, *Ber.*, **72**, 798 (1939).

4) M. Baron and D. P. Hollis, *Rec. Trav. Chim. Pays-Bas*, **84**, 1109 (1965).

5) M. Farines and J. Soulier, *Bull. Soc. Chim. Fr.*, **1970**, 332.

6) N. J. Turro, S. S. Edelson, J. R. Williams, and T. R. Darling, *J. Amer. Chem. Soc.*, **90**, 1926 (1968).

7) In a paper recently published, Cort and Stewart gave the same assignment on the basis of the PMR spectra of the phenyl rings as well as on that of the dipole-moment measurements of Compound (I). Since they obtained an equal value for the *cis* and *trans* coupling of the long-range couplings between 2-H and 5-H, they claimed that the characteristic long-range couplings could not be used for assignment in the stereochemistry of these compounds. However, our results on the long-range couplings are different from theirs. See L. A. Cort and R. A. Stewart, *J. Chem. Soc. C*, **1971**, 1386.

Table 1. The PMR spectral data of the compounds

Compound		Chemical shift (τ)[a] 2-H *cis*[b]	2-H *trans*[c]	5-H *cis*[d]	5-H *trans*[e]	Phenyl protons	Coupling constant, J (Hz) $\lvert J_{2H-5H}\rvert$	$\lvert J_{gem}\rvert$
I	*trans*	4.03		4.43		*ca.* 2.63 s	1.4	
	cis		4.13		4.56	*ca.* 2.56 c	1.1	
II	*trans*	3.23		5.09		*ca.* 2.60 s	1.6	
	cis		3.58		5.11	*ca.* 2.55 c	1.1	
III		4.54	4.47	4.93		*ca.* 2.68 s	0.7	0.4
							0.4	
IV		3.55		5.80	5.47	*ca.* 2.55 s	1.0	15.0
							0.4	

a) in CCl_4. b) *cis* to the 5-substituent group. c) *trans* to the 5-substituent group. d) *cis* to the 2-substituent group. e) *trans* to the 2-substituent group. s: almost single peak. c: complicated multiplet.

two doublets are observed due to long-range couplings through the oxygen atoms ($|J|=1.4$ Hz) for expanded patterns of the 2-H and 5-H signals in the a-isomer; the 5-H doublet is further broadened because of the long-range couplings with the phenyl-ring protons. Similarly, the 2-H in the b-isomer gives a doublet ($|J|=1.1$ Hz), and the 5-H gives a more broadened signal than that shown in Fig. 1 for the same reason (see Fig. 2). Accordingly, the absolute magnitude of the long-range couplings between the 2-H and the 5-H *via trans*($|J|=1.4$ Hz) was found to be larger than that of the coupling *via cis*($|J|=1.1$ Hz). As is given in Table 1, the *trans* coupling ($|J|=1.6$ Hz) is, in a similar manner, larger than the *cis* coupling ($|J|=1.1$ Hz) in the 2-phenyl-5-trichloromethyl derivative (II), a structural isomer of Compound(I). As is given in Table 1, the 5-H and the 2-H signal in Compound(I) both appear at a slightly higher field in the *cis* than in the *trans* isomer, but the 5-H signals of both isomers of Compound(II) have equal chemical shifts. Therefore, the assignments of the isomers on the basis of the chemical shift seem very difficult. Although the magnitude of the long-range couplings between the 2-H and 5-H signals of these compounds and the differences between the two couplings, are very small, it is possible to distinguish between them, at least, by comparing them with each other in the samples containing both isomers.

This result is in accordance with one of the empirical generalizations for 2,5-dihydrofurans,[8,9] which may be considered to be isoelectronic with 1,3-dioxolan-4-ones. This coupling mechanism is regarded as the same as in 2,5-dihydrofurans in view of the contribution of the $C-\overset{\overset{O}{\|}}{C}-O-C \longleftrightarrow C-\overset{|}{C}=\overset{+}{O}-C$ of the planar lactone function[10,11] in the 1,3-dioxolan-4-one ring.[5] The assignment based on the long-range couplings on the methylene protons of the C-2 and C-5 signals of Compounds-(III) and (IV) was in accordance with that made on the basis of the deshielding effects of their phenyl group. Hardly no solvent effect was observed on the long-range couplings.

Experimental

Preparation of Materials. *2-Trichloromethyl-5-phenyl-1,3-dioxolan-4-one (I)*: This was prepared by the reaction of *dl*-mandelic acid, chloral, and phosphorus pentoxide in tetrachloroethane (at *ca.* 100°C); the *cis*, *trans* mixture was purified by recrystallization from CCl_4–ligroin. Mp 66—67°C. Yield, 51.3%. Each isomer was separated by preparative tlc[12] from the mixture, and was recrystallized from petroleum ether. The upper band (a-band, *trans* isomer) yielded colorless needles; mp 67—68°C. Found: C, 42.77; H, 2.73%. Calcd for $C_{10}H_7O_3Cl_3$: C, 42.67; H, 2.51%. The lower band (b-band, *cis* isomer) gave colorless plates; mp 88—89.5°C. Found: C, 42.16; H, 2.49%.

2-Phenyl-5-trichloromethyl-1,3-dioxolan-4-one (II): This was similarly prepared by the reaction of *dl*-β,β,β-trichlorolactic acid with benzaldehyde; then the excess benzaldehyde was removed by distillation under reduced pressure, and the residue was treated in the same manner as Compound (I). Mp 74—76°C. Yield, 52.8%. The upper band (*trans* isomer) on the tlc gave colorless needles; mp 86—87°C. Found: C, 42.50; H, 2.22%. The lower band (*cis* isomer) gave colorless plates; mp 88—89.5°C. Found: C, 42.75; H, 2.41%. 5-Phenyl-1,3-dioxolan-4-one (III, colorless liquid, bp 124—125 °C/5 mmHg) and 2-phenyl-1,3-dioxolan-4-one (IV, colorless liquid, bp 123—124°C/5 mmHg) were prepared from the corresponding α-hydroxycarboxylic acids and aldehydes by Gerhardt's method[2,3] with a slight modification; they were purified by repeated distillation before use.

Measurements. All the melting points and boiling points are uncorrected. The PMR spectra were measured with a Varian A-60 spectrometer and a JNM-4H-100 spectrometer at room temperature. Carbon tetrachloride, chloroform-*d*, acetone-d_6, and tetrachloroethylene were used as the solvents (the concentrations were about 60—70 mg/0.5 ml), and TMS was used as the internal reference; none of the samples were degassed.

8) C. Barbier, D. Gagnaire, and P. Vottero, *Bull. Soc. Chim. Fr.*, **1968**, 2330; D. Gagnaire and P. Vottero, *ibid.*, **1970**, 164.

9) M. Barfield, R. J. Spear, and S. Sternhell, *J. Amer. Chem. Soc.*, **93**, 5322 (1971).

10) G. A. Jeffrey and S. H. Kim, *Chem. Commun.*, **1966**, 211.

11) E. A. Noe and J. D. Roberts, *J. Amer. Chem. Soc.*, **93**, 7261 (1971), and the referencs cited therein.

12) Two-layer, one-dimensional tlc plates coated with Merck Silica gel HF_{254}-Kieselguhr G (the thickness was 0.5 mm) were used, and benzene or benzene–ligroin mixed solvents were used as the developers.

BULLETIN OF THE CHEMICAL SOCIETY OF JAPAN, VOL. 46, 663—664 (1973)

Aromatic Substitution of Olefins. XIX. Reaction of Five-membered Heterocyclic Aromatic Compounds with Styrene

Ryuzo ASANO, Ichiro MORITANI, Yuzo FUJIWARA, and Shiichiro TERANISHI
Faculty of Engineering Science, Osaka University, Toyonaka, Osaka

(Received July 27, 1972)

We reported on substitution reactions of olefins with benzene derivatives in the presence of palladium(II) salts to give aryl-substituted olefins, and demonstrated that a number of olefins undergo the substitution with benzene derivatives.[1] Ferrocene, a nonbenzenoid aromatic compound, undergoes the reaction with vinyl compounds to give alkenylferrocenes *via* direct substitution.[2] If the reaction is of general applicability, heterocyclic aromatic compounds such as furan, thiophene, selenophene, or *N*-methylpyrrole should react with an olefin to give alkenyl-substituted derivatives. We have found that styrene reacts with heterocyclic five-membered aromatic compounds to give styryl-substituted derivatives.

Results and Discussion

The heterocyclic compounds have greater aromatic reactivity than benzene.[3] Thus it is of interest to determine whether they also react with olefins.

A solution of furan, styrene (equal mole equiv. to furan), palladium(II) acetate (equal mole equiv. to furan) in acetic acid and dioxane was stirred under reflux for 8 hr, to give *trans,trans*-2,5-distyrylfuran (46%, all yields based on palladium(II) acetate) with *trans*-2-styrylfuran (15%). Reactions with other heterocycles such as thiophene, selenophene, or *N*-methylpyrrole were carried out under similar reaction conditions. The results are given in Table 1.

TABLE 1. REACTION OF STYRENE WITH FIVE-MEMBERED HETEROCYCLIC AROMATIC COMPOUNDS BY PALLADIUM(II) ACETATE[a)]

Aromatics	Products and yield, %[b)]	
Furan	*trans*-2-Styrylfuran	15
	trans,trans-2,5-Distyrylfuran	46
Thiophene	*trans*-2-Styrylthiophene	13
	trans,trans-2,5-Distyrylthiophene	36
Selenophene	*trans*-2-Styrylselenophene	9
	trans,trans-2,5-Distyrylselenophene	34
N-Methylpyrrole	*trans*-2-Styryl-*N*-methylpyrrole	11
	trans-3-Styryl-*N*-methylpyrrole	3
trans-2-Styryl-furan	*trans,trans*-2,5-Distyrylfuran	68
	trans,trans,trans-2,3,5-Tristyrylfuran	12

a) Equimolar amounts of aromatics, styrene, and palladium acetate were used, and all the reactions were carried out under reflux for 8 hr. b) Yields are based on palladium acetate.

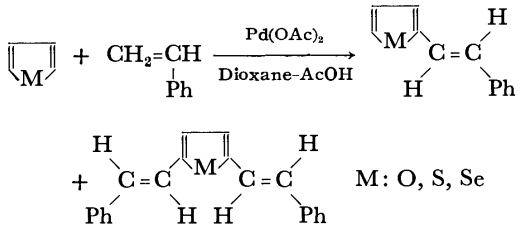

It was found that these heterocycles can easily react with styrene to give styryl-substituted heterocycles. Distyryl-substituted cyclic compounds are formed as a major product except for the case of *N*-methylpyrrole, suggesting that the mono-substituted derivative derived from a single-step alkenylation of the heterocycle undergoes further alkenylation reaction with styrene. This may be due to the higher reactivity of the mono-styryl-substituted compound in the present reaction. In fact, 2-styrylfuran reacts easily with styrene to afford 2,5-distyrylfuran in a good yield. This double-step alkenylation has not been observed in the reaction of benzenoid aromatic compounds with olefins.[1]

The substitution reaction appears to take place exclusively at positions 2 and 5 of the heterocycles except for *N*-methylpyrrole. This is consistent with the result obtained in electrophilic substitution reactions of these compounds.[4,5] *N*-Methylpyrrole seems to be of low reactivity since the aromatic character of the compound is destroyed by addition of acid.

The results provide a very convenient method for the synthesis of alkenylheterocyclic compounds.

Experimental

IR spectra were recorded on a Japan Spectroscopic Co. IR-E spectrometer. NMR spectra were obtained using a Japan Electron Optics JNM-4H-100 or JEOL C-60HL spectrometer, with tetramethylsilane as an internal standard.

Materials. Palladium (II) acetate was prepared from palladium sponge and acetic acid in the presence of concd. nitric acid. Selenophene (109—110°C) was prepared from butadiene and selenium metal according to the procedure of Yur'ev and Magdesieva.[6,7] Commercial aromatics and styrene were purified before use. Dioxane was refluxed with sodium metal and distilled. Acetic acid was dried over phosphorus pentoxide for 1 week and distilled. Light petroleum refers to a fraction of bp 38—60°C.

General Procedure for the Alkenylation of the Heterocycles. Solutions containing equimolar amounts of palladium(II)

1) Y. Fujiwara, I. Moritani, S. Danno, R. Asano, and S. Teranishi, *J. Amer. Chem. Soc.*, **91**, 7166 (1969).
2) R. Asano, I. Moritani, A. Sonoda, Y. Fujiwara, and S. Teranishi, *J. Chem. Soc. C*, **1971**, 3691, and prior papers of this series.
3) P. Linda and G. Marino, *Tetrahedron*, **23**, 1739 (1967).
4) P. Linda and G. Marino, *J. Chem. Soc. B*, **1968**, 392.
5) S. Clementi and G. Marino, *Tetrahedron*, **25**, 4599 (1969).
6) Yu. K. Yur'ev and N. N. Magdesieva, *Sb. IREA (Rept. Inst. Pure Chem. Reagents, USSR)*, No. 6, 6 (1962).
7) B. A. Arbuzov and E. G. Kataev, *Dokl. Akad. Nauk SSSR*, **96**, 983 (1954), *Chem. Abstr.*, **49**, 8907 (1955).

Table 2. Properties of styrylheterocycles

Compound	Mp (°C) (lit, mp)	Found (%)			Calcd (%)			IR (Nujol, cm^{-1}) and NMR spectra
		C	H	Other	C	H	Other	
trans-2-Styrylfuran	52.5—54 (54—55)[a]	84.73	6.01		84.68	5.92		1148, 1011, 965, 955, 924, 885, 804, 760, 741, 695; τ (CCl_4) 2.50—2.93 (5H: 1H,m), 3.04(1H, d, J=16Hz), 3.22 (1H,d, J=16 Hz), 3.60—3.83 (2H,m)
trans,trans-2,5-Distyrylfuran	144—145.5 (144—145.5)[a]	88.01	5.87		88.20	5.92		960, 792, 757, 696; τ(CCl_4) 2.47—2.94(10H,m), 2.97(2H,d, J=16 Hz), 3.23(2H,d, J=16 Hz), 3.73 (2H,s)
trans-2-Styrylthiophene	106.5—108 (112—113)[a]	77.61	5.62		77.38	5.41		965, 866, 845, 824, 760, 714, 698; τ (CCl_4) 2.54—3.16 (phenyl 5H: thiophenyl 3H, m), 3.00(1H, d, J= 16 Hz), 3.15(1H,d, J=16 Hz)
trans,trans-2,5-Distyrylthiophene	192.5—194 (196—198)[a]	82.99	5.61	11.09 (S)	83.29	5.59	11.12 (S)	954, 800, 753, 696; τ($CDCl_3$) 2.47—2.94(10H,m), 2.84 (2H, s), 2.92 (2H, d, J=16 Hz), 3.18 (2H, d, J=16 Hz)
trans-2-Styryl-selenophene	134—136	62.15	4.31		61.81	4.32		959, 825, 810, 759, 695; τ(CCl_4) 2.29 (1H,m), 2.51—3.04 (phenyl 5H: selenophenyl 2H: olefinic 1H, m), 3.29(1H,d)
trans,trans-2,5-Distyrylselenophene	220—221.5	71.48	4.67		71.64	4.81		948, 802, 753, 696; τ($CDCl_3$) 2.43—3.01 (phenyl 10H: olefinic 2H,m), 2.81(2H,s), 3.25(2H,d)
trans-2-Styryl-*N*-methylpyrrole	74.5—75.5 (73.5—75)[a]	84.88	7.14	7.61 (N)	85.20	7.15	7.65 (N)	1625, 1296, 1057, 957, 786, 725, 696; τ (CCl_4) 2.56—2.94 (5H, m), 3.16 (1H, d, J=15 Hz), 3.28 (1H,d, J= 15 Hz), 3.55 (1H, m), 3.69 (1H, m), 4.04 (1H,m), 6.32(3H,s)
trans-3-Styryl-*N*-methylpyrrole	97—98							1630, 1368, 1160, 1083, 968, 918, 788, 749, 715, 696; τ(CCl_4) 2.58—2.96 (5H,m), 3.15(1H,d, J=16 Hz), 3.39(1H,d, J=16 Hz), 3.41(1H,m), 3.57(1H,m), 3.76(1H,m), 6.36(3H,s)
trasn,trans,trans-2,3,5-Tristyrylfuran	150.5—151.5	89.57	6.04		89.80	5.92		1595, 1064, 953, 812, 754, 695; τ($CDCl_3$) 2.30—3.26 (phenyl 15H: olefinic 6H,m), 3.37 (1H,s)

a) Ref. 8.

acetate, styrene, and the heterocycle in acetic acid and dioxane were stirred for 8 hr under reflux. The resulting mixture was filtered to remove palladium metal. The filtrate was poured into water and the mixture was extracted with chloroform. The chloroform extract was washed with aqueous sodium bicarbonate and water, dried (Na_2SO_4) and then the solvent was evaporated. The products were isolated by alumina column or gas chromatography and identified by comparison (mixed mp, IR, and NMR spectra) with authentic samples. Analytical results and the properties of the styrylheterocycles are given in Table 2. A specific example of the reaction follows.

Reaction of Furan with Styrene. A solution of styrene (1.56 g, 15 mmol), furan (1.02 g, 15 mmol) and palladium(II) acetate (3.37 g, 15 mmol) in dioxane (160 ml) and acetic acid (40 ml) was stirred for 8 hr under reflux ($CaCl_2$ guard tube). After the work-up the residue was chromatographed on a column of alumina (130 g). Elution with light petroleum (900 ml) and recrystallization yielded *trans*-2-styrylfuran (0.38 g, 15%), which was identified by comparison with an authentic sample.[8] Further elution with benzene (500 ml) and recrystallization from ethanol gave *trans,trans*-2,5-distyrylfuran (0.92 g, 46%) which was identified by comparison with an authentic sample.[8] Finally elution with with ether (500 ml) and methanol gave tarry material (0.22 g) which was not further examined. Glc of the solvent evaporated off showed the presence of styrene and a trace amount of β-acetoxystyrene (*cis* and *trans* mixture).

8) E. J. Seus, *J. Heterocycl. Chem.*, **2**, 318 (1965).

BULLETIN OF THE CHEMICAL SOCIETY OF JAPAN, VOL. 46, 665—666 (1973)

The Ferrocenylation of Styrenes-β,β-d_2 with the Ferrocenylpalladium Compound

Akira KASAHARA and Taeko IZUMI

Department of Applied Chemistry, Faculty of Engineering, Yamagata University, Yonezawa, Yamagata

(Received June 16, 1972)

Recently, the arylation of olefin with arylpalladium compound (I), formed *in situ* by the exchange of arylmercuric compounds (II) with palladium salts, has been shown to be a useful reaction for the synthesis of various olefinic compounds [Eq. (1)].[1] Moreover, Heck[2] has reported that the reaction of olefin with I was stereospecific with internal olefin, giving products consistent with a *cis* addition of the organopalladium reagent to the olefin, followed by a *cis* elimination of a hydridopalladium(II) species. Henry[3] has also reported that the phenylpalladation of cyclohexene-3,3,6,6-d_4 (III) by phenylmercuric acetate and palladium acetate produces products (IV and V) which are consistent with the *cis* phenylpalladation, followed by *cis* palladium(II) hydride elimination and readdition [Eq. (2)]. On the other hand, Moritani *et al.*[4] have reported that, judging from the deuterium analyses of the *trans* stilbene formed, it seems that the phenylation of styrenes-β,β-d_2 (VI) with benzene in the presence of palladium acetate, without using a phenylmercuric compound, proceeds without any hydride shift. We ourselves have also reported that the reaction of benzo[*b*]furan with I results in the formation of 2-arylbenzo[*b*]furan, and that no hydride shift takes place in the reaction.[5]

Previously, we described the ferrocenylation of olefin with chloromercuriferrocene (VII) in the presence of palladium salts to produce alkenylferrocene derivatives.[6] Therefore, in order to study whether or not the hydride shift also occurs in the reaction of VI with VII, the reaction was performed in the presence of lithium chloropalladite. If the hydride shift occurs in the reaction, the reaction of VI with ferrocenylpalladium chloride (VIII), formed *in situ* from VII and palladium salts, will produce styrylferrocenes (IX) containing two and/or one deuterium as is shown by Eq. (3), and the deuterium content of IX will be 150%. Contrary to this, according to the no hydride shift mechanism,[4,5] the deuterium content of the product should be 100% [Eq. (4)]. The results are summarized in Table 1. Styrene-β,β-d_2, *p*-methylstyrene-β,β-d_2, and *p*-methoxystyrene-β,β-d_2 all resulted in the formation of IX, indicating that the deuterium content is *ca.* 150%, unlike the case of no hydride shift. These results clearly show that the hydride shift occurs in this reaction.

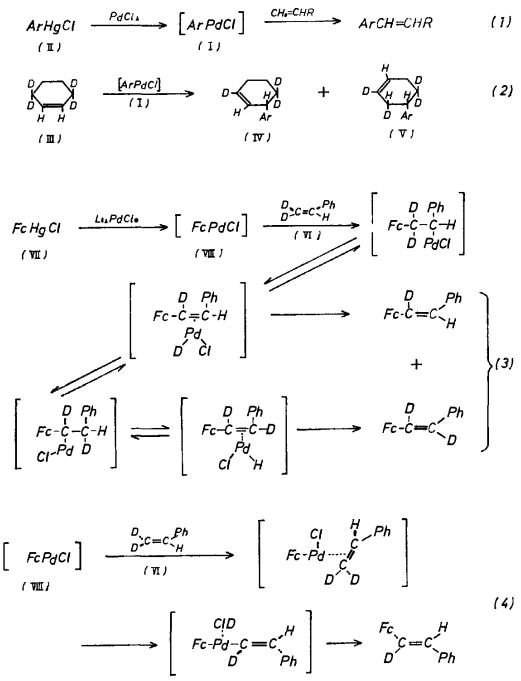

Fig. 1

Experimental

Analysis and Materials. All the melting points are uncorrected. The IR spectra were measured on KBr disks with a Hitachi EPI-S spectrometer, while the NMR spectra were obtained by means of a Hitachi H-60 NMR spectrometer at 60 MHz in $CDCl_3$, using tetramethylsilane as the internal standard. Their chemical shifts are presented in terms of ppm values, together with the splitting pattern and the relative integrated area. The letter designates the multiplicity of the signal: s, singlet; d, doublet; t, triplet; q, quadruplet; *m*, multiplet. The mass spectra were obtained on a Hitachi RMU6E mass spectrometer, using a direct inlet and an ionization energy of 70 eV.

The following compounds were synthesized by the methods described in the literature: chloromercuriferrocene,[7] styrene-β,β-d_2,[8] *p*-methylstyrene-β,β-d_2,[4b] and *p*-methoxystyrene-β,β-d_2.[4b]

General Procedure for the Ferrocenylation of Styrene-β,β-d_2. Lithium chloropalladite solutions were prepared by stirring 0.84 g (20 mmol) of anhydrous lithium chloride and 1.77 g (10 mmol) of palladium chloride overnight at room tempera-

1) R. F. Heck, *J. Amer. Chem. Soc.*, **90**, 5518 (1968), and following papers.
2) R. F. Heck, *ibid.*, **91**, 6707 (1969): *ibid.*, **93**, 6896 (1971).
3) P. M. Henry and G. A. Ward, *ibid.*, **94**, 673 (1972).
4) a) S. Danno, I. Moritani, and Y. Fujiwara, *Chem. Commum.*, **1970**, 610; b) S. Danno, I. Moritani, Y. Fujiwara, and S. Teranishi, *J. Chem. Soc., B*, **1971**, 196.
5) A. Kasahara, T. Izumi, T. Takeda, M. Yodono, R. Saito, and T. Sugawara, This Bulletin, in press.
6) A. Kasahara, T. Izumi, G. Saito, M. Yodono, R. Saito, and Y. Goto, This Bulletin, **45**, 894 (1972).
7) R. E. Fish and M. Rosenblum, *J. Org. Chem.*, **30**, 1253 (1965).
8) W. M. Schubert and Bo Lamm, *J. Amer. Chem. Soc.*, **88**, 120 (1966).

Table 1. The reaction of styrenes-β,β-d_2 with ferrocenylpalladium chloride

Olefin	Product	Mp °C	Yield %	D-content[a]	Chemical shift
Ph–CH=CD_2[b]	X	228—229	5		
	Styrylferrocene[e]	120—121	55	148±2	4.17 s 5, 4.32 q 2, 4.50 q 2 } –Fc
					6.74s 0.5 –CH=CFc
					7.37 m 5 Ph
p-$MeC_6H_4CH=CD_2$[c]	X	228—229	3		
	p-Methylstyryl-ferrocene[f]	130—131	48	145±2	2.32 s 3 $-CH_3$
					4.09 s 5, 4.24 q 2, 4.43 q 2 } –Fc
					6.64 s 0.5 –CH=CFc
					7.08 d 2, 7.31 d 2 } C_6H_4–
p-$MeOC_6H_4CH=CD_2$[d]	X	228—229	9		
	p-Methoxysty-rylferrocene	125—126	43	142±2	3.68 s 3 $-OCH_3$
					4.10 s 5, 4.24 q 2, 4.41 q 2 } –Fc
					6.67 s 0.5 –CH=CFc
					6.82 d 2, 7.32 d 2 } C_6H_4–

a) Calculated on the basis that D-content of product containing one olefinic deuterium is 100%, and by the comparison of the ratio of integrated area of olefinic proton with that of other protons in the 60 MHz spectrum. b) The mass spectrum showed this to be 98% deuteriated. c) The mass spectrum showed this to be 95% deuteriated. d) The mass spectrum showed this to be 96% deuteriated. e) Mp of an undeuteriated sample, 121—122°C. (P. L. Pauson and E. E. Watts, *J. Chem. Soc.*, **1963**, 2990). f) Mp of an undeuteriated sample, 131°C. (G. Drefahl, G. Ploctner, and I. Winnefeld, *Chem. Ber.*, **95**, 2788 (1962)). g) Mp of an undeuteriated sample, 125—126°C. (A. Kasahara and T. Izumi, unpublished work).

ture in 100 ml of ethanol. To these lithium chloropalladite solutions, mixtures of 4.20 g (10 mmol) of I and twice as much VI were added, after which the mixtures were stirred at room temperature for 12 hr. The products were isolated by filtering to remove a precipitated palladium, and by distilling under reduced pressure to remove the solvent. The residue was dissolved in benzene and chromatographed on alumina. The first elution with benzene and subsequent recrystallization from ethanol afforded deep yellow crystals (mp 228—229°C, 3—9% yields) which were identified as biferrocenyl (X)[9] by a comparison of the IR spectra and by a mixed-melting-point determination with an authentic sample. Further elution with benzene and recrystallization from ethanol afforded the respective ferrocenylation product (IX). The structures of the products were confirmed by the observation of the IR and NMR spectra. The deuterium-content of the products was also calculated from the NMR results (see Table).

9) H. Shechter and J. H. Helling, *J. Org. Chem.*, **26**, 1034 (1961).

The authors would like to express their thanks to Assistant Professor Kaoru Hanaya and Mr. Hideaki Kudo of Yamagata University for the measurements of the NMR spectra.

BULLETIN OF THE CHEMICAL SOCIETY OF JAPAN, VOL. 46, 667—669 (1973)

The Reaction of Acyl-substituted Sulfonium and Pyridinium Ylides with Diphenylthiirene Dioxide

Yosio HAYASI, Hideo NAKAMURA, and Hitosi NOZAKI
Department of Industrial Chemistry, Kyoto University, Yoshida, Kyoto

(Received July 28, 1972)

In contrast to the preceding paper,[1] which dealt with the reaction of sulfonium ylides with cyclopropenone, the present paper will report studies of the reactions of diphenylthiirene dioxide (I) as an electrophile with acyl-substituted sulfonium and pyridinium ylides.

Reaction with Sulfonium Phenacylides. The reaction of I with an equimolar quantity of dimethylsulfonium *p*-methylphenacylide (IIa) in benzene at reflux gave four crystalline products; the major one (67%) was a sulfur dioxide-elimination product, tolan, while the three minor products were identified as an oxathiin dioxide, IIIa (15%), a thiete dioxide, IVa (13%), and a dithiin, Va (12%). These products were identified from their spectral properties and from the results of elementary analyses. Thus, in the mass-spectrum fragmentation of IIIa, the elements of SO_2+CHO were lost from the molecular ion (*m/e* 374) to give a significant peak at *m/e* 281, probably because of a cyclopropenium ion. Meanwhile, the mass spectrum of IVa displayed a characteristic toluyl ion (*m/e* 119).

The formation of IIIa and IVa could be formulated by assuming the following sequences: (1) the benzoyl-migration in the VI adduct, giving intermediary ylides, VII;[2] (2) the subsequent isomerization to VIII, and finally (3) the ring closure of VIII with the elimination of dimethyl sulfide (Scheme 1). Remarkably, the carbon-to-carbon bond of the episulfone VII is preferentially broken instead of extruding sulfur dioxide.[3] The reaction pathway leading to Va is open to future research.

Analogously, the reaction of dimethylsulfonium phenacylide IIb with I afforded three crystalline products upon careful chromatography on silica gel. The spectroscopic and elementary analyses of the major product (36%) supported the structure IIIb; the very small amounts of the two minor products could be formulated as IVb (<5%) and Vb (6%) after a comparison of their spectra with those of IVa and Va respectively.

Reaction with Pyridinium and Related N-*Ylides.* 1,3-Dipolar cycloadditions of pyridinium and related heteroaromatic ylides with diethyl acetylenedicarboxylate, ethyl propiolate, and so on have been reported to give indolizine derivatives.[4] Diphenylthiirene dioxide (I) was found to behave similarly to *N*-ylides. Thus, pyridinium phenacylide (IX) reacted with an equimolar amount of I in benzene at room temperature to yield a yellow, crystalline solid, X (46%). The UV spectrum indicated the presence of cyclic conjugation systems.[4] The results of elementary analysis and the mass spectrum were in good accordance with the empirical formula of $C_{27}H_{19}NO$. The IR spectrum showed intense absorption bands at 1595, 1385, and 1210 cm^{-1}, which revealed the contribution of a charge-separated structure, *e.g.*, Xa, to the resonance hybrid. The structure of X was further confirmed by com-

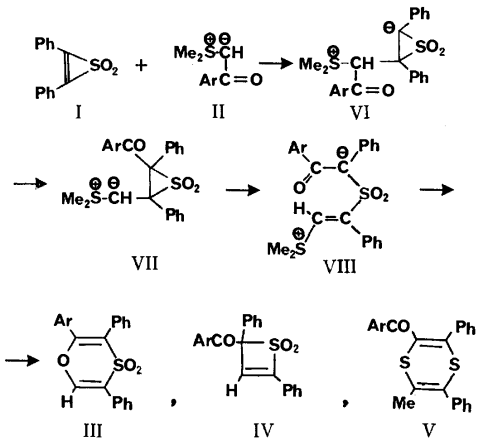

Ar=*p*-MeC_6H_4 (Series a), Ph (Series b)

Scheme 1. Reaction of I with sulfonium acylmethylides

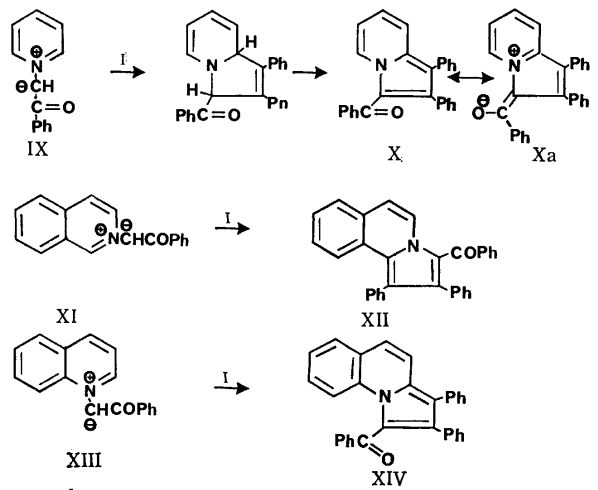

Scheme 2. Reaction of I with pyridinium acylmethylides

1) Y. Hayasi and H. Nozaki, *Tetrahedron*, **27**, 3080 (1971). See also T. Eicher, E. von Angerer, and A. M. Hansen, *Ann. Chem.*, **746**, 102 (1971).

2) a) H. Nozaki, Y. Hayasi, M. Takaku, and K. Kondo, *Tetrahedron*. **24**, 6563 (1968); b) M. Higo and T. Mukaiyama, *Tetrahedron Lett.*, **1970**, 2565.

3) For the C-C bond cleavage reaction of episulfone, see L. A. Paquette and S. Maiorane, *Chem. Commun.*, **1971**, 313.

4) a) T. Sasaki, K. Kanematsu, Y. Yukimoto, and S. Ochiai, *J. Org. Chem.*, **36**, 813 (1971), and references cited therein; b) J. E. Douglass and J. M. Wesolosky, *ibid.*, **36**, 1165 (1971); c) N. Basketter and A. O. Plunkette, *Chem. Commun.*, **1971**, 1578.

parison with an authentic sample, independently prepared from 1,2-diphenylindolizine by reaction with benzoyl chloride following the general method of Borrows.[5] It should be added that the attempted reaction of IX with tolan (1 : 1) at room temperature for 22 hr in benzene failed to afford the adduct X. A similar pattern was repeated using isoquinolinium (XI) and quinolinium (XIII) phenacylides to furnish two 3-benzoylindolizine derivatives XII and XIV respectively.

Experimental

All the melting points are uncorrected. The microanalyses were performed at the Elemental Analyses Center of Kyoto University. The NMR spectra were taken with JEOL C-60H and JNM-MH-60 spectrometers, and the chemical shifts are reported in δ values relative to TMS as the i nternal standard, unless otherwise stated. The abbreviations s and m refer to singlet and multiplet respectively. The UV absorption spectra were measured in 95% EtOH on a Shimadzu MPS-50L spectrometer, and the mass spectra, on a Hitachi RMU-6E instrument by the direct-injection method.

Reaction of Dimethylsulfonium p-*Methylphenacylide (IIa) with Diphenylthiirene Dioxide (I).* A solution of IIa (2.7 g, 13.6 mmol) and I (3.0 g, 12.4 mmol) in benzene (150 ml) was stirred at room temperature for 2 hr. The reaction mixture was then heated at reflux for 9 hr. The chromatographic separation of the crude products on a silica gel column (benzene and chloroform) gave tolan (1.5 g, 67%), IIIa (0.7 g, 15%), IVa (0.6 g, 13%), and Va (0.6 g, 12%).

3,5-Diphenyl-2-*p*-tolyl-1,4-oxathiin dioxide (IIIa): mp 183.5—185°C (PhH); λ_{max}^{EtOH} 233 (log ε 4.30), 238 (4.33) nm; IR (KBr) 1645, 1605, 1290, 1220, 1140 cm^{-1}; NMR ($CDCl_3$) 2.31 (s, 3), 7.2—7.8 (m, 15) ppm; MS *m/e* 376 (9), 375 (27), 374 (100, P), 311 (26), 310 (95), 282 (9), 281 (32), 193 (37), 192 (64), 191 (72), 190 (18), 184 (27), 165 (31), 119 (17), 91 (14), 89 (17), 77 (11).

Found: C, 74.0; H, 4.8%. Calcd for $C_{23}H_{18}O_3S$: C, 73.8; H, 4.9%.

2,4-Diphenyl-2-*p*-toluylthiete dioxide (IVa): mp 230—231°C (PhH); λ_{max}^{EtOH} 218 (4.35), 268 (4.35) nm; IR (KBr) 1680, 1610, 1280, 1150 cm^{-1}; NMR (DMSO-d_6) 2.5 (s, 3), 7.4—8.1 (m, 15) ppm; MS *m/e* 376 (1), 375 (4), 374 (13, P), 342 (5), 236 (6), 311 (22), 310 (77, P-SO_2), 205 (12), 191 (25), 189 (13), 165 (6), 120 (33), 119 (100), 105 (19), 91 (54), 77 (13), 64 (16).

Found: C, 74.0; H, 4.9%. Calcd for $C_{23}H_{18}O_3S$: C, 73.8; H, 4.9%.

2-Methyl-3,5-diphenyl-6-*p*-toluyl-1,4-dithiin (Va): mp 145—145.5°C (PhH); IR (KBr) 1655, 1605, 1280 cm^{-1}; NMR ($CDCl_3$) 2.30 (s, 3), 2.47 (s, 3), 7.2—8.2 (m, 14), ppm; MS *m/e* 402 (7), 401 (31), 400 (100, P), 285 (6), 367 (12), 309 (10), 295 (11), 262 (4), 234 (8), 220 (7), 154 (4), 121 (6), 119 (14), 91 (17).

Found: C, 74.5; H, 5.0; S, 15.5%. Calcd for $C_{25}H_{20}OS_2$: C, 75.0; H, 5.0; S, 16.0%.

Reaction of IIb with I. A solution of IIb (3.3 g, 18.2 mmol) and I (4.0 g, 16.5 mmol) in benzene (200 ml) was stirred at room temperature for 24 hr and then at reflux for 3 hr. After concentration, the residual oil was chromatographed on a silica gel column (benzene) to afford IIIb (2.4 g, 36%), IVb (0.3 g, 5%), and Vb (0.4 g, 6%).

2,3,5-Triphenyl-1,4-oxathiin dioxide (IIIb): mp 206—207°C (PhH); λ_{max}^{EtOH} 228 (4.35), 240 (4.32), 266 (4.12) nm; IR (KBr) 1650, 1283, 1220, 1135 cm^{-1}; NMR ($CDCl_3$) 6.9—7.8 (m) ppm; MS *m/e* 362 (3), 361 (7), 360 (23, P), 296 (40, P-SO_2), 268 (11), 267 (21), 178 (100), 177 (11), 176 (9), 152 (7), 149 (7), 105 (11), 102 (6),

Found: C, 73.2; H, 4.7%. Calcd for $C_{22}H_{16}O_3S$: C, 73.3; H, 4.5%.

4-Benzoyl-2,4-diphenylthiete dioxide (IVb); mp 142—143°C (PhH); IR (KBr) 1665, 1300, 1150 cm^{-1}; NMR ($CDCl_3$) 7.2—7.8 (m) ppm; MS *m/e* 362 (1), 361 (3), 360 (9, P), 297 (8), 296 (24, P-SO_2), 191 (14), 189 (7), 165 (10), 105 (100), 77 (19).

2-Benzoyl-3,5-diphenyl-6-methyl-1,4-dithiin (Vb): mp 111—112°C (PhH); λ_{max}^{EtOH} 244 (4.53), 286 (4.25) nm; IR (KBr) 1638, 1420, 1226, 1012 cm^{-1}; NMR ($CDCl_3$) 2.43 (s, 3), 6.8—7.5 (m, 15) ppm; MS *m/e* 388 (14), 387 (33), 386 (100, P), 372 (11), 371 (19), 353 (11), 309 (16), 295 (6), 262 (7), 234 (14), 221 (6), 193 (8), 154 (6), 145 (5), 121 (13), 105 (32), 77 (38).

Found: C, 74.6: H, 4.6; S, 16.5%. Calcd for $C_{24}H_{18}OS_2$: C, 74.6; H, 4.7; S, 16.5%.

Reaction of IX with I. A solution of IX (2.0 g, 10 mmol) and I (2.4 g, 10 mmol) in benzene (150 ml) was stirred at room temperature for 10 hr. After the solvent had then been removed *in vacuo*, the residual solids were chromatographed on a silica gel column (benzene) to give the unchanged I and yellow crystals (X, 1.7 g, 46%): mp 166—167°C (EtOH); λ_{max}^{EtOH} 251 (4.56), 286 (sh, 4.25), 400 (4.17) nm; IR (KBr) 1595, 1572, 1385, 1210 cm^{-1}; NMR ($CDCl_3$) 6.8—7.8 (m) ppm; MS *m/e* 375 (5), 374 (32), 373 (100, P), 344 (7), 296 (20), 268 (13), 267 (32), 239 (4), 186 (5), 177 (9), 133 (4), 105 (11), 77 (14).

Found: C, 86.6; H, 5.5; N, 3.6%. Calcd for $C_{27}H_{19}NO$: C, 86.8; H, 5.1; N, 3.8%.

1,2-Diphenylindolizine. A solution of 2-benzylpyridine (5.0 g, 30 mmol) and phenacyl bromide (5.9 g, 30 mmol) in ether was stirred at room temperature for 10 days. The resulting precipitates were filtered and then washed with ether to afford 1-phenacyl-2-benzylpyridinium bromide (quantitatively); mp 174—176°C (decomp.). The pyridinium bromide (0.6 g, 1.7 mmol) was dissolved in water (6 ml), $NaHCO_3$ (0.5 g) was added, and the mixture was brought to a boil. The resulting thick magma was recrystallized from ethanol to afford 1,2-diphenylindolizine (0.40 g, 94%); mp 112—113°C (EtOH).

Found: C, 89.0; H, 5.5; N, 5.4%. Calcd for $C_{20}H_{15}N$: C, 89.2; H, 5.6; N, 5.2%.

3-Benzoyl-1,2-diphenylindolizine (X). A mixture of 1,2-diphenylindolizine (0.40 g, 1.6 mmol) and benzoyl chloride (1.2 ml) was heated at 40°C for 24 hr. The cooled reaction mixture was triturated with petroleum ether (bp 30—50°C), and the resulting green solid was filtered off. Recrystallization from ethanol gave X (0.24 g, 35%); mp 166—167°C. Both specimens showed no depression upon a mixed-mp determination, and the IR spectra were completely superimposable.

Found: C, 86.7; H, 4.9; N, 3.9%. Calcd for $C_{27}H_{19}NO$: C, 86.8; H, 5.1; N, 3.8%.

Reaction of Isoquinolinium Phenacylide (XI) with I. A solution of isoquinolinium phenacylide (XI, 1.86 g, 7.5 mmol) and I (1.80 g, 7.4 mmol) in acetonitrile (300 ml) was heated at reflux for 39 hr. Chromatography (silica gel, benzene) afforded yellow crystals of 3-benzoyl-1,2-diphenylpyrrolo-[2,1-*a*]isoquinoline (XII, 1.95 g, 61%); mp 196—199.5°C (PhH); λ_{max}^{EtOH} 270 (4.57), 296 (4.19), 336 (3.94), 398 (4.23)

5) E. T. Borrows, D. O. Holland, and J. Kenyon, *J. Chem. Soc.*, **1946**, 1069.

nm; IR (KBr) 1605, 1592, 1365, 1198 cm^{-1}; NMR ($CDCl_3$) 6.75—7.8 (m) ppm; MS *m/e* 425 (6), 424 (36), 423 (100, P), 394 (4), 346 (19), 318 (10), 317 (20), 211 (9), 105 (10), 77 (7).

Found: C, 88.1; H, 5.1; N, 3.0%. Calcd for $C_{31}H_{21}NO$: C, 87.9; H, 5.0; N, 3.3%.

Reaction of Quinolinium Phenacylide (XIII) with I. A solution of quinolinium phenacylide (XIII, 0.93 g, 3.7 mmol) and I (0.90 g, 3.7 mmol) in benzene (150 ml) was stirred at room temperature for 2 days. Subsequent chromatography (silica gel, benzene) afforded yellow crystals of 1-benzoyl-2,3-diphenylpyrrolo[1,2-a]quinoline (XIV, 0.12 g, 8%): mp 218—219°C (PhH); λ_{max}^{EtOH} 266 (4.59), 292 (sh, 4.15), 332 (3.92), 380 (4.11), 394 (4.18) nm; IR (KBr) 1600, 1350, 1198, 890 cm^{-1}; NMR (CCl_4) 6.6—7.7 (m) ppm; MS *m/e* 424 (35), 423 (100, P), 394 (4), 346 (18), 318 (8), 316 (10), 211 (9), 105 (8), 77 (8).

Found: C, 87.9; H, 5.2; N, 3.0%. Calcd for $C_{31}H_{21}NO$: C, 87.9; H, 5.0; N, 3.3%.

BULLETIN OF THE CHEMICAL SOCIETY OF JAPAN, VOL. 46, 669—670 (1973)

A Convenient Method of Synthesizing Protected α-Amino-γ-butyrolactones

Hiroshi SUGANO and Muneji MIYOSHI

Research Laboratory of Applied Biochemistry, Tanabe Seiyaku Co., Ltd., Kashima-cho, Higashiyodogawa-ku, Osaka

(Received July 31, 1972)

α-Amino-γ-butyrolactone (homoserine lactone) is a key intermediate in the synthesis of amino acids, especially γ-substituted α-amino acids, such as cystathionine,[1,2] homolanthionine,[2] canaline,[3] canavanine,[4] phosphinothricin,[5] and selenium analogs of methionine and homocysteine.[6] Suitable synthetic methods for the preparation of an optically-active α-amino-γ-butyrolactone are, therefore, of importance in connection with the synthesis of such types of amino acids and of peptides containing a homoserine.

The known method for the preparation of an optically-pure *N*-protected α-amino-γ-butyrolactone involves a two-step sequence in which *N*-tosyl-glutamine is converted into *N*-tosyl-α,γ-diaminobutyric acid with potassium hypobromite, followed by diazotization.[1] However, the amino-protecting group in this method is limited to an acid-stable group, such as the tosyl and benzoyl groups.

It was reported previously, in connection with studies of the determination of amino acid sequences in peptides containing methionine, that a methionine residue is transformed into an α-amino-γ-butyrolactone residue by treatment with methyl iodide or cyanogen bromide, followed by hydrolysis.[7]

We will report in this paper the application of the above procedure on a preparative scale to the widely-used, optically-active α-amino-γ-butyrolactones, suitably protected for further elaboration in the synthesis. Thus, readily-available, optically-active *N*-acyl-methionines, such as *N*-benzyloxycarbonyl(Z)-, *N*-tosyl(Tos)-, *N*-benzoyl(Bz)-, and *N*-ethoxycarbonyl(Eoc)-methionine, were treated with methyl iodide in a mixture of acetic acid and formic acid to form sulfonium salts; they were then hydrolyzed under reflux at pH 6—7. The resulting *N*-acyl-α-amino-γ-hydroxybutyric acids were converted into the corresponding lactones with hydrogen chloride. The unreacted *N*-acyl-methionines were extracted out with a sodium bicarbonate solution; optically-pure *N*-acyl-α-amino-γ-butyrolactones are thus obtained in good yields (Eq. (1)).

The *N*-*t*-butyloxycarbonyl (Boc) derivative, in which the Boc-group was cleaved by formic acid, was methylated in acetic acid without the use of formic acid, but the yield was rather low because the cleavage of the Boc-group occurred during the hydrolysis.

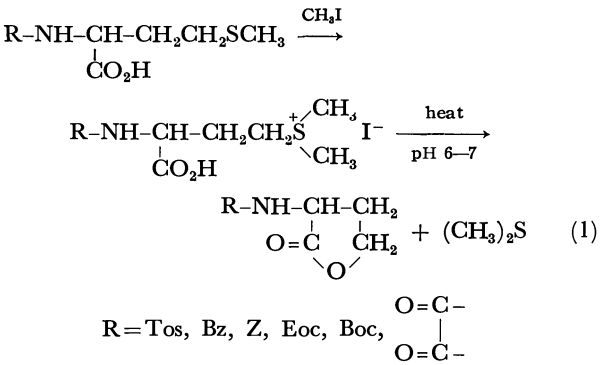

(1)

Bis-amide was obtained analogously from oxalyl bis-methionine. No appreciable racemization occurred during the procedure. The specific rotations of the derivatives synthesized above agreed with those of the derivatives which were obtained by the acylation of commercially-available optically-pure homoserine and by subsequent lactonization. The results are shown in Table 1.

Experimental

General Procedure. A solution of acyl-L-methionine

1) K. Jost and J. Rudinger, *Collect. Czech. Chem. Commun.*, **32**, 2485 (1967).
2) J. A. Stekol, *J. Biol. Chem.*, **173**, 153 (1948).
3) M. Kitagawa, *J. Agr. Chem. Soc. Jap.*, **12**, 871 (1936).
4) M. Kitagawa and T. Tomiyama, *J. Biochem.* (Tokyo), **11**, 265 (1929).
5) W. A. König and H. Zähner, *Helv. Chim. Acta*, **55**, 224 (1972).
6) E. P. Painter, *J. Amer. Chem. Soc.*, **69**, 232 (1947).
7) J. Bremner, *Biochem. J.*, **47**, 538 (1950).

TABLE 1. R–NH–C(=O)–O–C(=O)–CH$_2$–CH$_2$ (L-SERIES)

R	Yield (%)	Mp (°C)	$[\alpha]_D^{25}$ (c 1, MeOH)	Anal. (%) Calcd C	Calcd H	Calcd N	Found C	Found H	Found N
C_6H_5CO–	73	137—139	−29.0°	64.38	5.40	6.83	64.14	5.39	6.78
$CH_3C_6H_4SO_2$–	92	130—133	+8.0°	51.76	5.13	5.49	51.60	5.17	5.51
C_2H_5OCO–	81	88—89	−34.8°	48.55	6.40	8.09	48.35	6.46	8.12
$C_6H_5CH_2OCO$–	80	126—127	−30.5°	61.27	5.57	5.96	61.48	5.65	6.08
$(CH_3)_3COCO$–	29	125.5—126.5	−27.6°	53.72	7.51	6.96	53.68	7.47	6.95
O=C(–)–[a] O=C–	45	298—303	−25.0°[b]	46.88	4.72	10.93	45.94	4.75	10.81

a) This was not recrystallized. b) c 1, N NaOH.

(1 mol) in a mixture of acetic acid (300 ml), 80% formic acid (600 ml), and methyl iodide (110 ml) was allowed to stand in a dark place at room temperature for 10 hr. (In the case of Boc-L-methionine, formic acid was not used, and the mixture was allowed to stand for 48 hr). The mixture was then concentrated under reduced pressure below 40°C. The resulting oil was triturated with dry ether and dissolved in a N sodium hydroxide solution (1000 ml). The mixture was heated at 90°C with stirring for 3 hr. During the course of the reaction, the reaction mixture was kept at pH 6—7 by the addition of N sodium hydroxide. After cooling, the crystals which had appeared were collected by filtration, washed well with water, and dried. Recrystallization from ethyl acetate–petroleum ether gave an optically-pure *N*-acyl-α-amino-γ-butyrolactone. The mother liquor was adjusted to pH 2—3 with N hydrochloric acid and then allowed to stand at room temperature for 1 hr. The product was extracted with ethyl acetate, and the extract was washed with 4% sodium bicarbonate, N ammonia, and water, and dried over magnesium sulfate. The solvent was removed *in vacuo* and the crystals thus obtained were recrystallized from ethyl acetate–petroleum ether to afford an optically-pure *N*-acyl-α-amino-γ-butyrolacetone. The oxalyl derivative could not be recrystallized because of its low solubility in various solvents.

BULLETIN OF THE CHEMICAL SOCIETY OF JAPAN, VOL. 46, 670—671 (1973)

Studies on Nitro Sugars. IV.[1] The Synthesis of Benzyl 2-Deoxy-3,4-*O*-isopropylidene-2-nitro-β-D-arabino- and ribo-pyranoside

Tetsuyoshi TAKAMOTO, Minoru OHKI*, Rokuro SUDOH, and Toshio NAKAGAWA*

Department of Chemistry, Tokyo Institute of Technology, O-okayama, Meguro-ku, Tokyo 152

(Received August 10, 1972)

Recently, we reported the syntheses of 3- and 2-nitro furanoses[1-3] through the oxidation of sugar oximes with trifluoroperacetic acid. As an extension of our studies to the pyranose series, we have now examined the oxidation of the 2-oximino-pentopyranoside derivative to the corresponding 2-nitro compound by this method.

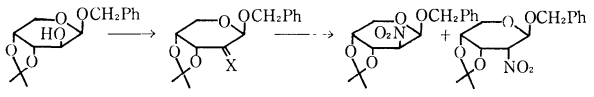

1 **2**: X=O, **3**: X=NOH **4** **5**

The dimethyl sulfoxide oxidation[4] of benzyl 3,4-*O*-isopropylidene-β-D-arabinopyranoside (**1**),[5] followed by distillation at 155—157°C/3 mmHg, afforded sirupy 2-ulose (**2**), showing 1756 cm^{-1} (neat); this was immediately converted to benzyl 3,4-*O*-isopropylidene-2-oximino-β-D-*erythro*-pentopyranoside (**3**) in the usual manner in a 27% overall yield from **1**. When **3** was treated with trifluoroperacetic acid in the presence of excess dibasic sodium phosphate as a buffer in acetonitrile, the corresponding 2-nito-pentoses, which consisted of benzyl 2-deoxy-3,4-*O*-isopropylidene-2-nitro-β-D-arabinopyranoside (**4**) and its 2-epimer (**5**) in the ratio of *ca.* 1: 1, were obtained in a 75% yield. The separation of both the products, according to the small difference in chromatographical mobility, could

* Department of Chemistry, Yokohama City University, Mutsuura-cho, Kanazawa-ku, Yokohama 236.

1) Part III; T. Takamoto, Y. Yokota, R. Sudoh, and T. Nakagawa, This Bulletin, in press.

2) T. Takamoto, R. Sudoh, Lnd T. Nakagawa, *Tetrahedron Lett.*, **1971**, 2053.

3) T. Takamoto, R. Sudoh, and T. Nakagawa, *Carbohyd. Res.*, in press.

4) J. S. Brimacombe, *Angew. Chem.*, **81**, 415 (1969).

5) H. G. Fletcher Jr., "Methods in Carbohydrate Chemistry," Vol. II, ed. by R. L. Whistler and M. L. Wolfrom, Academic Press, New York (1963), p. 386.

be achieved by using a long silica-gel column.

As is shown in Fig. 1, what was eluted later was identified as the *arabino*-isomer (**4**) on the basis of the coupling constant values, $J_{1,2}=3.7$, $J_{2,3}=8$, and $J_{3,4}=6$ Hz, which would mean a slightly twisted 1C conformation. On the other hand, the first-eluted component, *i.e.*, the *ribo*-isomer (**5**), showed $J_{1,2}=7$, $J_{2,3}=3$, and $J_{3,4}=7$ Hz, which would mean a twisted boat form, as is shown in Fig. 2.

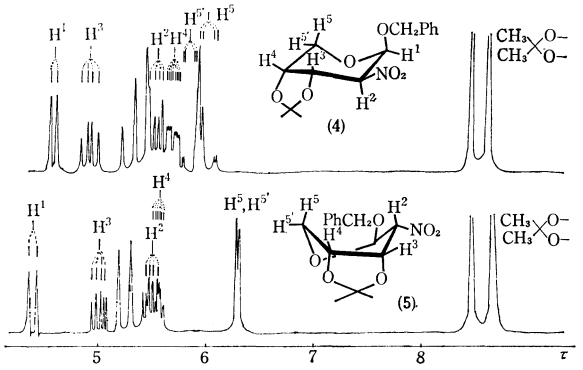

Fig. 1. 100 MHz NMR spectra (in $CDCl_3$).

As an explanation of the stereochemically-interesting results, it appears that an equatorially-oriented nitro group might be effective, but any detailed discussion must await further investigations concerning nitro sugars.

Experimental

The specific rotations were measured with a Carl Zeiss photoelectric polarimeter. The NMR spectra were recorded at 100 MHz with a spectrometer JNM-4H-100 (JEOL), using tetramethylsilane as the internal standard. Column chromatography was carried out on silica gel (100 Mesh, Mallinckrodt, St. Louis). All the evaporations were performed *in vacuo*.

*Benzyl 3,4-O-Isopropylidene-2-oximino-β-*D-erythro-*pentopyranoside (3).* To a solution of benzyl 3,4-*O*-isopropylidene β-D-arabinopyranoside (**1**) (58.6 g) in dimethyl sulfoxide (680 ml), acetic anhydride (452 ml) was added with manual stirring. After standing for 48 hr at room temperature, the mixture was evaporated below 60°C. A solution of the residue in chloroform (1 l) was washed with water four times, dried over calcium chloride, and evaporated. The sirup was distilled at 155—157°C/3 mmHg to give 2-ulose (**2**) contaminated with the starting material (**1**). The distilled sirup (43.8 g), showing an absorption band at 1756 cm^{-1} (C=O), was heated under reflux with hydroxylamine hydrochloride (21.9 g) in a mixture of pyridine (438 ml) and ethanol (438 ml) for 2 hr. The solution was evaporated to give a sirupy residue containing pyridine hydrochloride, which was then washed out with water several times. The sirup was crystallized and recrystallized from ethanol–petroleum ether to give crystalline **3** (16.7 g, 27%); mp 161.5—163.5°C (uncorrected); $[\alpha]_D^{20}$ −232° (*c* 1.02, $CHCl_3$); IR (KBr): 3320 cm^{-1} (OH). Found: C, 61.22; H, 6.27; N, 4.87%. Calcd for $C_{15}H_{19}NO_5$: C, 61.42; H, 6.53; N, 4.78%.

*Benzyl 2-Deoxy-3,4-O-isopropylidene-2-nitro-β-*D-*arabino-(4) and ribopyranoside (5).* Oxime **3** (100 mg) was stirred into an oxidizing agent, prepared by mixing successively 90% hydrogen peroxide (0.05 ml), trifluoroacetic anhydride (0.3 ml), acetonitrile (5 ml), dibasic sodium phosphate (1.15 g), and urea (5 mg), at room temperature. After 2 hr, the mixture was evaporated, then, the residue was dissolved in methylene chloride (100 ml). After it had been filtered, the solution was evaporated and chromatographed on silica gel with benzene to give a sirupy product (79 mg, 75%), which was subsequently rechromatographed on a silica-gel column (14×2.5 cm) developed slowly with benzene. The eluate was collected in 20 ml portions. Fractions No. 9—12 were combined and evaporated to give **5**, which was too hydroscopic and low-melting to be recrystallized; $[\alpha]_D^{20}$ −121° (*c* 1, $CHCl_3$); IR (neat): 1560 cm^{-1} (NO_2); NMR ($CDCl_3$): τ 4.39 (1H-*d*, $J_{1,2}=7$ Hz, H^1), 5.50 (1H-*q*, $J_{2,3}=3.5$ Hz, H^2), 5.01 (1H-*q*, $J_{3,4}=6.5$ Hz, H^3), 5.56 (1H-*sex*, $J_{4,5}=3.5$ Hz, H^4), 6.32 (2H-*d*, H^5, $H^{5'}$). Found: C, 58.21; H, 6.26; N, 4.45%. Calcd for $C_{15}H_{19}NO_6$: C, 58.24; H, 6.19; N, 4.53%.

The evaporation of Fractions No. 20—25 afforded sirupy **4**; $[\alpha]_D^{20}$ −200° (*c* 1, $CHCl_3$); IR (neat): 1560 cm^{-1} (NO_2); NMR ($CDCl_3$): τ 4.61 (1H-*d*, $J_{1,2}=3.7$ Hz, H^1), 5.55 (1H-*q*, $J_{2,3}=8$ Hz, H^2), 4.95 (1H-*q*, $J_{3,4}=6$ Hz, H^3), 5.71 (1H-*oct*, $J_{4,5}=2.5$ Hz, $J_{4,5'}=1.2$ Hz, H^4), 6.04 (1H-*q*, $J_{5,5'}=13.8$ Hz, H^5), 5.87 (1H-*q*, $H^{5'}$). Found: C, 58.20; H, 6.21; N, 4.40%

BULLETIN OF THE CHEMICAL SOCIETY OF JAPAN, VOL. 46, 672—673 (1973)

The Absolute Configulation of Dimethyl (−)-*erythro*-2-Ethyl-3-methylglutarate

Shosuke Ito and Yoshimasa Hirata

Department of Chemistry, Faculty of Science, Nagoya University, Chikusa-ku, Nagoya

(Received August 21, 1972)

In the course of the structure elucidation of a new antibiotic, ikarugamycin, dimethyl (−)-2-ethyl-3-methylglutarate, $[\alpha]_D^{25}$ −8.6° (*c* 0.64, $CHCl_3$), was obtained as an oxidation product of ikarugamycin.[2)]

The two diastereomeric forms of 2-ethyl-3-methylglutaric acid (IIa and IIIa) have been prepared by Michael and Moss,[3)] but their stereochemistry has yet been determined distinctly. On the other hand, the absolute configuration of 2-ethyl-3-methylsuccinic acid has recently been determined by Brockmann and Müller-Enoch.[4)] Therefore, (+)-*erythro*-2-ethyl-3-methylsuccinic acid (Ia), whose absolute configuration had been proved to be 2*R*, 3*S*,[4)] was converted into optically-active dimethyl *erythro*-2-ethyl-3-methylglutarate (IIb) and dimethyl *erythro*-3-ethyl-2-methylglutarate (IV) as follows:

The *cis*-anhydride derived from Ia by the known method[5)] was heated with methanol to give a mixture of monocarboxy-monomethyl esters. It was homologized by successive treatment with oxalyl chloride, diazomethane, and then silver oxide in methanol. The resulting mixture consisted of three esters, Ib, IIb, and IV, which could be separated by preparative glc.

The structures of (−)-IIb, $[\alpha]_D^{25}$ −14.9°, and IV, $[\alpha]_D^{25}$ +46.3°, were determined on the basis of the following NMR and mass spectral evidence: The NMR spectrum of IIb shows two C-methyl signals in a relatively high field (δ 0.89 and 0.93), and its mass spectrum exhibits a peak due to McLafferty rearrangement at *m/e* 102. These facts indicate the presence of the CH_3–CH_2–CH–COOMe group. On the other hand, the presence of the CH_3–CH–COOMe group in IV is confirmed by the appearance of a C-methyl doublet at δ 1.07 and a peak due to McLafferty rearrangement at *m/e* 88.

The optically-active dicarboxylic acid IIa could not be crystallized, but it formed a crystalline dicyclohexylamine salt. To obtain further proofs for the IIb structure, racemic IIb and IIIb were prepared as authentic samples. A mixture of synthetic IIa and IIIa was converted into a mixture of anhydrides, which could be separated by preparative glc. The hydrolysis of the anhydrides gave (±)-IIa, mp 97—98°C, and (±)-IIIa, mp 99—100°C, respectively. The latter could also be obtained by repeated recrystallizations of the crude mixture of dicarboxylic acids.

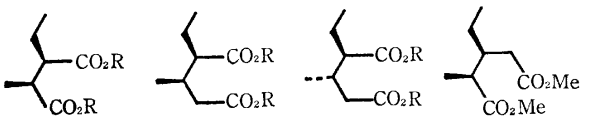

Ia: R=H Ib: R=Me IIa: R=H IIb: R=Me IIIa: R=H IIIb: R=Me IV

The IR spectra of the naturally-derived ester, the optically-active synthetic ester ((−)-IIb), and the racemic ester ((±)-IIb) were superimposable on one another. Thus, the absolute configuration of dimethyl (−)-*erythro*-2-ethyl-3-methylglutarate ((−)-IIb) was determined to be 2*R*, 3*R*.

Experimental

All the melting points are uncorrected. The IR spectra were recorded on a JASCO IR-S spectrometer. The NMR spectra were recorded on a Nihondenshi JNM-C60H spectrometer, using TMS as the internal reference. The mass spectra were measured on a Hitachi RMU-6D mass spectrometer operating with an ionization energy of 70 eV. The optical rotations were measured on a JASCO ORD/UV-5 spectrometer and a JASCO DIP-SL spectrometer. The glc were carred out on a Varian Aerograph 1828-4 instrument.

*Syntheses of Dimethyl (−)-*erythro*-2-ethyl-3-methylglutarate (IIb) and Dimethyl (+)-*erythro*-3-ethyl-2-methylglutarate (IV).* (+)-*erythro*-2-Ethyl-3-methylsuccinic acid (Ia)[6)] (290 mg) was converted into the *cis*-anhydride (255 mg) by the known method.[5)] A solution of the anhydride in methanol (5 ml) was refluxed for 4 hr, and then concentrated to give a mixture of half methyl esters ($\nu_{max}^{CCl_4}$ 1748, 1711 cm^{-1}); the NMR spectrum of this mixture showed it to consist of two isomers in the ratio of *ca.* 2:1. Into a solution of the half methyl esters in benzene (2 ml), oxalyl chloride (2 ml) was stirred in one portion at 0°C; the mixture was then stirred at the same temperature for 1 hr and at room temperature for 5 hr. The subsequent concentration of the mixture under reduced pressure gave crude acid chlorides (330 mg), which were then dissolved in benzene (5 ml). Into an ethereal diazomethane (30 ml), the solution was vigorously stirred, drop by drop, at −10°C over a period of 0.5 hr; the mixture was then stirred at −10—0°C for 0.5 hr and at room temperature for 5 hr. The excess diazomethane and the solvent were removed under reduced pressure to give crude diazoketones ($\nu_{xeu}^{CCl_4}$ 2130, 1742, 1649 cm^{-1}). A mixture of the diazoketones and silver oxide (freshly-prepared from 0.2 g of silver nitrate) in methanol (30 ml) was refluxed for 2 hr with stirring. The mixture was then treated with charcoal, filtered through celite, and washed with methanol. The filtrates were concentrated under reduced pressure to give a mixture (215 mg) of dimethyl esters, which was roughly separated by column chromatography on silica gel (10 g) with

1) A part of this work was preliminarily reported in Ref. 2b.

2) a) S. Ito and Y. Hirata, *Tetrahedron Lett.*, **1972**, 1185. b) S. Ito and Y. Hirata, *ibid.*, **1972**, 2557.

3) A. Michael and J. Moss, *J. Amer. Chem. Soc.*, **53**, 1150 (1931).

4) H. Brockmann, Jr. and D. Müller-Enoch, *Chem. Ber.*, **104**, 3704 (1971).

5) J. H. Golden and R. P. Linstead, *J. Chem. Soc.*, **1958**, 1732.

6) $[\alpha]_D^{25}$ +8.6° (*c* 2.5, EtOH); mp 179°C (lit,[4)] $[\alpha]_D^{20}$ +8.6° (*c* 2.5, EtOH); mp 180°C).

n-hexane–ether (9: 1) as the eluent. Further purification by repeated preparative glc (10% OV-17 column at 160°C) gave pure (+)-Ib (12 mg), (−)-IIb (35 mg), and (+)-IV (17 mg) as colorless oils. (+)-Ib: $[\alpha]_D^{25}$ +9.7° (*c* 1.0, $CHCl_3$). (−)-IIb: $[\alpha]_D^{25}$ −14.9° (*c* 1.13, $CHCl_3$); δ^{CCl_4} 0.89 (3H, d, J=6.8), 0.93 (3H, d, 6.3), 1.1—2.7 (6H, m), 3.61 (3H, s), 3.62 (3H, s); *m/e* 171 (M^+–OMe), 142, 129, 102, 101 (base peak), 87, 74. (+)-IV: $[\alpha]_D^{25}$ +46.3° (*c* 0.81, $CHCl_3$); δ^{CCl_4} 0.92 (3H, t, J=6.5), 1.07 (3H, d, 7.2), 1.1—1.6 (3H, m), 1.9—2.8 (3H, m), 3.61 (3H, s), 3.62 (3H, s); *m/e* 171 (M^+–OMe), 142, 129, 115, 88 (base peak), 73.

Dicyclohexylamine Salt of (−)-IIa. A solution of (−)-IIb (17 mg) in methanol (0.3 ml) was treated with 10% aqueous potassium hydroxide (0.3 ml) at 50°C for 2 hr. Working up as usual afforded 13 mg of (−)-IIa as an oil which could not be crystallized. Crude crystals of dicyclohexylamine salt of (−)-IIa were recrystallized from ethyl acetate–*n*-hexane to give 13 mg of needles; $[\alpha]_D^{25}$ −16.7° (*c* 0.72, MeOH). It showed no distinct melting point; mp *ca.* 103—108°C. Found: C, 67.59; H, 10.80; N, 3.94%. Calcd for $C_8H_{14}O_4C_{12}H_{23}N$: C, 67.57; H, 10.49; N, 3.94%.

Preparation of (±)-erythro-(IIa) and (±)-threo-2-ethyl-3-methylglutaric acid (IIIa). A mixture of (±)-IIa and (±)-IIIa was prepared according to the procedure of Snyder and Putnan.[7] A mixture of the acids (100 mg) and acetic anhydride (2 ml) was refluxed for 4 hr, and then concentrated under reduced pressure to give 80 mg of a mixture of *trans*- and *cis*-anhydrides. Separation with preparative glc (5% OV-17 column at 160°C) afforded 42 mg of *trans*-anhydride (93% pure) as an earlier fraction and 20 mg of *cis*-anhydride (80% pure) as a later fraction.

trans-Anhydride: $\nu_{max}^{CCl_4}$ 1821, 1772 cm^{-1}; δ^{CCl_4} 0.98 (3H, t, J=7.2), 1.13 (3H, d, 6.0).

cis-Anhydride: $\nu_{max}^{CCl_4}$ 1821, 1773 cm^{-1}; δ^{CCl_4} 0.98 (3H, d, J=6.0), 1.04 (3H, t, 6.6).

Each anhydride was hydrolysed by refluxing it in tetrahydrofuran–water (2: 1) for 2 hr; this gave crude acids. Several recrystallizations from ether–*n*-hexane gave pure (±)-IIIa (37 mg) and (±)-IIa (10 mg) as prisms respectively. The pure (±)-IIIa was also obtained by repeated recrystallization of a mixture of (±)-IIa and IIIa from ether–*n*-hexane.

(±)-IIIa: mp 99—100°C (lit, mp 100—101°C[3]). The dimethyl ester ((±)-IIIb): δ^{CCl_4} 0.89 (3H, t, J=6.8), 0.95 (3H, d, 6.8), 1.1—2.6 (6H, m), 3.62 (3H, s), 3.64 (3H, s).

(±)-IIa: mp 97—98°C (lit, 88°C[3]). The NMR and IR spectra of its dimethyl ester ((±)-IIb) were identical with those of the natural and synthetic (−)-IIb.

7) H. R. Snyder and R. E. Putnan, *J. Amer. Chem. Soc.*, **76**, 33 (1954).

BULLETIN OF THE CHEMICAL SOCIETY OF JAPAN, VOL. 46, 673—674 (1973)

The Reaction of 7-Methylenebicyclo[3.3.1]nonan-3-one and Bicyclo-[3.3.1]nonane-3,7-dione with Several Nucleophiles[1)]

Ryohei YAMAGUCHI, Kwan Her YANG, and Mituyosi KAWANISI

Department of Industrial Chemistry, Faculty of Engineering, Kyoto University, Yoshida, Kyoto 606

(Received August 14, 1972)

In connection with the current interest in bicyclo-[3.3.1]nonane system,[2-4)] we had occasion to examine the behavior of some nucleophiles towards 7-methylene-bicyclo[3.3.1]nonan-3-one (Ia) as well as bicyclo[3.3.1]-nonane-3,7-dione (Ib), reactions of which led to some novel products.

In the following reactions, transannular cyclization took place giving *adamantane* derivatives. In the reaction of Ia with aniline, Schiff's base (Ic) was not formed, but 3-phenylaminoadamantan-1-ol (IIa) was obtained as the sole isolable product in a 90% yield.

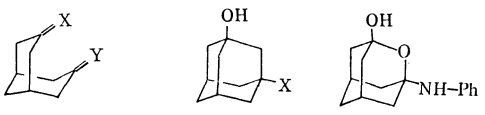

I II III

a: X=O; Y=CH_2
b: X=Y=O
c: X=Ph-N; Y=CH_2
d: X=Y=Ph-N
e: X=O; Y=Ph-N

a: X=Ph-NH
b: X=Ph-NMe
c: X=Ph-O
d: X=Ph-S

By the similar treatment of Ia with *N*-methylaniline, 3-*N*-methylphenylaminoadamantan-1-ol (IIb) was obtained in a 56% yield. The Eschweiler-Clarke methylation[5)] of IIa afforded IIb; thus, a structural correlation between IIa and IIb was established. *N,N*-Dimethylaniline did not react with Ia under the reaction conditions. With phenol, Ia afforded 3-phenyloxy-adamantan-1-ol (IIb) in a 38% yield, with thiophenol 3-phenylthioadamantan-1-ol (IId) in a 53% yield. The structures of these compounds were all supported by the spectral data. The transannular reaction described herein did not take place without molecular sieves. Stetter has pointed out that Ia cyclizes under acid

1) Part of this work was presented at the 24th Annual Meeting of the Chemical Society of Japan, Osaka, April, 1971.

2) For pertinent references, see G. Buchanan, "Topics in Carbocyclic Chemistry," D. Lloyd, ed., Vol. 1, Logos Press, London, p. 236; H. Kato, *J. Synth. Org. Chem. Japan*, **28**, 682 (1970).

3) a) H. Stetter, J. Gartner, and P. Tacke, *Chem. Ber.*, **98**, 3888 (1965), b) H. Stetter and J. Gartner, *Chem. Ber.*, **99**, 925 (1966), c) H. Stetter, J. Gartner, and P. Tacke, *Chem. Ber.*, **99**, 1435 (1969), d) A. R. Gagneux and R. Meier, *Tetrahedron Lett.*, **1969**, 1365, e) K. Kimoto and M. Kawanisi, *Chem. Ind.* (London) **1971**, 1174.

4) a) T. Mori, K. Kimoto, M. Kawanisi, and H. Nozaki, *Tetrahedron Lett.*, **1969**, 3653, b) A. G. Yurchenko, A. T. Voroschenko, and F. N. Stepanov, *Zh. Org. Khim.*, **6**, 189, (1970). T. Mori, K. H. Yang, K. Kimoto, and H. Nozaki, *Tetrahedron Lett.*, **1970**, 2419.

5) M. L. Moore, *Org. React.*, **5**, 301 (1949).

catalysis,[3d] and in the present case the molecular sieves probably act as an acidic catalyst.[6]

In the reaction of Ib with aniline, an *oxaadamantane* derivative, 3-phenylamino-2-oxaadamantan-1-ol (III), was formed as a labile product in a 28% yield. The structure of III was supported by its spectral data. The prolonged heating of Ib under the same conditions produced another product (Id) at the expense of III; this was confirmed by following the progress of the reaction by means of glc. We also observed that III was converted into Id by the reaction with aniline in the presence of molecular sieves. These observations suggest that III, a metastable hemiacetal, is dehydrated by the action of molecular sieves into an intermediate such as Ie, which subsequently condenses with aniline to give Id.

In the similar reaction of Ib with *o*-phenylenediamine, an intriguing cyclization took place to give IV, an *azaadamantane* derivative, in an 81% yield as a considerably unstable compound. The structure of IV could be assigned on the basis of the physical data. The NMR spectra, however, were not reproducible because of the instability of IV in solution. The formation of IV can be tentatively explained by the following scheme:

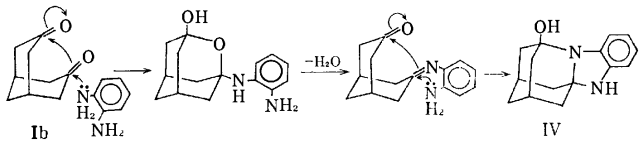

Experimental

All the melting points are uncorrected. The microanalyses were performed by Mrs. Kiyoko Fujimoto. The IR spectra were obtained on a Shimadzu IR-27 spectrophotometer. The mass spectra were taken using a Hitachi RMS-4 mass spectrometer. The NMR spectra were obtained on a JEOL C-60-H spectrometer in a $CDCl_3$ solution, with TMS as the internal standard.

Reagents. 7-Methylenebicyclo[3.3.1]nonan-3-one (Ia)[3d] and bicyclo[3.3.1]nonan-3,7-dione (Ib)[4b] were prepared according to the reported methods. The aniline, *N*-methylaniline, phenol, thiophenol, and *o*-phenylenediamine were of commercial reagent grade. The molecular sieves was of Type 3A.

Preparation IIa. A mixture of Ia (0.9 g), aniline (0.69 g), and molecular sieves (2 g) in benzene (20 ml) was refluxed for 26 hr, and then the molecular sieves were removed by filtration. The evaporation of the solvent yielded 1.69 g of a brown oil which gradually solidified. Recrystallization from benzene gave 1.43 g (90%) of pure IIa; mp 115—118°C. Found: C, 78.87; H, 8.64; N, 5.92%. Calcd for $C_{16}H_{21}NO$: C, 78.97; H, 8.70; N, 5.76%. IR (KBr): 3300, 3280, 2920, 1600, 1495, 1320, 1125, 1050, 910, 770, 740, 695 cm^{-1}. NMR: δ 1.33—1.93 (m, 12H), 2.27 (br. s, 2H), 2.73 (s, 2H), 6.67—7.33 (m, 5H). MS: *m/e* 243 (M^+), 93 (M^+—150: 100%).

Preparation of IIb. A mixture of Ia (0.9 g) *N*-methylaniline (0.65 g), and molecular sieves (2 g) in benzene (20 ml) was treated similarly; a subsequent work-up as described above gave a white solid (0.86 g; 56%). Recrystallization from petroleum ether (bp 40—60°C) yielded pure IIb; mp 114.5—116.5°C. Found: C, 79.08; H, 8.85; N, 5.45%. Calcd for $C_{17}H_{23}NO$: C, 79.33; H, 9.01; N, 5.44%. IR (KBr): 3240, 2920, 1595, 1490, 1445, 1305, 1260, 1100, 1010, 940, 800, 770, 695 cm^{-1}. NMR: δ 1.35—1.70 (m, 12H), 2.25 (br. s, 3H), 2.76 (s, 3H), 7.27 (s, 5H). MS: *m/e* 257 (M^+), 107 (M^+—150; 100%).

Methylation of IIa. A mixture of IIa (12 mg), formaldehyde (37%; 2 ml), and formic acid (99%; 1.5 ml) was heated under reflux for 24 hr. The base liberated by the addition of potassium hydroxide was extracted with ether and chloroform. The extracts were combined and dried (Na_2SO_4). Evaporation left a white solid, the sublimation of which gave pure IIb (58 mg; 88%); mp 115—117°C.

Reaction Ia with Phenol and Thiophenol. The similar reaction of Ia with phenol and with thiophenol afforded IIc (38%) and IId (53%) respectively. Analytical samples were obtained by preparative glc. The physical data of IIc and IId are as follows.

IIc; IR (KBr): 3370, 2950, 1595, 1495, 1115, 1030, 1010, 995, 675 cm^{-1}. NMR: δ 1.27—2.50 (m, 15H), 6.83—7.43 (m, 5H). MS: *m/e* 244 (M^+), 94 (M^+—150; 100%). mp 94—96°C. Found: C, 77.54; H, 8.27%. Calcd for $C_{16}H_{20}O_2$: C, 77.65; H, 8.25%. IId; IR (KBr): 3300, 2920, 1470, 1350, 1100, 1090, 975, 935, 750, 690 cm^{-1}. NMR: δ 1.43—1.90 (m, 12H), 2.03 (s, 1H), 2.23 (br. s, 2H), 7.40 (br. s, 5H). MS: *m/e* 260 (M^+), 151 (M^+—109; 100%). mp 131—133°C. Found: C, 73.67; H, 7.53%. Calcd for $C_{16}H_{20}OS$: C, 73.80; H, 7.74%.

Preparation of III. A mixture of Ib (618 mg), aniline (1.6 g), and molecular sieves (10 g) in benzene (15 ml) was refluxed for 6 hr. The usual work-up yielded a brown oil which solidified afterward. Recrystallizations from benzene gave a white solid (280 mg; 28%). This compound is exceedingly unstable and did not give satisfactory analysis. Mp 81.5—82.5°C. IR (KBr): 3300, 3260, 1605, 1500, 1340, 1190, 1155, 970, 930, 885, 745, 695, 680 cm^{-1}. NMR: δ 1.96—2.95 (m, 12H), 3.44 (s, 2H), 6.55—7.42 (m, 5H). MS: *m/e* 227 (M^+—18), 152 (M^+—93), 95 (M^+—150). The reaction of III and aniline in the presence of molecular sieves in benzene was effected similarly; the formation of Id described below was confirmed by glc.

Preparation of Id. A mixture of Ib (2 g), aniline (3.7 g), and molecular sieves (50 g) in benzene (30 ml) was refluxed for 28 hr. The usual work-up gave a brown oil, which immediately solidified. The solid was washed with ether and recrystallized from benzene, thus yielding pure Id (2 g; 51%); mp 190—191°C. Found: C, 83.28; H, 7.52; N, 9.11%. Calcd for $C_{21}H_{22}N_2$: C, 83.40; H, 7.33; N, 9.26%. IR (KBr): 3060, 2950, 1660, 1595, 1490, 1245, 1185, 1070, 905, 830, 785, 705 cm^{-1}. NMR: δ 1.80—2.85 (m, 14H), 6.70—7.45 (m, 10H). MS: *m/e* 302 (M^+), 170 (M^+ 132), 77 (M^+—225; 100%).

Preparation of IV. A mixture of Ib (110 mg), *o*-phenylenediamine (80 mg), and molecular sieves (2 g) in benzene (3 ml) was refluxed for 2 hr; the catalysts were then removed by filtration while the solution was hot. On cooling, colorless needles were obtained; these were collected by filtration and washed with chilled benzene. The azaadamantane derivative (IV) (141 mg; 81%) was obtained after drying *in vacuo*; mp 191—193.5°C (in nitrogen-sealed tube). Found: C, 74.67; H, 7.73; N, 11.46%. Calcd for $C_{15}H_{18}N_2O$: C, 74.35; H, 7.49; N, 11.56%. IR (KBr): 3390, 3290, 2930, 1594, 1489, 1295, 1145, 1085, 730 cm^{-1}. MS: *m/e* 242 (M^+), 132 (M^+—110; 100%).

6) For catalysis by molecular sieves in enamine formation, see K. Taguchi and F. H. Westheimer, *J. Org. Chem.*, **36**, 1570 (1971).

BULLETIN OF THE CHEMICAL SOCIETY OF JAPAN, VOL. 46, 675—677 (1973)

N-Isopropylidene- and *N-sec*-Butylideneanilines. I. Preparation and Characterization

Michiko TSUCHIMOTO, Shigeo NISHIMURA, and Hiizu IWAMURA*

Department of Industrial Chemistry, Tokyo University of Agriculture and Technology, Koganei, Tokyo

**Department of Chemistry, Faculty of Science, The University of Tokyo, Hongo, Tokyo*

(Received March 27, 1972)

In marked contrast to the chemistry of *N*-benzylideneanilines,[1] little is known of the ketimines from lower aliphatic ketones and aromatic amines because of the difficulty in preparing pure samples.[2] Recently some ketimines have been prepared from acetone and amines using a molecular sieve as dehydrating agent.[3]

In this paper we report syntheses of twenty-one new ketimines of acetone and ethyl methyl ketone with various anilines by means of a method using a molecular sieve as dehydrating agent. The course of the reaction was effectively monitored by the NMR spectra of the aliquots. It was found important to run the reaction at temperatures not higher than room temperature. Under these conditions, undesirable side reactions were minimized. The structure of the ketimines was confirmed by elemental analyses and IR and NMR spectra (Tables 1 and 2).

All the acetone anils showed two characteristic peaks due to the methyl groups in the NMR spectra as summarized in Table 2. Those from *p*-substituted anilines gave a symmetric NMR pattern characteristic of AA'XX' spin system for ring protons, showing the correct structure for ketimines. This also indicated that, while nitrogen inversion is sufficiently slow to give distinction between methyl groups *syn* and *anti* to the aromatic ring, the rotation around the *N*-Ar bond is fast relative to the time scale of the chemical shifts; otherwise the aromatic protons should give an ABXY pattern.

The assumption that the methyl group *syn* to the aromatic ring is the one with the resonance at higher field was verified by a study of the paramagnetic shifts induced by the addition of tris(dipivalomethanato)-europium(III) ($Eu(DPM)_3$). It was always the methyl signal at lower applied field which underwent a larger paramagnetic shift.

TABLE 1. CHARACTERISTICS OF *N*-ISOPROPYLIDENE- AND *N-sec*-BUTYLIDENEANILINES

X in 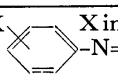	Bp or Mp, °C(mmHg)	IR $\nu_{C=N}$ (cm^{-1})	n_D^{25}	Yield (%)	Carbon, %		Hydrogen, %		Nitrogen, %	
					Calcd	Found	Calcd	Found	Calcd	Found
p-OH	mp 169—171[a]	1654		65	72.50	72.62	7.43	7.62	9.34	9.30
p-OCH_3	bp 95—97 (5)	1663	1.5426	66	73.59	73.32	8.03	8.25	8.58	8.40
m-OCH_3	bp 74—75 (10)	1663	1.5436	46	73.59	73.65	8.03	8.18	8.58	8.64
o-OCH_3	bp 60—62 (10)	1663	1.5478	52	73.59	73.35	8.03	8.25	8.58	8.82
p-NH_2	mp 107—108	1658		32	72.94	70.65	8.16	7.89	18.90	18.69
p-CH_3	bp 74—76 (5)	1663	1.5321	56	81.58	81.87	8.90	9.00	9.51	9.27
m-CH_3	bp 62—66 (5)	1663	1.5373	42	81.58	81.36	8.90	9.20	9.51	9.57
o-CH_3	bp 60—63 (5)	1663	1.5294	48	81.58	81.85	8.90	8.74	9.51	9.30
p-C_2H_5	bp 82—86 (5)	1663	1.5286	40	81.94	81.92	9.38	9.38	8.69	8.42
H	bp 66—67 (8)			69						
p-Cl[b]	bp 82—84 (5)	1663	1.5605	46	64.48	64.38	6.01	5.73	8.36	8.26
p-Br[c]	bp 98—102 (5)	1663	1.5824	47	50.97	50.70	4.75	4.79	6.60	6.83
p-$COOCH_3$	bp 110—118 (6)	1663	1.5560	47	69.09	68.80	6.85	6.66	7.33	7.30
p-$COCH_3$	bp 125—127 (4)	1670	1.5691	56	75.40	75.38	7.48	7.22	7.99	8.06
p-NO_2	bp 117—120 (8)	1663	1.5995	35	60.66	60.90	5.66	5.67	15.72	15.62
p-$N{=}C(CH_3)_2$	mp 128—130	1650		59	76.55	76.29	8.57	8.28	14.88	15.02
X in 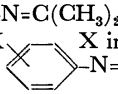										
p-OCH_3	bp 102—105 (6)	1660	1.5350	53	74.54	74.25	8.53	8.23	7.90	8.03
m-OCH_3	bp 107—110 (5)	1663	1.5372	52	74.54	74.35	8.53	8.62	7.90	8.12
o-OCH_3	bp 94—98 (5)	1663	1.5438	51	74.54	74.29	8.53	8.33	7.90	8.16
p-CH_3	bp 82—88 (5)	1660	1.5254	45	81.94	81.89	9.38	9.33	8.69	8.42
m-CH_3	bp 81—86 (5)	1663	1.5273	47	81.94	81.96	9.38	9.37	8.69	8.81
o-CH_3	bp 72—75 (5)	1665	1.5213	55	81.94	81.74	9.38	9.55	8.69	8.61
p-Cl[d]	bp 64—67 (4)	1660	1.5466	44	66.16	65.81	6.66	6.72	7.71	7.60

a) Reported mp 172—174°; A. Michaelis, *et al.*, *Ber.*, **27**, 3006 (1894). b) Cl: Found, 21.15% (Calcd, 21.19%). c) Br: Found, 37.80% (Calcd, 37.68%). d) Cl: Found, 19.52% (Calcd, 19.52%).

1) R. W. Layer, *Chem. Rev.*, **63**, 489 (1963).

2) P. A. S. Smith, "The Chemistry of Open-Chain Organic Nitrogen Compounds," Vol. 1, W. A. Benjamin, Inc., New York, Amsterdam (1965), p. 94, and the papers cited therein.

3) E. P. Kyba, *Org. Prep. Proced.*, **2**, 149 (1970).

TABLE 2. NMR DATA FOR *N*-ISOPROPYLIDENE- AND *N*-*sec*-BUTYLIDENEANILINES (δ values, ppm)

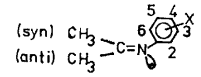

X	CH_3 (*anti*)	CH_3 (*syn*)	Rign proton			Other protons	
			2, (6)	3, (5)	4		
p-OH[a]	2.07	1.82	6.45	6.61		-OH	8.99
p-OCH_3[b]	2.15	1.82	6.68	6.78		-OCH_3	3.77
m-OCH_3	2.17	1.80	6.25	7.15	6.57	-OCH_3	3.77
o-OCH_3	2.22	1.75	6.7	6.9		-OCH_3	3.77
p-NH_2	2.11	1.80	6.50			-NH_2	3.33
p-CH_3[b]	2.15	1.77	6.63	7.05		-CH_3	2.32
m-CH_3	2.16	1.80	6.55	7.10	6.90	-CH_3	2.30
o-CH_3	2.22	1.70	6.57	7.10	6.92	-CH_3	2.03
p-C_2H_5	2.18	1.78	6.67	7.07		-CH_2 2.63	-CH_3 1.23
H[b]	2.15	1.77	6.70	7.31	7.07		
	(2.08[c])	(1.68[c])					
	(2.04[d])	(1.67[d])					
p-Cl[b]	2.15	1.78	6.63	7.20			
p-Br	2.15	1.78	6.62	7.32			
p-$COOCH_3$	2.19	1.80	6.75	7.97		-$COOCH_3$	3.90
p-$COCH_3$	2.19	1.82	6.77	7.90		-$COCH_3$	2.57
p-NO_2[a]	2.20	1.82	6.78	8.15			
p-N=$C(CH_3)_2$	2.13	1.82	6.63				

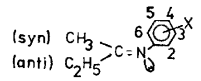

X	Proportional of *syn*-methyl isomer (%)	-CH_3		-CH_2-CH_3		-CH_2-CH_3		Ring proton			Other protons	
		anti	*syn*	*anti*	*syn*	*anti*	*syn*	2, (6)	3, (5)	4		
p-OCH_3	81.5	2.12	1.78	2.42	2.17	1.18	1.00	6.63	6.80		-OCH_3	3.77
m-OCH_3	81.8	2.12	1.77	2.40	2.17	1.18	0.92	6.25	7.17	6.53	-OCH_3	3.77
o-OCH_3	84.2	2.18	1.68	2.47	2.18	1.20	1.00	6.75	6.95		-OCH_3	3.75
p-CH_3	79.1	2.12	1.75	2.40	2.17	1.18	1.05	6.60	7.05		-CH_3	2.30
m-CH_3	80.9	2.12	1.77	2.38	2.15	1.18	1.07	6.52	7.16	6.84	-CH_3	2.30
o-CH_3	78.6	2.15	1.67	2.43	2.07	1.20	1.03	6.55	7.10	7.00	-CH_3	2.03
p-Cl	81.8	2.12	1.72	2.40	2.12	1.17	1.00	6.63	7.20			

a) 0.25 mmol/0.5ml D-DMSO b) Koga *et al.* previously reported NMR data of some *N*-isopropylideneanilines without obtaining the products in pure states; G. Koga, *et al.*, *5th NMR Symposium*, Abstract p. 28, Sendai (1966). c) H. A. Staab, *et al.*, *Tetrahedron Lett.*, **1965**, 697. d) D. Y. Curtin, *et al.*, *J. Amer. Chem. Soc.*, **88**, 2775 (1966).

The NMR spectra of *N*-*sec*-butylideneanilines are composed of two sets of peaks, one always about 4 times stronger than the other. From numerical comparison of the chemical shifts with those of *N*-isopropylidene derivatives and also from a shift reagent study, it is concluded that the presence of the *E* form is more prevalent than that of the *Z* isomer.

Experimental

Preparation. According to the standard procedure for the synthesis of *N*-isopropylideneaniline, 30 g of molecular sieve 4A (18—20 mesh, Gasukuro Kogyo Co., Ltd.) was added to a solution of 0.1 mol of acetone and 0.05 mol of aniline in anhydrous ether. The mixture was kept at 10°C for 24 hr. About 30% of the starting aniline was still found to remain unchanged. In order to complete the reaction, it was advisable to renew the molecular sieve at this stage of the reaction. It took about 48 hr to attain more than 95% completion of the reaction (the reaction was followed by observing the lower field signals of 3,5 ring protons by NMR spectra with 0.5 ml of aliquots). The reaction of *p*-chloro- and *p*-bromoaniline was sluggish and took 9 to 10 days to practically reach completion. *p*-Nitroaniline reacted exceedingly slowly under these conditions, only 50% conversion being attained after 10 days. It took 25 days to get more than 95% conversion by renewing the molecular sieve 4 times. After removing the molecular sieve by filtration and the solvent on a rotary evaporator, the residue was fractionally distilled, great care being taken to exclude moisture throughout the operation. The anils with the electronegative ring substituents are less stable, a slight decomposition being noted during the course of distillation. *N*-Isopropylidene-*p*-aminophenol was prepared by letting the solution of *p*-aminophenol in warm acetone to stand for about 15 min at room temperature, without using the molecular sieve. Mono acetone anil of *p*-phenylenediamine was prepared from the equimolar diamine and acetone, while the diacetone anil was obtained with the use of excess acetone. These anils were obtained as crystals and purified by recrystallization from ether–DMSO (20: 1).

N-sec-Butylideneanilines were similarly prepared by the reaction of ethyl methyl ketone with aromatic amines.

Nuclear Magnetic Resonance Spectra. NMR spectra were obtained on a JEOL C-60 HL (Japan Electron Optics Lab. Co., Ltd.) (60 MHz), with an internally-locked field-frequency stabilization control system. The samples (0.25 mmol) were dissolved in 0.5 ml of $CDCl_3$ and the chemical shifts were read relative to TMS as an internal reference at 25°C by an electronic-frequency counter in Hz. $Eu(DPM)_3$ was added to the above $CDCl_3$ solutions when required. The shift values for the ring protons (Table II) were obtained by a first order approximation from their peaks.

The authors wish to thank Mr. Shozo Masuda and members of his group, The University of Tokyo, for the elemental analyses.

BULLETIN OF THE CHEMICAL SOCIETY OF JAPAN, VOL. 46, 677—678 (1973)

Reactions of Hydrazinium Thiocyanate with Aldehydes and Ketones

Isamu ARAI, Shintaro ABE, and Akira HAGITANI

Department of Chemistry, College of Science, St. Paul's University (Rikkyo Daigaku), Nishi-Ikebukuro, Toshima-ku, Tokyo

(Received September 4, 1972)

In a previous paper,[1] we reported on the reactions of hydrazinium thiocyanate (I) with alcohols to give 1,2,4-triazolidine-5-thione derivatives (II). These reaction mechanisms were not clear but the structure of II suggested that II can also be prepared from the reactions of I with aldehydes and ketones. Sunner[2] and Futaki and Tosa[3] studied these reactions and obtained triazolo-triazole derivatives III, but they did not isolate II. We have reinvestigated these reactions and have found that fairly large quantity of II is obtained together with III. Formation of II is easily overlooked because II is not stable to heat, light and moisture, and readily hydrolyzes or decomposes by ring opening. In this paper, we report on preparation of II and its structure.

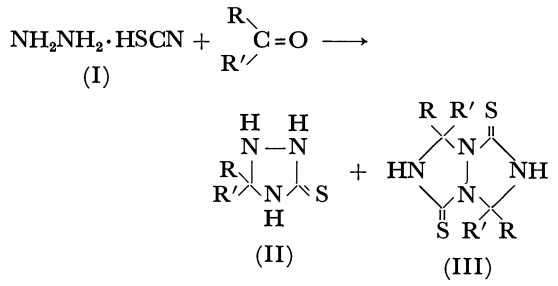

When an aqueous solution of (I) and acetaldehyde was allowed to stand at room temperature, white needles (IIa), mp 122°C (decomp.), were obtained together with 1,5-dimethyl-*s*-triazolidino [1,2-*a*]-*s*-triazolidine-3,7-dithione (triazolo-triazole compound (IIIa)[4]). The elemental analysis (Table 2) and MS spectral data of (IIa) gave a molecular formula $C_3H_7N_3S$. The IR spectrum showed absorption bands for NH, CH_3, and C=S groups; and the NMR spectrum indicated the presence of ethylidene group at τ 8.61 (3H, d, J=6.0 Hz) and 5.00 (1H, q, J=6.0 Hz). Thermolysis of IIa gave acetaldehyde thiosemicarbazone (IVa) and oxidation gave 3-methyl-5-mercapto-1,2,4-triazole (Va).

The following structure was deduced for IIa.

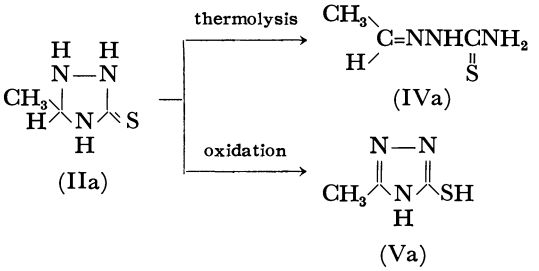

The mass spectrum also supported this structure *viz.*, it showed ions at *m/e* 117 (M), 116 (M−1), and 102 (M−15). The ion of *m/e* 58 generated by the loss of HSCN from the molecular ion indicated the presence of an –NH·CS– group in the molecule.

Other aldehydes and ketones were also treated with I to give 1,2,4-triazolidine-5-thione derivatives (II) in considerable yields (Table 1).

TABLE 1. REACTIONS OF HYDRAZINIUM THIOCYANATE (I) WITH ALDEHYDES AND KETONES[a]

Aldehyde	Yield (%) of II	Ketone	Yield (%) of II
CH_3CHO	34.36	CH_3COCH_3	6.85
C_2H_5CHO	40.76	$C_2H_5COCH_3$	26.62
n-C_3H_7CHO	32.21	*n*-$C_3H_7COCH_3$	49.28
		$C_2H_5COC_2H_5$	56.18
		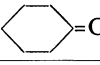	72.18

a) Water (ketone) or 50% aqueous methanol (aldehyde) was used as reaction solvent.

We considered that the 1,2,4-triazolidine-5-thione derivatives (II) was produced by the cycloaddition of thiocyanic acid to the hydrazones formed from aldehydes and ketones with hydrazine.

1) I. Arai, Y. Satoh, I. Muramatu, and A. Hagitani, This Bulletin, **42**, 2739 (1969).

2) S. Sunner, *Svensk Kem. Tidskr.*, **64**, 121 (1952).

3) K. Futaki and N. Tosa, *Chem. Pharm. Bull.*, (Tokyo), **6**, 58 (1958).

4) J. R. Bailey and A. T. McPherson, *J. Amer. Chem. Soc.*, **39**, 1322 (1917).

Table 2. 1,2,4-Triazolidine-5-thione 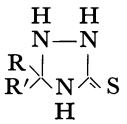 (II)

II	R	R′	Mp (°C) (decomp.)	Formula	Analysis (%) Calcd C	H	N	S	Found C	H	N	S
II a	CH_3	H	122	$C_3H_7N_3S$	30.75	6.03	35.86	27.36	30.75	6.42	35.29	—
II b	C_2H_5	H	110	$C_4H_9N_3S$	36.62	6.91	32.03	24.44	36.72	6.85	31.57	—
II c	n-C_3H_7	H	118	$C_5H_{11}N_3S$	41.36	7.64	28.93	22.08	41.50	7.46	28.36	—
II d	CH_3	CH_3	105	$C_4H_9N_3S$	36.62	6.91	32.03	24.44	36.63	6.84	32.08	—
II e	C_2H_5	CH_3	116	$C_5H_{11}N_3S$	41.36	7.64	28.93	22.08	41.00	7.60	29.40	21.60
II f	n-C_3H_7	CH_3	119	$C_6H_{13}N_3S$	45.26	8.23	26.39	20.13	45.64	7.53	26.55	20.09
II g	C_2H_5	C_2H_5	124	$C_6H_{13}N_3S$	45.26	8.23	26.39	20.13	44.92	7.80	26.54	20.32
II h			144	$C_7H_{15}N_3S$	49.09	7.65	24.54	18.72	49.45	7.38	24.18	18.86

Experimental

All melting points are uncorrected. The IR spectra were recorded from KBr pellets using a Shimadzu model IR-27B infrared spectrometer, and the NMR spectra were measured in a solution of deuteriomethanol with a Varian A-60 spectrometer. The mass spectra were obtained on a CEC 21-110B spectrometer at 70 eV.

Reaction of Hydrazinium Thiocyanate (I) with Acetaldehyde. Freshly prepared acetaldehyde (4.41 g, 0.1 mol) was added dropwise to a cooled solution of hydrazine monohydrochloride (6.85 g, 0.1 mol) and sodium thiocyanate (8.10 g, 0.1 mol) in 50% aqueous methanol (100 ml) with stirring. The solution was then stirred at room temperature for 24 hr under shield from light. The white precipitate (2.03 g) was filtered and recrystallized from methanol to give 1,5-dimethyl-*s*-triazolidino [1,2-*a*]-*s*-triazolidine-3,7-dithione (IIIa), mp 169°C (decomp.), (lit,[2] 168°C (decomp.)). The filtrate was evaporated to dryness under reduced pressure and the residue was extracted with methylene chloride. This extract was evaporated and the residue (3.87 g) gave 3-methyl-1,2,4-triazolidine-5-thione (IIa), mp 122°C (decomp.), from chloroform.

IR of (IIa): 3175, 2975, 2850, 1510, 1465, 1405, 1375, 1210, 1070, 945, 885 cm^{-1}.

MS of (IIa): *m/e* 117 ($C_3H_7N_3S^+$), 116 ($C_3H_6N_3S^+$), 115 ($C_3H_5N_3S^+$), 102 ($C_2H_4N_3S^+$), 101 ($C_2H_3N_3S^+$), 58 ($C_2H_6N_2^+$).

Thermolysis of 3-Methyl-1,2,4-triazolidine-5-thione (IIa). A solution of 0.5 g of (IIa) in 2-butanol (25 ml) was refluxed for 3 hr and then evaporated. The residue (0.5 g) was recrystallized from ethanol to give acetaldehyde thiosemicarbazone (IVa), mp 140°C, (lit,[5] mp 140°C).

Oxidation of 3-Methyl-1,2,4-triazolidine-5-thione (IIa). Oxygen was passed into a solution of one gram of (IIa) in 1N sodium hydroxide (50 ml) for 5 hr with stirring at room temperature. The solution was then acidified with 1N hydrochloric acid and concentrated under reduced presure. The white precipitate (0.64 g) was filtered and recrystallized from water to give 3-methyl-5-mercapto-1,2,4-triazole (Va), mp 270°C, identified by comparison (mixed mp and IR spectra) with an authentic sample.[6]

5) L. K. Evans and A. E. Gillam, *J. Chem. Soc.*, **1943**, 565.

6) R. G. Jones and Anisworth, *J. Amer. Chem. Soc.*, **77**, 1538 (1955).

BULLETIN OF THE CHEMICAL SOCIETY OF JAPAN, VOL. 46, 679—680 (1973)

Kinetic Studies of the Acid-catalyzed Amination of *p*-Nitrosoanisole with Anilines in Methanol

Yoshiaki FURUYA and Katsumi TERAOKA

Department of Industrial Chemistry, Faculty of Engineering, Kumamoto University, Kumamoto

(Received November 4, 1971)

The allelotrope of *p*-nitrosophenol[1] and/or another keto-enol tautomers[2,3] are easily etherified with an alcohol in the presence of inorganic acid, even at room temperature. Furthermore, the methoxy group of the methyl ether of the allelotrope, *p*-nitrosoanisole, can readily be replaced by an electro-negative atom with an unshared electron pair, such as the N-atom of amines. Thus, *p*-nitrosodiphenylamines are obtained by the title reaction in a favorable yield.[4]

In the present paper, we should like to propose a new reaction mechanism, though a mechanism has previously been speculated on the basis of the synthetic data.[4]

Experimental

Materials. The *p*-nitrosoanisole (abbreviated as PNA) was prepared by the reaction of the allelotrope of *p*-nitrosophenol (abbreviated as PNP) with methanol in the presence of sulfuric acid.[5] The blue crystals obtained by subsequent steam distillation were recrystallized twice from petroleum ether; yield, 50%; mp 23°C (lit, 23°C[6]). The product was kept at 0°C in a dark place for safe storage. Commercial *p*-nitrosodiphenylamine (abbreviated as PNDA) was recrystallized three times from benzene; mp 143—145°C (lit, 143°C,[7] 144—145°C[4]). The *p*-nitroso-*p'*- or -*m'*-substituted diphenylamines were prepared by the acid-catalyzed amination of *p*-nitrosoanisole with the corresponding *p*- or *m*-substituted anilines and were recrystallized from benzene and/or methanol; *p*-nitroso-*p'*-methoxydiphenylamine, mp 163—165°C (lit, 164—166°C[4]); *p*-nitroso-*p'*-methyldiphenylamine, mp 172—173°C (lit, 172—173°C[4]); *p*-nitroso-*p'*-chlorodiphenylamine, mp 158—159°C (lit, 157—160°C[4]); *p*-nitroso-*m'*-chlorodiphenylamine,[8] mp 148.5—149.5°C. Found: C, 62.04; H, 3.93; N, 12.05%. Calcd for $C_{12}H_9ClN_2O$: C, 61.95; H, 3.93; N, 12.04%. Commercial aniline, *p*-toluidine, *m*-chloroaniline, and *p*-chloroaniline were distilled twice under reduced pressure; aniline, bp 83°C/23 mmHg; *p*-toluidine, bp 95—95.5°C/22 mmHg; *m*-chloroaniline, bp 114—114.5°C/20 mmHg; *p*-chloroaniline, bp 115—116°C/21 mmHg. The *p*-anisidine was recrystallized from water and methanol–water; mp 58°C. Methanol as a medium was rectified; bp 65—65.5°C. The methanolic solution of hydrogen chloride was prepared by bubbling hydrogen chloride well dried with phosphorus pentoxide into the rectified methanol.

Reaction Product Criterion. A mixture (50 ml) of PNA (0.2M), aniline (0.5M), and hydrogen chloride (0.05N) in methanol was kept at 30°C for 11 hr, and then neutralized with methanolic potassium hydroxide. The mixture was filtered after adding water. PNDA was thus obtained; mp and mmp 143—145°C; yield 90%.

Ultraviolet Spectrophotometry and Chemical Analysis. The conversion percentages were calculated from the calibration curve which has been prepared by plotting the difference in extinction at 260, 290, and 340 nm, $(E_{260}-E_{340})$ *vs.* $(E_{290}-E_{340})$, and at 0 and 100% conversions. The difference between the conversion percentage obtained from the curve and that obtained from the composition of the mixture was within 1% at each attempted conversion percentage.

A Typical Run for the Rate Measurements. A two ml portion of methanolic solution of 1M PNA was poured into 8 ml of a methanolic solution containing 0.625M aniline and 0.0625N hydrogen chloride in order to start the reaction after both the solutions had attained the temperature equilibrium at 30°C. Aliquots (0.1 ml, each) were taken out at appropriate intervals of time and then diluted with methanol to a 4×10^{-5}M total concentration of PNA and PNDA. The conversion percentage was calculated graphically.

Results and Discussion

When the reaction product, PNDA, was kept at 30°C for 48 hr in methanol containing 0.01N hydrogen chloride, a slight side reaction tends to occur,[9] but the reverse reaction does not take place at all. There-

Table 1. The rate data for the acid-catalyzed amination of *p*-nitrosoanisole with aniline in the presence of 0.05 N hydrogen chloride in methanol

$[PNA]_0$ M	$[Aniline]_0$ M	Temp. °C	$k_{2obs}\times10^4$ $M^{-1}sec^{-1}$
0.2	0.2	30	4.81
0.2	0.3	30	4.88
0.2	0.4	30	4.82
0.2	0.5	30	4.85
0.2	0.6	30	4.80
0.1	0.5	30	4.80
0.3	0.5	30	4.85
0.4	0.5	30	4.89
0.2	0.5	20	3.12
0.2	0.5	25	3.79
0.2	0.5	35	6.16

E_a, 8.69 kcal mol^{-1} ΔS^*, −47.01 e.u.

1) Y. Furuya, I. Urasaki, K. Itoho, and A. Takashima, This Bulletin, **42**, 1922 (1969).

2) Y. Furuya, I. Urasaki, K. Itoho, and S. Miyazaki, *ibid.*, **42**, 1769 (1969).

3) Y. Furuya, K. Itoho, and K. Mori, Presented at the 21st Symposium of the Organic Reaction Mechanisms, Hiroshima, October, 1970.

4) J. T. Hays, H. L. Young, and H. H. Espy, *J. Org. Chem.*, **32**, 158 (1967).

5) See, for example, Y. Furuya, and R. Oda, *Kogyo Kagaku Zasshi*, **65**, 214 (1962).

6) A. Rising, *Ber.*, **37**, 44 (1904).

7) O. Fischer and E. Hepp, *Ber.*, **19**, 2991 (1886).

8) *m*-Chloroaniline was detected paper chromatographically in an ethereal solution extracted from an alkaline hydrolyzed mixture of this compound.

9) It is considered that azophenine is formed after a prolonged reaction; O. Fischer and E. Hepp, *Ber.*, **20**, 2479 (1887); **21**, 679, 2617 (1888).

fore, the amination reaction follows the irreversible second-order rate equation with PNA and aniline:

$$v = k_{2obs}[PNA][Aniline] \quad (1)$$

The rate was affected by the acidity. The plots of k_{2obs} *vs.* the square root of the concentration of hydrogen chloride gave a straight line passing through the point of origin, as is shown in Fig. 1. Therefore, the rate constant, k_{2obs}, may be expressed as follows:

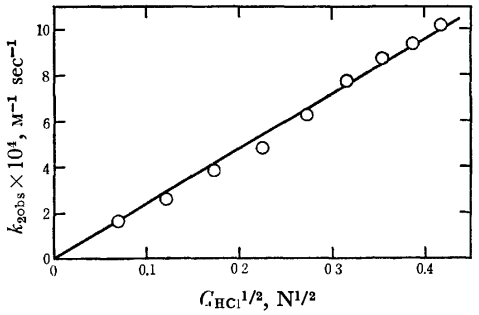

Fig. 1. The plot of k_{2obs} *vs.* square root of the concentration of hydrogen chloride in methanol for the amination of PNA with aniline at 30°C.
Initial concen. of PNA: 0.2M, Initial concen. of aniline: 0.5M

$$k_{2obs} = k_2 C_{HCl}^{1/2} \quad (2)$$

Here, $C_{HCl}^{1/2}$ is expressed as:

$$C_{HCl}^{1/2} = C_{H^+}/K^{1/2} \quad (3)$$

where K is the dissociation constant of hydrogen chloride in methanol. Therefore, the following relationship is obtained:

$$k_{2obs} = k_2 K^{-1/2} C_{H^+} \quad (4)$$

The pK_{BH^+} values of aniline, methanol, and the allelotrope of PNP in water are 4.6,[10] −2.5,[11] and −3.4,[1] respectively. As the σ_p value of the hydroxyl group (−0.357) is smaller than that of the methoxy group (−0.268), the pK_{BH^+} value of PNA may be smaller than that of the allelotrope of PNP. Thus, the order of ease for the protonation may be expressed as: aniline≫methanol>PNA. In other words, the protonated aniline exists in the medium predominantly.

On the other hand, the reaction was accelerated by the introduction of an electron-releasing group into the phenyl group of aniline, and retarded by the introduction of an electron-attracting group, as is shown in Table 2 and Fig. 2. The plot of the logarithm of the rate constant ratio, $\log k_2/k_{20}$, against Deno's σ^+ gives a straight line with a slope of −0.95 (r=0.994), as is

Table 2. Substituent effect of the hydrogen chloride-catalyzed amination of PNA with anilines in methanol at 25°C
Concn. of HCl: 0.05 N

Anilines	Deno's σ^+	$k_{2obs} \times 10^4$ M^{-1}sec^{-1}
p-Anisidine	−0.64	16.95
p-Toluidine	−0.27	8.50
Aniline	0	3.79
p-Chloroaniline	+0.08	3.27
m-Chloroaniline	+0.373	2.09

10) S. Patai, "The Chemistry of the Amino Group," Interscience Publishers, New York (1968), p. 182.
11) N. C. Deno and J. O. Turner, *J. Org. Chem.*, **31**, 1969 (1966).

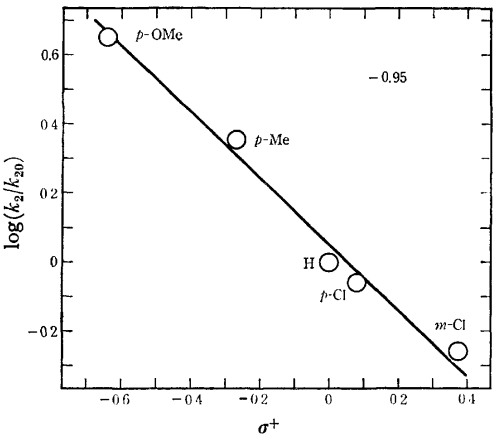

Fig. 2. Hammett plots for the acid-catalyzed amination of PNA with anilines at 25°C.
Concen. of HCl: 0.05N.

shown in Fig. 2.[12] These results suggest the participation of the anilinium ion in the formation of transition state of this reaction.

Moreover, the value of the activation entropy of the reaction (−47.01 e.u.) is much smaller than that in the ordinary protonation. Therefore, the transition state having a hydrogen-bonding annular construction of the protonated aniline, PNA, and a solvent molecule such as is illustrated below might be involved.[13] The over-all rate may be controlled by this step.

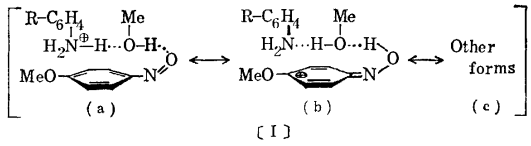

[I]

It is considered that the contribution of the Ib structure may be important because of the increase in the stability of the positive charge by diffusion into the benzene ring of PNA; hence, the nucleophilic attack of the N-atom of aniline on the positive C-atom of Ib may occur predominantly in the following step.

From these findings and considerations, a probable mechanism may be charted as below:

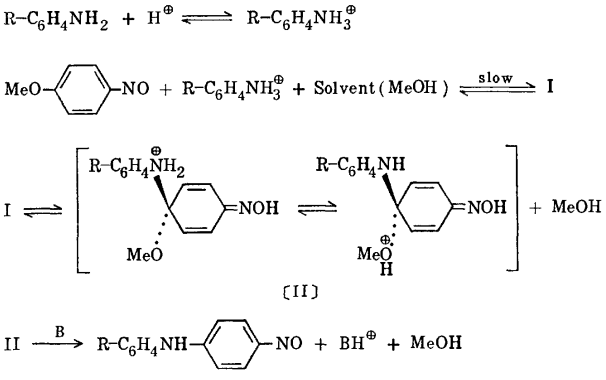

[II]

12) If the direct nucleophilic attack of aniline on the protonated PNA[4] occurs, σ values should be used in Hammett plot of this reaction.
13) See, for example, L. M. Litvimenko, D. M. Aleksandrova, and N. I. Pilyuk, *Ukrain. Khim. Zhur.*, **25**, 81 (1959); *Chem. Abstr.*, **53**, 21782i (1959).

BULLETIN OF THE CHEMICAL SOCIETY OF JAPAN, VOL. 46, 681—682 (1973)

^{18}O Tracer Studies of Catalytic Oxidations of Olefin over Transition Metal or Metal Oxide Catalysts. II. Oxidation of Propylene to Acrolein over Pd-Carbon Catalyst

Yoshihiko MORO-OKA, Tomohisa OHHATA, Yusaku TAKITA, and Atsumu OZAKI

Research Laboratory of Resources Utilization, Tokyo Institute of Technology, Ohokayama, Meguro-ku, Tokyo

(Received June 27, 1972)

In the first paper of this series, we reported a new type oxygen incorporation where oxygen atom in water molecule is incorporated into the oxidized products, *i.e.*,

$$A(olefin) + 1/2O_2 + H_2O^* \rightarrow AO^* + H_2O \quad (1)$$

We demonstrated by use of $H_2{}^{18}O$ tracer that the oxidation of propylene to acetone over SnO_2-MoO_3 catalyst follows Eq. (1) and called it oxyhydration.[1,2] Further study has been carried out to find new oxyhydrations. The route of oxygen incorporation was examined using $H_2{}^{18}O$ tracer in the catalytic oxidation of propylene to acrolein over Pd-carbon catalyst which was independently found by Fujimoto *et al.*[3] and by Seiyama *et al.*[4].

Experimental

Pd-carbon catalyst was prepared from activated charcoal and palladium chloride.[3] 10—20 mesh activated charcoal was boiled for 5 hr in dilute nitric acid solution and then washed with water until pH of the filtrate become higher than 4. This was impregnated with palladium chloride dissolved in 0.5 N HCl solution and allowed to stand for 24 hr. Palladium chloride supported on the activated charcoal (5 wt% $PdCl_2$) was reduced to metallic palladium by hydrogen gas at 250°C for 5 hr and activated by air at 230°C for 12 hr.

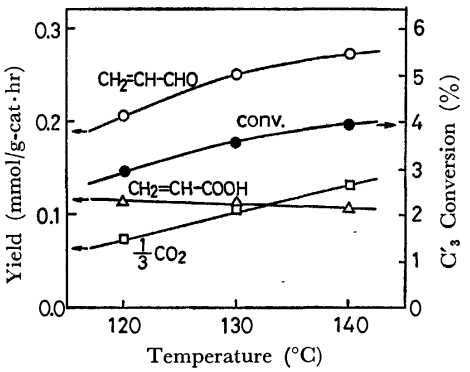

Fig. 1. One pass conversion of propylene and yields of oxidized products in the oxidation of propylene over Pd-carbon catalyst.

All the runs were carried out using a conventional flow system at atmospheric pressure. The reactor was a Pyrex tube of 8 mm diameter. The exit gases were cooled by water to separate gaseous and liquid phases, and analyzed by gas chromatography and mass spectrometry.

The ^{18}O content of the oxidized products was determined by mass spectrometry after separation and purification by gas chromatography. The mass spectra obtained at 80 V of ionization voltage were corrected for natural abundances, no isotope effect being assumed for the ionization efficiency. The ^{18}O content of acrolein was calculated from the peak height ratio, h_{58}/h_{56}, in the corrected mass spectra. The ^{18}O content of the unreacted oxygen was determined by mass spectrometry after it was converted into carbon dioxide by the reaction with the stoichiometric amount of carbon monoxide using a closed circulating reaction system and Pt-asbestos catalyst.

Results and Discussion

Propylene was oxidized at 120—140°C over Pd-carbon catalyst. 1.9 g of the catalyst was used in the fixed catalyst bed. The flow rates of each reactant gas were 10.0, 8.0, and 27.6 ml-STP/min for propylene, oxygen and water, respectively, GHSV being 530 ml-STP/ml-cat hr.

The activity of Pd-carbon catalyst and selectivity for each product changed gradually during the first few hours. They became constant after 10 hr and did not change any more in the subsequent runs. The main products were acrolein, acrylic acid, and carbon dioxide.[3] Although small amounts of acetone and acetaldehyde were produced, their total yield did not exceed 10% of the converted propylene. The values of one pass conversion of propylene and the yields of the main products at three different temperatures are shown in Fig. 1. The selectivity to acrolein was 50—55% of the converted propylene.

Tracer experiment was carried out at 130°C. Propylene was oxidized over Pd-carbon catalyst under the same conditions as mentioned above except that water in the reactant gas was replaced by water enriched with $H_2{}^{18}O$. The results are summarized in Table 1.

The values in the third column of Table 1 give ^{18}O content of the acrolein produced in the presence of 5.48% $H_2{}^{18}O$. In every run, ^{18}O tracer is found in acrolein with reasonably high concentrations. Thus, it is clear that the oxygen atom comes mostly from the water molecule. This suggests that acrolein is produced by an interaction between propylene and some active species derived from water on Pd-carbon cata-

1) Y. Moro-oka, Y. Takita, and A. Ozaki, *J. Catal.*, **27**, 177 (1972).

2) Y. Moro-oka, Y. Takita, and A. Ozaki, This Bulletin, **24**, 293 (1971).

3) K. Fujimoto, H. Yoshino, and T. Kunugi, 4th Oxidation Symposium (Tokyo), p. 111, (1970).

4) T. Seiyama, M. Aramaki, N. Takeyama, and N. Yamazoe, *Kogyo Kagaku Zasshi*, **74**, 672 (1971); T. Seiyama, N. Yamazoe, J. Hojo, and M. Hayakawa, *J. Catal.*, **24**, 173 (1972).

lyst. However, another possibility should be examined, *i.e.*, the incorporation of ^{18}O into the oxidized product results from the following exchange reactions.

$$^{16}O_2 + H_2{}^{18}O \rightleftharpoons {}^{16}O{}^{18}O + H_2{}^{16}O \quad (2)$$

$$CH_2{=}CH{-}CH^{16}O + H_2{}^{18}O \rightleftharpoons CH_2{=}CH{-}CH^{18}O + H_2{}^{16}O \quad (3)$$

These oxygen exchange reactions were also examined using $H_2{}^{18}O$ tracer. The ^{18}O contents of the unreacted oxygen are listed in the last column of Table 1. They suggest that a slight oxygen exchange reaction takes place between molecular oxygen and water under the conditions adopted in the runs. However, the values are too low to explain the ^{18}O contents found in the acrolein produced. Thus, the possibility that ^{18}O in the acrolein was incorporated from the $^{16}O{}^{18}O$ molecule formed by the exchange reaction as expressed in Eq. (2) can be rejected.

Table 1. ^{18}O content of the product in the oxidation of propylene to acrolein over Pd-carbon catalyst[a)]

Reaction	^{18}O content (atomic %)	
	$CH_2{=}CH{-}CHO$	O_2 (unreacted)
Oxidation	3.62	0.20
	4.36	0.22
	3.41	0.14
Exchange[b)]	0.75	—
	1.13	—

a) ^{18}O content of the reactant water is 5.48%.
b) Oxygen exchange reaction between acrolein and water.

Another oxygen exchange reaction between acrolein and water was examined using $H_2{}^{18}O$ tracer. The reaction conditions were the same as adopted in the oxidation runs, except that propylene in the reactant gas was replaced by nitrogen. The contact time of acrolein and its concentration in the reactant gas were adjusted to those produced in the oxidation runs. The results are shown in Table 1. Although some exchange reaction was observed under the conditions, the rate of exchange reaction was smaller than that of oxidation. The ^{18}O contents found in the produced acrolein are not attributable to the exchange reaction as given by Eq. (3). It seems reasonable that acrolein is produced by direct interaction between some active species of propylene and water, and that the oxidation of propylene on Pd-carbon catalyst is at least partly an oxyhydration.

Although the incorporation of ^{18}O into acrolein seems to be due to some direct interaction between the active species of propylene and water, ^{18}O content found in the acrolein was somewhat lower than that of water in the reaction system. The ^{18}O content of the issuing water was not determined because of inaccuracy of the mass spectrometry of water. However, since the conversion of propylene was lower than 4%, the ^{18}O content of the issuing water calculated on the mass balance of ^{18}O is higher than 5.30%. This indicates that the incorporation of oxygen into the acrolein also involves some active species originating from molecular oxygen as well as water. One possible explanation is that the oxidation to form acrolein involves a hydroxyl group which is formed by a reaction between atomic oxygen and propylene or some intermediate derived from propylene. If this is the case, the hydroxyl group formed on the catalyst surface would be indistinguishable from the active species of water, and the oxidation to form acrolein might be a sort of chain reaction.

A number of transition metal oxide catalysts have been developed for the oxidation of propylene to acrolein. Keulks[5)] and Wragg *et al.*[6)] have proved by using ^{18}O tracer that the oxygen ion in the oxide catalyst is incorporated into the oxidized acrolein over MoO_3-Bi_2O_3 catalyst. Our results demonstrate that the mechanism of the oxidation of propylene to acrolein over Pd-carbon catalyst differs from that of the oxidation of propylene to acrolein over the transition metal oxide catalyst such as MoO_3-Bi_2O_3 and strongly supports the mechanism proposed by Fujimoto *et al.*[3)] and Seiyama *et al.*[4)] They found that the rate of oxidation of propylene to form acrolein depends on the partial pressure of water,[3)] and estimated the following mechanism for this oxidation.

$$CH_2{=}CH{-}CH_3 \xrightarrow[-H]{} CH_2{=}CH{=}CH_2 \quad (4)$$

$$CH_2{=}C{=}HCH_2 \xrightarrow[+OH]{} CH_2{=}CH{-}CH_2OH \quad (5)$$

$$CH_2{=}CH{-}CH_2OH \xrightarrow[-2H]{} CH_2{=}CH{-}CHO \quad (6)$$

A hydrogen atom in methyl group of propylene is abstracted on the catalyst surface to form an allylic intermediate. Some active species of water such as hydroxyl group attacks one of the terminal carbon atoms of this intermediate to form allyl alcohol which is easily oxidized to acrolein.

The authors wish to thank Dr. K. Fujimoto and members of Prof. Kunugi's laboratory of the University of Tokyo for many useful suggestions.

5) G. W. Keulks, *J. Catal.*, **17**, 232 (1970).
6) R. D. Wragg, P. G. Ashmore, and J. A. Hockey, *ibid.*, **22**, 49 (1971).

BULLETIN OF THE CHEMICAL SOCIETY OF JAPAN, VOL. 46, 683—684 (1973)

The Phase Transitions of the Anion Radical Salts of $[(C_6H_5)_3PCH_3]_{1-x}^+$ $[(C_6H_5)_3AsCH_3]_x^+$ $(TCNQ)_2^-$, $(0 \leq x \leq 1)$, as Studied by the ESR Measurements

Yukio SUZUKI and Yôichi IIDA

Department of Chemistry, Faculty of Science, Hokkaido University, Sapporo

(Received August 28, 1972)

The prominent magnetic, electrical, and optical properties of the solid anion radical salts of 7,7,8,8-tetracyanoquinodimethane (TCNQ) have been the subject of many theoretical and experimental investigations over the past several years.[1-11] In particular, the anion radical salts containing the mixed cations represented by $[(C_6H_5)_3PCH_3]_{1-x}^+$ $[(C_6H_5)_3AsCH_3]_x^+$ $(TCNQ)_2^-$, $(0 \leq x \leq 1)$, show electron spin resonance (ESR) spectra characteristic of a triplet exciton state lying close to a singlet ground state.[1,3,11]

The salt of $[(C_6H_5)_3PCH_3]^+(TCNQ)^-$, $(x=0.00)$, undergoes a first-order phase transition at 315.7 K, where we earlier found anomalies in the temperature dependences of the ESR absorption and the electrical conductivity,[6,9] while the salt of $[(C_6H_5)_3AsCH_3]^+$ $(TCNQ)_2^-$, $(x=1.00)$, does not undergo such a phase transition.[5,8,10] The phase transitions of the anion radical salts containing the mixed cations have been studied, as a function of the composition parameter, by means of a differential scanning calorimeter (DSC) and by observing the anomalies in the temperature dependences of the magnetic susceptibility and the electrical conductivity.[5,8,10] The purpose of the present paper is to show that the measurements of the ESR absorption and its variation with the temperature are useful for investigating the phase transitions of these mixed crystals.

The six anion radical salts with the compositions of $x=0.00$, 0.20, 0.40, 0.60, 0.80, and 1.00 were prepared according to the method of Melby *et al.*[2] The ESR spectra of single crystals (5 mm × 5 mm × 1 mm) in the temperature range including the transition temperature were measured by means of a JES-ME X-band spectrometer with 100 KHz modulation. The temperature of the specimen was controlled to within ±1°C by its temperature equipment.

The ESR spectra of the triplet excitons in $[(C_6H_5)_3PCH_3]_{1-x}^+[(C_6H_5)_3AsCH_3]_x^+(TCNQ)_2^-$, $(0 \leq x \leq 1)$, have been shown from the anisotropic zero-field splitting at low temperatures.[1,3,11] Until the transition temperature, as the temperature is raised, the doublet components due to the zero-field splitting in the ESR spectra broaden and move together, eventually collapsing into a single line which becomes progressively sharper, while the temperature dependence of the ESR absorption intensity can be understood in terms of an equilibrium between a singlet ground state and a triplet state lying an energy (0.065 eV) above the ground state; this system has been established by Kepler from the temperature dependence of the static magnetic susceptibility.[5] However, striking discontinuities in the temperature dependence of the ESR spectra were found for all the salts except for that with $x=1.00$. At the temperature where the anomaly occurs, the linewidth of the ESR absorption becomes abruptly sharper, while the intensity discontinuously increases, in the higher temperature range. This change was found to be thermally reversible. In the region above this temperature, the linewidth is practically constant, while the intensity gradually decreases, as the temperature is raised.

As an example, the salt of $[(C_6H_5)_3PCH_3]_{0.80}^+$ $[(C_6H_5)_3AsCH_3]_{0.20}^+$ $(TCNQ)_2^-$, $(x=0.20)$, is described in some detail. At 59±1°C where the anomaly occurs, the ESR spectra of a single crystal for an arbitrary orientation were recorded just below and above this temperature, as is shown in Fig. 1. These spectra were obtained with the same spectrometer gain settings. In this salt, the intensity of the ESR absorption increased abruptly by a factor of about 1.2 in the

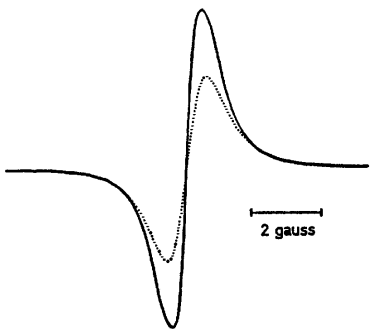

Fig. 1. The ESR spectra of a single crystal of $[(C_6H_5)_3PCH_3]_{0.80}^+[(C_6H_5)_3AsCH_3]_{0.20}^+(TCNQ)_2^-$, $(x=0.20)$, for an arbitrary orientation at 59±1°C, where a discontinuity occurs in the temperature dependence of the ESR absorption. The solid line and the broken line are the ESR spectra recorded just above and below this temperature, respectively, with the same spectrometer gain settings.

1) D. B. Chesnut and W. D. Phillips, *J. Chem. Phys.*, **35**, 1002 (1961).
2) L. R. Melby, R. J. Harder, W. R. Hertler, W. Mahler, R. E. Benson, and W. E. Mochel, *J. Amer. Chem. Soc.*, **84**, 3374 (1962).
3) M. T. Jones and D. B. Chesnut, *J. Chem. Phys.*, **38**, 1311 (1963).
4) W. J. Siemons, P. E. Bierstedt, and R. G. Kepler, *ibid.*, **39**, 3523 (1963).
5) R. G. Kepler, *ibid.*, **39**, 3528 (1963).
6) Y. Iida, M. Kinoshita, M. Sano, and H. Akamatu, This Bulletin, **37**, 428 (1964).
7) Y. Iida, *ibid.*, **42**, 71, 637 (1969).
8) Y. Iida, *ibid.*, **43**, 578 3685 (1970).
9) A. Kosaki, Y. Iida, M. Sorai, H. Suga, and S. Seki, *ibid.*, **43**, 2280 (1970).
10) Y. Iida, *J. Phys. Soc. Jap.*, **30**, 583 (1971); Y. Iida, *J. Chem. Phys.*, in press.
11) Y. Suzuki and Y. Iida, This Bulletin, to be published.

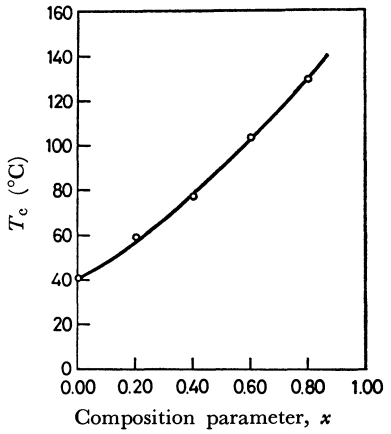

Fig. 2. The relation of the temperature, T_c, where the anomaly occurred in the temperature dependence of the ESR absorption, to the composition parameter, x, in $[(C_6H_5)_3PCH_3]_{1-x}^+[(C_6H_5)_3AsCH_3]_x^+(TCNQ)_2^-$, $(0 \leq x \leq 1)$.

higher-temperature range. Although the linewidth was found to be somewhat anisotropic, for a fixed orientation the linewidth of 1.1_2 gauss in the lower-temperature range abruptly sharpened to 0.8_4 gauss in the higher-temperature range.

In $[(C_6H_5)_3PCH_3]_{1-x}^+[(C_6H_5)_3AsCH_3]_x^+(TCNQ)_2^-$, $(0 \leq x \leq 1)$, the temperature, T_c, at which the anomaly occurred in the ESR spectra shifts progressively to higher temperatures as the value of the composition parameter, x, is increased. The relation of T_c to x was obtained as is illustrated in Fig. 2. This relation was found to be in good accordance with the relation of the phase-transition temperature to the composition parameter, as has been determined previously from the DSC measurements or from the electrical conductivity measurements.[8,10] On the other hand, the magnitude of the discontinuity of the ESR absorption intensity at T_c was found to decrease gradually as the value of x increased. This situation was good agreement with that investigated on the basis of static magnetic susceptibility measurements by Kepler.[5] However, in the salt of $[(C_6H_5)_3AsCH_3]^+$ $(TCNQ)_2^-$, $(x=1.00)$, no discontinuity in the temperature dependence of the ESR absorption was observed up to about 150°C.

At the transition temperature, the increase in the ESR absorption intensity and the decrease in the linewidth in the higher-temperature range can be understood by assuming that the abrupt reduction in the singlet-triplet energy separation is caused by the phase transition in the higher-temperature range.[12] In this case, at the transition temperature the ESR absorption will be markedly intensified in the higher-temperature range because the population of the paramagnetic triplet excitons is abruptly increased by the reduction of the singlet-triplet energy separation. Since the linewidth of the ESR absorption is narrowed by the exchange interaction due to the triplet exciton collisions,[3] the abrupt increase in the exciton population gives rise to a sharper linewidth of the ESR absorption in the higher-temperature range.

In view of these results, the application of the ESR absorption and its variation with the temperature brings valuable knowledge concerning the phase transitions of the $[(C_6H_5)_3PCH_3]_{1-x}^+$ $[(C_6H_5)_3AsCH_3]_x^+$ $(TCNQ)_2^-$, $(0 \leq x \leq 1)$, anion radical salts.

12) Y. Iida, This Bulletin, **46**, 320 (1973).

BULLETIN OF THE CHEMICAL SOCIETY OF JAPAN, VOL. 46, 684—685 (1973)

The Molecular Forms of the Rotational Isomers of Ethylmethylsilane

Michiro HAYASHI, Keiichi OHNO, and Hiromu MURATA

Department of Chemistry, Faculty of Science, Hiroshima University, Higashi-sendamachi, Hiroshima

(Received August 31, 1972)

In a previous note[1] on the rotational isomerism of ethylmethylsilane, the existence of two rotational isomers was reported. However, the molecular forms of the isomers could not be conclusively determined. In the gaseous state, one of the present authors has since found by microwave spectroscopy[2] that one of the isomers was in the *trans* form. However, since the microwave spectra of this substance were too weak for them to be assigned to another isomer, he could not find whether or not one of the isomers was in the *gauche* form.

In the present note, we will consider the unknown molecular form of the isomer, using the vibrational spectra of an asymmetrically-deuterated species of ethylmethylsilane.

Experimental

A sample of an asymmetrically-deuterated species of ethylmethylsilane was prepared by the method of reducing $CH_3CH_2SiCl_2CH_3$ with an equimolar mixture of $LiAlH_4$ and $LiAlD_4$ in *n*-butyl ether.[3] A mixture of $CH_3CH_2SiH_2CH_3$, $CH_3CH_2SiD_2CH_3$, and $CH_3CH_2SiHDCH_3$ was thus obtained and was used for the measurements without further attempts at isolation. In order to find the assignments of the spectra, the corresponding mixture of dimethylsilane and $(CH_3)_2SiH_2$ and $(CH_3)_2SiD_2$ were also prepared from dimethyldichlorosilane by a similar method.

1) M. Hayashi, K. Ohno, and H. Murata, This Bulletin, **45**, 298 (1972).

2) M. Hayashi and C. Matsumura, *ibid.*, **45**, 732 (1972).

3) A. E. Finholt, A. C. Bond, Jr., and H. I. Schlesinger, *J. Amer. Chem. Soc.*, **69**, 1199 (1947).

The infrared spectra in the region from 200 to 4000 cm^{-1} were recorded in the gaseous, liquid, and crystalline states with a Perkin-Elmer instrument (model 621), using the same technique as has been described in the previous note.

Results and Discussion

As is shown in Fig. 1, since the two *gauche* forms come not to be equivalent when one of the hydrogens of the SiH_2 group is replaced by a deuterium, the spectra of the *gauche* isomer are expected to be split into doublets, while the spectra of the *trans* isomer are singlets, without regard to the asymmetrical deuteration.

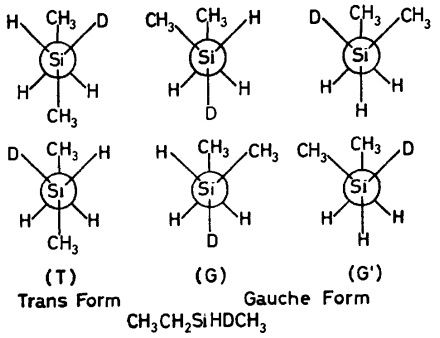

Fig. 1. Rotational isomers of $CH_3CH_2SiHDCH_3$.

In Fig. 2, the observed infrared spectra in the region from 300 to 600 cm^{-1} are shown for the mixture of $CH_3CH_2SiH_2CH_3$, $CH_3CH_2SiD_2CH_3$, and $CH_3CH_2SiHDCH_3$ species, where the solid and the dotted lines indicate the spectra in the liquid and in the crystalline states respectively. Since the pure sample of $CH_3CH_2SiHDCH_3$ can not be prepared at present, the spectra for this species must be found from the spectra of the mixture. For this purpose, the spectra in the liquid state for the corresponding species of dimethylsilane are considered as suitable references; they are also shown in Fig. 2.

The rocking mode of the SiH_2 group is expected around 480 cm^{-1}, which is probably well localized from the other modes; it is expected to be shifted to the region around 390 cm^{-1} for the deuterated species with the SiD_2 group. For dimethylsilane, it is found at 476 cm^{-1} for the SiH_2 species and at 385 cm^{-1} for the SiD_2 species. There are two additional bands at 496 and 415 cm^{-1} for the mixture besides the bands due to the SiH_2 and SiD_2 species. Therefore, they can be assigned to the SiHD deformation vibrations, which originate from the twisting and rocking modes.

For ethylmethylsilane, in the spectra for the mixture four bands are seen, at 422, 438, 486, and 513 cm^{-1},

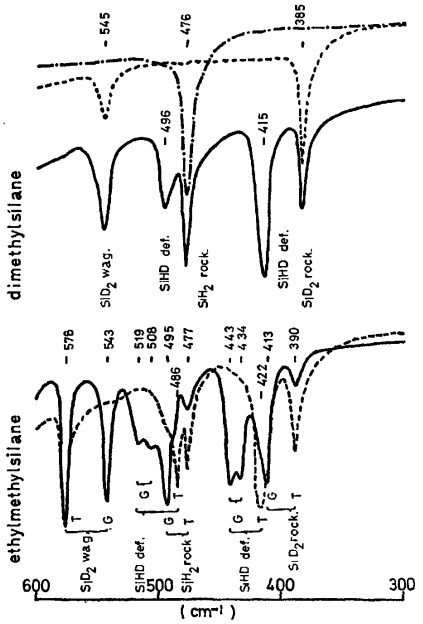

Fig. 2. Observed infrared spectra of dimethylsilane and ethylmethylsilane.
Upper: —— indicates the spectra of the mixture for $(CH_3)_2SiH_2$, $(CH_3)_2SiD_2$, and $(CH_3)_2SiHD$.
—•— indicates the spectra of $(CH_3)_2SiH_2$.
– – – indicates the spectra of $(CH_3)_2SiD_2$.
Lower: Solid and dotted lines indicate the spectra of the mixture for $CH_3CH_2SiH_2CH_3$, $CH_3CH_2SiD_2CH_3$, and $CH_3CH_2SiHDCH_3$ in the liquid and the crystalline states respectively.

attributable to the $CH_3CH_2SiHDCH_3$ species; the bands at 422 and 486 cm^{-1} are shoulders of the strong bands due to the other species. In the crystalline state, the bands at 422 and 486 cm^{-1} persist, while the two other bands at 438 and 513 cm^{-1} vanish. The persisting bands are obviously singlets, while the vanishing bands are doublets with spacings of 9 and 11 cm^{-1} respectively.

Therefore, it can be concluded that the isomer persisting in the crystalline state is definitely the *trans* and that the other isomer vanishing in the crystalline state is not the molecular form with a plane of symmetry such as the *trans* and *cis* forms, but is probably a *gauche* form, in which two hydrogens attached to the Si atom come not to be equivalent for the asymmetrically-deuterated species.

For the other modes, the assignments of the observed spectra seem to be difficult since the spectra due to three different species overlap. Therefore, no obvious evidence is obtained for the molecular form from these modes of vibrations.

BULLETIN OF THE CHEMICAL SOCIETY OF JAPAN, VOL. 46, 686 (1973)

The Addition of Nitrosyl Chloride to Nickel(0) Complexes. The Preparation of Nitrosyl Nickel Complexes

Masanobu HIDAI, Makoto KOKURA, and Yasuzo UCHIDA
Department of Industrial Chemistry, The University of Tokyo, Hongo, Tokyo

(Received September 30, 1972)

Several methods for preparing nitrosyl nickel complexes have been established.[1-5] During the course of a study of oxidative-addition reactions of covalent molecules to nickel(0) complexes,[6] we have found that nitrosyl chloride adds to nickel(0) complexes to yield a series of nitrosyl nickel complexes.

The nitrosyl complex, $NiCl(NO)(PPh_3)_2$, prepared by the reaction of $NiCl_2(PPh_3)_2$ with $NaNO_2$,[4] was obtained by the addition reaction of nitrosyl chloride to nickel(0) complexes such as $Ni(PPh_3)_4$ and $Ni(PPh_3)_2(COD)$ (COD=1,5-cyclooctadiene). The use of excess nitrosyl chloride afforded only $NiCl_2(PPh_3)_2$. The $NiCl(NO)(P(OPh)_3)_2$ complex was also prepared from $Ni(COD)_2$, triphenyl phosphite, and nitrosyl chloride. Hieber *et al.*[3] prepared similar nitrosyl complexes, $NiX(NO)(P(OPh)_3)_2$ (X=Br, I), by the reaction of triphenyl phosphite with $[NiX(NO)P(OPh)_3]_2$.

Nitrosyl chloride also added to $Ni(COD)_2$ in the presence of equimolar ditertiary phosphines *in ether* to afford new nitrosyl complexes, $NiCl(NO)(Ph_2P(CH_2)_nPPh_2)$ (n=1, 2, and 3). These nitrosyl complexes are fairly

$$Ni(COD)_2 + Ph_2P(CH_2)_nPPh_2 + NOCl \rightarrow NiCl(NO)(Ph_2P(CH_2)_nPPh_2)$$
$$n=1,\ 2,\ \text{and}\ 3$$

air-stable, but easily decompose in toluene or benzene at an ambient temperature. The nitrosyl complexes were, therefore, not obtained when the above reactions were carried out in benzene or toluene. Table 1 shows that ν_{N-O} shifts to a lower frequency with an increase in the length of the methylene chain of the ditertiary phosphines, as in the case of ν_{N-N} of $Mo(N_2)_2(Ph_2P(CH_2)_nPPh_2)_2$.[7] The reaction of nitrosyl chloride with $Ni(Ph_2P(CH_2)_nPPh_2)_2$ (n=1 and 2) at 90°C did not yield the nitrosyl complexes.

Table 1. Analytical and physical data for $NiCl(NO)(Ph_2P(CH_2)_nPPh_2)$

n	Mp (decomp.) °C	ν_{N-O} cm^{-1}	Analysis found (Calcd) (%) C	H	N	Cl
1	180	1750	60.45 (59.05)	4.48 (4.36)	2.62 (2.75)	7.01 (6.97)
2	198—199	1735	60.04 (59.76)	4.55 (4.63)	2.43 (2.68)	6.70 (6.78)
3[a]		1725				

a) The complex was not obtained in a pure state.

Experimental

All the reactions were carried out under a nitrogen atmosphere in a small Schlenk-type flask containing a magnetic stirring bar. Tetrakis(triphenylphosphine)nickel(0) $Ni(PPh_3)_4$[8] and bis(1,5-cyclooctadiene)nickel(0) $Ni(COD)_2$[9] were prepared by the published methods. All the operations for preparing nitrosyl nickel complexes are very similar, so only a few typical examples will be described below.

Preparation of $NiCl(NO)(PPh_3)_2$. To a solution of $Ni(PPh_3)_4$ (0.374 g, 0.337 mmol) in benzene (10 ml) was added a solution of nitrosyl chloride (0.337 mmol) in toluene (0.1 ml) at an ambient temperature. The colour of the solution turned dark blue. After stirring the solution for 2 hr at that temperature, hexane (20 ml) was added to the solution and $NiCl(NO)(PPh_3)_2$ was precipitated as blue crystals (0.139 g, 65%).

Found: C, 66.85; H, 4.84; N, 2.02; Cl, 5.84%. Calcd for $C_{36}H_{30}NOClNi$: C, 66.67; H, 4.63; N, 2.16; Cl, 5.47%.

Preparation of $NiCl(NO)(Ph_2PCH_2PPh_2)$. A suspension of $Ni(COD)_2$ (0.155 g, 0.56 mmol) and bis(diphenylphosphino)methane (0.215 g, 0.56 mmol) in ether (20 ml) was stirred at −15——20°C for 2 hr. To this yellow suspension was then added a solution of nitrosyl chloride (0.56 mmol) in toluene (0.17 ml) at that temperature, after which the reaction mixture was stirred for 2 hr. The colour of the mixture thus changed into purple. The purple precipitate was separated by filtration and recrystallized from tetrahydrofuran-hexane, thus affording $NiCl(NO)(Ph_2PCH_2PPh_2)$ as reddish-purple crystals (0.156 g, 53.5%).

1) T. S. Piper, F. A. Cotton, and G. Wilkinson, *J. Inorg. Nucl. Chem.*, **1**, 165 (1955).
2) W. P. Griffith, J. Lewis, and G. Wilkinson, *J. Chem. Soc.*, 2259 (1961).
3) W. Hieber and I. Bauer, *Z. Anorg. Allg. Chem.*, **321**, 107 (1963).
4) R. D. Feltham, *Inorg. Chem.*, **3**, 116 (1964).
5) H. Brunner, *Chem. Ber.*, **101**, 143 (1968).
6) M. Hidai, T. Kashiwagi, T. Ikeuchi, and Y. Uchida, *J. Organometal. Chem.*, **30**, 279 (1971).
7) M. Hidai, K. Tominari, and Y. Uchida, *J. Amer. Chem. Soc.*, **94**, 110 (1972).
8) G. Wilke, E. W. Müller, M. Kroner, P. Heimbach, and H. Breil, Ger. Pat., 1191375 (1965).
9) G. Wilke, *Angew. Chem.*, **72**, 581 (1960).

BULLETIN OF THE CHEMICAL SOCIETY OF JAPAN, VOL. 46, 687—688 (1973)

Reaction of Sulfenyl Chlorides with Sulfides. IV.[1] The Reaction with 1-Phenylvinyl Sulfides

Michinori Ōki and Keiji Kobayashi*

Department of Chemistry, Faculty of Science, University of Tokyo, Hongo, Tokyo

** Department of Chemistry, College of General Education, University of Tokyo, Komaba, Meguro, Tokyo*

(Received February 21, 1972)

The reaction of benzenesulfenyl chloride (**1**) with α-methylthiostyrene (**2**) gives no adducts but causes the formation of α-methylthio-β-phenylthiostyrene (**3**) in an almost quantitative yield.[2] Since styrene is known to react with sulfenyl chlorides to give the addition products,[3] the presence of a sulfur atom at the alpha-position of styrene appears to be essential for the displacement reaction on β-hydrogen by a phenylthio group to occur. This paper describes the results of an extended investigation on the reaction of 1-phenylvinyl sulfides with **1**.

The reaction of α-phenylthiostyrene (**4**) with one equivalent of **1** was examined at room temperature in carbon tetrachloride. Evolution of hydrogen chloride was observed and an isomeric mixture of *cis*- and *trans*-α,β-bis(phenylthio)styrene (**5**) was obtained in 70% yield.

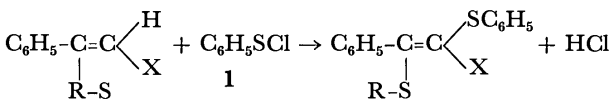

2; R=CH_3, X=H — **3**; R=CH_3, X=H
4; R=C_6H_5, X=H — **5**; R=C_6H_5, X=H
6; R=C_6H_5, X=Cl — **7**; R=C_6H_5, X=Cl

In a similar manner the reaction of α-phenylthio-β-chlorostyrene (**6**) with **1** led to the formation of α,β-bis(phenylthio)-β-chlorostyrene (**7**) in 48% yield. When 2,5-diphenyl-1,4-dithiin (**8**) was treated with two equivalents of **1** in chloroform, 2,5-diphenyl-3,6-bis(phenylthio)-1,4-dithiin (**9**) was obtained in 54% yield.

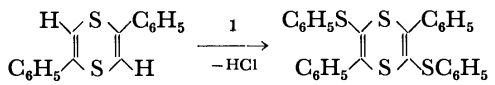

8 **9**

In contrast to the 1-phenylvinyl sulfides, the oxygen analog, α-methoxystyrene (**10**), afforded the Markownikoff-type adduct: the isolated product from the reaction of **10** with **1** was only α-phenylthioacetophenone (**11**), which would be formed by hydrolysis of the adduct **13** during the course of work-up. When the reaction mixture obtained from **10** and **1** was treated with triethylamine, α-methoxy-β-phenylthiostyrene

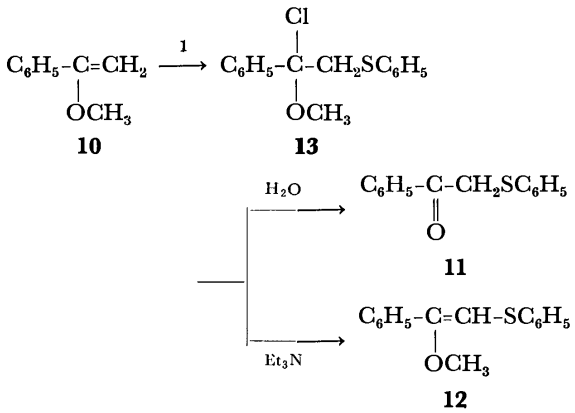

10 **13** **11** **12**

(**12**) was obtained in 63% yield. The marked difference in behavior between the sulfur analog and the oxygen analog is of interest for more detailed study.

In extending the β-phenylthio displacement reaction to **3**, a new chlorination reaction was found; the treatment of an isomeric mixture of **3** with one equivalent of **1** in carbon tetrachloride at room temperature led to the formation of an unexpected α-methylthio-β-phenylthio-β-chlorostyrene (**14**) in 34% yield. Although hydrogen chloride was evolved, the anticipated α-methylthio-β,β-bis(phenylthio)styrene was missing and *ca.* 40% of **3** was recovered. Diphenyl disulfide was also isolated in 81% yield. When **3** was treated with one equivalent of *p*-toluenesulfenyl chloride, the results were similar to those obtained from **1** except that di-*p*-tolyl disulfide was obtained in 67% yield instead of diphenyl disulfide. The results indicate that **14** arises according to the stoichiometry indicated below.

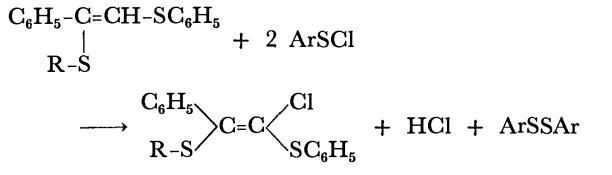

14; R=CH_3
7; R=C_6H_5

The reaction of **5** with **1** also afforded β-chlorinated product, α,β-bis(phenylthio)-β-chlorostyrene (**7**), in 22% yield. In this case, α,β,β-tris(phenylthio)styrene (**15**) was also isolated in 16% yield.

Treatment of **5** with two equivalents of methanesulfenyl chloride in carbon tetrachloride afforded **14** in 24% yield together with 61% methyl phenyl disulfide as detected by vpc analysis. Thus the chlorination reactions to give **14** may be supposed to involve the anti-Markownikoff addition of benzenesulfenyl

* To whom correspondence should be addressed.

1) Part III: M. Ōki and K. Kobayashi, This Bulletin, **43**, 1234 (1970).

2) M. Ōki and K. Kobayashi, *ibid.*, **43**, 1223 (1970).

3) W. L. Orr and N. Kharasch, *J. Amer. Chem. Soc.*, **75**, 6030 (1953); W. H. Mueller and P. E. Butler, *ibid.*, **90**, 2075 (1968); Y. Hayashi and R. Oda, *Nippon Kagaku Zasshi*, **89**, 1225 (1968).

chloride to **3** and methanesulfenyl chloride to **5**, giving rise to the formation of **16** as an intermediate.

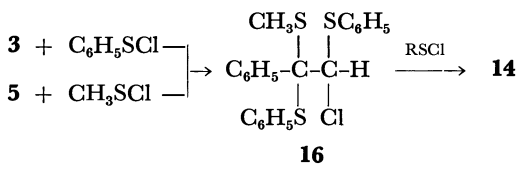

16

Experimental

*α,β-Bis(phenylthio)styrene (**5**).* To a mixture of **4**[4] (5.0 g, 0.023 mol) and carbon tetrachloride (100 ml), **1**[5] (3.5 g, 0.024 mol) was added at room temperature and the solution was stirred until it turned pale yellow and no further color change took place. The mixture was washed with saturated sodium bicarbonate, dried over anhydrous sodium sulfate and concentrated. The resulting yellow oil was chromatographed on alumina. Elution with petroleum ether–benzene (2 : 1) gave 5.3 g (70%) of **5** as viscous oil. M^+: 320; IR (cm^{-1}): 1580, 1540, 1025, 820, 760, 740, 690, 680; NMR (τ): 2.3—3.1 (m).

Found: C, 74.67; H, 4.91%. Calcd for $C_{20}H_{16}S_2$: C, 74.96; H, 5.03%.

An analytically pure sample of **5** showed the presence of two components attributed to the geometrical isomer on vpc.

*α,β-Bis(phenylthio)-β-chlorostyrene (**7**).* The reaction of **6**[6] with **1** was carried out as for **5**. The crude product mixture was chromatographed on alumina. Elution with benzene followed by recrystallization from petroleum ether–benzene (2 : 1) gave 48% of pure **7**, mp 89°C. M^+: 354; IR (cm^{-1}): 1580, 1540, 855, 750, 735, 690; NMR (τ): 2.90 (5H, s), 2.6—3.0 (10H, m).

Found: C, 67.93; H, 4.44; S, 17.87%. Calcd for $C_{20}H_{15}ClS_2$: C, 67.68; H, 4.26; S, 18.07%.

*2,5-Diphenyl-3,6-bis(phenylthio)-1,4-dithiin (**9**).* A solution of **8**[7] (1.5 g, 0.0056 mol) in chloroform (15 ml) was allowed to react with **1** (1.7 g, 0.012 mol) at room temperature for 30 min. The reaction mixture was washed, dried and concentrated. The residual oil was chromatographed on alumina. The yellow solid eluted with benzene was recrystallized from ethanol to give 1.4 g (54%) of **9**, mp 150—152°C. M^+: 484; IR (cm^{-1}): 1570, 1525, 1068, 1020 837, 775, 738, 692; NMR (τ): 2.72 (10H, s), 2.60—2.45 (6H, m), 2.32—2.28 (4H, m).

Found: C, 69.34; H, 3.98; S, 26.02%. Calcd for $C_{28}H_{20}S_4$: C, 69.38; H, 4.16; S, 26.46%.

*α-Methoxy-β-phenylthiostyrene (**12**).* To a solution of **10**[8] (13.4 g, 0.1 mol) in carbon tetrachloride (100 ml) was slowly added **1** (14.5 g, 0.1 mol) at 0°C and then triethylamine (18 g, 0.18 mol). Usual work-up and distillation under reduced pressure gave 15.2 g (63%) of **12**, bp 149—152°C/2 mmHg. M^+: 242; IR (cm^{-1}): 2820, 765, 740; 700; NMR (τ): 6.39 (3H, s), 3.99 (1H, s), 2.7 (10H, m) and 6.34 (3H, s), 4.61 (1H, s), 2.7 (10H, m).

Found: C, 74.08; H, 5.80; S, 13.35%. Calcd for $C_{15}H_{14}OS$: C, 74.35: H, 5.82; S, 13.23%.

*α-Methylthio-β-phenylthio-β-chlorostyrene (**14**).* To a solution of **3** (8.0 g, 0.031 mol) in carbon tetrachloride (50 ml) was added **1** (5.0 g, 0.035 mol). After decolorization of **1**, the mixture was washed with saturated sodium bicarbonate, dried and concentrated. The oily residue was chromatographed on alumina. Elution with petroleum ether gave 3.1 g (81%) of diphenyl disulfide and that with benzene afforded 3.1 g (34%) of **14**, mp 98—99°C. M^+: 292; IR (cm^{-1}): 1580, 1540, 858, 750, 735, 700, 692, 622; NMR (τ): 8.15 (3H, s), 2.80 (5H, s), 2.75 (5H, m).

Found: C, 61.57; H, 4.50; S, 22.01%. Calcd for $C_{15}H_{13}ClS_2$: C, 61.54; H, 4.44; S, 21.90%.

A similar treatment of **3** with *p*-toluenesulfenyl chloride gave 43% of **14** and 67% of di-*p*-tolyl disulfide.

*Reaction of **5** with **1**.* The reaction of **5** (5.7 g, 0.018 mol) with **1** (4.1 g, 0.028 mol) in carbon tetrachloride (15 ml) was carried out as described for the reaction of **3** with **1** to give 1.1 g of diphenyl disulfide, 1.4 g (22%) of **7**, and 1.3 g (16%) of α,β,β-tris(phenylthio)styrene, mp 79—80°C (lit,[9] 77—78°C).

4) S. H. Groen, R. M. Kellogg, J. Buta, and H. Wynberg, *J. Org. Chem.*, **33**, 2218 (1968).
5) H. Lecher and F. Holschneider, *Ber.*, **57**, 755 (1924).
6) W. H. Truce, H. E. Hill, and M. M. Boudakian, *J. Amer. Chem. Soc.*, **78**, 2760 (1956).
7) R. H. Barker and C. Barkenbus, *ibid.*, **58**, 262 (1936).
8) K. Alder and H. Niklas, *Ann. Chem.*, **585**, 109 (1954).
9) D. Seebach, A. K. Beck, and H. B. Stegmann, *Tetrahedron Lett.*, **1970**, 1933.

BULLETIN OF THE CHEMICAL SOCIETY OF JAPAN, VOL. 46, 688—689 (1973)

On the Cleavage of 2,4-Dibromo-5-methylanisole

Kazuo ADACHI

Osaka Institute of Technology, Omiya, Asahi-ku, Osaka

(Received June 13, 1972)

The phenolic hydroxyl group is sensitive to numerous reactions, but it may be protected in the ethers. On the treatment of phenol ethers with hydriodic or hydrobromic acid, the ether bond cleaves to the regenerated original phenols. This important reaction has been employed frequently in synthetic organic chemistry.[1)]

However, the refluxing of 2,4-dibromo-5-methylanisole (**2b**) with hydrobromic acid in acetic acid unexpectedly gave a mixture of 4-bromo-3-methylphenol (**1a**), 2,4-dibromo-5-methylphenol (**2a**), and 2,4,6-tribromo-3-methylphenol (**3a**). These three phenols, **1a**, **2a**, and **3a**, were methylated with dimethyl sulfate to give 4-bromo-3-methylanisole (**1b**), **2b**, and 2,4,6-tribromo-3-methylanisole (**3b**) respectively.

1) R. B. Wagner and H. D. Zook, "Synthetic Organic Chemistry," John Wiley & Sons, New York, N. Y. (1953), p. 171.

These results show that the cleavage of the methoxyl group of **2b** with hydrobromic acid is accompanied by bromination and debromination of **2a**.

In a recent paper, Kamikawa and his collaborators[2] described that the treatment of 2,4-dibromo-3,5-dimethylanisole with hydriodic acid gave 3,5-dimethylphenol. Similarly, the refluxing of **2b** with hydriodic acid in acetic acid gave *m*-cresol.

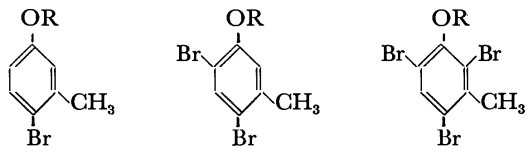

(**1a, b**) (**2a, b**) (**3a, b**)

a: R=H, **b**: R=CH_3

Experimental

*4-Bromo-3-methylanisole (**1b**) and 2,4-Dibromo-5-methylanisole (**2b**).* *m*-Cresol was brominated[3] to give 4-bromo-3-methylphenol (**1a**) containing 2,4-dibromo-5-methylphenol (**2a**).

*4-Bromo-3-methylphenol (**1a**)*: Needles from petroleum ether; mp 59—60°C (lit,[3] mp 56—57°C).

The crude bromo-*m*-cresol was methylated with dimethyl sulfate and then distilled. 4-Bromo-3-methylanisole (**1b**) and 2,4-dibromo-5-methylanisole (**2b**) were thus obtained.

*4-Bromo-3-methylanisole (**1b**)*: bp 91°C/4 mmHg (lit,[4] bp 81—83°C/4 mmHg).

*2,4-Dibromo-5-methylanisole (**2b**)*: Prisms from petroleum ether; mp 73—74°C (lit,[5] mp 73—74°C).

*Treatment of 2,4-Dibromo-5-methylanisole (**2b**) with Hydriodic Acid.* A mixture of **2b** (25.0 g), hydriodic acid (*d*, 1.7; 50 ml), and glacial acetic acid (50 ml) was refluxed with stirring for 4 hr. The reaction mixture was then diluted with water and extracted with benzene. The benzene layer was washed with aq. $NaHSO_3$ and then water, and extracted with aq. NaOH. The oil obtained by the subsequent acidification of the resulting alkaline solution with HCl was extracted with ether. The distillation of the crude product gave an oil boiling at 93—94°C/13 mmHg (5.7 g; 58.7%) which was identical with *m*-cresol (IR spectrum).

The removal of the solvent from the above benzene solution gave the unchanged **2b** (4.1 g).

*Treatment of **2b** with Hydrobromic Acid.* A mixture of **2b** (39.0 g), hydrobromic acid (*d*, 1.48; 280 ml), and glacial acetic acid (280 ml) was refluxed with stirring for 10 hr. The subsequent distillation of the phenolic components in the reaction mixture gave an oily mixture of bromo-*m*-cresols boiling at 83—130°C/6 mmHg (22.0 g; 57.9%) and 2,4,6-tribromo-3-methylphenol (**3a**) boiling at 130—166°C/6 mmHg (12.1 g; 31.9%), which solidified. The higher-boiling distillate was recrystallized to give **3a**.

*2,4,6-Tribromo-3-methylphenol (**3a**)*: Needles from petroleum ether; mp 81.5—82.5°C(lit,[6] mp 80—81°C).

By redistillation, the lower-boiling distillate was divided into three fractions, A, B, and C. The components in each fraction were confirmed by gas chromatography.

Fraction A (2.8 g), boiling at 85—120°C/7 mmHg, was a mixture of 4-bromo-3-methylphenol (**1a**), 2,4-dibromo-5-methylphenol (**2a**), and a trace of *m*-cresol.

From Fraction B (16.6 g), boiling at 120—127°C/7 mmHg, crystals (4.3 g) of **2a** and an oily mixture (11.9 g) of **1a** and **2a** were obtained. The crude crystals of **2a** were filtered and purified by recrystallization to give *2,4-dibromo-5-methylphenol (**2a**)*; needles from petroleum ether; mp 64—64.5°C (lit,[3] mp 65—66°C).

Fraction C (2.0 g), boiling at 127—136°C/7 mmHg, was a mixture of **1a**, **2a**, and **3a**. Fractions B and C contained two more components, which appeared to be isomers of **1a** and **2a** but which were not identified.

The methylation of **2a** and **3a** with dimethyl sulfate gave **2b** and 2,4,6-tribromo-3-methylanisole (**3b**) respectively. The oily mixture of bromo-*m*-cresols, obtained after the removal of **2a** from Fraction B, was methylated with dimethyl sulfate to give a mixture of **1b**, **2b**, and **3b**.

*2,4,6-Tribromo-3-methylanisole (**3b**)*: Microneedles from petroleum ether; mp 75.5—76.5°C. Found: C, 26.55; H, 1.94%. Calcd. for $C_8H_7Br_3O$: C, 26.77; H, 1.97%. IR: 6.89, 7.08, 7.40, 7.91, 9.56, 10.78, 11.58, and 13.00 μ.

*Treatment of **2b** with the Other Acids.* When **2b** (14.0 g) was refluxed with 20% HCl (140 ml) and also with 63% H_2SO_4 (140 ml) in glacial acetic acid (140 ml) with stirring for 10 hr, only a small amount of **2a** was obtained (0.6 g) in either case.

2) T. Kamikawa, M. Nakatani, and T. Kubota, *Tetrahedron*, **24**, 2091 (1968).

3) R. C. Huston and J. A. Hutchinson, *J. Amer. Chem. Soc.*, **54**, 1504 (1932).

4) M. S. Carpenter, W. M. Easter, and T. F. Wood, *J. Org. Chem.*, **16**, 586 (1951).

5) W. O. Kermack and T. W. Wight, *J. Chem. Soc.*, **1935**, 1421.

6) R. C. Huston and W. J. Peterson, *J. Amer. Chem. Soc.*, **55**, 3879 (1933).

BULLETIN OF THE CHEMICAL SOCIETY OF JAPAN, VOL. 46, 690—691 (1973)

Synthetic Photochemistry. II.[1] The Cycloaddition Reaction of Dehydroacetic Acid with Olefins

Hitoshi TAKESHITA,* Ryoko KIKUCHI, and Yoshikazu SHOJI
Department of Chemistry, Tohoku University, Sendai 980

(Received September 5, 1972)

As a part of the study of the photochemical cycloaddition reactions of α,β-unsaturated ketones bearing functional substituents, we have recently reported the reaction of methyl acetopyruvate with olefins.[1] According to the results thus obtained, the photoadducts have been directly formed by a reaction with the tautomer which exists in the ground state by means of remarkable regiospecific control. Dehydroacetic acid (I) possesses several tautomeric forms because of different orientations of enolization; this, from the preparative point of view, aroused our interest in examining the cycloaddition reaction with olefins.

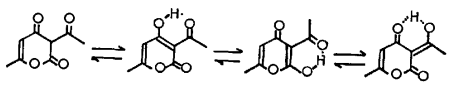

Chart 1.

During the course of our investigations, Kumamoto *et al.*[2] reported their results on the photochemical reactions of I with cyclohexene, acrylonitrile, and trimethylethylene. Our observations contain some novel features which we want to record in this brief paper.

The irradiation of I and cyclohexene in an ethyl acetate solution through a Pyrex glass filter by means of a 450 W high-pressure mercury lamp afforded several products, but the reaction could not be completed because of the production of a resious material. The products isolated by chromatography were II (pale yellow liquid (2%)), III(colorless needles, mp 85.5—87°(20%)), IV(colorless liquid (20%)), and V(colorless crystals, mp 215—216° (2.5%)).

Among these, III and V were identified, by comparisons of their physical data, as the 1 : 1 adduct previously obtained by Kumamoto,[2] and as the dimer formed by the solid-phase irradiation of I by Sugiyama,[3] respectively. The structure of II was deduced to be 3-(2-acetylcyclohexyl)-4-hydroxy-6-methyl-α-pyrone on the basis of NMR and IR spectral analyses, since the disappearance of the tricarbonyl-methane chromophore and the presence of a vinylic-methyl group and an olefinic proton were evident.

The structure of III has already been proposed by Kumamoto to be the *cis-cis-cis* isomer, mainly on the basis of his analysis of the NMR spectrum but his assignment of the stereochemistry seems unconvincing. The IV we obtained revealed physical properties very similar to those of III and was deduced to be a stereoisomer of III; therefore, the inspection of the NMR spectra of the two compounds might provide information on the point. When the NMR spectrum was measured in a benzene solution, the signal attributable to the C-5 methin proton clearly appeared as a doublet (J=9.3 Hz) at δ 2.35 indicating that the vicinal protons in the cyclobutane ring were in a *cis*-relationship. On the other hand, the NMR signal of the corresponding proton of IV had the same magnitude of the coupling constant, with a still-smaller spin-spin splitting (δ 3.09 dd, J=9, 2.5 Hz) in a carbon tetrachloride solution also showing a *cis*-relationship. In addition, the occurrence of only the long range coupling in IV would represent the *W*-letter-type relation for both the protons, and the *cis-cis*-configuration for three hydrogens at the A/B/C ring junctures. Therefore, III must be the *trans-cis* isomer. Moreover, the configuration of the methyl group and the hydrogen at the B/C ring should be a thermodynamically stable *cis*-configuration. Thus, the stereochemistry of III and IV has been deduced.

A few other products were isolated, but because of the limited quantity available for characterization and because of the instability to the isolation conditions, no further work was attempted.

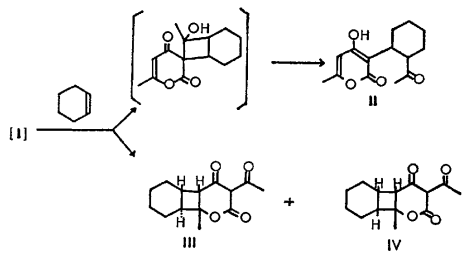

Chart 2.

A similar reaction of I with vinyl acetate also resulted in several products; among those fractionated from a complex mixture were VI (pale yellow liquid (21% as an isomeric mixture)), VII (pale yellow liquid (4.1%)), and VIII (colorless needles, mp 90.5—91°C (5.2%)).

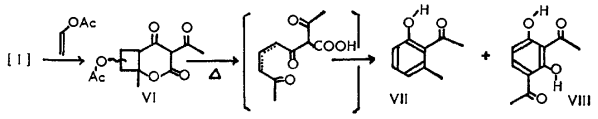

Chart 3.

* Present address: Research Institute of Industrial Science, Kyushu University, Hakozaki, Fukuoka 812.

1) Previous paper; H. Takeshita and S. Tanno, This Bulletin, in press (1973).

2) S. Kumamoto, K. Somekawa, and A. Tsuchida, Abstract Papers of 23rd Annual Meeting of Chemical Society of Japan(Apr., 1070, Tokyo), [III], 1300.

3) N. Sugiyama, T. Sato, H. Kataoka, and C. Kashima, This Bulletin, **44**, 555 (1971). In this paper, the authors described however I did not cause any photochemical change in solutions.

Although VI appeared as a single spot on thin-layer chromatograms, the NMR spectrum indicated it to be a mixture of all four of the possible stereo- and regio-isomers of the 1 : 1 adducts. Intensive efforts to separate them failed, except that the least polar component (VIa) could be obtained in an 80% purity, according to the NMR spectral analysis. VIa has shown a characteristic NMR signal for the tricarbonyl system, like I, indicating that a reaction has taken place at the C-5,6 position. The rest of the isomers also have very similar NMR spectral data for this reason.

The structure of VII was deduced to be 2-acetyl-3-cresol on the basis of the NMR and the other spectral properties. VIII was also identified as 2,4-diacetylresorcine.[4] Obviously, VII and VIII were formed by the aromatization of VI during the work-up. In fact, when a methanolic solution of VI was refluxed for a while, considerable amounts of VII and VIII were obtained.[5]

Thus, our results agree, in general, with those of Kumamoto. However, the formation of II shows a bi-functional nature in the photochemical cycloaddition.[6]

Experimental

Photochemical Reaction of Dehydroacetic Acid (I) and Cyclohexene. I (3.5 g) was dissolved in cyclohexene (70 ml) and ethyl acetate (80 ml), and then the solution was internally irradiated by means of a 450 W high-pressure mercury lamp through a Pyrex glass filter in a nitrogen atmosphere. The solution soon become dark brown and a polymeric material has deposited on the wall; therefore, irradiation was terminated after 5 hr. The reaction mixture was heated under reduced pressure to remove the solvent, and the residue was washed with a small amount of ligroin to recover the unreacted I, which weighed 0.63 g (22%) after collection. Then, the product mixture in ligroin was distilled *in vacuo* to give a yellow, viscous oil (2 g). This was fractionated by silica gel (200 g) column chromatography with benzene. After the elution of unidentified crystals (6 mg), II was isolated as a faintly colored liquid (bp 130°/0.5 mmHg (bath temp.), 80 mg). This sample showed a single spot on thin-layer chromatograms. (Found: C, 67.25; H, 7.40%). λ_{max}^{MeOH} 230 nm(sh.), 281 nm (6300). $\nu_{C=O}$ 1715 cm^{-1}(v. strong). δ_{CCl_4} 1.5(9H, m), 2.05(3H, s), 2.12 (3H, s), 2.86(1H, br.), and 5.50(1H, s).

Next several fractions containing a crystalline material were collected to give III (colorless needles; mp 85.5—87° (from ether-cyclohexane)(lit.[2] 88—89°C); weight, 120 mg). (Found: C, 67.83; H, 7.40%). δ_{CCl_4} 1.43(3H, s), 2.65 (3H, s), and 2.72(1H, d, J=9 Hz); $\delta_{C_6H_6}$ 1.03 (3H, s), 2.55(3H, s), and 2.35(1H, d, J=9.3 Hz).

Further elution with benzene-ethyl acetate gave on oily mixture of III and IV(1.87 g), which additionally yielded some crystalline III; repeated silica-gel chromatography with petroleum ether-benzene and preparative thin-layer chromatography finally yielded an enriched fraction of IV, together with some crystalline III. The NMR assay of the fraction still indicated the presence of III(*ca.* 5—10%), but a further attempt at its purification was not made. This specimen (colorless liquid, bp 120°C/0.5 mmHg(bath temp.)) showed an IR spectrum almost undistinguishable from that of III. (Found: C, 67.41; H, 7.44%). δ_{CCl_4} 1.53(3H, s), 2.67(3H, s), and 3.09(1H, dd, J=9, 2.5 Hz). The estimated yields of III and IV was both about 20% respectively.

Subsequent elution with benzene-ether gave mainly V and some unidentified compounds, from which V was isolated by fractional crystallization with cyclohexane as colorless needles(mp 215—216°C(from cyclohexane)(lit,[3] 214.5—215.5°C); weight, 75 mg).

Photochemical Reaction of I and Vinyl Acetate. I (3.5 g) was dissolved in vinyl acetate (35 ml) and ethyl acetate (250 ml), and the mixture was irradiated much as in the preceding reaction; again, the formation of a polymeric material prevented the completion of the reaction. The reaction mixture was evaporated under reduced pressure to remove most of the solvent and the unreacted vinyl acetate; the residue was washed with cold ligroin to separate the unreacted I (510 mg) and the products, which were distilled *in vacuo* to give a pale yellow liquid(bp 155—165°C/3 mmHg(bath temp.), 2.9 g) and separated by silica gel chromatography. The first fraction, eluted with benzene, contained VII, which was obtained in a pure form through preparative thin-layer chromatography as a pale yellow liquid(110 mg). (Found: C, 71.70; H, 6.87%). δ_{CCl_4} 2.59(3H, s), 2.64(3H, s), 6.72(1H, dd, J=7.5, 1.2 Hz), 6.83(1H, dd, J=7.8, 1.2 Hz), 7.28(1H, dd, J=7.8, 7.5 Hz), and 12.15(1H, OH).

The next fraction yielded VIII (colorless needles; mp 90.5—91°C(from ethyl acetate)(lit.[4] 88—90°C); weight, 189 mg). The following fraction, eluted with benzene-ether, contained VI and unidentified compounds; after repeated chromatography, VI(950 mg) was obtained as a colorless liquid(bp 120—130°C/1.5 mmHg(bath temp.)), whose least polar fraction, VIa, was obtained in a purity of *ca.* 80%. (Found: C, 56.69; H, 5.55%). δ_{CDCl_3} 1.58(3H, s), 2.00 (3H, s), 2.60(3H, s), 2.2—2.9(3H), and 4.87(1H, dd, J= 5.5, 3.5 Hz).

Aromatization of VI in Methanol. VI(30 mg, as a mixture of isomers) was heated in a methanol(10 ml) solution under reflux. The VI disappeared within 30 min, and after the removal of the solvent, VII(9 mg) and VIII(3 mg) were isolated by preparative thin-layer chromatography.

We wish to thank Professor S. Itô for his helpful suggestions, Mrs. H. Arai and Miss M. Suzuki for the elemental analyses, and T. Kondo for the NMR measurements. H. T. is also grateful to The Matsunaga Science Foundation for a research grant, by which a part of the expense has been defrayed.

4) G. Witting, *Ann. Chem.*, **446**, 155 (1926).

5) In this treatment, colorless needles (mp 87.5—87.5°) were obtained, and the structure was considered to be a monomethyl ether of VIII. However, no further characterization was attempted.

6) The formation of II can be regarded as another example of the cycloaddition reaction of α-acyl-β-diketone. The photochemical reaction of such a system has been successfully employed in the total synthesis of loganin; *cf.* G. Büchi, J. A. Carlson, J. F. Powell, Jr., and L. F. Tietze, *J. Amer. Chem. Soc.*, **92**, 2165 (1970).

BULLETIN OF THE CHEMICAL SOCIETY OF JAPAN, VOL. 46, 692 (1973)

One-step Synthesis of Putranjivic Acid from Friedelin

Reiko AOYAGI, Takahiko TSUYUKI, and Takeyoshi TAKAHASHI
Department of Chemistry, Faculty of Science, The University of Tokyo, Hongo, Bunkyo-ku, Tokyo

(Received September 11, 1972)

A triterpene, putranjivic acid, isolated from leaves of *Putranjiva roxburghii* (Euphorbiacea) has been characterized by spectral and chemical methods to be 10β-(2-carboxy)ethyl-5α-vinyl-des-A-friedelane (3,4-seco-friedel-4(23)-en-3-oic acid) (I) by Seshadri *et al.*[1-3] Very recently Sengupta and Dey[4] have described the synthesis and stereostructure of putranjivic acid (I). These authors have synthesized this acid from friedel-3-ene (II) through seven steps and established the configuration of all asymmetric centers in the acid.

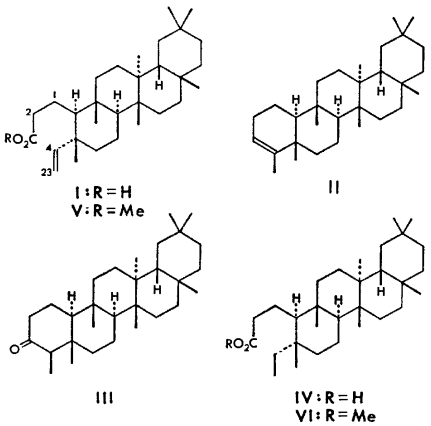

We now wish to report a one-step synthesis of putranjivic acid (I) from friedelin (III) by photochemical oxidation reaction. It is well-known that cyclohexanone derivatives are irradiated in the presence of oxygen to afford an unsaturated seco-acid and that this reaction was applied to syntheses of nyctanthic and roburic acids.[5]

Irradiation of friedelin (III) in benzene under oxygen atmosphere gave a complex mixture, which was subjected to column chromatographic separation. Acidic fractions were treated with diazomethane. The methyl esters were further separated by silver nitrate-impregnated silica gel tlc into unsaturated and saturated esters. The latter was shown to be methyl 3,4-seco-friedelan-3-oate (VI) by comparison with the authentic sample which was prepared by methylation of 3,4-seco-friedelan-3-oic acid (IV).[6] The former was hydrolyzed to an unsaturated acid. The olefinic acid and its methyl ester were identical with putranjivic acid (I) and its methyl ester (V), respectively, in respects to mp, IR, and MS.

The methyl ester (V) was catalytically hydrogenated to give a saturated ester, which was identical with methyl 3,4-seco-friedelan-3-oate (VI) in every respect. Thus the structure of the synthesized putranjivic acid (I) was confirmed.

Experimental

All melting points were determined on a hot block and uncorrected. IR and mass spectra were measured using Hitachi EPI-G2 and Hitachi RMU-6 mass spectrometers. NMR spectra were recorded in $CDCl_3$ on Hitachi Model R-24 NMR spectrometer at 60 MHz, using TMS as an internal standard.

Photo-oxidation of Friedelin (III). Friedelin (500 mg) was dissolved in benzene (700 ml) and irradiated with a high pressure mercury lamp for 11 hr with introduction of oxygen at room temperature. The concentrated solution was passed through a column (SiO_2, 95 g) and elution was continued with benzene (2.6 l) to give acidic fractions, which were combined and treated with diazomethane. After evaporation, the residue was separated by thin layer chromatography using 10% $AgNO_3$-impregnated silica gel, developed with a 3 : 1 mixture of petroleum ether and benzene. The unsaturated ester (V, R_f=0.23) was extracted with ether and recrystallized from methanol to yield 21 mg of V, mp 136.0—136.5°C; ν_{max}(Nujol) 1737, 1630, and 905 cm^{-1}; NMR: δ 3.65(s, $-COOC\underline{H}_3$) and 4.75—6.0($-C\underline{H}=C\underline{H}_2$); M^+ 456 ($C_{31}H_{52}O_2$) [lit,[1] mp 133—135°C, ν_{max}1754 cm^{-1}, $[\alpha]_D$ −8.3° (*c* 1.2, $CHCl_3$)].

V (13 mg) was heated under reflux with potassium hydroxide (10 mg) in methanol (7 ml) for 4 hr and then treated as usual. The unsaturated acid (I) was obtained (12 mg), mp 173.0—173.5°C; ν_{max}(Nujol) 1705, 1660, 990, and 905 cm^{-1}; $[\alpha]_D$ −12° (*c* 0.24, $CHCl_3$); NMR: δ 4.75—5.90($-C\underline{H}=C\underline{H}_2$) and 2.30(m, $-C\underline{H}_2-COOH$); Found: C, 81.45; H, 11.26%. Calcd for $C_{30}H_{50}O_2$: C, 81.39; H, 11.38%. M^+ 442 [lit,[1] mp 177—179°C, ν_{max} 1730 cm^{-1}, $[\alpha]_D$ −15° (*c* 0.4, $CHCl_3$)].

The saturated ester (VI, R_f=0.8) was extracted with ether from the $AgNO_3$-impregnated silica gel and recrystallized from methanol to give 18 mg of VI, whose spectral data [ν_{max}(Nujol) 1740 and 1163 cm^{-1}; NMR: δ 3.66(s, $-COOC\underline{H}_3$), M^+ 458 ($C_{31}H_{54}O_2$)] were identical with those of the authentic methyl 3,4-seco-friedelan-3-oate (VI), prepared by methylation of 3,4-seco-friedelan-3-oic acid (IV)[6] with diazomethane in ether.

The saturated methyl ester (VI) was hydrolyzed with potassium hydroxide in ethanol and recrystallized from methanol to afford 3,4-seco-acid (IV), mp 210.5—211.5°C. Mp, IR, NMR, MS, and tlc were identical with those of the authentic 3,4-seco-friedelan-3-oic acid (IV).[6]

Hydrogenation of Methyl Purtanjivate (V). The unsaturated methyl ester (V, 7 mg) was dissolved in ethanol (7 ml) and hydrogenated in the presence of 10% Pd-C. Recrystallization from methanol gave methyl 3,4-seco-friedelan-3-oate (VI), which was identical with the authentic sample, described above.

1) G. R. Chopra, A. C. Jain, and T. R. Seshadri, *Curr. Sci.*, **37**, 301 (1968); *Chem. Abstr.*, **69**, 93685q (1968).
2) G. R. Chopra, A. C. Jain, T. R. Seshadri, and G. R. Sood, *Indian J. Chem.*, **8**, 776 (1970); *Chem. Abstr.*, **74**, 1024a (1971).
3) G. R. Chopra, A. C. Jain, and T. R. Seshadri, *ibid.*, **7**, 1179 (1969); *Chem. Abstr.*, **72**, 67139g (1970).
4) P. Sengupta and A. K. Dey, *Tetrahedron*, **28**, 1307 (1972).
5) G. Quinkert and H.-G. Heine, *Tetrahedron Lett.*, **1963**, 1659.
6) T. Tsuyuki, S. Yamada and T. Takahashi, This Bulletin, **41**, 511 (1968); F. Kohen, A. S. Samson, and R. Stevenson, *J. Org. Chem.*, **34**, 1355 (1969).

BULLETIN OF THE CHEMICAL SOCIETY OF JAPAN, VOL. 46, 693—694 (1973)

Aromatic Nulceophilic Substitution. I. Preparation of Spiro Meisenheimer Complexes of Arenes

Shizen SEKIGUCHI and Takeo SHIOJIMA

Department of Synthetic Chemistry, Gunma University, Tenjincho, Kiryu, Gunma

(Received September 20, 1972)

Since Jackson and Gazzolo,[1] and Meisenheimer[2] synthesized the so-called Meisenheimer Complex I (R_1, R_2; alkyl), a large number of the complexes have been prepared.[3] We have recently found that the spiro Meisenheimer complexes (II, III) having the N–C_1–O bond could be isolated at room temperature (*ca.* 20°C) in the reaction of 1-[*N*-methyl-(2′-hydroxy)ethylamino]-2,4,6-trinitrobenzene (IV) or 1-[*N*-methyl-(2′-hydroxy)ethylamino]-2,4-dinitronaphthalene (V) with sodium methoxide.

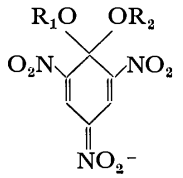

I

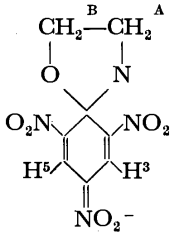

II

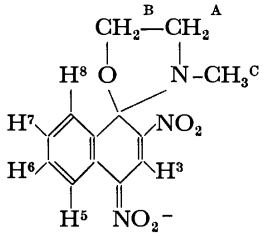

III

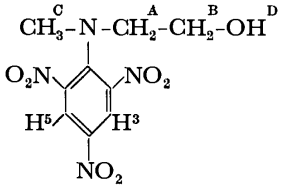

IV

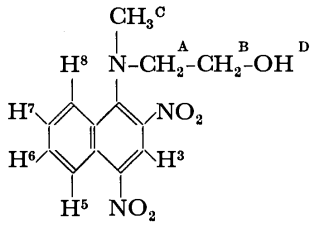

V

Preparation of II. When IV was treated with sodium methoxide in methanol at room temperature, II was formed. In the IR spectrum of V, the strong broad bands at 1220 and 1516 cm^{-1} could be assignable as the nitro group carrying the increased negative charge,[7] whereas these bands appeared at 1340 and 1516 cm^{-1} in that of IV. In the visible spectrum of II (3.47×10^{-5} mol/l), there are double maxima: λ_{max} 421 nm (ε 26100); λ_{max} 490 nm (sh, ε 16800). Not only the shape, but also the positions and intensities are similar to those of well-characterized Meisenheimer complexes.[3] In the NMR spectrum of II, the proton resonances at τ 1.41 (s, 2H), 5.77 (t, 2H), 6.62 (m, 2H), and 7.82 (s, 3H) are assignable as H^3 and H^5 (ring protons), H^B, H^A, and H^C ones, respectively, whereas H^3 and H^5 ones appeared at τ 1.17 (s, 2H) in that of IV. In the spectrum, a resonance appeared at τ 8.87 as a triplet. This resonance was due to the methyl group of diethyl ether, which was used for purification of II (see Experimental Section). The resonances of the methylene group of diethyl ether and the *N*-methylene one of II (or H_A resonance) overlapped each other at τ 6.62.

Preparation of III. Under the similar reaction condition to II, III was produced from V. In the IR spectrum of III, strong broad bands appeared at 1487 and 1150 cm^{-1}, assignable as the asymmetric and symmetric stretching absorptions of the nitro group,[8] whereas these bands appeared at 1510 and 1300 cm^{-1} in that of V. The visible spectrum of III (4.373×10^{-5} mol/l) has double maxima [λ_{max} 502 nm (ε 19400); λ_{max} 344 nm (ε 14200)], characteristic of 1,1-disubstituted 2,4-dinitronaphthalene σ-complexes.[4] Its shape, positions, and intensities are similar to those of VI, the presence of which was confirmed by Orvik and Bunnett.[9] The postulated structure of III was supported by its NMR spectrum. For III, H^3 and H^8 resonances appeared at τ 0.75 (s, 1H) and 1.18 (d, 1H), respectively, and H^5, H^6, and H^7 resonances overlapped at τ about 2.60 (m, 3H). These chemical shifts are different from those of V, in the NMR spectrum of which H^3 resonance appeared at τ 1.32 (s, 1H), H^5 and H^8 ones centered at τ 1.38 (m, 2H), and H^6 and H^7 ones centered at τ 2.07 (m, 2H).

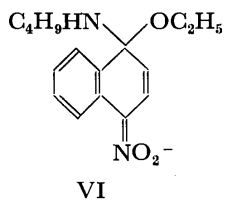

VI

Acid Decomposition of Meisenheimer Complexes (II and III). Acid decomposition of various Meisen-

1) C. J. Jackson and T. H. Gazzolo, *Amer. Chem. J.* **23**, 376 (1900).
2) J. Meisenheimer, *Ann. Chem.*, **323**, 205 (1902).
3) M. J. Strauss, *Chem. Rev.*, **70**, 667 (1970).
4) P. Caveng and H. Zoolinger, *Helv. Chim. Acta*, **50**, 861 (1961).
5) L. B. Clapp, H. Lacey, G. G. Beckwith, R. M. Srivastava, and N. Muhannad, *J. Org. Chem.*, **33**, 4262 (1968).
6) K. L. Servis, *J. Amer. Chem. Soc.*, **89**, 1508 (1967).
7) R. Foster, C. A. Fufe, and J. W. Morris, *Rec. Trav. Chim. Pays-Bas*, **84**, 516 (1965).
8) C. P. Conduit, *J. Chem. Soc.*, **1959**, 3273.
9) J. A. Orvik and J. F. Bunnett, *J. Amer. Chem. Soc.*, **92**, 2147 (1970).

heimer complexes have been reported.[10,11] Bunnett and Zahler[12] stated the formation of an anion by dissociation of a complex to depend upon the stability of the anion. The ease of anion seperation decreases in the order of alkoxide ions>amide ions. The decomposition of II and III with methanolic hydrochloric acid quantitatively gave IV and V, respectively. Our results are very consistent with the above order. Orvik and Bunnett[9] studied the nucleophilic substitution reaction of 2,4-dinitro-1-naphthyl ethyl ether (DNEE) with *n*- and *t*-butylamines in dimethyl sulfoxide solution, during the course of which VI, produced in the initial stage, was acid-catalyzed with butylammonium ion to seperate the alcohol. Our results are similar to those of Orvik and Bunnett.[9]

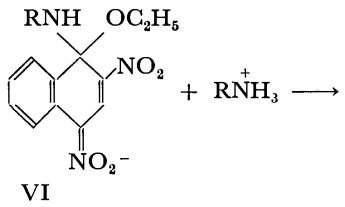

VI

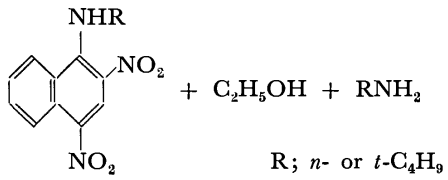

Experimental

Elemental analyses were performed in the Microanalytical Center of the University of Gunma. NMR spectra were recorded in DMSO-d_6 on a Varian A-60D spectrometer. IR spectra were measured in nujol mull on a Jasco DS-301 spectrophotometer. Visible spectra were recorded in methanol on a Hitachi-124 UV-VIS spectrophotometer. All melting points were uncorrected. The solvents and reagents were purified by the usual methods.

1-[N-*Methyl-(2'-hydroxy)ethylamino*]-*2,4,6-trinitrobenzene (IV)*. To a stirred solution of 3.2 g (0.043 mol) of *N*-methylethanolamine (NMEA) in 100 ml of acetone was added at room temperature 5.0 g (0.020 mol) of picryl chloride in 30 ml of acetone. After an additional 4 hrs' stirring at 40°C, the mixture was poured into 200 ml of ice-water, filtered, and dried. Recrystallization from methanol yielded 5.0 g of IV (86%, based on picryl chloride), mp 138.0—139.0 °C. IR (Nujol): ν_{OH} 3570, 3400 cm^{-1}, ν_{NO_2} 1516, 1332 cm^{-1}, ν_{Ar-N} 1352 cm^{-1}. NMR: τ_{Me_4Si} 5.46 (s, 1H, H^D).

The formation of 1-[2'-(*N*-methylamino)ethoxy]-2,4,6-trinitrobenzene was excluded by the evidence that in the IR spectrum of IV the band attributable to the ether bond [C(sp^2)-O-C(sp^3)] was not found by comparison of the spectrum of picryl ethyl ether.[13]

1-[N-*Methyl-(2'-hydroxy)ethylamino*]-*2,4-dinitronaphthalene (V)*. To a stirred solution of 3.2 g (0.043 mol) of NMEA in 50 ml of acetone was added at room temperature 5.0 g (0.020 mol) of 2,4-dinitro-1-naphthyl chloride (DNC) in 50 ml) of acetone. After the temperature had been raised to 40°C, the mixture was stirred for 8 hr. Then, the mixture was poured into 300 ml of ice-water. The aqueous mixture was extracted with three 50 ml portions of benzene. After drying of the benzene solution over calcium chloride, the distillation of benzene produced crude V. Further, chromatographic separation was carried out on a column of sicila gel. Recrystallization from diethyl ether-petroleum ether yielded 4.0 g (69%, based on DNC), mp 77.0—77.5°C. IR (Nujol): ν_{OH} 3518 cm^{-1}, ν_{NO_2} 1510, 1305 cm^{-1}, ν_{Ar-N} 1305 cm^{-1}. NMR: τ_{Me_4Si} 5.18 (s, 1H, H^D). Found: C, 53.33; H, 4.66%. Calcd for $C_{13}H_{13}N_3O_5$: C, 53.61; H, 4.50%.

The formation of 1-[2'-(*N*-methylamino)ethoxy]-2,4-dinitronaphthalene was excluded by comparison of IR spectra of IV and DNEE.[9]

Preparation of spiro Meisenheimer Complexes (II and III). A typical procedure is noted below in the case of III. When 7 ml (0.0045 mol) of methanolic sodium methoxide (0.638 mol/l) was added to a stirred solution of 1.310 g (0.0045 mol) of V in 30 ml of methanol at room temperature under nitrogen stream, the solution became red immediately. After an additional 30 mins' stirring, the solution was concentrated by evaporation of methanol at 30°C under reduced pressure. Further, the precipitate was filtered, washed with three 20 ml portions of diethyl ether in a dry box. After that, the precipitate was dried. Yield 1.0 g (71%, based on V). The complex (II) was obtained by the same method in a 65% yield. Found: C, 50.22; H, 3.62; N, 13.22%. Calcd for $C_{13}H_{12}N_2O_5Na$ (III): C, 49.84; H, 3.86; N, 13.41%. Found: C, 38.62; H, 4.01; N, 16.46%. Calcd for $C_9H_9O_7N_4Na\cdot\frac{1}{2}(C_4H_{10}O)$ (II): C, 38.26; H, 4.08; N, 16.23%.

Acid decomposition of spiro Meisenheimer Complexes (II and III). When an equimolar amount of hydrochloric acid in 10 ml of methanol was added to a stirred solution of 0.50 g (0.0014 mol) of II in 15 ml of methanol at room temperature, the mixture became immediately yellow. This mixture was poured into 200 ml of ice-water, filtered, and dried. Thin layer chromatography and mixed melting point test proved this compound to be IV. Yield 0.40 g (98%) for crude IV. The same treatment of 0.5 g (0.0016 mol) of III yielded 0.45 g (97%) of crude V.

10) R. C. Farmer, *J. Chem. Soc.*, **1959**, 3433.
11) J. B. Ainscough and E. F. Caldin, *ibid.*, **1956**, 2456.
12) J. F. Bunnett and R. E. Zahler, *Chem. Rev.*, **49**, 273 (1951).
13) R. Foster and C. A. Fyfe, *Tetrahedron*, **21**, 3363 (1965).

BULLETIN OF THE CHEMICAL SOCIETY OF JAPAN, VOL. 46, 695—696 (1973)

The Photochemical Reactions of Tetrahydrofuran and Tetrahydrothiophene with Sulfur Dioxide

Hiroshi TAKEUCHI*, Toshikazu NAGAI**, and Niichiro TOKURA

Department of Applied Chemistry, Faculty of Engineering, Osaka University, Suita, Yamada-kami, Osaka

(Received May 29, 1972)

The reaction of photochemically-excited sulfur dioxide (SO_2) with paraffins and olefins has been studied by a number of investigators.[1-7] Calvert and his co-workers[6,7] concluded that the excited triplet SO_2 molecule is the most important reactant leading to the product formation in the above systems. Though Dainton and Ivin[1] thought that sulfinic acids are the main products of the above reactions, there was no assurance that the products were thermally-unstable sulfinic acids. Dunken and Winde[8,9] reported the formation of a charge-transfer complex between ether and SO_2. We have initiated studies aimed at the confirmation of the photochemical products in the reaction of tetrahydrofuran (THF) with SO_2.

In the dark, no product was formed in the system of THF and SO_2, but a photochemical reaction in the above system yielded two new compounds, di-2-tetrahydrofurylsulfone (I) and 2-tetrahydrofuran-sulfinic acid (II). Since these products were unstable under atmospheric conditions, they were confirmed by the method to be described in the experimental section.

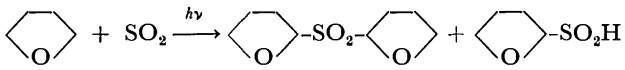

(I) (II)

The results are indicated in Table 1. The formation of I and II was observed in experiments using various irradiation sources under both degassed and aerial conditions.

The experiment using tetrahydrothiophene (THT) in place of THF was carried out to see if sulfone or sulfinic acid could be formed. The new compound, di-2-tetrahydrothiophenylsulfone (IV), was obtained in a low yield. In this reaction, the formation of sulfinic acid could not be observed. The mechanism of this reaction is ambiguous, but one possible explanation of the low reactivity of THT with SO_2 may depend upon the more reactive C–H bond at the transition state in the reaction of THF with SO_2 in comparison with the C–H bond in that of THT with SO_2.

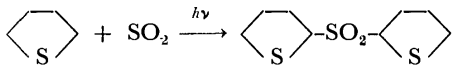

(IV)

Since the products, I, II, and IV, were formed by the selective reactions of SO_2 at the 2-positions of THF and THT, these ractions were interesting synthetically.

Experimental

A solution of THF and SO_2 in a quartz pressure-vessel was irradiated at 0°C under the conditions shown in Table 1. The solvent was distilled under reduced pressure, and the residue was recrystallized from cyclohexane to give di-2-tetrahydrofurylsulfone (I) (mp 68—70°C). Since product I was unstable under atmospheric conditions, it was immediately analyzed after drying under a vacuum. IR (Nujol):

TABLE 1. PHOTOCHEMICAL REACTION OF THF WITH SO_2

THF (g)	SO_2 (g)	Surrounding conditions	Irradiation source[a]	Irradiation time (hr)	Products (g)	
					I	Anilinium salt of II
106	42	Degassed	H 600 W	10	12.3	—
102	41	Degassed	H 300 W	15	8.6	3.7
80.5	24.5	Aerial	H 300 W[b]	10.5	3.5	0.9
130	46.5	Aerial	H 600 W	10	12.3	—
98	38.7	Aerial	H 600 W	5	2.7	13.5
89	35.1	Degassed	L 120 W	23	2.7	7.5

a) H: High-pressure mercury lamp. L: Low pressure mercury lamp. b) Use of a Pyrex filter.

* Present address: Department of Synthetic Chemistry, Faculty of Engineering, Shinshu University, Wakazato, Nagano.

** Present address: College of General Education, Osaka University, Toyonaka, Osaka.

1) a) F. S. Dainton and K. J. Ivin, *Trans. Faraday Soc.*, **46**, 374 (1950). b) F. S. Dainton and K. J. Ivin, *ibid.*, **46**, 382 (1950).

2) H. S. Johnston and K. D. Jain, *Science*, **131**, 1523 (1960).

3) Y. Ogata, Y. Izawa, and T. Tsuda, *Tetrahedron*, **21**, 1349 (1965).

4) Y. Ogata, Y. Izawa, and T. Tsuda, This Bulletin, **38**, 1984 (1965).

5) R. B. Timmons, *Photochem. Photobiol.*, **12**, 219 (1970).

6) C. C. Badcock, H. W. Sidebottom, J. G. Calvert, G. W. Reinhardt, and E. K. Damon, *J. Amer. Chem. Soc.*, **93**, 3115 (1971).

7) H. W. Sidebottom, C. C. Badcock, J. G. Calvert, B. R. Rabe, and E. K. Damon, *ibid.*, **93**, 3121 (1971).

8) H. Dunken and H. Winde, *Z. Physik. Chem.*, **56**, 303 (1967).

9) H. Dunken and H. Winde, *ibid.*, **58**, 246 (1968).

1140 and 1310 cm^{-1} (ν_{SO_2}), and 1060 cm^{-1} (ν_{C-O}); NMR in CCl_4 (τ): 4.8—5.1 (m, 2H, methine), 5.7—6.2 (m, 4H, $-OCH_2-$), and 7.4—8.3 (m, 8H, methylene); Found: C, 46.47; H, 6.92%; mol wt, 211 (by the vapor-pressure method) and 206 (by hydrolysis using aqueous *ca.* 0.3 N NaOH). Calcd for $C_8H_{14}O_4S$: C, 46.58; H, 6.84;% mol wt, 206.3. Mass spectrum: *m/e*; 188 (M^+-H_2O), 96, 70 (dihydrofuran$^{+\cdot}$), 64 ($\overset{+\cdot}{S}O_2$), 48 ($\overset{+\cdot}{S}O$), 41, and 39 (the cyclopropenium ion). The residue obtained after the separation of I was neutralized with aniline. The precipitate which there upon appeared was filtered off and crystallized from benzene to give an anilinium salt of 2-tetrahydrofuransulfinic acid (II), Compound III (mp 102—104°C). After it had been dried under a vacuum, the structure of III was

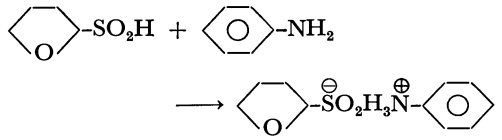

(III)

confirmed from the following data. IR (Nujol): 940 and 1020 cm^{-1} ($\nu_{\overset{\ominus}{SO_2}}$), and 1500 and 1610 cm^{-1} ($\nu_{\overset{\oplus}{NH_3}}$); NMR in $CDCl_3$ (τ): 1.6 (s, 3H, $-\overset{+}{N}H_3$), 2.7—2.9 (m, 5H, aromatic), 5.8—6.05 (t, $J=3$ Hz, 1H, methine), 6.1—6.4 (t, $J=6$ Hz, 2H, $-OCH_2-$), and 7.7—8.4 (m, 4H, methylene); Mass spectrum: *m/e*; 93 ($Ph\overset{+\cdot}{N}H_2$), 70 (dihydrofuran$^{+\cdot}$), 64 ($\overset{+\cdot}{S}O_2$), and 48 ($\overset{+\cdot}{S}O_2$); Found: C, 52.27; H, 6.53; N, 6.21%. Calcd for $C_{10}H_{15}NO_3S$: C, 52.38; H, 6.59; N, 6.11%. The neutralization equivalent was determined with NaOH in an aqueous solution; Found: 220. Calcd: 229.3.

A solution of THT (100 g) and SO_2 (24 g) in a quartz pressure vessel was irradiated by a high-pressure mercury lamp (600 W) for 7 hr at 0°C under degassed conditions. Di-2-tetrahydrothiophenylsulfone (IV) was thus obtained in a low yield (85 mg); mp 137—139°C (recrystallized from methanol). Th structure of IV was confirmed from the following data. IR (Nujol): 1130 and 1300 cm^{-1} (ν_{SO_2}); NMR in $CDCl_3$ (τ): 4.9—5.15 (m, 2H, methine), 6.8—7.15 (m, 4H, $-CH_2S-$), and 7.2—8.0 (m, 8H, methylene); Found: C, 40.35; H, 5.71%. Calcd for $C_8H_{14}O_2S_3$: C, 40.31; H, 5.92%. Mass spectrum: *m/e*; 238 (M^+), 174 (M^+-SO_2), 87, 86 (dihydrothiophene$^{+\cdot}$), 64 ($\overset{+\cdot}{S}O_2$), 59, 58, 53, and 45 ($^+S{\equiv}CH$).

BULLETIN OF THE CHEMICAL SOCIETY OF JAPAN, VOL. 46, 696—698 (1973)

Michael Cycloaddition of 2-Phenylethene-1-sulfonamide with Carbon Disulfide[1)]

Kiyoshi HASEGAWA, Tadashi SASAKI,* and Syuzi HIROOKA

Department of Industrial Chemistry, Faculty of Engineering, Toyama University, Takaoka-shi

** Institute of Applied Organic Chemistry, Faculty of Engineering, Nagoya University, Furo-cho, Chigusa-ku, Nagoya*

(Received November 1, 1972)

In the preceding paper,[2)] we reported that 2-phenylethene-1-sulfonamide **1** reacts with carbon disulfide and alkyl halide in the presence of base giving 3-alkylthio-5-phenyl-1,1-dioxo-5,6-dihydro-1,4,2-dithiazines **4**. The postulated mechanism for the formation of **4** involves an intermediary sodium salt of

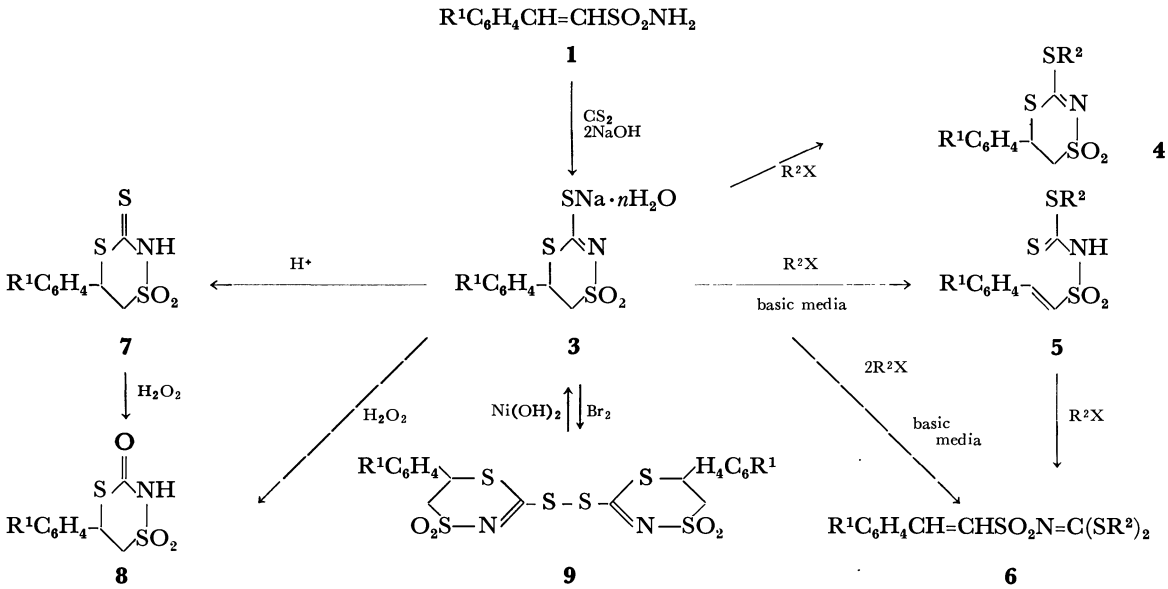

Scheme 1.

1) Presented at the 27th Annual Meeting of the Chemical Society of Japan, Nagoya, 12, October(1972). No. 2NO2.

2) K. Hasegawa and S. Hirooka, This Bulletin, **45**, 1567 (1972).

3-mercapto-5-phenyl-1,1-dioxo-5,6-dihydro-1,4,2-dithiazine **3**, which is intramolecular Michael cycloadduct of 2-phenylethene-1-sulfonyliminodithiocarbonate **2** ($R^1C_6H_4CH{=}CHSO_2N{=}C(S^-Na^+)_2$). This paper describes the isolation of **3** and the syntheses of some new derivatives from **3**. The process is outlined in Scheme 1.

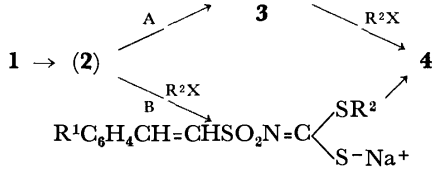

Results

The hydrates of the Michael cycloadducts **3** (n= 1,2) were isolated from the reaction mixture of **1**, sodium hydroxide and carbon disulfide. The results are given in Table 1. As regards the mechanism for the formation of **4**, the following two paths **A** and B are conceivable.

Isolation of **3** supports path **A** in which highly reactive intermediate **2** undergoes rapid ring-closure giving **3** followed by alkylation. The C–S bond in **3** could not be cleaved by strong bases, **3** being recrystallized from a 1 N sodium hydroxide solution. The structure of **3** was determined on the basis of analytical and spectral data. In the NMR pattern of **3a**, ring protons, $H_AH_CH_B$, showed an ABX spin system consisting of three quartets of H_A centered at δ 3.06, H_C 3.39 and H_B 4.79 (J_{AC}=13.5 Hz, J_{AB}=13.0 Hz, J_{BC}=3.6 Hz). Monoalkylation of **3** in 50% ethanol afforded **4** in a yield greater than 89% (R^1=H, p-Cl, p-Br, p-CH_3, R^2=CH_3), but the reverse Michael cycloadducts of **4**, *N*-(2-phenylethene-1-sulfonyl)-dithiocarbamates **5** were obtained in a strong alkali (R^1=H, p-Cl, p-CH_3, R^2=CH_3). Dialkylation of **3** in strongly basic media afforded alkyl 2-phenylethene-1-sulfonyliminodithiocarbonates **6** which were the same

Table 1. 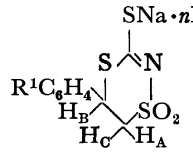 **3**

Compd.	R^1	Weight loss (%)[a] Found	Weight loss (%)[a] Calcd	n	Yield (%)	Mp (°C)	Found (%) C	Found (%) H	Found (%) N	Calcd (%) C	Calcd (%) H	Calcd (%) N
3a	H	12.1	11.3	2	67	245—247	33.92	3.70	4.37	34.06	3.81	4.41
3b	p-Cl	5.1	5.4	1	58	250—252	32.12	3.01	3.93	32.38	2.72	4.20
3c	p-Br	4.4	4.7	1	55	245—247	28.80	2.66	3.44	28.57	2.40	3.70
3d	p-CH_3	5.0	5.4	1	95	241—243	38.34	3.98	4.20	38.33	3.96	4.47

a) Mitamura 2-100-S type DTA apparatus was used and weight loss (%) was determined by heating hydrates **3** above 130°C.

Table 2. $R^1C_6H_4CH_B{=}CH_ASO_2N{=}C(SR^2)_2$ **6**

Compd.	R^1	R^2	Yield (%)	Mp (°C)	Found (%) C	Found (%) H	Found (%) N	Calcd (%) C	Calcd (%) H	Calcd (%) N
6a	H	CH_3	70	95— 96	45.76	4.42	4.97	46.00	4.56	4.88
6b	p-Cl	CH_3	72	129—130	41.35	3.77	4.50	41.10	3.76	4.36
6c	p-CH_3	CH_3	69	134—135	48.10	4.91	4.89	47.84	5.02	4.65

Table 3. 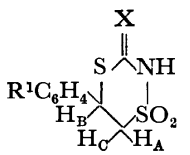 **7, 8**

Compd.	R^1	X	Yield (%)	Mp (°C)	Found (%) C	Found (%) H	Found (%) N	Calcd (%) C	Calcd (%) H	Calcd (%) N
7a	H	S	81	67— 69	41.49	3.40	5.38	41.71	3.50	5.40
7b	p-Cl	S	77	102—105	36.96	3.01	3.93	36.79	2.72	4.20
7c	p-CH_3	S	75	69— 71	44.23	3.98	5.02	43.96	4.06	5.13
8a	H	O	67	164—165	44.26	3.65	5.70	44.45	3.73	5.76
8b	p-Cl	O	68	172—173	39.03	2.91	5.30	38.92	2.90	5.04
8c	p-Br	O	73	159—161	33.82	2.51	4.43	33.56	2.50	4.35
8d	p-CH_3	O	83	170—171	46.98	4.29	5.32	46.70	4.31	5.45

TABLE 4. 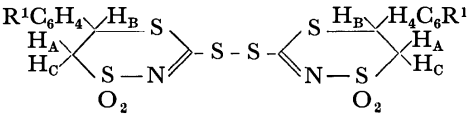 **9**

Compd.	R^1	Yield (%)	Mp (°C)	Found (%)			Calcd (%)		
				C	H	N	C	H	N
9a	H	98	215—218	41.86	3.29	5.35	41.84	3.12	5.42
9b	*p*-CH_3	93	208—210	44.34	3.89	5.30	44.09	3.60	5.14

as alkylation products of **5** (Table 2). Acidification of aqueous solution of **3** under cooling gave yellow analytically pure crystals of 3-thio-5-phenyl-2,3,5,6-tetrahydro-1,1-dioxo-1,4,2-dithiazines **7** (Table 3). Cycloadducts **3** and **7** were desulfurized with alkaline hydrogen peroxide to give 5-phenyl-2,3,5,6-tetrahydro-1,1,3-trioxo-1,4,2-dithiazines **8** (Table 3). Oxidation of **3** with bromine afforded 3,3'-bis(5-phenyl-1,1-dioxo-5,6-dihydro-1,4,2-dithiazinyl)disulfides **9** (Table 4) whose S–S bonds were cleaved by reduction with nickel hydroxide[3] in basic media to give **3** again. The structures of the new compounds **6**, **7**, **8**, and **9** were determined on the basis of analytical and spectral data.

Experimental

Sodium Salt of 3-Mercapto-5-phenyl-1,1-dioxo-5,6-dihydro-1,4,2-dithiazine ***3a***. To a stirred solution of **1** (5.50 g, 0.030 mol) in DMF (60 ml) was added a solution of NaOH (2.40 g, 0.060 ml) in water (4.0 ml) and then CS_2 (3.40 g, 0.045 mol) at 20—30°C. The reaction mixture was stirred for 2 hr at room temperature. Evaporation of the DMF *in vacuo* left a dark red residue, into which 1N NaOH solution (100 ml) was added, and the solution was cooled overnight. The crystal was collected to give 6.30 g (67%) of **3a** as dihydrate. Recrystallization from 1N NaOH solution gave a colorless crystal. IR(KBr): 3570 and 3440 (dihydrate), 1385, 1135, and 1110 (SO_2) cm^{-1}. NMR (acetone-d_6): δ 3.06 (q, 1H, H_A), 3.39 (q, 1H, H_C), 4.79 (q, 1H, H_B), J_{AC}=13.5 Hz, J_{AB}=13.0 Hz, J_{BC}=3.6 Hz, 7.35 (s, 5H, phenyl).

Dimethyl N-(2-p-chlorophenylethene-1-sulfonyl)iminodithiocarbonate ***6a***. To a stirred solution of **3b** (0.33 g, 0.0010 mol) in methanol (8 ml) and 0.5 N NaOH solution (4 ml) was added drop by drop two equivalents of dimethyl sulfate (0.28 g, 0.0022 mol) at 0—10°C, after which the reaction mixture was stirred for 2 hr at 0—10°C. The precipitate was collected to give 0.23 g (72%) of **6b**. IR (KBr): 3040 (=CH), 1620 (C=C), 1460 (N=C), 1305 and 1140 (SO_2) cm^{-1}. NMR ($CDCl_3$): δ 2.59 (6H, SCH_3), 6.88 (1H, H_A), 7.52 (1H, H_B), J_{AB}=15.2 Hz, 7.34 (s, 4H, phenyl). When one equivalent of dimethyl sulfate (0.14 g, 0.0011 mol) *vs* **3b** was used, 0.18 g (59%) of the dithiocarbamate was obtained on acidification of the alkaline aqueous layer. mp 113—116°C (lit.[2], 114—117°C).

3-Thio-5-phenyl-1,1-dioxo-2,3,5,6-tetrahydro-1,4,2-dithiazine ***7a***. IR (KBr): 3080 (NH, broad), 1330 and 1140 (SO_2) cm^{-1}. NMR (acetone-d_6): δ 3.81 (q, 1H, H_A), 3.98 (q, 1H, H_C), 5.09 (q, 1H, H_B), J_{AC}=13.8 Hz, J_{AB}=11.0 Hz, J_{BC}=5.8 Hz, 6.62 (1H, NH), 7.43±0.07 (5H, phenyl). MS *m/e*: 258.9783 (M^+, calculated for $C_{10}H_9NO_2S_3$: 258.9765).

5-Phenyl-1,1,3-trioxo-2,3,5,6-tetrahydro-1,4,2-dithiazine ***8a***. To a stirred solution of **3a** (0.48 g, 0.0015 mol) in acetone (2.0 ml) was added drop by drop a 30% hydrogen peroxide solution (0.21 g, 0.0060 mol) at 0—10°C, after which the reaction mixture was stirred for 3 hr at room temperature. The acetone was evaporated *in vacuo*, and the solution was acidified with concentrated hydrochloric acid to afford 0.24 g (67%) of **8a**. Analogously, **8a** was also formed in 59% yield from **7a** (0.26 g, 0.0010 mol), 0.5 N NaOH solution (6.0 ml) and 30% hydrogen peroxide solution (0.47 g, 0.0040 mol). IR (KBr): 2960 (NH), 1630 (C=O), 1330 and 1150 (SO_2) cm^{-1}. NMR (DMSO-d_6): δ 4.06 (q, 1H, H_A), 4.22 (q, 1H, H_C), 4.99 (q, 1H, H_B), J_{AC}=13.0 Hz, J_{AB}=10.8 Hz, J_{BC}=5.8 Hz, 5.77 (1H, NH), 7.46± 1.20 (5H, phenyl). MS *m/e*: 243 (M^+).

3,3'-Bis(5-phenyl-1,1-dioxo-5,6-dihydro-1,4,2-dithiazinyl) disulfide ***9a***. To a stirred solution of **3a** (0.66 g, 0.0021 mol) in DMF (5.0 ml) was added bromine (0.19 g, 0 0012 mol) at 0—10°C. After being stirred for 3 hr at 0—10°C, the reaction mixture was poured into ice water (100 ml) and kept overnight. The precipitate was collected to give 0.53 g (98%) of an analytically pure crystal. IR (KBr): 1520 (N=C), 1320 and 1140 (SO_2) cm^{-1}. NMR (DMSO-d_6): δ 4.09 (q, 2H, H_A), 4.41 (q, 2H, H_C), 5.43 (q, 2H, H_B), J_{AC}=14.0 Hz, J_{AB}=12.0 Hz, J_{BC}=4.1 Hz, 7.54± 0.03 (10H, phenyl).

3) S. Hirooka, K. Hasegawa, T. Kodama, K. Hisada, and H. Kodama, *Nippon Kagaku Zasshi*, **91**, 270 (1970).

BULLETIN OF THE CHEMICAL SOCIETY OF JAPAN, VOL. 46, 699—700 (1973)

The Decomposition Product of Ethyl 2-Cyano-3-mercapto-3-methylthioacrylate

Masataka YOKOYAMA* and Shigeki HONGO

Department of Chemistry, Faculty of Science, Chiba University, Yayoi-cho, Chiba

(Received October 2, 1972)

2-Cyano-3-mercapto-3-methylthioacrylamide is stable but the 2-cyano-3-mercapto-3-methylthioacrylic acid ethyl ester (**1**) obtained as colorless needles has been found to be unstable and to change easily into a stable yellow material after being left standing for several hours at room temperature.[1] The present work was undertaken in order to determine the structure of the yellow material derived from **1**.

It was found that heating solution (in EtOH or CS_2) of **1** gave yellow material (**2**), which was also synthesized by adding hydrogen sulfide to disulfide (**3**) prepared by oxidizing **1** with ammonium persulfate.

Structural assignments of **2** and **3** were made on the basis of elemental analysis, IR and NMR spectra. The NMR spectrum (DMSO-d_6) of **3** showed two signals due to two methylthio groups at δ 2.77 and δ 2.63, two quartet signals at δ 4.25 and δ 4.23, and two triplet signals at δ 1.27 and δ 1.25 which were assignable to the two ethyl groups. The following three structures can be considered for **3**.

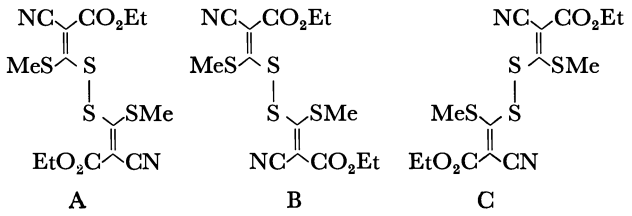

A B C

It was demonstrated by tlc that **3** was not a mixture of geometrical isomers. The above results supported the view that **3** has the structure of B, for only B has nonequivalent methylthio and ethyl groups. Hence, the structure of **3** was determined to be diethyl (1*Z*, 5*E*)-1,6-dicyano-2,5-bis(methylthio)-3,4-dithia-1,5-hexadiene-1,6-dicarboxylate.

In the IR spectrum (KBr) of **2**, the absorptions of 3305, 3190, 3150, and 2195 cm^{-1} suggested the presence of the amino group and the conjugated cyano group. The NMR spectrum (DMSO-d_6) of **2** showed two broad amino signals (δ 10.70 and 9.68) disappearing on deuterium exchange and two sharp singlet singlas (δ 2.87 and 2.33) due to two methylthio groups. The spectroscopic evidence revealed the presence of the two nonequivalent thiocarbamoyl groups. The result of tlc revealed that **2** existed as two geometrical isomers (see Experimental). Hence, the decomposition products were tentatively assigned to the structures of diethyl (1*E*, 5*E*)-6-cyano-2,5-bis(methylthio)-1-thiocarbamoyl-3,4-dithia-1,5-hexadiene-1,6-dicarboxylate (**2a**) and diethyl (1*Z*, 5*Z*)-6-cyano-2,5-bis(methylthio)-1-thiocarbamoyl-3,4-dithia-1,5-hexadiene-1,6-dicarboxylate (**2b**).

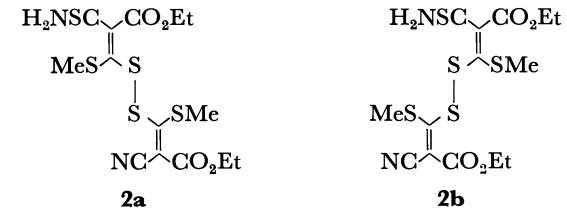

2a **2b**

Compounds **2a** and **2b** were not separated.

Pyridine cleaved both **2** and **3** to give pyridinium salt of **1** (**5**). Compounds **1**, **2**, and **3**, treated with phenylhydrazine, gave 5-amino-4-ethoxycarbonyl-3-methylthio-1-phenyl-1,2-pyrazole (**4**). The chemical reactivities also supported the structure of **2**.

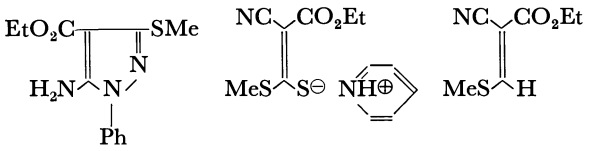

4 **5** **6**

The decomposition reaction of **1** could not be carried out in a sealed tube *in vacuo* without the irradiation of an ultraviolet ray (234 nm). On the other hand, the reaction could be depressed by the addition of hydroquinone as a radical trapping reagent. A small amount of ethyl (*E*)-2-cyano-3-methylthioacrylate (**6**) was isolated as a by-product of the decomposition reaction of **1**. This suggests that **1** is degraded by a radical mechanism.

Experimental

Compound **1** was prepared according to the method of Gompper and Töpfel.[2] The NMR spectra were recorded with a JNM-4H-100 MHz spectrometer, using tetramethylsilane as an internal standard. The IR, UV and mass spectra were recorded with Nihon Densi 403 G, Hitachi EPS-3T, and Hitachi Double Focus RMU-6E, respectively. Microanalyses were carried out at the Institute of Physical and Chemical Research.

*Preparation of **2a** and **2b**.* A mixture of **1** (7.55 g) and carbon disulfide or ethanol (100 ml) was refluxed for 1 hr. The crude material was collected by filtration, washed with ethanol and recrystallized from ethanol to give 1.40 g of yellow needles: yield 17%; mp 136—138°C; UV max (99% EtOH) 224 nm (log ε 4.25), 240 (sh, 4.16), 294 (sh, 4.14), 334 (4.53); NMR (DMSO-d_6) δ 10.70, 9.68 (br, 2, NH_2), 4.40, 4.38, 3.98, 3.96 (q, 2, CH_2, J=7.5 Hz), 2.89, 2.87, 2.33, 2.30 (s, 3, SCH_3), 1.35, 1.32, 1.15, 1.12 (t, 3, CH_3, J=7.5 Hz).

Found: C, 38.02; H, 4.15; N, 6.35; S, 36.52%; mol wt (Rast), 440. Calcd for $C_{14}H_{18}N_2S_5O_4$: C, 38.33; H, 4.15;

1) M. Yokoyama, This Bulletin, **44**, 1610 (1971).

2) R. Gompper and W. Töpfel, *Chem. Ber.*, **95**, 2861 (1962).

N, 6.38; S, 36.55%; mol wt, 438.62.

Compound **2** also was obtained when an ultraviolet light of 234 nm was irradiated on a sealed tube *in vacuo* containing **1** for 16 hr by using a minerallight UVSL-25 (Ultraviolet Products Inc. 13.8 W).

When **2** was examined by tlc with methanol and benzene (1 : 3) as a developing solvent, two spots (R_f: 0.72, 0.70) could be recognized.

*Conversion of **3** into **2**.* Compound **3** was prepared by the method of Gompper and Töpfel[2]: **1** (9.2 g, 45 mmol) was dissolved in 100 ml of 2% sodium hydroxide solution. To the resulting mixture was added aqueous ammonium persulfate solution (10.3 g of ammonium persulfate in 50 ml of water) dropwise under stirring. Stirring was continued for several minutes after the addition was complete. The solid product was collected and recrystallized from ethanol to give 3.5 g of colorless plates: yield 38%; mp 125—126°; UV max (99% EtOH) 255 nm (log ε 4.23), 335 (4.61); NMR (DMSO-d_6) δ 4.25, 4.23 (q, 2, C$\underline{H}_2$, J= 2.5 Hz), 2.77, 2.63 (s, 3, SC$\underline{H}_3$), 1.27, 1.25 (t, 3, C$\underline{H}_3$, J= 2.5 Hz).

Into a 200 ml acetone solution containing **3** (4.75 g) was gently passed hydrogen sulfide for 1 hr with stirring at room temperature. The whole was shaken for an additional 1 hr. The yellow crystals were collected and recrystallized from ethanol to give 2.8 g of yellow needles; yeild 54.2%. The IR spectrum coincided with that of **2**.

*Preparation of **4**.* A mixture of **3** (3.2 g, 8 mmol), phenylhydrazine (1.58 ml, 15.8 mmol), and ethanol (25 ml) was refluxed for 45 min. The colorless product was collected and recrystallized from ethanol-water to give 0.41 g of colorless needles; mp 98°C; UV max (99% EtOH) 248 nm (log ε 4.78); IR (KBr) 3440, 3340 (s), 3050 (w), 2985, 2920 (m), 1668 (vs), 1605 (vs), 1525 cm^{-1} (vs); NMR (DMSO-d_6) δ 7.50 (m, 5, C$_6\underline{H}_5$), 6.30 (br, 2, N$\underline{H}_2$), 4.20 (q, 2, C$\underline{H}_2$, J= 6 Hz), 2.38 (s, 3, SC$\underline{H}_3$), 1.25 (t, 3, C$\underline{H}_3$, J=6 Hz).

Found: C, 56.24; H, 5.44; N, 15.28; S, 11.52%; mol wt (Rast), 276. Calcd for $C_{13}H_{15}N_3SO_2$: C, 56.27; H, 5.49; N, 15.15; S, 11.56%. mol wt, 277.4.

*Preparation of **5**.* 11.35 g of **5** was obtained as yellowish prisms by dissolving **1** (9.75 g, 50 mmol) in pyridine, followed by the addition of ether. Compound **5** decomposed at 120—130°C; UV max (99% EtOH) 223.5 nm (log ε 4.73), 289 (4.57), 343.8 (5.06); IR (KBr) 3240, 3180 (m), 3080 (s), 2200 (vs), 1640 (vs), 1530 cm^{-1} (vs); NMR (DMSO-d_6) δ 8.65 (t, 2, C(2,6)$\underline{H}$, J=8 Hz), 8.10 (t, 3, C(3,4,5)$\underline{H}$, J= 8 Hz), 7.35 (br, 1, N$\underline{H}^{\oplus}$), 4.02 (q, 2, C$\underline{H}_2$, J=6 Hz), 2.38 (s, 3, SC$\underline{H}_3$), 1.18 (t, 3, C$\underline{H}_3$, J=6 Hz). The signal of δ 7.35 disappeared on deuterium exchange. Compound **1** was recovered by adding dilute hydrochloric acid to the aqueous solution of **5**. Compound **5** was also obtained by the above method from **2** and **3** in yields of 98% and 48%, respectively.

*Isolation of Ethyl (E)-2-cyano-3-methylthioacrylate (**6**).* A mixture of **1** (1.36 g) and 50 ml of ethanol was refluxed for 20 min. 0.82 g of **2** was filtered off and the resulting filtrate was evaporated with a vacuum evaporator to give a red oil, which was then extracted by shaking with two 50 ml portions of ether. A small amount of yellow crystal was obtained from the extracted ether and recrystallized from *n*-hexane to give yellowish plates; mp 68—69°C; UV max (99% EtOH) 304 nm (log ε 4.21); IR (KBr) 3005 (m), 2980, 2919 (m), 2210 (s), 1705 (vs), 1538 cm^{-1} (vs).

Found: C, 49.33; H, 5.02; N, 8.06; S, 18.63%; mol wt (mass spectrum) 171. Calcd for $C_7H_9NOS_2$: C, 49.11; H, 5.32; N, 8.18; S, 18.73%; mol wt, 171.23. A vinyl proton at δ 8.87 is just in the range expected for one of the *E*-form.[3]

*Geometrical Structure of **1**.* The NMR spectrum of **6** showed a singlet signal due to methylthio group at δ 2.70. The two singlet signals due to the two methylthio groups of ethyl 2-cyano-3,3-bis(methylthio)acrylate were observed at δ 2.72 and 2.52, which seem assignable to the *cis* methylthio group and the *trans* methylthio group with respect to the cyano group, respectively. This supports the conclusion that **1** in DMSO-d_6 can exist only in **1a** because the NMR spectrum of **1** shows a singlet signal at δ 2.70. The chemical shifts are summarized as follows:

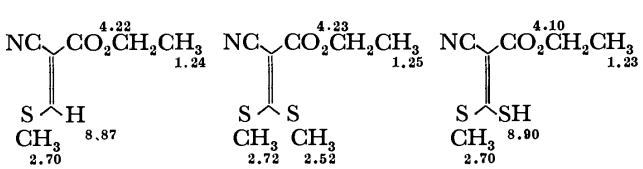

6 **1a**

3) V. E. Matter, C. Pascual, E. Pretsch, A. Pross, W. Simon, and S. Sternhell, *Tetrahedron*, **25**, 691 (1969).

Electron Spin Resonance Study on Photoinduced Changes of the Radicals Produced in Methyl Isocyanate Solid Irradiated with γ-Rays

Masato FUJIWARA, Naoyuki TAMURA,* and Hidefumi HIRAI

Department of Industrial Chemistry, Faculty of Engineering, The University of Tokyo, Bunkyo-ku, Tokyo
**Takasaki Radiation Chemistry Research Establishment, Japan Atomic Energy Research Institute, Takasaki*

(Received April 24, 1972)

Free radicals in the γ-irradiated solid of methyl isocyanate at -196°C have been studied by electron spin resonance (ESR) at $-196\sim-100$°C. An oriented solid of methyl isocyanate was prepared by solidification of methyl isocyanate around an aluminum rod under cooling. The original radical and trapped electron produced by γ-irradiation were recorded at -196°C in the dark. The original radical produced in the oriented solid gave a resonance pattern consisting of a triplet of triplets and was assigned to $\cdot CH_2NCO$ radical. This was converted completely into a new radical on irradiation with visible light for 90 min. The new resonance pattern consists of a triplet of triplets whose nitrogen and proton splitting constants are 20.0 and 87.4 gauss, respectively. The nitrogen hyperfine splitting was anisotropic and the proton splitting constant agreed with that of methylene imino radical ($H_2C{=}N\cdot$). The new radical was assigned to methylene imino radical. The resonance pattern of $\cdot CH_2NCO$ radical was restored when the temperature was raised up to -120°C. The mutual conversion between the two radicals by visible light and heat was concluded to be a decomposition of $\cdot CH_2NCO$ into $H_2C{=}N\cdot$ and CO, and a recombination of these two moieties.

Recently, several ESR studies on reversible changes of free radicals on irradiation of light and heating have been reported on allylic radical[1] in γ-irradiated polyethylene, isobutyl radical,[2] ethoxy radical,[3] and deuterated acetonitrile anion radical.[4] The photochemical changes of allylic and isobutyl radicals were attributed to an intramolecular transfer of hydrogen. On the other hand, the changes of ethoxy radical and deuterated acetonitrile anion radical were suggested to be decomposition and recombination reactions of the radicals.

The radical produced by γ-irradiation of methyl isocyanate at -196°C has been reported by Chung and Williams.[5] The electron spin resonance (ESR) spectrum was recorded at -196°C after the subsequent irradiation of visible light for a short period and ascribed to $\cdot CH_2NCO$ radical. They used the irradiation of visible light only for the purpose of obtaining a more symmetrical spectrum than that obtained in the dark. A slight orientation effect of the specimen was also noted by them. The change of the radical on irradiation of light and heating, however, has not so far been reported.

The object of this work is to study both the photochemical and thermal changes of the radical in γ-irradiated methyl isocyanate solid by ESR spectroscopy. The radical produced by γ-irradiation and the subsequent exposure to visible light are identified with the aid of the anisotropy of the spectrum and the deuteration of methyl isocyanate. The anisotropy is also examined by use of the oriented solid method which has been found to be useful for ESR measurement of vinyl acetate[6] and isocyanic acid,[7] whose melting points are too low for the preparation of single crystals.

Experimental

Methyl isocyanate (guaranteed reagent grade, Tokyo Chemical Industry Company Ltd.) was purified by vacuum distillation. Deuterated methyl isocyanate (CD_3NCO) was prepared in the following manner.[8] Deuterated acetyl chloride (CD_3COCl) was obtained by heating deuterated acetic acid (CD_3COOD) (degree of deuteration=99%, 20 g) with thionyl chloride under reflux. Sodium azide (24 g) dissolved in isoamyl ether (150 g) was added dropwise to the deuterated acetyl chloride, resulting in deuterated acetyl azide (CD_3CON_3) which was converted into deuterated methyl isocyanate by heating; Total yield=55.0%. The resulting deuterated methyl isocyanate was purified by gas chromatographic fractionation, using a 1 m column of Carbowax 1500. The degree of deuteration was determined as 98.5% with a Hitachi RMU-6 mass spectrometer.

An oriented solid of methyl isocyanate was prepared according to a procedure similar to that used for the preparation of an oriented solid of vinyl acetate.[6] Methyl isocyanate was solidified around an aluminum rod in a glass tube by cooling with liquid nitrogen and was irradiated with ^{60}Co γ-rays (8×10^5—8×10^6 rad) at -196°C.

After γ-ray irradiation, the solidified methyl isocyanate was cleft radially into several pieces, one of which was inserted in a crack of Teflon tube so as to hold the longitudinal axis of the piece, *i.e.* the axis of the mark of aluminum rod, horizontally. The angle between the longitudinal axis of the piece and the direction of the DC magnetic field is referred to as "orientation-angle." Orientation-angle 0 and 90° indicate the axes parallel and perpendicular, respectively, to the magnetic field. The ESR measurement was carried out using a Varian V-4502 X-band spectrometer with 100 KHz field modulation at several different temperatures between

1) S. Ohnishi, S. Sugimoto, and I. Nitta, *J. Chem. Phys.*, **39**, 2647 (1963).
2) M. Iwasaki and K. Toriyama, *ibid.*, **46**, 2852 (1967).
3) Quoted in a paper by V. V. Voevosdky, The 4th International Symposium on Free Radical Stabilization, B-V-1, 1959.
4) K. Takeda and F. Williams, *J. Phys. Chem.*, **74**, 4007 (1970).
5) Y. J. Chung and F. Williams, *ibid.*, **75**, 1893 (1971).
6) H. Hirai and M. Fujiwara, *Nippon Kagaku Kaishi*, **1972**, 986.
7) H. Hirai and M. Fujiwara, This Bulletin, to be published.
8) G. Schroter, *Ber.*, **B-42**, 3357 (1909).

−196 and −100°C. The method described above is referred to as the oriented solid method.

The γ-irradiated solid of methyl isocyanate was exposed to visible light (wave lengths>4000 Å) from an Ushio Denki HB 500/B high pressure mercury lamp in a transparent quartz Dewar vessel at −196°C, using a Dow Corning CS-3-75 filter.

Results

γ-Irradiated Methyl Isocyanate in the Dark. Figure 1 shows the ESR spectra of methyl isocyanate and deuterated methyl isocyanate irradiated with γ-rays (1×10^6 rad) and recorded at −196°C in the dark in a Spectrosil tube. Spectra 1a and 1b correspond to methyl isocyanate and deuterated methyl isocyanate, respectively. No changes in the pattern occurred when the Spectrosil tube was rotated about its longitudinal tube axis in the dc magnetic field. The spectra were unsymmetrical because of the overlapping of a singlet at the center of the spectra.

γ-Irradiated Methyl Isocyanate Exposed to Visible Light for a Short Period. The γ-irradiated methyl isocyanate and deuterated methyl isocyanate exposed subsequently to visible light for 1 min gave spectra 2a and 2b, respectively. Spectrum 2a consists of a set of nine lines which is grouped into a triplet of triplets. Spectrum 2b consists of seven lines with a relative intensity ratio of about 1: 3: 5: 9: 5: 3: 1, the line splitting being 3.5 gauss. The singlet centered at $g=2.002\pm0.001$ disappeared not only on subsequent exposure to visible light for 1 min but also on the storage in the dark at −196°C for a long period (20 hr). This singlet must be the absorption of trapped electron, since its behavior on irradiation of light and its g-value are analogous to those of the trapped electron.[9]

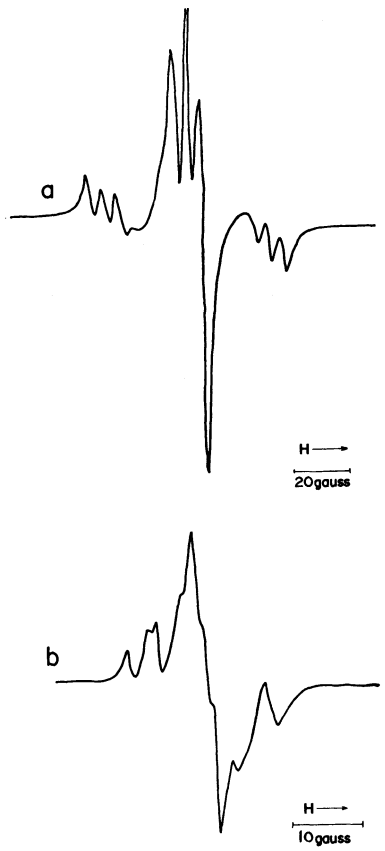

Fig. 1. ESR spectra of methyl isocyanate (a) and deuterated methyl isocyanate (b) irradiated with γ-rays (1×10^6 rad) at −196°C in a Spectrosil tube and measured in the dark.

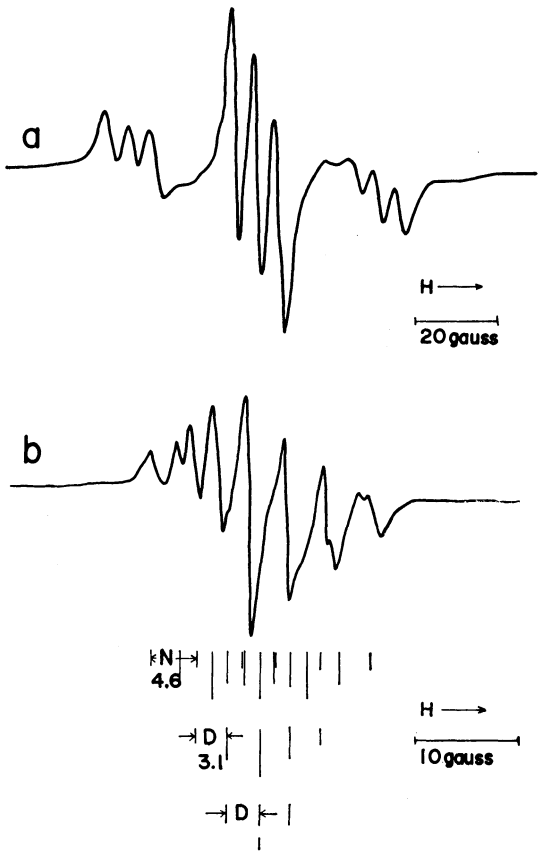

Fig. 2. ESR spectra of methyl isocyanate (a) and deuterated methyl isocyanate (b) irradiated with γ-rays and exposed subsequently to visible light for 1 min.

Theoretical intensity ratios of spectrum 2b whose nitrogen and deuteron splitting constants are 4.6 and 3.1 gauss, respectively, are reconstructed as shown at the bottom of Fig. 2. The line splitting, 3.1 gauss, corresponds to 1/6.65 of the proton splitting at orientation-angle 0°. The intensity ratios of the observed line agrees with theoretical ones.

Figure 3 shows the ESR spectra of the γ-irradiated oriented solid exposed subsequently to visible light for 1 min. The oriented solid method gives the anisotropic spectra when the specimen is rotated in the magnetic field keeping the longitudinal axis horizontal; the outer components of the spectra were anisotropic, while the three central lines were isotropic. The spectrum at orientation-angle 0° (Fig. 3a) consists of a triplet of triplets with a relative integral intensity ratio of 1: 2: 1. The larger triplet and the well-defined 1: 1: 1 triplet splittings were 20.6 and 4.6 gauss, respectively, at orientation-angle 0°. The larger triplet splitting at orientation-angle 45° and 90° could not

9) J. Lin, K. Tsuji, and F. Williams, *J. Amer. Chem. Soc.*, **90**, 2766 (1968).

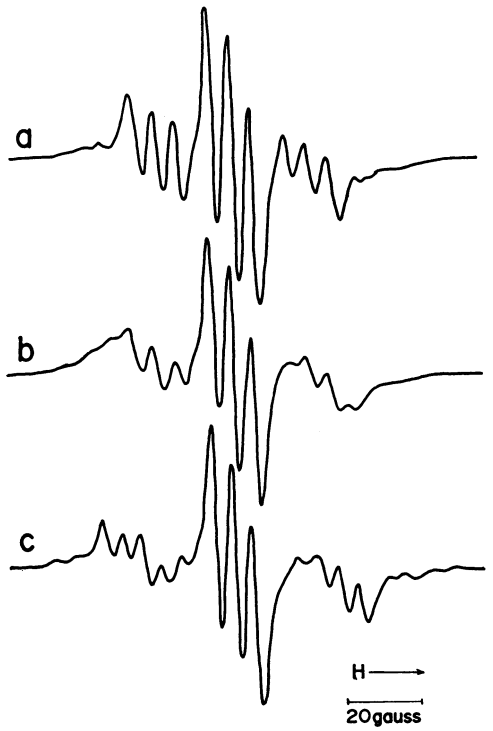

Fig. 3. ESR spectra of oriented solid of methyl isocyanate irradiated with γ-rays and exposed subsequently to visible light with orientation-angles 0° (a), 45° (b), and 90° (c).

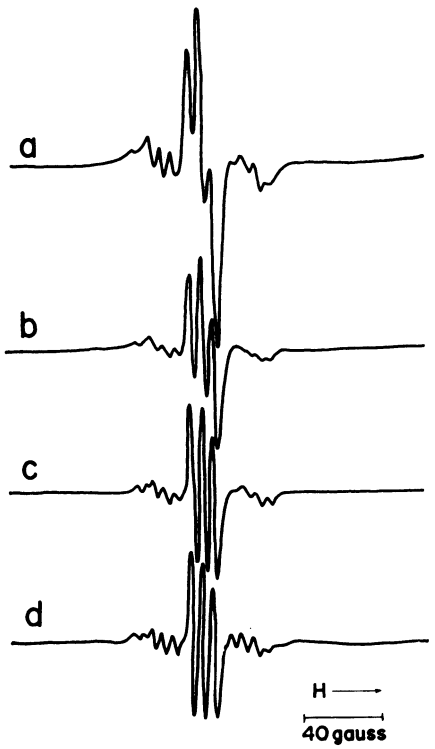

Fig. 4. ESR spectra of methyl isocyanate irradiated with γ-rays and measured at various temperatures; −196°C (a), −180°C (b), −150°C (c), and −120°C (d).

be determined because of broadening of the outer components, while the well-defined triplet splitting of the central components was 4.6 gauss. Elevation of temperature to about −100°C gave no changes in shape except that the singlet disappeared above −180°C as shown in Fig. 4. These results indicate that γ-irradiation of methylisocyanate solid gives only one species of radical, which is hereinafter referred to as Radical **1**.

γ-Irradiated Methyl Isocyanate Exposed to Visible Light for a Long Period. On continuing the irradiation of visible light to the γ-irradiation specimen, a new resonance pattern appeared gradually, accompanied by the disappearance of the original pattern, the changes being completed within 90 min (Fig. 5). The new resonance pattern shown in Fig. 5c was found to consist of a triplet of triplets with a relative integral intensity ratio 1:2:1. The main triplet splitting was 87.4 gauss, which agreed with that of the proton splitting constant of methylene imino free radical.[10] Each line of the main triplet was split into a secondary triplet whose splitting constant was 20.0 gauss. It was observed that the outer lines of each secondary triplet were weak and unsymmetrical, indicating that the hyperfine interaction responsible for this splitting is anisotropic. The new radical produced by the irradiation of visible light is referred to as Radical **2**. The concentration of Radical **1** obtained with spectrum 5a was almost equal to that of Radical **2** obtained with spectrum 5c.

Elevation of temperature of the γ-irradiated specimen exposed subsequently to visible light for 90 min showed a remarkable change in which the resonance pattern

Fig. 5. The changes of ESR spectra of methyl isocyanate irradiated with γ-rays and exposed subsequently to visible light for 5 min (a), 30 min (b), and 90 min (c).

10) E. L. Cochran, F. J. Adrian, and V. A. Bowers, *J. Chem. Phys.*, **36**, 1938 (1962).

of Radical **1** was regenerated, accompanied by the decrease of the pattern of Radical **2** (Fig. 6). The change was completed at −120°C. When the γ-irradiated specimen was warmed at about −120°C without the irradiation of visible light and subsequently exposed to visible light at −196°C for 90 min, the resonance pattern of Radical **2** appeared. This indicates that the mutual change between the two radiacls by visible light and heat was a reversible conversion of radical.

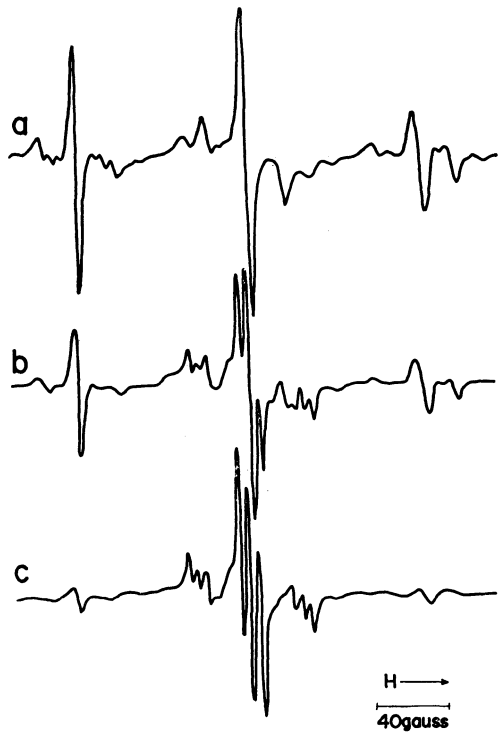

Fig. 6. The changes of ESR spectra of methyl isocyanate irradiated with γ-rays and exposed subsequently to visible light for 90 minutes at various temperatures; −196°C (a), −150°C (b), and −120°C (c).

The resonance pattern of deuterated methyl isocyanate also changes with the irradiation of visible light to the spectrum which consists of a quintuple of triplets (Fig. 7). The splitting of the main quintet with intensity ratio 1: 2: 3: 2: 1 was 13.1 gauss. Each line of the main quintet splits into a secondary triplet whose splitting constant is 20.0 gauss (Fig. 8). The value of this quintet splitting corresponds to 1/6.67 of the main triplet splitting of Radical **2** in methyl isocyanate and is ascribed to deuteron coupling. The secondary triplet splitting remains constant both for methyl isocyanate and for deuterated methyl isocyanate and is assigned to nitrogen coupling. Accordingly, the main triplet and the secondary triplet splitting of Radical **2** can be derived from the two protons and nitrogen coupling, respectively.

Determination of g-values of Radical 2. The shape of the ESR lines of deuterated Radical **2** (Fig. 8) clearly shows unsymmetrical absorption lines in the lower magnetic field and absorption lines separated into three lines in the higher magnetic field. The shape was ascribed to the broadening effect of the magnetic anisotropy similar to the case for DĊO

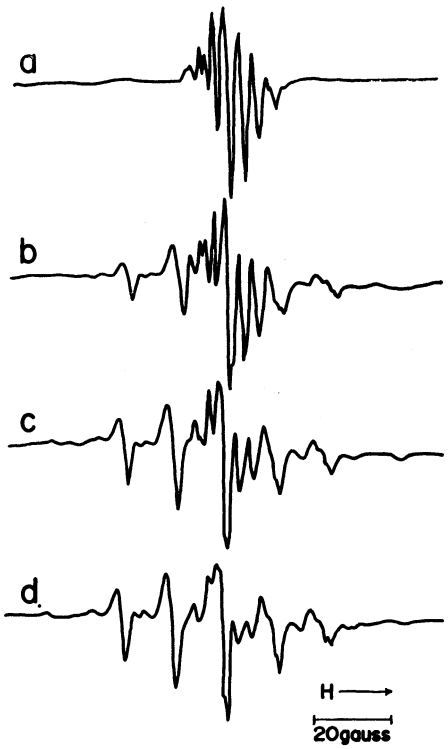

Fig. 7. The changes of ESR spectra of deuterated methyl isocyanate irradiated with γ-rays and exposed subsequently to visible light for 1 min. (a), 5 min (b), 30 min (c), and 90 min (d).

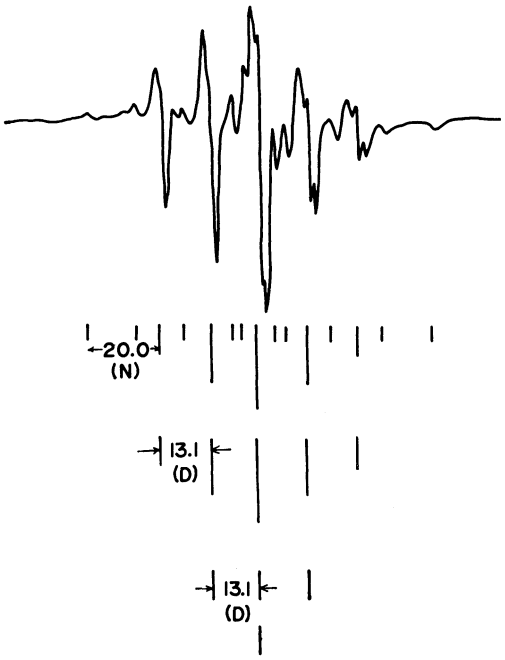

Fig. 8. ESR spectrum of deuterated methyl isocyanate irradiated with γ-rays and exposed to visible light for 90 min.

radical.[11] The line width between the strong five lines of the deuterated Radical **2** shows that the line broadening is due to the combination of anisotropic g-values and hyperfine interactions both with deuteron

11) F. J. Adrian, E. L. Cochran, and V. A. Bowers, *J. Chem. Phys.* **36**, 1661 (1962).

and nitrogen. In the spectra of deuterated Radical **2**, the central line broadening due to the anisotropy of *g*-value is large compared to the line width due to the other sources such as the anisotropic hyperfine interactions, since the magentic quantum numbers, M_I, both of nitrogen and of deuteron are zero. In this case, the principal *g*-values could be determined from the central strong line of the deuterated Radical **2**. The high- and low-field peaks of the derivative of the ESR absorption gave g_x and g_z, respectively, while g_y corresponded to the crossover point where the derivative vanished. The results are given in Table 1.

Table 1. Principal components of the *g*-value for radical **2**

$g_x=2.0038$
$g_y=2.0023$
$g_z=2.0015$

Discussion

Structure of Radical 1. The resonance pattern of spectrum 3a gives us the assignment of Radical **1**. The well-defined 1:1:1 triplet structure (4.6 gauss) is ascribed to the isotropic nitrogen coupling and the larger triplet structure (20.6 gauss) with a relative intensity ratio 1:2:1 to the coupling of the two equivalent protons. The anisotropy of spectra (Fig. 3) suggests that the protons of Radical **1** are α-protons. The outer components of spectra 3b and 3c consisted of many absorption lines due to the coalescence of the ESR absorption lines with different splitting constants caused by the anisotropic hyperfine interaction of α-protons. Accordingly, the nine-line spectrum can be assigned to $\cdot CH_2NCO$ radical. The two equivalent α-protons, as would be the case for a rotating methylene group,[12] give such characteristic hyperfine structures that the central component remains narrower and the outer components become broader. These characteristic structures which are typical of non-oriented specimen are found in spectrum 2a. Consequently, the methylene group of $\cdot CH_2NCO$ radical is assumed to be rotated around the C–N bond and the radical can be represented by the following formula;

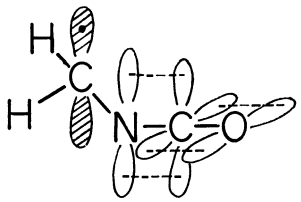

1

The unpaired electron occupies the carbon 2p orbital. The unpaired electron density on carbon atom ($=\rho_C$) which is estimated to be about 0.8 from the proton splitting may be reasonable, since the 2p orbital occupied by the unpaired electron is rotated around the C–N bond. The fact that the proton splitting is 20.6 gauss was confirmed by the result of deuterated methyl isocyanate; the ESR spectrum consists of fifteen-line, a quintuple of triplets (the bottom of Fig. 2b) and the splitting of quintet component of fifteen-line due to the deuteron coupling is 3.1 gauss, corresponding to 1/6.65 of proton splitting at orientation-angle 0°, while the splitting of triplet component due to the nitrogen coupling equals that of undeuterated specimen.

Structure of Radical 2. The proton splitting of Radical **2** gave the same value as that of methylene imino free radical[10] and the nitrogen splitting was anisotropic (Fig. 5). This suggests that the structure of Radical **2** is analogous to that of methylene imino radical. The unpaired electron of methylene imino radical occupies a nitrogen 2p orbital which is perpendicular to the C–N bond lying in the same plane as the C–H bonds.[10] Thus, three types of the structure might be proposed as shown in Structures **3**, **4**, and **5**;

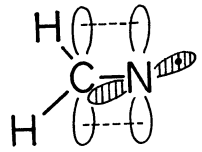

3

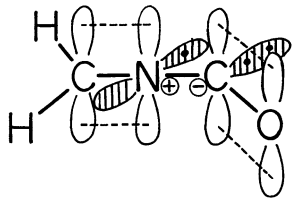

4

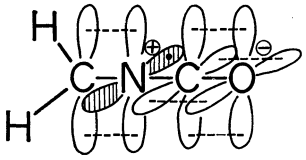

5

where Structure **3** is methylene imino radical itself and the radicals with Structures **4** and **5** are isomers of Radical **1**. The unpaired electron of Structure **3** occupies the nitrogen 2p orbital. In Structure **4**, it is located at an antibonding σ-molecular orbital (MO) consisting of sp^2 carbon hybrid orbital and nitrogen 2p orbital. In Structure **5**, it occupies a conjugated orbital consisted of nitrogen 2p orbital and π-orbital of carbonyl group.

The experimental values of nitrogen splitting and unpaired electron density on nitrogen atom ($=\rho_N$) are given by Adrian[13] for HCN^- radical. The unpaired electron occupies an antibonding σ-orbital similar to that of Structure **4** which consists of a sp^2 carbon hybrid orbital and a nitrogen 2p orbital. The observed

12) E. L. Cochran, F. J. Adrian, and V. A. Bowers, *ibid.*, **34**, 1161 (1961).

13) F. J. Adrian, E. L. Cochran, V. A. Bowers, and B. C. Weatherley, *Phys. Rev.*, **17**, 129 (1969).

value of nitrogen splitting (20.0 gauss) agrees with A_1 (20.9 gauss) of HCN^- radical. The value of ρ_N (=0.41) in HCN^- radical, however, is much smaller than that of Structure **3** (ρ_N=1). The unpaired electron of Structure **5** may be delocalized in the π-orbital of carbonyl group and ρ_N is estimated to be as large as that of allyl radical.[14] The delocalization of unpaired electron density can not give the large splitting of proton and nitrogen. Thus, Structures **4** and **5** are discarded. On the other hand, Structure **3** is acceptable for the interpretation of the large proton splitting and anisotropic nitrogen splitting. For the methylene imino radical in motion in the hydrogen cyanide matrix at −196°C, the nitrogen splitting has reported to be 11—21 gauss[15] which coincides with the observed value of spectrum 5c. Cochran reported that the nitrogen splitting was 34.4 gauss[10] in rigid argon matrix at 4.2°K. The matrix of methyl isocyanate should not be so rigid as to prohibit the motion of the radical at −196°C. Consequently, Structure **3** is most plausible for the assignment of Radical **2**. The authors had first considered that the mutual conversion between Radicals **1** and **2** was the isomerization between Radical **1** and the radical with Structure **4**, since Radical **1** changed quantitatively into Radical **2** on irradiation with visible light, and Radical **1** was regenerated as the temperature was raised.[16]

The mechanism of mutual conversion between Radicals **1** and **2** may be as follows. The decomposition of Radical **1** into $H_2C{=}N\cdot$ and CO, and the recombination of these two moieties $H_2C{=}N\cdot$ and CO might take place in the neighborhood of each other in the matrix of methyl isocyanate which is so rigid as to stabilize $H_2C{=}N\cdot$ at −120°C. This reaction can be represented by the formula

$$\cdot CH_2NCO \underset{\Delta}{\overset{h\nu}{\rightleftharpoons}} H_2C{=}N\cdot + CO$$

The authors wish to thank Dr. Hiroaki Sawai, the University of Tokyo, for his help in preparing deuterated methyl isocyanate.

14) R. W. Fessenden and R. H. Schuler, *J. Chem. Phys.*, **39**, 2147 (1963).

15) R. J. Egland and C. R. Symons, *J. Chem. Soc.*, *A*, **1970**, 1326.

16) The referee's suggestion that ρ_N of Structure **4** is too small to give the proton splitting (87.4 gauss), has been carefully investigated and accepted. The authors wish to thank the referee for his valuable suggestion.

BULLETIN OF THE CHEMICAL SOCIETY OF JAPAN, VOL. 46, 706—710 (1973)

The Carbon-13 Chemical Shift of *n*-Butane

Isao ANDO and Atsuo NISHIOKA

Department of Polymer Engineering, Tokyo Institute of Technology, Ookayama, Meguro-ku, Tokyo

(Received May 13, 1972)

The temperature dependence of the carbon-13 chemical shift of *n*-butane was calculated using the CNDO/2 method, taking into account the rotational isomers and assuming the Boltzmann distribution among them. The observed results could be well interpreted by assuming *ca.* 11.15 eV as the average excitation energy.

The chemical shifts of carbon-13 nuclei in saturated hydrocarbons have been studied systematically by the experiment of Grant *et al.*[1] Pople[2] has given a theory of the carbon-13 chemical shift, and has caluclated the shifts of ethane and other simple molecules. His approach is not convenient for calculating the carbon-13 chemical shift of a large molecule because of the tedious work involved. Then Sichel *et al.*[3] have reported empirically on an apparent correlation between the carbon-13 chemical shifts and the electron charge densities on the carbon atoms of hydrocarbons, as calculated by the extended Hückel method.[4] Yonezawa *et al.*[5] have interpreted theoretically the carbon-13 chemical shifts of various hydrocarbons by approximating Pople's theory[2] for the paramagnetic shielding of the carbon-13 nucleus, but the agreement between the calculated and observed chemical shifts is not good. This disagreement may be due mainly to the approximation, assuming the constancy of terms containing the bond orders between neighbouring atoms, the ambiguity of the value of the average excitation energy, and the neglect of the rotational isomers.

In this paper we will calculate the paramagnetic shielding constants of carbon atoms in *n*-butane based on Pople's theory, and will interpret the temperature dependence of the carbon-13 chemical shifts by estimating the diamagnetic shielding constant in addition to

1) E. G. Paul and D. M. Grant, *J. Amer. Chem. Soc.*, **85**, 1701 (1963), D. M. Grant and E. G. Paul, *ibid.*, **86**, 2984 (1964).
2) J. A. Pople, *Mol. Phys.*, **7**, 301 (1964).
3) J. M. Sichel and M. A. Whitehead, *Theoret. Chim. Acta*, **5**, 35 (1966).
4) R. Hoffmann, *J. Chem. Phys.*, **39**, 1397 (1963).
5) T. Yonezawa, I. Morishima, and H. Kato, This Bulletin, **39**, 1398 (1966).

its paramagnetic shielding constant, taking the rotational isomers into account also.

Experimental

The proton-decoupled carbon-13 NMR spectra of *n*-butane in neat liquid were measured at temperatures from −60 to 0°C at 25.25 MHz in the external-locked mode, using a Japan Electron Optics Laboratory, JEOL PS-100-type, spectrometer. The sample (purity: 99.9%) was obtained from the Tokyo Kasei Co., Ltd.

Calculation

The magnetic shielding constant of any specified carbon atom, A, in a molecule, σ_A, may be approximated by a sum of the following terms:[2]

$$\sigma_A = \sigma_{AA}^{dia} + \sigma_{AA}^{para} + \sigma' \quad (1)$$

where σ_{AA}^{dia} and σ_{AA}^{para} are the diamagnetic and paramagnetic contributions to the specified carbon atom, A, respectively, and σ', the contribution from the neighbouring atoms bonded to the A atom. Usually the effect of σ' on the carbon-13 chemical shift is known to be very small,[2] contributing less than a few parts per million. With Slater atomic orbitals, σ_{AA}^{dia} increases 14 ppm if a 2p electron is added, only about 10% of the width of the observed range of the carbon-13 chemical shifts. However, in this paper in order to discuss the carbon-13 chemical shift in detail we will take into account the terms of both the diamagnetic and paramagnetic shielding effects.

The value of σ_{AA}^{dia} is given by the formula:[6]

$$\sigma_{AA}^{dia} = (e^2/3mc^2)\sum_i \langle r_i^{-1} \rangle \quad (2)$$

where $\langle r_i^{-1} \rangle$ is the mean inverse distance of an electron from a nucleus; m, its mass; e, its charge and c, the velocity of light; the summation is over all the electrons on the atom being considered. The approximate value of σ_{AA}^{dia} for the carbon atom is given as:

$$\sigma_{AA}^{dia} = 4.45Z^*q \quad (3)$$

where:

$$Z^* = 3.25 - 0.35(q-4) \quad (4)$$

in which q is the total electron density around the carbon atom, and Z^*, the "effective nuclear charge" estimated according to Slater's rules.[7]

According to Pople's theory,[2] σ_{AA}^{para} is given as:

$$\sigma_{AA}^{para} = -(e^2\hbar^2/2m^2c^2\Delta E)\langle r^{-3} \rangle_{2p} \sum_{B(=A)} Q_{AB} \quad (5)$$

where:

$$Q_{AB} = \frac{4}{3}\delta_{AB}(P_{x_Ax_B} + P_{y_Ay_B} + P_{z_Az_B}) - \frac{2}{3}(P_{y_Ay_B}P_{z_Az_B} + P_{z_Az_B}P_{x_Ax_B} + P_{x_Ax_B}P_{y_Ay_B}) + \frac{2}{3}(P_{y_Az_B}P_{z_Ay_B} + P_{z_Ax_B}P_{x_Az_B} + P_{x_Ay_B}P_{y_Ax_B}) \quad (6)$$

$$\langle r^{-3} \rangle_{2p} = \frac{1}{24a_0^3}(3.25 - 0.35(q_{2p} - 3))^3 \quad (7)$$

$$q_{2p} = P_{x_Ax_B} + P_{y_Ay_A} + P_{z_Az_A} \quad (8)$$

In these formulae, ΔE is an averaged electronic excitation energy; $\sum_{B(=A)}$, a summation over all the atoms; $\langle r^{-3} \rangle_{2p}$, the mean inverse cube radius for carbon 2p orbitals; q_{2p}, the electron density of the 2p electrons; δ_{AB}, the Kronecker symbol, and a_0, the Bohr radius. $P_{x_Ax_B}$ is the element of the matrix for the $2p_x$ atom orbitals on the A and B atoms. When A=B, it is the charge density in $2p_x$ on the A atom, and When A≠B, it is the bond order between the two atomic orbitals.

σ_{AA}^{para} and σ_{AA}^{dia} were estimated by the CNDO/2 (Complete Neglect of Differential Overlap) molecular orbital method.[8]

In the *n*-butane molecule, three conformations are possible as the rotational isomerism (*trans*(T) and *gauche* (G or G′) with respect to the central bond). T, G, and G′ are defined as occuring at the rotational angles about 0, 120, and 240° respectively, by the clockwise rotation around the C–C bond, as expressed in the Newman projection. One of the three methyl protons was assumed to take the *trans* position in relation to the third carbon atom from the methyl carbon atom.

Then, obtaining the chemical shift of *n*-butane, we must average the calculated chemical shifts of the three possible isomers. For the averaging of the chemical shifts of the isomers, the following formula was used:[9]

$$\sigma_{AV} = \sum_{i=1}^{3} X_i \sigma_{A_i} \quad (9)$$

where σ_{AV} is the averaged chemical shift; σ_{A_i}, the chemical shift of the i-th isomer, and X_i, its fraction. X_i is expressed as:

$$X_i = e^{-\Delta E_i/RT} / \sum_{i=1}^{3} e^{-\Delta E_i/RT} \quad (10)$$

where R is the gas constant; T, the absolute temperature, and ΔE_i, the energy difference between the reference isomer (*trans*) and the i-th isomer. From the equations presented above, we can calculate the carbon-13 chemical shift and the temperature dependence of *n*-butane.

Here, the C–C and C–H bond lengths are set at 1.54 and 1.10 Å respectively, and both the C–C–C and the C–C–H bond angles are set at 109°28′.[10]

The numerical calculation was carried out by means of the HITAC-5020E computer of the Computer Center of the University of Tokyo.

Results and Discussion

n-Butane can take three rotational isomers, of one *trans* and two *gauche* forms; the total electron densities of the *trans* and *gauche* isomers are shown in Fig. 1. The electron densities and bond orders of the 2p electrons of the carbon atoms in these isomers are shown in Table 1. There is not much differences in the electronic states between the *trans* and *gauche* forms. Therefore, the large temperature dependence of the chemical shift of *n*-butane cannot be explained in terms of these

6) W. E. Lamb, *Phys. Rev.*, **60**, 817 (1941).
7) J. C. Slater, *ibid.*, **36**, 57 (1930).
8) J. A. Pople and G. A. Segal, *J. Chem. Phys.*, **43**, S 136 (1965).
9) H. S. Gutowsky, *ibid.*, **37**, 2196 (1962).
10) L. Pauling, "The Nature of the Chemical Bond," Cornell University Press (1960).

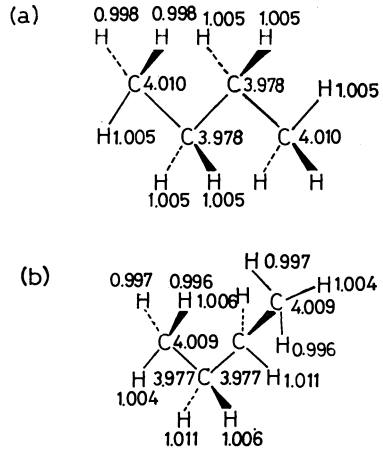

Fig. 1. The total electron density distribution of *n*-butane. (a): *trans* isomer, (b): *gauche* isomer.

total densities.

The carbon-13 chemical shifts of the *trans* and *gauche* isomers, and those averaged over these isomers, were calculated using Eqs. (1), (3), (5), and (9); they are shown in Table 2. The calculated and observed chemical-shift differences between the methyl and methylene carbons at 300K are also shown. Since there is no definite value for the average excitation energy (ΔE) published for *n*-butane, we first tried to use 10 eV for ΔE; this value was originally used by Pople[2] in the case of ethane.

As expected, and as Table 2 shows, σ_{AA}^{para} contributes mainly to the chemical-shift difference between the methyl and methylene carbons. The calculated chemical shifts of both methyl carbons in the *trans* and *gauche* isomers are nearly equal to each other, but those of the methylene carbon in the former appear at a slightly higher field than in the latter. This is due to the change in the electronic state of the methylene atom for the rotation around the central bond. Therefore, the chemical shift of the methylene carbon may be expected to depend upon the population of the rotational isomers, which is itself governed by the energy difference (ΔE_g) between the *trans* and *gauche* forms. It is known from spectroscopic studies that extensive results for liquid *n*-hydrocarbons confirm a value of 500 ± 100 cal/mol for ΔE_g.[11] Recently, on the basis of a laser-Raman spectroscopic study,[12] it has been reported that 600 cal/mol is more reasonable as

Table 1. The charge densities and bond orders of $2p_x$, $2p_y$, and $2p_z$ electrons on the carbon atoms of *n*-butane

(a) *Trans* form.

	$2p_x$				$2p_y$	
	$CH_3(1)$	$CH_2(2)$	$CH_2(3)$	$CH_3(4)$	$CH_3(1)$	$CH_2(2)$
$2p_x$ CH_3 (1)	1.0327	−0.6144	0.0053	−0.0525	0.0000	0.0000
CH_2 (2)	−0.6144	1.0146	0.1340	0.0053	0.0000	0.0000
CH_2 (3)	0.0053	0.1340	1.0148	−0.6144	0.0000	0.0000
CH_3 (4)	−0.0525	0.0053	−0.6144	1.0325	0.0000	0.0000
$2p_y$ CH_3 (1)	0.0000	0.0000	0.0000	0.0000	0.9765	0.1683
CH_2 (2)	0.0000	0.0000	0.0000	0.0000	0.1683	0.9600
CH_2 (3)	0.0000	0.0000	0.0000	0.0000	−0.0044	0.1641
CH_3 (4)	0.0000	0.0000	0.0000	0.0000	−0.0063	−0.0044
$2p_z$ CH_3 (1)	0.0177	−0.2707	−0.0380	−0.0209	0.0000	0.0000
CH_2 (2)	−0.2875	0.0061	−0.0139	−0.0110	0.0000	0.0000
CH_2 (3)	−0.0111	−0.0136	0.0062	−0.2873	0.0000	0.0000
CH_3 (4)	−0.0209	−0.0380	−0.2709	0.0177	0.0000	0.0000

	$2p_y$		$2p_z$			
	$CH_2(3)$	$CH_3(4)$	$CH_3(1)$	$CH_2(2)$	$CH_2(3)$	$CH_3(4)$
$2p_x$ CH_3 (1)	0.0000	0.0000	0.0177	−0.2875	−0.0111	−0.0209
CH_2 (2)	0.0000	0.0000	−0.2707	0.0061	−0.0036	−0.0380
CH_2 (3)	0.0000	0.0000	−0.0380	−0.0139	0.0062	−0.2709
CH_3 (4)	0.0000	0.0000	−0.0209	−0.0110	−0.2873	0.0177
$3p_y$ CH_3 (1)	−0.0044	−0.0063	0.0000	0.0000	0.0000	0.0000
CH_2 (2)	0.1641	−0.0044	0.0000	0.0000	0.0000	0.0000
CH_2 (3)	0.9600	0.1683	0.0000	0.0000	0.0000	0.0000
CH_3 (4)	0.1683	0.9764	0.0000	0.0000	0.0000	0.0000
$2p_z$ CH_3 (1)	0.0000	0.0000	0.9771	0.0544	−0.0300	−0.0011
CH_2 (2)	0.0000	0.0000	0.0544	1.0194	−0.7085	−0.0300
CH_2 (3)	0.0000	0.0000	−0.0300	−0.7085	1.0192	0.0544
CH_3 (4)	0.0000	0.0000	−0.0011	−0.0300	0.0544	0.9773

11) S. Mizushima, "Structure of Molecules and Internal Rotation," Academic Press (1954).

12) T. Fujishima, M. Tashumi, and T. Shimanouchi, Symposium on Polymer, 771 (1970) Kyoto.

(b) *Gauche* form.

	$2p_x$				$2p_y$	
	$CH_3(1)$	$CH_2(2)$	$CH_2(3)$	$CH_3(4)$	$CH_3(1)$	$CH_2(2)$
$2p_x$ CH_3 (1)	1.0301	−0.6124	−0.0087	−0.0143	−0.0001	0.0000
CH_2 (2)	−0.6124	1.0165	0.1495	−0.0056	−0.0003	0.0014
CH_2 (3)	−0.0087	0.1495	0.9704	−0.0272	0.0028	0.0049
CH_3 (4)	−0.0143	−0.0056	−0.0272	0.9910	0.0071	0.0046
$2p_y$ CH_3 (1)	−0.0001	−0.0003	0.0028	0.0071	0.9779	0.1677
CH_2 (2)	0.0000	0.0014	0.0049	0.0046	0.1677	0.9565
CH_2 (3)	−0.0059	0.0039	−0.0253	0.3376	−0.0065	0.1546
CH_3 (4)	0.0228	−0.0042	0.3379	−0.0226	0.0029	−0.0095
$2p_z$ CH_3 (1)	0.0168	−0.2705	−0.0403	−0.0029	−0.0002	−0.0006
CH_2 (2)	−0.2856	0.0099	0.0071	0.0094	0.0012	−0.0027
CH_2 (3)	−0.0155	−0.0136	−0.0073	0.1437	0.0020	0.0002
CH_3 (4)	0.0012	0.0165	0.1348	−0.0086	−0.0027	−0.0370

	$2p_y$		$2p_z$			
	$CH_2(3)$	$CH_3(4)$	$CH_3(1)$	$CH_2(2)$	$CH_2(3)$	$CH_3(4)$
$2p_x$ CH_3 (1)	−0.0059	0.0228	0.0168	−0.2856	−0.0155	0.0012
CH_2 (2)	0.0039	−0.0042	−0.2705	0.0099	−0.0136	0.0165
CH_2 (3)	−0.0253	0.3379	−0.0403	0.0071	−0.0073	0.1348
CH_3 (4)	0.3376	−0.0226	−0.0029	0.0094	0.1437	−0.0086
$2p_y$ CH_3 (1)	−0.0065	0.0029	−0.0002	0.0012	0.0020	−0.0027
CH_2 (2)	0.1546	−0.0095	−0.0006	−0.0027	0.0002	−0.0370
CH_2 (3)	1.0028	−0.4174	−0.0042	−0.0119	0.0073	−0.2348
CH_3 (4)	−0.4174	1.0168	−0.0003	−0.0124	−0.2466	0.0144
$2p_z$ CH_3 (1)	−0.0042	−0.0003	0.9770	0.0545	−0.0305	−0.0064
CH_2 (2)	−0.0119	−0.0124	0.0545	1.0192	−0.7082	−0.0305
CH_2 (3)	0.0073	−0.2466	−0.0305	−0.7082	1.0191	0.0545
CH_3 (4)	−0.2348	0.0144	−0.0064	−0.0305	0.0545	0.9771

Here *n*-butane was numbered like CH_3 (1)–CH_2 (2)–CH_2 (3)–CH_3 (4).

TABLE 2. THE CALCULATED σ_{AA}^{dia}, σ_{AA}^{para}, AND σ_A OF *n*-BUTANE AND ITS OBSERVED CARBON-13 CHEMICAL SHIFT

	trans isomer (ppm)			*gauche* isomer (ppm)			Averaged over the *trans* and *gauche* isomers (at 300K) (ppm)			Obsd[a] (at 300K) (ppm)
	σ_{AA}^{dia}	σ_{AA}^{para}	σ_A	σ_{AA}^{dia}	σ_{AA}^{para}	σ_A	σ_{AA}^{dia}	σ_{AA}^{para}	σ_A	
CH_3	57.93	−219.60	−161.67	57.92	−219.57	−161.65	57.93 (57.93)	−219.57 (−219.60)	−161.66[b] (−161.67)[c]	11.90
CH_2	57.67	−231.98	−174.31	57.66	−233.23	−175.57	57.67 (57.67)	−232.56 (−232.51)	−174.89[b] (−174.84)[c]	0
CH_3–CH_2	0.26	12.38	12.64	0.26	13.66	13.92	0.26 (0.26)	12.99 (12.91)	13.23[b] (13.17)[c]	11.90

a) Reference is the signal of the methylene carbon.
b) Calculated using 500 cal/mol as ΔE_g.
c) Calculated using 600 cal/mol as ΔE_g.

the ΔE_g value. Here, we have calculated the chemical shifts of the methyl and methylene carbons for both ΔE_g value, 500 and 600 cal/mol, at 300K. As may be seen from Table 2, the calculated chemical shifts between the methyl and methylene carbons using ΔE_g values of 500 and 600 cal/mol at 300K are 13.23 and 13.17 ppm respectively. There is only a slight difference (about 5%) between them.

The calculated and observed chemical-shift differences between the methyl and methylene carbons are 13.23 and 11.90 ppm respectively at 300 K. The agreement is good; the small difference is considered mainly to be due to the ambiguous estimation of the average excitation energy.

Now let us attempt to estimate an appropriate value of ΔE in order to interpret the observed chemical shift rigorously. As the first approximation, it may be considered that, according to Gutowsky's consideration,[9] the observed temperature dependence of the carbon-13 chemical shift of *n*-butane can be interpreted in terms of the temperature dependence of the fraction of rotational isomers. Therefore, if the ΔE_g and the

TABLE 3. THE OBSERVED CHEMICAL SHIFT DIFFERENCES BETWEEN THE METHYL AND METHYLENE CARBONS ($\Delta\sigma_{CH_3-CH_2}$) AND ΔE IN VARIOUS TEMPERATURES

T(K)	212	252	270	294	300
$\Delta\sigma_{CH_3-CH_2}$ (ppm)	11.75	11.77	11.84	11.86	11.90
ΔE (eV) (a)	11.19	11.23	11.16	11.17	11.10
ΔE (eV) (b)	11.13	11.15	11.12	11.13	11.17

a) ΔE_g=500 cal/mol, b) ΔE_g=600 cal/mol

temperature are determined, all the values of the chemical shifts observed for a wide range of temperatures can be estimated by a single value of ΔE.

The absolute measurement of the temperature dependence of the carbon-13 chemical shifts of the methyl or methylene carbons is very difficult because of some possible temperature drifts of the external or internal reference signal, whereas the temperature dependence of the chemical-shift difference ($\Delta\sigma_{CH_3-CH_2}$) between the methyl and methylene carbons is not affected by the temperature drifts of the reference signal. Thus, the values of $\Delta\sigma_{CH_3-CH_2}$ were measured at temperatures from 212 to 300 K, as is shown in Table 3; the values of ΔE were then calculated to fit the observed $\Delta\sigma$ value (where both 500 and 600 cal/mol were used as ΔE_g values). From the results, it was found that the observed values can be interpreted reasonably using the constant (ΔE) value of 11.16±0.04 and 11.14±0.02 eV in the cases of ΔE_g values of 500 and 600 cal/mol respectively. There is no significant difference between the two cases.

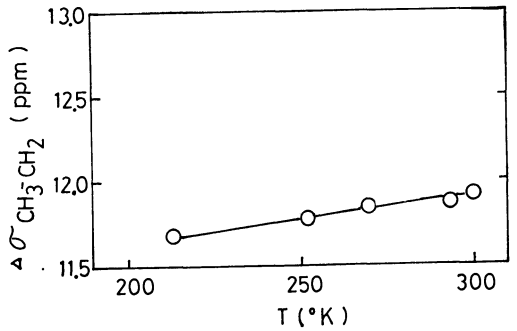

Fig. 2. The calculated and observed temperature dependences of the chemical shift difference between the methyl and methylene carbons of *n*-butane.
Drawn line: calculated using 11.16 eV as ΔE
○: observed

Next, in order to compare clearly the observed and calculated results, they are both shown in Fig. 2; the latter was obtained using 11.16 eV as ΔE and 500 cal/mol as ΔE_g. In this figure the observed data may be found to fit the calculated line better. Therefore, we may conclude that the temperature dependence of the carbon-13 chemical shift of *n*-butane may be interpreted using the rotational isomers and a single value of ΔE

BULLETIN OF THE CHEMICAL SOCIETY OF JAPAN, VOL. 46, 710—713 (1973)

Automatic Recording of Liquid Penetration through Filter Paper and Wetting Behavior of Liquids

Akio NAKAMURA, Tsutomu SEIMIYA, and Tsunetaka SASAKI

Department of Chemistry, Faculty of Science, Tokyo Metropolitan University, Tokyo

(Received May 16, 1972)

The penetration of liquid through a vertically suspended filter paper was studied by measuring the weight increase with a strain gauge tensiometer for several organic liquids and aqueous solutions. The plot of penetration rate $K=h/t^{1/2}$ (h, height of liquid rise and t, time) against $(\sigma/\eta)^{1/2}$ (σ, surface tension and η, viscosity coefficient of wetting liquids) showed two straight lines, one for organic liquids and the other for aqueous solutions of sodium dodecyl sulfate. Both these lines passed the origin, suggesting Lucas-Washburn formula to hold. The plots for ethyl alcohol–water mixtures showed behaviors intermediate between those two linear relations. The aqueous solutions caused swelling of fibers and reduced the mean capillary radius of the filter paper, resulting in a decrease of the penetration constant $P=K/(\sigma/\eta)^{1/2}$ but with a rather large K value. The plots for penetration of water through an untreated paper fell far below the straight line obtained for aqueous solutions of sodium dodecyl sulfate. The penetration was recovered by removing fatty contaminants from the filter paper using Soxhlet extractor with ether. The results of a simple test of unfolding a folded paper by touching it with liquids are also in line with those mentioned above.

A number of studies have since been made for the wetting of the fibrous and powder materials as a function of the porosity of fiber,[1-3] the degree of dispersion of powder, the surface treatment and the effect of surface-active agent[4] on these substances. The sinking time of solid sample may be used as a simple criterion of

1) R. Lucas, *Kolloid-Z.*, **21**, 105 (1917). E. W. Washburn, *Phys. Rev. Ser.* 2, **17**, 273 (1921).

2) P. L. Peek and D. A. McLean, *Ind. Eng. Chem. Anal. Ed.*, 85 (1934).

3) Z. E. Wolkowa, *Kolloid-Z.*, **67**, 280 (1934); J. M. Dallavalle, "Micromeritics," Second edition, Pitman Publishing Corporation, New York, London (1952).

4) A. M. Schwartz and J. W. Perry, "Surface Active Agent," Vol. 1, Interscience Publisher, New York (1957).

wetting power of surface-active agent,[5] while wettabilities of fibers,[6,7] filter papers[8,9] and powder materials[10,11] are measured by the penetration velocity or pressure of a liquid through the sample strip or the powders packed in a column. The rate of penetration should be a subject worth studying from both theoretical and practical interest. However, the frontal line of the ascending liquid is not easy to find visually because of its irregular and rapid movement, sepecially at the initial stage of penetration. This difficulty has been overcome by measuring the changes of the weight or the electrical capacity of the sample due to the liquid penetration, by torsion balance[6] or capacity meter.[11] In the present study, the weight increase was measured by a self-recording strain gauge tensiometer[12] which enabled a simple and accurate measurement of the kinetic process of penetration, especially at its early stage.

The penetration of filter paper by various liquids and solutions is described in the present paper to elucidate the different wetting and swelling behaviors of the filter paper towards water and organic liquids. Of the numerous studies of a similar nature[8] only little has been reported on these behaviors.[9]

Experimental

Materials. Ethyl alcohol, butyl alcohol, acetone, dioxane, *n*-hexane, and toluene were purified by dehydration and distillation.[13] Sodium dodecyl sulfate (SDS) was prepared by the sulfation of dodecyl alcohol free from its homologues, and was used after repeated purification.[14] Water used was obtained by refluxing ordinary distilled water first with acid permanganate, then distilling from alkaline permanganate solution, and finally distlling twice with a Hysil flask. The filter paper (No. 50 for chromatography, Toyo Filter Paper Co., Japan) was cut into strips 2×7 cm so as to make its total weight after the penetration within the maximum permissible load (300 mg) of the strain gauge. The paper was subjected to extraction with ether to remove fatty contaminants.

Apparatus and Measurement. A cantilever type self-recording strain gauge tensiometer[12] (Fig. 1) was used for the measurement of liquid penetration. A strip of filter paper was hung from the end of the tension arm, and the wetting liquid was introduced from the reservoir into the cell until it just touched the lower end of the filter paper. An increase of weight of the filter paper due to the penetration of liquid was converted into an electrical output by the strain gauge, and recorded with a 1 mV full scale recorder (QPD 33, Hitachi, Japan). The apparatus was kept at 30°C in a thermostat designed so as to keep the cell from outer environment and prevent the evaporation of solutions.[15] The reading of the recorder was calibrated to the height H of penetrating liquid from the electrical output of tensiometer for the liquid rise of unit length. The measurement was started after the saturation of the cell with the vapor of sample liquid. About five minutes of measurement was enough for analysis, since the approximate Eq. (2) was used which is only applicable for the early stage of penetration. A slight change of the surface tension with time and of the depth of paper in a liquid, caused a negligible error in the calculation of H. The viscosity of liquid was measured by an Ostwald viscometer, and the surface tension of liquid was measured by the same tensiometer using Wilhelmy's glass plate.[12] All measurements were made at 30°C.

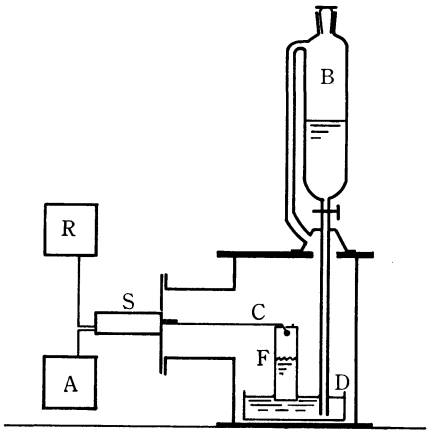

Fig. 1. Strain gauge tensiometer for penetration measurement.
A: DC Supply
B: Reservoir
C: Tension arm
D: Sample solution
F: Filter paper
R: Recorder
S: Strain gauge

Results and Discussion

The velocity of liquid ascending through fibrous material like filter paper was given by Peek and McLean[2] as

$$dh/dt = \bar{r}\sigma\cos\theta/4h\eta - \bar{r}^2dg/8\eta \quad (1)$$

where h denotes the height of liquid at time t, $\bar{r}$ the mean capillary radius, σ the surface tension, η the viscosity coefficient, d the density, g the gravity constant and θ the contact angle. At the initial stage of penetration Eq. (1) is approximated by

$$dh/dt = \bar{r}\sigma\cos\theta/4h\eta \quad (2)$$

which, after integration, gives Lucas-Washburn formula[1]

5) J. L. Moilliet and Collie, "Surface Activity," E. & F. N. Spon Ltd., London (1951), F. M. Fowkes, *J. Phys. Chem.*, **57**, 98 (1953); T. Hikota, K. Morohara, and K. Megro, This Bulletin, **43**, 3913 (1970); W. Yano, S. Takeo, and W. Kimura, *Yukagaku*, **11**, 241 (1962).
6) H. Sand, *Kolloid-Z.*, **183**, 57 (1961).
7) H. Sanuki, K. Kuri, and K. Ota, *Sen-i Gakkaishi*, **21**, 91 (1965); H. Sanuki, K. Ito, and K. Ota, *ibid.*, **21**, 506 (1965).
8) H. Fujita, *J. Phys. Chem.*, **56**, 625 (1952); T. Gillespie, *J. Colloid Sci.*, **13**, 32 (1958); M. Nakagaki and Osagawa, This Bulletin, **32**, 344 (1958); T. Gillespie, *J. Colloid Sci.*, **14**, 123 (1959); J. Szekely, A. W. Newmann, and Y. K. Chung, *ibid.*, **35**, 273 (1971); T. Kuwamura, E. Takahashi, and M. Oshima, *Yukagaku* **21**, 100 (1972).
9) T. Gillespie and T. Johnson, *J. Colloid Sci.*, **36**, 282 (1971).
10) F. E. Bartell and H. Y. Jenings, *J. Phys. Chem.*, **38**, 495 (1934).
11) M. Wada and N. Miyamoto, *Res. Inst. Dress. Met.*, **15**, 41 (1959). M. Wada and T. Yamamoto, *ibid.*, **21**, 53 (1965).
12) M. Koshinuma, A. Nakamura, T. Seimiya, and T. Sasaki, This Bulletin, **45**, 344 (1972).
13) A. Weissberger and E. S. Proskauer, "Technique of Organic Chemistry," Vol. 7, ed. by A. Weissberger, Interscience Publisher, New York, London (1955), pp. 318—379.
14) E. E. Dreger, *Ind. Eng. Chem.*, **36**, 610 (1944).
15) T. Seimiya and T. Sasaki, *J. Colloid Interfac. Sci.*, **21**, 229 (1966).

$$h = (\bar{r}\sigma \cos\theta/2\eta)^{1/2} t^{1/2} = Kt^{1/2} \quad (3)$$

Thus a plot of h *vs.* $t^{1/2}$ should give a straight line with a slope K, which is called hereafter the rate of penetration of liquid. If $\bar{r}$ is known, wetting tension $\sigma\cos\theta$ can be calculated from Eq. (3). We see also that in the case of constant $\bar{r}\cos\theta$, plot of K *vs.* $(\sigma/\eta)^{1/2}$ for various liquids should lie on the same straight line passing through the origin with a slope $P=(\bar{r}\cos\theta/2)^{1/2}$, which is called hereafter the penetration constant.

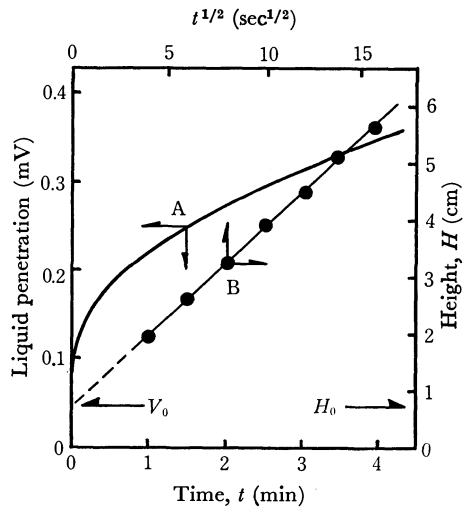

Fig. 2. Typical example of output against time and height against $t^{1/2}$ for water penetration.

Curve A in Fig. 2 shows a typical example of the liquid penetration process. The recorder reading increases along a parabolic curve with time, after an abrupt increase V_0, due to the pull by surface tension of liquid. The reading in terms of the apparent liquid rise H is plotted against $t^{1/2}$ as shown by the straight line B in Fig. 2. The value of H_0 (corresponding to V_0) was obtained by extrapolation as shown in the figure. Since $h=H-H_0$ is the true height of liquid rise, the straight line B with H_0 as zero point is taken as the h *vs.* $t^{1/2}$ plot. The linear relations are seen to hold for all systems so far studied, and show the Lucas-Washburn formula to hlod at least for the initial several minutes of the penetration process. Some typical results are shown in Fig. 3. The fair agreement with Lucas-Washburn formula might also imply the constancy of surface tension, presumably a dynamic one,[6,16] and the absence of chromatographic separation of solute at the ascending front in its initial stage. In the case of aqueous SDS solution, extrapolation to time zero was necessary to obtain the dynamic surface tension.

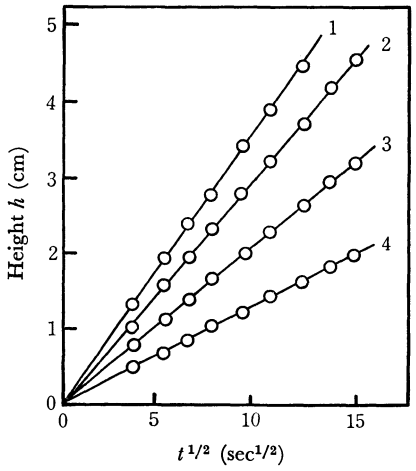

Fig. 3. Some plots of height against $t^{1/2}$.
1: acetone 2: water 3: aqueous SDS solution 1×10^{-2} (mol/l) 4: butyl alcohol

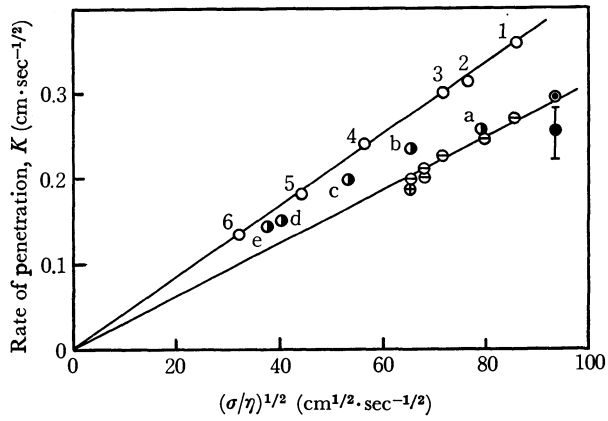

Fig. 4. Plots of rate of penetration against $(\sigma/\eta)^{1/2}$.
○: organic liquids, 1: acetone 2: *n*-hexane 3: toluene 4: dioxane 5: ethyl alcohol 6: butyl alcohol
◑: aqueous ethyl alcohol solutions (vol %), a: 5% b: 10% c: 20% d: 40% e: 60%
⊙: water, ●: water (untreated filter paper)
⊖: aqueous SDS solutions, ⊕: aqueous SDS solutions (untreated filter paper)

The plots of K *vs.* $(\sigma/\eta)^{1/2}$ are shown in Fig. 4. As expected, all plots for organic liquids tested fell on the same straight line passing through the origin with a slope $P=(\bar{r}\cos\theta/2)^{1/2}=4.3\times10^{-3}$ cm$^{1/2}$. Since $\bar{r}$ is considered to be constant for a given filter paper, the constancy of $\bar{r}\cos\theta$ means the constant θ, presumably zero degree, because most organic liquids are known to show zero contact angle against various compact solid surfaces.[2] The fact that Soxhlet extraction of the filter paper was immaterial for the penetration by organic liquids is quite reasonable, since the contact angles are unaffected by contamination and remain zero for these liquids. Figure 4 shows also that the plots for water and aqueous solutions considerably fall off the linear relation for the organic liquids. In the case of water penetration, removal of fatty contamination from the filter paper was seen to cause a remarkable increase of K value. The fact that the wetting of filter paper by aqueous SDS solution or organic liquids was not affected by the removal of fatty contamination of the paper also confirms this view. However, the increase of K due to the removal of contamination still does not bring the plots on the line obtained for the organic liquids. This can not be due to the incomplete removal of the contamination, since even a good wetting SDS solution can not bring the plots on the line of the organic liquids. This might suggest that the contact angle has already attained zero value, and that the decrease of $\bar{r}$ due to the swelling of fiber, for instance, affects the penetration by water or aqueous solutions.

16) H. Lange, *Kolloid-Z.*, **136**, 136 (1954).

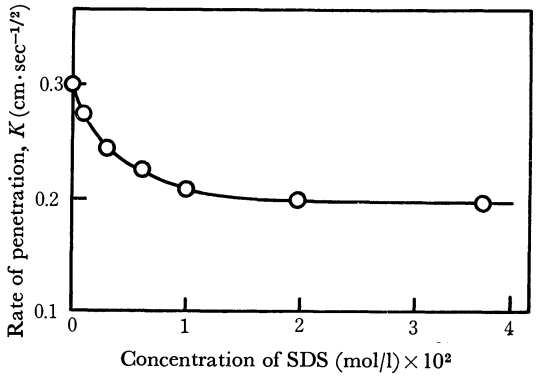

Fig. 5. Concentration dependence of rate of penetration K for aqueous SDS solutions.

The plots for aqueous SDS solutions and pure water lie on a straight line of smaller P than that for organic liquids. This may mean that the value of $\bar{r}$ for these aqueous systems is constant and smaller than that for organic liquids. The values of $\bar{r}$ estimated from the slope of straight lines in Fig. 4 are 3.4×10^{-5} cm for organic liquids, and 2.0×10^{-5} cm for both water and aqueous SDS solutions. The contact angle between pure water and the untreated filter paper is found to be 43°. The change of K with the concentration of SDS for clean filter paper is also shown in Fig. 5. The value of K decreased with increasing SDS concentration in contrast with the increased wetting of fibrous material contaminated with fatty substances.[14]

The penetration experiment of the filter paper by ethyl alcohol–water mixtures of various compositions revealed that the various states of swelling probably depend on the concentratration of ethyl alcohol. As seen in Fig. 4, the plots moved from the linear relation for aqueous solutions to that for organic liquids as the alcohol content increased. This may be caused by the increase of $\bar{r}$ with the decrease of water content and accordingly the decrease of the swelling. Curve A in Fig. 6 shows the regular increase of the P value with the concentration of ethyl alcohol in water, while the K value shows an irregular change with the alcohol concentration. Thus P is reasonably used as a measure of penetration.

As a simple demonstration of swelling, the rate of unfolding of a folded paper strip was measured by

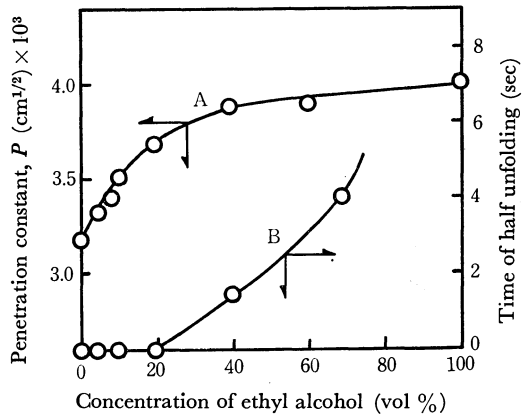

Fig. 6. Plots of penetration constant P and time of half unfolding against ethyl alcohol concentration.

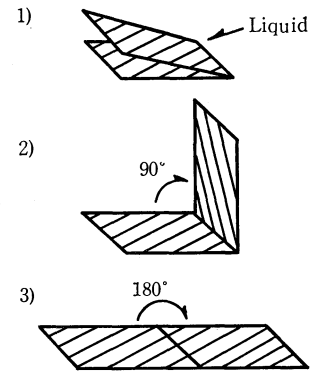

Fig. 7. Unfolding of filter paper strips.
1): no unfolding 2): half unfolding 3): full unfolding

applying a drop of liquid on the folded part of the paper (Fig. 7). No unfolding was observed for organic liquids tested, but for water and aqueous SDS solutions, it was full and instantaneous. The difference in unfolding also explains the difference in penetration shown by two straight lines in Fig. 4. Although the rate of penetration K is larger for n-hexane and acetone than that for water, the organic liquids neither cause swelling nor unfolding. The time for half-unfolding of the paper by aqueous solution of ethyl alcohol is also shown as curve B in Fig. 6. Unfolding and swelling were seen to be instantaneous in water-rich solutions. Half-unfolding angle of 90° was never reached at a concentration of ethyl alcohol higher than 80%. The tendency of non-unfolding presumed from a saturation of P value at higher concentration of ethyl alcohol seen in curve A of Fig. 6, is in line with the increasing tendency of unfolding time.

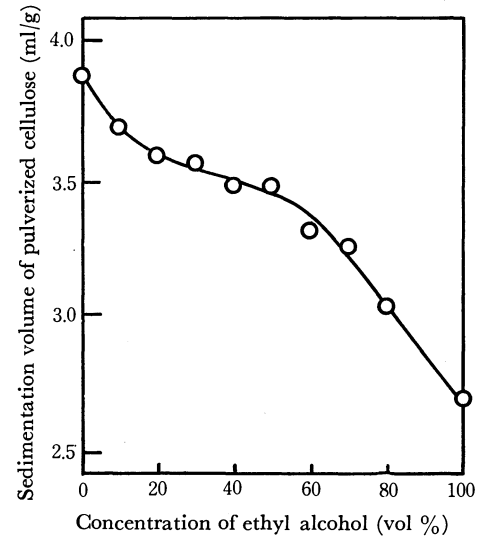

Fig. 8. Sedimentation volumes of *Avicel* in aqueous ethyl alcohol solutions.

The measurement of the sedimentation volume of pulverized cellulose in aqueous ethyl alcohol solution was carried out. The result shows that the tendencies of both swelling and non-swelling of cellulose depend on the concentration of ethyl alcohol. Figure 8 shows a decrease of sedimentation volume of pulverized cellulose (Avicel, Asahi Chemicals Inc., Japan) with increase of concentration of ethyl alcohol. This might also support the above view.

Charge-transfer and Proton-transfer in the Formation of Molecular Complexes. IV.[1] Picric Acid Complexes with Benzidine and Its Derivatives

Gunzi Saito and Yoshio Matsunaga
Department of Chemistry, Faculty of Science, Hokkaido University, Sapporo
(Received June 5, 1972)

The preparation of picric acid complexes with benzidine, *o*-tolidine, 3,3′-dichloro-*o*-tolidine, 3,3′-dibromo-*o*-tolidine, *o*-dianisidine, and *N,N,N′,N′*-tetramethylbenzidine was attempted in the following three solvents: benzene, chloroform, and ethanol. From benzene and chloroform, 3,3′-dibromo-*o*-tolidine forms a 1: 1 complex of the charge-transfer type, but the other five diamines give yellow salts formed by means of proton-transfer. Some complexes prepared in ethanol are of an unfamiliar nature. The spectroscopic examination of the 1: 1 complexes with *o*-tolidine, *o*-dianisidine, and tetramethylbenzidine revealed that a half of the diamine molecule acts as a proton-acceptor, while the other half has a charge-transfer interaction with the picrate ion. The simultaneous operation of charge-transfer and proton-transfer interactions was also demonstrated in the black-colored complex with benzidine of a 2: 1 composition.

Our earlier study of the vibrational and electronic spectra of the orange-colored α-naphthylamine-picric acid (2: 1) complex revealed that a proton is transferred from picric acid to α-naphthylamine, and that the interaction between the picrate ion and the second α-naphthylamine molecule is capable of producing a charge-transfer absorption band.[2] For brevity, such a complex may be denoted as a complex of the CPT type because of the simultaneous operation of charge-transfer (CT) and proton-transfer (PT) interactions between the component molecules.

When an aromatic diamine such as benzidine is combined with picric acid in a mole ratio of 1: 1, one may imagine the classification of the resulting complexes into the following three types. If the pK_a value of the diamine is low, a complex of the CT type may be formed.[1,3] On the other hand, the PT interaction may take place when the pK_a value of the diamine is high. In addition, a third possibility may be conceived on the basis of the observation of the above-mentioned naphthylamine complex; that is, a half of the diamine molecule acts as a proton-acceptor, while the other half has a CT interaction with the picrate ion. In this way, the complex of a 1: 1 composition can be of the CPT type (Case 1 of CPT complexes). Of course, the hydroxy group of the acid must be in the proximity of the amino group acting as a proton-acceptor to make the PT interaction feasible, and the molecular stacking must allow the picrate ion to superpose upon the unprotonated half of the adjacent diamine molecule. Two ways of stacking, (a) and (b), may be produced by the orientation of this diamine molecule.

In the *s*-trinitrobenzene (TNB) complexes of *N,N,N′,N′*-tetramethylbenzidine and *o*-dianisidine, the mole ratio of the diamine to TNB has been known to be 1: 2.[4,5] Because of the structural similarity between TNB and picric acid, the picric acid complexes of a 1: 2 composition and of the CT type may exist. It is also highly likely that the diamine molecule accepts two protons. In a situation intermediate between these two, a complex of the CPT type may be obtained; that is, one of the two picric acid molecules may be a proton-donor, and the other, an electron-acceptor (Case 2 of CPT complexes). As has been found with the 2,4-dinitrophenol and picric acid complexes of aromatic monoamines,[1,6] a delicate balance between the pK_a value of picric acid and those of the diamine may be the major factor governing the formation of such a complex.

By analogy to the α-naphthylamine-picric acid (2: 1) complex, the diamine complexes of a 2: 1 composition can also be expected to be of the CPT type (Case 3 of CPT complexes). The three cases imagined above for the picric acid (PiOH) complexes of the CPT type may be schematically shown as follows:

Case 1 (a) $H_2N{-}\phi{-}\phi{-}NH_3^+\cdots{}^-O{-}Pi$
⋮
$H_2N{-}\phi{-}\phi{-}NH_3^+\cdots{}^-O{-}Pi$

(b) $H_2N{-}\phi{-}\phi{-}NH_3^+\cdots{}^-O{-}Pi$
⋮ ⋮
$Pi{-}O^-\cdots{}^+H_3N{-}\phi{-}\phi{-}NH_2$

Case 2 $H_2N{-}\phi{-}\phi{-}NH_3^+\cdots{}^-O{-}Pi$
⋮
PiOH

Case 3 $H_2N{-}\phi{-}\phi{-}NH_3^+\cdots{}^-O{-}Pi$
⋮
$H_2N{-}\phi{-}\phi{-}NH_2$

This theorizing has led us to look into the picric acid complexes of benzidine and its five derivatives. As will be described below, the complexes belonging to most of the cases mentioned above, including Cases 1 and 3, were found by these combinations.

Experimental

Materials. The sources and handling of benzidine, *o*-tolidine, 3,3′-dichloro-*o*-tolidine, 3,3′-dibromo-*o*-tolidine, and *N,N,N′,N′*-tetramethylbenzidine have been described in a

1) Part III: N. Inoue and Y. Matsunaga, This Bulletin, **45**, 3478 (1972).
2) Y. Matsunaga and G. Saito, *ibid.*, **45**, 963 (1972).
3) E. Hertel, *Ann.*, **451**, 179 (1926).
4) J. J. Sudborough, *J. Chem. Soc.*, **109**, 1339 (1916).
5) T. Amano, H. Kuroda, and H. Akamatu, This Bulletin, **42**, 671 (1969).
6) G. Saito and Y. Matsunaga, *ibid.*, **44**, 3328 (1971).

previous paper of ours.[7] In addition to this series, *o*-dianisidine obtained commercially was used in this work. The complexes were prepared in the following three solvents of different polarities: benzene, chloroform, and ethanol. Generally, the complexes were precipitated by mixing equimolar amounts of the component compounds separately dissolved in a hot solvent. However, preparation with an excess of either the diamine or picric acid was also attempted when ethanol was used as the solvent.

Measurements. The vibrational spectra of the solid complexes in the region from 2000 to 4000 cm^{-1} were determined as hexachloro-1,3-butadiene mulls with a JASCO IR-G infrared spectrophotometer, and the electronic spectra in the visible region, with a Beckman DK-2A spectroreflectometer. The procedure in the latter measurements was similar to that described in a previous paper.[8] All the complexes with one exception decompose rather gradually. Therefore, the temperatures recorded as the decomposition points are only approximate.

Results and Discussion

The characteristics of the picric acid complexes obtained in this work are displayed in Table 1. Only the following pK_a values are available in the literature: 4.95 and 3.85 for the first and second pK_a values of benzidine, and 4.5 and 3.3 for those of *o*-tolidine.[9]

Table 1. Composition, color, and melting point of the picric acid complexes with benzidine and its derivatives

Diamine	Solvent		
	Benzene	Chloroform	Ethanol
N,N,N',N'-Tetramethyl-benzidine	2:3 Bright yellow 196°(decomp)	2:5 Yellow 199°(decomp)	2:5 Yellow 195°(decomp) 1:2 Greenish yellow 199°(decomp) 1:1 Tan 198°(decomp)
Benzidine	1:2 Yellow 230°(decomp)	1:2 Yellow 215°(decomp.)	1:2 Dull yellow 225°(decomp) 2:1 Black or brown 124°
o-Dianisidine	1:2 Yellow 230°(decomp)	2:3 Dark yellow 216°(decomp)	1:1 Orange 220°(decomp)
o-Tolidine	2:3 Yellow 215°(decomp)	2:3 Yellow 223°(decomp)	1:1 Brick red 190°(decomp)
3,3'-Dichloro-*o*-tolidine	1:1 Yellow 194°(decomp)	1:1 Yellow 195°(decomp)	1:1 Yellow 195°(decomp)
3,3'-Dibromo-*o*-tolidine	1:1 Jet black 190°(decomp)	1:1 Jet black 190°(decomp)	—[a]

a) Only the cation-radical salt could be isolated.

7) Y. Matsunaga and G. Saito, This Bulletin, **44**, 958 (1971).
8) K. Abe, Y. Matsunaga, and G. Saito, *ibid.*, **41**, 2852 (1968).
9) D. D. Perrin, "Dissociation Constants of Organic Bases in Aqueous Solution," Butterworths, London (1965), p. 120.

Therefore, the diamines in this table are arranged in the order in which the pK_a values of the related aniline derivatives decrease.

One may start a search for complexes of the CPT type by a visual examination. If the color is deeper than yellow, which arises from an absorption band due to the picrate ion, the presence of a CT interaction in some form is likely. As has been previously reported by us, the dissociation of picric acid does not much affect its electron affinity, which is close to that of TNB.[2,10] Consequently, the location of the CT absorption band in Case 3 of CPT complexes is expected to be not far from that of the corresponding TNB complex. On the other hand, a complex belonging to Case 1 or 2 cannot be so deep as the TNB complex because one of the two amino groups, which make the molecule a good electron-donor, is protonated.

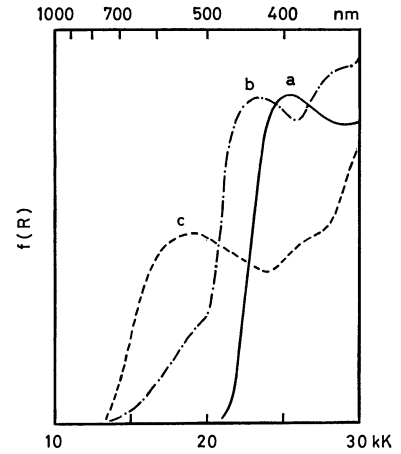

Fig. 1. Diffuse reflection spectra of a) the benzidine-picric acid (1:2) complex from benzene, b) the 2:1 complex from ethanol, and c) the corresponding TNB complex.

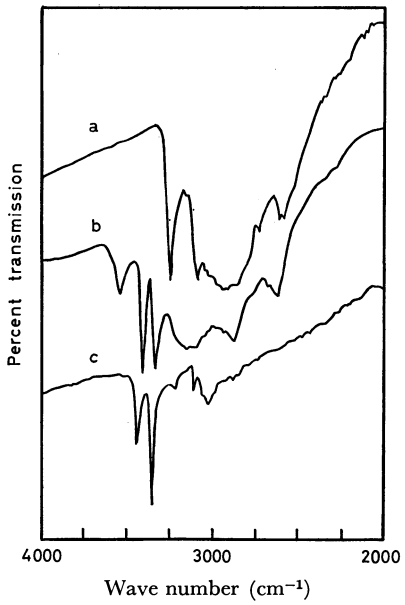

Fig. 2. Vibrational spectra of a) the benzidine-picric acid (1:2) complex from benzene, b) the 2:1 complex from ethanol, and c) the corresponding TNB complex.

10) G. Saito and Y. Matsunaga, This Bulletin, **45**, 2214 (1972).

The Benzidine Complexes (Figs. 1 and 2). A yellow-colored powder precipitates from all the three solvents when the component compounds are mixed in equimolar proportions. The mole ratio of the diamine to the acid was found to be 1:2. Found: C, 45.15; H, 2.93% (from benzene); C, 45.32; H, 2.96% (from chloroform); and C, 44.87; H, 3.03% (from ethanol). Calcd for $C_{12}H_{12}N_2 \cdot 2C_6H_3N_3O_7$: C, 44.86; H, 2.80%. Their electronic spectra are all the same. The absorption maximum located at about 25 kK can be assigned to the picrate ion (see Curve a in Fig. 1). Moreover, the vibrational spectra of all the three show the pattern characteristic of the picrates of primary amines, namely, broad bands in the region from 2500 to 3000 cm^{-1} and at about 3250 cm^{-1}.[11] This yellow-colored complex is undoubtedly a salt formed by the transfer of protons from two picric acid molecules to a diamine molecule.

When an excess of the diamine was employed in ethanol, the 2:1 complex was obtained as black needles or occasionally as a brown powder. Found: C, 61.70; H, 5.27%. Calcd for $2C_{12}H_{12}N_2 \cdot C_6H_3N_3O_7$: C, 60.30; H, 4.52%. As is shown in Fig. 1, this complex possesses an additional electronic absorption located below 20 kK. The comparison of this spectrum with that of the corresponding TNB complex clearly indicates that the diamine as a whole acts as an electron-donor. In this complex, the band to be assigned to the picrate ion appears at 23.5 kK. Such a location is not unusual, as we have seen in the cases of the α-naphthylamine- and pyridine-picric acid complexes.[2] The vibrational spectrum exhibits both the bands ascribed to the picrate of primary amine in the region from 2500 to 3250 cm^{-1} and those ascribed to the NH_2 group in the region from 3250 to 3500 cm^{-1}. The latter are well approximated by those in the spectrum of the TNB complex (see Curve c in Fig. 2). However, the assignment of the band appearing around 3500 cm^{-1} could not be settled. A sharp band at 3250 cm^{-1} observed in the 1:2 complex is not seen in the 2:1 complex. It may be added that a similar observation has been made in the α-naphthylamine-picric acid complexes.[2] These pieces of spectroscopic evidence lead to the conclusion that this 2:1 complex is of the CPT type. Moreover, the intensity of the absorption band appearing below 20 kK is consistent with our earlier observation that the weakness of the CT absorption is characteristic of the complexes with picrates.[2,10] The same 2:1 complex was isolated as black-colored plates when prepared in an aqueous solution containing a small amount of pyridine. Found: C, 60.87; H, 5.04%. It must be pointed out that the 2:1 complex melts at a temperature about 110°C lower than the 1:2 complex, reflecting the difference in the nature of intermolecular forces. The formation of the 1:1 and 1:2 complexes has been described by Rascanu.[12] Unfortunately, we could not obtain the former one, the melting point of which was reported to be 200—205°C.

The o-Tolidine Complexes (Figs. 3 and 4). The

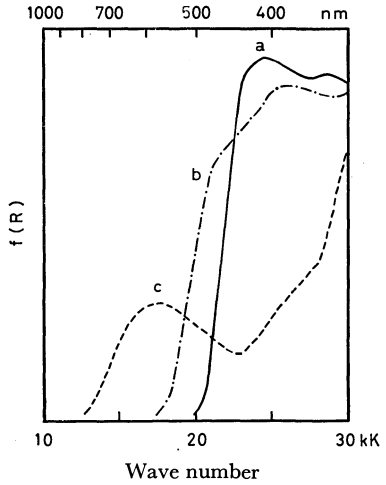

Fig. 3. Diffuse reflection spectra of a) the *o*-tolidine-picric acid (2:3) complex from benzene, b) the 1:1 complex from ethanol, and c) the corresponding TNB complex.

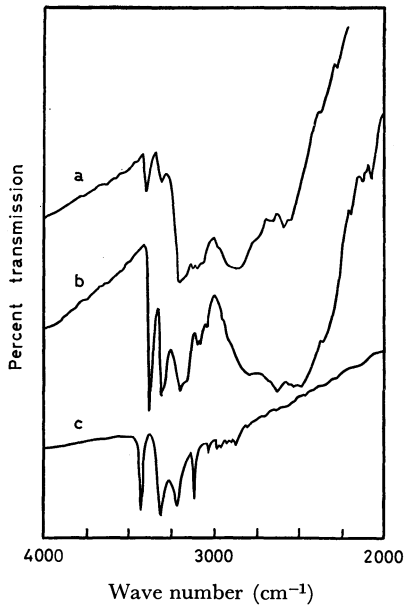

Fig. 4. Vibrational spectra of a) the *o*-tolidine-picric acid (2:3) complex from benzene, b) the 1:1 complex from ethanol, and c) the corresponding TNB complex.

complexes precipitated from benzene and chloroform are in the form of a yellow powder and have a mole ratio of 2:3, whereas the brick red-colored powder precipitated from ethanol is of a 1:1 composition. Found: C, 50.39; H, 3.78% (from benzene); C, 50.29; H, 4.10% (from chloroform), and C, 54.59; H, 4.48% (from ethanol). Calcd for $2C_{14}H_{16}N_2 \cdot 3C_6H_3N_3O_7$ and for $C_{14}H_{16}N_2 \cdot C_6H_3N_3O_7$: C, 49.68; H, 3.69% and C, 54.42; H, 4.31% respectively. As the spectra of the 2:3 complexes are identical, only that of the sample made in benzene is presented in Fig. 3. The bands above 23 kK are common to both 2:3 and 1:1 complexes and can be ascribed to the picrate ion. An extra absorption band at about 21 kK apparently accounts for the deep coloration of the 1:1 complex. A comparison with the spectrum of the corresponding TNB complex shown by Curve c indicates that the

11) R. P. Mariella, M. J. Gruber, and J. W. Elder, *J. Org. Chem.*, **26**, 3217 (1961).

12) R. Rascanu, *Ann. Sci. Univ. Jassy.*, **26**, 3 (1940), through *Chem. Abstr.*, **34**, 4385 (1940).

electron-donor is not a neutral *o*-tolidine molecule. If the electron-donor strength of the monoprotonated *o*-tolidine cation is essentially determined by that of the unprotonated half, the CT absorption is expected to appear near that of the *o*-toluidine-TNB complex, 23.1 kK. The close similarity of the locations strongly suggests that this 1:1 complex belongs to Case 1 of CPT complexes. This speculation is supported by the vibrational spectral analysis. Both the 2:3 and 1:1 complexes show patterns characteristic of the picrates of primary amines and also the NH_2 group. The latter pattern consists of bands appearing at 3300 and 3390 cm^{-1}, as evidenced by the spectrum of the corresponding TNB complex (see Fig. 4). The intensity of this pattern in the 2:3 complex is definitely weaker than that in the 1:1 complex; therefore, all the picric acid molecules in the former complex seem to participate in the PT interaction. Although the free amino group must be left in the 2:3 complex, no CT absorption could be detected.

The melting point observed by us for the 1:1 complex differs considerably from that reported by Rascanu, 110°C. Furthermore, we failed to obtain the 1:2 complex described by her.[12]

The 3,3'-Dichloro-o-tolidine Complexes. All the yellow-colored complexes precipitated from the three solvents were found to be of a 1:1 composition. Found: C, 47.31; H, 3.23% (from benzene); C, 46.67; H, 3.16% (from chloroform); and C, 47.16; H, 3.35% (from ethanol). Calcd for $C_{14}H_{14}N_2Cl_2 \cdot C_6H_3N_3O_7$: C, 47.06; H, 3.33%. Contrary to the case of the *o*-tolidine-picric acid (1:1) complex, no band to be assigned to the CT absorption could be detected. As would be expected from the color and the composition, the coexistence of the NH_3^+ and NH_2 groups is demonstrated by the vibrational spectrum.

By the prolonged heating of an ethanolic solution of the complex on a water-bath, a green powder of a 1:1 composition deposited. On the basis of the spectral behavior, we suppose that the product is a picrate of the 3,3'-dichloro-*o*-tolidine cation-radical.

The 3,3'-Dibromo-o-tolidine Complexes (Fig. 5). Jet black-colored needles were crystallized from benzene and chloroform. Their compositions appear to be 1:1. Found: C, 40.29; H, 2.90% (from benzene); C, 39.98; H, 2.92% (from chloroform). Calcd for $C_{14}H_{14}N_2Br_2 \cdot C_6H_3N_3O_7$: C, 40.08; H, 2.84%. Not only the electronic spectrum, but also the vibrational spectrum, strikingly resemble those of the TNB complex (see Fig. 5 for the reflection spectra). Thus, the complex is certainly of the CT type. In accordance with this conclusion, dibromo-*o*-tolidine is supposedly the poorest proton-acceptor among the diamines studied here.

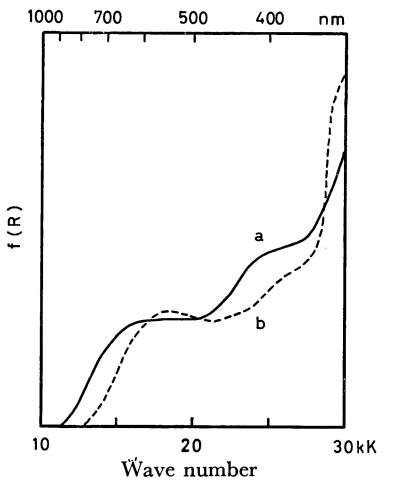

Fig. 5. Diffuse reflection spectra of a) the dibromo-*o*-tolidine-picric acid (1:1) complex and b) the corresponding TNB complex.

Upon storage for months in air, the color turned green. A bright green product was directly obtained if the component compounds were mixed in ethanol. These two samples show spectra similar to each other. The behavior of this and the above-mentioned diamine cation-radical salt will be reported in detail later.

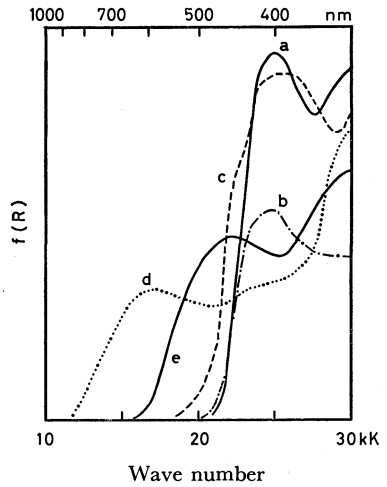

Fig. 6. Diffuse reflection spectra of the *o*-dianisidine-picric acid (1:2) complex from benzene, b) the 2:3 complex from chloroform, c) the 1:1 complex from ethanol, d) the corresponding TNB (1:2) complex, and e) the *o*-anisidine-TNB complex.

The o-Dianisidine Complexes (Fig. 6). The yellow-colored complex crystallized from a benzene solution has a 1:2 composition. Found: C, 44.35; H, 3.27%. Calcd for $C_{14}H_{16}N_2O_2 \cdot 2C_6H_3N_3O_7$: C, 44.44; H, 3.13%. The vibrational spectrum is dominated by the pattern to be ascribed to the NH_3^+ group, indicating that the two amino groups in an *o*-dianisidine molecule are protonated. This complex is undoubtedly of the same nature as the benzidine-picric acid (1:2) described above.

When chloroform is employed as the solvent, a yellow-colored powder was precipitated. The mole ratio is more complicated; namely, 2:3. Found: C, 47.05; H, 3.46%. Calcd for $2C_{14}H_{16}N_2O_2 \cdot 3C_6H_3N_3O_7$: C, 46.97; H, 3.49%. The presence of the NH_2 group is indicated by the appearance of vibrational bands at 3300 and 3380 cm^{-1}. Nevertheless, the electronic spectrum is essentially the same as that of the 1:2 complex. The possibility that this complex is a mixture of the 1:2 and the 1:1 complexes was ruled out by the X-ray diffraction measurements. Presumably this belongs to the same category as the *o*-tolidine complex of a 2:3 composition.

The 1:1 complex prepared in ethanol is orange-

colored. Found: C, 50.69; H, 4.14%. Calcd for $C_{14}H_{16}N_2O_2 \cdot C_6H_3N_3O_7$: C, 50.74; H, 4.02%. The reflection spectrum shown in Fig. 6 has an absorption in addition to those of the above-mentioned 1:2 and 2:3 complexes. This new band is at a location higher than the CT absorption band in the corresponding TNB complex, 17.3 kK, while close to that in the *o*-anisidine-TNB complex, 22.2 kK. Further evidence that the electronic absorption arises from the CT interaction between the monoprotonated *o*-dianisidine cation and the picrate anion comes from the coexistence of the vibrational patterns due to the NH_2 and NH_3^+ groups. This is a second example of Case 1 of CPT complexes.

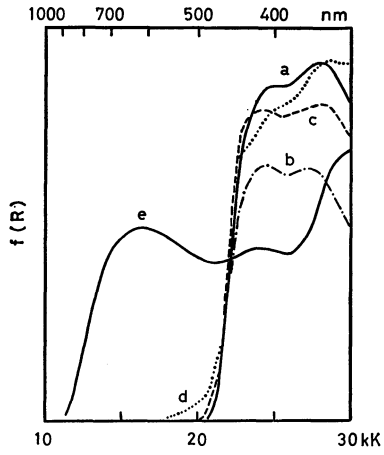

Fig. 7. Diffuse reflection spectra of a) the tetramethylbenzidine-picric acid (2:3) complex from benzene, b) the 2:5 complex from chloroform, c) the 1:2 complex from ethanol, d) the 1:1 complex from ethanol, and e) the corresponding TNB (1:2) complex.

The Tetramethylbenzidine Complexes (Fig. 7). The bright yellow complex deposited from benzene is of a 2:3 composition. Found: C, 51.21; H, 4.15%. Calcd for $2C_{16}H_{20}N_2 \cdot 3C_6H_3N_3O_7$: C, 51.41; H, 4.20%.

From chloroform a yellow-colored complex was precipitated. The mole ratio was found to be 2:5. Found: C, 45.43; H, 3.61%. Calcd for $2C_{16}H_{20}N_2 \cdot 5C_6H_3N_3O_7$: C, 45.78; H, 3.38%.

When ethanol was employed, the following three complexes were isolated, depending upon the ratio of the component compounds mixed. One of them was the 2:5 complex previously obtained from chloroform. Found: C, 45.93; H, 3.53%. The complex of a 1:2 composition is greenish yellow. Found: C, 47.39; H, 3.36%. Calcd for $C_{16}H_{20}N_2 \cdot 2C_6H_3N_3O_7$: C, 48.14; H, 3.72%. The last one has a 1:1 composition and is tan-colored. Found: C, 56.69; H, 5.09%. Calcd for $C_{16}H_{20}N_2 \cdot C_6H_3N_3O_7$: C, 56.29; H, 4.90%. The intensity of the electronic absorption unique to this complex is weak. However, its location is very clearly observable by the original recording in reflectance and can be well compared with that of the CT absorption in the solid *N,N*-dimethylaniline-TNB complex, 19.3 kK. Consequently, this may be considered as the third complex belonging to Case 1 of CPT complexes. Broad bands characteristic of the picrates of the tertiary amines in the region from 2300 to 2750 cm^{-1} are dominant in the vibrational spectra of all the complexes. Of course, the higher the picric acid content, the more dominant these bands are.

The ionization potentials of the diamines estimated by the energies of the CT absorption bands developed by mixing with *p*-chloranil in chloroform increase in this order: tetramethylbenzidine$<$*o*-dianisidine$\sim$*o*-tolidine$<$dibromo-*o*-tolidine$\sim$dichloro-*o*-tolidine$<$benzidine. The location of benzidine is dependent on the particular electron-acceptor chosen and is somewhat ambiguous.[13] The electron-donor strength seems to have no direct correlation with whether or not a diamine forms a solid complex of the CPT type. This is not at all surprising, since the stabilization by the CT interaction is only a minor fraction of the total ground-state binding energy in the complexes where both the CT and PT interactions simultaneously operate. The two which do not form such complexes are 3,3'-dihalo-*o*-tolidines; therefore, the steric effect of the two substituents introduced *ortho* to an amino group may be considered as a primary factor.

It must be noted that all the complexes of the CPT type were prepared in ethanol, the most polar solvent among the three. Even though the association of electron-donor and acceptor is expected to be poor in this solvent, the dissociation of the ion-pair formed by means of the PT interaction may facilitate the CT interaction between the picrate anion and the diamine molecule or the monoprotonated diamine cation.

No example of Case 2 of CPT complexes could be found in the present work. If the difference between the first and second pK_a values is as small as those in benzidine and *o*-tolidine, it may not be easy to find such a complex.

Very recently, Thewalt and Bugg have reported the crystal and molecular structures of red-colored serotonin picrate monohydrate.[14] The protonated serotonin cation and the picrate anion are arranged in alternatingly stacked arrays to form continuous columns. The interaction between these two components has been concluded by them to be of the CT type. This salt may be considered another example of Case 1 of CPT complexes.

13) G. Saito and Y. Matsunaga, This Bulletin, **44**, 1788 (1971).
14) U. Thewalt and C. E. Bugg, *Acta. Crystallogr.*, **B 28**, 82 (1972).

The Cation-radical Salts Derived from Benzo- and Dibenzo-phenothiazines

Yoshio MATSUNAGA and Yukio SUZUKI*

Department of Chemistry, Faculty of Science, Hokkaido University, Sapporo

(Received August 18, 1972)

The chloride, iodide, and perchlorate of benzo- and dibenzo-phenothiazine cation-radicals have been prepared by the reaction of an equimolar mixture of the thiazine and its *S*-oxide with an appropriate acid. The vibrational spectra of the products have been found to be in close agreement with those of the bromides made by the familiar oxidation of thiazines with bromine. The results of electronic spectral and ESR measurements have furnished further support for our conclusion that the thiazine cation-radical salts can be prepared by the above-mentioned reaction. The electronic spectra of the iodides of benzophenothiazines have been found to differ markedly from those of other salts and to bear a resemblance to those of the low-resistivity iodine complexes.

The cation-radical or semiquinoid salts derived from phenothiazine were described by Pummerer and Gassner and also by Kehrmann and Diserens over half a century ago.[1,2] These authors claimed the preparation of the following salts: bromide, periodide, sulfate, nitrate, perchlorate, and picrate. The first three salts were made by the oxidation of the parent compound with bromine, iodine, and concentrated sulfuric acid respectively. The next two were obtained as precipitates when the desired counter ion in an appropriate form was added to a dilute sulfuric acid solution of the sulfate thus prepared. The oxidation of phenothiazine with ferric chloride in the presence of picric acid resulted in the formation of the picrate. More recently, some new salts have been prepared by the oxidation of phenothiazine and its *N*-methyl derivative with antimony pentachloride.[3,4] Although halogens have been widely used as oxidizing agents in the preparation of cation-radicals, *e.g.*, those derives from aromatic diamines and tetrathiotetracene,[5–8] chlorine is not suited to the oxidation of either phenothiazine or diamines. Consequently, the use of ferric chloride has been proposed by Hatano *et al.* for the preparation of the chlorides of *p*-phenylenediamine and benzidine cation-radicals.[9] Moreover, the addition of iodine to phenothiazine has been known to produce a molecular complex with a 2: 3 mole ratio instead of the monoiodide.[10,11]

Earlier we studied the effects of iodine addition on the electrical resistivity and the electronic and vibrational spectra of the semiquinoid phenothiazine bromide.[12] A marked resistivity minimum was found to lie around the mole ratios from 1: 0.25 to 1: 0.30. The values in this composition range are from 4 to 5 ohm·cm, lower than those exhibited by the above-mentioned iodine complex, 13—20 ohm·cm.[10,12–14] The composition of this adduct corresponds approximately to (phenothiazine)$_2Br_2I$. As the mixed halide ion, Br_2I^-, is a well-known species, the formation of a complex cation-radical salt, (phenothiazine)$^+$(phenothiazine)$^0Br_2I^-$, is very likely. In order to examine systems consisting of iodine and the chloride or iodide, the method of preparing these halides must first be established. In this paper, we wish to present a method based on the following reaction:

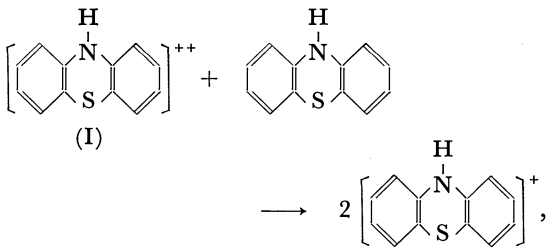

(I)

where the charge is proportionated between the protonated holoquinoid cation (I) and the phenothiazine molecule. The former species can be easily obtained when phenothiazine *S*-oxide is dissolved into strong acids.[1,2,15] A preliminary attempt to prepare the chloride and bromide by this reaction has already been reported by one of the present authors;[16] therefore, attention has here been directed towards the cation-radical salts derived from benzo[*a*]-, benzo[*c*]-, and dibenzo[*c,h*]-phenothiazines. As is indicated by the low energies of the charge-transfer absorptions in the *s*-trinitrobenzene and picric acid complexes listed in Table 1, the present compounds are expected to produce cation-radicals more easily than phenothiazine itself. The molecular orbital calculations made by Tyutyulkov *et al.* support this prediction.[17] In light of the size of the conjugated systems, the cation-radicals may be more stable than that of phenothiazine.

* Present address, Tokyo Shibaura Electric Co., Kawasaki.

1) R. Pummerer and S. Gassner, *Ber.*, **46**, 2310 (1913).
2) F. Kehrmann and L. Diserens, *ibid.*, **48**, 318 (1915).
3) Y. Sato, M. Kinoshita, M. Sano, and H. Akamatu, This Bulletin, **40**, 2539 (1967).
4) Y. Sato, M. Kinoshita, M. Sano, and H. Akamatu, *ibid.*, **42**, 548 (1969).
5) L. Michaelis and S. Granick, *J. Amer. Chem. Soc.*, **65**, 1747 (1943).
6) G. K. Hughes and N. S. Hush, *J. Proc. Roy. Soc. N. S. W.*, **81**, 48 (1947).
7) C. Marschalk and J. P. Niederhauser, *Bull. Soc. Chim. Fr.*, **1952**, 151.
8) J. Honzl, K. Ulbert, V. Hadek, and M. Tlustakova, *Chem. Commun.*, **1965**, 440.
9) K. Hatano, Y. Fujita, and T. Kwan, This Bulletin, **43**, 3022 (1970).
10) Y. Matsunaga, *Helv. Phys. Acta.*, **36**, 800 (1963).
11) F. Gutmann and H. Keyzer, *J. Chem. Phys.*, **46**, 1969 (1967).
12) Y. Matsunaga and K. Shono, This Bulletin, **43**, 2007 (1970).
13) M. Sano, K. Ohno, and H. Akamatu, *ibid.*, **44**, 3269 (1971).
14) Y. Matsunaga and Y. Suzuki, *ibid.*, **45**, 3375 (1972).
15) H. J. Shine and E. E. Mach, *J. Org. Chem.*, **30**, 2130 (1965).
16) Y. Matsunaga, *Nippon Kagaku Zasshi*, **89**, 905 (1968).
17) N. Tyutyulkov, D. Simov, and S. Stoyanov, *Compt. rend. Acad. bulg. Sci.*, **23**, 1095 (1970).

TABLE 1. ENERGIES OF CHARGE-TRANSFER ABSORPTION MAXIMA IN THE *s*-TRINITROBENZENE COMPLEXES IN CHLOROFORM AND IN THE SOLID PICRIC ACID COMPLEXES (IN kK) AND ENERGY COEFFICIENTS OF THE HIGHEST OCCUPIED MOLECULAR ORBITALS OF THE THIAZINES (IN β)

Donor	Acceptor		Energy coefficient of the HOMO[a]
	s-Trinitrobenzene	Picric acid	
Phenothiazine	19.1	17.1[b]	0.485
Benzo[*a*]-phenothiazine	*ca.* 18	16.2	0.382
Benzo[*c*]-phenothiazine	17.9	14.7	0.397
Dibenzo[*c,h*]-phenothiazine	17.4	14.1	0.346

a) Taken from Ref. 17.
b) 18.2 kK by Iida, Ref. 18.

Experimental

Materials. The examples cover only dibenzophenothiazine and its derivatives; however, they illustrate all of the preparative procedures which we employed.

Dibenzo[c,h]*phenothiazine*: β,β-Dinaphthylamine and sulfur were fused together in the presence of a small amount of iodine.[19] The product was then recrystallized from benzene.

Dibenzophenothiazine S-*Oxide*: Following the procedure described by Pummerer and Gassner for phenothiazine *S*-oxide,[1] dibenzophenothiazine, potassium hydroxide, and hydrogen peroxide in ethanol were gently heated for two hours. Subsequent recrystallization from ethanol gave yellow fine needles.

Dibenzophenothiazine Chloride and Iodide: An equimolar mixture of dibenzophenothiazine and its *S*-oxide was thoroughly ground in an agate mortar. The fine powder was spread in a beaker and moistened with concentrated hydrochloric acid. The reaction mixture was then dried in a vacuum desiccator containing potassium hydroxide pellets. Found: C, 67.2; H, 3.9; Cl, 10.0%. Calcd for $C_{20}H_{13}NS^+Cl^-\cdot H_2O$: C, 68.0; H, 4.3; Cl, 10.0%.

The iodide was prepared similarly. Found: C, 52.9; H, 2.9; N, 3.1; I, 32.8%. Calcd for $C_{20}H_{13}NS^+I_{1.15}^-$: C, 53.0; H, 2.9; N, 3.2; I, 32.8%.

Dibenzophenothiazine Bromide: The thiazine dissolved in a mixture of acetone and ether was cooled with an ice-salt mixture, and then bromine corresponding to less than one equivalent in cold ether was added, drop by drop. A black precipitate was then filtered out and washed with ether. Found: C, 63.1; H, 3.4; N, 3.2; Br, 21.5%. Calcd for $C_{20}H_{13}NS^+Br^-$: C, 63.3; H, 3.4; N, 3.7; Br, 21.1%.

Dibenzophenothiazine Perchlorates: An equimolar mixture of dibenzophenothiazine and its *S*-oxide was added to perchloric acid cooled with an ice-salt bath. A black precipitate appeared immediately. Found: C, 61.3; H, 3.3; N, 3.0%. Calcd for $C_{20}H_{13}NS^+ClO_4^-$: C, 60.2; H, 3.3; N, 3.5%.

If dibenzophenothiazine *S*-oxide alone is employed in place of the mixture, the holoquinoid perchlorate can be isolated. Found: C, 59.5; H, 3.0; N, 3.2; Cl, 9.2%. Calcd for $C_{20}H_{12}NS^+ClO_4^-$: C, 60.3; H, 3.0; N, 3.5; Cl, 8.9%.

Dibenzophenothiazine Picrate: The thiazine dissolved in ethanol was cooled with an ice-salt mixture and was then oxidized by adding it to an ethanolic solution containing an equimolar amount of ferric chloride and an excess of picric acid. The black picrate precipitated immediately. Found: C, 58.4; H, 2.8; N, 10.5%. Calcd for $C_{20}H_{13}NS^+C_6H_3N_3O_7^-$: C, 59.2; H, 2.9; N, 10.6%.

Measurements. The vibrational and electronic spectra of the solid salts were examined as have been reported elsewhere.[12] The ESR measurements were carried out by means of a JEOL model JES-ME-3X spectrometer in the temperature range from -100 to 100°C. The spin concentrations were estimated at room temperature by comparing the signal intensities due to the sample and the standard material, violanthrone (8.1×10^{19} spins/g) with the aid of a multimode cavity model JES-MCX-1.

Results and Discussion

Syntheses. Although the preparation of phenothiazine chloride by the above-mentioned reaction was not satisfactory,[16] the composition of the dibenzophenothiazine chloride agrees well with the calculated one. With the benzo derivatives the results were less satisfactory; those results were: C, 65.0; H, 4.1; N, 4.5; Cl, 10.9% for benzo[*a*]phenothiazine chloride, and C, 62.6; H, 4.0; N, 4.5; Cl, 10.7% for benzo[*c*]phenothiazine chloride. Calcd for $C_{16}H_{11}NS^+Cl^-\cdot H_2O$: C, 63.5; H, 4.3; N, 4.6; Cl, 11.7%.

A monoiodide hitherto unknown could be prepared by this method. In the case of benzo[*a*]phenothiazine, we obtained the following analytical results: C, 48.8; H, 2.6; N, 3.6; I, 35.3%. Calcd for $C_{16}H_{11}NS^+I_{1.07}^-$: C, 49.9; H, 2.9; N, 3.6; I, 35.3%. As for benzo[*c*]-phenothiazine iodide, C, 49.7; H, 2.8; N, 3.9; I, 34.8%. Calcd for $C_{16}H_{11}NS^+I_{1.05}^-$: C, 50.2; H, 2.9; N, 3.7; I, 34.9%. In all three, the presence of free iodine produced from hydroiodic acid during the preparation accounts for iodine contents higher than those expected for a 1:1 composition.

The reaction was also successfully applied to the preparation of the semiquinoid perchlorate. In addition to the dibenzophenothiazine perchlorate described above, we obtained the salts derived from benzo[*a*]- and benzo[*c*]-phenothiazines by the same technique. Found: C, 53.8; H, 3.0; N, 3.9; Cl, 10.5% for the former salt and C, 54.8; H, 3.1; N, 4.0% for the latter. Calcd for $C_{16}H_{11}NS^+ClO_4^-$: C, 55.1; H, 3.2; N, 4.0; Cl, 10.2%.

In the present work, the dibenzophenothiazine bromide was prepared by a method analogous to that reported by Pummerer and Gassner; however, it has already been shown that phenothiazine bromide can be obtained by the reaction described above.[16]

The present work seems to provide justification for our hypothesis that the addition of an equimolar mixture of a thiazine and its *S*-oxide to a strong acid is a convenient method for preparing the semiquinoid salts, provided that the cation-radical is stable in the acid. As will be discussed in the following sections, the physical properties of the salts so prepared support this conclusion.

Vibrational Spectra. If the chloride and iodide are indeed of the cation-radical, their vibrational spectra must be identical with that of the bromide prepared

18) Y. Iida, This Bulletin, **44**, 663 (1971).
19) E. Knoevenagel, *J. Prakt. Chem.*, (2) **89**, 1 (1914).

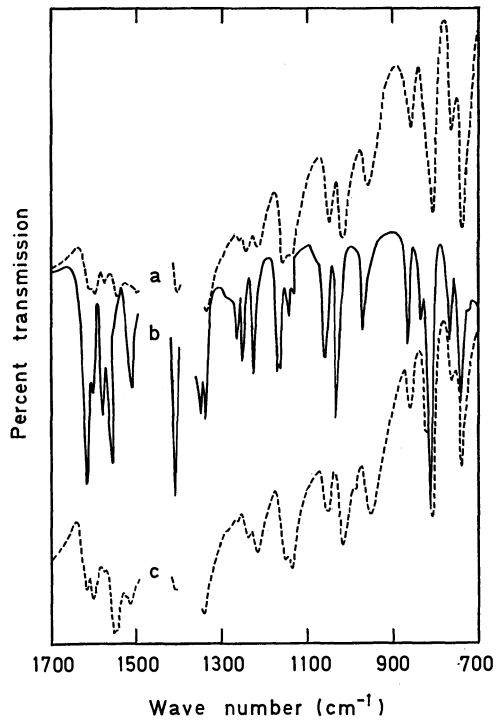

Fig. 1. Vibrational spectra of (a) dibenzophenothiazine chloride, (b) the bromide, and (c) the iodide.

by the authentic oxidation with bromine. The spectra of the three salts of dibenzophenothiazine are compared with each other in Fig. 1. As we noted earlier in the cases of phenothiazine and its benzo derivatives,[12,14] the bromide gives a spectrum distinctly different from that of the parent compound. The bands in the chloride and iodide are overlapped by the electronic absorption to be described later and are not well resolved; however, it is easy to see that their general features are in essential agreement with those of the bromide. The spectrum of the semiquinoid perchlorate is dominated by strong broad absorption bands due to the anion. Nevertheless, this is also in good accordance with that

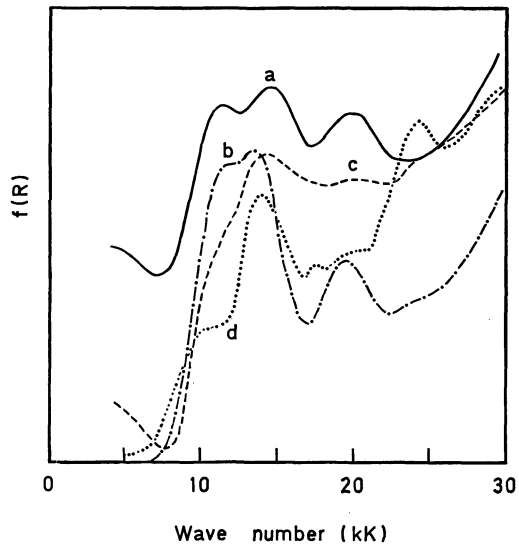

Fig. 2. Diffuse reflection spectra of (a) dibenzophenothiazine chloride, (b) the bromide, (c) the iodide, and (d) the picrate.

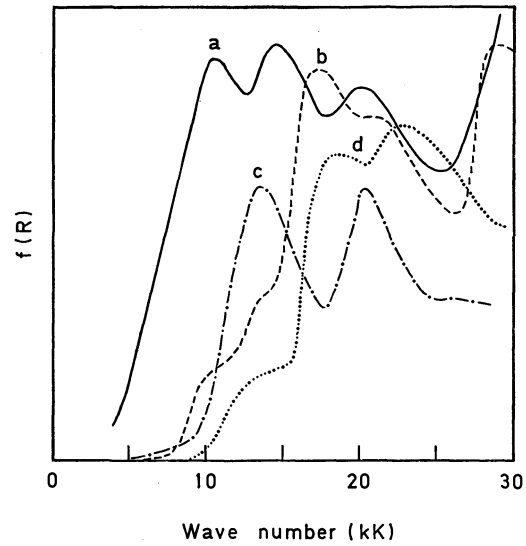

Fig. 3. Diffuse reflection spectra of (a) semiquinoid dibenzophenothiazine perchlorate, (b) the holoquinoid perchlorate, (c) semiquinoid phenothiazine perchlorate, and (d) the holoquinoid perchlorate.

of the bromide, as far as we can compare them. It must be added that the spectrum of the holoquinoid perchlorate differs appreciably from that of the corresponding semiquinoid salt. Thus, the vibrational spectra of the chloride, iodide, and perchlorate prepared by our method are definitely those of the cation-radical. This conclusion is also valid for the salts derived from benzophenothiazines.

Electronic Spectra. The dibenzophenothiazine cation-radical in hydrochloric acid-acetic acid (1: 1 by volume) exhibits absorption maxima at 14.3, 17.9, and 20.4 kK, with an intensity ratio of 1: 0.44: 0.52. The diffuse reflection spectra of the solid chloride, bromide, iodide, and picrate are presented in Fig. 2, and that of the perchlorate, in Fig. 3. The spectrum of the bromide includes bands at 11.6, 13.4, and 19.6 kK. The spectra of the chloride, iodide, and perchlorate prepared by our method also show bands around 11, 14, and 20 kK. Among the five, the picrate gives the most complicated spectrum, consisting of bands located at 10.3, 13.9, 17.4, about 20, and 24.2 kK. The last band can be assigned to the picrate anion. The locations of the second and third are close to those of the two strong ones observed in the solution spectrum; however, the one appearing around 11 kK is undoubtedly characteristic of the solid cation-radical salts. By analogy with the spectra of the phenothiazine cation-radical salts,[18] this band may arise from the pair-by-pair interaction between the cations. In addition to this, the chloride and iodide have bands located below 4 kK, indicating some difference in the mode of interaction. It must be noted that the relative intensities of the bands located at about 11 kK in the iodide and picrate are appreciably weaker than those in the other two. The nature of the extra band appearing at 17.4 kK in the picrate will be speculated on in connection with the ESR data.

In Fig. 3 the spectrum of the perchlorate of dibenzophenothiazine is compared with that of the holoquinoid

perchlorate. Although the holoquinoid salt absorbs also down to 10 kK, the intensities in the region below 15 kK are much diminished and the locations of the absorption maxima above 15 kK differ substantially from those of the cation-radical salt. A similar comparison is made for the semiquinoid and holoquinoid phenothiazine perchlorates in the same figure. The spectrum of this semiquinoid perchlorate is simpler than those of the phenothiazine bromide, bisulfate, and picrate reported earlier;[12,18] that is, a band near 23 kK common to the latter three is not observed here.

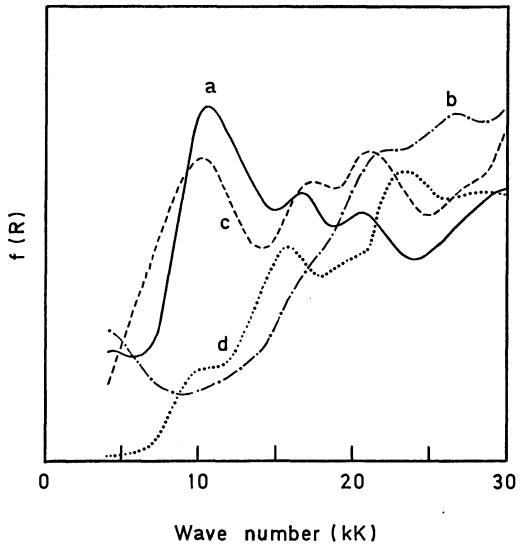

Fig. 4. Diffuse reflection spectra of (a) benzo[*c*]phenothiazine chloride, (b) the iodide, (c) the perchlorate, and (d) the picrate.

The diffuse reflection spectra of the cation-radical salts of benzo[*c*]phenothiazine prepared by our method are shown in Fig. 4, together with that of the picrate shown for the sake of comparison. The iodide was found to give a spectrum quite different from the others. This spectrum resembles that of the low-resistivity iodine complex presented in a previous paper.[14] The pattern of these two may be assigned to the cation-radicals in a more-than-by-pairs interaction. However, the band around 15 kK seen in the iodine complex is much diminished in the iodide. On the other hand, the absorption above 25 kK is intensified, resulting in the appearance of a maximum at 26.4 kK. Here again, bands at 16—17 and about 21 kK common to the chloride, perchlorate, and picrate are located close to the bands observed in the solution spectrum: 16.8 and 21.1 kK, with an intensity ratio of 1 : 0.70. The absorption located at about 10 kK is possibly due to the pair-by-pair interaction between the cation-radicals. A similarity in the spectrum was also noted between the iodide of benzo[*a*]phenothiazine and the iodine complex.

In spite of the coincidence in the locations of the absorption maxima, the whole spectrum of the solid salt varies considerably with the counter ion. Such pronounced variations are not unexpected in the solid-state spectrum of ion-radicals.[20,21]

Spin Concentrations. Electron-spin-resonance absorption was detected in all the salts which were supposed to be of cation-radicals, but not in the holoquinoid perchlorate. The absorptions are all symmetric except in the case of the benzo[*a*]phenothiazine perchlorate, where the *g*-values estimated by the method according to Kneubühl are as follows: $g_{//}=2.0027$ and $g_{\perp}=2.0074$.[22] The distance between the points of the maximum slope measured at room temperature are in the range from 7 to 12 Gauss, and the spin concentrations, in the range from 0.01 to 0.10 spins per molecule. Thus, the major fraction is diamagnetic. This finding is in accordance with the electronic spectral behavior discussed above. Besides, the concentrations were found to be temperature-independent; therefore, the observed spins must be ascribed to some imperfections and impurities in crystals. The dibenzophenothiazine picrate gave an exceptionally wide absorption; that is, a distance of 34 Gauss was observed. Moreover, a spin concentration as high as 0.30 was detected in this salt. One should recall the observation that this solid salt shows an electronic absorption maximum at 17.4 kK, corresponding to the weakest band in the spectrum of the monomeric cation-radical. The high spin concentration may be correlated with the appearance of this band in the solid-state spectrum. However, the weakness of the absorption at 10—11 kK is common in the solid picrates and cannot be correlated with the spin concentration. The benzo[*c*]phenothiazine salt has a spin concentration as low as 0.01.

The authors wish to express their thanks to Professor Minoru Kinoshita of the University of Tokyo for his gift of the sample of violanthrone. The ESR spectrometer was obtained with a grant-in-aid from the Ministry of Education.

20) Y. Iida and Y. Matsunaga, This Bulletin, **41**, 2615 (1968).
21) Y. Matsunaga and Y. Narita, *ibid.*, **45**, 408 (1972).
22) F. K. Kneubühl, *J. Chem. Phys.*, **33**, 1074 (1960).

The Crystal Structure of Di-π-allyl(dihydropentalenylene)dinickel

Yukishige KITANO, Michio KASHIWAGI, and Yukio KINOSHITA*

Basic Reseach Laboratories, Toray Industries, Inc., Tebiro, Kamakura 248

(Received June 8, 1972)

The crystal structure of di-π-allyl(dihydropentalenylene)dinickel, $(C_8H_6)Ni_2(C_3H_5)_2$, has been determined from three-dimensional single-crystal X-ray photographic data. The crystal of this compound is composed of discrete molecular units in the monoclinic space group $P2_1/a$, with two molecules per unit cell with dimensions of $a=8.451\pm0.004$, $b=12.691\pm0.005$, $c=5.976\pm0.006$ Å, and $\beta=108.81\pm0.05°$. The calculated and observed densities are 1.650 and 1.60 g·cm^{-3} respectively. The structure was deduced from a sharpened Patterson synthesis and was refined by means of the least-squares method to the final R index of 0.121 for 1151 independent non-zero reflections. The molecule has a crystallographic center of symmetry; therefore, two nickel atoms which are complexed in a sandwich fashion between the dihydropentalenylene ring and the π-allyl group take a *trans* configuration. The distances of the nickel atom from the ring carbons range from 2.03 to 2.27 Å, the closest approach being to the three non-bridging atoms of the five-membered ring. The orientation of the π-allyl groups with respect to the nickel atom is similar to those found in other π-allyl complexes.

In the reaction of (dihydropentalenylene)dilithium with allyl metal chlorides, Miyake and Kanai have newly synthesized π-allyl-dihydropentalenylene complexes of nickel, chromium, and zirconium.[1] The NMR spectra of the nickel derivative in C_6D_6 and benzene indicate the presence of the π-allyl group and the dihydropentalenylene ring. In order to confirm the configuration of the complex, the measurement of the dipole moment was attempted; however, because of its small value ($\mu=0.65\pm0.5$ D in benzene at 30°C), no definite conclusion was obtained. Thus, it is not certain whether the complex has a *cis* or a *trans* configuration; therefore, a single-crystal X-ray structure analysis of the complex was carried out in order to determine the molecular configuration and the mode of coordination of the π-allyl groups to the nickel.

Experimental

Di-π-allyl(dihydropentalenylene)dinickel, $(C_8H_6)Ni_2(C_3H_5)_2$, was prepared by the reaction of (dihydropentalenylene)-dilithium and bis π-allyl nickel chloride. The complex was recrystallized from an ether solution as extremely air-sensitive, deep green monoclinic plates elongated in the *b* direction. For the crystallographic analysis, the crystals were sealed into thin-walled glass capillary tubes, under an argon atmosphere; therefore, no serious crystal decomposition was found during the collection of the intensity data. The unit-cell dimensions were obtained by the least-squares procedure from measurements on Weissenberg photographs around the *b* and *c* axes. The density was measured by flotation in an aqueous solution of zinc chloride at 25°C. The crystal data are summarized in Table 1.

TABLE 1. CRYSTAL DATA

Di-π-allyl(dihydropentalenylene)dinickel, $Ni_2C_{14}H_{16}$
Molecular weight: 301.6
Monoclinic
$a=8.451\pm0.004$Å
$b=12.691\pm0.005$
$c=5.976\pm0.006$
$\beta=108.81\pm0.05°$
$V=606.77$ Å^3
$D_m=1.60$ g·cm^{-3}, $D_x=1.650$ g·cm^{-3} for $Z=2$
Systematic absences, $h0l$ with $h=2n+1$
$0k0$ with $k=2n+1$
Space group C_{2h}^5—$P2_1/a$ (No. 14)
Linear absorption coefficient for Cu$K\alpha$: $\mu=48.9$ cm^{-1}

The three-dimensional intensity data were collected from equi-inclination Weissenberg photographs taken with Ni-filtered Cu$K\alpha$ radiation. The multiple-film technique was used, and zero to seventh layers about the *b* axis and zero to fifth layers about the *c* axis were recorded. The intensities were estimated visually by comparison with a calibrated

TABLE 2. THE ATOMIC COORDINATES OF DI-π-ALLYL(DIHYDROPENTALENYLENE)DINICKEL, ALONG WITH ESTIMATED STANDARD DEVIATIONS IN PARENTHESES

Atom	*x/a*	*y/b*	*z/c*
Ni	0.2400(2)	0.0447(2)	0.2436(4)
C (1)	0.0310(20)	0.0080(22)	−0.0969(22)
C (2)	0.1818(24)	−0.0534(24)	−0.0510(28)
C (3)	0.2015(26)	−0.1100(26)	0.1537(28)
C (4)	0.0828(24)	−0.0789(24)	0.2633(26)
C (5)	0.4234(30)	0.1453(30)	0.2298(34)
C (6)	0.3192(28)	0.1835(28)	0.3535(32)
C (7)	0.3078(34)	0.1255(32)	0.5489(34)

TABLE 3. THERMAL PARAMETERS (Å^2) IN THE FORM OF $\exp\{-(B_{11}h^2+B_{22}k^2+B_{33}l^2+B_{12}hk+B_{13}hl+B_{23}kl)\}$ (each multiplied by 10^4, estimated standard deviations in parentheses)

Atom	B_{11}	B_{22}	B_{33}	B_{12}	B_{13}	B_{23}
Ni	33(2)	10(1)	106(5)	−10(2)	16(5)	− 8(4)
C (1)	42(14)	8(5)	85(30)	−12(14)	−30(34)	− 7(22)
C (2)	22(16)	6(6)	85(38)	− 1(16)	26(40)	−20(27)
C (3)	24(17)	5(7)	69(39)	−18(17)	−60(42)	30(28)
C (4)	30(15)	3(6)	55(35)	−15(16)	−11(38)	2(25)
C (5)	46(21)	15(8)	152(49)	−40(22)	54(53)	−21(34)
C (6)	46(20)	3(7)	144(49)	2(19)	1(51)	−26(31)
C (7)	90(27)	15(8)	143(50)	−43(25)	119(61)	−55(35)

* Present address: Ehime Laboratory, Toray Industries, Inc., Masaki, Ehime.

1) A. Miyake and A. Kanai, *Angew. Chem.*, **83**, 851 (1971); *Angew. Chem. internat. Edit.*, **10**, 801 (1971).

TABLE 4. OBSERVED AND CALCULATED STRUCTURE FACTORS
The table gives h, k, 10 $|F_0|$, and $10F_c$ in blocks of constant l.

H	K	FO	FC
	L = 0		
2	0	966	-1147
4	0	788	740
6	0	580	-499
8	0	117	133
10	0	109	-161
1	1	291	318
2	1	490	502
3	1	143	-121
4	1	118	-81
5	1	357	231
6	1	119	69
7	1	246	-243
9	1	155	196
10	1	116	-170
0	2	999	-1182
1	2	430	-555
2	2	525	-610
3	2	464	405
4	2	720	677
5	2	387	-326
6	2	510	-423
7	2	243	208
8	2	281	292
9	2	193	-216
10	2	184	-235
1	3	475	548
2	3	381	326
3	3	257	-173
4	3	66	57
5	3	298	218
6	3	25	-42
7	3	187	-177
8	3	49	61
10	3	145	-259
0	4	107	-26
1	4	310	-325
2	4	208	-145
3	4	694	711
4	4	474	376
5	4	603	-547
6	4	183	-146
7	4	457	457
8	4	268	286
9	4	357	-462
2	5	224	-182
3	5	317	225
4	5	191	158
5	5	72	20
6	5	268	-253
7	5	127	84
8	5	204	216
9	5	34	-16
0	6	42	-50
1	6	627	-687
2	6	232	202
3	6	741	721
5	6	606	-535
6	6	147	110
7	6	414	420
8	6	17	-7
9	6	290	-356
1	7	182	-123
2	7	88	-72
3	7	290	202
4	7	90	79
6	7	217	-212
7	7	236	245
8	7	172	206
9	7	58	-82
0	8	498	-367
1	8	743	-643
2	8	570	468
3	8	456	374
4	8	255	-212
5	8	529	-498
6	8	261	251
7	8	290	335
8	8	137	-166
1	9	79	28
2	9	104	-71
3	9	170	168
5	9	113	-111
6	9	38	-67
7	9	104	137
0	10	627	-505
1	10	257	-221
2	10	624	554
3	10	94	71
4	10	446	-393
5	10	269	-257
6	10	392	419
7	10	120	137
1	11	97	75
3	11	271	242
4	11	218	-190
5	11	201	-214
6	11	89	51
7	11	27	67
0	12	496	-475
1	12	91	72
2	12	586	632
3	12	113	-114
4	12	402	-425
5	12	121	144
6	12	192	245
1	13	74	72
3	13	90	100
4	13	85	-100
5	13	63	-90
0	14	271	-265
1	14	285	302
2	14	466	484
3	14	234	-280
4	14	190	-264
5	14	114	241
2	15	26	-27
3	15	55	75
0	16	62	88
1	16	164	287
	L = 1		
2	0	82	6
4	0	361	294
6	0	164	-165
8	0	252	812
-2	0	238	193
-4	0	133	-124
-6	0	327	207
-8	0	424	-337
-10	0	172	188
0	1	335	-375
1	1	673	-92
2	1	200	168
3	1	487	476
4	1	153	-113
5	1	431	-366
6	1	125	113
7	1	408	434
8	1	84	-97
9	1	133	-187
-1	1	1218	1436
-2	1	318	328
-3	1	767	861
-4	1	290	-244
-5	1	740	892
-6	1	204	159
-7	1	534	-553
-8	1	71	-74
-9	1	143	147
-10	1	76	95
0	2	381	391
1	2	575	703
2	2	360	-275
3	2	257	-159
4	2	[illegible]	[illegible]
5	2	281	-217
6	2	51	-62
7	2	94	95
8	2	161	197
9	2	176	-211
-1	2	113	-88
-2	2	214	181
-3	2	292	220
-4	2	39	-56
-5	2	76	-72
-6	2	282	239
-7	2	205	-157
-8	2	306	-309
-9	2	25	-32
-10	2	54	83
0	3	357	-379
1	3	207	-214
2	3	560	604
3	3	697	729
4	3	654	-575
5	3	430	-379
6	3	409	362
7	3	394	408
8	3	266	-316
9	3	221	-260
-1	3	392	473
-2	3	449	516
-3	3	449	-438
-4	3	464	-426
-5	3	409	319
-6	3	380	326
-7	3	394	-360
-8	3	333	-336
-9	3	262	255
-10	3	256	308
0	4	338	278
1	4	40	3
2	4	152	94
3	4	304	230
4	4	22	19
5	4	338	-279
6	4	145	67
7	4	152	170
8	4	75	67
9	4	131	-179
-1	4	94	-86
-2	4	20	-26
-3	4	215	235
-4	4	156	87
-5	4	225	-200
-6	4	43	41
-7	4	132	116
-8	4	117	-104
-9	4	69	-98
0	5	551	-636
2	5	815	1001
3	5	430	335
4	5	799	-797
6	5	439	393
7	5	154	126
8	5	338	-360
9	5	97	-122
-1	5	229	171
-2	5	651	820
-3	5	140	-88
-4	5	550	522
-5	5	64	-34
-6	5	383	335
-7	5	33	-34
-8	5	455	-420
-9	5	54	60
-10	5	238	329
0	6	132	-27
1	6	181	-140
2	6	577	461
3	6	242	197
4	6	135	57
5	6	257	-230
6	6	121	107
7	6	239	259
8	6	56	-54
-1	6	63	-32
-2	6	134	-85
-3	6	100	77
-5	6	90	-89
-6	6	211	-167
-7	6	222	229
-8	6	161	149
-9	6	133	-169
0	7	787	-880
1	7	406	350
2	7	776	750
3	7	168	-126
4	7	504	-478
5	7	287	247
6	7	349	321
7	7	135	-121
8	7	193	-201
-1	7	242	-230
-2	7	657	748
-3	7	345	292
-4	7	505	-469
-5	7	238	-189
-6	7	433	422
-7	7	121	121
-8	7	266	-243
-9	7	110	-102
2	8	295	168
3	8	153	117
4	8	248	170
5	8	186	-171
6	8	82	113
-1	8	25	1
-2	8	168	98
-3	8	182	144
-4	8	187	-113
-5	8	182	144
-6	8	109	-125
-7	8	141	146
-8	8	157	157
-9	8	74	111
0	9	479	-433
1	9	655	545
2	9	314	249
3	9	301	-258
4	9	288	-248
5	9	388	405
6	9	414	357
-1	9	507	-433
-2	9	320	244
-3	9	468	432
-4	9	261	-237
-5	9	437	-410
-6	9	412	447
-7	9	301	279
-8	9	146	-164
2	10	75	83
4	10	30	-50
5	10	40	25
6	10	107	114
-1	10	94	-74
-2	10	168	111
-3	10	160	114
-4	10	187	184
-5	10	63	41
-6	10	183	-190
-8	10	65	105
0	11	43	58
1	11	493	465
2	11	54	-73
3	11	391	-322
5	11	468	454
6	11	42	65
-1	11	442	-400
-3	11	531	530
-5	11	391	-524
-6	11	109	105
-7	11	333	366
2	12	128	110
3	12	144	-147
4	12	138	-134
5	12	185	201
6	12	116	164
-2	12	43	40
-3	12	114	-107
-4	12	162	192
-5	12	264	231
-6	12	132	-157
0	13	246	297
1	13	405	390
2	13	182	-220
3	13	249	-320
4	13	173	212
5	13	183	228
-1	13	391	-411
-2	13	139	-113
-3	13	473	627
-4	13	179	188
-5	13	188	-355
-6	13	113	-153
2	14	51	88
-1	14	193	214
-2	14	31	33
-3	14	64	-72
0	15	336	416
1	15	229	268
2	15	251	-331
3	15	251	-234
-1	15	147	-161
-2	15	211	-286
-3	15	186	233
	L = 2		
0	0	738	-940
2	0	688	656
4	0	407	-339
6	0	637	607
8	0	248	-202
-2	0	521	547
-4	0	771	-819
-6	0	727	723
-8	0	462	-455
-10	0	263	245
0	1	82	73
1	1	78	-84
2	1	196	-117
3	1	342	271
4	1	218	-143
5	1	114	-125
6	1	131	115
7	1	252	326
-1	1	89	71
-2	1	39	-22
-4	1	318	211
-5	1	140	-123
-7	1	127	124
-8	1	65	-20
-9	1	162	-284
-10	1	64	-76
0	2	534	-601
1	2	428	372
2	2	664	685
3	2	398	-305
4	2	476	-467
5	2	347	289
6	2	518	528
7	2	207	-228
8	2	213	-195
-1	2	361	-346
-2	2	447	480
-3	2	357	317
-4	2	37	-523
-5	2	328	-265
-6	2	481	438
-7	2	210	171
-8	2	467	-458
-9	2	137	-155
-10	2	250	237
0	3	[illegible]	-150
1	3	52	-1
2	3	121	-93
3	3	118	107
4	3	343	-272
5	3	165	75
6	3	168	152
7	3	176	215
8	3	21	-67
-1	3	191	-116
-2	3	127	73
-3	3	115	-84
-4	3	431	372
-5	3	49	-42
-6	3	186	-166
-7	3	75	71
-8	3	102	97
-9	3	107	-130
-10	3	121	-142
0	4	209	-196
1	4	646	636
2	4	525	460
3	4	763	-704
4	4	369	-278
5	4	481	426
6	4	258	247
7	4	267	-262
8	4	131	-145
-1	4	563	-613
-2	4	496	445
-3	4	647	732
-4	4	350	-290
-5	4	420	-362
-6	4	89	45
-7	4	359	336
-8	4	264	-264
-9	4	311	-344
-10	4	51	67
0	5	200	-125
1	5	426	326
2	5	356	262
3	5	156	-84
4	5	226	-186
5	5	85	40
6	5	166	154
7	5	126	111
8	5	99	-114
-1	5	180	-110
-2	5	46	18
-3	5	53	-17
-4	5	209	160
-5	5	57	-2
-6	5	241	-222
-7	5	265	-202
-8	5	121	206
-9	5	27	3
-10	5	93	-143
0	6	201	155
1	6	736	711
2	6	35	-34
3	6	559	-494
4	6	208	163
5	6	288	234
6	6	45	-22
7	6	175	-192
8	6	44	36
-1	6	762	-897
-2	6	32	-9
-3	6	857	1012
-5	6	583	-561
-6	6	184	-171
-7	6	403	403
-8	6	32	22
-9	6	251	-235
-10	6	103	-109
0	7	25	-18
1	7	140	96
2	7	220	172
3	7	153	76
4	7	192	-159
6	7	209	211
7	7	134	-154
-1	7	283	221
-3	7	35	43
-4	7	101	73
-5	7	223	-174
-6	7	101	-93
-7	7	169	-170
-8	7	155	161
-9	7	57	-31
0	8	523	422
1	8	628	565
2	8	321	-271
3	8	250	-208
4	8	343	325
5	8	310	275
6	8	177	-202
-1	8	671	-553
-2	8	446	-392
-3	8	575	451
-4	8	371	302
-5	8	541	-474
-6	8	352	-345
-7	8	330	354
-8	8	131	132
-9	8	114	-122
0	9	115	-70
1	9	161	-107
2	9	253	188
3	9	209	124
4	9	93	-90
5	9	175	182
-1	9	216	125
-2	9	32	19
-4	9	179	124
-5	9	111	-72
-6	9	99	-101
-8	9	162	170
0	10	583	450
1	10	290	225
2	10	481	-400
3	10	165	-135
4	10	510	527
5	10	341	324
6	10	392	-398
-1	10	34	-35
-2	10	358	-308
-3	10	34	-30
-4	10	318	307
-5	10	107	-106
-6	10	406	-420
-7	10	178	166
-8	10	216	247
0	11	181	124
	11	48	48
3	11	32	-54
4	11	165	154
5	11	210	252
-1	11	131	-118
-2	11	49	-34
-3	11	71	-72
-4	11	[illegible]	-71
-5	11	111	128
-6	11	83	63
-7	11	111	-132
0	12	334	329
1	12	107	-119
2	12	354	-370
3	12	82	72
4	12	463	509
-1	12	193	207
-2	12	387	-380
-3	12	46	-59
-4	12	337	354
-5	12	124	137
-6	12	332	-336
0	13	178	185
1	13	52	71
2	13	168	-172
4	13	212	253
-4	13	108	-124
-6	13	154	119
0	14	269	259
1	14	265	-266
2	14	240	-257
3	14	216	235
-1	14	352	384
-2	14	408	-437
-3	14	201	-223
-4	14	285	333
-5	14	233	279
-2	15	164	196
	L = 3		
0	0	142	-121
2	0	310	230
4	0	229	-201
6	0	253	282
-2	0	83	-80
-4	0	73	-40
-6	0	141	-136
-10	0	165	-180
0	1	261	241
1	1	673	771
2	1	212	-168
3	1	449	-384
4	1	178	147
5	1	434	423
6	1	140	-141
7	1	188	-211
-1	1	765	-870
-2	1	210	-212
-3	1	437	451
-4	1	268	214
-5	1	619	-664
-6	1	170	-135
-7	1	331	309
-8	1	56	50
-9	1	262	-288
-10	1	30	-49
0	2	126	-107
1	2	205	-122
2	2	308	245
3	2	65	14
4	2	117	-107
5	2	188	190
6	2	205	210
-1	2	176	-134
-2	2	162	-113
-3	2	71	-25
-4	2	106	-57
-5	2	137	87
-6	2	243	-222
-7	2	49	42
-8	2	74	84
-9	2	117	131
-10	2	92	-116
0	3	503	450
1	3	472	447
2	3	510	-482
3	3	482	-455
4	3	502	466
5	3	374	361
6	3	250	-281
7	3	101	-117
-1	3	477	-466
-2	3	480	-483
-3	3	330	313
-4	3	423	424
-5	3	348	-306
-6	3	300	-265
-7	3	197	179
-8	3	254	269
-9	3	266	-312
-10	3	196	-210
0	4	170	105
1	4	129	114
2	4	47	44
3	4	53	-53
4	4	33	-38
5	4	117	112
6	4	206	196
7	4	44	-76
-1	4	257	-190
-2	4	341	-272
-3	4	130	70
-4	4	35	37
-5	4	163	128
-6	4	199	-175
-7	4	175	-165
-8	4	84	-58
-9	4	220	221
0	5	445	393
2	5	498	-426
3	5	130	-103
4	5	515	463
5	5	152	132
6	5	255	-251
7	5	44	-46
-1	5	114	-75
-2	5	637	-671
-3	5	184	137
-4	5	656	627
-5	5	208	-154
-6	5	473	-458
-8	5	489	495
-9	5	139	-131
-10	5	229	-276
1	6	192	159
2	6	201	-176
3	6	165	-128
4	6	47	16
5	6	161	157
6	6	71	57
7	6	117	-150
-1	6	27	8
-2	6	35	-20
-3	6	43	22
-4	6	32	45
-5	6	100	80
-7	6	156	-154
-8	6	188	-181
-9	6	147	145
0	7	437	421
1	7	280	-225
2	7	286	-228
3	7	211	184
4	7	265	231
5	7	78	-70
6	7	252	-264
-1	7	241	204
-2	7	524	-489
-3	7	318	-250
-4	7	590	616
-5	7	118	95
-6	7	527	-585
-7	7	230	-216
-8	7	421	387
-9	7	49	39
0	8	272	-173
1	8	191	157
2	8	165	-130
3	8	89	-89
4	8	196	207
5	8	96	119
-1	8	97	-58
-2	8	316	238
-3	8	74	39
-4	8	190	-153
-5	8	35	27
-6	8	34	36
-7	8	48	-78
-8	8	48	-59
-9	8	118	122
0	9	500	479
1	9	440	-451
2	9	319	-287
3	9	378	382
4	9	262	259
5	9	312	-285
-1	9	422	371
-2	9	178	-131
-3	9	403	-376
-4	9	262	208
-5	9	291	263
-6	9	280	-265
-7	9	284	-298
-8	9	94	92
1	10	71	77
2	10	34	-42
3	10	93	30
4	10	291	246
5	10	106	-37
-1	10	35	37
-3	10	105	72
-4	10	255	-248
-5	10	33	-39
-6	10	31	30
-7	10	42	-67
-8	10	67	-90
0	11	183	161
1	11	523	-544
2	11	87	82
3	11	515	529
4	11	155	150
-1	11	483	440
-2	11	34	22
-3	11	397	-403
-4	11	33	-38
-5	11	197	206
-6	11	81	77
-7	11	229	-233
0	12	96	88
1	12	82	-81
3	12	110	112
4	12	162	177
-1	12	293	280
-2	12	106	-128
-4	12	124	-121
0	13	180	-181
1	13	267	-256
2	13	193	196
3	13	255	332
-1	13	345	350
-2	13	201	199
-3	13	470	-519
-4	13	150	-164
-5	13	215	204
-4	14	51	78
	L = 4		
0	0	523	537
2	0	357	-307
4	0	141	135
6	0	312	-360
-2	0	738	-635
-4	0	617	626
-6	0	669	-735
-8	0	235	240
-10	0	208	-230
0	1	131	-69
1	1	160	126
2	1	127	81
3	1	204	-191
4	1	132	147
5	1	95	112
6	1	117	-155
-1	1	168	-133
-2	1	88	76
-3	1	127	-97
-4	1	178	-156
-5	1	58	-30
-6	1	78	-44
-7	1	197	-187
-8	1	109	58
-9	1	82	94
0	2	474	444
1	2	322	-285
2	2	419	-414
3	2	285	282
4	2	260	256
5	2	196	-222
6	2	193	-203
-1	2	257	298
-2	2	426	-579
-3	2	331	-322
-4	2	413	377
-5	2	339	296
-6	2	448	-436
-7	2	215	-192
-8	2	204	200
-9	2	138	155
-10	2	261	-204
0	3	59	-9
1	3	154	121
2	3	129	74
3	3	143	-149
4	3	168	198
5	3	25	57
6	3	162	-220
-1	3	147	-136
-2	3	23	6
-3	3	70	-12
-4	3	153	-119
-6	3	72	-37
-7	3	292	-255
-9	3	79	79
-10	3	103	126
0	4	150	124
1	4	457	-425
2	4	333	-323
3	4	501	561
4	4	267	280
5	4	326	-338
6	4	106	-101
-1	4	454	449
-2	4	387	-349
-3	4	470	-451
-4	4	110	71
-5	4	303	234
-6	4	161	-127
-7	4	308	-291
-8	4	140	122
-9	4	323	329
-10	4	102	-113
0	5	112	75
1	5	118	-81
2	5	116	-86
3	5	54	-50
4	5	152	140
5	5	119	132
6	5	121	-140
-1	5	69	-57
-2	5	68	-37
-3	5	212	-162
-4	5	49	26
-5	5	68	39
-6	5	66	58
-7	5	75	-38
-8	5	127	-115
-9	5	50	-33
0	6	176	-164
1	6	373	-322
3	6	410	440
4	6	46	36
5	6	267	-310
-1	6	419	374
-2	6	47	2
-3	6	461	-398
-4	6	174	-126
-5	6	369	328
-7	6	394	-422
-8	6	44	-32
-9	6	348	355
0	7	105	88
1	7	245	-246
2	7	120	-116
3	7	151	166
4	7	141	151
-1	7	176	-108
-3	7	103	-96
-5	7	136	-112
-7	7	189	163
-8	7	66	-78
-9	7	66	-66
0	8	367	-335
1	8	372	-358
2	8	202	202
3	8	215	230
4	8	164	-182
-1	8	393	343
-2	8	228	215
-3	8	293	-232
-4	8	380	-332
-5	8	380	369
-6	8	213	190
-7	8	346	-309
-8	8	204	-177
1	9	197	-205
3	9	139	169
-5	9	275	-230
-7	9	147	122
-8	9	58	-78
0	10	475	-518
1	10	240	-243
2	10	282	366
3	10	130	115
4	10	212	-293
-1	10	278	266
-2	10	370	349
-3	10	116	-122
-4	10	436	-446
-5	10	182	164
-6	10	299	250
-7	10	46	-57
0	11	104	-75
1	11	64	-68
-1	11	116	104
-2	11	169	130
-3	11	70	-58
-5	11	183	-141
-6	11	33	26
0	12	334	-338
1	12	116	137
2	12	185	224
-2	12	385	395
-4	12	441	-479
-6	12	197	231
	L = 5		
0	0	58	21
2	0	192	-198
4	0	48	52
-2	0	110	-93
-4	0	83	-67
-8	0	118	-122
-10	0	84	108
0	1	118	-96
1	1	372	-385
2	1	133	107
3	1	130	147
4	1	101	-101
5	1	267	-330
-1	1	232	201
-2	1	85	85
-3	1	289	-338
-4	1	142	-133
-5	1	410	454
-6	1	123	144
-7	1	361	-433
-8	1	101	-97
-9	1	263	294
-10	1	71	85
0	2	45	-16
1	2	39	-66
2	2	158	-154
3	2	144	178
4	2	29	-10
5	2	204	-283
-1	2	73	67
-2	2	134	-147
-3	2	208	207
-4	2	73	61
-5	2	234	-219
-8	2	112	-105
-9	2	74	-77
0	3	313	-338
1	3	357	-363
2	3	319	342
3	3	232	229
4	3	235	-272
5	3	160	-203
-1	3	266	287
-2	3	323	388
-3	3	349	-409
-4	3	289	-308
-5	3	176	156
-6	3	180	176
-7	3	183	-204
-8	3	190	-210
-9	3	147	160
0	4	121	-72
1	4	88	-71
2	4	95	-95
3	4	129	145
4	4	12	15
5	4	136	-189
-1	4	91	69
-2	4	101	-85
-3	4	30	20
-5	4	110	-95
-6	4	27	-4
-8	4	30	-26
-9	4	87	-94
0	5	360	-409
1	5	157	-144
2	5	322	405
3	5	125	104
4	5	269	-319
-1	5	49	36
-2	5	442	533
-3	5	212	-199
-4	5	312	-368
-5	5	30	-25
-6	5	194	192
-7	5	65	-46
-8	5	251	-270
-9	5	51	52
0	6	91	-73
1	6	132	-104
2	6	24	17
3	6	147	137
-1	6	45	30
-2	6	64	-18
-3	6	95	-33
-4	6	197	-240
-5	6	35	-32
-6	6	34	-43
-7	6	31	39
-8	6	71	56
-9	6	39	-56
0	7	300	-328
1	7	89	63
2	7	275	274
3	7	141	-129
4	7	138	-179
-1	7	221	-219
-2	7	301	320
-3	7	93	90
-4	7	286	-343
-5	7	173	-198
-6	7	261	295
-7	7	130	130
-8	7	209	-259
0	8	98	-114
1	8	107	-35
2	8	112	96
3	8	106	97
-1	8	30	37
-2	8	87	-31
-4	8	142	-127
-5	8	42	-38
-6	8	126	-87
-8	8	62	72
0	9	295	-279
1	9	246	236
2	9	185	160
-1	9	337	-337
-2	9	147	141
-3	9	252	221
-4	9	235	-232
-5	9	317	-347
-6	9	213	216
-7	9	190	225
0	10	118	-116
2	10	67	-51
-1	10	68	-34
-5	10	35	-33
-6	10	58	-38
0	11	52	-27
1	11	179	216
-1	11	294	-331
-3	11	222	253
-4	11	[illegible]	[illegible]
-5	11	266	-329
-1	12	80	-73
	L = 6		
0	0	390	-406
2	0	254	264
-2	0	104	95
-4	0	206	-229
-6	0	293	282
-8	0	155	-153
0	1	115	-135
1	1	129	-145
2	1	44	63
3	1	43	34
-1	1	48	-33
-2	1	71	59
-3	1	49	-53
-4	1	95	77
-5	1	35	12
-6	1	51	-41
-7	1	48	64
-8	1	61	67
1	2	159	178
2	2	186	194
3	2	160	-168
-1	2	175	-188
-2	2	228	231
-3	2	175	190
-4	2	248	-262
-5	2	164	-166
-6	2	193	233
-7	2	110	106
-8	2	129	-152
0	3	140	-175
1	3	62	-85
2	3	41	74
-1	3	142	-106
-2	3	121	116
-3	3	32	-42
-4	3	76	41
-6	3	53	-49
-7	3	26	36
-8	3	99	98
0	4	204	-189
1	4	204	213
2	4	74	60
3	4	181	-234
-1	4	329	-366
-2	4	194	210
-3	4	356	413
-4	4	128	-203
-5	4	291	-279
-6	4	120	134
-7	4	213	231
-8	4	100	-122
0	5	86	-59
1	5	71	-100
2	5	56	59
-1	5	43	-24
-2	5	63	41
-3	5	86	50
-4	5	49	-31
-5	5	113	-94
-7	5	22	16
-8	5	43	43
1	6	127	160
2	6	69	68
-1	6	275	-267
-2	6	77	-54
-3	6	329	329
-5	6	316	-340
-7	6	244	315
0	7	91	-81
-1	7	78	49
-4	7	26	-25
-5	7	19	-32
-6	7	66	-58
-7	7	41	-29
	L = 7		
0	0	85	-91
0	1	74	71
-1	1	255	-277
-2	1	80	-78
-3	1	211	235
-4	1	81	85
-5	1	218	-247
-6	1	66	-67
-7	1	139	195
0	2	50	-60
-1	2	108	-131
0	3	125	149
-1	3	183	-208
-2	3	188	-250
-3	3	199	221
-4	3	197	213
-5	3	117	-134
-6	3	144	-176
0	4	50	-95
-1	4	51	-62
-4	4	56	50
-5	4	36	32
-6	4	52	-49
-1	5	36	-42
-2	5	210	-247
-3	5	64	63
-2	6	41	39
-4	6	56	65

intensity scale. The usual Lorentz and polarization corrections were applied to 1151 independent intensities. The crystals used for the intensity measurement had dimensions of $0.12\times0.25\times0.15$ and $0.13\times0.15\times0.30$ mm for the *b*-axis and *c*-axis Weissenberg photographs respectively, which were cut out from large crystals. No absorption correction was made.

Structure Determination

Since the unit-cell contains two molecules with the space group of $P2_1/a$, it is necessary for each molecule to lie on a crystallographic center of symmetry. The position of the nickel atom was readily deduced from a three-dimensional sharpened Patterson synthesis. The carbon atoms were found on successive Fourier syntheses phased initially by the nickel atom. The inclusion of these atoms in the structure-factor calculations reduced the conventional agreement index, $R(=\sum||F_o|-|F_c||/\sum|F_o|)$, from 0.36 to 0.28. The structure thus obtained was refined by the isotropic least-squares method; the *R* index fell to 0.20 after a few cycles of this refinement. The structure was further refined by several cycles of positional and anisotropic thermal parameters refinement, which led to the final *R* index of 0.121 for all the non-zero reflections. A difference Fourier synthesis was then computed in an attempt to find the positions of the hydrogen atoms. Some peaks appeared at or near the expected positions, but not all the hydrogen atoms could be located. Thus, contributions from the hydrogen atoms are not included in the structure-factor calculations. Throughout the refinement of the structure, equal weights were employed for all the reflections, and the atomic scattering factors were adopted from the International Tables for X-ray Crystallography.[2] The main part of the calculations was performed on the IBM7040 and 360 computers, with the use of the ERFR2 program for Fourier synthesis[3] and the HBLS program for structure-factor and least-squares refinement calculations.[4] The positional and anisotropic thermal parameters,along with their estimated standard deviations, are listed in Tables 2 and 3 respectively. The final observed and calculated structure factors are given in Table 4.

Results and Discussion

The principal interatomic bond distances and angles, along with their estimated standard deviations, are listed in Tables 5 and 6. A perspective view of the molecule is shown in Fig. 1, along with the atomic levels. Figure 2 represents the front and side views of the asymmetric unit of the molecule in order to show the mode of coordination of carbon atoms to the nickel.

The molecule has a crystallographic center of symmetry; therefore, two nickel atoms take a *trans* configuration, with a nickel-nickel distance of 4.31 Å. The nickel atom is bonded to the carbon atoms of the dihydropentalenylene ring and of the π-allyl group in a sandwich fashion. The nickel-carbon distances for the five-membered ring range from 2.03 Å to 2.27 Å, the closest nickel-carbon approach being to the non-bridging atoms of the ring. The mean Ni–C distance of 2.146 Å and the perpendicular distance from the nickel atom to the best plane of the ring carbons of 1.75 Å can well be compared with the corresponding ones observed in $(\pi\text{-}C_5H_5)Ni(P(C_6H_5)_3)C_6H_5$,[5] $(\pi\text{-}C_5H_5)Ni(P(C_6H_5)_3)C_6F_5$,[6] and other π-cyclopentadienyl nickel

Table 5. Principal interatomic lengths along with their estimated standard deviations in parentheses

Bond	Length	Bond	Length
Ni–C(1)	2.27(3)Å	C(1)–C(2)	1.44(3)Å
Ni–C(2)	2.08(3)	C(2)–C(3)	1.38(3)
Ni–C(3)	2.03(3)	C(3)–C(4)	1.42(3)
Ni–C(4)	2.08(3)	C(4)–C(1′)	1.45(3)
Ni–C(1′)	2.27(3)	C(1′)–C(1)	1.43(3)
Ni–C(5)	2.03(4)	C(5)–C(6)	1.41(4)
Ni–C(6)	1.92(4)	C(6)–C(7)	1.41(4)
Ni–C(7)	2.01(4)		

Table 6. Principal bond angles along with their estimated standard deviations in parentheses

	Angle
C(1)–C(2)–C(3)	107.2(1.2)°
C(2)–C(3)–C(4)	111.3(1.2)
C(3)–C(4)–C(1′)	105.5(1.2)
C(4)–C(1′)–C(1)	107.9(1.2)
C(1′)–C(1)–C(2)	107.5(1.3)
C(5)–C(6)–C(7)	118.5(1.5)
C(5)–Ni–C(7)	73.5(1.1)

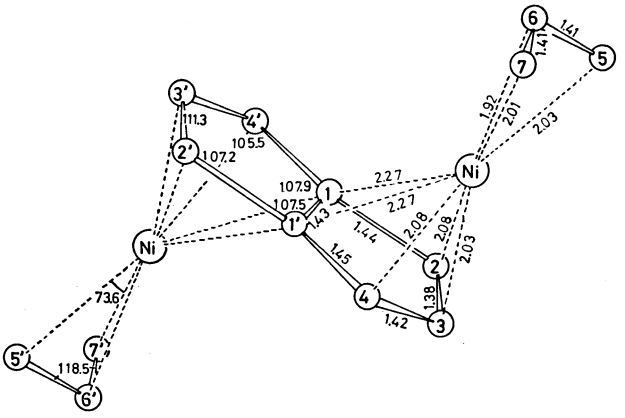

Fig. 1. A perspective view of the molecule.

2) "International Tables for X-ray Crystallography," Vol. 3, Kynoch Press, Birmingham (1962).

3) W. G. Sly, D. P. Shoemaker, and J. H. Van den Hende, ERFR2 Two and Three-Dimensional Crystallographic Fourier Summation Program, 1962.

4) T. Ashida, HBLS Universal Crystallographic Computation Program System (I) p. 65, The Crystallographic Society of Japan, 1967.

5) M. R. Churchill and T. A. O'Brien, *J. Chem. Soc.*, *A*, **1969**, 226.

6) M. R. Churchill and T. A. O'Brien, *ibid.*, *A*, **1968**, 2970.

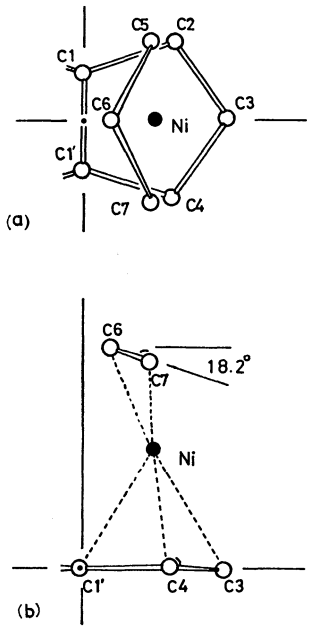

Fig. 2. (a) Front and (b) side views of the asymmetric unit of the molecule showing the mode of coordination of carbon atoms to the nickel. Center of symmetries are shown by dots.

complexes.[7-11] The dihydropentalenylene ring carbons are nearly coplanar. The best plane through the five-membered carbons of the ring is defined, with respect to the crystallographic axes, by this equation:

$$0.6605x + 1.1647y + 0.4975z = 0.0218.$$

The average displacement of atoms from the mean plane is 0.03 Å, with the maximum deviation of 0.05 Å for C(3). The mean carbon-carbon bond length of 1.424 Å, and the mean bond angle of 107.9° in the dihydropentalenylene ring, are comparable with those expected for the five-membered conjugated ring systems and are similar to the corresponding values found in π-cyclopentadienyl rings.[12]

As far as the allyl group is concerned, the mean distance of 1.99 Å of the carbon atoms of the π-allyl group from the nickel atom resembles those found in other allyl complexes of nickel[13-15] and palladium.[16-20]

The mean carbon-carbon bond length of 1.41 Å is within the range of those previously determined, and the bond angle of 118.5° is comparable with the values of 119.6° for dimeric 2-carboxyethyl-π-allylnickel bromide[13] and 118.9° for bis(1,2-diphenylphosphino)-

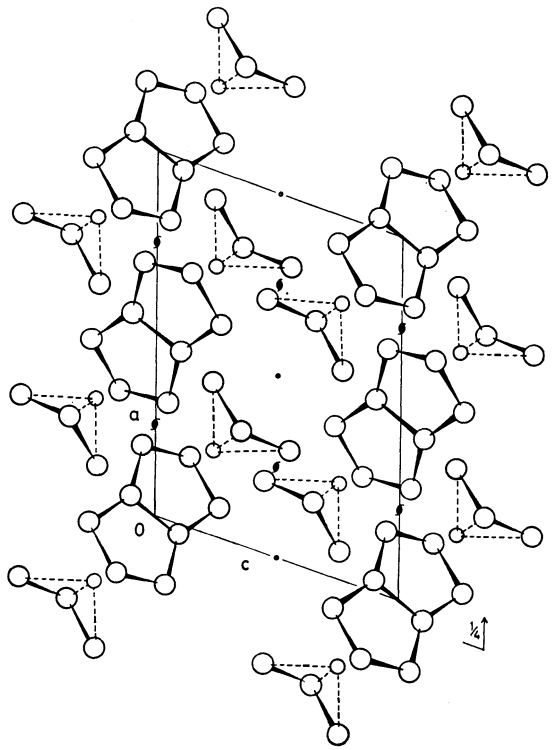

Fig. 3. The crystal structure projected along the *b* axis. Small and big circles represent nickel and carbon atoms, respectively.

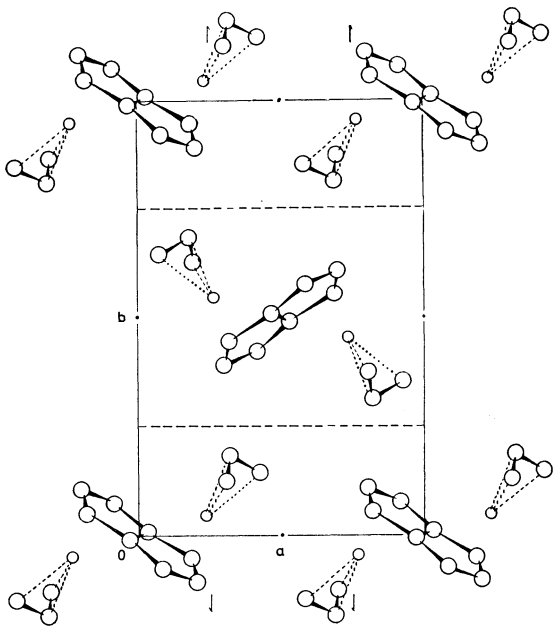

Fig. 4. The crystal structure projected along the *c* axis. Small and big circles represent nickel and carbon atoms, respectively.

7) R. M. Tuggle and D. L. Weaver, *Inorg. Chem.*, **10**, 150 (1971).
8) M. R. Churchill and T. A. O'Brien, *J. Chem. Soc., A*, **1970**, 161.
9) O. S. Mills and B. W. Shaw, *J. Organometal. Chem.*, **11**, 595 (1968).
10) W. Oberhansli and L. F. Dahl, *Inorg. Chem.*, **4**, 150 (1965).
11) L. F. Dahl and C. H. Wei, *ibid.*, **2**, 713 (1963).
12) P. J. Wheatley, "Perspectives in Structural Chemistry," Vol. 1, ed. by J. D. Dunitz and J. A. Ibers, John Wiley, New York (1967) p. 1.
13) M. R. Churchill and T. A. O'Brien, *Inorg. Chem.*, **6**, 1386 (1967).
14) M. R. Churchill and T. A. O'Brien, *Chem. Commun.*, **1968**, 246.
15) A. Sirigu, *Chem. Commun.*, **1969**, 256; *Inorg. Chem.*, **9**, 2249 (1970).
16) A. E. Smith, *Acta Crystallogr.*, **18**, 331 (1965).
17) W. E. Oberhansli and L. F. Dahl, *J. Organometal. Chem.*, **3**, 43 (1965).
18) G. R. Davies, R. H. B. Mais, S. O'Brien, and P. G. Owston, *Chem. Commun.*, **1967**, 1151.
19) R. Mason and D. R. Russel, *ibid.*, **1966**, 26.
20) Y. Kitano, T. Kajimoto, M. Kashiwagi, and Y. Kinoshita, *J. Organometal. Chem.*, **33**, 123 (1971).

ethane-π-metallylnickel bromide.[14] The equation for the best plane containing the π-allyl carbon atoms is:

$$0.7066x + 0.6097y + 0.4419z = 4.2586.$$

The dihedral angle between this plane and that containing the carbon atoms of the dihydropentalenylene ring is 18.2° (Fig. 2), which is comparable with the corresponding value found in bis(cyclopentadienyl)-2,2′-bi-π-allyl-bis(nickel).[21]

The molecular arrangements in the crystal viewed along the *b* and *c* axes are illustrated in Figs. 3 and 4 respectively. The crystal is built up of individual molecules of $(C_8H_6)Ni_2(\pi\text{-}C_3H_5)_2$, with the adjacent molecules held together by van der Waals forces. All interatomic contacts less than 4.0 Å were calculated. There are no abnormally short distances.

The authors are grateful to Dr. Akihisa Miyake and Mr. Atsuo Kanai for their kindness in supplying the compound, and to Mr. Susumu Arai for his aid in the reflection-data collection.

21) A. E. Smith, *Inorg. Chem.*, **11**, 165 (1972).

BULLETIN OF THE CHEMICAL SOCIETY OF JAPAN, VOL. 46, 727—736 (1973)

Electron-spin-resonance Studies of the Formation and Properties of the Trimeric Vanadyl Dibutylphosphate Complex

Mitsuo SATO, Teruo TAKAYANAGI, Yuzaburo FUJITA, and Takao KWAN

Faculty of Pharmaceutical Sciences, The University of Tokyo, Bunkyo-ku, Tokyo

(Received June 24, 1972)

The extraction of the vanadyl ion (VO^{2+}) from aqueous solutions by di-*n*-butylphosphoric acid ($(C_4H_9O)_2PO_2H$) in hexane has been studied by ESR. It has been found that monomeric and trimeric vanadyl di-*n*-butylphosphate complexes were present in the organic phase, and the equilibrium constant of the reaction involving monomeric and trimeric forms was determined. The ESR spectrum of the trimeric complex, characterized by 22 hf lines with a separation of 39 gauss, was interpreted as resulting from the magnetic exchange interaction between three vanadyl ions. A crystalline vanadyl complex was isolated from the hexane solution and found to be $(VOX_2)_3$, where X represents $(C_4H_9O)_2PO_2^-$. The properties of the complex were investigated by means of ESR, IR, and the optical absorptions. The mechanism of the extraction of VO^{2+} by $(C_4H_9O)_2PO_2H$ was discussed, and a cyclic model was proposed for the structure of $(VOX_2)_3$.

The extraction of the vanadyl ion (VO^{2+}) dissolved in aqueous solutions by di-(2-ethylhexyl)-phosphoric acid (HDEHP) in kerosene has been studied by several workers.[1,2] Accordingly, the vanadium/HDEHP ratios of the extracts ranged from 0.25 to 0.50, suggesting that at least two species of vanadyl complexes were formed. Moreover, it has been suggested[2] that polymeric vanadyl complexes are formed at lower HDEHP concentrations, while monomeric complexes are formed at higher HDEHP concentrations.

In the present study, the vanadyl complexes extracted from sulfuric acid solutions into the hexane phase by di-*n*-butylphosphoric acid (HDBP) have been investigated, with special interest being taken in the formation of polymeric species. Preliminary observations of extracts by electron spin resonance revealed that trimeric complexes rather than polymeric ones are formed. It was decided, therefore, to investigate first the conditions for the formation of the trimeric complex. Subsequently attempts were made to isolate the complex and to clarify the chemical stoichiometry and properties of the complex. The present paper will report the results of these investigations.

1) T. Rigg and J. O. Garner, *J. Inorg. Nucl. Chem.*, **29**, 2019 (1967).

2) T. Sato and T. Takeda, *ibid.*, **32**, 3387 (1970).

Experimental

Materials. HDBP (E.P. grade, Tokyo Kasei Kogyo Co.,) was used without further purification. The IR spectrum showed few impurities. Hexane (G.R. grade, Wako Junyaku Kogyo Co.,), which has previously been known to be the most effective diluent in the extraction of vanadium by HDEHP,[2] was used as the diluent after distillation. The vanadyl sulfate hydrate ($VOSO_4 \cdot nH_2O$) was obtained from Kishida Kagaku Co.; the colorimetric peroxide method indicated that the $VOSO_4$ content was 55 wt%. All the other reagents used were of a reagent grade and were commercially available.

Extraction of the Vanadyl Ion (VO^{2+}) by HDBP. The extraction of VO^{2+} from acidic aqueous solutions by HDBP in hexane was carried out in a 300 ml separating funnel, generally with equal volumes (100 ml) of the aqueous and organic phases. The two phases were mixed vigorously by shaking for about 10 min at the ambient temperature, and were then allowed to stand until the separation into two layers was complete. Little trouble was experienced with emulsions. The extractions were carried out under the following conditions:

initial HDBP concentrations as monomer in the organic phase: $C_{HX(i)} = 0.12—1.2M$

initial VO^{2+} concentrations in the aqueous phase: $C_{V(i)} = 0.02—1.5M$

final pH values in the aqueous phase: $pH_{(f)} = 0.8—5.5$

The variation in the final pH values in the aqueous phase was accomplished by adding the requisite amounts of H_2SO_4 or NaOH solutions either immediately before or during the mixing. The $pH_{(f)}$ values were determined by means of a Toadempa pH-meter (Model HM-5A) after the separation.

Isolation of the Trimeric Vanadyl Complex. The hexane phase was dehydrated with anhydrous sodium sulfate, and then the solvent was evaporated under a reduced pressure. The resulting blue viscous liquid was then chromatographed over a column packed with SiO_2, using benzene as the eluent; the blue fractions thus obtained were evaporated under a sufficiently reduced pressure (10^{-4} Torr) at 60°C for about 3 hr to give again a blue, oily liquid. After 1—2 weeks' standing in a refrigerator, a light blue crystalline material was obtained (mp 43°C).[3]

Measurements of ESR, IR, and Optical Spectra. The ESR spectra were recorded at room temperature with a JEOL spectrometer, Model JES P-10 (X-band), using 100 KHz field modulation. The magnetic field was calibrated with an ESR marker, MgO:Mn^{2+} powder, supplied by JEOL. Powdered DPPH was used as a reference in the determination of the *g*-values. Samples from the extracted organic phases were subjected to ESR measurements without any pretreatment, while those from isolated crystals were measured, generally *in vacuo*, after dissolving them in various organic solvents.

The IR spectra were recorded on a DS-402G grating spectrophotometer (Japan Spectroscopic Co.,) in Nujol mulls and in thin liquid films. The optical spectra were recorded on a Hitachi spectrophotometer (Model EPS-3T) in the range of 300—1200 nm.

Chemical Analyses. Vanadium was analysed by the colorimetric peroxide method.[4] Samples dissolved in hexane were back-extracted with 2N HCl, and color development was performed by the successive additions of 2N H_2SO_4, 85% phosphoric acid, and 30% hydrogen peroxide. The optical densities of the colorimetric solutions were determined at wavelength of 450 nm with a Shimadzu spectrophotometer (Model QV-50). The analyses of carbon and hydrogen were performed at the Microanalytical Center of our laboratory.

Molecular-weight Measurements and Differential Scanning Calorimetry. The molecular weights were determined in a chloroform solution at 35°C using a Hitachi Model 115 vapor-pressure osmometer calibrated with benzil. Scale readings were made 5 min after a drop of the solution had been placed on the thermistor. The concentrations of the solution were in the range of 10^{-2}—10^{-3}M. The DSC thermograms were recorded on a DSC-1B calorimeter (Perkin-Elmer) in an atmosphere of nitrogen.

Results and Discussion

ESR Spectra of Extracted Vanadyl Complexes. Hexane solutions of the extract were subjected to preliminary ESR measurements at room temperature in order to obtain some information about the states of the extracted vanadyl complexes.

Two types of spectrum were observed, depending upon the extraction conditions. As will be discussed below, one was assigned to a monomeric vanadyl species, and the other, to a trimeric one. Hereafter, the former will be denoted as the "M-spectrum", and the latter, as the "T-spectrum".

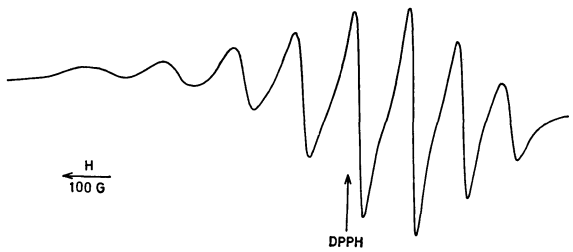

Fig. 1. ESR spectrum of the hexane phase (M-spectrum) obtained under the following extraction condition; $C_{HX(i)}$ = 1.20M, $C_{V(i)}$ = 0.30M, $pH_{(f)}$ = 0.8.

Assignment of M-spectrum: A typical M-spectrum obtained from the hexane solution extracted under the conditions; $C_{HX(i)} = 1.20$ M, $C_{V(i)} = 0.30$ M, and $pH_{(f)} = 0.8$, is shown in Fig. 1. The spectrum was characterized by eight resonance lines with unequal separations and linewidths. It is quite similar to the reported spectra[5] for many monomeric vanadyl complexes in liquid solutions, and can be interpreted by an isotropic spin Hamiltonian as:

$$\mathcal{H} = g_0\beta HS_z + a\boldsymbol{I}\cdot\boldsymbol{S} \qquad (1)$$
$$S=1/2,\ I=7/2$$

where the z axis is defined by the direction of the external magnetic field, where g_0 is the isotropic g value, where a is the isotropic hyperfine constant due to the vanadium nucleus, and where the other symbols have their usual meanings. The solution of the above Hamiltonian up to second order of a leads to the resonance condition described as:[5,6]

$$h\nu = g_0\beta H + am + \frac{a^2}{2g_0\beta H}\left(\frac{63}{4} - m^2\right) \qquad (2)$$
$$m=7/2,\ 5/2,\ 3/2,\ \cdots\cdots,\ -5/2,\ -7/2$$

The M-spectrum shown in Fig. 1 was then fitted to the equation to obtain the following parameters:

$$g_0 = 1.961 \qquad a = 119 \text{ gauss}$$

These values are in good agreement with those reported for monomeric vanadyl complexes coordinated with oxygen ligands, such as $VO(H_2O)_5^{2+}$,[6,7] $VO(Ac)_2$,[8] and VO(phthalic acid)$_2^{2-}$.[9]

On the other hand, it has generally been accepted that dialkylphosphoric acids ($(RO)_2PO_2H$) extract a

3) In some cases the crystallization did not take place even after a much longer period of standing. This was because of the contamination by a small amount of monomeric species in a blue oily liquid; the contamination was obvious from the ESR and molecular-weight measurements. It was necessary in such cases to wash the blue oily liquid after dissolving it in hexane with an appropriate amount of the 0.01N NaOH solution and then to repeat the treatment described above.

4) E. R. Wright and M. G. Mellon, *Ind. Eng. Chem., Anal. Ed.*, **9**, 375 (1937); A. Weissler, *ibid.*, **17**, 695 (1945).

5) H. A. Kuska and M. T. Rogers, "Radical Ions," ed. by E. T. Kaiser and L. Kevan, Interscience Publisher (1968), p. 579.

6) R. N. Rogers and G. E. Pake, *J. Chem. Phys.*, **33**, 1107 (1960).

7) N.S. Garifianov and B.M. Kozyrev, *Doklady Akad. Nauk SSSR*, **98**, 929 (1954); B. M. Kozyrev, *Discuss. Faraday Soc.*, **19**, 135 (1955).

8) H. R. Gersmann and J. D. Swalen, *J. Chem. Phys.*, **36**, 3221 (1962); I. Bernal and P. Reiger, *Inorg. Chem.*, **2**, 256 (1963).

9) K. Wuethrich, *Helv. Chim. Acta*, **48**, 1012 (1965).

number of metal cations by this ion-exchange reaction:[10]

$$M^{n+}_{(a)} + n(HX)_{2(o)} = M(X_2H)_{n(o)} + nH^+_{(a)} \quad (3)$$

in which X represents the anion $(RO)_2PO_2^-$; $(HX)_2$, the dimeric $(RO)_2PO_2H$; and (a) and (o), the aqueous and organic phases respectively. Furthermore, Sato *et al.*[2] have recently shown that the mechanism is applicable also in the case of the extraction of VO^{2+} by excess HDEHP, and they have confirmed the existence of $VO(X_2H)_2$, $X=(C_8H_{17}O)_2PO_2$, in kerosene from an analysis of the partition coefficients. Therefore, it is quite natural in our system also that the monomeric vanadyl complex $VO(X_2H)_2$, $X=(C_4H_9O)_2PO_2$, is formed in hexane *via* the reaction:

$$VO^{2+}_{(a)} + 2(HX)_{2(o)} = VO(X_2H)_{2(o)} + 2H^+_{(a)} \quad (4)$$

Consequently, the M-spectrum can be interpreted as resulting from the monomeric vanadyl complex, $VO(X_2H)_2$. This assignment may be further supported by the spin Hamiltonian parameters, and also by the experimental findings to be described in the later sections.

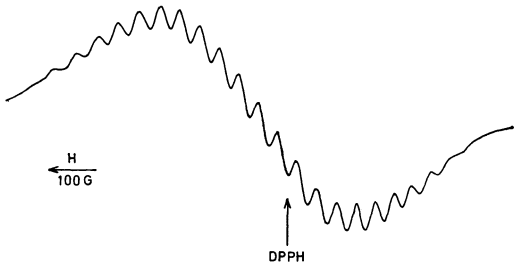

Fig. 2. ESR spectrum of the hexane phase (T-spectrum) obtained under the following extraction condition; $C_{HX(i)}=0.12M$, $C_{V(i)}=1.5M$, $pH_{(f)}=1.6$.

Assignment of T-spectrum: When the extraction was carried out under these conditions; $C_{HX(i)}=0.12$ M, $C_{V(i)}=1.5$ M, and $pH_{(f)}=1.6$, a typical T-spectrum was obtained. As is illustrated in Fig. 2, the T-spectrum has the following characteristics; (I) 22 resonance lines are found to be equally spaced with a separation almost equal to one-third of the average splitting found for the M-spectrum, (II) the resonance intensity for each line decreases with the line position almost symmetrically from the center of the spectrum to the outside. From such characteristics, it can readily be presumed that there are magnetic exchange interactions between three vanadyl ions.

In order to explain the observed T-spectrum qualitatively, we further assume that vanadium atoms of the trimer form equilateral triangular arrangements and that three vanadium ions of $S=1/2$ are exchange-coupled with an isotropic exchange Hamiltonian:

$$\mathcal{H}_{ex} = J(\boldsymbol{S}_1\cdot\boldsymbol{S}_2+\boldsymbol{S}_2\cdot\boldsymbol{S}_3+\boldsymbol{S}_3\cdot\boldsymbol{S}_1) \quad (5)$$

where J denotes the isotropic exchange integral and where $\boldsymbol{S}_1$, $\boldsymbol{S}_2$, and $\boldsymbol{S}_3$ are the spin operators for the respective vanadium ions. Thus, the total spin Hamiltonian describing the system becomes:[11]

$$\mathcal{H} = \mathcal{H}_1 + \mathcal{H}_2 + \mathcal{H}_3 + \mathcal{H}_{ex} \quad (6)$$

in which $\mathcal{H}_1$, $\mathcal{H}_2$, and $\mathcal{H}_3$ are each given by the form (1); it can be rewritten as:

$$\mathcal{H} = g_0\beta H(S_{1z}+S_{2z}+S_{3z}) + a(\boldsymbol{S}_1\cdot\boldsymbol{I}_1+\boldsymbol{S}_2\cdot\boldsymbol{I}_2+\boldsymbol{S}_3\cdot\boldsymbol{I}_3) + J(\boldsymbol{S}_1\cdot\boldsymbol{S}_2+\boldsymbol{S}_2\cdot\boldsymbol{S}_3+\boldsymbol{S}_3\cdot\boldsymbol{S}_1) \quad (7)$$

The eigen values of this Hamiltonian can readily be evaluated[12,13] by solving the secular determinant of the Hamiltonian on the assumption $|J|\gg|a|$; we then obtain the following ESR transitions[14] for the quartet state and for the two doublet states which are degenerate and which lie at a distance $3/2\,|J|$ from the quartet state.

Transitions for the quartet state:

$$h\nu = g_0\beta H + a/3(m_1+m_2+m_3) \quad (8)$$

Transitions for the two doublet states:

$$h\nu = g_0\beta H + a/3(m_1+m_2+m_3) \pm 2/3a(m_1^2+m_2^2+m_3^2-m_1m_2-m_2m_3-m_3m_1)^{1/2} \quad (9)$$

where m_1, m_2, and m_3 are the magnetic quantum numbers for each vanadium nucleus; each takes on the value of 7/2, 5/2, 3/2, ……, −5/2, −7/2.

Thus, it can be shown for the quartet-state spectrum that the 22 hf lines have the equal separation of $a/3$ and the intensity ratio of 1:3:6:10:15:21:28:36:42:46:48:48:46:42: ……, while the predicted spectrum for the doublet states consists of two sets of irregularly-spaced hf lines, both of which are symmetric to each other with respect to the magnetic filed defined by $h\nu=g_0\beta H$.

The characterisic (I) for the observed T-spectrum is quite consistent with the above expectation for the quartet-state spectrum. Furthermore, the observed intensity distribution of hf lines (Characteristic (II)), which is difficult to measure accurately, seems to follow approximately the expected one. One can, then, reasonably state that the T-spectrum results from the quartet-state transitions. On the other hand, it is not obvious at the moment why irregularly-spaced hf lines due to the doublet-state transitions are not observable.

The parameters determined from the T-spectrum on the basis of Eq. (8) are:

10) C. A. Blake, Jr., C. F. Baes, Jr., K. B. Brown, C. F. Coleman, and J. C. White, *Proc. 2nd. Int. Conf. on Peaceful Uses of Atomic Energy*, **28**, 289, Geneva (1958); C. A. Blake, Jr., C. F. Baes, Jr., and K. B. Brown, *Ind. Eng. Chem.*, **50**, 1763 (1958); D. F. Peppard, G. W. Mason, W. J. Driscoll, and R. J. Sironen, *J. Inorg. Nucl. Chem.*, **7**, 276 (1958).

11) G. F. Kokoszka and G. Gordon, *Transition Metal Chem.*, **5**, 181 (1969).

12) A. Hudson and G. R. Luckhurst, *Mol. Phys.*, **13**, 409 (1967).

13) A. Hasegawa, Y. Yamada, and M. Miura, This Bulletin, **42**, 846 (1969); A. Hasegawa, *J. Chem. Phys.*, **55**, 3101 (1971).

14) The second-order correction terms with respect to a must be added to Eqs. (8) and (9). The correction terms evaluated for (8) are as follows:

$$\frac{a^2}{18g_0\beta H}\{3I(I+1)-m_1^2-m_2^2-m_3^2\} + \frac{a^2}{18g_0\beta H}(2m_s-1)(m_1+m_2+m_3)$$

where $I=7/2$ and $m_S=3/2,\ 1/2,\ -1/2$. However, these terms are much smaller than that given in Eq. (2) and do not contribute to the line positions very much. Thus, the terms are ommitted from Eq. (8), although it seems that the terms are more or less related to the linewidth because of the superposition of resonance lines differing in m_S values.

$g_0 = 1.960$ $a/3 = 39$ gauss

These values are in good agreement with those obtained for the monomeric complex $VO(X_2H)_2$, indicating that our interpretation is valid. Moreover, the interpretation is consistent with that reported by Hasegawa *et al.*,[13] who studied the ESR of the trinuclear vanadyl pyrophosphate complex.

As will be described in the later section, a crystalline trimer was in fact isolated from the hexane solution. Thus, it can be concluded with reasonable certainty that the appearance of the T-spectrum results from a trimeric vanadyl complex.

Extraction Conditions for the Formation of the Trimeric Vanadyl Complex. In order to find how extracting conditions affect the selective formation of the trimeric or monomeric complex, the ESR measurements were further applied to hexane solutions obtained under systematically varied conditions. The results are summarized in Table 1.

TABLE 1. EXTRACTION CONDITIONS AND ESR SPECTRA OF HEXANE PHASES

Exp No	$C_{HX(i)}$ (M)	$C_{V(i)}$ (M)	$C_{HX(i)}/C_{V(i)}$	$pH_{(f)}$	Type of ESR spectra[a]
1		0.024	5.0		M
2		0.048	2.5		M≫T
3		0.096	1.25		M>T
4	0.12	0.24	0.50	1.3—1.4	T≫M
5		0.48	0.25		T≫M
6		1.20	0.10		T
7	0.012		0.10		T
8	0.060		0.50		T≫M
9	0.15	0.12	1.25	1.7—1.8	T>M
10	0.30		2.5		M>T
11	0.60		5.0		M≫T
12	0.03		0.3		M
13	0.10		1.0		M
14	0.20	0.10	2.0	0.9—1.0	M
15	0.40		4.0		M
16	1.0		10.0		M
17	0.03		0.3		T
18	0.10		1.0		T
19	0.20	0.10	2.0	3.6—4.0	T
20	0.40		4.0		T
21	1.0		10.0		T
22				0.9	M
23				1.3	M>T
24	0.40	0.20	2.0	1.9	T
25				2.9	T
26				4.6	T
27				0.8	M
28				1.7	M>T
29	1.0	0.15	6.7	3.4	T
30				4.3	T
31				5.7	T

a) Relative intensities of the M- and T-spectra are given roughly by an inequality.

Effect of $C_{V(i)}$: Extractions were carried out with $C_{V(i)}$ values varying from 0.024 to 1.2 M, while $C_{HX(i)}$ and $pH_{(f)}$ were kept constant as follows: $C_{HX(i)}=0.12$ M, $pH_{(f)}=1.3$—1.4 (Table 1, Exp. No. 1—6).

As is shown in the last column of Table 1, the M- and T-spectra were obtained for $C_{V(i)}=0.024$ and 1.2 M respectively. However, when $C_{V(i)}$ was intermediate between the above two extreme values, superimposed spectra of the M- and T-spectra with varying relative intensities were obtained. Some of the superimposed spectra are illustrated in Fig. 3.

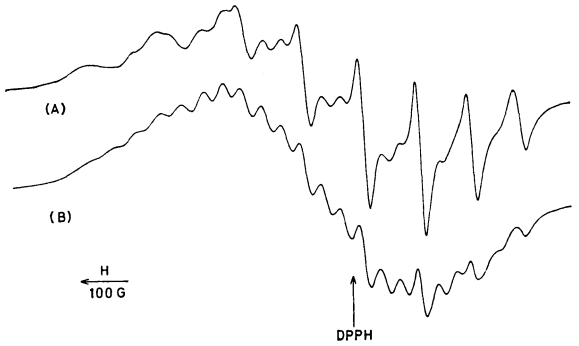

Fig. 3. ESR spectra of the hexane phases obtained under the following extraction conditions; (A) $C_{HX(i)}=0.12$M, $C_{V(i)}=0.096$M, $pH_{(f)}=1.4$; (B) $C_{HX(i)}=0.12$M, $C_{V(i)}=0.24$M, $pH_{(f)}=1.4$.

As can be seen from Table 1 (Exp. No. 1—6), an increase in $C_{V(i)}$ caused a progressive decrease in the ratio of the monomeric to the trimeric vanadyl complex; that is, $C_{V(i)}$ had a significant effect on the selective formation of the respective vanadyl complex.

Effect of $C_{HX(i)}$: As is obvious from Table 1 (Exp. No. 7—11), $C_{HX(i)}$ also had a singificant effect; the increase in $C_{HX(i)}$ favored the formation of the monomeric vanadyl complex. The increase in the ratio of $C_{HX(i)}$ to $C_{V(i)}$ resulted in a greater formation of monomeric vanadyl complex, but the decrease in the ratio resulted in that of trimeric one, as is evident from Table 1 (Exp. No. 1—11).

Such effects of $C_{HX(i)}/C_{V(i)}$ were closely correlated with the pH values of the final aqueous phase ($pH_{(f)}$) and were noted only in the $pH_{(f)}$ range from 1.0 to 2.0. For example, when the $pH_{(f)}$ values were kept constant at 0.9—1.0 (Table 1, Exp. No. 12—16), only the monomeric complex was formed for any value of $C_{HX(i)}/C_{V(i)}$, while the trimeric complex was selectively formed for $pH_{(f)}$ from 3.6 to 4.0 (Table 1, Exp. No. 17—21). Therefore, it appears that the effect of $C_{HX(i)}/C_{V(i)}$ is less significant than that of $pH_{(f)}$.

Effect of $pH_{(f)}$: Extractions were further carried out with $pH_{(f)}$ values varying from 0.8 to 5.7 and with a constant $C_{HX(i)}/C_{V(i)}$ (Table 1, Exp. No. 22—31). As expected, the extracted vanadyl complex was monomeric at $pH_{(f)}$ values below 1.0. The monomeric complex was, however, replaced by the trimeric one when $pH_{(f)}$ reached 1.3—1.8, while the trimeric complex was exclusively formed at higher $pH_{(f)}$ values. It is interesting to note that the coexistence of monmeric and trimeric complexes in the extracted hexane phase is limited to a narrow range of $pH_{(f)}$, where the effect of $C_{HX(i)}/C_{V(i)}$ is significant.

Distribution Ratios for Vanadium: Although we have not measured accurately the distribution ratios for vanadium ($D_V=[V_{(o)}]/[V_{(a)}]$) as functions of $C_{HX(i)}$, $C_{V(i)}$, and $pH_{(f)}$, it has been found that D_V depends rather sensitively upon $pH_{(f)}$. D_V increased markedly with the increase in $pH_{(f)}$ from 1.0 to 2.0. It reached a maximum at $pH_{(f)}$ about 2.0, and then decreased remarkably beyond $pH_{(f)}$ 3—4, accompanied by the

appearance of turbidity or a precipitate of hydrolyzed vanadyl ions in the aqueous phase. On the contrary, D_V was not markedly influenced by $C_{HX(i)}$ and $C_{V(i)}$ except in the $pH_{(i)}$ range below 2, where the increase in $C_{HX(i)}/C_{V(i)}$ brought about an increase in D_V.

Chemical Stoichiometry and Properties of Trimeric Vanadyl Complex. Isolation and Thermal Properties: As has already been described in the Experimental section, a light blue crystalline solid with a somewhat amorphous appearance was isolated from the hexane phase which exhibited the T-spectrum. The crystalline solid was stable to air and light. It melted at about 43°C to a blue, oily liquid, which was also stable in air but which decomposed to a dark brownish mass at higher temperatures (about 260—280°C).

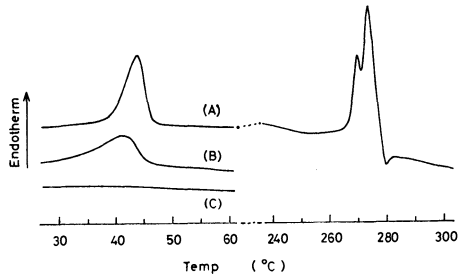

Fig. 4. DSC thermograms of trimeric vanadyl complex (sample S-II) crystallized from the oily state at the ambient temperature for different periods of time; (A) about 60 days, (B) 5 days, (C) 1 day.
(Heating rate and recorder sensitivity are 2°C/min and Range-4 for the low temperature region and 4°C/min and Range-16 for the high temperature region, respectively.)

Such thermal behavior of a crystalline sample is shown diagrammatically in the DSC thermograms (Fig. 4). The thermograms further indicated that the sample crystallizes with considerable difficulty. As is illustrated in Fig. 4, the crystallization took place very slowly when the crystalline sample was once melted to an oily liquid and then allowed to stand at the ambient temperature.

Table 2. Analytical data of the trimeric vanadyl complex

Sample[a] No	Elementary analyses V(%)	C(%)	H(%)	Molecular Weight
S-1	10.3	39.32	7.57	1385—1435
S-2	10.2	39.58	7.51	1365—1450
S-3	10.4	39.81	7.47	1390—1465
Calcd[b]	10.50	39.60	7.48	1456.1

a) Crystalline solids obtained from three independent preparations.
b) Calculated values for $(VOX_2)_3$

Chemical Stoichiometry: Three crystalline samples obtained from independent preparations were subjected to chemical analyses and molecular-weight measurements; the results are summarized in Table 2. No significant difference was found between the three samples, indicating that all the samples were chemically identical and of a high purity, in spite of the facts that they were obtained without further recrystallization and were somewhat different in the color and crystallinity from each other.

The chemical formulae determined from the results given in Table 2 were in close agreement with the following stoichiometry:

$$(VOX_2)_n;\ n=3$$

where n denotes the association value, and X, the di-*n*-butylphosphate anion $(C_4H_9O)_2PO_2^-$. The association value of 3 is consistent with the appearance of the T-spectrum.

Dissolved States of $(VOX_2)_3$ in Various Solvents: Although the crystalline sample of $(VOX_2)_3$ was insoluble in water and ethyleneglycol, it was highly soluble in most of the organic solvents. However, the dissolved state and stability of $(VOX_2)_3$ were found to be dependent upon the solvents.

As is summarized below, the solvents were classified roughly into two groups according to the type of ESR spectrum of the solution *in vacuo*:[15]

1) Non-polar or weakly polar solvents (hexane, *iso*-pentane, benzene, toluene, chloroform, methylenechloride, carbon disulfide, ethylacetate, acetone, ethylether, tetrahydrofuran, *etc.*): $(VOX_2)_3$ was dissolved in these solvents to give the T-type spectra. This means that, in these solvents, $(VOX_2)_3$ is present as the trimeric state.

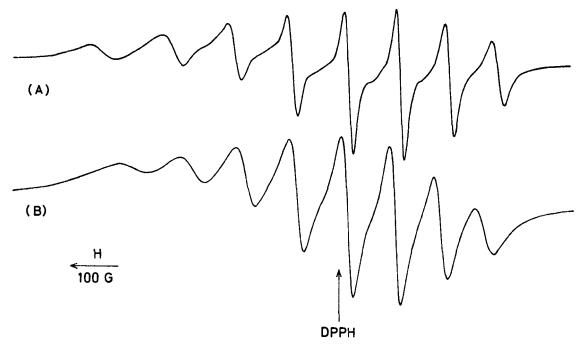

Fig. 5. ESR spectra resulting from methyl alcohol (A) and pyridine (B) solutions of $(VOX_2)_3$.

2) Polar solvents (methyl alcohol, ethyl alcohol, pyridine, picolines, *etc.*): In these solvents, the M-type spectra shown in Fig. 5 were observed with the disappearance of the T-type spectra. The ESR parameters for some of the M-type spectra were determined as follows:

$g_0=1.968$ $a=106$ gauss (for a pyridine solution)

$g_0=1.962$ $a=117$ gauss (for a methyl alcohol solution)

The results imply that $(VOX_2)_3$ reacts with these polar solvents to be converted into monomeric species. The reactions can presumably be expressed as follows:

$$(VOX_2)_3 + 6Py = 3VOX_2Py_2 \quad (10)$$

$$\left.\begin{aligned}(VOX_2)_3 + 6ROH &= 3VOX_2(ROH)_2\\ VOX_2(ROH)_2 + 2ROH &= VO(RO)_2(ROH)_2 + 2HX\end{aligned}\right\} \quad (11)$$

where Py denotes pyridine or picolines, and ROH, methyl or ethyl alcohol. Here, the di-*n*-butylphosphate

15) Although no spectral change with time was observed *in vacuo*, some of the solutions were found to show progressive spectral changes with time when the solutions were exposed to air. Work along this line is now in progress; the details will be reported in the future.

anion, X^-, in monomeric species is assumed to be coordinated as a monodentate ligand. The ESR parameters given above do not seem to be incompatible with these postulated monomeric species, because vanadyl complexes coordinated with nitrogen ligands usually give smaller hf constants than with oxygen ligands.

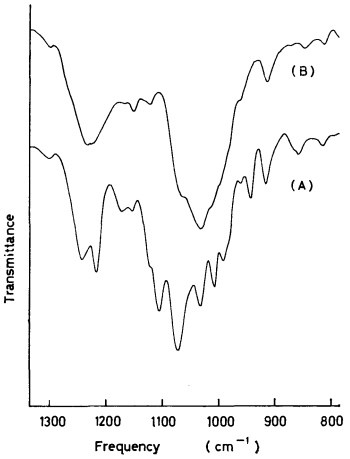

Fig. 6. Infrared spectra of $(VOX_2)_3$ as a Nujol mull (A) and of $(HX)_2$ as a thin liquid film (B).

IR Spectra: The spectrum of $(VOX_2)_3$ as a Nujol mull is given in Fig. 6, where it is compared with that of HDBP as a thin liquid film. As is shown in the literature,[16,17] the spectrum of HDBP shows the P=O stretching band at 1230 cm^{-1}, the superimposed bands due to P–O–(C), P–O–(H), and (P)–O–C stretching modes in the 1000—1070 cm^{-1} region, and three broad bands at *ca.* 2700, 2350, and 1700 cm^{-1} which are assignable to the vibrational modes of hydrogen-bonded hydroxyl groups in the HDBP dimer, $(HX)_2$.

It is seen, however, in the spectrum of $(VOX_2)_3$ that the P=O stretching band splits into two peaks at 1215 and 1240 cm^{-1}, with the complete disappearance of the hydrogen-bonded hydroxyl bands. Furthermore, the spectrum of $(VOX_2)_3$ shows a well-resolved structure in the 940—1100 cm^{-1} region with new bands at 945 and 1105 cm^{-1}, the former of which is presumed to be the V=O stretching vibration.[2,18]

Although an unambiguous assignment of each band is difficult, the above results may indicate that HDBP is coordinated to vanadium through two vacant oxygens as a result of the ionization of hydroxyl hydrogen atom, causing hence the spectral change from HDBP to $(VOX_2)_3$.

Visible Absorption Spectra: The visible absorption spectrum of the trimeric complex $(VOX_2)_3$ dissolved in hexane is presented in Fig. 7, along with that assignable to the monomeric complex $VO(X_2H)_2$. The latter spectrum was obtained from the hexane solution containing $(VOX_2)_3$ and a large excess of HDBP. The details will be described below.

16) D. F. Peppard, J. R. Ferraro, and G. W. Mason, *J. Inorg. Nucl. Chem.*, **7**, 231 (1958).

17) D. F. Peppard and J. R. Ferraro, *ibid.*, **10**, 275 (1959); J. Kennedy and A. M. Deane, *ibid.*, **19**, 142 (1961).

18) J. Selbin, L. H. Holmes, Jr., and S. P. McGlynn, *ibid.* **25**, 1359 (1963).

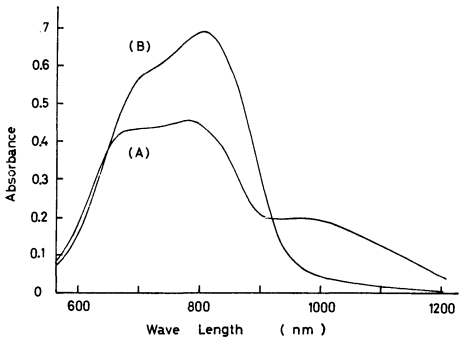

Fig. 7. Visible absorption spectra of $(VOX_2)_3$ (A) and $VO(X_2H)_2$ (B).

The following absorption maxima (with molar extinction coefficients given in parentheses) were derived from Fig. 7:

$(VOX_2)_3$	680 nm (40 $M^{-1}\cdot cm^{-1}$)
	780 nm (45 $M^{-1}\cdot cm^{-1}$)
	980 nm (19 $M^{-1}\cdot cm^{-1}$)
$VO(X_2H)_2$	700 nm (19 $M^{-1}\cdot cm^{-1}$)
	805 nm (23 $M^{-1}\cdot cm^{-1}$)

As will be shown below, $VO(X_2H)_2$ may have a local symmetry of C_{4v} with an unpaired electron in the $3d_{xy}$ orbital. Thus, according to the Ballhausen and Gray energy level scheme,[19] it seems probable that the absorption bands for $VO(X_2H)_2$ at 700 and 805 nm can be identified as $B_2(3d_{xy})\rightarrow B_1^*(3d_{x^2-y^2})$ and $B_2(3d_{xy})\rightarrow E_\pi^*(3d_{xz},3d_{yz})$ transitions respectively.

On the other hand, the situation in $(VOX_2)_3$ is more complicated, because exchange interactions among three vanadium ions exert a perturbing influence on the energy levels derived from the combination of three sets of monomeric energy levels. It is not within the scope of this paper to examine possible assignments for the visible spectra of $(VOX_2)_3$. However, it seems likely that the three absorption bands at 680, 780, and 980 nm originate from the perturbed d—d transitions, since the typical exchange energies for most of the polynuclear metal complexes thus far reported are of the order of a few hundred cm^{-1} or less.[11]

Equilibrium Reaction between $(VOX_2)_3$ and $VO(X_2H)_2$ in Hexane. In order to get information about the extraction mechanisms of $(VOX_2)_3$ and $VO(X_2H)_2$, the reaction of $(VOX_2)_3$ with HDBP in hexane was investigated at the ambient temperature (about 20°C) by both ESR and visible-absorption methods.

ESR Method: When HDBP was added, little by little, to a hexane solution of $(VOX_2)_3$, the ESR spectrum of the solution was found to show gradual changes from the T-spectrum to the M-spectrum with an increasing HDBP through such an intermediary spectrum as is given in Fig. 3. The change was reversed when $(VOX_2)_3$ was added to a HDBP solution. It was thus presumed that $(VOX_2)_3$ reacts reversibly with HDBP to form $VO(X_2H)_2$ according to:

$$(VOX_2)_3 + 3(HX)_2 = 3VO(X_2H)_2 \qquad (12)$$

19) C. J. Ballhausen and H. B. Gray, *Inorg. Chem.*, **1**, 111 (1962).

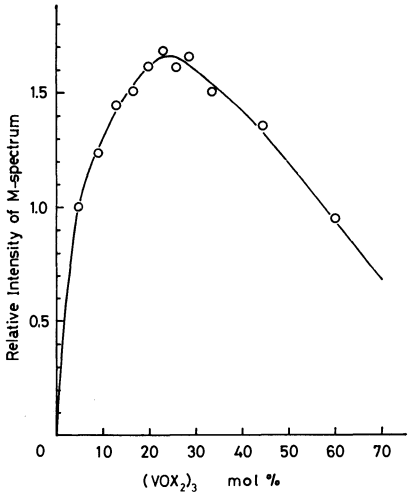

Fig. 8. Continuous variation method as applied to the $(VOX_2)_3$–$(HX)_2$ system by ESR measurements. $[(VOX_2)_3]+[(HX)_2]=2\times10^{-2}$M (const)

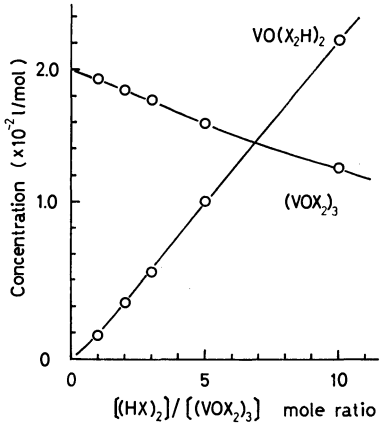

Fig. 9. Mole ratio method as applied to the $(VOX_2)_3$–$(HX)_2$ system by ESR measurements. $[(VOX_2)_3]=2\times10^{-2}$M (const)

where HDBP is assumed to exist as the dimer, $(HX)_2$, in hexane.

Then Job's method of continuous variations and the mole-ratio method[20] were applied to Eq. (12) in order to verify the validity of the assumed reaction and also to determine its equilibrium constant. Both results are presented graphically in Figs. 8 and 9. It is apparent from Fig. 8 that the signal intensity due to the M-spectrum, which is proportional to the concentrations of $VO(X_2H)_2$ formed, reaches a maximum at about 25 mol% of $(VOX_2)_3$, indicating that one mole of $(VOX_2)_3$ reacts with three moles of $(HX)_2$ in accordance with the presumed reaction scheme. On this basis, the equilibrium constant was evaluated directly from Fig. 9, where the equilibrated concentrations of $VO(X_2H)_2$ and $(VOX_2)_3$ are plotted as functions of the mole ratio of $(HX)_2$ to $(VOX_2)_3$. The equilibrium constant thus obtained is given by:

$$K=\frac{[VO(X_2H)_2]^3}{[(VOX_2)_3][(HX)_2]^3}=(1.0\pm0.5)\times10^{-1}\ \text{l/mol}$$

The rather poor accuracy of the value seems to have arisen from the inaccurate determination of the equilibrium concentrations because of the superposition of the M- and T-spectra.

Visible Absorption Method: The continuous-variation method was applied to the visible absorption spectra of the reaction system in a manner similar to that used in the case of the ESR measurements. Unfortunately, however, the method was found to be unusable for this system because the effective variation in the absorbance with a change in the mol% of $(VOX_2)_3$ was too small.

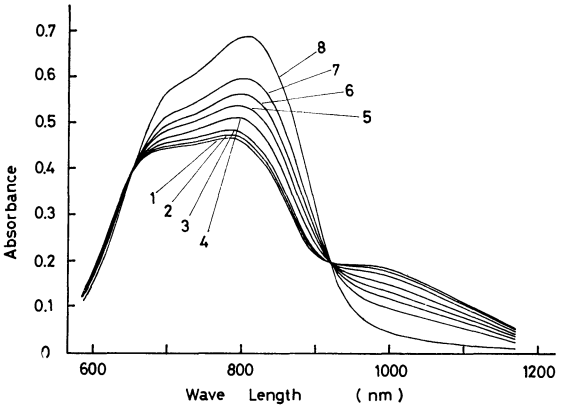

Fig. 10. Mole ratio method as applied to the $(VOX_2)_3$–$(HX)_2$ system by visible absorption measurements. $[(VOX_2)_3]=1\times10^{-2}$M (const.); $[(HX)_2]=2\times10^{-2}$M (1), 3×10^{-2}M (2), 5×10^{-2}M (3), 1×10^{-1}M (4), 1.5×10^{-1}M (5), 2×10^{-1}M (6), 3×10^{-1}M (7), $8\sim12\times10^{-1}$M (8).

On the other hand, the mole-ratio method was found to be successful in the evaluation of the equilibrium constant. A typical set of data is illustrated in Fig. 10, where a sharp isosbestic point is observed at 920 nm; this is consistent with our hypothesis of the presence of two absorbing species, $(VOX_2)_3$ and $VO(X_2H)_2$, in solutions.

The equation used for the calculation of the equilibrium constant was:[21]

$$K=\left\{\frac{3(A-A_0)}{3\varepsilon_M-\varepsilon_T}\right\}^3\Big/\left\{[(VOX_2)_3]_0-\frac{A-A_0}{3\varepsilon_M-\varepsilon_T}\right\}\times\left\{[(HX)_2]_0-\frac{3(A-A_0)}{3\varepsilon_M-\varepsilon_T}\right\}^3$$

where ε_T and ε_M are the molar extinction coefficients at the chosen wavelengths for $(VOX_2)_3$ and $VO(X_2H)_2$ respectively; A, the measured absorption at the wavelength ($A=\varepsilon_T[(VOX_2)_3]+\varepsilon_M[VO(X_2H)_2]$); A_0, the absorption of $(VOX_2)_3$ in the absence of $(HX)_2$ ($A_0=\varepsilon_T[(VOX_2)_3]_0$), and $[(VOX_2)_3]_0$ and $[(HX)_2]_0$, the initial concentrations of the two species.

The resulting K values were then averaged to give the following one, with a much smaller deviation than that determined by the ESR method:

$$K=(1.1\pm0.2)\times10^{-1}\ \text{l/mol}$$

20) A. Nakahara, "Jikken Kagaku Koza," Vol. 6, ed. by The Chemical Society of Japan, (1965), p. 184; H. Hosoya, "Jikken Kagaku Koza," Vol. 11, ed. by The Chemical Society of Japan (1965), p. 523.

21) R. L. Carlin and F. A. Walker, *J. Amer. Chem. Soc.*, **87**, 2128 (1965).

The extinction coefficient, ε_M, used for the calculation was approximated by that obtained from the spectra of the solution containing a large excess of $(HX)_2$, ranging from 80 to 120 times the amount of $(VOX_2)_3$. Under such conditions, the absorbance of the solution showed no significant change in relation to the variation in the $(HX)_2$ concentration, suggesting that $(VOX_2)_3$ is almost completely converted into $VO(X_2H)_2$. Consequently, one can consider the approximation in ε_M fairly good.

Mechanism of the Formation of $VO(X_2H)_2$ and $(VOX_2)_3$. It is well known that dialkyl phosphoric acids show a strong tendency to form dimers[16,22-24] in non-polar solvents similar to carboxylic acids. The proposed structure[16,22-24] of the dimer is illustrated in Fig. 11 (A), where an eight-membered ring structure is formed as the result of hydrogen bonding. If one of the acidic hydrogen atoms of this dimer is removed by ionization, and if the remaining hydrogen bond is not broken, the resulting, singly-charged dimeric anion should have the possibility of a relatively stable chelation with metal ions.

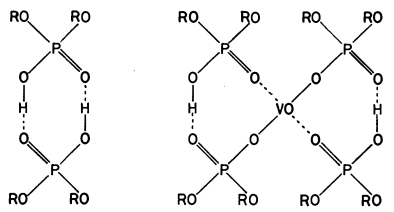

Fig. 11. Proposed structures of $(HX)_2$[16,22-24] and monomeric vanadyl complex $VO(X_2H)_2$[1].

From this point of view, it is well understandable that HDBP dimer extracts the vanadyl ion by the simple hydrogen ion-exchange reaction[10] given in Eq. (4), which then leads to the formation of a monomeric complex, $VO(X_2H)_2$, with the structure[1] shown in Fig. 11(B).

However, it should be noted here that the formation of $VO(X_2H)_2$ by this mechanism is strongly dependent upon the extraction conditions. As was described in the previous section, the monomeric complex $VO(X_2H)_2$ was selectively formed when the $pH_{(f)}$ was below 1. However, as the $pH_{(f)}$ increased from 1 to 2, the selective formation was suppressed by the simultaneous formation of the trimeric complex $(VOX_2)_3$; this was observed in this $pH_{(f)}$ region only when HDBP was present in excess. Furthermore, an increase in $pH_{(f)}$ values above 2 brought about the selective formation of $(VOX_2)_3$ in place of $VO(X_2H)_2$.

It is thus obvious that the simple ion-exchange mechanism is not applicable to all cases, and we are now in a position to take another mechanism into consideration in order to interpret the formation of $(VOX_2)_3$.

According to Rigg *et al.*,[1] who investigated the extraction isotherm for the vanadium-HDEHP system, a monomeric complex with the VOX_2 stoichiometry is formed at higher vanadium concentrations *via* this reaction:

$$VO^{2+}_{(a)} + VO(X_2H)_{2(o)} = 2VOX_{2(o)} + 2H^+_{(a)} \qquad (13)$$

where the formation of polymeric species is discounted on the ground that no increase in viscosity is noticeable in the solvent extracts. On the other hand, it has been postulated more recently by Sato *et al.*[2] that the formation of polymeric species is involved under the condition of a relatively low HDEHP concentration and that all the extraction reactions in the vanadium-HDEHP system can be described by the following general equilibrium reaction:

$$nVO^{2+}_{(a)} + (n+1)(HX)_{2(o)} = (VO)_nX_{2(n+1)}H_{2(o)} + 2nH^+_{(a)} \qquad (14)$$

where $n \geq 1$.

The latter mechanism, leading to the formation of a chain polymer of the $HX_2(VO)X_2(VO)X_2\cdots\cdots(VO)X_2(VO)X_2H$ type, is the most readily acceptable one if one remembers that Equation (14) is only an extension of the simple ion-exchange mechanism and that such a mechanism has already been accepted for the extraction of such metal ions as UO_2^{2+},[25,26] Th^{4+},[27] and Zr^{4+}.[28] In fact, the mechanism can interpret the extraction isotherm, because the $(VO)_nX_{2(n+1)}H_2$ chemical stoichiometry can be approximated to 1:2 for the vanadium-to-HDEHP mole ratio when n is large.

Unfortunately, the previous workers did not isolate the extracted vanadyl species. In view of the extraction conditions employed by the previous workers, it seems very likely that the postulated complex, VOX_2 or $(VO)_nX_{2(n+1)}H_2$, is identical with the trimeric complex, $(VOX_2)_3$, disclosed in the present work.

Equation (14) does not exclude the formation of trimeric species; according to this equation, many sorts of polymeric species, such as dimer, trimer, and tetramer, could be present. In this work we have observed no vanadyl species other than monomer and trimer. Furthermore, the chemical stoichiometry, $(VOX_2)_3$, determined for the isolated species was quite different from the formula, $(VO)_3X_8H_2$, expected from Eq. (14).

It has now become clear that Eqs. (13) and (14), proposed by previous workers, are inadequate for extractions at high $pH_{(f)}$ values and at high vanadium concentrations. Accordingly, the over-all reaction scheme under such conditions must be rewritten as follows:

$$3VO^{2+}_{(a)} + 3(HX)_{2(o)} = (VOX_2)_{3(o)} + 6H^+_{(o)} \qquad (15)$$

At the same time, one can obtain from Eqs. (4) and (15) such additional reactions as:

22) D. F. Peppard, J. R. Ferraro, and G. W. Mason, *J. Inorg. Nucl. Chem.*, **4**, 371 (1957).
23) D. Dyrssen, *Acta Chem. Scand.*, **11**, 1771 (1957).
24) D. Dyrssen and L. D. Hay, *ibid.*, **14**, 1091 (1960).
25) C. F. Baes, Jr., R. A. Zingaro, and C. F. Coleman, *J. Phys. Chem.*, **62**, 129 (1958).
26) T. V. Healy and J. Kennedy, *J. Inorg. Nucl. Chem.*, **10**, 128 (1959); T, Sato. *ibid.*, **27**, 1853 (1965).
27) T. Sato, *ibid.*, **27**, 1359 (1965).
28) T. Sato and T. Nakamura, *ibid.*, **33**, 1081 (1971).

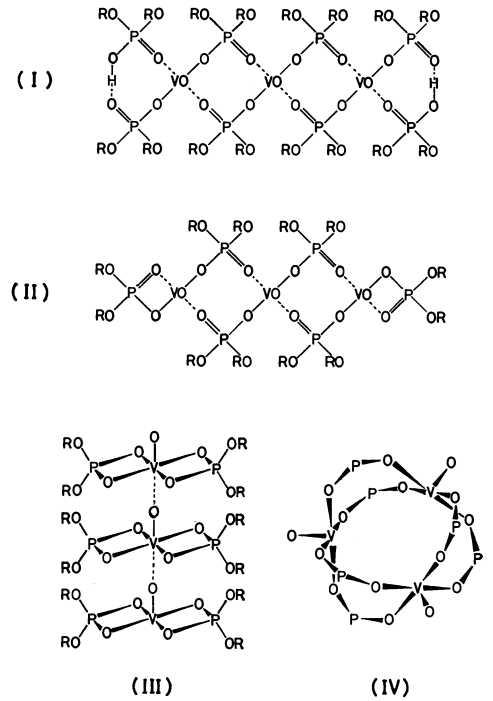

Fig. 12. Possible structures for trimeric vanadyl complex; (I) linear trimer for the stoichiometry $(VO)_3X_3H_2$, (II), (III) linear trimer for the stoichiometry $(VOX_2)_3$, (IV) cyclic trimer for the stoichiometry $(VOX_2)_3$, where each P represents $P(OR)_2$ with the two OR groups toward the outside.

in Fig. 12 (IV), where three vanadium atoms are assumed to be linked by the double-phosphate bridge in an equilateral triangle. A simple geometrical construction using a molecular structure model (HGS, D-type, Maruzen Co.), with the usual bond lengths, showed that this cyclic structure appeared reasonable, with no undue strain nor steric hindrance. Moreover, this cyclic structure can well explain the T-spectrum on the assumption that the magnitude of exchange interaction between vanadium ions satisfies the relation $|J| \gg |a|$.

A similar structural model has recently been proposed by Hasegawa *et al.*[13] for the trimeric vanadyl pyrophosphate complex, $Na_6(VOP_2O_7)_3 \cdot 12H_2O$, on the basis of ESR and magnetic susceptibility measurements, where magnetic electrons on the three vanadium atoms were found to interact antiferromagnetically with the exchange integral of $|J| \fallingdotseq 30\ cm^{-1}$. It can, therefore, be presumed that the exchange integral for $(VOX_2)_3$ does not differ greatly from that determined for $Na_6(VOP_2O_7)_3 \cdot 12H_2O$, and that the relation $|J| \gg |a|$ is valid. Thus, we can consider that the cyclic model (IV) is most probable for the structure of the trimeric vanadyl di-*n*-butylphosphate complex, $(VOX_2)_3$.

It is interesting to note that the proposed structure is closely related to those determined by X-ray single-crystal studies of such trimeric complexes as $Pd_3(CH_3COO)_6 \cdot 1/2H_2O$[31] and $Cr_3(CH_3COO)_6OCl \cdot 5H_2O$.[32] Our complex differs from $Pd_3(CH_3COO)_6 \cdot 1/2H_2O$ only in that the three metal ions are linked together by double-phosphate bridges rather than by double-acetate bridges. Needless to say, the final proof of the structure must await study by X-ray diffraction.

This work was supported in part by a grant of the Ministry of Education, to which the authors' grateful acknowledgements are made. The authors wish to thank Dr. T. Ohama for his kind advices on the molecular-weight measurements and Dr. H. Uchida for his invaluable help in the differential scanning calorimetries.

31) A. C. Skapski and M. L. Smart, *Chem. Commun.*, **1970**, 658.
32) B. N. Figgs and G. B. Robertson, *Nature*, **205**, 694 (1965).

The Effects of Ion-pair Formation on the ESR Spectra of the Anion Radicals of 4-Nitropyridine *N*-Oxide and 4-Nitropyridine[1]

Yoshiko KAWAMURA(née ŌISHI),[2] Koichi NISHIKIDA, and Tanekazu KUBOTA
Shionogi Research Laboratory, Shionogi & Co., Ltd., Fukushima-ku, Osaka 553
(Received June 26, 1972)

The effect of potassium ion-pair formation on the ESR spectra of the anion radicals of 4-nitropyridine and its *N*-oxide (4NPO) was studied at various temperatures lower than room temperature. The hyperfine splitting constant values due to hydrogen, nitrogen, and potassium nuclei were determined by applying the simulation technique. The above value arising from the potassium nucleus, decreased with a decrease in the temperature. Molecular orbital calculations covering the whole system of the $4NPO^{\cdot-}$–M^+ ion pair and employing the McLachlan modification for the spin-density calculation were carried out in order to discuss the configuration of the ion pairs and the temperature dependence of the hyperfine coupling constants. It was reasonably concluded that an alkali metal cation occupies the C_2 axis of the anion radicals and is in contact with the nitro-group oxygen atoms (the symmetry of the ion pairs is C_{2v}.). The temperature dependence of the hyperfine splitting constants was explained using the vibrational model of Atherton and Weissman.

In the foregoing paper we discussed the hydrogen-bonding effects on the electron spin resonance (ESR) spectra of 4-nitropyridine (4NP), 4-nitropyridine *N*-oxide (4NPO), and related *N*-oxide compounds from the experimental and theoretical viewpoints.[3] As part of a series of intermolecular interaction studies of free radicals, the effect of the alkalimetal ion-pair formation on the ESR spectra of the 4NPO and 4NP anion radicals will be reported in this paper.[4] It would be expected that the charge-transfer (CT) force and the electrostatic force may both play important roles[3] in the hydrogen bonding interaction and in the ion-pair formation of radical anions. Therefore, it seemed that it would be valuable to compare and discuss the effects of these two kinds of molecular interactions on the ESR spectra of 4NPO and 4NP anion radicals.

Experimental

Special-grade dimethoxyethane (DME) was carefully rectified and then dried, first with NaH and later with the Na–K alloy *in vacuo* (10^{-4}—10^{-5} mmHg). The solvent turned dark blue. Just before the use of DME as the solvent, degassing was done in the vacuum system by repeated freeze-thaw cycles at about the temperature of liquid nitrogen. In the present experiment, the ESR spectra due to the ion pair formed with the potassium ion alone were successfully obtained with a good resolution. The potassium was first purified by repeated distillation in a vacuum system, and finally a pure K film was prepared in the usual manner.[5,8] To obtain the high-resolution spectrum, the sample solution should be placed in contact with the above K film *in vacuo* as follows. After being placed in contact at room temperature, the glass apparatus, which had been sealed off from the vacuum system, was immersed overnight in liquid nitrogen. Then spectral observation at various temperatures lower than room temperature was carried out the next day. For 4NP, however, it was not necessary to leave the contact solution at the temperature of liquid nitrogen overnight. In turn, the spectra of electrochemically-generated free radicals in the DME solvent were adopted as an example of those where no ion-pair formation occurs.[6]

The ESR spectra were recorded with a Varian V-4502-15X-band spectrometer with a 100 KHz magnetic field modulation, the magnetic field being monitored with a Varian F-8 nuclear fluxmeter and a Takeda Riken TR-5578 frequency counter. The observed spectra were computer-simulated in order to verify the hyperfine coupling constant values.[6,7]

Results and Discussion

A well-resolved hyperfine splitting (hfs) due to the potassium nucleus was obtained at a temperature lower than 0°C. As an example Fig. 1 shows the ESR spectrum and a simulated one of the $4NPO^{\cdot-}$–K^+ ion pair obtained at −10°C, all the experimental data being collected in Table 1. The numbering of each atom in 4NPO and in 4NP is shown in Figs. 1 and 4 respectively. Here note that the lower the temperature, the smaller the values of a_K (the hfs value due to the potassium nucleus), $a_N^{NO_2}$, and a_{2H} for the $4NPO^{\cdot-}$–K^+ ion pair. However, the values of $a_N^{N\to O}$ and a_{3H} are almost independent of the temperature variation. By comparing the hfs values of the $4NPO^{\cdot-}$–K^+ ion pair with those of the 4NPO anion radical itself (see Table 1),

1) Presented in part at the 9th (Tokyo, Oct., 1970) Symposium of Electron Spin Resonance held by the Chemical Society of Japan.

2) Mrs. Kawamura has already left the Shionogi Research Laboratory. Any correspondence on this paper should be addressed to Dr. Kubota.

3) T. Kubota, Y. Ōishi, K. Nishikida, and H. Miyazaki, This Bulletin, **43**, 1622 (1970).

4) The ESR spectra of the anion radicals of 4NPO and 4NP produced by alkali-metal reduction were first reported by Itoh *et al.*, but the spectral resolution was low. Therefore, the effect of the ion-pair formation was not discussed by them. M. Itoh, T. Okamoto, and S. Nagakura, This Bulletin, **36**, 1665 (1963).

5) a) D. E. Paul, D. Lipkin, and S. I. Weissman, *J. Amer. Chem. Soc.*, **78**, 116 (1956). b) Y. Deguchi *et al.*, "Free Radicals in Solution," in "Electron Spin Resonance and Its Application to Chemistry," Kagaku Zōkan, **17**, ed. by Y. Deguchi, S. Ōnishi, and K. Morokuma (in Japanese), Kagaku Dojin (Kyoto) (1964), p. 43.

6) T. Kubota, K. Nishikida, H. Miyazaki, K. Iwatani, and Y. Ōishi, *J. Amer. Chem. Soc.*, **90**, 5080 (1968).

7) K. Nishikida, T. Kubota, H. Miyazaki, and S. Sakata, *J. Mag. Resonance*, **7**, 260 (1972).

8) N. M. Atherton and S. I. Weissmann, *J. Amer. Chem. Soc.* **83**, 1330 (1961).

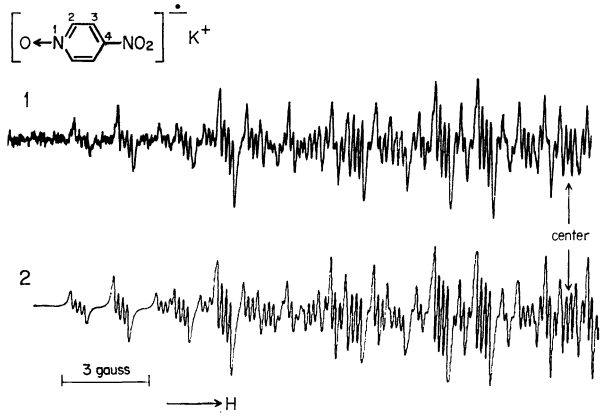

Fig. 1. Recorded (1) and simulated (2) ESR spectra of the potassium ion pair of 4-nitropyridine-*N*-oxide anion radical observed at −10°C. See also Table 1 footnote a.

TABLE 1. HYPERFINE SPLITTING CONSTANTS (IN GAUSS) OF THE K^+ COMPLEXES OF 4-NITROPYRIDINE *N*-OXIDE AND 4-NITROPYRIDINE ANION RADICALS AT VARIOUS TEMPERATURES

Temp (°C)	$a_N^{NO_2}$	$a_N^{N\to O}$	a_{2H}	a_{3H}	a_K	ΔH[a]
4-Nitropyridine-*N*-oxide anion radical itself[b]						
25	6.22	4.69	1.30	3.42	—	—
4-Nitropyridine-*N*-oxide anion radical-K^+ ion pair						
−10	7.35	4.40	1.45	3.51	0.160	0.110
−20	7.35	4.42	1.45	3.51	0.150	0.110
−40	7.23	4.40	1.43	3.51	0.140	0.100
−49	7.25	4.40	1.41	3.51	0.130	0.095
−59	7.22	4.40	1.40	3.51	0.120	0.095
4-Nitropyridine anion radical-K^+ ion pair						
−20	8.43	2.48	0.50	3.16	0.180	0.080
−30	8.31	2.47	0.49	3.13	0.160	0.080
−40	8.27	2.48	0.47	3.10	0.140	0.080
−50	8.23	2.49	0.46	3.10	0.120	0.080

a) Line width which was the most suitable for spectral simulation.
b) Obtained electrochemically in dimethoxyethane. See Fig. 's 1 and 4 for the numbering of each atom.

we can find that when the ion pair is formed, the values of $a_N^{NO_2}$, a_{3H}, and a_{2H} are increased, but the $a_N^{N\to O}$ value is decreased. Theoretically, these results proceed from the previously-reported MHMO calculation,[3] assuming that the Coulomb integral at the nitro-group oxygen atoms (α_0) comes out deeper[3] as a reslut of the ion-pair formation compared to that of the anion radical itself. Since the charge transfer may occur from the oxygen atoms to the K^+ ion, the deeper α_0 value seems reasonable. Therefore, it appears likely that the active center for the ion-pair formation is the nitro-group oxygen atoms. This result is in agreement with the active site for the 1:1 hydrogen-bonding interaction of $4NPO^{\dot{-}}$ and $4NP^{\dot{-}}$.[3] Next, it should be noticed that the hfs constants of the two *ortho*-protons and the two *meta*-protons in the ion-paired 4NPO and 4NP free radicals all become equivalent, as may be seen in Table 1. This means that the K^+ ion may, as a time average, lie on the σ_v plane, which contains the C_2 axis but which is vertical for the molecular plane (the symmetry of the ion pair may be C_s or C_{2v}). Summarizing the afore-mentioned discussions, the K^+ ion may occupy the position on the σ_v plane (perhaps on the C_2 axis) and near the NO_2-group oxygen atoms. This result can also explain the temperature dependence of the a_K value resonably in terms of the vibrational model of Atherton and Weissman[8] (*vide infra*).

Let us now consider quantitatively the structure of the ion pair and its behaviour. There have been reported several papers describing the theoreticl treatments of the structure of radical-ion pairs by applying the charge-transfer model or the electrostatic model, which more or less uses the perturbation technique.[9-12] Here we have treated the problem using the simple molecular orbital (SMO) method, which covers the whole system of the $4NPO^{\dot{-}}$–K^+ ion pair and which employs the McLachlan modification[13] for the spin density calculation.[14] The calculation procedure is as follows. The perturbation potential, V, due to a metal cation (the effective charge is Ze) on π or lone-pair orbitals is written by $V=-Ze^2/\varepsilon r_{M\mu}$, where $r_{M\mu}$ is the distance from the metal cation to an electron occupying the atomic orbital, ϕ_μ, in the radical anion. The ε is the dielectric constant of solvents, since the ion pair is embedded in the solvents[17] (see below). The mutual interaction of the alkali-metal cation with each $2p\pi$ atomic orbital and with the lone-pair orbitals of the nitro-group or *N*-oxide-group oxygen atoms in the anion radical is taken into account. Because the chemical orbital should be employed for the above mutual interaction, we assumed the lone-pair orbitals to be in the sp^2 hybridization. In addition, the charge transfer is considered to take place from the anion radical to the 2s, 3s, 4s, and 5s atomic orbitals of Li^+, Na^+, K^+, and Rb^+ cations respectively. Therefore, these s orbitals have been used for the present computation.

For the actual calculation, a zero-differential overlap approximation was adopted, so that the potential:[9]

$$V_{\mu\nu} = (-Ze^2/\varepsilon)\langle\phi_\mu|1/r|\phi_\nu\rangle \approx -2Ze^2S_{\mu\nu}/\varepsilon(r_{M\mu}+r_{M\nu})$$

is zero for $\mu \neq \nu$. Here, $S_{\mu\nu}=\langle\phi_\mu|\phi_\nu\rangle$ is the overlap integral. The parameters, k_a, in the form $\alpha+k_a\beta$, for the SMO calculation of the 4NPO anion radical are

9) B. J. McClelland, a) *Trans. Faraday Soc.*, **57**, 1458 (1961); b) *Chem. Rev.*, **64**, 301 (1964).
10) S. Aono and K. Oohashi, *Progr. Theor. Phys.*, **30**, 162 (1963); **32**, 1 (1964).
11) M. Iwaizumi, M. Suzuki, T. Isobe, and H. Azumi, This Bulletin, **40**, 1325 (1967); **41**, 732 (1968).
12) C. A. McDowell and K. F. G. Paulus, *Can. J. Chem.*, **43**, 224 (1965).
13) A. D. McLachlan, *Mol. Phys.*, **3**, 233 (1960).
14) This technique is convenient for the present case, because our previous calculation data[3,6,7] can extent to this kind of study. After we had presented this paper at the Symposium,[1] Goldberg and Bolton,[15] and Takeshita and Hirota[16] reported the theoretical calculation of several radical ion pairs. Their methods are somewhat similar to ours, but are more simplified than the present treatment.
15) I. B. Goldberg and J. R. Bolton, *J. Phys. Chem.*, **74**, 1965 (1970).
16) T. Takeshita and N. Hirota, *J. Amer. Chem. Soc.*, **93**, 6421 (1971).
17) M. Born, *Z. Phys.*, **1**, 45 (1920).

the same as those in the foregoing papers.[3,6] Here we employed the values[18] of $\alpha=-6.31$ eV and $\beta=-2.93$ eV. The electrostatic energies were expressed in β units, *i.e.*, $k_e\beta$. Thus, the total potential at each atom becomes $\alpha+(k_a+k_e)\beta$. The Coulomb integral due to the s orbital of alkali-metal cations is taken to be equal (as the absolute value) to the ionization potential of the neutral atoms;[19] thus, the values are: α_{Li} $(-5.39\text{ eV})=\alpha-0.314\,\beta$, α_{Na} $(-5.14)=\alpha-0.399\,\beta$, α_K $(-4.34)=\alpha-0.672\,\beta$, and α_{Rb} $(-4.18)=\alpha-0.727\,\beta$. In turn, we assumed that the energy of the lone-pair orbitals at the oxygen atoms of the 4NPO anion radical equals that of the corresponding oxygen π Coulomb integral.[20] The resonance integral between a metal cation s orbital and a π atomic orbital or a lone-pair orbital was estimated according to the $(\beta_{M-X}/\beta_{C=C})=(S_{M-X}/S_{C=C})$ relation at various metal positions (*vide infra*). Here note that the overlap integral, S_{K-X}, was obtained by the intrapolation method from the theoretical values using 1s, 2s, 3s, and 5s atomic Slater's orbitals, because $n-\delta=3.7$ in the atomic orbital parameter $\mu=(Z-\sigma)/(n-\delta)$ for the case of the 4s (potassium) orbital. In the present case the contact-ion pair was assumed, so that we take the sum of the ion radius and the Van der Waals radius for the distance[24] between the metal cation and each atom of the 4NPO anion radical, whose dimensions are put equal to those[21] of the neutral molecule.

Now we will solve the secular Eq. (1), to yield the necessary quantities for the discussion of the ion pairs:

$$|H_{\mu\nu}-E\delta_{\mu\nu}|=0 \tag{1}$$

where

$$H_{\mu\nu}=H^0_{\mu\nu}-Ze^2\langle\phi_\mu|1/r\varepsilon|\phi_\nu\rangle\delta_{\mu\nu} \tag{2}$$

$H^\circ_{\mu\nu}$ is for the SMO parameters of the 4NPO anion radical itself.[3,6] The above-mentioned calculation model represents the adoption of the π electron approximation; *i.e.*, the charge transfer of an odd π electron occurs to the vacant s orbital of alkali metal cations. The value of $\langle\phi_\mu|1/r_{M\mu}|\phi_\mu\rangle$ was theoretically calculated using the Slater orbital. The lone-pair orbitals in sp^2 hybridization are obtained explicitly in the usual manner; *i.e.*, they are first written out under a suitable coordinate at the oxygen atoms, and then these orbitals are transformed to those which are suitable for the coordinate of the whole molecule (see Fig. 2)[22] and are used for the calculation of S_{M-X} and the values of Eq. (2). Some integrals necessary here are given in the footnote.[23] The stabilization energy due to the ion-pair formation can thus be expressed by the equation:

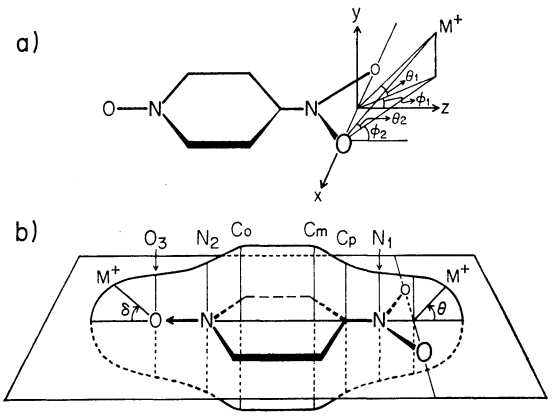

Fig. 2. a) The coordinate which has been used for the molecular orbital calculation of the whole system of the alkali metal ion pairs with 4-nitropyridine *N*-oxide (4NPO) anion radical. b) Each point on the circle, which is in the σ_V plane of 4NPO and drawn by keeping the distance of ion pair contact, is designated by θ, δ, N_1, Cp, *etc.* and employed for the abscissa in Fig. 3A. See text for detailed explanation.

$$\Delta E=\sum_i^{occ}n_i(E_i-E_i^0)+\sum_a\frac{ZZ_ae^2}{\varepsilon r_{Ma}} \tag{3}$$

Here, n_i is the electron number which occupies the i-th molecular orbital, E_i^0 being the i-th molecular orbital energy of the 4NPO anion radical itself. The last term in Eq. (3) stands for the nuclear repulsion energy between the nuclear cores a's (the core charge of the

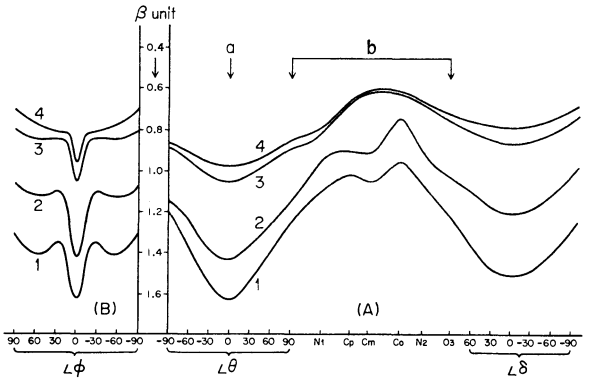

Fig. 3. The stabilization energies of alkali metal ion pairs with 4NPO anion radical. Curves 1, 2, 3, and 4 stand for the ion pairs with Li^+, Na^+, K^+, and Rb^+, respectively. See Fig. 2b and text on the explanation of the meaning of abscissa and "a and b" in the part A, respectively.

18) S. Mataga and N. Mataga, *Z. Phys. Chem., N.F.*, **33**, 374 (1962).

19) C. E. Moore, "Atomic Energy Levels," Natl. Bur. Standards (U. S. A.), Circ. No. 467, Vol. I–III; "American Institute of Physics Handbook, "McGraw-Hill, New York (1957).

20) Only for the ion pair with K^+ was the calculation made using a deeper Coulomb integral for the oxygen lone-pair orbitals (see below).

21) E. L. Eichhorn, *Acta Crystallogr.*, **9**, 787 (1956).

22) a) L. Pauling, "The Nature of the Chemical Bond" (Third Edition), Cornell University Press, Ithaca, New York (1960), p. 120. b) C. J. Ballhausen, "Introduction to Ligand Field Theory," McGraw-Hill, New York (1962), p. 54.

23)

$$-Ze^2\langle 2p\pi_a|1/r_{Ma}|2p\pi_a\rangle=-\frac{Ze^2}{R\rho^2}\left[-\frac{3}{2}+\rho^2+e^{-2\rho}\left(\frac{3}{2}+3\rho+2\rho^2+\frac{1}{2}\rho^3\right)\right]$$

$$-Ze^2\langle 2p\sigma_a|1/r_{Ma}|2p\sigma_a\rangle=-\frac{Ze^2}{R\rho^2}\left[3+\rho^2-e^{-2\rho}\left(3+6\rho+7\rho^2+\frac{11}{2}\rho^3+3\rho^4+\rho^5\right)\right]$$

$$-Ze^2\langle 2ps_a|1/r_{Ma}|2ps_a\rangle=-\frac{Ze^2}{R}\left[1-e^{-2\rho}\left(1+\frac{3}{2}\rho+\rho^2+\frac{1}{3}\rho^3\right)\right]$$

$$-Ze^2\langle 2p\sigma_a|1/r_{Ma}|2ps_a\rangle=-\frac{5Ze^2}{2\sqrt{3}R\rho}\left[1-e^{-2\rho}\left(1+2\rho+2\rho^2+\frac{6}{5}\rho^3+\frac{2}{5}\rho^4\right)\right]$$

In these equations R is the distance in atomic units between the metal cation and each atomic orbital in 4NPO$^-$, and $\rho=\mu_aR$.

atom a is $Z_a e$) of the conjugated system and the alkali metal cation (core charge: Ze). This term ought to be subtracted from the first electronic stabilization energy term. Here note that $Z_O^{NO_2}$, $Z_N^{NO_2}$, $Z_O^{N\to O}$, $Z_N^{N\to O}$, and Z_C of 4NPO are 5, 2, 5.3, 1.7, and 1 respectively. The calculated results are demonstrated in Fig. 3. In Part A of this figure, each point shown on the abscissa corresponds to that indicated in Fig. 2b. In Part B the ϕ angle is the same as that in Fig. 2a; *i.e.*, the metal cation occupies the $4NPO^{\pm}$ molecular plane and moves between $\phi=90$——$-90°$ by keeping the distance of the ion-pair contact constant.[24] It is now clear that, although the absolute value itself of the stabilization energy is not very accurate,[25] the most stable position of the metal cation is at $\theta=0$ and $\phi=0$; that is, the cation occupies the C_2 axis of the 4NPO anion radical and is in contact with the nitro-group oxygen atoms. In addition, the potential valley arising from the change in the ϕ angle is very narrow and quite deep (see Fig. 3). This may indicate that the metal cation can move more easily along the potential surface derived as a change in the θ angle, *i.e.*, in the direction deviating from the 4NPO molecular plane. These results support the previous qualitative discussions by other authors on the structure of the ion pairs of nitrobenzene, *etc.*[26-29]

Next, the calculated results depicted in Fig. 3 show that the stability of the alkali-metal ion pairs of $4NPO^{\pm}$ is in the order: $Li^+>Na^+>K^+>Rb^+$; the smaller the ion radius, the larger the stability. This conclusion is the same as that reported by Ling and Gendell[26] for the case of the alkali-metal ion pairs of nitrobenzene anion radical. On the other hand, they found a different behaviour in the Li^+ ion pair from the other alkali-metal ion pairs. For example, the hfs value due to the Li^+ nucleus (a_{Li}) has a tenednecy to increase with a decrease in the temperature. This behaviour can not be explained by the present calculations. On the basis of the small size of the Li^+ ion, there occurs more contact complex between Li^+ and the atoms of the nitro group. The terms, such as "spin polarization", other than the assumptions made here for the present calculations should also be taken into account in this kind of calculation.[30]

TABLE 2. CALCULATED HYPERFINE SPLITTING CONSTANTS OF ALKALI METAL-4-NITROPYRIDINE *N*-OXIDE ANION RADICAL ION PAIRS AS A FUNCTION OF THE ANGLE θ[a,b]

θ (°)	M^+	$a_N^{NO_2}$	$a_N^{N\to O}$	a_{2H}	a_{3H}	a_M	(ρ_M)[c]
0	Li	14.38	1.45	1.44	3.09	0.000	(0)
	Na	13.35	2.51	1.40	3.19	0.000	(0)
	K	12.37	3.12	1.34	3.22	0.000	(0)
	Rb	11.93	3.36	1.31	3.22	0.000	(0)
30	Li	15.11	1.01	1.43	3.03	1.079	(0.0075)
	Na	13.82	2.35	1.40	3.15	1.682	(0.0053)
	K	12.41	3.07	1.34	3.20	0.111	(0.0014)
	Rb	11.91	3.31	1.31	3.20	1.085	(0.0009)
45	Li	15.67	0.68	1.42	2.98	1.823	(0.0127)
	Na	14.24	2.16	1.40	3.11	3.105	(0.0098)
	K	12.45	2.95	1.34	3.15	0.442	(0.0054)
	Rb	11.86	3.25	1.31	3.18	2.450	(0.0020)
60	Li	16.03	0.34	1.40	2.90	2.053	(0.0143)
	Na	14.58	1.96	1.39	3.04	4.345	(0.0137)
	K	12.25	2.92	1.34	3.14	0.351	(0.0043)
	Rb	11.71	3.20	1.31	3.14	4.583	(0.0038)
90	Li	14.99	−0.16	1.36	2.72	0.844	(0.0059)
	Na	14.27	1.57	1.34	2.80	5.552	(0.0176)
	K	11.44	2.67	1.33	3.00	0.836	(0.0101)
	Rb	10.74	3.03	1.30	3.01	12.40	(0.0102)

a) For the actual calculations see text.
b) See text and Fig. 2 for the definition of the angle θ.
c) ρ_M indicates calculated spin density on metal cations.

Table 2 shows the calculated hfs values for hydrogen, nitrogen, and metal cations as a function of the θ angle, but at $\phi=0$. The equations combining the spin densities and the hfs values for the $a_N^{NO_2}$, $a_N^{N\to O}$, and a_H were the same as those reported previously.[3,6] The a_M values due to alkali metal cations were obtained using the equation $a_M=Q_M\rho_M$, where the Q_M values are:[31] $Q(^7Li)=143.3$, $Q(^{23}Na)=316.2$, $Q(^{39}K)=82.4$, $Q(^{87}Rb)=1219$. In Table 2 we can see that the increasing θ causes an increase in a_M and $a_N^{NO_2}$, although the $a_N^{NO_2}$ value again shows a tendency to decrease at $\theta>60°$. Therefore, the decreasing temperature, which corresponds to the decreasing θ, can be expected to bring about the decrease in the a_M and $a_N^{NO_2}$ values, since the metal ion in the ion pair would submerge to the bottom of the potential valley illustrated in Fig. 3.[8] These theoretical results explain well the experimental results previously mentioned, though, in our present treatment, the contributions from the effects of spin polarization, *etc.* to the a_M values were disregarded. Therefore, the spin density on alkali metal cations turns out to be zero when $\theta=0$. Here note that the linear relation is satisfied when the calculated values of $a_N^{NO_2}$ (see Table 2) are plotted against the values of $1/(R_M+C)$, where R_M is the ion radii of Li^+, Na^+, K^+, and Rb^+, and where C is a constant (1.4 Å in the present case). This kind of linear relation for radical-ion pairs was suggested by Nakamura[28] and by McClelland;[9a] the former author found this relation experimentally for

24) The ion and the Van der Waals radii (Å unit) used are shown in parentheses: Li^+ (0.6), Na^+ (1.0), K^+ (1.3), Rb^+ (1.5), 0 atom (1.4), N (1.5), and $2\pi p$ electron cloud of carbon (1.7).

25) One main reason for this may be the ε value, for which we used 3.0 as an average of the dielectric constants of ether-like solvents. After we had finished this work, Takeshita and Hirota[16] discussed the physical meaning of the ε value. They used it as an adjustable parameter in intimate correlation with the $r_{M\mu}$ value.

26) C. Ling and J. Gendell, *J. Chem. Phys.*, **47**, 3475 (1967).

27) J. M. Gross, J. D. Barnes, and G. N. Pillans, *J. Chem. Soc.*, *A*, **1969**, 109.

28) K. Nakamura, This Bulletin, **40**, 1 (1967).

29) Here note that there are two shallow potential minima at $\phi=50°$ and $-50°$ (see Fig. 3b), especially in the case of small-size alkali-metal ion pairs. These positions correspond to those where the lone-pair orbitals at each oxygen atom of the nitro group interact with an alkali ion. Previously, Nakamura[28] indicated the possibility of those potential minima in his qualitative discussion.

30) G. W. Canters, C. Corvaja, and E. de Boer, *J. Chem. Phys.*, **54**, 3026 (1971). In this paper it was theoretically emphasized that the charge-transfer process from doubly-occupied aromatic π MO's to the atomic orbitals (especially the ns orbital) of an alkali metal cation plays also a very important role in explaining the metal-spin density (particularly the negative spin density) in alkali-radical ion pairs.

31) H. Nishiguchi, Y. Nakai, K. Nakamura, K. Ishizu, Y. Deguchi, and H. Takaki, *Mol. Phys.*, **9**, 153 (1964).

the $a_N^{NO_2}$ values of alkali-metal ion pairs of halogen-substituted nitrobenzenes.

Now, let us turn to a discussion of the energy level of lone-pair orbitals. The calculation for the $4NPO^{\cdot-}$—K^+ ion pair indicated that the use of a deeper Coulomb integral for the oxygen lone-pair orbitals (α_l), compared to that of the carbon π orbital resulted in a smaller energy difference between two points, A (σ type ion pair) and B (π type ion pair), in Fig. 3A. The adoption of the deeper α_l value indicates a smaller interaction of lone-pair orbitals with the vacant s orbital of alkali-metal cations. Thus, the charge-transfer effect from the lone-pair orbitals to the s orbital becomes small, resulting in the structure of the above σ-type ion pair becoming unstable.

Last, we would like to add an experimental finding on the K^+ ion pair of the 4-nitropyridine ainon radical ($4NP^{\cdot-}$), the ESR spectrum of which is shown in Fig. 4 (see also Table 1 for the hfs values of each atom) and which was obtained under almost the same conditions as in the case of the $4NPO^{\cdot-}$–K^+ ion pair. The temperature dependence of the a_K and $a_N^{NO_2}$ values is quite similar to that of the $4NPO^{\cdot-}$–K^+ ion pair previously discussed in detail. Therefore, the nature of the $4NP^{\cdot-}$–K^+ ion pair seems to be the same as that of the $4NPO^{\cdot-}$–K^+ ion pair; *i.e.*, the K^+ ion would interact with the nitro-group oxygen atoms in the 4NP anion radical. This conclusion is the same as was derived from the study of the hydrogen-bonding effect on the ESR spectra of the 4NP anion radical,[3] where the active sites participating in the hydrogen-bonding interaction are nitro-group oxygen atoms.

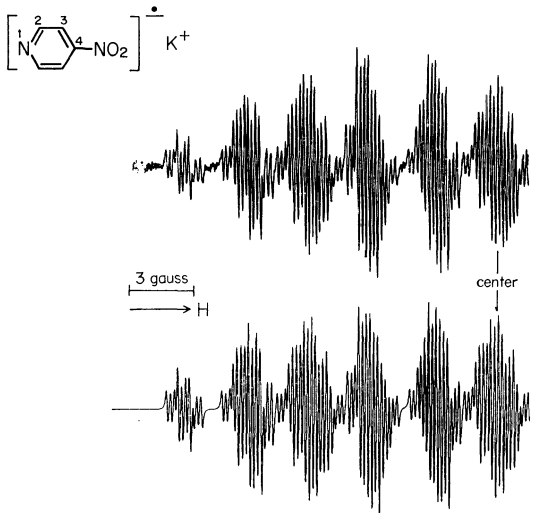

Fig. 4. Recorded (upper) and simulated (lower) ESR spectra of potassium ion pair of 4-nitropyridine anion radical observed at −20°C. See also Table 1 footnote a.

BULLETIN OF THE CHEMICAL SOCIETY OF JAPAN, VOL. 46, 741—744 (1973)

The Bromine Nuclear Quadrupole Resonance of Two Modifications of Indium Tribromide

Tsutomu OKUDA, Yoshihiro FURUKAWA, Hiroko SHIGEMOTO, and Hisao NEGITA

Department of Chemistry, Faculty of Science, Hiroshima University, Hiroshima

(Received June 29, 1972)

The bromine nuclear quadrupole resonance study of indium tribromide has revealed that there are at least two modifications in its solid state. The high-temperature modification shows the two ^{81}Br resonance lines of 85.985 and 86.205 MHz, with the relative intensity of 1 : 2 at 24.5°C. This modification was stable unless the temperature was lowered to ~15°C. The low-temperature modification shows one ^{81}Br resonance line, 86.915 MHz, at −196°C and was stable up to ~30°C. The directions of the z axes of the field gradient were determined by studying the Zeeman effect on each resonance line of the two modifications at room temperature. For the two resonance lines of the high-temperature modification, one and two directions, which had the asymmetry parameters of 0.362 and 0.400 respectively, were observed. The resonance line of the low-temperature modification showed three directions with the asymmetry parameter of 0.387. The crystal structures of the high- and low-temperature modifications were, therefore, concluded to be monoclinic and hexagonal respectively, from the numbers of resonance lines and of the nonequivalent directions of the z axes. The quadrupole coupling constants and asymmetry parameters were analyzed by means of the Townes-Dailey method.

Indium trihalides, InX_3 (X: Cl, Br, I), exist as dimers in the gaseous state,[1] but their crystal structures are not always the same. According to the X-ray diffraction analysis,[2] the crystal of $InCl_3$ has a layer structure in which every indium atom is octahedrally surrounded by chlorine atoms, and its space group is C2/m as in $AlCl_3$.[3] On the other hand, the crystal of InI_3 is made up of dimer molecules joined by iodine bridges,[4]

1) D. P. Stevenson and V. Schomaker, *J. Amer. Chem. Soc.*, **64**, 2514 (1942).

2) D. H. Templeton and G. F. Carter, *J. Phys. Chem.*, **58**, 940 (1954).

3) R. W. G. Wyckoff, "Crystal Structures," Interscience Publishers, Inc., New York (1948).

4) J. D. Forrester, A. Zalkin, and D. H. Templeton, *Inorg. Chem.*, **3**, 63 (1964).

as in the gaseous state. As for $InBr_3$, the X-ray analysis has not yet been reported, as far as we know.

The results of the nuclear quadrupole resonance (NQR) of bromine in $InBr_3$ were reported previously by Ludwig[5] and Barnes *et al.*,[6] but they are not completely consistent. Barnes *et al.* studied extensively the NQR on the trihalides of Group IIIb elements and found that all the NQR spectra consist of a singlet on the lower-frequency side and a doublet on the higher-frequency side.[6,7] The ^{81}Br NQR spectrum of $InBr_3$ consists of the singlet of 86.912 MHz and the doublet of 106.974 and 107.428 MHz at −196°C. The former is ascribed to the bridging bromine atoms, while the latter is assinged to the terminal ones.

On the other hand, Greenwood *et al.* have reported the infrared and Raman spectra of InX_3.[8] According to their results, the spectra of $InBr_3$ are more similar to those of $InCl_3$ than those of InI_3; that is, the crystal of $InBr_3$ has a layer structure. This is contrary to the NQR results presented above.

We re-examined the ^{81}Br NQR of $InBr_3$ and, furthermore, observed the Zeeman effect on the NQR. We obtained different spectra from those reported previously; our results can be satisfactorily explained by the layer structure suggested by Greenwood *et al.*

Also, the study of the temperature dependences of the NQR frequencies revealed the existence of at least two modifications in $InBr_3$ crystals. The high-temperature modification shows two resonance lines, while the low-temperature modification shows only one resonance line. The measurements of the NQR Zeeman effect were made on these two modifications.

Experimental

The sample of $InBr_3$ was purchased from Katayama Chemical Industries Co., Ltd., and was purified by sublimation. The single crystal necessary for the study of the Zeeman effect was grown by the Bridgman-Stockbarger method.

The NQR spectrometer used in these experiments was a super-regenerative oscillator with frequency modulation; the absorption lines were observed on an oscilloscope. The resonance frequencies were determined with a VHF signal generator and a frequency counter, TR-5578, from the Takeda Riken Industry Co., Ltd. The Zeeman effect was examined by means of the zero-splitting cone method used in a low-magnetic field. The magnetic field of about 200 G was applied by means of a Helmholtz coil, and the patterns of the zero-splitting loci were determined at room temperature. The temperature dependences of the resonance frequencies were measured by using a thermostat from the Takara Kogyo Co. After the sample had been cooled or heated at a fixed temperature for 30—60 min, the resonance frequencies were determined.

Results and Discussion

The ^{81}Br NQR frequencies of $InBr_3$ observed in our experiment are presented in Table 1. Those for ^{79}Br were observed at frequencies corresponding to the frequency ratio (1.197) of $\nu(^{79}Br)/\nu(^{81}Br)$. The crystals of $InBr_3$ commercially obtained or purified by sublimation always show two closely-spaced resonance lines at room temperature. The intensity ratio of the higher line (ν_{β_2}) to the lower (ν_{β_1}) is approximately 2: 1. These results indicate that there are two kinds of non-equivalent bromine atoms in the crystal and that their abundance ratio is 2: 1. On cooling, this modification is apparently transformed to the other one, which shows only one resonance line. Tentatively we will refer to the former as the β-modification and to the latter as the α-modification.

Table 1. ^{81}Br nuclear quadrupole resonance frequencies in the modifications of indium tribromide

Modification		Resonace frequency[a] (MHz)		
		−196°C	24.5°C	49°C
α	ν_α	86.915	85.962	.....
β	ν_{β_1}	.....	85.985 (1)[b]	85.867 (1)
	ν_{β_2}	.....	86.205 (2)	86.074 (2)

a) Experimental error is ±0.01 MHz.
b) The value in parenthesis is the relative intensity.

The resonance frequencies in Table 1 are close to that of the bridging bromine atom reported by Barnes *et al.*[6] Especially, the resonance frequency of the α-modification (ν_α) at −196°C is consistent within the limits of experimental error. We scanned carefully the frequency regions around 105 and 125 MHz, where the resonance frequencies of the terminal ^{81}Br and ^{79}Br atoms in the dimer have been reported by Barnes *et al.*,[6] but we could not detect any resonance line.[9] Therefore, we concluded that neither of the modifications observed here is composed of dimers.

The temperature dependences of the resonance frequencies were measured between −48 and 49°C, as is shown in Fig. 1. The transition point is hard to determine because of the large hysteresis. In the course of cooling the single crystal of the β-modification, an absorption line of the α-modification appeared at ~15°C. On warming, the signal of the α-modification was observed up to ~30°C. Using the powder sample, the region of the hysteresis spread as may be seen in Fig. 1. Furthermore, in the temperature range from −6 to −16°C, the absorption lines of both the α- and β-modifications were observed.

The β-Modification of Indium Tribromide. The single crystal of $InBr_3$ initially obtained had the β-modification, because it was crystallized from the melt. The patterns of zero-splitting were obtained on each resonance line. For the bromine atom (I=3/2), the

5) G. W. Ludwig, *J. Chem. Phys.*, **25**, 159 (1956).
6) R. G. Barnes, S. L. Segel, P. J. Bray, and P. A. Cassabella *ibid.*, **26**, 1345 (1957).
7) R. G. Barnes and S. L. Segel, *ibid.*, **25**, 180 (1956). S. L. Segel and R. G. Barnes, *ibid.*, **25**, 578 (1956).
8) N. N. Greenwood, D. J. Prince, and B. P. Straughan, *J. Chem. Soc., A*, **1968**, 1964.
9) The sensitivity of the spectrometer was confirmed by the detection of ^{127}I resonance line of InI_3 for 125 MHz region. The ^{79}Br resonance lines of $AlBr_3$ and also, of $InBr_3$ give the enough sensitivity for 105 MHz region.

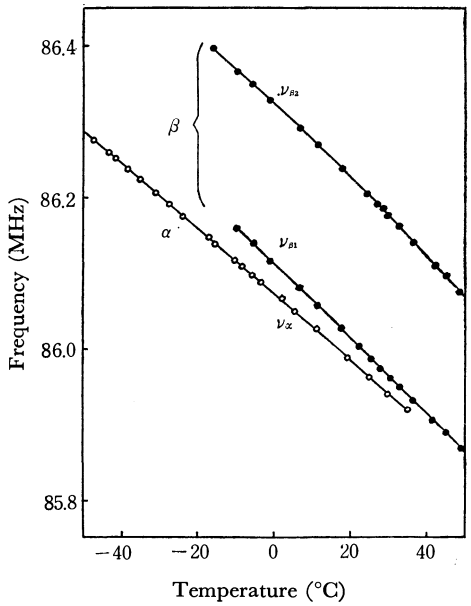

Fig. 1. Temperature dependences of ^{81}Br nuclear quadrupole resonance frequencies in indium tribromide.

zero-splitting occurs under the following conditions:[10]

$$\sin^2\theta = 2/(3-\eta\cos 2\varphi), \qquad (1)$$

where the orientation of the magnetic field is expressed by the polar coordinates (θ,φ) with respect to the coordinates of the principal axes (x, y, and z axes) of the field gradients at the resonant nuclei and where η is an asymmetry parameter of the field gradient. In this way, a cone about the z axis can be drawn by θ and φ which satisfies Eq. (1). The axes corresponding to $\varphi=0$ and $\varphi=\pi/2$ are shown by the x and y axes respectively. Only one zero-splitting pattern was obtained for ν_{β_1}, whereas two patterns were observed for ν_{β_2}. The experimental results are shown in Fig. 2, where Z_1, Z_{2A}, and Z_{2B} are the directions of the z axes at the bromine atoms contributing to ν_{β_1} and ν_{β_2}. From the number of the z axes of ν_{β_1} and ν_{β_2}, the symmetry of the β-modification must be lower than the tetragonal,

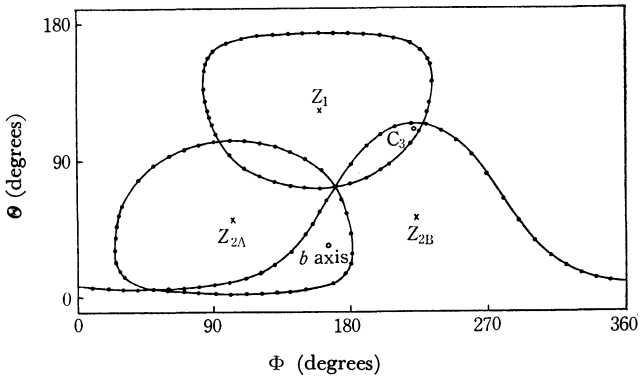

Fig. 2. Zero-splitting patterns of the Zeeman effect of the β-modification of indium tribromide. Θ and Φ are polar and azimuthal angles in the coordinates fixed to the sample respectively.

10) T. P. Das and E. L. Hahn, "Nuclear Quadrupole Resonance Spectroscopy," Solid State Physics, Suppl. 1, Academic Press, New York (1957).

but not the triclinic.[11] However, as a symmetry higher than the monoclinic is ruled out by the requirement for the angles between the z axes, it can be concluded that the β-modification belongs to the monoclinic space group. The asymmetry parameters of the field gradient were determined from Eq. (1) by the use of the least-squares method. As may be seen in Table 2, large values of η were obtained.

Table 2. Asymmetry parameters and quadrupole coupling constants for ^{81}Br in indium tribromide at room temperature

Modification		η	e^2Qq/h(MHz)	Up
α	(ν_α)	0.387±0.005	167.79	0.2609
β	(ν_{β_1})	0.362±0.002	168.33	0.2618
	(ν_{β_2})	0.400±0.007	167.99	0.2612

Greenwood *et al.* suggested that the crystal structure of $InBr_3$ is similar to that of $InCl_3$ or $AlCl_3$.[8] In the case of the $AlCl_3$-type structure, there are two non-equivalent halogen atoms which form slightly different bridges. Therefore, the low-resonance frequencies and the large asymmetry parameters may be attributed to the bridging bromine atoms in the β-modification. Also, it is reasonable, in view of this structure, that the β-modification shows two resonance lines with the intensity ratio of 1 : 2 and that the zero-splitting patterns observed are one for ν_{β_1} and two for ν_{β_2}. Table 3

Table 3. Angles between the z axes and the b axis in the β-modification of indium tribromide

	Z_1-Z_2	$Z_{2A}-Z_{2B}$	Z_1-b axis	Z_2-b axis
NQR	92°08′	88°16′	90°	44°08′
X-Ray[a]	90°27′	88°26′	90°	44°13′

a) These values were calculated from the atomic positions of $AlCl_3$. (Ref. 3).

shows the angles between the z axes and the b axis of the monoclinic lattice as determined by the Zeeman effect. The values in the second row are calculated from the atomic positions of $AlCl_3$,[3] because the data of X-ray analysis are not available for $InBr_3$. In this calculation, the z axis was assumed to be directed perpendicularly to the plane including M–X–M, as in the case of a bridging halogen atom of the dimer molecule.[12,13] The results of the NQR and those of the X-ray analysis are in good agreement, though the latter are derived for a related compound, $AlCl_3$. Accordingly, it seems most likely that the β-modification is isomorphous with $AlCl_3$. This conclusion is further supported by the fact that Zeeman patterns similar to those in Fig. 2 have been found in $ErCl_3$, which has an $AlCl_3$-type structure, by Carlson and Adams.[14]

11) K. Shimomura, *J. Phys. Soc. Jap.*, **12**, 652 (1957).
12) G. E. Peterson and P. M. Bridenbaugh, *J. Chem. Phys.*, **51**, 238 (1969).
13) T. Okuda, H. Terao, O. Ege, and H. Negita, *ibid.*, **52**, 5489 (1970).
14) E. H. Carlson and H. S. Adams, *ibid.*, **51**, 388 (1969).

The α-Modification of Indium Tribromide. When the single crystal of the β-modification mounted on the apparatus was cooled to about −50°C by means of a cold stream of nitrogen gas from liquid nitrogen, it was transformed to the single crystal of the α-modification. The measurements of the zero-splitting on this modification show three different directions of the z axes, indicating that the crystal of the α-modification has a threefold axis.[15] In Fig. 2, C_3 indicates the orientation of this threefold axis of the α-modification at the same coordinates of the β-modification. The compound that possesses three nonequivalent directions of the z axes belongs, in general, to the hexagonal (point group C_3 or C_{3i}) system or, in special cases, to another hexagonal or cubic system. In this case, however, the cubic system, which has three z axes orthogonal with one another,[11] can be excluded because the observed angle between the z axes is 92°13′.

The zero-splitting patterns of the α-modification are very similar to those of the β-modification. The directions of the z axes of the α-modification deviate from the relevant axes of the β-modification to a small degree. It can, therefore, be expected that the crystal structure of the α-modification is slightly different from that of the β-modification; that is, the crystal of the α-modification may be composed of a polymeric layer lattice like $AlCl_3$. In view of these results, it is likely to be of the BiI_3-type, the structure of which is closely related to the $AlCl_3$-type[16] and which has the space group $R\bar{3}$.[17] The ^{127}I NQR of BiI_3 indicates only a resonance line and a large asymmetry parameter of the field gradient.[18] The transition may occur between monoclinic and hexagonal systems, as in the case of $CrCl_3$ reported by Morosin and Narath.[19]

The crystal of $InBr_3$ is easily cloven along the plane perpendicular to the threefold axis, which may be parallel to the c axis of the hexagonal unit cell. The b axis of the monoclinic lattice of the β-modification was perpendicular to the threefold axis of the α-modification; that is, it was parallel to the cleavage plane.

It is interesting to notice that $InBr_3$ has a higher melting point (436°C) than those of the other Group IIIb trihalides which form dimers in the crystal (*e.g.*, 210°C for InI_3[20]) and that the ratio of the ionic radii for In^{3+}/Br^- is 0.42. This value is slightly larger than the lower limiting ratio, 0.414, for the octahedral coordination of the metal atom. In view of these points, $InBr_3$ can be expected to form an infinite layer lattice, as is proposed by this experiment.

Bond Character. The analyses of the Zeeman effect of $InBr_3$ reveal a close relation between the α- and β-modifications. Such a result as above can also be seen from Tables 1 and 2, *i.e.*, the resonance frequencies and the asymmetry parameters in both modifications are almost the same.

The observed x axis of the field gradient at the bromine atom is directed nearly along the bisector of In–Br–In and the y axis is parallel to the In–In direction. The z axis is perpendicular to the plane including In–Br–In, as has been explained before. From these coordinates of the principal field gradients, we can construct the hybrid orbitals of the bromine atom to bind with two indium atoms. Using the Townes and Dailey theory and appropriate approximations, the following two equations are found to hold for the NQR parameters:[21]

$$\eta = -3\cos\alpha, \tag{2}$$

$$Up(1+\eta/3) = 2 - a, \tag{3}$$

where a is the electron population in the bonding orbital directed to the indium atom and where α is the interbond angle, ∠In–Br–In. Up is the number of unbalanced p electrons and can be determined from the observed quadrupole coupling constant, e^2Qq_{obsd}:

$$h\nu = 1/2e^2Qq_{obsd}(1+\eta^2/3)^{1/2}, \tag{4}$$

$$Up = e^2Qq_{obsd}/e^2Qq_{atom} \tag{5}$$

where e^2Qq_{atom}/h is 643.03 MHz.[22]

Substituting the observed values of η and Up into Eqs. (2) and (3), we obtain $a=1.7$ as the mean value, which gives a negative charge of $0.4e$ on the bromine atom. This ionic character is smaller than the 55% expected from the electronegativity difference between indium and bromine. This discrepancy may be due to the crystal field exerted by the neighboring nuclei. The angles of In–Br–In are deduced to be 96°56′∼97°40′. These values are somewhat larger than the relevant angles, 94°20′ and 95°30′ for $AlCl_3$.

15) The NQR Zeeman analysis always introduces the center of symmetry. It is impossible to distinguish between the threefold rotation axis and the threefold inversion axis on the basis of the Zeeman analysis. (Ref. 11).

16) H. Krebs and P. H. L. Walter, "Fundamentals of Inorganic Crystal Chemistry," McGraw-Hill, London (1968).

17) J. Tretter and T. Zobel, *Z. Kristallogr.*, **123**, 67 (1966).

18) I. P. Biryukov, M. G. Voronkov, and I. A. Safin, "Tables of Nuclear Quadrupole Resonance Frequencies," Israel, IPST Press (1969).

19) B. Morosin and A. Narath, *J. Chem. Phys.*, **40**, 1958 (1964).

20) "Mukikagakuzensho X-2-1, Ga, In, Tl," Maruzen, Tokyo (1966).

21) E. A. C. Lucken, "Nuclear Quadrupole Coupling Constants," Academic Press, New York (1969).

22) V. Jaccarino and J. G. King, *Phys. Rev.*, **94**, 1610 (1945).

Photochemistry of Acridines. XIX. Photoreduction of Acridine in Mixed Solvents

Mikio HOSHINO and Masao KOIZUMI

Department of Chemistry, Faculty of Science, Tohoku University, Aoba, Aramaki, Sendai

(Received March 1, 1972)

The photoreduction of acridine has been investigated in three kinds of mixed solvents, benzene–isopropanol, benzene–methanol and benzene–cyclohexane, all in aerated and deaerated conditions. The following general tendensies have been found for the plot Φ_{rel} *vs.* mole fraction. It is approximately linear or slightly concave upward for molecular mechanism, while convex upward for radical mechanism. This indicates that for molecular mechanism a cage model trapping two radicals (*e.g.* C-radical and alcohol radical) is unsuitable while one act process involving two reactive sites is suitable.

Photoreduction of acridine in H-donating solvents occurs *via* dual mechanisms, molecular and radical. In general, the contribution of excited singlet state and triplet (n-π^*) state to each mechanism depends upon the nature of the solvent. In the case of isopropanol both mechanisms occur only in the singlet excited state, while in methanol both singlet and T(n-π^*) contribute to radical mechanism and molecular mechanism occurs mainly in the singlet excited state.[1] The case is essentially the same with ethanol and *n*-propanol. However, the feature is quite different in cyclohexane, radical mechanism occurring only in singlet excited state and molecular mechanism only in T(n-π^*).[2] The cause of such behavior still remains unclarified.

Concerning the meaning of radical and molecular mechanisms, the former is a mechanism in which half-reduced acridine is produced as an intermediate and is captured by the oridinary flash technique. In the latter no transient intermediate is observed by the flash technique in contrast to radical mechanism. It is still unknown whether it really occurs as one act or occurs *via* a transient intermediate too short-lived to be captured by the flash technique. Even the possibility that an intermediate in this mechanism is two radicals, *e.g.* acridine semiquinone and alcohol radical trapped in one cage is conceivable. In fact, Zanker and Prell[3] distinguished two mechanisms resembling radical and molecular ones and proposed a cage-like model for the photoreduction of 9-CH_3-acridine by ethanol.

To elucidate the problem, we have studied photoreduction in three mixed solvents, *i.e.*, 2-propanol, methanol and cyclohexane containing various amounts of benzene. They are the three H-donors which display distinct features of the reaction as listed below.

	Molecular mech.	Radical mech.
2-Propanol	singlet	singelt
Methanol	singlet, very littleT(n-π^*)	singlet, T(n-π^*)
Cyclohexane	T(n-π^*)	singlet

If the transient intermediate in molecular mechanism are two radicals trapped in a cage, the contribution of molecular and radical mechanisms will change with a certain correlation depending upon the composition of the solvent. Thus the stability of radicals trapped in the cage will depend upon its structure and nature which varies according to the composition of the solvent. Therfore, if the structure changes in such a way as to make it easy for the two radicals to separate from each other, the molecular mechanism will be transformed to radical mechanism by the amount determined by the cage structure. On the other hand, if the two mechanisms occur independent of each other, or if molecular mechanism occurs *via* a path completely different from the path involving semiquinone, they will show different dependencies upon the composition of the solvent, characteristic of each mechanism.

An outline is given on the method to determine the contribution of singlet excited state and T(n-π^*) state to molecular and radical mechanisms. The quantum yields due to radical (Φ_R) and molecular mechanism (Φ_M) can be discriminated in a simple way. Since the half-reduced acridine is oxidized back entirely to acridine in the aerated solution, the quantum yield experimentally obtained in the aerated solution gives Φ_M, and Φ_R can be obtained as the difference between the quantum yields in the aerated and deaerated solutions.

The contribution of singlet excited state and triplet state T(n-π^*) (the lowest T(π-π^*) of acridine is unreactive) to two mechanisms, $\Phi_M{}^S$, $\Phi_M{}^T$ ($\Phi_M=\Phi_M{}^S+\Phi_M{}^T$), $\Phi_R{}^S$ and $\Phi_R{}^T$ ($\Phi_R=\Phi_R{}^S+\Phi_R{}^T$) can be obtained from the quenching experiment using biacetyl as a quencher.[1,2] The triplet state of biacetyl being located a little lower than acridine T(n-π^*), the triplet energy transfer occurs from the latter to the former at fairly low concentrations of biacetyl. It was established[1] that the singlet excited state of acridine which is considered to be much shorter-lived than that of T(n-π^*) is also deactivated at higher concentrations of biacetyl. Thus, the quenching experiment with biacetyl in the aerated solution can, in principle, distinguish $\Phi_M{}^S$ from $\Phi_M{}^T$. Similarly $\Phi_M{}^T+\Phi_R{}^T$ and $\Phi_M{}^S+\Phi_R{}^S$ can be separated experimentally for the deaerated solution. Since $\Phi_{tot}=\Phi_M{}^S+\Phi_M{}^T+\Phi_R{}^S+\Phi_R{}^T$, $\Phi_M{}^S+\Phi_M{}^T$, $\Phi_M{}^S$, $\Phi_M{}^T$, $\Phi_M{}^T+\Phi_R{}^T$ and $\Phi_M{}^S+\Phi_R{}^S$ are determined experimentally, $\Phi_M{}^S$, $\Phi_M{}^T$, $\Phi_R{}^S$, and $\Phi_R{}^T$ can be evaluated in general. The procedures are more simplified in many cases.

Experimental

Acridine was purified by recrystallization twice from

1) M. Koizumi, Y. Ikeda, and H. Yamashita, This Bulletin, **41**, 1056 (1968).
2) M. Hoshino, S. Niizuma, and M. Koizumi *ibid.*, **45**, 2988 (1972).
3) V. Zanker and G. Prell, *Ber. Busenges.*, **73**, 791 (1969).

aqueous ethanol. Biacetyl was purified by distillation immediately before use. All the solvents used were purified by standard methods. As a light source of 365 nm, a 100 W high pressure mercury lamp was used with suitable filters. All the measurements were made at 25°C.

Results

Quantum Yields of the Photoreduction of Acridine in Mixtures of 2-Propanol–Benzene and Cyclohexane–Benzene. The quantum yields in the mixed solvents of various composition were measured for aerated and deaerated conditions, the former dealing with molecular mechanism. The quantum yields due to radical mechanism were calculated from the difference of the two. In

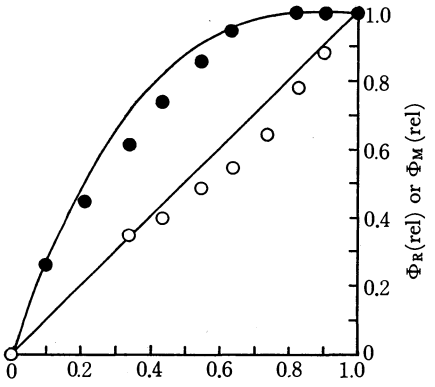

Fig. 1. Plots of Φ_R(rel) (●) and Φ_M(rel) (○) against the mole fraction of 2-propanol. A curve and a straight line are the calculated ones from the following equation by putting $n=3$ and 1 respectively.

$$\Phi_{rel}=1-(1-X)^n$$

Fig. 1, the relative values of Φ_M and Φ_R for a mixture of benzene and 2-propanol are plotted against the mole fraction. Only singlet excited state participates in the reaction and we have $\Phi_M=\Phi_M{}^S$ and $\Phi_R=\Phi_R{}^S$. It is seen that the former is approximately linear or a little concave upward and the latter convex upward. Figure 2 shows the results obtained for a mixture of benzene

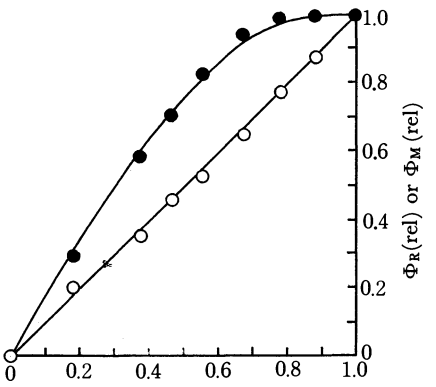

Fig. 2. Plots of Φ_R(rel) (●) and Φ_M(rel) (○) against the mole fraction of cyclohexane. A curve and a straight line are the calculated ones from the following equation by putting $n=3$ and 1 respectively.

$$\Phi_{rel}=1-(1-X)^n$$

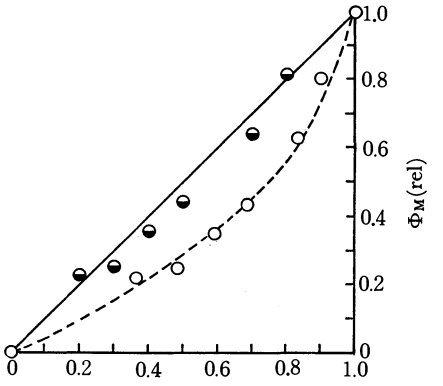

Fig. 3. Plots of Φ_M(rel) against the volume fraction of methanol (◒) and against the mole fraction of methanol (○).

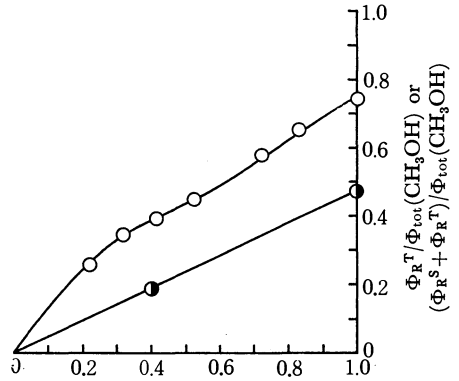

Fig. 4. Plots of $\Phi_R{}^T$ (◑) and $\Phi_R{}^S+\Phi_R{}^T$ (○) both divided by $\Phi_{tot}(CH_3OH)$, against the volume fraction of methanol.

and cyclohexane. The curves for Φ_M(rel) and Φ_R(rel) are very similar to the corresponding ones in Fig. 1. In this case we have $\Phi_M=\Phi_M{}^T$ and $\Phi_R=\Phi_R{}^S$. It is interesting that the characteristic feature of Φ_M(rel) is independent of the reactive state.

Quantum Yields of the Photoreduction of Acridine in a Mixture of Benzene and Methanol. The results are shown in Figs. 3 and 4. The plot for molecular mechanism resembles those of the above two systems though the degree of curvature is somewhat larger, but the plot for radical mechanism is quite different. The shape of the plot $(\Phi_R{}^T+\Phi_R{}^S)/\Phi_{tot}(CH_3OH)$ ($\Phi_{tot}(CH_3OH)$ is the value for pure methanol) suggests the superposition of the two components, one resembling the Φ_R plot of the previous systems (convex upward) and the other approximately a straight line.

Anticipating that this is due to the fact that T(n-π^*) in addition to singlet excited state contributes to radical mechanism, we have attempted to discriminate the two contributions $\Phi_R{}^T$ and $\Phi_R{}^S$. This has been done by examining the effect of the addition of biacetyl on the quantum yields of the photoreduction in the mixed solvent of composition, methanol: benzene=4:6, at which a component convex upward appears to approach a limiting value. In Fig. 5 the inverse of the relative quantum yield (in reference to the Φ-value in the absence of biacetyl) is plotted for the aerated and

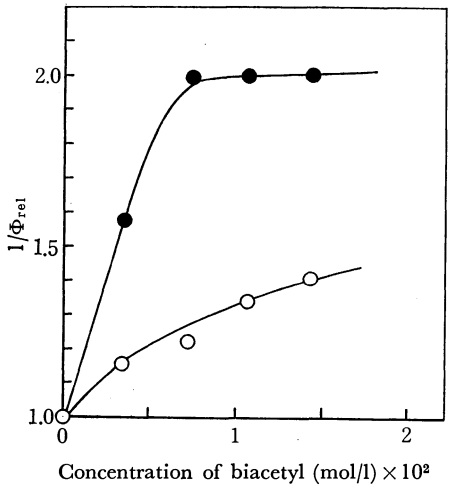

Fig. 5. Plots of $1/\Phi_{rel}$ for the degassed solution (●) and aerated solution (○) against the concentration of biacetyl. Solvent; methanol: benzene=4: 6 (in volume).

deaerated solutions, against biacetyl concentrations. The plot for the aerated solution deals with molecular mechanism to which singlet excited state mainly contributes. It is natural that the curve still increases at about 10^{-2}M. The plot for the deaerated solution apparently consists of two parts, one with a steep slope in the lower concentration region of biacetyl and the other with a very gradual slope in the higher concentration region. It is appropriate to relate the former to T(n-π^*) and the latter to the singlet excited state. We can estimate from the plot for the deaerated solution the value of Φ_R^T for the mixed solvent at methanol: benzene=4: 6, which was found to be 0.025_6. The value of Φ_R^T in pure methanol is 0.057—0.063.[1,2] The values of $\Phi_R^T/\Phi_{tot}(CH_3OH)$ are obtained by dividing the above two values by Φ_{tot} for pure methanol, 0.128.

It is seen that the contribution of T(n-π^*) to radical mechanism is approximately linear with respect to the volume fraction of methanol. Substracting this portion from the $(\Phi_R^R+\Phi_R^T)/\Phi_{tot}(CH_3OH)$, we obtain the Φ_R^S-values. The plots Φ_R^S(rel) *vs.* mole fraction and volume fraction are given in Fig. 6. The curves are convex upward and the limiting value is reached at a mole fraction of methanol of about 0.8.

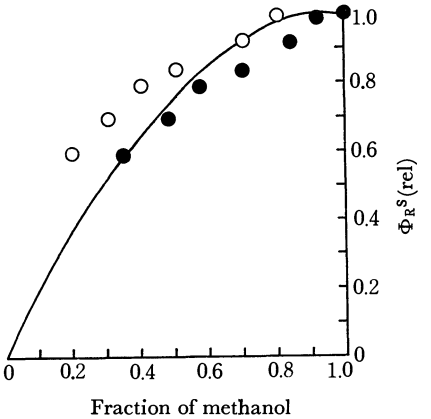

Fig. 6. Plots of Φ_R^S(rel) against the mole fraction (●) and against the volume fraction (○). The curve is a calculated one from the following equation by putting n=2.
$\Phi_{rel}=1-(1-X)^n$

Discussion

From the present results we can say that the Φ_R(rel) *vs.* X plot and the Φ_M(rel) *vs.* X plot are not related with each other at all and that the two plots show their own characteristic dependency on the mole fraction. Therefore a cage model involving two radicals can not be adopted. Since the concentration of H-donor is high enough under the present conditions (from X= 0.1 to pure solvent), the behavior of semiquinone will not be affected by the composition of the solvent in view of a long lifetime of semiquinone (>msec).[4] Accordingly the present results deal mainly with the characteristics of the primary processes for molecular and radical mechanisms, which essentially depend on the nature of H-donor.

A plausible model for molecular mechanism is either (1) a one act process involving two reactive sites (N and 9-C of acridine) or (2) a consecutive reaction with a very short-lived intermediate (first, N-atom and secondly 9-C atom react).

For the latter, it is likely that the step of intermediate formation is common to radical mechanism as written schematically below,

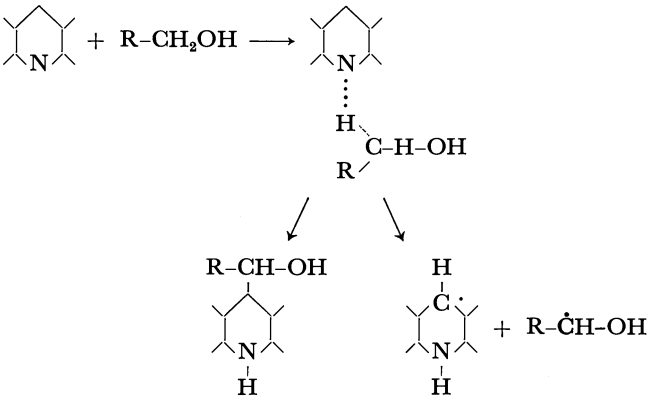

It is thus expected that M- and R-mechanisms are related to each other in a certain way. If the first step is essential in determining the feature of reaction, the solvent dependence should be common to both mechanisms, whereas if the second step is the key-process, a similar deduction to that for the cage model should hold. Both expectations contradict the experimental results and it is thus most likely that the M- and R-mechanisms occur *via* different paths from the start.

In order to discuss the solvent dependence of Φ_M and Φ_R quantitatively, we should know the lifetime of the excited state. However, acridine is nonfluorescent in nonpolar solvents and the lifetime of the singlet excited state cannot be measured. Still less knwon is the solvent dependence of the lifetime.

We have found that the feature in the solvent dependence of M- and R-mechanisms is not related to the existence of OH group in a H-donor molecule which

4) A. Kira, S. Kato, and M. Koizumi, This Bulletin, **39**, 1221 (1966).

is attached to N of acridine *via* H-bonding. This seems reasonable for M-mechanism for which two site reaction occurs as one step but not so for radical mechanism, since the existence of specific interaction in the form of H-bonding is suspected to favor the reaction in which N of acridine is attacked by H-atom. One is tempted to consider that the upward convex shape of the Φ_R *vs.* X plot is due to this specific interaction which suppresses the dilution effect of benzene. However, this view does not hold because a similar dependence of Φ_R on X has been obtained in the case of cyclohexane for which no such interaction exists. It is therefore inferred that the relative positions of acridine and H-donor together with their configurations necessary for R-mechanism to occur are taken newly after acridine is excited and irrespective of the ground state configuration. This is reasonable because a hydrogen atom to be detached from alcohol is a α-H atom and not one of the OH group. Thus it is considered that for the reaction to occur, a molecule of H-donor must occupy a specific site, orientation and configuration relative to N of acridine. When such an effective encounter is realized, the reaction will occur with certain probability. Assuming the constant lifetime of the excited state, the rate can be determined by the number of occurrences of such an encounter.

If such a view is adopted, the Φ_R *vs.* X relation will be treated approximately by a site-jumping model. Neglecting energy factor and assuming that the probability for H-donor to occupy this effective configuration is merely proportional to mole fraction, the relative quantum yield for radical mechanism can be given by

$$\Phi_{rel} = 1 - (1-X)^n$$

where X is a mole fraction and n is the number of effective encounters (number of jumping) during the excitation.

This model is too crude to treat the present results quantitatively, but it seems suitable as one step in a mathematical approach to the problem. If one applies the formula to the present results, the values of n for radical mechanism are evaluated as follows. The numbers in parentheses are the values of n when volume fractions are used instead of mole fractions.

2-propanol	$n = 3$ (3)
cyclohexane	$n = 2$ (2)
methanol	$n = 2$ (3)

The results appear to be reasonable.

If the same model is applied to molecular mechanism the value of n becomes 1 or less than 1. However, the concave upward curve may partially be due to the excess inhibiting action of benzene. For instance, a larger size of benzene molecule than of methanol will reduce the occurrence of effective encounter.

The results obtained strongly suggest that M- and R-mechanisms are two independent reactions occurring *via* different paths from the start. However, the reasons for the following behaviors still remain unclarified.

1) T(n-π^*) participates in the case of methanol but not isopropanol.

2) Only R-mechanism occurs in S* in the case of cyclohexane while both R- and M-mechanisms occur in S* in the case of methanol.

3) Only M-mechanism occurs in T(n-π^*) in the case of cyclohexane, while R-mechanisms mainly occurs in T(n-π^*) in the case of methanol.

4) Linear relation holds between Φ_R^T and the volume fraction for methanol in contrast to the convex upward curve of Φ_R^{S*} *vs.* volume fraction in general.

Interaction between Excited β-Naphthol and Pyridine. Hydrogen-bond Formation in S* and H-Transfer Reaction in T

Koichi KIKUCHI, Hitoshi WATARAI, and Masao KOIZUMI

Department of Chemistry, Faculty of Science, Tohoku University, Aoba, Aramaki, Sendai

(Received July 10, 1972)

The interaction between the excited β-naphthol and pyridine in cyclohexane has been investigated by an absorption-emission flash technique. The triplet naphthol has been found to be deactivated by pyridine with the rate constant of $1.5—1.9\times10^{9}$ $M^{-1}sec^{-1}$, yielding naphthoxyl radical. With 10^{-4} M pyridine the triplet naphthol is completely transformed into naphthoxyl radical. Above 10^{-1} M pyridine naphthol exists almost exclusively as a H-bonded species in the ground state, which is non-fluorescent and produces no transient species detectable by an ordinary flash apparatus. For $10^{-4}—10^{-1}$ M pyridine, the singlet excited naphthol undergoes collisional deactivation which most likely leads to a H-bonded species (rate constant, $1.2—1.4\times10^{10}$ $M^{-1}sec^{-1}$). At the same time naphthoxyl radical is also produced with about the same rate constant as that for the triplet state. The results strongly suggest that the mechanism for the internal conversion of the singlet excited state *via* H-bonding is a transient H-atom transfer.

An interesting feature of fluorescence of a hydrogen-bonded compound is that two π-electronic systems, fluorescer and quencher combined in conjugation *via* a hydrogen bond, such as naphthol–pyridine,[1c,5] carbazole–pyridine[4] and acridine dye–naphthol[1b] have no emissivity in general. This phenomenon was extensively studied in particular by Mataga and his coworkers,[1-4] and was attributed to the delocalization of π-electrons *via* H-bond, which may naturally involve charge transfer interaction as is expected from the mechanism proposed for hydrogen-bonding.[6] This was exemplified by one of the present authors (M.K.);[5] quinoline acting as an acceptor in C–T interaction quenches the fluorescence of β-naphthylmethylether (donor) in *n*-hexane although the quenching constant is about half that for β-naphthol which forms hydrogen bond with quinoline.

In the case of carbazole–pyridine in methylcyclohexane–isopentane at 77 K, Mataga *et al.* demonstrated that H-bonding significantly enhances internal conversion but not the intersystem crossing.[4] However, it is still unknown whether this conclusion generally holds or not.

On the other hand, Rehm and Weller[7] proposed on theoretical grounds that the mechanism of fluorescence quenching for naphthol–pyridine, benz(*c*)acridine–phenol is due to the transient hydrogen transfer. Thus it is desirable to study the effect of H-bonding on the two nonradiative processes in a more direct way at room temperature, and to study whether hydrogen transfer actually occurs and if so to study the correlation between H-bonding and H-transfer. In order to tackle these problems we have applied the absorption-emission flash technique[8] to the naphthol–pyridine system, measuring the triplet yield and the time-integrated fluorescence intensity of naphthol with one sample.

Experimental

Materials. β-Naphthol (G.R. grade, Wako Junyaku) was recrystallized twice from a mixed solvent of water and ethanol, and then sublimed twice *in vacuo*. β-Naphthylethylether synthesized by a standard method was recrystallized five times from ethanol and sublimed *in vacuo*. Cyclohexane and pyridine were purified by the standard method. Triethylamine (G.R. grade, Wako Junyaku) was used without further purification.

Apparatus and Procedure. Absorption spectra were measured with a Hitachi EPS-3T spectrophotometer. The fluorescence intensity was measured with a specially constructed fluorometer. The flash apparatus was modified so that two or three phenomena could be observed simultaneously. The energy of a flash was usually about 130 Joule and its half duration was about 10 μsec. A Hoya-U2 filter was used for excitation. All the measurements were made in cyclohexane solutions at room temperature; the solutions were degassed by pump and thaw method unless otherwise stated. The peak heights in the fluorescence spectra were used as a measure of fluorescence intensity since fluorescence spectra of β-naphthol were not affected by the addition of pyridine. The methods of measuring transient absorption spectra and the time-integrated fluorescence intensities during flashing were essentially the same as reported.[8]

Outline of Method. In principle, the absorption-emission flash technique is expected to be applicable for studying quantitatively the responsibility of internal conversion and intersystem crossing to the nonradiative process.

The triplet yield $[T]_0$ is related with the total quantity of light absorbed during one flash by

$$[T]_0 = \tilde{\phi}_{ST}\int I_{ab}dt \qquad (1)$$

and the time integrated fluorescence intensity (measured at λ') during a flash is given by

$$\int I_f(\lambda')dt = \alpha(\lambda')\tilde{\phi}_f\int I_{ab}dt \qquad (2)$$

where $\tilde{\phi}_f$ and $\tilde{\phi}_{ST}$ are the eventual fluorescence quantum

1) a) N. Mataga, Y. Kaifu, and M. Koizumi, *Nature*, **175**, 731 (1955), This Bulletin, **29**, 115 (1956); b) N. Mataga and S. Tsuno, *ibid.*, **30**, 368, 711 (1957); c) N. Mataga, *ibid.*, **31**, 481 (1958).

2) N. Mataga, Y. Torihashi, and Y. Kaifu, *Z. Physik. Chem. N.F.*, **34**, 379 (1962).

3) N. Mataga and K. Ezumi, This Bulletin, **40**, 1350 (1967).

4) N. Mataga, F. Tanaka, and M. Kato, *Acta. Phys. Polon.*, **34**, 733 (1968).

5) T. Miwa and M. Koizumi, This Bulletin, **36**, 1619 (1963).

6) S. Nagakura and M. Gouterman, *J. Chem. Phys.*, **26**, 881 (1957). H. Baba and S. Suzuki, *ibid.*, **35**, 1118 (1961).

7) D. Rehm and A. Weller, *Israel J. Chem.*, **8**, 259 (1970).

8) K. Kikuchi, H. Kokubun, and M. Koizumi, This Bulletin, **41**, 1545 (1968).

yield and intersystem crossing probability, respectively and $\alpha(\lambda')$ is a constant depending upon the setup of the apparatus and experimental conditions. It should be noted that $\tilde{\phi}_f$ and $\tilde{\phi}_{ST}$ are not constant but depend upon the composition of the solution. From (1) and (2) we have

$$[T]_0/\int I_f(\lambda')dt = \tilde{\phi}_{ST}/\alpha(\lambda')\tilde{\phi}_f \quad (3)$$

For the present system, the emitter of fluorescence is only the free naphthol molecule as verified experimentally. Thus, putting a fraction of light absorbed by free naphthol as δ and using the genuine ϕ_f, Eq. (2) can be rewritten as follows, where A is pyridine acting as a proton acceptor and k_q is the overall quenching constant.

$$\begin{aligned} &\int I_f(\lambda')dt = \alpha(\lambda')\delta\phi_f\int I_{ab}dt \\ &\phi_f = k_f/\{(k_d+k_f)+k_q[A]\} \\ &k_d = k_i + k_c \end{aligned} \quad (4)$$

(i, internal conversion; c, intersystem crossing)

The intersystem crossing is in general involved in the collisional quenching for free species, occurring also for the H-bonded species. Thus Eq. (1) is most generally rewritten as follows.

$$[T]_0 = \delta\int I_{ab}dt \times (k_{ST}+k_q^c[A])/(k_d+k_f+k_q[A]) + (1-\delta)\frac{k_c'}{k_i'+k_c'}\int I_{ab}dt \quad (5)$$

where k_q^c is the rate constant for the collision induced intersystem crossing, $k_c=k_{ST}$ and $'$ stands for hydrogen-bonded species. Hence

$$\frac{[T]_0}{\int I_f(\lambda')dt} = \frac{k_{ST}+k_q^c[A]}{k_f\alpha(\lambda')} + \frac{(1-\delta)}{\delta}\frac{k_c'}{\alpha(\lambda')k_f}\gamma \quad (6)$$

or

$$\tilde{\phi}_{ST}/\tilde{\phi}_f = (k_{ST}+k_q^c[A])/k_f + (1-\delta)k_c'\gamma/\delta k_f \quad (7)$$

where

$$\gamma = (k_d+k_f+k_q[A])/(k_i'+k_c')$$

On the basis of the above equation, we may obtain information on the rate constants k_q^c, k_i', and k_c', if we know some fundamental constants for the solution of β-naphthol including ϕ_{ST} and if we measure $[T]_0$ and $\int I_f(\lambda')\,dt$ at various pyridine concentrations.

Results and Discussion

First the ground state hydrogen bonding equilibrium of naphthol-pyridine in cyclohexane was investigated. The spectroscopic procedures and the method of evaluating the equilibrium constant K from them are similar to those in *n*-hexane.[5]

The value of K at 16°C was evaluated as $140M^{-1}$. This is compared with $K=125$, 61 in *n*-hexane at 21 and at 42°C respectively.[5]

Quenching of Fluorescence by Pyridine. The fluorescence behavior of β-naphthol influenced by the addition of pyridine in cyclohexane is also similar to that in *n*-hexane.[5] Thus the significant quenching occurs without any spectral change. Therefore, the same method of analysis can be applied if we assume the non-emissivity of hydrogen-bonded species. The equation[5]

$$\frac{F_0/F-1}{[A]} = \left(k_q\tau_0+\frac{\varepsilon'}{\varepsilon}K\right) + k_q\tau_0\frac{\varepsilon'}{\varepsilon}K[A] \quad (8)$$

can easily be derived from the scheme below. (In practice, the exciting wavelength was chosen so that $\varepsilon(\lambda)$ is equal to $\varepsilon'(\lambda)$. ε and ε' are the molar extinction coefficients of free naphthol and H-bonded species respectively.)

(I)
- i) $D + A \rightleftharpoons DA$ K (equilibrium constant)
- ii) $DA \xrightarrow{h\nu} DA^*$
- iii) $DA^* \longrightarrow DA$ $(k_i'+k_c')$
- iv) $D \xrightarrow{h\nu} D^*$
- v) $D^* \longrightarrow D + h\nu'$
- vi) $D^* \longrightarrow D$ $k_d = k_i + k_c$
- vii) $D^* + A \longrightarrow D + A$ k_q

Thus the collisional quenching vii) is superposed on the static quenching i) and iii). In a previous paper,[5] it was assumed simply that process vii) consists of the formation of hydrogen bond in the excited state followed by a rapid degradation of electronic energy.

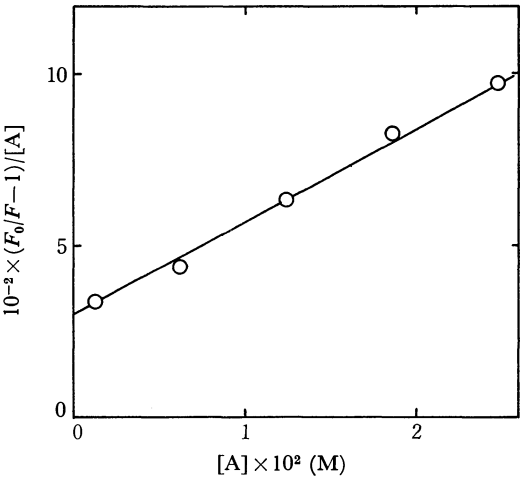

Fig. 1. The plot of $(F_0/F-1)/[A]$ *vs.* [A].

Figure 1 shows the plot of $(F_0/F-1)/[A]$ against [A]. By using $K=140M^{-1}$, we evaluate the value of $k_q\tau_0$ as $160—190M^{-1}$. This is compared with the previous $k_q\tau_0$-value of 120 (21°C) in *n*-hexane. Putting $\tau_0=13.3$ nsec,[9] we obtain $k_q=1.2—1.4\times10^{10}M^{-1}\,sec^{-1}$. Thus the collisional quenching occurs with the diffusion controlled rate constant.

Reaction between Triplet Naphthol and Pyridine. We first investigated the interaction between triplet naphthol and pyridine at low pyridine concentrations. Below $10^{-4}M$ of pyridine, the formation of H-bonded species in the ground state and the dynamic quenching of the singlet excited naphthol can be neglected as judged from the values of K, τ_0, and k_q obtained above.

Figure 2 gives a transient absorption spectrum obtained when the deaerated sloution of β-naphthol in cyclohexane is flashed; it does not appear in the aerated solution. This spectrum is attributed to the triplet-triplet absorption because of its close resemblance to the

9) J. B. Barlman, "Handbook of Fluorescence Spectra of Aromatic Molecules," Academic Press, New York, N.Y. (1965), p. 114.

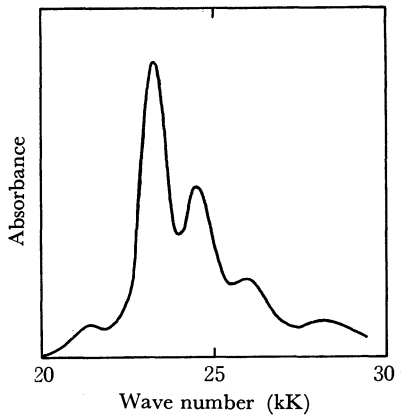

Fig. 2. T–T absorption spectrum of β-naphthol.

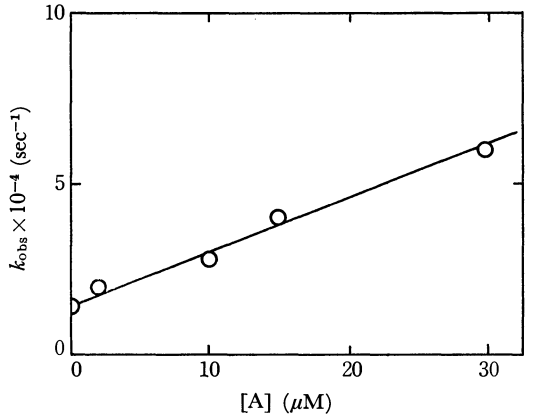

Fig. 3. The relation between the observed first order decay constant of β-naphthol triplet and pyridine concentration.

spectrum in literature.[10,11] For the sake of confirmation, T–T energy-transfer was ascertained to occur from β-naphthol to perylene. The decay was of first order with the rate constant 1.5×10^4 sec^{-1}.

The decay rate of triplet β-naphthol increased with increasing pyridine concentration. As shown in Fig. 3, the observed rate constant is satisfactorily linear with respect to [A].

$$k_{obs} = k_{dt} + k_{qt}[A]$$

where subscript t stands for triplet. From the intercept and inclination of the plot, we obtain

$$k_{qt} = 1.5\times10^9\ M^{-1}\ sec^{-1} \qquad k_{dt} = 1.5\times10^4\ sec^{-1}$$

For pyridine concentrations higher than 10^{-4}M, quite a different spectrum as shown in Fig. 4 completely replaces the T–T absorption spectrum. The spectrum decays as a second order process with the rate constant k/ε—1.9×10^6 cm sec^{-1} (at 470 nm). The yield measured at the end of flashing increases with increasing pyridine concentrations up to 10^{-4}M. Since in this concentration region of pyridine, neither the formation of H-bond species in the ground state nor the collisional quenching of singlet excited naphthol by pyridine scarcely occurs, there is no doubt that this species (R)

10) G. Jackson and G. Porter, *Proc. Roy. Soc. Ser. A.*, **260** 13 (1961).

11) E. J. Land, G. Porter, and E. Strachan, *Trans. Faraday Soc.*, **57**, 1885 (1961).

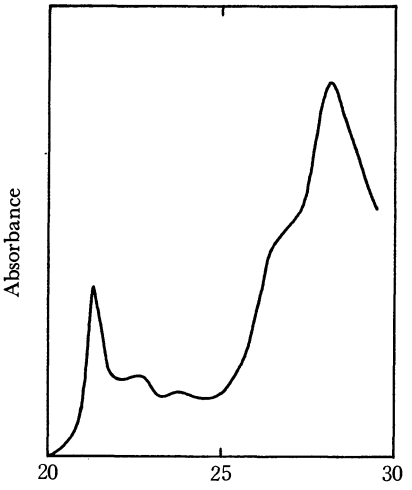

Fig. 4. The absorption spectrum of β-naphthoxyl radical.

is produced by the reaction between triplet naphthol and pyridine. In fact it was confirmed that at 10^{-4}M of pyridine, the decay of triplet is accompanied by the build-up of R. Assuming the scheme

$$\text{(II)}\quad \begin{cases} \left.\begin{array}{ll} \text{v)} & D \xrightarrow{h\nu} D^* \\ \text{viii)} & D^* \longrightarrow D^T \end{array}\right\} \phi_{ST} I_{ab} \\ \text{ix)} \quad D^T \xrightarrow{k_{dt}} D \\ \left.\begin{array}{ll} \text{x)} & D^T \xrightarrow{A} R \quad (k_{qt}^r) \\ & \searrow^{A} D + A \end{array}\right\} k_{qt} \end{cases}$$

the yield of R at the end of a flash is given as follows ($I_{ab}{}^0=\int I_{ab}dt$. $D_R{}^0$, optical density (at 470 nm) at the end of a flash).

$$[R]_0 = \frac{D_R{}^0}{\varepsilon_R d} = I_{ab}^0 \times \phi_{ST}\left(\frac{k_{qt}^r[A]}{k_{qt}[A]+k_{dt}}\right) \tag{9}$$

Hence

$$\frac{1}{D_R{}^0} = \frac{1}{\varepsilon_R d \phi_{ST} I_{ab}^0}\left(\frac{k_{qt}}{k_{qt}^r} + \frac{k_{dt}}{k_{qt}^r[A]}\right) \tag{10}$$

Figure 5 gives the $1/D_R{}^0$ *vs.* $1/[A]$ plot from which we obtain $k_{dt}/k_{qt}=7.9\times10^{-6}$ M. Inserting the value of $k_{dt}=1.5\times10^4$ sec^{-1}, we get $k_{qt}=1.9\times10^9$ M^{-1} sec^{-1} which agrees with the value of k_{qt} obtained from the effect of pyridine concentration on the triplet decay.

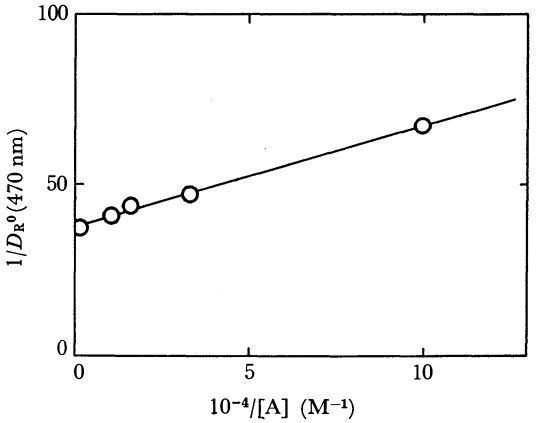

Fig. 5. The plot of $1/D_R{}^0$ *vs.* $1/[A]$.

It might be concluded that the interaction between triplet naphthol and pyridine mainly leads to the formation of R. R was identified to be a neutral naphthoxyl radical for the following reasons. Porter and Jackson reported the formation of this species upon flashing the solution of naphthol in liquid paraffin.[10] The peak position they observed was 465 nm which agrees with the present result. Further it was found that a similar reaction occurs between triplet acridine[12] and β-naphthol in cyclohexane and benzene. In this case the transient spectra are the superposition of that of acridine C-radical and that of β-naphthoxyl radical. Figure 6 shows the plot of the observed decay rate of acridine triplet state against naphthol concentration from which we obtain $k_q=2.9\times10^9M^{-1}sec^{-1}$. An analogous reaction is known to occur between phenol and eosin yielding phenoxy radical and semiquinone of dye.[13]

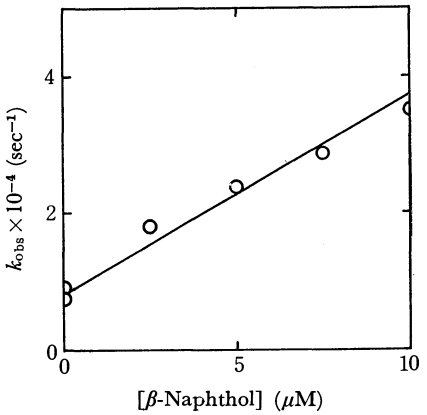

Fig. 6. The relation between the observed first order decay constant of acridine triplet and β-naphthol concentration.

Hence the reaction giving rise to this intermediate may be written as follows,[14]

xi) 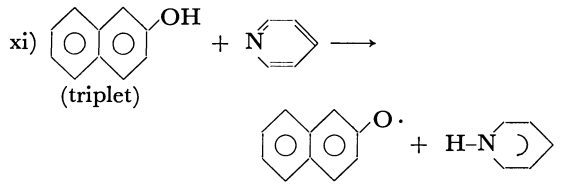

It is interesting that the same reaction occurs even in the aerated solution although the yield of the intermediate is less on account of the quenching action of oxygen upon triplet naphthol. The effect of oxygen concentration on the yield of naphthoxyl radical can be treated by adding the following reaction to shceme (II).

$$\text{xii)}\quad D^T + O_2 \xrightarrow{k_q'} D + O_2$$

However, since the concentration of pyridine is moderately high, we should use Eq. (6) instead of (9),

12) It is interesting that the lowest T(π-π^*) of acridine is involved in this photoreduction.

13) L. I. Grossweiner and E. F. Zwicker, *J. Chem. Phys.*, **34**, 1411 (1961).

14) It should be noted that another peak observed in the near ultraviolet region is also attributed to the same radical, since its decay feature is quite the same as that of the 470 nm peak both in deaerated and aerated solutions.

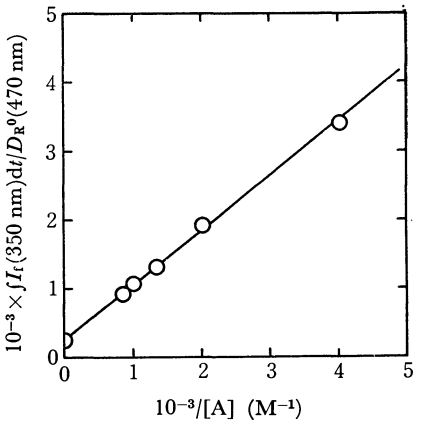

Fig. 7. The plot of $\int I_f(\lambda')dt/D_R^0$ *vs.* 1/[A].

$[T]_0$ being replaced by $[R]_0$. Under the present conditions, the second term and $k_q^c[A]$ on the right hand side of (6) are neglected for the reason described later. Since the condition $k_{dt}\ll k_q^r[A]$ is satisfied, Eq. (10) can be modified as follows.

$$\frac{\int I_f(\lambda')dt}{D_R^0}=\frac{\alpha(\lambda')k_f}{\varepsilon_R dk_{ST}}\left(\frac{k_{qt}}{k_{qt}^r}+\frac{k_q'[O_2]}{k_{qt}^r[A]}\right) \qquad (11)$$

Figure 7 gives the plot of $\int I_f(\lambda')dt/D_R^0$ against 1/[A]. The datum for 1/[A]=0 was taken from the result in the deaerated solution and is exactly on the line drawn through other experimental data for the aerated solution. From the slope and intercept we obtain

$$k_q'[O_2]/k_{qt}=3.3\times10^{-3}M$$

Inserting the value of $k_{qt}=(1.5\text{—}1.9)\times10^9M^{-1}sec^{-1}$ and $[O_2]=2.4\times10^{-3}M$ (from the soubility of oxygen in cyclohexane), we evaluated k'_q to be $2.6\times10^9M^{-1}sec^{-1}$. This is a reasonable value which supports scheme (II).

Table 1. The effect of addition of TEA on the decay rate of triplet naphthol

$[TEA]_M$	$k_{dt}(sec^{-1})$	D_T(432 nm)
0	1.5×10^4	0.212
3×10^{-5}	2.2×10^4	0.189
3×10^{-4}	2.2×10^4	0.189
2×10^{-2}	2.6×10^4	0.072

In contrast to pyridine, triethylamine (TEA) which cannot act as a hydrogen atom acceptor scarcely affects the decay of triplet naphthol below $3\times10^{-4}M$ as shown in Table 1. At $2\times10^{-2}M$ of TEA, the yield of triplet naphthol decreases to some extent. This might be due to the increase in the rate of internal conversion of H-bonded species as in carbazole-TEA.[4] For naphthylmethylether which is incapable of hydrogen bonding with pyridine, the decay rate of triplet state is scarcely affected by the addition of pyridine. To sum up, scheme (II) holds only for the system consisting of H-atom donor and acceptor.

Quenching Action of Pyridine on the Singlet Excited State of Naphthol. Since it has been established that triplet naphthol is converted into neutral radical at pyridine concentrations $\gtrsim10^{-4}M$, D_R^0 should be used instead of D_T^0 in order to investigate the quenching action of pyridine on the fluorescence of naphthol. $\int I_f(350)$

Table 2. Time integrated fluorescence intensity of naphthol and the yield of naphthoxyl radical

$[A]_0$, M	$\int I_f(350)dt$	$D_R^0(470)$	$\frac{D_R^0(470)}{\int I_f(350)dt}$
2.48×10^{-4}	1.97	0.051_3	0.026_2
2.48×10^{-3}	0.94_5	0.031_8	0.033_6
6.20×10^{-3}	0.48_5	0.018_7	0.038_6
1.24×10^{-2}	0.20_0	0.008_7	0.043_5
1.86×10^{-2}	0.08_5	0.004_8	0.056_5
2.48×10^{-2}	0.05_7	0.003_4	0.059_6
above 1×10^{-1}	0	0	

dt and D_R^0 (470 nm) were measured at various pyridine concentrations. The results are given in Table 2. It is seen that for $[A]_0 \gtrsim 10^{-1}$M, both $\int I_f(350)\,dt$ and $D_R^0(470)$ become zero. Since more than 90% of naphthol exists as hydrogen-bonded species, the remaining free naphhthol being almost completely quenched by pyridine in this concentration region of pyridine, it could be concluded that β-naphthol hydrogen bonded with pyridine scarcely undergoes intersystem crossing nor the reaction yielding naphthoxyl radical. Therefore the second term on the right hand side of Eqs. (6) and (5) can be neglected. However, there is a possibility of the formation of radical taking part in the collisional quenching of fluorescence, which may be discerned in the region of somewhat smaller pyridine concentrations. For this purpose, an analysis of the data in Table 2 was made by dividing process vii) in scheme (I) into three processes as follows.

$$\text{xv)}\quad D^* + A \xrightarrow{k_q^r} R$$

$$\text{xvi)}\quad D^* + A \xrightarrow{k_q^h} (D\cdots A)^* \text{ (H-bonded species)}$$

$$\text{xvii)}\quad D^* + A \xrightarrow{k_q^c} D^T + A$$

In other words, k_q in scheme (I) was assumed to be composed of three terms, $k_q = k_q^c + k_q^r + k_q^h$. However, since triplet naphthol if formed is quickly converted in to R under the present conditions, k_q^r and k_q^c cannot be discriminated experimentally. Therefore representing $(k_q^c + k_q^r)$ by k_q^r and replacing $[T]_0$ by $[R]_0$, we get from (6)

$$\frac{D_R^0(\lambda)}{\int I_f(\lambda')dt} = \frac{\varepsilon_R(\lambda)d}{\alpha(\lambda')k_f}(k_{ST} + k_q^r[A]) \qquad (12)$$

It is assumed that the triplet naphthol is converted into R completely.

The left hand side of Eq. (12) is plotted against pyridine concentration in Fig. 8. We see that the radical formation reaction takes part in the quenching process. From the plot we obtain $k_q^r/k_{ST} = 5.6\times 10\text{M}^{-1}$. Using the value of (τ_0) of the singlet excited naphthol, we obtain $(\tau_0)^{-1} = k_f + k_d + k_{ST} = 7.5_2\times10^7$ sec^{-1}, our preliminary result for ϕ_{ST} being 0.5—0.7. Therefore k_{ST} is 3.8—5.3×10^7, and k_q^r is evaluated as 2.1—3.0×10^9 $\text{M}^{-1}\,\text{sec}^{-1}$. Thus it is concluded that the formation of naphthoxyl radical occurs through the collisional interaction between singlet excited naphthol and pyridine, its rate constant being about the same as that in the triplet state. It is noteworthy that the value is significantly smaller than that of k_q, 1.2—$1.4\times10^{10}\text{M}^{-1}\text{sec}^{-1}$, which was evaluated from the quenching of naphthol fluorescence by pyridine.

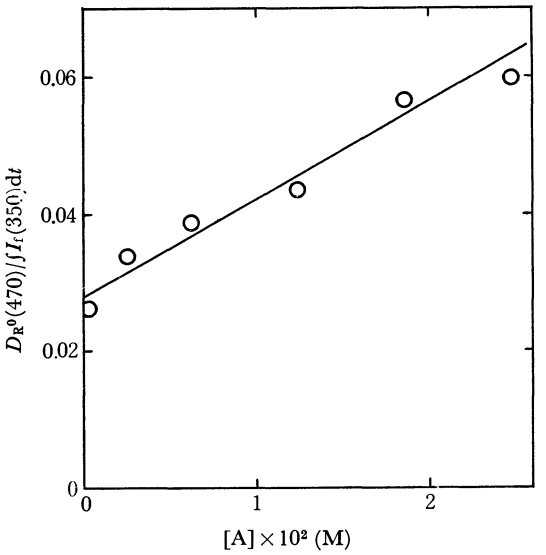

Fig. 8. The plot of $D_R^0(\lambda)/\int I_f(\lambda')dt$ *vs.* [A].

Critical Consideration

The rate constants of various elementary reactions pertaining to the singlet excited and triplet states of naphthol are listed in Table 3. Comments will be given on some of them, in particular k_q^h for excited free naphthol. k_i' and k_c' for the hydrogen-bond species were estimated as follows; k_i' from k_f[15] of free species multiplied by 10^3 on the basis of non-occurrence of fluorescence and intersystem crossing, and k_c' from the non-appearance of naphthoxyl radical.

Table 3. Rate constants of elementary reactions pertaining to the excited naphthol molecule in cyclohexane

	Singlet state		Triplet state
	free species	H-bonded species	
k_d	$k_i < 1.7\times10^7\ \text{sec}^{-1}$	$k_i' \gtrsim 2\times10^{10}\ \text{sec}^{-1}$	$k_{dt}\ 1.5\times10^4\ \text{sec}^{-1}$
	$k_c\ 3.8\text{—}5.3\times10^7\ \text{sec}^{-1}$	$k_c' < 10^7\text{—}10^8\ \text{sec}^{-1}$	
	$k_f\ 2.04\times10^7\ \text{sec}^{-1}$	$k_f' \sim 2\times10^7\ \text{sec}^{-1}$	
	$k_h\ 9\text{—}12\times10^9\ \text{M}^{-1}\,\text{sec}^{-1}$		
	$k_q^r\ 2.1\text{—}3.0\times10^9\ \text{M}^{-1}\,\text{sec}^{-1}$		$k_{qt}^r\ 1.5\text{—}1.9\times10^9$
	$1.2\text{—}1.4\times10^{10}\ \text{M}^{-1}\,\text{sec}^{-1}$		$\text{M}^{-1}\,\text{sec}^{-1}$

The present results demonstrate, that internal conversion is greatly enhanced by the formation of a hydrogen bond in the ground state. This is why the hydrogen-bonded species does not practically undergo intersystem crossing. The conclusion is essentially the same as that made by Mataga *et al.* on the carbazole–pyridine system.[4]

Next will be discussed the nature of k_q^r and k_q^h and the smaller value of k_q^r than that of k_q^h. There is no direct evidence for k_q^h being connected with the forma-

15) The absorption spectrum of the H-species dose not appreciably differ from that of the free species, and thus k_f' is equated to k_f.

tion of a H-bonded species, but this is highly plausible. According to Jackson and Porter,[10] acidity constants of β-naphthol in the ground, singlet excited and triplet states are respectively $pK_G=9.5$, $pK_{S*}=3.1$, and $pK_T=8.1$—8.3 (at 25°C). Since the strength of a hydrogen bond of an acid with a given base increases with the acidity, it is reasonable that hydrogen bond formation occurs much more easily in the singlet excited state[16] than in the ground and triplet states.

As regards k_q^r, it very likely occurs in the singlet excited state, although there is no direct experimental evidence, since if it connected with the reaction in the triplet state produced by the intersystem crossing of the excited H-bonded species, the value of k_q^r should be more than one order less than the observed value, as judged from the values of k_i' and k_c'.

Thus, such a model can be rejected, and we may conclude that the singlet excited and triplet states of naphthol have about equal reactivity toward hydrogen atom transfer, as demonstrated by the same values of k_q^r and k_{qt}. Further we may conclude that the significantly larger quenching constant of pyridine to naphthol fluorescence is mainly due to the formation of a H-bonded species, which does not occur in the triplet state. Perhaps radical formation and hydrogen bonding in the singlet excited state occur as competitive reactions and the latter overwhelms the former.

The above conclusions can be summarized by the scheme

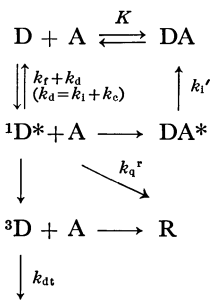

where the reaction between D* and pyridine is mainly the formation of a H-bonded species, whereas that of triplet naphthol is only a radical formation.

Such situations might exist in general, since acidity and basicity for the singlet excited state differ greatly from those for the ground state but not so for the triplet state. As is well-known, acridine in the singlet excited state abstracts a hydrogen atom from alcohol (a poor proton donor), playing a role in the quenching of fluorescence. However, if we use a stronger proton donor such as naphthol or phenol, it might be expected also for acridine that a hydrogen-bond formation participates in the quenching of fluorescence whereas radical formation is dominant in the triplet state.

As regards the mechanism of internal conversion *via* H-bonding, it has been attributed in the past to the delocalization of π electron which usually induces C–T interaction.[1-4] This is true in some systems[5] but in the present case H-atom transfer is more plausible. Since the occurrence of H-transfer has been established both in the singlet excited and triplet states, it seems natural to assume that in the hydrogen-bonded species a transient H-transfer is also occurring *via* charge transfer interaction followed by proton transfer, producing a certain kind of radical pair. The pair, being unstable without doubt, will quickly be reconverted into the initial compound. This is likely to be the cause of internal conversion *via* H-bonding in the present system and similar ones. The results support the theoretical argument of Rehm and Weller[7] who concluded the hydrogen transfer mechanism of quenching for naphtholpyridine, benz(*c*)acridine–phenol *etc.* It is to be noted, however, that the eventual hydrogen transfer occurs not *via* excited hydrogen-bonded species but as a one act bimolecular process which plays only a small role in the quenching action of pyridine on naphthol.

16) When the H-bonded species is fluoroscent as TEA–carbazole, the rate constant for its formation is known to be diffusion controled. (Ref. 4).

The Applicability of the Theory of R. A. Marcus to the Electron-Transfer Reactions between Polycyclic Aromatic Hydrocarbons and Their Anion Radicals

Kosaku SUGA and Shigeru AOYAGUI

Faculty of Engineering, Tokyo Institute of Technology, Ookayama, Meguro-ku, Tokyo

(Received July 13, 1972)

The rates of electron-transfer from the anthracene-anion radical to anthracene, 1,2-benzanthracene, and pyrene are measured by the electron spin resonance method, with a line-broadening procedure, under experimental conditions in which anion radicals are in a state of free ions or of loose ion pairs. The dependence of the observed rate constants on the standard free energy of reaction, the dielectric constant of the solvent, and the temperature are discussed on the basis of the theory of R. A. Marcus. The free energy of nuclear reorganization, as estimated from the $\Delta G°$-dependence of the rate constants, is much smaller than that predicted theoretically. The observed rate constants are almost independent of the dielectric constants of the solvents; consequently, the reorganization free energy of the solvent must be smaller than the theoretical value. The entropy term contributes to the activation energy to almost the same extent in the solvents with different dielectric constants; this is inconsistent with the theoretical prediction and requires a smaller value for the free energy of solvent reorganization than its theoretical value.

A number of rate constants for electron-transfer reactions between polycyclic aromatic hydrocarbons and their anion radicals have been measured by the electron spin resonance (ESR) method since the pioneering work of Ward and Weissman.[1] It has been revealed that these anion radicals form ion pairs with alkali ions and that the formation of such ion pairs affects the electron-transfer rates.[2] According to Hirota,[3] there can be two kinds of ion pairs, the tight ion pairs whose ESR spectra exhibit hyperfine splittings due to alkaki ions, and the loose ion pairs which yield ESR spectra without such hyperfine splittings. The rate constants of about 10^7 and $10^9 M^{-1}sec^{-1}$ were attributed to the tight and the loose ion pairs respectively. On the other hand, there is no difference between the rate constants of loose ion pairs and free ions;[3b] thus, it is not necessary to distinguish the loose ion pairs from free ions in the following discussion. They will be designated "free ions" in this paper for the sake of simplicity.

The electron-transfer reactions of hydrocarbon free anions can be pure electron-transfer reactions without the formation and/or rupture of chemical bonds; they resemble those of metal-complex ions with an outer-sphere mechanism. Thus, the theory of Marcus[4] is expected to be applicable to the former reactions, which have been scarcely discussed on the basis of the molecular theory. A test applying Marcus' theory to these reactions may be an approach to elucidating their microscopic mechanism. Moreover, such a test will serve to improve and refine the theory itself.

In this paper we will examine the applicabliity of the Marcus' theory to the electron-transfer reactions between hydrocarbon molecules and their radical anions when the latter reactants are in a free-ion state. The following aspects should be emphasized at the outset: first, the theoretical equation for the rate constant contains several parameters which can be specified experimentally; the standard free energy of reaction, the dielectric constant of the solvent, the temperature, and the molecular radii of the reactants; thus, the dependence of the rate constant on these parameters must be examined as a whole, not individually. Secondly, it is preferable that the measurements be made with at least two measuring techniques based on different principles. Such a comparative study as this is not only necessary for an examination of the reliability of the measuring technique itself, but it may inform us of the influence on the observed rate constants of the experimental conditions, which may be inevitably different from method to method.

This paper will deal with the $\Delta G°$, D_s, and T parameters.[5] A comparison between the ESR and the pulse-radiolysis methods will be made with regard to D_s. The $\Delta G°$-dependence obtained by the methods of pulse radiolysis, the quenching of the fluorescence, and ESR has already been discussed comparatively elsewhere.[7]

Experimental

Procedures. The electron-transfer rates were determined from the increase in the linewidth of the central hyperfine line in the ESR spectra of anthracene anion radicals after the addition of a known amount of neutral molecules. The rates of cross-electron-transfer reactions were evaluated with the procedure described in the preceding paper.[8] The con-

1) R. L. Ward and S. I. Weissman, *J. Amer. Chem. Soc.*, **79**, 2086 (1957).

2) P. J. Zandstra and S. I. Weissman, *ibid.*, **84**, 4408 (1962).

3) a) N. Hirota, *ibid.*, **90**, 3606 (1968). b) N. Hirota, R. Carraway, and W. Schook, *ibid.*, **90**, 3611 (1968).

4) a) R. A. Marcus, *J. Chem. Phys.*, **24**, 966 (1956). b) R. A. Marcus, *ibid.*, **43**, 679 (1965).

5) Spherical molecular shape of the reactants is assumed in the theory of Marcus,[4] but all the reactants in this investigation are planar. Thus the molecular radii of the reactants, a's, appearing in his theoretical expression for the rate constant cannot be well-defined quantities even when the molecular geometry is given. In fact we could not prove the a-dependence of the rate constant predicted theoretically.[6]

6) K. Suga, S. Ishikawa, and S. Aoyagui, This Bulletin, **46**, 808 (1973).

7) K. Suga, H. Mizota, Y. Kanzaki, and S. Aoyagui, "Current Topics of Kinetic Parameters of Electron-transfer Reactions," ed. by N. Tanaka, Tohoku University, (1972), p. 71; *J. Electroanal. Chem.*, in press.

8) K. Suga and S. Aoyagui, This Bulletin, **45**, 1375 (1972).

centration of the anthracene anion radicals was determined spectroscopically using the value for the extinction coefficient reported by Balk *et al.*[9]

Materials. All the aromatic hydrocarbons as well as the solvents used were commercially obtained. The anthracene (A), 1,2-benzanthracene (B), and pyrene (P) were recrystallized from benzene and ethanol. The solvents were purified to remove all traces of acidic materials, water and oxygene. The tetrahydrofuran (THF) and 1,2-dimethoxyethane (DME) were purified in a way described previously.[8] The *N,N*-dimethylformamide (DMF) was refluxed over calcium hydride, distilled, and then allowed to stand over calcium hydride in a vacuum for about two weeks; it was degassed after the evolution of hydrogen gas had ceased and then distilled into a glass ampoule containing solid sodium anthracenide in order to remove the residual water and oxygen.

Preparation of Radical Solutions. Only the anthracene radical anion was required in this experiment. A DME solution of its sodium salt was prepared by dissolving solid sodium anthracenide into DMF because of the reactivity of this solvent with sodium metals. The sodium anthracenide was prepared by the soidum reduction of anthracene in THF and was then made free from the solvent by distillation. The solutions in the DME–DMF mixed solvent were prepared by mixing the DME solution with DMF.

Measuring Devices. The ESR measurements were carried out on a JEOL Model JES-3BSX spectrometer operated at about 9.5 kMHz, with 100 kHz field modulation. The modulation amplitude was 0.03—0.08 Gauss. The temperature was maintained and controlled with a JEOL Model JES-UCT-2AX variable-temperature adaptor on the ESR cavity. All the measurements were made at 25°C unless otherwise stated.

Results and Discussion

According to the theory of Marcus,[4] the rate constant of the electron-transfer reaction, $R_1^- + R_2 = R_1 + R_2^-$, when the non-coulobmic interaction between reactants and between products can be neglected, is given by the following equation:

$$k = Z \exp(-\Delta G^*/RT), \quad (1)$$

with;

$$\Delta G^* = \lambda/4 + \Delta G^\circ/2 + (\Delta G^\circ)^2/4\lambda, \quad (2)$$

$$\lambda = \lambda_0 + \lambda_i, \quad (3)$$

$$\lambda_0 = e^2(1/2a_1 + 1/2a_2 - 1/r)(1/D_{op} - 1/D_s). \quad (4)$$

In these equations, Z is the bimolecular collission number of the hypothetical uncharged species in solution when they have a unit concentration; ΔG^* and ΔG° are the activation free energy and the standard free energy of the reaction respectively; λ is the free energy needed to reorganize both the solvent molecules and the reactants in forming the activated complex; λ_0 and λ_i are the contributions to λ from the reorganization of the solvent and of the bonds in the reactants respectively; e is the electronic charge; a_1 and a_2 are the radii of the reactants; D_s and D_{op} are the static and optical dielectric constants respectively, and r is the distance between the centers of the reactants in the activated complex.

Equation (1) can be rewritten in the form:

$$k = k_0 \exp(-\Delta G^\circ/2RT) \exp[-(\Delta G^\circ)^2/4RT], \quad (5)$$

with

$$k_0 = Z \exp(-\lambda/4RT), \quad (6)$$

where k_0 is the rate constant of the electron-exchange reaction with $\Delta G^\circ = 0$. In deriving Eq. (5), it is assumed that the values for λ of the cross-electron-transfer reaction and of the electron-exchange reactions, $R_1^- + R_1$ and $R_2^- + R_2$, are the same. The validity of this assumption will be discussed below.

Table 1. Observed rate constants, corrected forward rate constants and corrected backward rate constants for the electron transfer reactions $A^- + A$, $A^- + B$, and $A^- + P$ in DME at 25°C

Reactions	ΔG° (eV)	k_{obs} (M^{-1} sec^{-1})	$\vec{k}_a$ (M^{-1} sec^{-1})	$\overleftarrow{k}_a$ (M^{-1} sec^{-1})
$A^- + A = A + A^-$	0	$(1.8 \pm 0.2) \times 10^9$	2.4×10^9	2.4×10^9
$A^- + B = A + B^-$	0.052	$(5.4 \pm 1.0) \times 10^8$	5.9×10^8	4.5×10^9
$A^- + P = A + P^-$	0.113	$(9.6 \pm 1.5) \times 10^7$	9.7×10^7	7.8×10^9

ΔG°-Dependence of the Electron-transfer Rates. When the ΔG°-dependence of the electron-transfer rates are examined, the reaction rates between different mloecular species must be measured. Measurements were made on the A^-/B and A^-/P couples in the DME solvent. Plots of the increase in the linewidth *vs.* the concentration of added neutral molecules are illustrated in Fig. 1. The linearity of each plot is satisfactory. The rate constants of the cross-electron-transfer reactions calculated from the slopes of the straight lines in Fig. 1 are listed in Table 1, together with the rate constant of electron exchange between A^- and A.

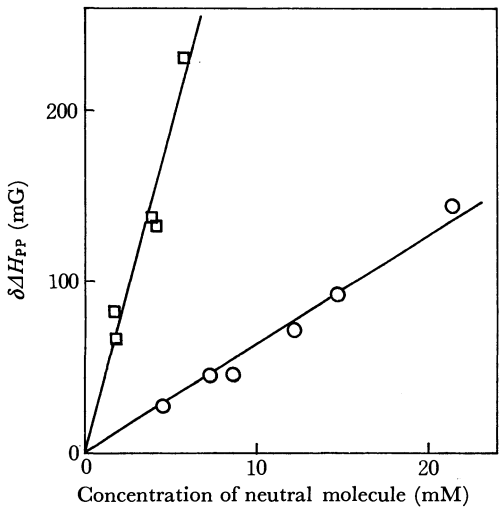

Fig. 1. Linewidth broadening ($\delta\Delta H_{PP}$) *vs.* concentration of neutral molecules in the cross electron transfer reactions in DME: □, $A^- + B = A + B^-$; ○, $A^- + P = A + P^-$.

Equation (2) shows that the rate constants of cross-electron-transfer reactions are dependent only on ΔG° when λ is a constant. According to the theory of Marcus, on the one hand, the λ value of the cross-electron-transfer reaction between A^- and B is approximately equal to the mean value of the λ's for two exchanging couples, A^-/A and B^-/B. On the other

9) P. Balk, G. J. Hoijtink, and J. W. H. Schreurs, *Rec. Trav. Chim.*, **76**, 813 (1957).

hand, the rate constants of the electron-exchange reactions between polycyclic aromatic hydrocarbons and their anion radicals generated by sodium reduction in DME are nearly equal: *e.g.*, $2.0\times10^{9}M^{-1}sec^{-1}$ for P^-/P[6] and $1.8\times10^{9}M^{-1}sec^{-1}$ for A^-/A. Although the electron-exchange rate of P^-/P has never been measured, it is quite probable that its rate constant is almost identical with those for A^-/A and P^-/P. Consequently, it is reasonable to assume that both cross-electron-transfer reactions treated in this paper have an λ value identical with that of the A^-/A couple. The λ value for an exchange reaction is obtainable experimentally with Eq. (6) and the observed k value when Z is given. In the following discussion, Z is taken to be 10^{11} and $10^{10}M^{-1}sec^{-1}$.

The observed k value must be corrected for diffusion. In the case of an activation-diffusion mixed control, the corrected or activation-controlled rate constant, k_a, is given by the equation:

$$1/k_a = 1/k - 1/k_d, \tag{7}$$

where k and k_d are the observed and the diffusion-controlled rate constants respectively. k_d can be estimated with the equation $k_d=4RT/3\eta$.[10] The observed k value for A^-/A, $1.8\times10^{9}M^{-1}sec^{-1}$, is of the same order of k_d, $7.2\times10^{9}M^{-1}sec^{-1}$, in DME at 25°C; this is a rate constant controlled by both the activation and the diffusion processes.

The rate constants for cross-electron-transfer reactions with negative ΔG° values are not obtainable in the present procedure. They are estimated with the ΔG° value of the reaction, the corrected forward rate constant, k_a, and the following equation:

$$\overleftarrow{k}_a = \overrightarrow{k}_a \exp(-\Delta G^\circ/RT) \tag{8}$$

Table 1 compiles the values for $\overleftarrow{k}_a$ and $\overrightarrow{k}_a$ thus obtained.

The λ value for the electron exchange reaction of anthracene, as calculated with the k_a in Table 1, is 8.8 kcal mol^{-1} when Z is assumed to be $10^{11}M^{-1}sec^{-1}$. The rate constants of electron-transfer reactions calculated with this λ value and Eq. (5) are drawn by dotted lines in Fig. 2. An identical plot with $Z=10^{10}M^{-1}sec^{-1}$ and, consequently, with $\lambda=3.4$ kcal mol^{-1} is shown by a dot-dash line. The solid straight line in the same figure shows the relation between k and ΔG° when the third term on the right-hand side of Eq. (2) is neglected; this line embodies the so-called "Linear Free Energy Relationship".[3]

The corrected observed rate constants are plotted with closed circles in Fig. 2. They fit best with the dot-dash line. However, it is rather unlikely that the collision number in solution is $10^{10}M^{-1}sec^{-1}$; according to recent reasoning, this is considered to be two or three times as large as the collision number in the gas phase, which is about $10^{11}M^{-1}sec^{-1}$.

Dependence of the Electron-transfer Rates on the Dielectric Constant of Solvents. The ESR measurements of the electron-transfer rates of aromatic hydrocarbon anion radicals have been made almost exclusively in solvents with low dielectric constants, *e.g.*, in DME

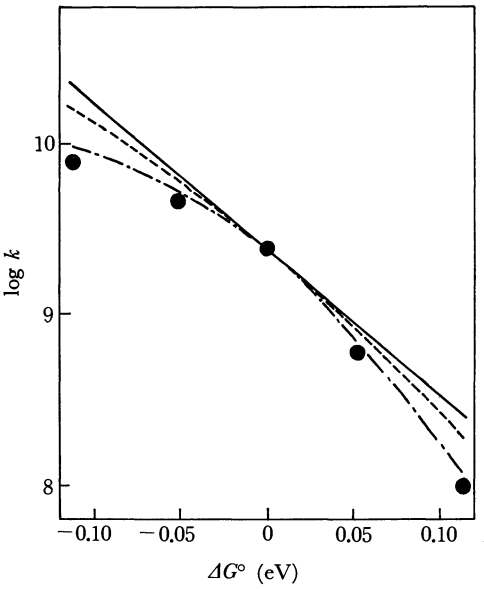

Fig. 2. ΔG°-dependence of electron transfer rates: ●, corrected observed values for rate constants in DME; ——, k *vs.* ΔG° plotted according to Eq. (5), the quadratic term in ΔG° neglected; —— and -·-·-, k *vs.* ΔG° plotted according to Eq. (5) with λ of 8.8 and 3.4 kcal mol^{-1} respectively.

($D_s=7.2$ at 25°C), even when free anion radicals were studied. There is one exception: a measurement in DMF ($D_s=36.7$ at 25°C) with electrolytically-generated radical anions.[11] Because of the large amount of supporting electrolytes indispensably present in the solution, however, it may be meaningless to compare the results with those obtained in solutions which do not contain such electrolytes.

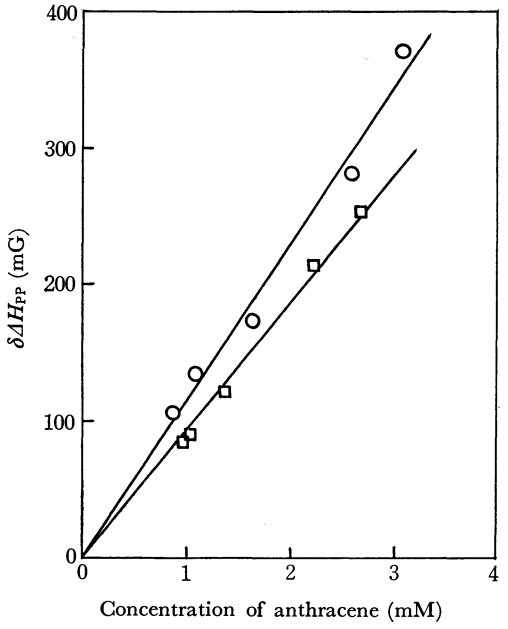

Fig. 3. Linewidth broadening *vs.* concentration of A in the electron exchange reaction between A^- and A: ○, in DME; □, in DMF.

10) M. P. Eastmen, R. G. Kooser, M. R. Das, and J. H. Freed, *J. Chem. Phys.*, **51**, 2690 (1969).

11) P. A. Malachesky, T. A. Miller, T. Layloff, and R. N. Adams, "Exchange Reactions," Proceeding of International Symposium on Exchange Reactions held at Upton, 1966, p. 157.

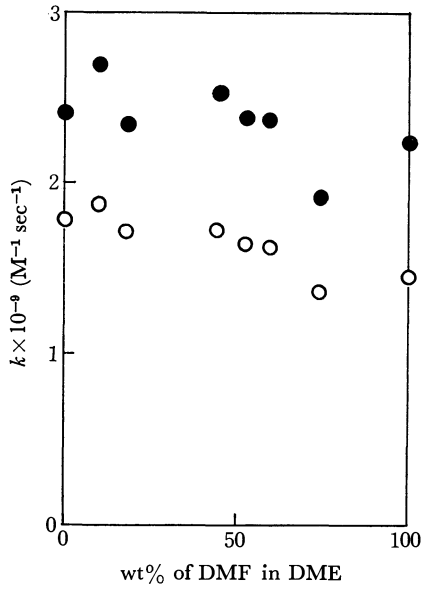

Fig. 4. Rate constants of electron exchange between A^- and A *vs.* weight percent of DMF in the mixture of DME and DMF: ○, observed values; ●, diffusion-corrected values.

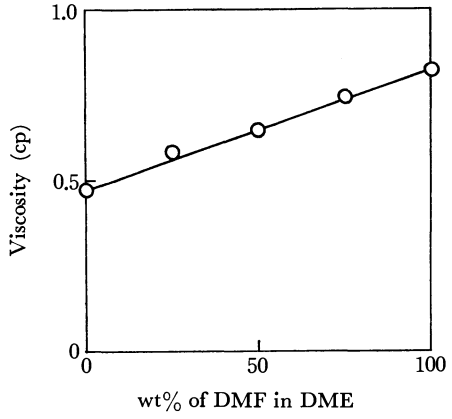

Fig. 5. Viscosities of DME–DMF mixtures.

The electron-exchange rates between anthracene and its anion radical were measured in several mixtures of DME and DMF. The correction of the linewidth for the decrease in the radical concentration was made in the same way as in the measurements of the cross-electron-transfer rates. Figure 3 illustrates the relations between the linewidth increase and the concentration of anthracene added in DMF and in DME respectively. The rate constants thus obtained are plotted in Fig. 4 with open circles against the weight percent of DMF in the mixed solvent. The corrected rate constants are shown with closed circles. The data for the viscosity of the DME–DMF mixture required in the correction are shown in Fig. 5; it is found that they depend almost linearly on the ratio of the composites.

Figure 4 shows that the corrected rate constants are nearly constant within the limits of experimental error. According to Eq. (4), the rate constant depends on D_s through the dependence of λ_0 on D_s. In the electron transfer of aromatic hydrocarbon-anion radicals, the contribution of λ_i to λ can be neglected; λ_0 is then

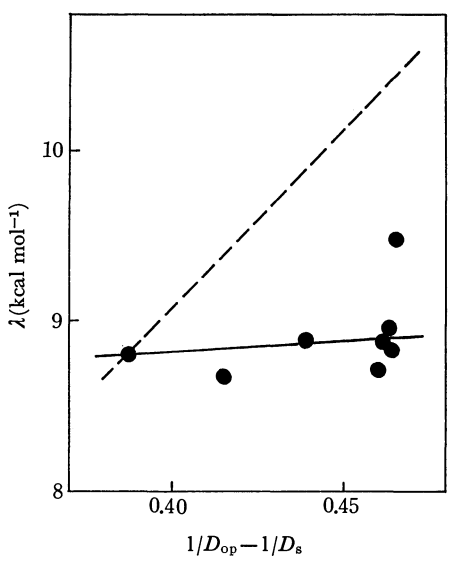

Fig. 6. Dependence of λ on the dielectric constants of solvents: ●, λ values calculated from Eq. (6) with corrected observed values for rate constants; ——, λ *vs.* $1/D_{op}-1/D_s$ plotted according to Eq. (4), the terms in the first parentheses estimated semi-empirically from λ values in DME.

approximately proportional to $(1/D_{op}-1/D_s)$. Since the D_{op} of each solvent is almost fixed, the value for λ, and consequently that for the rate constant also, are both substantially dependent only on D_s. The dotted line in Fig. 6 shows a theoretical plot of λ against $(1/D_{op}-1/D_s)$ drawn semi-empirically with the λ value and the slope calculated from the rate constant obtained in DME. The corrected observed λ values are plotted with closed circles in the same figure. The data for D_s in a DME–DMF mixture were not available. They were estimated from the D_s values of both solvents on the assumption that the D_s for the mixture depends linearly on the mixing ratio. The latter assumption was based on the fact that the viscosity of the mixture behaves in this manner without any molecular association at any specific mixing ratio, as is shown in Fig. 5. Figure 6 shows that λ depends on D_s to a much smaller extent than was predicted theoretically. This might be due to the neglect of the dielectric saturation in estimating the contribution to the activation free energy from solvent reorganization. This point will be discussed further later.

There has been an investigation examining the dependence of the rate constant on the dielectric constant of solvents with the pulse-radiolysis method.[12] Measurements were made on the electron-transfer from the pyrene anion to 9,10-dimethylanthracene; it was found that the results supported the theory of Marcus. However, it must be noticed that, on the one hand, the observed value for k is close to the diffusion-controlled one in this experiment. Consequently, errors in both the k_d and k values would seriously affect the accuracy of the corrected k_a values. On the other hand, the value for k_d was taken as that of the rate constant for

12) a) S. Arai, D. Grev, and L. M. Dorfman, *J. Chem. Phys.*, **46**. 2572 (1967). b) J. R. Brandon and L. M. Dorfman, *ibid.*, **53**, 3849 (1970).

reactions with sufficiently large negative ΔG° values, *e.g.* $6.7\times10^9 M^{-1}sec^{-1}$ in isopropanol. This is about four times the value calculated from $k_d=4RT/3\eta$; the validity of this relation has recently been reexamined in the ESR investigation of the Heisenberg spin-exchange process between tetracyanoethylene mononegative ions.[10] Moreover, the rate constants reported of the reactions with positive ΔG° values, *e.g.*, A^-/P, are as small as about one-tenth of that obtained by the ESR method. It is rather close to the value for an electron transfer from the anthracene$^-$-tetrabuthylammonium$^+$ ion pair to pyrene.[8] This suggests the ion pair (not loose ion pair) formation of the anthracene anion with some organic cationic species generated by electron-beam irradiation.

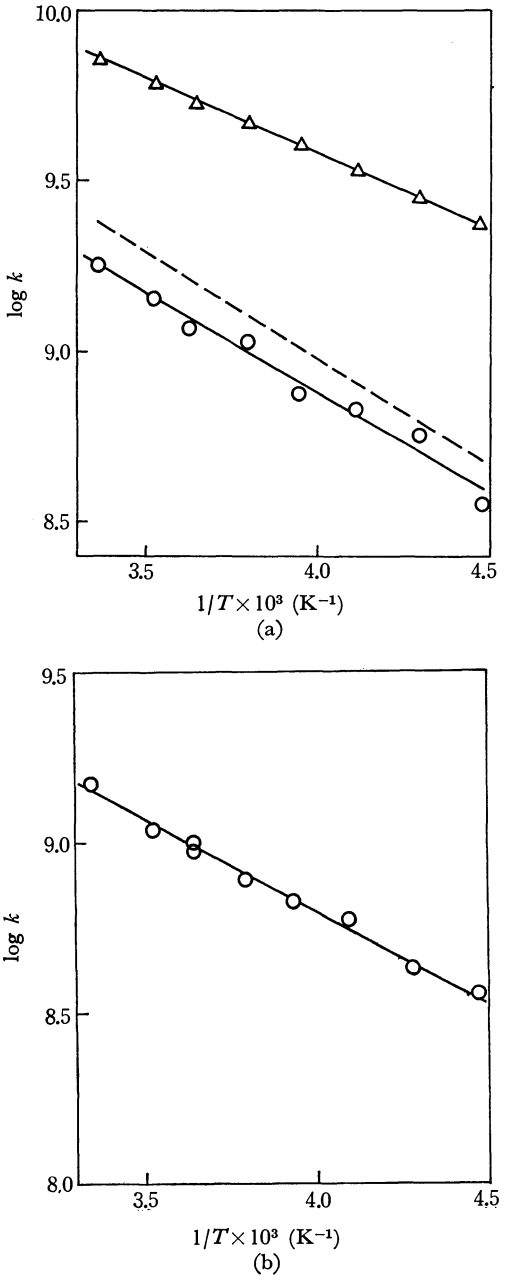

Fig. 7. Temperature dependence of rate constants of electron exchange between A^- and A in (a) DME and (b) DMF: ○, observed values; △, calculated values for k_d; ——, diffusion-corrected rate constants.

Temperature Depencence of the Electron-transfer Rates. Figures 7a and 7b show the temperature dependence of the rate constants of the electron-exchange reactions between anthracene and its anion radical in DME and DMF respectively. The observed rate constants are shown by open circles. The calculated k_d values and the corrected rate constants are shown in Fig. 7a by triangles and a dotted line respectively. The activation energies obtained from Fig. 7 are listed in Table 2.

Table 2. Semi-empirical estimate of activation enthalpy and observed activation energy of the reaction A^-+A in DME and DMF
(energies in kcal mol^{-1})

Solvents	$Z=10^{11}$ M^{-1} sec^{-1}		$Z=10^{10}$ M^{-1} sec^{-1}		E_a
	ΔH^*	ΔG^*	ΔH^*	ΔG^*	
DME	3.34	2.21	1.28	0.84	2.7±0.3
DMF	2.45	2.24	0.94	0.85	2.6±0.2

The corrected activation energy is nearly equal to the apparent one. The activation energy obtained from the calculated diffusion controlled rate constants in DME is 2.25 kcal mol^{-1}. The results in DMF could not be corrected, because the data for the viscosity of DMF at low temperatures were not available. The apparent activation energy in this solvent was assumed to be equal to the corrected one.

The activation energies in DME and in DMF are nearly equal; they are rather smaller than the activation energy obtained by Hirota in DME, 3 kcal mol^{-1}.[13]

Table 3. Non-empirical estimate of λ_0
(λ's in kcal mol^{-1})

Solvents	$(\lambda_0)_{calc}$ $a=5.15$ Å $r=10.3$ Å	$(\lambda_0)_{calc}$ $a=2.85$ Å $r=5.70$ Å	λ_{obs}
DME	12.5	22.5	8.81
DMF	14.9	26.8	8.84

The activation enthalpy of the electron-transfer reactions can be expressed in terms of the activation free energy in the sense of Marcus' theory, ΔG^*, as follows:

$$\Delta H^* = \Delta G^* - T(\partial \Delta G^*/\partial T).$$

It is ΔH^* that should be compared with the experimental activation energy, E_a. When λ_i is assumed to be negligible, ΔH^* is expressed as follows:

$$\Delta H^* = (1/4)[\lambda_0 - T(\partial \lambda_0/\partial T)].$$

In view of the fact that only D_s depends on the temperature in Eq. (4), the above equation can be rewritten in the following form:

$$\Delta H^* = (1/4)\left[\lambda_0 + T\frac{\lambda_0}{1/D_{op}-1/D_s}\frac{\partial}{\partial T}\left(\frac{1}{D_s}\right)\right]. \quad (9)$$

The temperature dependence of the dielectric constant of solvents is expressed by the empirical equations:

13) a) N. Hirota, *J. Phys. Chem.*, **71**, 127 (1967). b) N. Hirota, "Radical Ions," ed. by E. T. Kaiser and L. Kevan, Interscience Publishers, New York (1968), p. 35.

$D_s(\mathrm{DME}) = -2.83 + 2950/T$[14] and $D_s(\mathrm{DMF}) = -24.8 + 18300/T$.[15] The λ_0 values are obtainable from the observed rate constants using an appropriate value for Z. Table 2 shows the values for ΔH^* calculated from Eq. (9) with Z values of 10^{11} and $10^{10}\mathrm{M^{-1}sec^{-1}}$. The values for ΔG^* and E_a are also included in the table.

It may be seen from Table 2 that ΔH^* agrees with E_a fairly well when Z is $10^{11}\mathrm{M^{-1}sec^{-1}}$. Moreover, it may be noticed that the experimental activation energies in the two solvents are nearly equal; this differs from the theoretical prediction that the extent of the contribution to ΔH^* from the entropy term would be different in DME and DMF solutions.

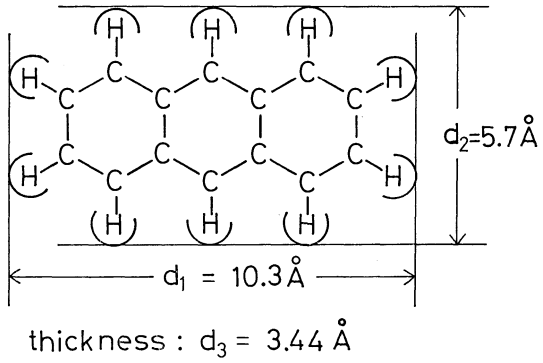

Fig. 8. Molecular geometry and dimensions of anthracene.

Non-empirical Estimate of λ_0. In the above discussion, the λ values were determined semi-empirically from the observed rate constants with an appropriate value for Z. According to Marcus' theory, λ_0 can be estimated non-empirically using Eq. (4) when λ_i is negligible. In deriving Eq. (4) Marcus assumed the reactants to be spherical. The reactants in the present discussion, *i.e.*, anthracene and its anion, however, have planar structures; the molecular radii must be estimated in an arbitrary way from the molecular geometry. Figure 8 shows the molecular geometry and dimensions of anthracene. In estimating d_1 and d_2 in Fig. 8, the van der Waals radii were taken into account besides the bond distances. The thickness, d_3, is rather indefinite. Because of the possible closest approach of reactants which may put the anthracene molecular planes face to face, it is assumed that the thickness is equal to the distance between the molecular layers in graphite, 3.44 Å. The value for λ_0 was calculated on the assumption that $a=a_1=a_2=r/2$. The value of a was tentatively taken as $d_1/2$ and $d_2/2$. Table 3 shows that even with the largest a val ue possible, *i.e.*, 5.16 Å, the calculated λ_0 values do not agree with the observed values. The agreement will be even less satisfactory for smaller a values.

Concluding Discussion. The following aspects were pointed out in the above examination of experimental results made on the basis of the Marcus' theory. First, the observed rate constants depend on ΔG° in such a way as is predicted theoretically when λ takes the value of 3.4 kcal mol^{-1}; this λ value is much smaller than that predicted by Eq. (4) with $Z=10^{11}\mathrm{M^{-1}sec^{-1}}$, 8.8 kcal mol^{-1}. Secondly, the rate constant is almost independent of D_s against the theoretical prediction. Thirdly, there is no difference between the experimental activation energies in DME and in DMF; thi might be a result of the difference in D_s; in other words, the activation entropy contributes to E_a to almost the same extent in solvents with different D_s values. The second and the third points require that the contribution of λ_0 to the activation free energy be smaller than that predicted theoretically. The inclusion of λ_i into λ cannot provide any successful elucidation: the situation that λ_0 is small, while $\lambda=\lambda_0+\lambda_i$ is large, is not probable in view of the first point.

The inconsistency between the theoretical predictions and the experimental results might be removed by reasoning as follows: when the non-coulombic interactions between reactants as well as products, which were neglected in deriving Eq. (2), are taken into consideration, the activation free energy can be expressed by:[4b]

$$\Delta G^* = (w^r + w^p)/2 + \lambda/4 + \Delta G^\circ/2 + (\Delta G^\circ + w^p - w^r)^2/4\lambda, \quad (10)$$

where w^r and w^p are the reversible work to bring two reactants together and two products together respectively, from the bulk of solution to the positions they would occupy in the activated complex. Generally, w's can be coulombic and/or non-coulombic. Here, one of the reactants as well as the products being neutral, they are non-coulombic. If $w^r=w^p=w$ is assumed for the sake of simplicity, Eq. (10) becomes:

$$\Delta G^\circ = w + \lambda/4 + \Delta G^\circ/2 + (\Delta G^\circ)^2/4\lambda. \quad (11)$$

Let $w=1.4$ kcal mol^{-1} and $\lambda=3.4$ kcal mol^{-1}, in view of the following facts: the observed ΔG^* for the A^-/A couple is 2.2 kcal mol^{-1} when Z is $10^{11}\mathrm{M^{-1}sec^{-1}}$, and the ΔG°-dependence of the observed rate constants can be elucidated by taking λ as 3.4 kcal mol^{-1}. Then, λ_0 can be quite small; this is consistent with the requirements of the second and third points.

Such a small λ value, however, cannot agree with that estimated non-empirically from Eq. (4), 12 kcal mol^{-1}. The agreement might be expected if the value of $1/D_{op}-1/D_s$ is one-fourth to one-third smaller than that calculated with the macroscopic D_s value or, consequently, if D_s is as small as 2 or 3. However, it is hardly probable that such a strong dielectric saturation occurs in the vicinity of hydrocarbon anions, which have an extensively-spread charge distribution.

In conclusion, the observed rate constants for the electron-transfer reactions between aromatic hydrocarbons and their anions depend on the parameters, *i.e.*, the standard free energy of reaction, the dielectric constant of the solvent, and the temperature, as a whole in some different way from that predicted by the theory of Marcus. This is inconsistent with the results of the previous investigations, which treated the parameters individually.[12b,16]

14) C. Carvajal, K. J. Tolle, J. Smid, and M. Szwarc, *J. Amer Chem. Soc.*, **87**, 5548 (1965).

15) J. A. Riddick and W. B. Bunger, "Organic Solvents," Wiley-Interscience, New York (1970), p. 446.

16) D. Rehm and A. Weller, *Ber. Bunsenges. Phys. Chem.*, **73**, 834 (1969).

There is some possibility that the most fundamental assumption in the Marcus' theory, *i.e.*, the small overlap of the wave functions of reactants, might not be completely fulfilled in the reactions in which the aromatic hydrocarbons participate.

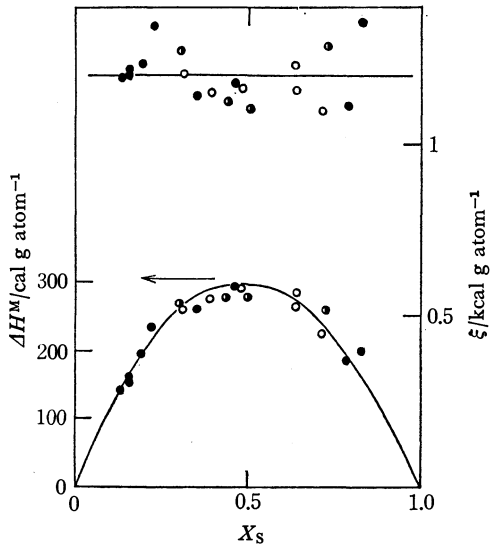

Fig. 1. Enthalpies of mixing of sulfur + selenium.
○: 345 °C, sulfur (inner ampoule)*
●: 460 °C, sulfur (inner ampoule)
◑: 460 °C, sulfur (outer ampoule)
* See text for charging method.

TABLE 1. ENTHALPIES OF MIXING AND INTERACTION PARAMETERS OF SULFUR+SELENIUM

Mole fraction X(S)	Total moles	ΔH^M cal/g atom	$\xi^M=\frac{\Delta H}{X(1-X)}$ cal/g atom
	345 °C		
	Sulfur: inner ampoule		
0.314	0.0420	260	1210
0.392	0.0429	275	1150
0.485	0.0435	291	1170
0.636	0.0419	285	1240
0.639	0.0425	266	1150
0.714	0.0460	224	1100
	460 °C		
	Sulfur; inner ampoule		
0.138	0.0513	142	1190
0.157	0.0290	159	1200
0.158	0.0561	153	1230
0.196	0.0340	195	1240
0.224	0.0319	234	1350
0.355	0.0246	262	1140
0.462	0.0416	294	1180
0.788	0.0401	185	1110
0.824	0.0465	198	1370
	Sulfur; outer ampoule		
0.303	0.0319	269	1270
0.349	0.0321	277	1130
0.504	0.0432	277	1110
0.725	0.0426	258	1290

not observed within the range of experimental scattering. The ξ-function of this system is almost constant over the entire composition range. In view of the small difference in the electronegativity values of sulfur and selenium, the enthalpies seem to be attributable to the transformation of the covalent bonding, that is, to

$$\text{-S-S-} + \text{-Se-Se-} \longrightarrow 2\ \text{-S-Se-}$$

in rings or chains, and to minor effects from the change in the van der Waals interaction among the rings and chains of various chain compositions. Although the equilibria between ring and chain molecules of various lengths will shift on mixing, the heat effects due to this transformation can not be estimated at the present stage of knowledge.

Sulfur+Tellurium. In this system, the enthalpy of mixing is positive on the sulfur- and tellurium-rich sides, but negative in the intermediate composition ranges. The composition at which the minimum appears is about 0.25, by the suflur atomic fraction. The ξ-function of this system was divided conveniently into three straight lines. The least-squares method leads to the following results:

$$0 \leq X_s \lesssim 0.25\text{: } \xi = 2880 - 19890X_s,$$

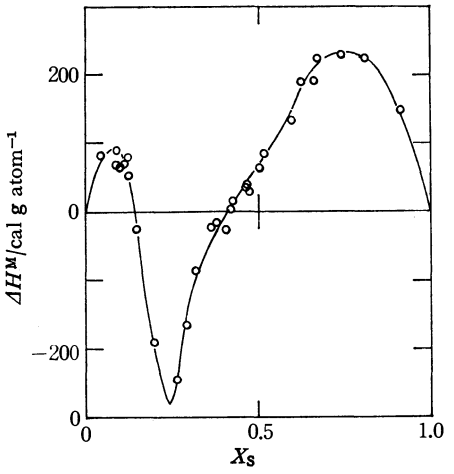

Fig. 2. Enthalpies of mixing of sulfur + tellurium at 468 °C.

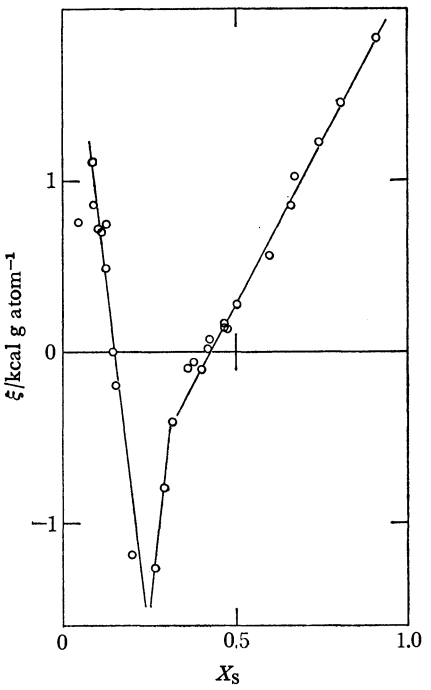

Fig. 3. ξ-functions of sulfur + tellurium. Experimental points and the straight lines by the least squares method.

Table 2. Enthalpies of mixing and interaction parameters of sulfur+tellurium at 468 °C

Mole fraction X(S)	Total moles	ΔH^M cal/g atom	$\xi^M=\frac{\Delta H}{X(1-X)}$
	Sulfur; inner ampoule		
0.045	0.0438	83	755
0.090	0.0510	70	855
0.090	0.0416	91	1110
0.102	0.0403	65	724
0.115	0.0415	72	707
0.125	0.0422	83	755
0.126	0.0481	54	489
0.150	0.0481	−25	−196
0.200	0.0412	−190	−1190
0.263	0.0494	−244	−1260
0.291	0.0229	−164	−794
0.315	0.0343	−88	−406
0.362	0.0389	−23	−100
0.380	0.0433	−14	−59
0.404	0.0593	−27	−112
0.419	0.0376	3	12
0.424	0.0453	17	70
0.464	0.0440	36	145
0.466	0.0455	40	161
0.474	0.0386	32	128
0.503	0.0436	63	272
0.512	0.0375	85	340
0.597	0.0421	133	553
0.624	0.0481	192	818
0.660	0.0350	191	851
0.670	0.0330	224	1010
0.742	0.0253	231	1200
0.807	0.0256	224	1440
0.912	0.0246	147	1830

$$0.25 \lesssim X_s \lesssim 0.30: \quad \xi = -5500 + 16160X_s,$$

and:

$$0.30 \lesssim X_s \lesssim 1.0: \quad \xi = -1620 + 3825X_s,$$

where X_s is the atomic fraction of sulfur.

The above equations are helpful in calculating the partial molar enthalpies of mixing. The forms of the ξ-functions is similar to that of binary systems in which the associated species are formed on mixing, for example, in the $MgCl_2$+KCl system studied by Kleppa.[5] The activity of each component can be calculated from the equilibrium-phase diagram.[6] With the data of the heat of fusion and the melting point of tellurium,[7] and on the assumption that the solid solution of sulfur in tellurium is ideal with respect to the tellurium solvent, the activity of tellurium on the liquidus temperature was derived. Further, the present enthalpy data permitted us to calculate the change in activity with the temperature. The acitivity of tellurium and that of sulfur derived from the former by means of the Gibbs-Duhem relation were combined with the present enthalpy values in order to evaluate the entropy of mixing. The free energy from the activities and the entropy are shown in Fig. 4, together with the enthalpy values. Although the free energy curve is smooth, the entropy value is less than that of the ideal solution and shows a minimum at $X_s=0.25$. These curves are similar to those of mixtures which generate the associated complex on mixing. From the trends of the entropy as well as from the enthalpy, some sorts of orderings can be suspected in the mixture around $X_s=0.25$. In order to interpret this entropy, let us consider for a moment a pseudo-binary mixture consisting of Te_3S and excess tellurium or sulfur, like thallium+tellurium.[8] The configurational entropies of the pseudo-binary mixture can be calculated on the basis of the quasi-crystalline lattice model. When $X_s>0.25$, the mixture consists of Te_3S and S and the entropy of mixing is given by:

$$-\Delta S^M/R = X_s[(1-X_2)\ln\phi_1 + X_2\ln\phi_2]$$

in which

$$X_2 = (1-X_s)/3X_s$$

and

$$\phi_2 = 1-\phi_1 = rX_2/[(1-X_2)+rX_2] \quad (r=4 \text{ in this case})$$

and for Te_3S+Te ($X_s<0.25$) by:

$$-\Delta S^M/R = (1-3X_s)[(1-X_2)\ln\phi_1 + X_2\ln\phi_2]$$

in which

$$X_2 = X_s/(1-X_s).$$

The entropies based upon above model are shown in Fig. 4 as a broken line. The agreement between the experimental and calculated values is satisfactory. One may note, however, that this does not necessarily mean that any molecule like Te_3S is present in the mixture. Considering the small enthalpy of mixing, the idea of the compound formation is far from reality. Rather,

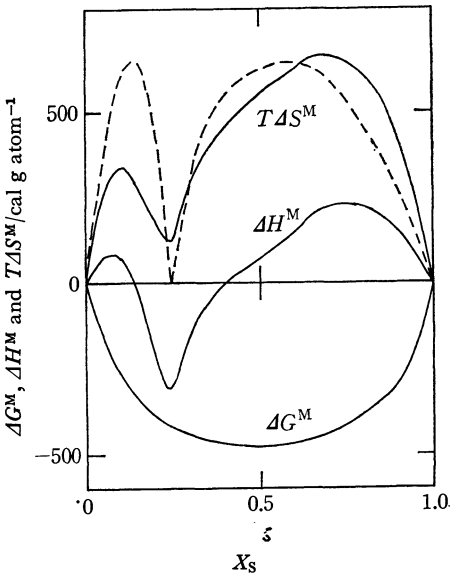

Fig. 4. The thermodynamic fuctions of sulfur + tellurium. The broken line; calculated values at 468 °C.

5) O. J. Kleppa and F. G. McCarty, *J. Phys. Chem.*, **70**, 1249 (1966).

6) M. Hansen and K. Anderko, "Constitution of Binary Alloys," McGraw-Hill, New York, (1958).

7) O. Kubaschewski, E. LL. Evans and C. B. Alcock, "Metallurgical Thermochemistry," Chap. 5, Pergamon Press, Oxford (1967).

8) Y. Nakamura and M. Shimoji, *Trans. Faraday Soc.*, **67**, 1270 (1971).

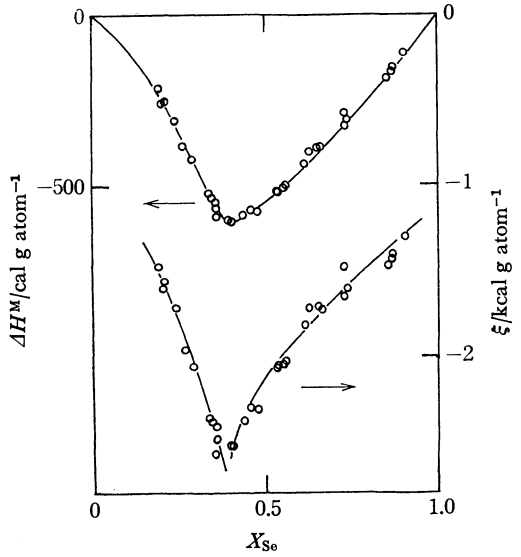

Fig. 5. The enthalpies of mixing of selenium + tellurium at 460°C.

Table 3. Enthalpies of mixing and interaction parameters of selenium + tellurium at 460 °C

Mole fraction X(Se)	Total moles	ΔH^M cal/g atom	$\xi^M=\frac{\Delta H}{X(1-X)}$ cal/g atom
0.193	0.0464	−229	−1470
0.206	0.0480	−263	−1610
0.209	0.0344	−257	−1550
0.239	0.0447	−312	−1720
0.265	0.0465	−382	−1960
0.290	0.0495	−424	−2060
0.333	0.0294	−524	−2360
0.342	0.0508	−536	−2380
0.357	0.0412	−550	−2400
0.357	0.0312	−569	−2480
0.358	0.0326	−592	−2580
0.394	0.0347	−599	−2510
0.403	0.0340	−607	−2520
0.438	0.0356	−584	−2370
0.454	0.0484	−571	−2300
0.474	0.0349	−576	−2310
0.532	0.0417	−515	−2070
0.537	0.0403	−517	−2060
0.552	0.0424	−509	−2060
0.554	0.0512	−499	−2020
0.611	0.0380	−433	−1820
0.624	0.0438	−403	−1710
0.651	0.0408	−390	−1720
0.660	0.0456	−389	−1730
0.726	0.0378	−292	−1470
0.729	0.0492	−329	−1670
0.735	0.0392	−313	−1610
0.853	0.0430	−184	−1470
0.864	0.0418	−168	−1430
0.866	0.0436	−163	−1400
0.900	0.0493	−117	−1300

the sulfur atoms seem to be preferably surrounded by three tellurium atoms when $X_S<0.25$. The positive enthalpies of mixing on the two sides of the composition may be attributable to positive heats effects, such as the difference in size between sulfur and tellurium.

Selenium+Tellurium. In this system, the enthalpy is negative throughout the composition range. The minimum of the enthalpies of mixing appears at the composition of 0.4, by the atomic fraction of selenium. The electronegativity difference between selenium and tellurium is the largest among the three combinations. Therefore, the enthalpies of mixing of this system are expected to be the most exothermic, in agreement with the experimental results. The ξ-function of this system can also be divided into two portions. Though there are no thermodynamic functions available except the present enthalpy data, the ordered structure may be constructed in the same manner as in the sulfur+tellurium system.

As has been shown by many authors, liquid sulfur has the so-called transition temperature, above which long chains with various chain lengths are formed in addition to the S_8 ring.[9] Liquid selenium can also be understood similarly, though the transition temperature lies below its melting point.[10] Since the experimental temperatures of the present work are higher than the transition temperatures, we must consider the presence of these species. In contrast to sulfur and selenium, liquid tellurium has only a short chain structure at low temperatures. However, it has recently been shown that liquid tellurium has a three-dimensional network structure. This idea is proposed on the basis of the experimental evidence that the numbers of the nearest neighbors in liquid tellurium are not two but three, even as high as above the temperature of 950 °C, as determined by the neutron diffraction measurement.[11] Therefore, the mixing process of these elements involve ring opening, chain scission, and the formation of co-ring and co-polymer chains.[12] The observed enthalpies of mixing are related to these processes. Therefore, the mixture cannot be simply treated like a usual metallic solution. A further aspect to be noted is the fact that the present enthalpy-composition curves are similar to those of metal+chalcogen systems. In the binary mixture of tellurium with sulfur or selenium, tellurium perhaps functions as a metal-like component. The theoretical evaluation of the thermodynamic functions depends on a certain structural model of the mixture. Unfortunately, such information is not available at the present time and a quantitative discussion was not attempted in this work. At the end of this paper, it may be noted that, in the selenium+tellurium system, the mixture is conventionally divided into two distinct portions, according to recent NMR studies.[13]

9) V. Tobolsky and E. Eisenberg, *J. Amer. Chem. Soc.*, **81**, 871 (1959).
10) A. Eisenberg and V. Tobolsky, *J. Polym. Sci.*, **46**, 19 (1960).
11) B. Cabane and J. Friedel, *J. Phys.*, (Paris), **32**, 73 (1971).
12) R. Cooper and J. V. Culka, *J. Inorg. Nuclear Chem.*, **29**, 1217 (1967); **29**, 1877 (1967); **31**, 685 (1969).
13) E. F. W. Seymour and D. Brown, The Second International Conference on the Properties of Liquid Metals, Tokyo, Japan, September, 1972.

In the region in which the compositions of tellurium are higher than 70 at. per cent, the mixture behaves in a metallic manner. On the other hand, in the lower composition range, the valence electrons are localized in the chain molecules. Although the composition of the minimum ΔH observation is slightly different from the above boundary, our opinions that an ordered structure is present and that the system is divided into two portions in the mixture are consistent with this view.

BULLETIN OF THE CHEMICAL SOCIETY OF JAPAN, VOL. 46, 765—769 (1973)

The Reflection Spectra of Würster's Salts

Yukako Oohashi and Tadayoshi Sakata*

The Institute for Solid State Physics, The University of Tokyo, Roppongi, Minato, Tokyo

(Received July 17, 1972)

The reflections of *N,N*-dimethyl-*p*-phenylenediamine (WR) perchlorate, bromide, and iodide, and also of *p*-phenylenediamine (PD) perchlorate and bromide were measured over the range from 5000 to 42000 cm^{-1} by Avery's method. The absolute absorption intensity and the refractive index of these solids were obtained by computer analysis. The absorption intensity of the solid was found to be, as a whole, larger than that of the dimer in solution; in particular, the CT band becomes broader and splits in a solid. Further, the anion was found to have a large effect on the electronic structure in the crystal. By taking account of these features of the spectrum and other experimental results, the WR salts were classified into two types according to their way of packing: Type I takes the dimer-unit structure (WRP) and Type II, the equidistantly-overlapped form (WRB and WRI).

It is known that an equilibrium exists between monomer and dimer ions in the solutions of some radical ion salts and that the charge-transfer (abbreviated hereafter to CT) band pertinent to the dimer appears at low temperatures.[1)]

In the crystalline state, *N,N,N',N'*-tetramethyl-*p*-phenylenediamine perchlorate (WBP) shows its phase transition at 186K; below the transition point, the ESR signal due to the triplet exciton[2)] appears, and the CT band intensity is sensitive to the temperature. These observations were found to be consistent with the dimerization mechanism of the phase transition,[3)] and to contradict the disproportionation mechanism presented by Kommandeur and Pott.[4)]

At room temperature, the crystalline spectra of *N,N,N',N'*-tetramethyl-*p*-phenylenediamine (WB) radical salts show only weak CT bands and rather resemble the spectra of the corresponding monomers in solution.[1b,5)] The crystals of *N,N*-dimethyl-*p*-phenylenediamine (WR) and *p*-phenylenediamine (PD) radical salts, however, show vivid CT bands, and their spectra are similar to those of the corresponding radical dimers in solution.[6)] This means that the CT interaction is stronger for the WR and PD crystals than for the WB crystal.

In comparison with the solution spectra of radical dimers, the solid-state spectra were found to be broader; in particular, the CT bands become broad and split into two peaks. The absolute intensities of the crystalline absorption bands, however, were difficult to determine because of the difficulty of measuring the thickness of the very thin crystals. This fact prevents us from making a detailed discussion of the interaction between the radical ions, including the effect of the counter anion. In the present investigation, we measured, at various wavelengths, the reflection intensities of the pressed pellets of WR and PD radical salts and determined the refrative index (n) and the extinction coefficient (k). On the basis of the experimental results of the absolute absorption intensities, we will discuss the electronic structures of these radicals in the solid state.

Experimental

Materials. Würster's red perchlorate (WRP), bromide (WRB), *p*-phenylenediamine perchlorate (PDP), and bromide (PDB) were prepared and purified by the method described in the literature.[7)] Würster's red iodide (WRI) was prepared by a method analogous with that used for WRB. (WRI; Calcd: C, 36.52; H, 4.56; N, 10.65; I, 48.27%. Found: C, 36.42; H, 4.59; N, 10.68; I, 48.84%). The radical salts are considerably stable in the air, and the measurements were carried out within a few days after the syntheses.

Measurements. Several methods have been used for the determination of the optical constants of the crystals from the reflection measurements. We constructed the apparatus on the basis of the method of Avery[8)] and measured the

* Present address: Department of Chemistry, Faculty of Engineering Science, Osaka University, Toyonaka, Osaka.

1) (a) K. H. Hausser and J. N. Murrell, *J. Chem. Phys.*, **27**, 500 (1957). (b) K. Uemura, S. Nakayama, Y. Seo, and Y. Ooshika, This Bulletin, **39**, 1348 (1966). (c) K. Kimura, H. Yamada, and H. Tsubomura, *J. Chem. Phys.*, **48**, 440 (1968). (d) R. H. Boyd and W. D. Phillips, *ibid.*, **43**, 2928 (1965).

2) D. D. Thomas, H. Keller, and H. M. McConnell, *ibid.*, **39**, 2321 (1963).

3) T. Sakata and S. Nagakura, This Bulletin, **42**, 1497 (1969); *Mol. Phys.*, **19**, 321 (1970).

4) G. T. Pott and J. Kommandeur, *J. Chem. Phys.*, **47**, 395, 401 (1967).

5) Y. Iida and Y. Matsunaga, This Bulletin, **41**, 2615 (1968).

6) J. Tanaka and M. Mizuno, *ibid.*, **42**, 1841 (1969).

7) L. Michaelis and S. Granick, *J. Amer. Chem. Soc.*, **65**, 1747 (1943).

8) D. G. Avery, *Proc. Phys. Soc.*, **B65**, 425 (1952).

reflections at the incident angles of 50 and 70°. The characteristics of the method are to measure the ratio of the reflecting powers by the use of lights polarized parallel and perpendicular to the incident plane, and to suppress the scattering effect. Kondo[9] showed, taking fuchsine as an example, that this method gives the same refractive index and extinction coefficient for the crystal and the pressed pellet. Therefore, this method is useful for the measurement of Würster's salts, for which it is difficult to obtain a crystal large enough for the reflection measurement.

The light sources were a tungsten lamp for the range of 5000—30000 cm^{-1} and a deuterium-discharged lamp for the range of 25000—42000 cm^{-1}. The polarizers were a Polaroid HR for the range of 5000—11000 cm^{-1} and a Glan-Thompson prism for the visible and ultraviolet regions. A photomultiplier, HTV 7102 or 1P28, was used as a detector. Corrections were made for the polarization of the incident light caused by the optical systems. The samples were ground by means of an agate mortar and were pressed by a KBr disc presser at about 10 kbar.

Analysis. The following relation exists for the isotropic solid with the complex refractive index of $N=n-ik$:

$$I = \frac{r_p}{r_s} = \frac{a^2+b^2-2a\sin\beta\tan\beta+\sin^2\beta\tan^2\beta}{a^2+b^2+2a\sin\beta\tan\beta+\sin^2\beta\tan^2\beta}$$

$$a^2 + b^2 = \{(n^2-k^2-\sin^2\beta)^2+4n^2k^2\}^{1/2}$$

$$a = \left\{\frac{1}{2}(n^2-k^2-\sin^2\beta)+\frac{1}{2}[(n^2-k^2-\sin^2\beta)^2 + 4n^2k^2]^{1/2}\right\}^{1/2}$$

where r_p and r_s are the reflecting power by the incident light polarized, respectively, parallel and perpendicular to the incident plane, and β is the incident angle. We determined n and k from the I's at $\beta=50$ and 70° by means of the Newtonian approximation for two variables using the electronic computer. The larger the absorption intensity, the smaller the experimental error; when the molar extinction coefficient $\kappa(\nu)$ is larger than 3000 $(mol/l)^{-1}cm^{-1}$, the error is estimated from repeated measurements to be less than 10%. The following equation represents the relation between $k(\nu)$ and $\kappa(\nu)$:

$$\kappa(\nu)C = \frac{4\pi k(\nu)\nu}{2.303c}$$

where $I(z)=I(0)10^{-\kappa Cz}$, C is the concentration (mol/l), and c is the light velocity. On the other hand, the oscillator strength is calculated from $n(\nu)$ and $k(\nu)$:[10]

$$f = \frac{m}{e^2 n_0}\int 4n(\nu)k(\nu)\nu d\nu$$

where n_0 is the number of molecules in a unit volume.

In order to discuss the difference in the absorption intensity between the solid and the solution, the oscillator strengths must be compared.[11] Here, the $4\pi n(\nu)k(\nu)\nu/2.303Cc$ value will be plotted to show the wave number dependence of the absorption intensity. For the solution, $n(\nu)$ is reasonably approximated as 1.0. Some other physical constants of the solid can be calculated from $k(\nu)$ and $n(\nu)$. The complex dielectric constant, $\varepsilon(\nu)=\varepsilon'(\nu)+i\varepsilon''(\nu)$, is related to $k(\nu)$ and $n(\nu)$ as follows:

$$\varepsilon'(\nu) = n(\nu)^2 - k(\nu)^2$$

$$\varepsilon''(\nu) = \frac{2\sigma(\nu)}{\nu} = 2n(\nu)k(\nu)$$

$\sigma(\nu)$ is the electric conductivity constant.

Results and Discussion

Figure 1 shows the solid-state spectra of WRP, WRB, and WRI determined from the reflection measurements of pressed pellets, together with the low-temperature spectrum of an ethanol solution of WRP. The low-temperature spectrum of the ethanol solution was assigned to the WR cation dimer.[1b] The band at 15000 cm^{-1} has mainly the character of the CT band between WR cations (CT band), and the bands at 24500, 27500, 35300, and 39000 cm^{-1} are the locally (within the WR cation)-excited (LE) bands (the LEI, LEII, LEIII, and LEIV bands).[1c] The solid-state spectra, which are similar to the solution spectrum of the dimer, have the characteristics that the absorption intensity is, as a whole, stronger than that of the solution dimer, and that the CT band becomes remarkably broad and splits in a solid.[5] Furthermore, the solid-state spectrum is changed by the counter anion, while the solution spectrum is insensitive to it. These characteristics are also seen in PDP and PDB (see Fig. 2).

The Absorption Intensity of the Solid-state Spectrum. The oscillator strengths (f) are listed for the WR and

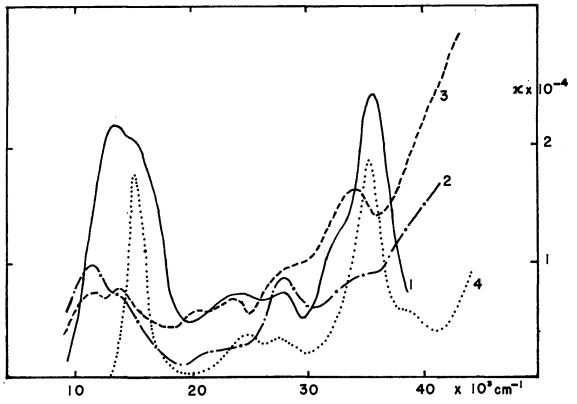

Fig. 1. The absorption spectra of WR salts. Solid (from the reflection measurements): 1 WRP, 2 WRB, 3 WRI; the ethanol solution of WRP at 110 K: 4.

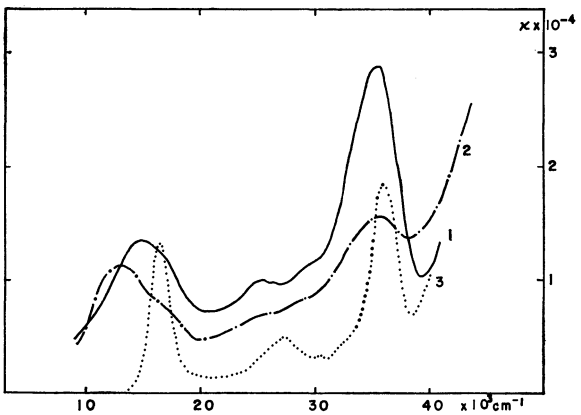

Fig. 2. The absorption spectra of PD salts. Solid (from the reflection measurements): 1 PDP, 2 PDB; the ethanol solution of PDP at 110 K: 3.

9) Y. Kondo, *Bussei*, **5**, 184 (1964).
10) J. M. Ziman, "Principles of the Theory of Solids," Cambridge Univ. Press, London (1963).
11) D. L. Dexter, *Phys. Rev.*, **101**, 48 (1956).

Table 1. The absorption spectra of WR radical salts
(s: shoulder)

	WRP		WRB		WRI		WRP in ethanol at 77 K	
	$\nu(cm^{-1})$	f	$\nu(cm^{-1})$	f	$\nu(cm^{-1})$	f	$\nu(cm^{-1})$	f
CT	13300 (15800)^s	0.61	11200 (14000)^s	0.25	11400 13800	0.23	14500	0.15
LEI LEII	24000 27800 (32000)^s	0.37	22000 27800	0.19	20000 23500 (28000)^s	0.4	25000 27500	0.10
LEIII	35600	0.46	(34000)^s	0.3	34000	0.4	35300	0.28
LEIV							39000	
$\sum f$		1.4		0.7		1.0		0.53

Table 2. The absorption spectra of PD salts

	PDP		PDB		PDP in ethanol at 77 K	
	$\nu(cm^{-1})$	f	$\nu(cm^{-1})$	f	$\nu(cm^{-1})$	f
CT	15000 (17000)^s	0.46	13000 (17000)^s	0.41	16500	0.12
LEI LEIII	25400 (29000)^s	0.4	26000 28000	0.3	27300 (32500)^s	0.15
LEII	35300	0.64	35500	0.5	36000	0.25
$\sum f$		1.5		1.2		0.52

PD radical salts in Tables 1 and 2 respectively. The value for each CT band was calculated with respect to the broad peak with splittings. The CT band is stronger for the solid radical salts than for the corresponding dimers in solution—4 times for WRP, 1.6 times for WRB and WRI, and 3—4 times for PD salts. Furthermore, the $f_{CT}/\sum_{I}^{III} f_{LE}$ ratios are 1.9, 1.4, 0.7, 1.5, and 1.9 times larger for the solid WRP, WRB, WRI, PDP, and PDB salts respectively than for the corresponding dimers in solution. Thus, the intensity increase in the solid state is more remarkable for the CT band than for the LE bands except for WRI, for which the tail of the strong absorption above 40000 cm^{-1} makes it difficult to calculate f_{LE} accurately.

The crystal structures of Würster's salts have been reported for WBP,[12] WBB,[6] WBI,[13] and WRB;[14] all of them contain a one-dimentional column of equidistantly-overlapped cation radicals. Theoretically, it was concluded that, in the infinite column, the intensity of the CT band is twice as large as that of the isolated dimer, and that the intensity of the LE band shows no increase, as long as the interaction between the LE states and CT states is negligibly small.[15] The observed increase in the intensity of the CT band for the solid WRB and WRI compared with that for their solutions is of a reasonable magnitude and is caused by the influence of the infinite column.

The intensity of the LE band is influenced by the degree of the mixing of the corresponding LE state with the lowest CT state. As WRB has a very short interplanar distance of the cation radicals (3.105 Å),[14] the interaction between the CT state and the LE state is not completely neglected. Moreover, the higher LE and CT states have complicated effects on the intensity in the crystalline state. On the other hand, WRP has a remarkably strong CT band, and its absorption spectrum as a whole resembles that of the dimer in solution. Taking into consideration the reported experimental results that WBP takes the dimer form in the low-temperature phase[12] and that WR salts show a stronger intercationic interaction than the WB salts in the crystalline state,[5] we can safely anticipate that the WRP radical will take the same molecular packing form as the low-temperature phase of WBP. The zeroth and the first-layer Weissenberg photographs of the WRP single crystal show the extinction rule that $h0l$ and $0kl$ (l=0,1) are absent when h and k are odd[16] (a=10.19, b=13.00, c=7.01 Å, Z=4, orthorhombic). This extinction rule supports the dimer form of WRP because, if the radicals were arranged in the unit cell equidistantly, the resulting interradical distance would become too large compared with those previously reported for Würster's salts. Furthermore, the ESR study of the temperature dependency of WRP powder reported of the triplet signal[17] that its intensity increases as the temperautre increases. From the above-mentioned results, it may be concluded that WRP takes the dimer form in the crystalline state and that the large increases in the CT band intensity compared with that of the dimer in solution is mainly attributable

12) J. L. DeBoer and A. Vos, *Acta Crystallogr.*, **B28**, 835 (1972).
13) J. L. DeBoer, A. Vos, and K. Huml, *ibid.*, **B24**, 542 (1968).
14) J. Tanaka and S. Sakabe, *ibid.*, **B24**, 1345 (1968).
15) T. Sakata and S. Nagakura, This Bulletin, **43**, 1346 (1970).
16) Yūji Ohashi, Private communication.
17) M. Itoh, This Bulletin, **44**, 2886 (1971).
18) T. Sakata and S. Nagakura, *ibid.*, **43**, 2414 (1970).

to the increase in the intercationic interaction, accompanied by the change in the molecular configuration. PDP and PDB both show strong CT bands, and the LEIII band is especially strong for PDP. There being no other experimental data, any detailed discussion is now impossible: however, PDP and PDB seem to show the optical properties similar to those of WRP and WRB respectively.

Table 3. The bandwidth and splitting of CT band

	Solid	Solution dimer	Splitting in solid
WRP	6500 cm^{-1}	1800 cm^{-1}	Yes
WRB	6500		Yes
WRI	7500		Yes
PDP	8500	1600	Yes
PDB	8800		Yes
WBP[3]	2500[a]	2500	No
WBB[18]	3000[a]		No
WBC[18]	3400[a]		No
N-EP[3]	2700[a]	1700	Yes

a) Calculated from the transmission spectra of the quartz plates smeared with the samples at 77 K and 50 K.

The Splitting of the CT Band. Table 3 shows the bandwidths of the CT bands of the solid-state spectra and the low-temperature solution spectra, and the presence of the splitting of the CT band in the solid. The values of the second column show the width of the wave numbers, which correspond to half of the peak-absorption intensity, because a reasonable deconvolution of CT band is impossible. The fact taht the values of PD salts are larger than those of WR salts seems to be due to the larger splitting of the CT band. For comparison, Table 3 also shows the bandwidths of WB salts (P: perchlorate, B: bromide, and C: chloride) and *N*-ethylphenazyl (*N*-EP), which have weak intercationic interaction in the crystalline state. The origin of this splitting has been explained before as being due to the forbidden CT state appearing by means of the intensity borrowing through vibrational or other kinds of perturbations.[6] However, as may be seen in Table 3, WR and PD salts, with strong intercationic interaction, have the splittings, while WB salts, with weak interaction, have not. Thereofre, the explanation can not be denied at present that a new absorption occurs due to the long-range interaction between the cation radicals characteristic of the strong intercationic interaction.

The Effect of the Anion Species. The third characteristic of the solid-state spectra of WR and PD salts is the remarkable difference produced by the change of the anion species. In the case of WR salts, the following classification is possible. The conclusion that a salt of Type I has the dimer unit in the crystal is supported by the ESR and X-ray studies. From the characteristics of the salts of Type II (the extroadinary broadning of the solid-state spectra with strong higher energy absorptions, the large red shift of CT band, and the lack of a triplet signal), it is conceivable that the salts of Type II contain a one-dimensional column of equidistantly-overlapped cation radicals in the crystalline state.

Table 4. Classification of WR salts

	Type I (WRP)	Type II (WRB, WRI)
Red shift of CT band from that of dimer in solution	1200 cm^{-1}	3000cm^{-1}
Splitting of CT band	Less clear	Clear
Absorption higher than 40000 cm^{-1}	No tail	Strong tail
ESR	Triplet signal	No signal[a]

a) Preliminary study by M. Itoh found only the impurity signal.

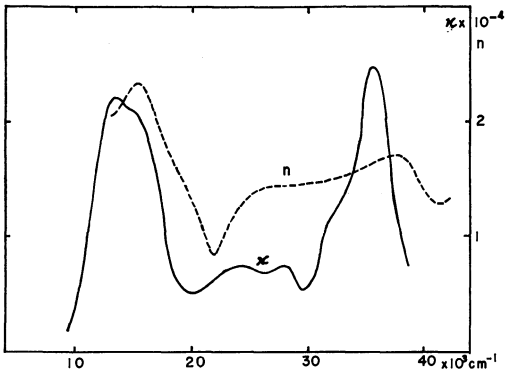

Fig. 3. The molar extinction coefficient and the refractive index of WRP solid determined by the reflection measurement.

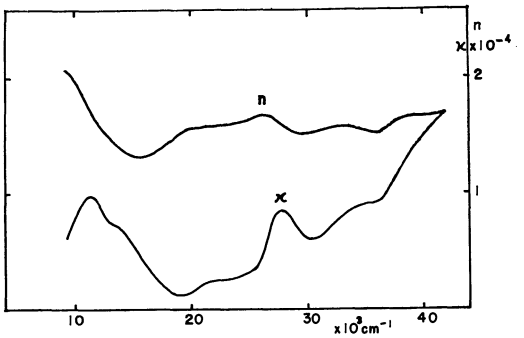

Fig. 4. The molar extinction coefficient and the refractive index of WRB solid determined by the reflection measurement.

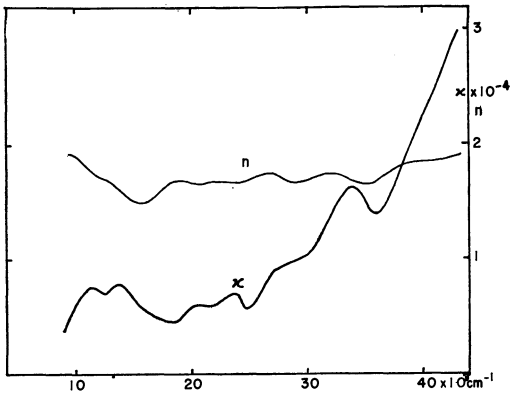

Fig. 5. The molar extinction coefficient and the refractive index of WRI solid determined by the reflection measurement.

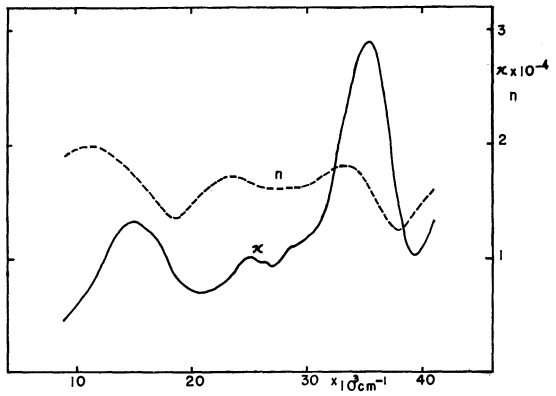

Fig. 6. The molar extinction coefficient and the refractive index of PDP solid determined by the reflection measurement.

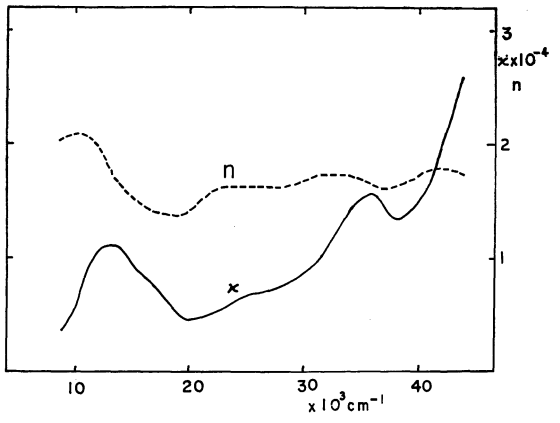

Fig. 7. The molar extinction coefficient and the refractive index of PDB solid determined by the reflection measurement.

The Determinations of the Optical Constants. Figures 3, 4, 5, 6, and 7 show the wave number dependence of the refractive index, $n(\nu)$, together with the molar extinction coefficients of WR and PD salts. At the wave number near the CT band, $k(\nu)$ takes the maximum value, and the wave number dependence of $n(\nu)$ is especially large. This suggests that the absorption maximum determined by the transmission measurement must be modified by taking the reflection effect into account. Figures 8 and 9 show the real and imaginary parts of the dielectric constant. The very small value of the real part of WRP near 17000 cm^{-1} causes the remarkably strong reflection.

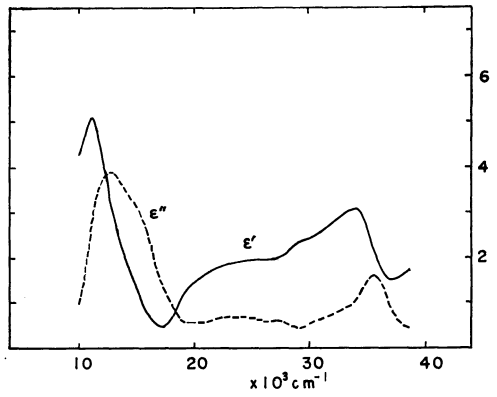

Fig. 8. The real and imaginary parts of the dielectric constant of WRP solid.

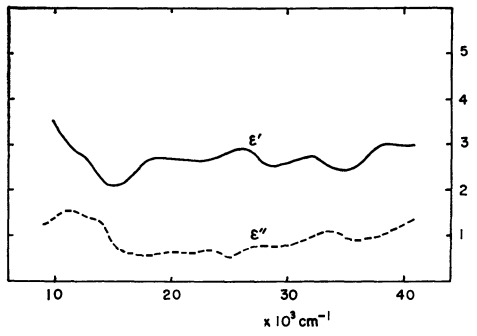

Fig. 9. The real and imaginary parts of the dielectric constant of WRI solid.

The authors would like to express their deep gratitude to Professor Saburo Nagakura of this Institute for giving them the chance to do this work and for his helpful discussions and critical reading of the manuscript. The authors are also grateful to Professor Shogen Nakahara, Rikkyo University, for his kind advice on the measurements of the reflection spectra.

The Preparation and Crystal Structure of Ternary Rare Earth Borides, RCo_3B_2

Koichi NIIHARA and Seishi YAJIMA

The Research Institute for Iron, Steel and Other Metals, Tohoku University, Sendai

(Received July 24, 1972)

In the ternary system of rare earth-cobalt-boron, RCo_3B_2 compounds (R=rare earth elements) were prepared by arc-melting methods. Their crystal structure was investigated by X-ray diffraction methods. These ternary borides, RCo_3B_2, crystallize in a hexagonal lattice. The lattice parameters are $a=5.020\pm0.002$ Å and $c=3.027\pm0.002$ Å for YCo_3B_2 and $a=5.066\pm0.003$ Å and $c=3.022\pm0.002$ Å for $GdCo_3B_2$. The good agreement between the X-ray diffraction intensities observed and calculated shows that the ternary borides, YCo_3B_2 and $GdCo_3B_2$, crystallize in the $CaZn_5$-type structure. The space group and atomic positions are as follows: P6/mmm (D^1_{6h}), 1R in 1(a), 3Co in 3(g), and 2B in 2(c). It can be seen from these results that the ternary borides, RCo_3B_2, have a superstructure in which two Co atoms in the 2(c) site of intermetallic compounds, RCo_5, with the $CaZn_5$-type structure are replaced by two B atoms. The B atoms in this structure are situated at the center of a trigonal prism formed by six Co atoms. The interatomic distances between B and the six Co atoms are 2.11—2.10 Å and are fairly constant, although the radii of the rare earth atoms are changed according to the lanthanide contraction. We have also found RCo_3B_2 compounds to be isostructural with YCo_3B_2 and $GdCo_3B_2$, where R= Ce, Sm, Tb, Dy, Ho, and Er. Efforts to prepare $LaCo_3B_2$, $PrCo_3B_2$, and $NdCo_3B_2$ by arc-melting were unsuccessful.

Only recently have ternary metal-boron compounds been reported.[1-9] The most interesting borides are the family of the borides with the $Cr_{23}C_6$-type structure, found when the works that led to the perovskite carbides and nitrides were extended to include boron. The composition of the ternary boride varies from system to system and can best be symbolized by the $T_{23-m}M_mB_6$ formula. Here, T represents one of the d-transition metals, cobalt or nickel, M is a nontransitional metal or, a IVth or Vth-group transition metal, and B is boron. Roughly, m ranges from 2 to 3.5. There also exist some other ternary phases, such as Mo_2CoB_2,[10] Mo_2FeB_2,[11] W_2CoB_2,[12] $MoFeB_4$,[13] $ThWB_4$,[14] and $Mo_2Fe_{13}B_5$.[14] However, there have been few investigations concerning any ternary rare earth borides except $YCrB_4$.[15]

Recently we reported[16,17] that, in the system of rare earth-cobalt-boron, there exist two ternary compounds, RCo_2B_2 and $RCo_{12}B_6$, with tetragonal and rhombohedral structures respectively, where R represents a rare earth atom. In the present paper, we will describe the preparation and the crystal structure of another ternary rare earth boride, RCo_3B_2, of a hexagonal $CaZn_5$-type[18] structure in systems of rare earth-cobalt-boron.

Experimental

Materials. The cobalt metal and the crystalline boron were obtained from Wako Pure Chemical Industries, Ltd., Tokyo. The purities were 99.99 and 99.9% respectively. All the rare earth metals[19] except samarium were prepared in our laboratory by the calcium-metal reduction of rare earth trifluorides. The samarium metal was prepared from samarium oxide by lanthanum-metal reduction. These metal rods were refined by arc-melting. The purity of the metals obtained by these methods was 99.8%. The main impurities were oxygen and carbon.

Preparation of Alloys. The alloys were prepared by co-melting mixtures of the rare earth metal, the cobalt metal, and crystalline boron in an arc furnace under an inert gas atmosphere. Each sample was remelted three times to prove its homogeneity. After melting, some of the alloy buttons were analysed by chemical methods; it was found that the rare earth metals lost during the melting process were negligible except for samarium. In the case of samarium, 10—15 wt% of the samarium metals were vaporized during the melting process.

In order to establish the thermal equilibrium, some of the alloy buttons were annealed at 1150°C for 96 hr in tantalum crucibles sealed into quartz tubes under a reduced pressure of purified argon.

The densities of the samples were determined at 24.5°C by the flotation technique using CCl_4.

X-Ray and Chemical Analytical Procedures. The samples

1) H. H. Stadelmarer, *Z. Metallk.*, **52**, 758 (1961).
2) H. H. Stadelmarer and A. C. Fraker, *Metall.*, **16**, 212 (1962).
3) H. H. Stadelmarer and R. A. Gregg, *ibid.*, **16**, 407 (1962).
4) H. H. Stadelmarer, J. D. Schobel, and L. T. Jordon, *Metall.*, **16**, 752 (1962).
5) H. H. Stadelmarer and L. T. Jordon, *Z. Metallk.*, **53**, 719 (1962).
6) H. H. Stadelmarer and R. B. Fitts, *Metall.*, **16**, 773 (1962).
7) H. H. Stadelmarer, J. D. Schobel, and J. R. Sagmuller, *ibid.*, **18**, 23 (1964).
8) H. H. Stadelmarer and T. S. Yun, *Z. Metallk.*, **53**, 754 (1962).
9) H. H. Stadelmarer and F. M. Lee, *Metall.*, **18**, 111 (1964).
10) W. Rieger, H. Nowotony, and F. Benesovsky, *Mh. Chem.*, **97**, 378 (1966).
11) W. Rieger, H. Nowotony, and F. Benesovsky, *ibid.*, **95**, 1502 (1964).
12) W. Rieger, H. Nowotony, and F. Benesovsky, *ibid.*, **96**, 844 (1965).
13) H. Haschke, H. Nowotony, and F. Benesovsky, *ibid.*, **97**, 1461 (1966).
14) H. Haschke, H. Nowotony, and F. Benesovsky, *ibid.*, **97**, 1459 (1966).
15) Yu. B. Kuzma, *Soviet Physics-Crystallography.*, **15**, 312 (1970).
16) K. Niihara, T. Shishido, and S. Yajima, This Bulletin, **44**, 3214 (1971).
17) K. Niihara and S. Yajima, *Chem. Lett.*, **1972**, 875.
18) J. H. Wernick and S. Geller, *Acta Crystallogr.*, **12**, 662 (1959).
19) K. Niihara, K. Sasaki, and S. Konno, Tecknical Report, The Research Institute for Iron, Steel, and Other Metals, Tohoku University, **1**, 54 (1969).

for X-ray and chemical analyses were generally taken from the most homogeneous part of annealed specimens. They were crushed in an agate mortar under toluene in order to avoid unnecessary oxidation and then divided for X-ray and chemical analyses.

After the solution obtained by dissolving the samples into aqua regia was fumed with conc. $HClO_4$, the precipitates of RF_3 obtained by the addition of conc. HF were submitted to a gravimetrical determination of the rare earth content. The analyses of the Co metal were performed by means of X-ray fluorescence analysis. The boron content was determined by a method[20] previously reported.

All the X-ray powder patterns were taken with a Debye-Scherrer camera (114.6 mm in diameter) which corrected using standard silicon powder. Mn-filtered Fe ($K\alpha_1$=1.9360 Å, $K\alpha_2$=1.9399 Å, and $K\bar{\alpha}$=1.9373 Å) radiation was employed. The lattice parameters were determined by the Nelson-Riley extraporation method. The observed X-ray diffraction intensities were obtained by measuring the peak areas which were produced using a diffractometer in combination with an NaI(Tl) scintillation counter and a pulse-height analyser.

Results and Discussion

In investigating the phase equilibria in the system of Y–Co–B, a ternary compound was found by chemical and X-ray analyses. This compound was, at 1150°C, in equilibrium with YCo_2, YCo_5, and the ternary compounds YCo_2B_2[16] and $YCo_{12}B_6$.[17] The chemical analyses of the samples in the single-phase region showed that the new ternary compound existed in the region (at.%): Y(16.5—16.7), Co(50.0—50.4), and B(33.2—33.3). The stoichiometric composition of YCo_3B_2 was proposed on the basis of the results of X-ray and chemical analyses and density measurements. Ternary compounds with a similar composition were also prepared by the arc-melting method in the systems of (Ce, Sm, Gd, Tb, Dy, Ho, and Er)–Co–B. However, efforts to prepare $LaCo_3B_2$, $NdCo_3B_2$, and $PrCo_3B_2$ by arc-melting were unsuccessful.

Table 2. X-ray diffraction data for $GdCo_2B_2$

hkl	d_{obs}(Å)	d_{cal}(Å)	I_{obs}	I_{cal}
100	4.388	4.387	38.6	39.8
001	—	3.022	0	0
110	2.530	2.533	15.3	18.2
101	2.488	2.489	98.7	96.6
200	2.193	2.194	75.8	77.9
111	1.940	1.941	55.2	53.5
201	—	1.775	0	0.1
210	1.658	1.658	6.5	5.8
002	1.512	1.511	7.9	8.5
300	1.460	1.462	3.2	2.9
211	1.453	1.454	30.9	34.5
102	1.429	1.429	21.5	18.5
301	1.318	1.316	19.8	16.5
112	1.300	1.298	6.0	4.6
220	1.268	1.267	14.2	16.7
202	1.244	1.244	26.6	28.7
310	1.217	1.217	21.8	14.2
221	—	1.168	0	0.1
311	1.129	1.129	24.0	25.9
212	1.117	1.117	5.0	6.5
400	1.097	1.097	17.4	15.4
302	1.052	1.051	8.1	5.9
401	—	1.031	0	0
320	1.007	1.007	7.3	5.8
003		1.007		0
103	0.983	0.982	35.2	38.3

B (the temperature factor)=0.87, R=0.130

Table 1. X-ray diffraction data for YCo_3B_2

hkl	d_{obs}(Å)	d_{cal}(Å)	I_{obs}	I_{cal}
100	4.346	4.347	5.6	5.9
001	3.029	3.027	6.0	5.7
110	2.509	2.510	4.3	6.2
101	2.484	2.484	89.4	90.8
200	2.174	2.174	100.1	96.7
111	1.934	1.932	45.2	53.9
201	1.766	1.766	10.6	10.2
210	—	1.643	0	1.1
002	1.514	1.514	8.6	11.1
300	—	1.449	0	1.0
211	1.445	1.444	42.0	30.9
102	—	1.429	0	0.7
301	1.307	1.307	15.6	16.2
112	1.297	1.296	2.3	1.7
220	1.255	1.255	19.8	21.2
202	1.244	1.242	42.2	35.7
310	—	1.206	0	0.8
221	—	1.159	0	1.7
311	1.121	1.120	26.5	23.5
212	1.112	1.113	1.0	1.4
400	1.088	1.087	15.7	19.4
302	1.046	1.047	1.5	2.3
401	1.024	1.023	5.2	4.8

B (the temperature factor)=0.64, R=0.122

The Crystal Structure of YCo_3B_2 and $GdCo_3B_2$. The X-ray powder pattern for YCo_3B_2 was indexed on the basis of a hexagonal unit cell. The d-values are shown in Table 1. As is shown in this table, the observed d-values are in good agreement with those calculated. The lattice parameters for YCo_3B_2 were a=5.020±0.002 Å, c=3.027±0.002 Å, and c/a=0.603. The calculated and measured densities were 4.35 g/cm³ and 4.29 g/cm³ respectively. Therefore, the unit cell contains one formula unit of YCo_3B_2.

The crystal structure of the YCo_3B_2 compound was considered to be of a type similar to that of the intermetallic compound $CaZn_5$,[18] because the X-ray diffraction pattern of YCo_3B_2 appeared to be similar. $CaZn_5$ has the following atomic positions, according to the International Table for X-ray Crystallography:[21] space group P6/mmm (D^1_{6h}), 1Ca in 1(a), 3Zn in 3(g), and 2Zn in 2(c). Therefore, it was assumed that the Y, Co, and B atoms of YCo_3B_2 occupy the following positions: 1Y in 1(a), 3Co in 3(g), and 2B in 2(c). The X-ray diffraction intensities were calculated according to the formula;

20) K. Niihara, This Bulletin, **44**, 963 (1971).

21) International Tables for X-ray Crystallography., Vol. 1, p. 298. The Kynoch Press, Birmingham, England 1968.

TABLE 3. CRYSTALLOGRAPHIC DATA FOR YCo_3B_2 AND $GdCo_3B_2$ COMPOUNDS.

	YCo_3B_2	$GdCo_3B_2$
Symmetry	Hexagonal	Hexagonal
Lattice parameters (Å)	$a=5.020+0.002$ $c=3.027+0.002$ $c/a=0.603$	$a=5.066+0.003$ $c=3.022+0.002$ $c/a=0.597$
Molecules per unit cell	1	1
Density (g/cm^3)	$\rho_{obsd}=4.29$ $\rho_{calcd}=4.35$	$\rho_{obsd}=5.25$ $\rho_{calcd}=5.30$
Space group	$P6/mmm(D^1_{6h})$	$P6/mmm(D^1_{6h})$
Atom position	1Y in 1(a) (0,0,0) 3Co in 3(g) $(\frac{1}{2}0\frac{1}{2})$ $(0\frac{11}{22})$ $(\frac{111}{22\bar{2}})$ 2B in 2(c) $(\frac{12}{33}0)$ $(\frac{12}{3\bar{3}}0)$	1Gd in 1(a) (0,0,0) 3Co in 3(g) $(\frac{1}{2}0\frac{1}{2})$ $(0\frac{11}{22})$ $(\frac{111}{22\bar{2}})$ 2B in 2(c) $(\frac{12}{3\bar{3}}0)$ $(\frac{21}{3\bar{3}}0)$
Interatomic distance in coordination polyhedron of B. (Å)	6Co–B=2.10 3Y–B=2.90 4Co–Co=2.51 2Co–Co=3.03	6Co–B=2.10 3Gd–B=2.93 4Co–Co=2.53 2Co–Co=3.02

$$\mathbf{I}_{cal} = A \cdot |\mathbf{F}|^2 \cdot M \cdot Lp \cdot \theta$$

in which A, $\mathbf{F}$, Lp, M, and θ represent the scaling factor, the structure factor, the multiplicity, the Lorentz polarization factor, and the overall temperature factor respectively. In the structure-factor calculation, the atomic scattering factor for the neutral atoms listed in the International Table for X-ray Crystallography and the anomalous dispersion corrections for the Y and Co atoms of Cromer[22] were employed.

In this structure, the positions of all the atoms are fixed by symmetry. Thus, the only variable parameter is the temperature factor.

The temperature factors were found by a least-squares solution of the plot of $\log |I_c/I_0|$ *vs.* $(\sin/\lambda)^2$. Using an overall temperature factor of 0.64, the calculated and observed X-ray diffraction intensities obtained for YCo_3B_2 are given in Table 1. The reliability factor, $R=\sum_{hkl}|I_{cal}-I_{obs}|/\sum_{hkl}I_{obs}$, amounts to 0.122 for this structure. From this result, it can be considered that the Y and Co atoms occupy the 1(a) and 3(g) sites respectively. However, from only the value of the R-factor it cannot be evaluated accurately whether or not the assumption concerning the positions of the B atoms is reasonable because of the small atomic scattering factor of the B atoms. It is impossible, however, that B atoms occupy the 2(d) and 2(e) sites in the P6/mmm space group, considering the atomic sizes of Y, Co, and B, and the coordination of the B atoms. Generally, B atoms of metal-rich borides, such as Re_3B, Pd_3B, Cr_5B_3, and Pd_5B_3,[23] are surrounded by nine metal atoms, situated at the six corners of a trigonal prism and outside the three lateral faces of this prism. Thus, with these simple geometrical arguments it is reasonable to think that the B atoms in YCo_3B_2 occupy the 2(c) site. In the ternary system of Gd–Co–B, a ternary boride $GdCo_3B_2$ with the $CaZn_5$-type structure was synthesized by arc-melting. The lattice parameters and densities are shown in Table 3. In order to calculate the X-ray diffraction intensities for $GdCo_3B_2$, it was assumed that the crystal structure of this compound was the same as that of YCo_3B_2. The final results are compared with the observed intensities in Table 2, using a temperature factor of 0.87. The

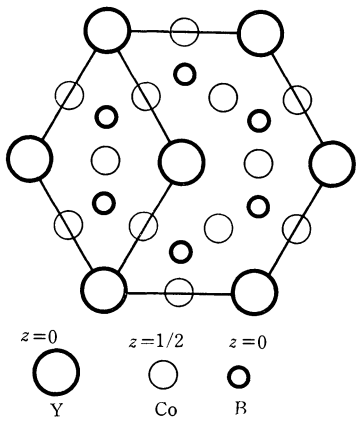

Fig. 1. The projection of YCo_3B_2 structure on (001).

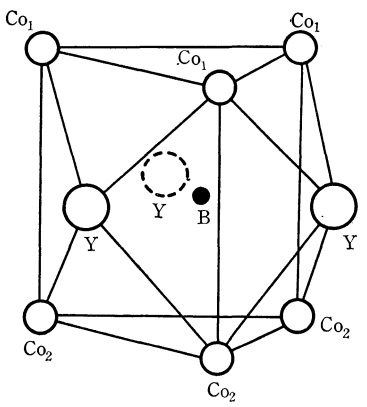

Fig. 2. The coordination polyhedron of boron atom in YCo_3B_2 structure.

22) D. T. Cromer, *Acta Crystallogr.*, **18**, 17 (1965).

23) B. Aronsson, "Borides, Silicides and Phosphides," Edited by B. Aronsson, Methuen and Co. Ltd., London (1965), p. 46.

TABLE 4. THE X-RAY DIFFRACTION DATA FOR $CeCo_3B_2$, $SmCo_3B_2$, $TbCo_3B_2$, $DyCo_3B_2$, $HoCo_3B_2$, AND $ErCo_3B_2$

hkl	Int	$CeCo_3B_2$		$SmCo_3B_2$		$TbCo_3B_2$		$DyCo_3B_2$		$HoCo_3B_2$		$ErCo_3B_2$	
		d_{obsd}	d_{calcd}	d_{obsd}	d_{calcd}	d_{obsd}	d_{calcd}	d_{obsd}	d_{calcd}	d_{obsd}	d_{calcd}	d_{obsd}	d_{calcd}
100	m	4.376	4.380	4.398	4.398	4.377	4.373	4.359	4.357	4.344	4.346	4.332	4.335
001	vvw	—	3.040	3.029	3.031	—	3.009	—	3.021	—	3.023	—	3.024
110	m	2.528	2.529	2.536	2.539	2.523	2.525	2.514	2.516	2.506	2.509	2.503	2.503
101	s	2.497	2.497	2.495	2.496	2.476	2.479	2.480	2.483	2.483	2.482	2.482	2.480
200	vs	2.189	2.190	2.200	2.199	2.187	2.187	2.178	2.178	2.174	2.173	2.168	2.168
111	s	1.943	1.944	1.945	1.947	1.933	1.934	1.932	1.933	1.930	1.931	1.927	1.928
201	m	1.777	1.777	1.783	1.780	1.768	1.769	1.765	1.767	—	1.764	—	1.762
210	vvw	1.654	1.656	1.663	1.662	1.652	1.653	1.647	1.647	1.640	1.643	1.638	1.639
002	m	1.520	1.520	1.514	1.516	1.504	1.503	1.511	1.511	1.513	1.512	1.512	1.512
211	s	1.454	1.454	1.459	1.458	1.450	1.449	1.447	1.446	1.445	1.443	1.441	1.441
102	vw	—	1.436	1.433	1.433	1.422	1.423	1.425	1.427	—	1.428	—	1.428
301	m	1.317	1.316	1.318	1.320	1.312	1.312	1.310	1.309	1.307	1.306	1.304	1.304
112	w	—	1.303	1.302	1.301	1.291	1.292	1.295	1.295	1.294	1.295	—	1.294
220	m	1.266	1.265	1.270	1.270	1.262	1.263	1.259	1.258	1.255	1.255	1.252	1.252
202	s	1.249	1.249	1.250	1.248	1.239	1.239	1.241	1.241	1.242	1.241	1.240	1.240
310	vw	—	1.215	1.220	1.220	1.213	1.213	1.211	1.208	1.204	1.205	—	1.156
221	vvw	—	1.168	—	1.171	—	1.164	—	1.161	—	1.159	1.202	1.202
311	m	1.129	1.128	1.134	1.132	1.125	1.125	1.123	1.122	1.120	1.120	1.118	1.117
212	w	—	1.120	1.122	1.120	1.113	1.113	1.111	1.113	1.113	1.112	—	1.111
400	m	1.095	1.095	1.100	1.100	1.093	1.093	1.089	1.089	1.086	1.086	1.084	1.084
302	vw	—	1.053	1.053	1.054	1.047	1.047	1.047	1.047	1.046	1.046	1.044	1.045

reliability factor, R, is 0.130. The crystallographic data for YCo_3B_2 and $GdCo_3B_2$ are summarized in Table 3. Figure 1 indicates the projection of the YCo_3B_2 structure on the (001) plane. The coordination polyhedron of the B atoms was formed by the combination of a trigonal prism and three rectangular pyramids on its lateral faces. In other words, the boron atom is surrounded by six Co atoms and three Y atoms, situated at the corners of a trigonal prism and outside the lateral faces of the prism respectively. Figure 2 shows the polyhedron of the B atom in the 2(c) site of the YCo_3B_2 structure. The ternary boride YCo_3B_2 has a superstructure in which two Co atoms in the 2(c) site of the intermetallic compound YCo_5[24] with the $CaZn_5$-type structure are replaced by two B atoms.

The interatomic distances between the B and the six nearest Co stoms are 2.10 Å for both YCo_3B_2 and $GdCo_3B_2$. This distance is closer to the sum of the Goldschmidt metallic radii[23] for the 12-coordination of B (0.88 Å) and Co (1.16 Å) than to the sum of the Pauling metallic radii[25] for the 12-coordination of B (0.98 Å) and Co (1.25 Å). The distances between the B atom and three rare earth atoms in the next-nearest neighbor are 2.90 and 2.93 Å for YCo_3B_2 and $GdCo_3B_2$ respectively.

The Structure of Ternary Rare Earth Borides, RCo_3B_2 (R=Ce, Sm, Tb, Dy, Ho, and Er). The crystal structure of RCo_3B_2 compounds (R=Ce, Sm, Tb, Dy, Ho, and Er) is isostructural with YCo_3B_2 and $GdCo_3B_2$. The powder X-ray data are shown in Table 4 for $CeCo_3B_2$, $SmCo_3B_2$, $TbCo_3B_2$, $DyCo_3B_2$, $HoCo_3B_2$, and $ErCo_3B_2$. As is shown in this Table, there is a good agreement between the observed and calculated interplanar spacings. The lattice parameters of RCo_3B_2 compounds are summarized in Table 5. The change in the a parameter against the atomic number of the rare earth elements plotted in Fig. 3 is characteristic of the well-known lanthanide contraction. The c para-

TABLE 5. THE LATTICE PARAMETERS FOR RCo_3B_2 COMPOUNDS (R=Y, Ce, Sm, Gd, Tb, Dy, Ho, Er)

R	Lattice parameters (Å)		Density (g/cm³)	
	a	c	ρ_{obsd}	ρ_{calcd}
Y	5.020±0.002	3.027±0.002	4.29	4.35
Ce	5.058±0.002	3.040±0.002	4.96	5.03
Sm	5.079±0.003	3.031±0.002	5.20	5.28
Gd	5.066±0.003	3.022±0.002	5.25	5.30
Tb	5.050±0.003	3.009±0.002	5.32	5.38
Dy	5.031±0.003	3.021±0.002	5.45	5.45
Ho	5.018±0.003	3.023±0.002	5.50	5.51
Er	5.006±0.003	3.024±0.002	5.57	5.57

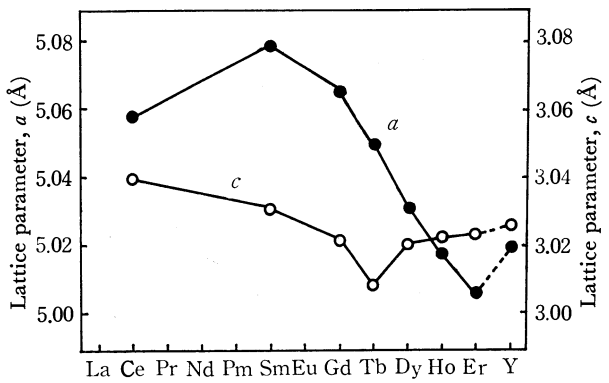

Fig. 3. The lattice parameters of the hexagonal RCo_3B_2 compounds as a function of atomic number of rare earth elements. ○: the c parameter, ●:the a parameter.

24) J. Schweizer and F. Tasset, *Mat. Res. Bull.*, **4**, 369 (1969).
25) L. Pauling, "The Nature of the Chemical Bond," 3rd ed., Cornell University Press, (1960), Chap. 11.

meter is fairly constant, increasing slightly with the atomic number of the rare earth element from the $TbCo_3B_2$ compound onwards.

The parameters of the $CeCo_3B_2$ compound are an exception. They are similar to those of the compound at the second series of lanthanides. It may be seen that the Ce atom has a relatively small radius in this structure. Various authors[26-28] have attributed this contraction of the Ce atom to the loss of the 4f electron to the compound's conduction band.

A similar variation in the *c* parameter has been observed in the case of RCo_5,[29] which has the $CaZn_5$-type structure. The *c* parameters of the RCo_3B_2 compounds do not indicate the lanthanide contraction, probably because of: (a) the effect of the nonstoichiometric composition in RCo_3B_2 compounds and (b) the fairly constant interatomic distances between the B and Co atoms in the trigonal prism. With reference to (b), the interatomic distances, B–6Co, in the trigonal prism of RCo_3B_2 (Fig. 2) are 2.11—2.10 Å and are fairly constant, although one rare earth is replaced by another small rare earth. Figure 4 shows the variation in the interatomic distances in the coordination polyhedron of the B atom in the RCo_3B_2 structure (Fig. 2) against the atomic number of the rare earth elements and the variation in the corresponding distances of RCo_5 compounds. As is shown in Fig. 4, the interatomic distances of B–3R, Co_1–Co_1, and R–4Co indicate an acceptable lanthanide contraction. The Co_1–Co_2 distance has its minimum at $TbCo_3B_2$. From these results, it may be seen that, in the compounds at the end of the second rare earth series, the Co_1–Co_1 distance decreases and the Co_1–Co_2 distance increases in order to preserve the stable Co–B interatomic distance (2.11—2.10) in the trigonal prism of the RCo_3B_2 structure, when one rare earth element is replaced by other small rare earth elements.

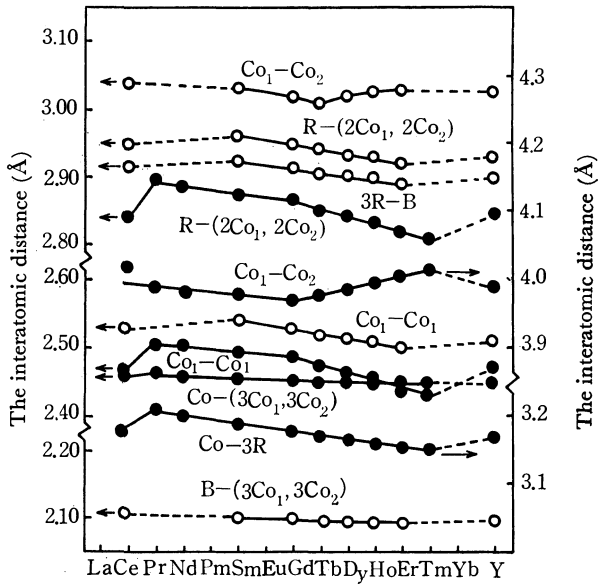

Fig. 4. The interatomic distances in the coorinatidon polyhedron of B and Co atoms situated at the 2(c) sites of RCo_3B_2 and RCo_5 structure, respectively (Ref. Fig. 2).
○: RCo_3B_2; ●: RCo_5.

Similar phenomena were observed in the RCo_5 compounds,[29] as is shown in Fig. 4. The nonstoichiometric and magnetic properties of these borides will provide additional data which may be useful in the interpretation of the nature of bonding. These data will be the subject of a separate paper.

26) A. W. Lawson and T. Y. Tangs, *Phys. Rev.*, **76**, 301 (1949).
27) L. F. Bates and M. M. Newman, *Proc. Roy. Soc.*, **72**, 345 (1958).
28) K. A. Gshneider and R. Smduchowski, *J. Less-Common Metals.* **5**, 374 (1963).
29) R. Lemaire, *Cobalt*, **32**, 132 (1966).

Theoretical Calculations and Assignments of Electronic Absorption Spectra of Cation Radicals of *o*-, *m*-, and *p*-Disubstituted Benzenes Having Amino and Hydroxyl Groups

Shunji KATSUMATA and Katsumi KIMURA

Physical Chemistry Laboratory, Institute of Applied Electricity, Hokkaido University, Sapporo

(Received August 3, 1972)

Calculations have been carried out on the electronic spectra and electronic structures of the cation radicals of *o*-, *m*-, and *p*-disubstituted benzenes having the amino and hydroxyl groups, by an open shell SCF MO CI method involving some doubly excited electron configurations. Assignments of the electronic absorption spectra of these cation radicals have been made on the basis of resulting transition energies and oscillator strengths. The results are in good agreement with experimental data. Effects of methyl-substitution on the cation spectra are discussed. Spin densities of these cation radicals have also been calculated and compared with experimental data.

Kimura *et al.*[1-3] observed the electronic absorption spectra of cation radicals of various disubstituted benzenes, *i.e.*, *p*-aminophenol$^+$, *m*-aminophenol$^+$, and their *N*- and *O*-methyl derivatives, by ultraviolet irradiation in rigid glasses at 77K. The electronic absorption spectra of hydroquinone$^+$ and several of its *O*-methyl derivatives have also been measured in concentrated sulfuric acid by Kimura and Yamada.[4] For EPA glasses containing *m*-aminophenol$^+$, *m*-anisidine$^+$, and *m*-phenylenediamine$^+$, appreciable blue shifts of the electronic absorption bands due to trapped electrons have been observed.[5] It has been pointed out that the mangitudes of such spectral shifts depend largely on electronic structures of the cations.

The open shell SCF MO method involving configuration interaction (CI) is now generally known to be advantageous for calculating electronic spectra and structures of organic free radicals having an odd electron. Using a method which combines the open shell SCF procedure of Longuet-Higgins and Pople[6] with CI, Ishitani and Nagakura[7,8] have extensively studied the electronic structures and spectra of the anion radicals of substituted benzenes having nitro, nitroso, and cyano groups and the anion radical of paracyclophane. Zahradnik and Carsky[9] have employed a similar theoretical method for studying the electronic spectra of the free radicals of various alternant hydrocarbons in more detail. Shida and Iwata[10] have recently carried out CI calculations of nitro-substituted aromatic anion radicals in order to explain experimental absorption spectra, by including some doubly excited electronic configurations.

However, as regards the cation radicals of disubstituted benzenes with electron donating groups such as amino and hydroxyl groups, only a few fragmentary reports have been given on their theoretical assignments; by Monkhorst and Kommandeur[11] for the electronic absorption spectrum of *N*,*N*,*N*′,*N*′-tetramethyl-*p*-phenylenediamine$^+$ and by Kimura and Mataga[12] for that of *p*-phenylenediamine$^+$, with the open shell MO CI calculation.

In connection with our previous works,[1-5] the present authors used the open shell SCF MO CI method to carry out theoretical studies on the cation radicals of a series of substituted benzenes having amino and hydroxyl groups, in order to clarify the electronic absorption bands already known for these cations and to predict those still unknown in experiment. It is especially interesting to compare the electronic transition of isomers of the disubstituted benzenes.

Method of Calculation

The SCF MO CI method was used in the calculation of cation radicals of *o*-, *m*-, and *p*-disubstituted benzenes having OH and NH_2 groups, and also that of monosubstituted benzenes such as phenol$^+$ and aniline$^+$. Numberings of carbon atoms in the cations are illustrated in Fig. 1.

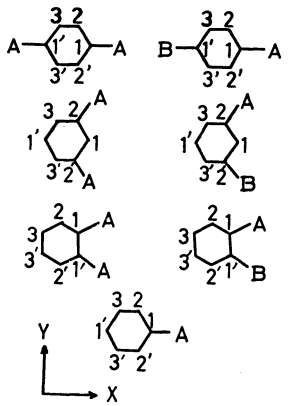

Fig. 1. Numbering of the carbon atoms in the cations of substituted benzenes, A and B indicating substituents.

1) K. Kimura, H. Yamada, and H. Tsubomura, *J. Chem. Phys.* **48**, 440 (1968).
2) K. Kimura, K. Yoshinaga, and H. Tsubomura, *J. Phys. Chem.*, **71**, 4485 (1967).
3) A. Egawa, K. Kimura, and H. Tsubomura, This Bulletin, **43**, 944 (1970).
4) K. Kimura and H. Yamada, *ibid.*, **42**, 3032 (1969).
5) K. Kimura, S. Katsumata, and K. Sawada, *J. Phys. Chem.*, **76**, 639 (1972).
6) H. C. Longuet-Higgins and J. A. Pople, *Proc. Phys. Soc. Ser. A*, **68**, 591 (1955).
7) A. Ishitani and S. Nagakura, *Theoret. Chim. Acta*, **4**, 236 (1966).
8) A. Ishitani and S. Nagakura, *Mol. Phys.*, **12**, 1 (1967).
9) R. Zahradnik and P. Carsky, *J. Phys. Chem.*, **74**, 1235, 1240, 1249 (1970).
10) T. Shida and S. Iwata, *ibid.*, **75**, 2591 (1971).
11) H. J. Monkhorst and J. Kommandeur, *J. Chem. Phys.*, **47**, 391 (1967).
12) K. Kimura and N. Mataga, *ibid.*, **51**, 4167 (1969).

TABLE 1. THEORETICAL RESULTS OF ANILINE$^+$ AND *o*-, *m*-, AND *p*-PD$^+$

Symmetry	Energy (eV)	Configurations mainly contributing (%)
		Aniline$^+$
$^2B_1$	−0.584	ground (95)
$^2A_2$	0.640	3→4 (93)
$^2B_1$	2.298	2→4 (73), 4→6 (15), 3→5 (4)′
$^2B_1$	3.747	4→6 (50), 3→5 (23)′, 3→5 (10), 1→4 (6)
$^2A_2$	3.898	4→5 (67), 3→6 (18)′
		o-PD$^+$
$^2B_1$	−0.572	ground (94)
$^2A_2$	0.700	4→5 (91)
$^2B_1$	2.518	3→5 (66), 5→6 (16), 4→7 (4)
$^2A_2$	3.283	5→7 (60), 4→6 (13), 4→6 (11), 2→5 (9)
$^2B_1$	3.892	5→6 (50), 4→7 (29), 3→5 (8)
		m-PD$^+$
$^2A_2$	−0.581	ground (95)
$^2B_1$	0.143	4→5 (92)
$^2B_1$	1.869	3→5 (77), 5→6 (11), 4→7 (5)′
$^2A_2$	3.414	5→7 (54), 4→6 (14), 4→6 (12)′, 2→5 (8)
$^2B_1$	3.707	5→6 (46), 4→7 (32), 4→5, 4→6 (5)
		p-PD$^+$
$^2B_{2g}$	−0.608	ground (95)
$^2B_{3u}$	1.923	3→5 (72), 5→7 (18)
^2A_u	3.206	5→6 (83), 3→5, 3→6 (5), 4→7 (4)′
$^2B_{3u}$	3.418	5→7 (58), 4→6 (21)′, 3→5 (6), 4→6 (6)
$^2B_{3u}$	5.021	4→6 (53), 1→5 (17), 5→7 (9), 3→5 (6)

We used a computer program in which a total of 40 configurations was chosen for each symmetry from the first 100 low-energy configurations of one- and two-electron excitations.[13]

The Coulomb repulsion integrals of the type $(pp|qq)$ were calculated by using the Pariser-Parr approximation. The valence state ionization potentials and electron affinities were taken from literature[14] as follows: $I_C=11.22$ eV, $A_C=0.62$ eV, $I_N{}^+=28.88$ eV, $A_N{}^+=12.28$ eV, $I_O{}^+=34.43$ eV, $A_O{}^+=14.97$ eV. Nuclear charge values $Z_C=1$, $Z_N=2$, and $Z_O=2$ were used for carbon, nitrogen, and oxygen atoms, respectively. The penetration integrals were neglected, and core resonance integrals parametrized as $\beta_{\mu\nu}$. Bond lengths r(C–C)= 1.39 Å and r(C–N)=r(C–O)=1.36 Å were used throughout this work. The calculations were carried out with a FACOM 230-60 electronic computer in Hokkaido University using a computer program prepared by Iwata and Katsumata.[13]

Results and Discussion

Calculated results for energies of the ground and lower electronic excited states of aniline$^+$ and *o*-, *m*-, and *p*-phenylenediamine$^+$ are given in Table 1, together with electron configurations contributing to the various states by more than 4% (those of doubly excited configurations are underlined). Electronic configurations having doublet states are distinguished from each other with a prime, configurations $(i\to k)$ and $(i\to k)'$ designating $\sqrt{1/2}(|im\bar{k}|-|i\bar{m}k|)$ and $6^{-1/2}(-2|\bar{i}mk|+|im\bar{k}|+|i\bar{m}k|)$, respectively. The resulting transition energies, oscillator strengths and directions of transition moments are summarized in Table 2 together with experimental data available for comparison.

Cations of o-, m-, *and* p-*Phenylenediamines* (o-, m-, *and* p-*PD*$^+$). Electronic transition energies and oscillator strengths of *m*- and *p*-PD$^+$ were calculated for different β_{CN} values from −2.40 to −3.60 eV with an interval of 0.2 eV. The resulting transition energies were plotted against the β_{CN}'s and compared with experimental data available, as shown in Fig. 2. The electronic transition to the excited state to which the (4→5) configuration mainly contributes is forbidden in *p*-PD$^+$ because of molecular symmetry (D_{2h}), whereas

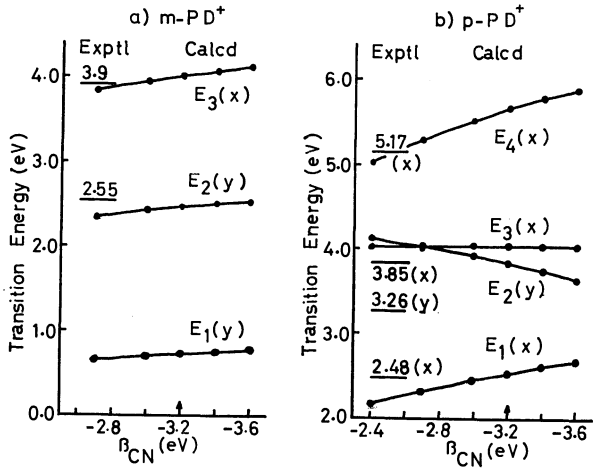

Fig. 2. Transition energies plotted against β_{CN}.

13) The program was prepared by S. Iwata and S. Katsumata, and used in the calculation of Ref. 10.

14) H. Hosoya, *Kagaku No Ryoiki*, **21**, 47 (1967). The values are essentially the same as those given by G. Pilcher and H. A. Skinner, *J. Inorg. Nucl. Chem.*, **24**, 937 (1962).

TABLE 2. THEORETICAL RESULTS OF ELECTRONIC TRANSITION ENERGIES (OSCILLATOR STRENGTHS, AND DIRECTION OF TRANSITION MOMENTS) OF THE CATIONS, COMPARED WITH AVAILABLE EXPERIMENTAL DATA

(E IN eV)

o-PD$^+$		m-PD$^+$		
E_{calcd}	(f_{calcd})	E_{calcd}	(f_{calcd})	E_{exptl}[a]
1.27	(0.01, y)	0.72	(0.01, y)	
3.09	(0.05, x)	2.45	(0.06, y)	2.55
3.86	(0.03, y)	4.00	(0.03, x)	3.90
4.46	(0.10, x)	4.29	(0.00, y)	

p-PD$^+$			
E_{calcd}	(f_{calcd})	E_{exptl}[b]	(f_{exptl})[b]
2.53	(0.10, x)	2.48, 2.67	(0.11)
3.81	(0.04, y)	3.26	(0.06)
4.03	(0.18, x)	3.85	(0.31)
5.63	(0.14, x)	5.17	(0.2)

DMPD$^+$			TMPD$^+$		
E_{calcd}	(f_{calcd})	E_{exptl}	E_{calcd}	(f_{calcd})	E_{exptl}[c] (f_{exptl})[c]
2.36	(0.00, y)		2.16	(0.08, x)	2.19 (0.19, x)
2.42	(0.09, x)	2.37	3.61	(0.04, y)	3.13 (0.05, y)
3.71	(0.04, y)	3.26	3.95	(0.30, x)	3.82 (0.32, x)
4.10	(0.20, x)	3.83	5.52	(0.16, x)	4.80 (0.1)
5.40	(0.11, x)	4.96			

o-AP$^+$		m-AP$^+$			p-AP$^+$		
E_{calcd}	(f_{calcd})	E_{calcd}	(f_{calcd})	E_{exptl}[d]	E_{calcd}	(f_{calcd})	E_{exptl}[e]
1.15	(0.00_5)	0.78	(0.00_4)		1.72	(0.00_0, y)	
3.11	(0.05)	2.67	(0.06)	2.65	2.72	(0.09, x)	2.78
4.06	(0.04)	4.21	(0.04)	4.0	4.00	(0.04, y)	3.50
4.76	(0.00_8)	4.67	(0.00_2)	4.6	4.1	(0.14, x)	4.10

o-DHB$^+$		m-DHB$^+$		p-DHB$^+$		
E_{calcd}	(f_{calcd})	E_{calcd}	(f_{calcd})	E_{calcd}	(f_{calcd})	E_{exptl}[f]
0.88	(0.00_4, y)	0.60	(0.00_2, y)	2.75	(0.09, x)	2.95
2.91	(0.05, x)	2.55	(0.06, y)	4.18	(0.03, y)	
4.08	(0.05, y)	4.21	(0.04, x)	4.22	(0.10, x)	
4.66	(0.00_0, x)	4.57	(0.00_4, y)	5.54	(0.20, y)	

Phenol$^+$		Aniline$^+$		
E_{calcd}	(f_{calcd})	E_{calcd}	(f_{calcd})	E_{exptl}[g]
0.78	(0.00_1, y)	1.22	(0.00_3, y)	
2.84	(0.06, x)	2.88	(0.06, x)	2.88
4.43	(0.06, x)	4.33	(0.06, x)	
4.56	(0.00_0, y)	4.48	(0.00_4, y)	

a) Ref. 5. The value 3.90 eV has recently been obtained. b) Ref. 12. c) Ref. 18. d) Ref. 5. The values 4.0 and 4.6 eV have recently been obtained. e) Ref. 2. f) Ref. 4. g) Ref. 15.

it is allowed in o- and m-PD$^+$. We see that E_1, E_2, and E_4 in p-PD$^+$ are considerably sensitive to β_{CN}, while E_3 in p-PD$^+$ and E_1 to E_3 in m-PD$^+$ are insensitive. The E_1 transition energy of p-PD$^+$ corresponding to the first visible absorption band was found to be well reproduced at $\beta_{CN}=-3.20$ eV. This value was therefore employed throughout the present work, and the transition energies and oscillator strengths shown in Table 2 are those calculated with it.

Contributions of nitrogen AO's to SCF MO's (ϕ_3–ϕ_7) of o-, m-, and p-PD$^+$ are as follows. In p-PD$^+$, the contributions of (N_1+N_2) to $\phi_3(b_{3u})$ and $\phi_7(b_{3u})$ are 21 and 7%, respectively, and that of (N_1-N_2) to $\phi_5(b_{2g})$ is 16%. There are no nitrogen contributions to $\phi_4(b_{1g})$ and $\phi_6(a_u)$ corresponding to the e_{1g} and e_{2u} MO's of benzene, respectively. In m-PD$^+$, contributions of (N_1+N_2) to ϕ_3, ϕ_4, and ϕ_6 in symmetry b_1 are 10, 14, and 2%, respectively, and those of (N_1-N_2) to ϕ_5 and ϕ_7 in symmetry a_2 are 11 and 6%, respectively. In o-PD$^+$, contributions of (N_1+N_2) to ϕ_3, ϕ_5, and ϕ_6 in symmetry b_1 are 8, 16, and 2%, respectively, and those of (N_1-N_2) to ϕ_4 and ϕ_7 in symmetry a_2 are 6 and 1%, respectively.

The electronic absorption spectrum of p-PD$^+$ was interpreted by Kimura and Mataga[12] with the open shell MO CI method using Hückel MO's. However, in the present work, much better results were obtained for transition energies and oscillator strengths (see Table 2).

In p-PD$^+$, electron configurations with the largest contributions are (3→5), (5→6), (5→7), and (4—6) in Ψ_1 to Ψ_4, respectively (Table 1).

The calculated results of m-PD$^+$ are also in good agreement with the experimental ones (Table 2). For o-PD$^+$, however, there are no experimental values reported. It is interesting to note that the present calculations of o- and m-PD$^+$ predict that the first transitions $\Psi_0\rightarrow\Psi_1$ (f=0.01) should cause weak absorption bands in near infrared region, although no such absorption bands have so far been reported.

Cations of o-, m-, *and* p-*Aminophenols (*o-, m-, *and* p-*AP*$^+$*).* Transition energies of p-AP$^+$ were calculated with various β_{CO} values from −2.40 to −3.60 eV with an interval of 0.20 eV. By plotting the resulting transition energies against β_{CO}, it was found that E_2 corresponding to the visible absorption band is fairly sensitive to β_{CO} and the experimental value of this second transition energy is reproduced at $\beta_{CO}=-3.20$ eV. This β_{CO} value and the β_{CN} value (−3.20 eV) previously determined were used in the calculation of all the isomers (Table 2).

The electronic absorption spectra of p-AP$^+$ and its *N*- and *O*-methyl derivatives are known to consist of three bands in a wavelength region greater than about 250 nm.[2] We see that agreement between the calculated and experimental transition energies is excellent for m- and p-AP$^+$.

Cations of o-, m-, *and* p-*Dihydroxybenzenes (*o-, m-, *and* p-*DHB*$^+$*).* The electronic absorption spectra of cation radicals of several p-dialkoxybenzenes (hydroquinone, p-methoxyphenol, p-dimethoxybenzene, p-ethoxyphenol, p-diethoxybenzene, and 2,3,5-trimethylhydroquinone) were measured in concentrated sulfuric acid by Kimura and Yamada.[4] Our calculation (Table 2) indicates that the first allowed transition of p-DHB$^+$ (hydroquinone$^+$) occurs at E=2.75 eV, in good agreement with the experimental value of 2.95 eV obtained from the 420 nm band.

Phenol$^+$ *and Aniline*$^+$. Electronic spectra of phenol$^+$ and aniline$^+$ were also calculated with the same parameter values as mentioned above. The visible absorp-

tion bands of aniline$^+$,[15] *N*-methylaniline$^+$,[16,17] and *N,N*-dimethylanilinc$^+$ [15-17] have been reported in the region 400—450 nm. According to the present results, such absorption bands may be interpreted as transition $\Psi_0 \rightarrow \Psi_2$ (f=0.06), which is mainly due to configuration (2→4).

No absorption data concerning phenol$^+$ are available. The present calculation predicts that a visible band should be located around 440 nm (2.84 eV) with f= 0.06.

Cations of N,N-*Dimethyl*-p-*Phenylenediamine and* N,N,N′,N′-*Tetramethyl*-p-*Phenylenediamine (DMPD$^+$ and TMPD$^+$).* The electronic absorption spectrum of TMPD$^+$ (so-called Würster's blue cation) has been studied in solution and crystalline state by many workers, this being the only cation whose experimental polarization has been reported.[18] Thus, it is of particular interest to compare the calculated results of TMPD$^+$ with experiment. In the present calculations of DMPD$^+$ and TMPD$^+$, the effect of methyl substitution was taken into account in such a way that the valence state ionization potential of the methyl-substituted nitrogen atom is reduced by 2.0 eV[19] and β_{CN} is made equal to −3.05 eV proportional to $1/2\,(I_N+I_C)$. Very good agreement was obtained between theory and experiment (Table 2).

The first transition of DMPD$^+$ is not symmetry-forbidden, but its intensity is very low. The first visible absorption band can be assigned to the second transition.

Effect of Methyl Substitutions. It was indicated[2] that the experimental shifts of the absorption bands of

Table 3. Shifts (in eV) of the first visible bands of the cations due to methyl substitutions

Methyl derivatives of *p*-PD$^+$					
Substituent	NH_2	NH_2	NHMe	NHMe	$N(Me)_2$
	NH_2	$N(Me)_2$	NHMe	$N(Me)_2$	$N(Me)_2$
Calcd	−0.15	−0.31	−0.31	−0.46	−0.61
Exptl[a]	−0.16	−0.30	−0.29	−0.40	−0.50
Methyl derivatives of *p*-AP$^+$					
Substituent	NH_2	NHMe	$N(Me)_2$	NHMe	
	OMe	OH	OH	OMe	
Calcd	−0.17	−0.12	−0.24	−0.41	
Exptl[b]	−0.04	−0.10	−0.25	−0.37	
Methyl derivatives of *p*-DHB$^+$					
Substituent	OH	OMe			
	OMe	OMe			
Calcd	−0.13	−0.26			
Exptl[c]	−0.14	−0.27			

a) Obtained from the data reported by Y. Iida and Y. Matsunaga, This Bulletin, **41**, 2535 (1968).
b) Obtained from the data of Ref. 2.
c) Obtained from the data of Ref. 4.

Table 4. Comparison of calculated and experimental spin densities

Cation	Atom	C(1) C(1′)	C(2) C(2′)	C(3) C(3′)	N	O
o-PD$^+$	Calcd	0.185	−0.030	0.114	0.231	
m-PD$^+$	Calcd	−0.049	0.052	0.373	0.142	
p-PD$^+$	Calcd	0.158	0.058	0.058	0.226	
	Exptl[20]		0.076	0.076	0.236	
DMPD$^+$	Calcd	0.088	0.074	0.028	0.390	
					0.177[a]	
TMPD$^+$	Calcd	0.088	0.047	0.047	0.318[a]	
	Exptl[21]		0.070	0.070	0.270[a]	
o-AP$^+$	Calcd	0.223	0.003	0.075	0.248	0.092
		0.230	−0.060	0.190		
m-AP$^+$	Calcd	−0.001	0.139	0.282	0.212	0.025
		−0.061	−0.037	0.367		
p-AP$^+$	Calcd	0.158	0.093	0.026	0.266	0.107
		0.229				
	Exptl[22]		0.143	0.021	0.332	
o-DHB$^+$	Calcd	0.249	−0.047	0.162		0.135
m-DHB$^+$	Calcd	−0.056	0.124	0.359		0.083
		−0.078				
p-DHB$^+$	Calcd	0.243	0.062	0.062		0.133
	Exptl[23]		0.080	0.080		0.158
Phenol$^+$	Calcd	0.243	0.128	−0.004		0.165
		0.343				
Aniline$^+$	Calcd	0.135	0.150	−0.024	0.317	
		0.295				

a) Spin density on the N atom belonging to the $N(CH_3)_2$ group

15) K. D. Cadogan and A. C. Albrecht, *J. Phys. Chem.*, **73**, 1868 (1969).
16) E. J Land and G Porter, *Trans. Faraday Soc.*, **59**, 2027 (1963).
17) S. Arimitsu, K. Kimura, and H. Tsubomura, This Bulletin, **43**, 1858 (1969).
18) A. C. Albercht and W. T. Simpson, *J. Amer. Chem. Soc.*, **77**, 4454 (1955).
19) Since the first ionization potentials of NH_3, CH_3NH_2, and, $(CH_3)_2NH$ are 10.16, 9.18, and 8.36 eV, respectively (A. D. Baker, D. P. May, and D. W. Turner, *J. Chem. Soc.*, **B 1968**, 22), it is inferred that the change in the valence state ionization potential of the nitrogen atom per one CH_3 group is about −0.9 eV.

p-aminophenols$^+$ from that of *p*-phenylenediamine$^+$ are approximately interpreted in terms of differences in valence-state ionization potentials of the substituents by using the first-order perturbation theory. In the present work, using the SCF MO's for the parent cations as unperturbed systems, we applied this perturbation method in order to explain the experimental band shifts of the various methyl substituted cations. The shifts of the first visible bands for the methyl derivatives of *p*-PD$^+$, *p*-AP$^+$, and *p*-DHB$^+$ (Table 3) may be given by $\{-0.0765(\Delta I_{N_1}+\Delta I_{N_2})\}$, $\{-0.0591\Delta I_N-0.0597\Delta I_o\}$, and $\{-0.0438(\Delta I_{o1}+\Delta I_{o2})\}$, where $\Delta I_N=2.0$ eV and $\Delta I_o=3.0$ eV were used. We see that calculated shifts are in good agreement with the experimental shifts of the longest wavelength absorption bands.

Spin Densities. Spin densities in cation radicals are obtainable from an analysis of hyperfine splittings of ESR spectra. Since hyperfine ESR splittings of *p*-PD$^+$,[20] TMPD$^+$,[11,21] *p*-AP$^+$,[22] and *p*-DHB$^+$ [23] have already been measured, we carried out theoretical calculations of the spin densities of these cation radicals and other related cations, obtained from the McLachlan relationship[24] using the experimental hyperfine splittings and appropriate Q values.[25] The calculated results are shown in Table 4. As far as comparison is possible, the calculated spin densities are in agreement with the experimental ones.

Effect of Doubly Excited Configurations. It should be mentioned that all the singly excited electron configurations are included for all the compounds studied except for aminophenols, in which a few of the singly excited configurations with high energies are excluded because of the low molecular symmetries. Contribution of the doubly excited configurations is less than a few percent in the lower states of the cations as underlined in Table 1.

20) M. T. Melchior and A. H. Maki, *J. Chem. Phys.*, **34**, 471 (1961).
21) J. R. Bolton, A. Carrington, and J. dos Santos-Veiga, *Mol. Phys.*, **5**, 615 (1962).
22) W. M. Fox and W. A. Wates, *J. Chem. Soc.*, **1964**, 6010.
23) P. D. Sullivan, *J. Amer. Chem. Soc.*, **89**, 4294 (1967).
24) A. D. McLachlan, *Mol. Phys.*, **1**, 233 (1958).
25) $Q_{C-H(ring)}=-28$ Gauss, $Q_{N-H}=Q_{N-CH_3}=25$ Gauss, and $Q_{O-H}=20.8$ Gauss.

BULLETIN OF THE CHEMICAL SOCIETY OF JAPAN, VOL. 46, 779—781 (9173)

The Magnetic Properties of Some Iminoxyl Polyradicals. IV. The Paramagnetic Susceptibilities of the Diluted Crystals of the TEMPAD Biradical

Akira NAKAJIMA

Department of Chemistry, Faculty of Science, Kyoto University, Kyoto

(Received August 15, 1972)

The paramagnetic susceptibilities of the diluted crystals of bis(2,2,6,6-tetramethylpiperidine-4)azine-1,1′-dioxyl (the TEMPAD biradical) have been measured from 1.8 to 77.3 K. The χ_M-T curves obey the Curie-Weiss law in the high and low temperature regions, and two kinds of the Weiss constant were found. The Weiss constant in the high-temperature region, which is caused by the strong inter-molecular exchange interaction, varies with the radical concentration from -8.5 to -15 K. The Weiss constant in the low-temperature region is of the order of magnitude of -1 K and reveals the existence of a weak intra-molecular exchange interaction. We can assume that the TEMPAD biradicals are distributed randomly in the matrix of the diamine and that they form either an isolated portion in which the weak intra-molecular exchange interaction exists only, or a clustering portion coupled by a strong inter-molecular exchange interaction besides the intra-molecular one. Then, the concentration dependence of the χ_M-T curves can be explained as the superposition of the contributions from these two portions. The curves caluclated on the assumption of the random distribution agreed with the experimental results.

There are many works concerned with the magnetic properties of organic stable free radical solids, which were introduced in Part II of the present series.[1] In these works some short-range ordering effects caused by exchange interaction among the unpaired electron spins were observed, and the linear chain or the spin-cluster model was applied. These two models are based on the localized spin treatment as in the case of the transition-metal ion salts. In iminoxyl radicals the unpaired electron is localized around the N–O bond, so they can also be treated as localized spin systems.

Previously the present author and his colleagues reported on these magnetic study of bis(2,2,6,6-tetramethylpiperidine-4)azine-1,1′-dioxyl (the TEMPAD biradical) and bis(2,2,6,6-tetramethylpiperidine-4)sulfite-1,1′-dioxyl (the sulfite biradical), and concluded that the strong inter-molecular exchange interaction has a

1) A. Nakajima, H. Ohya-Nishiguchi, and Y. Deguchi, This Bulletin, **44**, 2120 (1971). Please refer the added two works. J. Yamauchi, This Bulletin, **44**, 2301 (1971). W. Duffy, Jr., J. F. Dubach, P. A. Pianneta, J. F. Deck, D. L. Strandburg, and A. R. Miedema, *J. Chem. Phys.*, **56**, 2555 (1972).

short-range ordering effect in both biradicals.[2,3]

In this paper the author will report on the paramagnetic susceptibilities of the diluted crystals of the TEMPAD biradical and will discuss the intra- and inter-molecular exchange interactions in these systems.

Experimental

The TEMPAD biradical and bis(2,2,6,6-tetramethylpiperidine-4)azine (the diamine corresponding to the TEMPAD biradical), shown in Fig. 1, were prepared from 2,2,6,6-tetramethyl-4-piperidone supplied by the Aldrich Chemicals Co.; this substance was introduced in a previous paper.[3]

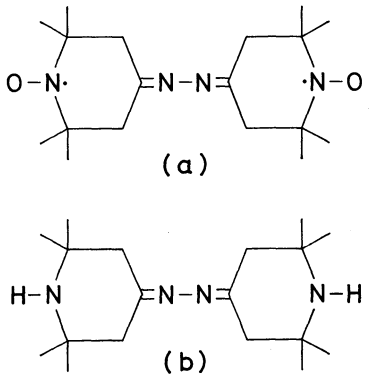

Fig. 1. Molecular structure of the TEMPAD biradical (a) and the corresponding diamine (b).

The space groups and the lattice constants of the TEMPAD biradical and the corresponding diamine listed in Table 1 are nearly equal to each other, so the diluted crystals of the TEMPAD biradical in its diamine can be prepared in various concentration ratios. The diluted crystals with 75, 50, and 25 mol% were crystallized from their ether solutions, and their elementary analyses agreed with the calculations.

TABLE 1. THE SPACE GROUPS AND THE LATTICE CONSTANTS FOR THE DIAMINE AND THE TEMPAD BIRADICAL

Name	Diamine	TEMPAD
Space-group	Monoclinic C_c	Monoclinic C_c or $C_{2/c}$
a	29.0 Å	29.1 Å
b	12.6	12.8
c	10.4	10.5
β	~90°	~90°

The paramagnetic susceptibility measurements were carried out using a torsion balance with powder samples from 77.3 to 1.8 K, the details of which have been described in the previous paper.[3] The diamagnetic contributions of the TEMPAD biradical and the diamine were calculated at -2.37×10^{-4} and -2.33×10^{-4} emu/mol respectively. The diamagnetic contributions of the diluted crystals were estimated as the sum of the aforementioned two values multiplied by each concentration ratio.

2) A. Nakajima, H. Nishiguchi, and Y. Deguchi, *J. Phys. Soc, Jap.*, **24**, 1175 (1968).

3) A. Nakajima, H. Ohya-Nishiguchi, and Y. Deguchi, This Bulletin, **45**, 713 (1972).

Results and Discussion

The inverse paramagnetic susceptibilities of the 100, 75, 50, and 25 mol% TEMPAD biradicals versus the temperature are shown in Fig. 2. Each curve obeys the Curie-Weiss law above 30K and below 4K except for the 100% case. The paramagnetic Curie constants and the Weiss constants of each concentration in these temperature regions are listed in Table 2.

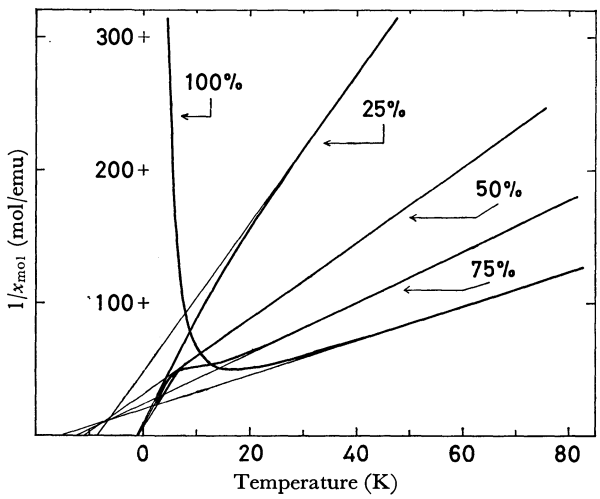

Fig. 2. Temperature dependence of the inverse paramagnetic susceptibilities of the diluted crystals of the TEMPAD biradical for 100, 75, 50, and 25 mol %.

TABLE 2. THE EXPERIMENTAL AND THE THEORETICAL MAGNETIC CONSTANTS FOR EACH CONCENTRATION. THE LATTERS ARE IN THE CASE OF $|J_1|/k=12.8$K AND $\alpha=1/20$.

n (%)	Experimental				Calculation	
	C_L	C_H	θ_L	θ_H	C_H	θ_H
25	0.131	0.181	−1.0	−8.5	0.189	− 3.20
50	0.158	0.368	−1.0	−11.0	0.378	− 5.25
75	0.146	0.537	−1.1	−12.5	0.574	− 7.95
100	—	0.770	—	−15.0	0.772	−10.8

C_H and C_L: the paramagnetic Curie constants
θ_H and θ_L: the Weiss constants (K).

The Weiss constant generally indicates the magnitude of the exchange interaction among the coupled magnetic spins. In the diluted crystals of the TEMPAD biradical, two kinds of Weiss constant were found, in the high- and in the low-temperature regions. The Weiss constant in the high-temperature region, which is of

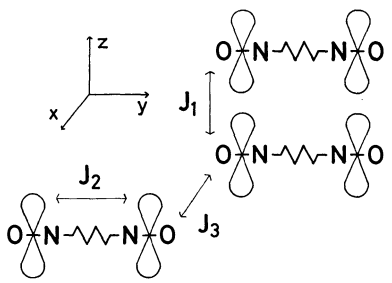

Fig. 3. Simplified molecular stack model for the TEMPAD biradical.

the order of magnitude of -10K, must be caused by the strong exchange interaction. On the other hand, the Weiss constant in the low-temperature region is of the order of magnitude of -1K.

By the dilution of the monoradical the inter-molecular exchange interaction can generally be eliminated, thus leading to the disappearance of the broad maximum in the χ_M-T curve. In the TEMPAD biradical two kinds of exchange interaction exist (see Fig. 3);[4] one is the strong inter-molecular exchange interaction (J_1), which causes the short-range ordering effect in the 100% case.[2] The other is the weak intra-molecular exchange interaction (J_2), which affects the hyperfine structure of the EPR in the dilute solution.[3] In the diluted crystals of the TEMPAD biradical, we can assume that the biradicals are distributed randomly in the matrix of the diamine and that they form two portions magnetically different in microscopical scale; one is the isolated portion in which the weak intra-molecular exchange interaction exists alone, and the other is the clustering portion coupled by the strong inter-molecular exchange interaction besides the intra-molecular one. Then the paramagnetic susceptibility of the diluted crystals may be considered to the superposition of the contributions from these two portions. If we adopt the pair model for the clustering portion and apply the Weiss molecular-field approximation for the weak intra-molecular exchange interaction, the theoretical susceptibility can be calculated on the assumption of the following random distribution:

$$|J_1|\chi_M/N_0(g\beta)^2 = 2[n^2x/(3+e^{2x})+n(1-n)x/4]/(1+\alpha x),$$

where $x=|J_1|/kT$; $\alpha=|J_2/J_1|$; N_0 is the Avogadro number; g, the g-value (2.0060 for the TEMPAD biradical[5]); β, the Bohr magneton, and n, the mole concentration of the biradical. The first term is the susceptibility of the pair model (the clustering portion), and the second term is that of the isolated portion. The theoretical $1/\chi_M-T$ curves for $|J_1|/k\simeq 12.8$K and $\alpha=1/20$ are shown in Fig. 4, while the theoretical paramagnetic Curie constants and the Weiss constants are listed in Table 2. They are in good qualitative agreement with the experimental results.

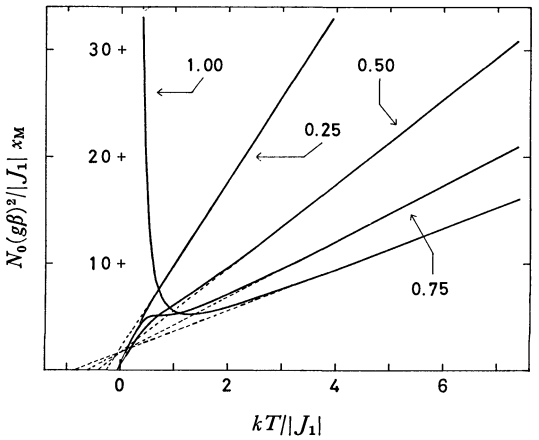

Fig. 4. Theoretical curves of the inverse paramagnetic susceptibility of the diluted systems for $n=1.0$, 0.75, 0.50, and 0.25 in the case of $\alpha=|J_2/J_1|=1/20$.

The exchange energy estimated from the Weiss constants in the low-temperature region is still larger than the value estimated from the EPR spectra in the dilute solution.[3] This is possibly caused by the difference in magnitude of the intra-molecular exchange interaction (J_2 in Fig. 3), which results from the distinction of the molecular conformation between the solid state and the dissolved state, and by the existence of another inter-molecular exchange interaction, *e.g.*, J_3 in Fig. 3.

The pair model was applied to the clustering portion on the basis of the random distribution, but the experimental results are different from those calculated—the value of χ_M deviates from the pair model near T_{max} ($=16.5$K) in the 100% case[2] and the Weiss constants of the high-temperature region are different from the calculated values (Table 2). If the TEMPAD molecules are distributed randomly enough in the diamine host, we must consider the higher-order clusters (trimers, tetramers, and so on) besides the pairs. As the data were explained qualitatively by the pair-model at so high a concentration, it may be suggested that the systems are fairly uniform.

The author wishes to thank Professor Yasuo Deguchi, Dr. Hiroaki Ohya-Nishiguchi, Dr. Jun Yamauchi, and their collaborators for their helpful advice and discussions. He is also indebted to Professors Hideo Takaki and Mamoru Mekata for their continuous guidance and encouragement during this work.

4) From the crystal structure, the distance between unpaired electrons in x-, y-, and z-directions are thought to be nearly equal to each other. Then the overlap integral will be the largest in the z-direction, namely $|J_1|>|J_2|$, $|J_3|$. The study of the dipolar interaction in ESR spectra also support this assumption.[5]

4) A. Nakajima, to be published.

The Infrared Spectra of α-Chlorinated Acetamides

Yoshiyuki MIDO

Department of Chemistry, Faculty of Science, Kobe University, Nada-ku, Kobe 657

(Received August 16, 1972)

The polarized infrared spectra of α,α,α-trichloroacetamide (TCA) and its deuterated compound (TCA-*d*) have been measured in the 400—4000 cm^{-1} region, and the infrared spectra of the series, $CCl_nH_{3-n}CONH_2$ (n= 0—3), and their deuterated compounds have been observed in the solid state. On the basis of the results, the vibrational assignments, the orientation of TCA, the intermolecular hydrogen bonds, and the inductive effect of the introduction of the chlorine atom, and the conformation of TCA have been discussed. It has been proposed that TCA in the solid state has two conformations, which are in linear-chain associations through hydrogen bonds.

The infrared spectra and vibrational analyses of acetamide[1-5] and *N*-alkylacetamides[6-8] have been extensively studied, with special interest taken in them as model molecules of polypeptides and proteins. However, the infrared spectra of α-chlorinated acetamides have been less widely studied than those of acetamide and *N*-alkylacetamides. Herman and Bièvre[9] have observed the infrared spectra of α-chlorinated acetamides in the solid state, but their spectra are in the sodium chloride region and the spectra of their *N*-deuterated compounds have not been reported. There is a spectroscopic study of chlorinated acetamides in a carbon tetrachloride solution as a part of the study of primary acid amides,[10] in which their molecular structure has been discussed by analogy with the intramolecularly-bonded structure of *N*-alkyl-α-chlorinated acetamides offered by Nyquist.[11]

As α,α,α-trichloroacetamide (TCA) grows into considerably large plate crystals by recrystallization from an ether solution, we were able to prepare the oriented crystal of TCA between potassium bromide plates.

In this paper, we will describe our findings on the polarized infrared spectra of TCA and TCA-*d* and on the infrared spectra of chlorinated acetamides and their *N*-deuterated compounds in the $CCl_nH_{3-n}CONH_2$ series (n=0—3).

Experimental

Materials. The TCA, DCA (α,α-dichloro-), MCA (α-monochloro-), and NCA (nonchloro-acetamide) were obtained from Nakarai Chemicals, Ltd., and each sample was purified by repeated recrystallization from an aqueous solution. The deuteration of MCA was done by a usual method,[12] while those of DCA and TCA were done by the method for water-insoluble compounds described in a previous paper.[13]

The oriented crystals of TCA and TCA-*d* were obtained by allowing the molten sample to crystallize between potassium bromide plates, with a temperature gradient. We observed through a microscope many long crystals arranged parallel to each other.

Infrared Spectra. The infrared absorption measurements in the 400—4000 cm^{-1} region were made by use of a Hitachi EPI-2G Infrared Grating Spectrophotometer. The spectra in the solid state were measured as potassium bromide discs and Nujol mulls. The spectra in the liquid state of TCA and TCA-*d* were obtained by the use of a cell with an electrically-heated and beam-transparent box, in which the solid sample between the window plates was heated to *ca.* 145°C, which is slightly higher than its melting point (141°C). The dichroic measurements of the oriented crystals were made with a pair of silver chloride polarizers.

Results and Discussion

Vibrational Assignment of TCA. The observed bands in the infrared spectra of TCA and TCA-*d* were assigned by observing the changes in the spectra according to the state of aggregation (Table 1) and by comparing them with the spectra of NCA, MCA, and DCA (Fig. 1).

As expected,[6,14] with the change in state from the solid to the liquid, the frequencies of a few $\nu(NH_2)$ bands in the 3μ region and the ν(C=O) band around 1700 cm^{-1} increase, but the frequencies of the other amide bands decrease more or less.

On deuteration, the two bands at 1379 and 1351 cm^{-1} are replaced by a band at 1395 cm^{-1} and a shoulder band at 1370 cm^{-1} assignable to the ν(C–N) modes, while, instead of a sharp $\delta(NH_2)$ band at 1616 cm^{-1} in TCA, a new band appears at 1159 cm^{-1} assignable to the $\delta(ND_2)$ mode. The upward frequency-shift of the ν(C–N) bands by deuteration may be due to the decoupling of the contribution of the $\delta(NH_2)$ mode, just as in NCA.[2] The bands at 1105, 922, and 437 cm^{-1} correspond to the bands at 1155, 875, and 464 cm^{-1} in NCA, which have been assigned by Suzuki[2] to the $\delta r(NH_2)$, ν(C–C′), and δ(C′–C=O) modes respectively. The strong bands near 825 cm^{-1}

1) M. Davies and H. E. Hallam, *Trans. Faraday Soc.*, **47**, 1170 (1951).
2) I. Suzuki, This Bulletin, **35**, 1279 (1962).
3) W. Kutzelnigg and R. Mecke, *Spectrochim. Acta*, **18**, 549 (1962).
4) a) T. Uno, K. Machida, and Y. Saito, This Bulletin, **42**. 897 (1969). b) T. Uno, K. Machida, and Y. Saito, *Spectrochim. Acta*, **27A**, 833 (1971). c) K. Machida, S. Kojima, and T. Uno, *ibid*, **28A**, 235 (1972).
5) S. T. King, *ibid.*, **28A**, 165 (1972).
6) T. Miyazawa, T. Shimanouchi, and S. Mizushima, *J. Chem. Phys.*, **24**, 408 (1956); **29**, 611 (1958).
7) B. Schneider, A. Horeni, H. Pivcova, and J. Hozl, *Collect. Czech. Chem. Commun.*, **30**, 2196 (1965); **33**, 643 (1968).
8) J. Jakes and S. Krimm, *Spectrochim. Acta*, **27A**, 35 (1971).
9) M. A. Herman and P. De Bièvre, *Bull. Soc. Chem. Belg.*, **68**, 558 (1959).
10) P. J. Krueger and D. W. Smith, *Can. J. Chem.*, **45**, 1611 (1967).
11) R. A. Nyquist, *Specrtochim. Acta*, **19**, 509 (1963).
12) Y. Mido and H. Murata, This Bulletin, **42**, 3372 (1969).
13) Y. Mido, *Spectrochim. Acta*, **28A**, 1503 (1972).
14) L. J. Bellamy, The Infrared Spectra of Complex Molecules, 2nd Ed. Chap. 23, Methuen (1958).

TABLE 1. INFRARED FREQUENCIES (cm^{-1}) OF TRICHLOROACETAMIDE

I CCl_3CONH_2						
Solid (KBr disk)	Dichroism (Oriented crystal) ⊥	∥	Solid (103°C)	Liquid (145°C)	$CHCl_3$ soln	Assign.
					3519	$\nu as(NH_2)$, free
3393(s)	s	s	3400(s)	3480(s)	3485	ν(N–H)
					3404	$\nu s(NH_2)$, free
3338(s)	s <	s	3340(s)	3355(s)	3325	
3260(s)	s	s	3250(s)	3300(sh)	3250	ν(N–H)
3196(s)	s	s	3200(s)	3175(sh)	3165	
2783(w)	vw	w	2800(w)			1694+1105=2799
2695(w)	w <	w	2700(vw)			1348×2=2696
1740(sh)	w	—				922+825=1747
1694(s)	w	s	1694(s)	1714(s)	1736	ν(C=O)
1616(s)	s >	s	1602(s)	1582(s)	1580	$\delta(NH_2)$
1379(s)	s	m	1374(s)	1352(s)	1358	ν(C–N)
1351(m)	s	m	1342(sh)	1334(sh)	1335	
1270(vw)	w	m				646×2=1292
1220(vw)	—	—				615×2=1230
1105(s)	m	s	1095(s)	1093(m)	1098	$\delta r(NH_2)$
922(m)	m	m	917(m)	906(w)	908	ν(C′–C)
850(sh)					844	437×2=874
825(s)	s	s	818(s)	819(s)	822	ν(C–Cl)
820(sh)						
746(s)	s	m	740(m)	680(m)	680	$\pi(NH_2)$, π(C=O)
646(s)	s	m	640(s)	617(m)	614	π(N–C=O)
615(s)	s	vw	592(w,sh)	490(w)	?	$\pi(NH_2)$
437(m)	s	—	426(m)	420(vw)	?	δ(C′–C–N)

II CCl_3COND_2					
Solid (KBr disk)	Dichroism (Oriented crystal) ⊥	∥	Solid (100°C)	Liquid (145°C)	Assign.
3065(vw)					1683+1395=3078
2930(vw)					?
2840(vw)					1683+1159=2842
2780(vw)					1395× 2 =2790
2510(s)	s	s	2548(s)	2600(s)	$\nu as(ND_2)$
2380(s)	s	s	2396(s)	2427(s)	$\nu s(ND_2)$
2360(sh)			(sh)	(sh)	
2345(sh)					
1683(s)	w	s	1694(s)	1710(s)	ν(C=O)
1500(w)	w	m	1493(w)	1480(w)	Amide I
1395(s)	—	s	1387(s)	1361(s)	ν(C–N)
1370(sh)	m	—	—	—	
1159(m)	m	m	1156(m)	1142(w)	$\delta(ND_2)$
940(m)	w	s	940(m)	940(m)	$\delta r(ND_2)$
884(s)	s	s	884(s)	878(s)	ν(C′–C)
821(s)	sh	s	820(s)	818(s)	ν(C–Cl)
817(sh)	s	sh			
678(s)	s	w	676(m)	669(s)	π(C=O)
591(s)	s	s	585(s)	554(s)	δ(N–C=O)
517(m)	m	w	500(vw,sh)	—(vw,b)	$\pi(ND_2)$
460(s)	m	w	426(w,b)	—(vw,b)	$\pi(ND_2)$
406(w)					δ(C′–C–N)

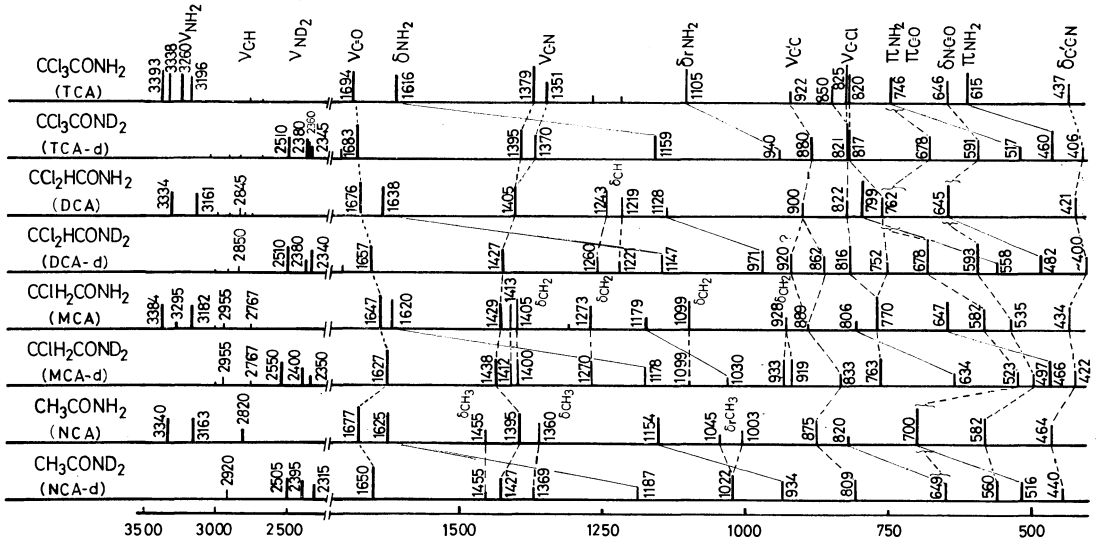

Fig. 1. Observed frequencies and relative intensities of $CCl_nH_{3-n}CONH_2$ ($n=0-3$) and these *N*-deuterated compounds. Bands combined with a solid line between an undeuterated and its deuterated compounds are related to a vibration due to NH_2 or ND_2 group, and among their compounds these bands are not combined with any lines. Data for NCA-*d* are by Suzuki (Ref. 2).

which are unshifted on deuteration and on the change in state are associated with the ν (C–Cl) vibrations.

In the 500—800 cm^{-1} region, four amide bands are predicted; a δ(N–C=O), a π(C=O), and two $\pi(NH_2)$ bands. In the observed spectra, only three bands are observed for TCA, whereas four bands are observed for TCA-*d*. The bands at 746 and 615 cm^{-1}, which disappear on deuteration, are assigned to the two $\pi(NH_2)$ modes, since these bands are very broad and the most sensitive to the change in state (see Table 1), just like the amide V band (mainly the π(N–H) vibration) of secondary amides[6] and dialkylureas.[12,13] The band at 646 cm^{-1} and an undetectable band probably covered by the higher $\pi(NH_2)$ band[12,13,15] may be associated with the δ(N–C=O) and π(C=O) modes respectively.

The observed frequencies and the vibrational assignment obtained are in agreement with those obtained by Herman and Bièvre[9] except for the assignment of the band at 746 cm^{-1}, which we assigned to the $\pi(NH_2)$ mode since this band disappears on deuteration.

Polarized Infrared Spectra of TCA and TCA-d.

The polarized infrared spectra of TCA and TCA-*d* are shown in Fig. 2. The ν(C=O) band exhibits a definitely parallel dichroism in both samples. This means that the direction of the C=O bond is parallel to the long direction of the oriented crystal and that the association of TCA shown below is acceptable. The parallel ν(C=O) band is contrasted with the ν(C=O) band of benzamide[16] at 1656 cm^{-1}, having an indistinguishable dichroism. The structure of the associated molecules of benzamide[17] has a chain association of dimer units, with a center of symmetry, in which the C=O bonds are placed in an inclined position to the

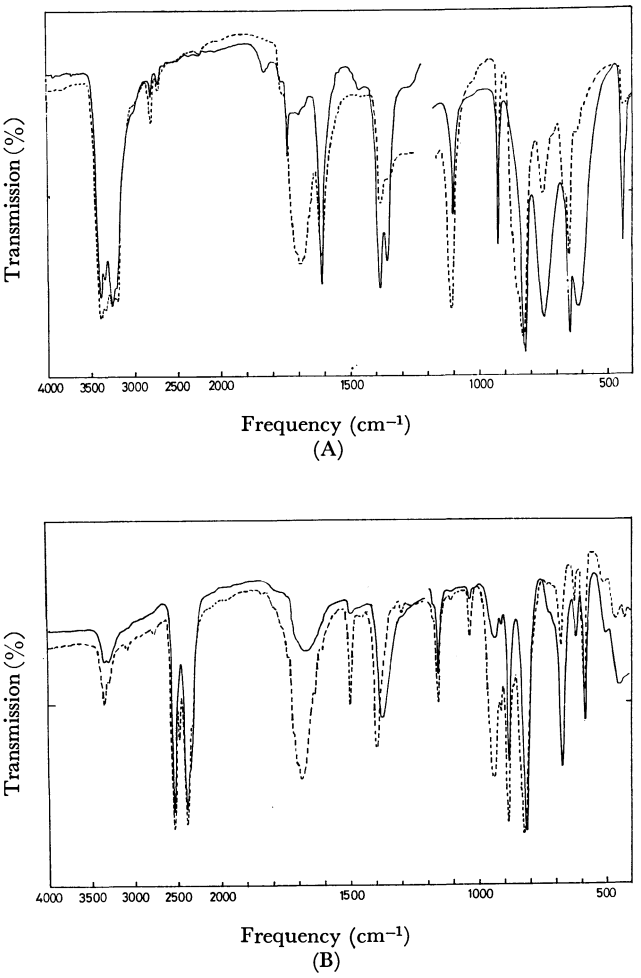

Fig. 2. The polarized infrared spectra of TCA (A) and TCA-*d* (B) with the electric vector of the incident infrared beam being parallel (broken line) or perpendicular (solid line) to the long direction of the oriented crystal.

15) J. Jakes and S. Krimm, *Spectrochim. Acta*, **27A**, 19 (1971).
16) S. Weckherlin and W. Luttke, *Z. Electrochem.*, **64**, 1228(1960).
17) B. R. Penfold and J. C. B. White, *Acta Crystallogr.*, **12**, 130 (1959).

Table 2. The CO stretching frequencies (cm^{-1}) in the carbon tetrachloride solution and the solid state

	CH_3CONH_2 (NCA)	$CH_2ClCONH_2$ (MCA)	$CHCl_2CONH_2$ (DCA)	CCl_3CONH_2 (TCA)
Free (CCl_4 soln.)	1711[a)]	1724	1731	1751
Associated (Solid)	1677	1647	1676	1694
Difference	34	77	55	57

a) E. A. Cutmore and H. E. Hallam, *Spectrochim. Acta.*, **25A**, 1767 (1969).

oriented axis;

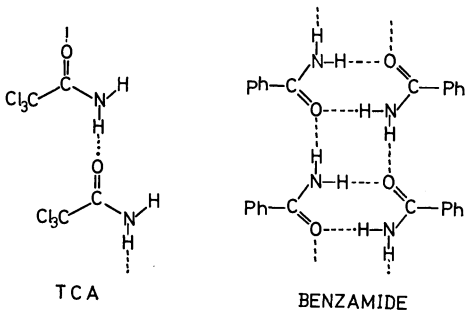

From the above figure, one can understand the indistinguishable dichroic property of ν(C=O) band of benzamide, and can see that the structure of TCA is not like that in benzamide. If such a chain association of TCA is assumed, it may be expected that $\nu a(NH_2)$ and $\delta r(NH_2)$ bands will exhibit a rather parallel dichroism, whereas $\nu s(NH_2)$, $\delta(NH_2)$, ν(C–N), and ν(C–C′) bands will exhibit a rather perpendicular dichroism. The polarized spectra of TCA almost satisfy the above expectation. This indicates that the assumed chain association model of TCA is reasonable. The dichroic properties of some bands of TCA-*d* do not satisfy the expectation. The unsatisfactory dichroism may be due to the insufficient deuteration and/or orientation. All bands related to out-of-plane vibrations exhibit a perpendicular dichroism in both samples, as expected. This indicates that the assignment of these bands is correct, and that the chain association suggested is also reasonable.

Amide Bands and Their Frequency Changes in $CCl_nH_{3-n}CONH_2$. The correlation among the observed frequencies for $CCl_nH_{3-n}CONH_2$ (n=0—3) and their *N*-deuterated compounds are graphically summarized in Fig. 1. With the successive introduction of a chlorine atom into the methyl group of NCA, the frequencies of the ν(C=O) and ν(C–N) bands sensitively and regularly move upwards and downwards respectively, and the frequencies of three NH_2 deformation bands (but not the $\delta(NH_2)$ band) also move downwards. These frequency changes may be explained as being due to the changes in the electronic state of the amide structure and the intermolecular hydrogen bonds.

The difference in the free ν(C=O) frequency (in nonpolar solvent) among the α-chlorinated acetamides may be due to the inductive effect of the α-substituent, which tends to raise its frequency.[14] The frequency-difference between the free ν(C=O) band and the associated ν(C=O) band (solid state) may be considered to be a qualitative measure of the strength of the hydrogen bonds. In Table 2, it can be understood that, with the α-successive introduction of a chlorine atom, the inductive effect regularly becomes larger; the more chlorine atoms are introduced to the methyl group, the larger the double bond character of the C=O bond becomes, at the expense of that of the C–N bond. Table 2 also indicates that α-chlorinated acetamides have stronger intermolecular hydrogen bonds than acetamide and that the frequency lowering of 37 cm^{-1} (1677—1640) from NCA to MCA in the solid state may be due mainly to the stronger hydrogen bonds of α-chlorinated acetamides.

The two $\pi(NH_2)$ bands seem to receive the inductive effect of chlorine atoms regularly. The behavior of the π(C=O) and δ(N–C=O) bands, on the other hand, is rather complicated.

Conformation of TCA. Contrary to our expectations for two ν(N–H) bands, four ν(N–H) bands appear definitely in TCA in the solid state. Also, two ν(C–N) bands are observed. These facts suggest that TCA has two different conformations in the solid state, just as

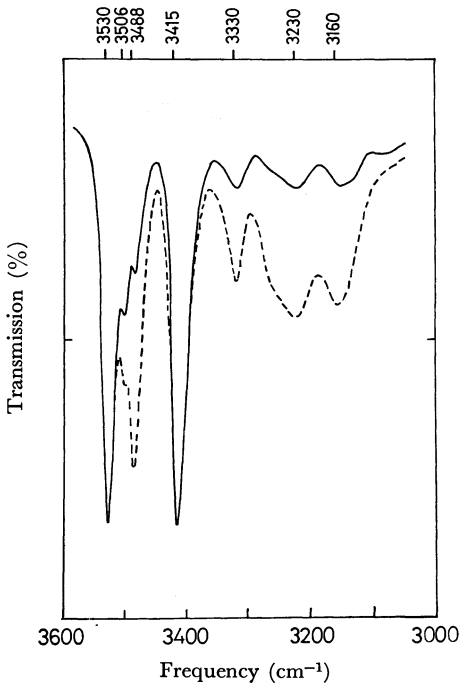

Fig. 3. The N–H stretching bands of TCA in carbon tetrachloride solution; ——: 1×10^{-3}M (10 cm cell), ------: 5×10^{-3}M (2 cm cell).

TABLE 3. THE N–H STRETCHING FREQUENCIES (cm^{-1}) OF α-CHLORINATED ACETAMIDES IN CARBON TETRACHLORIDE SOLUTION AT A CONCENTRATION OF 0.005 M

	Free $\nu as(NH_2)$	Associated ν(N–H)[a]			Free $\nu s(NH_2)$	2ν(C–O)	Typical associated ν(N–H)		
		A	B	C					
TCA	3530		3506	3488[b]	3415		3330	3230	3160
(Solid)				(3393)			(3338)	(3260)	(3196)
DCA	3528		3503	3481[b]	3413		3310	3210	3160
(Solid)							(3334)		(3161)
MCA	3529		3504	3479[b]	3413		3295	3200	3160
(Solid)				(3384)			(3295)	(3182)	
NCA	3540		3503[b]		3422	3362	3295	3228	3181
NCA[a]	3540.5	3518	3504[b]	3486	3420.5				
(Solid)							(3340)		(3170)
(Ar matrix)[c]	(3557)				(3436)				
			(3515)						(3140)
	(3554)				(3434)				

a) Bands named by Krueger and Smith in Ref. 10 and their data for NCA.
b) Concentration-dependent band.
c) The data obtained by King in Ref. 5; $\nu as(NH_2)$ and $\nu s(NH_2)$ bands alike are a doublet.

in *N*-methyl-α-monochloroacetamide.[18] This suggestion is supported by the chlorine NQR studies[19] of chlorinated acetamides from 77K to the melting point. In those studies, six lines in TCA, two lines in DCA, and one line in MCA are observed. They can be classified into two types on the basis of the different temperature coefficients of the NQR frequency (the slope); the two lines of DCA and the one line of MCA belong to the different types, while of the six lines of TCA, three lines belong to one type and remaining three lines to the other type. These NQR data indicate that TCA has two crystallographically-inequivalent CCl_3 groups.

In the infrared spectra of TCA in a dilute carbon tetrachloride solution, we observed two additional bands on the lower-frequency side of the $\nu as(NH_2)$ band at 3530 cm^{-1}, as is shown in Fig. 3. With an increase in the concentration, the intensity of the lower band at 3488 cm^{-1} increases more sensitively than the higher band at 3506 cm^{-1} and the typical associated N–H bands in the 3150—3350 cm^{-1} region. Also, the other chlorinated acetamides show similar spectral behavior, as is shown in Table 3. The lower band corresponds to the C band of three additional bands, at 3518 (named the A band), 3504 (B), and 3486 cm^{-1} (C), in the solution spectra of NCA, interpreted as being due to a cyclic dimer, a trimer, and a higher polymer of NCA with a free N–H bond and a bridged N–H bond respectively.[10]

In the solution spectra of NCA, we observed a concentration-dependent band at 3504 cm^{-1}, porbably corresponding to the B band. In the infrared spectra of NCA in the argon matrix, King[5] has observed only two bands in the 3500—3600 cm^{-1} region and assigned the lower band at 3515 cm^{-1} to the ν(N–H) mode due to a dimer species of the associated polymers. With due consideration of the frequency-differences (*ca.* 15 cm^{-1}) between the free $\nu as(NH_2)$ or $\nu s(NH_2)$ band in the matrix and in the solution, the 3515 cm^{-1} band in the matrix may be said to correspond to the B band. The lower frequency of the concentration-dependent band of chlorinated acetamides (the C band) than that of NCA (the B band) indicates that chlorinated acetamides may be in a higher polymer than in a dimer in the carbon tetrachloride solution.

With the change in state from the solution, through the liquid, to the solid state, the frequency of the corresponding C band of TCA is lowered and reaches 3393 cm^{-1} in the solid state, as is listed in Tables 1 and 3. The highest band at 3393 cm^{-1} in the solid state may be also characterized by the higher polymer of TCA with a weakly hydrogen-bonded N–H bond and a bridged N–H bond, but not by the associated polymer of dimer units, such as in benzamide. Considering the results of the previous NQR studies, two of the remaining three ν(N–H) bands of TCA in the solid state may be due to another higher polymer with two bridged N–H bonds.

The author wishes to express his deep gratitude to Dr. Katsunosuke Machida of Kyoto University, Dr. Hiroatsu Matsuura of Osaka University, and Mr. Masao Hashimoto of Kobe University for their very helpful discussions and suggestions.

18) Y. Koyama and T. Shimanouchi, *Acta Crystallogr.*, **B27**, 940 (1971).
19) M. Hashimoto, Preprints for the 24th Annual Meeting of the Chemical Society of Japan (Osaka, April 1971), 14401; I. V. Izmestev and G. B. Soifer, *Opt. Spectrosk.*, **30**, 479 (1971).

The Coupled Perturbed Hartree-Fock Calculations of the Magnetic Susceptibility for Some Nonbenzenoid Aromatic Hydrocarbons

Yasushi MIKAMI, Seiko MIYAI, and Takeshi NAKAJIMA
Department of Chemistry, Faculty of Science, Tohoku University, Aramaki, Sendai
(Received August 24, 1972)

The semi-empirical SCF MO method is applied to the calcutations of the magnetic susceptibility of the π-electron systems of several nonbenzenoid aromatic hydrocarbons. To avoid origin-dependent results, a method actually equivalent to Hall and Hardisson's one which is currently called the coupled perturbed Hartree-Fock method is used. With the best-fit parameters, the calculated results are in good agreement with the available experimental values except for the case of aceheptylene.

The diamagnetic susceptibilities of aromatic hydrocarbons are so anisotropic that they do not follow Pascal's sum rule. The first quantitative explanation of this anisotropy was given by Pauling,[1] who introduced the idea of the ring current in π-electron systems. The concept of the ring current, which should be replaced by the more suitable term "*delocalization susceptibility*,"[2] has survived in spite of corrections from the quantum-mechanical point of view.[3] The first attempt to treat the delocalization susceptibility quantum-mechanically was made by London.[4] In his method, the Hückel molecular orbital theory was generalized to include the gauge-invariant atomic orbitals, and the variation method was used to obtain the orbital energies in a magnetic field.

The semi-empirical aspect of the molecular orbital theory for conjugated molecules has been developed by Pariser and Parr[5] and by Pople.[6] They included the electron repulsion explicitly and used the zero-differential overlap approximation. All of the atomic integrals concerned were reduced to empirical parameters or were neglected completely. This semi-empirical scheme is quite simple, but it yields quantitative results which are in good agreement with the experimental values.

Advanced methods of the calculation of the anisotropy corresponding to the development of the molecular orbital theory should obtain more satisfactory results. However, it is well known that the self-consistent version of the molecular orbital theory leads to results which show an obvious origin-dependence[7] resulting from the approximate nature of wavefunctions. To overcome this diffrculty, two methods have been suggested. One is the coupled perturbed Hartree-Fock method which was first employed for aromatic hydrocarbons by Hall and Hardisson.[8] The other, simpler one is the uncoupled Hartree-Fock method,[7] in which the geometric approximation[9] is used instead of the complicated coupling procedure. These methods have given satisfactory results, mainly for benzenoid aromatic hydrocarbons.

The purpose of this paper is to show that, taking several examples, one can apply the above method to calculations of the delocalization susceptibility of nonbenzenoid aromatic hydrocarbons. It has been known that some of these molecules exhibit unusual magnetic properties, that is, a paramagnetic delocalization susceptibility. For actual calculations, the coupled perturbed Hartree-Fock method is adopted, though it is rather more tedious than the uncoupled one. The semi-empirical SCF MO method[10] combined with the variable bondlength technique, which is a variation of the Pariser-Parr-Pople theory, is adopted. The molecules examined are azulene, fulvene, heptafulvene, pentalene, heptalene, aceazulylene, and aceheptylene.

Theory

The Hamiltonian of a π-electron system in a magnetic field can be written as:

$$\mathcal{H} = \sum_a \left\{ -\frac{1}{2}(\nabla_a + i\alpha \mathbf{A}_a)^2 + \sum_\eta V_\eta(\mathbf{r}_a) \right\} + \sum_{a>b} \frac{1}{r_{ab}} \qquad (1)$$

where $\mathbf{A}_a$ is the vector potential of the magnetic field at the point occupied by the a-th electron, α, the fine structure constant, V_η $(\mathbf{r}_a)$, the potential due to the σ-core associated with the atom, η, and the last term, the interaction energy between π-electrons. Atomic units will be used throughout this paper.

We assume that the wavefunction for the ground state of a molecule with $2n$ π-electrons is the Hartree-Fock single determinant:

$$\Psi = \frac{1}{\sqrt{2n!}} |\tilde{\phi}_1(\mathbf{r}_1)\alpha\tilde{\phi}_2(\mathbf{r}_2)\beta \cdots \tilde{\phi}_{2n-1}(\mathbf{r}_{2n-1})\alpha\tilde{\phi}_{2n}(\mathbf{r}_{2n})\beta| \qquad (2)$$

in which $\tilde{\phi}_i$ is the i-th molecular orbital with spin functions of α or β in the presence of the magnetic field. Following London, $\tilde{\phi}_i$ is written as a linear combination of the gauge-invariant atomic orbitals:

$$\tilde{\phi}_i = \sum_\mu \tilde{C}_{i\mu}\omega_\mu, \qquad (3)$$

where:

$$\omega_\mu = \chi_\mu \exp(-i\alpha \mathbf{A}_\mu \cdot \mathbf{r}), \qquad (4)$$

1) L. Pauling, *J. Chem. Phys.*, **4**, 673 (1936).
2) D. W. Davies, "The Theory of the Electric and Magnetic Properties of Molecules," John Wiley and Sons, London, 1967.
3) J. I. Musher, *J. Chem. Phys.*, **43**, 4081 (1965).
4) F. London, *J. Phys. Rad.*, **8**, 397 (1937)
5) R. Pariser and R. G. Parr, *J. Chem. Phys.*, **21**, 466, 767 (1953).
6) J. A. Pople, *Trans. Faraday Soc.*, **49**, 1375 (1953).
7) A. T. Amos and H. G. Ff. Roberts, *J. Chem. Phys.*, **50**, 2375 (1969).
8) G. G. Hall and A. Hardisson, *Proc. Roy. Soc., Ser. A*, **268**, 328 (1962).
9) J. M. Schulman and J. I. Musher, *J. Chem. Phys.*, **49**, 4845 (1968).
10) H. Yamaguchi, T. Nakajima, and T. Kunii, *Theor. Chem. Acta*, **12**, 3491 (1968).

where $\mathbf{A}_\mu$ is the vector potential at the μ-th atomic site. The equations for the coefficients, $\tilde{C}_{i\mu}$, are:

$$\sum_\mu \tilde{F}_{\mu\nu}\tilde{C}_{i\mu} = E_i \sum_\mu \tilde{S}_{\mu\nu}\tilde{C}_{i\mu}, \tag{5}$$

Following the Pariser-Parr-Pople approximation, we neglect the overlap integrals, $\tilde{S}_{\mu\nu}$, and the matrix elements, $\tilde{\mathscr{H}}_{\mu\nu}$, except for those between the nearest neighbours, unless $\mu=\nu$. Thus, the Fock element, $\tilde{F}_{\mu\mu}$, is expressed as:

$$\tilde{F}_{\mu\mu} = \tilde{\mathscr{H}}_{\mu\mu} + \frac{1}{2}\tilde{P}_{\mu\mu}\gamma_{\mu\mu} + \sum_{\eta(\neq\mu)}(\tilde{P}_{\eta\eta}-\zeta_\eta)\gamma_{\mu\eta}, \tag{6}$$

$$\tilde{F}_{\mu\nu} = \tilde{\mathscr{H}}_{\mu\nu} - \frac{1}{2}\tilde{P}_{\mu\nu}\gamma_{\mu\nu}, \qquad (\mu\neq\nu), \tag{7}$$

where:

$$\tilde{\mathscr{H}}_{\mu\nu} = \int w_\mu^*(\mathbf{r})\left\{-\frac{1}{2}(\nabla+i\alpha\mathbf{A})^2+\sum_\eta V_\eta(\mathbf{r})\right\}w_\nu(\mathbf{r})d\mathbf{r}, \tag{8}$$

$$\gamma_{\mu\nu} = \int w_\mu^*(\mathbf{r}_1)w_\nu^*(\mathbf{r}_2)\frac{1}{r_{12}}w_\mu(\mathbf{r}_1)w_\nu(\mathbf{r}_2)d\mathbf{r}_1d\mathbf{r}_2$$
$$= \int \chi_\mu^*(\mathbf{r}_1)\chi_\nu^*(\mathbf{r}_2)\frac{1}{r_{12}}\chi_\mu(\mathbf{r}_1)\chi_\nu(\mathbf{r}_2)d\mathbf{r}_1d\mathbf{r}_2, \tag{9}$$

$$\tilde{P}_{\mu\nu} = \sum_i^{occu} 2\tilde{C}_\mu\tilde{C}_{i\nu} \tag{10}$$

and where ζ_η is the effective charge of the σ-core of the ζ atom. For hydrocarbons, $\zeta_\eta=1$. According to London,[4] the matrix element, $\tilde{\mathscr{H}}_{\mu\nu}$, is simplified as follows. The $(\mathbf{A}-\mathbf{A}_\mu)^2$ term is neglected and $\exp[(i\alpha(\mathbf{A}_\mu-\mathbf{A}_\nu)\cdot\mathbf{r}]$ is replaced by $\exp[i\alpha(\mathbf{A}_\mu-\mathbf{A}_\nu)-(\mathbf{r}_\mu+\mathbf{r}_\nu)/2]$, where $\mathbf{r}_\mu$ and $\mathbf{r}_\nu$ are the position vectors at the μ-th and ν-th atomic sites respectively. One thus obtains:

$$\tilde{\mathscr{H}}_{\mu\nu} = \exp\{i\alpha(\mathbf{A}_\mu-\mathbf{A}_\nu)\cdot(\mathbf{r}_\mu+\mathbf{r}_\nu)/2\}\beta_{\mu\nu}$$
$$= \exp(i\alpha HL_{\mu\nu})\beta_{\mu\nu}, \tag{11}$$

where $\beta_{\mu\nu}$ is the usual resonance integral:

$$\beta_{\mu\nu} = \int \chi_\mu^*(\mathbf{r})\left\{-\frac{\nabla^2}{2}+\sum_\eta V_\eta(\mathbf{r})\right\}\chi_\nu(\mathbf{r})d\mathbf{r}, \tag{12}$$

and where $L_{\mu\nu}$ is the signed area of the triangle formed by the point of origin and the nuclei, μ, ν. The diagonal matrix element, $\mathscr{H}_{\mu\mu}$, is also simplified by a similar approximation:

$$\tilde{\mathscr{H}}_{\mu\mu} = \int \chi_\mu^*(\mathbf{r})\left\{-\frac{\nabla^2}{2}+V_\mu(\mathbf{r})\right\}\chi_\mu(\mathbf{r})d\mathbf{r} = \alpha_\mu, \tag{13}$$

where α_μ is the Coulomb integral.

Following Hall and Hardisson, each term related to the magnetic field is expanded into a series in the descending order of the field strength, H:

$$\tilde{F}_{\mu\nu} = F_{\mu\nu} + iHF_{\mu\nu}^{(1)} - H^2F_{\mu\nu}^{(2)} - \cdots, \tag{14}$$
$$\tilde{C}_{i\mu} = C_{i\mu} + iHC_{i\mu}^{(1)} - H^2C_{i\mu}^{(2)} - \cdots, \tag{15}$$
$$\tilde{E}_i = E_i + iHE_i^{(1)} - H^2E_i^{(2)} - \cdots, \tag{16}$$
$$\tilde{\mathscr{H}}_{\mu\nu} = \beta_{\mu\nu}\left\{1+i\alpha L_{\mu\nu}-\frac{1}{2}\alpha^2H^2L_{\mu\nu}{}^2+\cdots\right\}, \tag{17}$$
$$\tilde{P}_{\mu\nu} = P_{\mu\nu} + iHP_{\mu\nu}^{(1)} - H^2P_{\mu\nu}^{(2)} - \cdots, \tag{18}$$

The actual expressions, say $F_{\mu\nu}$[1], *etc.*, are shown in Table 1. The self-consistent Eq. (5) become, to the zeroth order:

Table 1. Expressions for quantities in matrix elements

$$F_{\mu\nu} = \beta_{\mu\nu} - \frac{1}{2}P_{\mu\nu}\gamma_{\mu\nu} + \delta_{\mu\nu}\left(\sum_\eta P_{\eta\eta}\gamma_{\eta\mu} - \sum_{\eta(\neq\mu)}\gamma_{\eta\mu}\right)$$
$$F_{\mu\nu}^{(1)} = \alpha L_{\mu\nu}\beta_{\mu\nu} - \frac{1}{2}P_{\mu\nu}^{(1)}\gamma_{\mu\nu}$$
$$F_{\mu\nu}^{(2)} = \frac{1}{2}\alpha^2L_{\mu\nu}\beta_{\mu\nu} - \frac{1}{2}P_{\mu\nu}^{(2)}\gamma_{\mu\nu} + \delta_{\mu\nu}P_{\eta\eta}^{(2)}\gamma_{\eta\mu}$$
$$P_{\mu\nu} = 2\sum_i^{occu} C_{i\mu}C_{i\nu}$$
$$P_{\mu\nu}^{(1)} = 2\sum_i^{occu}(C_{i\mu}^{(1)}C_{i\nu} - C_{i\mu}C_{i\nu}^{(1)})$$
$$P_{\mu\nu}^{(2)} = 2\sum_i^{occu}(C_{i\mu}^{(2)}C_{i\nu} - C_{i\mu}^{(1)}C_{i\nu}^{(1)} + C_{i\mu}C_{i\nu}^{(2)})$$

$$\sum_\mu (F_{\mu\nu}-\delta_{\mu\nu}E_i)C_{i\mu} = 0 \qquad (\nu = 1, 2, \cdots, 2n), \tag{19}$$

to the first order:

$$\sum_\mu (F_{\mu\nu}-\delta_{\mu\nu}E_i)C_{i\mu}^{(1)} = \sum_\mu (E_i^{(1)}\delta_{\mu\nu} - F_{\mu\nu}^{(1)})C_{i\mu}$$
$$(\nu = 1, 2, \cdots, 2n), \tag{20}$$

and to the second order:

$$\sum_\mu (F_{\mu\nu}-\delta_{\mu\nu}E_i)C_{i\mu}^{(2)} = \sum_\mu (E_i^{(1)}\delta_{\mu\nu} - F_{\mu\nu}^{(1)})C_{i\mu}^{(1)}$$
$$+ \sum_\mu (E_i^{(2)}\delta_{\mu\nu} - F_{\mu\nu}^{(2)})C_{i\mu}$$
$$(\nu = 1, 2, \cdots, 2n). \tag{21}$$

The expression of the π-electron energy, E_π, is:

$$\tilde{E}_\pi = \frac{1}{2}\sum_{\mu\nu}\tilde{P}_{\mu\nu}\{\tilde{\mathscr{H}}_{\mu\nu}+\tilde{F}_{\mu\nu}\}$$
$$= \sum_i \tilde{E}_i + \frac{1}{2}\sum_{\mu\nu}\{\tilde{\mathscr{H}}_{\mu\nu} - \sum_{\eta(\neq\mu)}\gamma_{\mu\nu}\delta_{\mu\nu}\} \tag{22}$$

where the relation:

$$\sum_i^{occu}\tilde{E}_i = \frac{1}{2}\sum_{\mu\nu}\tilde{P}_{\mu\nu}\tilde{F}_{\mu\nu} \tag{23}$$

is used. As E_i is an eigenvalue of $F_{\mu\nu}$, Eq. (20) can be solvend only if:

$$\sum_{\mu\nu} C_{i\nu}(E_i^{(1)}\delta_{\mu\nu} - F_{\mu\nu}^{(1)})C_{i\mu} = 0, \tag{24}$$

but since $F_{\mu\nu}$[1] is skew, this implies that

$$E_i^{(1)} = 0. \tag{25}$$

The corresponding relation for Eq. (21) is:

$$E_i^{(2)} = \sum_{\mu\nu} F_{\mu\nu}^{(2)}C_{\mu i}C_{\nu i} + \sum_{\mu\nu} F_{\mu\nu}^{(1)}C_{\mu i}^{(1)}C_{\nu i}, \tag{26}$$

so that:

$$\sum_i^{occu} E_i^{(2)} = \frac{1}{2}\sum_{\mu\nu}F_{\mu\nu}^{(2)}P_{\mu\nu} + \frac{1}{4}\sum_{\mu\nu}F_{\mu\nu}^{(1)}P_{\mu\nu}^{(1)}. \tag{27}$$

On the other hand, from Eq. (23), we obtain:

$$\sum_i^{occu} E_i^{(2)} = \frac{1}{2}\sum_{\mu\nu}F_{\mu\nu}^{(2)}P_{\mu\nu} + \frac{1}{2}\sum_{\mu\nu}F_{\mu\nu}^{(1)}P_{\mu\nu}^{(1)}$$
$$+ \frac{1}{2}\sum_{\mu\nu}F_{\mu\nu}P_{\mu\nu}^{(2)}, \tag{28}$$

therefore:

$$\sum_{\mu\nu}F_{\mu\nu}^{(1)}P_{\mu\nu}^{(1)} = -2\sum_{\mu\nu}F_{\mu\nu}P_{\mu\nu}^{(2)}. \tag{29}$$

Since the magnetic susceptibility is of the second order in H, we need the energy expression of this order. From Eq. (22), we may express it as:

$$E_\pi^{(2)} = \sum_i^{occu} E_i^{(2)} + \frac{1}{2}\sum_{\mu\nu}[\{\beta_{\mu\nu} - \sum_{\eta(\neq\mu)} \gamma_{\eta\nu}\delta_{\mu\nu}\}P_{\mu\nu}^{(2)} + L_{\mu\nu}\beta_{\mu\nu}P_{\mu\nu}^{(1)} + \frac{1}{2}L_{\mu\nu}^2\beta_{\mu\nu}P_{\mu\nu}. \quad (30)$$

This expression can be simplified by the use of Eqs. (27) and (29) to:

$$E_\pi^{(2)} = \frac{1}{2}\alpha^2\sum_{\mu\nu}L_{\mu\nu}^2H_{\mu\nu}P_{\mu\nu} + \frac{1}{2}\alpha^2\sum_{\mu\nu}L_{\mu\nu}H_{\mu\nu}P_{\mu\nu}^{(1)}. \quad (31)$$

Therefore, in the presence of the magnetic field, the total π-electron energy of the molecule is:

$$E_\pi = E_\pi - H^2E_\pi^{(2)} + \cdots\cdots, \quad (32)$$

since the linear term in H vanishes for a normal molecule with doubly-occupied orbitals. The magnetic susceptibility of a π-electron system is:

$$K_z^\pi = -\partial^2E_\pi/\partial H^2 = 2E_\pi^{(2)} = 2\alpha^2\sum_{\mu\nu}L_{\mu\nu}^2\beta_{\mu\nu}P_{\mu\nu} + 2\alpha\sum_{\mu\nu}L_{\mu\nu}\beta_{\mu\nu}P_{\mu\nu}^{(1)}. \quad (33)$$

This gives the delocalization susceptibility required.

Method of Calculation

The first step of our calculations is to solve the zeroth-order Eq. (19). The method used here is a modification of the Pariser-Parr-Pople method, in which the bond lengths and, consequently, the resonance and Coulomb repulsion integrals are allowed to vary with the bond order at each iteration until self-consistency is reached. The bond length is calculated from the bond order by the relationship:[10]

$$r_{\mu\nu}(\text{Å}) = 1.520 - 0.186P_{\mu\nu} \quad (34)$$

The Coulomb repulsion integrals are calculated using the Nishimoto-Mataga formula. The resonance integrals are evaluated by the relation:

$$\beta_{\mu\nu} = \beta_0 \exp\{a(r_0 - r_{\mu\nu})\} \quad (35)$$

where β_0 and r_0 are the resonance integral and the C–C bond distance for benzene respectively. The a=2.5 value has been adopted, because it reproduces well the experimental C–C bond distances and dipole moments of a number of aromatic hydrocarbons.[10]

The second step is to solve the first-order perturbation, Eq. (20). We must consider the additional condition that the perturbed eigenfunction is orthogonal to the unperturbed one, *i.e.*:

$$\sum_\mu C_{\mu i}^{(1)}C_{\mu i} = 0 \quad (36)$$

If the matrix, $F_{\mu\nu}^{1)}$, is assumed to be known, the set of Eqs. (20) and (36) can be solved as linear equations for various $C_{i\mu}$ values. These $C_{i\mu}$ values are then used to produce a new $F_{\mu\nu}^{1)}$ and the linear equations are iteratively solved until this matrix element becomes self-consistent.

The computations were done on the NEAC-2200 computer at Tohoku University.

Results and Discussion

The calculations following the method given in the previous sections have been carried out by varying the positions of the point of origin. These positions, shown in Fig. 1, are various H-atomic sites, C-atomic sites, the midpoint of the C–C bond, and the center of an odd-membered ring. The calculated delocalization susceptibilities, K_z^π, are given in Table 2 in units of the K_z^π of benzene. It turns out that, for all of the molecules concerned, K_z^π is actually origin-independent. The small variation in the values with the displacement

Table 2. Origin dependence of the delocalization susceptibility

Molecule	Position of origin[a)]	K_z^π/K_z^π (benzene)
Azulene	1	2.30
	2	2.30
	3	2.30
	4	2.30
	5	2.30
	6	2.30
	7	2.30
Fulvene	1	0.02
	2	−0.01
	3	−0.03
	4	−0.02
	5	−0.03
Heptafulvene	1	−0.07
	2	−0.06
	3	−0.06
	4	−0.05
	5	−0.06
	6	−0.06
Pentalene	1	−1.31
	2	−1.24
	3	−1.37
	4	−1.35
	5	−1.39
Heptalene	1	−1.85
	2	−1.86
	3	−1.86
	4	−1.89
	5	−1.89
Aceazulylene	1	2.24
	2	2.25
	3	2.24
	4	2.22
	5	2.14
	6	2.15
	7	2.27
Aceheptylene	1	1.74
	2	1.85
	3	1.93
	4	1.82
	5	1.71
	6	1.74
	7	1.71
	8	1.71

a) Each position is shown in Fig. 1.

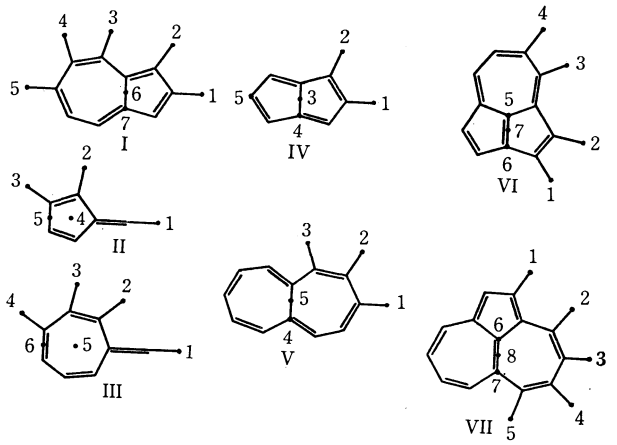

Fig. 1. The positions of the origin taken in this work.
I: Azulene, II: Fulvene, III: Heptafulvene, IV: Pentalene, V: Heptalene, VI: Aceazulylene, VII: Aceheptylene.

of the point of origin seems to be within the limits of unavoidable error arising from the termination of higher-order terms in the calculating processes. Azulene, aceheptylene, and aceazulylene are predicted to be diamagnetic, while heptalene and pentalene, classified as the $4n$-electron system, are predicted to be paramagnetic so far as the delocalization susceptibility is concerned. There exists an uncertainty about the sign of K_z^{π} of fulvene. However, this does not indicate a serious defect of the method, because the variation in the sign may be due to unavoidable errors since the absolute value of K_z^{π} is approximately zero. Contrary to the predictions of earlier works,[11,12] heptafulvene has a paramagnetic K_z^{π}. For azulene, the value (2.30) is in good agreement with the result (2.28) obtained by Hall and Hardisson. The discrepancy may be due to slightly different integral values in the two calculations.

In order to compare the calculated results with the experimental ones, we should add the local contributions to K_z^{π}. The most direct result obtained from the experiment on gaseous molecules is the mean susceptibility, K^{m}, which can be written as:

$$K^{\mathrm{m}} = \frac{1}{3}(K_x + K_y + K_z + K_z^{\pi}), \tag{37}$$

where we assume that:

$$K_x = K_y = N_C K_C^{\mathrm{m}} + N_H K_H^{\mathrm{m}}, \tag{38}$$

and that:

$$K_z = N_C K_C^{\perp} + N_H K_H^{\perp}. \tag{39}$$

In these expressions, N_H and N_C are the numbers of hydrogen and carbon atoms in a molecule respectively. For the Pascal constants of carbon and hydrogen atoms for the field perpendicular to the plane, we have used the Amos[7] values, $K_C^{\perp} = -8.5$, $K_H^{\perp} = -2.1$ (in units of 10^{-6} cgs emu), which are obtained from the original Hoarau[13] values by slight modifications. For the local values of the in-plane susceptibility, we take the values of $K_C^{\mathrm{m}} = -3.23$, and $K_H^{\mathrm{m}} = -2.69$. These values have been successfully used elsewhere.[7] The mean susceptibilities thus obtained are given in Table 3, together with the experimental results. For aceazulylene and aceheptylene, experimental values are available only for their derivatives. The calculations of the mean susceptibilities of these molecules were carried out on the assumptions that the methyl group contributes only to local effects and that the phenyl group gives one-half of the mean susceptibility of biphenyl. We have no experimental values for heptafulvene and pentalene.

TABLE 3. MEAN SUSCEPTIBILITY χ_{m}
(cgs emu 10^{-6}cm^3 mol^{-1})

Molecule	Theoretical	Experimental[a]
Benzene	54.94	54.8
Azulene	93.10	91.0
Fulvene	42.40	43.0
Heptafulvene	56.69	
Pentalene	41.93	
Heptalene	65.93	72±7
Aceazulylene	102.48	
its derivative[b]	(170.44)	179±4
Aceheptylene	113.10	
its derivative[c]	(131.35)	112±3

a) H. J. Dauben *et al.*, *J. Amer. Chem. Soc.*, **91**, 1991 (1969).
b) 2-phenyl-5,7-demethylaceazulylene.
c) 3, 5-dimethylaceheptylene.

A comparison of the theoretical and experimental values shows a good agreement in general, except for the case of aceheptylene. As for aceheptylene, no accurate comparison is possible unless the delocalization susceptibility of the derivative can be calculated on a reasonable basis. Moreover, there still remains an ambiguity in the allocated values of the local effects. Subtracting their own local effects, Dauben *et al.*[14] obtained 0.0 as the exaltation value (corresponding to the delocalization susceptibility) of aceheptylene. However, our calculation does not support this conclusion, because no choice of parameters could lead to the vanishing of the exaltation. It is, therefore, hoped that the experimental value of aceheptylene will be reexamined.

Finally, we may conclude that the coupled perturbed Hartree-Fock method gives satisfactory and gauge-invariant results on the delocalization susceptibility, K_z^{π}, for nonbenzenoid aromatic hydrocarbons as well as benzenoid ones.

11) B. Pullman and A. Pullman, "Les Theories Electroniques de la Chimie Organique," Masson et Cie., Paris, 1952.
12) T. Nakajima, T. Toyota, and H. Yamaguchi, "Aromaticity, Pseudo-Aromaticity, Antiaromaticity," Eds. E. D. Bergmann and B. Pullman, Academic Press, New York, 1971, p. 227.
13) J. Hoarau, *Ann. Chem.*, **13**, 544 (1956).
14) H. J. Dauben, J. D. Wilson, and J. L. Laity, *J. Amer Chem. Soc.*, **71**, 1991 (1969).

Light Scattering Studies on the Thermal Denaturation of Bovine Serum Albumin[1]

Masayuki NAKAGAKI and Yoh SANO

Faculty of Pharmaceutical Sciences, Kyoto University, Sakyo-ku, Kyoto

(Received September 4, 1972)

Thermal denaturation of bovine serum albumin (BSA) was studied by means of light scattering and viscosity measurements. The degree of denaturation ($w_D°$) was measured by using HABA, an anionic dye. The values of intrinsic viscosity, weight-average molecular weight and radius of gyration showed no appreciable changes when $w_D°$ was within 85 percent, but increased remarkably when $w_D°$ exceeded 85 percent. Thus, it has been concluded that the thermal denaturation proceeds in two steps, *i.e.*, intramolecular denaturation in the earlier stage and intermolecular association in the later stage. Analysis of the light-scattering data showed that the aggregated molecule was in a rod-like shape, whose length increased almost linearly with the weight fraction of the aggregated molecule w_n, the latter being obtained by analysis of the refractive index increment. On the other hand, the diameter did not change with the degree of denaturation, and its value was about 140 Å, which is almost equal to the largest dimension of the native BSA molecule. It has been concluded that the BSA molecules form aggregates by side-by-side association, whose length is about 2910 Å and diameter about 140 Å.

The thermal denaturation of proteins has been studied by many investigators with the use of the solubility method,[2] Tiselius electrophoresis,[3] ultracentrifugation,[3] optical density difference,[4] and acrylamide gel electrophoresis.[5] From the results of these investigations, it was concluded that the polar groups of the inner parts of BSA are exposed to the surface of the molecule and the mechanism of the thermal denaturation of BSA differs at the initial stage from that at the later stage, some fractions of BSA aggregating while some remain undenatured. However, such points as the percentage of the aggregates in the solution and its variation with heating time and the dimension of the aggregated molecules, have not been clarified. With particular attention to these points, we have studied the mechanism of thermal denaturation of BSA by means of light scattering and viscosity measurements.

Experimental

Materials. The bovine serum albumin (here after called BSA) used was made by Armour Co., Ltd., (Fraction V, No. G5715, D. 1092), as in the previous paper.[6] A solution containing about 0.25 percent BSA in 0.05M phosphate buffer (pH 7.2) was heated at the desired temperature between 25 and 90°C for the desired length of time in test tube fitted with a lid. It was dipped, into cold water in order to stop thermal denaturation.[2-5] Under these conditions, turbidity did not increase very much. Phosphate buffer solution (pH regions 6.2—7.4) is said to be more suitable than acetate buffer solution, because the BSA in it shows less turbidity. The concentration of BSA was determined by measuring the optical density at 278 mμ. Water used was distilled, refined by ion-exchange resin, and distilled again with an all-glass still.[6]

Degree of Denaturation. It is well-known[7] that an anionic dye, 2-(4′-hydroxyphenylazo) benzoic acid (abbreviated HABA) is specifically bound to the native BSA and causes a remarkable optical change giving a new absorption band at 482 mμ at pH=7.2. The degree of denaturation was therefore determined with HABA by using the difference of optical density at 482 mμ from a blank solution of the same dye concentration as a reference, with a Shimadzu photoelectric photometer QR-50 with quartz cells 1 cm thick. A stock solution of 10^{-3}M HABA, stable for at least 10 months, was diluted to 5×10^{-4}M with a phosphate buffer. The dilute solution was stable for at least two weeks. Protein and dye reacted immediately and the colour of the complex was stable for several hours. Concentration of HABA used was 5×10^{-4}M and that of BSA about 0.1 percent or below. In these concentration regions, Beer's rule was satisfied. The degree of denaturation, $w_D°$, was obtained experimentally by the relation

$$w_D° = 1 - \Delta E/\Delta E_N \quad (1)$$

where ΔE is the optical density difference between the heat-denatured solution and the reference solution and ΔE_N is that of the native BSA.

Intrinsic Viscosity. Viscosity of BSA solution denatured at various temperatures and at various times was measured by the Ostwald type viscometer, the flow time of the clean water being about 120 sec at 25°C. The viscometer was cleaned immediately before use by chromate mixture, rinsed with distilled water many times to remove all traces of the acid, and then dried with acetone which had been distilled three times. Measurements were carried out in a thermostat kept at 25°C. The intrinsic viscosity, $[\eta]$ (ml/g), was determined according to the Huggins equation

$$\eta_{sp}/c = [\eta] + k[\eta]^2c \quad (2)$$

where η_{sp} is the specific viscosity of the solution, c the concentration of the BSA in g/ml, and k the Huggins constant.

Light Scattering Measurements. The method of measurements was the same as that given in a previous paper.[8] A

1) This paper was presented at the 24 th Annual Meeting of the Chemical Society of Japan, Gifu, November, 1971.

2) R. C. Warner and M. Levy, *J. Amer. Chem. Soc.*, **80**, 5735 (1958).

3) S. Stokrova and J. Sponar, *Collect. Czech. Chem. Commun.*, **27**, 2516 (1962); S. Stokrova, P. Bartl, and J. Sponar, *ibid.*, **25**, 1258 (1960).

4) M. F. Kerekes, *Naturwissenschaften*, **17**, 537 (1963).

5) A. Aoki, K. Hiramatsu, K. Kimura, S. Kaneshima, Y. Nakamura, and K. Sano, *Bull. Inst. Chem. Res., Kyoto Univ.*, **47**, 274 (1969).

6) Nakagaki and Y. Sano, This Bulletin, **45**, 2100 (1972).

7) D. R. Rustein, E. F. Ingenito, W. E. Reynolds, and J. M. Burke, *J. Clin. Invest.*, **33**, 211 (1954); H. T. Wrenn and T. V. Feichtmeir, *Amer. J. Clin. Pathol.*, **26**, 960 (1956).

8) M. Nakagaki and Y. Sano, This Bulletin, **45**, 1011 (1972).

Shimadzu electrophotometric light scattering photometer PG-21 was used at 436 mμ and at 25°C. The reduced scattering intensity for unpolarized incident light was obtained and examined by the Zimm plot method. The solutions and solvent were made optically clean by ultrafiltration with Membrane Filter No. 15 from Sartorious Co. Ltd. It has been ascertained that the concentration of the thermally denatured BSA does not change by ultrafiltration.

Refractive Index Increment. Measurements were carried out with a Shimadzu photoelectric differential refractometer DR-3 (Brice type) at 436 mμ and at 25°C.

Density. A picnometer of about 35 ml was used at 25°C.

Results

Degree of Denaturation. The weight fraction of denatured BSA, $w_D°$, was obtained by using HABA for the solutions heated at various temperatures for various lengths of time. The results are shown in Figs. 1 and 2. We see from Fig. 1 that the value of $w_D°$ increases with time and seems to reach a final value determined by the temperature. When the temperature was below 53°C, the $w_D°$ value reaches, at most 25 percent, while at or above 80°C it reaches 90 percent in about 20 min. At 56—60°C, it increases gradually with time.

The $w_D°$ values obtained at various temperatures at the constant heating time of 100 min are plotted in Fig. 2. The value was less than 10 percent below 50°C but increased remarkably in the temperature range 50—60°C. Thus, $w_D°$ reached about 80 or 85 percent when the BSA solution was heated at 60°C for 100 min.

Intrinsic Viscosity. Two samples obtained by heating (A) at various temperatures for 100 min, and (B) at 60°C for various lengths of time, were studied, the values of the intrinsic viscosity [η] being obtained for the BSA of various degrees of denaturation, $w_D°$. The results are shown in Fig. 3, where open circles denote

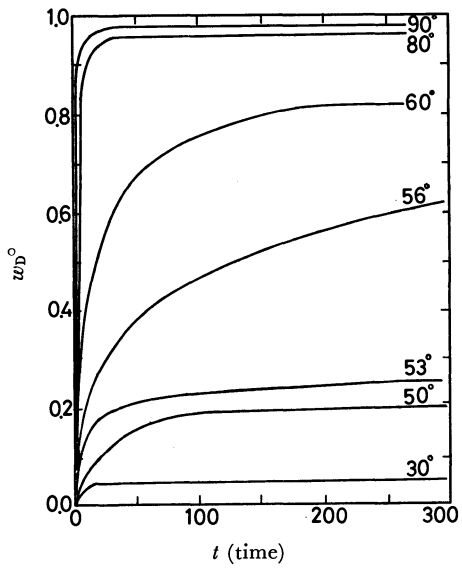

Fig. 1. Degree of denaturation, $w_D°$, obtained at various heating temperatures and heating times, with HABA (at 482 mμ) in 0.05M phosphate buffer at pH 7.2.

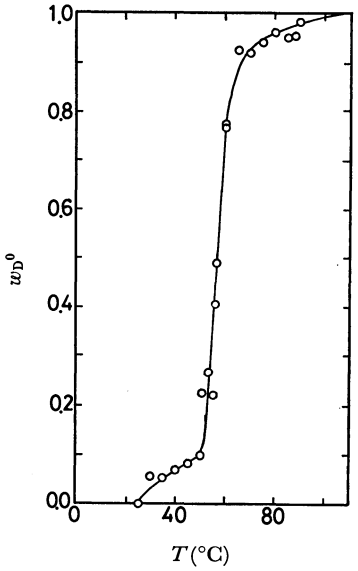

Fig. 2. Degree of denaturation, $w_D°$, obtained at various heating temperatures for 100 min.

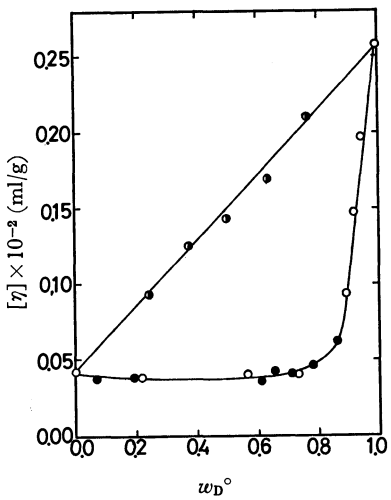

Fig. 3. Intrinsic viscosities, $10^{-2}[\eta]$, (ml/g) obtained by heating (A) at various temperatures for 100 min. (open circles) and (B) at 60°C for various times (closed circles) and (C) for the mixed solution of the native BSA and the denatured BSA, the latter having been heated at 90°C for 100 min. (half-open circles).

the BSA heated at various temperatures for 100 min (case A), and closed circles that heated at 60°C for various lengths of time (case B). Both plots lie on the same curve when plotted against w_D^0. This suggests that the state of BSA molecules and therefore the mechanism of the thermal denaturation in heated solutions does not depend on the method of heating but only on the degree of denaturation $w_D°$.

Half-open circles in Fig. 3 show the values of intrinsic viscosity obtained for the mixture of the solutions of untreated native BSA and of the almost fully denatured BSA, the latter being obtained by heating at 90°C for 100 min. It is seen that the additivity of the intrinsic viscosity against $w_D°$ holds for the mixed solution, and that the value of [η] of the mixture is entirely different from that of the partially denatured solutions. It is thus concluded that the actual solution is not a simple

mixture of fully denatured BSA and native BSA.

The curve $[\eta]$ *vs.* $w_D°$ is bent at about $w_D°=0.85$. When $w_D°$ was below 85 percent, the intrinsic viscosity showed no appreciable change but it increased remarkably when $w_D°$ exceeded 85 percent. The data indicate that the mechanism of thermal denaturation differs for below and above 85 percent of $w_D°$. In the initial stage of heating, intramolecular denaturation which does not affect the value of $[\eta]$ would mainly occur, while in the later stage, intermolecular aggregation which gives rise to an increase of $[\eta]$ would mainly occur. Light scattering measurements were carried out in order to clarify the results.

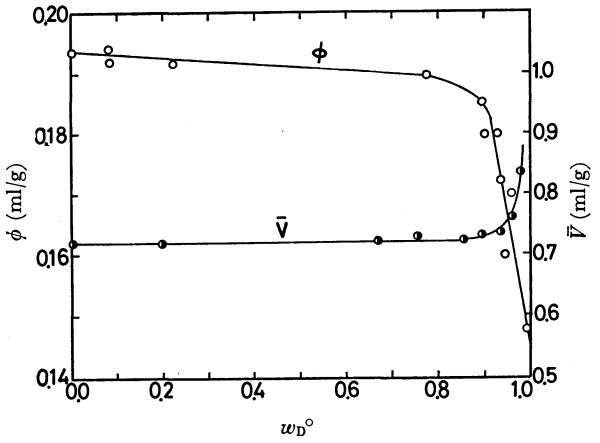

Fig. 4. Refractive index increment, ϕ, (ml/g) and the partial specific volume, $\bar{V}$, (ml/g) at various degree of denaturation.

Refractive Index Increment. The refractive index of the thermally denatured solution n was found to be linear with respect to BSA concentration c (g/ml). As the inclination of the straight lines, the value of the refractive index increment ϕ (ml/g) was determined for each thermally denatured solution and the result is given in Fig. 4. The quantity ϕ is the apparent refractive increment defined as follows.

$$\phi = (\mathrm{d}n/\mathrm{d}c)$$

We see that ϕ does not change appreciably for $w_D°$ values less than 85 percent but decreases remarkably at values exceeding 85 percent. This is in line with the variation of intrinsic viscosity.

Light Scattering. The reduced scattering intensity for unpolarized incident light, R_θ, was measured as a function of the scattering angle θ at various BSA concentration c (g/ml), in 0.05M phosphate buffer as a solvent. According to the Zimm plot method, apparent values of the weight-averaged molecular weight M, the radius of gyration R_g and the second virial coefficient A_2 are obtained on the basis of the following equation:

$$\frac{K'\phi^2 c}{R_\theta} = \frac{1}{M}\left(1+\frac{16\pi^2 n_0^2}{3\lambda_0^2}R_g^2 \sin^2\frac{\theta}{2}\right) + 2A_2 c \qquad (3a)$$

where

$$K' = 2\pi^2 n_0^2/N_0\lambda_0^4 \qquad (3b)$$

Here, N_0 is Avogadro's number, λ_0 is the wavelength in a vacuum, the value used in this experiment being 4360 Å.

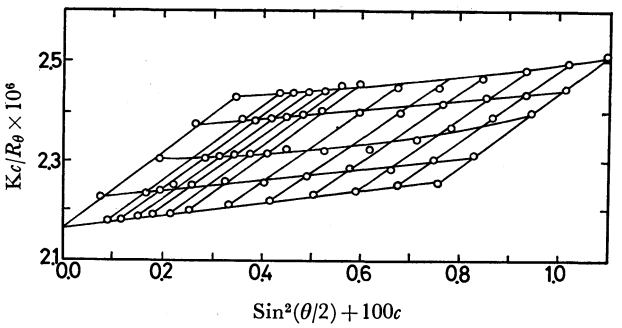

Fig. 5. Zimm plot for the thermally-denatured BSA at 60°C for 100 min.

It has been reported[8] that the Zimm plot of native BSA in 0.01M sodium chloride solution (pH=5.40) is narrow because the value of the second virial coefficient A_2 is nearly equal to zero, and that the value of the molecular weight M is 71900, which is in good agreement with the value reported.[9] The Zimm plot of the BSA thermally denatured by heating at 60°C for 100 min is shown in Fig. 5 as an example. The plots obtained by the extrapolation to zero of θ are linear against c. From the straight line, the apparent molecular weight M and the second virial coefficient A_2 can be calculated according to Eq. (3). The curves of the reduced scattering intensity against $\sin^2(\theta/2)$ at finite concentration are slightly concave upwards, but the curve obtained by the extrapolation to zero of c is almost linear against $\sin^2(\theta/2)$. The apparent radius of gyration R_g can therefore be obtained from the inclination of the straight line. The values of M, R_g, and A_2 thus obtained are given in Tables 1 and 2, which give the results obtained by the methods of heat treatment A and B, respectively, and Fig. 6 which gives the results of M and R_g plotted as a function of the degree of denaturation $w_D°$. We see that the increase of M is relatively small when $w_D°$ exceeds this value. Similarly, the value of R_g is nearly constant when $w_D°$

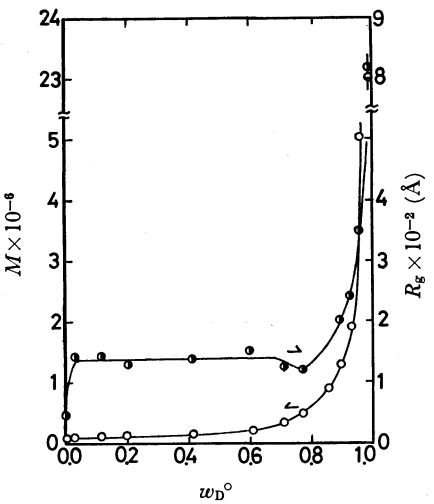

Fig. 6. Apparent molecular weight, M, and apparent radius of gyration, R_g, obtained at various degree of denaturation.

9) J. T. Edsall, H. Edelhoch, R. Lontie, and P. R. Morrison, *J. Amer. Chem. Soc.*, **72**, 464 (1950).

TABLE 1. RESULTS OF LIGHT SCATTERING, INTRINSIC VISCOSITY AND SPECIFIC VOLUME OF DENATURED BSA HEATED AT VARIOUS TEMPERATURES FOR 100 min

T°C	Native	55°C	60°C	65°C	70°C	80°C	90°C
$M\times10^{-6}$	0.0719	—	0.4628	1.263	1.890	5.025	23.04
$A_2\times10^{5}$ (mole ml/g^2)	0	—	3.08	1.93	1.50	0.638	0.175
R_g(Å)	45	—	116	201	242	354	816
$[\eta]\times10^{-2}$ (ml/g)	0.0405	0.0395	0.0475	0.0940	0.1468	0.1974	0.2582
ϕ (ml/g)	0.1935	—	0.1896	0.1850	0.1799	0.1702	0.1475
$\bar{V}$(ml/g)	0.7165	0.7190	0.7200	0.7338	0.7353	0.7577	0.8362
w_D°	0	0.400	0.770	0.895	0.930	0.960	0.990

TABLE 2. RESULTS OF LIGHT SCATTERING, INTRINSIC VISCOSITY, AND SPECIFIC VOLUME OF DENATURED BSA HEATED AT 60°C FOR VARIOUS TIMES

Time (min)	15	30	65	200
$M\times10^{-6}$	0.1296	0.1907	0.3397	0.8800
$A_2\times10^{5}$ (mol. ml/g^2)	0.169	0.288	0.203	2.02
R_g (Å)	177	153	153	163
$[\eta]\times10^{-2}$ (ml/g)	0.0398	0.0352	0.0407	0.0623
ϕ (ml/g)	0.1921	0.1902	0.1899	—
$\bar{V}$ (ml/g)	0.7180	0.7200	0.7200	—
w°_D	0.196	0.610	0.710	0.856

is below 85 percent, and increases remarkably when w_D° exceeds this value.

Discussion

Mechanism of Denaturation. It is thought that the mechanism of denaturation changes at about 85 percent of the degree of denaturation. No appreciable change in $[\eta]$, ϕ, and R_g and relatively small increase of M, observed at the earlier stage of heating, would suggest intramolecular denaturation in the range where w_D° is less than 85 percent. When w_D° exceeds 85 percent, the values of M, R_g, and $[\eta]$ increased and ϕ decreased remarkably, from which the intermolecular aggregation of denatured molecules could be suggested. There will, therefore, be at least three components in the solutions, that is, native (N), intramolecularly denatured (D), and intermolecularly aggregated (D_n) components. The following reaction would occur between them:

$$n\mathrm{N} \longrightarrow n\mathrm{D} \longrightarrow \mathrm{D}_n \qquad (4)$$

Component D is mainly formed in the stage where w_D° is less than 85 percent. The value of $[\eta]$, R_g, ϕ, M, and $\bar{V}$ of this component are nearly the same as those of the native BSA, although the component differs from that of native BSA in conformation. Component D_n is formed by the intermolecular aggregation of the intramolecularly denatured BSA mainly in the stage where $w_D{}^0$ exceeds 85 percent. Many papers have dealt with qualitative studies of aggregation of denatured proteins,[2-5] but not much with quantitative studies.

Weight Fraction of Denatured Components. The following equation is derived for the refractive index increment of a solution containing z macromolecular components at constant temperature T, and at constant pressure P.

$$\left(\frac{\partial n}{\partial c}\right)_{T,P} = \sum_{i=1}^{i=z}\left(\frac{\partial n}{\partial c_i}\right)_{T,P,c_{j\neq i}} \cdot \left(\frac{\partial c_i}{\partial c}\right)_{T,P} \qquad (5)$$

where

$$c = \sum_{i=1}^{i=z} c_i \quad \text{and} \quad w_i = c_i/c, \qquad (6)$$

n being the refractive index of the solution and c the concentration for the total solutes g/ml, related to the concentration of i-th component according to Eq. (6) where w_i is the weight fraction of the i-th component. If the refractive index increment by the i-th component $(\partial n/\partial c_i)_{P,T,c_j}$ is expressed by ϕ_i, Eq. (5) can be written as follows.

$$\phi = \sum_{i=1}^{i=z} \phi_i w_i \qquad (7)$$

where ϕ is the apparent refractive index increment obtained for the total solutes in the mixed solution. The following equations can be obtained for a mixed solution of three macromolecular solutes N, D, and D_n mentioned above:

$$1 - w_D{}^{\circ} = w_N \qquad (8a)$$

$$w_D{}^{\circ} = w_D + w_n \qquad (8b)$$

$$\phi = \phi_N w_N + \phi_D w_D + \phi_n w_n \qquad (8c)$$

where the subscripts N, D, and n represent N, D, and D_n, and w_D° is the degree of denaturation obtained experimentally by using HABA according to Eq. (2).

Since the value of ϕ in Fig. 4 showed no appreciable change when w_D° was within 85 percent, it may be proper to assume that the value of the refractive increment of component D is nearly equal to that of native BSA, *viz.*, $\phi_N \fallingdotseq \phi_D$. Thus, according to Eq. (8):

$$w_n = (\phi - \phi_N)/(\phi_n - \phi_N) \qquad (9a)$$

$$w_D = w_D{}^{\circ} - w_n \qquad (9b)$$

The results obtained are shown in Fig. 7 by using the values ϕ_n=0.1422(ml/g) and ϕ_N=0.1935(ml/g). The curve of w_D has a maximum point as expected for the intermediate component of a successive reaction as Eq. (4). The maximum point is for w_D°=85 percent. On the other hand, w_n showed no appreciable increase when w_D° is less than 85 percent. When w_D° exceeds this value, w_D increased remarkably as a result of the intermolecular aggregation.

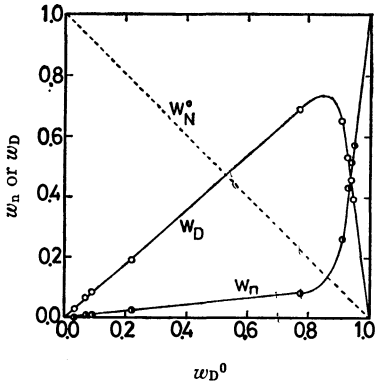

Fig. 7. Weight fraction of the monomeric, denatured BSA, W_D, and of the aggregate, W_n, at various degree of denaturation W_D°.

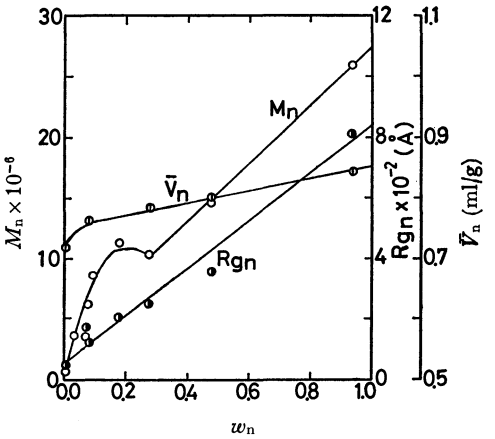

Fig. 8. Molecular weight, M_n, radius of gyration, R_{gn}, and partial specific volume, $\bar{V}_n$, of the aggregate at various degree of denaturation.

Physico-chemical Properties of Aggregated Molecules. For the light scattering of a solution containing z macromolecular components, the following equation derived by the theory of fluctuation of the chemical potential was used in the previous paper,[8]

$$\frac{K'c}{R_\theta} = \frac{1}{\sum_{i=1}^{i=z} M_i w_i \phi_i^2}\left\{1 + \frac{16\pi^2 n_0^2}{3\lambda_0}\left(\frac{\sum_{i=1}^{i=z} M_i w_i \phi_i^2 R_{gi}^2}{\sum_{i=1}^{i=z} M_i w_i \phi_i^2}\right)\sin^2\frac{\theta}{2}\right\} + 2c\frac{\sum_{i=1}^{i=z}\sum_{j=1}^{j=z} A_2^{(ij)} M_i M_j P_i(\theta) P_j(\theta) w_i w_j \phi_i \phi_j}{\left(\sum_{i=1}^{i=z} M_i P_i(\theta) w_i \phi_i^2\right)^2} \quad (10)$$

where R_θ is the reduced scattering intensity of the solution containing z macromolecular components, $P_i(\theta)$ the interference factor of the i-th macromolecular component, $A_2^{(ij)}$ the second virial coefficient describing the interaction between the i-th and j-th components, w_i the weight fraction of the i-th component in the total solute, M_i the weight-average molecular weight of the i-th component, ϕ_i the refractive increment of the i-th component, n_0 is the refractive index of the solvent and λ_0 the wavelength in a vaccum (the value 4360 Å was used). From this equation the following equations can be obtained for a mixed solution of three macromolecular species, N, D, and D_n,

$$M\phi^2 = M_N w_N \phi_N^2 + N_D w_D \phi_D^2 + M_n w_n \phi_n^2 \quad (11a)$$

$$R_g^2 M\phi^2 = R_{gN}^2 \phi_N^2 M_N w_N + R_{gD}^2 \phi_D^2 M_D w_D + R_{gn}^2 \phi_n^2 M_n w_n \quad (11b)$$

where M, ϕ, and R_g are experimental values.

From Eq. (11a) and the relations $M_D \fallingdotseq M_N$, and $\phi_D \fallingdotseq \phi_N$, the value of M_n can be obtained:

$$M_n = \{M\phi^2 - (1-w_n)M_N\phi_N^2\}/(w_n\phi_n^2) \quad (12)$$

The results are given in Fig. 8 and Table 3. The degree of association n can be obtained as (M_n/M_N).

It is seen that the value of M_n increases remarkably with the increase of w_n, the increase being almost linear when w_n exceeds 0.3. The last column of Table 3 shows values obtained by the extrapolation of w_n to 1, according to the data shown in Fig. 8. We see that the weight-average molecular weight of the aggregate is 27.2×10^6 at the maximum, and the aggregate is composed of 378 molecules of denatured BSA.

The conformation of the intramolecularly denatured BSA, D, is expected to differ more or less from that of the native BSA. The result given in Fig. 6, however, shows that the radius of gyration remains constant in the initial stage of thermal denaturation where w_D° is less than 85 percent. The radius of gyration of the component D, R_{gD}, is therefore assumed to be nearly equal to that of native BSA, R_{gN}. The value of the radius of gyration of the aggregate, R_{gn}, can then be obtained according to the equation easily derived from Eq. (11b):

$$R_{gn}^2 = \{R_g^2 M\phi^2 - R_{gN}^2 M_N \phi_N^2 (1-w_n)\}/(w_n M_n \phi_n^2) \quad (13)$$

The results are shown in Fig. 8 and Table 3. We see that R_{gn} increases almost linearly with the increase of w_n. The value of the radius of gyration of the aggregate itself was about 841 Å at the maximum, as obtained by extrapolation of w_n to 1. This value is about 19 times larger than that of the native BSA.

For the partial specific volume of polymer mixtures, the additivity rule is usually assumed. In the present case of three solutes,

$$\bar{V} = \bar{V}_N w_N + \bar{V}_D w_D + \bar{V}_n w_n \quad (14)$$

The value of $\bar{V}$ remains almost constant in the region of w_D° less than 85 percent, where the intramolecular denaturation mainly takes place. The partial specific volume of the denatured, monomeric BSA, $\bar{V}_D$, is therefore assumed to be nearly equal to that of the

Table 3. Results of light scattering and specific volume of the aggregates

w_n	0.0791	0.1724	0.2759	0.4726	0.9331	1.000
$M_n \times 10^{-6}$	6.42	7.73	10.3	14.7	25.8	27.2
R_{gn} (Å)	126	206	249	355	816	841
n	89.3	108	143	205	359	378
$\bar{V}_n$ (ml/g)	0.7607	0.7710	0.7847	0.8037	0.8448	0.8990

native BSA, $\bar{V}_N$. If $\bar{V}_D \fallingdotseq \bar{V}_N$ in Eq. (14), the value of the partial volume of the aggregate $\bar{V}_n$, can be obtained. The results are shown in Table 3 and Fig. 8. We see from Fig. 8 that values of $\bar{V}_n$ increase almost linearly with increase of w_n and that the value of $\bar{V}_n$ is 0.8990 ml/g at the maximum association state where w_n is equal to 1.

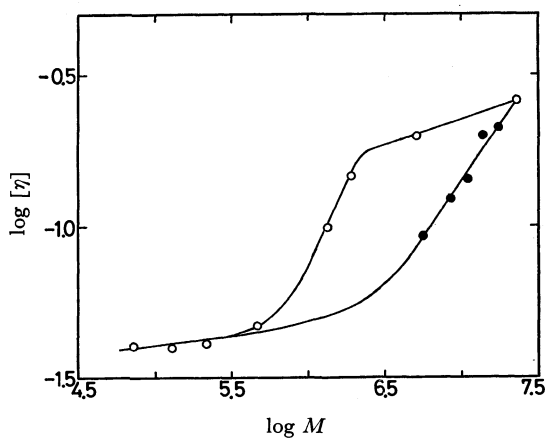

Fig. 9. Log-log plots of intrinsic viscosity against apparent molecular weight.

Dependence of $[\eta]$ *and* R_g *on* M. The log-log plots showing the dependency of the intrinsic viscosity on weight average molecular weight are given in Fig. 9. Open circles denote the experimental values obtained for variously denatured solutions and closed circles those obtained for the mixed solutions of the native BSA and completely denatured BSA. The latter was obtained heating at 90°C for 100 min, its molecular weight being 2.30×10^7. The exponent a in the Kuhn-Mark equation $[\eta]=KM^a$ was obtained from the slope of curves in Fig. 9. In the former, three values of the exponent a 0.054, 1.1, and 0.166 are obtained for lower, intermediate and higher M values, respectively. In the latter mixed solutions, the values of a are 0.055 and 0.75 for lower and higher M-values, respectively.

Log-log plots of R_g *vs.* M for the results from thermally treated solutions (open circles) and for calculated values of the aggregated molecules themselves (closed circles) are shown in Fig. 10. The relations are linear and expressed by the empirical equation: $R_g=K'M^b$. The value of the constants, $K'=0.185 \times 10^{-8}$ and $b=0.496$, were obtained for the solutions, and $K'=1.68 \times 10^{-17}$ and $b=1.578$ for the aggregates.

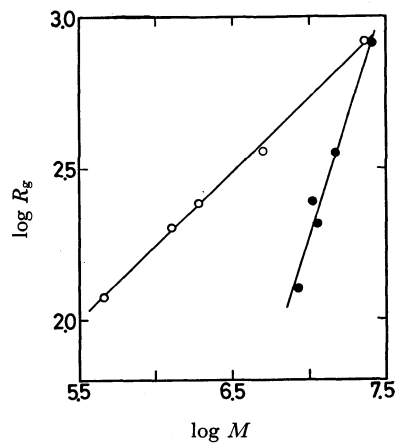

Fig. 10. Log-log plots showing dependence of radius of gyration on molecular weight for the mixture solutes (open-circles) and for the aggregate (closed circles).

The results indicate that native and intramolecularly denatured species are approximated with a compact, comparatively spherical shape because of the low a and b values, while the intermolecularly aggregated species is approximated with rigid, cylindrical rod molecules because of the relatively large a and b values.

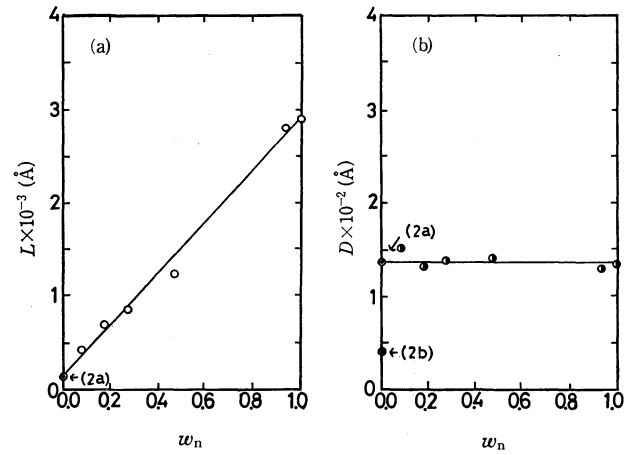

Fig. 11. Variation of molecular length L and diameter D by association.

TABLE 4. MOLECULAR DIMENSIONS OF THE AGGREGATES AS CYLINDRICAL RODS

w_n	L (Å)	D (Å)	p	L/n
0.0791	435	154	2.8	4.87
0.1724	715	133	5.4	6.65
0.2759	862	141	6.1	5.32
0.4726	1231	142	8.7	6.02
0.9331	2828	128	22.1	7.88
1.000	2913	133	21.9	7.70
		average		average
		139		6.41

Size and Shape of Aggregated Molecules. If the aggregate is assumed to be rigid and the mass is distributed uniformly all over the volume of the aggregate, the size and shape of the aggregate can be calculated from the above data of M_n, $\bar{V}_n$, and R_{gn}. The dimensions and axial ratio of the aggregates as cylindrical rod molecules are given in Fig. 11 and Table 4, where L and D are the length and diameter, respectively, of the rod molecule, and p is the axial ratio ($=L/D$). The diameters of the native BSA as a rigid prolate spheroid with major axis a and minor axis b are $2a=$ 140 Å and $2b=70$ Å as shown in Fig. 11 by double circles at $w_n=$zero. We see from Fig. 11a that the length L increases almost linearly with the increase of the weight fraction of the aggregate w_n. The value of the length of the aggregate obtained by extrapolation of w_n to zero agreed with the length of the native BSA: $2a=140$ Å. The length per one BSA in an aggregate

L/n (n is the degree of association) is about 6.41 Å, irrespective of the value of w_n (Table 4).

On the other hand, the diameter of the aggregated molecule D was almost constant irrespective of w_n (Fig. 11b). The average value of diameter D thus obtained was 140 Å, which is equal to the length of the native BSA, $2a$, instead of the diameter $2b$. This would indicate that the aggregate is formed by side-by-side association, so that the diameter of the aggregate is almost constant, but the length of the aggregate increases linearly with the degree of aggregation. At $w_n=1$, the length and diameter of the aggregate are 2910 and 140 Å, respectively, and one aggregate consists of 378 molecules.

BULLETIN OF THE CHEMICAL SOCIETY OF JAPAN, VOL. 46, 797—804 (1973)

The Molecular Vibrations and the Rotational Isomerism of (Chloromethyl)methylsilane

Michiro HAYASHI, Keiichi OHNO, and Hiromu MURATA

Department of Chemistry, Faculty of Science, Hiroshima University, Higashi-sendamachi, Hiroshima

(Received September 6, 1972)

The infrared spectra of (chloromethyl)methylsilane and its deuterated species have been measured in the gaseous, liquid, and crystalline states. The normal vibration calculation has been carried out using a modified Urey-Bradley force field. It has been concluded that, in the gaseous and liquid states, there exist both the *trans* and *gauche* isomers, while only the former persists in the crystalline state. For $ClCH_2SiD_2CH_3$, a different spectral pattern has sometimes been recorded in the crystalline state before the sample has been annealed enough. It has been concluded that the persisting isomer is in the *gauche* form in this metastable crystalline state. The *trans* and *gauche* isomers have been found, from the temperature dependence of the relative intensities of the spectra, to have nearly the same energy in the liquid state. From the solvent effects of the spectra, the *trans* isomer has been found to be more polar than the *gauche* isomer. Therefore, if the C–Cl bond moment is assumed to have the direction of C^+–Cl^-, the group moment of the C_2SiH_2 part of the molecule must be in the direction of

on the bisector of the C–Si–C angle. The vibrational assignments have been worked out taking into account the results of the normal vibration calculations and the reported assignments for chloromethylsilane, dimethylsilane, and ethylmethylsilane.

Recently, we have worked out the vibrational assignments and the rotational isomerism for alkylsilane. The vibrational assignments and the normal vibration calculations for halogenomethylsilane,[1] methylsilane,[2] dimethylsilane,[2] ethylsilane,[2] and ethylmethylsilane[3] have already been reported. In this paper, the vibrational assignments of (chloromethyl)methylsilane will be dealt with in relation to the rotational isomerism around the C–Si bond as an axis.

The normal vibrations of this molecule have been calculated using modified Urey-Bradley force constants transferred from those of chloromethylsilane and dimethylsilane.

The direction of the group moment of the C_2SiH_2 part of the molecule will be discussed using the results of the solvent effects of the spectra.

Experimental

The samples of (chloromethyl)methylsilane and its deuterated species were prepared by the reduction of a commercial product of $ClCH_2SiCl_2CH_3$ (Pierce Chem. Co. U.S.A.) with $LiAlH_4$, $LiAlD_4$, or an equimolar mixture of $LiAlH_4$ and $LiAlD_4$ in *n*-butyl ether.[4] The purities of the samples of $ClCH_2SiH_2CH_3$ and $ClCH_2SiD_2CH_3$ were checked by means of the infrared spectra and gas chromatography.

The infrared spectra in the region from 200 to 4000 cm^{-1} were recorded on a Perkin-Elmer instrument (model 621). For the measurements in the crystalline state, the vapors of the samples were directly condensed on a CsI plate in a cell cooled with liquid nitrogen in a vacuum and were then annealed several times in order to keep the samples from being in a supercooled state. The spectra in the gaseous state were measured with one-meter and 10 cm gas cells with CsI windows.

In order to measure the relative intensity changes in the infrared spectra, the solution spectra were also measured using a sealed KRS-5 cell (0.2 mm thick), with carbon disulfide and acetonitrile as the solvents.

Rotational Isomerism

In this substance, two rotational isomers are expected around the C–Si bond, as is shown in Fig. 1.

The observed infrared spectra of $ClCH_2SiH_2CH_3$ and $ClCH_2SiD_2CH_3$ in the region from 300 to 1000 cm^{-1}

1) K. Ohno and H. Murata, This Bulletin, **45**, 3333 (1972).

2) K. Ohno, M. Hayashi, and H. Murata, *J. Soc. Hiroshima Univ., Ser A.*, **36**, XXX (1972).

3) M. Hayashi, K. Ohno, and H. Murata, This Bulletin, **45**, 298 (1972); **46**, 684 (1973).

4) M. Kumada, M. Ishikawa, and S. Maeda, *J. Organometal. Chem.*, **2**, 478 (1964).

TABLE 1. INFRARED SPECTRA OF $ClCH_2SiH_2CH_3$

Gas		Liquid		Crystal		Assignment
cm^{-1}	Int.	cm^{-1}	Int.	cm^{-1}	Int.	
2982 2976 2970	ms	2966	m	2975	m	CH_2 antisym. str. T,G, CH_3 asym. str. (A′, A″) T,G
2948 2942 2936	ms	2942	m	2950	m	CH_2 sym. str. T,G
		2913 b 2905 b	vw vw	2912 b	vw	CH_3 sym. str. T,G
2182 sh	vs					
2174	vs	2156	vs	2155	s	SiH_2 antisym. str. T,G
2154 2148 2142	vs			2130	s	SiH_2 sym. str. T,G
1440 1431 1422	m	1416 b	mw	1421 sh 1416	w m	CH_3 asym. def. (A′,A″) T,G
				1411 sh	w	
1409 1402 1394	ms	1394	m	1400 1388	vw m	CH_2 sci. T,G
				1350	vw	
				1309	vw	
1267 1257	s	1256	s	1249	s	CH_3 sym. def. T,G
1184 1179 1173	m	1179	m	1170	ms	CH_2 wag. T,G
1142 b	w					
1113 1107 1101	m	1109	m	1111	m	CH_2 twist. T,G
				987 981	mw	
952 948 941	vs	940	vs	961 951	vs	SiH_2 sci. T,G
				920 sh	s	
912 905 899	vs	895	vs	908 b 887 b	vs vs	SiH_2 wag. T,G
875	s					
867	s	867	s	867	vs	CH_3 rock. (A″) T,G
				828 sh	m	
816 809	s	809	s	814	s	CH_2 rock. T
772	s					
759 748	s	761	s	766	s	CH_3 rock. (A′) T,G, CH_2 rock. G
740 sh	ms	745	vvw	745	s	C–Si str. T
728	ms	736	ms	—		C–Si str. G
706 701 694	ms	699	s	699	vs	C–Cl str. T
685	m	685	mw	—		C–Cl str. G
620	ms	617 sh	m	—		SiH_2 twist. G
612	ms	607	m	607	s	C–Si str. T
585 579 574	ms	579	m	—		C–Si str. G
490 485 478	s	487	s	492	s	SiH_2 rock. T, G

Int. =intensity ; s, m, w=strong, medium, weak;
v=very; sh=shoulder; b=broad;
T=*trans* form; G=*gauche* form.

TABLE 2. INFRARED SPECTRA OF $ClCH_2SiD_2CH_3$

Gas		Liquid		Crystal A		Crystal B		Assignment
cm^{-1}	Int.	cm^{-1}	Int.	cm^{-1}	Int.	cm^{-1}	Int.	
2975	s			2977	w			CH_2 antisym. str.,
2962	s	2967	mw	2967	w	2966	mw	CH_3 asym. str. (A′,A″)
2948, 2944, 2937	s	2935	mw	2931	w	2944	mw	CH_2 sym. str.
2905	mw	2908	w	2909	vw	2904	w	CH_3 sym. str.
1591 sh								
1584, 1578	vs			—		1581	s	SiD_2 antisym. str.
1571		1573	s	1576, 1570	vs	—		
1566, 1560	vs			—		1567, 1559	s	SiD_2 sym. str.
1552	vs	1553	s	1555	s	—		
						1427	ms	
1422, 1415	ms	1416	m	1422, 1416	w	1420	ms	CH_3 asym. def. (A′A″)
1409						—		
1401	ms	1396	m	1409	mw	—		
				1398	m	1396	ms	CH_2 sci.
				1388	w			
1346, 1335	vw			1333	vw			
				1274	vw			
1267, 1257	s	1253	ms	1250, 1246	ms	1250	s	CH_3 sym. def.
1182, 1177, 1172	w	1175	w	1178	w	1168	mw	CH_2 wag.
1110, 1105, 1099	w	1103	w	1111	w	1107	w	CH_2 twist.
				887	vw	884	vw	
				879	vw	876	vw	
				856	vw	—		
				850	vw	—		
827				826	vs			
824	vs	815	vs	818		819 b	vs	CH_3 rock. (A′)
817				813	vs	814	vs	CH_3 rock. (A″)
797, 786	vs	783	vs	788, 780	vs	784	w	CH_2 rock.
749, 743	s	735	ms	732	ms	747	s	C–Si str.
734						—		
728, 722	s	724	ms	—		722 b	s	SiD_2 sci.
		689	m	699, 695	ms	—		C–Cl str.
694				682	s	—		SiD_2 sci.
687	vs	681	s	679				
680						675	s	C–Cl str.
651		668 sh	ms					
646	mw	644	w	—		648	w	C–Si str.
640		637	w	637	m	—		
571, 565, 560	s	567	ms	—		570	s	SiD_2 wag.
544, 538, 533	s	537	ms	535	s	—		SiD_2 wag.
477, 472, 466	w	475	mw	479	mw	—		SiD_2 twist.
406								
400	s	401	s	401	s	—		SiD_2 rock.
395		389 sh	w	—		392	m	
				240	m	—		Skeletal bend.

Crystal A: The metastable crystalline state, where the *gauche* isomer persists alone.
Crystal B: The stable crystalline state, where the *trans* isomer persists alone.

are shown in Figs. 2 and 3 respectively, where (a) and (b) indicate the spectra in the liquid and in the crystalline states respectively,

TABLE 3. INFRARED SPECTRA OF THE MIXTURE OF $ClCH_2SiHDCH_3$, $ClCH_2SiH_2CH_3(-d)$, AND $ClCH_2SiD_2CH_3(-d_0)$[a]

Liquid		Crystal		Assignment[b]
cm^{-1}	Int.	cm^{-1}	Int.	
803 sh	s	805	vs	CH_2 rock. T
783	s	785	vs	$-d_2$
761	ms	766	m	$-d_0$
		750	m	C–Si str. T
747	ms	746	m	$-d_0$, $-d_2$
724	ms	727	m	$-d_2$
710	ms	714	s	Si–H def. T
700	ms	700	m	$-d_0$
682	s	687	m	C–Cl str. T
668 sh	m	675	m	$-d_2$
644	w	646	w	$-d_2$
637 sh	w	—		$-d_2$
617 sh	w	—		$-d_0$
607	m	607	m	$-d_0$
595 sh	w	—		C–Si str. G
579 sh	w	—		$-d_0$
567	m	568	m	$-d_2$
539	m	—		$-d_2$
502 sh	mw	—		Si–D def. G
494	m	498	m	Si–D def. T
487	m	489	m	$-d_0$
475 sh	mw	—		$-d_2$
433	m	—		SiHD rock. G
425	m	423	m	SiHD rock. T
401	m	—		$-d_2$
389 sh	w	391	m	$-d_2$

a) The region from 810 to 4000 cm^{-1} is omitted.
b) Assignments for the d_0 and d_2 species are omitted.

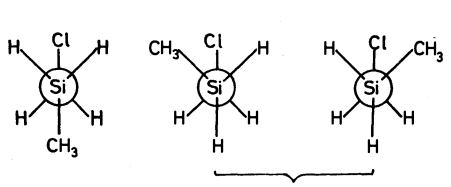

Fig. 1. Molecular forms of (chloromethyl)methylsilane.

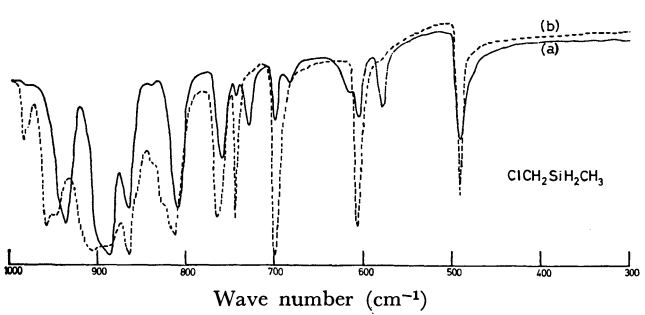

Fig. 2. Infrared spectra of $ClCH_2SiH_2CH_3$.
(a): in the liquid state,
(b): in the crystalline state.

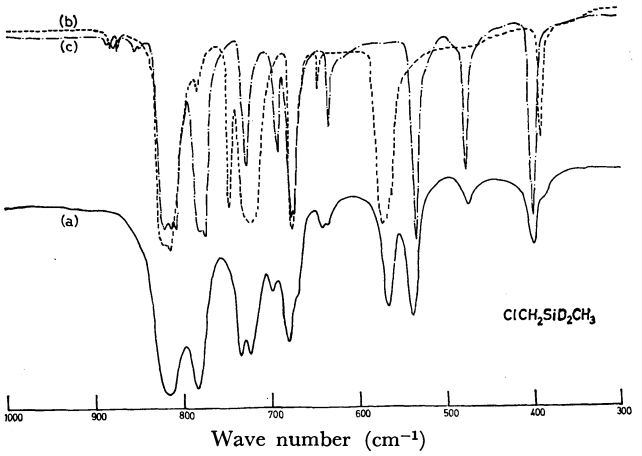

Fig. 3. Infrared spectra of $ClCH_2SiD_2CH_3$.
(a): in the liquid state,
(b): in the stable crystalline state,
(c): in the metastable crystalline state.

A comparison of the observed spectra in the liquid state with those in the crystalline state reveals the existence of rotational isomers in this substance, since some of the infrared bands vanish in the crystalline state.

Especially, it is to be noted that, for $ClCH_2SiD_2CH_3$, a different spectral pattern is sometimes obtained in the crystalline state before annealing the sample enough, as is shown in (c) of Fig. 3; furthermore, the superposition of these two kinds of spectral patterns, (b) and (c), coincides with the spectral pattern in the liquid state.

This is understandable if the persisting isomer has different molecular forms for $ClCH_2SiD_2CH_3$ in the metastable and stable crystalline states.

In the cases of ethylmethylsilane and its deuterated species, the existence of the rotational isomers has been proved from the lower-frequency mode of two Si–C stretchings and the SiH_2 rocking, SiD_2 rocking, and SiD_2 wagging modes appearing in the region from 300 to 650 cm^{-1}.[3] The spectra assigned to these modes have been observed for ethylmethylsilane as pairs which consist of two bands attributable to the *trans* and *gauche* isomers respectively.

These modes are also expected for (chloromethyl)-methylsilane in the same region as those for ethylmethylsilane; that is, for $ClCH_2SiH_2CH_3$, the lower-frequency mode of the two C–Si stretchings and the SiH_2 rocking mode are expected around 620 and 490 cm^{-1} respectively, and for $ClCH_2SiD_2CH_3$, the C–Si stretching, the SiD_2 wagging, and the SiD_2 rocking modes are expected around 640, 560, and 400 cm^{-1} respectively. In this region, for $ClCH_2SiH_2CH_3$ three bands are seen in the liquid state; one of them accompanies a shoulder on the higher-frequency side, while two bands persist in the crystalline state.

For $ClCH_2SiD_2CH_3$ five bands are seen in the liquid state; two of them accompany a shoulder on the lower-frequency side, while there are four and three bands persisting in the metastable and stable crystalline states respectively.

Although some of these bands can be regarded as pairs, only single bands can be found for the other

modes. However, these single bands can be regarded as unresolved pairs of two bands, since these bands are reduced in their relative intensities in the crystalline state; this fact can be understood if one of two unresolved bands vanishes in the crystalline state. The possibility of the unresolved bands in a pair is also supported by the fact that even the resolved bands in a pair actually have much smaller spacings than those for ethylmethylsilane.[3]

Because of the smallness of the spacing of the bands in the pair, the existence of the rotational isomers cannot be concluded from the SiH_2 rocking mode for $ClCH_2SiH_2CH_3$. However, for $ClCH_2SiD_2CH_3$, definite evidence is obtained from the SiD_2 wagging and the SiD_2 rocking modes. The pair at 567 and 537 cm^{-1} assigned to the SiD_2 wagging mode, and that at 401 and 389 cm^{-1} assigned to the SiD_2 rocking mode, are seen in the liquid state, where the bands at 537 and 401 cm^{-1} disappear in the stable crystalline state. This is the same as in the case of ethylmethylsilane.

Therefore, if the bands in the pair appear in the same order as in the case of ethylmethylsilane, the bands disappearing in the stable crystalline state are attributable to the *gauche* isomer and the bands persisting in the stable crystalline state are attributable to the *trans* isomer.

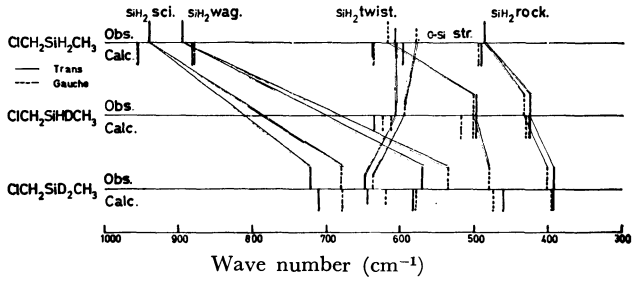

Fig. 4. Observed and calculated frequencies of the SiH_2, SiD_2, and SiHD deformation modes and the lower frequency C–Si stretching mode.

As is shown in Fig. 4, this conclusion is also confirmed by the normal vibration calculation, as will be described later.

The pair at 608 and 579 cm^{-1} for $ClCH_2SiH_2CH_3$ and that at 644 and 637 cm^{-1} for $ClCH_2SiD_2CH_3$ are seen in the liquid state, where one of two bands in each pair (579 and 637 cm^{-1}) disappears in the crystalline state. These are assigned to the lower-frequency mode of C–Si stretching from the results of the calculations.

Usually, the spectra of an asymmetrically deuterated species such as $ClCH_2SiHDCH_3$ give difinite experimental evidence on the molecular forms of the rotational isomers. For $ClCH_2SiHDCH_3$ and $CH_3CH_2SiHDCH_3$, since the two *gauche* forms come to be not equivalent, the spectra of the *gauche* isomer are expected to be split into doublets, while the spectra of the *trans* isomer remain singlets.

This is actually the case with ethylmethylsilane.[3] For the present case of $ClCH_2SiHDCH_3$, however, this is not actually the case.

As is shown in Fig. 5 although the doublet at 433

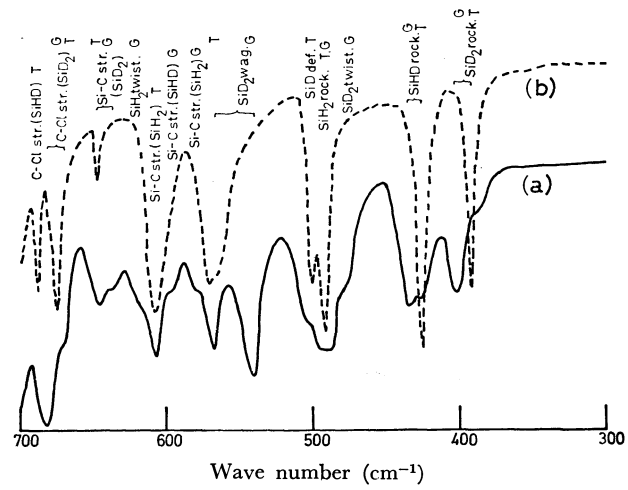

Fig. 5. Infrared spectra of the mixture of $ClCH_2SiHDCH_3$, $ClCH_2SiH_2CH_3$, and $ClCH_2SiD_2CH_3$.
(a): in the liquid state,
(b): in the crystalline state.

and 425 cm^{-1} assigned to the SiHD rocking mode is seen in the liquid state, one of the components, that at 433 cm^{-1}, disappears in the crystalline state. This component can be regarded as two unsplit bands due to two different pairs of *gauche* forms.

The existence of the rotational isomers in the gaseous state can also be proved from a comparison of the spectra in the gaseous and liquid states.

In the case of $ClCH_2SiD_2CH_3$, in the crystalline state it is concluded from the above discussions of the molecular forms of the isomers that the *gauche* isomer persists alone in the metastable state, while the *trans* isomer persists alone in the stable state.

As no appreciable changes in the relative absorption intensities between the spectra at low temperatures (*ca.* −100°C) and those at room temperature (*ca.* 23°C) were observed, the energy difference between the isomers can be disregarded in the liquid state. In the gaseous state, the larger overlapping of the key bands prevents the measurement of the relative intensities of the bands.

The Solvent Effects of the Spectra

The solvent effects of the spectra were measured using the pair of Si–C stretching bands at 608 and 579 cm^{-1} for $ClCH_2SiH_2CH_3$ and the pair of SiD_2 wagging bands at 567 and 537 cm^{-1} for $ClCH_2SiD_2CH_3$, where the higher-frequency bands of each pair are due to the *trans* isomer and the lower bands are due to the *gauche* isomer.

The bands for the *trans* isomer increase in their relative intensities when a mixture is made with a polar solvent such as acetonitrile, while the bands for the *gauche* isomer increase in their relative intensities in a mixture with a non-polar solvent such as carbon disulfide, as is shown in Fig. 6. Therefore, it can be concluded that the *trans* isomer is more polar than the *gauche* isomer.

From these results, if the C–Cl bond moment is assumed to have the direction of $C^+–Cl^-$, the group

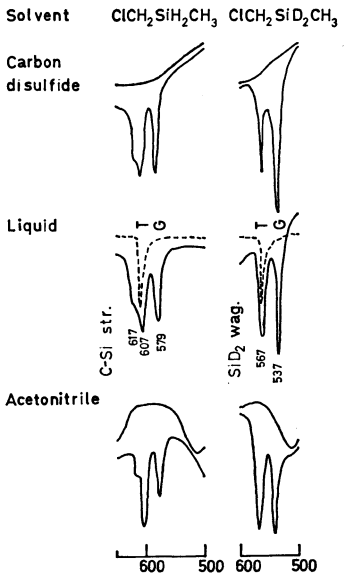

Fig. 6. Solvent effects of the infrared spectra for (chloromethyl)-methylsilane.

moment of the C_2SiH_2 group should be in the direction of $+\begin{smallmatrix} C\diagdown & \diagup H \\ & Si \\ C\diagup & \diagdown H \end{smallmatrix}-$ on the bisector of the C–Si–C angle.

The Normal Vibration Calculation and the Vibrational Assignments

In order to confirm the molecular forms of the rotational isomers and the assignments of the observed spectra, the normal vibration calculation for (chloromethyl)methylsilane was carried out using a modified Urey-Bradley force field.

The force constants used were transferred from those for chloromethylsilane[1] and dimethylsilane[2] except for the two force constants of H(Cl–C–Si) and F(Cl···C···Si), which were adjusted in order to predict the observed Cl–C–Si bending vibration, which had not been observed for chloromethylsilane.

The modified Urey-Bradley force field used in the calculation was the same type as in the cases of chloromethylsilane and dimethylsilane, where the internal rotation force constants for the CH_3–Si and CH_2–Si groups were taken so as to predict the observed barrier height of 1.65 kcal/mol for dimethylsilane[5] by microwave spectroscopy.

The structural parameters were transferred from those of chloromethylsilane[6] and dimethylsilane[5] determined by microwave studies. However, the valency angles were assumed to be tetrahedral without regard to the reported values.

The force constants used in the calculation are listed in Table 4. The observed and calculated frequencies of (chloromethyl)methylsilane and its deuterated species are given in Tables 5—7, together with their predominant symmetry coordinates in the potential energy

5) L. Pierce, *J. Chem. Phys.*, **34**, 498 (1960).
6) R. H. Schwendeman and G. D. Jacobs, *ibid.*, **36**, 1251 (1962).

TABLE 4. FORCE CONSTANTS FOR (CHLOROMETHYL)-METHYLSILANE[a]

K(C–H), CH_2	4.390	$\kappa(CH_2)$	0.027
K(C–H), CH_3	4.403	$\kappa(CH_3)$	0.014
K(Si–H)	2.462	$\kappa(SiH_2)$	0.104
K(C–Cl)	1.697	Y(C–Si)	0.051
K(C–Si)	1.991	p(C–H)	−0.084
H(Si–C–Cl)	0.030	F(Si·C·Cl)	0.280
H(Si–C–H), CH_2	0.104	F(Si·C·H), CH_2	0.271
H(Cl–C–H)	0.147	F(Cl·C·H)	0.558
H(H–C–H)	0.349	F(H·C·H)	0.200
H(C–Si–C)	0.133	F(C·Si·C)	0.040
H(C–Si–H), CH_3	0.092	F(C·Si·H), CH_3	0.149
H(C–Si–H), CH_2	0.113	F(C·Si·H), CH_2	0.149
H(H–Si–H)	0.180	F(H·Si·H)	0.041
H(Si–C–H), CH_3	0.102	F(Si·C·H), CH_3	0.271
t(Si–C–Cl, SiH_2)[b]	0.017	t(C–Si–C, CH)[b]	0.030
t(CH_2, SiH_2)[b]	0.082	t(CH_3, SiH_2)[b]	0.057

a) Force constants are transferred from those of dimethylsilane and chloromethylsilane except H (Si–C–Cl) and F(Si·C·Cl) which are adjusted so as to reproduce the observed frequency of the Si–C–Cl bending mode. The units of the force constants are in mdyn/Å for the streching, K; the bending, H; the repulsion, F; and the bond interaction, p, and in mdyn·Å for the internal rotation, Y; the *trans* coupling, t; and the intramolecular tension, k.
b) The *gauche* coupling constants are assumed to be $g=-0.5t$.

TABLE 5. OBSERVED AND CALCULATED FREQUENCIES OF $ClCH_2SiH_2CH_3$

	No.	*Trans* form Obsd	*Trans* form Calcd	*Gauche* form Obsd	*Gauche* form Calcd	P. E. D.[a]
A'	1	2966	2964	2966	2964	CH_3 asym. str.
	2	2942	2949	2942	2949	CH_2 sym. str.
	3	2913	2901	2913	2901	CH_3 sym. str.
	4	2156	2147	2156	2147	SiH_2 sym. str.
	5	1416	1413	1416	1413	CH_3 asym. def.
	6	1394	1420	1394	1421	CH_2 sci.
	7	1256	1254	1256	1254	CH_3 sym. def.
	8	1179	1168	1179	1168	CH_2 wag.
	9	940	955	940	956	SiH_2 sci.
	10	895	882	895	879	SiH_2 wag., CH_3 rock.
	11	761	777	761	770	CH_3 rock., SiH_2 wag.
	12	745	730	736	729	C–Si str., C–Cl str.
	13	699	688	685	695	C–Cl str., C–Si str.
	14	608	639	579	606	C–Si str., C–Cl str.
	15	—	212	—	251	Skeletal bend.
	16	—	158	—	148	Skeletal bend.
A''	17	2966	2994	2966	2993	CH_2 antisym. str.
	18	2966	2964	2966	2964	CH_3 asym. str.
	19	2156	2148	2156	2148	SiH_2 antisym. str.
	20	1416	1413	1416	1413	CH_3 asym. def.
	21	1109	1109	1109	1112	CH_2 twist.
	22	867	846	867	842	CH_3 rock., SiH_2 twist.
	23	809	824	761	776	CH_2 rock., CH_3 rock., SiH_2 twist.
	24	—	597	618	637	SiH_2 twist., CH_2 rock.
	25	487	492	487	496	SiH_2 rock.
	26	—	169	—	178	CH_3–Si torsion
	27	—	66	—	67	CH_2–Si torsion

a) Only the predominant symmetry coordinates are shown.

TABLE 6. OBSERVED AND CALCULATED FREQUENCIES OF $ClCH_2SiD_2CH_3$

	No.	*Trans* form Obsd	*Trans* form Calcd	*Gauche* form Obsd	*Gauche* form Calcd	P. E. D.[a]
A'	1	2966	2964	2967	2964	CH_3 asym. str.
	2	2944	2949	2931	2949	CH_2 sym. str.
	3	2904	2901	2909	2901	CH_3 sym. str.
	4	1563	1536	1555	1536	SiD_2 sym. str.
	5	1420	1413	1409	1413	CH_3 asym. def.
	6	1396	1420	1398	1421	CH_2 sci.
	7	1250	1254	1248	1254	CH_3 sym. def.
	8	1168	1167	1178	1166	CH_2 wag.
	9	819	822	822	823	CH_3 rock.
	10	747	749	732	731	C–Si str.
	11	722	711	680	678	SiD_2 sci.
	12	675	672	697	712	C–Cl str., C–Si str.
	13	648	645	637	619	C–Si str.
	14	570	582	535	578	SiD_2 wag.
	15	—	210	240	248	Skeletal bend.
	16	—	154	—	145	Skeletal bend.
A''	17	2966	2994	2977	2993	CH_2 antisym. str.
	18	2966	2964	2967	2964	CH_3 asym. str.
	19	1581	1552	1573	1552	SiD_2 antisym. str.
	20	1427	1413	1419	1413	CH_3 asym. def.
	21	1107	1107	1111	1110	CH_2 twist.
	22	814	817	815	816	CH_3 rock.
	23	784	780	784	759	CH_2 rock.
	24	—	460	479	474	SiD_2 twist.
	25	392	393	401	395	SiD_2 rock.
	26	—	168	—	175	CH_3–Si torsion
	27	—	65	—	65	CH_2–Si torsion

a) Only the predominant symmetry coordinates are shown.

TABLE 7. OBSERVED AND CALCULATED FREQUENCIES OF $ClCH_2SiHDCH_3$

	No.	*Trans* form Obsd	*Trans* form Calcd	*Gauche* form(G)[a] Obsd	*Gauche* form(G)[a] Calcd	*Gauche* form(G')[b] Obsd	*Gauche* form(G')[b] Calcd	P. E. D.[c]
A	1		2994		2993		2993	CH_2 antisym. str.
	2		2964		2964		2964	CH_3 asym. str.
	3		2964		2964		2964	CH_3 asym. str.
	4		2949		2949		2949	CH_2 sym. str.
	5		2901		2901		2901	CH_3 sym. str.
	6		2148		2147		2147	Si–H str.
	7		1544		1544		1544	Si–D str.
	8		1420		1421		1421	CH_2 sci.
	9		1413		1413		1413	CH_3 asym. def.
	10		1413		1413		1413	CH_3 asym. def.
	11		1254		1254		1254	CH_3 sym. def.
	12		1168		1166		1168	CH_2 wag.
	13		1108		1112		1110	CH_2 twist.
	14		869		876		855	SiHD sci.
	15		858		857		858	CH_3 rock., SiHD def.
	16		812		814		812	CH_3 rock.
	17	805	794		715		723	CH_2 rock. [d]
	18	750	753		746		731	C–Si str. [d]
	19	714	703		762		769	Si–H def. [d]
	20	687	686		668		690	C–Cl str. [d]
	21	607	636	595	613	595	624	C–Si str., C–Cl str.
	22	498	498	502	519	502	502	Si–D def.
	23	425	425	433	430	433	425	SiHD rock.
	24		211		248		251	Skeletal bend.
	25		168		176		176	CH_3–Si torsion
	26		156		146		147	Skeletal bend.
	27		66		66		66	CH_2–Si torsion

a) The chlorine atom occupies the *trans* position to the deuterium of the SiHD group.
b) The chlorine atom occupies the *trans* position to the hydrogen of the SiHD group.
c) Only the predominant symmetry coordinates are shown.
d) These four frequencies have the complicated mixing modes of the four symmetry coordinates of the CH_2 rocking, C–Si stretching, Si–H deformation, and C–Cl stretching. However, the correspondence of the observed frequencies to these symmetry coordinates can be found as is shown in the table from the comparison with those for the other species.

distribution.

A fair agreement is obtained between the observed and calculated frequencies. The deviation is within 3% for almost all of the modes. However, a little larger deviations (~5%) are seen for the C–Si and C–Cl stretching modes for $ClCH_2SiH_2CH_3$ and $ClCH_2SiHDCH_3$ and for the SiD_2 wagging mode for $ClCH_2SiD_2CH_3$. Although these larger deviations indicate the limitation of the transferability of the force constants, further adjustments of the force constants were not attempted.

From the calculated potential energy distribution, the mixings of the modes were found to be complicated among the C–Si and C–Cl stretchings and some of the hydrogen deformation modes of the CH_3, CH_2, and SiH_2 groups.

As is shown in Tables 1 and 2, according to the present assignments the frequency differences between the CH_3 rocking modes belonging to the A′ and A″ species are found to be more than 100 cm^{-1} for $ClCH_2SiH_2CH_3$ in both the *trans* and *gauche* forms, while those for $ClCH_2SiD_2CH_3$ are less than 10 cm^{-1}. The situation is the same with the CH_3 rocking modes for dimethylsilane[2] and ethylmethylsilane,[3] as has been reported in previous papers.

This is understandable for the following reasons. For $ClCH_2SiH_2CH_3$, as the SiH_2 wagging mode is found at a frequency close to the expected frequency for the CH_3 rocking mode belonging to the A′ species, the CH_3 rocking mode receives a strong coupling from the SiH_2 wagging mode and is pushed down to the lower-frequency side. On the other hand, for $ClCH_2SiD_2CH_3$, as the SiD_2 wagging mode is far from the frequency for the CH_3 rocking mode, the coupling becomes negligible.

This is also supported by the calculated potential energy distribution for these modes.

As has been already pointed out in the cases of dichlorosilane,[7] dimethylsilane,[2] and ethylmethylsilane,[3] for $ClCH_2SiHDCH_3$ the calculated potential energy distribution also shows that the SiHD rocking mode keeps its original mode, while the SiHD twisting mode should be more properly called the SiD deformation mode.

The vibrational assignments for the other modes can be obtained by taking into account the results of the normal vibration calculations and by comparing the observed spectra with those of similar molecules, such as dimethylsilane,[8–10] chloromethylsilane,[1] and ethylmethylsilane.[3] The results are shown in Tables 1—3.

7) to be published.

8) E. A. V. Ebsworth, M. Onyszchuk, and N. Sheppard, *J. Chem. Soc.*, **4**, 1453 (1958).

9) D. F. Ball, P. L. Goggin, D. C. McKean, and L. A. Woodward, *Spectrochim. Acta*, **16**, 1358 (1960).

10) I. F. Kovalev, *Opt. Spectrosk.*, **8**, 166 (1960).

BULLETIN OF THE CHEMICAL SOCIETY OF JAPAN, VOL. 46, 804—808 (1973)

The Crystal and Molecular Structure of *p*-Hydroxybenzoic Acid Monohydrate

Keiichi FUKUYAMA, Kenji OHKURA*, Setsuo KASHINO, and Masao HAISA
Department of Chemistry, Faculty of Science, Okayama University, Tsushima, Okayama

(Received September 25, 1972)

The crystal and molecular structure of *p*-hydroxybenzoic acid monohydrate has been determined by a single crystal X-ray analysis. The crystals are monoclinic, space group $P2_1/a$, $Z=4$, with $a=17.79$, $b=6.39$, $c=6.79$ Å, and $\beta=105.6°$. The structure was solved by the Patterson and Fourier methods, and refined by the block-diagonal least-squares method to a final R value of 0.086 for 806 non-zero reflections. Pairs of acid molecules form dimers by the hydrogen bonds between carboxyl groups (2.678 Å). The dimers are held together by the hydrogen bonds between phenolic hydroxyl groups and water molecules (2.595 and 2.823 Å); these hydrogen bonds extend around two-fold screw axes to make up layers of the dimers parallel to the (401). The layers are linked by the additional hydrogen bonds between carbonyl oxygens and water molecules (2.823 Å).

As a part of the investigation of the addition compounds of amines with carboxylic acids,[1] determination of the crystal and molecular structure of the title compound has been undertaken. This compound is of interest not only in hydrogen bonding scheme in the crystal, but also in molecular geometry of benzoic acids.

* Present address: Kyowa Carbon Co. Ltd., Ushimado, Okayama.

1) S. Kashino, Y. Sumida, and M. Haisa, *Acta Crystallogr.*, **B28**, 1374 (1972).

Experimental

Crystals prepared by slow evaporation from acetone solution were transparent plates elongated along the c axis. Cell constants were obtained from the oscillation and Weissenberg photographs taken with Cu$K\alpha$ radiation ($\lambda=1.5418$ Å). Space group was uniquely determined to be $P2_1/a$ from systematic absences; $h0l$ when h is odd, $0k0$ when k is odd. Elementary analysis and density measurement showed that the crystals contained four water molecules per unit cell.

TABLE 1. CRYSTAL DATA

p-HO-$C_6H_4COOH \cdot H_2O$ $FW=156.1$
Monoclinic $P2_1/a$
$a=17.79\pm0.05$ Å $b=6.39\pm0.02$ Å $c=6.79\pm0.01$ Å
$\beta=105.6\pm0.2°$
$D_m=1.38_6$ g cm^{-3} (by flotation)
$D_x=1.395$ g cm^{-3} (for $Z=4$)
$\mu=10.0$ cm^{-1} for Cu $K\alpha$ radiation
$F(000)=328$

The crystal data are listed in Table 1. Intensities were collected with Cu$K\alpha$ radiation by means of the multiple-film equi-inclination Weissenberg techniques for the layers $hk0$ to $hk5$. A total of 807 non-zero independent reflections were measured visually. The intensities were corrected for the Lorentz and polarization factors, and for spot shape.

Structure Determination and Refinement

The approximate positional parameters of p-hydroxybenzoic acid molecule were determined by the interpretation of a three-dimensional sharpened Patterson map and Harker section. The Fourier map based on the positional parameters of the acid molecule revealed the oxygen atom of water molecule. The structure thus obtained was refined by the block-diagonal least-squares calculations with isotropic temperature factors. For a time reflections 211, 311, 401, and $\bar{4}03$ were rejected because of strong extinction effect. A difference map revealed all peaks corresponding to eight hydrogen atoms. The least-squares refinement was made with anisotropic temperature factors for carbon and oxygen atoms including the hydrogen atoms with fixed parameters, which are shown in Table 2. The positional parameters of the hydrogen atoms were calculated by assuming suitable geometries, and their temperature factors were assumed to be equal to those of the heavy atoms to which they are attached. This refinement reduced an R value to 0.096. An extinction correction, $I_{corr}=I_o/(1-gI_o)$, was applied for strong reflections including 211, 311, and $\bar{4}03$, but inaccurate 401 was omitted. Further least-squares refinement for the non-hydrogen atoms gave the final R value of 0.086 for 806 non-zero reflections. The following weighting scheme was applied;

$$\sqrt{w} = 0.0 \text{ for } F_o = 0,$$
$$\sqrt{w} = 0.5 \text{ for } 0 < F_o < F_{min} \ (2.5),$$
$$\sqrt{w} = 1.0 \text{ for } F_{min} \leqq F_o \leqq F_{max} \ (22.6)$$

and

$$\sqrt{w} = F_{max}/F_o \text{ for } F_{max} < F_o.$$

The final atomic parameters are listed in Table 3. The final electron density map is shown in Fig. 1(a).

TABLE 2. THE ASSUMED ATOMIC PARAMETERS OF HYDROGEN ATOMS

Atom	x/a	y/b	z/c	B(Å^2)
H(1)	0.060	0.442	0.607	3.0
H(2)	0.121	0.525	0.344	3.4
H(3)	0.196	−0.096	0.345	2.9
H(4)	0.135	−0.175	0.611	3.0
H(5)	−0.012	0.177	0.961	3.6
H(6)	0.188	0.408	0.102	3.4
H(7)	0.142	0.730	−0.028	4.2
H(8)	0.231	0.678	−0.043	4.2

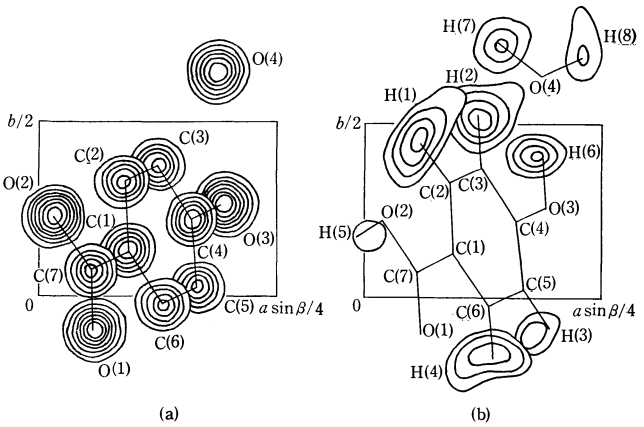

Fig. 1. (a) The final electron density map. Inaccurate 401 reflection was involved. Contours are at equal intervals of 1.0 e.Å^{-3} starting at about 2.4 e.Å^{-3}. (b) The difference electron density map. Contours are at equal intervals of 0.1 e.Å^{-3} starting at 0.2 e.Å^{-3}. The molecular frames are based on the coordinates in Table 2 and 3.

TABLE 3. THE FINAL ATOMIC PARAMETERS ALONG WITH THEIR E.S.D.'S WITHIN PARENTHESES

The anisotropic temperature factors are of the form;
$\exp(-B_{11}h^2-B_{22}k^2-B_{33}l^2-B_{12}hk-B_{13}hl-B_{23}kl)$.
All values of B_{ij} should be multiplied by 10^{-4}.

Atom	x/a	y/b	z/c	B_{11}	B_{22}	B_{33}	B_{12}	B_{13}	B_{23}
C (1)	0.0939(3)	0.1273(8)	0.6358(8)	18(2)	224(14)	185(16)	1(8)	43(8)	10(23)
C (2)	0.0898(3)	0.3286(8)	0.5548(9)	27(2)	198(13)	240(18)	13(8)	71(9)	28(23)
C (3)	0.1232(3)	0.3748(8)	0.3964(9)	32(2)	173(13)	299(20)	14(8)	83(10)	80(25)
C (4)	0.1603(3)	0.2179(8)	0.3160(8)	22(2)	207(13)	179(16)	−6(8)	64(8)	7(22)
C (5)	0.1660(3)	0.0201(8)	0.3954(8)	29(2)	219(14)	188(16)	18(9)	73(9)	16(24)
C (6)	0.1315(3)	−0.0247(8)	0.5520(8)	28(2)	195(13)	203(17)	−8(8)	38(9)	1(23)
C (7)	0.0556(3)	0.0736(8)	0.7987(8)	18(2)	235(14)	194(17)	2(8)	36(8)	49(22)
O (1)	0.0590(2)	−0.0999(6)	0.8736(6)	29(1)	242(11)	277(13)	29(6)	87(7)	119(18)
O (2)	0.0162(2)	0.2253(6)	0.8545(6)	29(2)	271(11)	270(13)	47(6)	88(7)	77(18)
O (3)	0.1924(2)	0.2546(6)	0.1589(6)	32(2)	257(11)	247(12)	14(7)	104(7)	75(18)
O (4)	0.1888(2)	0.6348(7)	0.0223(7)	35(2)	291(12)	423(16)	59(7)	147(8)	309(23)

TABLE 4. OBSERVED AND CALCULATED STRUCTURE FACTORS ($\times 10$)[a]

K	FO	FC	K	FO	FC	K	FO	FC	K	FO	FC	K	FO	FC	K	FO	FC	K	FO	FC	K	FO	FC	K	FO	FC
H,L= 0	0		1	61	68	1	50	-49	H,L=-18	1		3	45	41	1	83	79	H,L= 14	3		5	17	20	H,L= -1	4		5	26	-24
2	208-251		H,L= 1	1		H,L= -1	1		4	75	-89	H,L= 17	2		2	122	115	1	40	-44	H,L=-14	3		1	96	-90	6	25	16
4	30	-22	1	168	190	1	115	-116	H,L= 0	2		1	36	-41	3	33	26	2	71	-82	0	198	-198	2	60	54	H,L= 1		5
6	49	-42	2	160	-165	2	284	329	0	183	177	3	39	-40	4	172	-179	3	15	-21	1	50	53	3	92	92	1	32	24
8	62	57	3	204	-232	3	101	-102	2	154	156	H,L= 18	2		H,L=-15	2		H,L= 15	3		2	92	81	6	52	-51	2	79	-76
H,L= 1	0		4	46	36	4	70	-58	3	95	-88	1	37	40	1	36	32	1	69	-76	3	47	-39	7	35	-27	3	91	92
1	440	525	5	117	-119	5	45	41	4	108	-105	H,L= -1	2		2	86	-85	2	27	-34	4	105	110	H,L= -2	4		5	40	35
2	83	-85	6	21	23	6	51	-47	5	54	55	1	222	-261	4	58	61	3	36	37	5	25	28	1	256	-294	H,L= 2		5
3	90	80	H,L= 2	1		7	54	-47	6	96	88	2	96	-87	5	25	-27	H,L= 16	3		H,L=-15	3		2	42	34	0	51	41
4	40	41	1	859	858	H,L= -2	1		7	41	42	3	184	186	H,L=-16	2		0	24	-33	1	92	-102	4	85	86	1	122	-112
7	60	-55	2	256	290	1	40	33	H,L= 1	2		4	92	-84	2	59	57	2	19	20	2	43	-46	6	46	48	2	17	-17
H,L= 2	0		4	71	-59	2	93	-99	1	49	-35	5	35	-36	3	93	101	3	50	-65	H,L=-16	3		H,L= -3	4		3	18	-8
0	160	172	5	40	-34	3	337	-414	2	148	-135	6	85	87	5	85	-81	H,L= -1	3		1	188	-214	1	115	122	4	74	78
1	600	-580	6	36	-42	4	221	232	3	163	163	7	45	47	H,L=-17	2		1	212	-236	3	22	21	2	49	35	5	19	-24
2	48	45	7	30	-27	5	231	254	4	67	-57	H,L= -2	2		3	27	33	2	100	98	4	72	-80	3	96	92	H,L= 3		5
3	178	178	H,L= 3	1		6	33	-31	5	88	80	1	78	-73	5	50	50	3	74	71	H,L=-17	3		4	27	-31	1	57	-47
4	108	-90	1	713	861	H,L= -3	1		6	156	176	2	236	-267	H,L=-18	2		4	106	-98	1	163	-179	6	35	-26	3	25	23
6	43	-39	2	86	83	1	122	121	H,L= 2	2		3	240	-275	3	46	-43	5	80	81	2	26	-30	7	16	11	H,L= 4		5
H,L= 3	0		3	70	-69	3	21	9	0	65	-46	4	103	100	4	80	79	6	37	-33	3	32	30	H,L= -4	4		0	153	-152
1	117	112	5	46	-44	4	112	-103	1	301	324	5	35	32	H,L= 0	3		H,L= -2	3		H,L=-18	3		0	186	165	1	111	-108
2	249	262	6	44	44	5	159	160	2	44	35	6	35	46	0	181	-159	1	15	-18	2	89	-102	1	151	156	H,L= 5		5
3	316	-347	H,L= 4	1		6	141	149	3	202	-217	H,L= -3	2		1	48	43	2	58	50	H,L= 0	4		2	87	84	1	66	-64
4	41	-32	1	301	300	H,L= -4	1		4	62	48	1	35	-32	2	111	97	4	50	47	0	336	-351	4	51	-47	2	44	-32
5	136	-131	2	167	-156	0	216	-217	5	148	151	2	218	-239	3	194	-199	H,L= -3	3		1	39	-34	H,L= -5	4		3	31	34
H,L= 4	0		3	82	-71	1	161	165	6	35	-37	3	188	-191	4	134	-129	1	154	-154	2	76	68	1	73	-57	H,L= 6		5
0	512	-514	4	61	48	2	124	116	7	34	-30	4	71	-68	5	85	-84	2	46	39	3	44	37	2	74	-64	0	78	-65
1	76	-59	5	58	55	3	102	-89	H,L= 3	2		5	32	-30	6	68	61	3	41	26	4	19	-19	3	28	21	2	31	23
2	262	-260	6	32	-30	5	61	60	2	235	257	6	58	-65	H,L= 1	3		4	28	-28	6	32	32	4	173	171	H,L= 7		5
3	195	-193	H,L= 5	1		6	108	106	3	148	-154	7	65	59	1	93	-84	6	29	30	H,L= 1	4		5	68	-68	2	33	-34
4	79	74	1	43	30	H,L= -5	1		4	60	-60	H,L= -4	2		2	243	-271	7	39	44	1	142	-134	H,L= -6	4		H,L= 8		5
5	150	140	2	116	105	1	455	-499	5	46	-41	0	415	-500	3	91	-78	H,L= -4	3		2	106	-91	0	32	-27	1	38	-37
6	87	-69	3	124	109	2	207	-222	6	32	-31	1	332	399	4	29	-24	0	769	-642	3	48	44	1	19	-18	H,L= -1		5
7	45	-30	4	33	33	3	172	179	7	35	-39	2	90	71	6	48	-47	1	229	225	6	29	28	2	96	89	2	38	-25
H,L= 5	0		7	77	-66	4	102	-100	H,L= 4	2		3	193	-194	7	30	29	2	166	173	7	26	31	3	206	220	4	93	103
1	125	-121	H,L= 6	1		5	50	42	0	26	25	4	26	-20	H,L= 2	3		3	101	98	H,L= 2	4		4	233	-277	6	27	-22
2	85	75	0	359	357	6	107	116	1	157	-151	5	68	-68	0	199	-202	4	18	18	0	235	-250	5	48	-45	H,L= -2		5
4	42	-40	1	226	-228	H,L= -6	1		2	178	-176	6	74	77	1	72	73	7	54	-56	2	47	33	7	27	24	0	115	-111
5	118	108	2	176	-163	0	112	82	4	24	-21	H,L= -5	2		2	40	-38	H,L= -5	3		4	52	50	H,L= -7	4		1	82	-84
H,L= 6	0		3	144	140	1	70	-56	5	29	39	1	323	-315	3	149	-152	2	64	-51	5	36	-36	1	109	88	3	165	193
0	261	300	4	148	-149	2	385	-397	6	94	-102	2	105	95	4	52	51	3	111	108	7	12	-20	2	104	93	4	100	-106
1	36	26	5	47	-39	3	156	-160	H,L= 5	2		3	77	71	5	27	25	4	18	-5	H,L= 3	4		3	148	-146	5	38	-28
2	193	-214	6	24	-21	6	45	53	1	126	113	4	53	-37	H,L= 3	3		5	23	23	1	29	-20	4	127	119	6	16	-18
3	247	250	7	26	-25	7	45	-42	2	204	197	5	98	107	1	62	53	6	22	-22	2	12	-12	5	65	-61	H,L= -3		5
4	249	259	H,L= 7	1		H,L= -7	1		3	69	-56	H,L= -6	2		2	103	-87	7	16	-15	4	101	-107	6	26	-32	1	68	73
5	199	-210	1	191	-166	1	138	-119	4	31	32	0	159	-132	3	58	49	H,L= -6	3		5	30	24	7	16	-14	2	88	80
H,L= 7	0		2	39	28	2	33	28	5	78	-80	1	179	155	4	18	-11	0	139	138	H,L= 4	4		H,L= -8	4		3	175	-210
2	194	-197	3	133	-132	3	110	-100	6	23	-31	2	72	63	5	85	-93	1	269	-290	0	71	-69	0	122	113	4	75	70
4	57	45	4	28	-29	4	54	-47	H,L= 6	2		3	16	18	6	58	59	2	140	145	1	98	-84	1	105	-85	5	51	-44
5	211	215	5	59	-52	6	73	-73	0	104	93	4	50	-47	7	57	60	3	63	43	2	60	55	2	35	-31	H,L= -4		5
6	69	-51	7	17	-16	7	43	41	1	398	400	7	43	39	H,L= 4	3		4	22	-11	3	113	-111	3	181	195	1	51	38
H,L= 8	0		H,L= 8	1		H,L= -8	1		2	253	267	H,L= -7	2		1	94	-80	5	43	-33	4	77	-81	4	98	106	2	94	-95
0	339	-356	0	386	-391	0	378	-388	3	76	66	1	208	-199	2	130	120	6	50	50	5	53	-50	5	33	-34	3	156	172
3	139	123	1	27	26	1	326	343	4	78	-78	2	277	289	3	39	-30	7	16	-14	6	30	32	6	72	-67	4	79	75
4	80	70	2	106	-95	2	56	-49	5	33	-30	3	97	83	4	46	-39	H,L= -7	3		H,L= 5	4		H,L= -9	4		6	77	-70
5	110	-113	3	153	-137	3	160	-157	H,L= 7	2		4	19	-20	5	80	77	1	172	169	1	28	-31	1	238	250	H,L= -5		5
6	68	67	4	106	114	4	91	89	1	377	405	H,L= -8	2		6	54	54	2	205	207	2	97	-87	2	58	48	1	112	116
H,L= 9	0		5	96	92	6	56	60	3	33	-31	0	427	-438	7	47	44	3	116	117	3	28	-23	3	63	-47	2	123	122
1	230	-229	7	33	-31	H,L= -9	1		5	20	-16	1	233	211	H,L= 5	3		4	49	-42	6	37	-40	H,L=-10	4		4	22	14
2	117	109	H,L= 9	1		2	132	120	6	57	56	2	196	188	1	60	-54	5	73	-65	H,L= 6	4		1	77	68	H,L= -6		5
4	82	69	2	135	133	3	69	-57	7	32	29	4	40	42	3	143	139	6	39	-36	2	30	29	2	157	151	0	125	116
5	43	27	4	115	-121	5	42	38	H,L= 8	2		5	25	20	6	93	96	H,L= -8	3		3	53	-49	4	49	40	2	132	131
6	79	-71	5	75	71	H,L=-10	1		0	377	392	6	30	-26	H,L= 6	3		0	165	159	4	31	-33	5	32	37	5	51	53
H,L= 10	0		H,L= 10	1		1	263	267	1	303	310	7	68	-63	0	27	10	1	29	25	H,L= 7	4		6	17	16	6	57	44
0	104	93	0	128	117	2	73	62	2	61	-52	H,L= 9	2		1	194	190	2	57	37	1	51	44	H,L=-11	4		H,L= 7		5
2	241	-245	1	43	-27	3	74	72	3	34	-31	1	216	195	2	38	37	3	46	-32	2	71	-69	1	115	-105	2	112	97
3	35	-42	2	153	-142	4	36	-41	4	72	77	2	129	-105	3	55	-49	4	50	-44	4	51	49	2	26	19	3	103	103
4	48	-38	4	198	232	5	25	-26	5	32	30	3	26	4	4	75	-79	5	92	83	5	55	-51	3	97	91	6	54	-39
5	72	56	5	73	-73	7	37	31	6	24	-23	4	50	-38	5	62	56	H,L= -9	3		6	35	38	6	30	-26	H,L= -8		5
6	46	39	H,L= 11	1		H,L=-11	1		7	28	-26	H,L=-10	2		H,L= 7	3		1	39	37	H,L= 8	4		H,L=-12	4		0	20	-8
7	59	60	1	62	-60	1	139	-124	H,L= 9	2		0	47	42	1	65	-49	2	22	-21	0	58	-42	0	102	-103	1	256	-266
H,L= 11	0		2	90	-78	2	160	162	1	25	-3	1	77	-61	2	90	81	3	33	-31	2	56	54	1	306	-352	2	91	-92
1	137	-121	5	170	164	3	103	100	2	30	36	2	211	217	3	68	-61	4	133	128	3	31	33	2	75	-63	3	85	89
6	50	31	H,L= 12	1		H,L=-12	1		H,L= 10	2		3	88	79	5	22	-25	5	142	-159	5	51	50	3	31	26	4	18	-14
H,L= 12	0		0	148	-135	1	120	92	0	131	127	4	46	-44	H,L= 8	3		H,L=-10	3		H,L= 9	4		4	85	-83	5	30	-27
0	47	32	1	24	25	2	138	127	1	119	-105	5	55	-53	2	72	-58	0	24	-29	1	28	-19	6	23	24	H,L= -9		5
1	181	-169	2	20	-17	3	89	-90	2	156	-154	6	18	20	3	51	47	1	133	113	2	31	25	H,L=-13	4		1	119	-108
2	84	-73	3	96	97	4	25	-25	4	81	-84	7	51	-41	5	25	32	2	160	164	3	47	45	1	165	-162	2	166	-179
3	80	70	5	119	-103	5	20	24	H,L= 11	2		H,L=-11	2		6	62	-63	3	167	167	5	31	-32	2	97	-93	3	70	-73
4	38	31	H,L= 13	1		6	52	-46	1	160	-176	1	142	118	H,L= 9	3		4	257	-309	H,L= 10	4		3	28	-27	6	21	18
H,L= 13	0		1	94	-82	H,L=-13	1		2	29	-22	2	99	88	1	80	83	5	40	-46	0	24	-26	H,L=-14	4		H,L=-10		5
1	113	97	2	21	-29	1	159	156	3	21	22	3	94	87	2	173	183	H,L=-11	3		1	69	67	0	59	54	0	117	103
2	136	-136	3	55	-58	2	40	-25	H,L= 12	2		4	59	-55	5	47	-51	1	35	22	4	49	-52	1	88	-73	1	44	34
3	79	-70	4	54	40	3	21	-18	0	142	-138	5	64	-62	6	47	-41	2	43	-35	H,L= 11	4		2	172	-186	2	188	-206
H,L= 14	0		H,L= 14	1		4	51	-46	3	93	-93	6	21	23	H,L= 10	3		3	19	-12	1	51	-57	3	31	-27	3	70	-66
1	145	-153	1	21	19	6	25	-23	4	27	33	H,L=-12	2		0	38	33	4	105	112	2	46	42	4	70	74	4	28	27
2	37	26	2	96	-97	H,L=-14	1		5	26	21	0	215	208	1	96	99	5	37	-36	5	21	-4	H,L=-15	4		5	41	-34
H,L= 15	0		3	32	-35	2	145	145	H,L= 13	2		1	64	-50	2	152	155	H,L=-12	3		H,L= 12	4		2	167	-182	6	36	-32
2	31	-14	4	23	-23	H,L=-15	1		3	28	24	3	84	-75	3	27	27	0	192	180	1	26	23	5	46	41	H,L=-11		5
3	43	38	5	38	35	1	126	110	4	106	-106	4	91	-96	4	26	-31	1	122	-117	3	42	46	H,L=-16	4		1	24	-12
H,L= 16	0		H,L= 15	1		2	33	-35	5	47	43	5	93	104	H,L= 11	3		2	48	42	H,L= 13	4		1	59	55	2	156	-164
0	85	88	2	25	28	4	51	-47	H,L= 14	2		6	19	-28	1	130	135	3	124	127	1	30	43	2	51	55	5	29	32
1	37	-40	H,L= 16	1		5	49	-53	2	50	-54	H,L=-13	2		2	27	29	4	19	28	2	68	76	3	25	-30	6	44	35
2	64	55	0	130	132	H,L=-16	1		3	54	-57	1	58	53	H,L= 12	3		5	64	-67	H,L= 14	4		5	28	-19	H,L=-12		5
3	71	64	1	61	-70	3	28	-26	4	152	159	2	101	96	0	75	72	6	24	-27	2	63	77	H,L= 0	5		1	56	-34
H,L= 17	0		2	48	-57	4	75	-80	H,L= 15	2		3	29	-33	1	135	157	H,L=-13	3		H,L= 15	4		0	137	130	2	57	70
1	52	47	H,L= 17	1		5	66	60	4	26	-35	4	55	41	3	28	-29	1	187	182	1	65	53	1	87	78	3	82	-85
H,L= 18	0		1	47	45	H,L=-17	1		H,L= 16	2		5	139	-161	H,L= 13	3		2	50	50	2	20	25	2	82	82	4	26	17
2	63	66	2	49	-54	2	73	76	0	43	-42	H,L=-14	2		2	41	-49	3	19	-22	H,L= 16	4		3	30	-33			
H,L= 19	0		H,L= 18	1		5	73	-87	2	31	-31	0	77	-74	3	38	-37	4	19	-16	1	36	46	4	44	-42			

a) The reflection 401 ($F_o \times 10 = 832$, $F_c \times 10 = 1703$) is omitted.

Difference electron density map, for which the contributions of the hydrogen atoms were excluded from the calculated structure factors, is shown in Fig. 1(b). A list of the observed and calculated structure factors is given in Table 4.

The atomic scattering factors were taken from International Tables for X-ray Crystallography.[2] The computations were performed on a HITAC 5020E computer at the Computer Center of the University of Tokyo using the UNICS program system,[3] and on a NEAC 2200-N700 computer at the Computation Center of Osaka University using the program for block-diagonal least-squares calculation (HBLS–IV) written by Okaya

2) "International Tables for X-ray Crystallography," Vol. III, The Kynoch Press, Birmingham, (1962), p. 201.

3) "The Universal Crystallographic Computing System," The Crystallographic Society of Japan, Tokyo, (1967).

and Ashida[4] and that for Lorentz and polarization factors and spot shape corrections written by Yasuoka.

Description of the Structure and Discussion

The bond lengths and angles are listed in Table 5. Unlike terephthalic acid[5] or *p*-toluic acid,[6] *p*-hydroxybenzoic acid shows significant difference in the two C–O bond lengths of the carboxyl group, 1.214 and 1.310 Å, as found in *p*-nitrobenzoic acid,[7] 1.222 and 1.319 Å, in *p*-bromobenzoic acid,[8] 1.225 and 1.307 Å, and in anisic acid,[9] 1.233 and 1.290 Å. The difference is more significant than that in potassium hydrogen di-*p*-hydroxybenzoate,[10] 1.232 and 1.284 Å. The bond length of C(1)–C(7) is 1.486 Å, which agrees with the corresponding bond length in terephthalic acid,[5] 1.483 Å and in *p*-toluic aicd,[6] 1.476 Å, but is somewhat shorter than that found in potassium hydrogen di-*p*-hydroxybenzoate,[10] 1.504 Å, and in *p*-nitrobenzoic acid,[7] 1.501 Å. The C(4)–O(3) bond length is 1.359 Å. This value agrees with phenolic C–O bond length in α- and β-modifications of *p*-nitrophenol,[11,12] 1.351 and 1.361 Å respectively, but is smaller than that in potassium hydrogen di-*p*-hydroxybenzoate,[10] 1.385 Å and in *p*-cresol,[13] 1.395 and 1.387 Å. Although the bond lengths of both C(1)–C(7) and C(4)–O(3) agree with those in the compounds reported to have quinoid character, no significant deviations of any bond lengths in the benzene ring from the mean value of 1.387 Å could be observed except for C(4)–C(5) bond length. The angle of C(5)–C(4)–O(3), 117.8°, is smaller than that of C(3)–C(4)–O(3), 121.8°. Such an inequality of the two C–C–O angles has been observed in many phenols, such as catechol,[14] α- and β-modifications of *p*-nitrophenol[11,12] and *p*-cresol.[13]

The least-squares plane of the benzene ring is

Table 5. Bond lengths (Å) and angles (°) along with their e.s.d.'s within parentheses

Bond	Length	Bond	Angle
C(1)–C(2)	1.393(8)	C(6)–C(1)–C(2)	117.7(5)
C(2)–C(3)	1.393(9)	C(1)–C(2)–C(3)	120.9(6)
C(3)–C(4)	1.390(9)	C(2)–C(3)–C(4)	119.7(6)
C(4)–C(5)	1.367(8)	C(3)–C(4)–C(5)	120.3(5)
C(5)–C(6)	1.393(8)	C(4)–C(5)–C(6)	119.3(5)
C(6)–C(1)	1.386(8)	C(5)–C(6)–C(1)	122.0(5)
C(1)–C(7)	1.486(8)	C(2)–C(1)–C(7)	121.4(5)
C(7)–O(1)	1.214(7)	C(6)–C(1)–C(7)	120.8(5)
C(7)–O(2)	1.310(7)	C(1)–C(7)–O(1)	122.8(5)
C(4)–O(3)	1.359(7)	C(1)–C(7)–O(2)	115.6(5)
		O(1)–C(7)–O(2)	121.6(5)
		C(3)–C(4)–O(3)	121.8(5)
		C(5)–C(4)–O(3)	117.8(5)

Table 6. Deviations from the least-squares planes

Atom	Deviation(Å)	Atom	Deviation(Å)
a) Deviations from the benzene ring plane			
C(1)	−0.002	C(6)	0.008
C(2)	−0.001	C(7)	0.060
C(3)	−0.004	O(1)	0.045
C(4)	0.010	O(2)	0.159
C(5)	−0.012	O(3)	0.034
b) Deviations from the plane through carboxyl group and C(1)			
C(1)	0.002	O(1)	0.003
C(7)	−0.007	O(2)	0.002

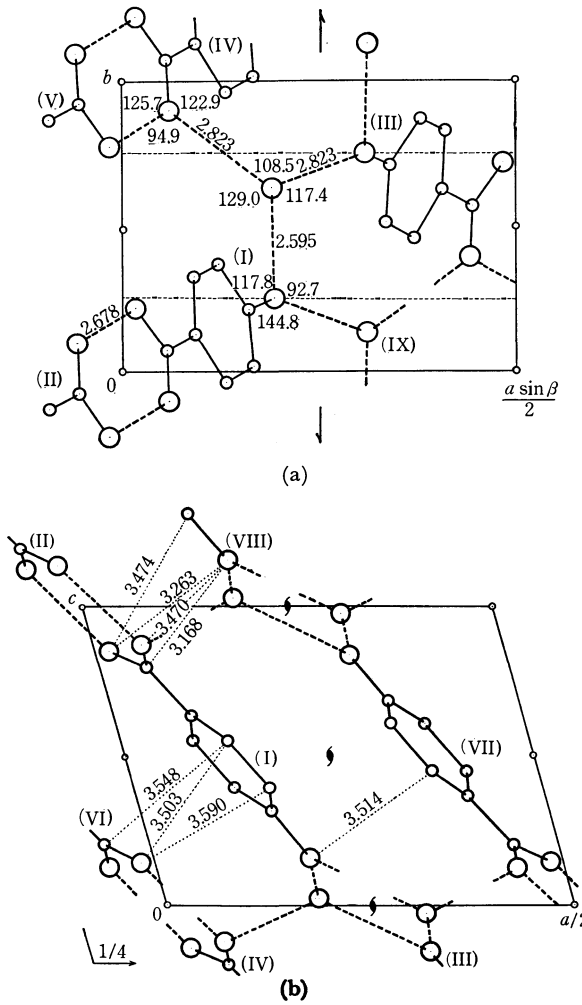

Fig. 2. Crystal structure of *p*-hydroxybenzoic acid monohydrate; (a) viewed along [001], (b) viewed along [010]. Broken lines show hydrogen bonds, and dotted lines show intermolecular contacts.

Key for molecules (I) $x/a, y/b, z/c$ (given in Table 2) (II) $-x/a, -y/b, 2-z/c$ (III) $1/2-x/a, 1/2+y/b, -z/c$ (IV) $x/a, 1+y/b, -1+z/c$ (V) $-x/a, 1-y/b, 1-z/c$ (VI) $-x/a, -y/b, 1-z/c$ (VII) $1/2-x/a, 1/2+y/b, 1-z/c$ (VIII) $x/a, y/b, 1+z/c$ (IX) $1/2-x/a, -1/2+y/b, -z/c$

4) Y. Okaya and T. Ashida, HBLS IV, The Universal Crystallographic Computing System (I), p. 65. The Crystallographic Society of Japan, Tokyo, (1967).
5) M. Baily and C. J. Brown, *Acta Crystallogr.*, **22**, 387 (1967).
6) M. G. Takwale and L. M. Pant, *ibid.*, **B27**, 1152 (1971).
7) T. D. Sakore and L. M. Pant, *ibid.*, **21**, 715 (1966).
8) K. Ohkura, S. Kashino, and M. Haisa, This Bulletin, **45**, 2651 (1972).
9) R. F. Bryan, *J. Chem. Soc. B*, **1967**, 1311.
10) L. Manojlović, *Acta Crystallogr.*, **B24**, 326 (1968).
11) P. Coppens and G. M. J. Schmidt, *ibid.*, **18**, 62 (1965).
12) P. Coppens and G. M. J. Schmidt, *ibid.*, **18**, 654 (1965).
13) C. Bois, *ibid.*, **B26**, 2086 (1970).
14) C. J. Brown, *ibid.*, **21**, 170 (1966).

represented by the equation:

$$-0.7077X - 0.2327Y - 0.6671Z + 3.3222 = 0,$$

where X, Y, and Z are the lengths (in Å) along the a, b, and c^* axes, respectively. The deviations of the atoms of the acid molecule from the plane are given in Table 6. The least-squares plane of the carboxyl group and C(1) is represented by the equation:

$$-0.6590X - 0.2726Y - 0.7010Z + 3.4743 = 0.$$

The deviation of the atoms of the carboxyl group and C(1) from the plane are also given in Table 6. The dihedral angle between the two planes is 4.1°, while the corresponding angle in potassium hydrogen di-*p*-hydroxybenzoate[10] is 9.5°. The C(1)–C(7) and C(4)–O(3) bonds bend to the same side out of the benzene ring plane.

The crystal structure is shown in Fig. 2. Pairs of acid molecules are linked through the hydrogen bonds (2.678 Å) between carboxyl groups to form dimers. The dimers in the crystal are held together by the hydrogen bonds between phenolic hydroxyl groups and water molecules (2.595 and 2.823 Å); these hydrogen bonds extend around two-fold screw axes to make up layers of the dimers parallel to the (401). The layers are linked by the additional hydrogen bonds between carbonyl oxygens and water molecules (2.823 Å). The two hydrogen atoms, H(7) and H(8), of the water molecule are accepted by the carbonyl oxygen, $O(1^{IV})$, and the phenolic oxygen,O (3^{III}), respectively, and the hydrogen atom of the phenolic hydroxyl group, H(6), is accepted by the oxygen atom of the water molecule $O(4^{I})$. The $O(4^{I})$ deviates only by 0.35 Å from the plane through $O(3^{I})$, $O(1^{IV})$, and $O(3^{III})$. The angle, $O(3^{III})$–$O(4^{I})$–$O(1^{IV})$, is 108.5° and is close to the H–O–H angle in a water molecule.

The intermolecular distances shorter than 3.6 Å are shown in Fig. 2(b), indicating no abnormal short contact.

The authors thank to Dr. Tamaichi Ashida of the Institute for Protein Research of Osaka University and Dr. Noritake Yasuoka of Faculty of Engineering of Osaka University for permission of using their programs.

BULLETIN OF THE CHEMICAL SOCIETY OF JAPAN, VOL. 46, 808—812 (1973)

The Dependence of the Electron-transfer Rates of Aromatic Hydrocarbon Anion Radicals upon the Molecular Radii of the Reactants

Kosaku SUGA, Shin-ichi ISHIKAWA, and Shigeru AOYAGUI

Faculty of Engineering, Tokyo Institute of Technology, Ookayama, Meguro-ku, Tokyo

(Received September 22, 1972)

The applicability of the theory of R. A. Marcus is tested, the behavior of the rate constant being examined as a function of the molecular radii of the reactants. The rate constants of the electron-transfer reactions from the anion radicals of pyrene, perylene, and tetracene to their respective parent molecules are measured under experimental conditions in which the anion radicals are in a free ion or loose ion-pair state. The rate constants thus obtained and subsequently corrected for diffusion are 2.8×10^9, 3.0×10^9, and 2.6×10^9 $M^{-1}sec^{-1}$ respectively, in 1,2-dimethoxyethane at 25°C. These rate constants, as well as others obtained elsewhere for naphthalene and anthracene, are compared with those predicted theoretically, assuming a spherical and an oblate spheroidal molecular shape. The consistence between the theoretical and experimental results is not satisfactory; the variation in the observed rate constants with the molecular radii of the reactants is much smaller than that expected theoretically. The spin-exchange rate constants for anion radicals of pyrene, perylene, and tetracene are also determined to be 7.0×10^9, 5.1×10^9, and 4.8×10^9 $M^{-1}sec^{-1}$ respectively, in the same solvent at 25°C.

The theoretical expression of R. A. Marcus for the rate constants of electron-transfer reactions contains the following parameters, adjustable experimentally: the standard free energy of reaction, the dielectric constant of the solvent, the temperature, and the molecular radii of the reactants.[1] In the preceding paper,[2] we have discussed the applicability of this theory to the electron transfer from polycyclic aromatic hydrocarbon anion radicals to their respective parent molecules by examining the dependence of the rate constants on the following three parameters: the standard free energy of reaction, the dielectric constant of the solvent, and the temperature. It has been revealed that the contribution to the activation free energy from the nuclear reorganization energy, especially from the reorganization energy of the solvent, is smaller than that predicted theoretically.

This paper will deal with the dependence of the rate constants of the last parameter mentioned above, *i.e.*, the molecular radii of the reactants, in the homogeneous electron-transfer reactions; the rate constants of elec-

1) R. A. Marcus, *J. Chem. Phys.*, **24**, 966 (1956).
2) K. Suga and S. Aoyagui, This Bulletin, **46**, 755 (1973).

tron-transfer reactions from the pyrene, perylene, and tetracene anion radicals to their respective parent molecules are measured in 1,2-dimethoxyethane (DME) under experimental conditions in which the anion radicals are in a free ion or loose ion-pair state. A theoretical estimate of the rate constants is made on the assumption of spherical and non-spherical molecular shapes.

Experimental

The pyrene was purified in a way similar to that described previously.[2] G.R.-grade perylene and tetracene were obtained from the Tokyo Kasei Kogyo Co. and were used without further purification. The hydrocarbons were reduced with sodium metals in DME. The purification of the solvent and the preparation of radical solutions as well as the determination of their concentrations were performed in the same way as in the preceding paper.[2]

The rates of the electron-exchange reactions were determined ESR-spectroscopically by the conventional line-broadening method. Since the hyperfine lines in the ESR spectra of the anion radicals of perylene and tetracene were not perfectly resolved, their linewidth was determined by a computer-simulation method described elsewhere.[3] The linewidth parameter, l_2/l_1, was taken in this case in the way shown in Fig. 1. Figure 1(a) typically illustrates the central portion of the ESR spectra of the perylene anion radical, while (b) illustrates that with added perylene. In Fig. 2 the calculated l_2/l_1 values of the simulated spectra are plotted by triangles *versus* ΔH^t_{pp}, the given width of the hypothetical, unoverlapped hyperfine lines. The apparent linewidths of

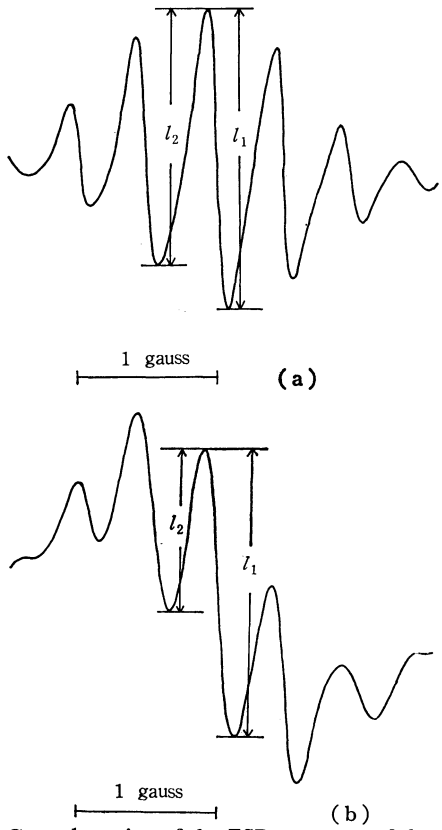

Fig. 1. Central portion of the ESR spectrum of the perylene anion radical: (a) without perylene added, (b) with perylene added.

3) T. Saji and S. Aoyagui, This Bulletin, in press.

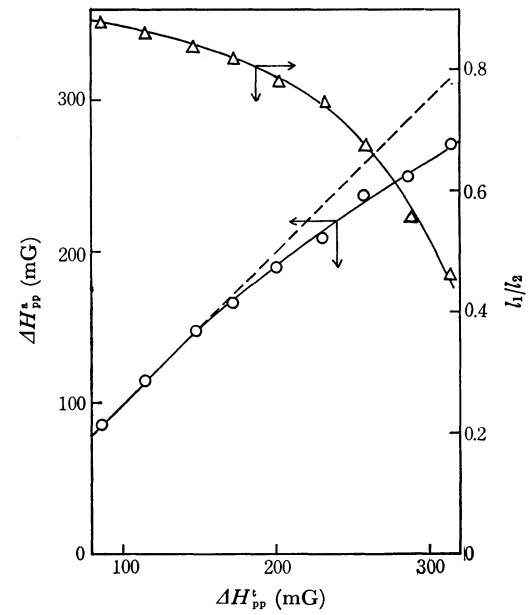

Fig. 2. Calculated l_2/l_1 values of the simulated spectra and the apparent linewidth (ΔH^a_{pp}) *vs.* the given linewidth of the hypothetical unoverlapped hyperfine lines (ΔH^t_{pp}).

the overlapped hyperfine lines obtained from the simulated spectra are designated as ΔH^a_{pp} and are shown by circles in the same figure. The latter plot shows that the direct measurement of the linewidth is not practicable when the observed or apparent linewidth is larger than 0.15 Gauss in the case of perylene. Simulation was performed on a JEOL JRA-5 spectrum computer. As for the pyrene anion, on the other hand, its linewidth was determined according to a procedure described previously.[2]

All the measurements were carried out at 25°C.

Results

Figures 3, 4, and 5 illustrate the increase in linewidth due to electron exchange plotted against the concentrations of perylene, pyrene, and tetracene respec-

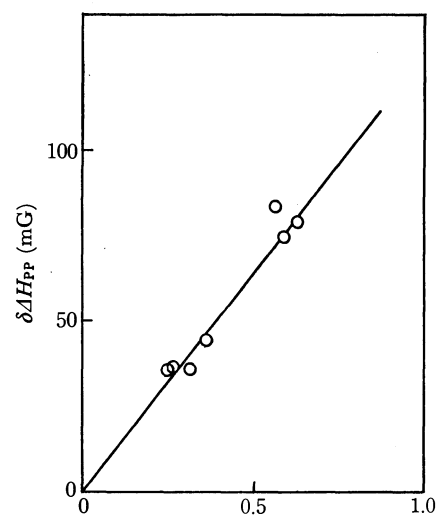

Fig. 3. Increase in the linewidth of the ESR spectrum of perylene anion due to electron exchange ($\delta\Delta H_{PP}$) *vs.* concentration of added perylene.

Table 1. Rate constants of electron exchange reactions between aromatic hydrocarbons and their respective anion radicals, and molecular dimensions of reactants

Hydrocarbon	$k_{obs}(M^{-1}\,sec^{-1})$	$k_a(M^{-1}\,sec^{-1})$	d_1 (Å)	d_2 (Å)	d_3 (Å)
Naphthalene	1.6×10^{9} a)	2.1×10^{9}	7.85	5.7	3.44
Anthracene	1.8×10^{9} b)	2.4×10^{9}	10.3	5.7	3.44
Tetracene	1.9×10^{9}	2.6×10^{9}	12.75	5.7	3.44
Pyrene	2.0×10^{9}	2.8×10^{9}	9.87	7.85	3.44
Perylene	2.1×10^{9}	3.0×10^{9}	9.87	7.85	3.44

a) R. Change and C. S. Johnson, Jr., *J. Amer. Chem. Soc.*, **88**, 2338 (1966). b) Ref. 2.

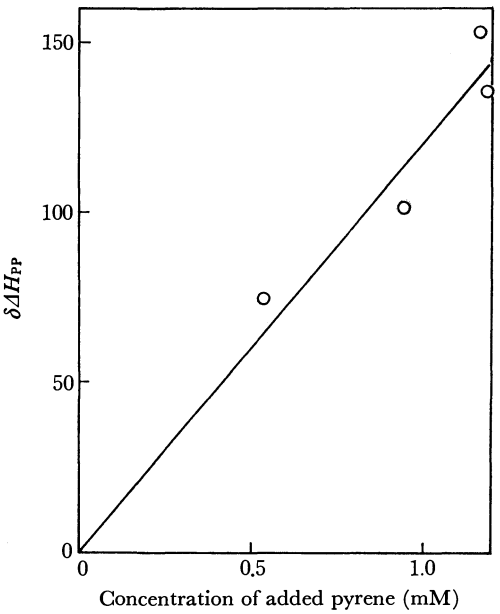

Fig. 4. Increase in the linewidth of the ESR spectrum of pyrene anion due to electron exchange ($\delta\Delta H_{PP}$) *vs.* concentration of added pyrene.

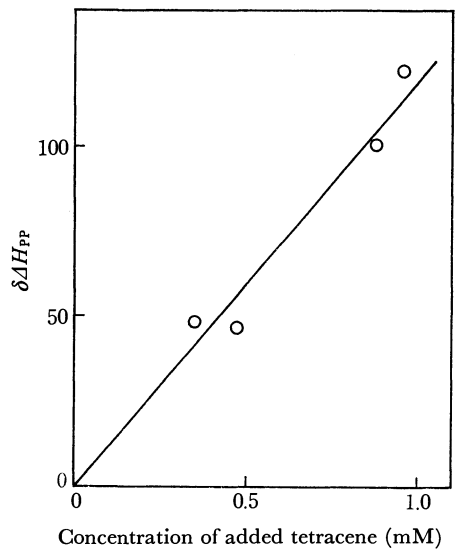

Fig. 5. Increase in the linewidth of the ESR spectrum of tetracene anion due to electron exchange ($\delta\Delta H_{PP}$) *vs.* concentration of added tetracene.

tively. The rate constants with and without correction for diffusion were determined from these figures according to the procedure described previously. They are presented in Table 1, designated as k_a and k_{obs} respectively. The values for the linewidth determined from the l_2/l_1 values of the observed spectra are typically plotted by circles *versus* the concentration of the perylene anion radicals in Fig. 6. The linearity of the plot was satisfactory; it supports this procedure in linewidth determination. The plot shown by triangles in the same figure is the linewidth from which the contribution due to electron exchange is eliminated; it corresponds to pure electron exchange. The second-order rate constant of a spin-exchange process between anion radicals can be determined from the slope of the latter plot.[4,5] The rate constants of the spin-exchange process thus determined are listed in Table 2. The diffusion-con-

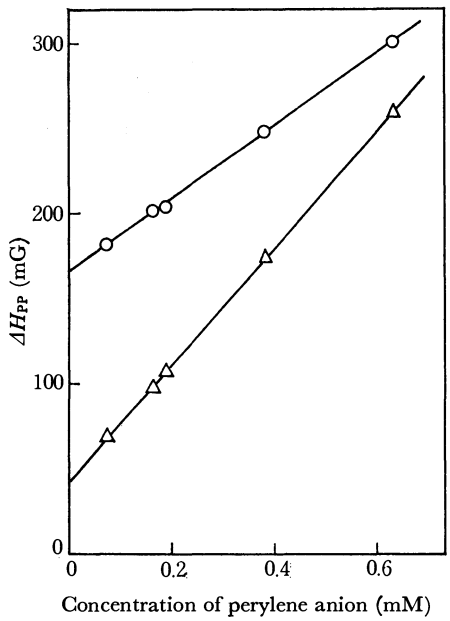

Fig. 6. Linewidth determined from the l_2/l_1 values of the observed spectra (ΔH_{PP}) *vs.* concentration of perylene anion radical. ○: observed linewidth for the solution containing both perylene and its anion radical ([Per$^-$]+[Per]= 0.95 mM), △: linewidth subtracted by the contribution due to electron exchange between perylene and its anion radical.

Table 2. Rate constants of spin exchange process

Hydrocarbon anion radical	k ($M^{-1}\,sec^{-1}$)
Pyrene$^-$	7.0×10^{9}
Perylene$^-$	5.1×10^{9}
Tetracene$^-$	4.8×10^{9}

4) M. P. Eastman, R. G. Kooser, M. R. Das, and J. H. Freed, *J. Chem. Phys.*, **51**, 2690 (1969).
5) K. Suga and S. Aoyagui, This Bulletin, **45**, 1375 (1972).

trolled rate constant calculated theoretically is $7.2\times 10^9 M^{-1}sec^{-1}$.[4,5] The agreement between the experimental and theoretical values was satisfactory. This may be another support of the present procedure of linewidth determination.

Discussion

According to the theory of Marcus,[1,6] the rate constant of an electron-exchange reaction, whose standard free energy is zero, is dependent on the molecular radii of the reactants. When the contribution to the activation free energy from the reorganization free energy of the inner-coordination shell can be neglected, the rate constant is expressed by the following equation:

$$k = Z\exp(-\Delta G^*/RT) \quad (1)$$

with:

$$\Delta G^* = (e^2/4)(1/2a_1+1/2a_2-1/r)(1/D_{op}-1/D_s) \quad (2)$$

where Z is the bimolecular collision number of the hypothetical uncharged reactants in solution at a unit concentration (it is assumed to be $10^{11}M^{-1}sec^{-1}$ in this paper); ΔG^* is the activation free energy; a_1 and a_2 are the molecular radii of the reactants; r is the distance between the centers of the reactants within the activated complex, and D_{op} and D_s are the static and the optical dielectric constants of the solvent respectively.

In deriving the equations above, Marcus assumed the reactants to be spherical. However, in the electron-transfre reactions discussed here the reactants, *i.e.*, the aromatic hydrocarbons and their anion radicals, are not spherical but planar. Hence, we shall examine the dependence of the electron-transfer rates on the molecular radii of reactants using two models, the spherical and the non-spherical models. In each case, a knowledge of the geometry and dimensions of the reactant molecules is required. Table 1 shows the molecular dimensions of several polycyclic aromatic hydrocarbons. The d_1, d_2, and d_3 dimensions have been defined previously.[2]

Spherical Model. In this model, the reactants are assumed to be spherical. If $a_1=a_2=r/2=a$ is assumed as usual, the activation free energy is given by the following equation:

$$\Delta G^* = (1/8)(1/D_{op}-1/D_s)(e^2/a) \quad (3)$$

Consequently, the activation free energy can be expected to be inversely proportional to a, the molecular radius of the reactants.

The values for the rate constant, k_{calc}, calculated from Eqs. (3) and (1) with $a=\sqrt{d_1d_2/2}$ and $Z=10^{11}$ $M^{-1}sec^{-1}$ assumed, are shown in Table 3. They are considerably smaller than the corresponding values for the corrected observed rate constants. Furthermore, the variation in the calculated rate constants with the molecular radii of the reactants is larger than that in the observed values.

The behavior of the observed rate constants might agree with that of the calculated ones, when it is assumed that the solvent around the reactants is dielectrically saturated to have a dielectric constant of about 3. Such a strong saturation, however, probably cannot be realized in the present reactions, in which the reactants have a π-electron distribution spread extensively. The idea of a spherical model for a planar molecule must be discarded.

Non-spherical Model. In this model each reactant is assumed to be an oblate spheroid. In the theoretical estimate of ΔG^* according to Marcus, the free energy of the non-equilibrium polarization of a solvent must be calculated.[1] Such a calculation is quite difficult when the shape of reactants is not spherical. Hush[7] has derived an expression for ΔG^* almost identical with that of Marcus. His theory, however, is based on an assumption of an equilibrium polarization of the solvent. His reasoning is: the electron-transfer occurs through the activated complex, in which the probability of the electron being on one of the reactants is intermediate between the probabilities it has in the initial and final states; the solvent around the reactants stays in thermal equilibrium with the ionic charge. Consequently, if the non-spherical ions are in thermal equilibrium with the solvent and if their free energy of solvation can be calculated, the ΔG^* value for non-spherical reactants can be obtained.

According to Soma and Yamagishi,[8] the solvation free energy of an oblate spheroid, with a major axis of length of $2a$ and a minor axis of length of $2c$, is given by;

$$\Delta G_{solv} = -(q^2/2\sqrt{a^2-c^2})(1-1/D_s)\tan^{-1}\sqrt{(a^2-c^2)/c^2} \quad (4)$$

where q is the charge of the spheroid. If an aromatic hydrocarbon is considered as an oblate spheroid with

Table 3. Comparison of corrected observed rate constants with calculated rate constants based on two models

Hydrocarbon	$\sqrt{d_1d_2/2}$ (Å)	a^* (Å)	k_{calc} (M^{-1} sec^{-1}) Spherical model $a=\sqrt{d_1d_2/2}$	Non-spherical model $r=d_3$	Non-spherical model $r=2d_3$	k_a (M^{-1} sec^{-1})
Naphthalene	3.35	2.70	2.55×10^7	1.45×10^9	5.37×10^5	2.1×10^9
Anthracene	3.88	3.05	6.90×10^7	1.34×10^9	6.50×10^6	2.4×10^9
Tetracene	4.27	3.30	1.42×10^8	5.26×10^{10}	1.78×10^7	2.6×10^9
Pyrene	4.40	3.42	1.72×10^8	9.51×10^{10}	3.52×10^7	2.8×10^9
Perylene	4.40	3.42	$1.72\times10_8$	9.51×10^{10}	3.52×10^7	3.0×10^9

6) R. A. Marcus, *J. Chem. Phys.*, **43**, 679 (1965).
7) N. S. Hush, *Trans. Faraday Soc.*, **57**, 557 (1967).
8) M. Soma and H. Yamagishi, presented at the 23rd Annual Meeting of the Chemical Society of Japan, Tokyo, April, 1970.

$a=\sqrt{d_1 d_2/2}$ and $c=d_3/2$, ΔG^* can be calculated from the following equation:

$$\Delta G^* = (e^2/4)(1/2a_1^* + 1/2a_2^* - 1/r)(1/D_{op} - 1/D_s) \quad (5)$$

with:

$$1/a^* = (1/\sqrt{a^2-c^2}) \tan^{-1} \sqrt{(a^2-c^2)/c^2} \quad (6)$$

The a^* values of each reactant have been calculated from the values of d_1, d_2, and d_3 in Table 1 and are listed in Table 3. Considering that r is fixed rather indefinetely in this case, this quatity is just an adjustable parameter even in the non-empirical calculations. The values for k_{calc} calculated from Eqs. (5), (6), and (1) with $r=d_3$ or $r=2d_3$ are tabulated in Table 3. When r is assumed to be d_3, on the other hand, the values for k_{calc} are much smaller than those for k_a. In either case, the variation in the calculated values with the molecular radii of the reactants is larger than that in the observed values. Consequently, even if r takes an appropriate value between d_3 and $2d_3$, k_{calc} does not agree with k_a.

Thus, the theory of Marcus, in both its original form (spherical model treatment) and its modified form (non-spherical model treatment), has failed to predict the experimental behavior of the rate constant as a function of the molecular radius. This suggests that the contribution to the activation free energy from the reorganization free energy of the solvent is again smaller than that predicted theoretically, as was seen in the previous paper concerning other parameters.

BULLETIN OF THE CHEMICAL SOCIETY OF JAPAN, VOL. 46, 812—817 (1973)

Isothermal Decay of Trapped Electron in Irradiated 2-Methyltetrahydrofuran Glass

Tsuneki ICHIKAWA, HIROSHI YOSHIDA, and Koichiro HAYASHI
Faculty of Engineering, Hokkaido Universtiy, Kita-ku, Sapporo

(Received October 3, 1972)

The isothermal decay of the electron trapped in gamma-irradiated 2-methyltetrahydrofuran glass was studied by electron spin resonance measurements at 92—95 K. Shape of the decay curves was found to be independent not only of radiation dose but also of temperature if they were plotted on the time scale in unit of half-life at each temperature studied. Although the decay follows neither a first order nor a second order reaction, the activation energy is able to be determined uniquely to be 0.8 eV. These results indicate that the mobilization of trapped electron is caused by repeated sequences of detrap-retrap due to thermal distortion or destruction of traps and that the evolution of decay is determined by the initial distribution of the electron-cation separation. On the basis of Nernst-Einstein assumption, the normalized distribution of the separation distance is numerically obtained and found to be close to a Gaussian function, though the absolute value of distance is unable to be determined because of the lack of knowledge of diffusion coefficient for the migration of electron in the glass. The effect of partial photobleaching of the trapped electron on the isothermal decay for the rest of electron was also studied and found to be the same as that of partial thermal bleaching.

2-Methyltetrahydrofuran (MTHF) glass is one of the glassy matrices where the nature of radiation-formed trapped electron has been most extensively studied by a number of techniques such as electron spin resonance (ESR) and optical absorption measurements.[1-4] The radiation-formed intermediates observed in this glass are mostly trapped electron and free radical. The former is characterized by an ESR sharp single line spectrum and a broad optical absorption spectrum with the maximum at about 1200 nm. The latter shows a seven line ESR spectrum, which is interpretable as due to the free radical formed by the cleavage of a hydrogen atom attached to tertiary carbon atom of MTHF molecule[5] or alternatively due to radical cation formed by the intramolecular hydrogen transfer reaction in the primary cation.[6] Although further studies seem needed to distinguish between these two possible interpretations, the present authors suggested that the decay of the trapped electron (at least, a considerable part of it) is caused by the charge neutralization process between the electron and the radical

1) L. Kevan, "Actions Chimiques et Biologiques des Radiations, 15éme sèrie," ed. M. Haissinsky, Masson et Cie., Editeurs, Paris (1971), p. 81. Almost all papers published before 1969 are collected in this review paper.

2) (a) D. P. Lin and L. Kevan, *J. Chem. Phys.*, **55**, 2629 (1971); (b) D. P. Lin, P. Hamlet, and L. Kevan, *J. Phys. Chem.*, **75**, 1226 (1972); (c) D. P. Lin, and L. Kevan *ibid.*, **76**, 636 (1972); (d) T. Huang, I. Eisele, D. P. Lin, and L. Kevan, *J. Chem. Phys*,. **56**, 4702 (1972).

3) (a) K. F. Baverstock and P. J. Dyne, *Can. J. Chem.*, **48**, 2182 1970); (b) F. P. Sargent, *ibid.*, **48**, 3453 (1970); (c) C. Chachaty,, A. Forchioni, J. Désalos, and M. Aris, *Int. J. Radiat. Phys. Chem.* **2**, 69 (1970); (d) J. R. Moller, *J. Chem. Phys.*, **56**, 5173 (1972).

4) (a) H. Yoshida and T. Higashimura, *Can. J. Chem.*, **48**, 504 (1970). (b) T. Shiga, T. Warashina, H. Yoshida, and S. Okamura, *Ann. Repts. Res. Reactor Inst. Kyoto Univ.*, **3**, 19 (1970); (c) M. Irie, K. Hayashi, S. Okamura, and H. Yoshida, *J. Phys. Chem.*, **75**, 476 (1971); (d) H. Yoshida, M. Ogasawara, T. Warashina, and T. Higashimura, *J. Chem. Phys.*, **56**, 4234 (1972).

5) (a) F. S. Dainton and G. A. Salmon, *Proc. Roy. Soc. Ser. A*, 285, 319 (1965); (b) F. S. Dainton, G. A. Salmon, J. Tepley, and J. P. Keene, *Proc. Chem. Soc.*, London, **1964**, 265.

6) (a) D. R. Smith and J. J. Pieroni, *Can. J. Chem.*, **43**, 876 (1965); (b) D. R. Smith and J. J. Pieroni, *ibid.*, **43**, 2141 (1965).

cation, by measuring the recombination luminescence.[7]

The isothermal decay of the trapped electron in this glass was studied by optical absorption[5] and ESR measurements.[6] The decay is now known to be independent of radiation dose and to be a composite first order reaction, which suggests that electron is trapped in close proximity of its partner positive charge to recombine with. However, the decay at about 77K was too slow to determine the exact shape of the decay curve.[6] Recently, Ogasawara *et al.* studied the decay at temperatures higher than 95.6K.[8] They found also, that the decay was independent of the radiation dose. In this study it was difficult to observe the whole shape of decay curves because the decay was very rapid.

Photobleaching of the trapped electron and photo-induced conductivity were also studied by Baverstock and Dyne,[3a] and Huang *et al.*[2d] These investigations gave an insight into the nature of electron traps in the glass. The electron is released from its trap to the conduction level by the absorption of light and then migrate to cationic entities to recombine with. The low quantum efficiency for the photobleaching suggested that electron undergoes detrap-retrap sequences repeatedly until it disappears. However, the migration of electron has not been studied well when it is thermally mobilized.

Smith and Pieroni studied the paramagnetic relaxation of the trapped electron in this glass, and estimated the separation distance between paramagnetic species at 77K.[6a] This result gave an evidence of the non-uniform spatial distribution of the radiation-formed intermediates, though it was not known which is important between the distance between trapped electrons or the distance between trapped electron and other paramagnetic intermediates in determining the relaxation process studied. Kevan *et al.* presumed the relaxation depending upon the interdistance between the trapped electrons and estimated the radius of spur (probably assumed that a spur contains more than one electron) to be 63 Å.[2a] Recent study of electron-electron double resonance of the irradiated MTHF glass showed that the cross relaxation between the trapped electron and the entity giving the seven line ESR spectrum played an important role in the paramagnetic relaxation process in the glass.[9] This suggests that the trapped electron is closely correlated with the free radical (or the radical cation).

If one assumes that the composite first order decay of the trapped electron is dependent upon the time required for it to migrate to its partner cation, precise determination of the decay curve may give another approach to study the distribution of electron-cation separation. On the basis of differential equation of diffusion under the influence of Coulombic attraction between oppositely charged ions, Ludwig showed a mathematical way to correlate the evolution of decay with the distribution of separation distance of isolated ion pairs in liquids.[10] Hamill and his co-workers studied the recombination luminescence in viscous liquids after pulse irradiation and examined it in terms of the initial distribution of ion pair separations.[11] Such an approach seems essentially applicable to the thermal decay of the trapped electron in the glassy matrices.

With this respect, it will be worth determining the shape of the isothermal decay of trapped electron at the temperature where the decay is appropriately fast to be studied precisely and conveniently. In the present investigation, the MTHF glass was chosen, because the nature of trapped electron has been well elucidated and the trapped electron decays at temperatures controlled rather easily.

Experimental

MTHF was purified as described elsewhere.[7] It was dried with sodium-potassium alloy under vacuum and sealed in ESR sample tubes of pure quartz (inner diameter: 0.3 cm) also under vacuum. Irradiation was carried out with ^{60}Co gamma-rays at the dose rate of 7×10^{17} eV/g min at 77K in dark.

The irradiated sample was quickly transferred into a variable temperature Dewar insert attached to the ESR resonant cavity, of which temperature was adjusted beforehand by flowing cold nitrogen gas from liquid. The intensity of the trapped electron ESR spectra were repeatedly recorded at constant temperature with a conventional X-band ESR spectrometer (JEOL JES-ME-2X) using a modulation width of 0.8 G and a microwave power level of 0.1 mW. The temperature was monitorred with a thermocouple positioned at the bottom of the sample tube with the accuracy of ±0.1 K. The temperature monitor was calibrated by comparing with the temperature measured by another thermocouple burried in the sample.

Photobleaching of the trapped electron was carried out with light of an incandescent lamp through a cut-off filter ($\lambda>660$ nm). During the photobleaching, the sample was rotated to avoid a spatially inhomogeneous bleaching.

The absorption spectrum of the trapped electron was recorded with a conventional recording spectrophotometer (Hitachi, EPS-3) for the sample in a rectangular quartz cell of 1.0×1.0 cm^2 immersed in liquid nitrogen.

Results

ESR spectral shape observed from irradiated MTHF glass is composed of a sharp single line spectrum due to trapped electron and a seven line spectrum due to free radical superposing each other. Although both spectra are stable at 77K, the former spectrum decays rapidly at temperatures higher than 90K accompanying a partial decay of the latter.[3b,4c,6a,8] Isothermal decays of the trapped electron were obtained at several temperatures between 92.2 and 95.0K by observing the change in intensity of the single line spectrum (correction was made for the free radical spectrum superposing on the trapped electron spectrum.)

Dependence of the decay upon radiation dose was studied in the range of $0.7—2.0\times10^{19}$ eV/g, as shown in Fig. 1. Immediately after warming the samples from 77K to a proper temperature, the intensity of the

7) T. Ichikawa, H. Yoshida, and K. Hayashi, *J. Nucl. Sci. Tech.*, in press.

8) M. Ogasawara, K. Ohno, K. Hayashi, and J. Sohma, *J. Phys. Chem.*, **74**, 3221 (1070).

9) H. Yoshida, D-F. Feng, and L. Kevan, *J. Chem. Phys.*, in press.

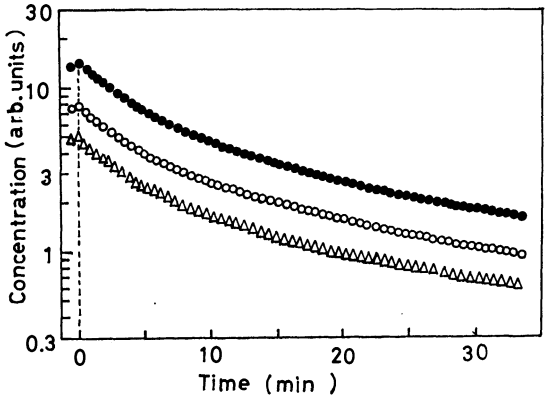

Fig. 1. Isothermal decay of trapped electron in MTHF glass irradiated to (●) 2×10^{19}, (○) 1×10^{19} and (△) 0.7×10^{19} eV/g at 77K and measured at 93.4K.

spectrum shows a slight increase. It may be caused by shorter paramagnetic relaxation times (especially spin-lattice relaxation time) at higher temperature. Under the present condition of ESR measurements, the microwave power level is a little too high to avoid a partial saturation of the trapped electron spectrum. Therefore, the intensity increases more or less when the relaxation times becomes shorter. It was assumed that the temperatures where the isothermal decay should be studied were reached when the observed decay curves reached the maximum. So the zero time for the isothermal bleaching was arbitrarily selected as shown in Fig. 1.

Depending on the radiation dose, the initial concentration of the trapped electron changes. However, the semilogarithmic plots of the decays can be completely superimposed if normalized at the initial concentration, which indicates that the rate of decay is independent of the radiation dose or the concentration of trapped electron. The decay does not follow an exponential curve nor is resolved into a few exponential curves.

Figure 2 shows the dependence of the isothermal decay upon temperature. The zero time was chosen as was done in Fig. 1. The scale of abscissas was chosen, so that the half-life ($t_{1/2}$, the time for the decay to 50% of the initial concentration), of the trapped electron has a fixed length for all temperatures examined.

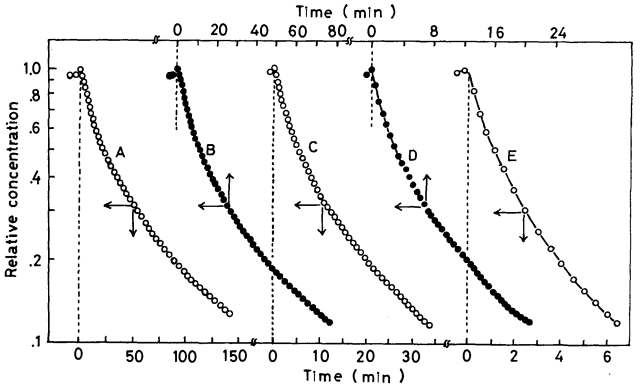

Fig. 2. Isothermal decay of trapped electron in MTHF glass irradiated to 1×10^{19} eV/g at 77K and measured at (A) 92.2, (B) 92.8, (C) 93.4, (D) 94.0, and (E) 95.0K.

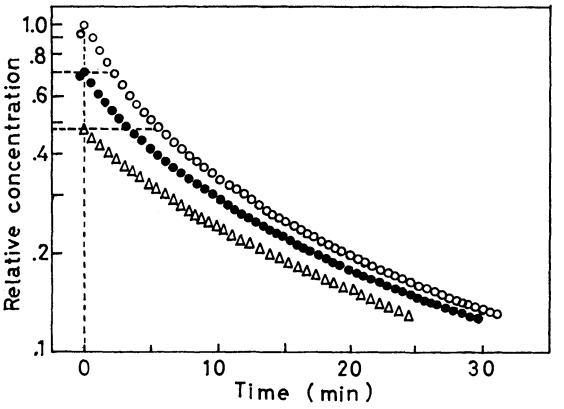

Fig. 3. Isothermal decay of trapped electron in MTFH glass irradiated to 1×10^{19} eV/g and measured at 93.4K after a partial photobleaching of trapped electron with light of $\lambda>660$ nm to (●) 70% and (△) 47% of its initial concentration. The decay without the photobleaching (○) is shown for comparison.

The concentration of trapped electron was also normalized to be unity at $t=0$. The decay becomes much faster with increasing temperature. However, the observed decay curves are again superimposed on each other, except a slight deviation observed for the curve at 95.0K, the highest temperature examined.

The decay curves were examined also after a partial photobleaching of the trapped electron with light of wavelength longer than 660 nm. They are shown in Fig. 3 as well as the decay curve obtained without the photobleaching. Evidently, the decay behavior after the partial photobleaching is the same as that after partial thermal bleaching. The curves A and B, obtained after the partial photobleaching, can be superposed on the curve C without photobleaching when they are horizontally shifted. Partial bleaching either thermally or by light affects equally on the decay behavior of the rest of trapped electron.

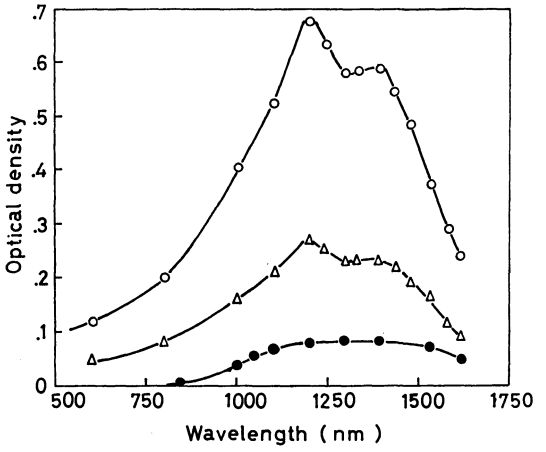

Fig. 4. Optical absorption spectra of trapped electron in MTHF glass irradiated to 7×10^{17} eV/g and measured at 77K (○) before and (△) after a partial photobleaching to 40% of its initial concentration. The spectra shown were obtained by subtracting the spectrum of the glass completely photobleached from those of the glasses containing the trapped electron. The residual spectrum (●) was determined as the difference in absorption between the glass irradiated and completely photobleached and the unirradiated glass.

Optical absorption spectrum of the trapped electron was studied immediately after the irradiation and after subsequent partial photobleaching of the trapped electron to 40% of its initial concentration both at 77 K. The results shown in Fig. 4 was obtained by subtracting the absorption of the sample irradiated and completely photobleached from that of the sample with trapped electron. It should be noted that a broad absorption was found at the wavelength region of 800—1600 nm, even after the complete photobleaching of trapped electron. This unidentified absorption disappeared when the irradiated glass was melted. The results clearly indicate that the absorption spectrum of trapped electron does not change in its shape during its decay.

Discussion

Activation Energy for the Decay of Trapped Electron. Since the decay curves show the same shape independent of the radiation dose and temperature, they can be characterized by a single parameter, for example, half-life. This implies that the apparent activation energy can be defined uniquely for the whole decay cruves. In other words, the activation energy remains unchanged during the decay.

The Arrhenius plot of the half-life is shown in Fig. 5, where the half-life appeared in the previous literatures are included for comparison. A good linear relationship is found in the temperature range studied in the present investigation. The present results seem consistent with the previous ones cited, though the activation energy tends to decrease with decreasing temperature.

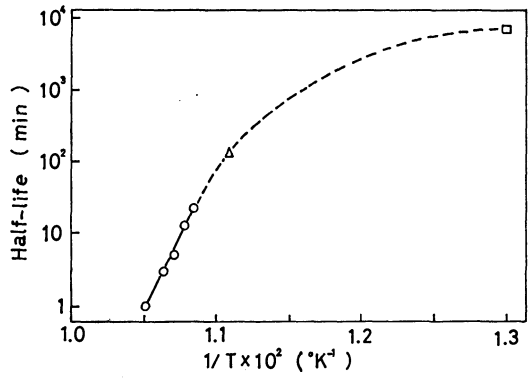

Fig. 5. Arrhenius plot of the half-life of trapped electron in irradiated MTHF glass when isothermally bleached. Half-lives estimated from the previous literatures (△) by Dainton and Salmon and (□) by Smith and Pieroni are also shown for comparison.

The activation energy is determined to be 0.8 eV (19 kcal/mol) from Fig. 5 in the temperature range of 92—95 K. The value is compared with the activation energy 14 kcal/mol determined in the same temperature range by Dainton *et al.* from the optical absorption measurements. They used the sample in a optical absorption cell of the cross section of 0.5×1.5 cm^2 and they mentioned that it took about 2.5 min to attain thermal equilibrium.[5a] In addition, the sample temperature is thought to have been inhomogeneous during rapid warming of a big sample. These factors may fortuitously cause a smaller activation energy. It should be noted also that the time 0.5 min of the transient rise of the sample temperature in the present investigation may have been a little too long to study the fast isothermal decay at 95 K and caused the slight distortion of the decay curve.

Ogasawara *et al.* studied previously the isothermal decay of the trapped electron in irradiated MTHF glass at temperatures higher than 95.6 K and obtained the activation energy of 6.1 kcal/mol.[8] The reason why the activation energy suddenly changes at around 95 K is not known well, though it may be attributed to the glass transition point of the MTHF glass.[12]

Decay Process of Trapped Electron. A unique value of activation energy for the whole decay process indicates that a single kind of migration process as well as a single kind of trap is responsible for the decay of trapped electron. In the MTHF glass, the primary cationic entity is believed to be stabilized by the intermolecular protonation or the intramolecular hydrogen transfer reaction.[5,6] The free radicals in this glass disappear in recombining with each other at about 100K somewhat higher than the temperature where the trapped electron decays very rapidly.[6a,8] This indicates that the stabilized cationic entity with the same size as MTHF molecule cannot migrate in the temperature range studied in the present investigation. Accordingly, the moving entity during the isothermal decay of trapped electron is the electron itself released from its trap.

The activation energy of 0.8 eV is considerably higher than that for the decay of trapped electron in irradiated 3-methylhexane glass caused by the migration of electron, 0.13 eV.[13] However, it is apparently less than the energies corresponding the absorption maximum of trapped electron and the threshold wavelength for its photobleaching.[2d,3a] Release of electron from its trap is very probably caused by the thermal distortion or destruction of the trap but not by the vertical transition up through the conduction level. Among the three possbile models for the mechanism of thermal mobilization of the trapped electron proposed by Kevan,[1] (1) diffusion of the matrix solvated electron as an entity, (2) tunneling between matrix traps due to matrix diploe reorientation, or (3) diffusion of a quasi-free electron, the present results support the second possibility. The strong temperature dependence does not indicate quantum tunneling of electron[3d,14] from electron trap to cation. With this respect, it may be interesting to compare the activation energy for the electron decay with that obtained from the temperature dependence of the viscosity of MTHF glass, 0.88 eV, in the temperature range of 92.0—101.5 K.[15]

10) P. K. Ludwig, *J. Chem. Phys.*, **50**, 1787 (1969).
11) (a) J. A. Leone and W. H. Hamill, *ibid.*, **49**, 5294, 5304 (1968). (b) T. Sawai and W. H. Hamill, *ibid.*, **56**, 5524 (1972).
12) M. Bodard and R. Marx, *J. Polymer Sci.*, **C16**, 4241 (1968).
13) H. Yoshida, *Ann. Repts. Res. Reactor. Inst. Kyoto Univ.*, **3**, 153 (1970).
14) M. Irie, H. Yoshida, K. Hayashi, and S. Okamura, This Bulletin, **45**, 2347 (1972).
15) A. G. Ling and J. E. Willard, *J. Chem. Phys.*, **72**, 1918 (1968).

Irrespective of the radiation dose and the temperature, all observed isothermal decay curves are superimposed on each other. A non-exponential decay indicates that the decay is not determined by a single thermally activated process of releasing electron from its original trap but by a sequence of detrap-retrap processes which the electron undergoes until it reaches at the predestined cation to recombine with. Therefore, the distribution of the life time of trapped electron is determined by the distribution of the number of detrap-retrap processes required for the electron to encounter the cation. An alternative interpretation may be that the decay was determined by the distribution of trap depth and the charge neutralization process involved a single thermally activated process of detrapping from the original trap. However, this is excluded by the observed constancy of the activation energy throughout the whole evolution of decay.

It was well established by the study of low temperature pulse radiolysis measurements[16] and by the study of irradiation at 4 K[4a,17] that the electorn formed in the MTHF glass is trapped primarily in a shallow trap and then the trap depth is deepened by the orientation of the matrix molecules at 77 K. However, the absorption spectrum of trapped electron stable at 77 K exhibits a structure attributable to two different depth of trap, and the shallow trap transforms to the deep one by warming the glass up to 85 K.[18] In the present measurements at higher temperature, the decay of deeply trapped electron may have been observed after the complete transformation of the shallow trap to the deep one, so that only one value of the activation energy may have been determined. After the partial photobleaching at 77 K, no change was found in the shape of the absorption spectrum. Therefore, the trapped electrons both in the shallow and deep traps are equally bleached by light of continuous spectrum ($\lambda>660$ nm). After that, the shallow trap may have been deepened by warming to the temperature of subsequent isothermal decay.

Electron-Cation Separation. On the basis of the assumption of isolated electron-cation pair and the neutralization time proportional to migration path length of electron or the number of detrap-retrap cycles before encountering with its partner cation, the evolution of electron decay can be correlated with the separation distance between the electron and the cation by the well known Smoluchowski equation.[10,19] However, if we assume that the migration of electron is to a large extent determined by the Coulombic interaction only, it is described simply by the Nernst-Einstein relationship,[20]

$$-\frac{dr}{dt} = \frac{Dr_c}{r^2} \tag{1}$$

where r is the distance between electron and cation, D is the diffusion coefficient of electron, and r_c is Onsager length defined as

$$r_c = \frac{e^2}{\varepsilon kT} \tag{2}$$

By integrating Eq. (1) under the initial condition $r=r_i$ at $t=0$, the following relationship is obtained between r and t:

$$r_i^3 - r^3 = 3Dr_c t \tag{3}$$

This gives the recombination time t_r for the electorn initially at r_i as

$$t_r = \frac{r_i^3}{3Dr_c} \tag{4}$$

which turns out to be $dr_i/dt_r = Dr_c/r_i^2$. Consequently, the survival probability of electron, P, is defined by the probability density of finding electron at r_i at $t=0$, $W(r_i)$, which is the initial distribution of separation distance between trapped electron and cation:

$$-\frac{dP}{dt_r} = W(r_i)\cdot\frac{dr_i}{dt_r} = \frac{Dr_c}{r_i^2}\cdot W(r_i) \tag{5}$$

The left-hand side of the above equation is the decay rate obtained from the normalized decay curve of the trapped electron. If one transforms t_r and r_i to dimensionless parameters $\tau=t_r/t_{1/2}$ and $x_i=(Dt_{1/2}r_i)^{-1/3}$. r_i, the following relation is obtained:

$$-x_i^2\cdot\frac{dP(\tau)}{d\tau} = W(x_i) \tag{6}$$

Equation (6) gives straightforwards the initial distribution of separation $W(x_i)$ from the observed decay curve by using the relationship $3\tau=x_i^3$. The distribution is temperature independent because not only the product $Dt_{1/2}$ but also r_c remains unchanged in a small range of temperature studied.

The initial distribution is numerically obtained from the whole evolution of the electron decay. In the same way, the probability of finding electron at reduced distance x at reduced time $\tau=\tau_1$ during the isothermal decay can be obtained from the evolution of decay in the region of τ larger than τ_1, using the relationship

$$-x^2\cdot\frac{dP(\tau+\tau_1)}{d\tau} = W(x,\tau_1) \tag{7}$$

Thus obtained distribution of the initial separation distance as well as those during the isothermal decay[21] is shown in Fig. 6.

The initial distribution qualitatively agrees with the Gaussian distribution, $W(x_i)=x_i^2\exp(-\alpha x_i^2)$, which was used to estimate the average separation between ion pair in irradiated liquid hydrocarbon.[22] The disagreement at large x_i values is much improved if the Smoluchowski equation is rigorously applied in the present analysis.[23] It should be noted that the maximum of distribution function and the average separation increase during the isothermal decay. This is

16) J.T. Richard and J.T. Thomas, *J.Chem. Phys.*, **54**, 298 (1970).
17) H. Hase, M. Noda, and T. Higashimura, *ibid.*, **54**, 2975 (1971).
18) T. Sawai and W. H. Hamill, *J. Phys. Chem.*, **73**, 3452 (1969).
19) A. Mozumdar, *J. Chem. Phys.*, **48**, 1659 (1968).
20) F. Williams, *J. Amer. Chem. Soc.*, **86**, 3954 (1964).
21) Computations were carried out at the Computing Center of Hokkaido University.
22) S. Sato, This Bulletin, **41**, 304 (1968).
23) T. Ichikawa, H. Yoshida, and K. Hayashi, to be published.

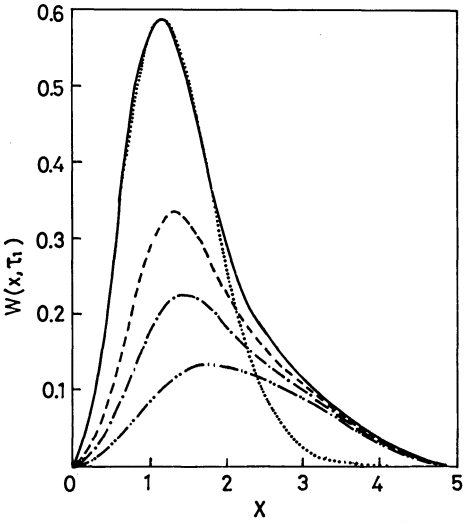

Fig. 6. Distribution of electron-cation separation distance in irradiated MTHF glass before and during the thermal decay of trapped electron determined from its isothermal decay curves. $W(x,\tau_1)$ is the probability density of finding electron at the reduced distance x at the reduced time τ_1. The distribution is shown for $\tau_1=0$ (——), 1/2 (– – –), 1 (–·–), and 2 (–··–). The definition of x and τ is given in the text. Gaussian distribution (·····) is also shown for comparison.

due to relatively short life time of electron at short distance from cation (see equation 3). This trend is more pronounced when the diffusion term in the Smoluchowski equation is taken into account in deriving the distribution.[23]

The quantum efficiency for the photobleaching of trapped electron in the MTHF glass was found to be much smaller than unity.[2d,3a,24] This implies that the electron undergoes several detrap-retrap cycles until it recombines with cation when photobleached. The present results of the effect of partial photobleaching on the subsequent isothermal decay (see Fig. 3) gives another evidence of the detrap-retrap cycles under the bleaching light. It indicates that the change in $W(x, \tau_1)$ during the photobleaching is the same as that during the isothermal decay of electron which is characterized by the migration of electron described by equation (1) but not by the single thermal activation process of detrapping from the original trap.

The decrease in the quantum efficiency of photobleaching with bleaching time was attributed to two class of trapped electron: one is electron trapped in proximity with cation and another is that trapped homogeneously in the glass.[24] However, such a classification of trapped electron seems unnecessary. The average distance between unbleached electron and cation increases longer and longer during the photobleaching, so that the number of detrap-retrap cycles required for the electron to recombine with the cation increases with photobleaching time, which results in a smaller quantum efficiency.

Lin and Kevan observed the increase in the paramagnetic relaxation times of trapped electron in the MTHF glass by a partial photobleaching, if the glass was irradiated to the dose at which the spurs did not overlap with each other.[2c] They thought that this result gave an evidence that a spur contains more than one trapped electron. However, if one presumes that the stabilized cationic entity is still paramagnetic (radical cation),[6,7] the observed change in the paramagnetic relaxation times during the photobleaching is interpreted by the increase in average distance between electron and the cation as shown in Fig. 6. Although the change in the separation distance seems to be slight, the spin-spin dipolar interaction depends on the inverse cube of the distance and very sensitive to the change in the distance.

24) P. J. Dyne and O. A. Miller, *Can. J. Chem.*, **43**, 2696 (1965).

Kinetics and Mechanism of the Reaction of Iodine Mono Chloride with Some Alcohols

C. R. Das and A. N. Bose*

Department of Chemistry, Ravenshaw College, Cuttack-3, India
**Department of Chemistry, R.C.E, Ajmer, Rajsthan, India*

(Received December 14, 1971)

Kinetics of the reaction of ICl with some aliphatic alcohols, methanol to *n*-butanol and isobutyl alcohol and isopropyl alcohol, have been studied by the conductance method at five different temperatures. Arrhenius parameters have been determined. Plot of log *k* against the reciprocal of dielectric constant has been drawn to test the applicability of the Amis and Jaffé equation. Energy of activation has been correlated with polarity of alcohols. The IR analysis of the product shows a sharp peak at 1620 cm^{-1}, which confirms a (O–I) bond stretching in the product. From these results a reasonable mechanism has been suggested as follows:

$$ICl \xrightarrow{\text{fast}} I^+ + Cl^- \quad (1)$$

$$R\text{–}O\text{–}H + I^+ \xrightarrow{\text{slow}} R\text{–}O\text{–}I + H^+ \quad (2)$$

Iodination reactions by ICl have been studied by various workers.[1–6] Lambourne and Robertson[7] studied the kinetics of iodination of various aromatic compounds using glacial acetic acid or chloro benzene as solvents. Kinetics of iodination of *p*-Cl $C_6H_4NH_2$ with ICl in water containing excess of chloride and H^+ ions has been studied by Berliner.[8] He suggested that the reaction involves free amine and hypo-iodous acidium ion (H_2OI^+). Irent'ev and Yanovskaya[9] have found that iodo derivatives are formed in the case of reactions of acids and resorcinol with ICl.

In the present investigation kinetics of the reaction of ICl with aliphatic alcohols, methanol to *n*-butyl alcohol, isobutyl alcohol, and 2-propanol has been studied systematically. It has been found that the reaction takes place according to the equation, provided

$$R\text{–}O\text{–}H + ICl = R\text{–}O\text{–}I + H^+ + Cl^-$$

no other complexities arise due to the impurities present either in alcohols or ICl. This has been confirmed in several ways. Infrared analysis confirms the presence of a (O–I) bond in the product. Gravimetric estimation of Cl^- ions confirms that Cl^- ions are not consumed during the course of the reaction. The aim of the present work is (a) to find out Arrhenius parameters, (b) to correlate rate constants with dielectric constant of the medium, (c) to find out the relationship between energy of activation (E) and polarity (μ) of the substance and (d) to suggest a reasonable mechanism for such reactions.

Experimental

(a) Materials. Iodine monochloride, E. Merck, E. P., was used for the experiment. It was kept in a vacuum desiccator to avoid moisture contamination.

The alcohols were of B. D. H. Analar quality. All the substances were dried with anhydrous calcium chloride and then distilled several times. Adequate precautions were taken to keep the sample dry.

Since ions were formed during the course of the reaction, kinetics was studied by conductance measurements most accurately with the help of a Beckman model RC 16 B 1 conductivity bridge and a cathod ray oscilloscope as a null point detector. This method was used in preference to the usual titriometric methods since it involves minimum number of operations and can be conveniently followed with the help of a small amount samples.

Fresh solutions were prepared every time before the experiment. First anhydrous alcohols were kept in glass stoppered tubes in a thermostat for one hour to attain the temperature of the bath. Calculated quantity of ICl was then taken by means of a perfectly dry syringe and accurately weighed inside the coloured glass conductivity cell as quickly as possible. 10 m*l* of the alcohol that had previously been kept in the thermostat was added to the cell. Thus a solution of ICl in alcohol of exactly 0.099M was immediately obtained in the cell. Rate of the reaction was then followed by measuring the resistance at different time intervals. Pseudo unimolecular rate constants were determined[10] at five different temperatures ranging from 15 to 35°C by applying the least square method from which Arrhenius parameters were determined.

Test for I^+ Ion. The presence of I^+ in the reaction mixture after completion of the reaction was tested by the method adopted by Arotsu *et al.*[11] When a drop of the reaction mixture was added to oleum, no blue colouration was observed, which proved the absence of I^+.

Effect of HCl. In order to find out if HCl has any catalytic effect, 0.05 ml of M/10 HCl was added to the reaction mixture of ICl and methanol, and then the rate of the reaction was followed by the conductance method. The rate constant was calculated. It was found that at 25°C

1) G. Willgerodt and E. Arnold, *J. Amer. Chem. Soc.*, **34**, 3343 (1901).
2) A. E. Bradfield and K. J. P. Orton and others, *J. Chem. Soc.* **1928**, 782.
3) E. White and P. W. Robertson, *ibid.*, 1509 (1939).
4) A. N. Glazer and F. Sanger, *J. Biol. Chem.*, **90**(i), **92**, (1964)
5) G. N. Zakharova, R. E. Avoyan, and Yu. T. Struchkov, *Zh. Strukt. Khim.*, **9**(6), 928(1963).
6) F. M. Vainstein, E. I. Tomilenko, and E. A. Shilov, *Kinet. Katal.* **7**, 33 (1966).
7) L. J. Lambourne and P. W. Robertson, *J. Chem. Soc.*, **1947**, 1167
8) E. Berliner, *J. Amer. Chem. Soc.*, **78**, 3632 (1956).
9) A. P. Irent'ev and L. A. Yanovskaya, *J. Gen. Chem. USSR* **24**, 1251 (1954).
10) A. Frost and R. G. Pearson, "Kinetics and Mechanism," 2nd Edn. John Wiley and Sons Inc. N.Y. (1961), p. 36.
11) J. Arotsu, H. C. Mishra, and M. C. R. Symon, *J. Chem. Soc.*, **1961**, 12.

$k=35.97\times10^{-4}$ min^{-1} with HCl and $k=36.02\times10^{-4}$ min^{-1} at 25°C without HCl. The little difference was within experimental error.

Effect of Water. To find out whether water has any effect on the rate of the reaction, 0.05 ml of water was added to the reaction mixture at the beginning and then the rate was followed. It was found that a small amount of water had no effect.

Estimation of Cl$^-$ Ion. The amount of Cl$^-$ was estimated gravimetrically[12] as AgCl before and after the reaction. It was found that the amount of Cl$^-$ after the reaction was the same as at the beginning. This proved that Cl$^-$ was not consumed during the course of the reaction.

Results and Discussion

It is of interest that in all cases the reaction was completed when a reactant (*i.e.* -alcohol) was present in a large excess.

This was further verified by the method given by Arotsu *et al.* (loc. cit.), from the fact that no free I$^+$ (iodonium ion) remained after the reaction was over.

Table 1. Values of μ, E, and log PZ

Alcohol	μ	E (kcal/g mol)	log PZ (min)
Methanol	1.70	11060	5.61
n-Butanol	1.69	13200	7.65
Ethanol	1.68	14700	8.45
Propanol	1.67	16400	9.82
2-Propanol	1.60	26700	16.98
Isobutyl alcohol	—	20300	12.92

From the results given in Table 1, it is observed that the frequency factor (log PZ) and energy of activation (E) both vary in the case of reactions of methanol to *n*-butyl alcohol, 2-propanol, and isobutyl alcohol. The variation of frequency factor A can be explained in terms of collision theory. A is made up of two factors probability factor P and collision number Z. They may be identified in the following form as has been described by Stern and Eyring.[13]

$$P \approx (f_v/f_r)^5$$

$$\text{and } Z \approx kT/h(f_r^2/f_t^3)$$

where f_v, f_r, and f_t are the partition functions for vibrational, rotational, and translational degrees of freedom, respectively. At ordinary temperature f_v is of the order of unity while f_r may vary from 10 to 100 in case of complex molecules. If the molecules are less complex, the smaller will be the value of f_r and so the factor P will be high, which will help raise the values of 'PZ'. In the present case it can be seen from Table 1 that the higher values of PZ may be due to the increase in the probability factor P. But if the complexity of the molecules increases with solvation, P will have lower values and consequently factor A will be low. According to collision theory we have

$$Z = N^2\sigma_{AB}^2[8\pi RT(1/M_A+1/M_B)]^{1/2}C_AC_B \quad (1)$$

In the present case, M_B the molecular weight of ICl is constant and M_A, the molecular weight of alcohols, does not vary much from methanol to *n*-butanol; so the factor 'Z' is constant.

Effect of Dielectric Constant on Reaction Velocity. Many equations[14] have been derived to correlate the dielectric constant of the medium with reaction velocity. Amis and Jaffé[15] gave the following equation for the ion-dipole interaction:

$$\ln k' = \ln k'_{r=0} + \frac{\xi Z_B \cos\theta_0}{DkTr_0^2}\left(\mu_0+\frac{\mu^*(1+Xr_0)}{e^{Xr_0}}\right) \quad (2)$$

In the limiting case of the direct approach of an ion to a dipolar molecule, Eq. (2) was modified by Amis[16] as follows:

$$\ln k'_{D=D} = \ln k'_{D=\infty} + \frac{Zc\mu}{DkTr^2} \quad (3)$$

According to this equation, the rate decreases with the increase of dielectric constant for a positive ionic reaction. Recently Laidler and Landskroener[17] developed the following general equation incorporating the corrections due to non-electrostatic forces.

$$\ln k = \ln k_0 + \frac{\xi^2}{2kT}\left(\frac{1}{D}-1\right)\left[\frac{Z_A^2}{b_A}+\frac{Z_B^2}{b_B}-\frac{(Z_A+Z_B)^2}{b_*}\right] + \frac{3\xi^2}{8kT}\left(\frac{2}{D}-1\right)\left[\frac{G_A}{b_A^3}+\frac{G_B}{b_B^3}-\frac{G_*}{b_*^3}\right] \quad (4)$$

This also, predicts a linearity between log k and the reciprocal of the dielectric constant.

Table 2. Values of $k_{25°C}$ and $100/D$ for the reaction of ICl with alcohols

Alcohol	$k_{25°C}\times10^4$ (min^{-1})	$100/D$
Methanol	36.02	3.062
Ethanol	54.81	4.110
Propanol	76.11	4.975
2-Propanol	92.12	5.464
n-Butanol	109.85	5.848
Isobutyl alcohol	132.10	6.330

In the present case of the reaction between ICl and alcohols, it has been found that log k increases with the decrease of the dielectric constant (Table 2) and the plot of log k against $100/D$ is a straight line (Fig. 1). This is in agreement with the Amis equation (2).

It can therefore be concluded that it is an ion-dipolar reaction.

Correlation of Polarity and Energy of Activation. Many equations have been derived by Amis,[16] Ingold and Nathan[18] and Evans, Gordon and Watson[19] connecting energy of activation and polarity of the solvents. Moelwyn-Hughes[20] has explained similar rela-

12) A. I. Volgel, "A text book of quantitative Inorganic analysis', Longmans Green & Co., 3rd ed. (1961), p. 460.
13) E. Stern and H. Eyring, *J. Chem. Phys.*, **5**, 113 (1937).
14) K. J. Laidler and H. Eyring, *Ann. N. Y. Acad. Sci.*, **39**, 303 (1940).
15) E. S. Amis and C. Jaffé, *J. Chem. Phys.*, **10**, 598 (1942).
16) E. S. Amis, *J. Chem. Educ.*, **30**, 351 (1953).
17) K. J. Laidler and P. A. Landskroener, *Trans. Faraday Soc.*, **52**, 200 (1956).
18) C.K. Ingold and W. S. Nathan, *J. Chem. Soc.*, **1936**, 222.
19) D. P. Evans, J. J. Gordon, and H. B. Watson, *ibid.*, **1973**, 1430.
20) E. A. Moelwyn-Hughes, "Physical Chemistry," Pergamon Press, N.Y., (1957), Chapter XXIV.

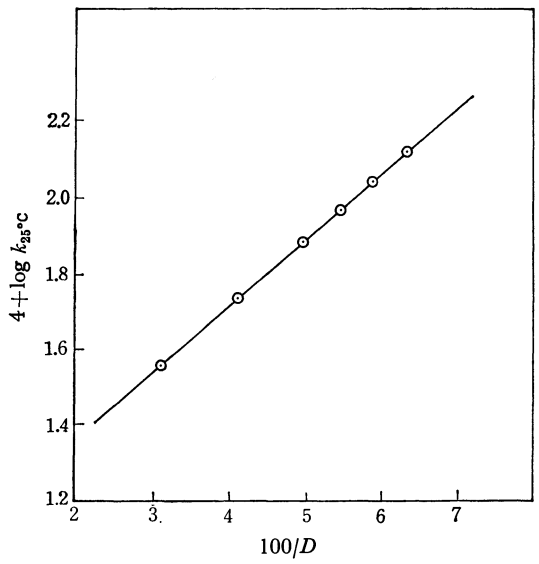

Fig. 1. Plot of log $k_{25°C}$ *vs.* $100/D$ for the reaction of ICl with alcohols.

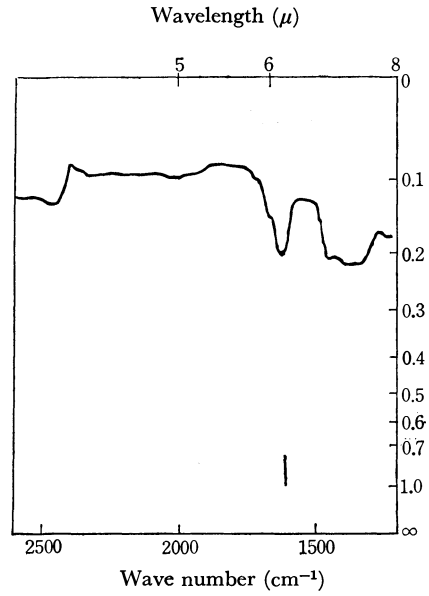

Fig. 3. IR spectrum.

tion ships in terms of electrostatic principles and for head on-alignment of ion and dipole, the equation becomes

$$E_s = E_\mu - \frac{N_Z \mu}{D_r^2} \qquad (5)$$

According to this equation, when the energy of activation is plotted against the dipole moment of dipolar molecules reacting with ions, the plot should be linear with a negative slope if the reacting ion is positive in charge, and with a positive slope if the ion is negative in charge.

In the present case, though the difference of dipole moments of alcohols is less, energy of activation has been plotted against 'μ'. It can be seen from that the plot is a straight line with a negative slope (Fig. 2), which means in this case the reacting ion is a positively charged I^+ ion reacting with a dipolar molecule like alcohol ($CH_3OH \rightleftharpoons CH_3O^- + H^+$). This also proves that in the case $ICl \rightleftharpoons I^+ + Cl^-$, a product like CH_3OI is expected not to be a chloride derivative. This has also been confirmed by the estimation of Cl^- ions, as AgCl, that no Cl^- ions are consumed during the course of the reaction.

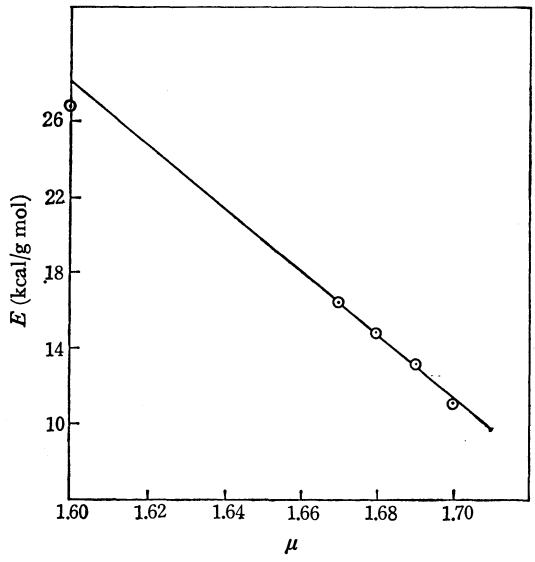

Fig. 2. Plot of E *vs.* μ for the reaction of ICl with alcohols.

Product Identification. The product in each case has been identified by IR spectrum (Fig. 3). A sharp peak at 1620 cm^{-1} confirms a (O–I) bond stretching[21] in the product. This confirms that iodo derivative of the type R–O–I is formed.

Mechanism. ICl being a highly reactive species and a polar compound, it is easily ionized in a medium of alcohols having high dielectric constants according to either of the following equations.

$$ICl \longrightarrow I^+ + Cl^- \qquad (1)$$

$$I_2Cl_2 \longrightarrow I^+ + ICl_2^- \qquad (2)$$

The interpretation will be the same whether ionization takes place according to Eq. (1) or (2). The iododichloride ion (ICl_2^-) has been ruled out, since the iodinating agent with the iodine in the middle of the structure of (ICl_2^-) has an unfavourable geometry for substitution.[22] Ionization (1) is favoured at high dielectric constants, as has been observed by Bearcraft and Nachtrich.[23]

Alcohols are also polar compounds and it is quite reasonable to predict that alcohols combine with highly reacting species like I^+ ions according to the reaction

$$CH_3OH + I^+ = CH_3OI + H^+ \qquad (3)$$

showing that this is an ion-dipole type of reaction.

If step (1) were the rate determining step of the present reaction, then the rate of the reaction would have increased with the increase of dielectric constant of the medium. In the present case (Table 2), however it was observed that as the dielectric constant decrease, from methanol to butanol, the rate of the reaction

21) Nakanishi, "Infrared absorption spectroscopy practical" Holden day (1962).
22) R. W. C. Wyckoft, *J. Amer. Chem. Soc.*, **42**, 1100 (1920).
23) D. Dearcraft and N. H. Nachtrich, *J. Phys. Chem.*, **71** (13), 400 (1967).

increases. This has also been confirmed from the straight line plot of $\log k$ against $100/D$.

It is also seen that addition of HCl does not change the specific reaction rate constant in these cases. Thus a reaction of the type $ICl+HCl=HICl_2$ is ruled out in this case, or if such a reaction takes place at all, the rate of reaction is extremely slow and indistinguishable kinetically.

The proposed mechanism is thus

$$ICl \xrightarrow{\text{fast}} I^+ + Cl^- \quad (1)$$

$$CH_3OH + I^+ \xrightarrow{\text{slow}} CH_3OI + H^+ \quad (2)$$

Step (2) is the rate determining step of the reaction as step (1) is an ionization process and very fast. A similar mechanism can be given for other alcohols.

The authors are grateful to Prof. E. Pickett, University of Missouri, U.S.A. and Prof. C. R. Kanekar of TIFR, Bombay, India for their kind help in carrying our IR analysis and supplying the pure ICl sample.

BULLETIN OF THE CHEMICAL SOCIETY OF JAPAN, VOL. 46, 821—825 (1973)

Electronic Structures and Spectra of Pyridinyl Hetero Diradicals. Charge-transfer Interaction between Two Different Radicals

Michiya Itoh

Faculty of Pharmaceutical Sciences, The University of Tokyo, Bunkyo-ku, Tokyo

(Received October 14, 1972)

Pyridinyl hetero diradicals, Py(Ac)·$(CH_2)_n$ Py(Car)·, (in which Py(Ac)· and Py(Car)· are 4-$CH_3OCC_5H_4N$· and 4-$CH_3OOCC_5H_4N$·, respectively, and $n=3$, 4, and 5) were obtained. Equilibrium between the open and closed forms in the hetero diradical $n=3$ was directly observed by temperature dependence of absorption spectra ($-\Delta H=5.6$ kcal and $\Delta S=-10.5$ e.u.). Electronic absorption spectroscopy and SCF–CI molecular orbital calculation reveal that the closed form shows a strong charge-transfer band from Py(Car)· to Py(Ac)· moieties. The electronic structure of the hetero diradical was discussed in relation to the electronic interaction between two different radicals.

Molecular complexes between two different free radicals, the hetero radical dimers may be considered to be a special case of the electron-donor-acceptor complex, both components of which are electron excess systems. From the viewpoint of the electronic structure, the hetero radical dimers may be isoelectronic with hetero nuclear diatomic molecule, although the hetero dimer involves no covalent bond between radical moieties.

While numerous investigations of the radical dimers[1-3] have been carried out, only few spectroscopic studies of the electronic interaction between two different radicals have been reported.[4,5] Recently, Yamazaki and Kimura[5,6] have demonstrated the complex formation of tetracene and perylene cation radicals in concentrated sulfuric acid at low temperature, where the cation dimers of each component were also observed.[7] In the previous papers, Itoh and Kosower[8] reported a strong intramolecular interaction of two pyridinyl moieties in the 1,3-dipyridinylpropane, Py(Car)·$(CH_2)_3$Py(Car)·. Subsequently, Itoh[9] demonstrated that the closed form of the pyridinyl cation radical, Py(Car)$^+(CH_2)_3$Py(Car)· was regarded to be the dimer cation which could not be observed in the mixed solution of the pyridinyl and pyridinium salt without tri- or tetramethylenes. On the other hand, importance and efficiency of the trimethylene group for the intramolecular interaction have been also emphasised in the excimer formation,[10,11] energy transfer[12] and fluorescence quenching.[13]

This paper presents a study of a new series of pyridinyl hetero diradicals; CH_3OOC- 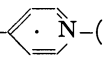 -$(CH_2)_n$- 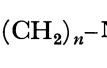 -C-

1) K. H. Hausser and J. N. Murrell, *J. Chem. Phys.*, **27**, 500 (1957).

2) M. Itoh and S. Nagakura, *J. Amer. Chem. Soc.*, **89**, 3959 (1967); *Tetrahedron Lett.*, **1966**, 227.

3) See references in Ref. 2.

4) K. Takemoto, S. Nakayama, and K. Suzuki, This Bulletin, **41**, 1974 (1968).

5) T. Yamazaki and K. Kimura, *ibid.*, **44**, 298 (1971).

6) T. Yamazaki and K. Kimura, *J. Phys. Chem.*, **76**, 1549 (1972). The author is indebted to Professor K. Kimura for showing a copy of the manuscript prior to publication.

7) K. Kimura, T. Yamazaki, and S. Katsumata, *J. Phys. Chem.*, **75**, 1768 (1971).

8) M. Itoh and E. M. Kosower, *J. Amer. Chem. Soc.*, **89**, 3955 (1967); **90**, 1843 (1968).

9) M. Itoh, *ibid.*, **93**, 4750 (1971).

10) F. Hirayama, *J. Chem. Phys.*, **42**, 3163 (1965).

11) E. A. Chandross and C. J. Dempster, *J. Amer. Chem. Soc.*, **92**, 3586 (1970).

12) O. Schnepp and M. Levy, *ibid.*, **84**, 172 (1962).

13) T. G. Scott, R. D. Spencer, N. J. Leonard, and G. Weber, *ibid.*, **92**, 687 (1970).

OCH_3, $n=3$, 4, and 5 which exhibit intramolecular charge-transfer interaction between two different pyridinyl radicals in solution at room temperature. Electronic structure of the closed form of the hetero diradical which is considered to be a hetero radical dimer was calculated by the aid of the SCF-CI method. Spectroscopic and theoretical results for the hetero diradical were compared with those for the diradicals, Py(Car)·$(CH_2)_3$Py(Car)·[8] and Py(Ac)·$(CH_2)_3$Py(Ac)··[14] (abbreviated to Car-3-Car, and Ac-3-Ac, respectively.).

Results and Discussion

Electronic Absorption Spectra. The pyridinyl hetero diradicals (**3** for $n=3$, **4** for 4, and **5** for 5) were prepared by reduction of the corresponding diiodides or bromides in the manner previously described.[8,9] The electronic absorption spectra of the 2-methyltetrahydrofuran (abbreviated to MTHF) solutions of **3**, **4**, and **5** were determined at room temperature (27—28°C), as shown in Fig. 1. While the spectra of **4** and **5** are very much

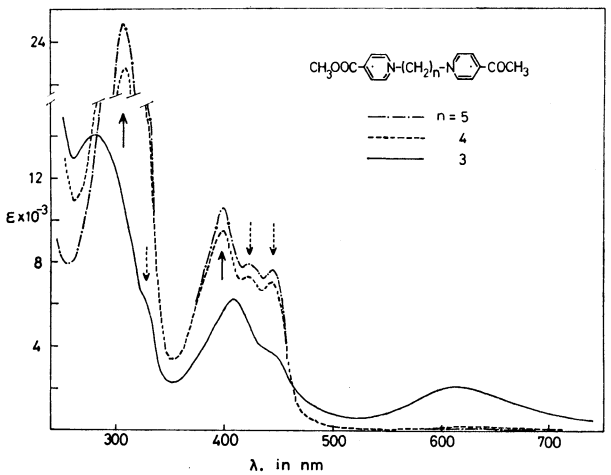

Fig. 1. The absorption spectra of the hetero diradical, **3**, **4**, and **5** in MTHF at room temperature (27—28°C); ←— and ←— show absorption bands due to 4-carbomethoxy- and 4-acetylpyridinyl moieties, respectively.

similar to the sum of the spectra of 1-methyl-4-carbomethoxy-[2,15] and 1-methyl-4-acetylpyridinyls,[15] **3** shows a remarkable absorption band in 600—650 nm region. Concentration independence of the spectrum of **3** at room temperature (1×10^{-3}—5×10^{-5}M) suggests that the spectrum of **3** may be ascribed to an intramolecular interaction. From spectroscopic behavior of **3** in comparison with that of the diradical, Car-3-Car reported in the previous paper, the visible absorption band at 615 nm may be a charge-transfer band between two kinds of pyridinyl moieties. This assignment is supported by the theoretical consideration based on the SCF-CI calculation, as will be mentioned later. Yamazaki and Kimura[6] reported two charge-transfer bands between tetracene and perylene cations at 800—950 nm region. In this paper, theoretical study suggests that a strong charge-transfer band from Py(Car)· to Py(Ac)· moieties and another very weak charge-transfer band in the reverse direction may appear by the electronic interaction between two different pyridinyl radicals. However, only one strong absorption band was observed as mentioned above.

An absorption maximum at 400—420 nm region appears in the MTHF solution of **3**, and a band at 300—340 nm region due to the pyridinyl moiety shifts to the shorter wavelength region compared to **4** and **5**, as shown in Fig. 1. These two absorption bands in the UV region which seem to be due to shifted local excitations decrease in intensity compared with those of the hetero diradicals **4** and **5**. Similar decrease of intensity at UV region was also observed in the diradicals, Car-**3**-Car and Ac-**3**-Ac. Leonard *et al.*[16] demonstrated the hypochromism in the absorption spectra of a series of dinucleotide analogs in which the bases are connected by a trimethylene; B-C_3-B or B-C_3-B′. It seems that the decrease of the intensity in the UV region in the diradicals is attributed to the hypochromism, and/or intensity borrowing by the charge-transfer band.[17]

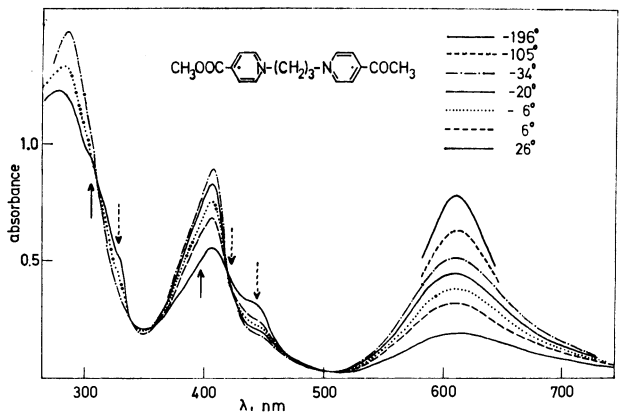

Fig. 2. Temperature dependence of the spectrum of **3** in MTHF. Concentration is 0.85×10^{-4}M: ←— and ←--- show absorption bands due to 4-carbomethoxy- and 4-acetylpyridinyl moieties, respectively. A visible absorption band at −196°C is shown as an extreme case of the equilibrium.

As mentioned in the previous communication,[18] the spectrum of the MTHF solution of **3** shows a remarkable temperature dependence (Fig. 2). The intensities of the 615 and 319 nm bands increased with decreasing temperature, while the absorption due to the each pyridinyl moiety decreased. This temperature dependence of the spectrum was ascribed to an equilibrium of the open and closed forms in **3** (an analog of the monomer dimer equilibrium). The thermodynamic data ($-\Delta H=5.6$ kcal and $\Delta S=-10.5$ e.u.) are compared with those on the complex formation of tetracene and perylene cations ($-\Delta H=7.7$ kcal and $\Delta S=-1.6$ e.u. at 20°C.[6] The complex formation of two different pyridinyls in **3** (the closed form) seems to be more

14) M. Itoh, *Chem. Pharm. Bull.* (Tokyo), **21**, 634 (1973).
15) M. Itoh and S. Nagakura, This Bulletin, **39**, 369 (1966).
16) D. T. Browne, J. Eisinger, and N. J. Leonard, *J. Amer. Chem., Soc.*, **90**, 7302 (1968).
17) Especially, a mixing between the charge-transfer and the local excitation appears in the slided model.
18) M. Itoh, *J. Amer. Chem. Soc.*, **94**, 1034 (1972).

TABLE 1. SPECTROSCOPIC AND CALCULATED DATA OF ELECTRONIC TRANSITIONS IN PYRIDINYL HETERO DIRADICAL **3**

Obsd	Calcd					
ΔE, eV	ΔE, eV	f-value[a]	μ_X[b]	μ_Y	μ_Z	Character[c]
—	1.69	0.01	−0.09	0.02	0.28	0.989(10→11)
2.02 (7800)[d]	1.74	0.85	−0.25	−0.10	−2.34	0.989(10→12)
3.04 (11500)[d]	3.47	0.17	0.07	0.74	−0.08	0.855(10→14) −0.495 (9→11)
4.35 (14000)[d]	4.35	0.95	−0.06	1.57	0.09	0.791 (9→11) 0.441(10→14) 0.343(10→15)

a) Oscillator strength. b) Transition moment, x, y and z are the molecular axes shown in Fig. 3. c) Only configurations whose coefficients in the total wave function exceed 0.3 are shown in the table. d) Molar coefficient of absorption maximum in **3** at 77 K, because the diradical is assumed to be in the purely closed form at the temperature.

efficient than that without any methylene chain of which the open form may be more predominant on the energetic ground. Similar equilibrium between the open and closed forms was observed in the diradical, Ac–**3**–Ac.[14] In the diradical Car–**3**–Car reported in the previous paper, a strong charge-transfer interaction of two moieties seems to make the diradical to be in the closed form, and to prevent direct observation of the equilibrium mentioned above.

Electronic Structure of Pyridinyl Hetero Diradical. In the previous paper,[2] Itoh and Nagakura reported molecular orbital calculation of the pyridinyl radical, and semiquantitatively estimated the transition energy of the charge-transfer band in the pyridinyl dimer. In order to bear out the quantitative discussion on the charge-transfer interaction between two different radicals in the hetero diradical, the SCF–CI calculations were made. Most of the calculations of the radical dimers[7,19,20] and/or dimer radical[21] have been made with the method of "composite molecule", which consists of configuration interaction including the charge-transfer configuration between two SCF MO's of the radical monomers. In this paper, molecular orbitals (closed shell) were considered to be delocalized over two different radicals (open shell).[22]

The standard program for restricted SCF–CI procedures was used in the diradicals as well as in the hetero diradical.[23,24] Interatomic overlap integrals between two pyridinyl moieties were calculated by the aid of the data in Clementi's Table.[25] Both intra- and intermolecular electron-electron repulsions were approximated by the Nishimoto-Mataga formula. The calculated results of the electronic transitions in the hetero diradical are summarized in Table 1, in comparison with the spectral data of **3**, where the molecular

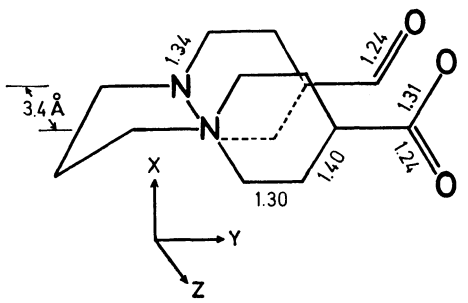

Fig. 3. Molecular geometry of the hetero diradical, **3** assumed in the calculation. A molecular model says that two pyridinyls are non-parallel in the spacing of ~3.4 Å.[2,14]

geometry was assumed to be a sandwich structure as shown in Fig. 3. Several other sandwich structures such as a twisted model[26] and a slided model along x axis were assumed for calculation. However, the results suggested that the structure shown in Fig. 3 was the most reasonable both in their transition energies and intensities. For the sake of simplicity, the results calculated based on the structure shown in Fig. 3 are discussed in this paper. The transition energies show fairly good agreement with the spectral data of the hetero diradical **3**, although no parameterization in SCF–CI calculation was made for adjusting the theoretical results to the spectral data. Similar molecular orbital calculations were done for the diradicals, Car–**3**–Car and Ac–**3**–Ac. These calculated results are shown in Fig. 4, together with the absorption spectra.

Comparison of both theoretical and spectral results in the hetero diradical with those in two diradicals, Ac–**3**–Ac and Car–**3**–Car, suggests that the electronic interaction between two different radicals seems to be rather similar to that in the same radical species. This argument may be justified by the following consideration from the results in SCF–CI calculation of the pyridinyl mono radicals, Py(Ac)· and Py(Car)·, which are components of the hetero diradical. Figure 5 demonstrates the energy levels of two pyridinyls and the hetero diradical. Energy difference of half-occupied

19) J. Tanaka and M. Mizuno, This Bulletin, **42**, 1841 (1969).
20) K. Kimura and N. Mataga, *J. Chem. Phys.*, **51**, 4167 (1969).
21) A. Ishitani and S. Nagakura, *Mol. Phys.*, **12**, 1 (1967).
22) T. Shida and S. Iwata, *J. Chem. Phys.*, **56**, 2858 (1972).
23) H. C. Longuet-Higgins and J. A. Pople, *Proc. Phys. Soc. Sec. A*, **68**, 591 (1955).
24) The computer program of the SCF-CI calculation used here was developed by Dr. S. Iwata.
25) E. Cleminti, *Tables of Atomic Functions* (IBM Co, San Jose, Calif., 1965).
26) Two pyridinyls were twisted in the molecular planes by 10—20° around a z-axis through a center of pyridinyl ring. M. Itoh, *Chem. Phys. Lett.*, **2**, 371 (1968).

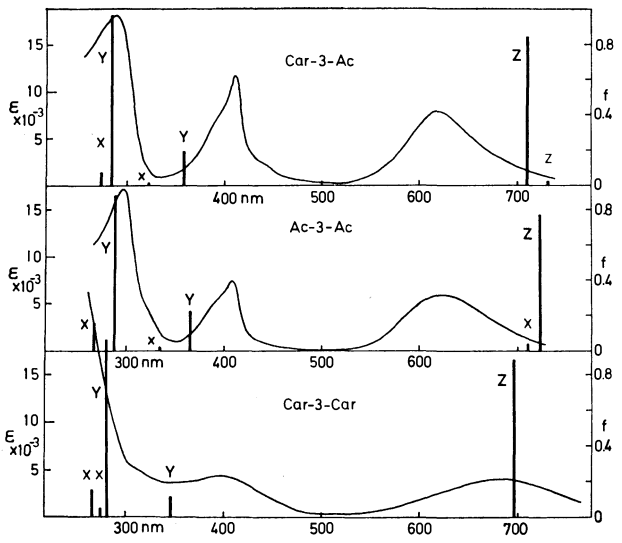

Fig. 4. Electronic absorption spectra of the MTHF solutions of **3** (at 77 K), Ac–**3**–Ac (at 77 K), and Car–**3**–Car (at room temperature), respectively. The sticks represent the calculated transition energies and osscillator strengths.

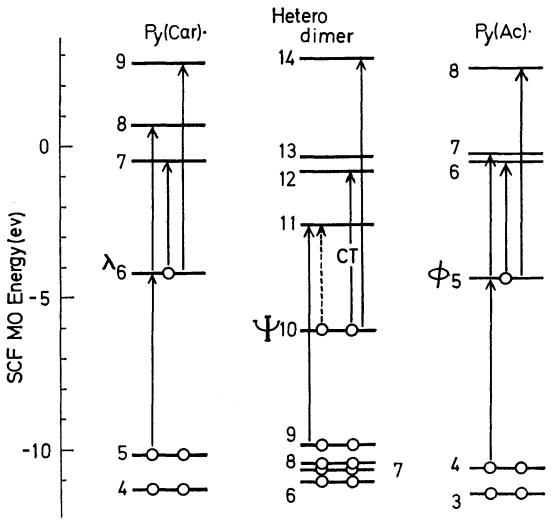

Fig. 5. Energy levels of molecular orbitals in the pyridinyl mono radicals and hetero diradical, respectively. In Py(Car)·, (6→7) is corresponding to ~640 nm (ε:<100) band, (5→6) and (6→7) are ~390 nm (4500), and (6→8) and (6→9) are 295 nm (11000), respectively. Electronic transitions in Py(Ac)• are very much similar to those in Py(Car)•.

molecular orbitals in two pyridinyls (ϕ_5 and λ_6) is unexpectedly only 0.185 eV. In the complex of tetracene$^+$–perylene$^+$ system, the energy difference of two half-occupied MO's was also very small. The half-occupied MO's in both radical components in the diradical (radical dimer) are degenerate, and only one charge-transfer band in the dimer is an allowed transition, which is from the ground state to the antisymmetric combination in the following equations;[1)]

$$\frac{1}{\sqrt{2}}[\Psi(R_1^+, R_2^-) \pm \Psi(R_1^-, R_2^+)]$$

where (R_1^-, R_2^+) is the charge-transfer configuration in the radical pair. Yamazaki and Kimura[6)] estimated two charge-transfer energies in the complex mentioned above from the following conventional equations; $I_I - A_P + C_{TP} = CT_1$ and $I_P - A_T + C_{PT} = CT_2$, where I and A are the ionization potential and electron affinity of the cations, respectively, and C is electrostatic force. However, they did not mention about the intensity of the charge-transfer bands. In this paper, theoretical results which was calculated by assuming electron delocalization over radical moieties show a strong charge-transfer transition from Py(Car)· to Py(Ac)· moieties, and another very weak charge-transfer in the reverse direction. These electronic transitions (energy, f-value and transition moment) and electronic configurations are summarized in Table 1. Then, the strong charge-transfer band observed at 615 nm in the hetero diradical **3** can be ascribed to transition, $\Psi_{10} \rightarrow \Psi_{12}$, of which MO's are shown in Fig. 6. Figure 6 clearly demonstrates a strong charge-transfer mentioned above, while $\Psi_{10} \rightarrow \Psi_{11}$ has a very small f-value with the reverse direction compared with that of $\Psi_{10} \rightarrow \Psi_{12}$.

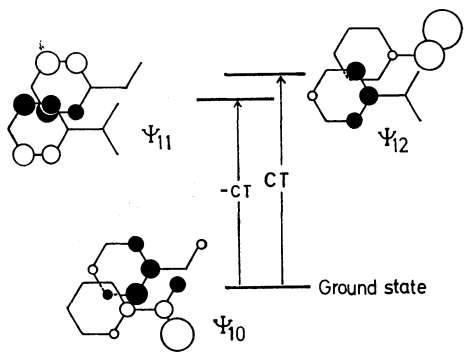

Fig. 6. Highest occupied orbitals of the ground (Ψ_{10}) and two charge-transfer states (Ψ_{11} and Ψ_{12}).

On the other hand, the electron transfer reaction from 1-methyl-4-carbomethoxypyridinyl to 1-methyl-4-acetylpyridinium occurred by adding the latter to an acetonitrile solution of the former. This suggests that Py(Ac)· may be an electron acceptor in the hetero diradical. The argument is successfully consistent with the direction of the charge-transfer mentioned above. Furthermore, total electron density on the each pyridinyl moiety in the diradical **3** demonstrates ~5% charge-transfer structure in the ground state;

$$\text{Py(Car)}^+ - \text{Py(Ac)}^- \sim 5\%$$
$$\text{Py(Car)}\cdot - \text{Py(Ac)}\cdot \sim 95\%.$$

If two different radical species (R_1 and R_2) of which the energy levels of each half-occupied MO are sufficiently different from each other, a complete electron transfer in this radical pair would occur to produce an ion pair (R_1^+,R_2^-) in the ground state. Conclusively, it seems that only two radical species where the half-occupied MO's are nearly degenerate have a possibility to make the molecular complex between them. In this molecular complex, *i.e.*, the hetero radical dimer with a conceivable conformational structure, a strong charge-transfer band and another very weak transition (nearly forbidden) in the reverse direction might be observed in the visible or near IR region.

Experimental

Materials. Three α-(4-carbomethoxypyridinium)-ω-(4-acetylpyridinium) alkane diiodides were prepared from 4-carbomethoxy- and 4-acetylpyridines, and three corresponding alkyl diiodides or bromides. 1-(4-Carbomethoxypyridinium)-3-(4-acetylpyridinium)propane dibromide, mp 150—151°C. Found: C, 43.94; H, 4.77; N, 5.88%. Calcd for $C_{17}H_{20}O_3N_2Br_2$: C, 44.34; H, 4.34; N, 6.08%. 1-(4-Carbomethoxypyridinium)-4-(4-acetylpyridinium)butane diiodide, mp 203°C. Found: C, 38.03; H, 4.00; N, 4.48%. Calcd for $C_{18}H_{22}O_3N_2I_2$: C, 38.05; H, 3.88; N, 4.93%. Non-crystalline products of 1-(4-carbomethoxypyridinium)-5-(4-acetylpyridinium)pentane diiodide and dibromide were used. The structure and purity were checked by IR, UV, and NMR spectroscopies. Purification of the solvents was mentioned in the previous papers.

Preparation of Hetero Diradicals. α,ω-Dipyridinium diiodides (~0.02 g) and 3% sodium amalgam (~0.2 g) were sealed into the reaction tube. After evacuating to 10^{-5} Torr, degassed acetonitrile (~7 ml) was introduced by using a vacuum line. The reaction tube was shaken several times for about 3—5 hr at room temperature. The solvent was removed by using a vacuum line, and the diradical was extracted with MTHF (~10 ml).

Measurements. Electronic absorption spectra were determined with a Cary Model 11 recording spectrophotometer. A quartz dewar with windows was used for low-temperature spectra. ESR measurements were made with JEOLCO P-10 ESR spectrometer with 100 kHz modulation. Determinations of concentration of the diradical and of relative spin concentration were done using the same procedures as described in the previous papers.

The author expresses his sincere thanks to Professor S. Nagakura for permission to use the computer center of the Institute of Physical and Chemical Research, and for reading the manuscript. The author is indebted to Dr. S. Iwata for supplying the computer program.

BULLETIN OF THE CHEMICAL SOCIETY OF JAPAN, VOL. 46, 825—829 (1973)

Spin Trapping by Use of Nitroso-Compounds. VII.[1] β-Fluorine Splitting Constants in Nitroxides

Shigeru TERABE and Ryusei KONAKA

Shionogi Research Laboratory, Shionogi & Co., Ltd. Fukushima-ku, Osaka, 553

(Received November 1, 1972)

Hyperfine splitting constants of β-fluorine atoms in aryl perfluoroalkyl nitroxides, $ArN(R_f)O\cdot$, where Ar= 2,4,6-tri-*t*-butylphenyl, phenyl, pentafluorophenyl, and 2,3,5,6-tetramethylphenyl and R_f=trifluoromethyl, pentafluoroethyl, and heptafluoroisopropyl were explored. The temperature dependence of hyperfine splitting constants was studied in the cases of 2,4,6-tri-*t*-butylphenyl and pentafluorophenyl nitroxides. In the former nitroxides the conformation of β-fluorine atoms are rigid and dihedral angles between the C_β–F bonds and p_z orbitals are 30 and 0° when perfluoroalkyl groups are ethyl and isopropyl, respectively. The conformational dependence of β-fluorine splitting constants are discussed, and it is concluded that the $\cos^2\theta$ law, $a_\beta^F=(B_0+B\cos^2\theta)\rho^\pi$, is also applicable to β-fluorine splitting constants in a series of nitroxides. The values of B_0 and B seem significantly dependent on the compound.

The conformational dependence and the origin of β-hydrogen splitting constants have been well established.[2,3] However, several different proposals[4-13] have recently been advanced concerning those of the β-fluorine atom. It is desirable for the elucidation of the dependence of β-fluorine splitting constants on conformation to investigate the ESR spectra of radicals having β-fluorine atoms in known conformations. Such radicals may include those in single crystals and rigid cyclic radicals. A few studies[9,13-16] along these lines have been reported, although in most of these cases the assumed conformations of the alkyl group containing the β-fluorine atoms have not always been unequivocal.

We have previously found during the spin trapping study[17] of 2,4,6-tri-*t*-butylnitrosobenzene that the ethyl and isopropyl groups in these adducts have substantially rigid conformations wherein the dihedral angles between

1) Part VI, S. Terabe, K. Kuruma, and R. Konaka, *J. C. S. Perkin II*, in press.

2) C. Heller and H. M. McConnell, *J. Chem. Phys.*, **32**, 1535 (1960).

3) D. H. Geske, *Progr. Phys. Org. Chem.*, **4**, 125 (1967).

4) See, *e.g.*, D. Holtz, *ibid.*, **8**, 1 (1971) and references cited therein.

5) E. T. Strom and A. L. Bluhm, *Chem. Commun.*, **1966**, 115.

6) W. R. Knolle and J. R. Bolton, *J. Amer. Chem. Soc.*, **93**, 3337 (1971) and references cited therein.

7) J. L. Gerlock, E. G. Janzen, and J. K. Ruff, *ibid.*, **92**, 2037 (1970) and references cited therein.

8) K. Morokuma, *ibid.*, **91**, 5412 (1969).

9) D. Kosman and L. M. Stock, *ibid.*, **92**, 409 (1970).

10) K. J. Klabunde, *ibid.*, **92**, 2427 (1970).

11) G. R. Underwood, V. L. Vogel, and I. Krefting, *ibid.*, **92**, 5019 (1970).

12) M. Iwasaki, *ibid.*, **92**, 6348 (1970); *Mol. Phys.*, **20**, 503 (1971).

13) C. Chachaty and M. Shiotani, *J. Chim. Phys.*, **68**, 300 (1971) and references cited therein.

14) M. T. Rogers and D. H. Whiffen, *J. Chem. Phys.*, **40**, 2662 (1964); L. D. Kispert and M. T. Rogers, *ibid.*, **54**, 3326 (1971).

15) R. J. Rontz, *ibid.*, **45**, 1339 (1966).

16) J. L. Gerlock and E. G. Janzen, *J. Phys. Chem.*, **72**, 1832 (1968).

17) S. Terabe and R. Konaka, *J. C. S. Perkin II*, in press; *J. Amer. Chem. Soc.*, **93**, 4306 (1971).

the C_β–H bonds and p_z orbitals containing the odd electron on the nitrogen atom are 30 and 0°, respectively. These conformational situations would be expected to remain unchanged if the *N*-alkyl groups are replaced by perfluoroalkyl groups. Hence perfluoroalkyl 2,4,6-tri-*t*-butylphenyl nitroxides were chosen to elucidate the dependence of β-fluorine splitting constants on conformation and a few other substituted phenyl perfluoroalkyl nitroxides were also prepared and studied for comparison.

Results

Substituted phenyl perfluoroalkyl nitroxides were produced by the photolysis of perfluoroalkyl iodides in the presence of substituted nitrosobenzenes.[10]

$$R_fI + ArNO \xrightarrow{h\nu} Ar\text{–}N(O\cdot)\text{–}R_f$$

I Ar: 2,4,6-$Bu^t_3C_6H_2$
II Ar: C_6H_5
III Ar: C_6F_5
IV Ar: 2,3,5,6-$(CH_3)_4C_6H$

R_f: a) CF_3 b) CF_2CF_3 c) $CF(CF_3)_2$

TABLE 1. ESR TEMPERATURE STUDY OF 2,4,6-TRI-*t*-BUTYLPHENYL PERFLUOROALKYL NITROXIDES IN *n*-HEXANE

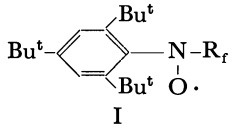

I

R_f	Temp. °C	*g* Value	Hyperfine splitting constants (G) $\lvert a^N\rvert$	$\lvert a_\beta^F\rvert$	$\lvert a_\gamma^F\rvert$	$\lvert a_m^H\rvert$
CF_3 (Ia)	60		9.44	9.44	—	0.70
	25	2.0066	9.44	9.44	—	0.70
	0		9.41	9.41	—	0.70
	−30		9.37	9.37	—	0.72
	−60		9.30	9.30	—	0.73
	−90		9.22	9.22	—	0.71
CF_2CF_3 (Ib)	60		9.64	27.02	0.68	0.68
	25	2.0065	9.63	27.21	0.69	0.69
	0		9.55	27.51	0.70	0.70
	−30		9.51	27.82	0.75	0.75
	−60		9.42	28.14	a)	a)
	−90		9.37	28.31	a)	a)
$CF(CF_3)_2$ (Ic)	25	2.0066	9.73	48.4	a)	a)

a) Hyperfine splittings were not resolved because of line broadening.

g Values and the temperature dependence of hyperfine splitting constants of the nitroxides Ia, Ib, and Ic are shown in Table 1. The photolysis of 2-iodoheptafluoropropane in the presence of 2,4,6-tri-*t*-butylnitrosobenzene produced *N*-perfluoroisopropoxy-2,4,6-tri-*t*-butylanilino radical (VI) as the major product

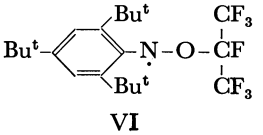

VI

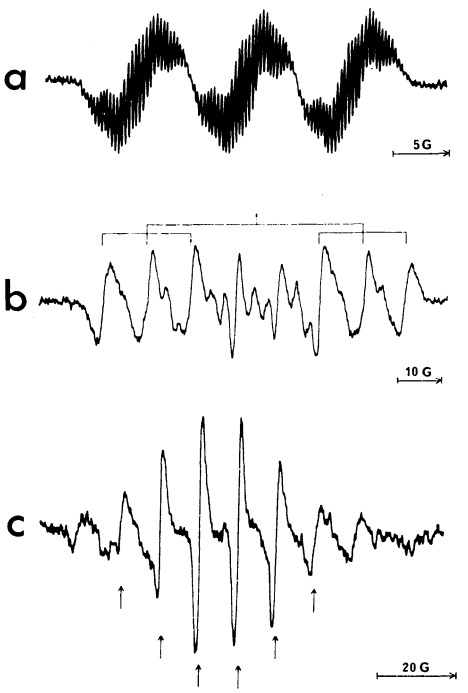

Fig. 1. ESR spectra obtained by the photolysis of 2-iodoheptafluoropropane in the presence of 2,4,6-tri-*t*-butylnitrosobenzene in *n*-hexane at 25°C. Intensities of these three spectra dose not show their relative concentrations because gains of the spectrometer were not equal in each measurement. In b and c, couplings of *meta*-hydrogens and γ-fluorines were not observed because of a high modulation amplitude.
a) Spectrum of *N*-heptafluoroisopropoxy-2,4,6-tri-*t*-butylanilino radical (VI).
b) Six lines indicated by the stick diagram demonstrate the absorption lines by 2,4,6-tri-*t*-butylphenyl heptafluoroisopropyl nitroxide (Ic). See text also.
c) Six lines indicated by arrows correspond to the absorption lines due to 2,4,6-tri-*t*-butylphenyl trifluoromethyl nitroxide (Ia). See text also.

whose spectra (g=2.0034) consisted of a triplet (a^N= 9.36 G) of multiplets having 0.30 G spacings (Fig. 1a) and the nitroxide Ic as minor ones together with other unknown radicals whose spectra could not be analyzed because of the superposition of the complex and strong spectrum of VI. However, since the anilino radical VI was less stable than the nitroxide Ic the former VI disappeared completely on standing in solution for a day and permitted the ESR spectra of minor radicals to be obtained (Fig. 1b), and it was inferred that at least three radicals existed in the solution. The main six lines shown in Fig. 1b are considered to be due to the nitroxide Ic because *g* value and the nitrogen splitting constant are very similar to those of Ia and Ib. Further standing of the solution for a total of three days gave the spectrum shown in Fig. 1c which

TABLE 2. HYPERFINE SPLITTING CONSTANTS (G) AND *g* VALUES OF PHENYL PERFLUOROALKYL NITROXIDES IN BENZENE AT 25°C

R_f in PhN(R_f)O·	*g* Value	$\lvert a^N\rvert$	$\lvert a_\beta^F\rvert$	$\lvert a_\gamma^F\rvert$	$\lvert a_{o,p}^H\rvert$	$\lvert a_m^H\rvert$
CF_3 (IIa)	2.0060	9.68	10.60	—	1.96	0.78
CF_2CF_3 (IIb)	2.0062	9.63	17.29	0.66	1.90	0.66
$CF(CF_3)_2$ (IIc)	2.0062	10.93	4.95	1.81	1.81	0.83

Table 3. ESR temperature study of pentafluorophenyl perfluoroalkyl nitroxides in perfluoro(methylcyclohexane)

R_f in $C_6F_5N(R_f)O\cdot$	Temp. °C	g Value	Hyperfine splitting constants (G)				
			$\|a^N\|$	$\|a_\beta^F\|$	$\|a_\gamma^F\|$	$\|a_{o,p}^F\|$	$\|a_m^F\|$
CF_3 (IIIa)	40		9.41	7.78	—	a)	a)
	25	2.0068	9.52	7.75	—	0.96	0.30
	0		9.48	7.68	—	0.96	0.29
	−30		9.45	7.62	—	0.98	0.30
CF_2CF_3 (IIIb)	40		9.38	11.59	1.56	0.94	0.31
	25	2.0069	9.32	11.54	1.60	0.95	0.32
	0		9.30	11.39	1.63	0.97	0.32
	−30		9.16	11.29	1.72	1.00	0.33
$CF(CF_3)_2$ (IIIc)	40		10.10	4.71	1.67	1.03	0.32
	25	2.0068	10.09	4.53	1.64	1.01	0.32
	0		10.08	4.32	1.65	1.02	0.32
	−30		10.08	4.04	1.68	1.02	0.32

a) The nitroxide IIIa was unstable at this temperature, and small hyperfine splitting constants could not be determined.

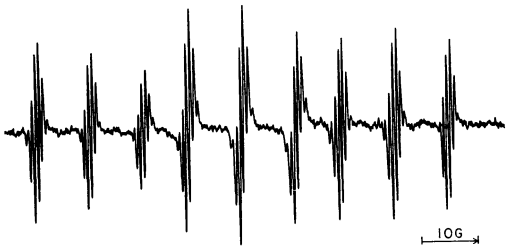

Fig. 2. ESR spectrum of 2,4,6-tri-*t*-butylphenyl pentafluoroethyl nitroxide (Ib) in *n*-hexane at 25°C.

indicated that trifluoromethyl nitroxide Ia was the major radical and Ic was the minor one. This result implies that a minor radical observed in Fig. 1b is Ia. The concentration of Ic was too low to observe *meta*-hydrogen and γ-fluorine splittings and to study the temperature dependence of β-fluorine splitting.

The ESR spectrum of the pentafluoroethyl nitroxide Ib is shown in Fig. 2. The rather low peak heights of the three central multiplets suggest that the two β-fluorine atoms are not completely equivalent, but they could not be distinguished within this experiment.

Spectral data at room temperature (25°C) of the nitroxides IIa, IIb, and IIc and those of the nitroxides IVa, IVb, and IVc are given in Tables 2 and 4, respectively. The temperature study of the nitroxides IIIa, IIIb, and IIIc and that of the 2,4,6-tri-*t*-butylphenyl alkyl nitroxides (V)[17] are summarized in Tables 3 and 5. The latter study was undertaken for the confirmation of the expected conformation of *N*-alkyl groups.

Table 4. Hyperfine splitting constants (G) and g values of 2,3,5,6-tetramethylphenyl perfluoroalkyl nitroxides in benzene at 25°C

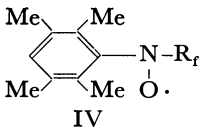

IV

R_f	g Value	$\|a^N\|$	$\|a_\beta^F\|$	$\|a_\gamma^F\|$
CF_3 (IVa)	2.0066	10.15	9.38	—
CF_2CF_3 (IVb)	2.0067	10.31	17.64	0.95
$CF(CF_3)_2$ (IVc)	2.0066	11.10	13.27	1.55

Table 5. ESR temperature study of 2,4,6-tri-*t*-butylphenyl alkyl nitroxides in *n*-hexane

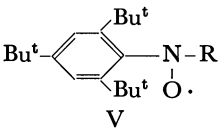

V

R	Temp. °C	g Value	Hyperfine splitting constants (G)			
			$\|a^N\|$	$\|a_\beta^H\|$	$\|a_\gamma^H\|$	$\|a_m^H\|$
CH_3 (Va)	90		12.82	11.97	—	0.81
	65		12.81	12.01	—	0.81
	25	2.0061	12.78	12.04	—	0.78
	0		12.80	12.17	—	0.80
	−30		12.70	12.27	—	0.82
	−60		12.62	12.38	—	0.81
	−90		12.58	12.58	—	0.81
CH_2CH_3 (Vb)	90		13.34	17.03	a)	0.83
	65		13.30	17.22	a)	0.83
	25	2.0061	13.26	17.58	a)	0.81
	0		13.25	17.84	a)	0.80
	−30		13.20	18.11	a)	0.79
	−60		13.22	18.53	a)	0.82
	−90		13.17	18.88	a)	0.77
$CH(CH_3)_2$(Vc)	90		13.24	21.04	0.36	0.72
	65		13.16	21.33	0.38	0.75
	25	2.0061	13.07	21.68	0.38	0.76
	0		13.03	22.11	0.37	0.73
	−30		13.02	22.26	0.39	0.79
	−60		13.01	22.52	a)	b)

a) No splitting observed for γ-protons.
b) *meta*-Hydrogen splittings were not resolved because of line broadening.

The ESR spectrum of IIIb is shown in Fig. 3. Some other substituted phenyl perfluoroalkyl nitroxides have been described previously.[1]

Discussion

2,4,6-Tri-t-buthylphenyl Perfluoroalkyl Nitroxides. The nitrogen splitting constant of each 2,4,6-tri-*t*-butylphenyl alkyl nitroxide increases with increase in tem-

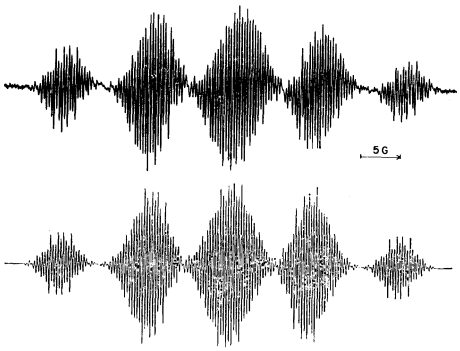

Fig. 3. ESR spectrum of pentafluorophenyl pentafluoroethyl nitroxide (IIIb) in perfluoro(methylcyclohexane) at 25°C. The upper spectrum is experimental and the lower is a simulation based on the splitting constants given in Table 3 and Lorentzian line shapes.

perature as shown in Table 5, and this observation is expected from the results of MO calculations[18] which have shown that the nitrogen splitting constant increases with the torsion of the nitroxide group. The decrease in the β-hydrogen splitting constant of the methyl nitroxide Va with temperature is also consistent with MO calculations[18] which have predicted that the β-hydrogen hyperfine splittings for free rotating hydrogens decrease as the out-of-plane torsion angle of the N–O bond increases. Slightly larger variations of β-hydrogen splitting constants in the nitroxides Vb and Vc with temperature than that in the nitroxide Va would mainly be attributable to the conformational changes of β-hydrogens.

The β-hydrogen splitting constants have been well known to obey the $\cos^2\theta$ law,[2,3,19]

$$a_\beta^{\mathrm{H}} = (B_0 + B\cos^2\theta)\rho^\pi \qquad (1)$$

where B_0 and B are constants, θ is the dihedral angle between the C_β–H bond and the p_z orbital containing an odd electron, and ρ^π is the π electron spin density. The value of B_0 is known to be small and is regarded to be zero in this consideration, and ρ^π is assumed to be constant among the nitroxides Va, Vb, and Vc, although the three nitroxides have slightly different values for nitrogen splitting constants. Then, Eq. (1) becomes

$$a_\beta^{\mathrm{H}} = B\cos^2\theta\rho^\pi_{\mathrm{N}} \qquad (2)$$

The methyl group on the nitrogen in Va is considered as freely rotating which leads to $\cos^2\theta = 1/2$. Taking $a_\beta^{\mathrm{H}} = 12.83$ G for Va at −60°C Eq. (2) gives $B\rho^\pi_{\mathrm{N}} = 24.76$ G. On substituting this value in turn into Eq. (2), dihedral angles at −60°C for Vb and Vc are found to be 30 and 17°, respectively. Examination of molecular models of Vb and Vc has predicted the angles are 30 and 0°, respectively, as described previously.[17] These values are in fair agreement with those obtained above. Although the value (17°) obtained by the above considerations for Vc seems large as compared with the predicted one from a molecular model, the difference between the magnitude of β-hydrogen splitting constants is only 1.4 G.

It will be reasonable to assume that the perfluoroalkyl groups in 2,4,6-tri-*t*-butylphenyl perfluoroalkyl nitroxides have the same conformations as the alkyl groups in 2,4,6-tri-*t*-butylphenyl alkyl nitroxides. A molecular model of the heptafluoroisopropyl nitroxide Ic indicates that steric repulsion between two *t*-butyl groups at the *ortho* positions and two trifluoromethyl groups in the heptafluoroisopropyl group is very large. This is probably the reason why the concentration of the nitroxide Ic formed was very low as mentioned above. The temperature effect on nitrogen splitting constants in the nitroxides Ia and Ib was similar to that in the corresponding alkyl nitroxides Va, Vb, and Vc in the direction and magnitude of variations. Changes of β-fluorine splitting constants with temperature were less than those of β-hydrogen splitting constants in the corresponding alkyl nitroxides.

The applicability of the $\cos^2\theta$ law (Eq. (3)) to the

$$a_\beta^{\mathrm{F}} = (B_0 + B\cos^2\theta)\rho^\pi_{\mathrm{N}} \qquad (3)$$

β-fluorine splitting constant is evaluated on the nitroxides shown in Table 1. Spin densities on nitrogens are assumed to be constant among the three nitroxides, although, in fact, nitrogen splitting constants differ slightly. We can take the values $a_\beta^{\mathrm{F}} = 9.44$ G (25°C) and $\cos^2\theta = 1/2$ for the nitroxide Ia, and $a_\beta^{\mathrm{F}} = 48.4$ G and $\theta = 0°$ for the nitroxide Ic. Hence, Eq. (3) gives $B_0\rho^\pi_{\mathrm{N}} = -29.52$ G and $B\rho^\pi_{\mathrm{N}} = 77.92$ G. On substituting these values and $\theta = 30°$ into Eq. (3), the β-fluorine splitting constant for Ib is found to be 28.92 G, which is close to the observed value (27.21 G). The assumed dihedral angle (0°) for Ic is chosen for convenience, but it must be near to zero-degrees. A change of even 10° does not affect the results seriously. The results obtained reveal that the Eq. (3) can relate β-fluorine splitting constants to dihedral angles at least in the series of nitroxides shown in Table 1. If we assume arbitrarily $\rho^\pi_{\mathrm{N}} = 0.30$, B_0 and B are found to be −98 G and 260 G, respectively. The negative value of B_0 is unequivocal so long as the β-fluorine splitting constant is taken to be positive. The negative value of B_0 has also been deduced by INDO calculations.[11] Large β-fluorine splitting constants have also been found in some other nitroxides where the dihedral angles are assumed to be small by Janzen and co-workers.[20,21]

Phenyl Perfluoroalkyl Nitroxides. Free rotation about the C_β–N bond is possible in the nitroxides shown in Table 2, so that the conformation of the β-fluorine atom is not definite. β-Hydrogen splitting constants decrease in the order methyl>ethyl>isopropyl in phenyl alkyl nitroxides.[19,22] This observation implies that the average dihedral angle θ increases reversely in that order. The conformational analogy between phenyl alkyl nitroxides and *t*-butyl alkyl nitroxides has been known.[19,22] In *t*-butyl perfluoroalkyl nitroxides, however, the conformational preference has been inferred to be somewhat different.[10,11] Trifluoromethyl and heptafluoroisopropyl groups are considered

18) J. Duady, Y. Ellinger, A. Rassat, R. Subra, and G. Berthier, *Mol. Phys.*, **17**, 217 (1969).
19) G. Chaplet-Letourneux, H. Lemaire, R. Lenk, M.-A. Maréchal, and A. Rassat, *Bull. Soc. Chim. Fr.*, **1968**, 3963.
20) E. G. Janzen, *Accounts Chem. Res.*, **4**, 31 (1971).
21) E. G. Janzen, private communication.
22) E. G. Janzen, *Topics Stereochem.*, **6**, 177 (1971).

to have similar conformational preference to the corresponding alkyl groups in *t*-butyl nitroxide, but pentafluoroethyl group is assumed to lie in the averaged dihedral angle less than 45°.[10,11]

The conformational analogy between *t*-butyl perfluoroalkyl nitroxides and phenyl perfluoroalkyl nitroxides should be valid. We assume averaged dihedral angles of β-fluorine atoms in the nitroxides IIa, IIb, and IIc to be 45, 35, and 80°, respectively, though the choice of the latter two values is rather arbitrary. Spin densities on nitrogens are assumed constant among IIa, IIb, and IIc. Substitution of β-fluorine splitting constants and dihedral angles for IIa and IIc into Eq. (3) gives $B_0\rho^{\pi}_N=-5.95$ G and $B\rho^{\pi}_N=33.10$ G. These values and $\theta=35°$ are in turn substituted into Eq. (3) to give the β-fluorine splitting constant of 16.26 G, which is fairly close to the observed value for IIb. By taking ρ^{π}_N as 0.30, B_0 and B are found to be −25 and 110 G, respectively. In the above consideration the β-fluorine splitting constant of IIc is assumed to be negative. If we assume it to be positive, we cannot relate the observed results through Eq. (3). Evidently it is possible to apply Eq. (3) to phenyl perfluoroalkyl nitroxides, although the interpretation is not unequivocal.

Pentafluorophenyl Perfluoroalkyl Nitroxides. The temperature dependence of the hyperfine splitting constants shown in Table 3 is small. It will be reasonable to expect that preferred conformations of these nitroxides are similar to those of phenyl perfluoroalkyl nitroxides. Average dihedral angles of IIIa, IIIb, and IIIc are assumed to be the same as in the corresponding phenyl perfluoroalkyl nitroxides. The same treatment utilizing hyperfine splitting constants at −30°C as mentioned above gives $B_0\rho^{\pi}_N=-4.79$ G and $B\rho^{\pi}_N=24.82$ G, thus $a_\beta^F=11.86$ G for $\theta=35°$. The calculated value is close to observed value for IIIb. B_0 and B are found to be −19 and 100 G, respectively, if $\rho^{\pi}_N=0.25$. The β-fluorine splitting constant of IIIc is assumed similarly to be negative.

2,3,5,6-Tetramethylphenyl Perfluoroalkyl Nitroxides. β-Hydrogen splitting constants of corresponding methyl, ethyl, and isopropyl nitroxides are 12.17, 10.97, and 6.92 G, respectively.[1] These values are similar in tendency to phenyl alkyl nitroxides but the magnitude of differences is not large. It is difficult to deduce suitable average dihedral angles for 2,3,5,6-tetramethylphenyl perfluoroalkyl nitroxides because the steric effect of two *ortho*-methyl groups on *N*-substituents is very subtle,[1] so that the validity of Eq. (3) cannot be tested

Conclusion

The conformations of β-fluorine atoms in Ib and Ic are rigid, and related to β-fluorine splitting constants through Eq. (3), where a negative value of B_0 is essential. For phenyl and pentafluorophenyl perfluoroalkyl nitroxides the application of Eq. (3) is possible although some ambiguity exists. Three series of perfluoroalkyl nitroxides studied give different values of B_0 and B. The validity of Eq. (3) is also confirmed concerning *t*-butyl perfluoroalkyl nitroxides[10,11] though the agreement between the calculated and observed values is not so good as in examples described above. The dihedral angle of 90° in perfluoro-2-azopropane radical anion[7] which shows very large β-fluorine splitting constant seems questionable because second order splittings will possibly be observed even at $\theta=0°$.[23] If this interpretation is correct β-fluorine splitting constants in perfluoroazoalkane radical anions can be successfully related to dihedral angles through Eq. (3) to give $B_0\rho^{\pi}_N=-26.93$ G and $B\rho^{\pi}_N=88.38$ G.

The results concerning B are consistent with SCF-MO calculations by Morokuma[8] which show that B depends on the particular molecule but that B_0 is near zero. Chachaty and co-workers[13] have proposed the values of B_0 and B to be ~-20 and −80 G, respectively for some perfluoroalkyl radicals. The meaning of B_0 is obscure at present.

Experimental

Trifluoromethyl iodide, pentafluoroethyl iodide, and heptafluoroisopropyl iodide were purchased from PCR, Incorp., and used without further purifications. Preparation of nitroso-compounds have been described previously.[1,17] For the preparation of perfluoroalkyl nitroxides,[10] 0.005—0.01 M deoxygenated solution of a nitroso-compound containing a suitable amount of a perfluoroalkyl iodide was irradiated by the light from a high pressure mercury lamp in the cavity of a spectrometer until an appropriate concentration of the nitroxide was attained. All spectra were recorded on a Varian V-4502-15 X-band spectrometer with 100 kHz magnetic field modulation. Temperature study was achieved with a Varian V-4557 variable temperature accessory in a 3 mm o.d. quartz cell, and temperature was calibrated by a thermometer. Hyperfine splitting constants and *g* values listed in Tables are the average values of at least three measurements. Measurements of magnetic field and microwave frequency, and ESR simulation have been given previously.[24]

The authors are grateful to Professor E. G. Janzen and Dr. K. Nishikida for helpful discussions and to Mr. S. Sakata for his assistance in the ESR experiments.

23) Dr. K. Nishikida suggested that two β-fluorine atoms will be almost completely equivalent in the conformation shown below,

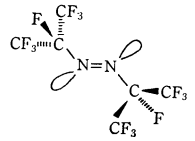

where perfluoro-2-azopropane radical anion shows possibly second order splittings.

24) S. Terabe and R. Konaka, *J. C. S. Perkin II*, **1972**, 2163.

Effect of Halogens on the Ionization of Alkali Metals in the Hydrogen Flame Ionization Detector for Ultra-Micro Analysis of Alkali and Alkaline Earth Metals

Masaaki YAMADA, Shigetaka SUZUKI, and Shun ARAKI

Department of Industrial Chemistry, Faculty of Engineering, Tokyo Metropolitan University, Setagaya-ku, Tokyo

(Received March 21, 1972)

Quantitative treatment of alkali metals in a small hydrogen flame in the presence or absence of halogens was studied. The proportionality of the ion current to the concentration of alkali metals was found to depend on the applied potential of the electrodes. On adding halogens, the concentration of free neutral alkali atoms decreased. Addition of bromine and iodine increased the ionization of alkali metals, while fluorine decreased it slightly. Addition of chlorine increased or decreased the ionization. The thermionic detection mechanism of halogen-containing compounds in TID of gas chromatograph was discussed.

Ultra-micro analysis of alkali and alkaline earth metals by the hydrogen flame ionization method was developed by the authors.[1-3] The method, in which an electric current caused by ionization of these metals in the hydrogen flame is measured by applying an electric field, has a high sensitivity. It was observed that the ionization of alkali metals was enhanced or suppressed by the addition of hydrogen chloride gas to the flame. Behavior of alkali metals in the small diffusion hydrogen flame without an electric field, distribution of free neutral atoms and charged particles and the mobility of charged particles were also studied.[4] In investigations carried out on the ionization of alkali metals in the presence of halogens,[5-7] large, flat and pre-mixed flames were used, no electric field being applied.

On the other hand, a high sensitive and selective gas chromatographic detector has been used[8,9] for halogen- and phosphorus-containing compounds, known as a thermionic or alkali flame detector. It is a modification of the flame ionization detector making use of different ionization processes in the flame in the presence of an alkali metal. The mechanism of response was discussed from the point of view that halogens and phosphorus increase the ionization or volatilization of alkali metals.

This paper deals with the quantitative treatment of the ionization of alkali metals when halogens are added or not added to a small diffusion flame to which electric field is applied. The study is also related with the thermionic detection mechanism.

Experimental

A double jet type hydrogen flame ionization detector was used, the flow rates of hydrogen and oxygen and also the instrument being the same as those used previously.[4] The electric field is applied to the ionizing flame by two parallel plane electrodes, 5.5×3.5 cm nickel plates plated with silver and gold. The applied potential and distance between the electrodes are variable. The flame photometric method was applied for studying the effect of halogens on the concentration of free neutral atoms.

Alkali metals were intermittently supplied to the ionizing flame (the upper flame) by inserting the tip of a platinum wire coated with 10^{-9}—10^{-11} mol alkali chloride into the evaporating flame (the lower flame). Halogens were continuously added to the ionizing flame by introducing them into the hydrogen gas stream for the ionizing flame. Chlorine was added as hydrogen chloride from a cylinder. Iodine, bromine, and fluorine were added as methyl iodide, diethyl bromide, and fluorobenzene, respectively, from a heated reservoir.

Results and Discussion

In the Absence of Halogens. Alkali chlorides MCl react with hydrogen atoms in the flame as follows:

$$MCl + H \rightleftarrows M + HCl; \text{ eq. const. } K_1.$$

This gives alkali atoms M which can be readily ionized. Alkali atoms are ionized by collisional process with B, major constituent of the gas products (water molecule in this case):

$$M + B \xrightarrow{k_1} M^+ + e^- + B. \qquad (I)$$

The activation energy of reaction (I) is equal to the ionization potential.[10] Since the concentration of water molecule is constant in a given flame, the reaction is considered to be of first order, depending only on the alkali atom concentration. This indicates that the ionization occurs *via* a thermal rather than a chemical path. If the process completely follows this reaction, then we have

$$\frac{d[M^+]}{dt} = k_1[M][B],$$

1) S. Araki, S. Suzuki, and T. Hobo, *Bunseki Kagaku*, **15**, 27 (1966).
2) S. Araki, S. Suzuki, T. Hobo, T. Yoshida, K. Yoshizaki, and M. Yamada, *ibid.*, **17**, 847 (1968).
3) S. Araki, S. Suzuki, T. Hobo, and M. Yamada, *ibid.*, **19**, 493 (1970).
4) M. Yamada, S. Suzuki, and S. Araki, This Bulletin, **45**, 1093 (1972).
5) E. M. Bulewicz, L. F. Phillips, and T. M. Sugden, *Trans. Faraday Soc.*, **57**, 921 (1961).
6) P. J. Padley, F. M. Page, and T. M. Sugden, *ibid.*, **57**, 1552 (1961).
7) A. N. Hayhurst and T. M. Sugden, *ibid.*, **63**, 1375 (1967).
8) V. V. Brazhnikov, M. V. Gurev, and K. I. Sakodynsky, *Chromatog. Rev.*, **12**, 1 (1970).
9) M. Krejci and M. Dressler, *ibid.*, **13**, 1 (1970).
10) D. E. Jensen and P. J. Padley, *Ttans. Faraday Soc.*, **62**, 2140 (1966).

where k_1 is the rate constant of reaction (I), [M] and [B] are concentrations of alkali atom and water molecule, respectively. If the recombination in the electric field is neglected, the ion current i which flows into the outer circuit will be proportional to $d[M^+]/dt$:

$$i \propto \frac{d[M^+]}{dt} = k_1[M][B]. \quad (1)$$

If $[M]_0$ and $[Cl]_0$ are total concentrations of metal and chlorine atom, whether combined or free, then

$$[M]_0 = [M] + [MCl] + [MOH], \quad (2)$$

$$[Cl]_0 = [M]_0 = [MCl] + [HCl] + [Cl], \quad (3)$$

where [MCl] is the concentration of undissociated alkali chloride, [MOH], [HCl], and [Cl] are concentrations of alkali hydroxide, hydrogen chloride and chlorine atom, respectively, formed in the flame. Formation of MOH and HCl is governed by the reversible reactions:

$$M + H_2O \rightleftarrows MOH + H,$$

$$Cl + H_2 \rightleftarrows HCl + H.$$

Putting $[MOH]/[M]=\phi$, Eq. (2) becomes

$$[M]_0 = [M]\left(1+\frac{[MCl]}{[M]}+\phi\right)$$

$$= [M]\left(1+\frac{[HCl]}{K_1[H]}+\phi\right). \quad (4)$$

From the previous results, the value of ϕ was 0.1—0.3 for lithium and $\phi \ll 1$ for the other alkali mtals.[4] Equations (2) and (3) give

$$[M](1+\phi) = [HCl]\left(1+\frac{[Cl]}{[HCl]}\right).$$

Since $[Cl]/[HCl] \ll 1$, this becomes

$$[M](1+\phi) = [HCl]. \quad (5)$$

From Eqs. (4) and (5), we obtain

$$[M] = \frac{2[M]_0}{(1+\phi)\{\sqrt{1+4[M]_0/K_1[H](1+\phi)}+1\}}. \quad (6)$$

In our experiment, the amounts of alkali metals added were 10^{-11}—10^{-9} mol. Thus we get for $[M]_0$ 10^{-8}—10^{-6} atm (partial pressure), for $K_1[H](1+\phi)$ about 10^{-2} atm for lithium and 10^{-3} atm for cesium. Equation (6) can therefore be simplified as

$$[M] = \frac{[M]_0}{1+\phi}. \quad (7)$$

This holds also for the other halides of alkali metals. Thus, we have from Eqs. (1) and (7)

$$i \propto \frac{[M]_0}{1+\phi}.$$

This indicates that the ion current is proportional to the total concentration of alkali metals. The experimental results are shown in Fig. 1.

The plot of lithium alone shows a straight line. A deviation from the straight line would be due to the space charge effect caused by insufficient applied potential. The relationship between the saturated ion current i_s and the minimum applied potential V_s at which i_s is obtained is shown in Fig. 2. The slope of straight lines is found to be 2 and i_s-V_s relation is represented by the equation. Since the coefficient a is correlated

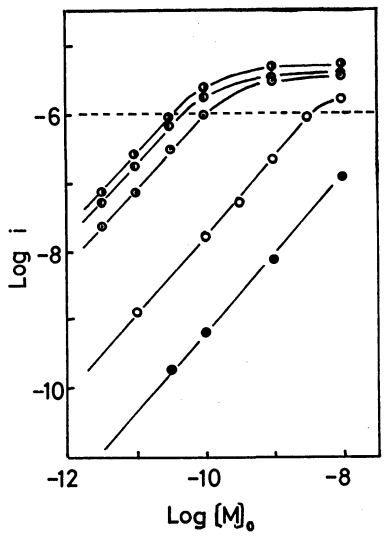

Fig. 1. Relationship between i and $[M]_0$.
i and $[M]_0$ are represented by ampere and mole, respectively. Applied potential: 1000 V; Distance between the electrodes d(cm): 1.8; Sample: ● LiCl, ○ NaCl, ⊙ KCl, ◐ RbCl, ◑ CsCl.

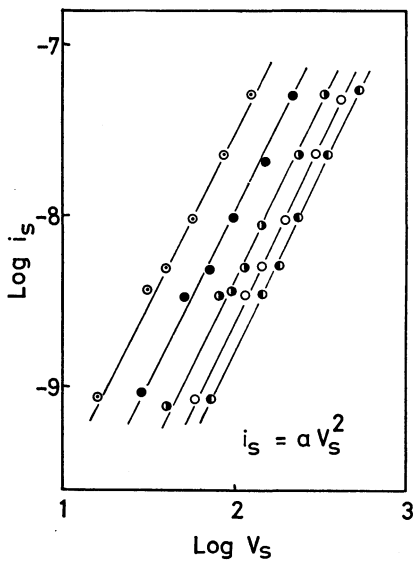

Fig. 2. Relationship between i_s and V_s.
i_s and V_s are represented by ampere and volt, respectively. Distance between the electrodes d(cm): ⊙ 1.4, ● 1.8, ◑ 2.2, ○ 2.6, ◐ 3.0; Sample (mol): NaCl 1×10^{-10}.

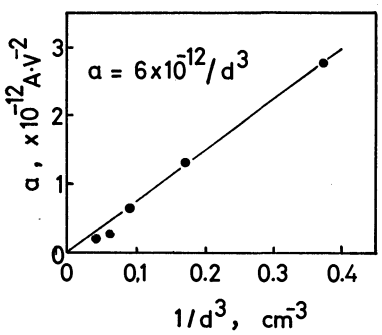

Fig. 3. Relationship between a and $1/d^3$.

with the distance between the electrodes d as shown in Fig. 3, we obtain

$$i_s = 6 \times 10^{-12} \frac{V_s^2}{d^3} (\mathrm{A}). \quad (8)$$

This shows that the saturated ion current depends on the applied potential, if d is kept constant. Under the conditions shown in Fig. 1, where V_s is 1000 V and d 1.8 cm, i_s is calculated to be 1.0×10^{-6} A. This value is represented by a horizontal dotted line. Above this line, linear relation can not be obtained because the applied potential is not sufficient. When the applied potential is larger, the plots should be linear if the secondary ionization do not occur. The working curves became non-linear in the range of large amounts of halide (for example, 10^{-10} mol in sodium chloride).[3] The applied potential was about 300 V, and the linear dynamic ranges of the working curves were not more than 100. These results show that the applied potential was apparently low.

In the Presence of Halogens. On adding halogens, the ionization can be considered to be the following reactions in the electric field:

$$\mathrm{M} + \mathrm{B} \xrightarrow{k_1} \mathrm{M^+} + \mathrm{e^-} + \mathrm{B}, \quad (\mathrm{I})$$

$$\mathrm{M} + \mathrm{X} \xrightarrow{k_2} \mathrm{M^+} + \mathrm{X^-}, \quad (\mathrm{II})$$

and halogens take part in two reversible bimolecular reactions,

$$\mathrm{MX} + \mathrm{H} \rightleftarrows \mathrm{M} + \mathrm{HX}; \text{ eq. const. } K_2, \quad (\mathrm{III})$$

$$\mathrm{H_2} + \mathrm{X} \rightleftarrows \mathrm{H} + \mathrm{HX}; \text{ eq. const. } K_3, \quad (\mathrm{IV})$$

where X is a halogen atom. In reaction (II), it is expected to increase the ion current, and in reaction (III), to decrease the ion current, since ionizable alkali atoms are removed as gaseous alkali halides.

If reaction (II) is of second order, the ion current i' is given by

$$i' \propto \frac{\mathrm{d}[\mathrm{M^+}]'}{\mathrm{d}t} = k_1[\mathrm{M}]'[\mathrm{B}] + k_2[\mathrm{M}]'[\mathrm{X}]', \quad (9)$$

where $[\mathrm{M^+}]'$ and $[\mathrm{M}]'$ are concentrations of the metal ion and the free atom, respectively, in the presence of added halogen, and $[\mathrm{X}]'$ that of atomic halogen. [B] remains constant because of the buffer effect of the flame gases. From Eqs. (1) and (9), the ion current ratio i'/i is obtained:

$$\frac{i'}{i} = \frac{[\mathrm{M}]'}{[\mathrm{M}]}\left(1 + \frac{k_2[\mathrm{X}]'}{k_1[\mathrm{B}]}\right). \quad (10)$$

If $[\mathrm{M}]_0$ and $[\mathrm{X}]'_0$ are the concentrations of total alkali metals and halogens, respectively, the material balance is given by

$$[\mathrm{M}]_0 = [\mathrm{M}]' + [\mathrm{MOH}]' + [\mathrm{MX}]', \quad (11)$$

$$[\mathrm{X}]_0' = [\mathrm{X}]' + [\mathrm{HX}]'. \quad (12)$$

Ions are ignored in the metal balance since the degree of ionization is small. $[\mathrm{MX}]'$ is neglected in the halogen balance since $[\mathrm{X}]'_0 \gg [\mathrm{M}]_0$. Equation (12) is rewritten as

$$[\mathrm{X}]_0' = [\mathrm{X}]'\left(1 + \frac{[\mathrm{HX}]'}{[\mathrm{X}]'}\right) = [\mathrm{X}]'\left(1 + \frac{K_3[\mathrm{H_2}]}{[\mathrm{H}]}\right). \quad (13)$$

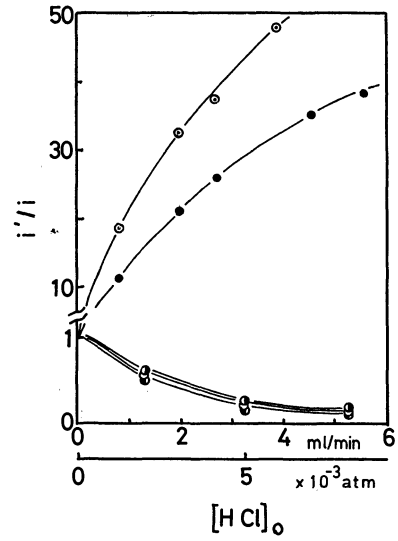

Fig. 4. Plots of i'/i against $[\mathrm{HCl}]_0$.
Applied potential: 1000 V; Distance between the electrodes d(cm): 1.8; Sample (mol): ⊙ LiCl 1×10^{-10}, ● NaCl 1×10^{-11}, ◑ KCl 1×10^{-11}, ○ RbCl 1×10^{-11}, ◐ CsCl 1×10^{-11}

Equation (10) then becomes

$$\frac{i'}{i} = \frac{[\mathrm{M}]'}{[\mathrm{M}]}\left\{1 + \frac{k_2[\mathrm{X}]_0'}{k_1(1 + K_3[\mathrm{H_2}]/[\mathrm{H}])[\mathrm{B}]}\right\}. \quad (14)$$

Change of i'/i, on addition of a few milliliters per minute of hydrogen chloride (an order of 10^{-3} atm in partial pressure), is shown in Fig. 4. We see that the ion currents for lithium and sodium increase, while those for the other alkali metals decrease. This is because $[\mathrm{M}]'/[\mathrm{M}]$ in Eq. (14) decreases the ion current, while the second term in the brace increases it. That is to say, in the case of lithium and sodium, the second term in the brace is much larger than 1, while in the case of other alkali metals, it is much smaller than 1.

Equation (11) is rewritten as

$$[\mathrm{M}]_0 = [\mathrm{M}]'\left(1 + \frac{[\mathrm{MOH}]'}{[\mathrm{M}]'} + \frac{[\mathrm{MX}]'}{[\mathrm{M}]'}\right) = [\mathrm{M}]'\left(1 + \phi + \frac{[\mathrm{HX}]'}{K_2[\mathrm{H}]}\right).$$

We have from Eqs. (12) and (13)

$$[\mathrm{M}]_0 = [\mathrm{M}]'\left\{1 + \phi + \frac{[\mathrm{X}]_0'}{K_2[\mathrm{H}](1 + [\mathrm{H}]/K_3[\mathrm{H_2}])}\right\}. \quad (15)$$

ϕ, [H], and $[\mathrm{H_2}]$ remain constant because of the buffer effect of the flame gases. Since $[\mathrm{Cl}]'/[\mathrm{HCl}]' \ll 1$, Eq. (15) for chlorine becomes

$$[\mathrm{M}]_0 = [\mathrm{M}]'\left(1 + \phi + \frac{[\mathrm{Cl}]_0'}{K_2[\mathrm{H}]}\right). \quad (16)$$

From Eqs. (6) and (16), the concentration ratio of free alkali atoms in the presence or absence of added hydrogen chloride is given by

$$\frac{[\mathrm{M}]}{[\mathrm{M}]'} = \frac{2\{1 + [\mathrm{Cl}]_0'/(1+\phi)K_2[\mathrm{H}]\}}{1 + \sqrt{1 + 4[\mathrm{M}]_0/(1+\phi)K_2[\mathrm{H}]}}. \quad (17)$$

$[\mathrm{M}]/[\mathrm{M}]'$ is equal to I/I', where I and I' are emission intensities of alkali atoms in the absence and presence of added hydrogen chloride. Plots of I/I' against $[\mathrm{Cl}]'$ and of $(I - I')$ against I give straight lines as shown in

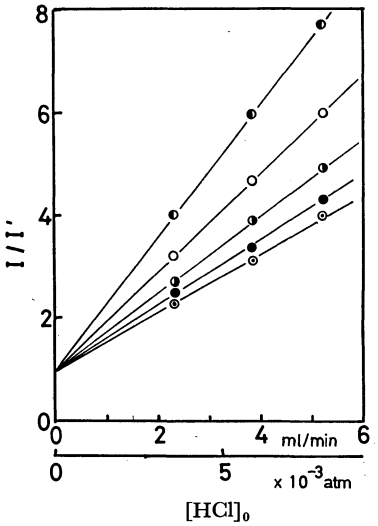

Fig. 5. Plots of I/I' against $[HCl]_0$.
Sample (mol): ⊙ LiCl 1×10^{-9}, ● NaCl 1×10^{-10}, ◑ KCl 1×10^{-8}, ○ RbCl 1×10^{-8}, ◐ CsCl 1×10^{-8}

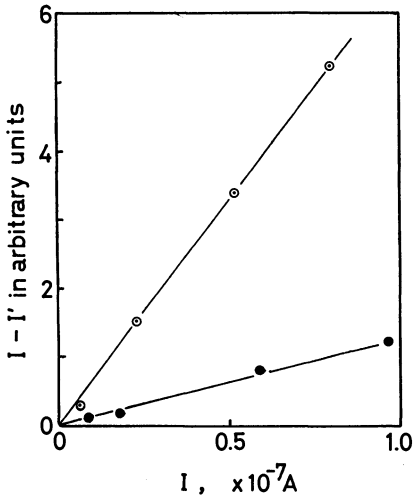

Fig. 6. Plots of $(I-I')$ against I.
Alkali metals were continuously supplied to the flame, while one milliliter of hydrogen chloride was intermittently injected to the hydrogen gas stream. Sample: ⊙ LiCl, ● NaCl

Figs. 5 and 6, respectively. Thus, $4[M]_0/(1+\phi)K_2[H]$ is considered to be negligible compared with 1. Thus Eq. (17) is simplified to

$$\frac{[M]}{[M]'} = 1 + \frac{[Cl]_0'}{(1+\phi)K_2[H]}.$$

Therefore, $(1+\phi)K_2[H]$ can be determined from the slope of straight lines in Fig. 5. They were 10^{-2} atm for lithium and 10^{-3} atm for cesium. The concentration of free alkali atoms was reduced because of the formation of MCl, and $[M]'/[M]$ was in the order of magnitude of 10^{-1}.

The second term in the brace in Eq. (14) should next be considered. The expression for the rate constant k_1 of reaction (I) is

$$k_1 = \pi r_{M-B}^2 \sqrt{\frac{8kT(m_M+m_B)}{m_M m_B}} \exp\left(-\frac{E_M}{RT}\right), \qquad (18)$$

where r_{M-B} is the collision diameter, m_M and m_B are respectively the atomic and molecular weight of the metal and water and E_M is the ionization potential of the metal. The collision cross-sections πr^2_{M-B} are greater than the normal gas kinetic values by several orders of magnitude and were deduced experimentally.[10] The results indicate that, although reaction (I) seems to be of first order with respect to the metal, it can not be a simple single-step process as given by reaction (I). Nevertheless, Eq. (18) with the appropriate values of the collision cross-sections can still be used to estimate the rate at which alkali metals are ionized.

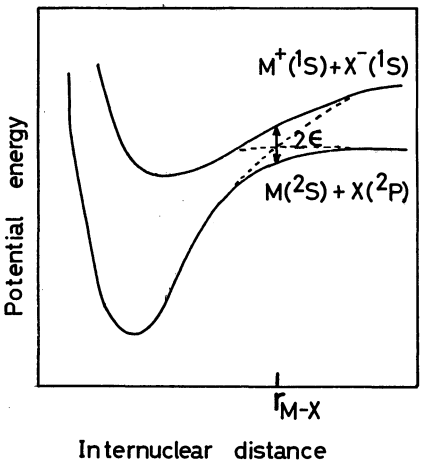

Fig. 7. Potential energy curves for electron transfer reaction.

Electron transfer reaction (II) may be considered with referring to the simple diagram of Fig. 7, which represents the potential curves for the two lowest states of the MX molecule. The rate constant k_2 of reaction (II), with a transition complex in the region of r_{M-X}, is reduced to

$$k_2 = \kappa\pi r_{M-X}^2 \sqrt{\frac{8kT(m_M+m_X)}{m_M m_X}} \exp\left(-\frac{E_M-E_X}{RT}\right), \qquad (19)$$

Where κ is a transmission coefficient, r_{M-X} the distance between the nuclei of alkali metal and halogen at the crossing point and E_X the electron affinity of halogen atom. The potential energy relative to the separated ions is approximately the same as at infinity, *i.e.*, E_M-E_X. Hence we have at the crossing point

$$r_{M-X} = \frac{e^2}{E_M-E_X}, \qquad (20)$$

where e is the electronic charge. The values of r_{M-X} calculated from Eq. (20) give the effective collision diameters for the reaction between the various alkali metals and halogen atoms.

If χ is the probability of crossing from the lower to the upper potential energy surface, then

$$\kappa = 2\chi(1-\chi).$$

The following Landau-Zener formula gives χ in terms of 2ε:

$$\chi = \exp\left(-\frac{4\pi^2\varepsilon^2}{hv|s_i-s_f|}\right),$$

where 2ε is the energy equivalent to the closest distance between the upper and lower curves. Thus ε is the resonance energy in the activated state, v the velocity

TABLE 1. CALCULATED VALUES OF k_2/k_1

	F			Cl		
	1400 K	1600 K	1800 K	1400 K	1600 K	1800 K
Li	1.5×10^{10}	3.9×10^{8}	1.6×10^{7}	5.3×10^{10}	1.0×10^{9}	5.4×10^{7}
Na	3.6×10^{9}	1.0×10^{8}	4.7×10^{6}	2.8×10^{10}	6.0×10^{8}	3.2×10^{7}
K	$<10^{4}$	$<10^{2}$	<10	10^{2}	1	10^{-1}
Rb	$<10^{4}$	$<10^{2}$	<10	$<10^{2}$	<1	$<10^{-1}$
Cs	$<10^{4}$	$<10^{2}$	<10	$<10^{2}$	<1	$<10^{-1}$

	Br			I		
	1400 K	1600 K	1800 K	1400 K	1600 K	1800 K
Li	$10^{9a)}$	$10^{7a)}$	$10^{6a)}$	$10^{4b)}$	$10^{3b)}$	$10^{2b)}$
Na	$10^{9a)}$	$10^{7a)}$	$10^{6a)}$	$10^{4b)}$	$10^{3b)}$	$10^{2b)}$
K	1.5×10^{9}	2.8×10^{7}	2.1×10^{6}	3.1×10^{6}	2.2×10^{5}	1.6×10^{4}
Rb	4.3×10^{7}	8.1×10^{5}	5.9×10^{4}	4.3×10^{7}	2.4×10^{6}	2.0×10^{5}
Cs	$\ll10^{7}$	$\ll10^{5}$	$\ll10^{4}$	5.3×10^{8}	2.4×10^{7}	1.1×10^{6}

a) $\epsilon\approx100$ cal/mol., b) $\epsilon\approx1000$ cal/mol.

with which the system passes through this configuration, and $|s_i-s_f|$ is the absolute magnitude of the difference between the slopes of the two common tangents to the curves. There will be little error in taking v as the classical mean velocity, $\sqrt{kT(m_M+m_X)/2\pi m_M m_X}$, s_i as e^2/r^2_{M-X}, and s_f as zero. Magee[11] calculated ε using the Slater one-electron wave functions. Equations (18) and (19) give the rate constant ratio of reactions (I) and (II) as

$$\frac{k_2}{k_1}=\frac{\kappa r^2_{M-X}}{r^2_{M-B}}\sqrt{\frac{(m_M+m_X)m_B}{(m_M+m_B)m_X}}\exp\frac{E_X}{RT}.$$

The calculated values of k_2/k_1 are given in Table 1.

The equilibrium constant of reaction (IV), K_3, was obtained by statistical calculations (Table 2):

TABLE 2. EQUILIBRIUM CONSTANT K_3

	1400 K	1600 K	1800 K
HF	6.9×10^{4}	1.8×10^{4}	6.7×10^{3}
HCl	1.5	1.6	1.7
HBr	5.4×10^{-3}	1.4×10^{-2}	2.6×10^{-2}
HI	3.6×10^{-5}	1.8×10^{-4}	3.8×10^{-4}

$$K_3=\frac{f_{HX}f_H}{f_{H_2}f_X}\exp\left\{\frac{D(HX)-D(H_2)}{RT}\right\},$$

where the fs are partition functions; D_{HX} and D_{H_2} are the heats of dissociation (positive) of HX and H_2, respectively, at 0 K. $[H_2]/[H]$ was obtained by calculating[12] the composition of the flame gases at a given temperature, assuming a stoichiometric H_2–O_2 flame. It was in the order of magnitude of 10^3 at 1400—1800 K. The concentration of water molecule, [B], was about 0.6 atm, considering the water vapor

TABLE 4. EXPERIMENTAL VALUES OF i'/i ON ADDING HALOGENS[a)]

Amounts of added metal (mol)		F	Cl	Br	I
Li	1×10^{-9}	1.0	22	31	7.1
Na	1×10^{-10}	1.0	11	84	16
K	1×10^{-11}	0.9	0.7	4.5	6.5
Rb	1×10^{-11}	0.9	0.6	3.5	4.4
Cs	1×10^{-11}	0.9	0.6	1.5	1.3

a) Added halogens: C_6H_5F 2.1×10^{-3} atm; HCl 2.0×10^{-3} atm; CH_2BrCH_2Br 4.0×10^{-3} atm; CH_3I 1.6×10^{-3} atm

TABLE 5. PREDICTIONS OF THE EFFECTS OF HALOGEN ADDITION ON ION CURRENT

	F	Cl	Br	I
Li	±	+	+	+
Na	±	+	+	+
K	±	−	+	+
Rb	±	−	+	+
Cs	±	−	+	+

+: Increase, −: Decrease, ±: A little, decrease, or no change

TABLE 3. ORDERS OF MAGNITUDE OF $k_2[X]'_0/k_1\,(1+k_3[H_2]/[H])\,[B]$

	F			Cl			Br			I		
	1400 K	1600 K	1800 K	1400 K	1600 K	1800 K	1400 K	1600 K	1800 K	1400 K	1600 K	1800 K
Li	10^{-1}	10^{-1}	10^{-2}	10^{5}	10^{4}	10^{2}	10^{6}	10^{3}	10^{2}	10^{3}	1	10^{-1}
Na	10^{-1}	10^{-2}	10^{-3}	10^{4}	10^{3}	10	10^{6}	10^{3}	10^{2}	10^{3}	1	10^{-1}
K	$<10^{-1}$	$<10^{-2}$	$<10^{-3}$	$\ll1$	$\ll1$	$\ll1$	10^{6}	10^{3}	10^{2}	10^{5}	10^{5}	10^{2}
Rb	$<10^{-1}$	$<10^{-2}$	$<10^{-3}$	$\ll1$	$\ll1$	$\ll1$	10^{4}	10^{2}	10	10^{6}	10^{6}	10^{3}
Cs	$<10^{-1}$	$<10^{-2}$	$<10^{-3}$	$\ll1$	$\ll1$	$\ll1$	$\ll10^{4}$	$\ll10^{2}$	$\ll1$	10^{7}	10^{7}	10

11) J. L. Magee, *J. Chem. Phys.*, **8**, 687 (1940).
12) A.G. Gaydon and H.G. Wolfhard, "Flames: Their Structure, Radiation, and Temperature," Chapman and Hall, London (1953), p. 264.

Table 6. Calculated values of i'/i for TID

	F		Cl		Br		I	
	1000 K	1200 K	1000 K	1200 K	1000 K	1200 K	1000 K	1200 K
Li	1	1	10^4—10^7	10—10^4	10^5—10^8	10^2—10^5	1—10^3	1
Na	1	1	10^4—10^7	10—10^4	10^5—10^8	10^2—10^5	1—10^3	1
K	1	1	1	1	10^6—10^9	10^2—10^5	10^3—10^6	1—10^3
Rb	1	1	1	1	10^4—10^7	10—10^4	10^4—10^7	10^2—10^5
Cs	1	1	1	1	$<10^4$—10^7	$<$10—10^4	10^6—10^9	10^3—10^6

produced in the evaporating (lower) flame. The total concentration of added halogens, $[X]_0'$, was in the order of 10^{-3} atm. Thus the second term in the brace in Eq. (14) was calculated as given in Table 3.

The results shown in Fig. 4 can be easily understood from Table 3 and the values of $[M]'/[M]$ in Fig. 5. The results from the presence of 10^{-3} atm of halogens are given in Table 4. $[M]'/[M]$ was in the order of 10^{-1} for bromine, and was nearly equal to 1 for fluorine and iodine. It can be predicted from the data of Table 3 whether the addition of halogens increases or decreases ion current. The predicted results are compatible with the experimental results as shown in Table 5. The experimental values of i'/i fairly differ from those predicted from the data in Table 3. Exact prediction is difficult in this experiment in which the diffusion flame is used. It is necessary to consider ionization not only from the ground states but also from electronically excited levels.

On TID Response. It has been found that the thermionic detector (TID) has a high sensitivity to halogen-containing compounds in gas chromatography. Karmen[13–15] proposed a TID with two burners placed one above the other and separated by a platinum screen treated with an alkali metal salt. This detector essentially consists of a combination of two self-contained detectors: a flame ionization (lower) detector and a thermionic (upper) detector. It is believed that the TID response depneds on the increase in ionization or volatilization of alkali metals. Karmen explained the sensitivity of the TID to halogen-containing compounds by the increase in volatilization. However, we see from Table 3 that the effect of halogens on ionization can not be neglected. The TID response will be discussed by means of Eq. (14).

Working conditions of the gas chromatographic detector required for the calculations were assumed as follows: the flow rates of hydrogen, air, and carrier gas (nitrogen) are 30, 400, and 40 ml/min, respectively; the flame is a stoichiometric one; mono-halogenated benzenes as halogen-containing compounds are supplied in the rate of 10^{-10}—10^{-7} g/sec (10^{-8}—10^{-5} atm in partial pressure) to the TID. Temperature of the flame used for the TID may be lower than that used for this experiment. It may be about 1000—1200 K.[16] Since $[X]_0'$ is very small, $[M]'/[M]$ is assumed to be nearly equal to 1. Calculated values of i'/i are given in Table 6.

We see that chlorine, bromine, and iodine appear to increase the ionization of all or some alkali metals, while fluorine appears to be ineffective. Karmen showed that the relative sensitivity to butyl bromide, chloride and iodide varied somewhat when screens treated with different alkali metals were used, and that the sensitivity to butyl bromide was greater than that to butyl chloride or butyl iodide for each of the screens. The sensitivity to fluorine-containing compounds was much less, but a definite response was obtained, particularly when a screen treated with a cesium salt was used. These results are consistent with the data in Table 6. However, Karmen also found that when a potassium-treated screen was used, the relative sensitivity to butyl chloride was higher than those treated with any of the other alkalis. This indicates that the increase in the volatilization of alkali metals plays an important role in the increase in sensitivity. It is almost certain that the sensitivity to fluorine-containing compounds and to chlorine-containing compounds when potassium-, rubidium-, and cesium-screens are used is due to the increase in the volatilization of alkali metals. In the case of other combinations of halogen-containing compounds and alkali metals, the response is considered to arise from the increase not only in the volatility, but also in the ionization. The increment of evaporation and ionization should be known in order to study the detection mechanism of TID in detail.

13) A. Karmen, *Anal. Chem.*, **36**, 1416 (1964).
14) A. Karmen, *J. Gas. Chromatog.*, **3**, 336 (1965).
15) A. Karmen, *J. Chromatog. Sci.*, **7**, 541 (1969).
16) V. V. Brazhnikov, M. V. Gurev, and K. I. Sakodynsky, *Chromatographia*, **3**, 53 (1970).

The Ion-exchange Behavior of the Ammonium Ion on Crystalline Zirconium Phosphate

Yoshitsugu HASEGAWA and Hisashi AOKI

Department of Industrial Chemistry, Faculty of Engineering, Tokyo University of Agriculture and Technology, Nakamachi, Koganei, Tokyo 184

(Received May 24, 1972)

The ion-exchange behavior of the ammonium ion on crystalline zirconium phosphate (c-ZrP) was studied by pH titration and X-ray powder diffraction. The ion-exchange capacity of c-ZrP was 4.4 meq/g in an acidic solution and 6.6 meq/g in an alkaline solution. At an exchange of 66% the $Zr(NH_4PO_4)_{1.33}(HPO_4)_{0.67}\cdot H_2O$ phase was present and at an exchange of 100% $Zr(NH_4PO_4)_2\cdot H_2O$ phase was present. The forward and backward titration curves exhibited a hysteresis loop. This results from the presence of the different phases in the titration of each direction. Through the ion-exchange cycle, the crystallinity of c-ZrP was maintained.

Since the crystalline zirconium phosphate ion-exchanger (referred to as c–ZrP hereafter) was prepared by Clearfield and Stynes,[1] the ion-exchange behavior of the compound has been investigated extensively. Especially for alkali-metal cations, the distribution coefficients, (K_d), the dependence of K_d on pH, and the pH titrations have been studied.[2,3] Clearfield and Smith prepared a single crystal of zirconium bis(monohydrogen orthophosphate) monohydrate, $Zr(HPO_4)_2\cdot H_2O$, and suggested a crystal structure for it.[4–6]

However, the ion-exchange behavior of the ammonium ion on c–ZrP has scarcely been studied at all. Only the composition of the ammonium form of c–ZrP, its interplanar spacing, and a simple thermal analysis have been reported.[1,7]

In the present study, the capacity and reversibility of the ion exchange were measured by pH titrations, and the structural change of c–ZrP was examined by means of the X-ray powder diffraction. A chemical analysis of the ammonium forms of c–ZrP was also carried out.

Experimental

Reagents. All the reagents were of a reagent grade and were used without further purification. The c-ZrP was prepared by refluxing a gelatinous zirconium phosphate in 6.7M phosphoric acid for 120 hr.[3]

pH-Titrations. The titrations were carried out by batch as follows: 250 mg of c-ZrP was placed in contact with 25 ml of an NH_4OH+NH_4Cl solution in a thermostat regulated at 25°C. The composition of the solution was chosen so that the total ammonium concentration was equal to 0.1N, and the ratio of OH^-/Cl^- was varied from 0/0.1 to 0.1/0N. The mixtures were shaken continuously until equilibration. After equilibration, the pH values of the supernatants were measured on a Model MG-1 pH meter (Denki Kagaku Keiki Co., Ltd.) with a glass electrode. The equilibrated pH was attained about 2 hr after the start of shaking. Usually the pH's were determined after the reaction mixtures had been shaken for 12—24 hr.

The analysis of the exchanger obtained at the end-point of the pH titration showed that the composition of the compound was $Zr(NH_4PO_4)_2\cdot H_2O$. Taking the difference in molecular weight from c-ZrP into consideration, in the backward titration 278 mg of the ammonium-form exchanger was placed in contact with the solution of $HCl+NH_4OH$. The ammonium hydroxide added was adjusted to 3.29 meq/g c-ZrP, since 6.6 meq NH_4^+/g c-ZrP was already included in the exchanger, and the amount of added hydrochloric acid was varied.

In confirmation of the ion-exchange capacity, the titrations were carried out with NH_4OH alone and with HCl alone in separate runs.

Analytical Procedure. The ammonium forms of the exchanger were analysed as follows. Zr; A weighed sample (*ca.* 100 mg) and 1.5—2.0 g of sodium peroxide powder were mixed. To the mixture 25 ml of water was added in an ice bath. After a few minutes, the slurry was placed on a water bath and the precipitated zirconium hydroxide was aged for 2—3 hr. After filtration, the precipitate was dissolved in 3N HCl. Then the zirconium was re-precipitated as cupferronate and ignited to ZrO_2. PO_4; The phosphorus was determined gravimetrically by the method described by Kolthoff and Sandell.[8] NH_4^+; The ammonium ion was determined gravimetrically to be tetraphenyl borate.[9]

X-Ray Powder Diffraction. X-Ray powder patterns were obtained with Ni filtered copper X-rays using a Geigerflex (Rigaku Denki Co., Ltd.).

Results and Discussion

pH *Titration Curves.* The titration curves obtained for NH_4OH–NH_4Cl solution media are shown in Fig. 1. The forward titration curve can apparently be divided into two regions. The first region of the ion exchange extends from zero exchange to 4.4meq/g c–ZrP ammonium ion uptake. In the second region, the ion-exchange reaction proceeds slowly and the end-point of neutralization is not observed claerly. The titration curve in Fig. 2(a) also shows that the ion-exchange capacity of c–ZrP for the ammonium ion in

1) A. Clearfield and J. A. Stynes, *J. Inorg. Nucl. Chem.*, **26**, 117 (1964).
2) J. Albertsson, *Acta Chem. Scand.*, **20**, 1679 (1966).
3) Y. Hasegawa and I. Tomita, This Bulletin, **43**, 3011 (1970).
4) A. Clearfield and G. D. Smith, *Inorg. Chem.*, **8**, 431 (1969).
5) A. Clearfield and G. D. Smith, *J. Colloid & Interface Sci.*, **28**, 325 (1968).
6) for example, A. Clearfield and A. S. Medina, *J. Phys. Chem.*, **75**, 3750 (1970).
7) A. Dyer, D. Leigh ,and F. T. Ocon, *J. Inorg. Nucl. Chem.*, **33**, 3141 (1971).
8) I. M. Kolthoff and E. B. Sandell, "Textbook of Quantitative Inorganic Analysis" 3rd. edition. The MacMillan Company, (1952), pp. 377—383.
9) F. E. Crane, Jr. and E. A. Smith, *Chemist-Analyst*, **49**, 38 (1960).

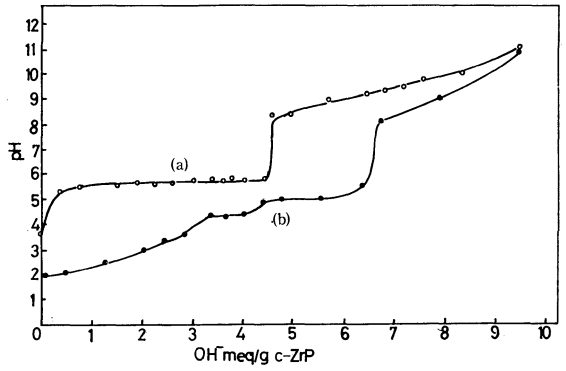

Fig. 1. pH titration curves for c-ZrP. Titrant: forward direction (—○—), 0.1N NH_4OH+0.1N NH_4Cl, backward direction (—●—), 0.1N HCl+NH_4Cl.

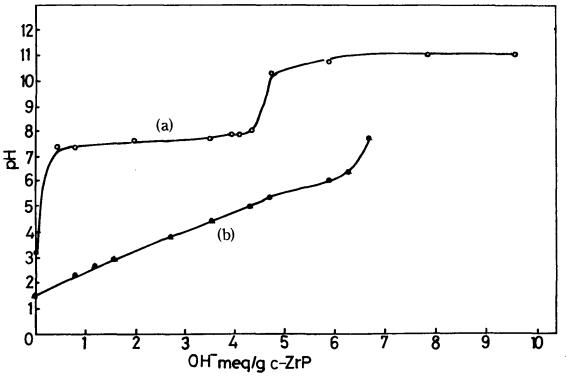

Fig. 2. pH titration curves for c-ZrP. Titrant: forward direction (—○—), 0.1N NH_4OH only, backward direction (—●—), 0.1N HCl only.

an acidic solution is equal to about 4.4 meq/g. As the theoretical ion-exchange capacity of c-ZrP is 6.6 meq/g, the value of 4.4 meq corresponds to a 66% exchange.

In the backward titration (Fig. 1(b)), it was found that the ion-exchange reaction took place in two stages. The first stage extended from an exchange of 100% to 67%, and the second stage, from 66 to 0%. That is, 0—33% of the ammonium ion in the exchanger was re-exchanged with the hydrogen ion at pH 5.5—5.0 and 34—100% over the pH range from 5.0 to 2.0. The second stage might be further divided into two steps if one takes account of the plateau found at an exchange of around 34—50% at pH 4.5. From Figs. 1(b) and 2(b) it turns out that the total ion-exchange capacity for the ammonium ion is equal to 6.6 meq/g c-ZrP experimentally.

The titration curves in Fig. 1 show the irreversibility of the ammonium-hydrogen ion exchange on c-ZrP; it results in a hysteresis loop of the curves. These may be due to the presence of different phases in the forward and backward titrations (the details will be presented later).

The ion exchange of the ammonium ion on c-ZrP resembles that of the lithium ion in some respects. Clearfield and Troup, and Nancollas and Harvie, have reported, respectively, that lithium-ion exchange takes place in two stages and that the ion-exchange capacity of c-ZrP for the lithium ion is 4.4 in an acidic solution and 6.6 meq/g in an alkaline solution.[10,11] This is what was observed for the ammonium ion.

It has already been established that c-ZrP works as a dibasic exchanger to the sodium ion and that the two groups of phosphate protons exist in the ratio of 1 to 1.[12] This can reasonably be expected from the $Zr(HPO_4)_2 \cdot H_2O$ formula. For ammonium exchange, this is not the case; *i.e.*, the two groups of phosphate protons seems to exist in the ratio of 2 to 1. This phenomenon was also observed in the lithium-ion exchange.[10,11]

The compositions of the 66%-exchange phase (Phase I) and 100%-exchange phase (Phase II) are as follows. Phase I, Found: Zr; 28.3, PO_4; 57.6, NH_4; 7.2, ignition loss; 18.0%. Calcd for $Zr(NH_4PO_4)_{1.33}(HPO_4)_{0.67} \cdot H_2O$, Zr; 28.2, PO_4; 58.6, NH_4; 7.43, ignition loss; 18.1%. Phase II, Found: Zr; 27.4, PO_4; 54.9, NH_4; 10.8, ignition loss; 21.1%. This corresponds to $Zr(NH_4PO_4)_2 \cdot H_2O$ (Calcd for Zr; 27.2, PO_4; 56.7, NH_4; 10.8, ignition loss: 20.9%).

X-Ray Diffraction. In Figs. 3 and 4, the X-ray diffraction patterns of the samples taken from the titration experiments are shown schematically. In Table 1, the interplanar spacing (*d* values) of c-ZrP, Phase I and Phase II, are shown. The *d* values of Phase II agreed with that reported by Clearfield and Stynes,[1] but did not agree with that reported by Dyer *et al.*[7]

At the initiation of the forward titration, a new reflection at d=9.49 Å was observed. In the ion-exchange process, the relative strength of this reflection increased and the reflection of 7.60 Å, which is the first one in c-ZrP, decreased. Beyond an exchange of

Table 1. *d* Values of c-ZrP, Phase I and Phase II

c-ZrP		Phase I		Phase II	
d(Å)	I/I_0	*d*(Å)	I/I_0	*d*(Å)	I/I_0
		9.49	s	9.49	vs
7.49	vs	7.58	vs		
7.01	vw			4.72	vw
				4.67	w
				4.62	vw
4.47	w	4.48	w	4.46	w
4.42	vw	4.43	w		
		3.97	w	4.00	s
		3.66	w	3.68	m
3.55	s	3.56	s	3.57	vw
3.52	m	3.53	m		
3.21	vw				
		3.12	vw	3.14	m
				2.89	vw
				2.72	vw
2.64	vw	2.64	w	2.66	vw
2.62	vw	2.62	vw		
2.40	vw	2.41	vw		

10) A. Clearfield and J. Troup, *J. Phys. Chem.*, **74**, 314 (1970).
11) S. J. Harvie and G. H. Nancollas, *J. Inorg. Nucl. Chem.*, **32**, 3923 (1970).
12) A. Clearfield, W. L. Duax, A. S. Medina and J. R. Thomas, *J. Phys. Chem.*, **73**, 3424 (1969).

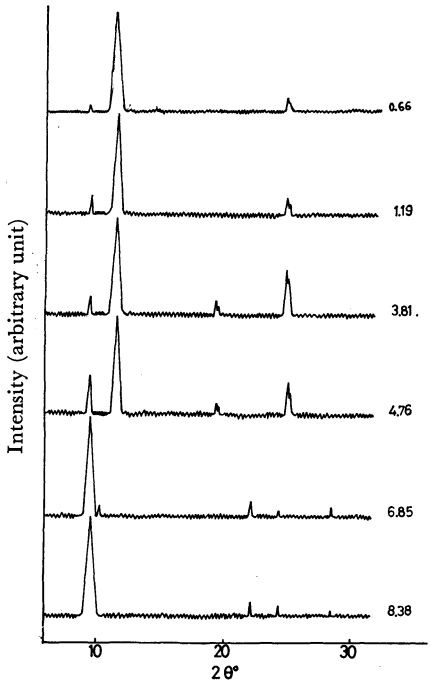

Fig. 3. Schematic diagrams of X-ray diffraction patterns for the ammonium forms of c–ZrP in forward titration. Numerals correspond to that of abscissa in Fig. 1.

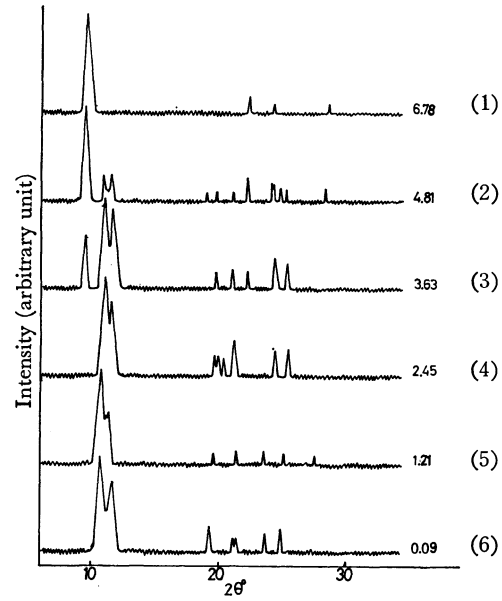

Fig. 4. Schematic diagrams of X-ray diffraction patterns for the ammonium forms of c–ZrP in backward titration. Numerals correspond to that of abscissa in Fig. 1.

66%, these two reflections were both observed. Finally, the latter reflection diminished.

Crystalline zirconium phosphate is known to have a layered structure, the interlayer distance is represented by the first reflection in the X-ray powder pattern. The change in the interplanar distance is found to be shorter than that to be expected from the ionic radius of the ammonium ion. Clearfield and Stynes[1] suggested that the shorter d value for the first reflection of the ammonium form might be due to hydrogen-bond formation between the ammonium ion and the phosphate group.

It is not possible to deduce, from the obtained diffractograms alone, whether the phases accompanied by the ion exchange are entirely different from that of c–ZrP or whether they are a mixture of two phases, c–ZrP and the ammonium-form exchanger. By analogy with the lithium-ion exchange, however, the existence of two phases is very likely, Phase I just at an exchange of 66% and Phase II at 100%.

The X-ray diffraction patterns of the samples which were taken from the backward titration were different from those of the forward titration. On the re-exchange of the ammonium ion with the hydrogen ion, the first reflection (d=9.50 Å) decreased and the second (d=8.20 Å) and third reflections (d=7.60 Å) appeared. The third reflection is identical with the first one of c–ZrP. The first reflection was not observed in Sample (4). It corresponds to the third reflection at 3.3 meq OH^-/g c–ZrP in the titration curve of Fig. 1(b). At the end of the backward titration, the exchanger was no longer identical with the original one, c–ZrP.

As has been stated above, the structural change in the exchanger is irreversible through the whole range of the ion exchange. This is the cause of the hysteresis loop in the titration curves.

In the ion-exchange cycle for the lithium ion, gelatinous zirconium phosphate was formed.[10] When the ammonium ions in the exchanger were replaced by protons, the crystallinity was maintained.

The authors would like to acknowledge the continuous guidance and helpful discussion of Professor Shuji Abe. One of the authors, Y. H., also wishes to thank Professors Kozo Nagashima and Isao Tomita of Tokyo Kyoiku University for their encouragement.

Estimation of the Thermal Yields in the Reaction with Methanes of ^{80}Br Activated by (n, γ) Process

Masakatsu SAEKI and Enzo TACHIKAWA

Division of Reactor Chemistry, Japan Atomic Energy Research Institute, Tokai, Ibaraki

(Received June 26, 1972)

The Estrup-Wolfgang Kinetic theory has been applied to the results obtained from the reactions of ^{80}Br activated by the (n,γ) process with two methanes, CH_4 and CD_4. With suitable assumptions, the most probable kinetic parameters, I's and α's have been obtained. The thermal yields of the products have been estimated as a function of the m.f. of the Kr moderator as the differences between the yields predicted by the kinetic theory with these kinetic parameters and those experimentally obtained. The thermal $CH_3{}^{80}Br$ and $CD_3{}^{80}Br$ yields are strongly affected by the m.f. of Kr in such a way that they are not important in the range from zero to around 0.7 m.f. of Kr, but become significant over 0.7 m.f. of Kr. On the other hand, the thermal $CH_2{}^{80}BrBr$ and $CD_2{}^{80}BrBr$ yields are much less sensitive to the m.f. of Kr and are almost constant at 0.5% over the whole moderator range of Kr.

In the recoil chemistry of the gaseous phase, the excess kinetic energy processes are depressed by the addition of an inert gas as a kinetic energy moderator to the reaction system. At 1.0 m.f. of an inert gas moderator, the yields of the energetic processes should be extrapolated to zero. If the extrapolated value is finite, the value is usually considered to be the yield of the kinetic-energy-independent processes in an unmoderated system. In our recent work on the reaction with CH_4 of ^{80}Br activated by the (IT) process, however, we found that the addition of a large excess of inert gases to a reaction system sometimes causes an increase in the yield.[1] In such a case, it is necessary for a detailed analysis of the data to establish how the kinetic energy-independent-processes are affected by the addition of inert gases.

This complex phenomenon is primarily due to the charges imparted to the ^{80}Br atom at the time of the nuclear reaction; it is also due to the relatively low ionization potential of Br. Thus, it could also be anticipated in the reaction of ^{80}Br activated by the (n,γ) process with methane.

Rack and Gordus have examined the above reaction and reached the conclusion that the ^{80}Br atom from the (n,γ) activation reacts with CH_4 principally *via* energetic processes in the whole m.f. range of the moderators.[2] However, a detailed examination of the same reaction system using Kr as the additive has clearly shown that the kinetic-energy-independent process also contributes to the observed organic yields.[3]

In this paper we will apply the Estrup-Wolfgang kinetic theory[4,5] to the data obtained in the reaction of ^{80}Br activated by the (n,γ) process with two methanes, CH_4 and CD_4; with suitable assumptions, the most probable kinetic parameter I's and α's will be determined. The thermal yields of the products have, then, been determined as a function of the m.f. of the Kr moderator as the differences between the yields predicted by the kinetic theory and those experimentally determined.

Experimental and Results

The experimental procedure has been described in detail in a previous paper.[3] Samples were prepared in 18.5 ml silica ampoules. In all cases, the Br_2/CH_4 or CD_4 ratio was 0.02, and the total pressure was kept constant at 500 ± 10 mmHg. Energetic ^{80}Br was formed by irradiating the samples for 5—60 sec in a JRR-4 reactor. The thermal neutron flux at the irradiation port was 2×10^{12} n/cm^2/sec.

The present experimental data, as well as those in Ref. 3, have been used for the present kinetic treatment. The agreements between them are reasonably good. A small difference, however, can be seen in the yield of $CH_3{}^{80}Br$ at a high moderation. All the results are included in Figs. 1 and 2. The most sig-

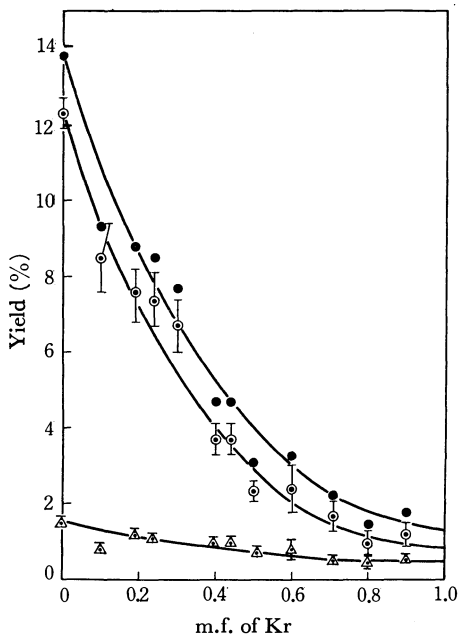

Fig. 1. Product distributions from the reaction system, ^{80}Br+CH_4+Kr.
●: total organic yield, ⊙: $CH_3{}^{80}Br$, △: $CH_2{}^{80}BrBr$.

1) K. Numakura, M. Saeki, and E. Tachikawa, This Bulletin, **46**, 1 (1973).
2) E. P. Rack and A. A. Gordus, *J. Phys. Chem.*, **65**, 944 (1961).
3) M. Saeki, K. Numakura, and E. Tachikawa, This Bulletin, **45**, 1715 (1972).
4) P. J. Estrup and R. Wolfgang, *J. Amer. Chem. Soc.*, **82**, 2665 (1960).
5) R. Wolfgang, *J. Chem. Phys.*, **39**, 2983 (1963).

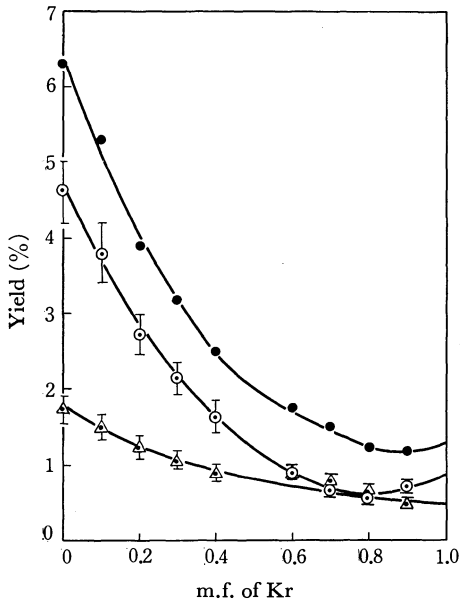

Fig. 2. Product distributions from the reaction system, $^{80}Br+CD_4+Kr$.
●: total organic yield, ⊙: $CH_3{}^{80}Br$, △: $CH_2{}^{80}BrBr$.

nificant error in the present data has been introduced in the measurement of the total ^{80}Br activities; it amounts to $\pm 10\%$ in some cases. The uncertainties in the figures indicate the standard deviations among the several measurements.

Application of Kinetic Theory

Estrup and Wolfgang have developed a kinetic theory of hot atom reactions partially based on the mathematics of neutron-cooling processes.[4,5] Although the exact solutions for the kinetic theory must be valid only for highly restricted special cases, they can furnish appropriate forms for the treatment of the experimental data. Three assumptions are involved in this kinetic treatment.[5] The first is that the energy loss occurs by collisions, in which the collision partners can be treated as elastic spheres. The second is that the initial energy of the atom, E_0, is sufficiently large so that the atom has made a number of collisions before reaching the upper limit of the reaction zone, E_2, thus providing a statistically well-defined distribution of energies for the hot atoms in the region of interest. The third is that the minimum energy required for the reaction, E_1, is still large compared to the thermal energies. The validity of these assumptions has been discussed in various systems, and the theory has been successfully applied to the hot atom reactions of halogens[2,6-8] as well as tritium.[5,9]

In the present systems, difficulties arise for at least two reasons. One is related to the initial energy of the ^{80}Br atom, in connection with the second assumption. Since the present knowledge of the spectrum of γ-rays emitted after the neutron capture of ^{79}Br is not sufficient, we only known that the maximum initial kinetic energy of ^{80}Br is 179 eV, which is low compared with those of (n,p)-activated tritium atoms (in the order of 10^5 eV). Thus, it can be considered that an appreciable fraction of the ^{80}Br atoms will be born with a low kinetic energy, in or near the reactive zone.[10] Rack and Gordus applied this theory to the reaction of ^{80}Br with gaseous methane.[2] Later, its application was extended further to the reaction of ^{80}Br[11,12] or ^{82}Br[6] activated by isomeric transition in various systems. These successful applications in both gaseous and liquid phases[8] can be taken as indicating that this assumption is reasonably justified in our present system. The other concerns the fact that no information is available about the Br-to-HBr abstraction reaction probability for the present reaction system, since no experimental procedure can serve for measuring $H^{80}Br$. Because of the low organic yield in the $^{80}Br+CH_4$ system, we could expect the inorganic yield to be comparable, causing no difficulty in the use of the kinetic theory treatment for a case of low reactivity.

According to the developed kinetic theory, the total energetic yields, P, in the moderator experiments have been expressed in terms of two kinetic parameters, I, reactivity integral and, α, average logarithmic energy loss, as follows:

$$-\frac{1}{\ln(1-P)} = \frac{\alpha_{react}}{I} + \frac{\alpha_{mod}}{I}\cdot\frac{1-f}{f} \qquad (1)$$

When the total probability of a hot reaction, P, is low, as in the present case, the developed equation for the yield of individual products from the hot reaction with a reactant in the moderated system, P_i (hot), can be simply expressed as:

$$P_i(\text{hot}) = (I_i/\alpha_{react})(1+\alpha_{mod}/\alpha_{react}(1/f-1))^{-1} \qquad (2)$$

If we know the values of I_i/α_{react} and $\alpha_{react}/\alpha_{mod}$, we can calculate P over the whole range of moderators using Eq. (1).

In the actual application of the kinetic theory to the results shown in Figs. 1 and 2, we have to consider the contribution of the thermal yield involved. It is possible to express the observed yield of individual products as the summation of the yields due to the energetic process and the thermal process at any m.f. of Kr. Thus, the following equation can be derived:

$$P_i = (I_i/\alpha_{CH_4})(1+\alpha_{Kr}/\alpha_{CH_4}(1/f-1))^{-1} + P_{i(\text{thermal})} \qquad (3)$$

The first term is for the energetic yield, and the second, for the thermal yield. It is known only that $P_{i(\text{thermal})}$ is equal to the extrapolated value, $P^{\infty}_{i(\text{thermal})}$, at 1.0 m.f. of Kr. Three cases can be considered, depending upon how the $P_{i(\text{thermal})}$ varies with the m.f. of Kr:

6) J. B. Nicholas and E. P. Rack, *J. Chem. Phys.*, **48**, 4058 (1968).
7) E. P. Rack and A. A. Gordus, *ibid.*, **34**, 1855 (1961).
8) M. Milman, *Radiochim. Acta*, **2**, 180 (1964).
9) R. T. K. Baker, M. Silbert, and R. Wolfgang, *J. Chem. Phys.*, **52**, 1120 (1970).
10) Using the random-walk equations, Rack *et al.* tried to calculate the kinetic energy spectra for (n,γ)-activated ^{128}I atoms, which have the maximum initial kinetic energy of 194 eV. The results showed that an appreciable fraction of the ^{128}I species are born with kinetic energy, near the reaction zone. M. Yoog, Y. C. Pao, and E. P. Rack, COO-1617-30 (1971).
11) E. Tachikawa and K. Yanai, *Radiochim. Acta*, **17**, 138 (1972).
12) K. Numakura and E. Tachikawa, This Bulletin, **46**, 346 (1972).

Case 1. $P_{i(thermal)}$ is constant over the whole m.f. range of Kr. In this case, $P_{i(thermal)}$ is simply equal to $P^{\infty}_{i(thermal)}$ and can be experimentally found.

Case 2. $P_{i(thermal)}$ is zero with no additive, but rises with an increase in the m.f. of Kr.

Case 3. This involves both cases, 1 and 2. $P_{i(thermal)}$ increases with the m.f. of Kr from a non-zero value to $P^{\infty}_{i(thermal)}$.

In the first case, the addition of an inert gas simply reduces the average kinetic energy of the ^{80}Br atom, resulting in a reduction of the energetic yiled without influencing the thermal yield. This is the case which is usually expected in recoil chemistry. In the other cases, however, the physical properties other than the kinetic energy of the recoil atom, such as the charge or electronic excitation energy state, are also affected by the addition of an inert gas, and the extrapolated value, $P_{i(thermal)}$, at 1.0 m.f. of Kr does not reflect the true thermal yield in the unmoderated system.

Unfortunately, without any *a priori* basis to know which category the present case belongs to, we can only assume that the thermal yield does not exceed the $P^{\infty}_{i(thermal)}$-value at any m.f. of Kr. Thus, the contribution of the total thermal yield ($P_{thermal}=\sum P_{i(thermal)}$) to the observed yield (P) is probably not significant at low m.f. values of Kr. As a first step to the kinetic treatment, therefore, the total organic yields obtained from zero to about 0.4 m.f. of Kr were subjected to Eq. (1), with the assumptions that, in this range of the m.f. of Kr, the total thermal yield is of only minor importance and that practically all the products are formed *via* energetic processes. The results obtained were shown graphically in Figs. 3 and 4 for the ^{80}Br–CH_4–Kr and ^{80}Br–CD_4–Kr systems. The ratio of the intercept to the slope gives $\alpha_{CH_4}/\alpha_{Kr}=0.33$ in Fig. 3 and $\alpha_{CD_4}/\alpha_{Kr}=0.37$ in Fig. 4.

If the I_i/α_{react} values are obtained by subtracting the thermal yield, $P^0_{i(trermal)}$, from the observed yield, P_i, in an unmoderated system, we can calculate the energetic yield of the individual products at any m.f. of Kr using Eq. (2). Then, the difference (ΔP_i) between the calculated yield and the experimentally-obtained

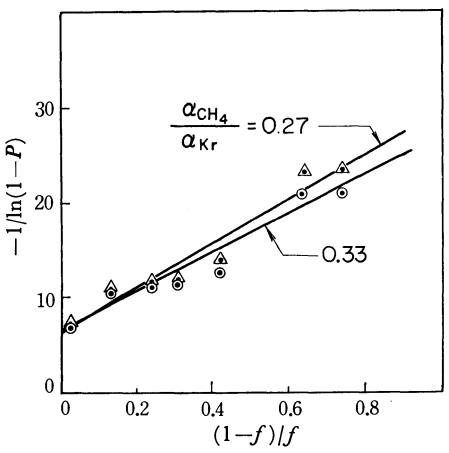

Fig. 3. Plot corresponding to equation 1) for the reaction system, ^{80}Br+CH_4+Kr.
⊙: calculated with the total organic yields, △: calculated with the values subtracted 0.5% from the total organic yields.

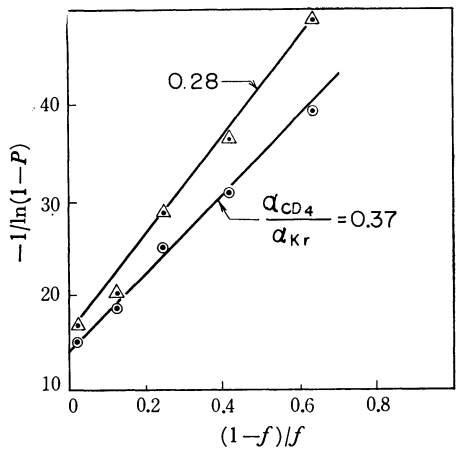

Fig. 4. Plot corresponding to equation 1) for the reaction system, ^{80}Br+CD_4+Kr.
⊙: calculated with the total organic yields, △: calculated with the values subtracted 0.5% from the total organic yields.

yield can be assumed to be the kinetic-energy-independent yield. Without a knowledge of the true $P^0_{i(thermal)}$ value, however, we can choose any value from zero to the limiting yield at 1.0 m.f. of Kr, $P^{\infty}_{i(thermal)}$. If a proper value is taken for $P^0_{i(thermal)}$, ΔP_i as a function of the m.f. of Kr should belong to one of three classes, depending upon the Cases 1, 2, or 3 discussed above. In Case 1, ΔP_i will be equal to the chosen value at any m.f. of Kr, while in Case 2 or 3 ΔP_i will increase with the m.f. of Kr from zero or a non-zero value to the $P^{\infty}_{i(thermal)}$. A set of calculations with the results for $CH_3{}^{80}Br$ and $CD_3{}^{80}Br$ show that when we use a $P^0_{i(thermal)}$ value other than zero the ΔP_i value obtained always shows a concave curve *vs.* the m.f. of Kr and has a minimum around 0.5 m.f. of Kr. Such a behavior of the thermal yield is very unrealistic, since the thermal process yield should not be reduced by the addition of an inert gas. On the other hand, when $P^0_{i(thermal)}$ is set as zero, the ΔP_i converges from around zero up to 0.7 m.f. of Kr. This ΔP_i curve shows a behavior consistent with the Case 2, indicating that the thermal yields of $CH_3{}^{80}Br$ and $CD_3{}^{80}Br$ in the present system are not important in the range from zero to around 0.7 m.f. of Kr, but become significant at a higher moderation.

A similar treatment of the results for $CH_2{}^{80}BrBr$ and $CD_2{}^{80}BrBr$ leads to the conclusions that, when $P^0_{i(thermal)}$ is chosen as 0.5%, ΔP_i is almost constant at 0.5 any mole fraction of Kr. This accords with the results expected in Case 1.

Those results were fed back to the recalculation of $\alpha_{react}/\alpha_{mod}$ using Eq. (1). In this feed-back calculation, the total organic yields less 0.5% were used as the P values. The results obtained are also plotted in Figs. 3 and 4 in the $-1/\ln(1-P)$ *vs.* $(1-f)/f$ relation. The ratio of the intercept to the slope of the lines gives $\alpha_{CH_4}/\alpha_{Kr}=0.27$ for the CH_4–Kr system and $\alpha_{CD_4}/\alpha_{Kr}=0.28$ for the CD_4–Kr system. Using new values for $\alpha_{react}/\alpha_{mod}$, the calculation of the energetic yields of the individual products were performed in a manner similar to that described above. The results are summarized in Fig. 5 for methyl bromides, $CH_3{}^{80}Br$ and $CD_3{}^{80}Br$, and in Fig. 6 for methylene bromide, CH_2-

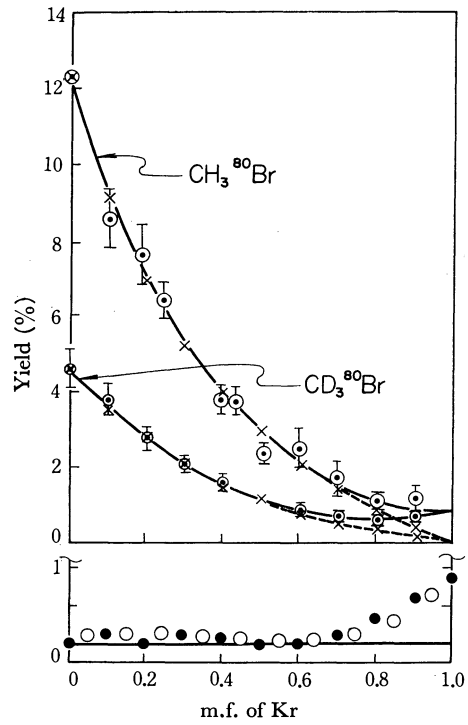

Fig. 5. Difference between the experimental yields and calculated ones of $CH_3{}^{80}Br$ and $CD_3{}^{80}Br$: estimation of their thermal yields.
in the upper figure.
⊙: experimental yields of $CH_3{}^{80}Br$ or $CD_3{}^{80}Br$
×: calculated yields of $CH_3{}^{80}Br$ or $CD_3{}^{80}Br$
in the lower figure
●: estimated thermal yields of $CH_3{}^{80}Br$
○: estimated thermal yields of $CD_3{}^{80}Br$

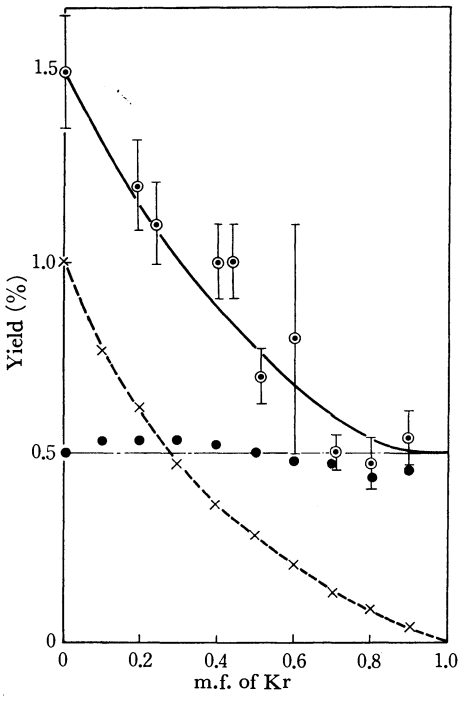

Fig. 6. Difference between the experimental yields and calculated ones of $CH_2{}^{80}BrBr$.
estimation of the thermal yields.
⊙: experimental yields of $CH_2{}^{80}BrBr$
×: calculated yields of $CH_2{}^{80}BrBr$
●: estimated thermal yields of $CH_2{}^{80}BrBr$

$^{80}BrBr$. The calculated energetic yields are shown by broken lines, in comparison with the experimental data, which are expressed by circles, with the experimental error and are connected by a solid line. The differences between two lines are assumed to be the thermal yields and are shown in the same figures by solid circles for $CH_3{}^{80}Br$ and $CH_2{}^{80}BrBr$ and by open circles for $CD_3{}^{80}Br$. The thermal yields of $CD_2{}^{80}BrBr$ obtained by a similar treatment, which are not included in the figure, were just the same as that obtained for $CH_2{}^{80}BrBr$, showing no significant difference in the contribution of the thermal process to the observed yield between $CH_2{}^{80}BrBr$ and $CD_2{}^{80}BrBr$.

It can be said that the thermal yield of methyl bromide is not significant and that it is substantially zero in the m.f. range of Kr from zero to around 0.7, but it starts to rise with a further increase in the m.f. of Kr and can reach to around 0.8% at 1.0 m.f. of Kr. On the other hand, the thermal yield of methylene bromide, $CH_2{}^{80}BrBr$ or $CD_2{}^{80}BrBr$, is almost constant at 0.5% over the whole m.f. range of Kr and no noticeable effect has been observed upon the addition of Kr.

In order to confirm the above hypotheses, a further investigation has been carried out on the isotope effect in $CH_3{}^{80}Br/CD_3{}^{80}Br$. The following assumptions have been introduced:

1) The thermal yield of the methyl bromide is related to the m.f. of Kr in the form of X_{Kr}^{n} (X_{Kr} is the m.f. of Kr, and n is a constant), and no isotope effect exists in the $CH_3{}^{80}Br/CD_3{}^{80}Br$ system as far as the thermal yields are concerned.
2) The values of the isotope effect in the energetic yield do not vary significantly from 2.7 over the whole moderator range of interest.

The first assumption is primarily based on the findings of the above kinetic treatments of the results. Although any other possible function might be used, it is convenient to use the present simple function, since there is almost no knowledge about the dependence of the thermal yield on the concentration of Kr except the present results. The non-existence of the isotope effect on the thermal processes has also been noticed in the reaction of ^{80}Br activated by the isomeric transition.[11] Thus, this is a reasonable starting assumption for the subsequent considerations. The second assumption is a rather crude one. Strictly speaking, this assumption is well justified only in a situation where the possible reaction energy range is the same for both reactions to form $CH_3{}^{80}Br$ and $CD_3{}^{80}Br$ and where the ratio of the probability of a successful reaction per collision for $CH_3{}^{80}Br$ relative to that for $CD_3{}^{80}Br$ is constant over the whole reaction energy range. This situation is a case of the reactivity integral isotope effect. However, the distinction of this situation from the others is not possible, and we can only assume this is the case.

On these assumption, the following equation can be derived for the isotopic variation in the yield of methyl bromide:

$$Y_{(n)} = \frac{(I_i/\alpha_{CH_4})(1+\alpha_{Kr}/\alpha_{CH_4}(1/f-1))^{-1}+X_{Kr}^{n}A}{(I_i/\alpha_{CD_4})(1+\alpha_{Kr}/\alpha_{CD_4}(1/f-1))^{-1}+X_{Kr}^{n}A'} \quad (4)$$

If n=zero, Eq. (4) can be simplified to;

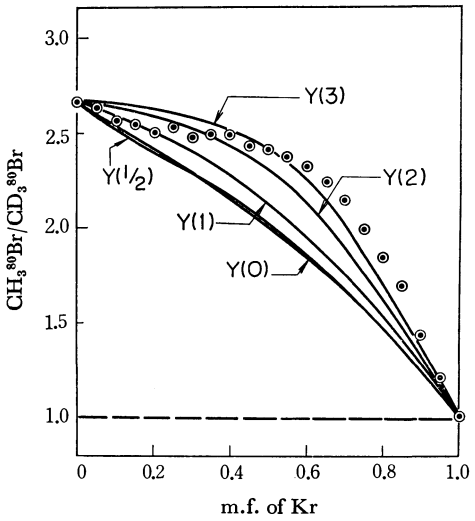

Fig. 7. Plot corresponding to Eqs. (4) and (5) with the experimental values. (details in the text.)

$$Y_{(n)} = \frac{(I_i/\alpha_{CH_4}-A)(1+\alpha_{Kr}/\alpha_{CH_4}(1/f-1))^{-1}+A}{(I_i/\alpha_{CD_4}-A')(1+\alpha_{Kr}/\alpha_{CD_4}(1/f-1))^{-1}+A'} \quad (5)$$

At the limiting condition at 1.0 m.f. of Kr, $A=P^{\infty}_{CH_3{}^{80}Br\,(thermal)}$ and $A'=P^{\infty}_{CD_3{}^{80}Br\,(thermal)}$. Since the limiting yield is roughly equal to 0.85% for both $CH_3{}^{80}Br$ and $CD_3{}^{80}Br$, $A'=A$. On the other hand, at zero m.f. of Kr, I_i/α_{CH_4} and I_i/α_{CD_4} are equal to $P^0_{CH_3{}^{80}Br}$ and $P^0_{CD_3{}^{80}Br}$ and are 12.3 and 4.6% respectively. Figure 7 shows Eq. (4) (for n equal to 1/2, 1, or 2) and Eq. (5) (for n equal to zero). The plots of the $CH_3{}^{80}Br/CD_3{}^{80}Br$ ratio obtained from the interpolated curves in Figs. 1 and 2 for $CH_3{}^{80}Br$ and $CD_3{}^{80}Br$ are also shown in the same figure. It is obvious that the experimental curve is far from the prediction for n=zero, although it does not show a good fit with either of the calculated cruves.

In view of the limits, accuracy of the present experimental results, it is very hard to discuss the results quantitatively and to find a function to fit the experimental results. One conclusion we can draw from the present calculations is that the contribution of the thermal process in producting methyl bromide is affected by the concentration of Kr. This conclusion accords with the finding in the early part of this paper.

Comparison of the Kinetic Parameter. I. Here it is interesting to evaluate the I value in the present reaction system and to compare it with those found in other reaction systems, such as in the reaction with the methane of ^{80}Br activated by isomeric transition.[1] This comparison will provide qualitative information concerning the reactivity of the recoil atom activated by various nuclear reactions.

By expanding Eq. (1), the following can be obtained:

$$P = (f/\alpha)I - (f/\alpha)^2K + (f/\alpha)^3L \cdots \quad (6)$$

In the case of a low reactivity, the total probability, P, may be well approximated by the first two terms, because these series will converge rapidly. A plot of $(\alpha/f)P$ *vs.* f/α should give a straight line, with an intercept of I and a slope of K. The values for I obtained by the plots are tabulated in Table 1, with along the α_{CH_4} and α_{CD_4} values. The I_i values obtained using Eq. (2) were also included. Those are all expressed in units of α_{Kr}.

Nicholas and Rack have also applied the kinetic theory to the total organic yield in the reaction of ^{82}Br activated by the (IT) process with CH_4.[6] In their calculation, the kinetic energy yield was obtained simply by subtracting the limiting yield at 1.0 m.f. of the moderator from the observed yield at various m.f. values of the moderator; $\alpha_{CH_4}=0.098\ \alpha_{Kr}$ and $I_{CH_3{}^{82}Br}=0.004\ \alpha_{Kr}$ were thus obtained.

However, a recent detailed examination of the reaction of ^{80}Br activated by the (IT) process with CH_4[1,14] has revealed that an additional yield due to the kinetic-energy-independent process becomes noticeable at a high moderation. A similar trend can also be expected in Rack's experiment. We consider that these reported values are strongly affected by the kinetic-energy-independent yield.

Although the α value should be an energy-dependent term, it is not conceivable that the value changes drastically in the reaction of the (IT)-induced ^{80}Br or ^{82}Br atom. The treatment of the results in Ref. (1) using the α value obtained in this work, $\alpha_{CH_4}=0.27\ \alpha_{Kr}$, gave $I_{CH_3{}^{80}Br}=0.018\ \alpha_{Kr}$, which is also included in Table 1. The $I_{CH_3{}^{80}Br}$ value in the $(n,\gamma)^{80}Br$–CH_4 system is roughly three times that in the ^{80m}Br–CH_4 system under the present kinetic treatment.

Discussion

The above calculations show that, within the limits of experimental error, the kinetic theory appears to be applicable to the present system as far as the energetic reactions are concerned; it also seems to be an adequate

Table 1. Parameters of kinetic theory
(expressed in units α_{Kr})

Reaction system	α	I(total)	I(product)	Reference
$^{79}Br(n,\gamma)^{80}Br+CH_4$	$\alpha_{CH_4}=0.266$	0.043	$I_{CH_3{}^{80}Br}=0.04$	Present work
	$(\alpha_{CH_4}=0.3)^{a)}$	0.057	.....	Ref. 2
$^{79}Br(n,\gamma)^{80}Br+CD_4$	$\alpha_{CD_4}=0.280$	0.020	$I_{CD_3{}^{80}Br}=0.015$	Present work
$^{80m}Br(IT)^{80}Br+CH_4$	$\alpha_{CH_4}=0.266$	.....	$I_{CH_3{}^{80}Br}=0.018$	Ref. 1
$^{82m}Br(IT)^{82}Br+CH_4$	$\alpha_{CH_4}=0.098$	.....	$I_{CH_3{}^{80}Br}=0.004$	Ref. 6

a) calculation with Kr moderation data in Ref. 2.
b) calculation based on the present α value.

13) J. O. Hirschfelder, C. F. Curtiss, and R. B. Bird, "Molecular Theory of Gases and Liquids" John Wiley & Sons, Inc., New York (1954), p. 1110.
14) E. Tachikawa and T. Kahara, This Bulletin, **43**, 1293 (1970).

framework for the entire range of data. In other words, it appears that the assumptions of the kinetic theory are reasonably satisfied, in that the treatment is sufficiently insensitive to the approximations that are inherent in these assumptions.

However, some question still remains as to the value used as the total energetic yield. The abstraction of hydrogen by the recoil atom is a very common reaction mode; it must also be taken into account in the present system. In the recoil tritium reactions, the ratio of the hydrogen-abstraction yield to the hydrogen-substitution-reaction yield has been well established as 0.79 for CH_4,[15] and it tends to increase with the number of carbon atoms in the reactant molecule.[16] Recently Root *et al.* examined the energetic F-to-HF abstraction yield in the reaction of recoil ^{18}F with CH_3CF_3 and reported the value of 51% for the primary yield.[17]

Without any available experimental data for the Br-to-HBr abstraction reaction, we assigned various yields for this abstraction yield and tried to determine the trend shown by the results drawn from the kinetic treatment. Assuming, for example, that the energetic $H^{80}Br$ yield is equal to the total organic yield, the kinetic treatment gave $\alpha_{CH_4}/\alpha_{Kr}=0.26$, which is quite similar to the value found in the preceeding calculation. Thus, the conclusion reached above is hardly affected by a correction for the total organic yield, considering the energetic $H^{80}Br$ yield.

The identity of the thermal processes is primarily ascribed to the thermal ionic processes, considering the physical state of ^{80}Br at the time of formation from the nuclear reaction. However, when we compared the limiting yield at 1.0 m.f. of Kr between the present case and the ^{80m}Br–CH_4,[1] a similar value was found for $CH_3{}^{80}Br$ but not for $CH_2{}^{80}BrBr$. This can not be easily explained with the presently available knowledge, as has been suggested in an earlier report of this series,[18] the role of interaction between ^{80}Br and Kr might also be considered.

15) J. W. Root and F. S. Rowland, *J. Chem. Phys.*, **46**, 4299 (1967).
16) E. Tachikawa and F. S. Rowland, *J. Amer. Chem. Soc.*, **90** 4767 (1968).
17) N. J. Parks, K. A. Krohn, and J. W. Root, *J. Chem. Phys.*, **55**, 2690 (1971).
18) E. Tachikawa, This Bulletin, **43**, 63 (1970).

BULLETIN OF THE CHEMICAL SOCIETY OF JAPAN, VOL. 46, 844—847 (1973)

Synthesis and Metal Chelate Stability of *N,N'*-Ethylenebis(aminomalonic) Acid

Misao MASHIHARA*, Takeshi ANDO, and Ichiro MURASE

Laboratory of Chemistry, College of General Education, Kyushu University, Ropponmatsu, Fukuoka 810

(Received July 20, 1972)

N,N'-Ethylenebis(aminomalonic) acid (EAMA) has been synthesized, and its acid dissociation constants and the stability constants of its alkaline earth metal complexes were determined potentiometrically at 25°C in a medium of ionic strength of 0.10 (KNO_3) with the following results: $pK_1=2.1$, $pK_2=2.72$, $pK_3=6.56$, $pK_4=9.69$; $\log K_{MY}$ and $\log M_{MHY}$ for Ca(II) respectively, 5.45 and 2.02; for Mg(II) respectively 4.93 and 1.80. The exact stability constants of Cu(II) and Ni(II) chelates of this ligand were not obtained on account of its decomposition in low pH solution, but the order of relative stability has been established. From a comparison of the stability of Ca(II) and Mg(II) chelates with those of the analogous complexane, the function of the malonate group in the chelate formation has been discussed. Zn(II) and Co(II) chelates of this ligand have been obtained and their probable structures are proposed.

Aminomalonic acid investigated by Schwarzenbach[1] as a chelating ligand has three functional groups in metal chelate formation. However, it is sterically impossible for these three groups to coordinate to the metal ion forming two chelate rings. The ligand functions as a bidentate ligand in which the amino nitrogen and one carboxylate participate in chelate formation. This was evidenced by the fact that the stability of the metal chelates of aminomalonic acid is lower than that of iminodiacetic acid which can act as a terdentate ligand to form two chelate rings with the metal ion.

N,N'-Ethylenebis(aminomalonic) acid (EAMA) (I) is a tetrabasic acid having six donor groups including two basic nitrogen atoms.

(I)

However, it is considered to act as a quadridentate ligand in metal chelate formation as in aminomalonic acid, being expected to exhibit behavior analogous to that of ethylenediamine-*N,N'*-diacetic acid.

This paper deals with the synthesis and chemical behavior of EAMA, the potentiometric determination of acid dissociation constants, and metal chelate stability. A discussion is given on the function of the

* Present address: Ube Technical College, Tokiwadai, Ube.

1) G. Schwarzenbach, E. Kampitsch, and R. Steiner, *Helv. Chim. Acta*, **28**, 1133 (1945).

malonate moieties in metal chelate formation and stability in comparison with analogous ligands such as ethylenediaminetetraacetic acid (EDTA), ethylenediamine-*N,N'*-diacetic acid (EDDA), and ethylenediamine-*N,N'*-di(α-propionic) acid (EDDMA). The structure of the insoluble chelates with Co(II) and Zn(II) ion has been determined by means of infrared spectroscopy.

Experimental

Material. N,N'-*Ethylenebis(aminomalonic) acid (EAMA)*: To a solution of 9.2 g (0.05 M) of bromomalonic acid dissolved in 30 ml of water and neutralized with 30% aqueous sodium hydroxide at 5°C was added 1.5 g (0.025 M) of 98% ethylenediamine and the mixture was heated at 70°C. The pH of the solution was kept at 9—11 for 1 hr by dropwise addition of 30% aqueous sodium hydroxide. On cooling, it was brought to 1—2 by careful addition of dilute hydrochloric acid and the resulting precipitates were filtered and washed with water and methanol. For purification, the crude product was dissolved in aqueous alkali, filtered and precipitated by adjusting the pH of the filtrate at nearly 1 with dilute hydrochloric acid. The procedure was repeated three times and a pure sample was dried over calcium chloride in a vacuum. The acid undergoes decarboxylation at 166—169°C and melts at 202—204°C with decomposition.

Found: C, 33.62; H, 5.33; N, 10.03%. Cacld for $C_8H_{12}N_2O_8 \cdot H_2O$: C, 34.05; H, 5.00; N, 9.93%.

Disodium Salt of EAMA: To a suspension of 6 g of free EAMA in 100 ml of water was added 30% aqueous sodium hydroxide until the pH of the solution reached 8 and the solution was filtered. The filtrate was diluted with 300 ml of ethanol and the resulting precipitates were filtered. The product was dissolved in a minimum amount of water, filtered, and precipitated by the addition of a large amount of ethanol. The procedure was repeated and the product was dried over calcium chloride in a vacuum.

Found: C, 28.14; H, 4.04; N, 8.55%. Calcd for $C_8H_{10}N_2O_8Na_2 \cdot 2H_2O$: C, 27.92; H, 4.10; N, 8.14%.

Decarboxylation of EAMA: A suspension of 6 g of free EAMA in 60 ml of water was refluxed for 2 hr, while the acid gradually dissolved into solution accompanied by evolution of carbon dioxide. The resulting clear solution was concentrated to 20 ml in a vacuum and diluted with 60 ml of ethanol. After being left overnight in a refrigerator, the resulting crystals were filtered. Recrystallization twice from dilute ethanol gave a pure sample of ethylenediamine-*N,N'*-diacetic acid, mp 210—211°C (decomp.).

Found: C, 40.56; H, 7.12; N, 15.84%. Calcd for $C_6H_{12}N_2O_4$: C, 40.91; H, 6.82; N, 15.90%.

The filtrate from which crude EDDA was obtained was evaporated to dryness and the residue was recrystallized three times from methanol. The compound was determined to be ethylenediamine-*N,N'*-diacetic acid lactam. It melts at 222°C with decomposition. IR (KBr) 1645 cm^{-1} (lactam C=O), 1586 cm^{-1} (COO^-).

Found: C, 44.02; H, 6.58; N, 17.29%. Calcd for $C_6H_{10}N_2O_3 \cdot 1/3\ H_2O$: C, 43.90; H, 6.55; N, 17.06%.

Co(II) Complex of EAMA: A 100 ml aqueous solution of 0.01 M disodium salt of EAMA was mixed with 90 ml of 0.01 M $Co(NO_3)_2$ aqueous solution, to which was added 20 ml of 0.1 N HNO_3. After being left overnight, the resulting precipitates were filtered and washed with water and methanol and dried over calcium chloride in a vacuum. Pink crystalline powder, mp>280°C.

Found: C, 25.43; H, 4.24; N, 7.77; Co, 15.85%. Calcd for $C_8H_{10}N_2O_8Co \cdot 3H_2O$: C, 25.61; H, 4.30; N, 7.47; Co, 15.72%.

Zn(II) Complex of EAMA: The procedure was the same as in the preparation of Co(II) complex except that zinc nitrate was used in place of cobalt nitrate. Colorless crystalline powder, mp>280°C.

Found: C, 25.18; H, 4.03; N, 7.48; Zn, 17.20%. Calcd for $C_8H_{10}N_2O_8Zn \cdot 3H_2O$: C, 25.18; H, 4.23; N, 7.34; Zn, 17.13%.

Measurements and Calculation. The method consists of potentiometric titration of the ligand in the absence of the metal ion for the acid dissociation constant and in the presence of the metal ion for the chelate stability. A carbonate free 0.1M KOH was used for the titration. All measurements were carried out at 25±0.1°C in a medium of ionic strength of 0.10 (KNO_3) with a Hitachi Horiba model F-5 pH meter.

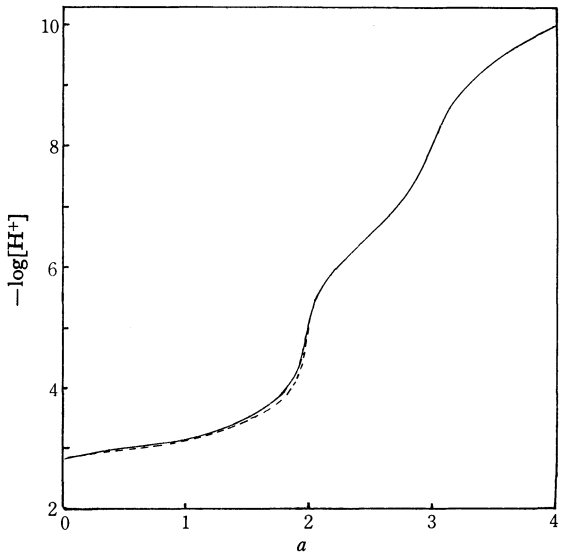

Fig. .1 Titration of EAMA and EAMA–2Na, ------ EAMA–2Na+0.1M HCl; —— EAMA+0.1M KOH (after the neutralization of EAMA–2Na). The concentration of the acid is 0.001 M.

It should be substantiated that no decomposition of the ligand occurs during the course of titration, since EAMA turns to decarboxylate in solution at low pH. Thus the solution of disodium salt of EAMA was titrated with 0.1M HCl until two equivalent of the acid had been added and the solution was retitrated with 0.1M KOH until four equivalent of the base had been added. As seen in Fig. 1, the titration curves coincide with each other within experimental error, provided that the effect of increasing volume is taken into consideration. Therefore, it has been proved that no decomposition occurred.

The acid dissociation constants were calculated by the method of Schwarzenbach and Ackermann.[2] Determination of the stability constants of the Ca(II) and Mg(II) chelates was also accomplished by the same method. For the determination of the stability of Ni(II) and Cu(II) chelates, attempts were made to apply the method of Anderegg used for measuring the stability constants of moderately stable chelates of complexanes.[3] However, the stability constants could not be calculated owing to possible partial decomposition of the ligand. Thus the calculation was made by Bjerrum's

2) G. Schwarzenbach and H. Ackermann, *ibid.*, **31**, 1029 (1947).
3) F. L'Eplattenier and G. Anderegg, *ibid.*, **47**, 1792 (1964).

procedure on the assumption that EAMA would form 1:1 chelates with both metal ions almost exclusively. The procedure was applied by Chaberek and Martell[4] to measure the stability of transition metal chelates of ethylenediamine-*N*,*N*'-diacetic-*N*,*N*'-dipropionic acid. In the present case, the relative precision of the obtained data was very low.

The equilibrium constants are expressed as follows:

Acid dissociation constants,

$$K_n = [H^+][H_{4-n}Y^{n-}]/[H_{4-n+1}Y^{(n-1)-}]$$

Stability constants,

$$K_{MHY} = [MHY^-]/[M^{2+}][HY^{3-}]$$

$$K_{MY} = [MY^{2-}]/[M^{2+}][Y^{4-}]$$

where H_4Y and M represent EAMA and metal ion, respectively.

Results and Discussion

Titration Curves. The titration curve of EAMA (Fig. 2) has buffer regions at about pH 4 and 7 followed by inflections at two equivalents and three equivalents of base respectively per mole of the amino acid. Thus the free acid, the divalent anion and the trivalent anion exist in a relatively pure state in solution, whereas the tetraalkali metal salt is extensively hydrolyzed.

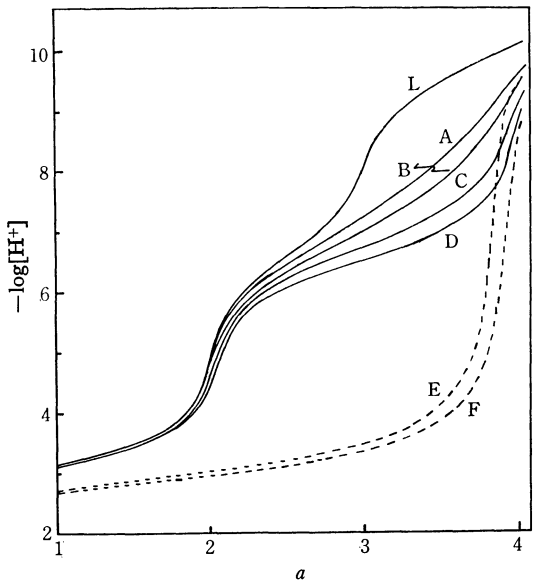

Fig. 2. Titration of EAMA with 0.1M KOH in the presence of metal ions. L, 0.001M free acid; A, B, E, and F, same as L with equimolar Mg(II), Ca(II), Ni(II), and Cu(II) respectively; C and D, with about ten times excess of Mg(II) and Ca(II) respectively. (All metal salts are the nitrate)

The titration curves in the presence of metal ions, shown in Fig. 2, indicate relatively weak chelate formation with alkaline earth metals but strong interaction with transition metals.

The free amino acid tends to decompose in acidic solution due to decarboxylation of the malonic acid moiety to yield ethylenediamine-*N*,*N*'-diacetic acid. In the absence and presence of alkaline earth metal ions, however, such decomposition process could not be observed during the course of titration. On the other hand, in the titration curves with Cu(II) and Ni(II) ions, the inflection deviates from the exact stoichiometry at $a=4$ indicating the decomposition of the ligand.

Table 1. Acid dissociation constants
$t=25°C$; $\mu=0.10$ (KNO_3)

	pK_1	pK_2	pK_3	pK_4
EAMA	2.1	2.72	6.56	9.69
EDTA[6]	2.0	2.67	6.16	10.27
			pK_1	pK_2
EDDA[5]			6.48	9.57
EDDMA[7]			6.69[a]	9.58[a]

a) These were measured at 20°C, $\mu=0.10$(KCl)

Acid Dissociation and Metal Chelate Stability Constants. The first and second acid dissociation constants (pK_1 and pK_2) of EAMA, listed in Table 1 are almost the same as the corresponding values for EDTA, indicating that they are due to the dissociation of the free carboxylic acid in (I) and (II).

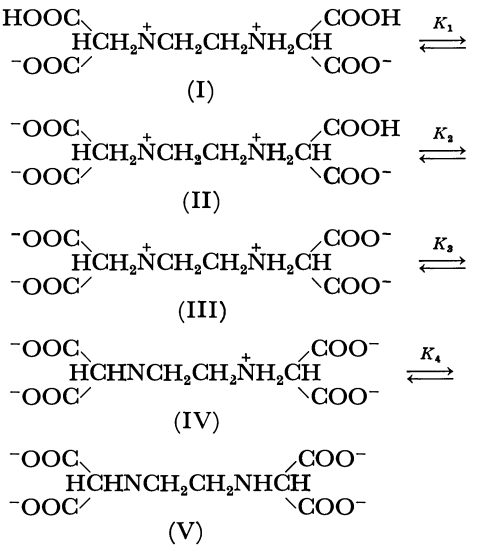

The third dissociation of a proton is the liberation from the $-\overset{+}{N}H_2-$ in (III). It is greatly influenced by positive charge of the adjacent ammonium group. The pK_3 value is higher than that of EDTA by 0.4 log unit and almost comparable to that of EDDA as seen in Table 1.

The difference between the acidity of the last proton to dissociate from (IV) and that of corresponding anion of EDTA may be explained on the basis of the relative electrostatic effects in these anions. The pK_4 value of EAMA is lower than that of EDTA by *ca.* 0.6 log unit. We see that the inductive effect of two carboxylate anions through one $-CH<$ group in EAMA is smaller than that of the two carboxylate anions through each $-CH_2-$ group in EDTA. However, a larger inductive effect of the malonate anion than that of single acetate

4) S. Chaberek, Jr., and A. E. Martell, *J. Amer. Chem. Soc.*, **74**, 6228 (1952).

5) L. C. Thompson, *J. Inorg. Nucl. Chem.*, **24**, 1083 (1962).

6) R. Skochdopole and S. Chaberek, Jr., *ibid.*, **11**, 222 (1959).

7) H. Irving, R. Shelton, and R. Evans, *J. Chem. Soc.*, **1958**, 3540.

TABLE 2. STABILITY CONSTANTS OF EAMA AND SOME RELATED CHELATES (μ=0.10)

	logK_{MY} for				log K_{MHY} for		Temp. (°C)	Medium
	Ca (II)	Mg(II)	Cu(II)	Ni (II)	Ca (II)	Mg(II)		
EAMA	5.45	4.93	(13)	(12)	2.02	1.80	25	KNO_3
EDTA	10.59	8.69	18.3	18.4	3.51	2.28	20	KCl
EDDA[4]		3.9	16.2	13.5			30	KCl
EDDMA[7]		2.8	15.2	12.2			20	KCl

group is observed in comparing the pK_4 value with pK_2 value in EDDA.

The stability constants of EAMA with alkaline earth metal ions are much lower than those with EDTA as seen in Table 2. Although EAMA carries six coordination sites in the molecule, it will be sterically impossible for the two carboxylate groups in each malonate moiety to coordinate to the metal ion at the same time. Since the presence of the binuclear chelate is not observed from titration in the presence of large excess of the metal ion (log $K_{M_2Y}\approx 0$), the most probable structure of the alkaline earth metal chelates will be one in which a carboxylate group in each malonate moiety is free and the remaining coordination sites are occupied by water molecules as shown in Fig. 3.

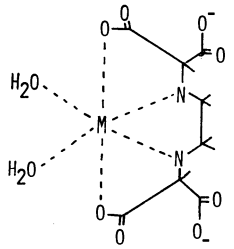

Fig. 3. Probable structure of the alkaline earth metal chelate.

We see from a comparison of log K_{MY} of Mg(II) chelate of EAMA with that of EDDA that the stability for the former is higher by one log unit. This may be partly due to higher basicity of the nitrogen atoms. However, the main contribution lies on the entropy effect of the two malonate groups, which results from an increase of the probability of attaining a spatial orientation required for chelation with the central metal ion. This is also evidenced by the comparison with EDDMA in which one carboxylate of both malonate groups in EAMA is replaced by a methyl group. Although the basicities of the two nitrogen atoms are comparable to those of EAMA (Table 1), the stability of Mg(II) chelate is lower than that of EAMA and even that of EDDA (Table 2). The methyl groups functioned only as a bulky group to exert a steric hindrance to the chelate formation.

A strong interaction of EAMA with Cu(II) and Ni(II) ions is observed from the titration curves. However, the chelate formation with these ions is accompanied by decomposition of the ligand, and the stability constants obtained suggest only a relative order of their magnitude. Considering the above chelate effect the true stability constants might assume any values between those of EDDA and EDTA provided the structures of these chelates are the same as those of the alkaline earth chelates. Decomposition will be due to a lowering of pH by the chelate formation and the metal ion in the chelate also may catalyze the decomposition.

Structure of Co(II) and Zn(II) Chelates. Titration of EAMA with Co(II) and Zn(II) ions was impossible because they formed insoluble precipitates before titration. It was found that the lower pH was favorable for the formation of precipitates. The metal-ligand composition is exactly 1:1 for both compounds as suggested by elementary analysis.

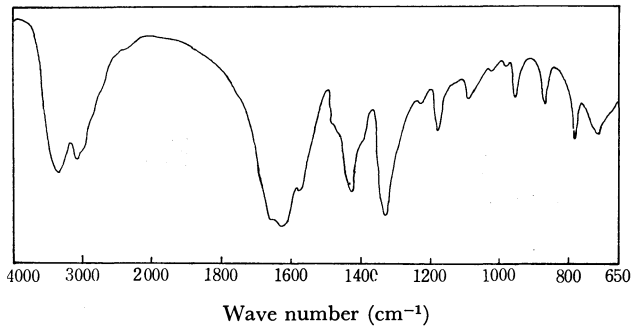

Fig. 4. Infrared spectrum of Zn(II) chelate.

Infrared spectra of both compounds are superimposal (Fig. 4). A very strong and broad band was observed around 1640 cm^{-1}, due to a symmetric stretching vibration of the carboxylate group. A stretching vibration of ammonium group appears around 3000—2500 cm^{-1}. In the free ligand, the carboxylate absorption is at the same position, but the carbonyl vibration of the free carboxylic acid is observed as a sharp absorption at 1754 cm^{-1}. Thus the compound might be a neutral metal chelate polymer in which the ligand molecules are bridged together with the metal ion at the terminal malonate groups and all imino nitrogens are protonated (Fig. 5).

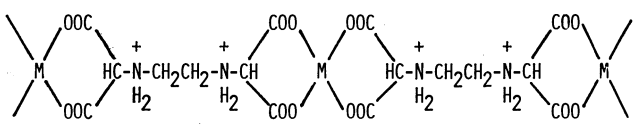

Fig. 5. Structure of Co(II) and Zn(II) chelates.

The chelate polymer is insoluble in water and soluble in alkaline solution. This can be explained by the positive charges on the ammonium nitrogens being neutralized by the hydroxide anion and the unit molecule carring −2 charge.

Photochromism of Thallium Chloride

Sumio SAKKA and J. D. MACKENZIE*

Department of Industrial Chemistry, Faculty of Engineering, Mie University, Tsu, Mie
**School of Engineering and Applied Science, University of California, Los Angeles, California, USA*

(Received July 26, 1972)

The ultraviolet-induced darkening and subsequent bleaching of crystalline thallium chloride was investigated in order to study the processes occurring in a photochromic glass containing TlCl crystalline particles. Doping with a small amount of copper, silver or indium ion was found to be effective in promoting darkenability of TlCl crystals. Exposure to visible light causes bleaching of UV-induced coloring of TlCl crystals. Almost no fading occurs, however, when TlCl crystalline pieces are kept in darkness at room temperature or higher temperatures up to about 70°C, where very quick fading in color is observed in the case of TlCl crystals embedded in a glassy matrix.

Much attention has been drawn to photochromic silver halide glass[1,2] since its discovery. The glass darkens when it is exposed to UV light and returns reversibly to the original non-colored state when kept in darkness. The active agents inducing such behavior are silver halide crystalline particles embedded in a glassy matrix. The reversibility of color change was explained by the reasoning that silver halide particles do not lose halogens since they are surrounded by impermeable and inert glassy matrix.[1]

Thallium monohalides are supposed to be similar to silver halides in some respects[3] and it is considered that photochromic glasses could be made with the use of thallium halides as active agents. This was actually found to be the case.[4] Experimental results on the photosensitive and photochromic behavior of TlCl crystalline pieces and a comparison with the behavior of TlCl crystals in glass are given in this paper. The photolytic behavior of silver halide crystal has been extensively investigated, because of its importance in the field of photography, but not that of thallium halide crystal. It is known that the presence of impurity Ag or Pb promotes the photosensitivity of TlCl,[5] although, according to Renz,[6] even very pure TlCl becomes dark by prolonged UV irradiation. Optical absorption measurements[7,8] show that TlCl has a few large absorption bands with the absorption edge reaching 400 mμ and a broad visible absorption band peaking at 535 mμ before and after UV irradiation, respectively. The crystal shows selective bleaching, to which Hilsch and Pohl attributed the presence of colloids.

Christy and Dimock[9] suggested that no color centers were formed by X-ray irradiation in a pure large crystal of TlCl. This is also the case for AgCl crystal. A large AgCl crystal showed almost no coloration upon irradiation when it was very pure, the addition of copper being necessary to give the UV coloration.

A small amount of chalcogen impurities such as S^{2-} and Se^{2-} produced an absorption peak near 400 mμ when a TlCl crystal is quenched from high temperatures without irradiation. The peak disappeared and another band (colloidal band) appeared near 600 mμ when the crystal was kept at room temperature. The study made by Christy and Dimock[9] and other previous works[5-8] would imply that a large TlCl crystal should contain some kind of impurity if it is colored by UV irradiation and that there is a possibility for the formation of Tl colloids in TlCl crystal.

Experimental

Preparation of TlCl Crystal. TlCl crystals were prepared by melting TlCl powder (Alfa Inorganics, Inc., U.S.A.). The powder was heated in a small pyrex beaker in an electrically heated furnace in air at 500°C. The molten mass of TlCl was slowly cooled down in the furnace. From the clear but slightly greyish solidified mass of TlCl crystal, rectangular pieces, about $20 \times 10 \times 1$ mm^3, were cut off with a razor blade, and, to make the surface smooth, were remelted between two thin sheets of glass which were easily peeled off after cooling. The thickness of plate samples was 1.0—1.4 mm. To incorporate a given impurity cation into "pure" TlCl, a given amount of the corresponding metal chloride was mixed with TlCl powder before the first melting.

Preparation of Glass. Composition, preparation, and properties of photochromic glasses containing TlCl crystallites were described in detail in a separate paper.[4]

For the present suty, a batch mixture consisting of KPO_3 25, $Ba(PO_3)_2$ 25, $Al(PO_3)_3$ 50, TlCl 12, NaCl 6, Cu_2O 0.03 parts by weight was melted in a platinum crucible at 1200°C for 20 min. A glass plate 8 mm × 20 mm × 1 mm was heated at 420°C for 10 hr to precipitate TlCl crystallites, and then subjected to measurement.

Light Exposure and Transimission Measurement. A black ray lamp with main emission peak at 3660 Å (General Electric Model F6T5) was used as UV-light source. The sample plate was placed at a distance of 4 cm from the lamp. An infrared heating lamp of 250 watts was used as a visible light source to cause bleaching of darkened samples. The sample was placed at a distance of 36 cm from the lamp, with filters which permitted light of wavelengths 530—680 mμ. To avoid possible temperature rise in the sample during exposure air was blown to the sample by an electric fan. Transmission measurements were made with a recording spectrophotometer Model Spectronic 505 of Bausch and Lomb Company. For the sake of simplicity "absorption"

1) W. H. Armistead and S. D. Stookey, *Science*, **144**, 150 (1964).
2) G. P. Smith, Paper 108, 7th Intern. Congr. Glass, Brussels, Belgium, July 1965.
3) F. Seitz, *Rev. Modern Phys.*, **23**, 328 (1951).
4) S. Sakka and J. D. Mackenzie, *J. Amer. Ceram. Soc.*, **55**, 553 (1972).
5) J. W. Mellor, Treatise on Inorganic and Theoretical Chemistry, Vol. V, p. 438 (1924).
6) C. Renz, *Helv. Chim. Acta*, **2**, 704 (1919).
7) H. Fesefeldt, *Z. Phys.*, **64**, 741 (1930).
8) R. Hilsch and R. W. Pohl, *ibid.*, **64**, 606 (1930).
9) R. W. Christy and J. D. Dimock, *Phys. Rev.*, **141**, 806 (1966).

or "absorbance" will be used throughout this paper to indicate the increment of absorption or absorbance over that of the samples before UV irradiation. Throughout the experiments, the samples were kept in darkness in a dessicator to avoid possible effects of room lights and diffuse sunlight.

Results

Preliminary Results for the Effect of Impurity on Darkenability. A small amount (0.05 mol%) of various chlorides was incorporated into TlCl by melting powder mixture and the resultant doped TlCl mass was exposed to UV light. The chlorides tried were $CaCl_2$, VCl_3, $MnCl_2$, $FeCl_2$, $NiCl_2$, CuCl, $CuCl_2$, $SrCl_2$, AgCl, $CdCl_2$, $PbCl_2$, $BiCl_3$, InCl, $CeCl_3$, and $SmCl_2$. Some of these chlorides gave grey, yellow, or brown color to the TlCl mass before irradiation. In spite of this original discoloration, it was possible to tell the effect of impurity on UV darkenability qualitatively. It was found that Cu, Ag, and In have a remarkable effect in promoting the coloring of the TlCl crystal induced by UV irradiation. "Pure" TlCl and Cu-doped TlCl crystalline pieces will be used for further experiments.

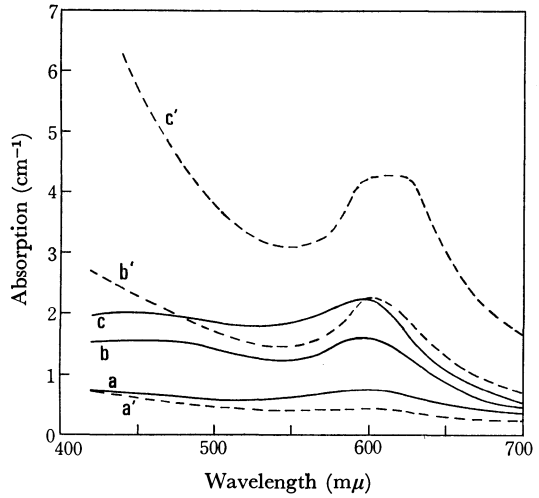

Fig. 1. Absorption spectra of TlCl crystals darkened by UV exposure. Solid lines (a′, b′, c′): "Pure" TlCl. Broken lines (a′, b′, c′): Cu-doped TlCl. Time of exposure: a 6 min, a′ 1 min, b and b′ 30 min, c and c′ 60 min.

Darkening by UV Irradiation. TlCl samples were exposed to UV light for different periods of time ranging from one to 60 min. Some examples of the absorption curves are shown in Fig. 1. The increase in absorption coefficient due to irradiation is plotted as a function of wavelength. In TlCl: Cu sample, darkening was quite remarkable on the surface facing the UV light source. In the "pure" TlCl sample, no particularly dark surface layer was detected. In spite of the difference, plots were given with the use of nominal absorption coefficient for a comparison of the darkenabilities.

We see that an absorption band is developed with a peak around 600 mμ and, at the same time, the absorption increases in the range of wavelengths shorter than 500 mμ. The increase in the latter absorption is particularly remarkable in Cu-doped sample.

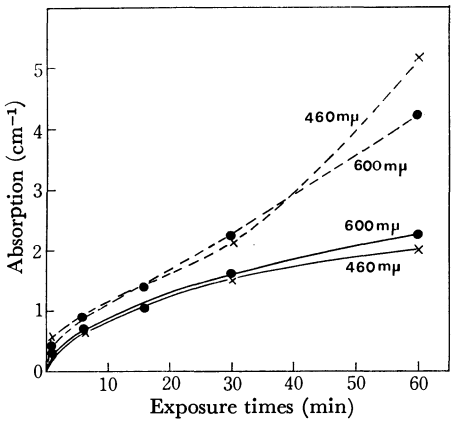

Fig. 2. Absorption change of TlCl crystals with increasing time of exposure to UV. Solid lines: "Pure" TlCl. Broken lines: Cu-doped TlCl.

Figure 2 shows the growth of a peak near 600 mμ and a band less than 500 mμ as a function of exposure time. The absorption coefficient at 600 mμ was chosen as a measure of absorption for the former and that at 460 mμ for the latter. We see that TlCl: Cu darkens at a faster rate than "pure" TlCl. The growth of the absorption at 460 mμ is almost parallel to that at 600 mμ, although the former grows slightly faster in Cu-doped TlCl when exposure time is long (30—60 min).

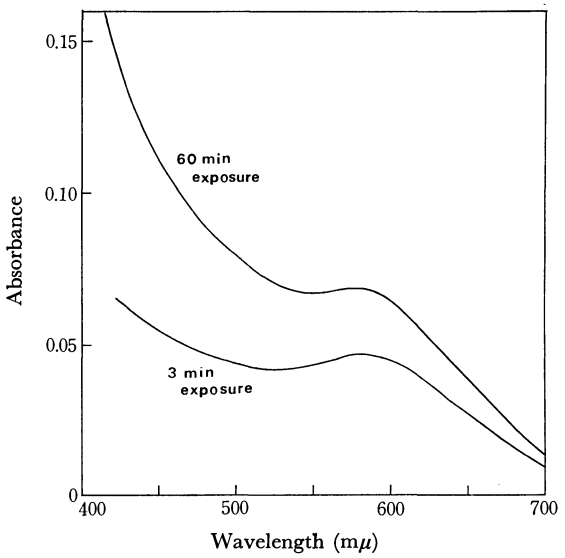

Fig. 3. Absorption spectra of glass darkened by UV exposure. Thickness of the sample: 0.67 mm.

Figure 3 shows the absorption in the TlCl-containing photochromic glass caused by UV irradiation. It can be seen that the general shape of the absorption curve is similar to that of TlCl crystals, especially TlCl: Cu sample. There is an absorption band with a peak at 580 mμ, which is a little shorter than those (600—610 mμ) for TlCl crystals, but pretty close. In the range of the wavelengths smaller than 500 mμ, there is another band.

Exposure of Darkened Samples to a Longer Wavelength Light. Irradiation of UV colored samples by a visible light causes the bleaching in color. Absorption

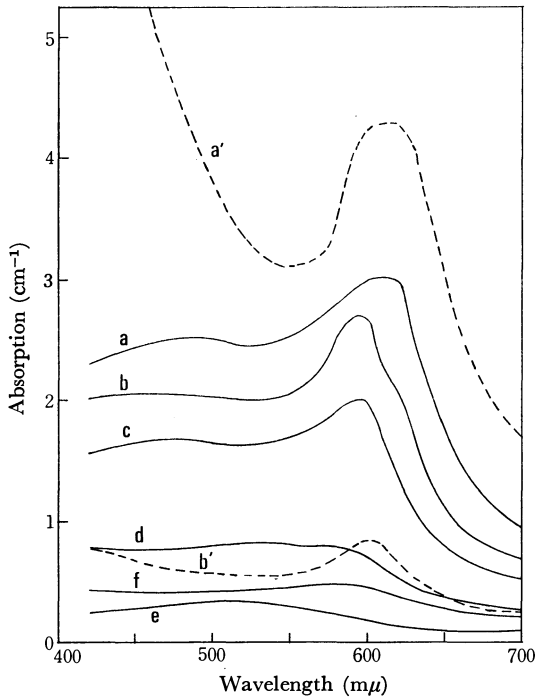

Fig. 4. Fading of color by visible light exposure. a: "Pure" TlCl after UV exposure of 2 hr (before bleaching). b: 1 min bleaching by visible light through filters. c: 2 min bleaching. d: 16 min bleaching. e: 26 min bleaching. f: 1 min bleaching by visible light without filters. a': Cu-doped TlCl after UV exposure of 1 hr. b': 20 min bleaching by visible light through filters.

curves obtained in the process of bleaching by a visible light containing rays ranging from 530 to 680 mμ are shown in Fig. 4.

From a series of cruves for "pure" TlCl (solid line), it can be seen that the band with a peak at 600 mμ becomes weak at a greater rate than in the absorption at shorter wavelengths. Thus the curves d and e have no distinct absorption peak around 600 mμ, while there is some absorption left around 500 mμ. It is true, however, that all absorption is decreased by irradiation and disappears eventually. When the sample is exposed to light without filters which permit only 530—580 mμ, the 600 mμ peak is found to remain more or less noticeable (see curve f). On the other hand, no preferential decrease in absorption is found in the case of TlCl: Cu from the curve b' which has a distinct 600 mμ-band.

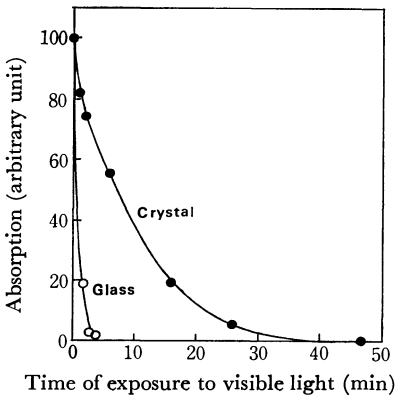

Fig. 5. Fading of UV-colored TlCl crystal and TlCl-containing glass upon visible light exposure.

Figure 5 shows the absorption change at 600 mμ with time of exposure to the bleaching light for "pure" TlCl crystal and the TlCl-containing glass. Both the crystal and glass are bleached, the rate being larger for the glass.

Heating of Darkened Samples. Fading is accelerated by heating the darkened samples. "Pure" TlCl and Cu-doped TlCl samples were heated at 40, 55, and 66°C for 30 to 60 min, but no fading occurred. The absorption spectra remained the same.

On the other hand, it was found that the darkened TlCl glass was bleached slowly at room temperature and rapidly at higher temperatures.

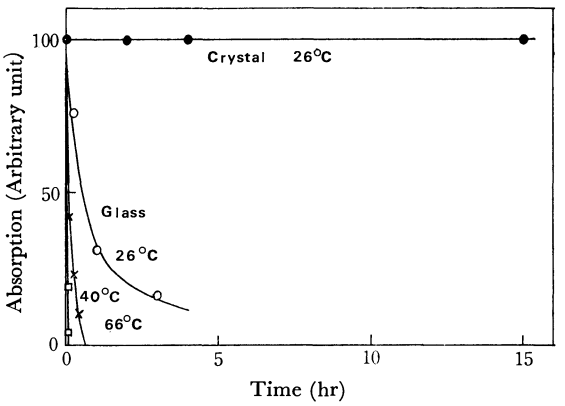

Fig. 6. Fading of UV-colored TlCl crystal and TlCl-containing glass in darkness.

Figure 6 shows the change in absorption at 600 mμ with time for the UV-colored crystalline TlCl plate and TlCl-glass sample kept at room temperature (26°C) in darkness. It is seen that with the TlCl plate sample no change in absorption is observed in 15 hr, while the darkened glass sample loses 50% of its absorption in about half an hour (b). Other curves show that the rate of fading of the glass increases sharply as the temperature rises.

Discussion

Effect of Impurity. Some impurity ions promote the darkenability of a TlCl crystal remarkably. For an explanation of the effect of copper ion the results obtained by Moser *et al.*[10] on silver chloride might be useful. They found that the presence of a small amount of cuprous ions promotes the darkenability of a silver chloride crystal noticeably and suggested that the cuprous ion might act as a trap for a positive hole produced by UV irradiation, changing into a cupric ion. If there is no cuprous ion, positive holes may be easily recombined with electrons and, as a result,the darkenability of a silver chloride crystal will be low. They also suggested that it is possible to interpret the photolytic absorption curve of a copper containing AgCl crystal as the sum of the absorptions due to dissolved cupric ions and photolytic silver. The absorption of cupric ions in an AgCl crystal can be described by a

10) F. Moser, N.R. Nail, and, F. Urbach, *J. Phys. Chem. Solids*, **9**, 217 (1959).

curve which is high in intensity at 400—450 mμ, becoming low rather rapidly with increasing wavelength toward 600—700 mμ.

A similar mechanism seems to be applied to the action of copper ion in a TlCl crystal. The absorption of TlCl: Cu increased remarkably in the wavelength range of 420—500 mμ upon UV irradiation compared with "pure" TlCl (Fig. 1). This can be attributed to the formation of Cu^{2+} ions from Cu^{+} ions in the TlCl: Cu crystal. The non-irradiated TlCl: Cu crystal had a little higher absorption in this wavelength region than the non-irradiated "pure" TlCl crystal, which can be attributed to possible presence of Cu^{2+} ions even before irradiation. It will be reasonable to assume that there are Cu^{+} ions as well as Cu^{2+} ions in the non-irradiated TlCl: Cu crystal, the Cu^{+} ions working as trapping centers for positive holes and promoting darkenability of the TlCl crystal.

Fading of Darkened Crystals by Visible Light. Darkened TlCl crystals are bleached by visible light (530—680 mμ), restoring then to their original state. A process reverse to the darkening by UV irradiation is believed to occur. Thallium atoms or their small aggregates (colloids) will absorb the light quanta and release electrons, which will be recombined with positive holes.

It should be noted, however, that the change in absorption spectra with increasing exposure of the crystal to the bleaching light is not monotonic (Fig. 4). Namely, the absorption near 600 mμ disappears faster than the absorption at shorter wavelength region. This is interpreted in terms of preferential (selective) bleaching.[8)]

For bleaching, the visible light of wavelengths 530—680 mμ was used. The centers which absorb this light must have been destroyed preferentially. It was found that bleaching by light covering the whole visible region was less preferential (Fig. 4, curve f).

In contrast to "pure" TlCl, Cu-doped TlCl crystal showed no such preferential bleaching. The cause of the difference has not been clarified. A possible explanation may be that some of the light quanta are absorbed by Cu^{2+} ion sites because these ions have absorption also in the range 530—680 mμ, and the light energy is transferred to the centers responsible for the absorption at shorter wavelength region, destroying the centers. This will give relatively less preferential bleaching.

Comparison of the Behavior of a TlCl Crystal with TlCl-Containing Glass. From Figs. 3, 5, and 6 it is clear that the darkening behavior of a glass can be explained on the basis of that of a TlCl crystal. Like the TlCl crystal the TlCl-containing glass becomes dark upon UV irradiation, giving an absorption curve with a peak near 600 mμ. The increase of absorption in the region 420—500 mμ will be explained by the presence of copper ion since a TlCl crystal shows the same tendency when doped with copper ion.

The quick bleaching of a darkened glass by visible light exposure would also be explained by a similar behavior of a TlCl crystal, although the rate appears different, the glass being bleached much faster. It is interesting to note that there is a great difference in thermal fading behavior. The darkened TlCl crystals show almost no thermal fading under the experimental conditions, 15 hr at room temperature and 2 hr at 66°C, while the darkened TlCl-containing glass is bleached by 50% in 30 min at room temperature and by 100% in 5 min at 66°C (Fig. 6).

If we assume that thermal fading and optical bleaching is initiated by the release and migration of positive holes (Cl°) which have been produced as a result of UV irradiation in darkening process and trapped somewhere in the TlCl crystal and TlCl-containing glass, trapping sites would be crystalline defects or crystal grain boundaries in the case of TlCl crystals and crystal-glass interfaces in the case of the photochromic glass. In the glass the size is too small for the crystallites to have dislocation or grain boundaries. There is no reason for considering that the bonding of the UV-induced reaction products (electrons, holes, Ag and Cl atoms) with crystalline defects is stronger than that with crystal-glass interfaces. Such a situation may be justified, however, if it is considered that glass is generally chemically inert near room temperature and its composition is quite different from that of the TlCl crystal or possible reaction products.

Our results indicate that the above view is reasonable, *viz.*, the effect of the presence of glassy matrix is shown.

We acknowledge the support of the Glass Division of PPG Industries, Inc., U.S.A.

Detosylation of *N*-Tosyl Amino Acids and Peptides by Electrolytic Reduction[1,2]

Tameo Iwasaki,[3] Kazuo MATSUMOTO,[4] Manabu MATSUOKA, Takeo TAKAHASHI, and Kentaro OKUMURA

Department of Synthetic Chemistry, Research Laboratory of Applied Biochemistry Tanabe Seiyaku Co., Ltd. Kashima-cho, Higashiyodogawa-ku, Osaka

(Received March 4, 1972)

An electrolytic reductive cleavage of tosyl group in *N*-tosyl amino acids was carried out by the use of 2 mol equivalent of NaCl or KCl as an electrolyte to the tosyl amino acids and of lead as a cathode in methanol–water. The procedure was applicable to the cleavage of *N*-tosyl peptides with preservation of the peptide bond, and with retention of their optical activity. No cleavage of the other protecting groups such as urethane type group and benzyl group was observed. The optimum conditions for reductive cleavage were found to be pH 11, lead being preferable to other cathode metals.

N-*p*-Toluenesulfonyl (tosyl) amino acids are easily prepared from the reaction of *p*-toluenesulfonyl chloride with amino acids in good yields and with retention of their optical activity.

Removal of the *N*-tosyl group with a warm phosphonium iodide–hydroiodic acid mixture was first reported by Fischer[5] in 1915. This drastic method was subsequently applied by Schönheimer[6] to obtain a free peptide from the tosyl peptide.

Since du Vigneaud[7] demonstrated in 1937 that the tosyl group was readily cleaved by reduction in sodium-liquid ammonia, the tosyl group has been employed for peptide synthesis, and is especially useful for the protection of the ω-amino groups in lysine and ornithine peptides.

The *N*-tosyl group was also removed by heating with 48% hydrobromic acid in the presence of phenol[8] and with 30% hydrobromic acid in acetic acid.[9] However, these methods have not been accepted for amino acid and peptide syntheses, since they involve drastic conditions for the cleavage of tosyl amino acids and peptides. Actually they seem to involve a side reaction in the case of hydrolysis of unstable amino acids such as hydroxy amino acid, the concomitant cleavage of peptide bond being often observed. Most of them were not applicable to the detosylation of *N*-tosyl serine because of a partial decompsoition of the resulting serine.

Recently, Horner and Neumann[10] reported a method of electrolytic reductive cleavage of the *N*-tosyl group by the use of tetramethylammonium (TMA) amalgam. The method was new for organic synthesis on a laboratory scale, but the use of TMA and mercury did not make it practicable for carrying out the procedure on a large scale. They stated that cleavage of the tosyl group had not been observed with the use of electrolyte and cathode materials other than TMA and mercury respectively. If a real convenient method with milder conditions could be developed, the tosyl group would serve as a useful protecting group of amino acids and peptides.

We previously reported a method for the cleavage of the tosyl group in various amino acids and peptides by an electrolytic reduction.[11] In the present paper, we wish to report in detail on the electrolytic reduction of tosyl amino acids and peptides.

The reductive cleavage of *N*-tosyl-L-serine under various conditions in particular was investigated. We chose tosyl serine for preparing L-serine practically, the latter being an unstable amino acid under drastic conditions such as heat and strong acid or alkali. Satisfactory results for the preparation of L-serine from tosyl serine readily prepared from *N*-tosyl-L-aspargine[12] have not been obtained.

Results and Discussion

Cathode Material. Experiments on the tosyl serine were carried out with the electrode materials given in Table 1. A lead cathode gave the highest yield of serine under the same conditions, and was used in the investigations.

Electrolyte. Reductive cleavage of the tosyl serine

TABLE 1. EFFECT OF ELECTRODE MATERIAL ON THE ELECTROLYSIS OF TOSYL SERINE AT pH 11 IN 20% MeOH

Electrode	Pb	Zn	Ti	Sn	Cu	C	Porous Zn	amalgamated Pb
Yield(%)	88	7	5	20	0	26	61	42

Cathodic solution: tosyl serine (0.1 mol) and NaCl (0.2 mol) dissolved in 20% MeOH (500 ml); Anodic solution: 20% HCl; Anode: C; Current density: 3.2 A/dm^2; Current concentration: 8 A/L; Temp.: 25°C; Time: 5 hr.

1) Formation of optically active amino acids. I.
2) Presented at the 24th Annual Meeting of the Chemical Society of Japan, Osaka 3rd, April, 1971.
3) Present Address: Institute of Molecular Evolution and Department of Chemistry, University of Miami, 521 Anastasia, Coral Gables, Fla., 33134 U.S.A.
4) To whom inquiries should be addressed.
5) E. Fisher, *Ber.*, **48**, 93 (1915).
6) R. Schönheimer, *Z. Physiol. Chem.*, **154**, 203 (1926).
7) V. du Vigneaud and O. K. Behrens, *J. Biol. Chem.*, **117**, 27 (1937).
8) H. R. Synder and R. H. Heckert, *J. Amer. Chem. Soc.*, **74**, 2006 (1952).
9) H. Ohle and G. Haesseler, *Chem. Ber.*, **69**, 2324 (1936).
10) L. Horner and H. Neumann, *ibid.*, **98**, 3462 (1965).
11) K. Okumura, T. Iwasaki, M. Matsuoka, and K. Matsumoto, *Chem. Ind.* (London), **1971**, 929.
12) N. Yoneda, T. Fujii, M. Umeda, Y. Yasuo, and K. Okumura, *Yakugaku Zasshi*, **98**, 98 (1969).

Table 2. Effect of electrolyte on the elecrolysis of tosyl serine at pH 11 in 20% MeOH

Electrolyte	Yield(%)
NaCl	88.0
KCl	87.4
LiCl	67.3
NH_4Cl	0
$CH_3NH_2 \cdot HCl$	19.8
$(CH_3)_2NH \cdot HCl$	8.2
$(CH_3)_3N \cdot HCl$	12.0
$(CH_3)_4N \cdot Cl$	62.3

Cathodic solution: tosyl serine (0.1 mol) and NaCl (0.2 mol) dissolved in 20% MeOH (500 ml); Cathode: Pb; Anodic solution: 20% HCl; Anode: Carbon; Current density: 3.2 A/dm²; Current concentration: 8A/L; Temp.: 25°C; Time: 5 hr.

was performed with the electrolytes shown in Table 2. NaCl and KCl gave high yields in methanol–water solvent.

Ammonium chloride, monomethylamine hydrochloride, dimethylamine hydrochloride, and trimethylamine hydrochloride did not give good results, but reduction with tetramethylammonium chloride afforded a relatively good yield.

The electrolytic reduction was carried out with the use of 1.2 mol equivalent of the electrolyte to the tosyl serine. It was found that reaction temperature rose since resistance of the cathodic solution increased. In the case of a large amount of the electrolyte, treatment after the reaction was troublesome.

Reaction was achieved successfully with 2 mol equivalent of the electrolyte such as NaCl or KCl.

Effect of pH in the Cathodic Solution. The electrolytic reduction of various organic compounds such as ketone,[13,14] alkyl halide[15] *etc.* is often observed to a great extent depend on the pH of the cathodic solution. We found this to be strongly so in our electrolytic reduction of the tosyl serine.

The reduction at pH 11 gave the best result (Fig. 1); a considerably lower yield being obtained in either higher or lower pH regions. In a higher pH region the resulting serine was partially decomposed and racemization took place, whereas in a lower one unreacted tosyl serine markedly appeared on the membrane. In curve E, the pH was adjusted to 11.0 before electrolytic reduction, and was not controlled during the course of the reduction. The pH gradually shifted to alkaline region with the lapse of time, and the final concentration of sodium hydroxide in cathodic compartment was about 0.5 N after 5 hr. Hardly any reaction took place during last one hour. The results suggest that cleavage of the tosyl group cannot be performed in a higher pH region than 13.

In the water–methanol system, an adequate amount of methanol was needed to dissolve the tosyl amino

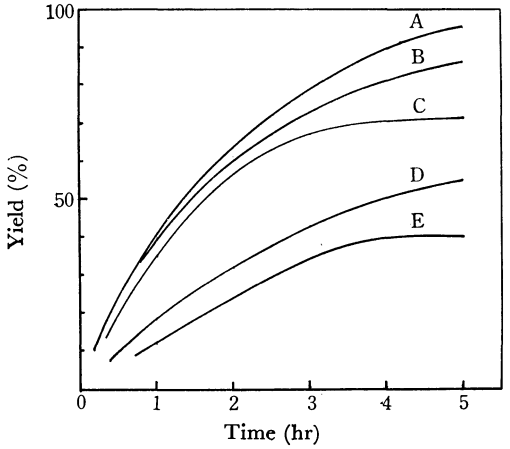

Fig. 1. Effect of pH on the electrolysis of tosyl serine. Cathodic solution: tosyl serine (0.1 mol) and NaCl (0.38 mol) dissolved in 20% MeOH (500 ml); Cathode: Pb; Anodic solution: 20% HCl; Anode: C; Current density: 3.2 A/dm²; Current concentration: 8 A/L; Yield: Analytical value. A: pH 10.8—11.2; B: pH 9.6—10.0; C: pH 12.6—13.0; D: pH 7.0—9.0; E: No controlled pH.

acid deposited on a membrane during the course of electrolysis. In the case of tosyl serine, 20% methanol was required.

Cathodic Erosion of Lead. The reductive cleavage of 0.1 mol of L-tosyl serine was carried out by the use of 0.2 mol of NaCl and lead cathode in 20% methanol. After 5 hr, L-serine was obtained in 88% yield. However, the cleavage of 0.2 mol of the tosyl serine in the presence of 0.4 mol of NaCl did not proceed sufficiently. The yield of L-serine was only 45%, even when the reaction was allowed to continue for 10 hr. This might be attributed to incorporation of alkali metal into the lead cathode.[16–19] It can also be understood from the fact that use of the lead cathode renewed by washing with 5% nitric acid after 5 hr resulted again in a high yield of the cleavage of the tosyl serine.

In these experiments the electrode potential of the lead cathode showed −2.08 V *vs.* SCE in the initial stage of reaction. After 5 hr, the potential shifted to −1.95 V *vs.* SCE. When the electrode was washed with 5% nitric acid, the potential returned to −2.08 V *vs.* SCE. This result is in line with that of Chernomorskii.[20]

Thus a potential of −2.0 V *vs.* SCE would be required at least in the reductive cleavage of the tosyl serine.

The current density was 3.2 A/dm² at 25°C. A current density greater than 5 A/dm² was not needed, since intensive erosion of lead took place by the incorporation of Na^+ into the cathode and temperature rose markedly in the cathodic solution.

13) M. J. Allen, "Organic Electrode Processes," Champan and Hall, London (1958), p. 58.
14) P. J. Elving and B. Pullman, "Advences in Chemical Physics," Vol. 1, ed. by I. Prigogine, Interscience Publishers, New York (1961), p. 1.
15) F. D. Popp and H. P. Schultz, *Chem. Rev.*, **61**, 19 (1961).
16) B. N. Kabanov, I. G. Kiseleva, I. I. Astakhov, and N. N. Tomashova, *Electrokhimiya*, **1**, 1023 (1965).
17) B. N. Kabanov, *Electrochim. Acta.*, **13**, 19 (1968).
18) B. N. Kabanov, O. I. Leikis, I. G. Kiseleva, I. I. Astakhov, and D. P. Aleksandrova, *Dokl. Akad. Nauk. SSSR.*, **144**, 1085 (1962).
19) I. G. Kiseleva, N. N. Tomashova, and B. N. Kabanov, *Zh. Fiz. Khim.*, **38**, 1188 (1964); *Chem. Abstr.* **57**, 10917f.
20) A. I. Chernomorskii, I. G. Kiseleva, and B. N. Kabanov, *Electrokhimiya*, **6**, 429 (1970).

Electrolytic Reductive Cleavage of the Other N-*Tosyl Amino Acids and Peptides.* The above method was applied to various optically active tosyl amino acids and peptides. The results are given in Table 3. All electrolyses were carried out under the same conditions as for tosyl serine.

TABLE 3. ELECTROLYTIC REDUCTIVE CLEAVAGE OF TOSYL-L-AMINO ACIDS AND PEPTIDES

Run	Tos-	Method	Yield[a] (%)	Observed $[\alpha]_D^{25}$deg.	Literature[b] $[\alpha]_D^{25}$deg.
1	Ser–OH	A	88	+14.5	+14.5 (N-HCl
2	Thr–OH	A	91	−28.3	−28.3 (H_2O)
3	Phe–OH	A	66	−34.2	−34.8 (H_2O)
4	Ala–OH	A	84	+13.9	+14.5 (6N-HCl)
5	Val–OH	A	77	+28.6	+28.8 (6N-HCl)
6	Leu–OH	A	84	+15.3	+14.9 (6N-HCl)
7	ILeu–OH	A	85	+41.2	+40.8 (5N-HCl)
8	Glu–OH	A	84	+31.6	+31.6 (2N-HCl)
9	Asp–OH	A	79	+25.5	+25.0 (6N-HCl)
10	Cys(Bzl)–OH	A	78	−26.5	−27.0 (N-HCl)[c]
11	Lys(Z)–OH	B	92	+14.1	+14.4 (2N-HCl)[d]
12	Ala–Gly–OH	A	74	+22.1	+22.6 (0.5N-HCl)[e]
13	Val–Gly–OH	A	83	+102.2	+102.0 (H_2O)[f]
14	*S*–Bzl–glutathione	B	92	−9.7(3N-HCl)	—
15	β-Cl–Ala–OH	A	33[g]	+14.1	+14.5 (6N-HCl)

a) Amino acids obtained were paper-chromatographically pure and agreed with authentic specimens.
b) Amino acids (run 1–9, and run 15): "Chemistry of Proteins," Vol. 1, ed. S. Akabori and S. Mizushima, Kyoritsu Shuppan Co. Ltd., (1954) p. 112.
c) L. Zervas, I. Photaki, and N. Ghllis, *J. Amer. Chem. Soc.*, **85**, 1337 (1963).
d), e), f) J. P. Greenstein and M. Winitz, "Chemistry of the Amino Acids," Vol. 2, John Wiley & Son, Inc, (1961) p. 893, p. 1203, p. 1228, respectively.
g) Alanine was obtained.

In the case of tosyl-L-β-chloroalanine,[12] simultaneous fission of sulfur-nitrogen bond and carbon-chlorine bond occurred to give L-alanine.

Urethane type protecting groups such as benzyloxycarbonyl (Z), *t*-amyloxycarbonyl, and *t*-butyloxycarbonyl and *S*-benzyl (S–Bzl) group were not cleaved under the above conditions, but the benzoyl group was attacked.[21] Z and Bzl groups could be cleaved in the electrolytic reduction under basic conditions using other electrode material.[21] Thus, N^{ε}–Z–L-lysine and *S*–Bzl-L-cysteine were obtained by the selective electrolytic reduction of N^{α}-tosyl-N^{ε}-Z-L-lysine and *N*-tosyl-*S*-Bzl-L-cysteine, respectively. *N*-Tosyl-*S*-Bzl-glutathione was treated to give *S*-Bzl-glutathione without cleavage of the *S*-Bzl group.

Reaction Mechanism. In connection with cleavage of the tosyl group in the TMA–mercury–methanol system, Horner and Neumann[22] stated that the radical (stable in the presence of mercury) obtained by reducing TMA cation on the mercury cathode cleaved the tosyl group, and that other electrolytes such as Na or K formed the corresponding amalgam without appreciable cleavage of this group.

In the polarographic reduction of benzenesulfonylamide, Manousék *et al.*[23] stated that benzene and sulfurous acid monoamide resulting from carbon-sulfur bond cleavage were produced in the initial stage of the reaction, and that the reaction mechanism as represented in the following Scheme was very similar to that of the reduction with sodium-liquid ammonia as reported by Kovacs Ghatak.[24,25]

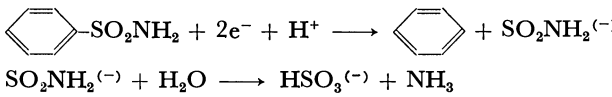

$$SO_2NH_2^{(-)} + H_2O \longrightarrow HSO_3^{(-)} + NH_3$$

However, in our electrolytic reductive cleavage of tosyl amino acids, *p*-toluenesulfinic acid was isolated from the reaction mixture in a good yield. *p*-Thiocresol was not detected at all even by iodometric titration of the cathodic solution after electrolytic reduction. The electrolytic reduction of *p*-toluenesulfinic acid was not observed under the same conditions as for tosyl amino acids and peptides, although it was reported that *p*-toluenesulfinic acid was reduced to *p*-thiocresol.[26]

The reaction in the electrolytic reduction of tosyl amino acids and peptides under our conditions should proceed *via* two electrons transfer to give sulfur-nitrogen bond cleavage as shown in the following Scheme;

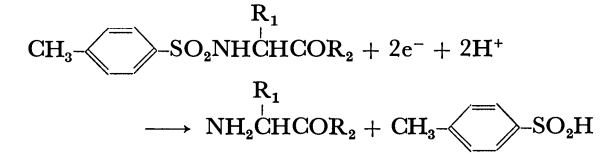

R_1=Amino acid side chains
R_2=OH or amino acid residues

Experimental

Apparatus. A Yanagimoto controlled potential electrolyser was used as a D.C. source. A 600 ml electrolysis cell with a cathode, anode, cellular membrane, thermometer, and a pH autocontroller was used (Fig. 2). Commercial metal plates sufficiently polished before use were used as electrode.

A glass electrode of pH meter was rounded with platinum

21) T. Iwasaki, K. Matsumoto, M. Matsuoka, and M. Miyoshi, unpublished data.
22) L. Horner and H. Neumann, *Chem. Ber.*, **98**, 1715 (1965).
23) O. Manousék, O. Exner, and P. Zuman, *Collect. Czech. Chem. Commun.*, **33**, 4000 (1968).
24) J. Kovacs and U. R. Ghatak, *Chem. Ind.* (London), 913 (1963).
25) J. Kovacs and U. R. Ghatak, *J. Org. Chem.*, **31**, 119 (1966).
26) S. Takagi, T. Suzuki, and J. Date, *Yakugaku Zasshi*, **71**, 126 (1951).

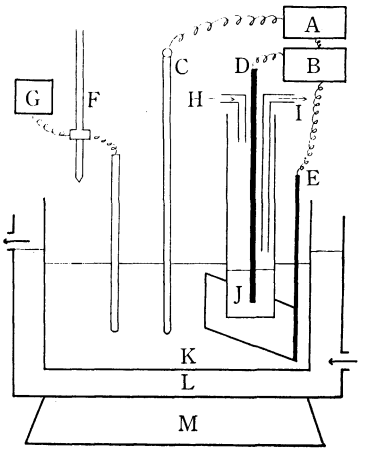

Fig. 2. Apparatus.
A: Recorder, B: DC source, C: Thermometer, D: Carbon anode, E: Lead cathode, F: Automatic buillette, G: pH controller, H: Anodic solution poured, I: Anodic solution drained, J: Anodic compartment, K: Cathodic compartment, L: Cooled water, M: Stirrer.

wire to prevent disturbance on accurate pH value from the electric current for the anode and cathode.

The pH of the cathodic solution was controlled to the desired value within ± 0.1 using a Toa Denpa pH autocontroller equipped with a buret.

Temperature in the cathodic compartment was maintained at 25°C with circulating water cooled by a Yamato cool line model BL-11 around the electrolysis cell. Current, voltage and temperature were recorded on the same chart by a Yokogawa multipoint model ERB, and the pH by a Toa Denpa multipoint pH recorder model HMR-3.

The anodic compartment, in which the anolyte was exchanged at a constant velocity with a fresh solution with a Mitsui Kagaku model SJ-1200, was clamped in position so that the anolyte and catholyte were on the same level. All optical rotations were measured with a Perkin-Elmer 141 polarimeter.

Method. Typical cases *A* and *B* are shown. *A*. Experiments on the effect of pH, electrolyte and cathode material were carried out by the following procedure. After a mixture of 26 g tosyl-L-serine and 12 g of sodium chloride dissolved in 500 ml of 20% methanol was placed in a cathodic compartment, pH of the cathodic solution was adjusted to the desired value with 1N sodium hydroxide solution. On the other hand, 20% hydrochloric acid was put in an anodic compartment with a carbon anode. The anode and cathode compartments were separated by a membrane. An electric current 4A (4—6 V), with density 3.2 A/dm^2, was then passed through the solution at 25°C. The pH of the cathodic solution was maintained at the desired value with 5% hydrochloric acid during the course of electrolytic reduction. The anodic solution was exchanged continuously with 20% hydrochloric acid.

The yield of L-serine was determined by the method of formol titration within an error of 3% in the follwoing way. A 10—20 ml sample taken out from the reaction mixture was adjusted to pH 7.0 with 0.1N hydrochloric acid. To this was added 10 ml of 37% formaldehyde, and pH of the solution was then adjusted to 8.3 with 0.1N sodium hydroxide solution. The amount of L-serine was calculated from that of the consumption of 0.1N sodium hydroxide solution.

For the preparation of L-serine, the cathodic solution was acidified with 20% hydrochloric acid. After removal of the unreacted compound and *p*-toluenesulfinic acid by extraction with ethyl acetate, the aqueous solution was treated with Dowex 50×2 column (H^+ form) and non-amino acid acidic components were eluted with distilled water, then amino acid was eluted with 5% ammonia. The solution was evaporated to dryness *in vacuo* to give a crude serine. The product was recrystallized from water to afford paper-chromatographically and optically pure L-serine as shown in Table 3.

B. A mixture of 55.0 g (0.1 mol) of *N*-tosyl-*S*-Bzl-glutathione, 7.0 g of potassium chloride and 500 ml of 20% methanol was placed in a cathodic compartment with a lead cathode, and potassium hydroxide solution was then added to adjust the pH of the cathodic solution at 11. The anodic solution in an anodic compartment with a carbon anode was exchanged continuously with 20% hydrochloric acid. A membrane was used, and electric current 4A (4—6 V), current density 3.2 A/dm^2, was passed through the solution at 25°C for 5 hr. The pH of the cathodic solution was maintained at 11 with 20% hydrochloric acid during the course of reduction. On completion of electrolysis, the cathodic solution was adjusted to pH 3—4 with hydrochloric acid. The precipitated crystals were collected by filtration and the crude product was washed with methanol. After recrystallization from water, 36 g (92%) of *S*-Bzl-glutathione was obtained, mp 204—205°C (decomp.),[27] $[\alpha]_D^{25}$ −9.7° (*c* 0.70, 3N-HCl). The material showed a single spot when subjected to paper chromatography (Toyo filter paper No. 50), R_f 0.58 (*n*-BuOH–AcOH–H_2O=3:1:1). Found: C, 51.24; H, 5.93; N, 10.87; S, 7.81%. Calcd for $C_{17}H_{23}O_6N_3S$: C, 51.36; H, 5.85; N, 10.57; S, 8.06%.

Isolation of p-*Toluenesulfinic Acid.* The cathodic solution subjected to the above treatment was acidified with hydrochloric acid. After removal of methanol under reduce pressure, the hydrochloric acid solution was extracted with ethyl acetate. The ethyl acetate solution was evaporated to dryness under reduced pressure. The residue was recrystallized from water to obtain *p*-toluenesulfinic acid (80% yield). The crystal showed mp 84—85°C, which was consistent with an authentic specimen.

27) Melting point is uncorrected.

Liquid-phase Oxidation Catalyzed by Cu(II)-Cl System. I. Oxidation of Cyclohexene

Sei-Ichiro IMAMURA, Toshiaki BANBA, and Yoshinobu TAKEGAMI*

Department of Chemistry, Kyoto Institute of Technology, Sakyo-ku, Kyoto

**Department of Hydrocarbon Chemistry, Kyoto University, Sakyo-ku, Kyoto*

(Received May 4, 1972)

Oxidation of cyclohexene catalyzed by Cu(II)–Cl systems was carried out in glacial acetic acid. The oxidation of cyclohexene with cupric chloride was highly accelerated by addition of various alkali chlorides. The decomposition of cyclohexenyl hydroperoxide, an intermediate product of the oxidation, was also accelerated by this catalyst system. Salts other than alkali chlorides had little effect. It was concluded that the activation of copper catalyst was due to the chloride ions which form a complex with copper. In the course of the reaction the catalyst loses its activity through ligand exchange with solvent molecule, acetic acid.

It is well known that the solubility of cupric salt is increased by the formation of complexes with alkali chlorides in acetic acid or acetonitrile. These catalyst systems are often used in the chlorination of olefines.[1] Tamura used these systems in the synthetic reaction of vinyl acetate and discussed the form of the catalyst and its behaviour.[2]

We have studied the oxidation of cyclohexene in detail to clarify the effect of various alkali chlorides on the catalytic activity of cupric chloride.

Experimental

Cyclohexene was synthesized by the dehydration of cyclohexanol.[3] The crude cyclohexene was washed with 5% aqueous sodium hydroxide, distilled twice and stored under nitrogen. Cyclohexenyl hydroperoxide was obtained by the autooxidation of cyclohexene. Cyclohexenol was obtained by the reduction of cyclohexenyl hydroperoxide with triphenylphosphine and cyclohexenone by the decomposition of cyclohexenyl hydroperoxide with cupric chloride–pyridine system.[4] Acetic acid was purified by the standard method. Cupric chloride and other reagents (anhydrous, GR grade) were used without further purification.

Oxidation was carried out using a reactor equipped with an atmospheric pressure gas burette. Fifteen ml of the mixture of cyclohexene and acetic acid containing a catalyst was warmed to the desired temperature (60°C) in a nitrogen atmosphere. Nitrogen was then replaced with oxygen and the reaction started. The decomposition of cyclohexenyl hydroperoxide was carried out in a nitrogen atmosphere and the rate of reaction was followed by iodometric titration of the remaining hydroperoxide.

Analysis of oxidation products was carried out using a Hitachi gas chromatograph 063 equipped with a flame-ionization detector. The column packing was *n*-decyl phthalate (1 m length) and the column temperature was 70—120°C (5°C/min). Visible spectra were measured by means of a Toshiba-Beckman UV spectrophotometer DBG.

Results and Discussion

Catalytic Activity of Cu(II)–Cl System. The effect of lithium chloride on the catalytic activity of cupric chloride was investigated and the results are shown in Fig. 1 and Table 1. In all cases, retardation of the reaction occurs after some uptake of oxygen. During the constant uptake of oxygen the reacting system is yellowish green or green but a deep blue colour appears

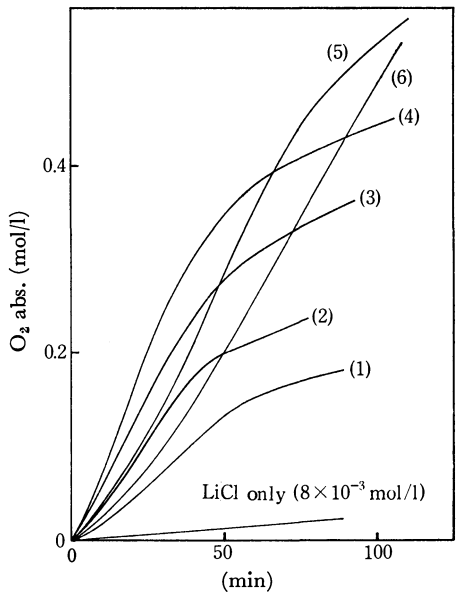

Fig. 1. Effect of LiCl on the oxidation catalyzed by $CuCl_2$. AcOH: 10 ml. Cyclohexene: 5 ml. $CuCl_2$: 8×10^{-3}mol/l. 60°C. LiCl ($\times10^3$mol/l) (1) 0, (2) 8, (3) 24, (4) 48, (5) 80, (6) 200.

TABLE 1. R_m AND MAXIMA OF ABSORBED O_2

LiCl ($\times10^3$M)	R_m ($\times10^3$M/min)	Max. O_2absd(M)
0	3.82	0.136
8	6.82	0.164
24	8.45	0.237
48	10.90	0.306
80	9.13	0.461
200	6.90	0.821

AcOH: 10 ml.
Cyclohexene: 5 ml.
$CuCl_2$: 8×10^{-3}mol/l. 60°C.

1) K. Ichikawa, S. Uemura, Y. Takagaki, and T. Hiramoto, *Bull. Jap. Petrol. Inst.*, **12**, 77 (1970).

2) M. Tamura and A. Yasui, *Kogyo Kagaku Zasshi*, **72**, 558 (1969).

3) H. Gilman, "Organic Synthesis," Coll. Vol. I, p. 183, (1956).

4) Cyclohexenone is obtained exclusively in the decomposition of cyclohexenyl hydroperoxide by cupric chloride in pyridine solution. This was reported by T. Banba, S. I. Imamura, and Y. Takegami at the 5th Oxidation Symposium in Osaka. (December 3, 1971).

after the retardation of oxygen uptake. Though the maximum rate of oxygen absorption (R_m) increases with an increase in the amount of lithium chloride added, a large excess (more than seven parts to one part of copper) results in a decrease in the rate. On the other hand, the maximum quantity of absorbed oxygen defined as the quantity of oxygen absorbed before the retardation occurs, increases linearly with the increase in the concentration of lithium chloride added. It is clear that lithium chloride increases and maintains the activity of the catalyst. As shown in Fig. 1 lithium chloride without copper salt has little activity.

Table 2. R_m and maxima of absorbed O_2

Additive	($\times 10^3$M)	R_m($\times 10^3$ M/min)	Max. O_2absd(M)
LiCl	8	6.32	0.161
	24	8.45	0.238
	48	10.90	0.306
$MgCl_2$	8	5.13	0.185
	24	7.68	0.202
	48	8.28	0.328
NaCl	8	6.72	0.196
	24	10.17	0.311
	48	11.37	0.518
KCl	8	9.73	0.184
	24	13.25	0.390
	48	14.00	0.546
LiBr	8	6.22	0.112
	24	6.32	0.131
	48	4.12	0.136
LiF	8	4.82	0.161
	24	5.60	0.109
	48	5.78	0.098
Li_2CO_3	8	6.22	0.136
	24	6.45	0.169
	48	6.03	0.174
$LiNO_3$	8	6.22	0.145
	24	7.98	0.145
	48	8.98	0.147

AcOH: 10 ml. Cyclohexene: 5 ml.
$CuCl_2$: 8×10^{-3} mol/l. 60°C.

The effects of various alkali metal chlorides and lithium salts on the catalytic activity of the cupric chloride were investigated and the results are shown in Table 2. We see that the addition of magnesium chloride, sodium chloride, or potassium chloride increases the maximum quantity of absorbed oxygen and the maximum rate of oxygen absorption (R_m) as in the case of lithium chloride, but the addition of lithium fluoride, lithium bromide, lithium carbonate, and lithium nitrate has little effect. It has been reported that lithium salts, which have a considerable covalent character, have a catalytic activity for oxidation through the activation of a molecular oxygen[5] or through the homolysis of a peroxide.[6] However, in our experiments no such general effect could be seen with lithium salts except for lithium chloride as mentioned above. The order of the effect is found to be KCl>NaCl>LiCl≒$MgCl_2$. The greater the ionic character of the added chloride, the more effective for the oxidation. It can be said that the effect of the additives on the catalytic activity of copper salt is due to the anionic part, namely chloride ion, the activity of copper salt increasing through complex formation with chloride ions. In Table 3 the activity of various copper compounds–lithium chloride systems is shown together with the visible spectra. All copper salts tested are inactive with the exception of cupric chloride. However, oxidation takes place on addition of lithium chloride to these salts. The visible spectra of the inactive copper salts show an absorption at about 670 mμ, while the active catalyst systems containing lithium chloride have absorption in a wavelength region greater than 710 mμ The absorption seems to indicate the formation of various types of complexes. The effect of chloride ion on the catalytic activity of transition metals other than copper was also studied. In Table 4 the effect of lithium chloride on the catalytic activity of cobalt, nickel, and manganese chlorides is given. Hardly any or no effect can be seen for chlorides of other transition metals.

Table 3. Oxidation activity and λ_{max} of copper salt-LiCl system

Catalyst	Activity	λ_{max}(mμ)
$CuCl_2$	○	—
+LiCl	○	760
$Cu(acac)_2$	×	673
+LiCl	○	710
CuF_2	×	672
+LiCl	○	674
$Cu_3(PO_4)_2 3H_2O$	×	—
+LiCl	○	780
$CuCO_3$	×	—
+LiCl	○	—
Cu-st*	×	675
+LiCl	○	770

* st: stearate

The accumulation of cyclohexenyl hydroperoxide in the reaction system was measured at oxygen uptake

Table 4. Oxidation of cyclohexene with MCl_2–LiCl system

Catalyst	LiCl ($\times 10^2$mol/l)	R_m ($\times 10^3$mol/l·min)
$CuCl_2$	0	2.61
	2.4	8.45
$CoCl_2$	0	12.91
	2.4	14.41
$NiCl_2$	0	1.26
	2.4	1.24
$CrCl_2$	0	1.49
	2.4	1.51
$MnCl_2$	0	3.16
	2.4	3.55

AcOH: 10 ml. Cyclohexene: 5 ml, 60°C.
[Catalyst]: 8×10^{-3}mol/l.

5) K. Ohkubo and T. Yamabe, *Bull. Jap. Petrol. Inst.*, **12**, 123 (1970).
6) J. K. Kochi, B. M. Graybill, and M. Kurz, *J. Amer. Chem. Soc.*, **86**, 5257 (1964).

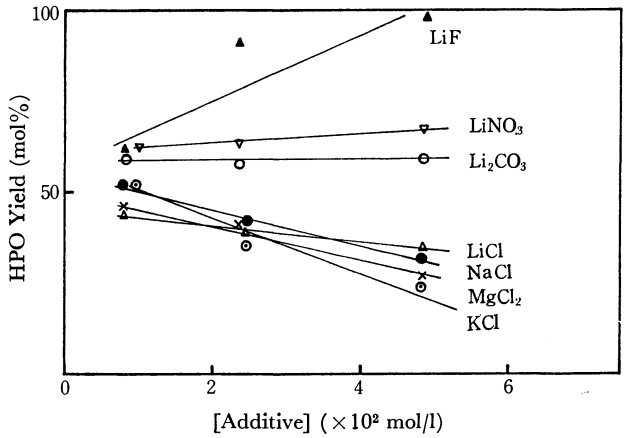

Fig. 2. Effect of additives on hydroperoxide (HPO) yield.
AcOH: 10 ml. Cyclohexene: 5 ml. $CuCl_2$: 8×10^{-3}mol/l. 60°C O_2absd: 0.136 mol/l.

of 0.136 mol/l. The results are given in Fig. 2. The addition of lithium carbonate or lithium nitrate has no effect upon the hydroperoxide yield, but in the case of various chlorides, the higher the concentration of the chloride, the lower the yield.

Product Distribution. The product distribution of the cyclohexene oxidation catalyzed by cupric chloride-lithium chloride system was investigated. Main products were cyclohexenyl hydroperoxide, cyclohexenol, and cyclohexenone. Two unknown high boiling products, I and II, were detected. Product I showed an infrared absorption at 1730 cm^{-1} due to carbonyl group and the product II at 3450 cm^{-1} due to hydroxyl group.[7] It was found that the product II contained chlorine. The relation between the product distribution at the point where the oxygen uptake amounted to 0.136 mol/l and the quantity of lithium chloride added is shown in Fig. 3. We see that as the concentration of lithium chloride increases, the yield of the hydroperoxide decreases and that of cyclohexenone increases. The higher the concentration of lithium chloride, the lower the total yield of these products and on the contrary, the higher the total yield of the unknown products; which is not shown in the figure. Thus it seems that the chloride ion is consumed by the chlorination of the reaction product.[8]

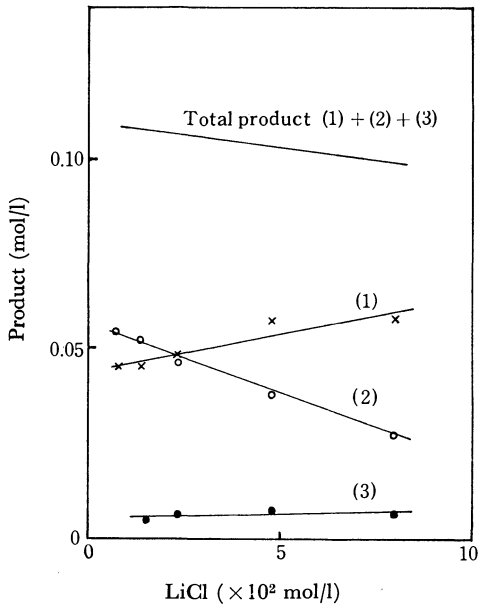

Fig. 3. Effect of LiCl on the product distribution.
AcOH: 10 ml. Cyclohexene: 5 ml. $CuCl_2$: 8×10^{-3}mol/l. 60°C O_2absd.: 0.136 mol/l. (1) Cyclohexenone, (2) Cyclohexenyl hydroperoxide, (3) Cyclohexenol.

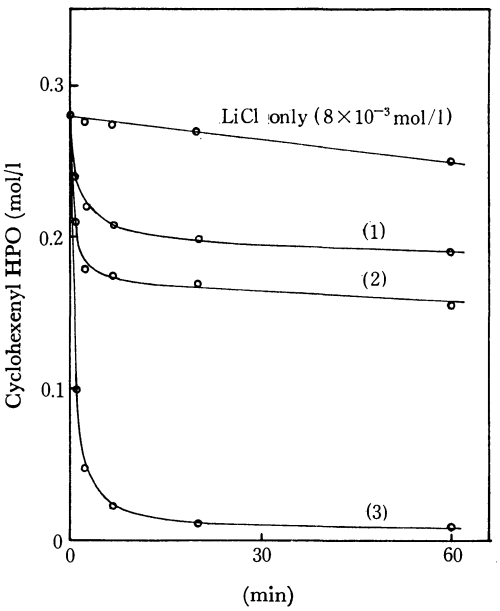

Fig. 4. Decomposition of cyclohexenyl HPO catalyzed by $CuCl_2$–LiCl.
AcOH: 10 ml. Cyclohexane: 10 ml. $CuCl_2$: 8×10^{-3}mol/l. 60°C LiCl (mol/l) (1) 0, (2) 8×10^{-3}, (3) 8×10^{-2}.

Decomposition of Cyclohexenyl Hydroperoxide Catalyzed by Cu(II)–Cl System. It was found that the addition of alkali chlorides decreased the yield of hydroperoxide, and thus the effect of lithium chloride on the decomposition of hydroperoxide catalyzed by copper salt was investigated. The result is given in Fig. 4. In this case also, lithium chloride increases the catalytic activity of the cupric chloride remarkably. Decomposition of hydroperoxide in the presence of lithium chloride alone does not proceed so much. The promotion of the catalytic activity by lithium chloride seems to be caused by the complex formation with copper. The decomposition curves resemble that of the oxidation of cyclohexene, *viz.*, retardation occurs after the decomposition of a certain amount of hydroperoxide, the colour of the solution turning from yellowish green to deep blue. The quantity of the hydroperoxide decomposed by the time retardation occurs is proportional to the concentration of lithium chloride added. It seems that lithium chloride increases the rate of decomposition of hydroperoxide and consequently increases that of oxidation.

7) By comparison with standard sample, substances I and II proved not to be 3-chlorocyclohexanone or 3-chlorocyclohexanol formed by the chlorination of the conjugated cyclohexenone which is one of the oxidation products. Moreover, they both did not correspond to 2-chlorocyclohexanone or cyclohexyl acetate.

8) After the retardation occurred, chloride ion was scarcely detected in the solution with silver nitrate.

Change of the Dissolved State of the Catalyst System. In the oxidation of cyclohexene, the colour of the solution changes from yellowish green to green and finally to deep blue in the course of the reaction. Thus the visible spectra of the reaction system were observed and the effect of lithium chloride upon the change of the state of the catalyst was discussed. At the beginning of the reaction a feeble absorption is observed at 760 mμ which seems to be due to the Cu(II)–Cl complex.[2] Soon after oxidation takes place, the absorption disappears and a new absorption appears at 680 mμ. From a comparison with the standard reagent, the absorption proved to be due to the cupric acetate which seemed to be formed through the ligand exchange of the catalyst with the solvent molecule, acetic acid. The time dependence of absorption is given in Fig. 5.

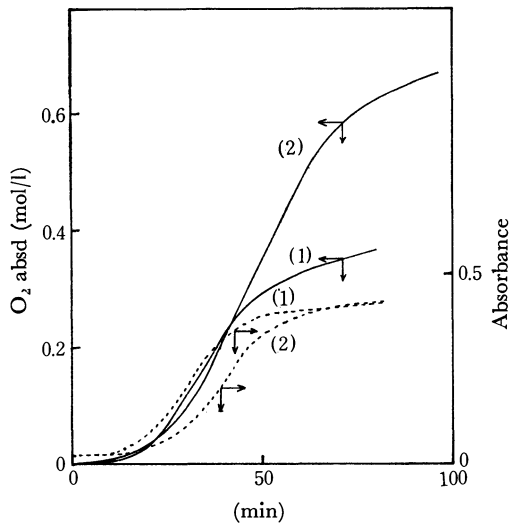

Fig. 5. Time dependence of the visible spectrum (λ_{max}=680mμ)
AcOH: 10 ml. Cyclohexene: 5 ml. $CuCl_2$: 8×10^{-3}mol/l. 60°C LiCl (mol/l) (1) 8×10^{-3}, (2) 4.8×10^{-2}.

We see that the absorbance increases during the reaction until the point where the rate of the oxidation begins to decrease and then remains constant. It seems that all the copper turns to cupric acetate at the end of the reaction. When the quantity of the lithium chloride increases, the time is lengthened at which the absorbance becomes constant [Curve (2), Fig. 5]. At the point where the catalyst became deactivated, addition of more lithium chloride recovered the activity of the system. This shows that the inactive cupric acetate is partly changed to the active Cu(II)–Cl complex. It can thus be concluded that lithium chloride contributes to maintain the activity of the catalyst and deactivation is caused by the consumption of chloride ions and the solvent molecules enter into the ligand site of the copper forming inactive cupric acetate.

Effect of the Catalyst Concentration. Dependence of the oxidation rate on the catalyst concentration was investigated. When the concentration of the copper catalyst is increased at a constant concentration of lithium chloride, R_m increases but reaches its maximum value at the concentration of copper about 2.4×10^{-2} mol/l, then remains constant [Curve (1), Fig. 6]. When

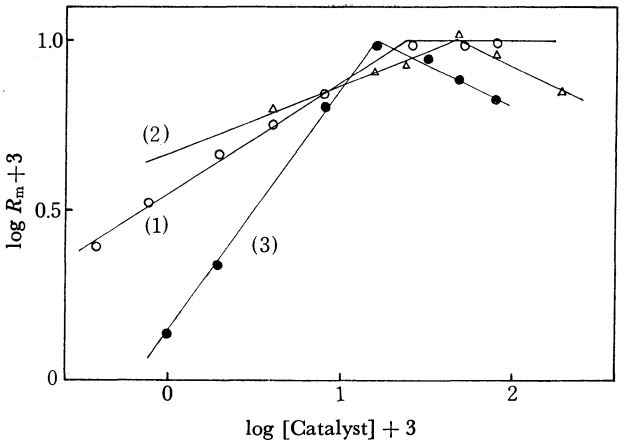

Fig. 6. R_m *vs.* catalyst concentration.
AcOH: 10 ml. Cyclohexene: 5 ml. 60°C.
(1) [$CuCl_2$] Dependence, [LiCl] 8×10^{-3}mol/l.
(2) [LiCl] Dependence, [$CuCl_2$] 8×10^{-3}mol/l.
(3) $\left[\begin{smallmatrix}CuCl_2\text{–}LiCl\\ 1:1\end{smallmatrix}\right]$ Dependence

the concentration of lithium chloride was made to vary at a constant concentration of copper [Curve (2)], R_m reaches the maximum value for a mole ratio of lithium to copper, *ca.* 7: 1, then begins to decrease. The concentration of the Cu(II)–Cl was made to vary at constant lithium to copper concentration of unity. It is shown that R_m also reaches the maximum value at the complex concentration of about 2.0×10^{-2} mol/l and then decreases [Curve (3)]. In all cases the maximum value of R_m is about 1.0×10^{-2} mol/l·min. From curves (2) and (3), it seemes that excess lithium chloride retards the reaction. An explanation for the phenomenon may be that excess lithium chloride blocks the active sites of the copper catalyst and prevents hydroperoxide molecules from approaching them. Another explanation may be that while the active species is $CuCl_3^-$, excess lithium chloride forms a complex of the type $CuCl_4^{2-}$[9] which retards the reaction.

Oxidation Scheme. From the results so far obtained, the oxidation mechanism is schematically drawn as follows.

$$CuCl_2 + Cl^- \rightleftarrows CuCl_3^- (CuCl_4^{2-}) \quad (1)$$

$$RH \longrightarrow R\cdot \quad (2)$$

$$R\cdot + O_2 \longrightarrow ROO\cdot \quad (3)$$

$$ROO\cdot + RH \longrightarrow ROOH + R\cdot \quad (4)$$

$$ROOH + CuCl_3^- (CuCl_4^{2-}) \longrightarrow ROO\cdot \text{ or } RO\cdot \quad (5)$$

$$CuCl_3^- (CuCl_4^{2-}) \xrightarrow[O_2,\,S]{AcOH} Cu(OAc)_2 + \text{Chlorination product} \quad (6)$$

$$\downarrow Cl^-$$

$$Cu(Cl)(OAc),\ CuCl_2,\ CuCl_3^-,\ CuCl_4^{2-} \quad (7)$$

In reaction (1) the copper salt forms a complex with chloride ions. It seems that the complex is not of a single form but a mixture of various forms. In reactions (2)—(4) cyclohexenyl hydroperoxide is formed.

9) C. L. Jenkins and J. K. Kochi, *J. Org. Chem.*, **36**, 3103 (1971).

In reaction (5) the hydroperoxide is decomposed by the Cu(II)–Cl complex. The increase in the rate of oxidation seems to be due to the high activity of the complex to promote the step. As shown in reaction (6), during oxidation, presumably in the decomposition of hydroperoxide, some ligand exchange occurs through the chlorination of a third body (cyclohexene or its oxidation product), represented by S in reaction (6), and cupric acetate is formed causing deactivation of the catalyst system. In reaction (7) addition of alkali metal chlorides to the deactivated system restores the activity of the system.

In conclusion, it can be said that in acetic acid solvent, chloride ion increases and maintains the catalytic activity of the copper salt as its ligand.

The authors are very much indebted to Professor Hiroshi Teranishi for his guidance and encouragement through this work. They also wish to thank Dr. Sakae Uemura for his helpful advice and discussions.

BULLETIN OF THE CHEMICAL SOCIETY OF JAPAN, VOL. 46, 860—863 (1973)

Studies of Organo Sulfur Compounds. II. The Preparation and Reactions of Benzoyl Benzenethiosulfonates

Shinzi KATO and Masateru MIZUTA
Faculty of Engineering, Gifu University, Kagamihara, Gifu

(Received May 31, 1972)

Some mixed sulfonic thiocarboxylic anhydrides (II, R, R′: Aryl) were obtained from the reactions of potassium substituted-thiobenzoate with benzene- or *p*-toluenesulfonyl chlorides. The reactions of benzoyl benzenethiosulfonate were examined in comparison with those of the corresponding mixed sulfonic carboxylic anhydrides.

Although a few reports[1-8] have been recorded on the mixed sulfonic carboxylic anhydride (I), there have been no reports for the mixed sulfonic thiocarboxylic anhydride (II). In this paper an attempt at the syntheses and reactions of mixed sulfonic carboxylic anhydride (II) will be described.

I II

R, R′: Alkyl, Aryl

The reaction of benzoyl chloride with potassium *p*-toluenethiosulfonate gave no benzoyl *p*-toluenethiosulfonate. However, it was found that the reactions of potassium substituted thiobenzoate with benzene- or *p*-toluenesulfonyl chloride gave the corresponding aroyl

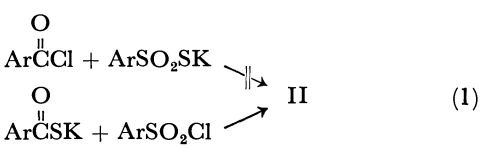

(1)

benzenethiosulfonate (Eq. (1)). We attempted to react the mixed sulfonic thiocarboxylic anhydride thus obtained with several reagents (*cf.* Chart 1).

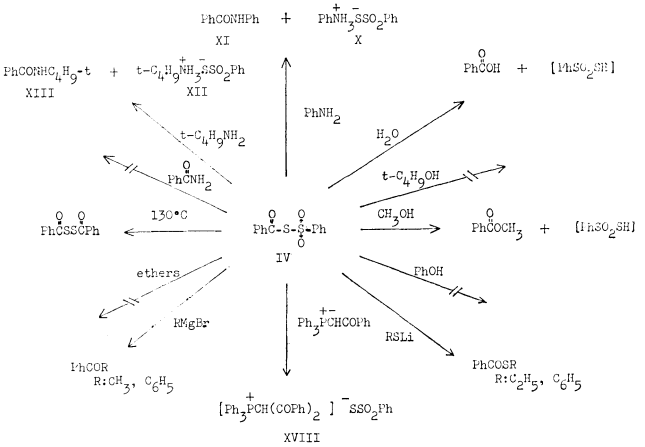

Chart 1. Reactions of benzoyl benzenethiosulfonate.

Results and Discussion

Potassium thiobenzoate and an equimolar amount of benzenesulfonyl chloride in dry acetonitrile (or THF) reacted exothermically. From the reaction mixture, benzoyl benzenethiosulfonate (IV), dibenzoyl disulfide (V), potassium benzenesulfonate (VI), benzoic anhydride, and potassium chloride were isolated in 31, 40, 20, trace, and 65% yields (based on the potassium thiobenzoate used) respectively. The structure IV was confirmed by the result of elemental analyses and by the IR spectrum. On the other hand, V and VI were identified by elemental analyses and by comparisons of the IR spectra with those of authentic samples. By an

1) A. Fahlberg, *Chem. Ber.*, **22**, 757 (1889).
2) A. Baroni, *Atti Acad, Naz. Lincei, Mem., Cl. Sci. Fis., Mat. Nature.*, **17**, 1081 (1933).
3) C. G. O. Overberger and E. Salo, *J. Amer. Chem. Soc.*, **85**, 2446 (1963).
4) G. A. Olah and S. J. Kuhn, *J. Org. Chem.*, **27**, 2667 (1962).
5) H. Böhme and K. H. Meyer-Dulheuer, *Justus Liebigs, Ann. Chem.*, **688**, 78 (1965).
6) M. H. Karger and Y. M. Mazur, *J. Amer. Chem. Soc.*, **90**, 3781 (1968).
7) M. H. Karger and Y. M. Mazur, *ibid.*, **91**, 5663 (1969).
8) M. H. Karger and Y. M. Mazur, *J. Org. Chem.*, **36**, 528 (1971).

analogous treatment of potassium thiobenzoate with *p*-toluenesulfonyl chloride, and of potassium *p*-methylthiobenzoate with benzenesulfonyl chloride, *p*-methylbenzoyl benzenethiosulfonate (IX) and benzoyl *p*-toluenethiosulfonate (XI) were obtained in 22.9 and 20.5% yields respectively.

The thiosulfonates were a slightly yellow oil or a semi-solid which could not be crystallized and which showed a strong carbonyl absorption band at 1690 cm^{-1}. They were fairly stable under anhydrous conditions below 130°C,[9] but were hydrolyzed by moisture when the THF solution was stood in air at room temperature; the absorption at 1690 cm^{-1} disappeared completely after 6 hr. Furthermore, the addition of a few drops of water to IV, IX, and XI accelerated their decomposition.

One of the most interesting reactivities of these anhydrides is their ability as acylating reagents. Benzoyl benzenethiosulfonate (VI) reacted with aniline exothermally in ether to give benzanilide (VIII) and anilinium benzenethiosulfonate (VIII) quantitatively. Furthermore, the reaction of IV with *n*-, or *t*-butylamine gave *N*-*n*(or *t*)-butylbenzamide (XVI or XIII), and *n*(or *t*)-butylammonium benzenethiosulfonate (XV or XIII) in good yields, respectively. However in contrast to benzoyl benzenesulfonate,[3] it did not react with phenol, *t*-butyl alcohol and benzamide. Recently, Karger and Mazur[10] have reported the powerful acylating ability of mixed sulfonic carboxylic anhydrides or the basis of their facile cleavage of ethers (*n*-butyl ether, benzyl ether, THF, *etc*). However, the reactions of IV with propylene oxide, tetrahydrofuran, tetrahydropyran, 1,4-dioxane, dibenzyl ether, and di-*n*-butyl ether did not occur even under more severe conditions than that of Karger.[10]

It has been known that stable phosphoranes[11] and sulforanes[12] are C-acylated by acid anhydrides to give other stable ylides. The anhydride IV reacted with phenacylidenetriphenyl phosphorane at room temperature to give the stable adducts, α,α′-dibenzoylmethyltriphenylphosphonium benzenethiosulfonate (XVIII),

$$\underset{\text{IV}}{PhCOSSO_2Ph} + Ph_3\overset{+}{P}-\overset{-}{C}HCOPh \xrightarrow[CH_2Cl_2]{rt} \left[Ph_3\overset{+}{P}-CH(COPh)_2\right]\overset{-}{S}SO_2Ph \quad (2)$$

XVIII

in a 56% yield (Eq. (2)). The XVIII structure was confirmed by elemental analyses by the IR spectrum, which a strong new peak at 1670 cm^{-1} due to carbonyl stretching, and the formation of α,α′-dibenzoylmethyltriphenyl phosphorane (XIX) through a reaction with 5% aqueous sodium hydroxide (Eq. (3)):

$$\text{XVIII} \xrightarrow{5\%\ NaOH} Ph_3\overset{+}{P}-\overset{-}{C}(COPh)_2 \quad (3)$$

XIX

Moreover, the anhydride (IV) in petroleum ether reacted exothermally with methyl- and phenylmagnesium bromide to give acetophenone (41%), and benzophenone (46%) respectively. In addition, the treatment of the anhydrides (IV) with lithium ethane- and benzenethiolate gave 52% of *S*-ethyl thiobenzoate and 33% of *S*-phenyl thiobenzoate.

Experimental

All the melting points are uncorrected. The IR spectra were measured on a JASCO Grating Infra-red spectrophotometer IR-G.

Materials. Benzene- and *p*-toluenesulfonyl chloride were purified by distillation before use. The potassium substituted thiobenzoate was prepared according to the directions in the literature.[13] The phenacylidenetriphenyl phosphorane was prepared according to the procedure of Ramirez and Dershowitz;[14] mp 185.2—186.5°C. The solvents were rigorously dried and distilled before use.

Reactions and the manipulations of the samples were carried out under dry nitrogen.

Benzoyl Benzenethiosulfonate (IV). A suspended solution of potassium thiobenzoate (8.4 g, 0.05 mol) in acetonitrile (100 ml) was added to a solution of benzenesulfonyl chloride (8.4 g, 0.05 mol) in acetonitrile (50 ml), after which the mixture was stirred for 5 hr at room temperature. After the acetonitrile had been evaporated from the organic layer, the residue was washed with two 20 ml portions of dichloromethane.

The concentration of the washings and subsequent chromatographic separation on silica gel [*n*-hexane–ether (9.5: 0.5)] under dark conditions gave 6.3 g (30.6%) of IV from the second effluent, which showed one spot on thin-layer chromatography. IR (neat): ν C=O 1690 cm^{-1}, ν SO_2 1382 (asym) and 1180 (sym) cm^{-1}, Found: C, 56.01; H, 3.42; S, 22.60%. Calcd for $C_{13}H_{10}O_3S_2$: C, 56.11; H, 3.30; S, 22.90%. An effluent insoluble in the dichloromethane insoluble parts were recrystallized from benzene–*n*-hexane to give 3.6 g of dibenzoyl disulfide (V) as colorless crystals. The melting point, the result of sulfur analysis, and the IR spectrum coincided exactly with those of an authentic sample obtained by the reaction of potassium thiobenzoate with iodine. Mp 134—135°C, IR (KBr): ν C=O 1700 and 1680 cm^{-1}, Found: S, 25.70% (Calcd for $C_{14}H_{10}O_2S_2$: S, 26.06%). On the other hand, the acetonitrile insoluble parts (solid) was extracted with five 30 ml portions of hot methanol. The subsequent evaporation of the methanol from the extracts left 4 g (25% based on the benzenesulfonyl chloride used) of potassium benzenesulfonate (VI). The results of elemental analyses and the spectrum were identical with those of an authentic sample prepared from benzenesulfonic acid and potassium hydroxide. IR (KBr): ν SO_2 1200 and 1190 cm^{-1}. Found: C, 35.62; H, 2.63; S, 14.49% (Calcd for $C_6H_5O_3SK$: C, 35.58; H, 2.50; S, 14.24%). The methanol insoluble part contains 95% KCl, as determined by Standard Volhard potentiometric titration (65%, based on the potassium thio-

9) Heating of IV in glass ampoule at 150°C for 3 hr under nitrogen atmosphere gave a 63% of dibenzoyl disulfide together with intractable oil.

10) M. H. Karger and Y. M. Mazur, *J. Org. Chem.*, **36**, 532 (1971).

11) P. A. Chopard, R. J. G. Searle, and F. H. Devitt, *ibid.*, **30**, 1015 (1965).

12) a) H. Nozaki, M. Takaku, and K. Kondo, *Tetrahedron*, **22**, 2145 (1966). b) A. W. Johnson, and R. T. Amel, *J. Org. Chem.*, **34**, 1240 (1969).

13) P. Noble and D. S. Tarbell, "Organic Syntheses" Coll. Vol. IV, p. 924.

14) F. Ramirez and S. Dershowitz, *J. Org. Chem.*, **22**, 41 (1957).

benzoate used).

p-*Methylbenzoyl Benzenethiosulfonate (VII).* Yield, 22.9%: IR (neat) ν C=O 1691 cm^{-1}, ν SO_2 1388 (asym) and 1190 (sym) cm^{-1}. Found: C, 57.44; H, 4.01; S, 21.74%. Calcd for $C_{14}H_{12}O_3S_2$: C, 57.39; H, 4.19; S, 21.90%.

Benzoyl p-*Toluenethiosulfonate (VIII).* Yield 20.5%: IR (neat) ν C=O 1691 cm^{-1}, ν SO_2 1385 (asym) and 1197 (sym) cm^{-1}. Found: C, 57.50; H, 4.20; S, 21.98%. Calcd for $C_{14}H_{12}O_3S_2$: C, 57.39; H, 4.19; S, 21.90%.

Reaction of the Anhydride IV with Methanol. A methanol solution (20 ml) of IV (1.08 g, 0.04 mol) was refluxed for 10 hr. After the evaporation of the excess methanol from the reaction mixture, vacuum distillation of the residue gave 0.3 g (41% based on the IV used) of methyl benzoate (IX): bp 55°C/0.04 mmHg. The IR spectrum was identical with that of an authentic sample. The treatment of the distillation residue with 4 ml of aqueous 5% potassium hydroxide, the evaporation of the water from the reaction mixture, and subsequent recrystallization of the evaporation residue from methanol gave 0.3 g (96%) of potassium benzenesulfonate, which was identified by a comparison of the IR spectrum with that of an authentic sample.

Reaction of Benzoyl Benzenethiosulfonate (IV) with Aniline. When a solution of 0.4 g (0.04 mol) of aniline in 2 ml of ether was added to a solution of 0.56 g (0.002 mol) of IV in 10 ml of ether, the reaction began immediately and gave the precipitates. After the reaction mixture had been stirred at room temperature for 10 min, the insoluble parts were filtered out and washed four times with 3 ml portions of hot ether to give 0.45 g (50.5% based on the IV used) of anilinium benzenethiosulfonate (X), mp 171—172°C. IR (KBr): ν-NH_3 3100 cm^{-1} (strong, broad absorption), 1540 cm^{-1}, ν SO_2 1160 and 1038 cm^{-1}. Found: C, 54.12; H, 4.80; N, 5.11; S, 23.94%. Calcd for $C_{12}H_{13}NO_2S_2$: C, 54.14; H, 4.89; N, 4.89; S, 24.00%. The structure X was comfirmed by elemental analyses and by the IR spectrum. From the ether soluble parts, a 1.3 g portion of benzanilide (XI, mp 162.5—163.5°C) was obtained. The mp and IR spectrum were identical with those of the commercially obtained compound.

Reaction of the Anhydride IV with t-*Butylamine.* A solution of 0.29 g (0.04 mol) of *t*-butylamine in 2 ml of ether was added to a solution of 0.56 g (0.002 mol) of IV in 10 ml of ether and the mixture was stirred at room temperature for 15 min. The precipitates were filtered, washed four times with 3 ml portions of ether, and recrystallized from ethanol to give 0.37 g (79%, based on the IV used) of *t*-butylammonium benzenethiosulfonate (XII) as colorless crystals. Mp 196—197°C, IR (KBr): ν-NH_3 3100 cm^{-1} (strong, broad absorption), ν SO_2 1185 and 1050 cm^{-1}. Found: C, 50.93; H, 7.03; N, 5.48; S, 26.84%. Calcd for $C_{10}H_{17}NO_2S_2$: C, 50.84; H, 7.20; N, 5.51; S, 27.12%. The XII structure was comfirmed by elemental analyses and by the IR spectrum. From the ether-soluble parts, 0.29 g (81%, based on the IV used) of *N*-*t*-butylbenzamide (XIII) was obtained. Mp 128—129°C, IR (KBr), ν NH 3300 cm^{-1}, ν C=O 1630 cm^{-1}. The mp and the IR spectrum were identical with those of an authentic sample prepared from benzoyl chloride and *t*-butylamine.

Reaction of the Anhydride IV with n-*Butylamine.* An analogous treatment of IV (0.002 mol) with *n*-butylamine (0.004 mol) gave 0.32 g (68%, based on the IV used) of *n*-butylammonium benzenethiosulfonate (XV) and 0.3 g (78%, based on the IV used) of *N*-*n*-butylbenzamide (XVI). XV: mp 168—170°C, IR (KBr), ν-NH_3 3100 cm^{-1} (strong-broad absorption), ν SO_2 1170 and 1040 cm^{-1}. Found: C, 50.62; H, 7.12; N, 5.44; S, 27.03%. Calcd for $C_{10}H_{17}NO_2S_2$: C, 50.48; H, 7.20; N, 5.51; S, 27.12%. XVI: mp 69—71°C, IR (KBr), ν NH 3300 cm^{-1}, ν C=O 1630 cm^{-1}. The mp and the IR spectrum were identical with that of an authentic sample prepared from benzoyl chloride and *n*-butylamine.

Reaction of the Anhydride IV with Phenol. A mixture of IV (0.52 g, 0.002 mol) and phenol (0.18 g, 0.002 mol) was heated in a glass ampoule at 100°C for 20 hr. Phenol (0.17 g, 92%) was subsequently recovered from the mixture by distillation.

Reaction of Anhydride IV with Benzamide. A solution of benzamide (0.94 g, 0.008 mol) and IV (1.04 g, 0.004 mol) in ether (30 ml) was refluxed for 24 hr. The subsequent concentration of the reaction mixture gave 0.88 g of colorless crystals; was 94% of the recovered benzamide. The mp and the IR spectrum of the crystal consisted with those of benzamide obtained commercially.

Hydrolysis of the Anhydride IV. A benzene-solution (20 ml) of IV (1.05 g, 0.004 mol) was stirred for 6 hr at room temperature. After the evaporation of the solvent from the reaction mixture, the extraction of the residue with small portions of hot water and the cooling of the extracts gave 0.3 g of benzoic acid (XVII); mp 121—123°C.

On the other hand, the treatment of the hot water insoluble parts with 5 ml of aqueous potassium hydroxide gave 0.6 g of potassium *p*-toluenesulfonate.

Reaction of the Anhydride IV with Phenacylidenetriphenyl Phosphorane. A solution of 1.52 g (0.004 mol) of phenacylidenetriphenyl phosphorane and 1.05 g (0.004 mol) of IV dissolved in 10 ml of dichloromethane (1.05 g, 0.004 mol) was stirred for 12 hr at room temperature. After the subsequent concentration of the reaction mixture, the residue was crystallized from a small portion of acetone, subsequent recrystallization from dichloromethane–acetone containing minimum amount of *n*-hexane gave 1.5 g (56%) of α,α'-dibenzoylphenacyltriphenylphosphonium benzenethiosulfonate (XVIII) as slightly yellow crystals; mp 245—247°C, IR (KBr): ν C=O 1670 cm^{-1}. Found: C, 71.53; H, 4.74; P, 4.60; S, 9.61%. Calcd for $C_{39}H_{31}O_4PS_2$: C, 71.69; H, 4.71; P, 4.58; S, 9.60%.

Treatment of α,α'-*Dibenzoylmethyl Triphenylphosphonium Benzenethiosulfonate (XVIII) with Base.* The treatment of XVIII (1.3 g, 0.02 mol) with an aqueous 5% sodium hydroxide solution according to the usual method gave 0.86 g (85%) of α,α'-dibenzoylmethyl triphenylphosphorane (XIX), which was identified by a comparison of the mp and the IR spectrum with those of an authentic sample prepared according to the literature;[14] mp 191—193°C, IR (KBr) ν C=O 1520 cm^{-1}.

The Reaction of the Anhydride IV with Grignard Reagents.

a) Methylmagnesium Bromide: An ether solution of methylmagnesium bromide (0.01 mol) was added to an equimolar amount (2.8 g) of IV in the same solvent (10 ml) at 0°C, and the mixture was stirred at room temperature for 30 min. After the removal of the insoluble parts from the reaction mixture by filtration, the vacuum evaporation of the solvent from the filtrate and the distillation of the residue gave 0.49 g of acetophenone, bp 201—202°C (lit,[15] 202°C), IR (neat) ν C=O 1680 cm^{-1}. The boiling point and the IR spectrum coincided with those of an authentic sample which had been obtained commercially.

b) Phenylmagnesium Bromide. The similar treatment of the anhydride IV with phenylmagnesium bromide gave 0.83 g of benzophenone, bp 99°C/0.2 mmHg (lit,[16] 108°C/1 mmHg), IR (CCl_4) ν C=O 1664 cm^{-1}. The IR spectrum was quite similar to that of an authentic sample.

15) "The Merck Index" 7 ed. Merck and Co. INC. p. 9 (1960).
16) *ibid.*, p. 134 (1960).

Treatment of the Anhydride IV with Thiolates. *a) Lithium Ethanethiolate*: An ether solution of IV (2.78 g, 0.01 mol) was slowly added to a petroleum ether solution of lithium ethanethiolate (0.01 mol), which had been prepared from *n*-butyllithium and ethanethiol, at 0°C, and the mixture was stirred at room temperature for 1 hr. After filtrating the insoluble parts had been filtered from the reaction mixture, the evaporation of the solvent and vacuum distillation gave 0.85 g of *S*-ethyl thiobenzoate. Bp 79—80°C/2 mmHg (lit,[17] 83—84°C/2.5 mmHg). IR (neat) ν C=O 1669 cm^{-1}. The IR spectrum was identical with that of an authentic sample prepared from benzoyl chloride and lithium ethanethiolate.

b) Lithium Benzenethiolate: A similar treatment of IV (0.01 mol) with lithium benzenethiolate (0.01 mol) in petroleum ether gave *S*-phenyl thiobenzoate (0.69 g), mp 55—58°C (lit,[18] 56°C), IR (KBr) ν C=O 1685 cm^{-1}. The IR spectral data was quite similar to that of an authentic sample prepared from benzoyl chloride and lithium benzenethiolate in petroleum ether.

The authors wish to thank Professor Yoshio Hirabayashi and Mr. Hideharu Ishihara of Gifu University for their discussions, and wish to express also their hearty gratifude to Professor Yoshio Ishii of Nagoya University for his encouragement.

17) L. E. Wolinski, H. Tieckelmann, and H. W. Post, *J. Org. Chem.* **16**,, 1134 (1951).

18) H. Böhme and H. Schram, *Ber.*, **82**, 453 (1949).

BULLETIN OF THE CHEMICAL SOCIETY OF JAPAN, VOL. 46, 863—871 (1973)

The Crystal and Molecular Structure of Vitamin B_6 Derivatives. I. Pyridoxal Phosphate Hydrate and Pyridoxal Phosphate Methyl Hemiacetal

Takaji FUJIWARA

Faculty of Pharmaceutical Sciences, Osaka University, Toneyama, Toyonaka, Osaka

(Received June 2, 1972)

Pyridoxal phosphate hydrate (PLPHYD) was crystallized from an aqueous solution in the form of monoclinic needles; space group $P2_1/c$ with $a=10.503$, $b=13.608$, $c=7.488$ Å, $\beta=93.71°$ and four molecules in the unit cell. Prism-shaped crystal of pyridoxal phosphate methyl hemiacetal (PLPMHA) was obtained by dissolving the pyridoxal phosphate hydrate crystals into 90% methanol; space group $P\bar{1}$, with cell dimensions, $a=9.42$, $b=10.61$, $c=6.20$ Å, $\alpha=105.6°$, $\beta=95.7°$, and $\gamma=99.7°$, and two molecules per cell. Intensity data were collected on an automated diffractometer for PLPHYD and photographically for PLPMHA. Crystal structures have been determined by the symbolic addition method. Refinements were done by the block-diagonal least-squares procedures, the final R value being 0.093 for PLPHYD and 0.112 for PLPMHA. The free aldehyde group of pyridoxal phosphate interacts with water molecule to form *gem-diol* in the crystalline state of PLPHYD and the *gem-diol* group of PLPHYD with methanol to form methyl hemiacetal. One of the two hydrogen atoms on a phosphate group is liberated and protonated to the pyridine ring nitrogen atom, resulting in the zwitterionic structure for both PLPHYD and PLPMHA molecules. All hydrogen bonds in PLPHYD are intermolecular ones, but in PLPMHA there is one OH–O intramolecular hydrogen bond.

Vitamin B_6 is found in natural foods in various forms as pyridoxine, pyridoxamine, pyridoxal, pyridoxamine-5′-phosphate and pyridoxal-5′-phosphate (PLP). Of these, PLP is the most important coenzyme form of vitamin B_6; that is, as the form of 'co-decarboxylase' or 'co-transaminase', it participates in a vast number of enzyme systems associated with nitrogen metabolisms. A great many PLP-dependent enzymes have been isolated in a crystalline state and a number of mechanisms have been proposed as regards substrate-enzyme interactions, but many substantial points are still obscure.[1-2] In order to elucidate the relationship between the structure and function of PLP-dependent enzymes, it is necessary to determine the molecular structure of the coenzyme PLP.

This paper deals with a detailed X-ray diffraction analysis of two forms of PLP; pyridoxal phosphate hydrate (PLPHYD) and pyridoxal phosphate methyl hemiacetal (PLPMHA); a preliminary report has been published.[3]

Experimental

The yellowish needle crystals of PLPHYD were obtained by dissolving the sample (labelled 'Pyridoxal Phosphate Monohydrate', Sigma Chemicals) into ion-exchanged distilled water (pH=6.5) at room temperature, and then by keeping the solution at 7°C in the dark.

PLPMHA was obtained in the form of transparent yellow prism-shaped crystals by dissolving PLPHYD into about 90% methanol aqueous solution by heating up to boiling point, cooling at room temperature and then standing the solution at 5°C.

Unit cell parameters of PLPHYD were obtained with a

1) Y. Morino and E. E. Snell, *J. Biol. Chem.*, **242**, 2800 (1967).

2) P. Fasella, *Ann. Rev. Biochem.*, **36**, 185 (1967).

3) T. Fujiwara and K. Tomita, *Tetrahedron Lett.*, **1969**, 2819.

Rigaku Denki four-circle diffractometer and those of PLPMHA from zero-layer Weissenberg photographs about b and c, calibrated with superimposed aluminum powder pattern and precession photographs of the reciprocal a^*c^* and b^*c^* planes. The density was measured by flotation in a benzene and ethylene dibromide mixture for PLPHYD and in a benzene and carbon tetrachloride mixture for PLPMHA. The crystal data are listed in Table 1.

Table 1. Crystal data of pyridoxal phosphate hydrate (PLPHYD) and pyridoxal phosphate methyl hemiacetal (PLPMHA)

Compounds	PLPHYD	PLPMHA
Chemical formula	$C_8H_{12}O_7NP$	$C_9H_{14}O_7NP$
Mol. wt.	265.2	279.0
a(Å)	10.503±0.006	9.42±0.01
b(Å)	13.608±0.009	10.61±0.01
c(Å)	7.488±0.003	6.20±0.02
α(°)	90	105.6±0.2
β(°)	93.71±0.04	95.7±0.2
γ(°)	90	99.7±0.2
V(Å^3)	1067.97	580.7
Space group	$P2_1/c$	$P\bar{1}$
Z	4	2
D_m(g·cm^{-3})	1.635±0.003	1.587±0.004
D_c(g·cm^{-3})	1.649	1.595
μ(cm^{-1}) for Cu Kα	26.75	24.95

Intensity data of PLPHYD were collected with a crystal of dimensions $0.04\times0.18\times0.07$ mm^3, on a Rigaku Denki four-circle computer-controlled diffractometer using nickel-filtered Cu$K\alpha$ radiation and ω-2θ scanning technique. Scanning speed (2θ) was 2°/min and scanning width was taken as $\Delta\omega=1°+0.015\tan\theta$. Background was counted for ten seconds. 1912 independent reflections with $\sin\theta/\lambda$ less than 0.600 Å^{-1} were measured.

Three-dimensional intensity data for PLPMHA were collected from equi-inclination Weissenberg photographs with nickel-filtered Cu$K\alpha$ radiation. X-ray photographs for layers ($hk0$) to ($hk5$), and ($h0l$) to ($h8l$) were taken with two crystals, $0.31\times0.40\times0.31$ mm^3 and $0.24\times0.31\times0.38$ mm^3, respectively. The intensity was estimated visually by comparison with a standard scale, and corrected for spot size, and Lorentz and polarization factors. Independent 2526 reflections were measured.

The observed structure factors for both compounds were put on an absolute scale by Wilson statistics, and normalized structure factors ($|E_h|$) were computed.[4]

Phase Determination

Both PLPHYD and PLPMHA structures were solved by the symbolic addition method[5] for the centrosymmetric system (program DPD).

With the normalized structure factors for both compounds, the $\sum_2$ listings[4] were made for reflections with $|E_h|\geqq1.5$ and with probability larger than 97%, using a computer program SIGMA.

The starting set for PLPHYD is shown in Table 2,

Table 2. Starting set for the application of $\sum_2$ formula to PLPHYD

h	k	l	E_h	Sign	NINT[a]
5	10	−1	3.228	+	26
7	1	−4	3.040	+	36
10	8	−3	3.225	+	26
6	9	3	3.120	A	28
9	1	0	3.224	B	32
4	8	1	3.408	C	41
4	10	0	3.151	D	31
0	0	2	2.260	—	18

a) Number of $\sum_2$ interaction pairs.

where the sign of (002) reflection is uniquely determined by the $\sum_2$ listing. After three cycles of phase determination, the following relations were found to be predominant; A=−, AC=+, AD=+, BC=+, BD=+, CD=+, and ABC=−, which were reduced to A=B=C=D=−. Out of 261 reflections with $|E_h|\geqq1.5$, phases of 140 reflections were determined, and a subsequent E map revealed the appropriate peak height for all seventeen non-hydrogen atoms at proper positions. Two large spurious peaks were thought to come from insufficient number of E_h per atom, when it was compared with that of the empirical criterion by Karle.[4]

Table 3. Starting set for the application of $\sum_2$ formula to PLPMHA

h	k	l	Sign	E_h	NINT[a]
6	−10	5	+	2.547	24
−7	4	2	+	3.176	37
−1	1	5	+	3.281	34
0	−6	2	+	3.263	38
6	−2	3	A	3.091	39
4	2	5	B	2.175	8
5	−6	5	C	2.496	12
7	6	0	D	3.928	42

a) Number of $\sum_2$ interaction pairs.

Direct phase determination of PLPMHA was initiated by the starting set of eight reflections as listed in Table 3, where a positive sign of reflection (0−62) was uniquely determined from the $\sum_1$ formula[5] with a probability of 0.99. After three cycles of the symbolic addition procedure, the signs of 253 reflections were determined out of 328 reflections with $|E_h|\geqq1.5$. From relationship occurring between the letters A to D, it seemed probable that A=−, B=+, C=−, and D=−. Three dimensional E map calculated by this combination clearly elucidated the molecular structure of PLPMHA.

Refinement of the Structure

Refinement was done by the successive Fourier synthesis and then by a block-diagonal least-squares method (program BLLS).

PLPHYD. The molecular structure derived from the E map was quite different from the expected one which consists of one pyridoxal phosphate molecule

4) J. Karle and I. L. Karle, *Acta Crystallogr.*, **21**, 849 (1966).
5) H. Hauptman and J. Karle, "Solution of the Phase Problem" I. The Centrosymmetric Crystal. A.C.A. Monography No. 3. Polycrystal Book Service, Pittsburgh (1953).

and one water molecule of crystallization. The peculiar *gem-diol* structure was confirmed by the two Fourier syntheses, one using the phases except for two oxygen atoms of *gem-diol*, and the other the phases of all non-hydrogen atoms (R=0.28). Further refinement of the positional and thermal parameters was carried out by the least-squares calculation wihch minimized $\sum\omega_i(k|F_o|-|F_c|)^2$, where ω_i, the weight of ith reflection, was zero for $|F_o|=0$ and unity for $|F_o|\neq 0$. Several cycles of refinement employing anisotropic temperature factors for all non-hydrogen atoms reduced the R index to 0.11. At this stage, a difference Fourier synthesis was computed, and all of twelve hydrogen atoms were found to occupy the appropriate positions. Final three cycles of refinement including the hydrogen atoms with isotropic thermal factors reduced the R index to 0.106 (R=0.093 with non-zero reflections). The final atomic positional and thermal parameters are listed in Tables 4 and 5, respectively.

PLPMHA. Refinement of the structure by the least-squares method with isotropic thermal parameters brought the R value from 0.21 to 0.16 after five cycles of refinement. A difference Fourier synthesis was calculated at this stage. Out of 14 hydrogen atoms, thirteen could be located at the peak positions in the difference map. Five cycles of refinement were done

Table 4. Final fractional coordinates and the estimated deviations (in Å) of PLPHYD

Atom[a)]	x/a	$\sigma(x)$	y/b	$\sigma(y)$	z/c	$\sigma(z)$	Atom[a)]	x/a	$\sigma(x)$	y/b	$\sigma(y)$	z/c	$\sigma(z)$
P	0.2447	0.001	0.1549	0.001	0.2186	0.001	C7	0.9394	0.006	0.3795	0.006	0.2009	0.007
O1	0.6133	0.004	0.0173	0.004	0.1367	0.004	C8	0.7101	0.006	0.0534	0.005	0.2565	0.006
O2	0.6879	0.005	0.0261	0.004	0.4326	0.004							
O3	0.9202	0.004	0.1641	0.004	0.1716	0.005	O6H	0.180	0.07	0.191	0.08	0.483	0.07
O4	0.3745	0.004	0.2147	0.004	0.2394	0.004	C1H1	0.486	0.08	0.101	0.08	0.312	0.08
O5	0.1523	0.004	0.2212	0.004	0.1149	0.004	C1H2	0.462	0.08	0.179	0.08	0.479	0.08
O6	0.2023	0.004	0.1381	0.004	0.4128	0.004	C6H	0.531	0.07	0.362	0.08	0.348	0.07
O7	0.2664	0.004	0.0554	0.004	0.1397	0.004	NH	0.723	0.08	0.432	0.08	0.289	0.08
N	0.7172	0.005	0.3648	0.004	0.2769	0.005	O3H	0.999	0.08	0.194	0.08	0.135	0.08
C1	0.4799	0.005	0.1689	0.006	0.3457	0.006	C8H	0.798	0.07	0.027	0.07	0.221	0.07
C2	0.8241	0.005	0.3192	0.005	0.2315	0.006	O1H	0.665	0.08	−0.016	0.09	0.026	0.08
C3	0.8194	0.006	0.2155	0.006	0.2197	0.006	O2H	0.725	0.09	−0.034	0.09	0.479	0.08
C4	0.7080	0.005	0.1663	0.005	0.2571	0.005	C7H1	0.928	0.09	0.417	0.09	0.095	0.09
C5	0.6012	0.005	0.2187	0.005	0.3003	0.005	C7H2	1.020	0.09	0.337	0.10	0.174	0.09
C6	0.6081	0.006	0.3201	0.006	0.3096	0.006	C7H3	0.957	0.09	0.429	0.09	0.286	0.09

a) Name of the hydrogen atom; for example, C7H3 shows the third hydrogen atom attached to the C7 atom.

Table 5. Final thermal parameters of PLPHYD. Anisotropic temperature factors are in the form of exp $\{-(B_{11}h^2+B_{22}k^2+B_{33}l^2+B_{12}hk+B_{13}hl+B_{23}kl)\}$ and their standard deviations ($\times 10^5$)

Atom	B_{11}	$\sigma(B_{11})$	B_{22}	$\sigma(B_{22})$	B_{33}	$\sigma(B_{33})$	B_{12}	$\sigma(B_{12})$	B_{13}	$\sigma(B_{13})$	B_{23}	$\sigma(B_{23})$
P	284	11	142	7	796	24	37	15	189	26	59	22
O1	624	43	387	27	1207	86	−287	56	−167	97	−416	77
O2	1061	55	283	26	887	79	293	59	46	105	409	72
O3	370	37	238	24	2252	108	22	49	725	101	−145	82
O4	375	35	187	22	1208	79	−69	44	−101	85	−1	67
O5	328	34	227	22	1239	80	108	44	140	84	415	68
O6	612	39	156	21	821	71	100	46	457	85	41	61
O7	618	41	131	20	1046	76	92	46	277	89	−291	63
N	481	44	175	26	980	89	−84	54	13	102	30	75
C1	284	46	297	34	1104	110	54	65	30	114	395	100
C2	351	49	173	30	1272	116	69	60	178	120	175	91
C3	328	49	225	32	1275	117	24	63	155	122	19	97
C4	339	47	170	29	933	100	−112	61	−7	110	−61	88
C5	421	50	146	28	840	98	−71	60	−219	112	−1	84
C6	385	51	261	33	969	109	27	65	147	119	−47	93
C7	533	59	188	33	2117	156	−204	72	387	154	−12	113
C8	441	52	118	28	1539	125	−120	63	155	129	−106	95

Atom	B(isotropic)	Atom	B(isotropic)
O6H	1.6	C8H	1.4
C1H1	2.0	O1H	3.2
C1H2	2.3	O2H	3.8
C6H	1.8	C7H1	4.6
NH	3.4	C7H2	5.2
O3H	2.8	C7H3	3.8

Table 6. Final fractional coordinates and the estimated standard deviations (in Å) of PLPMHA

Atom	x/a	$\sigma(x)$	y/b	$\sigma(y)$	z/c	$\sigma(z)$	Atom	x/a	$\sigma(x)$	y/b	$\sigma(y)$	z/c	$\sigma(z)$
P	0.7538	0.001	1.0394	0.001	0.9790	0.001	C9	1.0730	0.007	0.6582	0.009	0.4407	0.009
O1	0.9232	0.004	0.6245	0.004	0.3580	0.005							
O2	0.9497	0.004	0.6839	0.005	0.0062	0.004	NH	0.361	0.10	0.776	0.11	0.119	0.11
O3	0.6919	0.004	0.5871	0.005	−0.1998	0.005	O3H	0.812	0.12	0.627	0.12	−0.157	0.12
O4	0.6879	0.004	0.9206	0.005	0.7523	0.004	O2H	1.039	0.10	0.744	0.11	0.008	0.11
O5	0.6281	0.003	1.0373	0.004	1.1143	0.004	C6H	0.496	0.07	0.856	0.08	0.477	0.08
O6	0.7922	0.004	1.1663	0.004	0.9190	0.005	C1H1	0.841	0.08	0.824	0.08	0.635	0.08
O7	0.8848	0.004	1.0042	0.004	1.0959	0.004	C1H2	0.850	0.10	0.966	0.10	0.576	0.10
N	0.4535	0.004	0.7422	0.005	0.1416	0.005	C8H	0.969	0.07	0.825	0.07	0.287	0.07
C1	0.7788	0.005	0.8787	0.007	0.5901	0.006	C7H1	0.300	0.09	0.564	0.09	−0.186	0.09
C2	0.5023	0.005	0.6722	0.006	−0.0331	0.006	C7H2	0.467	0.11	0.533	0.11	−0.350	0.10
C3	0.6479	0.005	0.6608	0.006	−0.0157	0.006	C7H3	0.350	0.11	0.683	0.11	−0.325	0.11
C4	0.7403	0.005	0.7272	0.005	0.1891	0.005	C9H1	1.106	0.09	0.629	0.09	0.301	0.09
C5	0.6827	0.005	0.8007	0.006	0.3690	0.006	C9H2	1.110	0.10	0.742	0.10	0.512	0.10
C6	0.5361	0.005	0.8066	0.006	0.3431	0.006	C9H3	1.074	0.09	0.603	0.09	0.570	0.09
C7	0.3975	0.007	0.6090	0.008	−0.2530	0.007	O5H	0.5		1.0		1.0	
C8	0.9027	0.005	0.7251	0.006	0.2133	0.006	O7H	1.0		1.0		1.0	

Table 7. Final thermal parameters of PLPHA. Anisotropic temperature factors are in the form of exp $\{-(B_{11}h^2+B_{22}k^2+B_{33}l^2+B_{12}hk+B_{13}hl+B_{23}kl)\}$ and their standard deviations ($\times 10^5$)

Atom	B_{11}	$\sigma(B_{11})$	B_{22}	$\sigma(B_{22})$	B_{33}	$\sigma(B_{33})$	B_{12}	$\sigma(B_{12})$	B_{13}	$\sigma(B_{13})$	B_{23}	$\sigma(B_{23})$
P	323	12	723	14	1482	34	337	21	12	32	606	35
O1	630	45	853	48	3815	164	385	74	90	136	1836	146
O2	703	48	1029	53	2635	138	241	80	485	130	238	135
O3	935	55	1185	59	2360	136	508	90	223	137	−89	140
O4	576	44	1229	57	2280	128	401	80	147	120	120	135
O5	419	38	956	47	2140	116	326	67	322	105	933	118
O6	526	42	871	47	3375	149	363	70	242	125	1661	138
O7	501	41	996	49	2698	132	497	72	−313	116	1407	132
N	477	46	705	49	2333	141	392	75	15	127	1116	135
C1	473	57	984	72	2605	188	281	101	40	163	255	183
C2	702	61	725	59	1862	152	294	95	−243	152	897	153
C3	603	58	694	59	2381	173	330	93	−10	159	697	162
C4	504	52	585	52	2046	152	405	84	126	142	808	144
C5	487	53	702	57	2065	156	297	86	186	144	959	153
C6	594	57	695	57	2145	161	450	92	151	152	688	154
C7	915	77	1193	84	2214	187	319	128	−376	189	642	199
C8	557	57	739	60	2416	173	479	93	188	157	813	164
C9	820	77	1423	99	4506	294	693	140	−120	238	2776	286

Atom	B(isotropic)	Atom	B(isotropic)	Atom	B(isotropic)
NH	6.3	C1H2	5.6	C9H1	4.8
O3H	7.5	C8H	2.3	C9H2	5.3
O2H	6.3	C7H1	3.0	C9H3	5.0
C6H	2.5	C7H2	2.6	O5H	2.9
C1H1	3.1	C7H3	4.9	O7H	2.6

with anisotropic temperature factors for non-hydrogen atoms and with isotropic for 13 hydrogen atoms. A subsequent difference Fourier synthesis revealed no plausible peak for the one remaining hydrogen atom attached to the phosphate oxygen atom. This might be due to uncertainty of the hydrogen position; the two P–O bond lengths (P–O5=1.519 Å and P–O7=1.520 Å) were equal within the estimated standard deviation (0.005 Å) and the oxygen-oxygen distances related by a center of symmetry (O5–O5=2.555 Å and O7–O7=2.580 Å) indicated the existence of the symmetrical hydrogen bonding. The final five cycles on the least-squares refinement were carried out by keeping the one hydrogen atom at two centers of symmetry with a half weight, and the R index dropped to 0.112. The final positional and thermal parameters are listed in Tables 6 and 7, respectively.

A list of the observed and calculated structure factors for both crystals is kept as Document No. 7308 at the office of the Chemical Society of Japan.

All the numerical computations were done on an NEAC 2200—500 of the Computing Center of this University, a FACOM 230—60 of the Data Processing Center, Kyoto University and HITAC 5020E of the Computer Centre, the University of Tokyo. Computer programs SIGMA, BLLS, and DAPH were written by

Dr. Tamaichi Ashida and others by the author. The atomic scattering factors were taken from 'International Tables for X-ray Crystallography'.[6]

Discussion

The bond lengths and angles were calculated using the computer program DAPH and are shown in Fig. 1 for PLPHYD and Fig. 2 for PLPMHA.

Phosphate Group. Four P–O bond lengths of 1.587, 1.565, 1.503, and 1.501 Å in PLPHYD are in good agreement with the following average values[7] found in the other known monoanionic phsophates:[7–10] P–OC=1.602, P–OH=1.554, P–O$^-$=1.502, and P=O=1.490 Å, respectively. The P–O4 bond length of 1.600 Å and the P–O6 bond length of 1.487 Å in PLPMHA are very close to the above P–OC and P=O distances, respectively, whereas the P–O5 (1.519 Å) and the P–O7 (1.520 Å) bond lengths associated with the symmetrical hydrogen atom are intermediate to the normal P–OH and P=O bond lengths, similar P–O bond lengths of 1.522 and 1.530 Å being found in DL-*O*-serine phosphate monohydrate.[11] The correla-

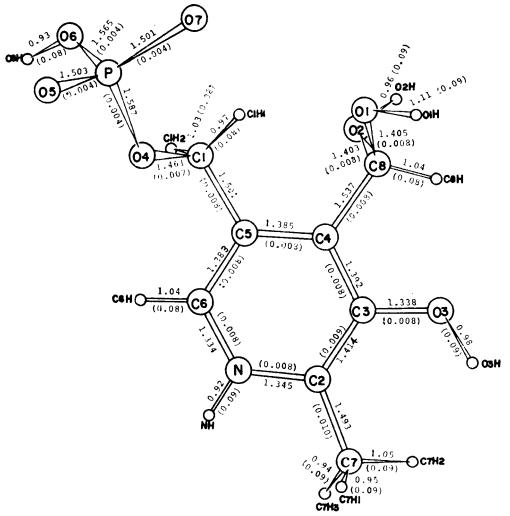

Fig. 1(a). Bond lengths and their standard deviations in parentheses (in Å) of PLPHYD. The molecule is projected on the plane of the pyridine ring.

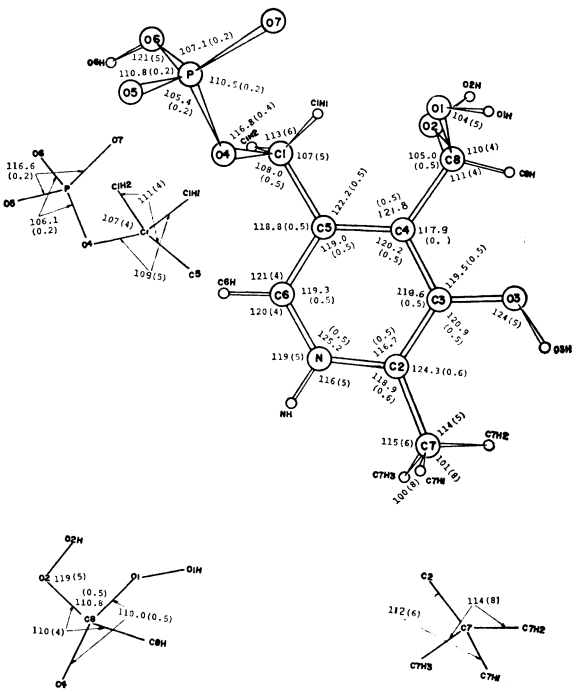

Fig. 1(b). Bond angles and their standard deviations in parentheses (in degree) of PLPHYD.

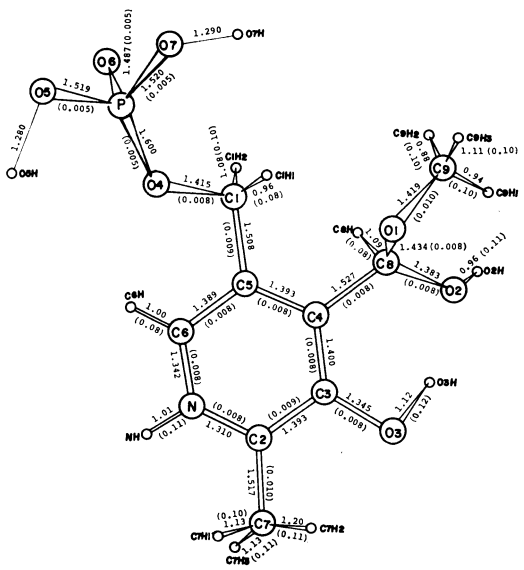

Fig. 2(a). Bond lengths and their standard deviations in parentheses (in Å) of PLPMHA. The molecule is projected on the plane of the pyridine ring.

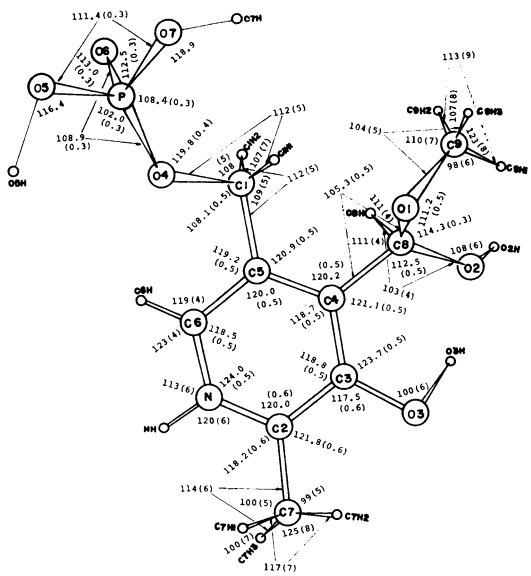

Fig. 2(b). Bond angles and their standard deviations in parentheses (in degree) of PLPMHA.

6) "International Tables for X-ray Crystallography," Vol. III, Kynoch Press, Birmingham (1962), p. 202.
7) M. Sundaralingam and E. F. Putkey, *Acta Crystallogr.*, **B26**, 790 (1970).
8) J. Kraut, *ibid.*, **14**, 1146 (1961).
9) J. Kraut and L. H. Jensen, *ibid.*, **16**, 79 (1963).
10) M. Sundaralingam, *ibid.*, **21**, 495 (1966).
11) E. Putkey and M. Sundaralingam, *ibid.*, **B26**, 782 (1970).

tion of each four O–P–O angles of PLPHYD and PLPMHA is explainable by considering the repulsive force between two adjacent oxygen atoms;[9] the larger bond angle is found between the two shorter bonds.

TABLE 8. DEVIATIONS OF THE ATOMS FROM THE LEAST-SQUARES PLANE (IN Å)

Atom	PLPHYD	PLPMHA	PINHCL[a]	PLPOXM[b]
The atoms involved in the calculation of the least-squares plane				
C2	0.000	−0.005	−0.009	−0.019
C3	0.008	0.007	0.009	0.003
C4	−0.010	−0.002	−0.001	0.014
C5	0.004	−0.005	−0.007	−0.017
C6	0.006	0.007	0.007	0.003
N	−0.008	−0.002	0.001	0.016
The atoms excluded in the calculation of the least-squares plane				
C1	−0.047	−0.072	−0.015	−0.068
C7	−0.031	−0.067	−0.037	−0.082
C8	−0.107	−0.075	−0.033	0.020
O3	0.046	0.011	0.015	−0.050
C6H	−0.03	0.06		
NH	−0.05	−0.31		
C8H	−0.11	−0.85		
O3H	0.13	−0.36		
O4	1.021	0.204	−0.029	−0.000

a) Pyridoxine hydrochloride[12]
b) Pyridoxal phosphate oxime[13]

Pyridine Ring. Figures 1 and 2 show the molecular projection on the plane of the pyridine ring for PLPHYD and PLPMHA, respectively. The deviations of the individual atoms from the least-squares plane, together with the corresponding values of similar compounds, pyridoxine hydrochloride[12] and pyridoxal phosphate oxime[13] are listed in Table 8. The pyridine ring is exactly planar and C1, C7, C8, O3, and two hydrogen atoms (C6H and NH) are nearly in the plane of the ring, both in PLPHYD and PLPMHA. The equations of the best plane passing through the ring atoms are as follows:

for PLPHYD, $-0.24677X+0.06189Y-0.96709Z+3.51217=0$,
for PLPMHA, $-0.11690X-0.94425Y+0.30779Z+7.16397=0$.

The bond lengths and the angles in the pyridine ring are listed in Table 9, together with those of the related compounds. In the pyridine ring of PLPHYD and PLPMHA, the average C–C bond length is 1.394 Å and the C–N bond length is 1.330 Å. Three $C(sp^2)$–$C(sp^3)$ bond lengths have a mean value of 1.515± 0.009 Å, which is comparable to a standard value of 1.50 Å for a $C(sp^2)$–$C(sp^3)$ single bond. The bond angles, C2–N–C6 of 125.2 and 124.0° for PLPHYD and PLPMHA indicate that an extra-annular hydrogen atom attaches to the ring nitrogen as suggested by Singh[14] and the position of the attached hydrogen atom is confirmed by the difference Fourier synthesis.

TABLE 9. BOND LENGTHS AND ANGLES OF THE PYRIDINE SKELETON

	PLP-HYD	PLP-MHA	PIN-HCL[a]	PLP-OXM[b]
BOND LENGTHS (IN Å)				
C2–C3	1.414	1.393	1.368	1.41
C3–C4	1.392	1.400	1.379	1.38
C4–C5	1.385	1.393	1.409	1.41
C5–C6	1.383	1.389	1.358	1.36
C6–N	1.334	1.342	1.325	1.34
N –C2	1.345	1.310	1.345	1.35
C2–C7	1.493	1.517	1.483	1.51
C4–C8	1.537	1.527	1.490	1.44
C5–C1	1.501	1.508	1.497	1.55
C3–O3	1.338	1.345	1.354	1.35
e. s. d.	0.009	0.009	0.005	0.02
BOND ANGLES (IN degree)				
N –C2–C3	116.7	120.0	118.1	117
N –C2–C7	118.9	118.2	119.4	119
C7–C2–C3	124.3	121.8	122.5	124
C2–C3–C4	119.6	118.8	120.1	121
C2–C3–O3	120.9	117.5	115.8	116
O3–C3–C4	119.5	123.7	124.1	123
C3–C4–C5	120.2	118.7	118.8	117
C3–C4–C8	117.9	121.1	123.0	122
C8–C4–C5	121.8	120.2	118.2	121
C4–C5–C6	119.0	120.0	119.6	122
C4–C5–C1	122.2	120.9	121.4	119
C1–C5–C6	118.8	119.2	119.0	120
C5–C6–N	119.3	118.5	118.9	119
C6–N –C2	125.2	124.0	124.5	124
e. s. d.	0.5	0.5	0.3	1

a)–b) See footnete a—b, Table 8.

Molecular Conformation. The conformational angles of PLPHYD and PLPMHA molecule are shown in Fig. 3. The torsion angle around the C1–O4 bond (162.2° for PLPHYD and 198.0° for PLPMHA) indicates that the P–O4 bond of the two compounds is almost symmetrical with each other with respect to the plane passing through C5, C1, and O4. The torsion angle around the C1–C5 bond (52.1° for PLPHYD and 13.5° for PLPMHA) means that the O4 atom of PLPHYD deviates appreciably from the plane of the pyridine ring (1.02 Å) but the O4 atom of PLPMHA is roughly in the plane (0.20 Å). As for the O4 atom, it is found that the C1–O4 bond distance of PLPHYD is significantly greater than that of PLPMHA. A large conformational change between PLPHYD and PLPMHA around the C8–C4 bond is probably due to the difference in the type of hydrogen bonding. Both two oxygen atoms (O1 and O2) in the *gem-diol* of PLPHYD are situated symmetrically at both sides of the pyridine ring plane as donors of the intermolecular hydrogen bonds, and the two C–O bonds with nearly equal length of 1.403 and 1.405 Å are in the *gauche-gauche* conformations with regard to the C4–C5 bond. On the other hand, of two oxygen atoms attached to the C8 atom of PLPMHA, O1 is of a methyl hemiacetal group and O2 is of a hydroxyl group, and the formation

12) F. Hanic, *Acta Crystallogr.*, **21**, 332 (1966).
13) A. N. Barret and R. A. Palmer, *ibid.*, **B25**, 688 (1969).
14) C. Singh, *Acta Crystallogr.*, **19**, 861 (1965).

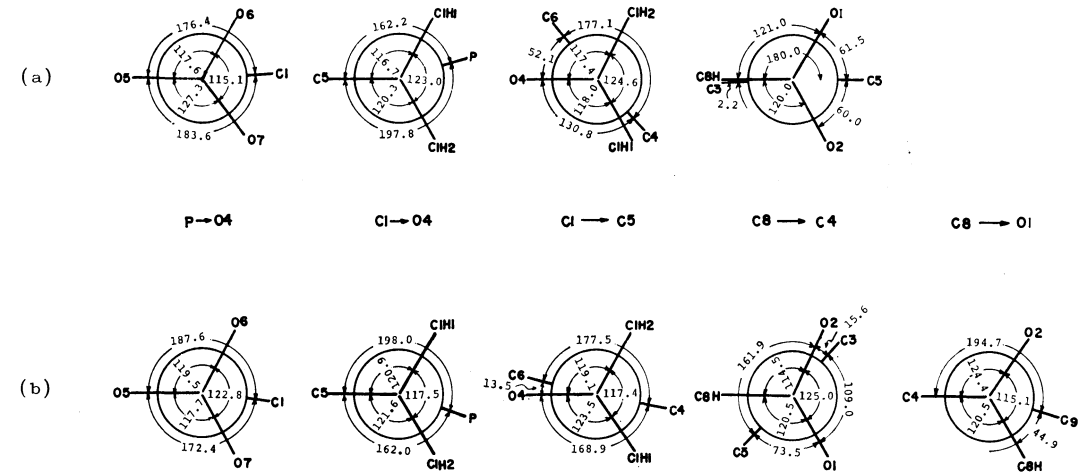

Fig. 3. Molecular conformations of PLPHYD (a) and PLPMHA (b). Torsion angles are in degree.

of the intramolecular hydrogen bond between O2 and O3 restricts the torsion angle between the C8–O2 and C4–C3 bonds to be 15.6°.

Pyridoxal phosphate has been determined to form a stable *gem-diol* type crystalline hydrate in PLPHYD. The reason for the *gem-diol* formation of the pyridoxal phosphate is ascribable to the electron attracting character of the protonated pyridine ring; the withdrawal of electron from the carbon atom of the carbonyl group causes this atom to have a relatively positive charge and hence to be attacked by hydroxide ion, as in the formation of chloral hydrate[15] by chloral. It is also indicated that the reaction from PLPHYD to PLPMHA is not the addition reaction between an aldehyde and a molecule of methyl alcohol but the dehydration reaction between a *gem-diol* and a molecule of methyl alcohol. On the other hand, from NMR spectra measurement of pyridoxal phosphate in D_2O solution at pD=7.8,[16] the ratio of the hydrated form (*gem-diol*) to the free aldehyde form has been calculated to be 0.86, and a similar ratio of 0.66 was estimated from the ultraviolet absorption measurement of 5-deoxypyridoxal at pH=6.88.[17]

Cystal Structure. The projections of the crystal structure and the hydrogen bondings in PLPHYD viewed along the *c* and *b* axes, respectively, are shown in Figs. 4 and 5, and the crystal structure of PLPMHA projected along the *c* axis in Fig. 6. The hydrogen bond distances and angles are listed in Tables 10 and 11 for PLPHYD and PLPMHA, respectively. All the

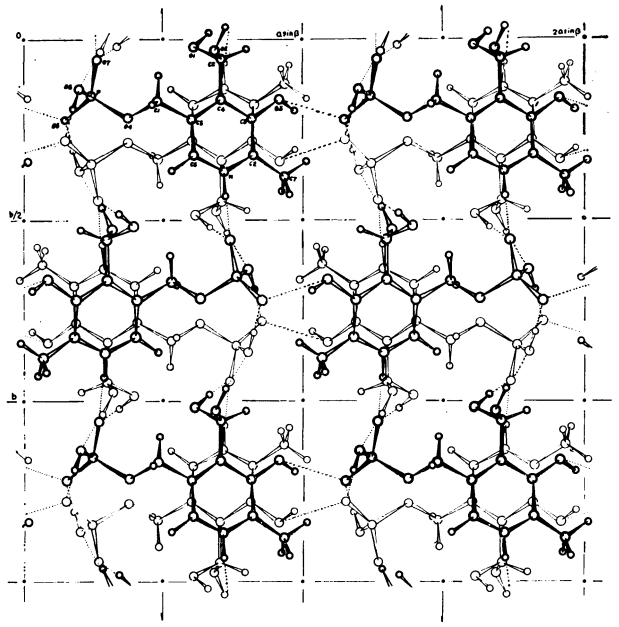

Fig. 4. A projection of PLPHYD structure along the *c* axis. Hydrogen bonds are indicated by the broken lines.

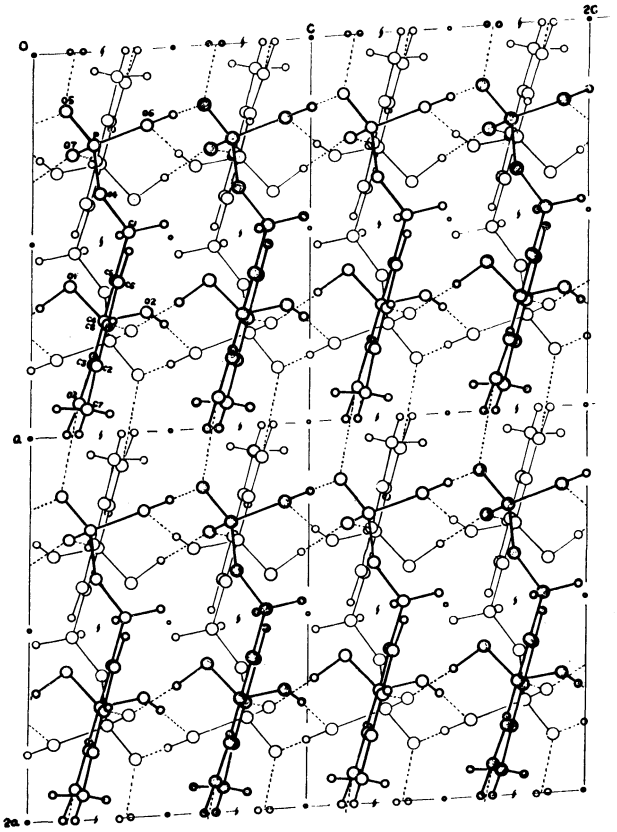

Fig. 5. A projection of PLPHYD structure along the *b* axis. Hydrogen bonds are indicated by the broken lines.

15) K. Ogawa, This Bulletin, **36**, 610 (1963).
16) W. Korytnyk and R. P. Singh, *J. Amer. Chem. Soc.*, **85**, 2813 (1963).
17) D. E. Metzler and E. E. Snell, *ibid.*, **77**, 2431 (1955).

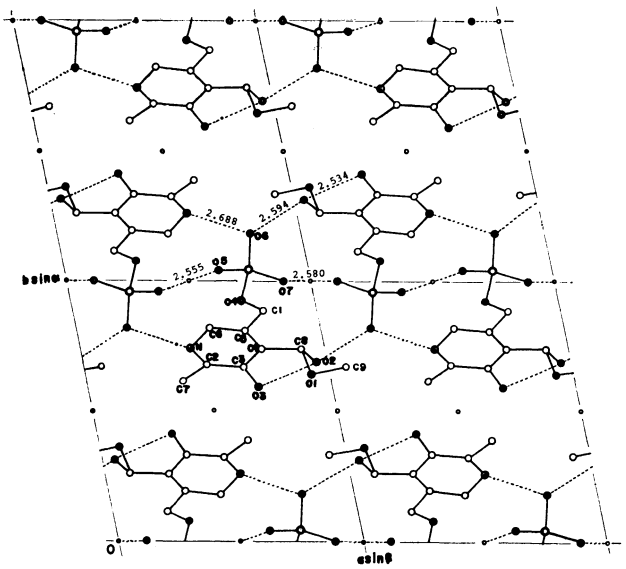

Fig. 6. A projection of PLPMHA structure along the *c* axis. Hydrogen bonds (in Å) are indicated by the broken lines.

hydrogen bonds in PLPHYD are intermolecular ones, whereas in PLPMHA there is one intramolecular hydrogen bond of 2.534 Å between O2 and O3. Phosphate oxygen atoms of both compounds participate in hydrogen bond formation. It is of interest that O5 and O7 atoms of PLPMHA form the symmetrical hydrogen bonds of 2.555 and 2.580 Å, respectively. The shortest OH···O hydrogen bond distance of 2.517 Å found on P–OH···O=P of PLPHYD is comparable to 2.492 Å of L-serine phosphate.[7] The ester oxygen atom O4 in both compounds and O1 in PLPMHA are not involved in the hydrogen bonding. The protonated nitrogen atom in the pyridine ring also takes part in the hydrogen bonding of NH···O type in both compounds. PLPHYD molecules are fixed by three dimensional networks of hydrogen bonding and the large overlaps of the pyridine rings with spacing of 3.7 Å are found among the molecules related by the *c* glide plane symmetry. Molecular arrangement in the PLPMHA crystal can be described as a layered structure parallel to the *ac* plane. The L and D antipodes

TABLE 10. HYDROGEN BOND DISTANCES AND ANGLES IN PLPHYD

Distances (Å)		Angles (degree)	
Donor Acceptor			
O3(S2)—O5(S1)	2.619(0.006)[a]	C3–O3(S2)—O5(S1)	130.5(0.4)[a]
		P –O5(S1)—O3(S2)	108.3(0.2)
O6(S1)—O5(S3)	2.517(0.006)	P –O6(S1)—O5(S3)	122.1(0.2)
		P –O5(S3)—O6(S1)	127.9(0.2)
O2(S4)—O6(S1)	2.737(0.006)	C8–O2(S4)—O6(S1)	122.0(0.3)
		P –O6(S1)—O2(S4)	112.0(0.2)
O1(S5)—O7(S1)	2.677(0.006)	C8–O1(S5)—O7(S1)	105.5(0.4)
		P –O7(S1)—O1(S5)	136.7(0.3)
N (S1)—O7(S6)	2.671(0.006)	C2–N (S6)—O7(S1)	117.7(0.4)
		C6–N (S6)—O7(S1)	116.3(0.4)
		P –O7(S1)—N (S6)	142.5(0.3)

S1	x	y	z
S2	$x-1$	y	z
S3	x	$1/2-y$	$1/2+z$
S4	$1-x$	$-y$	$1-z$
S5	$1-x$	$-y$	$-z$
S6	$1-x$	$-1/2+y$	$1/2-z$

a) Estimated standard deviations are in parentheses.

TABLE 11. HYDROGEN BOND DISTANCES AND ANGLES IN PLPMHA

Distances (Å)		Angles (degree)	
Donor Acceptor			
O3(S1)—O2(S1)	2.534(0.007)[a]	C3–O3(S1)—O2(S1)	86.7(0.4)[a]
		C8–O2(S1)—O3(S1)	92.5(0.4)
O2(S2)—O6(S1)	2.594(0.007)	P –O6(S1)—O2(S2)	125.9(0.3)
		C8–O2(S2)—O6(S1)	101.9(0.4)
N (S3)—O6(S1)	2.688(0.007)	P –O6(S1)—N (S3)	108.0(0.3)
		C6–N (S3)—O6(S1)	113.0(0.4)
		C2–N (S3)—O6(S1)	120.1(0.4)
O5(S1)—O5(S4)	2.555(0.009)	P –O5(S1)—O5(S4)	116.4(0.3)
O7(S1)—O7(S5)	2.580(0.009)	P –O7(S1)—O7(S5)	118.8(0.3)

S1	x	y	z
S2	$2-x$	$2-y$	$1-z$
S3	$1-x$	$2-y$	$1-z$
S4	$1-x$	$2-y$	$2-z$
S5	$2-x$	$2-y$	$2-z$

a) Estimated standard deviations are given in parentheses.

of PLPMHA related by a center of symmetry are held together by the network of hydrogen bonds in each layer, whereas between the adjacent layers the methyl group acts mainly as a spacer. As the number of intermolecular short contacts is greater in PLPHYD than in PLPMHA, it can be said that PLPHYD molecules are in closer packing arrangement than PLPMHA, which explains well the larger observed density of the former ($1.635\ g \cdot cm^{-3}$) than that of the latter ($1.587\ g \cdot cm^{-3}$).

The author wishes to express his sincere thanks to Professor Masao Kakudo and Dr. Ken-ichi Tomita for their encouragement and helpful discussions in the course of this study. Thanks are also due to Dr. Tamaichi Ashida for the use of his computer programs.

BULLETIN OF THE CHEMICAL SOCIETY OF JAPAN, VOL. 46, 871—876 (1973)

Solvolysis of Organic Phosphates. VI. Intramolecular Catalysis in the Hydrolysis of 2-Pyridylalkyl Phosphates[1)]

Yukito MURAKAMI, Junzo SUNAMOTO, and Naomi KANAMOTO

Department of Organic Synthesis, Faculty of Engineering, Kyushu University, Fukuoka 812

(Received June 5, 1972)

The spontaneous hydrolysis of 2-pyridylethyl, 2-pyridylpropyl, and 6-methyl-2-pyridylmethyl phosphates was investigated at 80—95°C in aqueous media with an ionic strength of 0.10. The reactions followed apparent first-order kinetics with respect to the phosphate species, and the maximum rates were observed at $-\log[H^+]$ 2—3 with a shoulder around 5—6. The participation of intramolecular catalysis played by the pyridinium group in the hydrolysis of the above pyridylalkyl phosphates as well as in that of 2-pyridylmethyl phosphate was investigated from the LFER viewpoint. For the evaluation of LFER, the acid dissociation constant was employed as the most reasonable structural parameter. As a result, the intramolecular pyridinium catalysis was found to takes place in the zwitterion hydrolysis for 2-pyridylmethyl, 2-pyridylethyl, and 6-methyl-2-pyridylmethyl phosphates. This indicates the importance of the geometry around the reaction center for the intramolecular catalytic action. The isokinetic relationship was established for the hydrolysis of pyridylalkyl phosphates with the exception of 6-methyl-2-pyridylmethyl phosphate. The anomalous behavior in the hydrolysis of the latter was attributed to the activation entropy effect which may have been caused by defreezing of solvation in the transition state.

We have investigated the extent of intramolecular catalysis in the hydrolysis of aryl and alkyl phosphates containing a hetero-aromatic ring system around the reaction center. An intramolecular general acid catalysis has been confirmed in the spontaneous hydrolysis of 2-pyridylmethyl,[2)] 8-quinolyl,[3)] and 3-hydroxy-2-pyridylmethyl phosphates.[4)] From the results so far obtained a question arose as to whether acidity of the catalytic group or the geometry around the reaction center contributes to the intramolecular catalysis in the hydrolysis.

In this work, we intend to clarify the effect of structural environment on the intramolecular catalysis by studying the hydrolysis of 2-pyridylalkyl phosphates. If both 2-pyridylethyl and 2-pyridylpropyl phosphates secure the rate enhancement in their hydrolyses due to the intramolecular catalysis by the pyridinium group as in the case of 2-pyridylmethyl phosphate **1**, a six-membered ring **2** and a seven-membered one **3**, respectively, would be formed in their transition states.

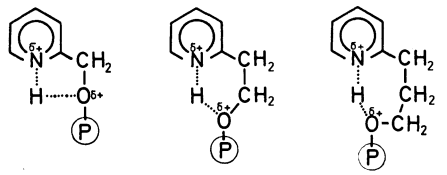

1 2 3

The stability of these ring conformations yielded in the hydrolysis of the above three phosphates will be discussed in connection with the intramolecular catalysis. The electronic and steric effects due to the methyl-substituent on the intramolecular-proton transfer mechanism were investigated in the hydrolysis of 6-methyl-2-pyridylmethyl phosphate.

Experimental

Materials. 2-Pyridylethyl and 2-pyridylpropyl phosphates were prepared by the phosphorylation of the corresponding alcohols with pyrophosphoric acid.

Pyridylethanol (2-(β-hydroxyethyl)pyridine) (CP grade, Wako Pure Chemical Ind., Ltd., Osaka) was purified by vacuum distillation. Fractions distilled at 66.5°C/0.20—0.25 mmHg were combined and used for the phosphorylation. Pyridylpropanol (2-(γ-hydroxypropyl)pyridine) (Schuchard Chemische Fabrik, München) was purified by distillation, the distillates at 95°C/0.35 mmHg being used for the phos-

1) Contribution No. 269 from the Department of Organic Synthesis, Faculty of Engineering, Kyushu University.

2) Y. Murakami and M. Takagi, *J. Amer. Chem. Soc.*, **91**, 5130 (1969).

3) Y. Murakami and J. Sunamoto, This Bulletin, **44**, 1939 (1971).

4) Y. Murakami, J. Sunamoto, and H. Ishizu, *ibid.*, **45**, 590 (1972).

phorylation. Phosphorylation of both pyridylalcohols was carried out according to the previous method.[5,6] Phosphorylated products were purified by the cation exchange column-chromatographic technique and further purified by recrystallization from aqueous ethanol.

2-Pyridylethyl Phosphate. Found: C, 40.58; H, 5.11; N, 6.78; P, 14.3%. Calcd for $C_7H_{10}NO_4P$: C, 41.34; H, 4.96; N, 6.90; P, 15.3%. IR[7] (KBr disk): ν_{O-H}, ~3200; $\nu_{P=O}$, 1254, 1156, and 1075; $\nu_{P-O-C(alk)}$, 1050, 1030, and 933 cm^{-1}. UV (10^{-4}M in water): λ_{max} 262 mμ (ε=7140). Neutralization equivalence; 102.15 (calcd., 101.57).

2-Pyridylpropyl Phosphate. Found: C, 44.01; H, 5.51; N, 6.33%. Calcd for $C_8H_{12}NO_4P$: C, 44.25; H, 5.57; N, 6.45%. IR[7] (KBr disk); ν_{O-H}, ~3400; $\nu_{P=O}$, 1295, 1280, 1175, 1158, and 1080; $\nu_{P-O-C(alk)}$, 1045, 1030, and 920 cm^{-1}. UV (10^{-4}M in water): λ_{max} 263 mμ (ε=7760). Neutralization equivalence; 107.72 (calcd., 108.58).

Preparation and purification of 2-pyridylmethyl[5] and 6-methyl-2-pyridylmethyl phosphates[6] were described previously.

Kinetic and Potentiometric Measurements. The apparatus and experimental procedures were essentially the same as those described previously,[2-4] except for the hydrolysis of 2-pyridylpropyl phosphate at 85, 90, and 95°C, and of 2-pyridylethyl phosphate at 95°C. For the hydrolysis of 2-pyridylpropyl and 2-pyridylethyl phosphates at higher temperatures, a 10 ml Pyrex test tube with a ground Pyrex stopper was used. An aliquot of sample solution containing a substrate, an inorganic salt to maintain the ionic strength constant, and perchloric acid to adjust the hydrogen ion concentration at an appropriate value was placed in the test tube. Several test tubes containing a sample solution of the same constituents were dipped in a water bath regulated to a given temperature. At an appropriate time interval one of them was drawn out and the sample was analyzed for inorganic phosphate liberated during the course of reaction. Since all runs using the Pyrex test tubes were carried out to cover a pH range 1—3 where the phosphate exists predominantly in a neutral zwitterion form, the pH-deviation during the course of hydrolysis reaction did not exceed ±0.02. The observed rate constant in each run was retained within an accuracy of ±2% while the reaction temperature was controlled within ±0.1—0.05°C.

Acid Dissociation Constants and Specific Rate Constants. Acid dissociation constants of the present phosphates at 80°C were obtained by the potentiometric determination[2] and/or by the dynamic (kinetic) method. Specific rate constants assigned to the reactive substrate species were calculated from the apparent first-order rate constants obtained at various pH values. The calculation procedures were described previously.[3,4]

Results

Acid Dissociation Constants. Acid dissociation constants obtained are summarized in Table 1. The acid dissociation constant for the 1-pyridinium proton is represented by K_{H_2A}, and that for the second phosphate proton by K_{HA}.

Table 1. Acid dissociation constants of the pyridylalkyl phosphates at μ=0.10 (KNO_3) as determined by potentiometric titration[a]

Phosphate	pK_{H_2A}		pK_{HA}	
	25°C	80°C	25°C	80°C
6-Methyl-2-pyridylmethyl	4.74[b]	4.50 (4.34)[f]	6.64[b]	6.36 (6.08)[f]
2-Pyridylmethyl	4.42[c]	4.15[d] (4.03)[e,f]	6.29[c]	6.54[d] (6.46)[e,f]
2-Pyridylethyl	5.31	4.84	6.83	6.79
2-Pyridylpropyl	5.60	5.09	6.90	6.75
3-Pyridylmethyl	4.86[c]	4.43[d]	6.23[c]	6.48[d]

a) Estimated error is within 0.02. Values in parentheses were evaluated by kinetic method using Eq. (1).
b) Cited from Ref. 6.
c) Cited from Ref. 5.
d) Cited from Ref. 2.
e) Cited from Ref. 3.
f) At 90°C.

Introduction of a methyl group at the 6-position of 2-pyridylmethyl phosphate resulted in an increase of both pK_{H_2A} and pK_{HA}. Similarly, the extension of the methylene-chain from 2-pyridylmethyl through 2-pyridylpropyl group brought about the lowering of acidity of both groups. Since the temperature dependency of the ionization constant varies according to the nature of the structural environment of the acid, the above trend would not necessarily be the case at a higher temperature.

Specific Rate Constants. All runs followed good first-order kinetics. The pH-rate profile for the hydrolysis of 6-methyl-2-pyridylmethyl phosphate at 90°C is illustrated in Fig. 1 as a typical example. The rate maximum in the pH-rate profile was observed at −log[H+] 2—3. This indicates that the most reactive species is in the neutral zwitterion form followed by the monoanionic one. This holds true also for the cases of 2-pyridylethyl and 2-pyridylpropyl phosphates.

The solid line in Fig. 1 is the theoretical curve calculated from the following equation:

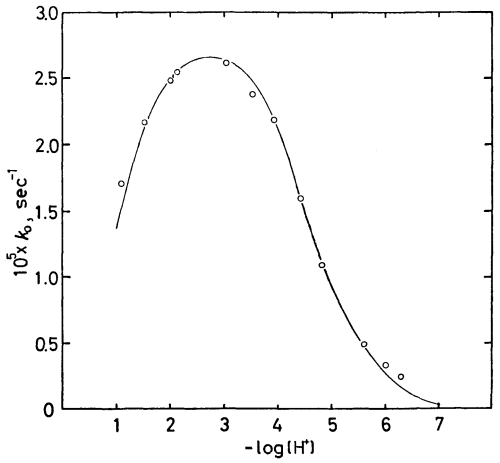

Fig. 1. pH-rate profile for the spontaneous hydrolysis of 6-methyl-2-pyridylmethyl phosphate at 90°C and μ=0.10. Solid line is a theoretical curve calculated from values listed in Tables 1 and 3 by using Eq. (1).

5) Y. Murakami, M. Takagi, and H. Nishi, This Bulletin, **39**, 1197 (1966).
6) Y. Murakami, J. Sunamoto, H. Sadamori, H. Kondo, and M. Takagi, *ibid.*, **43**, 2518 (1970).
7) Assignments of infrared absorption bands were made by referring to: J. Nakayama, *Yuki Gosei Kagaku Kyokai Shi*, **25**, 132 (1971).

$$k_0 = k_{H_2A}X_{H_2A} + k_{HA}X_{HA} \quad (1)$$

where X_{H_2A} and X_{HA} stand respectively for the mole fractions of neutral zwitterionic and monoanionic species, and k_0, k_{H_2A}, and k_{HA} are the overall first-order rate constant and the specific rate constants, respectively, of the above two reactive phosphate species. The calculation procedures of these parameters were the same as those described previously.[2-4] The agreement between the observed and the calculated rate constants was quite satisfactory.

Table 2. Apparent first-order rate constants for the spontaneous hydrolysis of pyridylalkyl phosphates under various conditions[a]

Temp °C[b]	$-\log[H^+]$[c]	$k_{obs}\times10^5$, sec^{-1}[d]	$k_{cal}\times10^5$, sec^{-1}[e]
6-Methyl-2-pyridylmethyl phosphate			
90.0	1.09	1.71	1.53
	1.53	2.17	2.12
	2.01	2.48	2.49
	2.15	2.54	2.55
	3.03	2.61	2.63
	3.53 (±0.03)	2.38	2.47
	3.92	2.19	2.21
	4.42 (±0.04)	1.60	1.63
	4.84	1.09	1.09
	5.60	0.481	0.529
	6.01 (±0.03)	0.337	0.341
	6.30	0.252	0.225
85.0	3.57	1.41	1.39
	3.79	1.29	1.31
	5.82	0.208	0.208
80.0	3.75	0.727	0.754
	3.48	0.784	0.802
2-Pyridylethyl phosphate			
95.0	1.91	0.986	0.997
90.0	2.01	0.582	0.582
	1.92	0.591	0.591
85.0	2.07	0.325	0.326
	1.99	0.320	0.320
2-Pyridylpropyl phosphate			
95.0	1.99	0.543	0.621
	1.98	0.535	0.619
	2.96	0.672	0.673
90.0	1.87	0.331	0.329
	1.89	0.331	0.331
	2.98	0.404	0.367
	2.99	0.413	0.367
85.0	2.96	0.205	0.210
	2.93	0.196	0.196

a) The initial concentration of the phosphates was 2.0×10^{-3}M in all runs. The ionic strength was maintained at 0.10 with $HClO_4$–$NaClO_4$ at a pH range lower than 3.5 and with KNO_3 at a range higher than 3.5.
b) Controlled within ±0.1°C.
c) Variation was maintained within ±0.02 except for the cases cited in parentheses.
d) Standard deviations in individual rate constants do not exceed ±2%.
e) Calculated from the experimental data by the aid of Eq. (1) and the pK-values listed in Table 1. Mole fractions of ionic species at 80—95°C were calculated with the use of the pK-values obtained at 80°C, except for the hydrolysis of 6-methyl-2-pyridylmethyl phosphate at 90°C where the specific rate constants and the pK-values were simultaneously obtained by dynamic procedures.

Table 3. The specific rate constants of the spontaneous hydrolyses for the pyridylalkyl phosphates[a]

Temp °C	$k_{H_2A}\times10^5$, sec^{-1}	$k_{HA}\times10^6$, sec^{-1}
6-Methyl-2-pyridylmethyl phosphate		
90.0	2.74	5.63
85.0	1.54	2.02
80.0	0.873	0.962
2-Pyridylethyl phosphate		
95.0	1.11	——[b]
90.0	0.640	——[b]
85.0	0.350	——[b]
2-Pyridylpropyl phosphate		
95.0	0.685	——[b]
90.0	0.374	——[b]
85.0	0.200	——[b]

a) Calculated by Eq. (1) with the aid of the acid dissociation constants listed in Table 1; μ=0.10.
b) Because of the extremely low hydrolysis rate, assignment of the rate constant was not performed.

For the hydrolysis of 6-methyl-2-pyridylmethyl, 2-pyridylethyl, and 2-pyridylpropyl phosphates, the apparent first-order rate constants and the reaction conditions are listed in Table 2. The calculated specific rate constants for the present phosphates are summarized in Table 3. We could not obtain reliable specific rate constants for the hydrolysis of 2-pyridylethyl and 2-pyridylpropyl phosphates in their monoanionic forms, for the reaction was extremely slow even at 90°C. However, participation of the intramolecular catalysis in hydrolysis can be studied for the zwitterionic species. Thus, the above data are not necessarily required for the present purpose.

Activation Parameters. Each specific rate constant satisfactorily followed the Arrhenius law. The activation parameters for the hydrolysis of the neutral zwitterion species, along with the data for 3-pyridylmethyl and 2-pyridylmethyl phosphates,[2] are listed in Table 4.

Table 4. Activation parameters for the hydrolyses of 6-methyl-2-pyridylmethyl, 2-pyridylmethyl, 2-pyridylethyl, and 2-pyridylpropyl phosphates in their zwitterion forms[a]

Phosphate	E_a kcal mol^{-1}	$\Delta H^{\neq}$ kcal mol^{-1}	$\Delta S^{\neq}$ e. u.
6-Methyl-2-pyridylmethyl	29.1±0.1	28.4±0.1	−1.6±0.3
2-Pyridylmethyl	28.2±0.1	27.5±0.1	−4.3±0.3
2-Pyridylethyl	30.6±0.1	29.8±0.1	−0.5±0.3
2-Pyridylpropyl	32.0±0.1	31.3±0.1	+2.4±0.2
3-Pyridylmethyl	29.3±0.1	28.6±0.1	−3.0±0.3

a) Errors for these parameters were calculated from the standard error of rate constant and errors ascribed to the reaction conditions such as reaction temperature and pH-values.

Discussion

Acid Dissociation Constants. The hydrolysis of alkyl and aryl phosphates has been provided with

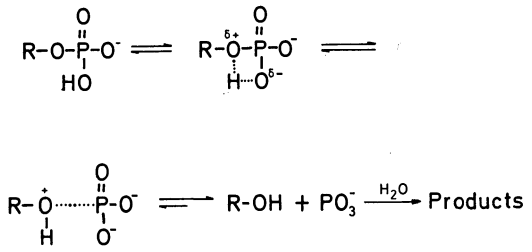

Scheme 1.

many evidences for an unimolecular P–O bond cleavage upon intramolecular general acid catalysis.[8,9] The state of affairs is shown in Scheme 1 for the monoanionic phosphate species. The extent of intramolecular general acid catalysis can be evaluated by referring to the acid dissociation constant of the corresponding alcohol (the leaving group)[8] and that of the second phosphate proton.[10] The latter, represented by K_{HA}, may reflect the donability of the proton from the phosphate moiety, while the former may be related to the proton acceptability of ester oxygen at the transition state. Both values may refer to the P–O bond strength in the transition state as well.

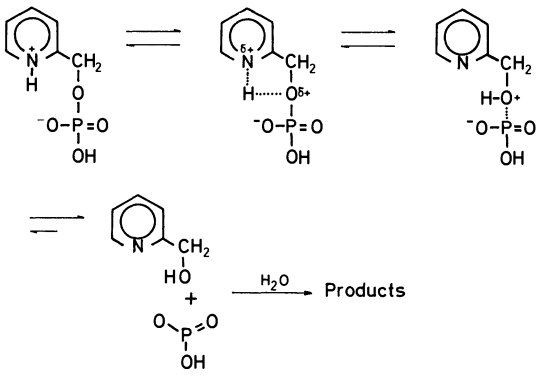

Scheme 2.

When a nitrogen atom exists in its leaving group as in the hydrolysis of the pyridylalkyl phosphates, the most reactive species is in the neutral zwitterion form and a general acid catalysis occurs intramolecularly with participation of the 1-pyridinium proton[2] as shown in Scheme 2. We understand, therefore, that the acid dissociation constant of ionic substrate is an important structural parameter for a study of the structure-reactivity correlation in its hydrolysis.

Substitution with the electron-donating methyl group at the 6-position of 2-pyridylmethyl phosphate resulted in an increase of pK_{H_2A} and pK_{HA}. The electron donability of the methyl group seems to prevent the dissociation of both protons, on the pyridine nitrogen and on the phosphate oxygen. Similarly, the extension of the methylene-chain in the 2-pyridylalkyl phosphates may result in the increase of basicity of both pyridyl nitrogen and phosphate moiety. These trends on both pK_{H_2A} and pK_{HA} values are obvious from the data given in Table 1.

Intramolecular Catalysis. We have already proposed a mechanism for the intramolecular general acid catalysis in the hydrolysis of 2-pyridylmethyl phosphate[2] and of 8-quinolyl phosphate[3] in their zwitterion forms. The catalysis was played by 1-pyridinium and 8-quinolinium groups, respectively. In the hydrolysis of 3-hydroxy-2-pyridylmethyl phosphate in its monoanion and dianion species, a unique intramolecular general acid catalysis by the 3-hydroxy group has also been clarified.[4] In all cases, the catalytic action has certainly been dependent upon the location of the catalytic site relative to the reaction center. Thus, a functional group of catalytic ability being located sterically in the proximity of ester oxygen, the hydrolysis rate is promoted through intramolecular proton transfer. In order to know whether an intramolecular catalysis takes place also in the hydrolysis of 2-pyridylalkyl phosphates, and to evaluate the extent of catalytic effect if any, we studied LFER on the hydrolysis of pyridylalkyl phosphates in their zwitterion forms. The acid dissociation constant of the second phosphate proton pK_{HA} was considered to be the most reasonable structural parameter for the present LFER study, as obvious from the preceding discussion on this parameter.[10] The linear relationship between pK_{HA} at 80°C and the logarithm of the specific first-order rate constant for the zwitterion hydrolysis at 90°C (log k_{H_2A}) is illustrated in Fig. 2.[11]

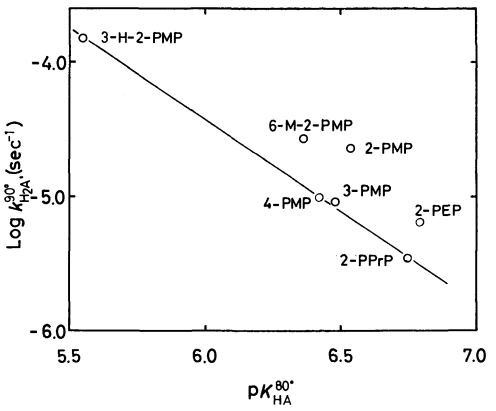

Fig. 2. Correlation between first-order rate constants at 90°C for hydrolyses of pyridylalkyl phosphates in their zwitterion forms and pK_{HA}'s of the phosphates at 80°C. Abbreviations: 3-H-2-PMP, 3-hydroxy-2-pyridylmethyl phosphate; 6-M-2-PMP, 6-methyl-2-pyridylmethyl phosphate; 2-PMP, 2-pyridylmethyl phosphate; 3-PMP, 3-pyridylmethyl phosphate; 4-PMP, 4-pyridylmethyl phosphate; 2-PEP, 2-pyridylethyl phosphate; 2-PPrP, 2-pyridylpropyl phosphate.

Judging from the location of the pyridinium group relative to the ester oxygen, the neutral zwitterions of 3-hydroxy-2-pyridylmethyl,[4] 3-pyridylmethyl, and 4-pyridylmethyl[2] phosphates can not secure an intramolecular catalysis due to the pyridinium group. Thus,

8) T. C. Bruice and S. J. Benkovic, "Bioorganic Mechanisms," Vol. 2, W. A. Benjamin Inc., New York (1966).

9) C. A. Bunton, *Accounts Chem. Res.*, **3**, 257 (1970).

10) Y. Murakami, J. Sunamoto, and N. Kanamoto, presented at the 22nd Annual Symposium on Organic Reaction Mechanisms, Nagoya, October, 1971.

11) Reliabilities of the present linear relationship and of the structural parameters used are scheduled to be discussed in a forthcoming paper along with more extensive investigations.

a straight line can be drawn in Fig. 2 through the plots for these phosphates as a reference for which the reaction proceeds without the pyridinium catalysis. 6-Methyl-2-pyridylmethyl, 2-pyridylmethyl, and 2-pyridylethyl phosphates apparently deviate upward from this line, while 2-pyridylpropyl phosphate lies on it. The significant rate enhancement of the former three phosphates, with reference to those expected from the simple LFER, may be ascribed to some additional catalysis. Thus, it can be seen that the intramolecular general acid catalysis takes place not only in the hydrolysis of 2-pyridylmethyl phosphate but also in that of 2-pyridylethyl and 6-methyl-2-pyridylmethyl phosphates in their zwitterion forms. As a result, we can conclude that formation of either a five-membered (**1**) or a six-membered ring (**2**) at the pre-equilibrium stage of the hydrolysis reaction is in favor of the intramolecular catalysis by the pyridinium group, but that formation of a seven-membered ring (**3**) is no longer favorable for such a catalysis. For the hydrolysis of 2-pyridylpropyl phosphate zwitterion, thus, we may propose a mechanistic pathway *via* an intramolecular proton transfer from the phosphate moiety, not from the pyridinium nitrogen as seen in Scheme 3, analogous to the cases of the usual alkyl phosphates.[8,9]

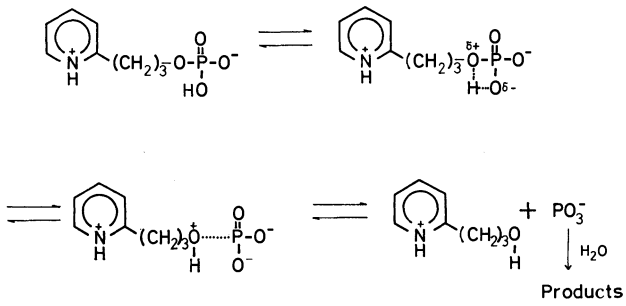

Scheme 3.

There exists another question as to the extent of their rate enhancement. In a series of 2-pyridylalkyl phosphates, the extents of the rate enhancement are 2.5-fold for $-CH_2-$, 2.0-fold for $-CH_2-CH_2-$, and 1.0-fold for $-CH_2-CH_2-CH_2-$ in their alkyl chains, respectively, relative to the corresponding rates expected from LFER without any additional effect as shown in Fig. 2. In reference to our previous postulate on the reaction mechanism,[2,3] the first energy barrier in this reaction pathway may exist at the stage, where the proton-transfer from the hetero-aromatic nitrogen atom or the terminal phosphate oxygen to the ester oxygen occurs, *viz.*, the pre-equilibrium protonation step. The second barrier may be located in the reaction coordinate at the stage where the P–O bond cleavage takes place to give products; this may most likely correspond to the rate-determining step, as justified by the kinetic solvent isotope effect,[3] and/or by the extent of activation parameters.[2-4,8] This phenomenon is illustrated by a typical schematic representation in Fig. 3. The fact that the linear free energy relationship between pK_{HA} and $\log k_{A_2A}$ was established apparently suggests that the rate-limiting step almost consists of an unimolecular P–O bond fission.

Isokinetic Relationship. The differential thermodynamic activation parameters for the hydrolysis of 2-pyridylalkyl phosphates, with 2-pyridylmethyl phosphate taken as the standard reactant, are plotted in Fig. 4. It is, therefore, most reasonable to assume that these phosphates undergo hydrolysis through essentially the same mechanistic pathway. At first sight, the isokinetic relationship obtained does not appear to be consistent with the mechanistic criteria on the intramolecular proton-transfer path. However, entropy and enthalpy of activation obtained in the present reaction system are mostly concerned with the unimolecular P–O bond fission of the protonated species. It is not necessary to consider from where the proton was transferred at the pre-equilibrium stage. An exception was noticed for the hydrolysis of 6-methyl-2-pyridylmethyl phosphate. The presence of the 6-methyl group seems to perturb the transition state. Contrary to what would be expected, Table 3 and Fig. 2 indicate that the zwitterionic species of 6-methyl-2-pyridylmethyl phosphate is more rapidly hydrolyzed than that of 2-pyridylmethyl phosphate. This was similarly observed in the hydrolysis of monoanionic species; $k_{HA}=5.63\times10^{-3}$

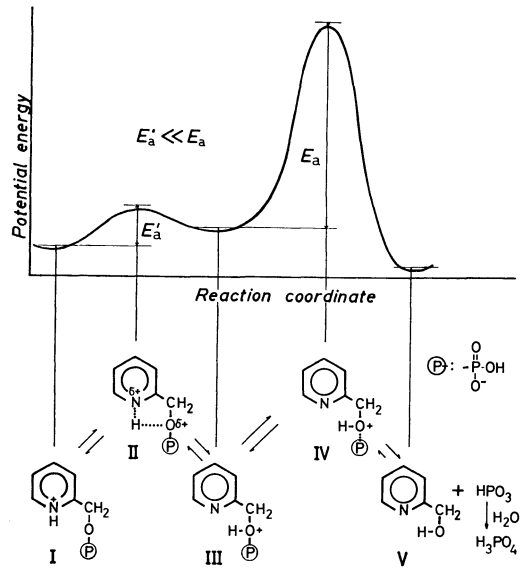

Fig. 3. Schematic representation of unimolecular mechanism in terms of potential energy *vs.* reaction coordinate as a typical intramolecular catalysis acted in the 2-pyridylmethyl phosphate hydrolysis.

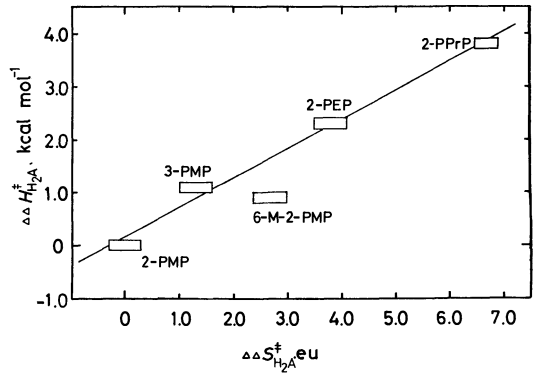

Fig. 4. The isokinetic relationship for the spontaneous hydrolyses of pyridylalkyl phosphate zwitterions. Abbreviations are the same as those used in Fig. 2.

sec^{-1} at 90°C for 6-methyl-2-pyridylmethyl phosphate, and 4.14×10^{-3} sec^{-1} at 90°C for 2-pyridylmethyl phosphate. A question of what is the driving force to bring about the rate enhancement must be solved. A clue can be found in Fig. 4 and Table 4. Only 6-methyl-2-pyridylmethyl phosphate showed deviation downward from the linear relationship of enthalpy-entropy compensation, being different from other pyridylalkyl phosphates. The electron-donating effect of the methyl group must be reflected in terms of activation enthalpy for the hydrolysis of 6-methyl-2-pyridylmethyl phosphate, partially in the pre-equilibrium protonation stage and mostly in the P–O bond cleavage step. The increase of activation enthalpy by 900 cal mol^{-1} was, in fact, observed as an evidence. Thus, the rate-enhancement and deviation in the isokinetic relationship caused by methyl-substitution should be attained from the activation entropy term and therefore the cause of a larger activation entropy ($\Delta\Delta S^{\neq}=2.7$ e.u.) should be considered. It may be most reasonable to postulate that a bulky alkyl-substituent in the neighborhood of the reaction center interferes significantly with the solvation, *viz.*, "defreezing" of solvation, in the transition state.

BULLETIN OF THE CHEMICAL SOCIETY OF JAPAN, VOL. 46, 876—880 (1973)

The Synthesis of 3-Amino-3-deoxy-D-allose and Related Substances[1]

Shinkiti KOTO, Noboru KAWAKATSU, and Shonosuke ZEN
School of Pharmaceutical Sciences, Kitasato University, Shirokane, Minato-ku, Tokyo

(Received June 15, 1972)

Starting from methyl 2,4,6-tri-*O*-benzyl-α-D-glucopyranoside, a facile synthesis of 3-amino-3-deoxy-D-allose was carried out; some new *O*-benzyl derivatives of 3-amino-3-deoxy-D-allopyranose are also described.

A variety of derivatives of 3-amino-3-deoxy-D-allose has been synthesized by various methods.[2-9] Recently, an alternative method of preparing this sugar has been reported.[10] In a practical sense, the synthesis demonstrated by Coxon and Hough[11] may be most convenient for getting this aminosugar. However, the known methods for the preparation of the derivative of this aminosugar with the pyranose-ring system[5-7] seem to be rather unpromising. This paper will be concerned with another route to 3-amino-3-deoxy-D-allose as well as with the *O*-benzyl derivative of 3-amino-3-deoxy-D-allopyranose. Recently, the *O*-benzyl derivative of aminosugars has frequently been synthesized as an useful synthetic intermediate.[11]

Methyl 2,4,6-tri-*O*-benzyl-α-D-glucopyranoside,[12] obtained by the one-step benzylation of readily-available methyl α-D-glucopyranoside, was treated with *p*-toluenesulfonyl chloride in pyridine to give the corresponding 3-*O*-*p*-toluenesulfonate (I), which, after debenzylation and acetylation, gave known methyl 2,4,6-tri-*O*-acetyl-3-*O*-*p*-toluenesulfonyl-α-D-glucopyranoside[13] (II), which was the starting material for the synthesis of 3-amino-3-deoxy-D-glucose (kanosamine).[14]

The nucleophilic displacement of the sulfonyloxy group of the sulfonate (I) by the azide ion encountered some difficulties. The nucleophilic substitution of the sulfonyloxy group of the benzylated sugar by the azide residue has been investigated by Stevens and his coworkers.[15] They have successfully utilized moist *N*,*N*-dimethylformamide (DMF) as a solvent. More recently, other high basic dipolar aprotic solvents, such as dimethylsulfoxide (DMSO)[16] and hexamethylphosphoric triamide (HMPA),[17] have been used and found to be excellent solvents for nucleophilic displacement reactions in the carbohydrate field. However, in the case of the replacement reaction of the sulfonate (I) with an azide ion, practically no reaction at all took place under those conditions. However, in DMSO or HMPA, the displacement did proceed under rather

1) Presented at the 25th Annual Meeting of the Chemical Society of Japan, Hiratsuka, April, 1972; Preprint, Vol. III, p. 1602, (1972).

2) K. Freudenberg, O. Burkhart ,and E. Braun, *Chem. Ber.*, **59**, 714 (1926); R. U. Lemieux and P. Chu, *J. Amer. Chem. Soc.*, **80**, 4745 (1958).

3) B. Coxon and L. Hough, *J. Chem. Soc.*, **1961**, 1643.

4) U. G. Nayak and R. L. Whistler, *J. Org. Chem.*, **34**, 3819 (1969).

5) B. Lindberg and O. Theander, *Acta Chem. Scand.*, **13**, 1226 (1959).

6) A. C. Richardson and H. O. L. Fischer, *J. Amer. Chem. Soc.*, **83**, 1132 (1961).

7) B. R. Baker and R. E. Schaub, *J. Org. Chem.*, **16**, 646 (1954).

8) J. Kovář and H. H. Baer, *Can. J. Chem.*, **49**, 3203 (1971).

9) T. Takamoto, R. Sudoh, and T. Nakagawa, *Tetrahedron Lett.*, **1971**, 2053.

10) J. Jary, Z. Kefurtova, and J. Kovář, *Coll. Czech. Chem. Commun.*, **34**, 1452 (1969).

11) R. Harrison and H. G. Fletcher, Jr., *J. Org. Chem.*, **30**, 2317 (1965); S. Koto, T. Tsumura, Y. Kato, and S. Umezawa, This Bulletin, **41**, 2765 (1968); T. Ueno, N. Kurihara, S. Hashimoto, and M. Nakajima, *Agr. Biol. Chem.*, (Tokyo), **31**, 1346 (1967); A. Hasegawa, N. Kurihara, D. Nishimura, and M. Nakajima, *ibid.*, **32**, 1123 (1968).

12) S. Koto, Y. Takebe, and S. Zen, This Bulletin, **45**, 291 (1972).

13) S. Peat and L. F. Wiggins, *J. Chem. Soc.*, **1938**, 1088.

14) S. Peat and L. F. Wiggins, *ibid.*, **1938**, 1810; S. Umezawa, Y. Ito, and S. Koto, This Bulletin, **35**, 1718 (1962).

15) C. L. Stevens, P. Blumbergs, and D. H. Otterbach, *J. Org. Chem.*, **31**, 2817 (1966); C. L. Stevens, P. Blumbergs, F. A. Daniher, D. H. Otterbach, and K .G. Taylor, *ibid.*, **31**, 2822 (1966).

16) W. M. zu Reckendorf, *Tetrahedron Lett.*, **1970**, 287.

17) Y. Ali and A. C. Richardson, *J. Chem. Soc., C*, **1968**, 1764.

Table 1. S_N2 reaction of the sulfonates I and Ia with NaN_3

Materials (w:w:v)	Solv.	Temp. (°C)	Time (hr)	Results
I:NaN_3:solv.				
1:4:10	DMF[a)]	150	70	——
1:4:10	DMA	150	50	——
1:4:10	DMSO	100	50	−−
1:4:10	DMSO	130	20	−
1:1:10	DMSO	150	20	+−
1:2:10	DMSO	150	20	+
1:4:10	DMSO	150	20	++
1:4:10	HMPA	100	20	−
1:4:10	HMPA	130	20	+−
1:1:10	HMPA	150	20	+
1:4:10	HMPA	150	20	++
Ia:NaN_3:solv.				
1:4:10	HMPA	100	20	+−
1:1:10	HMPA	130	20	+
1:4:10	HMPA	130	20	++

a) containing water (3%)
—— no reaction
−− I or Ia≫product
− I or Ia>product
+− I or Ia≃product
+ I or Ia<product
++ I or Ia≪product

compulsive conditions to give methyl 3-azide-2,4,6-tri-*O*-benzyl-3-deoxy-α-D-allopyranoside (III) (Table 1). The reaction was monitored by thin-layer chromatography of the reaction mixture. HMPA gave slightly better results.

The azide (III) was treated with lithium aluminium hydride in dioxane[15] to give methyl 3-amino-2,4,6-tri-*O*-benzyl-3-deoxy-α-D-allopyranoside (IV), which was characterized as a crystalline 2,4-dinitrophenyl derivative (V). The corresponding *N*-acetyl and *N*-carbobenzoxy compound of IV could not be crystallized. The amine (IV) was converted into known methyl 2-acetamido-2,4,6-tri-*O*-acetyl-3-deoxy-α-D-allopyranoside (VI)[7] by catalytic hydrogenolysis, followed by acetylation. The treatment of V with a warm suspension of an anionic resin in moist acetone regenerated the amine (IV), which was then converted into Compound VI. Thus, as might be expected, the substitution of the sulfonyloxy group by the azide ion proceeded with an inversion of the configuration at the reaction center.

The observed lack of reactivity of the sulfonyloxy group in the nucleophilic substitution reaction might be explained, at least, by the idea that the formation of the transition state, which requires the backside approach of the azide anion to C-3, would be interfered with by the 1,3-diaxial interactions by the axial methoxy group at the anomeric center.[18]

We have applied these conditions to another sulfonate, 3-*O*-*p*-toluenesulfonyl-1,2:5,6-di-*O*-isopropylidene-α-D-glucofuranose[19] (Ia), which has been mentioned as having little susceptibility to nucleophilic substitution reactions.[20] The replacement reaction of this sulfonate with sodium azide was recently carried out in moist DMF, in which heating was continued for 15 days a 115°C.[4] When this was treated with sodium azide in hot HMPA, however, the replacement reaction proceeded well above 125°C and was completed after 24 hr. This result showed that the sulfonate was slightly more susceptible to the replacement with the azide anion under those reaction conditions than was the sulfonate I.

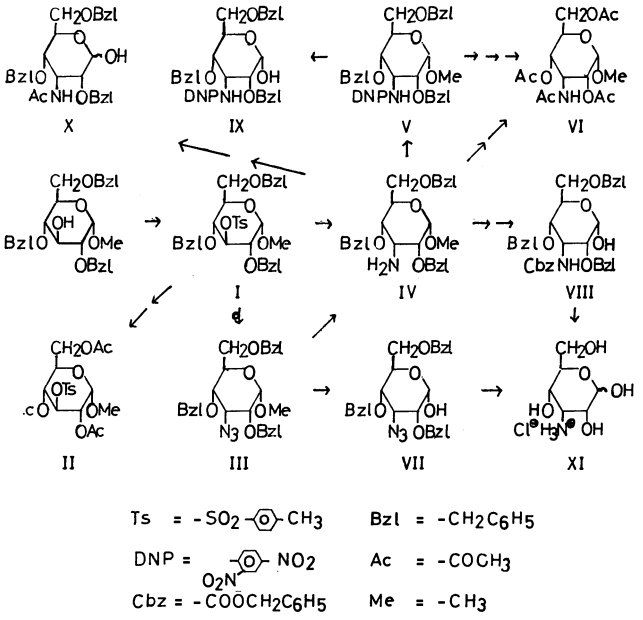

Chart 1.

The difference between the susceptibilities of these sulfonates might be interpreted on the basis of the recent conformational findings[21] that the most stable conformer of methyl α-D-glucopyranoside and its related substances in various solvents is one whose methyl group is oriented to have a *gauche* relationship with the ring oxygen and the C-2 carbon. Therefore, it is conceivable that the access of the azide anion to the reaction center from the opposite side of the leaving sulfonyloxy group would allow the aglycon to rotate to have an unfavorable eclipse relationship to the ring oxygen (Chart 2). On the other hand, the sulfonate (Ia) would not encounter such barriers.

By the way, the nucleophilic replacement of the sulfonyloxy group of syrupy methyl 3-*O*-methanesul-

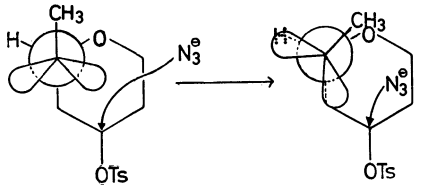

Chart 2.

18) N. A. Hughes and P. R. H. Speakman, *J. Chem. Soc.*, **1965**, 2236; H. J. Jennings and J. K. N. Jones, *Can. J. Chem.*, **43**, 2372 (1965).

19) K. Freudenberg and O. Ivers, *Ber.*, **55**, 929 (1922).

20) M. L. Wolfrom, J. Bernsmann, and D. Horton, *J. Org. Chem.*, **27**, 4505 (1962).

21) R. U. Lemieux, A. A. Pavia, J. C. Martin, and K. A. Watanabe, *Can. J. Chem.*, **47**, 4427 (1969); A. J. de Hoog, H. R. Buys, C. Altona, and E. Havingh, *Tetrahedron*, **25**, 3365 (1969); R. U. Lemieux and J. C. Martin, *Carbohydrate Res.*, **13**, 139 (1970).

fonyl-2,4,6-tri-*O*-benzyl-α-D-glucopyranoside by the azide ion was of no practical use.

The amination of the sulfonate (I) was also carried out by ammonolysis in methanol at 150°C for 30 hr; this gave the amine (IV).

The azide compound (III) was hydrolyzed to furnish a fine crystalline reducible compound (VII), which was then smoothly hydrogenolyzed over palladium-black in the presence of hydrochloric acid to gave the hydrochloride of 3-amino-3-deoxy-D-allose. This aminosugar was also obtained *via* the *N*-carbobenzoxy derivative (VIII).

Two other C-1 free compounds, the *N*-acetyl derivative (X) and the *N*-2,4-dinitrophenyl derivative (IX), were also synthesized. All the crystalline hydrolyzed products (VII, VIII, and IX) were assigned the α-configuration on the basis of their mutarotative behavior.[22] It should be noted that the concentration of the strong acid in the mixed acid used in these hydrolyses was lower than that used in the hydrolyses of the *O*-benzyl sugar with the gluco configuration[11] (Table 2).

Table 2. Hydrolyses of *O*-benzyl sugars

Product	H_2SO_4 in aq. Acetic Acid (N)	Temp. (°C)	Time (hr)	Yield (%)
VII	0.26	100	2.5	54
VIII	0.14	90	8.0	28
IX	0.28	90	11.0	48
X	0.14	100	2.0	27

Experimental

General Procedures. The solvent systems used for the column chromatography over silica gel (Kanto Chemical Co.) or the tlc (Silica Gel G; Merck) were as follows: A, benzene–2-butanone; B, benzene–acetone. The melting points were determined by means of a Yanagimoto micro-melting point apparatus; uncorrected values are given. The specific rotation was measured in a 1-dm tube by means of an Atago Polux apparatus. The IR spectra were determined by means of a JASCO IRA-1 infrared spectrophotometer. The PMR spectra were measured with a Varian S-60T apparatus in $CDCl_3$, with TMS as the internal standard. The elemental analyses were made by means of a Perkin-Elmer Model 240 Elemental Analyser apparatus.

Methyl 2,4,6-Tri-O-benzyl-3-O-p-toluenesulfonyl-α-D-glucopyranoside (I). A solution of methyl 2,4,6-tri-*O*-benzyl-α-D-glucopyranoside[12] (13 g) and *p*-toluenesulfonyl chloride (15 g) in pyridine (26 ml) was kept standing for 4 days at 28°C. The mixture was then diluted with benzene, and the solution was thoroughly washed by aqueous sodium carbonate and then by water. The yellow syrup thus obtained (18 g) was crystallized with cyclohexane to give crude crystals (14 g, 81%), which were then recrystallized from diisopropyl ether to give colorless crystals (10 g, 58%), mp 96—97°C, $[\alpha]_D^{25}$ +34° (*c* 1.9, $CHCl_3$), ν_{max}^{KBr} (cm^{-1}): 1365 and 1171 (sulfonyl). δ (ppm): 2.29 (3H, singlet; C<u>H</u>$_3$C$_6$H$_4$SO$_2$–), 3.31 (3H, singlet; C<u>H</u>$_3$O–), 7.27 and 7.32 (15H, quasi singlets; C$_6$<u>H</u>$_5$CH$_2$O–).

Found: C, 67.54; H, 6.29%. Calcd for $C_{35}H_{38}O_8S$: C, 67.94; H, 6.19%.

Methyl 2,4,6-Tri-O-acetyl-3-O-p-toluenesulfonyl-α-D-glucopyranoside[13] *(II).* I (0.20 g) was hydrogenolyzed over palladium-on-carbon (5%, 30 mg) in methanol (7 ml) at room temperature under atmospheric pressure. The glass thus obtained was then heated with acetic anhydride (6 ml) and sodium acetate (0.1 g) at 95°C for 3 hr. A crude acetate (0.16 g) was recrystallized from diisopropyl ether to afford colorless crystals (0.10 g, 65%); mp 95—96°C, $[\alpha]_D^{25}$ +91° (*c* 1.7, $CHCl_3$). The mp admixed with an authentic sample showed no depression. The IR spectrum (KBr) of II could be superimposed upon that of the authentic sample.

Methyl 2,4,6-Tri-O-benzyl-3-(2,4-dinitroanilino)-3-deoxy-α-D-allopyranoside (V). *Via the Replacement Reaction in DMSO*: A suspension of I (1.0 g) and sodium azide (4.0 g) in DMSO (10 ml) was vigorously stirred on an oil bath (150°C) under reflux for 15 hr. Another portion (1.0 g) of the azide was then added to the mixture, which was further stirred for 5 hr at the same temperature. The mixture was then diluted with benzene, and the insoluble matters were filtered off. The filtrates were concentrated and then evaporated under reduced pressure (3 mmHg) at 70°C to give a dark brown residue, which was chromatographed over the silica gel, developed with the A solvent system (40: 1). After the elution of some by-products as well as the unchanged starting material, the main product appeared; it gave a homogeneous syrup (0.54 g, 68%) of methyl 3-azido-2,4,6-tri-*O*-benzyl-3-deoxy-α-D-allopyranoside (III); ν_{max}^{film} 2155 cm^{-1}. The oily azide (III) (0.58 g) was immediately refluxed with lithium aluminum hydride (0.08 g) in dioxane (10 ml) for 2 hr.[15] After the decomposition of the excess hydride with water the mixture was extracted with benzene to afford a ninhydrin-positive syrup (0.50 g, 91%) of methyl 3-amino-3-deoxy-2,4,6-tri-*O*-benzyl-α-D-allopyranoside (IV). The traces of the by-products were removed by means of column chromatography over silica gel using B solvent system (1: 1). A mixture of the amine (IV) (0.28 g), 2,4-dinitrofluorobenzene (0.10 ml), and triethylamine (0.10 ml) in DMF (2 ml) was kept standing at room temperature overnight. The red solution was then evaporated at 55°C under reduced pressure to give a dark red residue, which was subsequently chromatographed over silica gel, elution being done with the A solvent system (20: 1). The yellow glass thus obtained was crystallized with diisopropyl ether to give yellow crystals (0.23 g, 60%; mp 120—122°C). Two recrystallizations from the same solvent gave an analytical sample; mp 122—123°C, $[\alpha]_D^{25}$ +124° (*c* 0.9, $CHCl_3$), ν_{max}^{KBr} (cm^{-1}): 1620, 1590, 1528, 1500, and 1333 (NHDNP), 1070 (ether).

Found: C, 64.64; H, 5.66; N, 6.63%. Calcd for $C_{34}H_{35}N_3O_9$: C, 64.85; H, 5.60; N, 6.67%.

Via the Replacement Reaction in HMPA: A suspension of I (1.0 g) and sodium azide (4.0 g) in HMPA (10 ml) was stirred at 145°C for 15 hr. Another portion (1.0 g) of the azide was then added to the mixture, after which it was further stirred at 155°C for 5 hr. The mixture was treated in the manner described in Method A to give an oil (0.58 g, 73%) of III, which was then treated with lithium aluminum hydride (0.13 g) in dioxane (13 ml) to give the amine (IV) (0.49 g, 89%).

The amine (IV) (73 mg) was treated with 2,4-dinitrofluorobenzene (50 mg) and triethylamine (33 mg) in DMF (0.7 ml) to give yellow crystals (55 mg, 55%). The mp of this compound was not depressed by admixture with V.

Via Ammonolysis: I (0.30 g) and a solution of ammonia (12 g, saturated at 0°C) in methanol (30 g) was charged in an autoclave, and then the mixture was heated at 155°C

22) O. T. Schmidt, T. Auer, and H. Schmadel, *Chem. Ber.*, **93**, 556 (1960).

for 30 hr with stirring. The resulting mixture was concentrated, diluted with methanol, and then passed through a column of Amberite IRA-400 (OH type, stored in methanol). The ninhydrin-positive fractions gave an oil (0.15 g, 67%) of IV. The amine (IV) (0.13 g) was treated with 2,4-dinitrofluorobenzene (0.05 ml) and triethylamine (0.05 ml) in DMF. The yellow crystals thus obtained (0.12 g, 68%) were recrystallized from diisopropyl ether to give a pure sample. The mp of this compound was not depressed by admixture with V.

Methyl 2-Acetamido-2,4,6-tri-O-acetyl-3-deoxy-α-D-allopyranoside[7] *(VI).* *From V*: A mixture of V (130 mg) and Dowex 1×2 (OH type, 4 ml) in acetone (40 ml) was stirred at 55°C for 50 hr under reflux, with the occasional addition of water (up to 5 ml). The subsequent evaporation of the solvent afforded a syrup which was diluted with methanol (3 ml) and then treated with acetic anhydride (3 ml). The crude syrup was chromatographed over silica gel and developed with the A solvent system (5: 1) to give a homogeneous syrup which was subsequently hydrogenolyzed in methanol in the presence of palladium-on-carbon (5%, 50 mg) under atmospheric pressure. The hydrogenolyzed product was heated with acetic anhydride (1 ml) in the presence of sodium acetate (0.1 g) to give a crude acetate (mp130—131°C). Recrystallization from diisopropyl ether gave a pure sample (37 mg, 50%); mp 134—135°C $[\alpha]_D^{25}$ +90° (*c* 2.3, $CHCl_3$). The mp of this compound admixed with the authentic specimen showed no depression. The IR and PMR spectra of the two compounds were superimposable.

Via the Catalytic Hydrogenolysis of IV: A sample (100 mg) of oily IV was hydrogenolyzed over palladium-on-carbon (5%, 20 mg) in methanol (6 ml) containing 0.02 ml of concd hydrochloric acid at room temperature under atmospheric pressure. A colorless glass (52 mg) thus obtained was subsequently heated with acetic anhydride (4 ml) in the presence of sodium acetate (0.4 g). A crude acetate (74 mg, 95%) thus obtained was crystallized with diisopropyl ether. The mp of this compound was not depressed by admixture with VI.

Via the N-Acetylation and Reduction of IV: A sample (200 mg) of oily IV was treated with acetic anhydride (1 ml) in methanol (4 ml) for 2 hr at 25°C to give a ninhydrin-negative syrup, which was dissolved in liquid ammonia (30 ml) and then treated with small pieces of sodium at −80°C until a blue color remained. The reduced mixture was acetylated by heating with acetic anhydride (8 ml) and sodium acetate (0.2 g). The crude acetate was chromatographed over silica gel with the A solvent system (1: 1) to give a pure acetate (94 mg; 60%). The mp admixed with VI showed no depression.

3-Azido-2,4,6-tri-O-benzyl-3-deoxy-α-D-allopyranose (VII). A mixture of oily III (0.23 g), acetic acid (4 ml), and dilute sulfuric acid (2N; 0.6 ml) was heated on a boiling-water bath for 2.5 hr. The mixture was then extracted with benzene to give a brown syrup (0.19 g), which was subsequently chromatographed over silica gel irrigated with the A solvent system (20: 1). After the recovery of a small quantity of the unreacted starting material, the main product was eluted. A homogenous colorless syrup was crystallized with *n*-hexane to give long needles (0.12 g; 54%), which were then recrystallized from the same solvent to afford an analytical sample; mp 108—109°C, $[\alpha]_D^{25}$ +26° (*c* 1.0, $CHCl_3$), $[\alpha]_D^{25}$ +30° (*c* 1.1, pyridine)→+25° (90 hr), $[\alpha]_D^{25}$ +29° (*c* 1.1, pyridine-phenol (8: 1, v/v])→+14° (20 hr). ν_{max}^{KBr} (cm^{-1}): 3410 (OH), 2123 (N_3), 1093 (ether), 820, 754, 733, and 692 (phenyl).

Found: C, 68.07; H, 5.97; N, 8.61%. Calcd for $C_{27}H_{29}N_3O_5$: C, 68.19; H, 6.15; N, 8.84%.

2,4,6-Tri-O-benzyl-3-carbobenzoxyamino-3-deoxy-α-D-allopyranose (VIII). To a mixture of III (0.21 g) in pyridine (4 ml), a solution (1.5 g) of carbobenzoxy chloride in toluene (30%) was added in three portions under cooling; after having been stirred for 18 hr at 25°C, the mixture was treated with a little water and extracted with benzene to gave an orange syrup which was subsequently chromatographed over silica gel irrigated with the A solvent system (20: 1). Homogeneous ninhydrin-negative oil (0.20 g, 74%) was immediately hydrolyzed by heating in a mixed acid prepared from acetic acid (6 ml) and dil. sulfuric acid (1N, 1 ml) at 90°C for 8 hr. The tlc of the hydrolyzate showed the presence of at least six products. A crude mixture which was chromatographed over silica gel was developed with the A solvent system (10: 1). After the elution of the unchanged material as well as other by-products, the aniline phthalate-positive main product (R_f 0.32; the A solvent system [5: 1]) was eluted to give a syrup which was subsequently crystallized with diisopropyl ether to afford a colorless solid (0.07 g, 28%). Recrystallization from the same solvent gave a pure sample; mp 152—153°C, $[\alpha]_D^{25}$ +34° (*c* 0.6, $CHCl_3$), $[\alpha]_D^{25}$ +61° (*c* 1.1, pyridine)→+51° (70 hr), $[\alpha]_D^{25}$ +61° (*c* 0.6, pyridine-phenol [8: 1])→+40° (180 min). ν_{max}^{KBr} (cm^{-1}): 3410 (OH), 3326, 1727, 1517 (NH–Cbz), 1052 (ether), 736, 733, and 690 (phenyl).

Found: C, 72.31; H, 7.24; N, 2.48%. Calcd for $C_{35}H_{37}NO_7$: C, 72.02; H, 6.39; N, 2.40%.

2,4,6-Tri-O-benzyl-3-deoxy-3-(2,4-dinitroanilino)-α-D-allopyranose (IX). A mixture of VI (0.30 g), acetic acid (6 ml), and dil sulfuric acid (2N, 1 ml) was heated at 90°C for 11 hr. The mixture was then treated in the manner described for VII to give an yellow syrup which was subsequently, chromatographed on silica gel with the irrigation of the A solvent system (5: 1). After the elution of the unchanged starting material, the hydrolyzed product (IX) (0.14 g, 48%) was obtained; recrystallization from diisopropyl ether furnished a pure sample, mp 164—165°, $[\alpha]_D^{25}$ +89° (*c* 1.1, $CHCl_3$), $[\alpha]_D^{25}$ +103° (*c* 0.4, pyridine–phenol [8: 1], 45 min)→+96° (7 hr), ν_{max}^{KBr} (cm^{-1}): 3290, 1621, 1592, 1505, 1334 (NH–DNP), 1075 (ether).

Found: C, 64.06; H, 5.43; N, 6.91%. Calcd for $C_{33}H_{33}N_3O_9$: C, 64.38; H, 5.40; N, 6.83%.

3-Acetamido-3-deoxy-2,4,6-tri-O-benzyl-D-allopyranose (X). The acetylation of the amine (IV) (0.21 g) with acetic anhydride (1 ml) in dry methanol (4 ml) at 25°C for 1 hr gave quantitatively a ninhydrin-negative syrupy *N*-acetate, to which was added acetic acid (6 ml) containing dil sulfuric acid (1N, 1 ml). After having been heated over a boiling-water bath for 2 hr, the reaction mixture was treated in the same manner as in the case of VII to give a crude syrup, which was then chromatographed over silica gel, with irrigation with the A solvent (5: 1). After the recovery of the unchanged *N*-acetate of IV (0.10 g), the product appeared to be a homogeneous hard syrup (0.06 g, 27%), $[\alpha]_D^{25}$ +19.3° (*c* 2.9, $CHCl_3$), ν_{max}^{film} (cm^{-1}): 1650, 1530 (NH–Ac), δ(ppm): 1.99 (3H, singlet; $\underline{CH_3}COO$).

Found: C, 69.96; H, 6.71; N, 2.83%. Calcd for $C_{29}H_{33}NO_6$: C, 70.86; H, 6.71; N, 2.85%.

3-Amino-3-deoxy-D-allose Hydrochloride[10] *(XI).* *From VII*: VII (60 mg) was hydrogenolyzed over palladium black (20 mg) in methanol (8 ml) containing a calculated amount of hydrochloric acid under the pressure (10 lb/in²) of hydrogen. The colorless glass thus obtained was taken up with a small volume of ethanol and then precipitated by the addition of excess diisopropyl ether to give an amorphous hygroscopic mass; (23 mg; 85%); mp 157—160° (decomp.), $[\alpha]_D^{25}$ +25° (*c* 0.7, water). R_{f3AG}[23]=1.08±0.01 (*n*-butanol: pyridine:

23) 3AG=3-amino-3-deoxy-D-glucose hydrochloride.

water: acetic acid=6: 4: 3: 1), Toyo filter paper No. 50; developed at 20°C for 50 hr in the descending manner and sprayed with ninhydrin in pyridine (0.3%) and aniline hydrogen phthalate in aqueous *n*-butanol (2.5%). The authentic sample[10] had the same value of R_{f3AG}.

From VIII: A small sample was hydrogenolyzed in the manner just described. The paper chromatogram of the hydrogenolyzed solution showed the existence of a single product, detectable by spraying with ninhydrin as well as aniline hydrogenphthalate, which had the same R_{f3AG} value as authentic 3-amino-3-deoxy-D-allose hydrochloride.[10]

3-Acetamido-3-deoxy-1,2: 5,6-di-O-isopropylidene-α-D-allofuranose[3] *(XII)*. A mixture of 3-*O*-*p*-toluenesulfonyl-1,2: 5,6-di-*O*-isopropylidene-α-D-glucofuranose (Ia)[19] (1.0 g) and sodium azide (4.0 g) in HMPA (10 ml) was vigorously stirred at 130°C for 24 hr. The crude mixture was then chromatographed over silica gel using the A solvent system (20: 1) gave a pure oil (0.49 g, 71%), which was subsequently reduced by the treatment with lithium aluminum hydride (0.1 g) in hot dioxane (10 ml). The amine (0.38 g, 85%) thus obtained was acetylated with acetic anhydride (0.15 ml) in methanol (4 ml) at 25°C for 2 hr to furnish Compound XII (0.38 g, 86%); mp 132—134°C, $[\alpha]_D^{25}$ +67° (*c* 1.3, $CHCl_3$). The mp admixed with the authentic sample showed no depression. The IR and PMR spectra of XI were identical with those of an authentic specimen.

BULLETIN OF THE CHEMICAL SOCIETY OF JAPAN, VOL. 46, 880—883 (1973)

Synthetic Photochemistry. I. The Cycloaddition Reaction of Methyl Acetopyruvate with Olefins

Hitoshi TAKESHITA* and Shimaho TANNO

Department of Chemistry, Faculty of Science, Tohoku University, Sendai 980

(Received June 15, 1972)

The photochemical cycloaddition reaction of methyl acetopyruvate, an unsymmetrical β-diketone, with olefins afforded the single 1: 1 molar adducts in good yields. A ready method of the cyclization of the adducts to the β-methoxycarbonyl-$\Delta^{\alpha,\beta}$-cyclohexenones has preparative values.

Unsaturated carbonyl compounds with various types of structural modifications have been reported to undergo a cycloaddition reaction with olefins upon ultraviolet light irradiation, and the mechanistic features of this method have been intensively investigated.[1,2] The cycloaddition reaction of acetylacetone (I), a typical enolizable β-diketone, has also been shown to yield aldolic adducts which dealdolyze spontaneously to heptane-2,6-diones.[3,4]

The absence of intermolecular hydrogen abstraction from the olefins or solvents, a distinctive feature of this particular instance, was in sharp contrast with the phenomenon observed in ordinary carbonyl irradiations, and could be interpreted as the intervention of intramolecular γ-hydrogen abstraction. Since I is a symmetrical molecule, one could not distinguish the difference between Ia and Ib; it is thus not possible to ascertain the reactivity of Ib, a species derived after the hydrogen shift, for the photochemical reaction.

In addition, since the photochemical adducts were convertible to cyclohexenone derivatives under very mild conditions, it has been considered that these would be useful as building blocks for the construction of certain types of alicyclic systems. The presence of two orientations of cyclization, however, could reduce the usefulness of the photoadducts.

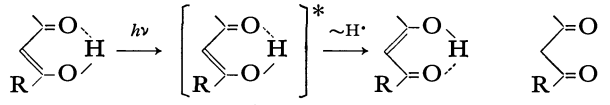

I: R=Me II: R=COOMe

Chart 1

We have carried out a study of the photochemical cycloaddition reaction of methyl acetopyruvate (II) with various types of olefins in connection with the above points and have obtained some new findings, which will be described herein.

Results and Discussion

The irradiation of an ethereal solution of II in cyclohexene with high-pressure mercury lamp through a Pyrex glass filter smoothly afforded a single photoadduct (III) in a nearly quantitative yield.[5] The presence of an acetyl group as well as a methoxycarbonyl group in III was evident from the NMR[δ 2.03 (3H, s) and 3.82 (3H, s)] and IR[$\nu_{C=O}$ 1730—1710

* Present address: Research Institute of Industrial Science, Kyushu University, Hakozaki, Fukuoka 812.

1) P. E. Eaton, *Accounts Chem. Res.*, **1**, 50 (1968).

2) P. de Mayo, *ibid.*, **4**, 41 (1971).

3) P. de Mayo and H. Takeshita, *Can. J. Chem.*, **40**, 440 (1963).

4) Since our early investigation was made, several reports on the photochemical cycloaddition of enolizable β-diketones appeared. Ref. 4a has shown the reaction occurred *via* n–π^* triplet of I by quenching experiment. 4a) H. Nozaki, M. Kurita, T. Mori, and R. Noyori, *Tetrahedron*, **24**, 1821 (1968). 4b) G. Büchi, J. A, Carlson, J. F. Powell, Jr., and L. F. Tietze, *J. Amer. Chem. Soc.*, **92** 2165 (1970).

5) In this case, the formation of 3,3-bi(cyclohexenyl), due to the intermolecular hydrogen abstraction by an n–π^* triplet, was not recognized (gas-liquid chromatogram).

cm^{-1} (strong)] spectra. The former also indicated the composition of II to be that of a 1:1 adduct. The cyclization of III in the presence of catalytic amounts of *p*-toluenesulfonic acid yielded IV, which was shown to be an epimeric mixture of β-methoxycarbonyl-$\Delta^{\alpha,\beta}$-cyclohexenone derivatives by the IR [$\nu_{C=O}$ 1730 and 1667 cm^{-1}, and δ_{CH_2} 1413 cm^{-1}] and NMR[δ 3.76 (s) and 3.78 (s), the total of both the signals integrated for 3H, 6.53 (br. s) and 6.28 (d, J=2.1 Hz), the total of the two signals integrated for 1H] spectra, although a silica-gel, thin-layer chromatogram showed only one spot. These observations permitted us to suggest the structure IVa or IVb for the cyclization product; those structures are analogous to those for the adducts from the reaction with I. The selection of the correct structure from the above two was made on the basis of the following evidence, first, zinc, and acetic acid reduction of IV afforded a dihydro-derivative (V) which subsequently gave a mixture of deuterio-derivatives by the ordinary procedure and by subsequent reesterification. The occurrence of a pentadeuterio-derivative among the products, confirmed by mass-spectral analysis, requires that Va be at least one of the components of V, even when it consists of an undetectable mixture of isomers. Secondly, palladium dehydrogenation after the lithium aluminum hydride reduction of IV yielded α-methylnaphthalene as the sole aromatized compound, which was characterized as the picrate. Since it has been established that the mixture of α- and β-methylnaphthalenes can not be fractionated by this procedure,[6] the absence of β-methylnaphthalene clearly excludes the possibility of the structures of III, IV, and V being IIIb, IVb, and Vb respectively.

A similar reaction of II with cyclohexa-1,4-diene afforded the corresponding photoadduct (VI), which was then catalytically reduced to III. The acid cyclization of VI yielded the corresponding cyclohexenone (VII), parallel to the case of the conversion of III to IV. The spectral data of VI[δ 2.03 (s) and 2.06 (s), the total of these two integrated for 3H, 3.82 (3H, s) and 5.63 (2H, br.), $\nu_{C=O}$ 1735 cm^{-1} (strong)] and VII[δ 3.78 (s) and 3.79 (s), the total of these two signals also integrated for 1H, $\nu_{C=O}$ 1738 and 1675 cm^{-1}, and δ_{CH_2} 1412 cm^{-1}] also supported the respective structures as depicted.

As examples of the unsymmetrical olefins, vinyl acetate and isobutyl vinyl ether were taken for the reaction with II; they again afforded the single adducts, VIII and IX, in each case.[7] Their structures were clearly deduced from the spectral evidence. In particular, the appearance of the triplets at δ 5.63 (1H, J=7 Hz) in VIII and at δ 4.32 (1H, J=7 Hz) in IX excluded the alternative structures. This electronic selectivity in the reaction is remarkable, and it may have a potential usefulness in synthesis.

Now, obvious points of interest in the relation between the structures of the products and the major tautomer of II in the ground state have to be considered.[8]

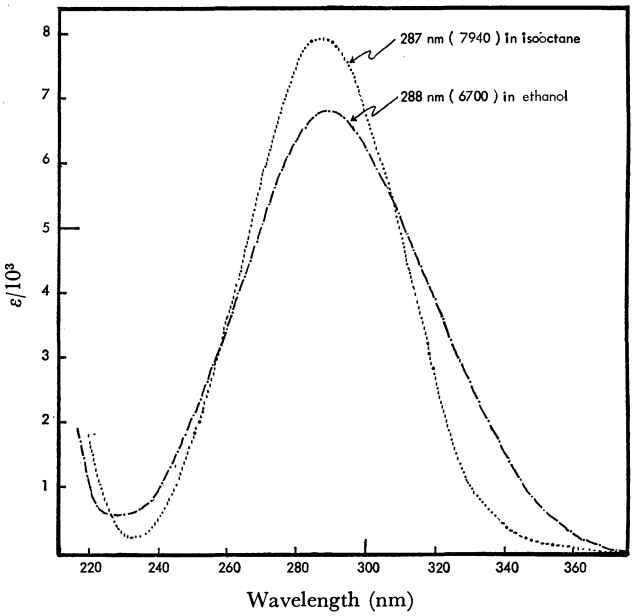

Fig. 1. UV absorption spectrum of II.

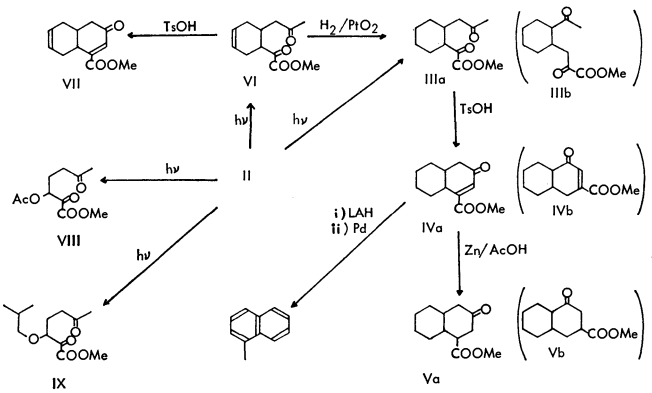

Chart 2.

The NMR spectrum of II [δ 2.22 (3H, s), 3.83 (3H, s), 6.27 (1H, s), and 13.5 (1H, br.)] in a carbon tetrachloride solution indicates that II is at least 95% enolized, showing no signal due to the diketonic tautomer (IIc). In addition to this, the UV spectrum of II (Fig. 1) in an isooctane solution showed an absorption maximum at 287 nm (ε=8000), suggesting that, even in a dilute solution, the enol form is substantial. Since the linearly conjugated tautomer (IIa) should be more stable than the other one (IIb),[9] it can be concluded that all of the above adducts were derived from the reaction of the major tautomer (IIa) in a straightforward manner, and that IIb, produced after a possible intramolecular hydrogen shift through photochemically-excited IIa, was being deactivated and was unreactive. The exclusive formation of VIII and IX from the oxygen-bearing olefins, a result in contrast with the reaction of I and isopropenyl acetate, might, with the reactants, be attributable to a hydrogen-bonding or

6) R. Meyer and H. Fricke, *Ber.*, **47**, 2770 (1914).

7) No indication for the intermolecular hydrogen abstraction. process was obtained in the reaction of II with cyclohexa-1,4-diene, vinyl acetate or isobutyl vinyl ether.

8) The reactive state of the reaction will be a subject of independent studies.

9) There would be no reason to reveal a marked difference in the contents of enolic tautomers between I and II, if II indeed exists as IIb.

a dipole-dipole interaction; II could form a more rigid complex than I leading to photoadducts with the observed orientation.

Finally, it may be mentioned that the yields of the products are quite high; even in the case of cyclohexa-1,4-diene, the 1:1 adduct VI was obtained in satisfactorily high yield. Since these adducts possess only one acetyl group, the cyclization naturally leads to a single product in each case. These two points make this procedure practical for certain alicyclic syntheses.

Experimental

The mps, determined with a Fisher-Jones apparatus, were uncorrected. The UV spectra were measured in a methanol solution unless otherwise stated. The IR spectra were obtained for either KBr disks or a carbon tetrachloride solution. The NMR spectra were determined at 60 MHz for a solution in carbon tetrachloride, with tetramethylsilane as the internal standard, and the chemical shifts were expressed in δ values.

The Reaction of Methyl Acetopyruvate (II) and Cyclohexene; The Formation of Methyl 2-Acetonylcyclohexylglyoxalate (III). II (5.76 g) was dissolved in a mixture of cyclohexene (40 ml) and ether (120 ml) and irradiated by a 450 W high-pressure mercury lamp through a Pyrex glass filter in a nitrogen atmosphere; the reaction was monitored by submitting an aliquot to a color reaction with a ferric chloride solution. After the completion of the reaction, the mixture was evaporated *in vacuo*; the residual oil was purified by distillation to yield a colorless liquid; bp 128°C/2 mmHg; 8.58 g (95%).

Found: C, 63.55; H, 8.21%. Calcd for $C_{12}H_{18}O_4$: C, 63.70; H, 8.02%. λ_{max} 232 nm (8700).

The Bis-Semicarbazone of III. Colorless needles; mp 240—242°C (from ethanol).

Found: C, 49.22; H, 6.95; N, 24.23%. Calcd for $C_{14}H_{24}O_4N_6$: C, 49.40; H, 7.11; N, 24.69%.

The Dehydration of III; The Formation of 4-Methoxycarbonyl-Δ^3-octalone-2 (IV). III (800 mg) was heated with *p*-toluenesulfonic acid (10 mg) in a benzene solution for 5 hr; then, the reaction mixture was passed through an alumina column and evaporated. The distillation of the residue on a cold finger yielded a colorless liquid; bp 105°C/0.2 mmHg (bath temp.); 750 mg (86%). This was homogeneous in gas-liquid chromatograms.

Found: C, 68.89; H, 7.58%. Calcd for $C_{12}H_{16}O_3$: C, 69.21; H, 7.74%.

The 2,4-Dinitrophenylhydrazone of IV. Yellow-orange needles; mp 176—177°C (from ethanol).

Found: C, 55.11; H, 6.30; N, 14.09%. Calcd for $C_{18}H_{24}O_6N_4$: C, 55.09; H, 6.17; N, 14.28%. λ_{max} 385 nm (18800).

The Reduction of IV by Zinc and Acetic Acid; The Formation of 4-Methoxycarbonyldecalone-2 (V). IV (200 mg) was reduced by an excess amount of zinc in acetic acid to give a colorless liquid; 140 mg; bp 125°C/0.2 mmHg (bath temp.).

Found: C, 68.41; H, 8.55%. Calcd for $C_{12}H_{18}O_3$: C, 68.54; H, 8.63%.

The 2,4-Dinitrophenylhydrazone of V. Yellow needles; mp 121—123°C (from ethanol).

Found: 55.49; H, 5.77; N, 14.11%. Calcd for $C_{18}H_{22}O_6N_4$: C, 55.38; H, 5.68; N, 14.35%. λ_{max} 363 nm (18100).

The Deuterium Oxide Treatment of V. V (60 mg) was converted to a mixture of deuterio-derivatives by the use of deuterium oxide (0.2 ml) in dioxane (1.2 ml) containing a trace amount of sodium deuteroxide. After the reesterification of the product by diazomethane, a colorless liquid (43 mg) was obtained by cold-finger distillation.

Mass spectrum: M^+/e; 210 (7.7), 211 (13.2), 212 (24.0), 213 (31.2), 214 (19.7), and 215 (4.2%).

The Dehydrogenation of the Lithium Aluminum Hydride Reduction Product of IV. IV (200 mg) was reduced by the use of lithium aluminum hydride (50 mg) in ether. After the usual work-up, the product was placed in a dehydrogenation tube containing 5% palladium carbon (500 mg) and heated at 220°C for 16 hr in a nitrogen atmosphere. Then, the mixture was extracted by ethanol and filtered. A saturated solution of picric acid was poured into the extract to precipitate naphthalenes. The yellow crystals (45 mg) thus obtained were purified by recrystallization from ethanol to give fine yellow needles; mp 141—142°C, which was undepressed on admixture with authentic α-methylnaphthalene picrate. Every fraction of the recrystallizations showed the absence of β-methylnaphthalene on NMR-spectral analysis.

The Photochemical Reaction of II with Cyclohexa-1,4-diene; The Formation of Methyl 2-Acetonylcyclohex-4-enylglyoxalate (VI). II (2.88 g) was dissolved in a mixture of cyclohexa-1,4-diene (50 ml) and ether (70 ml) and irradiated similarly as in the case of cyclohexene. The product was then purified by distillation to yield a colorless liquid (bp 132°C/0.2 mmHg (bath temp.)), whose homogeneity was proved by gas-liquid chromatograms; 4.08 g (91%).

Found: C, 64.55; H, 7.38%. Calcd for $C_{12}H_{16}O_4$: C, 64.26; H, 7.19%.

The Bis-Semicarbazone of VI. Colorless needles; mp 235—237°C (from methanol).

Found: C, 49.81; H, 6.43; N, 24.60%. Calcd for $C_{14}H_{22}O_4N_6$: C, 49.69; H, 6.55; N, 24.84%.

The Catalytic Reduction of VI. a): VI (25 mg) was hydrogenated in an ethyl acetate solution containing 10% palladium carbon (50 mg). After the reaction had ceased, the product was isolated by the filtration of the catalyst and by distillation with a cold finger to give a colorless liquid (15 mg), which was a 50:50 mixture of III and IV, as confirmed by NMR-spectral and gas-liquid-chromatographic analyses.

b): VI (55 mg) was reduced in acetic acid with platinum oxide. The product isolated after the usual work-up afforded a colorless liquid (45 mg) which was found to be homogeneous by gas-liquid-chromatographic determination and which was identified as IV.

The 2,4-Dinitrophenylhydrazone of the Reduction Product of VI. A part of the above sample was converted to 2,4-dinitrophenylhydrazone, which was identified with that of IV by a direct comparison.

The Acid Catalyzed Cyclization of VI; The Formation of 4-Methoxycarbonyl-$\Delta^{3,6}$-hexalone (VII). VI (200 mg) was heated with *p*-toluenesulfonic acid (5 mg) in benzene for 3 hr, and the product purified by cold-finger distillation was a colorless liquid (165 mg) which was gas-liquid chromatographically homogeneous.

Found: C, 70.21; H, 6.55%. Calcd for $C_{12}H_{14}O_3$: C, 69.88; H, 6.84%. λ_{max} 231 nm (7300).

The 2,4-Dinitrophenylhydrazone of VII. Yellow-orange needles; mp 176—177°C (from ethanol).

Found: C, 55.67; H, 4.37; N, 14.82%. Calcd for $C_{18}H_{18}O_6N_4$: C, 55.95; H, 4.70; N, 14.50%. λ_{max} 387 nm (19400).

The Photochemical Reaction of II with Vinyl Acetate; The Formation of Methyl 3-Acetoxy-2,6-dioxoheptanoate (VIII). II (77 mg) was sealed in a Pyrex glass tube with vinyl acetate (7 ml) and placed for an external irradiation. After 3 hr, the mixture was evaporated and the residue was distilled on a cold finger to yield a colorless liquid; 95 mg (82%). This was homogeneous in thin-layer chromatograms and in NMR spectroscopic analysis.

Found: C, 52.22; H, 6.27%. Calcd for $C_{10}H_{14}O_6$: C, 52.17; H, 6.13%.

The Photochemical Reaction of II with Isobutyl Vinyl Ether; *The Formation of Methyl 2,6-Dioxo-3-isobutoxyheptanoate (IX).* II (77 mg) was dissolved in a mixture of isobutyl vinyl ether (2 ml) and ethyl acetate (5 ml) and was externally irradiated in a sealed Pyrex tubing. A colorless liquid; 103 mg (84%), obtained after a cold-finger distillation, was homogeneous in thin-layer chromatograms and in NMR spectral analysis.

Found: C, 58.81; H, 8.33%. Calcd for $C_{12}H_{20}O_5$: C, 59.00; H, 8.25%.

We thank Professor S. Itô for a stimulating discussion, Mrs. H. Arai and Miss M. Suzuki for elemental analyses, and Messrs. K. Sasaki and T. Kondo for NMR measurements. H. T. is also grateful to The Matsunaga Science Foundation for a research grant by which a part of the expense has been defrayed.

BULLETIN OF THE CHEMICAL SOCIETY OF JAPAN, VOL. 46, 883—888 (1973)

The Dimerization of Acrylonitrile to 2-Methyleneglutaronitrile with Metal Halide and Trialkylamine

Yoshihisa WATANABE and Makoto TAKEDA

Central Research Laboratory, Mitsubishi Petrochemical Company Ltd., Ami-machi, Ibaraki

(Received June 19, 1972)

Acrylonitrile is dimerized to 2-methyleneglutaronitrile by the binary catalyst system of metal halide and trialkylamine. The catalytic activities of metals are in this order: Co(II)≥Zn(II)≫Fe(II)>Al(III)≫V(III)> Cd(II)>Ti(IV), while that of halogens is I>Br>Cl. Triethylamine is particularly effective for the reaction. The kinetic features are discussed, and a reaction mechanism for the catalyst system of zinc chloride and triethylamine is proposed.

The catalytic dimerization of acrylonitrile has been extensively investigated. When phosphines are used as the catalysts, 2-methyleneglutaronitrile is selectively obtained; a reaction mechanism has been proposed by Baizer *et al.*[1] It is generally acecpted that Lewis bases can catalyze the reaction; many catalysts such as trialkylstibine, trialkylarsine,[2] triethylenediamine,[3] and phosphine-coordinated metal carbonyls[4] have been reported. Saegusa has also reported metal-isocyanide complexes as a new type of catalyst.[5] These catalysts are, however, effective only in the presence of protic solvents.

We have found that acrylonitrile is readily dimerized to 2-methyleneglutaronitrile under mild conditions by the binary catalysts; metal halide and tertiary amine.[6] With these catalyst systems, a protic solvent is not necessary. On the contrary, its presence hinders the reaction. In the present work, various metal halides and amines have been examined; the kinetic features will be discussed in detail.

Results and Discussion

Catalytic Activity of Metal Halide and Amines. The dimerization reaction of acrylonitrile was investigated using various metal halides and amines. The results are shown in Table 1.

Acrylonitrile was catalytically converted to methyleneglutaronitrile; only a small amount of the trimeric product was formed as a by-product. Gas-chromatographic analysis showed that no other acrylonitrile oligomers were formed. The reaction products were isolated by fractional distillation. Two fractions, with bp's of 97°C/3 mmHg and 202°C/4 mmHg, were identified as 2-methyleneglutaronitrile and 2,4,6-tricyanohexene-1 respectively by the molecular weight measurement, infrared and NMR spectroscopy.

Table 1 shows that the order of the catalytic activity is Co(II)≥Zn(II)≫Fe(II)>Al(III)≫V(III)>Cd(II) >Ti(IV) for metals and I>Br>Cl for halogens. In our investigation, only metal halides could catalyze the reaction; all the other metal compounds, such as acetates, stearates, oxides, carbonates, sulfates and acetylacetonates of zinc, cobalt and iron, did not catalyze the dimerization reaction.

Primary and secondary amines showed no catalytic activity when coupled with various metal halides, but an addition reaction to the double bond of acrylonitrile occurred. Polyamines such as triethylenediamine and hexamethylenetetramine were also found to be undesirable since the chelation to the metal halide proceeded and inhibited the dimerization reaction. From these results, it is quite probable that only tertiary amines can be used as catalyst components. Especially it was found that only three amines, triethylamine, tri-*n*-propylamine, and tri-*n*-butylamine, were effective. Triphenylamine, tribenzylamine, and tricyclohexylamine, when coupled with zinc chloride or cobaltous chloride, did not show any catalytic activity. Also, *N*,*N*-diethylaniline and diethylcyclohexylamine, which are quite

1) M. M. Baizer and J. D. Anderson, *J. Org. Chem.*, **30**, 1357 (1965).
2) U. S. 2675372 (1954) (Eastman Kodak Co.).
3) Japan. 13924 (1969) (I.C.I. Ltd.).
4) Fr. 1411003 (1965) (Shell Inter. Res.).
5) T. Saegusa, Y. Ito, H. Kinoshita, and S. Tomita, This Bulletin, **43**, 877 (1970).
6) Japan. 6892 (1971), 15492 (1971) 8287 (1972), [Ger. Off. 1922017 (1969)] (Mitsubishi Photochemical Co.).

TABLE 1. THE DIMERIZATION OF ACRYLONITRILE CATALYZED BY METAL HALIDES AND AMINES[a]

Metal[b] halide	Amine	(ml)	Reaction temp., °C	Reaction time, hr	Conv. %	Yield[c] MGN[d]	Yield[c] TCH[e]
CoI_2	$(C_2H_5)_3N$	(25)	20	6	76.9	73.5	3.4
$CoBr_2$	$(C_2H_5)_3N$	(25)	20	6	71.5	68.3	3.2
$CoCl_2$	$(C_2H_5)_3N$	(25)	20	6.5	59.3	56.0	3.2
$CoCl_2$	$(n\text{-}C_3H_7)_3N$	(34)	20	5	5.8	5.4	0.4
ZnI_2	$(C_2H_5)_3N$	(15.8)	20	4	72.4	68.5	3.9
$ZnBr_2$	$(C_2H_5)_3N$	(15.8)	20	6	67.1	63.7	3.4
$ZnCl_2$	$(C_2H_5)_3N$	(15.8)	20	6	50.8	48.5	2.3
$ZnCl_2$	$(n\text{-}C_3H_7)_3N$	(15.8)	30	6	8.5	8.1	0.4
$ZnCl_2$	$(n\text{-}C_4H_9)_3N$	(15.8)	30	6	3.6	3.4	0.2
$ZnCl_2$	$(C_6H_5CH_2)_3N$	(16.2)	30	6	—	—	—
$ZnCl_2$	$(C_6H_{11})_3N$	(15.8)	30	6	—	—	—
$ZnCl_2$	$(C_6H_5)_3N$	(15.8)	20	6	—	—	—
$ZnCl_2$	$(C_6H_5)_2(C_6H_{11})N$	(15.8)	20	6	—	—	—
$ZnCl_2$	$(C_2H_5)_2(C_6H_5)N$	(15.8)	20	6	—	—	—
$FeCl_2$	$(C_2H_5)_3N$	(25)	20	7	27.0	26.4	0.6
$AlCl_3$	$(C_2H_5)_3N$	(15.8)	30	6	17.1	14.9	2.2
VCl_3	$(C_2H_5)_3N$	(15.8)	30	6	2.7	2.5	0.2
$CdCl_2$	$(C_2H_5)_3N$	(15.8)	30	6	2.1	2.0	0.1
$TiCl_4$	$(C_2H_5)_3N$	(15.8)	30	6	1.7	1.6	0.1

a) In all the reactions, a 100 ml portion of acrylonitrile was employed. b) The same amount (2.77×10^{-2} mol) was employed. c) Based on the acrylonitrile originally fed in (%). d) 2-Methyleneglutaronitrile. e) 2,4,6-Tricyanohexene-1.

TABLE 2. DIMERIZATION OF VARIOUS ACRYLATES AND CO-DIMERIZATION OF ACRYLONITRILE AND ACRYLATES CATALYZED BY ZINC CHLORIDE AND TRIETHYLAMINE[a]

Monomer (ml)	Reaction time (hr)	Product (Yield,[b] %)	
CH_2=CH–CN (100)	6	$NC-\overset{CH_2}{\overset{\|\|}{C}}-CH_2-CH_2-CN$ (MGN)	(61.0)
CH_2=CH–CO_2Me (100)	50	$MeOC-\overset{O}{\overset{\|\|}{C}}-\overset{CH_2}{\overset{\|\|}{C}}-CH_2-CH_2-\overset{O}{\overset{\|\|}{C}}-OMe$	(0.82)
CH_2=CH–CO_2Et (100)	50	$EtOC-\overset{O}{\overset{\|\|}{C}}-\overset{CH_2}{\overset{\|\|}{C}}-CH_2-CH_2-\overset{O}{\overset{\|\|}{C}}-OEt$	(0.59)
CH_2=CH–CN (50)	50	$NC-\overset{CH_2}{\overset{\|\|}{C}}-CH_2-CH_2-\overset{O}{\overset{\|\|}{C}}-OMe$	(2.61)
CH_2=CH–CO_2Me (50)		$MeO-\overset{O}{\overset{\|\|}{C}}-\overset{CH_2}{\overset{\|\|}{C}}-CH_2-CH_2-CN$	(0.46)
		MGN	(4.32)
CH_2=CH–CN (50)	31	$NC-\overset{CH_2}{\overset{\|\|}{C}}-CH_2-CH_2-\overset{O}{\overset{\|\|}{C}}-OEt$	(1.51)
CH_2=CH–CO_2Et (50)		$EtO-\overset{O}{\overset{\|\|}{C}}-\overset{CH_2}{\overset{\|\|}{C}}-CH_2-CH_2-CN$	(0.23)
		MGN	(1.93)
CH_2=CH–CN (50)	50	$NC-\overset{CH_2}{\overset{\|\|}{C}}-CH_2-CH_2-\overset{O}{\overset{\|\|}{C}}-OBu$	(3.34)
CH_2=CH–CO_2Bu (50)		$BuO-\overset{O}{\overset{\|\|}{C}}-\overset{CH_2}{\overset{\|\|}{C}}-CH_2-CH_2-CN$	(0)
		MGN	(9.56)

a) Reaction condition: $ZnCl_2$; 2.77×10^{-2} mol, Et_3N; 11.4 $\times10^{-2}$mol, React. Temp.; 30°C.
b) Based on the monomers originally fed in (%).

analogous to triethylamine, did not catalyze the dimerization reaction. Many amines form complexes with halides of cobalt or zinc, and it has been reported[7,8] that acrylonitrile also forms complexes with halides of cobalt or zinc. It is probable that zinc halide forms a complex with triethylamine and acrylonitrile and that this complex catalyzes the dimerization reaction.

Catalytic Dimerization of Other Olefinic Compounds by Zinc Chloride and Triethylamine. Many olefinic compounds, such as methacrylonitrile, crotononitrile, various acrylates, styrene, butadiene, and vinyl chloride, were examined, but no dimer was obtained except for acrylates. The rates of the dimerization of acrylates were smaller than that of acrylonitrile. The co-dimerizations of acrylonitrile and various acrylates were also attempted. These results are shown in Table 2.

In all the co-dimerization experiments, the dimer of acrylate was not detected and the dimerization of acrylonitrile was fairly much inhibited. This suggests that acrylates are more strongly coordinated to zinc chloride than to acrylonitrile.

Effect of Acrylonitrile Concentration. The relation of the 2-methyleneglutaronitrile obtained and the reaction time at various acrylonitrile concentrations is shown in Fig. 1.

The rate of 2-methyleneglutaronitrile formation was calculated from the initial gradient of the curves in Fig. 1. The result is plotted against the concentration of acrylonitrile in Fig. 2. A straight line with an inclination of +2 as observed in Fig. 2 suggests a second-order reaction with the acrylonitrile concen-

7) T. Ikegami and H. Hirai, *Chem. Commun.*, **1969**, 159.
8) M. F. Farona and G. R. Tompkin, *Spectrochim. Acta, A*, **24**, 788 (1968).

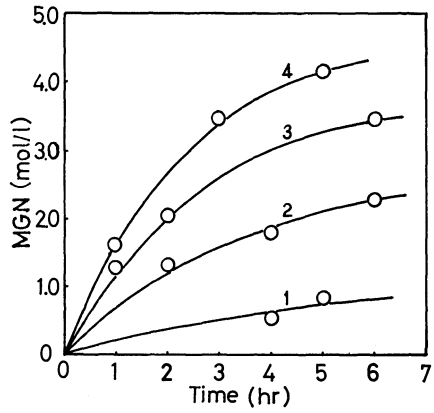

Fig. 1. The relation between amount of 2-methyleneglutaronitrile and reaction time at various acrylonitrille concentration.
Temperature: 20°C, $ZnCl_2$: 0.18 mol/l, Triethylamine: 2.40 mol/l, Acrylonitrile concentration: (1) 2.02 mol/l, (2) 4.05 mol/l, (3) 6.07 mol/l, (4) 8.09 mol/l.

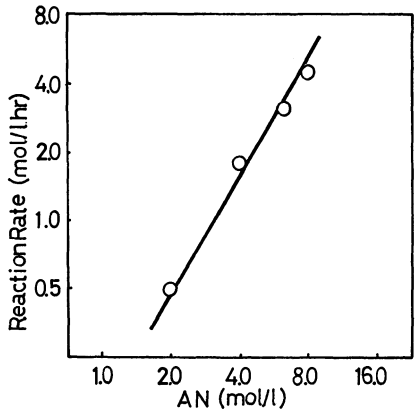

Fig. 2. Dependence of dimerization rate on concentration of acrylonitrile.
Temperature: 20°C, $ZnCl_2$: 0.18 mol/l, triethylamine: 2.40 mol/l.

tration.

The Reaction Paths of the Acrylonitrile Trimer. As is shown in Fig. 3, the trimeric product was found even in the very eary stages and exhibited a pattern of increase similar to that of the dimeric product. If the trimer is formed only from the dimer and the monomer by the consecutive reaction mechanism, its amount will be very small at first, but will show a rapid increase as the dimer increases. Such a pattern was not observed, however, even after more than half of the acrylonitrile was converted to the dimeric product. Therefore, two parallel paths for the trimeric product were postulated: one, a successive reaction of the dimer with the monomer, and the other, a simultaneous reaction from three molecules of acrylonitrile.

In order to confirm the assumption, the simulation of the rate process of the reaction was attempted by means of an analog computer (Melcom Model EA-716). The results of the simulation agree satisfactorily with the experimental results. An example is shown in Fig. 3; the results of the simulation are shown by solid lines, while the experimental values are illustrated symbols.

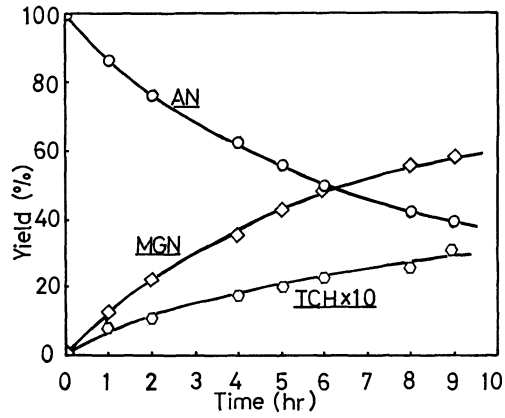

Fig. 3. Comparison of experimental yields with computer simulation. Solid lines are results of simulation (k_1: 0.180, k_2: 0.004, k_3: 0.009) and symbols are experimental values: ○ unreacted acrylonitrile, ◇ yield of methyleneglutaronitrile, ⟨⟩ yield of 2,4,6-tricyanohexene-1. Temperature: 20°C, acrylonitrile: 13.1 mol/l, $ZnCl_2$: 0.18 mol/l, triethylamine: 0.98 mol/l.

We may conclude that the reaction of acrylonitrile catalyzed by zinc chloride and triethylamine is composed of the following reactions:

$$2CH_2{=}CH{-}CN \xrightarrow{k_1} CH_2{=}C(CH_2{-}CH_2{-}CN){-}CN \quad (1)$$

$$CH_2{=}CH{-}CN + NC{-}\overset{CH_2}{\overset{\|}{C}}{-}CH_2{-}CH_2{-}CN \xrightarrow{k_2} CH_2{=}C(CH_2{-}CH(CH_2{-}CH_2{-}CN){-}CN){-}CN \quad (2)$$

$$3CH_2{=}CH{-}CN \xrightarrow{k_3} CH_2{=}C(CH_2{-}CH(CH_2{-}CH_2{-}CN){-}CN){-}CN \quad (3)$$

The rate expression of the above reaction is as follows. The concentration of the dimer and the trimer are reduced to those of the acrylonitrile consumed:

$$-d[A_1]/dt = k_1[A_1]^2 + k_2[A_1][A_2] + k_3[A_1]^3$$
$$d[A_2]/dt = k_1[A_1]^2 - k_2[A_1][A_2]$$
$$d[A_3]/dt = k_1[A_1][A_2] + k_3[A_1]^3$$

A_1=acrylonitrile unreacted, A_2=acrylonitrile converted to 2-methyleneglutaronitrile, A_3=acrylonitrile converted to 2,4,6-tricyanohexene-1.

Temparature Dependence on the Reaction Rate. The rate constants calculated by means of the analog computer will be used hereafter.

Figure 4 shows, the k_1, k_2, and k_3 logarithms *vs.* $1/T$. The apparent activation energies, as calculated from Fig. 4, are 3.4, 2.8, and 2.3 kcal/mol for Reactions (1), (2), and (3) respectively.

These unusually small activation energy values suggest the existence of an exothermal partial equilibrium prior to the rate-determining step. Therefore, it is assumed that the apparent activation energies can be observed as the differences in the real activation energies and the reaction heats of the equilibrium reaction.

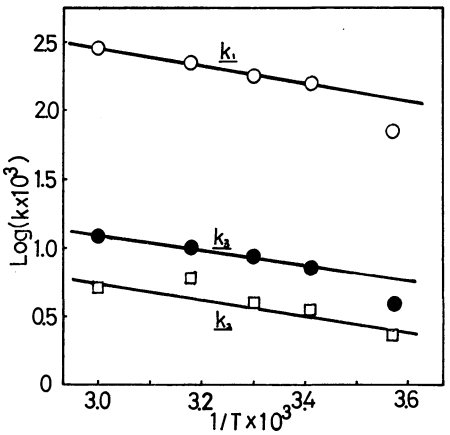

Fig. 4. Dependence of reaction rate on reaction temperature.
Acrylonitrile: 13.1 mol/l, $ZnCl_2$: 0.18 mol/l, triethylamine: 0.98 mol/l.

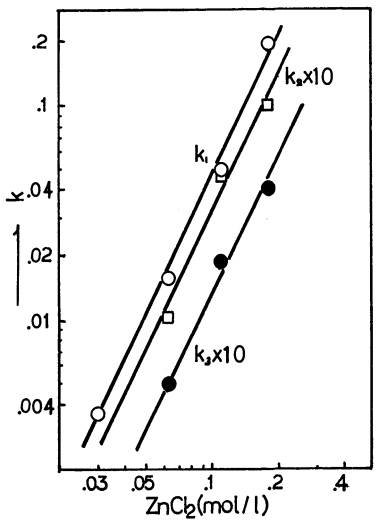

Fig. 5. Reaction rate as a function of $ZnCl_2$ concentration.
Temperature: 20°C, Acrylonitrile: 10.1 mol/l, Triethylamine: 2.40 mol/l.

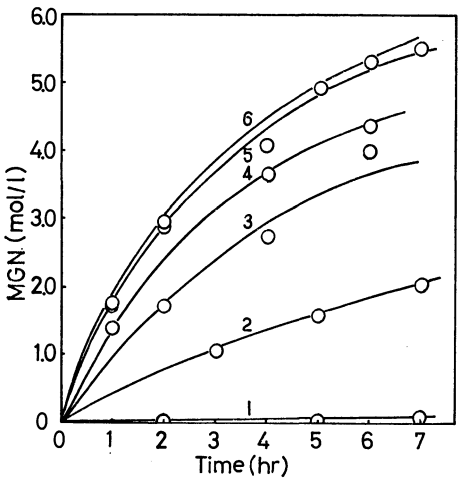

Fig. 6. The relation between amount of 2-methyleneglutaronitrile and reaction time at various triethylamine concentration.
Temperature: 20°C, Acrylonitrile: 10.1 mol/l, $ZnCl_2$: 0.18 mol/l, Triethylamine: (1) 0.19 mol/l, (2) 0.48 mol/l, (3) 0.96 mol/l, (4) 1.46 mol/l, (5) 1.94 mol/l, (6) 2.40 mol/l.

Effect of the Catalyst Concentration. The dependence of the zinc chloride concentration on the rate constants, k_1, k_2, and k_3, is shown in Fig. 5. The straight lines with the gradient of +2 for all the k's suggest that the reaction is of the second order with relation to the concentration of zinc chloride. This suggests that the zinc chloride complex exists in the dimeric form.

The relations of the 2-methyleneglutaronitrile and the reaction time obtained at various triethylamine concentrations are shown in Fig. 6. As is evident from Fig. 6, the catalytic activity is very small when the molar ratio of zinc chloride to triethylamine is less than unity, while it is almost constant when the ratio is over ten.

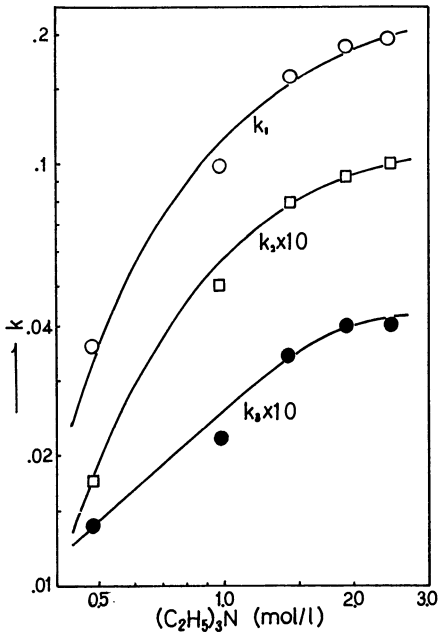

Fig. 7. Plots of reaction rates *vs.* concentration of triethylamine.
Temperature: 20°C, Acrylonitrile: 10.1 mol/l, $ZnCl_2$: 0.18 mol/l.

The logarithms of k_1, k_2, and k_3 are plotted against the logarithm of the triethylamine concentration in Fig. 7. The maximum gradient of each line was calculated as follows: about +2 for k_1 and k_2, and about +1 for k_3. In other words, the concentration of triethylamine influences Reactions (1) and (2) in the second order and Reaction (3) in the first order.

Reaction Mechanism. Summing the experimental results, we get: (1) zinc chloride, triethylamine, and acrylonitrile form a complex, and this complex catalyzes the reaction; (2) the trimer is formed through two different paths; (3) an exothermal partial equilibrium exists prior to the rate-determining step, and (4) the kinetic order of each catalyst component was determined and the product distribution in the co-dimers of acrylonitrile and acrylates was investigated.

The following reaction scheme is proposed on the basis of the experimental results:

i) Formation of methyleneglutaronitrile:

$$2ZnCl_2 + 2Et_3N + AN \rightleftarrows [Zn_2Cl_4(Et_3N)_2(AN)] \quad (4)$$

$$[Zn_2Cl_4(Et_3N)_2(AN)] + AN \xrightarrow{\text{-A-}} [Zn_2Cl_4(Et_3N)_2(MGN)] \quad (5)$$

$$[Zn_2Cl_4(Et_3N)_2(MGN)] + AN \xrightarrow{\text{fast}} [Zn_2Cl_4(Et_3N)_2(AN)] + MGN \quad (6)$$

ii) Formation of 2,4,6-tricyanohexene-1:

a) Successive reaction from methyleneglutaronitrile:

$$2ZnCl_2 + 2Et_3N + AN \rightleftarrows [Zn_2Cl_4(Et_3N)_2(AN)]$$

$$[Zn_2Cl_4(Et_3N)_2(AN)] + MGN \xrightarrow{\text{-A-}} [Zn_2Cl_4(Et_3N)_2(TCH)] \quad (7)$$

$$[Zn_2Cl_4(Et_3N)_2(TCH)] + AN \xrightarrow{\text{fast}} [Zn_2Cl_4(Et_3N)_2(AN)] + TCH \quad (8)$$

b) Direct formation from acrylonitrile:

$$2ZnCl_2 + Et_3N + 2AN \rightleftarrows [Zn_2Cl_4(Et_3N)(AN)_2] \quad (9)$$

$$[Zn_2Cl_4(Et_3N)(AN)_2] \xrightarrow{\text{fast}} [Zn_2Cl_4(Et_3N)(MGN)] \quad (10)$$

$$[Zn_2Cl_4(Et_3N)(MGN)] + AN \xrightarrow{\text{-A-}} [Zn_2Cl_4(Et_3N)(TCH)] \quad (11)$$

$$[Zn_2Cl_4(Et_3N)(TCH)] + 2AN \xrightarrow{\text{fast}} [Zn_2Cl_4(Et_3N)(AN)_2] + TCH \quad (12)$$

or

$$[Zn_2Cl_4(Et_3N)(TCH)] + AN + Et_3N \xrightarrow{\text{fast}} [Zn_2Cl_4(Et_3N)_2(AN)] + TCH \quad (13)$$

AN: acrylonitrile, MGN: 2-methyleneglutaronitrile, TCH: 2,4,6-tricyanohexene-1, Et_3N: triethylamine.

The above mechanism requires that zinc chloride be in the dimeric form and that the molar ratios of chlorine, acrylonitrile and triethylamine to zinc in the catalytic complex (Scheme 4) be 2, 1, and 1/2 respectively. We have tried to separate the catalytic complex and have succeeded in obtaining an orange precipitate by adding a small amount of toluene to the reactive solution.

The precipitate was examined by elemental analysis and by IR and NMR spectroscopy, and was shown to contain zinc, chlorine, acrylonitrile, triethylamine, and toluene as components. However, the integral stoichiometry was not determined (except that the ratio of chlorine to zinc is 2), since the complex was rather unstable in the air.

The dimeric form of zinc chloride may be supported by the fact that cadmium chloride forms an autocomplex like $Cd[CdCl_4]$, though the same structure has not been established for zinc chloride. Thus, according to the above mechanism, the structure of the catalytic complex may be postulated to be as follows:

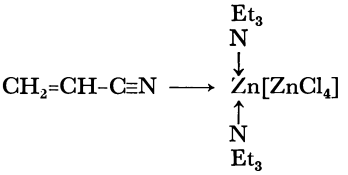

However, the real stoichiometry and the autocomplex structure were not proved in our experiments; these problems are left to further investigations.

Experimental

Materials and Reagents. As the reaction was strikingly hindered by the presence of water, it was carefully removed from all the reagents. The acrylonitrile and amines were dried over molecular sieves (4A) and distilled under nitrogen. The water content of the acrylonitrile after the purification was less than 10 ppm, while that of triethylamine was less than 20 ppm.

All the commercially-obtained metal halides except titanium tetrachloride were dried by heating them under nitrogen or gaseous hydrogen chloride.

The Reaction of Acrylonitrile. The following procedure was carried out under a nitrogen atmosphere.

About 3.6 g of zinc chloride were dissolved in 100 ml of acrylonitrile in a 200 ml three-necked flask provided with a stirrer, and then 16 ml of triethylamine were added. The flask was set in a water bath, and the temperature was controlled by means of a "Coolnics circulator" (Yamato Kagaku Co. Ltd.). The mixture was kept at the prescribed temperature for a certain number of hours. During the reaction, if desired, a portion of the reaction mixture was sampled by operating a micro syringe through the serum cap and was analyzed by gas chromatography.

NMR and IR Spectra of Reaction Products.

$NC-\underset{\underset{CH_2}{\|}}{C}-CH_2-CH_2-CN$: NMR (in CCl_4) τ 3.98 and 4.18 (s, 2H, CH_2=), 7.38 (s, 4H, $-C\underline{H}_2-C\underline{H}_2-$); IR (neat) 2265 and 2245 (-C≡N), 1625 and 953 cm^{-1} (C=C).

$CH_2=\underset{\underset{CN}{|}}{C}-CH_2-\underset{\underset{CN}{|}}{CH}-CH_2-CH_2-CN$: NMR (in CCl_4) τ 3.82 and 3.92 (s, 2H, $C\underline{H}_2$=), 6.87 (m, 1H, $-C\underline{H}-$), 7.29 (t, J= 6 Hz, 2H, $-CH_2-C\underline{H}_2-CN$), 7.38 (d, J=7.2 Hz, 2H, $CH_2=\underset{\underset{CN}{|}}{C}-C\underline{H}_2-$), 7.59, (q, J=6.6 Hz, 2H, $-\underset{\underset{CN}{|}}{CH}-C\underline{H}_2-CH_2-$); IR (neat) 2250 and 2230 (-C≡N), 1620 and 955 cm^{-1} (C=C).

$CH_3O-\underset{\underset{O}{\|}}{C}-\underset{\underset{CH_2}{\|}}{C}-CH_2-CH_2-\underset{\underset{O}{\|}}{C}-OCH_3$: NMR (in CCl_4) τ 3.86 and 4.40 (s, 2H, $C\underline{H}_2$=), 6.24 and 6.35 (s, 6H, $-COOC\underline{H}_3$), 7.46 (s, 4H, $-C\underline{H}_2-C\underline{H}_2-$); IR (neat) 1735 (C=O), 1630 cm^{-1} (C=C).

$C_2H_5O-\underset{\underset{O}{\|}}{C}-\underset{\underset{CH_2}{\|}}{C}-CH_2-CH_2-\underset{\underset{O}{\|}}{C}-OC_2H_5$: NMR (in CCl_4) τ 3.83 and 4.36 (s, 2H, $C\underline{H}_2$=), 5.80 (m, J=7 Hz, 4H, $CH_3-C\underline{H}_2-O-$), 7.46 (m, 4H, $-C\underline{H}_2-C\underline{H}_2-$), 8.70 (m, J=7 Hz, 6H, $C\underline{H}_3-CH_2-O-$); IR (neat) 1720 (C=O), 1625 cm^{-1} (C=C).

$CH_3O-\underset{\underset{O}{\|}}{C}-CH_2-CH_2-\underset{\underset{CH_2}{\|}}{C}-CN$: NMR (in CCl_4) τ 3.69 and 3.78 (s, 2H, $C\underline{H}_2$=), 6.06 (s, 3H, $-COOC\underline{H}_3$), 7.24 (s, 4H, $-C\underline{H}_2-C\underline{H}_2-$); IR (neat) 2230 (-C≡N), 1740 (C=O), 1621 and 945 cm^{-1} (C=C).

$CH_3O-\underset{\underset{O}{\|}}{C}-\underset{\underset{CH_2}{\|}}{C}-CH_2-CH_2-CN$: NMR (in CCl_4) τ 3.23 and 3.77 (s, 2H, $C\underline{H}_2$=), 5.94 (s, 3H, $-COOCH_3$), 7.25 (s, 4H, $-C\underline{H}_2-C\underline{H}_2-$); IR (neat) 2255 (-C≡N), 1721 (C=O), 1630 and 955 cm^{-1} (C=C).

Gas-chromatographic Analysis of the Products. For the analysis of acrylonitrile, methyleneglutaronitrile and 2,4,6-tricyanohexene-1, a column of 1-m Triton-x-305 (5% on Chamelite F.K.) was used.

The authors would like to thank Professor K. Tanabe (Hokkaido University) and Dr. H. Shinohara for their helpful discussion and advice and to Mr. S. Yoshida for his careful reading of the manuscript and valuable comments. We are also indebted to Mr. H. Kinoshita for his experimental skill and assistance. Finally, we thank to Mitsubishi Petrochemical Co. for permission to publish this paper.

BULLETIN OF THE CHEMICAL SOCIETY OF JAPAN, VOL. 46, 888—892 (1973)

The Synthesis and Absolute Configuration of Optically Active Tricyclo[4.3.0.0^{3,8}]nonane (Twist-brendane)

Koichiro NAEMURA and Masao NAKAZAKI

Department of Chemistry, Faculty of Engineering Science, Osaka University, Toyonaka, Osaka

(Received June 19, 1972)

(−)-Tricyclo[4.3.0.0^{3,8}]nonane ("twist-brendane") was synthesized *via* (−)-tricyclo[4.3.0.0^{3,8}]nonan-2-one ("twist-brendan-2-one"). The absolute configuration, (1*R*,3*S*,6*S*,8*R*)-tricyclo[4.3.0.0^{3,8}]nonane was assigned to (−)-twist-brendane by correlating with (−)-*endo*-5-carboxybicyclo[2.2.1]heptane.

Of the hydrocarbons with tricyclodecane skeleton, only tricyclo[4.4.0.0^{3,8}]decane ("twistane") (**1**) and tricyclo[4.4.0.0^{3,8}]dec-4-ene ("twistene") (**2**) are known in optically active modifications, their absolute configurations having been established.[1,2]

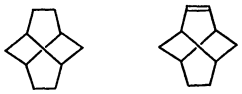

(**1**) (**2**)

"Twist-brendane" (**3**), brexane (**4**), brendane (**5**), and noradamantane (**6**) are the members of tricyclononane,[3-8] the next lower homolog of tricyclodecane, and are free from strain. We see from their structure formula that twist-brendane (**3**) and brexane (**4**) may be called "nortwistane" retaining the chiral twist boat cyclohexane moiety of their parent compound.

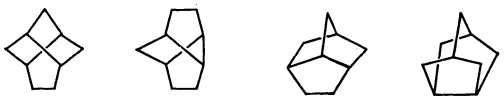

(**3**) (**4**) (**5**) (**6**)

Having succeeded in the synthesis of optically active twistane (**1**) and establishment of its absolute configuration,[1] we directed our studies toward the syntheses of the chiral hydrocarbons. This paper reports the synthesis and assignment of the absolute configuration of optically active twist-brendane (**3**).

endo-5-Carboxybicyclo[2.2.1]hept-2-ene (**7a**) is convenient as starting material since the absolute configuration and the absolute rotation have been determined by Berson and his co-workers.[9,10]

Pure *endo*-carboxylic acid (**7a**) was obtained from an *endo-exo* mixture of carboxylic acid (**7a**) and **7b** by the known method.[10-12]

Since the Arndt-Eistert reaction of the unsaturated carboxylic acid (**7a**) to give the higher homolog failed, the following stepwise procedure was adopted.

Reduction of carboxylic acid (**7a**) with lithium aluminium hydride in ether afforded *endo*-5-hydroxymethylbicyclo[2.2.1]hept-2-ene (**9**) which was converted into *p*-toluenesulfonate (**10**). *endo*-5-Cyanomethylbicyclo-[2.2.1]hept-2-ene (**11**) prepared from *p*-toluenesulfonate (**10**) was hydrolyzed by heating with potassium hydroxide in ethylene glycol to yield the desired higher homologous carboxylic acid (**12**).

We next spanned the ethano-bridge between 3 and 6 positions of norbornane by using, with a slight modification, the scheme for the synthesis of optically active twistane (**1**).

Iodolactonization of the unsaturated carboxylic acid (**12**) with iodine-iodide in aqueous sodium bicarbonate solution secured iodolactone (**13**), which was heated, without further purification, with 10% aqueous sodium hydroxide to give 3-oxo-5-*endo*-carboxymethylbicyclo-[2.2.1]heptane (**14**), mp 96—97°C.[13]

After esterification of carboxylic acid (**14**) with diazomethane followed by protection of the keto group

1) K. Adachi, K. Naemura, and M. Nakazaki, *Tetrahedron Lett.*, **1968**, 5467.
2) M. Tichy and L. Sicher, *ibid.*, **1969**, 4609.
3) B. R. Vogt, *ibid.*, **1968**, 1579.
4) R. R. Sauers and L. A. Whittle, *J. Org. Chem.*, **34**, 3579 (1969).
5) A. Nickon, H. Kwasnik, T. Swartz, R. O. Williams, and J. B. DiGiorogio, *J. Amer. Chem. Soc.*, **87**, 1613, 1615 (1965).
6) P. von R. Schleyer and E. Wiskott, *Tetrahedron Lett.*, **1967**, 2845.
7) B. R. Vogt and J. R. E. Hoover, *ibid.*, **1967**, 2841.
8) A. Nickon, G. D. Pandit, and R. O. Williams, *ibid.*, **1967**, 2851.
9) J. A. Berson, J. S. Walia, A. Remanick, S. Suzuki, P. Reynolds-Warnhoff, and D. Willner, *J. Amer. Chem. Soc.*, **83**, 3986 (1961).
10) J. A. Berson and D. A. Ben-Efraim, *ibid.*, **81**, 4083 (1959).
11) K. Alder, G. Stein, M. Liebmann, and E. Rolland. *Ann. Chem.*, **514**, 197 (1934). J. D. Roberts, E. R. Trumbull, Jr., W. Bennett, and R. Armstrong, *J. Amer. Chem. Soc.*, **72**, 3116 (1959).
12) E. E. van Tamelen, and M. Shamma, *ibid.*, **77**, 2315 (1955).
13) S. Beckmann, H. Geiger, and M. Schaber-Kiechle, *Chem Ber.*, **92**, 2419 (1959). S. Beckmann and H. Geiger, *ibid.*, **92**, 2411 (1959).

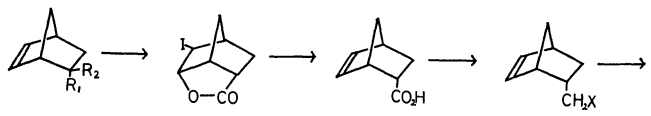

(**7a**) $R_1=CO_2H$ $R_2=H$ (**8**) (−)-(**7a**) (−)-(**9**) X=OH (**10**) X=OTs
(**7b**) $R_1=H$ $R_2=CO_2H$

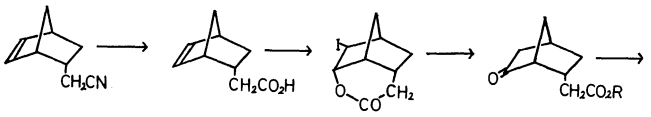

(−)-(**11**) (−)-(**12**) (**13**) (**14**) R=H (+)-(**15**) R=CH_3

by ketal formation with ethylene glycol, the resulting ketal-ester (**16**) was treated with lithium aluminium hydride in ether to yield ketal-alcohol (**17**), hydrolysis of which with *p*-toluenesulfonic acid in acetone gave 3-oxo-5-*endo*-(2-hydroxy)ethylbicyclo[2.2.1]nonane (**18**) Since the procedure which proved satisfactory in twistane synthesis gave a very poor yield (about 2%) for intramolecular alkylation of ketomethanesulfonate (**19**),[1] the conditions were modified as follows.

Prolonged heating (22 hr) at 60°C with excess sodium hydride in dry dimethylformamide in a nitrogen atmosphere converted the methanesulfonate (**19**) into a mixture from which twist-brendan-2-one, tricyclo-[4.3.0.0^{3,8}]nonan-2-one (**20**), mp 174—175°C was obtained after chromatographic purification and sublimation.

Although various evidences, including elemental analysis, mass spectrum (molecular ion peak, *m/e* 136) and infrared spectrum (1750 cm^{-1}) clearly supported the structure, conclusive proof was obtained by its conversion into the known twist-brendane.

The Wolff-Kishner reduction of the ketone (**20**) gave a product which was purified by column chromatography on neutral alumina followed by sublimation to provide a crystalline hydrocarbon, mp 159—160°C.

Its mass spectrum showed peaks at *m/e* 122, 93, 81, 80, 79, 67, 41, and 39. The NMR spectrum exhibited two broad singlets at τ 7.75 and 8.16 and a poorly resolved multiplet around 8.30—8.90. These spectra are found to be in line with those reported for twist-brendane (**3**) by Vogt.[3]

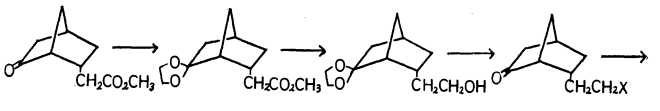

(+)-(**15**) (+)-(**16**) (**17**) (+)-(**18**) X=OH (**19**) X=OMs

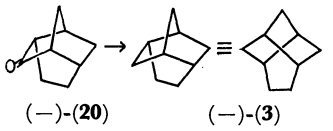

(−)-(**20**) (−)-(**3**)

The same reaction scheme outlined above provided optically active twist-brendan-2-one (**20**), mp 169—171°C, $[\alpha]_D^{21}$ −240° and twist-brendane (**3**), mp 157.5—159°C, $[\alpha]_D^{18}$ −235° from (−)-*endo*-5-carboxybicyclo-[2.2.1]hept-2-ene (**7a**), $[\alpha]_D^{20}$ −119° (82% optical purity), which was obtained by optical resolution of racemate *via* cinchonidine salt.

Since the absolute configuration of (−)-unsaturated carboxylic acid (**7a**) has been established by correlating with (−)-fenchone, (−)-twist-brendan-2-one (**20**) and (−)-twist-brendane (**3**) should be (−)-(1*R*,3*R*,6*S*,8*R*)-tricyclo[4.3.0.0^{3,8}]nonan-2-one and (−)-(1*R*,3*S*,6*S*,8*R*)-tricyclo[4.3.0.0^{3,8}]nonane, respectively.

The cyclohexanone moiety of twist-brendan-2-one which is indicated by the shaded past in the projection formula (**21**) has a "right-handed" twist boat form according to the definition of Djerassi and Klyne who drew the general conclusion that the twist boat form of this type exhibits a strong positive CD curve around 300 mμ.[15]

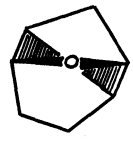

(**21**)

Contrary to expectation, (−)-twist-brendan-2-one (**20**) shows a negative maximum ([θ] 1.50×10^4) at 289 mμ (Fig. 1).

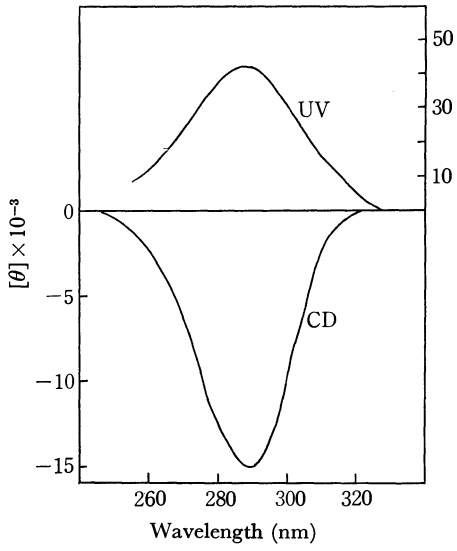

Fig. 6. UV and CD spectra.

This suggests that proper caution should be paid in applying this rule, which has been proved valid in steroid, to this type of cage compound.

Experimental[16]

(±)-endo-5-Hydroxymethylbicyclo[2.2.1]hept-2-ene (9) and Its Tosylate (10). *endo*-5-Carboxybicyclo[2.2.1]hept-2-ene

14) The structure formula indicated refers to the enantiomers which eventually give (−)-twist-brendane.

15) C. Djerassi and W. Klyne, *Proc. Nat. Acad. Sci. U.S.*, **48**, 1093 (1962).

16) Melting points and boiling points are uncorrected. NMR measurements were carried out on a JEOLC-60 H. Optical rotations were measured with a JASCO DIP-SL automatic polarimeter. Mass spectra were measured with a Hitachi RMS-4 spectrometer.

(**7a**) (35.6 g), which was prepared by the method of Berson,[10] was refluxed for 4.5 hr with 9.8 g of lithium aluminium hydride in 300 ml of dry ether. After addition of aqueous sodium sulfate, a separated solid was filtered off and the filtrate was washed with saturated aqueous sodium carbonate, saturated aqueous sodium chloride and dried. After removal of the solvent, the residue was distilled to give 28.3 g of *endo*-5-hydroxymethylbicyclo[2.2.1]hept-2-ene (**9**), bp 100—104°C/18 mmHg, n_D^{18} 1.5000.

IR (neat film): 3320, 1030, and 720 cm^{-1}.

NMR (CCl_4): τ 3.88—4.20 (2H, s), 6.00 (1H, s), 6.55—7.00 (2H, m), 7.05—7.35 (2H, m), 7.50—8.00 (1H, m), 8.00—8.50 (1H, m), 8.55—8.90 (2H, m), 9.40—9.70 (1H, m).[17]

A solution of 25.1 g of unsaturated alcohol (**9**) and 42.4 g of *p*-toluenesulfonyl chloride in 80 ml of dry pyridine was kept at room temperature for 24 hr. The reaction mixture was poured into chilled hydrochloric acid and extracted with ether. The extract was washed with dilute hydrochloric acid, aqueous sodium bicarbonate, saturated aqueous sodium chloride and dried. After removal of the solvent, crude *p*-toluenesulfonate (**10**) was recrystallized from *n*-hexane to give needles (50.4 g), mp 47—48°C.

Found: C, 64.47; H, 6.45; S, 11.64%. Calcd for $C_{15}H_{18}O_3S$: C, 64.73; H, 6.52; S, 11.50%.

(±)-endo-*5-Cyanomethylbicyclo[2.2.1]hept-2-ene (11).* A mixture of 55.9 g of *p*-toluenesulfonate (**10**) and 29.7 g of sodium cyanide in 330 ml of dry dimethylformamide was heated at 110—120°C for 2 hr and then at 130—140°C for further 8 hr. After cooling, a solid was filtered off and the filtrate was concentrated under reduced pressure. The residue was poured into chilled water and extracted with ether. The extract was washed with dilute hydrochloric acid, saturated aqueous sodium bicarbonate, saturated aqueous sodium chloride and dried over magnesium sulfate. After filtration and removal of the solvent, distillation gave *endo*-5-cyanomethylbicyclo[2.2.1]hept-2-ene (**11**) (20.7 g), bp 106—107°C/19 mmHg, n_D^{18} 1.4864.

IR (neat film): 2250 and 720 cm^{-1}.

Found: C, 80.75; H, 8.38; N, 10.32%. Calcd for $C_9H_{11}N$: C, 81.16; H, 8.33; N, 10.52%.

(±)-endo-*5-Carboxymethylbicyclo[2.2.1]hept-2-ene (12).* A mixture of 19.5 g of *endo*-5-cyanomethylbicyclo[2.2.1]hept-2-ene (**11**), 25.0 g of potassium hydroxide and 200 ml of ethylene glycol was heated at 130—140°C for 1 hr and then at 150—160°C for further 6 hr. After cooling, the reaction mixture was diluted with water and washed with ether. The aqueous solution was then acidified and extracted with ether. The extract was washed with saturated aqueous sodium chloride and dried over magnesium sulfate. After removal of the solvent, distillation gave 20.5 g of *endo*-5-carboxymethylbicyclo[2.2.1]hept-2-ene (**12**), bp 118—119°C/3 mmHg, n_D^{18} 1.4970.

IR (neat film): 1700 and 720 cm^{-1}.

Found: C, 70.74; H, 8.01%. Calcd for $C_9H_{12}O_2$: C, 71.02; H, 7.95%.

*(±)-3-Oxo-5-*endo-*carboxymethylbicyclo[2.2.1]heptane (14).* To a solution of 19.7 g of *endo*-5-carboxymethylbicyclo[2.2.1]-hept-2-ene (**12**) in 860 ml of 0.5N aqueous sodium bicarbonate was added a solution of 40 g of iodine and 158 g of potassium iodide in 470 ml of water and the mixture was kept for 24 hr in a dark place. A dark oil was separated by decantation and dissolved in chloroform and the water layer was extracted with chloroform. A combined chloroform solution was washed with aqueous sodium thiosulfate, saturated aqueous sodium bicarbonate, saturated aqueous sodium chloride and dried over magnesium sulfate. After filtration, the solvent was removed to give a crystalline iodolactone (**13**), which, without purification, was dissolved in 10% aqueous sodium hydroxide (800 ml). The mixture was heated at 100°C for 1 hr and then washed with ether. The alkaline solution was acidified and extracted with ether. The extract was washed with saturated aqueous sodium chloride and dried over magnesium sulfate. Filtration and removal of the solvent afforded a crystalline substance which was recrystallized from *n*-hexane–benzene to give 16.5 g of 3-oxo-5-*endo*-carboxymethylbicyclo-[2.2.1]heptane (**14**), mp 96—97°C.

IR (nujol): 1730 and 1700 cm^{-1}.

Found: C, 64.62; H, 7.23%. Calcd for $C_9H_{12}O_3$: C, 64.27; H, 7.19%.

*(±)-3-Oxo-5-*endo-*methoxycarbonylmethylbicyclo[2.2.1]heptane (15).* To a solution of 8.40 g of 3-oxo-5-*endo*-carboxymethylbicyclo[2.2.1]heptane (**14**) in ether was added a solution of diazomethane in ether at 5—0°C and the mixture was stirred for 2 hr at the same temperature. The solvent and excess diazomethane were then removed under reduced pressure and the residue was distilled to give 8.36 g of the methyl ester (**15**), bp 128—129°C/5 mmHg, n_D^{18} 1.4787.

IR (neat film): 1740 cm^{-1}.

NMR (CCl_4): τ 6.40 (3H, s), 7.3—7.6 (3H, m), 7.7—7.8 (2H, d), 8.0—8.1 (2H, d), 8.2—8.3 (3H, m), 8.85—9.20 (1H, d).

2,4-Dinitrophenylhydrazone: mp 95—96°C.

Found: C, 53.14; H, 5.02; N, 15.37%. Calcd for $C_{16}H_{18}O_6N_4$: C, 53.03; H, 5.01; N, 15.46%.

*(±)-3-Ethylenedioxy-5-*endo-*methoxycarbonylbicyclo[2.2.1]heptane (16).* A mixture of 32.6 g of 3-oxo-5-*endo*-methoxycarbonylmethylbicyclo[2.2.1]heptane (**15**), 560 ml of ethylene glycol, 2.10 g of *p*-toluenesulfonic acid and 2.5 l of benzene was refluxed for 21 hr. During this period the water generated was separated as benzene azeotrope from the reaction mixture. After cooling, the benzene layer was separated from ethylene glycol layer, which was poured into water and extracted with benzene. A combined benzene solution was washed with saturated aqueous sodium bicarbonate, saturated aqueous sodium chloride and dried over magnesium sulfate. After removal of the solvent, distillation gave 30.7 g of 3-ethylenedioxy-5-*endo*-methoxycarbonylmethylbicyclo[2.2.1]heptane (**15**), bp 127—131°C/4 mmHg, n_D^{18} 1.4829.

IR (neat film): 1735, 1175, 1100, and 1020 cm^{-1}.

Found: C, 63.51; H, 7.97%. Calcd for $C_{12}H_{18}O_4$: C, 63.70; H, 8.02%.

*(±)-3-Oxo-5-*endo-*(2-hydroxy)ethylbicyclo[2.2.1]heptane (18).* A solution of 30.5 g of 3-ethylenedioxy-5-*endo*-methoxycarbonylbicyclo[2.2.1]heptane (**16**) in 240 ml of dry ether was added to a suspension of 7.6 g of lithium aluminium hydride on 240 ml of dry ether and the mixture was refluxed for 4.5 hr. Saturated aqueous sodium sulfate was added to the chilled reaction mixture and a solid was filtered off. The filtrate was washed with saturated aqueous sodium chloride and dried over magnesium sulfate. After filtration, the solvent was removed to give ketalalcohol (**17**), which was stirred at room temperature for 5 hr with *p*-toluenesulfonic acid (4.4 g) in 1.8 l of acetone. After neutralization with sodium bicarbonate the acetone was removed and then a residue was diluted with ether. The resulting mixture was washed with saturated aqueous sodium chloride and dried over magnesium sulfate. After removal of the solvent, distillation gave 3-oxo-5-*endo*-(2-hydroxy)ethylbicyclo[2.2.1]-heptane (**18**) (14.1 g), bp 118—120°C/1.5 mmHg, n_D^{18} 1.4968.

IR (neat film): 3400, 1735, and 1050 cm^{-1}.

NMR (CCl_4): τ 6.23 (1H, s), 6.51 (2H, m), 7.50 (1H, s),

17) R. G. Foster and M. C. McIvor, *Chem. Commun.*, **1967**, 280.

7.8—9.1 (10H, m).

2,4-Dinitrophenylhydrazone: mp 124.5—125°C.

Found: C, 53.76; H, 5.35; N, 16.64%. Calcd for $C_{15}H_{18}O_5N_4$: C, 53.88; H, 5.43; N, 16.76%.

(±)-Tricyclo[4.3.0.0^{3,8}]nonan-2-one (**20**). To a solution of 4.34 g of 3-oxo-5-*endo*-(2-hydroxy)ethylbicyclo[2.2.1]heptane (**18**) in 16 ml of dry pyridine was added 6.9 g of methanesulfonyl chloride at 5—0°C. After stirring at the same temperature for 2 hr, the reaction mixture was kept at room temperature for 24 hr and then poured into chilled hydrochloric acid. The mixture was extracted with ether and the extract was washed with dilute hydrochloric acid, saturated aqueous sodium bicarbonate, saturated aqueous sodium chloride and dried over magnesium sulfate. After filtration, the solvent was removed to give methanesulfonate (**19**), which, without purification, was dissolved in 50 ml of dry dimethylformamide. The solution was added to a suspension of 4.00 g of sodium hydride on 100 ml of dry dimethylformamide and the mixture was heated at 60°C for 21.5 hr under a nitrogen atmosphere. The reaction mixture was poured into chilled water and extracted with ether. The extract was washed with dilute hydrochloric acid, saturated aqueous sodium bicarbonate, saturated aqueous sodium chloride and dried over magnesium sulfate. After removal of the solvent, the residue was chromatographed on neutral alumina (activity III). An elution with *n*-pentane gave a semisolid which was sublimed to yield 0.89 g of tricyclo[4.3.0.0^{3,8}]nonan-2-one (**20**), mp 174—175°C (in a sealed tube).

IR (CCl_4 solution): 1750 cm^{-1}.

NMR (CCl_4): τ 7.37 (1H, m), 7.60 (2H, s), 7.85 (1H, m), 8.0—8.6 (8H, m).

Mass spectrum: *m/e* 136, 93, 80, 79, 67, 66, 58, 54, 41, and 39.

Found: C, 79.38; H, 9.00%. Calcd for $C_9H_{12}O$: C, 79.37; H, 8.88%.

2,4-Dinitrophenylhydrazone: mp 137—139°C.

Found: C, 56.81; H, 5.00; N, 17.61%. Calcd for $C_{15}H_{16}O_4N_4$: C, 56.96; H, 5.10; N, 17.71%.

(±)-Tricyclo[4.3.0.0^{3,8}]nonane (**3**). A solution of 220 mg of tricyclo[4.3.0.0^{3,8}]nonan-2-one (**20**), 0.13 g of potassium hydroxide and 0.22 ml of 80% hydrazine hydrate in 2 ml of triethylene glycol was heated at reflux for 1.5 hr. Water was then allowed to boil out of the mixture as the temperature approached 200°C. The resulting mixture was heated at reflux for further 4 hr during which time a white solid collected in the condenser. After cooling, the solid was rinsed out with *n*-hexane and the triethylene glycol solution was extracted with *n*-pentane. A combined solution was washed with saturated aqueous sodium chloride and dried over magnesium sulfate. After filtration, removal of the solvent gave a solid which was chromatographed on neutral alumina (activity III). Sublimation of a solid eluted with *n*-pentane gave 85 mg of tricyclo[4.3.0.0^{3,8}]nonane (**3**), mp 159—160°C (in a sealed tube) (lit, mp 165—166°C,[3] 140°C[4]).

NMR (CCl_4): τ 7.75 (2H, s), 8.16 (2H, s), 8.30—8.90 (10H, m).

Mass spectrum: *m/e* 122, 93, 81, 80, 79, 67, 41, and 39.

Found: C, 87.68; H, 11.48%. Calcd for C_9H_{14}: C, 88.45; H, 11.55%.

(−)-endo-5-Carboxybicyclo[2.2.1]hept-2-ene (**7a**). To a boiling mixture of 50.0 g of cinchonidine in 3 l of acetone was added 24.0 g of pure *endo*-5-carboxybicyclo[2.2.1]hept-2-ene (**7a**). Cooling of the clear solution produced a salt $[\alpha]_D^{20}$ −84.8° (*c* 1.1, 99% ethanol), (47.0 g). Recrystallization six times from acetone gave the salt $[\alpha]_D^{19}$ −122° (*c* 1.2, 99% ethanol), (11.7 g). The salt was treated with 10% aqueous sodium hydroxide at room temperature. After acidification, the solution was extracted with ether and the extract was washed with saturated aqueous sodium chloride and dried over magnesium sulfate. After filtration and evaporation of the solvent, the residue was distilled to give 2.64 g of (−)-*endo*-5-carboxybicyclo[2.2.1]hept-2-ene (**7a**), bp 139—140°C/20 mmHg, $[\alpha]_D^{20}$ −119° (*c* 1.4, 95% ethanol), (lit, $[\alpha]_D^{26}$ −70.4°, *c* 1.4, 95% ethanol[10]).

Found: C, 69.45; H, 7.37%. Calcd for $C_8H_{10}O_2$: C, 69.54; H, 7.30%.

(−)-endo-5-Hydroxymethylbicyclo[2.2.1]hept-2-ene (**9**). (−)-*endo*-5-Carboxybicyclo[2.2.1]hept-2-ene (**7a**) (23.7 g) was reduced with lithium aluminium hydride in ether by the same procedure as described for the racemate to give 20.1 g of (−)-*endo*-5-hydroxymethylbicyclo[2.2.1]hept-2-ene (**9**), bp 92—96°C/14 mmHg, $[\alpha]_D^{23}$ −70.0° (*c* 1.0, 99% ethanol), n_D^{18} 1.4999.

Found: C, 77.27; H, 9.74%. Calcd for $C_8H_{12}O$: C, 77.37; H, 9.74%.

(−)-endo-5-Cyanomethylbicyclo[2.2.1]hept-2-ene (**11**). (−)-*endo*-5-Hydroxymethylbicyclo[2.2.1]hept-2-ene (**9**) (20.0 g) was treated with 34.4 g of *p*-toluenesulfonylchloride and 65 ml of dry pyridine to give *p*-toluenesulfonate (**10**), which, without purification, was heated with 27.0 g of sodium cyanide in 300 ml of dry dimethylformamide at 130—140°C for 12 hr to give 16.5 g of (−)-*endo*-5-cyanomethylbicyclo-[2.2.1]hept-2-ene (**11**), bp 100—102°C/15 mmHg, $[\alpha]_D^{18}$ −92.1° (*c* 0.75, 99% ethanol), n_D^{18} 1.4869.

Found: C, 80.69; H, 8.36; N, 10.30%. Calcd for $C_9H_{11}N$: C, 81.16; H, 8.33; N, 10.52%.

(−)-endo-5-Carboxymethylbicyclo[2.2.1]hept-2-ene (**12**). Hydrolysis of 16.5 g of (−)-*endo*-5-cyanomethylbicyclo[2.2.1]-hept-2-ene (**11**) with potassium hydroxide in ethylene glycol gave 18.7 g of (−)-*endo*-5-carboxymethylbicyclo[2.2.1]hept-2-ene (**12**), bp 102—105°C/1 mmHg, $[\alpha]_D^{24}$ −61.5° (*c* 0.68, 99% ethanol), n_D^{18} 1.4911.

Found: C, 70.69; H, 8.00%. Calcd for $C_9H_{12}O_2$: C, 71.02; H, 7.95%.

*(+)-3-Oxo-5-*endo*-methoxycarbonylmethylbicyclo[2.2.1]heptane* (**15**). Iodolactone (**13**) which was prepared from 18.5 g of (−)-*endo*-5-carboxymethylbicyclo[2.2.1]hept-2-ene (**12**) by the same procedure as described for racemate was, without purification, treated with 10% aqueous sodium hydroxide at 100°C for 1 hr to give 32.3 g of 3-oxo-5-*endo*-carboxymethylbicyclo[2.2.1]heptane (**15**). Without purification, the ketocarboxylic acid (**14**) was treated with diazomethane in ether to give 17.9 g of (+)-3-oxo-5-*endo*-methoxycarbonylbicyclo[2.2.1]heptane (**15**), bp 106—108°C/2 mmHg, $[\alpha]_D^{14}$ +16.5° (*c* 1.2, 99% ethanol), n_D^{18} 1.4790.

Found: C, 65.45; H, 7.67%. Calcd for $C_{10}H_{14}O_3$: C, 65.91; H, 7.74%.

*(+)-3-Ethylenedioxy-5-*endo*-methoxycarbonylmethylbicyclo-[2.2.1]heptane* (**16**). Treatment of 17.5 g of (+)-3-oxo-5-*endo*-methoxycarbonylmethylbicyclo[2.2.1]heptane (**15**) with 300 ml of ethylene glycol and 1.38 g of *p*-toluenesulfonic acid in 1.34 l of benzene gave 18.7 g of (+)-3-ethylenedioxy-5-*endo*-methoxycarbonylmethylbicyclo[2.2.1]heptane (**16**), bp 112—115°C/1 mmHg, $[\alpha]_D^{23}$ +22.1° (*c* 1.1, 99% ethanol), n_D^{18} 1.4833.

Found: C, 63.28; H, 7.88%. Calcd for $C_{12}H_{18}O_4$: C, 63.70; H, 8.02%.

*(+)-3-Oxo-5-*endo*-(2-hydroxy)ethylbicyclo[2.2.1]heptane* (**18**). Reduction of 18.6 g of (+)-3-ethylenedioxy-5-*endo*-methoxycarbonylmethylbicyclo[2.2.1]heptane (**16**) with lithium aluminium hydride in ether gave 3-ethylenedioxy-5-*endo*-(2-hydroxy)ethylbicyclo[2.2.1]heptane (**17**), which, without purification, was treated with *p*-toluenesulfonic acid in acetone to

give 8.79 g of (+)-3-oxo-5-*endo*-(2-hydroxy)ethylbicyclo-[2.2.1]heptane (**18**), bp 122—123°C/1.5 mmHg, $[\alpha]_D^{22}$ +17.2° (*c* 1.1, 99% ethanol), n_D^{18} 1.5007. The substance was very hygroscopic.

Found: C, 69.22; H, 8.20%. Calcd for $C_9H_{14}O_2$: C, 70.10; H, 9.15%.

*(−)-Tricyclo[4.3.0.0^{3,8}]nonan-2-one (**20**).* Methanesulfonate (**19**), prepared from 4.26 g of (+)-3-oxo-5-*endo*-(2-hydroxyethyl)bicyclo[2.2.1]heptane (**18**), was heated at 60°C for 25 hr with 4.00 g of sodium hydride in 150 ml of dry dimethylformamide. The product was chromatographed on neutral alumina (activity III) and a semisolid eluted with *n*-pentane was sublimed to yield 789 mg of (−)-tricyclo-[4.3.0.0^{3,8}]nonan-2-one (**20**), mp 169—171°C (in a sealed tube), $[\alpha]_D^{21}$ −240° (*c* 0.58, 99% ethanol).

UV: λ_{max}^{MeOH} 289 mμ (ε 43).

CD (*c* 3.03×10^{-3}, methanol): $[\theta]_{320}$ 0, $[\theta]_{289}$ -150×10^2, $[\theta]_{245}$ 0.

Found: C, 78.72; H, 8.92%. Calcd for $C_9H_{12}O$: C, 79.37; H, 8.88%.

*(−)-Tricyclo[4.3.0.0^{3,8}]nonane (**3**).* The Wolff-Kishner reduction of 450 mg of (−)-tricyclo[4.3.0.0^{3,8}]nonan-2-one (**20**) was carried out by the same procedure as described for racemate. The product was purified by chromatography and sublimation to give 208 mg of (−)-tricyclo[4.3.0.0^{3,8}]-nonane (**3**), mp 157.5—159°C (in a sealed tube), $[\alpha]_D^{18}$ −235°, $[\alpha]_{436}^{20}$ −483° (*c* 0.52, 99% ethanol).

Found: C, 87.76; H, 11.49%. Calcd for C_9H_{14}: C, 88.45; H, 11.55%.

The authors are grateful to Dr. K. Kuriyama for measurement of the CD curve.

BULLETIN OF THE CHEMICAL SOCIETY OF JAPAN, VOL. 46, 892—897 (1973)

Cyclopropanes from Olefins by the Oxygen-accelerated Zinc-carbenoid Reaction

Sotaro MIYANO and Harukichi HASHIMOTO

Department of Applied Chemistry, Faculty of Engineering, Tohoku University, Aramaki, Sendai

(Received June 28, 1972)

Oxygen greatly accelerates the cyclopropanation of olefins by the diethylzinc-chloroiodomethane or -diiodomethane system. Olefins, including cyclohexene, cyclooctene, 1-heptene, 1-octene, 2-heptene, indene, *n*-butyl vinyl ether, styrene, and methyl oleate, gave the corresponding cyclopropanes in yields of *ca.* 70—100%. The methylene addition to *cis*- and *trans*-2-butene proceeded in a stereospecific manner in the presence of oxygen. Methyl methacrylate gave no appreciable amount of cyclopropanated product, but polymerization proceeded. Styrene inhibited the formation of the zinc-carbenoid reagent from diethylzinc and dihalomethanes under a nitrogen atmosphere. AIBN and UV light initiated the cyclopropanation of styrene with diethylzinc and chloroiodomethane. A free-radical-chain mechanism is proposed for the formation of the zinc-carbenoid reagent from diethylzinc and dihalomethanes.

Furukawa *et al.* explored the cyclopropanation of olefins by the zinc-carbenoid reagents obtained from diethylzinc and *gem*-diiodoalkanes.[1] α-Iodoalkylethylzinc and bis(α-iodoalkyl)zinc are said to be active intermediates in the cyclopropanation reactions.[1c] Little attention has been paid to the mechanism of the formation of these carbenoid species from diethylzinc and *gem*-diiodoalkanes.

Since diethylzinc is highly sensitive to oxygen,[2] Furukawa's cyclopropanation reaction was carried out under a nitrogen atmosphere.[1] On the other hand, we ourselves have previously reported that oxygen greatly accelerates the cyclopropanation of olefins with diethylzinc and diiodomethane[3] or chloroiodomethane.[4] In the present paper we will report the details of the synthesis of cyclopropanes from olefins and will propose a plausible mechanism for the accelerating effect of oxygen on the zinc-carbenoid reaction with diethylzinc and dihalomethanes.

Results and Discussion

Accelerating Effect of Oxygen on the Formation of Norcarane from Cyclohexene, Diethylzinc, and Chloroiodomethane. Figure 1 shows that chloroiodomethane reacts with diethylzinc to form norcarane from cyclohexene under a nitrogen atmosphere. After 6 hr, the yield of norcarane was 61% based on the cyclohexene. By passing dry air into the free space above the reaction mixture after the addition of chloroiodomethane, the reaction was completed within only 30 min to give norcarane in a 99% yield (Fig. 2). Thus, oxygen greatly accelerates the formation of norcarane. Product analysis showed that the molar amount of ethyl iodide and propyl iodide formed was almost equal to that of the chloroiodomethane consumed, irrespective of the reaction atmosphere. This suggests that the zinc-carbenoid reagent is formed from chloroiodomethane by the selective cleavage of a carbon–iodine bond. Both

1) (a) J. Furukawa, N. Kawabata, and J. Nishimura, *Tetrahedron*, **24**, 53 (1968). (b) J. Furukawa, N. Kawabata, Y. Ueda, and J, Nishimura, *Kogyo Kagaku Zasshi*, **71**, 164 (1968). (c) J. Furukawa, N. Kawabata, T. Taniguchi, and J. Nishimura, *ibid.*, **72**, 1673 (1969).

2) G. E. Coates and K. Wada, "Organometallic Compounds," Vol. 1, Methuen & Co. Ltd., London, 3rd ed., (1967), p. 129.

3) S. Miyano and H. Hashimoto, *Chem. Commun.*, **1971**, 1418.

4) S. Miyano, J. Yamashita, and H. Hashimoto, This Bulletin, **45**, 1946 (1972).

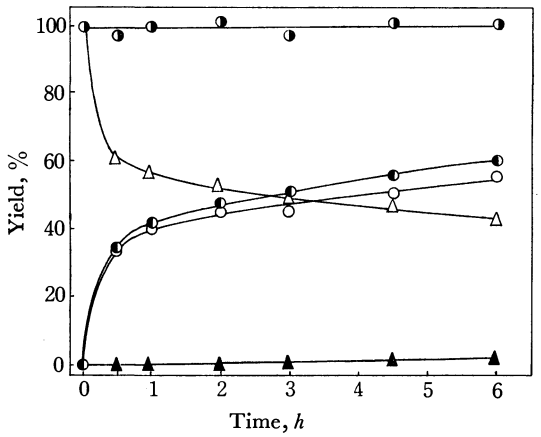

Fig. 1. Reaction of cyclohexene (25 mmol) with diethylzinc (25 mmol) and chloroiodomethane (38 mmol) in benzene (20 ml) at 40°C under a nitrogen atmosphere.
◐: norcarane, ○: ethyl iodide, ▲: propyl iodide, △: unchanged chloroiodomethane, ◑: total iodide.

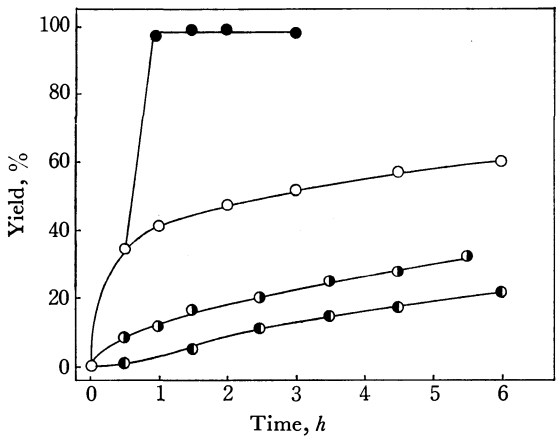

Fig. 2. Accelerating effect of oxygen and inhibiting effect of styrene and diphenylamine on the formation of norcarane from cyclohexene (25 mmol) with diethylzinc (25 mmol) and chloroiodomethane (38 mmol).
Benzene, 20 ml, at 40°C. ○; under a nitrogen atmosphere, ●; air was introduced at a rate of 10 ml/min after 0.5 h, ◐: styrene, 1.3 mmol, ◑: diphenylamine, 1.8 mmol.

zinc-ethyl bonds of diethylzinc seem effective in the zinc-carbenoid formation in the presence of oxygen from the fact that, upon passing air through, more than 1 mol of chloroiodomethane reacted with 1 mol of diethylzinc. However, under a nitrogen atmosphere the second zinc–ethyl bond seems not so reactive as the first one to chloroiodomethane[5] (Fig. 1 and Table 1). Similar results were obtained for the reaction of diethylzinc with diiodomethane.[1]

Dibromomethane gave only 4% of norcarane after air had been passed through for 3 hr, and 83% of the starting halide was recovered (Table 2). Bromochloromethane did not give norcarane under similar reaction conditions, and it was recovered almost quantitatively.

Table 1. Effect of the amount of diethylzinc for the cyclopropanation of cyclohexene[a]

CH_2ClI mmol	Et_2Zn mmol	Cyclohexene mmol	Reacted CH_2ClI mmol	Norcarane Yield (%)
10	8	10	8.2	62
10	10	10	9.6	65
10	15	10	9.2	60
38[b]	25	25	22	61

a) Reactions were carried out under nitrogen atmosphere for 6 h at 35°C in 30 ml of benzene.
b) In 20 ml of benzene at 40°C.

Cyclopropanation of Olefins. The accelerating effect of oxygen in the zinc-carbenoid reaction with diethylzinc and chloroiodomethane was utilized for the cyclopropanation of several olefins (Table 2). While the scope of the reaction has not been fully investigated with respect to the type of olefin and the reaction variables, it can be seen that the procedure described in this paper is useful for the cyclopropane synthesis. In general, chloroiodomethane gave better yields of cyclopropanes than did diiodomethane. This is partly due to the fact that diiodomethane gave more propyl iodide as a side-product than did chloroiodomethane.

Simple olefins gave the corresponding cyclopropanes in very good yields within rather short reaction periods. A satisfactory yield of a cyclopropane was obtained with 1 mol of diethylzinc and 1.2—1.5 mol of a dihalomethane for 1 mol of an olefin. Styrene gave a somewhat poor yield of phenylcyclopropane because of the polymerization of styrene and probably also because of the electron-withdrawing effect of the phenyl substituent on the ethylene bond. *n*-Butyl vinyl ether gave a high yield of *n*-butyl cyclopropyl ether under a nitrogen atmosphere, and the accelerating effect of oxygen was also observed. Methyl methacrylate gave no appreciable amount of a cyclopropanated product, but polymerized products were obtained. The stereospecific nature of the methylene transfer of the oxygen-accelerated zinc-carbenoid reaction was confirmed as follows. From *cis*- and *trans*-2-butene, *cis*- and *trans*-1,2-dimethylcyclopropane were obtained respectively. The NMR spectra of the products are consistent with the assumption that the methyl group linked to the cyclopropane ring shields the *cis* ring proton more than the *trans* proton.[1a,7] The glc analysis of each reaction mixture showed the presence of only unchanged olefin and a single cyclopropane, showing that no isomerization of the olefins and cyclopropanes occurred during the reaction. Methyl *cis*-9,10-methyleneoctadecanoate was obtained in an almost quantitative yield from methyl oleate (Eq. (1)):

5) This implies that the Schlenk equilibrium
$$Et_2Zn + ZnCl_2 \rightleftarrows 2EtZnCl$$
lies substantially in the right hand side. This is the case for ethylzinc iodide, but unambiguous result is not yet obtained for ethylzinc chloride.[6]

6) (a) R. E. Dessy and G. R. Coe, *J. Org. Chem.*, **28**, 3592 (1963). (b) M. H. Abraham and R. H. Rolfe, *J. Organometal. Chem.*, **7**, 35 (1967). (c) J. Boersma and J. G. Noltes, *ibid.*, **8**, 551 (1967). (d) D. F. Evans and I. Wharf, *J. Chem. Soc., A*, **1968**, 783. (e) D. F. Evans and G, V. Fazakerley, *ibid.*, **1971**, 182.

7) D. Seyferth, J. M. Burlitch, R. J. Minasz, J. Yick-pui Mui, H. D. Simmons, Jr., A. K. H. Treiber, and S. R. Dowd, *J. Amer. Chem. Soc.*, **87**, 4259 (1965).

Table 2. Cyclopropanation of olefins[a]

Olefin		Et_2Zn	CH_2X_2		Solvent ml	Reaction Time (hr)	Cyclopropane Yield (%)
	10^2 mol	10^2 mol		10^2 mol			
Cyclohexene	5.1	6.5	CH_2I_2	7.5	30	1[b]	91
	5.2	6.0		6.1	30[c]	1[d]	35
	10	6.0		12	50	20[e]	93
	5.2	4.0		6.0	30	20[e]	92
	9.9	10	CH_2ClI	12	50	20[e]	91
	2.6	2.5		3.8	20	1.5	99
	2.5	2.5	CH_2Br_2	4.0	20	3	4.2
	2.6	2.5	CH_2BrCl	3.8	20	3	0
Styrene	5.1	9.0	CH_2I_2	10	30	6	79
	5.0	5.0		6.1	30	5.5	62, 59, 58[f]
	5.0	5.0		6.1	30	2[g]	57
	5.0	5.0	CH_2ClI	6.0	30	2[g]	63
	2.5	2.5		3.8	20	1.5[g]	65, 70[f]
1-Heptene	10	10	CH_2I_2	15	50	2	66
	2.5	2.5		3.7	20	1	66
	2.5	5.0		5.0	20	1	94
	2.6	2.5	CH_2ClI	3.8	20	1	79
1-Octene	2.7	2.5	CH_2I_2	3.9	20	1	66
	2.5	2.5	CH_2ClI	3.8	20	1	88
2-Heptene[h]	3.6	3.5	CH_2I_2	5.2	20	1	90[h]
	2.5	2.5	CH_2ClI	3.8	20	1	94[h]
Cyclooctene	10	13	CH_2I_2	15	50	1	98
	5.1	6.5	CH_2ClI	7.5	30	1	99
Indene	10	10		15	50	3	77
n-Butyl vinyl ether	15	15		15	100[c]	1[i]	89
	2.5	2.5		3.8	20[c]	1	94

a) Solvent; benzene. The yield of cyclopropane is based on the olefin and determined by glc. Dry air was introduced into the space above the reaction mixture at a rate of 10 ml/min for the indicated reaction period at 50°C.
b) 40°C. c) Solvent; Ether. d) 35°C.
e) After the addition of the dihalomethane was complete, nitrogen stream was stopped, and the reaction mixture was allowed to stand at room temperature. f) Duplicate run. g) Oxygen was introduced at a rate of 10 ml/min.
h) Mixture of *cis*-, and *trans*-isomer. i) Under nitrogen atmosphere.

Table 3. AIBN or photochemically induced cyclopropanation of styrene[a]

Styrene 10^2 mol	Et_2Zn 10^2 mol	CH_2ClI 10^2 mol	Catalyst	Temp (°C)	Time (hr)	Ph-  Yield (%)	Reacted CH_2ClI (%)
2.5[b]	2.5	3.8	—	50	3	0	0
5.0	5.0	6.0	—	70	4	0	7.5
					7	3.7	10.5
		CH_2I_2					CH_2I_2
5.0	5.0	61	—	50	6	0	3.0
10[c]	10	10	—	80	24	26	
2.5[b]	2.5	38	O_2, 10 ml/min	50	1.5	70	100
5.0	0	6.1	AIBN, 2.4 mmol	70	7	0	1.9
5.0	5.0	6.1	0.52	50	7	0	15
5.0	5.0	6.0	0.51	70	4.5	9.1	49
5.1	5.0	6.1	2.5	70	4.5	22	74
5.0	5.0	6.1	4.5	70	4.5	24	87
5.0	5.0	9.4	2.5	70	4.5	46	64
5.0[d]	0	6.0	*hν*[e]	23	7	0	5.4
5.0[d]	5.0	6.0	*hν*[e]	23	1.5	73	100

a) Solvent; benzene 50 ml. b) Solvent; benzene 20 ml. c) From Ref. 1e.
d) Solvent; 150 ml. e) A hight pressure mercury lamp (100 W) was used.

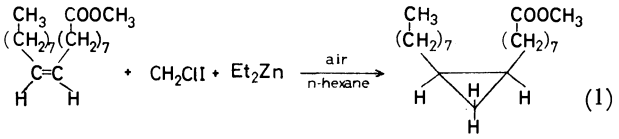

(1)

Inhibition by Styrene of the Zinc-carbenoid Formation from Diethylzinc and Chloroiodomethane. Styrene was allowed to react with diethylzinc and chloroiodomethane in benzene under a nitrogen atmosphere at 50°C. No phenylcyclopropane was obtained in 3 hr, but the starting styrene and chloroiodomethane were recovered unchanged (Table 3). When oxygen was introduced into the reaction mixture, cyclopropanation was completed within 1.5 hr, giving phenylcyclopropane in a 66% yield. When oxygen was introduced just after the completion of the addition of chloroiodomethane, the reaction was also completed within 1.5 hr, giving phenylcyclopropane in a 70% yield. These facts indicate that the presence of styrene inhibits the formation of the zinc-carbenoid reagent from diethylzinc and chloroiodomethane. When diiodomethane is used as the methylene source, styrene is cyclopropanated under a nitrogen atmosphere, but a higher temperature and a longer reaction period are necessary.[1] The presence of only 5% of styrene (based on cyclohexene) retarded the formation of norcarane from cyclohexene, chloroiodomethane, and diethylzinc (Fig. 2).

The AIBN- and Photochemically-initiated Cyclopropanation of Styrene. The accelerating effect of oxygen and the inhibiting effect of styrene suggest that the zinc-carbenoid formation from diethylzinc and dihalomethanes proceeds by means of a free radical mechanism. This assumption is supported by the facts that AIBN and UV light also initiate the cyclopropanation of styrene (Table 3). Without diethylzinc, chloroiodomethane did not cyclopropanate styrene in the presence of AIBN or UV light, though peroxides or UV light initiate the cyclopropanation of olefins with diiodomethane.[8,9]

The irradiation of a mixture of styrene, chloroiodomethane, and diethylzinc in *n*-hexane with a high-pressure mercury lamp at −70°C gave the zinc-carbenoid reagent under a nitrogen atmosphere, while the styrene remained unchanged. When the light was turned off and the temperature of the reaction mixture was allowed to rise to room temperature, an exothermic reaction took place and phenylcyclopropane was obtained in a 50% yield within 1 hr. On the addition of an ethereal solution of iodine to an irradiated mixture at −70°C, chloroiodomethane (32.3%) and diiodomethane (63.3%) were obtained. This shows that the zinc-carbenoid species[10] in the reaction mixture contained a Cl–CH_2–Zn– unit. Wittig *et al.* reported that diiodomethane was formed preferentially when $(ClCH_2)_2Zn$ was allowed to react with iodine because of the rapid exchange of iodide ions for chlorine atoms in chloromethyl groups.[11,12] The possibility that the zinc-carbenoid species contain the –Zn–CH_2–Zn– unit is excluded by the fact that the "$CH_2(ZnI)_2$" species does not cyclopropanate olefins.[13–15]

Oxygen also initiated the formation of the zinc-carbenoid reagent from diethylzinc and chloroiodomethane in the presence of styrene at −70°C, but the cyclopropanation of styrene did not occur at this temperature. After the reaction vessel had been flushed with nitrogen, the reaction mixture was allowed to stand at room temperature to give phenylcyclopropane in a 66% yield within 1 hr.

Mechanistic Consideration of the Accelerating Effect of Oxygen. Recently Brown *et al.* have shown that the addition of triethylborane to α,β-unsaturated carbonyl compounds proceeds by a radical-chain mechanism and that the reaction is initiated by oxygen, UV light, or peroxides.[16] Davies and Roberts proposed that the autoxidation of diethylzinc involves a radical-chain mechanism[17] rather than an ionic one.[18] It is known that a combination of diethylzinc and oxygen or polyhalometanes initiates the radical polymerization of vinyl monomers even in the presence of conventional radical inhibitors.[19,20] The reactivity order of dihalomethanes towards diethylzinc is: $CH_2I_2 > CH_2ClI > CH_2Br_2 > CH_2BrCl$. This reactivity sequence is in accordance with that of radical halogen-abstraction reactions from dihalomethanes.[21]

These facts suggest that the zinc-carbenoid reagent may be formed from diethylzinc and dihalomethanes *via* radical processes (Eqs. (2)—(4)) (X; Cl or I, R; Et or X):

$$EtZnR \xrightarrow{\text{Initiator}} Et\cdot \quad (2)$$

$$Et\cdot + CH_2IX \longrightarrow EtI + \cdot CH_2X \quad (3)$$

$$\cdot CH_2X + EtZnR \longrightarrow XCH_2ZnR + Et\cdot \quad (4)$$

Styrene or methyl methacrylate may easily react with the ethyl or halomethyl radical and stop the radical

8) L. Kaplan, *ibid.*, **89**, 4566 (1967).

9) D. C. Blomstrom, K. Hering, and H. E. Simmons, *J. Org. Chem.*, **30**, 959 (1965).

10) (a) S. Miyano, *Yuki Gosei Kagaku Kyokai Shi*, **27**, 11 (1969). (b) J. Furukawa, N. Kawabata, and J. Nishimura, *Kagaku no Ryoiki*, Zokan, No. 89, 235 (1970).

11) G. Wittig and K. Schwarzenbach, *Ann. Chem.*, **650**, 1 (1961).

12) G. Wittig and F. Wingler, *ibid.*, **656**, 18 (1962).

13) (a) P. Turnbull, K. Syhora, and J. H. Fried, *J. Amer. Chem. Soc.*, **88**, 4764 (1966). (b) I. T. Harrison, R. J. Rawson, P. Turnbull, and J. H. Fried, *J. Org. Chem.*, **36**, 3515 (1971).

14) S. Miyano, T. Ohtake, H. Tokumasu, and H. Hashimoto, *Nippon Kagaku kaishi*, **1973**, 381.

15) *Cf.* C. Fauveau, Y. Gault, and F. G. Gault, *Tetrahedron Lett.*, **1967**, 3149.

16) (a) G. W. Kabalka, H. C. Brown, A. Suzuki, S. Honma, A. Arase, and M. Itoh, *J. Amer. Chem. Soc.*, **92**, 710 (1970). (b) H. C. Brown and G. W. Kabalka, *ibid.*, **92**, 712 (1970). (c) H. C. Brown and G. W. Kabalka, *ibid.*, **92**, 714 (1970).

17) A. G. Davies and B. P. Roberts, *J. Chem. Soc., B*, **1968**, 1074.

18) (a) G. Sosnovsky and J. H. Brown, *Chem. Rev.*, **66**, 529 (1966). (b) H. Hock, H. Kropf. and F, Ernst, *Angew. Chem.*, **71**, 541 (1959).

19) L. Leich and A. Schindler, "Polymer Review," Vol. 12, Polymerization by Organometallic Compounds, Interscience Publishers, New York, (1966), p. 452.

20) J. Furukawa, N. Kawabata, and J. Nishimura, *Kobunshi Kagaku*, **25**, 36 (1968).

21) (a) E. M. Kosower and I. Schwager, *J. Amer. Chem. Soc.*, **86**, 5528 (1964). (b) L. W. Menapace and H. G. Kuivila, *ibid.*, **86**, 3047 (1964). (c) R. J. Fox, F. W. Fox, and M. Szwarc, *Trans. Faraday Soc.*, **57**, 1915 (1961).

chain. Among the radical inhibitors examined, diphenylamine retarded the formation of norcarane (Fig. 2), but galvinoxyl and hydroquinone were ineffective. Davies and Roberts reported that galvinoxyl did not inhibit the initial step of the autoxidation of diethylzinc.[17] Diphenylamine is almost inactive towards diethylzinc in the absence of a ligand such as bipyridine,[22] and it might retain its activity as a radical inhibitor in the zinc-carbenoid reaction. As the behavior of radical inhibitors has not yet been fully studied in the presence of organometallics, the results with galvinoxyl or hydroquinone do not exclude the proposed above reaction paths.

Though the exact nature of the zinc-carbenoid species formed in the oxygen-accelerated reaction of diethylzinc and CH_2IX (X; Cl or I) is not yet clear, XCH_2ZnEt and $(XCH_2)_2Zn$ seem to be the active methylene transferring reagents to judge from the results of Furukawa *et al.*,[1] Wittig *et al.*,[11,23] and Blanchard and Simmons.[24] Once the zinc-carbenoid species are formed, the methylene-transferring step to olefins seems to be a conventional one-step, three-centered carbenoid reaction in view of the stereospecific methylene addition to olefins, the absence of a C–H insertion product, and the fact that the zinc-carbenoid species formed can cyclopropanate styrene without any free radical initiator.

Experimental

Analytical Instruments. The glc analysis was carried out on a Shimadzu GC 3AF apparatus equipped with hydrogen-flame detectors and two 3 m×3 mm stainless steel columns packed with Diasolid M coated with Silicone DC 550 and Silicone DC 410 respectively. The infrared spectra were obtained with a JASCO Model IR-E spectrophotometer. The NMR data were obtained with a Varian Associates HA-60 instrument. All the chemical shifts are relative to the internal TMS or chloroform reference (*ca.* a 5 wt% solution in CCl_4).

Materials. The chloroiodimethane[25] (bp 108—109°C) and diiodomethane[26] (bp 65—67°C/13 mmHg) were synthesized as has been described before and were stored over tin pellets in the dark. Commercial diethylzinc was distilled under reduced pressure (bp 64°C/111 mmHg—66°C/125 mmHg). The galvinoxyl was obtained according to the method described by Bartlett and Funahashi,[27] and was recrystallized twice from ethanol; mp 152—153°C (lit,[27] 153.2—153.6°C). The AIBN was recrystallized from methanol, dried under reduced pressure, and stored in the dark in a refrigerator (decomp. 101°C). The hydroquinone and diphenylamine were of commercial origin and were used without further purification. The other materials were reagent-grade chemicals and were purified as usual before use. Distillation or recrystallization was carried out under a nitrogen atmosphere. The materials were stored under nitrogen.

Experimental Procedure. The following example is representative. The reaction was carried out in a 100 ml round-bottomed flask equipped with a magnetic stirrer, a reflux condenser, a pressure-equilibrating dropping funnel topped with a gas inlet cock, a thermometer, and an inlet with a rubber septum cap. The flask was flushed with prepurified nitrogen. In the flask, 20 ml of benzene, 25 mmol of cyclohexene, 3.3 g of ethylbenzene, and 2.5 ml of diethylzinc (25 mmol) were placed; the mixture was stirred and then warmed to 40°C. Chloroiodomethane (38 mmol) was added, drop by drop, over a 30 min period at 40°C under a nitrogen atmosphere. Samples (*ca.* 1 ml) were withdrawn at various times through the septum cap by means of a hypodermic syringe, and quenched under a nitrogen atmosphere with 3 ml of a dilute hydrogen chloride solution saturated with nitrogen. After three extractions of the aqueous layer with benzene, the combined organic phase was analysed by glc. The amounts of the products were estimated from the peak areas, using ethylbenzene as the internal standard.

Acceleration of the Formation of Norcarane with Oxygen. After the addition of chloroiodomethane had been completed, dry air was introduced at a rate of 10 ml/min into the space above the reaction mixture through the gas inlet cock and the side arm of the dropping funnel. The subsequent exothermic reaction was observed to be accompanied by fuming and by the precipitation of white solids, but it subsided within about 10 min. The products were then analyzed as above. Norcarane (25.8 mmol), ethyl iodide (33.3 mmol), and propyl iodide (3.2 mmol) were formed from cyclohexene (26 mmol), diethylzinc (25 mmol), and chloroiodimethane (37.8 mmol) after air had been passed through for 1 hr.

In another experiment, after the addition of chloroiodomethane the nitrogen inlet was replaced by a calcium chloride tube. The reaction mixture was then allowed to stand overnight (20 hr) at room temperature (see Table 2).

Zinc-carbenoid Formation at a Low Temperature. By means of a microfeeder, a 140 ml portion of oxygen was bubbled for 5 hr into a mixture of diethylzinc (40 mmol), chloroiodomethane (38 mmol), and styrene (25 mmol) in *n*-hexane (20 ml) at −70°C. Chloroiodomethane was consumed by the formation of ethyl iodide (37 mmol), but the cyclopropanation of styrene did not occur at this temperature. When the temperature of the mixture was then allowed to rise to room temperature, a 16.5 mmol portion of phenylcyclopropane was obtained within 1 hr.

Synthesis of Cyclopropanes. *Norcarane*: For the identification of norcarane, a controlled reaction was carried out according to the above procedure except that reaction scale was 4 times larger and ethylbenzene was not added. After air had been passed through at a rate of 10 ml/min for 1 hr, the reaction mixture was treated as has been described by Furukawa *et al.*[18] Repeated distillation through a Widmer column gave 0.7 g of an analytical sample boiling at 116—117°C (lit,[28] 116.5°C). The spectral data were identical with those of norcarane. IR (liq. film): 3090, 3010, 1020 cm^{-1} for the characteristic absorption of the cyclopropane ring.[29] NMR: δ 2.2—1.5 (4H, broad), 1.5—1.0 (4H, m), 1.0—0.7 (3H, m), 0.9——0.2 (1H, m). Found: C, 87.35; H, 12.90%. Calcd for C_7H_{12}: C, 87.42; H, 12.58%.

A similar procedure gave the following cyclopropanes (see Table 2 for the reaction conditions).

22) S. Inoue and T. Yamada, *J. Organometal. Chem.*, **25**, 1 (1970).
23) G. Wittig and F. Wingler, *Chem. Ber.*, **97**, 2146 (1964).
24) E. P. Blanchard and H. E. Simmons, *J. Amer. Chem. Soc.*, **86**, 1337 (1964).
25) S. Miyano and H. Hashimoto, This Bulletin, **44**, 2864 (1971).
26) S. Miyano, M. Hida, and H. Hashimoto, *Kogyo Kagaku Zasshi*, **69**, 2134 (1966).
27) P. D. Bartlett and T. Funahashi, *J. Amer. Chem. Soc.*, **84**, 2596 (1962).
28) H. E. Simmons and R. D. Smith, *ibid.*, **81**, 4256 (1959).
29) H. E. Simmons, E. P. Blanchard, and H. D. Hartzler, *J. Org. Chem.*, **31**, 295 (1966).

Phenylcyclopropane: Bp 83—83.5°C/38 mmHg (lit,[30] bp 79—80°C/37 mmHg). IR (liq. film): 1025, 1050 cm^{-1}. NMR: δ 7.1 (5H, m), 2.1—1.2 (1H, m), 1.1—0.5 (4H, m). Found: C, 91.16; H, 8.49%. Calcd for C_9H_9: C, 91.47; H, 8.53%. After the distillation of the reaction mixture, a resinous substance was obtained; it was dissolved in a small amount of benzene and precipitated with methanol. The white precipitate gave IR absorption spectra (KBr) apparently identical with those of polystyrene film over the wave range from 650 to 3200 cm^{-1}.

n-*Amylcyclopropane*: Bp 128—129°C (lit,[28] 128—129°C). NMR: δ 3.2—2.8 (8H, broad), 2.8—2.6 (3H, broad), 2.3—1.9 (3H, m), 1.8—0.5 (2H, m). Found: C, 85.76; H, 14.24%. Calcd for C_8H_{16}: C, 85.63; H, 14.37%.

n-*Hexylcyclopropane*: Bp 148—151°C (lit,[28] 148°C). IR (liq. film): 3090, 1045 cm^{-1}. NMR: δ 1.4—1.1 (10H, broad), 1.1—0.6 (3H, broad), 0.6—0. 2(3H, m), 0.2——0.2 (2H, m). Found: C, 85.31; H, 14.64%. Calcd for C_9H_{18}: C, 85.63; H, 14.37%.

1-n-*Butyl-2-methylcyclopropanes*: A mixture of *trans*- (27%) and *cis*-2-heptene (73%) gave a reaction mixture containing 26% of *trans*- and 74% of *cis*-1-*n*-butyl-2-methylcyclopropane. Distillation gave a portion boiling at 123—128°C which consisted of 84% of the *cis* and 16% of the *trans* isomer. In a glc analysis, the *cis* isomer gave the retention time of 7.4 min, while the *trans* isomer gave one of 5.9 min (Silicone DC 550 column, 110°C, nitrogen-carrier flow rate of 35 ml/min). NMR: δ 0.7—0.5, −0.3——0.4 (ring protons of the *cis* isomer), 0.35—0 (ring protons of the *trans* isomer). Found: C, 85.69; H, 14.31%. Calcd for C_8H_{16}: C, 85.63; H, 14.37%.

Benzobicyclo[*3.1.0*]*hex-2-ene*: A portion boiling at 84—88°C/22 mmHg (lit,[31] 104°C/40 mmHg) was finally purified by preparative glc (Shimadzu GC 2B, Apiezon Grease L). IR (liq. film): 3050, 1020 cm^{-1}. NMR: δ 7.3—6.9 (4H, m), 3.1—2.9 (3H, t), 2.5—2.1 (1H, m), 2.0—1.6 (1H, m), 1.2—0.8 (1H, m), 0.2——0.1 (1H, m).

Bicyclo[*6.1.0*]*nonane*: Bp 78°C/42 mmHg (lit,[32] 89°C/66 mmHg). IR (liq. film): 3035, 1030, 1010 cm^{-1}. NMR: δ 2.1—2.0 (1H, broad), 2.0—1.8 (1H, broad), 1.8—1.0 (9H, broad), 0.9—0.4 (4H, broad), −0.2——0.4 (1H, m).

n-*Butyl Cyclopropyl Ether*: Bp 121—121.5°C (lit,[18] 122—123°C). IR (liq. film): 3100, 1025 cm^{-1}. NMR: δ 3.6—3.3 (2H, m), 3.3—2.9 (1H, m), 1.7—1.1 (4H, m), 1.1—0.7 (3H, m), 0.6—0.2 (4H, m). Found: C, 74.01; H, 12.63%. Calcd for $C_7H_{14}O$: C, 73.63; H, 12.36%.

cis- *And* trans-*1,2-Dimethylcyclopropane*: *cis*-2-Butene (7.0 g, 125 mmol) was distilled into a sealed tube. To the cooled liquid, toluene (10 ml), diethylzinc (4 ml, 40 mmol), and chloroiodomethane (60 mmol) were added. The reaction mixture was allowed to stand at room temperature for 1 hr with stirring. Then, 200 ml of oxygen was injected into the reaction mixture. After the fuming had subsided, the reaction mixture was treated as usual. Glc analysis was carried out with a Silicone DC 550 column operated at 51°C with a nitrogen-carrier flow rate of 17 ml/min. The yields of *cis*- and *trans*-1,2-dimethylcyclopropane were not determined because of their volatility. NMR of the *cis* isomer: δ 1.2—1.0 (6H, m), 0.9—0.6 (3H, broad), 0.5——0.2 (1H,m). NMR of the *trans* isomer: δ 1.1—0.9 (6H, d), 0.6—0 (4H, m).

Methyl cis-*9,10-Methyleneoctadecanoate*: Methyl oleate (15 g, 53 mmol), chloroiodomethane (75 mmol), and diethylzinc (50 mmol) were allowed to react in 50 ml of *n*-hexane by passing air through (10 ml/min) for 1 hr at 50°C. Distillation gave two portions, boiling at 160—180°C/2 mmHg (6.2 g) and 180—186°C/2 mmHg (10 g) (lit,[33] bp 188.7—189°C/3 mmHg). Both portion showed NMR spectra identical with those of methyl *cis*-9,10-methyleneoctadecanoate. NMR: δ 3.6 (3H, s), 2.3 (2H, t), 1.7—1.1 (26H, broad), 1—0.8 (3H, t), 0.7—0.5 (3H, broad), −0.3——0.4 (1H, broad). IR (liq. film): 3060, 1020 cm^{-1}. Found: C, 77.68; H, 12.59%. Calcd for $C_{20}H_{38}O_2$: C, 77.37; H, 12.25%. Hydrolysis with methanol–KOH gave a free acid, mp 37.5—39°C (lit,[33] 39.7—40.5°C). Found: C, 76.46; H, 12.90%. Calcd for $C_{19}H_{36}O_2$: C, 76.96; H, 12.24%.

Attempted Cyclopropanation of Methyl Methacrylate: A mixture of methyl methacrylate (0.10 mol) and chloroiodomethane (0.15 mol) was added, drop by drop, to diethylzinc (10 ml) in *n*-hexane (50 ml) over a 30 min period under a nitrogen atmosphere. Oxygen was then passed through at a rate of 10 ml/min at 50°C for 1 hr. The subsequent usual work-up gave 8.9 g of a residue after distillation. From the distillate, ethyl iodide, propyl iodide, and unchanged methyl methacrylate and chloroiodomethane were detected by glc and NMR spectra, but the presence of cyclopropanated product was not detected. The residue was dissolved in acetone and precipitated with methanol. The white precipitate seemed to be polymethyl methacrylate, judging from its NMR spectra and the results of elemental analysis. NMR: δ 3.4 (3H, broad), 2.2—1.9 (2H, broad), 1.5—0.9 (3H, broad). Found: C, 59.55; H, 7.83%. Calcd for $(C_5H_8O_2)_n$: C, 59.98; H, 8.05%. The methanol-soluble part showed NMR spectra similar to the above spectra except for the new signals at 1.3—1.2 and 1.1 ppm, and it seemed to be a oligomerizied product.

This work was partly supported by a grant of the Ministry of Education of Japan. The authors wish to thank Assistant Professor Junzo Yamashita for his valuable discussions, and Professor Kyohei Yamashita and Professor Makoto Imaizumi for their interest.

30) F. H. Case, *J. Amer. Chem. Soc.*, **56**, 715 (1934).
31) A. L. Goodman and R. H. Eastman, *ibid.*, **86**, 908 (1964).
32) A. C. Cope and G. L. Woo, *ibid.*, **85**, 3601 (1963).
33) K. Hofmann, O. Jucker, W. R. Miller, A. C. Young, Jr., and F. Tausig, *ibid.*, **76**, 1799 (1954).

Oxidation of Diphosphine Dioxides, Disulfides and Phosphinothioite and Photolysis of Diphosphine Disulfides. Formation of Phosphinic and Phosphinothioic Anhydrides

Tateki EMOTO, Renji OKAZAKI, and Naoki INAMOTO

Department of Chemistry, Faculty of Science, The University of Tokyo, Hongo, Bunkyo-ku, Tokyo 113

(Received July 1, 1972)

Oxidation of tetraphenyldiphosphine dioxide with an equimolar amount of peroxybenzoic acid (III) gave diphenylphosphinic anhydride in a good yield. Similarly, diphosphine disulfides (II) with 1.5—2.0 mol times of III, gave the corresponding phosphinothioic anhydrides (V), together with the corresponding phosphinic acid and sulfur. II gave V in air in refluxing xylene or *o*-dichlorobenzene. The yields of V increased with reaction temperature and with reaction time, indicating a homolytic fission of the P(S)–P(S) bond. Reaction of tetraphenyldiphosphine disulfide with sulfur in refluxing *o*-dichlorobenzene gave bis(diphenylphosphinothioyl) sulfide. Photolysis of II with a low pressure mercury lamp gave phosphinic acid and sulfur under oxygen, and gave phosphine sulfide and *O*-methyl phosphinothioate in methanol. Phenyl diphenylphosphinothioite gave diphenyl disulfide and diphenylphosphinic acid with silver nitrate.

Diphosphine dioxides (I) and disulfides (II) undergo heterolytic cleavage of the P–P bond with various reagents.[1] Phosphinic anhydrides are considered to be the intermediate in the oxidation of diphosphines[2] and the corresponding disulfides (II),[3–5] with oxidizing reagents such as hydrogen peroxide and mercuric oxide to the corresponding phosphinic acids.

It has been reported that II inserts ethylene molecules between their phosphorus atoms.[6] In the course of unsuccessful attempts to insert heterocumulenes into the P(S)–P(S) bond of II, it was found that phosphinothioic anhydrides were always obtained in small yields in refluxing benzene or xylene in air.

We thus carried out oxidation of I and II with peroxybenzoic acid, anticipating the formation of the corresponding anhydrides through Baeyer-Villiger type reaction[7] and the air oxidation of II. This paper describes the results, photolysis of II and also oxidation of phenyl diphenylphosphinothioite with silver nitrate.

Results and Discussion

Oxidation of Diphosphine Dioxide (I) and Disulfides (II) with Peroxybenzoic Acid (III). Tetraphenyldiphosphine dioxide (Ia) was chosen as a sample of diphosphine dioxide, since tetraalkyldiphosphine dioxides are scarcely known.

When Ia was allowed to react with an equimolar amount of peroxybenzoic acid (III) in dichloromethane for 40 min at room temperature, diphenylphosphinic anhydride (IVa) was obtained in 83% yield.

Longer reaction time or use of excess amounts of III gave mainly diphenylphosphinic acid. The low yields of IVa may be attributed to decomposition of IVa by benzoic acid produced during the reaction or by excess of III. Anhydride (IVa) could not be purified by column chromatography or by recrystallization, because of easy hydrolysis with moisture.

$$\underset{\text{I, X=O}\quad\text{II, X=S}}{R_2P(=X)\text{-}P(=X)R_2} + \underset{\text{III}}{PhCO_3H} \longrightarrow R_2P(=X)\text{-}O\text{-}P(=X)R_2 + PhCO_2H$$

IV, X=O; V, X=S

a, R=Ph; b, R=Et

A similar oxidation of diphosphine disulfides (II) gave phosphinothioic anhydrides (V). Typical results are listed in Table 1.

V was obtained in poor yield with an equimolar amount of III, but in fairly good yield with 1.5—2.0 mol times of III. Phosphinic acid and sulfur were always produced in small yields, indicating that the oxygen atom insertion into the P(S)–P(S) bond competes with the oxidative desulfurization of the P=S groups. Therefore, use of the above 3 mol times of III gave no V but the corresponding phosphinic aicd and sulfur.

In order to clarify the oxidative desulfurization of the P=S group, triphenylphosphine sulfide was oxidized with III as a model compound under similar conditions. The reaction products were triphenylphosphine oxide and sulfur. It is known that triphenylphosphine sulfide is oxidized to the corresponding oxide with various oxidizing reagents.[8]

Recently the oxidation of diethyl aroylphosphonates with III has been reported to produce aroyl diethyl phosphates.[9] The present reactions are also explained by the Baeyer-Villiger type reaction.

However, the structures VI and VII may be considered to be the actual structures of so-called "diphosphine dioxides and disulfides", respectively.

$$\underset{\text{VI}}{R_2P(O)\text{-}OPR_2} \qquad \underset{\text{VII}}{R_2P(S)\text{-}SPR_2}$$

Both samples of Ia prepared by air oxidation of tetraphenyldiphosphine[2] and by air oxidation of diphenylphosphinous chloride in the presence of *t*-amine

1) A. H. Cowley, *Chem. Rev.*, **65**, 617 (1965).
2) W. Kuchen and H. Buchwald, *Chem. Ber.*, **91**, 2871 (1958).
3) W. Kuchen and H. Buchwald, *Angew. Chem.*, **71**, 162 (1959).
4) L. Maier, *ibid.*, **71**, 575 (1959).
5) L. Maier, *Chem. Ber.*, **94**, 3051 (1961).
6) G. W. Parshall, *J. Inorg. Nucl. Chem.*, **14**, 291 (1960).
7) For preliminary report see: N. Inamoto, T. Emoto, and R. Okazaki, *Chem. Ind.* (London), **1969**, 832.
8) L. Maier, *Helv. Chim. Acta*, **49**, 1258 (1966).
9) M. Sprecher and E. Nativ, *Tetrahedron Lett.*, **1968**, 4405.

Table 1. Oxidation of diphosphine disulfides (II) with peroxybenzoic acid (III) in dichloromethane

II	Temp. (°C)	Time (hr)	III/II (mol/mol)	Mol % $[R_2P(S)]_2O$	Mol % $R_2P(O)OH$	Mol % S
IIa R=Ph	18—35	2	1.2	13	22	11
	ca. 2	2	2.0	54	4	3
IIb R=Et	*ca.* 7	24	3.8	0	58	46
	ca. −50	5	1.5	37	25	33
	18—31[a]	14	2.0	40	17	21

a) In benzene.

and water,[10] and those of IIa or IIb prepared by sulfurization of diphosphines[2] and reaction of ethylmagnesium bromide with diphenylphosphinothioyl chloride[11] or phosphorus thioxychloride,[12] were quite the same as each other with respect to melting point, IR spectrum, and reactivity toward III. Uncertainty as to structure was thus eliminated.

Air Oxidation of Diphosphine Disulfides (II). When diphosphine disulfides (II) were refluxed in toluene, xylene or *o*-dichlorobenzene in the air for a longer time, phosphinothioic anhydrides (V) were obtained but not under nitrogen. Typical data are summarized in Table 2.

Table 2. Phosphinothioic anhydrides (V) from diphosphine disulfides (II)

II	R	Solvent	Temp. (°C)	Time (hr)	V (%)
IIa	Ph	PhH	80	24	8
		PhMe	110	64	45
		Xylene	140	72	98
IIb	Et	PhH	80	29	0
		Xylene	140	93	12
		o-$Cl_2C_6H_4$	180	33	35
IIc	*n*-Bu	*o*-$Cl_2C_6H_4$	180	42	48

We see that both higher temperature and longer reaction time favor the formation of V. No V was formed in benzene at room temperature after a longer period even under oxygen stream. These observations suggest the homolytic cleavage of the P(S)–P(S) bond in II.

$$\underset{\text{II}}{R_2P(S)\text{–}P(S)R_2} \xrightarrow{\Delta} 2R_2\dot{P}\text{=}S \xrightarrow{O_2} \underset{\text{V}}{R_2P(S)\text{–}O\text{–}P(S)R_2}$$

a, R=Ph; b, R=Et; c, R=*n*-Bu

IIa reacts at lower temperature because of the formation of more stable $Ph_2P(S)\cdot$ radical.

In the cases of aliphatic diphosphine disulfides, especially IIc, the formation of unidentified decomposition products was observed by tlc.

Thus, ethylene insertion reaction of II[6] is considered to proceed through homolysis of the P(S)–P(S) bond followed by the addition of $R_2P(S)\cdot$ radicals to ethylene, since the reaction is carried out at 275°C for 48 hr.

Similarly the reaction of IIa with sulfur gave bis(diphenylphosphinothioyl) sulfide (VIII) in refluxing *o*-dichlorobenzene under nitrogen.

$$\underset{\text{IIa}}{Ph_2P(S)\text{–}P(S)Ph_2} \longrightarrow 2Ph_2\dot{P}\text{=}S \xrightarrow{S_8} \underset{\text{VIII}}{Ph_2P(S)\text{–}S\text{–}P(S)Ph_2}$$

Photolysis of Diphosphine Disulfides (II). It has been reported that tetraphenyldiphosphine undergoes homolysis on irradiation of light or on heating at above 180°C,[13,14] but there is no report on the homolytic fission of II, except for the above results.

In the photolysis of II, evidences for the homolytic fission of the P(S)–P(S) bond were also obtained.

At room temperature, no Vb could be detected on irradiation of IIb with a high pressure mercury lamp in carbon disulfide or in methanol for 18—28 hr, even in the presence of rose bengal as a sensitizer, and IIb was recovered. On the other hand, irradiation of IIb in benzene with a low pressure (LP) mercury lamp for 19 hr under oxygen gave 59% of sulfur and 18% of diethylphosphinic acid, along with a trace amount of Vb.

The result is explained by a homolytic cleavage of the P(S)–P(S) bond and oxidative desulfurization of the P=S groups.

$$\underset{\text{IIb}}{Et_2P(S)\text{–}P(S)Et_2} \xrightarrow{\text{LP } h\nu} 2Et_2\dot{P}\text{=}S \xrightarrow{O_2} \underset{\text{Vb}}{[Et_2P(S)\text{–}O\text{–}P(S)Et_2]}$$

$$\xrightarrow[O_2]{h\nu} 1/4S_8 + [Et_2P(O)\text{–}O\text{–}P(O)Et_2] \xrightarrow{H_2O} 2Et_2P(O)OH$$

Although IIb did not react with α,α′-azobisisobutyronitrile (AIBN) in refluxing benzene under irradiation with a high pressure mercury lamp, IIb gave a small amount of diethyl-1-cyano-2-methylethylphosphine sulfide (IX) on irradiation with a low pressure mercury lamp. Sulfide (IX) could not be isolated in pure state, but its presence was determined by IR (2240 cm^{-1}) and MS (*m/e* 189, M^+).

$$\underset{\text{IIb}}{Et_2P(S)\text{–}P(S)Et_2} + \left(Me_2C(CN)\text{–}N\text{=}\right)_2 \xrightarrow{\text{LP } h\nu} \underset{\text{IX}}{Et_2P(S)\text{–}CMe_2CN}$$

When IIa was irradiated in methanol under nitrogen for 6 hr with a low pressure mercury lamp, 52% of diphenylphosphine sulfide and 65% of *O*-methyl diphenylphosphinothioate were obtained. This reaction is also explicable in terms of homolysis as follows.

10) L. D. Quin and H. G. Anderson, *J. Org. Chem.*, **31**, 1206 (1966).
11) N. K. Patel and H. J. Harwood, *ibid.*, **32**, 2999 (1967).
12) H. Niebergall and B. Langenfeld, *Chem. Ber.*, **95**, 64 (1962).
13) U. Schmidt, K. Kabitzke, K. Markau, and A. Müller, *Chem. Ber.*, **99**, 1497 (1966).
14) R. S. Davidson, R. A. Sheldon, and S. Trippett, *J. Chem. Soc., C*, **1966**, 722.

$$Ph_2P(S)-P(S)Ph_2 \xrightarrow{LP\ h\nu} 2Ph_2\dot{P}=S$$

$$Ph_2\dot{P}=S + MeOH \longrightarrow \left[\begin{array}{c} Ph_2\dot{P}-\overset{+}{O}-Me \\ {}^{-}\!S\ \ H \end{array}\right]$$

$$\xrightarrow{Ph_2\dot{P}=S} Ph_2P(S)OMe + Ph_2P(S)H$$

A similar reaction has been reported in photolysis or thermolysis of tetraphenyldiphosphine in alcohols.[14]

The above results indicate that II undegoes homolytic cleavage of the P(S)–P(S) bond on irradiation with a low pressure mercury lamp, and are reasonable from the fact that the disulfides (II) in methanol exhibit absorption maximum at 236—248 nm.

Oxidation of Phenyl Diphenylphosphinothioite (X) with Silver Nitrate. When X was allowed to react with silver nitrate in carbon disulfide at room temperature, silver metal (70%), diphenyl disulfide (87%), and diphenylphosphinic acid (60%) were obtained. The reaction might be attributed to electron transfer from X to silver ion.

$$\underset{X}{Ph_2P\text{–}SPh} + AgNO_3 \longrightarrow \underset{XI}{[Ph_2P\text{–}SPh]^{\cdot+}} + Ag + NO_3^-$$

$$[Ph_2P\text{–}SPh]^{\cdot+} \longrightarrow Ph_2P^+ + PhS\cdot$$

$$2PhS\cdot \longrightarrow PhS\text{–}SPh$$

$$Ph_2P^+ + NO_3^- \longrightarrow \underset{XII}{[Ph_2PONO_2]} \xrightarrow[H_2O]{O_2} Ph_2P(O)OH$$

The formation of diphenylphosphinic acid is explained by oxidation of an intermediate XII followed by hydrolysis during isolation.

A similar reaction of trimethylsilyldiphenylphosphine with silver halides has been reported.[15] The reaction is also considered to proceed through a similar mechanism.

$$\underset{XIII}{Ph_2P\text{–}SiMe_3} + AgX \longrightarrow [Ph_2P\text{–}SiMe_3]^{\cdot+} + Ag + X^-$$

$$[Ph_2P\text{–}SiMe_3]^{\cdot+} \longrightarrow [Me_3Si^+] + Ph_2P\cdot$$

$$\downarrow X^- \qquad \downarrow$$

$$Me_3SiX \quad 1/2\ Ph_2P\text{–}PPh_2$$

In the radical cations (XI and XIII), it is shown that more electronegative group generates the free radical.

Experimental

Materials. The following compounds were prepared by the methods given in literature: tetraphenyldiphosphine dioxide[2,10] (mp 164—165°C), tetraethyl-[12,16] (mp 76—76.5°C), tetra-*n*-butyl-[12,16] (mp 71—72°C), tetraphenyldiphosphine disulfides[11] (mp 170—171.5°C), phenyl diphenylphosphinothioite[17] (mp 46—48°C) and peroxybenzoic acid.[18]

Oxidation with Perbenzoic Acid (III). Only typical examples are given.

a) Tetraphenyldiphosphine Dioxide (Ia): To 10 g (25 mmol) of Ia in 100 ml of dichloromethane was added dropwise III (30 mmol) in 150 ml of dichloromethane at room temperature for 40 min under stirring. The reaction was exothermic. When addition was completed, III had been almost consumed. After removal of the solvent, the residual solid was extracted with ether to remove benzoic acid. Crude anhydride thus obtained was dissolved in carbon tetrachloride followed by precipitation with petroleum ether, mp 137—138°C (lit,[19] 142—143°C), *m/e* 418 (M^+); yield 9.2 g (83%).

b) Tetraphenyldiphosphine Disulfide (IIa): To 4.35 g (10 mmol) of IIa in 100 ml of dichloromethane was added dropwise III (20 mmol) in 100 ml of dichloromethane at room temperature over a period of 2 hr. The mixture was stirred for further 30 min and extracted with 5% aqueous sodium carbonate. The organic layer was washed three times with 400 ml of water and dried with anhydrous sodium sulfate. After removal of the solvent, the residual tarry material was dissolved in benzene and the solution was concentrated to give crude anhydride. After removal of the solvent from the filtrate, the residue gave 18.5 mg (3%) of sulfur as the insoluble in dichloromethane. The solution was separated by preparative tlc. In total, 2.4 g (54%) of anhydride (Va), mp 192—194°C (lit,[19] 196—198°C), *m/e* 450 (M^+), was obtained and 0.62 g (14%) of IIa was recovered. The first aqueous layer was acidified with hydrochloric acid to give 0.187 g (4.3%) of diphenylphosphinic acid, mp 190—191°C (lit,[20] 194—196°C).

c) Tetraethyldiphosphine Disulfide (IIb): To 4.85 g (20 mmol) of IIb in 100 ml of dichloromethane was added dropwise III (30 mmol) in 100 ml of dichloromethane at about −50°C over a period of 2 hr under stirring. 5% of III remained after addition was completed. After standing for 3 hr at this temperature, the reaction mixture was extracted with 5% aqueous sodium bicarbonate. The organic layer was dried with anhydrous magnesium sulfate and the solvent was removed. The oily residue was chromatographed on alumina to separate sulfur (0.42 g, 33%), unchanged IIb (1.2 g, 25%) and anhydride (Vb). Crude anhydride thus obtained was again chromatographed on silica gel, and recrystallized repeatedly from petroleum ether, mp 34—36°C (lit,[21] 42.5°C), *m/e* 258 (M^+); yield 1.9 g (37%)(Found: C, 36.92; H, 8.14%). The aqueous alkaline layer was acidified with hydrochloric acid, and extracted with dichloromethane. After removal of dichloromethane the residue was extracted with water, and dried to give viscous liquid (1.2 g, 25%). The IR spectrum was superimposable with that of diethylphosphinic acid.

d) Triphenylphosphine Sulfide: To 1.47 g (5 mmol) of triphenylphosphine sulfide in 10 ml of dichloromethane was added dropwise III (15 mmol) in 15 ml of dichloromethane at room temperature under stirring. After standing for 6 days, the solvent was removed. The residue was washed with ether and then aqueous sodium bicarbonate, and recrystallized from benzene to give triphenylphosphine oxide (0.98 g, 71%), mp 154—155°C (lit,[22] 156°C). The ethereal washings were washed with 10% aqueous sodium bicarbonate to give 98 mg (61%) of sulfur.

Air Oxidation of Diphosphine Disulfides (II). *a) Tetraphenyl Derivative (IIa)*: A solution of IIa (4.4 g, 10 mmol)

15) E. W. Abel, R. A. N. McLean, and I. H. Sabherwal, *J. Chem. Soc., A*, **1968**, 2371.
16) K. A. Pollart and H. J. Harwood, *J. Org. Chem.*, **27**, 4444 (1962).
17) B. E. Job, R. A. N. McLean, and D. T. Thompson, *Chem. Commun.*, **1966**, 895.
18) G. Braun, "Organic Syntheses," Coll. Vol. I, p. 431 (1958).
19) N. Kreutzkamp, J. Pluhatsch, H. Schindler, and H. Kayser, *Arch. Pharm.*, **295**, 81 (1962); *Chem. Abstr.*, **57**, 11229 (1962).
20) "Inorganic Syntheses," **8**, 71 (1966).
21) W. Kuchen, K. Strolenberg, and H. Buchwardt, *Chem. Ber.*, **95**, 1703 (1962).
22) C. Screttas and A. F. Isbell, *J. Org. Chem.*, **27**, 2573 (1962).

in xylene (40 ml) was refluxed for 72 hr. Removal of the solvent under reduced pressure and washing of the residue, with ether gave 4.4 g (98%) of crude anhydride (Va), which was recrystallized from benzene, mp 198—199°C (lit,[19] 197—198°C), 3.9 g (87%).

b) Tetraethyl Derivative (IIb): A solution of IIb (0.72 g 3.0 mmol) in *o*-dichlorobenzene (30 ml) was refluxed for 33 hr. After removal of the solvent *in vacuo*, the residual brown oil (0.96 g) was chromatographed on silica gel. Elution with petroleum ether gave colorless oily material. Recrystallization from petroleum ether gave 0.27 g (35%) of Vb, mp 31—32°C (lit,[21] mp 42.5°C). The IR spectrum and R_f value on tlc were in agreement with those of an authentic sample.

c) Tetra-n-butyl Derivative (IIc): A solution of IIc(0.60g, 1.7 mmol) in *o*-dichloromethane (30 ml) was refluxed for 42 hr. After removal of the solvent *in vacuo*, the residual brown tarry material (0.64 g) was purified by means of preparative tlc (silica gel, with petroleum ether–acetone (8: 2)) to obtain pure Vc (0.30 g, 48%), which was oily. IR (liquid film), ν_{max} 920 (P–O–P) and 520 cm^{-1} (P=S); *m/e* 370 (M^+, 41%), 314 ($M^+-C_4H_8$, 28), 257 ($M^+-C_4H_8-C_4H_9$, 80), 193 ($Bu_2P(S)O^+$, 77), and 177 (Bu_2PS^+, 100).

Found: C, 52.02; H, 9.62%. Calcd for $C_{16}H_{36}OP_2S_2$: C, 51.85; H, 9.81%.

Reaction of IIa with Sulfur. A mixture of IIa (0.55 g, 1.3 mmol) and sulfur (58 mg, 1.8 mg-atom) in *o*-dichlorobenzene (50 ml) was refluxed for 8 hr under nitrogen. After removal of the solvent *in vacuo*, the residual brown solid was purified by preparative tlc (silica gel, with *n*-hexane–benzene (1: 1)). Crude sulfide (VIII) (0.45 g) was recrystallized twice from 2-propanol, mp 120—121°C (lit,[23] 118—121°C), 0.39 g (66%).

Photochemical Oxidation of IIb. The disulfide (IIb) (0.86 g, 3.55 mmol) in benzene (50 ml) was irradiated with a low pressure mercury lamp (10 W) under oxygen at room temperature for 19 hr. After removal of the solvent, a small amount of benzene was added for the purpose of obtaining sulfur. The solution was chromatographed on silica gel to give sulfur (in total, 0.134 g, 59%), a small amount of Vb and diethylphosphinic acid (0.142 g, 18%) with petroleum ether and ether as eluent, respectively. The IR spectrum of diethylphosphinic acid was superimposable with that of an authentic sample.[20]

Photolysis of IIb in the Presence of AIBN. A mixture of IIb (1.2 g, 5 mmol) and AIBN (5.1 g, 31 mmol) in dichloromethane (100 ml) was irradiated for 10 hr with a low pressure mercury lamp (160 W) under nitrogen. After removal of the solvent and sublimation of tetramethylsuccinodinitrile *in vacuo*, the oily residue containing about ten components was separated by silica gel dry column chromatography (with petroleum ether–acetone (3:2)). The fraction of R_f 0.66 exhibited a peak at *m/e* 189, corresponding to the parent peak of diethyl-1-cyano-1-methylethylphosphine sulfide, and a weak band at 2240 cm^{-1} (C≡N). The fraction was also impure and further purification was difficult.

Photolysis of IIa in Methanol. A solution of IIa (0.54 g, 1.2 mmol) in absolute methanol (80 ml) and dichloromethane (40 ml) was irradiated with a low pressure mercury lamp (10 W) for 5 hr with water-cooling under nitrogen. After removal of the solvent, the residual viscous oil was separated into two components by silica gel dry column chromatography (with chloroform). One component was *O*-methyl diphenylphosphinothioate (0.20 g, 65%) mp 82—84°C (from *n*-hexane) (lit,[24] 84.5—85.5°C), and the other was diphenylphosphine sulfide (0.14 g, 52%), mp 93—95°C (lit,[25] 95—97°C).

Oxidation of Phenyl Diphenylphosphinothioite (X) with Silver Nitrate. To a solution of X (0.81 g, 2.76 mmol) in carbon disulfide (20 ml) was added under nitrogen silver nitrate (0.48 g, 2.8 mmol), the surface of which turned yellow at first and then black. After being stirred at room temperature overnight, a black precipitate containing mainly metallic silver and a small amount of silver diphenylphosphinate (by IR), was filtered off and the filtrate was evaporated. The residue was extracted with ether to leave 0.36 g (60%) of diphenylphosphinic acid, mp 190—191°C. The extract gave 0.26 g (87%) of diphenyl disulfide, mp 58—60°C.

23) T. R. Hopkins and P. W. Vogel, *J. Amer. Chem. Soc.*, **78**, 4447 (1956).

24) T. A. Mastryukova, T. A. Melent'eva, and M. I. Kabachnik, *Zh. Obshch. Khim.*, **35**, 1197 (1965); *Chem. Abstr.*, **63**, 11605 (1965).

25) G. Peters, *J. Amer. Chem. Soc.*, **82**, 4751 (1960).

A Novel Degradation Pathway of L-Ascorbic Acid under Non-oxidative Conditions[1]

Kazuaki GOSHIMA, Norihide MAEZONO, and Kanji TOKUYAMA
Shionogi Research Laboratory, Shionogi & Co., Ltd., Fukushima-ku, Osaka 553
(Received July 7, 1972)

The degradation of L-ascorbic acid (**1**) in methanol was studied in the presence of boron trifluoride-etherate under non-oxidative conditions. Two epimeric compounds containing an acetal group (**7a** and **7b**) were isolated as the intermediates and 2-methoxalylfuran (**13**) the final product. From the result, the degradation pathway of **1** in methanol was proposed to be **1**→**7**→**13**. By analogy with the proposed pathway, one in an aqueous acid was also presented.

It is well known that L-ascorbic acid (**1**) decomposes to 2-furaldehyde (**4**) and carbon dioxide in aqueous acids under non-oxidative conditions.[2,3] Many extensive studies have been reported on the mechanism of this degradation reaction.[3-9] From the kinetic point of view, Regna and Caldwell[5] and Yamamoto and Yamamoto[3] have concluded that the degradation does not proceed *via* L-xylo-2-hexulosonic acid (**2**),[2] the hydrolyzed product of **1**, as an intermediate. Several pathways have been proposed in which that conclusion was expanded.[6,7] However, no experimental proofs on their proposed pathways have been provided. On the other hand recently, Kurata and Sakurai[9] have succeeded in the first isolation of an intermediate, 3-deoxy-L-2-pentosulose (**3**), and proposed a novel pathway of **1**→**2**→**3**→**4**.

Although the isolation of **3** was very important, their conclusion as to the degradation pathway seemed to be in conflict with the kinetic results from which a possible pathway of the degradation can be presented as (**2**→)**1**→**3**→**4**. This disagreement in the interpretation of the role of **3** prompted us to study the degradation of **1**. For the purpose, the degradation of **1** in methanol containing boron trifluoride-etherate was studied as a model reaction.

When **1** in methanol was refluxed in the presence of boron trifluoride for about 10—15 hr, three spots appeared in the tlc, though some of the starting material, **1**, remained unchanged. From the product, **7a**, **7b**, and 2-methoxalylfuran (**13**)[8] were successfully isolated by means of preparative thin-layer chromatography. Compounds **7a** and **7b** had correct analyses for **1** plus one mole of methanol minus one mole of water.

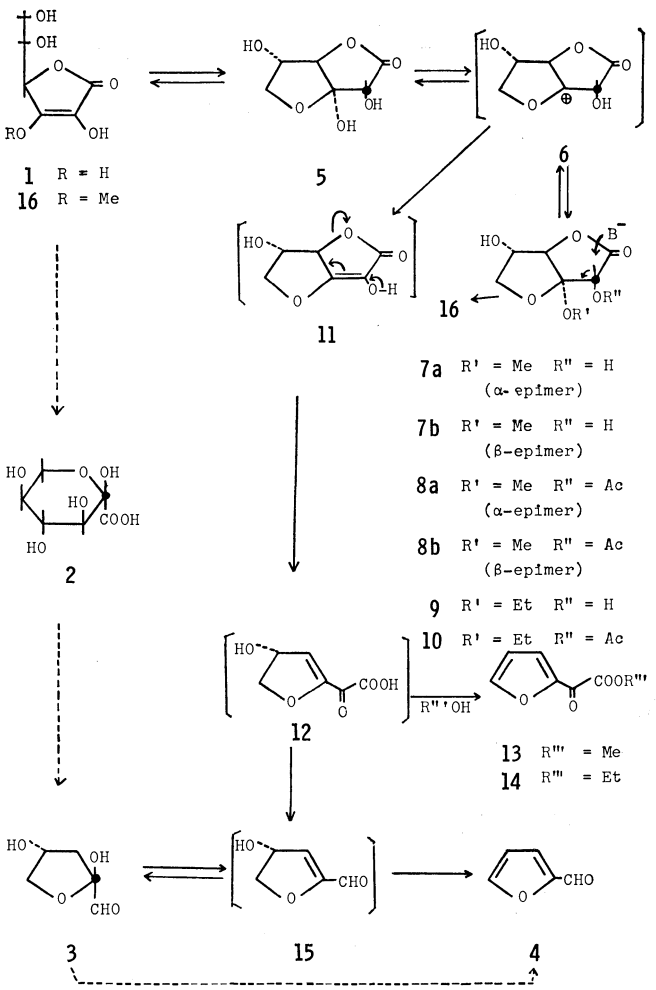

They showed the characteristic bands due to hydroxyl and γ-lactone groups in the IR spectra. Their acetylation gave diacetates, **8a** from **7a** and **8b** from **7b**, which showed the absence of a hydroxyl group in the IR spectra and a singlet due to one methoxy group in the NMR. By the deacetylation of **8a** with a potassium carbonate solution, **7a** was recovered; further, small amounts of **7b** and 3-*O*-methyl-L-ascorbic acid (**16**)[10] were detected. A similar result was obtained for the deacetylation of **8b**, which gave **7b** as the major product and **7a** and **16** as minor products. Therefore,

1) Sorboses Part 22. For part 21, see Ref. 8. A part of this paper was reported in a preliminary form: K. Tokuyama, K. Goshima, N. Maezono, and T. Maeda, *Tetrahedron Lett.*, **1971**, 2503.
2) T. Reichstein and A. Grussner, *Helv. Chim. Acta*, **17**, 311 (1934).
3) R. Yamamoto and E. Yamamoto, *Yakuzaigaku*, **25**, 42 (1965).
4) S. Kamiya, *Nippon Nogeikagaku Zasshi*, **33**, 398 ,402 (1959); **34**, 13 (1960).
5) P. P. Regna and B. P. Caldwell, *J. Amer. Chem. Soc.*, **66**, 246 (1966).
6) A. Cier, C. Nofre, and B. Drevon, *Bull. Soc. Chim. Fr.*, **1959**, 74.
7) P. Finholt, R. B. Paulsen, and T. Higuchi, *J. Pharm. Sci.*, **52**, 948 (1963); **54**, 181 (1965).
8) K. Goshima, N. Maezono, and K. Tokuyama, This Bulletin, **45**, 3692 (1972).
9) T. Kurata and Y. Sakurai, *Agr. Biol. Chem.*, **31**, 170 (1967).
10) W. N. Haworth, E. L. Hirst, and F. Smith, *J. Chem. Soc.*, **1934**, 1556.

Table 1. Chemical shifts and coupling constants

Compound	Solvent	Chemical shift (τ)						Coupling constant (Hz)			
		H_2	H_4	H_5	H_6	$H_{6'}$	MeO	$J_{4,5}$	$J_{5,6}$	$J_{5,6'}$	$J_{6,6'}$
8a	$CDCl_3$	4.27	5.25	4.79	5.28	5.50	6.62	0.5	7.0	5.0	10.0
	C_6D_6	4.28	5.27	5.01	5.88	6.27	6.87				
8b	$CDCl_3$	5.20	5.02	4.37	5.49	6.01	6.62	0.5	7.0	5.0	10.0
	C_6D_6	5.23	5.12	4.93	5.95	6.43	6.93				
10	$CDCl_2$	4.29	5.21	4.78	5.45	6.01					
	C_6D_6	4.29	5.49	5.95	5.75	6.20					

7a and **7b** must be epimers to each other.

The formation of **16** was interesting; it occurred by the further reactions of **7a** and **7b**, initially formed by the deacetylation, with the base employed. The fact that the alkaline treatment of **7a** easily afforded **16** supports this idea and suggests that the position of the methoxy group of **7** corresponds to the C_3-position of **1**. Therefore, the structures of **7a** and **7b** were determined to be the acetal derivatives of **1**, as is shown in the chart.

The structures were confirmed by the NMR spectra, the data of which are reported in Table 1. In the NMR spectrum of **8a** in chloroform-*d* at 60 MHz, three singlets due to one methoxy and two acetoxy groups, a singlet due to H_2 and signals appearing as the pattern of an ABXY system due to H_6, H_6', H_5, and H_4 were observed. The NMR spectrum of **8b** was similarly assigned.

The easy exchange of the methoxy group of **7a** with an ethoxy group also supported the idea of the existence of an acetal group in **7**. When **7a** in ethanol was refluxed in the presence of boron trifluoride, the ethoxy analog of **7a** (**9**) and 2-ethoxalylfuran (**14**) were obtained. The structure of **9** was determined by its conversion into its diacetate (**10**), whose NMR spectrum was assigned in a way similar to that used for **8a** (see Table 1). The structure of **14** was established from the IR and mass spectra, which are quite similar to those of **4**[11] and **13**.[8] Another compound was detected on the tlc. It was considered to be the ethoxy analog of **7b**, but an attempt of its isolation was unsuccessful because of its limited amount.

We will now describe how the epimeric structures of **7a** and **7b** were determined. It is quite natural to consider that the configuration of the 3-methoxy group should be α, since a *cis*-form is more stable in bicyclo-[3.3.0]octanes.[12] Therefore, **7a** should be the C_2-epimer of **7b**. In the acid treatment of **1**, the yield of **7a** was always higher than that of **7b**. Further, in the acid-catalyzed epimerization of **7**, the yield of **7a** was always higher, too. These facts demonstrate that **7a** is a stable epimer. Therefore, the configuartion of the 2-hydroxyl group of **7a** must be α, since the compound with the OH-*exo* configuration to the tetrahydrofuran ring is more stable than that with the OH-*endo* configuration, from the stereochemical point of view.

The CD curves for **7a** and **7b** in UV spectral region have peaks at 236 and 231 nm, respectively. The positive Cotton effect of **7a** suggests that the β-atom of the lactone exists above the lactone plane and the negative one of **7b** suggests the opposite conformation.[13,14] On the other hand, their diacetates, **8a** and **8b**, show a positive Cotton effect. The difference in conformations of the lactone ring between **7b** and the other compounds supported the above-described epimeric structures. The conformation of **7b** must be affected by the presence of a hydrogen bond between the 2-hydroxy group and the oxygen atom of the tetrahydrofuran ring; the presence of the hydrogen bond cannot be considered in the cases of the other compounds. When the hydrogen bond of **7b** disappears upon the acetylation of the 2-hydroxy group, the conformation may be effected to be transformed a conformation similar to the others; that is, the sign of the Cotton effect in **8b** was in accord with those of **7a** and **8a**. The presence of the hydrogen bond in **7b** was also evidenced by the IR spectrum in chloroform.

When **1** was treated in methanol containing boron trifluoride, the spots of **7a** and **7b** appeared on the tlc at the initial stages of the reaction, and then there appeared **13**, which increased at the expense of **7**. Therefore, the reaction was concluded to proceed *via* the pathway of **1**→**7**→**13**. This apthway was further supported by the fact that the acid treatment of **7** afforded **13**. In this treatment, a small amount of **1** was also detected, so the presence of an equilibrium between **1** and **7** was confirmed.

In conclusion, on the basis of the above results, the acid-catalyzed degradation of **1** in methanol may be said to proceed *via* the pathway of **1**→**5**→**6**→**11**→**12**→**13** as is shown in the chart. By analogy with this conclusion, the possible pathway of the degradation of **1** in water can be proposed to be **1**→**5**→**6**→**11**→**12**→**15**→**4**, as is shown in the chart. The interesting intermediate, **3**, reported by Kurata and Sakurai[9] can reasonably be explained as the hydrate of a possible intermediate, **15**.

Experimental

All the melting points were recorded on a Kofler block and have not been corrected. The NMR spectra were taken with a Varian A-60-A spectrometer, using tetramethylsilane as the internal reference; the data are reported in

11) K. Heynes, R. Stute, and H. Scharmann, *Tetrahedron*, **22**, 2223 (1966).
12) J. W. Barrett and R. P. Linstead, *J. Chem. Soc.*, **1936**, 611.
13) H. Wolf, *Tetrahedron Lett.*, **1965**, 1075; **1966**, 5151.
14) A. F. Beecham, *ibid.*, **1968**, 2355, 3591.

Table 1. Thin-layer chromatography was performed on a silica-gel plate using acetone and chloroform [5: 5, v/v (Solvent A) and 6: 4, v/v (Solvent B)] as the solvent for both detection and preparation. The separated materials were developed with either iodine vapor or UV light. The R_f-values are shown in Table 2. In the case of preparative thin-layer chromatography (ptc), the developed zones were extracted with acetone. The evaporation of the acetone under reduced pressure gave the materials.

Table 2. R_f-values of products

Compound	Solvent A	Solvent B
1	0.13—0.18	
7a	0.50—0.59	0.48—0.49
7b	0.53—0.63	—0.57
13	0.84—0.91	0.28—0.40
16	—0.20	

Reaction of L-*Ascorbic Acid (1) in the Presence of Boron Trifluoride-etherate.* (i) A solution of **1** (5.0 g) in absolute methanol (100 ml) containing boron trifluoride-etherate (5 ml) was refluxed for 10 hr and neutralized with triethylamine (7.5 ml), and then the solvent was removed. The preparative thin-layer chromatography of the residue with Solvent A afforded a mixture syrup of **7a** and **7b** (1.20 g) and crystals of **13** (0.3 g). The further ptc of the mixture syrup with Solvent B yielded **7a** (449 mg) and **7b** (169 mg) in pure states.

7a: mp 167—169°C. $[\alpha]_D^{26}$ +2.7 (*c* 1.031, methanol). CD (methanol) $[\phi]_{251}$ 0, $[\phi]_{226}$ +1351. $IR_{cm^{-1}}^{Nujol}$ 3480, 3390 (OH), 1790 (γ-lactone). Found: C, 44.24; H, 5.42%. Calcd for $C_7H_{10}O_6$: C, 44.21; H, 5.30%. **7b**: mp 94—95°C. $[\alpha]_D^{21.5}$ +73.9 (*c* 1.016, methanol), CD (methanol) $[\phi]_{257}$ 0, $[\phi]_{231}$ −1698, $IR_{cm^{-1}}^{Nujol}$ 3360, 3160 (OH), 1780 (γ-lactone). $IR_{cm^{-1}}^{CHCl_3}$ 3607 (free OH), 3578 (bonded OH). Found: C, 44.47; H, 5.19%. Calcd for $C_7H_{10}O_6$: C, 44.21; H, 5.30%.

(ii) A solution of **1** (2.0 g) in methanol (40 ml) containing boron trifluoride-etherate (2 ml) was refluxed for 15 hr and neutralized with triethylamine, and then the solvent was removed. The residue was washed with acetone. The remaining crystals (702 mg) were identified as **1**. The repeated preparative thin-layer chromatography of the acetone-soluble part with Solvents A and B afforded **1** (377 mg), **7a** (275 mg), **7b** (82 mg), and **13** (103 mg).

Reaction of **7a**. *1) Acetylation*: To a solution of **7a** (4.0 g) in pyridine (20 ml) we added acetic anhydride (20 ml) under cooling, after which the solution was left in a refrigerator overnight. The solution was evaporated to dryness and the residue was recrystallized from ether and petroleum ether. The acetate of **7a** (**8a**) was thus obtained. The yield was 5.68 g. Mp 105—106°C. $[\alpha]_D^{21}$ +58.9 (*c* 1.025, chloroform). CD (methanol) $[\phi]_{250}$ 0, $[\phi]_{216}$ +9100. $IR_{cm^{-1}}^{Nujol}$ 1806, 1740 (C–O), $IR_{cm^{-1}}^{CCl_4}$ 1820, 1760 (C=O). Found: C, 48.37; H, 5.18%. Calcd for $C_{11}H_{14}O_8$: C, 48.18; H, 5.15%.

2) Deacetylation of **8a**: To a solution of **8a** (600 mg) in methanol (12 ml) we added a solution of potassium carbonate (600 mg) in water (3 ml). The solution was left at room temperature for 1 hr, neutralized with Amberlite IR-120 (H^+) (25 ml), and then evaporated to dryness. The preparative thin-layer chromatography of the residue with Solvent B afforded **7a** (373 mg), **7b** (39 mg), and **16** (44 mg).

3) Base-catalyzed Reaction: A solution of potassium carbonate (700 mg) in water (3.5 ml) was added to a solution of **7a** (700 mg) in methanol (14 mg). The solution was allowed to stand at room temperature for 2.5 hr, neutralized with Amberlite IR 120 (H^+) (25 ml), and then evaporated to dryness. The preparative thin-layer chromatography of the residue with Solvent B afforded **7a** (499 mg), **7b** (57 mg), and **16** (67 mg).

4) Acid-catalyzed Reaction: (i) Methanol as a solvent: A solution of **7a** (700 mg) in absolute methanol (14 ml) containing boron trifluoride-etherate (0.7 ml) was refluxed for 15 hr, neutralized with triethylamine (0.5 ml), and then evaporated to dryness. The preparative thin-layer chromatography of the residue with Solvent A afforded **1** (105 mg), **7a** (349 mg), **7b** (22 mg), and **13** (118 mg).

(ii) Ethanol as a solvent: A solution of **7a** (1.0 g) in absolute alcohol (20 ml) containing boron trifluoride-etherate (1.0 ml) was refluxed for 6 hr. The solution was neutralized with triethylamine (1 ml) and then the solvent was removed. The preparative thin-layer chromatography of the residue with a mixture of acetone and chloroform (6: 4, v/v) afforded **1** (47 mg, R_f 0.06), **9** (493 mg, R_f 0.46), and **7a** (211 mg, R_f 0.85). **9**: Mp 144—145.5°C. $[\alpha]_D^{21}$ −2.5 (*c* 1.021, methanol). $IR_{cm^{-1}}^{Nujol}$ 3570, 3450 (OH), 1815 (C=O). Found: C, 47.33; H, 5.96%. Calcd for $C_8H_{12}O_6$: C, 47.06; H, 5.92%. **14**: Mp 29—29.5°C. $IR_{cm^{-1}}^{CCl_4}$ 1735, 1677 (C=O), C=C), 886 (furan).[15] Found: C, 56.39; H, 4.85%. Calcd for $C_8H_8O_4$: C, 57.14; H, 4.80%.

Compound **9** was acetylated in a way similar to that used in the acetylation of **7a**. The acetate of **9** (**10**): syrup. $[\alpha]_D^{20}$ +48.2 (*c* 0.901, chloroform). IR $_{cm^{-1}}^{CCl_4}$ 1815, 5757. Found: C, 50.00; H, 5.60%. Calcd for $C_{12}H_{12}O_8$: C, 50.02; H, 5.61%.

Reaction of **7b**. *1) Acetylation*: Acetic anhydride (5 ml) was added to a solution of **7b** (1.0 g) in pyridine (5 ml) under cooling. The solution was left overnight in a refrigerator and then evaporated to dryness. The recrystallization of the residue from acetone and ether gave **8b** (1.2 g). Mp 98.5—100°C. $[\alpha]_D^{26}$ +155.8 (*c* 1.053, chloroform). CD (methanol) $[\phi]_{265}$ 0, $[\phi]_{223}$ +4824, $[\phi]_{205}$ +2396. IR $_{cm^{-1}}^{Nujol}$ 1788, 1750 (C=O). IR $_{cm^{-1}}^{CCl_4}$ 1810, 1760 (C=O). Found: C, 47.99; H, 5.34%. Calcd for $C_{11}H_{14}O_8$: C, 48.18; H, 5.15%.

2) Deacetylation of **8b**: A solution of potassium carbonate (1.0 g) in water (5 ml) was added to a solution of **8b** (1.0 g) in methanol (20 ml). The mixture was allowed to stand at room temperature for 1 hr and then neutralized with Amberlite IR 120 (H^+) (40 ml). After the removal of the solvent, the residue was fractionated by ptc (Solvent A) to give 128 mg of **7a**, 261 mg of **7b**, and 20 mg of **16**.

3) Acid-catalyzed Reaction: A solution of **7b** (700 mg) in absolute methanol (14 ml) containing boron trifluoride-etherate (0.7 ml) was refluxed for 15 hr and then worked up in a way similar to that used for **7a** (Reaction of **7a**, *4*). L-Ascorbic acid **1** (157 mg), **7a** (98 mg), **7b** (85 mg, and **13** (74 mg) were thus obtained.

15) A. R. Katritzky and L. M. Logowsky, *J. Chem. Soc.*, **1959**, 657.

Autoxidation of Aromatic Hydrocarbons Catalyzed with Cobaltic Acetate in Acetic Acid Solution. II. Oxidation of Ethylbenzene and Cumene[1)]

Yoshio KAMIYA and Mikito KASHIMA
Faculty of Engineering, The University of Tokyo, Hongo, Bunkyo-ku, Tokyo
Polymer Research Laboratory, Ube Ind. Ltd., Goi, Ichihara, Chiba

(Received July 12, 1972)

The oxidation of ethylbenzene and cumene catalyzed with cobaltic acetate in acetic acid was studied kinetically in order to elucidate the reaction mechanism and the roles of cobaltic salt. The maximum absorption rate of oxygen as well as the maximum reduction rate of Co(III) in the oxidation of ethylbenzene or cumene were of first order with respect to the initial concentration of hydrocarbon, of inverse first order with respect to the initial concentration of Co(II), and of second order with respect to the initial concentration of Co(III). The kinetic equations are therefore just the same as in the case of toluene, but $d[Co(III)]/d[O_2]$ gave a quite different average value of 3.8, showing that almost no regeneration of Co(III) from Co(II) due to oxidation with peroxidic compounds occurred. Both rates were remarkably accelerated by the addition of sodium acetate and also influenced by a small amount of water. The order of oxygen absorption rate in oxidation was toluene>ethylbenzene>cumene in contrast to the order of hydrogen abstraction rate by peroxy radicals. The apparent activation energy for these hydrocarbons was found to be 10.1 kcal mol^{-1}.

Many papers have appeared on the mechanism of the initiation step in the autoxidation of ethylbenzene[1-3)] and cumene.[4-9)] The main role of transition metal salts established in the autoxidation of hydrocarbons with secondary and primary C–H bond is to decompose hydroperoxide[10-12)] into radicals by the following reactions.

$$M^{n+} + ROOH \longrightarrow M^{n+1} + RO\cdot + OH^-$$
$$M^{n+1} + ROOH \longrightarrow M^{n+} + ROO\cdot + H^+$$

However, another role of transition metal salts has been clarified recently, in which the hydrogen abstraction from hydrocarbon with a higher valence metal ion plays an important role in the reaction of methylbenzenes as follows.

$$M^{n+1} + RH \longrightarrow R\cdot + M^{n+} + H^+$$

We reported on the oxidation of toluene with cobaltic acetate either in the presence and the absence of oxygen and proposed that the reaction was initiated by an electron transfer equilibrium between cobaltic acetate and toluene.[13,14)]

The present kinetic study was undertaken in order to elucidate the reaction mechanism in the oxidation of ethylbenzene and cumene catalyzed with cobaltic acetate in acetic acid solution. The results were compared with those obtained in the oxidation of toluene.

Experimental

Materials. Ethylbenzene, cumene, benzene, and chlorobenzene were repeatedly shaken with concentrated sulphuric acid until no coloration was observed. They were then fractionally distilled after being washed with water and dried over calcium chloride. Acetic acid and cobaltous acetate were of reagent grade. Cobaltic acetate was prepared by the same method as in Part I[14)] and its concentration was determined by potentiometric titration.[13)] The amount of water in the solution was measured by Karl-Fischer titration. Ordinary reaction mixture containing 1.5—2.0M water was prepared unless otherwise stated.

Procedure. The oxidation apparatus and method were the same as in Part I.

Analysis. The solution after oxidation was poured into water of equal volume and extracted with ether. The extract was washed with aqueous sodium hydroxide and analyzed by gas chromatography with a Shimadzu model GC-20 with a 2.2 m column packed with D.O.P. on Celite 545; helium flow rate, 50 ml-min^{-1}, at 140°C. Analysis confirmed the formation of acetophenone and a small amount of α-phenylethanol and α-phenylethyl acetate in the oxidation of ethylbenzene. The main products in the oxidation of cumene were acetophenone, cumylalcohol and α-methylstyrene.

Results and Discussion

Oxidation of Cumene. Cumene can be easily oxidized with oxygen in acetic acid at 60°C, when cobaltic acetate is employed as a catalyst. Oxidation proceeded without induction period, the initial absorption rate of oxygen becoming the maximum rate of oxidation.

The initial oxidation rate and its rate constant in the oxidation of cumene are given in Table 1. The initial rate of oxidation was of first order with respect to the initial concentration of cumene, and of inverse first

1) W. S. Emerson, *J. Amer. Chem. Soc.*, **71**, 1742 (1949).
2) G. A. Russell, *ibid.*, **78**, 1047, 1506 (1956).
3) Y. Kamiya, *Kogyo Kagaku Zasshi*, **68**, 897 (1966).
4) H. S. Blanchard, *J. Amer. Chem. Soc.*, **82**, 2014 (1960).
5) H. Kropf, *Ann. Chem.*, **637**, 73 (1960).
6) D. G. Hendry, *J. Amer. Chem. Soc.*, **89**, 5433 (1967).
7) A. I. Minkov and N. P. Keier, *Kinet. Katal.*, **8**, 160 (1967).
8) T. G. Traylor and G. A. Russell, *J. Amer. Chem. Soc.*, **87**, 3698 (1965).
9) J. A. Howard, K. U. Ingold, and M. Symonds, *Can. J. Chem.*, **46**, 1017 (1968).
10) A. E. Woodward and R. B. Mesrobian, *J. Amer. Chem. Soc.*, **75**, 6189 (1953).
11) Y. Kamiya and K. U. Ingold, *Can. J. Chem.*, **41**, 2020, 2034 (1963).
12) Y. Kamiya, This Bulletin, **43**, 830 (1970).
13) K. Sakota, Y. Kamiya, and N. Ohta, *Can. J. Chem.*, **47**, 387 (1969).
14) M. Kashima and Y. Kamiya, *J. Catal.*, **25**, 326 (1972).

TABLE 1. INITIAL RATE AND RATE CONSTANT IN OXIDATION OF CUMENE AT 60°C, O_2: 1 atm

ϕ-$CH(CH_3)_2$ (M)	Co(III) (M)	Co(II) (M)	$-d[\dot{O}_2]/dt$ (M/sec)	$k\times10^{-5}$ (l/M·sec)
0.083	0.134	0.035	8.60×10^{-7}	2.02
0.440	0.134	0.035	4.30×10^{-6}	1.90
0.830	0.134	0.035	8.80×10^{-6}	2.07
1.65	0.134	0.035	2.00×10^{-5}	2.36
				2.09
0.553	0.014	0.002	8.50×10^{-7}	1.47
0.553	0.029	0.004	1.80×10^{-6}	1.51
0.553	0.083	0.011	4.90×10^{-6}	1.41
0.553	0.168	0.022	1.02×10^{-5}	1.44
				1.46
0.553	0.168	0.022	1.20×10^{-6}	1.69
0.553	0.168	0.050	5.40×10^{-5}	1.73
0.553	0.168	0.096	2.90×10^{-5}	1.78
0.553	0.168	0.165	1.45×10^{-5}	1.53
				1.68

order with respect to the initial concentration of cobaltous ion. The initial rate also was of first order with respect to the total cobalt ion, when the molar ratio of cobaltic to total cobalt ions was kept constant. However, when the inverse first order dependence of the initial rate on the initial concentration of cobaltous ion is taken into account, the over-all reaction should be of second order with respect to cobaltic ion concentration. Although the rate constants present good accordance within each set of experiment, they show a considerable discrepancy between individual sets. This may be mainly due to the difference of water concentration in the course of Co(III) preparation, since water remarkably influences the initial rate of oxidation.

The initial absorption rate of oxygen can be expressed as follows.

$$-d[O_2]/dt = k[\phi\text{-}CH(CH_3)_2][Co(III)]^2[Co(II)]^{-1}$$

The initial reduction rate of Co(III) and its rate constant in the typical oxidation of cumene with cobaltic acetate in acetic acid at 60°C are given in Table 2. The result is similar to that in Table 1.

Thus, the initial reduction rate of Co(III) can be expressed as follows.

TABLE 2. CONSUMPTION RATE OF Co(III) AND RATE CONSTANTS IN OXIDATION OF CUMENE, 60°C, O_2: 1 atm

ϕ-$CH(CH_3)_2$ (M)	Co(III) (M)	Co(II) (M)	$-d[Co(III)]/dt$ (M/sec)	$k'\times10^5$ (l/M·sec)
0.120	0.170	0.030	0.76×10^{-5}	6.57
0.240	0.170	0.030	1.98	8.56
0.360	0.170	0.030	2.66	7.67
0.480	0.170	0.030	3.40	7.35
				7.54
0.479	0.134	0.027	1.82×10^{-5}	5.71
0.479	0.134	0.050	0.98	5.69
0.479	0.134	0.077	0.67	5.99
0.479	0.134	0.128	0.36	5.36
				5.69

$$-d[Co(III)]/dt = k'[\phi\text{-}CH(CH_3)_2][Co(III)]^2[Co(II)]^{-1}$$

The reduction rate takes the value of 4.0×10^{-6} mol·l^{-1}·sec^{-1}, when cumene concentration is extrapolated to zero. This suggests that self-decomposition of Co(III) takes place in the early stage of reaction. Although it is considered that methyl radical ($\cdot CH_3$) or carboxymethyl radical ($\cdot CH_2COOH$) may be produced with self-decomposition of Co(III), they will not significantly contribute to the initial rate of oxidation and the initial reduction rate of Co(III) at higher concentration of cumene. In this case also there is an appreciable difference between rate constants of the two sets of experiment. This may be due to the concentration of water in the solution varies to some extent according to preparation condition of Co(III).

TABLE 3. INITIAL RATE AND RATE CONSTANTS IN OXIDATION OF ϕ-CH_2CH_3 AT 60°C, O_2: 1 atm

ϕ-CH_2CH_3 (M)×10	Co(III) (M)×10	Co(II) (M)×10^3	$d[O_2]/dt$ (M/sec)	k (l/M·sec)
0.13	1.66	2.00	0.65×10^{-6}	3.63×10^{-5}
0.20	1.66	2.00	1.05	3.81
0.34	1.66	2.00	1.65	3.53
0.68	1.66	2.00	3.30	3.52
				3.62
6.79	1.71	15.9	0.38×10^{-5}	3.05×10^{-5}
6.79	1.71	8.48	0.90	3.85
6.79	1.71	2.92	2.60	3.83
				3.58
7.42	0.84	2.50	0.60×10^{-5}	2.87×10^{-5}
7.42	1.27	2.50	1.75	3.66
7.42	1.70	2.50	2.75	3.21
7.42	2.20	2.50	4.60	3.20
				3.24

Oxidation of Ethylbenzene. The initial rate of oxidation and its rate constant in the oxidation of ethylbenzene with cobaltic acetate in acetic acid at 60°C are given in Table 3. The absorption rate of oxygen can be expressed by a similar equation to that obtained in the oxidation of toluene and cumene:

$$-d[O_2]/dt = k''[\phi\text{-}CH_2CH_3][Co(III)]^2[Co(II)]^{-1}$$

The initial reduction rate of Co(III) in the oxidation of ethylbenzene can also be expressed by a similar equation to that obtained in the oxidation of toluene and cumene.

$$-d[Co(III)]/dt = k'''[\phi\text{–}CH_2CH_3][Co(III)]^2[Co(II)]^{-1}$$

Reaction Products. When cobaltic acetate was employed as a catalyst, the main products in the oxidation of cumene were acetophenone, cumyl alcohol and α-methylstyrene. The product distribution differs considerably from that obtained in the autoxidation of cumene, *viz.*, the molar ratio of acetophenone to (cumyl alcohol+α-methylstyrene) is about 1.2 (Fig. 1). However, the difference in the ratio of ketone to alcohol can be attributed to the effect of dilution.[12]

Figure 2 shows a comparison of consumption curves of Co(III) under oxygen atmosphere with those under argon atmosphere in the oxidation of toluene, ethylbenzene, and cumene. The regeneration of Co(III)

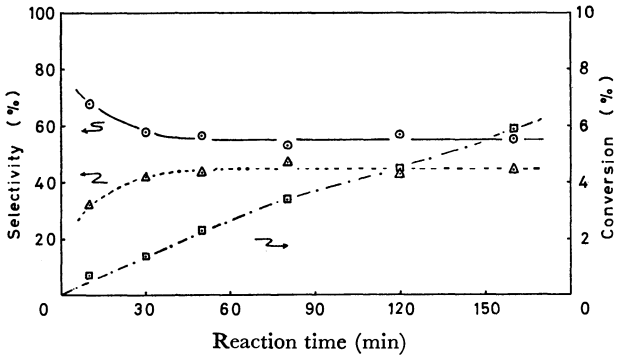

Fig. 1. Products distribution in oxidation of cumene
ϕ-$CH(CH_3)_2$: 0.553M, Co(III): 0.166M, Co(III): 0.017M, 60°C, O_2: 1 1 atm.
⊙: Acetophenone, △: Cumyl alcohol + α-Methylstyrene

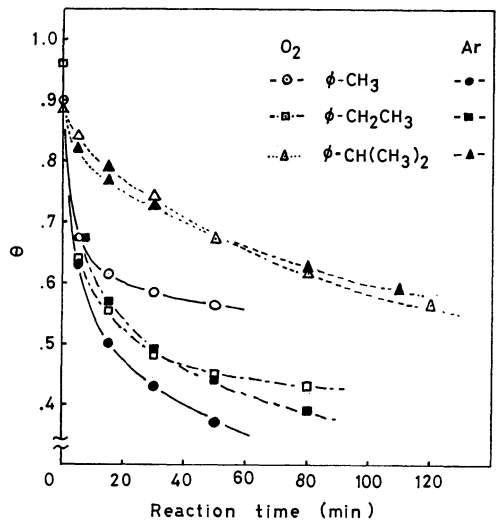

Fig. 2. Consumption curves of Co(III) in oxidn. of ϕ-CH_3, ϕ-CH_2CH_3 and ϕ-$CH(CH_3)_2$ at 60°C.

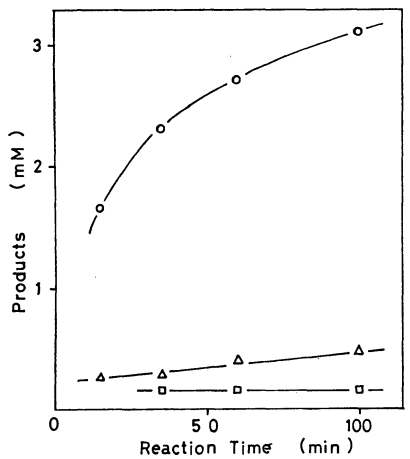

Fig. 3. Products distribution in Co(III) oxidn. of ϕ-CH_2CH_3.
ϕ-CH_2CH_3: 1.36M, Co(III): 0.19M, Co(II): 0.04M, 60°C, O_2: 1 atm.
○: $\phi COCH_3$, △: ϕ-$CH(OH)CH_3$, □: ϕ-$CH(OAc)\ CH_3$

was not observed in the oxidation of ethylbenzene or cumene in contrast to toluene.

The main products in the oxidation of ethylbenzene with Co(III) were acetophenone, α-phenylethanol and α-phenylethyl acetate (Fig. 3). The salient point of product distribution is that the molar ratio of ketone to alcohol is large in comparison to that obtained in the autoxidation of ethylbenzene. This is probably due to the subsequent oxidation of α-phenylethanol and the reaction of peroxy radical with cobaltic acetate.

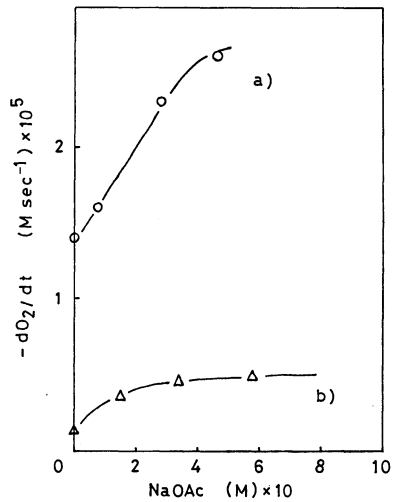

Fig. 4. Effect of NaOAc on initial rate
a) ϕ-CH_2CH_3: 1.26M, Co(III): 0.166M, Co(II): 0.017M.
b) ϕ-$CH(CH_3)_2$: 0.599M, Co(III): 0.153M, Co(II): 0.040M

Effect of Sodium Acetate. In the oxidation of cumene and ethylbenzene with cobaltic acetate in acetic acid, the initial rate of oxidation as well as the initial reduction rate of Co(III) were remarkably accelerated by the addition of sodium acetate (Fig. 4).

Table 4. Solvent effect
Co(III): 0.106M, Co(II): 0.080M, 60°C

ϕ-CH_2CH_3 (ml)	AcOH (ml)	ϕ-Cl (ml)	ϕ-H (ml)	$-dO_2/dt$ ($M \cdot sec^{-1}$)
5.0	60	—	—	1.01×10^{-5}
5.0	45	15	—	1.57
5.0	30	30	—	2.45
5.0	30	—	30	1.78

This can be explained as follows. Since the dissociation constant of sodium acetate in acetic acid is relatively large (1.3×10^{-6}),[15] a cobaltic ion is easily coordinated with an extra acetate anion and forms an active cobalt ion with coordination number greater than three.[16,17]

Solvent Effect. A remarkable positive solvent effect is observed in oxidizing ethylbenzene with cobaltic acetate, when a part of acetic acid is replaced with benzene or chlorobenzene. The initial rate of oxidation increases linearly as the amount of benzene or chlorobenzene is increased (Table 4). This suggests that the solvation of acetic acid around Co(III) is relieved by the addition of neutral solvent and it becomes easy for cobaltic ion to interact with ethylbenzene and the initial rate of oxidation is enhanced

15) R. J. L. Martin, *Aust. J. Chem.*, **15**, 409 (1962).
16) P. J. Proll, L. H. Sutcliff, J. Walkley, *J. Phys. Chem.*, **65**, 455 (1961).
17) E. I. Heiba, R. M. Dessau, W. J. Koehl, *J. Amer. Chem. Soc.*, **91**, 6830 (1969).

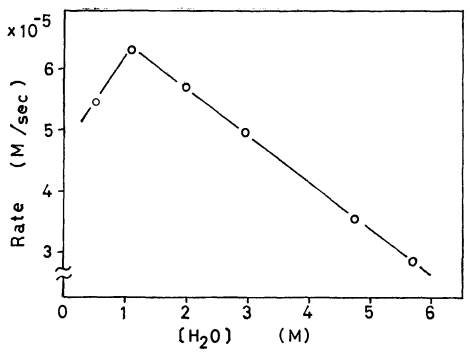

Fig. 5. Plots of initial rate *vs.* $[H_2O]_0$
ϕ-CH_2CH_3: 0.74M, Co(III): 0.21M, Co(II): 0.01M, 60°C, O_2: 1 atm.

by the dilution of acetic acid.

When alkylbenzenes are oxidized with cobaltic acetate in acetic acid, water remarkably influences the initial rate of oxidation. The initial rate in the oxidation of ethylbenzene increases as water concentration increases and reaches the maximum value at water concentration of about 1.0 mol·l^{-1} (Fig. 5). This can be explained as follows. The presence of a small amount of water makes the concentration of monohydroxide of cobaltic acetate increase which is more active than triacetate. When the concentration of water becomes very high, however, the deactivation effect of cobaltic ion with water will overcome the activation effect.

Effect of Reaction Temperature. The Arrhenius plot for the oxidation of toluene, ethylbenzene, and cumene with cobaltic acetate is shown in Fig. 6. The apparent activation energies (10.1 kcal·mol^{-1}) were found to be the same. The order of relative reactivities was toluene>ethylbenzene>cumene, a complete reverse of that expected from the C–H bond energy, *viz.*, the rate constant was profoundly affected in an inverse way to the case of oxidation by free radicals. The results are not explicable in terms of the C–H bond rupture process, but support the view that the electron transfer process is rate-determining.

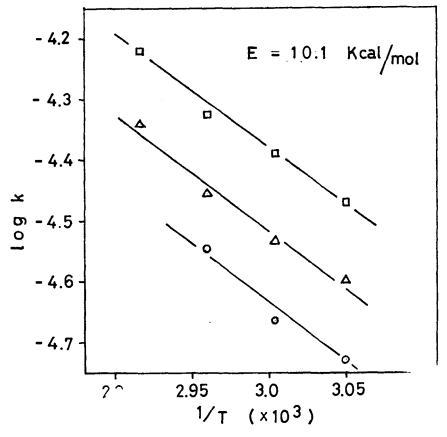

Fig. 6. Effect of reaction temp. on rate of aromatic hydrocarbon oxidn.
RH: 1.0M, Co(III): 0.13M. Co(II): 0.03M, O_2: 1 atm.
(—○—): ϕ-$CH(CH_3)_2$, (—△—): ϕ-CH_2CH_3, (—□—): ϕ-CH_3

Reaction Mechanism. We proposed that the active species of cobalt ion is a dimer of cobaltic ion or quadrivalent cobalt ion because the absorption rate of oxygen is of second order with respect to cobaltic ion and of inverse first order to cobaltous ion concentration.[14] We also postulated the following electron transfer equilibrium in the early stage of reaction.

$$Co(III)_2 + RH \rightleftarrows [RH^+AcO^-Co(III)] + Co(II)$$

$$[RH^+AcO^-Co(III)] \longrightarrow R\cdot + Co(III) + AcOH$$

The electron transfer equilibrium can be applied to the oxidation of ethylbenzene or cumene. The following reactions will mainly contribute to the oxidation of ethylbenzene or cumene with cobaltic acetate in the early stage of reaction.

$$2Co(III) \overset{K_1}{\rightleftarrows} Co(III)_2 \quad (1)$$

$$Co(III)_2 + RH \overset{K_2}{\rightleftarrows} [RH^+AcO^-Co(III)] + Co(II) \quad (2)$$

$$[RH^+AcO^-Co(III)] \overset{k_3}{\longrightarrow} R\cdot + Co(III) + AcOH \quad (3)$$

$$R\cdot + O_2 \overset{k_4}{\longrightarrow} ROO\cdot \quad (4)$$

$$ROO\cdot + Co(III) \overset{k_5}{\longrightarrow} \text{ketone} + H^+(\text{or } CH_3^+) + Co(II) + \frac{1}{2}O_2 \quad (5)$$

where R· is ϕ-$CHCH_3$ or ϕ-$C(CH_3)_2$ and ROO· is the corresponding peroxy radical. The difference in reactivities toward cobaltic acetate may be ascribed to that of the entropy decrease of the hydrocarbon in the transition state. When the rate determining step is reaction (3), the rate of oxygen absorption in the early stage of reaction can be expressed as follows.

$$-d[O_2]/dt = \frac{1}{2}K_1K_2k_3[RH][Co(III)]^2[Co(II)]^{-1}$$

The rate of Co(III) reduction in the early stage of reaction can be calculated as follows.

$$-d[Co(III)]/dt = 2K_1K_2k_3[RH][Co(III)]^2[Co(II)]^{-1}$$

Thus, the ratio of $d[Co(III)]/d[O_2]$ is 4. The value is nearly equal to that obtained from Tables 1 and 2 and would be comparable with the value of 1.7 in the case of toluene, in which the regeneration of Co(III) by oxidation product takes place.

Linear Conjugated Systems Bearing Aromatic Terminal Groups. XI. Syntheses and Electronic Spectra of α,ω-Diphenanthrylpolyenes

Yasuhira TAKEUCHI, Akio YASUHARA, Shuzo AKIYAMA, and Masazumi NAKAGAWA

Department of Chemistry, Faculty of Science, Osaka University, Toyonaka, Osaka 560

(Received July 21, 1972)

The syntheses of α,ω-di(2-phenanthryl)-, di(3-phenanthryl)-, and di(9-phenanthryl)polyenes (I_n, I_n', and I_n'', $n=1$—6) by means of the Wittig reaction are described. Formylphenanthrenes (II, II′, II″), phenanthrylpropenals (III′, III″), phenanthrylpentadienals (IV, IV′, IV″) and muconaldehyde (VIII) were used as carbonyl components in the reaction. Phenanthrylmethyl-, phenanthrylpropenyl- and phenanthrylpentadienyltriphenylphosphonium bromides and 1,4-bis(triphenylphosphonium)-2-butene dibromide were converted into phosphoranes (V, V′, V″, VI, VI′, VII″, IX, IX′, IX″, VII) by a reaction with phenyllithium. The reaction of carbonyl components with phosphoranes with a proper combination yielded diphenanthrylpolyenes (I_n, I_n', I_n''). 2- and 3-Phenanthryl derivatives (I_n and I_n') exhibited electronic spectra with well-defined vibartional fine structure, whereas 9-phenanthryl derivative (I_n'') showed broad and structureless absorption curves. It was found that the plots of the longest-wavelength maxima (λ_{max}) of I_n and I_n' against $n^{0.6}$ and $n^{0.8}$ give excellent straight lines which can be given by the empirical formulas:

I_n: $\lambda_{max} = 57.9n^{0.6} + 303$ nm (in tetrahydrofuran)

I_n': $\lambda_{max} = 30.3n^{0.8} + 348$ nm (in tetrahydrofuran)

A linear relationship between the square of wavelength of the longest-wavelength absorption maxima (λ_{max}) and the number of ethylenic bond (n) [$\lambda^2_{max} \propto n$, *i.e.*, $\lambda_{max} \propto n^{0.5}$] has been recognized for the electronic spectra of several series of all-*trans*-polyenes.[1] However, the bathochromic shift of λ_{max} of α,ω-di(2-naphthyl)polyenes was found to be linearly proportional to $n^{0.7}$ suggesting a marked influence of the terminal groups on the electronic excitation of polyene chromophore.[2] Thus we considered it desirable to prepare other series of diarylpolyenes to get information on the role of terminal groups on the electronic spectral regularity. The present paper deals with the syntheses of α,ω-di(2-phenanthryl)-(I_n), α,ω-di(3-pehnanthryl)- (I_n'), and α,ω-di(9-phenanthryl)-polyenes (I_n''), and the spectral regularity of the former two series of polyenes (I_n and I_n').

Syntheses. The reaction sequence used in the syntheses of α,ω-diphenanthrylpolyenes (I_n, I_n', I_n'') is outlined in the Scheme. Phosphoranes were prepared by the reaction of phenyllithium with the corresponding triphenylphosphonium bromides. I_1, I_1', and I_1'' were obtained by the reaction of II, II′, and II″ with V, V′, and V″, respectively. III, III′, and III″ were prepared from II, II′, and II″ by a modified Arens and van Dorp method.[3] I_2 could be obtained from II and VI. The reaction of III′ and III″ with V′ and V″ afforded I_2' and I_2'', respectively. Treatment of IV and IV′ with V and V′ yielded I_3 and I_3'. I_3' was also prepared by the reaction of II′ with VII derived from 1,4-dibromo-2-butene.[4] The reaction of III″ with VI″ gave I_3''. The Wittig reaction of muconaldehyde (VIII) with V, V′, and V″ yielded I_4, I_4', and I_4'', respectively. IV, IV′, and IV″ were treated with IX, IX′, and IX″ to yield I_5, I_5', and I_5''. I_6, I_6', and I_6'' were obtained from VI, VI′, and VI″ and VIII.

1. RCHO (II, II′, II″) + $RCH{=}PPh_3$ (V, V′, V″) ⟶ RCH=CHR (I_1, I_1', I_1'')

2. RCHO (II) + $RCH{=}CHCH{=}PPh_3$ (VI) ⟶ $R(CH{=}CH)_2R$ (I_2)

   RCH=CHCHO (III′, III″) + $RCH{=}PPh_3$ (V′, V″) ⟶ $R(CH{=}CH)_2R$ (I_2', I_2'')

3. $R(CH{=}CH)_2CHO$ (IV, IV′) + $RCH{=}PPh_3$ (V, V′) ⟶ $R(CH{=}CH)_3R$ (I_3, I_3')

   RCHO (II′) + $Ph_3P{=}CHCH{=}CHCH{=}PPh_3$ (VII) ⟶ $R(CH{=}CH)_3R$ (I_3')

   RCH=CHCHO (III″) + $RCH{=}CHCH{=}PPh_3$ (VI″) ⟶ $R(CH{=}CH)_3R$ (I_3'')

4. $2RCH{=}PPh_3$ (V, V′, V″) + $OCH(CH{=}CH)_2CHO$ (VIII) ⟶ $R(CH{=}CH)_4R$ (I_4, I_4', I_4'')

5. $R(CH{=}CH)_2CHO$ (IV, IV′, IV″) + $R(CH{=}CH)_2CH{=}PPh_3$ (IX, IX′, IX″) ⟶ $R(CH{=}CH)_5R$ (I_5, I_5', I_5'')

6. $RCH{=}CHCH{=}PPh_3$ (VI, VI′, VI″) + $OCH(CH{=}CH)_2CHO$ (VIII) ⟶ $R(CH{=}CH)_6R$ (I_6, I_6', I_6'')

Roman numerals with no prime, single prime and double prime denote the 2-phenanthryl, 3-phenanthryl and 9-phenanthryl isomers, respectively.

Scheme 1. Synthetic route of diphenanthrylpolyenes.

* For Part X of this series, see Ref. 2.

1) L. N. Ferguson, *Chem. Revs.*, **43**, 408 (1948) and references cited therein; F. Sondheimer, D. A. Ben-Efraim, and R. Wolovsky. *J. Amer. Chem. Soc.*, **83**, 1675 (1961).

2) A. Yasuhara, S. Akiyama, and M. Nakagawa, This Bulletin, **45**, 3638 (1972).

3) O. Isler, M. Montavon, R. Rüegg, and P. Zeller, *Helv. Chim. Acta*, **39**, 259 (1956).

4) S. W. Heitman, J. H. S. Weiland, and H. O. Huisman, *Koninkl. Ned. Akad. Wetenshap., Proc. Ser. B*, **64**, 165 (1961).

TABLE 1. PHYSICAL PROPERTIES OF DIPHENANTHRYLPOLYENES

n	I_n			I_n'			I_n''		
	Color	Mp(°C)	δ (cm^{-1})	Color	Mp(°C)	δ (cm^{-1})	Color	Mp(°C)	δ (cm^{-1})
1	colorless	315—316	965	pale greenish yellow	288—289	980	pale greenish yellow	271—273	960
2	greenish yellow	296—297	983	greenish yellow	286	992	greenish yellow	270—272	975
3	yellow	287—288	993	yellow	295—296	1000	yellow	243—244	992
4	yellow	283	998 1000	yellow	284—285	1005	yellow	263	1000
5	orange yellow	300	965 1005	orange yellow	275—276	1008	orange yellow	233—236	1000
6	yellow	293—294		orange	286—287	1008	orange	231—232	1000

TABLE 2. ELECTRONIC SPECTRAL DATA OF DI(2-PHENANTHRYL)POLYENES (I_n)

n	λ_{max} (log ε) in nm in tetrahydrofuran							
1	277 (4.80)	285 (4.91)	298.5 (4.90)	337[a]	348 (4.89)	360[a]	375[a]	
2	287 (4.67)	295 (4.65)	354 (4.88)	371 (5.01)	392 (4.89)			
3	285 (4.56)	296 (4.55)	312 (4.26)	371 (4.93)	390 (5.08)	414 (4.95)		
4	255 (4.60)	284 (4.47)	294 (4.53)	319 (4.24)	371[a]	388 (4.99)	408 (5.15)	436 (5.06)
5	260 (4.90)	266 (4.84)	297 (4.46)	382[a]	404 (5.05)	426 (5.18)	455 (5.10)	
6	270 (4.82)	292[a]	350 (4.20)	417 (4.99)	441 (5.16)	471.5 (5.09)		

a) shoulder.

TABLE 3. ELECTRONIC SPECTRAL DATA OF DI(3-PHENANTHRYL)POLYENES (I_n')

n	λ_{max} (log ε) in nm in tetrahydrofuran								
1	251.5 (4.81)	272.5 (4.68)	279[a]	291[a]	304.5 (4.23)	345[a]	357 (4.75)	379 (4.62)	
2	253[a]	280 (4.53)	299 (4.33)	313.5 (4.24)	360 (4.79)	378 (4.91)	399 (4.82)		
3	255[a]	279 (4.40)	289 (4.41)	309 (4.24)	324 (4.27)	359[a]	377 (4.87)	396 (5.02)	420 (4.91)
4	253 (4.89)	296 (4.32)	319 (4.18)	334 (4.30)	372[a] (4.69)	391 (4.93)	414 (5.09)	440 (5.00)	
5	255 (4.89)	301 (4.28)	329 (4.26)	345 (4.42)	375 (4.66)	407 (4.92)	428 (5.07)	458 (5.00)	
6[b]					356 (4.40)	421 (5.01)	443 (5.13)	474 (5.03)	

a) shoulder. b) measured in a glass cell.

The color of the crystals, melting points and wave number of IR absorption due to C–H out-of-plane deformation (δ) of *trans*-double bond are summarized in Table 1. Regular increase in melting point with increase in the chain length in α,ω-diphenylpolyenes[5] could not be observed in the series of diphenanthrylpolyenes (I_n, I_n', I_n'') as in di(1-anthryl)-[6] and di(2-naphthyl)polyenes.[2] The higher members of I_n were found to be scarcely soluble in usual organic solvents. Shift of δ to a higher wave number with the increase of n was observed in the three series of diphenanthrylpolyenes (I_n, I_n', I_n'') (Table 1). The same trend has been observed in the IR spectra of dianthryl-[6] and dinaphthylpolyenes.[2]

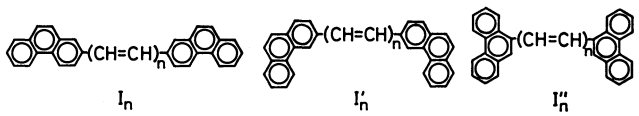

I_n I_n' I_n''

Electronic Spectra. Numerical data of the electronic spectra of I_n and I_n' are summarized in Tables 2 and 3. Absorption curves with well-developed fine structure were obtained for I_n and I_n', but broad and structureless ones for I_n'' (Figs. 1 and 2). The difference can be reasonably attributed to violation of coplanarity of the molecules of I_n'' caused by the steric interference between the hydrogen atoms at 1-, 1'-, 8-, and 8'-positions of the aromatic nuclei and β- and β'-positions of the ethylenic bonds. The same spectral behavior has been observed in other series of sterically hindered diarylpolyenes[2,5,7] and explained in

5) R. Kuhn and A. Winterstein, *Helv. Chim. Acta*, **11**, 87 (1928).
6) Y. Takeuchi, S. Akiyama, and M. Nakagawa, This Bulletin, **45**, 3183 (1972).
7) G. Wettermark, L. Tegner, and O. Mörtensson, *Arkiv. för Kemi*, **30**, 185 (1969).

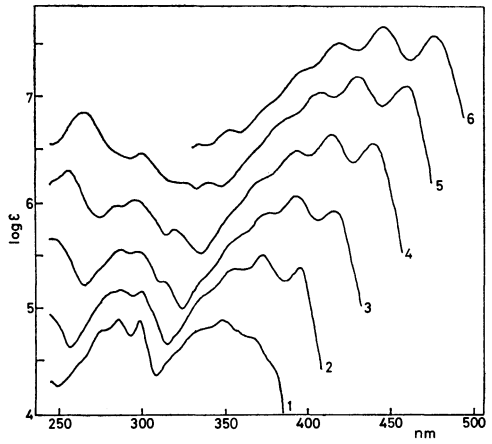

Fig. 1. Electronic spectra of di(2-phenanthryl)polyenes (I_n) in tetrahydrofuran. Each curve, except for the lowest one, has been displaced upward by a 0.5 log ε unit increment from one immediately below.

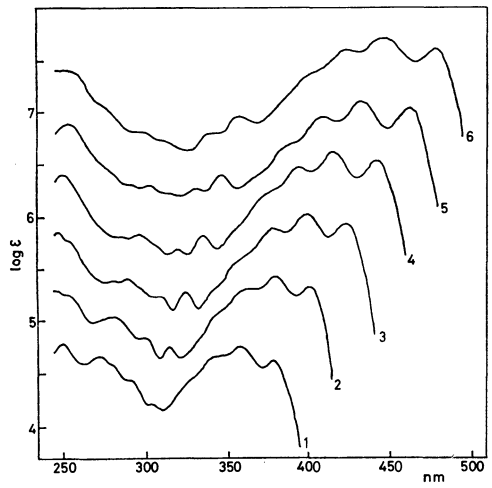

Fig. 2. Electronic spectra of di(3-phenanthryl)polyenes (I_n') in tetrahydrofuran. Each curve, except for the lowest one, has been displaced upward by a 0.5 log ε unit increment from one immediately below.

terms of nonplanarity of molecule.[7] The longest-wavelength absorption band consisting of three vibrational sub-bands seems to arise from an interaction of ^{1}La band of the terminal group with the absorption of polyene chromophore. The difference of wavelength $\Delta\lambda$ of the longest-wavelength sub-bands between a member of I_n or I_n' and the next higher member, I_{n+1} or I'_{n+1} decreases with the increase in the number of n. The same trend of bathochromic shift has been observed in various series of linear polyenes[1,2,5] in contrast with the increase of $\Delta\lambda$ in several series of diarylpoly-ynes.[8] This suggests the possibility that the mode of interaction of aromatic terminal groups with polyene chromophore differs from that with polyyne chromophore.

Discussion on spectral regularity is limited to I_n and I_n', owing to difficulty of estimation of the exact location of longest-wavelength sub-band (λ_I) or next

8) M. Nakagawa, S. Akiyama, K. Nakasuji, and K. Nishimoto, *Tetrahedron*, **27**, 5401 (1971).

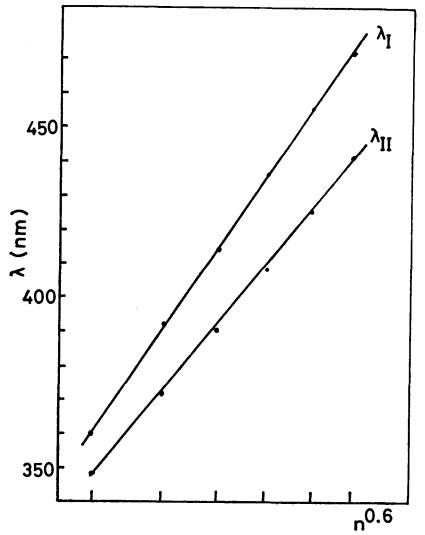

Fig. 3. Plot of λ_{max} *vs.* $n^{0.6}$ for di(2-phenanthryl)polyenes (I_n). λ_I: longest-wavelength maxima λ_{II}: second-longest-wavelength maxima

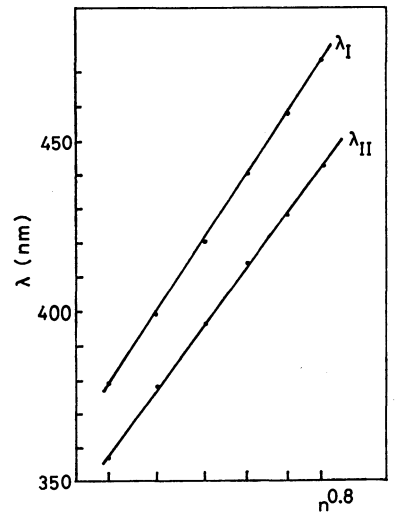

Fig. 4. Plots of λ_{max} *vs.* $n^{0.8}$ for di(3-phenanthryl)polyenes (I_n'). λ_I: longest-wavelength maxima λ_{II}: second-longest-wavelength maxima

longest-wavelength sub-band (λ_{II}) of I_n'' because of the broad and structureless feature of their absorption curves. The longest-wavelength bands of I_n and I_n' are considered to shift linearly with the xth power of the number of ethylenic linkage (n).[2] It was revealed that the plots of λ_I and λ_{II} of I_n *versus* $n^{0.6}$ and those of I_n' *versus* $n^{0.8}$ give good straight lines (Figs. 3 and 4). The linear relationships can be well represented by the following empirical formulas:

$$\lambda = An^x + B$$

I_n: $\lambda_I = 57.9n^{0.6} + 303$ nm (in tetrahydrofuran)

$\lambda_{II} = 48.6n^{0.6} + 298$ nm (in tetrahydrofuran)

I_n': $\lambda_I = 30.3n^{0.8} + 348$ nm (in tetrahydrofuran)

$\lambda_{II} = 27.1n^{0.8} + 330.5$ nm (in tetrahydrofuran)

The spectral regularity of acetylenic analogues of I_n and I_n', 2,2'-diphenanthrylpoly-ynes and 3,3'-diphenan-

thrylpoly-ynes, could be expressed by $\lambda_I = 13.9\ n^{1.3} + 333$ and $\lambda_I = 10.8\ n^{1.4} + 347$, respectively.[9] The value of constant B was found to be similar in both series, but that of coefficient A to be much larger in the polyene series than in poly-yne analogues.

Experimental

All the melting points are not corrected. The electronic spectra were measured with a Hitachi EPS-3T spectrophotometer using a well-matched pair of 1 cm quartz cells. The IR spectra were obtained on a Hitachi EPI-2 spectrophotometer by KBr disk method. Pure and anhydrous solvents were used. Preparation of phosphoranes was carried out under nitrogen atmosphere using ethereal solution of phenyllithium as a base. The Wittig reaction was performed under shielding from light.

1,2-Diphenanthrylethylenes (I_1, I_1', and I_1''). (a) 1,2-Di(2-phenanthryl)ethylene (I_1). To a suspension of 2-phenanthrylmethyltriphenylphosphonium bromide[10] (0.64 g, 1.2 mmol) in benzene (20 ml) was added phenyllithium (0.175N, 6.8 ml). After stirring for 1 hr at room temperature, a solution of II[2] (0.21 g, 1.0 mmol) in benzene (10 ml) was added to the resulting orange red solution of phosphorane (V). The solvent was removed after the mixture had been stirred for 24 hr. The residue was digested with boiling benzene and the solution was passed through a short column of alumina. Pure I_1 was obtained as colorless crystals, mp 315—316°C, 0.109 g (28.7%) by concentration of the filtrate. Further concentration of the filtrate afforded the second crop of I_1, mp 309—312°C, 0.02 g (5.2%).

(b) 1,2-Di(3-phenanthryl)ethylene (I_1'). By a similar method to that used in the preparation of I_1, I_1' (mp 284—287°C, 0.258 g, 67.9%) was obtained from V' [from the corresponding phosphonium bromide[10] (0.65 g, 1.2 mmol) and phenyllithium (0.69N, 1.7 ml)] and II'[9] (0.21 g, 1.0 mmol). Pure I_1', pale yellow needles, mp 288—289°C (from benzene).

(c) 1,2-Di(9-phenanthryl)ethylene (I_1''). The reaction of II'[9] (0.35 g, 1.5 mmol) with V'' [from 9-phenanthrylmethyltriphenylphosphonium bromide[10] (0.80 g, 1.5 mmol) and phenyllithium (0.09N, 16.6 ml)] afforded I_1'', mp 271—273°C (from toluene), $\lambda_{max}^{benzene}$ (log ε): 301 (4.27), 340 (4.30) nm.

Found: I_1, C, 94.58; H, 5.28%. I_1', C, 94.86; H, 5.38%. I_1'', C, 94.35; H, 5.28%. Calcd for $C_{30}H_{20}$: C, 94.70; H, 5.30%.

3-Phenanthryl-2-propenals (III, III', and III''). The preparation of 2-phenanthryl isomer (III) is described as a representative example, III' and III'' being prepared by a similar procedure.

(a) 3-(2-Phenanthryl)-2-propenal (III). To a solution of lithium ethoxyacetylide prepared from 2-chlorovinyl ethyl ether (7.0 g, 0.066 mol) in tetrahydrofuran (20 ml) and lithium amide (from lithium 0.9 g, 0.13 g-atom) in liquid ammonia (130 ml) was added a solution of II[9] (4.0 g, 0.019 mol) in tetrahydrofuran (50 ml). After the mixture had been stirred for 48 hr at the boiling point of liquid ammonia, ammonium chloride (10 g) was added and the ammonia was allowed to evaporate. The residue was mixed with water and extracted with benzene. The extract, after being washed and dried, was concentrated to give crude ethoxyethynylcarbinol as a brown liquid. A solution of the crude carbinol in tetrahydrofuran (40 ml) was added to a suspension of lithium aluminum hydride (2.9 g, 0.078 mol) in the same solvent (50 ml). After being stirred for 2 hr at room temperature, the reaction mixture was treated with ethyl acetate (15 ml), water (10 ml), and 2N sulfuric acid (120 ml), successively. Crude III obtained as a brown liquid was dissolved in benzene-tetrahydrofuran and the solution was shaken with a saturated solution of sodium hydrogen sulfite to precipitate sulfite adduct of III. Decomposition of the adduct with 10% hydrochloric acid afforded pale yellow crystals, mp 118—123°C (1.19 g, 26.4%) which were recrystallized from benzene to give pure III, colorless cubes, mp 132—133°C.

(b) 3-(3-Phenanthryl)-2-propenal (III'). Crude III' (0.87 g, 19.3%) obtained in crystalline state from II'[9] (4.0 g) was recrystallized from ethanol to afford pure III', colorless plates, mp 114—115°C.

(c) 3-(9-Phenanthryl)-2-propenal (III''). Pale yellow needles (5.7 g, 37.2%) obtained from II'[9] (13.6 g) were recrystallized from benzene to yield pure III'', colorless needles, mp 158—159°C.

Found: III, C, 87.63; H, 5.23%. III', C, 87.94; H, 5.06%. III'', C, 87.88; H, 5.70%. Calcd for $C_{17}H_{12}O$: C, 87.90; H, 5.21%.

3-Phenanthryl-2-propen-1-ols. Phenanthrylpropenols were obtained by the sodium borohydride reduction of III, III', and III''. The preparation of 2-phenanthryl isomer is described as a typical example.

(a) 3-(2-Phenanthryl)-2-propen-1-ol. A suspension of sodium borohydride (1.20 g, 3.2 mmol) in methanol (20 ml) was added to a stirred solution of III (1.48 g, 6.4 mmol) in tetrahydrofuran (16 ml) and methanol (8 ml) at room temperature. After being stirred for 1.5 hr, dilute hydrochloric acid was added to the reaction mixture and extracted with benzene. The extract was washed, dried and treated with active charcoal at room temperature. Pale yellow crystals, mp 157—162°C, 1.31 g (87.9%) obtained by concentration of the extract were recrystallized from benzene to yield pure alcohol, pale yellow plates, mp 167—168°C.

(b) 3-(3-Phenanthryl)-2-propen-1-ol. Crude alcohol (0.30 g) obtained from III' (0.30 g) and sodium borohydride (0.30 g) were recrystallized from benzene to give 3-phenanthrylpropenol, colorless plates, mp 130.5—131.1°C.

(c) 3-(9-Phenanthryl)-2-propen-1-ol. Reduction of III'' (2.3 g) with sodium borohydride (2.3 g) yielded 9-phenanthrylpropenol (2.2 g, 96%) which was recrystallized from benzene to give pure material, colorless needles, mp 143—144°C.

Found: 2-isomer, C, 87.08; H, 6.03%. 3-isomer, C, 87.30; H, 5.99%. 9-isomer, C, 86.99; H, 5.96%. Calcd for $C_{17}H_{14}O$: C, 87.15; H, 6.02%.

3-Phenanthryl-2-propenyltriphenylphosphonium Bromides. The synthesis of 2-phenanthryl isomer is described as a representative example, the preparation of phenanthryl-2-propenyltriphenylphosphonium bromides being performed under similar reaction conditions.

(a) 3-(2-Phenanthryl)-2-propenyltriphenylphosphonium Bromide. To a solution of 3-(2-phenanthryl)-2-propen-1-ol (1.0 g, 4.3 mmol) in chloroform (50 ml) containing 4 drops of pyridine was added a solution of phosphorus tribromide (0.8 g, 3.0 mmol) in chloroform (10 ml) under cooling with an ice-salt bath, and the mixture was stirred for 30 min at the same temperature. After being stirred for 30 min at room temperature, the reaction mixture was poured onto ice-water. The organic layer, after being washed and dried, was treated with active charcoal at room temperature. Fine pale

9) S. Akiyama and M. Nakagawa, This Bulletin, **44**, 2237 (1971).

10) S. Akiyama, K. Nakasuji, and M. Nakagawa, *ibid.*, **44**, 2231 (1971).

yellow crystals obtained by evaporation of the solvent were mixed with triphenylphosphine (1.3 g, 5.0 mmol) and benzene (30 ml) and the mixture was refluxed for 19 hr. The phosphonium bromide deposited as colorless plates, mp 235—241°C, 2.12 g (88.7%).

(b) 3-(3-Phenanthryl)-2-propenyltriphenylphosphonium Bromide. 3-Phenanthrylpropenol (0.217 g, 0.93 mmol) was converted into bromide with phosphorus tribromide (0.20 g, 0.73mmol). Treatment of the bromide with triphenylphosphine afforded phosphonium bromide, colorless crystals, mp 223—226°C, 0.309 g (59.4%).

(c) 3-(9-Phenanthryl)-2-propenyltriphenylphosphonium Bromide. The reaction of the bromide obtained from 9-phenanthryl-2-propenol (1.50 g, 6.4 mmol) and phosphorus tribromide (1.2 g, 4.4 mmol) with triphenylphosphine (1.9 g, 7.5 mmol) gave phosphonium bromide, colorless crystals, mp 144—146°C (from ethanol), 3.55 g (93.6%).

Found: C, 74.92; H, 5.11; Br, 14.55%. Calcd for $C_{35}H_{28}BrP$: C, 75.15; H, 5.01; Br, 14.30%.

5-Phenanthryl-2,4-pentadienals (IV, IV', and IV''). As the three isomeric aldehydes were prepared by similar procedures, only IV is described in some detail.

(a) 5-(2-Phenanthryl)-2,4-pentadienal (IV). To a stirred solution of ethylmagnesium bromide in tetrahydrofuran [from ethyl bromide (4.4 g) and magnesium (0.70 g, 28 mg-atom)] was added a solution of 1-methoxy-1-buten-3-yne (3.2 g, 38.9 mmol) in tetrahydrofuran (12 ml). After being stirred for 30 min at 40°C and then for 30 min at room temperature, a solution of II[9] (4.0 g, 19.4 mmol) in the same solvent (20 ml) was added dropwise under cooling. After stirring for 12 hr at room temperature, ethanol (1.3 ml) and lithium aluminum hydride (1.1 g, 29 mmol) were added to the stirred mixture. After 2 hr, water (4 ml) and 4N sulfuric acid (100 ml) were added successively to the reaction mixture and stirring was continued for 2 hr. The reaction mixture was worked up in the usual way. Crude IV (3.89 g, 77.8%, mp 159—161°C) was recrystallized from ethanol to give pure IV, yellow needles, mp 161°C.

(b) 5-(3-Phenanthryl)-2,4-pentadienal (IV'). The reaction product obtained from the Grignard derivative of methoxybutenyne (5.0 g, 61 mmol) and II'[9] (6.2 g, 30 mmol) was reduced with lithium aluminum hydride (1.7 g, 35 mmol) and the reduction product was treated with 4N sulfuric acid. The aqueous layer was extracted with benzene. The combined organic layer was shaken with a saturated sodium hydrogen sulfite solution to precipitate sulfite adduct. Decomposition of the adduct with a dilute hydrochloric acid afforded yellow crystalline powder (5.7 g, 73.5%, mp 90—94°C) which was recrystallized from ethyl acetate to give pure IV', yellow rods, mp 102°C.

(c) 5-(9-Phenanthryl)-2,4-pentadienal (IV''). Crude IV'', yellow crystalline powder, 2.50 g (32.3%), mp 170—173°C obtained from II''[9] (6.20 g, 0.030 mol), the Grignard derivative of methoxybutenyne (6.1 g, 0.074 mol) and lithium aluminum hydride (1.7 g, 0.035 mol) was rcerystallized from benzene to yield pure IV'', yellow rods, mp 177—178°C.

Found: IV, C, 88.03; H, 5.48%. IV', C, 88.34; H, 5.47%. IV'', C, 88.16; H, 5.47%. Calcd for $C_{19}H_{14}O$: C, 88.34; H, 5.46%.

5-Phenanthryl-2,4-pentadien-1-ols. Reduction of IV, IV', and IV'' in tetrahydrofuran-methanol with sodium borohydride followed by treatment of the products with a dilute hydrochloric acid afforded phenanthrylpentadienols.

(a) 5-(2-Phenanthryl)-2,4-pentadien-1-ol. IV (1.50 g, 5.8 mmol) in the mixed solvent (3: 1, 40 ml) and the hydride (0.45 g, 12 mmol) in methanol (10 ml) gave fairly pure 2-phenanthrylpentadienol, colorless crystals, mp 89—100°C, 1.45 g (96.2%) which were used directly in the following reaction.

(b) 5-(3-Phenanthryl)-2,4-pentadien-1-ol. Pale yellow crystalline powder, mp 143—149°C, 0.94 g (quantitative) obtained from IV' (0.90 g, 3.5 mmol), the mixed solvent (2: 1, 12 ml) and the hydride (0.27 g, 6 mmol) in methanol (8 ml) was recrystallized from chloroform, yielding pure alcohol, yellow plates, mp 149—150°C.

(c) 5-(9-Phenanthryl)-2,4-pentadien-1-ol. IV'' (0.394 g, 1.5 mmol), the mixed solvent (2: 1, 30 ml) and the hydride (0.120 g, 3.2 mmol) in methanol (10 ml) gave colorless needles, mp 119—124°C, 0.399 g (quantitative) which were recrystallized from benzene–cyclohexane (1:1) to give pure material, colorless needles, mp 125°C.

Found: 3-isomer, C, 87.30; H, 6.07%. 9-isomer, C, 87.43; H, 6.18%. Calcd for $C_{19}H_{16}O$: C, 87.66; H, 6.19%.

5-Phenanthryl-2,4-pentadienyltriphenylphosphonium Bromides. The preparation of 9-phenanthryl isomer is described as a typical example.

(a) 5-(9-Phenanthryl)-2,4-pentadienyltriphenylphosphonium Bromide. To a solution of 5-(9-phenanthryl)-2,4-pentadien-1-ol (0.60 g, 2.3 mmol) in chloroform (30 ml) containing a drop of pyridine was added a solution of phosphorus tribromide (0.68 g, 2.5 mmol) in chloroform (10 ml) under cooling on an ice-salt bath. After being stirred for 1 hr at room temperature, the reaction mixture was poured onto ice–water. The organic layer, after being washed and dried, was evaporated and the residue was mixed with benzene (52 ml) and triphenylphosphine (0.76 g, 2.9 mmol). Phosphonium bromide, pale yellow crystals, mp *ca.* 117°C, 0.64 g (47.6%) crystallized out on standing the mixture overnight at room temperature. The filtrate was refluxed for 6 hr, giving a second crop of phosphonium bromide, mp 137—143°C, 0.567 g (42.1%). The combined crystals were recrystallized from ethanol to yield pure material, colorless cubes, mp 190—191.5°C.

Found: C, 74.48; H, 5.28; Br, 13.60%. Calcd for $C_{37}H_{30}BrP \cdot 1/2C_2H_5OH$: C, 75.00; H, 5.47; Br, 13.13%.

(b) 5-(2-Phenanthryl)-2,4-pentadienyltriphenylphosphonium Bromide. The reaction of triphenylphosphine (0.36 g, 1.4 mmol) with the bromide derived from 2-phenanthrylpentadienol (0.24 g, 0.92 mmol) and phosphorus tribromide (0.26 g, 0.97 mmol) afforded phosphonium bromide, light yellow crystals, mp 160—164°C, 0.27 g (50%). This was used without purification in the following reaction.

(c) 5-(3-Phenanthryl)-2,4-pentadienyltriphenylphosphonium Bromide. 3-Phenanthrylpentadienol (1.5 g, 5.77 mmol) was converted into the corresponding bromide by the reaction with phosphorus tribromide (1.8 g, 6.68 mmol). The bromide was refluxed with triphenylphosphine (2.3 g, 8.8 mmol) in benzene (40 ml) to give phosphonium bromide (1.27 g) which was used without purification in the subsequent reaction.

1,4-Diphenanthryl-1,3-butadienes (I_2, I_2', and I_2''). (a) 1,4-Di(2-phenanthryl)-1,3-butadiene (I_2). A suspension of 3-(2-phenanthryl)-2-propenyltriphenylphosphonium bromide (0.67 g, 1.2 mmol) in benzene (25 ml) was mixed with phenyllithium (0.73N, 1.6 ml) to give a dark red solution of phosphorane (VI). A solution of II[9] (0.21 g, 1.0 mmol) in benzene (11 ml) was added and the mixture was stirred for 24 hr at room temperature. The residue obtained by evaporating the solvent was extracted with hot benzene and the hot extract was passed through a short column of alumina. Concentration of the filtrate gave pure I_2, greenish yellow crystals, mp 296—297°C, 0.132 g. Further concentration of the filtrate afforded a slightly impure second crop of I_2, mp 288—297°C, 0.020 g (total yield 37.5%).

(b) 1,4-Di(3-phenanthryl)-1,3-butadiene (I_2'). To a yellow solution of V′ prepared from 3-phenanthrylmethyltriphenylphosphonium bromide (1.10 g, 2.07 mmol) in benzene (20 ml) and phenyllithium (0.31N, 6.7 ml) was added a solution of III′ (0.322 g, 1.38 mmol) in the same solvent (15 ml), and the mixture was stirred for 28 hr at room temperature. The residue obtained by evaporating the solvent was extracted with hot benzene. I_2', mp 280—284°C, 0.174 g (31.1%) obtained by concentration of the extract was redissolved in hot benzene, and the hot solution was passed through a short column of alumina to give pure I_2', greenish yellow plates, mp 286°C.

(c) 1,4-Di(9-phenanthryl)-1,3-butadiene (I_2''). To a solution of V″ prepared from 9-phenanthrylmethyltriphenylphosphonium bromide (0.80 g, 1.5 mmol) and phenyllithium (0.15N, 10.0 ml) was added a solution of III″ (0.350 g, 1.5 mmol) in benzene (18 ml). Greenish yellow crystalline powder obtained after stirring the mixture for 6 hr at room temperature was triturated with a small amount of benzene, and the powder was extracted with hot toluene. Greenish yellow needles, mp 269—171°C, 0.557 g (25.8%) deposited on cooling the extract were dissolved in hot toluene and the hot solution was percolated through a thin layer of alumina to give pure I_2'', greenish yellow needles, mp 270—272°C, $\lambda_{max}^{benzene}$ (log ε): 367 (4.56) nm.

Found: I_2, C, 94.67; H, 5.63%. I_2', C, 94.54; H, 5.62%. I_2'', C, 94.33; H, 5.46%. Calcd for $C_{32}H_{22}$: C, 94.54; H, 5.46%.

1,6-Diphenanthryl-1,3,5-hexatrienes (I_3, I_3', and I_3''). (a) 1,6-Di(2-phenanthryl)-1,3,5-hexatriene (I_3). To a solution of V prepared from 2-phenanthrylmethyltriphenylphosphonium bromide (0.80 g, 1.5 mmol) in benzene (25 ml) and phenyllithium (0.38N, 4.0 ml) was added a solution of IV (0.322 g, 1.25 mmol) in the same solvent (25 ml). After the mixture had been stirred for 24 hr at room temperature, the product was extracted with hot benzene and the hot extract was passed through a short column of alumina. Concentration of the filtrate afforded I_3, yellow plates, mp 287—288°C. Further concentration of the filtrate yielded a sceond crop of I_3, mp 276—279°C, total 0.386 g (71.5%).

(b) 1,6-Di(3-phenanthryl)-1,3,5-hexatriene (I_3'). From 3-Phenanthrylmethyltriphenylphosphonium Bromide. A solution of IV′ (0.26 g, 1.0 mmol) in benzene (12 ml) was added to a solution of V′ in the same solvent (20 ml) prepared from 3-phenanthrylmethyltriphenylphosphonium bromide (0.64 g, 1.2 mmol) and phenyllithium (0.69N, 1.7 ml). After being stirred for 72 hr at room temperature, the product was extracted with hot toluene. Fine yellow crystals, mp 295—296°C, 0.15 g (34.9%) obtained by concentrating the extract were dissolved in hot toluene and passed through a short column of alumina to yield I_3', yellow plates, mp 295—296°C.

From 3-Formylphenanthrene (II′) and Bis-phosphorane (VII). To an ice-cooled solution of 1,4-bis(triphenylphosphonium)-2-butene dibromide[4] (0.75 g, 1.0 mmol) in ethanol (26 ml) were added simultaneously over a 12 min period a solution of lithium methoxide (from lithium, 0.14 g, 0.02 g-atom and methanol, 28 ml) and a solution of II′ (0.45 g, 2.2 mmol) in ethanol (42 ml) and the mixture was stirred for 4 hr at 0°C. Fine yellow crystals, mp 285—291°C, 0.068 g (15.8%) deposited after stirring overnight at room temperature were washed with ethanol and recrystallized from benzene to yield pure I_3', yellow plates, mp 294.5°C.

(c) 1,6-Di(9-phenanthryl)-1,3,5-hexatriene (I_3''). To a solution of VI″ in benzene (15 ml) prepared from 3-(9-phenanthryl)-2-propenyltriphenylphosphonium bromide (0.840 g, 1.5 mmol) and phenyllithium (0.17N, 17.6 ml) was added a solution of III″ (0.348 g, 1.5 mmol) in the same solvent (20 ml). After being stirred overnight at room temperature, the product was washed with a small amount of benzene and extracted with hot toluene. The hot extract was percolated through a thin layer of alumina and the filtrate was concentrated to yield pure I_3'', yellow needles, mp 243—244°C, $\lambda_{max}^{benzene}$ (log ε): 384 (4.67) nm.

Found: I_3, C, 94.15; H, 5.57%. I_3' (from IV′), C, 94.15; H, 5.57%. I_3' (from II′), C, 94.04; H, 5.59%. I_3'', C, 94.30; H, 5.55%. Calcd for $C_{34}H_{24}$: C, 94.41; H, 5.60%.

1,8-Diphenanthryl-1,3,5,7-octatetraenes (I_4, I_4', and I_4''). (a) 1,8-Di(2-phenanthryl)-1,3,5,7-octatetraene (I_4). To a solution of V in benzene (20 ml) obtained from 2-phenanthrylmethyltriphenylphosphonium bromide (0.64 g, 1.2 mmol) and phenyllithium (0.18N, 6.8 ml) was added a solution of VIII (0.055 g, 0.50 mmol) in benzene (7 ml). After the mixture had been stirred overnight at room temperature, the product was digested with boiling benzene. Concentration of the extract afforded yellow crystals (0.0935 g). The mother liquor was passed through a short column of alumina and the filtrate was concentrated to yield a second crop of yellow crystals (0.013 g). The combined crude crystals (mp 280—281°C) dissolved in hot benzene were percolated through a short column of alumina to give pure I_4, yellow plates, mp 283°C.

(b) 1,8-Di(3-phenanthryl)-1,3,5,7-octatetraene (I_4'). A mixture of VIII (0.056 g, 0.5 mmol) and V′ derived from 3-phenanthrylmethyltriphenylphosphonium bromide (0.64 g, 1.2 mmol) and phenyllithium (0.69N, 1.7 ml) was stirred for 24 hr at room temperature. The product dissolved in hot toluene was passed through a short column of alumina. Fine yellow crystals, mp 279—285°C, 0.0935 g (20.4%) obtained from the filtrate were dissolved in hot toluene and percolated through a thin layer of alumina to yield pure I_4', yellow plates, mp 284—285°C.

(c) 1,8-Di(9-phenanthryl)-1,3,5,7-octatetraene (I_4''). To a solution of V″ in benzene (15 ml) prepared from 9-phenanthrylmethyltriphenylphosphonium bromide (0.800 g, 1.5 mmol) and phenyllithium (0.14N, 10.7 ml) was added a solution of VIII (0.056 g, 0.5 mmol) in benzene (6 ml). After being stirred for 6 hr at room temperature, crystalline powder deposited was washed with benzene and digested with hot toluene. Concentration of the extract afforded yellow needles, mp 255—257°C, 0.107 g (46.7%). A second crop of yellow needles, mp 236—241°C, 0.065 g (28.3%) was obtained from the filtrate on concentration. A hot toluene solution of the first crop was percolated through a short column of alumina to give pure I_4'', yellow needles, mp 263°C, $\lambda_{max}^{benzene}$ (log ε): 296 (4.52), 403 (4.83) nm.

Found: I_4, C, 94.00; H, 5.69%. I_4', C, 94.33; H, 5.68%. I_4'', C, 94.40; H, 5.67%. Calcd for $C_{36}H_{26}$: C, 94.28; H, 5.72%.

1,10-Diphenanthryl-1,3,5,7,9-decapentaenes (I_5, I_5', and I_5''). (a) 1,10-Di(2-phenanthryl)-1,3,5,7,9-decapentaenes (I_5). A solution of IV (0.136 g, 0.53 mmol) in benzene (18 ml) was added to a benzene solution (20 ml) of IX prepared from 5-(2-phenanthryl)-2,4-pentadienyltriphenylphosphonium bromide (0.34 g, 0.59 mmol) and phenyllithium (0.97N, 0.6 ml) and the mixture was stirred for 27 hr at room temperature. Yellow solid obtained by evaporation of the solvent was digested with hot toluene. Concentration of the extract afforded yellow plates, mp 284—288°C, 0.086 g (33.7%) which were redissolved in hot toluene and passed through a short column of alumina to give pure I_5, orange yellow plates, mp 300°C.

(b) 1,10-Di(3-phenanthryl)-1,3,5,7,9-decapentaene (I_5'). To a solution of IX′ in benzene (20 ml) prepared from 5-(3-

phenanthryl)-2,4-pentadienyltriphenylphosphonium bromide (0.70 g, 1.2 mmol) and phenyllithium (0.098N, 9.6 ml) was added a solution of IV′ (0.26 g, 1.0 mmol) in benzene (15 ml). After being stirred for 49 hr at room temperature, the reaction product was extracted with hot toluene. Concentration of the extract yielded I_5', orange yellow plates, mp 275—276°C, 10 mg.

(c) 1,10-Di(9-phenanthryl)-1,3,5,7,9-decapentaene (I_5''). A solution of IV″ (0.214 g, 0.83 mmol) in benzene (20 ml) was added to a solution of IX″ in the same solvent (30 ml) obtained from 5-(9-phenanthryl)-2,4-pentadienyltriphenylphosphonium bromide (0.480 g, 0.83 mmol) and phenyllithium (0.16N, 5.2 ml). After being stirred for 19 hr at room temperature, crystalline solid deposited was washed with benzene and extracted with hot toluene. The hot extract was percolated through a short column of alumina. Orange yellow needles, mp 233—236°C, 0.070 g (17.4%) obtained on concentration of the filtrate were redissolved in hot toluene and again passed through a thin layer of alumina to yield pure I_5'', yellow needles, mp 248—249°C, $\lambda_{max}^{benzene}$ (log ε): 305 (4.43), 420 (4.81) nm.

Found: I_5, C, 93.55; H, 5.83%. I_5', C, 93.71; H, 5.82%. I_5'', C, 93.86; H, 5.90%. Calcd for $C_{38}H_{28}$: C, 94.18; H, 5.82%.

1,12-Diphenanthryl-1,3,5,9,11-dodecahexaenes (I_6, I_6', and I_6'').

(a) 1,12-Di(2-phenanthryl)-1,3,5,7,9,11-dodecahexaene (I_6). A solution of VIII (0.052 g, 0.5 mmol) in benzene (10 ml) was added to a solution of VI in the same solvent (25 ml) prepared from 3-(2-phenanthryl)-2-propenyltriphenylphosphonium bromide (0.714 g, 1.3 mmol) and phenyllithium (0.84N, 1.5 ml) and the mixture was stirred for 21 hr at room temperature. The reaction product was extracted with hot toluene. Orange crystals obtained by concentrating the extract were dissolved in hot toluene and percolated through a thin layer of alumina to give pure I_6, orange crystals, mp 293—294°C.

(b) 1,12-Di(3-phenanthryl)-1,3,5,7,9,11-dodecahexaene (I_6'). By a similar procedure to that for I_6, 3-(3-Phenanthryl)-2-propenyltriphenylphosphonium bromide (0.309 g, 0.56 mmol), phenyllithium (0.19N, 2.9 ml) and VIII (0.030 g, 0.28 mmol) afforded I_6', orange rods, mp 286—287°C (from toluene), 11.5 mg (8.2%).

(c) 1,12-Di(9-phenanthryl)-1,3,5,7,9,11-dodecahexaene (I_6''). A solution of VI″ in benzene (15 ml) prepared from 3-(9-phenanthryl)-2-propenyltriphenylphosphonium bromide (0.670 g, 1.2 mmol) and phenyllithium (0.135N, 8.9 ml) was mixed with a solution of VIII (0.044 g, 0.4 mmol) in benzene (7 ml). After being stirred overnight at room temperature, the reaction product was extracted with hot toluene. Orange crystals, mp 217—220°C, 0.117 g (57.4%) obtained by concentrating the extract were redissolved in hot toluene. Percolation of the hot solution through a short column of alumina afforded pure I_6'', orange needles, mp 231—232°C, $\lambda_{max}^{benzene}$ (log ε): 314 (4.35), 434 (5.17) nm.

Found: I_6, C, 93.97; H, 5.88%. I_6', C, 93.89; H, 5.94%. I_6'', C, 93.93; H, 5.97%. Calcd for $C_{40}H_{30}$: C, 94.08; H, 5.92%.

BULLETIN OF THE CHEMICAL SOCIETY OF JAPAN, VOL. 46, 915—920 (1973)

Optically Active 9,10-Dihydro-9,10-etheno and -ethanoanthracenes. I. Syntheses of Optically Active 1,5-Disubstituted-9,10-dihydro-9,10-etheno and -ethanoanthracenes.

Hitoshi TATEMITSU, Fumio OGURA, and Masazumi NAKAGAWA

Department of Chemistry, Faculty of Science, Osaka University, Toyonaka, Osaka 560

(Received July 21, 1972)

1,5-Dimethoxycarbonyl-9,10-dihydro-9,10-ethenoanthracene was synthesized by the reaction of 1,5-dimethoxycarbonylanthracene with dichloroethylene followed by dechlorination with zinc-copper couple. Optical resolution of 1,5-dicarboxy-9,10-dihydro-9,10-ethenoanthracene prepared from the dimethyl ester could be achieved by strychnine to give optically pure (−)-dicarboxylic acid and (+)-diacid with an optical purity of 87.3%. Catalytic reduction of (−)-dicarboxylic acid afforded (−)-ethano-dicarboxylic acid. Transformation of the carboxyl groups in various substituent groups to give optically active C_2-symmetrical etheno- and ethanoanthracene derivatives belonging to the same series of absolute configuration as that of the starting material is described.

The present authors have studied the relation of structure and optical rotatory properties of a number of optically active triptycene derivatives bearing various substituents at various positions of the benzene rings.[1] The absolute configurations of optically active 2,5-dimethoxy-7-substituted- and 2,7-disubstituted-triptycenes have been studied by both X-ray analysis[2] and chemical correlation.[3] It was found that the cautious analyses of CD spectra of these triptycene derivatives lead to antipodal absolute configurations.[4,5]

1) a) A. Sonoda, F. Ogura, and M. Nakagawa, This Bulletin, **35**, 853 (1962); b) F. Ogura, Y. Sakata, and M. Nakagawa, *ibid.*, **45**, 3646 (1972); c) F. Ogura and M. Nakagawa, *ibid.*, **46**, 651 (1973): d) M. Kuritani, Y. Sakata, F. Ogura, and M. Nakagawa, *ibid.*, **46**, 605 (1973).

2) N. Sakabe, K. Sakabe, K. Ozeki-Minakata, and J. Tanaka, presented at the 9th International Congress of Crystallography (Kyoto), (1972), *Acta. Crystallogr.*, **B28**, 3441 (1972).

3) M. Kuritani, Y. Sakata, F. Ogura, and M. Nakagawa, *Chimia*, **1972**, 470.

4) J. Tanaka, F. Ogura, M. Kuritani, and M. Nakagawa, *ibid.*, **1972**, 471.

5) J. Tanaka, K. Ozeki-Minakata, F. Ogura, and M. Nakagawa, *Nature, Phys. Sci.*, (London), **241**, 22 (1973).

9,10-Dihydro-9,10-etheno- and ethanoanthracenes (I and II) prepared by Cristol[6] are stable compounds with a fairly rigid cage structure. 9,10-Dihydro-9,10-etheno- and ethanoanthracene derivatives substituted dissymmetrically in the benzene rings should be resolved in the optical antipodes. In fact, optical resolution and CD spectral properties of some etheno- and ethanoanthracene derivatives have been reported.[7] Considering the direction of polarization of transition of benzene chromophores,[8] we have carried out the syntheses and optical resolution of a series of 9,10-dihydro-9,10-etheno- and ethanoanthracenes bearing the same substituent groups at 1,5-positions (III and IV). It is contemplated that systematic studies on the CD spectral properties of series of III and IV with the same absolute configuration may afford valuable information on the relation of structure and rotatory properties.

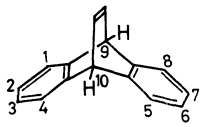

I

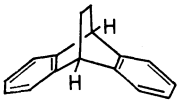

II

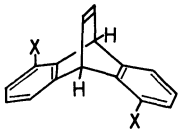

III

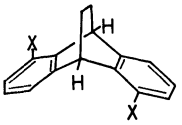

IV

The present paper deals with the synthesis and optical resolution of 1,5-dicarboxy-9,10-dihydro-9,10-ethenoanthracene (X) and the transformation of carboxyl groups in optically active X in various substituents to give a series of optically active 1,5-disubstituted derivatives with the same absolute configuration. The reaction sequence of the synthesis of X and ethanoanalogue (XII) starting from 1,5-dichloroanthraquinone is outlined in Fig. 1. The reaction of *cis*- or *trans*-dichloroethylene with 1,5-dimethoxycarbonylanthracene (V) derived from dichloroanthraquinone was carried out in a sealed tube at 180—190°C. As expected, *cis*-dichloroethylene gave an adduct (VI) and the *trans*-isomer afforded two kinds of adducts which could be separated on silica gel column chromatography into crystalline VII and VIII. Treatment of the adduct (VI or VII or VII or a mixture of VII and VIII) with zinc-copper couple in boiling methanol by the reported method[9] yielded the same 1,5-dimethoxycarbonyl-9,10-dihydro-9,10-ethenoanthracene (IX) in a good yield. Hydrolysis of IX gave dicarboxylic acid

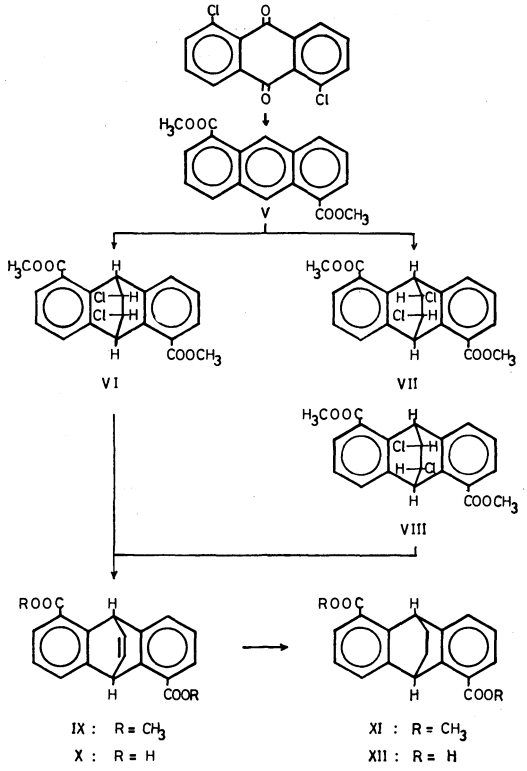

Fig. 1. Synthesis of 1,5-dicarboxy-9,10-dihydro-9,10-etheno- and ethanoanthracenes (X and XII).

(X). Catalytic hydrogenation of IX and X afforded ethano-derivatives (XI and XII), respectively.

The optically resolution of X could b eachieved by strychnine. A solution of X and equimolar strychnine in 99% ethanol was refluxed to give crystalline salt. Optically pure salt obtained by repeated recrystallization of the salt from ethanol was treated with aqueous 50% acetic acid to yield (−)-X. Decomposition of crude salt obtained by concentration of the mother liquor of first recrystallization with aqueous 50% acetic acid afforded (+)-X with an optical purity of 87.3%.[10]

The reaction sequence of the transformation of carboxyl groups in optically active X in various substituents is shown in Fig. 2. X was converted into diamino derivative (XIII) by the Curtius reaction *via* acid chloride, azide, and isocyanate. Hydrogenation of XIII over platinum catalyst gave diamino-ethano derivative (XIV). XIV in chloroform was oxidized with peracetic acid to give dinitro-ethanoanthracene (XVIII). (−)-Diamino derivative (XIII) was converted into (−)-dihydrobromide (XV) and the single crystal of (−)-XV was subjected to X-ray structure analysis by the Bijvoet method to determine the absolute configuration. Diazotization of XIII in acetic acid with sodium nitrite followed by hydrolysis afforded etheno-phenol (XVI) which was converted into etheno-dimethyl ether (XVII) by the reaction with dimethyl sulfate. 1,5-Dimethoxycarbonyl-ethenoanthracene (IX) obtained from dicarboxylic acid (X) was treated with lithium aluminum hydride to give bis-hydroxymethyl deriva-

6) S. J. Cristol and N. L. Hause, *J. Amer. Chem. Soc.*, **74**, 2193 (1952).

7) M-J. Brienne and M. J. Jaques, *C. R. Sci. Acad. Paris, Ser C*, **272**, 1889 (1971); S. Hagishita and K. Kuriyama, *Tetrahedron*, **28**, 1435 (1972).

8) J. R. Platt, *J. Chem. Phys.*, **19**, 263 (1951); J. Petruska, *ibid.*, **34**, 1111 (1961); A. C. Albrecht and W. T. Simpson, *ibid.*, **23**, 1480 (1955); J. Tanaka, This Bulletin, **36**, 833 (1963).

9) S. J. Cristol and D. C. Lewis, *J. Amer. Chem. Soc.*, **89**, 1476 (1967); S. J. Cristol and W. Y. Lin, *J. Org. Chem.*, **34**, 1 (1969).

10) Attempts to resolve (±)-X with cinchonidine resulted in (−)-X with poor optical purity (5.13%).

tive (XIX). The reaction of thionyl chloride with XIX resulted in bis-chloromethyl-etheno derivative (XX). Bis-iodomethyl-etheno compound (XXI) obtained on treatment of XX with sodium iodide in acetone was reduced by lithium aluminum hydride in tetrahydrofuran to give dimethylethenoanthracene (XXII). Catalytic reduction of XXII afforded dimethyl-ethano compound (XXIII).

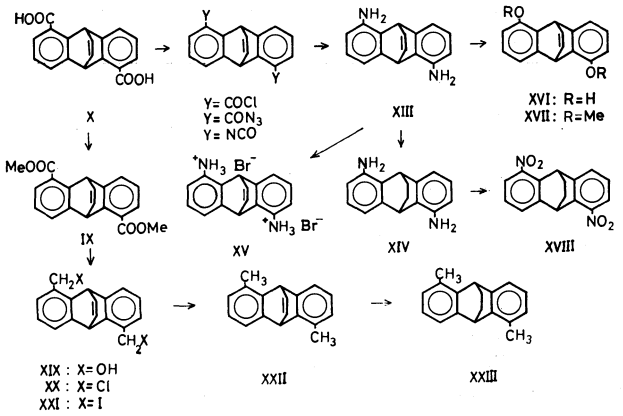

Fig. 2. Transformation of X into 1,5-disubstituted-9,10-dihydro-9,10-etheno- and ethanoanthracenes.

Optically active 1,5-disubstituted-9,10-dihydro-9,10-etheno- and ethanoanthracenes thus prepared clearly belong to a series of the same absolute configuration as that of starting X, because the rigid cage structure of the molecule excludes the possibility of occurrence of the Walden inversion and racemization during the course of transformation.

Experimental

The melting points below 260°C were determined on a Mettler FP2 apparatus and those over 260°C on a Shimadzu Kofler micro hot stage, and are not corrected. Anhydrous pure solvents were used unless otherwise stated. Ligroin with bp 60—80°C was used. The IR and UV spectra were obtained on Hitachi EPI-2, JASCO DS-301 and Hitachi EPS-3T spectrophotometers, respectively. A Yanagimoto ORD-185 and a JASCO J-20 with CD attachment spectropolarimeters were used for the measurements of rotation and CD spectra, respectively. Inflection or shoulder is denoted by an asterisk. Methanol or ethanol containing 10 vol% of 0.1N hydrochloric acid (MeOH–HCl or EtOH–HCl) was used for the measurements of UV, ORD, and CD spectra in an acidic medium. The UV, ORD, and CD spectral data are summarized in Tables 1, 2, and 3. The NMR spectra in deuteriochloroform were measured on a Varian A-60 spectrometer using TMS as an internal standard. Chemical shifts are given in τ-unit.

*1,5-Dimethoxycarbonyl-9,10-dihydro-9,10-(*cis*-11,12-dichloro)-ethanoanthracene (VI).* A mixture of 1,5-dimethoxycarbonylanthracene[1d] (V, 6.54 g, 0.0222 mol) and *cis*-dichloroethylene (18.75 g, 0.2065 mol) in a sealed tube was heated to 180—185°C for 3 days. The crystals deposited on standing the reaction mixture overnight were washed with benzene to give colorless crystals (6.46 g). The residue obtained by evaporating the combined washings and filtrate was dissolved in carbon tetrachloride–benzene (1:1) and the solution was passed through a column of alumina (150 g), yielding an additional amount of crystals, 1.23 g (total 7.69 g, 88.9%). The combined crystals were recrystallized twice from carbon tetrachloride to give pure VI, mp 204.8—205.2°C, IR (KBr-disk): 1718 ($\nu_{C=O}$) cm^{-1}, NMR: 1.98—2.73 (m, 6H, aromatic), 3.83 (m, 1H, bridgehead), 4.09 (m, 1H, bridgehead), 5.50 (t, 2H, bridge), 6.02 (s, 6H, $-COOCH_3$), UV: $\lambda_{max}^{dioxane}$ (ε) 291 (4430), 227* (23000), 211 (39500) nm.

Found: C, 61.23; H, 4.14; Cl, 18.22%. Calcd for $C_{20}H_{16}Cl_2O_4$: C, 61.39; H, 4.12; Cl, 18.13%.

1,5-Dimethoxycarbonylanthracene (V, 0.9 g) was recovered from benzene eluate of the alumina column.

*1,5-Dimethoxycarbonyl-9,10-dihydro-9,10-(*trans*-11,12-dichloro)-ethanoanthracene (VII and VIII).* A mixture of V[1d] (5.0 g, 0.017 mol) and *trans*-dichloroethylene (16.5 g, 0.170 mol) in a sealed tube was heated to 180—190°C for 48 hr. Treatment of the reaction mixture by a similar method to that used for VI afforded pale yellow crystals (6.33 g, 95.2%) along with recovered V (0.02 g). A solution of the crystals (5.364 g) in benzene–carbon tetrachloride (1:1) was passed through a column of silica gel (300 g) and eluted with the same mixed solvent. The eluate was divided into 36 fractions, each fraction being 100 ml. As fractions 10—16 gave a spot at the same R_f on tlc (silica gel), they were combined and evapo-

Table 1. UV spectra of etheno- and ethanoanthracenes

Compound	Solvent	λ_{max} in nm (ε)
(±)-IX	MeOH	306 (6610), 284* (2840), 243* (16400), 223 (31100), 205 (33500)
(−)-X	MeOH	305 (6440), 222 (33200), 205 (35100)
(±)-XI	MeOH	290.5 (5270), 230 (21100), 202 (46400)
(±)-XII	MeOH	291 (5130), 263* (1500), 259.5* (1600), 257 (1700), 253.5 (2430), 229 (20700), 210.5 (29100), 206.5 (29400), 202 (30400), 197.5 (38300)
(−)-XIII	MeOH	296 (3140), 224 (41300), 207* (30900), 204 (32700), 200 (31800)
	MeOH–HCl	295* (100), 278 (2510), 270 (1680), 215 (42600), 211* (38500)
(−)-XIV	MeOH	288 (3610), 232* (20800), 212* (35900), 199 (48800)
	EtOH–HCl	290 (210), 270 (1110), 263 (1010), 250* (950), 209* (35000)
(+)-XVII	99% EtOH	285 (2440), 277 (2290), 219 (42000)
(−)-XVIII	EtOH	309* (4210), 262 (11100), 217 (14600)
(−)-XIX	MeOH	284 (3430), 276 (1990), 267* (1050), 257* (1160), 220 (44100), 215* (38700), 207* (35500), 203* (37500), 200* (38300), 196* (41700), 193* (42600)
(−)-XXII	isooctane	281 (1260), 273 (830), 237* (4270), 220 (53300), 215* (38900), 195 (30000)
(−)-XXIII	isooctane	274 (460), 268* (580), 265* (660), 260.5 (1060), 254.5 (1210), 249 (980), 243 (970), 215* (40200), 207.5 (58000), 204 (63700), 200.5 (65000), 196* (71200), 194* (78000), 192* (93300)

TABLE 2. ORD SPECTRA OF ETHENO- AND ETHANOANTHRACENE AT 20°C

Compound	Solvent	Concentration (g/100 ml)	[α] (λ_{max} in nm)
(−)-X	dioxane	0.237	−333.3° (D), −411.0° (546)
	MeOH	0.004925	−7920° (312), −3860° (297), −6090° (287), −1750° (272), −29250° (236)
(−)-XIII	MeOH	0.00615	−1040° (436), −1580° (405), −2340° (365), −8730° (310), +2930° (289), −63400° (242)
	MeOH–HCl	0.00745	−820° (365), −1260° (308), +5130° (279), −7070° (275), −6640° (273), −12300° (266*), −12700° (260), −11000° (252)
(−)-XIX	MeOH	0.00589	−760° (365), −1150° (304), +2170° (285), −6210° (280), −5980° (278), −9120° (270), −7560° (257), −63800° (224)

TABLE 3. CD SPECTRA OF ETHENO- AND ETHANOANTHRACENES

Compound	Solvent	λ_{max} ($\Delta\varepsilon$) in nm
(−)-IX	MeOH	307 (−5.5), 282 (−7.4), 226 (−65.0), 205 (+46.0)
(−)-X	MeOH	307 (−5.0), 281 (−6.4), 226 (−65.0), 204 (+47.0)
(−)-XI	MeOH	293 (−9.7), 242* (−16.0), 222 (−22.6), 209 (−31.7), 196 (+22.0)
(−)-XIII	MeOH	297 (−8.69), 276 (+3.35), 260 (+3.20), 228 (−11.1), 206 (+80.8)
	MeOH–HCl	294 (−0.24), 276 (+6.73), 269 (+4.78), 239* (−7.23), 215 (−40.3), 195 (+10.1)
(−)-XIV	MeOH	292 (−8.35), 272 (+1.57), 237 (−35.1), 214 (−30.5), 201 (+39.0)
	MeOH–HCl	291 (−0.17), 270 (+2.02), 264 (+1.63), 230* (−6.39), 222 (−6.87), 207 (−24.2)
(+)-XVII	99% EtOH	285 (+5.85), 277 (+4.85), 250 (−14.44), 223 (+153.43), 203 (−82.52)
(−)-XVIII	EtOH	318 (−8.03), 285 (−6.50), 258 (+0.15), 238 (−5.93), 227 (+1.09), 204 (−10.70)
(−)-XIX	MeOH	283 (+5.83), 274 (+3.01), 265 (−1.12), 257 (−1.75), 251 (−1.53), 241 (+0.67), 220 (−103.7), 198 (+40.8)
(−)-XXII	Isooctane	281 (+4.89), 274 (+3.29), 266 (+2.70), 255 (+1.47), 245 (+1.78), 222 (−50.03), 214 (−28.72), 202 (+25.01)
(−)-XXIII	Isooctane	274 (+3.13), 268* (+2.56), 265 (+2.71), 260* (+1.91), 232* (−11.19), 214 (−37.69), 200 (+9.33)

rated to give crystals (2.733 g) which were recrystallized from benzene–ligroin to afford colorless needles, mp 211.6—211.7°C, 2.136 g. Fractions 17—23 gave two spots on tlc indicating that they contain VII and VIII. Fractions 24—36 gave a spot on tlc and were therefore combined and evaporated, yielding crystals (1.225 g). Recrystallization from benzene–ligroin afforded colorless granulous crystals, mp 256.3—256.4°C 0.925 g.

Lower Melting Isomer: IR (KBr-disk): 1720 ($\nu_{C=O}$) cm^{-1}, NMR: 2.00—2.87 (m, 6H, aromatic), 4.13 (t, 2H, bridgehead), 5.77 (m, 2H, bridge), 6.02 (s, 6H, $-COOCH_3$), UV: $\lambda_{max}^{dioxane}$ (ε) 290 (4260), 228 (24100), 211 (37200) nm.

Found: C, 61.65; H, 4.18; Cl, 18.12%. Calcd for $C_{20}H_{16}Cl_2O_4$: C, 61.39; H, 4.12; Cl, 18.13%.

Higher Melting Isomer: IR (KBr-disk): 1715 ($\nu_{C=O}$) cm^{-1}, UV: $\lambda_{max}^{dioxane}$ (ε) 292 (4200), 287* (4140), 230* (23200), 211.5 (43500) nm.

Found: C, 61.19; H, 4.01; Cl, 18.09%. Calcd for $C_{20}H_{16}Cl_2O_4$: C, 61.39; H, 4.12; Cl, 18.13%.

1,5-Dimethoxycarbonyl-9,10-dihydro-9,10-ethenoanthracene (IX). From cis*-Adduct (VI).* Zinc-copper couple[11] (76 g) was added to a solution of VI (3.00 g, 7.67 mmol) in methanol (400 ml) and benzene (140 ml). The mixture was refluxed for 4 days under stirring. The hot reaction mixture was filtered and the insoluble material was washed successively with hot methanol and hot benzene. The combined filtrate and washings were concentrated and mixed with water (1000 ml) and extracted with benzene. The extract, after washing and drying, was evaporated under reduced pressure to give colorless crystals 2.43 g (95.3%) which were recrystallized from methanol to yield pure IX, mp 150.5—151.0°C, IR (KBr-disk): 1724 ($\nu_{C=O}$) cm^{-1}, NMR: 2.27—3.16 (m, 8H, aromatic and olefinic), 3.30—3.55 (m, 2H, bridgehead), 6.03 (s, 6H, $-COOCH_3$).

Found: C, 75.25; H, 4.99%. Calcd for $C_{20}H_{16}O_4$: C, 74.99; H, 5.03%.

From Lower Melting trans*-Adduct (VII or VIII).* A mixture of lower melting *trans*-adduct (0.301 g, 0.77 mmol), zinc-copper couple[10] (7.6 g), methanol (40 ml) and benzene (15 ml) was refluxed under stirring for 48 hr. The reaction mixture was worked up according to a procedure similar to that used for VI, and the crude IX in benzene was chromatographed on alumina (15 g). Colorless crystals 0.288 g (92.2%) obtained from the first benzene eluate (300 ml) were recrystallized twice from methanol, yielding pure IX as colorless rhomboids, mp 151.4—151.7°C. The IR spectrum was found to be identical with that of IX derived from *cis*-adduct.

Found: C, 74.97; H, 5.13%. Calcd for $C_{20}H_{16}O_4$: C, 74.99; H, 5.03%.

From Higher Melting trans*-Adduct (VII or VIII).* Zinc-copper couple[11] (7.6 g) was added to a mixture of higher melting *trans*-adduct (0.297 g, 0.76 mmol), methanol (40 ml) and benzene (30 ml), and the mixture was refluxed for 77.5 hr under stirring. Crystals obtained on working up the reaction mixture by a similar procedure to that used for *cis*-adduct were found to be contaminated with the starting chloro compound (25% on the basis of NMR spectrum). The crystals in benzene (20 ml) and methanol (60 ml) were treated with zinc-copper couple[10] (8.0 g) for further 28 hr. Working up the reaction mixture yielded colorless crystals, 0.143 g (58.8%), which were recrystallized 3 times from methanol to give pure IX, mp 149.8—151.1°C. The IR spectrum was identical with that of IX obtained from *cis*-adduct.

11) R. D. Smith and H. E. Simmons, "Organic Syntheses," Vol. 41, p. 72 (1961).

Found: C, 74.97; H, 5.03%. Calcd for $C_{20}H_{16}O_4$: C, 74.99; H, 5.03%.

A mixture of VII and VIII gave IX under the same reaction conditions.

1,5-Dicarboxy-9,10-dihydro-9,10-ethenoanthracene (X). A solution of potassium hydroxide (100 g) in water (200 ml) was added to a solution of IX (4.305 g, 13.44 mmol) in methanol (300 ml) and the mixture was refluxed for 5 hr. After the methanol had been removed by distillation, the mixture was made acidic to Congo red with concentrated hydrochloric acid under cooling. Colorless precipitate formed was washed thoroughly with cold water and dried *in vacuo* at 100°C to give X, 3.86 g (98.4%). This material was recrystallized successively from acetic acid and methanol to afford pure X, colorless crystals, mp 303—309°C (decomp.), IR (KBr-disk): 1678, 1691 ($\nu_{C=O}$) cm^{-1}.

Found: C, 73.50; H, 4.21%. Calcd for $C_{18}H_{12}O_4$: C. 73.96; H, 4.14%.

X could be converted into IX on heating with methanol and sulfuric acid.

1,5-Dimethoxycarbonyl-9,10-dihydro-9,10-ethanoanthracene (XI), Dimethyl ester (IX, 0.324 g, 1.011 mmol) in dioxane (50 ml) was reduced over platinum oxide (21.4 mg). The crystals (0.316 g) obtained on evaporation of the solvent were recrystallized twice from methanol to yield pure XI, colorless crystals, mp 140.1—140.3°C, IR (KBr-disk): 1713 ($\nu_{C=O}$) cm^{-1}, NMR: 2.15—3.03 (m, 6H, aromatic), 4.34 (m, 2H, bridgehead), 6.06 (s, 6H, $-COOCH_3$), 8.27 (t, 4H, ethane bridge).

Found: C, 74.36; H, 5.06%. Calcd for $C_{20}H_{18}O_4$: C, 74.52; H, 5.63%.

Hydrolysis of XI under the similar reaction conditions used for IX afforded ethano-dicarboxylic acid (XII).

1,5-Dicarboxy-9,10-dihydro-9,10-ethanoanthracene (XII). Catalytic hydrogenation of X (0.0987 g, 0.338 mmol) in methanol (40 ml) over platinum oxide (14.9 mg) afforded XII as colorless crystals (0.1024 g) which were recrystallized twice from methanol to give pure XII, mp 318—327°C (decomp.), IR (KBr-disk): 1690 ($\nu_{C=O}$) cm^{-1}.

Found: C, 73.30; H, 5.02%. Calcd for $C_{18}H_{14}O_4$: C, 73.46; H, 4.80%.

XII could be converted into XI on treatment with methanol and sulfuric acid.

Optical Resolution of (±)-1,5-Dicarboxy-9,10-dihydro-9,10-ethenoanthracene (X). A solution of equimolar strychnine (4.58 g, 0.0137 mol) in 99% ethanol (600 ml) was added to a solution of (±)-X (4.00 g, 0.0137 mol) in the same solvent (3500 ml). After being refluxed for 3 hr, the mixture was concentrated to *ca.* 1000 ml and allowed to stand overnight. Crystalline salt deposited (3.43 g) was recrystallized 4 times from 99% ethanol to give optically pure salt, mp 322—326°C (decomp.), 1.43 g.

Found: C, 74.41; H, 5.45; N, 4.43%. Calcd for $C_{39}H_{34}N_2O_6$: C, 74.74; H, 5.47; N, 4.47%.

Since the measurement of rotation of the strychnine salt was difficult owing to its poor solubility in organic solvents, the increase in optical purity of the salt was followed by measurements of rotation of dicarboxylic acids obtained from the mother liquors of recrystallization on acidification with acetic acid.

Optically pure salt thus obtained was decomposed with aqueous 50% acetic acid to yield optically pure (−)-X, mp 315—322°C (decomp.), 0.65 g.

Found: C, 73.45; H, 4.24%. Calcd for $C_{18}H_{12}O_4$: C, 73.96; H, 4.14%.

The mother liquor of the first recrystallization was concentrated to give crystalline salt (5.05 g). Decomposition of the salt with aqueous 50% acetic acid afforded (+)-enantiomer, 2.35 g, $[\alpha]_D$ +291.2° (*c*, 0.215, dioxane), optical purity, 87.3%.

(−)-1,5-Dimethoxycarbonyl-9,10-dihydro-9,10-ethenoanthracene (IX). Concentrated sulfuric acid (3 ml) was added to a solution of (−)-X (0.196 g) in methanol (30 ml) and the mixture was refluxed for 16.5 hr. The reaction mixture was worked up by the usual way to afford (−)-etheno-diester (IX), 0.198 g (92.4%). Pure (−)-IX was obtained by recrystallization from methanol, mp 151.5—151.8°C, $[\alpha]_{405}$ −1160° (*c* 0.00546, methanol).

Found: C, 75.22; H, 5.14%. Calcd for $C_{20}H_{16}O_4$: C, 74.99; H, 5.03%.

(−)-1,5-Dimethoxycarbonyl-9,10-dihydro-9,10-ethanoanthracene (XI). Reduction of (−)-IX (22.6 mg) in dioxane (10 ml) over platinum oxide (6.6 mg) yielded colorless liquid which could be crystallized on trituration with methanol. Recrystallization from methanol gave pure (−)-XI, colorless crystals, mp 121.8—122.4°C, 19.4 mg, $[\alpha]_{405}$ −1170° (*c* 0.00600, methanol).

Found: C, 74.21; H, 5.66%. Calcd for $C_{20}H_{18}O_4$: C, 74.52; H, 5.63%.

(−)-1,5-Diamino-9,10-dihydro-9,10-ethenoanthracene (XIII). A mixture of (−)-X (0.441 g, 1.508 mmol), thionyl chloride (5 ml) and tetrahydrofuran (40 ml) was refluxed for 3 hr. Crude acid chloride (0.716 g) obtained by evaporation of volatile material under reduced pressure was dissolved in tetrahydrofuran (16 ml), and a solution of sodium azide (0.359 g, 5.521 mmol) in water (8 ml) was added under ice-cooling. After being stirred for 3 hr at the same temperature, the reaction mixture was mixed with ice-water and extracted with benzene. The extract, after washing and drying, was concentrated under reduced pressure to give crystalline acid azide. Thoroughly dried acid azide (0.561 g) in benzene (40 ml) was refluxed for 5 hr. Isocyanate (0.584 g) obtained as a brown liquid on evaporation of the solvent under reduced pressure was mixed with a solution of potassium hydroxide (3 g) in 99% ethanol (35 ml) and water (8 ml). After the mixture had been refluxed for 12 hr, the reaction mixture was poured onto ice-water and extracted with benzene. Concentration of the extract, after washing and drying, afforded crude diamine (XIII, 0.281 g) as a brown solid. A solution of the crude XIII in benzene–ether (9: 1) was passed through a column of silica gel (30 g) and the filtrate was chromatographed on the same adsorbent. Elution with dichloromethane afforded (−)-XIII (0.128 g, 79.1%) which was recrystallized from ether-ligroin to give pure (−)-XIII, mp 188.3—189.6°C (racemate, mp 187.6—189.5°C), IR (Nujol mull): 3320, 3230 (ν_{N-H}), 1627 (δ_{N-H}) cm^{-1}, NMR: 2.72—3.75 (m, 8H, aromatic and olefinic), 4.85 (t, 2H, bridgehead), 6.45 (s, 4H, $-NH_2$).

Found: C, 81.89; H, 6.10; N, 11.81%. Calcd for $C_{16}H_{14}N_2$: C, 82.02; H, 6.02; N, 11.96%.

(−)-1,5-Diamino-9,10-dihydro-9,10-ethanoanthracene (XIV). Hydrogenation of (−)-XIII (0.167 g, 0.712 mmol) in methanol (20 ml) over platinum oxide afforded crude (−)-XIV (0.158 g) which was chromatographed on silica gel and eluted with benzene–ether (9: 1) to yield (−)-XIV (0.146 g, 86.7%). Recrystallization of this material from benzene-ligroin gave pure (−)-XIV, mp 213.3—213.8°C (racemate, mp 188.8—188.9°C), IR (Nujol mull): 3340, 3230 (ν_{N-H}), 1625 (δ_{N-H}) cm^{-1}, NMR: 2.90—3.43 (m, 6H, aromatic), 5.68 (s, 2H, bridgehead), 6.60 (s, 4H, $-NH_2$), 8.30 (t, 4H, bridge).

Found: C, 81.49; H, 6.84; N, 11.73%. Calcd for $C_{16}H_{16}N_2$: C, 81.32; H, 6.83; N, 11.86%.

(−)-1,5-Diamino-9,10-dihydro-9,10-ethenoanthracene Dihydrobro-

mide (XV). A mixture of hydrobromic acid (47%, 2 ml) and water (2 ml) was added to a solution of (−)-XIII (0.0211 g) in 99% ethanol (10 ml). Homogeneous solution obtained on warming the mixture was allowed to stand at room temperature. Fine needles deposited after a week were dissolved on addition of the same solvent (5 ml) under warming. The homogeneous solution in a loosely stoppered flask was kept in a dark place at room temperature. After 3 months, single crystal of (−)-XV was obtained as a rod.

Found: C, 46.54; H, 4.53; Br, 38.22%. Calcd for $C_{16}H_{16}Br_2N_2 \cdot H_2O$: C, 46.40; H, 4.38; Br, 38.59%.

(−)-1,5-Dinitro-9,10-dihydro-9,10-ethanoanthracene (XVIII). To a warm solution of peracetic acid prepared by heating a mixture of chloroform (0.1 ml), 90% hydrogen peroxide (0.15 ml), concentrated sufuric acid (2 drops) and acetic anhydride (0.1 ml) was added dropwise a solution of (−)-XIV (51.7 mg) in chloroform (5 ml). After the mixture had been refluxed for 2.5 hr under stirring, the reaction mixture was poured onto water and extracted with chloroform. The extract, after washing and drying, was concentrated under reduced pressure to afford crystals (37.1 mg, 57.2%). A solution of the crystals in carbon tetrachloride–benzene (1:1) was passed through a column of alumina (7 g). The crystals (23.3 mg) obtained from the early filtrate (150 ml) were recrystallized twice from benzene–methanol to give pure (−)-XVIII, feather-like crystals, 10.7 mg, mp 206.3—207.3°C (racemate, mp 225.1—225.6°C), IR (Nujol mull): 1532 ($\nu_{as\ N-O}$), 1347 ($\nu_{s\ N-O}$) cm^{-1}, NMR: 2.00—2.90 (m, 6H, aromatic), 4.47 (broad s, 2H, bridgehead), 8.15 (broad s, 4H, ethane bridge).

Found: C, 64.71; H, 4.13%. Calcd for $C_{16}H_{12}N_2O_4$: C, 64.86; H, 4.08%.

(+)-1,5-Dimethoxy-9,10-dihydro-9,10-ethenoanthracene (XVII). To a solution of (+)-XIII (0.0573 g, 0.2446 mmol) in acetic acid (2 ml) was added dropwise a solution of sodium nitrite (0.047 g, 0.6812 mmol) in water (1.0 ml) under ice-cooling. After being stirred for further 1.5 hr at the same temperature, the solution of diazonium salt was added dropwise to boiling 6N sulfuric acid (24 ml) and reflux was continued for 1.5 hr. The reaction mixture was repeatedly extracted with ether. The ethereal extract, after washing and drying, was concentrated under reduced pressure. Crude (+)-phenol (XVI, 0.0434 g, 75.1%) obtained as a brown solid was methylated without purification. In the case of racemate, crude XVI was converted into diacetate by the usual method, and treated with lithium aluminum hydride in tetrahydrofuran to give pure (±)-XVI.

(±)-Diacetate: mp 176.7—177.1°C. Found: C, 74.99; H, 5.03%. Calcd for $C_{20}H_{16}O_4$: C, 74.99; H, 5.03%.

(±)-Phenol (XVI): mp 231.4—234.8°C (decomp.). Found: C, 81.05; H, 5.08%. Calcd for $C_{16}H_{12}O_2$: C, 81.34; H, 5.12%.

A mixture of crude (−)-XIV (43.4 mg), dimethyl sulfate (0.15 g), potassium carbonate (0.75 g) and acetone (13 ml) was refluxed for 18.5 hr. The reaction mixture was worked up in the usual way to give crude crystals (46.6 mg, 72% based on (+)-XIII). The crude crystals dissolved in carbon tetrachloride–benzene (1:1) were passed through a column of alumina (20 g). Colorless crystals (15.3 mg) obtained from the early eluate (200 ml) were recrystallized from methanol–benzene to yield pure (+)-XVII, colorless needles, 9.3 mg, mp 206.9—207.3°C (sealed tube) (racemate 210.0—210.4°C), NMR: 3.60—2.77 (m, 8H, aromatic and olefinic), 4.43 (t, 2H, bridgehead), 6.23 (s, 6H, $-OCH_3$).

Found: C, 82.13; H, 6.09%. Calcd for $C_{18}H_{16}O_2$: C, 81.79; H, 6.10%.

(−)-1,5-Bis(hydroxymethyl)-9,10-dihydro-9,10-ethenoanthracene XIX). A solution of (−)-IX (0.158 g, 0.494 mmol) in tetrahydrofuran (10 ml) was added to a suspension of lithium aluminum hydride (0.295 g) in the same solvent. After refluxing for 21 hr, ethyl acetate (5 ml), ice-water (5 ml) and 6N sulfuric acid (60 ml) were added successively to the reaction mixture under ice-cooling, and then extracted with ether. The extract, after washing and drying, afforded yellow liquid (0.143 g) on evaporation under reduced pressure. The liquid was chromatographed on silica gel (10 g) and eluted with benzene–ether (9: 1) to give pale yellow liquid (0.113 g, 86.7%) which could be crystallized from benzene–acetone, yielding pure (−)-XIX, colorless crystals, 0.0454 g, mp 154.5—155.1°C (racemate, mp 204.5—205.5°C), IR (Nujol mull): 3260 (ν_{O-H}) cm^{-1}.

Found: C, 81.72; H, 6.10%. Calcd for $C_{18}H_{16}O_2$: C, 81.79; H, 6.10%.

(−)-1,5-Dimethyl-9,10-dihydro-9,10-ethenoanthracene (XXII). To a solution of (−)-XIX (79.1 mg, 0.2993 mmol) in benzene (20 ml) was added thionyl chloride (2 ml). After the mixture had been refluxed for 10 hr, the volatile material was removed under reduced pressure to give crude XX (84.9 mg). Crude (−)-XX thus prepared was used in the following reaction. (±)-XX was recrystallized from ligroin to give pure material, mp 195.6—197.5°C, NMR: 2.47—3.23 (m, 8H, aromatic and olefinic), 4.41 (t, 2H, bridgehead), 5.23 (s, 4H, $-CH_2Cl$).

Found: C, 71.71; H, 4.78%. Calcd for $C_{18}H_{14}Cl_2$: C, 71.77; H, 4.69%.

Crude (−)-XX (84.9 mg) in acetone (15 ml) was refluxed for 6 hr with sodium iodide (0.2 g) under shielding from light. Crude crystals of (−)-XXI (102.4 mg) obtained by working up the reaction mixture in the usual way were dissolved in tetrahydrofuran (40 ml) and the solution was added to a stirred suspension of lithium aluminum hydride (0.2 g) in the same solvent (40 ml). After being refluxed for 25 hr, the reaction mixture was treated successively with ethyl acetate, water and 6N sulfuric acid and extracted with ether. The extract, after being washed and dried, was concentrated under reduced pressure. The resulting colorless liquid (58.6 mg, 84.3%) was distilled *in vacuo* to give pure (−)-XXII, bp 90—100°C/15 mmHg (bath temp.) which gave a spot on tlc, NMR: 2.72—3.36 (m, 8H, aromatic and olefinic), 4.66 (t, 2H, bridgehead), 7.58 (s, 6H, $-CH_3$).

(±)-XXII was obtained as crystals, mp 159.4—162.9°C (from methanol) which gave an identical UV spectrum in isooctane with that of (−)-XXII.

Found: C, 92.82; H, 7.03%. Calcd for $C_{18}H_{16}$: C, 93.06; H, 6.94%.

(−)-1,5-Dimethyl-9,10-dihydro-9,10-ethanoanthracene (XXIII). (−)-XXII (21.1 mg) in 99% ethanol was reduced over platinum oxide. The product dissolved in carbon tetrachloride was chromatographed on alumina (10 g). Crude crystals obtained from the early eluate (100 ml) were recrystallized from methanol to give pure (−)-XXIII, mp 92.4—94.7°C (racemate, mp 49.0—55.0°C), NMR: 2.79—3.18 (m, 6H, aromatic), 5.46 (s, 2H, bridgehead), 7.59 (s, 6H, $-CH_3$), 8.36 (t, 4H, ethane bridge).

Found: C, 91.99; H, 7.83%. Calcd for $C_{18}H_{18}$: C, 92.26; H, 7.74%.

Stereochemical Studies on the Halogenation of Sulfoxides. I. The Chlorination of Cyclic Sulfoxides[1]

Shinobu IRIUCHIJIMA, Mariko ISHIBASHI, and Gen-ichi TSUCHIHASHI

Sagami Chemical Research Center, Nishiohnuma, Sagamihara, Kanagawa 229

(Received June 5, 1972)

The cyclic sulfoxides, thiane 1-oxide, *cis*- or *trans*-4-chlorothiane 1-oxide, and *cis*- or *trans*-4-phenylthiane 1-oxide, were chlorinated with *t*-butyl hypochlorite, sulfuryl chloride, and chlorine in the presence of potassium acetate or pyridine. The stereoformulas of the products, together with those of the isomers having an inverted sulfoxide configuration, were determined by means of the IR and NMR spectral data and the R_f-values in the tlc. Consequently, it has been found that chlorination occurs when the sulfinyl oxygen is equatorial and that chlorine is always introduced at a *trans*-position to the sulfinyl lone pair to give rise to the *cis*-products. A mechanism accommodating these results is proposed. The conformation of the substituted thiane 1-oxide rings is also discussed.

The configurational stability of sulfoxides has been confirmed by the resolution of three sulfoxides,[2] and examples of geometrical isomerism attributable to the sulfinyl group has been reported.[3] Recently, a simple synthetic method of the optically active sulfoxides has been established,[4] and there has been much interest in the stereochemical aspects of sulfoxides.[5]

The α-halogenation of sulfoxides with halogenating agents in the presence of base is known to be a stereoselective reaction. For example, in the halogenation of benzyl methyl sulfoxide with iodobenzene dichloride or bromine in the presence of pyridine, it has been shown that the proton diastereotopic to the proton which is preferentially exchanged by deuterium in the presence of NaOD in D_2O is replaced with halogen stereospecifically.[6] The stereoselectivity was also observed in the chlorination of benzyl phenyl sulfoxide with *t*-butyl hypochlorite.[7]

In this and the following papers we would like to report on our stereochemical studies of the halogenation of the cyclic sulfoxides, designed to ascertain the stereochemical course of the reaction. The cyclic sulfoxides used were thiane 1-oxide, *cis*- or *trans*-4-chlorothiane 1-oxide,[8] and *cis*- or *trans*-4-phenylthiane 1-oxide.[9] The chlorination with *t*-butyl hypochlorite,[7] sulfuryl chloride,[10] and chlorine[11] in the presence of potassium acetate or pyridine will be described here, while the bromination with bromine/*N*-bromosuccinimide in the presence of pyridine[12] will be reported in the following paper.[13]

Results and Discussion

The Chlorination of Thiane 1-Oxide with t-*Butyl Hypochlorite.* The chlorination of six-membered thiane 1-oxide (**1**) with *t*-butyl hypochlorite in the presence of anhydrous potassium acetate in dichloromethane produced, stereospecifically, *cis*-2-chlorothiane 1-oxide (**2**) (Fig. 1) (mp 65.5—66.5°C) in an 88% yield. The inversion of the sulfoxide configuration of **2** with triethyloxonium tetrafluoroborate(Et_3OBF_4)[14] furnished *trans*-2-chlorothiane 1-oxide (**3**) (mp 43—44 °C) in a 74% yield.

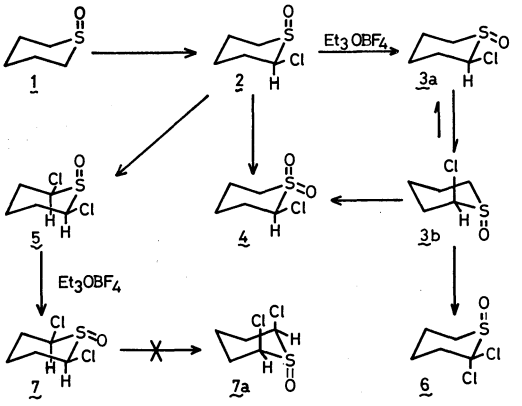

Fig. 1.

The stereoformulas of **2** and **3** were determined as follows. Aromatic solvent-induced shifts(ASIS; $\Delta = \delta_{CCl_4} - \delta_{C_6H_6}$), known as a useful method in deriving stereochemistry, are also applicable to the sulfoxides, as has been shown in the cases of penicillin sulfoxides,[15]

1) G. Tsuchihashi, S. Iriuchijima, and M. Ishibashi, Abstracts of the Third International Congress of Heterocyclic Chemistry: B, Sendai, Japan (1971), p. 624.

2) P. W. B. Harrison, J. Kenyon, and H. Phillips, *J. Chem. Soc.*, **1926**, 2079.

3) E. V. Bell and G. M. Bennett, *ibid.*, **1927**, 1798.

4) K. K. Andersen, *J. Org. Chem.*, **29**, 1953 (1964).

5) For example, C. R. Johnson and C. W. Schroeck, *J. Amer. Chem. Soc.*, **93**, 5303 (1971), T. Durst, R. Viau, R. Van Den Elzen, and C. H. Nguyen, *Chem. Commun.*, **1971**, 1334, and K. Nishihata and M. Nishio, *ibid.*, **1971**, 958.

6) M. Cinquini, S. Colonna, and F. Montanari, *ibid.*, **1969**, 607 and M. Cinquini and S. Colonna, *Boll. sci. Fac. Chim. ind. Bologna*, **27**, 201 (1969).

7) S. Iriuchijima and G. Tsuchihashi, *Tetrahedron Lett.*, **1969**, 5259.

8) J. C. Martin and J. J. Uebel, *J. Amer. Chem. Soc.*, **86**, 2936 (1964).

9) B. J. Hutchinson, K. K. Andersen, and A. R. Katritzky, *ibid.*, **91**, 3839 (1969).

10) G. Tsuchihashi, K. Ogura, S. Iriuchijima, and S. Tomisawa, *Synthesis*, **1971**, 89.

11) G. Tsuchihashi and S. Iriuchijima, This Bulletin, **43**, 2271 (1970).

12) S. Iriuchijima and G. Tsuchihashi, *Synthesis*, **1970**, 588.

13) S. Iriuchijima and G. Tsuchihashi, This Bulletin, **46**, 929 (1973).

14) C. R. Johnson and D. McCants, Jr., *J. Amer. Chem. Soc.*, **87**, 5404 (1965).

15) R. D. G. Cooper, P. V. DeMarco, J. C. Cheng, and N. D. Jones, *ibid.*, **91**, 1408 (1969); R. D. G. Cooper, P. V. DeMarco, D. O. Spry, *ibid.*, **91**, 1528 (1969); D. H. R. Barton, F. Comer, and P. G. Sammes, *ibid.*, **91**, 1529 (1969).

TABLE 1. NMR SPECTRAL DATA OF H-C_2 OF 2-CHLOROTHIANE 1-OXIDES (**2** AND **3**). $\Delta=\delta_{CCl_4}-\delta_{C_6H_6}$.

Solvent	**2**	**3**
CCl_4	4.88 q(ax) J=3.2, 9.3	4.72 m(eq)
C_6H_6	4.23 q(ax) J=3.1, 9.6	4.29 m(eq)
$CDCl_3$	4.91 oct(ax) J=1, 3, 8	4.69 m(eq)
CD_3CN	4.95 oct(ax) J=1, 3.3, 10	—
D_2O	5.71 oct(ax) J=1, 4, 8.3	5.36 q(ax) J=3.4, 8.7
CF_3COOH	5.33 oct(ax) J=1.5, 2.7, 6.6	5.02 q(ax) J=3, 7.5
CD_3OD	—	4.84 oct(ax) J=1, 3, 7.5
Δ	0.65	0.43

biotin sulfoxides,[16] and thiolane 1-oxide.[17] According to ASIS for the sulfoxides, the proton *trans* to the sulfinyl oxygen is more shielded and has a larger Δ-value than the proton *cis* to the sulfinyl oxygen, because aromatic systems like benzene coordinate at electron-deficient sites, avoiding a strongly negative sulfinyl oxygen atom (and probably a negative halogen atom, also). Therefore, the chlorinated product with a larger Δ-value(Δ=0.65) (Table 1) should possess a *cis*-form(**2**), while the inverted isomer with a smaller Δ-value(Δ=0.43) should possess a *trans*-form(**3**). This assignment is supported by the facts that the IR C–Cl stretching frequency of **2** is observed at 763 cm^{-1}(C-Cl_{eq}) while that of **3** is observed at 696 cm^{-1}(C-Cl_{ax})[18] in carbon disulfide, and that **3** is detected higher than **2** on a thin-layer plate of silica gel, indicating that **3** is a less polar substance than **2**. Moreover, in the polar solvents (CD_3CN, D_2O, and CF_3COOH), the H-C_2 of **3** was observed as axial, while in the non-polar solvents(CCl_4, $CDCl_3$, and C_6H_6), it was observed as equatorial rather than axial, whereas the H-C_2 of **2** was always observed as axial regardless of whether the solvent was polar or not (Table 1). This phenomenon can be well explained by saying that **2** has a stable *cis*-form possessing a preferable axial sulfinyl oxygen[8,19] and equatorial chlorine. On the other hand, since **3** has an unstable *trans*-form, its conformation changes with the solvent polarity; the polar conformation **3a** is favored in the polar solvents, while the less polar conformation **3b** dominates in the non-polar solvents. The possibility that **3**, which might be formed by the chlorination of **1**, was isomerized to the thermodynamically stable isomer(**2**) during the reaction was excluded by the fact that **2** was not produced at all when **3** was kept in the chlorination condition with 0.5 equivalent of *t*-butyl hypochlorite. After treatment with concentrated hydrochloric acid (1 volume) in dioxane (2 volumes), which is known to cause the complete racemization of sulfoxides,[20] **3** was recovered unchanged, whereas *cis*-4-chlorothiane 1-oxide(**10**) or *trans*-isomer(**8**) was equilibrated to a 47.5 : 52.5 mixture of **10** and **8**.[21] Therefore, **3** is a configurationally stable compound, and it is evident that **2** is directly formed by the chlorination of **1**.

The hydrogen peroxide oxidation of both **2** and **3** in acetic acid gave 2-chlorothiane 1,1-dioxide(**4**) (mp 68—69.5°C).

Further chlorination of **2** and **3** gave results which are quite informative of the reaction mechanism. The chlorination of **2** gave a mixture from which 2e,6e-dichlorothiane 1a-oxide(**5**) (mp 134—135°C), was subsequently isolated in a 37% yield as the major product, whereas the chlorination of **3** produced 2,2-dichlorothiane 1-oxide(**6**) (mp 34.5—36°C) in a 67% yield. The transformation of **5** with Et_3OBF_4 afforded 2e,6e-dichlorothiane 1e-oxide(**7**) (mp 129—130°C) in a 60% yield. The stereochemistry of **5** and **7** has been established on the basis of the NMR coupling constants, ASIS(Table 2), and tlc; **5** is detected higher than **7** on a thin-layer plate. According to the general rule which we found in a series of studies, a sulfoxide having an axial sulfinyl oxygen is observed higher on a thin-layer plate than the isomer having an equatorial oxygen if the other parts of the structures are the same.

TABLE 2. NMR SPECTRAL DATA OF H-C_2(AND H-C_6) OF 2,6-DICHLOROTHIANE 1-OXIDES (**5** AND **7**), 2-CHLORO-4-PHENYLTHIANE 1-OXIDES(**17** AND **18**), AND 2,6-DICHLORO-4-PHENYLTHIANE 1-OXIDES(**20** AND **21**). $\Delta=\delta_{CCl_4}-\delta_{C_6H_6}$.

	5	**7**	**17**	**18**	**20**	**21**
δ_{CCl_4}	4.45 ax	4.97 ax	5.14 eq	4.75 eq	4.52 ax	4.80 eq
$\delta_{C_6H_6}$	3.82	4.49	4.65	4.20	3.81	4.28
Δ	0.63	0.48	0.49	0.55	0.71	0.52

The Chlorination of 4-Chlorothiane 1-Oxides and 4-Phenylthiane 1-Oxides with t-*Butyl Hypochlorite.* The chlorination of *trans*-4-chlorothaine 1-oxide(**8**) gave, stereospecifically, 2e,4a-dichlorothiane 1a-oxide(**9**) (mp 72.5—74°C) in a 70% yield, while *cis*-4-chlorothiane 1-oxide(**10**) furnished, in a 66% yield, a 67 : 33 mixture of **9** and 2e,4e-dichlorothiane 1a-oxide(**11**) (mp 110—111.5°C) (Fig. 2). The inversion of **9** with Et_3OBF_4 gave 2a,4e-dichlorothiane 1a-oxide (**12**) (mp 92—93.5°C) in an 83% yield. The stereochemical structures of **9**, **11**, and **12** were established by means of the NMR coupling constants of H-C_2 and H-C_4, ASIS (Table 3), and by comparison with the corresponding bromo-derivatives.[13]

The oxidation of a mixture of **9** and **12** produced *trans*-2,4-dichlorothiane 1,1-dioxide(**13**) (mp 131.5—

16) R. Lett and A. Marquet, *Tetrahedron Lett.*, **1971**, 2855.
17) E. T. Strom, B. S. Snowden, Jr., and P. A. Toldan, *Chem. Commun.*, **1969**, 50.
18) K. Kojima and K. Sakashita, This Bulletin, **31**, 796 (1958).
19) J. B. Lambert and R. G. Keske, *J. Org. Chem.*, **31**, 3429 (1966).
20) K. Mislow, T. Simmons, J. T. Melillo, and A. L. Ternay, Jr., *J. Amer. Chem. Soc.*, **86**, 1452 (1964).
21) On the contrary to C. R. Johnson and D. McCants, Jr., *ibid.* **87**, 1109 (1965), in which a 65 : 35 mixture of **10** and **8** was obtained.

Table 3. NMR spectral data of H-C_2 and H-C_4 of 2,4-dichlorothiane 1-oxides(**9**, **11**, and **12**)

	9		**11**		**12**	
δ_{CCl_4}	4.94 ax	4.52 eq	4.32 ax	3.76 ax	4.83 eq	4.17 ax
$\delta_{C_6H_6}$	4.40	3.61	3.28	—	4.15	3.64
Δ	0.54	—	1.04	—	0.68	—

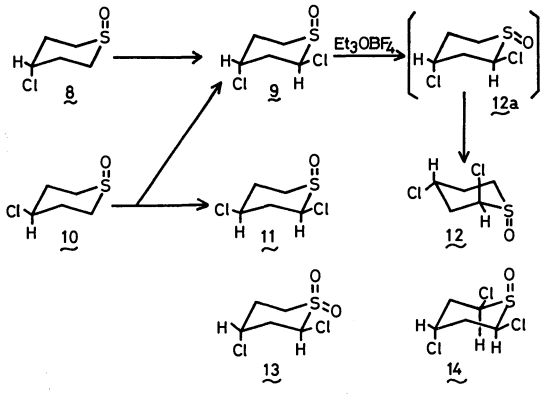

Fig. 2.

132°C) in a 71% yield.

The chlorination of conformationally rigid *trans*-4-phenylthiane 1-oxide(**15**) and *cis*-4-phenylthiane 1-oxide (**16**) in the presence of potassium acetate gave a single identical product, 2a-chloro-4e-phenylthiane 1e-oxide (**17**) (mp 160—160.5°C), in 83% and 66% yields respectively (Fig. 3). In the presence of pyridine, *cis*-oxide(**16**) gave **17** in a 45% yield. The product (**17**) was converted with Et_3OBF_4 into 2a-chloro-4e-phenylthiane 1a-oxide (**18**) (mp 94.5—95°C) in an 82% yield. The stereoformulas (**17** and **18**)[22] were based on the NMR (Table 2) and tlc; compound **18** possessing an axial oxygen is higher than **17**, which possesses an equatorial one. After treatment with concentrated hydrochloric acid in dioxane, compound

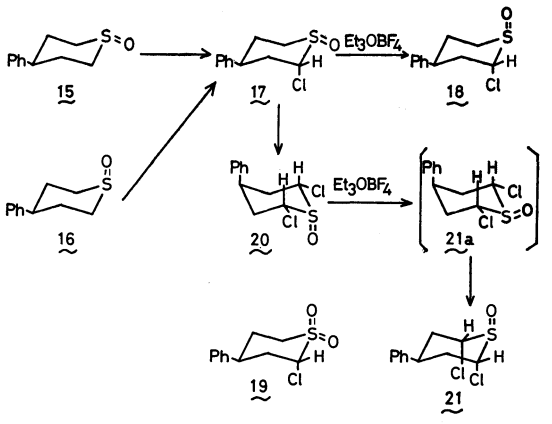

Fig. 3.

22) The stereoformulas of **17** and **18** together with **15** and **16** were unambiguously determined by the use of the shift-reagent, Eu(DPM)$_3$, and the decoupling study in the NMR spectra. M. Fukuyama, K. Sato, M. Fukuyama, S. Iriuchijima, and G. Tsuchihashi, Abstracts of the 26th Meeting of the Chemical Society of Japan: III, Kanagawa, Japan (1972). p. 1438.

17 was recovered quantitatively.

The oxidation of **17** gave *trans*-2-chloro-4-phenylthiane 1,1-dioxide(**19**) (mp 157.5—158.5°C) in a 93% yield.

The chlorination of **17** with 2.4 equivalents of *t*-butyl hypochlorite gave 2e,6e-dichloro-4a-phenylthiane 1a-oxide(**20**) (mp 119—120°C) in an 87% yield; this was then converted with Et_3OBF_4 into 2a,6a-dichloro-4e-phenylthiane 1a-oxide (**21**) (mp 101.5—102°C) in a 34% yield. The structures of **20** and **21** were established by the complete assignments of all their protons in the NMR spectra.

Mechanism of the Chlorination with t-*Butyl Hypochlorite.* The chlorination of the thiane 1-oxides(**1**, **2**, **3**, **8**, **10**, **15**, **16**, and **17**) with *t*-butyl hypochlorite described above gives products in which chlorine was always introduced at a *cis*-position to the sulfinyl oxygen, and it seems to occur when the oxygen is equatorial; compounds **15** and **17**, which possess an equatorial oxygen, are chlorinated at a *cis*-position to the oxygen, as is shown in Fig. 4. Compounds **1** and **8** which can easily take the conformations **1a** and **8a** by the inversion of the ring, are chlorinated at a *cis*-position to the equatorial oxygen in **1a** and **8a**. Compounds **2** and **3** seem to be chlorinated mainly in a manner similar to **1** and **8**. Compound **10**, the ring of which is appreciably fixed by an equatorial chlorine at C_4, is chlorinated partly by passing through the conformation **10a** (Route *a* in Fig. 4) and partly by passing through **8a**, with an inversion of the sulfoxide configuration (Route *b* in Fig. 4) to produce a mixture of **11** and **9**. The possibility of the intermediacy of **8a** is supported by the fact that the isomerization of

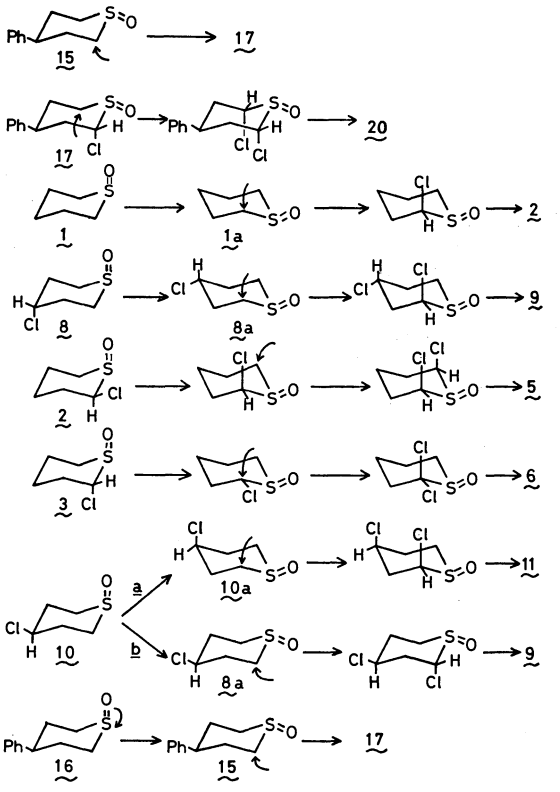

Fig. 4.

10 to **8** was observed in the chlorination of **10** with 0.3 equivalent of *t*-butyl hypochlorite. Compound **16**, the ring of which is rigidly fixed by a phenyl group, gives product **17**, accompanied by a complete sulfoxide inversion. Compound **16** might be chlorinated mainly *via* **15**, because the isomerization of **16** to **15** was observed in the chlorination of **16** with 0.5 equivalent of *t*-butyl hypochlorite.

It has been proposed that α-chlorosulfoxides can be obtained from the chloro-oxosulfonium ions *via* the ylids, either by a concerted rearrangement[23] or by an elimination-addition sequence analogous to a Pummerer-type rearrangement.[24] Our result is not compatible with the concerted rearrangement because the formation of the *trans*-product (**26**) should be expected by the process, as is shown in Fig. 5. Here, we would like to propose the mechanism shown in Fig. 6. The first step is the formation of the chloro-

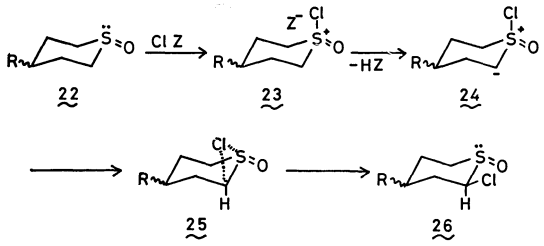

Fig. 5. Z=*t*-BuO, Cl; R=H, Cl, Ph.

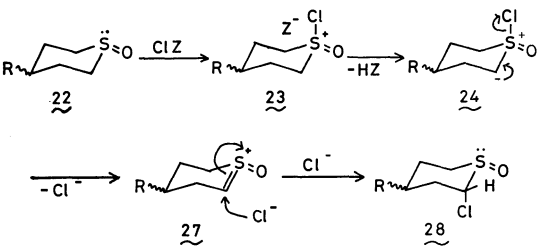

Fig. 6. Z=*t*-BuO, Cl; R=H, Cl, Ph.

oxosulfonium ion(**23**) by the attack of a positive chlorine of *t*-butyl hypochlorite on the sulfinyl lone pair. The second step is the formation of the hypothetical intermediate (**27**); the chloro-oxosulfonium ion (**23**) gives the ylid (**24**) by the action of the counter anion Z^-, which, in the present case, is the *t*-butoxide anion, and then **24** gives rise to **27** by the elimination of the chloride ion. The final step is the addition of the chloride ion to **27**, thus producing the α-chlorosulfoxide(**28**), in which the chlorine atom and sulfinyl lone pair are in the *trans* relationship. Although we do not have any direct evidence of the intervention of the chloride ion, an analogous mechanism has been proposed in the Pummerer rearrangement.[25] We have stated that chlorine is always introduced at a *cis*-position to the sulfinyl oxygen, but according to this mechanism we should say that chlorine is always introduced at a *trans*-position to the sulfinyl lone pair.

The Conformational Stability of the Substituted Thiane 1-Oxides. It is known that thiane 1-oxide(**1**)[19] and *trans*-4-chlorothiane 1-oxide(**8**)[8] exhibit a conformational preference for the forms with the sulfoxide oxygen axial, and that, in 4-substituted thiane 1-oxides such as **15** and **16**, the isomer bearing the axial oxygen is more stable.[26] In addition to this knowledge, we have found that a preferable conformer of **3** is **3a** in the polar solvents and **3b** in the non-polar solvents. Moreover, **7** is a preferable conformer to **7a**, probably because **7a** possesses two axial chlorine atoms which are highly unfavorable because of a 1,3-diaxial relationship, although it possesses a favorable axial oxygen. In **17** an equatorial phenyl group can hold the ring against the unfavorable equatorial sulfinyl oxygen and axial chlorine. In **20**, however, the phenyl group cannot hold the ring against the 1,3-diaxial chlorine atoms and equatorial oxygen; instead, the diequatorial chlorine atoms and axial oxygen keep the ring against the unfavorable axial phenyl group. In compound **21** which was obtained by the inversion of the sulfoxide configuration of **20** with Et_3OBF_4, the equatorial phenyl group and the axial oxygen together keep the ring against the 1,3-diaxial chlorine atoms. Thus, in the thiane 1-oxide ring, (1) an equatorial phenyl group keeps both a sulfinyl oxygen equatorial and a chlorine atom axial (Ph> >S=O+Cl); (2) the combination of 1,3-diequatorial chlorine atoms and an axial sulfinyl oxygen keeps a phenyl group axial(1,3-diCl+ >S=O> Ph), and (3) the combination of an euqatorial phenyl group and an axial sulfinyl oxygen keeps two chlorine atoms diaxial (Ph+ >S=O>1,3-diCl).

The Chlorination with Other Chlorinating Agents. The chlorination of **15** with 0.8 equivalent of sulfuryl chloride in the presence of pyridine produced, stereospecifically, **17**, the same product as was obtained with *t*-butyl hypochlorite, in a 79% yield. The chlorination of **16** with 0.8 equivalent of sulfuryl chloride furnished the same product(**17**) in a 62% yield, while with 1.2 equivalent it gave a mixture of **17** (79% yield) and **20** (16% yield).

The chlorination of **1** with chlorine in the presence of pyridine gave a mixture of **2**(54.5% yield) and **5** (18% yield), though 19% of **1** was also recovered. The chlorination of **8** afforded **9** in a 68% yield, together with **11**(7% yield), while **10** gave, in an 87% yield, a mixture of **9** and **11** in a 3 : 7 ratio, a converse ratio to that obtained in the chlorination with *t*-butyl hypochlorite. In the reaction with *t*-butyl hypochlorite in the presence of potassium acetate, **10** was chlorinated, mainly *via* Route *b*, to produce **9** as the major product, whereas with chlorine in the presence of pyridine **10** was chlorinated, mainly *via* Route *a*, to give **11** as the major component. Compound **15** furnished **17** in a 63% yield, plus small amounts of **20**. **16** also gave **17** in 80% and 62% yields, plus small amounts of **20**.

The chlorination of the cyclic sulfoxides with sul-

23) M. Cinquini, S. Colonna, and F. Montanari, *Chem. Commun.*, **1970**, 1442.
24) T. Durst and K.-C. Tin, *Can. J. Chem.*, **49**, 2374 (1971).
25) C. R. Johnson and W. G. Phillips, *J. Amer. Chem. Soc.*, **91**, 682 (1969).
26) C. R. Johnson and D. McCants, Jr., *ibid.*, **86**, 2936 (1964)

furyl chloride or chlorine in the presence of pyridine seems to be nearly the same as the reaction with *t*-butyl hypochlorite, except that dichlorides can be easily obtained and that the ratio of the isomers (if any are obtained) may be different. Accordingly, the mechanism shown in Fig. 6 can also be applied to the reaction with sulfuryl chloride or chlorine (Z=Cl) in the presence of pyridine.

Experimental

Unless otherwise noted, the NMR spectra were measured with a Varian HA-100 spectrometer and/or a Hitachi R-20B spectrometer in a concentration of 40—50 mg in 0.4 ml of $CDCl_3$, while the IR spectra were recorded with a KBr pellet using a Hitachi EPI-G3 spectrometer. HHW in the NMR spectral data means half-height width. In the crystallization solvents, B, C, and H stand for benzene, cyclohexane, and hexane respectively, and B/C/H means that the crystal was dissolved in benzene, followed by the successive addition of cyclohexane and hexane.

*Chlorination of Thiane 1-Oxide(**1**) to* cis*-2-Chlorothiane 1-Oxide(**2**) with* t*-BuOCl.* *(a) In the Presence of Potassium Acetate*: To a stirred mixture of **1**(405 mg, 3.16 mmol) and potassium acetate(0.82 g, 8.4 mmol) in 20 ml of CH_2Cl_2 was added 0.34 ml(3.1 mmol) of *t*-BuOCl at 0°C. After the mixture had then been stirred for 2 hr, 20 ml of water was added. The mixture was extracted with CH_2Cl_2, and the extract was dried over Na_2SO_4 and evaporated to give white crystals. Recrystallization from C/H afforded 423 mg(2.78 mmol; 88%) of **2**, which was then recrystallized to give mp 65.5—66.5°C. IR: 755, 1050(S=O) cm^{-1}. IR(5% in CS_2): 763(C-Cl_{eq}), 1047, 1080(S=O) cm^{-1}. NMR($CDCl_3$): 1.2—3.4(8H), 4.91(1H, octet, J=1, 3, 8). NMR(CCl_4): 1.2—3.3(8H), 4.88(1H, q, J=3.2, 9.3). NMR(C_6H_6): 0.4—2.75(8H), 4.23(1H, q, J=3.1, 9.6). NMR(D_2O): 1.85—3.8(8H), 5.71(1H, octet, J=1, 4, 8.3). NMR(CD_3CN): 1.3—3.1(8H), 4.95(1H, octet, J=1,3.3, 10). NMR(CF_3COOH): 1.5—3.65(8H), 5.33(1H, octet, J=1.5, 2.7, 6.6). Mass: *m/e* 152(M^+), 41 (base peak). Found: C, 39.59; H, 6.13; Cl, 23.34%. Calcd for C_5H_9ClOS: C, 39.35; H, 5.94; Cl, 23.23%.

(b) In the Presence of Pyridine: To a stirred solution of **1**(0.50 g, 3.91 mmol) and pyridine(0.63 ml, 7.82 mmol) in 20 ml of CH_2Cl_2 at 0°C was added *t*-BuOCl(0.43 ml, 3.91 mmol). The solution was stirred for 1.5 hr, and then 25 ml of 0.5 N aqueous sulfuric acid was added and it was extracted with CH_2Cl_2. The subsequent evaporation of the solvent and the crystallization of the residue from B/C gave 407 mg(2.67 mmol; 68.2%) of **2**, identified by means of mp, IR, NMR, and tlc.

*Transformation of **2** to* trans*-2-Chlorothiane 1-Oxide(**3**) with Et_3OBF_4.* 1.2 g(6.3 mmol) of Et_3OBF_4 was added to a solution of 625 mg(4.1 mmol) of **2** in 5 ml of CH_2Cl_2. After the mixture had been stirred at room temperature for 1 hr, 40 ml of anhydrous ether was added at 0°C to give oily ethoxysulfonium salt as a precipitation. After the mixture had been stirred for 2 hr, the solvents were removed by decantation, and to the residue was added 20 ml of a 0.5 N NaOH solution. The mixture was then extracted with CH_2Cl_2. The solvent was dried over Na_2SO_4 and evaporated to give a residue which was subsequently chromatographed on silica gel with benzene. Elution with benzene containing 2% ethyl acetate then furnished 465 mg(3.05 mmol; 74.3%) of **3**. The continuation of the elution gave a small amount of **2**. **3** is eluted faster and is detected higher than **2** on a thin-layer plate. Recrystallization from B/C/H at 0°C gave mp 43—44°C. **3** is hygroscopic. IR(Nujol): 697, 954, 1029, 1059(S=O) cm^{-1}. IR(5% in CS_2): 696 (C-Cl_{ax}), 950, 1030, 1063(S=O) cm^{-1}. NMR($CDCl_3$): 1.45—3.28 (8H), 4.69(1H, m, HHW=11). NMR(CCl_4): 1.43—3.2 (8H), 4.72(1H, m, HHW=10). NMR(C_6H_6): 0.8—2.7 (8H), 4.29(1H, m, HHW=11). NMR(CF_3COOH): 1.5—3.65(8H), 5.02(1H, q, J=3, 7.5). NMR(CD_3OD): 1.42—3.4(8H), 4.84(1H, octet, J=1, 3, 7.5). NMR(D_2O): 1.8—4.03(8H), 5.36(1H, q, J=3.4, 8.7). Mass: *m/e* 152 (M^+). Found: C, 39.60; H, 6.07; Cl, 23.23%. Calcd for C_5H_9ClOS: C, 39.35; H, 5.94; Cl, 23.23%.

*Oxidation of **2** to 2-Chlorothiane 1,1-Dioxide (**4**).* The oxidation of **2** by the usual method with 30% H_2O_2 in acetic acid gave **4**. Recrystallization from B/C/H afforded mp 68—69.5°C. IR(Nujol): 1127, 1161, 1280, 1312 cm^{-1}. NMR: 1.3—3.7(8H), 4.75(1H, octet, J=2, 3.5, 6.5). Mass: *m/e* 168(M^+), 42(base peak). Found: C, 35.95; H, 5.36%. Calcd for $C_5H_9ClO_2S$: C, 35.61; H, 5.38%.

*Chlorination of **2** with* t*-BuOCl.* 153 mg(1 mmol) of **2** was chlorinated with 0.13 ml(1.15 mmol) of *t*-BuOCl in the presence of potassium acetate(0.32 g, 3.26 mmol) in 5 ml of CH_2Cl_2 at room temperature for 2 hr. The NMR spectrum of the crude extract after the usual work-up indicated that 2e,6e-dichlorothiane 1a-oxide (**5**) was obtained as the major product. Crystallization from B/C at 0°C gave 0.70 g(0.374 mmol; 37.4%) of **5**. Recrystallizations from CCl_4 gave mp 134—135°C. IR(Nujol): 752, 1060(S=O) cm^{-1}. NMR: 1.3—2.7(6H), 4.69(2H, q, J=3.8, 12.2). NMR(7 mg in 1 ml of CCl_4): 4.45(q, J=3, 12). NMR(25 mg in 0.3 ml of C_6H_6): 0.45—1.60(4H), 1.80—2.60(2H), 3.82(2H, q, J=3.5, 12). Mass: *m/e* 186(M^+), 75(base peak). Found: C, 32.18; H, 4.27; Cl, 37.89%. Calcd for $C_5H_8Cl_2OS$: C, 32.10; H, 4.31; Cl, 37.90%.

*Chlorination of **3** with* t*-BuOCl.* *(a) With 1.1 equiv of* t*-BuOCl*: 177 mg(1.16 mmol) of **3** was chlorinated with 0.145 ml(12.8 mmol) of *t*-BuOCl in the presence of potassium acetate(0.34 g, 3.48 mmol) in 10 ml of CH_2Cl_2 at room temperature for 1 hr. The NMR of the extract showed the major product to be 2,2-dichlorothiane 1-oxide (**6**). Chromatography with benzene/hexane (7 : 3), followed by elution with a (8 : 2) mixture, afforded 145 mg(0.775 mmol; 66.7%) of **6**, which was then crystallized at −20°C. Recrystallization from hexane at 0°C gave mp 34.5—36°C. IR (Nujol): 776, 945, 958, 1034, 1080, 1411 cm^{-1}. NMR: 1.55—3.37(8H) [1.55—2.6(5H), 2.75—3.37 (3H)]. Mass: *m/e* 186(M^+), 151(base peak). Found: C, 32.24; H, 4.31; Cl, 37.64%. Calcd for $C_5H_8Cl_2OS$: C, 32.10; H, 4.31; Cl, 37.90%.

(b) With 0.5 equiv of t*-BuOCl*: A mixture of **3**(101 mg, 0.665 mmol), potassium acetate(40 mg, 0.41 mmol), and *t*-BuOCl(0.036 ml, 0.33 mmol) in 10 ml of CH_2Cl_2 was stirred at room temperature for 3 hr. The usual work-up gave 98 mg of the white crystals, in which **2** was not detected by studying the NMR spectrum.

*Transformation of **5** to 2e,6e-Dichlorothiane 1e-Oxide (**7**).* A solution of **5**(425 mg, 2.27 mmol) and Et_3OBF_4(0.65 g, 3.4 mmol) in 3 ml of CH_2Cl_2 was stirred at room temperature for 2 hr. The usual work-up gave a residue, which was then crystallized on standing. Recrystallization from B/C/H gave 255 mg(1.36 mmol; 60.0%) of **7**, showing mp 129—130°C(sintered at *ca.* 100°C) on further recrystallization. IR(Nujol): 758, 1071(S=O) cm^{-1}. NMR: 1.5—2.25(4H) 2.35—2.65(2H), 4.72(2H, q, J=3.5, 11). NMR(12 mg in 0.7 ml of CCl_4): 1.7—2.2(4H), 2.3—2.65(2H), 4.97(2H, J=3, 10.5). NMR(12 mg in 0.3 ml of C_6H_6): 0.5—2.0 (6H), 4.49(2H, q, J=4, 10.5). NMR(CF_3COOH): 1.7—

3.0(6H), 5.05(2H, q, J=3.5, 11.5). Found: C, 32.23; H, 4.10%. Calcd for $C_5H_8Cl_2OS$: C, 32.10; H, 4.31%.

Chlorination of **8** *to 2e,4a-Dichlorothiane 1a-Oxide (***9***) with* t-*BuOCl.* To a stirred, suspended solution of **5**(454 mg, 2.98 mmol) and potassium acetate (322 mg, 3.28 mmol) in 15 ml of CH_2Cl_2 at 0°C was added 0.36 ml(3.28 mmol) of *t*-BuOCl. The mixture was stirred at 0°C for 4 hr. The usual work-up gave a residue, which was then chromatographed with benzene. Elution with 1% ethyl acetate in benzene gave 0.39 g(2.09 mmol; 70.0%) of **9**. 80 mg(0.53 mmol) of **8**(containing 10% of **10**) was recovered with benzene–ethyl acetate(85 : 15). The recrystallizations of **9** with B/H gave mp 72.5—74°C. IR: 570, 688, 780, 1000—1090 cm^{-1}. IR(5% in CS_2): 572, 692, 787, 1076 cm^{-1}. NMR($CDCl_3$): 1.80—3.17(6H), 4.51(1H, m, HHW=9), 5.00(1H, q, J=3, 11). NMR(CCl_4): 4.52(1H, m, HHW=8.5), 4.94(1H). NMR(C_6H_6): 3.61(1H, m, HHW=9), 4.40(1H). NMR(CF_3COOH): 4.52(1H, m, HHW=11), 5.27(1H). Mass: *m/e* 186(M^+), 101(base peak). Found: C, 32.06; H, 4.24; Cl, 38.07%. Calcd for C_5H_8ClOS: C, 32.10; H, 4.31; Cl, 37.90%.

Chlorination of **10** *with* t-*BuOCl.* *(a) With 1.1 equiv of* t-*BuOCl*: To a stirred mixture of **10** (465 mg, 3.04 mmol) and potassium acetate (0.33 g, 3.36 mmol) in 15 ml of CH_2Cl_2 was added 0.37 ml (3.36 mmol) of *t*-BuOCl at 0°C. The mixture was stirred at 0°C for 2 hr. The NMR spectrum of the crude extract obtained by the usual work-up showed it to be a 67 : 33 mixture of **9** and 2e, 4e-dichlorothiane 1a-oxide(**11**). Chromatography with benzene, followed by elution with 1% ethyl acetate–benzene, gave 375 mg(2.0 mmol; 65.7%) of a mixture of **9** and **11**, while 108 mg(0.71 mmol) of a 35 : 65 mixture of **8** and **10** was recovered with a 1 : 1 mixture of benzene and ethyl acetate. Since **9** is eluted faster than **11** in silica gel chromatography, **9** was isolated from the first fractions, while **11** was isolated from the last. **9** was identified by mp, IR and NMR(CCl_4). **11** has mp 110—111.5°C from B/H. IR: 730, 792, 1000—1090 cm^{-1}. NMR: 1.80—3.43(6H), 3.96(1H, septet, J=4, 4, 8, 8), 4.62(1H, q, J=4.5, 11). NMR(4 mg in 0.4 ml of CCl_4): 3.76(1H), 4.32(1H). NMR(8 mg in 0.4 ml of of C_6H_6): 0.96—2.99(7H), 3.28(1H). NMR(8 mg in 0.5 ml of CF_3COOH): 3.95(1H), 4.78(1H). Mass: *m/e* 186(M^+), 101(base peak). Found: C, 32.10; H, 4.30; Cl, 38.09%. Calcd for $C_5H_8Cl_2OS$: C, 32.10; H, 4.31; Cl, 37.90%.

(b) With 0.3 equiv of t-*BuOCl*: A solution of **10** (100 mg, 0.655 mmol), potassium acetate (30 mg, 0.33 mmol), and *t*-BuOCl (0.023 ml, 0.204 mmol) in 8 ml of CH_2Cl_2 was stirred for 1.5 hr. The NMR spectrum of the extract showed that **8**, **9**, and **10** were obtained in a ratio of 35 : 89 : 100. A 26.5 : 73.5 mixture (33 mg) of **8** and **10** was recovered by chromatography.

Transformation of **9** *to 2a,4e-Dichlorothiane 1a-Oxide (***12***).* A solution of **9**(185 mg, 0.99 mmol) and Et_3OBF_4 (0.38 g, 1.99 mmol) in 3 ml of CH_2Cl_2 was stirred for 1 hr. The usual work-up gave white crystals at −20°C. Recrystallization from B/H afforded 153 mg(0.82 mmol; 82.7%) of **12**, with mp 92—93.5°C.

IR: 580, 650, 700, 800, 1000—1100 cm^{-1}. NMR(CDCl): 2.00—3.50(6H), 4.25(1H, nonet, J=3.5, 3.5, 11, 11), 4.86 (1H, m, HHW=10). NMR(CCl_4): 4.17(1H), 4.83(1H, m, HHW=7.5). NMR(C_6H_6): 3.64(1H), 4.15(1H, m, HHW=10). NMR(CF_3COOH): 4.38(1H, septet, J=3.5, 3.5, 7, 7), 5.31(1H, q, J=3.5, 8). Mass: *m/e* 186(M^+). Found: C, 32.17; H, 4.41; Cl, 38.02%. Calcd for $C_5H_8Cl_2OS$: C, 32.10; H, 4.31; Cl, 37.90%.

trans-*2,4-Dichlorothiane 1,1-Dioxide (***13***).* A solution of **9** (63 mg), **12**(65 mg), and 30% H_2O_2 (0.11 ml; 1.1 mmol) in 2 ml of acetic acid was kept at 45°C for 15 hr. The subsequent addition of Na_2CO_3, followed by extraction with CH_2Cl_2 and the evaporation of the solvent, gave 0.11 g (0.545 mmol; 71.0%) of **13** as white crystals. Recrystallizations from $CHCl_3$/H gave mp 131.5—132°C. IR: 1150, 1323 cm^{-1}. NMR: 2.66(4H, m), 3.40(2H, t, J=6, 6), 4.51(1H, quintet, J=5—6, 5—6, 5—6, 5—6), 5.00(1H, q, J=5.5, 8). Mass: *m/e* 202(M^+), 75(base peak). Found: C, 29.39; H, 3.98; S, 15.60%. Calcd for $C_5H_8Cl_2O_2S$: C, 29.57; H, 3.97; S, 15.79%.

*2e,4a,6e-Trichlorothiane 1a-Oxide (***14***).* To a stirred mixture of **8**(0.12 g, 0.785 mmol), **10**(0.12 g, 0.785 mmol), and potassium acetate(0.62 g, 6.3 mmol) in 15 ml of CH_2Cl_2 was added 0.69 ml (6.28 mmol) of *t*-BuOCl at 0°C, and the mixture was stirred for 1.5 hr. The usual work-up gave 0.33 g(1.49 mmol; 94.9%) of the white crystals (**14**). Recrystallizations from B/H gave mp 139.5—140.5°C. IR: 1056 cm^{-1}. NMR: 2.35(2H, sextet, J=3.5, 3.5, 15), 2.82(2H, septet, J=3.5, 12, 15), 4.52(1H, quintet, J=*ca.* 3.5, 3.5, 3.5, 3.5), 5.07(2H, q, J=3.5, 12). Mass: *m/e* 220(M^+), 135(base peak). Found: C, 27.33; H, 3.27; S, 14.52%. Calcd for $C_5H_7Cl_3OS$: C, 27.11; H, 3.19; S, 14.47%.

Chlorination of **15** *to 2a-Chloro-4e-phenylthiane 1e-Oxide (***17***) with* t-*BuOCl.* To a stirred mixture of **15**(159 mg, 0.815 mmol) and potassium acetate(0.16 g, 1.63 mmol) in 10 ml of CH_2Cl_2 was added 0.09 ml(0.82 mmol) of *t*-BuOCl at 0°C, and the mixture was stirred at 0°C for 2 hr. The usual work-up gave yellowish white crystals, which were later recrystallized from B/H to give 154 mg(0.675 mmol; 82.8%) of **17**. Further recrystallization from B/H gave mp 160—160.5°C. IR(Nujol): 689, 710, 773, 1072(S=O) cm^{-1}. NMR($CDCl_3$): 1.92—2.20 (2H), 2.30—2.25 (2H), 2.97—3.43 (3H), 5.30(1H, m, HHW=8), 7.23(5H, m). NMR(CCl_4): 5.14 (1H, m, HHW=8). NMR(C_6H_6): 4.65(1H, m, HHW=8.5). NMR(CF_3COOH): 5.64(1H, m, HHW=8). Mass: *m/e* 228(M^+), 117(base peak). Found: C, 57.53; H, 5.84; Cl, 15.77%. Calcd for $C_{11}H_{13}ClOS$: C, 57.76; H, 5.73; Cl, 15.50%.

Chlorination of **16** *to* **17** *with* t-*BuOCl.* *(a) With 1.0 equiv of* t-*BuOCl*: A mixture of **16** (0.15 g, 0.77 mmol), potassium acetate(0.15 g, 1.54 mmol), and *t*-BuOCl(0.085 ml, 0.77 mmol) in 10 ml of CH_2Cl_2 was stirred at 0°C for 3.5 hr. The NMR spectra($CDCl_3$ and C_6H_6) of the crude crystals obtained by the usual work-up revealed that **17** was the sole product. Recrystallization from B/H gave 117 mg(0.51 mmol; 66.4%) of **17**, identified by mp, IR, NMR, and tlc.

(b) With 0.5 *equiv of* t-*BuOCl in the Presence of Potassium Acetate*: A solution of **16** (200 mg, 1.03 mmol), potassium acetate(51 mg, 0.52 mmol), and *t*-BuOCl (0.06 ml, 0.53 mmol in 10 ml of CH_2Cl_2 was stirred for 3 hr. The usual work-up followed by chromatography gave 120 mg (0.53 mmol) of **17** and 73 mg of a 23 : 77 mixture of **15** and **16**.

(c) In the Presence of Pyridine: A mixture of **16** (154 mg, 0.79 mmol), pyridine (0.14 ml, 1.74 mmol), and *t*-BuOCl (0.90 ml, 0.80 mmol) in 10 ml of CH_2Cl_2 was stirred at 0°C for 3 hr. The usual work-up followed by chromatography gave 81 mg (0.356 mmol; 45.0%) of **17**, eluted with 1% ethyl acetate in benzene.

Transformation of **17** *to 2a-Chloro-4e-phenylthiane 1a-Oxide (***18***).* A solution of **17**(148 mg, 0.647 mmol) and Et_3OBF_4 (0.25 g, 1.31 mmol) in 3 ml of CH_2Cl_2 was stirred at room temperature for 1 hr. The usual work-up gave a white solid, which was subsequently crystallized from C/H to afford 121 mg(81.6%) of **18**. Chromatographic purifi-

cation with benzene–ethyl acetate(99 : 1), followed by recrystallization from B/H gave, a pure sample with mp 94.5—95.0°C. IR: 691, 1053, 1497, 1602 cm^{-1}. NMR-($CDCl_3$): 1.65—3.43(7H), 4.89(1H, m, HHW=7), 7.25(5H, s). NMR(CCl_4): 4.75(1H, m, HHW=7). NMR(C_6H_6): 4.20(1H, m, HHW=6.5). Mass: *m/e* 228(M^+). Found: C, 57.51; H, 5.79; Cl, 15.75%. Calcd for $C_{11}H_{13}ClOS$: C, 57.76; H, 5.73; Cl, 15.50%.

*Treatment of Chlorothiane 1-Oxides(**2**, **3**, **8**, **10**, and **17**) with Concentrated Hydrochloric Acid(1 vol) in Dioxane (2 vol).*

*(a) **2***: To a stirred solution of **2** (50 mg) in 6 ml of dioxane was added 3 ml of concentrated HCl at room temperature, after which the mixture was stirred for 1 hr. The addition of water and subsequent extraction with CH_2Cl_2 gave 48 mg of white crystals, the NMR spectrum of which showed that **2** was recovered unchanged.

*(b) **3***: A solution of **3**(92 mg) in a mixture of concentrated HCl(3 ml) and dioxane (6 ml) was stirred at room temperature for 1 hr. The usual work-up gave 89 mg of white crystals, the NMR spectrum of which showed that **3** was recovered quantitatively.

*(c) **8***: A solution of **8** (50 mg) in the same reagent(9 ml) was stirred for 1 hr. The usual work-up gave a 52 : 48 mixture (49 mg) of **8** and **10**.

*(d) **10***: A solution of **10** (52 mg) in 9 ml of the reagent was stirred for 1 hr. A work-up gave a 53 : 47 mixture (47 mg) of **8** and **10**.

*(e) **17***: A solution of **17**(56 mg) in 9 ml of the reagent was stirred for 1 hr. A work-up afforded 52 mg of **17**.

*Oxidation of **17** to trans-2-Chloro-4-phenylthiane 1,1-Dioxide (**19**).* A solution of **17**(0.19 g, 0.83 mmol) and 30% H_2O_2(0.18 ml, 1.76 mmol) in 2 ml of acetic acid was kept at 45°C for 15 hr. The subsequent addition of water furnished white crystals, which were then filtered off, washed with water, and dried under a vacuum to give 188 mg(0.77 mmol; 93%) of **19**. Recrystallizations from B/H gave mp 157.5—158.5°C. IR: 1136, 1330 cm^{-1}. NMR: 2.10—3.97(7H), 4.82(1H, q, J=3.5, 6), 7.28(5H, s). Mass: *m/e* 244(M^+), 117(base peak). Found: C, 53.90; H, 5.42; S, 13.01%. Calcd for $C_{11}H_{13}ClO_2S$: C, 53.98; H, 5.35; S, 13.10%.

*Chlorination of **17** to 2e,6e-Dichloro-4a-phenylthiane 1a-Oxide (**20**) with t-BuOCl.* A mixture of **17**(250 mg, 1.09 mmol), potassium acetate(215 mg, 2.18 mmol), and *t*-BuOCl 0.12 ml, 1.06 mmol) in 15 ml of CH_2Cl_2 was stirred for 1 hr. An additional 0.06 ml(0.53 mmol) of *t*-BuOCl was then added, and after 1 hr's stirring, 0.10 ml(0.885 mmol) of *t*-BuOCl was added. After stirring for 1 more hr, the usual work-up furnished white crystals, which were recrystallized from $CHCl_3$/H to give 252 mg(0.95 mmol; 87.2%) of **21**. Further purification by chromatography and recrystallizations from $CHCl_3$/H gave an analytical sample with mp 119—120°C. IR: 1078, 1495, 1598 cm^{-1}. NMR: 2.25—3.70(5H), 4.73(2H, q, J=4, 10). NMR(15 mg in 0.6 ml of CCl_4): 2.47(H_{eq}–C_3 and –C_5, sextet, J=3—4, 3—4, 14), 2.89(H_{ax}–C_3 and –C_5, octet, J=3—4, 12, 14), 3.41(H_{eq}–C_4, quintet, J=3—4, 3—4, 3—4, 3—4), 4.52(H_{ax}–C_2 and –C_6, q, J=3—4, 12). NMR(25 mg in 0.4 ml of C_6H_6): 1.98(2H), 2.60(2H), 2.64(1H), 3.81(2H). Mass: *m/e* 262(M^+), 115 (base peak). Found: C, 49.97; H, 4.56; S, 12.24%. Calcd for $C_{11}H_{12}Cl_2OS$: C, 50.20; H, 4.60; S, 12.18%.

*Conversion of **20** to 2a,6a-Dichloro-4e-phenylthiane 1a-Oxide (**21**).* A solution of **20**(132 mg, 0.50 mmol) and Et_3O-BF_4(0.20 g, 1.05 mmol) in 4 ml of CH_2Cl_2 was stirred for 1 hr. The subsequent recrystallization from $CHCl_3$/H of the crude crystals obtained by the usual work-up gave 45 mg (0.172 mmol; 34.2%) of **21**, with mp 101.5—102°C. IR: 1052, 1493, 1600 cm^{-1}. NMR(CCl_4): 2.16(H_{eq}–C_3 and –C_5, sextet, J=3, 3, 15.5), 2.93(H_{ax}–C_3 and –C_5, octet, J=3, 11, 15.5), 3.47(H_{ax}–C_4, nonet, J=3, 3, 11, 11), 4.80 (H_{eq}–C_2 and –C_6, m). NMR(C_6H_6): 1.68(2H), 2.60(2H), 3.32 (1H), 4.28(2H). Mass: *m/e* 262(M^+). Found: C, 50.21; H, 4.64; S, 12.15%. Calcd for $C_{11}H_{12}Cl_2OS$: C, 50.20; H, 4.60; S, 12.18%.

*Chlorination of **15** to **17** with SO_2Cl_2.* To a stirred solution of **15** (120 mg, 0.617 mmol) and pyridine (0.15 ml, 1.86 mmol) in 15 ml of CH_2Cl_2 was added 0.04 ml(0.494 mmol) of SO_2Cl_2 at 0°C, after which the mixture was stirred for 1 hr. The usual work-up gave crude white crystals which were subsequently dissolved in 1.0 ml of $CDCl_3$ with 36.0 mg(0.153 mmol) of bromomethyl phenyl sulfone as the standard. The NMR spectrum of the solution showed that **17** was produced, and through the NMR integral of the H–C_2 of **17** and the –CH_2– of bromomethyl phenyl sulfone, the yield of **17** was estimated to be 79%.

*Chlorination of **16** with SO_2Cl_2. (a) With 0.8 equiv of SO_2Cl_2*: A solution of **16** (120 mg, 0.617 mmol), pyridine (0.15 ml, 1.86 mmol), and SO_2Cl_2(0.04 ml, 0.494 mmol) in 15 ml of CH_2Cl_2 was stirred at 0°C for 2 hr. The NMR spectrum of the reddish crystals obtained by the usual work-up showed that **17** was produced in a 61.7% yield, by the same method as has been described above.

(b) With 1.2 equiv of SO_2Cl_2: A solution of **16** (256 mg, 1.32 mmol), pyridine(0.32 ml, 4.0 mmol), and SO_2Cl_2(0.13 ml, 1.61 mmol) in 15 ml of CH_2Cl_2 was stirred at 0°C for 4 hr. The NMR spectrum of the crude crystals obtained by the usual work-up showed that **17** and **20** were produced in a ratio of 8 : 2. The mixture was chromatographed with benzene/hexane(8 : 2). 43 mg(0.162 mmol; 15.7%) of **20** was eluted with benzene, and 187 mg (0.814 mmol; 79.1%) of **17** was eluted benzene–ethyl acetate (98 : 2). **17** and **20** were identified by means of the mp, IR, and NMR spectra.

*Chlorination of **1** with Cl_2.* To a stirred solution of **1** (4.86 g, 41.2 mmol) and pyridine (9.9 ml, 123.6 mmol) in 50 ml of CH_2Cl_2 was added at 0°C a solution of Cl_2(more than 2.48 g; 35 mmol) in 35 ml of CCl_4 over a 0.5-hr period. The mixture was stirred for 1 hr. The usual work-up, followed by chromatography with benzene, gave 1.38 g (7.37 mmol; 17.9%) of **5** with benzene, and 3.43 g (22.5 mmol; 54.3%) of **2** with benzene containing 1—5% ethyl acetate. 0.91 g (7.7 mmol; 18.7%) of **1** was recovered by elution with benzene/ethanol (95 : 5). **2** and **5** were identified by means of mp, IR, and NMR spectra.

*Chlorination of **8** with Cl_2.* To a stirred solution of **8** (50 mg, 0.328 mmol) and pyridine(0.08 ml, 1.0 mmol) in 10 ml of CH_2Cl_2 was added a solution of Cl_2(more than 20.6 mg; 0.29 mmol) in 0.29 ml of CCl_4 at 0°C, after which the mixture was stirred for 2 hr. Further addition of 0.088 mmol of Cl_2 in CCl_4, followed by 2.5 hr's stirring; the usual work-up gave a crude residue which was dissolved in 0.5 ml of $CDCl_3$, with 69.6 mg(0.312 mmol) of dichloromethyl 4-methylphenyl sulfoxide as the standard. The NMR spectrum of the solution showed that a 91 : 9 mixture of **9** and **11** was produced in a 75% yield.

*Chlorination of **10** with Cl_2.* To a stirred solution of **10**(48 mg, 0.314 mmol) and pyridine(0.08 ml, 1.0 mmol) in 10 ml of CH_2Cl_2 was added a solution of Cl_2(ca. 0.29 mmol) in 0.29 ml of CCl_4 at 0°C, after which the mixture was stirred for 3 hr. The usual work-up, followed by NMR spectral measurement with 70.5 mg(0.316 mmol) of dichloromethyl 4-methylphenyl sulfoxide, showed that a 3 : 7 mixture of **9** and **11** was obtained in an 86.6% yield.

*Chlorination of **15** with Cl_2.* To a stirred solution of **15** (122 mg, 0.627 mmol) and pyridine(0.15 ml, 1.87 mmol)

in 15 ml of CH_2Cl_2 was added a solution of 0.55 mmol of Cl_2 in 0.55 ml of CCl_4 at 0°C, after which the mixture was stirred for 1.5 hr. The addition of 0.088 mmol of Cl_2(1.5 hr's stirring) and the further addition of 0.055 mmol of Cl_2 1.5 hr's stirring), followed by the usual work-up, gave 140 mg of white crystals. Their NMR spectrum with 36.2 mg (0.154 mmol) of bromomethyl phenyl sulfone showed that **17** and **20** were produced in 62.7% and 6.3% yields respectively.

Chlorination of ***16*** *with* Cl_2. *(a)*: To a stirred solution of **16** (247 mg, 1.27 mmol) and pyridine(0.3 ml, 3.75 mmol) in 15 ml of CH_2Cl_2 was added a solution of Cl_2(1.27 mmol) in 1.27 ml of CCl_4, after which the mixture was stirred for 2.5 hr. The usual work-up followed by crystallization from $CHCl_3$/H gave 234 mg(1.02 mmol; 80.3%) of **17**.

(b): To a stirred solution of **16** (121 mg, 0.622 mmol) and pyridine(0.15 ml, 1.87 mmol) in 15 ml of CH_2Cl_2 was added a solution of 0.50 mmol of Cl_2 in 0.50 ml of CCl_4 at 0°C, after which the mixture was stirred for 2.5 hr. An additional 0.13 mmol of Cl_2 in CCl_4 was added, and stirring was continued for 1.5 hr. The NMR measurement after the usual work-up showed that **17** was obtained in a 61.8% yield.

Synthesis of trans-*4-Chlorothiane 1-Oxide (8) and* cis-*4-Chlorothiane 1-Oxide (10)*. To a stirred solution of 4-chlorothiane[27] (0.58 g, 4.25 mmol) in 100 ml of methanol was added a solution of $NaIO_4$(955 mg, 4.46 mmol) in 100 ml of water at 0°C. The mixture was stirred at 0°C for 5 hr and then at room temperature for 5 hr. 100 ml of water was added, and the mixture was extracted with CH_2Cl_2. The evaporation of the solvent gave 595 mg(3.9 mmol; 91.7%) of the white crystals which were a 60 : 40 mixture of **8** and **10** on the basis of the NMR spectrum.

4.20 g(30.8 mmol) of 4-chlorothiane was oxidized similarly, followed by chromatography with benzene. Elution with benzene–ethyl acetate(90 : 10) afforded 1.62 g(10.6 mmol; 34.4%) of **8**, 863 mg(5.65 mmol; 18.4%) of a mixture of **8** and **10**, and 1.295 g(8.48 mmol; 27.5%) of **10** containing a very small amount of **8** successively. The solubilities of **8** and **10** in cyclohexane at room temperature were 6 mg/ml and 1 mg/ml respectively. Accordingly, **10** can be easily isolated from a mixture of **8** and **10**. Recrystallization of **8** from B/C/H gave mp 108—109.5°C (sintered at *ca.* 85°C) (lit,[8] mp 104—105°C). IR(3.5% in CS_2): 573, 719, 980, 1055 cm^{-1}. NMR: 1.65—3.2(8H), 4.51(1H, m, HHW=9). Found: C, 39.45; H, 6.08%. Calcd for C_5H_9ClOS: C, 39.35; H, 5.94%. Recrystallization of **10** from C/H gave mp 120—121°C (lit,[8] mp 120—121°C). IR(0.5% in CS_2): 726, 753, 938, 1019, 1066 cm^{-1}. NMR($CDCl_3$): 1.85—3.40(8H), 4.12(1H, m, HHW=16—21.5).

Synthesis of 4-Phenylthiane. 4-Phenylthiane was prepared by a modification of a method previously reported.[28] A solution of 4-hydroxy-4-phenylthiane(2.32 g, 12 mmol) and *p*-toluenesulfonic acid monohydrate(0.30 g) in 15 ml of isopropyl acetate was refluxed for 10 hr, while being monitored by tlc. The subsequent evaporation of the solvent gave 2.11 g (12 mmol; 100%) of a crystalline residue, which was then treated with charcoal in cyclohexane.

A solution of dehydrated product(1.58 g, 8.96 mmol) in 30 ml of 99.5% ethanol was stirred with 2.37 g of 5% Pd-charcoal under H_2 for 40 hr at 100—120 atm/40—50°C. The mixture was filtered, and the filtrate was concentrated to a residue which was treated with charcoal in cyclohexane. The crystallization of the product from hexane at 0°C gave 0.95 g of 4-phenylthiane. The mother liquor was cooled to −20°C to furnish 0.32 g of the product. The total yield was 1.27 g(7.13 mmol; 79.5%). Recrystallization from methanol at −20°C gave mp 52—53°C (lit,[28] mp 55°C).

Synthesis of trans-*4-Phenylthiane 1-Oxide (15) and* cis-*4-Phenylthiane 1-Oxide (16)*. To a stirred solution of $NaIO_4$(2.79 g, 13.0 mmol) in 300 ml of water was added a solution of 4-phenylthiane(2.07 g, 11.6 mmol) in 900 ml of methanol at 0°C; the mixture was stirred at 0°C for 5 hr and then at room temperature for 14 hr. It was then filtered, and the filtrate was concentrated to 400 ml which was subsequently extracted with CH_2Cl_2. The usual work-up gave 2.122 g(10.93 mmol; 94.2%) of white crystals, which were a 26 : 74 mixture of **15** and **16**, as determined by means of the 100 MHz NMR spectrum.[9] Fractional crystallization from cyclohexane gave 0.89 g (39.6%) of **16** with mp 148.5—149°C(lit,[9] mp 150—151°C).

A 2.82-g portion of a 1 : 1 mixture of **15** and **16** was chromatographed with benzene. After successive elutions with 1, 2, 4, 6, 8, 10, and 15% of ethyl acetate in benzene, elution with 15—20% of ethyl acetate, followed by fractional crystallizations from cyclohexane, afforded 867 mg(30.8%) of **16**, 834 mg(29.6%) of **15** with mp 121—123°C(lit,[9] mp 137—138.5°C), and 1.11 g(39.3%) of a 1.1 : 1 mixture of **15** and **16**.

The authors wish to thank the Kawakami Memorial Foundation for its partial financial support of this work. They are also grateful to the members of the Analytical Laboratory of this research center for the microanalyses and for the NMR and mass spectra measurements.

27) E. Adlerová and M. Protiva, *Collect. Czech. Chem. Commun.*, **24**, 1268 (1959).

28) M. J. Cook, H. Dorn, and A. R. Katritzky, *J. Chem. Soc., B*, **1968**, 1467.

Stereochemical Studies on the Halogenation of Sulfoxides. II. The Bromination of Cyclic Sulfoxides[1]

Shinobu IRIUCHIJIMA and Gen-ichi TSUCHIHASHI

Sagami Chemical Research Center, Nishiohnuma, Sagamihara, Kanagawa 229

(Received July 26, 1972)

The cyclic sulfoxides, thiane 1-oxide, 4-chlorothiane 1-oxides, and 4-phenylthiane 1-oxides, were brominated with a mixture of bromine and *N*-bromosuccinimide in the presence of pyridine. The stereoformulas of the products, together with those of the isomers with an inverted sulfoxide configuration, were determined by means of the IR and NMR spectral data and by a comparison of the R_f-values in the tlc. As a result, it has been revealed that the bromination reaction gives products in which a bromine atom is introduced stereospecifically at a *trans*-position to the sulfinyl lone pair, in a manner similar to that of the chlorination reaction reported previously. The same mechanism as in the chlorination is proposed for the main reaction course.

The α-halogenation of sulfoxides with the halogenating agents in the presence of base is known to be a stereoselective reaction.[2,3] In the preceding paper[4] we have reported on the chlorination of the cyclic sulfoxides with *t*-butyl hypochlorite, sulfuryl chloride, and chlorine in the presence of potassium acetate or pyridine. In the present paper we would like to describe our stereochemical study on the bromination of the cyclic sulfoxides,[4] thiane 1-oxide, *cis*- or *trans*-4-chlorothiane 1-oxide, and *cis*- or *trans*-4-phenylthiane 1-oxide, with a mixture of bromine and *N*-bromosuccinimide[5] in the presence of pyridine.

Results and Discussion

Bromination of Thiane 1-Oxide. The bromination of six-membered thiane 1-oxide (**1**) with a mixture of 0.5 equiv of bromine and 1.0 equiv of *N*-bromosuccinimide[5] in the presence of pyridine in dichloromethane produced, stereospecifically, *cis*-2-bromothiane 1-oxide(**2**) (mp 61—62°C) (Fig. 1) in an 80% yield. The inversion of the sulfoxide configuration of **2** with triethyloxonium tetrafluoroborate (Et_3OBF_4)[6] furnished *trans*-2-bromothiane 1-oxide(**3**) (mp 59.5—60°C) in a 68% yield.

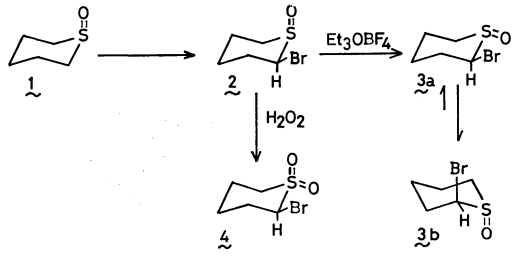

Fig 1.

The stereoformulas of **2** and **3** were determined in the same way as the corresponding chloro-derivatives described in the preceding paper:[4] the aromatic solvent-induced shifts (ASIS; $\Delta=\delta_{CCl_4}-\delta_{C_6H_6}$) are also a useful method in determining the stereoformulas of sulfoxides. Since a proton *trans* to the sulfinyl oxygen is more shielded and has a larger Δ-value than a proton *cis* to the sulfinyl oxygen, the product obtained by bromination, which has a larger Δ-value ($\Delta=0.64$)(Table 1), should possess a *cis*-form (**2**), while the inverted isomer, with a smaller Δ-value ($\Delta=0.43$), should possess a *trans*-form (**3**). This assignment was supported by the following facts: the H-C_2 of **3** was observed as axial in the polar solvents (CD_3OD, D_2O, CF_3COOH, and CD_3SOCD_3) and as equatorial rather than axial in the nonpolar solvents (CCl_4, $CDCl_3$, and C_6H_6), whereas the H-C_2 of **2** was always observed as axial, regardless of whether the solvent was polar or not(Table 1). This observation can be explained as follows. The product (**2**) has a thermodynamically stable *cis*-form possessing a preferable axial sulfinyl oxygen and equatorial bromine. On the other hand, since **3** has an unstable *trans*-form, its conformation changes with the solvent polarity;

Table 1. NMR spectral data of H-C_2 of 2-bromothiane 1-oxides(**2** and **3**). $\Delta=\delta_{CCl_4}-\delta_{C_6H_6}$

Solvent	**2**	**3**
CCl_4	5.14 q(ax) J=3.5, 9	4.78 m(eq)
C_6H_6	4.50 oct(ax) J=1, 3, 9.5	4.35 m(eq)
$CDCl_3$	5.09 oct(ax) J=1, 3.5, 8	4.76 m(eq)
CD_3OD	—	4.93 oct(ax) J=1, 3.2, 7.4
CD_3CN	5.13 oct(ax) J=1, 3.5, 9.5	—
CD_3SOCD_3	—	5.12 q(ax) J=3.5, 7.5
D_2O	5.84 oct(ax) J=0.5, 4, 8.5	5.43 q(ax) J=3.5, 8.3
CF_3COOH	5.37 oct(ax) J=1.6, 3.4, 7	5.09 q(ax) J=3, 7.2
Δ	0.64	0.43

1) G. Tsuchihashi, S. Iriuchijima, and M. Ishibashi, Abstracts of the Third International Congress of Heterocyclic Chemistry: B, Sendai, Japan(1971), p. 624.

2) M. Cinquini, S. Colonna, and F. Montanari, *Chem. Commun.*, **1969**, 607. M. Cinquini and S. Colonna, *Boll. Sci. Fac. Chim. Ind. Bologna*, **27**, 201 (1969).

3) S. Iriuchijima and G. Tsuchihashi, *Tetrahedron Lett.*, **1969**, 5259.

4) S. Iriuchijima, M. Ishibashi, and G. Tsuchihashi, This Bulletin, **46**, 921 (1973).

5) S. Iriuchijima and G. Tsuchihashi, *Synthesis*, **1970**, 588.

6) C. R. Johnson and D. McCants, Jr., *J. Amer. Chem. Soc.*, **87**, 5404 (1965).

TABLE 2. NMR SPECTRAL DATA OF H-C_2 AND H-C_4 OF 2-BROMO-4-CHLOROTHIANE 1-OXIDES(**6**, **7**, **9**, AND **10**)

	6		**7**		**9**		**10**	
	H-C_2	H-C_4	H-C_2	H-C_4	H-C_2	H-C_4	H-C_2	H-C_4
δ_{CCl_4}	5.10 ax	4.47 eq	4.87 eq	4.17 ax	4.51 ax	3.80 ax	4.90 ax	4.16 ax
$\delta_{C_6H_6}$	4.57	3.63	4.17	—	3.56	—	4.20	3.28
Δ	0.53	—	0.70	—	0.95	—	0.70	—

the polar conformation, **3a**, is favored in the polar solvents, while the less polar conformation, **3b**, dominates in the non-polar solvents. Moreover, the fact that, in thin-layer chromatography, **3** was found at a higher position than **2** indicates that **3** has a less polar structure than **2**. The possibility that **3**, which might be formed by the bromination of **1**, was isomerized to the stable isomer (**2**) during the reaction was excluded by the fact that **2** was not produced when **3** was kept under the bromination conditions for 3 hr.

The halogenation of **1** in the presence of base[7] proved to give, stereospecifically, the *cis*-halogenated product in both chlorination[4] and bromination.

The hydrogen peroxide oxidation of **2** in acetic acid gave 2-bromothiane 1,1-dioxide (**4**) (mp 89—90°C), in a 95% yield.

Bromination of 4-Chlorothiane 1-Oxide. The bromination of *trans*-4-chlorothiane 1-oxide(**5**) afforded, stereospecifically, 2e-bromo-4a-chlorothiane 1a-oxide(**6**) (Fig. 2) (mp 48—49°C) in an 81% yield. The bromination of *cis*-4-chlorothiane 1-oxide (**8**), however, furnished, in an 85% yield, a 20 : 80 mixture of **6** and 2e-bromo-4e-chlorothiane 1a-oxide (**9**) (mp 102—103°C). This fact indicates that **8** is brominated, mainly, not *via* **5** but *via* the ring inversion, unlike as in the chlorination with *t*-butyl hypochlorite in the presence of potassium acetate.[4] The competitive bromination of **5** and **8** showed that **8** is brominated approximately five times faster than **5**. This is a somewhat unexpected result, which remains unexplained.

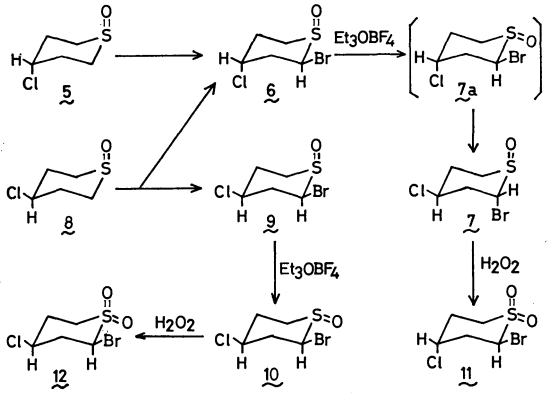

Fig. 2.

The products, **6** and **9**, were transformed with Et_3OBF_4 to 2a-bromo-4e-chlorothiane 1a-oxide (**7**) (mp 73.5—75°C) in an 86% yield and 2e-bromo-4e-chlorothiane 1e-oxide (**10**) (mp 93—94.5°C) in an 85% yield respectively.

The stereochemical structures of **6**, **7**, **9**, and **10** were established by means of the NMR coupling constants of H-C_2 and H-C_4, ASIS shown in Table 2 (the isomer **9** is expected to have the largest Δ-value), and the behavior on a thin-layer plate; the compound **7** was observed higher, than **6** and **9** which were themselves higher than **10**. According to the axial-equatorial sulfinyl oxygen rule,[8] the compound **9**, which possesses an axial oxygen, is expected to be higher on a thin-layer plate than **10**, which possesses an equatorial one.

The oxidation of **7** and **10** with hydrogen peroxide in acetic acid yielded *trans*-2-bromo-4-chlorothiane 1,1-dioxide (**11**) (mp 105—108°C) in a 93% yield and *cis*-2-bromo-4-chlorothiane 1,1-dioxide (**12**) (mp 124—125°C) in a 93.5% yield respectively.

Bromination of 4-Phenylthiane 1-Oxides. The bromination of conformationally rigid *trans*-4-phenylthiane 1-oxide (**13**) with a mixture of bromine (0.5 equiv) and NBS(1.0 equiv) for 0.5 hr furnished, in an 86% yield, a 63 : 37 mixture of 2a-bromo-4e-phenylthiane 1e-oxide (**14**) (mp 143—144°C) and 2e-bromo-4e-phenylthiane 1a-oxide (**15**) (mp 132—133°C), while *cis*-4-phenylthiane 1-oxide (**18**) with bromine (0.5 equiv) and NBS (2.2 equiv) for 23 hr afforded, in only a 48.5% yield, a 81 : 19 mixture of **14** and **15** (Fig. 3), with a 44% recovery of **18**. This fact, indicating that **13** is much more easily brominated than **18**, is in agreement with the result of the competitive bromination that **13** is brominated approximately five times faster than **18**. The bromination of both **13** and **18** produced an all-*cis* product

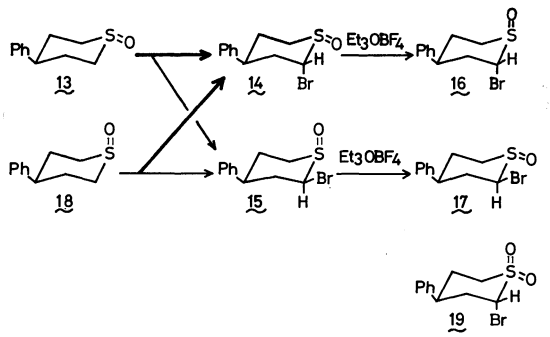

Fig. 3.

7) In the absence of base, non-stereoselectivity was observed. K.-C. Tin and T. Durst, *Tetrahedron Lett.*, **1970**, 4643.

8) A sulfoxide which possesses an axial oxygen is observed higher on a thin-layer plate than a sulfoxide which possesses an equatorial one, when the other part of their structures is the same.[4]

Table 3. NMR spectral data of H-C_2 of 2-bromo-4-phenylthiane 1-oxides(**14**, **15**, **16**, and **17**)

	14	**15**	**16**	**17**
δ_{CCl_4}	5.23 eq	4.71 ax	4.86 ex	4.61 ax
$\delta_{C_6H_6}$	4.80	4.16	4.42	4.30
Δ	0.43	0.55	0.44	0.31

(**15**) as a minor component, while the corresponding chloro-derivative was never detected in the chlorination.[4]

The products, **14** and **15**, were isomerized with Et_3OBF_4 to 2a-bromo-4e-phenylthiane 1a-oxide (**16**) (mp 93°C) in an 83% yield and 2e-bromo-4e-phenylthiane 1e-oxide (**17**) (mp 133—143°C) in a 59% yield respectively. The assignment of the stereoformulas of **14**, **15**, **16**, and **17**, is based on the NMR spectral data shown in Table 3 (the isomer **15** is expected to have the largest Δ-value) and the comparison of the R_f-values in the tlc: the isomer **16** was observed higher than **15**, which was itself higher than **14** and **17** on a thin-layer plate; according to the rule (see above), the isomer **16** which possesses an axial sulfinyl oxygen is expected to be higher than **14** which possesses an equatorial oxygen, and **15** is expected to be higher than **17** as well.

The inverted isomer **16** was not isomerized to **14** when it was placed in the bromination condition. Moreover, since the both compounds **14** and **16** were recovered unchanged after treatment with concentrated hydrochloric acid(1 vol) in dioxane(2 vol),[9] they are configurationally-stable compounds.

The oxidation of **14** gave *trans*-2-bromo-4-phenylthiane 1,1-dioxide(**19**) (mp 149—151°C) in an 82.5% yield.

Mechanism of the Bromination with Bromine/N-Bromosuccinimide in the Presence of Pyridine. The bromination of the thiane 1-oxides(**1**, **5**, **8**, **13**, and **18**) with bromine/NBS in the presence of pyridine proved to give products in which bromine was introduced at a *trans*-position to the sulfinyl lone pair, mainly in the same manner as in the chlorination.[4] Consequently, the mechanism postulated for the chlorination[4] is also applicable to the bromination reaction as shown in Fig. 4; the bromo-oxosulfonium ion (**21**), which is formed by the attack of a positive bromine of a bromine molecule on the sulfinyl lone pair, gives the ylid (**22**) by the action of the bromide ion, and then **22** gives rise to the hypothetical intermediate (**23**) by the elimination of the bromide ion. The final step is the addition of the bromide ion to **23**, producing the α-bromosulfoxides (**24**), in which the bromine atom and sulfinyl lone pair are in a *trans* relationship.

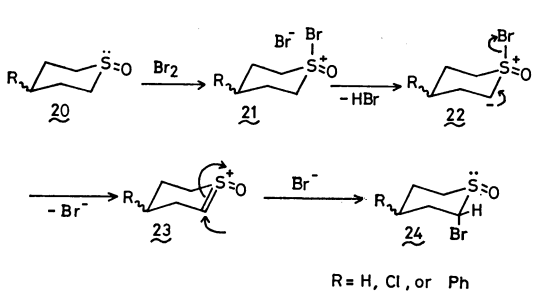

Fig. 4.

9) K. Mislow, T. Simmons, J. T. Melillo, and A. L. Ternay, Jr., *J. Amer. Chem. Soc.*, **86**, 1452 (1964).

Experimental

Unless otherwise stated, the NMR spectra were measured with a Varian HA-100 spectrometer (100 MHz) and/or a Hitachi R/20B spectrometer (60 MHz) in a concentration of 40—50 mg in 0.4 ml of $CDCl_3$, while the IR spectra were recorded with Nujol mull using a Hitachi EPI-G3 spectrometer. In the NMR spectral data, J(coupling constant) is expressed in Hz, and HHW means a half-height width or the sum of the coupling constants. In the crystallization solvents, B, C, and H stand for benzene, cyclohexane, and hexane respectively, and the expressions B/C/H, *etc.* mean that the crystallization was carried out by dissolution in benzene, followed by the successive addition of cyclohexane and hexane.

*Bromination of Thiane 1-Oxide (**1**) to* cis*-2-Bromothiane 1-Oxide (**2**).* A solution of Br_2(0.6 g, 3.75 mmol) in 5 ml of CH_2Cl_2 and *N*-Bromosuccinimide (NBS) (1.34 g, 7.5 mmol) was added to a stirred solution of **1** (0.89 g, 7.55 mmol) and pyridine (0.61 ml, 7.6 mmol) in 30 ml of CH_2Cl_2. After stirring at room temperature for 1 hr, 30 ml of water, 10 ml of a 1M aqueous Na_2CO_3 solution, and 10 ml of a 1M Na_2SO_3 solution were added; the mixture was then extracted with CH_2Cl_2. The organic phase was dried over anhydrous Na_2SO_4 and then concentrated to an oily residue which was subsequently chromatographed on silica gel with benzene. Elution with benzene containing 2—5% ethyl acetate afforded 1.20 g (0.608 mmol; 80.5%) of the white crystals (**2**). Recrystallization from B/C/H gave mp 61—62°C. IR: 697, 946, 953, 1002, 1040 (S=O), 1058, 1068 cm^{-1}. IR (5% in CS_2): 700, 1078 (S=O) cm^{-1}. NMR: 1.2—3.4(8H), 5.09 (1H, octet, J=1, 3.5, 8). NMR (CCl_4): 1.3—3.1 (8H), 5.14(1H, q, J=3.5, 9). NMR(C_6H_6): 0.6—2.8 (8H), 4.50(1H, octet, J=1, 3, 9.5). NMR(CD_3CN): 5.13 (1H, octet, J=1, 3.5, 9.5). NMR(HCOOH): 1.5—3.5(8H), 5.40(1H, octet, J=1, 3.8, 8). NMR(D_2O): 2.0—3.7(8H), 5.84(1H, octet, J=0.5, 4, 8.5). NMR(CF_3COOH): 1.5—3.55(8H), 5.37(1H, octet, J=1.6, 3.4, 7). Mass: *m/e* 196(M^+), 117(base peak). Found: C, 30.59; H, 4.58; Br, 40.49%. Calcd for C_5H_9BrOS: C, 30.47; H, 4.60; Br, 40.54%.

*Transformation of **2** to* trans*-2-Bromothiane 1-Oxide(**3**).* To a stirred solution of **2** (0.885 g; 4.5 mmol) in CH_2Cl_2 (5 ml) *ca.* 1.5 g (7.9 mmol) of triethyloxonium tetrafluoroborate (Et_3OBF_4) was added. After the mixture had been stirred at room temperature for 1 hr, 40 ml of anhydrous ether was added at 0°C to give the oily ethoxysulfonium salt as a precipitation. After standing for 2 hr, the solvents were removed by decantation, and to the residue was added 20 ml of a 0.5M NaOH solution. The mixture was then extracted with CH_2Cl_2. The solvent was dried over Na_2SO_4 and evaporated to the residue, which was then chromatographed on silica gel with benzene. Elution with benzene containing 2% ethyl acetate yielded 0.60 g (3.06 mmol; 67.8 %) of a colorless oil (**3**) which was crystallized on standing. Recrystallizations from B/C/H at 0°C gave mp 59.5—60°C. **3** was detected with iodine higher than **2** on a thin-layer plate, using ethyl acetate: 95% ethanol (95 : 5). IR: 1016, 1023, 1050(S=O) cm^{-1}. IR(2% in CS_2): 1059 cm^{-1}.

IR(CCl_4): 1058 cm^{-1}. NMR: 1.4—3.6(8H), 4.76(1H, m, HHW=10.5). NMR(CCl_4): 1.4—3.45(8H), 4.78(1H, m, HHW=9). NMR(CS_2): 1.35—3.45(8H), 4.70(1H, m, HHW=9). NMR(C_6H_6): 0.7—2.95(8H), 4.35(1H, m, HHW=10). NMR(Et_3N): 4.98 (1H, m, HHW=10). NMR(Et_2O): 4.88(1H, m, HHW=8.5). NMR(pyridine): 1.1—3.5(8H), 5.08(1H, octet, J=1, 3.2, 6.3). NMR(CF_3COOH): 1.5—4.0(8H), 5.09(1H, q, J=3, 7.2). NMR (CD_3SOCD_3): 1.3—3.5, 5.12(1H, q, J=3.5, 7.5). NMR-(CD_3OD): 1.4—3.5, 4.93(1H, octet, J=1, 3.2, 7.4). NMR(CD_3COCD_3): 1.45—3.4, 4.91(1H, octet, J=1.2, 3, 7). NMR(D_2O): 1.9—4.12, 5.43 (1H, q, J=3.5, 8.3). Mass: *m/e* 196(M^+), 117(base peak). Found: C, 30.48; H, 4.59; Br, 40.27%. Calcd for C_5H_9BrOS: C, 30.47; H, 4.60; Br, 40.54%.

Oxidation of ***2*** *to 2-Bromothiane 1,1-Dioxide (****4****).* A solution of **2** (0.89 g; 4.51 mmol) and 30% H_2O_2(1 ml; 10 mmol) in acetic acid (10 ml) was kept at 45°C for 15 hr. The subsequent addition of water (40 ml) gave crystals which were then filtered off and recrystallized from B/C/H to yield 0.92 g (4.3 mmol; 95%) of **4**. Recrystallization from the same solvents gave mp 89—90°C. IR: 1122, 1155, 1279, 1309 cm^{-1}. NMR: 1.3—3.8 (8H), 4.82(1H, octet, J=2, 4, 8). Mass: *m/e* 212 (M^+), 41(base peak). Found: C, 28.19; H, 4.28; Br, 37.46%. Calcd for $C_5H_9BrO_2S$: C, 28.18; H, 4.26; Br, 37.50%.

Bromination of trans*-4-Chlorothiane 1-Oxide(****5****) to 2e-Bromo-4e-chlorothiane 1a-Oxide (****6****).* To a stirred solution of **5** (347 mg; 2.28 mmol) and pyridine (0.2 ml; 2.5 mmol) in CH_2Cl_2 (20 ml) were added NBS (405 mg; 2.28 mmol) and a solution of Br_2(0.18 g; 1.14 mmol) in CH_2Cl_2 (5 ml). The mixture was then stirred at room temperature for 22 hr. The usual work-up gave a residue, which was subsequently chromatographed on silica gel with benzene. Elution with benzene containing 4% ethyl acetate afforded 0.43 g (1.86 mmol; 81.5%) of the white crystals (**6**), which were then recrystallized from B/C at 0°C to give mp 48—49°C. IR: 965, 1031(S=O) cm^{-1}. IR (2% in CS_2): 982, 1073 (S=O) cm^{-1}. NMR: 1.7—3.35 (6H), 4.48 (1H, m, HHW=9), 5.13 (1H, q, J=3.6, 11). NMR (CCl_4): 1.82—3.40 (6H), 4.47 (1H, m, HHW=9), 5.10 (1H, q, J=3.3, 11.5). NMR (C_6H_6): 1.03—1.45 (1H), 1.78—2.4 (4H), 2.54—2.85 (1H), 3.63 (1H, m, HHW=9), 4.57 (1H, q, J=3.2, 11.2). NMR (CF_3COOH): 1.92—3.67 (6H), 4.53 (1H, m, HHW=9.5), 5.38 (1H, m, HHW=19). Mass: *m/e* 230 (M^+), 151 (base peak). Found: C, 26.43; H, 3.59; S, 13.76%. Calcd for $C_5H_8BrClOS$: C, 25.94; H, 3.48; S, 13.85%.

45 mg (13.0%) of **5** was recovered by elution with benzene: ethyl acetate (9 : 1).

Transformation of ***6*** *to 2a-Bromo-4e-chlorothiane 1a-Oxide (****7****).* To a stirred solution of **6** (365 mg; 1.58 mmol) in CH_2Cl_2 (5 ml) was added 0.45 g (2.37 mmol) of Et_3OBF_4, and the mixture was then stirred at room temperature for 1 hr. The addition of anhydrous ether (40 ml) gave rise to a white solid as a precipitation. The solvent was removed by decantation, and to the residue a 0.2M NaOH solution (25 ml) was added. The mixture was extracted with CH_2Cl_2. The evaporation of the solvent afforded an oil which was subsequently crystallized from B/C/H at −20°C to give 315 mg (86.6%) of **7**. Recrystallizations gave mp 73.5—75°C. IR: 762, 832, 870, 921, 1012, 1023, 1054 (S=O) cm^{-1}. IR (5% in CS_2): 970, 1022, 1064 (S=O) cm^{-1}. NMR: 2.0—3.44 (6H), 4.24 (1H, nonet, J=4, 4, 10, 10), 4.88 (1H, m, HHW=10). NMR (CCl_4): 1.95—3.38 (6H), 4.17 (1H, nonet, J=4, 4, 11, 11), 4.87 (1H, m, HHW=9.5). NMR (C_6H_6): 3.66 (1H, m, HHW=29.5), 4.17 (1H, m, HHW=9.5). NMR (CF_3COOH): 2.1—3.77 (6H), 4.33 (1H, septet, J=*ca.* 4, 4, 8, 8), 5.29 (1H, q, J=3.4, 7.4). NMR (CD_3OD): 2.0—3.72 (6H), 4.39 (1H, septet, J=*ca.* 4.3, 4.3, 8.6, 8.6), 5.19 (1H, m, HHW=10). NMR (CD_3CN): 1.85—3.60 (6H), 4.37 (1H, septet, J=4.3, 4.3, 8.6, 8.6), 5.02 (1H, m, HHW=10.5). Mass: *m/e* 230 (M^+). Found: C, 25.93; H, 3.56; S, 13.95%. Calcd for $C_5H_8BrClOS$: C, 25.94; H, 3.48; S, 13.85%.

Bromination of cis*-4-Chlorothiane 1-Oxide (****8****).* To a stirred solution of **8** (0.42 g, 2.75 mmol) and pyridine (0.33 ml, 4.1 mmol) in CH_2Cl_2 (10 ml) were added bromine (0.22 g, 1.38 mmol) and *N*-bromosuccinimide (0.49 g, 2.75 mmol). The mixture was stirred at room temperature for 6 hr. The NMR spectrum of the extract after the usual work-up showed it to be a 80 : 20 mixture of 2e-bromo-4e-chlorothiane 1a-oxide (**9**) and **6**. Crystallization from $CHCl_3$/B/C/H at 0°C gave 0.39 g (1.684 mmol; 61.2%) of **9**. The chromatography of the mother liquor gave 46 mg of **6** and 104 mg of a mixture of **6** and **9**, by elution with benzene containing 2% ethyl acetate. **6** was identified by mp, IR, and NMR. The total yield of **6** and **9** became 84.7%. Recrystallization of **9** from B/C gave mp 102—103°C (decompn.). IR: 681, 925, 1010, 1042, 1059 (S=O) cm^{-1}. IR (0.6% in CS_2): 917, 1079, 1086 (S=O) cm^{-1}. NMR: 1.95—3.38 (6H), 3.91 (1H, m, axial H), 4.68 (1H, q, J=4, 12). NMR (15 mg in 0.4 ml C_6H_6): 3.56 (1H, q, J=3, 12), NMR (CF_3COOH): 2.25—3.35 (5H), 3.61 (1H, sextet, J=3.5, 3.5, 15), 4.01 (1H, m, HHW=30, axial H), 4.90 (1H, q, J=7.2, 8.8). NMR (5 mg in 0.4 ml CCl_4+0.1 ml $CDCl_3$): 3.80 (1H, m, axial H), 4.51 (1H, q, J=4, 12). Mass: *m/e* 230 (M^+), 151 (base peak). Found: C, 26.04; H, 3.64; S, 13.74%. Calcd for $C_5H_8BrClOS$: C, 25.94; H, 3.48; S, 13.85%.

Transformation of ***9*** *to 2e-Bromo-4e-chlorothiane 1e-Oxide (****10****).* A solution of **9** (0.33 g, 1.43 mmol) and 0.42 g (2.2 mmol) of Et_3OBF_4 in CH_2Cl_2 (5 ml) was stirred at room temperature for 1 hr. The usual work-up and chromatography gave 282 mg (85.5%) of **10**, eluted with benzene containing 2% ethyl acetate. Recrystallization from B/C/H gave mp 93—94.5°C. IR: 490, 643, 674, 850, 931, 1051 (S=O) cm^{-1}. IR (1% in CS_2): 988, 1063 (S=O), 1078 cm^{-1}. NMR: 1.87—3.19 (5H), 3.53 (1H, octet, J=3, 7, 13), 4.12 (1H, nonet, J=4, 4, 9.5, 9.5), 4.65 (1H, q, J=3.6, 10). NMR (25 mg in CCl_4 0.4 ml): 1.82—3.14 (5H), 3.40 (1H, octet, J=3, 7, 12.5), 4.16 (1H, nonet, J=4, 4, 9.5, 9.5), 4.90 (1H, q, J=4, 10.5). NMR (C_6H_6): 1.11—2.52 (5H), 2.71 (1H, octet, J=3, 6, 13), 3.28 (1H, nonet, J=4, 4, 10, 10), 4.20 (1H, q, J=4, 11). NMR (CF_3COOH): 1.95—3.40 (5H), 3.80 (1H, octet, J=3, 5.7, 13), 4.11 (1H, nonet, J=4, 4, 10.5, 10.5), 5.02 (1H, q, J=3.8, 11.5). Mass: *m/e* 230 (M^+). Found: C, 26.12; H, 3.56; S, 13.84%. Calcd for $C_5H_8BrClOS$: C, 25.94; H, 3.48; S, 13.85%.

Oxidation of ***7*** *to* trans*-2-Bromo-4-chlorothiane 1,1-Dioxide(****11****).* A solution of **7** (0.26 g, 1.12 mmol) and 30% hydrogen peroxide (0.3 ml, 2.94 mmol) in 3 ml of acetic acid was kept at 45°C for 15 hr. The subsequent evaporation and crystallization from B/C gave 257 mg (1.04 mmol; 92.7%) of **11**. Recrystallization from B/C gave mp 105—108°C. IR: 485, 718, 1004, 1119, 1143, 1155, 1288, 1313 cm^{-1}. NMR: 2.1—3.1 (4H), 3.15—3.85 (2H), 4.47 (1H, quintet, J=*ca.* 4, 4, 4, 4), 5.08 (1H, q, J=6, 8.2). Mass: *m/e* 246 (M^+), 131 (base peak). Found: C, 24.32; H, 3.50; S, 13.10%. Calcd for $C_5H_8BrClO_2S$: C, 24.26; H, 3.26; S, 12.95%.

Oxidation of ***10*** *to* cis*-2-Bromo-4-chlorothiane 1,1-Dioxide(****12****).* A solution of **10** (83 mg, 0.354 mmol) and 30% H_2O_2 (0.1 ml, 1 mmol) in 3 ml of acetic acid was kept at 45°C for 15 hr. The subsequent evaporation of the solvent afforded white

crystals, which were recrystallized from B/C/H to give 82 mg (0.33 mmol; 93%) of **12**. The recrystallization gave mp 124—125°C. IR: 1139, 1280, 1320 cm^{-1}. NMR: 2.05—3.70 (6H), 4.14 (1H, m, HHW=30.5), 4.83 (1H, q, J=5.1, 11.1). Mass: *m/e* 246 (M^+). Found: C, 24.23; H, 3.29; S, 12.89%. Calcd for $C_5H_8BrClO_2S$: C, 24.26; H, 3.26; S, 12.95%.

Bromination of trans-*4-Phenylthiane 1-Oxide (**13**).* To a stirred solution of **13** (0.36 g, 1.85 mmol) and pyridine (0.23 ml, 2.8 mmol) in 10 ml of CH_2Cl_2 were added Br_2 (0.15 g, 0.94 mmol) and NBS (0.48 g, 2.7 mmol). The mixture was stirred at room temperature for 30 min. The NMR spectrum of the crystalline residue, obtained by the usual work-up, showed it to be 63 : 37 mixture of 2a-bromo-4e-phenylthiane 1e-oxide (**14**) and 2e-bromo-4e-phenylthiane 1a-oxide (**15**). Crystallization from B/CCl_4 followed by recrystallization from B/C/H gave 0.12 g (0.44 mmol; 23.7%) of **14**. Recrystallizations from B/C/H gave mp 143—144°C. IR: 710, 771, 1065 cm^{-1}. NMR: 1.7—3.4 (7H), 5.39 (1H, m, HHW=9), 7.20 (5H, m). NMR (C_6H_6): 1.0—3.2 (7H), 4.80 (1H, m, HHW=9). NMR (3 mg in 0.4 ml CCl_4): 5.23 (1H, m, HHW=8). Mass: *m/e* 272 (M^+), 193 (base peak). Found: C, 48.30; H, 4.77; S, 11.78%. Calcd for $C_{11}H_{13}BrOS$: C, 48.36; H, 4.80; S, 11.74%.

The combined mother liquors were chromatographed with benzene. Elution with benzene containing 1% ethyl acetate furnished 0.157 g (0.574 mmol; 31%) of **15**, and then 0.158 g (0.578 mmol; 31.2%) of **14**. Recrystallizations of the former (**15**) from B/C gave mp 132—133.5°C. IR: 699, 751, 921, 1011, 1037, 1055 cm^{-1}. NMR: 1.7—3.35 (7H), 4.77 (1H, q, J=3.5, 12.2), 7.20 (5H, m). NMR (C_6H_6): 0.8—3.4 (7H), 4.16 (1H, q, J=3.2, 12). NMR (6 mg in 0.4 ml CCl_4): 4.71 (1H, q, J=3.5, 12). Mass: *m/e* 272 (M^+). Found: C, 47.84; H, 4.84; S, 11.75%. Calcd for $C_{11}H_{13}BrOS$: C, 48.36; H, 4.80; S, 11.74%.

Bromination of cis-*4-Phenylthiane 1-Oxide (**18**).* *(a) With 1.0 equiv of NBS*: A solution of **18** (0.25 g, 1.29 mmol), pyridine (0.21 ml, 2.6 mmol), Br_2 (0.1 g, 0.64 mmol), and NBS (0.23 g, 1.29 mmol) in 10 ml of CH_2Cl_2 was stirred for 3 hr at room temperature. Chromatography after the usual work-up gave 128 mg (0.47 mmol; 36.0%) of a 77 : 23 mixture of **14** and **15**, eluted with benzene containing 1—2% ethyl acetate, and 0.15 g (60%) of **18** containing *ca.* 5% of **13** eluted with benzene–ethyl acetate (1 : 1).

(b) With 2.2 equiv of NBS: To a stirred solution of **18** (0.42 g, 2.16 mmol) and pyridine (0.26 ml, 3.24 mmol) in 10 ml of CH_2Cl_2, were added Br_2(0.17 g, 1.06 mmol) and NBS (0.46 g, 2.58 mmol). After the mixture had then been stirred at room temperature for 18 hr, more NBS (385 mg, 2.16 mmol) and pyridine (0.26 ml, 3.24 mmol) were added and the reaction was continued for 5 hr. The NMR spectrum of the extract from the usual work-up showed that a 81 : 19 mixture of **14** and **15** was obtained. Chromatography gave 45 mg (0.165 mmol; 7.6%) of **15**, with benzene containing 1% ethyl acetate, and then 0.245 g (0.90 mmol; 41.5%) of **14**, with 1—4% ethyl acetate. **14** and **15** were identified by mp, IR, NMR, and tlc. 185 mg (44.0%) of **18** was recovered by the elution of benzene containing 5% methanol.

*Transformation of **14** to 2a-Bromo-4e-phenylthiane 1a-Oxide (**16**).* A solution of **14** (0.38 g, 1.39 mmol) and 0.53 g (2.8 mmol) of Et_3OBF_4 in 5 ml of CH_2Cl_2 was stirred at room temperature for 30 min. The addition of ether at 0°C gave a crystalline ethoxysulfonium salt, which was decomposed with 20 ml of a 0.2M NaOH solution and extracted with CH_2Cl_2. The chromatography of the extract afforded 315 mg (1.15 mmol; 82.8%) of **16** with 1% ethyl acetate in benzene. Recrystallizations from B/H gave mp 93°C. IR: 703, 750, 1016, 1049 cm^{-1} (S=O) cm^{-1}. NMR: 1.65—3.50 (7H), 4.91 (1H,m, HHW=7), 7.23 (5H, m). NMR (C_6H_6): 0.95—3.15 (7H), 4.42 (1H, m, HHW=7.5). NMR (CCl_4): 1.55—3.41 (7H), 4.86 (1H, m, HHW=7), 7.18 (5H, s), NMR (CF_3COOH): 1.7—4.0 (7H), 5.29 (1H, m, HHW=7). Found: C, 48.51; H, 4.92; S, 11.67%. Calcd for $C_{11}H_{13}BrOS$: C, 48.36; H, 4.80; S, 11.74%.

*Transformation of **15** to 2e-Bromo-4e-phenylthiane 1e-Oxide (**17**).* A solution of **15** (205 mg, 0.75 mmol) and Et_3O-BF_4 (285 mg, 1.5 mmol) in 3 ml of CH_2Cl_2 was stirred at room temperature for 1 hr. The usual work-up furnished a crystalline extract, which was subsequently recrystallized from B/H to give 0.12 g (59%) of **17**. Several recrystallizations from B/H gave mp 133—143°C (decompn.). IR: 703, 750, 1016, 1049 (S=O) cm^{-1}. NMR: 1.8—3.2 (6H), 3.60 (1H, sextet, J=3.6, 3.6, 13), 4.74 (1H, q, J=4, 11.3), NMR (3 mg in 0.4 ml CCl_4+0.05 ml $CDCl_3$): 4.61 (1H, q, J=4, 12). NMR (5 mg in 0.4 ml C_6H_6): 4.30 (1H, q, J=4, 12). Found: C, 47.76; H, 4.87; S, 11.66%. Calcd for $C_{11}H_{13}BrOS$: C, 48.36; H, 4.80; S, 11.74%.

*Oxidation of **14** to* trans-*2-Bromo-4-phenylthiane 1,1-Dioxide (**19**).* A solution of **14** (0.24 g, 0.88 mmol) and 0.2 ml (2.0 mmol) of 30% H_2O_2 in 5 ml of acetic acid was kept at 50°C for 15 hr. The subsequent evaporation of the solvent followed by passage through silica gel with benzene, gave 0.21 g (0.725 mmol; 82.5%) of **19**. Recrystallization from B/H gave mp 149—151°C (sintered at 144°C). IR: 1110, 1287, 1314 cm^{-1}. NMR: 1.93—3.87 (7H), 4.85 (1H, q, J=3.2, 6.4), 7.22 (5H, m). Mass: *m/e* 288 (M^+), 209 (base peak). Found: C, 45.80; H, 4.60; S, 11.14%. Calcd for $C_{11}H_{13}BrO_2S$: C, 45.68; H, 4.53; S, 11.09%.

*Competitive Bromination of **13** and **18**.* A solution of **13** (197 mg), **18** (180 mg), pyridine (0.12 ml, 1.5 mmol), Br_2 (80 mg, 0.5 mmol), and NBS (0.18 g, 1 mmol) in 10 ml of CH_2Cl_2 was stirred at room temperature for 40 min. The NMR spectrum of the residue, which had been obtained by the usual work-up, showed that **14** and **15** were obtained in a 65 : 35 ratio. Chromatography gave 53 mg of **15** and 125 mg of **14**, together with 243 mg of a 37 : 63 mixture of **13** and **18**. Accordingly, in this bromination reaction, 107 mg of **13** was consumed, while only 27 mg of **18** was used, showing that **13** is brominated approximately five times faster than **18**.

*Treatment of 2-Bromo-4-phenylthiane 1-Oxides (**14** and **16**) with Concentrated Hydrochloric Acid (1 vol) in Dioxane (**2** vol).*

*(a) **14***: To a stirred solution of **14** (117 mg) in 4 ml of dioxane, 2 ml of concentrated HCl were added. The mixture was then stirred at room temperature for 24 hr. After the usual work-up, **14** was recovered unchanged, as was confirmed by the NMR and mass spectra and by tlc.

*(b) **16***: A solution of **16** (53 mg) in 6 ml of the reagent was stirred at room temperature for 2 hr. After the usual work-up, **16** was recovered quantitatively, as estimated by means of the NMR spectrum and tlc.

Kinetics and Mechanism of Aziridine Synthesis from Ketoxime with Lithium Aluminum Hydride[1]

Hiroshi TANIDA, Tetsuo OKADA, and Katsumi KOTERA

Shionogi Research Laboratory, Shionogi & Co., Ltd., Fukushima-ku, Osaka 553

(Received July 29, 1972)

The stoichiometry and rate of the reaction of dibenzyl ketoxime (**1**) with lithium aluminum hydride in tetrahydrofuran leading to *cis*-2-benzyl-3-phenylaziridine (**2**, 92%) and 2-amino-1,3-diphenylpropane (**3**, 8%) were determined by gas meter and vpc. It was found that the aziridine formation proceeds with an immediate evolution of 1 mole of hydrogen followed by a slow liberation of a second mole of hydrogen and an accommodation of 1 equiv. of hydride into the molecule. Also, the formation has an induction period and there is a catalytic acceleration effect by the concurrently-formed minor product **3**. Combination of the previously-reported results and the present findings leads us to propose a mechanism by which an aluminum derivative rapidly obtained on addition of **1** to the solution of lithium aluminum hydride undergoes slow hydrogen elimination to afford an azirine intermediate, followed by reduction to the aziridine. Making use of the catalytic effect discovered, the reaction rate and yield of aziridine were increased by the addition to the reaction mixture of an amine, particularly a secondary amine such as *n*-butylmethylamine.

Although the principal products from the reductions of ketoximes with lithium aluminum hydride (LAH) had been reported to be the corresponding primary amines,[2] we observed some years ago that the reactions of certain aryl ketoximes and bridged benzocyclene oximes mainly yielded the aziridine derivatives.[3] Since then, this reaction has been considerably developed as a simple and convenient method for aziridine synthesis.[4-6] During this development, some characteristic features of the reaction have been revealed. First, the reaction produces only *cis* aziridine. For example, dibenzyl ketoxime (**1**) leads to *cis*-2-benzyl-3-phenylaziridine. Secondly, aziridine ring-closure takes place on the side syn to the oxime configuration preferably to the side anti to it.[7] This is entirely different from the Neber rearrangement, which has been reported to proceed independently of oxime configuration.[8] Thirdly, aziridine ring-closure at a benzylic position is favored over that at an aliphatic position.[6,7] Fourthly, when lithium aluminum deuteride (LAD) is used, one deuterium atom is incorporated into the carbon originally carrying the oximino function, but not at all into other carbons.[3,4d,6] Fifthly, no aziridine is formed from *N*-(α-methylphenethyl)hydroxylamine so that it is very unlikely that the reaction proceeds through a hydroxylamine intermediate.[9] With these findings in mind, we undertook a kinetic investigation in order to get further insight into the mechanism of this reaction and also to improve the reaction from a synthetic viewpoint.

Results and Discussion

As reported earlier,[4,5] dibenzyl ketoxime (**1**) undergoes the reaction affording *cis*-2-benzyl-3-phenylaziridine (**1**) and 2-amino-1,3-diphenylpropane (**3**) in the isolated yields of 71—78% and about 8%, respectively. The present procedure was essentially the same as that reported, but it involved the use of a reaction mixture of LAH (0.25 M, 1.00 M in hydride) and **1** (0.167 M) in tetrahydrofuran.[10] When reaction was complete, the mixture was treated with water to destroy the excess hydride and analyzed by vpc, showing the formation of **2** in 92% yield and **3** in 8% yield.

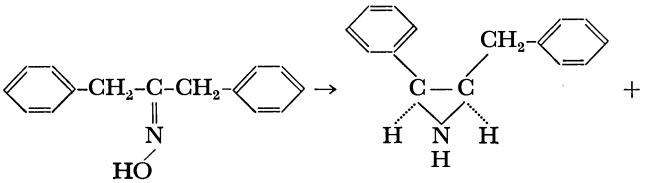

1 **2**

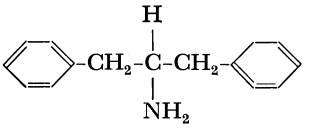

3

The rate and stoichiometry were determined by measurement of evolving hydrogen with a gas meter and the results obtained are presented in Table 1 and Fig. 1. It is noted that about 1 mol (the amount actually found was 1.13 mol) of hydrogen is evolved very rapidly on mixing **1** with the LAH solution, the reaction then proceeding with slow evolution of a second

1) Presented in part at the 19th Organic Reaction Mechanism Symposium of the Chemical Society of Japan in Yamagata, Oct., 1968.

2) N. G. Gaylord, "Reduction with Complex Metal Hydrides," Interscience Publishers, New York, N. Y. (1956).

3) K. Kitahonoki, K. Kotera, Y. Matsukawa, S. Miyazaki, T. Okada, H. Takahashi, and Y. Takano, *Tetrahedron Lett.*, **1965**, 1059.

4) a) K. Kotera, M. Motomura, S. Miyazaki, T. Okada, and Y. Matsukawa, *Tetrahedron*, **24**, 1727 (1968). b) K. Kotera, S. Miyazaki, H. Takahashi, T. Okada, and K. Kitahonoki, *ibid.*, **24**, 3681 (1968). c) K. Kitahonoki, Y. Takano, and H. Takahashi, *ibid.*, **24** 4605 (1968). d) K. Kotera, Y. Matsukawa, H. Takahashi, T. Okada, and K. Kitahonoki, *ibid.*, **24**, 6177 (1968).

5) K. Kotera and K. Kitahonoki, "Organic Syntheses," Vol. 48, p. 20 (1968).

6) K. Kotera and K. Kitahonoki, *Organic Preparations and Procedures*, **1**, 305 (1969).

7) K. Kotera, T. Okada, and S. Miyazaki, *Tetrahedron Lett.*, **1967**, 841; *Tetrahedron*, **24**, 5677 (1968).

8) H. O. House and W. F. Berkowitz, *J. Org. Chem.*, **28**, 307, 2271 (1963).

9) Footnote 26 in Ref. 5.

10) It is convenient to discuss the utilization of the reagent in terms of moles of hydride consumed per mole of compound.

Table 1. Kinetic analysis by gas meter[a)]

Reaction time hr	Hydrogen evolved	Hydride consumed	Hydride utilized for reduction
0	1.13	1.21	0.08
0.5	1.14	1.27	0.13
1.0	1.19	1.51	0.32
3.0	1.75	2.53	0.78
6.0	2.10	3.17	1.07
12.0	2.12	3.36	1.24

a) Units: mol for hydrogen and mol equiv for hydride.

1 mol of hydrogen (in total, 2.12 mol were evolved before cessation of reaction). At appropriate time intervals, the reaction mixture was hydrolyzed by addition of dilute sulfuric acid and the hydrogen evolved was determined to calculate the hydride consumed; this is shown in the second column of Table 1. The difference between the hydride consumed and the hydrogen evolved corresponds to the hydride taken up by the molecule of **1** for reduction; this is 1.24 mol equiv. at 100% reaction. It has been reported that the reduction of cyclohexanone oxime to cyclohexylamine requires 4 equiv of hydride, 2 for reaction and 2 for hydrogen evolution, and also that the reaction proceeds with a rapid evolution of 1 equiv. of hydrogen followed by a slow utilization of 2 equiv. of hydride for reduction and slow liberation of a second mole of hydrogen.[11] In this connection, 100% formation of aziridine would require, after an immediate evolution of 1 mol of hydrogen, a slow utilization of 1 equiv of hydride for reduction and a slow liberation of a second mole of hydrogen. It is obvious that the first step in both the reactions with **1** and cyclohexanone oxime is the formation of an O–Al bond, as evidenced by the immediate evolution of hydrogen corresponding to the active hydrogen on the oxime function.[2,12] If an aziridine is then formed as the only product, since the molecular formula is equal to that of an imine, the stoichiometry

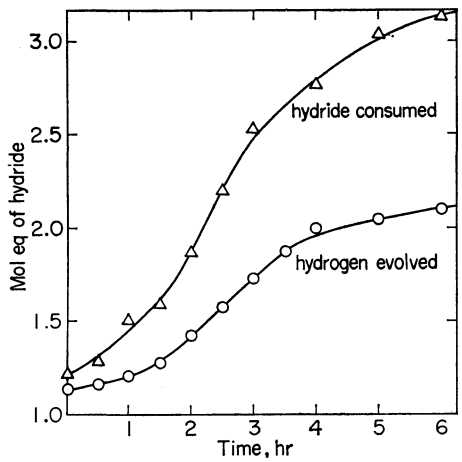

Fig. 1. Kinetic analysis by gas meter. At $t=0$, [**1**]=0.167 M and [LAH]=0.25 M in THF; reaction temp., 25°C.

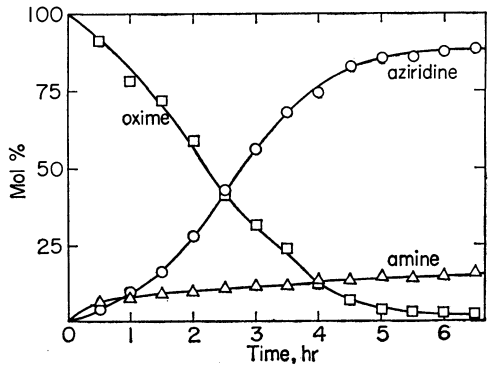

Fig. 2. Kinetic analysis by vapor phase chromatography. At $t=0$, [**1**]=0.167 M and [LAH]=0.25 M in THF; reaction temp., 26°C.

will involve utilization of 1 equiv. of hydride for reduction and the liberation of a second mole of hydrogen. Therefore, the stoichiometric difference between the formation of amine and that of aziridine will be indicated by the amount of hydride utilized for reduction; 2 equiv. or 1 equiv. In this connection, the results in Table 1 (1.24 mol equiv were utilized at the completion of reaction) are understood if one considers the formation of a mixture consisting of mostly **2** with a minor amount of **3**.

The results obtained by monitoring the reactant and products by vpc are shown in Fig. 2. Of note are the existence of an induction period in the reaction and the close resemblance between the curve for the slow evolution of hydrogen in Fig. 1 and that for the production of aziridine in Fig. 2. The vpc data were analyzed in our laboratory[13] by a Melcom EA-7410 analog computer and it was found possible to accommodate the data by the following kinetic equations. An important implication of these equations

$$\text{Oxime} + \text{LAH} \xrightarrow{\text{very fast}} I_1 + H_2$$

$$I_1 \xrightarrow{k_1} \text{Amine} \qquad I_1\text{: Intermediate}$$

$$I_1 \xrightarrow{k_2 C_{\text{Amine}}} \text{Aziridine}$$

is that the amine formed by k_1 has a catalytic acceleration effect upon the formation of aziridine with

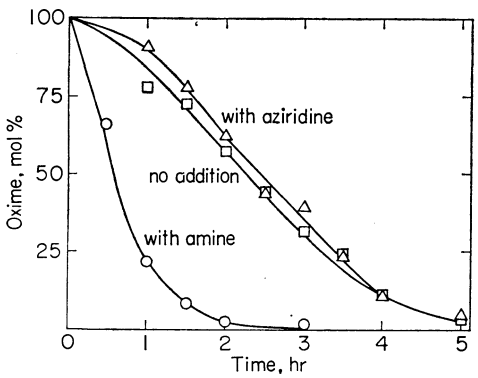

Fig. 3. Demonstration of catalytic effect by the amine. At $t=0$, [1]=0.167 M and [LAH]=0.34 M in THF; reaction temp., 26°C. The concentrations of **2** and **3** added were 0.167 M.

11) H. C. Brown, P. M. Weissman, and N. M. Yoon, *J. Amer. Chem. Soc.*, **88**, 1458 (1966).

12) W. T. Borden, *ibid.*, **90**, 2197 (1968).

13) We thank Dr. T. Takahashi and Mr. M. Shudo for the aid.

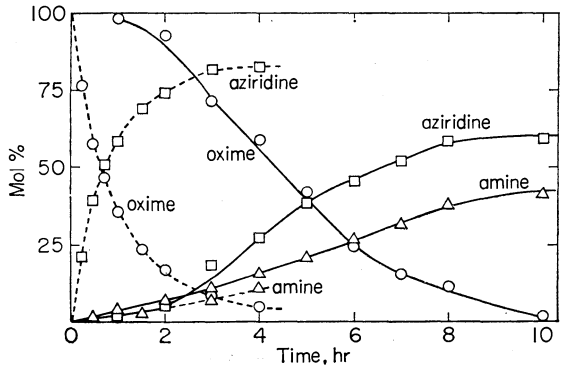

Fig. 4. Reaction of acetophenone oxime; solid lines for results without addition of *n*-butylmethylamine, dotted lines for those with addition. At $t=0$, [oxime]=0.167 M and [LAH]=0.30 M in THF; reaction temp., 40°C.

the rate coefficient $k_2\ C_{\text{Amine}}$. Indeed, it was confirmed that addition of **3** to the reaction mixture enhances the reaction rate and shortens the induction period though the addition of **2** has no effect; these experiments are shown in Fig. 3.

Similar experiments were carried out for the reaction of *anti*-acetophenone oxime.[14] Figure 4 shows

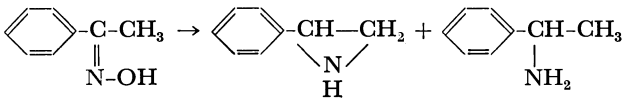

the results monitored by vpc. Again, treatment by the computer yielded equations of the same type as the above and suggested a positive catalytic effect by the by-product amine. The yield of 2-phenylaziridine was raised to 80% by addition of an amine, *n*-butylmethylamine, although it had been reported as 60% without the addition.

In the reaction with **1**, variation of the concentration of LAH did not affect the reaction rate or the aziridine yield. Therefore, the transition state in the rate-determining step must be of an intramolecular nature. Transformation of certain α,β-unsaturated carboxylic acids or esters into the corresponding cyclopropanes by reduction with LAH may be a related reaction. The ring-closing steps in these reactions have been suggested as intramolecular nucleophilic displacement reactions.[17,18]

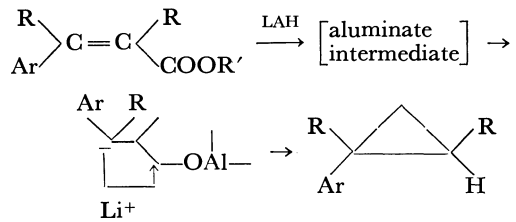

(or concerted displacement)

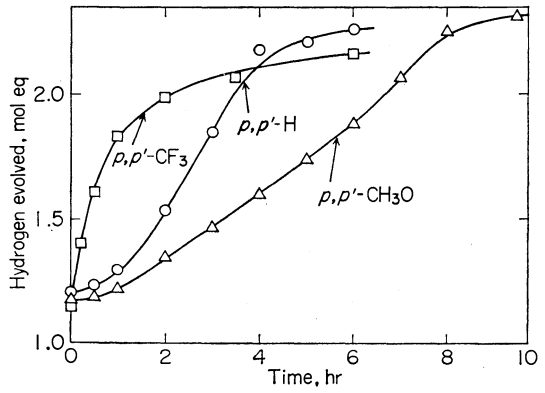

Fig. 5. Substituent effects. At $t=0$, [oxime]=0.167 M and [LAH]=0.25 M in THF; reaction temp., 26°C.

Studies of substituent effects were carried out with *p,p'*-di-(trifluoromethyl) and *p,p'*-dimethoxyl derivatives of **1** and the results obtained are shown in Fig. 5.

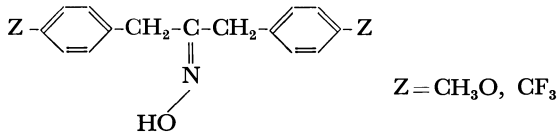

Shortening of the induction period and enhancement of the rate are noted with introduction of the electron-withdrawing trifluoromethyl substituents and a rate decrease is noted with that of the electron-donating methoxy substituents. Therefore, increasing capability of the proton α to the aryl group for elimination increases the overall rate.

On the basis of the present data and previous findings (see Introduction) we propose that the aziridine formation proceeds by the rapid formation of an aluminate intermediate **4** on addition of the oxime to the LAH solution, followed by a concerted intramolecular displacement to give an azirine and, finally, saturation to the aziridine. This may be depicted as follows.

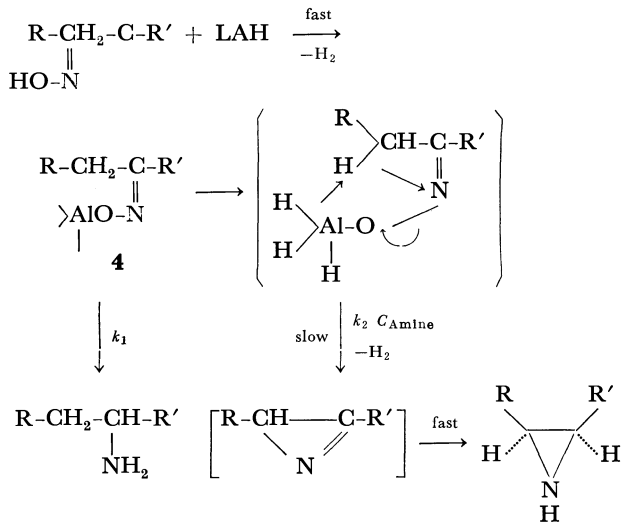

14) The anti configuration has been reported by Karabatsos and Taller.[15] We have determined by NMR that the aluminate of this oxime has the same configuration and no alternation of it at the reaction temperature.[16]

15) G. J. Karabatsos and R. A. Taller, *Tetrahedron*, **24**, 3347 (1968).

16) We thank Mr. Y. Terui for this determination.

17) M. J. Jorgenson and A. W. Friend, *J. Amer. Chem. Soc.*, **87**, 1815 (1965).

18) R. Y. Uyeda and D. J. Cram, *J. Org. Chem.*, **30**, 2083 (1965)

Table 2. Solvent effect

Solvent	Product, %		Half life, hr	pK_a of conjugated acid[a]
	Amine	Aziridine		
Tetrahydrofuran	13	86	2.3	−2.08
2-Methyltetrahydrofuran	23	68	3.3	−2.65
Tetrahydropyran	21	71	3.0	−2.79
Dimethoxyethane	9	86	3.5	−3.27(−2.97)
Diethyl ether	70	25	4.5	−3.59

a) E. M. Arnett and C. Y. Wu, *J. Amer. Chem. Soc.*, **84**, 1684 (1962).

Table 3. Effects of added *n*-butylmethylamine[a]

Ketoxime	With addition		Without addition	
	Aziridine, %	Amine, %	Aziridine, %	Amine, %
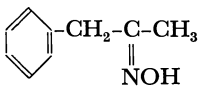	75	15	30	60
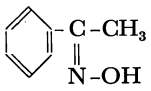	82	11	57	47
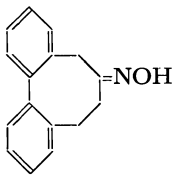	50	20	12	60
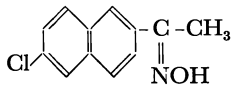	51		10	
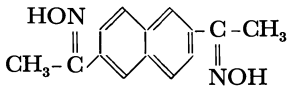	30		2	
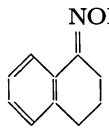	60	35	20	75

a) One mol of the amine was added per mol of lithium aluminum hydride.

The by-product amine is considered to activate one of the aluminate hydrogens in **4** thereby facilitating proton elimination. Reduction of the azirine with LAH will take place from a sterically less hindered side resulting in the *cis* aziridine.[2-6,19] Since according to the proposed mechanism hydrogen is incorporated in the steps from the azirine to the aziridine and from **4** to the amine, the results obtained with LAD (Introduction)[3,4d,6] are reasonably accommodated.

Solvent Effects. Various solvents were tested in the reaction with **1**. Yields of products and half-lives of the reaction were as shown in Table 2. Relatively high yields of **2** were found in solvents having high solvation ability such as tetrahydrofuran and dimethoxyethane, while a low yield was found in ether, which has a low solvation ability.

Influence of Added Amine on Yield. Several kinds of amine were added to the reaction mixture to improve the reaction; the results obtained are shown in Fig. 6. Of the amines tested, secondary *n*-butylmethylamine gave the best result. Reactions with

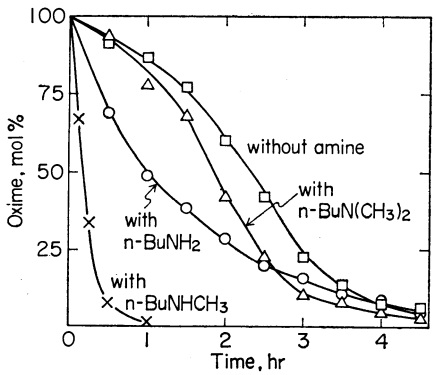

Fig. 6. Catalytic effects by various amines. At $t=0$, [**1**]= 0.167 M, [LAH]=0.70 M, and [amine catalyst]=0.30 M in THF; reaction temp., 26°C.

19) A Hassner and W. Fowlen, *J. Amer. Chem. Soc.*, **90**, 2869 (1968).

and without added *n*-butylmethylamine were carried out with the oximes listed in Table 3. It is clearly seen that the addition increases the yield of aziridine and decreases the yield of amine; with benzylmethyl ketoxime, for example, aziridine increases from 30% to 75% and amine decreases from 60% to 15%.

None of the experimental results so far obtained are inconsistent with the above-proposed mechanism.

Experimental

Materials. Purification of lithium aluminum hydride was carried out by the method of Davis *et al.*[20] Forty grams of LAH purchased from Metal Hydrides Inc. was added to 500 ml of anhydrous ether, refluxed for several days under argon atmosphere, and filtered. The filtrate was concentrated to a volume of 50 ml under reduced argon atmosphere, mixed with anhydrous benzene which had been distilled over LAH, and stored for several hours in an ice bath to deposit 23 g of prismatic crystals. LAH thus purified was completely soluble in THF. Commercially available THF was refluxed for three days over LAH under argon atmosphere and distilled. Two further distillations over LAH then provided THF suitable for the present use.

Dibenzyl Ketoxime. A solution of 50 g of dibenzyl ketone (Tokyo Kasei, GR. grade) in 100 ml of pyridine was added to a solution of 10 g of hydroxylamine hydrochloride in 30 ml of water and 30 ml of alcohol. After being stirred for 2 hr at room temperature, the reaction mixture was poured into water and extracted with ether. The ether layer was washed with dilute hydrochloric acid, dilute sodium carbonate, and water, and dried over sodium sulfate. Evaporation of the solvent followed by recrystallization from a mixture of hexane and ether yielded 50 g of dibenzyl ketoxime, mp 123—124°C.

Vapor Phase Chromatography. Concentrations of the reactants and reaction temperatures in the reactions analyzed by vpc are indicated in the captions of the figures. The analyses were carried out on a Hitachi gaschromato Model K-53 equipped with a hydrogen flame ionization detector using a 1 m × 3 mm stainless steel column.

Procedure-A: A column packed with 4% KF-54 on 60—80 mesh Chromosorb W was used for analysis of **1**, **2**, and **3**; benzyl *p*-methylbenzyl ether was used as an internal reference. The retention times of benzyl *p*-methylbenzyl ether, **3**, **2**, and **1** were 6.8, 9.0, 13.0, and 16.5 min, respectively, at 170°C with 1.0 kg/cm^2 of N_2.

Procedure-B: A column packed with 10% KF-54 on 80—100 mesh Chromosorb W was used for analysis of acetophenone oxime, 2-phenylaziridine, and 1-phenylethylamine, using pentamethyl benzene as an internal reference. The retention times of the amine, the aziridine, pentamethylbenzene, and the oxime were 7.0, 16.2, 26.0, and 41.3 min, respectively, at 70°C with 1.4 kg/cm^2 of N_2.

Kinetic Analysis by Gas Meter. Hydrogen Evolved. A 100 ml three-necked flask equipped with a magnetic stirrer was kept in a constant temperature bath. A glass tube connected one neck of the flask to a trap which was kept at −50°C in a dry ice-acetone bath, and an exit to the trap was connected to a buret adjusted by a water level. The flask was flushed with argon and stoppered with a gum cap. When the water level of buret became constant, 15.0 ml of the LAH solution was injected into the flask through the gum cap, then the oxime solution was added over a period of 2 min under stirring. A control experiment was performed by addition of the reaction solvent containing no oxime to the LAH solution. Concentrations of the reactants and reaction temperatures are shown in the captions of the figures. Hydrogen evolved was measured at appropriate time intervals with the buret.

Hydride Consumed. A known volume of the reaction mixture was injected through the gum cap and decomposed by 5% sulfuric acid with ice-water cooling. Hydrogen liberated was measured with the buret. Subtraction of the amount of hydrogen thus-liberated at a given reaction time from the amount liberated at zero reaction time corresponds to the amount of hydride consumed.

We are indebted to Dr. K. Kitahonoki for his encouragement.

20) W. D. Davis, L. S. Mason, and G. Stegeman, *J. Amer. Chem. Soc.*, **71**, 2775 (1949).

The Structures of the Reoxidation Products of 7,8-Dihydroneopterin

Katsura SUGIURA and Miki GOTO

Department of Chemistry, Gakushuin University, Toshima-ku, Tokyo

(Received August 3, 1972)

On the reduction of D-*erythro*-neopterin with sodium dithionite, after which it was let stand in neutral pH, three colorless compounds, I, II, and III, and two yellow compounds, I and II, were obtained. On the reduction of D-*erythro*-neopterin with Fe dust in 25% acetic acid, after which it was let stand at a neutral pH, two yellow compounds, II and III, were obtained. From UV and NMR spectral data as well as from the chemical reactions, the structures for these compounds were identified, Colorless Compound I is 2-amino-4-hydroxy-6-(1′,3′-dihydroxypropyl)pteridine; Colorless Compound II, 2-amino-4-hydroxy-6-(D-*erythro*-1′,2′,3′-trihydroxypropyl)-pteridine; Colorless Compound III, 2-amino-4-hydroxy-6-(D-*threo*-1′,2′,3′-trihydroxypropyl)pteridine; Yellow Compound I, 2-amino-4-hydroxy-6-(1′-oxo-3′-sulfopropyl)-7,8-dihydropteridine; Yellow Compound II, 2-amino-4-hydroxy-6-(1′-oxo-3′-hydroxypropyl)-7,8-dihydropteridine, and Yellow Compound III, 2-amino-4-hydroxy-6-(1′-oxo-2′,3′-dihydroxypropyl)-7,8-dihydropteridine.

The biological function of a phosphate of 2-amino-4-hydroxy-6-(D-*erythro*-1′,2′,3′-trihydroxypropyl)-7,8-dihydropteridine (7,8-dihydro-D-*erythro*-neopterin) was proved to serve as a key compound for the biosynthesis of folic acid and the biopterin group of co-factors.[1-3] Recently, the enzymic transformation of 7,8-dihydro-D-*erythro*-neopterin to D-*threo*-neopterin has been demonstrated.[4] Kaufman has reported that 7,8-dihydrobiopterin is obtained from biopterin by treatment with Fe dust in an acidic solution, and the synthetic 7,8-dihydrobiopterin has been demonstrated by using purified rat liver extract to be the phenylalanine-hydroxylation co-factor.[5] Fukushima and Akino have reported that neopterin and biopterin give 7,8-dihydroneopterin and 7,8-dihydrobiopterin respectively by treatment with sodium dithionite.[6]

For the study of the biosynthesis of pteridines, we prepared 7,8-dihydro-D-*erythro*-neopterin by treating it with sodium dithionite or Fe dust in 25% acetic acid, as has been described by the above authors. On the reduction of D-*erythro*-neopterin, followed by its purification on a Sephadex column, we did not get pure 7,8-dihydro-D-*erythro*-neopterin, but some unknown compounds were always produced together with 7,8-dihydro-D-*erythro*-neopterin.[2] The yields of these unknown compounds were increased when the reduced solutions were kept standing in a neutral pH for a longer time. The present paper will report on the structures of these compounds.

On the reduction of D-*erythro*-neopterin by treatment with sodium dithionite, after which it was let stand in a nuetral pH, three colorless and two yellow substances were obtained, *i.e.*, colorless Compounds I, II, and III, and Yellow Compounds I and II. On the reduction of D-*erythro*-neopterin by treatment with Fe dust in 25% acetic acid, after which it was let stand in a neutral pH, the products were two yellow substances, Yellow Compounds II and III.

On the basis of UV and NMR spectral data as well as the chemical reactions, the structures for these compounds were deduced to be as follows:

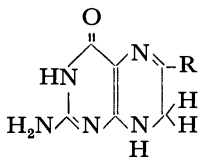

R; $-CO-CH_2-CH_2SO_3H$
Yellow Compound I

R; $-CO-CH_2-CH_2OH$
Yellow Compound II

R; $-CO-\underset{\displaystyle OH}{\underset{|}{CH}}-CH_2OH$
Yellow Compound III

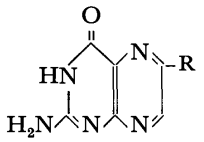

R; $-CHOH-CH_2-CH_2OH$
Colorless Compound I

R; $-\underset{\displaystyle OH}{\underset{|}{CH}}-\underset{\displaystyle OH}{\underset{|}{CH}}-CH_2OH$
Colorless Compound II

R; $-\underset{\displaystyle OH}{\underset{|}{CH}}-\underset{\displaystyle OH}{\underset{|}{CH}}-CH_2OH$
Colorless Compound III

Experimental

Reduction of D-erythro-*Neopterin by Treatment with Sodium Dithionite and the Isolation of the Products.* D-*erythro*-Neopterin (140 mg) was suspended in 2 ml of water, and then 2M sodium hydroxide was added until a clear solution was obtained. After the addition of sodium dithionite (400 mg), the solution was left at 90—95°C for 15 min, then, after the addition of 6M hydrochloric acid (1 ml), the solution was heated at 90—95°C. The solution was neutralized with ammonia, and the excess sodium dithionite was removed by means of a Sephadex G-25 (fine) column (3×25 cm, developer; water) and the eluate was concentrated to 200 ml by means of a rotary evaporator below 40°C. The solution was left standing for 48 hr at room temperature in the dark. The solution was acidified with acetic acid, and then it was placed on a 3×25 cm column of Florisil; the column was subsequently washed with 0.001M acetic acid, and 20% aqueous acetone successively. Colorless matters were eluted by the first solvent, and yellow matters by the second solvent. The colorless substances were separated into two fluoresent bands by means of a cellulose column (4×25 cm, developer; 2-propanol—1% ammonia; 2 : 1). The eluate of the

1) K. Sugiura and M. Goto, *Biochem. Biophys. Res. Commun.*, **28**, 687 (1967).
2) K. Sugiura and M. Goto, *J. Biochem.* (Tokyo), **64**, 657 (1968).
3) J. B. Mathis and G. M. Brown, *J. Biol. Chem.*, **245**, 3015 (1970).
4) G. M. Brown, "Chemistry and Biology of Pteridines," ed. by K. Iwai, M. Akino, M. Goto and Y. Iwanami, International Academic Printing Co., Tokyo (1970), p. 243.
5) S. Kaufman, *Proc. Natl. Acad. Sci. U. S.*, **50**, 1085 (1963).
6) T. Fukushima and M. Akino, *Arch. Biochem. Biophys.*, **128**, 1 (1968).

first was concentrated and the residue was recrystallized from water to give colorless needles; 12 mg (8.6%); this was Colorless Compound I. The eluate of the second was purified by chromatographic method using six sheets of paper (40×40 cm, Toyo Roshi Co. Ltd., No. 54, developer; 2-propanol—1% ammonia: 2 : 1). The fluorescent bands were then cut out, and the materials were eluted from it with water. The eluates were subsequently evaporated to dryness. There was a trace of the (R_f, 0.21) fraction; this was Colorless Compound III. The residue of the (R_f, 0.31) fraction was recrystallized from water to give colorless needles; 29 mg (21%); this was Colorless Compound II. The yellow substances were separated into two fluorescent bands by means of a cellulose column (3×20 cm, developer; 0.05% ammonia). The eluate of the first was concentrated, the residue was purified by means of a Sephadex G-25 (fine) column (3×25 cm, developer; water), the eluate was concentrated to dryness *in vacuo*, and the residue was recrystallized from 50% ethanol to give yellow needles; 48 mg (25%); this was Yellow Compound I. The eluate of the second such substance was concentrated, the residue was purified by means of a DEAE-cellulose column (3×25 cm, developer; water), the eluate was concentrated to dryness *in vacuo*, and the residue was recrystallized from water to give yellow needles; 25 mg (18%); this was Yellow Compound II. The samples were dried at 70—80°C/0.01 mmHg for 12 hr over P_2O_5 for analysis.

Colorless Compound I:

Found: C, 44.02; H, 4.50; N, 29.55%. Calcd for $C_9H_{11}O_3N_5 \cdot 0.5H_2O$: C, 43.90; H, 4.88; N, 28.46%.

UV: $\lambda_{max}^{0.1M\ NaOH}$ mμ (ε), 255 (23.1×10³), 368 (7.77×10³); $\lambda_{min}^{0.1M\ NaOH}$ mμ (ε), 232 (9.28×10³), 302 (1.4×10³); $\lambda_{max}^{H_2O}$ mμ (ε), 236 (13.2×10³), 275 (14.8×10³), 348 (6.8×10³); $\lambda_{min}^{H_2O}$ mμ (ε), 254 (8.0×10³), 296 (2.36×10³); $\lambda_{max}^{0.1M\ HCl}$ mμ (ε), 246 (1.15×10³), 324 (8.47×10³); $\lambda_{min}^{0.1M\ HCl}$ mμ (ε), 275 (2.1×10³).

Yellow Compound I:

Found: C, 32.08; H, 3.95; N, 20.45; S, 8.94%. Calcd for $C_9H_{11}O_5N_5S \cdot 2H_2O$: C, 32.05; H, 4.48; N, 20.77; S, 9.50%.

UV: $\lambda_{max}^{0.1M\ NaOH}$ mμ (ε), 268 (1.74×10³), 438 (14.2×10³); $\lambda_{min}^{0.1M\ NaOH}$ mμ (ε), 234 (4.6×10³), 340 (1.8×10³); $\lambda_{max}^{H_2O}$ mμ (ε), 267(17.6×10³), 418 (11.3×10³); $\lambda_{min}^{H_2O}$ mμ (ε), 238 (7.0×10³), 325 (1.2×10³); $\lambda_{max}^{0.1M\ HCl}$ mμ (ε), 248 (11.0×10³), 406 (9.2×10³), $\lambda_{min}^{0.1M\ HCl}$ mμ (ε), 256 (6.4×10³), 316 (1.2×10³).

NMR (CF_3COOD) : δ3.56 (bs, 4H), 4.61 (s, 2H).

Yellow Compound II:

Found: C, 44.21; H, 4.61; N, 28.56%. Calcd for $C_9H_{11}O_3N_5 \cdot 0.5H_2O$: C, 43.90; H, 4.88; N, 28.46%.

UV: $\lambda_{max}^{0.1M\ NaOH}$ mμ (ε), 269 (17.3×10³), 440 (12.3×10³), $\lambda_{min}^{0.1M\ NaOH}$ mμ (ε), 237 (5.0×10³), 340 (1.3×10³); $\lambda_{max}^{H_2O}$ mμ (ε), 267 (18.1×10³), 417 (10.4×10³); $\lambda_{min}^{H_2O}$ mμ (ε), 240 (6.9×10³), 340 (1.5×10³); $\lambda_{max}^{0.1M\ HCl}$ mμ (ε), 282 (11.8×10³), 408 (8.0×10³); $\lambda_{min}^{0.1M\ HCl}$ mμ (ε), 254 (7.1×10³), 340 (1.7×10³).

NMR (CF_3COOD): δ 3.33 (t, J=5.8 Hz, 2H), 4.14 (t, J=5.8 Hz, 2H), 4.56 (s, 2H).

Bromine Oxidation of Yellow Compound I. A suspension of Yellow Compound I (40 mg) in 2M hydrochloric acid (20 ml) was treated with bromine (*ca.* 1 g) for a few minutes at room temperature. The mixture was then concentrated to 10 ml by means of a rotary evaporator and the solution was treated with charcoal (1 g). The adsorbed fluorescent compound was eluted with a mixture of 3% aqueous ammonia and ethanol (3 : 1). The eluate was purified by the chromatographic method, using a cellulose column (3×25 cm, developer; 50% ethanol). The eluate was evaporated to dryness, and the residue was crystallized from 50% ethanol (yellow powder, 36 mg, 74%; this was Yellow Compound I·Br_2). The sample was dried at 70—80°C/0.01 mmHg for 3 hr over P_2O_5 for analysis.

Found: C, 29.26; H, 3.11; N, 19.86; S, 8.46%. Calcd for $C_9H_9O_5N_5S \cdot 3.5H_2O$: C, 29.83; H, 4.41; N, 19.33; S, 8.83%.

UV: $\lambda_{max}^{0.1M\ NaOH}$ mμ (ε), 277 (16.2×10³), 316 (7.4×10³), 372 (11.5×10³); $\lambda_{min}^{0.1M\ NaOH}$ mμ (ε), 240 (4.58×10³), 308 (7.3×10³), 332 (6.8×10³); $\lambda_{max}^{0.1M\ HCl}$ mμ (ε), 234 (9.72×10³), 270 (11.7×10³), 318 (10.6×10³); $\lambda_{min}^{0.1M\ HCl}$ mμ (ε), 230 (9.70×10³), 250 (8.8×10³), 291 (7.12×10³).

NMR (CF_3COOD): δ 4.00 (m, 4H), 9.16 (s, 1H).

2,4-Dinitrophenylhydrazone of Yellow Compound II. An aqueous solution of Yellow Compound II reacted immediately with 2,4-dinitrophenylhydrazine in 2M hydrochloric acid to give a dark-red precipitate. This was collected, washed with water, and dried at 70—80°C/0.01 mmHg for 12 hr over P_2O_5 for analysis.

Found: C, 42.99; H, 3.48; N, 29.64%. Calcd for $C_{15}H_{15}O_6N_9$: C, 43.17; H, 3.60; N, 30.22%.

The Reduction of D-erythro-*Neopterin by Treatment with Fe Dust in* 25% *Acetic Acid and the Isolation of the Products.* To a solution of D-*erythro*-neopterin (2 g) in 200 ml of 25% acetic acid, Fe dust was added. The mixture was shaken for 30 min at 50—60°C. The Fe dust was then removed, and the solution was neutralized with ammonia and left standing for 12 hr at room temperature in the dark. The solution was subsequently acidified with acetic acid, and then the solution was placed on a 3×25 cm column of Florisil; the yellow substances were adsorbed at the top of the column. The column was washed well with 0.01% acetic acid, and the yellow substances were eluted with 20% aqueous acetone. The eluate was concentrated. The yellow substances were purified by means of a chromatographic method, using a cellulose column (7.5×35 cm, developer; water) and a DEAE-cellulose column (2.5×25 cm, developer; water). For the exclusion of Yellow Compound II, the eluate was placed on a 7.5×25.0 cm column of cellulose and the column was eluted with *n*-butanol–ethanol–water (2 : 1 : 1). The eluate of the second substance was concentrated to dryness, and the residue was recrystallized from water to give a yellow powder; 453 mg (23%); this was Yellow Compound III. The sample was dried at 70—80°C/0.01 mmHg for 2 hr over P_2O_5 for analysis.

Found: C, 41.23; H, 4.54; N, 27.06%. Calcd for $C_9H_{11}O_4N_5.0 \cdot 5H_2O$: C, 41.22; H, 4.96; N, 26.71%.

UV: $\lambda_{max}^{0.1M\ NaOH}$ mμ (ε), 270 (17.5×10³), 446 (12.8×10³); $\lambda_{min}^{0.1M\ NaOH}$ mμ (ε), 240 (6.2×10³), 350 (1.4×10³); $\lambda_{max}^{H_2O}$ mμ (ε), 268 (17.9×10³), 424 (10.3×10³); $\lambda_{min}^{H_2O}$ mμ (ε), 236 (6.4×10³), 340 (1.4×10³); $\lambda_{max}^{0.1M\ HCl}$ mμ (ε), 273 (12.8×10³), 416 (8.4×10³); $\lambda_{min}^{0.1M\ HCl}$ mμ (ε), 254 (8.2×10³), 340 (1.6×10³).

NMR: (CF_3COOD): δ 4.55 (bs, 2H), 4.73 (s, 2H), 5.70 (bs, 1H). ($(CD_3)_2SO$-D_2O): δ 3.68 (d, J=5.2 Hz, 2H), 4.15 (s, 2H), 5.00 (t, J=5.2 Hz, 1H).

The R_f values of the pteridines are given in Table 1.

Results and Discussion

Yellow Compound II gives ultraviolet spectra similar to those of isosepiapterin.[7] The analytical data indicate that the empirical formula for the compound is

7) H. S. Forrest, C. Van Baalen and J. Myers, *Arch. Biochem. Biophys.*, **83**, 508 (1959).

$C_9H_{11}O_5N_5$. The yellow compound contains a keto group on the side chain, since the compound forms a 2,4-dinitrophenylhydrazone. The NMR spectrum of the compound in CF_3COOD has two triplets, at 3.33 ppm and 4.14 ppm, and a singlet at 4.56 ppm, the proton ratio of the signals being 2 : 2 : 2. The two triplet signals (4.56 ppm and 3.33 ppm) showed that this compound has a $-CH_2-CH_2-$group. The signal at 4.56 ppm was assigned to the methylene protons at the 7 position. The triplet signal at 3.33 ppm was assigned to the methylene protons adjacent to a keto group, and the triplet signal at 4.14 ppm, to the methylene protons adjacent to a hydroxyl group; this couples with the signal (3.33 ppm) of the neighboring methylene protons (J=5.8 Hz), and *vice versa* (J= 5.8 Hz). Therefore, the structure of Yellow Compound II was determined to be 2-amino-4-hydroxy-6-(1′-oxo-3′-hydroxypropyl)-7,8-dihydropteridine.

When Yellow Compound II was reduced with sodium borohydride after treatment with bromine in an acidic solution, Colorless Compound I was obtained in an almost quantitative yield. Thus, Colorless Compound I is 2-amino-4-hydroxy-6-(1′,3′-dihydroxypropyl)pteridine.

Colorless Compound II was indistinguishable from authentic *erythro*-neopterin,[8] and Colorless Compound III was identical with authentic *threo*-neopterin,[8] as determined by a study of the ultraviolet spectra and R_f values. It remains to be decided which configurations the products have, although it is most probable that Colorless Compound II and III are D-isomers.

Yellow Compound I gives ultraviolet spectra similar to those of isosepiapterin, and it has an acidic group. The permanganate oxidation to 2-amino-4-hydroxy-6-carboxypteridine shows that the compound is a 6-substituted pteridine. On treatment with bromine in acidic solution, Yellow Compound I yielded a new compound, Yellow Compound I·Br_2, which gives ultraviolet spectra similar to those of 2-amino-4-hydroxy-6-acetyl-7-methylpteridine.[9] Accordingly, Yellow Compound I has the keto group on carbon 1′ of the side chain, and its ring system has the 7,8-dihydro structure. Yellow Compound I contains a $-CH_2SO_3H$ group, but does not contain a $-CH_2OSO_3H$ group, since the compound remained unchanged by the acidic hydrolysis. The NMR spectrum of Yellow Compound I in CF_3COOD has a broad singlet at 3.56 ppm and a singlet at 4.61 ppm; the proton ratio of the signals is 4 : 2. The NMR spectrum of Yellow Compound I·Br_2 in CF_3COOD has a broad singlet at 3.5—4.0 ppm and a singlet at 9.16 ppm; the proton ratio of the signals is 4 : 1. The signal of Yellow Compound I at 4.16 ppm was assigned to the methylene protons at the 7 position, while in the spectrum of Yellow Compound I·Br_2 its signal (4.16 ppm) was transferred to 9.16 ppm as a vinyl proton. The signal of Yellow Compound I at 3.56 ppm and that of Yellow Compound I·Br_2 at 3.5—4.0 ppm were assigned to the protons of a $-CH_2-CH_2-$ group on the side chain, because their spectra could be explained by the A_2B_2 spin system and the slight chemical-shift difference between the methylene adjacent to a keto group and the methylene adjacent to a sulfonic acid group. These findings suggest that Yellow Compound I is 2-amino-4-hydroxy-6-(1′-oxo-3′-sulfopropyl)-7,8-dihydropteridine.

Table 1. Paper chromatography and electrophoresis of pteridines

Compounds	R_f in Solvents[a]				
	A	B	C	D	E
2-Amino-4-hydroxy-pteridine (pterin)	0.52	0.36	0.36	0.45	0
Pterin-6-carboxylic acid	0.40	0.16	0.14	0.51	−28
D-*erythro*-Neopterin	0.55	0.31	0.15	0.64	0
Colorless Compound II					
D-*threo*-Neopterin	0.52	0.28	0.15	0.63	0
Colorless Compound III					
Colorless Compound I	0.60	0.40	0.30	0.61	0
Yellow Compound I	0.46	0.26	0.03	0.48	−28
Yellow Compound II	0.43	0.31	0.26	0.28	0
Yellow Compound III	0.41	0.23	0.16	0.31	
Yellow Compound I $-Br_2$	0.47	0.28	0.03	0.62	−32
Isosepiapterin	0.52	0.49	0.58	0.24	0

a) Solvents: A, 2-Propanol-2% ammonium acetate (1:1); B, 2-Propanol-1% ammonia (2:1); C, *n*-Butanol-acetic acid-water (4:1:1); D, 3% Ammonium chloride; E, Distance to anode in electrophoresis; buffer: 0.05 M acetic acid-sodium acetate (pH 4.25); 30 min and 500 V/25 cm.

Yellow Compound III gives ultraviolet spectra similar to those of sepiapterin.[10] The analytical data indicate that the empirical formula for the compound is $C_9H_{11}O_4N_5$. The reduction of the compound with sodium borohydride, followed by oxidation with manganese oxide to *erythro*-neopterin and *threo*-neopterin, shows that Yellow Compound III has a side chain of a $-CO-CHOH-CH_2OH$ or $-CHOH-CO-CH_2OH$ group. The NMR spectrum of Yellow Compound III in $(CD_3)_2SO-D_2O$ has a doublet at 3.68 ppm, a singlet at 4.15 ppm, and a triplet at 5.00 ppm, the proton ratio of the signals being 2 : 2 : 1. The signals (a doublet signal at 3.18 ppm (J=5.2 Hz) and a triplet signal at 5.00 ppm (J=5.2 Hz)) show that Yellow Compound III has a $=CH-CH_2-$ group. The signal at 3.68 ppm was assigned to the methylene protons adjacent to a hydroxyl group; the signal at 5.00 ppm, to the methylene group adjacent to a hydroxyl group and a keto group, and the signal at 4.15 ppm, to the methylene protons at the 7 position. Accordingly, the structure of Yellow Compound III is determined to be 2-amino-4-hydroxy-6-(1′-oxo-2′,3′-dihydroxypropyl)-7,8-dihydropteridine.

It may be concluded that these compounds are not produced by the process of the reduction of D-*erythro*-neopterin, but by the process of the reoxidation of 7,8-dihydro-D-*erythro*-neopterin. When the reaction mixture of sepiapterin and the sepiapterin reductase was

8) K. Sugiura, H. Yamashita, and M. Goto, This Bulletin, **45**, 3564 (1972).

9) K. Sugiura and M. Goto, *ibid.*, **42**, 2662 (1969).

10) S. Nawa, *ibid.*, **33**, 1555 (1960).

treated with diluted acid after an almost complete reduction of the pteridine, biopterin was produced together with isosepiapterin.[11] This fact is not inconsistent with the above observation. This type of reaction including epimerization, oxidation, and reduction, is similar to certain reactions of carbohydrates. The relation of the C=N bond at 5 and 6 positions to the polyhydroxyalkyl group at the 6 position of 7,8-dihydroneopterin is similar to that in a keto and polyhydroxyalkyl group in carbohydrates.

11) S. Katoh and M. Akino, *Experientia*, **22**, 793 (1966).

BULLETIN OF THE CHEMICAL SOCIETY OF JAPAN, VOL. 46, 942—946 (1973)

The Photochemistry of 2-Quinolinecarbonitriles. I. The Photochemical Reactions of 2-Quinolinecarbonitriles with Alcohols, Ethers, or Carboxylic Acids

Norisuke HATA, Isao ONO, Satoru MATONO, and Harutoshi HIROSE

Department of Chemistry, College of Science and Engineering, Aoyama Gakuin University, Chitosedai, Setagaya-ku, Tokyo

(Received August 19, 1972)

The photochemical reactions of 2-quinolinecarbonitriles with alcohols, diethyl ether, or aliphatic carboxylic acids in an atmosphere of oxygen or nitrogen were found to result in the replacement of the cyano group by 1-hydroxyalkyl, 1-ethoxyethyl, or alkyl group. However, the irradiation of 2-quinolinecarbonitrile in an alcoholic solvent except for the case of *tert*-butyl alcohol under a nitrogen atmosphere gave an unidentified substance (probably, a certain triazapentaphene) in addition to the photosubstitution product. The photoinduced substitution reaction found in the present experiment was revealed to proceed through the excited singlet state of 2-quinolinecarbonitrile, whereas the lowest triplet state was responsible for the formation of an unidentified substance in a deaerated alcohol.

Photoalkylation reactions of *N*-heterocyclic compounds have been extensively studied from both a synthetic and mechanistic point of view during the past few years.[1] In order to investigate the effect of an electron-withdrawing group on such photoinduced reactions, the present authors have started photochemical studies of cyano-substituted N-heteroaromatics. As has been briefly reported in a preliminary communication,[2] 2-quinolinecarbonitrile in an alcoholic solvent has been found, interestingly, to be converted into 2-(1-hydroxyalkyl)quinoline upon irradiation by ultraviolet light longer than 300 nm under an oxygen atmosphere. The purpose of the present paper is to present the experimental data on the photochemical reactions of 2-quinolinecarbonitriles with alcohols, ethers, or carboxylic acids.

Photochemical Reactions of 2-Quinolinecarbonitriles with Alcohols. A 2×10^{-2} M solution of 2-quinolinecarbonitrile (I) in an alcoholic solvent (II) (350 ml of ethanol, 1-propanol, 2-propanol, or *tert*-butyl alcohol was irradiated with ultraviolet light longer than 300 nm in an atmosphere of oxygen at room temperature. As a result, white, crystalline solids (III) depending on the reaction medium were isolated as the main product. The UV absorption spectra of the photoproducts (III) were quite similar to that of quinaldine. The IR spectra of III in KBr showed absorptions at about 3250 cm^{-1} (O–H stretching) and ~2900 cm^{-1} (aliphatic C–H stretching), while the peak at 2230 cm^{-1} characteristic of the C≡N group was completely missing. The NMR spectra in $CDCl_3$ indicated the presence of a 1-hydroxyalkyl group, which corresponds to the alcohol used as a reaction medium, at the 2-position of a quinoline. In addition to the UV, IR, and NMR spectra, the structural determinations of the products (III) were made on the basis of the mass spectra as well as by means of elemental analysis; the results are summarized in Table 1. It was concluded from these results that the 2-quinolinecarbonitrile (I) changed photochemically in an alcoholic solvent (IIa—d) to yield 2-(1-hydroxyalkyl)quinoline (IIIa—d). In the case of 4-methylquinoline-2-carbonitrile, also a similar photosubstitution reaction was found to take place to afford 2-(1-hydroxyalkyl)-4-methylquinoline in a good yield; the analytical data for 2-(1-hydroxyethyl)-4-methylquinoline (III'a) are listed in Table 1.

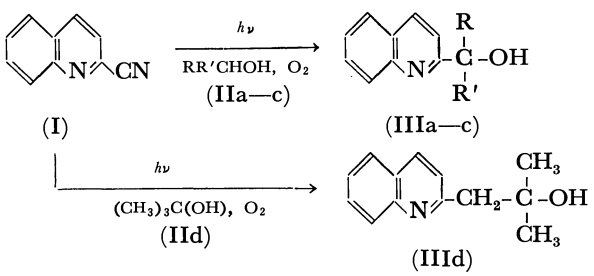

IIa and IIIa: R=CH_3, R'=H
IIb and IIIb: R=C_2H_5, R'=H
IIc and IIIc: R=CH_3, R'=CH_3

1) (a) M. Ochiai and K. Morita, *Tetrahedron Lett.*, **1967**, 2349; M. Ochiai, E. Mizuta, Y. Asahi, and K. Morita, *Tetrahedron*, **24**, 5861 (1968). (b) H. Nozaki, M. Kato, R. Noyori, and M. Kawanishi, *Tetrahedron Lett.*, **1967**, 4259; R. Noyori, M. Kato, M. Kawanishi, and H. Nozaki, *Tetrahedron*, **25**, 1125 (1969). (c) F. R. Stermitz, R. P. Seiber and D. E. Nicodem, *J. Org. Chem.*, **33**, 1136 (1968). (d) F. R. Stermitz, C. C. Wei, and C. M. O'Donnell, *J. Amer. Chem. Soc.*, **92**, 2745 (1970). (e) E. F. Travecedo and V. I. Stenberg, *Chem. Commun.*, **1970**, 609.

2) N. Hata, I. Ono, and S. Ogawa, This Bulletin, **44**, 2286 (1971).

TABLE 1. ANALYTICAL DATA FOR THE PHOTOPRODUCTS III AND VIII

Product	Mp (°C)	Yield (%)[a]	Mass (M^+)	NMR[b] (δ, ppm)	Elemental analysis Found (%)	Calc (%)
IIIa	79—80	35(54)[c]	173	7.2—8.2 (m, 6H, aromatic) 6.15 (s, 1H, -O*H*, deuterium exchangeable) 5.08 (q, J=7 Hz, 1H, -C*H*(CH_3)OH) 1.55 (d, J=6.5 Hz, 3H, -CH(C*H*$_3$)OH)	C 76.22 H 6.44 N 8.07	C 76.30 H 6.36 N 8.09 (for $C_{11}H_{11}NO$)
IIIb	68—69	45(30)[c]	187	7.4—8.3 (m, 6H, aromatic) 4.90 (t, J=4.5 Hz, 1H, -C*H*(OH)C_2H_5) 4.82 (s, 1H, -O*H*, deuterium exchangeable) 1.6—2.2 (m, 2H, -CH(OH)C*H*$_2$$CH_3$) 0.98 (t, J=7 Hz, 3H, -CH(OH)CH_2C*H*$_3$)	C 76.57 H 6.49 N 7.83	C 77.01 H 6.95 N 7.49 (for $C_{12}H_{13}NO$)
IIIc	69—70	40(20)[c]	187	7.3—8.3 (m, 6H, aromatic) 4.75 (s, 1H, -O*H*, deuterium exchangeable) 1.62 (s, 6H, -C(C*H*$_3$)$_2$OH)	C 76.75 H 6.85 N 8.06	C 77.01 H 6.95 N 7.49 (for $C_{12}H_{13}NO$)
IIId	49—50[d]	14(35)[c]	201	7.5—8.2 (m, 6H, aromatic) 5.95 (s, 1H, -O*H*, deuterium exchangeable) 3.10 (s, 2H, -C*H*$_2$C(CH_3)$_2$OH) 1.30 (s, 6H, -CH_2C(C*H*$_3$)$_2$OH)	C 77.36 H 7.46 N 6.78	C 77.58 H 7.51 N 6.95 (for $C_{13}H_{15}NO$)
III'a	82.5	41(62)[c]	187	7.4—8.2 (m, 5H, aromatic) 5.22 (s, 1H, -O*H*, deuterium exchangeable) 4.99 (q, J=6.5 Hz, 1H, -C*H*(OH)CH_3) 2.62 (s, 3H, -C*H*$_3$) 1.55 (d, J=6.8 Hz, 3H, -CH(OH)C*H*$_3$)	C 77.08 H 6.98 N 7.77	C 77.01 H 6.95 N 7.49 (for $C_{12}H_{13}NO$)
VIII	109—110[e]	32(59)[c]	201	7.4—8.3 (m, 6H, aromatic) 4.74 (q, J=7 Hz, 1H, -C*H*(CH_3)O-) 3.48 (q, J=7.3 Hz, 2H, -OC*H*$_2$$CH_3$) 1.56 (d, J=6.7 Hz, 3H, -CH(C*H*$_3$)O-) 1.23 (t, J= 7 Hz, 3H, -OCH_2C*H*$_3$)	C 52.74[e] H 4.24[e] N 12.70[e]	C 53.03[e] H 4.22[e] N 13.02[e] (for $C_{19}H_{18}N_4O_8$)

a) Represents the yield in an oxygen atmosphere. b) Measured in $CDCl_3$ solution using a TMS as an internal standard. c) The value in bracket represents the yield in HCl acidified solution. d) Mp of the picrate: 141—142°C. e) The picrate.

Such a photochemical hydroxyalkylation of 2-quinolinecarbonitrile was demonstrated to take place in an HCl-acidified alcoholic solution as well, although the yield of III was appreciably different from that in the solution without acid. On the other hand, Stermitz *et al.*[1d] have reported that the irradiation of quinoline in HCl-acidified ethanol resulted in the ethylation of the 2- or 4-position of a quinoline, indicating that there exists a striking difference in the photoreactivity between 2-quinolinecarbonitrile and quinoline in an acidified alcohol.

When the irradiation of 2-quinolinecarbonitrile in alcohols different from *tert*-butyl alcohol was carried out, with nitrogen being bubbled in instead of oxygen, the solution became reddish-violet[3] and two products were separated; one was the product (III) depending on the reacting solvent, while the other was a compound (IV) with a mp of 215°C (decomp), irrespective of the alcohol used as a reaction medium. The yields of III and IV in various alcohols are as follows: 36% and 17% in ethanol, 30% and 25% in 1-propanol, and 26% and 20% in 2-propanol. However, the product (IV) was not formed in an acidified alcohol, nor was it in the case of 4-methylquinoline-2-carbonitrile. When the *tert*-butyl alcohol was used as a reaction medium, only the product (IIId) was isolated as the major product in a 14% yield, while the formation of the product (IV) was not observed. The IR spectrum of the photoproduct (IV) in KBr indicated that the peak at 2230 cm^{-1} characteristic of a C≡N group was absent, whereas absorptions around 3060 cm^{-1} (aromatic C–H stretching), 1505, 1590 cm^{-1} (ring vibration), and 830, 755 cm^{-1} (aromatoc C–H out-of-plane) were observed. The NMR spectrum showed only multiplet signals due to aromatic protons around 7.5—8.5 ppm ($CDCl_3$, TMS); also, the predominantly strong peaks corresponding to M^+= 281 and $(M-1)^+$=280 were observed in the mass spectrum. Figure 1 shows the UV absorption spectrum of the product (IV), which is interestingly very similar to that of pentaphene in maximum wavelength and in molar extinction coefficient.[4] In addition to these data, the elemental analysis led to a conclusion that the product (IV) might be a certain triazapentaphene; Found, C 80.22, H 3.96; N 14.99%, Calcd for $C_{19}H_{11}N_3$, C 81.22, H 3.92, N 14.95%.

3) The reddish-violet color disappeared rapidly by the introduction of air (or oxygen) or the addition of DPPH into the irradiated solution.

4) H. H. Jaffé and M. Orchin, "Theory and Applications of Ultraviolet Spectroscopy", John Wiley & Sons Inc., London, (1962) Chapter 13.

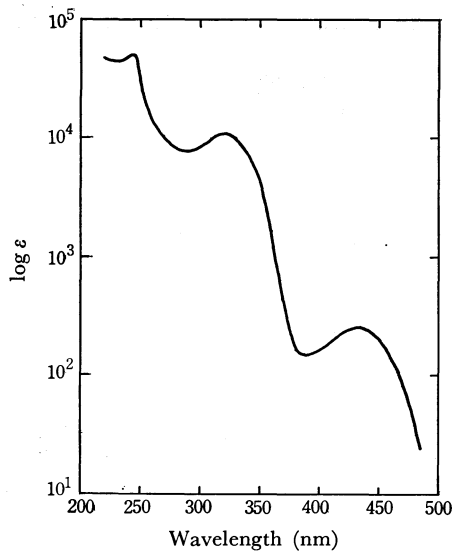

Fig. 1. The UV absorption spectrum of photoproduct (IV) in ethanol.

Although the location of nitrogen atoms on the pentaphene nucleus is entirely ambiguous at present, (A) or (B) seems to be a plausible structure for the reason to be discussed below.

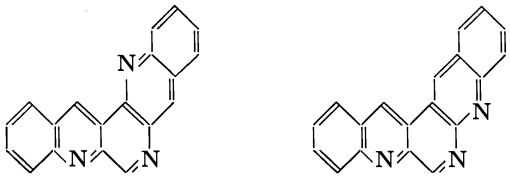

Judging from the fact that the photochemical conversion I→IV did not occur in *tert*-butyl alcohol or benzene, the light absorption of 2-quinolinecarbonitrile (I) appears first to cause a hydrogen-atom abstraction from an alcohol to give V. If V thus formed reacts photochemically with I to yield an azomethine compound (VIa) or (VIb), followed by photochemical cyclization, A or B may be expected to be formed.

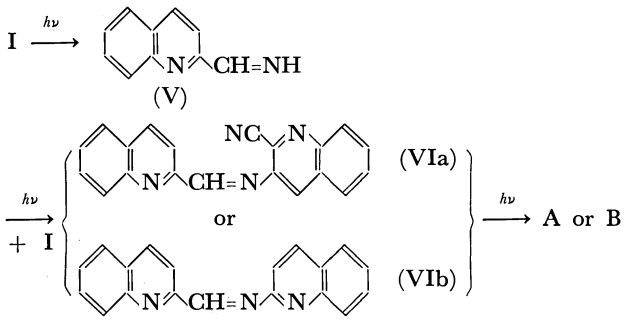

As has been described above, the product (III) was formed under an oxygen or nitrogen atmosphere, while the product (IV) resulted only in an atmosphere of nitrogen. This implies that the reactive state responsible for the formation of the product (III) is probably the excited singlet state of 2-quinolinecarbonitrile, whereas the triplet state is involved in the formation of the product (IV). In order to make this clear, a quenching experiment on the lowest triplet state of 2-quinolinecarbonitrile was thus undertaken

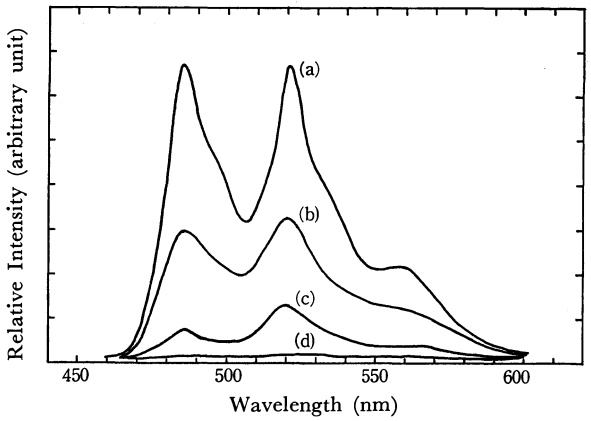

Fig. 2. The phosphorescence spectrum of 2-quinolinecarbonitrile in ethanol at 77K (concentration of 2-quinolinecarbonitrile: 5.0×10^{-4} M).
(a) [Piperylene]: 0 M, (b) [Piperylene]: 5.0×10^{-2} M, (c) [Piperylene]: 4.0×10^{-1} M, (d) [Piperylene]: 1.0 M

in deaerated ethanol. Figure 2 shows the phosphorescence spectrum of 2-quinolinecarbonitrile in ethanol at 77K. It was estimated, from the first maximum of the phosphorescence spectrum (484 nm), that the lowest triplet state of 2-quinolinecarbonitrile has an excitation energy of about 59 kcal·mol^{-1}. Accordingly, the piperylene (E_T=57 kcal·mol^{-1}) may be expected to be usable as a triplet quencher for 2-quinolinecarbonitrile. As is shown in Fig. 2, the addition of piperylene to an ethanol solution of 2-quinolinecarbonitrile in amounts much greater than the molar equivalence led to the complete disappearance of the phosphorescence of 2-quinolinecarbonitrile. The photochemical reaction of 2-quinolinecarbonitrile in deaerated ethanol at room temperature was, therefore, carried out in the presence of varying amounts of piperylene. As can be seen from Fig. 3, the photochemical conversion from I to IIIa was not affected by the addition of piperylene, while the formation of the product (IV) decreased linearly with the in-

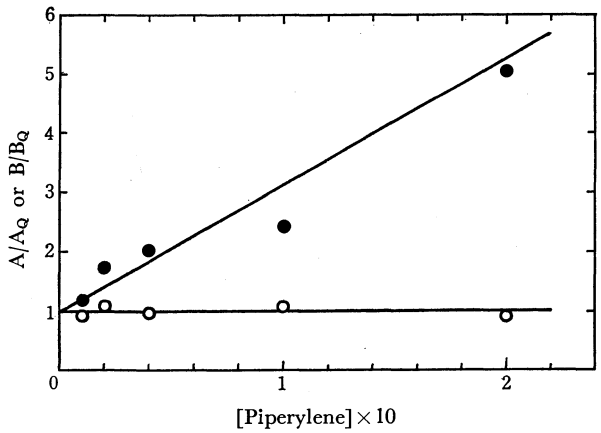

Fig. 3. The Effect of piperylene on the photochemical reaction of 2-quinolinecarbonitrile in ethanol under nitrogen atmosphere at 20°C. A (or B) and A_Q (or B_Q) represent, respectively, the amounts of the product (IIIa) (or (IV)) in the absence and in the presence piperylene.
Initial amount of 2-quinolinecarbonitrile: 100 mg (in 70 ml ethanol). Irradiation time: 60 min. A: 25 mg. B: 16 mg. ○: product (IIIa). ●: product (IV).

creased concentration of piperylene. These results indicate that the photochemical substitution reaction I→III proceeds through the excited singlet state of 2-quinolinecarbonitrile, whereas the photochemical formation of IV involves the lowest triplet state.

Photochemical Reactions of 2-Quinolinecarbonitriles with Diethyl Ethers. In the same manner as in the case of an alcoholic solution, the ultraviolet irradiation of 2-quinolinecarbonitrile was carried out in diethyl ether under an oxygen or nitrogen atmosphere. As a result, an oily, colorless substance (VIII) was obtained as the main product; the yield was 32% in an oxygen atmosphere, while it was only 21% in a nitrogen atmosphere. The UV absorption spectrum of the product (VIII) was very similar to that of quinaldine. The IR spectrum in liquid showed peaks at about 3050 cm^{-1} (aromatic C–H stretching), 2960, 2930, 2850 cm^{-1} (aliphatic C–H stretching), 1100 cm^{-1} (C–O–C stretching), and 828 and 705 cm^{-1} (aromatic C–H out-of-plane), while a peak due to the C≡N group (2230 cm^{-1}) was missing. The analytical data of the product (VIII) are listed in Table 1. Consequently, the C≡N group of 2-quinolinecarbonitrile was revealed to be replaced by an 1-ethoxyethyl group as follows:

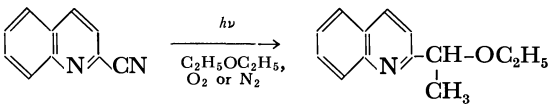

(I) (VII) (VIII)

Differing from the case of an alcoholic solution, neither a deep coloration of the solution nor the formation of a triazapentaphene-like substance was detected in an atmosphere of nitrogen. The photosubstitution reaction also took place in the solution saturated with HCl gas; the yield was good (59%).

Photochemical Reactions of 2-Quinolinecarbonitriles with Aliphatic Carboxylic Acids. 2-Quinolinecarbonitriles (0.5 g) dissolved in 70 ml of benzene containing carboxylic acid (IX) (2 g of acetic acid, propionic acid, butyric acid, isobutyric acid, or trimethylacetic acid) in a Pyrex vessel were irradiated with ultraviolet light under a nitrogen or oxygen atmosphere. As a result, two products, X and XI, were separated as the main products; the yields of these products in an atmosphere of nitrogen are shown in Table 2. On the basis of the UV, IR, and NMR spectra as well as the melting points of the picrates, the products (X) were identified as known 2-alkylquinolines[1b] corresponding to the carboxylic acid used in the photoreaction. The UV absorption spectra of the products (XI) closely resembled that of 2-quinolinecarbonitrile (I), and the IR spectra in KBr showed peaks at about 3050 cm^{-1} (aromatic C–H stretching), 2220 cm^{-1} (C≡N stretching), and ~2900 cm^{-1} (aliphatic C–H stretching). Table 3 summarizes the analytical data for the products (XI).

Table 2. Yields of the photoproducts X and XI

Products	Yield (%)				
	a	b	c	d	e
X	4	11	18	17	13
XI	trace	9	15	14	5

It was concluded from these results that the 2- or 4-alkylquinolines were formed as a result of the photochemical reaction of 2-quinolinecarbonitrile with an aliphatic carboxylic acid in benzene as follows:

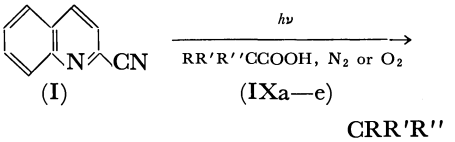

(I) (IXa—e)

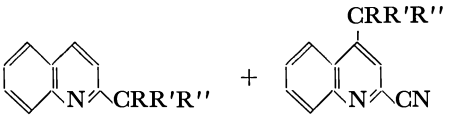

(Xa—e) (XIa—e)

IXa, Xa and XIa: R=H, R'=H, R''=H
IXb, Xb and XIb: R=CH_3, R'=H, R''=H
IXc, Xc and XIc: R=C_2H_5, R'=H, R''=H
IXd, Xd and XId: R=CH_3, R'=CH_3, R''=H
IXe, Xe and XIe: R=CH_3, R'=CH_3, R''=CH_3

Table 3. Analytical data for the photoproducts XI

Product	Mp (°C)	Mass (M^+)	NMR[a] (δ, ppm)	Elemental analysis	
				Found (%)	Calcd (%)
XIb	121	182	7.5—8.3 (m, 5H, aromatic) 3.15 (q, J=7 Hz, 2H, $-CH_2CH_3$) 1.40 (t, J=7.5 Hz, 3H, $-CH_2CH_3$)	C 78.26 H 5.26 N 15.27	C 79.12 H 5.49 N 15.38 (for $C_{12}H_{10}N_2$)
XIc	66	196	7.4—8.2 (m, 5H, aromatic) 3.72 (h, J=6.5 Hz, 1H, $-CH(CH_3)_2$) 1.39 (d, J=6.8 Hz, 6H, $-CH(CH_3)_2$	$C_{13}H_{12}N_2$[b]	
XId	107	196	7.5—8.3 (m, 5H, aromatic) 3.10 (t, J=7.5, 2H, $-CH_2CH_2CH_3$) 1.5—2.2 (m, $-CH_2CH_2CH_3$) 1.06 (t, J=7 Hz, 3H, $-CH_2CH_2CH_3$)	C 78.85 H 5.96 N 13.97	C 79.59 H 6.12 N 14.29 (for $C_{13}H_{12}N_2$)
XIe	104	210	7.6—8.6 (m, 5H, aromatic) 1.64 (s, 9H, $-C(CH_3)_3$)	$C_{14}H_{14}N_2$[b]	

a) Measured in $CDCl_3$ solution using a TMS as an internal standard. b) Estimated from the result of the mass analysis performed with a JEOL JMS-OISG-2 mass spectrometer.

Such a photochemical alkylation was not inhibited by the addition of piperylene.

Further studies for the elucidation of the primary photochemical process as well as the reaction mechanism are now in progress and will be reported soon.

Experimental

The UV absorption and the phosphorescence spectra were respectively, measured with a Hitachi recording spectrophotometer EPS–3T and a Hitachi fluorescence spectrophotometer MPF–2A with a phosphorescence accessory attached. The IR spectra were determined with a JASCO infrared spectrophotometer IR–G. The NMR spectra were taken in deuteriochloroform with a Hitachi-Perkin Elmer NMR spectrometer R–20 at 60 MHz, using a TMS as the internal standard. The mass spectra were obtained with a Hitachi RMU–6L or a JEOL JMS–O1SG–2 mass spectrometer.

Materials. The 2-quinolinecarbonitrile and 4-methylquinoline-2-carbonitrile used in this experiment were prepared according to the method given in the literature;[5] these compounds were purified by recrystallization from ethanol several times. The aliphatic carboxylic acids and all the solvents for the irradiation experiments were reagent-grade products of Wako Pure Chemical Industries, all of which were used without further purification. Reagent-grade piperylene was purified by distillation several times.

Photochemical Reactions of 2-Quinolinecarbonitriles with Alcohols under an Oxygen Atmosphere. 2-Quinolinecarbonitrile (1.0 g) dissolved in 350 ml of alcohol (ethanol, 1-propanol, 2-propanol or *tert*-butyl alcohol in a Pyrex vessel was irradiated with a 100 W high-pressure immersion mercury lamp (Riko Kagaku Sangyo Co.) for 10 hr while oxygen was being bubbled in. After the removal of the solvent under reduced pressure, the residue was chromatographed on a silica-gel column by elution with a mixture of *n*-hexane and diethyl ether (1 : 1). A white, crystalline solid (III) was isolated as the main product. When the HCl-acidified alcohol was used as the reaction medium, a 350–ml alcoholic solution with 2-quinolinecarbonitrile (1.0 g), dissolved in it, to which 3.0 ml of concentrated HCl had been added, was irradiated for 10 hr under an oxygen atmosphere. The irradiated solution was concentrated *in vacuo*, and the concentrate was neutralized with a sodium carbonate aqueous solution. The aqueous solution was then extracted with chloroform, dried with anhydrous sodium sulfate, and the inorganic salts were removed by filtration. The chloroform solution was then concentrated under reduced pressure to afford a crystalline mass, which was subsequently chromatographed over silica gel to isolate the product (III).

Photochemical Reactions of 2-Quinolinecarbonitriles with Alcohols under a Nitrogen Atmosphere. A solution of 1.0 g 2-quinolinecarbonitrile in 350 ml of alcohol (ethanol, 1-propanol, or 2-propanol) was irradiated with a 100W high-pressure immersion mercury lamp, where half an hour before the irradiation was started nitrogen had been bubbled through the solution; this was continued constantly during the irradiation. When the irradiation was performed for *ca.* 15 min, the solution became reddish-violet. After the solution had been irradiated for 5 hr, the solvent was evaporated to dryness *in vacuo*. The residue was subjected to silica-gel chromatography (with dichloromethane used as the eluent) to afford the starting material, the products (III) and (IV). III or IV was purified by silica-gel chromatography using a mixture of *n*-hexane and diethyl ether (1 : 1) or a mixture of dichloromethane, *n*-hexane, and diethyl ether (10 : 1 : 1) as the eluent. The product (IV) thus obtained was further purified for the analysis by recrystallization from ethanol several times.

Photochemical Reactions of 2-Quinolinecarbonitriles with Diethyl Ether under a Nitrogen or Oxygen Atmosphere. A solution of 1.0 g of 2-quinolinecarbonitrile in 350 ml of diethyl ether was irradiated in a Pyrex vessel under cooling at 5—10°C in an ice-bath, and with a 100W high-pressure immersion mercury lamp in an atmosphere of oxygen or nitrogen. After having been irradiated for 10 hr, the solution was concentrated under reduced pressure; the residue was chromatographed on a silica-gel column by elution with dichloromethane to isolate the product (VIII). The product (VIII) thus obtained was further purified by using a mixture of *n*-hexane and diethyl ether (1 : 1) as the eluent.

Photochemical Reactions of 2-Quinolinecarbonitriles with Aliphatic Carboxylic Acids in Benzene under a Nitrogen or Oxygen Atmosphere. A solution of 2-quinolinecarbonitrile (0.5 g) and carboxylic acid (2 g of acetic acid, propionic acid, butyric acid, isobutyric acid, or trimethylacetic acid) in 70 ml of benzene was irradiated in a Pyrex vessel with a 100W high-pressure immersion mercury lamp for 6 hrs while nitrogen or oxygen was being bubbled in. After the removal of the solvent under reduced pressure, a 30-ml portion of water was added to the residue; the solution was then neutralized with sodium carbonate. After the extraction with chloroform or dichloromethane, the solution was concentrated *in vacuo*. The concentrate was chromatographed on a silica-gel column by elution with a mixture of *n*-hexane and ethyl acetate (9 : 1) to separate the starting material, the products (X) and (XI). These products were then further purified by alumina chromatography using the same eluent as before.

In conclusion, the authors wish to thank Professor Juji Yoshimura of Tokyo Institute of Technology for his kind discussions and Dr. Teiki Iwaoka of Sankyo Co. for his mass-spectral measurement of the photoproduct (IV).

5) H. Menze, *Ber.*, **69**, 1566 (1936).

When VII was subjected to thermal decarboxylation, it gave a compound which was found to be identical with Va. Esterification of dicarboxylic acid with ethanol and hydrogen chloride afforded half ester (VIII), which is isomeric with VII. When the esterification of VI was carried out by refluxing ethanol–benzene solution of VI in the presence of *p*-toluenesulfonic acid with continuous removal of water, a mixture of both esters (Va and VIII) was obtained.

Condensation of I with acetylacetone could be accomplished by heating the reaction mixture at 120°C in the absence of condensing agent, an intermediate hydrazone (IIId) being obtained. The hydrazone, when treated with alcoholic sodium hydroxide, gave a new compound, 4-acetyl-3-methyl-1,5-diphenylpyrazole (Vd). Compound Vd readily condensed with benzaldehyde in the presence of sodium hydroxide to give 4-cinnamoyl-3-methyl-1,5-diphenylpyrazole (IX).

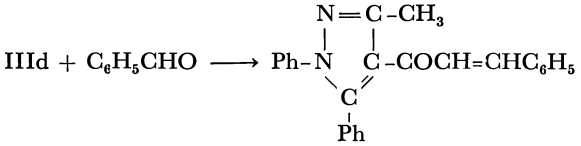

IX

The procedures for preparation of 4-carboxyl-1,5-diphenylpyrazol-3-ylacetic acid and all its possible esters were found to be satisfactory and compounds with interesting synthetical possibilities are now available.

Experimental

Preparation of Hydrazone (IIIa). To a solution of 4.25 g (0.02 mol) of I in 100 ml of benzene was added 2.6 g (0.02 mol) of ethyl acetoacetate and 2 g of phosphorus pentoxide. The mixture was refluxed on a water bath for 5 hr. The hot benzene solution was separated by decantation and the solvent was removed under reduced pressure. The residual oily product was triturated with a small amount of ethanol and the resulting solid was recrystallized from ethanol to afford colorless crystals, mp 142°C. 5.8 g (90%).

Found: C, 70.20; H, 5.98; N, 8.55%. Calcd for $C_{19}H_{20}O_3N_2$: C, 70.53; H, 6.09; N, 8.64%.

Cyclization of IIIa to Pyrazole (Va). Two milliliters of 2M sodium hydroxide was added dropwise at room temperature with vigorous stirring to a solution of IIIa (1 g) in 50 ml of ethanol. Stirring was continued until the yellow color disappeared completely. Fifty milliliters of water was then added. The precipitate was collected by filtration and recrystallized from ethanol to give colorless crystals, mp 121°C (lit. mp 122°C). Yield 95%.

Found: C, 74.35; H, 5.77; N, 9.28%. Calcd for $C_{19}H_{18}O_2N_2$: C, 74.49; H, 5.92; N, 9.15%.

4-Carbethoxy-1,3,5-triphenylpyrazole (Vb). Hydrazone (IIIb) was prepared from 1-benzoyl-1-phenylhydrazine (4.2 g) and ethyl benzoylacetate (3.8 g) by the same method as for the preparation of IIIa. The hydrazone (6.2 g), obtained as an oily product, was dissolved in 100 ml of ethanol, to which 5 ml of 2 M sodium hydroxide solution was gradually added. The solution was then stirred for 10 min, diluted with water and the precipitate formed was collected to give 4.8 g of Vb which was recrystallized from ethanol to give colorless crystals, mp 143—144°C (lit. mp 145—146.5°C).

Found: C, 77.97; H, 5.60; N, 7.58%. Calcd for $C_{24}H_{20}O_2N_2$: C, 78.24; H, 5.42; N, 7.60%.

Ethyl 4-Carbethoxy-1,5-diphenylpyrazol-3-ylacetate (Vc). To a solution of 1-benzoyl-1-phenylhydrazine (4.2 g) and diethyl acetonedicarboxylate (4.1 g) in 100 ml of benzene was added 2 g of phosphorus pentoxide and the mixture was refluxed on a water bath for 5 hr. The hot benzene solution was separated by decantation and concentrated *in vacuo*. The residual oil (6.8 g) was dissolved in 100 ml of ethanol and to the resulting solution was added gradually 5 ml of 2 M sodium hydroxide solution at 10—15°C with stirring. Stirring was continued for 30 min at room temperature, after which water was added to precipitate Vc which was recrystallized from dilute ethanol to give colorless crystals (4.5 g), mp 67.5—68°C.

Found: C, 69.50; H, 5.65; N, 7.51%. Calcd for $C_{22}H_{22}O_4N_2$: C, 69.82; H, 5.86; N, 7.40%. IR: 1743, 1693 cm^{-1}.

Preparation of Hydrazone (IIId). A mixture of acetylacetone (1 g) and 1-benzoyl-1-phenylhydrazine (2.1 g) was heated in an oil bath at 120°C for about 30 min. After cooling, the solid product was recrystallized from ethanol to afford IIId as colorless crystals, mp 147—148°C.

Found: C, 73.35; H, 5.91; N, 9.70%. Calcd for $C_{18}H_{18}O_2N_2$: C, 73.45; H, 6.16; N, 9.52%.

4-Acetyl-3-methyl-1,5-diphenylpyrazole (Vd). To a solution of 2 g of the hydrazone (IIId) in 50 ml of ethanol was added 5 ml of 2 M sodium hydroxide solution. This was left to stand at room temperature for 1 hr and then diluted with water. The precipitates were collected, washed with water, and recrystallized from dilute ethanol to give Vd, colorless crystals, mp 93—95°C.

Found: C, 77.94; H, 5.98; N, 10.21%. Calcd for $C_{18}H_{16}ON_2$: C, 78.23; H, 5.84; N, 10.14%, IR: 1660 cm^{-1}.

4-Cinnamoyl-3-methyl-1,5-diphenylpyrazole (IX). To a solution of 2.8 g of Vd and 1.1 g of benzaldehyde in 50 ml of ethanol was added gradually with stirring 10 ml of aqueous sodium hydroxide solution (40%). The reaction mixture was left to stand for 2 hr at room temperature and then diluted with water. Precipitates were collected, washed thoroughly with water and recrystallized from ethanol to give IX, pale yellow crystals, mp 157—158°C. 3.2 g.

Found: C, 82.10; H, 5.65; N, 7.73%. Calcd for $C_{25}H_{20}ON_2$: C, 82.39; H, 5.53; N, 7.68%. IR: 1650 cm^{-1}.

4-Carboxy-1,5-diphenylpyrazol-3-ylacetic Acid (VI). A solution of the diethyl ester (Vc, 3 g) in ethanol (25 ml) containing potassium hydroxide (2.5 g) and water (5 ml) was refluxed at 100°C for 30 min and concentrated, cooled, and acidified with dilute hydrochloric acid. The product was collected and washed with water, and then crystallized from dilute acetic acid (80%) to give dicarboxylic acid (VI) in colorless prisms, mp 251—252°C with decomposition.

Found: C, 66.85; H, 4.37; N, 8.57%. Calcd for $C_{18}H_{14}O_4N_2$: C, 67.07; H, 4.38; N, 8.69%. IR: 3500—2500, 1710, 1665 cm^{-1}.

4-Carbethoxy-1,5-diphenylpyrazol-3-ylacetic Acid (VII). Ethyl 4-carbethoxy-1,5-diphenylpyrazol-3-ylacetat (4 g) was dissolved at room temperature in ethanol (30 ml) containing potassium hydroxide (3.5 g) and water (2 ml). After 30 min dipotassium salt of the dicarboxylic acid (0.5 g) was separated by filtration and the filtrate was diluted with water and acidified with dilute hydrochloric acid to precipitate VII which was recrystallized from ethanol to give 2.6 g of colorless plates, mp 195—196°C.

Found: C, 68.65; H, 5.04; N, 8.16%. Calcd for $C_{20}H_{18}O_4N_2$: C, 68.56; H, 5.18; N, 8.00%. IR: 3300—

2500, 1743, 1715 cm^{-1}.

The above half ester (2 g) was heated at 190—200°C in an oil bath until evolution of carbon dioxide was over. The residue solidified on treating with ethanol, and by recrystallization from ethanol, the compound Va (1 g) was obtained in colorless crystals, mp 120—121°C.

Ethyl 4-Carboxy-1,5-diphenylpyrazol-3-ylacetate (VIII). (i) Dry hydrogen chloride was passed into a suspension of 2 g of VI in 20 ml of absolute ethanol until VI dissolved completely (15 min). The reaction mixture was allowed to stand at room temperature for 2 hr. Crystals separated out were collected and washed to give 1.2 g of the crude half ester VIII. Recrystallization from benzene gave colorless prisms, mp 185—186°C.

Found: C, 68.30; H, 4.93; N, 7.97%. Calcd for $C_{20}H_{18}O_4N_2$: C, 68.56; H, 5.18; N, 8.00%. IR: 3200—2500, 1740, 1665 cm^{-1}.

(ii) To a suspension of 2 g of VI in anhydrous benzene (50 ml) and absolute ethanol (1 ml) was added 0.5 g of *p*-toluenesulfonic acid. The mixture was refluxed for 5 hr using a water separator. Benzene was removed and the oily residue was boiled in petroleum ether (bp 40—60°C) and cooled, and the precipitates were collected and recrystallized from benzene to give 0.7 g of VIII. Mixed melting point measurement with an authentic sample showed no depression.

Evaporation of the petroleum ether filtrate and recrystallization of the residue from dilute ethanol gave 0.6 g of diester (Vc), mp 67—68°C.

The authors are grateful to the International Post-Graduate University Course in Chemistry and Chemical Engineering, organized by Tokyo Institute of Technology and Japanese National Commission for UNESCO, for support of this work.

BULLETIN OF THE CHEMICAL SOCIETY OF JAPAN, VOL. 46, 949—954 (1973)

Chemical Studies on Tuberactinomycin. V.[1] Structures of Guanidino Amino Acids in Tuberactinomycins[2]

Tateaki WAKAMIYA, Tetsuo SHIBA, Takeo KANEKO,*
Hideo SAKAKIBARA,** Toshiharu NODA,** and Teruo TAKE**
Department of Chemistry, Faculty of Science, Osaka University, Toyonaka, Osaka
** *The Research Laboratories, Toyo Jozo Co., Ltd., Ohito, Shizuoka*

(Received September 26, 1972)

Tuberactidine (III) is a guanidino amino acid component of antitubercular peptides, tuberactinomycin A and B, while the known guanidino amino acid capreomycidine (V) is involved in tuberactinomycin N and O. The structure of tuberactidine was assigned to be α-(4-hydroxy-2-iminohexahydro-6-pyrimidinyl)glycine and its stereochemistry was also established. During isolation of tuberactidine from an eluate in the column chromatography of tuberactinomycin hydrolyzate, it was converted to N^{α}-formyltuberactidine dimer (I). In this dimer, structural alternation between a carbinolamine form of cyclol type and an amide lactone form was noticed depending to a pH of the solution. I was hydrolyzed to tuberactidine and viomycidine (IV) with hydrobromic acid. In addition, a plausible pathway for the formation of viocidic acid (VII), one of the artifacts formed during hydrolysis of tuberactinomycin, was proposed.

Tuberactinomycins are antitubercular peptides isolated from the broth filtrate of *Streptomyces griseoverticillatus* var. *tuberacticus*[3] and its mutant.[4] A family of this antibiotic comprises four congeners, A, B, N and O. Among them, tuberactinomycin B was found to be the same to the one known as viomycin.[4] Amino acid compositions of these four peptides were listed in Table 1.

Acid hydrolyzate of tuberactinomycin A was separated by ion-exchange column chromatography, using a buffer solution of pyridine and formic acid as an eluent. Serine, α,β-diaminopropionic acid, a mixture of guanidino amino acids, *i.e.*, viomycidine, tuberactidine and viocidic acid, and finally γ-hydroxy-β-lysine[1] were eluted in this order. In the case of viomycin, a similar elution pattern was obtained except a replacement of γ-hydroxy-β-lysine with β-lysine. As a guanidino amino acid in viomycin, viomycidine (IV) has already been isolated from its hydrolyzate by many workers,[5] and its structure was determined by Büchi and Raleigh as shown in Fig. 1.[6] From hydrolyzates of tuberactinomycin N and O, capreomycidine (V) was obtained as a guanidino amino acid component. First isolation of this amino acid from the known

* Present address: Shiseido Laboratory, Nippa-cho, Kohoku-ku, Yokohama.

1) Part IV: T. Wakamiya, T. Shiba, and T. Kaneko, This Bulletin, **45**, 3668 (1972).

2) Presented at the 24th Annual Meeting of the Chemical Society of Japan, Osaka, April, 1971; p. 1783. A part was reported: T. Wakamiya, T. Shiba, T. Kaneko, H. Sakakibara, T. Take, and J. Abe, *Tetrahedron Lett.*, **1970**, 3497.

3) A. Nagata, T. Ando, R. Izumi, H. Sakakibara, T. Take, K. Hayano, and J. Abe, *J. Antibiotics*, **21**, 681 (1968).

4) R. Izumi, T. Noda, T. Ando, T. Take, and A. Nagata, *ibid.*, **25**, 201 (1972).

5) a) T. H. Haskell, S. A. Fusari, R. P. Frohardt, and Q. Bartz, *J. Amer. Chem. Soc.*, **74**, 599 (1952). b) J. H. Bowie, A. W. Johnson and G. Thomas, *Tetrahedron Lett.*, **1964**, 863. c) J. R. Dyer, H. B. Hayes, E. G. Miller, Jr., and R. F. Nassar, *J. Amer. Chem. Soc.*, **86**, 5363 (1964). d) T. Takita and K. Maeda, *J. Antibiotics*, **21**, 512 (1968).

6) G. Büchi and J. A. Raleigh, *J. Org. Chem*, **36**, 873 (1971). J. A. Raleigh, Ph. D. Dissertation, Massachusetts Institute of Technology, Oct. 1966.

Table 1. Amino acid compositions of tuberactinomycins (TUM)

TUM	Molecular Formula	Ser	Dpr	Uda	Tbd	Cpd	γ-Hy-β-lys	β-Lys
A	$C_{25}H_{43}O_{11}N_{13}$	2	1	1	1	—	1	—
B	$C_{25}H_{43}O_{10}N_{13}$	2	1	1	1	—	—	1
N	$C_{25}H_{43}O_{10}N_{13}$	2	1	1	—	1	1	—
O	$C_{25}H_{43}O_9N_{13}$	2	1	1	—	1	—	1

Ser: L-serine, Dpr: L-α,β-diaminopropionic acid, Tbd: L-tuberactidine, Cpd: L-capreomycidine, γ-Hy-β-lys: γ-hydroxy-L-β-lysine, β-Lys: L-β-lysine, Uda: 3-ureidodehydroalanine

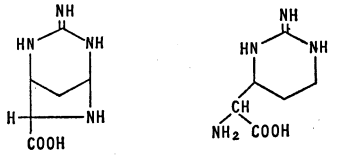

Fig. 1. Structures of viomycidine(IV) and capreomycidine(V).

antibiotic capreomycin had been reported by Herr and its structure was decided as above (Fig. 1).[7]

The existence of 3-ureidodehydroalanine as a composite amino acid in the antibiotics was confirmed not only by X-ray analysis in the case of tuberactinomycin O,[8] but also by the chemical evidences and NMR data[9] which were coincided with those reported in the studies of viomycin by Bycroft and his colleagues.[10] However, this moiety could not be isolated from the hydrolyzate because of ease of decomposition to NH_3 and CO_2 during acid hydrolysis.

For the isolation of tuberactidine (III), fractions of a positive Sakaguchi reaction in the eluates of column chromatography were combined and evaporated to give colorless prisms. Although the original eluate containing tuberactidine gave positive reactions both for ninhydrin and Sakaguchi reactions, the crystals obtained above were found to be negative for both reactions. Molecular formula of $C_{14}H_{20}O_6N_8$ (I) was deduced to the compound from the results of elemental analysis and molecular peak (396) in the mass spectrum. This molecular weight was supported by the results of mass spectrum of its diacetyl derivative $C_{18}H_{24}O_8N_8$ (480) (II).

When I was treated with 15% hydrobromic acid at 50°C, it was degradated to tuberactidine (III) and viomycidine (IV), in almost equal amounts, both of which were isolated separately by fractional crystallization from aqueous ethanol. As reported in the preliminary form, we decided the structure of tuberactidine on the basis of NMR (Fig. 2) and ORD spectrum (Fig. 3) to α-(4-hydroxy-2-iminohexahydro-6-pyrimidinyl)glycine (4S, 6R, 7S) (Fig. 4).[2] The signals of the NMR spectrum in D_2O could be assigned as follows: a triplet at δ 5.26 (1H, J=3.0 Hz) is ascribed to C-4 equatorial proton: a multiplet at δ 4.40 (1H, J=3.0, 3.45, 6.9 Hz) to C-6 axial proton; a doublet at δ 3.91 (1H, J=3.0 Hz) to C-7 proton; a multiplet at δ 2.45 (1H, J=3.45, 6.9, 14.7 Hz) to C-5 axial proton; a multiplet at δ 2.12 (1H, J=3.45, 3.45, 14.7 Hz) to C-5 equatorial proton.

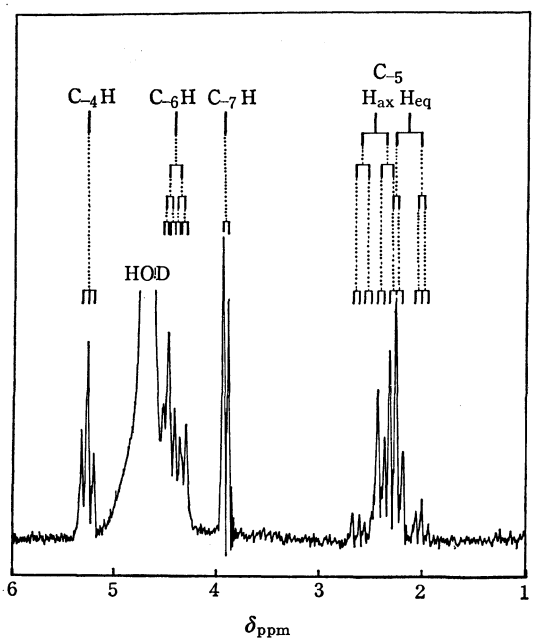

Fig. 2. NMR spectrum of tuberactidine in D_2O.

The ORD spectrum of tuberactidine showed a positive Cotton effect at 221 nm ([Φ]+807 pk, 0.1 M hydrochloric acid) which is characteristic of L-α-amino acid. In connection with this observation, ORD curves of a series of guanidino amino acids obtained from tuberactinomycins were measured (Fig. 3). Tuberactidine, capreomycidine and dihydroviomycidine showed a positive Cotton effect characteristic of L-α-amino acids whereas viomycidine a negative effect characteristic of L-α-imino acids as proline or hydroxy proline.

The structure of viomycidine was determined by X-ray analysis as shown in Fig. 4. The unit cell of crystalline hydrobromide was orthorhombic with a=9.37, b=12.49, c=15.41Å, Z=8, ρ_c=1.865, and

7) E. B. Herr, Jr., Antimicr. Agents and Chemoth. 1962, **1963**, 201.

8) H. Yoshioka, T. Aoki, H. Goko, K. Nakatsu, T. Noda, H. Sakakibara, T. Take, A. Nagata, J. Abe, T. Wakamiya, T. Shiba, and T. Kaneko, *Tetrahedron Lett.*, **1971**, 2043.

9) Tuberactinomycin A, N and viomycin show a olefin proton signal ascribed to -NH-C(=H)-CO- at δ 8.01, 8.01 and 8.10 in NMR

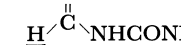

respectively. When tuberactinomycin A, N and viomycin were hydrogenated with palladium on charcoal catalyst, urea was liberated and hydrogenated compounds were hydrolyzed to produce one mole of alanine newly.

10) B. W. Bycroft, D. Cameron, L. R. Croft, A. Hassanali-Walji, A. W. Johnson, and T. Webb, *Tetrahedron Lett.*, **1968**, 5901.

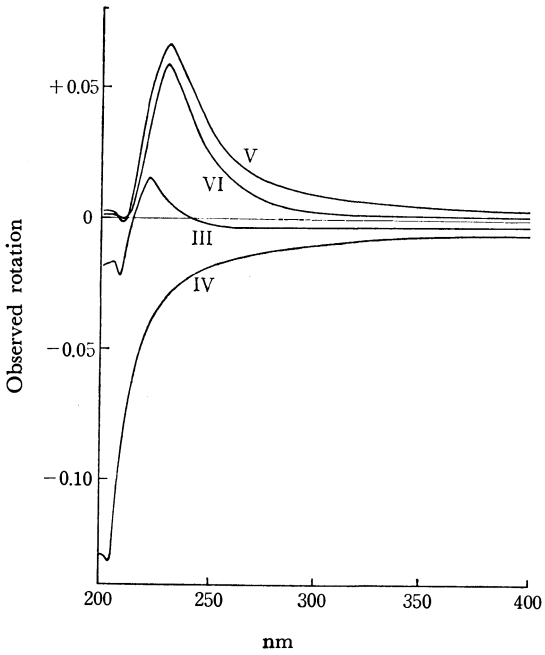

Fig. 3. Observed ORD curves of guanidino amino acids, *i.e.* tuberactidine (III), viomycidine (IV), capreomycidine (V) and dihydroviomycidine (VI). Molecular rotations [Φ] were calculated to +807° (III, 221 nm), −5373° (IV, 204 nm), +3992° (V, 229 nm), and +3926° (VI, 229 nm) respectively.

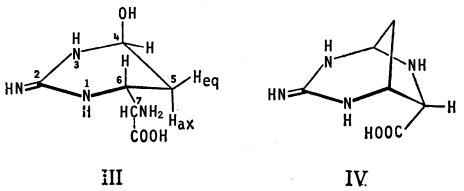

Fig. 4. The absolute structure of tuberactidine(III) and viomycidine(IV).

space group $C222_1$. The result was consistent with that reported by other investigators.[11]

The facts obtained above indicated that I could be a condensed product of two molecules of formyl derivative of tuberactidine or viomicidine. From the measurement of pK_a', it was shown that free amino group is not present in the molecule of I. In the NMR spectrum of I as shown in Fig. 7, two signals ascribed to formyl protons were recognized at the position centered at δ 8.5. However, no more useful data for the structural determination of I were obtained from I itself at the stage of the investigation. In the meantime, hydrobromide (II), $C_{14}H_{20}O_6N_8 \cdot 2HBr$, of I was readily prepared. It showed the absorption of carbonyl of either ester or lactone at 1740 cm^{-1} and 1760 cm^{-1} in IR spectrum, while no absorption was recognized in I between 1700 cm^{-1} to 1800 cm^{-1} (Fig. 5). Moreover, when an aqueous solution of II was neutralized with pyridine, it was reconverted to I.

The peculiar interconversion between I and II reminded us of lactone-lactal equilibrium in tetrodotoxin,[12] cyclol-amide lactone carbonyl interaction in ergotamine[13] or depsipeptides,[14] and amide-ortho-amide transannular interaction in cyclic peptides,[15] all of which were realized rather recently in the field of chemistry of natural compounds. By an application of the above concept to our observation, the reversible structural alternation between I and its hydrobromide II was concluded to be interconversion of cyclic carbinolamine form of cyclol type and amide lactone form (Fig. 6).

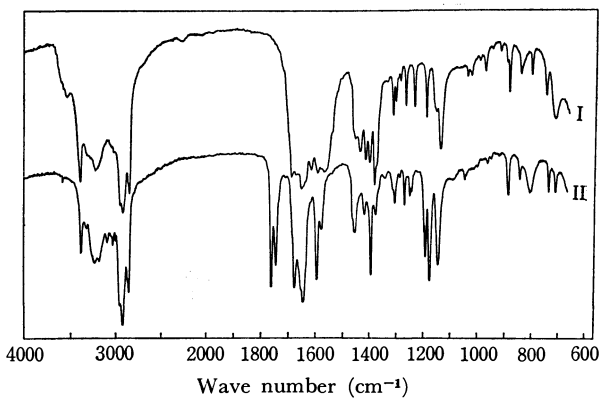

Fig. 5. IR Spectra of I and its hydrobromide II.

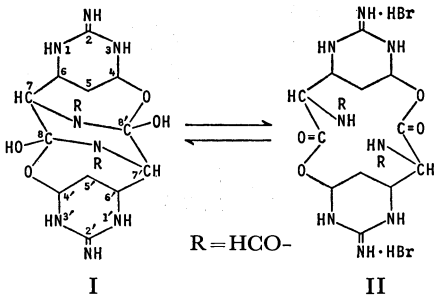

Fig. 6. Structures and interconversion of I and II.

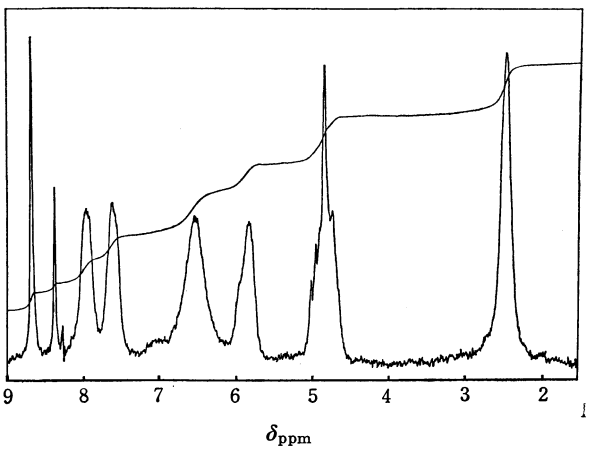

Fig. 7. NMR spectrum of I in TFA.

11) a) J. C. Floyd, J. A. Bertrand, and J. R. Dyer, *Chem. Commun.*, **1968**, 998. b) G. Koyama, H. Nakamura, S. Omoto, T. Takita, K. Maeda, and Y. Iitaka, *J. Antibiotics*, **22**, 34 (1969).

12) T. Goto, Y. Kishi, S. Takahashi, and Y. Hirata, *Tetrahedron*, **21**, 2059 (1965).

13) A. Hofmann, H. Ott, G. Griot, P. A. Stadler, and A. J. Frey, *Helv. Chim. Acta*, **46**, 2306 (1963).

14) M. M. Shemyakin, V. K. Antonov, A. M. Shkrob, V. I. Shchelokov, and Z. E. Agadzhanyan, *Tetrahedron*, **21**, 3537 (1965).

15) A. Prox, J. Schmid, and H. Ottenheym, *Ann. Chem.*, **722**, 179 (1969).

On the basis of the proposed structure, the signals of the NMR spectrum of I in TFA (Fig. 7) could be now assigned as follows: 4H protons at δ 2.5 were ascribed to C-5 and C-5′ methylene; 4H at δ 4.85 to C-6, C-6′, C-7 and C-7′ methine; 2H at δ 5.8 to C-4 and C-4′ methine; 4H at δ 6.5 to =NH bearing on C-2 and C-2′, and -OH on C-8 and C-8′; 2H at δ 7.6 to N-1 and N-1′ protons; 2H at δ 7.95 to N-3 and N-3′ protons; 2H centered at δ 8.5 to two formyl protons.

Splitting of the formyl protons at δ 8.36 and 8.66 could be presumably accounted for by the equilibrium of two types of hydrogen bonding between two formyl groups as shown in Fig. 8. Thus the upfield signal may be due to non-hydrogen bonded proton and the lowfield to hydrogen bonded one. In fact, the latter is relatively stronger than the former.

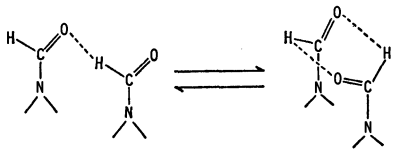

Fig. 8. Hydrogen bonding in formyl groups.

A mechanism for the formation of I was assumed from its structure as follows. Tuberactidine was first formylated with formic acid and pyridine in the eluate during concentration and then two molecules of them were condensed each other by dehydration followed by cyclization. However, a possibility of the formation of I through N^{α}-formylviomycidine could not be excluded, because I was actually obtained when the solution of viomycidine alone in the above buffer solution was evaporated. In addition to this, tuberactidine was easily converted to viomycidine with dehydration in the aqueous solution. Therefore, it is not clear at this stage whether N^{α}-formyltuberactidine or N^{α}-formylviomycidine is the real intermediate in the formation of I.

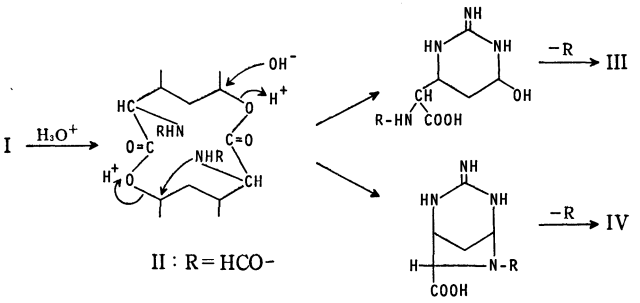

Fig. 9. Degradation of I to tuberactidine(III) and viomycidine(IV).

On the other hand, degradation of I to tuberactidine and viomycidine could be explained by concerted hydrolysis mechanism through II as shown in Fig. 9.

As mentioned previously,[2] it was contended that tuberactidine is a true constituent of tuberactinomycin A and viomycin, and viomycidine is possibly an artifact derived from tuberactidine during the isolation process. This assumption was supported by the following facts. First, tuberactidine as well as tuberactinomycin A and viomycin showed a positive Sakaguchi reaction whereas viomycidine gave a negative one. Secondly, when tuberactinomycin A was reduced with sodium borohydride in alkaline medium followed by acid hydrolysis, a hydroxy compound VI was obtained (Fig. 10). Physical properties such as mp, $[\alpha]_D$ and NMR spectrum in D_2O of monohydrochloride of VI were virtually identical with those of dihydroviomycidine hydrochloride which was obtained by reduction of viomycin in similar manner by Maeda *et al.*[16] The formation of VI can be elucidated by the interconversion between tuberactidine and its amino-aldehyde form in alkaline solution.

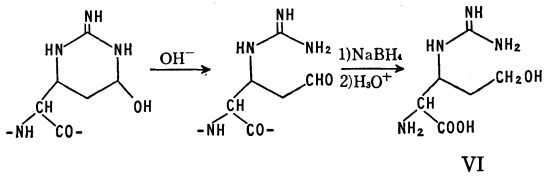

Fig. 10. Isolation of dihydroviomycidine(VI) from tuberactinomycin A.

The presence of the amino-aldehyde form in alkaline solution of tuberactidine can also explain a positive Sakaguchi reaction of tuberactidine, since this reaction should work on mono substituted guanidino compound like amino-aldehyde form derived from tuberactidine but not on disubstituted derivative like tuberactidine itself. Thus, it may be reasonable that VI gave a positive Sakaguchi reaction while viomycidine and capreomycidine were negative.

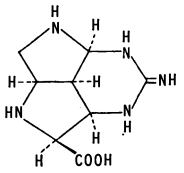

Fig. 11. Structure of viocidic acid(VII)

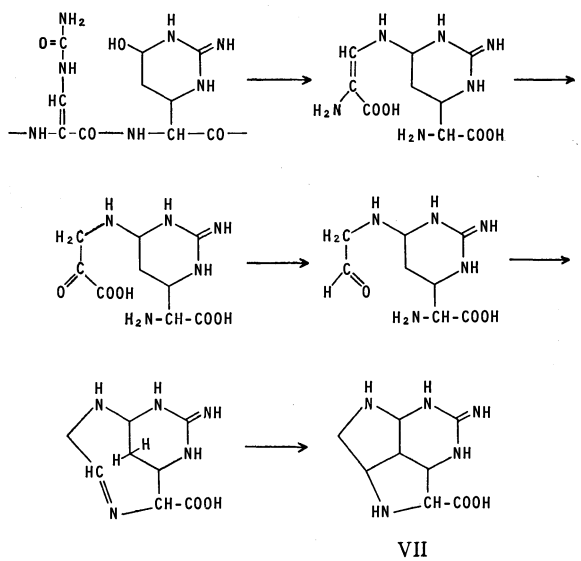

Fig. 12. Presumed formation pathway of viocidic acid(VII)

16) T. Takita and K. Maeda, *J. Antibiotics*, **22**, 39 (1969).

In several runs of column chromatography of the hydrolyzate of tuberactinomycin A, viocidic acid (VII), the other artifact formed during the hydrolysis, was eluted after viomycidine and tuberactidine. Viocidic acid had been also isolated from the hydrolyzate of viomycin, and the structure was determined using X-ray analysis by Bycroft *et al.* (Fig. 11).[17]

Pathway for the formation of viocidic acid remains unexplained as yet. However, it may be possibly interpreted by assuming the participation of 3-ureidodehydroalanine moiety as shown in Fig. 12, although the clarification of this problem must be left to a future investigation.

Experimental

All melting points are uncorrected. The infrared spectra were obtained in Nujol mull with a Hitachi EPI-G3 spectrophotometer. The NMR spectra were obtained with a Hitachi NMR R-20 spectrometer at 60 MHz in trifluoroacetic acid and deuterium oxide. Tetramethylsilane (TMS) was used as an internal reference in trifluoroacetic acid solution, and sodium 2,2-dimethyl-2-silapentane-5-sulfonate (DSS) in the case of deuterium oxide solution. The ORD curves were obtained with a Yanagimoto ORD-185 spectropolarimeter in 0.1 M hydrochloric acid. The specific rotations were obtained with a Perkin-Elmer 141 polarimeter in water and 1 M hydrochloric acid. Amino acids were analyzed with a JEOL-JLC-5AH amino acid analyzer. Thin-layer chromatography was carried out by the ascending method on silica gel G using developing solvents of phenol–water–28% ammonium hydroxide (30 : 10 : 0.6) and *n*-butanol–acetic acid–water (4 : 1 : 2). Paper electrophoresis was carried out at 750 volt and 10 mA for 1.5 hr on Toyo Roshi No. 51 paper using a buffer solution of pyridine–acetic acid–water (30:4:966).

Isolation of Viomycidine (IV). A solution of 20 g of tuberactinomycin A hydrochloride or viomycin hydrochloride in 180 ml of 6 M hydrochloric acid was heated at 135—140°C under reflux for 20 hr. Hydrochloric acid was evaporated *in vacuo* and the residue was dissolved in water. The evaporation was repeated three times after addition of water. The solution of the residue obtained in a small amount of water was applied on a column (2.5×65 cm) of Dowex 50W×2 ion exchange resin which was previously equilibrated with buffer solution of 0.2 M pyridine and formic acid (pH 3.1). Fractions of a positive Sakaguchi reaction were collected and evaporated *in vacuo*. The residue was dissolved in diluted hydrochloric acid and evaporated again. Ethanol and ether were added and a powder thus obtained was recrystallized from water and ethanol two times. Colorless prisms of viomycidine (IV) hydrochloride were obtained, yield 500 mg, mp 215—219°C (decomp.), Lit, mp 200—208°C (decomp.)[5c], $[\alpha]_D^{13}$ −89° (*c* 0.5, H_2O), Lit, $[\alpha]_D^{22}$ −85° (*c* 0.11, H_2O).[18]

Found: C, 34.89; H, 5.61; N, 26.84; Cl, 16.97%. Calcd for $C_6H_{10}O_2N_4 \cdot HCl$: C, 34.87; H, 5.37; N, 27.12; Cl, 17.16%.

Isolation of N^{α}*-Formyltuberactidine Dimer (I).* The same fraction of a positive Sakaguchi reaction in the eluate at another run of the above column chromatography was concentrated without acidification. Ethanol was added to the residue to make it powder. It was filtered off and crystallized from water. Colorless prisms of N^{α}-formyltuberactidine dimer (I) were obtained, yield 540 mg, mp 230°C (darkened) −245°C (decomp.). For analysis sample was dried *in vacuo* at 100°C.

Found: C, 42.19; H, 5.41; N, 28.09%. Calcd for $C_{14}H_{20}O_6N_8$: C, 42.42; H, 5.09; N, 28.27%.

Isolation of Viocidic Acid (VII). Mother liquor of I was evaporated *in vacuo* and the residue was dissolved in diluted hydrobromic acid. The acidic solution was concentrated and the residue was treated with ethanol to make it powder. It was recrystallized from aqueous ethanol several times to give colorless needles of viocidic acid (VII) dihydrobromide in a low yield, mp 208—210°C (decomp.), Lit. mp of trihydrate 222—225°C,[18] $[\alpha]_D^{25}$ −27° (*c* 0.5, H_2O).

Found: C, 25.70; H, 4.16; N, 18.64; Br, 42.71%. Calcd for $C_8H_{13}O_2N_5 \cdot 2HBr$: C, 25.70; H, 4.05; N, 18.77; Br, 42.84%.

N^{α}*-Formyltuberactidine Dimer from Viomycidine.* In a buffer solution of 0.2 M pyridine and formic acid (pH 3.1), 90 mg of viomycidine hydrochloride was dissolved. The solution was evaporated *in vacuo* at 50—60°C. The oily residue was treated with ethanol to make it powder. It was recrystallized from water to give colorless prisms. Melting point and infrared spectrum were virtualy identical with I obtained above.

Capreomycidine (V) from Tuberactinomycin N and O. A solution of 7 g of tuberactinomycin N hydrochloride in 21 ml of 6 M hydrochloric acid was heated at 100—110°C in a sealed tube for 24 hr. Hydrolyzate treated as mentioned above was column chromatographed on Dowex 50W×2 ion exchange resin (200—400 mesh, 2.5×25 cm) with a buffer solution of 0.2 M pyridine and acetic acid (pH 3.6). Fractions containing capreomycidine were evaporated and the residue was purified by column chromatography again with the same buffer solution. Crude capreomycidine hydrochloride was recrystallized from water and ethanol, yield 666 mg, mp 242—248°C (decomp.), Lit. mp 241°C (decomp.),[5] $[\alpha]_D^{25}$ +21° (*c* 1, H_2O), Lit, $[\alpha]_D$ +16.1° (*c* 1, H_2O).[7]

Found: C, 34.21; H, 6.17; N, 26.40; Cl, 17.17%. Calcd for $C_6H_{12}O_2N_4 \cdot HCl$: C, 34.54; H, 6.28; N, 26.85; Cl, 16.99%.

Detection of capreomycidine in a hydrolyzate of tuberactinomycin O was carried out by comparison with authentic sample chromatographically. Amino acid analysis, thinlayer chromatography and paper electrophoresis also characterized this guanidino amino acid in the hydrolyzate of tuberactinomycin O.

Hydrobromide of N^{α}*-Formyltuberactidine Dimer.* Crystals of 210 mg of I were dissolved in 1 ml of 25% hydrobromic acid, and then immediately 10 ml of ethanol and 20 ml of ether were added. After allowing to stand at room temperature until some crystals precipitated, it was stored in refrigerator overnight. Colorless needles were filtered off and washed with ethanol and ether thoroughly, yield 190 mg, mp 227°C (decomp.).

Found: C, 30.10; H, 4.04; N, 19.92; Br, 28.49%. Calcd for $C_{14}H_{20}O_6N_8 \cdot 2HBr$: C, 30.12; H, 3.97; N, 20.08; Br, 28.63%.

To the solution of the hydrobromide in a small amount of water, enough pyridine was added. Excess of pyridine was neutralized with formic acid. When it was allowed to stand for some time, I was recovered as a precipitate

17) a) B. W. Bycroft, D. Cameron, L. R. Croft, A. W. Johnson, T. Webb, and P. Coggon, *Tetrahedron Lett.*, **1968**, 2925. b) P. Coggon, *J. Chem. Soc., B*, **1970**, 838.

18) B. W. Bycroft, L. R. Croft, A. W. Johnson, and T. Webb, *J. Chem. Soc., Perkin I*, **1972**, 820.

Acetyl Derivative of N^{α}*-Formyltuberactidine Dimer.* In 25 ml of pyridine, 470 mg of I was suspended and 13 ml of acetic anhydride was added. After stirring overnight at room temperature, a clear solution obtained was poured on ice and concentrated *in vacuo*. The residue was dissolved in water and evaporation was repeated. Residual oil was dissolved in ethanol and allowed to stand, yield of crystals 390 mg. Analytical sample was obtained by recrystallization from water, mp 217—220°C (decomp.).

Found: 42.07; H, 5.26; N, 22.06%. Calcd for $C_{18}H_{24}O_8N_8 \cdot 2H_2O$: C, 41.86; H, 5.46; N, 21.70%.

Recrystallization from water and ethanol gave fine plates, mp 194—196°C (decomp.).

Found: C, 44.00; H, 5.68; N, 20.84%. Calcd for $C_{18}H_{24}O_8N_8 \cdot H_2O \cdot C_2H_5OH$: C, 44.11; H, 5.92; N, 20.58%

Degradation of I to Viomycidine and Tuberactidine. Crystals of 1.1 g of I were dissolved in 4.5 ml of 15% hydrobromic acid and evaporated *in vacuo* at about 50°C. The residue was dissolved in water and evaporation was repeated several times. The oily residue was dissolved in ethanol and allowed to stand in refrigerator overnight. Precipitate was filtered off and crystallized from water and ethanol to give colorless prisms of viomicidine hydrobromide, yield 350 mg, mp about 210°C (decomp.), Lit, mp 202—204°C (decomp.),[11b] $[\alpha]_D^{25}$ −63° (*c* 0.5, H_2O).

Found: C, 28.63; H, 4.61; N, 22.24; Br, 31.77%. Calcd for $C_6H_{10}O_2N_4 \cdot HBr$: C, 28.70; H, 4.42; N, 22.31; Br, 31.83%.

Mother liquor from viomycidine was evaporated. The residue was dissolved in ethanol and stored in refrigerator for a long time. Tuberactidine hydrobromide was obtained and recrystallized from aqueous ethanol repeatedly, if necessary, with addition of ether, yield 100 mg, mp about 182°C (decomp.), $[\alpha]_D^{13}$ −25.8° (*c* 0.5, H_2O).

Found: C, 26.98; H, 4.81; N, 20.94; Br, 29.65%. Calcd for $C_6H_{12}O_3N_4 \cdot HBr$: C, 26.78; H, 4.87; N, 20.82; Br, 29.70%.

Dihydroviomycidine (VI). In 100 ml of 0.3 M sodium hydroxide, 20 g of tuberactinomycin A hydrochloride was dissolved and 5 g of sodium borohydride in 70 ml of 0.3 M sodium hydroxide was added dropwise with stirring magnetically at 45°C for 8 hr. After stirring for 24 hr, 5 g of sodium borohydride was added by portions for 10 hr. Reaction mixture was acidified with hydrochloric acid and concentrated *in vacuo*. The residue was dissolved in 100 ml of concentrated hydrochloric acid and insoluble inorganic substance was filtered off. Filtrate was diluted with 100 ml of water and heated under reflux at 135°C for 8 hr. Hydrolyzate was column chromatographed as mentioned above. Next fraction to that of diaminopropionic acid showed a positive Sakaguchi reaction but was differentiated from those of viomycidine or tuberactidine. It was concentrated *in vacuo*, and the residue was dissolved in water. Evaporation was repeated and residual oil obtained was allowed to stand overnight. Crystalline product thus obtained was dissolved in a small amount of diluted hydrochloric acid, and then ethanol and ether were added. After allowing to stand overnight in a refrigerator, colorless needles were obtained. Recrystallization from water and ethanol gave 93 mg of hydroxy compound as hydrochloride, mp 180°C (decomp.), Lit, mp 182°C (decomp.),[5d] $[\alpha]_D^{15}$ +33° (*c* 0.5, 1 M HCl), Lit. $[\alpha]_D^{25}$ +25° (*c* 0.7, 6 M HCl).

Found: C, 30.90; H, 7.06; N, 23.59%. Calcd for $C_6H_{14}O_3N_4 \cdot HCl \cdot 1/2H_2O$: C, 30.58; H, 6.84; N, 23.77%.

BULLETIN OF THE CHEMICAL SOCIETY OF JAPAN, VOL. 46, 954—959 (1973)

S_N2 Reactions in Dipolar Aprotic Solvents. III. Chlorine Isotopic Exchange Reactions of Cinnamyl Chlorides and 3-Aryl-2-propynyl Chlorides. Effect of the Unsaturated Group Adjacent to the Reaction Center

Jun-ichi HAYAMI,[1] Nobuo TANAKA, and Aritsune KAJI
Department of Chemistry, Faculty of Science, Kyoto University, Kyoto

(Received October 6, 1972)

Chlorine isotopic exchange reactions of substituted cinnamyl chlorides and 3-aryl-2-propynyl chlorides with tetraethylammonium chloride-^{36}Cl were studied in acetonitrile. In both cases, the electron-donating groups accelerated the reaction. An acceptable linear Hammett relationship was found for the propynyl chlorides. Cinnamyl chlorides gave a linear relationship for the *m*-substituted compounds superposed by a concaved U-shaped relationship of *p*-substituted compounds. Both classes of compounds showed 10^{2-3} times of rate enhancement, compared with 2-arylethyl chlorides in the similar isotopic exchange reaction. Features of these S_N2 reactions are discussed.

Many works have been carried out to further our understanding of the bimolecular nucleophilic substitution at a saturated carbon atom,[2] an important reaction in organic chemistry.

Of the bimolecular nucleophilic substitutions at a saturated carbon atom, the Finkelstein reaction is one of the most thoroughly studied.[3] However, not many works have been carried out dealing with the Hammett type analysis to reveal the electronic requirement of the reaction center in a transition state.

The authors presented an example of a Hammett analysis in which the heteroatom adjacent to the S_N2

1) To whom the correspondence should be addressed.

2) a) C. K. Ingold, "Structure and Mechanism in Organic Chemistry," 2nd Edition, Cornell Univ. Press, Ithaca, New York (1969) p. 418. b) C. A. Bunton, "Nucleophilic Substitution at a Saturated Carbon Atom," Elsevier Pub. Co., London (1963). c) A. Streitwieser, Jr., "Solvolytic Displacement Reactions," McGraw-Hill Book Co., New York (1962).

3) For instance, P. B. D. de la Mare, *J. Chem. Soc.*, **1955**, 3169, and succeeding papers.

reaction center accelerates the reaction by a conjugative stabilization of the transition state.[4] The authors also showed that, in the Finkelstein reaction with benzyl chloride, chloride and fluoride anions behave similarly and the substituent effect can be rationalized in terms of the importance of the approach of a nucleophile superposed by the stabilization of the transition state.[5]

The rate enhancing effect of the unsaturated bond in an S_N2 reaction is well-known.[6] However, a further advance can be anticipated from systematic studies of the symmetrical exchange reaction of these classes of compounds.

The authors studied the chlorine-chlorine isotopic exchange reactions of the nuclear substituted cinnamyl chlorides and 3-aryl-2-propynyl chlorides in solvent acetonitrile to examine the effect of the carbon to carbon multiple bond adjacent to the S_N2 reaction center. Comparison was made with the results obtained for the other modified methyl chlorides to reveal the dominating factors of these reactions.

Results and Discussion

Nine kinds of nuclear substituted cinnamyl chlorides and eight kinds of 3-aryl-2-propynyl chlorides were treated with tetraethylammonium chloride-^{36}Cl in dry acetonitrile, as shown in the following scheme.

$$X\text{-}Ph\text{-}Y\text{-}CH_2Cl + (C_2H_5)_4N\overset{*}{Cl} \rightleftharpoons X\text{-}Ph\text{-}Y\text{-}CH_2\overset{*}{Cl} + (C_2H_5)_4NCl$$

I Y: $CH^{t}{=}CH$, X: a) p-NO_2, b) m-NO_2, c) m-CF_3, d) m-Cl, e) p-Cl, f) H, g) m-CH_3, h) p-CH_3, i) p-OCH_3

II Y: C≡C, X: a) p-NO_2, b) m-CF_3, c) m-Cl, d) p-Cl, e) H, f) m-CH_3, g) p-CH_3, h) p-OCH_3

The advantage of using the dipolar aprotic solvent has been reported.[7] In the present cases, a good second-order kinetics holds, the second-order rate coefficients remaining virtually constant in varying concentration of nucleophile and also on addition of an inert salt, tetraethylammonium perchlorate (Table 1).

The results are given in Table 2 together with the rate coefficients for the Finkelstein reaction of benzyl chloride with chloride ion and fluoride ion.

The rate data for the unsubstituted modified methyl chlorides are collected in Table 3 to show the relative effectiveness of the group adjacent to the S_N2 reaction center.

A significant rate enhancement as compared with the chlorine-chlorine isotopic exchange reaction of 2-arylethyl chloride was observed for the three classes of compounds in Table 2. Thus benzyl chloride, cinnamyl chloride, and 3-aryl-2-propynyl chloride showed fairly similar reactivity, and all reacted about 10^2 times more rapidly in the S_N2 isotopic exchange reaction than 2-arylethyl chloride. However, the double bond in cinnamyl chloride seemed to exert a more pronounced effect than the triple bond and direct linkage in other classes. Sulfur atom in the chloromethyl aryl sulfides seemed to be more effective than the unsaturated groups in Table 3 in accelerating the Finkelstein reaction.

Electron-donating groups on the phenyl ring faciliated the chlorine-chlorine exchange reaction of cinnamyl chlorides as well as the same reaction of 3-aryl-2-propynyl chlorides. The rate data are plotted against Hammett σ to give the relationships given in Figs. 1 and 2.

As is shown in Fig. 2, the Hammett plot for the 3-aryl-2-propynyl chlorides gives an acceptable linear relation ($\rho=-0.19$, $r=0.919$[8]). Similarly, the m-substituted cinnamyl chloride gives a straight line ($\rho=-0.19$, $r=0.962$[8]) superposed by a concaved U-

Table 1. Effect of the chloride ion concentration on the rate of chlorine exchange in the presence and absence of tetraethylammonium perchlorate

	Y	X	T°C	[RCl]	[Cl$^-$]	[ClO_4^-]	$k\times10^2$ l/mol·min
Ie	CH=CH	p-Cl	20	0.10	0.10	—	2.63
				0.10	0.03	—	2.72
				0.10	0.01	—	2.80
				0.10	0.03	0.07	2.56
				0.10	0.01	0.09	2.55
Ii	CH=CH	p-OCH_3	20	0.10	0.10	—	7.42
				0.05	0.10	—	7.40
IId	C≡C	p-Cl	30	0.10	0.10	—	3.32
				0.10	0.03	—	3.36
				0.10	0.01	—	3.48
				0.10	0.03	0.07	3.15
				0.10	0.01	0.09	3.17

4) J. Hayami, N. Tanaka, S. Kurabayashi, Y. Kotani, and A. Kaji, This Bulletin, **44**, 3091 (1971).

5) J. Hayami, N. Tanaka, and N. Hihara, *Bull. Inst. Chem. Res., Kyoto Univ.*, **50**, 354 (1972).

6) a) L. F. Hatch, L. B. Gordon, and J. J. Russ, *J. Amer. Chem. Soc.*, **70**, 1093 (1948). b) L. F. Hatch and H. E. Alexander, *ibid.*, **72**, 5643 (1950). c) L. F. Hatch and V. Chiola, *ibid.*, **73**, 360 (1951). d) C. A. Vernon, *J. Chem. Soc.*, **1954**, 4462.

7) a) A. J. Parker, *Advan. Org. Chem.*, **5**, 1 (1965). b) A. J. Parker, *Quart. Rev.* (London), **1962**, 163.

8) The correlation factor obtained for these compounds is not satisfactory, but the rather poor linearity does not affect a general discussion of the present work. Jaffé reported that there were not enough examples of good linear relationship for systems with $|\rho|\leqq0.2$.[9]

9) H. H. Jaffé, *Chem. Rev.*, **53**, 191 (1953).

TABLE 2. SECOND ORDER RATE COEFFICIENTS OF FINKELSTEIN REACTIONS (X-Ph-Y-CH_2Cl + Halide) AT 20°C. $k \times 10^2$ l/mol·min

X \ Y	CH=CH	C≡C	None[a] Cl⁻	None[a] F⁻
p-NO_2	2.34	0.90	3.47	—
m-NO_2	1.93	—	2.46	5.71
m-CF_3	1.96	0.841	1.76	2.94
m-Cl	2.13	0.860	1.35	1.59
p-Cl	2.63	0.964	1.81	2.29
H	2.54	0.914	1.23	1.59
m-CH_3	2.64	1.07	1.25	1.48
p-CH_3	3.18	1.15	1.83	2.29
p-OCH_3	7.42	1.15	4.52	3.26

a) Ref. 5.

TABLE 3. EFFECT OF THE GROUP ADJACENT TO THE REACTION CENTER. RELATIVE RATE OF FINKELSTEIN REACTIONS OF MODIFIED METHYL CHLORIDES (20°C)

Y	Halide	$k \times 10^2$ (l/mol·min)	Relative rate
O	Cl	1500[a,b]	400000
S	Cl	3.81[b]	1020
CH=CH	Cl	2.54	680
C≡C	Cl	0.914	250
None	Cl	1.23[c]	330
None	F	1.59[c]	430
CH_2	Cl	0.00372[a,b]	1

a) Calculated from the the data at other temperatures.
b) Ref. 4. c) Ref. 5.

shaped line for *p*-substituted compounds.

In discussing the results, three factors are conceivable in determining the rate of the S_N2 reactions. Besides the solute-solvent interactions and steric effects, which are similar or essentially similar to those of all the reaction systems studied, the following factors have been proposed and successfully applied to rationalize the S_N2 reactions:[10] a) approach of the nucleophile; b) stabilization of the transition state by the electron-donating conjugation with the incipient pseudo-p-orbital; and c) the "neighboring orbital overlap," an interaction which involves both the substrate and nucleophile.

The rate determining approach of a nucleophile is a characteristic feature of the S_N2 reaction, a dominating factor when there is no group that stabilizes the transition state of such a reaction. An example was presented for the Finkelstein reaction of 2-arylethyl chlorides where a good linear Hammett relationship with positive value of ρ was obtained.[4] For modified methyl chlorides, at least for the examples studied in the present paper, the nucleophilic approach may be rather a common factor while the other two effects should be discriminating. The polar effect alone cannot account for the rate differences between 2-

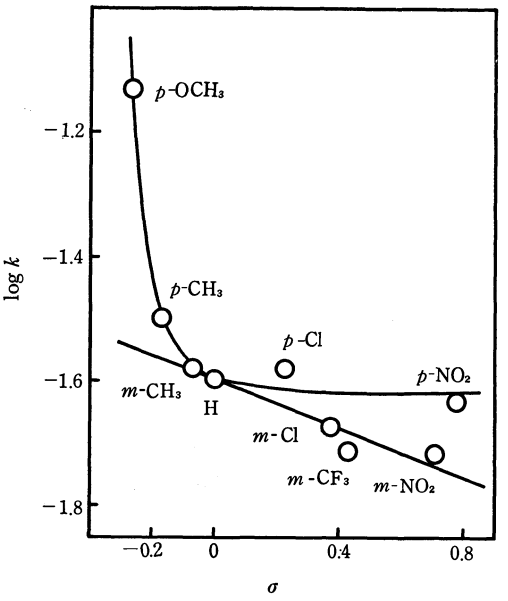

Fig. 1. Hammett plot for the chlorine exchange of substituted cinnamyl chlorides (I) at 20°C.
$\rho = -0.19$, $r = 0.962$

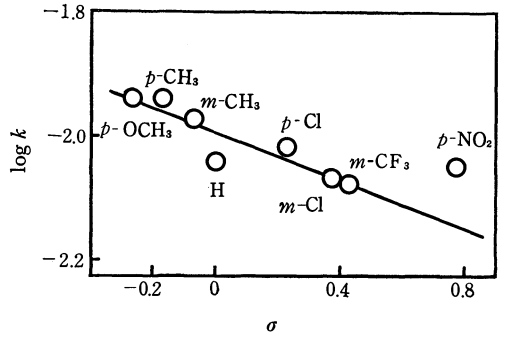

Fig. 2. Hammett plot for the chlorine exchange of 3-aryl-2-propynyl chlorides (II) at 20°C. $\rho = -0.19$, $r = 0.919$

phenylethyl chloride and benzyl chloride.[11] Thus the rate enhancement should be attributed to the conjugative interaction involving the reaction center.

Negative ρ values found for the cinnamyl and 3-aryl-2-propynyl chlorides indicate that an electron-donating effect is dominant in these reactions. Stabilization would be attributed to an electron-donating conjugation. The cinnamyl system seems to exert a somewhat larger effect than the 3-aryl-2-propynyl system does. Taking into account the fact that an acceptable linear Hammett relationship holds for both of the *p*- and *m*-substituted 3-aryl-2-propynyl chlorides and that the ethynylic linkage is a rather poor transmitter of the conjugative effect but a good transmitter of the polar effect,[12] the effect in this system should be ascribed to the electron-donating conjugation of the triple bond itself with the reaction center.

10) Ref. 2c. pp. 26—29.

11) The difference in $\sigma^*(\sigma^*_{Ph} - \sigma^*_{PhCH_2} = 0.4)$ predicts a rate enhancement not more than several times for a conceivable reaction parameter ($\rho = 1$—2) for such a reaction.

12) For a reaction involving the rate determining approach of an anion, a triple bond exerts an almost similar effect as a double bond as long as there is no pronounced effect of conjugation. Thus for the base catalyzed hydrolysis of ethyl cinnamate, ρ was reported to be 1.3 while the same reaction with ethyl 3-arylpropiolate gave $\rho = 1.1$. (cf. R. M. O'Ferrall and S. I. Miller, *J. Amer. Chem. Soc.*, **85**, 2440 (1963), and I. J. Solomon and R. Filler, *ibid.*, **85**, 3492 (1963).)

Table 4. Comparison of the rate of Finkelstein reaction of benzyl chlorides with chloride and fluoride[a)]

	p-OCH_3	p-CH_3	m-CH_3	H	p-Cl	m-CF_3	m-NO_2	p-NO_2
k_{Cl^-}/k_{F^-}	1.39	0.80	0.84	0.77	0.79	0.60	0.43	<0.60[b)]

a) Ref. 5. b) $k_{Cl^-}(p\text{-}NO_2)/k_{F^-}(m\text{-}NO_2)$

The U-shaped Hammett plot for the p-substituted cinnamyl chlorides suggests an operation of an additional conjugation through the double bond, an effect not operative in the present instance of the ethynylic linkage. This additional rate enhancement definitely shows that the cinnamyl system is a good transmitter of a conjugative effect even in the S_N2 transition state. A similar observation for the benzyl chloride is common, an example having been given[13] (Table 2).

The increment of the rate constant from the value predicted by the ρ-σ relationship for m-substituted compounds is a measure of the perturbing effect of a p-substituent. Such increments for the benzyl chlorides[14] are plotted against a similar increment observed in the cinnamyl chlorides, and shown in Fig. 3.

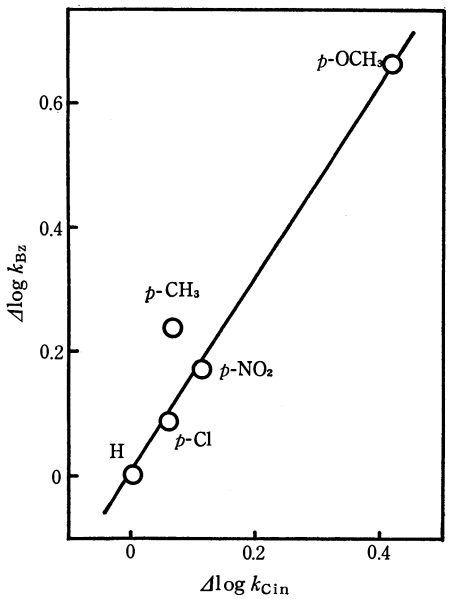

Fig. 3. Rate increment by p-substituents. Comparison of benzyl chlorides ($\Delta\log k_{Bz}$) with cinnamyl chlorides ($\Delta\log k_{Cin}$).

A fairly good linear relationship was obtained which implies the common nature of the reactivity of two classes of compounds. A most interesting observation is that the linear relationship also includes p-nitro substituent which shows a rate enhancement hardly interpreted.

The concept of "neighboring orbital overlap" is quite attractive to rationalize the rate accelerating effect by p-cyano and p-nitro substituents.[10] The trend has often been reported and is also observed in the present cases (Figs. 1 and 2).

In a trial to reveal the contribution of the effect, the reaction of benzyl chlorides with fluoride anion in acetonitrile[5] has quite an important bearing.

If the "neighboring orbital overlap" is operative in the present instances of chlorine-chlorine isotopic exchange reaction, the overlap should serve as a retarding factor for the organic halides with an electron-donating substituent, while the S_N2 reaction with fluoride anion should be essentially free of this overlap.[15]

Thus the ratio of the second-order rate coefficients of these two Finkelstein reactions, k_{Cl^-}/k_{F^-}, should be lower for benzyl chlorides with effective electron-donating substituent and higher for benzyl chlorides with strongly electron-attracting substituent whose rate enhancement due to the overlap is expected. This is not the case with the two Finkelstein reactions of the substituted benzyl chlorides (Table 4). The finding would be an indication against the operation of the "neighboring orbital overlap."

However, there can be another explanation for the rate ratio in Table 4. Tightening of the transition state, which is possibly brought about by the involvement of a very "hard" nucleophile (fluoride anion), should result in a lower k_{F^-} for compounds with electron-donating substituent and a higher k_{F^-} for compounds with electron-attracting substituent. Thus, the effect of "neighboring orbital overlap" can be counteracted, or could be apparently counterbalanced depending upon the degree of tightening. In an extreme case, in which tightening is overwhelming, importance of the approach of a nucleophile becomes dominating and the contribution of conjugative stabilization plays only a minor role. The effect of the overlap can thus easily be masked.

Table 5. Activation parameters for Finkelstein reactions of modified methyl chlorides[a)]

Y	X	E_a kcal/mol	$\Delta S^{\neq}$ e.u. (20°C)
O[b)]	H	14.0	−14.9
O[b)]	p-NO_2	17.7	−5.6
S[b)]	H	18.0	−13.8
S[b)]	p-NO_2	20.1	−10.0
CH=CH	H	19.6	−9.1
CH=CH	p-Cl	19.3	−10.1
C≡C	H	20.6	−7.7
C≡C	p-Cl	21.0	−6.2
None	H	18.1	−15.8
None[c)]	H	17.1	−16.5
CH_2[b)]	H	24.0	−6.8
CH_2[b)]	p-NO_2	24.2	−4.1

a) Reaction with chloride ion. b) Ref. 4. c) Reaction with fluoride ion. Ref. 5.

13) G. M. Bennett and B. Jones, *J. Chem. Soc.*, **1935**, 1815.

14) A linear relationship ($\rho=0.36$, $r=0.905$) was tentatively given from the data for the benzyl chlorides with m-substituent (m-NO_2, m-CF_3, m-Cl, and H, m-CH_3).

15) It is commonly accepted that the rate-controlling effect of this nature is more pronounced in cases in which the entering and leaving groups are not first row elements. (*cf.* Ref. 2c, p. 28).

TABLE 6. PHYSICAL CONSTANTS OF SUBSTITUTED CINNAMYL CHLORIDES

	X	bp °C/mmHg (mp°C)	Solvent	(lit)
Ia	*p*-NO_2	(56.0—56.5)	CH_3OH	(58.5—59.5)[a] (58—60)[b]
Ib	*m*-NO_2	(83.0—83.5)	CH_3OH	(78)[a]
Ic	*m*-CF_3	79.0—79.5/3		
Id	*m*-Cl	112.0—113.0/6		90/0.1[a]
Ie	*p*-Cl	(41.0—41.5)	CH_3OH	95/0.6[a]
If	H	116.0—118.0/16 (7.0—8.0)		94/2[c] (7—8)
Ig	*m*-CH_3	86.5—87.0/3		
Ih	*p*-CH_3	(38.5—39.0)	*n*-C_6H_{14}-C_6H_6	(39.5—40.0)[d]
Ii	*p*-OCH_3	(73.0—74.0)	*n*-C_6H_{14}-C_6H_6	(71.5—73.0)[e]

a) Ref. 20. b) Ref. 21. c) Ref. 6b. d) Ref. 22. e) Ref. 19.

However, the use of the fluoride anion failed to substantiate the tight transition state as is proved by the U-shaped Hammett plot concave upward of the reaction with benzyl chlorides.[16]

As to the relative effectiveness of the group adjacent to the S_N2 reaction center in promoting the reactions of the modified methyl chlorides, the present work furnishes the order O≫S>CH=CH>None (benzyl)≳C≡C≫CH_2. This can be rationalized in terms of the relative effectiveness of the conjugative stabilization of the transition state, oxygen and sulfur atom being more effective than the unsaturated group. The data of activation energy support this explanation (Table 5).

As the rate enhancement due to the effective conjugation implies loose transition state,[17] a study of the secondary deuterium isotope effect should be quite interesting. The work is now in progress and the results will be the subject of the forthcoming paper.[18]

Experimental

Preparation of Materials. Cinnamyl chloride (If) and *p*-nitrocinnamyl chloride (Ia) were prepared from the corresponding cinnamyl alcohols by the standard method with thionyl chloride in dry benzene. Other cinnamyl chlorides (Ib, c, d, e, g, h) were prepared from the corresponding 1-arylallyl alcohols[19] by passing gaseous hydrogen chloride through their ethereal solutions. After being passed through a short column of alumina with *n*-hexane-benzene mixture as an eluent, cinnamyl chlorides were purified by distillation under reduced pressure or by recrystallization from the solvent listed in Table 6.

TABLE 7. PHYSICAL CONSTANTS OF 3-ARYL-2-PROPYNYL DERIVATIVES

	X	Chloride bp°C/mmHg (mp°C)	Alcohol bp°C/mmHg (mp°C)
IIa	*p*-NO_2	(65.5—66.0)	
IIb	*m*-CF_3	80.0—80.5/4	103.5—105.0/3
IIc	*m*-Cl	108.0—108.5/6.5	122.5—124.0/3
IId	*p*-Cl	99.5—100.5/2.5 (26.4—26.6)[a]	138—140/6 (78.0—78.5)
IIe	H	78.5—79.0/5[b]	139—141/18[e]
IIf	*m*-CH_3	97.0—98.0/5.5	115.5—117.0/4
IIg	*p*-CH_3	92.0—92.5/4	116.5—117.5/4 (25.0—26.0)
IIh	*p*-OCH_3	126—129/3[c] (22.5—23.0)[d]	146—148/4 (62.0—63.0)

a) CH_3OH. b) Ref. 23. c) Crude material. d) *n*-hexane-benzene. e) Ref. 20 and 24.

3-Aryl-2-propynyl chlorides. 3-Aryl-2-propynyl alcohols were prepared from the corresponding arylacetylenes. As an example, phenylacetylene (20 g, 0.20 mol) in 50 ml of ether was added to ethereal solution of 0.22 mol of ethyl magnesium bromide in 150 ml of ether. The resulting solution was stirred overnight at room temperature. Powdered paraformaldehyde (10 g, 0.33 mol as CH_2O), dried in a vacuum dessicator for a few days, was added to this solution in small portions. After being refluxed for three hours, the solution was worked up as usual. Distillation gave 16.5 g (63%) of 3-phenyl-2-propynyl alcohol. 3-Aryl-2-propynyl chlorides (IIb—IIh) were obtained from the corresponding alcohols by the reaction with thionyl chloride.

3-*p*-Nitrophenyl-2-propynyl chloride (IIa) was prepared by nitration of 3-aryl-2-propynyl chloride (IIe). Under vigorous stirring 1g of IIe was added slowly into 20 ml of fuming nitric acid (d. 1.50) at −30°C. After the addition was complete, the solution was stirred for another minute,

16) The observed trend that the rate ratio is slightly larger for the strongly electron-donating substituent and smaller for the strongly electron-attracting substituent was pointed out previously.[5] This can be a reflection of the tightening of the transition state, although it is not overwhelming.

17) A. J. Parker, *Chem. Rev.*, **69**, 1 (1969).

18) Normal isotope effects were found; 5% for *p*-methyl and *p*-methoxy benzyl chloride, about 10% for chloromethyl aryl ethers and sulfides. Cinnamyl chloride also exhibited about 5% isotope effect. The positive effect definitely supports the concept of loose transition state and a conjugative interaction. cf. Preprint p. 21, 23rd Symposium on Organic Reaction Mechanism, Kobe, October 1972 and also N. Tanaka, A. Kaji, and J. Hayami, *Chem. Lett.*, **1972**, 1223.

19) W. N. White and W. K. Fife, *J. Amer. Chem. Soc.*, **83**, 3846 (1961).

20) G. Cignarella, E. Occelli, and E. Testa, *J. Med. Chem.*, **8**, 326 (1965).

21) N. V. Smirnova, A. P. Arendaruk, D. D. Smolin, and A. P. Skoldinov, *Med. Prom. S. S. S. R.*, **12**, 31 (1958).

22) P. J. C. Fierens, G. Geuskens, and G. Klopman, *Bull. Soc. Chim. Belges*, **68**, 177 (1959).

23) M. Nagawa, H. Ito, and A. Terada, Jap., 10919 (1964).

24) a) E. B. Bates, E. R. H. Jones, and M. C. Whiting, *J. Chem. Soc.*, **1954**, 1854. b) C. Moureu and H. Desmots, *C. R. Acad. Sci. Paris*, **132**, 1224 (1901).

and the mixture was poured into ice water. The organic compounds were extracted with benzene. The benzene extract was dried with anhydrous magnesium sulfate and the solution was concentrated under reduced pressure. The residue was chromatographed on silica gel with *n*-hexane–benzene as an eluent. Recrystallization from methanol gave pure IIa.

These chlorides decomposed gradually on standing. Fresh samples were therefore used for the kinetic experiment immediately after purification. Purification was affected by column chromatography on alumina followed by distillation or recrystallization.

The structures of these unsaturated chlorides were confirmed by their NMR and IR spectra. Physical constants are summarized in Tables 6 and 7.

Preparation and purification of tetraethylammonium salts and acetonitrile were undertaken as described previously.[4]

Kinetic Measurements. Batch method was utilized. A modification was made by use of toluene as an extracting solvent instead of benzene.

Tracer experiments were carried out at Radioisotope Research Center of Kyoto University. Sincere thanks are due to the staff of this institution. The work was supported by the Ministry of Education and Saneyoshi Shogakkai.

BULLETIN OF THE CHEMICAL SOCIETY OF JAPAN, VOL. 46, 959—963 (1973)

4-Epifriedelin and 4-Epishionone. Structure and Reflex Effect[1]

Reiko AOYAGI, Shūzō YAMADA, Takahiko TSUYUKI, and Takeyoshi TAKAHASHI

Department of Chemistry, Faculty of Science, The University of Tokyo, Hongo, Bunkyo-ku, Tokyo

(Received October 13, 1972)

4-Epifriedelin (III) and 4-epishionone (VII) were prepared by photoepimerization of friedelin (I) and shionone (VI), respectively. On base treatment, III and VII were completely isomerized into I and VI, respectively; this observation was discussed based on reflex effect.

Friedelin (I), a pentacylic triterpene bearing 3-oxo-4-methyl substituents in A-ring, is widely distributed in the plant kingdom.[2] Especially it is well-known as one of the major constituents of cork.

Biosynthetic pathway of friedelin from squalene has been described.[3] Friedelin in enol form (II) may be derived from the protonated β-amyrin type intermediate by a sequence of 1,2-shifts of methyl groups and hydrogen atoms, followed by deprotonation in the last step.[3] It is, therefore, reasonable that the formation of 4α(axial)-methyl epimer (III, 4-epifriedelin) as well as that of friedelin (I) would be expected. Friedelin and several friedelin derivatives have been isolated from a large number of plants. However, isolation of 4-epifriedelin (III) from natural source has never been reported.

Ramirez and Stafiej described that D-homosteroid (IV) and its 17aα-methyl epimer (V) existed in a ratio of 70 : 30 under equilibrating conditions.[4] On the other hand, Ourisson *et al.* showed that friedelin (I) did not contain 4-epifriedelin (III) at equilibrium and this observation was explained by reflex effect.[5] The deformation of ring B caused by 1,3-diaxial interaction between the 5β- and 9β-methyl groups of III produces reflex effect which brings the 4α-methyl group nearer to the 10α-hydrogen atom, resulting in destabilization of III.[5] In the 17aα-methyl epimer (V), the corresponding 1,3-diaxial interaction (between 13β-methyl and 8β-hydrogen) should cause the reflex effect less severe.[5] These considerations were also supported by the equilibrating experiment on shionan-3-one (VI, with saturated side chain) with alkali; the 4α-epimer (VII, with saturated side chain) was not detectable at equi-

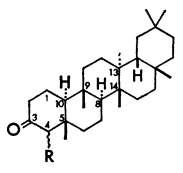

(I) R = β - CH_3
(III) R = α - CH_3

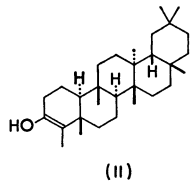

(II)

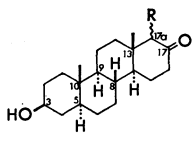

(IV) R = β - CH_3
(V) R = α - CH_3

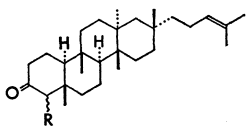

(VI) R = β - CH_3
(VII) R = α - CH_3

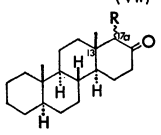

(VIII) R = β - CH_3
(IX) R = α - CH_3

1) A preliminary account of this paper: T. Tsuyuki, R. Aoyagi, S. Yamada, and T. Takahashi, *Tetrahedron Lett.*, **1968**, 5263.

2) *Cf. e. g.*, P. Boiteau, B. Pasich, and A. R. Ratsimamanga, "Les Triterpénoides en Physiologie végétale et animale," Ganthier-Villars, Paris (1964), p. 174.

3) A. Eschenmoser, L. Ruzicka, O. Jeger, and D. Arigoni, *Helv. Chim. Acta*, **38**, 1890 (1955).

4) F. Ramirez and S. Stafiej, *J. Amer. Chem. Soc.*, **77**, 134 (1955); **78**, 644 (1956).

5) C. Sandris and G. Ourisson, *Bull. Soc. Chim. Fr.*, **1958**, 1524; *cf.* E. Eliel, N. L. Allinger, S. J. Angyal, and G. A. Morrison, "Conformational Analysis," Interscience, New York, (1965), p. 345,

librium.[6a] This seems, therefore, to be the reason why neither the preparation of III[7] (and VII) nor the isolation of III (and VII) from natural source has yet been described.

In order to verify the exertion of the reflex effect in 4-epifriedelin (III) and 4-epishionone (VII), equilibration of these two compounds, as well as that of 17aβ- and 17aα-D-homo-5α-androstan-17-ones (VIII and IX) as comparative compounds, was examined.

We have briefly reported a photochemical reaction of I in ethanol, in which III has been isolated together with A-norfriedelane, ethyl 3,4-seco-friedelan-3-oate, friedelin and 3β- and 3α-friedelanols.[8] Friedelin (I) in ethanol, *n*-hexane or diethyl ether was irradiated with a high pressure mercury lamp under a nitrogen atmosphere at room temperature. The reaction products were subjected to silica gel column chromatographic separation and a ketone fraction was collected. The ketone fraction consisted of two components; the tlc examination showed two spots. A ketone with R_f 0.52 was shown to be identical with I. The other ketone (R_f 0.45), recrystallized from petroleum ether, showed mp 257.5°C, IR ν_{max} (Nujol) 1706 cm^{-1}. The molecular formula of $C_{30}H_{50}O$ was determined by the appearance of M^+ peak at *m/e* 426 in the mass spectrum, whose fragmentation pattern was very similar to that of I. These observations suggest that the photoepimerized ketone would be 4-epifriedelin (III). IR spectrum of III together with that of I is given in Fig. 1.

Further confirmation of the structure (III) was given by isomerization reaction of III. 4-Epifriedelin (III) in benzene was adsorbed on alumina overnight and then eluted with benzene to afford an isomerized product which was found to be identical (mp, mixed mp, IR, tlc and glc) with I, and no original ketone (III) was detectable by tlc examination. When silica gel was used no isomerization occurred. When III was treated with sodium methoxide in methanol–dioxane under reflux, it was completely isomerized to I. 4-Epifriedelin (III) was also thermally isomerized; on glc (Diasolid H-523, at 250°C) it gave two peaks at 36.6 and 41.1 min, due to III and I, respectively. These observations firmly confirm the Ourisson's reflex effect and lead to assignment of 4α(axial)-methyl configuration (X) for 4-epifriedelin (III).

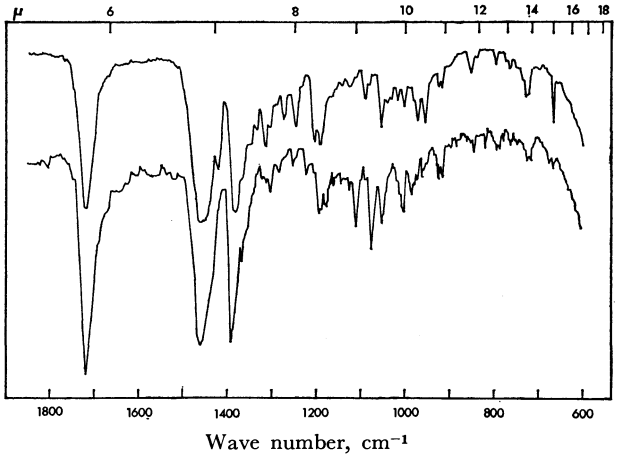

Fig. 1. IR spectra of friedelin (I, lower) and 4-epifriedelin (III, upper).

This assignment for III is compatible with optical rotatory dispersion (ORD) curve of III when compared with that of I(Fig. 2a). Both ORD curves show negative Cotton effect and the amplitude[9] of III ($a=-43$) is smaller than that of I($a=-126$). If one assumes a chair comformation such as X for both rings A and B, this evidence could be interpreted as that, while 4β-methyl group of I lies on octant plane, 4α-methyl group of III contributes to the positive octant (Xa), resulting in reduction of absolute value of the amplitude for III. As positive Cotton effect is expected for conformations (X′ and X″) with ring A in boat form, these conformations can be excluded for III.

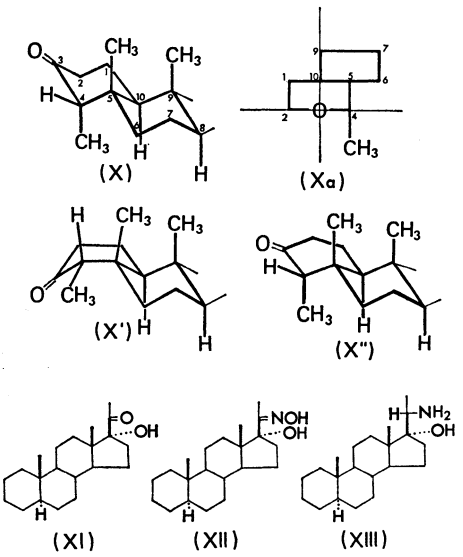

4-Epishionone (VII) was prepared by photoepimerization of shionone (VI).[1] The same observations were obtained for VII as in the case of 4-epifriedelin (III), except the isomerization with alumina; VII was not isomerized with alumina. ORD curves of VI and VII are shown in Fig. 2b.

17aβ- and 17aα-methyl-D-homo-5α-androstan-17-one (VIII and IX) were prepared as follows. Oximation of 17α-hydroxy-5α-pregnan-20-one (XI)[10] gave an oxime (XII), which on hydrogenation yielded 17α-

6) a) Y. Tanahashi, T. Takahashi, F. Patil, and G. Ourisson, *Bull. Soc. Chim. Fr.*, **1964**, 584. b) Y. Moriyama, Y. Tanahashi, T. Takahashi, and G. Ourisson, *ibid.*, **1968**, 2890; T. Tsuyuki, T. Hoshino, M. Ito, and T. Takahashi, *ibid.*, **1968**, 2895; and the references cited therein.

7) *Cf.* T. Brunn, *Acta Chem. Scand.*, **8**, 76 (1954). The corresponding hydrocarbon, "friedelane-II," was described. However, there seems to be lacking in spectral evidences to confirm this structure.

8) T. Tsuyuki, S. Yamada, and T. Takahashi, This Bulletin, **41**, 511 (1968).

9) The previously reported values (Ref. 1) were corrected by reinvestigation of ORD measurement.

10) J. C. Danielwicz and W. Klyne, *J. Chem. Soc.*, **1962**, 4950.

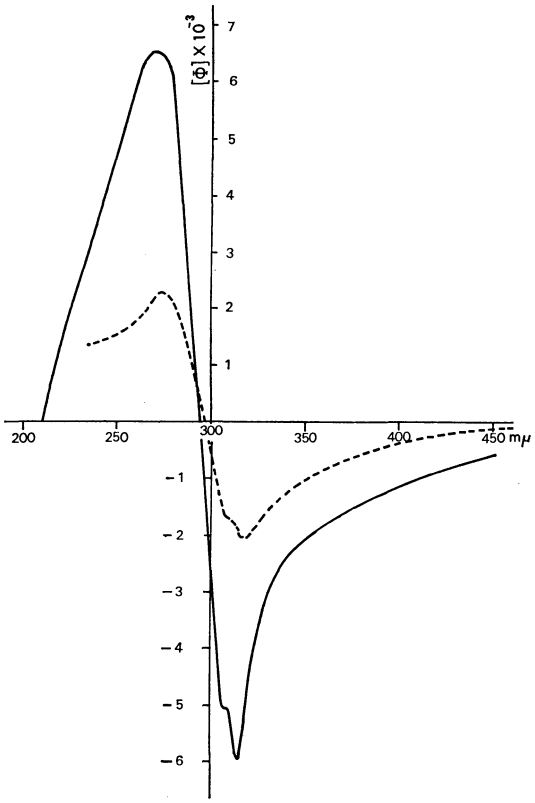

Fig. 2a. ORD curves of friedelin (I, solid line) and 4-epifriedelin (III, dotted line).

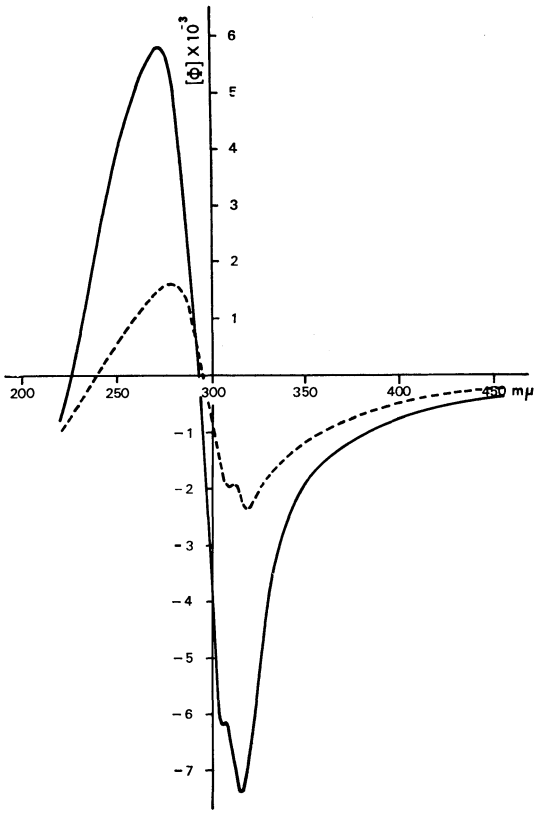

Fig. 2b. ORD curves of shionone (VI, solid line) and 4-epishionone (VII, dotted line).

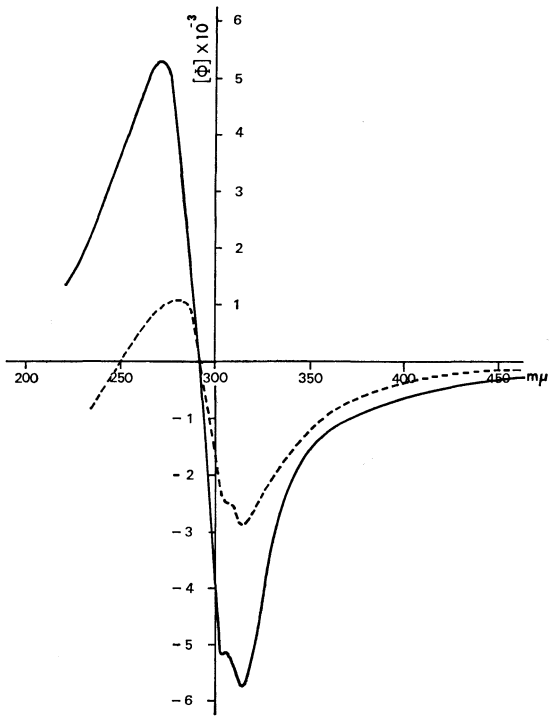

Fig. 2c. ORD curves of 17aβ-methyl-D-homo-5α-androstan-17-one (VIII, solid line) and 17aα-methyl epimer (IX, dotted line).

hydroxy-20α-amino-5α-pregnane (XIII).[11] As in the case of the corresponding 3α-hydroxy derivative[4] of XIII, when treated with nitrous acid XIII underwent the Demjanov ring enlargement to give 17aα(axial)-methyl-D-homo-5α-androstan-17-one (IX).[13] This ketone (IX) was treated with potassium hydroxide in ethanol under reflux to afford a mixture of 17aα- and 17aβ-methyl-D-homo-5α-androstan-17-ones (IX and VIII). The same equilibrating mixture was also obtained by treatment of 17aβ-methyl-D-homo-5α-androstan-17-one (VIII) with alkali. The equilibrating mixture was separated into each component. ORD curves of VIII and IX are

11) The configuration at C-20 of XIII was deduced from the formation of 17aα-methyl-D-homosteroid (IX) on nitrosation of XIII (*cf.* Ref. 4 and 12).

12) D. N. Kirk and M. P. Hartshorn, "Steroid Reaction Mechanisms," Elsevier, Amsterdam (1968), p. 304.

13) The location of ketone group on C-17 (not on C-17a) for IX was shown as follows. The mass spectrum of the ethylene ketal (XIV) of 17aβ-methyl epimer (VIII) showed the presence of a characteristic peak at *m/e* 99 due to fragmentation "a" and absence of peak at *m/e* 113 due to fragmentation "b", which would be responsible for an alternative structure (XV). The 17aα-(axial)-methyl configuration of IX was deduced from equilibration experiments.

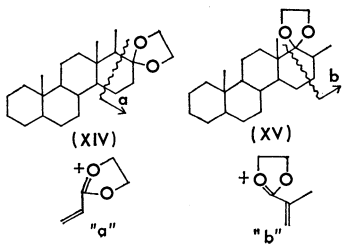

Table 1. PMR spectral data[a)]

		δ_{CDCl_3}	$\delta_{C_6D_6}$	Δ		δ_{CDCl_3}	$\delta_{C_6D_6}$	Δ		δ_{CDCl_3}	$\delta_{C_6D_6}$	Δ
I	4β-CH_3	0.87	0.97	−0.10	5β-CH_3	0.72	0.63	+0.09	9β-CH_3	0.87	0.74	+0.13
III	4α-CH_3	1.11	0.86	+0.25	5β-CH_3	0.87	0.69	+0.18	9β-CH_3	0.92	0.85	+0.07
VI	4β-CH_3	0.87	0.92	−0.05	5β-CH_3	0.71	0.60	+0.11	9β-CH_3	0.88	0.74	+0.14
VII	4α-CH_3	1.11	0.86	+0.25	5β-CH_3	0.90	0.74	+0.16	9β-CH_3	0.90	0.83	+0.07
VIII	17aβ-CH_3	0.87	0.98	−0.11	13β-CH_3	0.60	0.51	+0.09	10β-CH_3	0.72	0.66	+0.06
IX	17aα-CH_3	1.08	0.85	+0.23	13β-CH_3	0.81	0.70	+0.11	10β-CH_3	0.77	0.66	+0.11

a) Chemical shifts are expressed in δ_{ppm} downfield from TMS; $\Delta = \delta_{CDCl_3} - \delta_{C_6D_6}$.

given in Fig. 2c. The equilibrating mixture was shown to consist of 28% of 17aα- and 72% of 17aβ-isomers from ORD data. The fact that the amplitude of 17aα-methyl isomer (IX, $a=-40$) is smaller than that of 17aβ-methyl isomer (VIII, $a=-108$), indicates that 17aα(axial)-methyl group of IX contributes to the positive octant and 17aβ(equatorial)-methyl group of VIII lies on octant plane just as same as in the cases of friedelin and shionone series.

PMR spectral data of I, III, VI, VII, VIII, and IX are given in the Table. The solvent shift for a signal due to methyl group adjacent to carbonyl is well documented.[14] Each of 4α-, 4α- and 17aα-methyl resonances of III, VII and IX, respectively, suffers an appreciable upfield shift ($\Delta=\delta_{CDCl_3}-\delta_{C_6D_6}=+0.23\sim+0.25$ ppm) on passing from deuteriochloroform to deuteriobenzene solution, showing that these methyl groups are in axial conformation. However, in I, VI and VIII, 4β-, 4β- and 17aβ-methyl resonances, respectively, suffer a small downfield shift ($\Delta=-0.05\sim-0.11$ ppm), suggesting an equatorial nature for these methyl groups. As to the other methyl signals, the solvent shifts (Δ) of 5β- or 13β-methyl resonances are within $+0.09\sim+0.11$ ppm for I, VI or VIII, and within $+0.11\sim+0.18$ ppm for III, VII or IX. An upfield shift ($\Delta=+0.06\sim+0.14$ ppm) is observed for 9β- or 10β-methyl resonances of I, III, VI, VII, VIII or IX.

These observations exclude boat conformations of ring A for these six compounds, in agreement with the results obtained from ORD data. In conclusion, the most probable conformation of ring A of III and VII, and that of ring D of IX should be a deformed chair conformation.

Experimental[15]

1. Friedelin Series. Isolation of 4-Epifriedelin (III). Friedelin[2] (I, 2.01 g) in ethanol (750 ml) was heated under reflux with introduction of nitrogen for 30 min and the resulting solution was irradiated with a high pressure mercury lamp under a nitrogen atmosphere at reflux temperature. After evaporation of the solvent under reduced pressure, the residue was dissolved in petroleum ether–benzene (1 : 1) and passed through a column (silica gel, 60 g). The elution with the same solvent gave hydrocarbons, ethyl 3,4-seco-friedelan-3-oate, ketones, and 3β- and 3α-friedelanols. The ketone fraction consisted of two components. A ketone (R_f 0.52) which was eluted from the column, was collected and recrystallized from ethyl acetate to give 788 mg of white crystals which were shown to be identical with friedelin (I) in every respect. Further elution with the same solvent gave another ketone (R_f 0.45), which was recrystallized from petroleum ether to afford 4-epifriedelin (III, 53.7 mg, 2.7%); IR (Nujol): $\nu_{C=O}$ 1706 cm^{-1}; Found: C, 84.31; H, 11.97%. Calcd for $C_{30}H_{50}O$: C, 84.44; H, 11.81%. MS: *m/e* 426 (M^+), 341 [$(M-85)^+$] and 302 [$(M-124)^+$]; PMR ($CDCl_3$): δ 0.87, 0.92, 0.95, 0.99, 1.00, 1.04, 1.17 (each singlet due to *t*-CH_3), 1.11 ppm (d, $J=7.0$ Hz, *sec*-CH_3); PMR (C_6D_6): δ 0.69, 0.85, 0.94, 1.01, 1.03, 1.09, 1.22 (each singlet due to *t*-CH_3), 0.86 ppm (d, $J=6.0$ Hz, *sec*-CH_3), ORD: $[\Phi]_{589}$ 0°, $[\Phi]_{318}^{trough}$ −2070°, $[\Phi]_{309}$ −1680° (sh), $[\Phi]_{275}^{peak}$ +2280° and $[\Phi]_{214}$ +1180°. Friedelin (I, 1.00 g) in *n*-hexane (500 ml) was irradiated under the same conditions. By the same separation procedure, 4-epifriedelin (III, 47 mg, 4.7%) was isolated from the photoreaction mixture.

Isomerization of 4-Epifriedelin (III) into Friedelin (I).

a) With Sodium Methoxide: 4-Epifriedelin (III, 5 mg) in dioxane (5 ml) and methanol (5 ml) was heated under reflux with sodium methoxide under a nitrogen atmosphere for 5.5 hr. The residue, after removal of the solvent, was extracted with ether. The ethereal extract was dried over sodium sulfate. Tlc (SiO_2) examination showed only one spot with R_f 0.52, which corresponded to that of friedelin. The presence of 4-epifriedelin (III) was not detectable.

The isomerized product was isolated by SiO_2 preparative tlc to give friedelin (I), which was identified with an authentic sample by mp, IR and glc.

b) With Alumina: 4-Epifriedelin (III) was dissolved in benzene and the solution was divided into two portions. Each portion was poured into alumina (Showa Chemical, neutral) and silica gel columns, respectively, and adsorbed overnight. On elution with benzene, friedelin (I) was isolated from the eluent from the alumina-packed column. In the benzene eluent from the silica gel column, no friedelin (I) was detected; 4-epifriedelin (III) was recovered unchanged.

c) Thermal Isomerization in Gas Chromatography: 4-Epifriedelin (III) in acetone was injected into a column packed with Diasolid H-523 at 250°C. There appeared two peaks; one peak at t_R 36.6 min due to III was exceedingly weak compared with the other one at t_R 41.1 min due to friedelin

14) N. S. Bhacca and D. H. Williams, "Applications of NMR Spectroscopy in Organic Chemistry," Holden-Day (1964), pp. 164—169.

15) IR and mass spectra were measured using Hitachi EPI-G2 and Hitachi RMU-6 spectrometers, respectively. PMR spectra were taken on a JEOL-JNM-C-60 spectrometer at 60MHz using TMS as an internal standard. ORD measurement was carried out on a JASCO ORD/UV-5 spectrometer in dioxane solution (*c*: 2 mg/ml). All melting points were determined on a hot block and reported uncorrected. Silica gel column and thin layer chromatographies were carried out on Wakogel C-200 (Wako Pure Chem.) and Kieselgel G nach Stahl (E. Merck), respectively.

(I).

2. Shionone Series. Isolation of 4-Epishionone (VII) A solution of shionone[6] (VI, 1.00 g) in *n*-hexane (500 ml) was irradiated under the same conditions (*cf.* friedelin series) for 7 hr. This procedure was repeated and the combined residue, after the solvent had been removed, was chromatographed on silica gel. By the same procedures described for friedelin series, shionone (VI, R_f 0.52) and 4-epishionone (VII, R_f 0.45) were isolated. The latter (VII) was purified by recrystallization from ethyl acetate to give 93.1 mg of 4-epishionone (4.7%), mp 153.5—154°C; IR (Nujol): $\nu_{C=O}$ 1706 cm^{-1}; Found: C, 84.63; H, 11.61%. Calcd for $C_{30}H_{50}O$: C, 84.44; H, 11.81%. MS: *m/e* 426 (M^+); PMR ($CDCl_3$): δ 0.90, 0.92 (each singlet due to $2\times t$-CH_3), 1.15 (s, *t*-CH_3), 1.11 (d, J=7.0 Hz, *sec*-CH_3), 1.60, 1.67 ppm (each singlet, $C{=}C\langle^{CH_3}_{CH_3}$); PMR ($C_6D_6$): δ 0.74, 0.98, 1.10 (each singlet, *t*-CH_3), 0.83 (s, $2\times t$-CH_3), 0.86 (d, J=6.5 Hz, *sec*-CH_3), 1.62, 1.70 ppm (each singlet, $C{=}C\langle^{CH_3}_{CH_3}$); ORD: $[\Phi]_{589}$ −130°, $[\Phi]^{trough}_{319}$ −2370°, $[\Phi]_{310}$ −1990° (sh), $[\Phi]^{peak}_{278}$ +1620° and $[\Phi]_{220}$ −1010°.

Isomerization of 4-Epishionone (VII) into Shionone (VI).

a) With Sodium Methoxide: 4-Epishionone (VII, 5 mg) was dissolved in a mixture of dioxane (5 ml) and methanol (5 ml) and the solution was heated with sodium methoxide under a nitrogen atmosphere for 5.5 hr. The reaction products were worked up as usual and examined by silica gel tlc. The presence of VII was not detectable and the spot due to VI appeared on tlc.

b) With Alumina: 4-Epishionone (VII) in benzene was adsorbed on alumina and silica gel, respectively, for 24 hr. The compound eluted with benzene from each column was shown to be identical with the starting material (VII), by tlc. In the case of 4-epishionone (VII), it was shown that alumina did not bring about isomerization of VII.

3. D-Homosteroid Series. 17α-Hydroxy-20-hydroxyimino-5α-pregnane (XII). A mixture of 17α-hydroxy-5α-pregnan-20-one[10] (X, 1.69 g), ethanol (60 ml), hydroxylamine hydrochloride (4.0 g) sodium acetate (4.7 g) and water (20 ml) was heated under reflux for 6 hr. On evaporation of some amount of solvent followed by cooling, crystals precipitated from the concentrated solution. Recrystallization from ethanol gave the oxime (XII, 1.59 g), mp 212.0—212.5°C; IR (Nujol): 3450 cm^{-1} (broad). Found: C, 75.55; H, 10.67; N, 3.94%. Calcd for $C_{21}H_{35}O_2N$: C, 75.63; H, 10.58; N, 4.20%.

17α-Hydroxy-20α-amino-5α-pregnane (XIII). 17α-Hydroxy-20-hydroxyimino-5α-pregnane (XII, 1.59 g) in acetic acid (180 ml) was hydrogenated in the presence of platinum oxide with addition of two drops of concentrated hydrochloric acid (*cf.* Ref. 4). After the acetic acid had been removed under reduced pressure, the residue was washed with chloroform and recrystallized from methanol. The product XIII gave one spot on tlc, mp 290°C (with decomposition), IR (Nujol): 3300 and 3260 cm^{-1}. From the chloroform washings, the starting material (XII, 50 mg) was recovered.

17aα-Methyl-D-homo-5α-androstan-17-one (IX). A solution of 17α-hydroxy-20α-amino-5α-pregnane (XIII, 318 mg) in acetic acid (15 ml) and water (13 ml) was kept at 0°C. To this solution was added dropwise, with stirring, a solution of sodium nitrite (1.0 g) in water (5 ml). The mixture was stirred for 4 hr at 0°C and allowed to stand at room temperature for 10 hr. The reaction mixture was filtered and the precipitate was washed with chloroform. The filtrate and the washings were combined and neutralized with aqueous sodium hydrogen carbonate solution (*cf.* Ref. 4). After an usual work-up, recrystallization from acetone yielded 181 mg of a ketone (IX), mp 138.0—138.5°C; IR (Nujol): 1710 cm^{-1}; Found: C, 83.26; H, 11.49%. Calcd for $C_{21}H_{34}O$: C, 83.38; H, 11.33%. MS: *m/e* 302 (M^+) and 230 [$(M-72)^+$; base peak]; PMR ($CDCl_3$): δ 0.77, 0.81 (s, *t*-CH_3), 1.08 ppm (d, J=7.0 Hz, *sec*-CH_3); PMR (C_6D_6): δ 0.66. 0.70 (s, *t*-CH_3), 0.85 ppm (d, J=7.5 Hz, *sec*-CH_3); ORD: $[\Phi]_{589}$ −170°, $[\Phi]^{trough}_{318}$ −2870°, $[\Phi]_{308}$ −2410° (sh), $[\Phi]^{peak}_{280}$ +1120°, and $[\Phi]_{234}$ −420°.

17aβ-Methyl-D-homo-5α-androstan-17-one (VIII). A solution of 17aα-methyl-D-homo-5α-androstan-17-one (XI, 91.6 mg) and potassium hydroxide (400 mg) in ethanol (47 ml) was refluxed under nitrogen for 16 hr. The solution was concentrated, treated with 1 M-hydrochloric acid and diluted with water. The precipitate was extracted with ether and the ethereal extract was washed with water, dried over sodium sulfate and evaporated to dryness giving rise to 88 mg of product. This showed two spots (R_f 0.5 and 0.4) on silica gel tlc developed with benzene and the lower spot was found to be identical with that of the starting material (IX). The mixture was separated by silica gel column chromatography into 17aα-methyl epimer (IX, 16.8 mg) and 17aβ-methyl epimer (VIII, 69 mg). The 17aβ-methyl epimer (VIII) showed mp 143.5°C; Found: C, 83.51; 11.44%. Calcd for $C_{21}H_{34}O$: C, 83.38; H, 11.33%. MS: *m/e* 302 (M^+) and 230 [$(M-72)^+$; base peak]; PMR ($CDCl_3$): δ 0.62, 0.72 (s, *t*-CH_3), 0.87 ppm (d, J=6.0 Hz, *sec*-CH_3); PMR (C_6D_6): δ 0.51, 0.66 (s, *t*-CH_3), 0.98 ppm (d, J=7.0 Hz, *sec*-CH_3); ORD: $[\Phi]_{589}$ −180°, $[\Phi]^{trough}_{312}$ −5740°, $[\Phi]_{304}$ −4980° (sh), $[\Phi]^{peak}_{270}$ +5010° and $[\Phi]_{222}$ +1660°.

Equilibration of 17aβ-Methyl-D-homo-5α-androstan-17-one (VIII) with Alkali. 17aβ-Methyl-D-homo-5α-androstan-17-one (VIII, 11.3 mg) was treated with potassium hydroxide (100 mg) in ethanol (2 ml) and subjected to equilibration for 17 hr. The equilibrating products were extracted and the ketone fraction was washed with water, dried and used for ORD measurement. ORD: $[\Phi]_{589}$ −175°, $[\Phi]^{trough}_{314}$ −4980°, $[\Phi]_{303}$ −3930° (sh), $[\Phi]^{peak}_{270}$ +3930° and $[\Phi]_{230}$ +1130°. These data show that the equilibrated ketone mixture consisted of 28% of 17aα- and 72% of 17aβ-epimers. On preparative tlc separation, the equilibrating mixture gave 17aα-methyl epimer (IX, 2.6 mg) and 17aβ-methyl epimer (VIII, 7.4 mg).

Ethylene Ketal (XIV) of 17aβ-Methyl-D-homo-5α-androstan-17-one (IX). 17aβ-Methyl-D-homo-5α-androstan-17-one (VIII, 10 mg) was dissolved in benzene (10 ml) and heated under reflux with ethylene glycol (4 ml) and *p*-toluenesulfonic acid (150 mg) for 13.5 hr under a nitrogen atmosphere. The reaction products were subjected to silica gel column chromatography and the ethylene ketal (XIV, 6.7 mg, recrystallized from acetone), mp 163°C; MS: *m/e* 346 (M^+) and 99 (fragment "a", base peak), was obtained.

Mesoionic 5-Acylimino-2-methylthiothiazoles

Toshie SHIBA and Hiroshi KATO*

Okaya Works, Kyorin Pharmaceutical Co., Okaya 394

**Department of Chemistry, Faculty of Science, Shinshu University, Asahi, Matsumoto 390*

(Received October 27, 1972)

Treatment of 5-acylamino-4-thiazoline-2-thiones (**6**) with methyl iodide followed by treatment with an alkali gave the corresponding mesoionic 5-acylimino-2-methylthiothiazoles (**8**) instead of the corresponding thiazolium salts. The reactions of 2-methylthiothiazoles (**8**) with nucleophiles gave 2-substituted 5-acylamino-4-thiazolines.

We reported[1] on the preparation of mesoionic 5-acyliminothiazoles (**1**) by treatment of 3-substituted 5-acylaminothiazolium chlorides (**2**) with an alkali. Cook and Cox[2] claimed the preparation of 5-acetamido-2-methylthio-3-isopropylthiazolium hydroxide (**3**) by the reaction of 5-acetamido-3-isopropyl-4-thiazoline-2-thione and methyl iodide in the presence of sodium hydroxide. Although their results of elemental analyses agreed with those of thiazolium hydroxide structure, the substance might be assumed to actually have the corresponding anhydro-base or mesoionic structure, since the method of preparation is similar in principle to the one we employed for the preparation of mesoionic 5-iminothiazoles. The present study was initiated with the view of establishing the structure of the product obtained by Cook and Cox.

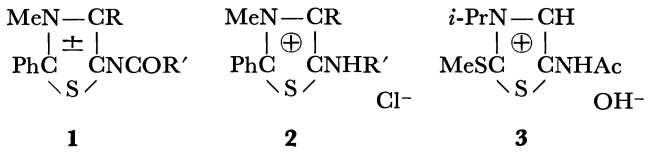

1 **2** **3**

The reactions between aminoacetonitriles (**4a—c**) and carbon disulfide gave 5-amino-4-thiazoline-2-thiones (**5a—c**), which, on treatment with acetic anhydride or benzoic anhydride, gave the corresponding acylamino-4-thiazoline-2-thiones (**6a—d**). Treatment of **6a—d** with methyl iodide gave the corresponding 5-acylamino-2-methylthiothiazolium iodides (**7a—d**), which gave the free bases **8a—d** on treatment with aqueous alkali.

The elemental analyses of the final products agreed with the anhydro-bases **8** but not with the thiazolium hydroxides of type **3**. A considerable bathochromic shift of the ultraviolet absorption maxima is observed with **8** in comparison with iodides **7**. The infrared spectra of **7** show an amide carbonyl band at 1650—1675 cm^{-1} whereas the free bases **8** show no carbonyl band above 1600 cm^{-1}.

From the results including spectral data (Table 2), we might conclude that the compounds obtained by treatment of iodides **7** with alkali are mesoionic 5-acylimino-2-methylthiothiazoles (**8**).

The same **8a** was isolated when **6a** was treated with methyl iodide in aqueous sodium hydroxide as described by Cook and Cox.[2] Treatment of **8a** with water did not afford hydroxide **3**. The melting points of **8a** (178—179°C) and its hydriodide **7a** (159—160°C) did not agree with the reported values (83°C and 182—183°C respectively).

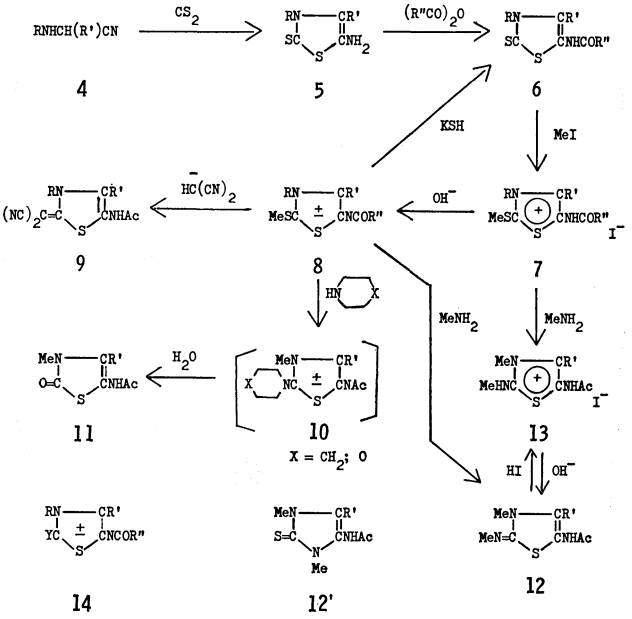

a: R=*i*-Pr, R′=H, R″=Me
b: R=Me, R′=Me, R″=Me
c: R=Me, R′=Ph, R″=Me
d: R=Me, R′=Ph, R″=Ph

The NMR chemical shifts of the substituents of **8** (Table 2) appear at a region close to the values of the corresponding thiazolium salts **7**. The signal for the methylthio group of **8** is also shifted downfield in comparison with thioanisole (δ 2.47) and 2-methylthiopyrimidines (δ around 2.5).[3] These spectral values are very close to those of mesoionic 2-phenyl-5-acyliminothiazoles.[1] For the sake of comparison, 5-acetylimino- and 5-benzoylimino-3,4-dimethyl-2-phenylthiazole (**1b**: R=R′=Me; **1c**: R=Me, R′=Ph) were prepared by the method reported,[1] and the results are shown in Tables 1 and 2. The NMR data, together with the solvent dependent electronic spectra (See Table 2) and the lack of infrared carbonyl absorption in the normal infrared region suggest that the ring bears a considerable positive charge, and the acylimino group is strongly polarized; *i.e.*, there is a large contribution from resonance structures such as **8′** and **8″**.

1) T. Shiba and H. Kato, This Bulletin, **44**, 1864 (1971).
2) A. H. Cook and S. F. Cox, *J. Chem. Soc.*, **1949**, 2337.
3) N. S. Bhacca, L. F. Johnson, and J. N. Schoolery, "NMR Spectra Catalog," Varian Associates, Palo Alto, Calif., Vol. 1 (1962); Vol. 2 (1963).

TABLE 1. PROPERTIES OF 5-AMINOTHIAZOLE AND 5-AMINO-4-THIAZOLINE DERIVATIVES

Compd.	Appearance	Solvent of Recryst.	Yield %	Mp °C	Formula	Anal. Found / Calcd. C	H	N
5b	colorless needles	dimethylformamide	77	263.5—264	$C_5H_8N_2S_2$	37.80 37.50	4.85 5.04	17.15 17.50
5c	yellow needles	ethyl acetate	79	138—139	$C_{10}H_{10}N_2O_2$	53.79 54.01	4.50 4.54	12.82 12.60
6b	colorless needles	methanol	91	214.5—215.5	$C_7H_{10}N_2OS_2$	41.32 41.56	5.20 4.98	13.39 13.69
6c	colorless prisms	acetone	88	272—272.5	$C_{12}H_{12}N_2OS_2$	54.68 54.55	4.61 4.58	10.32 10.60
6d	pale yellow needles	dimethylformamide	93	273—274	$C_{17}H_{14}N_2OS_2$	62.56 62.55	4.35 4.32	8.88 8.58
7a	colorless leaflets	ethanol	91	159—160[g]	$C_9H_{15}N_2OS_2I$	30.08 30.18	4.27 4.22	7.54 7.82
7b	colorless prisms	methanol	88	183.5—184.5	$C_8H_{13}N_2OS_2I$	28.13 27.92	3.88 3.81	7.99 8.14
7c	yellow prisms	ethanol	96	267.5—268	$C_{13}H_{15}N_2OS_2I$	38.52 38.44	3.81 3.72	6.61 6.90
7d	pale yellow needles	dimethylformamide	75	268—270	$C_{18}H_{17}N_2OS_2I$[i]	45.87 46.17	3.42 3.66	6.23 5.98
8a	colorless prisms	ethyl acetate	90	178—179[h]	$C_9H_{14}N_2OS_2$	46.67 46.97	6.24 6.13	11.80 12.17
8b	pale yellow needles	acetone	88	175—176	$C_8H_{12}N_2OS_2$	44.34 44.44	5.52 5.55	12.51 12.91
8c	yellow prisms	ethanol	96	212—213	$C_{13}H_{14}N_2OS_2$	56.46 56.11	5.32 5.07	9.77 10.07
8d	yellow leaflets	dimethylformamide	73	244.5—246	$C_{18}H_{16}N_2OS_2$	63.62 63.50	4.63 4.74	8.18 8.23
2a[a]	yellow prisms	2-propanol	57	243—244 dec	$C_{11}H_{13}N_2SCl$	54.70 54.81	5.55 5.44	11.64 11.64
2a, pic[b]	yellow needles	ethanol		150.5—151	$C_{17}H_{15}N_5O_7S$	47.22 47.11	3.52 3.52	15.79 16.16
2b[c]	colorless prisms	ethanol–acetone	90	228—230	$C_{13}H_{15}N_2OSCl$	55.01 55.31	5.48 5.31	9.62 9.92
2b, pic[b]	yellow needles	ethanol		167.5—168	$C_{19}H_{17}N_5O_8S$	48.30 48.00	3.81 3.60	14.56 14.73
2c[d]	colorless prisms	ethanol	58	175—176	$C_{18}H_{17}N_2OSCl$	62.36 62.70	5.20 4.97	7.96 8.13
2c, pic[b]	yellow prisms	ethanol		182—183	$C_{24}H_{19}N_5O_8S$	53.98 53.63	3.20 3.57	13.21 13.02
1b[c]	yellow prisms	ethanol	48	218.5—219	$C_{13}H_{14}N_2OS$	63.12 63.38	5.83 5.74	11.10 11.37
1c[d]	yellow needles	methanol	90	250—251	$C_{18}H_{16}N_2OS$	68.89 70.12	5.12 5.23	8.80 9.09
9a	colorless needles	dimethylformamide	89	>350	$C_{11}H_{12}N_4OS$	53.50 53.22	5.10 4.88	22.27 22.57
9b	colorless needles	dimethylformamide	74	307—308	$C_{10}H_{10}N_4S$	51.42 51.28	4.19 4.30	24.12 23.92
9c	colorless needles	ethanol	89	212.5—213.5	$C_{15}H_{12}N_4OS\cdot H_2O$[j]	57.05 57.30	4.75 4.50	18.12 17.82
11b	pale yellow prisms	ethanol	84[e]; 98[f]	186—187	$C_7H_{10}N_2O_2S$	44.91 45.14	5.54 5.41	14.57 15.01
11c	colorless needles	ethanol	72[e]; 81[f]	200—201	$C_{12}H_{12}N_2O_2S$	58.34 58.04	4.82 4.87	10.93 11.28
12b	colorless prisms	acetone	72	156—157	$C_8H_{13}N_3OS$	47.99 48.23	6.52 6.58	20.95 21.09
12c	colorless prisms	acetone	81	180—182	$C_{13}H_{15}N_3OS$	59.51 59.76	5.53 5.79	16.29 16.08
13b	colorless prisms	ethanol	80	303—304.5	$C_8H_{14}N_3OSI$	29.16 29.37	4.22 4.31	13.15 12.85
13c	colorless prisms	ethanol	79	230—232	$C_{13}H_{16}N_3OSI$	40.18 40.12	4.41 4.14	10.78 10.81

a) 5-Amino-3,4-dimethyl-2-phenylthiazolium chloride; R=Me, R′=H. b) The corresponding picrate. c) R=R′=Me. d) R=Me, R′=Ph. e) From piperidine. f) From morpholine. g) Reported mp: 182—183°C.[2] h) Reported mp for the corresponding hydroxide: 83°C.[2] i) This contains a molecule of dimethylformamide of crystallization before being dried in a vacuum at 200°C. j) Water content: 5.6% (Karl Fisher; calcd 5.73%).

Table 2. Spectra of 5-aminothiazole and 5-amino-4-thiazoline derivatives

Compd.	λ_{max}^{EtOH} (nm) (log ε)	NMR (δ) of substituents at respective positions 2	3	4	5	IR (cm^{-1})
7a	319 (4.036)	2.97	1.64 d[d] 4.73 sept	8.68	2.40	~3420 (NH), 1675 (C=O)
7b	324 (4.042)	3.00	3.92	2.62	2.28[e]	3085—2990 (NH), 1660 (C=O)
7c	264 (3.852) 322 (4.056)					3010—2880 (NH), 1660 (C=O)
7d						3200—2800 (NH), 1650 (C=O)
8a	264 (3.717)[c]	2.80	1.56 d[d] 4.82 sept	7.40	2.25	1560 (C=N or C=O)
8b	262 (3.804)[c] 363 (3.885)	2.77	3.83	2.62	2.28	1580 (C=N or C=O)
8c	234 (3.910)[c] 305 (3.915) 362 (3.970)	2.82	3.71	7.52	2.20	1555 (C=N or C=O)
8d	230 (4.303) 330 (4.061) 382 (4.211)	2.77	3.70	7.30—7.75 m (8H) 8.20—8.35 m (2H)		1540 (C=N or C=O)
1b[a]	250 (3.975) 365 (3.929)	7.58	3.88	2.67	2.30	1560 (C=N or C=O)
1c[b]	298 (3.855) 382 (4.250)	7.58	3.92	2.96	7.40—7.70m (3H) 8.35—8.50m (2H)	1560 (C=N or C=O)
11b			3.25	2.11	2.02	3400—2800 (NH), 1675 (C=O), 1660 (C=O), 1615 sh, 1600 (C=C)
11c			3.08	7.25—7.60m	1.99	3300—2800 (NH), 1670 (C=O), 1640 (C=O), 1600, 1590 sh (C=C)
12b		2.96	3.22	2.10	1.97	3240—3050, 2900 (NH), 1655 (C=O), 1635 (C=N), 1610 (C=C)
12c		3.03	3.08	7.30—7.63m	2.01	3300—2700 (NH), 1680 (C=O), 1640 (C=N), 1605 (C=C)
13b		3.06	3.57	2.37	2.18[e]	3350—2800 (NH), 1665, 1655 sh (C=O)
13c		3.19	3.71	—[f]	2.14	3400—2700 (NH), 1655 (C=O)

a) R=R′=Me. b) R=Me, R′=Ph. c) λ_{max} in pyridine: **8a**: 377 (4.047); **8b**: 391 (4.074); **8c**: 327 (3.929), 387 (4.030). λ_{max} in tetrahydrofuran: **8a**: 382 (4.055); **8b**: 395 (4.091); **8c**: 326 (3.970), 392 (4.031). d) J=7 Hz. e) In $CDCl_3$—DMSO-d_6 (2 : 3). f) Because of the low solubility of **13c**, this multiplet signal could not be measured with accuracy.

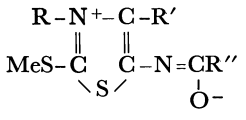

8′

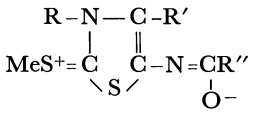

8″

The mass spectra (see Experimental) of **8b** and **8c** show, besides the molecular ion peak, prominent fragmentation peaks corresponding to $(MeSCS)^+$, $(MeNCSMe)^+$, and $(MeNCR')^+$ as well as peaks of fragmentation at the ring substituents. It is to be noted that both **8b** and **8c** give fragment ion peaks corresponding to (M—133) with a considerable relative intensity.[4]

Since the spectral study suggested that the thiazole ring is positively charged, it was expected that the methylthio group of **8** would be readily replaced by nucleophiles.

Mesoionic 5-acylimino-2-methylthiothiazoles (**8a**—**c**) readily reacted with potassium hydrosulfide at room temperature to give the corresponding 5-acetamido-4-thiazoline-2-thiones (**6a**—**c**). The reaction between **8a**—**c** and dicyanomethide ion also gave the corresponding 2-dicyanomethylene derivatives **9a**—**c**. Methylthiothiazoles **8b** and **c** and their hydriodides **7b** and **c** reacted with piperidine and morpholine on heating in ethanol. However, the expected mesoionic 2-piperidino and 2-morpholino derivatives **10b** and **c** were not isolated, which apparently underwent hydrolysis to give the corresponding 5-acetamido-4-thiazolin-2-ones (**11b** and **c**) as the final products.

Although **8b** and **8c** did not react with aniline even on heating, they reacted with methylamine to give substitution products, the elemental analyses of which agreed with 2-methylimino derivatives (**12b** and **c**). However, an imidazoline-2-thione structure **12′** should also be considered as a possible structure of the reaction products since a similar skeletal rearrangement has been observed by the reactions of 5-methylthiothiazolium[5] and 5-methylthiothiadiazolium[6] salts and methylamine.

4) The high resolution mass spectrum of **8c** measured by Prof. Fukiko Yamada, Kansai University, gave the composition $C_9H_9N_2$ for this fragment.

5) T. Shiba and H. Kato, This Bulletin, **43**, 3491 (1970); P. B. Talukdar, S. K. Sengupta, and A. K. Datta, *Chem. Commun.*, **1972**, 696.

6) M. Ohta, H. Kato, and T. Kaneko, This Bulletin, **40**, 579 (1967).

Comparison of the NMR spectra of the reaction products and their hydriodides, formed either by the treatment of **12b** and **c** with hydriodic acid or directly by the reaction of methylthiothiazolium iodides **7b** and **c** and methylamine, shows that one methyl signal is shifted to a considerably lower magnetic field in going from the free base to the hydriodide, but the other remains almost unchanged. This suggests that one methyl group is substituted on a ring nitrogen atom while the other is substituted on an exocyclic nitrogen atom. This, together with the lack of infrared bands often observed with an N-C=S group,[6,7] supports the view that the reaction products have a 2-methyliminothiazoline structure **12b** and **c**. Although the mass spectra of **12b** and **c** do not provide information as to the choice of structure between **12** and **12'**, they show a strong peak corresponding to (M−116) which probably has the same composition as the (M−133) peak of **8**.

That the products of nucleophilic displacement reactions have 5-acetamido-4-thiazoline structures (**6**, **9**, **11**, **12**) rather than the corresponding mesoionic 2-substituted 5-acetyliminothiazole structures (**14**) was supported, *inter alia*, by the presence of the amide carbonyl band at a normal infrared region and the presence of an NH stretching frequency band. This shows that 4-thiazoline structures are thermodynamically more stable than the corresponding mesoionic thiazole structures.

Experimental[8]

*5-Amino-4-thiazoline-2-thiones (**5**).* A solution of 0.21 mol of aminoacetonitriles (**4**) and 16 g (0.21 mol) of carbon disulfide in 150 ml of ethyl acetate was allowed to stand at room temperature for two days. The solvent was concentrated and the residue was recrystallized. IR: **5b**: ~3300 (NH), 1620 (C=C), 1092, 1300 (C=S); **5c**: 3380—3300 (NH), 1620 (C=C), 1105, 1295 (C=S).

*5-Acylamino-4-thiazoline-2-thiones (**6**).* One part of 5-aminothiazolinethione (**5**) was dissolved in 20 parts of acetic anhydride and the resulting precipitate was collected. Benzoylation of **5c** was effected by heating equimolar amounts of **5c** and benzoic anhydride in benzene for twenty minutes. IR: **6a**: 3200—3100 (NH), 1665 (C=O), 1595 (C=C) 1075, 1290 (C=S); **6b**: ~3280 (NH), 1670 (C=O), 1630 (C=C), 1105, 1275 (C=S); **6c**: ~3320 (NH), 1650 (C=O), 1610 (C=C), 1120, 1294 (C=S); **6d**: ~3210 (NH), 1660 (C=O), 1610 (C=C), 1105, 1294 (C=S).

*5-Acylamino-5-methylthiothiazolium Iodides (**8**).* A solution of 5-acylamino-4-thiazoline-2-thione (**6**) and two molar equivalents of methyl iodide in methanol was heated under reflux; the solvent was concentrated and the residue was recrystallized.

*Mesoionic 5-Acylimino-2-methylthiothiazoles (**8**).* An aqueous solution (or suspension) of 5-acylamino-2-methylthiothiazolium iodide (**7**) was made alkaline with potassium carbonate and the crystals which separated out were collected and recrystallized. MS: **8b**: 216 (30) M, 201 (41) [M-Me], 91 (73) MeSCS, 88 (21) MeNCSMe, 83 (30) [M−MeSCS−Ac+H], 56 (88) MeNCMe, 43 (100) Ac. **8c**: 278 (41) M, 263 (38) [M−Me], 145 (19) [M−MeSCS−Ac+H], 118 (80) MeNCPh, 91 (97) MeSCS, 88 (32) MeNCSMe, 77 (48) Ph, 43 (100) Ac.

*Mesoionic 5-Acylimino-3,4-dimethyl-2-phenylthiazoles (**1**).* The compounds were prepared by methods similar to those described earlier.[1]

*Reactions of **8a–c** with Potassium Hydrosulfide.* To a solution of 0.5 g of **8** in 15 ml of ethanol was added a solution of two molar equivalents of potassium hydrosulfide in 10 ml of ethanol, and the resulting solution was stirred at room temperature for one hour. The reaction mixture was poured into water and the precipitate was collected, recrystallized and identified to be 5-acetamido-4-thiazoline-2-thiones (**6**) by mixed mp and comparison of their infrared spectra. Yields: 99, 96, and 87% from **8a**, **b**, and **c** respectively.

*5-Acetamido-2-dicyanomethylene-4-thiazolines (**9**).* One gram of **8a–c** was added under an atmosphere of nitrogen to a solution of dicyanomethide anion in 20 ml of dimethyl sulfoxide prepared from an equimolar amount of malononitrile and sodium hydride. The resulting solution was stirred at room temperature for two hours, and poured into 20 ml of water. The precipitate was collected and recrystallized. IR: **9a**: 3300—2700 (NH), 2200, 2175 (CN), 1670 (C=O), 1625 (C=C); **9b**: 3260—2840 (NH), 2200, 2165 (CN), 1680 (C=O), 1640 (C=C); **9c**: 3700—2900 (NH), 2200, 2170 (CN), 1665 (C=O), 1630 (C=C).

*5-Acetamido-4-thiazolin-2-ones (**11**).* A solution of **8** or **7** and an equimolar amount of piperidine or morpholine was heated under reflux for ten hours. The solvent was concentrated and the crystals which separated out were collected.

*5-Acetamido-2-methylimino-4-thiazolines (**12**).* A solution of 0.5 g of **8** and 1.5 ml of 30% ethanolic methylamine in 10 ml of ethanol was stirred at room temperature for ten hours. The reaction mixture was concentrated and the crystals which separated out were collected and recrystallized. MS: **12b**: 199 (56) M, 156 (29) [M−Ac], 83 (78) [M−MeNCS−Ac], 56 (100) MeNCMe, 43 (60) Ac; **12c**: 261 (49) M, 219 (15) [M−Ac+H], 218 (10) [M−Ac], 145 (36) [M−MeNCS−Ac], 118 (100) MeNCPh, 77 (42) Ph, 43 (29) Ac.

*5-Acetamido-2-methylaminothiazolium Iodides (**13**).* The compounds were prepared either by the action of hydroiodic acid on **12**, or by treatment of **7** with an excess of ethanolic methylamine at room temperature for ten hours. The yields given in Table 1 refer to those from **7**. The free bases **12** were formed by treatment of **13** with potassium carbonate.

We are indebted to the staff of Kyorin Chemical Laboratories for elemental analyses and mass spectral measurements.

7) T. G. Stewart and L. B. Kier, *J. Pharm. Sci.*, **54**, 731 (1965); P. B. Talukdar and S. K. Sengupta, *J. Indian Chem. Soc.*, **47**, 49 (1970); and references cited therein.

8) The melting points were determined on a micro hot stage and are not corrected. The ultraviolet spectra were recorded on a Hitachi model ESP-2U spectrophotometer, and the infrared spectra were recorded as KBr disks on a Hitachi model EPI-SII spectrophotometer. Unless otherwise stated, the NMR spectra were obtained on a JEOLCO JNM-4H-100 (100 MHz) spectrometer in deuteriochloroform, and the chemical shifts are recorded (ppm) downfield from internal TMS. The mass spectra were measured on a Hitachi RMU-6 spectrometer at 75 eV using a direct inlet technique. The yields, properties and elemental analyses are given in Table 1, and the spectral data of some compounds in Table 2.

Synthesis of a Gramicidin S Analog Containing δ-Aminovaleric Acid, [4–5-δ-Aminovaleric Acid]-Gramicidin S

Shōsuke SŌFUKU

Department of Chemistry, College of Science, Rikkyo (St. Paul's) University, Nishi-Ikebukuro, Tokyo, Japan

(Received July 6, 1972)

In order to investigate the contribution of amide bond in peptide to its activity and conformation, a new type of analog of gramicidin S, [4–5-δ-aminovaleric acid]-gramicidin S, was synthesized, in which one of the D-phenylalanyl-L-proline residues of gramicidin S was replaced with δ-aminovaleric acid residue. The analog peptide has antimicrobial activity and shows similar ORD and CD spectra to those of gramicidin S. The linear peptide (Val-Orn-Leu-δAva-Val-Orn-Leu-D-Phe-Pro) has no activity and its ORD and CD spectra are nearly the same as those of random coil of polypeptide.

Since the primary structure of antibiotic cyclodecapeptide gramicidin S (GS) from *Bacillus brevis* was confirmed by means of successful total synthesis by Schwyzer and Sieber,[1] a number of investigations have been undertaken to determine the higher structure of the antibiotic. Hodgkin and Oughton[2] proposed some possible models for GS from X-ray diffraction analysis. One of them, an antiparallel β-pleated sheet model, was favored by Schwyzer,[3] and supported by the results of nuclear magnetic resonance by Stern *et al.*[4] and others.[5,6] Several studies on optical rotatory dispersion (ORD)[7–9] and circular dichroism (CD)[7,10,11] of GS have also been undertaken to reveal the conformation in solution. A considerable number of analogs of GS have been prepared by Izumiya *et al.* in an effort to elucidate the relationship between structure and antimicrobial activity. In almost all cases, each amino acid residue of the natural peptide was replaced with a residue having a different side chain. Their results[12] suggested some fundamental significance of the presence of side chains of constituent amino acids, especially basic amino acid.[13] It was found that the analogs formed by replacing the L-proline residues of GS with glycine[14] or sarcosine[15] residues had an activity similar to that of GS. For determining the relation between ring-size of cyclic peptide and activity, cyclic pentapeptide (half-size compounds of GS[16] and some analogs[12,17]), cyclo-(Val-Orn-Leu-D-Phe-Pro-Gly),[18,19] cyclo (Val-Orn-Leu-D-Phe-Pro-Gly-Gly),[19,20] and [5,5′-βAla]-GS[21] were synthesized by Izumiya and his co-workers,but found to show no activity. It is consequently presumed that the ring-size of such an analog is an important factor in determining whether or not the analog possesses activity.

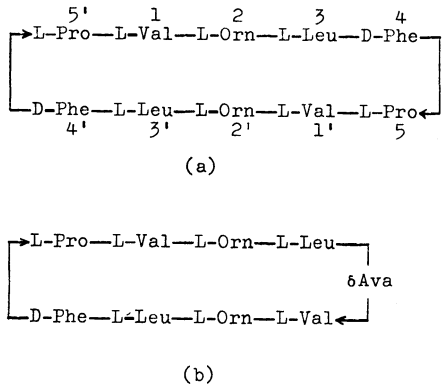

Fig. 1. Structure of GS (a) and [δAva$^{4-5}$]−GS (b).

Participation of amide bonds through hydrogen bonds between L-valine and L-leucine residues in holding the rigid ring structure of the peptide was confirmed by nmr studies.[4,5] However, it has not been ascertained whether all the amide bonds are indispensable for the function and conformation of the antibiotic. In order to determine this, we synthesized a new type of GS analog containing δ-aminovaleric acid residue (δAva). In this peptide, one of the D-phenylalanyl-L-proline residues of GS is replaced with δAva and, consequently, one amide group is displaced with an ethylene group (–CH_2–CH_2–) which has almost the same length as –CO–NH– but does not participate in the hydrogen bond. Since this analog and the

1) R. Schwyzer and P. Sieber, *Helv. Chim. Acta*, **40**, 624 (1957).
2) D. C. Hodgkin and B. M. Oughton, *Biochem. J.*, **65**, 752 (1957).
3) R. Schwyzer, Ciba Foundation Symp. Amino Acids and Peptides with Antimetabolic Activity, 171 (1958); R. Schwyzer, *Chimia* **12**, 53 (1958).
4) A. Stern, W. A. Gibbons, and L. C. Craig, *Proc. Nat. Acad. Sci. U. S.*, **61**, 734 (1968).
5) M. Ohnishi and D. W. Urry, *Biochem. Biophys. Res. Commun.*, **36**, 194 (1969).
6) R. Schwyzer and U. Ludescher, *Biochemistry*, **7**, 2519 (1968); R. Schwyzer and U. Ludescher, *Helv. Chim. Acta*, **52**, 2033 (1969).
7) D. Balasuburamanian, *J. Amer. Chem. Soc.*, **89**, 5445 (1967).
8) L. C. Craig, *Proc. Nat. Acad. Sci. U. S.*, **61**, 152 (1968).
9) T. Kato, M. Waki, S. Matsuura, and N. Izumiya *J. Biochem.* (Tokyo), **68**, 751 (1970).
10) F. Quadrifoglio and D. W. Urry, *Biochem. Biophys. Res. Commun.*, **29**, 785 (1967).
11) S. Laiken, M. Printz, and L. C. Craig, *J. Biol. Chem.*, **244**, 4454 (1969).
12) M. Kondo and N. Izumiya, This Bulletin, **40**, 1975 (1967).
13) M. Waki, O. Abe, R. Okawa, T. Kato, S. Makisumi, and N. Izumiya, *ibid.*, **40**, 2904 (1967).
14) H. Aoyagi, T. Kato, M. Ohno, M. Kondo, M. Waki, S. Makisumi, and N. Izumiya, *ibid.*, **38**, 2139 (1965).
15) H. Aoyagi and N. Izumiya, *ibid.*, **39**, 1747 (1966).
16) M. Waki and N. Izumiya, *ibid.*, **40**, 1687 (1967).
17) H. Aoyagi, M. Kondo, T. Kato, S. Makisumi, and N. Izumiya, *ibid.*, **40**, 1685 (1967).
18) T. Kato, M. Kondo, M. Ohno, and N. Izumiya, *ibid.*, **38**, 1202 (1965).
19) Abbreviations with no prefix show L-amino acid residues.
20) O. Abe, K. Kuromizu, M. Kondo, and N. Izumiya, This Bulletin, **43**, 914 (1970).
21) S. Matsuura, M. Waki, S. Makisumi, and N. Izumiya, *ibid.*, **43**, 1197 (1970).

natural peptide have the same number of members in the ring although the side chains inevitably differ, it is expected that the analog peptide may have a similar ring structure and antimicrobial activity as those of the natural peptide if the amide group between phenylalanine and proline is not involved in any intramolecular hydrogen bond. We recently reported on the antimicrobial activity of this analog toward certain microorganisms,[22] giving details of the syntheses of the cyclic analog peptide and the related linear nonapeptide (Val-Orn-Leu-δAva-Val-Orn-Leu-D-Phe-Pro)[19] and their properties in comparison with GS.

Results and Discussion

Synthesis. The synthesis of the GS analog is shown in Schemes 1 and 2. The conventional coupling methods could be applied to the synthesis of peptide containing δAva as well as α-amino acid. Two fragments VI and XII were synthesized without racemization by using the procedure of stepwise elongation with the mixed anhydride method improved by Anderson *et al.*[24] The latter was saponified to XIII. After the removal of the *N*-protecting group of XIII, the resulting peptide XIV was coupled with VII to the linear nonapeptide XV by the Rudinger modification[25] of the azide method. Preparation of XV by hydrolyzing the ethyl ester (XX) of the peptide was unsuccessful under various of conditions. Cyclization of XV was carried out following the method of Schwyzer *et al.*[1,16] for the synthesis of GS. The cyclic peptide XVI was obtained in a good yield (70%) regardless of the presence of δAva in the middle of the linear peptide. This result might indicate that the conformation of the active ester of XV is so arranged as to be favorable for the cyclization as well as the synthesis of GS.[3] The desired [4-5-δAva]-GS XVII was obtained as a crystalline dihydrochloride by means of hydrogenolysis of benzyloxycarbonyl groups on ornithine residues of the cyclic peptide XVI in the presence of hydrogen chloride, followed by lyophilization in water.

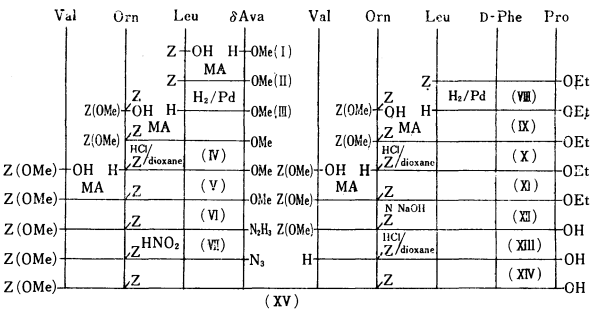

Scheme 1.[19,23]

The linear nonapeptide trihydrochloride XVIII was prepared from peptide XV. *N*-Protecting groups of XV were removed with hydrogen bromide in acetic acid, and the hydrobromide of the product was transformed into trihydrochloride XVIII.

Characterization. Thin layer chromatography of each of the synthetic peptides XVII and XVIII gave one ninhydrin-positive spot. The chromatogram of paper electrophoresis is shown in Fig. 2. The linear peptide XVIII has three amino groups and hence moves faster than the others.

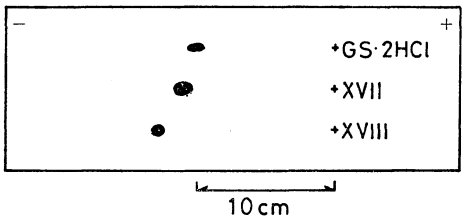

Fig. 2. Paper electrophoresis of cyclic analog (XVII), linear peptide (XVIII), and gramicidin S dihydrochloride (GS) (HCOOH-AcOH-H_2O; 4 : 15 : 180 v/v, pH 1.9, Toyo No. 50 15×40 cm, 600 v, 2 hours).

The free amino groups of the analog peptide XVII were detected by the DNS method in the usual manner.[26] After coupling the peptide with 1-dimethylamino-naphthalene-5-sulphonyl chloride (DNS-chloride) and hydrolyzing the DNS derivative, only the

XV ⟶ Linear nonapeptide (XVIII)

↓ $SO(OC_6H_4NO_2)_2$

Z(OMe)-Val-Orn(δ-Z)-Leu-δAva-Val-Orn(δ-Z)-Leu-D-Phe-Pro-ONp

↓ CF_3COOH

H-Val-Orn(δ-Z)-Leu-δAva-Val-Orn(δ-Z)-Leu-D-Phe-Pro-ONp·CF_3COOH

↓ in pyridine

Cyclo-(Val-Orn(δ-Z)-Leu-δAva-Val-Orn(δ-Z)-Leu-D-Phe-Pro) (XVI)

↓ H_2/Pd, HCl

Cyclo-(Val-Orn-Leu-δAva-Val-Orn-Leu-D-Phe-Pro)·2HCl (XVII)

Scheme 2. Diagram of the synthesis of XVII[19,23]

22) I. Muramatsu, S. Sōfuku, and A. Hagitani, *J. Antibiot.*, **25**, 189 (1972).

23) The following abbreviations are from *Biochemistry*, **5**, 2485 (1966): Z-, benzyloxycarbonyl; Z(OMe)-, *p*-methoxybenzyloxycarbonyl; -ONp, *p*-nitrophenoxy; -OMe, methoxy; -OEt, ethoxy.

24) G. W. Anderson, J. E. Zimmerman, and F. M. Callahan, *J. Amer. Chem. Soc.*, **89**, 5012 (1967).

25) K. Hofmann, W. Haas, M. J. Smithers, R. D. Wells, Y. Wolman, N. Yanaihara, and G. Zanetti, *ibid.*, **87**, 620 (1965); J. Honzl and J. Rudinger, *Collect. Czech. Chem. Commun.*, **26**, 2333 (1961).

26) G. Pataki, "Dünnschichtchromatographie in der Aminosäure- und Peptid-Chemie," Walter de Gruyter & Co., Berlin (1966), p. 167.

N^{δ}-DNS-ornithine was detected on thin layer chromatograms,[27] which proves that the analog has a cyclic form. The IR spectrum of XVII was measured as a KBr disk and the absorption bands of amide I (1640 cm^{-1}) and II (1530 cm^{-1}) were in good agreement with those of GS. The IR spectrum of XVIII had a band at 1727 cm^{-1} (-COOH) besides bands I and II.

On the Structure and Biological Activity. Analog XVII has an antimicrobial activity in the range from the same to half that of GS toward certain microorganisms, and about one third of the acute toxicity of GS in mice when given intravenously.[22] Linear nonapeptide XVIII has no activity toward the same microorganisms. To obtain information on the conformation of this biological active analog, ORD and CD were measured. ORD studies on GS and several other GS analogs had been carried out by Craig,[8] Balasuburamanian,[7] and Kato *et al.*[9] Kato *et al.* pointed out that GS and biological active analogs showed negative Cotton effect at 232 mμ and inactive analogs gave curves differing from that of GS. The ORD of the new analog has a trough similar to GS at 232 mμ in both ethanol and water (Fig. 3). In the case of XVIII, a trough is found at 210 mμ with hypsochromic shift. The trough corresponded to that of random structure of polypeptide.[28] The CD spectra of XVII and XVIII are shown in Fig. 4. The minimum value of XVII appears at 203 mμ and a shoulder at 216 mμ. This band is observed at a wavelength slightly shorter than that of the band of GS (at 206 mμ). Laiken *et al.*[11] found that the CD of modified GS, in which D-phenylalanine residues were hydrogenated, showed two minima in the same region as that of GS. They supposed that the two minima are attributable to the common backbone conformation of both peptides. The CD of XVIII is regarded as that of random structure[29,30] in the same manner as ORD. Thus, the CD band of XVII in the region of 203—216 mμ seems to be attributable to the backbone conformation. The CD spectrum resembles one typical of the α-helix conformation of polypeptide but the wavelength of the minimum differs from that of α-helix and also β-structure.[29,30] It seems reasonable to assume that the CD of GS or its analog is characteristic for such cyclic oligopeptides. The CD spectra in the region near 260 mμ were measured and the bands[31] caused by phenylalanine residue were found. We might conclude that the analog XVII has a conformation similar to that of GS both from the results of ORD and CD measurements and from a valuation of the biological activity. The results also support the antiparallel β-pleated sheet structure of GS proposed by Stern *et al.* and Schwyzer, in which amide groups of phenylalanylproline residues do not take part in any intramolecular hydrogen bond.

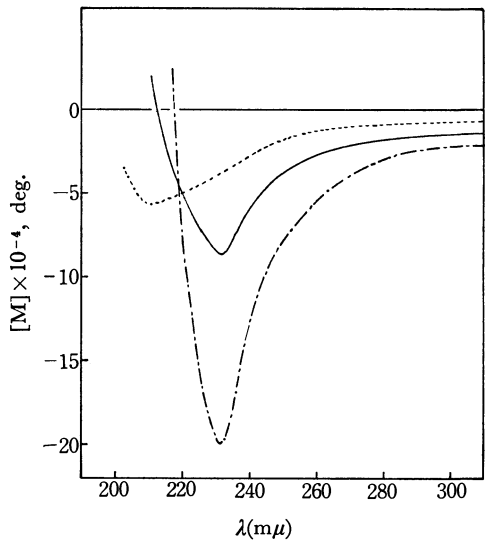

Fig. 3. Optical rotatory dispersions of cyclic analog (XVII), linear peptide (XVIII), and gramicidin S dihydrochloride (GS) in water, XVII (—), XVIII (·····), and GS (—·—). Measurments were made using a 1 mm quartz cell at room temperature.

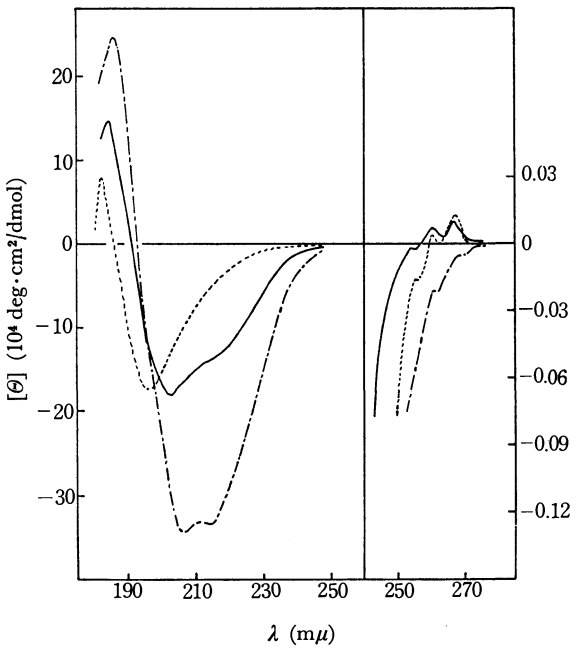

Fig. 4. Circular dichroism spectra of cyclic analog (XVII), linear peptide (XVIII), and gramicidin S dihydrochloride (GS) in water, XVII (——), XVIII (·····), and GS(———). Measurments were made using 0.5 mm (<250 mμ) and 10 cm (>240 mμ) quartz cells at room temperature.

Experimental

All melting points are uncorrected. ORD measurements were performed with a JASCO model UV/ORD-5 and the results were expressed in terms of molar optical rotations.

27) DNS-amino acid was detected as a green spot under UV (254 mμ). R_f values of δ-DNS-ornithine were 0.5 on silica gel plate with *n*-butanol-acetic acid-water (10 : 1 : 1, v/v) and 0.3 on polyamide plate with benzene-acetic acid-*n*-butanol (9 : 2 : 1, v/v).

28) E. R. Blout, I. Schmier, and N. S. Simmons, *J. Amer. Chem. Soc.*, **84**, 3193 (1962).

29) G. Holzwarth and P. Doty, *ibid.*, **87**, 218 (1965).

30) R. Townend. T. F. Kumosinski, S. N. Timasheff, G. D. Fasman, and B. Davidson, *Biochem. Biophys. Res. Commun.*. **23**, 163 (1966).

31) M. Shiraki, *Sci. Papers College of Gen. Education, Univ. of Tokyo*, **19**, 151 (1969).

CD spectra were measured with a JASCO model J-20 and represented by molar ellipticity values. IR spectra were recorded on a Hitachi grating infrared spectrophotometer model 215. The molecular weight of XVI was determined with a Hitachi-Perkin-Elmer vapor pressure osmometer model 115, using methanol. Amino acid analyses were carried out with an automatic amino acid analyzer,[32] after hydrolysis of XVII and XVIII in 6 N hydrochloric acid for 19 hours at 110°C. The purity of the peptide derivatives at each step was confirmed by thin layer chromatography on a silica gel plate with the following solvent systems (v/v): Solv. 1, chloroform–methanol–acetic acid (95 : 5 : 3); Solv. 2, chloroform–methanol (9 : 1); Solv. 3, chloroform–methanol–acetic acid–pyridine (95 : 5 : 3 : 4); Solv. 4, chloroform-methanol–acetic acid (12 : 1 : 1); Solv. 5, *n*-butanol–acetic acid–water (4 : 1 : 1); Solv. 6, *n*-butanol –acetic acid–pyridine–water (4 : 1 : 1 : 2). Compounds possessing free amino groups were detected by spraying ninhydrin reagent. *N*-Protected compounds were also detected with ninhydrin after deblocking with concd. hydrobromic acid.

Methyl δ-Aminovalerate Hydrochloride (I). A solution of δ-valerolactam (45.0 g) in 500 ml of methanol was saturated with dry hydrogen chloride and refluxed for 3 hours. The reaction mixture was concentrated *in vacuo* to an oily residue which was dissolved in methanol. The colorless product was crystallized by the addition of ethyl ether, and collected by filtration; yield, 58.0 g (76.2%). This ester was also obtained by Fischer's esterification from δ-aminovaleric acid in a 95% yield. Mp 145—146°C (lit,[33] mp 145—146°C); Tlc: 0.75 (Solv. 6). (Found: C, 42.94; H, 8.32; N, 8.65%).

Methyl Benzyloxycarbonyl-L-leucyl-δ-aminovalerate (II). Benzyloxycarbonyl-L-leucine obtained from the corresponding dicyclohexylammonium salt[34] (9.0 g, 20.0 mmol) was dissolved in 100 ml of tetrahydrofuran, and 1.74 ml of *N*-methylmorpholine and 2.68 ml of isobutyl chloroformate were added at −15°C. After 5 min, a chilled mixture of 3.34 g (21.5 mmol) of I and 2.8 ml of triethylamine in 15 ml of chloroform was added at −15° to a solution of the mixed anhydride prepared in the preceding step. The reaction mixture was stirred at 5°C for one hour and then at room temperature for one hour. After removal of insoluble materials by filtration, the filtrate was concentrated *in vacuo*. The residue was dissolved in ethyl acetate, and the solution was washed successively with 5% sodium bicarbonate, water, 0.5 N hydrochloric acid and water, and then dried over sodium sulfate. After the solvent was evaporated *in vacuo*, the product was recrystallized from ethyl acetate and petroleum ether. Yield, 5.40 g (71.4%); mp 89—90°C; $[\alpha]_D^{22}$ −15.3° (*c* 1.5, ethanol); Tlc: R_f 0.7 (Slolv. 1).

Found: C, 63.37; H, 8.27; N, 7.64%. Calcd for $C_{20}H_{30}N_2O_5$: C, 63.47; H, 7.99; N, 7.40%.

Methyl L-Leucyl-δ-aminovalerate Hydrochloride (III). II (4.5 g, 11.9 mmol) was hydrogenolyzed in the usual manner over 0.2 g of palladium black in a mixture of 40 ml of ethanol and 6 ml of 2 N hydrochloric acid. After 4 hours, the filtrate from the catalyst was concentrated to dryness *in vacuo*. The oily product was obtained in a theoretical yield. Tlc: R_f 0.1 (Solv. 1).

Methyl N^{α}-p-*Methoxybenzyloxycarbonyl-*N^{δ}*-benzyloxycarbonyl-L-ornithyl-L-leucyl-δ-aminovalerate (IV).* This was prepared from N^{α}-*p*-methoxybenzyloxycarbonyl-N^{δ}-benzyloxycarbonyl-L-ornithine[35] (30.0 mmol) and III (30.0 mmol) by a method similar to that for the synthesis of II. The product was recrystallized from ethanol. Yield, 14.56 g (73.9%); mp 154—157°C; $[\alpha]_D^{20}$ −7.7°C (*c* 1, dimethylformamide); Tlc: R_f 0.6 (Solv. 1).

Found: C, 62.42; H, 7.44; N, 8.40%. Calcd for $C_{34}H_{48}N_4O_9$: C, 62.17; H, 7.37; N, 8.53%.

Methyl N^{α}*-Benzyloxycarbonyl-L-ornithyl-L-leucyl-δ-aminovalerate Hydrochloride (V).* To a solution of IV (5.5 g, 8.4 mmol) in 33 ml of chloroform were added 3.73 N hydrogen chloride in dioxane (11.3 ml) and 2.5 ml of anisole. The solution was stirred at room temperature for 10 min and then concentrated *in vacuo*. The residue was washed several times with ethyl ether and dried *in vacuo*. The product was obtained in a theoretical yield. Tlc: R_f 0.65 (Solv. 5).

Methyl p-*Methoxybenzyloxycarbonyl-L-valyl-*N^{δ}*-benzyloxycarbonyl-L-ornithyl-L-leucyl-δ-aminovalerate (VI).* *p*-Methoxybenzyloxycarbonyl-L-valine[35] (12.0 mmol) was coupled with V (8.4 mmol) by the mixed anhydride method. After removal of the precipitate in the reaction mixture by filtration, the filtrate was concentrated to dryness *in vacuo*. The residue washed with petroleum ether by decantation was combined with the above precipitate. The solids were washed on a filter funnel successively with water, 5% sodium bicarbonate, water, 10% citric acid and water, and dried under reduced pressure. The product was recrystallized from methanol and ethyl ether. Yield, 4.93 g (77.2%); mp 204—205°C; $[\alpha]_D^{20}$ −8.5° (*c* 2, dimethylformamide); Tlc: R_f 0.9 (Solv. 6).

Found: C, 61.82; H, 7.56; N, 9.21%. Calcd for $C_{39}H_{57}N_5O_{10}$: C, 61.97; H, 7.60; N, 9.27%.

p-*Methoxybenzyloxycarbonyl-L-valyl-*N^{δ}*-benzyloxycarbonyl-L-ornithyl-L-leucyl-δ-aminovaleryl Hydrazine (VII).* To a solution of 2.27 g (3.0 mmol) of VI in 18 ml of dimethylformamide was added 5.63 g (90 mmol) of 80% hydrazine hydrate and the solution was stirred for 2 days at room temperature. The hydrazide, precipitated by the addition of 340 ml of water, was filtered and washed with water. A white product dried under reduced pressure was obtained in a yield of 2.26 g (99.6%). Mp 215—217.5°C; $[\alpha]_D^{18}$ −9.0° (*c* 1, hexamethylphosphoramide); Tlc: R_f 0.7 (Solv. 1).

Found: C, 60.17; H, 7.84; N, 12.92%. Calcd for $C_{38}H_{57}N_7O_9$: C, 60.38; H, 7.60; N, 12.97%.

Ethyl N^{α}-p-*Methoxybenzyloxycarbonyl-*N^{δ}*-benzyloxycarbonyl-L-ornithyl-L-leucyl-D-phenylalanyl-L-prolinate (X).* Ethyl L-leucyl-D-phenylalanyl-L-prolinate hydrochloride (IX)[36] obtained from VIII (31.0 mmol) by hydrogenolysis was coupled with N^{α}-*p*-methoxybenzyloxycarbonyl-N^{δ}-benzyloxycarbonyl-L-ornithine[35] (31.5 mmol) by the mixed anhydride method. The product was purified in a manner similar to that for II and weighed 19.47 g (77.0%). Mp 135—138°C; $[\alpha]_D^{30}$ −52.4° (*c* 1, methanol); Tlc: R_f 0.55 (Solv. 1).

Found: C, 64.59; H, 7.17; N, 8.58%. Calcd for $C_{44}H_{57}N_5O_{10}$: C, 64.77; H, 7.04; N, 8.58%.

Ethyl N^{δ}*-Benzyloxycarbonyl-L-ornithyl-L-leucyl-D-phenylalanyl-L-prolinate Hydrochloride (XI).* To a solution of X (12.24 g, 15 mmol) in 120 ml of dioxane was added 5.5 M hydrogen chloride in dioxane (68.2 ml) in an ice bath, and the solution was stirred at room temperature. After 45 min a white precipitate appeared and the reaction was completed in

32) D. H. Spackman, W. H. Stein, and S. Moore, *Anal. Chem.* **30**, 1190 (1958).
33) W. Oelofsen and C. H. Li, *J. Org. Chem.*, **33**, 1581 (1968).
34) E. Klieger, E. Schröder, and H. Gibian, *Ann. Chem.*, **640**, 157 (1961).
35) S. Sōfuku, M. Mizumura, and A. Hagitani, This Bulletin, **43**, 177 (1970).
36) M. Ohno, T. Kato, S. Makisumi, and N. Izumiya, *ibid.*, **39**, 1738 (1966).

4 hours. The product, a white hygroscopic precipitate, was obtained in a reasonable yield after evaporation of the solvent *in vacuo* and washing with ethyl ether by decantation. Mp 126—130°C; Tlc: R_f 0.05 (Solv. 1).

Ethyl p-*Methoxybenzyloxycarbonyl*-L-*valyl*-N$^{\delta}$-*benzyloxycarbonyl*-L-*ornithyl*-L-*leucyl*-D-*phenylalanyl*-L-*prolinate (XII).* This was obtained from *p*-methoxybenzyloxycarbonyl-L-valine[35] (15.0 mmol) and XI (15.0 mmol) by the method for VI. The crude product was recrystallized from ethyl acetate. Yield 12.27 g (89.4%); mp 153—156°C; $[\alpha]_D^{23}$ −29.5° (*c* 1, dimethylformamide), (lit,[16] mp 149—150°C; $[\alpha]_D^{24}$ −26.8° (*c* 2, dimethylformamide)), Tlc: R_f 0.65 (Solv. 3). (Found: C, 64.33; H, 7.38; N, 9.02%).

p-*Methoxybenzyloxycarbonyl*-L-*valyl*-N$^{\delta}$-*benzyloxycarbonyl*-L-*ornithyl*-L-*leucyl*-D-*phenylalanyl*-L-*proline (XIII).*[16] XII (2.29 g, 2.5 mmol) was saponified according to Ref. 16. The reaction mixture was acidified to pH 4.2 with 25 ml of 2.2% citric acid on cooling, and concentrated *in vacuo*. The residue was washed with 5% citric acid and water, and dried under reduced pressure. Recrystallization from methanol and ethyl ether gave 1.75 g (78.8%) of the product. Mp 149—150.5°C; $[\alpha]_D^{21}$ −31.9° (*c* 1, dimethylformamide); Tlc: R_f 0.5 (Solv. 3).

Found: C, 62.68; H, 7.19; N, 9.54%. Calcd for $C_{47}H_{62}N_6O_{11}\cdot H_2O$: C, 62.36; H, 7.13; N, 9.29%.

L-*Valyl*-N$^{\delta}$-*benzyloxycarbonyl*-L-*ornithyl*-L-*leucyl*-D-*phenylalanyl*-L-*proline Hydrochloride (XIV).* When XIII (1.24 g, 1.6 mmol) was subjected to the same treatment as for V, the product was obtained in a theoretical yield. Mp 153—157°; Tlc: R_f 0.1 (Solv. 1).

p-Methoxybenzyloxycarbonyl-L-*valyl*-N$^{\delta}$-*benzyloxycarbonyl*-L-*ornithyl*-L-*leucyl*-δ-*aminovaleryl*-L-*valyl*-N$^{\delta}$-*benzyloxycarbonyl*-L-*ornithyl*-L-*leucyl*-D-*phenylalanyl*-L-*proline (XV).* To a suspension of 1.21 g (1.6 mmol) of VII in 26 ml of dimethylformamide were added 5.5 N hydrogen chloride in dioxane (1.12ml) and 0.43 ml of *n*-butyl nitrite.[37] To this mixture a solution of 1.6 mmol of XIV and 0.44 ml of triethylamine in 38 ml of dimethylformamide was added dropwise at −20——30°C, and the stirring was continued at this temperature for 15 min and at 0°C for 2 days. The crude product precipitated on pouring the reaction mixture into 500 ml of cold water was filtered and washed with cold 5% citric acid and water and dried. It was dissolved in 130 ml of dimethylformamide and the insoluble material was removed by filtration. The product was precipitated by addition of ethyl ether into the filtrate. After filtering off and drying it weighed 1.614 g (69.7%). Mp 225—227°C (decomp.). It was then recrystallized from a large quantity of methanol. Yield, 1.354 g (58.5%); mp 226°C (decomp.); $[\alpha]_D^{21}$ −34.4° (*c* 0.5, dimethylformamide); Tlc: R_f 0.55 (Solv. 4).

Found: C, 63.19; H, 7.73; N, 10.69%. Calcd for $C_{76}H_{107}N_{11}O_{17}$: C, 63.09; H, 7.46; N, 10.65%.

Cyclo-L-*valyl*-N$^{\delta}$-*benzyloxycarbonyl*-L-*ornithyl*-L-*leucyl*-δ-*aminovaleryl*-L-*valyl*-N$^{\delta}$-*benzyloxycarbonyl*-L-*ornithyl*-L-*leucyl*-D-*phenylalanyl*-L-*prolyl (XVI).* The reaction of XV (723 mg, 0.5 mmol) and dinitrophenylsulfite[38] (1.62 g, 5 mmol) in a mixture of pyridine (6 ml) and dimethylformamide (20 ml) at room temperature for 41 hours gave the *p*-nitrophenyl ester of XV. After evaporation of the reaction mixture *in vacuo* and treatment of the residue with a mixture of *n*-hexane and ethyl ether (1 : 1), the dried colorless product was dissolved in trifluoroacetic acid (5 ml) containing anisole (0.8 ml) in an ice-salt bath. After 20 min, the reaction mixture was concentrated *in vacuo* at 0°C. The residue was triturated with ethyl ether and the supernatant liquid removed by decantation. A solution of the residue in dimethylformamide (10 ml) containing acetic acid (0.13 ml) was added dropwise into 330 ml of anhydrous pyridine with stirring at 58—60°C over 2.5 hours. The reaction mixture was further stirred for 5 hr at this temperature and then evaporated to dryness *in vacuo*. The yellow residue was dissolved in a mixture of methanol and water (7 : 1) and this solution was passed successively through columns of Dowex-1 (OH^- form) and Dowex-50 (H^+ form) which had been washed with the same solvent. The effluent (total 300 ml) was concentrated to dryness *in vacuo* and a white crystalline product was obtained in a 81% yield, mp 212—215°C. It was recrystallized from 90% methanol. Yield, 446.7 mg (70.6%); mp 221—223°C; $[\alpha]_D^{27}$ −207.0° (*c* 0.5, methanol); Tlc: R_f 0.6 (Solv. 1), 0.65 (Solv. 4), 0.95 (Solv. 6); MW, Found: 1224.5 (Calcd for $C_{67}H_{97}N_{11}O_{13}$: 1264.6).

Found: C, 63.43; H, 7.87; N, 11.93%. Calcd for $C_{67}H_{97}N_{11}O_{13}$: C, 63.64; H, 7.73; N, 12.18%.

Cyclo-L-*valyl*-L-*ornithyl*-L-*leucyl*-δ-*aminovaleryl*-L-*valyl*-L-*ornithyl*-L-*leucyl*-D-*phenylalanyl*-L-*prolyl Dihydrochloride (XVII).* XVI (252.9 mg, 0.2 mmol) in *ca.* 8 ml of methanol containing 0.89 N methanolic hydrogen chloride (0.68 ml) was hydrogenolyzed in the presence of palladium black (30 mg) for 8 hours. After removal of the catalyst, the filtrate was concentrated to dryness *in vacuo*. The residue was dissolved in water and the solution was filtered through active charcoal. A white crystalline product was obtained by lyophilization of the filtrate which was dried in a desiccator over calcium chloride. Yield, 192.9 mg (90.2%); mp 251—252 °C (decomp.); $[\alpha]_D^{28}$ −204.0° (*c* 0.1, ethanol); Tlc: R_f 0.75 (Solv. 6); IR: 1530, 1640 cm^{-1} (KBr). Amino acid ratios: Val, 2.09; Orn, 1.90; Leu, 2.09; Phe, 1.00; δAva, 0.83. When the sample dried in a vacuum over phosphorous pentoxide at 105°C for 6 hours was left standing in the air, it rapidly absorbed moisture. The increase in weight was 9.6%, which was in good agreement with one (10.5%) calculated from change of the anhydrous form to the heptahydrate.

Found: C, 51.16; H, 8.59; N, 12.71; Cl, 6.38%. Calcd for $C_{51}H_{87}N_{11}O_9Cl_2\cdot 7H_2O$: C, 51.24; H, 8.52; N, 12.89; Cl, 5.93%.

L-*Valyl*-L-*ornithyl*-L-*leucyl*-δ-*aminovaleryl*-L-*valyl*-L-*ornithyl*-L-*leucyl*-D-*phenylalanyl*-L-*proline Trihydrochloride (XVIII).* XV (434 mg, 0.3 mmol) was added into 25% hydrogen bromide in acetic acid (2.5 ml) in an ice bath. The solution was shaken at room temperature for one hour and concentrated *in vacuo*. Treatment of the oily residue with cold ethyl ether afforded a hygroscopic solid, which was collected by filtration and dried rapidly under reduced pressure. An aqueous solution of the product was charged to a column (1.5 × 13 cm) of Dowex-50 (H^+ form) and the column was washed with water. Pyridine-acetate buffer was used for elution and the effluent was collected in *ca.* 7 ml fractions, each of which was tested by thin layer chromatography with ninhydrin. Buffers[39] of pH 4.87, 4.96, and 5.13 were used for fraction numbers 1—37, 38—50, 51—65, respectively. Fraction nos. 21—65 were combined and concentrated *in vacuo*. Addition of water to the residue and evaporation were repeated several times to remove pyridine and acetic acid completely. The product was dissolved in a small amount of methanol. Hydrogen chloride in tetrahydrofuran (4.09 N, 3 ml) was added to it. The solution was

37) W. A. Noyes, "Organic Syntheses," Coll. Vol. II, p. 108 (1943).

38) B. Iselin and R. Schwyzer, *Helv. Chim. Acta*, **43**, 1760 (1960).

39) J. L. Bailey, "Techniques in Protein Chemistry," Elsevier Publishing Co., Amsterdam (1967), p. 105.

concentrated to dryness *in vacuo* and the residue was recrystallized from methanol and ethyl ether. Yield, 223 mg (66.2%); mp 223—225°C (decomp.); $[\alpha]_D^{18}$ −46.3° (*c* 0.2, ethanol); Tlc: R_f 0.1 (Solv. 5), 0.8 (Solv. 6); IR: 1531, 1640, 1727 cm^{-1} (KBr). Amino acid ratios: Val, 1.85; Orn, 1.91; Leu, 2.06; Phe, 1.00; δAva, 1.11.

Found: C, 50.43; H, 8.27; N, 12.69; Calcd for $C_{51}H_{90}N_{11}O_{10}Cl_3 \cdot 5H_2O$: C, 50.47; H, 8.30; N, 12.96%.

Antimicrobial activity of XVIII for some microorganisms (*Bacilus subtilis*, *Staphylococcus aureous*, *Micrococcus flavus*, *Sarcina lutea*, *Proteus vulgaris etc.*) was examined by the agar dilution method, but no inhibition was observed in concentrations below 100 μg/ml.

Ethyl L-*Valyl*-N$^{\delta}$-*benzyloxycarbonyl*-L-*ornithyl*-L-*leucyl*-D-*phenylanalyl*-L-*prolinate Hydrochloride (XIX).* To a solution of XII (2.29 g, 2.5 mmol) in 20 ml of dioxane was added 3.73 N hydrogen chloride in dioxane (20 ml). The solution was stirred at room temperature for 3 hours and then concentrated to dryness *in vacuo*. The product was obtained as oil in a theoretical yield. Tlc: R_f 0.35 (Solv. 2).

Ethyl p-*Methoxybenzyloxycarbonyl*-L-*valyl*-N$^{\delta}$-*benzyloxycarbonyl*-L-*ornithyl*-L-*leucyl*-δ-*aminovaleryl*-L-*valyl*-N$^{\delta}$-*benzyloxycarbonyl*-L-*ornithyl*-L-*leucyl*-D-*phenylalanyl*-L-*prolinate (XX).* VII (1.89 g, 2.5 mmol) was dissolved in 60 ml of dimethylformamide containing 10 ml of acetic acid; 190 mg of sodium nitrite in 4 ml of water and 7.5 ml of 1 N hydrochloric acid were then added at 0—5°C under vigorous stirring. After 15 min, the reaction mixture was poured into cold water (700 ml). In a cold room the white precipitate was filtered and washed on a funnel successively with cold water, 5% sodium bicarbonate, and water. This peptide azide was dried in a desiccator over phosphorous pentoxide. The azide was added to a solution of XIX (2.5 mmol) and 0.35 ml of triethylamine in 85 ml of dimethylformamide, and the mixture was stirred for 7 days at 0°C. The insoluble substance was removed by filtration and the filtrate was poured into water. The precipitate was collected, and washed with 5% citric acid, water, 5% sodium bicarbonate, and water. After drying, the product was purified from dimethylformamide and ethyl ether. Yield, 2.18 g (59.2%); mp 218—225°C (decomp.); $[\alpha]_D^{21}$ −32.4° (*c* 0.5, dimethylformamide); Tlc: R_f 0.6 (Solv. 2).

Found: C, 63.52; H, 7.59; N, 10.45%. Calcd for $C_{78}H_{111}N_{11}O_{17}$: C, 63.64; H, 7.85 N, 11.29%.

The author wishes to express his sincere gratitude to Professor I. Muramatsu for his suggestions and support in this work, and to Professor A. Hagitani for his encouragement. He also wishes to thank Mr. T. Takakuwa, Applied Research Laboratory of the Japan Spectroscopic Co., for the measurements of CD and ORD, and the members of the Research Laboratories of Toyo Jozo Co., for elementary and amino acid analyses and microbiological assays.

BULLETIN OF THE CHEMICAL SOCIETY OF JAPAN, VOL. 46, 973—977 (1973)

The Syntheses of Heterocyclic Compounds by the Ternary Condensation of Malononitrile, Salicylaldehyde, and Aliphatic Ketones in the Presence of Ammonium Acetate

Akio SAKURAI, Yoshito MOTOMURA,* and Hiroshi MIDORIKAWA

The Institute of Physical and Chemical Research, Wako-shi, Saitama

(Received July 28, 1972)

Various 2-amino-6-alkyl (or 5,6-dialkyl)-4-aryl-4,5-dihydronicotinonitriles (**1**) were readily prepared by the ternary condensation of malononitrile, salicylaldehyde (or 3-methoxysalicylaldehyde), and aliphatic ketones in the presence of ammonium acetate. The resulting **1** was transformed into the corresponding 3-carbamoyl derivatives (**3**) *via* their 2-acetamino derivatives (**2**). In addition, the reaction of **3** with acetic anhydride led to [2,3-*d*]pyridopyrimidine derivatives (**4**).

In a previous paper,[1] the syntheses of benzopyranopyrido-pyrimidine and benzopyranopyridine derivatives by the ternary condensation of malononitrile, salicylaldehyde, and aromatic ketones in the presence of ammonium acetate were reported.

The present paper will deal with the syntheses of substituted 4,5-dihydronicotinonitriles (**1**), 1,4,5,6-tetrahydro-[2,3-*d*] pyridopyrimidines (**4**), and 4,4a,5,6,7,8-hexahydroquinolines (**8**) by the ternary condensation of malononitrile, salicylaldehyde (or 3-methoxysalicylaldehyde), and aliphatic ketones, *e. g.*, acetone, methyl ethyl-, methyl *n*-propyl, and diethyl ketone, and cyclohexanone in the presence of ammonium acetate.

The reaction of malononitrile, 3-methoxysalicylaldehyde, and the *n*-alkyl ketone (molar ratio of 1 : 1 : 1) in the presence of ammonium acetate (1 mol or a slight excess) gave 2-amino-6-alkyl (or 5,6-dialkyl)-4-(2-hydroxy-3-methoxyphenyl)-4,5-dihydronicotinonitriles (**1**) in 13—23% yields. The subsequent treatment of the resulting **1** with acetic anhydride led to the corresponding 2-acetamino derivatives (**2**), which were then further transformed into 3-carbamoyl derivatives (**3**) by the action of acetic acid in refluxing ethanol. The further treatment of **3** with boiling acetic anhydride afforded cyclization products, such as 5-(2-hydroxy-3-methoxyphenyl)-2,7-dimethyl (or 2,6,7-trimethyl)-4-oxo-1,4,5,6-tetrahydro[2,3-*d*]pyridopyrimidines (**4**), as is indicated in Scheme 1. On the other hand, **2b** (**2**, R_1=OCH_3, R_2=H, R_3=CH_3) was converted directly to **4a** (**4**, R_1=OCH_3, R_2=H,

* Present address: Kurita Central Laboratory, Hodogaya-ku, Yokohama, Kanagawa.

1) A. Sakurai, Y. Motomura, and H. Midorikawa, *J. Org. Chem*, **37**, 1523 (1972).

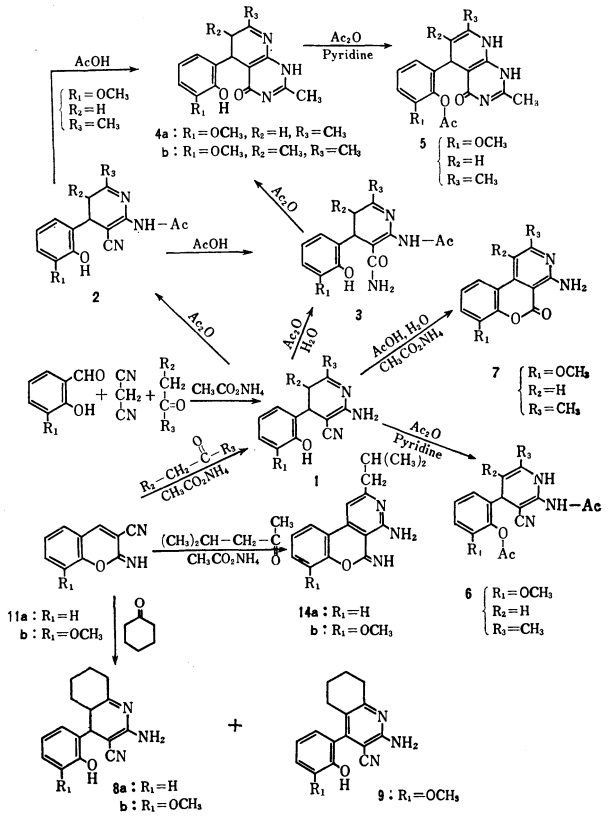

Scheme 1.

$R_3=CH_3$) by treatment with acetic acid in boiling ethanol. The acetylation of **4a** with acetic anhydride in boiling pyridine afforded 5-(2-acetoxy-3-methoxyphenyl)-2,7-dimethyl-4-oxo-1,4,5,8-tetrahydro[2,3-*d*]pyridopyrimidine (**5**). The acetylation of **1b** with acetic anhydride gave **2b**, while the same reaction of **1b** with acetic anhydride-pyridine gave 2-acetamino-4-(2-acetoxy-3-methoxyphenyl)-6-methyl-1,4-dihydronicotinonitrile (**6**). On the other hand, when heated with acetic acid containing a few drops of water in the presence of ammonium acetate, **1b** was cyclized to 4-amino-7-methoxy-2-methyl-5-oxo-[1]benzopyrano-[3,4-*c*]pyridine (**7**),[2] which was proved, on the basis of the spectral studies, to be identical with that previously-reported substance obtained by the condensation of ethyl cyanoacetate, 3-methoxysalicylaldehyde, and acetone. Type 1 compounds were also obtained in 13—33% yields by the condensation of 3-cyanocoumarinimide (**11**) with *n*-alkyl ketones. The reaction of cyclohexanone with **11a** afforded 16% of 2-amino-3-cyano-4-(2-hydroxyphenyl)-4,4*a*,5,6,7,8-hexahydroquinoline (**8a**), while the same reaction with 11b gave a mixture of **8b** (27%) and its 5,6,7,8-tetrahydro derivative **9** (7%) under the same reaction conditions (Scheme 1). When a methyl isoalkyl ketone such as the methyl isobutyl ketone was employed as the ketone reactant, ring-opening did not occur. For example, the condensation of **11b** with methyl isobutyl ketone afforded 4-amino-5-imino-2-isobutyl-7-methoxy-[1]-benzopyrano[3,4-*c*]pyridine (**14b**), which was then hydrolyzed to the corresponding 5-oxo compound.[2]

2) A. Sakurai, H. Midorikawa, and Y. Hashimoto, This Bulletin, **43**, 2925 (1970).

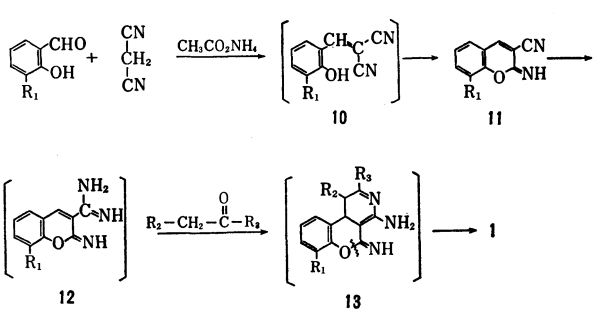

Scheme 2.

It seems reasonable to assume that the formation of 1 may be achieved by the following process. Malononitrile is first condensed with salicylaldehyde in the presence of ammonium acetate to give **10**, which is then readily converted to **11**. This is further transformed into amidine-type **12**. Then, **12** condenses with the *n*-alkyl ketone to form **13**, which immediately undergoes ring-opening to yield **1** (Scheme 2).

In the IR spectra of **1**, **2**, and **8**, C≡N stretching bands were shifted to lower frequencies at 2160—2150 cm^{-1} (**1**), 2170 cm^{-1} (**2**), and 2170—2140 cm^{-1} (**8**) respectively, whereas the stretching bands of **6** and **9** appeared at 2200 cm^{-1}. The NMR spectra of **1a-e** in $(CD_3)_2SO$ showed a methyl singlet due to three protons in the 1.5—1.7 ppm region. In addition, **1c** (from methyl ethyl ketone) gave a methyl doublet, centered at 0.98 ppm, due to three protons. These NMR data suggest that the methylene group adjacent to the carbonyl group of the ketones, such as the methyl ethyl-, methyl *n*-propyl-, and diethyl ketone, is involved in this cyclization. The structural assignment of **1**, therefore, was based on the above spectral data and the fact that **1b** gave the expected compound, **7**. The IR spectrum of **3a** (obtained when **2b** was heated with acetic acid in ethanol) gave no absorption band due to a C≡N stretching, but new bands appeared at 3440, 3350, 3320, and 3180 cm^{-1}. In the spectrum of **4a**, however, the primary amino stretching bands disappeared and only the absorption at 3310 cm^{-1} was observed in this region. The NMR spectrum in CF_3CO_2H revealed two singlets, at 2.0 and 2.8 ppm, due to three protons. The former was assigned to a methyl proton at the 7-position by means of a NMR comparison of the methyl protons in **1b**, **2b**, and **3a** (Tables 1, 2, and 3). The latter signal, therefore, was assigned to a methyl proton of the 2-position. The NMR spectrum in $(CD_3)_2SO$ of **5** (derived from **4a**) gave a new methyl singlet at 2.24 ppm, and the IR spectrum showed a new absorption band at 1755 cm^{-1} attributable to acetoxy carbonyl. These observations show that the hydroxy group of **3a** is independent of the cyclization to **4a**. The NMR spectrum of **5** exhibited signals of methine doublets at 4.24 and 4.62 ppm, each corresponding to one proton, but no signal for the methylene group was observed in Compound **4a**. This suggests that compound **5** is predominantly in the 1,4,5,8-tetrahydro form rather than in the 1,4,5,6-tetrahydro form of [2,3-*d*]pyridopyrimidine. Similarly, **6** (derived from **1b**) is predominantly in the 1,4-dihydro form of ni-

Table 1. Substituted 2-amino-4-aryl-4,5-dihydronicotinonitriles (**1**)

Compd	R_1	R_2	R_3	Mp, °C	Yield, %	IR (KBr), cm^{-1}		NMR δ (ppm)[b]			
						νNH_2, OH	$\nu C{\equiv}N$	CH_3	CH_2	CH	NH_2
1a	H	H	CH_3	226—229 (decomp.)	**8**	3420, 3350, 3340, 3220	2160				
1b	OCH_3	H	CH_3	250—253 (decomp.)	23	3430, 3360, 3320, 3230	2150	1.66(s, 3H)	1.92(d, 2H)	3.4 (t, 1H)	5.28(s, 2H)
1c	OCH_3	CH_3	CH_3	233—236 (decomp.)	17	3470, 3340, 3210	2150	0.98(d, 3H) 1.56(s, 3H)		1.8—2.1(m, 1H) 3.08(d, 1H)	5.26(s, 2H)
1d	OCH_3	C_2H_5	CH_3	232—235 (decomp.)	28[a]	3450, 3350, 3220	2160				
1e	OCH_3	n-C_3H_7	CH_3	217—219 (decomp.)	13[a]	3450, 3370, 3340, 3210	2160				
1f	OCH_3	CH_3	C_2H_5	236—238 (decomp.)	17	3450, 3340, 3330, 3220	2160	0.96(d, 3H) 1.0 (t, 3H)	1.87(q, 2H)[c]	1.8—2.1(m, 1H) 3.1 (d, 1H)	5.31(s, 2H)

a) Yield based on **11b**. b) Parts per million downfield from tetramethylsilane in $(CD_3)_2SO$; s, singlet; d, doublet; t, triplet; q, quartet; m, multiplet c) Overlapped with CH (δ 1.8—2.1), 3H.

Table 2. Substituted 2-acetamino-4-aryl-4,5-dihydronicotinonitriles (**2**)

Compd	R_1	R_2	R_3	Mp, °C	Yield, %	IR (KBr), cm^{-1}			NMR δ (ppm)[a]				
						νNH, OH	$\nu C{\equiv}N$	$\nu C{=}O$	CH_3	CH_2	CH	OH	NH
2a	H	H	CH_3	206—208	69								
2b	OCH_3	H	CH_3	210—213	90	3290, 3230	2170	1690	1.7 (s, 3H) 1.96(s, 3H)	1.9—2.1(d, 2H)[b]	3.6(t, 1H)	8.42(s, 1H)	9.6—9.9(br, 1H)
2c	OCH_3	C_2H_5	CH_3	205—207	78	3290, 3220	2170	1690	1.0 (t, 3H) 1.63(s, 3H) 1.95(s, 3H)	1.5—2.0 (CH_2 and CH, 3H)	3.5(d, 1H)	8.33(br, 1H)	9.7—9.9(br, 1H)

a) Parts per million downfield from tetramethylsilane in $(CD_3)_2SO$; s, singlet; d, doublet; t, triplet; br, broad. b) Overlapped with CH_3 (δ 1.96), 5H.

Table 3. Substituted 2-acetamino-4-aryl-3-carbamoyl-4,5-dihydropyridines (**3**)

Compd	R_1	R_2	R_3	Mp, °C	Yield,[a] %	IR (KBr), cm^{-1}		NMR δ (ppm)[b]			
						νNH_2, NH, OH	$\nu C{=}O$	CH_3	CH	NH_2	OH
3a	OCH_3	H	CH_3	254—256 (decomp.)	59	3440, 3350, 3320, 3180	1660	1.7 (s, 3H) 1.98(s, 2H)	4.05(t, 1H)	7.03(br, 2H)	9.03(s, 1H)
3b	OCH_3	CH_3	CH_3	266—268 (decomp.)	67	3420, 3350, 3310, 3170	1660	0.95(d, 3H) 1.64(s, 3H) 2.0 (s, 3H)	2—2.2(m, 1H) 3.82(d, 1H)	7.1 (br, 2H)	9.0 (s, 1H)
3c	OCH_3	C_2H_5	CH_3	242—245 (decomp.)	48						
3d	OCH_3	CH_3	C_2H_5	238—240 (decomp.)	41	3430, 3350, 3300, 3170	1660				

a) Yield based on **1**. b) Parts per million downfield from tetramethylsilane in $(CD_3)_2SO$; s, singlet; d, doublet; t, triplet; br, broad. In **3a** spectrum, δCH_2 1.8—2.1 ppm, overlapped with CH_3 (δ 1.98), 5H.

cotinonitrile, judging from the NMR spectrum, which has methine doublets at 4.27 and 4.43 ppm, each corresponding to one proton. On the other hand, the IR spectra of the compound, **14**, obtained by the condensation of **11** with methyl isobutyl ketone gave no absorption attributable to a C≡N group, and the NMR spectra showed no signal for the methyl singlet observed in Compound **1**—**6**, as has been mentioned above. This shows that the methyl group adjacent to the ketone carbonyl was involved in this cyclization.

Experimental

All the melting points are uncorrected. The IR spectra were determined by means of potassium bromide pellets. The NMR spectra were determined in deuterodimethylsulfoxide or trifluoroacetic acid at 100 MHz, using tetramethylsilane as the internal standard. The chemical shifts are reported as parts per million downfield from TMS.

Reaction of Malononitrile, 3-Methoxysalicylaldehyde (or Salicylaldehyde), and n-*Alkyl Ketones.* A mixture of malononitrile (0.06 mol), aldehyde (0.06 mol), ketone (0.06 mol), and ammonium acetate (0.06—0.07 mol) in ethanol (30 ml) was refluxed for 1 hr. The pale yellow crystals which precipitated during the reaction were collected and washed with hot ethanol. Recrystallization from dimethyl sulfoxide–ethanol gave **1a**–**c** and **1f**. The experimental results and spectral data are summarized in Table 1.

Found: C, 68.76; H, 5.79; N, 18.65%. Calcd for $C_{13}H_{13}N_3O$ (**1a**): C, 68.70; H, 5.77; N, 18.49%. Found: C, 65.54; H, 5.65; N, 16.60%. Calcd for $C_{14}H_{15}N_3O_2$ (**1b**): C, 65.35; H, 5.88; N, 16.33%. Found: C, 66.47; H, 6.35; N, 15.55%. Calcd for $C_{15}H_{17}N_3O_2$ (**1c**); C, 66.40; H, 6.32; N, 15.49%. Found: C, 67.05; H, 6.86; N, 14.43%. Calcd for $C_{16}H_{19}N_3O_2$ (**1f**): C, 67.34; H, 6.71; N, 14.73%

*Reaction of 8-Methoxy-3-cyanocoumarinimide (**11b**)*[1] *and* n-*Alkyl Ketones.* A mixture of **11b** (0.02 mol), ketone (0.02 mol), and ammonium acetate (0.04 mol) in ethanol (20 ml) was refluxed for 0.5 hr. After the mixture had cooled, the resulting precipitate was collected and recrystallized from ethanol–dimethyl sulfoxide to afford **1d** and **1e** (Table 1).

Found: C, 67.26; H, 6.48; N, 14.48%. Calcd for $C_{16}H_{19}N_3O_2$ (**1d**): C, 67.34; H, 6.71; N, 14.73%. Found: C, 67.82; H, 7.15; N, 13.82%. Calcd for $C_{17}H_{21}N_3O_2$ (**1e**): C, 68.20; H, 7.07; N, 14.04%.

*Formation of **2** by the Reaction of **1** and Acetic Anhydride.* Acetic anhydride (15—18 ml) was added to **1** (0.02 mol) and heated for a few minutes. Pale yellow crystals thereupon began to separate from the solution (Table 2).

Found: C, 66.74; H, 5.59; N, 15.65%. Calcd for $C_{15}H_{15}N_3O_2$ (**2a**): C, 66.90; H, 5.61; N, 15.61%. Found: C, 64.08; H, 5.73; N, 14.15%. Calcd for $C_{16}H_{17}N_3O_3$ (**2b**): C, 64.20; H, 5.72; N, 14.04%. Found: C, 66.04; H, 6.51; N, 12.72%. Calcd for $C_{18}H_{21}O_3N_3$ (**2c**): C, 66.03; H, 6.47; N, 12.84%.

*Formation of **3** by the Reaction of **1** with Acetic Anhydride and Water.* Acetic anhydride (5—8 ml) was added to **1** (4 mmol), and the mixture was heated for a few minutes. After cooling, a few drops of water were added to the reaction mixture; a crystalline precipitate was thus formed. Recrystallization from acetic acid–ethanol afforded colorless crystals (Table 3).

Found: C, 60.41; H, 5.96; N, 13.15%. Calcd for $C_{16}H_{19}N_3O_4$ (**3a**): C, 60.55; H, 6.04; N, 13.24%. Found: C, 61.62; H, 6.39; N, 12.55%. Calcd for $C_{17}H_{21}N_3O_4$ (**3b**) C, 61.62; H, 6.39; N, 12.68%. Found: C, 62.81; H, 6.47; N, 12.26%. Calcd for $C_{18}H_{23}N_3O_4$ (**3c**): C, 62.59; H, 6.71; N, 12.17%. Found: C, 62.36; H, 6.68; N, 12.04%. Calcd for $C_{18}H_{23}N_3O_4$ (**3d**): C, 62.59; H, 6.71; N, 12.17%.

*Formation of **4a** by the Reaction of **3a** and Acetic Anhydride.* Acetic anhydride (3 ml) was added to **3a** (1 mmol) and heated for 0.5 hr. After the mixture had cooled, the deposited crystals were collected and recrystallized from dimethyl sulfoxide–ethanol to afford white crystals (mp 276—278°C (decomp.)) in a 63% yield; ν_{max}^{KBr} 3310 (NH), 1650 cm^{-1} (C=O); NMR (CF_3CO_2H) 2.0, 2.8 (CH_3, singlet, 3H each), 3.97 (OCH_3, singlet, 3H), 2.35 (CH_2, doublet, 2H), 4.55 (CH, triplet, 1H), 7.7—8.2 ppm (NH, broad, 1H).

Found: C, 64.21; H, 5.86; N, 13.89%. Calcd for $C_{16}H_{17}N_3O_3$: C, 64.20; H, 5.72; N, 14.04%.

Similarly, the same reaction with **3b** gave **4b** (mp 273—274°C (decomp.)) in a 72% yield; NMR (CF_3CO_2H) peaks at 1.15 (CH_3, doublet, 3H), 1.92, 2.8 (CH_3, singlet, 3H each), 3.97 (OCH_3, singlet, 3H), 2.4—2.7 (CH, multiplet, 1H), 4.25 (CH, doublet, 1H), 7.5—8.2 ppm (NH, broad, 1H).

Found: C, 64.99; H, 6.11; N, 13.09%. Calcd for $C_{17}H_{19}N_3O_3$: C, 65.16; H, 6.11; N, 13.41%.

*5-(2-Acetoxy-3-methoxyphenyl)-2,7-dimethyl-4-oxo-1,4,5,8-tetrahydro[2,3-d]pyridopyrimidine (**5**).* A mixture of **4a** (1.1 g) and acetic anhydride (5 ml) in pyridine (4 ml) was heated for 2 hr. When the reaction mixture was then left to stand overnight, pale yellow crystals were obtained. Recrystallization from ethanol gave 0.7 g of colorless needles (mp 225—227°C); ν_{max}^{KBr} 3360 (NH), 1755, 1660 cm^{-1} (C=O); NMR spectrum (DMSO-d_6) gave signals at 1.64, 2.16 (CH_3, singlet, 3H each), 2.24 (O–Ac, singlet, 3H), 3.72 (OCH_3, singlet, 3H), 4.24, 4.62 (CH, doublet, 1H each), 8.5, 11.59 ppm (NH, singlet, 1H each).

Found: C, 63.20; H, 5.73; N, 12.42%. Calcd for $C_{18}H_{19}N_3O_4$: C, 63.33; H, 5.61; N, 12.31%.

*2-Acetamino-4-(2-acetoxy-3-methoxyphenyl)-6-methyl-1,4-dihydronicotinonitrile (**6**).* To a solution of **1b** (0.8 g) dissolved in pyridine (3 ml), acetic anhydride (3 ml) was added, after which the mixture was heated for 5 min. After the mixture had then been allowed to stand at room temperature, the resulting precipitate was washed with dilute methanol and recrystallized from ethanol–dimethyl sulfoxide to afford 0.5 g of colorless crystals (mp 224—227°C); NMR (DMSO-d_6) 1.66 (6-CH_3, singlet, 3H), 2.0 (NH–Ac, singlet, 3H), 2.28 (O–Ac, singlet, 3H), 3.76 (OCH_3, singlet, 3H), 4.27, 4.43 (CH, doublet, 1H each), 8.68, 9.9 ppm (NH, singlet, 1H each); ν_{max}^{KBr} 3260, 3220(NH), 2200 (C≡N), 1760 (O–Ac), 1690 cm^{-1} (NH–Ac).

Found: C, 63.13; H, 5.62; N, 12.22%. Calcd for $C_{18}H_{19}N_3O_4$: C, 63.33; H, 5.61; N, 12.31%.

*Reaction of **1b** and Acetic Acid.* A mixture of **1b** (0.4 g), acetic acid (5 ml), water (1 ml), and ammonium acetate (1 g) was refluxed for 1 hr. The pale yellow crystals which were thus precipitated were collected and recrystallized from ethanol–dimethyl sulfoxide to give 0.2 g of 4-amino-7-methoxy-2-methyl-5-oxo-[1]benzopyrano[3,4-*c*]pyridine (**7**) (mp 230—232°C).[2] This compound was proved by IR spectral studies to be identical with that obtained by the condensation of ethyl cyanoacetate, 3-methoxysalicylaldehyde, and acetone in the presence of ammonium acetate.

*Reaction of **11** and Cyclohexanone.* To a mixture of **11a**[1] (2.38 g, 0.014 mol) and cyclohexanone (1.37 g, 0.014 mol) in ethanol (10 ml), ammonium acetate (2 g, 0.026 mol) was added. After having been refluxed for 1 hr, the reaction mixture afforded 0.6 g (16%) of 2-amino-3-cyano-4-(2-hydroxyphenyl)-4,4a,5,6,7,8-hexahydroquinoline (**8a**).

(mp 223—225°C (decomp.)); ν_{max}^{KBr} 3440, 3350, 3220 (NH_2, OH), 2140 cm^{-1} (C≡N).

Found: C, 71.89; H, 6.26; N, 15.98%. Calcd for $C_{16}H_{17}N_3O$: C, 71.88; H, 6.41; N, 15.72%.

When **11b** was used instead of **11a**, the condensation afforded 27% of **8b** (mp 230—233°C (decomp.)) and 7% of 2-amino-3-cyano-4-(2-hydroxy-3-methoxyphenyl)-5,6,7,8-tetrahydroquinoline (**9**) (mp 241—244°C); ν_{max}^{KBr} 3470, 3370, 3220 (NH_2, OH), 2200 cm^{-1} (C≡N).

Found: C, 68.99; H, 5.46; N, 14.58%. Calcd for $C_{17}H_{17}N_3O_2$: C, 69.13; H, 5.80; N, 14.23%.

The IR spectrum (KBr) of **8b** gave bands at 3440, 3340, 3220 (NH_2, OH), and 2170 cm^{-1} (C≡N).

Found: C, 68.53; H, 6.42; N, 14.19%. Calcd for $C_{17}H_{19}N_3O_2$: C, 68.66; H, 6.44; N, 14.13%.

*Reaction of **11** and Methyl Isobutyl Ketone.* To a mixture of **11b** (3 g, 0.015 mol) and methyl isobutyl ketone (1.8 g, 0.018 mol) in ethanol (10 ml), ammonium acetate (2.31 g, 0.03 mol) was added, and the mixture was refluxed for 1 hr. This mixture afforded 1 g (22%) of **14b** (mp 180—182°C); ν_{max}^{KBr} 3300, 3130 (NH_2, NH), 1645 cm^{-1} (C=N); NMR (CF_3CO_2H) peaks at 1.15 (CH_3, doublet, 6H), 2.05—2.55 (CH, multiplet, 1H), 2.95 (CH_2, doublet, 2H), 4.13 (OCH_3, singlet, 3H).

Found: C, 68.90; H, 6.48; N, 14.02%. Calcd for $C_{17}H_{19}N_3O_2$: C, 68.66; H, 6.44; N, 14.13%.

When **11a** was used instead of **11b**, the condensation afforded 18% of **14a** (mp 184—186°C); ν_{max}^{KBr} 3295; 3125 (NH_2, NH), 1645 cm^{-1} (C=N).

Found: C, 71.84; H, 6.35; N, 15 44%. Calcd for $C_{16}H_{17}N_3O$: C, 71.88; H, 6.41; N, 15.72%.

*Reaction of **14b** and Hydrochloric Acid.* To a solution of **14b** (0.2 g) suspended in ethanol (7 ml), hydrochloric acid (3 ml) was added. After the reaction mixture has then been refluxed for 1 hr, a crystalline precipitate was yielded. Recrystallization from ethanol gave 0.1 g of 4-amino-2-isobutyl-7-methoxy-5-oxo-[1]benzopyrano[3,4-*c*]pyridine(mp 196—197°C).[2] This compound was identified with that obtained by the reaction of ethyl cyanoacetate, 3-methoxysalicylaldehyde, and methyl isobutyl ketone by a study of their IR spectra.

The authors wish to express their thanks to Dr. Taro Hayashi and Dr. Tatsuo Takeshima for their kind advice. Thanks are also due to Dr. Haruo Homma and his staff for their microanalyses, to Mr. Jun Uzawa for his measurements of the NMR spectra, and to Mr. Hironori Ogawa for his measurements of the IR spectra.

BULLETIN OF THE CHEMICAL SOCIETY OF JAPAN, VOL. 46, 977—985 (1973)

Studies of Peptide Antibiotics. XXVIII.[1] Syntheses of Sesquigramicidin S and Digramicidin S[2,3]

Shuji MATSUURA, Michinori WAKI, Tetsuo KATO, and Nobuo IZUMIYA

Laboratory of Biochemistry, Faculty of Science, Kyushu University, Hakozaki, Fukuoka

(Received September 6, 1972)

Two macro-ring analogs of gramicidin S, namely *cyclo*(–L-Val–L-Orn–L-Leu–D-Phe–L-Pro–)$_3$ (sesquigramicidin S) and *cyclo*(–L-Val–L-Orn–L-Leu–D-Phe–L-Pro–)$_4$ (digramicidin S), were prepared to investigate the influence of the ring size of gramicidin S for antibacterial activity. Several linear analogs such as H–(L-Val–L-Orn–L-Leu–D-Phe–L-Pro)$_n$–OH (n=2, 3 and 4) were also prepared as reference compounds. All these macro-ring and linear analogs showed weaker activity than gramicidin S and synergistic property when each of the analogs is mixed with gramicidin S. Measurements of optical rotatory dispersion were made with these analogs and gramicidin S in solvents of ethanol and 8 M aqueous urea. From these experiments, it was suggested that the mode of antibacterial action of the macro-ring analogs and their conformations are similar to those of the linear analogs.

In studies of the relationship between chemical structure and antibacterial activity of gramicidin S (GS), various analogs have been synthesized.[5] Particularly in regard to the ring size, several cyclic peptides with smaller ring size than that of GS were prepared, but none of them were active.[4,6] As only one analog with a larger ring size than GS, [β-Ala$^{5,5'}$]-GS was synthesized, but this compound was also inactive.[7] In order to determine further the influence of larger ring size on the activity, we have designed the syntheses of sesquigramicidin S[3] and digramicidin S[3] which contain decapeptide sequence of GS.

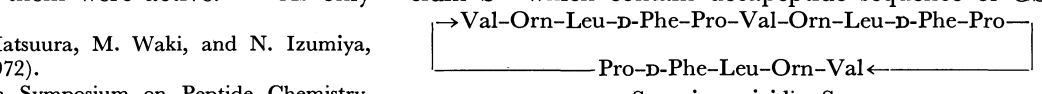

Sesquigramicidin S

1) Part XXVII: S. Matsuura, M. Waki, and N. Izumiya, This Bulletin, **45**, 863 (1972).

2) Presented at the 9th Symposium on Peptide Chemistry, Shizuoka, November, 1971. Part of this work has been briefly communicated: S. Matsuura and N. Izumiya, *Experientia*, **28**, 1402 (1972).

3) We introduced the naming of cyclosemigramicidin S for *cyclo*(-Val-Orn-Leu-D-Phe-Pro-) primarily,[4] but changed this naming as semigramicidin S in the recent review.[5] Therefore, we employ the namings of sesquigramicidin S and digramicidin S for *cyclo*(-Val-Orn-Leu-D-Phe-Pro-)$_3$ and *cyclo*(-Val-Orn-Leu-D-Phe-Pro-)$_4$, respectively.

4) M. Waki and N. Izumiya, This Bulletin, **40**, 1687 (1967).

5) T. Kato and N. Izumiya, "Chemistry and Biochemistry of Amino Acids, Peptides, and Proteins," Vol. 2, B. Weinstein, Ed., Marcel Dekker, New York (1972), in press.

6) N. Izumiya, T. Kato, Y. Fujita, M. Ohno, and M. Kondo, This Bulletin, **37**, 1809 (1964); T. Kato, M. Kondo, M. Ohno, and N. Izumiya, *ibid.*, **38**, 1202 (1965); O. Abe, K. Kuromizu, M. Kondo, and N. Izumiya, *ibid.*, **43**, 914 (1970).

7) S. Matsuura, M. Waki, S. Makisumi, and N. Izumiya, *ibid.*, **43**, 1197 (1970).

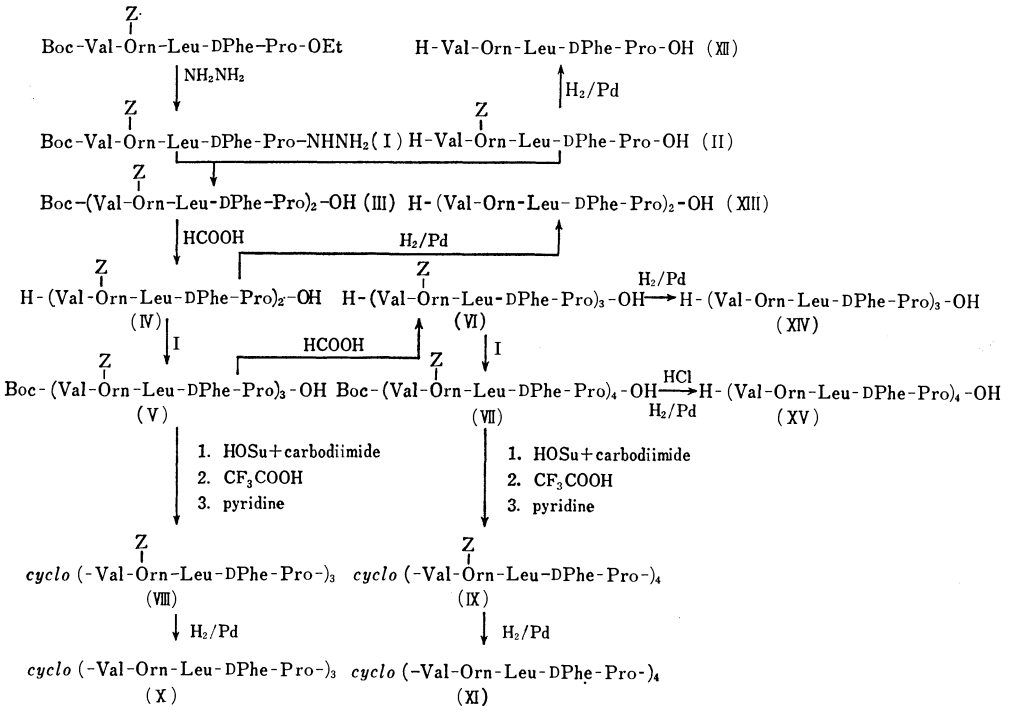

Scheme 1.

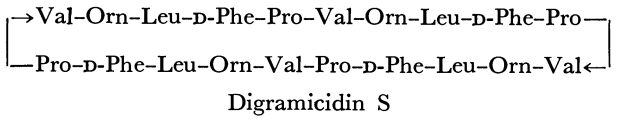

Digramicidin S

This paper describes the syntheses, antibacterial properties and ORD[8] measurements of two macro-ring analogs of GS besides those of several linear analogs.

Scheme 1 indicates the routes for syntheses of the macro-ring and linear analogs. The azide derived from Boc–pentapeptide hydrazide (I) was condensed with a neutral pentapeptide (II), and the resulting acyl-decapeptide acid (III) was converted to a neutral decapeptide (IV) by the action of formic acid. The azide derived from I was again condensed with VI, the resulting Boc–pentadecapeptide acid (V) was transformed to Boc–pentadecapeptide *N*-hydroxysuccinimide ester by the action of HOSu and water soluble carbodiimide, and its Boc group was removed with trifluoroacetic acid. Pentadecapeptide ester trifluoroacetate thus obtained was treated with pyridine for the cyclization reaction.[9] The reaction mixture yielded a pure Z-substituted cyclic pentadecapeptide (VIII) with a fairly good yield. The hydrogenolysis of VIII afforded the desired sesquigramicidin S (X) as a crystalline trihydrochloride. In a similar manner, the desired digramicidin S (XI) was prepared as a crystalline tetrahydrochloride as shown in Scheme 1.

The linear penta- (XII), deca- (XIII), and pentadecapeptide (XIV) were prepared from the corresponding Z-substituted peptides by hydrogenolysis.

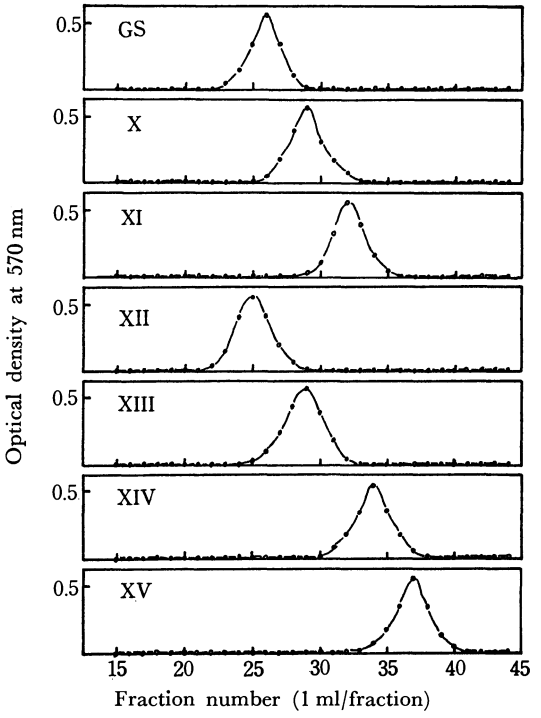

Fig. 1. CMC column chromatography of macro-ring and linear analogs of GS.

8) Abbreviations according to IUPAC-IUB Commission on Biochemical Nomenclature, *J. Biol. Chem.*, **247**, 977 (1972), are used. Additional abbreviations are as follows: ORD, optical rotatory dispersion; CMC, carboxymethyl cellulose; HOSu, *N*-hydroxysuccinimide; TEA, triethylamine; DMF, dimethylformamide. Amino acid symbols except D-Phe denote the L-configuration.

9) For the cyclization reaction we have used very often linear peptide *p*-nitrophenyl esters. However, we recognized recently that the cyclization of linear peptide *N*-hydroxysuccinimide ester gives better yield than that of *p*-nitrophenyl ester in many cases. Some features using *N*-hydroxysuccinimide ester for the cyclization were presented at the 24th Annual Meeting of the Chemical Society of Japan, Tokyo, April, 1971.

Table 1. Antibacterial activity of the compounds (Minimum inhibitory concentration, μg/ml)

Compound[a,b]	Medium for assay[c]	*Staphylococcus aureus*	*Bacillus subtilis*
semiGS	B, S	>100	>100
GS	B	5	2
	S	5	5
X (sesquiGS)	B	50	20
	S	50	50
XI (diGS)	B	20	10
	S	20	10
XII (penta)	B, S	>100	>100
XIII (deca)	B	50	50
	S	100	20
XIV (pentadeca)	B	50	50
	S	100	20
XV (eicosa)	B	20	10
	S	20	20
GS+X[d]	B	10	2
	S	5	5
GS+XI[d]	B	5	2
	S	5	2
GS+XIII[d]	B	5	5
	S	5	5
GS+XIV[d]	B	5	5
	S	5	5
GS+XV[d]	B	5	5
	S	5	5

a) The μg in the minimum inhibitory concentration refers net weight of a peptide without either HCl or H_2O in the compound. b) All compounds showed no activity for *Echerichia coli*. c) B, usual bouillon agar medium of pH 7.0. S, synthetic Stephensen-Whetham's medium of pH 7.0. d) A mixture was prepared with 1 : 1 weight ratio of GS and an analog.

The eicosapeptide (XV) was derived from α-Boc-δ-Z-substituted eicosapeptide (VII) by successive treatments of hydrogen chloride in ethyl acetate and hydrogenolysis. The purities of these macro-ring and linear analogs were ascertained by CMC column chromatography (Fig. 1) besides other experiments such as elemental analysis.

The antibacterial activities of the macro-ring and linear analogs toward microorganisms were tested (Table 1). As like that semigramicidin S was inactive,[4] the corresponding linear pentapeptide (XII) was also inactive. The linear decapeptide (XIII) showed weak activity as reported previously.[10,11] It is interesting to note that a level of the activity of sesquigramicidin S and digramicidin S was approximately same with that of the corresponding linear peptides, XIV, and XV, respectively. Furthermore, it seems that level of the specific activity increased with an increase of molecular size in both the macro-ring and linear analogs. Erlanger and Goode observed that some linear decapeptides such as XIII reveal synergistic activity with GS against microorganism, and noted that the mode of antibacterial action by XIII may differ from that of GS.[12] As shown in Table 1, a mixture of GS and each of macro-ring and some linear analogs showed the same activity as GS itself; these analogs revealed synergistic activity with GS. We thus assumed that the mode of antibacterial action of the macro-ring analogs is similar to that of the linear analogs, and differ from that of GS.

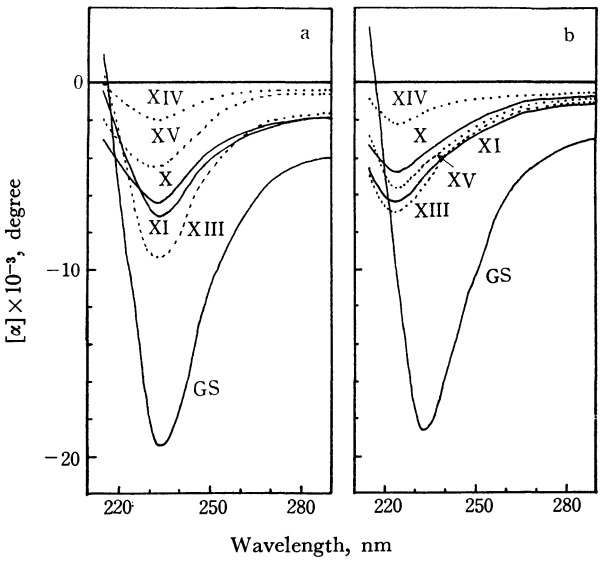

Fig. 2. ORD curves of macro-ring and linear analogs of GS. Solvent; a, ethanol; b, 8 M urea.

The assumption mentioned is favored by the experiments of ORD. The ORD curves measured in a solvent of ethanol are shown in Fig. 2-a. The macro-ring and linear analogs have similar shaped curves with a negative trough at 232 nm as GS possesses the same. In a solvent of 8 M aqueous urea which causes denaturation of some polypeptides,[13] the troughs of the peptides except GS were moved to 225 nm whereas that of GS remained constant (Fig. 2-b). The results may indicate that a conformation of the macro-ring analogs is similar to that of the linear analogs, whereas that of GS is very stable even in 8 M aqueous urea. In this connection, it would be noteworthy that GS has the rigid β-pleated sheet structure having an antiparallel tripeptide sequence with four hydrogen bondings.[14] In conclusion, the presented data suggest that a cyclic character in a pentadeca- or eicosapeptide which contains a sequence of GS is not essential to exhibit the activity, whereas in a linear decapeptide sequence in GS, the cyclic character is important to form the rigid structure and consequently to exhibit a strong and characteristic antibacterial activity.

10) B. F. Erlanger and L. Goode, *Nature*, **174**, 840 (1954).
11) S. Makisumi, M. Waki, and N. Izumiya, This Bulletin, **44**, 143 (1971).
12) B. F. Erlanger and L. Goode, *Science*, **131**, 669 (1960).
13) B. Jirgensons, "Optical Rotatory Dispersion of Proteins and Other Macromolecules," Springer-Verlag, Berlin (1969).
14) D. C. Hodgkin and B. M. Oughton, *Biochem. J.*, **65**, 752 (1957); W. A. Gibbons, J. A. Sogn, A. Stern, and L. C. Craig, *Nature*, **227**, 840 (1970); F. Quadrifoglio and D. W. Urry, *Biochem. Biophys. Res. Commun.*, **29**, 785 (1967); S. L. Laiken, M. P. Printz, and L. C. Craig, *Biochemistry*, **8**, 519 (1969).

Experimental

Thin layer chromatography was carried out on Merck silica gel G with the following solvent systems: R_f^1, *n*-butanol–acetic acid–pyridine–water (4 : 1 : 1 : 2, v/v); R_f^2, chloroform–methanol (5 : 1, v/v); R_f^3, *sec*-butanol–formic acid–water (4 : 1 : 1, v/v).

Boc–Val–Orn(Z)–Leu–D-Phe–Pro–NHNH$_2$ (I). A solution of Boc–Val–Orn(Z)–Leu–D-Phe–Pho–OEt[15] (8.72 g, 10.3 mmol) and hydrazine hydrate (9.9 ml, 205 mmol) in DMF (35 ml) was allowed to stand at room temperature for 7 days. The solution was evaporated *in vacuo*, and then water (150 ml) was added to the residue. The resulting crystals were collected by filtration and recrystallized from methanol–ether; yield, 7.73 g (90%); mp 183—185°C; $[\alpha]_D^{15}$ −19.2° (*c* 0.5, DMF); R_f^1 0.67, R_f^2 0.60.

Found: C, 60.75; H, 7.88; N, 13.53%. Calcd for $C_{43}H_{64}O_9N_8 \cdot 1/2H_2O$: C, 61.04; H, 7.74; N, 13.25%.

Boc–(Val–Orn(Z)–Leu–D-Phe–Pro)$_2$–OH (III). I (2.23 g, 2.66 mmol) was dissolved in DMF (10 ml) and 2 N hydrogen chloride in dioxane (2.7 ml). To the solution at −30°C was added isoamyl nitrite (0.45 ml, 3.2 mmol). After some 10 min, disappearance of the hydrazide was ascertained by the detection method for hydrazide.[16] To the reaction mixture was added TEA (0.74 ml, 5.3 mmol). After 5 min at 0°C, a solution of H–Val–Orn(Z)–Leu–D-Phe–Pro–OH·HCOOH (II·HCOOH)[11] (2.46 g, 3.2 mmol) in DMF containing TEA (0.9 ml) was added to the mixture. After 3 days at 4°C, the reaction mixture was added to cold 0.2 M citric acid (1000 ml). The resulting solid was recrystallized from methanol–ether–petroleum ether; yield, 3.49 g (86%); mp 173—175°C; $[\alpha]_D^{25}$ −105° (*c* 1, MeOH). The same compound was prepared already from Boc–Val–Orn(Z)–Leu–D-Phe–Pro–OH and II by the method of HOSu plus DCC; $[\alpha]_D^{23}$ −109° (MeOH).[11] No depression of melting point was observed on a mixture of III with the previous product.[11]

H–(Val–Orn(Z)–Leu–D-Phe–Pro)$_2$–OH (IV). A solution of III (2.57 g, 1.68 mmol) in 99% formic acid (30 ml) was allowed to stand for 5 hr at room temperature. The solvent was removed by evaporation, and the residue was dissolved in a mixture of TEA (12 ml) and methanol (70 ml). The solution was evaporated, and the resulting crystals were collected by filtration with the aid of water;[17] yield, 2.19 g (87%); mp 155—157°C; $[\alpha]_D^{25}$ −21.8° (*c* 0.3, DMF); R_f^1 0.80, R_f^2 0.70. Hygroscopic monohydrochloride of IV was prepared previously.[11]

Found: C, 60.86; H, 7.51; N, 11.17%. Calcd for $C_{76}H_{106}O_{15}N_{12} \cdot 4H_2O$: C, 60.86; H, 7.66; N, 11.20%.

Boc–(Val–Orn(Z)–Leu–D-Phe–Pro)$_3$–OH (V). I (515 mg, 0.62 mmol) in DMF (5 ml) was treated with isoamyl nitrite (0.1 ml, 0.74 mmol) as in the case of III. To the azide solution was added a solution of IV (1.02 g, 0.68 mmol) in DMF (4 ml) containing TEA (0.095 ml). After being stirred for 5 days at 4°C, the reaction mixture was added to 0.2 M citric acid (300 ml). The resulting solid was collected and recrystallized from methanol–ether–petroleum ether; yield, 1.13 g (80%); mp 150—152°C; $[\alpha]_D^{25}$ −22.8° (*c* 0.5, DMF); R_f^1 0.98, R_f^2 0.64.

Found: C, 62.64; H, 7.54; N, 11.22%. Calcd for $C_{119}H_{166}O_{24}N_{18} \cdot 3H_2O$: C, 62.49; H, 7.58; N, 11.03%.

H–(Val–Orn(Z)–Leu–D-Phe–Pro)$_3$–OH (VI). This was prepared from V (2.26 g, 0.99 mmol) with 99% formic acid (60 ml) as in the case of IV: yield, 1.96 g (90%); mp 158—160°C; $[\alpha]_D^{25}$ −77.4° (*c* 0.5, DMF); R_f^1 0.90, R_f^2 0.65.

Found: C, 61.85; H, 7.52; N, 11.37%. Calcd for $C_{114}H_{158}O_{22}N_{18} \cdot 4H_2O$: C, 62.10; H, 7.50; N, 11.44%.

Boc–(Val–Orn(Z)–Leu–D-Phe–Pro)$_4$–OH (VII). The azide solution was prepared from I (1.04 g, 1.24 mmol) as in the case of III. To this was added a solution of VI (2.11 g, 0.96 mmol) in DMF (15 ml) containing TEA (0.13 ml). The solid was obtained as in the case of V and recrystallized from methanol–ether–petroleum ether; yield, 2.38 g (82%); mp 151—154°C; $[\alpha]_D^{25}$ −47.6° (*c* 1.0, DMF); R_f^1 0.90, R_f^2 0.70.

Found: C, 62.40; H, 7.67; N, 11.09%. Calcd for $C_{157}H_{218}O_{31}N_{24} \cdot 5H_2O$: C, 62.28; H, 7.59; N, 11.10%.

cyclo*(–Val–Orn(Z)–Leu–D-Phe–Pro–)$_3$ (VIII).* To a solution of V (320 mg, 0.14 mmol) in dichloromethane (2 ml) and DMF (1 ml) at 0°C, *N*-hydroxysuccinimide (32 mg, 0.28 mmol) and 1-ethyl-3-(3-dimethylaminopropyl)carbodiimide hydrochloride[18] (54 mg, 0.28 mmol) was added. After 12 hr at 4°C, the mixture was evaporated. The residual solid was collected by filtration with the aid of cold water; yield, 314 mg. To Boc–pentadecapeptide *N*-hydroxysuccinimide ester obtained, trifluoroacetic acid (3 ml) was added at 0°C. After 20 min, the solution was evaporated, and the residual powder was collected by filtration with the aid of ether. Pentadecapeptide *N*-hydroxysuccinimide ester trifluoroacetate obtained was dissolved in DMF (5 ml), and the solution was added into pyridine (50 ml) at room temperature. The stirring was continued for 2 hr. The solvent was removed, and the residue was dissolved in a mixture of methanol (50 ml) and water (10 ml). The solution was passed through columns (1.9×20 cm, each) of Dowex 1 (OH^- form) and Dowex 50 (H^+ form). The columns were washed with the same solvent (200 ml), the combined effluent was evaporated, and the product was collected by filtration with the aid of water. The product was further purified by a column (2.4×115 cm) with Sephadex LH-20; the product dissolved in methanol (3 ml) was applied to the column, and developed with methanol. Main fractions were evaporated, and the residual solid was recrystallized from methanol-ether-petroleum ether; yield, 144 mg (47% from V); mp 128—130°C; $[\alpha]_D^{25}$ −15.6° (*c* 0.3, DMF); R_f^1 0.90, R_f^2 0.75.

Found: C, 62.39; H, 7.49; N, 11.34%; mol wt 2110.[19] Calcd for $C_{114}H_{156}O_{21}N_{18} \cdot 4H_2O$: C, 62.61; H, 7.56; N, 11.53%; mol wt 2186.

cyclo*(–Val–Orn(Z)–Leu–D-Phe–Pro–)$_4$ (IX).* VII (1.91 g, 0.63 mmol) was converted to IX as described for the preparation of VII; yield, 911 mg (50% from VII); mp 153—155°C; $[\alpha]_D^{25}$ −23.0° (*c* 0.5, DMF); R_f^1 0.98, R_f^2 0.75.

Found: C, 63.00; H, 7.32; N, 11.37%; mol wt 2900.[19] Calcd for $C_{152}H_{208}O_{28}N_{24} \cdot 4H_2O$: C, 63.13; H, 7.53; N, 11.63%; mol wt 2891.

cyclo*(–Val–Orn–Leu–D-Phe–Pro–)$_3$ (Sesquigramicidin S) (X).* A solution of VIII (39 mg, 0.018 mmol) in 0.01 N methanolic hydrogen chloride (6 ml) was subjected to hydrogenolysis in the presence of palladium black, and the filtrate was evaporated. The product was recrystallized from methanol-ether–petroleum ether; yield of air-dried product (X·3HCl·

15) M. Ohno, T. Kato, S. Makisumi, and N. Izumiya, This Bulletin, **39**, 1738 (1966).

16) H. Ertel and L. Horner, *J. Chromatog.*, **7**, 268 (1962).

17) In the case of H-Val-Orn(Z)-Leu-D-Phe-Pro-OH (II), the neutral peptide (II) was never solidified, whereas monohydrochloride of II was obtained as nice crystals.

18) J. C. Sheehan, P. A. Cruickshank, and G. L. Boshart, *J. Org. Chem.*, **26**, 2525 (1961).

19) Molecular weight was determined on a Hitachi Osmometer, type 115, using methanol as a solvent.

BULLETIN OF THE CHEMICAL SOCIETY OF JAPAN, VOL. 46, 981—985 (1973)

Synthetic Studies of Amino Acids by the Use of Copper(II) Complex. III. Syntheses of Several 2-Amino-2-deoxyaldonic Acids by the Use of Bisglycinato- and *N*-Pyruvylideneglycinatoaquocopper(II)

Shohji OHDAN, Toshiro OKAMOTO, Sadao MAEDA, Tetsuya ICHIKAWA, Younosuke ARAKI, and Yoshiharu ISHIDO

Department of Chemistry, Faculty of Science, Tokyo Institute of Technology, O-okayama, Meguro-ku, Tokyo

(Received September 16, 1972)

A comparative study of the relative reactivity of bisglycinatocopper(II) and *N*-pyruvylideneglycinatoaquocopper(II) in a base-catalyzed condensation reaction with aldehydo sugar derivatives concluded that the latter complex is much more reactive than the former. This reaction was found to proceed with a considerably high stereoselectivity to afford blocked 2-amino-2-deoxyaldonic acids with a *threo* configurational relationship between *C*–2 and *C*–3, and between *C*–3 and *C*–4. The resultant products were converted to the corresponding free 2-amino-2-deoxyaldonic acids in good yields by deblocking them with Amberlite IR–120B(H form).

In the preceding papers,[1] a new procedure for synthesizing β-hydroxy amino acids and 2-amino-2-deoxyaldonic acids involving the base-catalyzed condensation reaction of *N*-pyruvylideneglycinatocopper(II) complexes with a variety of aldehyde species has been reported. An investigation of the syntheses of some 2-amino-2-deoxyaldonic acids by the above

1) a) T. Ichikawa, S. Maeda, Y. Araki, and Y. Ishido, *J. Amer. Chem. Soc.*, **92**, 5514 (1970); b) T. Ichikawa, T. Okamoto, S. Maeda, S. Ohdan, Y. Araki, and Y. Ishido, *Tetrahedron Lett.*, **1971**, 79; c) T. Ichikawa, S. Maeda, T. Okamoto, Y. Araki, and Y. Ishido, This Bulletin, **44**, 2779 (1971).

procedure was undertaken on the basis of the fact that the reaction is applicable to aldehydes susceptible to isomerization or polymerization under strongly basic conditions,[1] and the discovery of polyoxins,[2] which have been demonstrated to involve 2-amino-2-deoxy-L-xylonic acid and 5-amino-5-deoxy-D-alluronic acid as their constituents.

Results and Discussion

The Condensation Reaction with Bisglycinatocopper(II). To elucidate the excellence of the procedure utilizing *N*-pyruvylideneglycinatoaquocopper(II)[1] (**1**) in comparison with that utilizing bisglycinatocopper(II)[3] (**2**), the base-catalyzed condensation reactions of **2** with 2,3-*O*-isopropylidene-D-glyceraldehyde (**3**) and with 2,4-*O*-ethylidene-*al*-D-erythrose (**4**) were examined first.

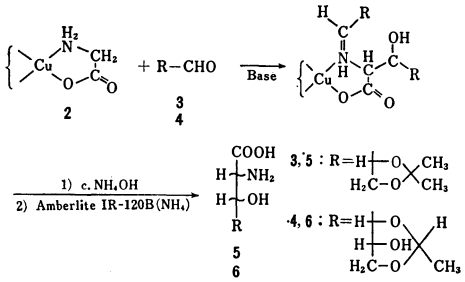

The reaction of **2** (10 mmol) with **3** (80 mmol) was carried out at 48—50°C, keeping the pH of the mixture at 10.7 by the drop-by-drop addition of an aqueous sodium hydroxide solution during the reaction; this gave 2-amino-2-deoxy-4,5-*O*-isopropylidene-D-aldopentonic acid (**5**) in a 31% yield. Similarly, 2-amino-2-deoxy-4,6-*O*-ethylidene-D-aldohexonic acid (**6**) was obtained in a 22% yield from the reaction of **2** with **4**. The application of **2** to the reaction involving such aldehydo sugars was abandoned since the reaction requires an excess amount of the aldehyde species because of the formation of a Schiff-base-type intermediate in the course of the reaction, and since the yields of the reactions are not very good.

The Condensation Reaction with N-*Pyruvylideneglycinatoaquocopper(II).* On the basis of the above results, the syntheses of 2-amino-2-deoxyaldonic acids were scrutinized by the base-catalyzed condensation reaction of **1** with almost equimolar amounts of **3**, **4**, 2,3-*O*-isopropylidene-L-glyceraldehyde (**7**), and 2,3;4,5-di-*O*-isopropylidene-*al*-D-arabinose (**8**) respectively. In contrast with the reaction of **2**, in which an excess amount of aldehyde species have been utilized, the reaction of **1** with all these aldehydes was completed within 60 min, even at pH 9.5, at room temperature to afford the corresponding 2-amino-2-deoxyaldonic acids with blocking groups in good yields. These results are summarized in Table 1. **3** (Run 1), **4** (Run 2) and **8**(Run 4) gave **5**, **6**, and 2-amino-2-deoxy-4,5;6,7-di-*O*-isopropylidene-D-aldoheptonic acid (**9**) in 70, 70, and 60% yields respectively. On the other hand, the reaction of **1** with **7**(Run 3) assumed a different aspect in contrast with those with other aldehydro sugars. Raw **7**, which was prepared by the lead-tetraacetate oxidation of 4,5-*O*-isopropylidene-L-arabinose dibenzyl dithio acetal,[4] followed by the condensation of the solution *in vacuo*, gave no product. This fact was deduced to arise from the decomposition of **1** by interaction with glyoxal 1,1-dibenzyl dithio acetal (**10**), which was co-produced in the course of the oxidation. On the basis of this fact, a variety of attempts at the separation of **7** from **10** were made. 2-Amino-2-deoxy-4,5-*O*-isopropylidene-L-aldopentonic acid(**11**) was obtained in a 36% yield by the use of a raw sirup of **7** which had been prepared by the concentration of a lead diacetate-free benzene solution of **7**, followed by repeatedly removing the viscous precipitates produced during the evaporation of methanol from the methanolic aqueous solution of the above residual sirup. No more effective procedure was evolved in spite of further attempts at the purification of **7**. The purification by high-vacuum distillation or by chromatography on a column of silica gel gave a material no longer reactive in the condensation reaction. An attempt at the removal of **10** by treating the oxidation mixture with such metal halides as cupric chloride or mercuric bromide was unsuccessful, and the extraction of **7** from the raw sirup with methylene chloride or benzene also resulted in failure. Fortunately, no such trouble accompanied the reactions of **4** or **8** with **1** since they were easily separated from the co-produced sodium formate by repeating the treatment of the raw sirup with ethanol followed by filtration and concentration, or were easily separated from formaldehyde by extraction with methylene chloride from the periodate oxidation mixture.

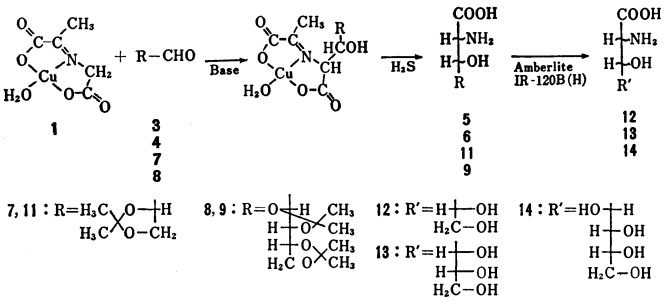

Subsequently, we attempted to remove blocking groups of the above 2-amino-2-deoxyaldonic acid derivatives by the use of Amberlite IR-120B(H form) in water. By the treatment of **5**, **6**, and **9** with the resin, 2-amino-2-deoxy-D-aldopentonic acid(**12**), -D-aldohexonic acid(**13**), and -D-aldoheptonic acid(**14**) were obtained in 87, 85, and 76% yields respectively. **12**, **13**, and **14** were prepared similarly from **3**, **4**, and **8** without the isolation of **5**, **6**, and **9** by the base-catalyzed condensation reaction, followed by this deblocking procedure; this resulted in 22, 60, and 65% yields respectively. In the first case, the filtrate of crystallization was found by tlc examination still to contain a considerable amount of **12**;

2) K. Isono, K. Asahi, and S. Suzuki, *J. Amer. Chem. Soc.*, **91**, 7490 (1969).

3) M. Sato, K. Okawa, and S. Akabori, This Bulletin, **30**, 937 (1957).

4) S. B. Baker, *J. Amer. Chem. Soc.*, **74**, 827 (1952).

Table 1. Base-catalyzed condensation reaction of *N*-pyruvylideneglycinatoaquocopper(II) with *aldehydo*-sugar derivatives[a]

Run	*aldehydo*-Sugars	Molar Ratio, R-CHO/**1**	Reaction Time, min	Products			
					Mp(decomp), °C	$[\alpha]_D$(*c* 1.0, H_2O) (at t°C)	Yield, %
1	**3**[b]	1.1	60	**5**	198	+0.2°(25°C)	70
2	**4**	1.1	40	**6**	209	−0.3°(25°C)	70
3	**7**	1.1	60	**11**	198	−0.2°(20°C)	36
4	**8**	1.2	40	**9**	212	+1.3°(20°C)	60

a) These reactions were carried out by the use of 9 mmol of *N*-pyruvylideneglycinatoaquocopper(II) (**1**) at pH 9.5.
b) The yield of this reaction has been reported in a previous paper (*cf.* 1c).

Table 2. Deblocking of 2-amino-2-deoxy-4,5-*O*-isopropylidene-D-xylonic acid (**5**), -4,6-*O*-ethylidene-D-gluconic acid(**6**), and -4,5;6,7-di-*O*-isopropylidene-D-aldoheptonic acid (**9**) by the use of amberlite IR-120B (H form)

Materials	Products	Mp(decomp), °C	Specific Rotation in H_2O	Yield,[a] %
5	2-Amino-2-deoxy-D-xylonic acid(**12**)	160	$[\alpha]_D^{20}$ −3.9° (*c* 1.9)	82(22)
6	2-Amino-2-deoxy-D-gluconic acid(**13**)	245	$[\alpha]_D^{20}$ +3.7° (*c* 1.0)	85(60)
9	2-Amino-2-deoxy-D-aldoheptonic acid(**14**)	180	$[\alpha]_{546}^{22}$ +0.2° and $[\alpha]_{578}^{22} \simeq 0°$ (*c* 2.0)	76(65)

a) The data in parentheses are the yields in the preparations without isolation of **5**, **6**, or **9** from the reaction of **1** with the corresponding *aldehydo*-sugars followed by the deblocking procedure.

Table 3. Stereoisomeric composition in the reaction products calculated from the area of chromatograms obtained by the amino acid analysis

Observed Peaks[a]	*aldehydo*-Sugar Derivative Used for the Reaction					
	3[b]	**3**[c]	**4**[b]	**4**[c]	**8**[b]	**8**[c]
A	0.03	0.02	0.02	0.01	0.15	—
B	0.17	0.17	0.12	0.02	0.20	0.05
C	1 (**5**)	1 (**12**)	1 (**6**)	1 (**13**)	1 (**9**)	1 (**14**)
D	0.13	0.14	—	—	0.09	0.07

a) The terms of A, B, C, and D are arbitrary given to the peaks in the chromatograms in the order of their appearence, and C always stands for the main peaks.
b) These mixtures were obtained by the condensation reaction of **1** with *aldehydo*-sugar derivatives.
c) These mixtures were obtained by the condensation reaction followed by the deblocking procedure.

however, no more crystalline product could be obtained. These results are summarized in Table 2.

Subsequently, the stereoisomeric composition of each product was examined by amino-acid analysis in order to examine the possibility that the potential four stereoisomers, which are expected to be formed in this reaction, might be detected easily. These results are summarized in Table 3. Three or four peaks were obviously detected in every chromatogram; the ratios demonstrated in the table were calculated from the ratios of area in the corresponding chromatogram of amino-acid analysis. In view of these data, and supposing that these ratios stand for the actual compositions in each product, it is very interesting that all the reactions proceed with a considerably high stereoselectivity; hence, an important clue for the elucidation of the steric course of the reaction may be obtained by determining the configuration at *C*-2 and *C*-3 in each main product. **12** was confirmed to be 2-amino-2-deoxy-D-xylonic acid on the basis of its behavior in the amino-acid analysis (it behaved just like 2-amino-2-deoxy-L-xylonic acid),[2] and **13** was identified with 2-amino-2-deoxy-D-gluconic acid[5] by a mixed-melting-point determination and by IR spectroscopy. On the basis of these facts, the stereochemistry in **12** and **13** among *C*-2, *C*-3, and *C*-4 were confirmed; they are all *threo* to each other.[6] The stereochemistry in **9** or **14**, in analogy with the above facts, was thought to have the same relation, although there is no decisive evidence at present.[7] These products were found by amino-acid analysis to be identical with the main products observed in each chromatogram.

5) M. L. Wolfrom and M. J. Cron, *ibid.*, **74**, 1715 (1952).
6) Further investigations with close attention to some potential factors were required to elucidate the steric course of the reaction mechanism involving a variety of aldehydes which are variously substituted. A tentative proposal on the mechanism has been made in Dr. Thesis of T. Ichikawa, Tokyo Institute of Technology (1971, March).
7) The stereochemistry of this compound will be confirmed by deriving into the corresponding 2-amino-2-deoxy-D-aldoheptose. The investigation is now in progress along with **12** and **13**.

Experimental

All the melting points are uncorrected. Amino-acid analyses were carried out by means of a Hitachi KLA-3B Amino-acid Analyzer. The specific rotations were determined by means of a Carl-Zeiss Photoelectric Precision Polarimeter (0.005°) at 546 and 578 nm, and the $[\alpha]_D$ values were calculated by the use of Drude's equation.

The Condensation Reaction with Bisglycinatocopper(II). *The Reaction of Bisglycinatocopper(II) (**2**) with 2,3-O-Isopropylidene-D-glyceraldehyde (**3**).* To a solution of 1,2;5,6-di-*O*-isopropylidene-D-mannitol[8] (10.4 g, 40 mmol) in water (120 ml), we added, portion by portion, sodium metaperiodate (8.8 g, 40 mmol), keeping the temperature at 25°C; the solution was then stirred at room temperature for 30 min. The precipitated sodium iodate was filtered off, and the filtrate was concentrated *in vacuo* below 40°C almost to a sirup. When the sirup was treated with ethanol (20 ml), the sodium iodate further precipitated was removed by filtration. This operation was repeatedly carried out in order to remove the small amount of sodium iodate remaining in the sirup. To a solution of the resultant sirup in water (total volume: 60 ml), we added **2**[3] (2.30 g, 10 mmol); the resultant mixture was stirred for 1 hr at room temperature, keeping the pH at 10.7 by the drop-by-drop addition of a 1 M aqueous sodium hydroxide solution. Then, the resultant mixture was treated with a concentrated aqueous ammoniacal solution to decompose the complex of 2-amino-2-deoxy-4,5-*O*-isopropylidene-D-xylonic acid (**5**), after which the solution was treated on a column (2.5×7 cm) of Amberlite IR-120B (NH_4 form). The column was then washed with water (500 ml). The light yellow effluent was evaporated *in vacuo* to a volume of *ca.* 20 ml, and the concentrate was extracted with methylene chloride (10 ml×3). The aqueous layer was further concentrated *in vacuo* to a volume of *ca.* 5 ml, and the concentrate was treated with several milliliters of methanol to afford **5** (1.27 g, 31%). Mp 201—202°C (decomp.) [lit.[1c] 198°C (decomp.)].

*The Reaction of **2** with 2,4-O-Ethylidene-al-D-erythrose (**4**).* To a solution of 4,6-*O*-ethylidene-D-glucopyranose[9] (8.4 g, 40 mmol) in water (100 ml), sodium metaperiodate (17.6 g, 80 mmol) was portion by portion added, under cooling with ice water. During this operation, the pH of the mixture was kept at 4—5 by the addition of crystalline sodium bicarbonate. After the removal of the resultant salts in the same way as above, the solution of **4** was similarly subjected to the reaction with **2**. When the resultant mixture was treated in a similar manner, 2-amino-2-deoxy-4,6-*O*-ethylidene-D-gluconic acid (**6**) (0.96 g, 22%) was obtained. Mp 209°C (decomp.). Found: C, 43.54; H, 6.97; N, 6.54%. Calcd for $C_8H_{15}NO_6$: C, 43.43; H, 6.84; N, 6.33%.

*The Condensation Reaction with N-Pyruvylideneglycinatoaquocopper(II). The Reaction of N-Pyruvylideneglycinatoaquocopper(II) (**1**) with 2,3-O-Isopropylidene-L-glyceraldehyde (**7**):* To a solution of 4,5-*O*-isopropylidene-L-arabinose dibenzyl dithio acetal[4] (4.2 g, 10 mmol) in benzene (80 ml), we added lead tetraacetate (4.7 g, 11 mmol); the solution was then stirred at room temperature for about 30 min. The precipitate was filtered off, and the filtrate was concentrated *in vacuo* below 40°C to a sirup. After the dissolution of the sirup in methanol (20 ml), distilled water (20 ml) was added. The solution was concentrated again *in vacuo* below 40°C to a volume of *ca.* 20 ml. The resultant sirupy precipitate was filtered off, and the filtrate was concentrated to a volume of 10 ml. To a solution of L-glyceraldehyde thus prepared, **1** (2.30 g, 9 mmol) was added together with water (30 ml); the pH of the resultant mixture was adjusted to 9.5 by the addition of a 2 M aqueous sodium hydroxide solution. Then, the mixture was stirred at room temperature for 1 hr, keeping its pH at 9.5. After the reaction, the resultant solution was adjusted at pH 4.5 with a 2 M aqueous hydrochloric acid solution and treated with hydrogen sulfide gas; the resultant precipitate was filtered off. The filtrate was immediately treated on a column (2.5×9 cm) of Amberlite IR-45 (OH form), and the column was washed with water (100 ml). The effluent was concentrated to a volume of *ca.* 50 ml, and the concentrate was treated on a column (2.5×9 cm) of Amberlite IR-120B (NH_4 form). Then, the column was washed with water (100 ml). The effluent was concentrated to a volume of *ca.* 50 ml, and the concentrate was washed with methylene chloride (10 ml×3). The aqueous layer was then concentrated *in vacuo* to a volume of *ca.* 10 ml. The treatment of the concentrate with several milliliters of ethanol gave raw crystals, which were subsequently recrystallized from aqueous ethanol to give 2-amino-2-deoxy-4,5-*O*-isopropylidene-L-aldopentonic acid (**11**) (0.65 g, 36%).

Mp 198°C (decomp.). $[\alpha]_D^{20}$ −0.2° (*c* 1.0, H_2O). Found: C, 46.61; H, 7.51; N, 6.66%. Calcd for $C_8H_{15}NO_5$: C, 46.82; H, 7.37; N, 6.83%.

*The Reaction of **1** with 2,4-O-Ethylidene-al-D-erythrose (**4**):* To a solution of **4**, which had been prepared from 4,6-*O*-ethylidene-D-glucopyranose (2.1 g, 10 mmol) in the way described previously, in water (50 ml), we added **1** (2.30 g, 9 mmol) together with water (30 ml); the mixture was then stirred at room temperature for 40 min, keeping the pH at 9.5 by the drop-by-drop addition of a 1 M sodium hydroxide solution. After the reaction, the resultant mixture was treated in the same way described in the previous experiment, and the resultant raw crystals were recrystallized from aqueous ethanol to give **6** (1.40 g, 67%). Mp 209°C (decomp.).

*The Reaction of **1** with 2,3;4,5-Di-O-isopropylidene-al-D-arabinose (**8**):* To a solution of 1,2;3,4-di-*O*-isopropylidene-D-mannitol (2.6 g, 10 mmol)[10] in water (50 ml) we added sodium metaperiodate (2.2 g, 10 mmol); the solution was then stirred at room temperature for 30 min, keeping the pH at 4—4.5 by the addition of sodium bicarbonate. The solution was then extracted with methylene chloride (50 ml×10), and the extract was concentrated *in vacuo* below 40°C almost to a sirup. The resultant sirup was subjected to a reaction with **1** (2.30 g, 9 mmol) (reaction time: 40 min) and treated in the same way as above to give 2-amino-2-deoxy-4,5;6,7-di-*O*-isopropylidene-D-aldoheptonic acid (**14**) (1.85 g, 60%).

Mp 212°C (decomp.) (recrystallized from aqueous ethanol). Found: C, 50.86; H, 7.56; N, 4.78%. Calcd for $C_{13}H_{23}NO_7$: C, 51.14; H, 7.59; N, 4.59%.

*Deblocking of **5**:* An aqueous solution of **5** (2.83 g, 13.7 mmol) in water (200 ml) was treated on a column of Amberlite IR-120B (H form) (3×9 cm), after which the column was washed with water (2000 ml). Then, the column was eluted with a 0.5 M aqueous ammoniacal solution (2000 ml), and the effluent was concentrated *in vacuo* to a volume of *ca.* 10 ml. The concentrate was treated with methanol (10 ml) to give crystals of 2-amino-2-deoxy-D-xylonic acid (**12**) (1.98 g, 87%). Mp 160°C (decomp.). $[\alpha]_D^{25}$ −3.4° (*c* 1.9, H_2O).

Found: C, 36.41; H, 6.95; N, 8.48%. Calcd for $C_5H_{11}NO_5$: C, 36.36; H, 6.71; N, 8.48%.

8) D. Horton, J. B. Hughes, and J. K. Thompson, *J. Org. Chem.*, **33**, 728 (1968).

9) R. Barket and D. L. MacDonald, *J. Amer. Chem. Soc.*, **82**, 2301 (1960).

10) L. F. Wiggings, *J. Chem. Soc.*, **1946**, 13.

Deblocking of ***6***: To a solution of **6** (10g, 45 mmol) in water (300 ml), we added Amberlite IR-120B (H form) (200 ml); the mixture was then stirred at room temperature for 24 hr.[11] The complete adsorption of **6** to the resin was examined by means of the ninhydrin test. The resin was then packed in a column (d: 2.5 cm), and the column was washed with water (1000 ml) and subsequently eluted with a 1 M aqueous ammoniacal solution (500 ml). The effluent was concentrated *in vacuo* to a volume of about 10 ml, and the concentrate was treated with several milliliters of ethanol to give 2-amino-2-deoxy-D-gluconic acid (**13**) (7.5 g, 85%). Mp 245°C (decomp.). This sample showed no depression on admixture with an authentic specimen.[5] $[\alpha]_D^{20}$ +3.7° (*c* 1.0, H_2O). The IR spectrum of this sample was also in complete agreement with that of the specimen.[5] Found: C, 36.64; H, 6.82; N, 7.17%. Calcd for $C_6H_{13}NO_6$: C, 36.92; H, 6.71; N, 7.18%.

Deblocking of ***9***: A solution of **9** (3.0 g, 10 mmol) in water (200 ml) was treated in the same way as has been described for the deblocking of **5** to give 2-amino-2-deoxy-D-aldopentonic acid (**14**) (1.7 g, 76%). Mp 180°C (decomp.). $[\alpha]_{546}^{22}$ +0.2° and $[\alpha]_{578}^{22} \simeq 0°$ (*c* 2.0, H_2O). Found: C, 37.21; H, 6.49; N, 6.36%. Calcd for $C_7H_{15}NO_7$: C, 37.33; H, 6.71; N, 6.22%.

Preparation of ***12***, ***13***, *and* ***14*** *without the Isolation of* ***5***, ***6***, *and* ***9*** *Respectively.* *Preparation of* ***12***: The mixture resulting from the base-catalyzed condensation reaction of **1** with **3**, which has been described in a previous paper,[1c] was adjusted at pH 4.5 with a 5 M aqueous acetic acid solution and then treated with hydrogen sulfide gas. The precipitated cupric sulfide was removed by filtration, and the filtrate was treated on a column of Amberlite IR-120B (H form) (3×9 cm). The column was washed with water (1000 ml) and then eluted with a 0.5 M aqueous ammoniacal solution (1000 ml). The effluent was concentrated *in vacuo* to a volume of *ca.* 10 ml, and the concentrate was treated as has been described previously to give **12** in a 22% yield.

Preparation of ***13***: The mixture resulting from the reaction of **1** with **4**, which has been described as the fourth example in this section, was treated in the same way as above, except that the washing procedure after the adsorption of **6** on the resin was done with 5000 ml of water. Yield, 60%.

Preparation of ***14***: The mixture resulting from the reaction of **1** with **8**, which has been described as the fifth example in this section, was treated in the same way as that used in the preparation of **12**. Yield, 65%.

11) Unless this operation is done under possibly gentle stirring, the resin was ground into small particles, and the washing and the elution procedures got into difficulties. Moreover, these operations came to need much voluminous solvents, and the yield of **13** was considerably lowered.

The authors are grateful to Professor Juji Yoshimura, Tokyo Institute of Technology, and Dr. Kiyoshi Isono, the Institute of Physical and Chemical Research, for their kind gifts of 2-amino-2-deoxy-D-gluconic acid and 2-amino-2-deoxy-L-xylonic acid respectively for the identification. They also wish to express their thanks to the members of the Laboratory of Elemental Analysis, Tokyo Institute of Technology, and Dr. Tadatoshi Seino and Miss Yoshimi Koike, Central Research Laboratories, Ajinomoto Co., Inc., for their assistance in the elemental and amino acid analyses respectively. Moreover, they are grateful to the Ministry of Education, Japanese Government, for a Scientific Research Grant-in-aid.

BULLETIN OF THE CHEMICAL SOCIETY OF JAPAN, VOL. 46, 985—990 (1973)

Stereospecific Syntheses and Acid Dissociations of 2,3-Diaminotetralins and 2,3-Diamino-*trans*-decalins[1)]

Tairoku YANO, Hiroshi KOBAYASHI, and Keihei UENO

Department of Organic Synthesis, Faculty of Engineering Kyushu University, Fukuoka, Japan 812

(Received September 29, 1972)

cis- and *trans*-2,3-Diaminotetralins and 2(*e*),3(*e*)-, 2(*e*),3(*a*)-, and 2(*a*),3(*a*)-diamino-*trans*-decalins were stereospecifically synthesized from 1,4-dihydronaphthalene and *trans*-Δ^2-octalin, respectively. The stepwise acid dissociation constants of the decalin derivatives were determined by potentiometric method and discussed in relation to their configurations.

In the course of investigations into steric effect on the chelate formation equilibria of complexane type ligands,[2,3)] we required stereochemically pure samples of three kinds of 2,3-diamino-*trans*-perhydronaphthalenes. Since reasonable separation of the isomers was unlikely, we were obliged to synthesize each diamine separately *via* a stereospecific route, using a starting material of known stereochemistry. This paper deals with such routes and their applications to the synthesis of related *cis*- and *trans*-2,3-diamino-1,2,3,4-tetrahydronaphthalenes, as well as their proton dissociation behaviors in aqueous solutions.

2,3-Diamino-trans-*perhydronaphthalenes.* The three kinds of configurational isomers are denoted as *trans*-2(*a*),3(*a*)-,*cis*-2(*a*),3(*e*), and *trans*-2(*e*),3(*e*)-diamines. The sequences of their preparations are outlined in Scheme 1. Of the three routes, the first two are essentially the same as those reported by Swift and Swern.[4)] The last one, however, required some modifications in order to control the number of inversions

1) Contribution No. 286 from the Department of Organic Synthesis, Kyushu University.

2) N. Okaku, K. Toyota, Y. Moriguchi, and K. Ueno, This Bulletin, **40**, 2326 (1967).

3) Y. Yanagihara, T. Yano, H. Kobayashi, and K. Ueno, *ibid.*, **45**, 554 (1972).

4) G. Swift and D. Swern, *J. Org. Chem.*, **32**, 511 (1967).

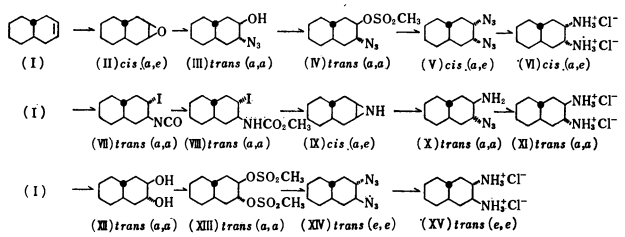

Scheme 1.

in the synthetic route. Our starting material for each synthesis was *trans*-octahydronaphthalene (I). Epoxidation of olefin (I) with perbenzoic acid gave *cis*-epoxide (II), which was ring-opened, with inversion, to *trans*-3(*a*)-azido-2(*a*)-ol(III) in a quantitative yield by the reaction with sodium azide in aqueous ethanol. Hydroxy function of the resulting azido-alcohol (III) was mesylated with methanesulfonyl chloride in pyridine to yield 3(*a*)-azido-*trans*-2(*a*)-perhydronaphthyl methanesulfonate (IV) in 86% yield. Sulfonate (IV) was treated with sodium azide in aqueous dimethylformamide to displace the methanesulfonate function, with inversion, to give oily *cis*-2(*e*), 3(*a*)-diazide (V) in 79% yield. It was then hydrogenated at room temperature over Adam's catalyst to yield the *cis*-diamine, which was immediately converted into *cis*-2(*e*),3(*a*)-diamino-*trans*-perhydronaphthalene dihydrochloride (VI) in 77% yield, melting above 250°C. Acetylation of the *cis*-diamine gave the bisacetyl derivative melting at 245—255°C.

On the other hand, iodine isocyanate, generated *in situ* from silver cyanate and iodine, was added olefin (I), and the resulting *trans*-iodoisocyanate (VII) was converted, without isolation, into *trans*-2(*a*)-iodo-3(*a*)-carbamate (VIII) in 32% yield. Highly purified carbamate (VIII) was ring-closed, with inversion, to *cis*-aziridine (IX) in 72% yield by warming with alcoholic potassium hydroxide. Aziridine (IX) was then converted into *trans*-2(*a*)-amino-3(*a*)-azide (X) in 72% yield by ring cleavage accompanied by inversion, with sodium azide in aqueous ethanol. Aminoazide (X) gave *trans*-2(*a*),3(*a*)-diamino-*trans*-perhydronaphthalene dihydrochloride (XI) in 27% yield by hydrogenation over Adam's catalyst at room temperature, followed by treatment with ethanolic hydrochloric acid. Dihydrochloride (XI) melted with decomposition above 200°C, while the bisacetyl derivative of the *trans*-diamine showed melting point at 245—250°C, which was very close to that of bisacetyl-*cis*-diamine. A mixed melting point test of both bisacetyl derivatives, however, showed considerable depression, mp 213—220°C.

trans-2(*e*),3(*e*)-Diamine was prepared through a sequence involving simultaneous two inversions in contrast to the sequences leading to the other two isomers, which involved successive two inversions *via* three-membered ring intermediates. Olefin (I) was oxidized with performic acid to *trans*-2(*a*),3(*a*)-diol (XII) in 42% yield, followed by mesylating with methanesulfonyl chloride in pyridine to afford *trans*-2(*a*),3(*a*)-bismethanesulfonate (XIII) in 54% yield. Bissulfonate (XIII) was then treated with sodium azide in aqueous dimethylformamide to displace both sulfonate functions at the same time, with inversions. Resulting 2(*e*),3(*e*)-diazide (XIV) was, without further purification, hydrogenated over Adam's catalyst at room temperature, followed by treatment with ethanolic hydrochloric acid to give *trans*-2(*e*),3(*e*)-diamino-*trans*-perhydronaphthalene dihydrochloride (XV) in 29% yield.

TABLE 1. ACID DISSOCIATION CONSTANTS OF 1,2-DIAMINES

Diamine	pK_{a_1}	pK_{a_2}
(VI) (*a*, *e*)[a]	6.36±0.01	9.93±0.01
(XV) (*e*, *e*)[a]	6.68±0.01	10.08±0.01
(XI) (*a*, *a*)[a]	6.97±0.01	9.97±0.01
cis-Cyclohexane-1,2-diamine[b]	6.41	9.99
trans-Cyclohexane-1,2-diamine[b]	6.72	9.89
Ethylenediamine[b]	7.48	10.18
Propane-1,2-diamine[c]	7.13	10.00
dl-Butane-2,3-diamine[d]	6.91	10.00

a) Measured at 25.0±0.1°C and μ=0.10 (KNO_3).
b) Measured at 20°C and μ=0.1 (KCl), G. Schwarzenbach and R. Bauer, *Helv. Chim. Acta*, **39**, 722 (1956).
c) Measured at 25°C and μ=0.5 (KNO_3), F. Basolo, R. K. Murmann, and Y. T. Chen, *J. Amer. Chem. Soc.*, **75**, 1478 (1953).
d) Measured at 25°C and μ=0.5 (KNO_3), F. Basolo, Y. T. Chen, and R. K. Murmann, *ibid.*, **76**, 956 (1954).

The apparent pK_a values of the conjugate acids (VI), (XI), and (XV) were measured potentiometrically in water at 25°C under an ionic strength of μ=0.1 (KNO_3). The obtained values are summarized in Table 1 along with those of some related diamine hydrochlorides.

At the first dissociation step, the mutual field effect between the vicinal di-cation seems to be predominant in affecting the pK_{a_1} values of the three conjugate acids, since the inductive effect is considered to be equal among such isomeric systems to a first approximation. As expected from the order of the distance between the vicinal di-cation,[5] the isomer which shows the highest pK_{a_1} value is assigned to be the *trans*-(*a*,*a*)-diamine. The difference in pK_{a_1} values of the remaining two is of a similar extent, as observed between *cis*- and *trans*-cyclohexanediamine, and may be rationalized by steric hindrance among the axial ammonium and the axial hydrogens on the same six-memberes ring.[6] If this is the case, the isomer of the lowest

5) Studies with Dreiding molecular models show that the nitrogen atoms in the *trans*-(*a*,*a*)-diamine are separated by approximately 3.7 Å, and those of *trans*-(*e*,*e*)- and *cis*-(*a*,*e*)-isomers by 2.8 Å.

6) The steric effect might act as a direct steric repulsion between ammonium hydrogen and the adjacent axial hydrogens, or as a buttressing effect of the axial hydrogens upon the axial ammonium group, causing a much shorter distance and consequently an increased field effect between the vicinal ammonium group in the *cis*-(*a*,*e*)-diamine than that of the *trans*-(*e*,*e*)-homologue. Alternately, such congestion around the axial ammonium function causes steric hindrance preventing solvation by polar solvent molecules which, otherwise, would stabilize the charged site by dielectric shielding: G. Schwarzenbach and R. Bauer, *Helv. Chim. Acta*, **39**, 722 (1956). Other workers also recognized and increased acidity of protonated amines in overcrowded steric environments: T. Sasaki, S. Eguchi, and T. Kiriyama, This Bulletin, **44**, 3410 (1971).

pK_{a_1} should be assigned to the *cis*-(*a*,*e*)-homologue. Assignations of the three conformational isomers are consistent with the consequences considered from their respective synthetic routes. Of the two conjugate cations in the *cis*-(*a*,*e*)-isomer, the axial ammonium dissociates preferentially to the equatorial function, and the assignment is compatible with the fact that the pK_{a_1} values of axial conjugate acids are smaller than those of the corresponding equatorial ones.[7] It seems also ascribable to the 1,3-diaxial steric hindrance that the *trans*-(*a*,*a*)-diamine shows a much lower pK_{a_1} value than ethylene diamine, the value being rather close to that of *dl*-butane-2,3-diamine in which the ammonium group is under considerable steric hindrance of the methyl group in the *guache* position.

In the second acid dissociation constants pK_{a_2} we expected rather large differences among the three isomeric diamines, depending upon the relative easiness of forming an intramolecular hydrogen bonding between the ammonium and the vicinal amino group. However, differences in the observed pK_{a_2}'s are very small as shown in Table 1. Each IR spectrum of the diamines measured at high dilution exhibits a sharp peak at 3380—3385 cm^{-1} and a broad peak at 3300 cm^{-1}, which are ascribable to a free amino group. Similarity of the spectra of the diamines, as shown in Fig. 2, indicates that intramolecular hydrogen bonding on the *trans*-(*e*,*e*)-diamine, though stereochemically quite possible, is unlikely to be formed even in a non-polar solvent such as tetrachloroethylene.[8] Thus, the absence of intramolecular hydrogen bonding in the three isomeric diamine mono-cations, may be partly responsible for the resemblance in their second dissociation constants. However, the cause for their rather similar pK_{a_2} values, which were determined in aqueous media and found to be contrary to ones expected from a stereochemical standpoint, can be rationalized only with additional experimental data such as an equilibrium study in aqueous organic solvents.

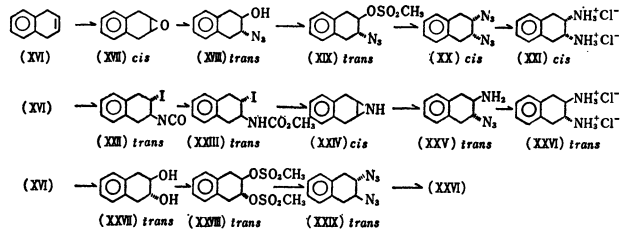

Scheme 2.

2,3-Diamino-1,2,3,4-tetrahydronaphthalenes. The reaction sequences shown in Scheme 1 were then applied to the preparation of vicinal diamines having a tetralin skeleton as outlined in Scheme 2. Dihydrochloride (XXVI) of the *trans* isomer obtained from 1,4-dihydronaphthalene (XVI) *via* the aziridine (XXIV), was identical with the diamine dihydrochloride obtained from the same starting material (XVI) *via* the *trans*-diazide (XXIX). Two possible configurations of the *trans* vicinal diamine would be readily equilibrated on the flexible tetralin skeleton, so that they cannot be isolated separately, whereas the vicinal diamine groups on the rigid *trans*-decalin framework retain their configurations, two *trans* diamino isomers (XI) and (XV) being individually isolated. This also provides an evidence for the simultaneous displacement of the vicinal two sulfonate functions with azide groups, with inversions.

It should be noted that in the route leading to *trans*-diamine (XXVI), aziridine (XXIV) could be obtained only from the extremely purified iodocarbamate (XXII), otherwise the carbamate gave only naphthalene.

Experimental

trans-Δ^2-Octalin(I),[9] 2,3-epoxy-*trans*-decalin(II),[9] 2(*a*),3(*a*)-dihydroxy-*trans*-decalin(XII),[10] 1,4-dihydronaphthalene (XVI),[10] 2,3-epoxytetralin(XVII),[11] and *trans*-2,3-dihydroxytetralin(XXVII)[12] were prepared according to literature. Melting and boiling points were not corrected. Infrared spectra were determined with JASCO DS-301 and DS-403G spectrophotometers. NMR spectra were recorded with a Varian A-60 and JOEL JNM-PS-100[13] in heavy water solutions using *t*-butanol as an internal reference (at 72 Hz downfield from TMS) unless otherwise stated.

2(a)-Hydroxy-3(a)-azido-trans-*decalin (III).* 2,3-Epoxy-*trans*-decalin(II) (14 g, 0.092 mol) was refluxed for 24 hr in 80% aqueous ethanol(200 ml) with sodium azide (7.4 g, 0.114 mol) and ammonium chloride (5.65 g, 0.114 mol). The reaction mixture was poured into water and extracted with ether. The ether layer was evaporated to give an oil which solidified gradually on cooling. Yield: 18.0 g, almost quantitative. Analytical sample was purified by sublimation under reduced pressure. Mp 36—38°C. IR: ν_{OH} 3310 cm^{-1}, ν_{N_3} 2120 cm^{-1}. Found: C, 62.14; H, 8.63; N, 20.69%. Calcd for $C_{10}H_{17}ON_3$: C, 61.59; H, 8.72; N, 21.54%.

3(a)-Azido-2(a)-trans-*decahydronaphthyl Methanesulfonate (IV).* Methanesulfonyl chloride (18 g, 0.158 mol) was gradually added to a solution of *trans*-azidohydrine(III) (18.0 g, 0.092 mol) in pyridine (100 ml) at 0—5°C with stirring for 3 hr. Stirring was continued for 1.5 hr without cooling. The reaction mixture was allowed to stand overnight at room temperature(14—25°C). The resulting solution was poured into water (1 liter) and the crystalline precipitate was recrystallized from methanol to give colorless needles(22 g, 86%). An analytical sample was purified by sublimation. Mp 56—58°C. IR: ν_{N_3} 2120 cm^{-1}, $\nu_{OSO_2CH_3}$ 800—1000 cm^{-1}. Found: C, 48.21; H, 6.97; N, 14.62%. Calcd for $C_{11}H_{19}N_3O_3S$: C, 48.35; H, 6.96;

7) J. Sicher, M. Tichý, F. Šipoš, M. Svoboda, and J. Jonáš, *Collection Czechoslov. Chem. Commun.*, **29**, 1561 (1964).

8) The result is in line with the conclusion that in a series of monoprotonated diamines $(H_2N(CH_2)_nN^+H_3)$ in acetonitrile, the intramolecular hydrogen bonding contributes very little to the increase of pK_a value of the diamines with $n=2$ or $n>5$. J. F. Coetzee and G. R. Padmanabjan, *J. Amer. Chem. Soc.*, **87**, 5005 (1965).

9) W. S. Johnson, V. J. Bauer, J. L. Magrave, M. A. Frisch, L. H. Dreger, and W. N. Hubbard, *ibid.*, **83**, 606 (1961).

10) H. B. Henbest, M. Smith, and A. Thomas, *J. Chem. Soc.*, **1958**, 3293.

11) E. S. Cook and A. J. Hill, *J. Amer. Chem. Soc.*, **62**, 1995 (1961).

12) R. Huisgen, E. Laschtuvka, I. Ugi, and A. Kammermeier, *Ann*, **630**, 128 (1960).

13) Measured by Mr A. Kito at the Government Industrial Research Institute, Osaka, to whom the authors are very grateful.

N, 15.38%.

2(e),3(a)-Diamino-trans-*decalin Dihydrochloride (VI).* A mixture of the azidomethanesulfonate (IV) (35 g, 0.13 mol) and sodium azide (17 g, 0.26 mol) in 85% aqueous dimethylformamide (420 ml) was refluxed for 6 hr. The resulting solution was poured into water (1 l) and extracted with ether. Evaporation of the ethereal extract gave an oily diazide (23 g, 79%). Diazide (V) (23 g, 0.1 mol) was dissolved in absolute ethanol (150 ml) and hydrogenated in an autoclave, under 80 kg/cm² over Adam's catalyst (0.43 g) for 90 hr at room temperature. The resulting solution was acidfied with hydrochloric acid (100 ml) and the solvent was evaporated off. The residue was dissolved in water (200 ml) and washed with ether. The aqueous solution was treated with activated charcoal and evaporated off. The residual solid was recrystallized from water–ethanol to yield diamine dihydrochloride(19.3 g, 76.5%). Mp above 254°C. NMR(in D_2O):[14] 1.2—2.4 ppm(14H), 3.8—4.2 ppm(2H). Found: C, 49.66; H, 9.26; N, 11.62%. Calcd for $C_{10}H_{22}N_2Cl_2$: C, 49.79; H, 9.12; N, 11.62%. The bisacetyl derivative of (VI) had mp 246—250°C. Found: C, 66.60; H, 9.53; N, 10.94%. Calcd for $C_{14}H_{24}N_2O_2$: C, 66.67; H, 9.52; N, 11.11%.

Methyl-2(a)-iodo-trans-*decalin-3(a)-carbamate (VIII).* *trans*-Δ^2-Octalin (I) (7 g, 0.05 mol) and iodine (12.7 g, 0.05 mol) were dissolved in dry ether (120 ml) at 0—5°C and silver cyanate[15] (12 g, 0.075 mol) was added in one portion with stirring. After continuous stirring for 2 hr, an additional silver cyanate (6 g) was added. The resulting light yellow mixture was then kept under stirring for further 15 hr with cooling at 0—5°C. It was filtered and the filtrate was evaporated to dryness. The residue, dissolved in absolute methanol (100 ml), was refluxed for 3 hr and kept standing overnight to give colorless needles (5.4 g, 32%), which were recrystallized from methanol. Mp 134.5°C. IR: ν_{NH} 3280 cm^{-1}, $\nu_{C=O}$ 1690 cm^{-1}. Found: C, 42.67; H, 6.11; N, 4.05%. Calcd for $C_{12}H_{20}NO_2I$: C, 42.73; H, 5.93; N, 4.15%.

2,3-Imino-trans-*decalin (IX).* A solution of potassium hydroxide (7 g) in water (15 ml) was added into a solution of the methylcarbamate (VIII) (8 g, 0.024 mol) in ethanol (60 ml). After being refluxed for 2 hr, the reaction mixture was poured into water (700 ml). The aqueous mixture was extracted with ether and the ethereal extract was evaporated off to give (IX) (2.6 g, 72%). An analytical sample was purified by sublimation. Mp 42—47°C. IR: ν_{NH} 3170 cm^{-1}. Found: C, 78.40; H, 11.06; N, 8.65% Calcd for $C_{10}H_{17}N$: C, 79.54; H, 11.26; N, 9.27%.

2(a)-Amino-3(a)-azido-trans-*decalin Hydrochloride (X).* A solution of (IX) (10 g, 0.07 mol), sodium azide (9.15 g, 0.14 mol), and ammonium chloride (7.56 g, 0.14 mol), in ethanol (160 ml) and water (40 ml) was refluxed for 24 hr, and then poured into water. The aqueous mixture was adjusted to be slightly alkaline and extracted with ether. The ethereal extract was evaporated off to give an oil (10.8 g, 84%) which was subjected to hydrochlorination to yield (X). Hydrochloride (X) was recrystallized from ethanol–ether for an analytical sample. Mp 190—197°C. IR: (free HCl) ν_{NH_2} 3320 cm^{-1}, ν_{N_3} 2120 cm^{-1}. Found: C, 52.11; H, 8.27; N, 24.04%. Calcd for $C_{10}H_{19}N_4Cl$: C, 52.06; H, 8.24; N, 24.30%.

2(a)-3(a)-Diamino-trans-*decaline Dihydrochloride (XI).* Aminoazide compound (X) (10.8 g, 0.055 mol) was hydrogenated in a similar manner to that described for VI. Yield, 5.2 g (39%). Mp 197—230°C (decomp.). NMR (in D_2O):[14] 1.2—2.2 ppm (14H), 4.00 ppm (2H). Found: C, 47.55; H, 9.15; N, 11.03%. Calcd for $C_{10}H_{22}N_2Cl_2 \cdot 0.7H_2O$: C, 47.30; H, 9.24; N, 11.05%.

The bisacetyl derivative of XI had mp 245—250°C. Found: C, 66.37; H, 9.40; N, 10.86%. Calcd for $C_{14}H_{24}N_2O_2$: C, 66.67; H, 9.52; N, 11.11%.

2(a),3(a)-Dihydroxy-trans-*decalin(XII).* Into a mixture of 99% formic acid(110 g) and 30% hydrogen peroxide (13 g), was gradually added *trans*-Δ^2-octalin (I) (13.6 g, 0.1 mol) at 40—45°C with stirring and the stirring was continued for 9 hr. After the remaining performic acid was decomposed with sodium sulfite, formic acid was removed by evaporation and the residue was refluxed together with ethanol (50 ml) and sodium hydroxide (15 g) in water (30 ml) for 5 hr. The resulting mixture was acidified and again evaporated under reduced pressure. The residual precipitate was washed with water and recrystallized from benzene. Yield was 15.7 g. Mp 164—165.5°C. (lit,[9] 163—164°C). IR: ν_{OH} 3280 cm^{-1}. Found: C, 70.62; H, 10.56%. Calcd for $C_{10}H_{18}O_2$: C, 70.58; H, 10.58%.

trans-*Decahydro-2(a),3(a)-naphthalene Bismethanesulfonate (XIII)* was prepared from XII (12.8 g, 0.076 mol) in a similar manner to that for IV. Methanesulfonate (XIII) was purified by repeated recrystallization from methanol. Yield, 23 g (93%). Mp 129—130°C. IR: $\nu_{OSO_2CH_3}$ 800—1000 cm^{-1}. Found: C, 43.85; H, 6.86%. Calcd for $C_{12}H_{22}O_6S_2$: C, 44.17; H, 6.75%.

2(e),3(e)-Diamino-trans-*decalin Dihydrochloride (XV).* Methanesulfonate (XIII) (19.7 g, 0.06 mol) dissolved in 85% aqueous dimethylformamide (210 ml) was refluxed for 5.5 hr together with sodium azide (16.0 g, 0.25 mol). Reaction mixture was treated subsequently in a similar manner to that for VI. The oily diazidodecalin was separated as a fraction soluble in petroleum ether (100 ml, boiling region 38—43°C). Yield, 8.6 g (64%). Without further purification, the product (XIV) was hydrogenated over Adam's catalyst in absolute ethanol (100 ml) at room temperature under 100 Kg/cm² for 72 hr. The resulting ethanol solution was acidified with hydrochloric acid, ethanol being removed by evaporation. The residue was dissolved in water and washed with ether. The final aqueous solution was evaporated and the residue was recrystallized from water–ethanol to yield diamine dihydrochloride(XV) (2.7 g, 28.5%). Mp 265—270°C. NMR(in D_2O):[14] 1.2—2.4 ppm (14H), 3.6—3.8 ppm (2H). Found: C, 49.44; H, 9.10; N, 11.20%. Calcd for $C_{10}H_{22}N_2Cl_2$: C, 49.79; H, 9.10; N, 11.62%.

The bisacetyl derivative of XV had mp above 290°C. Found: C, 66.49; H, 9.55; N, 11.08%. Calcd for $C_{14}H_{24}N_2O_2$: C, 66.67; H, 9.52; N, 11.11%.

trans-*3-Azido-2-hydroxytetralin (XVIII).* 2,3-Epoxytetralin (XVII) (27.3 g, 0.187 mol) dissolved in 80% aqueous ethanol (380 ml), was refluxed for 24 hr together with sodium azide (15 g, 0.23 mol) and ammonium chloride (12.3 g, 0.23 mol). The reaction mixture was poured into water (1 liter) and a cystalline precipitate was recrystallized from benzene–petroleum ether. The yield was nearly quantitative. Mp 66—67°C. IR: ν_{OH} 3300 cm^{-1}, ν_{N_3} 2124 cm^{-1}. Found: C, 63.58; H, 5.83; N, 22.08%. Calcd for $C_{10}H_{11}N_2O$: C, 63.49; H, 5.82; N, 22.02%.

trans-*3-Azido-2-tetrahydronaphthyl Methanesulfonate (XIX).* *trans*-Azidohydrin (XVIII) (40.8 g, 0.217 mol), dissolved in pyridine (155 ml) was treated with methanesulfonyl chloride in a similar manner to that for III. The yield was nearly quantitative. An analytical sample was recrystallized from methanol. Mp 76—76.5°C. IR: ν_{N_3} 2120 cm^{-1}, $\nu_{OSO_2CH_3}$

14) The proton signal in D_2O was used as a reference and set at 5.0 ppm downfield from TMS.

15) R. G. Neville and J. J. McGee, "Inorganic Syntheses" Vol. 8, p. 23 (1966) McGraw-Hill, New York.

820—980 cm^{-1}. Found: C, 49.14; H, 4.94; N, 15.42%. Calcd for $C_{11}H_{13}N_3O_3S$: C, 49.43; H, 4.87; N, 15.73%.

cis-*2,3-Diazidotetralin (XX).* A mixture of azidomethanesulfonate (XIX) (17 g, 0.064 mol) and sodium azide (8.5 g, 0.13 mol) was treated in a similar manner to that for V, to give the oily product (XX) (7.5 g, 54.5%). IR: ν_{N_3} 2120 cm^{-1}.

cis-*2,3-Diaminotetralin Dihydrochloride (XXI).* Diazide (XX) (7.5 g, 0.035 mol) in absolute ethanol (100 ml) was hydrogenated in a similar manner to that for VI. Dry hydrogen chloride was passed into the resulting ethanol solution at 0—5°C to give a colorless precipitate, which was recrystallized from water–ethanol to yield diamine dihydrochloride (XXI) (7 g, 85%). Mp 243°C. NMR(in D_2O): 2.05 ppm (4H), 2.97 ppm (2H), 6.06 ppm (4H). Found: C, 51.17; H, 6.93; N, 11.73; Cl, 29.4%. Calcd for $C_{10}H_{16}N_2Cl_2$: C, 51.06; H, 6.83; N, 11.90; Cl, 30.2%.

trans-*Methyl-2-iodo-3-tetrahydronaphthylcarbamate (XXIII).* 1,4-Dihydronaphthalene (XVII) (13 g, 0.1 mol) and iodine (25.4 g, 0.1 mol) were dissolved in dry ether (170 ml) at 0—5°C. To this solution was added silver cyanate (15 g, 0.1 mol) in one portion. The mixture was stirred for 24 hr and filtered. The filtrate was evaporated to dryness. The solid residue was dissolved in absolute methanol (300 ml), and refluxed for 3 hr. The solution was treated with sodium thiosulfate in order to remove the remaining iodine and then evaporated to about 100 ml. The concentrated solution was poured into water (3 l) to give precipitate which was recrystallized from methanol. Mp 138—140°C. IR: ν_{NH} 3320 cm^{-1}, $\nu_{C=O}$ 1700 cm^{-1}. Found: C, 43.23; H, 4.33; N, 4.12%. Calcd for $C_{12}H_{14}NO_2I$: C, 43.50; H, 4.23; N, 4.23%.

cis-*2,3-Iminotetralin (XXIV).* A solution of potassium hydroxide (18 g) in water (35 ml) was added into a solution of methanesulufonate (XXIII) (20 g, 0.06 mol) in ethanol (170 ml). After being refluxed for 2 hr, the reaction mixture was concentrated to about 100 ml and poured into water (300 ml). The aqueous mixture was extracted with ether and the ethereal extract was evaporated and distilled to give an oil (5 g, 57%) boiling at 70—80°C/0.17 mmHg, which solidified immediately. Mp 72°C. IR: ν_{NH} 3238 cm^{-1}. Found: C, 81.81; H, 7.52; N, 9.12%. Calcd for $C_{10}H_{11}N$: C, 82.75; H, 7.59; N, 9.66%.

trans-*3-Azido-2-aminoteralin Hydroazide (XXV).* A mixture of imine (XXIV) (5 g, 0.036 mol), sodium azide (11.5 g, 0.174 mol) and ammonium chloride (9.5 g, 0.147 mol) in 80% aqueous ethanol (220 ml) was refluxed for 17 hr, and then poured into water. A solid product was obtained by extraction of the aqueous mixture with ether, followed by evaporation to dryness. Recrystallization from methanol gave the product melting at 88°C. Yield, 5.5 g (68%). IR: ν_{N_3} 2040 and 2140 cm^{-1}, (free HN_3) ν_{N_3} 2110 cm^{-1}, ν_{NH_2} 3320 and 3380 cm^{-1}. Found: C, 52.21; H, 5.70; N, 42.36%. Calcd for $C_{10}H_{13}N_7$: C, 51.94; H, 5.63; N, 42.42%.

trans-*2,3-Diaminoteralin Dihydrochloride (XXVI).* *trans*-3-Azido-2-aminotetralin (XXV) (4.5 g, 0.025 mol) was hydrogenated and was worked up in a similar manner to that for *cis*-diamine (XXI). Yield, 3.2 g (57%). Mp 270°C. NMR(in D_2O): 2.00 ppm (4H), 2.75 ppm (2H), and 6.07 ppm (4H). Found: C, 51.11; H, 6.93; N, 11.67%. Calcd for $C_{10}H_{16}N_2Cl_2$: C, 51.06; H, 6.83; N, 11.90%.

1,2,3,4-Tetrahydro-trans-*2,3-naphthalene Bismethanesulfonate (XXVIII).* *trans*-Glycol (XXVII) (21.1 g, 0.13 mol) was mesylated in a similar manner to that for III and XIII, to give the bismethanesulfonate (XXVIII) (39.4 g, 95%) which was recrystallized from methanol. Mp 138°C. IR: $\nu_{OSO_2CH_3}$ 825—1000 cm^{-1}. Found: C, 44.65; H, 5.05%. Calcd for $C_{12}H_{16}O_7S_2$: C, 44.95; H, 5.02%.

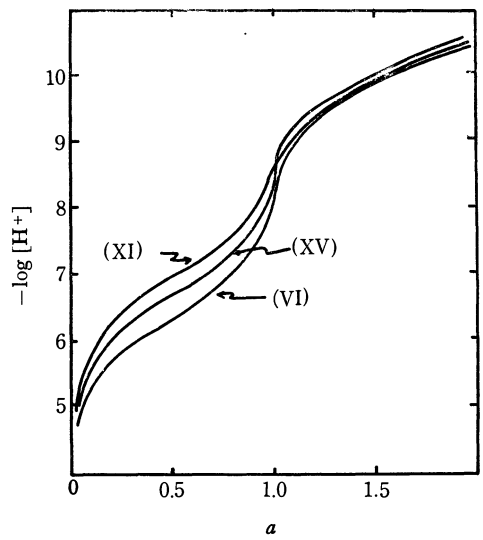

Fig. 1. Titration curves of diaminodecalins. Concn of ligands: 2×10^{-3} M.

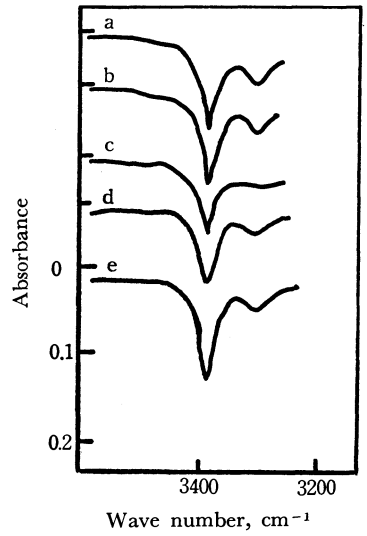

Fig. 2. N-H streching vibration of diamines in dilute C_2Cl_4 solutions (1×10^{-3} M).
a) *cis*-2(*a*),3(*e*)-diamine, b) *trans*-2(*e*),3(*e*)-diamine
c) *trans*-2(*a*),3(*a*)-diamine, d) *cis*-diaminotetralin
e) *trans*-diaminotetralin

trans-*2,3-Diazidotetralin (XXIX).* Bismethanesulfonate (7.4 g, 0.023 mol) was refluxed in a mixture of dimethylformamide (60 ml) and water (10 ml) for 5 hr together with sodium azide (5.1 g, 0.091 mol), to afford diazide (XXIX) (2 g, 40%), which was recrystallized from methanol. Mp 55°C. IR: ν_{N_3} 2120 cm^{-1}. Found: C, 56.49; H, 4.75; N, 39.20%. Calcd for $C_{10}H_{10}N_6$: C, 56.07; H, 4.67; N, 39.25%. Hydrogenation of the diazide (6 g, 0.03 mol) followed by subsequent working up yielded diaminodihydrochloride (XXVI) (4.5 g, 68%).

Determination of Acid Dissociation Constants. The potentiometric measurements were carried out at 25°C and under a constant ionic strength (μ=0.100) with potassium nitrate, using a Horiba pH meter model P equipped with 1026 glass and 2010 calomel electrodes. The pH-meter reading was calibrated under the same titration conditions by referring to the hydrogen ion concentration cal-

culated from the acetic acid–potassium hydroxide titration system.

Calculation. The titration curves of diamine dihydrochlorides are shown in Fig. 1, from which the dissociation constants were calculated according to the standard procedure by Schwarzenbach *et al.*[16] as typical dibasic acids. The result for the present diamines are summarized in Table 1 along with the values of related compounds.

Infrared Spectra in Highly Diluted Solutions. Sample solutions were prepared as follows. To a solution of 20 mg of diamine hydrochloride in 0.5 ml of water were added three drops of 50% aqueous potassium hydroxide. The resulting alkaline solution was extracted with two 1.5 ml portions of tetrachloroethylene which had been purified by passing through a column of activated alumina. The combined extract was dried over anhydrous sodium sulfate. IR spectra were measured with matched pairs of 1.0, 5.0, and 10.0 cm quartz cells using a JASCO-DS-403G spectrophotometer at room temperature. Concentrations of the solutions were in the range 2×10^{-2}—6×10^{-4} M, where intermolecular association of these compounds can be neglected. The results are shown in Fig. 2.

16) G. Schwarzenbach, A. Willi, and R. O. Bach, *Helv. Chim. Acta*, **30**, 1303 (1947).

The authors are grateful to the Ministry of Education for financial support.

BULLETIN OF THE CHEMICAL SOCIETY OF JAPAN, VOL. 46, 990—992 (1973)

The Peroxide-induced Addition of Acetic Acid to Olefins

Yasuo SUHARA

National Chemical Laboratory for Industry, Honmachi, Shibuya-ku, Tokyo

(Received May 20, 1972)

The peroxide-induced addition of acetic acid to ethylene gave straight-chain fatty acids, such as butyric, hexanoic, octanoic, decanoic, lauric, myristic, and palmitic acids. Some α-branched-chain fatty acids were also formed. Di-*t*-butyl peroxide (DTBP) was an effective initiator in forming fatty acids. To obtain the 1 : 1-telomer acids, it was preferable that a 20—10 : 1 : 0.25 (mol) mixture of acetic acid, ethylene, and DTBP be heated at 150°C for 6 hr. Straight-chain fatty acids were also obtained by the reaction of acetic acid to 1-olefins under similar conditions.

The radical addition to 1-olefins gives anti-Markownikoff's products,[1] and α-branched-chain fatty acids are generally formed by the addition of fatty acids to 1-olefins.[2-4] It is expected that straight-chain fatty acids can be obtained by the radical addition of acetic acid to ethylene or 1-olefins. However, the removal of a hydrogen atom from the α-position of acetic acid is much more difficult than that of other fatty acids.[2,3,5,6] Consequently, the yields of the addition products of acetic acid to olefins are generally poor.[5,6] A few papers[3,5,7,8] have reported on the addition of acetic acid to olefins. However, the addition of acetic acid to ethylene has been considered in only two patents.[6,9] Therefore, the details of the reaction have not been made clear.

In the present study, in order to find preferable conditions for the formation of fatty acids, the acidic products of the radical addition of acetic acid to ethylene and 1-olefins under various conditions were investigated. The peroxides used were di-*t*-butyl peroxide (DTBP), *t*-butyl hydroperoxide (TBHP), benzoyl peroxide (BZPO), and dilauroyl peroxide (DLPO). The reaction was carried out in an autoclave, and the products were identified by GLC, GC–MS, and IR, and determined by GLC.

When BZPO or DLPO was used in the reaction temperature range of 60—180°C, no fatty acids were formed. When DTBP or TBHP was employed, however, the addition product was a mixture of acidic and neutral substances, and DTBP was the best initiator for the reaction forming fatty acids. No succinic acid formed by the radical dimerization of acetic acid was found in any products, although a small amount of succinic acid was obtained by heating acetic acid with DTBP in the absence of an olefin.

In the case of the addition of acetic acid to ethylene, no acidic product was separated from the reaction mixture, because butyric acid formed by the reaction is easily soluble in water. However, the compositions of the acidic products could be determined by GLC. The addition product contained acetic, butyric (1 : 1-telomer), 2-ethylbutyric, hexanoic, (2 : 1-telomer), 2-ethylhexanoic, octanoic (3 : 1-telomer) 2-ethyloctanoic, decanoic (4 : 1-telomer), lauric (5 : 1-telomer), myristic (6 : 1-telomer), and palmitic (7 : 1-telomer) acids, various hydrocarbons, and a small amount of an ester

1) J. C. Smith, *Chem. Ind.* (London), **1937**, 833; *ibid.*, **1938**, 461; J. C. Allen, J. I. G. Cadogan, B. W. Harris, and D. H. Hey, *J. Chem. Soc.*, **1962**, 4468.

2) G. I. Nikishin, Yu, N. Ogibin, and A. D. Petrov, *Izv. Akad. Nauk SSSR, Otd. Khim. Nauk*, **1961**, 1487.

3) J. C. Allen, J. I. G. Cadogan, and D. H. Hey, *Chem. Ind.* (London), **1962**, 1621.

4) W. C. Ault, T. J. Micich, A. J. Stirton, and R. J. Bistline, Jr., *J. Amer. Oil Chem. Soc.*, **42**, 233 (1965); T. J. Micich, E. A. Diamond, R. G. Bistline, Jr., A. J. Stirton, and W. C. Ault, *ibid.*, **43**, 539 (1966).

5) A. Steitz, Jr., and T. P. Moote, Jr., *Ind. Eng. Chem. Process Des. Develop.*, **1**, 132 (1962).

6) F. W. Banes, Wm. P. FitzGerald, and F. F. Nelson, U. S. 2585723 (1952); *Chem. Abstr.*, **47**, 2767e (1953).

7) E. Roe, D. A. Konen, and D. Swern, *J. Amer. Oil Chem. Soc.*, **42**, 457 (1965).

8) J. C. Allen, J. I. G. Cadogan, and D. H. Hey, *J. Chem. Soc.*, **1965**, 1918.

9) D. H. Hey and J. I. G. Cadogan, Belg. 621365 (1963); *Chem. Abstr.*, **59**, 9807c (1963).

Table 1. Addition of acetic acid to ethylene

Run No.	Molar ratio AcOH	C_2H_4	Peroxide (A, DTBP) (B, TBHP)	Reaction Temp. (°C)	Time (hr)	Yield from 1 kg of acetic acid (g) Fatty acid Straight-chain C_4	C_6	C_8	C_{10}	C_{12}	C_{14}	Total	Branched-chain	Total	Neutral product
1	20	1	A 0.25	150	6	5.9	4.5	2.6	1.9	1.2	0.8	16.9	12.1	30.0	3.4
2	10	1	A 0.25	130	6	6.0	3.4	1.9	1.4	0.7	0.3	13.7	14.2	27.9	16.1
3	10	1	A 0.15	150	6	1.5	1.5	1.4	0.7	0.5	0.1	5.7	4.5	10.2	7.9
4	10	1	A 0.20	150	6	7.2	4.0	2.5	1.4	0.5	0.3	15.9	13.5	29.4	9.7
5	10	1	A 0.25	150	4	6.7	2.8	1.7	0.9	0.3	0.1	12.5	9.1	21.6	8.8
6	10	1	A 0.25	150	6	8.5	4.1	2.6	1.5	0.9	0.4	18.0	13.1	31.1	10.3
7	10	1	A 0.25	150	11	5.3	6.3	2.6	1.9	1.2	0.5	17.8	17.9	35.7	14.3
8	10	1	A 0.25	170	6	8.1	4.8	2.4	1.3	1.0	0.4	18.0	14.8	32.8	13.8
9	10	1	A 0.25	190	6	8.5	4.6	1.9	1.1	0.5	0.2	16.8	13.8	30.6	16.5
10	5	1	A 0.25	150	6	4.4	4.1	3.5	1.6	0.9	0.4	14.9	16.2	31.1	28.0
11	3	1	A 0.25	150	6	7.3	6.1	4.3	2.6	1.6	0.4	22.3	21.9	44.2	53.0
12	10	1	B 0.25	150	6	7.2	3.0	2.2	1.9	1.3	0.7	16.3	13.5	29.8	22.5
13	10	1	B 0.25	170	6	6.7	3.2	2·0	1.8	1.4	0.9	16.0	15.2	31.2	26.7

a) Small amounts of palmitic acid were detected except Runs 3, 5, and 9.

of acetic acid. 2-Ethylbutyric, 2-ethylhexanoic, and 2-ethyloctanoic acids are presumably formed by the adition of butyric, hexanoic, and octanoic acids respectively to ethylene. 2-Ethylhexanoic acid may also be formed by the addition of ethylene to a radical formed by the addition of butyric acid to ethylene. The ester of acetic acid may be formed by the ionic addition of acetic acid to ethylene.[10]

The reaction conditions and the yields of the addition products of acetic acid to ethylene are shown in Table 1. The best yield of straight-chain fatty acids was given by Run 11 (the conversion of ethylene to straight-chain fatty acid: 7.0%), but very large amounts of neutral substances were also formed in this case. On the other hand, the autoclave was a little injured at reaction temperatures above 70°C. Judging from the conversions of ethylene, the yields of the products, and the reaction time and the temperature, the conditions of Runs 1 and 6 are preferable (the conversions of ethylene to straight-chain fatty acids were 35.2% in Run 1 and 17.2% in Run 6).

The telomerization for the formation of fatty acids with reasonable yields required 20—25 mol % of a peroxide to olefin; the amount of the peroxide was much larger than the amount employed usually as an initiator. This fact shows that the kinetic chain lengths are rather short.

The addition of acetic acid to 1-olefins was carried out under conditions similar to those in the case of Run 6, and the acidic and neutral products were separated from each other. The acidic addition product of acetic acid to 1-octene was a mixture of hexanoic, heptanoic, 3-methylnonanoic (Markownikoff's product), decanoic (1 : 1-telomer), 4-hexyldodecanoic 2 : 1-telomer), and 4,6-dihexyltetradecanoic (3 : 1-telomer) acids. It is noteworthy that Markownikoff's product[11] and lower fatty acids were also formed, although their yields were quite low.

Gas chromatograms of the acidic addition products of acetic acid to other 1-olefins resembled that of the acidic addition product of acetic acid to 1-octene. Thus, the formations of 1 : 1-, 2 : 1-, and 3 : 1-telomers, and of small amounts of lower fatty acids and Markownikoff's products, were observed. The following acids (1 : 1-telomers) with purities of more than 95% could be obtained from the acidic products of the addition of acetic acid to the corresponding 1-olefins by distillation or recrystallization: octanoic (from 1-hexene), decanoic (from 1-octene), lauric (from 1-decene), myristic (from 1-dodecene), palmitic (from 1-tetradecene), stearic (from 1-hexadecene),

Table 2. Conversion of 1-olefin in addition of acetic acid to 1-olefin

Acetic acid : 1-olefin : DTBP=10 : 1 : 0.25 (mol)
Reaction temperature : 150°C. Reaction time: 6 hr.

Olefin	Conversion of 1-olefin (%) Telomer 1 : 1	2 : 1	3 : 1	M* a)	Neutral product
1-Hexene	28.9	10.0	4.1	0.3	40.8
1-Octene	28.3	9.7	2.5	0.5	45.7
1-Decene	30.7	8.7	2·8	0.6	46.6
1-Dodecene	29.6	6.0	2.1	0.8	45.5
1-Tetradecene	28.5	6.1	1.7	0.8	48.2
1-Hexadecene	28.9	6.0	—	0.8	47.0
1-Octadecene	26.7	4.9	—	0.7	44.4

a) M: Markownikoff's product

10) G. I. Nikishin, R. I. Mustafaev, and A. D. Petrov, *Izv. Akad. Nauk SSSR., Otd. Khim. Nauk*, **1963**, 359.

11) V. D. Vorob'ev and G. I. Nikishin, *ibid.*, **1966**, 138; G. I. Nikishin, M. G. Vinogradov, and R. V. Kereselidze, *ibid.*, **1967**, 1624; D. Elad and J. Rokach, *J. Org. Chem.*, **29**, 1855 (1964); G. I. Nikishin, M. G. Vinogradov, and R. V. Kereselidze, *Zh. Org. Khim.*, **2**, 1918 (1966).

and eicosanoic (from 1-octadecene) acids.

The conversions of 1-olefins are shown in Table 2. Allen *et al.* obtained decanoic acid in a 70% yield from a 300 : 1 : 0.15 (mol) mixture of acetic acid, 1-octene, and DTBP.[3] Although the yield based on the moles of 1-octene employed was very high, only 6.7 g of decanoic acid were obtained from 1 kg of acetic acid under the above conditions. According to the conditions shown in Table 2, however, 81.2 g of decanoic acid were obtained from the same amount of acetic acid. Therefore, the present conditions were preferable practically.

Dimers and trimers of the 1-olefins employed and esters of acetic acid were found in the neutral products.

Experimental

GLC was carried out with a Hitachi Gas Chromatogram 063 equipped with dual columns (3 mm × 2 m) packed with 15% SE 30-Chromosorb WAW (70→300°C, 10°C/min) or 20% DEGS-Chromosorb WAW (50→220°C, 10°C/min).

GC-MS was carried out with a Shimadzu LKB-9000 Gas Chromatograph-Mass Spectrometer with a column packed with 15% SE 30-Chromosorb WAW, and the ionization intensity was 70 eV.

The IR spectra were measured in a liquid film with a Hitachi EPI-S2 Infarared Spectrophotometer, a sodium chloride cell being used.

Identification of Products. The acidic products were identified by deriving them into their butyl esters, and by comparing the retention times of the esters in GLC with those of authentic esters using two columns packed with SE 30 and DEGS. In the cases of the addition products of acetic acid to ethylene, both butyl and amyl esters of the products were used in order to distinguish between acidic and neutral substances. In addition, the correction factor for GLC and mass spectrum of each butyl ester were measured.

The derivation into butyl and amyl esters was done as follows: Ten milliliters of 1-butanol or 1-pentanol containing 0.2 ml of sulfuric acid was added to 1 g of a sample, and the solution was warmed for 1 hr on a water bath. Then, a solution saturated with both sodium carbonate and sodium chloride was added to the reaction mixture until the mixture was free from sulfuric acid; the upper layer of the mixture was then ready to submit to GLC.

The neutral products were analyzed by means of GLC and IR without pretreatment.

Materials. The purity of ethylene was more than 99%. Each gas chromatogram of acetic acid and 1-olefins showed a single peak. The 1-olefins used were 1-hexene, 1-octene, 1-decene, 1-dodecene, 1-tetradecene, 1-hexadecene, and 1-octadecene. The peroxides were all commercial products.

Addition of Acetic Acid to Ethylene. A typical procedure (Run 6) was as follows: Ninety milliliters of acetic acid and 5.70 g of DTBP were put in a 200-ml autoclave, after which ethylene was fed into the autoclave until the pressure gauge showed 36 kg/cm² at 20°C (the pressure was calculated by presuing that ethylene was an ideal gas and that it was insoluble in acetic acid). When stirring was begun, the pressure quickly dropped to 13.5 kg/cm². The reaction mixture was heated at 150°C under stirring. The pressure rose to 26 kg/cm² with an increase in the temperature, and then it gradually decreased to 18 kg/cm². After 6 hr, the reaction mixture was cooled and distilled to remove most of the unreacted acetic acid.

A part of the residue was esterified for identification. Most of the residue was dissolved in ether, and the ethereal solution was washed successively with water, a 5% aqueous potassium carbonate solution, and water. The ethereal solution was dried over anhydrous sodium sulfate, and the ether was distilled off to obtain neutral substances.

The conversions of ethylene and the yields of fatty acids were calculated from the results of GLC, and the amounts of the residue and neutral substances.

Addition of Acetic Acid to 1-Olefins. A mixture of acetic acid (2.0—1.5 mol), and 1-olefin, and DTBP (molar ratio, 10 : 1 : 0.25) was stirred in a 200-ml autoclave at 150°C for 6 hr. Then, unreacted acetic acid was distilled off from the reaction mixture, and the residue was dissolved in ether. The ethereal solution was washed successively with water, a 5% aqueous potassium carbonate solution, and water. After being dried over anhydrous sodium sulfate, the ether was distilled off to obtain neutral product. The washings obtained above were combined and then acidified with hydrochloric acid. The acidic product separated from the washings was extracted with ether. The ethereal solution was washed with water and dried over anhydrous sodium sulfate. The ether was distilled off, and acidic product was thus obtained. A part of the acidic product was esterified to make identification possible.

The isolation of 1 : 1-telomer acids from the acidic products was carried out by distillation (C_8—C_{12} acids) or by three recrystallizations (C_{14}—C_{20} acids) from petroleum benzin (bp 60—85°C).

The author is grateful to Mr. Yasuhiko Kubota for recording the GC-MS, and to Mr. Yutaka Inoue and Mr. Mitsuru Tanaka for their assistance in the experimental work.

NOTES

BULLETIN OF THE CHEMICAL SOCIETY OF JAPAN, VOL. 46, 993—994 (1973)

Further Study on the Course of Olefin Dimerization Catalyzed by σ-Aryl Nickel(II) Compound-Boron Trifluoride Etherate

Ken-ichi MARUYA, Tsutomu MIZOROKI, and Atsumu OZAKI

Research Laboratory of Resources Utilization, Tokyo Institute of Technology, Ohokayama, Meguro-ku, Tokyo

(Received September 22, 1972)

The codimerization of ethylene with propylene catalyzed by the catalyst systems composed of bis(triphenylphosphine)bromo(σ-aryl)nickel(II) and boron trifluoride etherate was investigated to know the course of the reaction from the product distribution. 2-Pentene and 2-methyl-1-butene are mainly formed in the first stage of the codimerization. Their formations are in consistent with the process of the insertion of propylene into ethyl-nickel bond to form 1-methylbutyl- and 2-methylbutyl-nickel complexes followed by elimination of β-hydrogen to give 2-pentene and 2-methyl-1-butene respectively.

It was reported that a new catalyst system composed of a σ-aryl nickel(II) compound and boron trifluoride etherate is highly active and selective for ethylene dimerization[1] and the codimerization of ethylene with styrene[2] to give butene and 3-phenyl-1-butene respectively. From the study on the isotopic exchange between C_2H_4 and C_2D_4 and the dimerization of C_2D_4 using this catalyst system, it has been concluded that a nickel hydride is responsible for dimerization of ethylene and that the hydrogen is supplied by dissociative addition of ethylene.[3] In the previous paper,[4] two possible processes(1-1 and 1-2) were left undiscriminated on the course of dimerization of ethylene with the same catalyst.

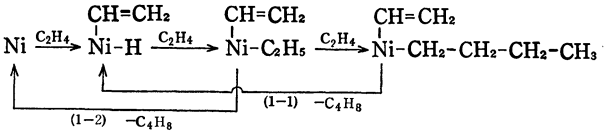

The isomer distribution of pentene obtained from the codimerization of ethylene with propylene, however, is helpful to discriminate them, because the isomer distribution of pentene formed depends on the processes expected for 1-1 and 1-2.

The present work was undertaken to clarify the course of olefin dimerization catalyzed by bis(triphenylphosphine) bromo(1-naphthyl)nickel(II) in the presence of boron trifluoride etherate by investigating the product distribution of the codimerization of ethylene with propylene.

Experimental

Dried bis(triphenylphosphine)bromo(1-naphthyl)nickel (II) (1 mmol) prepared according to the method described in the literature[5] was dissolved in a dried methylene dichloride (30 ml) at 0°C under nitrogen atmosphere, using a two necked flask (50 ml), followed by adding a given amount of benzene solution of purified boron trifluoride etherate (10% in volume) with vigorous stirring. The nitrogen in the flask was, then, evacuated before propylene (300 ml at S. T. P.) was introduced into the flask at 0°C and the pressure was kept constant at 40 cmHg for a given period of time by supplying ethylene during the run. The codimerization was terminated by cooling the flask with liquid nitrogen. All volatile materials such as ethylene, propylene, butenes, pentenes, solvent *etc.* in the flask were transferred into another flask cooled with liquid nitrogen and their amounts were determined by a gas chromatograph equipped with VZ-7 columun (8 m).

Results and Discussion

The mole ratio of propylene to ethylene in the solution was separately estimated from their solubilities in methylene dichloride under the same condition. On addition of propylene (300 ml S. T. P.) to the methylene dichloride solution(30 ml) of 1-$C_{10}H_7Ni(P\phi_3)_2Br$ in the absence of boron trifluoride etherate, 249 ml of propylene was dissolved leaving a 20 cmHg of propylene in the gas phase. On a further addition of ethylene to this solution up to a total pressure of 40 cmHg including 20 cmHg of propylene and 15 cmHg of the solvent vaper, 13 ml (S. T. P.) of ethylene was dissolved. Thus the mole ratio, C_3H_6/C_2H_4, in the solution is calculated to be about 23, a fairly large excess of propylene. This ratio could be assumed to be unchanged during the early period of the reaction time. Since ethylene was absorbed almost linearly with respect to the reaction time, the rate of ethylene absorption was obtained from its amount consumed within a given reaction time. This rate can be regarded as the rate of reaction of ethylene under large excess of propylene dissolved. The rate increases linearly with increasing the mole ratio as was observed in the dimerization of ethylene.[4] In Fig. 1, the product distribution at the same temperature and concentrations of ethylene and propylene are plotted against the amount of ethylene consumed, which depends on the reaction time and the mole ratio of $BF_3 \cdot OEt_2$ to 1-$C_{10}H_7Ni(P\phi_3)_2Br$. This indicates that the product distribution neither depends on the amount of ethylene consumed, nor on the mole ratio of the catalyst. Accordingly, both butene and pentene are catalytically formed by the same active species and its amount increases almost

1) K. Maruya, T. Mizoroki, and A. Ozaki, This Bulletin, **43**, 3630 (1970).
2) N. Kawata, K. Maruya, T. Mizoroki, and A. Ozaki, *ibid.*, **44**, 3217 (1971).
3) K. Maruya, T. Kuroki, T. Mizoroki, and A. Ozaki, *ibid.*, **44**, 2002 (1971).
4) K. Maruya, T. Mizoroki, and A. Ozaki, *ibid.*, **45**, 2255 (1972).
5) J. Chatt, and B. L. Show, *J. Chem. Soc.*, **1960**, 1718.

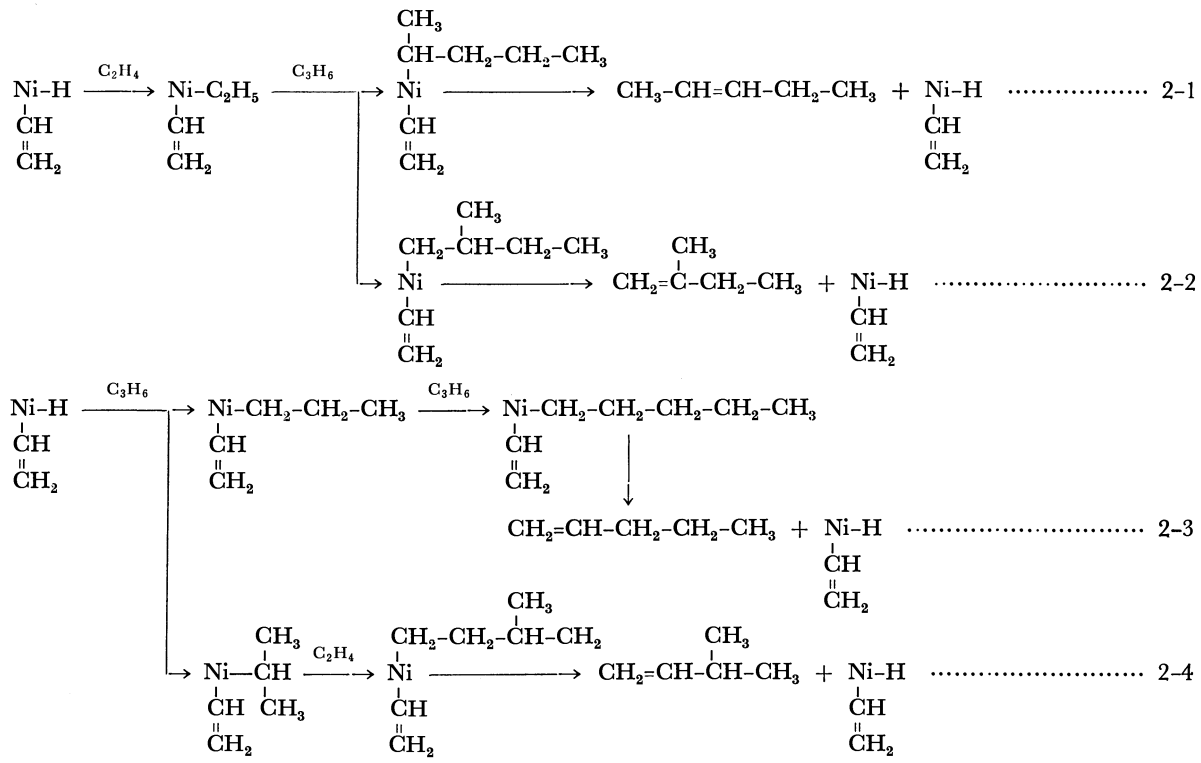

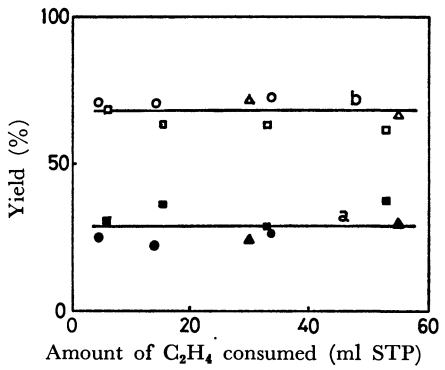

Fig. 1. Yields of butene and pentene based on the amount of ethylene consumed.
a: pentene, b: butene, ●,○: $BF_3 \cdot OEt_2$ 0.8 mmol, ■,□: $BF_3 \cdot OEt_2$ 1.6 mmol, △,▲: $BF_3 \cdot OEt_2$ 2.4 mmol

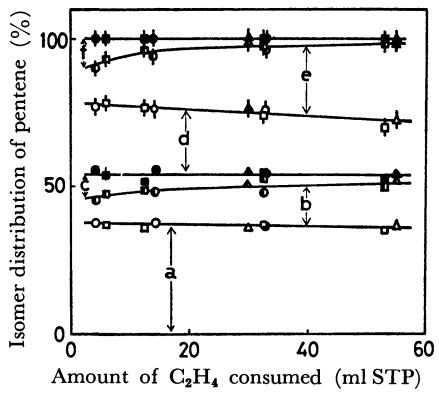

Fig. 2. Product distribution of the codimerization of ethylene with propylene.
a: 2-methyl-1-butene, b: 2-methyl-2-butene, c: 3-methyl-1-butene, d: *cis*-2-pentene, e: *trans*-2-pentene, f: 1-pentene. ○,◐,●,◇,◈,◆: $BF_3 \cdot OEt_2$ 0.8 mmol, □,◧,■,▯,▮,▬: $BF_3 \cdot OEt_2$ 1.6 mmol, △,◭,▲,△,◭,▲: $BF_3 \cdot OEt_2$ 2.4 mmol

linearly with increasing the amount of boron trifluoride etherate as was discussed in the previous paper.[4] The isomer distribution of pentene is shown in Fig. 2 as a function of the amount of ethylene consumed. The initial products of the codimerization are mainly 2-pentene and 2-methyl-1-butene. The fraction of isopentene in total pentene is nearly 54±1%, independent of the amount of ethylene consumed and the mole fraction of the catalyst. Since the sum of the selectivities to butene and pentene reaches near 100%, a secondary reaction of butene and pentene with ethylene is negligible. The coordination equilibrium between olefin and the active species is evidently more favorable for ethylene than for propylene, because butene is preferably formed even in the presence of a large excess of propylene. This is also supported by the strong inhibition of the dimerization of propylene caused by ethylene.

If pentene is formed through the following processes (2-1～4) expected for 1-1, four isomers of pentene, 2-methyl-1-butene, 1-pentene and 3-methyl-1-butene, will be initially formed. If it does through the other processes expected for 1-2, neither 2-pentene, nor 2-methyl-1-butene will be initially formed. Figure 2 indicates that pentene should be formed predominantly through the processes of 2-1～4, since 2-pentene (d and e) and 2-methyl-1-butene(a) are main products, where the formation of small amounts of 1-pentene and 3-methyl-1-butene can be attributed to the disadvantage of propylene for its coordination to the active species of the catalyst. Thus this results supports that butene is formed through the process of 1-1. At present, there is no evidence to support the existence of vinyl ligand on nickel atom during the reaction. All attempts to detect the vinyl and its coupling compounds were unsuccessful.

BULLETIN OF THE CHEMICAL SOCIETY OF JAPAN, VOL. 46, 995—996 (1973)

The Distribution of Benzene and Its Monosubstituted Derivatives between Hexane and Water

Tatsuya SEKINE, Yasuo SUZUKI, and Naohiko IHARA

Department of Chemistry, Science University of Tokyo, Kagurazaka, Shinjuku-ku, Tokyo

(Received April 14, 1972)

The liquid-liquid distribution equilibria of benzene and its eight monosubstituted derivatives have been investigated in order to study the effect of the substituted atom or atom group on the distribution behavior. The results are compared with the solubilities of the materials in water.

Experimental

All of the reagents used were of a reagent grade. The purity was checked by spectrometry and, in some cases, by gas chromatography. All of the procedures were carried out in a thermostatted room at 25±0.3°C. A weighed portion of the material was dissolved in hexane. The concentration of aniline was further checked by titration with a standard acid solution.

The distribution experiments were done as follows. A portion of a hexane solution of the material and a portion of water (in the case of benzoic acid, 0.03M perchloric acid in order to prevent dissociation) were placed in a stoppered glass vessel. The two phases were shaken vigorously by hand for three minutes, and then the hexane phase was transferred into a stoppered glass tube and centrifuged. When the distribution ratio was too high, a portion of this aqueous phase was also shaken with a portion of hexane, and then this hexane phase was transferred into another glass tube and centrifuged. The concentration of the material in the hexane phase was determined by spectrometry.

Results and Discussion

The distribution ratio of the material, M, was defined as follows:

$$D = \frac{[M]_{org,total}}{[M]_{total}} \quad (1)$$

The subscript "org" denotes the species in the organic phase, while the absence of a subscript denotes that in the aqueous phase.

The distribution ratios of all these materials except benzoic acid were independent of their concentrations. Thus, it was concluded that these materials undergo no dissociation in the aqueous phase and that there is no association in the organic phase under these experimental conditions.

For this reason, the distribution constant;

$$M \rightleftharpoons M_{(org)}, \quad K_D = \frac{[M]_{org}}{[M]} \quad (2)$$

for these materials is identical with the distribution ratio. The constants obtained are listed in Table 1.

The distribution ratio of benzoic acid is given in Fig. 1 as a function of its concentration in the aqueous phase. Since the aqueous phase is 0.03M perchloric acid, the dissociation of benzoic acid (pK_a=4.0[1] μ=0.1 25°C)) is negligible. Furthermore, this distribution ratio was unaffected by perchloric acid within the concentration range from 0.003M to 0.03 M.

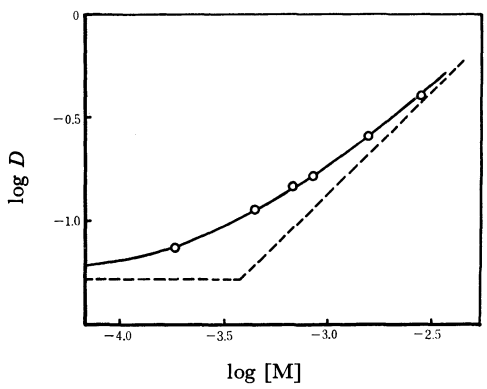

Fig. 1. Distribution ratio of benzoic acid which is denoted by M, between hexane and 0.03 M $HClO_4$ as a function of the solute concentration in the aqueous phase. The solid curve represents:
$\log D = \log(K_D + 2K_{dim(org)}K_D^2[M])$
$= \log(5.13\times10^{-2} + 1.32\times10^{2}[M])$
The two dotted lines represent the asymptotes for the extraction curve.

Thus, the distribution ratio of benzoic acid can be written as;

$$D = \frac{[M]_{org} + 2[(M)_2]_{org}}{[M]} \quad (3)$$

The dimerization constant in the organic phase can be written as;

$$2M_{(org)} \rightleftharpoons (M)_{2(org)}, \quad K_{dim(org)} = [(M)_2]_{org}/[M]^2_{org} \quad (4)$$

By introducing the distribution constant and this dimerization constant, Eq. (3) can be rewritten as;

$$D = K_D + 2K_{dim(org)}K_D^2[M] \quad (5)$$

The K_D and $2K_{dim(org)}K_D^2$ values can be determined by a curve-fitting method.[2] The value of $K_{dim(org)}$ obtained from these values is listed in Table 1. The table also lists the solubilities of these materials reported in the literature.[3]

The solubility in water has sometimes been employed as an index of the aquophilic tendency of molecular substances; when a molecule has an aquophilic group, it is usually estimated to be more soluble in water than those which have no such group. However, this is only a rough approximation, because the introduction of such a group into a nonpolar molecule increases

1) M. Yasuda, K. Yamasaki, and H. Ohtaki, This Bulletin, **33**, 1067 (1960).

2) F. J. C. Rossotti and H. Rossotti, "The Determination of Stability Constants" McGraw-Hill, New York (1961).

3) H. Stephen and T. Stephen, "Solubility of Inorganic and Organic Compounds" Vol. I, Pergamon Press, Oxford (1963).

TABLE 1. DISTRIBUTION CONSTANTS BETWEEN HEXANE AND WATER (25°C) AND OTHER PROPERTIES OF BENZENE AND ITS MONOSUBSTITUTED DERIVATIVES

Material	Distribution (25°C)		Solubility (30°C)	
	K_D[a]	$K_D/K_D(C_6H_6)$	S[b] (M)	$S(C_6H_6)/S$
Benzene	2.8×10^{2}	1	2.4×10^{-2}	1
Toluene	9.7×10^{2}	3.5	6.2×10^{-3}	3.9
Fluorobenzene	3.0×10^{2}	1.1	1.6×10^{-2}	1.5
Chlorobenzene	9.5×10^{2}	3.4	4.3×10^{-3}	5.6
Bromobenzene	1.2×10^{3}	4.5	2.8×10^{-3}	8.6
Nitrobenzene	3.1×10	1.1×10^{-1}	1.7×10^{-2}	1.4
Aniline	9.0×10^{-1}	3.3×10^{-3}	4.1×10^{-1}	5.9×10^{-2}
Phenol	1.3×10^{-1}	4.9×10^{-4}	9.8×10^{-1}	2.4×10^{-2}
Benzoic acid[c]	5.1×10^{-2}	1.9×10^{-4}	3.4×10^{-1}	7.1×10^{-2}

a) The values for benzoic acid, *cf.* Fig. 1. b) The values of solubility by wt% are summarized in Ref. 3. They are converted into molarity assuming that the density of the solution at this temperature is 1.0. c) The dimerization constant in Eq. (4) was obtained to be 2.5×10^{4} in hexane.

not only the interaction between the solute and water molecules in the solution, but also the interaction among the molecules in the pure solute phase. For example, as can be seen from Table 1, the solubility of nitrobenzene in water in the molar units is even lower than that of benzene; this is probably caused by the strong interaction among the molecules in the water-saturated nitrobenzene phase.

The increase in the distribution ratio of toluene may mainly be attributed to the increase in the molecular volume. It was reported by Collander[4] that the distribution ratio of organic compounds between diethyl ether and water increases by a factor of from two to four for each new CH_2 group introduced into the molecule in a homologous series. The solubility of normal aliphatic alcohols in water was found by Kinoshita, Ishikawa, and Shinoda[5] to decrease by a factor of four when a CH_2 group is added to the hydrocarbon chain; an increase in the distribution ratio of aliphatic alcohols between benzene and the aqueous phase by a factor of around four was also reported by Tanaka and Kojima.[6] The increase in the distribution ratio by a factor of 3.5 by the replacement of a hydrogen atom of benzene with a methyl group in the present study is quite similar to these previous results.

The effect on the distribution of the replacement of a hydrogen atom with a halogen atom is not very clear. However, the effect of the replacement with one of the four aquophilic atom groups, $-NO_2$, $-NH_2$, -OH, and -COOH, seems to be very clear. The replacement increases the molecular volume, but it also increases the interaction with water very much, and the distribution ratio is very much decreased by the latter.

Since the interaction between the solute molecules in the pure solute phase has no effect on the distribution ratio, the effect of the replacement on the distribution is not parallel with that on the solubility, as may be seen from Table 1; the introduction of an aquophilic group does not so increase the solubility into water as it increases the distribution into the aqueous phase.

The dimerization of benzoic acid in the organic phase is very important for its distribution. As can be seen from Fig. 1 and from the value of K_D, the effect of the dimerization becomes negligible only when the concentration is very low.

4) A. A. Collander, *Acta Chem. Scand.*, **3**, 717 (1949).
5) K. Kinoshita, H. Ishikawa, and K. Shinoda, This Bulletin, **31**, 1081 (1958).
6) M. Tanaka and I. Kojima, *J. Inorg. Nucl. Chem.*, **27**, 1769 (1967).

BULLETIN OF THE CHEMICAL SOCIETY OF JAPAN, VOL. 46, 997—998 (1973)

Rise Times of Triplet-Triplet Absorptions of Some Aromatic Hydrocarbons

Naohiko MIKAMI, Yasuo UDAGAWA, Ikuo HAYASHI, Koji KAYA, and Mitsuo ITO

Department of Chemistry, Faculty of Science, Tohoku University, Aramaki, Sendai

(Received July 4, 1972)

Recent development of lasers has given the chemist short-lived sources of excitation which are powerful enough to observe excited singlet species by absorption spectroscopy.[1-5] This technique has been called "laser photolysis" and applied to know higher excited singlet levels. Analyses of the growth rate of triplet state and the decay process of singlet state which occur during scores of nanoseconds are possible by the similar technique and give informations about dynamic behavior of energy relaxation. Especially, if the rate constant of the growth of the triplet state is determined, it provides information on the initial state of the relaxation process to the triplet state. In this note we report the rise times of the triplet states of phenanthrene, 3,4-benzpyrene and 1,2,3,4-dibenzanthracene in 2-methyltetrahydrofuran at room temperature. The transient spectra and the decay times of the singlet states of these compounds were already reported by Porter and Topp.[4] In order to make a comparison, we also measured the decay times of their excited singlet states on the same experimental condition for the triplet states.

A coaxial type pulsed N_2 laser constructed in our laboratory was used as a pumping source. A 12 nsec, 0.2 mJ. pulse of light of wavelength of 3371 Å is produced with a repetition rate of *ca.* 30 Hz. In spite of the small peak power of our N_2 laser used here, sufficient amount of excited singlet molecules for observation of the transient process can be accumulated by focusing the laser beam on a very small area.

A probe light must be intense on account of the low sensitivity of wide band detection system. When fluorescence overlaps S–S or T–T absorption region, monitoring light has to be more intense than the fluorescence by the order of two or more. A CRL 52B cw Ar ion laser which has total output power of 4 W was used for this purpose. This laser has eight lasing lines between 4579 Å and 5145 Å and the molecules studied here have both S–S and T–T absorptions in this region.[4] The two laser beams were made to coincide strictly by employing the experimental setup shown in Fig. 1. The greater part of the light from N_2 laser passed through a quartz plate Q, while a portion

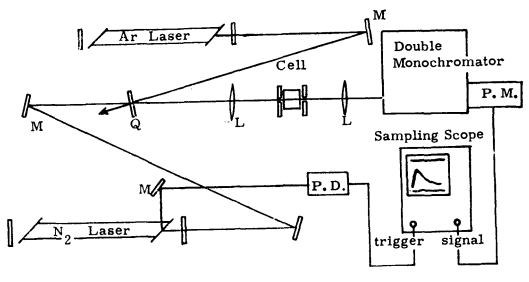

Fig. 1. Schematic diagram of the apparatus.

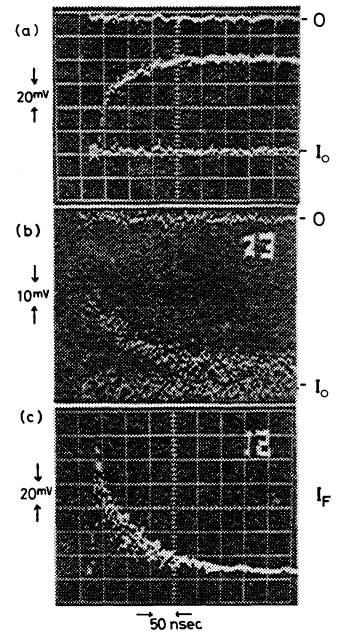

Fig. 2. Oscilloscope tracings (50 ns/div.) of 5×10^{-3} mol/l phenanthrene in 2-methyltetrahydrofuran. (a) Rise of the T_1–T_n absorption at 4880 Å. (b) Decay of the S_1–S_n absorption at 5145 Å. (c) Decay of the fluorescence at 4200 Å.

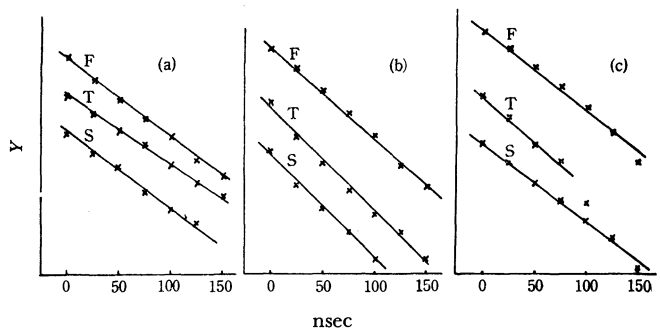

Fig. 3. First order decay curves of the singlet absorption (S); $Y=\log(\text{O.D.})^{S-S}$ and the fluorescence (F); $Y=\log I_F$, and first order increase of the triplet absorption (T); $Y=\log((\text{O.D.})^{T-T}_{max}-(\text{O.D.})^{T-T})$. (a): phenanthrene, (b): 3,4-benzopyrene, (c): 1,2,3,4-dibenzanthracene.

1) J. R. Novak and M. W. Windsor, *Proc. Roy. Soc., Ser. A*, **308**, 95 (1968).
2) R. Bonneau, J. Faure, and J. Joussot-Dubien, *Chem. Phys. Lett.*, **2**, 65 (1968).
3) R. McNeil, J. T. Richards, and J. K. Thomas, *J. Phys. Chem.*, **74**, 2290 (1970).
4) G. Porter and M. R. Topp, *Proc. Roy. Soc., Ser. A*, **315**, 163 (1970).
5) D. S. Kliger and A. C. Albrecht, *J. Chem. Phys.*, **53**, 4059 (1970).

Table 1. Rise times of triplet–triplet absorption, decay times of singlet–singlet absorption, and lifetimes of fluorescence in 2-methyltetrahydrofuran

		Rise time of T–T absorption	Decay time of S–S absorption	Decay time of fluorescence
Phenanthrene	This work	78 ns (4880 Å)	74 ns (5145 Å)	71 ns (4200 Å)
	Porter and Topp[a,c]		65 ns	67.2 ns
3,4-benzpyrene	This work	53 ns (4765 Å)	53 ns (5145 Å)	60 ns (4140 Å)
	Porter and Topp[b,c]		49.1 ns	57.5 ns
1,2,3,4-dibenzanthrecene	This work	62 ns (4579 Å)	71 ns (4880 Å)	71 ns (4100 Å)
	Porter and Topp[b,c]		51.2 ns	53.5 ns
	Lavalette *et al.*[a,d]	58 ns	56 ns	61 ns

a) In polymethyl methacrylate. b) In cyclohexane. c) Ref. 4. d) Ref. 6.

of the Ar ion laser beam was reflected and the two beams were adjusted to coincide exactly. Although the reflectivity of the quartz plate is low, reflected Ar ion laser beam was still intense enough. After adequate diaphragms the two beams were focused through the sample cell and refocused onto the entrance slit of a Nalumi 0.3-m double monochromator.

The repeated pulsed N_2 laser enabled us to employ sampling technique which is suitable for high speed phenomena. A probe beam emerging from the exit slit of the monochromator was detected by a 1P28 photomultiplier with a load resistance of 50 Ω. The output of the photomultiplier at a centain time after triggering was displayed on a Tektronix 564A sampling oscilloscope.

Fig. 2 shows the rise curve of the T–T absorption of 5×10^{-3} mol/l deaerated solution of phenanthrene in 2-methyltetrahydrofuran taken at 4880 Å and decay curve of the S–S absorption at 5145 Å. Upper traces are with the monitoring light off and lower traces are with the exciting light off. Assuming first order processes, triplet rise time and singlet decay time are determined by plotting log $((O.D.)^{T-T}_{max}-(O.D.)^{T-T})$ and log $(O.D.)^{S-S}$ *vs.* time, respectively. Fig. 3 shows that they are described well as first order processes and the results are tabulated in Table 1. The rise times of the T–T absorption and the decay times of the S–S absorption coincide with each other within experimental errors and also agree well with the fluorescence lifetimes. These agreements apparently show that the initial states of the energy relaxation process of these molecules to their triplet states are the fluorescent states. In this table, the rate times obtained in this work are somewhat different from those of the literatures.[4,6] It is probably due to the difference of the solvent used.

The method described here is considered to be of wide applicability to the study of the dynamic behaviors of the excited state molecules. For example, intermediate species formed after the photolysis can be detected, and the rate of formation can be determined. Recently it has been suggested that intersystem crossing of electron-donor-acceptor complex[7] or photoionization of organic molecules[8] may occur from excited Franck-Condon state, not from fluorescent state. Such problems can be dissolved by the comparison of the rise time of triplet state or ionized molecules with the decay time of singlet state, both of which are determined with high accuracy by this technique.

6) D. Lavalette, C. J. Werkhaven, D. Bebelaar, J. Langelaar, and J. D. W. Van Voorst, *Chem. Phys. Lett.*, **9**, 230 (1971).

7) H. Masuhara, N. Tsujino, and N. Mataga, *ibid.*, **12**, 481 (1972).

8) M. Ottolenghi, *ibid.*, **12**, 339 (1972).

BULLETIN OF THE CHEMICAL SOCIETY OF JAPAN, VOL. 46, 998—999 (1973)

Charge-transfer and Proton-transfer in the Formation of Molecular Complexes. V.[1] Tryptophan Picrate

Yoshio MATSUNAGA

Department of Chemistry, Faculty of Science, Hokkaido University, Sapporo

(Received July 11, 1972)

In connection with our work on molecular complexes in which charge-transfer and proton-transfer interactions operate simultaneously between the component molecules, and also in connection with a recent report on the crystal and molecular structures of red-colored serotonin picrate monohydrate by Thewalt and Bugg,[1-3] a spectroscopic examination of the tryptophan picrate has been undertaken. The preparation of this picrate was reported by Mayeda as early as 1907.[4] He noted also that the color is similar to that of the indole picrate.

The tryptophan picrate was crystallized from water following the procedure described by Mayeda, and

1) Part IV: G. Saito and Y. Matsunaga, This Bulletin, **46**, 714 (1973).

2) Y. Matsunaga and G. Saito, *ibid.*, **45**, 963 (1972).

3) U. Thewalt and C. E. Bugg, *Acta Crystallogr., B*, **28**, 82 (1972).

4) M. Mayeda, *Z. Physiol. Chem.*, **51**, 263 (1907).

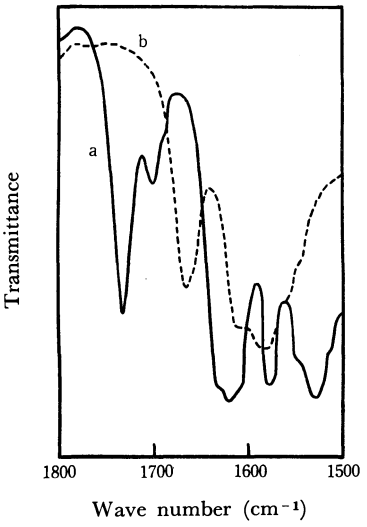

Fig. 1. Vibrational spectra of a) the tryptophan picrate and b) tryptophan.

the indole picrate, from chloroform. As was pointed out by Briegleb and Delle,[5] the infrared spectrum of the latter complex, well approximated by the superposition of the spectra of the component compounds, clearly indicates the absence of proton transfer.

Tryptophan is in the form of the zwitter ion; therefore, the vibrational spectrum in the region from 2000 to 4000 cm^{-1} is dominated by the pattern due to the NH_3^+ group. Although this pattern remains through the picrate formation, a big change is observed in the region from 1500 to 1800 cm^{-1} (see Fig. 1). A strong band located at 1740 cm^{-1} in the picrate should be assigned to the carbonyl stretching vibration. These pieces of evidence indicate that the proton-transfer from picric acid to tryptophan occurs in the following way:

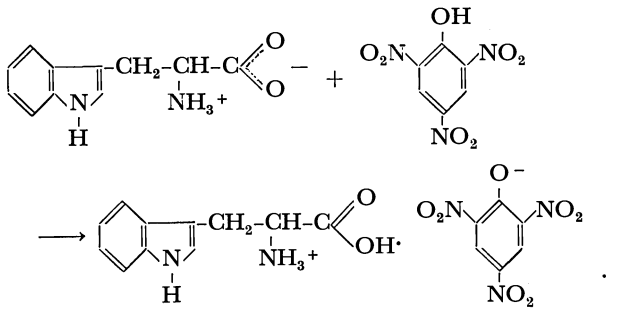

Both of the complexes are reddish orange. Their visible spectra, measured by the diffuse reflectance method, are plotted using the Kubelka-Munk function in Fig. 2. Indole and its derivatives have been shown to be electron donors.[6] The charge-transfer absorption in the indole-*s*-trinitrobenzene complex in carbon tetrachloride is expected to appear around 26 kK by the extrapolation of the plot of the energies corresponding to the band maxima of indole with each of a series of acceptors against the energy maxima

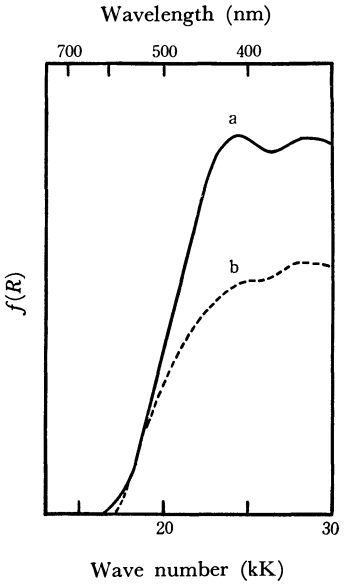

Fig. 2. Diffuse reflection spectra of a) the tryptophan picrate and b) the indole picrate.

of the spectra of the corresponding hexamethylbenzene-electron-acceptor complexes. As the electron-acceptor strength of picric acid is comparable with that of *s*-trinitrobenzene, the absorption maximum observed at about 25 kK in the solid indole picrate may be attributed to the charge-transfer interaction. The intense maximum located at 24.4 kK in the tryptophan picrate is possibly due to the picrate ion; however, the contribution from this yellow-colored anion must end by 21 kK.[7] No absorption beyond this limit is present in either component species alone. As the indole nucleus and the functional groups in protonated tryptophan are separated by the $-CH_2-CH-$ group, the electron-donating ability is expected to be essentially determined by that of the indole nucleus. Moreover, we have shown that the picrate anion is as strong as picric acid itself as an electron-acceptor.[1,2,7] Because of the intense absorption due to the picrate ion, the maximum of the charge-transfer absorption band in the tryptophan picrate cannot be located. Nevertheless, the similarity in the spectrum below 20 kK between the indole and tryptophan complexes strongly supports the assumption that the color of the tryptophan complex arises from the charge-transfer interaction between the indole nucleus and the picrate anion.

Thewalt and Bugg have found that protonated serotonin cation, which is very closely related to the protonated tryptophan cation, and the picrate anion are arranged in alternatingly stacked arrays to form continuous columns in the red-colored crystal. On the basis of its color and those crystallographic observations, they have concluded that the picrate is a complex of the electron donor-acceptor type.[3] The results of the present spectroscopic study of the tryptophan picrate seem to be in conformity with their conclusion.

5) G. Briegleb and H. Delle, *Z. Elektrochem.*, **64**, 347 (1960).
6) R. Foster and P. Hanson, *Trans. Faraday Soc.*, **60**, 2189 (1964).
7) G. Saito and Y. Matsunaga, This Bulletin, **45**, 2214 (1972).

BULLETIN OF THE CHEMICAL SOCIETY OF JAPAN, VOL. 46, 1000—1001 (1973)

The Fractionation of Tritiated Water in Several Hydrated Chlorides

Haruhiko TANAKA,* Michifumi TANGA, and Hisao NEGITA

Department of Chemistry, Faculty of Science, Hiroshima University, Higashisenda-machi, Hiroshima

(Received July 14, 1972)

The fractionation of tritiated water (HTO) on the crystallization of various hydrated sulfates from their aqueous solutions has been reported in our recent papers.[1,2] It may also be worthwhile to examine such a fractionation in other hydrated salts, because more data seem to be necessary in order for us to study the fractionation in a systematic way. In the present investigation, hydrated chlorides of cobalt, strontium, and barium have been chosen for study.

The results have been discussed on the basis of the crystal-growth mechanism and an ionic process in the solution in a way similar to that described in a previous paper.[1] Furthermore, other factors such as the dehydration temperature of the chloride have been taken into account. For this purpose, thermal analyses, *i.e.*, the DTA and TGA of the hydrated chlorides, were studied, since no exact dehydration temperatures have yet been determined, as far as we know.

Experimental

Crystal Growth. The chlorides, of commercial origin, were purified by recrystallization. The purified salts were put into the solvent, which consisted of twice-distilled water containing a trace of tritiated water (HTO). The well-developed single crystal of the hydrated chloride was grown from a very slightly super saturated aqueous solution by evaporating the solvent gradually. At the same time, the temperature of the solution was lowered in a narrow range in order to suppress the formation of stray crystals. The temperature ranges were 38.3—37.9°C for $CoCl_2 \cdot 6H_2O$, 40.3—39.7°C for $SrCl_2 \cdot 6H_2O$, and 37.7—37.3°C for $BaCl_2 \cdot 2H_2O$.

Recovery of Water and Analysis of the β-Activity. Water from both the mother liquor and the hydrated single crystal was recovered by heating them under identical conditions. The β-activity of the sample water was measured with a liquid scintillation counter, as has been described in a previous paper.[1]

Thermal Analysis. TGA and DTA were carried out simultaneously with a thermal analyzer, Model 8002 TG-DTA, of the Rigaku Denki Co., Ltd., using a sample of *ca.* 20 mg and heating it at the rate of 5°C/min.

Results and Discussion

The separation factor of HTO, S, on the crystal growth of a hydrated salt from a slightly supersaturated aqueous solution is given as follows:

$$S = N_s/N_l, \quad (1)$$

where N_s and N_l are the mole fractions of HTO in the water of crystallization and in the mother liquor respectively. Table 1 gives the S values for the hydrated chlorides, together with the net cpm due to HTO in the water. It can be seen that an appreciable dilution of HTO occurs in the crystalline water of the chlorides. The dilution in $SrCl_2 \cdot 6H_2O$ may be compared with the S value of deuterated water (mostly HDO), which has been determined to be 0.977± 0.005 by Barrer and Denny.[3]

TABLE 1. THE SEPARATION FACTOR, S, OF HTO FOR HYDRATED CHLORIDES

Crystal	Net cpm of HTO[a]		S_{obsd}
	N_s	N_l	
$CoCl_2 \cdot 6H_2O$	23688±188	24244±229	0.977±0.008
$SrCl_2 \cdot 6H_2O$	20328± 88	21472± 83	0.947±0.004
$BaCl_2 \cdot 2H_2O$	17929±191	19311±115	0.928±0.008

a) Averaged for several measurements using 0.1 g of the sample water recovered from the hydrated crystal of 2—3 g.

It was reported in a previous paper that the appreciable dilution of HTO in the hydrated crystal might be attributed to the surface-diffusion model of the crystal growth and to an ionic process in an aqueous solution.[1] The S value of the free water can thus be approximately calculated as 0.949 ($= (18/20)^{1/2}$) for the surface diffusion, provided that a possible fractionation of HTO in the hydration water of an ion from bulk water is disregarded.[4]

According to this treatment, the S value for $CoCl_2 \cdot 6H_2O$ can be derived as *ca.* 0.975, assuming that half of the hydration water of $Co(OH_2)_6^{2+}$ in the solution becomes free to integrate into the crystal.[1] On the other hand, it can be assumed in the cases of $SrCl_2 \cdot 6H_2O$ and $BaCl_2 \cdot 2H_2O$ that practically all of the water of crystallization comes from free water in the solution, because the half-lives, τ, of $Sr(OH_2)_6^{2+}$ and $Ba(OH_2)_6^{2+}$ in the solution[6] are much smaller than the relaxation times of these ions needed to integrate themselves into the crystal from the solution.[7] Accordingly, the S values for $SrCl_2 \cdot 6H_2O$ and $BaCl_2 \cdot 2H_2O$ are

* Present address: Shinonome Branch School, Faculty of Education, Hiroshima University, Shinonome, Hiroshima.

1) H. Tanaka and H. Negita, This Bulletin, **43**, 3079 (1970).

2) H. Tanaka, *J. Sci. Hiroshima Univ., Ser. A*, **36**, 31 (1972).

3) R. M. Barrer and A. F. Denny, *J. Chem. Soc.*, **1964**, 4677.

4) The disregard of the fractionation may be allowable in the present study, because no appreciable fractionation or a slight enrichment, if at all, in the hydration water seems to result.[5]

5) C. G. Swain and R. F. W. Bader, *Tetrahedron*, **10**, 182 (1960); C. J. Collins and N. S. Bowman, "Isotope Effects in Chemical Reactions," Van Norstand Reinhold Co., New York (1971), p. 254; H. G. Hertz, *Angew. Chem. Int. Ed. Engl.*, **9**, 124 (1970).

6) M. Eigen, *Pure Appl. Chem.*, **6**, 97 (1963).

7) P. Bennema, Thesis, The Technical University of Delft (1965).

Table 2. The calculated S value together with the τ, r_c, and T_d values

Crystal	S_{calc}	τ (sec)[a]	r_c (Å)	T_d (°C)
$CoCl_2 \cdot 6H_2O$	0.975	10^{-6}	0.72	185
$SrCl_2 \cdot 6H_2O$	0.949	10^{-9}	1.13	145
$BaCl_2 \cdot 2H_2O$	0.949	$10^{-9.5}$	1.35	120

a) Taken from Ref. 4.

derived as *ca.* 0.949 by means of the surface-diffusion model. Table 2 gives the estimated S values, together with the half-lives of the hydrated cations, τ.

It may be noticed here that the observed S values are in good agreement with the estimated ones for $CoCl_2 \cdot 6H_2O$ and $SrCl_2 \cdot 6H_2O$, but not for $BaCl_2 \cdot 2H_2O$. Although the cause of the discrepancy can not be ascertained at this stage, it is interesting to note that the observed S value decreases with an increase in the cationic radius, r_c, of the chloride (*cf.* the fourth column of Table 2). The increase in the radius leads to a hydrated ion with a shorter half-life in the solution,[8] which in turn gives more free water in the process of diffusion onto the crystal surface.[9] The S value should thus decrease with an increase in the mole fraction of free water in the solution according to the present assumption that free water is largely responsible for the dilution of HTO in the crystal.

The too small S value for $BaCl_2 \cdot 2H_2O$ seems likely to be caused by the following factors of (1) and/or (2):

(1) As has been pointed out in Ref. 1, the minimum S value estimated should be regarded as an approximate one, because some approximation and assumption are included in the derivation. A small deviation of the estimated value from the observed one seems to be inevitable, as was the case with the few other inorganic hydrates.[1,10] From the viewpoints of the crystal-growth mechanism and the ionic process, however, the direction of the dilution may be significant in our study.

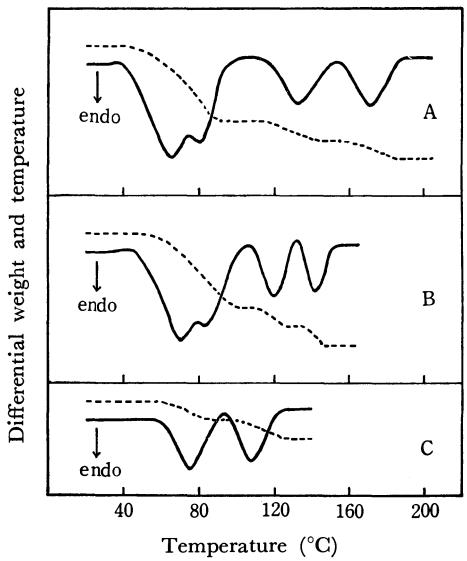

Fig. 1. Curves of the simultaneous DTA and TGA for the dehydration of the hydrated chlorides of cobalt (A), strontium (B), and barium (C).
——: DTA, ----: TGA, and endo: endothermic

(2) The dehydration temperature, T_d, of the barium chloride dihydrate is considerably lower than those of the other chlorides (*cf.* the last column of Table 2), as may be seen from the DTA and TGA curves in Fig. 1. This fact shows that the bonding of the crystalline water is relatively weak; this might be related to the too small S value, since the content of a heavier isotope in a given chemical species is known to decrease as the bonding becomes weaker in the case of an exchange reaction of isotopes.

We still believe that the major cause of the observed dilution in the chloride is the surface-diffusion mechanism of the crystal growth, since the possible enrichment, if any, of HTO in the hydration water of the Ba^{2+} ion in the solution seems to be negligible.[5]

The authors wish to express their thanks to Dr. Osamu Yamamoto for his help in analyzing the activity of tritium.

8) F. Basalo and R. C. Johnson, "Coordination Chemistry," W. A. Benjamin, Inc., New York (1964), p. 153.
9) H. Tanaka, This Bulletin, **45**, 339 (1972).
10) H. Tanaka, T. Kado, and H. Negita, *ibid.*, **45**, 3342 (1972).

BULLETIN OF THE CHEMICAL SOCIETY OF JAPAN, VOL. 46, 1001—1003 (1973)

A CNDO Treatment of the Strucures of the Grignard Reagents

Hiroshi KATO and Shigeru TSURUYA*

Department of General Education, Nagoya University, Chikusa-ku, Nagoya

** Department of Chemical Engineering, Faculty of Engineering, Kobe Univrsity, Nada-ku, Kobe*

(Recieved August 18, 1972)

Although many experimental studies of the structures of Grignard reagents have been accumulated[1], there have been few approaches from the point of view of the molecular orbital consideration of the structures of these organomagnesium compounds.[2]

The purpose of this note is to examine the plausible

1) E. C. Ashby, *Quart. Revs.* (London), **21**, 259 (1967); G. E. Parris and E. C. Ashby, *J. Amer. Chem. Soc.*, **93**, 1206 (1971).

2) K. Ohkubo and F. Watanabe, This Bulletin, **44**, 2869 (1971).

structures of Grignard reagents on the basis of their energies obtained by the CNDO/2 method[3], which does not consider the outer d-AO of the Mg atom. The following monomer-dimer equilibrium has been observed as the composition of Grignard reagents in diethyl ether[1]:

$$\underset{\text{(III)}}{R\text{-}Mg\langle^{X}_{X}\rangle Mg\text{-}R} \rightleftharpoons \underset{\text{(I)}}{2RMgX} \rightleftharpoons \underset{\text{(IV)}}{R\text{-}Mg\langle^{X}_{R}\rangle Mg\text{-}X}$$

$$\underset{\text{(VI)}}{\left(X\text{-}Mg\langle^{R}_{R}\rangle Mg\text{-}X\right)}$$

$$\rightleftharpoons \underset{\text{(II)}}{R_2Mg} + \underset{}{MgX_2} \rightleftharpoons \underset{\text{(V)}}{^{R}_{R}\rangle Mg\langle^{X}_{X}\rangle Mg}$$

$$\underset{\text{(VII)}}{\left(^{R}_{R}\rangle Mg\text{-}X\text{-}Mg\text{-}X\right)}$$

$$\underset{\text{(VIII)}}{\left(^{R}_{R}\rangle Mg\text{-}Mg\langle^{X}_{X}\right)}$$

For the sake of simplicity, the smallest molecules showing the essential properties are chosen that is $R=CH_3$ and $X=Cl$. The geometries of the above compounds are taken to be Mg–Cl=2.5 Å, Mg–C=2.2 Å, and Mg–Mg=2.8 Å(bridge type)[6] through all the compounds considered (the adopted valence angle for R–Mg–R, R–Mg–X, and X–Mg–X in dimers and bent monomers are determined by the use of the above atomic distances).

The relative energies of various compounds appearing in the above equilibrium are illustrated graphically in Fig. 1, in which the total energies of linear and bent CH_3–Mg–Cl monomers are doubled for the sake of comparison with those of the dimeric species, and in which the sum of the energies of the linear $Mg(CH_3)_2$ and $MgCl_2$ is taken as a reference for the energy di-

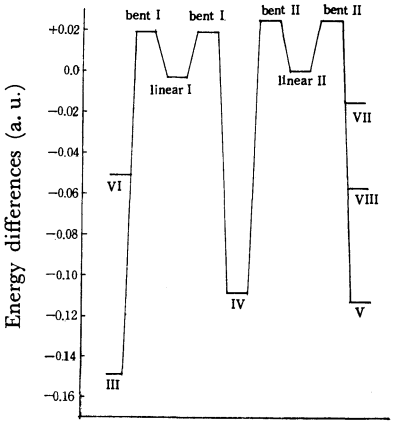

Fig. 1. The energy diagram of various compounds appearing in the equilibrium of Grignard reagents.

Table 1. The calculated results of the net charges of atoms and energy differences

Compounds	Net charges[a]			Energy differences ΔE (a. u.)
	Mg	$R=CH_3$	$X=Cl$	
MgR_2 linear (II)	+0.562	−0.281	——	0.0
MgX_2 linear (II)	+0.826	——	−0.413	
RMgX linear (I)	+0.689	−0.279	−0.410	+0.003
MgR_2 bent (II)	+0.603	−0.301	——	+0.025
MgX_2 bent (II)	+0.842	——	−0.421	
RMgX bent (I)	+0.711	−0.339	−0.401	+0.019
$^{R}_{R}\rangle Mg^1\text{-}X^1\text{-}Mg^2\text{-}X^2$ (VII)	+0.439(+0.935)	−0.347	−0.309(−0.385)	−0.014
$X\text{-}Mg\langle^{R}_{R}\rangle Mg\text{-}X$ (VI)	+0.594	−0.183	−0.421	−0.051
$^{R}_{R}\rangle Mg^1\text{-}Mg^2\langle^{X}_{X}$ (VIII)	+0.336(+0.548)	−0.135	−0.306	−0.057
$X^1\text{-}Mg^1\langle^{R^1}_{X^2}\rangle Mg^2\text{-}R^2$ (IV)	+0.602(+0.464)	−0.109(−0.274)	−0.420(−0.264)	−0.109
$^{R}_{R}\rangle Mg^1\langle^{X}_{X}\rangle Mg^2$ (V)	+0.208(+0.884)	−0.301	−0.244	−0.113
$R\text{-}Mg\langle^{X}_{X}\rangle Mg\text{-}R$ (III)	+0.498	−0.275	−0.223	−0.149

a) The values in parentheses are referred to the atoms with the number 2.

3) J. A. Pople, D. P. Santry and G. A. Segal, *J. Chem. Phys.*, **43**, s 129 (1965); J. A. Pople and G. A. Segal, *ibid.*, **44**, 3289 (1966); D. P. Santry and G. A. Segal, *ibid*, **47**, 158 (1967).

4) The SCF procedures for many solvated compounds did not converge.

5) Some results for the energy differences in solvated species which are calculated to be considerably unstabilized by the coordinated water molecules, are given as as follows:

$$\left[^{R}_{R}\rangle Mg\langle^{OH_2}_{OH_2} + {}^{H_2O}_{H_2O}\rangle Mg\langle^{X}_{X}\right]\left[{}^{H_2O}_{X}\rangle Mg\langle^{X}_{R}\rangle Mg\langle^{R}_{OH_2}\right]$$

ΔE 0.0 −0.068

$$\left[{}^{H_2O}_{R}\rangle Mg\langle^{X}_{X}\rangle Mg\langle^{R}_{OH_2}\right]$$

−0.081 (a. u.)

where the energy reference is the one-half of the sum of the total energies of the two monomers in the first bracket. From the above results, the solvated states seem to be situated in the narrower energy region than the isolated state as in Fig. 1.

6) These distances are taken as the sum of the covalent radius estimated by Prithard and Skinner (*Chem. Rev.*, **55**, 177 (1955)).

agram (in atomic units). The dimer types are energetically more favored than the monomer types, as is indicated in Fig. 1. The calculated results for the net charge of the atoms are presented in Table 1, together with their energy differences. It seems in this table that the net charges of Mg atoms coordinated by three or four atoms in dimers are generally smaller than in monomers, and that these excess charges are transferred from the bridge-head atoms or groups. That is, the stability of the dimer forms, especially of the bridge structures, is mainly dependent on the electro-dificient character of the magnesium atom as well as on the electron-rich character of the bridge-head atoms and the methyl groups which act as the electron donor. The exchange of alkyl groups can be explained by the existence of an intermediate mixed alkyl-halogen bridge structure(IV), as has suggested earlier.[1] Figure 1 indicates that the stability of this mixed bridged dimer is considerably larger than those of monomers; this is in accordance with the above experimental considerations. It should be noted, however, that our results are obtained by neglecting the solvent effects,[4] and also that the experiment shows that the dimer forms are present in equilibrium states in "weak" solvents such as diethyl ether, and not in "strong" solvents such as tetrahydrofuran. Thus, it may be said that both the experimental and calculated results prove that the mixed structure is favored at the monomer-dimer equibrium in the case of weak interaction with solvent molecules;[5] also, there is no doubt that the solvent strongly influences the structures of Grignard reagents.

For the solvated state in these compounds, further treatments are desired.

We wish to acknowlege the help of Mr. Ishida in these CNDO calculations, and also that of the Computer Center of Kyoto University and of Nagoya University.

BULLETIN OF THE CHEMICAL SOCIETY OF JAPAN, VOL. 46, 1003—1004 (1973)

The Formation of β-Glycine in the Thermal Decomposition of a Solid Complex of Aminomalonic Acid with Glycine

Jujiro NISHIJO and Toshio KINUGASA*

Kobe Women's College of Pharmacy, Higashinada-ku, Kobe

** Department of Chemistry, Faculty of Science, Kobe University, Nada-ku, Kobe*

(Recived September 5, 1972)

In a previous paper,[1] we reported that aminomalonic acid reacted with glycine to form a solid complex with a 1 : 1 molar ratio on crystallization from an aqueous solution, and that the solid complex decarboxylated at a higher temperature and at a slower rate than did aminomalonic acid, as was established by means of the DTA–TGA of the solid complex at a heating rate of 1°C/min in air. Moreover, it was found, by the aid of X-ray analysis, that an unstable unknown substance was formed, together with α- and γ-glycine, in the course of the thermal decomposition of the solid complex, and that this substance changed to either α- or γ-glycine above 150°C. At the stage where this substance is formed, however, the coexistence of a remaining solid complex and the α- and γ-glycine produced made it difficult for us to study the unstable substance. Here, an investigation was carried out into the conditions for the formation of the unstable unknown substance and on its formation mechanism.

Experimental

To a mixture of 1.19 g of a recrystallized aminomalonic acid and 0.75 g of glycine of a reagent grade, was added 30 ml of pure water and then 30 ml of methanol. The resulting solution was kept overnight in a refrigerator (7—8°C) to yield scaly crystals. The yield was 1.90 g (90%).

Found: C, 30.86%; H, 5.36%. Calcd for $C_5H_{10}O_6N_2$ (aminomalonic acid : glycine=1 : 1) : C, 30.93%; H, 5.15%. The X-ray diffraction pattern, the infrared spectrum, and the DTA-TGA of this substance agreed well with those of the crystalline powder[1] obtained by the concentration of an aqueous solution.

The solid complex was decomposed in a Riken-type sample dryer. The infrared spectra were observed with a Nihon Bunko Grating Infrared Spectrometer, type DS-402G, by means of the Nujol-mull method. X-ray analysis was carried out with the same apparatus as had previously been reported.[1] In order to represent the amount of the decomposition products semi-quantitatively, the ratio of the height of diffraction peak was used. Also, a sample holder was used throughout this work.

Results and Discussion

The unstable unknown substance changed either α- or γ-glycine at temperatures above 150°C.[1] On the assumption that the unknown substance may be formed in a large amount at a lower temperature, thermal decomposition was carried out at a temperature in the neighborhood of 122°C.

The decarboxylation proceeded extremely slowly and required about 45 hours for completion. The product in this period was only an unknown sudstance in many cases, but in some cases a small amount of α- and γ-glycine was also formed at the completion of the reaction. On further heating, the intensity of the dif-

1) T. Kinugasa, J. Nishijo, G. Hashizume, and I. Imanishi, This Bulletin, **44**, 2035 (1971).

Table 1. Decomposition products of solid complex and aminomalonic acid

Reactant	Reaction temperature (°C)	Reaction time (hours)	Fraction of decomposition (%)	Decomposition products	Relative amount of product[a]
Complex	122±1	25	70	unknown	0.51
		45	100	unknown	1.00
		90	100	unknown	0.13
				γ-glycine	0.93
				α-glycine	0.16
Aminomalonic acid	115±1	4	100	γ-glycine	

a) The ratio of the height of the diffraction peak due to each product in the reaction mixture to the height of the diffraction peak due to each compound alone at the respective diffraction angles.
α-glycine: at 29.3 (2θ), unknown: at 17.9 (2θ), γ-glycine: at 21.8 (2θ).

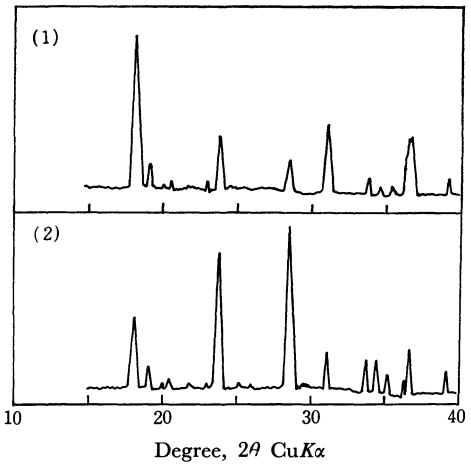

Fig. 1. X-ray diffraction patterns of (1) β-glycine and (2) the unknown.

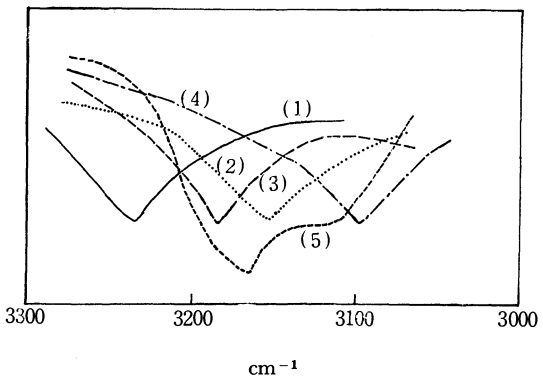

Fig. 2. Infrared spectra.
(1): complex. (2): α-glycine. (3): β-glycine. (4): γ-glycine. (5): aminomalonic acid.

fraction peak of the unknown substance decreased and γ-glycine was formed in a large amount, accompanied by the formation of a small amount of α-glycine. The infrared spectrum of the unknown substance differs slightly from that of α- or γ-glycine. These properties resemble those of β-glycine. The X-ray diffraction pattern of the unknown substance was compared with that of β-glycine which had been prepared according to Iitaka method[2] (Fig. 1). Although different in the relative intensities of the diffraction peaks, they agree with each other in the angles of the diffraction peaks. It was thus proved that the unknown substance produced in the thermal decomposition of the solid complex was β-glycine. The difference between them in the relative intensities of the diffraction peaks may result from the difference in the orientation of the crystals which is caused according to the method of preparation.

The formation mechanism of β-glycine, the most unstable among three polymorphic forms of glycine, will be discussed below. When aminomalonic acid decomposed slowly at the temperature in the neighborhood of 115°C, not β- but γ-glycine was detected in the decomposition product (Table 1). This is consistent with the findings that, as was reported previously,[3] aminomalonic acid decarboxylates, with the disintegration of the crystal lattice to amorphous glycine, and that the amorphous glycine crystallizes to γ-glycine, which is the most stable against the thermal processes.

On the other hand, scarcely no thermal change due to the crystallization of the decomposition products was in the decarboxylation of the solid complex.[1] This fact suggests that the decarboxylation of the complex occurs with no disintegration, but with only a slight displacement of the crystal lattice. Moreover, the observation that the crystal lattice is not disintegrated may be explained as follows. Since each stretching vibration of NH_3^+ in the aminomalonic acid and α-glycine is observed near 3165 cm^{-1} and 3154 cm^{-1} respectively and near 3233 cm^{-1} in the complex, the intermolecular hydrogen bond has been formed between aminomalonic acid and glycine by forming the solid complex (Fig. 2). Hence, when the solid complex decarboxylates at a low temperature and at a very slow rate, the intermolecular hydrogen bond may remain to some extent, and the disintegration of the crystal lattice of the complex may not occur. Therefore, the formation of an unstable compound such as β-glycine may be possible.

The authors wish to thank Professor Isamu Imanishi and Dr. Genzo Hashizume for their advice and interest.

2) Y. Iitaka, *Acta Crystallogr.*, **13**, 35 (1960).

3) T. Kinugasa, J. Nishijo, and G. Hashizume, *Nippon Kagaku Zasshi*, **70**, 584 (1969).

BULLETIN OF THE CHEMICAL SOCIETY OF JAPAN, VOL. 46, 1005—1006 (1973)

Ion-exchange Equilibria on a Crystalline Zirconium Phosphate Exchanger

Hiroko SEKINO and Isao TOMITA

Department of Chemistry, Faculty of Science, Tokyo Kyoiku University, Otsuka, Tokyo

(Received August 25, 1972)

Ahrland and Albertsson have suggested that the zirconium phosphate gels contain, besides the ordinary phosphate groups, small amounts of a functional group capable of interacting more or less strongly with various cations.[1] They studied the ion selectivity by plotting the logarithm of the distribution coefficients, K_d, as a function of the pH at a constant value of the load.

Albertsson extended the study to the sorption of Na^+, Cs^+, Sr^{2+}, UO_2^{2+} and Ce^{3+} ions on a crystalline zirconium phosphate.[2] The log K_d *vs.* pH curves for Na^+ and Cs^+ have the theoretical slopes, but the slopes for UO_2^{2+} and Ce^{3+} curves have somewhat lower values than those expected. Strontium ion behaves peculiarly, and the sorption by no means proceeds *via* a perfect ion exchange.

The aim of the present experiment is the further investigation of the ion-exchange equilibria of divalent ions such as Zn^{2+} on a crystalline zirconium phosphate, $Zr(HPO_4)_2 \cdot H_2O$ (abbreviated as α-ZP). The equilibrium of the Cs^+ ion was also reexamined. Both Cs^+ and Zn^{2+} ions have appreciably high K_d values in acidic-solution media and are suitable for the study.

Theoretical

If α-ZP behaves as a monofunctional exchanger, the mass action law can be applied to the following equilibrium:

$$n\overline{AH} + M^{n+} \rightleftharpoons \overline{AnM} + nH^+$$

$$K_d = \frac{[\overline{AnM}]}{[M^{n+}]} = K \cdot \frac{[\overline{AH}]^n}{[H^+]^n} \quad (1)$$

where the bar denotes the exchanger phase; A, an anionic functional group; M^{n+}, metal ions, and K, an equilibrium constant. When the load is sufficiently small, $[\overline{AH}]$ is nearly equal to the H^+ ion concentration before loading, $[\overline{AH}]_0$. Thus, the plots of log K_d *vs.* pH should result in a straight line with a slope of n.

If the exchanger contains some kinds of functional groups, A_1, whose affinities for cations are different from each other, K_d is expressed as follows:

$$K_d = \frac{\sum[\overline{A_{1n}M}]}{[M^{n+}]} = \frac{\sum(K_1 \cdot [\overline{A_1H}]^n)}{[H^+]^n}$$

$$\log K_d = \log (\sum K_1 \cdot [\overline{A_1H}]^n) + n\,\mathrm{pH} \quad (2)$$

When one functional group is of an amount comparable to the load, but has an appreciable affinity for the cations involved, the first term of Eq. (2) is no longer constant and the log K_d *vs.* pH plot does not give a straight line with a slope of n. This is actually the case for zirconium phosphate gels.

As a simple case, let us consider an exchanger containing two kinds of functional groups, A and B, where A is a major component with an equilibrium constant of K_A, and where B is a minor component with K_B and $K_B \gg K_A$. We obtain:

$$K_d = \frac{1}{[H^+]^n}\{K_B[\overline{BH}]^n + K_A[\overline{AH}]^n\}$$

Now that the load is kept sufficiently low in comparison with the exchange capacity, *i.e.*, $[\overline{AH}] \gg [\overline{A_nM}]$, the above equation can be re-written as follows:

$$K_d = \frac{1}{[H^+]^n}[K_B\{[\overline{BH}]_0 - [\overline{B_nM}]\}^n + K_A[\overline{AH}]_0{}^n] \quad (3)$$

where the subscript 0 denotes the concentration before loading. Further, the following cases can be considered under these conditions:

i) If the initial amount of $\overline{BH}$ is larger than the load, C_M, the latter is considered to be equal to $[\overline{B_nM}]$. Then

$$K_d = \frac{1}{[H^+]^n}[K_B\{[\overline{BH}]_0 - C_M\}^n + K_A[\overline{AH}]_0{}^n] \quad (4)$$

ii) If $C_M > [\overline{BH}]_0$, then $[\overline{B_nM}] = [\overline{BH}]_0$ and

$$K_d = \frac{1}{[H^+]^n} \cdot K_A[\overline{AH}]_0{}^n \quad (5)$$

This value is constant when pH is kept constant.

From the above considerations, it is at least possible to deduce whether or not the exchanger in question is monofunctional from the general shape of the K_d *vs.* C_M curve determined experimentally.

Experimental

Exchanger. α-ZP was prepared and treated as has been reported previously.[3] The particle sizes range from 100 to 200 mesh. Identification was made by means of X-ray powder diffraction.

Distribution Coefficients. All the measurements were carried out at 25°C using 250 mg of α-ZP and 25 ml of a contact solution in the same manner as before.[3] The hydrogen-ion concentrations were adjusted with hydrochloric acid for the cesium chloride solution and with nitric acid for the zinc nitrate solution. Radioactive tracers such as ^{65}Zn and ^{137}Cs with known specific activities were used to determine the concentrations of the cations. The radioactivities were measured with a well-type NaI(Tl) scintillation counter.

Usually, three runs were carried out under the same conditions and the mean values of the K_d values thus obtained were taken.

Results and Discussion

In general, it is difficult to keep the experimental media at a constant ionic strength in this kind of ion-

1) S. Ahrland and J. Albertsson, *Acta Chem. Scand.*, **18**, 1861 (1964).

2) J. Albertsson, *ibid.*, **20**, 1689 (1966).

3) Y. Hasegawa and I. Tomita, This Bulletin **43**, 3011 (1970).

exchange study because small amounts of functional groups might have an unusual affinity for cations other than those in question. In this experiment, the variation in the involved activity coefficients is disregarded over the pH range studied, but this does not seem to have influenced the discussion given below.

Dependence of K_d upon C_M at a Constant pH. Figure 1 shows typical examples of the plots of K_d *vs.* C_M

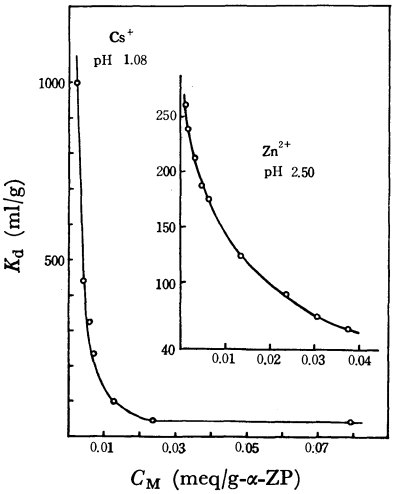

Fig. 1. The plot of K_d *vs.* C_M at constant pH values.

at constant pH values for the Cs^+ and Zn^{2+} ions respectively. Similar curves have been obtained at pH values of 0.70, 1.08. 1.58, and 2.03 for Cs^+, and at 1.59, 2.08, 2.50, and 2.99 for Zn^{2+} ions. In the region of very low loading, the K_d values decrease rapidly with an increase in C_M for both metal ions. This is what is to be expected from Equation (4). However, as the value of C_M increases further, the K_d values still decrease slowly and do not attain constant values over the C_M range studied. It is not easy to judge from the results whether or not the left part of the cesium curve is rectilinear or whether or not that of the zinc curve is parabolic. There might be an oversimplification of the assumptions in deriving Eq. (3)~(5), and the possible existence of more than one kind of functional group with a high affinity can not be excluded. However, it is possible roughly to estimate the upper limit of concentration of the B group by intercepting the extrapolated parts of the left- and right-hand sides of each curve. Values of about 0.01 meq/g α-ZP for cesium and of about 0.05 meq/g α-ZP for zinc were thus obtained. The total exchange capacity of α-ZP is theoretically 6.64 meq/g, and the quantity of the high-affinity group is less than 1%. This makes the chemical identification and characterization of the group extremely difficult.

The purity of the exchanger used is good, and so is the crystallinity. Thus, the existence of any functional group other than the phosphate group is not likely. However, the incorporation of amorphous zirconium

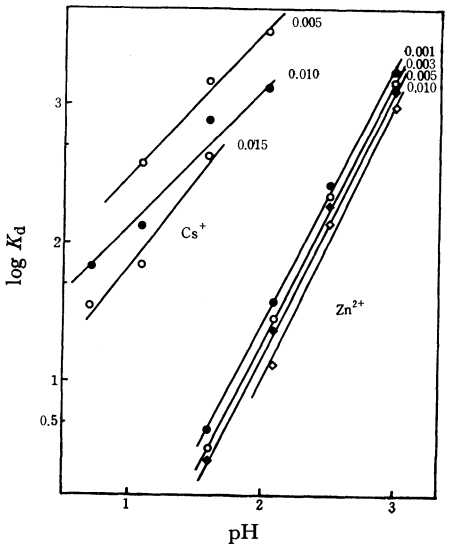

Fig. 2. The plot of log K_d *vs.* pH at constant C_M values. Numerical value beside each line denotes C_M in meq/g α-ZP.

phosphate into the crystals is probable, because the crystals have been prepared from the gels by refluxing them in phosphoric acid. Further, from steric considerations,[4] the phosphate groups on the crystal surface should have a higher affinity for Cs^+ and Zn^{2+} ions than those inside the crystal. Even inside the crystal, there might be small amounts of sorption sites which occupy particular positions leading to a different acidity of the phosphate protons from that of a majority of the monohydrogen phosphate groups. If each of the above-mentioned phosphate groups is responsible for the sorption of cations, but to a different extent, K_d values which are independent of the C_M can not be attained within the range of the present experiment, in which the extent of the exchanged sites is only about 1% of that of the total exchangeable ones.

The log K_d vs. pH Plots at Constant Loads. From the curves of K_d *vs.* C_M at different constant pH values, it is possible to find the K_d values for a constant C_M. The logarithm of the values were then plotted against the pH, as is shown in Fig. 2. The slopes of the resulting straight lines were calculated by a least-squares method. For cesium, these values are 1.01, 1.02, and 1.24 for the C_M values (meq/g α-ZP) of 0.005, 0.010, and 0.015 respectively. With regard to zinc, the slopes are 1.86, 1.91, 1.97, and 2.05 for the C_M values of 0.001, 0.003, 0.005, and 0.010 respectively. The approximate values of +1 for cesium and +2 for zinc are what can reasonably be expected from their normal valency states. Figure 2 also shows the parallel displacement of straight lines with the change in the C_M values. This is again to be expected from Eq. (4).

The authors wish to express their thanks to Professor Kozo Nagashima for his interest and encouragement. They are also indebted to Mr. Yoshitsugu Hasegawa for his valuable discussions. Finally, they are grateful to Mr. Yasuhiko Saito for his help with the experiments.

4) The ion-sieving property of α-ZP is known for relatively large ions, such as cesium and rubidium. A strongly hydrated polyvalent ion is considered also to be hindered to a considerable extent.

BULLETIN OF THE CHEMICAL SOCIETY OF JAPAN, VOL. 46, 1007—1008 (1973)

The Photoreaction of 2,6-Diphenyl-4*H*-thiopyran-4-one 1,1-Dioxide

Hiromu AOYAMA, Yoshiaki SATO, Takehiko NISHIO, and Noboru SUGIYAMA

Department of Chemistry, Faculty of Science, Tokyo Kyoiku University, Otsuka, Tokyo

(Received July 19, 1972)

Previously, we have reported that the irradiation of 2,6-diphenyl-4*H*-thiopyran-4-one (Ia) in non-polar solvents gave a head-to-tail anti-dimer[1] and in polar solvents gave photooxidized products,[2] while that of 2,6-diphenyl-4*H*-pyran-4-one (Ib) gave the corresponding cage dimer.[2] This paper will be concerned with the photoreaction of 2,6-diphenyl-4*H*-thiopyran-4-one 1,1-dioxide (II).

The irradiation of II in a methanol solution (0.02 mol/l) with a high-pressure mercury lamp under a nitrogen atmosphere gave a methanol-adduct (III) (mp 208—210°C) in a 14% yield and a trace of benzoic acid. The structure of III was determined as follows. The NMR spectrum of III showed a singlet at δ 3.51 (3H) assignable to methoxy protons and a singlet at δ 4.86 (2H) assignable to methylene protons. The IR spectrum of II showed a carbonyl band at 1640 cm^{-1}, but that of III showed it at 1690 cm^{-1}. The mass spectrum of III showed a peak at *m/e* 328 (M^+, $C_{18}H_{16}O_4S$) and base peaks at *m/e* 134 ($M-C_9H_6O_3S$) and 264 ($M-SO_2$). The hydrogenation of III in a mixture of acetic acid and ethanol by means of palladium-charcoal gave IV. Its NMR spectrum exhibited a pair of doublets at δ 4.42 (1H) and 4.73 (1H) due to methylene protons at C-3. The irradiation of II in benzene gave an intractable mixture.

When a mixture of II and cyclohexene in benzene was irradiated under the same conditions for 4 hr, a 1 : 1-adduct (V) was obtained in a 93% yield. The NMR spectrum of V showed two doublets at δ 6.59 (0.75 H) and 6.52 (0.25 H) assignable to an olefinic proton. The product V was therefore considered to be a mixture of stereoisomers at the cyclobutane ring. Furthermore, the results of the elemental analysis confirmed that V was a 1 : 1-adduct, and the UV and IR spectra indicated the presence of an enone system.[3] Also, the hydrogenation of V afforded VII quantitatively. The NMR spectrum of VII exhibited a multiplet at δ 4.94 (1H) attributable to the methine proton at C-2. The IR spectrum also indicated a saturated carbonyl band at 1710 cm^{-1}.

When a mixture of II and cyclooctene in benzene was irradiated under the same conditions for 5 hr, a 1 : 1-adduct (VI) was also obtained in a 50% yield. The structure of VI was determined on the basis of its elemental analysis and spectral data. The product VI also seems to be a mixture of stereoisomers at the cyclobutane ring like V, for the NMR spectrum of VI exhibited two doublets at δ 6.57 (0.55 H) and 6.47 (0.45 H) assignable to an olefinic proton.

Experimental

Material. 2,6-Diphenyl-4*H*-thiopyran-4-one 1,1-dioxide (II)[4] was synthesized by Arndt's method,[5] mp 143—144.5°C (lit,[5] 144—145°C).

Irradiation of II. A solution of 600 mg of II in 100 ml of methanol was irradiated with a high-pressure mercury lamp through a Pyrex filter under nitrogen for 6 hr. After the removal of the solvent, the residue was chromatographed on a silica-gel column. Elution with benzene–ethyl acetate (19 : 1) yielded 86 mg of II and 91 mg of III. Recrystallizations of III from benzene afforded colorless prisms. Found: C, 65.69; H, 4.94%. Calcd for $C_{18}H_{16}O_4S$: C, 65.85; H, 4.91%. UV: λ_{max}^{EtOH} nm (ε), 217 (21,700) and 292 (9,900). IR: ν_{max}^{KBr} cm^{-1}, 1690 (C=O). NMR: (δ in $CDCl_3$) 7.85—7.33 (m, 10H, phenyl), 6.54 (s, 1H, olefinic), 4.86 (s, 2H, methylene), 3.51 (s, 3H, methoxy).

Hydrogenation of III. When 40 mg of III was hydrogenated in 10 ml of acetic acid and 5 ml of ethanol with 30 mg of palladium-charcoal, IV was quantitatively obtained. Recrystallizations of IV from benzene afforded colorless prisms; mp 231—232°C. Found: C, 65.43; H, 5.61%. Calcd for $C_{18}H_{18}O_4S$: C, 65.44; H, 5.49%. IR: ν_{max}^{KBr} cm^{-1}, 1728 (C=O), 1312, 1113 (SO_2). NMR: (δ in $CDCl_3$) 7.40 (s, 10H, phenyl), 4.73 (d, 1H, J=15, methylene at C-3) and 4.42 (d, 1H, J=15, methylene at C-3), 4.43 (d, 1H, J=3.5, methine), 3.80 (d, 1H, J=15, methylene at C-5) and 3.02 (dd, 1H, J=15, J=3.5, methylene at C-5), 3.37 (s, 3H, methoxy).[6] When the signal of the methine proton at δ 4.43 was irradiated, the signal of the methylene protons at δ 3.80 and 3.02 changed into a pair of doublets (AB q.) at δ 3.12 and 2.89.

Irradiation of the Mixture of II and Cyclohexene. A solution of 500 mg of II and 2 ml of cyclohexene in 30 ml of benzene was irradiated under the same conditions as have been described above for 4 hr. After the solvent had been removed, the residue was chromatographed on a silica-gel column with benzene–*n*-hexane (9 : 1). The evaporation of the solvent from the eluted fraction gave a crude product as a pale yellow crystals, which were then collected, and washed with *n*-hexane to afford colorless prisms; 594 mg of V; mp 175.5—177°C. Found: C, 72.79; H, 5.97%. Calcd for $C_{23}H_{22}O_3S$: C, 73.00; H, 5.86%. UV: λ_{max}^{EtOH} nm (ε), 220 (16,200) and 294.5 (10,600). IR: ν_{max}^{KBr} cm^{-1}, 1685 (C=O), 1308, 1135 (SO_2). NMR: (δ in $CDCl_3$) 7.50—7.25 (m, 10H, phenyl), 6.59 (d, 0.75H, olefinic

1) N. Sugiyama, Y. Sato, H. Kataoka, C. Kashima and K. Yamada, This Bulletin, **42**, 3005 (1969).

2) N. Sugiyama, Y. Sato, and C. Kashima, *ibid.*, **43**, 3205 (1970).

3) *E. g.*, H. E. Zimmerman and D. I. Schuster, *J. Amer. Chem. Soc.*, **84**, 4527 (1962).

4) UV: λ_{max}^{EtOH} nm (ε), 226 (sh. 16,200), 314 (11,700) and 327 (sh. 11200). IR: ν_{max}^{KBr} cm^{-1}, 1640 (C=O), 1305, 1128 (SO_2). NMR: (δ in $CDCl_3$) 7.97—7.63 (m, 10H, phenyl), 6.63 (s, 2H, olefinic).

5) F. Arndt, P. Nachtwey and J. Pusch, *Ber.*, **58**, 1633 (1925).

6) This assignment was determined by comparing the NMR spectrum of IV with that of 2,6-diphenyl-2,3,5,6-tetrahydro-4*H*-thiopyran-4-one 1,1-dioxide. δ ($CDCl_3$) 7.39(s, 10H, phenyl), 4.52 (dd, 2H, J=15, J=3.5, methine), 3.67 (dd, 2H, J=15, J=15, methylene), 2.90 (br d, 2H, J=15, methylene).

and 6.52 (d, 0.25H, olefinic), 3.82—2.92 (m, 3H, methine), 2.80—0.88 (m, 8H, methylene).

Hydrogenation of V. When a 300-mg portion of V was hydrogenated in 25 ml of acetic acid and 40 ml of ethanol with 50 mg of palladium-charcoal, VII was quantitatively obtained. Recrystallizations of VII from benzene afforded colorless prisms; mp 178—179°C. Found: C, 72.88; H, 6.36%. Calcd for $C_{23}H_{24}O_3S$: C, 72.61; H, 6.36%. IR: ν_{max}^{KBr} cm^{-1}, 1710 (C=O), 1305, 1125 (SO_2). NMR: (δ in $CDCl_3$) 7.5—6.9 (m, 10H, phenyl), 4.94 (m, 1H, methine at C-2), 3.92—3.2 (m, 5H, methylene at C-3 and methine), 2.95—1.0 (m, 8H, methylene). When the signal of the methine proton at δ 4.94 was irradiated, the signal of the methylene protons at C-3 appeared as a broad singlet at δ 3.38.

Irradiation of the Mixture of II and Cyclooctene. A solution of 500 mg of II and 5.5 ml of cyclooctene in 30 ml of benzene was irradiated under the same conditions as have been described above for 5 hr. After the solvent had been removed, the residue was chromatographed on a silica-gel column. Elution with benzene–ethyl acetate (9 : 1) yielded 203 mg of VI. Recrystallizations of VI from *n*-hexane afforded colorless prisms; mp 209—211°C. Found: C, 73.53; H, 6.48%. Calcd for $C_{25}H_{26}O_3S$: C, 73.86; H, 6.45%. UV: λ_{max}^{EtOH} nm (ε), 220.5 (19,500) and 293.5 (11,000). IR: ν_{max}^{KBr} cm^{-1}, 1692 (C=O), 1300, 1125 (SO_2). NMR: (δ in $CDCl_3$) 7.48—7.05 (m, 10H, phenyl), 6.57 (d, 0.55H, olefinic) and 6.47 (d, 0.45H, olefinic) 3.8—3.0 (m, 3H, methine), 2.1—0.85 (m, 12H, methylene).

BULLETIN OF THE CHEMICAL SOCIETY OF JAPAN, VOL. 46, 1008—1009 (1973)

The Synthesis of 2-(Diphenylcyclopropenylidene)cyclobutane-1,3-dione (1,2-Diphenylbutatriafulvalene-3,5-dione)[1]

Toyonobu Asao,* Morio Yagihara, and Yoshio Kitahara
Department of Chemistry, Faculty of Science, Tohoku University, Aoba, Aramaki, Sendai 980

(Received August 4, 1972)

Recently, 4-diphenylmethylene-1,2-diphenylbutatriafulvalene-3,5-dione (**1**)[2] and heptabutafulvalenedione derivatives (*e.g.*, **2**)[3] have been synthesized, and their spectral data have been discussed.

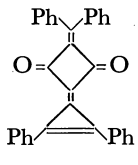

(**1**)

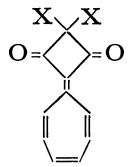

(**2**) X=Cl, Me

In the course of synthetic studies of fulvalenes, we have prepared 2-(diphenylcyclopropenylidene)cyclobutane-1,3-dione (1,2-diphenylbutatriafulvalene-3,5-dione); the results will be reported herein.

The reaction of cyclobutane-1,3-dione and 1,2-diphenyl-3-ethoxycyclopropenylium tetrafluoroborate in methylene chloride in the presence of a minute amount of pyridine afforded pale yellow needles (**3**) (mp 225—230°C (decomp.)) in a 14% yield; the structure of 2-(diphenylcyclopropenylidene)cyclobutane-1,3-dione was inferred from the following spectroscopic data as well as from the results of elemental analyses.

Compound **3** exhibits the mass-spectral parent ion at *m/e* 272 (relative intensity 69), and fragment ions at 257 (14), 230 (100), 216 (18), 215 (19), 202 (88), 178 (23), and 165 (27); IR (KBr) 1840 (m) (methylenecyclopropene), 1660 (s) (C=O), 1600 (w), and 1510 (s) cm^{-1}; UV λ_{max}^{EtOH} 225^{sh} (log ε 4.23), 266 (4.28), and 325 nm (4.65); NMR ($CDCl_3$) δ 3.5 (2H, s, methylene protons), 7.6—7.8 (6H, m, Hb and Hc), and 8.35—8.55 (4H, m, Ha).

The strong deshielding of Ha by the diamagnetic anisotropy of the carbonyl group is similarly observed in compound **1**[2] and diphenylpentatriafulvalenedione derivatives.[4]

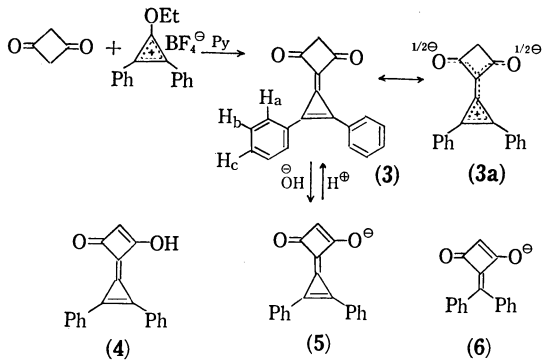

From the facts that the C=O stretching frequency appears at 1660 cm^{-1}, and that methylene protons in NMR appear at δ 3.5 as a singlet, compound **3** must be stabilized by a contribution of a dipolar structure **3a**; it seems that an enol structure **4** does not contribute to the structure.

Compound **3** is not soluble in aqueous sodium hydrogen carbonate, but it is soluble in NaOH–EtOH. The ultraviolet absorption curve in a dilute acidic medium does not change from that in ethanol. However, in an alkaline solution, the curve shows absorption maxima at 265 (log ε 4.12), 328 (4.39), and 342 nm (4.37); this curve is reversibly backed to the original curve by the addition of an acid. From these data, an enolate

* Present Address: College of General Education, Tohoku University, Kawauchi, Sendai 980.

1) Presented at the 24th Annual Meeting of the Chemical Society of Japan, Osaka, April, 1971.

2) F. Toda, *Chem. Lett.*, **1972**, 621.

3) N. Morita, T. Asao, and Y. Kitahara, *ibid.*, **1972**, 927.

4) I. Agranat, R. M. J. Loewenstein, and E. D. Bergmann, *J. Amer. Chem. Soc.*, **90**, 3278 (1968).

anion **5** may be assigned for compound **3** in an alkaline solution. A similar anion **6** has been assigned for 2-diphenylmethylenecyclobutane-1,3-dione.[2)]

Experimental

*2-(Diphenylcyclopropenylidene)cyclobutane-1,3-dione (**3**).* To a stirred solution of cyclobutane-1,3-dione (42 mg) and diphenylethoxycyclopropenylium tetrafluoroborate (320 mg) in anhydrous methylene chloride (6 ml), 3 drops of pyridine were added at room temperature. After 30 min, the color of the solution turned red. Water was added, and the solution was extracted with methylene chloride and dried over anhydrous magnesium sulfate, the subsequent removal of the solvent left an oil, which was chromatographed on silica gel to give pale yellow crystals (225 mg). An ether-insoluble part of the crystals was recrystallized from a mixture of methanol and methylene chloride to give 18 mg (14%) of pale yellow needles (**3**) (mp 225—230°C (decomp.)). From the ether-soluble part diphenylcyclopropenone was obtained.

Found: C, 83.42; H, 4.28%. Calcd for $C_{19}H_{12}O_2$: C, 83.80; H, 4.44%.

BULLETIN OF THE CHEMICAL SOCIETY OF JAPAN, VOL. 46, 1009—1010 (1973)

Photochemical Type II Elimination of Diisobutyl Trichloromethylphosphonate*

Yoshio OGATA, Yasuji IZAWA, and Toshiyuki UKIGAI

Department of Applied Chemistry, Faculty of Engineering, Nagoya University, Chikusa-ku, Nagoya

(Received August 12, 1972)

The type II photo-elimination of carbonyl compounds containing γ-hydrogen to form olefins and degradated carbonyl compounds *via* a cyclic transition state is well known.[1] However, little information is available on the analogous photochemistry of phosphoryl group. In view of the strongly polar character of P^+–O^- bond in ordinary phosphorus compounds, no absorption of the P=O group appears in the near UV region.[2]

We reported previously that no reduction of the phosphoryl portion occurred in photoreduction of carbonyl group of dialkyl β-ketophosphonates (I) to β-hydroxyphosphonates (II) (Eq. (1)). The quantum yield for disappearance of ketones were 0.6—0.7.[3]

$$\underset{\text{I}}{RCOCH_2P(O)(OR')_2} \rightarrow \underset{\text{II}}{RCH(OH)CH_2P(O)(OR')_2} \quad (1)$$

a, $R=CH_3$, $R'=C_2H_5$
b, $R=C_2H_5$, $R'=C_2H_5$
c, $R=C_2H_5$, $R'=(CH_3)_2CH$

The extent of $p\pi-d\pi$ character of the P=O bond may be determined by the overlap integral and the electron affinity of the bonded atoms at phosphorus. Thus, the electronegativity of substituent on the phosphorus atom may exert a considerable effect on the $p\pi-d\pi$ overlap integral and hence on its bond energy.[4] Electron-withdrawing groups on phosphorus compete with a double-bonded oxygen atom to attract electron, resulting in a stiffer P=O bond and a higher frequency.[5]

The values of bond orders of some phosphoryl compounds have been reported, *e. g.*, $P(O)Br_3$: 1.92, $P(O)Cl_2$: 1.95, $P(O)(CF_3)_3$: 2.00, $P(O)FCl_2$: 2.05, $P(O)F_2Cl$: 2.11, and $P(O)F_3$: 2.22.[4]

Consequently, the absorption spectrum of the phosphoryl group is expected to appear in a near UV region, if a strongly electron-withdrawing group is present on phosphorus. In fact, diisobutyl trichloromethylphosphonate (III)[6] shows a new absorption (shoulder) at $\lambda_{max}^{n\text{-hexane}}$ 253.7 nm ($\varepsilon\sim2$). The present paper reports on photochemical type II decomposition of III to give the corresponding half ester and isobutylene.

A solution of III (1.5 g, 0.25 M) in *n*-hexane was irradiated with a low-pressure Hg lamp in a quartz tube for 60 hr and the photoproducts were separated by column chromatography, giving colorless crystals (IV), mp 104—105°C, in an 11% yield and viscous liquid (V)[7] (0.18 g). The IR spectrum of IV showed strong bands of P–OH at 1640 and 1110 cm^{-1}. The mass spectrum showed the fragment ions *m/e* 83 [34%, $HP^+(OH)_3$], 137 (22%), 199 (12%), and 56 (100%, $C_4H_8^+$), although the expected parent peaks did not appear. Accurate mass numbers of

* Contribution No. 167.

1) For comprehensive reviews see (a) N. J. Turro, "Molecular Photochemistry," Benjamine, New York, N. Y. (1965), p. 154; b) J. G. Calvert and J. N. Pitts, Jr., "Photochemistry," John Wiley & Sons, New York, N. Y. (1966) p. 377; c) N. C. Yang in "Reactivity of the Photoexcited Organic Molecule," John Wiley & Sons, New York, N. Y. (1967) p. 145.

2) R. P. Buck, S. Singhadaja, and L. B. Rogers, *Anal. Chem.*, **26**, 1240 (1954).

3) H. Tomioka, Y. Izawa, and Y. Ogata, *Tetrahedron*, **24**, 1501 (1969).

4) O. P. Craig, A. Maccoll, R. S. Nyholm, L. E. Orgel, and L. E. Sutton, *J. Chem. Soc.*, **1954**, 332.

5) N. B. Colthup, L. H. Daly, and S. E. Wiberley, "Introduction to Infrared and Raman Spectroscopy," Academic Press, New York, N. Y. (1964) p. 298.

6) III: bp 109—110°C (1 mm); IR (film) 1280 (P=O), 1020 (P–O–C), 765 (P–C), 545 (C–Cl), 1370, and 1395 cm^{-1} ($CH(CH_3)_2$); NMR ($CDCl_3$) isobutyl methyl H (δ 1.10, d, J=7.5 Hz), isobutyl methine H (δ 2.11, m), and isobutyl methylene H (δ 4.20, t, J=6.6 Hz); mass *m/e*, P: 31.0 (20%), fragment ions: 199 [55%, $Cl_3CP^+(OH)_3$], 137 (60%, $P^+(OH)(O)(OC_4H_9)$], 117 (15%, CCl_3^+), 83 [10%, $HP^+(OH)_3$], and 56 (100%, $C_4H_8^+$).

7) Although V showed similar IR and NMR spectra to that of III, its structure is not clear. V is not identical with III because of its mass spectrum, M^+ 500.

ions at *m/e* 137 and 199 were 137.037 and 198.889, respectively. Hence, the former is due to $P^+(O)(OH)(OC_4H_9)$ (calcd 137.036), the latter to $C^{35}Cl_3P^+(OH)_3$ (calcd 198.899). In the mass spectrum of III, no peak corresponding to $Cl_3CP^+(OH_2)(OC_4H_9)$ ion was observed. In support of this, a β-scission to P=O group under electron impact is knwon.[8]

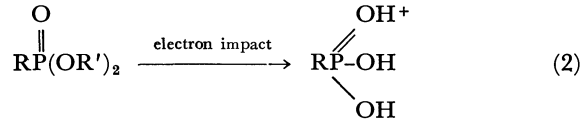

(2)

Thus it is certain that $Cl_3CP^+(OH)_3$ ion for IV is produced *via* electron impact fragmentation of $Cl_3CP(O)(OH)(OC_4H_9)$. On the basis of this fact as well as in spectroscopic property, the photoproduct (IV) was identified to be $Cl_3CP(O)(OH)(OC_4H_9)$. If IV is produced *via* a type II cleavage of III, isobutylene should be simultaneously formed as a photoproduct. In fact, it was isolated by means of glpc using di-*n*-butyl maleate-β,β'-oxydipropionitrile on C–22.

Thus, it is probably valid to write the process for the photochemical cleavage of III in analogy with the type II cleavage for ketones.

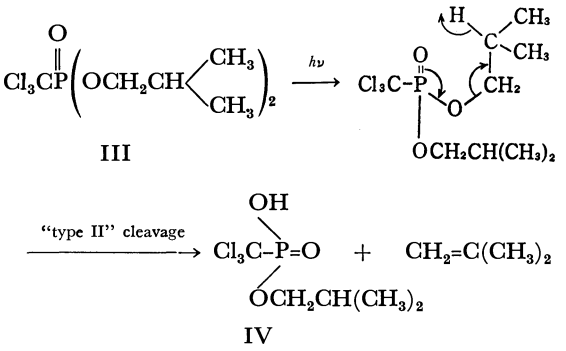

III

(3)

IV

Indeed, no decomposition was observed in 54 hr irradiation of dimethyl ester, $Cl_3CP(O)(OCH_3)_2$,[9] in which a six-membered transition state for hydrogen abstraction is impossible. No isobutane was detected in the photodecomposition of III.

8) a) J. L. Occolowitz and G. L. White, *Anal. Chem.*, **35**, 1971 (1963); b) T. Nishikawa, *Tetrahedron*, **22**, 1383 (1966).

9) Bp 120—126°C (12 mm); IR (film) 1280 (P=O), 1185 (P–O–CH_3), 760 (P–C), and 555 cm^{-1} (C–Cl); NMR ($CDCl_3$) methyl H (δ 4.07, d, J=10.8 Hz).

BULLETIN OF THE CHEMICAL SOCIETY OF JAPAN, VOL. 46, 1010—1011 (1973)

Sesquiterpene Hydrocarbons of the Liverwort, *Scapania parvitexta*

Akihiko MATSUO, Mitsuru NAKAYAMA, and Shûichi HAYASHI

Department of Chemistry, Faculty of Science, Hiroshima University, Higashisenda, Hiroshima 730

(Received September 7, 1972)

The liverworts (*Hepaticae*), which are phylogenetically placed between the vascular plants and the algae, and which contain several oil bodies in each cell, form a unique division in the plant kingdom. About 8500 species of the plants are distributed throughout the world. The essential oils of liverworts have hardly been investigated at all to date because of the difficulty of collecting a sufficient amount of the plants to examine their constituents. In the course of our studies of the constituents of *Hepaticae*,[1] the present investigation was undertaken on the essential oil of a leafy liverwort, *Scapania parvitexta* Steph. (Japanese name, Koamimehishakugoke), belonging to the *Scapaniaceae* family; we were able to identify nine sesquiterpene hydrocarbons.

The hexane extract of the liverwort was subjected to fractional distillation under reduced pressure, followed by elution chromatography; we thus obtained a hydrocarbon fraction, which showed thirteen peaks in gas chromatography with a Golay column, as is shown in Fig. 1. Since the fraction was very small in amount, its analysis depended upon a method combining a gas chromatograph and a mass spectrometer (GC-MS); by a comparison of the mass spectra thus obtained (*cf.* Table 1) with the previously-reported data, nine sesquiterpene hydrocarbons of β-bourbonene,[2] β-ylan-

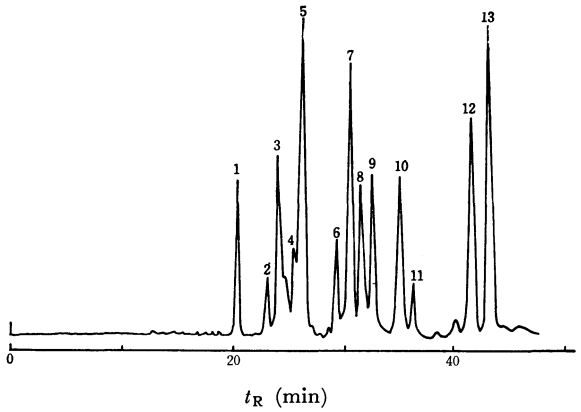

Fig. 1. Gas chromatogram of the sesquiterpene hydrocarbon fraction of *Scapania parvitexta*.
1. β-bourbonene 2. $C_{15}H_{24}$ 3. $C_{15}H_{24}$ 4. β-ylangene 5. β-cubene 6. $C_{15}H_{24}$ 7. $C_{15}H_{24}$ 8. γ-cuprenene 9. calamenene 10. β-chamigrane 11. β-selinene 12. bazzanene 13. cuparene

1) Chemical constituents from *Hepaticae*, Part XII: Part XI, A. Matsuo, M. Nakayama, J. Ono, and S. Hayashi, *Z. Naturforsch.*, *B*, **27**, 1437 (1972).

2) K. Morikawa and Y. Hirose, Abstract of the 14th Symposium on the Chemistry of Terpenes, Essential Oils, and Aromatics, Kitami, p. 27 (1970).

Table 1. Abundant ions in mass spectra of identified sesquiterpene hydrocarbons[a)]

Compound	M (%)	H_1	H_2 (%)	H_3 (%)
β-Bourbonene	204 (9)	81	80 (74)	123 (63)
β-Ylangene	204 (35)	161	41 (82)	204 (35)
β-Cubebene	204 (45)	161	119 (60)	105 (55)
γ-Cuprenene	204 (25)	119	93 (53)	105 (40)
Calamenene	202 (12)	159	157 (35)	142 (18)
β-Chamigrene	204 (55)	189	41 (90)	93 (75)
β-Selinene	204 (100)	204	41 (85)	105 (80)
Bazzanene	204 (5)	109	108 (52)	67 (31)
Cuparene	202 (15)	132	131 (42)	145 (30)

a) Percentages in parentheses represent the relative abundance.

gene,[3] β-cubebene,[4] γ-cuprenene,[4] calamenene,[5] β-chamigrene,[6] β-selinene,[7] bazzanene,[8] and cuparene,[9] were identified.

The biogenetic pathways of the hydrocarbons may be shown as in Chart 1: β-chamigrene (VI), γ-cuprenene (VII), bazzanene (VIII), and cuparene (IX) are synthesized from *cis*-farnesol (I) *via* the (III) cation, and β-ylangene (X), β-cubebene (XI), and calamenene (XII), from the same precursor *via* the (IV) cation, whereas the other compounds, β-selinene (XIII) and β-bourbonene (XIV), are synthesized from *trans*-farnesol (II) *via* the (V) cation. Although most of these biogenetic courses have already been known in higher plants,[10,11] it is very interesting that so many kinds of sesquiterpene hydrocarbons were also detected in the liverwort.

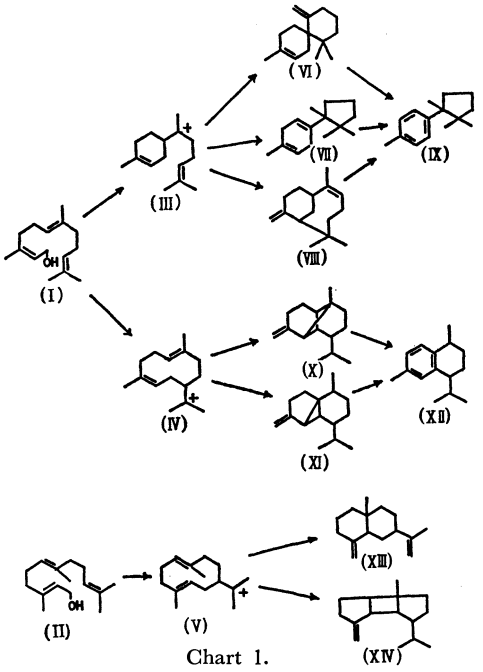

Chart 1.

Experimental

Separation of a Sesquiterpene Hydrocarbon Fraction. Liverwort collected at Yaku Island in Kagoshima Prefecture (October, 1969) was dried in the shade for a week; the plants (3.85 kg) were then digested with hexane (15 l) to obtain a dark brown, viscous matter (5.3 g) in a 0.14% yield. This matter was subjected to distillation under reduced pressure by using a small-type distillation column packed with single-turn spirals of stainless steel. The distillate (bp 70—90°C/2 mm Hg; 0.45 g) thus obtained was then chromatographed over a silica gel column (1.5×25 cm) to collect a hydrocarbon fraction (0.37 g), which was then quickly eluted with hexane.

Gas Chromatography. The gas chromatograms were taken on a Hitachi K-53 gas chromatograph equipped with a flame-ionization detector in connection with a Golay column (coating, PEG-20 M; 0.5 mm×45 m): the column temperature was programmed from 120 to 170°C at a rate of 2°C/min, and the carrier (nitrogen gas) had a pressure of 1.0 kg/cm^2.

An Apparatus Combining a Gas Chromatograph and a Mass Spectrometer. The hydrocarbon fraction described above was analyzed with an instrument combining a gas chromatograph and a mass spectrometer, Hitachi RMU-6E Model, using a Golay column (PEG-20 M, 0.5 mm×45 m); the gas-chromatograph part was operated under the same conditions as above, except that helium was used instead of nitrogen gas as the carrier gas. The column effluent was admitted to an ion source *via* a heated line and a Watson-Biemann-type helium separator. The mass spectrometer part was operated under the following conditions: 70 eV, ionization voltage; 100 μA, total emission; 1800 eV, ion-accelerating voltage, and 220°C, ion source temperature.

Mass Spectrum of Each Constituent. From the mass spectra thus taken, four abundant ions of molecular (M), base (H_1), second-highest (H_2), and third-highest (H_3) ions and their abundance were read, as is shown in Table 1. These spectral patterns were then a compared with the respective reported spectra, and the listed sesquiterpene were identified.

The authors are indebted to Drs. Yoshio Hirose and Kumiko Morikawa, The Institute of Food Chemistry, for sending the mass spectra.

3) G. C. K. Hunter and W. B. Brogden, Jr., *J. Org. Chem.*, **29**, 2100 (1964).
4) Y. Hirose, *Shitsuryo Bunseki*, **15**, 162 (1965).
5) S. Hayashi, N. Hayashi, K. Yano, M. Okano, and T. Matsuura, This Bulletin, **41**, 234 (1968).
6) Y. Ohta and Y. Hirose, *Tetrahedron Lett.*, **1968**, 2483.
7) M. G. Moshonas and E. D. Lund, *Flavor Industry*, **1**, 375 (1970).
8) S. Hayashi, A. Matsuo and T. Matsuura, *Experientia*, **25**, 1139 (1969); A. Matsuo, *Tetrahedron*, **27**, 2759 (1971).
9) C. Enzell and H. Erdtman, *ibid.*, **4**, 361 (1958).
10) L. Ruzicka, *Experientia*, **9**, 367 (1953).
11) J. B. Hendrickson, *Tetrahedron*, **7**, 82 (1959).

BULLETIN OF THE CHEMICAL SOCIETY OF JAPAN, VOL. 46, 1012—1013 (1973)

Palladium-catalyzed Exchange of Allylic Groups of Ethers and Esters with Carboxylic Anhydrides

Kuniyuki TAKAHASHI*, Go HATA, and Akihisa MIYAKE

Basic Research Laboratories, Toray Industries, Inc., Tebiro, Kamakura

(Received October 12, 1972)

Previously we have reported[1,2] the palladium-catalyzed exchange reaction of allylic groups of ethers and esters with active-hydrogen compounds. In the course of the studies, it has been found that the reaction of the allylic compounds (I) with carboxylic anhydrides in the presense of palladium catalysts also gives the exchanged products (II and III) of allylic groups.

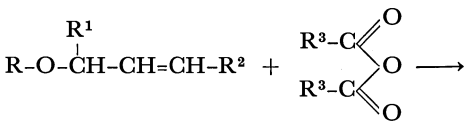

I

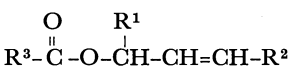

II

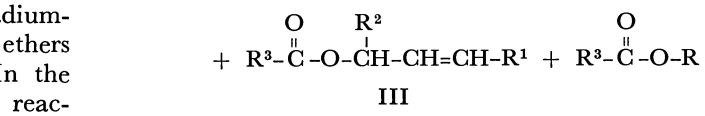

III

$R = C_6H_5$, CH_3CO, CH_3CH_2CO
$R^1 = H$, $CH_2CH_2CH_2CH{=}CH_2$
$R^2 = H$, $CH_2CH_2CH_2CH{=}CH_2$
$R^3 = CH_3$, C_6H_5

An active and easily available catalyst is prepared by mixing palladium acetate and triphenylphosphine. Tetrakis(triphenylphosphine)palladium(0) is also an effective catalyst. However, the catalytic activity of the combination of dichlorobis(triphenylphosphine)-palladium (II) and sodium phenoxide is much smaller than that of the above two catalysts. Some platinum catalysts also showed the catalytic activity, but it was smaller than that of palladium catalysts.

The results on the reaction of allylic ethers and

Table 1. Reactions of allylic ethers and esters with carboxylic anhydlides[a]

Anhydride (mol)	Allylic compound (mol)	Catalyst (mmol)	Time (hr)	Products[e] and yields[f] (%)
$(CH_3CO)_2O$	$C_6H_5OC_8H_{13}$[b]	$Pd(OCOCH_3)_2$-Ph_3P	40	CH_3CO_2X, 57 CH_3CO_2Y 24
$(CH_3CO)_2O$	$C_6H_5OC_8H_{13}$[b]	$PdCl_2(Ph_3P)_2$-PhONa	40	CH_3CO_2X, 18 CH_3CO_2Y 8
$(CH_3CO)_2O$	$C_6H_5OC_8H_{13}$[b]	$Pd(Ph_3P)_4$	40	CH_3CO_2X, 36 CH_3CO_2Y 15
$(CH_3CO)_2O$	$C_6H_5OC_8H_{13}$[b]	$PtCl_2(Ph_3P)_2$-PhONa	40	CH_3CO_2X, 10 CH_3CO_2Y 2
$(CH_3CO)_2O$	$C_6H_5OC_8H_{13}$[b]	$Pt(Ph_3P)_4$	40	CH_3CO_2X, 33 CH_3CO_2Y 14
$(C_6H_5CO)_2O$	$C_6H_5OC_8H_{13}$[b]	$Pd(OCOCH_3)_2$-Ph_3P	40	$C_6H_5CO_2X$, 42 $C_6H_5CO_2Y$ 14
$(C_6H_5CO)_2O$	$C_6H_5OCH_2CH{=}CH_2$*	$Pd(OCOCH_3)_2$-Ph_3P	40	$C_6H_5CO_2CH_2CH{=}CH_2$ 17
$(CH_3CO)_2O$	$C_2H_5CO_2C_8H_{13}$[c]	$Pd(OCOCH_3)_2$-Ph_3P	16	CH_3CO_2X, 55 CH_3CO_2Y 22
$(C_6H_5CO)_2O$	$CH_3CO_2C_8H_{13}$[d]	$Pd(OCOCH_3)_2$-Ph_3P	16	$C_6H_5CO_2X$, 50 $C_6H_5CO_2Y$ 25
$(C_6H_5CO)_2O$	$CH_3CO_2CH_2CH{=}CH_2$	$Pd(OCOCH_3)_2$-Ph_3P	16	$C_6H_5CO_2CH_2CH{=}CH_2$ 33

a) Reaction conditions: anhydride 0.05 mol, allylic compound 0.025 mol (* 0.05 mol), palladium and platinum complex 0.05 mmol, Ph_3P 0.2 mmol, PhONa 0.5 mmol, reaction temperature 85°C, dimethylformamide 5 ml.
b) 1-Phenoxy-2,7-octadiene containing 1.3% of 3-phenoxy-1,7-octadiene.
c) A mixture of $C_2H_5CO_2X$(69%) and $C_2H_5CO_2Y$(31%).
d) A mixture of CH_3CO_2X(76%) and CH_3CO_2Y(24%).
e) $X = -CH_2CH{=}CHCH_2CH_2CH_2CH{=}CH_2$, $Y = -CH(CH{=}CH_2)CH_2CH_2CH_2CH{=}CH_2$.
f) Based on the allylic compound employed.

1) G. Hata, K. Takahashi, and A. Miyake, *Chem. Commun.*, **1970**, 1392.

2) K. Takahashi, A. Miyake, and G. Hata, This Bulletin, **45**, 230 (1972).

esters with carboxylic anhydrides are shown in Table 1.

Experimental

Reagents. $Pd(OAc)_2$[3], $PdCl_2(Ph_3P)_2$,[4] $Pd(Ph_3P)_4$,[4] $PtCl_2(Ph_3P)_2$[5] $Pt(Ph_3P)_4$,[5] 1-phenoxy-2,7-octadiene,[6] 1-phenoxy-2-propene,[7] octadienyl carboxylate[8] were prepared by previously reported methods. Carboxylic anhydrides and allyl acetate were purified by distillation. Dimethylformamide was dried on calcium hydride and purified by distillation.

Reaction Procedure. All the reactions were carried out under an argon atmosphere. In a 50 ml two necked flask, catalysts, reagents, and dimethylformamide were charged and the reaction mixture was stirred at 85°C. The reaction products were characterized by elemental analysis, molecular weight measurement, and IR and NMR spectral measurement or by comparison with authentic samples. The gas chromatography was used for the quantitative analysis of products.

3) T. Matsuda, T. Mitsuyasu, and Y. Nakamura, *Kogyo Kagaku Zasshi*, **72**, 1751 (1969).
4) L. Malatesta and M. Angolleta, *J. Chem. Soc.*, **1957**, 1866.
5) L. Malatesta and C. Cariells, *ibid.*, **1958**, 2323.
6) E. J. Smutny, *J. Amer. Chem. Soc.*, **89**, 6793 (1968).
7) W. M. Iaver and W. F. Filbert, *ibid.*, **58**, 1388 (1936).
8) S. Hattori, H. Munakata, T. Suzuki, and N. Imaki, Netherland Patent, 6816008 (1969).

BULLETIN OF THE CHEMICAL SOCIETY OF JAPAN, VOL. 46, 1013—1014 (1973)

Synthesis of Sugar Derivatives of *N*-Methyl-*N*-nitrosourea

Tomoya MACHINAMI and Tetsuo SUAMI

Department of Applied Chemistry, Faculty of Engineering, Keio University, Hiyoshi, Yokohama

(Received October 27, 1972)

Streptozotocin is a broad spectrum antibiotic and possesses antitumor,[1,2] mutagenic,[3] and diabetogenic[2,4–9] activities. Its isolation from a fermentation broth of *Streptomyces achromogenes var. streptozoticus* was reported in 1960[10–13], and the structure has been established to be *N*-carbamyl-*N'*-methyl-*N'*-nitroso-D-glucosamine along with the synthesis.[14,15]

In previous papers, a synthesis of methyl glycosides of this antibiotic[16] and that of the analogs in which D-glucosamine was substituted for aminocyclitols[17] were described. In the present note, we wish to report the analogs of methyl 6-amino-6-deoxy-α-D-glucopyranoside and methyl 2,6-diamino-2,6-dideoxy-α-D-glucopyranoside.

Methyl 6-amino-6-deoxy-α-D-glucopyranoside hydrochloride (**1**)[18] and methyl 2,6-diamino-2,6-dideoxy-α-D-glucopyranoside dihydrochloride (**4**) were used as starting materials. **1** and **4** were treated with methyl isocyanate in the presence of silver carbonate giving respective *N*-carbamyl-*N'*-methyl derivatives (**2**) and (**5**) in 75 and 65% yield. Nitrosation of **2** and **5** were carried out with sodium nitrite in aqueous acetic acid to give *N*-nitroso derivatives (**3**) and (**6**) in 49 and 67% yield respectively. **3** and **6** were active against Ehrlich ascites tumor in mice.

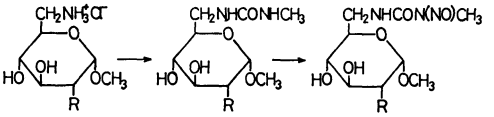

Experimental

General. Melting points were determined in capillary tubes and are uncorrected. Solutions were evaporated below 50°C under reduced pressure.

*Methyl 6-Amino-6-deoxy-α-D-glucopyranoside hydrochloride (**1**).* This compound was prepared by the method of Cramer.[18]

Methyl N-*Carbamyl*-N'-*methyl-6-amino-6-deoxy-α-D-glucopyranoside (**2**).* A 502 mg portion of **1** was dissolved in 65% aqueous acetonitrile (72 ml). To the solution, silver carbonate (363 mg) and methyl isocyanate (0.16 ml) were added and the mixture was heated for 1 hr under reflux. After cooling, the mixture was filtered and the filtrate was evaporated. The residue was crystallized in acetonitrile to give a crude product (426 mg, 78%). Recrystallization from *n*-propanol yielded crystals of mp 176—177°C. $[\alpha]_D^{22}$ +99° (*c* 1.0, methanol).

1) F. R. White, *Cancer Chemother. Rep.*, **30**, 49 (1963).
2) J. S. Evans, G. C. Gerritsen, K. M. Mann, and S. P. Owen, *ibid.*, **48**, 1 (1965).
3) F. Reusser, *J. Bacteriol.*, **105**, 580 (1971).
4) N. Rakieten, M. L. Rakieten, and M. V. Nadkarni, *Cancer Chemother, Rep.*, **29**, 91 (1963).
5) A. Junod, A. E. Lambert, L. Orci, R. Pictet, A. E. Gonet, and A. E. Renold, *Proc. Soc. Exp. Biol. Med.*, **126**, 201 (1967).
6) P. S. Schein, D. A. Cooney, and M. L. Vernon, *Cancer Res.*, **27**, 2324 (1967).
7) M. Brosky and J. Logothetopoulos, *Diabetes*, **18**, 606 (1969).
8) R. M. Pitkin and W. A. Reynolds, *ibid.*, **19**, 85 (1970).
9) L. Sadoff, *Cancer Chemother. Rep.*, **54**, 457 (1970).
10) J. J. Vavra, C. Deboer, A. Dietz, L. J. Hanka, and W. T. Sokolski, *Antibio. Ann.*, **1959—1960**, 230 (1960).
11) R. R. Herr, T. E. Eble, M. E. Bergy, and H. K. Janke, *ibid.*, **1959—1960**, 236 (1960).
12) W. T. Sokolski, J. J. Vavra, and L. J. Hanka, *ibid.*, **1959—1960**, 241 (1960).
13) C. Lewis and A. R. Barbiers, *ibid.*, **1959—1960**, 247 (1960).
14) R. R. Herr, H. K. Janke, and A. D. Argoudelis, *J. Amer. Chem. Soc.*, **89**, 4808 (1967).
15) E. Hardegger, A. Meier, and A. Stoos, *Helv. Chim. Acta*, **52**, 2555 (1969).
16) T. Suami and T. Machinami, This Bulletin, **43**, 3013 (1970).
17) T. Suami and T. Machinami, *ibid.*, **43**, 2953 (1970).
18) F. D. Cramer, "Methods in Carbohydrate Chemistry," Vol. 1, Academic Press, New York (1963), p. 242.

Found: C, 42.91; H, 6.93; N, 11.13%. Calcd for $C_9H_{18}N_2O_6$: C, 43.19; H, 7.25; N, 11.20%.

Methyl N-*Carbamyl*-N'-*methyl*-N'-*nitroso*-6-*amino*-6-*deoxy*-α-D-*glucopyranoside* (**3**). **2** (120 mg) was dissolved in 5.6% aqueous acetic acid (18 ml) under ice cooling. 0.1 M Sodium nitrite solution (6.5 ml) was added to the solution and the mixture was settled overnight at room temperature. After sodium ions were removed by treating with Amberlite IR-120 (H^+ type), the solution was lyophilized. The residue was crystallized in ethanol under ice cooling to give the product (65 mg, 49%), mp 106—107°C. $[\alpha]_D^{22}$ +82.0° (*c* 0.5, methanol).

Found: C, 39.08; H, 6.20; N, 14.80%. Calcd for $C_9H_{17}N_3O_7$: C, 38.71; H, 6.14; N, 15.05%.

Methyl N-*benzyloxycarbonyl*-6-O-*tosyl*-α-D-*glucosaminide*. The product was prepared by the method of Foster *et al.*[19].

Methyl 2,6-*Diamino*-2,6-*dideoxy*-α-D-*glucopyranoside dihydrochloride* (**4**). A mixture of methyl *N*-benzyloxycarbonyl-6-*O*-tosyl-α-D-glucosaminide[19] (7.3 g) and sodium azide (5.4 g) in 70% aqueous 2-methoxyethanol (140 ml) was heated for 21 hr under reflux. The solution was evaporated and the residue was extracted with warm acetone. The acetone extracts were evaporated and the residue was hydrogenated in ethanol (55 ml) with 5% palladium on carbon and conc hydrochloric acid (1.7 ml) at 3.4 kg/cm² hydrogen pressure for 21 hr. After the catalyst was removed by filtration, the solution was evaporated to give a crude product (1.97 g, 49%), mp 198—201°C (decomp.). Recrystallization from ethanol–methanol gave hygroscopic crystals with the same decomposition point. $[\alpha]_D^{21}$ +125° (*c* 1.28, water). The product showed a ninhydrin-positive single spot on paper chromstography (R_f 0.26) in *n*-butanol–pyridine–water (6 : 4 : 3) system in an ascending development (R_f D-glucosamine hydrochloride 0.36).

Found: C, 31.59; H, 6.73; N, 10.56; Cl, 24.82%. Calcd for $C_7H_{18}N_2O_4Cl_2$: C, 31.71; H, 6.84; N, 10.57; Cl, 26.75%.

Methyl Di-N,N'-(N-*methyl*-*carbamyl*)-2,6-*diamino*-2,6-*dideoxy*-α-D-*glucopyranoside* (**5**). To a solution of **4** (911 mg) in 70% aqueous acetonitril (45 ml), methyl isocyanate (0.5 ml) and silver carbonate (1.4 g) were added and the mixture was heated for 1 hr under reflux. After cooling, the mixture was filtered and the filtrate was evaporated to give a crude product (684 mg, 65%). Recrystallization from ethanol afforded an analytically pure sample, mp 247—249°C. $[\alpha]_D^{22}$ +108° (*c* 0.88, water).

Found: C, 43.02; H, 7.30; N, 18.30%. Calcd for $C_{11}H_{22}N_4O_6$: C, 43.14; H, 7.24; N, 18.29%.

Methyl Di-N,N'-(N-*methyl*-N-*nitroso*-*carbamyl*)-2,6-*diamino*-2,6-*dideoxy*-α-D-*glucopyranoside* (**6**). **5** (684 mg) was treated with 0.5 M sodium nitrite solution (7.6 ml) in 5.7% aqueous acetic acid (26.5 ml) as described in **3**. After the solution was settled overnight, the crystals were collected by filtration to give a first crop of the product (338 mg), mp 154—156°C. The mother liquor was treated with Amberlite IR-120 (H^+ type) and then lyophilized. The residue was crystallized in ethanol to give a second crop of the product (204 mg), mp 154—156°C. Total yield was 67%. Recrystallization from methanol afforded a sepcimen for analysis, mp 154.5°C (decomp.). $[\alpha]_D^{22}$ +106° (*c* 0.75, methanol).

Found: C, 36.25; H, 5.66; N, 22.94%. Calcd for $C_{11}H_{20}N_6O_8$: C, 36.26; H, 5.53; N, 23.07%.

The authors wish to thank Professor Sumio Umezawa for his helpful advice and Mr. Saburo Nakada for his elementary analysis.

19) A. B. Foster, M. Stacey, and S. V. Vardheim, *Acta Chem. Scand.*, **13**, 281 (1959).

BULLETIN OF THE CHEMICAL SOCIETY OF JAPAN, VOL. 46, 1014—1016 (1973)

Synthesis of Planteose

Tetsuo SUAMI, Toshiki OTAKE,* Tatsuo NISHIMURA, and Toshihide IKEDA

Department of Applied Chemistry, Faculty of Engineering, Keio University, Hiyoshi, Yokohama

** Nippon Electric Varian Co., Ltd., Azabu Iigura-cho, Minato-ku, Tokyo*

(Received November 22, 1972)

Planteose[1] was first isolated by Wattiez and Hans[2] in 1943 from the seeds of *Plantago major* and *Plantago ovata*. The structure has been established by French and his coworkers[3] in 1953 as *O*-α-D-galactopyranosyl-(1→6)-*O*-β-D-fructofuranosyl-(2→1)-α-D-glucopyranoside. The presence of this nonreducing trisaccharide in other plant sources was descirbed by Wada and Yamazaki[4] and by French and Wild.[5]

In connection with previous papers on sucrose chemistry[6–9], we have attempted to synthesize planteose (**4**) by a chemical method. The attractive starting material in this attempt was 2,3,4,6,1′,3′,4′-hepta-*O*-acetylsucrose (**2**) which was described by Otake[10] and more recently by Buchanan *et al.*[11]. **2** was condensed with tetra-*O*-benzyl-α-D-galactopyranosyl chloride[12] (**1**) giving *O*-(2,3,4,6-tetra-*O*-benzyl-α-D-ga-

1) D. French, "Advances in Carbohydrate Chemistry," Vol. 9, Academic Press Inc., New York (1954), p. 169.

2) N. Wattiez and M. Hans, *Bull. Acad. Roy. Med. Belg.*, **8**, 386 (1943); *Chem. Abstr.*, **39**, 4849 (1945).

3) D. French, G. M. Wild, B. Young, and W. J. James, *J. Amer. Chem. Soc.*, **75**, 709 (1953).

4) E. Wada and K. Yamazaki, *J. Agr. Chem. Soc. Jap.*, **24**, 398 (1951).

5) D. French and G. M. Wild, *J. Amer. Chem. Soc.*, **75**, 2612 (1953).

6) T. Suami, T. Otake, S. Ogawa, T. Shoji, and N. Kato, This Bulletin, **43**, 1219 (1970).

7) T. Suami, N. Kato, M. Kawamura, and T. Nishimura, *Carbohyd. Res.*, **19**, 407 (1971).

8) T. Suami, T. Otake, N. Kato, T. Nishimura, and T. Ikeda, *ibid.*, **21**, 451 (1972).

9) T. Suami, T. Otake, T. Nishimura, and T. Ikeda, *ibid.*, in press.

10) T. Otake, This Bulletin, **43**, 3199 (1970).

11) J. G. Buchanan, D. A. Cummerson, and D. M. Turner, *Carbohyd. Res.*, **21**, 283 (1972).

12) P. W. Austin, F. E. Hardy, J. G. Buchanan, and J. Baddiley, *J. Chem. Soc.*, **1964**, 2128.

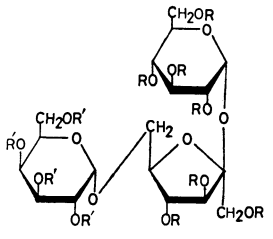

3 R=Ac R'=Bu
4 R=H R'=H
5 R=Ac R'=Ac

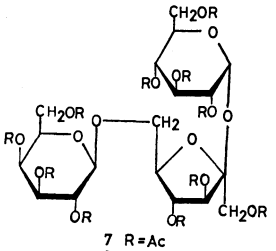

7 R=Ac
8 R=H

lactopyranosyl)-(1→6)-*O*-(1,3,4-tri-*O*-acetyl-β-D-fructofuranosyl)-(2→1)-2,3,4,6-tetra-*O*-acetyl-α-D-glucopyranoside (**3**) as an amorphous solid in 59% yield. Deacetylation of **3** in 0.1 M methanolic sodium methoxide and subsequent catalytic hydrogenolysis afforded a crude product of **4** in 44% yield.

The PMR spectrum of **4** revealed two doublets at δ 5.02 (J=2.7 Hz) and 5.46 (J=3.5 Hz) which were attributed to an anomeric proton of the α-D-galactopyranosyl group and that of the α-D-glucopyranosyl group respectively. The assignment of the signals was reasonably acceptable, because the corresponding proton of the α-D-galactopyranosyl group in melibiose showed its signal at δ 4.96 (J=2.9 Hz)[13] and that of the α-D-glucopyranosyl group in sucrose at δ 5.45 (J=3.2 Hz).[8,13]

4 was acetylated in the usual manner to give the crystalline undecaacetate (**5**) in 32% yield. The mp and the optical rotation were in good agreement with those described in the literature.[3] The PMR spectrum of **5** revealed eight sharp signals for the eleven acetoxy groups and a doublet at δ 5.75 (J=3.6 Hz) for an anomeric proton of the α-D-glucopyranosyl group, since the corresponding proton of sucrose octaacetate[14] and raffinose undecaacetate[9] resonated at δ 5.68 (J=3.5—3.7 Hz). Also a signal of the methylene bridge was observed at δ 3.69 and 3.98 supporting an existence of a bond between 0-6′ of sucrose and D-galactosyl residue, because the methylene bridge in 1-kestose undecaacetate was observed at δ 3.67 ($J_{geminal}$=9.5 Hz).[14]

On the other hand, when **2** was condensed with tetra-*O*-acetyl-α-D-galactopyranosyl bromide[15] (**6**) in nitromethane, an isomeric trisaccharide undecaacetate (**7**) was obtained in 22% yield.

The PMR spectrum of **7** revealed seven sharp signals in the δ 1.98—2.15 region for the eleven acetoxy groups and two doublets at δ 4.62 (J=7.5 Hz) and 5.60 (J=3.5 Hz) for an anomeric proton of the β-D-galactopyranosyl group and that of the α-D-glucopyranosyl group respectively. Because the corresponding proton of the β-D-galactopyranosyl group in β-allolactose octaacetate[9] showed its signal at δ 4.55 (J=7.4 Hz) as a doublet.

The undecaacetate **7** was deacetylated in 0.1 M methanolic sodium methoxide to give a trisaccharide (**8**).

The PMR spectrum of **8** revealed two doublets at δ 4.48 (J=7.2 Hz) and 5.44(J=3.4 Hz) which were attributed to an anomeric proton of the β-D-galactopyranosyl group and that of the α-D-glucopyranosyl group respectively, since the corresponding proton of the β-D-galactopyranosyl group in *O*-β-D-galactopyranosyl-(1→6)-*O*-α-D-glucopyranosyl-(1→2)-β-D-fructofuranoside[9] and allolactose[9,16] revealed their signals at δ 4.44 (J=7.5—7.9 Hz) as a doublet.

Experimental

General. Melting points were determined in capillary tubes and are corrected. Optical rotations were measured with a Japan Spectroscopic DIP-SL polarimeter. The PMR spectra were recorded at 100 MHz with a Varian HA-100D and at 60 MHz with a Varian A-60D spectrometer in deuteriochloroform or deuterium oxide with tetramethylsilane or sodium trimethylsilylpropanesulfonate as an internal standard. The peak positions are given in δ-values. Tlc was performed on silica gel plates (Wakogel B-10). Solutions were evaporated below 40°C under diminished pressure.

*Tetra-O-benzyl-α-D-galactopyranosyl Chloride (**1**).* The product was prepared by the method of Austin *et al.*[12]

*2,3,4,6,1′,3′,4′-Hepta-O-acetylsucrose (**2**).* The crude product was prepared by the method of Otake.[10] Recrystallization from toluene afforded the crystalline product of mp 159—160°C. $[\alpha]_D^{20}$ +50.1° (*c* 1.46, chloroform). Lit,[11] mp 160°C, $[\alpha]_D^{20}$ +49.5° (*c* 0.4, chloroform).

*O-(2,3,4,6-Tetra-O-benzyl-α-D-galactopyranosyl)-(1→6)-O-(1,3,4-tri-O-acetyl-β-D-fructofuranosyl)-(2→1)-2,3,4,6-tetra-O-acetyl-α-D-glucopyranoside (**3**).* To a solution of **1** (994 mg, 1.8 mmol) and **2** (498 mg, 0.8 mmol) in dry benzene (30 ml), mercuric cyanide (1.4 g, 5.5 mmol) and "Drierite" (1.4 g) were added and the mixture was heated for 40 hr under reflux with an exclusion of moisture. The reaction mixture was filtered and the filtrate was evaporated. The residue was dissolved in benzene, washed with water and again evaporated to give a residue (1.10 g). The residue was chromatographed on a silica gel column (Wakogel C-200, 4 g, 1.5×45 cm) in butanone-toluene (1 : 10, v/v). Fractions which showed a single spot on tlc at R_f 0.21 in the same solvent were combined and evaporated to give a solid product (538 mg, 59%). $[\alpha]_D^{20}$ +53,5° (c 0.93, chloroform). PMR (60 MHz, $CDCl_3$): δ 2.01 (s, 3H, OAc), 2.015 (s, 6H, OAc×2), 2.02 (s, 3H, OAc), 2.06 (s, 3H, OAc), 2.11 (s, 3H, OAc), 2.16 (s, 3H, OAc), 5.03 (d, 1H, J 3.6 Hz, H^{α}_{gal}—1), 5.80 (d, 1H, J 3.5 Hz, H^{α}_{glu}—1) and 7.25—7.34 (m, 20H, phenyl).

*O-α-D-Galactopyranosyl-(1→6)-O-β-D-fructofuranosyl-(2→1)-α-D-glucopyranoside (**4**).* **3** (538 mg) was dissolved in 0.1 M methanolic sodium methoxide (20 ml) and the solution was settled for 16 hr at room temperature. The solution was deionized with Amberlite IR-120 (H^+ type) until pH 7 and the solution was subsequently hydrogenated

13) J. M. van der Veen, *J. Org. Chem.*, **28**, 564 (1963).
14) W. W. Binkley, D. Horton, and N. S. Bhacca, *Carbohyd. Res.*, **10**, 245 (1969).
15) H. Ohle, W. Marecek, and W. Bourijau, *Ber.*, **62**, 833 (1929).
16) B. Helferich and G. Sparmberg, *ibid.*, **66**, 806 (1933).

with palladium black under hydrogen pressure (3.4 kg/cm²) for 22 hr. The mixture was filtered to remove the catalyst and the filtrate was evaporated to give a solid product (211 mg), which showed a single spot on tlc at R_f 0.20 in chloroform–methanol (5 : 4, v/v). The product was dissolved in water, decolorized with active charcoal and again evaporated. The residue was dissolved in a small amount of water and ethanol was added to the solution. The solution was settled in a refrigerator to give precipitates (104 mg, 44%) which were collected by filtration. Mp 120—123°C, $[\alpha]_D^{20}$ +122.5° (*c* 1.42, water). PMR (60 MHz, D_2O): δ 5.02 (d, 1H, *J* 2.7 Hz, $H^{\alpha}_{gal}-1$) and 5.46 (d, 1H, *J* 3.5 Hz, $H^{\alpha}_{glu}-1$). The sample for an analysis was obtained by drying over phosphorus pentoxide at 75°C *in vacuo* overnight. The product did not reduce a Fehling's solution.

Found: C, 42.53; H, 6.35%. Calcd for $C_{18}H_{32}O_{16}$: C, 42.86; H, 6.39%.

Lit,[3] mp 124°C, $[\alpha]_D$ +129.0° (c 4, water).

*Planteose Undecaacetate (**5**).* **4** (112 mg) was acetylated with acetic anhydride and pyridine in the usual manner to give a glassy solid (179 mg). Recrystallization from *n*-butanol yielded **5** (69 mg, 32%), mp 134—135°C, $[\alpha]_D^{25}$ +97.2° (*c* 1.03 chloroform). PMR (100 MHz, $CDCl_3$): δ 1.99 (s, 3H, OAc), 2.01 (s, 3H, OAc), 2.04 (s, 6H, OAc×2), 2.08 (s, 9H, OAc×3), 2.10 (s, 3H, OAc), 2.135 (s 3H, OAc), 2.14 (s, 3H, OAc), 2.15 (s, 3H, OAc), 5.75 (d, 1H, *J* 3.6 Hz, $H^{\alpha}_{glu}-1$) and 3.69, 3.98 (o, 2H, $J_{geminal}$ 9.1, *J* 4.2, 5.6 Hz, CH_2 bridge).

Found: C, 49.47; H, 5.63%. Calcd. for $C_{40}H_{54}O_{27}$: C, 49.68; H, 5.63%.

Lit,[3] mp 135°C, $[\alpha]_D^{26}$ +97° (c 1, chloroform).

*Tetra-O-acetyl-α-D-galactopyranosyl Bromide (**6**).* The product was prepared by the method of Ohle *et al.*[15]

*O-(2,3,4,6-Tetra-O-acetyl-β-D-galactopyranosyl)-(1→6)-O-(1,3,4-tri-O-acetyl-β-D-fructofuranosyl)-(2→1)-2,3,4,6-tetra-O-acetyl-α-D-glucopyranoside (**7**).* A mixture of **6** (526 mg, 1.3 mmol), **2** (468 mg, 0.7 mmol), "Drierite" (1.1 g), mercuric cyanide (1.1 g, 4.4 mmol) and nitromethane (17 ml) was agitated for 24 hr at room temperature in the dark with an exclusion of moisture. Insoluble matters were removed from the mixture and the solution was evaporated. The residue was dissolved in chloroform (40 ml) and the solution was washed with water, dried over anhydrous sodium sulfate and evaporated. The residue was acetylated as usual and the acetylated product was chromatographed on a silica gel column (Wakogel C–200, 40 g, 1.5×45 cm) in butanone–toluene (1 : 5, v/v). Each fraction was monitored by tlc with the same solvent. Fractions having a single spot at R_f 0.34 were combined and evaporated to give a glassy solid (387 mg, 54%). The product was dissolved in a warm mixture of *n*-butanol and 50% aqueous ethanol (3 : 1, v/v) and the solution was settled in a refrigerator to give an amorphous product (157 mg, 22%), mp 87—89°C, $[\alpha]_D^{25}$ +44.9° (c 2.51, chloroform). PMR (100 MHz, $CDCl_3$): δ 1.98 (s, 3H, OAc), 2.02 (s, 3H, OAc), 2.04 (s, 6H, OAc×2), 2.06 (s, 3H, OAc), 2.09 (s, 3H, OAc), 2.11 (s, 9H, OAc×3), 2.15 (s, 6H, OAc×2), 4.62 (d, 1H, 7.5 Hz, $H^{\beta}_{gal}-1$) and 5.60 (d, 1H, *J* 3.5 Hz, $H^{\alpha}_{glu}-1$).

Found: C, 49.82; H, 5.95%. Calcd. for $C_{40}H_{54}O_{27}$: C, 49.68; H, 5.63%.

*O-β-D-Galactopyranoyl-(1→6)-O-β-D-fructofuranosyl-(2→1)-α-D-glucopyranoside (**8**).* **7** (235 mg) was deacetylated in 0.1 M methanolic sodium methoxide analogously as described in **4** to give a crude product (101 mg, 82%), $[\alpha]_D^{18}$ +51.3° (*c* 1.6, water). The product did not reduce Fechling's solution. PMR (60 MHz, D_2O): δ 4.48 (d, 1H, *J* 7.2 Hz, $H^{\beta}_{gal}-1$) and 5.44 (d, 1H, *J* 3.4 Hz, $H^{\alpha}_{glu}-1$). A sample for analysis was obtained by drying over phosphorus pentoxide at 50°C for 3 days *in vacuo*.

Found: C, 42.65; H, 6.45%. Calcd. for $C_{18}H_{32}O_{16}$: C, 42.86; H, 6.39%.

This work has been supported financially in part by the grant of the Japanese Ministry of Education. We thank Professor Sumio Umezawa for his helpful advice and Mr. Saburo Nakada for performing elementary analysis.

BULLETIN OF THE CHEMICAL SOCIETY OF JAPAN, VOL. 46, 1016—1018 (1973)

Cationic Arylation. VI. Phenylation of Arenes with Benzenediazonium Trifluoroacetate

Nobumasa KAMIGATA, Ryuki HISADA,* Hiroshi MINATO, and Michio KOBAYASHI

Department of Chemistry, Faculty of Science, Tokyo Metropolitan University, Fukazawa, Setagaya, Tokyo

** Faculty of Education, University of Shizuoka, Shizuoka*

(Received December 20, 1972)

Nesmeyanov *et al.* first reported that the decomposition of aryldiazonium tetrafluoroborate in aromatic solvents yields aryl cation as a reactive intermediate which attacks the aromatic nucleus, forming biaryls.[1] However, concerning the substitution of arenes with aryl cation only few papers have been published, mainly by Abramovitch *et al.*[2]

The investigations carried out in our laboratories on cationic arylation have established that phenyl cation can readily be generated by one of the following three routes; a) thermal decomposition of benzenediazonium tetrafluoroborate in aprotic polar solvents,[3] b) thermal decomposition of phenylazo *p*-tolyl sulfone in the presence of trifluoroacetic acid,[4] and c) thermal decomposition of phenylazotriphenylmethane in tri-

1) A. N. Nesmeyanov, L. G. Makarova, and T. P. Tolustaya, *Tetrahedron*, **1**, 145 (1957).

2) R. A. Abramovitch and J. G. Saha, *Can. J. Chem.*, **23**, 3269 (1965); R. A. Abramovitch and F. F. Gadallah, *J. Chem. Soc., B*, **1968**, 497.

3) M. Kobayashi, H. Minato, E. Yamada, and N. Kobori, This Bulletin, **43**, 215 (1970).

4) M. Kobayashi, H. Minato, and N. Kobori, *ibid.*, **43**, 219 (1970).

fluoroacetic acid.[5]

a) PhN_2BF_4

b) $PhN{=}N{-}S(=O)(=O){-}C_6H_4{-}CH_3$ $\xrightarrow{CF_3CO_2H}$ $C_6H_5{+}$

c) $PhN{=}NCPh_3$ $\xrightarrow{CF_3CO_2H}$

Benzenediazonium trifluoroacetate (I) was first prepared and isolated by Pettit *et al.*[6] They concluded that phenyl radical was an intermediate simply because biphenyl was found in 24% yield when I was decomposed in benzene. This conclusion contradicts with our hypothesis that in the decomposition of phenylazo *p*-tolyl sulfone[4] or phenylazotriphenylmethane[5] in trifluoroacetic acid I is formed in the first step and subsequently degrades, not to phenyl radical, but to phenyl cation. Since I may exist either in the covalent diazoacetate structure ($Ph{-}N{=}N{-}O_2CCF_3$) which will give aryl free radical or in the ionic diazonium ion pair form ($PhN_2^+CF_3CO_2^-$) which should yield aryl cation, its decomposition mechanism can be formulated in terms of these two reactive species.

In order to clarify the mechanism of the decomposition of I, phenylation of arenes by I has been investigated, and the isomer distributions and partial rate factors in the phenylation have been determined. The results are described in this paper.

Results and Discussion

Phenylation of Arenes. I is insoluble in aromatic solvents and soluble in water and such aprotic polar solvents as acetonitrile and nitromethane. Therefore, I was decomposed in arene–acetonitrile mixture in order to carry out the phenylation in homogeneous solution. The isomer distributions and partial rate factors determined are compared in Tables 1 and 2 with the data reported in the literature. The isomer distributions of phenylarenes are quite similar to those obtained in the phenylation with benzenediazonium tetrafluoroborate,[3] phenylazo *p*-tolyl sulfone in the presence of trifluoroacetic acid,[4] and phenylazotriphenylmethane in trifluoroacetic acid,[5] but significantly differ from the values observed in the phenylation with *N*-nitrosoacetanilide.[7] Namely, in the former cases the methoxy, ethyl and chloro groups behaved as *o,p*-directors and nitro group behaved as a *m*-director, whereas in the latter case the nitro group behaved as an *o,p*-director.

The partial rate factors observed with I are also similar to the values in the phenylation with benzenediazonium tetrafluoroborate,[3] phenylazo *p*-tolyl sulfone[4] or phenylazotriphenylmethane[5] in trifluoroacetic acid but different from the figures reported for phenylation with *N*-nitrosoacetanilide.[7] These results clearly show that the decomposition of I does not yield phenyl radical, but yields phenyl cation. Thus, I is a new reagent for production of phenyl cation, and one can choose from PhN_2BF_4, $PhN_2O_2SAr{+}CF_3CO_2H$, $PhN_2CPh_3{+}CF_3CO_2H$, and $PhN_2O_2CCF_3$ (I).

$$PhN_2^+CF_3CO_2^- \longrightarrow Ph^+ + N_2 + CF_3CO_2^-$$

$$\xrightarrow{PhX} Ph{-}C_6H_4{-}X + CF_3CO_2H$$

Reaction with Oxygen[18]*-enriched Water.* When I was dissolved in water and decomposed at 25°C, phenol was obtained in 60—65% yield. This finding further supports the ionic decomposition mechanism and the formation of phenyl cation as a reactive intermediate. The reaction seems to be a convenient method for preparation of phenols, especially for preparation of ^{18}O-labeled phenols. When I was decomposed in water containing 1.3 atom % excess ^{18}O, phenol with 0.89 atom % excess ^{18}O was obtained in

Table 1. Isomer distributions of phenylarenes produced by phenylation of arenes with various phenylating agents

X	Position	PhC_6H_4X produced (%) by				
		$PhN_2^+CF_3CO_2^-$	$PhN_2^+BF_4^-$[3]	PhN_2Ts in CF_3CO_2H[4]	PhN_2CPh_3 in CF_3CO_2H[5]	$PhN(NO)Ac$[7]
$-OCH_3$	*o*	61.6	51.0	45.6	43.9	69
	m	9.7	6.6	8.2	8.1	18
	p	28.7	42.4	46.2	48.0	13
$-C_2H_5$	*o*	45.5	39.6	41.1	20.7	71[a]
	m	28.1	21.0	20.7	10.6	18[a]
	p	26.4	39.4	38.2	68.7	11[a]
$-Cl$	*o*	55.2	47.9	39.2	58.1	64
	m	19.9	12.1	14.4	10.5	21
	p	24.9	40.0	46.4	31.4	15
$-NO_2$	*o*	27.8	27.0	17.6	21.3	62
	m	69.4	40.6	37.3	72.3	8
	p	2.8	32.4	45.1	6.4	30

a) Isomer distribution of $PhC_6H_4CH_3$.

5) N. Kamigata, M. Kobayashi, and H. Minato, *ibid.*, **45**, 1231 (1972).

6) M. R. Pettit, M. Stacey, and J. C. Tatlow, *J. Chem. Soc.*, **1953**, 3081; M. R. Pettit and J. C. Tatlow, *ibid.*, **1954**, 1941.

7) R. Ito, T. Migita, N. Morikawa, and O. Simamura, *Tetrahedron*, **21**, 955 (1965).

Table 2. Partial rate factors in the phenylation of C_6H_5X with various phenylating agents

Arenes	Position	Partial rate factor in the reaction with				
		$PhN_2^+CF_3CO_2^-$	$PhN_2^+BF_4^-$ [3]	PhN_2Ts in CF_3CO_2H [4]	PhN_2CPh_3 in CF_3CO_2H [5]	PhN(NO)Ac [7]
$C_6H_5OCH_3$	*o*	2.66	1.77	1.72	1.52	3.56
	m	0.42	0.23	0.31	0.28	0.93
	p	2.48	1.47	1.74	1.66	1.29
$C_6H_5C_2H_5$	*o*	1.46	1.45	1.57	1.80	3.7[a]
	m	0.90	0.77	0.79	0.92	0.9[a]
	p	1.69	1.44	1.46	5.99	1.1[a]
C_6H_5Cl	*o*	0.83	0.67	0.60	0.89	3.09
	m	0.30	0.17	0.22	0.16	1.01
	p	0.75	0.56	0.71	0.48	1.48
$C_6H_5NO_2$	*o*	0.10	0.10	0.09	0.10	9.38
	m	0.25	0.15	0.19	0.34	1.16
	p	0.02	0.12	0.23	0.03	9.15

a) Partial rate factor with toluene.

61% yield.

Oxygen-18 labeled phenols could be produced by such methods as 1) $ArMgX+{}^*O_2$, 2) $ArSO_3Na+Na^*OH$, 3) $ArX+Na^*OH$ and 4) $ArN_2BF_4+CH_3C^*O_2H\rightarrow Ar^*OAc\rightarrow Ar^*OH$. The method 1) requires ^{18}O-enriched oxygen gas which is not commercially available. The method 2) and 3) require Na^*OH and rather high temperatures. The method 4) requires large excess of $CH_3C^*O_2H$ which is also not commercially available. Hydrolysis of $PhN_2^+BF_4^-$ or $PhN_2^+Cl^-$ in $H_2{}^*O$ needs high temperature and tends to give phenol with a lot of tarry mixture. On the contrary, the reaction between I and $H_2{}^{18}O$ proceeds smoothly at room temperature, the procedure is very simple, and therefore, one can say that this method is most convenient for preparation of ^{18}O-labeled phenol.

Experimental

Materials. I was prepared by diazotization of aniline with a concentrated aqueous solution (*ca.* 40%) of sodium nitrite in trifluoroacetic acid at 0—5°C. The crystals formed were filtered off, washed with small quantities of ice-water, and then dried for several hours *in vacuo* at 0°C over phosphorus pentoxide.[6] Purification of benzene and several arenes and preparation of authentic samples of substituted biphenyls were described previously.[3]

General Procedure for Determination of the Relative Reactivities of PhX toward Benzenediazonium Trifluoroacetate in Acetonitrile. A solution of I (2.0 g) in acetonitrile (2.0 g) was diluted with an equimolar mixture of PhH and PhX (the molar ratio (PhH+PhX)/I was 75). The homogeneous solution was placed in a bath at 20±0.1°C, and the decomposition was followed by evolution of nitrogen. After the evolution of nitrogen ceased, the reaction mixture was washed with water, a 5% sodium hydroxide solution, water, and then dried over anhydrous magnesium sulfate. The amounts of substituted biphenyl isomers were determined by a Hitachi Gas Chromatograph K–53 (Apiezon L 10% on Chromosorb W).

Not benzene but chlorobenzene was used as the standard for the competitive phenylation of PhOMe, PhEt, and $PhNO_2$, since unsubstituted biphenyl easily sublimes during the evaporation of arenes.[3-5]

Preparation of ^{18}O-labeled Phenol. Dry I (53 g) was dissolved in 70 ml of water (1.3 excess atom % ^{18}O) and spontaneously decomposed at 25°C. After the evolution of nitrogen ceased, the reaction mixture was diluted with ether, washed with water and dried over anhydrous magnesium sulfate. Oxygen-18 excess phenol was isolated by distillation under reduced pressure, bp 70°C/30 mmHg, yield 6.2 g (61%).

Determination of Oxygen-18 Contents. Phenol was brominated to 1,3,5-tribromophenol, which was purified by sublimation three times, and then converted into carbon dioxide according to the method of Rittenberg and Ponticorvo[8] for determination of the oxygen-18 contents. The ^{18}O-contents of the carbon dioxide was determined by use of a Hitachi RM–50 Type Mass Spectrometer.

8) D. Rittenberg and L. Ponticorvo, *Int. J. Appl. Radiat. Isotopes*, **1**, 208 (1956).

BULLETIN OF THE CHEMICAL SOCIETY OF JAPAN, VOL. 46, 1019—1020 (1973)

Synthetic Studies of Amino Acids by the Use of the Copper(II) Complex. IV.[1d] A Facile Procedure for Isolating Amino Acids from Their Copper(II) Complexes by Means of Amberlite IR-120B

Shohji OHDAN, Tetsuya ICHIKAWA, Younosuke ARAKI, and Yoshiharu ISHIDO

Department of Chemistry, Faculty of Science, Tokyo Institute of Technology, O-okayama, Meguro-ku, Tokyo

(Received September 27, 1972)

It has been shown in a series of investigation[1)] that the base-catalyzed condensation reaction of *N*-pyruvylideneglycinatoaquocopper(II) with a variety of aldehydes is useful for the preparation of β-hydroxy amino acids and 2-amino-2-deoxyaldonic acids. The isolation of the resultant amino acids from the corresponding copper(II) complexes has been performed by the treatment of their aqueous solutions with hydrogen sulfide gas or sodium sulfide, followed by the filtration of the precipitated cupric sulfide, adsorption on a column of Amberlite IR-120B(H form), and elution with a dilute aqueous ammoniacal solution. However, treatment with sodium sulfide makes the resultant solution strongly alkaline, and an alkaline condition is unsuitable for such amino acids as 2-amino-2-deoxyaldonic acids susceptible to isomerization. Moreover, hydrogen sulfide gas is, if anything, unsuitable for the isolating procedure in view of its toxicity. In these connections, an investigation was undertaken in order to establish a more favorable procedure for the isolation of amino acids by the use of some reagents;[2)] the application of Amberlite IR-120B(H form) was proved to afford amino acids in high yields quite simply.

A solution of *N*-pyruvylideneglycinatoaquocopper-(II)[1c)] (10 mmol) in distilled water (100 ml) was treated on a column (3×9 cm) of the resin, washed with distilled water, and then eluted with a dilute

TABLE 1. AN EXAMINATION ON THE WASHING PROCEDURE WITH DISTILLED WATER PRIOR TO THE ELUTION WITH AQUEOUS AMMONIACAL SOLUTION[a)]

Run	The volume of water for washing, l	Yield of isolated glycine	
		g	%
1	5	0.732	97.6
2	3	0.727	96.9
3	1	0.702	93.6

a) All the examinations were carried out by the use of 10 mmol of *N*-pyruvylideneglycinatoaquocopper(II) dissolved in distilled water (100 ml). In each case, the elution was carried out with 2000 ml of 0.5 M aqueous ammoniacal solution.

TABLE 2. AN EXAMINATION ON THE ELUTING PROCEDURE WITH 0.5 M AQUEOUS AMMONIACAL SOLUTION AFTER THE WASHING WITH DISTILLED WATER[a)]

Fractions[b)]	Yield of isolated glycine	
	g	%
1	0.722	96.3
2	0.005	0.7
3	0.003	0.3
4	0.002	0.3

a) All the examinations were carried out by the use of 10 mmol of *N*-pyruvylideneglycinatoaquocopper(II) dissolved in distilled water (100 ml). Prior to the elution, the column was washed with distilled water (5000 ml). b) The eluate was divided into the fractions of 500 ml, and the fractions were numbered in turn in the order of eluting-out.

TABLE 3. ISOLATION OF AMINO ACIDS FROM THE CORRESPONDING COPPER(II) COMPLEXES BY THE USE OF AMBERLITE IR-120 B[a)]

Copper(II) complexes	Mol. weight	Yield of isolated glycine or alanine	
		g	%
N-Pyruvylidene-glycinatoaquocopper(II)[b)]	260	0.732	97.6
Bisglycinatocopper(II)[c)]	230	1.485	99.0
N-Salicylidene-glycinatoaquocopper(II)[d)]	278	0.564	75.2
N-Pyruvylidene-glycinatopyridinecopper(II)[e)]	339	0.705	94.0
Bisalaninatocopper(II)	258	1.768	98.6

a) All the isolations were carried out by the use of 10 mmol of the corresponding copper(II) complexes and the column (3×9 cm) of the resin(H form). b) On removing the copper(II) ion by treating with hydrogen sulfide gas prior to the treatment on the column, glycine was obtained in 82.1% yield. c) Glycine was obtained in 97.5% yield by decomposing the complex with concentrated aqueous ammoniacal solution prior to the treatment on the column. d) The yield is considered to be arisen from the low solubility of the complex. e) On treating the complex as described in b), glycine was obtained in 82.0% yield.

1) a) T. Ichikawa, S. Maeda, Y. Araki, and Y. Ishido, *J. Amer. Chem. Soc.*, **92**, 5514 (1970); b) T. Ichikawa, T. Okamoto, S. Maeda, S. Ohdan, Y. Araki, and Y. Ishido, *Tetrahedron Lett.*, **1971**, 79; c) T. Ichikawa, S. Maeda, T. Okamoto, Y. Araki, and Y. Ishido, This Bulletin, **44**, 2779 (1971); d) S. Ohdan, T. Okamoto, S. Maeda, T. Ichikawa, Y. Araki, and Y. Ishido, *ibid.*, **46**, 981 (1973).

2) a) The copper(II) complex was not decomposed by a concentrated aqueous ammoniacal solution, although it has been well known that bisglycinatocopper(II) can be decomposed by the solution; b) The separation of the excess amines from glycine could not be achieved distinctly by the same ion-exchange resin-column technique, although the complex was decomposed by the use of 1.5—2.0 equivalents of ethylenediamine, diethylenetriamine, and triethylenetetramine respectively; c) Amberlite IR-120B (H form) was used since *N*-salicylideneglycinatoaquocopper-(II) has been shown to be decomposed by 6 M aqueous hydrochloric acid [K. Harada and J. Oh-hashi, *J. Org. Chem.*, **32**, 1103 (1967)].

Table 4. Isolation of glycine from *N*-pyruvylideneglycinatoaquocopper(II) in alkaline solution by the treatment with amberlite IR-120 B[a]

Run	Solvent system	Conditions		Yield of isolated glycine	
		pH[b]	Treating time, hr	g	%
1	H_2O (100 ml)	9.5	0	0.677	90.3
2	H_2O–DMF(80+80 ml)	9.0	0	0.715	95.3
3	H_2O–DMF(80+80 ml)	9.0	2	0.511	68.1

a) All the isolations were carried out by the use of *N*-pyruvylideneglycinatoaquocopper(II) and a column (3×9 cm) of the resin(H form). The washing of the column and the elution were carried out with distilled water (5000 ml) and 0.5 M aqueous ammoniacal solution (2000 ml), respectively. b) These conditions were adjusted by the use of a pH meter and by the addition of 1 M aqueous sodium hydroxide solution.

aqueous ammoniacal solution; the eluate was then concentrated *in vacuo* to give white crystals of glycine in a 97.6% yield. Incidentally, the amounts of solvents necessary for the washing and the elution were found to be 1000 ml and 500 ml respectively by such examinations as are shown in Tables 1 and 2. By the application of best condition, the isolation of glycine and alanine were attempted with respect to bisglycinatocopper(II),[3] *N*-salicylideneglycinatoaquocopper(II),[4] *N*-pyruvylideneglycinatopyridinecopper (II),[1c] and bisalaninatocopper(II);[5] they were proved to give the corresponding amino acids in 99.0, 75.2, 94.0, and 98.6% respectively, under the conditions summarized in Table 3. Except in the case of *N*-pyruvylideneglycinatopyridinecopper(II), these results are greatly improved in comparison with those obtained by conventional procedures. On the basis of these results, the isolation of glycine with respect to *N*-pyruvylideneglycinatoaquocopper(II) treated under the conditions(pH 9.5) previously used in the base-catalyzed condensation reaction;[1] glycine was thus obtained in a 90.3% yield, as is shown in Table 4. Furthermore, the base-catalyzed condensation reaction of the complex with some aldehydes can not be carried out even in aqueous methanol because of their low solubility; it is thus necessary to examine the application of other solvents to the reaction. The isolation of glycine from the complex in aqueous *N,N*-dimethylformamide was attempted as is shown in the table as a model experiment postulating the case that the condensation reaction was carried out in the solvent system. The yield is also fairly good in this case (95.3%).[6] On the other hand, the treatment of the complex under the same condition for 2 hr was proved to afford glycine in a 68.1% yield, and it was concluded that the condensation reaction can be carried out in aqueous *N,N*-dimethylformamide since the extent of the degradation of glycine in the complex is comparable with that observed in an aqueous solution.[1c]

It can thus be concluded that the isolating procedure involving a simple treatment on a column of Amberlite IR-120B(H form) is facile and useful for the isolation of amino acids from the corresponding copper(II) complexes.

Experimental

Isolation of Glycine from the Aqueous Solution of N-*Pyruvylideneglycinatoaquocopper(II).* A solution of *N*-pyruvylideneglycinatoaquocopper(II)[1c] (2.600 g, 10 mmol) in distilled water (100 ml) was treated on a column(3×9 cm) of Amberlite IR-120B(H form). This column was then washed with distilled water(5000 ml) and eluted with a 0.5 M aqueous ammoniacal solution(2000 ml). The eluate was concentrated *in vacuo* almost to dryness and subsequently triturated with ethanol(10 ml) to give glycine(0.732 g, 97.6%); mp 232°C (decomp.). The IR spectrum of this product was identical with that of the authentic specimen.

Incidentally, the alkaline solution was prepared by the addition of a 1 M aqueous sodium hydroxide solution, and its pH was adjusted by the use of a pH meter.

Isolation of Amino Acids from Bisglycinatocopper(II),[3] N-*Salicylideneglycinatoaquocopper(II),*[4] N-*Pyruwylideneglycinatopyridinecopper(II),*[1c] *and Bisalaninatocopper(II).*[5] The isolations were accomplished under the conditions described in each table in the same way as has been described for the preceeding experiment.

3) M. Sato, K. Okawa, and S. Akabora, This Bulletin, **30**, 937 (1957).

4) A. Nakahara, *ibid.*, **32**, 1195 (1959).

5) Z. E. Gol' braikh, *Zh. Neorg. Khim.*, **1**, 1739 (1956); *Chem. Abstr.*, **51**, 2446c (1957).

6) When the solution was treated with hydrogen sulfide gas according to the conventional procedure, the resultant fine precipitates of cupric sulfide could not be filtered off; they passed through the filter cell on filtration. The cupric sulfide remained in the isolated glycine in spite of the filtration and treatment on a column of the resin.

The Crystal Structure of *d,l*-1,1,4aα-Trimethyl-2α-hydroxy-8α-acetoxy-1,2,3,4,4a,5,6,7,8,9-decahydrophenanthrene

Akio FURUSAKI, Nobuyuki HAMANAKA, and Takeshi MATSUMOTO
Department of Chemistry, Faculty of Science, Hokkaido University, Sapporo
(Received August 24, 1972)

The conformation of *d,l*-1,1,4aα-trimethyl-2α-hydroxy-8α-acetoxy-1,2,3,4,4a,5,6,7,8,9-decahydrophenanthrene has been studied by means of X-ray methods. The crystals are triclinic, with two molecules in a unit cell with the dimensions of $a=11.463$, $b=11.509$, $c=7.430$ Å, $\alpha=84°42'$, $\beta=102°47'$, and $\gamma=115°40'$. The space group is $P\bar{1}$. The intensity data were collected on an automatic four-circle diffractometer with Cu$K\alpha$ radiation. The structure was solved by the symbolic-addition method, and was refined by the block-diagonal-matrix least-squares method with anisotropic temperature factors for all the non-hydrogen atoms. From a difference Fourier map, all the 28 hydrogen atoms were also found. Further least-squares refinement including these hydrogen atoms reduced the R factor to 5.4%. In the present molecule, the cyclohexene ring has the normal half-chair conformation, and does not show the unusual behavior found in the *p*-bromobenzoate of 1,1,4aα-trimethyl-2α-hydroxy-8β-methoxy-1,2,3,4,4a,5,6,7,8,9-decahydrophenanthrene. The 8α-acetoxyl group, like the 8β-methoxyl group in the *p*-bromobenzoate, takes the axial orientation notwithstanding the inversion of the configuration. Such a conformation seems to be the preferred one for a cyclohexene ring which has a methoxyl or an acetoxyl group at the allylic position.

It has recently been found that the Birch reduction of 1,1,4aα-trimethyl-2α-hydroxy-8-acetoxy-1,2,3,4,4a,9-hexahydrophenanthrene, I, affords an unusual product, II, and that, in the acetolysis of II, the methoxyl group is much more easily replaced with an acetoxyl group than those in usual allyl methyl ethers.[1] On the other hand, for the purpose of inquiring into the cause of the high reactivity, the stereostructure of II has been studied by means of the X-ray crystallographic analysis of its *p*-bromobenzoate derivative, III.[2] The study has revealed not only that the methoxyl group is axially bonded to the cyclohexene ring with a considerably flattened half-chair form, but also that the two carbon atoms in the ring vibrate vigorously in a direction almost perpendicular to the mean plane of the ring. In order to examine whether or not these remarkable features are also observed in the acetolysis product, IV, and to establish the configuration of the acetoxyl group, an X-ray analysis of IV has now been carried out.

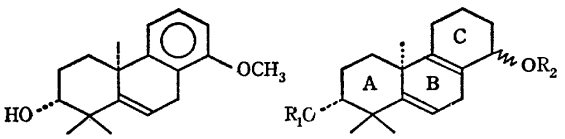

I

II $R_1=H$, $R_2=CH_3$
III $R_1=BrC_6H_4CO$, $R_2=CH_3$
IV $R_1=H$, $R_2=CH_3CO$

Experimental

Colorless, single crystals of IV (racemate), $C_{19}H_{28}O_3$, mp 146—7°C, were grown in an ether solution. A sample with dimensions of about $0.1\times0.2\times0.4$ mm was cut out of one of the single crystals and used for the X-ray measurement. The crystal data are summarized in Table 1. The cell dimensions were measured by using a single-crystal diffractometer with Cu$K\alpha$ radiation ($\lambda=1.54178$ Å). The space group was assumed to be $P\bar{1}$ at the beginning of the study; this choice was confirmed later by successful refinement. The intensities of reflections with 2θ values up to 140° were collected on an automatic four-circle diffractometer at this University, using Cu$K\alpha$ radiation monochromatized with a LiF crystal. The intensity measurement was made by the use of the ω-2θ scanning technique. The scan rate was about 0.5°(ω)/min, and the background was measured for each reflection for 30—60 s at the beginning and end of each scanning range. The intensity data were corrected for the usual Lorentz and polarization factors, but not for the absorption effect. Out of the structure factors thus obtained, 2769 above $2\sigma(F)$ were selected for the structural study.

TABLE 1. THE CRYSTAL DATA

Crystal system Space group	Triclinic $P\bar{1}$
a	11.463±0.003 Å
b	11.509±0.003
c	7.430±0.003
α	84°42'±3'
β	102°47'±3'
γ	115°40'±3'
Z	2
D_x	1.173 g/cm³

Structure Determination

The structure was elucidated by means of the symbolic addition method[3] on the basis of 585 $|E|$ values above 1.30. After 286 phases had been expressed by three symbols, A, B, and C, the values of the R factor ($R=\Sigma||E_o|-|E_c||/\Sigma|E_o|$) were calculated for all eight possible combinations of the numerical values of the symbols. Since it was certain that the set ($A=B=C=0$) with the lowest R value, 0.171, did not lead to the true structure, an E-Fourier synthesis was carried

1) N. Hamanaka, T. Okuno, T. Nakajima, A. Furusaki, and T. Matsumoto, *Chem. Lett.*, **1972**, 1037.
2) A. Furusaki, N. Hamanaka, and T. Matsumoto, This Bulletin, **46**, 434 (1973).
3) J. Karle and I. L. Karle, *Acta Crystallogr.*, **21**, 849 (1966).

Table 2. The final atomic parameters with their standard deviations

(a) The non-hydrogen atoms

The parameters are multiplied by 10^4.

(1) The fractional coordinates

Atom	x/a	y/b	z/c	Atom	x/a	y/b	z/c
O(1)	3613(2)	3557(2)	2033(2)	C(9)	8460(2)	3017(2)	3046(2)
O(2)	10612(1)	2007(1)	5789(2)	C(10)	6967(2)	2618(2)	2483(2)
O(3)	12079(3)	2850(3)	8346(3)	C(11)	9247(2)	3517(3)	1533(3)
C(1)	6709(2)	3594(2)	1058(2)	C(12)	10544(2)	3386(3)	1981(4)
C(2)	5281(2)	3413(2)	640(2)	C(13)	11289(2)	3936(2)	3873(4)
C(3)	4895(2)	3569(2)	2376(3)	C(14)	10496(2)	3234(2)	5326(3)
C(4)	4981(2)	2554(2)	3863(2)	C(15)	4770(2)	2958(3)	5637(3)
C(5)	6346(1)	2531(2)	4144(2)	C(16)	3870(2)	1212(2)	3303(4)
C(6)	6964(2)	2383(2)	5829(2)	C(17)	6361(2)	1273(2)	1556(3)
C(7)	8281(2)	2355(2)	6272(3)	C(18)	11403(2)	1940(3)	7335(3)
C(8)	9040(2)	2872(2)	4757(2)	C(19)	11409(4)	652(4)	7594(6)

(2) The anisotropic temperature factors

These are expressed as

$$\exp[-(B_{11}h^2+B_{22}k^2+B_{33}l^2+B_{12}hk+B_{23}kl+B_{31}lh)].$$

Atom	B_{11}	B_{22}	B_{33}	B_{12}	B_{23}	B_{31}
O(1)	114(2)	227(3)	234(3)	223(4)	−14(4)	23(4)
O(2)	107(1)	100(1)	264(3)	116(2)	−65(3)	−73(3)
O(3)	206(3)	217(3)	329(5)	266(5)	−178(6)	−234(6)
C(1)	96(2)	106(2)	140(3)	107(3)	33(3)	56(3)
C(2)	102(2)	133(2)	151(3)	136(3)	24(4)	14(4)
C(3)	86(2)	120(2)	180(3)	117(3)	−10(4)	22(3)
C(4)	77(2)	113(2)	171(3)	81(3)	5(4)	52(3)
C(5)	74(1)	75(1)	142(3)	60(2)	4(3)	41(3)
C(6)	94(2)	115(2)	140(3)	90(3)	22(3)	57(3)
C(7)	104(2)	139(2)	152(3)	123(3)	38(4)	10(4)
C(8)	77(1)	79(1)	179(3)	70(2)	−28(3)	18(3)
C(9)	77(1)	81(1)	167(3)	72(2)	2(3)	51(3)
C(10)	77(1)	78(1)	130(3)	71(2)	−11(3)	27(3)
C(11)	106(2)	163(3)	226(4)	145(4)	91(5)	133(5)
C(12)	118(2)	163(3)	338(6)	162(4)	111(7)	197(6)
C(13)	77(2)	119(2)	422(7)	84(3)	45(6)	82(5)
C(14)	82(2)	89(2)	265(4)	84(3)	−63(4)	−31(4)
C(15)	122(2)	204(3)	202(4)	189(5)	26(6)	117(5)
C(16)	79(2)	129(2)	335(6)	37(3)	12(6)	65(5)
C(17)	112(2)	97(2)	210(4)	90(3)	−81(4)	12(4)
C(18)	103(2)	151(3)	254(5)	154(4)	−25(5)	−30(5)
C(19)	197(4)	177(4)	436(9)	234(7)	75(9)	−62(10)

(b) The hydrogen atoms

The positional and thermal parameters are multiplied by 10^3 and 10 respectively.

Atom	x/a	y/b	z/c	B	Atom	x/a	y/b	z/c	B
H(1-1)	729(2)	449(2)	157(3)	23(4)	H(14)	1085(3)	377(2)	639(4)	29(5)
H(1-2)	695(2)	353(2)	−4(4)	26(4)	H(15-1)	559(4)	384(3)	622(5)	51(7)
H(2-1)	519(2)	405(2)	−23(3)	23(4)	H(15-2)	400(3)	307(3)	535(4)	39(6)
H(2-2)	469(3)	255(2)	10(4)	27(4)	H(15-3)	468(4)	227(4)	656(5)	54(7)
H(3)	556(2)	447(2)	298(3)	24(4)	H(16-1)	395(4)	56(4)	421(6)	57(8)
H(6)	657(3)	226(2)	686(4)	28(5)	H(16-2)	308(4)	122(4)	326(5)	53(7)
H(7-1)	822(3)	150(3)	655(4)	32(5)	H(16-3)	384(3)	91(3)	210(5)	45(6)
H(7-2)	880(4)	285(4)	740(5)	51(7)	H(17-1)	539(3)	100(3)	97(4)	39(6)
H(11-1)	869(3)	306(3)	37(5)	45(7)	H(17-2)	644(3)	66(3)	250(4)	36(5)
H(11-2)	943(3)	449(3)	127(4)	42(6)	H(17-3)	688(3)	130(3)	64(4)	39(6)
H(12-1)	1109(4)	389(3)	100(5)	53(7)	H(19-1)	1120(7)	30(7)	873(10)	108(16)
H(12-2)	1036(3)	244(3)	195(4)	42(6)	H(19-2)	1059(6)	−2(6)	704(8)	90(13)
H(13-1)	1212(3)	394(3)	419(4)	42(6)	H(19-3)	1207(7)	58(7)	779(10)	112(16)
H(13-2)	1143(3)	489(3)	391(4)	41(6)	H(O)	327(4)	328(4)	96(6)	61(8)

out using 558 phases based on the set ($A=B=0$, $C=\pi$) with the second lowest R, 0.199. As was expected, the resulting E-map yielded the locations of all the non-hydrogen atoms. The structure thus obtained was refined by the block-diagonal-matrix least-squares method, first with individual isotropic temperature factors and then with anisotropic thermal parameters for all the atoms. In this way, the value of the discrepancy factor, $R(R=\Sigma||F_o|-|F_c||/\Sigma|F_o|)$, dropped to 11.2%. After the 28 hydrogen atoms were located in a difference Fourier map, the least-squares refinement was further repeated including these hydrogen atoms with isotropic temperature factors. In this refinement, the following weighting scheme was used:

$$W = 1/\{\sigma(F_o)^2 \exp(AX^2+BY^2+CXY+DX+EY)\},$$

where $X=|F_o|$, $Y=\sin\theta/\lambda$. The $\sigma(F_o)$ values were calculated from the counting statistics. The intensity data were grouped with constant intervals along two coordinates, $|F_o|$ and $\sin\theta/\lambda$. The coefficients, A, B, C, D, and E, were determined by the least-squares fit so as to give as equal values of $<W\Delta|F|^2>$ for all the groups as possible. The final R factor was 5.4%. The atomic parameters thus obtained are listed in Table 2.

The calculations in the present study were carried out on a FACOM 230—60 computer at the Computer Center of Hokkaido University using our own programs. The atomic scattering factors were taken from the International Tables for X-ray Crystallography (1962), Vol. III.

Tables of the observed and calculated structure factors are preserved by the Chemical Society of Japan. (Document No. 7309).

Results and Discussion

The molecular framework of IV thus obtained is shown in Fig. 1. First of all, it is found that the acetoxyl group has the *cis* relation with the angular methyl,

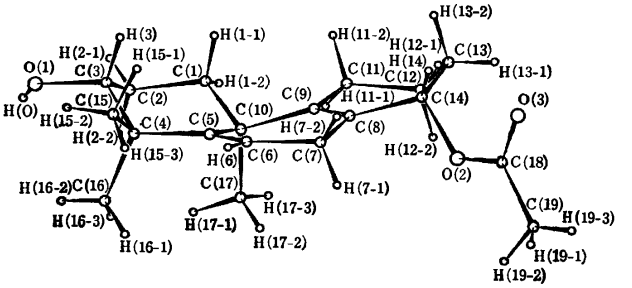

Fig. 1. The molecular framework of IV and the numbering system of the atoms.

Table 3. The bond distances with their standard deviations (Å)

(a) The bond distances between the non-hydrogen atoms

Bond	D	σ	Bond	D	σ
C(1)-C(2)	1.520	0.003	C(8)-C(9)	1.329	0.002
C(1)-C(10)	1.549	0.003	C(8)-C(14)	1.503	0.003
C(2)-C(3)	1.502	0.003	C(9)-C(10)	1.534	0.002
C(3)-C(4)	1.552	0.003	C(9)-C(11)	1.513	0.003
C(3)-O(1)	1.429	0.003	C(10)-C(17)	1.552	0.003
C(4)-C(5)	1.544	0.003	C(11)-C(12)	1.520	0.004
C(4)-C(15)	1.537	0.004	C(12)-C(13)	1.507	0.004
C(4)-C(16)	1.537	0.003	C(13)-C(14)	1.510	0.004
C(5)-C(6)	1.330	0.002	C(14)-O(2)	1.477	0.003
C(5)-C(10)	1.531	0.002	C(18)-C(19)	1.480	0.005
C(6)-C(7)	1.487	0.003	C(18)-O(2)	1.316	0.003
C(7)-C(8)	1.496	0.003	C(18)-O(3)	1.203	0.003

(b) The bond distances involving the hydrogen atoms

Bond	D	σ	Bond	D	σ
C(1)-H(1-1)	1.01	0.02	C(14)-H(14)	0.94	0.03
C(1)-H(1-2)	0.93	0.03	C(15)-H(15-1)	1.08	0.03
C(2)-H(2-1)	0.95	0.03	C(15)-H(15-2)	0.93	0.04
C(2)-H(2-2)	0.99	0.02	C(15)-H(15-3)	0.98	0.04
C(3)-H(3)	1.05	0.02	C(16)-H(16-1)	0.98	0.04
C(6)-H(6)	0.94	0.03	C(16)-H(16-2)	0.90	0.05
C(7)-H(7-1)	0.96	0.03	O(16)-H(16-3)	0.97	0.04
C(7)-H(7-2)	0.98	0.03	C(17)-H(17-1)	1.02	0.03
C(11)-H(11-1)	0.99	0.03	C(17)-H(17-2)	0.97	0.03
C(11)-H(11-2)	1.06	0.04	C(17)-H(17-3)	0.99	0.04
C(12)-H(12-1)	1.04	0.04	C(19)-H(19-1)	0.94	0.08
C(12)-H(12-2)	1.02	0.04	C(19)-H(19-2)	0.95	0.05
C(13)-H(13-1)	0.93	0.04	C(19)-H(19-3)	0.77	0.09
C(13)-H(13-2)	1.04	0.04	O(1)-H(O)	0.84	0.04

Table 4. The bond angles with their standard deviations (°)

	Angle	σ		Angle	σ
C(2)-C(1)-C(10)	113.4	0.2	C(5)-C(6)-H(6)	121	2
C(1)-C(2)-C(3)	110.0	0.2	C(7)-C(6)-H(6)	114	2
C(2)-C(3)-C(4)	112.7	0.2	C(6)-C(7)-H(7-1)	112	2
C(2)-C(3)-O(1)	112.4	0.2	C(6)-C(7)-H(7-2)	109	2
C(4)-C(3)-O(1)	110.1	0.2	C(8)-C(7)-H(7-1)	108	2
C(3)-C(4)-C(5)	109.4	0.2	C(8)-C(7)-H(7-2)	109	2
C(3)-C(4)-C(15)	106.6	0.2	H(7-1)-C(7)-H(7-2)	105	3
C(3)-C(4)-C(16)	110.8	0.1	C(9)-C(11)-H(11-1)	109	2
C(5)-C(4)-C(15)	111.6	0.2	C(9)-C(11)-H(11-2)	110	2
C(5)-C(4)-C(16)	110.6	0.2	C(12)-C(11)-H(11-1)	111	2
C(15)-C(4)-C(16)	107.7	0.2	C(12)-C(11)-H(11-2)	110	2
C(4)-C(5)-C(6)	119.9	0.2	H(11-1)-C(11)-H(11-2)	105	3
C(4)-C(5)-C(10)	120.3	0.1	C(11)-C(12)-H(12-1)	108	2
C(6)-C(5)-C(10)	119.7	0.2	C(11)-C(12)-H(12-2)	110	2
C(5)-C(6)-C(7)	124.8	0.2	C(13)-C(12)-H(12-1)	110	2
C(6)-C(7)-C(8)	113.4	0.2	C(13)-C(12)-H(12-2)	110	2
C(7)-C(8)-C(9)	121.9	0.2	H(12-1)-C(12)-H(12-2)	110	3
C(7)-C(8)-C(14)	115.0	0.2	C(12)-C(13)-H(13-1)	113	2
C(9)-C(8)-C(14)	123.0	0.2	C(12)-C(13)-H(13-2)	109	2
C(8)-C(9)-C(10)	122.3	0.2	C(14)-C(13)-H(13-1)	110	2
C(8)-C(9)-C(11)	120.8	0.2	C(14)-C(13)-H(13-2)	106	2
C(10)-C(9)-C(11)	116.8	0.2	H(13-11)-C(13)-H(13-2)	107	3
C(1)-C(10)-C(5)	110.3	0·2	C(8)-C(14)-H(14)	110	2
C(1)-C(10)-C(9)	109.2	0.1	C(13)-(14)-H(14)	108	2
C(1)-C(10)-C(17)	109.3	0.1	O(2)-C(14)-H(14)	109	2
C(5)-C(10)-C(9)	112.1	0.1	C(4)-C(15)-H(15-1)	112	2
C(5)-C(10)-C(17)	109.6	0.1	C(4)-C(15)-H(15-2)	108	2
C(9)-C(10)-C(17)	106.2	0.1	C(4)-C(15)-H(15-3)	110	2
C(9)-C(11)-C(12)	113.1	0.2	H(15-1)-C(15)-H(15-2)	110	3
C(11)-C(12)-C(13)	109.5	0.3	H(15-1)-C(15)-H(15-3)	108	3
C(12)-C(13)-C(14)	111.0	0.2	H(15-2)-C(15)-H(15-3)	109	3
C(8)-C(14)-C(13)	114.8	0.2	C(4)-C(16)-H(16-1)	111	2
C(8)-C(14)-O(2)	105.5	0.2	C(4)-C(16)-H(16-2)	110	3
C(13)-C(14)-O(2)	109.7	0.2	C(4)-C(16)-H(16-3)	115	2
O(2)-C(18)-O(3)	122.8	0.3	H(16-1)-C(16)-H(16-2)	107	4
O(2)-C(18)-C(19)	111.9	0.3	H(16-1)-C(16)-H(16-3)	107	3
O(3)-C(18)-C(19)	125.2	0.3	H(16-2)-C(16)-H(16-3)	107	4
C(14)-O(2)-C(18)	118.5	0.2	C(10)-C(17)-H(17-1)	111	2
C(2)-C(1)-H(1-1)	109	1	C(10)-C(17)-H(17-2)	108	2
C(2)-C(1)-H(1-2)	109	2	C(10)-C(17)-H(17-3)	109	2
C(10)-C(1)-H(1-1)	108	1	H(17-1)-C(17)-H(17-2)	109	3
C(10)-C(1)-H(1-2)	110	2	H(17-1)-C(17)-H(17-3)	112	3
H(1-1)-C(1)-H(1-2)	108	2	H(17-2)-C(17)-H(17-3)	108	3
C(1)-C(2)-H(2-1)	109	2	C(18)-C(19)-H(19-1)	111	5
C(1)-C(2)-H(2-2)	110	1	C(18)-C(19)-H(19-2)	113	3
C(3)-C(2)-H(2-1)	109	2	C(18)-C(19)-H(19-3)	120	7
C(3)-C(2)-H(2-2)	110	1	H(19-1)-C(19)-H(19-2)	87	6
H(2-1)-C(2)-H(2-2)	109	2	H(19-1)-C(19)-H(19-3)	94	8
C(2)-C(3)-H(3)	109	1	H(19-2)-C(19)-H(19-3)	122	7
C(4)-C(3)-H(3)	105	1	C(3)-O(1)-H(O)	105	3
O(1)-C(3)-H(3)	106	1			

$C(17)H_3$; this shows that the acetolysis of II proceeds with an inversion of the configuration at the C(14) atom. Thus, Compound IV can be fully expressed by the name: *d,l*-1,1,4aα-trimethyl-2α-hydroxy-8α-acetoxy-1,2,3,4,4a,5,6,7,8,9-decahydrophenanthrene.

The torsion angles for the tricyclic system are given in Fig. 2. The A and B rings take, respectively, distorted chair and boat forms very similar to those found in III.[2] On the other hand, the C ring has the ordinary half-chair form, which is nearly as puckered

Table 5. The intramolecular H···H contacts (Å)

	D	σ		D	σ
H(1-1)···H(2-1)	2.34	0.03	H(6)···H(7-2)	2.29	0.05
H(1-2)···H(2-1)	2.31	0.05	···H(15-3)	2.14	0.06
···H(2-2)	2.36	0.04	H(7-2)···H(14)	2.39	0.05
···H(11-1)	2.23	0.05	H(11-1)···H(12-2)	2.37	0.06
H(2-1)···H(3)	2.39	0.04	···H(17-3)	2.21	0.04
···H(O)	2.33	0.06	H(11-2)···H(12-1)	2.34	0.07
H(2-2)···H(16-3)	2.30	0.04	H(12-1)···H(13-1)	2.40	0.05
···H(17-1)	2.25	0.05	H(13-1)···H(14)	2.36	0.05
···H(O)	2.34	0.07	H(13-2)···H(14)	2.21	0.04
			H(16-3)···H(17-1)	2.09	0.06

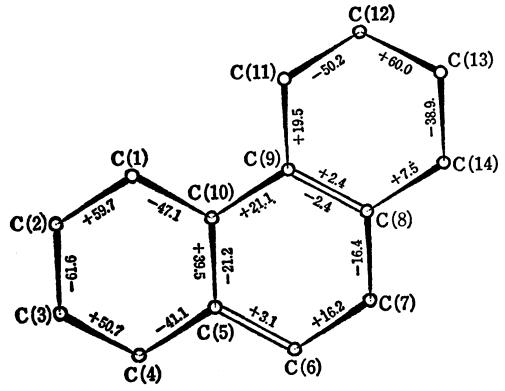

Fig. 2. The torsion angles (°) for the tricyclic system.

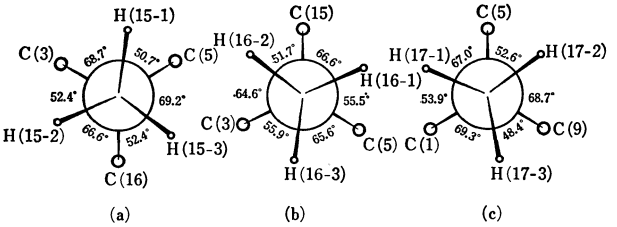

Fig. 3. The Newman projections along the bonds, (a) C(4)-C(15), (b) C(4)-C(16), and (c) C(10)-C(17).

as those in many other cyclohexene derivatives. The acetoxyl group, like the methoxyl group in III, is axially oriented by the flipping of the C ring, although the configuration at the C(14) atom is inverted. The bond lengths and angles calculated with the final coordinates are listed in Tables 3 and 4 respectively. These values are all reasonable, considering their estimated standard deviations. Table 5 gives the intramolecular H···H distances smaller than 2.40 Å.

It may be said that the A ring in the present molecule is still less puckered than that in III, because the average torsion angle for the former, 50.0°, is about 2.2° smaller than that for the latter. Out of the corresponding torsion angles in these two rings, those around the C(3)-C(4), C(4)-C(5), and C(5)-C(10) bonds especially differ by about 4° to 6°. These differences may be attributable partly to the replacement of the benzoyl group with the hydrogen atom, but seem to arise mainly from the flipping of the C ring. Considering the fact that, in IV, the hydrogen atoms attached to the C(1) and C(11) atoms keep distances of at least 2.23 Å without any great distortion of the C ring, the flipping of the C ring would remarkably lessen the steric repulsion between the A and C rings. Consequently, the two axial methyl groups, C(16)H_3 and C(17)H_3, would be allowed to become somewhat more distant from each other by the conformational change in the A and B rings. In fact, as may be seen in Fig. 3, the deviations of the C(16)H_3 and C(17)H_3 groups from the staggered conformation, 6° and 8°, are somewhat smaller than the corresponding values for III, 13° and 10° respectively, although the H(16—3) and H(17—1) atoms keep a distance of about 2.09 Å, which is nearly equal to that in III, 2.05 Å. On the contrary, the C(15)H_3 group is forced to rotate by about 8° from the staggered arrangement, so that the H(15-3) atom may be separated at a distance of about 2.14 Å from the H(6) atom. This rotation angle is about 5° larger than the corresponding angle for III. The O(1)-H(O) bond takes approximately the eclipsed conformation with the C(2)-C(3) bond, the deviation being about 14°. This conformation seems to be caused by the hydrogen-bond formation of the hydroxyl group with the acetyl oxygen atom of another molecule, O(3′). Because of the unstable eclipsed conformation of the hydroxyl group, the angle between the O(1)-H(O) and O(1)···O(3′) directions is reduced to about 12°. It is interesting to notice that the alternate valence angles in the A ring are significantly larger than the usual tetrahedral angle. This may show a way in which a cyclohexene ring is distorted by forming an exocyclic double bond.

The conformation of the B ring is almost symmetrical with respect to the plane which approximately bisects the C(6)-C(7)-C(8) and C(5)-C(10)-C(9) angles. The two nonconjugated double bonds in the ring, C(5)=C(6) and C(8)=C(9), are both twisted to some extent. The deviations of the atoms from the least-squares best planes through the C(4), C(5), C(6), C(7), and C(10) atoms and through the C(7), C(8), C(9), C(10), C(11), and C(14) atoms are given in Table 6. The two planes make a dihedral angle of about 20°; this is about 5° larger than the corresponding angle for III.

In the present molecule, the C ring does not show the unusual behavior found in III.[2] The thermal motions of the C(12) and C(13) atoms as well as the bond distances and angles related to these atoms are normal,as

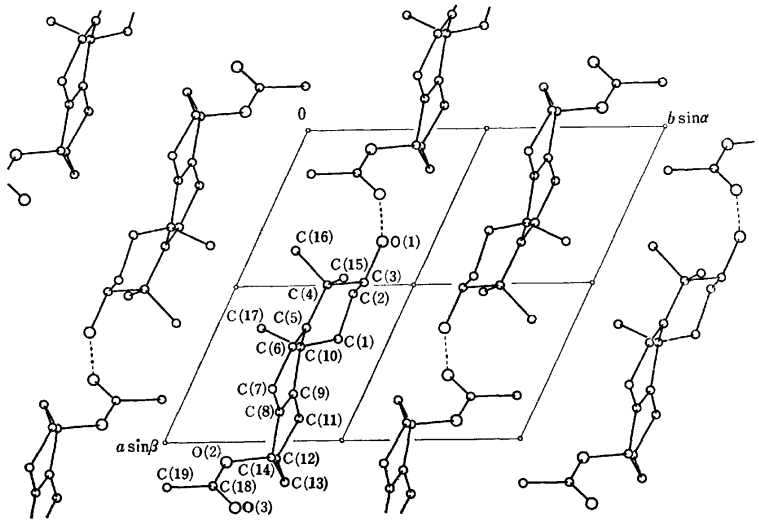

Fig. 4. The molecular arrangement viewed along the *c* axis.

TABLE 6. THE DEVIATIONS OF THE ATOMS FROM THE LEAST-SQUARES PLANES

Plane I		Plane II	
Atom	Deviation, Å	Atom	Deviation, Å
C(4)	0.000	C(7)	−0.003
C(5)	0.013	C(8)	−0.002
C(6)	−0.013	C(9)	0.020
C(7)	0.006	C(10)	−0.007
C(8)[a)]	0.440	C(11)	−0.008
C(9)[a)]	0.462	C(12)[a)]	−0.525
C(10)	−0.006	C(13)[a)]	0.206
H(6)[a)]	−0.07	C(14)	−0.001

a) The atoms indicated with asterisks were omitted from the calculations of the least-squares planes.

TABLE 7. THE SHORT INTERMOLECULAR DISTANCES (Å)
The standard deviations are given in parentheses.

(1) I···II (III···I)		(5) I···IX (IX···I)	
C(12)···O(1)	3.429(4)	C(6)···C(16)	3.848(3)
C(13)···O(1)	3.447(4)	C(7)···C(16)	3.791(3)
C(18)···C(15)	3.978(4)	(6) I···X (X···I)	
(2) I···IV (V···I)		C(11)···C(11)	3.875(4)
O(3)···C(12)	3.758(5)	(7) I···XI (XI···I)	
C(15)···C(2)	3.684(3)	O(2)···C(19)	3.709(4)
(3) I···VI (VII···I)		C(17)···C(19)	3.971(6)
O(3)···C(2)	3.489(3)	(8) I···XII (XII···I)	
···O(1)	2.881(3)	C(6)···C(13)	3.825(3)
(4) I···VIII (VIII···I)			
C(17)···C(17)	3.715(3)		

I: $x/a, y/b, z/c$ (given in Table 2). II: $1+x/a, y/b, z/c$. III: $-1+x/a, y/b, z/c$. IV: $x/a, y/b, 1+z/c$. V: $x/a, y/b, -1+z/c$. VI: $1+x/a, y/b, 1+z/c$. VII: $-1+x/a, y/b, -1+z/c$. VIII: $1-x/a, -y/b, -z/c$. IX: $1-x/a, -y/b, 1-z/c$. X: $2-x/a, 1-y/b, -z/c$. XI: $2-x/a, -y/b, 1-z/c$. XII: $2-x/a, 1-y/b, 1-z/c$.

compared with those in III. The C ring has a somewhat unsymmetrical half-chair form, the displacements of the C(12) and C(13) atoms from the mean plane through the C(8), C(9), C(11), and C(14) atoms being 0.51 and 0.22 Å respectively. The sum of these deviations, 0.73 Å, is in good agreement with that in cyclohexene, 0.7346 Å.[4] The distance between the H(1-2) and H(11-1) atoms is about 2.23 Å; this is nearly equal to the H(1-2)···H(11-2) distance in III, 2.17 Å. As has already been mentioned, the acetoxyl group in the present molecule, like the methoxyl group in III, takes the axial orientation. The fact that, independently of the configuration at the C(14) atom, the C ring has a half-chair conformation with these axially-oriented groups implies that such a conformation may be the preferred one of a cyclohexene ring which has a methoxyl or an acetoxyl group at the allylic position. It is also of interest that the internal valence angles of the sp^3 type at the C(11) and C(14) atoms, 113.1° and 114.8°, lie between those of the sp^2 type at the C(9) and C(8) atoms, 120.8° and 123.0°, and those of the sp^3 type at the C(12) and C(13) atoms, 109.5° and 111.0°, respectively. This may show a typical distribution of strains in a cyclohexene ring. The acetyl group is located at such a position that the torsion angles, O(3)-C(18)-O(2)-C(14) and C(18)-O(2)-C(14)-H(14), are about −3.4° and −15° respectively. Consequently, the O(3) atom is very close to the H(14) atom; the distance between them is only about 2.30 Å. This close contact suggests that the negatively-charged carbonyl oxygen atom and the more or less positively-charged hydrogen atom may exert quite strong attractive forces on each other.

The molecular arrangement viewed along the *c* axis is shown in Fig. 4. The short intermolecular distances are also given in Table 7. The molecules are connected by an intermolecular hydrogen bond, O(1)···O(3′), at a distance of 2.881 Å, forming a linear chain parallel to [101]. These molecular chains are further held together mainly by the usual van der Waals interactions.

4) J. F. Chiang and S. H. Bauer, *J. Amer. Chem. Soc.*, **91**, 1898 (1969).

Studies of Ionic Association. I. Alkali Halide and Sodium Nitrate in the Butyl Alcohol-Water System

Norio Yui, Yōichi Kurokawa, and Masami Nakayama

Department of Applied Science, Faculty of Engineering, Tohoku University, Aoba, Aramaki, Sendai

(Received October 28, 1971)

It has previously been reported that the dissociation of alkali halide and sodium nitrate between butanol and water phases could be explained reasonably if they were dissociated into free ions in each phase. The present investigation was undertaken to see to what extent dissociation occurs in the butanol phase. Conductometric measurements were carried out on solutions of LiBr, NaBr, NaCl, KCl, RbCl, and $NaNO_3$ in the *n*-butanol–water system and on the solution of NaCl in the *t*-butyl alcohol–water system at 20°C or 25°C. These data were analyzed by using the Fuoss-Onsager equation for associated electrolytes, and the association constants were calculated to be as follows: NaBr 250, NaCl 600, KCl 610, RbCl 1850, $NaNO_3$ 180, and NaI 220 in the *n*-butanol–water (11 wt%) system at 25°C (except NaBr), and NaCl; 590, 160, and 75 for water wt% 30, 45, and 60 in the *t*-butyl alcohol–water system at 25°C, respectively. The association constants of NaCl in the *t*-butyl alcohol–water system were explained in terms of the simple electrostatic theory. The results were discussed briefly in comparison with conductance data reported in the literature.

The solvent extraction of various species has been widely investigated and reviewed by Marcus and by Diamond and Tuck.[1,2] However, the investigations have been restricted to systems involving a distribution of the species between aqueous and organic solvents immiscible with water. These distributions have, in general, been interpreted in terms of the association of ions in organic solvents. We reported previously that the distribution of alkali halide and sodium nitrate between *n*-butanol and water phases could be explained most reasonably if they were treated as dissociating into free ions.[3] The present investigation was undertaken to see to what extent dissociation occurs in the butanol–water system. Many authors have studied the conductometric behavior of strong electrolytes in binary mixtures of solvents in order to establish the effect of ion-solvent interaction.[4] However, there is insufficient information on the behavior of electrolytes in the butanol–water system. Butanol, which is an associated solvent with a low vapor pressure and with a moderate value of the dielectric constant at 25°C, offers an interesting solvent for the study of ion-ion and ion-solvent interactions.

Experimental

Materials. The conductivity water used in the present study was prepared by the passage of distilled water through mixed-bed ion exchange resin. The specific conductance of this water was below 5×10^{-7} ohm^{-1} cm^{-1}. We treated *n*-butanol with a sodium bisulfite solution, then we boiled it for 4 hours with a 10% solution of NaOH, washed the separated butanol with water, and neutralized it to remove any NaOH. The butanol was boiled with fresh lime for 3 hr. The butanol was decanted from the lime and refluxed with magnesium turning. Then, we collected the middle of a distillation under an atmospheric pressure.[5] The salts and t-butanol were of a reagent grade and were used without further purification. The salts were dried at 110°C before use.

Procedure. The electric equipment, conductance cell (flask type), and general techniques were essentially the same as had been previously described[6] except for the conductance bridge, which was of a YOKOGAWA BV-Z-103B type. A quartz flask cell with lightly platinized electrodes was used. The cell constant was determined by means of an aqueous KCl solution to be 0.1893 cm^{-1}. The solvents and solutions were prepared by weight. All the measurements were carried out in a thermostat of 25±0.01°C or 20±0.01°C. The conductance of the solution was determined by subtracting the conductance of the solvent. Since the specific conductance of solvent was below 10^{-6} ohm^{-1}·cm^{-1} at 25°C, no solvent correction was necessary even for the most dilute solution. Relative viscosity measurements were made by using an Ostwald viscometer immersed in a thermostat of 25±0.01°C or 20±0.01°C.

Results and Discussion

Alkali Halide in n-*Butanol–Water System.* The properties of *n*-butanol–water solvents are listed in Table 1. The conductances were determined in the range of salt concentration of 0.5—10×10^{-3} mol/l. The salts used in this investigation were LiBr, NaCl, KCl, $NaNO_3$, and NaI. The distributions of these salts have all previously been studied except for $NaNO_3$. The solvent compositions are in the range of the upper phase (rich in *n*-butanol) compositions that correspond to the composition of the separation of the two phases. Because of solubility limitations, many data were not available in the precision required.[7] The addition of salt above the

1) Y. Marcus, *Chem. Rev.*, **63**, 139 (1963).

2) R. M. Diamond and D. C. Tuck, "Progress in Inorganic Chemistry" F. A. Cotton ed., Interscience Publishers Inc., New York (1960), p. 109.

3) Y. Kurokawa and N. Yui, *Nippon Kagaku Zasshi*, **89**, 487 (1968).

4) J. B. Ezell and W. R. Gilkerson, *J. Phys. Chem.*, **72**, 144 (1968). A. S. Quist and W. L. Marshall, *ibid.*, **72**, 684 (1968). T. C. Wehman and A. L. Popov, *ibid.*, **72**, 4031 (1968). D. F. Evans and T. L. Broadwater, *ibid.*, **72**, 1037 (1968). D. F. Evans and P. Gardam, *ibid.*, **73**, 158 (1969).

5) J. A. Riddik and E. E. Toops, "Technique of Organic Chemistry Vol VII Organic Solvents" Interscience Publishers, Inc., New York (1955), p. 346.

6) N. Yui, Y. Kurokawa, M. Sono, and T. Hiramoto, *Nippon Kagaku Zasshi* **89**, 483 (1968); T. Shedlovsky, *J. Amer. Chem. Soc.*, **54**, 1411 (1932).

7) The solubilities of salts in pure *n*-butanol are all very small except for NaI.

TABLE 1. PROPERTIES OF *n*-BUTANOL-WATER MIXTURE

Water (wt%)	η (poise)	ε[a)]	Temp. (°C)
5.0	0.02250	20.0	20
9.0	0.02360	22.3	20
11.0	0.02593	24.0	25
15.0	0.02487	26.0	20

a) They were estimated from the values for pure water and pure *n*-butanol by assuming that the dielectric constant of mixtures is a linear function of the weight fraction by analogy with the behavior of water-ethanol mixture. H. S. Harned and B. B. Owen, "The Physical Chemistry of electrolytic Solutions" Reinhold Publishing Co. (1964), p. 161.

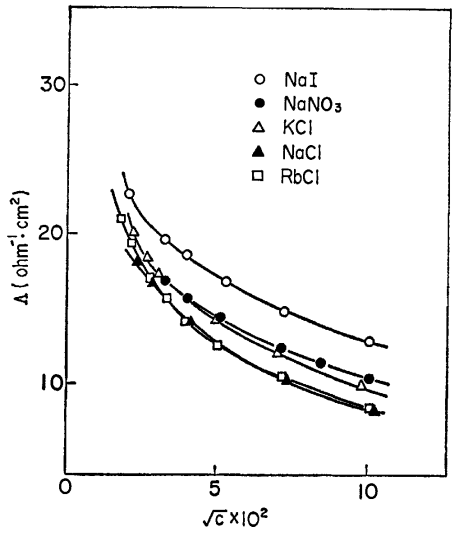

Fig. 1. Conductance *vs.* square root of concentration for alkali halide in *n*-butanol-water system at 25 °C.

extent of solubility brought about the separation of the solution into two phases. The values of conductance Λ (ohm^{-1} cm^2), are presented in Table 2. The measurements temperatures were 20 °C for LiBr and NaBr, and 25 °C for the others. Λ *vs.*$\sqrt{c}$ plots for each salt are shown in Fig. 1. The curves are similar in form and show the same behavior as weak electrolytes. It is considered from these results that the salts are considerably associated.

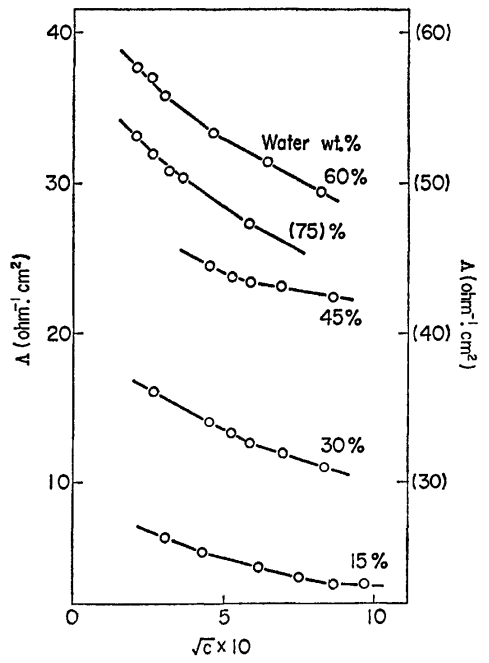

Fig. 2. Conductance *vs.* square root of concentration for NaCl in *t*-butyl alcohol-water system at 25 °C.

TABLE 2. CONDUCTANCE OF ALKALI SALTS IN *n*-BUTANOL-WATER SYSTEM

(A) LiBr; 20 °C water 11%		(B) NaBr; 20 °C water 15%		(C) NaBr; 20 °C water 9%		(D) NaCl; 25 °C water 11%	
$c\times10^3$	Λ	$c\times10^3$	Λ	$c\times10^3$	Λ	$c\times10^3$	Λ
1.542	12.03	1.522	14.97	1.569	17.06	0.4967	17.91
2.348	11.01	2.684	12.98	2.497	15.58	0.6903	16.69
3.504	9.86	3.478	12.39	3.677	14.47	0.9938	15.95
4.778	9.89	5.087	11.14	5.002	13.66	1.492	14.05
5.829	9.44	6.439	10.57	6.261	13.35	2.486	12.40
7.224	9.03	7.483	10.42	7.924	12.51	4.972	10.28
9.396	8.40	10.00	9.50	9.804	11.86	9.945	8.30

(E) KCl; 25 °C water 11%		(F) NaI; 25 °C water 11%		(G) $NaNO_3$; 25 °C water 11%		(H) RbCl; 25 °C water 11%	
$c\times10^3$	Λ	$c\times10^3$	Λ	$c\times10^3$	Λ	$c\times10^3$	Λ
0.472	19.99	0.404	22.61	0.4962	17.24	0.3078	20.88
0.661	18.21	1.009	19.51	0.9925	16.54	0.4104	19.38
0.944	17.21	1.513	18.52	1.489	15.55	0.5130	18.54
1.416	15.84	2.523	16.86	2.481	14.11	0.7183	17.03
2.360	14.00	5.045	14.89	4.962	12.07	1.026	15.52
4.721	11.80	10.09	12.83	6.947	11.12	1.539	14.09
9.443	9.70	100.9	8.19	9.925	10.34	2.565	12.36
						5.130	10.19
						10.66	8.20

NaCl in t-Butyl Alchohol–Water System. The other butanols have dielectric constants above 18, while *t*-butyl alcohol has a dielectric constant of 11.8 and yet is the only butanol completely miscible with water at 25°C.[8] Appropriate conductance measurements provides a useful indication of ion-solvent interaction, but conductance studies over the range of solvent composition have not been previously published for the *t*-butyl alcohol–water system at 25 °C. The properties of the solvents are summarized in Table 3.

Table 3. Properties of *t*-butyl alcohol–water mixture at 25°C

Water content (wt%)	η (poise)	ε	Density (g/cm^3)
15	0.04569	14.3	0.8154
30	0.04845	21.4	0.8519
45	0.05105	31.5	0.8869
60	0.03757	43.9	0.9023
75	0.02568	57.1	0.9567
100	0.008937	78.5	0.9971

The viscosity reaches its maximum in the vicinity of a water content of 40%, as in the cases of water–methanol, –ethanol, and –propanol. The values of Λ are represented in Table 4 and show a sharp increase in the conductance with an increase in water content. As shown in Fig. 2, the values of Λ change smoothly with the increase in water content, despite the maximum in viscosity. Obviously, ion mobility is not predominantly controlled by the bulk viscosity.

Calculation. In order to ascertain whether any variation in the conductance could be due to ion-pair formation, the limiting equivalent conductance and the ion-pair formation constants, K_A were calculated by the Fuoss and Fuoss-Onsager methods. The data were initially treated by the method of Fuoss.[9]

$$F(z)/\Lambda = 1/\Lambda^0 + (K_A \cdot c\Lambda f_\pm^2)/(F(z)/\Lambda^{02}) \quad (1)$$

where $F(z)$ is the Fuoss function and where $f_\pm^2$ is calculated from the Debye-Hückel theory. The initial value of Λ° was obtained by the extrapolation of Λ *vs.* $\sqrt{c}$ plot to an infinite dilution. After we had obtained the apparent Λ^0 and value of K_A, the data were analyzed by the Fuoss-Onsager extended equation for associated electrolytes in this form.[10]

$$\Lambda = \Lambda^0 - S(c\gamma)^{1/2} - Ec\gamma \log c\gamma + Jc\gamma - K_A c\gamma \Lambda f_\pm^2 \quad (2)$$

Here, γ is the degree of dissociation, S is the Onsager limiting slope, and both E and J are the parameters as defined in the Fuoss-Onsager equation. In computing the Λ' defined by the equation:

$$\Lambda' = \Lambda + S(c\gamma)^{1/2} - Ec\gamma \log c\gamma \quad (3)$$

the following variables are defined thus;

$$\Delta\Lambda = \Lambda' - \Lambda^0 \quad (4)$$

$$y = \Delta\Lambda/c\gamma \quad (5)$$

$$x = f_\pm^2 \Lambda \quad (6)$$

Then, Eq. 2 is transformed into Eq. 7;

$$y = J - K_A x \quad (7)$$

If Λ° was known, y could be calculated, then a plot of y against x should be linear and K_A could be evaluated.[10] The association constans, K_A, obtained by the above two methods are given in Table 5. The values of K_A calculated by the Fuoss method are approximately twice as large as those calculated by the Fuoss-Onsager method.[11] As can be seen in Table 5, K_A increases in the order of NaCl<KCl<RbCl with an increase in the size of the cation, and increases in the order of NaI<NaBr<NaCl with a decrease in the size of the anion. That is, RbCl, in spite of its greater size, is more associated than the others. This means that the cations are hydrated, while halide ions are not. This is in agreement with the order found by Kay and Fuoss for the alkali halide in various hydrogen-bonded solutions.[12,13] That is, the association increases in this order; Li<Na<K<Rb<Cs. Fuoss and his co-workers have found the same order for alkali halides in a dioxane–water system, and Smith has reported that KNO_3 is more associated than $LiNO_3$ in pure ethanol.[14] However, Evans has reported that tetraethyl ammonium salts in alcohol do not exhibit the simple dependence upon the order of association predicted by the electrostatic theory, that is, K_A increases with an increase in the anion size.[4]

Table 4. Conductance of NaCl in *t*-butyl alcohol–water system at 25 °C

(A) water 15%		(B) water 30%		(C) water 45%		(D) water 60%		(E) water 75%	
$c\times10^3$	Λ	$c\times10^3$	Λ	$c\times10^3$	Λ	$c\times10^3$	Λ	$c\times10^3$	Λ
0.951	6.273	0.712	15.98	1.391	24.96	0.4234	37.68	0.4131	53.14
1.902	5.532	1.423	14.14	2.086	24.27	0.6774	37.30	0.6884	51.95
3.805	4.677	1.993	13.77	2.781	23.73	0.8468	35.88	0.9638	50.76
5.707	3.783	2.135	13.48	3.476	23.29	2.117	33.45	1.377	50.48
7.610	3.414	3.559	12.66	4.867	23.37	4.234	31.72	3.422	47.30
9.512	3.409	4.982	11.91	6.953	22.30	6.774	29.50		
		5.694	11.85						
		7.117	11.23						

8) Ref. 5, p. 90.
9) R. M. Fuoss, *J. Amer. Chem. Soc.*, **57**, 478 (1935).
10) R. M. Fuoss and F. Accasina, "Electrolytic Conductance" Interscience Publishers, Inc. (1959), p. 225.
11) E. Kubota and M. Yokoi, *Nippon Kagaku Zasshi*, **86**, 894 (1965).
12) J. L. Fabry and R. M. Fuoss, *J. Phys. Chem.*, **68**, 971 (1964).
13) J. L. Hawes and R. L. Kay, *ibid.*, **69**, 2420 (1965).
14) G. D. Parfitt and A. L. Smith, *Trans. Faraday Soc.*, **59**, 57 (1963).

TABLE 5. ASSOCIATION CONSTANT OF ALKALI HALIDE IN *n*-BUTANOL–WATER SYSTEM

	K_A		Λ^0	Temp. (°C)
	Fuoss	Fuoss-Onsager		
$NaNO_3$	350	180	20.7	25
NaI	490	220	25.5	25
NaCl	1170	600	23.0	25
KCl	1140	610	24.0	25
RbCl	4060	1850	29.0	25
NaBr(1)		250	25.57	20
NaBr(2)		280	20.83	25

(1) and (2) in NaBr indicate 15 and 9 water content (wt%), respectively.

The coulombic theory predicts that a plot of log K_A against $1/\varepsilon$ for any given salt will be a straight line with a slope proportional to $1/a_K$.[10] Such a plot

$$K_A = K_A^0 \exp(e^2/a_K \cdot \varepsilon \cdot kT) \quad (8)$$

for NaCl in the *t*-butanol–water system is shown in Fig. 3. An approximately straight line is obtained, and the value of a_K, 5.6 Å is calculated from the slope of the line. The point for NaCl in the *n*-butanol–water(11 wt%) system seems to fall on the line. Therefore, it seems that the solvent structure

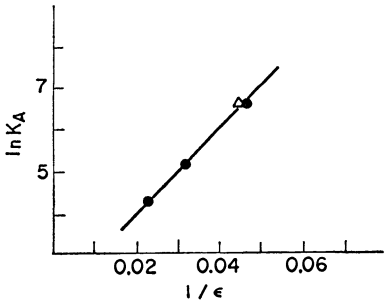

Fig. 3. Logarithm of association constant *vs.* reciprocal of dielectric constant for NaCl in *t*-butyl alcohol–water system at 25°C. △: NaCl in *n*-butanol–water (11 wt%)

plays a negligible role in the association process. Water molecules in the primary solvation shell are not easily replaced by butanol molecules. This hydrated ion is further solvated either by more water molecules or by the butanol molecules through hydrogen-bonding, thus forming the secondary solvation shell.

In conclusion, we can say that the alkali halide is partly associated in the *n*-butanol phase which is equilibrated with the aqueous phase at 20°C or 25°C, and that the Fuoss and Fuoss-Onsager equation describe the behavior of alkali halide.

BULLETIN OF THE CHEMICAL SOCIETY OF JAPAN, VOL. 46, 1030—1035 (1973)

Excitation Transfer in the Radiolysis of Solid Alkane Mixtures at 77 K

Tetsuo MIYAZAKI, Terunobu WAKAYAMA, Mitsuharu FUKAYA, Yoshiyuki SAITAKE, and Zen-ichiro KURI

Department of Synthetic Chemistry, Faculty of Engineering, Nagoya University, Chikusa-ku, Nagoya

(Received March 10, 1972)

The radiolysis of isobutane–propane (less than 5 mol %) or neopentane–alkane (5 mol%) mixtures has been studied at 77 K by means of ESR spectroscopy. When these alkane mixtures are γ-irradiated, the solute radicals are mainly formed by energy transfer from γ-irradiated isobutane or neopentane to the solutes. It is discussed whether the energy transfer is due to a proton transfer, a positive-charge transfer, or an excitation transfer, and it is concluded, for the following reasons, that the energy tranfser is probably due to the excitation transfer and that the excitation transfer may occur *via* highly-excited states of isobutane or neopentane; (i) The ionization potentials and the energies of the first singlet-excited states of the some additives are higher than those of isobutane or neopentane. (ii) The decrease in the solvent radical yields and the increase in the solute radical yields upon the addition of the solutes to the isobutane or neopentane amount approximately to 2—2.5 G-units. (iii) The yields of hydrogen increase sharply upon the addition of cyclopentane in the radiolysis of solid neopentane. (iv) It was concluded in previous studies that the formation of the solvent radical in the radiolysis of solid isobutane is due to the fragmentation of excited isobutane produced directly by γ-irradiation.

It was reported in previous studies that, while the fragmentation of excited ions plays an important role in the radiolysis of isobutane in the gas[1] and liquid[2] phases, the fragmentation of excited molecules is an important process in the solid phase at 77 K.[3] It was found that the physical conditions of the matrix appreciably affects the radiolysis in the solid phase; this is the case for isobutane,[4] phenylacetate,[5] and succinic

1) T. Miyazaki, *J. Phys. Chem.*, **71**, 4282 (1967).

2) K. Tanno, S. Shida, and T. Miyazaki, *ibid.*, **72**, 3496 (1968).

3) a) T. Wakayama, T. Miyazaki, K. Fueki, and Z. Kuri, This Bulletin, **42**, 1164 (1969). b) T. Wakayama, T. Kimura, T. Miyazaki, K. Fueki, and Z. Kuri, *ibid.*, **43**, 1017 (1970). c) T. Miyazaki, T. Yamada, T. Wakayama, K. Fueki, and Z. Kuri, *ibid*, **44**, 934 (1971).

4) a) T. Miyazaki, T. Wakayama, K. Fueki, and Z. Kuri, *ibid*, **42**, 2086 (1969). b) T. Wakayama, T. Miyazaki, K. Fueki, and Z. Kuri, *J. Phys. Chem.*, **74**, 3584 (1970). c) Y. Saitake, T. Wakayama, T. Kimura, T. Miyazaki, K. Fueki, and Z. Kuri, This Bulletin, **44**, 301 (1971).

5) Y. Noro, M. Ochiai, T. Miyazaki, A. Torikai, K. Fueki, and Z. Kuri, *J. Phys. Chem.*, **74**, 63 (1970).

acid.[6]

Then, we have indicated that two important problems must be solved in order to elucidate the cause of the peculiar phenomena in the radiolysis of solid hydrocarbons. One is the problem of the extent to which the formation of an exciton plays an important role; the other is how the state of the solid matrix, such as the phase and the defects, affects the fate of the exciton.

It was previously concluded that, in the radiolysis of solid isobutane at 77 K,[3] C–H bond rupture occurs by way of the fragmentation of an excited isobutane molecule produced directly by γ-irradiation. This conclusion is based on the following observation:

i) The yields of the C_4H_9 radical in the radiolysis of polycrystalline isobutane are not changed by the presence of conventional electron scavengers, such as phenyl iodide, ethyl iodide, nitrous oxide, and sulfur hexafluoride.

ii) The yields of the C_4H_9 radical do not increase upon the photobleaching of toluene anions in the γ-irradiated isobutane–toluene (5 mol/100 mol of i-C_4H_{10}) mixture in the polycrystalline state.

iii) The yields of the C_4H_9 radical do not increase upon the photo-bleaching of electron trapped in the γ-irradiated isobutane–methylcyclohexane (4 mol/100 mol of i-C_4H_{10}) mixture in the glassy state or upon the photobleaching of benzene anions in the γ-irradiated isobutane–methylcyclohexane (4 mol/100 mol of i-C_4H_{10})–benzene (5 mol/100 mol of i-C_4H_{10}) mixture in the glassy state.

iv) The yields of H_2 in the radiolysis of glassy isobutane are not changed at all by the presence of conventional electron scavengers, such as nitrous oxide and sulfur hexafluoride.

Since the yields of the C_4H_9 radical and H_2 decrease upon the addition of CCl_4 or toluene, it was suggested that the migration of an exciton to the solutes may be an important process in the radiolysis of solid isobutane. The role of the exciton was also studied by the measurement of the luminescence from eleven kinds of alkanes containing toluene (2 mol %) during γ-irradiation at 77 K.[7]

In this paper we will report clearer results suggesting the excitation transfer in the radiolysis of isobutane and neopentane in the solid phase.

Experimental

The ethane, propane, and isobutane were supplied by the Takachiho Shoji Co. and were of a high purity; the isobutane was more than 99.7% pure. The cyclopentane, methylcyclopentane, *n*-hexane, and cyclohexane supplied by the Tokyo Kagaku Seiki Co. were more than 99.0% pure. They were passed through a 30-cm column packed with activated alumina and were used after distillation on a vacuum line. The neopentane was more than 99.9% pure.

Samples were sealed into a quartz cell and irradiated at 77 K with γ-rays from Co-60 at a dose rate of 7.6×10^5 rad/hr. The total doses were 3.8×10^5 rad for the ESR measurements and 1.0×10^7 rad for the product analysis. The ESR spectra of irradiated samples were measured at 77 K on a JES-3BX ESR spectrometer. H_2 and CH_4 were analyzed by a gas burette connected to a Toepler pump and a copper oxide furnace kept at 240°C.

Results

Figure 1a shows the ESR spectrum of γ-irradiated pure isobutane, which is assigned to an isobutyl radical. Figure 1b shows the ESR spectrum of γ-irradiated isobutane containing 4.8 mol% propane. It may be seen from Figures 1a and 1b that there is a drastic difference in the spectra. The spectra in Fig. 1b represent those assigned to two species; the main spectrum is ascribed to the i-C_3H_7 radical.

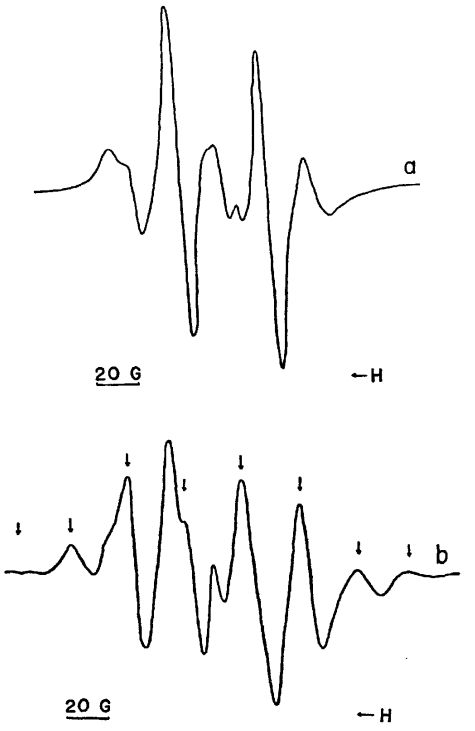

Fig. 1. a) ESR spectrum of γ-irradiated isobutane at 77 K. b) ESR spectrum of γ-irradiated isobutane-propane(4.8 mol%) at 77 K. The arrows indicate signals of C_3H_7 radical.

When pure neopentane is γ-irradiated at 77 K, t-C_4H_9 and *neo*-C_5H_{11} radicals are formed; their ESR spectra are shown in Fig. 2a.[8] The spectrum of eight narrow lines is ascribed to the t-C_4H_9 radical. The spectrum of three broad lines is ascribed to the *neo*-C_5H_{11} radical. When neopentane containing a small amount of alkane is γ-irradiated at 77 K, a solute radical and a neopentyl radical are formed, while the t-C_4H_9 radical disappears completely. The ESR spectra of γ-irradiated neopentane–ethane, propane,

6) a) T. Miyazaki, S. Okada, T. Wakayama, K. Fueki, and Z. Kuri, This Bulletin, **43**, 1907 (1970). b) T. Miyazaki, Y. Fujitani, T. Wakayama, K. Fueki, and Z. Kuri, *ibid.*, **44**, 984 (1971).

7) T. Miyazaki, Y. Saitake, M. Fukaya, T. Wakayama, and Z. Kuri, Japanese Conference on Radiation Chemistry, Sapproo, Japan, Sept. 1971.

8) B. Smaller and M. S. Matheson, *J. Chem. Phys.*, **28**, 1169 (1958).

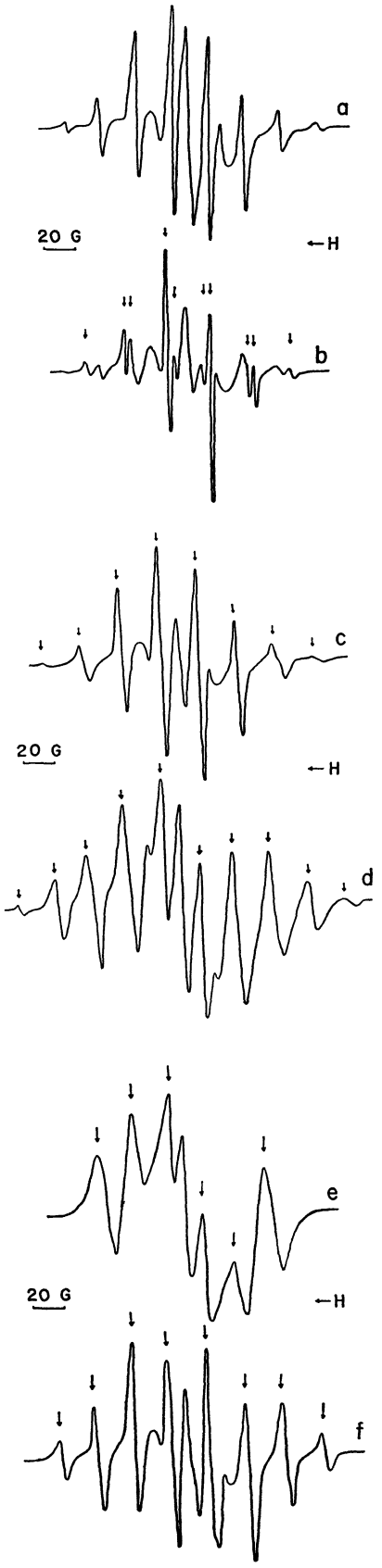

Fig. 2. ESR spectra of γ-irradiated neopentane and neopentane-alkane mixtures at 77 K. The arrows indicate signals of solute alkane radicals.
a) pure neopentane. b) neopentane-ethane (4.8 mol%). c) neopentane-propane(4.9 mol%). d) neopentane-methylcyclopentane(4.9 mol%). e) neopentane-cyclohexane(6.5 mol%). f) neopentane-cyclopentane(4.7 mol%)

Table 1. Formation of solute radical in the radiolysis of neopentane containing alkane at 77 K

Solute alkane	Solute radical	Splitting, Gauss: This work	Splitting, Gauss: Other work
Ethane	$\cdot CH_2CH_3$	$\alpha^{a)}$: 22.9 $\beta^{a)}$: 27.1	$\alpha^{a)}$: 22.4[b] $\beta^{a)}$: 26.9[b]
Propane	$CH_3\dot{C}HCH_3$	24.1	24.8[c]
2,3-dimethylbutane	$\cdot CH_2CH(CH_3)$-$CH(CH_3)_2$	22.7	22[d]
Cyclopentane	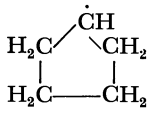	23.7	23.8[c]
Cyclohexane	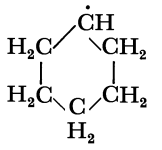	21.4	21[e]

a) Splittings by α-proton and β-proton are represented by α and β respectively.
b) R. W. Fessenden and R. H. Schuler, *J. Chem. Phys.*, **39**, 2147 (1963).
c) P. B. Ayscough and C. Thomson, *Trans. Faraday Soc.*, **58**, 1477 (1962).
d) M. Fukaya, T. Wakayama, T. Miyazaki, Y. Saitake, and Z. Kuri, This Bulletin, **46**, 1036 (1973).
e) B. Smaller and M. S. Matheson, *J. Chem. Phys.*, **28**, 1169 (1958).

methylcyclopentane, cyclohexane, and cyclopentane systems are shown in Figs. 2b, c, d, e, and f respectively. When neopentane containing a small amount of isobutane, 2,3-dimethylbutane, or *n*-hexane is γ-irradiated, solute radicals are mainly formed also. The structures and splittings of the solute radicals formed in the radiolysis of neopentane-alkane mixtures are shown in Table 1. The splittings of the radicals formed by other methods are also shown there.

The effect of propane on the formation of radicals in the radiolysis of solid isobutane is shown in Fig. 3. The i-C_4H_9 radical decreases sharply upon the addition

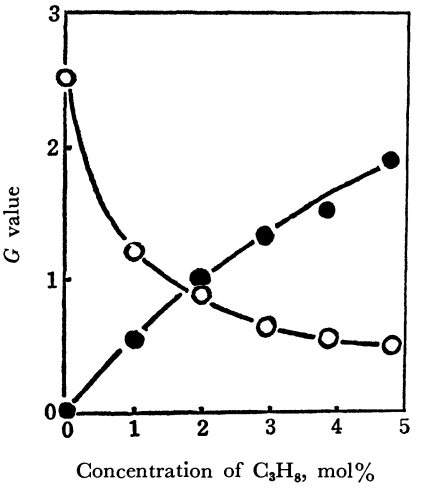

Fig. 3. Effect of propane on the formation of isobutyl radical in the radiolysis of isobutane at 77K.
○: i-C_4H_9 radical ●: i-C_3H_7 radical

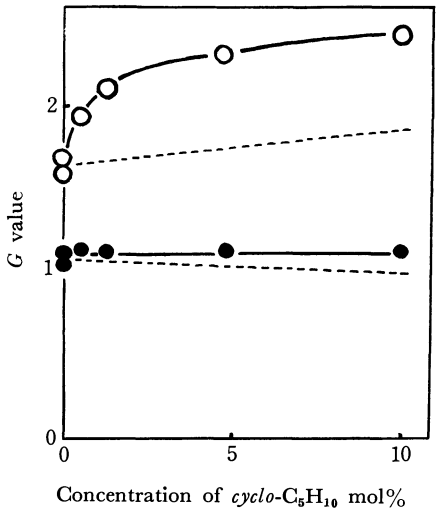

Fig. 4. Effect of cyclopentane on the radiolysis of neopentane in the solid phase at 77 K.
○: H_2 ●: CH_4

of propane, while the C_3H_7 radical increases complementally. The sum of $G(C_3H_7)$ and $G(i\text{-}C_4H_9)$ decreases slightly upon the addition of 1 mol% propane. It is uncertain whether this result is due to experimental errors or to some characteristic phenomena upon the addition of C_3H_8.

The yields of H_2 and CH_4 in the radiolysis of *neo*-C_5H_{12}–*cyclo*-C_5H_{10} mixtures in the solid are shown in Fig. 4.

Discussion

The C_4H_9 radical decreases sharply upon the addition of propane in the radiolysis of isobutane, while the C_3H_7 radical increases complementally (Fig. 1b and Fig. 3). Since the electron fraction of propane is smaller than 0.04 in the experimental concentration, the results represent some type of energy transfer from γ-irradiated isobutane to propane. Since the electron fraction of the solutes is about 0.05 in the radiolysis of neopentane–solute mixtures, the formation of solute radicals also represents the energy transfer from γ-irradiated neopentane to the solute (Fig. 2). We will discuss here whether the energy transfer is due to a proton transfer, a positive-charge transfer, or an excitation transfer.

Proton-transfer Reaction in γ-irradiated Alkane Mixtures in the Solid Phase. Willard *et al.* proposed that the solvent radical may be formed by the proton-transfer reaction in the radiolysis of 3-methylpentane in the solid phase.[9] According to this mechanism, the formation of the solute radical in the radiolysis of neopentane (or isobutane) may be represented as follows:

$$\textit{neo}\text{-}C_5H_{12} \rightsquigarrow C_5H_{12}^+ + e^- \quad (1)$$

$$C_5H_{12}^+ + C_5H_{12} \longrightarrow C_5H_{11}\cdot + C_5H_{13}^+ \quad (2)$$

$$C_5H_{12}^+ + RH \longrightarrow R\cdot + C_5H_{13}^+ \quad (3)$$

where RH represents an alkane as a solute. These mechanisms, however, seem unlikely because for the following three reasons: i) Though the proton-transfer reaction of polar molecules has been found in the mass spectrometer, the reaction cannot be detected in any alkane systems except for methane and ethane. The reaction seems to become more difficult as the molecular weight of alkane increases.[10] Recently it has been reported, from a study of the high-pressure mass spectrometry of propane, that the protonated alkane ion ($C_3H_9^+$) was not detected at all, but only a clustered parent ion ($(C_3H_8)_2^+$).[11] The formation of a clustered parent ion was also reported in the high-pressure mass spectrometry of butane.[12]

ii) Only the fragmentation of the parent ion ($C_4H_{10}^+$ or $C_5H_{12}^+$) has been observed in the radiolysis of isobutane and neopentane in the liquid phase.[2,13,14] The existence of the parent ion (*cyclo*-$C_5H_{10}^+$ or *cyclo*-$C_6H_{12}^+$) has been also shown in the radiolysis of cyclopentane or cyclohexane in the liquid phase.[15]

Since the proton-transfer reaction between *neo*-$C_5H_{12}^+$ and *neo*-C_5H_{12} (Reaction (2)) does not occur in the liquid phase, Reaction (2) may be endothermic; in it the heat of reaction is taken as ΔH_2 kcal/mol. Therefore, the heat of hydrogen-transfer reaction between $C_5H_{12}^+$ and C_2H_6 (Reaction (4)) may be expected to be $\Delta H_2+3.7$ kcal/mol:

$$\textit{neo}\text{-}C_5H_{12}^+ + C_2H_6 \longrightarrow C_5H_{13}^+ + C_2H_5\cdot \quad (4)$$

Therefore, Reaction (4) is also endothermic and its occurrence may be more difficult than that of Reaction (2).

The same conclusion can be obtained also from the results in the radiolysis of an ethane–neopentane mixture in the liquid phase.[6] It has been shown that the proton-transfer reaction between $C_2H_6^+$ and *neo*-C_5H_{12} (Reaction (5)) does not occur:

$$C_2H_6^+ + \textit{neo}\text{-}C_5H_{12} \longrightarrow C_2H_5 + C_5H_{13}^+ \quad (5)$$

Reaction (5) is expected to be an endothermic reaction and the heat of its reaction is taken to be ΔH_5 kcal/mol. The heat of Reaction (4) may, then, be expected to be ΔH_5+30 kcal/mol. Therefore, the occurrence of Reaction (4) may be more difficult than that of Reaction (5).[17,18]

iii) When neopentane containing cyclopentane

9) a) M. Shirom and J. E. Willard, *J. Phys. Chem.*, **72**, 1702 (1968).
b) D. Timm and J. E. Willard, *ibid*, **73**, 2403 (1969).

10) F. P. Abramson and J. H. Futrell, *ibid*, **71**, 3791 (1967).
11) L. W. Sieck, S. Searles, and P. Ausloos, *J. Chem. Phys.*, **54**, 91 (1971).
12) T. A. Milne, J. E. Beachey, and F. T. Greene, Annual Conference on Mass Spectrometry and Applied Topics, 17th ASTM Committee, E-14, Dallas Tex., U. S. A., May, 1969.
13) K. Tanno, T. Miyazaki, K. Shinsaka, and S. Shida, *J. Phys. Chem.*, **71**, 4290 (1967).
14) G. J. Collin and P. Ausloos, *J. Amer. Chem. Soc.*, **93**, 1336 (1971).
15) P. Ausloos, A. A. Scala, and S. G. Lias, *ibid.*, **89**, 3677 (1967).
16) J. A. Stone and G. Matsushita, *Can. J. Chem.*, **49**, 3287 (1971).
17) Neopentane has a solid phase transition at 140 K (J. G. Aston and G. H. Messerly, *J. Amer. Chem. Soc.*, **58**, 2354 (1936); E. O. Stejskal, D. E. Woessner, T. C. Farrar, and H. S. Gutowsky, *J. Chem. Phys.*, **31**, 55 (1959)), but it has no phase transition near 77 K. The reaction (4) is not facilitated at 77 K by the phase transition.

(5 mol%) is γ-irradiated at 77 K, the cyclopentyl radical is mainly formed (Fig. 2f). If the formation of the cyclopentyl radical is due to Reaction (3), the amounts of the $C_5H_{13}^+$ ion do not change upon the addition of cyclopentane. $C_5H_{13}^+$ ion may produce a H atom or a H_2 molecule upon neutralization with an electron:

$$C_5H_{13}^+ + e^- \longrightarrow C_5H_{12} + H\cdot \quad (6)$$

$$\searrow\ C_5H_{11}\cdot + H_2 \quad (7)$$

$$H\cdot + H\cdot \longrightarrow H_2 \quad (8)$$

Therefore, it may be expected from Reactions (1)—(3) and (6)—(8) that the yields of hydrogen do not change upon the addition of cyclopentane if the proton-transfer reaction is responsible for the formation of the cyclopentyl radical. The experimental results, however, show that the yields of hydrogen increase sharply upon the addition of cyclopentane in the radiolysis of solid neopentane (Fig. 4). This result suggests that the C–H bond rupture of cyclopentane is accelerated by the energy transfer from γ-irradiated neopentane to cyclopentane.

Positive-charge Transfer in the γ-irradiated Alkane Mixtures in the Solid Phase. Isobutane Containing Propane: Though a positive-charge transfer is generally proposed in the γ-irradiated alkane mixtures in the liquid phase,[16,19] such a mechanism (Reactions (7)—(10)) cannot be adopted here for the following two reasons:

$$C_4H_{10} \rightsquigarrow C_4H_{10}^+ + e^- \quad (7)$$

$$C_4H_{10}^+ + e^- \longrightarrow C_4H_9\cdot + H\cdot \quad (8)$$

$$C_4H_{10}^+ + C_3H_8 \longrightarrow C_4H_{10} + C_3H_8^+ \quad (9)$$

$$C_3H_8^+ + e^- \longrightarrow C_3H_7\cdot + H\cdot \quad (10)$$

i) As has been described in the Introduction, the C_4H_9 radical is not formed by the neutralization reaction between the butane cation and the electron.

ii) Though the gas-phase ionization potentials may be different from the condensed-phase ionization potentials, the charge-transfer reaction in the liquid alkane mixtures can be discussed by using the gas-phase ionization potentials.[16,19] The ionization potential of an alkane ion is always higher than that of a charge acceptor. Therefore, the relative magnitude of the gas-phase ionization potentials of alkanes may hold even in the condensed phase. Since the ionization potential of isobutane is lower than that of propane (Table 2), it is impossible for a charge transfer from the isobutane cation in a ground state to propane to occur.

Table 2. Energies of first electronic excited state and ionization potentials of alkanes

	Energies of first electronic excited state,[a] eV	Ionization potentials,[b] eV
C_2H_6	9.3	11.65
C_3H_8	9.0	11.07
i-C_4H_{10}	7.7	10.57
cyclo-C_5H_{10}	8.3	10.53
neo-C_5H_{12}	7.9	10.35
cyclo-C_6H_{12}	7.8	9.88

a) J. W. Raymonds and W. T. Simpson, *J. Chem. Phys.*, **47**, 430 (1967).
b) K. Watanabe, T. Nakayama, and J. Mottl, *J. Quant. Spectrosc. Radiat. Transfer*, **2**, 369 (1962).

If the energy transfer in the γ-irradiated i-C_4H_{10}–C_3H_8 mixture is due to a charge-transfer reaction, we will have to introduce a mechanism of a charge-transfer *via* the excited state of the solvent cation, as has been suggested by Hamill *et al.*[20] Since our information about the excited cation produced by γ-irradiation is very scanty at present, the energy transfer *via* the excited cation and its chemical reaction cannot be discussed in detail. There are, however, some drawbacks to this mechanism. First, the yields of the excited alkane ion may amount only to 20% of the total alkane ions.[21,22] The G-value of the excited ion is likely to be 0.8 if we take the G-value for ion-pair production as the gas-phase value of about 4. This value is much smaller than the decrement ($G\sim2.0$) in the i-C_4H_9 radical or the increment ($G\sim1.9$) in the C_3H_7 radical upon the addition of propane in the radiolysis isobutane (Table 3). Second, a migration of the excited isobutane ion is considered to be rather difficult, for the toluene cation was not observed at 77 K in the γ-irradiated isobutane containing toluene.[3b] Third, supposing the excited isobutane ion is formed, it may decompose in the period of one vibration because of the fact that the C–C bond of the isobutane ion is very weak.[2,21] It is highly unlikely, judging from the mass spectrum of isobutane, that the i-C_4H_9 radical is formed by the fragmentation of an excited isobutane ion:

$$i\text{-}C_4H_{10}{}^{+*} \longrightarrow i\text{-}C_4H_9\cdot + H^+ \quad (11)$$

Neopentane Containing Alkanes: When neopentane containing ethane, propane, cyclopentane, or methylcyclopentane is γ-irradiated at 77 K, ethyl, propyl, cyclopentyl, or methylcyclopentyl radicals are mainly formed respectively (Fig. 2). Since these additives have higher ionization potentials than that of neopentane (Table 2), it is not possible that a charge transfer from the neopentane cation in a ground state to the additive occurs. The yields of the solute radicals amount to approximately 2.5 G-units (Table 3),

18) The possibility of Reaction (4) was diminished by the recent experiments (M. Ito, T. Miyazaki, Y. Saitake, and Z. Kuri, Japanese Conferrence on Radiation Chemistry, Osaka, Japan, Oct. 1972). The addition of CCl_4, which is an efficient electron scavenger and an excitation quencher, to the *neo*-C_5H_{12}–C_2H_6 mixture suppresses the formation of C_2H_5 radical in the solid radiolysis. If the formation of C_2H_5 radical is due to the Reaction (4), the yield of C_2H_5 radical should not decrease upon the addition of CCl_4.

19) a) J. Hardwick, *J. Phys. Chem.*, **66**, 2132 (1962). b) T. Kudo and S. Shida, *ibid*, **71**, 1971 (1967). c) J. A. Stone, *Chem. Commun.*, **1968**, 1677.

20) W. H. Hamill, "Ionic Process in Irradiated Organic Solids", a chapter in "Radical Ions", E. T. Kaiser and L. Kevan, Eds., John Wiley and Sons, New York, N. Y., 1968.

21) W. A. Chupka and M. Kaminsky, *J. Chem. Phys.*, **35**, 1991 (1961).

22) R. H. Partridge, *ibid.*, **52**, 2491 (1970).

Table 3. Yields of radicals in the γ-irradiated alkane at 77 K[a)]

γ-Irradiated system	G(solvent radical)	G(solute radical)
i-C_4H_{10}	2.5	0
i-C_4H_{10}-C_3H_8 (4.8%)	0.5	1.9
neo-C_5H_{12}	2.3	0
neo-C_5H_{12}-C_2H_6 (4.8%)	0.9	0.9
neo-C_5H_{12}-C_3H_8 (4.9%)	0.4	1.3
neo-C_5H_{12}-*cyclo*-C_5H_{10} (4.7%)	0.9	2.0
neo-C_5H_{12}-C_6H_{12}[b)] (4.9%)	0.3	2.3
neo-C_5H_{12}-*cyclo*-C_6H_{12} (6.5%)	0.2	2.6
neo-C_5H_{12}-*n*-C_6H_{14} (4.8%)	0.5	2.4

a) G value of the radicals were determined by assuming G(radical) = 1.6 for the radicals produced in the γ-irradiated 3-methylpentane at 77 K. (M. Shirom and J. E. Willard, *J. Phys. Chem.*, **72**, 1702 (1963)) The errors of radical yields are about 20%. When neopentane–alkane mixtures are irradiated, neopentyl and solute radicals are formed. A standard ESR spectrum of neopentyl radical was obtained by the γ-irradiation of neopentane containing N_2O. (*cf.* J. Lin and F. Williams, *J. Phys. Chem.*, **72**, 3707 (1968)). The yields of neopentyl radical were obtained from the height of central peak in the ESR spectrum and the standard spectrum of neopentyl radical. The yields of solute radical was obtained by subtracting the yields of neopentyl radical from the total radical yields.

b) C_6H_{12} represents methylcyclopentane.

which may be much higher than the yields of the mobile excited cations. Even if the excited neopentane cation is formed, it may decompose in the period of one vibration[13,14)] before transferring its charge to the additive.

Excitation-transfer Reaction in γ-irradiated Alkane Mixtures in the Solid Phase. It seems from the above discussions that the energy transfer from γ-irradiated isobutane or neopentane to the solutes cannot be ascribed to the ionic processes, although the possibility of a transfer *via* the excited cation cannot be excluded completely. The excitation transfer reaction may be responsible for the energy transfer in the radiolysis of an alkane mixture, as in the radiolysis of the *i*-C_4H_{10}–CCl_4 (or $C_6H_5CH_3$) system:[3)]

$$\textit{neo}\text{-}C_5H_{12} \sim\!\!\sim\!\!\sim C_5H_{12}^* \quad (12)$$

$$C_5H_{12}^* \longrightarrow C_4H_9\cdot + CH_3\cdot \quad (13)$$

$$\searrow\ C_5H_{11}\cdot + H\cdot \quad (14)$$

$$C_5H_{12}^* + RH \longrightarrow C_5H_{12} + RH^* \quad (15)$$

$$RH^* \longrightarrow R\cdot + H\cdot \quad (16)$$

where $C_5H_{12}^*$ represents an excited molecule. CH_3 radicals are not observed by ESR spectroscopy, although their formation is expected from Eq. (13). This is because the CH_3 radical may migrate in the neopentane matrix even at 77 K and may recombine with other CH_3 radicals or H atoms.

When the *i*-C_4H_{10}–C_3H_8 or *neo*-C_5H_{12}–C_2H_6, C_3H_8, or *i*-C_4H_{10} systems are γ-irradiated at 77 K, solute radicals are mainly formed. As is shown in Table 2, it is impossible for an excitation transfer from isobutane or neopentane in the first excited state to the solute alkanes to occur. Therefore, the excitation transfer may occur by way of the highly-excited states of isobutane or neopentane.

Yields of Hydrogen in the Radiolysis of Neopentane Containing Cyclopentane at 77 K in the Solid Phase. The effect of cyclopentane on the yields of H_2 and CH_4 in the radiolysis of neopentane at 77 K in the solid phase is shown in Fig. 4. The yields of H_2 increase sharply upon the addition of a small amount of cyclopentane, while the yields of CH_4 are not affected. The broken line indicates the yields which may be expected when the energy transfer between neopentane and cyclopentane does not occur.

Since the cyclopentyl radical is the main radical formed in the radiolysis of the solid neopentane–cyclopentane (5 mol %) system (Fig. 2f), the large yields of H_2 upon the addition of cyclopentane may be due to an excitation transfer from highly-excited neopentane to cyclopentane (*cf.* Reactions (12)—(16)). Since the increase in H_2 becomes approximately constant above 2 mol % of cyclopentane, the excitation transfer occurs entirely below this concentration. The increase in the cyclopentyl radical shows the same concentration dependency in the radiolysis of the solid neopentane–cyclopentane mixture.[23)] Though it is expected from the ESR study that the yields of the CH_3 radical decrease upon the addition of cyclopentane (*cf.* Reactions (13) and (15)), the yields of CH_4 do not decrease. Therefore, methane may be formed mainly *via* a non-radical process, such as molecular detachment from neopentane.

23) M. Fukaya, T. Miyazaki, and Z. Kuri, unpublished results.

Effect of Matrix on the Formation of Solvent Radicals in the Radiolysis of Alkanes in the Solid State at 77 K

Mitsuharu FUKAYA, Terunobu WAKAYAMA, Tetsuo MIYAZAKI*,
Yoshiyuki SAITAKE, and Zen-ichiro KURI

Department of Synthetic Chemistry, Faculty of Engineering, Nagoya University, Chikusa-ku, Nagoya

(Received March 10, 1972)

The effect of the matrix on the radiolysis of 2,3-dimethylbutane, neopentane, 2,2-dimethylbutane, and isobutane in the solid state has been studied at 77 K by means of ESR spectroscopy. Though only the $\cdot CH_2CH(CH_3)CH(CH_3)_2$ radical is formed by the γ-irradiation of 2,3-dimethylbutane in the I crystal, the $CH_3\dot{C}(CH_3)CH(CH_3)_2$ radical is formed by the γ-irradiation of 2,3-dimethylbutane in the II crystal. Though the t-C_4H_9 and neo-C_5H_{11} radicals are formed by the γ-irradiation of pure neopentane, the formation of radicals is affected appreciably by the addition of a small amount of alkanes. When neopentane containing ethane, *etc.* is γ-irradiated, the solute radical is mainly formed by energy transfer form the γ-irradiated neopentane to the solute. Most of the solutes have a spherical molecular structure like that of neopentane or are smaller than neopentane. When neopentane containing 3-methylpentane, *etc.* is γ-irradiated, only the neopentyl radical is formed. The molecular structures of the solutes are very different from that of neopentane. The formation of the solvent radical in the radiolysis of 2,2-dimethylbutane is affected by the addition of 3-methylpentane or methylcyclohexane. The formation of the butyl radical in the radiolysis of isobutane is also changed drastically by addition of alkanes. It is concluded that the formation of solvent radicals in the radiolysis of solid alkane is appreciably affected by the conditions of the matrix.

It has previously been found that the isobutyl radical is formed by the radiolysis of isobutane in the polycrystalline state, while the t-C_4H_9 radical is formed in the transparent solid state.[1] The study of the radiolysis of isobutane-2-d_1 showed that the phase change affects the primary process of the C–H bond rupture in the radiolysis of solid isobutane.[2] The phase effect was also reported in the radiolyses of phenyl acetate[3] and disodium succinate[4] in the solid state. Recently it was found in the radiolysis of solid succinic acid that the $G(CO+H_2)$ from the powder is much higher than that from the single crystal. It was suggested that the exciton produced by the γ-irradiation of solid succinic acid migrates to a surface or a defect of the powder and thus produces CO and H_2.[5] It was also been reported that, in the radiolysis of alkanes at 77 K, solvent radicals are formed by the fragmentation of excited molecules produced directly by γ-irradiation.[6]

Therefore, we have proposed that two important problems must be solved in order to elucidate the mechanism of the solid-phase radiolysis. One is the problem of the extent to which the formation of an exciton plays an important role: the other is how the condition of the matrix affects the reaction in the solid phase. Here we will report about the latter problem in the radiolyses of 2,3-dimethylbutane, neopentane, 2,2-dimethylbutane, and isobutane in the solid phase.

Experimental

The isobutane was more than 99.7% pure. The neopentane was more than 99.9% pure. The 2,3-dimethylbutane and 2,2-dimethylbutane were more than 99.0% pure and were passed through a 30-cm column packed with activated alumina. They were used after distillation on a vacuum line. The additives, such as ethane, propane, n-hexane, cyclohexane, and methylcyclohexane, were the same as those which had been used before.[6d] The additives, such as n-pentane, n-octane, isooctane, and *trans*-decaline, were Tokyo Kagaku Seiki's guaranteed reagents. The n-heptane, n-decane, n-hexadecane, isopentane, cyclooctane, adamantane, and carbon tetrachloride were Nakarai Chemicals' guaranteed reagents. The n-butane and nitrous oxide were supplied by Takachiho Shoji Co. and were of a high purity. The 3-methylpentane (Aldrich Chemical Co.) was washed with concentrated sulfuric acid. After this treatment the specimen was separated from the sulfuric acid solution by distillation.

Samples were sealed into a silica cell and irradiated at 77 K with γ-rays from Co-60 at a dose rate of 7.6×10^5 rad/hr. The total dose was 3.8×10^5 rad. The ESR spectra of the irradiated samples were measured at 77 K on a JES-3BX ESR spectrometer.

Results and Discussion

Effect of Phase on the Formation of Radicals in the Radiolysis of 2,3-Dimethylbutane at 77 K. Recently Adachi, Suga, and Seki have reported a calorimetric

* To whom correspondence should be addressed.

1) a) T. Miyazaki, T. Wakayama, K. Fueki, and Z. Kuri, This Bulletin, **42**, 2086 (1969). b) T. Wakayama, T. Miyazaki, K. Fueki, and Z. Kuri, *J. Phys. Chem.*, **74**, 3584 (1970).

2) Y. Saitake, T. Wakayama, T. Kimura, T. Miyazaki, K. Fueki, and Z. Kuri, This Bulletin, **44**, 301 (1971).

3) Y. Noro, M. Ochiai, T. Miyazaki, A. Torikai, K. Fueki, and Z. Kuri, *J. Phys. Chem.*, **74**, 63 (1970).

4) a) H. M. Vyas, J. Janecka, and M. Fujimoto, *Can. J. Chem.*, **48**, 2804 (1970). b) M. Fujimoto and W. A. Seddon, *ibid*, **48**, 2809 (1970).

5) a) T. Miyazaki, S. Okada, T. Wakayama, K. Fueki, and Z. Kuri, This Bulletin, **43**, 1907 (1970). b) T. Miyazaki, Y. Fujitani, T. Wakayama, K. Fueki, and Z. Kuri, *ibid.*, **44**, 984 (1971).

6) a) T. Wakayama, T. Miyazaki, K. Fueki, and Z. Kuri, *ibid*, **42**, 1164 (1969). b) T. Wakayama, T. Kimura, T. Miyazaki, K. Fueki, and Z. Kuri, *ibid*, **43**, 1017 (1970). c) T. Miyazaki, T. Yamada, T. Wakayama, K. Fueki, and Z. Kuri, *ibid.*, **44**, 934 (1971). d) T. Miyazaki, T. Wakayama, M. Fukaya, Y. Saitake, and Z. Kuri, *ibid*, **46**, 1030 (1973).

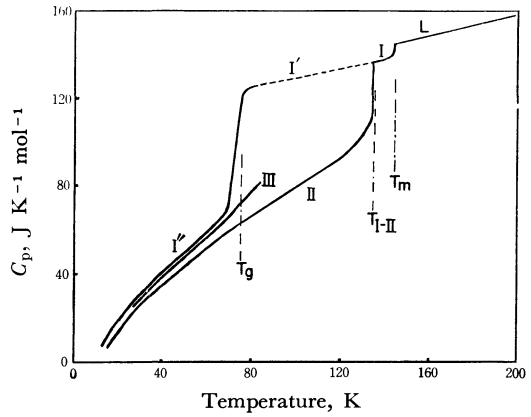

Fig. 1. The heat capacity curves of 2,3-dimethylbutane measured by Adachi *et al.*[7]
L, the liquid; I, the crystal–I; I′, the supercooled crystal–I; I″, the glassy crystal–I; II, the crystal–II; III, the crystal–III:
T_m, the melting point (145 K); T_{I-II}, the phase transition temperature between crystal–I and II (136 K); T_g, the glass transition temperature (76 K).

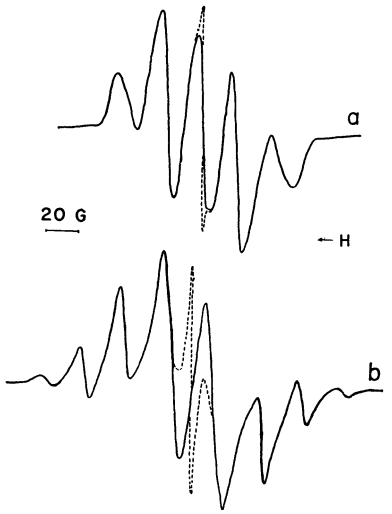

Fig. 2. a) ESR spectrum of γ-irradiated 2,3-dimethylbutane in crystal–I at 77 K.
b) ESR spectrum of γ-irradiated 2,3-dimethylbutane in crystal–II at 77 K.
Dotted lines represent the spectra of trapped electrons which are easily bleached by illumination with visible light.

study of 2,3-dimethylbutane in the solid state.[7] The heat-capacity curves measured by them are shown in Fig. 1. 2,3-Dimethylbutane has three crystalline phases: a high-temperature form (the I crystal) which is stable at temperatures between 136 K to 145 K, a low-temperature form (the II crystal) which is stable below 126 K, and a metastable intermediate phase (the III crystal).[8] When 2,3-dimethylbutane is cooled repidly at 77 K, it forms a supercooled crystal (I′ in Fig. 1), which is a transparent solid.[9] When the supercooled I crystal is warmed to some temperature lower than 136 K and then cooled to 77 K, and when annealing is repeated several times, it forms a II crystal.

The ESR spectrum of γ-irradiated 2,3-dimethylbutane in the supercooled I crystal at 77 K is shown in Fig. 2a. The spectrum consists of five lines, with a splitting of 22 G, which is approximately consistent with the reported value of 21 G for the $\cdot CH_2CH(CH_3)CH_3$ radical.[10] The spectrum may be assigned to the $\cdot CH_2CH(CH_3)CH(CH_3)_2$ radical which is formed by the rupture of a primary C–H bond.

A quite different ESR spectrum is, however, obtained by the γ-irradiation of 2,3-dimethylbutane in the II crystal form at 77 K (Fig. 2b). The spectrum consists of eight lines, with a splitting of 24 G. The spectrum may be assigned to the $CH_3\dot{C}(CH_3)CH(CH_3)_2$ radical which is formed by the rupture of a tertiary C–H bond, or to the C_3H_7 radical which is formed by the rupture of a C–C bond. The yield of H_2 in the radiolysis of 2,3-dimethylbutane in the II crystal at 77 K is the same as that in the radiolysis of 2,3-dimethylbutane in the I crystal. The spectrum of eight lines coincides well with that of the $CH_3\dot{C}(CH_3)CH(CH_3)_2$ radical which is produced by H-atom abstraction from 2,3-dimethylbutane during the UV illumination of a 2,3-dimethylbutane-hydrogen iodide mixture at 77 K in the II crystal.[11] Therefore, it is probable that the solvent radical of γ-irradiated 2,3-dimethylbutane in the II crystal may be the $CH_3\dot{C}(CH_3)CH(CH_3)_2$ radical.

The following two conclusions are obtained from the results of the radiolysis of 2,3-dimethylbutane at 77 K. First, in the previous studies of the effect of the phase on the radiolysis of solid isobutane[1,2] the phase change was caused by the addition of alkane and the phase change was not ascertained by the calorimetric measurements. The present results for the radiolysis of solid 2,3-dimethylbutane, however, clearly show that quite different radicals are formed in the two different phases, as determined by calorimetric measurement.

Second, it was proposed that, in the radiolysis of isobutane,[1b] the phase effect on the formation of the solvent radical may be explained by the cage effect. The present results, however, show that the phase effect on the radiolysis of solid 2,3-dimethylbutane cannot be explained by the cage effect. In effect, since the C–C bond of the $CH_3\dot{C}(CH_3)CH(CH_3)_2$ radical is formed by sp^2-hybrid orbitals, two CH_3 groups and $CH(CH_3)_2$ group constitute a planar structure. Therefore, a structural rearrangement of C–C bonds would be necessary for the formation of the $CH_3\dot{C}(CH_3)CH(CH_3)_2$ radical from the 2,3-dimethylbutane molecule, while such a change would not be necessary for the formation of the $\cdot CH_2CH(CH_3)CH(CH_3)_2$ radical. Therefore, it would be expected from the hypothesis of the cage effect that the for-

7) K. Adachi, H. Suga, and S. Seki, This Bulletin, **44**, 78 (1971).
8) Unfortunately, the crystal structures of crystal–I, II and III are unknown at present. X-Ray analysis of these crystals is desirable in future.
9) The terms "glass" or "glassy state" were often used in the previous studies by the present authors.[1,2,5,6] These terms, however, mean only that the solid is in the transparent state.
10) P. B. Ayscough and H. E. Evans, *J. Phys. Chem.*, **68**, 3066 (1964).

mation of the C–C bonds may be suppressed in the II crystal, which is more rigid than the I crystal (i.e., the plastic crystal). The experimental results, however, show that the $CH_3\dot{C}(CH_3)CH(CH_3)_2$ radical is formed only in the II crystal.

The phenomenon that different solvent radicals are formed selectively by the change in the phase is quite mysterious for us. When a solvent radical is formed by H-atom abstraction from 2,3-dimethylbutane during the UV illumination of a 2,3-dimethylbutane-hydrogen iodide mixture at 77 K, the $\cdot CH_2CH(CH_3)CH(CH_3)_2$ radical is formed in the I crystal, while the $CH_3\dot{C}(CH_3)CH(CH_3)_2$ radical is formed in the II crystal.[11] Therefore, the effect of the phase on the H-atom abstraction reaction is similar to the effect on the radiolysis. The results suggest that the matrix of 2,3-dimethylbutane itself possesses a selectivity for the formation of the solvent radical.

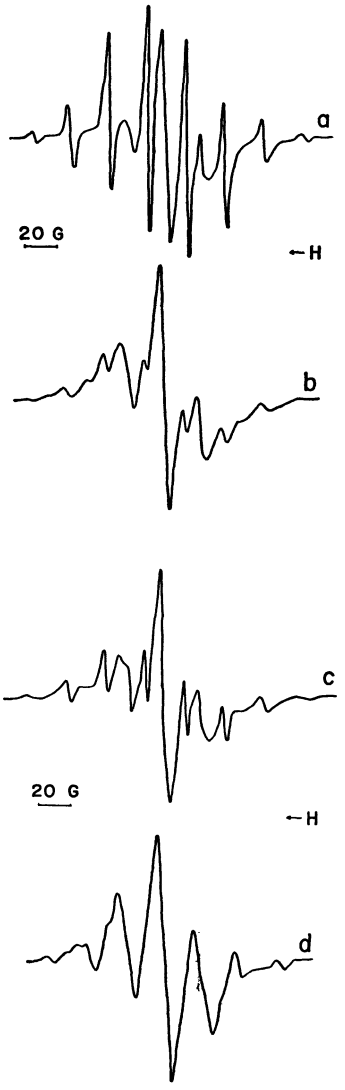

Fig. 3. ESR spectra of γ-irradiated neopentane and neopentane-alkane mixture at 77 K.
a) pure neopentane b) neopentane–3-methylpentane (4.5 mol%) c) neopentane–isooctane (4.8 mol%) d) neopentane–*n*-butane (6.2 mol%)

Effect of the Addition of Alkanes on the Formation of Radicals in the Radiolysis of Neopentane at 77 K.
When pure neopentane is γ-irradiated at 77 K in the solid phase, the ESR spectrum of the radicals is as is shown in Fig. 3a.[12] The spectrum of eight narrow lines is ascribed to the t-C_4H_9 radical. The spectrum of three broad lines is ascribed to the *neo*-C_5H_{11} radical. When neopentane containing a small amount of alkane is γ-irradiated at 77 K, a quite different ESR spectrum is obtained. The effects of the addition of alkanes may be classified into two types. Type A is as follows: when neopentane containing ethane *etc.* is γ-irradiated, the solute radical is mainly formed by excitation transfer from the γ-irradiated neopentane to the solute. The details of Type A were reported in a previous study.[6] Type B is as follows: when neopentane containing 3-methylpentane, *etc.* is γ-irradiated, only a neopentyl is formed, while the formation of the t-C_4H_9 radical and the solute radical is suppressed. A small quantity of solute radicals, however, seems to be formed in a few cases. The ESR spectra of γ-irradiated neopentane containing 3-methylpentane, isooctane, and *n*-butane are shown in Figs.

TABLE 1. EFFECTS OF ADDITIVES ON THE RADIOLYSIS OF SOLID NEOPENTANE AT 77 K

	Additives	
	Alkanes	Other
Type A	○ C-C ○ C-C-C C-C-C-C-C-C ● 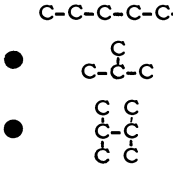 ●	●  ● 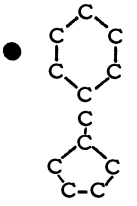
Type B	C-C-C-C C-C-C-C-C C-C-C-C-C-C *n*-$C_{10}H_{22}$ *n*-$C_{16}H_{34}$ 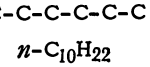 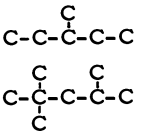 	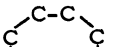 ● 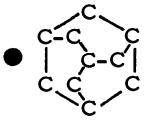 	N_2O CH 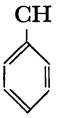

●: spherical molecules
○: Its size is smaller than that of neopentane.

11) T. Wakayama, T. Miyazaki, K. Fueki, and Z. Kuri, unpublished results.

12) B. Smaller and M. S. Matheson, *J. Chem. Phys.*, **28**, 1169 (1958).

3b, c, and d respectively. A small amount of the *t*-C_4H_9 radical is formed in the radiolysis of neopentane containing isooctane (Fig. 3c).

The effects of various alkanes on the radiolysis of neopentane are classified in Table 1. Most of the alkanes of Type A have approximately spherical molecular structures, like that of neopentane, or are smaller than neopentane. The molecular structures of the additives of Type B, however, are very different from that of neopentane. Although adamantane is spherical like neopentane, it is larger than that of neopentane.

Since the information on the radiolysis of solid alkane is very scanty at present, it is difficult to explain why the effects of alkane mixtures fall into two types. The phenomena may be related to the behavior of an exciton formed by γ-irradiation, the local crystalline structure near the additive, or some such thing.

It is noted that when neopentane containing 4 mol% nitrous oxide is γ-irradiated at 77 K, only the *neo*-C_5H_{11} radical is formed. Lin and Williams ascribed this phenomenon to the electron-scavenging effect of nitrous oxide.[13] Since the solvent radical may be formed by the fragmentation of an excited neopentane molecule,[6] and since a decrease in the *t*-C_4H_9 radical is also observed upon the addition of alkanes, it is possible that nitrous oxide acts similarly to the addition-effect of alkanes in the radiolysis of solid neopentane.

Effects of the Addition of Alkane on the Formation of Radicals in the Radiolysis of 2,2-*Dimethylbutane at* 77 *K.* The ESR spectrum of γ-irradiated pure 2,2-dimethylbutane in the solid state is shown in Fig. 4a. The spectrum consists mainly of three lines, with a splitting of 23 G, which is consistent with that of 23 G for the $\cdot CH_2C(CH_3)_2CH_3$ radical. The spectrum may be assigned to the $\cdot CH_2C(CH_3)_2CH_2CH_3$ radical.

When 2,2-dimethylbutane containing 5 mol% of 3-methylpentane is γ-irradiated at 77 K, the spectrum of the triplet decreases, while the very small peaks on both sides of the triplet are not affected by the addition of 3-methylpentane. Therefore, the spectrum of γ-irradiated 2,2-dimethylbutane containing 3-methylpentane consists of five lines, as is shown in Fig. 4b. The assignment of the quintet ESR spectrum is not possible at present. A similar effect is also observed upon the addition of methyl-cyclohexane.

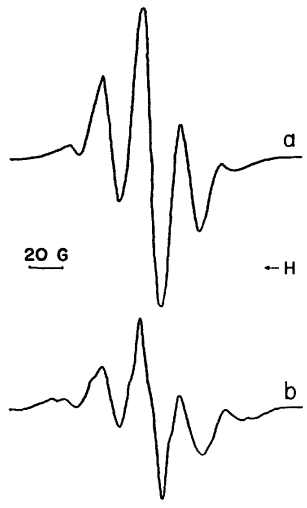

Fig. 4. a) ESR spectrum of γ-irradiated pure 2,2-dimethylbutane at 77 K.
b) ESR spectrum of γ-irradiated 2,2-dimethylbutane-3-methylpentane (4.9 mol%) at 77 K.

Effect of the Addition of Alkane on the Formation of Radicals in the Radiolysis of Isobutane at 77 *K.* When pure isobutane is γ-irradiated at 77 K in the solid state, the isobutyl radical is formed,[6a,b] while a quite different ESR spectrum is obtained in the radiolysis of isobutane containing a small amount of alkane at 77 K.[1] The effects of the addition of alkanes on the radiolysis of solid isobutane may be classified into two types. When isobutane containing propane is γ-irradiated at 77 K, the propyl radical is mainly formed, while the formation of the isobutyl radical is suppressed. As was discussed in a previous study,[6d] the exciton by the γ-irradiation of isobutane migrates to propane to produce the propyl radical. We could not, however, find any other alkanes which behave like propane in the radiolysis of solid isobutane.

When isobutane containing other alkanes is γ-irradiated at 77 K, the formation of the isobutyl radical is suppressed without the solute radical appearing, while the *t*-C_4H_9 radical is formed as has been shown in the previous reports.[1]

Table 2. Effects of additives on the radiolysis of soid isobutane at 77 K

	Alkanes as additives
Type A	○ C-C-C
Type B	C-C-C-C-C C-C-C-C-C-C C-C-C-C-C-C-C C C-C-C-C C C-C-C C C C C-C-C-C C C-C-C-C-C C C C-C-C-C C C/C\C C\C/C C C/C\C C\C/C

○: Its size is smaller than that of isobutane.

13) J. Lin and F. Williams, *J. Phys. Chem.*, **72**, 3707 (1968).

The effects of various alkanes on the radiolysis of isobutane are shown in Table 2. It may be noted that propane is smaller than isobutane, while the other alkanes of Type B are larger than isobutane.

It may be concluded that the radiolysis of alkane in the solid phase is appreciably affected by the condition of the matrix. The effect is characteristic of the solid phase; further studies are desired for the elucidation of the solid kinetics.

BULLETIN OF THE CHEMICAL SOCIETY OF JAPAN, VOL. 46, 1040—1045 (1973)

The Proton Chemical Shift of *n*-Pentane

Isao ANDO and Atsuo NISHIOKA

Department of Polymer Engineering, Tokyo Institute of Technology, Ookayama, Meguro-ku, Tokyo

(Received April 8, 1972)

The temperature dependence of the proton chemical shift of *n*-pentane was calculated by the CNDO/2 method, taking into account the possible preferred conformations and the contributions from the diamagnetic, paramagnetic, and bond anisotropy terms. It was found that the bond anisotropy term contributes predominantly, while the diamagnetic term is not negligible, and that the paramagnetic term is negligible in comparison with these terms. The observed temperature dependence of the chemical shift can be reasonably explained by calculations using 570 cal/mol as the energy difference between the *trans* and *gauche* conformations, and also using 9.1×10^{-30} cm^3 as the magnetic anisotropy of the C–C bond.

So far quantum-chemical calculations of the shielding constants in the chemical shifts of hydrocarbons have been done for some typical simple molecules, such as methane, acetylene, and ethylene,[1,2] by the LCAO MO method, but for more complex molecules which have some rotational isomers, *e. g.*, the *n*-pentane under consideration, these rigorous calculations becomes virtually impossible. Thus, for estimating the chemical shift of such molecules we must make some approximations by dividing the shielding constant into contributions from electrons localized on atoms and in the chemical bond.

According to Pople,[3] the shielding constant, σ_A, of a nucleus A is written as:

$$\sigma_A = \sigma_A^{dia} + \sigma_A^{para} + \sum_{B(\neq A)} \sigma_{AB} \qquad (1)$$

where the σ_A^{dia} term arises from induced diamagnetic currents on the A atom, depending upon the electron density around the nucleus, A; where σ_A^{para} is the contribution of induced paramagnetic currents on A, and where σ_{AB} is the contribution arising from locally-induced currents on the atoms, B's, other than A in the molecule, referred to as the neighbour anisotropy effect. In estimating these terms, we will use the electron density calculated by the CNDO/2 (Complete Neglect of Differential Overlap) method[4] for σ_A^{dia}, and will apply Marshall and Pople's theory[5] to the evaluation of σ_A^{para}, which is here assumed to be contributed by the excess or deficient charges on the carbon atom bonded to the specified proton; we will also calculate the bond anisotropy term[6] for σ_{AB}, because it is difficult to obtain exactly information about the excitation energy which is used in the point dipole equation.[3]

Many attempts using the LCAO MO method have been made to estimate the proton and the ^{13}C chemical shift of hydrocarbon molecules by calculating the electron density. Yonezawa *et al.*[7] calculated the electron densities on hydrogen atoms of hydrocarbons by the simple LACO MO method for the σ electron system, and estimated the chemical shifts. The calculated results are consistent with the observed ones, but the simple LCAO MO method is too simple for a discussion of the proton chemical shift of *n*-pentane, which can take various conformations. Sichel and Whitehead[8] calculated the electron density on atoms of hydrocarbons using the extended Hückel theory, which can take into account the molecular conformations; they found that the calculated electron densities on the carbon atoms correspond well to the observed ^{13}C chemical shifts, but that those on the hydrogen atom do not correspond to the proton chemical shift. Baird and Whitehead[9] discussed the correlation between the proton chemical shift of hydrocarbons and the electron density calculated by the electronegativity equation method, and found that the ^{13}C chemical shift reasonably corresponds to the charge on the carbon atom, while the proton chemical shift does not correspond to that on the hydrogen atom.

As has been described above, a good correlation between the calculated electron densities on the hy-

1) M. J. Stephen, *Proc. Roy. Soc.*, **243**, 264 (1957).
2) M. Fixaman, *J. Chem. Phys.*, **35**, 679 (1961).
3) J. A. Pople, W. G. Schneider, and H. J. Bernstein, "High resolution nuclear magnetic resonance", McGraw-Hill Book Co., Inc., New York (1957) Section 7. 4.
4) J. A. Pople and G. A. Segal, *J. Chem. Phys.*, **44**, 3289 (1966).
5) T. W. Marshall and J. A. Pople, *Mol. Phys.*, **1**, 199 (1958).
6) H. M. McConnell, *J. Chem. Phys.*, **27**, 226 (1957).
7) T. Yonezawa, H. Kato, and K. Fukui, "Introduction to quantum chemistry", Kyoritsu Book Co., Inc., Tokyo (1964) p. 520.
8) J. M. Sichel and M. A. Whitehead, *Theoret. Chim. Acta*, **5**, 35 (1966).
9) N. C. Baird and M. A. Whitehead, *ibid.*, **5**, 167 (1966).

drogen atoms and the chemical shifts of proton in hydrocarbons has not been obtained. One cause may be the neglect of the second and third terms in Eq. (1). In the proton chemical shift of non-polar hydrocarbon molecules, it is usually conjectured that the contribution of the second term to the chemical shift is negligible in comparison with those of the other terms. Generally discussing the chemical shift of such molecules, we will report that the third term is important.

It is the purpose of this paper to calculate the proton chemical shift of *n*-pentane, considering the various conformations, and to estimate plausible values of the *trans-gauche* potential barrier and the magnetic bond anistropy of the C–C bond, $\Delta\chi_{C-C}$, by comparing the observed temperature dependences of the proton chemical shifts with the calculated ones.

Experimental

The NMR spectra of *n*-pentane (99.9%) were measured in neat liquid at temperatures from −70 °C to +60 °C, using a JEOL 4H-100 type spectrometer (100 MHz). Tetramethylsilane (TMS) was used as the internal standard. The chemical shift is expressed in ppm downfield.

Calculation

In estimating the chemical shift of *n*-pentane, we calculate separately the first, second, and third terms in Eq. (1).

The first term[10] is expressed as;

$$\sigma_A^{dia} = \frac{e^2}{3mc^2} = \langle 0 \left| \sum_k \frac{1}{r_k} \right| 0 \rangle \tag{2}$$

where e is the electron charge; m, the mass of the electron; c, the velocity of light, and r_k the distance of the k-th electron from the nucleus, and where $|0\rangle$ refers to the electronic ground state of the molecule. σ_A^{dia} is fairly easy to calculate, since it depends only on the electron distribution in the electronic ground state. Thus, in practice, we used the following equation[3] to estimate the proton chemical shift;

$$\sigma_A^{dia} = k \cdot \rho \tag{3}$$

where we used 17.8 ppm[3] as k and where ρ is the electron density of the atom under consideration, being calculated by the CNDO/2 method.

The second term, the paramagnetic one, which represents the effect of the mixing of the ground and excited states by the magnetic field, is usually more difficult to evaluate. Thus, we will evalute this term by the following expression, proposed by Marshall and Pople,[5] which was obtained from a calculation of the nuclear magnetic shielding in a hydrogen nucleus placed in an electric field, due to the excess or deficient charge on the carbon atom bonded to the hydrogen atom, neglecting any effect of the spin of the electron:

$$\sigma_A^{para} = k \cdot \sigma_\perp^{para} \sin^2\theta \tag{4a}$$

$$\sigma_\perp^{para} = -\frac{233}{144}\frac{a^3E^2}{mc^2} \tag{4b}$$

where $\sigma_\perp^{para}$ is the paramagnetic shielding constant in the case of H (magnetic field) perpendicular to E (electric field); σ_A^{para}, the value of σ for an intermediate direction making an angle of θ with E, and a, the Bohr radius. Therefore, when we evaluate σ_A^{para}, one must average all the θ angles. Thus, σ_A^{para} becomes:

$$\sigma_A^{para} = \frac{1}{2}\sigma_\perp^{para} = -\frac{1}{2}\cdot\frac{233}{144}\frac{a^3E^2}{mc^2} \tag{5}$$

When we estimate E in any specified hydrogen nucleus, we assume that the hydrogen nucleus experiences the electric field of the carbon atom bonded to it, which arises from its excess electron charge.

As to the third term, although the point dipole equation proposed by Pople[3] should be used, it is difficult to estimate the equation because the excited states are not known. Thus, we used approximately the McConnell equation[6], neglecting only the small contribution from the C–H bond.

$$\sigma_{AB} = \frac{\Delta\chi_{C-C}}{3r^3}(1 - 3\cos^2\theta_M) \tag{6}$$

in which $\Delta\chi_{C-C}(=\chi_\parallel - \chi_\perp)$ is the magnetic anisotropy of the C–C bond, where r is the distance between any specified proton and the midpoint of the C–C bond, and where θ_M is the angle between the directions of r and the C–C bond. So far, although various values for the magnetic anisotropy of the C–C bond have been reported,[11] the most reliable value is not known at present. However, to promote the discussion, we adopted tentatively the value of 5.5×10^{-30}cm^3 reported by Bothner-By and Narr-Colin.[11] We will discuss the value of $\Delta\chi_{C-C}$ in a later chapter.

Here, the rotational isomeric states of *trans*(T) and *gauche* (G and G′) are defined to occur at the rotational angles about 0°, 120°, and 240° respectively by the clockwise rotation around the C–C bond as expressed in the Newman projection.

We numbered the carbon atoms in pentane as follows:

$$CH_3(1)\text{-}CH_2(2)\text{-}CH_2(3)\text{-}CH_2(4)\text{-}CH_3(5)$$

The C–C and C–H bond lengths are set as 1.54 Å and 1.10 Å respectively, and both of the C–C–C and C–C–H bond angles are set at 109°28′.[12]

10) N. F. Ramsey, *Phys. Rev.*, **78**, 699 (1950).

11) a) A. A. Bothner-By and C. Narr-Colin, *Ann. New York Acad, Sci.*, **70**, 833 (1958). b) M. T. Rogers and R. T. Narasimhan, *J. Chem. Phys.*, **31**, 1302 (1959). c) J. I. Musher, *ibid.*, **35**, 1159 (1961). d) R. F. Zürcher, *Helv. Chim. Acta*, **44**, 1755 (1961). e) R. F. Zürcher, *J. Chem. Phys.*, **37**, 2421 (1962). f) A. G. Moritz and N. Sheppard, *Mol. Phys.*, **5**, 361 (1962). g) G. S. Reddy and J. H. Goldstein, *J. Chem. Phys.*, **38**, 2736 (1963). h) J. I. Musher, *Mol. Phys.*, **6**, 93 (1963), i) L. D. Hall, *Tetrahedron Lett.*, **1964**, 1457. j) D. W. Davis, *Mol Phys.*, **6**, 489 (1963), k) J. W. ApSimon, W. G. Craig, P. V. Demarco, D. W. Mathieson, L. Saunders, and W. B. Whalley, *Chem. Commun.*, **1966**, 359, l) J. Homer and D. Callaghan, *J. Chem. Soc., A*, **1968**, 439.

12) L. Pauling, "Nature of Chemical Bond", Cornell University Press, New York (1960).

The numerical calculations were carried out by means of the HITAC-5020E of the Computer Center of the University of Tokyo.

Results and Discussion

n-Pentane can take seven isomeric states (TT, TG, TG′, GT, G′T, GG and G′G′), where GG′ and G′G were ignored due to the large steric hindrance. Because the observed chemical shift is usually considered to be the average of the chemical shifts of rapidly interconverting rotamers, the chemical shift, $\sigma(j)$, of the j-th proton in *n*-pentane should be expressed as follows:

$$\sigma(j) = \sum_{i=1}^{7} X_i \sigma_i(j) \tag{7}$$

where X_i and σ_i are the fraction and the chemical shift of the i-th isomer respectively. X_i is expressed as:

$$X_i = e^{-\Delta E_i/RT} / \left(\sum_{i=1}^{7} e^{-\Delta E_i/RT}\right) \tag{8}$$

where R is the gas constant; T, the absolute temperature, and ΔE_i the energy difference between TT and the i-th conformation.

Now, let us discuss the electron-density distributions of *n*-pentane in Fig. 1, we show the electron densities of the protons in the TT, TG and GG conformations as obtained by the CNDO/2 method; one of the three protons of the methyl group is assumed to take the *trans* position in relation to the central carbon atom. The electron density of the methyl protons is averaged by the three protons in the methyl group, since it may be considered that the methyl group rotates freely, and the parameters used in the CNDO/2 calculation are the same as those proposed by Pople.[4] The electron densities of the protons in the other conformations can be at once obtained from those of the TT, TG and GG conformations. The calculated total energies of these conformations were −1221.4326, −1221.4136, and −1221.3698 eV respectively. Thus, the energy difference between the *trans* and *gauche* conformations, ΔE_g, is *ca.* 440 cal/mol in an isolated pentane. This agrees fairly well with the value (450±60 cal/mol) obtained by the spectroscopic method,[13] the value (*ca.* 500 cal/mol) obtained by an inherent bond potential, and the energy of interaction between nonbonded substituents.[14] This is one of several successful cases[15] of the application of the CNDO/2 method to problem of the energy difference between the rotational isomers. Recently Fujiyama *et al.*[16] reported obtaining a value of 600 cal/mol by laser-Raman spectroscopy, and Ishikawa and Nagai.[17] obtained *ca.* 800 cal/mol by means of the

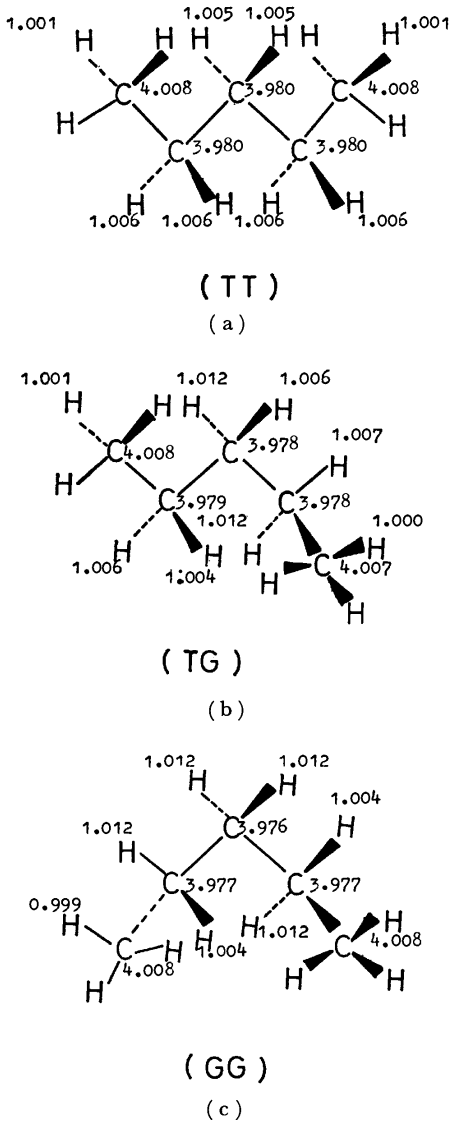

Fig. 1. The electron densities on the atoms of *n*-pentane in (a) TT, (b) TG, (c) GG conformations.

electro-optical effect. Our value is more or less lower than the experimental ones shown above. We will discuss this point below.

The temperature dependences of the proton diamagnetic shielding constants calculated by using Eqs. (3), (7), and (8) are shown in Fig. 2, in which the 440 and 600 cal/mol obtained by the CNDO/2 method and the laser-Raman spectroscopy respectively as described above are used as ΔE_g, and in which the $CH_2(2)$ and the $CH_2(4)$ are equivalent to each other. For reference, the values at 22°C are listed in Table 1. The temperature dependences of the chemical shifts calculated with 440 and 600 cal/mol as ΔE_g differ considerably from each other; the finding that the methyl protons are less shielded than the methylene groups is opposite to the observed one, as is shown in Fig. 3. This is true over a wide temperature range, as is shown in Fig. 4. Thus, the proton chemical shift of *n*-pentane cannot be explained by the first term only, but it is noticeable that there is a small and detectable chemical shift between the $CH_2(2)$

13) N. Sheppard and G. J. Szasz, *J. Chem. Phys.*, **17**, 86 (1949).
14) A. Abe, R. L. Jernigan and P. J. Flory, *J. Amer. Chem. Soc.*, **88**, 631 (1966).
15) For example, a) M. S. Gordon, *ibid.*, **91**, 3122 (1969). b) N. J. S. Dewar and M. Shanshal, **91**, 3654 (1969). c) L. Random and J. A. Pople, *ibid.*, **92**, 4786 (1970).
16) T. Fujiyama, M. Tasumi, and T. Shimanouchi, Symposium on Polymer, 771 (1970) Kyoto.
17) T. Ishikawa and K. Nagai, *Polymer J.*, **2**, 213 (1971).

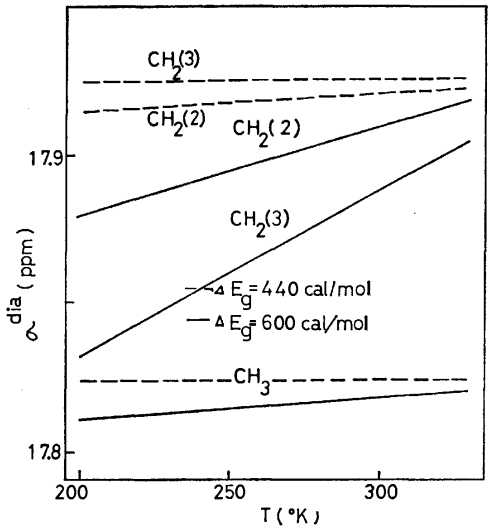

Fig. 2. The temperature dependences of the diamagnetic shielding term of *n*-pentane used 440 cal/mol and 600 cal/mol as ΔE_g.

TABLE 1. THE DIAMAGNETIC SHIELDING TERM σ^{dia} MAGNETIC ANISOTROPY EFFECT TERM σ_{C-C} AND THEIR SUM σ OF *n*-PENTANE AT 22 °C

	σ^{dia} (ppm)	σ_{C-C} (ppm)	σ (ppm)
ΔE_g=440 cal/mol			
$CH_3(1)$	17.825	−0.308	17.517
$CH_2(2)$	17.925	−0.588	17.337
$CH_2(3)$	17.926	−0.549	17.377
ΔE_g=600 cal/mol			
$CH_3(1)$	17.818	−0.306	17.512
$CH_2(2)$	17.910	−0.601	17.309
$CH_2(3)$	17.880	−0.538	17.342

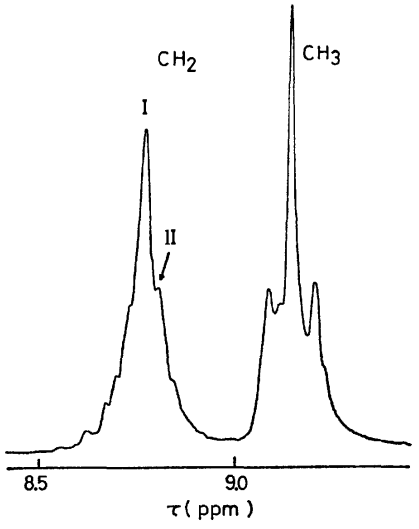

Fig. 3. The NMR spectrum of *n*-pentane. (at 22 °C and 60 MHz).

and $CH_2(3)$ protons in this calculation.

The second term, the paramagnetic contribution, was calculated according to Eq. (4), estimating E at any specified proton by the excess or deficient charge from the neutral one at the carbon atom bonded to the proton; the results are shown in Table 2. As expected, the contribution of the paramagnetic term to the proton chemical shift of *n*-pentane is almost negligible in comparison with the diamagnetic one shown in Table 1. It may be considered that the formation of the *S*-state electron localized around the hydrogen nucleus resulting from the adjacent carbon atom, is very small in *n*-pentane. Thus, we may neglect this term.

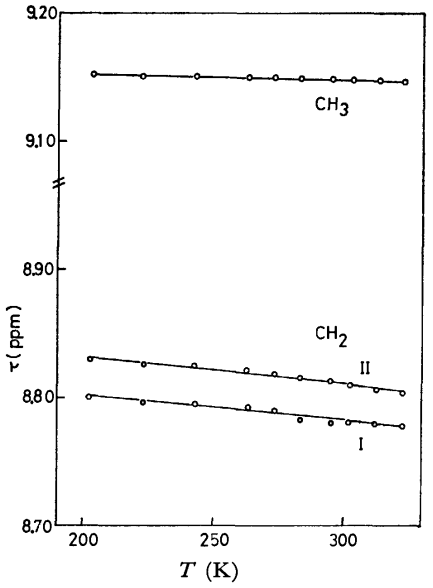

Fig. 4. The temperature dependence of the observed chemical shift of *n*-pentane.

TABLE 2. THE PARAMAGNETIC TERM σ^{para} OF THE TT, TG AND GG CONFORMATIONS OF *n*-PENTANE.

Preferred conformation	TT (ppm)	TG (ppm)	GG (ppm)
$CH_3(1)$	−0.00029	−0.00029	−0.00029
$CH_2(2)$	−0.00180	−0.00179	−0.00243
$CH_2(3)$	−0.00180	−0.00226	−0.00265
$CH_2(4)$	−0.00180	−0.00220	−0.00243
$CH_3(5)$	−0.00029	−0.00023	−0.00029

Next, we shall discuss the third term, which was calculated by assuming the C–C bond anisotropy effect. The results obtained are shown in Fig. 5, in which 440 and 600 cal/mol are used as ΔE_g. It has been found that the order of the arrangement of the calculated chemical shifts of each proton agrees fairly well with those observed over a wide temperature range, the temperature dependences of the chemical shifts of the CH_3 and $CH_2(2)$ groups differing from each other, and the contribution of this term to the chemical shift of *n*-pentane is larger than that of the diamagnetic term. Then, summing up σ^{dia} and $\Delta\chi_{C-C}$ contributions, we obtained the results shown in Figure 6. For reference, the sum of both contributions at 22 °C is listed in Table 1, which reveals that the chemical shifts of the $CH_2(2)$ and $CH_2(3)$

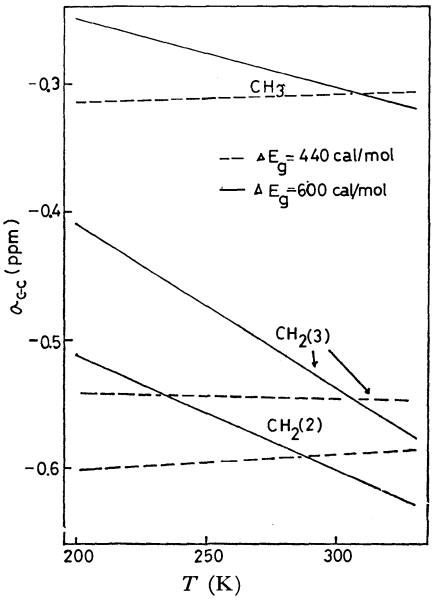

Fig. 5. The temperature dependence of the bond anisotropy term used 440 and 600 cal/mol as ΔE_g.

differ from each other slightly. The spectrum shown in Figure 3 suggests that the signal of the CH_2 group shows a weak shoulder, II,[18] on the higher-field side of the main peak, I, with a chemical-shift difference of 0.058 ppm, and that the ratio of the intensities of the peaks, I to II, is about 2 : 1. Moreover, it is found that the calculated temperature dependences of the chemical shifts for CH_3, $CH_2(2)$, and $CH_2(3)$, shown in Fig. 6, correspond qualitatively to those of these peaks, I and II, which shift to a lower field with an increase in the temperature. Comparing these observed and calculated results, it may tentatively be assumed that the peaks, I and II, are assignable to the $CH_2(2)$ and $CH_2(3)$ groups respectively. However, taking into account the effect of the spin-spin coupling, this assignment is more or less tentative; a detailed and more reliable assignment of these protons could be obtained by using some deuterated compounds and spectrum simulation.

As may be seen from Table 1, the chemical shifts between the CH_3 and $CH_2(2)$ groups in the cases of ΔE_g=440 cal/mol and 600 cal/mol are 0.180 and 0.210 ppm respectively, and those between the CH_3 and $CH_2(3)$ groups in the cases of ΔE_g=440 and 600 cal/mol are 0.140 and 0.170 ppm respectively. The quantitative agreement between the observed and the calculated values is not good. As to the temperature dependence of the chemical shift, it is found that the sign of the slope of the chemical shift of the $CH_2(3)$ group calculated using 440 cal/mol as ΔE_g coincides with that observed, while those of the CH_3 and $CH_2(2)$ groups do not, and that those of the CH_3, $CH_2(2)$ and $CH_2(3)$ groups derived by taking 600 cal/mol as ΔE_g coincide with those observed. Thus, the results calculated for 600 cal/mol agree with the observed values better than those calculated for 440 cal/mol in neat liquid. This is natural because 440 cal/mol for ΔE_g is the value calculated in an isolated n-pentane molecule. From these calculations, it may be seen that the slopes of the chemical shifts against the temperature depend on the magnitude of ΔE_g. For discussing the slope and ΔE_g, we plotted the observed and calculated chemical-shift differences between the CH_3 and $CH_2(2)$ groups ($\Delta\sigma_{CH_3-CH_2(2)}$) and the CH_3 and $CH_2(3)$ ($\Delta\sigma_{CH_3-CH_2(3)}$) against the temperature in Fig. 7. This figure also shows that 600 cal/mol is better than 440 cal/mol for ΔE_g. The

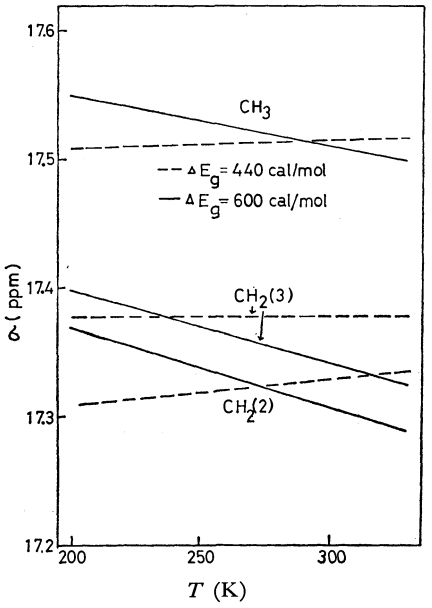

Fig. 6. The temperature dependence of the sum of the diamagnetic and the bond anisotropy terms used 440 and 600 cal/mol as ΔE_g.

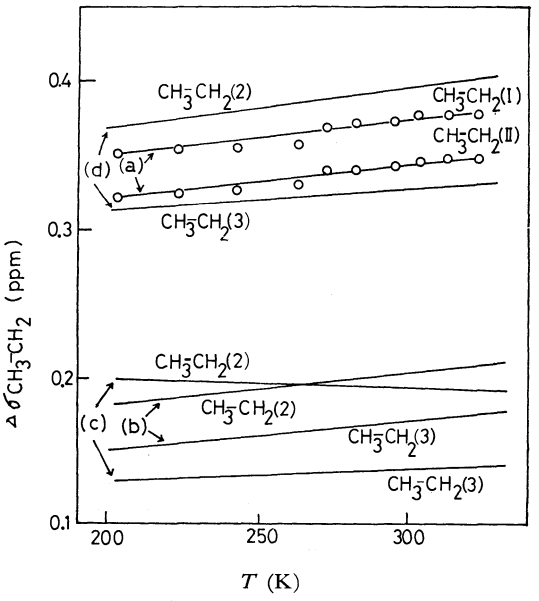

Fig. 7. The temperature dependence of the chemical shift difference between the CH_3 and CH_2 (2) groups.
(a) observed. (b) calculated with 440 cal/mol and (c) 600 cal/mol for ΔE_g, and 5.5×10^{-30} cm^3 for $\Delta\chi_{C\text{-}C}$. (d) calaclated with 570 cal/mol for ΔE_g and 9.1×10^{-30} cm^3 for $\Delta\chi_{C\text{-}C}$.

18) This peak splits more clearly in benzene, pyridine and α-chloronaphthalene than in this case (neat liquid).

best-fitting calculated slope to the observed one can be obtained by taking 570 cal/mol for ΔE_g, as is shown in Fig. 7(c), but the quantitative agreement between the chemical shifts observed and calculated is not satisfactory. The discrepancy may be caused by our choice of the value of $\Delta\chi_{C-C}$. As may be seen from Figure 8, the observed chemical shift differences $\Delta\sigma_{CH_3-CH_2}$ $(=\sigma_{CH_3}-\sigma_{CH_2})$ can be fitted by choosing 8.5—9.7×10^{-30} cm^3 as $\Delta\chi_{C-C}$. Thus, using 9.1×10^{-30} cm^3 at its averaged value of $\Delta\chi_{C-C}$ and 570 cal/mol as ΔE_g, the calculated temperature dependence

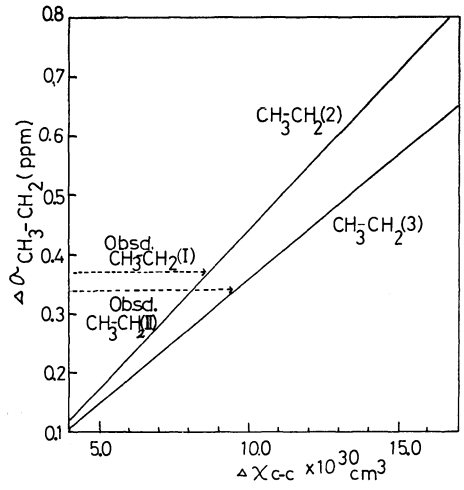

Fig. 8. The chemical shift dependences (CH_3–CH_2 (2) and CH_3–CH_2 (3)) on $\Delta\chi_{C-C}$. ----→: observed results.

of the chemical shift difference, $\Delta\sigma_{CH_3-CH_2}$, is shown in Fig. 7(d). It is found that the calculated results agree fairly well with the observed ones. However, the chemical-shift difference between the CH_2(2) and CH_2(3) groups disagrees slightly. We consider that this is partly due to the ambiguity of the assignment of the CH_2 (II) group. It is necessary to use some deuterated compounds and to simulate the NMR spectrum, taking the spin-spin coupling into account, in order to obtain a more reliable assignment. The above value of $\Delta\chi_{C-C}$, 9.1×10^{-30} cm^3, is near to the value, 10.0×10^{-30} cm^3, proposed by Moritz and Shappard.[11f] However, Homer and Callaghan[11] reported 7.26×10^{-30} cm^3 as the $\Delta\chi_{C-C}$ value of the magnetic anisotropy, but neglected the effect of electron density. If we neglect the contribution of the diamagnetic effect in order to fit the observed results with the calculated ones, we obtain 7.0×10^{-30} cm^3 as $\Delta\chi_{C-C}$. This value is nearly equal to that proposed by Homer and Callaghan. However, we consider that it is better to adopt 9.1×10^{-30} cm^3 as $\Delta\chi_{C-C}$ in *n*-pentane because the diamagnetic contribution to the chemical shift depends upon the conformation.

The authors gratefully acknowledge the helpful comments made by Dr. N. Nakagawa of the University of Electro-Communication and by Dr. T. Yonemoto of the Electrotechnical Laboratory, and the use of the program of the CNDO/2 method made by Dr. T. Hirano of the University of Tokyo.

BULLETIN OF THE CHEMICAL SOCIETY OF JAPAN, VOL. 46, 1045—1048 (1973)

The Crystal and Molecular Structure of *meso*-2,4-Pentanediol Borate

Shunsuke KURIBAYASHI

Government Industrial Research Institute, Osaka, Midorigaoka, Ikeda

(Received April 12, 1972)

The crystals of *meso*-2,4-pentanediol borate are monoclinic with a space group of C2/c. There are eight molecules in the unit cell with dimensions of: $a=15.36$, $b=13.53$, $c=7.68$ Å, and $\beta=113.3°$. The crystal structure was determined by the X-ray method. The final discrepancy index is 0.121 for 1030 non-zero reflections. The molecule has a six-membered ring composed of one boron, three carbon, and two oxygen atoms. The borate group and the two carbon atoms of the pentane group are nearly co-planar. The five carbon atoms are also co-planar, and they are in *trans* positions. The molecule was proved to be of the *meso* type.

In the course of our investigation of model compounds of polymers, the molecular and crystal structure of 2,4-pentanediol seemed of great interest for us as a model compound for polyvinyl alcohol.

As has been reported earlier,[1,2] chemically-synthesized 2,4-pentanediols are composed of three components, of the *meso*, *d*, and *l* types. They are separated into two components by column chromatography; one of them is assumed to be of the *meso* form, and the other, of the racemic form.

When eluted by chromatography, the compounds are separated in a form of borate. The present paper will report the crystal and molecular structure of *meso*-2,4-pentanediol borate.

Experimental

The sample was prepared by a method reported earlier.[1] The crystals are monoclinic and colorless. They crystallize in the form of needles elongated along the *c*-axis or in a lozenge shape. The cell dimensions were determined by the method of least-squares for a *c*-axis oscillation photograph, using Si powder as the standard. The systematic

1) M. Shiraki and E. Nagai, *Nippon Kagaku Zasshi*, **81**, 976 (1960).

2) E. Nagai, S. Kuribayashi, M. Shiraki, and M. Ukita, *J. Polym. Sci.*, **35**, 295 (1959).

TABLE 1. CRYSTAL DATA

$C_5O_3BH_{11}$	Systematic absences
$a=15.36$ (6) Å	of the reflections
$b=13.53$ (2)	$h+k=2n+1$ for $h\,k\,l$
$c=7.68$ (6)	$l=2n+1$ for $h\,0\,l$
$\beta=113.3$ (4)°	$\rho_c=1.17$ g·cm^{-3}
Mol. wt. 129.	$\rho_0=1.17$—1.19 g.cm^{-3}
$Z=8$	mp 87°C
Space group C2/c	
V=1465 Å^3	

absences showed that the space group was C2/c or Cc. The former was chosen on the basis of the Wilson statistics. The measured density was about 1.17—1.19, which is in good agreement with the density calculated assuming that the unit cell contains eight molecules. It was difficult to determine the accurate density of the crystal by the ordinary flotation method, as this compound is very hygroscopic and is easily dissolved in nearly all kinds of solvents. The crystal data are shown in Table 1.

Multiple-film equi-inclination Weissenberg photographs were taken about the c-axis, with Ni-filtered Cu$K\alpha$ radiation from zero to the sixth layer. Oscillation and precession photographs were also taken about the b-axis using Zr-filtered Mo$K\alpha$ radiation; they were used mainly for the scaling of the structure amplitudes obtained from the Weissenberg photographs. The intensities were estimated visually by comparison with a standard scale prepared by the same crystal. They were corrected for the Lorentz, polarization, and spot-shape factors. No absorption correction was made. 1030 non-zero structure factors were obtained by these procedures.

Structure Determination

A Patterson projection along the c-axis and a consideration of the packing offered us effective clues for analyzing the structure. Reflections with $l=2n$ are generally stronger than those with $l=2n+1$. Especially, the $\bar{3}12$ and $\bar{2}02$, reflections are extremely strong. From these facts, a trial structure was deduced; it was then refined by the Fourier method in the (001) projection. By these procedures, the discrepancy index, R, became 0.217 for $F(h\ k\ 0)$. At this stage, the z parameters were introduced for every atom, on the assumption that the planar molecule lies nearly on the $(\bar{3}12)$ plane. The block-diagonal least-squares method with isotropic temperature factors was applied, using a program written by N. Yasuoka for the OKITAC 5090 C. After 6 cycles of iterations, the discrepancy index, R, for all the observed reflections decreased from 0.253 to 0.179. Then, a block-diagonal least-squares procedure with anisotropic temperature factors was applied on a TOSBAC 3400-41 using a program, HBLS IV, written by T. Ashida.[3] The function to be minimized was $\Sigma w\Delta^2$, where the weighting scheme used was:

$w=(25.0/|F_o|)^2$ for $|F_o|\geq 25.0$

$w=1$ for $25.0>|F_o|\geq 5.0$, and

$w=0.2$ for $|F_o|<5.0$

After five cycles of interactions, the R factor decreased to 0.134.

With these positional parameters and temperature factors, a difference Fourier map was synthesized, but hydrogen atoms were not found clearly in this map. Therefore, the co-ordinates of hydrogen atoms were assumed to have C–H bond lengths of 1.09 Å and bond angles of 109.5°. They were included in the structure-factor calculation, and the R value was reduced to 0.121. The final atomic co-ordinates and temperature factors, with their estimated standard deviations, are shown in Tables 2 and 3. A list of

TABLE 2. POSITIONAL PARAMETERS IN FRACTIONAL CO-ORDINATES AND ESTIMATED STANDARD DEVIATIONS (in Å)

Atom	x/a	$\sigma(x)$	y/b	$\sigma(y)$	z/c	$\sigma(z)$
C (1)	0.0941	0.009	0.2525	0.007	0.0319	0.009
C (2)	0.1378	0.008	0.1772	0.007	0.1904	0.009
C (3)	0.2439	0.007	0.1671	0.006	0.2632	0.007
C (4)	0.2805	0.008	0.0833	0.008	0.4047	0.008
C (5)	0.3854	0.008	0.0633	0.008	0.4802	0.009
O (1)	0.0934	0.004	0.0811	0.003	0.1222	0.004
O (2)	0.2319	0.004	−0.0081	0.004	0.3235	0.004
O (3)	0.0976	0.004	−0.0930	0.003	0.1285	0.004
B	0.1414	0.006	−0.0047	0.007	0.1932	0.006

TABLE 3. ANISOTROPIC TEMPERATURE FACTORS OF NONHYDROGEN ATOMS IN THE FORM $\exp\{-10^{-4}\times(h^2\beta_{11}+k^2\beta_{22}+l^2\beta_{33}+hk\beta_{12}+hl\beta_{13}+kl\beta_{23})\}$.
Their estimated standard deviations are given in parenthesis.

Atom	β_{11}	β_{22}	β_{33}	β_{12}	β_{13}	β_{23}
C (1)	128 (6)	63 (4)	383 (24)	−5 (4)	36 (10)	35 (8)
C (2)	86 (5)	73 (5)	466 (26)	−14 (4)	45 (9)	−26 (9)
C (3)	74 (4)	81 (4)	291 (18)	−15 (3)	64 (7)	5 (7)
C (4)	82 (5)	100 (6)	391 (23)	−12 (4)	20 (8)	7 (10)
C (5)	71 (4)	131 (7)	423 (25)	−21 (5)	43 (8)	−20 (11)
O (1)	62 (2)	49 (2)	229 (10)	−9 (2)	31 (3)	−2 (3)
O (2)	64 (2)	66 (2)	234 (9)	−10 (2)	18 (3)	−0 (4)
O (3)	62 (2)	50 (2)	260 (11)	−5 (2)	33 (4)	6 (4)
B	55 (3)	58 (3)	158 (13)	−2 (3)	41 (5)	6 (7)

3) "Universal Crystallographic Computation Program System," ed. by Tosio Sakurai, Crystallographic Society of Japan, Tokyo (1967).

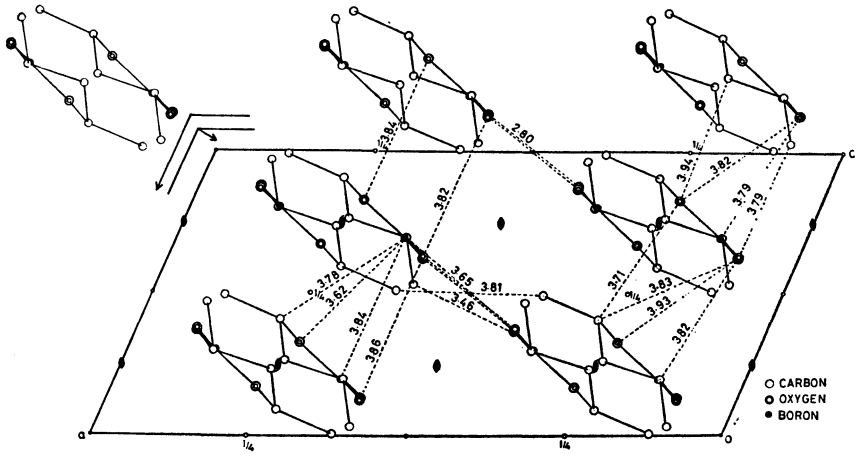

Fig. 1. The crystal structure projected onto the ac plane, with some distances shorter than 4.0 Å.

the observed and calculated structure factors is given in Table 6.[4]

Results and Discussion

The crystal structure projected along the b- and c-axes is shown in Figs. 1 and 2. The molecular structure is shown in Figs. 3 and 4. In Table 4, the bond lengths and angles are listed. As was assumed in the earlier report,[5] the five carbon atoms are in a *trans* position and the molecule is of the *meso* type.[1,2]

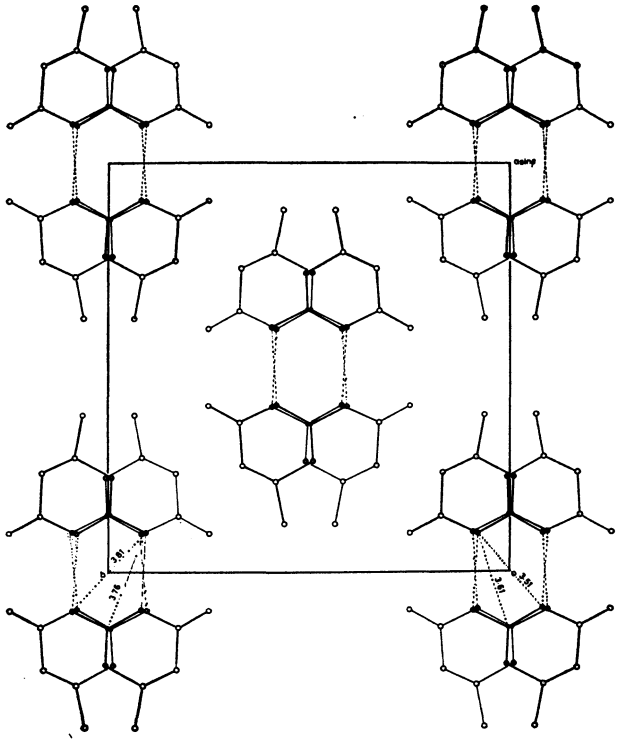

Fig. 2. The crystal structure projected onto ab plane, with some distances shorter than 4.0 Å. The broken lines which connect two oxygen atoms indicate the hydrogen bonds.

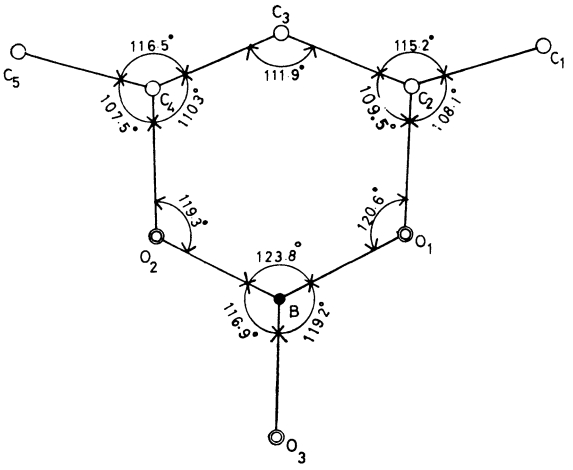

Fig. 3. The molecular shape looking along the direction normal to the molecular plane. The bond angles are also shown.

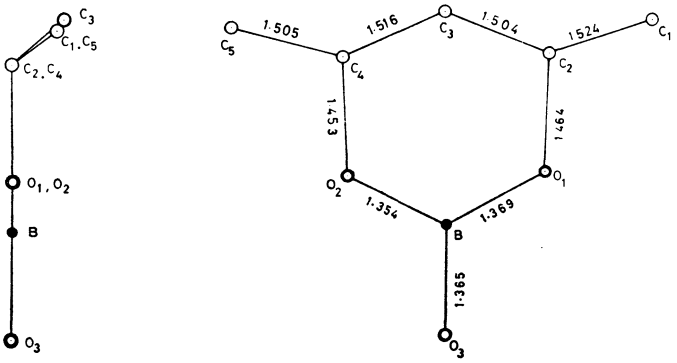

Fig. 4. The molecular shape looking along the direction normal to the molecular plane and the side view, with bond lengths.

All the C–C bond lengths (mean value, 1.51 Å) are a little shorter than the ordinary single bond, and the corresponding length in *dl*-2,4-pentanediol diacetate is 1.52 Å.[6] The C–O bond distances are very close to the values found in various compounds. The B–O bond lengths are the same as those observed

4) Table 6 has been submitted to, and is kept by the office of the Chemical Society of Japan, 1–5 Kanda Surugadai, Chiyoda-ku, Tokyo. (Document No. 7310).

5) S. Kuribayashi, This Bulletin, **39**, 2784 (1966).

6) K. Tichý, *Acta Crystallogr.*, **20**, 865 (1966).

TABLE 4. COVALENT BOND LENGTHS (Å) AND ANGLES (°)
Estimated standard deviations are given in parenthesis.

Bond	Length	Bond angles	
C (1) - C (2)	1.524 (10)	C (1) - C (2) - C (3)	115.2 (0.7)
C (2) - C (3)	1.504 (10)	C (2) - C (3) - C (4)	111.9 (0.6)
C (3) - C (4)	1.516 (10)	C (3) - C (4) - C (5)	116.5 (0.7)
C (4) - C (5)	1.505 (11)	C (1) - C (2) - O (1)	108.1 (0.5)
C (2) - O (1)	1.464 (7)	C (3) - C (2) - O (1)	109.5 (0.5)
C (4) - O (2)	1.453 (8)	C (5) - C (4) - O (2)	107.5 (0.6)
O (1) - B	1.369 (7)	C (3) - C (4) - O (2)	110.3 (0.5)
O (2) - B	1.354 (6)	C (2) - O (1) - B	120.6 (0.4)
C (3) - B	1.365 (7)	C (4) - O (2) - B	119.3 (0.5)
		O (1) - B - O - (2)	123.8 (0.5)
		O (1) - B - O (3)	119.2 (0.4)
		O (2) - B - O (3)	116.9 (0.5)

for H_3BO_3 and HBO_2.[7,8] The C(1)–C(2)–C(3) and C(3)–C(4)–C(5) bond angles are remarkably larger than those found for ordinary aliphatic compounds. Similar results have been also reported for *dl*-2,4-pentanediol diacetate.[6] The five carbon atoms are nearly co-planar, but C(3) is a little apart from this plane in the direction opposite of that for C(1) and C(5). This plane is expressed by the equation:

$$-0.1549x + 0.6848y + 0.7151z = 2.3405,$$

where x, y, and z are in Å units with repect to the crystallographic axes. The C(2), C(4), O(1), O(2), O(3), and B atoms are also co-planar. The equation of this plane is:

$$-0.6959x - 0.0085y + 0.9349z = -0.1248.$$

As can easily be realized from the co-efficients of the equation, this plane is nearly parallel to the b-axis. The deviations of atoms from these planes are listed in Table 5. The boron atom is surrounded by three oxygen atoms, which form an almost equilateral triangle about the boron.

TABLE 5. DEVIATION OF EACH ATOM FROM PLANES
Plane (I) (five carbon atoms)
Plane (II) (C(2), C(4), O(1), O(2), O(3) and B)

Atom	Deviation (Å)	Atom	Deviation (Å)
C (1)	−0.0488	C (2)	−0.0016
C (2)	0.0198	C (4)	0.0228
C (3)	0.0741	O (1)	−0.0056
C (4)	−0.0121	O (2)	−0.0312
C (5)	−0.0329	O (3)	0.0151
		B	0.0006

Surrounding the center of symmetry, two molecules are linked together by hydrogen bonds. The hydrogen-bond distances are 2.80 Å. The van der Waals distances shorter than 4.0 Å are shown in Figs. 1 and 2. The nearest intermolecular B–B and B–O distances are 3.84 and 3.61 Å respectively. These values are a little longer than the shortest distances found for H_3BO_3 and HBO_2.[7,8] The bond lengths, bond angles, van der Waals distances, and coefficients of the best planes were computed by means of a program written by T. Sakurai for the UNICS.[3]

The author wishes to express his thanks to Dr. T. Ashida, Dr. T. Sakurai, and Dr. N. Yasuoka for providing him with computing facilities. The author is also indebted to Dr. M. Shiraki for supplying the sample.

7) W. H. Zachariasen, *Acta Crystallogr.*, **16**, 385 (1963).
8) W. H. Zachariasen, *ibid.*, **7**, 305 (1954).

BULLETIN OF THE CHEMICAL SOCIETY OF JAPAN, VOL. 46, 1048—1053 (1973)

Mercury-Photosensitized Decomposition of Ethylbenzene

Hitoshi MIKUNI, Azuma TAKASE*, Motohiro MURANO** and Makoto TAKAHASI

Department of Pure and Applied Sciences, College of General Education, University of Tokyo, Komaba, Meguro-ku, Tokyo

(Received April 28, 1972)

The decomposition of ethylbenzene sensitized by $Hg(^3P_1)$ was studied in gas phase. Hydrogen, methane and ethane were obtained as the main gaseous products. Their rates of formation were determined as a function of the pressure of ethylbenzene or xenon. To decide whether methyl or ethyl radical is the primary product in the photolysis, ethylbenzene-β-d_1 was photolyzed. It was concluded that methyl radical is the primary product, since methane-d_1 and ethane-d_2 were obtained as products. A probable reaction mechanism is proposed to interpret the effect of pressure and light intensity on the rate of formation of ethane and methane. It is suggested that a biphotonic process is involved, which can explain the fact that the rate of formation of ethane is proportional to the square of light intensity.

Studies on the decomposition of organic compounds by excited mercury atoms have been reported by many authors.[1] The mechanism of the reaction is generally classified into two types; (a) the abstraction of hydrogen atom by excited mercury atom as found in the decomposition of alkanes, and (b) the excitation transfer from excited atoms to organic compounds as in the decomposition of unsaturated compounds such as ethylene and butenes. In (b), the acceptor compound should have its triplet state below the level of $Hg(^3P_1)$.

* Present Address: Sanyo Chemical Industry Co., Ltd.
** Present Address: Sony Co., Ltd.

1) R. J. Cvetanović, "Progress in Reaction Kinetics," Vol. 2, Pergamon Press, London (1964), p. 39.

Unsaturated compounds generally have larger cross sections than saturated ones. Until recently, the formation of triplet state of unsaturated compounds by mercury-sensitization was only presumed from the spin conservation rule and relatively long lifetime of the intermediate. Recently Burton and Hunzicker[2] gave direct evidence of the formation of triplet benzene and toluene by excitation transfer from $Hg(^3P_0)$, by means of modulation type kinetic spectroscopy. However, not many studies have been made on the mercury-sensitized decomposition of aromatic compounds, probably due to their low vapor pressure, and details of the mechanism have not been clarified yet. Scott and Steacie[3] reported the mercury-photosensitized reaction of benzene, and Sehon and Darwent[4] proposed a mechanism involving two types of excited toluene in the reaction of toluene with $Hg(^3P_1)$. Hentz and Burton[5] studied the photochemistry of toluene, mesitylene and ethylbenzene in comparison with radiation chemistry. The present authors[6] reported preliminary results of mercury photosensitized decomposition of ethylbenzene. Yamamoto *et al.* also photolyzed ethylbenzene with mercury and investigated the reaction products.[7] We report herewith on the study of mercury-photosensitized decomposition of ethylbenzene, taking into consideration the effects of pressure of ethylbenzene and xenon and light intensity on the rate of formation of gaseous products. Since the compound has both alkyl and phenyl groups in one molecule, it may be interesting to decide whether abstraction of hydrogen or excitation transfers reaction plays the more important role in a single molecule in mercury-photosensitized decomposition.

Experimental

Materials. Commercial ethylbenzene was purified by gas chromatographic separation through a DOP column, dried with sodium and distilled in a reaction cell. Ethylbenzene-β-d_1 was prepared from 2-phenylethyl bromide by the Grignard reaction with deuterium oxide of 99.9% isotopic purity, and fractionated by gas chromatography. No impurity was found either in ethylbenzene or ethylbenzene-β-d_1 by FID through the DOP column. Isotopic purity of ethylbenzene-β-d_1 was determined to be about 90% by reduced ionization voltage technique of mass spectrometer. Xenon (Takachiho Co.) was used without further purification.

Apparatus. We constructed a low pressure spiral type mercury lamp, its light intensity being determined occasionally by mercury-photosensitized decomposition of propane, and found to be $9.7—12\times10^{15}$ photon/sec. Variation in lamp intensity in a series of experiments was small. A slight gradual decrease of absorbed light was due to the decrease of transparency of the quartz window of the reaction cell caused by the deposition of reaction products. The reaction cell, a cylindrical one of 1 cm length and 5 cm diameter and connected to a glass bulb of 500 ml was placed in an electric furnace with temperature regulated to ±1°C. A filter (Toshiba UVD 25) placed in front of the reaction cell removed 184.9 nm light. The pressure of ethylbenzene was measured with a glass Bourdon gauge outside the furnace. Ethylbenzene with mercury vapor was circulated with a glass fan and a mercury booster pump. The pressure of mercury was not determined, but was presumed to be fairly high from the temperature of the furnace. Two metal valves are fitted to the inlet and outlet parts of the reaction system. In order to control incident light intensity, single or double blackened gauzes were inserted in front of the reaction cell. Transmission of the gauze was calibrated both by spectrophotometry and actinometry with mercury-photosensitized decomposition of propane. Both methods gave almost the same ratios of transmission.

Analysis of Reaction Products. After irradiation, the reaction mixture was passed through two helical traps kept at -196 °C. Hydrogen and methane were collected in Toepler gauge, and the combined amount of hydrogen and methane was measured first. Hydrogen was oxidized to water in copper oxide combination tube at 300 °C, and unoxidized gas was assumed to be methane. Ethane was pumped out by warming the traps up to -140 °C with a refrigerant mixture. In the quenching experiment with Xe, the quantitative determination of ethane was carried out by gas chromatography with FID, but the amounts of methane and hydrogen were not determined.

Results and Discussion

Long Irradiation Experiment and Direct Photolysis of Ethylbenzene. The rate of decomposition of ethylbenzene with mercury at 253.7 nm at room temperature is too small to be measured. Reactions at 150—300 °C gave hydrogen, methane and ethane as main products of low boiling point with a small amount of propane, but no ethylene was detected. The formation of toluene and styrene was confirmed by gas-chromatography, but not conclusive. Yamamoto *et al.*[7] reported on the formation of benzene, toluene, isopropylbenzene, bibenzyl, and 1,2-diphenylpropane, but not styrene. A detailed comparison of the present results with theirs may be not appropriate, since the experimental conditions differ. However, as far as gaseous products are concerned, qualitative results of both experiments seem to be in good agreement. In Fig. 1, the rates of formation of hydrogen, methane and ethane (R_{H_2}, R_{CH_4}, $R_{C_2H_6}$[8]) are plotted against irradiation time under 1.9 Torr of ethylbenzene at 150 °C. $R_{C_2H_6}$ is constant for 3 hr, and R_{CH_4} is also almost constant irrespective of time. It seems that R_{H_2} decreases gradually with time. This may be explained as being caused by internal scavenging by some unsaturated product as known in mercury-

2) C. S. Burton and H. E. Hunzicker, *Chem. Phys. Lett.*, **6**, 352 (1970).

3) E. J. Scott and E. W. R. Steacie, *Can. J. Chem.*, **29**, 233 (1951).

4) A. H. Sehon and B. deB Darwent, *J. Chem. Phys.*, **23**, 822 (1959).

5) R. R. Hentz and M. Burton, *J. Amer. Chem. Soc.*, **73**, 532 (1951).

6) A. Takase, M. Murano, H. Mikuni, and M. Takahasi, Preprints of International Conference on Photochemistry, Tokyo, (1965), p. 39.

7) Y. Yamamoto, S. Takamuku, and H. Sakurai, This Bulletin, **44**, 574 (1972).

8) $R_{C_2H_6}$ is proportional to the square of light intensity. Thus, we use rate instead of quantum yield. The apparent quantum yield of ethane at 2 Torr of ethylbenzene, 1.2×10^{16} photon and 150 °C is 0.04.

photosensitized decomposition of alkanes.[9] However, since our result on styrene formation was not conclusive, it is left for future investigation.

It was confirmed that no pure thermal reaction of ethylbenzene took place up to 300°C. Since ethylbenzene has an absorption band below 270 nm, the direct photolysis of ethylbenzene may be involved to some extent in the mercury-photosensitizing reaction system. Although quantitative determination of the relative amounts of light by mercury and ethylbenzene is not possible, the amount of light absorbed directly by ethylbenzene is presumed to be much less than that by mercury. For the sake of comparison, ethylbenzene of 10 Torr was photolyzed at 25°C in the reaction system where the contamination of mercury vapor was carefully avoided. It was found that $R_{C_2H_6}$ was 0.93×10^{-10} mol/sec, fairly less than the value 5.7×10^{-10} mol/sec obtained in the mercury photosensitizing reaction system (Fig. 1). Hentz and Burton[5] reported the rough quantum yields of gaseous products in the direct photolysis of ethylbenzene to be the order of 10^{-4}. We may presume that the mercury photosensitizing reaction predominates in the present reaction system, but we can not eliminate completely the possibility of involvement of direct photolysis.

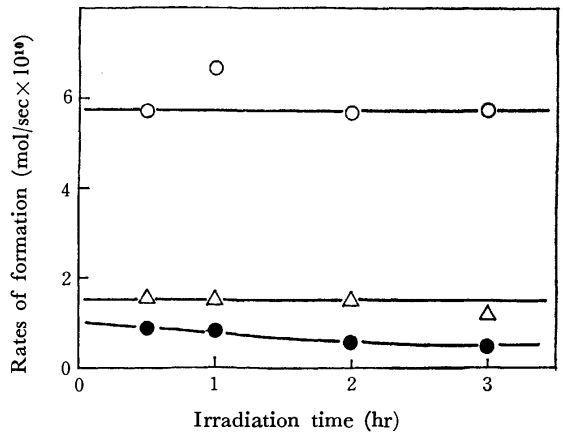

Fig. 1. The variations of $R_{C_2H_6}$, R_{CH_4} and R_{H_2} with irradiation time.
○ ethane, △ methane, ● hydrogen.

Except for long irradiation experiments, we carried out our experiments keeping the conversion below 10% to avoid complication of internal scavenging.

Mercury-Photosensitized Decomposition of Ethylbenzene-β-d_1. In order to decide whether methyl or ethyl radical is the primary reaction entity to give ethane, ethylbenzene-β-d_1 was irradiated for 3 hr at 150°C under pressure of 2 Torr of ethylbenzene-β-d_1. The mole ratios of deuterium substituted methanes and ethanes were determined by mass spectrometry. The results are given in Table 1.

TABLE 1. MOLE RATIOS OF DEUTERIUM SUBSTITUTED METHANES AND ETHANES PRODUCED BY MERCURY-SENSITIZED PHOTOLYSIS OF ETHYLBENZENE-β-d_1

CH_4	CH_3D	C_2H_6	C_2H_5D	$C_2H_4D_2$
15	85	0	20	80

It is seen that the main primary product in the reaction is methyl radical considering the following reaction scheme.

$$C_6H_5CH_2CH_2D(\text{excited}) \rightarrow C_6H_5CH_2\cdot + CH_2D\cdot$$
$$CH_2D\cdot + C_6H_5CH_2CH_2D \rightarrow CH_3D + C_6H_5\dot{C}HCH_2D$$
$$2\ CH_2D\cdot \rightarrow CH_2DCH_2D$$

The presence of about 20% C_2H_5D in the products can be explained by the reaction of undeuterated ethylbenzene contained in the reactant.

Effect of Pressure of Ethylbenzene and Xenon on $R_{C_2H_6}$, R_{CH_4} and R_{H_2}. The effect of pressure of ethylbenzene on $R_{C_2H_6}$, R_{CH_4} and R_{H_2} was investigated at 150°C. The variable range of pressure of ethylbenzene was limited in a narrow range due to its low vapor pressure, but we see that a maximum exists in $R_{C_2H_6}$ at 1 Torr, but no maximum for R_{CH_4} and R_{H_2} (Fig. 2). Sehon and Darwent[4] observed a similar maximum in the quantum yield of hydrogen at 2 Torr, but no maximum for methane and ethane in the mercury-photosensitized decomposition of toluene. An interpretation of the decrease of the rates of formation below 1 Torr may not be so simple, as Cvetanović pointed out.[1] The incomplete quenching of excited mercury atom by ethylbenzene and/or the inefficient absorption of radiation due to the decrease of pressure broadening[10] might cause the fall-off. The decrease of $R_{C_2H_6}$ above 1 Torr is understood in terms of the collisional deactivation of excited ethylbenzene of relatively long lifetime by normal ethylbenzene as proposed in the case of ethylene[11] and toluene.[4] A good linearity was obtained by plotting $1/R_{C_2H_6}{}^{1/2}$ against pressure of ethylbenzene, although the pressure is

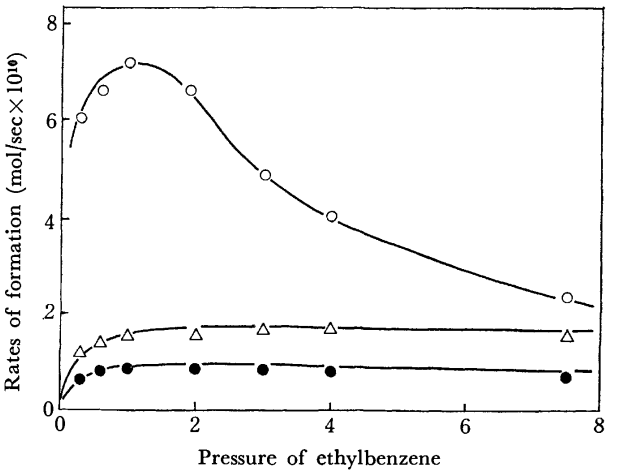

Fig. 2. The variations of $R_{C_2H_6}$, R_{CH_4} and R_{H_2} in terms of pressure of ethylbenzene.
○ ethane, △ methane, ● hydrogen.

9) See, for example, a) R. A. Back, *Can. J. Chem.*, **37**, 1834 (1959), b) K. R. Jennings and R. J. Cvetanović, *J. Chem. Phys.*, **35**, 1233 (1961).

10) K. Yang, *J. Amer. Chem. Soc.*, **86**, 3941 (1964).

11) A. B. Callear and R. F. Cvetanović, *J. Chem. Phys.*, **24**, 873 (1956).

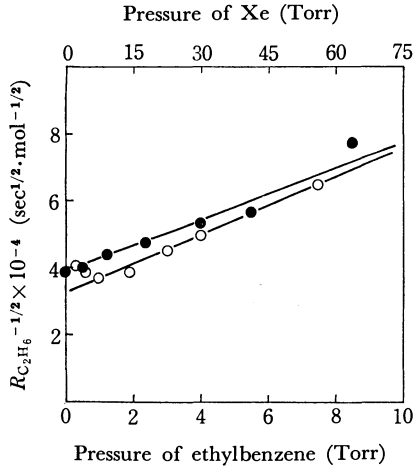

Fig. 3. Plots of $R_{C_2H_6}^{-1/2}$ against pressure of ethylbenzene and Xe.
○ for change of pressure of ethylbenzene. ● for change of pressure of Xe.

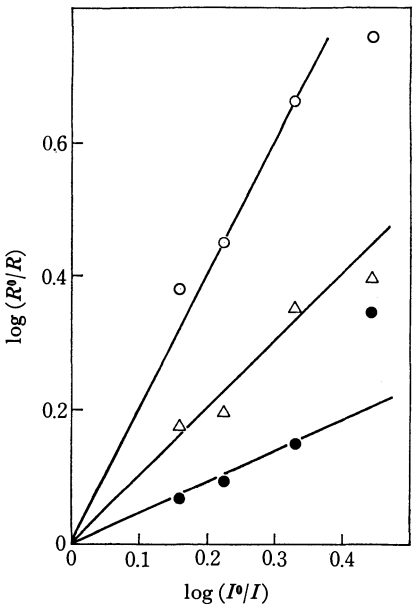

Fig. 4. The dependence of $R_{C_2H_6}$, R_{CH_4} and R_{H_2} against light intensity in log–log plot.
○ ethane, △ methane, ● hydrogen.

limited to a narrow range. We investigated the effect of pressure of Xe on $R_{C_2H_6}$ up to 66 Torr, keeping the pressure of ethylbenzene at 2.0 Torr at 150 °C. A good linearity was also obtained between $1/R_{C_2H_6}$ and the pressure of Xe, as shown in Fig. 3. The fact that $R_{C_2H_6}$ decreased with the increase of the pressure of ethylbenzene or of Xe indicates that the concentration of methyl radical decreased with the increase of pressure of these quenching substances. R_{CH_4} is almost constant above 1 Torr of ethylbenzene. This might be qualitatively interpreted by considering the compensation of the decrease of methyl radical concentration by the increase of ethylbenzene (see equation (3)). The behavior of R_{H_2} against the pressure of ethylbenzene is apparently similar to that of R_{CH_4}, but the mechanism of hydrogen formation may be more complicated.

Dependence of $R_{C_2H_6}$, R_{CH_4} and R_{H_2} on Light Intensity. $R_{C_2H_6}$, R_{CH_4} and R_{H_2} were measured at 150 °C at 2 Torr of ethylbenzene, varying the light intensity with blackened copper gauzes. When log R^0/R is plotted against log I^0/I, where R^0 and I^0 are the reaction rate and light intensity, respectively, without gauze, a good linearity for $R_{C_2H_6}$, R_{CH_4} and R_{H_2} each is obtained. Each slope gives 2 for ethane, 1 for methane and 0.5 for hydrogen. The findings that $R_{C_2H_6}$ is proportional to square of light intensity and that R_{CH_4} is proportional to light intensity suggest that some biphotonic process may be involved.

Many studies have been reported[12] on photophysical and photochemical processes by flash technique involving biphotonic processes. However, even in steady irradiation experiments with usual lamps several studies[13a-d] indicate the participation of some biphotonic process. Strausz and Gunning[13d] reported that in the mercury-photosensitized decomposition of carbon dioxide at 253.7 nm the rate of decomposition of carbon dioxide is proportional to the square of light intensity. Considering that the mechanism of formation of ethane is most simple in the present system, we will discuss mainly the mechanism of formation of methyl radical. In order to interpret result where $R_{C_2H_6}$ is proportional to the square of light intensity, the following three mechanisms are considered for a possible biphotonic process to produce methyl radicals.

$Hg + h\nu \rightarrow Hg^*$	I_a	common to all three processes below
$Hg^* \rightarrow Hg + h\nu$	k_2	
$Hg^* + E \rightarrow Hg + E^*$	k_3	
$E^* + E \rightarrow 2E$	k_4	
$E^* + Xe \rightarrow E + Xe$	k_5	
(a) $E^* + h\nu' \rightarrow E^{**}$ (triplet)		possible three processes
or		
(b) $E^* + Hg^* \rightarrow E^{**}$ (singlet or triplet) + Hg		
or		
(c) $E^* + E^* \rightarrow E^{**}$ (singlet or triplet) + E	k_6	
$E^{**} \rightarrow C_6H_5CH_2\cdot + CH_3\cdot$	k_7	common to all three processes
E^{**}(singlet) $\rightarrow E + h\nu''$	k_8	
$CH_3\cdot + CH_3\cdot \rightarrow C_2H_6$	k_9	
$CH_3\cdot + E \rightarrow CH_4 + C_6H_5\dot{C}HCH_3$	k_{10}	

(E is ethylbenzene)

At present, we have no conclusive evidence to select one mechanism from these three, but process (c) seems to be most suitable to interpret our experimental results. In process (2), T-T absorption of 253.7 nm

12) *Cf. e. g.*, "Photophysics of Aromatic Molecules," by J. B. Birks, John Wiley & Sons, (1970).

13) a) A. Terenin, "Recent Progress in Photobiology", ed. by E. J. Bowen, Oxford, 1965, p. 3, b) A. Proch, M. Djibelian and S. Sullivan, *J. Phys. Chem.*, **71**, 3378 (1967), c) B. Brocklehurst, W. A. Gibbons, F. T. Lang, G. Porter, and M. I. Savadatti, *Trans. Faraday Soc.*, **62**, 1793 (1966), d) O. P. Strausz and H. E. Gunning, *Can. J. Chem.*, **39**, 2244 (1961).

by triplet ethylbenzene is assumed. Burton and Hunzicker[2] reported the absorption spectra of triplet benzene and toluene formed by $Hg(^3P_0)$. T–T absorption spectrum of toluene covers the region 210—370 nm. A similar absorption spectrum can be expected for ethylbenzene. However, the amount of light absorbed by triplet ethylbenzene under our experimental conditions should be very small, considering the fact that our light source consists of atomic lines of a low pressure mercury lamp and that the molar extinction coefficient of triplet ethylbenzene may be much less than that of mercury. Assuming process (a) or (b), the rate equations in terms of pressure of ethylbenzene or Xe and light intensity were derived, but they were not in line with our experimental results. If process (c) is assumed, the following expression is derived.

$$R_{C_2H_6} = \frac{k_3^2 k_6 [E]^2 I_a^2}{(k_2 + k_3[E])^2 (k_4[E] + k_5[Xe])^2} \quad (2)$$

In this derivation we assumed that $k_4[E]+k_5[Xe] \gg k_6[E^{**}]$ and $[CH_3]^2 k_9 \gg [CH_3][E]k_{10}$. The first assumption may be justified if we consider that the quantum yields of ethane and methane are fairly small (less than 0.10). The second assumption is generally used in the competitive reactions of abstraction and recombination of methyl radical. We also neglected the radiative process of E**, but this is not essential in the interpretation of pressure and light dependence in the rate expression. The above expression is consistent with the results where $R_{C_2H_6}$ is proportional to the square of light intensity, and the linear relationship between $1/R_{C_2H_6}^{1/2}$ and pressure of ethylbenzene or Xe is satisfied. From the slope of the plot in Fig. 4, we can calculate k_4/k_5 to be about 39, indicating that ethylbenzene is much more efficient as a quencher than Xe. In a similar way, we can derive the following expression for R_{CH_4}.

$$R_{CH_4} = \frac{k_{10}}{k_4}\left(\frac{k_3 k_6}{k_9}\right)^{1/2} \frac{I_a[E]}{(k_2 + k_3[E])} \quad (3)$$

This is consistent with the experimental result where R_{CH_4} is proportional to light intensity and approaches a constant value at high pressure of ethylbenzene.

Comparison of the Rate of Formation of Methyl Radical with That of Hydrogen Atom. A comparison of excitation transfer process with hydrogen atom abstraction process might be of interest, if both processes actually take place in ethylbenzene. There can be no doubt that methyl radical formation proceeds through excited ethylbenzene, but the mechanism of hydrogen formation in the present system is not conclusive. For the formation of atomic hydrogen, the following two processes are possible, (a) abstraction of hydrogen atom from ethylbenzene by excited mercury atom, and (b) decomposition of excited ethylbenzene to produce hydrogen atom. At present, we have no evidence to differentiate the two processes from a consideration of our experimental results, and we therefore can not eliminate the possibility of simultaneous occurrence of excitation transfer process and abstraction process. We tentatively calculated the values $(R_{CH_4}+2R_{C_2H_6})/R_{H_2}$ under various pressures of ethylbenzene, considering the values may correspond to the ratio of rate of production of methyl radical to that of hydrogen atom. Since R_{CH_4} and R_{H_2} do not vary remarkably with pressure of ethylbenzene above 1 Torr (Fig. 2), the value $(R_{CH_4}+2R_{C_2H_6})/R_{H_2}$ mainly depends on the change of $R_{C_2H_6}$, which gradually increases with the decrease of pressure. We obtained the value of about 17 for the ratio in the pressure range 0.6—2 Torr.

The Effect of the Reaction Temperature on $R_{C_2H_6}$, R_{CH_4} and R_{H_2}. We investigated the change of $R_{C_2H_6}$, R_{CH_4} and R_{H_2} with respect to reaction temperatures 100—350 °C at constant light intensity. The pressure of ethylbenzene was kept at 2 Torr at each temperaute. $R_{C_2H_6}$ increases first up to 250 °C and begins to decrease above 250 °C, while R_{CH_4} increases gradually in the whole temperature range. The behavior of $R_{C_2H_6}$ is not completely understood, but its increase up to 250 °C indicates that the rate constant of decomposition of excited ethylbenzene (k_7) is dependent on the reaction temperature, considering that the rate constant of recombination of methyl radicals is almost independent of temperature. Although the amounts of energy contained in E* and E** are not known, it is rather surprising that the decomposition of E** is dependent on temperature, since the bond energy of $C_6H_5CH_2$–CH_3 is reported to be only 63 kcal/mol.[14] The amount of energy of E* must be in the range from the lowest triplet level of ethylbenzene (probably ~85 kcal/mol) up to 112 kcal/mol, which is the maximum amount of energy transferable from $Hg(^3P_1)$. The decrease of $R_{C_2H_6}$ above 250 °C may be partly interpreted by considering the increase of R_{CH_4} with temperature, but the fact that the sum of $2R_{C_2H_6}+R_{CH_4}$ still decreases above 250 °C is not understood yet.

In order to calculate the activation energy of hydrogen abstraction process by methyl radical from ethylbenzene, we derived the following equation by combining equations (2) and (3), assuming $E_9 \cong 0$

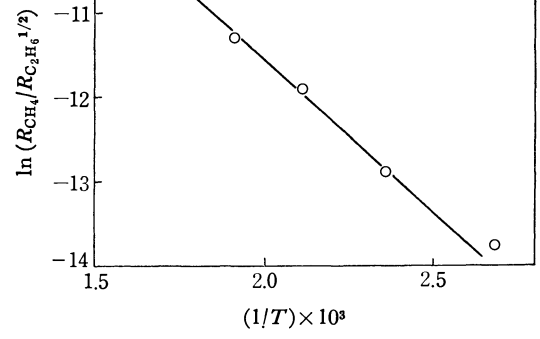

Fig. 5. Arrhenius plot of $R_{CH_4}/R_{C_2H_6}^{1/2}$ at a constant concentration of ethylbenzene in the temperature range from 100 to 350°C.

14) M. Szwarc, *J. Chem. Phys.*, **17**, 431 (1949).

$$R_{CH_4}/R_{C_2H_6}{}^{1/2}[E] = k_{10}/k_9,$$

or

$$\log k_{10}/k_9 = R_{CH_4}R_{C_2H_6}{}^{1/2}[E] = E_{10}/RT + \log A_{10} - \tfrac{1}{2}\log A_9$$

$\log k_{10}/k_9 = \log R_{CH_4}/R_{C_2H_6}{}^{1/2}[E] = E_{10}/RT + \log A_{10} - 1/2 \log A_9$. Thus, $R_{CH_4}/R_{C_2H_6}{}^{1/2}$ obtained keeping the pressure of ethylbenzene at 2 Torr at each temperature should be recalculated by dividing it by [E] at each temperature. The Arrhenius plot, recalculated log $R_{CH_4}/R_{C_2H_6}{}^{1/2}$ against $1/T$, gives a good linearity (Fig. 5). From the slope we obtained 7.1 kcal/mol for the activation energy of abstraction of methyl radical, comparable with the reported values of the abstraction of methyl radical from toluene, which are rather scattered as 7[15 a)], 7.3[b)], 9.5[c)] and 11.0[d)] kcal/mol according to the source of radicals and to the authors. It is found that R_{H_2} also depends on temperature, but since we cannot obtain a unique rate expression for R_{H_2}, we tentatively calculated an apparent activation energy from the Arrhenius plot of R_{H_2} which gives the value of 4.1 kcal/mol.

We would like to thank Mr. H. Horiguchi for valuable comments and also Mr. S. Hirano and Mr. M. Takakubo for their assistance in the experiments.

15) a) H. S. Taylor and J. O. Smith, *ibid.*, **8**, 543 (1940), b) R. E. Rebbert and E. W. R. Steacie, *ibid.*, **21**, 1723 (1953), c) M. Cher, *J. Phys. Chem.*, **70**, 877 (1966), d) M. Szwarc and J. S. Roberts, *Trans. Faraday Soc.*, **46**, 625 (1950).

BULLETIN OF THE CHEMICAL SOCIETY OF JAPAN, VOL. 46, 1053—1055 (1973)

The Temperature Dependence of the Nuclear Quadrupole Resonance of ^{35}Cl in $KClO_3$, $AgClO_3$, $Ba(ClO_3)_2 \cdot H_2O$, and $Cu(ClO_3)_2 \cdot 6H_2O$

Masahiko SUHARA

Department of Chemistry, Faculty of Science, Kanazawa University, Maru-no-uchi, Kanazawa

(Received May 8, 1972)

The nuclear quadrupole resonance (NQR) frequencies of ^{35}Cl in $KClO_3$, $AgClO_3$, $Ba(ClO_3)_2 \cdot H_2O$, and $Cu(ClO_3)_2 \cdot 6H_2O$ have been measured as a function of the temperature in the range from 77 to 350 K at a constant (atmospheric) pressure. These data have then been analyzed by the method of Brown. The torsional frequencies of the ClO_3^- ion in the crystals have been determined by fitting the experimental data with the Bayer theory, modified by taking into account the anharmonicity in torsional oscillation. The low barrier height obtained in Cu salt indicates that a freer rotational motion of the chlorate ion is to be expected in this crystal.

Many attempts have been carried out to investigate the torsional oscillation in crystals through the NQR experiments. One approach is to determine the torsional frequency by measuring the temperature and the pressure dependences of the NQR frequencies by means of the theoreis developed by Bayer,[1] Kushida,[2] and Kushida, Benedek and Bloembergen.[3] Another approach is to study the characteristics of the torsional or reorientational motion by measuring the NQR linewidth or the relaxation times as a function of the temperature.

The present investigation is of the former type. At lower temperatures, the Bayer theory (if there is a small torsional amplitude, so that the harmonic oscillation approximation is valid) gives a reliable torsional frequency in many cases, though not at very low temperatures. At higher temperatures, a large discrepancy appears between the theory and the experimental results. The purpose of the present work is to estimate the magnitude of the anharmonicity, using the quasi-harmonic approximation and assuning that the discrepancy originates from the anharmonic character of the torsional oscillation.

Experimental

The NQR signal was detected by means of a Kushida-type regenerative oscillator detector,[4] with a Zeeman modulation of an antisymmetric sinusoidal magnetic field of 30 Hz. The detected signals were suitably amplified by means of an audio-amplifier and automatically recorded on a chart (Hitachi Model QPD-33) through a lock-in-amplifier (NF Circuit Design Block Co., Model LI-572A). The resonance frequency was measured by means of pip marks at 1-kHz intervals on a chart which was generated by a frequency counter (Matsushita Communication Ind. Co., Model VP-0428). The details of the spectrometer system have been reported elsewhere.[5]

The accuracy in the frequency measurement is ± 0.1 kHz at the temperature of liquid nitrogen or at the freezing temperature of coolants, and is $\pm(0.2 \sim 0.1)$ kHz when the temperature is regulated by letting in cold nitrogen gas evaporated from the liquid-nitrogen container by heating it with a small heater. Combining with a chart-recorder voltmeter (Shimadzu Seisakusho, Ltd., Model A-521) for recording the junction voltage, a copper-constantan thermocouple was used to measure the temperature; it was affixed to the sample tube, which had been calibrated by the boiling temperatures of liquid nitrogen, benzene, and water,

1) H. Bayer, *Z. Physik*, **130**, 227 (1951).
2) T. Kushida, *J. Sci. Hiroshima Univ. Ser. A*, **19**, 327 (1955).
3) T. Kushida, G. B. Benedek, and N. Bloembergen, *Phys. Rev.*, **104**, 1364 (1956).
4) T. Cole, T. Kushida and H. C. Heller, *J. Chem. Phys.*, **38**, 2915 (1963).
5) M. Suhara, *Sci. Rep. Kanazawa Univ.*, **17**, 7 (1972).

the sublimation temperature of dry ice, and the triple point of water. The error in the temperature measurement was ±0.5 K, which causes an ambiguity in the resonance frequency of ±1 kHz.

The calculation of the best-fitting parameters in the theoretical equation was carried out by using a digital computer, FACOM 230-35, at Kanazawa University. The errors in the calculated parameters were estimated by assuming the condence coefficient to be 0.99.

The $AgClO_3$ was prepared by mixing hot aqueous solutions of 0.5 M of $AgNO_3$ and 0.5 M of $NaClO_3$, cooling the mixture in a refrigerator, filtering the crystals, and repeating the recrystallization. The sample must be kept in the dark. The $KClO_3$ and $Ba(ClO_3)_2 \cdot H_2O$ were commericial grade materials purified by repeating the recrystallization from hot water. The $Cu(ClO_3)_2 \cdot 6H_2O$ was obtained by mixing a hot aqueous solution of 1 M of $CuSO_4 \cdot 5H_2O$ and $Ba(ClO_3)_2 \cdot H_2O$, filtering off the $BaSO_4$ by means of No. 50 filterpaper, evaporating the blue filtrate at room temperature by a vacuum pump, filtering the crystals, and then repeating the recrystallization from cold water.

Results and Discussion

The NQR of ^{35}Cl in K, Ag, Ba, and Cu chlorates has been detected from 77 K to 350 K. The observed spectrum of each chlorates consists of a single line. This fact indicates that all the chlorate ions in a unit cell are located in crystallographically-equivalent positions; this could be expected from the crystal structure except for the Cu salt, whose structure has not been known. The resonances of the K and Ag salts were rather more intense than others throughout the temperature region examined.

The temperature dependence of the resonance frequency is shown in Fig. 1, together with the results of the previous works. The resonance frequencies of these four chlorates at the temperature of liquid nitrogen were in good agreement with the reported data, but at room temperature there was a large discrepancy between Moshier's results[6] and the present ones except in the case of K salt. When the temperature variation was repeated (by increasing or decreasing it), the temperature dependence showed a good reproducibility, so the phase transitions have not been detected in all the chlorates. The intensity of each line decreased with an increase in the temperature.

The experimental data were analyzed by the method of Brown,[7] in which the temperature dependence of the resonance frequency is represented by a polynomial of the form:

$$\nu(T) = a_0 + a_1 T + a_2 T^2 \qquad (1)$$

where:

$$a_0 = \nu_0$$
$$a_1 = -3ka_0/(4\pi^2 \nu_{t0}^2 \Theta)$$
$$a_2 = 2a_1 g$$

$\nu(T)$ and ν_0 are the NQR frequencies at T and 0 K respectively, Θ is a constant moment of inertia, and ν_{t0}, a torsional oscillation frequency. In this analysis,

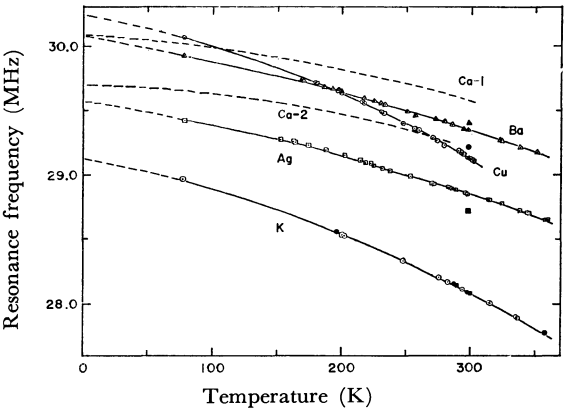

Fig. 1. Temperature dependence of the NQR frequencies of ^{35}Cl in several chlorates.
The quoted data are indicated by the corresponding solid symbols except Ca salt, for which the broken lines are used.

Chlorates	Literatures	
K	a, b, c, d, e	a) T. C. Wang, C. H. Townes, A. L. Schawlow, and A. N. Holden, *Phys. Rev.*, **86**, 809 (1952).
		b) H. Zeldes and H. Livingston, *J. Chem. Phys.*, **26**, 1102 (1957).
Ag	f	c) Ref. (3) in text.
		d) N. Negita and S. Saton, This Bulletin, **29**, 426 (1956).
Ba	f, g	e) P. J. Bray and R. G. Barnes, *J. Chem. Phys.*, **22**, 2023 (1954).
		f) Ref. (6) in text.
Cu	f, h	g) P. J. Bray and P. J. Ring., *J. Chem. Phys.*, **21**, 2226 (1953).
		h) P. J. Bray, *ibid.*, **23**, 703 (1955).
Ca	i	i) Ref. (9) in text.

a quasi-harmonic approximation for the anharmonic oscillation is used; the temperature variation in the torsional frequency is assumed to be:[8]

$$\nu_t = \nu_{t0}(1 - gT) \qquad (2)$$

with g a small positive constant. From the experimentally-determined values of a_0, a_1, and a_2, the values of ν_{t0} and g have been evaluated, using 83×10^{-40} g·cm² as the value of Θ. The results are summarized in Table 1. together with the values for Ca salt obtained by Kumar and Nageswara Rao.[9] The uncertainties in the g and ν_t values were $\pm 0.2 \times 10^{-4}$ K^{-1} and ± 2 cm^{-1} respectively. The a_1 values for the four chlorates are of the same order of magnitude, but the a_2 values for Ag and Ba salts are rather smaller than those of the others. On the other hand, the a_1 value in Ca salt is significantly smaller than those of the four chlorates, although the a_2 values lie in the middle between them. Since the values of a_0 in all the chlorates considered are 29~30 MHz, the difference in the coefficient, a_1, indicates the difference in the torsional frequency at 0 K, when all the chlorate ions have the same value of the moment of inertia. The torsional frequencies at 0 K and 300 K are also shown in Table 1.

6) R. W. Moshier, *Inorg. Chem.*, **3**, 199 (1964).
7) R. J. Brown, *J. Chem. Phys.*, **32**, 116 (1960).
8) I. Ichishima, *Nippon Kagaku Zassi*, **71**, 607 (1950)., A. A. Maradudin and R. F. Wallace, *Phys. Rev.*, **125**, 1277 (1962).
9) U. V. Kumar and B. D. Nageswara Rao, *Phys. Stat. Solid.*, **B44**, 203 (1971).

TABLE 1. VALUES OF THE FITTING PARAMETERS; a_0, a_1 AND a_2, AND CALCULATED VALUES; $\langle g \rangle$, ν_t AND V_0.

	$KClO_3$	$AgClO_3$	$Ba(ClO_3)_2 \cdot H_2O$	$Cu(ClO_3)_2 \cdot 6H_2O$	$Ca(ClO_3)_2 \cdot 2H_2O$[a]	
					ν_1	ν_2
a_0 (kHz)	29131.9 ±1.6	29576.6 ±4.0	30080.9 ±3.4	30241.5 ±3.2	30087.6 ±1.2	29699.5 ±1.3
a_1 (kHz/K)	−1.861 ±0.007	−1.584 ±0.015	−1.719 ±0.013	−1.768 ±0.013	−0.665 ±0.013	−0.211 ±0.015
a_2 (10^{-3} kHz/K^2)	−5.48 ±0.03	−2.80 ±0.05	−2.51 ±0.04	−6.51 ±0.05	−3.41 ±0.03	−4.67 ±0.04
$\langle g \rangle$ (10^{-4} K^{-1})	14.7	8.8	7.3	18.4	25.64	110.7
ν_t (cm^{-1}) 0 K	148	162	156	155	178	325
ν_t (cm^{-1}) 300 K	81	114	122	70	44[b]	—
V_0 (kcal/mol) 77 K	140	185	178	143	164[b]	19[b]
V_0 (kcal/mol) 300 K	56	106	122	39	15[b]	—

a) Ref. 9 in text.
b) Calculated from the results of Ref. 9 in text.

Using different assumptions and methods, the temperature dependence of the resonance frequency of ^{35}Cl in $KClO_3$ has been analyzed in various temperature regions by three authors.[3,10,12] The torsional frequency thus obtained has been compared with the room-temperature values[11] of the Raman lines; 54, 82, 98, 127, and 145 cm^{-1}.

From the present analysis, which differs from the above three the torsional frequency at room temperature, was found to be $\nu_t(300)=81$ cm^{-1}, which was in agreement with the observed Raman line[11] at 82 cm^{-1} at 297 K. The g value was found to be 1.47×10^{-3} K^{-1}, which was larger than the 2×10^{-4} K^{-1} for the 98 cm^{-1} line; the temperature coefficient for the 82 cm^{-1} line has not been measured, however.

Recently, the temperature dependence of the resonance frequency in $Ba(ClO_3)_2 \cdot H_2O$ has been independently measured by Ramanohan and Sobhanadri.[13] The same procedure as that in the present study has been employed to analyze the experimental data. The parameters obtained by them give the values of 30039.7 kHz, −1.45 kHz/K, and -3.28×10^{-3} kHz/K^2 for a_0, a_1, and a_2 respectively; these values are in agreement with the present results. The torsional frequency of 125 cm^{-1} at 300 K is also in good agreement with the present finding.

If a simple sinusoidal potential for the torsional oscillation in crystal is assumed, the frequency, ν_t, is given by:[14]

$$\nu_t = (n/2\pi)\sqrt{V_0/(2\Theta)} \qquad (3)$$

where V_0 is the height of the potential barrier with an n-th-fold symmetry. In Table 1, the calculated V_0 values are shown. The potential barrier substantially decreases with an increase in the temperature. This indicates that the chlorate ion may rotate at the crystal site at room temperature; then the torsional oscillation has a large amplitude, so anharmonic motion takes place. In Ag and Ba salts it can be seen that the torsional motion of the chlorate ion as a whole hardly occurs, even at room temperature. On the other hand, a freer rotational motion can be expected in Ca and Cu salts from the low barrier height, which is of nearly the same order as, or several times larger in magnitude than that in organic molecular crystals—*i.e.*, it is of the order of 10 kcal/mole.[15] In Ca salt, it is clear from the results reported by Kumar *et al.*[9] that ν_2 has an anomalous temperature dependence. A very large g value gives a negative $(1-gT)$ factor at room temperature. Although Kumar *et al.* did not discuss this fact, it can be suggested that the present method for the analysis of the experimental results can not be used to illustrate the motion of the chlorate ion in the crystal site corresponding to ν_2.

The author wishes to thank Professor S. Aono for his encouragement and Mr. H. Ichikawa for the preparation of the sample.

10) J. Vanier, *Can. J. Phys.*, **38**, 1397 (1960).
11) C. S. Kumari, *Proc. Indian Acad. Sci.*, **23A** 177 (1950).
12) D. B. Utton, *J. Chem. Phys.*, **47**, 371 (1967).
13) C. V. Ramanohan and J. Sobhanadri, *Mol. Phys.*, **22**, 575 (1971).
14) G. Herzberg, "Molecular Spectra and Molecular Structure", II, D. Van Nostrand, New York (1949), p. 226.
15) B. L. Barton, *J. Chem. Phys.*, **51**, 4670 (1969).

Line Shapes of the ^{35}Cl Nuclear Quadrupole Resonance in $KClO_3$, $AgClO_3$, $Ba(ClO_3)_2 \cdot H_2O$, and $Cu(ClO_3)_2 \cdot 6H_2O$

Masahiko SUHARA and Ken-ichi SHIMIZU*

Department of Chemistry, Faculty of Science, Kanazawa University, Maru-no-uchi, Kanazawa 920

(Received May 8, 1972)

The nuclear quadrupole resonance (NQR) of ^{35}Cl in $KClO_3$, $AgClO_3$, $Ba(ClO_3)_2 \cdot H_2O$, and $Cu(ClO_3)_2 \cdot 6H_2O$ at room temperature has been measured by using a spectrometer system capable of reproducing with fidelity the line shape. The line-shape parameters were determined from the observed spectrum. All the line shapes of the four chlorates are of an intermediate character between Gaussian and Lorentzian. The line-width in K and Ag salts seems to originate from the inhomogeneity of the electric-field gradient, itself a result of the imperfection of the crystal. In Ba salt, it was found that the line-width is determined by the magnetic dipole-dipole interaction between chlorine and protons in the water of crystallization. The Lorentzian is the superior component of the line shape in Cu salt. This is explained in terms of the anharmonicity of the torsional oscillation of the ClO_3^- group.

Most of the works on the NQR line shape have dealt with the line-width rather than with the actual line shape. This is also the case in the investigations of NQR in chlorates. Wang[1] studied the temperature change of the full half-width in $NaClO_3$ and found that the width increases with a decrease in the temperature. Zeldes and Livingston[2] observed the full width between the flex of the second derivative of the spectrum in $NaClO_3$, $KClO_3$, and $Ba(ClO_3)_2 \cdot H_2O$, and found the sharpest line in $KClO_3$. Grechishkin[3] measured the full half-width in $Ba(ClO_3)_2$, $KClO_3$, and $NaClO_3$ by using a super-regenerative spectrometer, which does not generally give the actual line shape. More precise observations have been reported by Koi and his co-workers[4,5,6] on the Br NQR line in $NaBrO_3$ and $KBrO_3$ using a regenerative spectrometer. However, no precise line-shape study has been done in metal chlorate. We have now determined the line-shape parameters in several chrorates by using a spectrometer capable of reproducing the line shape with fidelity.

Experimental

The NQR line was detected by utilizing a Kushida-type regenerative oscillator[7] with a magnetic field modulation of a 200 Hz on-off field. The spectrum was recorded on a chart by means of a lock-in detection technique, together with pip marks at 1 kHz intervals. In order to obtain an undistorted line shape, the rf level was kept as weak as possible, the sweep rate was 2 kHz/min, and the time constant, 0.3 sec. Details of the spectrometer system have been given in a previous paper.[8] During the observation, the temperature of the sample was maintained within 0.01 K, which corresponds to the shift of the resonance frequency of ~0.05 kHz. The accuracy of the temperature measurement was ±0.5 K. The chlorates were prepared in the usual way.[9]

Line-shape Analysis

A block diagram of the process of the line-shape analysis from the observed spectrum is shown in Fig. 1, together with the line-shape parameters to be determined. The analysis was performed by means of a NEAC 2230 computer at Kanazawa University.

The In-put Data consisted of the reading of the out-put voltage on the recorded chart with a constant frequency interval (order of 10^{-2} kHz), the number

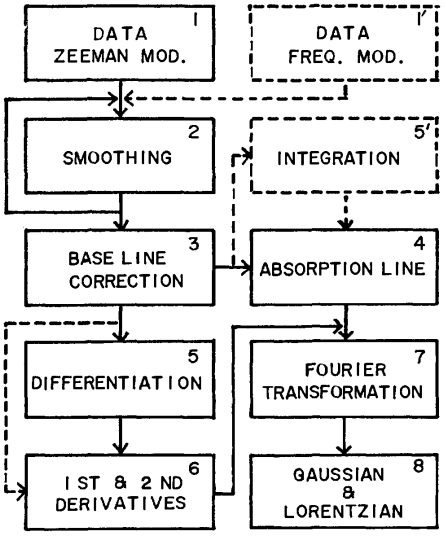

Fig. 1. Block diagram of the process of line shape analysis.
1, 1') Intensity of observed spectrum
Numbers of sample point
Frequencies of initial and final points
Frequency interval
2) Sensitivity improvement when poor S/N ratio.
3) When base line drift occures.
4) Area (M_0)
Peak intensity ($g(\nu_0)$)
Full half-line width ($\Delta\nu_{1/2}$)
First, second and fourth moments (M_1, M_2 and M_4)
6) Peak frequency (ν_0)
Width between maximum slope ($\Delta\nu_{msl}$)
Derivative half intensity (g'_{max})
8) Full half-line widths of Gaussian ($\Delta\nu_G$) and Lorentzian ($\Delta\nu_L$)

* Present address: Fukui Seiren Co., Fukui.

1) T. C. Wang, *Phys. Rev.*, **99**, 566 (1955).
2) H. Zeldes and R. Livingston, *J. Chem. Phys.*, **26**, 1102 (1957).
3) V. S. Grechishkin, *Zh. Eksp. Teor. Fiz.*, **36**, 630 (1959).
4) Y. Koi, A. Tsujimura and T. Fuke, *J. Chem. Phys.*, **23**, 1346 (1955).
5) Y. Koi, *J. Phys. Soc. Jap.*, **12**, 49 (1957).
6) Y. Koi, A. Tsujimura and Y. Imaeda, *J. Chem. Phys.*, **27**, 603 (1957).
7) T. Cole, T. Kushida and H. C. Heller, *ibid.*, **38**, 2915 (1963).
8) M. Suhara, *Sci. Rep. Kanazawa Univ.*, **17**, 7 (1972).
9) M. Suhara, This Bulletin, **46**, 1053 (1973).

of sample points (200~300), and the frequency at initial point.

Smoothing and Differentiation. When the observed spectrum has a poor S/N ratio, a least-squares smoothing technique (convolution method)[10] is employed to determine the smoothed spectrum. The m-th derivative of the original spectrum can also be obtained by a similar technique. Details of the technique were given by Savitzky and Golay.[11] The smoothing interval chosen is smaller than half of the full line-width at half-maximum intensity, seventeen sample points being included in this interval. Under these conditions, the line distortion error is expected to be smaller than 1%.[10] When a small base-line drift occurs, the true absorption spectrum can be obtained by subtracting the drift from the observed spectral intensity on a chart. The drift was assumed to be linear; by means of the least-squares method, the linear equation was determined using the ten data points, which consisted of two blocks of five successive sample points from both terminals of the frequency in the observed spectrum.

Separation of Gaussian and Lorentzian. Assuming the observed absorption curve to be a convolution of Gaussian and Lorentzian shape (Voigt profile), the full half-widths of each component ($\Delta\nu_G$ and $\Delta\nu_L$) can be determined by the Fourier transformation of the spectrum.[12] Using the least-squares method to fit the logarithm of cosine-transform of the observed spectrum to a quadratic function of the time, the linear and quadratic coefficients give the values of $\Delta\nu_L$ and $\Delta\nu_G$ respectively.

The reliability of the process and the results of the analysis were confirmed by checking the consistency between the observed value, $\Delta\nu_{1/2}$, and the calculated one, $\Delta\nu_{1/2}{}^c$. According to the steps:

(i) $a = \Delta\nu_L/[(\ln 2)^{-1/2}\Delta\nu_G]$, (ii) $a \xrightarrow[\text{Table}]{\text{Posener's}} \omega$,

(iii) $\Delta\nu_{1/2}{}^c = \Delta\nu_G\omega/(\ln 2)^{1/2}$,

the $\Delta\nu_{1/2}{}^c$ value was calculated from the $\Delta\nu_G$ and $\Delta\nu_L$ values by using the relationship between the a and ω parameters in the table[13] of the Voigt profile.

A Gaussian function was examined in order to check the error in the processes shown in Fig. 1. An excellent reproducibility of the line-shape parameters was obtained, as is shown in Table 1.

Results and Discussions

For all the chlorates, the S/N ratio of the observed spectrum was 10~20 even when using a slow sweep and a short time constant. An example is given in Fig. 2, in which the original spectrum and the true absorption line after smoothing and the base-line-drift correction are compared. The absorption line shapes of the four chlorates were almost symmetrical. The values of the first moment were smaller than ±0.1 kHz. The relative intensities of the chlorates of K and Ag were larger than those of Ba and Cu. The results of the measurement are summarized in Table 2. The full width between the half-maximum intensities ($\Delta\nu_{1/2}$), the full width between maximum slopes ($\Delta\nu_{msl}$), and second and fourth moments increase in the order (K, Ag), Ba, and Cu salts. The $\Delta\nu_L$ and $\Delta\nu_G$ values for each chlorate are also given in Table

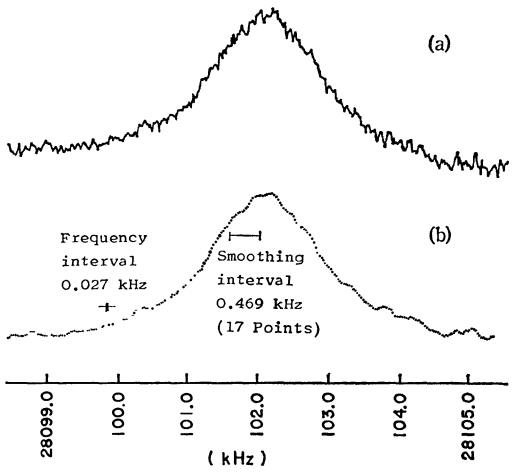

Fig. 2. (a) Observed resonance spectrum in $KClO_3$ (sweep rate 2 kHz/min, time constant 0.3 sec). (b) Spectrum after smoothing and base line correction.

Table 1. Reliability of the process of line shape analysis

Assumed function: Gaussian		Theoret	Calcd
$g(\nu)=g(\nu_0)\exp[-(\nu-\nu_0)^2\ln 2/(1/2\,\Delta\nu_{1/2})^2]$	ν_0	30000.000	30000.000_4
$\nu_0=30000.000$ kHz	M_0	2.1286	2.1289
$\Delta\nu_{1/2}=2.000$ kHz	M_2	0.721	0.720
$g(\nu_0)=1.000$	M_4	1.55	1·54
Data points 159	$g(\nu_0)$	1.000	1.000_1
Smoothing interval 0.85 kHz	$g(\nu_0+1/2\,\Delta\nu_{1/2})$	0.500	0.500_1
Differentiation interval 0.25 kHz	$g'(\nu_0+1/2\,\Delta\nu_{msl})$	0.7142	0.7113
	$\Delta\nu_{msl}$	1.698	1.70
	$\Delta\nu_G$	2.000	1.999_3
	$\Delta\nu_L$	0	0.000_7

10) R. R. Ernst, "Advances in Magnetic Resonance", Vol. 2, ed. by J. S. Waugh, Academic Press, New York, N. Y. (1966), p. 1.
11) A. Savitzky and M. J. E. Golay, *Anal. Chem.*, **36**, 1627 (1964).
12) B. D. Bartoro, "Optical Interaction in Solids", John Wiley & Sons, New York, N. Y. (1968), p. 326.
13) D. W. Posener, *Aust. J. Phys.*, **12**, 184 (1959).

TABLE 2. SPECTRAL PARAMETERS OF OBSERVED LINES

	$KClO_3$	$AgClO_3$	$Ba(ClO_3)_2 \cdot H_2O$	$Cu(ClO_3)_2 \cdot 6H_2O$
T (K)	297	297	300	300
ν_0 (kHz)	28102.03±0.10	28847.93±0.10	29335.80±0.10	29118.58±0.10
$\Delta\nu_{1/2}$ (kHz)	1.66±0.10	2.00±0.10	2.80±0.10	3.29±0.10
$\Delta\nu_{msl}$ (kHz)	1.51±0.10	1.34±0.10	1.87±0.10	2.53±0.10
M_2 ((kHz)^2)	0.87±0.3	1.6 ±0.1	2.3 ±0.5	3.4 ±0.5
M_4 ((kHz)^4)	3±1	10±3	19±7	36±7
$\Delta\nu_L$ (kHz)	0.26±0.1	0.9 ±0.5	1.3 ±0.2	2.3 ±0.2
$\Delta\nu_G$ (kHz)	1.8 ±0.1	1.6 ±0.3	2.0 ±0.1	1.4 ±0.2
$\Delta\nu_{1/2}{}^C$ (kHz)	1.9	2.1	2.8	3.0
Number of experiments	4	6	4	3

TABLE 3. COMPARISON OF CHARACTERISTIC PARAMETERS

Parameters	Gaussian	Lorentzian	$KClO_3$	$AgClO_3$	$Ba(ClO_3)_2 \cdot H_2O$	$Cu(ClO_3)_2 \cdot 6H_2O$
$\Delta\nu_{1/2}/\Delta\nu_{msl}$	1.177	1.732	1.1	1.5	1.5	1.3
$g(\nu_0)/(g'_{max}\Delta\nu_{msl})$	0.824	1.333	0.63	0.86	0.84	0.92
$M_0/(g(\nu_0)\Delta\nu_{1/2})$	1.064	1.571	1.18	1.22	1.25	1.35
$M_0/(g'_{max}\Delta\nu_{msl})$	1.033	3.628	1.2	2.1	2.9	3.5
a	0	∞	0.12	0.47	0.51	1.32

2, together with the values of $\Delta\nu_{1/2}{}^C$. The excellent agreement between $\Delta\nu_{1/2}$ and $\Delta\nu_{1/2}{}^C$ indicates that the values of $\Delta\nu_L$ and $\Delta\nu_G$ for the four chlorates we obtained are reliable. Thus, it was found that each of the resonance lines of the four chlorates has an intermediate character between Gaussian and Lorentzian. In K salt, the line shape is close to Gaussian. On the other hand, a large amount of Lorentzian contributes to the line shape in Cu salt. Several spectral parameters are compared in Table 3, in which a relation similar to that seen in Table 2 is found.

The possible mechanisms of the line broadening are as follows: (1) quadrupole spin-lattice relaxation, (2) magnetic dipole-dipole interaction, and (3) field fluctuation due to the crystal strain. From (1) a Lorentzian shape would result, and from (2), a Gaussian, if there are many interacting neighbours. The line shape due to (3) depends on the nature of the strain. However, the second and the third mechanisms are assumed to give a single Gaussian shape. Koi[5] found that the main cause of the line-width of the $NaBrO_3$ crystal is the magnetic dipole interaction and that the contribution from the relaxation to the line-width is very small, since the ratio of the line-width for the ^{79}Br and ^{81}Br isotopes is equal to 0.94, agreeing closely with 0.928, the ratio of their magnetic dipole moments. Koi *et al.*[6] also reported that, in $KBrO_3$, the crystal strain is primarily responsible for the observed Br NQR line-width. Hashi[14] found that the free-induction-decay curve on Br NQR in $NaBrO_3$ has a Gaussian shape and that its decay time, $T_2{}^*$, is mostly determined by the distribution of the electric-field gradients in the crystal due to strain, imperfections, or temperature gradient. For $KClO_3$ and $AgClO_3$, the line shape we observed was almost Gaussian. The mechanism which contributes to the line-width is probably due to mechanism (2) and/or (3). Weber[15] observed that the free induction signals of the Zeeman components, the α and α' resonances, exhibit an increased decay lifetime relative to the lifetime in the zero-field resonance. It was found that the observed increase agrees with the predicted value obtained from the second moment, $\langle\Delta\nu^2\rangle = 0.0127$ (kHz)^2, due to the magnetic dipole interaction, calculated by the equations of Abragam and Kambe.[16] The observed second moment in $KClO_3$ was greater than the calculated one by one order of magnitude. A similar calculation of the second moment in $AgClO_3$ gave the value of $\langle\Delta\nu^2\rangle = 0.0058$ (kHz)^2. calculated by using the crystal parameters of $AgClO_3$[17] by means of NEAC 2230. In $AgClO_3$ as well as in $KClO_3$, the calculated second moment is considerably smaller than the observed one. Even the second moment expected from the value of $\Delta\nu_G$ does not agree with the calculated one. It can, therefore, be concluded that the mechanism which contributes to the $\Delta\nu_G$ values in $KClO_3$ and $AgClO_3$ might be mainly due to the random distribution of the electric-field gradient originating from the strain in the crystal. Using the crystal parameters of $Ba(ClO_3)_2 \cdot H_2O$,[18,19] we found that the line-width, $\Delta\nu_G$, corresponding to the calculated second moment, is 2.5 kHz and that it is mainly determined by the protons in the water of crystallization. In contrast to K and Ag salts, the rough agreement between the calculated line-width and the observed one indicates that the dominant effect on the Gaussian width in Ba salt is the magnetic

14) T. Hashi, *J. Phys. Soc. Jap.*, **13**, 911 (1958).

15) M. J. Weber, *J. Phys. Chem. Solids*, **17**, 267 (1961).
16) A. Abragam and K. Kambe, *Phys. Rev.*, **91**, 894 (1953).
17) R. W. G. Wyckoff, "Crystal Structure", Interscience Publishers, New York (1957).
18) G. Kartha, *Acta Crystallogr.*, **5**, 845 (1952).
19) S. K. Sikka, S. N. Momin, H. Rajagopal, and R. Chidambaram, *J. Chem. Phys.*, **48**, 1883 (1968).

dipole interaction between the chlorine nucleus and the proton. Although the crystal parameters are not known in $Cu(ClO_3)_2 \cdot 6H_2O$, it is considered that the observed line-width also originates from the dipolar interaction, as in the case of Ba salt, since many protons in the water of crystallization can give a broad line-width.

It is reasonable to consider that the Lorentzian width is attributable to the lifetime in the energy states of the nuclear spin system. A general theory of line shape was developed by Freed and Fraenkel[20] in terms of a relaxation matrix theory. They have shown that a composite line arising from a set of degenerate nuclear-spin states should, in general, consist of a sum of superimposed lines of the Lorentzian shape with different widths rather than a single line with an overall Lorentzian shape. However, as a limiting case, a single Lorentzian line is still obtained when the torsional oscillation in the crystal is represented a simple model in which, in am olecular frame, the by field gradient has a cylindrical symmetry around the oz axis (since the asymmetry parameter in chlorates has the value of almost zero, all the chlorates satisfy this condition); the motion of this frame is the rotation of oz by a small angle, θ, around a position of stable equilibrium, oZ, in a plane perpendicular to the axis, oX, of the laboratory frame. The time-dependent perturbation responsible for the broadening of the NQR line is thus given by:[21]

$$H_1(t) = A\left\{-\frac{1}{2}(\theta^2-\overline{\theta^2})[3I_z^2-I(I-1)] - \frac{3}{4}(\theta^2-\overline{\theta^2})(I_+^2+I_-^2) - 3\theta(I_zI_y+I_yI_z)\right\} \quad (1)$$

where $A=e^2qQ/4I(2I-1)$ However, it is easy to prove that, for half-integral spins, the two transitions, $m\rightarrow(m-1)$ and $-m\rightarrow-(m-1)$, are actually uncoupled, all the off-diagonal elements of the relaxation matrix being zero for the Hamiltonian $H_1(t)$. Each $m\rightarrow(m-1)$ transition is thus a simple line that has the shape of a single Lorentzian. For $I=3/2$, the line width, $1/T_2$, is expressed in terms of the spectral density functions of the random functions, $\theta^2(t)-\overline{\theta^2}$ and $\theta(t)$. The non-adiabatic terms in Eq. (1) also cause a spin-lattice relaxation, the decay time (or relaxation time, T_1) of which is expressed in terms of the same spectral density functions as in the case of T_2. In view of the fact that the quadrupole resonance frequency is small relative to the reciprocal of the correlation time for the random functions, the spectral density is assumed to be independent of the frequency. By using a damped oscillator model for the effect of the thermal bath, when the frequency distribution of the torsional oscillation is relatively sharp, the relation between the Lorentzian width, $1/T_2$, and the reciprocal of the spin-lattice relaxation time, $1/T_1$, is given by:[22]

$$1/T_2 = (7/2)(1/T_1) \quad (2)$$

In ionic crystals the additional relaxation due to crystal lattice vibrations should be considered. Chang[23] developed a general theory of quadrupole spin-lattice relaxation in solids based on the interaction of the quadrupole moment of the nucleus with the fluctuating crystalline electric-field gradient produced by thermal lattice vibrations of neighboring electronic charges. Although the theory was confirmed by the measurement[24] of the temperature dependence of T_1, Weber[15] found that the measurement of T_1 does not provide a critical test of the correctness of the model and that the Chang theory is inadequate for the ^{35}Cl relaxation in ClO_3^- groups, whereas the Bayer theory is consistent with the measurement of the individual transition probabilities corresponding to $\Delta m=\pm1$ and $\Delta m=\pm2$ by using a selective excitation experimental technique.

If the observed line-width for a Lorentzian component were determined by the torsional oscillation of the ClO_3^- ion in $KClO_3$, we might obtain the spin-lattice relaxation time, T_1, as about 4 msec, which is shorter by a factor of 1/5 than the reported value,[15] $T_1=21$ msec, at 300 K. It seems that the present c. w. experiment gives a much broader Lorentzian width than the one to be expected from the transient measurements. This discrepancy is probably due to the following factors: (1) A single mechanism of broadening, *i.e.*, the torsional motion, was considered. (2) Simple assumptions were used to derive Eq. (2), which was then used to obtain the line-width. (3) In the transient experiment, a large departure from the thermal equilibrium was achieved. On the other hand, the c. w. measurement was carried out without saturation. (4) The distribution of the electric-field gradient due to the strain and the imperfection in the crystal, which determine the major part of the line-width, was assumed to be Gsussian. In Ba salt, a similar discrepancy was obtained. We can not discuss Ag and Cu salts in detail because of the lack of the T_1 values. However, it should be noted that in Cu salt the superior component of the line shape is not Gaussian, but Lorentzian. If the Lorentzian width originates from spin-lattice relaxation due to the torsional oscillation of the ClO_3^- group, T_1 is found to be 0.5 msec, which is much shorter than that of $KClO_3$. This may be explained as follows. The relaxation mechanism due to torsional oscillation is mainly the transition process of $\Delta m=\pm2$, as is shown by the Bayer theory. When the temperature increases and the torsional frequency ν_t decreases, the $h\nu_t/kT$ factor becomes much smaller than unity and the transition probability corresponding to $\Delta m=\pm2$ becomes large. This situation is achieved when the anharmonicity of torsional oscillation can not be neglected;[9] from it the large temperature dependence of the torsional frequency of the ClO_3^- group has been found

20) J. H. Freed and G. K. Fraenkel, *J. Chem. Phys.*, **39**, 326 (1963).
21) H. Bayer, *Z. Phys.*, **130**, 227 (1951).
22) Y. Ayant, *Ann. Phys.*, (Paris) Ser. 12, **10**, 487 (1955). A. Abragam, "The Principles of Nuclear Magnetism", Clarendon, Oxford, England (1961), Chap. X, Sec. VI.
23) C. H. Chang, U. S. Air Forse Office of Scientific Resarch Technical Note TN-55-401 (1955).
24) P. A. Bender, D. A. Jennings, and W. H. Tanttila, *J. Chem. Phys.*, **32**, 499 (1960).

in Cu salt. Since the temperature at which the linewidth measurement was carried out is relatively close to the melting point, 65°C, a vigorous lattice motion can be expected. Thus, the transition probability or the spectral function corresponding to $\Delta m=\pm 2$ must have a large value, and a large lifetime broadening can thus be expected. More detailed discussions will be possible when the temperature dependence of the line shape is investigated experimentally.

The authors wish to thank Professor S. Aono for his encouragement, Dr. A. Sado for his discussions, and Mr. H. Ichikawa for the preparation of the sample.

BULLETIN OF THE CHEMICAL SOCIETY OF JAPAN, VOL. 46, 1060—1063 (1973)

The Photoreduction of 2-Nitronaphthalene in 2-Propanol

Kinichi OBI, Jan W. BOTTENHEIM, and Ikuzo TANAKA

Department of Chemistry, Tokyo Institute of Technology, Ohokayama, Meguro-ku, Tokyo 152

(Received July 25, 1972)

The photoreduction of 2-nitronaphthalene in 2-propanol has been studied at 313 nm. The photoreduction is suppressed in the presence of dissolved oxygen or a triplet quencher such as 1,3-cyclohexadiene. The results are consistent with the triplet state of 2-nitronaphthalene being the reactive species. 2-Naphthylhydroxylamine is formed as the reaction product. The quantum yield for the disappearance of 2-nitronaphthalene is estimated to be 0.037. The low quantum yield results from the slow reaction rate of hydrogen abstraction by the $\pi\pi^*$ triplet state of 2-nitronaphthalene.

The photoreduction of simple aromatic nitrocompounds has been the subject of several recent publications.[1] Whereas the photoreduction occurs with good efficiency in the presence of protons[2,3] or such reducing agents as tri-*n*-butylstannane,[4] the reduction in alcoholic solvents is much less efficient. The photoreduction of nitrobenzene in 2-propanol[5] has been reported to occur with a low quantum yield ($\Phi \sim 0.01$). While several groups have studied the photoreduction of 1-nitronaphthalene,[3,6] no concordant conclusion has yet been obtained.

It has generally been agreed that the photoreduction of the aromatic nitrocompounds should take place through their triplet state in accordance with the aromatic carbonyl compounds, of which very extensive researches have been established rather conclusively that the $n\pi^*$ triplet state as the reacting state.[7] However, much less agreement exists as to the nature ($n\pi^*$ or $\pi\pi^*$) of the reacting triplet state of aromatic nitrocompounds.

The phosphorescence study[8] has suggested that the lowest triplet states of nitrobenzene are $n\pi^*$ and that those of 1- and 2-nitronaphthalenes are $\pi\pi^*$ states. The hydrogen abstraction reaction of the $n\pi^*$ triplet state has been widely understood, whereas generally that of the $\pi\pi^*$ triplet has not been observed or occurs at significantly lower reaction rates.

In this paper, we wish to report on the photoreduction of 2-nitronaphthalene in 2-propanol and to discuss the hydrogen abstraction reaction by the $\pi\pi^*$ triplet state of 2-nitronaphthalene.

Experimental

Chemicals. 2-Nitronaphthalene was obtained from K & K, Ltd., and was purified by recrystallization from hexane. Spectral-grade 2-propanol was obtained from Merck and was used as received.

Procedures. Unless otherwise specified, all the samples were thoroughly degassed on a high-vacuum line by freeze-pump-thaw cycles. A medium-pressure mercury lamp (Toshiba H-400P) was used as the 313 nm radiation source; it was equipped with a combination filter of a nickel sulfate solution and a Toshiba UV-31 filter, while a high-pressure mercury lamp (Toshiba SHL-1200) with a Pyrex filter was used for the ESR studies. The light intensity was measured with a potassium ferroxalate actinometer.

The disappearance of 2-nitronaphthalene was determined spectrophotometrically. The ultraviolet absorption spectra were taken with Hitachi 124 and EPS-2 spectrophotometers. The ESR spectra were measured by means of a JEOL JES-3BS-X.

Results and Discussion

The spectrum of the 2-propanol solution of 2-nitronaphthalene changed upon irradiation with 313 nm light, as shown in Fig. 1. The absorption bands of 2-nitronaphthalene at 254, 261, and 305 nm decreased, and new bands with maxima at 244 and *ca.* 280 nm appeared, as the irradiation time increased, with isosbestic points at 250, 270, and 288 nm and probably also at 330 and 340 nm. If the irradiated solution was allowed to stand for several days in contact with air,

1) H. A. Morrison "The chemistry of the nitro and nitroso groups" Part 1, Wiley, New York (1969), p. 165.
2) R. Hurley and A. C. Testa, *J. Amer. Chem. Soc.*, **89**, 6917 (1967).
3) W. Trotter and A. C. Testa, *J. Phys. Chem.*, **74**, 845 (1970).
4) W. Trotter and A. C. Testa, *J. Amer. Chem. Soc.*, **90**, 7044 (1968).
5) R. Hurley and A. C. Testa, *ibid.*, **88**, 4330 (1966).
6) S. Hashimoto and K. Kano, *Kogyo Kagaku Zasshi*, **72**, 188 (1969).
7) J. G. Calvert and J. N. Pitts, Jr., "Photochemistry", Wiley, New York (1966), p. 528.
8) R. Rusakowicz and A. C. Testa, *Spectrochim. Acta.* **27A**, 787 (1970).

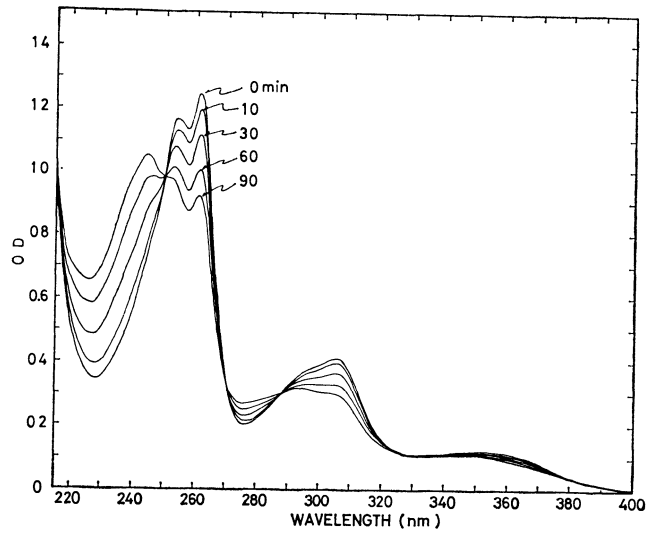

Fig. 1. Spectral change of 2-propanol solution of 2-nitronaphthalene on 313 nm irradiation.

the band of the products at 244 nm disappeared and a broad new band appeared around 520 nm assignable to the azoxy compound. By adding a small amount of hydrochloric acid to the irradiated solution, the absorption peak of the products disappeared and a new peak appeared at 233 nm, which corresponded to 2-naphthylamine hydrochloride. It has been established that N-aromatic-hydroxylamines are autoxidized to the corresponding azoxy compounds in contact with air,[9] and also undergo a reaction to give the corresponding amines when a small amount of hydrochloric acid is added.[10] Thus, a possible candidate for the products is thought to be 2-naphthylhydroxylamine. In the photolysis of 2-propanol solutions of nitrobenzene[5,10] and 1-nitronaphthalene,[6] the nitrocompounds are photoreduced to phenylhydroxylamine and 1-naphthylhydroxylamine respectively. The similar reaction is also observed in the photolysis of 4-nitropyridine-1-oxide.[11] Therefore, it is reasonable to consider the reaction product of 2-nitronaphthalene to be 2-naphthylhydroxylamine.

The quantum yields of the disappearance of 2-nitronaphthalene were measured. The yields decreased slightly with the irradiation time; the results are shown in Fig. 2. The small decline must come from the internal filter effects of the produdts. The initial quantum yield (Φ_0) of the disappearance of 2-nitronaphthalene was obtained by extrapolating it to the zero irradiation time. The 2-nitronaphthalene concentration did not affect the quantum yield, which was 0.037, as is shown in Fig. 3. In order to study the effects of the dissolved oxygen, the aerated solution was photolyzed. The results, however, showed no spectra change after a 120-min irradiation.

Quenching experiments with 1,3-cyclohexadiene were also carried out; the results are shown in Fig. 4.

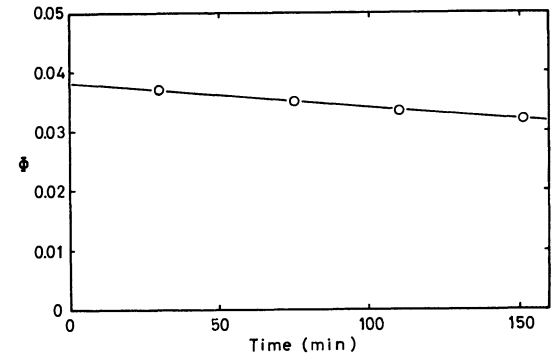

Fig. 2. Dependence of apparent disappearance quantum yields on irradiation time with 7.0×10^{-5} M 2-nitronaphthalene.

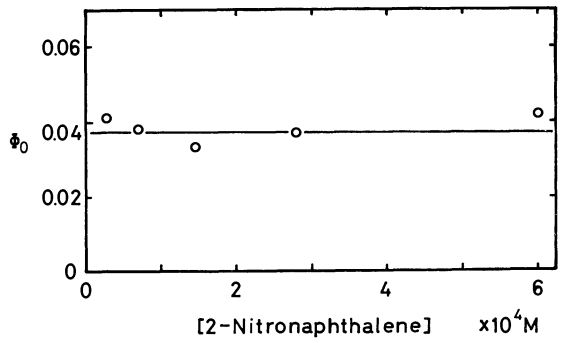

Fig. 3. Dependence of disappearance quantum yields on 2-nitronaphthalene concentration.

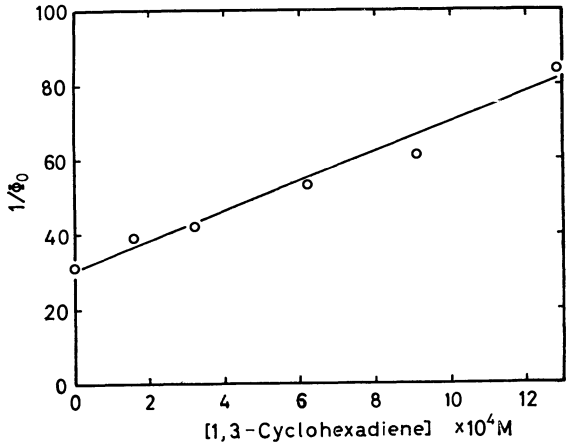

Fig. 4. Reciprocal of disappearence quantum yields *vs.* 1,3-cyclohexadiene concentration with 1.6×10^{-4} M 2-nitronaphthalene.

Since the triplet energy of 1,3-cyclohexadiene[12] (E_T= 54 kcal) is lower than that of 2-nitronaphthalene[8] (E_T=56.8 kcal), this compound is effective as a triplet quencher. The linear Stern-Volmer plots shown in Fig. 4 indicate that the triplet state of 2-nitronaphthalene plays an important role in the photoreduction. The absence of any product formation by the photochemical reaction in the aerated solution also supports the triplet mechanism.

9) Y. Ogata, M. Tsuchida and Y. Takagi, *J. Amer. Chem. Soc.*, **79**, 3397 (1957).

10) S. Hashimoto, J. Sunamoto, H. Fujii, and K. Kano, This Bulletin, **41**, 1249 (1968).

11) N. Hata, E. Okutsu and I. Tanaka, *ibid.*, **41**, 1769 (1968).

12) N. J. Turro, "Energy Transfer and Organic Photochemistry" Wiley, New York (1969), p. 133.

According to the above discussion, the following reaction scheme is obtained:

$$S_0 + h\nu \longrightarrow S_1 \quad (1)$$

$$S_1 \longrightarrow S_0 \quad (2)$$

$$S_1 \longrightarrow T_1 \quad (3)$$

$$T_1 \longrightarrow S_0 \quad (4)$$

$$T_1 + \text{IPA} \longrightarrow \text{products} \quad (5)$$

$$T_1 + Q \longrightarrow S_0 + {}^3Q \quad (6)$$

where S_0, S_1, and T_1 are the ground state, the excited singlet state,[13] and the lowest triplet state of 2-nitronaphthalene respectively, IPA is 2-propanol, and Q is 1,3-cyclohexadiene. This scheme leads to the following equation:

$$\frac{1}{\Phi_0} = \frac{1}{\Phi_T}\left\{1 + \frac{k_4 + k_6[Q]}{k_5[IPA]}\right\}$$

where Φ_T is the quantum yield of the 2-nitronaphthalene triplet. Using the value of $\Phi_T = 0.83$ given by Rusakowicz and Testa,[8] the following values are obtained:

$$k_4/k_5[IPA] = 24.3 \text{ and } k_6/k_5[IPA] = 3.19 \times 10^4\ M^{-1}$$

Since the flash photolysis of 2-nitronaphthalene in 2-propanol at room temperature showed no triplet-triplet absorption, the lifetime of the triplet state is probably less than 20 μ sec; that is, $\tau_T^{-1} = k_4 + k_5 \times [IPA] > 5 \times 10^4\ s^{-1}$. On the other hand, the 1,3-cyclohexadiene quenching of the triplet is thought to be diffusion-controlled at the most; $k_6 \leq 3 \times 10^9\ M^{-1}\ s^{-1}$. Using these relations, the following limits are obtained:

$$5 \times 10^4 < k_4 < 2 \times 10^6\ s^{-1}$$

$$2 \times 10^3 < k_5[IPA] < 8 \times 10^4\ s^{-1}$$

$$6 \times 10^7 < k_6 < 3 \times 10^9\ M^{-1}\ s^{-1}$$

The radiationless decay rate of the triplet 2-nitronaphthalene is roughly of the same order as that of benzophenone[14] ($5.3 \times 10^5\ s^{-1}$), while it is significantly slower than that of nitrobenzene[15] ($\sim 10^9\ s^{-1}$). On the other hand, the rate of Reaction (5), which is the hydrogen abstraction reaction, is much slower than those of benzophenone[16] ($k_5[IPA] = 1.3 \times 10^7\ s^{-1}$) and of nitrobenzene ($k_5[IPA] \simeq 1.7 \times 10^7\ s^{-1}$), which is estimated from the triplet yield[15] (0.67), the radiationless decay rate[15] ($\sim 10^9\ s^{-1}$), and the disappearance quantum yield[5] in 2-propanol (0.011) of nitrobenzene. Therefore, the slower abstraction rate of 2-nitronaphthalene results in the disappearance quantum yield of 2-nitronaphthalene being lower than that of benzophenone ($\Phi = 1$).

In order to study the reaction mechanism in more detail, the ESR spectrum of the reaction intermediates

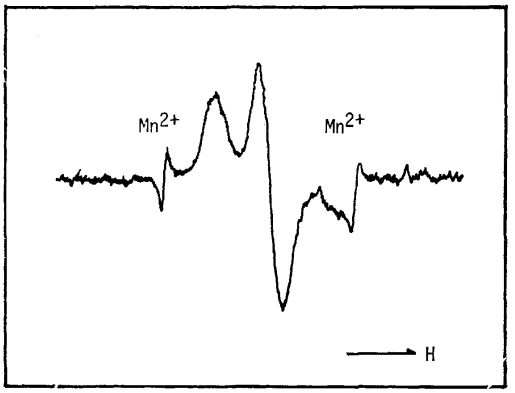

Fig. 5. ESR spectra obtained during the photolysis of 2-nitronaphthalene at −110 °C with 3.5×10^{-4} M 2-nitronaphthalene.

were measured at −110 °C. The spectrum observed at short irradiation time consists of three broad absorption lines and is shown in Fig. 5. The formation of this intermediate was saturated within about a 20-s irradiation, while no 2-propanol radicals were observed in this period. Since no radical was formed in the carbon tetrachloride solution of 2-nitronaphthalene at −110 °C, this radical is probably formed by the interaction between excited 2-nitronaphthalene and 2-propanol and would be the precursor of 2-naphthylhydroxylamine. Since the observed ESR spectrum did not give a hyperfine structure at −110 °C, it was difficult to identify the intermediate.

In the photolysis of nitrobenzene in alcohols at room temperature, $C_6H_5N(R)CH(O\cdot)OH$ and $C_6H_5NH(O\cdot)$ radicals have been observed in the primary and secondary alcohols respectively, while no alcohol radicals have been observed by means of the ESR technique.[17,18] The following reaction scheme is proposed.[18]

$$C_6H_5NO_2 + h\nu \longrightarrow C_6H_5NO_2^* \quad (7)$$

$$C_6H_5NO_2^* + RCH_2OH \rightarrow C_6H_5\dot{N}O_2H + R\dot{C}HOH \quad (8)$$

$$C_6H_5\dot{N}O_2H + R\dot{C}HOH \rightarrow \cdot OH + C_6H_5N(R)CH(O\cdot)OH \quad (9)$$

and if the alcohol is secondary, C_6H_5NOH radicals are formed. As no alcohol radicals appeared in the photolysis of nitrobenzene and 2-nitronaphthalene in 2-propanol, it seems reasonable to expect that similar reaction mechanisms are operative in the two systems. Therefore, the absence of 2-propanol radicals, which should be formed by the abstraction reaction, indicates their consumption by some secondary reactions similar to Reaction (9). However, the detailed reaction mechanism has not yet been determined.

Whereas the lowest triplet state of 2-nitronaphtha-

13) As the 313 nm absorption belongs to the second absorption band of 2-nitronaphthalene, S_1 does not mean the lowest excited singlet state.

14) H. L. Backstrom and K. Sandros, *Acta Chem. Scand.*, **14**, 48 (1960).

15) R. Hurley and A. C. Testa, *J. Amer. Chem. Soc.*, **90**, 1949 (1968).

16) A. Beckett and G. Porter, *Trans. Faraday Soc.*, **59**, 2038 (1963).

17) P. B. Ayscough, R. C. Sealy, and D. E. Woods, *J. Phys. Chem.*, **75**, 3454 (1971).

18) C. Chachaty and A. Forchioni, *Tetrahedron Lett.*, **3**, 307 (1968).

lene has been identified as $\pi\pi^*$ by the phosphorescence study,[8] the hydrogen abstraction reaction from 2-propanol occurs with a higher quantum yield (0.037) than that (0.01) for nitrobenzene, the lowest triplet state of which[15] is $n\pi^*$. The reaction rate of the hydrogen abstraction by 2-nitronaphthalene seems likely to be slower than those by such $n\pi^*$ triplet states as benzophenone and nitrobenzene. However, the longer triplet lifetime would compensate for the slower reaction rate and may result in the relatively high quantum yield.

BULLETIN OF THE CHEMICAL SOCIETY OF JAPAN, VOL. 46, 1063—1067 (1973)

Emission Spectra of Aromatic Halides by Controlled Electron Impact

Teiichiro OGAWA, Masaharu TSUJI, Minoru TOYODA, and Nobuhiko ISHIBASHI

Faculty of Engineering, Kyushu University, Hakozaki, Fukuoka 812

(Received July 29, 1972)

Fluorobenzene, chlorobenzene, and bromobenzene were excited at a very low pressure in the vapor phase by a controlled electron beam of 60—300 V. Their emission spectra were then measured and compared with those excited by the photon. Fluorobenzene showed a characteristic photoemission of the parent molecule in the 260—320 nm region. The band was assigned to the transition from the lowest excited state to the ground state, and its shape did not vary appreciably with the energy of the electron beam. Though the spectrum had some features of "resonance fluorescence," the vibrational structure of the band was not identical with that of any of the spectra obtained by photon impact between 4.7—4.9 eV. This seems to indicate that the molecule gave different spectra according to the excitation energy. However, the excitation by 60 V electrons and that by 300 V electrons did not produce any remarkable difference in the spectra under the resolution of the spectrometer used. Other aromatic halides failed to show any characteristic band of the parent molecules; instead, they showed weak lines due to Cl^+ or Br^+ and pronounced bands due to HCl^+ or HBr^+. This result was ascribed to the spin-orbit coupling effect and the predissociation of the excited parent molecules.

Photochemical investigations of the excited states of aromatic molecules have been carried out by various authors. The effects of pressures and exciting wavelengths on the fluorescence spectra and their lifetimes have given information on the relaxation processes. However, few studies have been carried out at very low vapor pressures, and ultraviolet radiation has been used for the excitation in most of the previous studies.

Electric-discharge methods of various sorts have been effective sources of molecular excitation. The complicated character of the discharge, however, disturbs the detailed studies of the mechanism of fragmentation and excitation. The crossed electron and molecular beam method was proposed to overcome the difficulties and the emission spectra of the OH radical upon electron impact were studied.[1] Since then various di- and tri-atomic molecules have been studied by this method. This method has recently been developed for the investigation of large molecules,[2] and the emission spectra of some aromatic molecules have been reported.[3] In this controlled electron impact method, the photoemission of excited species is obtained at a very low pressure where the effect of molecular collisions is greatly reduced. The energy of electrons can be controlled from the outside. Thus, the method has proved to be of great use in studying the excited states and the emission spectra of various molecules.

The ionization and the fragmentation of molecules by electron impact have also been studied by mass spectroscopy. The information thus obtained, however, has been restricted to the ionized species, and little is known on the excited species in the ionization chamber. Thus, spectroscopic studies of the excited species by electron impact in a high vacuum would be of use.

The fluorescence of fluorobenzene in the vapor phase has been measured by Bass and Sponer[4] and by Nakamura.[5] Both the fluorescence spectra and the quantum yield have been measured at various wavelengths of excited radiation, and the mechanism of energy relaxation has been discussed.[5] If the molecules are raised to a certain vibrational level of an upper electronic state on the absorption of monochromatic light, and if the gas pressures are sufficiently low so that practically no collisions occur during the lifetime of the excited molecules, the light emission of these molecules will show a resonance fluorescence and the shape of fluorobenzene band will vary according to wavelengths of the radiation used for excitation. However, the energy values in his study were confined between 253—266 nm.[5] In the electron excitation method, the impact energy can be varied easily over a wider range, though the experimental

1) T. Horie, T. Nagura and M. Otsuka, *J. Phys. Soc. Jap.*, **11**, 1157 (1956).

2) T. Ogawa, I. Fujita, M. Hatada, and K. Hirota, This Bulletin, **44**, 659 (1971); I. Fujita, M. Hatada, T. Ogawa, and K. Hirota, *ibid.*, **44**, 1751 (1971).

3) T. Ogawa, M. Tsuji, M. Toyoda, and N. Ishibashi, *Chem. Lett.*, **1972**, 233.

4) A. M. Bass and H. Sponer, *J. Opt. Soc. Amer.*, **40**, 389 (1950).

5) K. Nakamura, *J. Chem. Phys.*, **53**, 998 (1970).

difficulties prevented us from using an excitation energy of less than 60 V. Chloro- and bromobenzenes are known not to show any fluorescence; this is attributable to a heavy halogen atom inducing spin-orbit relaxation.[4]

In the present study, the emission spectra of fluoro-, chloro-, and bromobenzenes under electron impact excitation will be reported. The relations of the spectra under electron impact excitation with those under photon irradiation excitation will also be discussed.

Experimental

The sample vapor from a nozzle was crossed so as to collide with an electron beam in a chamber, as is shown schematically in Fig. 1. The details of the apparatus were described elsewhere.[6] The cell was made of glass; it was 4.5 cm in diameter and 40 cm in length. The electron beam (b) from a tungsten filament (a) was accelerated by grids (not shown in the figure) and was introduced into the chamber through a slit. The sample (c) was jetted through a nozzle 0.1—1.0 mm in diameter and was excited by electrons. The chamber was evacuated (e) continuously to a high vacuum; a penning gauge attached to the chamber indicated a pressure of the order 10^{-4}~10^{-5} mmHg during electron impact. The actual pressure in the impact region was expected to be higher than the above value and smaller than 10^{-2} mmHg. The photoemission (d) was observed through a quartz window.

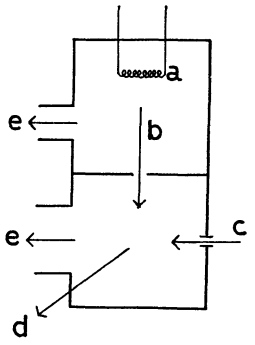

Fig. 1. Schematic diagram of the collision chamber. a; tungsten filament, b; electron beam, c; sample vapor, d; photoemission, e; to vacuum pump.

The spectra were obtained with a Jarrell-Ash JE 25 monochromator, which was equipped with two 1200 grooves/mm gratings blazed for 300 and 600 nm; it had a 100 μm slit and a reciprocal dispersion of about 33 Å/mm. The photometric measurements were carried out with an EMI 9558QB photomultiplier and a Burr-Brown 3421J OP amplifier. The mass spectrum was taken with a Hitachi RML-6E mass spectrometer. Fluorobenzene (Kishida, guaranteed grade), chlorobenzene (Kishida, guaranteed grade) and bromobenzene (Tokyo Kasei, guaranteed grade) were frozen and degassed in a high vacuum just before use.

Results and Discussion

A typical emission spectrum of fluorobenzene under electron-impact excitation is shown in Fig. 2. The

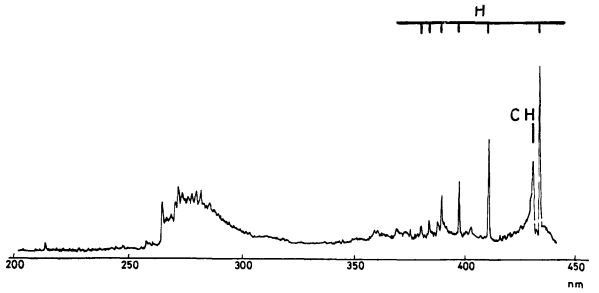

Fig. 2. Emission spectrum of fluorobenzene by electron impact. Impact voltage 200 V, electron beam current 1 mA.

band in the 260—320 nm region is similar to that of toluene,[3] which is identical to fluorobenzene in symmetry and which may, therefore, be expected to have similar vibronic interaction. The fluorine atom causes little change in the position of the absorption band around 260 nm, which is a typical band of aromatic molecules. The vibrational structure of the emission spectrum of fluorobenzene upon electron impact is similar to the fluorescence spectra in the vapor phase,[5] but not identical to any of them. Aromatic hydrocarbons such as benzene, toluene, xylenes and cumene show the band in a similar region in the electron-impact emission spectra[7] and in the fluorescence spectra,[8] as does fluorobenzene. Consequently, the observed band was assigned to the transition from the lowest excited singlet state to the ground state as in the cases of other hydrocarbons.[3,7] The other features in the spectrum in Fig. 2 were assigned to the hydrogen Balmer series and to the CH radical.

The intensities of the photoemission of fluorobenzene were determined for various amounts of incident electrons and for various gas pressures. The intensities of the emissions from H and CH were found to

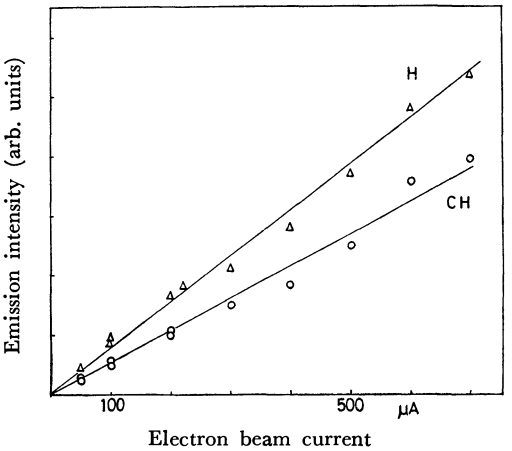

Fig. 3. Relationship between the emission intensity and the electron beam current. Hydrogen Balmer series (△) and CH radical (○). For the sake of clarity, 16 data for each species were omitted from the figure below 100 μA, all of which lay on the same straight line. Impact voltage 200 V.

6) T. Ogawa, M. Toyoda, M. Tsuji, and N. Ishibashi, *Technology Repts. Kyushu Univ.*, **45**, 427 (1972).

7) T. Ogawa, M. Tsuji, M. Toyoda, and N. Ishibashi, *Chem. Lett.*, **1972**, 1157; This Bulletin, submitted.

8) I. B. Berlman "Handbook of Fluorescence Spectra of Aromatic Molecules," 2nd ed., Academic Press, N. Y. (1971).

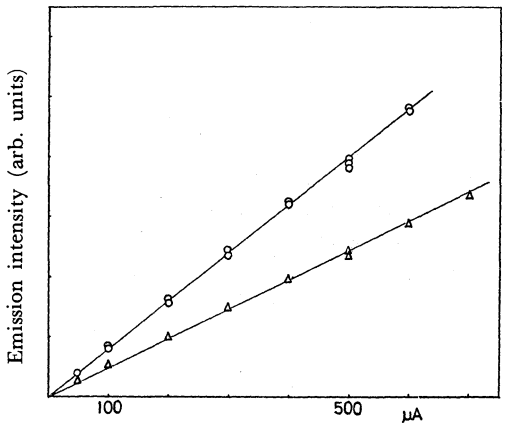

Fig. 4. Relationship between the emission intensity and the electron beam current. Intensities at 265 nm (△) and at 272 and 278 nm (○). For the sake of clarity, 12 data for each species were omitted from the figure below 100 μA, all of which lay on the same straight line. Impact voltage 200 V.

be proportional to the electron-beam current, as is shown in Fig. 3. This result is in agreement with that in the case of methane;[2] it shows that the fragmentation and the excitation of these species consist of a one-electron process. The relationship between the electron-beam current and the emission intensities of three peaks of the excited parent molecules in the 260—320 nm region is shown in Fig. 4. The excitation of a π electron of fluorobenzene was also concluded to be a one-electron process like the excitations of H and CH. The intensities of photoemissions of all species mentioned above were found to be proportional to the pressure in the gas reservoir, as is shown in Fig. 5. The pressure in the gas reservoir was estimated to be proportional to the pressure in the region of collisions by the use of a penning gauge attached to the impact chamber. Thus, inter-molecular quenching processes by collision seem to be unimportant. These results seem to indicate that the excitation

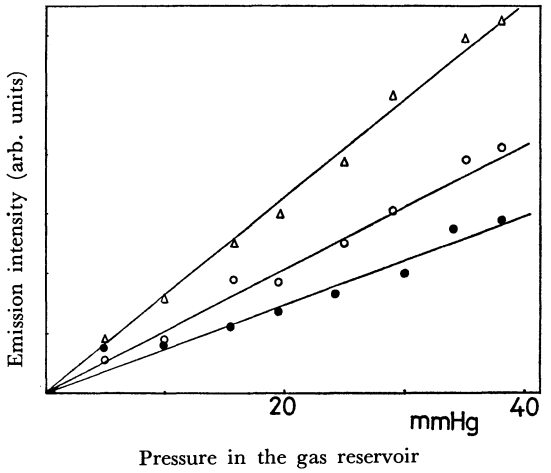

Fig. 5. Relationship between the emission intensity and the gas pressure in the gas reservior. Hydrogen Balmer series (△), CH radical (○) and the parent band at 264 nm (●). Impact voltage 200 V, electron beam current 50 μA.

and the fragmentation take place through one-electron processes, such as;

$$X \xrightarrow{e} X^* \tag{1}$$

$$X \xrightarrow{e} X^{**} \begin{cases} \xrightarrow{\text{fast}} X^* \\ \xrightarrow{\text{fast}} H,\ CH^* \cdots \end{cases} \tag{2}$$

where X stands for fluorobenzene, where ** indicates highly-excited states, and where * indicates the lower electronically-excited state from which the photoemission was observed. The relative importance of the two processes (1) and (2) could not be determined in the present study. X** would be a kind of superexcited state[9] which has excitation energy in excess of the first ionization energy. These superexcited states are considered to play an important role in the radiation chemistry[9] and in the fragmentation in mass spectrometry.[10]

The behavior of the first excited singlet state of fluorobenzene in the vapor phase was studied by Nakamura[5] by exciting the molecule with monochromatic light between 253 and 266 nm. The emission spectra varied in shape according to the wavelengths of incident radiation. The fluorescence spectra excited at longer wavelengths (*e.g.* 263 and 266 nm) were confined at wavelengths longer than the (0, 0) band (264 nm) and had the pronounced vibrational structure. The fluorescence spectra excited at shorter wavelengths (*e.g.* 253 and 258 nm), however, were broad and showed some emission at wavelengths shorter than the (0, 0) band. It was concluded that some resonance emission occurred at the shorter wavelengths of incident radiation.[5]

The present spectrum observed by the electron-impact excitation has some features at wavelengths shorter than the (0, 0) band; they probably arise from transitions which start at vibrational levels higher than those in statistical equilibrium with the surroundings. A comparison of the present emission spectra with those obtained by Nakamura reveals that the present spectra are close to those excited at the shorter wavelengths. However, the present spectrum, shown in Fig. 2, has a pronounced peak at 265 nm, whereas his spectrum, excited at 253 nm, has only a small peak at 265 nm; thus, the details of the vibrational structure of the present spectrum does not coincide with those of any of the fluorescence spectra. In the present study, the variation in the impact voltage between 60—200 V did not induce any appreciable change in the appearance of the spectrum under the present experimental resolution. It may be concluded that the molecule received enough excess energy and showed the resonance emission even when it was excited with electrons of 60 V, and that a similar resonance emission was observed for the excitation by electrons of higher energies.

A typical emission spectrum of chlorobenzene by electron impact and that of bromobenzene are shown

9) R. L. Platzman, *Radiation Res.*, **17**, 419 (1962).
10) K. Hirota, *Nippon Kagaku Zasshi*, **89**, 327 (1968); **91**, 585 (1970).

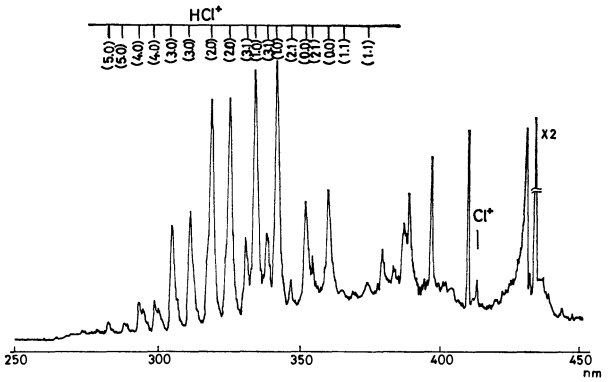

Fig. 6. Emission spectrum of chlorobenzene by electron impact. Impact voltage 300 V, electron beam current 300 μA.

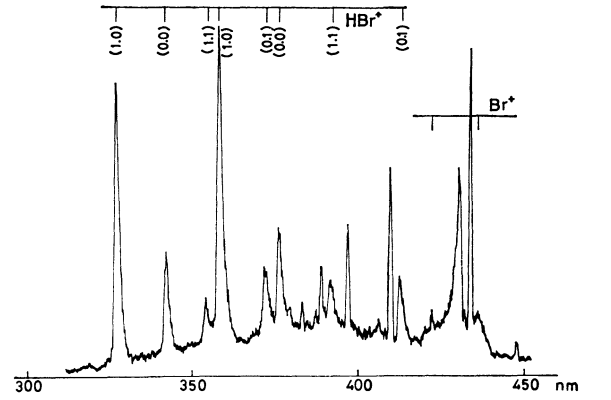

Fig. 7. Emission spectrum of bromobenzene by electron impact. Impact voltage 200 V, electron beam current 500 μA.

in Figs. 6 and 7 respectively. No appreciable bands of parent molecules could be detected in the spectra. Instead, they show strong bands of HCl^+ or HBr^+ and weak lines of Cl^+ or Br^+. Heavy atoms generally tend to reduce the fluorescence quantum yield through an spin-orbit coupling effect.[8] That is, the rate for intersystem crossing becomes large and competes effectively with the rate for fluorescence. Thus, the radiationless transition from the lowest excited singlet state to the triplet state should have a much higher probability when heavy substituents are involved. Bass and Sponer[4] tried to measure the fluorescence of fluoro- and chlorobenzenes in the vapor phase and observed no emission from the latter. The present finding that both chloro- and bromobenzenes did not show any remarkable photoemission under electron-impact excitation is consistent with the previous findings.

In addition to the spin-orbit coupling effect mentioned above, the predissociation of the carbon-halogen bond may have some effect on the disappearance of the photoemission of the parent species. The mass spectra of fluoro- and chlorobenzenes were taken in order to determine the relative probability of the cleavage of the carbon-halogen bond of the two molecules. The electron-accelerating voltage used was 80 V. In both cases, the peak of the parent cation was the strongest peak. The sum of the intensity of the phenyl cation peak and that of the halogen cation peak, which are peaks of the fragments produced by the cleavage of the carbon-halogen bond, was measured in relation to that of the parent peak. The relative intensities were 0.02 for fluorobenzene and 0.68 for chlorobenzene. Thus, it can be concluded that the carbon-chlorine bond is much weaker and more scissile by electron impact and that the predissociation of the excited chlorobenzene probably plays an important role. This is consistent with the bond energy of the carbon-halogen bond. Furthermore, this conclusion is supported by the presence of the emissions of HCl^+ and Cl^+ and by the absence of the emissions of F^+ and HF^+, as will be discussed below.

In the spectra of chloro- and bromobenzenes, pronounced doublet bands were observed in the 280—400 nm region, as is shown in Figs. 6 and 7 respectively. These bands were assigned to the HCl^+ $^2\Sigma$—$^2\Pi$ transition and the HBr^+ $^2\Sigma$—$^2\Pi$ transition respectively.[2,11-13] The bands are split by the coupling of rotation and electronic motions in the ground Π state. The vibrational assignment of the HCl^+ band was carried out by means of the following formula;[12]

$$v = \begin{Bmatrix} 28446 \\ 27788 \end{Bmatrix} + 1561p - 30.3p^2 - 2573n \qquad (cm^{-1})$$

where p is the vibrational quantum number of the upper electronic state and n that of the ground state. The order of intensities of transitions among various vibrational levels is $(1, 0) > (2, 0) > (3, 0) \fallingdotseq (0, 0)$ for HCl^+ and $(1, 0) > (0, 0)$ for HBr^+. No emission from HBr^+ above $p=1$ was observed clearly, probably because of predissociation.[14] On the other hand, the (0, 0) band was the strongest one in the study of the electric discharge.[11] Haugh measured the emission of HCl^+ in the collision of He^+ with HCl and found that the (0, 0) and (0, 1) transitions were by far stronger than any other transition.[15] The vibrational populations of the excited state of HCl^+ were also studied in the collision of $He^*(2^3S_1)$ with HCl, and the vibrational ground state of the upper electronic state of HCl^+ was found to be markedly populated.[16] Although the large difference in the internuclear lengths of the ground state (1.32 Å) and of the excited state (1.52 Å)[17] favors the present result as the calculated Franck-Condon factors[16] show, it is noteworthy that the relative intensity of the vibrational component of $HCl^+(^2\Sigma)$ varies with the method of excitation. Lines of Cl^+ and Br^+ were

11) R. W. B. Pearse and A. G. Gaydon "The Identification of Molecular Spectra," Chapman and Hall, London (1965).
12) B. A. Brice and F. A. Jenkins, *Nature*, **123**, 944 (1929).
13) F. Norling, *Z. Phys.*, **95**, 179 (1935); **104**, 638 (1937).
14) M. J. Haugh and K. D. Bayes, *J. Phys. Chem.*, **75**, 1472 (1971).
15) M. J. Haugh, *J. Chem. Phys.*, **56**, 4001 (1972).
16) W. C. Richardson, D. W. Setser, D. L. Albritton, and A. L. Schmeltckopf, *Chem. Phys. Lett.*, **12**, 349 (1971).
17) G. Herzberg, "Spectra of Diatomic Molecules" D. Van. Nostrand, Princeton, N. J. (1950), p. 534,

also observed in the 400—600 nm region, as is shown in part in Figs. 6 and 7. Neither HF^+ nor F^+ was observed in the spectrum of fluorobenzene. This is probably because the carbon-fluorine bond is stable against electron impact.

The authors wish to thank to Professor Tetsuro Seiyama and Dr. Makoto Egashira of Kyushu University for the measurement of the mass spectra and to Professor Emeritus Kozo Hirota of Osaka University for his encouragement.

BULLETIN OF THE CHEMICAL SOCIETY OF JAPAN, VOL. 46, 1067—1071 (1973)

A CNDO Study of Biphenyl

Akio TAJIRI, Shohji TAKAGI and Masahiro HATANO

The Chemical Research Institute of Non-aqueous Solutions, Tohoku University, Katahira, Sendai 980

(Received August 2, 1972)

The ground-state electronic structure of biphenyl were studied by the use of the CNDO/2 method. It was found that the lengthening of the central C–C bond in biphenyl gave a reasonable minimum point for the potential energy curve. A modified version of the CNDO/2 method was used in order to calculate the electronic spectra of biphenyl for three possible (planar, angular, and vertical) conformations. The method gave a reasonable interpretation of the spectral features of biphenyl.

The most important aspect of the CNDO/2 method[1–3] has been considered to lie in its usefulness for the predictions of the equilibrium nuclear arrangements and the stable conformations of various kind of molecules in their ground states. In fact, the CNDO/2 method has been shown to lead to reasonably successful predictions of the equilibrium bond angles and lengths of small molecules.[2,3] It has been theoretically illustrated for the H_2 molecule[4] that the approximate location of its potential energy minimum is established on a balance between the total Coulombic repulsion between the two atoms and the resonance integral. As for the predictions of the equilibrium bond lengths of relatively large conjugated hydrocarbons, composed of 10—15 carbon atoms,[5] the CNDO/2 method leads to satisfactory results comparable to those obtained from the more sophisticated LCAO-MO-SCF theory on the basis of the π-electron approximation, in which the σ-bond compression energies are taken into account.[6]

Unfortunately, however, several authors have failed in using the CNDO/2 method to calculate the rotational barriers and to predict the stable conformers in some conjugated systems. This is the case with biphenyl. The angle of twist around the central C–C bond in biphenyl is about 42°[7,8] in the gaseous phase, while the molecule is planar in the crystal.[9] Recently, Tinland[10] has calculated the total energy of biphenyl as a function of the twisting angle, θ (Fig. 1), by means of the CNDO/2 method, assuming the fixed bond length of 1.50 Å[11] observed for the twisted bond. The potential energy decreases as the twisting angle, θ, increases and is minimized at 90°, in disagreement with the experimental results.

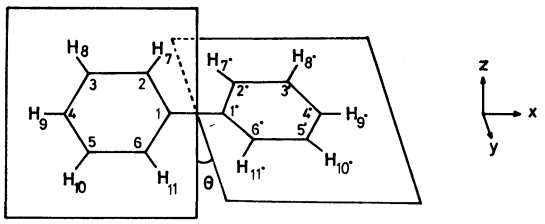

Fig. 1. Numbering of atoms and choice of axis in biphenyl.

More recently, Gropen and Seip[12] have given conclusive results for the CNDO/2 calculations aimed at making it possible to predict the stable conformation of the molecules. Their calculation for biphenyl has given the same result as Tinland's. Even for rather simple molecules such as glyoxal, the calculated total energy minimum was found for a torsional angle, θ, slightly above 90°, in disagreement with the experimental results.

In spite of the deficiencies of the CNDO/2 method pointed out, we venture to present this article out of our desire to elucidate the electronic spectra of biphenyl, which have long been of interest both to theoretical and experimental chemists, especially from a stereochemical point of view.

1) J. A. Pople, D. P. Santry, and G. A. Segal, *J. Chem. Phys.*, **43**, s129 (1965).
2) J. A. Pople and G. A. Segal, *ibid.*, **43**, s136 (1965).
3) J. A. Pople and G. A. Segal, *ibid.*, **44**, 3289 (1966).
4) G. A. Segal, *ibid.*, **47**, 1876 (1967).
5) A. Tajiri, N. Ohmichi, and T. Nakajima, This Bulletin, **44**, 2347 (1971).
6) H. Yamaguchi, T. Nakajima, and T. L. Kunii, *Theor. Chim. Acta*, **12**, 349 (1968).
7) O. Bastiansen and M. Treatterberg, *Tetrahedron*, **17**, 147 (1962).
8) A. Almenningen and O. Bastiansen, *Kgl. Norske Videnskab. Selskabs Skrifter*, **1958**, 4.
9) J. Trotter, *Acta Crystallogr.*, **14**, 1135 (1961).
10) B. Tinland, *Theor. Chim. Acta*, **11**, 452 (1968).
11) Tables of interatomic distances and configuration in molecules and ions. London: The Chemical Society 1958.
12) O. Gropen and H. M. Seip, *Chem. Phys. Lett.*, **11**, 445 (1971).

Method of Calculation

Although the calculation of the electronic transition energies of biphenyl is of much interest, it has been well established that the original CNDO/2 method predicts markedly high excitation energies, almost twice as high, of molecules.[13] Several authors[13-19] have proposed some modifications of the CNDO/2 method aimed at making it more useful for predicting and interpreting spectroscopic data. One of the present authors[5,20] has succeeded in interpreting the electronic spectra of some non-alternant conjugated hydrocarbons and heterocyclics by use of a modified version of the CNDO/2 method, using a new parametrization for the Del Bene-Jaffé's parameter, κ, for the π-bonds and the bonding parameter, β_x^0, which correlates with the two-center core matrix element, $\beta_{\mu\nu}$, by menas of the following equation:

$$\beta^{\sigma}_{\mu\nu} = \frac{1}{2}(\beta^0_A+\beta^0_B)S_{\mu\nu} \quad (1)$$

$$\beta^{\pi}_{\mu\nu} = \frac{\kappa}{2}(\beta^0_A+\beta^0_B)S_{\mu\nu} \quad (2)$$

where μ and ν denote the AO's on the A and B atoms respectively. The values of κ, β_C^0, and β_H^0 are chosen to be 0.75, -15.0 eV, and -8.0 eV so as to give the most consistent spectroscopic agreements for methane, ethylene and benzene. In this work, the above equation (2) is used to determine the value of the resonance integral for all π-type interactions, wherever they occur. It is also used to evaluate the π-component of the interaction of the two "2p" atomic orbitals which are part of the sigma framework, and to evaluate the interaction of the two "2p" orbitals which are perpendicular to the molecular plane. Only under these conditions could the symmetry of the nonplanar molecule hold; accordingly, this method could be used to study nonplanar molecules. One-center and two-center electron repulsion integrals are evaluated with the Sichel-Whitehead formula[21,22] and the Mataga-Nishimoto formula[23] respectively, and the local core matrix elements, with the Sichel-Whitehead procedures.

Results and Discussion

Ground-state Properties. As was dsecribed above, the CNDO/2 method has predicted a conformation with $\theta=90°$ instead of 42°.[7,8] It is apparent that this is mainly due to the overestimation of the core repulsions evaluated from the point-charge approximation between non-bonded atoms, especially between ortho-hydrogen atoms at the 7, 7′, 11, and 11′ positions; that is, if we assume the central bond length to be 1.50 Å, the change in the core-repulsion energy overcomes the change in the electronic energy in the neighbourhood of the expected equilibrium conformation of biphenyl. The minimum point of the potential energy curve no longer exists at $\theta=42°$, but at $\theta=90°$, where the core repulsions between non-bonded atoms have the smallest values. Of course, these repulsions will be reduced if the distance of the central bond is increased in the case of biphenyl, as was suggested by Tinland. A minimization of the total energy with respect to an angle variation is possible when we adopt a value of 1.54 Å for the central bond, in accordance with the results of Karle and Blockway.[24] This is shown in Fig. 2. It is interesting to note that the curve has a very shallow trough and that the energy difference between $\theta=0°$ and $\theta=42°$ is calculated to be 0.08 eV (about 1.8 kcal/mol). This is in good agreement with the experimentally-determined rotational potential barrier in biphenyl, 2 kcal/mol.[25]

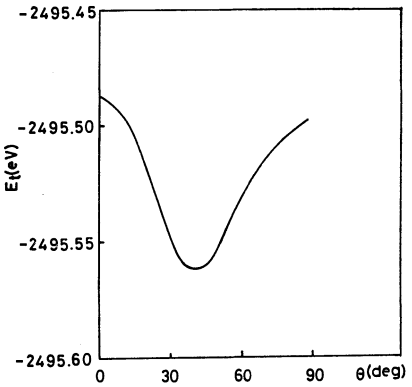

Fig. 2. Calculated potential energy curve for biphenyl with central C–C bond length 1.54 Å.

The calculated AO and atom populations calculated at this energy minimum point are summarized in Table 1. It should be stressed that the electron densities on the carbon atoms at the positions of 2, 6, 2′, and 6′ are larger than those on the other carbon atoms.

Excited-state Properties. The behavior of a so-called "conjugation band" has long been of interest to theoretical and experimental chemists. As early as 1936 Pickett[26] found a strong absorption band at

13) H. W. Kroto and D. P. Santry, *J. Chem. Phys.*, **47**, 792 (1967).
14) J. Del Bene and H. H. Jaffé, *ibid.*, **48**, 1807 (1968).
15) J. Del Bene and H. H. Jaffé, *ibid.*, **48**, 4050 (1968).
16) J. Del Bene and H. H. Jaffé, *ibid.*, **49**, 1221 (1968).
17) J. Del Bene and H. H. Jaffé, *ibid.*, **50**, 1126 (1969).
18) C. Giessner-Pretre and A. Pullman, *Theor. Chim. Acta*, **13**, 265 (1969).
19) C. Giessner-Pretre and A. Pullman, *ibid.*, **18**, 14 (1970).
20) A. Tajiri, T. Asano, and T. Nakajima, *Tetrahedron Lett.*, **1971**, 1785.
21) J. M. Sichel and M. A. Whitehead, *Theor. Chim. Acta*, **7**, 32 (1967). One center electron repulsion integrals are evaluated from averaging all intra-atomic electron repulsion integrals g_{ij} between AO's on atom A and can be written

$$g_{AA} = \frac{1}{16}\sum_i\sum_j g_{ij}$$

where g_{ij}'s are evaluated from atomic valence state energies.
22) J. M. Sichel and M. A. Whitehead, *ibid.*, **11**, 220 (1968).
23) N. Mataga and K. Nishimoto, *Z. Phys. Chem.*, **13**, 140 (1957).
24) I. L. Karle and L. O. Blockway, *J. Amer. Chem. Soc.*, **66**, 1974 (1944).
25) J. E. Katon and E. R. Lippincott, *Spectrochim. Acta*, **19**, 627 (1959).
26) L. W. Pickett, G. F. Walter, and H. France, *J. Amer. Chem. Soc.*, **58**, 2296 (1936).

TABLE 1. AO(q_{ao}) AND ATOM (q_{at}) POPULATIONS IN BIPHENYL

Atom	AO	q_{ao}	q_{at}
C_1	2s	0.994	3.979
	$2p_x$	0.985	
	$2p_y$	1.000	
	$2p_z$	1.000	
C_2	2s	1.014	4.005
	$2p_x$	1.003	
	$2p_y$	0.985	
	$2p_z$	1.003	
C_3	2s	1.013	3.986
	$2p_x$	1.007	
	$2p_y$	0.982	
	$2p_z$	0.984	
C_4	2s	1.011	3.995
	$2p_x$	0.958	
	$2p_y$	1.011	
	$2p_z$	1.011	
H_7	1s	1·007	1.007
H_8	1s	1.008	1.008
H_9	1s	1.008	1.008

about 250 nm characteristic of a series of biphenyl derivatives, and suggested a correlation between the location of this strong band and the conformation of biphenyl. It has also been shown[27] that the intensity of this band weakens as the conjugation of the two benzene rings decreases.

From the theoretical point of view, several authors[28–33] have tried to elucidate the spectral shift of the conjugation band with the conformational change of the biphenyl skeleton on the basis of the π-electron LCAO-MO method. Murrell and Longuet-Higgins[28] have calculated the lower singlet excitation energies by the use of the "molecules in molecules" method, while Gondo[31] and Grinter[32] have compared the transition energies calculated using a modified version of the PPP method[34,35] over a wide range of twisting angles, θ.

According to the above discussions, it seems to be appropriate to compare the results calculated over the wide range of θ values from $\theta=0°$ to $\theta=90°$ in order to clarify the spectral change in biphenyl. We have calculated the transition energies of biphenyl at each point corresponding to the planar ($\theta=0°$; D_{2h}), angular ($\theta=42°$; D_2), and vertical ($\theta=90°$; D_{2d}) conformations. In the CI calculations, 55 singly-excited configurations are taken into account for each conformation. Throughout the calculations, the central C–C bond length has been assumed to be 1.50 Å[11] and the C–C bond lengths of the two benzene rings to be equal and 1.40 Å.

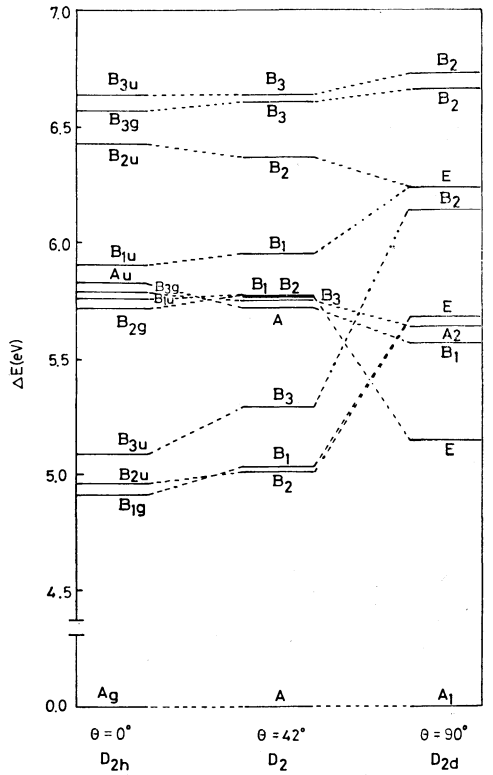

Fig. 3. The energies and symmetries of the lower excited states of three possible conformations of biphenyl.

Figure 3 shows a schematic diagram of the lower singlet states of biphenyl predicted for the three possible conformations. It is apparent from Fig. 3 that the conjugation band is to be assigned to the $A_g \rightarrow B_{3u}$ electronic transition in the D_{2h} conformation, to the $A \rightarrow B_3$ transition in the D_2 conformation, and to the $A_1 \rightarrow B_2$ transition in the D_{2d} conformation, respectively. Table 2 summarizes the calculated energies and symmetries of the lower singlet states of biphenyl, together with the oscillator strengths due to the transitions from the totally-symmetric ground state to the excited states.

In the D_{2h} conformation, the lowest $\pi \rightarrow \pi^*$ electronic transition energy is predicted to be 4.91 eV, corresponding to a symmetry-foribidden $A_g \rightarrow B_{1g}$ transition. The excitation energy corresponding to the next $\pi \rightarrow \pi^*$ electronic transition, $A_g \rightarrow B_{2u}$, is calculated to be 4.96 eV, with its moment directed along the short axis. As for the order of these two states, the results are in disagreement with those obtained by Grinter[32], who concluded that the B_{2u} state was lower than the B_{1g} state, while it is in agreement with the results of Suzuki.[30] An $A_g \rightarrow B_{3u}$ transition which gives rise to the conjugation band is predicted at 5.04 eV, and its oscillator strength is calculated to be 0.80. Although several transitions associated with σ-MO's are predicted to exist in the range of 5.5—5.6 eV, they are predicted to be forbidden by symmetry or very weak in intensity. It should be noted that the higher $\pi \rightarrow \pi^*$ transition energies, corresponding to the $A_g \rightarrow B_{2u}$ and $A_g \rightarrow B_{3u}$ electronic transitions, are

27) M. T. O'Shaughnessy and W. H. Rodebush, *ibid.*, **62**, 2096 (1940).
28) J. N. Murrell and H. C. Longuet-Higgins, *Proc. Phys. Soc.*, **A68**, 601 (1955).
29) J. N. Murrell, *J. Chem. Soc.*, **1956**, 3779.
30) H. Suzuki, This Bulletin, **32**, 1340 (1959).
31) Y. Gondo, *J. Chem. Phys.*, **41**, 3928 (1964).
32) R. Grinter, *Mol. Phys.*, **11**, 7 (1966).
33) A. Imamura and R. Hoffmann, *J. Amer. Chem. Soc.*, **90**, 5379 (1968).
34) R. Pariser and R. G. Parr, *J. Chem. Phys.*, **21**, 466, 767 (1953).
35) J. A. Pople, *Trans. Faraday Soc.*, **24**, 250 (1956).

TABLE 2. CALCULATED SINGLET TRANSITION ENERGIES ΔE(eV) AND OSCILLATOR STRENGTHS f(C.G.S)

$\theta=0°$		$\theta=42°$		$\theta=90°$	
Type	$\Delta E(f)$	Type	$\Delta E(f)$	Type	$\Delta E(f)$
$A_g \rightarrow B_{1g}$	4.91 (forb.)	$A \rightarrow B_2$	5.01 (0.02)	$A_1 \rightarrow E$	5.15 (0.04)
$A_g \rightarrow B_{2u}$	4.96 (0.01)	$A \rightarrow B_1$	5.03 (0.00)	$A_1 \rightarrow B_1$	5.57 (forb.)
$A_g \rightarrow B_{3u}$	5.04 (0.80)	$A \rightarrow B_3$	5.29 (0.68)	$A_1 \rightarrow A_2$	5.64 (forb.)
$A_g \rightarrow B_{2g}$	5.71 (forb.)	$A \rightarrow A$	5.72 (forb.)	$A_1 \rightarrow E$	5.67 (0.00)
$A_g \rightarrow B_{1u}$	5.75 (0.00)	$A \rightarrow B_3$	5.75 (0.01)	$A_1 \rightarrow B_2$	6.14 (0.41)
$A_g \rightarrow B_{3g}$	5.78 (forb.)	$A \rightarrow B_1$	5.76 (0.00)	$A_1 \rightarrow E$	6.22 (0.02)
$A_g \rightarrow A_u$	5.82 (forb.)	$A \rightarrow B_2$	5.76 (0.00)	$A_1 \rightarrow B_2$	6.65 (0.00)
$A_g \rightarrow B_{1u}$	5.90 (0.00)	$A \rightarrow B_1$	5.95 (0.00)	$A_1 \rightarrow B_2$	6.72 (1.52)
$A_g \rightarrow B_{2u}$	6.42 (0.67)	$A \rightarrow B_2$	6.36 (0.24)		
$A_g \rightarrow B_{3g}$	6.56 (forb.)	$A \rightarrow B_3$	6.60 (0.02)		
$A_g \rightarrow B_{3u}$	6.63 (0.90)	$A \rightarrow B_3$	6.63 (0.83)		

predicted to be 6.42 eV and 6.36 eV, with their moments directed along the short and long axes of biphenyl respectively.

The correlation between two point groups, D_{2h} and D_2, is easily found. The B_{1g} and B_{2u} states turn out to be B_1 and B_2 states respectively in an angular conformation. It should be noted that the B_2 state is lower than the B_1 state. It can clearly be seen from Fig. 3 that the conformational change in biphenyl is well reflected in the change both in the energy and in the intensity of the electronic transition, which has the same character as the $A_g \rightarrow B_{3u}$ transition in planar biphenyl. The excitation energy corresponding to this electronic transition is calculated to be 5.29 eV, with its moment directed along the long axis. Its oscillator strength is predicted to be 0.68, which is smaller than that of the corresponding transition in D_{2h} biphenyl because of the decrease in the conjugation of π-electrons in the two benzene rings. It is interesting to note that the higher $A \rightarrow B_3$ transition energy is unaffected by the conformational change in biphenyl.

In a vertical conformation, the lowest excitation energy corresponding to an electronic transition from the ground state, A_1, to a degenerate excited state, E, is predicted to be 5.15 eV, with a small value of oscillator strength, 0.04. This lowest degenerate excited state can be correlated to the nearly degenerate B_1 and B_2 states located near 5.8 eV in D_2 conformation, while in the study of Grinter the lowest E state come from the lowest B_1 and B_2 states. A long-axis polarized transition, $A_1 \rightarrow B_2$, in the D_{2d} conformation has come from the $A \rightarrow B_3$ electronic transition in the D_2 conformation. The effect of the twist is most evidently reflected in the blue-shift of this transition and in the oscillator strength. The higher B_2 state is little affected, as in the case of reduction from D_{2h} to D_2.

From the experimental point of view, many authors[26,27,36-42] have been interested in the electronic spectra of biphenyl and its derivatives. Unfortunately, however, we have no spectral data on biphenyl itself with a vertical conformation.

We are forced to compare the calculations for $\theta=0°$ and $\theta=42°$ with solid[43-47] and solution or vapor-phase[48,49] spectra of the unsubstituted biphenyl respectively.

With regard to the energy of the transition which gives rise to the conjugation band, it is unfortunate that the measurement of this band has not been made for crystalline biphenyl. Dale,[48] however, has measured the spectrum of solid biphenyl by the pressed KCl-disk technique and found an intense, structureless band with a maximum at 2530 Å (=4.94 eV). Suzuki[30] has suggested, after a correction for the normal red-shift observed when samples are measured in KCl-disks, that planar biphenyl which is free from intermolecular interactions should show the characteristic conjugation band at 2495 Å (=4.97 eV). This is in excellent agreement with the results of this calculation for $\theta=0°$, *i. e.*, 5.04 eV. Coffman and McClure[43,44] have reported bands at 33340 cm^{-1} (=4.13 eV, B_{1g}) and 33714 cm^{-1} (=4.18 eV, B_{2u}). The order of these states is in agreement with this calculation, while the predictions of their energy are too high.

The spectrum of biphenyl has also been measured in the vapor phase[50]; absorption maxima were found at 5.2 eV and 5.18 eV for the temperatures of 170° and 520°C respectively. In non-polar solvents, the

36) Steric effects in conjugated systems. E. A. Braude and W. F. Forbes, Butterworths Scientific Pub. London (1958), p. 22.
37) E. A. Braude and W. F. Forbes, *J. Chem. Soc.*, **1955**, 3776.
38) B. Williamson and W. H. Rodebush, *J. Amer. Chem. Soc.*, **63**, 3018 (1941).
39) R. A. Friedel, M. Orchin, and L. Reggel, *ibid.*, **70**, 199 (1948).
40) G. H. Beaven, D. M. Hall, and M. S. Lesslie, *J. Chem. Soc.*, 854 (1952).
41) T. M. Dunn and T. Iredale, *ibid.*, 1592 (1952).
42) G. H. Beaven, D. M. Hall, M. S. Lesslie, E. E. Turner, and G. R. Biard, *ibid.*, 131 (1954).
43) R. Coffman and D. S. McClure, *Canad. J. Chem.*, **36**, 48 (1955).
44) D. S. McClure, *ibid.*, **36**, 59 (1958).
45) E. Merkel and C. Weigand, *Z. Naturf.*, **B3**, 93 (1948).
46) T. M. Dunn, J. R. Gott, and C. Zauli, *Boll. Sci. Fac. Bologna*, **18**, 210 (1960).
47) A. R. Deb, *Ind. J. Phys.*, **27**, 305 (1953).
48) J. Dale, *Acta Chem. Scand.*, **11**, 650 (1957).
49) E. P. Carr and H. Stucklen, *J. Chem. Phys.*, **4**, 760 (1936).
50) F. Almasy and H. Laemmel, *Helv. Chim. Acta*, **33**, 2092 (1950).

Table 3. Singlet transition energies ΔE(eV) and oscillator strengths f(C.G.S.) calcuted at the point corresponding to the energy minimum in Fig. 2

Type	$\Delta E(f)$	Type	$\Delta E(f)$
$A\rightarrow B_2$	5.00(0.03)	$A\rightarrow B_2$	5.92(0.00)
$A\rightarrow B_1$	5.01(0.01)	$A\rightarrow B_1$	6.05(0.00)
$A\rightarrow B_3$	5.41(0.67)	$A\rightarrow B_3$	6.30(0.01)
$A\rightarrow A$	5.77(forb.)	$A\rightarrow B_2$	6.44(0.35)
$A\rightarrow B_3$	5.79(0.00)	$A\rightarrow B_3$	6.62(0.75)
$A\rightarrow B_1$	5.92(0.00)		

conjugation band is found at 2480 Å (=5.00 eV)[36], with an oscillator strength of 0.411.[50] These values are to be compared with the value of 5.29 eV determined here for $\theta=42°$. The agreement between theory and experiment seems to be fairly good.

Finally, we have listed the transition energies calculated with $\theta=42°$ and the central C–C bond length of 1.54 Å in Table 3. It is apparent from the table that the bond lengthening has little, if any, effect on the electronic spectra.

The authors wish to thank Professor Nakajima of Tohoku University for his encouragement and helpful discussions.

BULLETIN OF THE CHEMICAL SOCIETY OF JAPAN, VOL. 46, 1071—1076 (1973)

Orbital Symmetry Control in the Interaction of Three Systems

Hiroshi FUJIMOTO, Shigeki KATO, Shinichi YAMABE, and Kenichi FUKUI

Faculty of Engineering, Kyoto University, Sakyo-ku, Kyoto 606

(Received August 8, 1972)

Some perturbation equations for calculating the interaction energy of three independent systems have been derived in the frame of the simple Hückel MO approximation. The results of the numerical calculation of some typical interactions of three conjugated systems are presented in order to show the effect of the orbital symmerty upon the interaction energy. The role of the d orbitals of transition-metal catalysis olefin metathesis is examined.

Some important information on the nature of chemical interactions in unimolecular reactions has been derived by considering the conjugation between two parts of a molecule, using a partitioning technique.[1] To discuss the stability of a molecular system by means of the conjugation stabilization of the interaction of three or four parts of a molecule properly partitioned seems to be promising for the purpose of illuminating the essential features of complicated chemical reactions.[2] Recently, Goldstein and Hoffmann extended the concept of aromaticity to some multi-centric interactions of more than three systems.[3] They discussed the interaction of three systems by regarding it as two successive cyclic interactions of two systems, based upon the concept of orbital interaction between the highest occupied (HO) molecular orbital (MO) of one system and the lowest unoccupied (LU) MO of the other system. The applicability of the theory of the HOMO–LUMO interaction to predicting the favorable reaction paths has been verified in numerous cases.[1,4] Therefore, the generalization of aromaticity by Goldstein and Hoffmann may be accepted. Since such multi-centric interactions of three systems are highly related to the catalytic action of transition-metal complexes, we would like to present some simple formulae for the simultaneous cyclic interactions of three independent systems. These formulae will be useful for a semi-quantitative comparison of various types of interactions of three systems.

Interaction Energy

Longicyclic Interactions. First, let us consider the longicyclic interaction[3] of three systems, A, B,

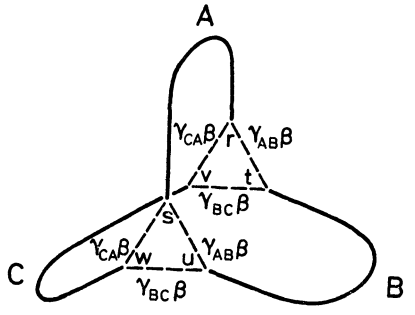

Fig. 1. Longicyclic interaction of three systems A, B and C.

1) a) K. Fukui and H. Fujimoto, "Mechanisms of Molecular Migrations," B. S. Thyagarajan, Ed., Interscience. New York, N. Y. (1969), pp. 117—190. b) K. Fukui, *Accounts Chem. Res.*, **4**, 57 (1971).

2) a) M. J. Goldstein, *J. Amer. Chem. Soc.*, **89**, 6357 (1967). b) H. E. Zimmerman, *Accounts Chem. Res.*, **4**, 272 (1971). c) R. Hoffmann and W. D. Stohrer, *J. Amer. Chem. Soc.*, **93**, 6941 (1971). d) L. A. Paquette, M. R. Short, and J. F. Kelly, *ibid.*, **93**, 7179 (1971).

3) M. J. Goldstein and R. Hoffmann, *J. Amer. Chem. Soc.*, **93**, 6193 (1971).

4) a) K. Fukui, "Molecular Orbitals in Chemistry, Physics, and Biology," P. -O. Löwdin and B. Pullman, Eds., Academic Press, New York, N. Y. (1964), pp. 513—537. b) K. Fukui, "Modern Quantum Chemistry. Istanbul Lectures, Part I," O. Sinanoğlu, Ed., Academic Press, New York, N. Y. (1965), pp. 49—84. c) K. Fukui, "Sigma Molecular Orbital Theory," O. Sinanoğlu and K. B. Wiberg, Eds., Yale University Press, New Haven, Conn. (1970), pp. 121—129. d) K. Fukui, *Fortschr. Chem. Forsch.*, **15**, 1 (1970). e) G. Klopman, *J. Amer. Chem. Soc.*, **90**, 223 (1968). f) L. Salem, *ibid.*, **90**, 543, 553 (1968). g) K. Fukui and H. Fujimoto, This Bulletin, **41**, 1989 (1968). h) K. Fukui and H. Fujimoto, *ibid.*, **42**, 3399 (1969). i) H. Fujimoto, S. Yamabe, and K. Fukui, *ibid.*, **44**, 2936 (1971). j) R. G. Pearson, *Theor. Chim. Acta*, **16**, 107 (1970).

and C, which are joined together at the AO's, r and s of A, t and u of B, and v and w of C. The interaction of these three systems is represented by the $\gamma_{AB}\beta$, $\gamma_{BC}\beta$, and $\gamma_{CA}\beta$, resonance integrals respectively, as is shown in Fig. 1. The simple Hückel secular equation for the system is given by:

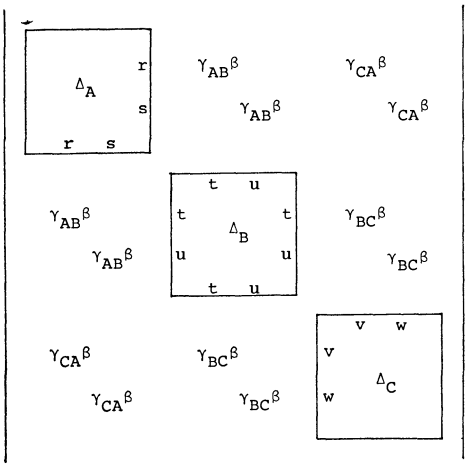

(1)

where $\Delta_A(\varepsilon)=0$, $\Delta_B(\varepsilon)=0$, and $\Delta_C(\varepsilon)=0$ are the secular equations for the A, B, and C systems respectively in their isolated states. By expanding Eq. (1) in the power series of the interaction integrals, $\gamma\beta$, we obtain:

$$\begin{aligned}&\Delta_A\Delta_B\Delta_C\\&-(\gamma_{AB}\beta)^2\{\Delta_{Arr}\Delta_{Btt}+\Delta_{Ass}\Delta_{Buu}+2(-1)^{r+s+t+u}\Delta_{Ars}\Delta_{Btu}\}\\&-(\gamma_{BC}\beta)^2\{\Delta_{Btt}\Delta_{Cvv}+\Delta_{Buu}\Delta_{Cww}+2(-1)^{t+u+v+w}\Delta_{Btu}\Delta_{Cvw}\}\\&-(\gamma_{CA}\beta)^2\{\Delta_{Cvv}\Delta_{Arr}+\Delta_{Cww}\Delta_{Ass}+2(-1)^{v+w+r+s}\Delta_{Cvw}\Delta_{Ars}\}\\&+\cdots\cdots\\&=0\end{aligned} \tag{2}$$

where Δ_{Ars}, for instance, is the minor of Δ_A with respect to the (r, s) element of the determinant. Assuming that $|\gamma_{AB}|$, $|\gamma_{BC}|$, $|\gamma_{CA}|$ are small in comparison with unity, we may expand the eigenvalues of the perturbed secular equation in the power series of the interaction integrals.[5] When the ith root, ε_{Ai}, of the secular equation, $\Delta_A(\varepsilon)=0$, is not simultaneously the root of $\Delta_B(\varepsilon)=0$ and $\Delta_C(\varepsilon)=0$, the perturbed eigenavlue of Eq. (1) is given by:

$$\begin{aligned}\varepsilon_{Ai}' = \varepsilon_{Ai} &- \sum_j^{all}\frac{(c_r^{(i)}c_t^{(j)}+c_s^{(i)}c_u^{(j)})^2}{\varepsilon_{Bj}-\varepsilon_{Ai}}(\gamma_{AB}\beta)\\&-\sum_k^{all}\frac{(c_r^{(i)}c_v^{(k)}+c_s^{(i)}c_w^{(k)})^2}{\varepsilon_{Ck}-\varepsilon_{Ai}}(\gamma_{CA}\beta)^2+\cdots\cdots\end{aligned} \tag{3}$$

where $C_r^{(i)}$, for instance, is the coefficient of the (AO) r atomic orbital in the MO i of A, and where j and k denote the MO's of B and C respectively. Similar equations can be derived for ε_{Bj}', and ε_{Ck}', corresponding to the jth root of $\Delta_B(\varepsilon)=0$ and the kth root of $\Delta_C(\varepsilon)=0$ respectively. When all of the three systems have closed-shell electronic structures, the conjugation stabilization energy due to the interaction is given by:

$$\begin{aligned}\Delta E\cong 2&\Big(\sum_i^{occ}\sum_j^{uno}-\sum_i^{uno}\sum_j^{occ}\Big)\frac{(c_r^{(i)}c_t^{(j)}+c_s^{(i)}c_u^{(j)})^2}{\varepsilon_{Ai}-\varepsilon_{Bj}}(\gamma_{AB}\beta)^2\\&+2\Big(\sum_j^{occ}\sum_k^{uno}-\sum_j^{uno}\sum_k^{occ}\Big)\frac{(c_t^{(j)}c_v^{(k)}+c_u^{(j)}c_w^{(k)})^2}{\varepsilon_{Bj}-\varepsilon_{Ck}}(\gamma_{BC}\beta)^2\\&+2\Big(\sum_k^{occ}\sum_i^{uno}-\sum_k^{uno}\sum_i^{occ}\Big)\frac{(c_v^{(k)}c_r^{(i)}+c_w^{(k)}c_s^{(i)})^2}{\varepsilon_{Ck}-\varepsilon_{Ai}}(\gamma_{CA}\beta)^2\end{aligned} \tag{4}$$

where the $\sum^{occ}$ and $\sum^{uno}$ symbols imply the summation over all the doubly-occupied and unoccupied MO's respectively. Equation (4) indicates that, as to the second-order perturbation energy, the conjugation stabilization due to the interaction of three systems is simply given by the sum of those of the interaction between two systems. By the use of the results of calculations for cyclic interaction between two systems presented in our previous paper,[6] we obtain the results shown in Table 1. The conjugation stabilization of the cyclic syn-interaction[6] of two systems is large when the number of electrons forming a cycle is 4n+2, while the stabilization is not large when the number of electrons is 4n.[1,6] When A is a 4n-electron system, both B and C should be (4n+2)-electron systems in order to make the conjugation stabilization due to the interaction between A and B and that between A and C large. When the A system is a (4n+2)-electron system, the case in which both B and C are 4n-electron systems leads to a large stabilization.

Table 1. The conjugation stabilization energy in longicyclic interaction of three conjugated systems

A[a]	B[a]	C[a]	$\Delta E/\gamma^2\beta$[b]
2	2	2	0.0
4	4	4	2.147
6	6	6	2.987
2	4	4	4.293
2	2	6	1.244
2	6	6	2.239
6	4	4	4.200
4	2	2	3.578
4	2	6	4.153
4	6	6	4.480

a) 2; ethylenic, 4; butadienic, 6; hexatrienic: by the term ethylenic, for instance, is meant the employment of the π MO's of ethylene.

b) $|\gamma_{AB}|=|\gamma_{BC}|=|\gamma_{CA}|=\gamma$: hereafter β is taken always negative.

In both the cases, however, the interaction between B and C does not produce a large stabilization. In this sense, the interaction can be classified into doubly-stabilized and unstabilized cases, following the notations introduced by Goldstein and Hoffmann.[3] Equation (4) supplies us with a simpler and even more quantitative means than the step-by-step method of Goldstein and Hoffmann to discuss the cyclic interactions of three independent systems.

5) a) K. Fukui, C. Nagata, T. Yonezawa, H. Kato, and K. Morokuma, *J. Chem. Phys.*, **31**, 287 (1959). b) K. Fukui, K. Morokuma, T. Yonezawa, and C. Nagata, This Bulletin, **33**, 963 (1960).

6) K. Fukui and H. Fujimoto, *ibid.*, **39**, 2166 (1966).

When one of the three systems, say A, has a singly-occupied MO, 0, the following additional term appears:

$$+\left(\sum_{j}^{\text{uno}}-\sum_{j}^{\text{occ}}\right)\frac{(c_r^{(0)}c_t^{(j)}+c_s^{(0)}c_u^{(j)})^2}{\varepsilon_{A0}-\varepsilon_{Bj}}(\gamma_{AB}\beta)^2$$
$$+\left(\sum_{k}^{\text{uno}}-\sum_{k}^{\text{occ}}\right)\frac{(c_r^{(0)}c_v^{(k)}+c_s^{(0)}c_w^{(k)})^2}{\varepsilon_{A0}-\varepsilon_{Ck}}(\gamma_{CA}\beta)^2$$

Laticyclic Interactions. The equation representing the conjugation stabilization energy of the laticyclic interaction[3] of A, B, and C is immediately derived from Eq. (4) by putting one of the three integrals, say $\gamma_{CA}\beta$, equal to zero. When B is interposed between A and C, as is shown in Fig. 2, we obtain:

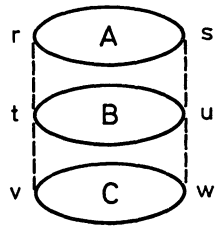

Fig. 2. Laticyclic interaction of three systems A, B and C.

$$\Delta E\cong 2\left(\sum_{i}^{\text{occ}}\sum_{j}^{\text{uno}}-\sum_{i}^{\text{uno}}\sum_{j}^{\text{occ}}\right)\frac{(c_r^{(i)}c_t^{(j)}+c_s^{(i)}c_u^{(j)})^2}{\varepsilon_{Ai}-\varepsilon_{Bj}}(\gamma_{AB}\beta)^2$$
$$+2\left(\sum_{j}^{\text{occ}}\sum_{k}^{\text{uno}}-\sum_{j}^{\text{uno}}\sum_{k}^{\text{occ}}\right)\frac{(c_t^{(j)}c_v^{(k)}+c_u^{(j)}c_w^{(k)})^2}{\varepsilon_{Bj}-\varepsilon_{Ck}}(\gamma_{AB}\beta)^2 \quad (5)$$

The results of the calculation for several laticyclic interactions of three conjugated systems are given in Table 2. We can see that the conjugation stabilization is large in the following two cases: (i) when A and C are (4n+2)-electron systems and B is a 4n-electron system, and (ii) when A and C are 4n-electron systems and B is a (4n+2)-electron system.

Table 2. The conjugation stabilization energy in laticyclic interaction of three conjugated systems

A[a]	B[a]	C[a]	$\Delta E/\gamma^2\beta^{b}$
2	2	2	0.0
2	2	4	1.789
2	4	2	3.578
2	4	4	2.504
4	2	4	3.578
2	2	6	0.622
2	6	2	1.244
4	4	4	1.431
2	4	6	3.531
2	6	4	2.364
6	2	4	2.411
2	6	6	1.617
6	2	6	1.244
4	4	6	2.458
4	6	4	3.483
4	6	6	2.738
6	4	6	3.484
6	6	6	1.991

a) 2; ethylenic, 4; butadienic, 6; hexatrienic.
b) $|\gamma_{AB}|=|\gamma_{BC}|=\gamma$

Pericyclic Interactions. Next, let us consider the pericyclic interaction[3] of the three systems, A, B, and C, as is shown in Fig. 3. The perturbed secular equation is:

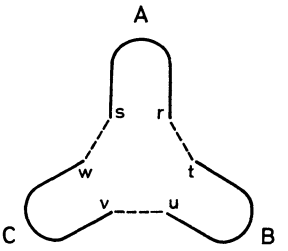

Fig. 3. Pericyclic interaction of three systems A, B and C.

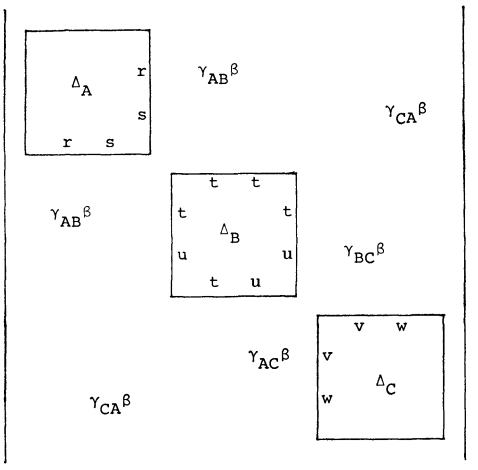

(6)

Expanding the perturbed MO energies in the power series of $\gamma\beta$, the second-order perturbation energy is given by:

$$\Delta E=2\left(\sum_{i}^{\text{occ}}\sum_{j}^{\text{uno}}-\sum_{i}^{\text{uno}}\sum_{j}^{\text{occ}}\right)\frac{(c_r^{(i)}c_t^{(j)})^2}{\varepsilon_{Ai}-\varepsilon_{Bj}}(\gamma_{AB}\beta)^2$$
$$+2\left(\sum_{j}^{\text{occ}}\sum_{k}^{\text{uno}}-\sum_{j}^{\text{uno}}\sum_{k}^{\text{occ}}\right)\frac{(c_u^{(j)}c_v^{(k)})^2}{\varepsilon_{Bj}-\varepsilon_{Ai}}(\gamma_{BC}\beta)^2$$
$$+2\left(\sum_{k}^{\text{occ}}\sum_{i}^{\text{uno}}-\sum_{k}^{\text{uno}}\sum_{i}^{\text{occ}}\right)\frac{(c_w^{(k)}c_s^{(i)})^2}{\varepsilon_{Ck}-\varepsilon_{Ai}}(\gamma_{CA}\beta)^2 \quad (7)$$

The results of the calculations are given in Table 3. Unfortunately, as to the second-order perturbation terms, we can not distinguish the 4n and (4n+2)-electron cycles. For example, the pericyclic interaction of the ethylenic, butadienic, and allyl cationic systems gives the same conjugation stabilization energy as the interaction of the ethylenic, butadienic, and allyl anionic system, 2+4+(3−1). The interaction energy of the third-order with respect to γ is given by:

$$\Delta E=8\left\{\sum_{i}^{\text{occ}}\sum_{j}^{\text{all}}\sum_{k}^{\text{all}}\frac{c_r^{(i)}c_s^{(i)}c_t^{(j)}c_u^{(j)}c_v^{(k)}c_w^{(k)}}{(\varepsilon_{Bj}-\varepsilon_{Ai})(\varepsilon_{Ck}-\varepsilon_{Ai})}\right.$$
$$+\sum_{j}^{\text{occ}}\sum_{k}^{\text{all}}\sum_{i}^{\text{all}}\frac{c_t^{(j)}c_u^{(j)}c_v^{(k)}c_w^{(k)}c_r^{(i)}c_s^{(i)}}{(\varepsilon_{Ck}-\varepsilon_{Bj})(\varepsilon_{Ai}-\varepsilon_{Bj})}$$
$$\left.+\sum_{k}^{\text{occ}}\sum_{i}^{\text{all}}\sum_{j}^{\text{all}}\frac{c_v^{(k)}c_w^{(k)}c_r^{(i)}c_s^{(i)}c_t^{(j)}c_u^{(j)}}{(\varepsilon_{Ai}-\varepsilon_{Ck})(\varepsilon_{Bj}-\varepsilon_{Ck})}\right\}\gamma_{AB}\gamma_{BC}\gamma_{CA}\beta^3 \quad (8)$$

Table 3. The conjugation stabilization energy in pericyclic interaction of three conjugated systems (second-order)

A[a]	B[a]	C[a]	$\Delta E/\gamma^2\beta$[b]
2	2	2	1.500
2	2	4	1.606
2	4	4	1.732
4	4	4	1.878
2	2	1−1	2.500
2	2	1+1	2.500
2	4	1−1	2.894
2	4	1+1	2.894
2	2	3−1	1.914
2	2	3+1	1.914
2	4	3−1	2.154
2	4	3+1	2.154

a) 2; ethylenic, 4; butadienic, 1−1; cation with single p AO, 1+1; anion with single p AO, 3−1; allyl cationic, 3+1; allyl anionic.
b) $|\gamma_{AB}|=|\gamma_{BC}|=|\gamma_{CA}|=\gamma$

Table 4. The conjugation stabilization energy in pericyclic interaction of three conjugated systems (third-order)

A	B	C	$\Delta E/\gamma^3\beta$[a]
2	2	1−1	−2.000
2	2	1+1	6.000
2	4	1−1	4.000
2	4	1+1	−4.000
2	2	3−1	4.000
2	2	3+1	0.000
2	4	3−1	−2.000
2	4	3+1	2.000

a) Degeneracy was removed by the method reported in Ref. 5 b).

The results of the calculations for several examples are given in Table 4. For instance, the third-order perturbation energy of the cycle composed of the ethylenic, butadienic, and allyl cationic systems is calculated to be $-2.000\,\gamma_{AB}\gamma_{BC}\gamma_{CA}\beta$, while that of the cycle composed of the ethylenic, butadienic and allyl anionic systems is $2.000\,\gamma_{AB}\gamma_{BC}\gamma_{CA}\beta$. Therefore, in order to make the stabilization large, $\gamma_{AB}\gamma_{BC}\gamma_{CA}$ should be negative in the former case, while it should be positive in the latter case. The cyclic conjugation of the three systems in which $\gamma_{AB}\gamma_{BC}\gamma_{CA}$ is positive obviously corresponds to the usual Hückel-type conjugation, while that in which $\gamma_{AB}\gamma_{BC}\gamma_{CA}$ is negative corresponds to the anti-Hückel or Möbius-strip-type conjugation.[7] The conclusions thus derived from the third-order perturbation energy, that the 2+4+(3−1) system favors the anti-Hückel interaction and that the 2+4+(3+1) system favors the Hückel interaction, are in agreement with the results obtained by Goldstein and Hoffmann.[3] However, it should

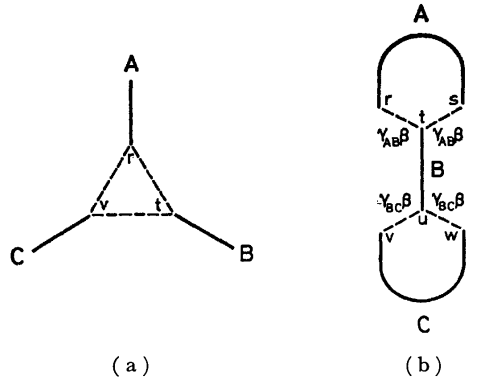

(a) (b)

Fig. 4. Other types of interactions of three systems A, B and C.

be noted here that whether or not a pericyclic interaction of three independent systems takes place preferentially in the Hückel-type or in the anti-Hückel-type interaction depends not on the symmetry properties of the MO's of the three independent systems, but on the number of electrons forming a cycle. This conclusion is completely consistent with that given in our previous paper,[8] and also with the theory of aromaticity.[9]

Other Kinds of Interactions. Let us now discuss some other kinds of interactions of three independent systems. The first case is the interaction of three systems at the r, t, and v termini, as is shown in Fig. 4(a). The interaction energy is given by:

$$\Delta E \cong 2\Big(\sum_{i}^{occ}\sum_{j}^{uno}-\sum_{i}^{uno}\sum_{j}^{occ}\Big)\frac{(c_r^{(i)}c_t^{(j)})^2}{\varepsilon_{Ai}-\varepsilon_{Bj}}(\gamma_{AB}\beta)^2 + 2\Big(\sum_{j}^{occ}\sum_{k}^{uno}-\sum_{j}^{uno}\sum_{k}^{occ}\Big)\frac{(c_t^{(j)}c_v^{(k)})^2}{\varepsilon_{Bj}-\varepsilon_{Ck}}(\gamma_{BC}\beta)^2 + 2\Big(\sum_{k}^{occ}\sum_{i}^{uno}-\sum_{k}^{uno}\sum_{i}^{occ}\Big)\frac{(c_v^{(k)}c_r^{(i)})^2}{\varepsilon_{Ck}-\varepsilon_{Ai}}(\gamma_{CA}\beta)^2 \quad (9)$$

The next case is the interaction of three systems, A, B, and C, in which the AO's r and s of A conjugate with the AO t of B and the AO's v and w of C conjugate with the AO u of B, as is shown in Fig. 4 (b). The conjugation stabilization energy is then given by:

$$\Delta E \cong 2\Big(\sum_{i}^{occ}\sum_{j}^{unc}-\sum_{i}^{uno}\sum_{j}^{occ}\Big)\frac{(c_r^{(i)}c_t^{(j)}+c_s^{(i)}c_t^{(k)})^2}{\varepsilon_{Ai}-\varepsilon_{Bj}}(\gamma_{AB}\beta)^2 + 2\Big(\sum_{k}^{occ}\sum_{j}^{uno}-\sum_{k}^{uno}\sum_{j}^{occ}\Big)\frac{(c_t^{(j)}c_v^{(k)}+c_t^{(j)}c_w^{(k)})^2}{\varepsilon_{Ck}-\varepsilon_{Bj}}(\gamma_{BC}\beta)^2 \quad (10)$$

The results of the calculations are given in Table 5. We can see that the number of electrons of the bridge, B, has little influence upon the interaction energy in the interaction of type (b). In addition, when B is neutral, as in the cases of ethylenic, butadienic, *etc.*, the conjugation stabilization does not depend on the number of electrons, *i. e.*, 4n or 4n+2, of A and of C. When B is cationic, the stabilization is large when both A and C have 4n+2 electrons. On the other hand, when B is anionic, when both A and C are

7) a) E. Heilbronner, *Tetrahedron Lett.*, 1923 (1964). b) H. E. Zimmerman, *J. Amer. Chem. Soc.*, **88**, 1564, 1566 (1966). c) M. J. S. Dewar, *Tetrahedron Suppl.* **8**, Part I, 75 (1966).

8) K. Fukui and H. Fujimoto, This Bulletin, **40**, 2018 (1967).

9) See, for instance, A. Strietwieser, Jr., "Molecular Orbital Theory for Organic Chemists," John Wiley & Sons, New York, N. Y. (1961), p. 256.

Table 5. The conjugation stabilization energy in the interaction of three conjugated systems shown in Fig. 4

	A[a]	B[a]	C[a]	$\Delta E/\gamma^2\beta$[b]
Type (a)	2	2	2	1.500
	2	2	4	1.606
	2	4	4	1.732
	4	4	4	1.878
Type (b)	2	2	2	2.000
	2	2	4	2.106
	2	4	2	2.211
	2	4	4	2.358
	4	2	4	2.211
	4	4	4	2.504
	2	3−1	2	4.828
	2	3+1	2	0.828
	2	3−1	4	3.203
	2	3+1	4	3.203
	4	3−1	4	1.578
	4	3+1	4	5.578

a) 2; ethylenic, 4; butadienic, 6; hexatrienic, 3−1; allyl cationic, 3+1; allyl anionic.
b) $|\gamma_{AB}|=|\gamma_{BC}|=|\gamma_{CA}|=\gamma$

4n-electron systems there will be a large conjugation stabilization. The results in Table 5 correspond to the case in which A, B and C interact through the π-like overlapping of terminal p AO's.

Interaction with d Orbitals

Numerous chemical reactions take place simultaneously with catalysis. In bimolecular reactions of two reactants, A and B, under the influence of a catalysis, C, we must consider the interaction of three independent systems, A, B, and C. Therefore, a theoretical means of handling three systems simultaneously is necessary in order to investigate the role of catalysis in chemical reactions. Recently, the important role of the d orbitals of transition-metal complexes in olefin metathesis was clearly recognized.[4d,10] Some theoretical papers have been published concerning this reaction.[10] However, these consider the process as an interaction between the orbitals of the transition metal and two weakly-coupled olefin molecules or tetramethylene. By the use of Eq. (4), we can examine the role of the d orbitals at the begining of the reaction. The modes of the orbital-overlap interactions are schematically illustrated in Fig. 5. We can see that the HOMO of olefin can interact with $d_{x^2-y^2}$ and that the LUMO can overlap with d_{xy}. Accordingly, the interaction between the d orbitals and π MO's of olefins will result in a net stabilization, although the interaction between two olefins is symmetry-unfavorable and does not lead to stabilization.[6,11] The donation of electrons from the occupied MO's of olefins to the unoccupied d orbital, and that from the occupied d orbital to the unoccupied MO's of olefins, will bring about a loosening of the π bonds of olefins. Consequently, the mixing of the chemically-induced excited state of olefins through the charge-transfer interaction with d orbitals will activate olefins and lessen the symmetry constraint. As the reaction proceeds, it is reasonable to regard the process as an interaction between the d orbitals and two weakly-coupled olefin molecules or a tetramethylene system.[10]

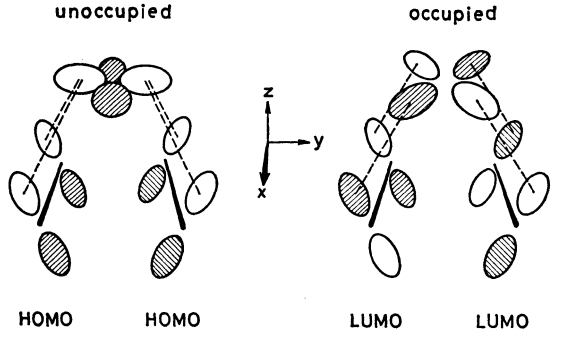

Fig. 5. A schematic representation of orbital overlap interactions in olefin metathesis.

Equation (4) suggests that the two reactants should have the same MO symmetry properties in order for both of them to be activated by the same pair of occupied and unoccupied d orbitals. Olefins metathesis is such a case. Polyenes with an even number of electrons can be classified into two classes; one possessing 4n electrons, and the other, 4n+2 electrons. The HOMO of a 4n-electron system is antisymmetric (A) and the LUMO is symmetric (S). The HOMO of a (4n+2)-electron system is S and the LUMO is A. Therefore, when one reactant is a 4n-electron system and the other is a (4n+2)-electron system, only one of them can be activated by one occupied d orbital and one unocupied d orbital of the central metal of catalysis. In order to activate both, more than two occupied and two unoccupied d orbitals should participate in the reaction. Thus, the important role of the d orbitals of transition-metal complex catalysis can be most clearly observed in the interactions of two conjugated systems belonging to the same class, such as the cases of (2+2), (4+4), (2+6), (6+6), ·····, which are thermally unfavored without catalysis.[1,6,11,12]

Some concenient equations have been derived for the purpose of calculating the stabilization energy of the simultaneous interaction of three independent systems. The stabilization energy for some types of interactions of three systems has been given in the second-order perturbation forms, using the energies and AO coefficients of the MO's of the isolated reactants. These equations can be used for the semi-

10) a) F. D. Mango and J. H. Schachtschneider, *J. Amer. Chem. Soc.*, **89**, 2484 (1967); **91**, 1030 (1969); **93**, 1123 (1971). b) F. D. Mango, *Tetrahedron Lett.*, **1971**, 505. c) W. Th. A. M. van der Lugt, *ibid.*, **1970**, 2281. d) G. S. Lewandos and R. Pettit, *ibid.*, **1971**, 789. e) See also, R. H. Grubbs and T. K. Brunck, *J. Amer. Chem. Soc.*, **94**, 2538 (1972).
11) a) R. Hoffmann and R. B. Woodward, *J. Amer. Chem. Soc.*, **87**, 2046 (1965). b) R. B. Woodward and R. Hoffman, *Angew. Chem. Int. Ed. Engl.*, **8**, 781 (1969).
12) K. Fukui, This Bulletin, **39**, 498 (1966).

quantitative estimation of the conjugation stabilization at the initial stage of three bodies interactions, regardless of whether or not some particular symmetry exists. The method presented here will be helpful for understanding the important role of the d orbitals of transition metals in complex formations and in the activation of organic molecules in chemical reactions. When the HOMO of one system happens to be degenerate with the LUMO of another, the HOMO-LUMO interaction can be expressed by a first-order perturbation term and comes to play a discriminatively important role.[12]

Appendix

In the case of longicyclie interaction, the third-order interaction energy with respect to $\gamma_{AB}\gamma_{BC}\gamma_{CA}$ is given by

$$\Delta E = 8\left\{\sum_{i}^{occ}\sum_{j}^{all}\sum_{k}^{all}\frac{(c_r^{(i)}c_t^{(j)}+c_s^{(i)}c_u^{(j)})(c_t^{(j)}c_v^{(k)}+c_u^{(j)}c_w^{(k)})(c_v^{(k)}c_r^{(i)}+c_w^{(k)}c_s^{(i)})}{(\varepsilon_{Bj}-\varepsilon_{Ai})(\varepsilon_{Ck}-\varepsilon_{Ai})}\right.$$
$$+\sum_{j}^{occ}\sum_{k}^{all}\sum_{i}^{all}\frac{(c_t^{(j)}c_v^{(k)}+c_u^{(j)}c_w^{(k)})(c_v^{(k)}c_r^{(i)}+c_w^{(k)}c_s^{(i)})(c_r^{(i)}c_t^{(j)}+c_s^{(i)}c_u^{(j)})}{(\varepsilon_{Ck}-\varepsilon_{Bj})(\varepsilon_{Ai}-\varepsilon_{Bj})}$$
$$\left.+\sum_{k}^{occ}\sum_{i}^{all}\sum_{j}^{all}\frac{(c_v^{(k)}c_r^{(i)}+c_w^{(k)}c_s^{(i)})(c_r^{(i)}c_t^{(j)}+c_s^{(i)}c_u^{(j)})(c_t^{(j)}c_v^{(k)}+c_u^{(j)}c_w^{(k)})}{(\varepsilon_{Ai}-\varepsilon_{Ck})(\varepsilon_{Bj}-\varepsilon_{Ck})}\right\}\gamma_{AB}\gamma_{BC}\gamma_{CA}\beta^3$$

In the case of laticyclic interaction, the third-order interaction energy does not appear.

BULLETIN OF THE CHEMICAL SOCIETY OF JAPAN, VOL. 46, 1076—1080 (1973)

The Polarized Phosphorescence Spectra of Phenazine in a Phenanthrene Crystal

Kasumi IKEGAMI, Naohiko MIKAMI, and Mitsuo ITO

Department of Chemistry, Faculty of Science, Tohoku University, Aramaki, Sendai

(Received September 1, 1972)

The polarized phosphorescence spectra of phenazine in phenanthrene was observed at 4.2 K. From the assignments of vibrations that were made on the basis of the results of polarized Raman spectra measurements for the single crystal, it was concluded that the possible mechanisms for the appearance of the vibronically-induced part of the spectrum are the following:

$$^3B_{1u}(\pi, \pi^*) \xrightarrow{\text{s. o.}} {}^1B_{3u}(n, \pi^*) \xrightarrow{\text{vib.}} {}^1B_{2u}(\pi, \pi^*)$$

$$^3B_{1u}(\pi, \pi^*) \begin{cases} \xrightarrow[\text{vib}]{} {}^3B_{3u}(n, \pi^*) \xrightarrow[\text{s.o.}]{} {}^1B_{1u}(\pi, \pi^*) \\ \xrightarrow[\text{s.o.}]{} {}^1B_{3u}(n, \pi^*) \xrightarrow[\text{vib}]{} {}^1B_{1u}(\pi, \pi^*) \end{cases}$$

Furthermore, it has been found that the vibrational modes which give rise to the more intense in-plane polarized bands are out-of-plane ring modes. These results seem to support the regularity found by Lim *et al.*

It is well known that the different vibronic bands associated with the phosphorescence spectra of organic molecules gain the intensity through different routes of spin-orbit and vibronic couplings. In order to determine the coupling routes, it is necessary to know the polarizations of the individual vibronic bands. Interesting contributions along this line have been made by several investigators. However, they have used mainly the method of photoselection, and this method has problems arising from the necessary use of a rigid glass solution—that is, the broadening of the vibronic bands, the restriction of the lowest temperature employed, and so on. These difficulties may be eliminated by polarization measurements for mixed crystals at very low temperatures.

In the present paper, we will report the polarized phosphorescence spectra of phenazine embedded in a single crystal of phenanthrene at 4.2 K. The results obtained were used to determine the possible coupling routes of the individual vibronic bands. The phosphorescence spectra of phenazine have been studied by Pavlopoulos by the method of photoselection.[1] He has associated some vibronic bands with the infrared active u-vibrations. In view of the results obtained here, his assignments should be revised. We also provide additional evidence supporting the regularity found by Lim *et al.* in the perturbing vibrations which appear in the phosphorescence spectra of polycyclic azine.[2]

Experimental

The phenazine was obtained from the Tokyo Kasei Co. and was purified by recrystallization from various solvents and by alumina-column chromatographic extraction. The phenanthrene which was used as a host crystal was treated with maleic anhydride to remove the contaminated anthracene, then it was subjected to extensive zone melting. The

1) T. G. Pavlopoulos, *J. Chem. Phys.* **51**, 2936 (1969).
2) E. C. Lim, R. Li, and Y. H. Li, *ibid.*, **50**, 4925 (1969).

phenanthrene crystal (3% phenazine concentration) was grown by the Bridgman method. The crystal was cleaved along the ab-plane, and then cut down perpendicular to it.

To measure the phosphorescence spectrum of phenazine in phenanthrene, the crystal was submerged in liquid helium and front-surface excitation of the crystal was provided by a mercury line of 365 nm from a 500 W high-pressure mercury lamp. A Toshiba UV39 glass filter and a 0.25 m Bausch & Lomb monochromator were used to filter to other mercury lines. The phosphorescence was collected in the same direction as that of excitation with a lens on the slit of a 0.75 m Nalumi double-grating monochromator (dispersion, 11A/mm) after having passed through a polarized sheet and a Babine plate. The spectrum was recorded with an EMI 9558BQ multiplier phototube and a photon-counting system.

The polarized Raman spectra of a phenazine single crystal were also measured with the exciting light of 4880Å of an Ar-ion laser and a Nalumi double-grating monochromator.

Results and Discussion

The phosphorescence spectrum of phenazine in a phenanthrene crystal at 4.2 K is shown in Fig. 1. The intense and sharp band at 15787 cm^{-1} is onsidered to be an 0-0 band. The vibrational analysis of the observed bands is shown in Table 1, in which the wave number differences from the 0-0 band are compared with the vibrational frequencies obtained from the Raman spectrum. Pavlopoulos[1] observed the phosphorescence spectrum of phenazine in *n*-heptane at 77 K and assigned the 0—486, 0—581, 0—761, 0—823 cm^{-1} bands in the phosphorescence spectrum to the 474, 596, 751, and 820 cm^{-1} infrared active

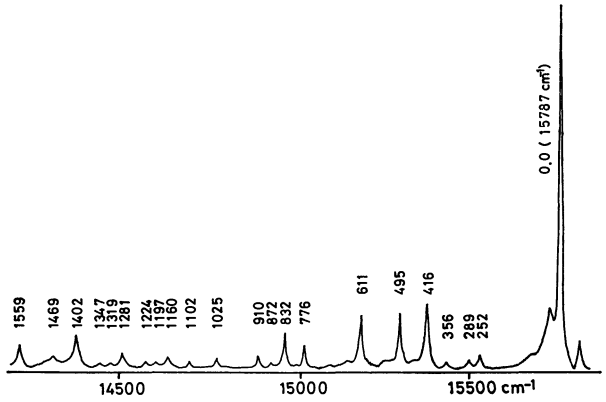

Fig. 1. Phosphorescence spectrum of phenazine in phenanthrene at 4.2 K.

u-vibrations respectively. The 0—486, 0—761, and 0—823 cm^{-1} bands in his spectrum correspond to the 0—495, 0—776, and 0—832 cm^{-1} bands in our spectrum; no band corresponding to his 0—581 cm^{-1} band was observed here. As is shown in Table 1, the 0—495 cm^{-1} band is assigned to the Raman line of 494 cm^{-1}, and it is more reasonable to assign the 0—776 and 0—832 cm^{-1} bands to 416+356 cm^{-1} and 416 $cm^{-1}\times 2$ respectively. Thus, Pavlopoulos' assignment of some vibronic bands to the infrared active u-vibrations should be revised. It is the Raman active vibrations which are associated with all the vibronic bands in the phosphorescence spectrum of phenazine.

Table 1 also gives the symmetry species of the Raman lines, which were determined from polarization mea-

Table 1. Vibrational analysis of the phosphorescence spectrum of phenazine in phenanthrene at 4.2 K and Raman frequencies of phenazine

Phosphorescence (cm^{-1})	Intensity	Difference from the 15787 cm^{-1} band	Assignment	Polarization	Raman frequencies	Symmetry species
15787	vvs	···		N		
15532	w	252	252	L	245	b_{1g}
15498	w	289	289	M	286	b_{2g}
15438	w	356	356	L?	358	
15371	s	416	416	N	415	a_g
15292	s	495	495	L	494	b_{1g}
15176	s	611	611	N	611	a_g
15011	m	776	416+356	L		
14955	m	832	416×2	N		
14915	w	872	611+252	L		
14877	w	910	416+495	L		
14762	w	1025	416+611	N		
14685	w	1102	611+495	L		
14627	m	1160	1160	N	1155	a_g
14590	w	1197	1197	N	1208	a_g
14563	w	1224	611×2	N		
14506	m	1281	1281	N	1278	a_g
14468	w	1319	416×2+495	L		
14440	m	1347	1347	N	1346	a_g
14379	m	1402	1402	N	1400	a_g
14318	w	1469	1469	N	1475	a_g
14228	m	1559	1559	N	1553	a_g

surements for the phenazine single crystal, as well as from depolarization factors for liquid phenazine obtained by melting. As for the nontotally symmetric lines, the Raman line at 494 cm^{-1} can definitely be assigned to the b_{1g} species on the basis of the polarization characteristics of the crystal spectra, while the Raman lines at 245 and 286 cm^{-1} remain ambiguous due to their weak Raman intensities. The latter probably correspond to the 243 and 290 cm^{-1} of anthracene, which belong to b_{1g} and b_{2g} respectively.[3] The 358 cm^{-1} line remains unassigned because of its weak intensity.

In order to determine the polarization directions of individual vibronic bands of the phosphorescence spectrum, the polarized phosphorescence spectra of phenazine were observed for the single crystal of phenanthrene containing 3% phenazine at 4.2 K. The phenanthrene crystal belongs to a monoclinic system with the space group $P2_1$. The bimolecular unit cell has dimensions of $a=12.967$ Å, $b=4.981$ Å, $c=7.056$ Å, and $\beta=109.0°$.[4] Table 2 gives the squared direction cosines of the L, M, and N-axes of the molecule (L, M, and N respersent the long molecular axis, the short molecular axis, and the normal to the molecular plane respectively) with respect to the a, b, and c* axes of the crystal respectively. If we assume that, in the mixed crystal, the phenazine molecules substitutionally occupy the molecular sites of the phenanthrene crystal in such a way that the, L, M, and N axes of the phenazine molecule are parallel to the corresponding axes of the phenanthrene molecule, Table 2 will predict that the vibronic bands of the phosphorescence spectrum of phenazine having transition moments parallel to the L, M, and N-axes should favorably appear along the c*, b, and a-axis spectra respectively. The polarized phosphorescence spectra from the ab and bc* planes are shown in Figs. 2 and 3 respectively. Although the polarization ratios deviate appreciably from the values expected from Table 2 because of the depolarization caused by the cryostat windows, the crystal surface, and so on, the directions of the polarization of the individual vibronic bands may be determined uniquely from Figs. 2 and 3. The 0—0, 0—416, and 0—611 cm^{-1} bands are polarized along the a-axis, so these bands are of the N-axis polarization. The 0—495 and 0—252 cm^{-1} bands are of the L-axis polarization, for these bands appear strongly in the c* axis spectrum. The 289 cm^{-1} band appears strongly along the b axis, and so it is of the M-axis polarization. Similarly, the polarization directions of all the vibronic bands observed were determined; these results are listed in the fifth column of Table 1.

TABLE 2. SQUARED DIRECTION COSINES BETWEEN THE MOLECULAR FIXED AXES L, M, AND N AND THE CRYSTAL AXES a, b, AND c* IN PHENANTHRENE CRYSTAL

	a	b	c*(⊥ab)
L	0.0648	0.0073	0.9279
M	0.1964	0.7676	0.0386
N	0.7406	0.2251	0.0343

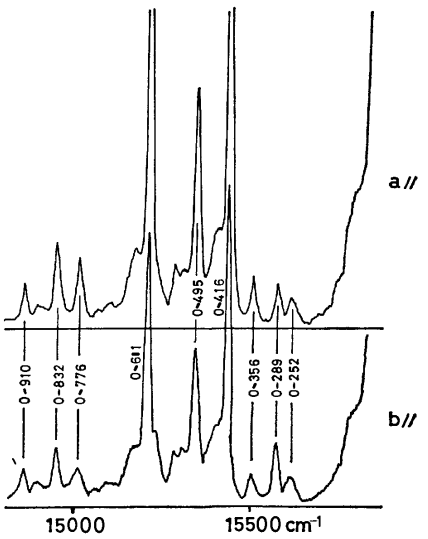

Fig. 2. Polarized phosphorescence spectra of phenazine in phenanthrene (ab face) at 4.2 K.

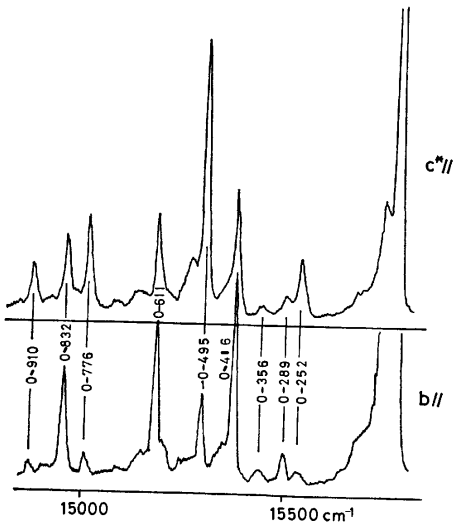

Fig. 3. Polarized phosphorescence spectra of phenazine in phenanthrene (bc* face) at 4.2 K.

To discuss the origin of vibronic bands appearing in the phosphorescence spectrum of phenazine, we need information about the electronic states of phenazine; the information can be obtained from the absorption studies by Mikami[5] and by Hochstrasser[6] for a phenazine single crystal. The crystal spectrum of phenazine has an n–π^* absorption at 20800 cm^{-1} and three strong π–π^* absorption at about 47600, 40000, and 27800 cm^{-1}. The n–π^* absorption at 20800 cm^{-1} is assigned to the symmetry-allowed $^1B_{3u}\leftrightarrow {}^1A_g$ transition. The π–π^* absorption at 47600 and 40000 cm^{-1} are attributed, respectively to a $^1B_{1u}\leftrightarrow {}^1A_g$

3) M. Suzuki, T. Yokoyama, and M. Ito, *Spectrochim. Acta*, **24A**, 1091 (1968).
4) J. Trotter, *Acta Crystallogr.* **16**, 605 (1963).
5) N. Mikami, *J. Mol. Spectry.* **37**, 147 (1971).
6) R. Hochstrasser, *J. Chem. Phys.* **36**, 1808 (1961).

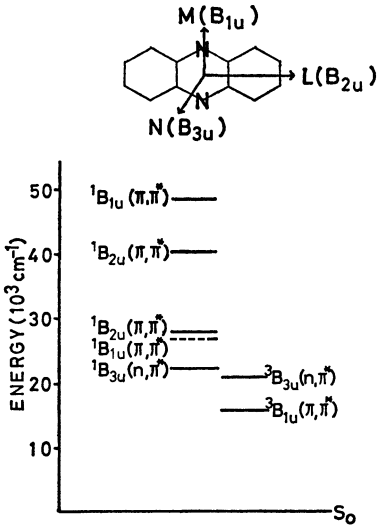

Fig. 4. The low lying singlet and triplet states of phenazine. (The location of the $^1B_{1u}$ (π,π^*) state shown by broken lines is not established.)

transition with the transition moment parallel to the short axis of the molecule and to a $^1B_{2u}\leftrightarrow{}^1A_g$ transition with the transition moment parallel to the long axis of the molecule. However, there are two alternatives for the assignment of the 27800 cm^{-1} π–π^* absorption; one is the assignment of the $^1B_{1u}\leftrightarrow{}^1A_g$ π–π^* transition with the transition moment parallel to the short axis of molecule, and the other is the superposition of two kinds of π–π^* transitions, $^1B_{1u}\leftrightarrow{}^1A_g$ and $^1B_{2u}\leftrightarrow{}^1A_g$. As for the triplet states, the lowest triplet states is known to be $^3B_{1u}(\pi, \pi^*)$. The second triplet state, studied recently by Mikami and Ito,[7] was assigned to $^3B_{3u}$ on the basis of the polarized absorption spectra of the single crystal. The low-lying electronic states of phenazine described above are shown in Fig. 4.

Now, we shall discuss the origin of each vibronic band, based on the vibronic spin-orbit interaction scheme. The Hamiltonian involving spin-orbit interaction[8] is written to the first order in nuclear displacement by:

$$\mathbf{H} = \mathbf{H}_o^\circ + \mathbf{H}_{so}^\circ + \sum_a \left\{\left(\frac{\partial \mathbf{H}_o}{\partial \mathbf{Q}_a}\right)^0 + \left(\frac{\partial \mathbf{H}_{so}}{\partial \mathbf{Q}_a}\right)^0\right\}\mathbf{Q}_a$$

where $\mathbf{H}_o^\circ$ is an unperturbed term, where $\mathbf{H}_{so}^\circ$ is a spin-orbit coupling operator, and where $\mathbf{Q}_a$ indicates a normal coordinate, the superscript zero referring to the equilibrium nuclear configurations. The vibronic wave function of the triplet state with which we are now concerned is thus written, according to the second-order perturbation theory, by:

$$\begin{aligned}{}^T\theta = {}^T\theta_o &+ \sum_S \frac{\langle S|\mathbf{H}_{so}^\circ|T\rangle}{E_{ST}}\,{}^S\theta_o + \sum_S \frac{\langle S|\mathbf{H}_{so}'|T\rangle}{E_{ST}}\,{}^S\theta_o \\ &+ \sum_S \sum_{S'} \frac{\langle S|\mathbf{H}_o'|S'\rangle}{E_{SS'}} \frac{\langle S'|\mathbf{H}_{so}^\circ|T\rangle}{E_{S'T}}\,{}^S\theta_o \\ &+ \sum_S \sum_{T'} \frac{\langle S|\mathbf{H}_{so}^\circ|T'\rangle}{E_{ST'}} \frac{\langle T'|\mathbf{H}_o'|T\rangle}{E_{TT'}}\,{}^S\theta_o\end{aligned}$$

where $\mathbf{H}_o'$ and $\mathbf{H}_{so}'$ represent $(\partial\mathbf{H}_o/\partial\mathbf{Q}_a)^\circ\mathbf{Q}_a$ and $(\partial\mathbf{H}_{so}/\partial\mathbf{Q}_a)^\circ\mathbf{Q}_a$ respectively. S′ and T′ indicate intermediate singlet and triplet states. The second term represents a usual spin-orbit coupling for a pure electronic state. The third term represents a "direct spin vibronic coupling". The fourth and last term are called "vibronic coupling in the singlet manifold with spin-orbit coupling" and "spin-orbit coupling with vibronic coupling in the triplet manifold" respectively.

It may be seen from Table 1 that the 0—0 band and the bands involving the totally symmetric vibrations are out-of-plane polarized. Since the lowest triplet state is $^3B_{1u}$, these bands borrow their intensities from the $^1B_{3u}\leftrightarrow{}^1A_g$ transition through usual spin-orbit coupling. The lowest n–π^* $^1B_{3u}$ state is considered to be most responsible for the coupling. This confirms the previous conclusions about the origin of the 0—0 band reached by many workers. As for the origin of the vibronic bands of the in-plane polarizations, that is, the 0—252, 0—289, and 0—495 cm^{-1} bands, we have to consider the spin-orbit coupling in the singlet manifold or triplet manifold (the third or fourth term of the above equation). Since the 0—252 and 0—495 cm^{-1} bands are long-axis polarized, they must borrow their intensity from the $^1B_{2u}\leftrightarrow{}^1A_g(\pi, \pi^*)$ transition. There are two low-lying $^1B_{2u}$ states in the 27800 and 40000 cm^{-1} regions, but energy considerations suggest that the intensity borrowing from the $^1B_{2u}\leftrightarrow{}^1A_g(\pi, \pi^*)$ transition in the 27800 cm^{-1} region contributes mainly to the long-axis polarized vibronic bands. Since the $^1B_{2u}(\pi, \pi^*)$ state can not couple effectively with $^3B_{1u}(\pi, \pi^*)$ state by means of spin-orbit coupling, and since all the long-axis polarized bands involve the b_{1g} vibrations, the following scheme is considered to be the most likely one:

$$^3B_{1u}(\pi, \pi^*) \xrightarrow[R_y]{\text{s.o.}} {}^1B_{3u}(n, \pi^*) \xrightarrow[b_{1g}]{\text{vib}} {}^1B_{2u}(\pi, \pi^*)$$

As for the short-axis polarized vibronic band of 0—289 cm^{-1}, it borrwos its intensity from the $^1B_{1u}\leftrightarrow{}^1A_g(\pi, \pi^*)$ transition. Either the $^1B_{1u}$ state of 47600 cm^{-1} or the $^1B_{1u}$ state of 27800 cm^{-1} must be responsible for it. Since the 0—289 cm^{-1} band involves the b_{2g} vibration, the most likely coupling routes are:

$$^3B_{1u}(\pi, \pi^*) \xrightarrow[b_{2g}]{\text{vib}} {}^3B_{3u}(n, \pi^*) \xrightarrow[R_y]{\text{s.o.}} {}^1B_{1u}(\pi, \pi^*)$$

$$^3B_{1u}(\pi, \pi^*) \xrightarrow[R_y]{\text{s.o.}} {}^1B_{3u}(n, \pi^*) \xrightarrow[b_{2g}]{\text{vib}} {}^1B_{1u}(\pi, \pi^*)$$

It is interesting to note here that all three schemes given above contain vibronic coupling between n–π^* and π–π^* states. Vibronic coupling between n–π^* and π–π^* states is realized only through and out-of-plane vibration. In the study of the perturbing vibrations of the phosphorescence spectra of polycyclic azines, Lim *et al.*[2] showed that the out-of-plane hydrogen wagging vibration of the CH group adjacent to the heteroatoms is responsible for the appearance of relatively strong in-plane polarized vibronic bands in the π–π^* phosphorescence of dibenzo (*f*, *h*) quinoxaline, while, in dibenzo (*a*, *c*) phenazine, where there is no CH group adjacent to the nitrogen atoms, the

7) N. Mikami, and M. Ito, This Bulletin **45**, 992 (1972)
8) A. C. Albrecht, *J. Chem. Phys.* **38**, 354 (1963).

vibrational modes which give rise to the more intense in-plane polarized vibronic bands are of the out-of-plane ring mode. In the case of phenazine, where there is no CH group adjacent to the nitrogen atoms, the out-of-plane ring mode should be active if the regularity found by Lim *et al.* applies in our case also. The active fundamental vibrations in the phosphorescence spectrum of phenazine are of frequencies less than 500 cm^{-1}. Therefore, they are not due to the CH vibration (their frequencies are too low), but are probably due to the out-of-plane ring mode. In our recent study of the polarized phosphorescence spectra of quinoxaline, phthalazine, and quinoline, whose molecules have the CH group adjacent to the nitrogen atoms, we found that the out-of-plane CH bending vibrations (872 cm^{-1} of quinoxaline and 921 cm^{-1} of phthalazine)[9] are active vibrations in the phosphorescence spectra. These facts seem to support the regularity found by Lim *et al.* for the perturbing vibrations in the phosphorescence spectra of polycyclic azines.

The authors wish to thank Mr. Isamu Suzuka for his assistance and encouragement during the course of this work.

9) K. Ikegami and M. Ito, unpublished result.

BULLETIN OF THE CHEMICAL SOCIETY OF JAPAN, VOL. 46, 1080—1084 (1973)

Kinetics of Oxygen Exchange between Selenate Ions and Water

Akiko OKUMURA and Nobukazu OKAZAKI

Department of Chemistry, Nara Women's University, Nara 630

(Received October 3, 1972)

The rate of oxygen exchange between selenate ions and solvent water has been measured by using oxygen-18 as a tracer. At 30°C in the concentration range of $[H_2SeO_4]=0.57$—1.5 M, and at 80°C in the region of pH= 1.0—2.3, the rate may be expressed as $R=k_1[H^+][HSeO_4^-]$. The values of the energy and entropy of activation are 23.1 kcal/mol and −5.0 e.u.(80°C) at pH=1.12, and 21.8 kcal/mol and −9.9 e.u.(30°C) at $[H_2SeO_4]=1.64$ M. An A-2 mechanism has been suggested for this path. Above *ca* 1.5 M H_2SeO_4, an additional rate term proportional to $[H_2SeO_4]^2$ comes into play.

Oxygen exchange between oxyanions and water has been the subject of many investigations, but the nature of the reaction is not fully understood. The kinetics of the oxygen exchange of oxyanions of typical elements of the fourth period has, except for that of bromine,[1] received hitherto relatively little attention. For a better understanding of the nature of the reaction, it seems desirable to obtain information on the exchange behaviour of oxyanions of these elements. To this end, we have studied the oxygen exchange reactions between oxyanions of selenium and water.

Experimental

Materials. Water enriched in oxygen-18(1.8 atom%) was obtained from a fractionating column of this laboratory. It was refluxed with alkaline permanganate, distilled three times, and used without normalizing its deuterium content (<1 atom %). The selenic acid (Especially pure) was used without further purification. It contained 98% (by weight) of selenic acid (as analysed by the hydrazine method[2]) and 1.7% of selenious acid (as analysed by the permanganate method[3]). The absence of a catalytic effect of selenious acid on the oxygen exchange of selenic acid has been checked by preliminary experiments. The results will be given in a later section. Guanidine hydrochloride (Special grade, JIS) was recrystallized from absolute methanol, dried at 110°C, and stored in a descicator. All the other chemicals were of an analytical-reagent grade and were used without further purification.

Procedure. The solutions used for kinetic runs in the pH region were prepared as follows. Weighed amounts of selenic acid and oxygen-18 water were sealed in a glass ampoule, and the ampoule was heated for *ca.* 2 hr at 100°C to equilibrate the oxygen-18 content of selenic acid with that of the water. This solution was used as a stock solution. In a measuring flask (25 ml), a weighed amount of the isotopically-equilibrated solution was diluted with water of a normal isotopic content to 25 ml, proper amounts of sodium perchlorate and of sodium hydroxide or perchloric acid being added to adjust the ionic strength and the pH of the solution. A portion of the solution was analysed to check its composition. The pH values of the solutions were measured with Hitachi-Horiba M-5- or F-5-type pH meter. For the runs in the more acidic region ($[H_2SeO_4]>0.5$ M), the following procedure was chosen to minimize the induced exchange upon mixing. Selenic acid was added to oxygen-18 water which had been frozen in a dry ice-ethanol bath, and the mixture was caused to melt in an ice-water bath. Even with this procedure, the zero time exchange amounted to *ca.* 20% of the total exchange. The concentrations of selenic acid and hydrogen ion in the solution were determined by titration. The amount of water in the solution was determined by density measurement.

Portions of the solution were sealed in glass ampoules and

1) T. C. Hoering, R. C. Butler, and H. O. McDonald, *J. Amer. Chem. Soc.*, **78**, 4829 (1956); M. Anbar and S. Guttmann, *ibid.*, **83**, 4741 (1961); H. Gamsjäger, A. Grütter, and P. Baertschi, *Helv. Chim. Acta*, **55**, 781 (1972); M. Anbar and H. Taube, *J. Amer. Chem. Soc.*, **80**, 1073 (1958).

2) B. Blanka, P. Hudec, P. Mosna, and J. Touzim, *Collection Czech. Chem. Commun.*, **28**, 3434 (1963).

3) S. Barabas and W. C. Cooper, *Anal. Chem.*, **28**, 129 (1956).

placed in a constant-temperature bath. At appropriate intervals an ampoule was removed and cooled rapidly, and the selenate ions were precipitated by adding a barium chloride solution. The precipitate was separated by centrifuge washed three times with absolute ethanol, and dried at 110°C. It was then converted into carbon dioxide by heating it at 400°C for 1 hr with guanidine hydrochloride in a borosilicate glass tube. This method[4] was originally proposed for the oxygen-18 analysis of water and of acid phosphates, and the reaction involved in the method is a hydrolytic one. In the present case, however, the reaction is of an oxidation-reduction type. The conversion of selenate oxygen into carbon dioxide was>60%. The carbon dioxide, being freed from ammonia and water vapour, was analysed on a Hitachi RMS-I-type mass spectrometer.

The rate of oxygen exchange in g atom per liter in unit of time was calculated by means of the formula:

$$R = -\frac{4[\mathrm{Se(VI)}][\mathrm{H_2O}]}{4[\mathrm{Se(VI)}]+[\mathrm{H_2O}]}\cdot\frac{1}{t}\cdot\ln(1-F),$$

$$F = (O_0 - O_t)/(O_0 - O_\infty),$$

where O_0, O_t, and O_∞ are the ^{18}O atom% of the selenate oxygen at time zero, t, and infinity respectively, and where [Se(VI)] and [H_2O] are the molar concentrations of the selenate ion and water respectively. For each run, 4 or 5 samples were taken at intervals over about two half-lives, and the infinity value was taken after ten half-lives. The McKay plots were satisfactorily linear over two half-lives.

Results and Discussion

Oxygen Exchange in the pH Region. This has been studied at 80°C in the pH region of 1.0—2.3 (Fig. 1). The total selenate concentrations were kept in the 0.064—0.068 M range, and the pH values were adjusted by the addition of a small amount of perchloric acid or of a sodium hydroxide solution. The ionic strengths of the solutions were not adjusted and were in the 0.08—0.16 M range. The pH values were measured at 80°C with solutions of the same compositions (but without oxygen-18 label) as those of the kinetic runs. Figure 1 shows that the pH dependence changes from first-order(pH<1.4) to second-order(pH>2.00) with the increase in the values of pH. The straight line through the four points on the left of the figure has a slope of $-(0.95\pm0.04)$, and the line through the three points on the right, one of $-(2.01\pm0.11)$. This change in kinetic order occurs in the region of the pK_2 value of selenic acid, which has been determined by potentiometric titrations with a glass electrode to be 1.93±0.01(at 80°C).

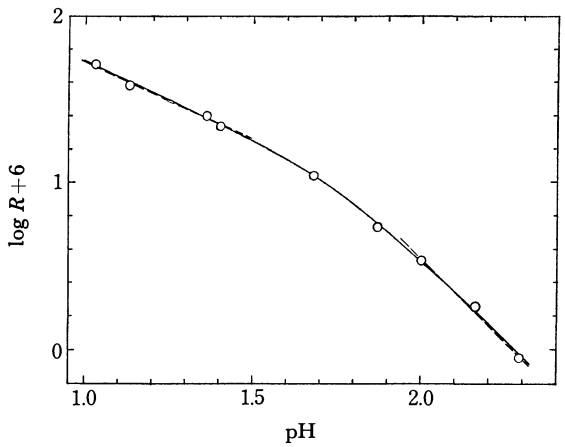

Fig. 1. Dependence of exchange rate on pH at 80 °C ([Se(VI)]=0.064—0.068 M).

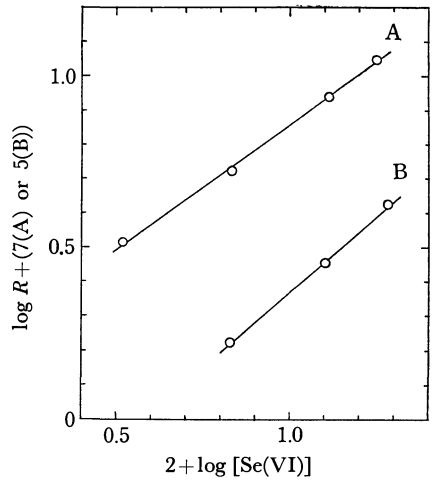

Fig. 2. Dependence of exchange rate on total concentration of selenate [Se(VI)] at 80 °C. The ordinate is 7+log R for A(pH=2.03) and 5+log R for B(pH=1.23).

The dependence of the exchange rate on the total selenate concentration has been studied at two fixed pH values at 80°C. The observed rates were corrected for small differences in pH values (<0.05) by the observed pH dependence. Plots of log R against log [Se(VI)] yield straight lines with slopes of 0.88±0.02 at pH=1.23(I=0.61 M) and of 0.73±0.01 at pH=2.03(I=1.15 M) (Fig. 2). It may be inferred that the exchange reaction is first-order with respect to the total selenate concentration over the entire pH range studied.

These results may be best interpreted in terms of the rate law:

$$R = k[\mathrm{H^+}][\mathrm{HSeO_4^-}] = k[\mathrm{H^+}][\mathrm{Se(VI)}]/(1+(K_2/[\mathrm{H^+}]))$$

$$\simeq k[\mathrm{H^+}][\mathrm{Se(VI)}], \qquad [\mathrm{H^+}]>K_2, \qquad (1)$$

$$\simeq (k/K_2)[\mathrm{H^+}]^2[\mathrm{Se(VI)}], \qquad [\mathrm{H^+}]<K_2. \qquad (1')$$

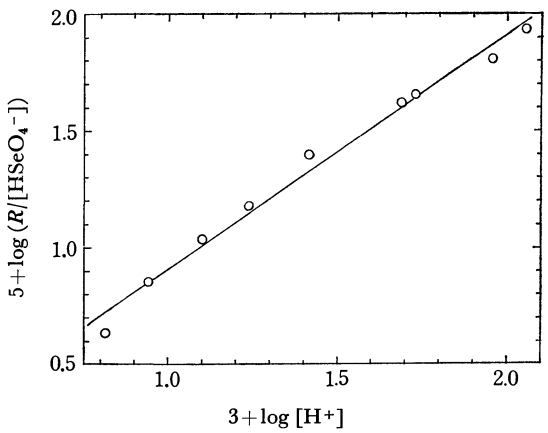

Fig. 3. $R/[\mathrm{HSeO_4^-}]$ as a function of log[H^+] at 80°C.

4) P. D. Boyer, D. J. Graves, C. H. Suelter, and M. E. Dempsey, *Anal. Chem.*, **33**, 1906 (1961).

Fig. 3 shows a plot of log $(R/[HSeO_4^-])$ against log $[H^+]$. The straight line through the points has a slope of 1.00±0.03. The exchange reaction is first-order in both hydrogen-ion and biselenate-ion concentrations, which is in agreement with the rate law. The least-squares treatment of the plots yields the rate constant of $k=(8.2\pm0.8)\times10^{-3}$ l mol^{-1} s^{-1}. In the above treatment, the concentrations of the selenate ion species at each pH value were calculated from [Se(VI)] and $K_2=a_{H^+}\cdot[SeO_4^{2-}]/[HSeO_4^-]$, and the values of K_2 by the formula:

$$pK_2^\circ = pK_2 + \log(f_{SeO_4^{2-}}/f_{HSeO_4^-}),$$

where pK_2° is the thermodynamic dissociation constant and where f's are the activity coefficients. The value of pK_2° at 80°C was obtained from Ghosh and Nair's results[5] by extrapolation, and the values of the activity coefficients were estimated by means of the Debye-Hückel equation by using the ion-size parameters tabulated by Kielland.[6] Succesive approximations yielded the pK_2 values of 2.03—1.93 for I=0.08—0.16 M, which are consistent with the experimentally-determined value; they were used to calculate $[HSeO_4^-]$.

The temperature dependence of the exchange rate has been studied at two fixed pH values, 1.12(at 60, 80, and 95 °C) and 1.81(80, 100, and 120 °C) (Fig. 4). These pH values were measured at room temperature and correspond to pH values of 1.36 and 2.30 at 80 °C. A batch of a solution with a fixed pH was divided into three portions, and each portion was brought to the appropriate reaction temperature. Thus, the observed temperature variation in the exchange rate includes a contribution from the variation in the pH with the temperature. The activation parameters were calculated in the usual way to be E_a=23.10± 0.19 kcal/mol and $\Delta S^\ddagger$=−5.0±0.6 e.u.(80 °C) at pH= 1.12 and E_a=17.18±0.17 kcal/mol and $\Delta S^\ddagger$=−23.4± 0.5 e.u.(80 °C) at pH=1.81. At pH=1.12, where the solution consists of aqueous selenic acid plus a small amount of perchloric acid, the dissociation of the biselenate ion changes little with the pH and contributes only a small fraction to the total hydrogen-ion concentration. Under these circumstances, the temperature variation in log R measures the variartion of log k with the temperature (Eq. (1)). On the other hand, at pH=1.81(buffer region), the temperature variation in log R may be expressed from Eq. (1′) as;

$$\frac{d\log R}{dT} = \frac{d\log k}{dT} - \frac{d\log K_2}{dT} + 2\frac{d\log a_{H^+}}{dT} - 2\frac{d\log f_{H^+}}{dT}$$

and the variation of a_{H^+} at a constant buffer ratio as;

$$\frac{d\log a_{H^+}}{dT} = \frac{d\log K_2^\circ}{dT} - \frac{d\log f_{SeO_4^{2-}}}{dT} + \frac{d\log f_{HSeO_4^-}}{dT}$$

The $d\log f/dT$'s terms may be ignored as compared with $d\log K_2/dT$.[7] Therefore,

$$E_a = E_a^\circ - \Delta H + 2\Delta H^\circ \simeq E_a^\circ + \Delta H^\circ,$$

where E_a° is the true activation energy of the exchange reaction and where ΔH° is the enthalpy of dissociation of the biselenate ion. The value of ΔH° is −5.70±0.2 kcal/mol.[5] Thus, the discrepancy between the activation energies at the two pH values seems quite reasonable.

The effect of the ionic strength has been studied at 80°C, pH=1.33, and [Se(VI)]=0.064 M, with solutions of I=0.82, 0.61, and 0.087 M. The observed rates were 1.47, 1.67, and 2.36×10^{-5} mol/l s respectively. The exchange reaction shows a negative salt effect which is probably due to an equilibrium salt effect on the dissociation of the biselenate ion.

The effect of selenious acid on the exchange rate is shown in the following table.

Table 1. The effects of selenious acid on the oxygen exchange rate of selenic acid at 80°C

Composition of the solution, M×10² [Se(VI)]	[Se(IV)]	pH	R(mol/l s)×10⁵
6.77	0.662	1.39	2.18±0.02
6.38	0	1.40	2.20±0.01
3.09	0.295	1.61	0.0391±0.0003
3.29	0	1.61	0.0370±0.0001

Oxygen Exchange in the Region, $[H_2SeO_4]$=0.56—5.46 M. Figure 5 shows a plot of log R against the logarithm of the total selenic acid concentration, log [Se(VI)], in the region of [Se(VI)]=0.56—5.46 M at 30°C. It may be seen that the [Se(VI)] dependence is nearly second-order up to 1.6 M, and approximately fourth-order above 3.8 M. As selenic acid is almost completely ionized into hydrogen and biselenate ions in this region, the concentrations of each of these ions may be taken to be proportional to [Se(VI)]. Thus, the rate law of the exchange reaction may be written;

$$R = k_1[H^+][HSeO_4^-] + k_2[H^+]^2[HSeO_4^-]^2. \quad (2)$$

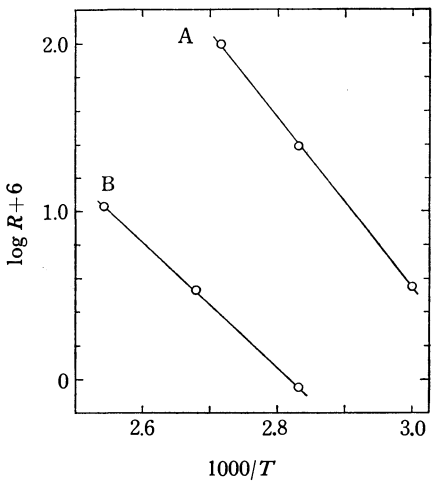

Fig. 4. Temperature dependence of exchange rate in the pH region. A: pH=1.36, [Se(VI)]=0.068 M, B: pH= 2.30, [Se(VI)]=0.067 M.

5) R. Ghosh and V. S. K. Nair, *J. Inorg. Nucl. Chem.*, **32**, 3041 (1970).

6) J. Kielland, *J. Amer. Chem. Soc.*, **59**, 1675 (1937).

7) R. G. Bates, "Determination of pH, Theory and Practice", John Wiley and Sons, New York, (1965), p. 116.

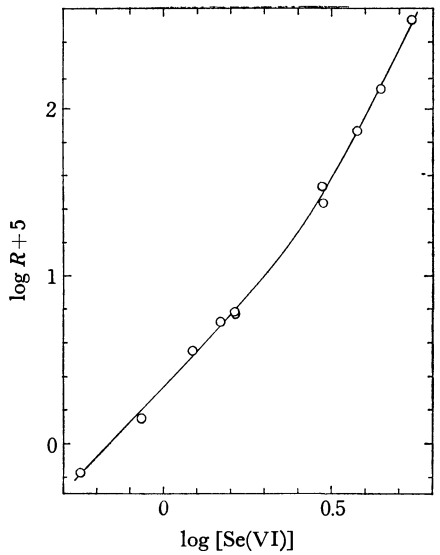

Fig. 5. Rate of oxygen exchange of selenic acid as a function of total concentration of selenic acid at 30°C.

The k_2 term may be interpreted as a bimolecular path involving two selenic acid molecules.

The dependence of the exchange rate on [Se(VI)] at a fixed hydrogen ion concentration has been studied at $[H^+]=3.92$ and 8.7 M. At $[H^+]=3.92$ M, [Se(VI)] was varied between 0.32 and 1.96 M by replacing a part of the selenic acid with an equivalent quantity of perchloric acid. The plot of $\log R$ against log[Se(VI)] is linear, with a slope of 1.09±0.03 at 60°C (Fig. 6-A). At $[H^+]=8.7$ M, selenic acid was replaced by an equivalent quantity of sulfuric acid, which has almost the same acid strength. In this case, the exchange was followed by measuring the decrease in the oxygen-18 content of water. After appropriate reaction times, about 70% of the water in the solution was recovered by the freeze-dry method and was analysed by the guanidine hydrochloride method. It had been confirmed preliminarily that no exchange of oxygen atoms of sulfuric acid occurs in these systems. Figure 6-B gives a plot of $\log R$ against log [Se(VI)] at 30°C. The observed rates were normalized to a hydrogen-ion concentration of 8.7 M.

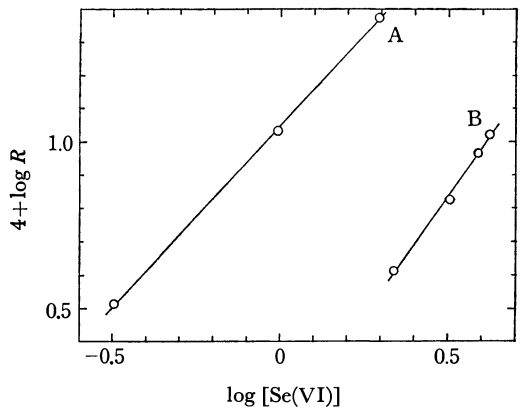

Fig. 6. Dependence of exchange rate on total concentration of selenic acid at constant hydrogen ion concentration.
A: $[H^+]=3.92$ M, 60°C; B: $[H^+]=8.7$ M, 30°C.

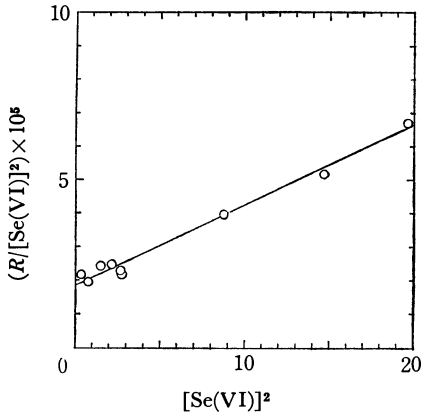

Fig. 7. $R/[Se(VI)]^2$ as a function of $[Se(VI)]^2$ at 30°C.

The least-squares treatment of the plots gives a straight line with a slope of 1.5±0.1. These results support the rate law given in Eq. (2).

Walrafen[8] has studied quantitatively the ionic species present in aqueous selenic acid by the Raman spectroscopic method. According to his results, the concentration of the H_2SeO_4 molecule is practically zero below *ca* 11 M, and from Fig. 3 of his paper, it may be estimated that, up to *ca* 4 M, the concentration of the selenate ion $[SeO_4^{2-}]$ is about three tenths of the total selenic acid concentration. Thus,

$$[HSeO_4^-] = [Se(VI)] - [SeO_4^{2-}] \simeq 0.7\,[Se(VI)],$$

$$[H^+] = [HSeO_4^-] + 2[SeO_4^{2-}] \simeq 1.3[Se(VI)],$$

and the rate law (2) becomes;

$$R/[Se(VI)]^2 = 0.91\,k_1 + 0.828\,k_2[Se(VI)]^2.$$

In Fig. 7, the data shown in Fig. 5 are replotted according to this equation, the points at [Se(VI)]= 5.64 and 2.99 M being ignored. The least-squares treatment yields the rate constants;

$$k_1 = (2.0_1 \pm 0.0_1) \times 10^{-5}\ \text{l/mol s} \quad (30°C),$$

$$k_2 = 0.3 \times 10^{-5}\ \text{l}^3/\text{mol}^3\ \text{s} \quad (30°C).$$

From the values of $k_1(=8.2\times10^{-3}$ l/mol s) and the activation energy(=23.10 kcal/mol) obtained in the pH region at 80°C, the rate constant at 30°C is calculated to be 3.6×10^{-5} l/mol s, which is in satisfactory agreement with the above value. This fact suggests that the exchange reaction has the same mechanism in both the pH and molar regions.

The temperature dependence of the exchange rate in the molar region has been studied at [Se(VI)]= 1.64 M and at 30, 40, and 50°C (Fig. 8). The energy and entropy of activation are calculated to be $E_a=$ 21.82±0.11 kcal/mol and $\Delta S^{\neq}=-9.9\pm0.4$ e.u.(30°C).

Mechanisms of the Exchange Reaction. The second-order rate term, $k_1[H^+][HSeO_4^-]$, suggests the following mechanism;

$$H^+ + HSeO_4^- \rightleftarrows H_2SeO_4, \quad (3)$$

$$H_2SeO_4^* + H_2O \rightleftarrows H_2SeO_4 + H_2O^*, \quad (4)$$

$$\text{or} \quad H_2SeO_4 \rightleftarrows H_2O + SeO_3. \quad (5)$$

8) G. E. Walrafen, *J. Chem. Phys.*, **39**, 1479 (1963).

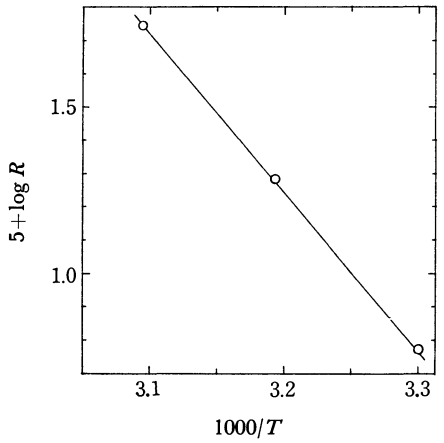

Fig. 8. Temperature dependence of exchange rate at [Se(VI)]=1.64 M.

The negative values of $\Delta S^{\neq}$ obtained for the reaction favour the bimolecular path (4).

Bunton and Hendy[9] have studied the acid hydrolysis of the methyl selenate ion. In contrast to the analogous reaction of the alkyl sulfate ion, the reaction is characterized by a negative value of the entropy of activation (−27 e.u.) and a relatively small deuterium solvent effect ($k_{D_2O}/k_{H_2O}=1.36$), and by a linear dependence of the hydrolysis rate on the hydrogen ion concentration. On the basis of these facts, these authors suggests an A-2 mechanism for the hydrolysis of the methyl selenate ion. Our results are not conclusive at present, but in view of the well-known analogy between the mechanisms of the oxygen exchange of oxyanions and the hydrolysis of its simple alkyl esters, it is probable that the oxygen exchange of the biselenate ion also proceeds through an A-2 mechanism (Path (4)). It is interesting to note that the plot of $\log(R/[\mathrm{Se(VI)}])$ against Hammett's acidity function $-H_0$ of selenic acid[10] gives a straight line with a slope of 0.66±0.01 over the entire range of acidity studied (up to 5.46 M, at 30 °C).

The fourth-order rate term, $k_2[H^+]^2[HSeO_4^-]^2$, which gains importance with an increase in the concentration of selenic acid, may be interpreted as a bimolecular path between two selenic acid molecules;

$$H_2SeO_4 + H_2SeO_4 \rightleftarrows H_2Se_2O_7 + H_2O.$$

The occurrence of $H_2Se_2O_7$ in water-free selenic acid has been suggested by Raman-spectroscopic and conductivity measurements.[11]

The authors wish to thank Professor Shinichi Kawaguchi of Osaka City University for helpful discussions, and Mrs. Masayo Yamamoto and Mrs. Junko Kajihara for their assistance.

9) C. A. Bunton and B. N. Hendy, *J. Chem. Soc.*, **1963**, 3130,

10) D. H. McDaniel and L. H. Steinert, *J. Amer. Chem. Soc.*, **88**, 4826 (1966).

11) R. Paetzold and H. Amoulong, *Z. Anorg. Allgem. Chem.*, **343**, 70 (1966).

BULLETIN OF THE CHEMICAL SOCIETY OF JAPAN, VOL. 46, 1084—1088 (1973)

Kinetics of Oxygen Exchange between Selenite Ions and Water

Akiko Okumura and Nobukazu Okazaki

Department of Chemistry, Nara Women's University, Nara 630

(Received October 3, 1972)

The rate of oxygen exchange between selenite ions and solvent water has been measured at 0°C over the pH range of 8.7—12.5. The rate of exchange, R, may be expressed by the rate law;

$$R = k_1[SeO_3^{2-}] + k_2[HSeO_3^-] + k_3[HSeO_3^-]^2 + k_4[HSeO_3^-][SeO_3^{2-}].$$

The observed rates were analysed in order to obtain the values of the rate constants. The over-all exchange reaction shows a negative salt effect; this has been shown to be an equilibrium salt effect on the dissociation of the hydrogen selenite ion.

No kinetic study of oxygen exchange between selenite ions and water has ever been reported. Earlier qualitative studies[1] have revealed that selenite ions exchange their oxygen atoms with water very rapidly even in a strongly alkaline solution. As a part of the study of oxygen exchange between water and oxyanions of selenium, we have studied the exchange of selenite ions.

Experimental

Materials. Sodium selenite(Special grade, JIS) was used without further purification. Water enriched in oxygen-18 and guanidine hydrochloride were treated as has been described in a previous paper.[2] The other materials were of an analytical reagent grade and were used without further purification.

Procedure. The procedures were almost the same as those used in the previous work.[2] Exchange was started by diluting an isotopically-equilibrated solution of sodium selenite in oxygen-18 water with a relatively large amount of isotopically-normal water. The pH was adjusted by the addition of hydrochloric acid or a sodium hydroxide solution, and the ionic strength, by the addition of sodium

1) N. F. Hall and O. R. Alexander, *J. Amer. Chem. Soc.*, **62**, 3455 (1940); A. I. Brodskii and N. A. Vysotzkaya, *Zh. Fiz. Khim.*, **32**, 1521 (1958).

2) A. Okumura and N. Okazaki, This Bulletin, **46**, 1080 (1973).

chloride. The reaction was carried out in an ice-water bath or in a low-temperature bath. At appropriate intervals, the reactant was precipitated by adding a barium chloride solution. For the runs at pH>11, care was taken to avoid contamination with atmospheric carbon dioxide. The water used for the preparation of the solution was boiled to exclude the dissolved carbon dioxide, and the operations were carried out in a nitrogen atmosphere freed from carbon dioxide. The precipitate, after being washed three times with absolute ethanol, was dried in an oven at 110°C, and then converted into carbon dioxide by the guanidine hydrochloride method.[3] The precipitate of barium selenite is not oxidized by air during the drying at 110°C. The isotopic analysis of the carbon dioxide was made on a Hitachi RMS-I-type mass spectrometer.

The rate of oxygen exchange in g atom per liter per unit of time was calculated by the relation;

$$R = -\frac{3[\mathrm{Se(IV)}][\mathrm{H_2O}]}{3[\mathrm{Se(IV)}]+[\mathrm{H_2O}]}\cdot\frac{1}{t}\cdot\ln\frac{O_t-O_\infty}{O_0-O_\infty}$$

where O_0, O_t, and O_∞ are the oxygen-18 atom per cent of the selenite ion at time 0, t, and infinity respectively, and where [Se(IV)] and [H_2O] are molar concentrations of selenite and water respectively. The McKay plots were linear over two half-periods.

For the analysis of the results, it is desirable to obtain the pK_2 values of selenious acid under the conditions of the kinetic runs. These were obtained by potentiometric titrations with a glass electrode.[4] The 0.053 M sodium selenite solution was titrated with 0.55 N hydrochloric acid with and without added sodium chloride, the values of the ionic strength at the half-neutralisation points being I=0.56 and 0.14 M respectively. The values of pK_2(at 0°C) obtained are $8.10_1\pm0.00_3$ at I=0.56 M, and $8.38_2\pm0.01_5$ at I=0.14 M.

Results and Discussion

pH Dependence of the Exchange Rate. Figure 1 shows the variation in the exchange rate with the pH

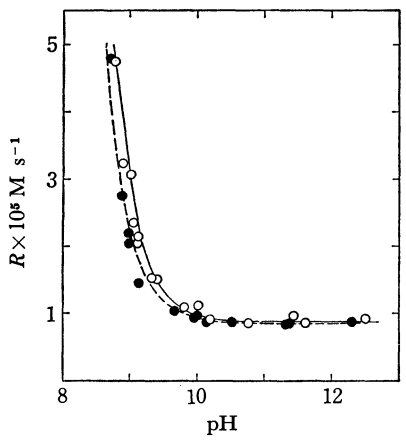

Fig. 1. Rate of oxygen exchange of selenite ions as a function of pH at 0°C. [Se(IV)]=0.055—0.059 M. Open circle: I=0.16 M, Solid circle: I=0.54 M. The curves show the calculated rates. Solid line: I=0.16 M, Broken line: I=0.54 M.

3) P. D. Boyer, D. J. Graves, C. H. Suelter, and M. E. Dempsey, *Anal Chem.*, **33**, 1906 (1961).

4) A. Albert and E. P. Serjeant, "Ionization constants of acids and bases. A laboratory manual." Translated by S. Matsuura, Maruzen, Tokyo (1963).

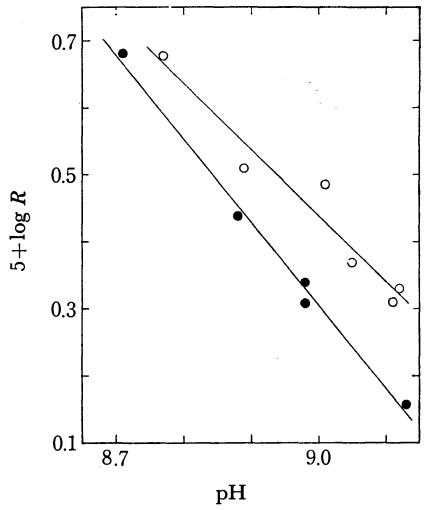

Fig. 2. Dependence of exchange rate on pH in the region of pH<9.1. Open circle: I=0.16 M, Solid circle: I=0.54 M.

at 0 °C and at a fixed total selenite concentration ([Se(IV)]=0.055—0.059 M). The exchange was studied at two different values of ionic strength, I=0.16(±0.02) M and I=0.54(±0.01) M. In the region of pH<9, plots of log R against pH for the runs at I=0.54 and 0.16 M are linear with slopes of 1.24±0.05 and 0.99±0.08 respectively (Fig. 2). On the other hand, above pH=11, the rate is practically independent of the pH.

To check the possibility of hydroxide-ion catalysis, the exchange reaction was studied in a strongly alkaline medium in the following way. A solution of sodium selenite was mixed with a solution of sodium hydroxide in oxygen-18 water in an ice-water bath. The mixed solution was 1.94 M in hydroxide ion and 2.21 M in sodium selenite. At appropriate intervals, a portion of the solution was removed and subjected to vacuum distillation to separate the water. The water thus obtained was analysed for its oxygen-18 content by the guanidine hydrochloride method. As a control, a solution containing an equivalent amount of sodium chloride instead of sodium hydroxide was also studied ([Se(IV)]=2.09 M). The rate observed were;

$$R(\mathrm{NaOH}) = (1.9\pm0.1)\times10^{-4}\ \mathrm{mol/l\,s},$$

and $$R(\mathrm{NaCl}) = (10.1\pm0.4)\times10^{-4}\ \mathrm{mol/l\,s}.$$

The value of R(NaOH) may be recalculated to the rate for [Se(IV)]=0.057 M by the observed first-order dependence on [Se(IV)]. The value thus obtained is 0.5×10^{-5} mol/l s, which compares well with the values obtained at pH=10—12 (see Fig. 1). These facts suggest the absence of hydroxide-ion catalysis.

Salt Effect. In the region of pH<9.5, the addition of sodium chloride exhibits a retarding effect on the exchange rate (see Fig. 1). The effect decreases with the increase in pH and above pH≃11 merges into the experimental errors. In Fig. 1, a plot at pH=8.98 and I=0.54 M was obtained with a solution the ionic strength of which was adjusted by the addition of sodium perchlorate instead of sodium chloride. The plot falls on a line with other plots. This fact

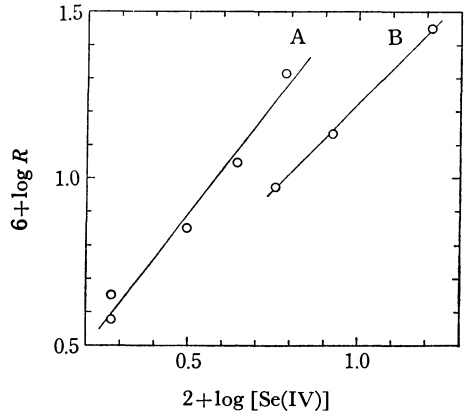

Fig. 3. Dependence of exchange rate on [Se(IV)]. I= 0.54 M. A: pH=9.19, B: pH=10.1.

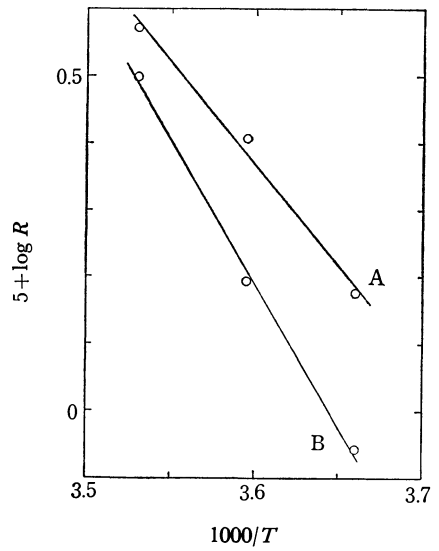

Fig. 4. Temperature dependence of the exchange rate. [Se(IV)]=0.052 M, I=0.54 M. A: pH=9.1, B: pH= 10.1.

shows the absence of any specific effects of these anions.

Dependence on [Se(IV)]. The dependence of the exchange rate on the total concentration of selenite [Se(IV)] was studied at 0°C and at a constant ionic strength (I=0.54 M) for two fixed values of pH (9.19 and 10.1) (Fig. 3). These pH values are representative of the two pH regions of different rate-pH relationships. The observed rates were corrected for the difference in pH values (<0.05 pH). The slopes of the plots of log R against log [Se(IV)] are 1.32±0.08 for pH=9.19 and 1.04±0.03 for pH= 10.1.

Activation Energies. Because of the rapidity of the exchange reaction, the temperature dependence of the exchange rate could be studied only over a limited temperature range (0—10°C) (Fig. 4). In Fig. 4 the rates observed at pH=9.1 are corrected for the difference in pH values (<0.1 pH). The values of the activation energy were calculated to be;

E_a=14.0±0.9 kcal/mol, at pH=9.1 and I=0.54 M,

and

E_a=19.6±0.8 kcal/mol, at pH=10.1 and I=0.54 M.

Analysis of the Exchange Rate. In the region of pH > *ca.* 10, where SeO_3^{2-} is the dominating ionic species and where the concentration of $HSeO_3^-$ is less than 1 per cent of the total selenite-ion concentration, the rate is independent of the pH and depends on the first power of the total selenite concentration. This fact, together with the finding that hydroxide ion catalysis is absent, suggests that the exchange occurs through the mechanism;

$$SeO^*_3{}^{2-} + H_2O \rightleftarrows SeO_3^{2-} + H_2O^*. \quad (1)$$

In the region of pH<*ca.* 9, the observed kinetic order with respect to the [Se(IV)] of 1.32 at pH=9.2 suggests bimolecular mechanisms between selenite ions as important paths;

$$HSeO_3^- + HSeO_3^- \rightleftarrows Se_2O_5^{2-} + H_2O, \quad (3)$$

$$HSeO_3^- + SeO_3^{2-} \rightleftarrows Se_2O_5^{2-} + OH^-. \quad (4)$$

The occurrence of the pyroselenite ion in aqueous solutions of alkali hydrogen selenite (0.5—4 M) has been demonstrated by Raman spectroscopic investigation.[5] Moreover, SeO_3^{2-} being still the major species, exchange occurs through Path (1), and Path (2);

$$HSeO^*_3{}^- + H_2O \rightleftarrows HSeO_3^- + H_2O^*, \quad (2)$$

should gain increasing importance with an increase in the biselenite-ion concentration. Thus, the rate law of the oxygen exchange of the selenite ion over the entire range studied may be written as;

$$R = k_1[SeO_3^{2-}] + k_2[HSeO_3^-] + k_3[HSeO_3^-]^2 + k_4[HSeO_3^-][SeO_3^{2-}]. \quad (I)$$

In the region of pH>10, we may, to a good approximation, ignore the occurrence of the k_2 and k_3 paths. The observed [Se(IV)] dependence of 1.04 at pH= 10.1 suggests some contribution to the exchange of the bimolecular path, k_4. The rate equation may be simplified as;

$$R = k_1[SeO_3^{2-}] + k_4[SeO_3^{2-}][HSeO_3^-],$$

or $$R/[SeO_3^{2-}] = k_1 + k_4[HSeO_3^-].$$

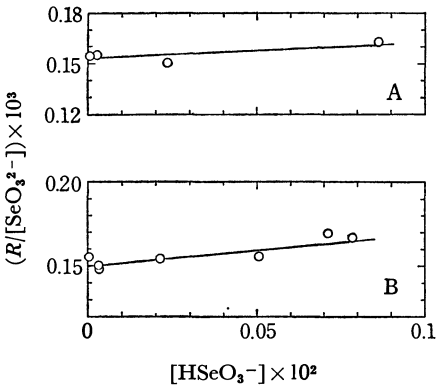

Fig. 5. Evaluation of the rate constants k_1 and k_4. A: I=0.16 M, B: I=0.54 M.

5) A. Simon and R. Paetzold, *Z. Anorg. Allgem. Chem.*, **303**, 46 (1960).

Fig. 5 shows the plots of $(R/[SeO_3^{2-}])$ against $[HSeO_3^-]$ for I=0.16 and 0.54 M. The values of $[SeO_3^{2-}]$ and $[HSeO_3^-]$ were calculated by using the appropriate values of pK_2 (see experimental part). From the intercepts and the slopes of the plots, the values of k_1 and k_4 have been obtained as;

$$k_1(0.16\text{ M}) = (0.15_3 \pm 0.00_2) \times 10^{-3}\ s^{-1},$$
$$k_1(0.54\text{ M}) = (0.15_0 \pm 0.00_2) \times 10^{-3}\ s^{-1},$$
$$k_4(0.16\text{ M}) = (0.10 \pm 0.04) \times 10^{-1}\ M^{-1}\ s^{-1},$$
$$k_4(0.54\text{ M}) = (0.21 \pm 0.03) \times 10^{-1}\ M^{-1}\ s^{-1}.$$

As may be expected, the k_1 path is free from the salt effect and the k_4 path shows a positive salt effect.

By using the $[Se(IV)] = [HSeO_3^-] + [SeO_3^{2-}]$ relation, Eq. (I) may be rewritten in the form;

$$(R - k_1[SeO_3^{2-}])/[HSeO_3^-] = (k_2 + k_4[Se(IV)]) + (k_3 - k_4)[HSeO_3^-]. \quad \text{(II)}$$

Fig. 6 shows the plots of $(R - k_1[SeO_3^{2-}])/[HSeO_3^-]$ against $[HSeO_3^-]$ at a constant [Se(IV)] for two values of the ionic strength. The least-squares treatment yields;

$$(k_2 + k_4[Se(IV)]) = (0.68 \pm 0.16) \times 10^{-3}\ s^{-1},$$
and $$(k_3 - k_4) = (1.16 \pm 0.16) \times 10^{-1}\ M^{-1}\ s^{-1},$$
for I=0.16 M, and
$$(k_2 + k_4[Se(IV)]) = (1.05 \pm 0.14) \times 10^{-3}\ s^{-1},$$
and $$(k_3 - k_4) = (1.54 \pm 0.25) \times 10^{-1}\ M^{-1}\ s^{-1},$$
for I=0.54 M. By using the values of k_4 obtained above, k_3 may be evaluated from the values of $k_3 - k_4$ as;

$$k_3(0.16\text{ M}) = (1.3 \pm 0.2) \times 10^{-1}\ M^{-1}\ s^{-1},$$
and $$k_3(0.54\text{ M}) = (1.8 \pm 0.3) \times 10^{-1}\ M^{-1}\ s^{-1},$$

As it is expected that the value of k_2 is only a small fraction of the value of $k_2 + k_4[Se(IV)]$, it is unadvisable to evaluate k_2 from $k_2 + k_4[Se(IV)]$. By using the relation, $[HSeO_3^-] = [Se(IV)]/(1 + (K_2/a_{H^+}))$, Eq. (II) may be rewritten in the form;

$$(R - k_1[SeO_3^{2-}])/[HSeO_3^-] = k_2 + S[Se(IV)], \quad \text{(III)}$$
$$S = (k_3 a_{H^+}/(K_2 + a_{H^+})) + (k_4 K_2/(K_2 + a_{H^+})).$$

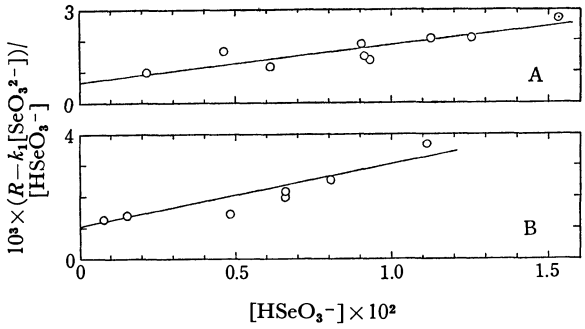

Fig. 6. $(R - k_1[SeO_3^{2-}])/[HSeO_3^-]$ as a function of $[HSeO_3^-]$. A: I=0.16 M, B: I=0.54 M.

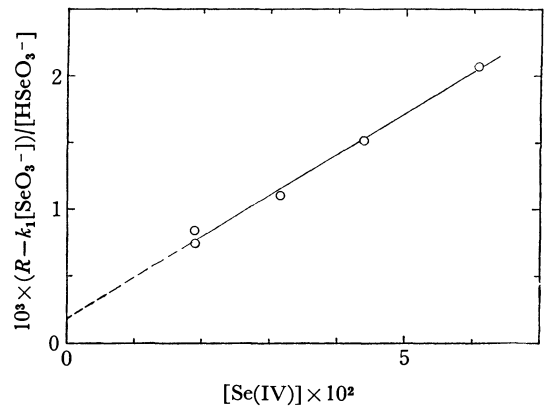

Fig. 7. Evaluation of the rate constant k_2 at I=0.54 M.

Figure 7 shows a plot of $(R - k_1[SeO_3^{2-}])/[HSeO_3^-]$ against [Se(IV)] at a constant pH(9.19) and ionic strength (0.54 M); here the data in Fig. 3 are replotted according to the equation above. The least-squares treatment of the plot yields the values;

$$k_2(0.54\text{ M}) = (0.19 \pm 0.04) \times 10^{-3}\ s^{-1},$$
$$S(0.54\text{M}) = (0.31 \pm 0.01) \times 10^{-1}\ M^{-1}\ s^{-1}.$$

As Path (2) may be expected to be free from any kinetic salt effect, the rate constant, k_2, at I=0.16 M should have almost the same value as k_2(0.54 M).

The values of k_4 calculated from the values of k_2 and $k_2 + k_4[Se(IV)]$ are $k_4(0.16\text{ M}) = 0.09 \times 10^{-1}$ and $k_4(0.54\text{ M}) = 0.15 \times 10^{-1}\ M^{-1}\ s^{-1}$. The value of $k_3(0.54\text{ M})$ may also be calculated from the values of k_4 and of the slope, S, of Eq. (III). The result is $k_3(0.54\text{ M}) = 1.5 \times 10^{-1}\ M^{-1}\ s^{-1}$. These values are in satisfactory agreement with the values of k_3 and k_4 obtained above. This fact gives evidence of the self-consistency of this analysis.

The values of the rate constants obtained are summarized in the following table. By using the rate law (I) and the values of the rate constants, the rates of oxygen exchange are recalculated and shown as curves in Fig. 1. The agreement of the calculated rates with the observed rates is satisfactory except at the acidic end of the curve for I=0.54 M.

The reactivities of the hydrogen-selenite and selenite ions towards water are almost equal, the former being somewhat larger. The hydrogen-selenite ion is about ten times as reactive as the selenite ion towards the

Table 1. The values of rate constants at 0°C

Exchange path	Rate const. (unit)	Ionic strength 0.16 M	Ionic strength 0.54 M
$SeO_3^{2-} + H_2O \rightleftarrows$	$k_1(s^{-1})$	0.15×10^{-3}	0.15×10^{-3}
$HSeO_3^- + H_2O \rightleftarrows$	$k_2(s^{-1})$	0.2×10^{-3}	(0.2×10^{-3})
$HSeO_3^- + HSeO_3^- \rightleftarrows Se_2O_5^{2-} + H_2O$	$k_3(M^{-1}\ s^{-1})$	1.3×10^{-1}	1.8×10^{-1}
$HSeO_3^- + SeO_3^{2-} \rightleftarrows Se_2O_5^{2-} + OH^-$	$k_4(M^{-1}\ s^{-1})$	0.1×10^{-1}	0.2×10^{-1}

hydrogen-selenite ion. This is in part due to the electrostatic repulsion between the reactants.

It may be seen from the table that none of the paths, (1)—(4), show a negative salt effect. Thus, the negative salt effect observed for the over-all oxygen exchange rate cannot be attributed to a kinetic origin. It must be due to an equilibrium salt effect on the dissociation of the biselenite ion. An increase in the ionic strength increases the dissociation of the biselenite ion and reduces the concentration of the reactive species, $HSeO_3^-$. The negative salt effect observed for the exchange of selenite[2] probably has the same origin.

The authors wish to thank Professor Shinichi Kawaguchi of Osaka City University for his helpful discussions and Mrs. Chiyoko Morimoto for her assistance.

BULLETIN OF THE CHEMICAL SOCIETY OF JAPAN, VOL. 46, 1088—1093 (1973)

The Electronic Structure of the Electron Donor-Acceptor Complex in Its Lowest Excited Singlet State. II

Hiroshi MASUHARA, Nobuyuki TSUJINO, and Noboru MATAGA

Faculty of Engineering Science, Osaka University, Toyonaka, Osaka 560

(Received October 4, 1972)

The electronic spectra of some 1,2,4,5-tetracyanobenzene complexes in the lowest excited singlet state at 77 K were obtained by laser photolysis method. The observed spectra can be well reproduced with the superposition of the bands similar to those of acceptor anion as well as donor cation, independent of donors. Comparing the spectra with those of ionic radical salts, it is concluded that the electronic structure of these complexes is quite polar and the fluorescent state is a contact ion-pair. The electronic structures of excited electron donor-acceptor systems have been discussed, on the basis of the interaction between donor cation and acceptor anion. The charge-transfer degree in the excited complexes was found to increase in the following order; 1,2,4,5-tetracyanobenzene-hexamethylbenzene complex in the phosphorescent state < hydrocarbon-amine heteroexcimers < the present complexes in the fluorescent state.

The electronic spectra of excited electron donor-acceptor (EDA) systems such as EDA complexes in the fluorescent as well as phosphorescent states and heteroexcimer have been investigated by laser photolysis method. The excited singlet-singlet ($S_n \leftarrow S_1$) absorption spectra of EDA complexes, which are stable in the ground state, were observed for the first time in the case of 1,2,4,5-tetracyanobenzene (TCNB) and pyromellitic dianhydride (PMDA) complexes with methylsubstituted benzenes.[1-3] The spectra were similar to those of acceptor anion, which indicated the quite polar structure of the lowest excited charge-transfer singlet (^{1}CT) state of EDA complexes. On the other hand, the absorption spectra of intermolecular as well as intramolecular heteroexcimers show numerous bands in the visible region, some of which were found to coincide with those of acceptor anion and donor cation.[4,5] The absorption spectra of the charge-transfer triplet (^{3}CT) state of EDA complex were found to be different from those of acceptor anion and donor cation. The triplet-triplet ($T_n \leftarrow T_1$) absorption spectra of naphthalene, pyrene as well as phenanthrene complexes are similar to those of the donor.[6-8] In the case of the $T_n \leftarrow T_1$ spectra of TCNB complexes with methylsubstituted benzenes, some bands which cannot be ascribed to those of the component triplet state have been reported.[7,9]

In view of the above results, the problems on the electronic structures of the excited EDA systems may be summarized as follows; (1) elucidation of the relation between the electronic spectra and CT degree in these systems, (2) investigation of the difference among the electronic structures of ^{1}CT as well as ^{3}CT states of EDA complexes and heteroexcimer, (3) theoretical study on energies as well as intensities of back CT transitions from acceptor anion to donor cation,[2] (4) investigation of the structural change, which occurs in the course of the relaxation from the excited Franck-Condon (FC) to fluorescent states.[2,10]

We have been studying the electronic spectra of some excited EDA complexes for elucidating the above problems. Although the $S_n \leftarrow S_1$ spectra of TCNB complexes with benzene, toluene and mesitylene were obtained at room temperature, the observation of the $S_n \leftarrow S_1$ spectra of TCNB complexes with α-methylstyrene, durene and hexamethylbenzene (HMB)

1) H. Masuhara and N. Mataga, *Chem. Phys. Lett.*, **6**, 608 (1970).
2) H. Masuhara and N. Mataga, *Z. Phys. Chem. N. F.*, **80**, 113 (1972); Part I of this series.
3) R. Potashnik and M. Ottolenghi, *Chem. Phys. Lett.*, **6**, 525 (1970).
4) R. Potashnik, C. R. Goldschmidt, M. Ottolenghi, and A. Weller, *J. Chem. Phys.*, **55**, 5344 (1971).
5) T. Okada, T. Fujita, M. Kubota, S. Masaki, N. Mataga, R. Ide, Y. Sakata, and S. Misumi, *Chem. Phys. Lett.*, **14**, 563 (1972).
6) G. Briegleb, H. Schuster, and W. Herre, *ibid.*, **4**, 53 (1969); G. Briegleb and H. Schuster, *Z. Phys. Chem. N. F.*, **77**. 269 (1972).
7) N. Tsujino, H. Masuhara, and N. Mataga, *Chem. Phys. Lett.*, **15**, 360 (1972).
8) Z. Teitelbaum, R. Potashnik, and M. Ottolenghi, *Mol. Photochem.*, **3**, 107 (1971).
9) S. Matsumoto, S. Iwata, J. Nakamura, and S. Nagakura, *Chem. Phys. Lett.*, **13**, 463 (1972).
10) N. Mataga and Y. Murata, *J. Amer. Chem. Soc.*, **91**, 3144 (1969).

donors was difficult because of their short lifetimes of the lowest excited singlet state. However, in rigid solutions the fluorescence lifetimes of the latter complexes become long enough for measurement of the $S_n \leftarrow S_1$ spectra. In the present paper, the $S_n \leftarrow S_1$ spectra of several TCNB complexes in polymethylmethacrylate (PMMA) at room temperature as well as in rigid glass at 77 K will be reported.

Experimental

The fluorescence intensities of the present TCNB complexes are stronger than the monitoring light intensity. Accordingly, the observation of the $S_n \leftarrow S_1$ spectra is difficult. However, we can obtain those spectra by the re-absorption method developed by us.[11] Namely, the $S_n \leftarrow S_1$ spectra have been obtained by comparing fluorescence spectra observed by laser excitation of low intensity (one three hundredth of high intensity) with those observed by laser excitation of high intensity which are partially re-absorbed by the complex in the fluorescent state. Some points should be noted on this method. The first one is the selection of the wave number, at which both fluorescence spectra are normalized. Secondly, it is difficult to obtain the $S_n \leftarrow S_1$ spectra in the wave number regions where the fluorescence intensity is about one tenth of its peak intensity, because in this case the noise of the out-put of photomultiplier is in the same order of magnitude as the signal and a slight fluctuation of fluorescence intensity out-put leads to a large uncertainty of the $S_n \leftarrow S_1$ spectra. Thirdly, it is necessary to remove the contribution of the absorption of ^{3}CT state from the observed spectra since ^{3}CT state of some TCNB complexes is confirmed to be formed from the excited FC state, competing with the formation of ^{1}CT state.[12] The wave number where we have normalized two fluorescence spectra obtained by high and low laser excitations, and the absorbances of the $T_n \leftarrow T_1$ transitions at those wave numbers respectively, are indicated in Table 1. At the longer wavelength regions, we have measured $S_n \leftarrow S_1$ spectra by usual nsec flash photolysis method.[13] The apparatus and the chemicals were the same as used before.[12,13]

Table 1. Normalization conditions of fluorescence spectra of some TCNB complexes, obtained by high and low intensity laser excitations

Donors	Wave number of normalization	Optical density of $T_n \leftarrow T_1$ spectra at the wave number of normalization
Toluene	20 kK	0.1
Mesitylene	24.8	~0 (neglected)
	18.9~19.2	~0 (neglected)
Durene	22.5	~0 (neglected)
HMB	17~18	~0 (neglcctcd)
Naphthalene	18.2	0.1

11) H. Masuhara and N. Mataga, This Bulletin, **45**, 43 (1972).
12) H. Masuhara, N. Tsujino, and N. Mataga, *Chem. Phys. Lett.*, **12**, 481 (1972); N. Tsujino, H. Masuhara, and N. Mataga, *ibid.*, **15**, 357 (1972).
13) H. Masuhara, M. Shimada, N. Tsujino, and N. Mataga, This Bulletin, **44**, 3310 (1971).

Results

Fluorescence spectra obtained by plotting the peak intensity at each wave number and the transient absorption spectra of excited TCNB complexes at 77 K are given in Figs. 1—5. Since we have shown that the intersystem crossing process to the triplet state

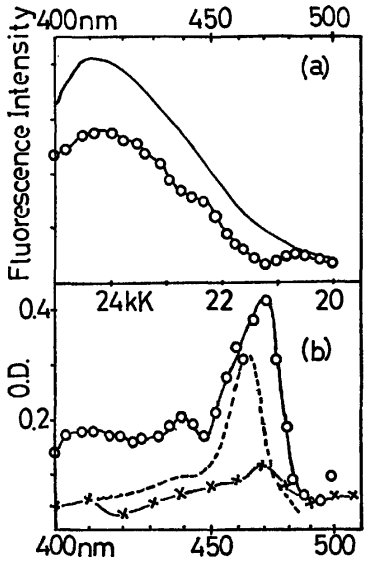

Fig. 1. Flurescence spectra and the transient absorption spectra of TCNB-toluene complex in rigid mixed solvent of *n*-propyl alcohol and isopropyl alcohol (*n*P–*i*P) with volume ratio of 2 : 3 at 77 K.
(a) Flurescence spectra obtained by laser excitation of high intensity (-O-O-) and by laser excitation of low intensity (——).
(b) The obtained transient absorption spectra (-O-O-) and the $T_n \leftarrow T_1$ spectra observed previously[7] (-×-×-). The absorption spectra of TCNB anion taken from literature[14] are included (----).

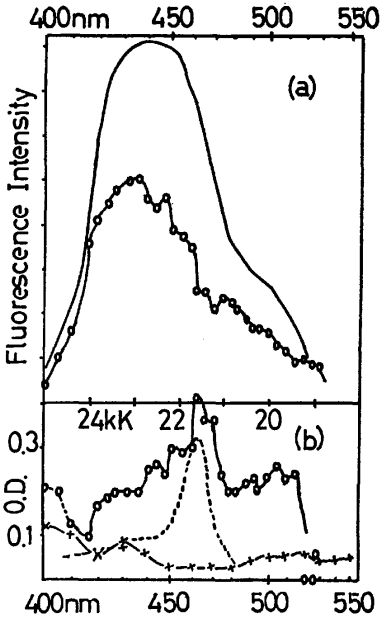

Fig. 2. Flurescence spectra and the transient absorption spectra of TCNB-mesitylene complex in *n*P–*i*P at 77 K. Notations are the same as described in Fig. 1.

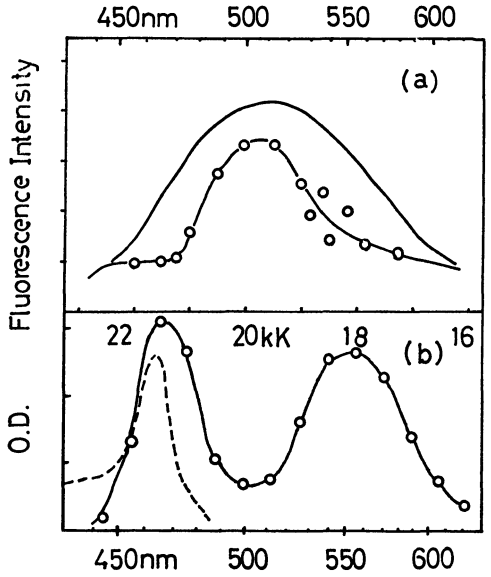

Fig. 3. Fluorescence spectra and the transient absorption spectra of TCNB-durene in PMMA at room temperature. Notations are the same as described in Fig. 1.

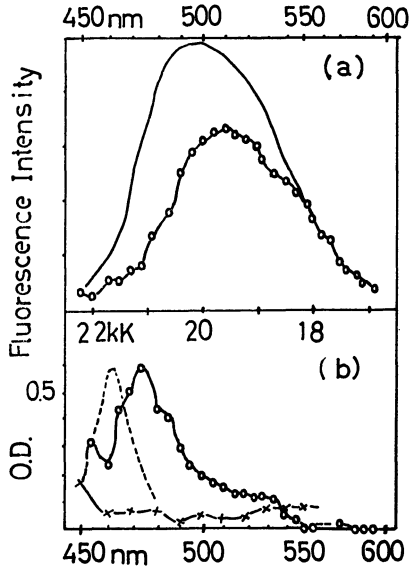

Fig. 4. Fluorescence spectra and the transient absorption spectra of TCNB-HMB complex in *n*P–*i*P at 77 K. Notations are the same as described in Fig. 1.

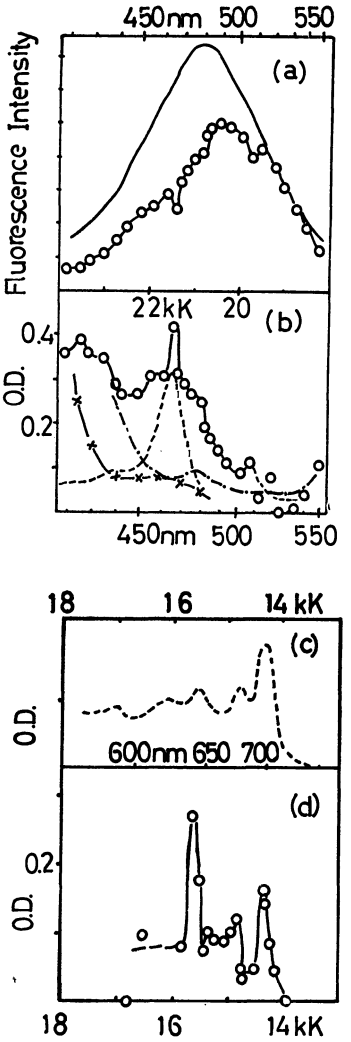

Fig. 5. Fluorescence spectra and the transient absorption spectra of TCNB-naphthalene complex in PMMA at room temperature.
(a) Fluorescence spectra obtained by laser excitation of high intensity (-O-O-) and by laser excitation of low intensity (——).
(b) The transient absorption spectra (-O-O-) and the $T_n \leftarrow T_1$ spectra observed previously[7] (-×-×-). The absorption spectra of TCNB anion[14] (----) as well as naphthalene cation (—·—·—)[16] are included.
(c) The absorption spectra of naphthalene cation at longer wavelengths.[16]
(d) The $S_n \leftarrow S_1$ spectra of TCNB-naphthalene complex observed by nsec flash photolysis method.

occurs from the excited FC state, the contribution of the $T_n \leftarrow T_1$ spectra to the observed transient spectra should be taken into consideration. The transient absorption band with maximum at about 21 kK cannot be ascribed to the TCNB anion produced by laser excitation, but is due to the fluorescent state of TCNB complexes which has a very polar structure, since the fluorescence at this wave number shows a particular nonexponential decay as shown in Fig. 6.

In the case of TCNB-toluene complex, the peak at 21.2 kK is similar to the band of TCNB anion.[14] A slight red shift and broadening of this band, compared to the case of the solution spectra of TCNB anion, can be noted. In the lower wave number region, no information is available by means of the present reabsorption method. In the present $S_n \leftarrow S_1$ spectra, one cannot observe any band which can be ascribed to the toluene cation.

In the transient spectra of TCNB-mesitylene system, the peak at 21.6 kK may be attributed to the TCNB anion-like component in the fluorescent state of the complex. In this case no red shift in comparison with the solution spectra of TCNB anion was observed. The broad band in the region of 22.4~24 kK may be attributed to the $T_n \leftarrow T_1$ transition, while the band at 20 kK may be ascribed to mesitylene cation-like

14) A. Ishitani and S. Nagakura, *Theoret. Chim. Acta (Berl.)*, **4**, 236 (1966).

component in the excited complex, since Badger and Brocklehurst have reported the cation band at 19.2 kK.[15]

Quite similar interpretation of the spectra may be possible also in the case of TCNB-durene-PMMA system. One can recognize a little broadening of 21.5 kK band. The band at about 18 kK may be related to the durene cation-like state in the fluorescent complex as well as the ^{3}CT state.[9]

In the case of TCNB-HMB complex, the bands in high wave number region cannot be obtained by the present re-absorption method. The band, 21.2 kK is similar to that of TCNB anion. The red shift and a little broadening of the latter band are observed. The absorption band in the low wave number region is almost identical with that of HMB cation.[15] The contribution of $T_n \leftarrow T_1$ absorption to the spectra is rather small.

The spectra of TCNB-naphthalene-PMMA system can be well reproduced by a superposition of the $T_n \leftarrow T_1$ spectra and the band similar to those of TCNB anion and naphthalene cation.[16] The peak at 21.4 kK and the shoulder at 20.8 kK are similar to those of TCNB anion and naphthalene cation, respectively. The strong broad band near 23 kK can be attributed to the superposition of the $T_n \leftarrow T_1$ spectra with large intensity and the $S_n \leftarrow S_1$ band similar to those of naphthalene cation. The similarity of the $S_n \leftarrow S_1$ band to the band of naphthalene cation can be observed clearly also in the low wavenumber region, where the spectra were measured by nsec flash photolysis method.[13]

These spectra are the first observations of the $S_n \leftarrow S_1$ spectra of EDA complexes at 77 K. Although the $S_n \leftarrow S_1$ spectra of TCNB complexes with benzene, toluene and mesitylene donors at room temperature have been reported,[1-3] the absorption spectra of TCNB complexes in the fluorescent state with rather strong donors such as durene, HMB and naphthalene are given for the first time in the present work.

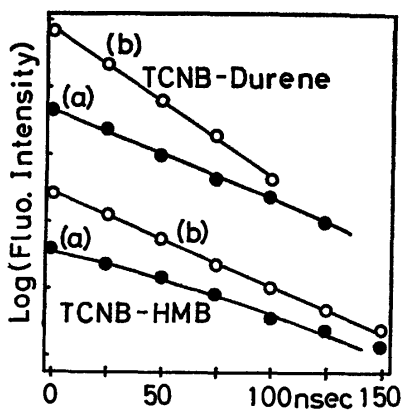

Fig. 6. Fluorescence decay curves of TCNB-durene and TCNB-HMB complexes. (a) 475 nm. (b) 515 nm. In the case of TCNB-mesitylene and TCNB-naphthalene complexes, similar results were obtained but the deviation from the exponential decay is small. The decay curve of TCNB-toluene complex in *n*P–*i*P has been reported in Ref. 12.

Discussion

The $S_n \leftarrow S_1$ spectra of the present TCNB complexes at 77 K can be well reproduced by the superposition of the bands similar to those of TCNB anion as well as donor cation. Although the wave numbers and bandwidths of the ion-like bands in the $S_n \leftarrow S_1$ spectra are a little different from those of the free ions in solution, the electronic structures of the fluorescent states may be concluded to be quite polar in general even at 77 K, irrespectively of the donors. This result is the same as that obtained from some TCNB complexes at room temperature. Since it can be expected theoretically[17] that the CT degree of the excited FC state is not so large as that of the fluorescent state and depends on the strength of the donor, there may exist a relaxation process involving structural changes as well as solvent re-orientation from the excited FC state to the fluorescent state, leading to the quite polar structure.[2]

The $S_n \leftarrow S_1$ spectra of the present complexes may be compared with the spectra of ionic radical salts, since the latter are deemed to be composed of donor cation and acceptor anion. The characteristics of the spectra of some ionic radical salts are summarized as follows.[18-20] (1) The blue shift of the bands associated with component ions is observed to be about 2~4 kK. (2) The absorption bands of the original ions are broadened. (3) The CT transition from acceptor anion to donor cation is observed in the near-infrared region, which is not obtained in solution spectra of both ions. The shift as well as the broadening of the bands of component ions in the present case of the TCNB complexes are rather different from those of the ionic radical salts. On the other hand, Kimura et al. have reported electronic spectra of ion-pair produced by irradiating EDA complexes and those of photoionized molecules in rigid solution and have pointed out a slight red shift of the ion bands in the ion-pair.[21] These comparisons suggest that the component ions in the fluorescent state of TCNB complexes does not interact with each other through the overlap integrals as in the case of ionic radical salts, but are influenced only by electrostatic interaction between both ions. Since fluorescence, which is accompanied with an electron transfer from anion to cation, is observed, it is concluded that the fluorescent state of these complexes at 77 K is not a solvent-shared but a contact ion-pair. However, the latter ion-pair

15) B. Badger and B. Brocklehurst, *Trans. Faraday Soc.*, **65**, 2582 (1969).
16) B. Badger and B. Brocklehurst, *ibid.*, **65**, 2588 (1969); T. Shida and W. H. Hamill, *J. Chem. Phys.*, **44**, 2375 (1966).
17) S. Iwata, J. Tanaka, S. Nagakura, *J. Amer. Chem. Soc.*, **88**, 894 (1966).
18) T. Amano, H. Kuroda, and H. Akamatu, This Bulletin, **41**, 83 (1968).
19) H. Kuroda, S. Hiroma, and H. Akamatu, *ibid.*, **41**, 2855 (1968).
20) Y. Iida, *ibid.*, **42**, 71 (1969).
21) K. Kimura, S. Katsumata, and K. Sawada, *J. Phys. Chem.*, **76**, 639 (1972); Y. Achiba, S. Katsumata, and K. Kimura, Preprint for the Symposium on EDA Complexes, Sendai, 1971.

may be strongly solvated, which leads to weak interaction. Although the CT band is reported in the case of ionic radical salts, we have observed no back CT transition from TCNB anion to donor cation in the $S_n \leftarrow S_1$ spectra. This result is consistent with the above conclusion.

Now it is interesting to discuss generally the electronic structure of the excited EDA systems such as ^{1}CT as well as ^{3}CT states of EDA complexes and heteroexcimer. In the case of heteroexcimer formed through the quenching of aromatic hydrocarbon by aromatic amines and nitriles, the polar character of the electronic structure has been confirmed by a number of investigations.[22] The direct observation of the electronic spectra of heteroexcimer has been made possible by nsec flash photolysis. Potashnik *et al.* reported the spectra of diethylaniline-aromatic hydrocarbon systems, which seem to be interpretable as originating from the local transitions in aromatic hydrocarbon anion as well as dietylaniline cation and the back CT transition from anion to cation.[4] Similar results have been obtained in the pyrene–dimethylaniline systems in various solvents and also in the case of the intramolecular EDA systems containing the aromatic hydrocarbon and dimethylaniline moieties in the same molecule.[5] In the case of ^{3}CT state of TCNB complexes with methylsubstituted benzene donors, the CT degree was concluded to increase with the decrease of ionization potential of donor.[23] The CT degree of TCNB-HMB complex in the phosphorescent state was calculated to be about 95%. Thus, its electronic structure is quite polar. Therefore, it seems to be appropriate to study on the electronic structure of ^{1}CT state of the present TCNB complexes, ^{3}CT state of TCNB-HMB complex and the above mentioned heteroexcimer, based on the interaction between donor cation and acceptor anion.

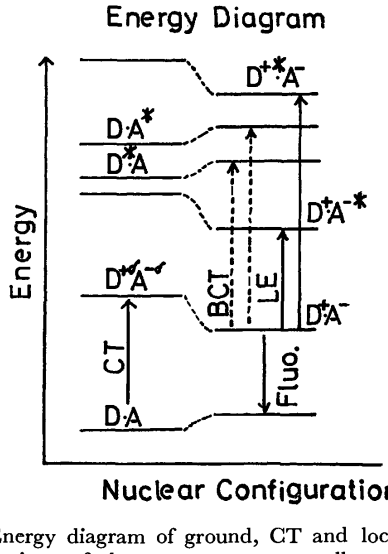

Fig. 7. Energy diagram of ground, CT and locally excited configurations of donor, acceptor as well as component ions. LE; local excitations of donor cation or acceptor anion. BCT; back CT transition from acceptor anion to donor cation.

We made a theoretical study on the fluorescent state by considering the configuration interactions (CI) among the ground, CT, back CT configurations and locally excited configurations of the acceptor anion-donor cation system.[2] This method may be useful also in analyzing ^{3}CT state of TCNB-HMB complex and the fluorescent state of heteroexcimer. The wave functions of several configurations may be given in the same form as in the previous paper.[2] The energies of the locally excited configurations of anion and cation may be taken from the observed values of the ions. It is rather difficult to estimate the energy of back CT transition from acceptor anion to donor cation. We have proposed a semiempirical method for obtaining the latter transition energy in terms of the rearrangement energy.[2] As indicated in Fig. 7, the transition energy can be given as

$$E(\text{back CT}) = E(\text{D*A}) \text{ or } E(\text{DA*}) - h\nu_{\text{f, 0-0}} + E_{\text{rea}}$$

where E(D*A) and E(DA*) represent the energies of locally excited configurations of donor and of acceptor, respectively, and $h\nu_{\text{f,0-0}}$ is the 0–0 band of fluorescence. E_{rea} is the rearrangement energy in question. Two methods for the evaluation of E_{rea} were proposed. In one method, it is assumed that E_{rea} involves the effects of the change of the geometrical structure and the CT degree in the higher excited state of the complex. In the other method, it is assumed that the contribution of the solvation energy to E_{rea} is overwhelming. The latter method is applied in the present work, since the problem of the structural change in the higher excited state is not yet elucidated. Putting E_{rea} as E_{des}, destablization energy in the FC ground state due to the solvent orientation, one can obtain the following equation.

$$\begin{aligned} E(\text{back CT}) &= E(\text{D*A}) \text{ or } E(\text{DA*}) - h\nu_{\text{f, 0-0}} + E_{\text{des}} \\ &= E(\text{D*A}) \text{ or } E(\text{DA*}) - h\nu_{\text{f, max}} \end{aligned}$$

where $h\nu_{\text{f,max}}$ represents the fluorescence maximum energy. The nondiagonal terms of CI secular equation should be evaluated theoretically using open shell MO.

Using the above theoretical treatment, we will now discuss the electronic structures of some excited EDA systems. In the first place, the $S_n \leftarrow S_1$ spectra of the present TCNB complexes and the absorption spectra of heteroeximers will be examined. The spectra of heteroexcimers were assigned to the transition associated with component ions and to the back CT transitions, where the intensities of both transitions are in the same order.[4] This assignment is consistent with theoretical model proposed by us. On the other hand, no large band due to back CT transition was observed

22) N. Mataga, T. Okada and N. Yamamoto, This Bulletin, **39**, 2562 (1966); H. Beens, H. Knibbe and A. Weller, *J. Chem. Phys.*, **47**, 1183 (1967); H. Beens and A. Weller, *Acta Phys. Polon.*, **34**, 593 (1968); D. Rehm and A. Weller, *Z. Phys. Chem. N. F.*, **69**, 183 (1970); A. Weller, "Nobel Symposium 5, Fast Reactions and Primary Processes in Chemical Kinetics," ed. by S. Claesson, Almqvist and Wiskell, Stockholm (1967), p. 413; T. Okada, H. Oohari, and N. Mataga, This Bulletin, **43**, 2750 (1970); N. Mataga, T. Okada, and K. Ezumi, *Mol. Phys.*, **10**, 201, 203 (1966).

23) H. Hayashi, S. Iwata, and S. Nagakura, *J. Chem. Phys.*, **50**, 993 (1969).

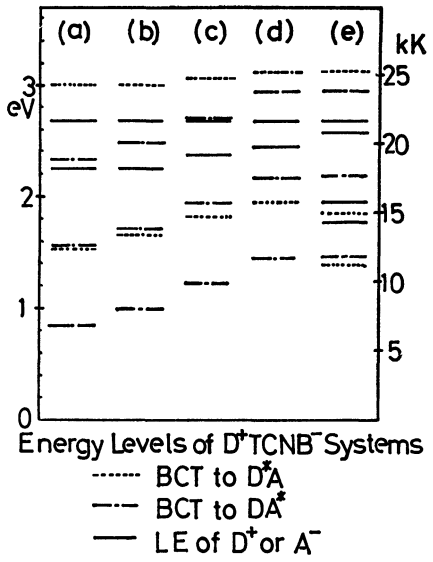

Fig. 8. Estimated energy levels for higher excited states of donor cation-TCNB anion system. The energy of fluorescent state of some TCNB complexes at 77 K was set as the standard. Donors are (a) benzene (b) toluene (c) mesitylene (d) HMB and (e) naphthalene. The energy levels of TCNB-durene complex are omitted since the precise value of higher excited state of durene is not known. However, almost the same values as in the case of TCNB-HMB complex are expected. Each value is estimated, using the data of Refs. 10, 24 and 25.

in the present work, which is the important difference between the ^{1}CT state of EDA complex and heteroexcimer. We have estimated the back CT transition energy using the above theoretical model and obtained the results as shown in Fig. 8. Here only *ungerade* states of locally excited configurations of donor as well as acceptor are included, although notations of *gerade* and *ungerade* are meaningless in the symmetry of the EDA complex. There may be more locally excited configurations, which corresponds to the *gerade* state of component molecules, and more back CT transitions may be expected. However, we have observed no absorption bands other than those due to the transitions associated with component ions. Since back CT transitions are forbidden without CI interaction the mixing of the back CT and locally excited configuration is required for the observation of these transitions. The fact that it is possible to observe the back CT transitions in the case of heteroexcimer means the more extensive mixing of both configurations than in the case of ^{1}CT state of the TCNB complexes. Hence, it may be concluded that ^{1}CT state of TCNB complexes at 77 K is more polar than heteroexcimer.

In the second, the $S_n \leftarrow S_1$ spectra of the present complexes and $T_n \leftarrow T_1$ spectra of TCNB-HMB complex will be discussed. Because the diagonal terms are the same in both cases, there may be nondiagonal matrix element that leads to the different electronic spectra. In the first approximation, the matrix elements between CT and other configurations may be important for elucidating the electronic structure of both of lowest singlet and triplet states. Under the condition of neglecting intermolecular differential overlap integrals, the matrix elements of the triplet state are identical with those of the singlet state and consist of one core attraction term.[7] Assuming the same geometrical structure in the fluorescent and phosphorescent states, it is expected that the $T_n \leftarrow T_1$ spectra are similar to $S_n \leftarrow S_1$ spectra. However, the observed results are different from this expectation and in the $T_n \leftarrow T_1$ spectra[7] we have found no band which coincides with that of TCNB anion. This result may be attributed to the difference of CT degree of the triplet state from that of the singlet state which may have different geometries, contrary to the above treatment.

We have made clear that the observed $S_n \leftarrow S_1$ spectra similar to those of TCNB anion can be explained statisfactorily when donor cation and acceptor anion are completely overlapped each other in C_{2v} symmetry or when both ions are loosely interacting with each other at a longer distance.[2] Moreover the CT degree was determined to be $\sim$100% in the case of these geometrical configurations. Thus, it is concluded that the CT degree in the phosphorescent state of TCNB-HMB complex is lower than that in the fluorescent state and the geometrical configurations of the former state are different from those of the latter. Moreover, the CT degree in the ^{3}CT state of the TCNB-HMB complex may be lower than that of heteroexcimer since any band similar to that of the acceptor anion was not observed in the case of the former system.

Now it is concluded that the CT degree increases in the following order; ^{3}CT state of TCNB-HMB complex < heteroexcimer < ^{1}CT state of some TCNB complexes.

24) T. Kobayashi, K. Yoshihara, and S. Nagakura, This Bulletin, **44**, 2603 (1971).

25) "UV Atlas of Organic Compounds," Butterworth, London (1966).

The Crystal and Molecular Structure of 5-Chloro-7-iodo-8-quinolinol, Chinoform

Setsuo KASHINO and Masao HAISA

Department of Chemistry, Faculty of Science, Okayama University, Tsushima, Okayama 700

(Received October 28, 1972)

Isomorphous crystals of 5-chloro-7-iodo- and 5,7-dibromo-8-quinolinols have been examined by X-ray analysis. Both compounds crystallize in the monoclinic space group $P2/a$ with four formula units in the unit cell. The cell dimensions are: $a=16.98$; $b=4.16$; $c=14.84$ Å, and $\beta=112.0°$ for 5-chloro-7-iodo-8-quinolinol, and $a=16.34$, $b=4.02$, $c=15.52$ Å, and $\beta=115.6°$ for 5,7-dibromo-8-quinolinol. The structure of the former, chinoform, has been determined by the Patterson methods from data collected with Mo$K\alpha$ radiation on Weissenberg photographs, and refined by the block-diagonal least-squares method, with anisotropic temperature factors. The final R value is 0.081 for 836 observed reflections. The quinolinol molecule is nearly planar. In the crystals, the molecules related by two-fold axis are held together by hydrogen bonds to form bent dimers, which are stacked closely by van der Waals forces along the b axis.

The derivatives of 8-quinolinol are widely used as chelating agents in analytical chemistry and a number of their complexes are investigated, especially by Prout and his coworkers,[1] by means of X-ray diffraction structure analysis in connection with the Mulliken's "overlap and orientation" principle.[2] 5-Chloro-7-iodo-8-quinolinol is medically important as so-called "chinoform". In this study the cell dimensions and the space group of 5-chloro-7-iodo- and 5,7-dibromo-8-quinolinols were determined, and the structure of the former compound was studied by X-ray diffraction analysis.

Experimental

5-Chloro-7-iodo-8-quinolinol (prepared by Tanabe Seiyaku Co., Ltd.) was recrystallized from ethanol. Crystals obtained by slow evaporation from ethanol solution were monoclinic needles elongated along the b-axis. Cell constants were determined from Weissenberg and oscillation photographs taken with Cu$K\alpha$ radiation ($\lambda=1.5418$ Å). Crystal data are given in Table 1 along with those of 5,7-dibromo-8-quinolinol, which have been determined by the same way as those of chinoform. Since crystals of 5,7-dibromo-8-quinolinol gave no suitable photographic spots for intensity measurements, the structure analysis was not tried. A possible space group of these two compounds is determined to be Pa or $P2/a$ from the absent spectra: $h0l$ when h is odd. Structure analysis of chinoform was made on the basis of the latter space group symmetry and gave a reasonable structure. The space group of 5,7-dibromo-8-quinolinol may also be $P2/a$ because its molecular symmetry is the same as that of chinoform.

Intensity data of chinoform were initially collected with Cu$K\alpha$ radiation by means of the equi-inclination Weissenberg photographs, for the layers of $h0l$ to $h3l$. However, in view of the large absorption effect the data were recollected, after the structure was determined, with Mo$K\alpha$ radiation, for the layers of $h0l$ to $h4l$ using a crystal of $0.11\times0.12\times0.60$ mm³. A total of 836 independent non-zero reflections were measured visually. The inter-layer scaling was made according to the exposure time. Corrections were made for the Lorentz and polarization factors, and for the spot shape.

Table 1. Crystal data

	5-Chloro-7-iodo-8-quinolinol C_9H_5NOClI	5,7-Dibromo-8-quinolinol $C_9H_5NOBr_2$
MW	305.5	303.0
Mp	172°C	196°C
Crystal system	Monoclinic	Monoclinlic
a	16.98(2) Å	16.34 Å
b	4.16(1)	4.02
c	14.84(1)	15.52
β	112.0(2)°	115.6°
V	971.9 Å³	919.3 Å³
D_c	2.088 g cm^{-3}	2.189 g cm^{-3}
D_m	2.08$_4$ (by flotation)	
Z	4	4
Absent spectra	$h0l$ when h odd	$h0l$ when h odd
Space group	$P2/a$	$P2/a$
μ for Cu$K\alpha$	285.5 cm^{-1}	120.8 cm^{-1}
μ for Mo$K\alpha$	35.6	93.0
$F(000)$	576	576

Structure Determination

Approximate positional parameters of all non-hydrogen atoms were easily determined from a three-dimensional Patterson map. The structure was then refined isotropically by the block-diagonal least-squares method.[3] An R value dropped from 0.24 for the trial structure to 0.18. The structure was refined anisotropically for the non-hydrogen atoms to the R value of 0.123 for the copper data. Using the positional parameters thus obtained and $B=5.35$ Å² from Wilson's method as initial parameters, an isotropic refinement was made with the molybdenum data. Thereafter the data of each layer were re-scaled on the basis of the ratio of $\Sigma|F_o|$ and $\Sigma|F_c|$. The refinement with anisotropic thermal parameters reduced the R value to 0.084. Three hydrogen atoms attached to a quinoline ring were located from a difference map, but the other two hydrogen atoms were not revealed. Assuming suitable geometries of the C–H bond (C–H=1.08 Å), the positional parameters of the four ring hydrogen atoms were computed. These parameters and an isotropic temperature factor, $B=4.5$ Å², were introduced as

1) E. Castellano and C. K. Prout, *J. Chem. Soc., A*, **1971**, 550.
2) R. S. Mulliken, *Rec. Trav. Chim.*, **75**, 845 (1956).
3) Y. Okaya and T. Ashida, "HBLS IV, The Universal Crystallographic Computing System (I)." The Crystallographic Society of Japan, Tokyo (1967) p. 65.

Table 2. Final atomic parameters

All values should be multiplied by 10^{-4}. The e.s.d.'s of atomic coordinates are shown in parentheses. The anisotropic thermal parameters are expressed as $\exp(-B_{11}h^2-B_{22}k^2-B_{33}l^2-B_{12}hk-B_{13}hl-B_{23}kl)$.

Atom	x/a	y/b	z/c	B_{11}	B_{22}	B_{33}	B_{12}	B_{13}	B_{23}
I	7638(1)	6246(4)	1773(1)	43	663	82	22	54	85
Cl	4277(3)	990(18)	776(4)	35	1023	43	−11	12	−38
O	7698(8)	3544(43)	3840(10)	37	915	65	−83	34	−9
N(1)	6461(9)	360(45)	4352(11)	31	801	46	69	37	69
C(2)	5893(14)	−1441(63)	4600(15)	48	795	52	125	21	−5
C(3)	5089(14)	−2223(64)	3912(16)	42	1025	60	−91	49	109
C(4)	4848(11)	−1358(57)	2970(16)	32	617	85	−102	61	−164
C(5)	5288(10)	1719(50)	1703(13)	20	648	40	23	−13	−48
C(6)	5866(11)	3498(49)	1474(13)	31	491	42	63	13	4
C(7)	6700(11)	3977(52)	2167(15)	34	454	71	−42	32	−36
C(8)	6915(13)	2986(48)	3159(15)	34	544	56	−56	6	−163
C(9)	6261(10)	1324(55)	3419(14)	25	566	65	1	37	−61
C(10)	5444(13)	617(49)	2677(14)	41	578	48	−11	11	−80

fixed parameters, and the parameters for all non-hydrogen atoms were refined anisotropically, using the following weighting scheme:

$\sqrt{w} = 1.0$, if $10.0 \leqq F_o \leqq 27.0$,

$\sqrt{w} = 27.0/F_o$, if $F_o > 27.0$,

and $\sqrt{w} = 0.0$ for unobserved reflections.

The final R value was 0.081 for the 836 non-zero reflections. The final atomic parameters are given in Table 2. A composite drawing of the final electron density map is shown in Fig. 1. The observed and calculated structure factors are listed in Table 3.

The atomic scattering factors used were those of Hanson, Herman, Lea, and Skillman.[4] The numerical calculations were performed with the aid of a HITAC 5020 E computer of the Computer Center of the University of Tokyo.

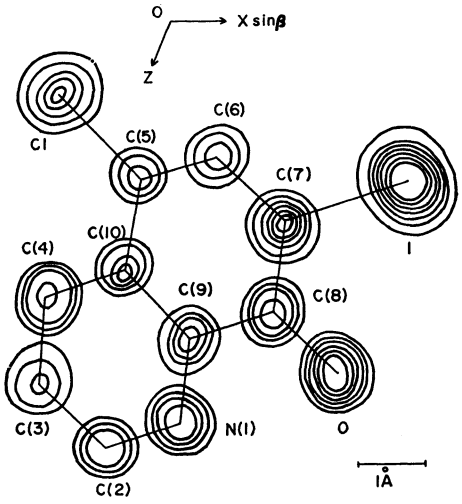

Fig. 1. Composite three-dimensional final electron-density map projected along the b axis. Contours are at intervals of 1 e Å^{-3} for C, N and O atoms, 5 e Å^{-3} for Cl atom and 10 e Å^{-3} for I atom, each starting at 3 e Å^{-3}.

4) H. H. Hanson, F. Herman, J. D. Lea, and S. Skillman, *Acta Crystallogr.*, **17**, 1040 (1964).

Results and Discussion

Bond lengths and angles are shown in Fig. 2. The average C–C bond length within the quinoline ring is 1.42 Å. Although the average standard deviation of the bond lengths amounts to 0.03 Å, the shortening of the C(3)–C(4) and C(5)–C(6) bonds and the lengthening of the C(4)–C(10) and C(8)–C(9) bonds may be significant. The results of semi-empirical SCF-MO calculation[5] and X-ray crystallographic studies[1,6,7] of quinoline and its derivatives have shown the similar shortening and lengthening of the corresponding bonds as compared in Table 4. The C–O bond length (1.36 Å) is almost the same as those

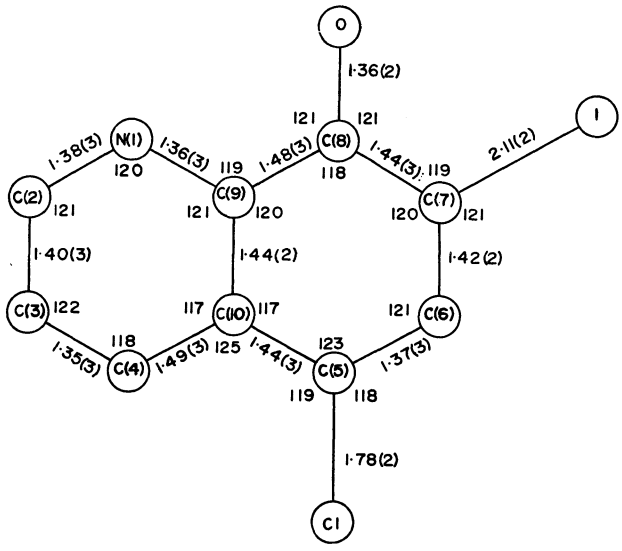

Fig. 2. Bond lengths(Å) and angles(°). The e.s.d.'s are shown in parentheses for bond lengths, and are 2° for all the bond angles.

5) M. J. S. Dewar and G. J. Gleicher, *J. Chem. Phys.*, **44**, 759 (1966).

6) M. Sax and R. Desiderato, *Acta Crystallogr.*, **23**, 319 (1967).

7) L. L. Merritt, Jr and B. Duffin, *ibid.*, **B26**, 734 (1970).

TABLE 3. OBSERVED AND CALCULATED STRUCTURE FACTORS

H	FO	FC	H	FO	FC	H	FO	FC	H	FO	FC	H	FO	FC	H	FO	FC	H	FO	FC	H	FO	FC	H	FO	FC
K,L=	0	0	-4	108	121	-2	23	26	0	142	118	-17	19	21	4	36	-35	-4	23	-22	-1	33	29	0	44	-46	-9	1/	-18
2	151	-112	-2	205	-179	2	24	26	1	157	128	-16	33	-34	5	18	-16	-3	155	-147	1	42	-42	1	52	54	-8	29	-28
4	202	165	0	88	77	4	13	-16	2	78	-78	-15	45	-45	7	23	20	-2	14	11	3	25	23	2	35	35	-7	36	33
6	184	-150	2	82	-83	K,L=	0	15	3	97	-93	-14	31	27	K,L=	1	12	-1	133	130	K,L=	2	10	3	33	-33	-6	36	33
8	72	75	4	78	78	-16	23	-21	4	141	119	-13	36	35	-15	15	-18	1	70	-77	-17	25	21	4	37	-27	-4	13	-20
10	63	-63	6	17	-17	-14	20	23	5	20	26	-12	49	-49	-14	25	26	2	13	17	-15	35	-33	5	33	31	-3	24	24
12	55	55	8	24	25	-10	31	35	6	33	-36	-11	43	-43	-13	24	24	3	90	96	-13	19	17	6	31	29	-2	20	19
K,L=	0	1	K,L=	0	7	-8	29	-30	7	63	-60	-10	27	30	-12	25	-27	4	16	15	-11	36	-33	7	31	-32	-1	32	-30
-18	32	-35	-20	29	29	-4	30	-29	8	22	25	-9	71	68	-11	53	-45	5	74	-74	-9	47	43	8	20	-20	0	14	-15
-16	37	38	-18	38	-38	2	19	14	9	12	13	-8	15	-28	-10	14	19	7	32	28	K,L=	2	11	9	25	22	1	17	17
-14	55	-57	-16	35	33	K,L=	1	0	10	39	-39	-7	38	-40	-9	34	34	9	40	-41	-9	18	-18	K,L=	3	4	2	17	18
-12	100	105	-14	70	-64	2	220	198	K,L=	1	4	-6	65	66	-8	35	-34	11	18	18	-5	24	-23	-15	24	23	3	18	-14
-10	88	-96	-12	44	47	3	85	85	-18	27	-26	-5	29	32	-7	19	-20	K,L=	2	4	-3	37	35	-14	24	21	K,L=	4	0
-8	89	92	-10	63	-69	4	135	-123	-17	20	-24	-4	10	-12	-6	23	24	-19	22	-21	-1	56	-51	-13	21	-19	2	29	34
-6	207	-178	-8	61	70	5	109	-98	-15	50	49	-3	51	-52	-5	43	40	-17	31	31	3	37	-31	-12	22	-23	4	31	-31
-4	91	99	-6	26	-24	6	69	71	-14	59	-54	-2	12	17	-4	26	-25	-15	41	-37	K,L=	2	12	-11	31	30	6	35	33
2	71	-69	-4	46	54	7	92	85	-13	43	-44	1	13	19	-3	16	-19	-13	62	60	-15	27	25	-10	28	25	8	19	-20
4	21	25	-2	13	14	8	68	-64	-12	66	60	2	19	-24	-2	42	42	-11	48	-46	-13	36	-31	-9	29	-29	K,L=	4	1
6	22	-27	6	42	42	9	21	-25	-11	68	62	5	51	52	-1	17	20	-9	58	61	-11	30	28	-8	27	-29	-12	19	-23
8	105	-101	10	24	28	10	25	29	-10	52	-51	7	13	-13	1	14	-15	-7	94	-87	-9	47	-40	-6	55	52	-10	21	25
10	24	27	12	19	-27	11	45	47	-9	68	-64	8	24	28	3	15	11	-4	24	21	-7	48	43	-5	53	-49	-8	19	-22
12	37	-40	K,L=	0	8	12	19	-26	-8	78	74	9	14	16	K,L=	1	13	-3	54	-61	-5	25	-23	-4	12	-16	-6	32	33
14	45	43	-20	17	16	14	23	27	-6	98	-94	11	19	-23	-14	27	24	-1	45	47	-3	35	32	-3	25	28	-4	22	-23
K,L=	0	2	-16	23	20	K,L=	1	1	-5	77	-74	K,L=	1	8	-11	21	-19	2	27	27	-1	23	-18	-2	19	20	-2	16	16
-18	32	-32	-14	14	-19	-17	19	21	-4	50	51	-12	16	-21	-10	18	19	7	39	-44	1	22	23	-1	12	-15	K,L=	4	2
-12	51	55	-6	62	64	-16	22	-25	-3	23	27	-11	22	24	-8	17	-19	11	25	-22	3	23	-17	1	19	21	-4	16	15
-4	116	-116	-2	61	66	-15	28	-30	-2	81	-82	-8	21	22	-3	17	19	13	31	28	K,L=	2	13	K,L=	3	5	-2	16	-18
0	177	-136	0	111	-107	-14	35	35	0	36	36	-7	44	42	K,L=	1	14	K,L=	2	5	-13	20	-21	-8	21	22	0	24	26
2	274	185	2	48	49	-13	18	21	2	19	20	-5	67	-66	-9	26	-22	-13	25	28	-9	19	-21	-6	17	-20	2	28	-27
4	164	-141	4	75	-77	-12	53	-48	4	33	35	-4	55	54	-7	14	15	-6	13	12	-1	23	22	-5	11	14	4	27	25
6	55	57	6	37	36	-11	64	-63	5	29	-33	-3	44	44	-6	18	-23	-5	52	-55	K,L=	2	14	-4	20	20	8	19	28
8	98	-101	8	23	-23	-10	89	86	6	13	15	-2	44	-40	-3	18	17	-4	20	-20	-7	25	-18	-3	26	-26	10	39	-18
10	48	50	10	32	34	-9	41	43	7	11	13	-1	68	-65	-2	18	-19	-3	36	38	-5	26	23	-2	28	-28	12	18	17
12	57	-55	12	17	-17	-8	91	-87	8	15	-17	0	11	17	0	19	21	-1	56	-55	-1	23	19	-1	23	23	K,L=	4	3
14	43	42	K,L=	0	9	-7	93	-92	9	23	-27	1	46	48	1	15	12	1	75	78	K,L=	2	15	0	42	39	-10	16	-20
K,L=	0	3	-18	30	26	-6	43	43	11	17	22	2	59	-59	K,L=	1	15	2	25	-22	-7	26	-20	1	11	-11	-8	22	22
-14	38	43	-16	16	-16	-5	73	70	12	24	-28	3	33	-30	-15	20	19	3	43	-44	-1	17	13	2	46	-40	-6	33	-30
-12	42	-45	-14	42	45	-4	53	-53	K,L=	1	5	4	36	36	-14	23	-19	5	61	60	K,L=	3	0	3	33	32	-4	32	34
-10	100	114	-12	72	-66	-3	129	-119	-20	17	14	5	44	44	-12	19	20	7	71	-65	2	56	-70	4	34	32	-2	29	-32
-8	78	-73	-10	50	50	2	49	49	-18	22	-28	6	36	-35	-11	19	17	9	20	18	3	40	43	5	27	-24	0	32	37
-6	105	104	-8	94	-96	5	13	-22	-15	14	14	7	45	-39	-9	15	-15	11	35	-31	4	42	41	6	35	-32	2	35	-36
-4	189	-161	-6	106	109	6	25	-28	-14	13	-17	8	17	22	-6	19	-25	13	28	24	5	50	-50	7	17	18	4	29	26
-2	152	134	-4	74	-74	7	30	-23	-8	17	11	K,L=	1	9	-5	15	-13	K,L=	2	6	6	39	-37	8	18	18	K,L=	4	4
0	211	-161	-2	67	74	8	17	-15	-7	13	-15	-17	19	-22	K,L=	2	0	-17	24	-24	7	41	39	9	38	-34	-12	17	22
2	214	160	0	81	-76	10	51	-47	-6	39	39	-16	21	20	3	121	-121	-15	22	22	8	23	19	10	23	-23	-10	28	-29
4	68	-69	4	93	-90	12	30	30	-5	32	33	-15	27	24	4	19	-18	-13	28	-28	10	20	-20	K,L=	3	6	-8	24	23
6	171	136	6	26	22	13	25	25	-4	58	-56	-14	24	-23	5	65	73	-11	63	59	11	20	21	-13	15	19	-6	23	-23
8	63	-63	K,L=	0	10	16	31	26	-3	61	-60	-13	39	-35	7	56	-57	-9	53	-51	K,L=	3	1	-12	31	29	-4	25	22
12	39	-40	-20	25	-23	K,L=	1	2	-2	41	42	-12	32	29	9	87	91	-7	62	65	-14	16	-17	-10	29	-29	-2	10	-10
K,L=	0	4	-18	48	45	-19	17	-15	-1	41	44	-11	43	42	K,L=	2	1	-5	102	-104	-13	19	21	-9	37	38	0	11	10
-20	20	-19	-16	20	-25	-17	19	22	0	126	-106	-10	57	-57	-15	40	40	-3	72	75	-12	28	30	-8	25	23	K,L=	4	5
-18	30	31	-14	43	45	-16	18	-21	1	62	-63	-9	39	-36	-13	51	-53	-1	76	-76	-11	34	-34	-7	25	-23	-4	11	-11
-16	73	-70	-12	54	-57	-15	17	-21	2	59	56	-8	64	59	-11	26	25	0	18	-21	-10	31	-33	-6	50	-48	-2	30	31
-14	24	25	-10	34	31	-14	24	26	3	77	78	-7	68	66	-9	83	-81	1	91	93	-9	24	26	-5	42	36	0	20	-21
-12	79	-75	-8	45	-49	-13	50	49	4	65	-60	-6	50	-47	-7	68	73	3	33	-35	-8	36	36	-4	40	40	2	28	27
-10	109	114	-6	34	39	-10	26	26	5	41	-41	-5	33	-33	-5	89	-94	5	47	45	-7	36	-35	-3	48	-50	4	32	-30
-8	152	-130	-2	22	26	-6	13	-17	6	79	79	-4	64	61	-3	125	117	7	38	-35	-6	32	-35	-2	40	-41	K,L=	4	6
-6	123	118	2	41	-43	-4	32	-30	7	35	38	-3	50	52	1	34	43	9	21	20	-5	36	38	-1	47	44	-12	15	-15
-4	197	-173	4	29	33	-3	157	134	8	40	-37	-2	49	-48	3	41	-47	K,L=	2	7	-4	28	30	0	28	27	-10	20	19
0	111	-90	8	25	27	-2	183	-142	9	47	-47	-1	50	-50	4	14	16	-19	18	16	-3	23	-24	1	26	-27	-8	41	-39
2	68	70	K,L=	0	11	0	113	99	10	31	33	0	39	39	11	22	18	-17	35	-32	-2	17	-16	2	24	-21	-6	27	26
4	50	51	-10	54	-59	1	117	104	12	33	-33	1	25	25	13	21	-18	-15	39	33	1	10	-13	3	38	37	-4	26	-24
10	54	-56	-8	15	17	2	31	-33	K,L=	1	6	2	61	-59	15	21	19	-13	52	-52	2	11	-11	K,L=	3	7	-2	32	28
12	14	17	-6	49	-50	3	83	-81	-18	16	17	6	24	-25	17	33	-22	-11	64	59	10	28	29	-15	26	-24	0	28	-25
K,L=	0	5	-4	49	58	4	68	68	-16	14	-18	8	18	20	K,L=	2	2	-9	50	-49	K,L=	3	2	-13	27	25	2	19	20
-20	20	-17	-2	32	-32	5	67	66	-15	17	-26	K,L=	1	10	-15	39	34	-7	47	50	-3	31	29	-11	27	-23	4	16	-17
-18	18	17	0	55	59	6	89	-84	-13	34	31	-17	19	-16	-13	20	-21	-5	50	-50	-2	32	34	-10	21	-22	K,L=	4	7
-16	48	-47	2	23	-25	7	111	-100	-12	43	-46	-16	42	37	-11	33	33	-1	25	-28	-1	10	-11	-9	30	31	-12	15	-17
-14	17	18	4	21	22	8	33	33	-11	48	-44	-15	22	22	-9	17	-18	3	22	22	0	33	-36	-8	13	12	-8	13	-16
-12	20	-25	6	39	-38	9	72	70	-10	82	78	-14	28	-28	-7	16	-17	7	40	41	1	33	33	-7	20	-21	-6	10	14
-8	67	73	8	16	19	10	70	-61	-9	62	62	-13	30	-30	-5	53	56	9	22	-20	2	31	32	-6	15	-17	-4	15	-17
-6	16	-17	K,L=	0	12	11	41	-37	-8	56	-54	-12	25	24	-4	16	-16	K,L=	2	8	3	48	-49	-4	12	-9	K,L=	4	8
-4	52	54	-18	17	-22	12	39	33	-7	79	-73	-11	32	27	-3	18	16	-9	30	29	4	41	-39	-3	30	-31	-6	11	-14
-2	158	-154	-16	33	33	13	45	42	-6	108	106	-10	34	-32	-2	21	-19	-7	32	-29	5	23	22	K,L=	3	8	-4	13	14
0	108	90	-14	28	-28	15	25	-26	-5	61	54	-8	15	19	-1	66	83	-5	48	47	6	50	45	-8	16	-16	0	22	21
2	151	-124	-10	47	-46	K,L=	1	3	-4	77	-75	-7	23	24	1	57	-64	-3	69	-67	7	59	-50	-5	16	-21	2	14	-14
4	167	148	-8	43	40	-17	15	-13	-3	119	-110	-6	29	-30	3	79	80	-1	44	41	9	26	24	-4	13	-15	4	17	19
6	53	-52	-6	56	-58	-16	15	10	-2	43	45	-4	29	31	5	110	-109	1	58	-60	10	27	25	-3	15	14	K,L=	4	9
8	84	83	-4	44	41	-15	33	31	-1	59	61	1	16	-17	7	67	67	3	55	57	K,L=	3	3	-2	36	38	-12	15	15
10	61	-63	0	39	39	-12	44	43	0	122	-106	K,L=	1	11	9	76	-72	5	26	-25	-12	20	-24	-1	32	-31	-10	18	-17
12	35	34	K,L=	0	13	-11	43	40	1	44	-45	-11	17	-18	11	59	55	7	41	37	-11	17	20	0	22	-20	-8	21	21
14	31	-31	-18	14	-17	-10	29	-26	2	54	55	-8	55	-49	13	32	-30	9	42	-35	-10	16	20	1	22	21	-6	24	-23
K,L=	0	6	-16	21	25	-9	79	-75	3	79	76	-7	22	-23	15	29	25	K,L=	2	9	-9	33	-38	2	26	26	-4	20	18
-20	17	15	-14	12	-16	-8	87	87	4	31	-31	-6	23	24	17	26	-21	-17	24	18	-8	39	-38	4	20	-20	-2	22	-24
-18	13	-12	-12	49	50	-7	85	82	5	29	-31	-5	30	33	K,L=	2	3	-15	33	-30	-7	36	37	5	29	28	0	16	17
-16	20	24	4	16	-13	-6	121	-110	6	43	44	-4	13	-18	-13	41	41	-13	35	33	-6	33	33	K,L=	3	9			
-14	63	-66	K,L=	0	14	-5	154	-129	7	27	26	-3	30	-31	-11	47	-49	-11	52	-45	-5	57	-56	-14	16	16			
-12	63	66	-14	16	17	-4	33	32	9	20	-22	-2	44	40	-9	58	61	-9	64	62	-4	36	-34	-13	23	-19			
-10	48	-56	-8	23	-28	-3	160	133	K,L=	1	7	-1	13	17	-7	90	-89	-7	27	-24	-3	50	50	-12	19	-17			
-8	180	165	-6	14	12	-2	105	-99	-19	20	-21	1	59	-56	-6	22	-24	-5	78	79	-2	43	44	-11	23	23			
-6	111	-108	-4	42	-46	-1	146	-125	-18	25	25	2	34	33	-5	144	114	-3	58	-56	-1	33	-34	-10	22	22			

found in 8-hydroxyquinoline–1,3,5-trinitrobenzene[1] and 8-hydroxyquinoline–chloranil[8] complexes (1.353 and 1.38 Å, respectively), and in phenols such as *p*-hydroxybenzoic acid monohydrate (1.359 Å),[9] α- and β-modifications of *p*-nitrophenol (1.351 and 1.361 Å, respectively).[10,11] No bond angles in a quinoline ring differ significantly from 120°.

As is shown in Table 5, the planes of a benzene ring, P(2), and a pyridine ring, P(3), are planar within 0.050 and 0.013 Å, respectively. The dihedral angle between these planes is only 3.2°, and the quinoline

8) C. K. Prout and A. G. Wheeler, *J. Chem. Soc., A*, **1967**, 469.

9) K. Fukuyama, K. Ohkura, S. Kashino, and M. Haisa, This Bulletin, **46**, 804 (1973).

10) P. Coppens and G. M. J. Schmidt, *Acta Crystallogr.*, **18**, 62 (1965).

11) P. Coppens and G. M. J. Schmidt, *ibid.*, **18**, 654 (1965).

Table 4. The comparison of bond lengths (Å) of quinoline and its derivatives

	CIQ[a]	AMNQ[b]	HQSA[c]	HQTNB[d]	Quinoline[e] (Theoretical)
N(1)–C(2)	1.38	1.314	1.334	1.318	1.314
C(2)–C(3)	1.40	1.408	1.406	1.411	1.424
C(3)–C(4)	1.35	1.365	1.365	1.352	1.374
C(4)–C(10)	1.49	1.416	1.422	1.426	1.424
C(10)–C(5)	1.44	1.422	1.440	1.418	1.429
C(5)–C(6)	1.37	1.379	1.386	1.364	1.373
C(6)–C(7)	1.42	1.410	1.386	1.429	1.426
C(7)–C(8)	1.44	1.371	1.388	1.380	1.370
C(8)–C(9)	1.48	1.416	1.425	1.411	1.436
C(9)–C(10)	1.44	1.423	1.413	1.431	1.409
C(9)–N(1)	1.36	1.370	1.387	1.372	1.352

a) 5-Chloro-7-iodo-8-quinolinol, this work. b) 5-Acetoxy-6-methoxy-8-nitroquinoline, Ref. 6. c) 2-Methyl-8-hydroxyquinoline-5-sulfonic acid monohydrate, Ref. 7. d) 1 : 1 complex of 8-hydroxyquinoline and 1,3,5-trinitrobenzene, Ref. 1. e) Ref. 5.

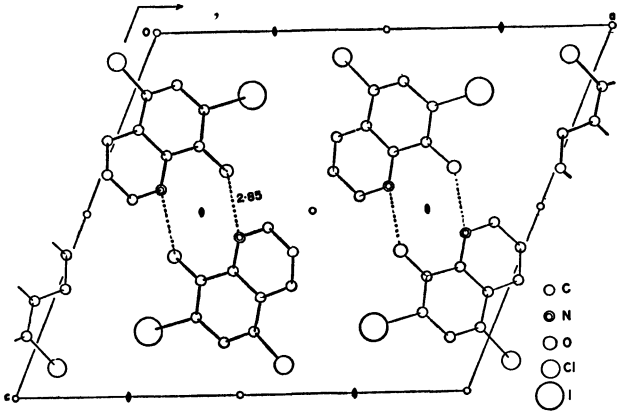

(a)

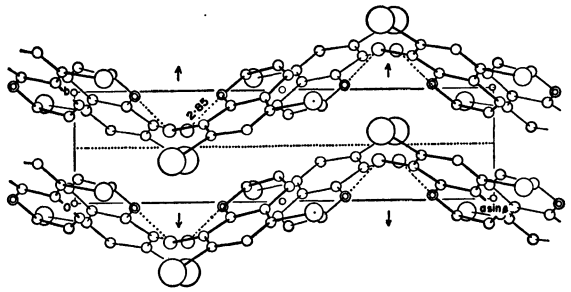

(b)

Fig. 3. (a) The projection of the crystal structure along the *b* axis. (b) The projection of the crystal structure along the *c* axis. Hydrogen bonds are shown by broken lines.

ring as a whole is substantially planar within the limit of experimental errors. Among three substituents, only iodine atom deviates significantly from the quinoline ring plane, P(1).

The arrangements of the molecules viewed along the *b* and *c* axes are shown in Fig. 3. In the crystals, the molecules related by the two-fold axis are held together by the hydrogen bonds between oxygen and nitrogen atoms to form bent dimers, which are stacked closely by van der Waals forces along the *b* axis. The hydrogen bond length is 2.85 Å, which is comparable to the intermolecular O–H···N hydrogen bond lengths in 8-hydroxyquinoline dimers in 8-hydroxyquinoline–chloranil[8] and 8-hydroxyquinoline–1,3,5-trinitrobenzene[1] complexes (2.80 and 2.914 Å,

Table 5. Distances from the least-squares plane (Å)

	P(1)	P(2)	P(3)
I	−0.218*	−0.138*	
Cl	0.041*	−0.032*	
O	−0.088*	−0.029*	
N(1)	0.047	0.040*	0.007
C(2)	−0.005		−0.006
C(3)	−0.022		0.010
C(4)	−0.041	−0.113*	−0.013
C(5)	0.005	−0.029	−0.017*
C(6)	0.052	0.050	
C(7)	−0.060	−0.030	
C(8)	−0.038	−0.009	−0.125*
C(9)	0.035	0.029	−0.011
C(10)	0.026	−0.012	0.013

P(1), the plane of quinoline ring; P(2), the plane of benzene ring; P(3), the plane of pyridine ring. The atom with asterisk is not included in the plane evaluation.

Table 6. Intermolecular distances

From molecule (I)	To atom	Of molecule	Translation			Distance (Å)
I	I	(I)	0	−1	0	4.16
I	C(7)	(I)	0	1	0	3.73
I	Cl	(II)	0	1	0	3.79
O	C(2)	(IV)	1	0	1	3.35
O	C(2)	(IV)	1	1	1	3.36
N(1)	N(1)	(IV)	1	0	1	3.33
C(2)	C(3)	(III)	1	0	1	3.57
C(3)	C(9)	(I)	0	−1	0	3.58
C(4)	C(10)	(I)	0	−1	0	3.56
O	N(1)	(IV)	1	0	1	2.85[a]

a) Hydrogen bond.
Key for molecules (I) $x/a, y/b, z/c$ (given in Table 2) (II) $x/a+1/2, -y/b, z/c$ (III) $-x/a, -y/b, -z/c$ (IV) $-x/a+1/2, y/b, -z/c$

respectively). The intramolecular N···O distance is 2.82 Å, close to the corresponding distances in the complexes (2.74 and 2.745 Å).[8,1)]

Some intermolecular distances are shown in Table 6. The intermolecular contacts are at the normal van der Waals distances. The dimension of the *b* axis is governed by the contact between atoms I and I (0 −1 0). In fact, in 5,7-dibromo-8-quinolinol, the lattice constant *b*, 4.02 Å, corresponds to the Br···Br van der Waals contact.

The authors are indebted to Dr. Shinji Ōmori and Professor Kyōji Tōei for supplying the materials.

BULLETIN OF THE CHEMICAL SOCIETY OF JAPAN, VOL. 46, 1098—1101 (1973)

The Kinetics of Association-Dissociation Reaction in an Aqueous Solution of *n*-Butylamine by Means of Ultrasonic Absorption

Sadakatsu NISHIKAWA and Tatsuya YASUNAGA

Department of Chemistry, Faculty of Science, Hiroshima University, Higashisenda-machi, Hiroshima 730

(Received October 30, 1972)

The ultrasonic absorptions of *n*-butylamine in aqueous solutions were measured at 25°C in the range of frequency from 15 to 220 MHz and of concentration from 0.698 to 3.00 M. The peak sound absorption was found. The mechanism of the observed peak sound absorption was attributed to the $4A \rightleftarrows A_4$ reaction where A and A_4 are the monomer and tetramer of the solute respectively. The rate constants of the forward and backward reaction were determined to be 2.2×10^6 M^{-3} sec^{-1} and 9.0×10^7 sec^{-1} respectively, and the standard volume change between the initial and final state in the reaction was calculated to be 14 ml mol^{-1}.

The method of ultrasonic absorption has been successfully applied to the investigation of reaction kinetics which occurs rapidly, since the relaxation time and excess absorption determined from the absorption data are related to the kinetic parameters.

It is well known that a number of binary liquid mixtures exhibit a maximum in their excess absorption at an intermediate concentration. Andreae and his coworkers[1] have summarized the data for these systems and developed a theory which is associated with the solute-solvent interactions. However, this analysis employs a rather unusually defined equilibrium constant and some of the stoichiometries reported appear to be implausible. Moreover, the data reported are insufficient for a reasonable analysis of the excess absorption mechanism.

It has reported that some amines also show the peak sound absorption phenomena at intermediate concentrations of their aqueous solutions.[1] The purpose of the present investigation is to report the ultrasonic absorption data on aqueous solutions of *n*-butylamine and to clarify the mechanism of the peak sound absorption using the relaxation theory.

Experimental

The *n*-butylamine was of a guaranteed reagent grade and was purified by distillation once. The purity was verified to be higher than 99.9% by the gas-chromatographic method. Deionized and distilled water was used as the solvent. The measurements of the ultrasonic absorption were made at the odd harmonic frequencies of 5 and 20 MHz X-cut quartz transducers by means of the pulse technique.[2] The frequency range of the measurement was from 15 to 220 MHz. The sing-around method was employed at 1.92 MHz to measure the sound velocity. The densities were measured by the standard pycnometer. The pH values of the solutions were measured by a Hitachi-Horiba type F-5 pH meter. All the measurements were made at 25°C.

Results

In Fig. 1 the plots of α/f^2 *vs.* the concentration are shown, where α is the sound absorption coefficient and f is the frequency. As may be seen in this figure, the absorption and the peak sound absorption concentration(P. S. A. C) depend on the frequency. This absorption behavior leads us to predict the existence of the relaxation phenomena.

In general, the sound absorption caused by the several relaxation processes can be described by the following equation:

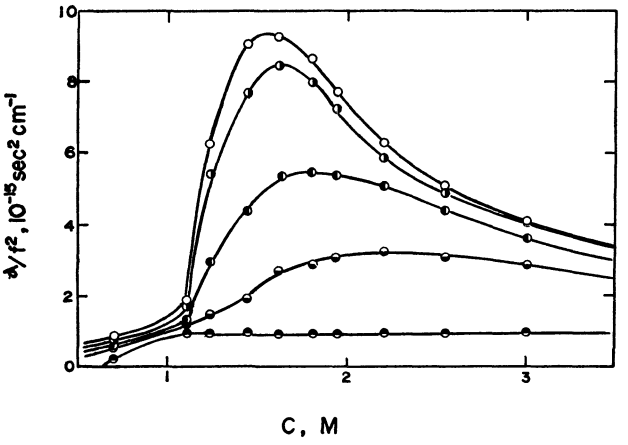

Fig. 1. The plots of α/f^2 *vs.* concentration in aqueous solutions of *n*-butylamine at 25 °C. ○: $f \rightarrow 0$, ◑: $f=15$ MHz, ◐: $f=45$ MHz, ◒: $f=100$ MHz, ◓: $f \rightarrow \infty$.

1) J. H. Andreae, P. D. Edmonds, and J. F. McKeller, *Acustica*, **15**, 74 (1965).

2) N. Tatsumoto, *J. Chem. Phys.*, **47**, 4561 (1967).

$$\alpha/f^2 = \sum_i \frac{A_i}{1+(f/f_{ri})^2} + B \quad (1)$$

where f_{ri} is the relaxation frequency for the i-th process and A_i and B are constants. In particular, for single and double relaxation processes Eq. (1) can be rewritten as:

$$\alpha/f^2 = \frac{A}{1+(f/f_r)^2} + B \quad (2)$$

and:

$$\alpha/f^2 = \frac{A_1}{1+(f/f_{r1})^2} + \frac{A_2}{1+(f/f_{r2})^2} + B \quad (3)$$

Figure 2 shows the representative ultrasonic absorption spectra of aqueous solutions of *n*-butylamine. All these spectra except the one at 1.10 M show the characteristic behavior due to the single relaxation process which is represented by Eq. (2). The spectrum at 1.10 M is represented by Eq. (3). The relaxation parameters were determined so as to obtain the best fit of the data of Eq. (2) or (3). As may be seen in this figure, the excess absorptions observed in more than 1.10 M are different from those in less than 1.10 M. The latter was attributed to hydrolysis, which was reported in a previous paper by the present authors.[3] In the concentrated solution, the experimental values of α/f^2 at high frequencies tend to be lower than the theoretical ones, as is shown in Fig. 2. This is because the excess absorptions associated with hydrolysis exist in a higher frequency range than that investigated here and the effect due to this relaxation process appears in the experimental values at high frequencies. However, the excess absorption in the concentrated solutions could be treated approximately as a single relaxation process. The concentration dependences of the sound velocity, c, and of the excess absorption, A, are shown in Fig. 3. The concentration at which the sound velocity shows its maximum is lower than that of the excess absorption. This kind of phenomenon has also been observed in binary mixtures.[1,4] The relaxation parameters and the sound velocity obtained are listed in Table 1, together with the density, the pH and the activity coefficient of ions, the last of which was calculated by Davis equation,

$$-\log \gamma = 0.5[\{\sqrt{I}/(1+\sqrt{I})\} - 0.3I].$$

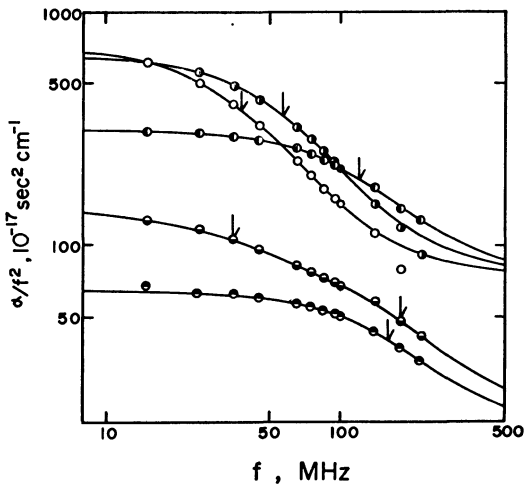

Fig. 2. Ultrasonic absorption spectra in aqueous solutions of *n*-butylamine at 25°C. ◓: 0.698 M, ◒: 1.10 M, ◑: 1.44 M, ○: 1.80 M, ◐: 3.00 M.

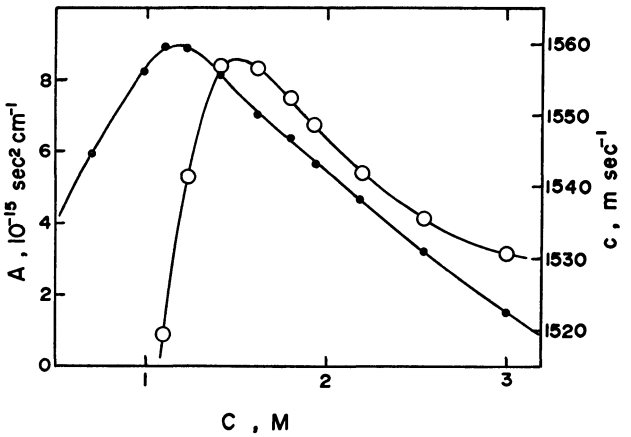

Fig. 3. Concentration dependence of the excess absorption and of the sound velocity. ○: A, ●: c.

Table 1. Relaxation parameters, sound velocity and density in the aqueous solution of *n*-butylamine at 25°C

C M	pH	γ	ρ g ml^{-1}	c m sec^{-1}	f_r MHz	A 10^{-17} sec^2 cm^{-1}	B
3.00	12.63	0.794	0.9460	1524.8	120	312	97.9
2.54	12.62	0.795	0.9534	1531.1	100	411	97.9
2.19	12.61	0.797	0.9604	1538.3	82	532	97.9
1.94	12.58	0.800	0.9653	1543.1	67	670	95.6
1.80	12.57	0.802	0.9718	1549.0	57	748	97.9
1.61	12.56	0.803	0.9721	1550.1	50	829	89.2
1.41	12.53	0.808	0.9757	1554.9	40	839	95.0
1.23	12.49	0.812	0.9796	1559.4	35	524	97.9
1.10	12.44	0.816	0.9834	1559.5	35, 180	86.3, 74.8	20.7
0.698	12.30	0.837	0.9884	1544.5	160	62.7	20.7

3) S. Nishikawa, T. Nakamoto, and T. Yasunaga, This Bulletin, **46**, 324 (1973).

4) R. N. Barfield and W. G. Schneider, *J. Chem. Phys.*, **31**, 488 (1959).

Interpretation of Results

Theoretical. The molecules which consist of hydrophilic and hydrophobic groups have a tendency to associate in an aqueous solution as in the case of surfactants.[5] Therefore, let us consider the reaction expressed by the next formula:

$$nA \underset{k_b}{\overset{k_f}{\rightleftharpoons}} A_n \tag{4}$$

where A is the monomer, A_n is the aggregate, n is the aggregation number, and k_f and k_b are the forward and backward rate constants respectively. If one denotes the molar concentrations of the components, A and A_n, by C_1 and C_2, the rate of return of the system to equilibrium is governed by the rate law:

$$\frac{dC_2}{dt} = k_f(C_1)^n - k_bC_2 \tag{5}$$

Provided that very small periodic perturbations are applied to the system, it may be assumed that the perturbed rate constants and the concentrations differ only slightly from their equilibrium values. One can write for the perturbed variables a series of relations such as:

$$\left.\begin{aligned} C_1 &= \bar{C}_1 + \delta C_1\cdot\exp(i\omega t), \quad C_2 = \bar{C}_2 + \delta C_2\cdot\exp(i\omega t), \\ k_f &= \bar{k}_f + \delta k_f\cdot\exp(i\omega t), \quad k_b = \bar{k}_b + \delta k_b\cdot\exp(i\omega t), \end{aligned}\right\} \tag{6}$$

where the equilibrium values of the rate constants and the concentrations are indicated by a bar over each symbol and the quantities δC_i and δk_i represent the amplitudes of the small variations associated with the sound wave. As the relation between δC_1 and δC_2 is $\delta C_1 = -n\delta C_2$, one obtains the next equation:

$$\delta C_2 = \frac{(\bar{C}_1)^n\delta k_f - \bar{C}_2\delta k_b}{i\omega + \bar{k}_f n^2(\bar{C}_1)^{n-1} + \bar{k}_b} \tag{7}$$

The relaxation time, τ, can be defined as:

$$\tau^{-1} = 2\pi f_r = \bar{k}_f n^2(\bar{C}_1)^{n-1} + \bar{k}_b \tag{8}$$

Since the equilibrium constant is $K = k_b/k_f = (C_1)^n/C_2$,

$$\delta K = \frac{\bar{k}_f\delta k_b - \bar{k}_b\delta k_f}{(\bar{k}_f)^2} \tag{9}$$

The thermodynamic dependence of the equilibrium constant on the pressure is given by the equation:

$$\left(\frac{\partial K}{\partial P}\right)_T \frac{1}{K} = -\frac{\Delta V^\circ}{RT} \tag{10}$$

where ΔV° is the standard volume change, R is the gas constant and T is the absolute temperature. The standard volume change, ΔV°, is defined by $\Delta V^\circ = \bar{V}_2 - n\bar{V}_1$ where $\bar{V}_1$ and $\bar{V}_2$ are the partial molar volumes of A and A_n respectively. The complex compressibility, defined as $\beta' = (-1/V)(\delta V/\delta P)_T$, is related to the relaxational compressibility, β_r:

$$\beta' = \frac{\beta_r}{1 + i\omega\tau} = -\frac{1}{V}\left(\frac{\partial V}{\partial C_2}\right)_T\left(\frac{\partial C_2}{\partial P}\right)_T \tag{11}$$

The relaxational compressibility in a reacting system close to the equilibrium is given by:

$$\beta_r = \frac{2\mu_{max}}{\pi\rho c^2} \tag{12}$$

where ρ is the density and μ_{max} is the maximum excess absorption per wavelength. Therefore, one obtains the next equation:

$$\mu_{max} = \frac{\pi\rho c^2}{2}\cdot\frac{(\Delta V^\circ)^2}{RT}\bar{k}_f(\bar{C}_1)^n\tau \tag{13}$$

Comparison with Experiment. In aqueous solutions of *n*-butylamine, there exists the following equilibrium in addition to that of Eq. (4):

$$R\text{-}NH_3^+ + OH^- \rightleftharpoons R\text{-}NH_2 + H_2O \tag{14}$$

The equilibrium constant, $\bar{K}_b$, is defined by:

$$K_b = \frac{\gamma^2[OH^-]^2}{[R\text{-}NH_2]} \tag{15}$$

where γ is the activity coefficient. Therefore, Eq. (8) may be rewritten as:

$$\tau^{-1} = 2\pi f_r = \bar{k}_f n^2\left(\frac{\gamma^2[OH^-]^2}{\bar{K}_b}\right)^{n-1} + \bar{k}_b \tag{16}$$

The value of n was determined so as to obtain the straight line of the plots of $2\pi f_r$ *vs.* $(\gamma^2[OH^-]^2)^{n-1}$; the result was $n=4$. Figure 4 shows the plots of $2\pi f_r$ *vs.* $(\gamma^2[OH^-]^2)^3$. The forward and backward rate

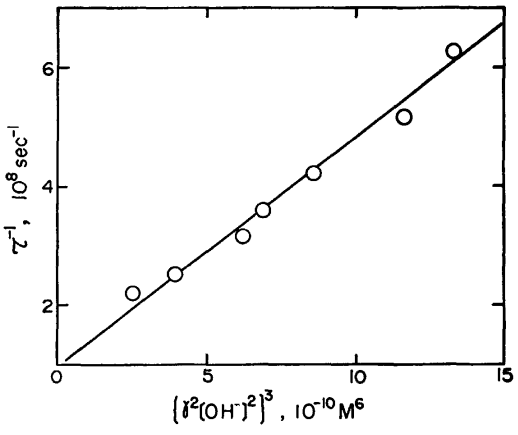

Fig. 4. The plots of τ^{-1} vs. $\{\gamma^2[OH^-]^2\}^3$.

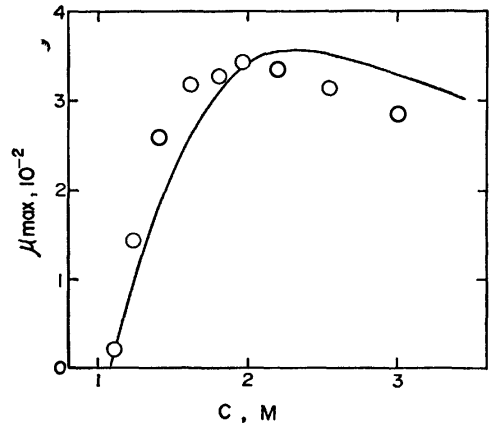

Fig. 5. Comparison of experimental values of μ_{max} with the theoretical ones.

5) K. Shinoda and T. Nakagawa, "Colloidal Surfactants," Academic Press, New York (1963).

constants were determined from the slope and the intercept of this line, using the equilibrium constant, $\bar{K}_b = 4.44 \times 10^{-4}$ M, in the literature.[6]

On the other hand, the maximum excess absorption per wavelength, μ_{max}, was calculated from Eq. (13). The result of the theoretical calculation of μ_{max} at $n=4$ is shown in Fig. 5, together with the experimental values. A considerably good agreement between the experimental and theoretical values was obtained, as is seen in this figure. The value of ΔV° was calculated from Eq. (13) by using the experimental value for μ_{max} at the concentration of 1.94 M. The rate constantes and the standard volume change obtained in the present investigation are $\bar{k}_f = 2.2 \times 10^6$ M^{-3} sec^{-1}, $\bar{k}_b = 9.0 \times 10^7$ sec^{-1} and $\Delta V^\circ = 14$ ml mol^{-1}.

Discussion

The phenomena that the excess absorption and velocity of ultrasonic wave exhibit the maximum in the intermediate concentration have previously been reported in many binary mixtures. The excess absorption mechanism has been explained in terms of the solute-solvent interaction.[1,4] The models are:

$$AA + BB \rightleftharpoons 2AB, \tag{17}$$

$$A + B_m \underset{k_b'}{\overset{k_f'}{\rightleftharpoons}} AB_m \tag{18}$$

where A is the solute molecule, B is the water molecule, B_m is the aggregate of water molecules and the AB or AB_m complex is formed by hydrogen bonding. First, if the mechanism of the excess absorption in the aqueous solution of *n*-butylamine is due to the perturbation of the equilibrium expressed by Eq. (17), P. S. A. C should be 0.5 mole fraction of the solute. However, the observed value of P. S. A. C is 0.04 mole fraction of amine for the aqueous solution of *n*-butylamine. Secondary, if the mechanism is associated with the model of Eq. (18), the relation between the relaxation time and the concentration is derived to be $\tau^{-1} = 2\pi f_r = \bar{k}_f' \sqrt{\{\bar{K}' + \bar{C}_a - (\bar{C}_b/m)\}^2 + (4\bar{C}_b/m)\bar{K}'}$ where $\bar{K}' = \bar{k}_b/\bar{k}_f'$ and $\bar{C}_a$ and $\bar{C}_b$ are the total concentrations of the solute and the solvent respectively. However, the concentration dependence of the relaxation time cannot be interpreted by this equation, since the reasonable parameters, $\bar{k}_f'$ and $\bar{K}'$ have not been determined unitarily. Therefore, these two mechanisms must be ruled out as the cause of the excess absorption in the aqueous solution of *n*-butylamine.

6) M. C. Cox, D. H. Everett, D. A. Landsman, and R. J. Munn, *J. Chem. Soc., B*, **1968** 1373.

The *n*-butylamine, which consists of hydrophilic and hydrophobic groups, is one of the surface active agent.[7,8] Therefore, the molecule has a tendency to aggregate in an aqueous solution. The aggregate is formed by hydrophobic bonding. Expressing Eq. (8) in terms of $C_0 = [R\text{-}NH_2] + n[(R\text{-}NH_2)_n]$ yields:

$$\tau^{-1} = 2\pi f_r = n\bar{k}_b\bar{K}_b \frac{C_0}{\gamma^2[OH^-]^2} + (1-n)\bar{k}_b \tag{19}$$

One can estimate the equilibrium constant, $\bar{K}_b$, from this equation. The value is $\bar{K}_b = (8 \pm 3) \times 10^{-4}$ M which is very close to the value in the literature.[6] This information also confirms that the cause of the excess absorption in the aqueous solution of *n*-butylamine is attributable to the perturbation of the equilibrium expressed by Eq. (4).

As there exist two types of equilibria in the solution, it may be necessary to consider precisely the two-step mechanism, that is, the reaction which is coupled by Eqs. (4) and (14). Therefore, the following formula may be considered:

$$A^+ + B^- \underset{k_{21}}{\overset{k_{12}}{\rightleftharpoons}} A \underset{k_{32}}{\overset{k_{23}}{\rightleftharpoons}} \frac{1}{n}A_n \tag{20}$$

The relaxation times are derived from the next determinant:[9]

$$\begin{vmatrix} a_{11} - \tau^{-1} & a_{12} \\ a_{21} & a_{22} - \tau^{-1} \end{vmatrix} = 0 \tag{21}$$

where $a_{11} = \bar{k}_{12}(\bar{C}_{A^+} + \bar{C}_{B^-}) + \bar{k}_{21}$, $a_{12} = n\bar{k}_{21}$, $a_{21} = \bar{k}_{23} \times (\bar{C}_A)^{n-1}$, and $a_{22} = \bar{k}_{32} + \bar{k}_{23}(\bar{C}_A)^{n-1}n^2$. If one denotes the relaxation time for the faster process by τ_1, and that for the slower process by τ_2, one obtains the next equation under the condition $\tau_1 \ll \tau_2$:

$$\tau_2^{-1} = \bar{k}_{23}(\bar{C}_A)^{n-1}\left\{\frac{n^2(\bar{C}_{A^+} + \bar{C}_{B^-})}{\bar{C}_{A^+} + \bar{C}_{B^-} + \bar{K}_b}\right\} + \bar{k}_{32} \tag{22}$$

Therefore, the contribution from the faster process to the slower one is expressed in terms of $(\bar{C}_{A^+} + \bar{C}_{B^-})/(\bar{C}_{A^+} + \bar{C}_{B^-} + \bar{K}_b)$ comparing with Eq. (8). The neglect of this term alters the calculated values of $\bar{k}_f$ and $\bar{k}_b$ in Eq. (4) by less than 2%.

Similar investigations for aqueous solutions of other amines will give an insight into the more detailed clarification of the cause of the phenomena associated with the peak sound absorption.

7) S. K. Sharma, *Kolloid-Z. Z. Polym.*, **233**, 962 (1969).
8) R. Wolff, *Kollid-Z.*, **138**, 181 (1954).
9) G. H. Czerlinski, "Chemical Relaxation," Marcel Dekker Inc., New York (1966).

Vibration-Rotation Interaction Constants, *l*-Type Doubling Constants and Cubic Force Constants of CH_3I and CD_3I

Hiroatsu MATSUURA and John OVEREND*

Institute for Protein Research, Osaka University, Yamada-kami, Suita, Osaka 565

**Molecular Spectroscopy Laboratory, School of Chemistry, University of Minnesota, Minneapolis, Minnesota 55455, U.S.A.*

(Received November 22, 1972)

The harmonic parts of the vibration-rotation interaction constants and the *l*-type doubling constants were calculated for CH_3I and CD_3I from the harmonic force field. The harmonic parts were subtracted from the experimental values to obtain the anharmonic parts which give relations among the cubic normal-coordinate force constants. Some of the individual values for the cubic force constants associated with the bending modes were obtained by using the derived relations and the previously estimated values for the stretch-stretch-stretch cubic force constants of the methyl group.

Spectroscopic data for CH_3I and CD_3I have been accumulated by the systematic studies of high-resolution infrared spectra and microwave spectra. The observed values of rotational constants in the ground vibrational state and a knowledge of the dependence of these rotational constants on each of the normal modes of vibration made it possible to determine accurately the equilibrium geometry of the methyl iodide molecule.[1] From the experimental values of the vibration-rotation interaction constants (α) and the *l*-type doubling constants (q), supplemented by the calculation of the harmonic contributions to these constants, relations among the cubic normal-coordinate force constants may be derived.[2,3] Although the determination of the individual force constants is not possible for this molecule,[4] these relations are still important in the estimation and discussion of vibrational anharmonicity in the methyl iodide molecule. In the present study, we have derived such relations for CH_3I and CD_3I from the α and q constants, and have used the relations together with the previously estimated cubic force constants of the CH stretching modes[5] to obtain some of the individual cubic force constants associated with the bending modes.

Vibration-Rotation Interaction Constants

The vibration-rotation interaction constants α_s^B and α_s^A are defined according to the relations[6]

$$B_{[v]} = B_e - \sum_s \alpha_s^B(v_s + d_s/2), \tag{1}$$

and

$$A_{[v]} = A_e - \sum_s \alpha_s^A(v_s + d_s/2). \tag{2}$$

The α_s^B and α_s^A constants consist of harmonic and anharmonic parts, namely

$$\alpha_s^B = \alpha_s^B(\text{harm}) + \alpha_s^B(\text{anharm}), \tag{3}$$

and

$$\alpha_s^A = \alpha_s^A(\text{harm}) + \alpha_s^A(\text{anharm}). \tag{4}$$

$\alpha_s^B(\text{harm})$ and $\alpha_s^B(\text{anharm})$ are given by the following general expressions[7]

$$\alpha_s^B(\text{harm}) = -\frac{2B_e^2}{d_s\omega_s} \times \sum_\sigma \left[\sum_{\substack{s'\sigma' \\ (s' \neq s)}} \frac{3\omega_s^2 + \omega_{s'}^2}{\omega_s^2 - \omega_{s'}^2} (\zeta_{s\tau,s'\sigma'}^{(y)})^2 + \frac{4}{3} \sum_\xi \frac{(a_{s\tau}^{(y\xi)})^2}{I_{\xi\xi}^{(e)}} \right], \tag{5}$$

and

$$\alpha_s^B(\text{anharm}) = -4\pi \frac{B_e^2}{d_s} \left(\frac{c}{h}\right)^{1/2} \times \sum_\sigma \left[\frac{3k_{sss}a_{s\sigma}^{(yy)}}{\omega_s^{3/2}} + \sum_{\substack{s'\sigma' \\ (s' \neq s)}} \frac{k_{sss'}a_{s'\sigma'}^{(yy)}}{\omega_{s'}^{3/2}} \right]. \tag{6}$$

$\alpha_s^A(\text{harm})$ and $\alpha_s^A(\text{anharm})$ are given by the corresponding expressions with A_e and z, in place of B_e and y, respectively. The harmonic parts of α_s^B and α_s^A may be rewritten into forms more convenient for the present case, as will be given below. k_{sss} and $k_{sss'}$ appearing in the anharmonic parts are the cubic force constants when the potential function of a molecule is expanded in terms of dimensionless normal coordinates q_s:

$$V(q)/hc = \frac{1}{2}\sum_s \omega_s q_s^2 + \sum_{s\leq s'}\sum_{s''} k_{ss's''}q_s q_{s'} q_{s''} + \sum_{s\leq s'}\sum_{s''\leq s'''}\sum_{s'''} k_{ss's''s'''}q_s q_{s'} q_{s''} q_{s'''} + \cdots\cdots \tag{7}$$

For the non-degenerate modes, $\alpha_s^B(\text{harm})$ and $\alpha_s^B(\text{anharm})$ are given by

$$\alpha_s^B(\text{harm}) = -\frac{2B_e^2}{\omega_s} \times \left[\sum_{t\in E} \frac{4\omega_t^2}{\omega_s^2 - \omega_t^2} (\zeta_{s,ta}^{(y)})^2 + 3\{1 - \sum_i (l_{t,s}^{(y)})^2\} \right], \tag{8}$$

and

$$\alpha_s^B(\text{anharm}) = -4\pi B_e^2 \left(\frac{c}{h}\right)^{1/2} \times \left[\frac{3k_{sss}a_s^{(yy)}}{\omega_s^{3/2}} + \sum_{\substack{s'\in A_1 \\ (s' \neq s)}} \frac{k_{sss'}a_{s'}^{(yy)}}{\omega_{s'}^{3/2}} \right], \tag{9}$$

1) H. Matsuura and J. Overend, *J. Chem. Phys.*, **56**, 5725 (1972).

2) Y. Morino, K. Kuchitsu, and S. Yamamoto, *Spectrochim. Acta*, **24A**, 335 (1968).

3) T. Oka, *J. Chem. Phys.*, **47**, 5410 (1967).

4) For molecules with more than three atoms, all of the independent cubic force constants cannot be determined from the experimental values of the α and q constants, since the experimental data are insufficient.

5) J. Overend and K. Machida, *Spectrochim. Acta*, **26A**, 1225 (1970).

6) G. Herzberg, "Molecular Spectra and Molecular Structure, II. Infrared and Raman Spectra of Polyatomic Molecules," D. Van Nostrand Co., Inc., New York (1945), p. 370.

7) For symbols and notation in the forthcoming expressions, see H. H. Nielsen, "Handbuch der Physik," Vol. 37, ed. by S. Flügge, Springer-Verlag, Berlin (1959), p. 173.

and for the doubly-degenerate modes

$$\alpha_t^B(\text{harm}) = -\frac{2B_e^2}{\omega_t}\left[\sum_{s\subset A_1}\frac{2\omega_s^2}{\omega_t^2-\omega_s^2}(\zeta_{s,ta}{}^{(y)})^2 + \sum_{\substack{t'\subset E\\(t'\neq t)}}\frac{4\omega_{t'}{}^2}{\omega_t^2-\omega_{t'}{}^2}(\zeta_{ta,t'a}{}^{(y)})^2 + 3\left\{1-\frac{1}{2}\sum_i[(l_{i,ta}{}^{(y)})^2+(l_{i,tb}{}^{(y)})^2]\right\}\right], \quad (10)$$

and

$$\alpha_t^B(\text{anharm}) = -4\pi B_e^2\left(\frac{c}{h}\right)^{1/2}\sum_{s\subset A_1}\frac{k_{tatas}a_s{}^{(yy)}}{\omega_s{}^{3/2}}. \quad (11)$$

Similarly for α_s^A(harm) and α_s^A(anharm); for the non-degenerate modes

$$\alpha_s^A(\text{harm}) = -\frac{2A_e^2}{\omega_s}\cdot 3[1-\sum_i(l_{i,s}{}^{(z)})^2], \quad (12)$$

and

$$\alpha_s^A(\text{anharm}) = -4\pi A_e^2\left(\frac{c}{h}\right)^{1/2} \times\left[\frac{3k_{sss}a_s{}^{(zz)}}{\omega_s{}^{3/2}}+\sum_{\substack{s'\subset A_1\\(s'\neq s)}}\frac{k_{sss'}a_{s'}{}^{(zz)}}{\omega_s{}^{3/2}}\right], \quad (13)$$

and for the doubly-degenerate modes

$$\alpha_t^A(\text{harm}) = -\frac{2A_e^2}{\omega_t}\left[\sum_{\substack{t'\subset E\\(t'\neq t)}}\frac{4\omega_{t'}{}^2}{\omega_t^2-\omega_{t'}{}^2}(\zeta_{ta,t'b}{}^{(z)})^2 - 3(\zeta_{ta,tb}{}^{(z)})^2 + 3\{1-\sum_i(l_{i,ta}{}^{(z)})^2\}\right], \quad (14)$$

and

$$\alpha_t^A(\text{anharm}) = -4\pi A_e^2\left(\frac{c}{h}\right)^{1/2}\sum_{s\subset A_1}\frac{k_{tatas}a_s{}^{(zz)}}{\omega_s{}^{3/2}}. \quad (15)$$

Since the harmonic parts, α_s^B(harm) and α_s^A(harm), are determined by only the quadratic force constants, we may calculate their values from the harmonic force field. That of methyl iodide is reasonably well known,[8-10] and we have used in the present calculations the hybrid-orbital force field determined by Russell, Needham and Overend.[9] The anharmonic parts, α_s^B(anharm) and α_s^A(anharm), are then obtained by subtracting the calculated values of α_s^B(harm) and α_s^A(harm) from the experimental values of α_s^B and α_s^A. The experimental values of α_s^B and α_s^A, the calculated values of α_s^B(harm) and α_s^A(harm), and α_s^B(anharm) and α_s^A(anharm) are listed in Tables 1 and 2.

Table 1. α_s^B and α_s^A for CH_3I, in cm^{-1}

s	α_s^B(obs)[a]	α_s^B(harm)	α_s^B(anharm)
1	0.00017	−0.000075	0.00024
2	0.000849[b]	0.000066[b]	0.000783
3	0.001811	−0.000657	0.002468
4	−0.000122	−0.000078	−0.000044
5	0.000058[b]	−0.000095[b]	0.000153
6	0.000787	0.000105	0.000682
s	α_s^A(obs)[a]	α_s^A(harm)	α_s^A(anharm)
1	0.0514	−0.0450	0.0964
2	−0.0222	−0.0137	−0.0085
3	−0.0038	−0.0003	−0.0035
4	0.0311	−0.0588	0.0899
5	0.0460	0.0504	−0.0044
6	−0.0347	0.0128	−0.0475

a) For sources, see Table I of Ref. 1.
b) Not affected by the Coriolis interaction between ν_2 and ν_5. In Table I of Ref. 1, footnote k should be given to the figures $+0.000849\pm0.000003$ and $+0.000058\pm0.000002$, but not to α_2^B and α_5^B.

Table 2. α_s^B and α_s^A for CD_3I, in cm^{-1}

s	α_s^B(obs)[a]	α_s^B(harm)	α_s^B(anharm)
1	0.000135	−0.000062	0.000197
2	0.00103	0.000605	0.00043
3	0.00126	−0.000425	0.00168
4	0.000086	−0.000070	0.000156
5	−0.000403	−0.000366	−0.000037
6	0.000494	0.000089	0.000405
s	α_s^A(obs)[a]	α_s^A(harm)	α_s^A(anharm)
1	0.0232	−0.0151	0.0383
2	−0.0078	−0.0058	−0.0020
3		−0.0000	
4	0.0135	−0.0192	0.0327
5	0.0148	0.0174	−0.0026
6	−0.0135	0.0025	−0.0160

a) For sources, see Table I of Ref. 1. Recently microwave spectra of CD_3I in the excited vibrational states have been measured and values for α_2^B, α_3^B, α_5^B, and α_6^B have been obtained (Y. Kawashima and K. Kozima, Symposium on Molecular Structure, Sendai, 1972).

The observed values of α_2^B and α_5^B for CH_3I have been corrected for the Coriolis interaction between ν_2 and ν_5[11]; we use the symbols $\alpha_2^{B'}$ and $\alpha_5^{B'}$ for these corrected quantities. Thus $\alpha_2^{B'}$ and $\alpha_5^{B'}$ are given by

$$\alpha_s^{B'} = \alpha_s^{B'}(\text{harm}) + \alpha_s^B(\text{anharm}) \quad (s=2 \text{ or } 5) \quad (16)$$

and $\alpha_s^{B'}$(harm) corresponds to the quantity obtained by dropping the term containing $\zeta_{2,5a}{}^{(y)}$ from the expression in Eq. (5).

l-Type Doubling Constants

The l-type doubling constant q_t consists of harmonic and anharmonic parts[3] like α_s^B and α_s^A;

$$q_t = q_t(\text{harm}) + q_t(\text{anharm}). \quad (17)$$

For CH_3X type molecules, q_t(harm) and q_t(anharm) are given by

$$q_t(\text{harm}) = \frac{2B_e^2}{\omega_t}\left[\sum_{s\subset A_1}\frac{3\omega_t^2+\omega_s^2}{\omega_t^2-\omega_s^2}(\zeta_{s,ta}{}^{(y)})^2 - \frac{3}{4}\frac{(a_{tb}{}^{(yz)})^2}{I_{zz}{}^{(e)}}\right], \quad (18)$$

which may be rewritten into

8) J. Aldous and I. M. Mills, *Spectrochim. Acta*, **19**, 1567 (1963).
9) J. W. Russell, C. D. Needham, and J. Overend, *J. Chem. Phys.*, **45**, 3383 (1966).
10) J. L. Duncan, A. Allan, and D. C. McKean, *Mol. Phys.*, **18**, 289 (1970).

$$q_t(\text{harm}) = \frac{2B_e^2}{\omega_t}\left[\sum_{s\subset A_1}\frac{4\omega_s^2}{\omega_t^2-\omega_s^2}(\zeta_{s,ta}{}^{(y)})^2 + 3\sum_i\{(l_{i,tb}{}^{(y)})^2-(l_{i,ta}{}^{(y)})^2\}\right], \quad (19)$$

and

$$q_t(\text{anharm}) = 8\pi B_e^2\left(\frac{c}{h}\right)^{1/2} \times\left[\frac{3k_{tatata}a_{ta}{}^{(yy)}}{\omega_t{}^{3/2}} + \sum_{\substack{t'\subset E\\(t'\neq t)}}\frac{k_{tatat'a}a_{t'a}{}^{(yy)}}{\omega_{t'}{}^{3/2}}\right]. \quad (20)$$

The observed value of q_5 for CH_3I does not include the effect of the Coriolis interaction between ν_2 and ν_5,[11] and its harmonic part, q_5'(harm), is obtained by dropping the term containing $\zeta_{2,5a}{}^{(y)}$ from the expression in Eq. (18), which is then rewritten as

$$q_5'(\text{harm}) = \frac{2B_e^2}{\omega_5}\left[\frac{4\omega_1^2}{\omega_5^2-\omega_1^2}(\zeta_{1,5a}{}^{(y)})^2 + \frac{4\omega_3^2}{\omega_5^2-\omega_3^2}(\zeta_{3,5a}{}^{(y)})^2 - 3(\zeta_{2,5a}{}^{(y)})^2 + 3\sum_i\{(l_{i,5b}{}^{(y)})^2-(l_{i,5a}{}^{(y)})^2\}\right]. \quad (21)$$

The harmonic parts of the l-type doubling constants were calculated from the harmonic force field of Russell *et al.*[9] and were subtracted from the observed values[12] to obtain the anharmonic parts of the l-type doubling constants, q_t (anharm) (Table 3).

TABLE 3. q_t FOR CH_3I AND CD_3I, IN cm^{-1}

	t	q_t(obs)	q_t(harm)	q_t(anharm)
	4		0.000073	
CH_3I	5	−0.000022[a,b]	−0.000012[b]	−0.000010
	6	−0.000200[c]	−0.000266	0.000066
	4		0.000078	
CD_3I	5	0.000580[d]	0.000516	−0.000064
	6	−0.000126[d]	−0.000204	0.000078

a) Ref. 11. b) Not affected by the Coriolis interaction between ν_2 and ν_5. c) H. Matsuura and J. Overend, *Spectrochim. Acta*, **27A**, 2165 (1971); see also footnote 18 of Ref. 11. d) D. R. Anderson and J. Overend, *Spectrochim. Acta*, **28A**, 1231 (1972). The signs of q_5 and q_6 of CD_3I listed in this table are opposite to and the values are twice those reported by Anderson and Overend, because of different definitions of the q_t constant used. The values in this table are in accord with Mills' sign convention[13] and Eqs. (18)—(20).

Cubic Force Constants

From the anharmonic parts of the $\alpha_s{}^B$, $\alpha_s{}^A$ and q_t constants, we obtain relations among the cubic normal-coordinate force constants through Eqs. (9), (11), (13), (15) and (20). $\alpha_s{}^B$(anharm) and $\alpha_s{}^A$(anharm) relate the cubic constants k_{ss1}, k_{ss2} and k_{ss3}, and q_t(anharm) relates k_{tt4}, k_{tt5} and k_{tt6}. Thus $\alpha_s{}^B$ and $\alpha_s{}^A$, and q_t are complementary in the anharmonic information they provide. Making use of the harmonic potential function[9] incalculating the $a_s{}^{(\xi\,\eta)}$ coefficients appearing in the equations, we obtain the following explicit relations[14] for CH_3I from the $\alpha_s{}^B$ constants:

$$\begin{aligned}
-0.08\,k_{111} + 0.08\,k_{112} - 2.83\,k_{113} &= 24\ cm^{-1},\\
-0.03\,k_{221} + 0.23\,k_{222} - 2.83\,k_{223} &= 78\ cm^{-1},\\
-0.03\,k_{331} + 0.08\,k_{332} - 8.50\,k_{333} &= 247\ cm^{-1},\\
-0.03\,k_{441} + 0.08\,k_{442} - 2.83\,k_{443} &= -4\ cm^{-1},\\
-0.03\,k_{551} + 0.08\,k_{552} - 2.83\,k_{553} &= 15\ cm^{-1},
\end{aligned}$$

and

$$-0.03\,k_{661} + 0.08\,k_{662} - 2.83\,k_{663} = 68\ cm^{-1}, \quad (22)$$

from the $\alpha_s{}^A$ constants:

$$\begin{aligned}
-0.54\,k_{111} - 0.24\,k_{112} - 0.08\,k_{113} &= 96\ cm^{-1},\\
-0.18\,k_{221} - 0.71\,k_{222} - 0.08\,k_{223} &= -9\ cm^{-1},\\
-0.18\,k_{331} - 0.24\,k_{332} - 0.24\,k_{333} &= -4\ cm^{-1},\\
-0.18\,k_{441} - 0.24\,k_{442} - 0.08\,k_{443} &= 90\ cm^{-1},\\
-0.18\,k_{551} - 0.24\,k_{552} - 0.08\,k_{553} &= -4\ cm^{-1},
\end{aligned}$$

and

$$-0.18\,k_{661} - 0.24\,k_{662} - 0.08\,k_{663} = -48\ cm^{-1}, \quad (23)$$

and from the q_t constants:

$$0.28\,k_{554} - 3.04\,k_{555} + 0.15\,k_{556} = -10\ cm^{-1},$$

and

$$0.28\,k_{664} - 1.01\,k_{665} + 0.44\,k_{666} = 66\ cm^{-1}. \quad (24)$$

Similar relations are obtained for CD_3I:

$$\begin{aligned}
-0.11\,k_{111} + 0.03\,k_{112} - 2.23\,k_{113} &= 20\ cm^{-1},\\
-0.04\,k_{221} + 0.09\,k_{222} - 2.23\,k_{223} &= 43\ cm^{-1},\\
-0.04\,k_{331} + 0.03\,k_{332} - 6.69\,k_{333} &= 168\ cm^{-1},\\
-0.04\,k_{441} + 0.03\,k_{442} - 2.23\,k_{443} &= 16\ cm^{-1},\\
-0.04\,k_{551} + 0.03\,k_{552} - 2.23\,k_{553} &= -4\ cm^{-1},
\end{aligned}$$

and

$$-0.04\,k_{661} + 0.03\,k_{662} - 2.23\,k_{663} = 41\ cm^{-1}, \quad (25)$$

$$\begin{aligned}
-0.31\,k_{111} - 0.14\,k_{112} - 0.02\,k_{113} &= 38\ cm^{-1},\\
-0.10\,k_{221} - 0.43\,k_{222} - 0.02\,k_{223} &= -2\ cm^{-1},\\
-0.10\,k_{441} - 0.14\,k_{442} - 0.02\,k_{443} &= 33\ cm^{-1},\\
-0.10\,k_{551} - 0.14\,k_{552} - 0.02\,k_{553} &= -3\ cm^{-1},
\end{aligned}$$

and

$$-0.10\,k_{661} - 0.14\,k_{662} - 0.02\,k_{663} = -16\ cm^{-1}, \quad (26)$$

$$0.38\,k_{554} - 4.79\,k_{555} + 0.10\,k_{556} = -64\ cm^{-1},$$

and

$$0.38\,k_{664} - 1.60\,k_{665} + 0.31\,k_{666} = 78\ cm^{-1}. \quad (27)$$

The signs of the k constants are in accord with those of the $\boldsymbol{L}$ matrix elements given in Table 4.[15]

11) H. Matsuura, T. Nakagawa, and J. Overend, *J. Chem. Phys.*, to be published. Detailed analysis of ν_5 of CH_3I.

12) The signs of the observed values for q_t, listed in Table 3, are in accord with Mills' sign convention[13] and are consistent with Eqs. (18)—(20).

13) I. M. Mills, *Pure Appl. Chem.*, **18**, 285 (1969); G. J. Cartwright and I. M. Mills, *J. Mol. Spectrosc.*, **34**, 415 (1970).

14) $k_{tts}=k_{tatas}=k_{tbtbs}$, $k_{ttt}=k_{tatata}=-(1/3)k_{tatbtb}$ and $k_{ttt'}=k_{tatat'a}=-k_{tbtbt'a}=-(1/2)k_{tatbt'b}$.

15) The geometry of the molecule and the internal-symmetry coordinates used in this study are the same as those of Russell *et al.*[9]

Table 4. Elements of the L matrix, in $amu^{-1/2}$

	L_{11}	L_{12}	L_{13}	L_{21}	L_{22}	L_{23}
CH_3I	1.007	0.011	0.004	−0.102	1.356	0.109
CD_3I	0.720	0.020	0.007	−0.150	1.040	0.023
	L_{31}	L_{32}	L_{33}	L_{44}	L_{45}	L_{46}
CH_3I	−0.045	0.100	0.282	1.051	0.026	−0.025
CD_3I	−0.066	0.149	0.255	0.781	0.006	−0.012
	L_{54}	L_{55}	L_{56}	L_{64}	L_{65}	L_{66}
CH_3I	0.106	1.522	−0.133	−0.068	0.254	0.910
CD_3I	0.188	1.113	−0.051	−0.103	0.111	0.679

The determination of individual values for the k constants is not possible from the above relations; the combination of Eqs. (22) and (23), or Eqs. (25) and (26) gives only relations between two k constants. For planar or pyramidal XY_3 molecules, the k constants appearing in the relations similar to Eqs. (22), (23), (25) and (26) can be determined uniquely, and some of the k constants have, in fact, been obtained from observed α_s^B and α_s^C for NH_3 and ND_3.[2]

Overend and Machida[5] have made a simple calculation of the anharmonic force constants of the CH stretching modes for the methyl group, assuming a Morse function for a CH bond. Their estimation of the cubic force constants may be used to obtain other force constants, making use of the relations derived in this study. While the stretch-stretch-stretch cubic force constants may be estimated relatively easily,[5] the estimation of the constants involving bending modes is not so simple, and the relations among the k constants are useful in estimating the latter. In Table 5 are listed the force constants estimated by Overend and Machida[5] and the new force constants of CH_3I and CD_3I determined in the present work. They are compared with the corresponding constants for NH_3 and ND_3. The values of k_{111}, k_{444}, and k_{441} (the CD stretch-stretch-stretch force constants) for CD_3I were derived from the corresponding values for CH_3I by multiplying by the factor $[(\mu_D+\mu_C)/(\mu_H+\mu_C)]^{3/4}\simeq 0.63$, where μ_H, μ_D, and μ_C are the reciprocals of the masses of H, D, and C atoms.

Table 5. Estimates of the cubic normal-coordinate force constants, in cm^{-1}, for CH_3I and CD_3I and corresponding constants for NH_3 and ND_3

	k_{111}	k_{112}	k_{113}	k_{441}	k_{442}	k_{443}
CH_3I	−173[a]	−10	−4	−518[a]	13	7
CD_3I	−109[b]	−33	−4	−326[b]	5	−2
NH_3[c]	−228	4		−603	136	
ND_3[c]	−153	−77		−382	89	
	k_{444}	k_{551}	k_{552}	k_{553}	k_{356}	
CH_3I	−122[a]	61	−26	−7	29.614[d]	
CD_3I	−77[b]					
NH_3[c]	−142	87	−36			
ND_3[c]	−89	22	−17			

a) Ref. 5. b) See text. c) Ref. 2. d) Absolute value.[11]

Duncan *et al.*[10] have estimated the interaction terms of the Fermi resonance between ν_1 and $2\nu_5$ of CH_3I from the intensities of these parallel bands. From the interaction term, the value of $|k_{551}|$ is found to be 61 cm^{-1}. By comparing with the corresponding value (+87 cm^{-1}) for NH_3,[2] it seems reasonable to take a positive sign for k_{551}. The values for k_{552} and k_{553} derived through the relations in Eqs. (22) and (23) are listed in Table 5. A value for k_{356} of CH_3I is also listed. This was obtained by the detailed analyses of the Fermi doublet, ν_5 and $\nu_3+\nu_6$.[11,16,17]

Discussion

There are 38 independent cubic normal-coordinate force constants for CH_3I or CD_3I. Of these, we have estimated or observed 11 constants for the former and 7 for the latter, as shown in Table 5. The stretch-stretch-stretch constants (k_{111}, k_{444} and k_{441}) previously estimated for the CH_3 and CD_3 groups[5] are of the reasonable magnitudes, compared with those of NH_3 and ND_3, and the systematic variations of the values from those of the ammonia molecule are related closely to the values of the quadratic internal-coordinate force constants (*i.e.*, 5.5 mdyn/Å for the methyl group and 7 mdyn/Å for ammonia).

In the present study, we have been able to estimate two stretch-stretch-bend interaction constants (k_{112} and k_{442}) of the CH_3 or CD_3 group. The values obtained for k_{442} for CH_3I and CD_3I are found to be about ten times smaller than the corresponding values for NH_3 and ND_3. This difference may be real and may reflect structural differences between the CH_3 group and ammonia. Alternatively it may stem from approximation made in our analysis and, with this possibility in mind, we refrain from further comments. It is interesting to note, on the other hand, that the bend-bend-stretch constant (k_{551}) and the bend-bend-bend constant (k_{552}) of CH_3I have magnitudes similar to those for NH_3.

The cubic constant k_{356} for CH_3I has been determined experimentally from the analyses of the perpendicular bands, ν_5 and $\nu_3+\nu_6$.[11,16,17] The value obtained is only an absolute one, but is very accurate, *i.e.*, $|k_{356}|=29.6144\pm0.0007$ cm^{-1}.[11] The same force constant has also been determined from the Fermi doublets, $\nu_5+\nu_6$ and $\nu_3+2\nu_6$, and $\nu_2+\nu_5$ and $\nu_2+\nu_3+\nu_6$, to be 29.572 ± 0.002 cm^{-1} and 29.1 ± 0.2 cm^{-1}, respectively.[18]

At the present time, we do not have individual values for the cubic force constants other than those listed in Table 5. However, the relations among the cubic force constants derived in the present study are useful in estimating other force constants and in discussing the vibrational anharmonicity in the methyl

16) Y. Morino, J. Nakamura, and S. Yamamoto, *J. Mol. Spectrosc.*, **22**, 34 (1967).
17) H. Matsuura and J. Overend, *J. Chem. Phys.*, **55**, 1787 (1971).
18) H. Matsuura and J. Overend, *Spectrochim. Acta*, **28A** 1203 (1972).

halide molecules.

Numerical calculations in the present study were carried out with a NEAC 2200—700 computer (Nippon Electric Co., Ltd.) at the Computer Center of Osaka University.

The authors wish to thank Professor Tatsuo Miyazawa of Osaka University, Dr. Toru Nakagawa of the University of Tokyo, and Dr. Katsunosuke Machida of Kyoto University for their valuable discussions and suggestions.

BULLETIN OF THE CHEMICAL SOCIETY OF JAPAN, VOL. 46, 1106—1111 (1973)

The Adiabatic Compressibility of Nonelectrolyte Aqueous Solutions in Relation to the Structures of Water and Solutions

Harumi ENDO

Department of Applied Physics, Defense Academy, Yokosuka 239

(Received May 23, 1972)

The sound velocity (V) and density of aqueous solutions of urea, dimethylurea, thiourea, acetamide, acetone, and dimethylformamide have been measured, and the adiabatic compressibility (β) has been calculated at various concentrations (μ: mole fraction). The β-μ curves and V-μ curves at various temperatures have a common intersection at the fixed concentrations of μ_c^β and μ_c^V respectively. At these concentrations, the compressibility (β_c) and the sound velocity (V_c) of a solution are independent of the temperature over a certain range. When β_c is plotted against the mole ratio, r_c^β=(water)/(solute) at μ_c^β, the plots for acetyl-derivatives fall on one straight line, and those for urea-derivatives, on another line. In the cases of acetone and ethanol, the r_c^β values of these solutes coincide with the number of water molecules constituting the framework of the solid clathrate hydrate. Also, for the other aqueous solutions, it may be reasonable to conclude that the r_c^β value corresponds to the number of water molecules constituting some other type of liquid-clathrate hydrate characteristic of each solute.

A number of papers have been published on the properties of nonelectrolyte aqueous solutions from the view point of the dependence of the sound velocity (V) on the concentration (μ: mole fraction). The V-μ curves for the aqueous solutions of methanol (Me), ethanol (Et), propanol (Pr), acetone (A), *etc.*, have been known to show some unusual behaviors.

The V-μ curves of these solutions at a constant temperature exhibit maxima (maximum sound velocity: V_p) at certain concentrations[1-3] (velocity peak concentration: C_p). As both V_p and C_p decrease with an increase in the temperature, the V-μ curves for two different temperatures meet at a certain concentration (μ_c^V) ($<C_p$). Usually, a number of the V-μ curves within a certain temperature range (ΔT_c^V) have a common intersection[4,5] at a fixed concentration (μ_c^V), although Kuhnkies and Schaaffs[6] have pointed out the gradual displacement of the point of intersection with the temperature range in the case of alcohol solutions, among others. This behavior of the V-μ curves is found not only for the aqueous solutions of liquids of simple molecules, but also for those of complicated molecules such as morpholine[7] (Mo) $O(CH_2CH_2)NH$, for which the V_c at μ_c^V=0.0369 is constant in the temperature range of 20—60 °C.

In the present study, the adiabatic compressibilities, (β) of aqueous solutions of urea (U), dimethylurea (DMU), acetamide (AA), acetone (A), and dimethylformamide (DMF) are determined over the temperature range of 20—50 °C, and that of thiourea (TU), in the 50—60 °C range, by measuring the density and the sound velocity.

From these results, it is found that the β-μ curves of various temperatures also show a common intersection at a characteristic concentration (μ_c^β). At this concentration, the adiabatic compressibility (β_c) is independent of the temperature over a certain temperature range (ΔT_c^β). The parameters such as V_c, β_c, ΔT_c^V, ΔT_c^β, μ_c^V and μ_c^β are determined for these solutes in order to examine their relation with the solution structure.

When β_c is plotted against the mole ratio, r_c^β=(water)/(solute), the plots for acetyl-derivatives fall on one straight line, and those for urea-derivatives, on another line. From these β_c—r_c^β curves, the properties and the dissolved state of solute in water are discussed. The reason why the peak concentration shifts to the lower-concentration side with an increase in the molecular weight in each homologue series is explained.

Experimental

Materials. The U, DMU, TU, and AA are purified by the recrystallization of reagent-grade products from absolute alcohol. To purify A and DMF, reagent-grade products are distilled twice before use.

1) O. Nomoto and H. Endo, This Bulletin, **43**, 2718 (1970).
2) W. Schaaffs, Landolt-Börnstein, Zahlenwerte und Funktionen. Gruppe II, Band5, "MolekularakustiK," Springer-Verlag, Berlin, Heidelberg, New York (1967), pp. 89—125.
3) J. Saneyoshi, K. Kikuchi, and O. Nomoto, "Tyonpa Gizutu Binran," Nikkan Kogyo Shinbunsha, Tokyo (1966), pp. 1254—1267.
4) A. Giacomini, *J. Acoust. Soc. Amer.*, **19**, 702 (1947).
5) N. V. Chekalin and M. I. Schakhparonov, *Soviet Phys. Acoust.* (English Transl.) **17**, 147 (1971).
6) R. Kuhnkies and W. Schaaffs, *Acustica*, **12**, 254 (1962).
7) K. Mallikharjuna Swamy and P. Sitramaswamy, *J. Phys. Soc. Jap.*, **28**, 535 (1970).

Apparatus. A crystal-controlled ultrasonic interferometer operating at a frequency of 5 MHz is used to measure the sound velocity. To determine the wavelength, one hundred standing waves are used. The measuring cell containing the solutions is immersed in an oil bath, the temperature of which is kept constant within ±0.1 °C.

Results

In Figs. 1—6, the sound velocity is plotted against the mole fraction for aqueous solutions of U, DMU, AA, A, and DMF respectively, over the temperature range of ΔT=20—50 °C, while that for TU is plotted

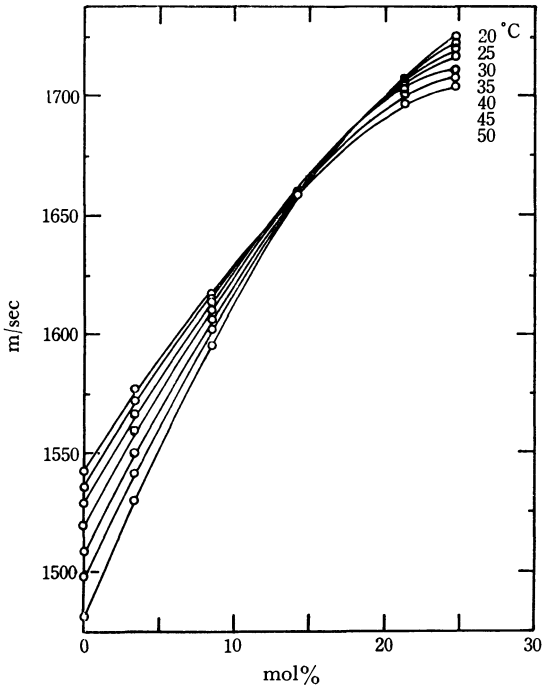

Fig. 1. Sound velocity *vs.* concentration of urea aqueous solutions.

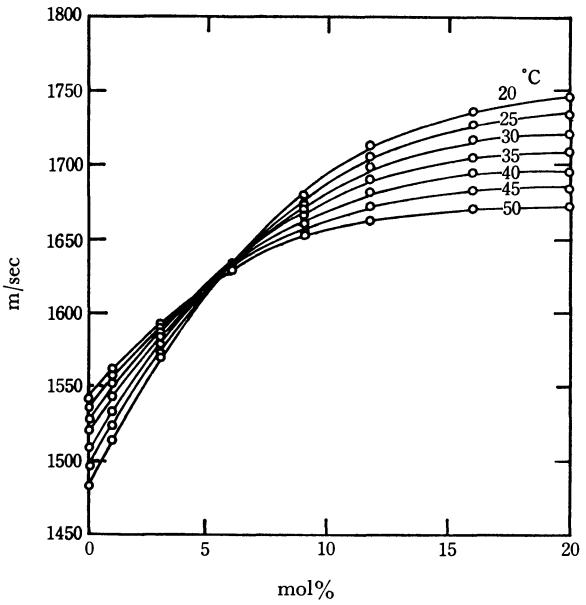

Fig. 2. Sound velocity *vs.* concentration of DMU aqueous solutions.

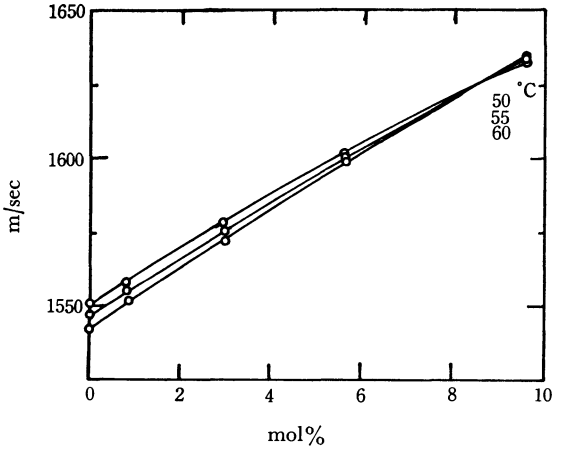

Fig. 3. Sound velocity *vs.* concentration of thiourea aqueous solutions.

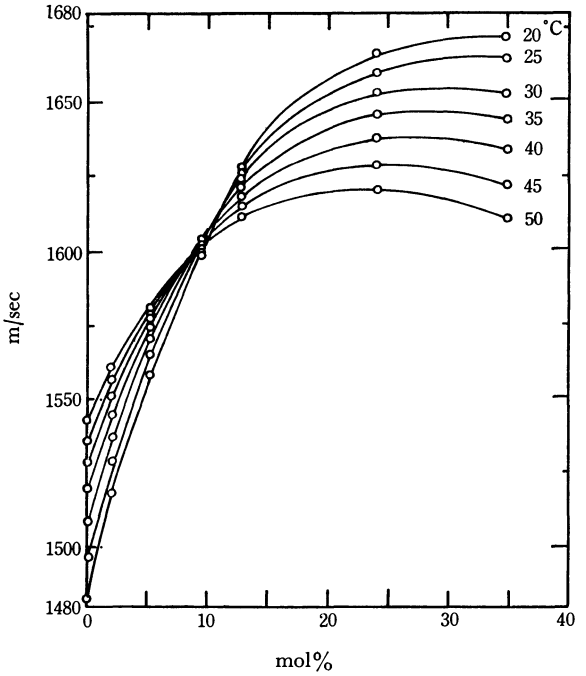

Fig. 4. Sound velocity *vs.* concentration of acetamide aqueous solutions.

over the range of ΔT=50—60 °C. The sound velocity always increases with an increase in the concentration, reaches a maximum, and then decreases. In the cases of U and TU, no maximum was observed within the concentration range measured because of the solubility limit. It is found that V_p gradually decreases and shifts towards the lower-concentration side with an increase in the temperature (*cf.* Fig. 5 and Ref. 1). At the higher temperatures, the V-μ curves show no maximum and decrease nearly linearly.

For the aqueous solutions of TU and DMF, the intersection points of V-μ curves of various temperatures converge at one point over the observed temperature range (20—50 °C) (Figs. 3 and 6). For the aqueous systems of U, DMU, AA, and A (Figs. 1, 2, 4, and 5), on the other hand, the converging temperature range is rather narrower. The V_c, ΔT_c^V, and μ_c^V values at the converging point in the V-μ curves are summarized in the left-hand half of Table 1.

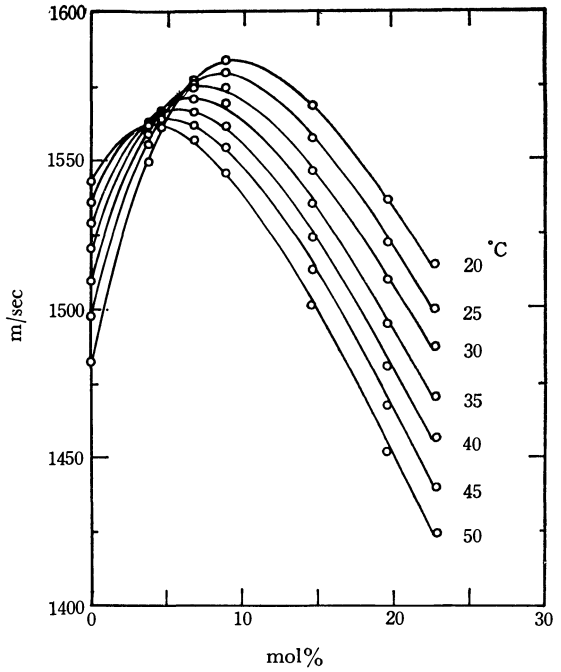

Fig. 5. Sound velocity *vs.* concentration of acetone aqueous solutions.

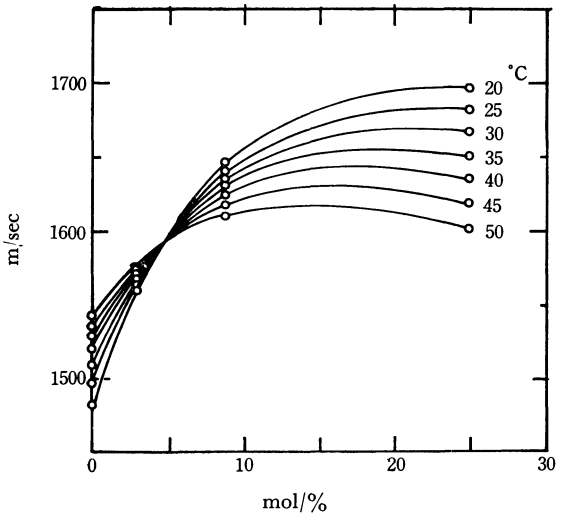

Fig. 6. Sound velocity *vs.* concentration of DMF aqueous solutions.

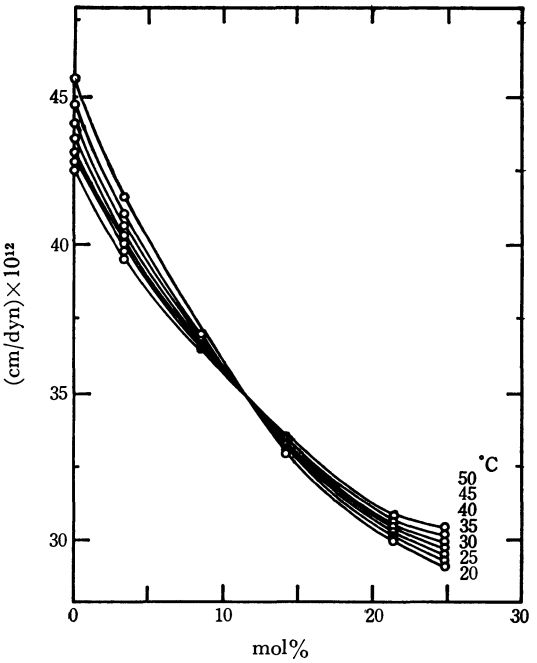

Fig. 7. Compressibility *vs.* concentration of urea aqueous solutions.

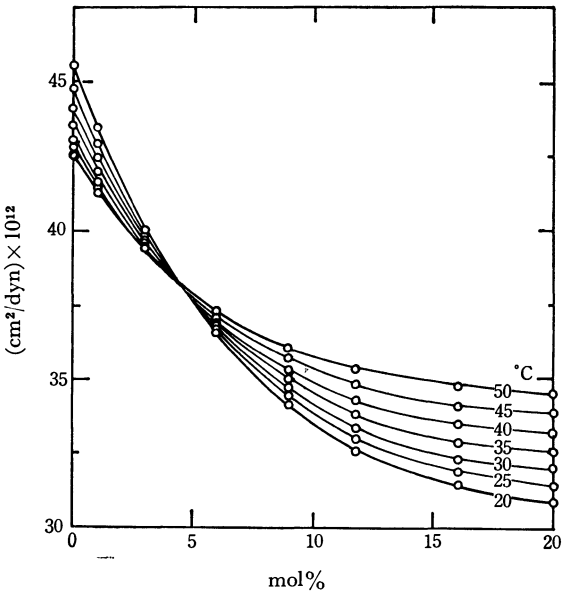

Fig. 8. Compressibility *vs.* concentration of DMU aqueous solutions.

Figures 7—12 show the β-μ curves for aqueous solutions of U, DMU, AA, A, and DMF respectively, over the observed temperature range of 20—50 °C, and that for TU, over the range of ΔT=50—60 °C. Similarly, the β-μ curves of various temperatures intersect at one common point. The numerical values of the μ_c^β values of the β-μ curves are slightly different from those of the μ_c^V values of the V-μ curves, and the converging temperature range, ΔT_c^β, is nearly the same as ΔT_c^V. The values of β_c, μ_c^β, r_c^β, and ΔT_c^β are reproduced in the right-hand half of Table 1. Table 1 also contains the data for alcohol homologues, obtained from the data of Larionov.[8]

In Fig. 13, β_c is plotted against r_c^β for various solutes. According to this plot, the solutes studied can be classified into two groups. One group consists of the urea-derivatives, for which

$$\beta_c = (0.22 r_c^\beta + 33.3) \times 10^{-12} \text{ (cm}^2\text{/dyn)} \quad (1)$$

while the other group consists of the acetyl-derivatives, for which

$$\beta_c = (0.49 r_c^\beta + 33.3) \times 10^{-12} \text{ (cm}^2\text{/dyn)} \quad (2)$$

They have a common intercept with the ordinate of $\beta_c^\circ = 33.3 \times 10^{-12}$ (cm²/dyn).

Figure 14 shows a similar plot of V_c *vs.* r_c^V (mole ratio,=(water)/(solute) at μ_c^β). Here, however, no

8) I. Larionov, Dissertation, MPPI (1951) in "The Use of Ultrasonic in Molecular Physics" by V. F. Nozdrev, translated from Russian by J. A. Carde, Pergamon Press, Oxford (1965), p. 354.

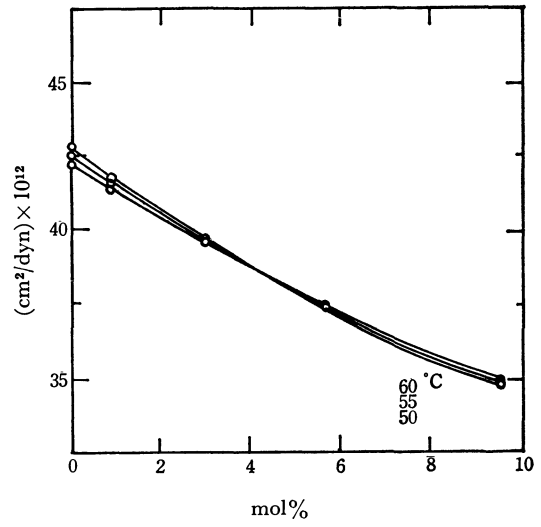

Fig. 9. Compressibility *vs.* concentration of thiourea aqueous solutions.

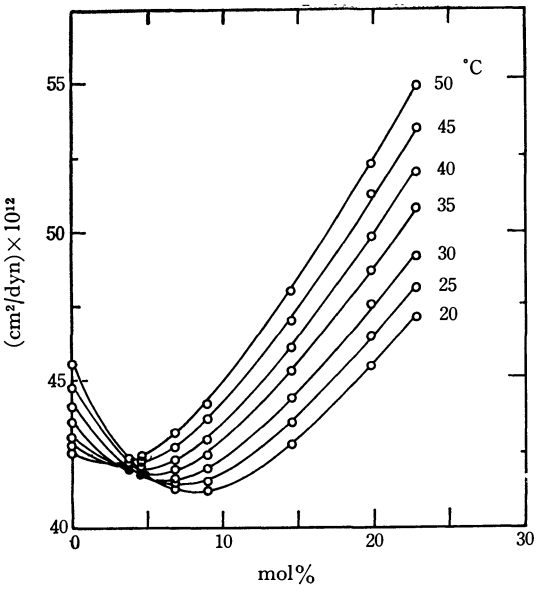

Fig. 11. Compressibility *vs.* concentration of acetone aqueous solutions.

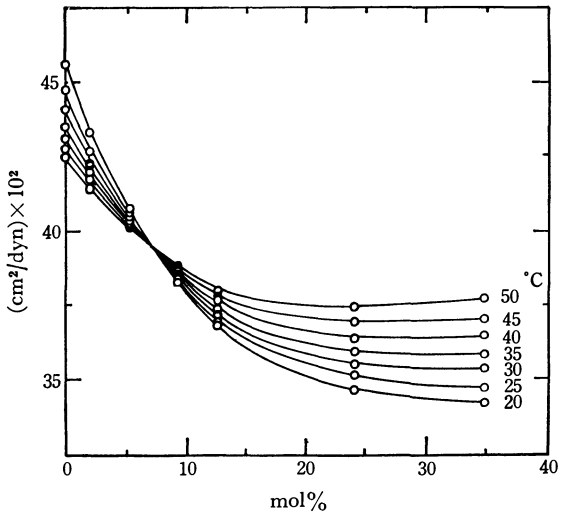

Fig. 10. Compressibility *vs.* concentration of acetamide aqueous solutions.

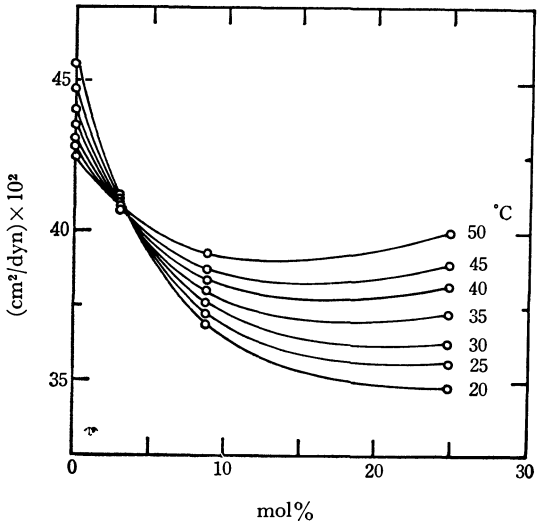

Fig. 12. Compressibility *vs.* concentration of DMF aqueous solutions.

Table 1. The parameters at a common intersection obtained from both curves $V-\mu$ and $\beta-\mu$.

	Data concerning sound velocity				Data concerning adiabatic compressibility			
	V_c m/sec	μ_c^V mol%	r_c^V	ΔT_c^V °C	β_c $\times 10^{-12}$ cm²/dyn	μ_c^β mol%	r_c^β	ΔT_c^β °C
U	1688	18.0	4.5	20—40	34.8	11.8	7.4	20—50
DMU	1641	6.5	14.3	20—35	37.5	5.2	18.2	20—40
TU	1628	8.8	10.3	50—60	38.7	4.0	24.0	50—60
AA	1615	11.2	7.9	20—35	39.0	8.0	11.5	20—35
A	1573	6.2	15.1	20—30	41.6	5.6	16.8	20—30
DMF	1591	4.7	20.3	20—50	39.9	4.2	22.8	20—40
Me[a]	1574	13.5	6.3	20—30	42.1	10.5	8.5	20—40
Et[a]	1605	6.8	13.7	20—40	40.7	5.5	17.2	20—30
Pr[a]	1580	5.2	18.2	0—20	41.7	4.1	23.4	10—30
Mo[b]	1565	3.7	26.1	20—60				

a) Ref. 8. b) Ref. 6.

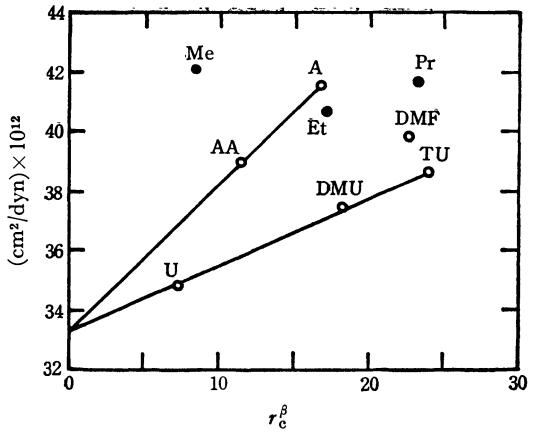

Fig. 13. β_c *vs.* r_c^β for various solutions.
○ present study, ● others study (*cf.* Ref. 8).

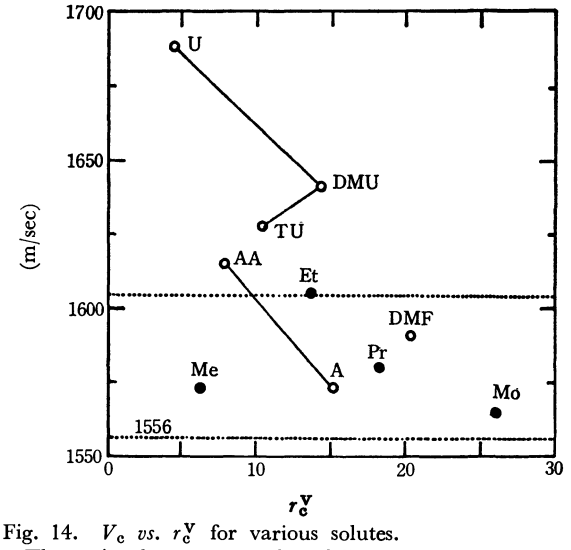

Fig. 14. V_c *vs.* r_c^V for various solutes.
The region between two dotted lines corresponds to that of 1580 m/sec ± 1.5%.
○ present study, ● others study (*cf.* Refs. 6 and 8)

clear relationship between them is found.

Discussion

As is well known, the X-ray diffraction studies of liquid water[9,10] suggest that it has a long-range ordered structure. The number of nearest neighbors in liquid water is slightly larger than in ice, and it increases slightly with an increase in the temperature. The framework of the structure of liquid water consists of a hexagonal ice-1 structure with numerous cavities, which can accommodate another species of water (non-hydrogen-bonded water); this structure is very stable against thermal agitation up to higher temperatures.

According to Hall,[11] the compressibility (β) of liquid water is given by:

$$\beta = \beta_\infty + \beta_{st} \tag{3}$$

where β_∞ is the instantaneous compressibility due to the compression of the molecules and the intermolecular distance, and where β_{st} is the structural compressibility due to the breakdown of intermolecular bonds accompanying the destruction of the open structure.

The mechanism of ultrasonic absorption in water has been studied by Hall[11] and by others.[12–14] By using the two-state-model theory of water, they have explained the bulk viscosity and the relaxational compressibility of water. In Hall's paper, it is assumed that β_∞ is independent of the temperature (T), *i.e.*, that $d\beta_\infty/dT=0$. On the basis of the X-ray diffraction data of liquid water obtained by Narten *et al.*[10], we[15] have previously studied the mechanism of ultrasonic absorption in water in relation to the liquid-water structure.

It is assumed that Eq. (3) is also applicable for nonelectrolyte aqueous solutions. The temperature derivatives of β in aqueous solutions are given by:

$$\frac{d\beta}{dT} = \frac{d\beta_\infty}{dT} + \frac{d\beta_{st}}{dT} \tag{4}$$

In the aqueous solutions at μ_c^β in ΔT_c^β, Eq. (4) leads to $d\beta/dT=0$. Accordingly, from the assumption that $d\beta_\infty/dT$ is zero, $d\beta_{st}/dT$ becomes zero also. For $\mu < \mu_c^\beta$, $d\beta/dT$ becomes negative from Figs. 7—12; therefore, $d\beta_{st}/dT$ also becomes negative. On the other hand, for $\mu > \mu_c^\beta$, $d\beta_{st}/dT$ is also equal to zero, because $d\beta_{st}/dT$ cannot become positive because of physical considerations. Therefore, it is found from Figs. 7—12 that $d\beta_\infty/dT>0$. A schematical illustration of the relationship between $d\beta/dT$ and μ is shown in Figs. 15 (a) and 15 (b).

It is assumed that the cavities contained in the framework of the water-cluster are gradually filled up by the solutes, or that the framework water in the lattice of clusters involves an exchange of solute molecules with an increase in the concentration up to μ_c^β with a maintenance of the structure of ice-1. This accompanies a decrease in the β_{st} and also in the $d\beta_{st}/dT$ of the solution. When a nonelectrolyte is dissolved in water, a new structure is formed of the water and solute molecules. This structure change accompanies a decrease in the compressibility of liquid water (*cf.* Fig. 15 (c)).

Also, it is assumed that the number of clusters of water molecules does not change appreciably up to μ_c^β. The instantaneous compressibility, β_∞, consists of two parts, one due to the compression of the clusters

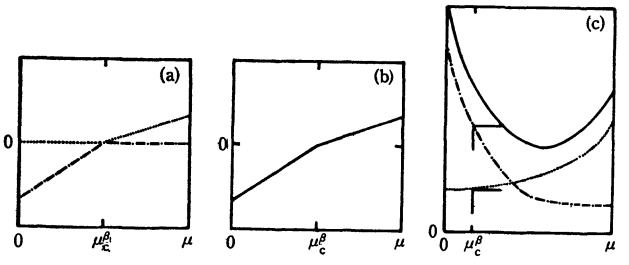

Fig. 15. $\frac{d\beta_\infty}{dT}$, $\frac{d\beta_{st}}{dT}$, $\frac{d\beta}{dT}$, β_∞, β_{st}, and β of aqueous solutions *vs.* concentration.
(a) ····· $\frac{d\beta_\infty}{dT}$, —·— $\frac{d\beta_{st}}{dT}$
(b) —— $\frac{d\beta}{dT}$, Here $\frac{d\beta}{dT}=\frac{d\beta_\infty}{dT}+\frac{d\beta_{st}}{dT}$
(c) —— β, —·— β_{st}, ····· β_∞, Here $\beta=\beta_\infty+\beta_{st}$

9) J. Morgan and B. E. Warren, *J. Chem. Phys.*, **6**, 666 (1938).
10) H. Narten, M. Danford and H. Levy, *Disscus. Faraday Soc.*, **43**, 97 (1967).
11) L. Hall, *Phys. Rev.*, **73**, 775 (1948).

and the other due to the compression of the intermolecular distance. The former does not change appreciably when we adopt the solute molecules in cavities because the elasticity of a cluster is mainly caused by the framework. Also, the latter does not change up to μ_c^β, because the number of the cluster does not change up to μ_c^β. Therefore, we may conclude that β_∞ is appreciably constant and that $d\beta_\infty/dT=0$ up to μ_c^β.

For higher concentrations, it is assumed that the increase in the number of solute molecules accompanies an increase in the number of clusters, thus decreasing β_{st} and increasing β_∞ (*cf.* Fig. 15 (c)). These two opposite effects serve to form a minimum of compressibility, or a maximum of sound velocity, at C_p.

A model of the structure of a solution has been proposed by Glew[16] on the basis of density measurements of an Et aqueous solution; there the name "solution hydrate" has been suggested. It seems better, however, that this structure of solution be named "liquid-clathrate hydrate," because the composition of this structure in Et is the same as that of the solid clathrate hydrate.[17] In this model, the solute is surrounded by a three-dimensionally hydrogen-bonded framework of water molecules. The solute molecules in the liquid-clathrate hydrate may be oriented in the cavity of a water-cluster hydrogen-bonded with framework-water molecules. In talking about the "solution hydrate"[16] or the "liquid-clathrate hydrate" in solution, it must be emphasized that the meaning of the definite composition in a hydrate does not indicate the hydration number of the solute, but is, rather, a structural unit.

It may be suggested here that the number of water molecules composing the framework of the liquid-clathrate hydrate corresponds to r_c^β for each solute. Also, the empirical relation between β_c and r_c^β may be indicative of the change in the water structure. From Eqs. (1) and (2), we obtained the following equations for the decrease in the strucutural compressibility in water caused by the solute. Here, the value of β_0, the compressibility of liquid water, is 45.6×10^{-12} cm²/dyn at 20 °C: for the urea-derivatives,

$$\Delta\beta=\beta_o-\beta_c=(12.3-0.22r_c^\beta)\times10^{-12}\ (\mathrm{cm^2/dyn}) \quad (5)$$

and for the acetyl-derivatives:

$$\Delta\beta=\beta_o-\beta_c=(12.3-0.49r_c^\beta)\times10^{-12}\ (\mathrm{cm^2/dyn}) \quad (6)$$

Since we have assumed that the number of clusters in water remains appreciably constant up to the concentration of r_c^β (μ_c^β mole fraction), the β_∞ values are nearly the same for both water and the solution at this concentration; therefore, $\Delta\beta$ indicates the difference in the structural compressibility of a solution, *i.e.*, $\Delta\beta_{st}$. For the solutes with larger r_c^β values, the water strucuture is less modified, or the cavities are less occupied, so the decrease in $\Delta\beta_{st}(=\Delta\beta)$ is smaller. This explains the negative signs of the coefficients of r_c^β in Eqs. (5) and (6). By comparing the urea-derivatives and the acetyl-derivatives, it is obvious from Eqs. (5) and (6) that the coefficient of r_c^β in the latter is nearly twice that for the former. This presumably indicates that the latter fills up the cavity only, while the former also collaborates to make the framework[18] as a constitutive part.

For Et[17] and A[19,20] aqueous solutions, it may be seen in Table 1 that r_c^β is equal to the composition in the Structure-II solid clathrate hydrate with the formula of $M\cdot17H_2O$.[21] Here, M is the guest molecule. Glew has proposed, in an Et aqueous solution over the temperature range of 0—30 °C, the existence of the liquid-clathrate-hydrate (Structure-II type of composition, $Et\cdot17H_2O$) to account for an anomaly molar volume at $\mu=ca.$ 0.06. For other aqueous solutions, it may be reasonable to assume that r_c^β corresponds to the number of water molecules constituting some other type of liquid-clathrate hydrate characteristic for each solute. Accordingly, the discussion and interpretation of results may be based on the following non-stoichiometric reaction scheme:

$$M+r_c^\beta H_2O \rightleftarrows M\cdot r_c^\beta H_2O \quad (7)$$

Since the number of water molecules constituting the liquid-clathrate hydrate in a homologues series increases with an increase in the molecular weight, r_c^β decreases with the molecular weight. Accordingly, μ_c^β (as well as C_p of aqueous solution) also shifts to a lower-solute concentration with an increase in the molecular weight of the homologue series.

It may be seen in Table 1 that the upper limiting temperature (T_c^u) of ΔT_c^β decreases with the addition of a non-polar group to the derivatives of urea and acetyl, so it may be reasonable to assume that the strength of the water-water hydrogen bond adjacent to the non-polar group is weaker than that of the polar group. Accordingly, it may be concluded that the framework of the liquid-clathrate hydrate adjacent to a non-polar group is selectively decomposed by the thermal agitation of molecules with a rise in the temperature. T_c^u is higher for the urea-derivatives than for the acetyl-derivatives for this same reason.

Chekalin *et al.*[5] report that V_c is independent of the sort of solute and that it is equal to 1580 m/sec within ±1.5% (*ca.* 1556—1604 m/sec). This rule is, however, not of universal validity, as may be seen in Fig. 14.

The author wishes to thank Prof. Tsunetaka Sasaki of the Tokyo Metropolitan University for his helpful discussions and generous support of this research and also Prof. Otohiko Nomoto of the Defense Academy for his valuable suggestions and discussions.

12) A. Smith and A. Lawson, *J. Chem. Phys.*, **22**, 351 (1954).
13) T. Litovitz and E. Carnevale, *J. Appl. Phys.*, **26**, 816 (1955).
14) C. Davis and T. Litovitz, *J. Chem. Phys.*, **42**, 2563 (1965).
15) O. Nomoto and H. Endo, This Bulletin, 44, 1519 (1971).
16) D. N. Glew, *Nature*, **195**, 698 (1962).
17) A. D. Potts and D. W. Davidson, *J. Phys. Chem.*, **69**, 996 (1965).
18) M. Abu-Hamidiyyah, *J. Phys. Chem.*, **69**, 2720 (1965).
19) A. S. Quist and H. S. Frank, *ibid.*, **65**, 560 (1961).
20) G. J. Wilson and D. W. Davidson, *Can. J. Chem.*, **41**, 264 (1963).
21) R. M. Barrer in "Non-Stoichiometric Compounds" ed. by L. Mandelcorn, Academic Press, New York and London (1964). p. 313.

Dielectric Relaxation and Molecular Structure. IV. Dielectric Relaxation and Hydrogen Bonding in Chloroanilines

J. K. VIJ* and K. K. SRIVASTAVA**

Physics Department, Panjabi University, Patiala, India

***Physics Department, Panjab University, Chandigarh, India*

(Received May 12, 1972)

Measurements of relative permittivity were carried out at 30.0 °C in *p*-dioxane at 1 MHz and at 9.48 GHz for *ortho* (A), *meta* (B), and *para* (C) chloroanilines. The results are interpreted in terms of hydrogen bonding between amino hydrogens and the oxygen atoms of the dioxane molecule, the dipole moments and dielectric relaxation time values being given. The relative behaviour of chloroanilines has been discussed. It seems that a finite probability of H-Cl bond formation exists between one of the amino hydrogens and the neighbouring chlorine atom in *o*-chloroaniline.

Curran and Estok[1] assume that hydrogen bonding between amino hydrogens and dioxane oxygens is a normal phenomenon. Few and Smith[2] incline to the view that hydrogen bonding occurs when the actual structure is that of resonance between several possible structures and that it also receives considerable contribution from highly polar structures. Chitoku and Higasi[3] showed, from dipole moment and dielectric relaxation study, that an increase in the dielectric relaxation time of certain anilines in dioxane is a measure of the strength of hydrogen bonds and have verified the viewpoint of Few and Smith[2] by concluding that the strength of hydrogen bonds depends upon the increment in mesomeric moment of amino group. Smith and Walshaw[4] had demonstrated that the mesomeric interaction and presumably the *p*-character of the lone pair orbital of nitrogen atom increases upon *n*-methylation of the amino group and with the introduction of the electro-negative substituent in the phenyl ring. Cumper and Singleton[5] have carried out measurements on dipole moments of a large number of systems including chloroanilines. Their results support the observations of Smith and Walshaw.[4] They interpret the '$\Delta\mu$' increment (*i.e.*, $\mu_D - \mu_B$) as the increase in mesomeric moment since their results for '$\Delta\mu$' and mesomeric interaction correspond with each other in most of the systems they studied. The behaviour of different isomers can be estimated by this method. We have made measurements[6] on *o*-, *m*-, and *p*-, chloroanilines for calculating both the dipole moments and dielectric relaxation times in benzene and dioxane with the hope that additional relaxation data for these molecules might give more information on their relative behaviour.

Experimental and Results

Benzene and *p*-dioxane were purified by standard methods. Purification of solutes, instruments, methods of measurement and of analysis were given previously.[7]

TABLE 1. VALUES OF a_0 (slope of ε *vs.* concn curve), a' (Slope of ε' *vs.* concn curve), a'' (slope of ε'' *vs.* concn curve), AND a_D (slope of n_D^2 *vs.* concn curve)

Solvent	a_0	a'	a''	a_D
		o-Chloroaniline		
Benzene	3.14	2.80±0.02	0.88±0.02	0.106
p-Dioxane	4.32	2.37±0.02	1.20±0.02	0.410
		m-Chloroaniline		
Benzene	6.25	4.44±0.03	2.33±0.04	0.220
p-Dioxane	9.00	2.90±0.02	2.69±0.04	0.450
		p-Chloroaniline		
Benzene	7.96	4.90±0.03	2.49±0.04	0.256
p-Dioxane	11.50	3.47±0.02	3.10±0.06	0.470

TABLE 2. VALUES OF THE DIPOLE MOMENT AND DIELECTRIC RELAXATION TIME

	Dipole moment in benzene μ_B (Debyes)		Dipole moment in dioxane μ_D (Debyes)		Dielectric relaxation time 10^{-12} s			
					τ_B		τ_D	
	Present	Literature	Present	Literature	$\tau(1)_B$	$\tau(2)_B$	$\tau(1)_D$	$\tau(2)_D$
o-Chloroaniline (A)	1.88	1.77 to 1.84[a]	2.00	1.97[d]	5.5	6.5	10.3	27.4
m-Chloroaniline (B)	2.67	2.66 to 2.70[a]	2.98	3.06[d]	9.3	13.0	18.5	38.2
p-Chloroaniline (C)	3.02	2.90 to 3.00[a]	3.40	3.39[b]	9.0	20.6	17.7	43.6
				3.37[c]				

a) A. L. McClellan, "Tables of Experimental Dipole Moments", Freeman and Co., San Francisco, (1963).
b) A. V. Few and J. W. Smith, *J. Chem. Soc.*, **1949**, 2781. c) Ref. 1.

* Present address: Engineering School, Trinity College, Dublin, 2, Ireland.

1) C. Curran and G. K. Estok, *J. Amer. Chem. Soc.*, **72**, 4575 (1950).
2) A. V. Few and J. W. Smith, *J. Chem. Soc.*, **1949**, 753, 2663.
3) K. Chitoku and K. Higasi, This Bulletin, **39**, 2160 (1966).
4) J. W. Smith, *J. Chem. Soc.*, **1952**, 3532; **1953**, 109; J. W. Smith and S. M. Walshaw, *ibid.*, **1957**, 3217; **1959**, 3748.
5) C. W. N. Cumper and A. Singleton, *J. Chem. Soc., B*, **1968**, 645.
6) These measurements formed a part of the Ph. D. thesis of one of the authors (J. K. Vij), Panjab University, Chandigarh, India, February 1969.
7) K. K. Srivastava and J. K. Vij, This Bulletin, **43**, 2307 (1970).

TABLE 3. VALUES OF THE SOLVENT INCREMENT AND THE RATIO OF DIELECTRIC RELAXATION TIMES

Substance	$(\mu_D-\mu_B)$ (Debye) *i.e.* Present	$(\mu_D-\mu_B)$ (Debye) *i.e.* Literature	Ratios of dielectric relaxation time	
			$\tau(1)_D/\tau(1)_B$	$\tau(2)_D/\tau(2)_B$
o-Chloronailine (A)	0.12±0.01	0.20[d]	1.9	4.2
m-Chloroaniline (B)	0.31±0.01	0.39	2.0	2.9
p-Chloroaniline (C)	0.38±0.01	0.37[e]	2.0	2.1
		0.39[d]		
Aniline (D)	—	0.25[f]	—	2.9[f]

d) Ref. 5. e) Ref. 10, Chap. X, p. 329. f) Ref. 3.

Both parts, real and imaginary, of relative permittivity were found, from observation, to be linear functions of solute concentration in the range studied.

The results have been discussed in terms of $\tau(1)$ and $\tau(2)$, which are the dielectric relaxation time values defined by the following two independent equations derived from the Debye equation for dilute solutions:

$$\tau(1) = \frac{1}{\omega}\frac{a''}{a'-a_D} \quad (1)$$

$$\tau(2) = \frac{1}{\omega}\frac{a_0-a'}{a''} \quad (2)$$

This method of analyzing the single frequency data has recently been proposed by Higasi *et al.*[8] and has been discussed in more detail.[9] The values of the "so-called slopes" for *o*-, *m*-, and *p*-, chloroanilines in *p*-dioxane are given in Table 1 along with those in benzene.[7] Possible errors in the value of the slopes are also indicated. Values for dipole moments and dielectric relaxation times are given in Table 2, and dipole moment increments (*i.e.*, $\Delta\mu=\mu_D-\mu_B$) and ratios of both $\tau(1)_D/\tau(1)_B$ and $\tau(2)_D/\tau(2)_B$ in Table 3.

Discussion

The values of moments show a close agreement with those in literature indicating the reliability of technique and purity of the chemicals.

A small increment in $\Delta\mu$ and consequently a small increase in mesomeric moment of amino group has been interpreted[5] as either of two possibilities:

(i) H–Cl bond between one of two amino hydrogens and the neighbouring chlorine atom, leaving the second hydrogen atom free for hydrogen bonding.

(ii) An electrostatic repulsion between the electronegative chlorine atom and the oxygen atoms of a dioxane molecule.

$\tau(1)$ at the experimental frequency is a combination of τ_1, and τ_2 whereas $\tau(2)$ corresponds very nearly to τ_1.[9] The relaxation data show that the ratio $\tau(1)_D/\tau(1)_B$ remains almost constant. This suggests that intramolecular relaxation time does not depend much on the solvent, whereas molecular relaxation time is affected possibly because of complex formation[3] of the molecule in *p*-dioxane. Intramolecular relaxation time seems to be independent as the result of its inversion mechanism postulated by Smyth.[10]

The ratio $\tau(2)_D/\tau(2)_B$ follows a decreasing trend in contrast to that observed from dipole moment studies and the ratio for *o*-chloroaniline, in particular, is large. This may imply that the system formed for this molecule in *p*-dioxane is relatively one with more complexities. It appears to favour (i), since (ii) would not lead to the large increase in the molecular relaxation time for *o*-chloroaniline in *p*-dioxane. Our observations support the postulates already made from the examination of the dissociation constants[11] and N–H stretching frequencies[12] in *o*-chloroanilines.

8) K. Higasi, Y. Koga, and M. Nakamura, This Bulletin **44**, 988 (1971).

9) J. K. Vij, Iqbal Krishan, and K. K. Srivastava, *ibid.*, **46**, 17 (1973).

10) C. P. Smyth, "Molecular Relaxation Processes," Chemical Society Publication No. 20, Academic Press, London (1966), p. 8.

11) D. H. McDaniel and H. C. Brown, *J. Amer. Chem. Soc.*, **77**, 3756 (1955).

12) P. J. Krueger, *Can. J. Chem.*, **40**, 2300 (1962).

Structure of Ethylene Oxide Oligomer Complexes. I. A 1:1 Complex of Tetraethylene Glycol Dimethyl Ether with Mercuric Chloride

Reikichi IWAMOTO

Government Industrial Research Institute, Osaka, Midorigaoka, Ikeda, Osaka 563

(Received March 11, 1972)

Molecular and crystal structure of a 1 : 1 molecular complex of tetraethylene glycol dimethyl ether $CH_3O(CH_2CH_2O)_4CH_3$ (TGM) with mercuric chloride has been determined by means of X-ray diffraction. The complex has a monoclinic unit cell with $a=14.29$, $b=15.10$, $c=7.84$ Å, and $\beta=97.0°$. The space group is $P2_1/n$. Four molecules of both TGM and mercuric chloride are contained in the unit cell. The structure was determined by the ordinary heavy atom method. The molecular conformation of TGM in the complex is approximately

$$\underset{T}{CH_3}\text{-}\underset{G}{O}\text{-}\underset{T}{CH_2}\text{-}\underset{T}{CH_2}\text{-}\underset{\bar{G}}{O}\text{-}\underset{T}{CH_2}\text{-}\underset{T}{CH_2}\text{-}\underset{G}{O}\text{-}\underset{T}{CH_2}\text{-}\underset{T}{CH_2}\text{-}\underset{\bar{G}}{O}\text{-}\underset{T}{CH_2}\text{-}\underset{T}{CH_2}\text{-}\underset{G}{O}\text{-}\underset{T}{CH_2}\text{-}\underset{T}{CH_2}\text{-}O\text{-}CH_3,$$

where T, G, and $\bar{G}$ indicate *trans*, *gauche*, and minus *gauche* forms, respectively. All the CH_2–O bonds are *trans*, while the CH_2–CH_2 bonds are *gauche* and minus *gauche* in the adjacent chemical units. The conformational unit of

$$\underset{T}{O}\text{-}\underset{G}{CH_2}\text{-}\underset{T}{CH_2}\text{-}\underset{T}{O}\text{-}\underset{\bar{G}}{CH_2}\text{-}\underset{T}{CH_2}\text{-}$$

was found to be very important and favorable for coordination between the O and Hg atoms. The molecule is circular but not closed, and the five oxygen atoms, which are nearly coplanar and located at the inner side of the circular molecule, enclose one $HgCl_2$ molecule with close interatomic distances (2.78—2.96 Å) between the O and Hg atoms.

The molecular complexes of polyethylene oxide (PEO) with $HgCl_2$ were previously investigated,[1,2] and it was found that they have two crystalline forms, one having the composition of CH_2CH_2O: $HgCl_2$= 4 :1 (type I) and the other that of CH_2CH_2O: $HgCl_2$= 1: 1 (type II). The conformation of PEO in the complexes is

$$\text{-}\underset{T}{O}\text{-}\underset{T}{CH_2}\text{-}\underset{T}{CH_2}\text{-}\underset{T}{O}\text{-}\underset{T}{CH_2}\text{-}\underset{G}{CH_2}\text{-}\underset{T}{O}\text{-}\underset{T}{CH_2}\text{-}\underset{T}{CH_2}\text{-}\underset{T}{O}\text{-}\underset{T}{CH_2}\text{-}\underset{\bar{G}}{CH_2}\text{-}$$

in type I and

$$\text{-}\underset{T}{O}\text{-}\underset{G}{CH_2}\text{-}\underset{G}{CH_2}\text{-}\underset{T}{O}\text{-}\underset{T}{CH_2}\text{-}\underset{\bar{G}}{CH_2}\text{-}$$

in type II, where T, G, and $\bar{G}$ denote *trans*, *gauche*, and minus *gauche*, respectively. These differ significantly from the conformation of PEO in the ordinary PEO,[3] which is helical consisting of a uniform succession of $\underset{T}{O}\text{-}\underset{T}{CH_2}\text{-}\underset{G}{CH_2}$. In the type I complex two of the four oxygen atoms in the identity period are coordinated with one Hg atom, while in the type II complex each oxygen atom is coordinated with two Hg atoms. In these complexes the interatomic interactions between the Hg and O atoms cause the complex formation and have important influence on the conformation of PEO.

On the other hand, according to Pedersen,[4,5] macrocyclic polyethers especially those containing CH_2CH_2O units form stable crystalline molecular complexes with many metal salts including $HgCl_2$. Investigations have recently been carried out on the crystal structures of some complexes in which an alkali ion is enclosed in a cavity surrounded by oxygen atoms of the molecule.[6,7] This spatial arrangement indicates the existence of strong interactions between oxygen and alkali ions. It was reported that there occurs specific solvation between dimethoxy ethane and $HgCl_2$ in solution.[8] Ethylene oxide oligomers, $CH_3O(CH_2CH_2O)_m$-CH_3, have specific solvation with alkali-carbanion ion pairs in solution and the solvation has significant influence on reactivity of the ion pairs, which are the initiators of living polymerization of styrene.[9-11] Dimethoxy ethane has specific interaction with alkali metals, also.[12,13]

These studies indicate that ethers composed of the CH_2CH_2O groups have a specific property to interact with metal salts or ions. In the structural studies of the PEO–$HgCl_2$ complexes,[1,2] it was not possible to determine the precise structure of PEO and to discuss the structure of the complexes in details on account of the small number of reflections and predominant contribution of $HgCl_2$ to the diffraction intensities. Recently it has been found that ethylene oxide oligomers, $RO(CH_2CH_2O)_mR$, form molecular complexes with $HgCl_2$ and some of the complexes give single crystals available for structural investigation by means of X-ray diffraction. It was hoped that the X-ray structure determination of the complexes would give important and more detailed information on the interaction between ethylene oxide groups and mercuric chloride and on the conformational change of the molecules. From this point of view structural studies of a series

1) R. Iwamoto, Y. Saito, H. Ishihara, and H. Tadokoro, *J. Polymer. Sci, A-2*, **6**, 1509 (1968).
2) M. Yokoyama, H. Ishihara, R. Iwamoto, and H. Tadokoro, *Macromolecules*, **2**, 184 (1969).
3) H. Tadokoro, Y. Chatani, T. Yoshihara, S. Tahara, and S. Murahashi, *Makromol. Chem.*, **73**, 109 (1964).
4) C. J. Pedersen, *J. Amer. Chem. Soc.*, **89**, 7017 (1967).
5) C. J. Pedersen, *ibid.*, **92**, 391 (1970).
6) D. Bright and M. R. Truter, *J. Chem. Soc., B*, **1970**, 1544.
7) M. A. Bush and M. R. Truter, *ibid.*, **1971**, 1440.
8) R. Iwamoto, *Spectrochim. Acta*, 27*A*, 2385 (1971).
9) R. V. Slates and M. Szwarc, *J. Amer. Chem. Soc.*, **89**, 604, (1967).
10) L. L. Chan and J. Smid, *ibid.*, **89**, 4547 (1967).
11) M. Shinohara, J. Smid, and M. Szwarc, *ibid.*, **90**, 2175 (1968).
12) F. Cafasso and B. R. Sundheim, *J. Chem. Phys.*, **31**, 809 (1959).
13) S. H. Glarum and J. H. Marshall, *ibid.*, **52**, 5555 (1970).

of the complexes of ethylene oxide oligomers, RO-$(CH_2CH_2O)_mR$, with $HgCl_2$ have been undertaken. The present paper deals with the $CH_3O(CH_2CH_2O)_4$-CH_3–$HgCl_2$ complex.

Experimental

Samples. Commercially available sample of tetraethylene glycol dimethyl ether (TGM) was used (Tokyo Kasei Kogyo Co., Ltd.). Crystals of the TGM–$HgCl_2$ complex were prepared by dissolving crystalline powder of $HgCl_2$ into an ethanol-TGM (about 10:1 volume ratio) mixture to saturation at about 35 °C and cooling the saturated solution to room temperature, single crystals of the complex being precipitated in solution. The crystals are transparent needles grown along the *c* axis. The melting point of the complex is 66 °C as determined microscopically. The density of the crystal was measured by the flotation method by use of a liquid mixture of CCl_4 and $CHBr_3$ as the flotation medium. The observed density was 1.96 g/cc. The composition of the complex was found to be TGM: $HgCl_2$=1:1 by elemental analysis (Found: Hg, 40.8%. Calcd for the 1:1 complex: Hg, 40.6%).

Table 1. Crystallographic and physical data of the TGM–$HgCl_2$ complex

Formula	$CH_3O(CH_2CH_2O)_4CH_3 \cdot HgCl_2$
MW	493.7
Mp	66 °C
Crystal system	monoclinic
Space group	$P2_1/n$-C_{2h}^5
a	14.29 Å
b	15.10 Å
c	7.84 Å
β	97.0°
Z	4
Vol.	1697.0 Å^3
D_c	1.95 g/cc
D_m	1.96 g/cc
μ (Cu$K\alpha$)	206.4 cm^{-1}
F(000)	944

Unit Cell and Space Group. The unit cell parameters were determined with a Weissenberg camera and calibrated by silicon powder. Systematic absences were observed with respect to reflections having indices $h0l$ with $h+l$ odd and $0k0$ with k odd. The space group, thus, is $P2_1/n$. The crystallographic data are given in Table 1 together with some physical constants.

Intensity Measurement. X-Ray diffraction photographs of the complex crystal were taken by using Cu$K\alpha$ radiation. The crystals used were about 0.2 mm × 0.2 mm × 0.2 mm in size. Intensity data were recorded on photographs by using equi-inclination Weissenberg multiple film method about the *c* axis from l=0 to 6 layers and about the *b* axis for a k=0 layer. The number of recorded reflections having non-zero intensities was 2455. The intensities were measured by visual comparison with standard intensity scales. Intensity data were corrected for the Lorentz and polarization factors. Although the absorption coefficient is very large (μ=206 cm^{-1} for Cu$K\alpha$ radiation), the intensity data were not corrected for absorption. The smallest possible crystal was used for collecting the intensities. When the crystal was exposed to radiation for longer than 100 hr under operation conditions of 35 kV and 20 mA, it became opaque and light brown, and the diffraction photographs were contaminated with Debye ring reflections due to the decomposed material. The crystal was renewed for each layer line.

Structure Determination

Since atomic scattering power of a Hg atom is much stronger than that of other atoms contained in the complex, the general feature of reflections can be explained approximately by considering the Hg atom only. The crystal structure has been determined according to the ordinary heavy atom method. Atomic scattering factors were taken from *International Tables of X-Ray Crystallography* (1962). The atomic parameters refined by the block diagonal least squares method[14] were set as the final result. For this, the

Table 2. Atomic coordinates and temperature factors in the TGM–$HgCl_2$ complex

atom	*x*	*y*	*z*	*B* or B_{11}	B_{22}	B_{33}	B_{12}	B_{13}	B_{23}
Hg	0.2386	0.0598	−0.0102	0.0023	0.0017	0.0124	−0.0002	0.0005	0.0009
Cl_1	0.3019	−0.0591	0.1500	0.0054	0.0031	0.0218	0.0014	0.0008	0.0051
Cl_2	0.1614	0.1706	−0.1701	0.0050	0.0025	0.0226	0.0013	−0.0028	0.0039
C_1	0.0461	−0.0248	0.2375	4.39A^2					
O_1	0.0865	0.0636	0.2140	4.31					
C_2	0.1131	0.1004	0.3759	4.71					
C_3	0.1692	0.1851	0.3295	3.24					
O_2	0.2612	0.1574	0.2928	2.76					
C_4	0.3259	0.2302	0.2765	3.54					
C_5	0.4153	0.1952	0.2185	3.70					
O_3	0.3940	0.1720	0.0490	2.95					
C_6	0.4748	0.1423	−0.0284	3.31					
C_7	0.4453	0.1197	−0.2161	3.53					
O_4	0.3875	0.0362	−0.2108	3.44					
C_8	0.3594	0.0087	−0.3933	5.18					
C_9	0.3050	−0.0813	−0.3535	3.13					
O_5	0.2203	−0.0588	−0.2968	3.29					
C_{10}	0.1638	−0.1345	−0.2635	4.67					

14) By the courtesy of Dr. Y. Chatani of Osaka University, the calculation was made at the computer center of the University according to the program programmed by T. Ashida.

R factor ($\Sigma||F_o|-|F_c||/\Sigma|F_o|$) for the structure taking the Hg and Cl atoms only into account was 21.5%. Consideration of the C and O atoms of TGM improved the R factor to 15.6%. The atomic parameters are given in Table 2.

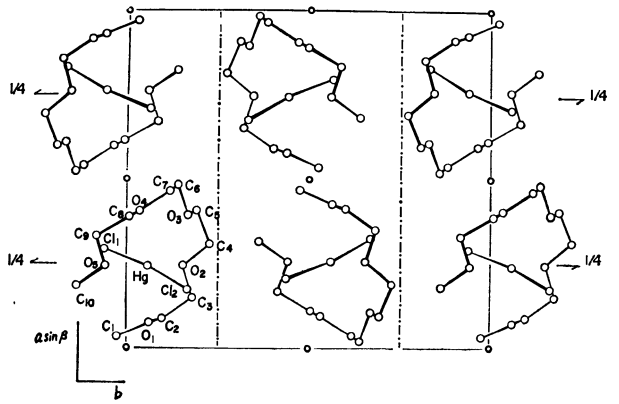

Fig. 1. Crystal structure of the TGM-$HgCl_2$ complex.

Table 3. Bond lengths (Å) and bond angles (°) and their estimated standard deviations in the TGM-$HgCl_2$ complex

Hg–Cl_1	2.311±0.013	Cl_1–Hg–Cl_2	174.2
Hg–Cl_2	2.291±0.013	C_1–O_1–C_2	108.3±3.7
C_1–O_1	1.47 ±0.06	O_1–C_2–C_3	101.7±3.8
O_1–C_2	1.40 ±0.06	C_2–C_3–O_2	108.3±3.5
C_2–C_3	1.58 ±0.07	C_3–O_2–C_4	113.9±3.1
C_3–O_2	1.44 ±0.05	O_2–C_4–C_5	109.6±3.5
O_2–C_4	1.45 ±0.05	C_4–C_5–O_3	106.7±3.6
C_4–C_5	1.50 ±0.07	C_5–O_3–C_6	113.2±3.2
C_5–O_3	1.37 ±0.05	O_3–C_6–C_7	109.7±3.5
O_3–C_6	1.44 ±0.05	C_6–C_7–O_4	104.4±3.4
C_6–C_7	1.52 ±0.06	C_7–O_4–C_8	106.8±3.3
C_7–O_4	1.51 ±0.06	O_4–C_8–C_9	97.4±3.7
O_4–C_8	1.50 ±0.06	C_8–C_9–O_5	108.4±3.6
C_8–C_9	1.62 ±0.07	C_9–O_5–C_{10}	113.2±3.4
C_9–O_5	1.38 ±0.05		
O_5–C_{10}	1.44 ±0.06		

Table 4. Internal rotation angles for the TGM molecule in the complex

C_1–O_1–C_2–C_3	171°
O_1–C_2–C_3–O_2	−77
C_2–C_3–O_2–C_4	−170
C_3–O_2–C_4–C_5	−174
O_2–C_4–C_5–O_3	72
C_4–C_5–O_3–C_6	176
C_5–O_3–C_6–C_7	−179
O_3–C_6–C_7–O_4	−71
C_6–C_7–O_4–C_8	−178
C_7–O_4–C_8–C_9	177
O_4–C_8–C_9–O_5	73
C_8–C_9–O_5–C_{10}	178

Results and Discussion

The crystal structure of the complex as a whole is shown in Fig. 1. Each TGM molecule encloses one $HgCl_2$ molecule in the crystal of the complex. Bond lengths and angles for the TGM molecules are listed in Table 3, together with those for the $HgCl_2$ molecule. These values are reasonable considering the fact that the Hg atoms contribute predominantly to the diffration intensities in the complex. Table 4 gives internal rotation angles around each bond of the TGM molecule in the complex. Internal rotation angles around the CH_2–O bonds are approximately *trans* (170—179°), while those around the CH_2–CH_2 bonds are nearly *gauche* with alternation of *gauche* and minus *gauche* in the succeeding chemical units (71—77°):

$$\underset{T}{-CH_2}\text{–}\underset{G}{CH_2}\text{–}O\text{–}\underset{T}{CH_2}\text{–}\underset{T}{CH_2}\text{–}O\text{–}\underset{\bar{G}}{CH_2}\text{–}\underset{T}{CH_2}\text{–}O\text{–}.$$

The conformation of the whole molecule is, therefore, denoted by

$$\underset{T}{CH_3}\text{–}O\text{–}\underset{G}{CH_2}\text{–}\underset{T}{CH_2}\text{–}O\text{–}\underset{T}{CH_2}\text{–}\underset{\bar{G}}{CH_2}\text{–}O\text{–}\underset{T}{CH_2}\text{–}\underset{T}{CH_2}\text{–}O\text{–}\underset{G}{CH_2}\text{–}\underset{T}{CH_2}\text{–}O\text{–}$$

$$\underset{\bar{G}}{CH_2}\text{–}\underset{T}{CH_2}\text{–}O\text{–}CH_3.$$

Figure 2 shows the molecular structure of TGM in the complex, where the molecule is projected on the plane formed by the five oxygen atoms. The molecule has an open circular structure and the five oxygen atoms are on the inner side, enclosing one Hg atom in the way shown in Fig. 3. Table 5 gives interatomic distances involving Hg atoms and angles for $O_i\cdots Hg\cdots O_{i+1}$, Cl_j–$Hg\cdots O_i$, and C_j–$O_i\cdots Hg$. Interatomic dis-

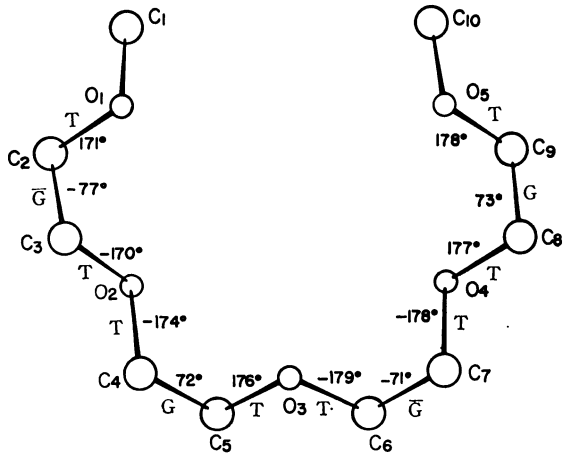

Fig. 2. Molecular conformation of TMG in the complex.

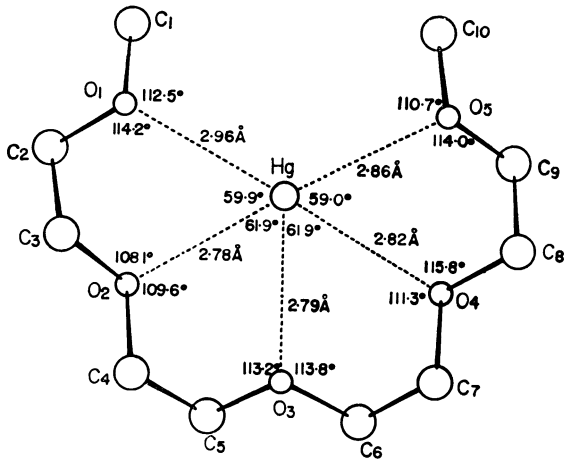

Fig. 3. Interactions between the O and Hg atoms in the TGM-$HgCl_2$ complex.

Table 5. Interatomic distances and angles for non-bonded atoms in the TGM-$HgCl_2$ complex

$O_1..Hg..O_2$	59.9°	$Hg..O_1$	2.96Å
$O_2..Hg..O_3$	61.9	$Hg..O_2$	2.78
$O_3..Hg..O_4$	61.9	$Hg..O_3$	2.79
$O_4..Hg..O_4$	59.0	$Hg..O_4$	2.82
		$Hg..O_5$	2.86
$Cl_1-Hg..O_1$	87.7		
$Cl_2-Hg..O_1$	88.4	$C_1-O_1..Hg$	112.5°
$Cl_1-Hg..O_2$	87.2	$C_2-O_1..Hg$	114.2
$Cl_2-Hg..O_2$	94.5	$C_3-O_2..Hg$	108.1
$Cl_1-Hg..O_3$	97.5	$C_4-O_2..Hg$	109.6
$Cl_2-Hg..O_3$	88.2	$C_5-O_3..Hg$	113.2
$Cl_1-Hg..O_4$	86.2	$C_6-O_3..Hg$	113.8
$Cl_2-Hg..O_4$	97.6	$C_7-O_4..Hg$	111.3
$Cl_1-Hg..O_5$	86.2	$C_8-O_4..Hg$	115.8
$Cl_2-Hg..O_5$	92.0	$C_9-O_5..Hg$	114.0
		$C_{10}-O_5..Hg$	110.7

tances between the Hg and O atoms range from 2.78 to 2.96 Å. All the angles of $Cl_j-Hg\cdots O_i$ are 86—98° and the five oxygen atoms of the TGM molecule enclose one Hg atom in the plane nearly perpendicular to the Cl-Hg-Cl direction and passing through the Hg atom. The angles of $O_i\cdots Hg\cdots O_{i+1}$ are 59—62°. The five oxygen atoms are located at the five corners of a hexagon with the remaining one corner empty, the Hg atom being located at the center of the hexagon. Since the $C_j-O_i\cdots Hg$ angles are 108—116° and nearly of a tetrahedral angle, the Hg atom is located at one of the tetrahedral directions of an oxygen atom with respect to the bonded carbon atoms. The above geometry of the coordination indicates that the circular structure of TGM is very favorable for coordination of the O atoms with the Hg atom. Figure 4 shows the structure of the complexed pair projected along the *a* axis.

The chain conformation of TGM in the complex is very similar to that of PEO[3] with respect to the single chemical unit of $O-CH_2-CH_2-$. However, since the CH_2-CH_2 bonds are alternately *gauche* and minus

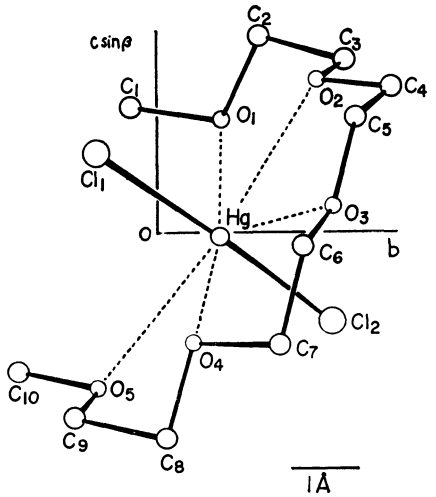

Fig. 4. Structure of one pair of the TGM-$HgCl_2$ complex projected along the *a* axis.

gauche in the adjacent CH_2CH_2O groups, the shape of the molecule as a whole becomes open circular in contrast to the helical conformation of PEO which consists of a uniform succession of $-\underset{T}{CH_2}-\underset{G}{CH_2}-\underset{T}{O}$. It has been shown that when PEO forms molecular complexes with $HgCl_2$, the conformation of the asymmetric unit changes either to $-\underset{T}{O}-\underset{T}{CH_2}-\underset{T}{CH_2}-\underset{T}{O}-\underset{T}{CH_2}-\underset{G}{CH_2}-$ (type I)[1] or to $-\underset{T}{O}-\underset{G}{CH_2}-\underset{G}{CH_2}-$ (type II).[2] It might be of interest to compare these conformations with that found in the complex $-\underset{T}{CH_2}-\underset{G}{CH_2}-\underset{T}{O}-\underset{T}{CH_2}-\underset{\bar{G}}{CH_2}-\underset{T}{O}-$. The stability of these conformations will be considered next. With respect to the CH_2-CH_2 bonds, the *gauche* form may be more stable by about 400 cal/mol than the *trans* form,[15] while for the CH_2-O bonds the *trans* form is more stable by 1.2 kcal/mol than the *gauche* one.[16] Consequently, the conformation of TGM in the present complex must be stable as an isolated molecule. The conformational stability of PEO in the type I complex,[1] which contains equal number of *gauche* and *trans* forms of the CH_2-CH_2 bond, must be next to the most stable form of $-\underset{T}{CH_2}-\underset{G}{CH_2}-\underset{T}{O}-\underset{T}{CH_2}-\underset{\bar{G}}{CH_2}-\underset{T}{O}-$. In contrast to this, the conformation of PEO in the type II complex is less stable as a single chain, since one half of the CH_2-O bonds is gauche. This may be clearly understood from Fig. 5, where the five possible conformations of $O-CH_2-CH_2-O-CH_2-CH_2-$ are given in the order of decreasing stability from the top to the bottom. The conformations of TGM and ordinary PEO correspond to A, the most stable one. PEO of type I complex corresponds to B, and PEO of type II complex to E.

	O—C—C—O—C—C—
A	T G T T G($\bar{G}$) T
B	T G T T T T
C	T T T T T T
D	T G T T G G
E	T G G T G($\bar{G}$) G($\bar{G}$)

Fig. 5. Possible five conformations for the $O-CH_2-CH_2-O-CH_2-CH_2-$ unit. $\bar{G}$ in parentheses indicates alternative possibility for G. A is the most stable and *E* is the least stable conformation.

It is interesting to compare the spatial configuration of the TGM-$HgCl_2$ complex with that of the complex of a cyclic ether with Rb and Na isothiocyanate.[6] In the latter complex, two kinds of molecules are contained in the crystal. One is complexed with the metal ion and the other is free. For the complexed molecule, a Rb or Na ion is enclosed by six oxygen atoms of the cyclic ether molecule, the six oxygen atoms being coplanar. The interatomic distances are 2.73—2.88 Å for Na···O and 2.86—2.93 for Rb···O. Thus, the

15) J. E. Mark and P. J. Flory, *J. Amer. Chem. Soc.*, **88**, 3702 (1966).

16) H. Wieser, W. G. Lailaw, P. T. Krueger, and H. Fuhrer, *Spectrochim. Acta*, **24** *A*, 1055 (1968).

way of coordination between the cyclic ether molecule and the metal ion is very similar to that found in the TGM–$HgCl_2$ complex.

The fact that the ethers composed of CH_2CH_2O, linear or cyclic, form complexes not only with $HgCl_2$ but also with many other metal salts[4] and that a metal ion is coordinated to coplanar five or six oxygen atoms might suggest that the complex is formed by electrostatic forces acting between positively charged metal atom or ion and the negatively charged O atoms, although the tetrahedral arrangement of Hg and O may indicate that some other factors contribute to the coordination.

The angle Cl–Hg–Cl is distorted to 174° from the complete linear form as in the case of the PEO–$HgCl_2$ complexes.[1,2]

The author would like to thank Professor H. Tadokoro, Dr. Y. Chatani, and Dr. M. Kobayashi, Osaka University, for their helpful discussions and encouragement. He is also indebted to Dr. S. Kuribayashi of this Institute for his helpful discussions.

BULLETIN OF THE CHEMICAL SOCIETY OF JAPAN, VOL. 46, 1118—1123 (1973)

Structure of Ethylene Oxide Oligomer Complexes. II. A 1:1 Complex of Tetraethylene Glycol Diethyl Ether with Mercuric Chloride

Reikichi IWAMOTO

Government Industrial Research Institute, Osaka, Midorigaoka, Ikeda, Osaka 563

(Received March 18, 1972)

Structure of a 1:1 complex of tetraethylene glycol diethyl ether $CH_3CH_2O(CH_2CH_2O)_4CH_2CH_3$ (TGE) with mercuric chloride has been investigated by means of X-ray diffraction. The complex has a cubic unit cell with $a=12.54$ Å and four molecules of both TGE and $HgCl_2$ are contained in the unit cell. The space group is Pa3-T_h^6. Four Hg atoms are located at the positions corresponding to the face centered arrangement. The TGE molecule is statistically arranged around the Hg atom located at the position having site symmetry $\bar{3}$. The following molecular conformation of TGE was suggested:

$$CH_3\text{-}\underset{T}{CH_2}\text{-}\underset{T}{O}\text{-}\underset{G}{CH_2}\text{-}\underset{T}{CH_2}\text{-}\underset{T}{O}\text{-}\underset{\bar{G}}{CH_2}\text{-}\underset{T}{CH_2}\text{-}\underset{T}{O}\text{-}\underset{G}{CH_2}\text{-}\underset{T}{CH_2}\text{-}\underset{T}{O}\text{-}\underset{\bar{G}}{CH_2}\text{-}\underset{T}{CH_2}\text{-}\underset{G}{O}\text{-}CH_2\text{-}CH_3,$$

where T, G, and $\bar{G}$ indicate *trans*, *gauche*, and minus *gauche* forms, respectively. The TGE molecule encloses the $HgCl_2$ molecule around the Hg atom with close interatomic distances between the Hg and O atoms.

Structure of the molecular complex of tetraethylene glycol dimethyl ether $CH_3O(CH_2CH_2O)_4CH_3$ (TGM) with $HgCl_2$ has been reported in a previous paper.[1] Tetraethylene glycol diethyl ether $CH_3CH_2O(CH_2CH_2O)_4CH_2CH_3$ (TGE) also forms a 1:1 molecular complex with $HgCl_2$. Replacement of CH_3 by CH_2CH_3 for the terminal groups causes a remarkable change in the symmetry of the unit cell: that is, the TGM–$HgCl_2$ complex has a monoclinic unit cell, while the TGE–$HgCl_2$ complex has a cubic unit cell. The occurrence of the cubic unit cell for the complex may be noticeable because, generally speaking, only simple or highly symmetric molecules form a cubic unit cell. In the present paper the structure of the TGE–$HgCl_2$ complex is described.

Experimental

Samples. TGE was synthesized according to the method of Fordyce, Lovell, and Hibbert.[2] The synthesized TGE was purified by distillation, the purity being checked by means of gas chromatography.

Crystals of TGE–$HgCl_2$ were prepared in the same way as for TGM–$HgCl_2$.[1] The crystal is transparent; the melting point is 88°C as determined microscopically. The density of the crystal was measured by the flotation method with the use of a liquid mixture of CCl_4 and $CHBr_3$ as the flotation medium. The observed density was 1.76 g/cc. The composition was found to be TGE: $HgCl_2$=1:1 by elemental analysis (Found: Hg, 38.3%. Calcd for the 1:1 complex: Hg, 38.2%).

Unit Cell and Space Group. At first the unit cell was mistaken as monoclinic but more detailed investigation revealed that the crystal has a three-fold symmetry axis along the direction perpendicular to the axis around which X-ray photographs were taken at an early stage. Finally, it was found that the unit cell is cubic. The unit cell para-

Table 1. Crystallographic and physical data of the TGE–$HgCl_2$ complex

Formula	$CH_3CH_2O(CH_2CH_2O)_4CH_2CH_3\cdot HgCl_2$
MW	521.7
Mp	88 °C
Crystal system	cubic
Space group	Pa3-T_h^6
a	12.54 Å
Z	4
Vol.	1971.9 Å^3
D_c	1.76 g/cc
D_m	1.76 g/cc
μ (Cu$K\alpha$)	177.8 cm^{-1}
F(000)	1008

1) R. Iwamoto, This Bulletin, **46**, 1114 (1973).

2) R. Fordyce, E. L. Lövell, and H. Hibbert, *J. Amer. Chem. Soc.*, **61**, 1095 (1939).

meter was measured by a powder camera with diameter of 11.46 cm and calibrated with silicon powder. The crystallographic data are given in Table 1, together with some physical constants. The assumption that the unit cell contains four molecules of both TGE and $HgCl_2$ gives the calculated density of 1.76 g/cc, which is reasonable as regards the observed density of 1.76 g/cc. The systematic absences observed are $h0l$ with l odd, $hk0$ with h odd, and $0kl$ with k odd. The space group is, therefore, $Pa3\text{-}T_h^6$.

Intensity Measurement. X-Ray diffraction photographs of the complex crystal were taken by using Cu$K\alpha$ radiation. The crystal used were about 0.2 mm × 0.2 mm × 0.2 mm. Intensity data of the complex were recorded on photographs, using equi-inclination Weissenberg multiple film method, around the [110] direction from the equator to the fifth layer line. The number of recorded reflections having non-zero intensities was 200. The intensities were measured by visual comparison with standard scales. Although the absorption coefficient ($\mu = 178\ cm^{-1}$ for Cu$K\alpha$ radiation) is large, the intensity data were not corrected for absorption. They were corrected only for Lorentz and polarization factors. The smallest possible crystals were used for collecting diffraction intensities. The crystal used for collection of intensity data was renewed for each layer line.

Infrared Measurement. Infrared spectra of the TGE–$HgCl_2$ and related complexes were measured by the Nujol mull method with a Japan Spectroscopic Co., Ltd. model IR-G and 402G infrared spectrometers.[3]

Structure Determination

Reflections having indices hkl with $h+k$ even, $k+l$ even, and $h+l$ even are selectively very strong and reflections of other indices are, in general, quite weak. These strong reflections decrease in intensity apparently only with increasing $\sin\theta/\lambda$. Since the general feature of the diffraction pattern was supposed to be regulated by the atomic position of Hg, the characteristic feature led to the conclusion that the four Hg atoms are located at such special positions as 0,0,0; 0,1/2,1/2; 1/2,0,1/2; 1/2,1/2,0. Thus, the contribution of the Hg atoms to a reflection having an index, hkl, is as follows.

$$F(hkl)_{Hg} = 4f_{Hg}(hkl)$$

for hkl with h even, k even, and l even, and

$$F(hkl)_{Hg} = -4f_{Hg}(hkl)$$

for hkl with h odd, k odd, and l odd. Thus, the Hg atoms do not interfere with each other among themselves for these reflections but contribute to them to their full scattering power, making the contribution of the Hg atoms to intensities of these reflections overwhelming as compared with that of the C and O atoms of TGE. The atomic position of Cl was easily determined by the Fourier method. However, due to the dominant contribution of the Hg atom, it was not possible to determine the atomic positions of the C and O atoms by the heavy atom method. Therefore, the conformation of the TGE molecule and the arrangement of the molecules in the crystal lattice was assumed by referring to the TGM–$HgCl_2$ complex[1] as described below.

In the first place, it seems reasonable to assume the following conformation of TGE which is similar to that of TGM[1];

$$CH_3\text{-}CH_2\text{-}O\text{-}CH_2\text{-}CH_2\text{-}O\text{-}CH_2\text{-}CH_2\text{-}O\text{-}CH_2\text{-}CH_2\text{-}O\text{-}CH_2\text{-}CH_2\text{-}O\text{-}CH_2\text{-}CH_3$$
$$T\ T\quad G\quad T\ T\quad \bar{G}\quad T\ T\quad G\quad T\ T\qquad \bar{G}\quad T\ T$$

However, this model gives the very short interatomic distance of 2.2 Å between the two C atoms of the terminal CH_3 groups. To overcome the difficulty, one of the internal rotation angles about the terminal CH_2–O bonds was changed to a gauche form (−80°) by referring to the angles of the *gauche* CH_2–O bond in the $CH_3CH_2O(CH_2CH_2O)_6CH_2CH_3$ (HGE)[4] and PEO of type II[5] in the complexes with $HgCl_2$ so that the molecular model gave reasonable distances between the terminal groups. The assumed model is shown in Fig. 1 for which the conformation of the bonds along the chain can be given approximately by

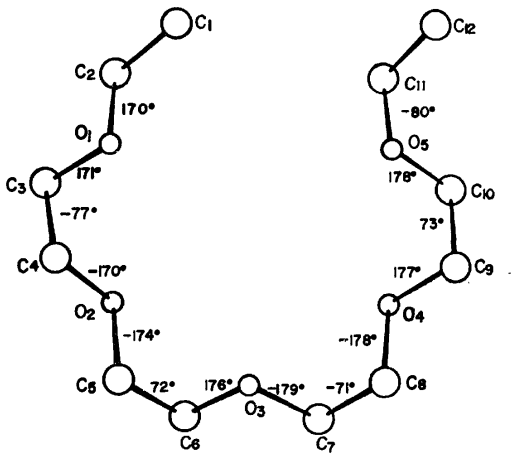

Fig. 1. The adopted molecular model for TGE in the complex.

$$CH_3\text{-}CH_2\text{-}O\text{-}CH_2\text{-}CH_2\text{-}O\text{-}CH_2\text{-}CH_2\text{-}O\text{-}CH_2\text{-}CH_2\text{-}O\text{-}CH_2\text{-}CH_2\text{-}O\text{-}CH_2\text{-}CH_3$$
$$T\ T\quad G\quad T\ T\quad \bar{G}\quad T\ T\quad G\quad T\ T\qquad \bar{G}\quad T\ G$$

For this model, the nearest distance between C_1 and

Table 2. Molecular constants for the adopted molecular model of the TGE molecule

C_1–C_2	1.54Å	C_1–C_2–O_1	109.5°	C_1–C_2–O_1–C_3	170°
C_2–O_1	1.47	C_2–O_1–C_3	108.3	C_2–O_1–C_3–C_4	171
O_1–C_3	1.40	O_1–C_3–C_4	101.7	O_1–C_3–C_4–O_2	−77
C_3–C_4	1.58	C_3–C_4–O_2	108.3	C_3–C_4–O_2–C_5	−170
C_4–O_2	1.44	C_4–O_2–C_5	113.9	C_4–O_2–C_5–C_6	−174
O_2–C_5	1.45	O_2–C_5–C_6	109.6	O_2–C_5–C_6–O_3	72
C_5–C_6	1.50	C_5–C_6–O_3	106.7	C_5–C_6–O_3–C_7	176
C_6–O_3	1.37	C_6–O_3–C_7	113.2	C_6–O_3–C_7–C_8	−179
O_3–C_7	1.44	O_3–C_7–C_8	109.7	O_3–C_7–C_8–O_4	−71
C_7–C_8	1.52	C_7–C_8–O_4	104.4	C_7–C_8–O_4–C_9	−178
C_8–O_4	1.51	C_8–O_4–C_9	106.8	C_8–O_4–C_9–C_{10}	177
O_4–C_9	1.50	O_4–C_9–C_{10}	97.4	O_4–C_9–C_{10}–O_5	73
C_9–C_{10}	1.62	C_9–C_{10}–O_5	108.4	C_9–C_{10}–O_5–C_{11}	178
C_{10}–O_5	1.38	C_{10}–O_5–C_{11}	113.2	C_{10}–O_5–C_{11}–C_{12}	−80
O_5–C_{11}	1.44	O_5–C_{11}–C_{12}	109.5		
C_{11}–C_{12}	1.54				

3) Infrared spectra at low temperature were measured by the courtesy of Professor H. Tadokoro and Mr. S. Ishikawa, Osaka University.

4) R. Iwamoto, This Bulletin, **46**, 1123 (1973).

5) M. Yokoyama, H. Ishihara, R. Iwamoto, and H. Tadokoro, *Macromolecules*, **2**, 184 (1969).

C_{11} is 3.84 Å (for the numbering of atoms, see Fig. 1). This value may be allowable in comparison with the van der Waals distance, 4.0 Å. The assumed molecular dimensions are listed in Table 2 and were taken from those of TGM–$HgCl_2$[1] except for the terminal C–C bonds.

Next, we have to consider the arrangement of the TGE molecules in the crystal lattice. By analogy with the case of TGM–$HgCl_2$,[1] it was assumed that the TGE molecule encloses one $HgCl_2$ molecule with nearly equal interatomic distances between Hg and five O atoms. The atomic parameters of the atoms were determined in the following way.

First, a Cartesian right-handed coordinate system fixed to the molecule was assumed and is denoted by X^m. In this coordinate system the x axis is along the first bond and the y axis is in the plane of the first and second bonds and perpendicular to the x axis. The z axis was chosen so as to be perpendicular to the x and y axes and to make the right-handed system. Here, a dummy oxygen atom was assumed to be bonded to the first C atom with the bond length of 1.43 Å, bond angle of 109°28′ and internal rotation angle of 70°. This was chosen to facilitate the setting of the origin of the following X_0^m coordinate system at the position equidistant from the five oxygen atoms. The dummy atom is denoted by O_0.

Secondly, the coordinate system X^m was transformed into the other Cartesian coordinate system X_0^m fixed to the molecule. In this system, the z axis was set along the direction of the following vector.

$$\overrightarrow{O_0O_1} \times \overrightarrow{O_1O_2} + \overrightarrow{O_1O_2} \times \overrightarrow{O_2O_3} + \overrightarrow{O_2O_3} \times \overrightarrow{O_3O_4} + \overrightarrow{O_3O_4} \times \overrightarrow{O_4O_5} + \overrightarrow{O_4O_5} \times \overrightarrow{O_5O_0} + \overrightarrow{O_5O_0} \times \overrightarrow{O_0O_1},$$

where O_i is the ith oxygen atom and each vector product $O_{i-1}O_i \times O_iO_{i+1}$ was normalized to a unit vector. The origin of the coordinate system was set at the center of gravity of the five oxygen atoms and the dummy atom. The x axis is perpendicular to the plane including the z axis and O_0; that is, it is parallel to the $\overrightarrow{O_gO_0} \times \vec{z}$ direction, where O_g is the center of gravity. The y axis is taken along the $\vec{z} \times \vec{x}$ direction as shown in Fig. 2.

Finally the X_0^m was transformed into the coordinate system fixed to the crystal lattice so that the molecular axis (z axis) is along [111] as shown in Fig. 3, where the TGE molecule was simply drawn around the $HgCl_2$ molecule located at the origin. This transformation was made according to the transformation matrix expressed by the Eulerian angles. The rotation angle around [111] is denoted by χ.

Figure 4 shows some of the symmetry elements existing in the space group Pa3-T_h^6. The Hg atoms are located at the positions having site symmetry $\bar{3}$. Since the TGE molecule enclosing the Hg atom has no symmetry, it should be assumed that the TGE molecules are rotated statistically around the Cl–Hg–Cl direction in order to satisfy the site symmetry. Figure

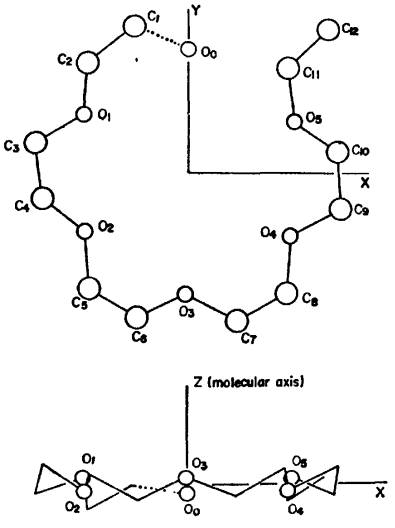

Fig. 2. Molecular coordinate system for the TGE molecule. The dummy atom O_0 was assumed to be bonded to C_1 in order to set the origin at the equi-distant position from the five oxygen atoms.

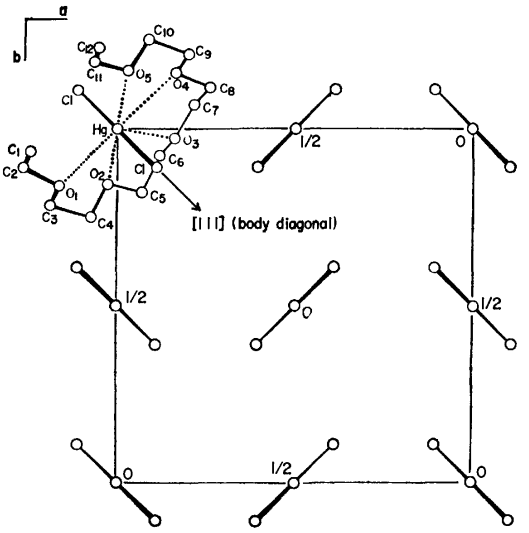

Fig. 3. Molecular arrangement of the TGE molecule in the complex crystal. Only one molecule around $HgCl_2$ at the origin is shown for simplicity.

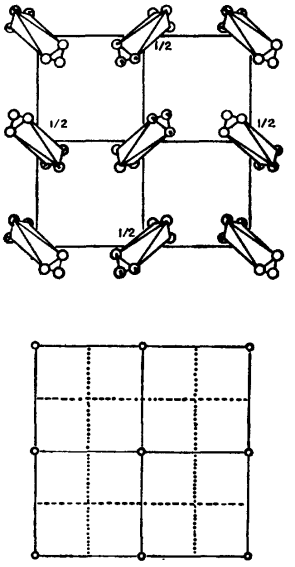

Fig. 4. Some of the symmetry elements in the space group Pa3–T_h^6.

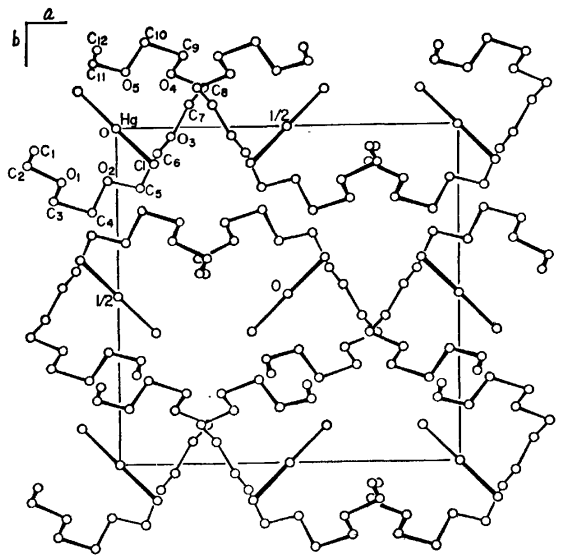

Fig. 5. Crystal structure of the TGE-$HgCl_2$ complex. The statistical arrangement of TGE molecules in the crystal lattice is not drawn for simplicity.

5 shows the crystal structure of the complex. However, the statistical arrangement of the TGE molecule is not shown in order to avoid complication of the figure. Structure factors of the TGE–$HgCl_2$ complex were calculated on the basis of the atomic coordinates deduced above assuming the statistical structure. It was found that the R factor ($\sum||F_o|-|F_c||/\sum|F_o|$) varies with χ. From this dependence the χ angle of 115° was found most reasonable.

Least squares refinement of isotropic approximation was applied to all the atoms except hydrogen and the resulting R factor was 11.0%. However, the resulting molecular dimensions for the TGE molecule were so distorted that they were not allowable in comparison with the ordinary bond lengths and angles. The atomic coordinates for TGE were, then, fixed and the least squared method was applied to the Hg and Cl atoms only, the resulting R factor being 12.3%. The $HgCl_2$ molecule was assumed to be linear. The atomic coordinates are given in Table 3.

Table 3. Atomic coordinates and temperature factors in the TGE–$HgCl_2$ complex

Atom	x	y	z	B
Hg	0.0	0.0	0.0	5.44 Å^2
Cl	0.1081	0.1081	0.1081	6.30
C_1	0.0627	−0.2414	0.1778	6.0
C_2	0.1101	−0.2611	0.0662	6.0
O_1	0.1609	−0.1625	0.0272	6.0
C_3	0.2185	−0.1869	−0.0647	6.0
C_4	0.2503	−0.0725	−0.1059	6.0
O_2	0.1582	−0.0255	−0.1561	6.0
C_5	0.1811	0.0723	−0.2136	6.0
C_6	0.0786	0.1212	−0.2519	6.0
O_3	0.0283	0.1619	−0.1637	6.0
C_7	−0.0686	0.2178	−0.1888	6.0
C_8	−0.1177	0.2619	−0.0872	6.0
O_4	−0.1575	0.1644	−0.0286	6.0
C_9	−0.2107	0.2034	0.0708	6.0
C_{10}	−0.2502	0.0888	0.1144	6.0
O_5	−0.1626	0.0339	0.1521	6.0
C_{11}	−0.1891	−0.0686	0.1971	6.0
C_{12}	−0.2317	−0.0534	0.3113	6.0

Discussion

Since it is not possible to determine the atomic positions of the C and O atoms directly by the heavy atom method, it is necessary to consider whether the adopted molecular model is reasonable.

Since the composition (TGE: $HgCl_2$) of the complex is 1 : 1 and all the four $HgCl_2$ molecules contained in the unit cell are symmetrically equivalent, one TGE molecule should enclose one $HgCl_2$ molecule. In the HGE–$HgCl_2$,[4] each half part of the HGE molecule enclosing one $HgCl_2$ has the conformation

$$\underset{T}{CH_3}-\underset{T}{CH_2}-O-\underset{G}{CH_2}-\underset{T}{CH_2}-O-\underset{G}{CH_2}-\underset{T}{CH_2}-O-\underset{G}{CH_2}-\underset{G}{CH_2}-O-.$$

It should be noted that this conformation and the spatial configuration are very similar to those of TGM in the complex,[1] indicating that the conformation is very stable and favorable to form coordination between the O and Hg atoms. Therefore, it seems reasonable to assume essentially the same conformation of TGE for TGM except for the terminal groups to which a *gauche* CH_2–O bond is assigned in order to avoid too close approach between the terminal groups.

Improvement of the R factor by 4% (from 16.4 to 12.3) by taking into account the TGE molecule having the adopted molecular conformation might indicate that the molecular model and the arrangement are reasonable. Although the 4% improvement for the TGE–$HgCl_2$ is smaller in comparison with 6% for the TGM–$HgCl_2$,[1] this may be accounted for by the fact that in the former complex the Hg atoms are located at special positions and contribute much more greatly to structure factors, while in the latter complex they are located at general positions.

In the present structure, the TGE molecule must be located around the position whose site symmetry is $\bar{3}$. However, the molecule does not have any symmetry and the statistical structure must be assumed, in which the six molecules having the structure shown in Fig. 1

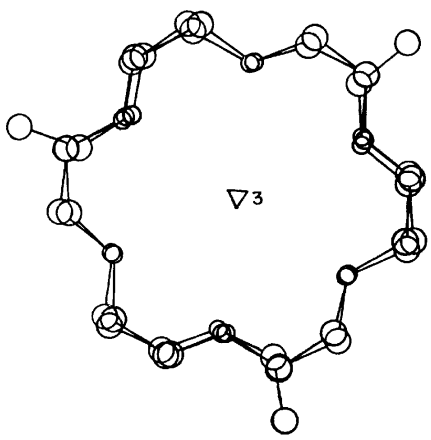

Fig. 6. Statistical sructure having the symmetry 3 produced by the three molecules of TGE.

are arranged around the Hg atom with the weight of 1/6 for each molecule, satisfying symmetry 3. Figure 6 shows the statistical arrangement in which the three TGE molecules are arranged so as to produce symmetry 3. In order to give the statistical arrangement having the $\bar{3}$ symmetry, another of these molecules related by $\bar{1}$ at the position of Hg should be superposed in the figure. It should be noticed that the molecules generated by the symmetry operation 3 coincide approximately with the original molecule if the molecular ends are neglected.

In the adopted molecular model of Fig. 1, a *gauche* form was fixed to the O_5–C_{11} bond in order to avoid the intramolecular steric hindrance, but there is no necessity of assigning the gauche CH_2–O bond to the O_5–C_{11} bond. Any CH_2–O bond of the TGE molecule can be *gauche* and furthermore there is a possibility that the *gauche* CH_2–O bond can move from time to time through the whole molecule; that is, the *gauche* CH_2–O bond may be delocalized over the whole molecule. The delocalization of the *gauche* CH_2–O bond may give rise to vigorous molecular motion of the TGE molecule around the Hg atom. Evidence of some kind of molecular motion is shown by the temperature dependence of the infrared spectra as discussed below. Combination of the molecular model in which the *gauche* CH_2–O bond moves through the whole molecule with time and the molecular motion around the Hg atom may produce the apparent site symmetry, $\bar{3}$, observed for the TGE–$HgCl_2$ complex.

Figure 7 shows infrared spectra of the TGE–$HgCl_2$ at room temperature and at a low temperature (liquid nitrogen). Absorption bands, even if they are weak or have shoulders at room temperature, become strikingly sharp and well-defined at low temperature in the whole region. On the other hand, for TGM–$HgCl_2$, temperature dependence of the infrared spectrum (Fig. 8) is not so marked as in the former. It should be noted that, although the nature of the spectral change in TGE–$HgCl_2$ is not clear, each absorption corresponds well between the two temperatures, even if some bands are very weak or have shoulders at room temperature.

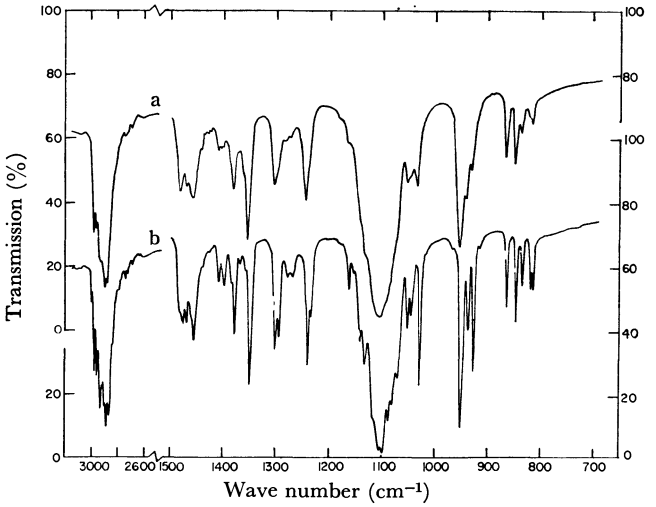

Fig. 7. Infrared spectra of the TGE–$HgCl_2$ complex at (a) room temperature and (b) a low temperature (liquid nitrogen).

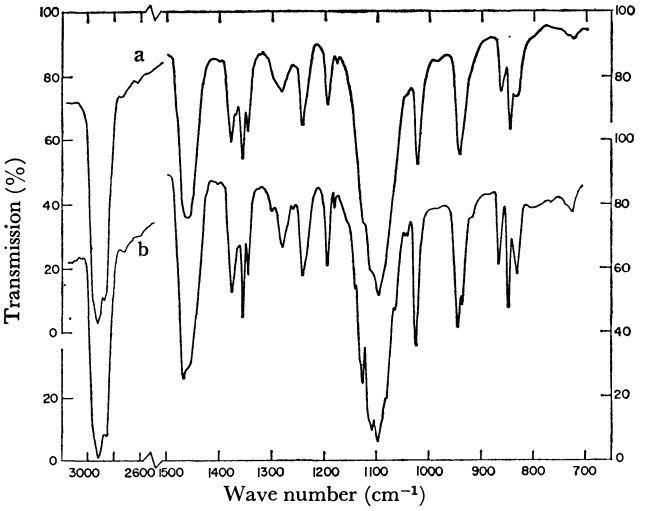

Fig. 8. Infrared spectra of the TGM–$HgCl_2$ complex at (a) room temperature and (b) a low temperature (liquid nitrogen).

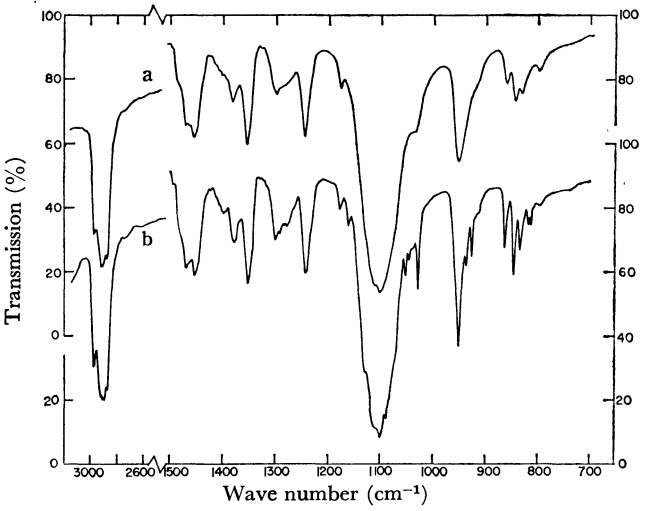

Fig. 9. Infrared spectra of the TGE–$HgBr_2$ complex at (a) room temperature and (b) a low temperature (liquid nitrogen).

Consequently, the observed spectral change is due to a molecular motion but not to a conformational change of the TGE molecule.

A similar spectral change is observed for the $HgBr_2$ complex of TGE as shown in Fig. 9, which has a monoclinic unit cell. The infrared spectrum of the TGE–$HgBr_2$ becomes sharp and well-defined at low temperature as observed in the $HgCl_2$ complex. Since it is considered that a TGE molecule encloses one Hg atom in TGE–$HgBr_2$, the same kind of intramolecular steric hindrance must occur between the terminal groups as was found in TGE–$HgCl_2$. These observations lead to the conclusion that too close approach between the terminal groups causes some kind of molecular motion of the chain in the complex crystal.

Since the $HgCl_2$ molecule is bent by 4—5° from the linear form both in the cases of TGM–$HgCl_2$ and HGE–$HgCl_2$,[1,4] it may be reasonable to consider that the $HgCl_2$ molecule is also deviated from the linear form in TGE–$HgCl_2$. This study gave no conclusive information as to whether the molecule is bent or not,

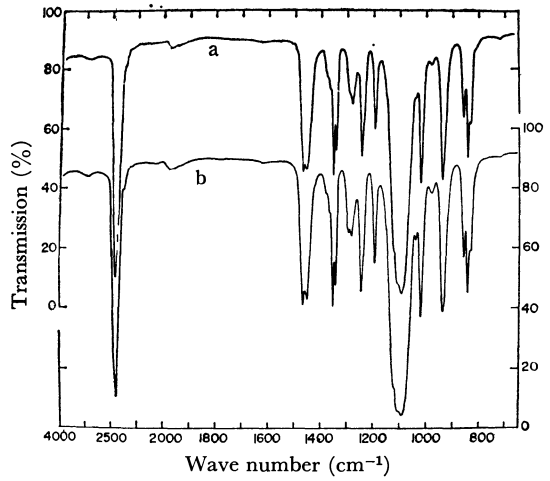

Fig. 10. Infrared spectra of (a) $HgCl_2$ and (b) $HgBr_2$ complexes of TGM at room temperature.

although the R factor was slightly improved for the structure having the bent $HgCl_2$.

It is interesting to note that the complex consisting of such fairly complicated molecules as TGE and $HgCl_2$ forms a cubic unit cell, while the $HgBr_2$ complex which should have the same situation as the $HgCl_2$ complex with respect to the intramolecular steric hindrance of the TGE molecule, has a monoclinic unit cell. The infrared spectrum of the TGE–$HgBr_2$ (Fig. 9) is similar to that of the $HgCl_2$ complex as a whole but they differ to some extent in detail in the whole region. On the other hand, the infrared spectra of the $HgCl_2$ and $HgBr_2$ complexes of TGM are quite the same in detail as shown in Fig. 10 but their unit cells differ. Therefore, the observed spectral difference between the $HgCl_2$ and $HgBr_2$ complexes of TGE must be closely correlated with the occurrence of the cubic unit cell for the $HgCl_2$ complex.

The author would like to thank Professor H. Tadokoro, Dr. Y. Chatani, and Dr. M. Kobayashi, Osaka University, for their helpful discussions and encouragement. He is much indebted to Mr. A. Ueda of Nippon Zeon Co., Ltd. for his valuable assistance in the synthesis of TGE, and also grateful to Dr. S. Kuribayashi of this Institute for his helpful discussions.

BULLETIN OF THE CHEMICAL SOCIETY OF JAPAN, VOL. 46, 1123—1127 (1973)

Structure of Ethylene Oxide Oligomer Complexes. III. A 1:2 Complex of Hexaethylene Glycol Diethyl Ether with Mercuric Chloride

Reikichi IWAMOTO

Government Industrial Research Institute, Osaka, Midorigaoka, Ikeda, Osaka 563

(Received March 24, 1972)

Molecular and crystal structure of a 1 : 2 complex of hexaethylene glycol diethyl ether $CH_3CH_2O(CH_2CH_2O)_6CH_2CH_3$ (HGE) with $HgCl_2$ has been determined by means of X-ray diffraction. The unit cell is monoclinic with $a=23.34$, $b=7.84$, $c=16.69$ Å, and $\beta=115.0°$. The space group is C2/c. The unit cell contains four HGE and eight $HgCl_2$ molecules. The HGE molecule in the complex has the conformation

$$CH_3\text{-}\underset{T}{CH_2}\text{-}\underset{T}{O}\text{-}\underset{G}{CH_2}\text{-}\underset{T}{CH_2}\text{-}\underset{T}{O}\text{-}\underset{\bar{G}}{CH_2}\text{-}\underset{T}{CH_2}\text{-}\underset{T}{O}\text{-}\underset{G}{CH_2}\text{-}\underset{G}{CH_2}\text{-}\underset{G}{O}\text{-}\underset{G}{CH_2}\text{-}\underset{T}{CH_2}\text{-}\underset{T}{O}\text{-}\underset{\bar{G}}{CH_2}\text{-}\underset{T}{CH_2}\text{-}\underset{T}{O}\text{-}\underset{G}{CH_2}\text{-}\underset{T}{CH_2}\text{-}\underset{T}{O}\text{-}CH_2\text{-}CH_3,$$

where T, G, and $\bar{G}$ denote *trans*, *gauche*, and minus *gauche*, respectively, two $HgCl_2$ molecules being coordinated with one HGE molecule. The asymmetric unit consists of a half of HGE and one $HgCl_2$ molecule. The four oxygen atoms of either half of HGE, which are coplanar, are coordinated with one Hg atom with close interatomic distances (2.66—2.91 Å) between the O and Hg atoms, the central oxygen atom of HGE being coordinated with two Hg atoms. The $HgCl_2$ molecule is distorted from the linear form by 4°.

Structures of the molecular complexes of tetraethylene glycol dimethyl ether $CH_3O(CH_2CH_2O)_4CH_3$ (TGM) and tetraethylene glycol diethyl ether $CH_3CH_2O(CH_2CH_2O)_4CH_2CH_3$ (TGE) with $HgCl_2$ were reported in previous papers.[1,2] It has been found that TGE is the limiting case in which one TGE molecule encloses one $HgCl_2$ without drastic change of the molecular conformation consisting of a succession of $\underset{T}{CH_2}\text{-}\underset{G}{CH_2}\text{-}\underset{T}{O}\text{-}\underset{\bar{G}}{CH_2}\text{-}\underset{T}{CH_2}\text{-}O$-. The present paper deals with the complex of hexaethylene glycol diethyl ether $CH_3CH_2O(CH_2CH_2O)_6CH_2CH_3$ (HGE) with $HgCl_2$.

1) R. Iwamoto, This Bulletin, **46**, 1114 (1973).
2) R. Iwamoto, *ibid.*, **46**, 1118 (1973).

Experimental

Samples. HGE was synthesized according to the method of Fordyce *et al.*[3] The synthesized HGE was purified by distillation and the purity was checked by gas chromatography.

The crystalline complex with $HgCl_2$ was prepared in quite the same way as the TGM–$HgCl_2$ complex.[1] The crystal is transparent and long along the *b* axis. The melting point was found to be 103°C by microscopy. The density of the crystal was measured by the flotation method with the use of a liquid mixture of $CHBr_3$ and CCl_4 as flotation medium.

3) R. Fordyce, E. L. Lovell, and H. Hibbert, *J. Amer. Chem. Soc.*, **61**, 1905 (1939).

The observed value was 2.13 g/cc. From elemental analysis with respect to Hg, the composition was found to be HGE: $HgCl_2$=1:2 (Found: Hg, 46.4%. Calcd for the 1:2 complex: Hg, 45.6%).

Unit Cell and Space Group. The unit cell parameters were determined with a Weissenberg camera and calibrated by silicon powder. Systematic absences were observed for *hkl* with $h+k$ odd and *h0l* with *l* odd. From the observed absences the possible space groups were C2/c and Cc, C2/c being finally chosen. The crystallographic data are given in Table 1, together with some physical constants.

Table 1. Crystallographic and physical data of the HGE–$HgCl_2$ complex

Formula	$CH_3CH_2O(CH_2CH_2O)_6CH_2CH_3 \cdot 2HgCl_2$
MW	881.3
Mp	103 °C
Crystal system	monoclinic
Space group	C2/c-C_{2h}^6
a	23.34 Å
b	7.84 Å
c	16.69 Å
β	115.0°
Z	4
Vol.	2767.9 Å
D_c	2.18 g/cc
D_m	2.13 g/cc
μ (Cu$K\alpha$)	256.9 cm^{-1}
F (000)	1656

Intensity Measurement. The X-ray diffraction photographs were taken by use of Cu$K\alpha$ radiation. The crystals used were about 0.2 mm×0.3 mm×0.2 mm in size. Intensity data were collected around the *b* axis from k=0 to 4 layer lines by equi-inclination Weissenberg multiple film method, the number of the observed reflections being 1491. The intensities were measured by visual comparison with standard scales. Intensity data were corrected only for Lorentz and polarization factors, although the absorption coefficient is very large (μ=257 cm^{-1} for Cu$K\alpha$ radiation). The smallest possible crystal was used for collecting the intensity data and was renewed for each layer line because of its decomposition under irradiation of X-rays.

Structure Determination

The atomic positions of the Hg and Cl atoms were easily determined by the Patterson method. The Patterson map showed strong peaks due to Hg at v=0.0. This suggested that the crystal lattice should have a two-fold symmetry axis along the *b* axis and the space group should be C2/c. Based upon the atomic positions of the Hg and Cl atoms, the atomic positions for all the C and O atoms of HGE, the asymmetric unit of which is a half, were determined by the difference Fourier method. Calculation of structure factors and the Fourier synthesis were made according to the space group C2/c. The results were quite reasonable. The space group was, thus, taken as C2/c. Atomic scattering factors were taken from the *International Table for X-Ray Crystallogrphy* (1962).

The atomic coordinates and temperature factors for all the atoms except hydrogen were refined by the least squares method of isotropic and diagonal approximation. The least squares method improved the *R* factor ($\Sigma||F_o|-|F_c||/\Sigma|F_o|$) to 14.0%. The resulting atomic coordinates and temperature factors are given in Table 2, and the molecular dimensions in Table 3.

Table 2. Atomic coordinates and temperature factors in the HGE–$HgCl_2$ complex

Atom	*x*	*y*	*z*	*B*
Hg	0.0844	0.0693	0.2487	3.76Å²
Cl_1	0.0008	0.2156	0.1419	4.40
Cl_2	0.1653	−0.0761	0.3635	4.55
O_1	0.0	−0.2002	0.2500	3.96
C_1	−0.0224	−0.3062	0.1678	4.64
C_2	0.0376	−0.3466	0.1461	3.86
O_2	0.0537	−0.1720	0.1221	4.09
C_3	0.1090	−0.1989	0.0936	5.02
C_4	0.1155	−0.0220	0.0591	4.27
O_3	0.1368	0.0736	0.1380	4.58
C_5	0.1540	0.2676	0.1163	5.88
C_6	0.1975	0.3324	0.2048	5.62
O_4	0.1689	0.3559	0.2693	4.56
C_7	0.2143	0.3954	0.3570	6.60
C_8	0.1747	0.4021	0.4177	6.20

Table 3. Bond lengths and bond angles in the HGE–$HgCl_2$ complex

Hg–Cl_1	2.298Å	Cl_1–Hg–Cl_2	175.9°
Hg–Cl_2	2.319	C_1'–O_1–C_1	111.2
O_1–C_1	1.47	O_1–C_1–C_2	107.6
C_1–C_2	1.61	C_1–C_2–O_2	102.2
C_2–O_2	1.51	C_2–O_2–C_3	106.4
O_2–C_3	1.56	O_2–C_3–C_4	102.1
C_3–C_4	1.53	C_3–C_4–O_3	104.1
C_4–O_3	1.40	C_4–O_3–C_5	111.9
O_3–C_5	1.59	O_3–C_5–C_6	102.0
C_5–C_6	1.46	C_5–C_6–O_4	114.3
C_6–O_4	1.48	C_6–O_4–C_7	112.2
O_4–C_7	1.41	O_4–C_7–C_8	104.4
C_7–C_8	1.62		

Results and Discussion

Figure 1 shows the crystal structure of the HGE–$HgCl_2$ complex. Table 4 gives the internal rotation angles for each bond of the asymmetric unit of the molecule. The CH_2–CH_2 bonds are approximately *gauche* (67—77°) and the CH_2–O bonds are nearly *trans* (169—176°) with the exception of the *gauche* CH_2–O bonds located at the center of the molecule, the angle of which is 88° and considerably deviated from the ordinary *gauche* angle. The conformation of the whole molecule is then denoted by

$$CH_3\text{-}\underset{T}{CH_2}\text{-}O\text{-}\underset{T}{CH_2}\text{-}\underset{G}{CH_2}\text{-}O\text{-}\underset{\bar{G}}{CH_2}\text{-}\underset{T}{CH_2}\text{-}O\text{-}\underset{T}{CH_2}\text{-}\underset{G}{CH_2}\text{-}O\text{-}$$

$$\underset{G}{CH_2}\text{-}\underset{T}{CH_2}\text{-}O\text{-}\underset{T}{CH_2}\text{-}\underset{\bar{G}}{CH_2}\text{-}O\text{-}\underset{T}{CH_2}\text{-}\underset{G}{CH_2}\text{-}O\text{-}\underset{T}{CH_2}\text{-}CH_3.$$

The HGE molecule encloses two $HgCl_2$ molecules in the way shown in Figs. 2 and 3, having the two-fold symmetry axis passing through the central O_1 atom. It should be noted that each half of HGE enclosing

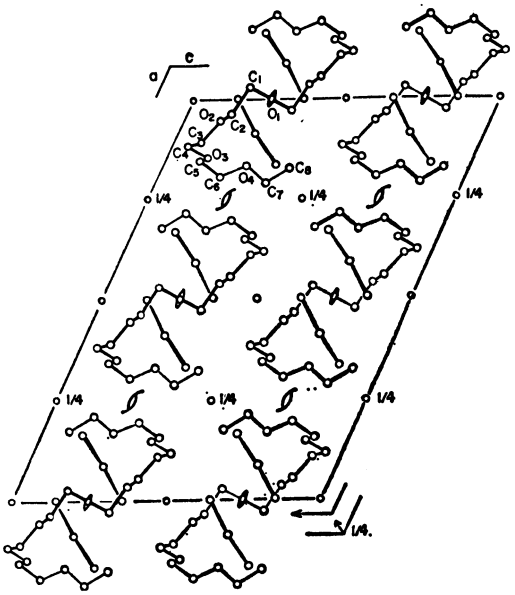

Fig. 1. Crystal structure of the HGE-$HgCl_2$ complex.

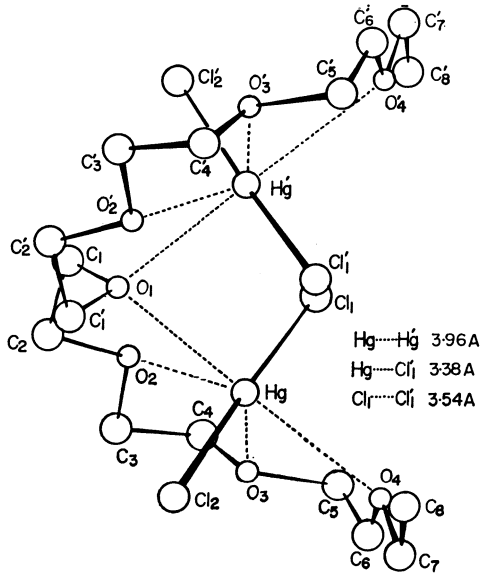

Fig. 3. Structure of one pair of the HGE-$HgCl_2$ complex projected along the *c* axis.

Table 4. Internal rotation angles for the HGE molecule in the complex

C_1'–O_1–C_1–C_2	−88°
O_1–C_1–C_2–O_2	−67
C_1–C_2–O_2–C_3	−176
C_2–O_2–C_3–C_4	173
O_2–C_3–C_4–O_3	77
C_3–C_4–O_3–C_5	−176
C_4–O_3–C_5–C_6	−169
O_3–C_5–C_6–O_4	−74
C_5–C_6–O_4–C_7	172
C_6–O_4–C_7–C_8	−176

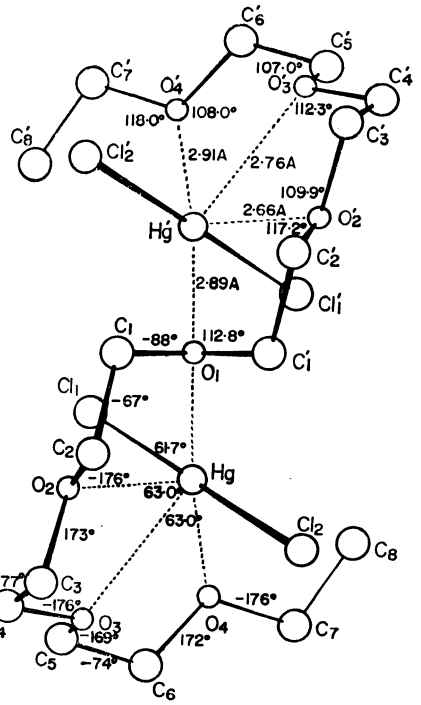

Fig. 2. Structure of one pair of the HGE-$HgCl_2$ complex projected on the *ac* plane.

one $HgCl_2$ consists of a sequence of the conformation $-\underset{T}{CH_2}-\underset{G}{CH_2}-O-\underset{T}{CH_2}-\underset{T}{CH_2}-\underset{G}{CH_2}-O-\underset{T}{CH_2}-$ as found in the TGM-$HgCl_2$[1] but the central part of HGE combining the two halves has the conformation $-\underset{T}{CH_2}-\underset{G}{CH_2}-\underset{G}{O}-\underset{G}{CH_2}-\underset{G}{CH_2}-O-\underset{T}{CH_2}-$.

Table 5. Interatomic distances and angles for non-bonded atoms in the HGE–HgCl complex

O_1··Hg··O_2	61.7°	Hg··O_1	2.89Å
O_2··Hg··O_3	63.0	Hg··O_2	2.66
O_2··Hg··O_4	63.0	Hg··O_3	2.76
		Hg··O_4	2.91
Cl_1–Hg··O_1	90.4		
Cl_2–Hg··O_1	87.7	C_1–O_1··Hg	112.8°
Cl_1–Hg··O_2	84.5	C_2–O_2··Hg	117.2
Cl_2–Hg··O_2	97.8	C_3–O_2··Hg	109.9
Cl_1–Hg··O_3	90.7	C_4–O_3··Hg	112.3
Cl_2–Hg··O_3	93.3	C_5–O_3··Hg	107.0
Cl_1–Hg··O_4	91.1	C_6–O_4··Hg	108.0
Cl_2–Hg··O_4	90.3	C_7–O_4··Hg	118.0
		Hg··O_1··Hg	86.3
		Hg··Hg	3.96Å

Table 5 gives the interatomic distances and angles for non-bonded atoms in HGE-$HgCl_2$. The four oxygen atoms contained in the half of HGE enclosing one Hg atom are nearly coplanar and the interatomic distances between the O and Hg atoms range from 2.66 to 2.91 Å. The angles O_i···Hg···O_{i+1} are nearly 60° (61.7—63.0°) and the angles C_j–O_i···Hg are nearly a tetrahedral angle. The spatial arrangement of the Hg and O atoms in the part enclosing one $HgCl_2$ is very similar to the case of TGM-$HgCl_2$.[1] In the HGE-$HgCl_2$, genearlly, one oxygen atom is coordinated to one Hg but the O_1 atom only is coordinated with two Hg atoms. It may be considered that the interatomic interactions between the Hg and O atoms

Table 6. Molecular constants of $HgCl_2$, interatomic distances Hg··O, the angles for O··Hg··O and Hg··O··Hg, the number of coordinating oxygen atoms per Hg(N), and the average number of coordination per oxygen atom (M) in the TGM–$HgCl_2$, TGE–$HgCl_2$, HGE–$HgCl_2$, and PEO–$HgCl_2$ complexes

	Hg–Cl (Å)	ClHgCl (°)	Hg··O (Å)	OHgO (°)	HgOHg (°)	N	M
TGM–$HgCl_2$[a]	2.29 2.31	174.2	2.78—2.96	59.9—62.0	—	5	1
TGE–$HgCl_2$[b]	2.35	180 (?)	(2.81—2.91)	(58.7—60.6)	—	5	1
HGE–$HgCl_2$	2.30 2.32	175.9	2.66—2.91	61.7—63.0	86.3	4	8/7
PEO–$HgCl_2$(I)[c]	2.30	176.6	2.62	62.9	—	2	1/2
PEO–$HgCl_2$(II)[d]	2.23 2.25	171.7	2.79	64.0	85.5	2	2
$HgCl_2$[e]	2.23 2.27	180					

a) See Ref. 1. b) See Ref. 2. c) See Ref. 4. d) See Ref. 5. e) See Ref. 6.

must have greater influence on the O_1 atom causing the two CH_2–O bonds involving the O_1 atom to take a *gauche* form.

Table 6 summarizes the molecular constants of $HgCl_2$,Hg···O interatomic distances, the angles for O···Hg···O and Hg···O···Hg, the number of coordination per Hg (N) and the average number of coordination per O (M) in the TGM–$HgCl_2$,[1] TGE–$HgCl_2$,[2] HGE–$HgCl_2$, and polyethylene oxide (PEO)–$HgCl_2$.[4,5] The molecular constants of $HgCl_2$ reveal some differences among these complexes. The longest bond length of Hg–Cl is 2.35 Å in the TGE–$HgCl_2$ and the shortest is 2.23 Å in the PEO–$HgCl_2$ of type II. The two Hg–Cl bonds of $HgCl_2$ are non-equivalent in the TGM–$HgCl_2$, HGE–$HgCl_2$, and PEO–$HgCl_2$ (type II), and they are significantly different in the bond length. The $HgCl_2$ molecule is, in general, deviated from the linear form in the complexes. The angle of the deviation ranges from 3.4 (PEO–$HgCl_2$ of type I) to 8.3° (PEO–$HgCl_2$ of type II). The interatomic distances between the O and Hg atoms are in the 2.66—2.96 Å range and the O···Hg···O angle is in the 59.9—64.0° range for all these complexes. The Hg···O···Hg angle is 86.3 and 85.5° in HGE–$HgCl_2$ and PEO–$HgCl_2$ (type II), respectively. The number of the coordinating oxygen atoms around a Hg atom (N) ranges from 2 to 5 among these complexes.

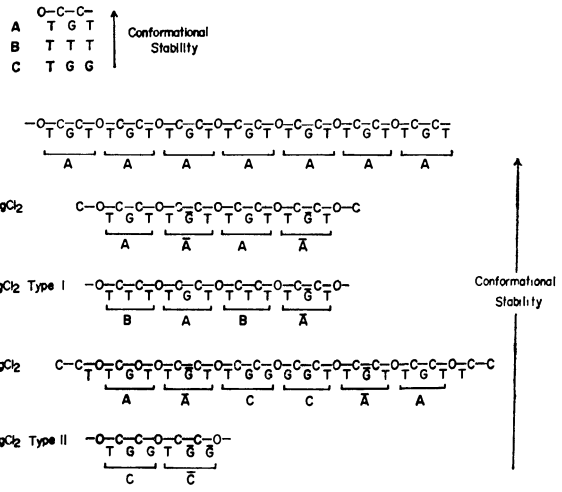

Fig. 4. Molecular conformations of TGM and HGE in the crystalline complex with $HgCl_2$, and of PEO in the ordinary polymer and the complexes with $HgCl_2$.

General Discussion

In the molecular conformations of $RO(CH_2CH_2O)_mR$ and PEO in the complexes with $HgCl_2$,[1,2,4,5] the *gauche* form of the CH_2–CH_2 bond is essentially favorable for coordination between the O and Hg atoms, while the CH_2–O bond takes either a *trans* or a *gauche* form depending on the situation, although the *gauche* form

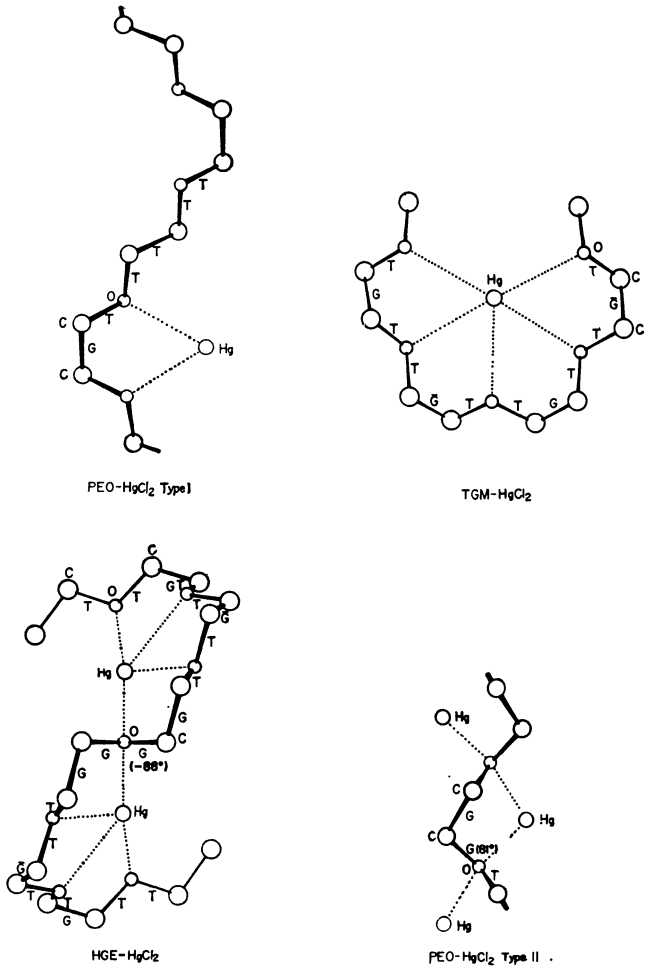

Fig. 5. Way of the interactions between the O and Hg atoms in the TGM–$HgCl_2$, HGE–$HgCl_2$, and PEO–$HgCl_2$ complexes.

4) R. Iwamoto, Y. Saito, H. Ishihara, and H. Tadokoro, *J. Polymer Sci.*, *A-2*, **6**, 1509 (1968).

5) M. Yokoyama, H. Ishihara, R. Iwamoto, and H. Tadokoro, *Macromolecules*, **2**, 184 (1969).

6) H. Bräkken and L. Harang, *Z. Krist.*, **68**, 123 (1928).

is considerably deviated from the ordinary *gauche* angle. These molecular conformations in the complexes may be considered to be governed by two factors: (i) conformational stability of a single chain and (ii) stabilization by the interactions between the O and Hg atoms.

Figure 4 gives the molecular conformations of TGM,[1] HGE in the $HgCl_2$ complexes and of PEO in the pure polymer[7] and the $HgCl_2$ complexes.[4,5] The three possible forms for the $O-CH_2-CH_2-$ group are TGT, TTT, and TGG in the order of conformational stability,[1] and are denoted as types A, B, and C, respectively, as shown in Fig. 4.

PEO in the pure polymer consists of type A only[7] and the TGM molecule is composed of alternations A and $\bar{A}$ ($\bar{A}$: minus A).[1] PEO in the type I complex is composed of A (or $\bar{A}$) and B,[4] and the HGE molecule has the $A\bar{A}CC\bar{A}A$ form. PEO in the type II complex is composed of type C only.[5] Therefore, from the viewpoint of conformational stability, these molecules can be arranged from top to bottom in the order of conformational stability as shown in Fig. 4. PEO in the pure polymer and TGM are the most stable as a single chain, while the PEO molecule in the type II complex is the least stable among these molecules.

The correlation of the conformational stability with the mode of coordination between the O and Hg atoms in the complexes is considered next. Figure 5 gives the way of coordination between the O and Hg atoms in the complexes. The numbers given under *M* in Table 6 indicate the average number of coordination per oxygen atom and are, therefore, a measure of the strength of the interactions between $HgCl_2$ and the oligomer or polymer molecules. In the PEO–$HgCl_2$ of type I,[4] only two of the four oxygen atoms in the fiber identity period are coordinated with one Hg atom and *M* is 1/2. In the case of the TGM–$HgCl_2$[1] all the five oxygen atoms are coordinated with one Hg and *M* is 1. In the HGE–$HgCl_2$, three oxgyen atoms of either half of HGE are coordinated with one Hg atom as in the TGM–$HgCl_2$[1] and the central oxygen atom between the two gauche CH_2-O bonds is coordinated to two Hg atoms, giving 8/7 for *M*. In the PEO–$HgCl_2$ of type II,[5] each oxygen atom is coordinated to two Hg atoms just as the central oxygen atom of HGE and *M* is 2. Thus, the strength of the interactions between ethylene oxide oligomers or polymer and $HgCl_2$ is least effective for the PEO–$HgCl_2$ of type I and most effective for the PEO–$HgCl_2$ of type II, increasing from upper left to down right in Fig. 5.

It is thus found that the less stable conformation has stronger interactions between the O and Hg atoms in the complexes. These interactions might cause the molecule to take a more favorable conformation for coordination between ethylene oxide oligomers or polymer and $HgCl_2$ in the complexes, which is usually less stable as a single chain. Thus, the two factors, conformational stability and stabilization by the interactions between the O and Hg atoms, are very important when we consider the resulting conformation of these molecules.

The author would like to thank Professor H. Tadokoro, Dr. Y. Chatani and Dr. M. Kobayashi, Osaka University, for their helpful discussions and encouragement. He is also much indebted to Mr. A. Ueda of Nippon Zeon Co., Ltd. for his valuable assistance in the synthesis of HGE, and to Dr. S. Kuribayashi of this Institute for his helpful discussions.

7) H. Tadokoro, Y. Chatani, T. Yoshihara, S. Tahara, and S. Murahashi, *Makromol. Chem.*, **73**, 109 (1964).

BULLETIN OF THE CHEMICAL SOCIETY OF JAPAN, VOL. 46, 1127—1129 (1973)

Structure of Ethylene Oxide Oligomer Complexes. IV. Infrared Study of $CH_3O(CH_2CH_2O)_mCH_3$-$HgCl_2$ Complexes

Reikichi IWAMOTO

Government Industrial Research Institute, Osaka, Midorigaoka, Ikeda, Osaka 563

(Received April 15, 1972)

Infrared spectra of $CH_3O(CH_2CH_2O)_mCH_3$ (m=1—4) in their crystalline complexes with $HgCl_2$ have been measured. There is no significant regular variation of band frequencies depending upon m. Molecular conformations of the compounds in the complexes have been concluded to be CH_3-O(T)-CH_2(G)-CH_2(T)-O(T)-CH_2($\bar{G}$)-CH_2(T)-O-CH_3 for m=2 and CH_3-O(T)-CH_2(G)-CH_2(T)-O(T)-CH_2($\bar{G}$)-CH_2(T)-O(T)-CH_2(G)-CH_2(T)-O-CH_3 for m=3 from molecular structures for m=1 and 4.

Molecular and crystal structures of the molecular complexes of $CH_3O(CH_2CH_2O)_4CH_3$,[1] CH_3CH_2O-$(CH_2CH_2O)_4CH_2CH_3$,[2] and $CH_3CH_2O(CH_2CH_2O)_6$-CH_2CH_3[3] with $HgCl_2$ have been studied by means of X-ray diffraction. It has been found that the conformational unit of O(T)-CH_2(G)-CH_2(T)-O(T)-CH_2($\bar{G}$)-CH_2(T)-O is favorable for the coordination between the molecules

1) R. Iwamoto, This Bulletin, **46**, 1114 (1973).
2) R. Iwamoto, *ibid.*, **46**, 1118 (1973).
3) R. Iwamoto, *ibid.*, **46**, 1123 (1973).

and $HgCl_2$. The ethylene oxide oligomer molecules enclose the $HgCl_2$ molecules with close interatomic distances between the Hg and O atoms (2.66—2.97 Å).[1-3]

According to Snyder and Zerbi[4] the molecular conformation of $CH_3OCH_2CH_2OCH_3$ in the crystalline state is of TGT form. In a previous paper,[5] the $CH_3OCH_2CH_2OCH_3$ molecule in the crystalline complex with $HgCl_2$ was concluded to have the TGT form from analogy with the molecular conformation of the $CH_3O(CH_2CH_2O)_4CH_3$–$HgCl_2$ complex[1] and from a comparison of the infrared spectrum of the $CH_3OCH_2CH_2OCH_3$–$HgCl_2$ complex with that of the pure crystalline compound of $CH_3OCH_2CH_2OCH_3$.[4] Therefore, the molecular structures of $CH_3O(CH_2CH_2O)_mCH_3$ for $m=2$ and 3 in the complexes with $HgCl_2$ may be inferred by infrared spectroscopy, since it has been found that the O_T–CH_{2G}–CH_{2T}–O_T–$CH_{2\bar{G}}$–CH_{2T}–O conformation is favorable for coordination between Hg and O in the complexes. From this view-point the infrared spectra of the $CH_3O(CH_2CH_2O)_mCH_3$–$HgCl_2$ complexes have been studied.

Experimental

Commercial $CH_3O(CH_2CH_2O)_mCH_3$ was used (Tokyo Kasei Kogyo Co., Ltd.). Crystalline complexes of these compounds with $HgCl_2$ were prepared by dissolving powdered crystals of $HgCl_2$ in an ethanol solution containing the compounds in volume ratio about 4:1 at 35 °C and by cooling the saturated solution to room temperature. In the case of $CH_3OCH_2CH_2OCH_3$, crystalline powder of $HgCl_2$ was dissolved directly in the pure liquid, the crystalline complex being precipitated in the solution. Infrared spectra were measured by a Japan Spectroscopic Co., Ltd. Model IR-G grating infrared spectrometer by means of Nujol mull method. Frequencies were calibrated by the standard bands of polystyrene.

Table 1. Infrared absorption bands of $CH_3O(CH_2CH_2O)_mCH_3$–$HgCl_2$ complexes in the 1500—700 cm^{-1} region[a]

$m=1$	$m=2$	$m=3$	$m=4$
1472 s	1469 s	1473 m	1471 m
1455 s	1453 s	1455 m	1454 m
1442 sh			
1414 m	1424 vw	1394 vw	1383 vw
1377 sh	1378 m	1382 vw	1370 vw
1371 m	1366 sh	1365 m	1355 m
	1346 m	1350 m	1345 m
1288 m	1283 m	1300 w	1296 w
		1288 m	1285 w
1243 s	1245 m	1250 m	1248 m
1202 sh	1200 m	1201 m	1198 m
1194 s			
1157 m	1160 w	1160 vw, sh	1160 vw, sh
1154 sh			
1123 vs	1129 s	1129 s	1126 s
1091 vs	1101 vs	1106 vs	1112 vs
	1095 sh		
	1078 vs	1085 vs	1096 vs
1064 sh	1051 vs, sh		
1028 m	1029 w	1030 sh	1044 vw
1016 s	1013 s	1023 m	1025 m
982 w		984 w	983 w
	940 m	944 m	943 m
		932 sh	937 sh
			921 sh
852 sh	859 s	861 m	862 m
841 vs	835 m	847 m	848 m
	831 m	834 m	835 m

a) vs: very strong, s: strong, m: medium, w: weak, vw: very weak, sh: shoulder.

Results and Discussion

Infrared spectra of the $CH_3O(CH_2CH_2O)_mCH_3$–$HgCl_2$ ($m=1$—4) complexes in the region 1500—700 cm^{-1} are shown in Fig. 1. The absorption bands are listed in Table 1. The absorption spectra of these complexes are, on the whole, very similar to each other.

The band around 940 cm^{-1} which is not observed for $m=1$ appears as a well-defined and fairly strong band when m is equal to or greater than 2. The band becomes stronger with increasing m, no significant frequency change being observed. The band is observed for crystalline diethyl ether.[4] The band should be characteristic when the chain molecule is composed of a sequence of two or more CH_2CH_2O units. The spectral feature around 850 cm^{-1} changes depending on m until $m=3$. The absorption bands are similar for $m=3$ and 4 in this region. In the other regions, the absorption bands of these complexes correspond to

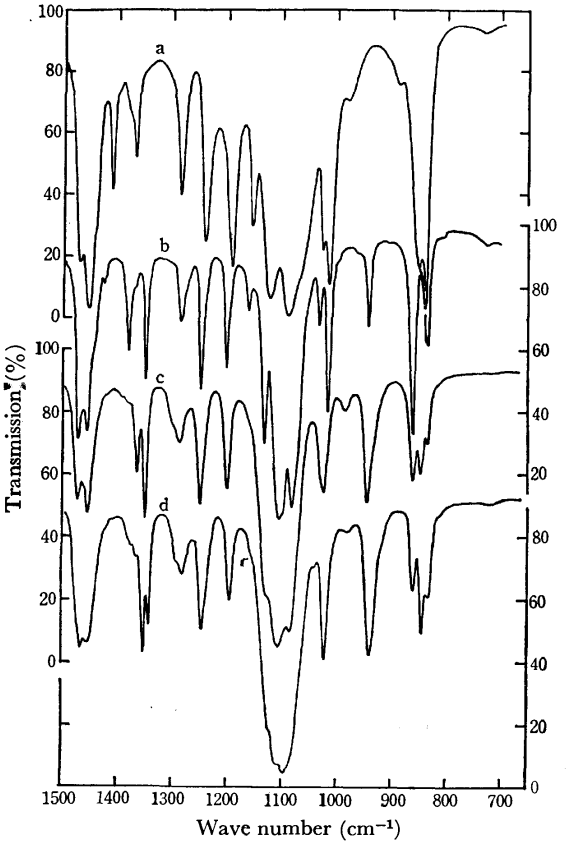

Fig. 1. Infrared spectra of $CH_3O(CH_2CH_2O)_mCH_3$-$HgCl_2$ complexes for (a) $m=1$, (b) $m=2$, (c) $m=3$, and (d) $m=4$ in the crystalline state.

4) R. G. Snyder and G. Zerbi, *Spectrochim. Acta*, **23A**, 391 (1967).
5) R. Iwamoto, *ibid.*, **27A**, 2385 (1971).

each other, especially when m is equal to or greater than 2. The two bands at 1150 and 1200 cm^{-1} are associated with the terminal CH_3 groups[4] and display different behavior with increasing m. The 1200 cm^{-1} band decreases in intensity very gradually with increasing m. It appears as a fairly strong and well-defined band even for $m=4$, while the 1150 cm^{-1}, band which is weak but well-defined for $m=1$ and 2, is hardly observable for $m=3$ and 4.

Thus, the infrared spectra of these complexes for $m=2$ and 3 are very similar to those of the $CH_3O(CH_2CH_2O)_4CH_3$–$HgCl_2$ complex in the whole region. In the $CH_3O(CH_2CH_2O)_4CH_3$–$HgCl_2$ complex, the conformation was found to be essentially a sequence of O_T–CH_{2G}–CH_{2T}–O_T–$CH_{2\bar{G}}$–CH_{2T}–O.[1] From the similarity of the infrared spectra of the members of $m=2$ and 3 to those of the $CH_3O(CH_2CH_2O)_4CH_3$–$HgCl_2$ complex, the following conformations can be assumed in the complexes:

$$CH_3\text{-}O_T\text{-}CH_{2G}\text{-}CH_{2T}\text{-}O_T\text{-}CH_{2\bar{G}}\text{-}CH_{2T}\text{-}O\text{-}CH_3$$

for $m=2$, and

$$CH_3\text{-}O_T\text{-}CH_{2G}\text{-}CH_{2T}\text{-}O_T\text{-}CH_{2\bar{G}}\text{-}CH_{2T}\text{-}O_T\text{-}CH_{2G}\text{-}CH_{2T}\text{-}O\text{-}CH_3$$

for $m=3$.

It has been found reasonable to consider that the molecular conformation of $CH_3O(CH_2CH_2O)_mCH_3$ ($m=4$) in the complexes with $HgCl_2$ consists of a sequence of O_T–CH_{2G}–CH_{2T}–O with alternation of G and $\bar{G}$ in the adjacent chemical units. It is noticed that "band progression" or regular variation of band frequencies depending on m is not observed for these complexes, but their infrared spectra can be reasonably interpreted in terms of group characteristic vibrations.

The author would like to thank Prof. H. Tadokoro and Dr. M. Kobayashi, Osaka University, for their helpful discussions and encouragement. He is also grateful to Dr. S. Kuribayashi of this Institute for his valuable discussions.

BULLETIN OF THE CHEMICAL SOCIETY OF JAPAN, VOL. 46, 1129—1134 (1973)

Magnetic Properties of Some Iminoxyl Polyradicals. V. EPR Studies of the TEMPAD Biradical

Akira NAKAJIMA

Department of Chemistry, Faculty of Science, Kyoto University, Kyoto 606

(Received September 20, 1972)

The EPR of pure and diluted crystals of bis(2,2,6,6-tetramethylpiperidine-4)azine-1,1′-dioxyl (the TEMPAD biradical) was studied. From the spectra of the diluted cyrstal, the intra- and inter-molecular dipole-dipole interactions were identified. The crystal-field parameters of the intra-molecular coupling determined for the EPR spectra were: $|D|/hc \simeq 0.00477$ cm^{-1} and $|E|/hc \simeq 0.00032$ cm^{-1} and two kinds of principal axes were found. As the z-axis of the intra-molecular dipole-dipole coupling is in the direction connecting two N–O bonds in a molecule, the TEMPAD molecules in a unit cell may be said to occupy two different sites. The crystal-field parameters of the inter-molecular dipole-dipole coupling were determined to be: $|D'|/hc \sim 0.012$ cm^{-1} and $|E'|/hc \sim 0.003$ cm^{-1} and the z-axis of the tensor was in the direction of the a-axis. The assumed molecular-stack model could account for the aforementioned results. The EPR spectra of the pure TEMPAD biradical are one symmetrical Lorentzian line in all the directions; the angular dependence of the peak-to-peak linewidths was explained by means of the term of the inter-molecular dipole-dipole interaction obtained from the spectra of the diluted crystal using the three-dimensional Anderson-Weiss formula. The exchange parameter for the best-fit curve was of the order of magnitude of the weak exchange interaction estimated roughly from the small Weiss constant appearing in the paramagnetic susceptibility of the diluted crystals.

There have been many investigations regarding the magnetic properties of organic, stable free-radical solids; they have been adequately discussed elsewhere.[1] In these works, some short-range ordering effects caused by the exchange interaction between unpaired electrons have been of special interest. On the other hand, the dipole-dipole interactions of organic free-radical solids have been little studied in spite of their importance for the spin correlation.

Recently, Takizawa *et al.* reported the EPR spectra of the radical pair of di-p-anisyl-nitric-oxide in the diamagnetic host, and assumed the structure of the radical pair in the host.[2] In the case of diluted biradicals, we can expect the existence of the intra- and inter-molecular radical pairs which will have an influence on the magnetic behavior of the dense system.

Previous magnetic studies of bis(2,2,6,6-tetramethylpiperidine-4)azine-1,1′-dioxyl (the TEMPAD biradical) have revealed two kinds of exchange interaction; one is the strong inter-molecular exchange interaction which produces the broad maximum in the paramagnetic susceptibility (χ_M) of the 100% case at the temperature of 16.5 K[3] and the large Weiss

1) A. Nakajima, H. Ohya-Nishiguchi, and Y. Deguchi, This Bulletin, **44**, 2120 (1971).

2) O. Takizawa, J. Yamauchi, H. Ohya-Nishiguchi, and Y. Deguchi, to be published.

3) A. Nakajima, H. Nishiguchi, and Y. Deguchi, *J. Phys. Soc. Jap.*, **24**, 1175 (1968).

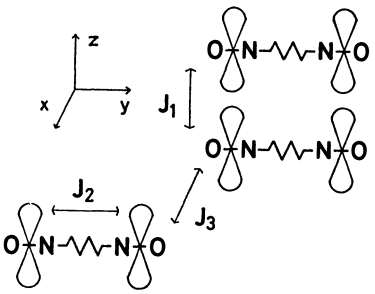

Fig. 1. Simplified molecular-stack model assumed from the $\chi_M - T$ results.

constant in the $\chi_M - T$ curves of the diluted crystals,[4] and the other is the weak intra-molecular exchange interaction which affects the hyperfine structure in the EPR spectrum in solution[5] and the small Weiss constant in the $\chi_M - T$ curves of the diluted crystals.[4] As the unpaired electron is localized around the N–O bond, the aforementioned results can be explained by the simplified molecular-stack model (shown in Fig. 1) on the basis of the localized spin treatment.[4] The EPR spectrum of the powdered TEMPAD biradical at room temperature was a symmetrical line, and new lines appeared on both sides of the central line at low temperatures. They have been explained in terms of the dipole-dipole interaction of the intra-molecular spin pair on the basis of the triplet exciton theory.[6]

In this paper, the author will report on his EPR studies of pure and diluted crystals of the TEMPAD biradical, determine the orientations of the intra- and inter-molecular radical pairs, and discuss the magnetic behavior of the dense system according to the assumed molecular-stack model.

Experimental

The TEMPAD biradical and bis(2,2,6,6-tetramethyl-piperidine-4)azine (the diamine), which are shown in Figs. 2(a) and 2(b) respectively, were prepared from 2,2,6,6-tetramethyl-4-piperidone supplied by the Aldrich Chemicals Co. following the method described by Rassat *et al.*[5,7] The single crystals of both the pure and diluted TEMPAD in the diamine host (less than 2 mol % in concentration) were crystallized from their ether solutions. The monoradical impurity, shown in Fig. 2(c), was formed in the diamine crystal by the air-oxidation, and its EPR spectra were used for the analysis of the hyperfine structure of the biradical spectra.[8]

The EPR measurements were carried out at room temperature using an X-band spectrometer, JEOLCO JES-ME-3X, equipped with a 100 kHz-field modulation for the first derivatives and an 80 Hz-field modulation for the second derivatives. As a standard sample, peroxylamine disulfonate, $[\cdot ON(SO_3)_2]^=$ (A_N=13.0 gauss and g=2.00537), was used. The mount for holding the crystals in the microwave cavity was made of Teflon, and it had a quartz rod; the crystals were fixed to the mount with silicon grease. The error in the measurements of the angle was about 2 degrees.

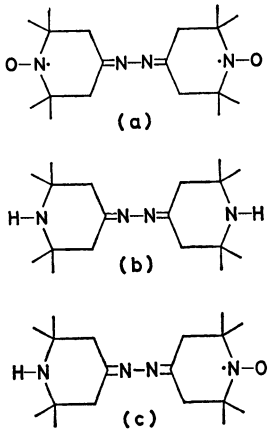

Fig. 2. Molecular structure of the TEMPAD biradical (a), the corresponding diamine (b), and the monoradical (c).

Results and Discussion

Diluted Crystal. The Hamiltonian of the biradical with a strong exchange interaction, introduced by Kurita,[9] is given by:

$$\mathcal{H} = \mathcal{H}_z + \mathcal{H}_{hf} + \mathcal{H}_{dip} + \mathcal{H}_{ex} + \mathcal{H}' \quad (1)$$

$$\mathcal{H}_z = \mu_B \sum_{ij} \bar{g}_{ij} H_i (S_{1j} + S_{2j}) \quad (2)$$

$$\mathcal{H}_{hf} = (1/2) g_0 \mu_B \sum_{ij} (A^{I}_{ij} I^{I}_j + A^{II}_{ij} I^{II}_j)(S_{1i} + S_{2i}) \quad (3)$$

$$\mathcal{H}_{dip} = (4\mu_B^2/R^3)[(\boldsymbol{S}_1 \cdot \boldsymbol{S}_2) - 3(\boldsymbol{S}_1 \cdot \boldsymbol{R})(\boldsymbol{S}_2 \cdot \boldsymbol{R})R^{-2}] \quad (4)$$

$$\mathcal{H}_{ex} = J(\boldsymbol{S}_1 \cdot \boldsymbol{S}_2) \quad (5)$$

$\mathcal{H}'$: inter-molecular term

where μ_B is the Bohr magneton and where the other notations are all the same as in Kurita's equation except for the last inter-molecular term in Eq. (1). In the case of the orthorohmbic symmetry, the term of the intra-molecular dipole-dipole interaction (Eq. (4)) can be rewritten as follows:

$$\mathcal{H}_{dip} = D_{xx} S_x^2 + D_{yy} S_y^2 + D_{zz} S_z^2$$
$$= D[S_z^2 - (1/3)S(S+1)] + E(S_x^2 - S_y^2) \quad (6)$$

where $S_j = S_{1j} + S_{2j}$ ($j = x, y$, and z),

S is the eigen value of the total spin: $\boldsymbol{S} = \boldsymbol{S}_1 + \boldsymbol{S}_2$,

$$D_{jj} = (1/2) g_0^2 \mu_B^2 \langle (R^2 - 3X_j^2)/R^5 \rangle \quad (X_j = X, Y, \text{and } Z) \quad (7)$$

$$D_{xx} = -D/3 + E, \; D_{yy} = -D/3 - E, \; D_{zz} = 2D/3 \quad (8)$$

where D and E are the crystal-field parameters of the biradical.

In a monoclinic crystal, some couples of sites exist in a unit cell and can be superposed upon each other by a symmetry transform of the crystal. When $\beta \simeq 90°$ in the case of the diamine host (see Table 1), we can adopt the *a*-, *b*-, and *c*-axes as the rectangular coordinate system (Fig. 3). Some typical EPR spectra with the static magnetic field at several orientations of the *ab*- and *ca*-planes are shown in Fig. 4. The observed positions of the EPR spectra in the *ca*-plane shown in Fig. 5 have two parts of the angular depend-

4) A. Nakajima, This Bulletin, **46**, 779 (1973).
5) A. Nakajima, H. Ohya-Nishiguchi, and Y. Deguchi, This Bulletin, **45**, 712 (1972).
6) J. Yamauchi, T. Fujito, A. Nakajima, H. Ohya-Nishiguchi, and Y. Deguchi, *ibid.*, **44**, 2263 (1971).
7) R. Briere, R. M. Duperyre, H. Lemaire, C. Morat, A. Rassat, and P. Rey, *Bull. Soc. Chem. Fr.*, **1965**, 3290.
8) A. Nakajima, unpublished work.

Table 1. The space groups and the lattice constants for the diamine and the TEMPAD biradical

	diamine	TEMPAD
space group	monoclinic C_c	monoclinic C_c or $C_{2/c}$
a	29.0 Å	29.1 Å
b	12.6	12.8
c	10.4	10.5
β	~90°	~90°
z	8	8

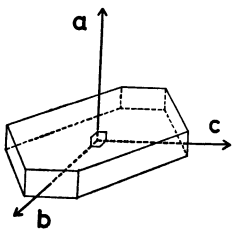

Fig. 3. System of the coordinates of the diamine host.

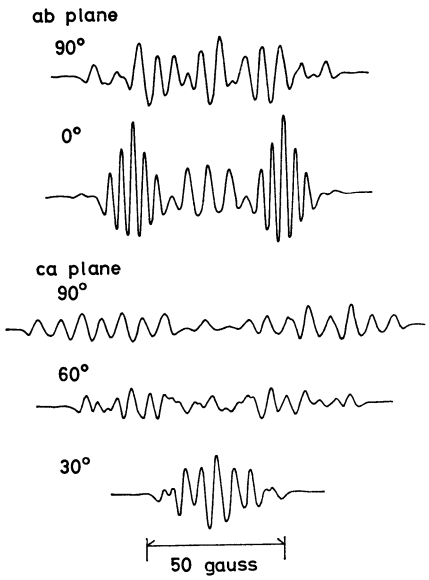

Fig. 4. Typical EPR spectra with the static magnetic field at some orientations in the *ab*- and *ca*-planes.

ence, namely, the intra- and the inter-molecular parts.

Intra-molecular Part: The g-value of the biradical is the mean-value, $\bar{g}_{ij}$, of the two radicals in a molecule.[9] As the angular dependence of the g-value is almost isotropic for the TEMPAD biradical, $\bar{g}_{ij}$ can be replaced by the $g_0=2.0060$ obtained from the EPR spectrum in solution. Although the principal axes of the tensor of the intra-molecular dipole-dipole interaction are nearly equal to those of the hyperfine tensor, it is difficult to analyze the spectra because of the complexity caused by the unequivalent molecules in a unit cell.

To solve this problem, the author chose the half-value of the hyperfine tensor of the monoradical formed

9) Y. Kurita, *Nippon Kagaku Zasshi*, **85**, 833 (1964).

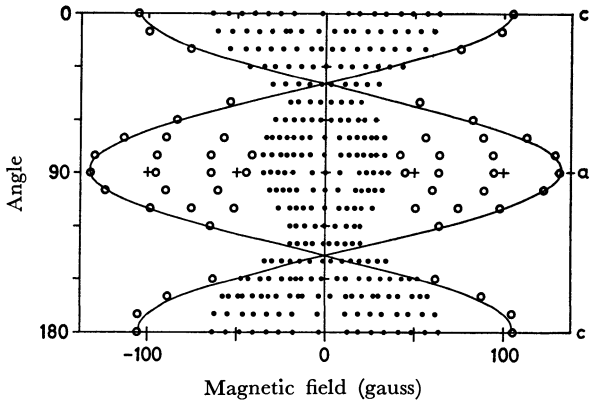

Fig. 5. Observed positions of the EPR spectra in the *ca*-plane; ●: intra-molecular part, ○: inter-molecular part. The solid curve is the calculated angular variation for the inter-molecular dipole-dipole interaction.

Table 2. The principal values and the direction cosines of the tensor of the intra-molecular dipole-dipole interaction with regard to the *abc*-system

Principal values			Direction cosines a	b	c
D_{xx}	$\pm(18.7\pm0.5)$ gauss	(p)	0.938	0.335	−0.094
		(q)	0.910	0.396	0.118
D_{yy}	$\pm(15.3\pm0.4)$	(p)	−0.346	0.866	−0.361
		(q)	−0.412	0.892	0.183
D_{zz}	$\mp(34.0\pm1.0)$	(p)	−0.040	0.371	0.928
		(q)	−0.033	−0.216	0.976
Crystal field parameter					
$\lvert D\rvert/g_0\mu_B$	51.0±1.5 gauss				
$\lvert E\rvert/g_0\mu_B$	3.4±0.9 gauss				

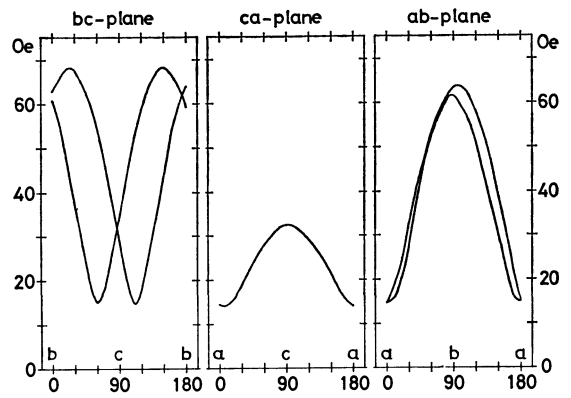

Fig. 6. Angular dependence of the hyperfine structure of the monoradical with regard to the abc-system.

in the diamine, as that of the biradical. The angular dependence of the hyperfine structure of the monoradical with regard to the *abc*-system is shown in Fig. 6.[8] Then, the principal values and the direction cosines of the tensor of the intra-molecular dipole-dipole interaction with regard to the *abc*-system, which are summarized in Table 2, could be determined. The calculated angular dependence on the *ca*-plane is shown in Fig. 7 in comparison with the experimental

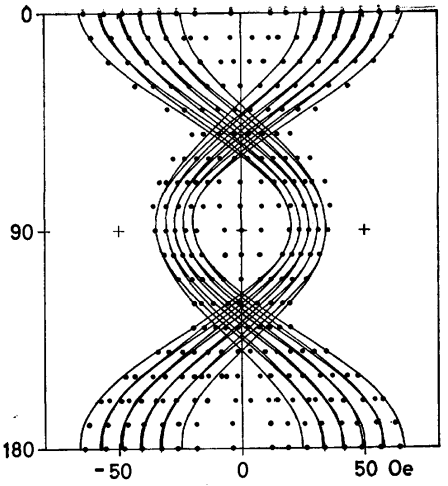

Fig. 7. Calculated angular dependence of the EPR spectra for the intra-molecular dipole-dipole interaction compared with the experimental results.

results. From Table 2 we can find that the tensor of the intra-molecular dipole-dipole interaction has two principal axes (p and q). As the z-axis of the tensor of the intra-molecular dipole-dipole coupling is in the direction connecting two N–O bonds in a molecule, the TEMPAD molecule in a unit cell occupies two different sites. A suitable molecular-stack model is shown in Fig. 8; each segment indicates the TEMPAD molecules, and the angles from the b-axis are about 22.0° and −12.5° for the p- and q-sites respectively. The distance between the two radicals in a molecule could be estimated from the equation: $|D| \sim 3\mu_B/R^3$, and then $R \sim 8.2$ Å.

Inter-molecular Part: Outside of the intra-molecular spectra broad lines appeared, apparently under the large field-modulation width (2—10 gauss). The angular dependence of the broad lines shown in Fig. 5 can be explained as a result of the inter-molecular dipole-dipole interaction between biradical molecules. According to the aforementioned molecular-stack model, the system of the coupled two biradicals can be shown as:

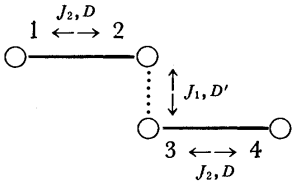

where J_1 and J_2 are the inter- and intra-molecular exchange interactions, and where D' and D are the inter- and intra-molecular dipole-dipole interactions. In the case of the TEMPAD biradical, $|J_1| \gg g_0\beta H_0 > |J_2| \simeq |D'| > |D|$; then, the spin Hamiltonian can be briefly given by:

$$\mathcal{H} \simeq g_0\beta \boldsymbol{H}_0 \cdot (\boldsymbol{S}_0 + \boldsymbol{S}_1 + \boldsymbol{S}_4) + \boldsymbol{S}_0 \cdot \boldsymbol{D}' \cdot \boldsymbol{S}_0 + \boldsymbol{S}_0 \cdot \boldsymbol{D} \cdot (\boldsymbol{S}_1 + \boldsymbol{S}_4) \quad (9)$$

where $\boldsymbol{S}_0 = \boldsymbol{S}_2 + \boldsymbol{S}_3$ and where $\boldsymbol{D}$ and $\boldsymbol{D}'$ are the tensors of the intra- and inter-molecular dipole-dipole interactions respectively. When $|D'| \gg |D|$, the system can be treated as one with one spin-pair (S_2 and S_3) and two monomers (S_1 and S_4). On this assumption, the principal values which are listed in Table 3 were roughly calculated: the z-axis of the tensor, $\boldsymbol{D}'$ was found to be in the direction of the a-axis. The calculated angular dependence, which is shown in Fig. 5, agreed with the experimental results except for the case of the ab-plane. The slight lack of agreement in the case of the ab-plane can be reduced by disregarding the $\boldsymbol{D}$-tensor. The distance between the radicals along the a-axis can be estimated from the value of D' at 6.0 Å, which agrees with the separation between the nearest neighbors in the direction of the a-axis, $a/4 = 7.2$ Å (Table 1).

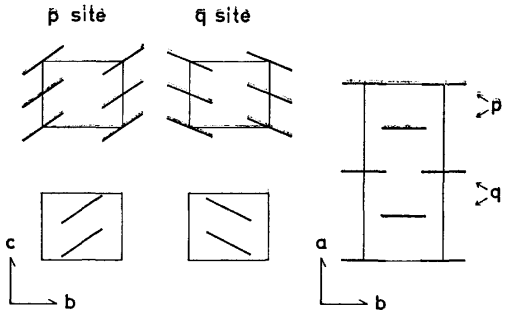

Fig. 8. Assumed stack model for the TEMPAD molecules in a unit cell. Each segment indicates the TEMPAD molecule and the angles from the b-axis are about 22.0° and −12.0° for the p- and q- sites, respectively.

TABLE 3. THE PRINCIPAL VALUES OF THE TENSOR OF THE INTER-MOLECULAR DIPOLE-DIPOLE INTERACTION WITH REGARD TO THE *abc*-SYSTEM AND THE CRYSTAL FIELD PARAMETERS

Principal values		Crystal field parameters	
D'_{xx}	±13 gauss	$\|D'\|/g_0\mu_B$	130 gauss
D'_{yy}	±73	$\|E'\|/g_0\mu_B$	30
D'_{zz}	∓86		

The EPR spectra with the static magnetic field around the a-axis showed three other kinds of weak broad lines, which can be explained as dipole-dipole interactions among the next nearest and further neighbors. The distances of these couplings were roughly estimated to be 6.6, 7.5, and 8.5 Å respectively.

The obtained crystal-field parameters of the intra- and inter-molecular dipole-dipole interactions are summarized in Table 4 in comparison with those of other triplet states. The order of magnitude of our results was in the class of the thermally-excited triplets or of the radical pair.

Pure Crystal. As the crystal structure of the TEMPAD biradical is nearly equal to that of the diamine (see Table 1),[4] we can adopt the same a-, b-, and c-axes as the rectangular coordinate system as in the case of the diamine (Fig. 9). The EPR spectra of the TEMPAD biradical have one absorption line in all the directions, and the angular dependence of the g-value is almost the same isotropically as in the diluted crystal. The absorption lines are all symmetrical Lorentzian, and the peak-to-peak linewidths, shown in Fig. 10, varied with the static magnetic field in the bc-,

Table 4. The crystal field parameters of the intra- and the inter-molecular dipole-dipole itneractions of the TEMPAD compared with other triplet states

Triplet states	D/hc(cm^{-1})	E/hc(cm^{-1})	Ref.
((Biradical))			
TEMPAD (Intra)	±0.00477	±0.00032	This
(Inter)	±0.012	±0.003	Work
((Optically excited triplets))			
Naphthalene (Durene)	+0.10119	−0.01411	10
Quinoxaline (Durene)	±0.1007	∓0.0182	11
((Ground state triplets))			
Diphenylmethylene (Benzophenone)	±0.40505	∓0.01918	12
Fluorenilidene (Diazofluorene)	±0.40923	∓0.02828	12
((Thermally excited triplets))			
$(\phi_3XCH_3)^+(TCNQ)_2^-$	0.0062	0.00098	13
$Cs_2^+(TCNQ)_3^{-2}$	±0.00936	±0.00151	14
[Morpholinium]$^+$· (TCNQ)$^-$	±0.0148	±0.00191	15
$(TMPD^+)_2$· $[Ni(nmt)_2]^{2-}$	±0.0204	±0.00266	16
((Radical pair))			
Dimethylglyoxime	0.0290	0.0	17

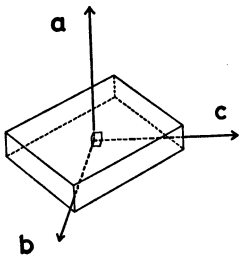

Fig. 9. System of the coordinates of the TEMPAD biradical same as the diamine host.

ca-, and *ab*-planes.

The strong inter-molecular exchange interaction (J_1 in Fig. 1), which determines the energy levels of the magnetic system, will never affect the linewidth. On the other hand the weak intra-molecular exchange interaction (J_2) will cause a narrowing of the linewidth. In the case of a narrowing, we can apply the usual three-dimensional Anderson-Weiss formula for a Lorentzian line:[18]

$$\Delta H_{pp} = \Delta H_d^2/\sqrt{3}H_{ex} + C, \quad (10)$$

where ΔH_{pp} is the peak-to-peak linewidth; ΔH_d^2, the second moment of the sum of the dipole-dipole interactions; H_{ex}, an effective exchange field, and C, a residual linewidth. As the angular dependence of the linewidth is smallest in the *bc*-plane, the inter-molecular dipole-dipole interaction along the *a*-axis is dominant in the second moment. Therefore the secular part of the second moment was calculated using the term of the inter-molecular dipole-dipole interaction obtained from the spectra of the diluted crystal. In Eq. (10), two adjustable parameters, H_{ex} and C, were estimated to be 4300 and 9.5 gauss respectively. The calculated curves are also shown in Fig. 10. The value of H_{ex} (~0.6 K) was of about the same order of magnitude as the weak intra-molecular interaction, 1 K, estimated from the $\chi_M - T$ curve of the diluted TEMPAD biradical.[4] The residual linewidth, C, represents all the broadening mechanisms besides the secular part of the inter-molecular dipole-dipole interaction: (1) the non-secular part of the inter-molecular dipole-dipole coupling, (2) the residual nuclear hyperfine broadening, and (3) the intra-molecular or long-range dipole-dipole couplings.

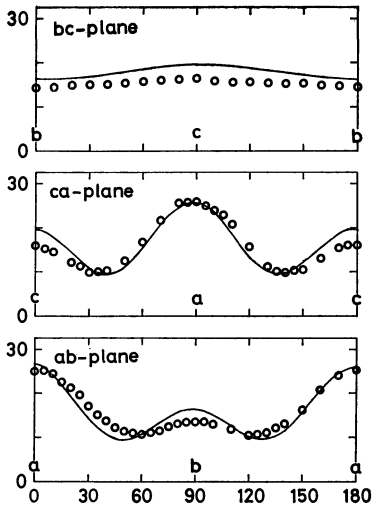

Fig. 10. The angular dependence of the EPR linewidths of the TEMPAD biradical. The solid curves are the calculated results using the three-dimensional Anderson-Weiss formula.

Summary

The EPR of the diluted and pure crystals of the TEMPAD biradical was studied at room temperature. From the spectra of the diluted crystal, the intra- and inter-molecular dipole-dipole interactions were identified. The crystal-field parameters of the dipole-dipole couplings were obtained as:

10) C. A. Hutchison, Jr. and B. W. Mangum, *J. Chem. Phys.*, **34**, 908 (1961); A. W. Hornig and J. S. Hyde, *Mol. Phys.*, **6**, 33 (1963); N. Hirota, C. A. Hutchison, Jr., and P. Palmer, *J. Chem. Phys.*, **40**, 3717 (1964).

11) J. S. Vincent and A. H. Maki, *J. Chem. Phys.*, **39**, 3088 (1963).

12) R. W. Brandon, G. L. Closs, and C. A. Hutchison, Jr., *ibid.*, **37**, 1878 (1962); R. W. Brandon, G. L. Closs, C. E. Davoust, C. A. Hutchison, Jr., B. E. Kohler, and R. Silbey, *ibid.*, **43**, 2006 (1965).

13) D. B. Chesnut and W. D. Phillips, *ibid.*, **35**, 1002 (1961).

14) D. B. Chesnut and P. Arthur, Jr., *ibid.*, **36**, 2969 (1962).

15) M. A. Marechal and H. M. McConnel, *ibid.*, **43**, 497 (1965).

16) M. J. Hove, B. M. Hoffman, and J. A. Ibers, *ibid.*, **56**, 3490 (1972).

17) Y. Kurita, *ibid.*, **41**, 3926 (1964).

18) T. Z. Huang, R. P. Taylor, and Z. G. Soos, *Phys. Rev. Lett.*, **28**, 1054 (1972). See also the following paper as the original work; P. W. Anderson and P. R. Weiss, *Rev. Mod. Phys.*, **25**, 269 (1953).

a) Intra-molecular couplings:

$|D|/hc \simeq 0.00477$ cm^{-1} and $|E|/hc \simeq 0.00032$ cm^{-1},

b) Inter-molecular coupling:

$|D'|/hc \sim 0.012$ cm^{-1} and $|E'|/hc \sim 0.003$ cm^{-1}.

In the assumed molecular-stack model, the TEMPAD molecules in a unit cell occupy two different sites (*p*- and *q*-sites), and the inter-molecular coupling is in the direction of the *a*-axis. The linewidth variation in the EPR spectra of the pure TEMPAD biradical could be explained in terms of the inter-molecular dipole-dipole interaction, using the three-dimensional Anderson-Weiss formula. The obtained exchange parameter was of the order of magnitude of the weak intramolecular interaction estimated from the $\chi_M - T$ of the diluted TEMPAD biradical.

The author wishes to thank Professor Yasuo Deguchi, Dr. Hiroaki Ohya-Nishiguchi, Dr. Jun Yamauchi and their collaborators for their helpful advice and discussions. He is also indebted to Professors Hideo Takaki and Mamoru Mekata for their continual guidance and encouragement during this work.

BULLETIN OF THE CHEMICAL SOCIETY OF JAPAN, VOL. 46, 1134—1136 (1973)

Study of the Poisoning Effect on Nickel and Nickel Boride Catalysts by Means of a Flow Microcalorimeter

Toshinobu IMANAKA, Yuriko NITTA, and Shiichiro TERANISHI

Department of Chemical Engineering, Faculty of Engineering Science, Osaka University, Osaka 560

(Received July 5, 1972)

The relation between the poisoning effect on nickel and nickel boride catalysts in the liquid-phase hydrogenation of styrene and the bond strength of inhibitors on the catalysts has been studied by means of liquid-phase chromatography using a thermal detector. The results show that the sequence of poisoning effect is in agreement with that of the adsorption heat of inhibitors, and that the adsorption heat of each inhibitor on nickel boride is smaller than that on nickel. Besides, this sequence is also in agreement with that of the bond strength of the central metal ion and the coordinated ligand of some manganese complexes in a homogeneous system. These facts indicate that the adsorption energy of inhibitors on a catalyst in a heterogeneous system corresponds to the bond strength of the ligand coordinated to metal complexes in a homogeneous system.

The poisoning effect on nickel and nickel boride catalysts in the liquid-phase hydrogenation of styrene has mainly been studied by the kinetic method, and it has previously been reported that the resistibility of the nickel boride catalyst was greater than that of the nickel catalyst.[1)]

Since the poisoning effect is assumed to be connected with the bond strength between a catalyst and an inhibitor, the adsorption heat of the inhibitor was measured by means of liquid-phase chromatography using a thermal detector.

The results showed that the sequence of the poisoning effect was in agreement with that of the adsorption heats of inhibitors on the catalysts. Besides, the resistibility to inhibition on nickel and nickel boride catalysts was also studied in relation to the adsorption heats of inhibitors on the catalysts. Each adsorption heat of inhibitor on nickel boride was smaller than that on nickel; accordingly, nickel boride can be said to exhibit a higher resistibility than that of nickel. Furthermore, the sequence of the poisoning coefficient estimated by taking the steric effect into account was in agreement with that of the bond strength of adsorption obtained with the thermal measurements; this sequence was also in agreement with that of the bond strength between the central metal ion and the ligand coordinated to some manganese complexes[2)] in a homogeneous system.

Experimental

Materials. The Ni_2B catalyst was prepared by adding $NaBH_4$ to a solution of $(CH_3COO)_2Ni$ (Ni=0.6 g), as has been desdribed in the previous publication;[1)] the precipitate was washed and centrifuged with ethanol. The BET surface area of the Ni_2B catalyst was 21.8 m^2/g. The Ni catalyst used was degassed by heating $(HCOO)_2Ni$ at about 250°C for 3—4 hr under a vacuum and cooled after charging in hydrogen gas; then ethanol was poured into the reaction vessel. The BET surface area of this Ni catalyst was 13.8 m^2/g.

The dichlorophenyl phosphine, trialkyl phosphites, and 2,3-dimercaptopropanol were used without further purification. The styrene was purified by distillation before use.

Procedures. The apparatus used for the thermal measurements is shown schematically in Fig. 1. The catalyst prepared was charged in the columns of both the detector and reference parts. In order to remove the oxygen soluted in the carrier liquid (99.5% ethanol), the hydrogen was saturated by bubbling it through the gas-adsorption vessel. Stable thermal measurements were made possible by this procedure. The inhibitors were injected into the carrier liquid from the inlet part as an ethanol solution of a certain

1) Y. Nitta, T. Imanaka, and S. Teranishi, *Kogyo Kagaku Zasshi*, **74**, 777 (1971).

2) R. J. Angelici and F. Basolos, *J. Amer. Chem. Soc.*, **84**, 2475 (1962).

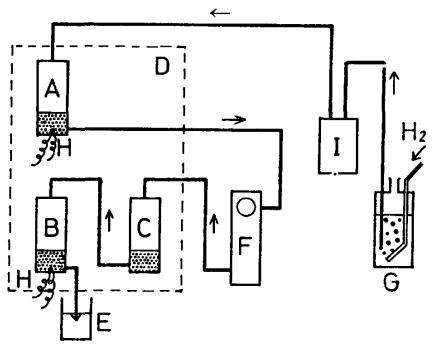

Fig. 1. Block diagram of the apparatus used.

A: Reference column, B: Detector column, C: Adsorption column, D: Water bath, E: Recovery vessel, F: Sample inlet, G: Hydrogen Saturator, H: Thermistor, I: Pump. Eluent: 99.5% ethanol, Flow rate: 0.62 ml/min, Pressure: 2—3 kg/cm², Temperature of the water bath: 35°C.

concentration of the inhibitor.

The exothermic value calculated from the peak area per unit of the catalyst was determined by means of liquid chromatography using a thermal detector (NIHON Electric Company, JLC-A). First, the heats of adsorption of inhibitors per unit of catalyst were determined against the amounts of inhibitors injected, without the adsorption column (C). Second, the amounts of injected inhibitors adsorbed by the catalyst in the detector column (B) were estimated by determining the heat effects produced by the same inhibitors after they had left an identical column (C), filled with the same catalyst and connected in series between the sample injection part (F) and the detector column (B). Since the residual inhibitor passing through the first column (C) subsequently entered the detector column (B) and produced a heat effect similar to those produced by the inhibitors injected directly, the amount of that inhibitor was obtained from the relations, determined previously, between different amounts of the inhibitors injected directly and the heat effects they produce.

Thus, the quantity of inhibitor adsorbed in the first column was determined by subtracting the amount obtained above from that of the inhibitor injected.[3] However, the adsorption heat of the inhibitor was corrected by subtracting the heat of dilution of the sample solution with ethanol.

The measurements of the rate of hydrogenation reaction were performed directly in the usual manner[4] at 30°C, using 1 ml of styrene as a reactant and 40 ml of ethanol as a solvent. In order to eliminate the change in catalytic activity arising from the preparation of the catalyst, the rate of hydrogenation on the catalyst without any inhibitor was at first measured using 1 ml of styrene. When the reaction was complete, the inhibitor was added to the reaction mixture; it was stirred for 10 min, and then the rate of hydrogenation was again measured by adding 1 ml of styrene. As the hydrogenation reaction proceed in zero-order in the styrene concentration, the rate of hydrogen uptake was used as the hydrogenation rate when 50% of the added styrene had been hydrogenated to ethylbenzene.

The catalytic activity was determined by means of the ratio of the hydrogenation rate on the catalyst with and without an inhibitor. In this case, it was confirmed that the catalyst was not poisoned with styrene or ethylbenzene, a hydrogenated substance, and that the activity of the catalyst without an inhibitor did not change with a repetition in the reaction.

3) A. J. Groszek, *ASLE Transactions*, **5**, 105 (1962).

4) Y. Murakami, S. Kishida, T. Imanaka, and S. Teranishi, *Nippon Kagaku Zasshi*, **89**, 263 (1968).

Results and Discussion

The relation between the exothermic value of trimethylphosphite, $P(OMe)_3$, as an inhibitor and the amount of inhibitor added to nickel and nickel boride catalysts is shown in Fig. 2. In these catalysts, the exothermic values are proportional to the amounts of several inhibitors. Figure 3 shows the amount of inhibitor added against the amount of triphenylphosphite, $P(Oph)_3$, adsorbed per unit of catalyst when the adsorption column is connected in series to the sample column. It was found that the amount of adsorption increases with an increase in the amount of inhibitor added. The fact that the amount of adsorption on nickel boride is more than that on nickel may be due to the difference in the surface areas of the catalysts. Table 1 shows the adsorption heats of several inhibitors on nickel and nickel boride catalysts against the modified poisoning coefficients, α'[1,5], calculated from the poisoning coefficients, α,

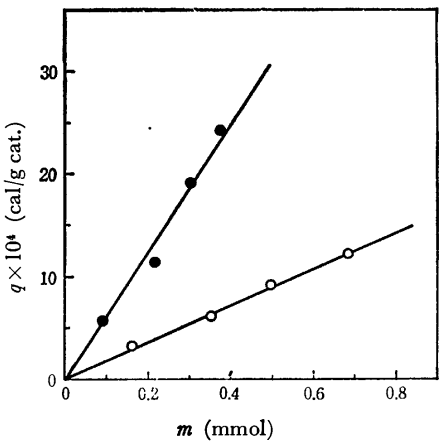

Fig. 2. Relation between exothermic value and the amount of added inhibitor.
○: Ni_2B, ●: Ni

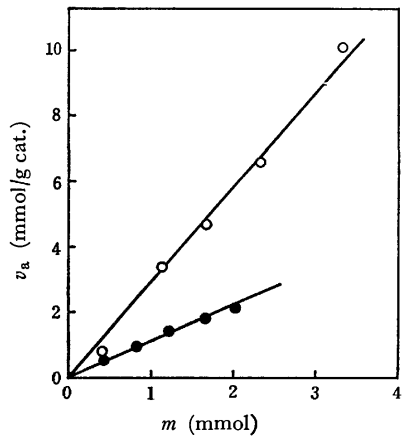

Fig. 3. Relation between the amount of adsorption and the amount of added inhibitor.
○: Ni_2B, ●: Ni

5) $\alpha' = \alpha/s$, s; the occupied area of adsorbed inhibitor molecule (Å²).

TABLE 1. HEAT OF ADSORPTION AND POISONING COEFFICIENT OF SEVERAL INHIBITORS

Inhibitor	Catalysts			
	Ni_2B		Ni	
	Heat of adsorp. (cal/mol)	Poisoning coeff. (gNi/mmol, Å²)	Heat of adsorp. (cal/mol)	Poisoning coeff. (gNi/mmol, Å²)
$CH_2(SH)CH(SH)CH_2OH$	84.2	0.169	104	1.41
$PPhCl_2$	124	0.341	142	1.73
$P(OCH_3)_3$	0.610		5.72	0.695
$P(OPh)_3$	0.332		4.31	0.203
$P(On\text{-}Bu)_3$	0.317		3.34	0.163

of the Maxted equation[6] $K_c=K_0(1-\alpha C)$, obtained from the hydrogenation rate of styrene [K_c, K_0; activity with or without an inhibitor, C; amount of added inhibitor(mmol/gNi)]. As has been shown in the preceding paper,[1] it was also found by means of thermal measurements that the resistibility to the inhibitor of nickel boride is more than that of nickel. The high resistibility to the poisoning of the nickel boride catalyst is probably due to the effect that the bonding electrons of the boron atom occupy the vacant d-orbitals of the nickel atom and make it difficult for the lone pairs of the inhibitors to coordinate with and so poison the nickel catalyst. Furthermore, the sequence of the poisoning coefficients for nickel and nickel boride catalysts was as follows;

$$PPhCl_2>CH_2(SH)CH(SH)CH_2OH>P(OCH_3)_3>P(OPh)_3>P(On\text{-}Bu)_3$$

In addition, the sequence of the adsorption heats of inhibitors for nickel and nickel boride catalysts obtained from the thermal measurements agrees completely with the preceding sequence; therefore, it was found that the poisoning coefficient for a catalyst is subject to the bond strength of the adsorption of the inhibitor.

6) E. B. Maxted, *Advan. Catal.*, **3**, 129 (1951).

It has previously been reported that the infrared spectra of some $Mn(CO)_4LX$ (X=Cl, Br, I)[2] complexes in the CO stretching region show an increase in the wave number of adsorption with the changes in L in this sequence:

$$P(C_6H_5)Cl_2\geq P(OCH_2)_3CCH_3>P(OC_6H_5)_3\geq P(OC_4H_9)_3>Sb(C_4H_9)_3\sim As(C_6H_5)_3\sim P(C_6H_5)_3>P(C_4H_9)_3$$

When styrene is used as the ligand of the manganese complex, it can be considered that the electron-attracting ability of styrene is weaker than that of the $P(C_4H_9)_3$ ligand.

The increase in the wave number of the C–O absorption suggests that the strong electron-attracting ligand results in less electron density on manganese, which means less back-donation of the d-orbital electron and, therefore, less Mn–C bond strength. The sequence of increase along the $P(C_6H_5)Cl_2\gg P(OC_6H_5)_3>P(OC_4H_9)_3$ series agrees completely with the sequence of the poisoning coefficients for nickel and nickel boride catalysts, as is shown in Table 1. This fact indicates that the magnitude of the adsorption energy of inhibitors on a catalyst in a heterogeneous system corresponds to the bond strength of the ligand coordinated to metal complexes in a homogeneous system.

The Crystal Data of Ternary Rare Earth Borides, RCo_2B_2

Koichi NIIHARA, Toetu SHISHIDO, and Seishi YAJIMA

The Research Institute for Iron, Steel and Other Metals, Tohoku University, Sendai 980

(Received July 19, 1972)

Compounds with the composition of RCo_2B_2 (R=La, Nd, Sm, Gd, Tb, Dy, and Y) were prepared by arc-melting methods. Their crystal structure was investigated by means of X-ray diffraction. These ternary rare earth borides crystallize in the tetragonal lattice. The lattice parameters are $a=3.616\pm0.003$ Å and $c=10.215\pm0.005$ Å for $LaCo_2B_2$ and $a=3.561\pm0.002$ Å and $c=9.358\pm0.005$ Å for YCo_2B_2. The good agreement between the X-ray diffraction intensities observed and those calculated shows that the ternary borides, $LaCo_2B_2$ and YCo_2B_2, crystallize in the $ThCr_2Si_2$-type structure. The crystallographic data obtained for $LaCo_2B_2$ and YCo_2B_2 are as follows: space group $14/mmm(D_{4h}^{17})$; 2R in 2(a), 4Co in 4(d), and 4B in 4(e) with $z\sim3/8$. The boron atoms in this structure are situated at the center of a trigonal prism formed by four rare earth atoms and two cobalt atoms. We also found the RCo_2B_2 compounds to be isostructural with $LaCo_2B_2$ and YCo_2B_2, where R=Nd, Sm, Gd, Tb, and Dy. However, efforts to prepare $CeCo_2B_2$ and $ErCo_2B_2$ by arc-melting were unsuccessful.

In the binary systems of rare earth–cobalt and cobalt–boron, there exist a series of intermetallic compounds, (R_3Co, R_3Co_2, RCo, R_2Co_3, RCo_2, RCo_3, RCo_5, R_2Co_7, R_2Co_{17}, Co_3B, Co_2B, and CoB), many of which possess interesting magnetic properties.[1-3] On the other hand, there are five compounds in the rare earth–boron system,[4] (RB_2, RB_4, RB_6, RB_{12}, and RB_{66}), which are interesting for their possible electric and high-temperature uses. Taking into consideration the properties of these binary compounds, the ternary system of the rare earth–cobalt–boron combination seems quite interesting. Unfortunately, there have been few investigations concerning this ternary system.

While investigating the phase equilibria in the Y–Co–B system, we found a new ternary compound with a composition close to YCo_2B_2.[5] The purpose of the present investigation is to prepare the ternary rare earth borides, RCo_2B_2 (R=rare earth elements), and to determine their crystal structures.

Experimental

Materials. All the rare earth metals[6] except samarium were prepared in our laboratory by the calcium-metal reduction of rare earth trifluorides. The samarium metal was prepared from samarium oxide by lanthanum-metal reduction. The purity of the metals obtained by these methods was 99.5%. Cobalt and crystalline boron were obtained from Wako Pure Chemical Industries, Ltd., Tokyo. The purities were 99.99% and 99.9% respectively.

Preparation of Samples. The ternary samples were synthesized by arc-melting mixtures of rare earth metal, cobalt, and boron in the atomic ratio of 1 : 2 : 2. Argon was used as a protective atmosphere in the arc-melting furnace, and the small amount of residual oxygen was eliminated prior to melting by fusing a button of titanium. The samples, weighing approximately 10 g, were melted three times to insure homogeneity. The fused samples were then wrapped with tantalum foil, sealed in quartz capsules under a vacuum, and annealed for 150 hr at 800°C. The samples were then pulverized in an agate motar under an inert gas atmosphere to prevent oxidation and examined by chemical and X-ray analyses. The chemical analyses for the content of rare earth metals and boron were preformed by a method previously reported.[7] The cobalt content was determined by X-ray fluorescence analysis. The losses of the rare earth metals, cobalt, and boron during the melting process were negligible for the ternary systems of (La, Nd, Gd, Tb, Dy, and Y)-Co-B. In the case of the Sm–Co–B system, though 10—15 wt% of the Sm metal vaporized during the melting process. Therefore, mixtures containing an excess of the Sm metal were melted by means of an arc-furnace.

The density of the samples was determined at 20.5°C by a floatation technique, using CCl_4.

X-Ray Diffraction Measurements. The X-ray diffraction patterns of the samples were taken with a Debye-Scherrer camera 114.6 mm in diameter. The correction of the diameter of the Debye-Scherrer camera was performed using standard silicon powder. Mn-filtered Fe ($K\alpha_1=1.9360$ Å, $K\alpha_2=1.9399$ Å, and $K\bar{\alpha}=1.9373$ Å) radiation was employed. The lattice parameters were determined by extrapolating the lattice parameters for $\cos^2\theta$ up to $\theta=90°$. The relative intensities were obtained by measuring the counts under the peaks which were produced using a diffractometer conbined with a scintillation counter and a pulse-height analyser. The scanning speed of the diffractometer was one-fourth degree (2θ) per minute.

Results and Discussion

A new compound was prepared by the arc-melting method in the ternary system of Y–Co–B. This compound was in equilibrium with YCo_2, YB_2, YCo_3B_2,[7] and YCo_4B_4[8] at 800°C. It was found by chemical analyses that the samples in the single-phase region had compositions of 17.3—20.7 at% Y, 40.3—41.5at%

1) K. I. Strnat, G. Hoffer, J. Olson, and W. Ostertag, *J. Appl. Phys.*, **38**, 1001 (1967).
2) W. A. J. J. Velge and K. H. J. Buschow, Proc. I. E. E. Conference, London, Sep. 1967.
3) K. I. Strnat, G. Hoffer, W. Ostertag, and J. Olson, *J. Appl. Phys.*, **37**, 1252 (1966).
4) G. V. Samsonov, Boride of the rare earth metals, "High temperature compounds of the rare earth metals with nonmetals," Edited by G. V. Samsonov, Consultants Bureau, New York (1965) p. 1.
5) K. Niihara, T. Shishido, and S. Yajima, This Bulletin, **44**, 3214 (1971).
6) K. Niihara, K. Sasaki, and S. Konno, Technical Report, The Research Institute for Iron, Steel and other Metals, Tohoku, University, Sendai, I. 54 (1969).
7) K. Niihara and S. Yajima, This Bulletin, to be published.
8) This compound has a composition close to YCo_4B_4 and crystallizes in a tetragonal lattice. The lattice parameters are $a=5.07$ Å and $c=7.13$ Å, respectively.

Co, and 39.6—42.3 at% B. The stoichiometric composition of YCo_2B_2 was proposed on the basis of the results of X-ray and chemical analyses and the density measurements. The ternary compounds with the same composition were also prepared for La, Nd, Sm, Gd, Tb, and Dy.

Y was used as a crystal chemical stand-in for heavy rare earths since its atomic radius is located between those of Tb and Dy.[9] It may be assumed that the ternary compounds (RCo_2B_2) of the lanthanides will be structurally similar if $LaCo_2B_2$ and YCo_2B_2 are found to be isostructural. Therefore, particular emphasis in this experiment was placed on the investigation of the La–Co–B and Y–Co–B systems.

The Crystal Structures of $LaCo_2B_2$ and YCo_2B_2. The X-ray diffraction patterns of both ternary borides, $LaCo_2B_2$ and YCo_2B_2, could be indexed on the basis of the tetragonal lattices. The lattice parameters were $a=3.616\pm0.003$ Å and $c=10.215\pm0.005$ Å for $LaCo_2B_2$, and $a=3.561\pm0.002$ Å and $c=9.358\pm0.005$ Å for YCo_2B_2. The agreement between the observed and calculated d-values is excellent, as is shown in Tables 1 and 2. The unit-cell content is $2RCo_2B_2$, and the densities observed are in good agreement with those calculated, as is shown in Table 3.

Table 1. X-Ray diffraction data for $LaCo_2B_2$

hkl	d_{obsd}(Å)	d_{calcd}(Å)	I_{obsd}	I_{calcd}
002	5.11	5.11	13.8	16.9
101	3.410	3.409	53.7	43.0
110	2.555	2.557	45.0	8.6
004		2.554		29.4
103	2.478	2.479	26.4	26.4
112	2.285	2.286	102.6	98.8
200	1.808	1.808	27.9	25.1
114		1.807		6.9
105	1.775	1.779	6.5	9.5
202	1.703	1.704	2.0	3.2
006		1.703		0.7
211	1.598	1.597	8.0	7.8
204	1.475	1.476	22.5	18.9
213	1.460	1.461	5.8	10.0
116	1.417	1.417	22.5	21.1
107	1.353	1.353	1.0	2.1
220	1.277	1.278	6.6	4.2
008		1.277		4.3
215	1.269	1.268	10.5	6.9
222	n. obs.	1.240	0	1.9
206	n. obs.	1.240	0	1.9
301	1.200	1.197	1.5	2.4
310	1.144	1.144	16.2	1.4
224		1.143		12.4
118	1.141	1.142	1.3	1.3
303	1.135	1.136	5.0	3.7
312	1.116	1.116	30.5	29.7
217	1.084	1.083	5.6	5.9
109		1.083		2.9
314	1.043	1.044	28.2	5.9
208		1.043		21.7
305	1.039	1.043	5.3	5.2
226	1.022	1.022	2.4	2.6

$B=0.85$, $R=0.148$

Table 2. X-Ray diffraction data for YCo_2B_2

hkl	d_{obsd}(Å)	d_{calcd}(Å)	I_{obsd}	I_{calcd}
002	4.678	4.679	5.5	4.3
101	3.319	3.328	43.2	47.4
110	n. obs.	2.518	0	0.1
103	2.344	2.346	63.6	24.2
004		2.340		29.0
112	2.215	2.217	93.8	95.1
200	1.781	1.781	23.4	25.7
114	n. obs.	1.714	0	1.1
202	n. obs.	1.664	0	0.3
105	1.656	1.657	9.3	8.8
211	1.570	1.570	4.3	6.9
006	n. obs.	1.560	0	0.1
213	1.418	1.418	25.1	11.0
204		1.417		18.5
116	1.326	1.326	24.6	18.1
220	1.258	1.259	5.3	9.5
107	1.251	1.252	3.4	2.8
222	n. obs.	1.216	0	0.1
215	1.213	1.213	6.4	8.5
301	1.177	1.178	4.2	2.8
206	n. obs.	1.173	0	0.1
008	1.169	1.170	6.2	4.4
310	n. obs.	1.126	0	0.0
303	1.109	1.109	25.6	4.6
224		1.109		17.2
312	1.094	1.095	15.4	35.3
118	n. obs.	1.061	0	0.2
217	1.025	1.024	8.1	8.4
314	n. obs.	1.015	0	1.0
305	1.002	1.002	10.5	8.2
109	0.997	0.998	4.2	5.8
312	0.982	0.982	17.5	16.5
226	n. obs.	0.980	0	0.3
208	0.978	0.978	64.5	66.4

$B=0.74$, $R=0.142$

Table 3.

It may be seen from Tables 1 and 2 that there is systematic absence of reflections when $h+k+l=2n+1$. Therefore, the possible space groups are 14, $1\bar{4}$, 14/m, 1422, 14 mm, 14 m2, and 14/mmm. The structures of $LaCo_2B_2$ and YCo_2B_2 were considered to be similar to that of $ThCr_2Si_2$ because the lattice parameters and X-ray diffraction intensities of these three compound appeared to be similar to one another. The structure of $ThCr_2Si_2$[10–13] belongs to the $BaAl_4$ type, whereby the two nonequivalent sites of aluminium are occupied by crominum and silicon. The X-ray diffraction intensities were calculated on the assumption, by analogy with the $ThCr_2Si_2$ structure, that the atomic

9) W. H. Zachariazen, *Acta Crystallogr.*, **4**, 231 (1951).

10) Z. Ban and M. Sikirica, *ibid.*, **18**, 594 (1965).

11) Z. Ban and M. Sikirica, *Z. Anorg. Allg. Chem.*, **356**, 96 (1967).

12) O. I. Bodak, E. I. Gladysheuskii and P. I. Kripyyakeuichi, *Izv. Akad. SSSR, Neorg. Mat.*, **2**, 2151 (1966).

13) O. S. Zarechnyuk, P. I. Kripyyakeuich, and E. J. Gladysheusku, *Sov. Phys. Chem.*, 9, 706 (1965).

configurations of $LaCo_2B_2$ and YCo_2B_2 are as follows: space group 14/mmm (D_{4h}^{17}), 2R in 2(a), 4Co in 4(d), and 4B in 4(e). In this structure, the positions of the rare-earth and cobalt atoms are fixed by symmetry and the only variable parameter is z, which defines the positions of the boron atoms. The value of the z-parameter was assumed to be 3/8 from the geometrical argument for $LaCo_2B_2$ and YCo_2B_2.

The calculated intensities were derived from:

$$\mathbf{I}(\text{cal}) \propto p \frac{1+\cos^2 2\theta}{\sin^2\theta \cdot \cos} |\mathbf{F}|^2$$

where p is the multiplicity, θ is the Bragg diffraction angle, and $\mathbf{F}$ is a structure factor. The structure factors were calculated from the atomic coordinates (x_n, y_n, z_n) and the total atomic scattering factors, f_n:

$$\mathbf{F} = \sum_n f_n \exp 2\pi i(hx_n + ky_n + lz_n)$$

$$f_n = f_0 + \Delta f_n' + i\Delta f_n''$$

where f_0 is the atomic scattering factor for radiation with a frequency much higher than any absorption edge, and where $\Delta f_n'$ and $\Delta f_n''$ are the real and imaginary dispersion corrections respectively. The respective values of $\Delta f_n'$ for Y, La, Co, and B were -0.56, -7.09, -1.74, and 0, while those of $\Delta f_n''$ were 3.08, 12.45, 0.84, and 0.[14] The correction of the absorption by the sample was not employed because the absorption does not depend on the diffraction angle in the case of the diffractometer. The temperature factor was found by a least-squares solution of the plot of $\log |\mathbf{I}_{cal}/\mathbf{I}_{ob}|$ *vs* $(\sin\theta/\lambda)^2$.

In the calculation of the X-ray diffraction intensities for YCo_2B_2[5] previously reported, we did not employ any corrections for the abnormal dispersion in the structure factor or for the temperature dependence. Therefore, the calculation in present paper is more accurate.

The observed and calculated intensities of $LaCo_2B_2$ and YCo_2B_2 are summarized in Tables 1 and 2. The temperature factors for $LaCo_2B_2$ and YCo_2B_2 were 0.85 and 0.74 respectively. The reliability factor, $R = \sum_{hkl} |I_{obs} - I_{cal}| / \sum_{hkl} I_{obs}$, is 0.148 and 0.142 for $LaCo_2B_2$ and YCo_2B_2 respectively.

From these results, it can be considered that the rare earth and cobalt atoms occupy the 2(a) and 4(d) sites respectively. The variable parameter, z, however, could not be evaluated with sufficient accuracy because of the small atomic scattering factor of the boron atoms. In general, the boron atoms of the binary borides,[15] such as Re_3B, Pd_3B, Cr_5B_3, and Pd_5B_3, are situated at the center of the trigonal prism formed by six metal atoms. In the ternary borides,[16] such as Mo_2CoB_2, Mo_2NiB_2, W_2FeB_2, W_2CoB_2, and W_2NiB_2, with U_3Si_2-type structure, the boron atoms are also situated at the center of the trigonal prism formed by two kinds of metals. On the other hand, it is impossible to consider that the boron atoms occupy the 4(c) site in the 14/mmm space group with respect to the atomic sizes of rare earth, cobalt, and boron, and the coordination of the boron atoms.

Thus, from these geometrical arguments it is reasonable to think that the boron atoms in $LaCo_2B_2$ and YCo_2B_2 occupy the 4(e) site and that the z-parameter is about 3/8. The crystallographic data for $LaCo_2B_2$ and YCo_2B_2 are summarized in Table 3.

Table 3. Crystallographic data for $LaCo_2B_2$ and YCo_2B_2

	$LaCo_2B_2$	YCo_2B_2
Symmetry	Tetragonal	Tetragonal
Lattice parameter (Å)	$a=3.616\pm0.003$ $c=10.215\pm0.005$ $c/a=2.825$	$a=3.561\pm0.003$ $c=9.358\pm0.005$ $c/a=2.628$
Molecule per unit cell	2	2
Density (g/cm^3)	$\rho_{obsd}=6.88$ $\rho_{calcd}=6.92$	$\rho_{obsd}=6.30$ $\rho_{calcd}=6.39$
Space group	14/mmm(D_{4h}^{17})	14/mmm(D_{4h}^{17})
Atom position	$\left(0,0,0;\frac{1}{2},\frac{1}{2},\frac{1}{2}\right)+$ 2La in 2(a) (0, 0, 0) 4Co in 4(d) $\left(0,\frac{1}{2},\frac{1}{4}\right)$ $\left(\frac{1}{2},0,\frac{1}{4}\right)$ 4B in 4(e) (0, 0, z) (0, 0, $\bar{z}$) $z\sim3/8$	$\left(0,0,0;\frac{1}{2},\frac{1}{2},\frac{1}{2}\right)+$ 2Y in 2(a) (0, 0, 0) 2Co in 4(d) $\left(0,\frac{1}{2},\frac{1}{4}\right)$ $\left(\frac{1}{2},0,\frac{1}{4}\right)$ 4B in 4(e) (0, 0, z) (0, 0, $\bar{z}$) $z\sim3/8$
Interatomic distances (Å)	La–Co=3.13 La–B=2.86 Co–B=2.21 B–B=2.55	Y–Co=2.94 Y–B=2.78 Co–B=2.13 B–B=2.34

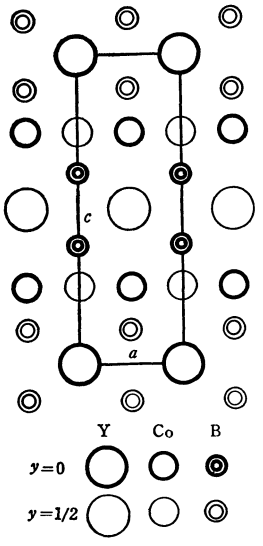

Fig. 1. The projection of RCo_2B_2 structure on (010).

14) D. T. Cromer, *Acta Crystallogr.*, **18**, 17 (1965).
15) B. Aronsson, "Borides, Silicides and Phosphides," Edited by B. Aronsson, Methuen and Co. Ltd., London (1965) p. 46.
16) W. Rieger, H. Nowotony, and F. Benesovsky, *Mh. Chem.*, **Bd. 97**, 379 (1965).

TABLE 4. X-RAY DIFFRACTION DATA FOR $NdCo_2B_2$, $SmCo_2B_2$, $GdCo_2B_2$, $TbCo_2B_2$, AND $DyCo_2B_2$

hkl	Int.	$NdCo_2B_2$		$SmCo_2B_2$		$GdCo_2B_2$		$TbCo_2B_2$		$DyCo_2B_2$	
		d_{obsd}	d_{calcd}	d_{obsd}	d_{calcd}	d_{obsd}	d_{calcd}	d_{obsd}	d_{calcd}	d_{obsd}	d_{calcd}
002	m	4.865	4.837	4.823	4.815	4.718	4.769	—	4.710	—	4.667
101	s	3.342	3.351	3.340	3.340	3.347	3.346	3.326	3.328	3.320	3.317
110	w	2.518	2.523	—	2.519	2.520	2.526	—	2.515	2.506	2.509
004	s	2.437	2.437	2.410	2.408	2.386	2.385	2.355	2.355	2.340	2.339
103	m	2.403	2.402	2.386	2.385	2.375	2.376		2.354		2.342
112	vs	2.243	2.241	2.232	2.232	2.233	2.233	2.219	2.219	2.210	2.210
200	m	1.786	1.784	1.782	1.782	1.784	1.787	1.777	1.779	1.774	1.773
105	w	1.710	1.711	1.695	1.694	1.684	1.683	1.663	1.665	1.652	1.655
211	w	1.574	1.575	1.572	1.572	1.575	1.576	1.568	1.569	1.563	1.564
204	m	1.439	1.440	1.431	1.432	1.427	1.430	1.418	1.419	1.415	1.413
213	w	1.432	1.432	1.429	1.427		1.428		1.419		1.414
116	m	1.366	1.366	1.353	1.354	1.345	1.346	1.334	1.322	1.323	1.324
107	vvw	1.299	1.297	1.257	1.260	1.271	1.273	1.258	1.259	1.249	1.251
220	vw	1.252	1.262		1.253	1.262	1.263		1.258	1.254	1.254
215	vvw	1.233	1.235	1.227	1.228	1.224	1.225	1.215	1.215	1.212	1.210
222	vw	1.220	1.221	1.221	1.219		1.221		1.215		1.211
008	vw		1.218	1.203	1.204	1.191	1.193	1.177	1.177	1.169	1.169
301	vvw	1.181	1.181	1.179	1.179	1.182	1.182		1.176	1.173	1.173
310	vvw	1.126	1.128	—	1.127	—	1.130	1.126	1.125	1.121	1.121
224	m	1.121	1.120	1.116	1.116	1.116	1.116	1.109	1.109	1.105	1.105
303	w	1.117	1.117	1.113	1.114		1.115		1.109		1.105
312	m	1.101	1.099	1.096	1.097	1.099	1.100	1.094	1.094	1.090	1.090
217	w	1.050	1.049	1.044	1.041	1.037	1.037	1.029	1.027	1.021	1.022

TABLE 5. LATTICE PARAMETERS OF TETRAGONAL RCo_2B_2

R	Lattice parameters (Å)		Density (g/cm³)	
	a	*c*	ρ_{obsd}	ρ_{calcd}
La	3.616±0.003	10.215±0.005	6.88	6.92
Nd	3.586±0.005	9.747±0.007	7.49	7.52
Sm	3.563±0.003	9.630±0.007	7.70	7.83
Gd	3.573±0.003	9.540±0.005	8.02	8.09
Tb	3.557±0.004	9.419±0.007	8.25	8.31
Dy	3.546±0.004	9.354±0.006	8.50	8.53
Y	3.561±0.003	9.358±0.005	6.30	6.39

Figure 1 shows the projection of the RCo_2B_2 structure on the (010) plane. As is shown in Fig. 1, each boron atom is situated at the center of a trigonal prism formed by the four rare earth atoms and the two cobalt atoms. The interatomic distances of 4R–B and 2Co–B in the trigonal prism are 2.86 and 2.21 for $LaCo_2B_2$, and 2.78 and 2.13 for YCo_2B_2. These values are close to the sum of the corresponding Pauling metallic radii for the 12-coordination of La(1.87 Å), Y(1.78 Å), Co(1.25 Å), and B(0.98 Å).

The X-Ray Diffraction Data for RCo_2B_2 (R=Nd, Sm, Gd, Tb, and Dy). The RCo_2B_2 compounds were found to be crystallized isostructurally with $LaCo_2B_2$ and YCo_2B_2, since the X-ray diffraction data of these samples were similar to those of $LaCo_2B_2$ and YCo_2B_2. The X-ray diffraction data are shown in Table 4 for $NdCo_2B_2$, $SmCo_2B_2$, $GdCo_2B_2$, $TbCo_2B_2$, and $DyCo_2B_2$. As is shown in this table, there is a good agreement between the observed and calculated *d*-spacings. Efforts to prepare $CeCo_2B_2$ and $ErCo_2B_2$ by arc-melting were unsuccessful. The failure to obtain these compounds may be caused by a decomposition process occurring during the arc-melting.

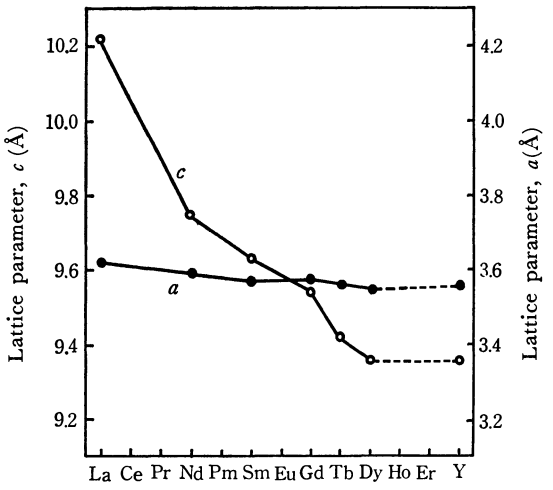

Fig. 2. The variation of the lattice parameters for RCo_2B_2 with the atomic number.
The open circles: the *c* parameter, The closed circles: the *a* parameter.

The lattice parameters of the RCo_2B_2 compounds obtained in this study are summarized in Table 5, while their variation with the atomic number is plotted in Fig. 2. The contraction in the *c* parameter against the atomic number of the rare earth elements is approximately 10 percent, about the same as that of the rare-earth metals. On the other hand, the *a* parameter is fairly constant, decreasing only slightly with the atomic number of the rare earth elements.

The Mechanism of the Lumiflavin-sensitized Photooxygenation of Tryptophan Accelerated by Adenine

Akio YOSHIMURA and Shunji KATO

Institute of Chemistry, College of General Education, Osaka University, Toyonaka, Osaka

(Received August 10, 1972)

It was found that the lumiflavin-sensitized photooxygenation of tryptophan in a dilute aqueous solution is greatly accelerated by the addition of adenine. This effect of adenine on the photosensitized oxygenation is specific for flavin dyes, and the quantum yield increases with the oxygen concentration at very low oxygen concentrations, but decreases at higher oxygen concentrations. Therefore, singlet oxygen can be excluded from the intermediates of this oxidative reaction. The oxygen adduct of the dye is considered to be a possible intermediate for the photooxygenation of tryptophan accelerated by adenine.

The photosensitized inactivation of various enzymes has been studied by many investigators[1] and is known to be a sort of photodynamic action. Uehara *et al.* have shown that the riboflavin-sensitized photoinactivation of yeast alcohol dehydrogenase [EC 1.1.1.1] is greatly accelerated by the addition of adenine.[2] The present authors expected that such a photoinactivation promoted by adenine might result from the photosensitized decomposition of some components which constitute the enzyme. After examining several substances, it was found that adenine similarly promotes the lumiflavin-photosensitized oxygenation of indoles, including tryptophan, indole-3-acetic acid, and serotonin, which are biologically important substances in dilute aqueous solutions. Therefore, in this paper we will examine this interesting phenomenon from the viewpoint of photochemical kinetics and will discuss the mechanism of the flavin-sensitized photooxygenation of indoles. Lumiflavin was chosen as the sensitizer in this research because it is much more stable against irradiation than such a flavin dye as riboflavin, which has a reducible ribityl side chain. The function of lumiflavin in the sensitized photooxygenation of indoles seems equal to that of other flavin dyes, such as riboflavin, flavin mononucleotide (FMN), and flavin adenine dinucleotide (FAD), because adenine promotes the photosensitizing action of these flavin dyes.

Experimental

Materials. Lumiflavin was prepared from riboflavin (Wako Pure Chemical Co., Ltd.) in the way described by Kuhn *et al.*,[3] and the purity was confirmed by paper chromatography with Toyo Roshi No. 51A paper (*n*-butanol: acetic acid: water, 4 : 1 : 5 by volume, ascending). (Found: C, 60.75; H, 4.70; N, 20.92%. Calcd for $C_{13}H_{12}N_4O_2$: C, 60.93; H, 4.72; N, 21.82%.) The other chemicals used were of G. R. grade. Redistilled water was used throughout.

Apparatus and Procedure. The photolysis was carried out in a quartz reaction cell (1×1×4 cm) with a glass tube inlet, set in a reaction apparatus as in Ref. (4), thermostated (30±0.1°C) with circulated water. Light from a Toshiba SHL-100UV-2 Hg lamp was passed through Toshiba filters VV-40 and VY-43, and an almost monochromatic radiation of 435.8 nm was obtained. The intensity of the illumination was determined by means of the potassium ferrioxalate actinometry described by Hatchard and Parker.[5]

All the experiments were carried out in a 0.05 M phosphate buffer at pH 7.2. The pH values of sample solutions were measured with a Hitachi-Horiba M-5 pH meter. The solution was bubbled before irradiation with a mixture of oxygen and nitrogen of a known composition, and the concentration of the dissolved oxygen was calculated by the use of Ostwald's absorption coefficient of oxygen in water, disregarding the effect of dissolved substances. The deaerated solution was prepared by five cycles of freezing-pumping-thawing by the use of a mercury diffusion pump.

The tryptophan concentration was followed by the fluorometric method, using a Hitachi MPF-2A fluorescence spectrophotometer. For the fluorometry, the exciting light was reduced enough so as not to cause photolysis during the measurement. Since the fluorescence of tryptophan is very sensitive to changes in the temperature,[6] care was taken to keep control solution in the thermostat and then to transfer it into the fluorometer compartment together with the samples. The excitation of dilute tryptophan for the fluorometry was done at its absorption maximum, 285 nm. In order to determine concentration of tryptophan higher than 50 μM, the sample solutions were diluted for every measurement of a fluorescence or a different wavelength with less absorbance was used as the exciting light, so that a linear relationship was kept between the fluorescence intensity and the concentration of tryptophan. It was confirmed that the reaction products do not quench the fluorescence of tryptophan. Accordingly, the fluorometry of the reaction system measures the true concentration of tryptophan in these experiments. The reaction quantum yields were always calculated from the initial reaction rate in order to avoid the effects of products, because such products retarded the photosensitized oxygenation of tryptophan.

Results and Discussion

Figure 1 shows the quantum yield of the lumiflavin-sensitized photooxygenation of tryptophan in solutions which contain 0—0.2 mM adenine, plotted against

1) A. D. McLaren and D. Shugar, "Photochemistry of Proteins and Nucleic Acids," Pergamon Press, Ltd., Oxford, England (1964), p. 156.

2) K. Uehara, M. Yonezawa, S. Hosomi, and R. Hayashi, *J. Biochem.* (Tokyo), **60**, 721 (1966).

3) R. Kuhn, H. Rudy, and T. Wagner-Jauregg, *Ber.*, **66**, 1950 (1933).

4) S. Kato, Y. Usui, and M. Koizumi, This Bulletin, **36**, 1523 (1963).

5) C. G. Hatchard and C. A. Parker, *Proc. Roy. Soc. Ser. A*, **235**, 518 (1956).

6) J. Eisinger and G. Navon, *J. Chem. Phys.*, **50**, 2069 (1969).

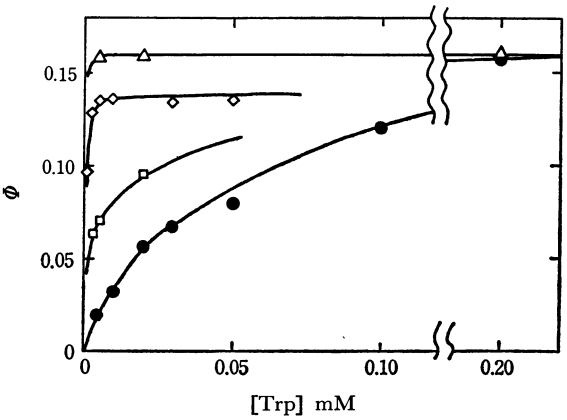

Fig. 1. Plots of quantum yields of photosensitized oxygenation of tryptophan by 2.5 μM lumiflavin against the concentration of tryptophan in 0.05 M phosphate buffer at pH 7.2, containing 0.23 mM oxygen and adenine: ● 0 mM, □ 0.04 mM, ◇ 0.1 mM, △ 0.2 mM.

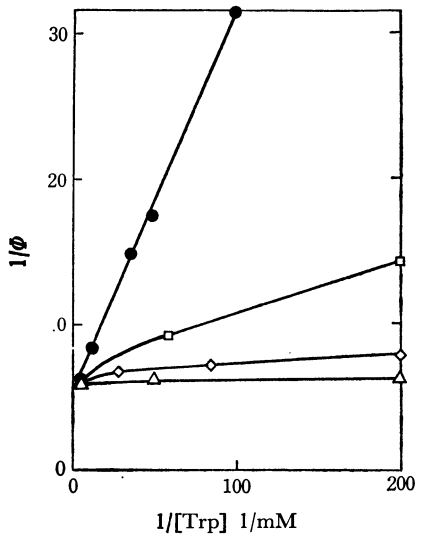

Fig. 2. $1/\Phi$ plotted against 1/[Trp].
$[O_2]$; 0.23 mM and [Adenine]; ● 0 mM, □ 0.04 mM, ◇ 0.1 mM, △ 0.2 mM.

the concentration of tryptophan. Figure 2 shows that a linear relationship holds between the reciprocal of the quantum yield of photooxygenation and the reciprocal of the tryptophan concentration in the absence of adenine. The acceleration of this reaction by the addition of adenine is shown as a decrease in the slope in Fig. 2. As is evident from these figures, the addition of adenine enhances the quantum yield greatly at a very low concentration of tryptophan, but it little affects the yield at a higher concentration. Adenine seems to act as a unit, keeping the memory of irradiation in the face of quenching actions until the oxygenation of tryptophan occurs.

Such an effect of adenine was observed for the photooxygenation of indoles when lumiflavin, riboflavin, FMN, or FAD (all these are flavin dyes), is used as the sensitizer, while it was not observed for the systems with rose bengal, methylene blue, thiopyronine, or fluorescein as the sensitizer, as is shown in Table 1. Table 1 also shows that this accelerating effect of adenine is

Table 1. Effect of 0.1 mM adenine on the photosensitized oxygenation of indoles containing 0.23 mM oxygen by various dyes

Substrate	Dye	Φ_0[a]	Φ_A/Φ_0[a]
Tryptophan[b]	Lumiflavin[d]	0.023	6.7
	Riboflavin[d]	0.024	6.4
	FMN[d]	0.022	7.4
	FAD[d]	0.006	6.2
	Rose bengal[e]	—	1.0
	Methylene blue[e]	—	0.9
	Thiopyronine[e]	—	1.0
	Fluorescein[e]	—	1.0
Indole[b]	Lumiflavin[d]	0.038	4.0
Serotonin[b]		0.026	5.6
Indole-3-acetic acid[b]		0.040	6.0
Bovin serum albumin[c]		—	11.3

a) Φ_0=quantum yield without adenine, Φ_A=quantum yield with adenine. b) [Substate]=5 μM. c) [BSA]=15 μg/ml ([Tryptophan residue]=0.5 μM). d) [Dye]=2.5 μM, Irradiation=436 nm. e) [Dye]=5 μM, Irradiation=through UV cut-off glass filter.

observed for the flavin-sensitized photooxygenation of such indoles as indole, tryptophan, serotonin, indole-3-acetic acid, and bovin serum albumin (BSA).

Although it is known that adenine forms a molecular complex with flavin in a concentrated solution, the association constant has been estimated to be about 100 l/mol and the addition of 0.2 mM adenine decreases the fluorescence of lumiflavin by only 2%. Therefore, such a large increment of the reaction quantum yield by the addition of adenine can be explained neither by the formation of a ground-state lumiflavin-adenine complex nor by the attack of adenine on the excited singlet state of lumiflavin.

This accelerating effect of adenine is not accounted for by the energy transfer mechanism to adenine, either, because the energy level of the adenine triplet state[7] is higher than that of lumiflavin.[8]

The mechanism of many dye-sensitized photooxygenation reactions have recently been considered to involve singlet oxygen.[9] Among the dyes examined in the present work, rose bengal and some others might sensitize the oxidation through singlet oxygen. However, flavin dyes cannot be the case, because adenine is effective only when flavin dyes is used as sensitizers.

When a solution of 5 μM tryptophan and 10 μM lumiflavin in a 0.05 M phosphate buffer (pH 7.2) was irradiated under deoxygenated conditions, the fluorescence of tryptophan increased by 15% and the photofading of lumiflavin occurred slowly. For a similar solution of 5 μM indole instead of tryptophan, a slow photofading of the lumiflavin and a very slight change in the fluorescence of indole took place. Photofading also occurred slowly when lumiflavin alone was irradiated under deoxygenated conditions. Therefore, it may be said that the cleavage of the indole ring does not occur in the deoxygenated conditions, and that

7) J. W. Longworth, R. O. Rahn, and R. G. Shulman, *J. Chem. Phys.*, **45**, 2930 (1966).
8) W. E. Kurtin and P. S. Song, *Photochem. Photobiol.*, **9**, 127 (1969).
9) K. Gollnick, *Adv. Photochem.*, **6**, 1 (1968).

the product of the oxidative deamination of tryptophan accompanied by the photoreduction of lumiflavin[10] fluoresces more than tryptophan.[11] This reaction under the deoxygenated condition was not affected by the addition of adenine; therefore, the reaction mechanism is considered to have no correlation with that for photosensitized oxygenation.

Oxygen is one of the substrates of the photosensitized cleavage reaction of the indole ring; the effect of the concentration of dissolved oxygen on the quantum yield of the photooxygenation is shown in Fig. 3. This figure shows that the quantum yield increases with the oxygen concentration at very low oxygen concentrations, but decreases at higher concentrations; that is, oxygen also acts as a quencher. An optimum oxygen concentration for the photosensitized oxygenation of 5 μM tryptophan was about 10 μM, which is much lower than that of an air-saturated solution (0.23 mM). Under such conditions, the fluorescence of lumiflavin was not actually quenched by oxygen. The possibility of a reaction mechanism including singlet oxygen generated by the lumiflavin triplet state was obviated by this retarding effect of oxygen as well as by the selective accelerating effect of adenine.

A similar dependence of a reaction's quantum yield on the oxygen concentration was found by Bellin and Yankus[12] in the photooxygenation of histidine by rose bengal, and by Knowles and Mautner[13] for the lumiflavin-sensitized photooxygenation of nucleotides. The former authors suggested the quenching of a reaction intermediate, "photoperoxide." The latter ones proposed that the primary reaction is between the dye triplet state and the nucleotide, and that oxygen is involved in a later stage.

The dependence of the reaction quantum yield on the oxygen concentration in the presence of adenine is also shown in Fig. 3. Adenine apparently prevents the reaction intermediate from being quenched by oxygen, but at higher oxygen concentrations the protecting effect is not complete. The retarding action of oxygen on the photooxygenation reaction was apparently observed when the tryptophan concentration was low, but it was not evident when the concentration was high or when adenine was added. This behavior of oxygen implies that the retarding action of oxygen competes with the oxidation process of tryptophan or with a process involving adenine, followed by the oxidation of tryptophan.

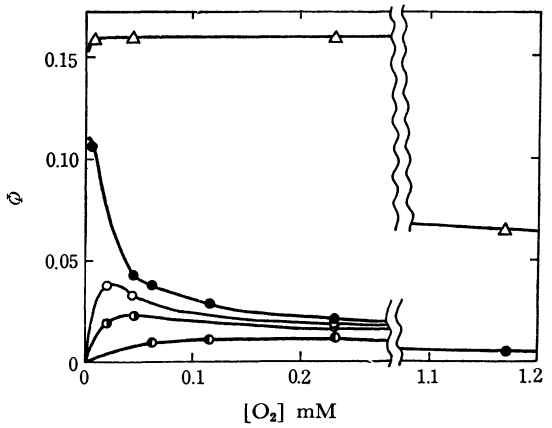

Fig. 3. Effect of dissolved oxygen concentration on the quantum yield of photosensitized oxygenation of 5 μM tryptophan with 2.5 μM lumiflavin in 0.05 M phosphate buffer at pH 7.2, ● alone, and containing △ 0.2 mM adenine, ○ 5 μM KI, ◑ 10 μM KI, ◐ 50 μM KI.

The fluorescence of lumiflavin is little affected by oxygen, tryptophan, or adenine, as has been mentioned above. Therefore, it can be expected that these reactions start from the triplet state of lumiflavin. This was confirmed by an experiment using the iodide ion as a triplet quencher. When potassium iodide is added to the reaction system, the quantum yield of the photooxygenation decreases, as is shown in Fig. 3. The fact that the quenching efficiency decreases with the oxygen concentration shows that oxygen attacks the triplet state of the dye, competing with the iodide ion. The variation in the ratio of the quantum yield (Φ_0/Φ) with the change in the concentration of KI is shown in Fig. 4; a Stern-Volmer-type relation is obtained. This figure also presents the following results.

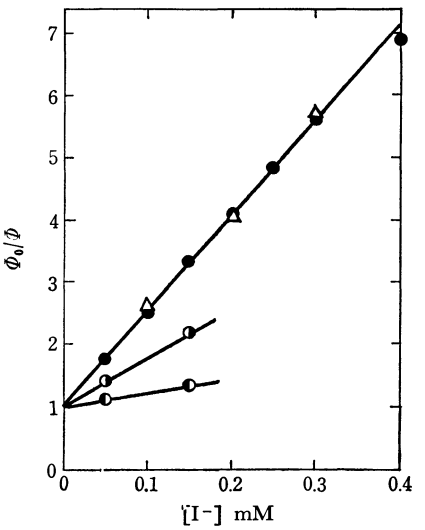

Fig. 4. Effect of KI upon the ratio of quantum yield (Φ_0/Φ) for photosensitized oxygenation of 0.005 mM (●, △), 0.05 mM (◑), and 0.5 mM (◐) tryptophan, alone (●, ◑, ◐), and with 0.2 mM adenine (△).

As the tryptophan concentration increases, the slopes of the plots decrease; that is, tryptophan as well as oxygen competes with the iodide ion. Moreover, the finding that adenine does not affect the quenching action of the iodide ion shows that adenine does not directly attack the triplet state of the dye. Under these conditions, the oxidation of the iodide ion to I_3^- was not detected by the iodine-starch reaction.

We now propose the following reaction scheme, which satisfies all the results mentioned above. In this scheme, D_0, $^1D^*$, and $^3D^*$ denote the ground state,

10) P. Byrom and J. H. Turnbull, *Photochem. Photobiol.*, **6**, 125 (1967).
11) R. W. Ricci, *ibid.*, **12**, 67 (1970).
12) J. S. Bellin and C. A. Yankus, *Arch. Biochem. Biophys.*, **123**, 18 (1968).
13) A. Knowles and G. N. Mautner, *Photochem. Photobiol.*, **15**, 199 (1972).

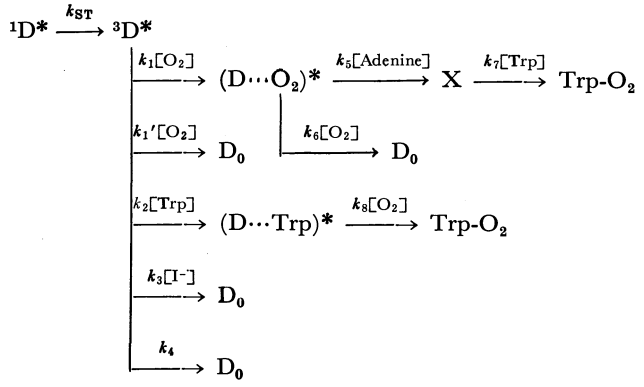

the first excited singlet state, and the triplet state of lumiflavin respectively. The triplet state of lumiflavn reacts with oxygen, tryptophan, and the iodide ion, but not with adenine, and a linear relationship between $1/\Phi$ and the inverse of the tryptophan concentration can be expected. From the kinetical data, it was estimated that $k_2 \approx k_3 \approx k_4(k_1+k_1')$ and $k_5 \approx 4k_6$. We have no other explicit evidence about $(D\cdots O_2)^*$, but it must be taken into consideration in explaining the accelerating effect of adenine. The intermediate, $(D\cdots O_2)^*$, reacts with adenine to form "X," which reacts finally with tryptophan with very great efficiency. From this reaction mechanism in the presence of adenine, the process in which $(D\cdots O_2)^*$ reacts directly with tryptophan may be possible, but was poorly proved.

In this investigation, the reaction could easily be followed in a very low concentration of the substrate because fluorometry is a sensitive method for analyzing indoles. This is the reason why the promoting effect of adenine on the photosensitized oxygenation was apparently observed and could be analyzed kinetically. In the case where the components of biochemical macromolecules, such as proteins and nucleic acids, are photochemically sensitive, the substrate concentration must usually be very low. This is the case in which Uehara found an anomalous promoting effect of adenine on the flavin-sensitized photoinactivation of enzymes. The authors are inclined to think that analogous phenomena will be found if kinetical experiments are done under very dilute conditions of the substrates.

The authors would like to express their gratitude to Professor Kihachiro Uehara for his helpful discussions.

BULLETIN OF THE CHEMICAL SOCIETY OF JAPAN, VOL. 46, 1144—1148 (1973)

ESR Study of γ-Irradiated Ammonia–Silica Gel System

Siro NAGAI

Osaka Laboratory for Radiation Chemistry, Japan Atomic Energy Research Institute, Mii, Neyagawa-shi, Osaka 572

(Received September 22, 1972)

Ammonia–silica gel system was γ-irradiated at -196 °C. ESR spectrum observed from samples with low ammonia content showed a marked linewidth anomaly in the hf lines at -196 °C and changed with temperature reversibly. The free radical responsible for the spectrum was assigned to NH_2 radical which undergoes a preferential rotation about an axis perpendicular to the radical plane at low temperatures and a substantially free rotation above -90 °C.

In the previous papers[1-4] of our ESR studies on the γ-irradiated adsorbed systems, we reported the structures of free radicals produced at -196 °C and also the effects of temperature on the ESR spectra. The investigation of the temperature effects on the spectra gave us some informations concerning not only to the structural change but also to the thermal motion of adsorbed radicals. The change of the structure was observed in adsorbed methylbenzenes where monomer cations formed by γ-irradiation at -196 °C change to the corresponding dimer cations by raising the temperature.[2] Restricted motion of adsorbed radicals was suggested from the asymmetry and/or linewidth variations appeared in the spectra.[2-4] More detailed analysis as for the motion on silica gel, however, can be made when we can observe ESR spectra of adsorbed radicals containing some nucleus with a larger anisotropy in the hf interaction. In this viewpoint, NH_2 radical is suitable for such study because of the large anisotropy in the nitrogen splitting.[5]

Experimental

NH_3 was obtained commercially from Takachiho Trading Co. Ltd. Deuterated ammonia ND_3 was synthesized from Mg_3N_2 and D_2O in an evacuated system. $^{15}NH_3$ was synthesized from $(^{15}NH_4)_2SO_4$ (^{15}N atom 90%) and NaOH. Silica gel was the same as that reported.[2] For deuteration of silica gel, the heat-treated gel was immersed in D_2O at 100 °C for 2—3 hr and then degassed at 500 °C *in vacuo*. The other procedures employed in the present study were the same as those described in the previous paper.[2]

1) S. Nagai, S. Ohnishi, and I. Nitta, *J. Phys. Chem.*, **73**, 2438 (1969).
2) S. Nagai, S. Ohnishi, and I. Nitta, This Bulletin, **44**, 1230 (1971).
3) S. Nagai, S. Ohnishi, and I. Nitta, *Chem. Phys. Lett.*, **13**, 379 (1972).
4) S. Nagai, S. Ohnishi, and I. Nitta, This Bulletin, **45**, 1934 (1972).
5) J. R. Morton and D. R. Smith, *Can. J. Chem.*, **44**, 1951 (1966).

Results and Discussion

ESR Spectra at Low Temperature. ESR spectra of adsorbed ammonia after γ-irradiation at −196°C were dependent on the ammonia content. In the samples with the content larger than the monolayer value 2×10^{-3} mol/g, the observed spectrum consists of poorly resolved nine lines and is similar to that of NH_2 radical in solid ammonia matrix.[6-8] When the ammonia content was below the monolayer coverage, the complex spectrum shown in Fig. 1a was observed predominantly. It consists of a dominant quintet with a central triplet splitted by 25 gauss and outermost broad signals, and several weak lines. The spectrum arises from single species in view of the thermal behavior to be discussed later. When the ammonia content became still lower, the spectrum showed additional weak signals other than the predominant one described above(see Fig. 1b). No change was observed in the overall feature of the spectrum when the adsorption amount was further reduced.

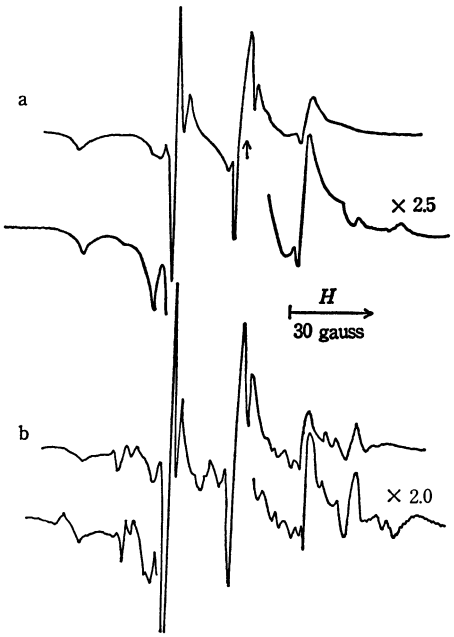

Fig. 1. ESR spectra of γ-irradiated ammonia-silica gel at $^{14}NH_3$ content, a; 1.1×10^{-3} mol/g, and b; 1.2×10^{-4} mol/g. The arrow in a denotes the position of DPPH signal.

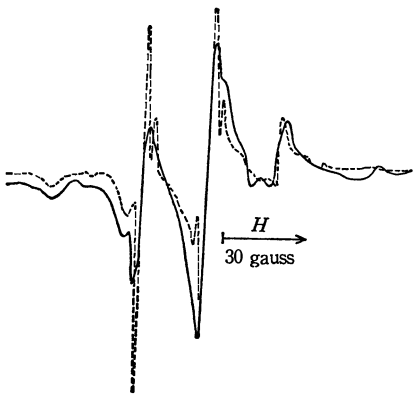

Fig. 2. A comparison of the predominant spectrum on silica gel (broken line) with that of γ-irradiated aqueous ammonia (solid line).

It should be noted that the central triplet in the dominant quintet shows a marked linewidth anomaly, linewidths being 1.9 gauss, 4.8 gauss, and 3.0 gauss from the low field side. A similar triplet spectrum has been previously observed from photolyzed hydrazoic acid in inert gas matrices.[9]

For comparison, frozen aqueous solutions of ammonia were γ-irradiated and examined at −196 °C. When the concentration of ammonia was 30%, the spectrum showed a quintet structure quite similar to that in Fig. 1a (see Fig. 2). ESR spectra of γ-irradiated aqueous ammonia have been previously observed and assigned to NH_2 radical by other workers.[10,11] Al-Naimy *et al.*[10] observed a triplet spectrum similar to the central triplet in our spectrum and assigned it to NH_2 radical with the assumption that the nitrogen splitting is quenched due to the hindered rotation of the radical. Tupikov *et al.*, [11] on the other hand, observed a poorly resolved five-line spectrum and obtained hf splitting values of 24.5 gauss for proton

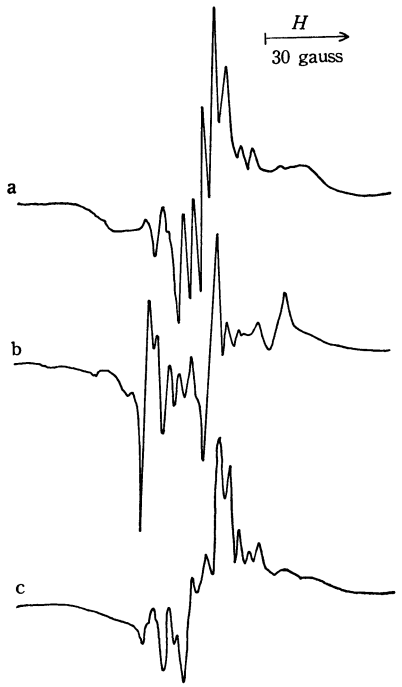

Fig. 3. ESR spectra of γ-irradiated ammonia-silica gel at −196 °C, a; ND_3-deuterated silica gel, b; NH_3-deuterated silica gel, and c; ND_3-silica gel.

6) R. Marx and J. Maruani, *J. Chim. Phys.*, **61**, 1604 (1964).
7) D. R. Smith and W. A. Seddon, *Can. J. Chem.*, **48**, 1938 (1970).
8) V. I. Tupikov, V. I. Tsivenko, S. Ya. Pshezhetskii, A. G. Kotov, and V. K. Milinchuk, *Zh. Fiz. Khim.*, **37**, 138 (1963), V. I. Tupikov and S. Ya. Pshezhetskii, *ibid.*, **37**, 1900 (1963).
9) P. H. H. Fischer, S. W. Charles, and C. A. McDowell, *J. Chem. Phys.*, **46**, 2162 (1967).
10) B. S. Al-Naimy, P. N. Moorthy, and J. J. Weiss, *J. Phys. Chem.*, **70**, 3654 (1966).
11) V. I. Tupikov and S. Ya. Pshezhetskii, *Zh. Fiz. Khim.*, **38**, 2511 (1964).

and 31 gauss for nitrogen. Their value for nitrogen, however, seems to be too large compared with that of the same radical in ammonia matrix.[7] The assignment of the splitting value should be made by taking into account an anisotropic motion of NH_2 radical as shown in the present investigation.

The deuterated samples showed ESR spectra as given in Fig. 3a, b, and c. Fig. 3a is the spectrum of ND_3 adsorbed on deuterated silica gel. The central part of the spectrum consists of five intense lines with a hf splitting value of 4 gauss which is about one-sixth of the value of the central triplet in Fig. 1. The triplet splitting in Fig. 1, therefore, is ascribed to two equivalent protons. Both the spectrum Fig. 3b for NH_3 on deuterated silica gel and the spectrum Fig. 3c for ND_3 on silica gel are well explained by appropriate superpositions of the non-deuterated spectra Fig. 1 and the deuterated spectrum Fig. 3a. The hydrogen-deuterium exchange reaction occurs to some extent.

Temperature Dependence of Spectra. On raising the temperature, the nine-line spectrum of high content samples diminished in intensity without any change of the feature. The spectrum observed from samples with low content, on the other hand, showed a remarkable temperature dependence as represented in Fig. 4. The linewidth anomaly in the central triplet as well as some weak lines observed at low temperature gradually disappeared at higher temperatures. The separation of the outermost broad signals became smaller with temperature while the splitting of the central triplet remained constant in the whole temperature range. Above −90 °C was observed only the narrowing of the widths of the hf lines. On recooling the sample, the lower temperature spectra were reproduced satisfactorily.

The sample with the lower content of adsorbed ammonia showed essentially the same reversible change of the spectrum (see Fig. 5). In addition, the four weak lines indicated by arrows in Fig. 5b increased in intensity at an early stage of the rise of temperature and then diminished above −150 °C. The four-line spectrum might be attributed to NH_3^+ [13] possibly formed by charge transfer reaction from silica gel to adsorbed ammonia. A similar reaction was found to play an important role in the formation of cation radicals of benzene on silica gel.[14]

Assignment of Spectra. The spectra observed above −90 °C consist of nine lines and may be assigned to NH_2 radical with hf splitting values of 25 gauss for proton and 19 gauss for nitrogen. The assignment is supported by studying the spectrum of adsorbed $^{15}NH_3$ after γ-irradiation. An apparent four-line spectrum shown in Fig. 6c is the same as that of $^{15}NH_2$ radical in solid $^{15}NH_3$ matrix.[7] Because the nine-line spectrum for $^{14}NH_2$ and the four-line one for $^{15}NH_2$ are explained by the isotropic values of hf splittings, the adsorbed NH_2 radicals are consi-

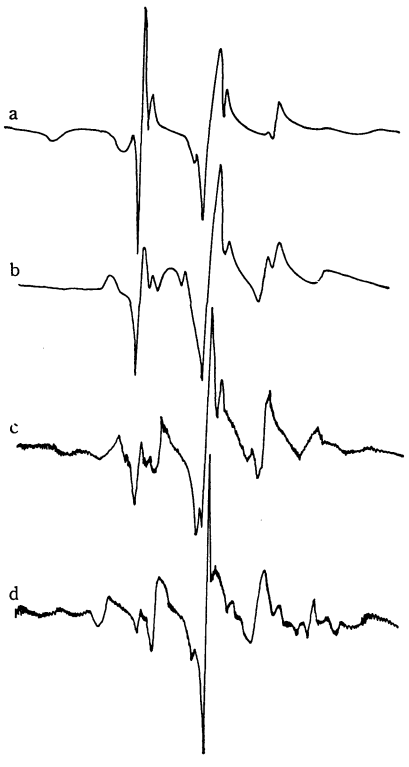

Fig. 4. Change of ESR spectrum of γ-irradiated $^{14}NH_3$–silica gel with $^{14}NH_3$ content; 1.1×10^{-3} mol/g. a; −196 °C, b; −125 °C, c; −90 °C, and d; −30 °C.

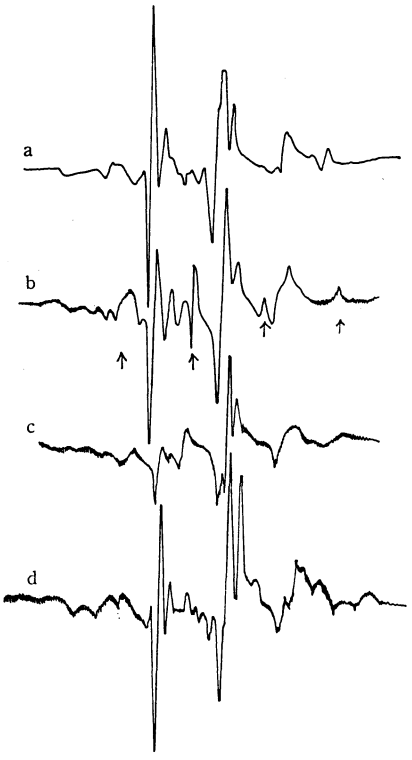

Fig. 5. Change of ESR spectrum of γ-irradiated $^{14}NH_3$–silica gel with $^{14}NH_3$ content; 1.2×10^{-4} mol/g. a; −196 °C, b; −135 °C, c; −90 °C, and d; −196 °C (recooled). Hf lines indicated by arrows in b are most likely due to NH_3^+, see text.

12) O. Kikuchi, This Bulletin, **42**, 1187 (1969).
13) J. S. Hyde and E. S. Freeman, *J. Phys. Chem.*, **65**, 1636 (1961).
14) S. Nagai, S. Ohnishi, and I. Nitta, *Shokubai*, **13**, 48 (1971).

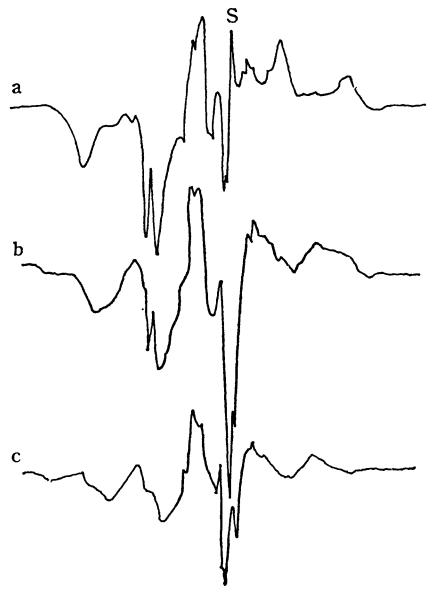

Fig. 6. Change of ESR spectrum of γ-irradiated $^{15}NH_3$–silica gel a; −196 °C, b; −150 °C, and c; −90 °C. A line designated by S in a is due to the silica gel defect.

dered to carry out a substantially free rotation at the relatively high temperatures. The reversible temperature dependence, therefore, arises from motional change of adsorbed NH_2 radicals from fixed or some restricted state at low temperatures to free rotation above −90 °C.

The low temperature spectrum in Fig. 1a can now be explained on the basis of the anisotropic data of NH_2 radical. The ESR data in the coordinate axis system in Fig. 7 are summarized in Table 1. Anisotropies in the proton hf splitting and in the g value are fairly small compared with the anisotropy in the nitrogen splitting. Since the central triplet is due to two protons and the splitting value is constant in the whole temperature range, the other part of the spectrum may be ascribed to the hf splitting of nitrogen. If the separation of the outermost broad signals~114 gauss is assumed to be a sum of hf splittings of proton and nitrogen, a_H and a_N, we obtain

Table 1. ESR data of NH_2 radical

	Isotropic	x	y	z	Ref.
a_N[a,b]	+13.3	−13.1	−12.9	+25.0	5
a_H[b]	−27.3	−4.1	+1.8	+2.3	5
g	2.0037	2.0029	2.0058	2.0023	12

a) Calculated values from $^{15}NH_2$ data in Ref. 5.
b) Splitting values are given in gauss.

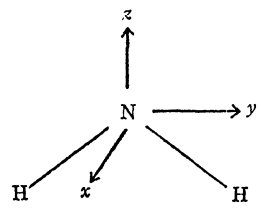

Fig. 7. A coordinate axis system of NH_2 radical.

32 gauss for a_N by taking 25 gauss for a_H from the splitting value of the central triplet. As can be seen from Table 1, such a large value of a_N is expected when the adsorbed NH_2 radical remains immobile or carries out a preferential rotation about z-axis. The rotation hypothesis seems to be more probable in view of the linewidth anomaly in the central triplet as well as the narrow linewidths.

Linewidth Anomaly. The linewidth anomaly similar to that in the central triplet has been often observed in the spectra of adsorbed radicals[2-4] and may arise from the modulation of the anisotropic hf and g tensor interactions coupled with molecular rotation. To shed some light on the nature of the tumbling of NH_2 radical, a qualitative analysis of the triplet was made according to the theory of ESR linewidth in solution.[15,16] The linewitdh of each line of the triplet can be written;

$$T_2^{-1}(M_H) = A + BM_H + CM_H^2 \quad (1)$$

where M_H is the total field-direction component of spin angular momentum for two protons, and A, B and C are parameters. The term B arises from the anisotropic g tensor in conjunction with the anisotropic hf interaction between the unpaired electron and the protons. The theoretical expression for B is given by

$$B = \frac{16}{3} j_H^{(DG_2)}(0) B_0, \quad (2)$$

where B_0 is the external magnetic field and $j_H^{(DG_2)}(0)$ is the spectral density due to the cross term between anisotropic hf and g tensor interactions. Equation (2) is valid for the case that a condition $\omega^2\tau_R^2 \gg 1$ holds, where ω is the angular resonance frequency of the electron, and τ_R the correlation time for molecular tumbling. This condition seems to be satisfied for the central triplet because of the narrow widths, 2—5 gauss.

Relative linewidth of $M_H=-1$ and $M_H=+1$ depends on the sign of B, that is, $T_2^{-1}(-1) < T_2^{-1}(+1)$ for $B>0$, and $T_2^{-1}(-1) > T_2^{-1}(+1)$ for $B<0$.

For the isotropic rotation, the spectral density $j_H^{(DG_2)}(0)$ is given by

$$j_H^{(DG_2)}(0)/\tau_R = \frac{1}{5}\sum_m F_{D,H}^{(m)} F_G^{(-m)}, \quad (3)$$

where $F_{D,H}^{(m)}$ and $F_G^{(-m)}$ are the irreducible tensor components corresponding to the anisotropic hf interaction and g tensor interaction, respectively.

Evaluation of the $F_{D,H}^{(m)}$ and $F_G^{(m)}$ using the values in Table 1 gives

$$\left.\begin{aligned} F_{D,H}^{(0)} &= 24.8 \times 10^6\ \text{sec}^{-1}, \\ F_{D,H}^{(\pm 2)} &= -26.0 \times 10^6\ \text{sec}^{-1}, \\ F_G^{(0)} &= 0.0074 \times 10^6\ \text{sec}^{-1}\ \text{gauss}^{-1}, \\ F_G^{(\pm 2)} &= 0.0065 \times 10^6\ \text{sec}^{-1}\ \text{gauss}^{-1}. \end{aligned}\right\} \quad (4)$$

The spectral density in Eq. (3) becomes using the results in Eq. (4) and $B_0=3260$ gauss as

$$j_H^{(DG_2)} B_0/\tau_R = -1.00 \times 10^{14}\ \text{sec}^{-2}. \quad (5)$$

15) J. H. Freed and G. K. Fraenkel, *J. Chem. Phys.*, **39**, 326 (1963).
16) J. H. Freed, *ibid.*, **41**, 2077 (1964).
17) B. L. Barton and G. K. Fraenkel, *ibid.*, **41**, 695 (1964).

Since $a_H<0$ and $j_H^{(DG_2)}(0)$ and B should have the same sign,[17] B should be negative for the isotropic rotation, which is inconsistent with our spectrum.

When anisotropic rotation is taken into account, the appropriate spectral density can be written in place of Eq. (3),[16]

$$j_H^{(DG_2)}(0) = \frac{1}{5}\sum_{m,m'} F_{D,H}^{(m)} F_G^{(m')} \lambda_{mm'}. \quad (6)$$

where $\lambda_{mm'}$ are functions of the principal values of the molecular diffusion tensor, R_1, R_2, and R_3. In our calculation, the principal axes of the diffusion tensor are chosen as molecule-fixed axes in Fig. 7, that is, R_1, R_2, and R_3 denote the principal values along x, y, and z axis, respectively.

We obtain using Eq. (4);

$$j_H^{(DG_2)}(0)B_0 = [1.20\lambda_{00} - 0.41\lambda_{02} - 2.20\lambda_{22} - 2.20\lambda_{2-2}] \times 10^{14}\,\mathrm{sec}^{-2}. \quad (7)$$

Results of our calculation of Eq. (7) using values $\lambda_{mm'}$ for various ratios of $R_1 : R_2 : R_3$ show that the sign of $j_H^{(DG_2)}(0)$ can be positive only when $R_3 > R_1$, R_2. For the special case of the axial rotation, *e.g.* $R_1 = R_2$, the third principal value R_3 should be larger than twice of R_1. A preferential rotation about z axis, therefore, may explain the observed linewidth anomaly, $T_2^{-1}(-1) < T_2^{-1}(+1)$.

Summary

The dominant species produced in γ-irradiated ammonia–silica gel system is assigned to NH_2 radical. The observed dependence of the ESR spectrum on both the ammonia content in the sample and temperature is due to the motional change of the radical on silica gel surfaces. The NH_2 radical in the high content samples is considered to carry out a substantially free rotation even at −196 °C. The radical produced in the low content samples, on the other hand, carries out a preferential rotation about the axis perpendicular to the radical plane at low temperatures and becomes free above −90 °C.

Finally, the observed dependence of the NH_2 radical spectrum on three matrices, silica gel, frozen aqueous ammonia and solid ammonia, is ascribed to the result of the different environments of the radical.

The author wishes to express his hearty thanks to Professor Isamu Nitta and Professor Shun-ichi Ohnishi for their helpful discussions.

BULLETIN OF THE CHEMICAL SOCIETY OF JAPAN, VOL. 46, 1148—1154 (1973)

Infrared Absorption Spectra of Aminobenzoic Acid Coordination Compounds

Tadaaki INOMATA and Takao MORIWAKI

Department of Chemistry, Faculty of Science and Technology, Sophia University, Chiyoda-ku, Tokyo 102

(Received October 3, 1972)

Several divalent metal–aminobenzoic acid coordination compounds were prepared in aqueous solutions and their thermal analyses, magnetic moments, and infrared spectra were investigated. These coordination compounds have the structure of ML_2 or $ML_2 \cdot nH_2O$ and are coordinated with amino and carboxyl groups of the ligand. Metal–*o*-aminobenzoic acid chelates give approximately the same infrared spectra but metal–*m*- and *p*-aminobenzoic acid coordination compounds are classified into two groups by their infrared spectra. Detailed assignments for the infrared absorption bands of the metal-coordination compounds have been made by a comparison of the spectra with those of the ligand and its related compounds.

The infrared spectra of aliphatic α-amino acid chelates have been investigated in great numbers but not those of metal aromatic amino acid coordination compounds. Hill and Curran[1] prepared several divalent metal–*o*-aminobenzoic acid coordination compounds in aqueous solutions, and showed them to have a *trans* square-planar configuration from their ultraviolet spectra and infrared spectra at about 3200 cm^{-1}.

Several stability constants of metal–*o*-aminobenzoic acid coordination compounds have been reported.[2,3] Decker and Frye[4,5] measured the infrared spectra of metal *N*- and ring- substituted *o*-aminobenzoic acid coordination compounds and studied the substituent effect on stability constants. They also prepared[6] metal coordination compounds of aminoterephthalic acid and 3-aminophthalic acid and indicated that the compounds have a dimer structure and nitrogen and oxygen are coordinated to the metal cations. In the former two carboxyl groups and one amino group are coordinated to each metal, but in the latter two amino groups and one carboxyl group are coordinated to one metal and three carboxyl groups to the other metal. Alyariya *et al.*[7] studied the infrared spectra of *o*-, *m*-, and *p*-aminobenzoic acid cadmium(II) coordination compounds and indicated that nitrogen and oxygen are coordinated to cadmium(II) in *o*-isomer but only

1) A. G. Hill and C. Curran, *J. Phys. Chem.*, **64**, 1529 (1960).
2) W. F. Harris and T. R. Sweet, *ibid.*, **60**, 509 (1956).
3) W. F. Harris and T. R. Sweet, *J. Amer. Chem. Soc.*, **77**, 2893 (1955).
4) J. S. Decker and H. Frye, *Z. Naturforschug*, **21b**, 527 (1966).
5) J. S. Decker and H. Frey, *ibid.*, **21b**, 522 (1966).
6) J. S. Decker and H. Frye, *ibid.*, **21b**, 626 (1966).
7) M. K. Alyariya, T. Saidaliev, and Y. T. Tashpulatov, *Zh. Neorgan Khim.*, **10**, 1493 (1965).

nitrogen is coordinated in *m*- and *p*-isomer. Aggarwal and Singh[8] prepared the tin(IV) coordination compounds of three isomers in many organic solvents and showed that coordination occurs through nitrogen only. Khakimow and Azizov[9] indicated that cobalt (II) coordination compounds of three isomers had the following molecular formulas. $[(o\text{-}C_7H_6NO_2)_2Co]$, $[(m\text{-}C_7H_6NO_2)_2Co]H_2O$, $[(p\text{-}C_7H_6NO_2)_2Co]\cdot 4H_2O$.

In this investigation, the infrared spectra of several divalent metal coordination compounds of the three isomers of aminobenzoic acid have been studied in the region 4000—200 cm^{-1} and detailed assignments for the observed bands have been made.

Experimental

Preparation of compounds. Bis(*o*-, *m*-, *p*-aminobenzonato) copper(II), zinc(II), nickel(II), cobalt(II), and cadmium(II) were prepared as follows. To a solution of 0.2 mol of aminobenzoic acid and 0.2 mol of sodium hydroxide dissolved in 200 ml of water was added 0.1 mol of metal chloride with stirring. The solution was heated to 80 °C and stirred for two days in the case of bis(*p*-aminobenzonato)-nickel, cobalt, zinc, and cadmium and for half an hour for all the other compounds.

Bis(*o*-aminobenzonato)-palladium (II) and bis(*m*-aminobenzonato)-palladium (II) were prepared by the same method as above but at room temperature. The resulting precipitate was filtered and washed several times with hot water and then with dioxane and was dried at 100 °C *in vacuo* for several hours.

o-Aminobenzoic acid chelates, Found: C, 49.96; H, 3.47; N, 8.42%. Calcd for $C_{14}H_{12}N_2O_4Cu$: C, 50.07; H, 3.60; N, 8.34%. Found: C, 49.60; H, 3.84; N, 8.28%. Calcd for $C_{14}H_{12}N_2O_4Zn$: C, 49.80; H, 3.58; N, 8.30%. Found: C, 43.50; H, 3.22; N, 7.25%. Calcd for $C_{14}H_{12}N_2O_4Cd$: C, 43.71; H, 3.14; N, 7.28%. Found: C, 50.90; H, 3.68; N, 8.21%. Calcd for $C_{14}H_{12}N_2O_4Ni$: C, 50.81; H, 3.65; N, 8.46%. Found: C, 50.82; H, 3.61; N, 8.55%. Calcd for $C_{14}H_{12}N_2O_4Co$: C, 50.77; H, 3.65; 8.46%. C, 44.45; H, 3.42; N, 7.46%. Calcd for $C_{14}H_{12}N_2O_4Pd$: C, 44.41; H, 3.19; N, 7.40%.

m-Aminobenzoic acid coordination compounds, Found: C, 50.04; H, 3.48; N, 8.50%. Calcd for $C_{14}H_{12}N_2O_4Cu$: C, 50.07; H, 3.60; N, 8.34%. Found: C, 48.38; H, 3.25; N, 8.07%. Calcd for $C_{14}H_{12}N_2O_4Zn1/2H_2O$: C, 48.51; H, 3.77; N, 8.10%. Found: C, 43.71; H, 3.26; N, 7.18%. Calcd for $C_{14}H_{12}N_2O_4Cd$: C, 43.71; H, 3.14; N, 7.28%. Found: C, 45.44; H, 4.22; N, 7.74%. Calcd for $C_{14}H_{12}N_2O_4Ni$ $2H_2O$: C, 45.82; H, 4.38; N, 7.63%. Found: C, 50.82; H, 3.61; N, 8.55%. Calcd for $C_{14}H_{12}N_2O_4Co$: C, 50.77; H, 3.65; N, 8.46%. Found: C, 40.53; H, 3.95; N, 7.06%. Calcd for $C_{14}H_{12}N_2O_4Pd$ $2H_2O$: C, 40.55; H, 3.88; N, 6.75%.

p-Aminobenzoic acid coordination compounds, Found: C, 50.04; H, 3.28; N, 8.13%. Calcd for $C_{14}H_{12}N_2O_4Cu$: C, 50.07; H, 3.60; N, 8.34%. Found: C, 38.17; H, 3.90; N, 6.45%. Calcd for $C_{14}H_{12}N_2O_4Cd$ $3H_2O$: C, 38.30; H, 4.14; N, 6.38%. Found: C, 46.01; H, 4.47; N, 7.78%. Calcd for $C_{14}H_{12}N_2O_4Ni$ $2H_2O$: C, 45.82; H, 4.38; N, 7.63%. Found: C, 43.75; H, 3.76; N, 7.57%. Calcd for $C_{14}H_{12}N_2O_4Pd$ $1/2H_2O$: C, 43.37; H, 3.38; N, 7.22%.

Deuteration of Compounds. The *N*-deuterated metal coordination compounds were prepared according to the same procedures as mentioned above in 99.7% deuterium oxide solution.

Absorption Measurements. The infrared spectra from 4000 to 200 cm^{-1} were recorded on Leitz 221, Hitachi EPI-G_2 and Hitachi EPI-L infrared spectrophotometers and were calibrated with polystyrene, 1,2,4-trichlorobenzene, carbon dioxide and water vapour. Samples were prepared as potassium bromide discs in the region 4000—700 cm^{-1} and nujol mulls in the region 700—200 cm^{-1}. All spectra were checked using nujol mulls.

Thermal Analysis. Thermal analysis was carried out with Rigaku Denki D. T. A. 8001 from room temperature to 400 °C in air, the decrease in weight being measured when an endothermic reaction occurred. The results coincided with those of elemental analyses.

Magnetic Moment. Magnetic susceptibility measurements were carried out on finely divided powdered samples using the conventional Gouy method. All determinations were made at room temperature(20 °C). The cell constants were obtained using $Hg(CoSCN)_4$ as a standard. The magnetic moments were calculated by the formula $\mu_{eff}=\sqrt{2.83\chi_g}$.

Rusults and Discussion

o-*Aminobenzoic Acid Chelates.* The infrared spectra of the copper(II) and cobalt(II) chelates and ligand are shown in Fig. 1. The infrared spectra of all other chelates are similar to those of copper(II) or cobalt(II) in the region 4000—500 cm^{-1}. In the case of copper(II) chelates, two peaks at 3234 and 3135 cm^{-1} shifted to 2432 and 2294 cm^{-1} on *N*-deuteration are about 300 cm^{-1} lower than those of ligand and ligand sodium salt and are assigned to NH_2 stretching vibrations of the coordinated NH_2 groups. The carboxylate stretching vibrations are assigned to the two bands at 1551 and 1384 cm^{-1}, since the observed bands in the region 1350—1660 cm^{-1} not disappearing on N-deuteration are COO^- and C=C stretching vibrations, and two peaks at 1551 and 1384 cm^{-1} are shifted with the variation of metals as shown in Table 1.

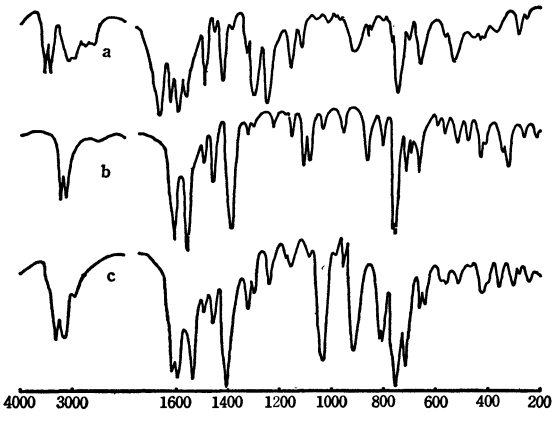

Fig. 1. Infrared absorption spectra of *o*-aminobenzoic acid and its chelateds in KBr discs.
(a): *o*-aminobenzoic acid, (b): Cu(II), (c): Co(II)

8) R. C. Aggarwal and P. P. Singh, *J. Inorg. Nucl. Chem.*, **27**, 2593 (1965).

9) K. Khakimow and H. Azizov, *Trudy Tashkent Farm. Inst.*, **2**, 279 (1960).

TABLE 1. OBSERVED FREQUENCIES AND ASSIGNMENTS FOR METAL-*o*-AMINOBENZOIC ACID CHELATES (cm^{-1})

Cd(II)	Ni(II)	Co(II)	Zn(II)	Cu(II)	Pd(II)	Assignments
3287 m	3298 s	3306 m	3294 m	3234 m	3165 s	NH_2 asym. str.
3137 m	3125 s	3138 m	3127 m	3135 m	3090 m	NH_2 sym. str.
1616 m	1614 s	1615 s	1614 s	1604 s	1620 s	C=C str.
1591 s	1592 s	1591 s	1592 s		1607 s	C=C str.
1534 vs	1545 vs	1535 vs	1542 s	1551 s	1555 m	COO^- asym. str.
1493 sh	1493 m	1493 w	1490 w	1491 w	1491 w	C=C str.
1457 m	1458 s	1458 m	1457 m	1459 m	1451 m	C=C str.
1404 vs	1410 vs	1409 vs	1407 vs	1384 s	1358 s	COO^- sym. str.
1327 w	1330 m	1326 m	1327 w	1327 w		
1300 w	1300 w	1300 w	1299 w	1301 vw	1303 w	
1237 w	1242 w	1241 w	1239 w	1231 w	1212 vw	C–N str.
	1178 vw	1178 vw	1175 vw	1177 vw	1194 vw	
1154 w	1154 w	1152 w	1152 w	1154 w	1157 w	
1082 w	1096 m	1087 w	1091 w	1085 w	1088 w	CH in plane def.
1024 m	1067 m	1035 s	1047 s	1108 m		NH_2 wagging
1002 m						
	1041 w			1037 w	1043 w	
	984 vw	983 vw	983 vw			
951 w	952 w	951 w	952 w	953 w	950 w	CH out of plane def.
864 m	869 s	868 m	868 m	866 m	882 m	
839 vw						
809 m	815 m	813 m	811 m	812 m	819 w	
801 m	809 m	807 m	808 m	807 m	803 w	COO^- scissors
754 s	753 vs	753 vs	753 s	756 s	742 s	CH out of plane def.
716 m	717 s	717 s	716 s	715 m	701 m	benzene ring def.
705 vw						
654 m	660 s	669 m	667 sh	669 m	668 m	benzene ring def.
668 sh	672 sh	645 w	650 w	698 m		NH_2 rocking
582 vw	589 w	585 w	586 w	590 vw	584 vw	benzene ring def.
559 vw	567 w	562 w	558 w	567 vw	535 w	COO^- wagging
516 w	519 m	516 m	515 w	516 w		
459 vw	474 m	466 vw	461 vw	478 w	481 m	COO^- rocking
407 m	426 w	419 m	416 m	412 m	400 m	benzene ring def.
400 sh	413 sh	410 sh				CN def.
333 w	312 w	300 m	405 sh	422 w	442 m	M–N str.
	365 m	355 m	347 w	342 w	345 w	CC def.
			290 w	328 w	335 w	
		280 vw	282 w			
270 w	261 w	245 w	248 w	266 w	273 w	CN def.
				210 w	222 w	M–O str.

Abbreviation: s=strong, m=medium, w=weak, sh=shoulder

The remaining bands can thus be assigned to C=C stretching vibrations.

The infrared spectra of copper(II) and palladium(II) chelates of *o*-aminobenzoic acid differ slightly from those of other metal chelates. However, the difference is not so great as in the case of *m*- and *p*-aminobenzoic acid coordination compounds. Curran and Hill reported that copper(II) chelate of *o*-aminobenzoic acid has a *trans* square planar configuration. The magnetic moment of nickel(II) chelate is 3.22 B.M. which shows that it has no *trans* square planar configuration. Nyholm[10] reported that the magnetic moments of nickel(II) chelates of various ligands having an octahedral configuration are 3.1—3.6 B.M.. Thus, from the similarity of their infrared spectra, we may assume that copper(II) and palladium(II) chelates have a *trans* square planar configuration and the other metal chelates an octahedral configuration. Since the sodium chloride region spectra of all chelates are approximately similar, absorption bands except for vibrations related with metal-ligand bonds should be observed at approximately the same position also in the far infrared region. Since the frequency shifts of carboxylate stretching vibrations by the difference of metals are smaller than those of amino stretching vibrations and in aliphatic α-amino acid metal

10) R. S. Nyholm, *Record Chem. Progr.*, **19**, 45 (1958).

chelates,[11,12] the metal-nitrogen and metal-oxygen stretching vibrations are observed in the region 450—300 cm^{-1} and 300—180 cm^{-1}, respectively. Thus the most metal sensitive band at about 380 cm^{-1} which is not observed in the ligand and ligand sodium salt[13] is reasonably assigned to metal-nitrogen stretching vibration and the bands at 222 cm^{-1} for palladium(II) and 210 cm^{-1} for copper(II) are assigned to metal-oxygen stretching vibration.

Detailed assignments were made by a comparison of the spectra of ligand, ligand sodium salt[13], *o*-chlorobenzoic acid,[14] *o*-chloroaniline,[15] and *o*-dichlorobenzene.[16] The results are shown in Table 1.

m-*Aminobenzoic Acid Coordination Compounds.* The infrared spectra of the copper(II) and cobalt(II) coordination compounds and ligand are shown in Fig. 2.

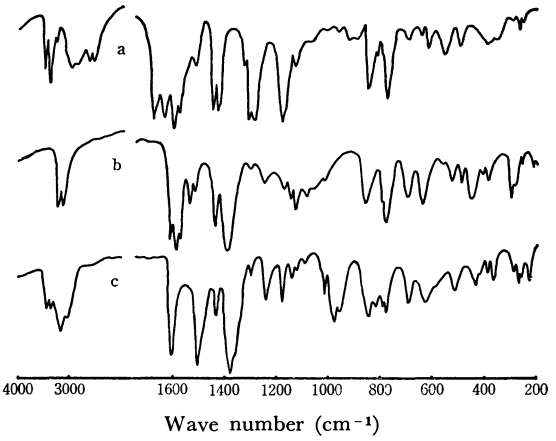

Fig. 2. Infrared absorption spectra of *m*-aminobenzoic acid and its coordination compounds in KBr discs.
(a): *m*-aminobenzoic acid, (b): Cu(II), (c): Co(II)

In the region 3400—2800 cm^{-1}, the important frequencies are those due to NH_2 stretching vibrations in the metal coordination compounds. Two peaks at 3255 and 3147 cm^{-1} in the copper(II) coordination compound are shifted on *N*-deuteration to 2428 and 2298 cm^{-1}, respectively, and the ratios (ν_{NH_2}/ν_{ND_2}) between NH_2 and ND_2 stretching vibrational frequencies of these two bands are 1.34 and 1.37, respectively, being similar to those of aliphatic α-amino acid chelates.[11,12] The two peaks are observed at frequencies lower than those of *m*-aminobenzoic acid sodium salt[13] by about 180—200 cm^{-1}, and are assigned to NH_2 stretching vibrations of the coordinated NH_2 groups. In the region 600—270 cm^{-1}, the spectra contain a new band at 382 cm^{-1} in addition to the vibrations in the spectra of ligand. The frequencies of NH_2 and COO^- stretching vibrations in the metal *m*-aminobenzoic acid coordination compounds are observed in approximately the same region as in *o*-isomer chelates, the frequency shifts due to the different metals being also approximately the same as in *o*-isomer chelates. Thus, it is reasonable to assign this band to the metal-nitrogen stretching vibration. The ligand can be assumed to be coordinated to copper through the nitrogen atom. The frequency shifts of the COO^- stretching vibrations on coordination in the copper(II) coordination compound are smaller than those of NH_2 stretching vibration. However, it can hardly be said that the carboxyl group is not coordinated to the metal and remains as a carboxylic acid as Alyariya *et al.*[7] reported with the cadmium coordination compound,[7] since OH and C=O stretching vibrations, the combination bands of OH in plane deformation and C–O stretching vibration are not observed in copper(II) *m*-aminobenzoic acid coordination compound (Fig. 2 and Table 2.). This is also inconsistent with the result of elemental analysis which excludes the existence of the carboxyl group as a sodium salt. A new band is observed at 223 cm^{-1} which is not present in the ligand. This band is assigned to the metal-oxygen stretching vibration by considering the results of metal *o*-aminobenzoic acid chelates and aliphatic α-amino acid chelates.[11,12] It is therefore concluded that the oxygen of the carboxyl group is also coordinated to copper atom. Similar conclusions can be drawn for the palladium(II) and Zinc(II) coordination compounds from the similarity of their infrared spectra to that of the copper(II) coordination compound as shown in Table 2.

The infrared spectrum of cobalt(II) coordination compound is shown in Fig. 2. This differs somewhat from that of the copper(II) coordination compound. In the region 1300—1650 cm^{-1} only four peaks are observed in cobalt(II) but seven in copper(II). In cobalt(II) the strong bands at 1006 and 989 cm^{-1} are observed instead of the strong bands around 1110 cm^{-1} in copper(II). In the region 600—800 cm^{-1} the number of bands are the same but their shapes differ. Nevertheless, these spectra indicate that the coordination to metal has occurred through both nitrogen and oxygen in the cobalt(II) coordination compound for the same reasons mentioned above.

The spectrum of cadmium(II) coordination compound is similar to that of cobalt(II). Though the nickel(II) coordination compound has two molecules of water as thermal and elemental analyses show, the spectrum of the nickel(II) dihydrate is also similar to that of cobalt(II). It is therefore concluded that the six metal coordination compounds of *m*-aminobenzoic acid have a coordination of both nitrogen and oxygen with metal. The result is inconsistent with that of Alyariya *et al.*[7] in which only nitrogen is coordinated to cadmium(II).

In the case of aliphatic α-amino acids chelates, the antisymmetric carboxylate stretching frequency increases and symmetric frequency decreases in comparison with those of ligand and ligand sodium salt,

11) J. F. Jackovitz and J. L. Walter, *Spectrochim., Acta*, **22**, 1393 (1966).
12) J. F. Jackovitz, J. A. Durkin and J. L. Walter, *ibid.*, **23A**, 67 (1967).
13) T. Inomata and T. Moriwaki, *Nippon Kagaku Zasshi*, **91**, 819 (1970).
14) E. Spinner, *J. Chem. Soc.*, **B**, **1967**, 874.
15) V. B. Singh, R. N. Singh, and I. S. Singh, *Spectrochim. Acta*, **22**, 927 (1966).
16) P. R. Griffiths and H. W. Thompson, *Proc. Royl. Soc., Ser. A*, **298**, 51 (1967); H. F. Shurvell, B. Dulaurens, and P. Pesteil, *Spectrochim. Acta*, **22**, 333 (1966).

TABLE 2. OBSERVED FREQUENCIES AND ASSIGNMENTS FOR METAL–*m*-AMINOBENZOIC ACID COORDINATION COMPOUNDS

Pd(II)	Cu(II)	Zn(II)	Ni(II)	Cd(II)	Co(II)	Assignments
3191 m	3255 m	3276 m	3348 m	3350 m	3356 m	NH_2 asym. str.
3093 m	3147 m	3240 m	3264 m	3270 m	3287 m	NH_2 sym. str.
		3105 w	3164 m			
			3059 m			
1620 s	1629 s	1632 s	1608 m	1588 m	1587 m	C=C str.
		1550 w		1608 w		NH_2 scissors
1582 vs	1572 vs	1569 vs	1542 vs	1541 vs	1538 vs	COO^- asym. str.
	1531 m					
1494 w	1495 w	1501 w				
1455 s	1459 m	1464 s	1453 s	1458 s	1454 m	C=C str.
1348 vs	1406 vs	1400 vs	1394 vs	1391 vs	1391 vs	COO^- sym. str.
	1386 vs					
1314 w	1325 w	1326 w	1316 w	1313 w	1323 w	
1298 w	1303 w	1305 w	1305 w	1301 w	1303 w	
1220 w	1240 w	1241 w	1244 m	1248 m	1242 m	CN str.
	1187 vw	1199 w				
1160 m	1153 m	1165 m				NH_2 wagging
1132 m	1128 m	1136 m				
1110 m	1106 m	1107 m		1119 w	1119 w	CH in plane def.
1074 m	1073 m	1076 m	1079 w	1074 w	1074 w	
1001 w	1001 w	1001 w	1152 w	1168 w	1163 w	
			1011 s	1007 s	1006 s	NH_2 wagging
			995 vs	988 vs	989 vs	
		933 m				
929 m	927 m	924 m	926 m	924 m	925 m	CH out of plane def.
886 m	889 m	877 m				
				917 m	914 m	
			902 m	905 m	903 m	
			883 m	902 m	896 m	
			818 w	825 w	822 w	
807 s	802 s	808 s	783 s	785 s	787 s	COO^- scissors
796 m	786 s	789 m				
758 s	759 s	760 s	769 vs	775 vs	776 vs	CH out of plane def.
				688 m	690 m	
678 s	677 s	677 s	683 m	683 m	683 m	COO^- wagging
670 m	668 sh	669 m	672 m	667 m	669 m	C=C def.
619 w	592 w	564 w				
			568 s	586 s	597 m	NH_2 rocking
			584 vs	561 vs	575 m	C=C def.
556 m	545 w	540 m	547 s	548 s	551 m	C=C def.
572 m	528 w	520 m	526 m	516 m	523 w	COO^- rocking
446 m	458 m	446 m	435 w	433 w	440 w	C=C def.
423 w	425 w	413 w	400 m	413 m	417 m	CN def.
391 w	387 w	370 w				C–C def.
			380 m	368 m	382 m	
470 sh	437 w	429 sh	350 w	360 w	369 m	MN str.
293 w	280 w		268 w		268 m	CN def.
271 w	244 m	252 w	245 w	243 w	250 m	C–C def.
227 w	223 w	209 w				MO str.

Abbreviations: s=strong, m=medium, w=weak, sh=shoulder

Rosenberg[17] showed that the nickel–oxygen bond is essentially ionic, and the frequencies of carboxylate stretching vibration are the same as those of an amino acid sodium salt. In the case of *m*-aminobenzoic acid, palladium(II), copper(II), and zinc(II) coordination compounds have a similar tendency but for nickel(II), cobalt(II), and cadmium(II) the frequencies of antisymmetric and symmetric carboxylate stretching vibrations shift to lower frequencies in comparison with those of the sodium salt[13] and the positions are

17) A. Rosenberg, *Acta. Chem. Scand.*, **10**, 840 (1956).

nearly the same for these compounds. This leads to conclusion that when the carboxyl group is coordinated to palladium(II), copper(II), and zinc(II) they have the structure $-C\begin{matrix}O-M\\O\end{matrix}$, and nickel(II), cobalt(II), and cadmium(II) derivatives can be represented as the structure $-C\begin{matrix}O\\O-M\end{matrix}$.

These coordination compounds can be divided into two groups which shows that each group has the same configuration. The magnetic moments of copper(II) (2.02 B.M.), cobalt(II) (5.08 B.M.), and nickel(II) (3.12 B.M.) indicate that both cobalt(II) and nickel (II) have an octahedral configuration (cobalt(II) has 4.8—5.2 B.M. and nickel(II) 3.1—3.6 B.M.[10]), but it is not easy to deduce the configuration from the magnetic moment alone.

Detailed assignments for observed bands were made by comparing them with ligand, ligand sodium salt,

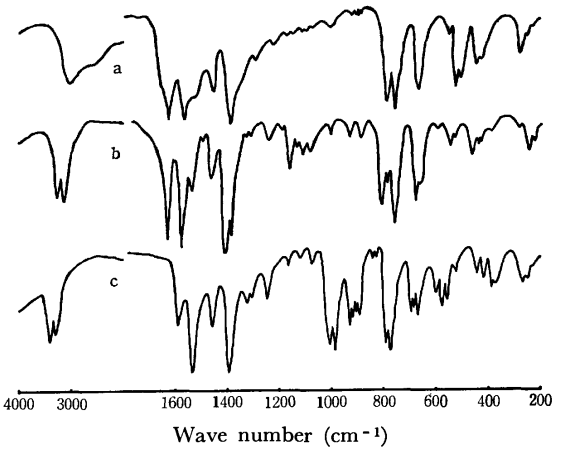

Fig. 3. Infrared absorption spectra of *p*-aminobenzoic acid and its coordination compounds in KBr discs.
a=*p*-aminobenzoic acid, *b*=Cu(II), *c*=Ni(II)

Table 3. Observed frequencies and assignments for metal-*p*-aminobenzoic acid coordination compounds (cm^{-1})

Ni(II)	Cd(II)	Cu(II)	Pd(II)	Assignments
3183 s	3350 m	3226 m	3178 m	NH_2 asym. str.
3030 sh	3140 sh	3177 m	3071 m	NH_2 sym. str.
1604 s	1605 s	1611 s		C=C str.
1504 vs	1511 s	1580 vs	1602 vs	COO^- asym. str.
		1571 s	1552 s	C=C str.
		1538 m	1507 s	
		1512 m		
1430 w	1423 sh	1437 s	1436 m	C=C str.
1372 vs	1389 vs	1385 vs	1349 vs	COO^- sym. str.
1300 vw	1304 vw	1302 vw	1303 sh	
1239 m	1255 w	1247 w	1250 w	CN str.
1176 m	1175 m	1175 w	1171 s	
1143 w	1139 vw	1146 w		
1091 vw	1091 w			CH in plane def.
1016 m	1015 w	1019 vw	1015 w	
972 s	954 sh	1124 m	1110 m	NH_2 wagging
954 m	935 m			
	864 m			
845 s	845 m	851 m	858 m	CH out of plane def.
816 m	804 w	782 sh	802 vw	
784 m	783 m	777 s	776 s	C=C def.
774 m				
693 m	698 m	695 m	696 m	C=C def.
628 m	626 m	639 s	632 m	C=C def.
		552 vw	542 m	
		527 w		
514 m	507 w	489 m	503 w	C=C def.
432 m	409 m	445 m	454 w	COO^- rocking
363 m		405 vw	441 w	MN str.
384 w		384 w	380 w	CN def.
			330 w	
288 w		298 m	296 w	CN def.
		281 sh		
264 m	266 m	259 vw	240 w	C–C def.
		211 w	223 v	MO str.

Abbreviations: s=strong, m=medium, w=weak, sh=shoulder

ligand hydrochloride,[13] deuterated compound of metal coordination compounds, *m*-chlorobenzoic acid,[14] *m*-cnloroaniline,[15] and *m*-dichlorobenzene.[16] The results are shown in Table 2.

p-*Aminobenzoic Acid Coordination Compounds.* The infrared spectra of copper(II) and nickel(II) *p*-aminobenzoic acid coordination compounds and ligand are shown in Fig. 3 and their detailed assignments in Table 3. The assignments have been made by the same method as for the metal *m*-aminobenzoic acid coordination compounds. These spectra indicate that the compounds are also classified into two groups, one group including palladium(II) and copper(II) and the other cadmium(II) and nickel(II).

By the same discussions as for metal *m*-aminobenzoic acid coordination compounds, such as the shifts of NH_2 and COO^- stretching vibrations, existence of new peaks due to metal–nitrogen and metal–oxygen stretching vibrations, disappearance of absorption bands due to COOH and the elemental analysis of these compounds, it is clear that the coordination with metal has occurred through both nitrogen and oxygen in metal *p*-aminobenzoic acid coordination compounds as in metal *m*-aminobenzoic acid. This also differs from the results of Alyariya *et al.*[7] in which the nitrogen was only coordinated to cadmium(II).

The magnetic moment of nickel(II) (3.37 B.M.) indicates that nickel(II) has an octahedral configuration[10] but the configuration could not be determined from magnetic moment alone.

BULLETIN OF THE CHEMICAL SOCIETY OF JAPAN, VOL. 46, 1154—1158 (1973)

Radiation Synthesis of Hydrogen Cyanide from Nitrogen-Ethylene System. Effect of Temperature, Gas Density, and Reactor Wall

Yasumasa IKEZOE, Shoichi SATO, and Akibumi DANNO

Japan Atomic Energy Research Institute, Tokai-mura, Ibaraki-ken 319-11

(Received November 1, 1972)

The rate of formation of hydrogen cyanide from the nitrogen–ethylene system by ^{60}Co gamma rays was found to depend on irradiation temperature, gas density, gas composition, and the nature of the wall surface of the reaction vessel. Above 100 °C, the G(HCN) value increased with the rise of temperature. Below 100 °C, the G(HCN) value remained constant down to −196 °C. In the temperature range from 400 °C to −196 °C, it increased with reduction of nitrogen gas density. The largest G(HCN) value obtained was 2.0. In certain cases, the wall surface influenced the suppression of hydrogen cyanide formation. As an active species responsible for hydrogen cyanide formation, excited nitrogen molecules are proposed in addition to nitrogen atoms. Excited nitrogen molecules are decomposed to nitrogen atoms with small activation energy or deactivated by collision with other molecules. They play an important role in cyanide formation at low pressures and at high irradiation temperatures.

Radiation reactions of activated nitrogen have been investigated in many systems. In the radiolytic isotopic exchange reaction of nitrogen, the G-value of the exchange reaction is in the range 9—19.[1-3] The large exchange G-value seems to indicate that nitrogen molecules are activated by radiation. Ammonia synthesis from the nitrogen–hydrogen system,[4] nitrogen fixation from the nitrogen–oxygen system[5] and ammonium synthesis from the air–water system[6] are also reported. The G-values of nitrogen fixation reactions in these systems are generally about one, and reach three at most.

As a radiation reaction involving activated nitrogen, formation of hydrogen cyanide from nitrogen–ethylene system has been studies by Oka *et al.*, and the G-values of about 0.5 and 0.2 were reported for the reactions in gas phase and in liquid nitrogen.[7-9] In order to elucidate the reactivity of the radiation activated nitrogen and attain higher yields of cyanide, we investigated in detail the effects of irradiation temperature, density, gas composition, and the nature of the wall surfaces of reaction vessels.

Experimental

Nitrogen gas (purity; 99.9995%, oxygen content; 0.5 ppm, Nihon Sanso Co.) was used after removal of condensable gases with a liquid nitrogen trap. Ethylene gas (purity; 99.9%, acetylene content; 1 ppm, oxygen content; 0 ppm, Nihon Sekiyukagaku Co.) was purified by trap to trap distillation in a vacuum line. The two gases mixed in a vacuum line were analysed with a mass spectrometer and the absence of oxygen, water or carbon dioxide was confirmed.

Four kinds of irradiation ampoules, *i. e.* 170 ml Pyrex glass, 64 ml Pyrex glass, 64 ml quartz glass, and 55 ml stainless

1) M. Anbar and P. Perlstein, *J. Chem. Phys.*, **68**, 1234 (1964).
2) D. H. Dawes and R. A. Back, *ibid.*, **69**, 2385 (1965).
3) R. Shimozawa and K. Oshima, Proceedings for the 10th Discussion Meeting of Radiation Chemistry, Hiroshima (October, 1967).
4) C. H. Cheek and V. J. Linnenbon, *J. Phys. Chem.*, **62**, 1475 (1958).
5) M. Steinberg, *Chem. Eng. Progr.*, **62**, (9) 105 (1966).
6) S. Sato and M. Steinberg, BNL-13692 (1969).
7) T. Oka, R. Kato, S. Sato, and S. Shida, This Bulletin, **41**, 2192 (1968).
8) T. Oka and S. Sato, *ibid.*, **42**, 582 (1969).
9) T. Oka, Y. Suda, and S. Sato, *ibid.*, **42**, 3083 (1969).

steel, were used. The glass ampoules were washed in two ways, by washing them thoroughly with only distilled water or by immersing them in concentrated nitric acid solution for several days and washing with distilled water four or five times. The stainless steel ampoules were immersed in a rust removing reagent (Dipsol ST-305 solution) for 5—10 minutes, washed with water, treated with 20% NaCN solution and washed with water again. The ampoules were evacuated to a vacuum of 1×10^{-4} Torr while they were being heated. Known amounts of gases were then charged into the ampoules, pressure being measured with a quartz Bourdon gage.

Irradiation of the gases was carried out with ^{60}Co-γ rays. The dose rate of γ-rays was measured with a Fricke dosimeter. The absorbed dose in nitrogen gas was estimated from the Fricke dosimetry corrected for the ratio of stopping power of nitrogen to that of glass against secondary electrons.[10-11] The absorbed dose in ethylene was neglected in the calculation of G(HCN). High temperature irradiation was carried out in an electric furnace, in which the temperature was controlled to an accuracy of ±2 °C. Low temperature irradiations were carried out in liquid nitrogen (−196 °C) and in dry ice (−78 °C).

Hydrogen cyanide was measured as follows. The product was trapped at the bottom of the irradiated ampoule with a liquid nitrogen trap. The top of the ampoule was then broken and 10 ml of 1/100 N NaOH solution quickly poured into the ampoule to dissolve hydrogen cyanide. In the case of high ethylene partial pressure, a device was connected to the top of the ampoule in order not to release hydrogen cyanide. After purging the dissolved ethylene and other hydrocarbons by bubbling with nitrogen gas about 5 minutes, hydrogen cyanide remaining in the 1/100 N NaOH solution was titrated with 10^{-4} M mercuric nitrate solution, using 1 ml of 38 ppm carbon tetrachloride solution of copper diethyldithiocarbamate[12] as an indicator. Hydrogen cyanide in the solution was also analysed with an electrode potentiometer (Cyanometer CN-IA, Toa Electronics Ltd.) for confirmation of the titration method. The two methods gave the same result.

Results

When nitrogen–ethylene mixtures are irradiated, acetylene, *n*-butane, ethane, and propane are formed besides hydrogen cyanide. Hydrogen cyanide formation was studied in connection with reaction of nitrogen activated by radiation. It was found to depend on the irradiation temperature, the density, and composition of the mixed gas and the nature of the wall.

The formation of hydrogen cyanide at various temperatures, shown in Fig. 1, is linear to the absorbed radiation energy in nitrogen gas. Estimated errors in titration are also given. The G(HCN) values calculated from the slopes were 1.9 at 400 °C, 1.5 at 300 °C, 0.8_0 at 100 °C and 0.7_3 at −196 °C. The G(HCN) value 0.7_3 at −196° C was very close to the one, 0.8_0 at 100 °C. This is of interest when we consider the small partial pressure of ethylene at −196 °C.[13]

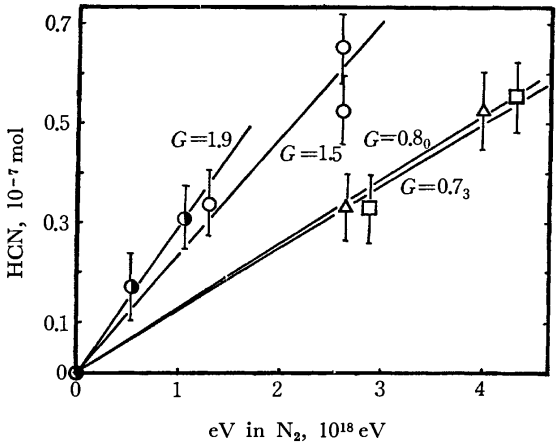

Fig. 1. HCN formation from N_2-C_2H_4 at various temperatures.
N_2; 0.11 g/l, C_2H_4=0.075, γ-rays; 6.8×10^5 R/hr, 0—6 hr irradiated.
◐; 400 °C, ○; 300 °C, △; 100 °C, □; −196 °C

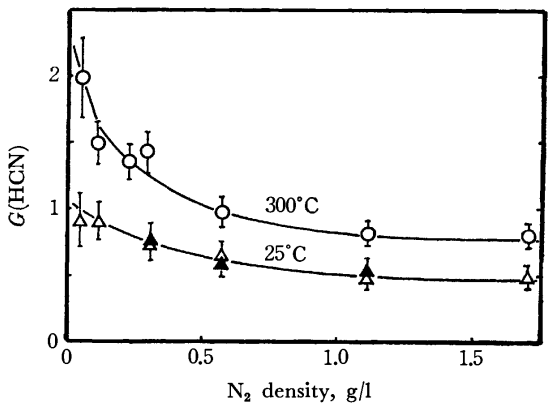

Fig. 2. N_2 gas density dependence of G(HCN).
γ-rays; 6.8×10^5 R/hr, 0—6 hr irradiated, C_2H_4/N_2=0.075.
○; irradiated at 300 °C in 170 ml Pyrex ampoule.
△; irradiated at 25 °C in 170 ml Pyrex ampoule.
▲; irradiated at 25 °C in 64 ml Pyrex ampoule.

The G(HCN) values at 300 °C and 25 °C are shown in Fig. 2 as a function of nitrogen gas density, for a constant C_2H_4/N_2 ratio of 0.075. At both temperatures the G-values depended on the density of gas and became larger as the density was reduced. At 25 °C and at high nitrogen gas density, the G-values converged to 0.5, in agreement with a reported value.[7] The density dependence might be attributed to heterogeneous reactions on the wall surface of the reaction vessels. Two kinds of Pyrex ampoules with different surface to volume ratios were used to examine the effect of heterogeneous reaction. However, no difference in density dependence of G(HCN) was seen between the two ampoules within the experimental error (Fig. 2).

At 300 °C, the G(HCN) value converged to 0.8 at high nitrogen gas density, becoming as large as 2.0

10) T. E. Burlin, "Radiation Dosimetry" Vol. 1, ed. by F. H. Attix, W. C. Roesch, and E. Tochilin, Academic press, New York (1968), p. 331.
11) G. R. A. Johnson, *J. Inorg. Nucl. Chem.*, **24**, 461 (1962); D. W. Huyton and T. W. Woodward, *Radiation Res. Rev.*, **2**, 205, (1970).
12) Y. Tanaka and S. Yamamoto, *Bunseki Kagaku*, **9**, 6 (1960).
13) At −196 °C the vapor pressure of ethylene becomes 6.5×10^{-4} Torr. Ethylene in the irradiation ampoules is condensed on the wall surface for the most part, and the C_2H_4/N_2 ratio in gas phase is equal to 3.3×10^{-5}, which is much smaller than the one, 7.5×10^{-2} at other temperatures.

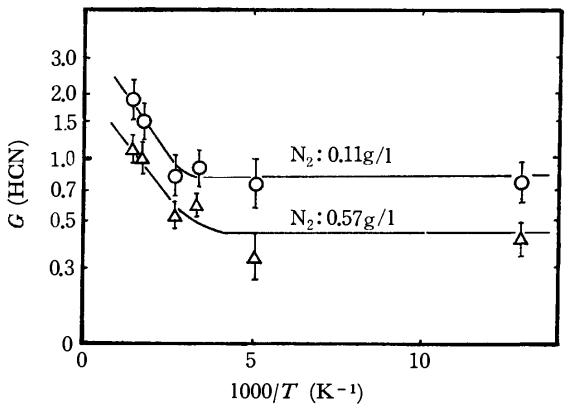

Fig. 3. Arrhenius' plot of G(HCN).
γ-rays; 6.8×10^6 R/hr, 0—6 hr irradiated, $C_2H_4/N_2=0.075$.
○; N_2 gas density=0.11 g/l.
△; N_2 gas density=0.57 g/l.

(±0.3) as the density was reduced to 0.054 g/l. The latter value is one of the greatest obtained experimentally. At both temperatures, a constant value was reached with high gas density, and became larger as the density was reduced. However, the extent of increase in G(HCN) at 300 °C was greater than that at 25 °C.

Arrhenius' plots of G(HCN) are shown in Fig. 3 for two nitrogen gas densities, 0.11 and 0.57 g/l, with a constant C_2H_4/N_2 ratio, 0.075. All the plotted G(HCN) values were obtained from the slopes of the cyanide formation as in Fig. 1. At low gas density, the G(HCN) values were larger than those at high density in the whole temperature range, —196—400 °C, but the temperature dependences corresponding to the two gas densities were similar. Above 100 °C, the G(HCN) values increased with an apparent activation energy of 1.2 kcal/mol, and below 100 °C, they were constant down to —196 °C. This indicates that the mechanism of hydrogen cyanide formation at high temperature differs from that at low temperature.

The G(HCN) value is known to be independent of ethylene partial pressure in the C_2H_4/N_2 ratio range 0.1—0.001.[7,14] The variation of G(HCN) with higher ethylene partial pressures is shown in Table 1. Since the ionization potential of nitrogen, 15.6 eV, is fairly larger than that of ethylene, 10.6 eV, it is not probable that nitrogen molecules are activated by the excited ethylene molecules to form hydrogen cyanide.[15] In the calculation of the G(HCN) value, only the energy absorbed by nitrogen was counted and that by ethylene neglected.

The G(HCN) values at 25 °C (Table 1) decreased from 0.6_4 to 0.3_0 as the C_2H_4/N_2 ratio was increased from 0.036 to 1.92. Decreasing G(HCN) values were obtained with both high nitrogen gas density and high ethylene partial pressure, the tendency being the same at 25 °C and at 300 °C.

Table 1. G(HCN)[a] dependence on C_2H_4/N_2 ratio at 300 and 25 °C

C_2H_4/N_2	G(HCN), 300 °C	G(HCN), 25 °C
0.036	—	0.6_4
0.075	0.9_4	0.6_1
0.36	—	0.5_2
0.72	—	0.4_6
1.09	—	0.3_9
1.92	0.6_7	0.3_0

γ-rays; 6.8×10^5 R/hr, 0—2 hr irradiated, N_2; 0.57 g/l in 170 ml ampoules.
a) Calculation of G(HCN) is based on the energy absorbed by the nitrogen.

Table 2. Wall effect

Reactor	G(HCN)
Pyrex A[a]	0.5±0.05
Pyrex B[b]	0.5±0.05
Quartz A[c]	0.5±0.1
Quartz B[d]	0.3±0.1
Steel[e]	0.3±0.1

$C_2H_4/N_4=0.07\pm0.02$, N_2; 1.1 g/l, γ-rays; 0—3×10^6 Rad, 25 °C.
a) 170 ml Pyrex ampoule washed with distilled water.
b) 64 ml Pyrex ampoule washed with distilled water.
c) 64 ml quartz ampoule washed with distilled water.
d) 64 ml quartz ampoule washed with concentrated nitric acid solution and distilled water.
e) 55 ml stainless steel ampoule, treated with rust removing reagent (Dipsol ST-305 solution) and with NaCN 20% solution, and then washed with water.

Ampoules of different size and material were used as the irradiation vessel to investigate the surface effect on hydrogen cyanide formation under the same experimental conditions. The results are shown in Table 2. In the Pyrex and quartz ampolues washed only with distilled water, the G(HCN) values were 0.5±0.1. In the quartz and stainless steel ampoules treated with nitric acid and washed with water, they were 0.3±0.1, reproducibility being poor.

Discussion

The results show that the formation of hydrogen cyanide depends on the irradiation temperature, the density, composition of the mixed gas and the wall. The mechanism of the formation of hydrogen cyanide will be discussed.

Nitrogen molecules are activated by radiation to form a variety of active species.[19-20]

14) Y. Ikezoe, O. Tokunaga, N. Moriyama, R. Shimozawa, T. Tamura, and A. Danno, JAERI-memo 3506 (1969).
15) Excitation spectrum of ethylene[16-17] shows that ethylene can be excited to higher energy levels than dissociation energy 9.76 eV, and ionization potential of nitrogen 15.6 eV. Such highly excited ethylene can dissociate or ionize a nitrogen molecule. However, the direct ionization, autoionization, and dissociation process of ethylene are much faster[18] than the nitrogen activation process by the excited ethylene in our experimental conditions. Thus, the ethylene molecules directly activated by radiation seem to make no contribution to cyanide formation.
16) Y. Hatano, This Bulletin, **41**, 1126 (1968).
17) E. N. Lassettre and S. A. Francis, *J. Chem. Phys.*, **40**, 1208 (1964).
18) S. Shida, *Radioisotopes*, **19**, 92 (1970).
19) S. Ya. Pshezhetskii and M. T. Dmitriev, *At. Energ. (U. S. S. R.)*, **3**, 350 (1957).
20) S. Dondes, P. Harteck, and C. Kunz, *Z. Naturforschg.* **19**, 6 (1964).

$$N_2 \text{ -WWW-} \rightarrow N_2^+, N^+, N, N_2^*, N_2^{+*}, e^- \quad (1)$$

Nitrogen molecule ions N_2^+ are thought to take no part in the formation of hydrogen cyanide, on account of their fast charge transfer reaction with ethylene.[7]

$$N_2^+ + C_2H_4 \longrightarrow N_2 + C_2H_4^+ \quad (2)$$

Thus an active species considered able to take part in the formation of hydrogen cyanide should be sought from nitrogen atoms, atom ions, excited nitrogen molecules, and excited molecule ions.

In the study of active nitrogen produced by electric discharge, hydrogen cyanide has been said to be formed by the following reactions.[21-23]

$$N + C_2H_4 \longrightarrow HCN + CH_3 \quad (3)$$

$$N + CH_3 \longrightarrow HCN + 2H \quad (4)$$

Reaction (4) is faster in electric discharge but can be neglected in the case of radiolysis, because of low concentration of active species.[24] As the reaction of hydrogen cyanide formation by radiation, the following reaction has been proposed by Oka *et al.*[7]

$$N(\text{or } N^+) + C_2H_4 \rightarrow HCN + CH_3\cdot(\text{or } CH_3^+) \quad (3')$$

They found the G(HCN) value to be independent of nitrogen pressure in the range 250—750 Torr and explained the phenomena by this reaction.

Our results, however, show that the G(HCN) value depends both on gas density and irradiation temperature. It therefore seems apparent that a mechanism other than reaction (3′) is important for our experimental conditions.

Absorbed Dose of Gas in an Ampoule at Low Gas Density. Before discussing the mechanism of hydrogen cyanide formation, absorbed dose at low gas density should be considered. Absorbed dose of high density gas in an ampoule is proportional to the electron density, and that of low density to the stopping power ratio to the secondary electrons.[10] In general, absorbed dose varies as the gas density varies. In the case of nitrogen gas in a glass ampoule, both the stopping power ratios of nitrogen and of glass are nearly equal, and the absorbed dose of nitrogen can be obtained from the electron density of nitrogen irrespective of nitrogen gas density.[11] The difference in the G(HCN) value at high and low nitrogen gas density in Fig. 3 can not be explained by the deviation of absorbed doses at low gas density.

Excited Nitrogen Molecule. Heterogeneous reactions on the wall of the Pyrex glass ampoules were not detected (Fig. 2). We might thus assume the following reactions to explain the gas density dependence of G(HCN) value.

$$N_2^* (\text{or } N_2^{+*}) \longrightarrow N + N (\text{or } N^+) \quad (5)$$

$$N_2^* (\text{or } N_2^{+*}) + M \longrightarrow N_2 + M (\text{or } M^+) \quad (6)$$

Reaction (5) is predominant at low gas density, and reaction (6) at high gas density.

Nitrogen atom formed by reaction (5) then reacts with ethylene to form hydrogen cyanide. This means excited nitrogen molecules and/or excited nitrogen molecule ions in addition to the atoms and/or the atom ions can be precursors of hydrogen cyanide. The difference in G(HCN) values at low and high nitrogen gas density, $\Delta G_{25\,^\circ C}=0.4$ and $\Delta G_{300\,^\circ C}=1.2$, can be explained if they correspond to the initial G-value of excitation of nitrogen molecules, $g(N_2^*$ or $N_2^{+*})$.[26]

It is of interest to see whether the excited nitrogen molecules form cyanide by reactions (5) and (3′) or directly by the following reaction.

$$N_2^* (\text{or } N_2^{+*}) + C_2H_4 \longrightarrow HCN + \text{others} \quad (7)$$

The result given in Table 1 indicates that reaction (7) does not take place at 25 °C and 300 °C, and the excited nitrogen molecules are deactivated by ethylene by the following reaction.

$$N_2^* (\text{or } N_2^{+*}) + C_2H_4 \rightarrow N_2 + C_2H_4^* (\text{or } C_2H_4^{+*}) \quad (6')$$

Excited nitrogen molecules can not directly form hydrogen cyanide but after reaction (5), they react to form hydrogen cyanide.

Irradiation Temperature Dependence. At temperatures above 100 °C, the G-values were dependent on temperature, but at lower temperatures they were independent of temperature (Fig. 3). This indicates that an elementary reaction which requires some activation energy is the rate-determining step in the cyanide formation reaction at high temperatures. The nitrogen gas density dependence of G(HCN)

21) G. Paraskevopoulos and C. A. Winkler, *J. Phys. Chem.*, **71**, 947 (1967).

22) J. T. Herron, *J. Phys. Chem.*, **69**, 2736, (1965).

23) B. Brocklehurst and K. R. Jennings, "Progress in Reaction Kinetics," Vol. 4 ed. by G. Porter, Pergamon Press, Oxford, p. 1.

24) Nitrogen atom concentration in our experimental conditions is estimated. When partial pressure of nitrogen is 1 atm, ethylene 0.1 atom, dose rate of γ-rays 10^6 Rad/hr, the initial G (N) value 0.5 and the rate constant of disappearance reaction of nitrogen atoms, reaction (3), ($k=1\times10^7$ litre mol^{-1} s^{-1})[23], the rate of nitrogen atom formation per one mole nitrogen κ, is

$\kappa=(10^6 \text{ Rad/hr})\times(1/3600 \text{ h/s})\times(6.24\times10^{13} \text{ eV/g Rad})$
$\times(28 \text{ g/N}_2 \text{ mole})\times(G(\text{N})/100 \text{ atom/eV})=4.85\times10^{15}\,G(\text{N})$
atom/N_2 mol sec$=2.43\times10^{15}$ atom/N_2 mol sec

The mean life time of nitrogen atom τ, is

$\tau=1/k[C_2H_4]=2.2\times10^{-5}$ s.

The mean concentration of nitrogen atom (N), is

$(\text{N})=\kappa\tau=5.4\times10^{10}$ atom/N_2 mol.

The ratio, $(\text{N})/(N_2)=5.4\times10^{10}/6\times10^{23}=0.9\times10^{-13}$. This value is much smaller than 1×10^{-1} in the electric discharge experiment.[25]

25) D. R. Safrany and W. Jaster, *J. Phys. Chem.*, **72**, 518 (1968).

26) It is possible to calculate a $g(N_2^*)$ value with an excitation energy range 11.4—13.6 eV, which lies between the dissociation energy and the ionization potential of nitrogen molecules. As the oscillator strength in the range is known to be 0.87,[27] the $g(N_2^*$, 11.4—13.6) value can be calculated by the equation.[28]

$$g(N_2^*,\ 11.4\text{—}13.6) = \frac{(M_{11.4-13.6})^2}{(M_i')^2}\times\frac{100}{W}$$

where $(M_{11.4-13.6})^2$ is the dipole matrix element squared for the excitation energy range and is equal to $fR/E(=0.95)$, R Rydberg constant, E excitation energy (taken as an average in the energy range), $(M_i')^2$ the dipole matrix element squared for ionization ($=3.85$), and W the average energy for an ion pair production ($=34.4$ eV). Thus $g(N_2^*$; 11.4—13.6) is calculated to be 0.72.

27) S. M. Silverman and E. N. Lassettre, *J. Chem. Phys.*, **42**, 3420 (1965).

28) C. E. Klots, "Fundamental Processes in Radiation Chemistry," ed. by P. Ausloos, Interscience Publishers, New York, N. Y. (1968), p. 1.

was more remarkable at high temperatures than at low. Thus, excited nitrogen molecules seem to play a more important role at high temperatures making reaction (5) require some activation energy.

G(HCN) values reached constant values at a high gas density, but differed with differing temperature (Fig. 2). The G(HCN) value became constant at low temperature, but also took a different value at a different gas density (Fig. 3). This seems to indicate that two kinds of nitrogen atoms, one directly formed by radiation according to reaction (1) and the other indirectly formed by radiation according to reactions (1) and (5), can not be distinguished clearly from each other.

Wall Effect. In glass ampoules washed with only distilled water, the G(HCN) value was constant irrespective of ampoule volume, but in glass ampoules and stainless steel ampoules treated with nitric acid solution, cyanide formation was suppressed. In the former case, the surface/volume ratio did not differ so much that it is difficult to say whether the wall surface affects cyanide formation at all. In the latter case, the suppression may be due either to the active species being trapped on the wall surface or to hydrogen cyanide formed being decomposed on the surface.

BULLETIN OF THE CHEMICAL SOCIETY OF JAPAN, VOL. 46, 1158—1161 (1973)

Formation of Uranium Nitride by the Reaction of Uranium Hydride with Nitrogen and Ammonia

Hiroaki TAGAWA

Japan Atomic Energy Research Institute, Tokai-mura, Ibaraki-ken 319-11

(Received June 23, 1972)

The hydrogenation of uranium metal and the nitrogenation of uranium and its hydride with either nitrogen or ammonia have been studied using thermogravimetry. The reactions were examined at different pressures of hydrogen, nitrogen, and ammonia. The reaction of uranium with hydrogen takes place at 200°C and proceeds quickly above 210°C. The conversion curve depends greatly on the hydrogen pressure. In the reaction of the hydride with nitrogen, the weight gain occurs at about 160°C and becomes fast above 240°C. The reaction is shown to proceed in two steps: the formation of the mononitride and that of the sesquinitride. The reaction between uranium hydride and ammonia begins at 150°C and becomes rapid above 300°C. The reaction proceeds monotonously, and no step is observed. The nitrogenation behavior of uranium hydride with ammonia is found to be quite different from that in reaction with nitrogen.

The phases in the uranium–nitrogen system were first characterized by Rundle *et al.*[1]: NaCl-type face-centered cubic UN, Mn_2O_3-type body-centered cubic U_2N_3, and CaF_2-type face-centered cubic UN_2. Another nitride was found by Mallett and Gerds[2] and by Vaughan,[3] and was indexed as La_2O_3-type hexagonal close-packed U_2N_3. The bcc and hcp U_2N_3 are designated as the α- and β-U_2N_3, respectively. The α-U_2N_3 phase exhibits a wide range of composition, and ordinarily contains more nitrogen than is represented by its chemical formula; *i. e.*, $UN_{1.54}$-$UN_{1.75}$. α-U_2N_3 is transformed into β-U_2N_3 above 800 °C near the decomposition pressure of the α phase. Uranium nitride, prepared at temperatures below 1300 °C in a nitrogen atmosphere, is usually the α phase. The composition depends on the fabrication conditions–the temperature and the nitrogen pressure. Uranium mononitride is obtained by decomposing α-U_2N_3 at 1500—1600 °C *in vacuo*.

Uranium nitride is prepared by the following methods:

1) $U+N_2$[2,4–7]
2) UH_3+N_2[4,8]
3) $U+NH_3$[4,9]
4) UO_2+C+N_2[8,10,11]
5) UCl_4+NH_3[12]
6) UX_4+Me+N_2(X=F, Cl; Me=Si Al)[13,14]

Methods (1) and (2) are commonly used for preparing the pure material, but the reaction process is not known well in detail. Method (4) is useful for producing the

1) R. E. Rundle, N. C. Baenzieger, A. S. Wilson, and R. A. McDonald, *J. Amer. Chem. Soc.*, **70**, 99 (1948).
2) M. W. Mallett and A. F. Gerds, *J. Electrochem. Soc.*, **102**, 292 (1955).
3) D. A. Vaughan, *J. Metals*, **8**, 78 (1956).
4) R. E. Rundle, N. C. Baenzieger, A. S. Newton, A. H. Daane, T. A. Butler, I. B. Johns, W. Tucker, and P. Figard, USAEC Report TID-5290, Book 1 (1958) p. 53.
5) C. Moreau and J. Philippot, *C. R. Acad. Sci. Paris*, **253**, 1100 (1961).
6) Y. Sasa and T. Atoda, *J. Amer. Ceram. Soc.*, **53**, 102 (1970).
7) R. Benz and W. B. Hutchinson, *J. Nucl. Mater.*, **36**, 135 (1970).
8) K. M. Taylor, C. A. Lenie, P. A. Smudski, L. N. Hailey, and T. J. Keaty, USAEC Report ORO-248 (1959).
9) R. E. Alire and J. H. McCrary, *J. Chem. Phys.*, **45**, 3958 (1966).
10) K. R. Hyde, D. A. Landsman, J. B. Morris, W. E. Seddon, and H. J. C. Tulloch, UKAEA Report AERE-R 4650 (1965).
11) J. R. McLaren, R. J. Dicker, J. D. L. Harrison, and L. E. Russell, UKAEA Report AERE-R 5710 (1968).
12) J. J. Katz and E. Rabinowitch, "The Chemistry of Uranium," Dover Pub. Inc., New York (1951).
13) T. Mitamura, M. Kanno, and T. Mukaibo, *J. Nucl. Sci. Tech.*, **5**, 60 (1968).
14) K. Yoshihara, M. Kanno, and T. Mukaibo, *ibid.*, **5**, 643 (1968).

nitride on an industrial scale. All the reactions except (4) produce the sesquinitride. The composition of α-U_2N_3 produced varies with the fabrication methods and the annealing conditions. This report describes a study of the behavior of the hydrogenation of uranium metal and of the nitrogenation of uranium and its hydride in thermogravimetry. Although TG does not give precise data on the kinetics, the use of TG will yield some valuable information on the kinetics of these reactions and on the preparations of hydride and nitride of uranium

Experimental

Apparatus and Procedures. The experimental apparatus for heating uranium metal or its hydride in either hydrogen, nitrogen, or ammonia was very similar to that described in an earlier paper reporting on the measurement of the equilibrium nitrogen pressure over a UN and U_2N_3 mixture.[15] It consisted of a Cahn RH-type automatic electrobalance, used as a thermobalance, a Kanthal resistance furnace, a pressure measurement system, a gas supply system, and vacuum pumps. The volume of the reaction system, including the balance chamber and mercury manometer, was 5550 ml. The reaction behavior was examined in a closed system in an atmosphere of hydrogen, nitrogen, or ammonia.

The balance was adjusted so as to have a maximum weight change of 500 mg and a sensitivity of 0.01 mg. A quartz crucible, 25 mm in height and 18 mm in outer diameter, was hung from the balance, and then a quartz tube of 30 mm in outer diameter was connected to the vessel containing the balance. After the connection, the system was evacuated to 5×10^{-6} mmHg or below.

The temperature of the specimen was measured by means of a Pt/Pt+13%Rh thermocouple placed close to the crucible inside the reaction tube. Most of the experiments were made by the thermogravimetric method, with a heating rate of 2 °C/min.

Materials. Pure uranium metal, in the form of chips 0.5 mm thick, 5 mm wide, the 7 mm long, was washed successively with 1 : 1 HNO_3, distilled water, and acetone. About 1 g of the bright metal thus prepared was quickly weighed; it was then placed in the quartz crucible and converted into the hydride and the nitride *in situ.*

High-purity nitrogen was further purified by passing it over a copper gauze heated at 520 °C, and then through a liquid nitrogen trap. The hydrogen was purified by passage through palladium asbestos heated at 300 °C and through a liquid nitrogen trap. The ammonia was solidified in a liquid nitrogen trap, and was then gasified after evacuating the trap.

Results and Discussion

Formation of Uranium Hydride. The bright uranium metal was placed in the quartz crucible, which was hung from one end of the balance arm. The reaction chamber was evacuated, and then hydrogen was admitted into the system. The hydrogen pressures applied were 75, 100, 150, and 300 mmHg. The temperature was raised at a rate of 2 °C/min. Some typical results are shown in Fig. 1. As seen in the figure, the temperature at which the hydrogenation begins depends on the hydrogen pressure. The temperatures are 200, 210, 220, and 260 °C at the hydrogen pressures of 300, 150, 100, and 75 mmHg, respectively. As the initial hydrogen pressure is lowered, the rate of the reaction becomes smaller. After the reaction terminated, the pressure of the hydrogen consumed was found to decrease by 20 mmHg from the initial level. At the hydrogen pressure of 100 mmHg or less, the hydrogenation did not terminate: the conversion into UH_3 was 87% at 100 mmHg and 20% at 75 mmHg. In these cases, the hydride once formed conversely decomposed into uranium and hydrogen above 350 °C before the hydrogenation was complete. The composition of the hydride was $UH_{3.00}$ at room temperature and $UH_{2.97}$ at temperatures between 200 and 400 °C. The values were in agreement with those obtained by equilibration.[12,16] The product was a fine black powder.

The reaction between uranium and hydrogen was found to occur at temperatures exceeding 200 °C, but the initiation temperature and the rate of the reaction were affected by the surface conditions, the shape of the metal-powder, the film or block, and the heating rate, as well as by the hydrogen pressure. When the oxide layer on metal surface was not completely removed, or when the surface was slightly oxidized, the temperature at which the hydrogenation began became obviously higher than that on the clean surface.

In the reactions at the hydrogen pressures of 100 and 75 mmHg, a plateau on the conversion curve appeared, as seen in Fig. 1. The formation of the hydride did not proceed any further beyond a certain temperature, resulting in a pseudo-equilibrium state. Its temperature was 325 °C at the hydrogen pressures of both 100 and 75 mmHg. Spedding *et al.*[17] and Albrecht and Mallett[18] have reported that the reaction

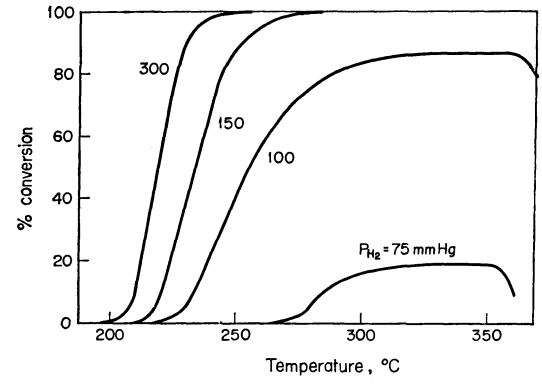

Fig. 1. Thermograms for the hydrogenation of uranium metal in hydrogen of various pressures in mmHg: a heating rate, 2 °C/min.

15) H. Tagawa, *J. Nucl. Mater.*, **41**, 313 (1971).

16) G. G. Libowitz, "Metal Hydrides," ed. by W. M. Mueller, J. P. Blackedge, and G. G. Libowitz, Academic Press, New York (1968), p. 490.

17) F. H. Spedding, A. S. Newton, J. C. Warf, O. Johnson, R. W. Nottorf, I. B. Johns, and A. H. Daane, *Nucleonics*, **4**, 4 (Jan. 1949).

18) W. M. Albrecht and M. W. Mallett, *J. Electrochem. Soc.*, **103**, 404 (1956).

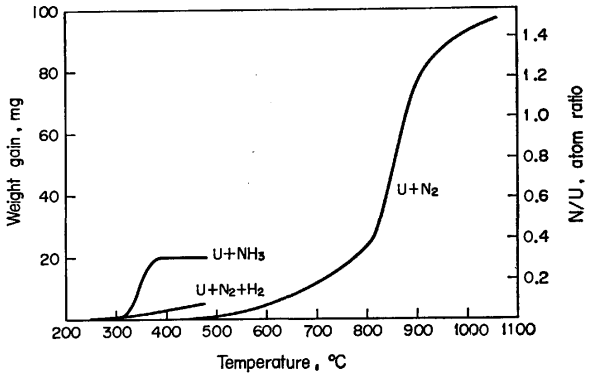

Fig. 2. Thermograms for the reactions of uranium metal with nitrogen and ammonia: the weight of uranium metal, 1.110 g; p_{N_2}, p_{NH_3}=300 mmHg; p_{H_2}=150 mmHg; a heating rate, 2 °C/min.

rate is a function of the $p-p_0$ value, i. e., $C(p-p_0)^{5/2}$ and $k(p-p_0)/p_0$, respectively, where p is the system pressure, p_0, the dissociation pressure of uranium hydride, and C and k, constants. In the present experiment, the $p-p_0$ values at 325 °C were 29 and 19 mmHg at the initial hydrogen pressures of 100 and 75 mmHg, respectively. The hydrogenation did not actually proceed before the value became zero.

Reaction between Uranium Metal and Nitrogen. As in the hydrogenation, 1 g of chips was heated in a nitrogen atmosphere at 300 mmHg up to 1000 °C. The results for the heating rate of 2 °C/min are shown in Fig. 2. The curve shows that the reaction begins at about 400 °C and that the weight changes rapidly in the temperature range between 800 and 900 °C. The temperature range with the maximum velocity did not vary, even if the heating rate was changed. Mallett and Gerds[2] found, in the reaction of uranium rods with nitrogen, that the Arrhenius plot of the reaction rate was made from two slopes below and above the temperature band of 750—775 °C and that the activation energy changed from 25.5 kcal/mol below 750 °C to 15.1 kcal/mol above 775 °C, where the reaction rate obeyed the parabolic law. If their results are plotted as the relation between the reaction rate and the temperature, the curve is similar to that in Fig. 2. The nitride formed on the metal surface was in the form of a film below 800 °C and coarse powder above 800 °C. The rapid increase in the reaction vleocity in the upper temperature region must be based on the formation of highly porous reaction layers, accompanied by spalled powders.

From the fact that the hydrogenation of uranium metal proceeds at a lower temperature than the nitrogenation of uranium with nitrogen, the nitride formation in the presence of hydrogen may be expected to occur more readily than in the absence of hydrogen. The reaction was examined in a mixture of hydrogen of 150 mmHg and nitrogen of 300 mmHg. The results are also shown in Fig. 2. The nitride formation proceeded slightly more rapidly, but it was not like the case for the hydrogenation in Fig. 1. The surface of the metal was covered with a grayish nitride film, and no powder such as that observed in the hydrogenation appeared. The hydrogenation of the metal, followed by the nitrogenation of the hydride, was scarcely found to occur; thus, the growing of the nitride film on the surface was inferred to be rather predominant over the hydrogenation.

When ammonia of 300 mmHg was used, the reaction began at about 250 °C, but the reaction was terminated at 380 °C, before it was complete. These results are also shown in Fig. 2. As in the case of the mixture of nitrogen and hydrogen, the metal surface was coated with a nitride film, and there existed a small amount of a fine black powder spalled at the bottom of the crucible.

Reaction between Uranium Hydride and Nitrogen. Uranium hydride was prepared in a crucible at about 280°C in a hydrogen atmosphere of 200 mmHg. The nitrogenation behavior was examined by varying the pressures of nitrogen and hydrogen. Figure 3 shows the reaction of uranium hydride with nitrogen of 75, 150, and 300 mmHg in the absence of hydrogen. The reaction began at about 160°C and became rapid above 240°C. In the case of each pressure, the slope of the curve appeared to vary sharply at about 290°C at a composition a little below $UN_{1.0}$. The temperature at the bend was lowered somewhat as the nitrogen pressure increased, but the shapes of the curves

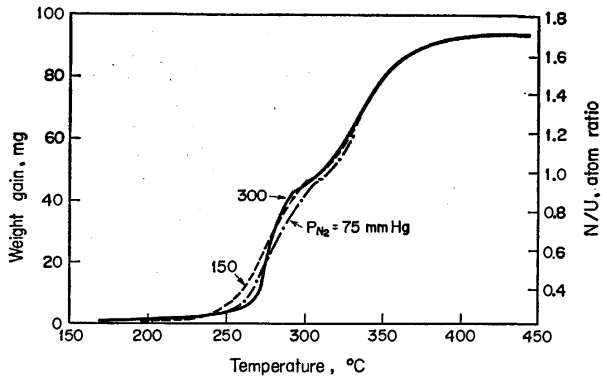

Fig. 3. Thermograms for the nitrogenation of uranium hydride in nitrogen of various pressures in mmHg: The weight of uranium metal, 1.070 g; a heating rate, 2 °C/min.

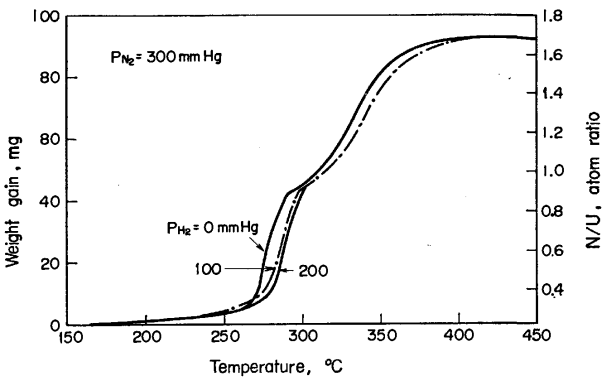

Fig. 4. Thermograms for the reaction of uranium hydride with nitrogen in the presence of hydrogen in mmHg: the weight of uranium metal, 1.070 g; p_{N_2}=300 mmHg; a heating rate, 2 °C/min.

were hardly altered at all by varying the nitrogen pressure. The change in the slope shows two steps of the reaction-the formation of the mononitride, followed by that of the sesquinitride. The nitrogen content increased as the temperature was raised to 420 °C. However, the nitride formed, having more nitrogen than that expressed by the chemical formula of U_2N_3, seemed not to be in an equilibrium state. When the nitride was kept at a temperature below 500 °C, the nitride observed to dissolve more nitrogen with the passage of time.

Figure 4 shows the effect of the pressure of hydrogen on the nitrogenation of the hydride at the nitrogen pressure of 300 mmHg. The hydrogen pressures used were 100 and 200 mmHg. The shape of the curve was not dependent on the variation in the hydrogen pressure. The temperature at which there was a sharp weight gain was 260 °C in the absence of hydrogen, but it shifted higher by about 10 °C when hydrogen was present in the system. The equilibrium hydrogen pressures over UH_3 have been reported to be 4.8, 6.6, and 10.0 mmHg at 250, 260, and 270 °C, respectively.[12,16] When hydrogen was not present, the reaction would occur between nitrogen and the uranium metal produced by the spontaneous thermal decomposition of the hydride. At 100 and 200 mmHg of hydrogen, however, the hydride reacted directly with nitrogen, because the decomposition pressure of the hydride was lower than the system pressure.

The reaction behavior of the hydride with nitrogen at a fixed temperature between 260 and 340 °C was examined by the procedure in which nitrogen of 300 mmHg was added a system which contained the hydride in a hydrogen atmosphere of 150 mmHg. The results are shown in Fig. 5. The velocity of the weight gain at $N/U<1$ is shown to be greater than that at $N/U>1$. The former corresponds to the formation of UN by the reaction of the hydride with nitrogen, and the latter to the formation of the sesquinitride by the reaction between the mononitride and nitrogen.

As mentioned above, the reaction sequence of the nitride formation is expressed as follows:

$$UH_3 + 1/2N_2 = UN + 3/2H_2, \quad \Delta H^\circ_{298} = -40.24 \text{ kcal}$$

$$UN + 1/4N_2 = 1/2U_2N_3, \quad \Delta H^\circ_{298} = -16.7 \text{ kcal}$$

$$U_2N_3 + x/2N_2 = U_2N_{3+x}$$

where the heats of formation, $-\Delta H^\circ_{f298}$, for UH_3,[16] UN,[19] and $1/2U_2N_{3.08}$[15] are 30.59, 70.59, and 86.3 kcal/mol, respectively. Thermochemically, the formation of the mononitride is indicated to take precedence over the sesquinitride in the early stage of the reaction. As seen in Fig. 5, the rate of the weight increase at $N/U<1$ is greater than that at $N/U>1$. Therefore, it may be deduced that the hydride converts to the mononitride, which then reacts with nitrogen to form the sesquinitride after the composition approaches $UN_{1.0}$.

Reaction between Uranium Hydride and Ammonia. The reaction was examined in an ammonia atmosphere

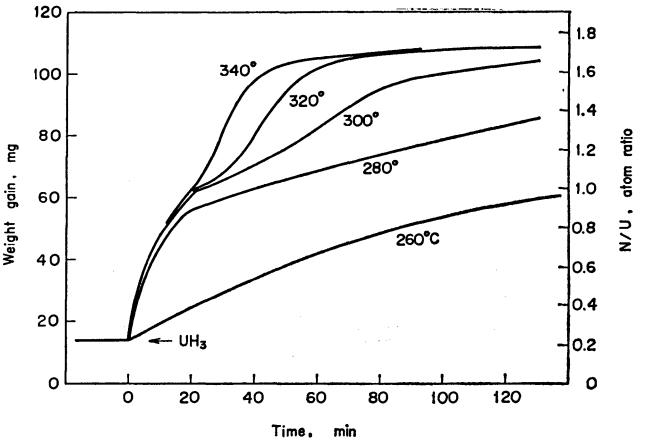

Fig. 5. Nitrogenation of uranium hydride in the mixture of nitrogen of 300 mmHg and hydrogen of 150 mmHg at constant temperatures between 260 and 340 °C: the weight of uranium metal, 1.070 g.

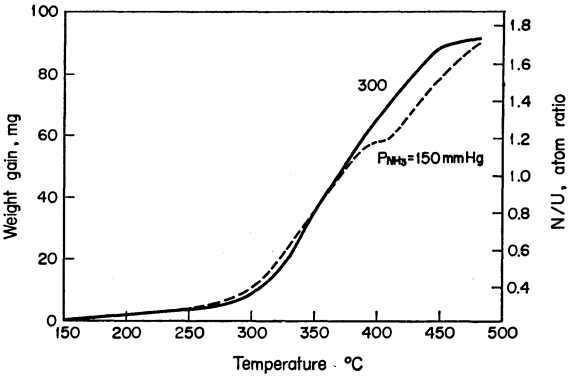

Fig. 6. Thermograms for the nitrogenation uranium hydride in ammonia of various pressures in mmHg: the weight of uranium metal, 1.030 g; a heating rate, 2 °C/min.

of 150 and 300 mmHg. The results are shown in Fig. 6. The reaction began at about 150 °C, and became fast above 250 °C. With ammonia of 300 mmHg, the shape of the curve was obviously different from that of the reaction between the hydride and nitrogen. The reaction is shown to form the sesquinitride directly. In ammonia of 150 mmHg, a plateau on the curve appeared around 400 °C. The plateau seems to indicate that the amount of ammonia becomes too small to continue the reaction with the hydride, but the further reaction of the more reactive uranium powder, produced by the decomposition of the hydride, with the residual ammonia takes place above 400 °C. This is because the partial pressure of hydrogen in the system is about 300 mmHg, and the hydride, of which the equilibrium pressure is 300 mmHg, does not yet proceed to decompose at 390 °C. When the equilibrium pressure is more than the system pressure as the temperature is raised, the thermal decomposition of the residual hydride occurs. As far as the pressure change was followed with time, the decomposition of ammonia was not seen to be catalysed by the nitride or the hydride.

19) Average value measured in calorimetry: H. Tagawa, *Nippon-Genshiryoku-Gakkai Shi*, **12**, 658 (1970).

The Determination of Beryllium in Several Alloys by Means of Atomic Absorption Spectrophotometry

Taketoshi NAKAHARA, Makoto MUNEMORI, and Sôichirô MUSHA

Department of Applied Chemistry, College of Engineering, University of Osaka Prefecture, Mozu-umemachi, Sakai 591

(Received June 24, 1972)

The atomic absorption spectrophotometric determination of beryllium in aqueous solutions and the effect of some water-miscible organic solvents were studied in a nitrous oxide-acetylene flame, using a Perkin-Elmer Model 303 atomic absorption spectrophotometer. The beryllium atomic absorptions were measured at the 234.9-nm resonance line of beryllium. The sensitivity for beryllium was 0.03 ppm for a 1% absorption. With the exception of palladium and silicon, none of the elements interfered with the determination of beryllium. Phosphoric acid caused an enhancement, while hydrochloric and nitric acids had a slight depressing effect. Furthermore, there seems to be a tendency for organic solvents with a higher ratio of the number of carbon atoms to that of oxygen atoms to cause greater enhancements in beryllium absorption, though there are a good number of exceptions. The atomic absorption method was applied to the determination of beryllium in several aluminum-, copper-, and magnesium-base alloys, with satisfactory results.

Since beryllium is one of the elements capable of forming highly refractory compounds, it cannot be atomized efficiently to give a measurable atomic absorption in low-temperature flames such as in air-acetylene flame, in which a sensitivity of 300 ppm for a 1% absorption has been reported.[1] Slavin and Manning[2] used a fuel-rich oxygen-acetylene flame in conjunction with an ethanolic solution of beryllium to obtain a sensitivity of 0.2 ppm for a 1% absorption. The introduction of a high-temperature and highly-reducing nitrous oxide-acetylene flame enabled Amos and Willis[3] to determine trace levels of beryllium (a sensitivity of 0.02 ppm for a 1% absorption) by means of atomic absorption spectrophotometry. Later Ramakrishna *et al.*[4] described that the nitrous oxide-acetylene flame was useful as well as an oxygen-acetylene flame at a 1 ppm level of beryllium and that the sensitivity was improved when an aqueous solution of 10% in diethylene glycol diethyl ether was used.

In this paper, the enhancement of depressant effects on the atomic absorption of beryllium in a nitrous oxide-acetylene flame will be described. Furthermore, the method was applied to the determination of beryllium in several aluminum-, copper-, and magnesium-base alloys with satisfactory results.

Experimental

Apparatus. All the atomic absorption signals were obtained by using a Perkin-Elmer Model 303 atomic absorption spectrophotometer, fitted with a 5-cm slot burner head for a premixed nitrous oxide-acetylene flame. A beryllium hollow-cathode lamp (Atomic Spectral Lamps Pty., Australia) was used as the source of radiation. A Yanagimoto GCG-252 chart recorder was used after modification so as to adapt it to the Perkin-Elmer instrument.

Reagents. The stock solution of beryllium, 1000 ppm, was prepared by dissolving 9.83 g of analytical-reagent grade beryllium sulfate tetrahydrate in distilled water and by then diluting it to 500 ml. Various concentrations were made by the appropriate dilution of the stock solution.

Results and Discussion

Operating Conditions. The optimum operating conditions listed in Table 1 were established with a 2.0-ppm solution of beryllium. The atomic absorptions for beryllium were measured at different flame heights under various flame conditions in an attempt to find the optimum flame conditions for beryllium. The results are shown in Fig. 1. Under these flame conditions, about 3-cm-long "red feather" zone was produced above the burner head, and the sample aspiration rate was about 13 ml/min.

Table 1. Operating conditions for the measurement of beryllium atomic absorption

Wavelength	234.9 nm
Slit width	0.3 mm
Spectral bandpass	0.2 nm
Lamp current	20 mA
Scale expansion	×1
Acetylene flow rate	8.1 l/min
Acetylene pressure	0.6 kg/cm²
Nitrous oxide flow rate	18.0 l/min
Nitrous oxide pressure	1.5 kg/cm²
Flame height	3—4 mm above the top of the burner head
Burner slot	0.48 mm × 50 mm

Calibration Graph and Sensitivity for Beryllium. Under the optimum operating conditions described above, a straight calibration graph passing through the point of origin was obtained over the concentration range of 0—5 ppm for beryllium aqueous solutions. A good linearity held to the relatively high absorbance of about 0.6. The sensitivity for beryllium was 0.03 ppm for a 1% absorption. In this range, beryllium absorbances were measured with a precision of a relative standard deviation of 2.1%.

Effects of Other Elements. It has already been presented that a number of foreign elements have no

1) J. E. Allan, *Spectrochim. Acta*, **18**, 259 (1962).
2) W. Slavin and D. C. Manning, *Anal. Chem.*, **35**, 253 (1963).
3) M. D. Amos and J. B. Willis, *Spectrochim. Acta*, **22**, 1325 (1966).
4) T. V. Ramakrishna, P. W. West, and J. W. Robinson, *Anal. Chim. Acta*, **39**, 81 (1967).

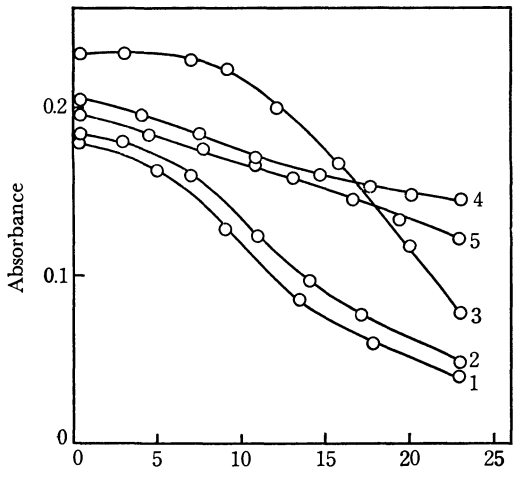

Fig. 1. Effect of flame composition and flame height on beryllium atomic absorption. Concentration of beryllium: 2 ppm. Nitrous oxide flow rate: 18.0 l/min. Acetylene flow rate: (1) 7.5 l/min; (2) 7.8 l/min; (3) 8.1 l/min; (4) 8.5 l/min; (5) 9.0 l/min.

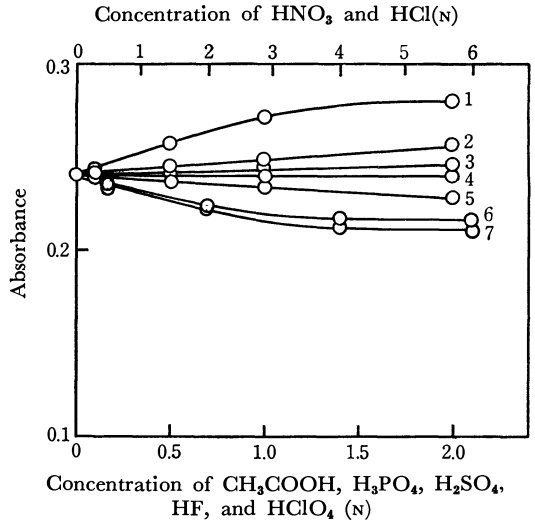

Fig. 2. Effect of acids on beryllium atomic absorption. Concentration of beryllium: 2 ppm.
1: Acetic acid, 2: phosphoric acid, 3: sulfuric acid, 4: hydrofluoric acid, 5: perchloric acid, 6: nitric acid, 7: hydrochloric acid.

effect on the beryllium atomic absorption.[3-5] In the present investigation, the effects of various elements were also examined. The concentration of beryllium was 2 ppm, and that of the element, 200 ppm. The elements examined were Al, As, Au, Ba, Bi, Ca, Cd, Co, Cr(III), Cs, Cu, Fe(III), Hg(II), In, La, Mg, Mn(II), Mo, Na, Ni, Pb, Pd, Sb, Se, Si, Sn(II), Sr, Te, Th, Ti, V, Zn, and Zr. These elements were added as chloride, nitrate, or sulfate in most instances. An element was considered to interfere with the beryllium atomic absorption when it produced a variation in the absorbance of more than twice the relative standard deviation for beryllium alone.

With the exception of palladium and silicon, none of the elements interfered with the determination of beryllium at this concentration level. Palladium and silicon depressed the beryllium absorbance by about 29 and 8% respectively. A large amount of aluminum, however, depressed the beryllium atomic absorption, as will be described later.

Effects of Acids. Amos and Willis[3] have reported no interference from 2.5 N sulfuric acid with, and a slight enhancement by phosphoric acid of the beryllium absorption. On the other hand, Fleet *et al.*[5] have described that no interference occurred from hydrochloric, hydrofluoric, nitric, and phosphoric acids at the 10000 ppm level with respect to Cl, F, N, and P respectively.

In this study, the effect of hydrochloric, hydrofluoric, nitric, perchloric, phosphoric, sulfuric, and acetic acids in the concentration range of 0—2.0 N or 0—6.0 N on the beryllium atomic absorption was studied for 2-ppm solutions of beryllium. The results are shown in Fig. 2. Phosphoric acid caused an enhancement, as has been reported by Amos and Willis.[3] Sulfuric acid caused, but in a somewhat different way and in a higher concentration, an enhancement such as has been described by Fleet *et al.*[5] Hydrochloric and nitric acids in the 0—6.0 N range had, contrary to expectations, a slight depressing interference. Acetic acid caused an enhancement. A similar effect has been observed on the atomic absorption of vanadium in a nitrous oxide-acetylene flame.[6] The enhancement by acetic acid may be considered to be a kind of organic-solvent effect, such as has been described by Ramakrishna *et al.*[4] and by Fleet *et al.*[5]

As has been mentioned above, somewhat different results for the interference effects have been observed in the several investigations in this field, including this study. This may be ascribable to the difference in the efficiency of the nebulizers employed in those investigations.

Effect of Water-miscible Organic Solvents. Ramakrishna *et al.*[4] have described that the addition of glycols considerably enhanced the beryllium atomic absorption and that the sensitivity for beryllium was increased by 25% in the presence of 5% of diethylene glycol diethyl ether, which was the most effective on the glycols. Fleet *et al.*[5] have reported that the presence of methanol, ethanol, and isopropyl alcohol in the concentration of 20 vol% enhanced by 11—20% the beryllium atomic absorption, while glycol had a depressing effect of 17%.

In this study, the effect of water-miscible organic solvents, *e.g.*, alcohols, ketones, and glycols, on the beryllium absorption was studied. Solutions of 1 ppm in beryllium and 5- or 10-% in commonly-available alcohols, ketones, or glycols were prepared. These solutions were nebulized into the flame, and the beryllium absorptions were measured. At the same time, sample aspiration rates were measured. The results are shown in Table 2. It can be seen from Table 2 that the enhancement in the presence of organic

5) B. Fleet, K. V. Liberty, and T. S. West, *Talanta*, **17**, 203 (1970).

6) T. Nakahara, M. Munemori, and S. Musha, *Nippon Kagaku Zasshi*, **90**, 697 (1969).

TABLE 2. EFFECT OF SOME WATER-MISCIBLE ORGANIC SOLVENTS ON THE ATOMIC ABSORPTION OF BERYLLIUM

Organic solvent	Molecular weight	Boiling point (°C)	5%-Addition		10%-Addition		C/O ratio
			Sample aspiration rate (ml/min)	Absorbance	Sample aspiration rate (ml/min)	Absorbance	
None	—	—	13.0	0.120	13.0	0.120	—
Ethylene glycol	62.07	197.7	12.4	0.122	11.4	0.124	1.0
1,4-Dioxane	72.11	79.6	12.3	0.128	11.9	0.146	2.0
Methanol	32.04	64.65	12.5	0.137	12.1	0.150	1.0
Acetone	58.08	56.3	12.3	0.146	11.6	0.161	3.0
Ethanol	46.07	78.3	12.0	0.153	11.4	0.165	2.0
Diethylene glycol diethyl ether	162.23	186.0	11.5	0.154	10.8	0.166	2.6
Isopropyl alcohol	60.10	82.4	11.5	0.163	11.1	0.185	3.0
Propyl alcohol	60.10	97.15	11.6	0.164	10.8	0.186	3.0
Diethylene glycol monobutyl ether	162.23	230.4	11.4	0.174	10.8	0.196	2.6
Isobutyl alcohol	74.12	108.0	10.9	0.210	10.4	0.252	4.0
Butyl alcohol	74.12	117.5	10.9	0.213	10.3	0.254	4.0

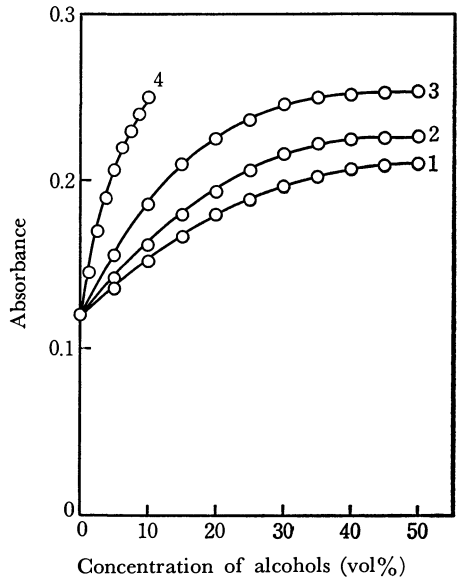

Fig. 3. Effect of alcohols on beryllium atomic absorption.
Concentration of beryllium: 1 ppm.
1: Methanol, 2: ethanol, 3: propyl and isopropyl alcohols, 4: butyl and isobutyl alcohols.

solvents has no relation to their molecular weights and boiling points. As for alcohols alone, however, the beryllium absorbance was increased in the order of the molecular weights and the boiling points. With an increase in the concentration of alcohols, the absorbance was increased as is shown in Fig. 3. Butyl alcohol was the most effective for the enhancement of the beryllium absorption, though its concentration was limited below 10% because of its solubility. Table 2 shows also that the absorbance was increased in the reverse order of the increase in the sample aspiration rate. If it can be assumed that the increase in the sample aspiration rate signifies an increase in the amount of the solution reaching the flame, the enhancement must be explained in terms of an increase in the efficiency of atomization. Perhaps a hotter or more reducing condition was created in the flame, with the result that the vaporization and dissociation of the metal compounds were increased.

The ratio of the number of carbon atoms to that of oxygen atoms (C/O ratio) in the flame is taken into account in determining the reducing properties of the flame.[7] L'vov[8] calculated the variation in the flame composition with a variation in the fuel-to-oxidant flow ratio for a total-consumption nebulizer-burner using an oxygen-acetylene flame and nebulizing aqueous or ethanolic solutions. According to L'vov's conclusions, optimum reducing properties of the flame are achieved when the composition of the flame, including the solvent, have a C/O ratio equal to unity. Solvents with a higher ratio of C/O increase the reducing properties of the flames more efficiently than ethanol. It should be remembered also that, when using organic solvents, the cooling effect due to an aspirated solution is decreased and a temperature rise takes place.[9] The C/O ratios of the organic solvents used are shown in Table 2. There seems to be a tendency for solvents with higher C/O ratios to cause greater enhancements, though there are a good number of exceptions. It may be concluded that the organic solvent provides a more reducing property for the flame, resulting in an increased production of beryllium atoms in the flame.

Application to the Determination of Beryllium in Several Aluminum-, Copper-, and Magnesium-base Alloys. The use of small amounts (0.01 to 0.5%) of beryllium as an additive to aluminum-, copper-, and magnesium-base alloys to improve their yield strength has created the need for a rapid and simple method for the determination of beryllium. For such a determination, atomic absorption spectrophotometry is the most

7) I. Rubeska in "Flame Emission and Atomic Absorption Spectrometry," Vol. 1, J. A. Dean and T. C. Rains, eds., Marcel Dekker, New York, N. Y. (1969), p. 325.

8) B. V. L'vov, "Atomic Absorption Spectroscopy" (Translated from the Russian), Israel Program for Scientific Translations, Jerusalem, Israel (1969), p. 133.

9) M. R. Baker and B. L. Vallee, *Anal. Chem.*, **31**, 2036 (1959)

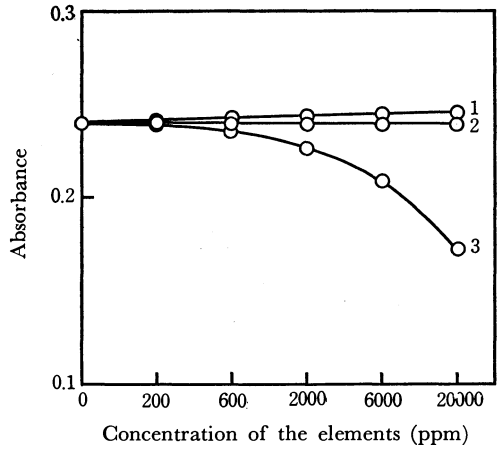

Fig. 4. Effect of a large amount of aluminum, copper, and magnesium on beryllium atomic absorption. Concentration of beryllium: 2 ppm.
1: Magnesium, 2: copper, 3: aluminum.

useful. In this investigation the determination of beryllium in several aluminum-, copper-, and magnesium-base alloys was studied.

The effect of a great amount of aluminum, copper, and magnesium, which are matrix elements in the sample alloys, on the beryllium atomic absorption was studied first. The effects observed in the actual concentration levels (200—20000 ppm) of these elements for 2 ppm of beryllium are shown in Fig. 4. Copper and magnesium showed no interference, but a great amount of aluminum (above 600 ppm of aluminum) had a depressing interference. At the 2000- and 20000-ppm aluminum levels, depressions of 6 and 28% respectively were observed. This depression must be taken into consideration in the case of the determination of trace beryllium in aluminum-base alloys; otherwise, serious errors will obviously result.

It has been already reported by Fleet *et al.*[5] that the depressing effect by aluminum can be overcome by the addition of oxine (8-hydroxyquinoline) to a solution containing beryllium and aluminum. The "masking" of aluminum by oxine, however, falls off steadily if the concentration of aluminum is increased to above 4000 ppm, and a corresponding increase in the oxine concentration to, say, 5% can not offset this.

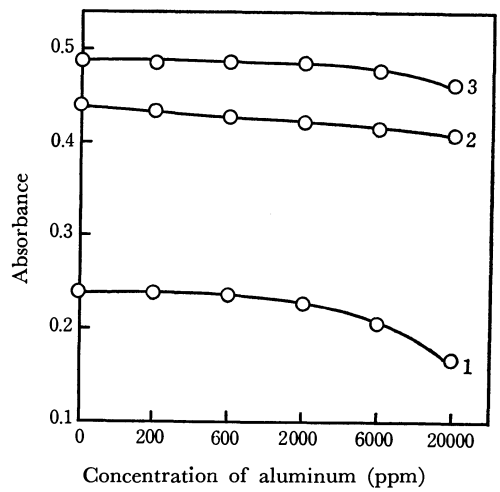

Fig. 5. Effect of aluminum in the presence of diethylene glycol monobutyl ether or butyl alcohol on beryllium atomic absorption. Concentration of beryllium: 2 ppm.
1: With no addition, 2: with the addition of diethylene glycol monobutyl ether(20 vol%), 3: with the addition of butyl alcohol(10 vol%).

In this study, another method for eliminating the interference from aluminum was examined; that is, beryllium absorptions were measured upon the addition of 20% of diethylene glycol monobutyl ether or 10% of butyl alcohol; such additions caused a relatively great enhancement, as is shown in Table 2, to 2-ppm beryllium solutions containing aluminum in the 200—20000 ppm range. The results are shown in Fig. 5. It can be seen that the addition of diethylene glycol monobutyl ether or butyl alcohol was effective not only in enhancing the beryllium absorption, but also in eliminating the depressing interference of aluminum. This fact also suggests that the organic solvents play an important role in the process of beryllium atom-production. However, the interference-suppressing effect of diethylene glycol monobutyl ether and butyl alcohol falls off slightly in the presence of a a greater amount (6000 ppm) of aluminum (as is is shown in Fig. 5); therefore, a standard addition technique in the presence of diethylene glycol monobutyl ether was employed in the determination of beryllium in aluminum-, copper-, and magnesium-base alloys.

The methods of preparing the sample solutions were as follows. Aluminum-base alloy: A 1-g sample was weighed precisely and dissolved in 25 ml of 6 N hydrochloric acid by gentle heating on a hot plate. After cooling, the resultant solution was transferred to a 100-ml volumetric flask and diluted to volume with distilled water. Copper-base alloy: A 1-g sample containing less than 0.1% of beryllium was weighed and dissolved in 10 ml of 6 N nitric acid, or a 0.1-g sample containing more than 0.1% of beryllium was weighed and dissolved in 4 ml of 2 N nitric acid by gentle heating on a hot plate. After cooling, the resulstant solutions were transferred to 100-ml volumetric flasks and diluted to volume with distilled water. Magnesium-base alloy: A 1-g sample was weighed

Table 3. Results of the determination of beryllium in aluminum-, copper-, and magnesium-base alloys

Sample	Beryllium content (%)			
	Colorimetric method	Atomic absorption method		
Aluminum-base alloy				
No. 1	0.06	0.06_5	0.06_2	0.06_3
No. 2	0.18	0.18_2	0.18_7	0.18_4
No. 3	0.43	0.43_5	0.43_3	0.43_6
Copper-base alloy				
No. 1	0.11	0.11_1	0.10_8	0.11_5
No. 2	0.24	0.23_8	0.24_5	0.24_0
Magnesium-base alloy				
No. 1	0.02	0.01_3	0.01_3	0.01_2

and dissolved in 25 ml of 6 N hydrochloric acid by gentle heating on a hot plate. After cooling, the resultant solution was transferred to a 100-ml volumetric flask and diluted to volume with distilled water.

Five 10-ml portions of the sample solutions and 5 ml of diethylene glycol monobutyl ether were taken into 25-ml volumetric flasks, 0-, 1-, 2-, 3-, and 4-ml portions of the 12.5 ppm standard solution of beryllium were added, and the mixtures were diluted to volume with distilled water. The solutions were sprayed into the nitrous oxide-acetylene flame, and the beryllium atomic absorption signals were measured under the optimum operating conditions. The determinations were performed three times on each aliquot of aluminum-, copper-, and magnesium-base alloys.

The beryllium contents in the samples were determined by using a standard addition method. The results are shown in Table 3. Table 3 shows the results of the colorimetric determination of beryllium with Arsenazo I[10] on the alloy samples. Atomic absorption spectrophotometry and colorimetry with Arsenazo I gave consistent results on the aluminum-, and copper-base alloys, but inconsistent results on the magnesium-base alloy. The latter results were possibly caused by the irrelevance of the application of the colorimetric method to such a sample, but, at any rate, they may be tolerable in view of the smallness of the beryllium content in the sample.

10) T. Hattori, I. Tsukahara, and T. Yamamoto, *Bunseki Kagaku*, **15**, 41 (1966).

BULLETIN OF THE CHEMICAL SOCIETY OF JAPAN, VOL. 46, 1166—1172 (1973)

The Atomic Absorption Spectrophotometric Determination of Bismuth in Premixed Inert Gas(Entrained Air)-Hydrogen Flames

Taketoshi NAKAHARA, Makoto MUNEMORI, and Sôichirô MUSHA

Department of Applied Chemistry, College of Engineering, University of Osaka Prefecture, Mozu-umemachi, Sakai 591

(Received June 26, 1972)

The atomic absorption spectrophotometric determination of bismuth in aqueous solutions was established in premixed inert gas(entrained air)-hydrogen flames with a "multi-flame" burner in conjunction with a Nippon Jarrell-Ash Model AA-1 atomic absorption/flame emission spectrophotometer. Under the optimum operating conditions, a straight calibration graph was obtained at 223.1 nm in the concentration range of 0–10 ppm and the bismuth sensitivity for a 1% absorption was 0.1 ppm. The effects of acids and other elements on the bismuth atomic absorption were examined. Phosphoric acid caused a considerable depressing effect on the bismuth absorption. Hydrochloric acid remarkably depressed the bismuth absorption at acid concentrations lower than 0.5 N, but it gave no interference in acid concentrations higher than 0.5 N, in which water-insoluble bismuth oxychloride was quickly dissolved in hydrochloric acid. Hydrofluoric, nitric, perchloric, and sulfuric acids had no effect on the bismuth absorption. Most of the elements examined, with the exception of aluminum, boron, cerium, silicon, and zirconium, gave no interference to the bismuth absorption. The depressing interferences due to some elements were removed in appearance by adding a large amount (2000 ppm) of magnesium (as chloride). Furthermore, it was found that most of the depressing interferences could be eliminated by adding a large amount (0.1 M) of ammonium salts (as chloride or perchlorate) to the sample solutions. Bismuth in the presence of magnesium chloride, ammonium chloride, or ammonium perchlorate could be determined without interference from various other elements. The atomic absorption spectrophotometric method was applied to the determination of bismuth in sulfide ores, aluminum-, tin-, and lead-base alloys with satisfactory results.

Bismuth is determined readily in an air-acetylene flame. The bismuth line at 306.8 nm is of limited usefulness, however, because it falls on the band head of the major hydroxyl band in the flame; moreover, the flame luminosity makes the atomic absorption measurement uncertain. The resonance line at 223.1 nm is usually the most useful. The best sensitivity for a 1% absorption in the determination of bismuth in an aqueous solution by atomic absorption spectrophotometry with an air-acetylene fiame is 0.7 ppm at the 223.1 nm line.[1] Kinser[2] has reported the determination of bismuth in biological samples with an air-acetylene flame without any interference from the materials found in the samples. Bismuth could be readily extracted from aqueous solutions into organic solvents with such chelating agents as ammonium pyrrolidine dithiocarbamate (APDC), dithizone, etc. An APDC-organic solvent extraction system has been used in the analysis of urine samples[3] and the lead-base and tin-base metals.[4] The dithizone-carbon tetrachloride system has been used in the determination of bismuth in ferrous alloys.[5] Furthermore, Headridge and Richardson[6] have reported on the use of a bismuth iodide-methyl isobutyl ketone system for the determination of bismuth in ferrous alloys. On the other

1) W. Slavin, "Atomic Absorption Spectroscopy," Interscience Publishers, New York, N. Y. (1968), p. 60.
2) R. E. Kinser, *Amer. Ind. Hyg. Assoc. J.*, **27**, 260 (1966).
3) J. B. Willis, *Anal. Chem.*, **34**, 614 (1962).
4) H. K. Y. Lau, H. A. Droll, and P. F. Lott, *Anal. Chim. Acta*, **56**, 7 (1971).
5) G. Kisfaudi and M. Lenhof, *ibid.*, **55**, 444 (1971).
6) J. B. Headridge and J. Richardson, *Analyst* (London), **95**, 930 (1970).

hand, McGee and Winefordner[7] have described the determination of bismuth using a modified long-path absorption cell and a xenon lamp as a continuum radiation source, with an argon-hydrogen flame. Burke[8] has studied the scavenger property of manganese (IV) oxide for the separation of less than 100 ppm of bismuth by atomic absorption spectrophotometry with an air-acetylene fiame.

Several authors have examined the so-called "cool" flames with respect to their use in flame methods of analysis. These flames are usually entrained air-hydrogen flames in which the combustible gas is diluted with an inert gas, such as nitrogen or argon. Winefordner *et al.*[9,10] have used an argon (entrained air)-hydrogen flame in the flame-emission spectrophotometric determination of 14 elements and have obtained limits of detection which are better than, or as good as, those obtained with an oxygen-hydrogen flame. Their success has been attributed to the low background noise associated with the argon-hydrogen fiame and also to possible chemiluminescence with certain elements. Dagnall *et al.*[11] have used a hydrogen flame diluted with nitrogen to observe the molecular band emission of S_2 in the determination of sulfur. The argon (entrained air)-hydrogen flame has also been used in atomic absorption spectrophotometry because of its low flame background absorption in the ultraviolet region; this has resulted in improving the atomic absorption sensitivities for several elements.[12]

This paper will decribe an investigation of the flame characteristics for bismuth in the premixed argon (entrained air)- and nitrogen(entrained air)-hydrogen flames produced using a specially-constructed "multi-flame" burner,[13] and an investigation of the interference with bismuth atomic absorptions. A depressing interference was observed over a wide range of concentration of several elements. It may, however, be noted that a large amount of magnesium can eliminate the depressing effect due to some of the elements examined. This was successfully applied to the determination of bismuth in several metallurgical samples.

Experimental

Apparatus. All the atomic absorption measurements were performed using a Nippon Jarrell-Ash Model AA-1 atomic absorption/flame emission spectrophotometer on a single-pass system. A "multi-flame" burner[13] was used in conjunction with a Techtron standard nebulizer-chamber. The height in the flame was taken as zero when the light beam from the hollow-cathode lamp just touched the top of the burner head. The analytical wavelength was 223.1 nm, and the light source was a bismuth high-spectral-output hollow-cathode lamp (Westinghouse, Type No. 45467), operated at 8 mA. The gas flow rates were carefully regulated and were monitored on calibrated flow meters.

Reagents. A stock solution of bismuth (1000 ppm) was prepared by dissolving 1.000 g of high-purity bismuth metal in 10 ml of concentrated nitric acid by gentle heating, and by then diluting it to 1000 ml with distilled water. It was necessary to keep the acid concentration high enough (pH 1) to prevent its hydrolysis. Lower concentrations of standard bismuth solutions were freshly prepared daily by diluting the stock solution.

All the other reagents used were either of a reagent grade or of the highest quality available. Blanks were run on each solution in the case of the interference study with the bismuth atomic absorption.

Results and Discussion

Bismuth Sensitivity in Various Flames. Slavin[1] and Kinser[2] have reported a sensitivity of 0.7 ppm for a 1% absorption in aqueous solutions with an air-acetylene flame at the wavelength of the 223.1 nm bismuth resonance line. The bismuth sensitivities for a 1% absorption in aqueous solutions were obtained in several flames produced with a "multi-flame" burner[13] under optimum flame and measuring conditions. They were 0.14, 0.80, 0.18, 1.00, 0.10, and 0.11 ppm in the premixed air-acetylene, nitrous oxide-acetylene, air-hydrogen, nitrous oxide-hydrogen, argon (entrained air)-hydrogen, and nitrogen(entrained air)-hydrogen flames respectively. The sensitivities in the inert gas(entrained air)-hydrogen flames were considerably better than those obtained in the other hydrogen or acetylene flames. Furthermore, it was found that the inert gas(entrained air)-hydrogen flames gave extremely low background absorptions at the 223.1 nm line compared with the other flames examined. These higher sensitivities indicated that such relatively volatile elements as arsenic, bismuth, cadmium, lead, selenium, tin, and zinc were sufficiently atomized, even in the low-temperature flames.

Effect of Flame Composition and Flame Height. At a fixed flow rate of argon or nitrogen as a nebulizing gas, the hydrogen flow rates were varied from 3.6 to 12.6 l/min and the absorptions were measured for 10 ppm of bismuth in various flame heights in order to find the optimum flame composition and flame height. The results obtained in the argon(entrained air)-hydrogen flame are shown in Fig. 1. It may be seen from Fig. 1 that the bismuth atomic absorption may be depends remarkably on both the flame composition and the flame height. Similar results were obtained in the nitrogen(entrained air)-hydrogen flame. The optimum conditions for bismuth atomic absorption are summarized as follows. Argon(entrained air)-hydrogen flame: hydrogen flow rate, 5.4 l/min; argon flow rate, 4.5 l/min; argon pressure, 1.5 kg/cm^2; height in the flame, 4 mm above the top of burner head. Nitrogen(entrained air)-hydrogen flame: hydrogen flow rate, 5.4 l/min; nitrogen flow rate 5.0 l/min; nitrogen pressure, 1.5 kg/cm^2; height in the flame,

7) W. W. McGee and J. D. Winefordner, *Anal. Chim. Acta*, **37**, 429 (1967).
8) K. E. Burke, *Anal. Chem.*, **42**, 1536 (1970).
9) K. Zacha and J. D. Winefordner, *Anal. Chem.*, **38**, 1539 (1966).
10) C. Veillon, J. M. Mansfield, M. L. Parsons, and J. D. Wineforder, *ibid.*, **38**, 204 (1966).
11) R. M. Dagnall, K. C. Thompson, and T. S. West, *Analyst* (London), **92**, 506 (1967).
12) H. L. Kahn and J. E. Schallis, *At. Absorption Newslett.*, **7**, 5 (1968).
13) T. Nakahara, H. Date, M. Munemori, and S, Musha, This Bulletin, **46**, 637 (1973).

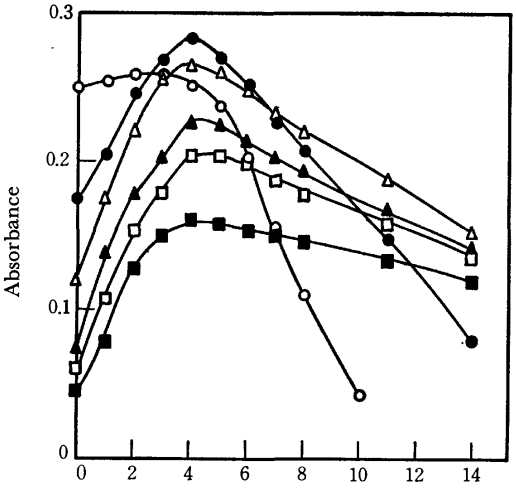

Fig. 1. Effect of flame composition and flame height on bismuth atomic absorption. Concentration of bismuth: 10 ppm.
Flame: an argon(entrained air)-hydrogen flame.
Hydrogen flow rate: (○) 3.6 l/min; (●) 5.4 l/min; (△) 7.2 l/min; (▲) 9.0 l/min; (□) 10.8 l/min; (■) 12.6 l/min.

5 mm above the top of the burner head. Under these conditions, both the flames were completely invisible and quiet.

Effect of Acids. No detailed study has been previously reported on the effect of acids on the determination of bismuth by atomic absorption spectrophotometry in either an air-acetylene flame or an air-hydrogen flame. The bismuth absorptions were, therefore, measured in inert gas(entrained air)-hydrogen, flames for 10 ppm of bismuth in the presence of acids, the concentrations of which were varied from 0.1 to 2.0 N. The acids examined included hydrochloric, hydrofluoric, nitric, phosphoric, perchloric, and sulfuric acids. The results obtained in the argon(entrained air)-hydrogen flame are shown in Fig. 2. Similar results were obtained in the nitrogen(entrained air)-hydrogen flame. Phosphoric acid had a considerable depressing effect on the bismuth atomic absorption. The effect of phosphoric acid may be due to the difficulty of the thermal decomposition of the phosphate in the low-temperature flame. On the other hand, hydrofluoric, perchloric, and sulfuric acids caused a slight enhancement of the bismuth atomic absorption.

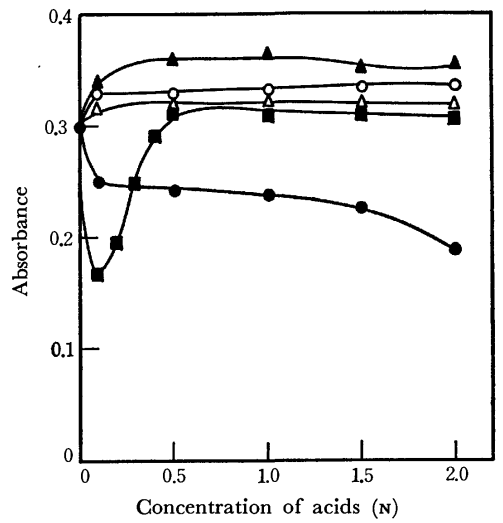

Fig. 2. Effect of acids on bismuth atomic absorption.
Concentration of bismuth: 10 ppm. Flame: an argon(entrained air)-hydrogen flame. (▲) Perchloric acid; (○) hydrofluoric and sulfuric acids; (△) nitric acid; (■) hydrochloric acid; (●) phosphoric acid.

Hydrochloric acid was found, as is shown in Fig. 2, to depress remarkably the bismuth atomic absorption in acid concentrations lower than 0.5 N, but this depressing interference disappeared in acid concentrations higher than 0.5 N because water-insoluble bismuth oxychloride is quickly dissolved in hydrochloric acid of a higher concentration. The bismuth solution containing hydrochloric acid at the 1.0 N level was used in all the later work, because the effect of hydrochloric acid caused the smallest interference in the determination of bismuth of all the acids examined.

Effect of Various Other Elements. Winefordner *et al.*[9,10] have described that an argon(entrained air)-hydrogen flame was useful for atomic fluorescence and flame emission spectrophotometry. Kirkbright and Ranson[14] have reported that the determination of some elements, such as arsenic and selenium, in the argon(entrained air)-hydrogen flame suffered from interference from foregin elements because of the inability of the cool flame to vaporize or atomize the other elements present in the sample solution.

The effects of various other elements on the atomic absorption spectrophotometric determination of bismuth were studied in detail at constant concentration levels: aqueous solutions containing 10 ppm of bismuth and 200 ppm of other elements. The results obtained in both the flames are shown in Table 1. Most elements, with the exception of aluminum, beryllium, silicon, etc., gave no interference, the deviation of the absorbance of bismuth being less than 5%. As is shown in Table 1, however, aluminum, beryllium, boron, cerium, silicon, and zirconium, which easily produce refractory metallic oxides in the flame, depressed the bismuth atomic absorption. These depressing effects on the bismuth absorption can not be satisfactorily explained.

Because the flame composition has been shown to be an important parameter in interference studies,[1,15,16] the hydrogen-flow rate and the flame height in inert gas(entrained air)-hydrogen flames were varied to see what effect, if any, would be thus produced on the depressing interference. For example, an aluminum depression showed a dependency on these parameters. As is shown in Fig. 3, this interference could be negative

14) G. F. Kirkbright and L. Ranson, *Anal. Chem.*, **43**, 1238 (1971).
15) J. A. Dean and T. C. Rains, "Flame Emission and Atomic Absorption Spectrometry," Vol. 1, Marcel Dekker, New York, N. Y. (1969).
16) R. Herrman and C. Th. J. Alkamade, "Chemical Analysis by Flame Photometry," 2nd. revised ed., Interscience Publishers, New York, N. Y. (1963).

Table 1. Effect of other elements on bismuth atomic absorption

	Argon(entrrained air)-hydrogen flame	Nitrogen(entrained air)-hydrogen flame
No interference	Ag[a], As[b], Au[c], Ba[a], Ca[a], Cd[a], Co[c], Cr[c], Cu[d], Fe[c], Hg[c], In[c], K[c], La[c], Li[c], Mg[c], Mn[a], Mo[e], Na[c], Ni[d], Pb[a], Rb[c], Sb[c], Se[b], Sn[c], Sr[a], Te[b], Ti[c], Tl[a], V[e], W[b], Y[a], Zn[a]	Ag[a], As[b], Au[c], Ba[c], Cd[a], Cu[d], Fe[c], Hg[c], In[c], K[c], La[c], Li[c], Mg[c], Mn[a], Mo[e], Na[c], Pb[a], Sb[d], Se[b], Sn[c], Te[b], Ti[c], Tl[a], V[e], W[b], Y[a], Zn[a]
Depression	Al[c], B[f], Be[d], Ce[d], Cs[c], Pd[c], Si[b], Zr[a]	Al[c], B[f], Be[d], Ca[a], Ce[d], Co[c], Cr[c], Cs[c], Ni[d], Pd[c], Si[b], Sr[a], Zr[a]
Enhancement	None	None

a) Added as nitrate. b) Added as sodium arsenite, selenite, silicate, tellurite or tungstate, respectively. c) Added as chloride. d) Added as sulfate. e) Added as ammonium molybdate or vanadate, respectively. f) Added as boric acid.

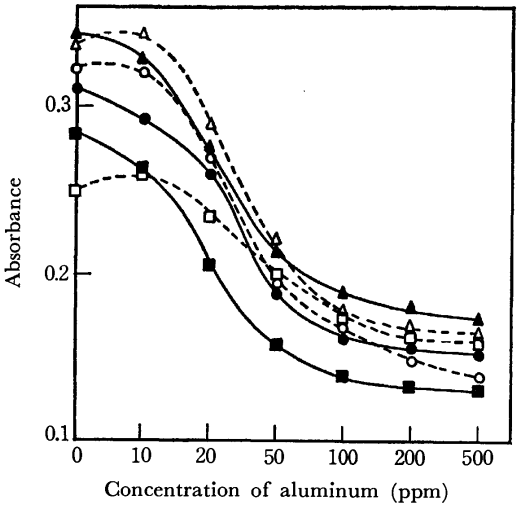

Fig. 3. Effect of hydrogen flow rate and flame height on the interference from aluminum with bismuth atomic absorption. Concentration of bismuth: 10 ppm. Flame: an argon(entrained air)-hydrogen flame.
Effect of hydrogen flow rate: (■) 4.5 l/min; (▲) 5.4 l/min; (●) 6.3 l/min. Effect of flame height above burner head: (○) 2 mm; (△) 4 mm; (□) 8 mm.

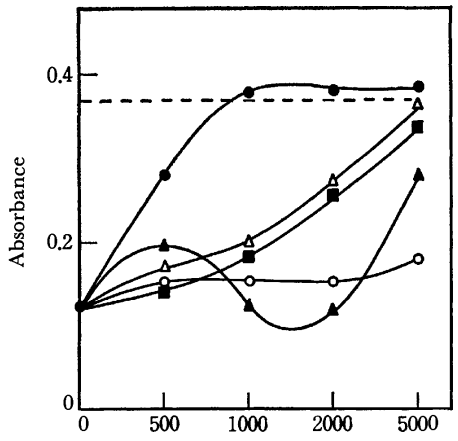

Fig. 4. Effect of non-interfering elements on the depressing interference from aluminum. Concentration of bismuth: 10 ppm. Concentration of aluminum: 2000 ppm. Flame: an argon(entrained air)-hydrogen flame. ---- Bismuth alone; (●) magnesium; (△) yttrium; (■) lanthanum; (▲) potassium; (○) mercury.

or occasionally positive, depending on the hydrogen flow rate and the flame height. This phenomenon can not be explained adequately, but it is possibly due to a perturbation of basic flame chemistry or it is possibly related to the specific chemistry of the elements and bismuth in the flame.

On the other hand, no element was found to enhance the bismuth atomic absorption.

Effect of Magnesium on the Depressing Interference. The depressing interference described above depends considerably on the concentration of the depressing elements, the flame composition, and the flame height. In an attempt to eliminate the depressing interference due to aluminum, beryllium, *etc.*, the effect of the further addition of such an element as gave no interference with the bismuth absorption, *i. e.*, mercury, potassium, lanthanum, magnesium, and yttrium, was examined on a bismuth solution containing interferents. The results on the aluminum interference are shown in Fig. 4. As is shown in Fig. 4, magnesium was the most effective in eliminating the depressing interference among the elements examined. Then, the bismuth (10 ppm) absorptions were measured in the presence

Table 2. Effect of magnesium on the depressing interference

Element	Relative absorbance			
	Argon(entrained air)-hydrogen flame		Nitrogen(entrained air)-hydrogen flame	
	In the absence of magnesium	In the presence of magnerium	In the absence of magnesium	In the presence of magnesium
None	1.00	1.00	1.00	1.00
Al	0.43	1.03	0.37	1.03
B	0.41	1.06	0.60	1.05
Be	0.62	1.07	0.59	1.05
Ca	0.96	1.06	0.76	1.05
Ce	0.43	0.45	0.16	0.25
Co	1.02	1.00	0.86	1.05
Cr	1.00	1.00	0.54	1.05
Cs	0.62	1.04	0.62	1.03
Ni	0.95	1.00	0.74	1.01
Pd	0.69	0.97	0.47	0.98
Si	0.42	1.06	0.26	1.04
Sr	0.97	1.02	0.79	1.01
Zr	0.18	1.05	0.07	1.04

The concentrations of bismuth, the elements added, and magnesium were 10, 200, and 1000 ppm, respectively.

of the depressing elements (200 ppm) with and without the addition of magnesium (as chloride) (1000 ppm). The results obtained in both the flames are shown in Table 2. The interference from all the depressing elements, with the exception of that of cerium, disappeared completely. This phenomenon could be applied to the atomic absorption spectrophotometric determination of bismuth without any interference from matrix elements.

The mechanism of the interference-elimination due to magnesium cannot be satisfactorily explained. If the interference from aluminum in the determination of bismuth is considered to be due to the formation of bismuth aluminate in the flame, the elimination of the interference by adding a large amount of magnesium may be explained in terms of the predominant formation of magnesium aluminate in the flame, resulting in a release of the bismuth atoms from the influence of aluminum.

Effect of the Ammonium Ion on the Interference. As is shown in Table 2, chromium depressed the bismuth absorption in the nitrogen(entrained air)-hydrogen flame, but it did not do so in the argon(entrained air)-hydrogen flame. This fact seemed to be very interesting; therefore, the interference from chromium in the nitrogen(entrained air)-hydrogen flame was studied with various kinds of chromium compounds. The results are shown in Fig. 5. The ammonium salts gave no interference with the bismuth atomic absorption, while the others remarkably depressed the bismuth atomic absorption. This fact indicated that the ammonium ion possibly plays an important role in the elimination of the depressing interference. Further investigation showed that the depressing interference from chromium could be eliminated with the addition of a large amount of ammonium chloride or ammonium perchlorate, as is shown in Fig. 6.

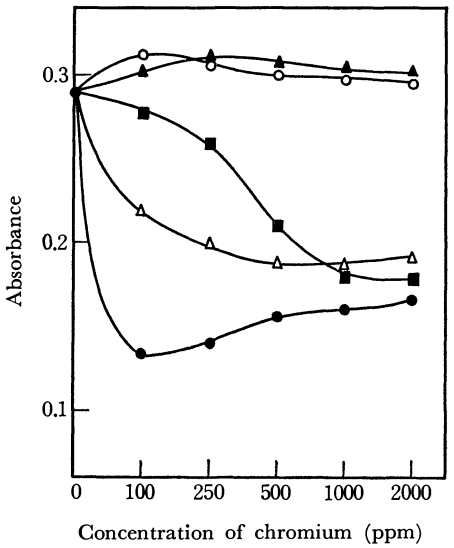

Fig. 5. Effect of chromium compounds on bismuth atomic absorption in the nitrogen(entrained air)-hydrogen flame. Concentration of bismuth: 10 ppm. (▲) Ammonium chromate; (○) ammonium dichromate; (■) potassium chromate; (△) potassium dichromate; (●) chromium(III) chloride.

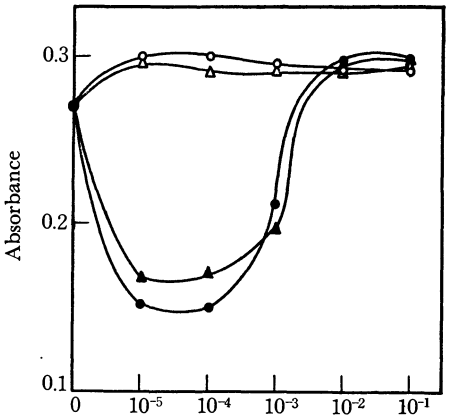

Fig. 6. Effect of ammonium salts on the depressing interference from chromium(III) chloride in the nitrogen (entrained air)-hydrogen flame. Concentration of bismuth: 10 ppm. (○) Ammonium perchlorate alone; (△) ammonium chloride alone; (●) ammonium perchlorate in the presence of chromium(III) chloride (Concentration of chromium: 1000 ppm); (▲) ammonium chloride in the presence of chromium(III) chloride (Concentration of chromium: 1000 ppm).

Then, the atomic absorptions were measured for a solution containing bismuth (10 ppm) and the depressing elements (200 ppm) in the presence of a large amount (0.1 M) of ammonium chloride or ammonium perchlorate in the inert gas (entrained air)-hydrogen flames. The results are shown in Table 3. The interferences from all the depressing elements appeared to disappear completely.

TABLE 3. EFFECT OF AMMONIUM CHLORIDE AND AMMONIUM PERCHLORATE ON THE DEPRESSING INTERFERENCE

Element	Relative absorbance			
	Argon(entrained air)-hydrogen flame		Nitrogen(entrained air)-hydrogen flame	
	In the presence of ammonium chloride	In the presence of ammonium perchlorate	In the presence of ammonium chloride	In the presence of ammonium perchlorate
None	1.00	1.00	1.00	1.00
Al	0.98	1.05	0.95	0.98
B	0.96	1.01	0.95	0.98
Be	0.97	0.99	0.96	0.98
Ca	0.96	0.97	0.95	0.98
Ce	0.94	0.93	0.90	0.95
Co	1.00	1.00	1.02	1.01
Cr	0.99	1.02	1.02	0.98
Cs	0.95	1.02	0.96	0.98
Ni	0.98	1.02	0.99	0.98
Pd	0.95	0.93	0.97	0.92
Si	1.02	1.00	1.05	0.95
Sr	1.02	0.99	0.98	0.98
Zr	1.02	0.97	1.05	0.98

The concentrations of bismuth, ammonium chloride, and ammonium perchlorate were 10 ppm, 0.1 M, and 0.1 M, respectively.

Effects of Organic Solvents. The effects of organic solvents on the bismuth atomic absorption were also examined. A series of primary alcohols were selected, and the concentrations of the alcohols added were from 10 to 50% by volume. The effect of the alcohols was found to be a depressing interference; that is, the bismuth atomic absorption was decreased with an increase in the alcohol concentrations in the sample solutions. A more detailed investigation was not made on the effects of organic solvents.

Calibration Graphs and Sensitivity. Typical calibration graphs for bismuth are shown in Fig. 7. With magnesium or ammonium chloride added, the same graph was obtained in the presence and in the absence of aluminum. The bismuth sensitivities for a 1% absorption were 0.10 and 0.11 ppm in the argon(entrained air)-hydrogen flame and the nitrogen(entrained air)-hydrogen flame respectively.

Application to the Determination of Bismuth in Sulfide Ores, Aluminum-, Tin-, and Lead-base Alloys. On the basis of the above-mentioned observations, the following procedures were followed for determination of bismuth in some practical samples, *e. g.*, sulfide ores, aluminum-, tin-, and lead-base alloys.

Sulfide Ores: A 2.5-g ore sample was weighed and dissolved in about 70 ml of dilute aqua regia by gentle heating on a hot plate. After the solution had then been cooled to room temperature, the insoluble matter was filtered out. The filtrate was transferred to a 100-ml volumetric flask and diluted to volume with distilled water. The final solution was adjusted to provide a concentration of about 1.0 N hydrochloric acid. The major constituents in the ore samples were found spectrographically to be copper, iron, silicon, and lead by means of a d. c. arc technique on a Shimadzu Type GE-340 Ebert mounting emission spectrograph. Furthermore, these elements were determined in a nitrous oxide-acetylene flame by using a Hitachi Model 207 atomic absorption spectrophotometer. As a result, the contents of the sulfide ore sample of A mine were found to be 18.3, 17.9, 14.0, and 3.9% for copper, iron, zinc, and lead respectively. The contents of the sulfide ore sample of B mine were found to be 83.0, 0.3, 0.2, and 0.1% for iron, copper, zinc, and lead respectively. The silicon and sulfur in the samples were separated as silicate and elementary sulfur from the sample solutions by filtration after the dissolution of the samples.

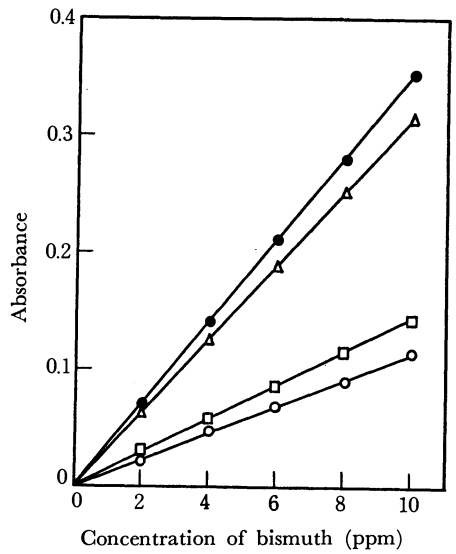

Fig. 7. Calibration graphs for bismuth. Flame: an argon (entrained air)-hydrogen flame. (○) In the presence of aluminum (2000 ppm); (□) in the presence of aluminum (1000 ppm); (●) in the presence of magnesium (2000 ppm) alone, magnesium (2000 ppm) and aluminum (1000 ppm), or magnesium (2000 ppm) and aluminum (2000 ppm); (△) bismuth alone.

Table 4. Results of the determination of bismuth in sulfide ores

Sample	Bismuth content (%)		
	Atomic absorption method		Colorimetric method
	$Ar-H_2$[a]	N_2-H_2[b]	
A mine ore (Cu conc.)	0.0041[c] 0.0038[d]	0.0044[c] 0.0042[d]	0.0039
B mine ore (S conc.)	0.0068[c] 0.0065[d]	0.0072[c] 0.0064[d]	0.0066

a) Argon(entrained air)-hydrogen flame.
b) Nitrogen(entrained air)-hydrogen flame.
c) Determined by using the calibration graph method.
d) Determined by using the standard addition method.

The bismuth in the ore samples was determined by the standard addition method and by the calibration graph method. Copper, iron, lead, and zinc did not interfere with the determination of bismuth, as has been described above. However, since small amounts of silicon and other interferents were presumably present in the samples, both sample and standard solutions were prepared so as to contain magnesium of 2000 ppm and hydrochloric acid of 1.0 N in the final solutions. The bismuth atomic absorptions were measured at 223.1 nm in the inert gas(entrained air)-hydrogen flames under optimum conditions. The results of the determinations are shown in Table 4. The results were compared with those obtained by the colorimetric method, in which the bismuth contents in sulfide ores were determined by a two-stage extraction with sodium diethyldithiocarbamate into carbon tetrachloride.[17]

Aluminum-base Alloys: As is shown in Fig. 3, the presence of aluminum caused a depressing interference with the bismuth atomic absorption. Therefore, a sufficient amount of magnesium (5000 ppm) was added to the sample solutions in order to eliminate the interference from the matrix element, *i. e.*, aluminum, in the determination of bismuth. A 0.5-g sample was dissolved in 20 ml of aqua regia by gentle heating on a hot plate. After cooling, the sample solution was transferred to a 100-ml volumetric flask and diluted to volume with distilled water. A 10-ml aliquot was taken out, 2.5 ml of a 50000 ppm magnesium solution and 5 ml of 5 N hydrochloric acid were added, and then the mixture was diluted to 25 ml with distilled

17) K. Yaguchi and J. Kaneko, *Bunseki Kagaku*, **19**, 705 (1970).

Table 5. Results of the determination of bismuth in aluminum-, tin-, and lead-base alloys

Sample	Bismuth content (%)		
	Cert. value	Atomic absorption method	
		$Ar-H_2$[a]	N_2-H_2[b]
Aluminum-base alloy			
No. 1	0.04	0.037[c]	0.043[c]
		0.042[d]	0.045[d]
No. 2	0.05	0.047[c]	0.049[c]
		0.048[d]	0.052[d]
Tin-base alloy			
No. 1	0.028	0.029[c]	0.028[c]
		0.027[d]	0.025[d]
No. 2	0.040	0.041[c]	0.038[c]
		0.038[d]	0.037[d]
Lead-base alloy			
No. 1	0.13	0.13_7[c]	0.13_6[c]
		0.14_0[d]	0.14_2[d]

a) Argon(entrained air)-hydrogen flame.
b) Nitrogen(entrained air)-hydrogen flame.
c) Determined by using the calibration graph method.
d) Determined by using the standard addition method.

water. The resultant solution was sprayed into the flame, and the determination of bismuth was carried out by both the standard addition method and the calibration graph method. The results are shown in Table 5. The results agreed closely with the certificate values.

Tin- and Lead-base Alloys: A 0.9-g sample was dissolved in 30 ml of 6 N acid by slowly heating it on hot plate. The acid employed was hydrochloric acid for tin-base alloys and nitric acid for lead-base alloy. After cooling the sample solution was transferred to a 100-ml volumetric flask and diluted to volume with distilled water. A 10-ml aliquot was taken out and diluted to 25 ml with distilled water. The resultant solution was sprayed into the flame, and the bismuth absorption was measured. Magnesium was not added to the solutions, because the matrix elements do not interfere with the bismuth absorption, as is shown in Table 1. The results are shown in Table 5. When hydrochloric acid was added to the solution of the lead-base alloy, lead chloride precipitated on cooling; then, the supernatant solution was used for the atomic absorption measurement. The determination of bismuth after the removal of lead as chloride was successful, since little or no bismuth was lost, as has been reported by Lau *et al.*,[4] who confirmed radiometrically the recovery of over 99% of the bismuth.

In the standard addition method, the concentrations of bismuth added to the sample solutions were 0, 2, 4, 6, and 8 ppm in the final solutions. The calibration graphs for bismuth were prepared in the concentration range of 0—8 ppm.

BULLETIN OF THE CHEMICAL SOCIETY OF JAPAN, VOL. 46, 1172—1177 (1973)

Determination of Titanium in Some Metallurgical Materials by Atomic Absorption Spectrophotometry

Taketoshi NAKAHARA, Makoto MUNEMORI, and Sôichirô MUSHA

Department of Applied Chemistry, College of Engineering, University of Osaka Prefecture, Mozu-umemachi, Sakai 591

(Received June 29, 1972)

The atomic absorption spectrophotometric determination of titanium was subject to interference by other elements in a nitrous oxide-acetylene flame with a Perkin-Elmer Model 303 atomic absorption spectrophotometer, fitted with a 5-cm long-path slot burner. The effects of various other elements, acids, and water-miscible organic solvents on the titanium atomic absorption were examined. Aluminum produced the greatest enhancement of the titanium absorption of all the elements examined. Both butyric acid (2.0 M) and diethylene glycol monobutyl ether (20%) enhanced the titanium absorption by about 100% in aqueous solutions. In the presence of 5000 ppm aluminum or 20% diethylene glycol monobutyl ether, the interferences from other elements appeared to be completely removed. Furthermore, the extraction of titanium with cupferron into methyl isobutyl ketone was successful in effecting an increase in the sensitivity of titanium and in eliminating, or at least diminishing the interferences from other elements. The atomic absorption method was then applied to the determination of titanium in ferric oxides, nickel-chromium steel, nickel alloy, and steels with satisfactory results.

Titanium is one of the elements which are difficult to determine by means of atomic absorption spectrophotometry because it forms a stable refractory oxide in the flame. However, after Amos and Willis[1] introduced a nitrous oxide-acetylene flame into atomic absorption spectrophotometry, many refractory elements including titanium have become determinable by means of atomic absorption spectrophotometry. Headridge and Hubbard[2] reported the atomic absorption spectrophotometric determination of titanium in steels, permanent magnet alloys, and cast iron with hydrofluoric acid solutions. Bowman and Willis[3] obtained satisfactory results in the determi-

1) M. D. Amos and J. B. Willis, *Spectrochim. Acta*, **22**, 1325 (1966).

2) J. B. Headridge and D. P. Hubbard, *Anal. Chim. Acta*, **37**, 151 (1967).

3) J. A. Bowman and J. B. Willis, *Anal. Chem.*, **39**, 1210 (1967).

nation of titanium in bauxite and steel. Amos and Willis[1] found that iron at the 2000 ppm level in the presence of 20% hydrofluoric acid considerably enhanced the titanium atomic absorption. Recently Kirkbright *et al.*[4] reported the sensitive, indirect determination of titanium by means of atomic absorption spectrophotometry, with the extraction of molybdotitanophosphoric acid into butyl alcohol.

The effect of organic solvents has been well studied on the atomic absorption of many elements, but scarcely not at all on the atomic absorption of titanium. In this investigation, the effects of various extraneous elements and water-miscible and immiscible organic solvents on titanium absorption in a nitrous oxide-acetylene flame were investigated. Many elements interfered with the titanium absorption, but effective means, including solvent extraction, were found to eliminate the interferences. This paper will also describe the results of the atomic absorption spectrophotometric determination of titanium in ferric oxides, steels, and a nickel-base alloy.

Experimental

Table 1. Operating conditions for titanium absorption

Wavelength	364.3 nm
Slit-width	0.3 mm
Spectral bandpass	0.2 nm
Lamp current	40 mA
Scale expansion	×1
Nitrous oxide flow rate under the pressure of 30 p.s.i.	14.0 l/min
Acetylene flow rate under the pressure of 8 p.s.i.	7.6 l/min for aqueous solution
	6.4 l/min for methyl isobutyl ketone
Flame height	3 mm above burner head
Burner slot	0.48 mm × 50 mm

Apparatus. A Perkin-Elmer Model 303 atomic absorption spectrophotometer, equipped with a nitrous oxide burner head, was used in this work. The experimental conditions are shown in Table 1. The titanium 364.3 nm line was slightly less intensive, but it was more strongly absorbed by titanium atoms, than the 365.4 nm line; therefore, the 364.3 nm line was chosen as the analytical absorption line. A Perkin-Elmer titanium hollow-cathode lamp was used as the radiation source. Under the optimum flame conditions, shown in Table 1, about a 3 cm long "red feather" was produced above the burner head, and the sample aspiration rate was about 8.6 ml/min.

Reagents. A stock solution of titanium(5000 ppm) was prepared by dissolving 5.000 g of high-purity titanium sponge (99.99%) with 50 ml of 6 N hydrochloric acid by heating on a hot plate and by then diluting to 1000 ml with distilled water. Various standard titanium solutions were prepared by suitably diluting the stock solution.

A cupferron solution (5%) was prepared by dissolving 5.0 g of cupferron with distilled water. The solution was prepared daily.

All the other chemicals used were of an analytical-reagent grade.

4) G. F. Kirkbright, A. M. Smith, and T. S. West, *Analyst*, **94**, 754 (1969).

Results and Discussion

Effects of Inorganic Acids. The effects of the inorganic acids generally used for sample decomposition were studied in the concentration range of 0—2.0 N on a 100 ppm titanium solution. The acids studied were hydrochloric, hydrofluoric, nitric, perchloric, phosphoric, and sulfuric acids. Hydrochloric and nitric acids had no effect on the titanium absorption, even at higher concentrations up to 6.0 N. The other acids enhanced the titanium atomic absorption, as is shown in Fig. 1.

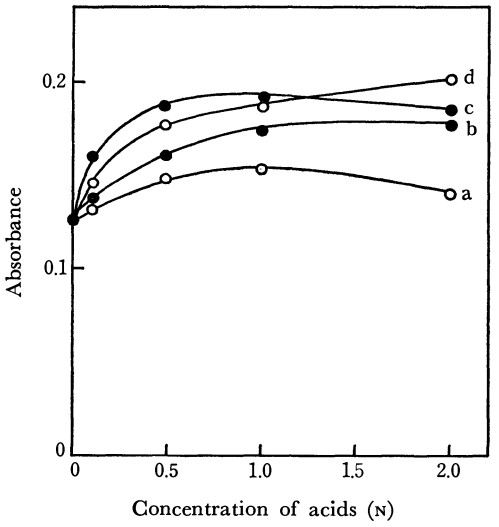

Fig. 1. Effect of inorganic acids on titanium atomic absorption.
Concentration of titanium: 100 ppm.
(a) Sulfuric acid; (b) phosphoric acid; (c) perchloric acid; (d) hydrofluoric acid.

As has been described by Amos and Willis,[1] the enhancement by hydrofluoric acid is possibly due to the inhibition of the formation of titanium monoxide in the flame by forming a more stable fluoro-complex, which decomposes easily at the temperature of the nitrous oxide-acetylene flame. Since sulfate and phosphate ions are known to form complexes with titanium, the enhancement by sulfuric and phosphoric acids may be explained, as in the case of hydrofluoric acid, in terms of the inhibition of monoxide formation, but the enhancement by perchloric acid, the extent of which is nearly equal to that by hydrofluoric acid, is difficult to explain because of its inability to form stable complexes with titanium. At any rate, when hydrofluoric acid and/or perchloric acid are used in the sample decomposition, the acid concentrations of the sample solution and the standard solution should match.

Effects of Organic Acids. The effects of monocarboxylic acids, *i.e.*, formic, acetic, trichloroacetic, propionic, and butyric acids, on the titanium absorption were also studied. The absorption measure-

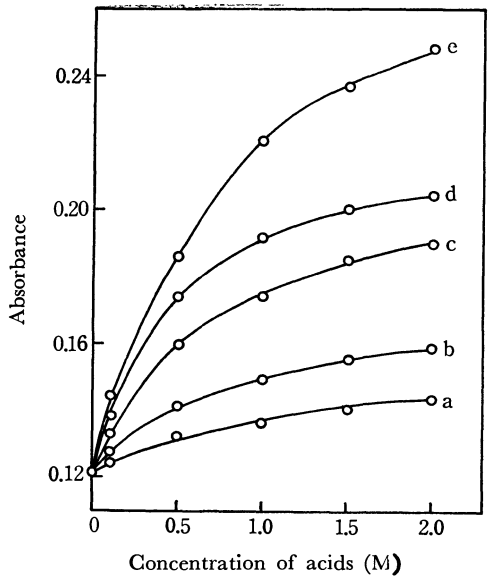

Fig. 2. Effect of organic acids on titanium atomic absorption.
Concentration of titanium: 100 ppm.
(a) Formic acid; (b) acetic acid; (c) propionic acid; (d) trichloroacetic acid; (e) butyric acid.

ments were made on a 100 ppm titanium solution in the presence of the acids, the concentrations of which were changed from 0.1 to 2.0 M. These acids produced an enhancement, and the titanium absorptions were increased, with an increase in the acid concentrations, as is shown in Fig. 2. Butyric acid was the most effective, enhancing the titanium absorption 2-fold at 2.0 M. The enhancing effect of these acids is probably due to the formation of stable complexes of titanium, which decompose easily in the flame. On the other hand, these acids may play the same role as organic solvents, as will be discussed later, since the enhancement in the presence of the acids increased with an increase in the carbon numbers, the molecular weight, and the boiling point except in the case of trichloroacetic acid.

Effects of Various Other Elements. Amos and Willis[1] have reported the enhancing effects of hydrofluoric acid and of iron in the determination of titanium. Headridge and Hubbard[2] have described that there is no interference from various foreign elements, such as chromium, cobalt, manganese, molybdenum, nickel, niobium, sulfur, tantalum, tungsten, and vanadium, in the presence of iron in the aqueous ethanolic hydrofluoric acid solution, and that aluminum interferes with the determination of titanium.

The effects of various other elements on the atomic absorption of titanium were studied at constant concentration levels in aqueous solutions. The elements examined and their effects on the atomic absorption of titanium are shown in Table 2. The concentration of titanium was 100 ppm, and that of the interferent, 1000 ppm. Table 2 indicates that most elements except for antimony and selenium enhanced the titanium absorption. It is also evident from Table 2 that such elements as aluminum, beryllium, cerium, lanthanum, and silicon, which are apt to form stable

Table 2. Effect of other elements on titanium absorption

Element	Recovery of Ti (%)		Element	Recovery of Ti (%)	
	Aqueous solution	Solvent extraction		Aqueous solution	Solvent extraction
None	100	100	Mn[d,f]	115	99
Al[a,f]	170	101	Mo[e,f]	141	62
As[b]	125	101	Na[a]	98	99
Au[a]	111	102	Ni[c,f]	104	99
Ba[a]	111	100	Pb[d]	105	102
Be[c]	140	98	Pd[a]	116	100
Bi[d,f]	107	99	Rb[a]	102	100
Ca[d,f]	135	99	Sb[a,f]	42	102
Cd[d,f]	109	100	Se[b]	25	101
Ce[c,f]	146	102	Si[b,f]	146	98
Co[d,f]	115	98	Sn[a,f]	117	103
Cr[d]	121	99	Sr[d]	105	99
Cs[a]	114	101	Te[b]	119	100
Cu[d,f]	116	102	Th[d,f]	127	95
Fe[a,f]	118	62	Tl[a]	109	99
Hg[a,f]	110	96	V[e,f]	121	55
In[a,f]	113	99	W[b,f]	105	95
K[a]	112	101	Y[b,f]	148	98
La[a,f]	148	99	Zn[a,f]	112	102
Li[a]	112	101	Zr[d,f]	130	35
Mg[d,f]	128	97			

Concentration of the elements added, 1000 ppm; titanium added, 100 ppm.
a) Added as chloride. b) Added as sodium arsenite, selenite, silicate, tellurite or tungstate, respectively. c) Added as sulfate. d) Added as nitrate. e) Added as ammonium molybdate or vanadate, respectively. f) Element chelating with cupferron.

oxides in the flame, produced a greater enhancement. Aluminum produced the greatest enhancement. Such an enhancement is possibly caused by competition between titanium and the other refractory elements to form stable oxides in the flame, as has been described in the case of aluminum[5] and vanadium[6] by Robinson *et al.*, but the enhancement cannot be explained completely satisfactorily. The decreasing effect of antimony and selenium is ascribable to the formation of insoluble precipitates in aqueous solutions. Although bismuth and thallium produced insoluble precipitates, they slightly enhanced the titanium absorption.

Thus, titanium absorption suffers serious interference from many elements, so a suitable means for eliminating or suppressing them must be found. Otherwise, atomic absorption will be of little analytical use. David[7] has already demonstrated that aluminum suppresses interferences from other elements in the determination of molybdenum in an air-acetylene flame. In this study, the suppressing effect of aluminum on the interferences with titanium absorption was studied. At first, the effect of an increase in the

5) T. V. Ramakrishna, P. W. West, and J. W. Robinson, *Anal. Chim. Acta*, **39**, 81 (1967).
6) S. L. Sachdev, J. W. Robinson, and P. W. West, *ibid.*, **37**, 12 (1967).
7) D. J. David, *Analyst* (London), **86**, 730 (1961).

concentration of aluminum was studied on 100 ppm of titanium; it was found that the titanium absorption was increased with an increase in the aluminum concentration until a constant enhancement was attained at more than 2000 ppm of aluminum. Then, in the presence of aluminum at 5000 ppm the effects of various other elements were studied at the 1000-ppm concentration level. None of the elements listed in Table 2 showed any more effect on the titanium absorption; thus, the interferences from other elements on titanium absorption appeared to disappear completely. Furthermore, the titanium absorption was measured in the presence of aluminum (5000 ppm) by varying the concentrations of the interferents. Figure 3 shows the results, with iron as an example. Similar results were obtained with other interferents.

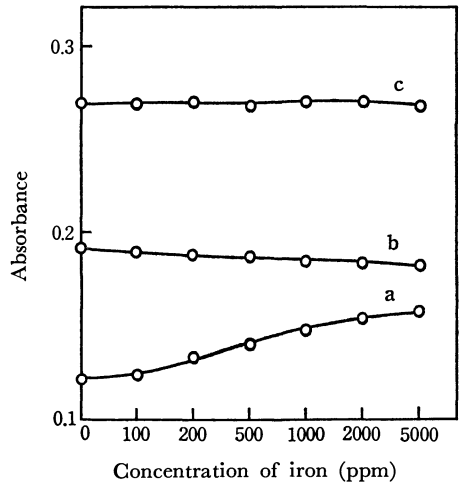

Fig. 3. Suppressing effect of aluminum and diethylene glycol monobutyl ether on the interference from iron with titanium atomic absorption.
Concentration of titanium: 100 ppm.
(a) With no addition; (b) with the addition of aluminum (5000 ppm); (c) with the addition of diethylene glycol monobutyl ether (20 vol%)

Effects of Water-miscible Organic Solvents. Atomic absorptions were measured on 100 ppm titanium solutions containing water-miscible organic solvents, such as alcohols, ketones, and glycols, at 10 vol%. The results are shown in Table 3. Among the alcohols, butyl alcohol produced the greatest enhancement, and very stable chart readings were obtained in its presence. Glycols produced greater enhancements. The greatest enhancement was produced by diethylene glycol monobutyl ether, which had previously reported to be very effective in the enhancement of vanadium absorption in a nitrous oxide-acetylene flame.[6] The effect of an increase in the concentration of diethylene glycol monobutyl ether on the titanium absorption was studied; it was found that about 20 vol% of diethylene glycol monobutyl ether increased the absorption by about 100% and that concentrations higher than 20 vol% did not produce further enhancement.

It can be seen from Table 3 that the organic solvents with higher boiling points and longer carbon chains increased the titanium absorption more, and that the absorption was contrary to the increase in the sample aspiration rate when the enhancement effect was compared in its extent among solvents of the same kinds.

Interferences from other elements with titanium

Table 3. Effect of water-miscible organic solvents on titanium absorption

Solvent	Molecular weight	Boiling point (°C)	Sample aspiration rate (ml/min)	Absorbance	Enhancement
None	—	—	8.6	0.125	1.00
Methanol	32.0	64.1	7.9	0.142	1.14
Ethanol	46.1	78.3	7.6	0.136	1.09
Isopropyl alcohol	60.1	82.4	7.2	0.145	1.16
Propyl alcohol	60.1	97.4	7.1	0.158	1.26
Isobutyl alcohol	74.1	107.9	6.6	0.176	1.41
Butyl alcohol	74.1	117.7	6.9	0.189	1.51
Acetone	58.0	56.5	8.1	0.133	1.06
1,4-Dioxane	88.1	101.1	6.0	0.143	1.14
Methyl ethyl ketone	72.1	79.6	8.2	0.177	1.42
Ethylene glycol	62.1	197.7	8.3	0.171	1.37
Ethylene glycol monomethyl ether	76.1	124.5	7.9	0.179	1.43
Ethylene glycol dimethyl ether	90.1	84.7	7.7	0.180	1.44
Ethylene glycol monoethyl ether	90.1	134.8	7.9	0.186	1.49
Diethylene glycol monoethyl ether	134.2	195	7.7	0.200	1.60
Diethylene glycol diethyl ether	162.2	186	7.2	0.224	1.79
Diethylene glycol monobutyl ether	162.2	230	7.2	0.253	2.02

Concentration of the solvents added, 10 vol%; titanium added, 100 ppm.

absorption were studied in the presence of 20 vol% of diethylene glycol monobutyl ether. As in the case of a large amount of aluminum, the interferences seemed to disappear completely. Some representative results are shown in Fig. 3. This fact suggests that diethylene glycol monobutyl ether competes with other elements, as aluminum does, in suppressing the formation of titanium monoxide by providing the flame with reducing properties through the burnt gases. The difference in titanium absorbance observed between Curves b and c in Fig. 3 is probably due to the difference in the efficiencies of the nebulizing sample solutions. It seems, therefore, that diethylene glycol monobutyl ether, a representative water-miscible organic solvent, plays a dual role, *i.e.*, as an atomizing aid and a nebulizing aid, in enhancing the titanium atomic absorption.

Extraction of Titanium Complexes into Organic Solvents. Extractions were carried out with the following reagents for titanium: cupferron,[8] 8-hydroxyquinoline,[9] *N*-benzoyl-*N*-phenyl hydroxylamine,[10] morin,[11] and quinalizarin.[12] Of these, the first three proved to be applicable to the atomic absorption spectrophotometric determination of titanium. The chelates of titanium with morin and quinalizarin were not extracted into methyl isobutyl ketone, which is well known to be suitable for atomic absorption measurements. Cupferron was finally selected as the best chelating reagent. The extraction procedure for titanium cupferrate was as follows: standard solutions containing 10, 20, 30, 40, and 50 μg/ml of titanium were prepared by diluting a stock solution of titanium. A 10-ml aliquot of each standard solution was then placed in a 100-ml separatory funnel, and 40 ml of 1.2 N hydrochloric acid was added. Then 2 ml of a 5% cupferron solution was added, and the titanium cupferrate formed in the solution was extracted into 10 ml of methyl isobutyl ketone with shaking for two minutes. The organic phase which was thus separated, after dehydration with anhydrous sodium sulfate, was sprayed into the flame. The titanium absorption was measured in the nitrous oxide-acetylene flame under the optimum operating conditions described in Table 1. As is shown in Fig. 4, the most sensitive results were obtained with cupferron.

Furthermore, the extractions of titanium cupferrate were carried out with mixed organic solvents of methyl isobutyl ketone containing 25% of oleic acid, as had been done by Sachdev *et al.*[13] in the case of vanadium using an oxygen-acetylene flame created by a total-consumption nebulizer-burner. However, the effects of mixed organic solvents were not as compared with that of methyl isobutyl ketone alone by aspirating the organic extract into the nitrous oxide-acetylene flame.

Effects of Other Elements: Some elements were extracted along with titanium under the conditions described above. Their effects on titanium absorption were studied by the following procedure: a 5-ml portion of a standard solution containing 100 μg/ml of titanium and 5 ml of other metal solutions (1000 μg/ml) was diluted to 50 ml with 1.2 N hydrochloric acid. The solution was then transferred into a 100-ml separatory funnel and extracted into 10 ml of methyl isobutyl ketone after adding 2 ml of a 5% cupferron solution. The absorption measured on the organic extract was compared with that measured on an organic phase containing the titanium chelate alone. The results are shown in Table 2. With the exception of the elements which can be extracted with cupferron, essentially no interference was observed from the other

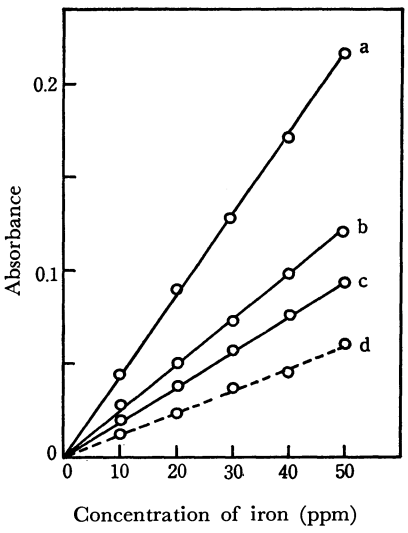

Fig. 4. Calibration graphs for titanium.
(a) Titanium cupferrate; (b) titanium *N*-benzoyl-*N*-phenyl hydroxylamine complex; (c) titanium oxinate; (d) titanium aqueous solutions.

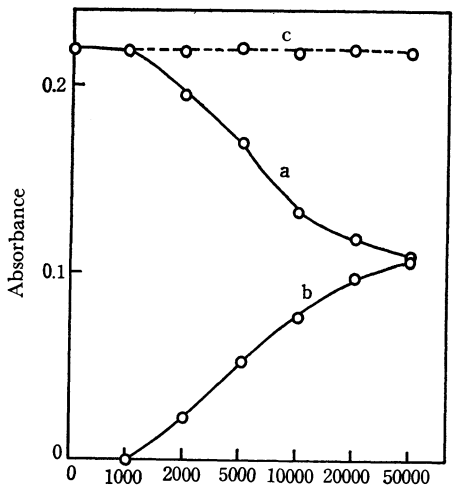

Fig. 5. Solvent extraction of titanium cupferrate in the presence of a large amount of iron.
Amount of titanium: 500 μg (in 10 ml of methyl isobutyl ketone.
(a) Absorbance for the first extraction; (b) absorbance for the second extraction; (c) total absorbance of the first and second extractions.

8) N. H. Furman, W. B. Mason, and J. S. Pekola, *Anal. Chem.*, **21**, 1325 (1949).
9) K. Gardner, *Analyst* (London), **76**, 485 (1951).
10) S. C. Chome, *ibid.*, **75**, 27 (1950).
11) E. B. Sandell, "Colorimetric Determination of Traces of Metals," 2nd edn., Interscience Pub., New York (1950), p. 127.
12) G. Beck, *Mikrochim. Acta*, **34**, 282 (1949).
13) S. L. Sachdev, J. W. Robinson, and P. W. West, *Anal. Chim. Acta*, **37**, 156 (1967).

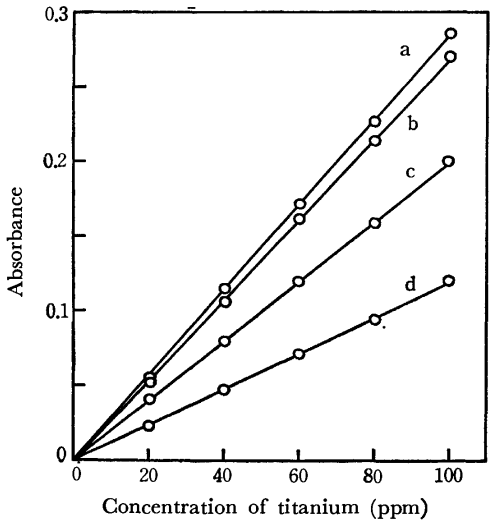

Fig. 6. Calibration graphs for titanium.
(a) In the presence of diethylene glycol monobutyl ether (20 vol%); (b) in the presence of butyric acid (2.0 M); (c) in the presence of aluminum (1000 ppm); (d) titanium alone.

elements present at a concentration 10 times that of titanium. Iron, molybdenum, vanadium, and zirconium, which can be extracted with cupferron, showed depressing effects on the titanium absorption, but the depressing interference could be completely eliminated by successive extractions with two 10-ml portions of methyl isobutyl ketone even if the interfering element was present at a concentration 100 times that of titanium in an aqueous solution, as is shown in Fig. 5. When the concentration of interfering elements was more than 100 times that of titanium, the extraction had to be repeated three times or more. However, a large amount of these interfering elements should preferably be separated before the titanium-cupferrate extraction. Iron, for example, can be extracted as the chloro-complex from 6 N hydrochloric acid solution with methyl isobutyl ketone.

Calibration Graphs for Titanium. Calibration graphs for aqueous titanium, aqueous titanium in the presence of aluminum, butyric acid, and diethylene glycol monobutyl ether, and titanium complexes extracted into methyl isobutyl ketone are shown in Figs. 4 and 6, respectively. Sensitivities for aqueous titanium alone, for aqueous titanium in the presence of aluminum, for aqueous titanium in the presence of butyric acid, for aqueous titanium in the presence of diethylene glycol monobutyl ether, and for titanium complexes with cupferron, *N*-benzoyl-*N*-phenyl hydroxylamine, and 8-hydroxyquinoline extracted into methyl isobutyl ketone were 3.2, 2.0, 1.5, 1.4, 0.8, 1.4, and 1.8 ppm for a 1% absorption respectively.

Application to the Determination of Titanium in Ferric Oxides, Steels, and a Nickel-base Alloy. The present method was then applied to the determination of titanium in ferric oxides, steels, and a nickel-base alloy. The sample was decomposed with the smallest necessary amount of hydrochloric acid and/or nitric acid. After the addition of the amount of aluminum, butyric acid, or diethylene glycol monobutyl ether necessary to bring the final concentration to 5000 ppm, 2.0 M, or 20% respectively, the solution was diluted with distilled water. The resultant solution was sprayed into the nitrous oxide-acetylene flame, and the absorption was measured. The results are shown in Table 4. The results with the methyl-isobutyl-ketone extraction of titanium cupferrate are also shown in Table 4. In this case, iron was separated from the 6 N hydrochloric acid solution with methyl isobutyl ketone before the titanium extraction. The determination was made by referring to the corresponding calibration graphs, shown in Figures 4 and 6. As a result, it was found that the atomic absorption spectrophotometric method could be applied to the determination of titanium in ferric oxides, steels, and a nickel-base alloy with satisfactory results.

Table 4. Results of the determination of titanium in a few kinds of materials

Sample	Titanium content (%)				
	Cert. value	Atomic absorption method			
		A	B	C	D
Ferric oxide					
No. 1	2.47	2.5_0	2.4_0	2.4_5	2.4_0
No. 2	0.20	0.19	0.19	0.21	0.18
NBS 348 Ni–Cr steel	2.24	2.2_5	2.2_1	2.2_7	2.1_9
BCS No. 310 Ni alloy	2.46	2.4_8	2.4_5	2.4_4	2.4_0
Steel					
No. 100—1	0.12	0.12	0.11	0.12	0.10
No. 102—1	0.24	0.23	0.25	0.24	0.21

A) Determined in the presence of 5000 ppm aluminum.
B) Determined in the presence of 2.0 M butyric acid.
C) Determined in the presence of 20 vol% diethylene glycol monobutyl ether.
D) Determined by the extraction of titanium cupferrate into methyl isobutyl ketone after separation of iron.

Formation of Zinc(II) Complexes with Several Carboxylic Acids and Their Extraction with Carbon Tetrachloride

Hiromitsu MORIYA and Tatsuya SEKINE

Department of Chemistry, Science University of Tokyo, Kagurazaka, Shinjuku-ku, Tokyo 162

(Received July 7, 1972)

The distribution of zinc(II) was determined between 0.1 M constant-ionic-strength media containing sodium perchlorate and/or carboxylate ions, A^-, and carbon tetrachloride containing a neutral ligand, quinonline, Q, or the dimer of the same carboxylic acid, $(HA)_2$. The distribution ratio was measured as a function of the concentration of carboxylate ions in the aqueous phase or of that of one of the above neutral ligands, in the organic phase. The extraction constant of the ZnA_2 species in the caproic acid system was found to be $K_{exA}=[ZnA_2]_{org}/[Zn^{2+}][A^-]^2=10^{-0.15}$, while that in the valeric or butyric acid system was too small to be determined. The distribution ratio of zinc(II) increased with an increase in the concentration of the ligand in the organic phase. These increases were explained by the formation of adducts in the organic phase; in the caproate system, the species found were ZnA_2Q and ZnA_2Q_2, ($\beta_{1(org)}=[ZnA_2Q]_{org}/[ZnA_2]_{org}[Q]_{org}=10^{1.92}$, $\beta_{2(org)}=[ZnA_2Q_2]_{org}/[ZnA_2]_{org}[Q]_{org}^2=10^{2.84}$) or $ZnA_2(HA)_4$ ($\beta_{2(org)}=[ZnA_2(HA)_4]_{org}/[ZnA_2]_{org}[(HA)_2]_{org}^2=10^{2.92}$). No polynuclear species was found in these organic phases when the initial zinc(II) concentration in the aqueous phase was less than 10^{-3} M.

Carboxylic acids, especially acetic acid, are widely employed as buffering agents in weakly acidic solutions because they buffer aqueous solutions at around pH 5 and they usually form only weak complexes with various metal ions.

For solvent extraction work, they are also useful buffering reagents. However, the equilibria of carboxylic acid in liquid-liquid distribution systems are rather complicated; in such systems, not only the dissociation of protons in the aqueous phase, but also the two-phase distribution of the acid and its dimerization in the organic phase, should be taken into account. The distribution and dimerization of several carboxylic acids have been studied in systems of carbon tetrachloride by the present authors[1] and in systems of benzene and various other solvents by Kojima, Yoshida, and Tanaka.[2]

The solvent extraction equilibria of metal ions with carboxylic acids are more complicated; the extracted metal species very often contain an undissociated form of the acid as well as the carboxylate anions, and in many cases, various types of polymerized metal species are also found in the organic phase, as has been reported by many authors.

The present study has been carried out in order to determine the distribution equilibria of zinc(II) in the carbon tetrachloride-aqueous system containing carboxylic acids; zinc(II) was extracted with these acids into carbon tetrachloride containing various amounts of quinoline. The results were statistically analyzed, and the equilibrium constants were evaluated. The results were considered on the basis of the present authors' previous work on the distribution equilibria of several carboxylic acids between carbon tetrachloride and the aqueous phase.[1] The extractability of this metal ion in these systems under vairous conditions was also considered.

Experimental

Reagents. The zinc-65 tracer was used throughout this study; it was obtained from the New England Nuclear Co. as a hydrochloric acid solution. In some experiments, a zinc(II) carrier which has been prepared by dissolving a reagent-grade zinc powder in perchloric acid was added. The stock solution of the tracer or of the carrier always contained 0.01 M perchloric acid. Analytical-grade butyric, valeric, and caproic acids were obtained from the Tokyo Kasei Co., the Kanto Chemical Co., or the Merck Co. (Germany). They were of a reagent grade and were distilled before use. The quinoline was obtained from the Merck Co. Carbon tetrachloride was washed three times with same volume of water before use. The other reagents were the same as those reported in previous paper.[1,3,4]

Procedures. All of the experiments were carried out in a thermostated room at 25°±0.3 °C. Five ml of carbon tetrachloride containing a carboxylic acid and, in some cases, quinoline, and 5 ml of an aqueous solution containing sodium hydroxide and sodium perchlorate (the total salt concentration was 1.0×10^{-1} M) and 10^{-3}—10^{-6} M zinc(II) (except when stated otherwise) were placed in stoppered glass tubes (volume, 20 ml); the two phases were agitated by hand or by means of a shaker until the distribution equilibrium was reached, after which the two phases were centrifuged. The distribution ratio of zinc(II) was determined from the γ-radioactivity of each phase. The details of the procedures were the same as those described in previous papers.[3,4] The distribution ratio is always defined as;

$$D=\frac{[Zn(II)]_{org.total}}{[Zn(II)]_{total}}=\frac{\gamma\text{-count-rate in 1 ml of the org. phase}}{\gamma\text{-count-rate in 1 ml of the aq. phase}}$$

Statistical

The complex formation equilibrium of zinc(II) in the aqueous phase with the anion of a carboxylic acid, HA, can be written as follows;

$$Zn^{2+}+nA^- \rightleftarrows ZnA_n^{2-n} \quad (1)$$

$$\beta_n=\frac{[ZnA_n^{2-n}]}{[Zn^{2+}][A^-]^n} \quad (2)$$

1) T. Sekine, M. Isayama, S. Yamaguchi, and H. Moriya, This Bulletin, **40**, 27 (1967).
2) I. Kojima, M. Yoshida, and M. Tanaka, *J. Inorg. Nucl. Chem.*, **32**, 987 (1970).
3) H. Moriya and T. Sekine, This Bulletin, **44**, 3347 (1971).
4) H. Moriya and T. Sekine, *ibid.*, **45**, 1626 (1972).

and the total concentration of zinc(II) in such an aqueous phase can be represented by;

$$[Zn^{2+}]_{total} = [Zn^{2+}](1 + \beta_1[A^-] + \beta_2[A^-]^2 + \cdots) \quad (3)$$

The extraction of zinc(II) as the uncharged complex with this anion into a nonpolar solvent can be represented as follows;

$$Zn^{2+} + 2A^- \rightleftarrows ZnA_2(org) \quad (4)$$

$$K_{exA} = \frac{[ZnA_2]_{org}}{[Zn^{2+}][A^-]^2} \quad (5)$$

When the extracted species, ZnA_2, can add n molecules of a neutral ligand, L, such as quinoline or dimerized acid molecule, in the organic phase, the equilibrium can be written as follows;

$$ZnA_2(org) + nL(org) \rightleftarrows ZnA_2L_n(org) \quad (6)$$

$$\beta_{n(org)} = \frac{[ZnA_2L_n]_{org}}{[ZnA_2]_{org}[L]_{org}^n} \quad (7)$$

The distribution ratio of zinc(II) in the presence of quinoline can be written as follows when the adduct formation with the dimer of the carboxylic acid is assumed to be negligible, and, furthermore, when only the first and the second quinoline adducts are formed in the organic phase, while only the first complex with the acid is formed in the aqueous phase;

$$D = \frac{[ZnA_2]_{org} + [ZnA_2Q]_{org} + [ZnA_2Q_2]_{org}}{[Zn^{2+}] + [ZnA^+]} \quad (8)$$

By introducing Eqs. (5) and (7) and the stability constant in Eq. (2), Eq. (8) can be rewritten as follows:

$$D = \frac{K_{exA}[A^-]^2(1 + \beta_{1(org)}[Q]_{org} + \beta_{2(org)}[Q]_{org}^2)}{1 + \beta_1[A^-]} \quad (9)$$

The distribution ratio of zinc(II) in the absence of quinoline can be rewritten as follows if the formation of only the first and second adducts in the organic phase, and that of only the first complex in the aqueous phase, are assumed:

$$D = \frac{[ZnA_2]_{org} + [ZnA_2(HA)_2]_{org} + [ZnA_2(HA)_4]_{org}}{[Zn^{2+}] + [ZnA^+]} \quad (10)$$

By introducing Eqs. (5) and (7), and the stability constant for the complexes in the aqueous phase, Eq. (10) can be rewritten as follows:

$$D = \frac{K_{exA}[A^-]^2(1 + \beta_{1(org)}[(HA)_2]_{org} + \beta_{2(org)}[(HA)_2]_{org}^2)}{1 + \beta_1[A^-]} \quad (11)$$

Since only the initial concentrations of the carboxylic acid and the hydroxide ion, and the equilibrium concentration of the hydrogen ion are usually obtained, the following treatments are necessary in order to calculate the other concentrations at equilibrium.

When the volumes of the two phases are the same, the following relation can be given for the total concentration of the carboxylic acid in the initial organic phase:

$$C_{HA(org)} = [A^-] + [HA] + [HA]_{org} + 2[(HA)_2]_{org} \quad (12)$$

The total concentration of the carboxylic acid in the aqueous phase can be written as follows:

$$[HA]_{total} = [A^-] + [HA] \quad (13)$$

By introducing the dissociation constant, $K_a = [H^+][A^-]/[HA]$, Eq. (13) can be written as:

$$[HA]_{total} = [A^-](1 + [H^+]/K_a) \quad (14)$$

When the sodium hydroxide concentration in the initial aqueous phase is denoted by C_{OH}, the $C_{OH} + [H^+] = [A^-] + [OH^-]$ relation is obtained; when the pH is not too high and not too low (for example, 10^{-10} M $< [H^+] < 10^{-4}$ M), this can be written as $C_{OH} = [A^-]$. The $[HA]_{total}$ value can be estimated from Eq. (14) by using this relation, the value of $[H^+]$ experimentally obtained, and the value of the dissociation constant.

The following relation is obtained from Eqs. (12) and (13):

$$[HA]_{org.total} = C_{HA(org)} - [HA]_{total} = 2[(HA)_2]_{org} + [HA]_{org} \quad (15)$$

By introducing the dimerization constant, $K_{dim(org)} = [(HA)_2]_{org}/[HA]_{org}^2$, Eq. (15) can be rewritten as:

$$[HA]_{org.total} = 2[(HA)_2]_{org} + \sqrt{[(HA)_2]_{org}/K_{dim(org)}} \quad (16)$$

However, when $[HA]_{org} \ll [(HA)_2]_{org}$ as under the conditions employed in this study (this will be discussed later), the following relation is obtained from Eq. (15):

$$[(HA)_2]_{org} = \frac{1}{2}[HA]_{org.total} \quad (17)$$

The experimental data of D at a given value of $[A^-]$, determined as a function of $[Q]_{org}$ or as a function of $[(HA)_2]_{org}$, can be transformed to the following equation:

$$\log y = \log c_0(1 + c_1x + c_2x^2) \quad (18)$$

The c_0, c_1, and c_2 constants can be obtained from the plot of the experimental data by a curve-fitting method, as has already been demonstrated.[3,4] The equilibrium constants in Eqs. (5) and (7) can be obtained from these values of c_0, c_1, and c_2.

Results

The experimental results were reproducible, and the recovery of zinc(II) from the two phases was quantitative within the limit of experimental accuracy.

It was found in another work of the present authors[5] that only the first zinc(II) complex is formed with the carboxylic acid in a 0.1 M sodium perchlorate constant ionic medium at 25 °C; the values for $\beta_1 = [ZnA^+]/[Zn^{2+}][A^-]$ are $10^{1.10}$(butyrate), $10^{1.10}$(valerate) and $10^{1.10}$(caproate). These values were used for the analysis of the experimental data of the present work.

The following equation can be written on the basis of the electrical neutrality:

$$[Na^+] + [H^+] + 2[Zn^{2+}] + [ZnA^+] = [OH^-] + [ClO_4^-]$$

Since the concentration of zinc(II) was very low (less than 10^{-5} M), the hydrogen-ion concentrations was in the range of 10^{-5} M $> [H^+] > 10^{-9}$ M (and thus $[H^+] \ll 0.1$ M and $[OH^-] \ll 0.1$ M), and the initial aqueous phase was a mixture of 0.1 M sodium

5) H. Moriya and T. Sekine, to be published.

perchlorate and 0.1 M sodium hydroxide at various mixing ratios, the following relation can be introduced:

$$0.1 \simeq C_{OH} + [ClO_4^-] = [A^-] + [CO_4^-]$$

The term of the concentration of the undissociated acid in the aqueous phase, [HA], can be regarded as negligible in the statistical analysis of the results of experiments with quinoline because the K_a values for these acids are about 10^{-5}(in 0.1 M sodium perchlorate at 25 °C, they are 1.51×10^{-5}(butyric acid), 1.41×10^{-5} (valeric acid) and 1.45×10^{-5}(caproic acid)),[2] it can be assumed that $[A^-]\gg[HA]$ when $-\log[H^+]$ is higher than 7 (in Figs. 1 and 2). For the experiments in the absence of quinoline, the $[H^+]$ values ranges from $10^{-5.5}$ to $10^{-6.5}$; thus, the [HA] term can not be neglected. This value was calculated from $[H^+]$, which was determined by potentiometry, $[A^-]$ (which is equal to C_{OH}), and K_a.

Extraction in the Presence of Quinoline. The distribution ratio of zinc(II) in an aqueous phase at a given $[A^-]$ is enhanced by the addition of quinoline to the organic phase. Since the distribution constant of quinoline is not small (77 between carbon tetrachloride and 3 M sodium perchlorate[6]), the $[Q]_{org\cdot initial}=[Q]_{org}$ relation can be assumed. Figure 1 shows the change in the distribution ratio with the change in the quinoline concentration when $[A^-]$ is 1.0×10^{-1} M and when the total concentration of carboxylic acid in the organic phase at equilibrium is less than 10^{-2} M. Figure 2 shows the dependence of

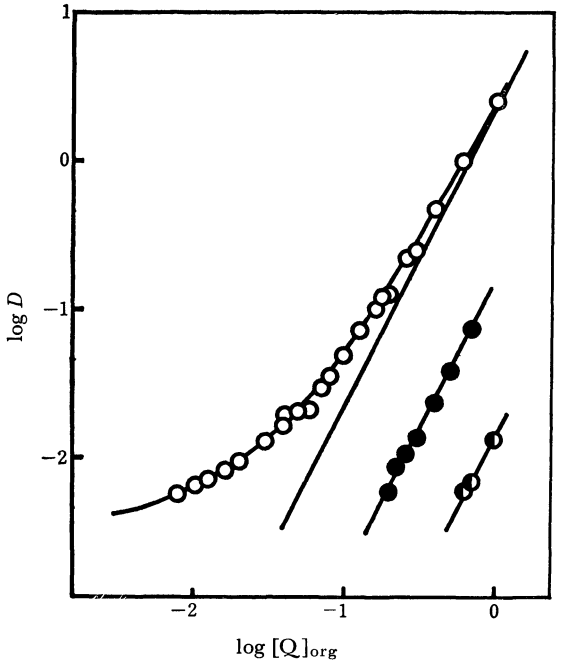

Fig. 1. Extraction as a function of quinoline concentration when the aqueous phase initially contains 1.0×10^{-1} M of caproate (○), valerate (●) and butyrate (◑) anion. The solid curve for caproate represents; $\log D=\log K_{exA}[A^-]^2(1+\beta_1[A^-])^{-1}(1+\beta_{1(org)}[Q]_{org}+\beta_{2(org)}[Q]_{org}^2)$ and the straight lines for these three acids represent; $\log D=\log K_{exA}[A^-]^2(1+\beta_1[A^-])^{-1}\beta_{2(org)}[Q]_{org}^2$. These constants are listed in Table 1.

6) P. Antikainen and D. Dyrssen, *Acta Chem. Scand.*, **14**, 86 (1960).

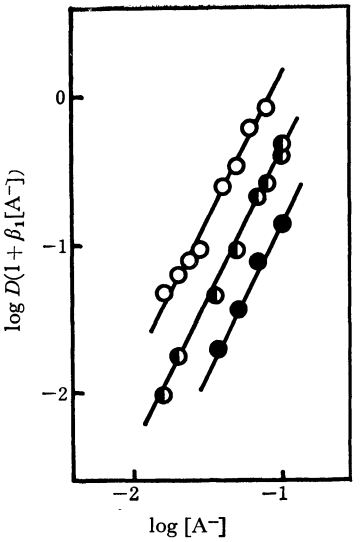

Fig. 2. Extraction as a function of the concentration of the caproate ion in the aqueous phase when the quinoline concentration in the organic phase is 0.5 M (○), 0.25 M (◐) and 0.1 M (●), the straight lines represent; $\log D(1+\beta_1[A^-])=\log K_{exA}[A^-]^2(1+\beta_{1(org)}[Q]_{org}+\beta_{2(org)}[Q]_{org}^2)$. These constants are listed in Table 1.

the distribution ratio on the concentration of the caproate anion in the aqueous phase when the organic phase contains less than 10^{-2} M of the carboxylic acid and a certain amount of quinoline (0.1 M, 0.25 M or 0.5 M). In this figure, the effect of the carboxylate complex in the aqueous phase has been corrected by plotting $\log D(1+\beta_1[A^-])$ instead of $\log D$ (*cf.* Eq. 9). As may be seen from Fig. 2, the extraction is proportional to the square of $[A^-]$; thus, it can be concluded that the metal species in these organic phases contains at least two carboxylate anions. Furthermore, as will be seen later, no adduct of zinc(II) caproate with the dimer of the acid is formed under these conditions, the distribution ratio can well be represented by Eqs. (8) and (9). Since the extraction with butyric and valeric acid is very poor in the absence of quinoline, the K_{exA} value in Eq. (5) for these extractions could not be determined and the distribution ratio could be given for these systems by the equation:

$$D=\frac{K_{exA}\beta_{2(org)}[A^-]^2[Q]_{org}^2}{1+\beta_1[A^-]} \qquad (19)$$

On the other hand, the distribution ratio in the caproate system in the absence of quinoline was $10^{-2.50}$ when $[A^-]$ is 0.1 M; it was enhanced by the increase in the quinoline concentration. Hence, the data can be concluded to be well represented by Eq. (9).

The constants for the butyrate and valerate systems were determined directly from the data in Fig. 1, but those for the caproate were determined by the curve-fitting. The constants are listed in Table 1.

Extraction in the Absence of Quinoline. The extraction of zinc(II) in the absence of quinoline was further studied by changing $[A^-]$, $[HA]_{org.total}$, or the total zinc(II) concentration.

Since the distribution and dimerization constants are knwon for butyric acid,[1] but are not known for valeric and caproic acids in carbon tetrachloride sys-

Table 1. Equilibrium constants for zinc(II) extraction with carboxylic acids (HA) in the presence and absence of quinoline at 25 °C

Org. phase: CCl_4

Aq. phase: 0.1 M $Na(A^-, ClO_4)$

[a] $K_{exA}=[ZnA_2]_{org}/[Zn^{2+}][A^-]^2=10^{-0.15}$ (for caproate ion)

$\beta_{n(org)}=[ZnA_2L_n]_{org}/[ZnA_2]_{org}[L]_{org}^n$

(a) In the presence of quinoline ($[HA]_{org.total}<10^{-2}$ M)

Acids	$\log K_{exA}\beta_{2(org)}$	$\log \beta_{1(org)}$	$\log \beta_{2(org)}$
caproic	2.69	1.92	2.84
valeric	1.53	—	—
butyric	0.47	—	—

(b) Adduct formation with dimer molecules of the acid in the absence of quinoline (10^{-2} M $<[(HA)_2]_{org}<9.0\times10^{-1}$ M)

Acids	$\log K_{exA}\beta_{2(org)}$	$\log \beta_{2(org)}$
caproic	2.77	2.92
valeric	1.20	—

a) The distribution ratio of zinc(II) between CCl_4 containing a very small amount of caproic acid and an aqueous phase containing 0.1 M caproate ion is $10^{-2.50}$.

b) The formation of the first adduct $ZnA_2(HA)_2$ is negligible.

tems, the concentrations of the monomer and of the dimer of these acids in the organic phase were treated as follows.

The dimerization constants for acetic, propionic, and butyric acids in carbon tetrachloride are 5.92×10^2, 9.40×10^2, and 2.91×10^3,[1] respectively. From these facts, it can reasonably be assumed that the dimerization constants for valeric and caproic acid are large; it should not be unreasonable to asume that the dimerization constants for these acids are higher than 3×10^3. From this assumption and Eq. (16), we find that even when $[HA]_{org.total}$ is only 5×10^{-2} M, less than 5% of the acid in the organic phase exists in the form of the monomer, and since the total concentration of the acid in the organic phase in the following experiments is always higher than 5×10^{-2} M, all the acid in the organic phase can be regarded as existing in the form of a dimer, —in other words, Eq. (17) can be used for these experimental results.

Figure 3 shows the change in the distribution ratio when the concentration of the anions, $[A^-]$, is kept at 9.6×10^{-2} M, but when the concentration of the dimer of the acid changes and when quinoline is absent. Figure 4 gives the dependence of the extraction on the concentration of the carboxylate anions in the aqueous phase. Since the total concentration, $[HA]_{org.total}$, is high (2M), it can be assumed as will be described later, that only the second adduct exists in the organic phase. In order to make a correction for the small change in the $[(HA)_2]_{org}$ and for the change in the complex formation in the aqueous phase, $\log D(1+\beta_1[A^-])[(HA)_2]_{org}^{-2}$ is plotted in this figure instead of $\log D$. As may be seen from Fig. 4, the extraction is proportional to the square of $[A^-]$; thus, it was concluded that the metal species in these organic phases also contains two carboxylate anions.

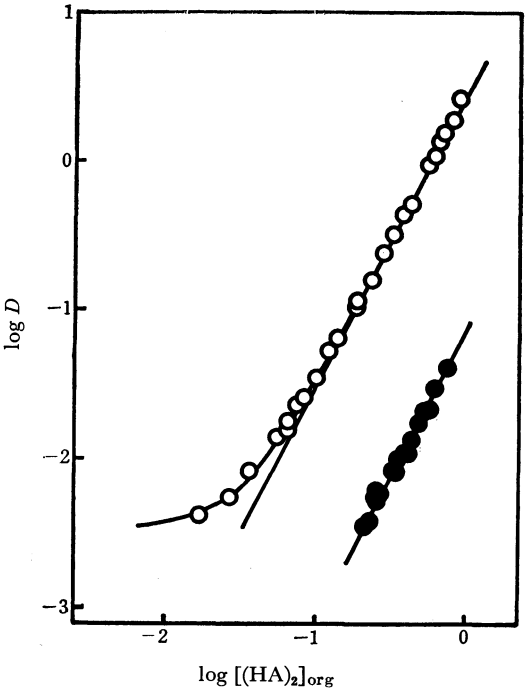

Fig. 3. Extraction in the absence of the quinoline as a function of the concentration of dimer of caproic acid (○) and valeric acid (●) in the organic phase when the concentration of $[A^-]$ is kept at 9.6×10^{-2} M. The solid curve for caproic acid represents; $\log D=\log K_{exA}[A^-]^2(1+\beta_1[A^-])^{-1}(1+\beta_{2(org)}[(HA)_2]_{org}^2)$ and the straight lines for the two acids; $\log D=\log K_{exA}[A^-]^2(1+\beta_1[A^-])^{-1}\beta_{2(org)}[(HA)_2]_{org}^2$.
These constants are listed in Table 1.

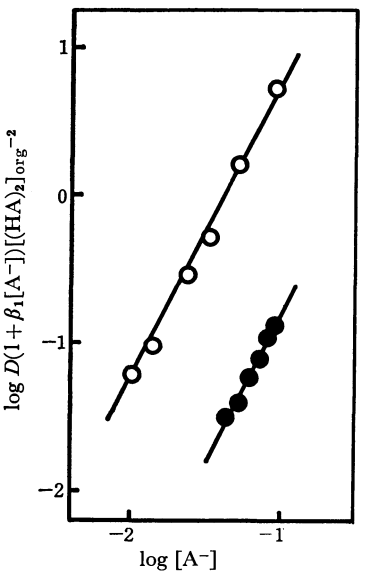

Fig. 4. Extraction in the absence of quinoline as a function of the concentration of caproate ion (○) and valerate ion (●) in the aqueous phase, the straight lines for the two acids; $\log D(1+\beta_1[A^-])[(HA)_2]_{org}^{-2}=\log K_{exA}[A^-]^2\beta_{2(org)}$.
These constants are listed in Table 1.

As may be seen from Fig. 3, the distribution ratio in the higher-acid-concentration region is proportional to the square of $[(HA)_2]_{org}$. This fact indicates that the zinc(II) species in the organic phase of this region

is $ZnA_2(HA)_4$. Furthermore, since the increase in the distribution ratio is very abrupt, we assumed that the first adduct was not formed. This was confirmed by the fact that the extraction curve can be well fitted with the standard-curve $Y=\log(1+v^2)$; $X=\log v$. The equilibrium constants obtained by the curve-fitting are also given in Table 1.

Since extractions of polynuclear species have very often been observed in systems containing carboxylic acid, the effect of the total metal concentration of zinc(II) on the distribution ratio was determined. It was found that when the acid is caproic, when $[HA]_{org,total}$ is 0.9 M, and when $[A^-]$ is 0.1 M, the distribution ratio of zinc(II) is constant in the range of $[Zn^{2+}]_{initial}$, 10^{-3}—10^{-6} M. Thus there was no extraction of polynuclear species within this range of metal concentrations.

Discussion

The chemical equilibria of metal extraction with carboxylic acids are generally very complicated because the distribution equilibria of the carboxylic acid are complicated as a result of dimerization in the organic phase and the extraction of polynuclear species combining various numbers of the dimer of the acid molecules. However, as has been described above, the chemical equilibria in the systems studied in this paper could be treated much more easily than those systems previously reported.

This is because of the following reasons: (i) The extraction of the ZnA_2 species could be determined separately. This was possible because the extraction could be carried out when $[A^-]$ was relatively high and $[HA]_{org,total}$ was small; in order to achieve this condition, the pH of the solution must be high (for example, when $[A^-]$ is 0.1 M and when $[HA]_{org,total}$ is less than 10^{-2} M, $[H^+]$ should be $10^{-6.5}$ M). Many other metal ions undergo hydrolysis at such high pH values, and thus the equilibria become very complicated. However, the hydrolysis of zinc(II) at this pH is fortunately negligible provided the metal concentration is very low.[7] (ii) It was possible to assume that all the acid in the organic phase can be regarded as existing as the dimers, judging from the results of Ref. 1. The dimerization constant in carbon tetrachloride is much larger than that, for example, in benzene; thus, the above assumptions are possible in the former solvent under the conditions employed. (iii) The fact that $C_{OH}\simeq[A^-]$ could be reasonably assumed under the conditions employed also simplified the analysis.

There have been several reports on the extraction of zinc(II) with carboxylic acids.[8–11] Among these, Schweizer and Clifford have made a systematic analysis of their extraction date and have concluded that the distribution ratio of zinc(II) increased (i) upon an increase in the molecular weight of the acid, (ii) upon an increase in the concentration of the acid, (iii) upon an increase in the concentration of 1-aminobutane added to the system, and (iv) upon a decrease in the hydrogen-ion concentration, but that the distribution ratio is independent of the metal concentration. These observations agree qualitatively with the present results. However, their interpretation of the results is different from that by the present authors, although the solvent of the present study is different from that employed in the previous work.[11] It seems difficult to explain why the conclusion in that work[11] is different from that of the present work. However, some oversimplified assumptions, such as that there is no formation of the zinc(II) carboxylate complex in the aqueous phase, might be one of the reasons.

Among the systems studied in the comprehensive series of papers on metal extraction with carboxylic acid carried out by Tanaka and his co-workers,[12–18] only lead(II)[18] was found to be extractable as a monomeric species over a wide range of metal concentrations. The extraction of zinc(II) is similar to that of lead(II) although only the $MA_2(HA)_4$ species was found to be extracted in addition to the MA_2 species. The extraction of the MA_2 species has not been found for the metal ions studied by the above workers.

As long as we are concerned only with the data obtained by distribution experiments, no information about the structure of the extracted metal species can be obtained. Thus, we do not know the nature of the bonds between the ZnA_2 species and the quinoline or the carboxylic acid in the organic phase. It is very remarkable that the stability constants for the second adduct, $\beta_{2(org)}$, with quinoline and carboxylic acid dimer are similar to each other.

The authors are grateful to Mr. Naohiko Ihara and and Mr. Yoshihiro Takahashi of the present laboratory for their experimental aid. Part of this work has been carried out in the Laboratory of Analytical and Nuclear Chemistry, Institute of Physical and Chemical Research. The authors are grateful to Professor Nobufusa Saito, the head of that laboratory.

7) T. Sekine, *Acta Chem. Scand.*, **19**, 1526 (1965).
8) L. M. Gindin, P. A. Bobikov, and A. M. Rosen, *Dokl. Akad. Nauk SSSR*, **128**, 295 (1959).
9) L. M. Gindin, P. A. Bobikov, and A. V. Bugaeva, *Russ. J. Inorg. Cem.*, **5**, 906 (1960).
10) R. Blumberg and P. Melzer, Int. Miner. Process. Congr., Tech. Pap., 7th, New York, **I** 139 (1965).
11) G. K. Schweitzer and F. C. Clifford, *Anal. Chim. Acta*, **45** 57 (1969).
12) M. Tanaka and T. Niinomi, *J. Inog. Nucl. Chem.*, **27**, 431 (1965).
13) M. Tanaka, N. Nakasuka, and S. Goto, "Solvent Extraction Chemistry" edited by D. Dyrssen, J. O. Liljenzin, and J. Rydberg, North-Holland, p. 154 (1967).
14) M. Tanaka, N. Nakasuka, and S. Sasane, *J. Inorg. Nucl. Chem.*, **31**, 2591 (1969).
15) I. Kojima, N. Uchida, and M. Tanaka, *ibid.*, **32**, 1333 (1970).
16) M. Tanaka, N. Nakasuka, and H. Yamada, *ibid.*, **32**, 2759 (1970).
17) M. Tanaka, N. Nakasuka, and H. Yamada, *ibid.*, **32**, 2791 (1970).
18) N. Nakasuka, M. Nakai, and M. Tanaka, *ibid.*, **32** 3667 (1970).

A Study of Silver(I) Complexes with Some π-Donors and n-Donors in Chloroform by the Solvent Extraction Method

Tatsuya SEKINE and Yoshihiro TAKAHASHI

Department of Chemistry, Science University of Tokyo, Kagurazaka, Shinjuku-ku, Tokyo 162

(Received July 17, 1972)

The solvent extraction of silver(I) in a 0.1 M constant-ionic-strength solution into chloroform with 2-thenoyltrifluoroacetone(TTA) and with caproic acid was studied by means of radiometry. It was found that these extractions are enhanced by the addition of aliphatic and cyclic alkenes, of aromatic hydrocarbons, and of some n-donors. The enhancement of the extraction was explained in terms of the formation of molecular complexes of the silver(I)-TTA chelate or of silver(I) caproate in chloroform. By an analysis of the experimental data, the stability constant of the silver(I)-TTA chelate in the aqueous phase, and the stability constants of the molecular complexes in the chloroform phase with these donors, were determined. Some consideration was made of these results and of the possibility of the application of these extraction systems to analytical chemistry.

Many workers have reported the complex formation of silver(I) with various n-donor ligands, and the stability constants have been determined by various experimental techniques.[1] At the same time, some workers have also reported that silver(I) can form complexes with π-donor ligands, such as unsaturated aliphatic or aromatic hydrocarbons.[2,3]

The complex formation equilibria of silver(I) with n-donor ligands have been determined, in most cases, in aqueous solutions because the complexes with n-donors which are usually anionic have often been of interest to analytical and inorganic chemists from the standpoint of the chemical behavior of silver(I) in aqueous solutions. The π-donors are, on the other hand, usually uncharged, and they are often relatively insoluble in water. However, the complex formation of silver(I) with these ligands has also been determined in aqueous solutions or mixed solutions of water and polar organic solvents, because silver(I) salts with ordinary inorganic anions are insoluble in nonpolar organic solvents.

The formation of various other molecular complexes, however, has been studied very often in nonpolar organic solvents such as carbon tetrachloride,[2,3] in many cases, the formation constants of molecular complexes seem to be affected by the nature of the solvent—they are usually larger in organic solvents than in water.[2] This could be due to a great interaction of water molecules with various ionic or molecular substances; the comparison of the formation constants of a given complex in water and in other kinds of solvents should give some information about that complex.

The present study has been undertaken from this standpoint. The present authors have determined the complex formation of silver(I) extracted from aqueous solutions into chloroform as a chelate complex with thenoyltrifluoroacetone(TTA) or as a complex with caproic acid. Thenoyltrifluoroacetone and caproic acid were used in order to make silver(I) extractable into the organic solvent, and the complex formation was determined from the enhancement of the extraction due to the formation of molecular complexes in the organic phase. The stability constants thus obtained were compared with those determined in aqueous solutions, the results obtained in these different solvents were discussed. The effect of the formation of these molecular complexes on the solvent extraction of silver(I) with the chelating reagent or with the fatty acid was considered, and the possibility of the application of such extractions to analytical chemistry was discussed.

Experimental

Reagents. The silver-110 m tracer was obtained from the New England Nuclear Corp. U. S. A., as silver nitrate in a dilute nitric acid solution. It was diluted with 0.1 M nitric acid and used as the stock tracer solution. The quinoline and caproic acid were obtained from the Merck Co. Germany. The tributyl phosphate (TBP) and unsaturated hydrocarbons were obtained from Tokyo Kasei Co., and the TTA and trioctylphosphine oxide (TOPO), from Dojindo Co. All of the reagents were of a reagent-grade. TBP was washed with 0.1 M perchloric acid, water, and 0.1 M sodium hydroxide, and then several times with water. Chloroform was washed three times with water just before use. The other reagents were used without further purification. The concentration of the sodium hydroxide solution was determined by means of acid titration, and the concentrations of the other solutions were determined by means of gravimetry.

Procedures. All of the procedures were carried out in a thermostatted room at 25 °C. Stoppered glass tubes (volume, 20 ml) were used to equilibrate the two phases. For the experiments on the silver(I)-TTA chelate, sodium perchlorate solutions containing sodium hydroxide and a chloroform solution of TTA were placed in the tubes. After the two phases has been equilibrated by shaking them for one minute by hand, a certain amount of a silver(I) solution labelled by silver-110 m was added; the two phases were then again agitated by hand for three minutes and centrifuged. For the experiments on the silver(I) caproate complex, aqueous solutions containing sodium perchlorate and/or sodium caproate, and chloroform were placed in the tubes and the labelled silver(I) was added. The two phases were agitated for three minutes by hand and then centrifuged. The initial volumes of the two phases were always 5.0 ml, and

1) "The Stability Constants of Metal-Ion Complexes," ed. by L. G. Sillén and A. E. Martell, The Chemical Society Special Publication, No. 17 (1964).

2) L. J. Andrews and R. M. Keefer, "Molecular Complexes in Organic Chemistry," Holden-Day Inc., San Francisco (1964).

3) G. Briegleb, "Elektronen-Donator-Acceptor-Komplexe", Springer, Berlin (1961).

the inoic strength of the aqueous phase was 0.1 M. The initial concentration of the silver(I) ion in the aqueous phase was 2×10^{-5} to 3×10^{-6} M. The concentration of TTA in the organic phase was 0.1 M. The concentration of caproate ions in the aqueous phase was 0.1 M unless otherwise stated. The pH of the aqueous phase at equilibrium was in a range from 7 to 8 in both cases.

A 2 ml portion was pipetted out from each equilibrated phase and transferred into a test tube. The γ-radioactivity was measured with a well-type(NaI) scintillation counter, and the distribution of silver(I) was calculated as follows;

$$D=\frac{[\mathrm{Ag(I)}]_{\mathrm{org,total}}}{[\mathrm{Ag(I)}]_{\mathrm{total}}}=\frac{\gamma\text{-count-rate per ml of the organic phase}}{\gamma\text{-count-rate per ml of the aqueous phase}}$$

Statistical

The extraction of silver(I) in an aqueous solution with an organophilic and acidic extracting reagent, HA, can be written as follows:

$$\mathrm{Ag^+ + HA(org) \rightleftarrows AgA(org) + H^+} \quad (1)$$

$$K_{\mathrm{ex}}=\frac{[\mathrm{AgA}]_{\mathrm{org}}[\mathrm{H^+}]}{[\mathrm{Ag^+}][\mathrm{HA}]_{\mathrm{org}}} \quad (2)$$

When the organic phase initially contains C_{HA}M of the extractant and when the volumes of the two phases are the same, the following equation can be used:

$$C_{\mathrm{HA}}=[\mathrm{HA}]_{\mathrm{org}}+[\mathrm{HA}]+[\mathrm{A^-}] \quad (3)$$

However, if the aqueous phase initially contains C_{OH}M of sodium hydroxide (which is smaller than C_{HA}M) and if the pH is not very high (that is, $[\mathrm{OH^-}]\ll 1$), the following equation can be used:

$$C_{\mathrm{OH}}\simeq[\mathrm{A^-}] \quad (4)$$

Thus, under such conditions, the concentration of the dissociated extractant anion, $[\mathrm{A^-}]$, in Eq. (4) can be calculated from the amount of sodium hydroxide added to the initial aqueous phase, regardless of the total concentration of the extractant in the system.

The distribution ratio of silver(I) into an inert solvent such as chloroform can be described as:

$$D=\frac{[\mathrm{Ag(I)}]_{\mathrm{org,total}}}{[\mathrm{Ag(I)}]_{\mathrm{total}}} \quad (5)$$

$$=\frac{[\mathrm{AgA}]_{\mathrm{org}}}{[\mathrm{Ag^+}]+[\mathrm{AgA}]+\cdots}=\frac{K_{\mathrm{dm}}\beta_1[\mathrm{A^-}]}{1+\beta_1[\mathrm{A^-}]+\cdots} \quad (6)$$

where β_1 is the stability constant of the silver(I) complex with the extractant in the aqueous phase and where K_{dm} is the distribution constant of the uncharged chelate between the two phases:

$$K_{\mathrm{dm}}=\frac{[\mathrm{AgA}]_{\mathrm{org}}}{[\mathrm{AgA}]} \quad (7)$$

From the acid dissociation constant and the distribution constant of HA, that is, $K_{\mathrm{a}}=[\mathrm{A^-}][\mathrm{H^+}]/[\mathrm{HA}]$ and $K_{\mathrm{d}}=[\mathrm{HA}]_{\mathrm{org}}/[\mathrm{HA}]$, we obtain:

$$[\mathrm{A^-}]=\frac{K_{\mathrm{a}}[\mathrm{HA}]_{\mathrm{org}}}{K_{\mathrm{d}}[\mathrm{H^+}]} \quad (8)$$

When no aqueous complex with $\mathrm{A^-}$ is formed, the following equation is obtained from Eqs. (6) and (8):

$$D=K_{\mathrm{dm}}\beta_1[\mathrm{A^-}]=K_{\mathrm{dm}}\beta_1K_{\mathrm{a}}K_{\mathrm{d}}^{-1}[\mathrm{HA}]_{\mathrm{org}}[\mathrm{H^+}]^{-1} \quad (9)$$

From Eqs. (2) and (9), we obtain:

$$K_{\mathrm{ex}}=K_{\mathrm{dm}}\beta_1K_{\mathrm{a}}K_{\mathrm{d}}^{-1} \quad (10)$$

When the metal complex forms molecular complexes with a neutral ligand, L, in the organic phase, the equilibrium can be written as:

$$\mathrm{AgA(org)} + n\mathrm{L(org)} \rightleftarrows \mathrm{AgAL}_n\mathrm{(org)} \quad (11)$$

$$\beta_n\mathrm{(org)}=\frac{[\mathrm{AgAL}_n]_{\mathrm{org}}}{[\mathrm{AgA}]_{\mathrm{org}}[\mathrm{L}]_{\mathrm{org}}^{\,n}} \quad (12)$$

where $\beta_{n(\mathrm{org})}$ is the over-all stability constant of the "n-th" molecular complex in the organic phase.

The distribution ratio in such a system can be written as:

$$D=\frac{[\mathrm{AgA}]_{\mathrm{org}}+[\mathrm{AgAL}]_{\mathrm{org}}+[\mathrm{AgAL_2}]_{\mathrm{org}}+\cdots}{[\mathrm{Ag^+}]+[\mathrm{AgA}]+\cdots} \quad (13)$$

From Eqs. (6), (12), and (13), the following equation is obtained:

$$D=\frac{K_{\mathrm{dm}}\beta_1[\mathrm{A^-}]}{1+\beta_1[\mathrm{A^-}]+\cdots}\times(1+\beta_{1(\mathrm{org})}[\mathrm{L}]_{\mathrm{org}}+\beta_{2(\mathrm{org})}[\mathrm{L}]_{\mathrm{org}}^{\,2}+\cdots) \quad (14)$$

If the concentration, $[\mathrm{L}]_{\mathrm{org}}$, is kept at a constant value, $\mathrm{L_1}$, Eq. (14) can be written as:

$$D=C_{\mathrm{L}}\times\frac{K_{\mathrm{dm}}\beta_1[\mathrm{A^-}]}{1+\beta_1[\mathrm{A^-}]+\cdots} \quad (15)$$

where C_{L} is a constant which is equal to $(1+\beta_{1(\mathrm{org})}\mathrm{L_1}+\beta_{2(\mathrm{org})}\mathrm{L_1}^2+\cdots)$

If the concentration, $[\mathrm{A^-}]$, is kept at a constant value, $\mathrm{A_1}$, the following equation can be obtained from Eqs. (6) and (14):

$$D/D_{\mathrm{A}}=(1+\beta_{1(\mathrm{org})}[\mathrm{L}]_{\mathrm{org}}+\beta_{2(\mathrm{org})}[\mathrm{L}]_{\mathrm{org}}^{\,2}+\cdots) \quad (16)$$

where D_{A} is a constant which is equal to $K_{\mathrm{dm}}\beta_1\mathrm{A_1}(1+\beta_1\mathrm{A_1}+\cdots)^{-1}$ in such a case.

The stability constants, β_n and $\beta_{n(\mathrm{org})}$, and the distributation constant, K_{dm}, can be determined from the experimental results by a curve-fitting method.[4]

If only the first complex is formed in the aqueous phase, the log D *vs.* log $[\mathrm{A^-}]$ plot of the data represented by Eq. (15) can be fitted with the standard curve represented by Eq. (17), while if only the first complex is formed in the organic phase, the log D/D_{A} *vs.* log $[\mathrm{L}]_{\mathrm{org}}$ plot of the data represented by Eq. (16) can be fitted with the standard curve represented by Eq. (18):

$$Y=-\log(1+v^{-1});\ X=\log v \quad (17)$$

$$Y=\log(1+v);\ X=\log v \quad (18)$$

If both the first and second complexes are formed in the organic phase, the plot can be fitted with the following family of standard curves:

$$Y=\log(1+pv+v^2);\ X=\log v \quad (19)$$

The equilibrium constants can be obtained from the parameters of the fitted curve.

4) T. Sekine and M. Ono, This Bulletin, **38**, 2087 (1965).

Results

TTA Extraction. The extraction of silver(I) with TTA in chloroform is poor. The open circles in Fig. 1 gives the distribution ratio of silver(I) between chloroform and the aqueous phase as a function of the concentration of the TTA anion. The extraction is less than 10 percent even when the aqueous phase contains nearly 0.1 M TTA anions.

This extraction is enhanced very much if a molecular complex-forming ligand is added to the chloroform phase. Figure 1 also gives the extraction curves when the chloroform phase contains 5×10^{-1} M toluene, 1×10^{-2} M cyclohexene, or 1×10^{-3} M quinoline. It also gives the extraction curve of silver(I) with TTA in benzene. As may be seen from Fig. 1, each plot has two asymptotes, with slopes of +1 and 0. This fact indicates that the data can be represented by Eq. (15). The equilibrium constants obtained by the curve-fitting method are listed in Table 1.

Figures 2 to 6 show the enhancement of the extraction of the silver(I)-TTA chelate by an addition

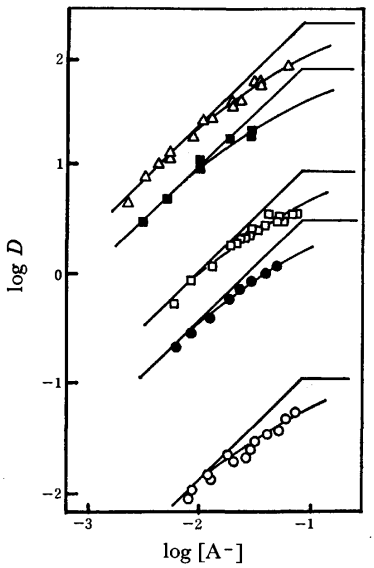

Fig. 1. Distribution ratio of Ag(I) as a function of the concentration of TTA anion. Org. phase: ○: $CHCl_3$, ●: $CHCl_3$ containing 5×10^{-1} M toluene, □: $CHCl_3$ containing 1×10^{-2} M cyclohexene, ■: benzene, △: $CHCl_3$ containing 1×10^{-3} M quinoline.

TABLE 1. EQUILIBRIUM CONSTANTS OBTAINED FROM Fig. 1

Organic solvent	$\log\beta_1$[a]	$\log K_{dm}'$[b]	$\log K_{ex}'$[c]
$CHCl_3$	1.10	−0.96	−7.94
$CHCl_3$ containing 5×10^{-1} M toluene	1.10	0.50	−6.48
$CHCl_3$ containing 1×10^{-2} M cyclohexene	1.10	0.94	−6.04
$CHCl_3$ containing 1×10^{-3} M quinoline	1.10	2.30	−4.68
C_6H_6	1.10	1.95	−4.78

a) $\beta_1=[AgA]/[Ag^+][A^-]$ in the aqueous phase where A^- is the dissociated TTA anion.
b) $K_{dm}'=K_{dm}C_L$ (K_{dm}, *cf.* Eq. (7) and C_L, *cf.* Eq. (15)).
c) $K_{ex}'=K_{ex}C_L$ (K_{ex}, *cf.* Eqs. (2) and (10) and C_L, *cf.* Eq. (15)).
These values are calculated from the values of K_{dm}' by using the following constants for TTA: $pK_a=6.23$, $\mu=0.1$[6] and $K_d=71$[5] ($CHCl_3$–0.1 M $NaClO_4$), $K_d=40$ (C_6H_6–0.1 M $NaClO_4$).[17]

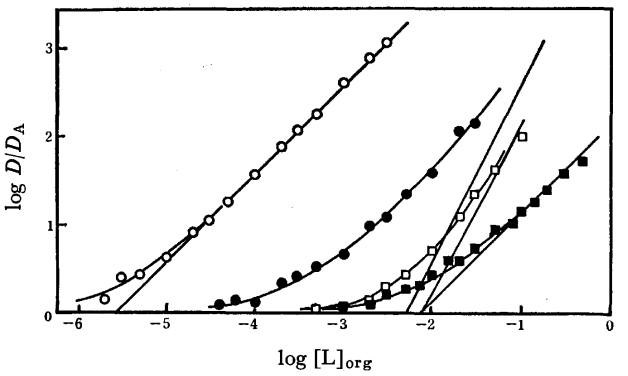

Fig. 2. Enhancement of Ag(I)-TTA extraction by an addition of one of the three ligands into $CHCl_3$. ○: quinoline, ●: TOPO, ■: TBP. Enhancement of Ag(I) caproate extraction by an addition of TOPO (□) into $CHCl_3$ is also shown.

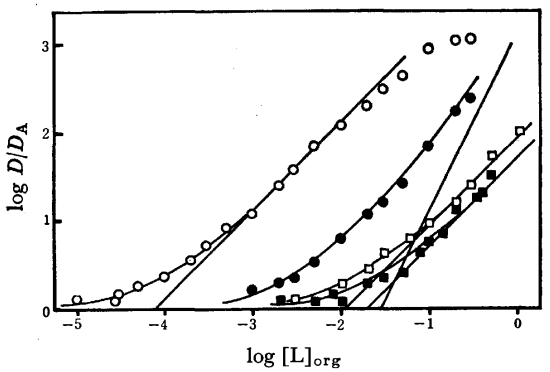

Fig. 3. Enhancement of Ag(I)-TTA extraction by an addition of one of the three ligands into $CHCl_3$. ○: 1-hexene, ●: mesitylene, ■: toluene. Enhancement of Ag(I) caproate extraction by an addition of 1-hexene (□) into $CHCl_3$ is also shown.

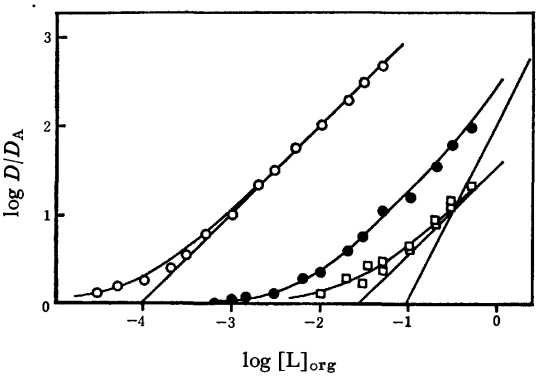

Fig. 4. Enhancement of Ag(I)-TTA extraction by an addition of one of the three ligands into $CHCl_3$. ○: cyclohexene, ●: *o*-xylene, □: benzene.

5) T. Sekine and Y. Hasegawa, "Solvent Extraction Research," ed. by A. S. Kertes and Y. Marcus, John Wiley & Sons (1969) p. 289.

6) J. C. Reid and M. Calvin, *J. Amer. Chem. Soc.* **72**, 2948 (1950).

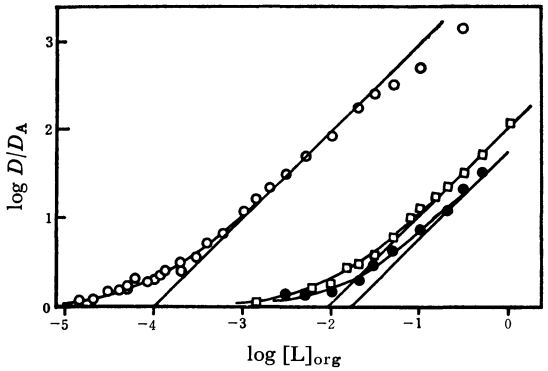

Fig. 5. Enhancement of Ag(I)-TTA extraction by an addition of one of the two ligands into $CHCl_3$. ○: 1-pentene, ●: *p*-xylene. Enhancement of Ag(I) caproate extraction by an addition of cyclohexene (□) into $CHCl_3$ is also shown.

of the molecular complex-forming ligand to the chloroform phase. By the curve-fitting, it was concluded that both the first and second complexes are formed with *o*-xylene, mesitylene, and TOPO, while only the first complex is formed with the other ligands. The stability constants of these complexes were determined from the parameters of the fitted standard curve; they are given in Table 2. Table 2 also lists the literature stability constants of silver(I) complexes with these ligands in an aqueous solution.

Caproate Extraction. The extraction of silver(I) with the caproate ion into chloroform is also poor. The distribution ratio was found to be only $10^{-2.29}$ even when the concentration of the caproate ion is

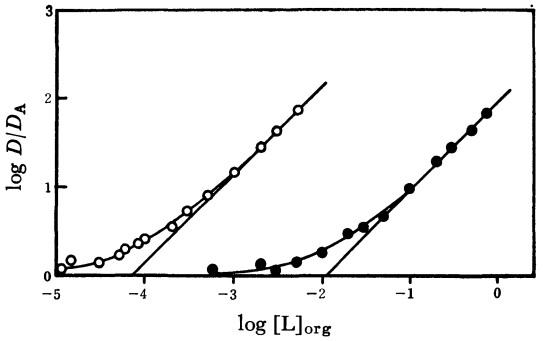

Fig. 6. Enhancement of Ag(I)-TTA extraction by an addition of one of the two ligands into $CHCl_3$. ○: 1-heptene, ●: *m*-xylene.

0.1 M.[12] This extraction is also enhanced by the addition of 1-hexene, cyclohexene, or TOPO. Figures 2, 3, and 5 also show the enhancement of the silver(I) caproate extraction caused by these ligands. The data were analyzed by the curve-fitting method. The constants thus obtained are also listed in Table 2.

Discussion

The results in Fig. 1 and Table 1 show that the stability of the silver(I) complex with the TTA anion in the aqueous phase is rather small and that the distribution constant of the silver(I)-TTA chelate between chloroform and the aqueous phase is very small. It is known that β-diketones are not effective extractants for silver(I) (see, for example, Ref. 13). This seems

TABLE 2. STABILITY CONSTANTS FOR THE MOLECULAR COMPLEXES OF Ag(I)–TTA CHELATE AND Ag(I)–CAPROATE IN CHLOROFORM OR FOR SILVER COMPLEXES IN AQUEOUS 1 M (K, Ag)NO_3 SOLUTIONS WITH SOME π-DONORS AND *n*-DONORS AT 25°C

Donors	Present work (in chloroform)				From literature (in aqueous soln.)		Ref.
	AgTTA		AgCap.		Ag^+		
	$\log \beta_{1(org)}$	$\log \beta_{2(org)}$	$\log \beta_{1(org)}$	$\log \beta_{2(org)}$	$\log \beta_1$	$\log \beta_2$[a]	
Propene	—	—	—	—	1.94	—	7
1-Butene	—	—	—	—	2.08	—	8
1-Pentene	4.01	—	—	—	—	—	
1-Hexene	4.11	—	1.96	—	2.93	—	9
1-Heptene	4.12	—	—	—	—	—	
Cyclohexene	4.03	—	2.15	—	1.90	—	9
Benzene	1.55	—	—	—	0.38	−0.29	10
Toluene	1.70	—	—	—	0.47	−0.20	10
o-Xylene	2.17	2.12	—	—	0.46	−0.04	10
m-Xylene	1.94	—	—	—	0.48	−0.01	10
p-Xylene	1.78	—	—	—	0.42	−0.06	10
Mesitylene	2.56	3.08	—	—	0.26	—	11
TBP	2.15	—	—	—	—	—	
TOPO	3.58	4.20	2.73	4.26	—	—	
Quinoline	5.56	—	4.65[b]	—	—	—	

a) The stability constant is given as $\beta_2=[Ag_2L^{2+}]/[Ag^+]^2[L]$. b) Taken from Ref. 12.

7) C. K. N. Trueblood and H. J. Lucas, *J. Amer. Chem. Soc.*, **74**, 1338 (1952).
8) F. R. Hepner, K. N. Trueblood and H. J. Lucas, *ibid.*, **74**, 1333 (1952).
9) S. Winstein and H. J. Lucas, *ibid.*, **60**, 836 (1938).
10) L. J. Andrews and R. M. Keefer, *ibid.*, **71**, 3644 (1949).
11) L. J. Andrews and R. M. Keefer, *ibid.*, **72**, 5034 (1950).
12) T. Sekine and D. Dyrssen, unpublished data.
13) J. Stary, "The Solvent Extraction of Metal Chelates," Pergamon Press, Oxford (1964).

to be because of this small distribution constants of of the silver(I) chelate. Since this distribution constant of the silver(I)-TTA chelate is much lower than that of the acid-form TTA (the distribution constant of TTA between chloroform and a 0.1 M sodium perchlorate solution has been reported to be 71[5]), it is assumed that the silver(I) ion in the TTA chelate interacts with water molecules in the aqueous phase rather strongly.

The results in Table 2 can be summarized as follows: (i) In all cases, the molecular complexes of silver(I) combined with the thenoyltrifluoroacetonate ion in chloroform are more stable than those with the caproate ion in chloroform and those of the silver(I) ion in aqueous solutions. (ii) The stabilities of the molecular complexes of the silver(I) TTA chelate with the three unsaturated aliphatic hydrocarbons and with cyclohexene are similar to one another. (iii) The stabilities of the molecular complexes with the aromatic hydrocarbons increase as the number of the methyl group increases. Among the three xylenes, the stability becomes larger in this order: ortho-, meta-, and para-xylene. On the other hand, the stability constants of the molecular complexes of Ag^+ in an aqueous solution with these ligands are not very different. (iv) The three n-donors also form stable molecular complexes. TOPO forms more stable complexes than does TBP, and quinoline forms the most stable first complex. (v) The stabilities of the molecular complexes of silver(I)-caproate with cyclohexene are similar to that of the silver(I) cyclohexene complex in an aqueous solution, but the molecular complex with 1-hexene in chloroform is somewhat less stable than the corresponding complex in the aqueous phase.

Although no information has been obtained about the structure of the complexes from only these distribution data, there is no doubt that TOPO, TBP, and quinoline form complexes through the lone-pair electrons on the oxygen or nitrogen atom, whereas the unsaturated hydrocarbons form complexes with the π-electrons.

It is remarkable that these donors form more stable complexes with the silver(I)-TTA chelate in chloroform than with the silver(I) ion in aqueous solutions. In the chloroform phase, the silver(I) in the TTA chelate is probably combined with the TTA anion through the lone-pair electrons on the two oxygens in the anion. At the same time, it is possible that both the complex and the ligand in the chloroform phase are combined with some molecules of water. In an aqueous solution, the silver(I) ion is probably hydrated with several water molecules; the ligands may also interact with some water molecules. The complex formation and the interaction of the silver atom and of the ligand with other molecules probably interfere with the formation of the molecular complexes to some extent. The stability constants are affected by many factors; thus, it seems to be very difficult to estimate the contributions of the interactions of TTA or of water molecules on the silver(I) or on the ligands. However, since the stability constants of the molecular complexes in the chloroform phase are much higher, even though the silver(I) is coordinated with TTA, the effect of the interactions with water molecules is probably very large.

In the present study, chloroform was employed as the organic solvent. However, as has been pointed out on the basis of various pieces of evidence, this solvent interacts with these molecular complex-forming ligands and probably also with the silver(I)-TTA chelate more strongly than do many other inert solvents, such as saturated hydrocarbons or carbon tetrachloride, and the stabilities of various molecular complexes in this solvent are usually lower than in the above other inert solvents. For example, in the adduct formation of various metal chelates with organophilic neutral ligands in solvent extraction systems, the stabilities of the molecular complexes are larger in carbon tetrachloride than in chloroform.[14] Thus, the stabilities of the molecular complexes studied in the present paper may also be larger in other non-polar solvents. It has also been reported that the stability of the molecular complexes of Ag^+ with alkenes is much lower in ethylene glycol than in water.[2] This can not be compared with the present results, however, because this alcohol may also interact with the silver(I) and with the donors.

It may be reasonable to assume that the length of the hydrocarbon chain does not have any significant effect on the stabilities of the molecular complexes with the 1-alkenes, as can be seen in the cases of many ther chemical properties. At the same time, it may also be reasonable to assume that the stabilities of the molecular complexes increase in the order of the increase in the density of the π-electrons in the aromatic ring; a similar order of the stabilities was pointed out among the complexes between Ag^+ and substituted benzenes in an equivalent molar mixture of water and methyl alcohol.[15] There seems to be no reasonable explanation of why this tendency of the stability of the molecular complexes does not appear in the complexes of Ag^+ with the same ligands in water (*cf.* Table 2).

The molecular complexes of various metal chelates, especially of TTA chelates, with these three n-donors have been determined from the enhancement of the metal-chelate extraction in solvent extraction systems, which is called "synergism".[14] It is known that TOPO forms more stable adducts than does TBP. However, it was found that quinoline forms a less stable adduct with europium(III)-TTA chelates in chloroform than does TOPO or TBP;[16] this seems to indicate that the stability order of adducts with ligands coordinating through an oxygen atom and through a nitrogen atom can be different when the central metal ion is different.

Carboxylic acids are said to form no chelate type complexes with various metal ions. Thus, the interaction

14) T. V. Healy, "Solvent Extraction Research" ed. by A. S. Kertes and Y. Marcus, Wiley-Interscience, New York (1969) p. 257.

15) N. Ogimachi, L. J. Andrews and R. M. Keefer, *J. Amer. Chem. Soc.*, **78**, 2210 (1956).

16) T. Sekine and D. Dyrssen, *J. Inorg. Nucl. Chem.*, **29**, 1475 (1967).

17) T. Sekine, Y. Hasegawa, and N. Ihara, *ibid.*, in press.

of silver(I) with the caproate anion should be weaker than in a complex with the TTA anion. This difference in the nature of the bond between silver(I) and the adjacent anion may cause a difference in the stability of the molecular complex of silver(I) with the donors studied in this work. However, since only the formation of molecular complexes with quinoline,[12] and that of cyclohexene, 1-hexene, and TOPO complexes with silver(I) caproate, have been studied, no final conclusion can be drawn with regard to this interesting problem; further information is necessary in order to make a detailed discussion.

The synergism due to the molecular complex formation has been studied in many metal chelate extraction systems by using various n-donors. It is very remarkable that the silver(I)-TTA chelate shows a synergism with both n-donors and π-donors. Such molecular complexes of silver(I) with π-donors can be used for some analytical purpose. For example, although the extraction of silver(I) with β-diketones in an inert solvent is usually poor,[13] the addition of 1×10^{-3} M quinoline makes the extraction quantitative, as may be seen from Fig. 1. When aromatic solvents such as benzene are used as the diluents of TTA, silver(I) can also be extracted nearly quantitatively (more than 90%).

The chelate extraction of silver(I) has often been carried out with dithizone or oxine. The dithizone extraction is excellent and is favorable for the colorimetry of silver, but it is interferred by many ions. The oxine extraction, on the other hand, is comparable with the present TTA extraction into, for example, benzene.[13] However, the oxine extraction is not very specific. The metal extraction with TTA is also not very specific. However, since only a few metal ions form π-complexes with aromatic hydrocarbons, the synergism of TTA extraction with aromatic hydrocarbons may occur in only a few cases. Thus, when a sample solution containing various metal ions is pretreated by extraction with TTA in chloroform ($[A^-]<10^{-2}$ M), only silver(I) and a small number of metal ions may remain in the aqueous phase; thus, when the solution is shaken twice with benzene or toluene containing 0.1 M TTA (and $[A^-]\simeq10^{-2}$ M), only silver(I) will be extracted from the residue in the aqueous phase, while the other metal ions, such as alkaline earths, will remain in the aqueous phase. Such an extraction method seems to be quite favorable for the separation of silver(I) from among many other metal ions.

BULLETIN OF THE CHEMICAL SOCIETY OF JAPAN, VOL. 46, 1188—1195 (1973)

The Oxidation of Iron(II) by Molecular Oxygen Catalyzed by Chloride Ion, Thiocyanate Ion, and Ethylenediamine in Dimethyl Sulfoxide

Yuriko UNNO and Goro WADA*

Department of Chemistry, Nara Women's University, Nara 630

(Received August 3, 1972)

The rates of the oxidation reactions of iron(II) to iron(III) by molecular oxygen in DMSO were measured under the catalyses of Cl^-, SCN^-, and en. The rate was proportional to the partial pressure of oxygen and was of the second order to [Fe(II)] in catalyses of Cl^- and SCN^-, while it was of the first order to [Fe(II)] in catalysis of en. The reaction rate was also linear to $[X]^2$ and $[H^+]$, where X represents Cl^- or SCN^-, indicating that the reaction proceeds via both the electron-transfer and hydrogen-atom-transfer mechanisms, side by side. The reaction order of [Fe(II)] depends upon which step is rate-determining among those of the oxygenation of Fe(II), its spontaneous decomposition, and its bimolecular reaction with another Fe(II) and, therefore, may be variable according to the concentrations of the reacting species. The autoxidation rate can be affected by the kinds of the catalyzing ligands. The autoxidation may be slow when an Fe(II) complex with low spin is oxidized to an Fe(III) complex with high spin and may be fast when from high spin type to low spin one. In the present cases of Cl^-, SCN^-, and en in DMSO, it seems to go from high spin type to high spin one with moderately large rates.

The autoxidation of iron(II) proceeds considerably slow in acidic aqueous solutions being catalyzed by a variety of existing anions and molecules as coordinating ligands. The rate equations for the oxidation of iron(II) in aqueous media are expressed in the first order with respect to the concentration of iron(II) when $H_2PO_4^-$,[1,2] $H_2P_2O_7^{2-}$,[2,3] F^-,[4] Cl^-,[5] ethylenediaminetetraacetic acid (EDTA),[6] or one of other specific chelating ligands[7,8] is present in the reaction system, while they are of the second order with respect to that of iron(II) when either of NO_3^-,[9] SO_4^{2-},[10,11]

* To whom correspondence should be addressed.

1) M. Cher and N. Davidson, *J. Amer. Chem. Soc.*, **77**, 793 (1955).

2) J. King and N. Davidson, *ibid.*, **80**, 1542 (1958).

3) S. Utsumi and K. Muroshima, *Nippon Kagaku Zasshi*, **86**, 593 (1965).

4) J. Weiss, *Experimentia*, **9**, 61 (1953).

5) A. M. Posner, *Trans. Faraday Soc.*, **49**, 382 (1953).

6) Y. Kurimura, R. Ochiai, and N. Matsuura, This Bulletin, **41**, 2234 (1968).

7) Th. Kaden, D. Walz, and S. Fallab, *Helv. Chim. Acta*, **43**, 1639 (1960).

8) Th. Kaden and S. Fallab, *ibid.*, **44**, 714 (1961).

9) J. R. Pound, *J. Phys. Chem.*, **43**, 955 (1939).

10) A. B. Lamb and L. W. Elder, *J. Amer. Chem. Soc.*, **53**, 137 (1931).

11) R. E. Huffman and N. Davidson, *ibid.*, **78**, 4836 (1956).

or ClO_4^- [12] is present in the reaction system, although ClO_4^- ion does not necessarily act as a coordinating ligand.

George pointed out[13] that the one-electron-transfer mechanism proposed first by Haber and Weiss[14,15] was not satisfactory to explain the cases in which the reaction took place at a rate of the second order with respect to the iron(II) concentrations. Weiss, then, revised his mechanism and extended it to the so-called two-electron-transfer mechanism. George, on the other hand, showed an idea on another novel mechanism of hydrogen-atom-transfer in which the oxidation occurred via transfer of a hydrogen atom from a water molecule coordinated with an iron(II) ion to FeO_2^{2+}, instead of considering a radical mechanism.[12] Fallab discussed the autoxidation of various transition metal ions by molecular oxygen on the basis of the redox potentials of oxygen.[16]

The autoxidation of iron(II) in alcohols is known to occur much faster than that in aqueous solutions,[17] although those in other non-aqueous solutions than alcohols are not known yet. In the present research, therefore, the reactions in dimethyl sulfoxide (DMSO) as catalyzed by Cl^-, SCN^- ions and ethylenediamine (en) were investigated. As the results, the reaction proceeded at a rate proportional to $[Fe(II)]^2$ when it was catalyzed by Cl^- or SCN^- ion, and at one proportional to [Fe(II)] when catalyzed by en. The reaction schemes in each case in DMSO will be developed below.

Experimental

Materials. Commercial DMSO was distilled in a reduced atmosphere of nitrogen at about 3 mmHg, dried over activated alumina overnight to remove water, distilled again in the same way as before, and stocked for use. Sodium chloride, ammonium thiocyanate, ammonium perchlorate, and sodium perchlorate of the guaranteed reagent grade were recrystallized twice from water. Ethylenediamine of the guaranteed reagent grade was used without further purification. Perchloric acid in DMSO was prepared by passing a DMSO solution of ammonium perchlorate through a column charged with cation-exchange resin Dowex 50 of H-type. Iron(II) perchlorate was prepared by dissolving pure iron wire in perchloric acid and recrystallizing it under an atmosphere of nitrogen to protect it from oxidation.

Procedure. The reaction was initiated by mixing a solution of iron(II) perchlorate in DMSO with that containing one of the catalyzing substances, Cl^-, SCN^- ion or en, and perchloric acid in DMSO. Two methods were adopted for the kinetic measurements. In a flow-method, air or a mixed gas of oxygen and nitrogen at various ratios was let to flow into the reaction solution at a constant flow rate and aliquots were taken out of the solution into quenching solutions for analyses at appropriate time intervals. When Cl^- ion or en was adopted as a catalyst, α,α′-bipyridyl was contained in the quenching solutions, forming $Fe(bipy)_3^{2+}$ at once which not only interupted further progress of the reaction but also was used for the spectrophotometric determination of iron(II) concentration at 522 nm at the individual reaction times. When SCN^- ion was adopted as a catalyst, on the other hand, aliquots of the reaction solution were diluted into a definite amount of water to slow down the reaction velocity and were soon used for the spectrophotometric determination of iron(III) concentration in the form of thiocyanato complex at 470 nm.

As a second method, a Warburg apparatus was used for the volumetric pursuit of oxygen gas consumed by oxidation. The procedure for the initiation of the reaction was the same with that of the flow method.

The ionic strength and the temperature of the reaction systems were always kept constant at 0.2 M and 25 °C respectively.

Photometry. A Hitachi-Perkin-Elmer UV-VIS spectrophotometer Model 139 and a Hitachi Recording spectrophotometer Model EPS-3T were used for the optical determinations of the concentrations of iron species and for the measurements of the absorption spectra of reaction solutions, respectively.

Results and Discussion

Catalyses by Cl^- and SCN^- Ions. Under a constant partial pressure of oxygen, p, the relationship of $(1/[Fe(II)]-1/[Fe(II)]_0)$ *vs.* time, t, was linear for reactions catalyzed by Cl^- or SCN^- ion, as is shown in Fig. 1, as an example at $[Fe(II)]_0=2\times10^{-2}$ M, $p=$ 0.2 atm, $\mu=0.2$ M, and 25°C, and at various $[Cl^-]$ and $[H^+]_0$. Here, $[Fe(II)]_0$ and $[H^+]_0$ represent the initial concentrations of Fe(II) and H^+. These linearities indicate that the reaction proceeds in the second order of the concentration of iron(II). When the partial pressure of oxygen, p, was varied under a fixed reaction condition except p, another proportionality between the reaction rate and p was recognized,

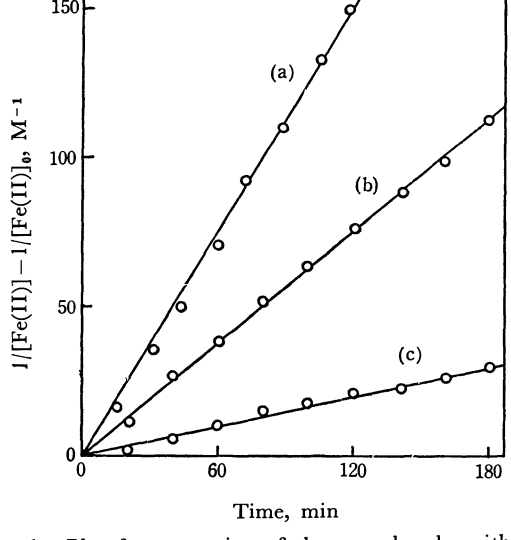

Fig. 1. Plot for a reaction of the second order with respect to [Fe(II)] at $[Fe(II)]_0=2.00\times10^{-2}$ M, $p=0.2$ atm., $\mu=0.2$ M, and 25°C.
(a) $[Cl^-]=3.52\times10^{-2}$ M, $[H^+]_0=3.00\times10^{-2}$ M
(b) $[Cl^-]=2.73\times10^{-2}$ M, $[H^+]_0=5.00\times10^{-2}$ M
(c) $[Cl^-]=1.82\times10^{-2}$ M, $[H^+]_0=1.00\times10^{-2}$ M

12) P. George, *J. Chem. Soc.*, **1954**, 4349.
13) P. George, *Adv. Catalysis*, **4**, 367 (1952).
14) F. Haber and J. Weiss, *Proc. Roy. Soc. Ser. A*, **147**, 332 (1934).
15) J. Weiss, *Naturwissenschaften*, **23**, 64 (1935).
16) S. Fallab, *Angew. Chem.*, **79**, 500 (1967).
17) J. R. Pound, *J. Phys. Chem.*, **43**, 969 (1939).

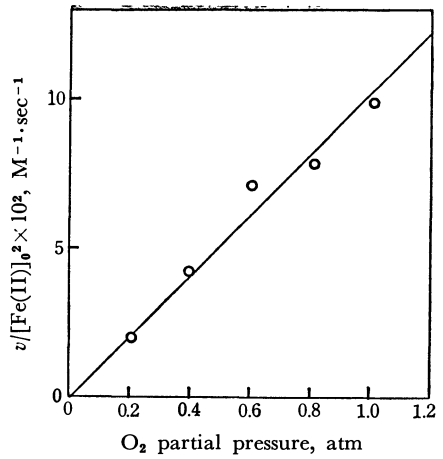

Fig. 2. The proportionality of the reaction rate with the partial pressure of oxygen at $[Fe(II)]_0 = 2.00 \times 10^{-2}$ M, $[Cl^-] = 3.50 \times 10^{-2}$ M, $[H^+]_0 = 3.00 \times 10^{-2}$ M, $\mu = 0.2$ M, and 25°C.

indicating that the reaction is of the first order with respect to p. This is shown in Fig. 2. Similar relationships were also observed in the case of SCN^- catalysis. Thus, the reaction rate equation for the both catalytic reactions is expressed in the form:

$$v = -\frac{d[Fe(II)]}{dt} = kp[Fe(II)]^2 \qquad (1)$$

The mole ratio of the reacting iron(II) to the consumed oxygen was found to be 4 : 1, indicating that one molecule of oxygen oxidizes four ions of iron(II) to iron(III). The spectral changes during the reaction supported this stoichiometric relation. A spectrum of an acidic solution containing iron(II) after the completion of the reaction coincided well with that containing iron(III) at the same concentration, as shown in Fig. 3. Therefore, the overall chemical equation of the reaction is written as follows:

$$4Fe(II) + O_2 + 4H^+ \rightarrow 4Fe(III) + 2H_2O \qquad (2)$$

The rate constant, k, defined in Eq. (1) was also observed to be dependent upon the concentrations of both acid and catalyzing ions. Approximate linear relationships of k with $[Cl^-]^2$ at various $[H^+]_0$ and with $[H^+]_0$ at various $[Cl^-]$ are shown in Figs. 4 and 5, respectively, although their linearities look like worse than those revised by theoretical treatment below.

The stoichiometry of the reaction in the case of SCN^- ion and the dependence of k upon $[SCN^-]^2$ and $[H^+]_0$ were quite similar to the case of Cl^- ion, although their plots corresponding to Figs. 1—5 are not shown here.

Reaction Schemes for Cl^- and SCN^- Catalyses. Since the reaction proceeds at rates linearly depending upon $[X]^2$ and $[H^+]_0$, k can be expressed empirically as below, where X stands for Cl^- or SCN^- and A, B, C,

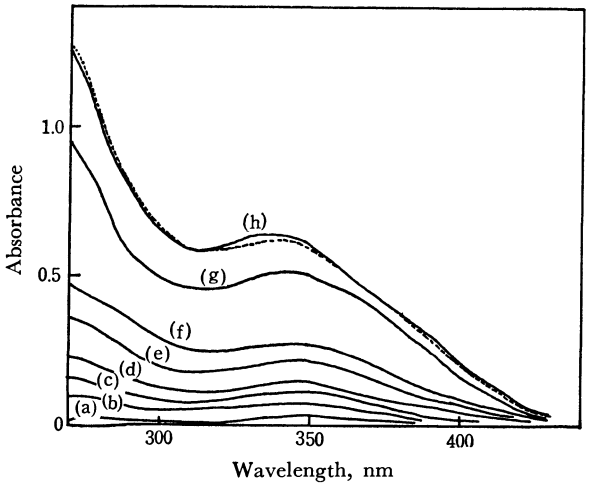

Fig. 3. Spectral changes during the reaction to complete oxidation at $[H^+]_0 = 1.00 \times 10^{-2}$ M, $[Cl^-] = 2.00 \times 10^{-2}$ M, and $\mu = 0.2$ M.
Solid curves: $[Fe(II)]_0 = 1.00 \times 10^{-4}$ M at times after the initiation of the reaction (a) 7 min, (b) 74 min, (c) 135 min, (d) 200 min, (e) 330 min, (f) 460 min, (g) 1400 min, (h) ∞
Dotted curve: $[Fe(III)] = 1.00 \times 10^{-4}$ M

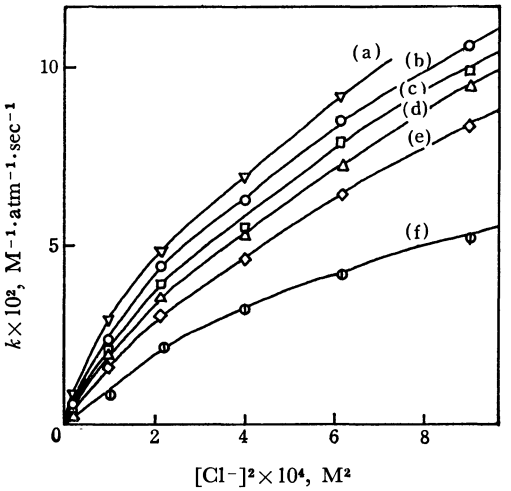

Fig 4. Relations between k and $[Cl^-]^2$ at $[Fe(II)]_0 = 2.00 \times 10^{-2}$ M, $\mu = 0.2$ M, and 25°C.
(a) $[H^+]_0 = 1.00 \times 10^{-1}$ M (b) $[H^+]_0 = 7.00 \times 10^{-2}$ M
(c) $[H^+]_0 = 5.00 \times 10^{-2}$ M (d) $[H^+]_0 = 3.00 \times 10^{-2}$ M
(e) $[H^+]_0 = 1.00 \times 10^{-2}$ M (f) $[H^+]_0 = 1.00 \times 10^{-3}$ M

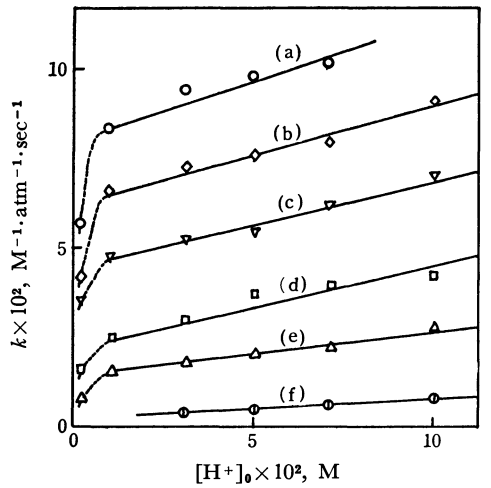

Fig. 5. Relations between k and $[H^+]_0$ at $[Fe(II)]_0 = 2.00 \times 10^{-2}$ M, $\mu = 0.2$ M, and 25°C.
(a) $[Cl^-] = 3.00 \times 10^{-2}$ M (b) $[Cl^-] = 2.50 \times 10^{-2}$ M
(c) $[Cl^-] = 2.00 \times 10^{-2}$ M (d) $[Cl^-] = 1.50 \times 10^{-2}$ M
(e) $[Cl^-] = 1.00 \times 10^{-2}$ M (f) $[Cl^-] = 5.00 \times 10^{-3}$ M

and D are constants:

$$k = A + B[X]^2 + C[H^+] + D[H^+][X]^2 \quad (3)$$

The following four paths from (a) through (d) are reasonably deduced corresponding to the respective four terms on the right-hand side of Eq. (3).

(a) $Fe^{2+} + O_2 \overset{K_0}{\rightleftharpoons} FeO_2^{2+}$ (a1)

$FeO_2^{2+} + Fe^{2+} \overset{k_a}{\longrightarrow} [Fe.O_2.Fe]^{4+}$

$\longrightarrow Fe^{3+} + O_2^{2-} + Fe^{3+}$ (a2)

(b) $Fe^{2+} + X^- \overset{K_1}{\rightleftharpoons} FeX^+$ (b1)

$FeX^+ + O_2 \overset{K_0'}{\rightleftharpoons} XFeO_2^+$ (b2)

$XFeO_2^+ + FeX^+ \overset{k_b}{\longrightarrow} [X.Fe.O_2.Fe.X]^{2+}$

$\longrightarrow FeX^{2+} + O_2^{2-} + FeX^{2+}$ (b3)

(c) $Fe^{2+} + O_2 \overset{K_0}{\rightleftharpoons} FeO_2^{2+}$ (c1), (a1)

$Fe^{2+} + H^+ \overset{K_H}{\rightleftharpoons} FeSH^{3+}$ (c2)

$FeO_2^{2+} + FeSH^{3+} \overset{k_c}{\longrightarrow} [Fe.O_2.HS.Fe]^{5+}$

$\longrightarrow Fe^{3+} + HO_2^- + Fe^{3+}$ (c3)

(d) $Fe^{2+} + X^- \overset{K_1}{\rightleftharpoons} FeX^+$ (d1), (b1)

$FeX^+ + O_2 \overset{K_0'}{\rightleftharpoons} XFeO_2^+$ (d2), (b2)

$FeX^+ + H^+ \overset{K_H'}{\rightleftharpoons} HSFeX^{2+}$ (d3)

$XFeO_2^+ + HSFeX^{2+} \overset{k_d}{\longrightarrow} [X.Fe.O_2.HS.Fe.X]^{3+}$

$\longrightarrow FeX^{2+} + HO_2^- + FeX^{2+}$ (d4)

Equilibrium constants and rate constants appearing in the individual steps are represented by respective symbols in the equations, and S stands for DMSO as solvated with iron ions which functions as a proton acceptor. The bracketed species shown in every path means activated complexes.

In the whole reaction, these four paths may be prevailing in parallel with one another; (a) and (b) involve two electron-transfer processes from two Fe(II) ions to an O_2, and (c) and (d) involve, on the other hand, a hydrogen-atom-transfer process from an Fe(II) to an O_2 as well as an electron-transfer process from another Fe(II) to the same O_2, producing O_2^{2-} and HO_2^- respectively.

The common products of the above reactions, O_2^{2-} and HO_2^-, will be followed by further reactions of their own, being finally reduced to H_2O in order to hold the stoichiometry as shown in the reaction (2).

(t) $O_2^{2-} + H^+ \longrightarrow HO_2^-$ (t1)

$HO_2^- + H^+ \longrightarrow H_2O_2$ (t2)

$H_2O_2 + Fe(II) \longrightarrow OH + OH^- + Fe(III)$ (t3)

$OH + Fe(II) \longrightarrow OH^- + Fe(III)$ (t4)

$H^+ + OH^- \longrightarrow H_2O$ (t5)

Thus, the overall rate constant of the reaction is expressed in a following form:

$$k = \frac{k_aK_0 + k_bK_0'K_1^2[X]^2 + k_cK_0K_H[H^+] + k_dK_0'K_H'K_1^2[H^+][X]^2}{\{1 + K_1[X] + K_H[H^+] + K_H'K_1[H^+][X] + K_0[O_2] + K_0'K_1[X][O_2]\}^2} \quad (4)$$

where the last two terms appearing in the denominator of the right-hand side of Eq. (4) are negligibly small as compared to the rest ones in it, because the solubilities of oxygen in the reaction media, $[O_2]$, are very small.[18]

When the denominator of the right-hand side of Eq. (4) is denoted by d^2 for brevity, kd^2, instead of k itself, should be linearly dependent upon $[X]^2$ at constant $[H^+]_0$ and upon $[H^+]_0$ at constant $[X]$.

$$kd^2 = 4k_aK_0 + 4k_bK_0'K_1^2[X]^2 + 4k_cK_0K_H[H^+] + 4k_dK_0'K_H'K_1^2[H^+][X]^2 \quad (5)$$

If d does not vary much within the concentration ranges of $[X]$ and $[H^+]_0$ employed under the present consideration, k will also show approximately linear relationships with $[X]^2$ and $[H^+]$, which are the cases of Eq. (3) and Figs. 4 and 5. In the case of Cl^- ion catalyst, the values of $K_1 = 20\ M^{-1}$ and $K_H = K_H' = 5\ M^{-1}$ give best fits for the linearities of kd^2 with $[Cl^-]^2$ and $[H^+]_0$, which are drawn in Figs. 6 and 7. As are clearly recognized in the figures, the linearities in Figs. 4 and 5 are fairly revised to give those in Figs. 6 and 7, respectively. In Fig. 7, the curves fail from the linearities at very low concentrations of hydrogen ion below 1.00×10^{-2} M, where the steps as controlled by $[H^+]$ might be rate-determining.

The straight lines at various hydrogen ion concentrations in Fig. 6 will give intercepts and slopes, indicating as follows:

$$\text{Intercept} = 4k_aK_0 + 4k_cK_0K_H[H^+] \quad (6)$$

$$\text{Slope} = 4k_bK_0'K_1^2 + 4k_dK_0'K_H'K_1^2[H^+] \quad (7)$$

Plotting of those slopes against $[H^+]$ will also give a

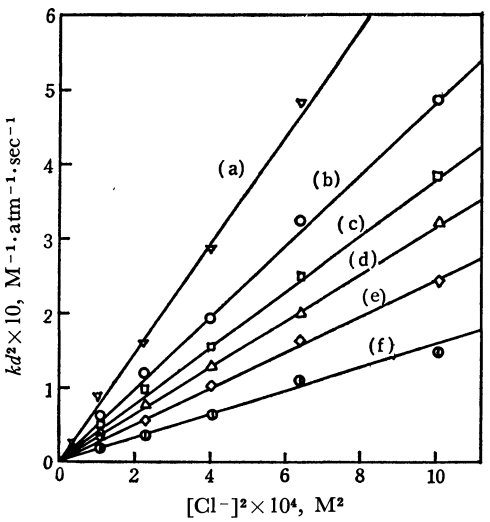

Fig. 6. Relations between kd^2 and $[Cl^-]^2$ at the same conditions with Fig. 4.

18) T. Fujinaga, K. Izutsu, and T. Adachi, This Bulletin, **42**, 140 (1969).

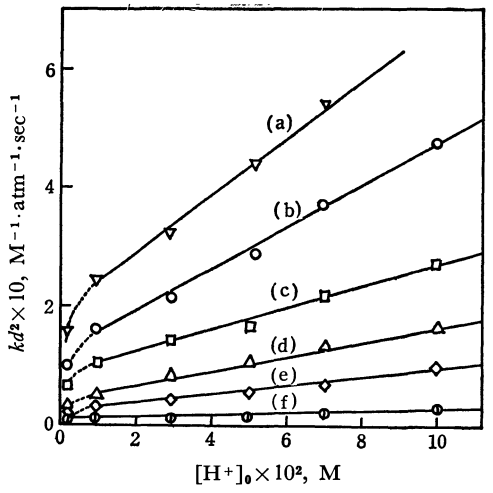

Fig. 7. Relations between kd^2 and $[H^+]_0$ at the same conditions with Fig. 5.

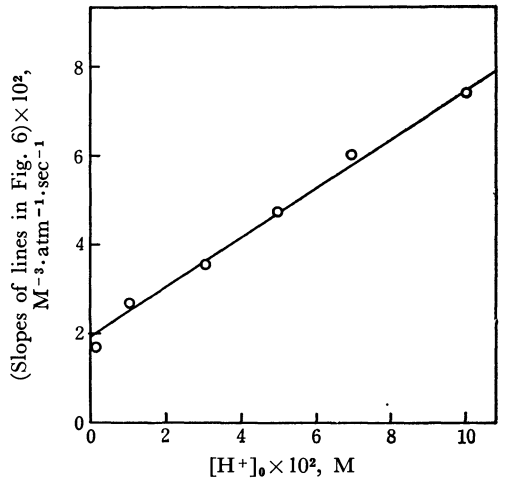

Fig. 8. Linear relationship of the slopes in Fig. 6 *vs.* $[H^+]_0$.

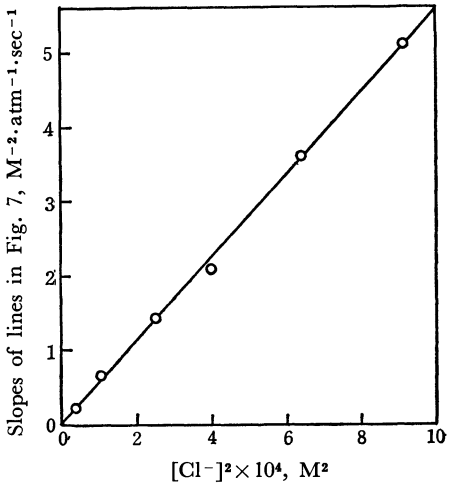

Fig. 9. Linear relationship of the slopes in Fig. 7 *vs.* $[Cl^-]^2$.

straight line having an intercept $4k_bK_0'K_1^2$ and a slope $4k_dK_0'K_H'K_1^2$, as shown in Fig. 8.

In quite a similar way, the straight lines in Fig. 7 give slopes at different Cl^- ion concentrations, and those slopes have also a linear relationship with $[Cl^-]^2$, as shown in Fig. 9. The intercept and the slope in Fig. 9 correspond to $4k_cK_0K_H$ and $4k_dK_0'K_H'K_1^2$, respectively.

Table 1. Various rate and equilibrium constants in the cases of Cl^- and SCN^- ions used as catalysts

Constants $M^{-1}\cdot atm^{-1}\cdot sec^{-1}$	Catalysts	
	Cl^-	SCN^-
k_aK_0	~0	~0
k_bK_0'	1.3×10^{-1}	7.5×10^{-3}
k_cK_0	1.0×10^{-3}	1.0×10^{-3}
k_dK_0'	6.8×10^{-1}	4.2×10^{-2}

Various linearities are similarly noticed in the case of SCN^- ion as a catalyst, as well as in that of Cl^- ion. Thus, constants obtained directly by means of the least-squares method from Eq. (5) are summarized in Table 1 in both catalysts. In the case of SCN^- ion, the values of $K_1=10\ M^{-1}$ and $K_H=K_H'=5\ M^{-1}$ were adopted for the best linearities.

Since neither K_0 nor K_0' can be estimated at the present stage, we have to compare rate constants multiplied by K_0 or K_0'. Fortunately, nevertheless, the ratios k_d/k_b are found to be almost equal, being 5.2 in Cl^- and 5.6 in SCN^-. It is worth noticing that, although the rate constant at each path seems smaller in SCN^- than in Cl^-, the acceleration ratio, k_d/k_b, of the oxidation due to the participation of the hydrogen-atom-transfer mechanism is approximately the same in both catalysts. Of course, k_a and k_c are indifferent to the kind of catalyzing ions because no catalyst is involved in the reaction scheme (a) and (c), and this is definitely proved by the results in the table, k_aK_0 and k_cK_0 being nearly zero and $1.0\times10^{-3}\ M^{-1}\cdot atm^{-1}\cdot sec^{-1}$ in both systems.

Catalysis by Ethylenediamine and its Reaction Scheme. When en is added in the reaction system, the oxidation reaction goes much faster than the cases catalyzed by Cl^- and SCN^- ions. Figure 10 indicates that the reaction is of the first order with respect to [Fe(II)] under

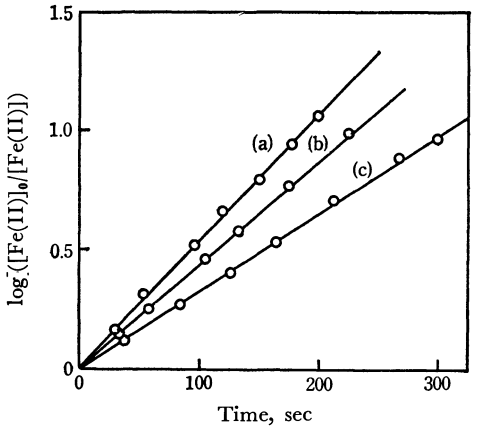

Fig. 10. Plot for a reaction of the first order with respect to [Fe(II)] at $[Fe(II)]_0=2.00\times10^{-2}$ M, $p=0.2$ atm, $\mu=0.2$ M, and 25 °C.
(a) $[en]_0=9.00\times10^{-2}$ M, $[H^+]_0=1.00\times10^{-2}$ M
(b) $[en]_0=1.20\times10^{-1}$ M, $[H^+]_0=3.00\times10^{-2}$ M
(c) $[en]_0=1.05\times10^{-1}$ M, $[H^+]_0=5.00\times10^{-2}$ M

a constant partial pressure of oxygen, because log-[Fe(II)] decreases linearly with the lapse of reaction time, being in contrast with the cases of Cl^- and SCN^- ions. The dependence of the reaction rate upon the partial pressure of oxygen, p, was found to be in a proportional correlation, as equally to the cases of Cl^- and SCN^- ions. Therefore, the rate equation is established as:

$$v = kp[\mathrm{Fe(II)}] \tag{8}$$

The absorption spectra of a reaction solution containing iron(II) and en were observed to vary with time and finally to agree with those of iron(III) at the same concentration with the initial one of iron(II). This observation shows that the reaction only goes by simple oxidation of iron(II) to iron(III) without any further chemical changes of the substances involved. The rate of consumption of oxygen also showed the stoichiometry of the overall reaction to be quite the same with the cases of Cl^- and SCN^- ions, as represented by Eq. (2).

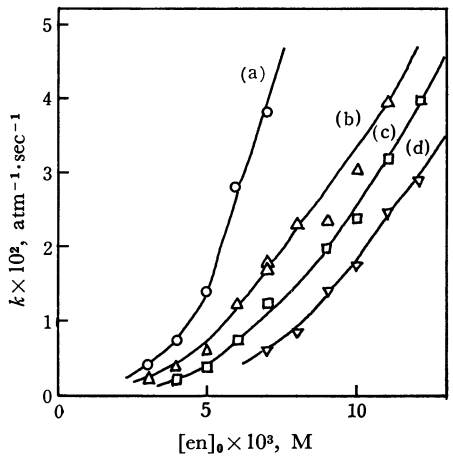

Fig. 11. The dependence of k upon $[en]_0$ and $[H^+]_0$ at $p=0.2$ atm, $\mu=0.2$ M, and 25 °C.
(a) $[H^+]_0=2.00\times10^{-3}$ M (b) $[H^+]_0=3.00\times10^{-3}$ M
(c) $[H^+]_0=4.00\times10^{-3}$ M (d) $[H^+]_0=6.00\times10^{-3}$ M

The apparent rate constant k in Eq. (8) is affected by the concentrations of both en and acid; the higher the concentration of en and the lower that of acid, the larger the rate constant, as is shown in Fig. 11. Judging from these experimental facts, the following reaction scheme (e) can be deduced in addition to those of (a) and (c), although the contribution due to (a) and (c) may be negligibly small.

(e) $\mathrm{Fe^{2+} + en \overset{K_1}{\rightleftharpoons} Fe.en^{2+}}$ (e1), (b1)

$\mathrm{Fe.en^{2+} + O_2 \overset{K_0'}{\rightleftharpoons} en.FeO_2^{2+}}$ (e2), (b2)

$\mathrm{en.FeO_2^{2+} \overset{k_e}{\longrightarrow}}$ (e3)

$\mathrm{en.FeO_2^{2+} + Fe.en^{2+} \longrightarrow}$ (e4)

$\mathrm{en + H^+ \overset{K_e}{\rightleftharpoons} enH^+}$ (e5)

Since the reaction is of the first order with respect to [Fe(II)], either the forward reaction of (e2) or (e3) may be rate-determining, with the rate constant k_0' or k_e, respectively. If (e2) is rate-determining, it may be followed by (e3) and/or (e4), and if (e3) is so, (e4) must not occur and (e2) establishes an equilibrium. Whichever the rate-determining step may be, they will produce O_2^{2-} and will be succeeded similarly by the reactions as shown in (t). Thus, k is expressed as follows:

$$k = \frac{EK_1[\mathrm{en}]}{1+K_1[\mathrm{en}]} \tag{9}$$

in which E represents $4k_0'$ or $4k_1K_0'$ according to whether the rate-determining step is (e2) or (e3). When the total concentration of en is expressed by $[en]_0$, the concentration of free en is defined approximately by

$$[\mathrm{en}]_0 = (1+K_e[H^+]+K_1[Fe^{2+}])[\mathrm{en}] \tag{10}$$

The values of log K_e in aqueous media is as large as about 10.[19] Although DMSO is more basic than water in nature,[20] log K_e in DMSO can be regarded to be still so large as compared with $(1+K_1[Fe^{2+}])$ and $K_1[en]_0$. Then, k is rewritten as:

$$k = \frac{EK_1[\mathrm{en}]_0}{K_e[H^+]} \tag{11}$$

At constant total acid concentrations, $[H^+]_0$, the hydrogen ion concentration $[H^+]$ decreases with increasing $[en]_0$. This is the reason why k exhibits no rigorous linear relationship with $[en]_0$ but a trend of abrupt increase with increasing $[en]_0$ as shown in Fig. 11. From the slope of the curve at very low $[en]_0$, EK_1/K_e is roughly estimated to be 3.5×10^{-4} $atm^{-1}\cdot sec^{-1}$.

General Consideration on the Order of the Reaction with Respect to [(Fe(II)]. In a reaction system, FeL^{2+}, $FeSH^{3+}$, and $HSFeL^{3+}$ can be considered to exist in individual equilibria with their composing species, where L stands for one of the catalyzing ligands, Cl^-, SCN^-, or en. If any one of these iron(II) complexes is simply denoted by Fe(II), the reaction schemes as have been described above are generalized as follows:

$$\mathrm{Fe(II) + O_2 \xrightarrow{(A)} Fe(II).O_2 \overset{(B)}{\underset{(C)}{\nearrow\!\searrow}} +Fe(II)}$$

Depending upon the rates of the reaction of passing the steps, (A), (B), and (C), there may possibly come out the following three cases:

(i) (A)<(B), (C)

(ii) (A)>(B), (C), and (B)≫(C)

(iii) (A)>(B), (C), and (B)≪(C)

The rate-determining step will be (A), (B), or (C) according to the case (i), (ii), or (iii), respectively. In the cases (i) and (ii), the reaction is of the first order with respect to [Fe(II)], while in the case of (iii), it is of the second order with respect to [Fe(II)]. When Cl^- and SCN^- ions are employed as ligands, the case (iii) must actually happen because of the fact that the reaction is of the second order. When en is used, on

19) "Stability Constants of Metal-Ion Complexes," ed. by L. G. Sillén and A. E. Martell, The Chemical Society Special Publication No. 17 (1964), p. 370.

20) G. Wada, This Bulletin, **42**, 890 (1969).

the other hand, the case must be (i) or (ii) although it is not decided yet which it is, at the present stage.

By taking into account all of the possible elementary reactions of the schemes from (a) through (e), and by using the steady-state method for the species appearing as intermediates, a set of probable elementary reactions and a rate equation can be drawn out as follows:

$$Fe^{2+} + L \rightleftharpoons FeL^{2+} \quad (K_1) \quad (b1, d1, e1)$$

$$Fe^{2+} + H^+ \rightleftharpoons FeSH^{3+} \quad (K_H) \quad (c2)$$

$$FeL^{2+} + H^+ \rightleftharpoons HSFeL^{3+} \quad (K_H') \quad (d3)$$

$$Fe^{2+} + O_2 \overset{k_0}{\rightleftharpoons} FeO_2^{2+} \quad (K_0) \quad (a1, c1)$$

$$FeL^{2+} + O_2 \overset{k_0'}{\rightleftharpoons} LFeO_2^{2+} \quad (K_0') \quad (b2, d2, e2)$$

$$FeO_2^{2+} \xrightarrow{k_1}$$

$$LFeO_2^{2+} \xrightarrow{k_e} \quad (e3)$$

$$FeO_2^{2+} + Fe^{2+} \xrightarrow{k_a} \quad (a2)$$

$$LFeO_2^{2+} + FeL^{2+} \xrightarrow{k_b} \quad (b3, e4)$$

$$FeO_2^{2+} + FeSH^{3+} \xrightarrow{k_c} \quad (c3)$$

$$LFeO_2^{2+} + HSFeL^{3+} \xrightarrow{k_d} \quad (d4)$$

$$v = \frac{4p\{\alpha + (\beta/\delta)[Fe(II)]\}\gamma[Fe(II)]}{\{\alpha + (\beta/\delta)[Fe(II)] + \gamma\}\delta} \quad (12)$$

$$\alpha = k_1K_0 + k_eK_0'K_1[L] \quad (13)$$

$$\beta = k_aK_0 + k_bK_0'K_1^2[L]^2 + k_cK_HK_0[H^+] + k_dK_H'K_0'K_1^2[H^+][L]^2 \quad (14)$$

$$\gamma = k_0 + k_0'K_1[L] \quad (15)$$

$$\delta = 1 + K_H[H^+] + K_1[L] + K_H'K_1[H^+][L] \quad (16)$$

Under limiting conditions, the following extreme three cases can be derived, corresponding to the three ones, (i), (ii), and (iii) respectively, as mentioned above and Eq. (12) results in typically simple forms.

(i) If $\alpha + (\beta/\delta)[Fe(II)] \gg \gamma$,

$$v = \frac{4\gamma}{\delta}p[Fe(II)] \quad (17), (8)$$

(ii) If $\alpha + (\beta/\delta)[Fe(II)] \ll \gamma$ and $\alpha \gg (\beta/\delta)[Fe(II)]$

$$v = \frac{4\alpha}{\delta}p[Fe(II)] \quad (18), (8)$$

(iii) If $\alpha + (\beta/\delta)[Fe(II)] \ll \gamma$ and $\alpha \ll (\beta/\delta)[Fe(II)]$

$$v = \frac{4\beta}{\delta^2}p[Fe(II)]^2 \quad (19), (1)$$

Equation (19) coincides with the empirical rate equation (1), which was seen in the cases of Cl^- and SCN^- catalysts, while Eqs. (17) and (18) coincide with the empirical one (8) under the catalysis of en.

In the cases (i) and (ii), it is possible to distinguish whether Eq. (17) or (18) is actually available, in the following manner. When [Fe(II)] is made larger, Eq. (17) remains unchanged as a function of the first order of [Fe(II)], while Eq. (18) becomes no longer useful and the reaction order with respect to [Fe(II)] gradually grows higher up to the second order, with increasing [Fe(II)]. Even in the case (iii), on the other hand, the reaction order may fall down from the second order to the first at the extremely low value of [Fe(II)] as is easily understood from Eq. (19). Unfortunately, we could not realize these extreme cases at very high and very low [Fe(II)] due to the experimental difficulties. Anyway, it is worth noticing that the reaction order is not definitely specific nor characteristic to the catalyzing ligands but depends upon their reaction conditions; a similar kind of thing to this is also known in the Lindemann mechanism in which a reaction of the first order at a certain concentration may become to be of the second order at a lower concentration than that with respect to a reacting species. Therefore, the order of the reaction itself is not essentially important, unless the reaction conditions are rigorously taken into account.

Ligand and Solvent Effects upon the Reaction Rates of Oxidation. Aquocobalt(II) ion in aqueous solution is thermodynamically stable and is, therefore, impossible to be oxidized to cobalt(III). However, when Co(II) is coordinated with ammonia,[21] en,[22] or histidine,[23] it forms a high spin complex which acts as an oxygen carrier and is rapidly oxidized to a Co(III) complex of low spin. In the cases of iron complexes, it is known that $Fe(bipy)_3^{2+}$ and $Fe(phen)_3^{2+}$ which are of low spin complexes in aqueous solution are very stable and inert against oxidation, whereas another low spin complex of iron(II), $Fe(CN)_6^{4-}$, is easily oxidized to produce $Fe(CN)_6^{3-}$ which is also of a low spin complex. The overall formation constants, $\log\beta$, of $Fe(bipy)_3^{2+}$, $Fe(phen)_3^{2+}$, and $Fe(CN)_6^{4-}$ are 17.6,[24] 21,[25] and 24[26] respectively, and those for their oxidized states are unknown for $Fe(bipy)_3^{3+}$ and 14.1 and 31 for $Fe(phen)_3^{3+}$ [25] and $Fe(CN)_6^{3-}$ [26], respectively. The oxidation of iron(II), therefore, results in the decrease in stabilities in the cases of bipy and phen complexes, while it results in the increase in stability in the case of cyano complex. This is likely to be the reason why only the cyano complex undergoes a rapid oxidation. Kurimura and others[6] found out that there exists a linear relationship between $\log k$ and $\log[\beta(III)/\beta(II)]$ among many iron complexes coordinated with organic ligands of various polyaminoacetic and other acids, where k, $\beta(III)$, and $\beta(II)$ stand for rate constant of oxidation reaction, overall formation constants of iron(III) and iron(II) complexes, respectively. This relationship is, in other words, a linear relation between the activation free energies and the thermodynamical standard free energies of the reaction, similar cases to which are also observed in the electron transfer reactions between iron(II) and iron(III) complexes coordinated with

21) J. Simplicio and R. G. Wilkins, *J. Amer. Chem. Soc.*, **91**, 1325 (1969).
22) F. Miller, J. Simplicio, and R. G. Wilkins, *ibid.*, **91**, 1962 (1969).
23) M. S. Michailidis and R. B. Martin, *ibid.*, **91**, 4683 (1969).
24) P. Krumholz, *Anais. Acad. Brasil de Cienco*, **22**, 2484 (1950).
25) T. S. Lee, I. M. Kolthoff, and D. L. Leussing, *J. Amer. Chem. Soc.*, **70**, 2348, 3596 (1948).
26) C. C. Stephenson and J. C. Morrow, *ibid.*, **78**, 275 (1956).

Table 2. Types of changes in electronic structures associated with the oxidation Fe(II)→Fe(III)

Types	Electronic configurations Fe(II) → Fe(III)	Examples of ligands
L→H	$t_{2g}^6e_g^0 \rightarrow t_{2g}^3e_g^2$	
L→L	$t_{2g}^6e_g^0 \rightarrow t_{2g}^5e_g^0$	CN^-, phen, bipy
H→H	$t_{2g}^4e_g^2 \rightarrow t_{2g}^3e_g^2$	en, Cl^-, SCN^-, H_2O
H→L	$t_{2g}^4e_g^2 \rightarrow t_{2g}^5e_g^0$	

various ligands.[27]

Summarizing the above-described considerations, as long as the linear free energy relation is available, four types of the autoxidation reaction in connection with the electronic structures of the reactants and products can be deduced, as shown in Table 2. On the basis of stability variations involved in the course of oxidation, a change in the electronic configuration from low spin to high spin (L→H) might be most difficult to take place, while a change of the reverse direction (H→L) might occur most easily, although such cases have not been found yet. Examples of L→L type are seen in the cases of bipy, phen, and CN^- ion, among which the former two are slow and the latter is fast.

The formation constants, log K_1, of $FeCl^{2+}$ and $FeSCN^{2+}$ in DMSO have been measured as 3.6 [28] and 2.9,[29] although those of iron(II) species with the same ligands were not determined due to their low stabilities. Moreover, those of Fe–en complexes for both oxidation states in DMSO are not known either. In spite of such lacks of data, it may be safely said that the autoxidation catalyzed by these three ligands, en, Cl^-, and SCN^- ions, in DMSO proceeds via H→H type, with moderately large reaction rates in the sequence of en>Cl^->SCN^-, being faster than L→H type and slower than H→L one.

The solvent effect that the reaction proceeds much faster in DMSO than in water can be attributed to the larger differences in the formation constants of the iron complexes between the two oxidation states in DMSO than those in water. The electrostatic repulsion between ions of like signs is clearly larger in DMSO of a lower dielectric constant than in water of a higher one. This effect should contribute toward the reaction disadvantageously and make the reaction proceed slower in DMSO than in water, this being not the case though. Consequently, the latter effect in repulsion must be conquered by the former in stability after all.

The authors are grateful to the Ministry of Education of Japan for a financial support.

27) K. Bächmann and K. H. Lieser, "Exchange Reactions," International Atomic Energy Agency, Vienna (1965), p. 29.
28) G. Wada, This Bulletin, **41**, 882 (1968).
29) G. Wada, N. Yoshizawa, and Y. Sakamoto, *ibid.*, **44**, 1018 (1971).

BULLETIN OF THE CHEMICAL SOCIETY OF JAPAN, VOL. 46, 1195—1198 (1973)

The Preparation and Spectroscopic Properties of Fumaronitrile Complexes of Palladium(0) and Platinum(0)

Keinosuke SUZUKI and Hideshi OKUDA

Inorganic Chemistry Laboratory, Faculty of Science, Nagoya University, Chikusa, Nagoya 464

(Received Septembet 11, 1972)

Fumaronitrile complexes, $M(FMN)(AsPh_3)_2$ (M=Pd, Pt and FMN=fumaronitrile), have been prepared. Various chelating agents replaced $AsPh_3$ in the complexes, giving M(FMN)L (L is a chelating agent containing N, P, or As as donor atoms). The chemical shift of the methine protons of these complexes increased in the order:

$$Pd\text{–}As < Pd\text{–}P < Pt\text{–}As < Pt\text{–}P.$$

This is probably the increasing order of the π-back donation in these complexes. The UV spectra of the complexes are also described.

In recent years, olefin complexes of transition metals in the low oxidation state have been the subjects of many studies.[1] These investigations have established that stable complexes are formed with olefins containing electronegative substituents (activated olefin). Fumaronitrile is a typical activated olefin and is expected to give stable complexes of Pd(0) and Pt(0). However, only two complexes, $Pd(FMN)(PPh_3)_2$[2] and $Pt(FMN)(PPh_3)_2$,[3] have been reported so far. In this paper we will describe the preparation, spectroscopic properties, and some ligand-exchange reactions of fumaronitrile complexes of zero-valent Pd and Pt. The effect of a donor atom, N, P, or As, on the metal-olefin bonding will also be discussed.

Results and Disucssion

Preparation and Ligand-exchange Reactions. The complex $Pt(FMN)(AsPh_3)_2$ was prepared by the reac-

1) B. Nelson and H. B. Jonassen, *Coord. Chem. Rev.*, **6**, 27 (1971) and refs. therein.

2) G. L. McClure and W. H. Baddley, *J. Organometal. Chem.*, **27**, 155 (1971).

3) G. La Monica, G. Navazio, P. Sandorini, and S. Cenini, *ibid.*, **31**, 89 (1971).

tion of $Pt(AsPh_3)_4$ with FMN in benzene. A corresponding palladium complex, $Pd(FMN)(AsPh_3)_2$, was synthesized by the reduction of $PdCl_2(AsPh_3)_2$ with hydrazine monohydrate in the presence of FMN. The similar reduction of $PdCl_2(PPh_3)_2$ also gave the complex $Pd(FMN)(PPh_3)_2$ reported by MaClure *et al.*[2]

The reactivities of these two arsine complexes towards bidentate ligands are very similar except for the reaction with the ligands (N–N) containing two nitrogen donor atoms. As is shown in the Scheme, all of the ligands (N–N) studied here replaced $AsPh_3$ in $Pd(FMN)(AsPh_3)_2$, thus forming Pd(FMN)(N–N), but only ethylenediamine (en) and cyclohexanediamine (cyhn) could react with $Pt(FMN)(AsPh_3)_2$. The other three ligands failed to replace $AsPh_3$ in the complex. Two factors are conceivable to explain the difference in their reactivities: the pK values and the steric factors of the bidentate ligands(N–N). Steric factors do not seem to be serious in the present case, because cyhn reacts with both palladium and platinum complexes; also two ligands, bipy and o-phen, replace $AsPh_3$ in $Pt(CF_2{=}CF_2)(AsPh_3)_2$, thus giving $Pt(CF_2{=}CF_2)L$ (L is bipy, o-phen), as has been reported by Kemmitt and Moore.[4] As is clear from Table 1, the pK values of en and cyhn are larger than those of the other three ligands. Thus, it may be reasonable to assume that the pK values of the ligands (N–N) are important in the ligand-exchange reactions studied here. The replacement of $AsPh_3$ in the perfluoroolefin complex may be due to the strong *trans*-effect of perfluoroolefin, which weakens the Pt–As bond and makes the substitution of $AsPh_3$ by the ligand with a small pK value possible.

Table 1. The pK values of bidentate ligands (N–N)[a]

	en	cyhn	o-phen	2,9-phen	bipy
pK_1	9.87	9.99(*trans*) 9.89(*cis*)	4.92	6.15	4.49

a) L. G. Sillen and A. E. Martell ed., "Stability Constants," Special Publication No. 17, The Chemical Society, London (1964).

$Pd(FMN)(EPh_3)_2$ (E=P, As) reacts with $SbPh_3$ to give white precipitates. The porduct of E=P was identified as $Pd(SbPh_3)_2(PPh_3)_2$ as reported by Takahashi *et al.*[5] on the basis of its analytical data and decomposition point. The analytical data of the compound of E=As corresponds to $Pd(SbPh_3)_3(AsPh_3)$, and the presence of $SbPh_3$ and $AsPh_3$ in the complex was confirmed by its far-infrared spectrum, which gave absorptions at 455(s), 270(s), and 260(s) cm^{-1} assignable to $SbPh_3$ and 472(m), 325(m), and 315(m) cm^{-1} assignable to $AsPh_3$.

PMR Spectra. The PMR spectra of fumaronitrile complexes were measured in $CDCl_3$, with TMS as the internal standard; the data are summarized in Table 2. Unfortunately, the spectra of the complexes formed with a bidentate ligand (N–N) were not obtained because of their low solubility in common organic solvents. As is clear from Table 2, the olefinic protons show the large high-field shift which is characteristic of the olefin coordinated to a transition metal in the low-oxidation state. The chemical shifts increased in the order:

$$Pd\text{-}As < Pd\text{-}P < Pt\text{-}As < Pt\text{-}P$$

for both monodenate ligands (PPh_3 and $AsPh_3$) and bidentate ligands (P–P and As–As), although the shifts of the complexes with monodentate ligands are always larger than those of the corresponding chelates. Cenini *et al.*[6] related this shift to the amount of π-back donation from the metal to the ligand. Therefore, the order seems to indicate the increasing ability of π-back donation of the ME_2 system (M=Pd, Pt and E=P, As).

Table 2. The PMR spectral data of the CH of fumaronitrile (FMN) and its complexes in $CDCl_3$ (23°C)

Complex	τ(CH)(ppm)	J(P-H)(Hz)	J(Pt-H)(Hz)
FMN	3.70(s)		
$Pd(FMN)(PPh_3)_2$	7.01(d)	4.5	
Pd(FMN)(P-P)	6.71(d)	6.8	
$Pd(FMN)(AsPh_3)_2$	6.65(s)		
$Pd(FMN)(As\text{-}As)_2$	6.10(s)		
$Pt(FMN)(PPh_3)_3$	7.54(dt)	6.4	59
Pt(FMN)(P-P)	7.23(dt)	7.8	62
$Pt(FMN)(AsPh_3)_2$	7.19(t)		68
Pt(FMN)(As-As)	6.93(t)		70

s=singlet, d=doublet, dt=doublet of triplet, t=triplet.

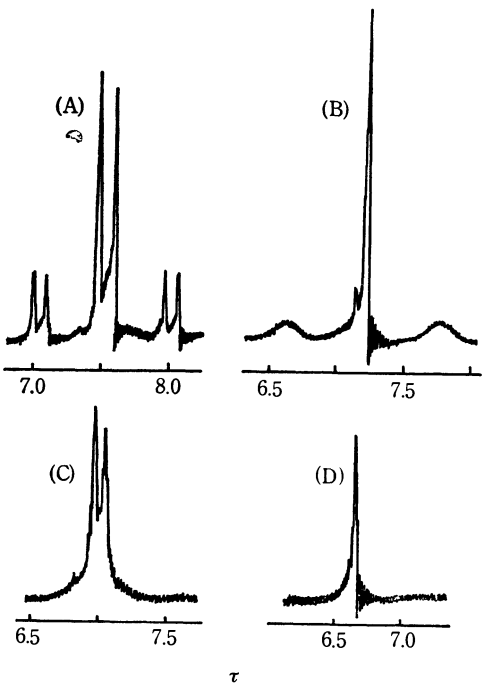

Fig. 1. The PMR spectra of the CH of the complexes M(FMN)L.
(A) $Pt(FMN)(PPh_3)_2$, (B) $Pt(FMN)(AsPh_3)_2$,
(C) $Pd(FMN)(PPh_3)_2$, (D) $Pd(FMN)(AsPh_3)_2$.

4) R. D. W. Kemmitt and R. D. Moore, *J. Chem. Soc., A*, **1971**, 2472.

5) S. Takahashi, K. Sonogashira, and N. Hagihara, *Nippon Kagaku Zasshi*, **87**, 610 (1966).

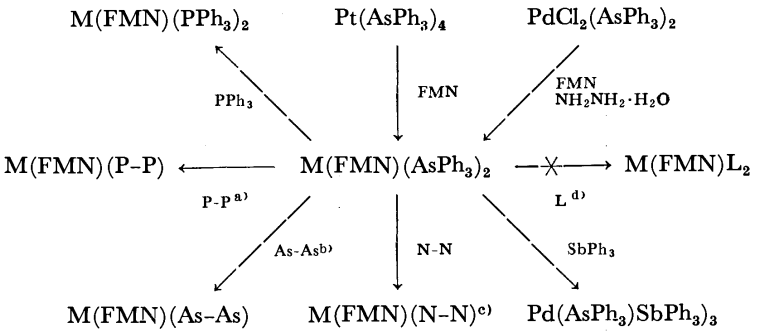

a) P-P=$Ph_2PCH_2CH_2PPh_2$
b) As-As=$Ph_2AsCH_2CH_2AsPh_2$
c) M=Pd N-N=αα′-bipyridyl (bipy), 1,10-phenanthroline (o-phen), 2,9-dimethyl-1,10-phenanthroline (2,9-phen), ethylenediamine (en), cyclohexanediamine (cyhn)
M=Pt N-N=en, cyhn
d) L=pyridine, SPh_2, $S(CH_3)_2$

Scheme.

one phosphorus atom is coupled with the methine protons, as is shown in Fig. 1, although the coupling of two phosphorus atoms to ^{19}F or ^{1}H has been reported in the complexes $Pt(CF_2{=}CF_2)(PPh_3)_2$[7], $Pt(CH_2{=}CH_2)(PPh_3)_2$[8], and $Pt(RC{\equiv}CH)(PPh_3)_2$.[1] Similar results are also obtained for $Pt(FMN)(PPh_3)_2$[3] and some other olefin complexes.[6] The phosphorus atom which couples with a methine proton is probably *trans* to the carbon atom of the methine group, as has been suggested by Cenini *et al.*[6] It is likely that the appearance of a doublet in our complexes is due to the small coupling constant of a *cis*-phosphorus atom with the olefinic proton, since Greaves *et al.*[9] observed that the 60 MHz spectrum of the methyl protons of $Pt(MeC{\equiv}CPh)(PPh_3)_2$ gave only a doublet, while the 100 MHz spectrum split the methyl doublet into symmetrical doublets.

The satellites of the complex $Pt(FMN)(AsPh_3)_2$ are very broad, but its central peak is sharp, as is shown in Fig. 1. A similar phenomenon is also observed in the PMR spectrum of $Pt(CH_2{=}CClCN)(AsPh_3)_2$.[10] Recently Mann *et al.*[11] reported the complex behaviour of the satellites of $Pt_2Cl_2(2\text{-methylallyl})_2$ with the temperature; they suggested the possibility of a partial contribution of a relaxation phenomenon of the platinum-195 nucleus. A similar consideration might explain the phenomenon observed here.

In the platinum complexes, J(Pt–H) was *ca.* 60 Hz for the phosphine complexes and ca. 70 Hz for the arsine complexes (Table 2). A decrease in J(Pt–H) with the change from As to P has also been reported for *trans*-$[Pt(Me)L(PMe_2Ph)_2]$ (L=PPh_3, $AsPh_3$).[12] This order is expected on the basis of the fact that

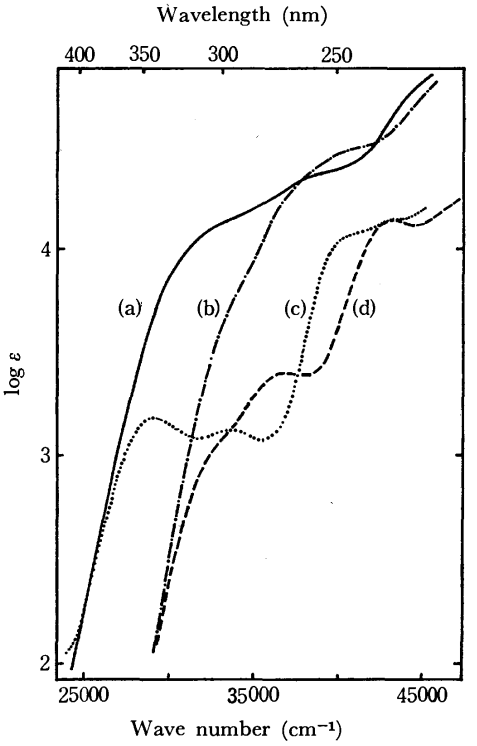

Fig. 2. The UV spectra of the complexes M(FMN)L.
(a) $Pd(FMN)(PPh_3)_2$, (b) $Pt(FMN)(AsPh_3)_2$,
(c) Pd(FMN)(cyhn), (d) Pt(FMN)(cyhn).

J(Pt–C–H) seems to have a close relation with the s-character of Pt,[13] and the Pt(6s) character in the Pt–olefin bond will be decreased by the coordination of a better σ-donor atom, as has been discussed by Church and Mays,[14] although Nelson and Jonassen[1] suggested that the contributions from terms other than the Fermi contact term are important.

UV Spectra. The UV spectra of M(FMN)(cyhn) (M=Pd, Pt) are shown in Fig. 2. Similar spectra are also obtained for the complexes M(FMN)(en). The bands in the 25000—38000 cm^{-1} region arise from the complex formation, because FMN do not show strong

6) S. Cenini, R. Ugo, and G. La Monica, *J. Chem. Soc., A*, **1971**, 409.
7) M. Green, R. B. L. Osborn, A. J. Rest, and F. G. A. Stone, *ibid.*, **1968**, 2525.
8) P. -T. Cheng, C. D. Cook, S. C. Nyburg, and K. Y. Wan, *Inorg. Chem.*, **10**, 2210 (1971).
9) E. O. Greaves, C. J. L. Lock, and P. M. Maitlis, *Can. J. Chem.*, **46**, 3879 (1968).
10) K. Suzuki and H. Okuda, This Bulletin, **45**, 1938 (1972).
11) B. E. Mann, B. L. Shaw, and G. Shaw, *J. Chem. Soc., A*, **1971**, 3536.
12) H. C. Clark and J. D. Ruddick, *Inorg. Chem.*, **9**, 1226 (1970).
13) F. H. Allen and A. Pidcock, *J. Chem. Soc., A*, **1968**, 2700. J. D. Ruddick and B. L. Shaw, *ibid.*, **1969**, 2801.
14) M. J. Church and M. J. Mays, *ibid.*, **1970**, 1938.

Table 3. Analytical data

M(FMN)L		Mp(dp) (°C)	Found (%)			Required (%)		
M	L		C	H	N	C	H	N
Pd	$(PPh_3)_2$	130—140	67.3	4.6	4.0	67.8	4.6	4.0
Pd	$(AsPh_3)_2$	155—165	60.1	4.1	3.5	60.3	4.1	3.5
Pd	(P-P)	170—185	61.6	4.7	4.6	61.8	4.5	4.8
Pd	(As-As)	190—205	53.7	3.8	4.0	53.7	3.9	4.2
Pd	bipy	155—165	47.9	2.7	15.7	49.4	3.0	16.5
Pd	o-phen	225—235	52.4	2.6	15.1	52.7	2.8	15.4
Pd	2,9-phen	235—245	54.8	3.7	14.2	55.1	3.6	14.3
Pd	en	120—130	29.3	4.1	22.6	29.5	4.1	22.9
Pd	cyhn	150—158	40.7	5.2	18.0	40.2	5.4	18.8
Pt	$(PPh_3)_2$	200—210	59.5	3.9	2.9	60.2	4.0	3.5
Pt	$(AsPh_3)_2$	179—185	53.7	3.6	2.6	54.3	3.6	3.2
Pt	(P-P)	250—255	53.5	3.8	4.1	53.7	3.9	4.2
Pt	(As-As)	200—210	47.8	3.7	4.3	47.4	3.5	3.7
Pt	en	230—242	22.6	3.2	17.5	21.6	3.0	16.8
Pt	cyhn	226—241	31.8	4.2	14.5	31.0	4.2	14.5

absorptions below 42000 cm^{-1}. Since the formal charge of Pd and Pt in the complexes is zero, these bands are probably due to charge transfer from the metal d-orbitals to the FMN π^*-orbital. In their spectroscopic study of *trans*-[(ol)$PtCl_2L$] (ol=olefin), Denning *et al.*[15] also reported that the transitions from metal d-orbitals to olefin π^* are observed in the 31000—45000 cm^{-1} range. The molar extinction coefficients of M(FMN)(cyhn) also support the above assignment, because they are $\sim 10^3$ and comparable to those reported for *trans*-[(ol)$PtCl_2L$].[15,16] For the other complexes studied here we could not find any bands assignable to charge transfer from metal d-orbitals to FMN π^* or vacant d-orbitals of a phosphorus atom[17] because of the strong absorption of the ligand other than FMN (Fig. 2).

Experimental

The PMR spectra were recorded with a JEOL-C-60H spectrometer. The UV spectra were recorded with a HITACHI 323 spectrophotometer, using acetonitrile as the solvent. All the reagents were commercially available and were used without further purification. The $Pd(PPh_3)_4$,[18] $Pt(PPh_3)_4$,[19] and $Pt(AsPh_3)_4$[20] were prepared by the methods reported in the literature.

Fumaronitrilebis(triphenylarsine)palladium(O). To an ethanol solution of $AsPh_3$ (3.2 g) we added an aqueous solution of K_2PdCl_4 (1.6 g) at 50—60°C. Fumaronitrile (0.5 g) and then 10 ml of an ethanol solution of $NH_2NH_2 \cdot H_2O$ (10%) were added slowly to the mixture at 50—60°C. About 20 min later, the pale yellow products were filtered off and washed with water, ethanol, and diethyl ether.

Fumaronitrilebis(triphenylarsine)platinum(O). $Pt(AsPh_3)_4$ (2.1 g) was stirred into a benzene solution (100 ml) of FMN (0.2 g). After the complete dissolution of the $Pt(AsPh_3)_4$, the solution was filtered and concentrated to about 10 ml *in vacuo*. The white precipitates formed by adding methanol were filtered off and washed with diethyl ether.

Fumaronitrile-1,2-bis(diphenylarsino)ethanepalladium(O). A solution of 1,2-bis(diphenylarsino)ethane (0.6 g) in benzene (20 ml) was added to a solution of $Pd(FMN)(AsPh_3)_2$ (0.8 g) in benzene (50 ml) at room temperature. The solution turned pale yellow; by adding ethanol to the concentrated solution, pale yellow materials were precipitated. Recrystallization from chloroform–diethyl ether gave pale yellow crystallines.

In a similar manner, Pd(FMN)(P-P), Pt(FMN)(As-As), and Pt(FMN)(P-P) were prepared.

Fumaronitrile(α,α'-bipyridyl)palladium(O). To a solution of $Pd(FMN)(AsPh_3)_2$ (0.8 g) in benzene (60 ml), we added a solution of α,α'-bipyridyl (0.3 g) in benzene (40 ml) at room temperature. The solution turned yellow-green and then gave pale yellow precipitates. It was filtered and washed with benzene. By analogous methods, Pd(FMN)L was prepared (L is o-phen and 2,9-phen).

Fumaronitrile(ethylendiamine)palladium(O). To a solution of $Pd(FMN)(AsPh_3)_2$ (0.8 g) in benzene (60 ml), we added a solution of ethylenediamine (0.1 ml) in benzene (40 ml). White materials started to precipitate in a few minutes. After the mixture had been stirred for 1 hr, the precipitates were filtered off and washed with benzene. Pt(FMN)(en), Pd(FMN)(cyhn) and Pt(FMN)(cyhn) were prepared in a similar way.

Triphenylarsinetris(triphenylantimony)palladium(O). A solution of triphenylantimony (1.4 g) in benzene (40 ml) was added to a solution of $Pd(FMN)(AsPh_3)_2$ (0.8 g) in benzene (60 ml) at room temperature. The solution turned yellow and then gave white precipitates. After 1 hrs' stirring, the precipitates were filtered off and washed with benzene and ether. Found: C, 58.0; H, 3.8.% Calcd for $C_{72}H_{60}AsPdSb_3$: C, 58.8, H, 4.1%.

The analytical data for the fumaronitrile complexes are summarized in Table 3.

15) R. C. Denning, F. R. Hartley, and L. M. Venanzi, *ibid.*, **1967**, 1322.
16) C. K. Jorgensen, "Absorption Spectra and Chemical Bonding in Complexes," Pergamon, Oxford (1962).
17) J. Chatt, G. A. Gamlen, and L. E. Orgel, *J. Chem. Soc.*, **1959**, 1047.
18) D. T. Rosevear and F. G. A. Stone, *J. Chem. Soc., A*, **1968**, 164.
19) W. L. Jolly, "Inorganic Syntheses" Vol. 11, McGraw-Hill, New York (1968), P. 105.
20) L. Malatesta and C. Cariello, *J. Chem. Soc.*, **1958**, 2323.

A Separation Scheme for the Analysis of Metal Ions Using Column Extraction Chromatography. Grouping of Nineteen Metal Ions into Six Fractions[1]

Ikuko AKAZA,* Takatoshi TAJIMA,** and Toshiyasu KIBA

Department of Chemistry, Faculty of Science, Kanazawa University, Kanazawa, Ishikawa

(Received October 3, 1972)

A new scheme for the quantitative group separation of 19 common cations by reversed-phase extraction column chromatography has been devised. The following six columns, in which the organic solvent was adsorbed on Daiflone(polytrifluorochloroethylene), were prepared: a TBP–2N HCl column for Fe(III), Hg(II), and Sn(IV); a TOA(CCl_4)–2N HCl column for Ag(I), Bi(III), Zn(II), and Cd(II); a TBP–6N HCl column for Sb(III); an AcAc($CHCl_3$)–pH 5.0 column for Cr(III) and Al(III); a TTA(MIBK)–pH 5.0 column for Cu(II), Co(II), Ni-(II), Pb(II), Mn(II), and Mg(II), and a TTA(MIBK)-pH 7.0 column for Ca(II), Sr(II), and Ba(II). After a test solution had been passed through the six columns successively in the above order, the metal ions are grouped and entirely retained on the specified columns.

Most of the investigations of the mutual separation of metal ions have been mainly concerned with the specific problems involved in separating some desired elements from their mixture, or in separating an important element from many other unimportant ones; therefore, a more general separation method for each ion from a mixture of various metals, of any composition, is much to be desired.

We aimed to establish a systematic scheme for the separation of many metals in macro to trace amounts; as the first report on our continuing study, this paper will present a quantitative grouping scheme for 19 common metals by reversed-phase extraction chromatography using six different columns.

A sequential separation scheme for the quantitative analysis of many different metal ions had been the object of much searching; recently, among the many kinds of separation techniques, the solvent extraction technique has been preferred for this purpose; there having been several reports on it, including those by Chalmers *et al.*[2–4] and more recently by Morsches and Tölg.[5]

Unless the distribution coefficients of metal ions differ remarkably from each other, multiple extraction steps such as counter-current extraction are required for any quantitative separation, and this is tedious. If reversed-phase extraction-column chromatography, which is closely related to liquid-liquid extraction in the batch system, could be adopted for the purpose, the multiple extraction would take place successively in the column; the extraction column technique can be used for trace to macro levels with a very simple apparatus, and this apparatus can, if necessary, be automatized. There have been a few reports in which the extraction chromatography has been used for the separation of a mixture involving many metals. Among these, one described the use of a α-benzoinoxime–$CHCl_3$–polytetrafluoroethylene bed,[6] and others, the use of a di(2-ethylhexyl)orthophosphoric acid–Kieselguhr column,[7,8] both being combined with an ion-exchange column; the metals were thus separated into several groups suitable for their gamma spectrometry. Recently, a comprehensive separation scheme has been devised by Fritz and Latwesen[9] for the separation of 27 metal ions with trioctyl phosphine oxide, isopropyl ether, and isobutylmethyl ketone columns in combination with an ion-exchange column; it seems an excellent work in our field of investigation. The procedure of Deing *et al.*,[10] involving extraction with a tri-*n*-butylphosphate and di(2-ethylhexyl)orthophosphoric acid column, has also been proposed for the separation of fission products of irradiated uranium. The present paper will describe the systematic and quantitative group separation of 19 common metal ions using six columns based on reversed-phase extraction chromatography; tri-*n*-butylphosphate(TBP)–6 N HCl, TBP–2 N HCl, tri-*n*-octylamine(TOA)–CCl_4–2 N HCl, acetylacetone(AcAc)–$CHCl_3$–pH 5.0, 2-thenoyltrifluoroacetone(TTA)–methyl isobutyl ketone–(MIBK)–pH 5.0, and TTA–MIBK–pH 7.0 columns. These columns were named the TBP-(1) column, the TBP-(2) column, the TOA column, the AcAc column, the TTA-(1) column, and the TTA-(2) column respectively. The grouping metal ions from a complex mixture of various metals in varying concentrations is the first step to a quantitative separation of each metal alone from the respective column.

The Selection of The Extraction System and The Construction of a Separation Scheme. It is necessary to select a good extractant, a suitable solvent, and the optimum conditions for the purpose from the wide variety of extraction systems which have been reported. The authors chose the extraction systems described above for those reasons. Extraction systems should

* Present address: Kanazawa Women's College, Kanazawa.

** Present address: Ishikawa Hygienic Laboratory, Kanazawa.

1) A part of this paper has been read at the 17th Annual Meeting of the Japan Society for Analytical Chemistry, 1968.

2) R. A. Chalmers and D. M. Dick, *Anal. Chim. Acta*, **31**, 520 (1964).

3) R. A. Chalmers and D. M. Dick, *ibid.*, **32**, 117 (1965).

4) R. A. Chalmers and G. Svehla, "Solvent Extraction Chemistry," eds. D. Dyrssen et al, p. 600, North-Holland, Amsterdam, 1967.

5) B. Morsches and G. Tölg, *Z. Anal. Chem.*, **250**, 81 (1970).

6) R. Malvano, P. Grosso, and M. Zanardi, *Anal. Chim. Acta*, **41**, 251 (1968).

7) K. Samsahl, *Analyst*, **93**, 101 (1968).

8) K. Samsahl, P. O. Wester, and O. Landström, *Anal. Chem.*, **40**, 181 (1968).

9) J. S. Fritz and G. L. Latwesen, *Talanta*, **17**, 81 (1970).

10) R. Denig, N. Trautmann, and G. Herrmann, *J. Radioanal. Chem.*, **6**, 331 (1970).

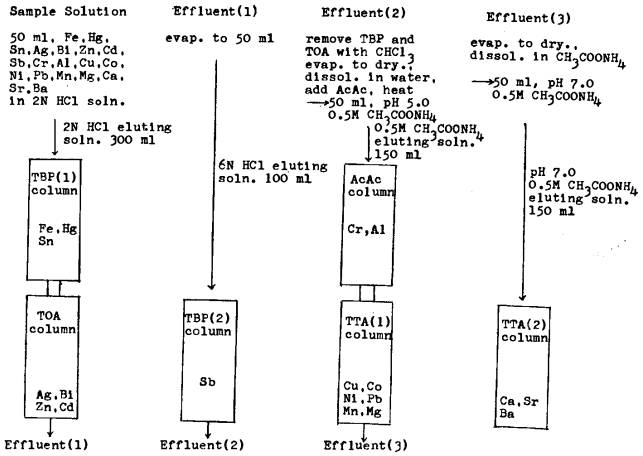

Fig. 1. Scheme of group separation.

be selective; that is, the extractability of the metal ions to be separated must be high enough for them to be retained on the upper part of the extraction column. The distribution of each metal ion should be markedly dependent on the acidity or pH of the aqueous medium; if so, the metal ions retained on the column can be eluted easily by varying the acidity or pH of the eluting solution. A simple medium in which no masking agent or nonvolatile salt exists is also preferred as an eluant, for its use will facilitate the subsequent determination of metals and the simple isolation of the compound.

The scheme shown in Fig. 1 was prepared for the group separation of 19 common cations by reversed-phase extraction column chromatography, with reference to sufficient information about the behavior of each element in the extraction system, taking the following points into consideration: (1) the extractions of the metal ions, readily hydrolyzable in a weakly acidic solution, were done in the earier stage of the separation process; (2) two columns in which eluting solutions of an identical acidity or pH could be used were joined together, and (3), the separation conditions were set up so as none of the retained metals could be released from the column even when a sample solution of a large volume flowed through.

Experimental

Reagents and Materials. *Daiflon*: Daiflon (a trade name of polytrifluorochloroethylene) M-300 moulding powder was purchased from the Daikin Kogyo Co.; 42-to 80-mesh powder was used.

Metals: Chlorides and nitrates of metals of an analytical reagent grade were dissolved in hydrochloric, nitric acid, or redistilled water.

Organic Reagents and Solvents: TTA, MIBK, chloroform, TOA, carbon tetrachloride, AcAc, and TBP were all of a chemically pure grade.

Radiochemicals: Several radionuclides were employed in order to ascertain the behavior of individual ions in the chromatography: Fe-59, Hg-203, Sn-113, Bi-207, Ag-110m, Zn-65, Cd-115m, Sb-124, Co-60, Ni-63, Sr-90, and Ca-45 were employed. The radiochemical purity of these nuclides was examined by measuring their half-lives, γ-ray spectra, and β-ray adsorption curves with aluminum foils.

Organic Solvent Solutions Available for the Stationary Phase of the Column. In each case the organic solvent solution used for the stationary phase should be in equilibrium with the eluting solution which comes in contact with the column.

100% TBP Solution for the TBP(1) and TBP(2) Columns: The TBP was equilibrated with 2 N (or 6 N) HCl.

20% TOA–CCl_4 Solution for the TOA Column: This solution was equilibrated with an equal volume of 2N HCl.

50% AcAc–$CHCl_3$ Solution for the AcAc Column: This solution was equilibrated with an equal volume of an 0.5 M ammonium acetate solution of pH 5.0 which had been saturated with an AcAc–$CHCl_3$ solution.

1.5 M TTA–MIBK Solution for the TTA(1) and TTA(2) Columns: This solution was equilibrated with an equal volume of an 0.5 M ammonium acetate solution of pH 5.0 (or 7.0) which had been saturated with MIBK.

Eluting Solutions. Each eluting solution was equilibrated with a proper organic solvent solution placed in the column.

Eluting Solution for the TBP(1) and TBP(2) Columns: 2 N (for Column 1) or 6 N (for Column 2) HCl which had been saturated with a small amount of TBP was used.

Eluting Solution for the TOA Column: 2 N HCl saturated with a TOA–CCl_4 solution was used.

Eluting Solution for the AcAc Column: Fifty milliliters of AcAc were placed in a 1-l separating funnel, and then 300 ml of water saturated with $CHCl_3$ and 125 ml of a 2 M ammonium acetate solution which had been saturated with $CHCl_3$ were added. The funnel was shaken, and a very small amount of the undissolved AcAc was rejected; then the aqueous phase was transferred into a measuring flask, and its volume was made up to 500 ml with water saturated with $CHCl_3$. The pH of this solution was then adjusted to 5.0 by adding 0.5 M acetic acid saturated with $CHCl_3$.

Eluting Solution for the TTA(1) Column: A TTA reagent (3.1 g) was dissolved, with shaking for 30 minutes, in 900 ml of a 0.5 M ammonium acetate solution which had been saturated with MIBK, then the pH of the solution was adjusted to 5.0 by adding 0.5 M acetic acid saturated with MIBK. The total volume was made up to 1 l with a solution of 0.5 M ammonium acetate solution saturated with MIBK.

Eluting Solution for the TTA(2) Column: With a TTA reagent (3.2 g), the eluting solution was prepared in the manner described just above, but the pH was adjusted to 7.0.

The amount of a TTA reagent to be dissolved in the eluting solution was determined in accordance with Reference 11.

Test Solutions. Stock solutions, each containing 0.5 mg of the metal ion in question per ml, were prepared. A test solution was prepared by diluting the stock solution so as it contained 1.0 mg of each element per 100 ml; in some cases, a radioactive tracer was added to the test solution. Fifty milliliters of the test solution were used for the column experiment. It is often desirable, but not in all cases, that the test solution have a composition similar to that of the eluting solution except for the metal ion. According to the variety of the metal ion in the sample solution to be tested, some part of the scheme shown in Fig. 1 may be omitted. Therefore, in such a case a test solution should have a composition similar to that of the eluting solution for the column from which the systematic separation starts.

The "test solution used for the AcAc column" was prepared as follows: Two milliliters of a stock solution (if necessary, with a radioactive tracer) were placed in a beaker and

11) I. Akaza, M. Kozaka, and T. Imamura, *Bunseki Kagaku*, **14**, 825 (1965).

diluted to about 20 ml with water saturated with AcAc–$CHCl_3$. The pH was adjusted to 5.0 by adding 0.5 M acetic acid or aqueous ammonia, both saturated with $CHCl_3$; 5 ml of AcAc were then added to this solution. The beaker was heated gently for an hour, and then cooled. Twenty-five milliliters of a 2 M ammonium acetate solution saturated with AcAc–$CHCl_3$ were added to this solution, and the pH was adjusted to 5.0 by adding 0.5 M acetic acid or aqueous ammonia, both saturated with $CHCl_3$. Finally, the solution was transferred into a measuring flask and its volume was made up to 100 ml with water of pH 5.0 which had been saturated with the AcAc–$CHCl_3$ solution.

Experimental Procedure. Column Preparation. A glass chromatographic column, 0.94 cm in diameter and 30 cm long, and with a coarse frit at the bottom, was used. The Daiflon powder (5.5 g) was placed in an Erlenmyer flask fitted with a stopper, and then a definite volume of a proper "organic solvent solution for the stationary phase" (described above) was poured in. The preferable volumes of the organic solvent are 6.0 ml of TBP, 7.0 ml of 20% TOA–CCl_4, 5.0 ml of 50% AcAc–$CHCl_3$ and 6.5 ml of 1.5 M TTA–MIBK for each 5.5-g portion of Daiflon; these volumes were derived from the results of other preliminary experiments, in which the adsorbable amount of each organic solution on Daiflon had been determined. The stoppered flask was shaken gently by hand and was then left to stand over three hours. A small volume of an adequate eluting solution was added, and the slurry was poured into the chromatographic column. Every time a small portion of slurry was added, the column bed was gently pressed with a glass rod; the bed length eventually reached about 20 cm. About 50-ml portion of an adequate eluting solution was passed through the column in order to remove any contaminant.

In such a way, the six columns were prepared.

Basic Chromatographic Procedure. Fifty milliliters of a test solution prepared as above were percolated through the column at the rate of about 0.3 ml per minute, and then an eluting solution of a definite composition was passed through at a flow rate of about 0.5 ml per minute. The effluent was taken in a fraction collector or in beakers.

In the chromatographic process, some metal ions in the test solution were retained on the column, while others passed through the column and went into the subsequent column.

Systematic Procedure for the Group Separation. One systematic procedure for the group separation of 19 common cations from their mixtures is based on the scheme shown in Fig. 1, in compliance with the basic chromatographic procedure described above. The following descriptions of the individual columns show that the method may be applicable for the grouping of 19 cations when the entire course of the scheme is followed. Nevertheless, if some part of the scheme is omitted when the ions which would be retained in the omitted column are known to be absent in a sample solution, the test solution should be prepared as described in the appropriate paragraph discussing the test solutions.

The test solution(a) for the TBP(1) column was fed into the TBP(1) column, which was joined with the TOA column. A 300-ml portion of the "eluting solution for the TBP(1) column" was run through both columns. The effluent(1) from the lower column was collected in a beaker and evaporated to a small volume, and then the volume was make up to 50 ml with water saturated with TBP (test soln. (b)). The test solution (b) was fed into the TBP(2) column, and then 100 ml of "the eluting solution for the TBP(2) column" was run through this column. The effluent (2) was collected, 1 ml of concentrated nitric acid was added, and then the solution was shaken, together with a small volume of chloroform, for a minute in order to remove the small amount of dissolved TBP and TOA from the aqueous solution. After that, the aqueous phase was collected and evaporated to dryness under an infrared lamp in order to expel the free nitric acid and hydrochloric acid. The residue was dissolved in about 20 ml of water saturated with AcAc–$CHCl_3$ solution. After the pH of this solution had been adjusted to 5.0, 2.5 ml of AcAc was added to this solution; then the mixture was heated gently for an hour until the completion of the formation of the AcAc-chelates with metal ions. After cooling, 12.5 ml of a 2 M ammonium acetate solution saturated with $CHCl_3$ was added to the solution, and the pH of the solution was adjusted again to 5.0. Finally, the volume was made up to 50 ml with water saturated with the AcAc–$CHCl_3$ solution (test soln. (c)). The test solution (c) was poured into the upper column of the combined set of AcAc and TTA(1) columns, and 150 ml of "the eluting solution for the AcAc column" was run through these combined columns. The effluent (3) from the lower column was collected in a beaker and evaporated to dryness. The residue was dissolved again in "the eluting solution for the TTA(2) column," and the volume was made up to 50 ml with the solution (test soln. (d)). The test solution (d) was placed in the TTA(2) column, and then 150 ml of "the eluting solution for the TTA(2) column" was run through the column in order to wash it (effluent (4)). Finally, the columns were separated from one another, and the metal ions retained on each column were eluted with a suitable solution or were removed from the column, together with the stationary phase, by washing the column with ethanol. The metal ions thus released were determined as will be described below.

Determination of Metal Ions. In general, the metal ions in the effluent from each column were determined colorimetrically, radiometrically, or flamephotometrically. The

Table 1. The analytical methods used for the determination of the metal ions

Metal	Method
Fe	Radiometric (Fe-59)
Hg	Radiometric (Hg-203)
Sn	Radiometric (Sn-113)
Bi	Radiometric (Bi-207)
Ag	Radiometric (Ag-110 m)
Zn	Radiometric (Zn-65)
Cd	Radiometric (Cd-115 m)
Sb	Radiometric (Sb-124)
Cr	Spectrophotometric as dichromate (440 mμ)
Al	Spectrophotometric as oxinate (390 mμ)
Cu	Spectrophotometric as diethyldithiocarbamate (435 mμ)
Co	Radiometric (Co-60)
Ni	Radiometric (Ni-63)
Pb	Spectrophotometric as dithizonate (510 mμ)
Mn	Spectrophotometric as permanganate (520 mμ)
Mg	Spectrophotometric as oxinate (380 mμ)
	Atomic adsorptiometric
Ca	Radiometric (Ca-45)
	Flamephotometric (554 mμ)
Sr	Radiometric (Sr-90)
	Flamephotometric (460.7 mμ)
Ba	Flamephotometric (515 mμ)

analytical method used for the determination of each metal ion is described in Table 1. In the case of colorimetric methods, MIBK, chloroform, and carbon tetrachloride were apt to be present in the effluent; they had to be removed by evaporation. A small amount of TBP and TOA in the effluent did not interfere with the colorimetric method, but TTA and AcAc did. When TTA or AcAc was present in the effluent, concentrated nitric acid was added to the solution and then the solution was evaporated to dryness to decompose the organic matter.

When the effluent was fractionated in the tubes of a fraction collector, each fraction was submitted to the determination of the metal ions. On the other hand, the whole effluent from one column was collected and evaporated to a small volume under an infrared lamp; then the final solution was made up to 50 ml with a suitable acidic solution. An aliquot of this solution was also pipetted out for the determination of the metal ions.

When a radioactive tracer was employed, each metal ion in the effluent or on the column was checked not only by means of its radioactivity, but also by means of its specific reagent.

Visuable colored bands appearing on a column during the elution (for example, on the AcAc and TTA(1) columns) generally provided a good measure for the column separation: TBP(1) column–Fe(yellow), Sn(yellow); TBP(2) colun–Sb(yellow); AcAc column–Cr(light violet-brown); TTA(1) column–Cu(green), Co(red-brown), Ni(light yellow-green), Pb(light yellow), Mn(orange-yellow).

Results and Discussion

Chromatographic Behavior of Metal Ions. If separation proceeds chromatographically on the basis of only the partition phenomenon, the chromatographic behavior of each metal ion on the column can be predicted by means of this equation: $E=D\cdot B+F$, where D is the batch distribution ratio, which has been otherwise obtained under conditions corresponding to those in the column extraction; E, the volume of the effluent before the emergence of the solute in a maximal concentration in the column; B, the volume of the stationary phase, and F, the volume of the mobile phase in the column.

Actually, the behavior of each metal ion was in good agreement with that predicted from the distribution ratio in the batch extraction. For example, in the TBP–HCl system, the extraction behavior of many metal ions against the concentration of HCl has been investigated in batch extraction by Ishimori *et al.*[12] and with reversed-phase thin layer chromatography by Bark *et al.*[13]; their extraction mechanisms have been also discussed by the latter. Their data, shown by the values of D or R_f, and the results we have obtained here are given in Fig. 2. The behavior of the metal ions in this reversed-phase chromatography agreed with those predicted from the data of the batch extraction and the thin-layer chromatography in relation to the concentration of HCl of the aqueous phase.

Retention of Individual Ions on the Column. To examine quantitatively the retention of each metal ion on a column, a 50-ml portion of a test solution containing a metal ion was first fed into the column, and then a 100-ml portion of an adequate eluting solution was passed through the column. The amounts of both the metal ion retained on the column and that in the effluent were determined, and the percentages of retention were calculated. No loss of metal ions was found in any column experiment; more than 99% of them could be recovered. The results obtained are illustrated in Table 2. Iron, mercury and tin were perfectly retained on the TBP(1) column from 2 N HCl, and Bi, Ag, Zn, and Cd were also retained on the TOA column from 2 N HCl; Sb was completely retained on the TBP(2) column from 6 N HCl. Chromium and aluminum were retained on the AcAc

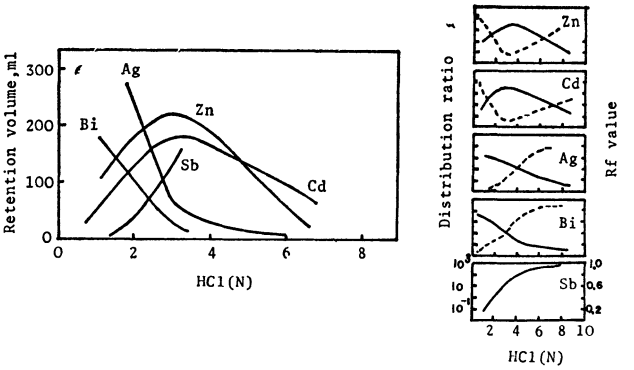

Fig. 2. The retention volume of TBP column and distribution ratio or R_f value as a function of HCl concentration.
—— Ishimori's data by liq.-liq. extraction.
---- Bark's data by reversed-phase thin layer chromatography.

TABLE 2. THE RETENTION OF INDIVIDUAL IONS ON THE COLUMNS, CONDUCTED SEPARATELY

Metal	Retained %					
	TBP(1) column	TOA column	TBP(2) column	AcAc column	TTA(1) column	TTA(2) column
Fe(III)	100	100	100			
Hg(II)	100	100	100			
Sn(IV)	100	100	100			
Bi(III)	1.0	100	0			
Ag	0.9	100	0			
Zn	43.2	100	2.1			
Cd	1.6	100	35.8			
Sb(III)	0	9.2	100			
Cr(III)	0	0	0	100		
Al	0	0	0	100		
Cu	0	0	0	0.5	100	
Co	0	0	0	0	100	
Ni	0	0	0	0	100	
Pb	0	0	0	0	100	
Mn(II)	0	0	0	0	100	
Mg	0	0	0	0	100	
Ca	0	0	0	0	0	100
Sr	0	0	0	0	0	100
Ba	0	0	0	0	0	100

12) T. Ishimori, K. Watanabe, and E. Nakamura, This Bulletin, **33**, 636 (1960).
13) L. S. Bark, G. Duncan and R. J. T. Graham, *Analyst*, **92**, 347 (1967).

column, and Cu, Co, Ni, Pb, Mn, and Mg on the TTA column from a 0.5 M ammonium acetate buffer solution of pH 5.0. Calcium, strontium, and barium were perfectly retained on the TTA column from a 0.5 M ammonium acetate solution of pH 7.0. The bismuth, silver, zinc, and cadmium on the TBP(1) column ($D=10$), Sb on the TOA column ($D=5$), Zn and Cd on the TBP(2) column ($D=15$) and Cu on the AcAc column ($D=8$) were not completely washed down from the column because of their relatively higher distribution ratios; they still remained on the lower part of the column. These metal ions could, however, be eluted from the column by the subsequent passing of an adequate eluting solution through the column.

The Bahavior of the Metal Ions in a Mixed Solution on Each Column. In achieving the group separation of cations, it is also necessary to examine the chromatographic behavior of the metal ion in question as well as that of all the other ions by passing mixed solutions through the respective columns in the scheme of group separation. Fig. 3 summarizes the features of the chromatographic behavior of each metal ion in the presence of all the others. This has been constructed of the data collected by many experiments carried out with 50-ml portions of test solutions containing all the metal ions except the metal ion in question. In such a case, the behavior of all the metal ions can not be defined simultaneously; therefore, only the behavior of the desired metal ion was followed by the use of its radioactive tracer, or by other methods, in the presence of all the others.

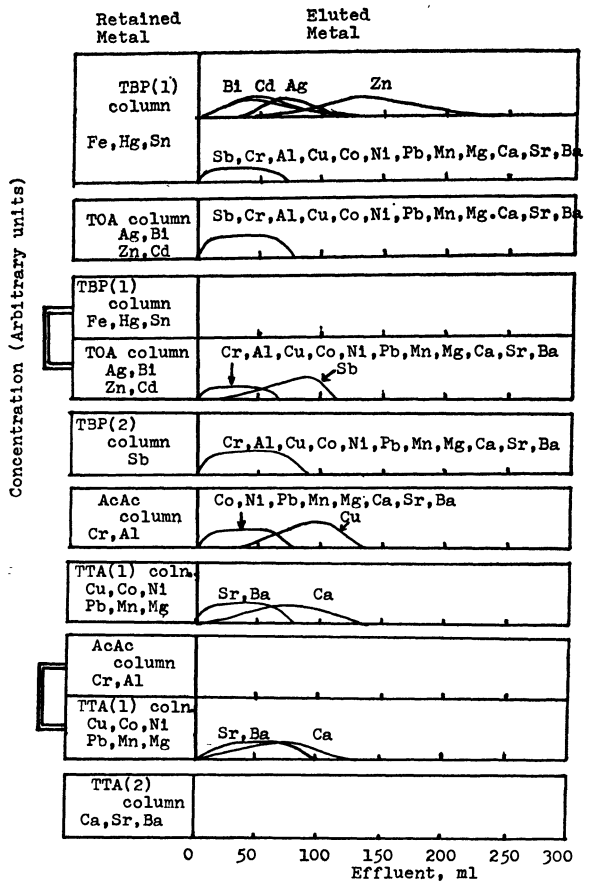

Fig. 3. The behavior of the 19 metal ions on each column. Sample solution: 50 ml, containing each 0.5 mg of cations.

As is shown at the left-hand side in Fig. 3, Fe, Hg, and Sn on the TBP(1) column, Ag, Bi, Zn, and Cd on the TOA column, Sb on the TBP(2) column, Cr and Al on the AcAc column, Cu Co, Ni, Pb, Mn, and Mg on the TTA(1) column, and Ca, Sr, and Ba on the TTA(2) column were retained completely on the upper part of the column, even after 300 ml of the eluting solution had been passed through. On the other hand, most of the other cations passed through each column easily; these data were represented by the elution curves. These results are in good agreement with those shown in Table 2; the results on the TTA(2) column are also in good agreement with those obtained in the previous paper.[14]

A Combined Column Consisting of the TBP(1) and the TOA Columns in Fig. 3: As has been mentioned above, the eluting solutions for both the TBP(1) and TOA columns were of the same acidity. Therefore, if the TBP(1) column could be joined to the top of the TOA column, the separation procedure would become simpler. Fifty milliliters of a test solution containing 19 cations were fed into the combined columns. After a 300-ml portion of the "eluting solution for the TBP(1) column" had been run through the two columns, the metal ions were determined in each fraction of the effluent. Finally, the two columns were disjoined and the metals retained on each column were determined respectively. The result was in good agreement with that obtained with a single column. Therefore, when both the TBP(1) and TOA columns must be employed, a combined column should always be used in the separation process.

The Combined Columns Consisting of the AcAc and TTA (1) Columns in Fig. 3: The acetylacetone column was joined to the top of the TTA(1) column for the same reason as in the case of the TBP(1) and TOA columns. Fifty milliliters of the test solution for the AcAc column were fed into the combined column, and then 200 ml of "the eluting solution for the AcAc column" was run through the column; each fraction of the effluent from the lower column was submitted to a determination of the metal ions. The columns were then disjoined from each other, and the retained metal ions were determined. The results agreed with those obtained in the experiment using the two columns were separately. Thus, it is possible to effect the group separation by using a combination of the AcAc column and the TTA column.

The Group Separation of 19 Common Cations. On the basis of the scheme shown in Fig. 1, the group separation of 19 common cations from their mixtures was carried out without a fraction collector in order to prove the practical usefulness of the method. After the entire course of the scheme had been finished, each column was separated from the other and the metal ions retained on each column were determined.

14) I. Akaza, This Bulletin, **39**, 980 (1966).

The actual separation into the six groups was successfully achieved; the results agreed well with the expectations mentioned in the previous paragraph. Consequently, it was clarified that the scheme devised by the present authors was useful and effective for the group separation of 19 common cations, and might also be useful for the practical analysis of a sample solution containing these cations.

BULLETIN OF THE CHEMICAL SOCIETY OF JAPAN, VOL. 46, 1204—1208 (1973)

The Catalytic Effect of the Bismuth Nitrate on the Autoxidation of Olefins

Fujio TSUCHIYA and Tsuneo IKAWA

Tokyo Institute of Technology, O-okayama, Meguro-ku, Tokyo

(Received March 9, 1972)

The catalytic effect of the bismuth nitrate on the autoxidation of olefins has been investigated. Nitrogen dioxide, oxygen atoms, and bismuth oxynitrate, which are the thermal decomposition products of the bismuth nitrate, are not involved in the initiation of the reaction. The bismuth nitrate is only effective on olefinic compounds, not on saturated hydrocarbons, and it does not decompose hydroperoxide. The catalysis of the bismuth nitrate is supposed to result from direct interaction with olefin.

Metal-ion catalysts have generally been used in autoxidation in the form of metal salts of organic acids, and the catalyses of metal ions on the autoxidation of hydrocarbons are classified into the following three effects on the initial step of the oxidation: the formation of alkoxy and alkylperoxy radicals by the metal-ion-catalyzed decomposition of hydroperoxide, the formation of alkyl radicals from hydrocarbons by a higher valent metal ion, and the formation of radicals by the metal-oxygen complex.[1]

In the previous paper,[2] it has been reported that the bismuth nitrate is the most effective catalyst among many bismuth compounds as an initiator for the oxidation of isobutene. In this paper, the mechanism of catalysis by the bismuth nitrate has been mainly investigated from the point of view of the character of the nitrate. The effect of nitrogen dioxide, oxygen atoms, and bismuth oxynitrate, which may be formed from bismuth nitrate by its thermal decomposition during the reaction, have been examined, but their formation and contribution have been negligibly small. Iodometric observation has been undertaken in order to ascertain whether or not the bismuth nitrate decomposes hydroperoxide to active free radicals; it has been found not to decompose hydroperoxide. The autoxidation of nonolefinic hydrocarbons, such as cumene and tetralin, has not been catalyzed by the bismuth nitrate. The catalysis of the bismuth nitrate can not be attributed to the three mechanisms mentioned above, but can be assumed to result from the direct interaction between the bismuth nitrate and the double bond of olefin.

Experimental

A stainless autoclave with a reservoir and a magnetic stirrer[2] was used for the autoxidation of olefins. The volume of the reaction mixture was kept at 50 ml; the total pressure, 20 kg/cm^2; the partial pressure of oxygen, 5 kg/cm^2, and the reaction temperature, 100°C. Acetonitrile was used as the solvent. The oxidation of cyclohexene and some saturated hydrocarbons has been carried out in an oxygen-absorption apparatus[3] under atmospheric pressure. Iodometry was carried out by means of the chloroform method.[4]

The gaseous olefins were 99.0% pure grade. Cyclohexene and other hydrocarbons were purified by distillation in a nitrogen atmosphere. The glycerol was of a chemical pure grade. The metal nitrates, stored in a dark ice box, were of a chemical pure grade and were used without further purification. The nitrogen dioxide was obtained by the thermal decomposition of the lead nitrate at 500°C and was stored in a dry ice box.

Gas chromatography was used to analyse the reacted and unreacted substances; the volatile substances using a 3-m column of polyethylene glycol(PEG) 1000 at 80°C; the nonvolatile substances using temperature-programed gas chromatography with a 3-m column of PEG 20M, and unreacted butenes using a 5-m column of benzyl cyanide-$AgNO_3$ at room temperature.

Results and Discussion

Decomposition of Hydroperoxide. The bismuth nitrate oxidized potassium iodide to iodine, and the

TABLE 1. IODOMETRY[4] OF BISMUTH NITRATE AND CUMYL HYDROPEROXIDE AT 50°C

$Bi(NO_3)_3$ (mol)	CHPO[a] (mol)	I_2[b] (mol)	$I_2/Bi(NO_3)_3$[c]
6.5×10^{-6}		9.0×10^{-6}	1.3
75.9		70.5	0.9
7.6	21.4×10^{-6}	33.9	1.2[d]
77.8	42.9	115.7	1.0[d]

a) Cumyl hydroperoxide. b) Isolated iodine. c) Molar ratio of isolated iodine to $Bi(NO_3)_3$. d) Molar ratio of isolated iodine to ($Bi(NO_3)_3$+CHPO).

1) Y. Kamiya, *Yuki Gosei Kagaku Kyokai Shi*, **26**, 957 (1968).
2) F. Tsuchiya, T. Sumi and T. Ikawa, *Kogyo Kagaku Zasshi*, **74**, 2074 (1971).
3) T. Ikawa, M. Muto and T. Shintani, *Bull. Jap. Petrol. Inst.*, **7**, 42 (1965).
4) Y. Ogata, "Chemistry of Organic Peroxide," p. 91, Nankodo, Tokyo (1971).
5) W. F. Brill and B. J. Barone, *J. Org. Chem.*, **29**, 140 (1964).

amount of iodine produced was measured by iodometry in a chloroform solution. The results are tabulated in Table 1. The iodine isolated increased with the increase in the amount of the bismuth nitrate, but the molar ratio of the iodine isolated to the initially-added bismuth nitrate was nearly constant. Then, the bismuth nitrate was added into an acetonitrile solution of cumyl hydroperoxide and iodemetry was carried out on this mixture. The amount of iodine thus isolated was equal to the sum of the quantities of iodine which were obtained in each iodometry of the bismuth nitrate and cumyl hydroperoxide (Table 1). These were increased in the amounts of the bismuth nitrate and cumyl hydroperoxide initially added, but the total amount of iodine was nearly equal to the sum of the individual quantities of iodine (Table 1). From these results, we consider that the bismuth nitrate does not decompose hydroperoxide in the atmosphere.

The Autoxidation of Nonolefinic Hydrocarbons in the Presence of the Bismuth Nitrate. The autoxidation of nonolefinic hydrocarbons, such as tetralin, cumene, and *p*-xylene, was carried out in the presence of the bismuth nitrate; the results are listed in Table 2. The induction periods were very long, even in the presence of the bismuth nitrate, on the autoxidation of saturated hydrocarbons. Although cumene has an active tertiary hydrogen atom, on which can easily be abstracted, no oxygen absorption was observed. This indicates that the bismuth nitrate promotes only the autoxidation of olefins and that the catalytic effect is not based on the direct hydrogen abstraction from an organic compound by a metal ion, such as a higher valence metal ion or a metal-oxygen complex.

Table 2. Autoxidation of nonolefinic hydrocarbons in the presence of bismuth nitrate; induction period

Hydrocarbons	Temp (°C)[a]	Induction period (min)	
Tetralin	70	125	A[b]
Cumene	70	154	A
p-Xylene	100	420	P[c]
Cyclohexanone	100	310	P
α-Methylstyrene	60	2	A
Cyclohexene	60	4	A
2-Hexene	60	4	A

a) Reaction temperature. b) Pressure: 1 atom of O_2.
c) Total pressure: 20 kg/cm², partial pressure of O_2; 5 kg/cm², Hydrocarbon: 4.9 mol/l, solvent: acetonitrile, Bismuth nitrate: 6.2×10^{-4} mol.

The Effect of Metal Nitrates. Metal nitrates such as cobaltous, manganous, ferric, and lead nitrates, were added to a solution of isobutene in order to investigate the effect of nitrates. The results are shown in Table 3. The nitrate effect was observed in the cases of ferric nitrate and the bismuth nitrate; some oxygen was absorbed, and some products, such as acetone and isobutene oxide, were obtained. The cobaltous and manganous nitrates scarcely promoted the oxidation, while these metal salts of organic acids are known to be effective catalysts for the autoxidation of hydrocarbons. This is interesting phenomenon and must be due to the ligand effect of a metal complex. The lead nitrate did not have promoting effect at all.

These nitrates oxidized potassium iodide to iodine; the results are tabulated in Table 4. The amounts of iodine isolated per mole of each metal nitrate were nearly equal to one another except for the ferric nitrate. For the ferric nitrate, the higher value of iodine may be due to the higher valence of the ferric ion. However, this oxidizing ability does not correspond to the promoting effect of the autoxidation.

The decomposition temperatures of the metal nitrates, which were taken from the literature, are also tabulated in Table 4. The promoting effect of the nitrate corresponded to the decomposition temperature of the nitrate except for the cobaltous nitrate; the bismuth nitrate and the ferric nitrate, which decompose at comparatively low temperatures, were effective promoters, and the lead nitrate, which decomposes at a very high temperature, did not have any promoting effect at all. From these results, it can be supposed that nitrogen dioxide, the oxygen atom, and bismuth oxynitrate, which may be formed by the thermal decomposition of the bismuth nitrate during the oxidation of hydrocarbons in the presence of the bismuth nitrate, will contribute to the initial step of the oxidation. Therefore, it became necessary to examine whether or not, nitrogen dioxide, the oxygen atom, and bismuth oxynitrate participate in the initiation of the reaction.

First of all, the effect of nitrogen dioxide was exa-

Table 3. The effect of metal nitrate on the autoxidation of isobutene

Metal nitrate	Conversion of *iso*-C_4H_8	Absorbed O_2	Products (Selectivity[a] mol%)					
			CH_3COCH_3	*iso*-BO[b]	*tert*-BuOH[c]	PO[d]	A[e]	E[f]
$Mn(NO_3)_2$	9.1%	3.0 mmol	5.9	—[g]	19.0	2.6	15.7	58.2
$Fe(NO_3)_3$	24.1	24.8	26.4	—	26.3	3.2	8.4	30.6
$Pb(NO_3)_2$	—	—	0	0	0	—	—	—
$Co(NO_3)_2$	5.0	6.4	8.4	—	—	—	0.4	52.3
$Bi(NO_3)_3$[h]	34.2	35.2	23.1	2.5	12.3	0.4	8.9	7.5

iso-C_4H_8: 3.4 mol/l, Metal nitrate: 0.01 mol, solvent: CH_3CN 100 ml, total pressure: 20 kg/cm², partial pressure of O_2: 5 kg/cm², reaction time; 160 min, reaction temp 100°C.
a) Calculated from the reacted butene. b) Isobutene oxide. c) *tert*-Butyl alcohol. d) Peroxide. e) Acid. f) Ester. g) Trace-amount. h) *iso*-Butandiol was produced (33.0 mol%).

Table 4. Iodometry and decomposition temperature of nitrates

Nitrates	I_2[a]	Decomposition temp (°C)[b]
$Mn(NO_3)_2 6H_2O$	2.3	129.4
$Fe(NO_3)_3 9H_2O$	9.8	47.2
$Pb(NO_3)_2$	1.5	470
$Co(NO_3)_2 6H_2O$	4.8	50
$Bi(NO_3)_3 5H_2O$	1.20	30

a) The molar ratio of I_2 isolated from KI by nitrate to the nitrate initially added, at 100°C. b) The value taken from those in Ref. 13.

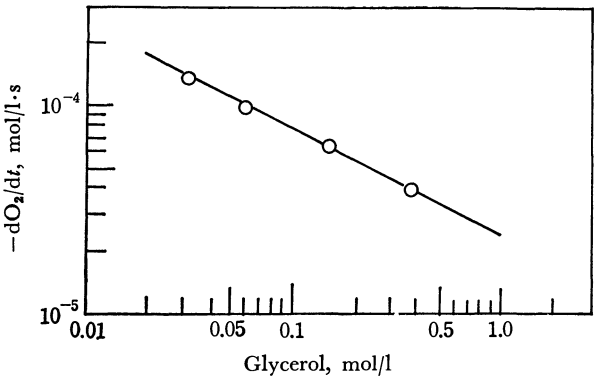

Fig. 1. Glycerol effect on the oxidation of C_6H_{10}. C_6H_{10}; 4.9 mol/l, 70°C, $Bi(NO_3)_3 5H_2O$; 2.2×10^{-4} mol solvent; acetonitrile, reaction mixture; 10 ml

mined; a blue solution of nitrogen dioxide–acetonitrile was introduced into the reaction mixture, after with oxygen was introduced at 100°C under a reaction pressure of 15 kg/cm². After few minutes of oxygen introduction, the absorption of oxygen began and some oxygenated products were obtained (Table 5). The distribution of these products was the same as Brill's[5] and Imamura's[6] reports. It is obvious that nitrogen dioxide initiates the reaction; this result corresponds to Titov's indication[7]: nitrogen dioxide adds to the double bond of olefin and form a radical. If the bismuth nitrate thermally decomposes to give nitrogen dioxide, the autoxidation will be initiated by nitrogen dioxide. On the other hand, when glycerol (2.7 mol/l) was added to the solution on the oxidation of isobutene in the presence of the bismuth nitrate, the absorption of oxygen was suppressed and oxygen absorption was not observed until about 70 min after the introduction of the oxygen. The inhibiting effect of glycerol was examined at 70°C(Fig. 1). The rate of oxygen absorption decreased with the increase in the amount of glycerol added. However, the apparent absorption of oxygen was observed a few minutes after oxygen introduction on the oxidation of butene in the presence of nitrogen dioxide, and oxygenated products were obtained (Table 5). These results indicate that glycerol only disturbs the oxidation of isobutene in the presence of the bismuth nitrate and does not inhibit the oxidation initiated by nitrogen dioxide. Moreover, nitrogen dioxide was not observed experimentally on the oxidation of olefin in the presence of the bismuth nitrate(Table 3). If the nitrogen dioxide is formed from the bismuth nitrate, it should be effective for the oxidation of cumene, for it has been reported by Nanba *et al.*[8] that nitrogen dioxide is able to abstract a hydrogen atom from cumene at 70°C. Judging from these results, it is difficult to take nitrogen dioxide as the active origin of the bismuth nitrate on the autoxidation of olefins. An oxygen atom in the triplet state is able to abstract hydrogen atom from hydrocarbons[9] and to initiate the autoxidation. A singlet oxygen atom can not abstract a hydrogen atom from hydrocarbons, but it can give rise to insertion reaction.[10] If the bismuth nitrate generates an oxygen atom by its thermal decomposition, the autoxidation of hydrocarbons will occur by hydrogen abstraction in case of the triplet oxygen atom generated. However, it is difficult to take the oxygen atom possibly generated from the nitrate as the active origin of the bismuth nitrate on the oxidation of olefins, because no catalytic effect of the bismuth nitrate was observed in the case of the oxidation of saturated hydrocarbons, such as cumene and tetralin (Table 2).

The effect of bismuth oxynitrate was examined by means of infrared absorption spectra. The IR spectra of the bismuth nitrate, $Bi(NO_3)_3 5H_2O$, is shown in Fig. 2; the characteristic absorption bands at 830, 1380, and 1620 cm^{-1} have been attributed to the modes of bending, stretching, and harmonics of the bending of the(N–O) bond respectively by Vratny.[11] The

Table 5. The effect of NO_2 on the oxidation of butenes at 100°C

Olefins	Conv. of olefin[a]	Absd. O_2[b]	Products (mmol)				
			CH_3COCH_3	CH_3CHO	Epoxide	PO[c]	Ester
iso-C_4H_8	24.4%	30.5 mmol	14.4		6.7	3.7	11.6
cis-2-C_4H_8	35.7	39.5		7.1	20.5	1.8	7.4
cis-2-C_4H_8[d]	33.5	44.2		8.0	18.6	2.5	10.1

C_4H_8: 3.4 mol/l, NO_2: 0.34 mol/l, solvent: CH_3CN 50 ml, reaction time: 160 min.
a) Conversion of olefin. b) Absorbed oxygen. c) Peroxide. d) Glycerol (2.7 mol/l) was added.

6) J. Imamura, M. Hirata, I. Kawase, and N. Ohta, *Kogyo Kagaku Zasshi*, **68**, 2391 (1965).
7) A. I. Titov, *Tetrahedron*, **19**, 557 (1963).
8) T. Yoshida, F. Yamamoto, and K. Nanba, *Kogyo Kagaku Zasshi*, **73**, 519 (1970).
9) A. Kato and R. J. Cvetanović, *Can. J. Chem.*, **45**, 1845 (1967).
10) Y. Moro-oka, *Shokubai*, **13**, 135 (1971).
11) F. Vratny, *Appl. Spectrosc.*, **13**, 59 (1959).

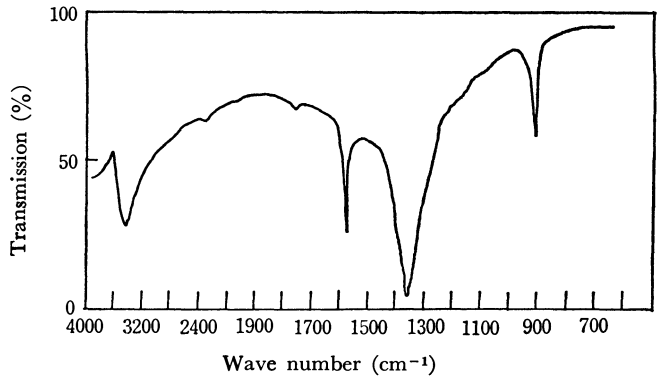

Fig. 2. Infrared spectra of $Bi(NO_3)_3 5H_2O$.
Before use for reaction in KBr pellet.

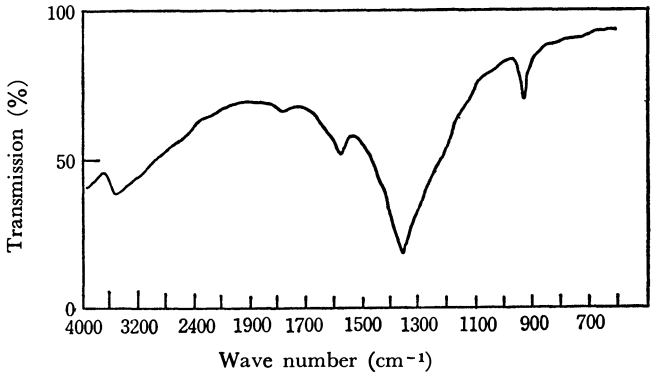

Fig. 3. Infrared spectra of white substance recovered from the reaction mixture.
100°C, 50 min, in KBr pellet.

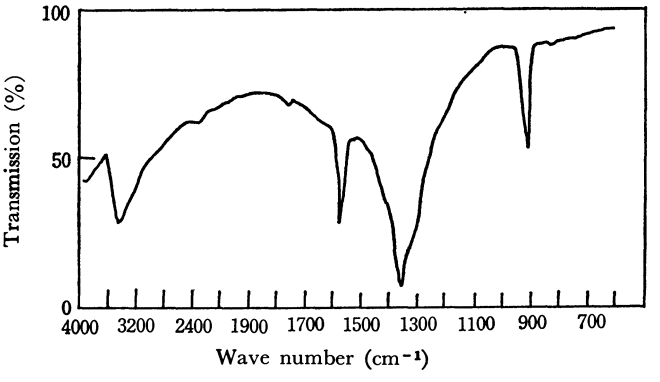

Fig. 4. Infrared spectra of $Bi(NO_3)_3 5H_2O$ treated in benzene at 80°C for 1 hr in KBr pellet.

absorption at 1620 cm^{-1} can also be attributed to the bending of H–O–H in the lattice. The IR spectra of the white substance recovered from the solution after a 50-min reaction using bismuth nitrate as the catalyst at 100°C are shown in Fig. 3. The absorptions at 830 and 1620 cm^{-1} decreased a little in their intensities, and the band at 1380 cm^{-1} became broad. However, the characteristic absorption were the same as those in Fig. 2. Cismaru *et al.*[12] indicate that the oxynitrate has split absorptions at 1320 and 1380 cm^{-1} as a result of an increase in the covalent bond-character of the (N–O) bond. Therefore, we can regard the recovered substance as a bismuth nitrate containing no bismuth oxynitrate. The spectra of the bismuth nitrate treated in benzene at 80°C for 1 hr were the same as those of the untreated one(Fig. 4). From these results, we can suppose that the bismuth nitrate is rather stable in circumstances, even if it is heated, and that the active origin of the bismuth nitrate is of itself.

cis-trans *Isomerization.* It has been reported in the previous paper[2] that the recovered *cis*-2-butene contained the *trans*-isomer after the oxidation of *cis*-2-butene at 100°C under a pressure of 20 kg/cm^2 in the presence of the bismuth nitrate. The isomerization of *cis*-2-butene was examined further in this paper. It was observed to take place in the presence of the bismuth nitrate with and without oxygen. It was also observed when nitrogen dioxide and bismuth trichloride were added; our findings are summarized in Table 6.

Glycerol did not prevent the isomerization so much, but it did prevent the oxidation. In the presence of glycerol, nitrogen dioxide promoted both the isomerization and the oxidation. The isomerization with the catalysts used here must be due to both protonic acid and to the coordinating of olefin to the bismuth

Table 6. Isomerization of *cis*-2-butene to *trans*-isomer

Catalyst	*cis*-/*trans*-2-C_4H_8[a]	
—[b]	1/[c]	100°C
$Bi(NO_3)_3 5H_2O$	1/1.5	40°C without O_2
$Bi(NO_3)_3 5H_2O$	1/1.6	100°C with O_2
$Bi(NO_3)_3 5H_2O$-Glycerol	1/1.1	100°C with O_2
$Co(NO_3)_2 6H_2O$	1/0.9	100°C with O_2
NO_2	1/0.9	100°C with O_2
$BiCl_3$	1/0.8	100°C without O_2
$AlCl_3$	1/0[c]	100°C without O_2

cis-2-C_4H_8: 3.4 mol/l, solvent: CH_3CN, catalyst: 0.01 mol, reaction time: 160 min. 1-Butene was not observed in each case.
a) Molar ratio of *cis*-2-C_4H_8 to isomerized *trans*-isomer. b) No catalyst was used. c) No isomerization was observed.

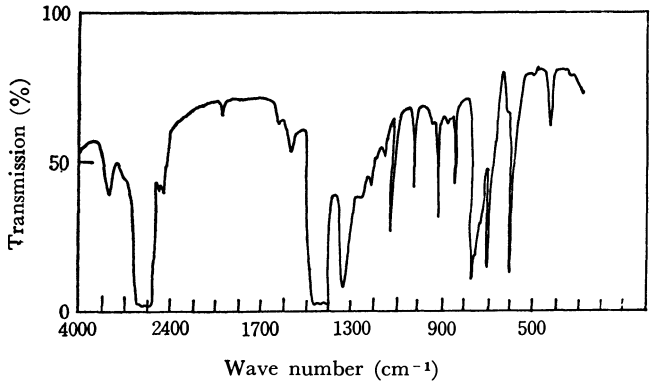

Fig. 5. Infrared spectra of $Bi(NO_3)_3 5H_2O$-cyclohexene solution. In Nujol. New absorptions were observed at 1880, 1000, 780, and 430 cm^{-1}.

12) D. Cismaru, Z. Cimons and C. Volanschi, *Rev. Roum. Chem.*, **9**, 681 (1964); *Chem. Abstr.*, **62**, 14047a (1965).

13) "Kagaku Benran Kisohen-1," Ed. by the Chemical Society of Japan, Maruzen, Tokyo (1966), p. 51.

nitrate. In the case of the oxidation, the coordination of olefin is probably prevented by the glycerol coordinated on the bismuth nitrate and the rate of oxidation is reduced. It can be assumed from above results that the initiation of the oxidation by the bismuth nitrate occurs by the direct interaction of the bismuth nitrate with olefin. The direct interaction was examined by studying the infrared spectra of the solution of bismuth nitrate–cyclohexene (Fig. 5). New bands, which were not observed on either the bismuth nitrate or cyclohexene, were observed at 430, 780, 1000, and 1880 cm^{-1}. Though the assignment of these bands is not clear, the newly-observed absorption, especially at 430 cm^{-1}, is significant because the absorption is near the characteristic absorption of Pt–C_2H_4(405 cm^{-1} in the Zeise salt. The coordination of cyclohexene is not clear in detail, but it is certain that the initiation of cyclohexene depends on this coordinated olefin. However, there is a possibility that a bismuth-oxygen complex may be formed during the reaction and that it contributes to the initiation by adding to the double bond of olefins. This possibility will be further investigated kinetically, and the direct interaction of the bismuth nitrate with olefin will be confirmed.

BULLETIN OF THE CHEMICAL SOCIETY OF JAPAN, VOL. 46, 1208—1211 (1973)

A Study of the Catalytic Partial Oxidation of Hydrocarbons. XVI. The Effect of the Bi_2O_3 Content in the MoO_3-Bi_2O_3-P_2O_5 Catalysts on the Oxidation of Various Olefins, Acids, and Aldehydes

Mamoru Ai and Sadao Suzuki

Research Laboratory of Resources Utilization, Tokyo Institute of Technology, Ookayama, Meguro-ku, Tokyo

(Received March 24, 1972)

The vapor-phase oxidation of various kinds of olefins, acids, aldehydes, etc. was carried out in a flow system over a series of MoO_3–Bi_2O_3–P_2O_5 catalysts with different Bi/Mo ratios (P/Mo=0.2 atomic ratio) under fixed reaction conditions, in order to elucidate how the oxidation of these compounds is affected by the Bi_2O_3 content in the catalysts. The oxidation activity for these compounds varies in different individual manners as the Bi_2O_3 content increases. The results were interpreted successfully on the basis of the acid-base nature of the reactant and the catalyst. Then, the relationship between the character of the partial oxidations and the nature of the catalysts was discussed.

The present authors have reported in recent papers[1,2] that the MoO_3–Bi_2O_3–P_2O_5 catalyst containing a high Bi_2O_3 content, which is well-known as an excellent catalyst for such an allylic oxidation as those of *n*-butene to butadiene and of propylene to acrolein, is inadequate for the oxidation of butene, butadiene, and furan to maleic anhydride, while a low-Bi_2O_3-content catalyst (Bi/Mo=0.1 atomic ratio) is quite good for the formation of maleic anhydride. Furthermore, it has also been proved that, with in increase in the Bi_2O_3 content in the catalyst, the oxidation activities for butene, butadiene, furan, and maleic anhydride vary, that the kinetics of both butene and butadiene is of about a 0.5 order in oxygen and a 0.8 order in olefin over the low Bi_2O_3 (Bi/Mo<0.15) catalysts, and that it becomes almost zero-order in oxygen and first-order in olefin over a high Bi_2O_3 (Bi/Mo> 0.5) catalyst.[2,3]

The authors have tried to interpret these results in terms of the acid-base nature of the catalyst and the reactant. With an increase in the Bi_2O_3 content, the basicity of the catalyst increases and its interaction with such electron donor-type compounds (base) as olefin decreases, while that with acids and oxygen increases. Thus it was interesting to confirm whether or not the oxidation aspects of other organic compounds could also be interpreted by the above-mentioned acid-base conception. In the present work, the oxidation of various kinds of organic compounds, including olefins, acids, and aldehydes, over a series of MoO_3–Bi_2O_3–P_2O_5 ternary catalyst system, while varying their Bi/Mo proportions in the presence of a large excess of oxygen, was performed in order to elucidate how the oxidation of these compounds is affected by the Bi_2O_3 content in the catalyst, and to obtain more detailed information about the oxidation over catalyst systems.

Experimental

The vapor-phase oxidation of various kinds of olefins, acids, aldehydes, etc., was carried out over a series of molybdenum-bismuth-phosphorus oxide catalysts with different Bi/Mo ratios (P/Mo=0.2 atomic ratio) in an ordinary continuous-flow-type reaction system, as has been described in an earlier paper.[4]

The concentration of the reactant was in the range of 0.6—1.5 mol% in air, the flow rate was kept at 1.5 l/min (at about 20°C), and the amount of the catalyst used was 40 ml; the contact time, which was shown by the volume of the catalyst (ml) per total flow rate (ml/s), was 1.6 s. The reaction temperature was increased at intervals of 10~20 from 250°C to 650°C, and the efflux from the reactor was analysed at each temperature until the conversion be-

1) M. Ai and S. Suzuki, This Bulletin, **44**, 3081 (1971).
2) M. Ai and S. Suzuki, *Nippon Kagaku Kaishi*, **1972**, 290.
3) M. Ai and S. Suzuki, *Shokubai*, **14**, 50 (1972).
4) M. Ai, T. Niikuni, and S. Suzuki, *Kogyo Kagaku Zasshi*, **73**, 165 (1970).

came more than 50%. Before the analysis, the feed flow was passed over the catalyst at the desired temperature for more than about 20 min in order to obtain the data under steady-state conditions. The experimental and the analytical procedures were also identical with those employed in the earlier works.[1-4]

The catalysts used in these experiments were the same as those used in some preceding works.[2,3] They were calcined under flowing air at 550°C for 5 hr. The surface area of these catalysts was of the order of 3 m^2/g, as determined by the BET method, and the variation in the Bi_2O_3 content had little effect on the surface area.

Results

Oxidation of Olefins. The oxidation of such olefins as *cis*-2-heptene, 2-hexene, 2-pentene, *cis*-2-butene, butadiene, propylene, and ethylene was examined over a series of MoO_3–Bi_2O_3–P_2O_5 catalysts with different Bi/Mo ratios (P/Mo=0.2 atomic ratio) under fixed reaction conditions. The relationship between the catalyst composition and the oxidation activity for such olefins as 2-heptene, 2-hexene, 2-pentene, and *cis*-2-butene is plotted in Fig. 1. The range of activity variation is so wide that it is hard to express it by a reaction rate at a constant temperature. Therefore, the value of $1000/T_{50}$ is adopted as a measure reflecting the oxidation activity, where T_{50} means the reaction temperature (K) corresponding to the reactant conversion of 50%.

The results indicate that the catalytic activity for these olefins, excluding propylene, varies similarly when the Bi_2O_3 content in the catalyst increases; the activity increases and goes through a maximum at a Bi/Mo atomic ratio of about 0.1, and then it decreases to the value of the Bi_2O_3 alone catalyst, which is extremely inactive for olefins. The higher the olefin, the higher becomes the reactivity over the whole range of Bi/Mo ratios. It is also clear that the difference in the reactivity among these olefins is relatively small in the range of low Bi_2O_3 content (Bi/Mo<0.15), but in the range of Bi/Mo=1—2, the difference becomes very significant—*i.e.*, the reactivity increases as the number of carbon atoms increases.

The activity for lower olefins, including *cis*-2-butene, propylene, and ethylene, is shown as a function of the Bi_2O_3 content in Fig. 2. In the case of olefins lower than butene, the reactivity decreases markedly with a decrease in the carbon number; besides, the maximum activity is not observed at Bi/Mo=0.1. The activity for propylene passes through a maximum at about Bi/Mo=1—2. The reactivity of ethylene is too low to obtain detailed information about it, but it appears

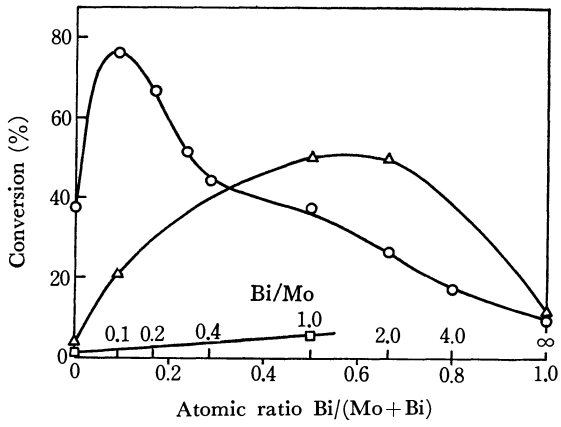

Fig. 2. Oxidation activity *vs.* the Bi_2O_3 content.
Contact time=1.6 s, olefin=0.67 mol% in air, ○: *cis*-2-butene at 430°C, △: propylene at 550°C, □: ethylene at 580°C.

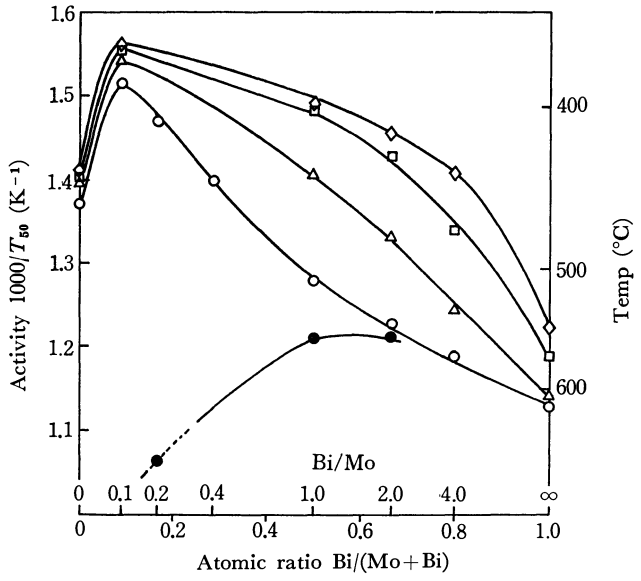

Fig. 1. Oxidation activity ($1000/T_{50}$) for olefins *vs.* the Bi_2O_3 content.
T_{50} is the temperature in K at which the conversion becomes 50%.
Olefin=0.67—1.5 mol% in air, contact time=1.6 s, ◇: *cis*-2-heptene, □: 2-hexene, △: *cis*-2-heptene, ○: *cis*-2-butene, ●: propylene.

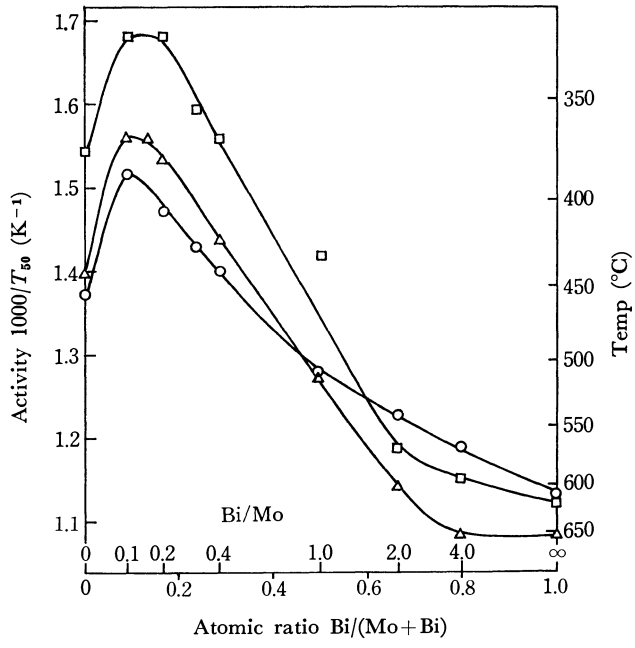

Fig. 3. Oxidation activity ($1000/T_{50}$) *vs.* the Bi_2O_3 content.
Contact time=1.6 s, reactant=0.67 mol% in air, ○: *cis*-2-butene, △: butadiene, □: furan.

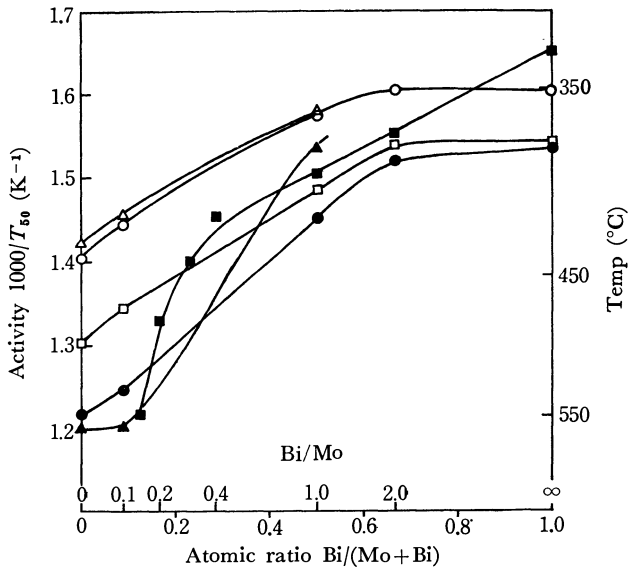

Fig. 4. Oxidation activity ($1000/T_{50}$) for acids *vs.* the Bi_2O_3 content.
Contact time=1.6 s, reactant=1.5 mol% in air, □: acetic acid, ○: propionic acid, △: butyric acid, ■: maleic anhydride, ●: acrylic acid, ▲: crotonic acid.

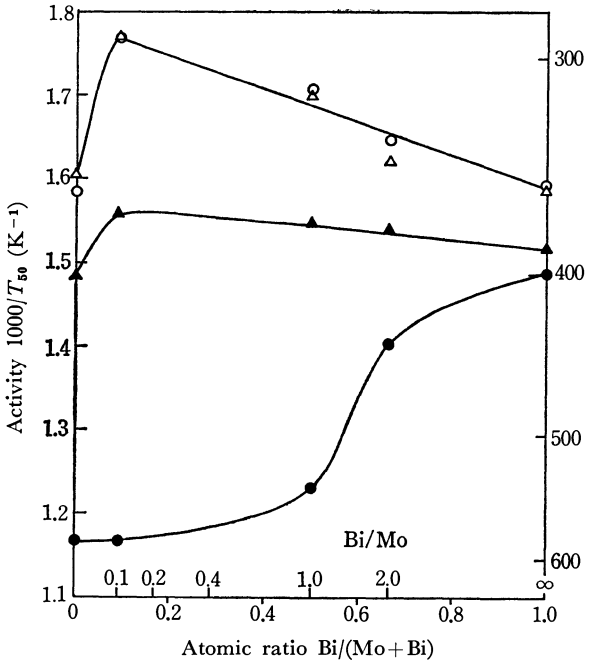

Fig. 5. Oxidation activity ($1000/T_{50}$) for aldehydes *vs.* the Bi_2O_3 content.
Contact time=1.6 s, reactant=1.5 mol% in air, ○: propionaldehyde, △: butyraldehyde, ●: acrolein, ▲: crotonaldehyde.

that the Bi_2O_3-rich catalyst is more active than the Bi_2O_3-poor catalyst.

The activities for unsaturated C_4 compounds, that is, *cis*-2-butene, butadiene, and furan, are compared in Fig. 3. As has been mentioned in an earlier paper,[2] the reactivity-order of these compounds varies with an increase in the Bi_2O_3 content.

Oxidation of Acids. The oxidation of both saturated and unsaturated carboxylic acids—acetic acid, propionic acid, butyric acid, acrylic acid, crotonic acid, and maleic anhydride—is performed under fixed reaction conditions. The activities obtained are plotted as a function of the Bi_2O_3 content and compared in Fig. 4.

The results reveal:

a) the low Bi_2O_3 catalyst is very inactive for the oxidation of carboxylic acid, especially for unsaturated acid, but the high Bi_2O_3 catalyst is fairly active for the oxidation.

b) the activity for the oxidation of carboxylic acid always increases steadily with an increase in the Bi_2O_3 content.

c) acetic acid is much more stable than the higher saturated acids.

d) the reactivities of propionic acid and butyric acid are almost the same.

e) unsaturated acids are fairly stable in comparison with the corresponding saturated acids.

Oxidation of Aldehydes. Figure 5 shows the activity for the oxidation of various aldehydes, including propionaldehyde, butyraldehyde, acrolein, and crotonaldehyde, as a function of the Bi/Mo ratio. The results indicate:

a) the saturated aldehydes are much more reactive over the catalyst system than the other compounds.

b) the reactivities of propionaldehyde and butyraldehyde are almost the same.

c) unsaturated aldehydes are much less reactive than the corresponding saturated aldehydes.

d) the activity-curves for propionaldehyde, butyraldehyde, and crotonaldehyde vary with the same trend as for olefins higher than propylene.

e) the activity for acrolein changes in a unique manner; at a relatively low content of Bi_2O_3(Bi/Mo<1), acrolein is very stable, but at a higher Bi_2O_3 content (Bi/Mo> 2), it increases sharply.

Discussion

First, we attempted to discuss the oxidation aspects of these organic compounds, by supposing that the rate of contact oxidation is mainly affected by these three factors: (1) the amount of species adsorbed on the catalyst surface, which is closely related to the interaction strength between the catalyst and the reactant; (2) the reactivity or stability of the adsorbed species of the reactants, and (3) the availability of surface oxygen.

When the Bi_2O_3 content in the catalyst increases, the oxidation activities for the olefins of C_4—C_7 vary in a fashion similar to the activity for the dehydration of alcohol to olefin, which was adopted as a measure of the acidity of the catalyst, assuming that the dehydration occurs at acid sites of the catalyst.[5] This indicates that the oxidation activities for higher olefins, as well as those for butene and butadiene,[2,3] are intimately related to the acidity of the catalyst. According to the closeness of their ionization potential, if the amount of the adsorption is of about the same

5) M. Ai and S. Suzuki, This Bulletin, **46**, 321 (1973).

order of magnitude in C_4—C_7 olefins, the difference in the activities for these olefins observed in the Bi_2O_3-rich composition (Bi/Mo=1—2) may be attributed to the difference in reactivity of their adsorbed species, presumably in the C–H bond-strength at the allylic position, as has been suggested by Adams *et al.*[6] In the cases of the low Bi_2O_3 content catalyst (Bi/Mo< 0.15), the difference in the oxidation rate of these olefins is not so great. Probably the rate is limited, to some extent, by the activation of oxygen because the adsorption of olefin is strong and almost reaches its saturation point, while that of oxygen is very weak.[3]

On the other hand, the activity for propylene and ethylene varies in a way different from the activity for higher olefins; this way cannot be explained directly by the adsorptive nature of the olefins. However, the fact that the interaction of the catalyst with oxygen increases with an increase in the Bi_2O_3 content[3] seems to suggest that the availability of surface oxygen increases with the Bi_2O_3 content. On this assumption, it may be considered that the lower olefins resist oxidation more strongly than the higher olefins, and that their oxidation requires more activated oxygen, that is, a higher Bi_2O_3 content catalyst.

The difference in the reactivity between butene and butadiene at various Bi/Mo ratios can be explained by the difference in their adsorption nature, that is, their basicity. As the ionization potential of butadiene (8.75—9.18 eV) is lower than that of butene (9.3—9.8 eV), the basicity of butadiene is presumably higher than that of butene. Thus, butadiene is adsorbed more strongly on the Bi_2O_3-poor catalysts and less strongly on the Bi_2O_5-rich catalysts, than is butene.

Regarding the oxidation of saturated carboxylic acids and aldehydes, it may be reasonable to consider that the carboxylic and carbonyl group play main roles in their adsorption. In the case of acid, since both acid and oxygen act as electron acceptors and since these adsorptions are promoted with an increase in the Bi_2O_3 content, the oxidation activity increases steadily with the Bi_2O_3 content. The high reactivity of the saturated aldehyde compounds may be attributed to the nature of their carbonyl group polarizing as $-C^+-O^-$, which can be attacked either by an electron-donor-type (basic) or by an electron-acceptor-type (acidic) reagent. The shapes of the curves in Fig. 5 follow the same trend as those for higher olefins. This suggests that the saturated aldehydes are, rather, basic compounds, and that they are inclined to be attacked by an electrophilic reagent.

The presence of a double bond in an aldehyde or an acid molecule increases their stability markedly. This may be, in part, due to a resonance-stabilization by their conjugated double bond, but it may be also attributed to the difference in the character of adsorption. As has been mentioned by Gorshkov *et al.*[7] some of these compounds, *e.g.*, acrolein, may be linked with the catalyst by a double bond and may thus form stable π-complexes. The stability of the adsorbed species is so great that the oxidation of acrolein may require highly activated oxygen—that is, a higher-Bi_2O_3-content catalyst.

Finally, according to the data obtained in this and past studies,[1,2,6,8,9] the relationship between the character of the partial oxidation of organic compounds and the nature of the catalyst can be generalized as follows:

a) Formation of acids from olefins and furan: an acidic catalyst (low Bi_2O_3 catalyst) is favarable, and a relatively good yield can be expected because the products is much more stable than the reactant.

b) Formation of diene from mono-olefin: the high Bi_2O_3 content catalyst has an advantage in selectivity, but the Bi_2O_3 content is limited from the point of view of the activity. Bi/Mo=1—2, therefore, is considered to be optimum.

c) Formation of acrolein from propylene: the Bi_2O_3 content of Bi/Mo=1—2 is favorable both in the activity and in the selectivity.

d) Formation of crotonaldehyde from olefin: it is difficult to get a good result, for crotonaldehyde is more reactive than olefin over every catalyst.

6) H. H. Voge and C. R. Adams, "Advance in Catalysis," Vol. 17, ed. by D. D. Eley, H. Pines, and P. B. Weisz, Academic Press, New York and London (1967), p. 151.

7) A. P. Gorshkov, I. K. Kolchin, A. M. Gribov, and L. Ya. Margolis, *Kinet. Katal.*, **9**, 1086 (1967).

8) M. Ai, *Kogyo Kagaku Zasshi*, **74**, 183 (1971).

9) Ph. A. Batist, B. C. Lippens, and G. C. A. Schuit, *J. Catal.*, **5**, 55 (1965).

The Condensation Reactions of 5-Azidotropolone Derivatives with Active Methylene Compounds[1)]

Hiroshi HORINO* and Takashi TODA

Department of Chemistry, Faculty of Science, Tohoku University, Aoba, Aramaki, Sendai

(Received April 20, 1972)

The reactions of 5-azidotropolone (I), its methyl ether (II), and tosylate (XIII) with active methylene compounds were investigated. Several tropolones and azulenes which possess the 1,2,3-triazole ring as a substituent were obtained. The order of reactivities in these reactions were found to be: tropolone tosyl groups>azido groups>tropolone methyl ether groups. The direction of the addition of the azido groups to active methylene compounds was also clarified.

In 1902, Dimroth reported that the reaction of phenyl azide with ethyl acetoacetate gave a 1,2,3-triazole derivative,[2)] and this type of reactions has been reviewed by Benson and Savell.[3)]

Recently, much attention has been focused on organic azido compounds, because of their interesting 1,3-dipolar characteristics, and on nitrene-formation reactions.[4)] We ourselves have also been interested in azido derivatives of troponoid compounds and have investigated several reactions of 5-azidotropolones.[1,5)]

Active troponoid compounds have been known to give azulene derivatives or their related compounds by reactions with active methylene compounds.[7)] As a part of our studies of azidotropolones, we have investigated the reactions of 5-azidotropolones with active methylene compounds in order to obtain the 1,2,3-triazole derivatives of troponoid and azulenoid compounds and to investigate their properties.

5-Azidotropolones possess two active centers in their molecules toward active methylene compounds. Therefore, their order of reactivity is interesting. Moreover, if the addition reactions take place, the direction of addition to the azido group must be determined, because the direction will indicate the degree of interaction between the azido group and tropolone moiety.

The treatment of 5-azidotropolone methyl ether (II) with an excess of ethyl cyanoacetate afforded a crystalline substance (III). The elemental analysis of III ($C_{21}H_{23}O_6N_5$) showed that III was a condensation product of II with three moles of ethyl cyanoacetate. The UV and visible spectra of III are agreeable to classifying it as an azulene derivative,[7)] and the NMR spectrum of III shows two peaks (2H, d, J=11 Hz respectively) at 9.10 and 7.46 ppm which correspond to adjacent hydrogens on the seven-membered ring moiety.[8)] The IR spectrum of III shows the existence of two different kinds of amino groups (3545, 3488, and 3380 cm^{-1}) and of ester groups (1680 and 1656 cm^{-1}). Therefore, the structure of III is 2-amino-1,3-diethoxycarbonyl-6*N*-(5′-amino-4′-ethoxycarbonyl-1,2,3-triazol-1-yl)azulene, and the attack of ethyl cyanoacetate takes place at the azido group and the tropolone moiety at the same time. Also, the reaction of II with malononitrile gave 2-amino-1,3-dicyano-6*N*-(5′-amino-4′-cyano-1,2,3-triazol-1-yl)azulene (IV).

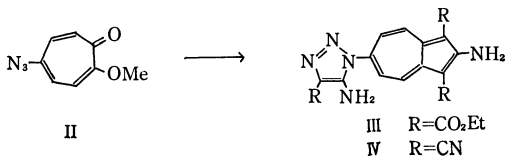

II

III R=CO_2Et
IV R=CN

When II was treated with a rather weak active methylene compound—diethyl malonate, a sodium salt (V) was obtained. The acid treatment of V afforded a yellow crystalline substance (VI), whose molecular formula was agreeable with $C_{13}H_{13}O_5N_3$; VI also showed a strong absorption at 2140 cm^{-1} in its IR spectrum. These data suggest that VI possesses an azido or diazo group.[9)] If the azido group of II was kept unchanged, VI might be 6-azido-3-ethoxycarbonyl-1-oxaazulan-2-one. However, the UV and visible spectra of VI are not of the oxaazulanone type,[6,7)] but are very similar with those of tropolone methyl ethers. Thus, the structure of VI is 5α-diazo-α-ethoxycarbonyl-acetylamino-2-methoxytropone, and V is the sodium salt of the ring-closed enol tautomer of VI. VI is interchangeable with V upon treatment with sodium hydroxide. This relaxation is also proved by the following fact: when the silver salt of VI was treated with methyl iodide, the enol ether of VI—5-(4′-ethoxycarbonyl-5′-methoxy-1,2,3-triazol-1-yl)-2-methoxytropone (VII)—was obtained. The existence of this type of ring-chain tautomer was suggested by Dimroth[10)] and proved by Leffler.[11)]

1) Presented at 18th Annual Meeting of the Chemical Society of Japan, Osaka, April, 1965.

* Present address: College of General Education, Tohoku University, Kawauchi, Sendai.

2) O. Dimroth, *Ber.*, **35**, 1029 (1902).

3) F. R. Benson and W. L. Savell, *Chem. Rev.*, **46**, 1 (1950).

4) G. Lâbbe, *ibid.*, **69**, 345 (1969), and the references cited therein.

5) T. Toda, H. Horino, and T. Nozoe, This Bulletin, **45**, 226 (1972).

6) T. Nozoe, K. Takase, and H. Matsumura, "Dai Yuki Kagaku," (Comprehensive Organic Chemistry), Vol. 13, ed. by M. Kotake, Asakura Shoten, Tokyo (1960), p. 178.

7) a) T. Nozoe and T. Asao, *ibid.*, p. 439. b) T. Nozoe, S. Seto, K. Takase, S. Matsumura, and T. Nakazawa, *Nippon Kagaku Zasshi*, **86**, 346 (1965), and the references cited therein.

8) H. Sugiyama, *Sci. Repts. Res. Inst. Tohoku Univ., Ser.. A*, **20**, 34 (1968).

9) L. J. Bellamy, "Advances in Infrared Group Frequencies," Methuen, London (1968), pp. 62—64.

10) O. Dimroth, *Ann.*, **373**, 349 (1910).

11) J. E. Leffler and S. K. Lim, *J. Amer. Chem. Soc.*, **78**, 1949 (1956).

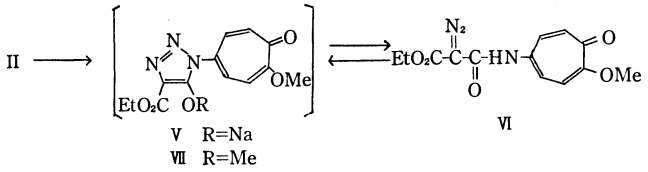

V R=Na
VII R=Me

VI

In order to obtain stable triazole derivatives, the reactions of II with suitable active methylene compounds which should not enolized at the C-5 position of the triazole ring were carried out. These compounds were ethyl acetoacetate, acetylacetone, ethyl benzoylacetate and dibenzoylmethane. The products obtained are listed in Table 1. Although the active methylene compounds were used in excess amounts, no azulene or oxaazulane formation was observed in any case. The methoxy groups in the tropone moieties of X and XI were replaced by the ethoxy group of the solvent used during the reactions.

Table 1.

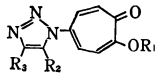

	R_1	R_2	R_3
VII	Me	OMe	CO_2Et
VIII	Me	Me	CO_2Et
IX	Me	Me	COMe
X	Et	Ph	CO_2Et
XI	Et	Ph	COPh

Under the same conditions as above, the reaction of I itself with malononitrile, cyano acetoacetate, and other active methylene compounds was examined. The reaction with malononitrile gave the corresponding triazolyltropolone (XII). However, with other active methylene compounds it did not give any condensation products, but resulted in the recovery of the starting substances. The reason why the reactivity of the azido group of I is lower than that of II is that the tropolone anion is formed under the reaction conditions and the electron density on the azido group become higher than that of II. This phenomenon is shown below as the resonance contribution of the anion:

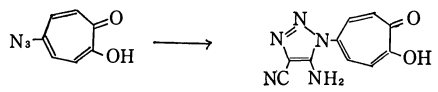

I XII

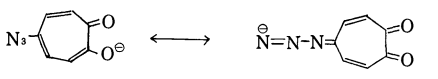

Thus, the condensation reaction did not take place except with a strong, active methylene compound such as malononitrile.

The reaction of the tosylate (XIII) of I with malononitrile afforded an azulene derivative (XIV) which differs from III. The IR spectrum of XII shows absorptions at 877 and 800 cm^{-1}. Those correspond to an isolated hydrogen and the three adjacent hydrogens on the seven-membered ring moiety[12] of XIV. It had previously been established that 2-halotropones and tropolone tosylates gave abnormal substitution products or addition products in those reactions.[7,13] The structure of XIV is 2-amino-1,3-dicyano-5*N*-(5′-amino-4′-cyano-1,2,3-triazol-1-yl)azulene.

When this reaction was carried out under controlled conditions, a minor product (XV) was also obtained in addition to XIV. The elemental analysis ($C_{12}H_6N_6$), the IR spectrum (2110 cm^{-1}, N_3: 872 and 787 cm^{-1}, an isolated hydrogen and three adjacent hydrogens respectively), and the UV and visible spectra (typical azulene type) all suggested that the structure of XV was 2-amino-5-azido-1,3-dicyanoazulene.

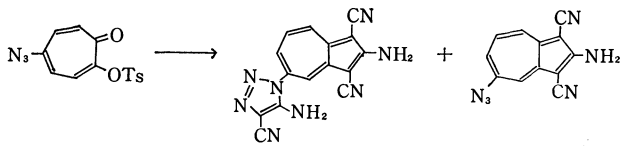

XIII XIV XV

The results obtained above indicate that the order of the reactivity of the each functional group with active methylene compounds is : the tosyl group> the azido group>the methyl ether group.

As far as the 1,3-dipolar character of the azido group is concerned,[4,14] there are two possible 1,2,3-triazole ring formation by the reaction of azidotropolones with acetive methylene compounds. In the cases of phenyl azides, it has been proved that the 1,2,3-triazole derivatives formed are of the A type.[4,15]

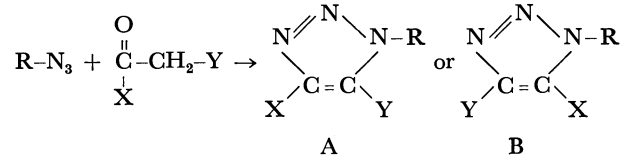

A B

No special interactions between the 5-azido groups and tropolone moieties were observed in several reactions of 5-azido tropolones.[5] Therefore, the direction of the addition of the above condensation might be similar to the case of phenyl azides. In order to clarify this question, the following experiments were carried out. The rearrangement of VIII with sodium ethoxide[16] and subsequent hydrolysis afforded *N*-phenyl-1,2,3-triazole dicarboxylic acid. On the other hand, the condensation reaction of methyl *p*-azido-

12) Y. Ikegami, Kagaku no Ryoiki, Special Issue, "Infrared Spectra," No. 8, Nanko-Do, Tokyo (1958), p. 33.

13) T. Sato, *Nippon Kagaku Zasshi*, **80**, 1342, 1345, 1349 (1959).
14) R. Huisgen, *Angew. Chem.*, **75**, 604 (1963).
15) M. E. Munk and Y. Y. Kim, *J. Amer. Chem. Soc.*, **80**, 2213 (1964).
16) T. Nozoe, K. Takase, and H. Matsumura, "Dai Yuki Kagaku," (Comprehensive Organic Chemistry), Vol. 13, ed. by M. Kotake, Asakura Shoten, Tokyo (1960), p. 186.

benzoate[17] with ethyl acetoacetate gave the *N*-phenyl-1,2,3-triazole dicarboxylic acid mentioned above. Therefore, the structure of VIII and the direction of the addition of active methylene compounds to II are proved.

When the methyl ether of XII was treated with malononitrile, IV was obtained in a good yield. Therefore, in this case the direction of the addition of the active methylene compounds is proved to be the same as in the case of phenyl azides. Therefore, the influence of the tropolone moiety on the azido group is not strong enough to change the direction of the addition of active methylene compounds to the azido group.

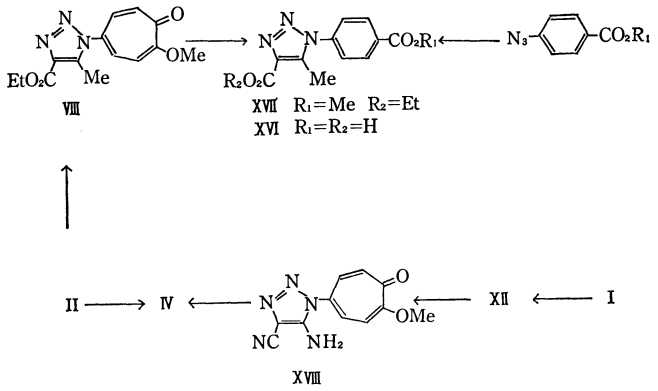

Experimental[18]

The Reaction of II with Ethyl Cyanoacetate. Into a solution of 2.1 g of ethyl cyanoacetate and 130 mg of sodium in 10 ml of absolute ethanol, 1.0 g of 5-azido-2-methoxytropone (II) was stirred; the mixture was then allowed to stand overnight. The precipitate formed was collected and extracted with hot benzene to give 1.14 g of yellowish-orange crystals of 2-amino-1,3-diethoxycarbonyl-6*N*-(5′-amino-4′-ethoxycarbonyl-1,2,3-triazol-1-yl)azulene (III), which were recrystallized from benzene; mp 237 °C (dec).

Found: C, 57.34; H, 5.61; N, 15.70%. Calcd for $C_{21}H_{23}O_6N_5$: C, 57.13; H, 5.25; N, 15.87%. λ_{max}, mμ(log ε); 246 (4.3), 332 (4.7), 418 (3.9). ν_{max}(KBr); 3546, 3485, 3380, 1680, 866, 844 cm^{-1}.

The Reaction of II with Malononitrile. Into a mixture of 270 mg of triethylamine and 270 mg of malononitrile in 3 ml of absolute ethanol, 200 mg of II was stirred while the mixture was being cooled in an ice bath. After the mixture had been allowed to stand for 4 hr, the precipitates formed were collected to yield 390 mg of a yellow powder of 2-amino-1,3-dicyano-6*N*-(5′-amino-4′-cyano-1,2,3-triazol-1-yl)azulene (IV), which was subsequently recrystallized from dimethylformamide; mp 280 °C (dec).

Found: C, 60.41; H, 2.75; N, 37.39%. Calcd for $C_{15}H_8N_8$: C, 59.99; H, 2.69; N, 37.32%. λ_{max}, mμ (log ε); 231 (4.49), 328 (5.29), 404 (3.75). ν_{max}; 3500, 3390, 3280, 2230, 858, 833 cm^{-1}.

The Reaction of II with Diethyl Malonate. Two hundred mg of II were dissolved in a solution of 650 mg of diethyl malonate and 35 mg of sodium in 3 ml of absolute ethanol. After the mixture had stood overnight, the precipitates were separated and washed with 2 M hydrochloric acid to leave 166 mg of yellow crystals of 5α-diazo-α-ethoxycarbonylacetylamino-2-methoxytropone (VI), which were subsequently recrystallized from ethanol; mp 144 °C.

Found: C, 53.46; H, 4.67; N, 14.43%. Calcd for $C_{13}H_{13}O_5N_3$: C, 53.61; H, 4.50; N, 14.43%. λ_{max}, mμ (log ε); 225 (4.41), 244 (4.33 sh), 340 (4.16). ν_{max}; 2140, 1685, 1630, 881, 857 cm^{-1}.

5-(4′-Ethoxycarbonyl-5′-methoxy-1,2,3-triazol-1-yl)-2-methoxytropone (VII). The precipitate made from a mixture of 1.30 g of II, 2.15 g of diethyl malonate, and 175 mg of sodium in 8 ml of absolute ethanol according to the above method was dissolved in 15 ml of water, and to this we added an excess aqueous solution of silver nitrate. The greenish gray deposits were collected, dried, and weighed (245 mg). A suspension of this precipitate and 460 mg of methyl iodide in 6 ml of acetone was then refluxed on a water bath for 5 hr. After it had been filtered, the solution was concentrated and the residue was recrystallized from ethanol to afford 87 mg of yellow crystals (VII); mp 211 °C.

Found: C, 54.69; H, 5.19; N, 13.60%. Calcd for $C_{14}H_{15}O_5N_3$: C, 55.08; H, 4.95; N, 13.77%. λ_{max}, mμ (log ε); 224 (4.41), 246 (4.41), 334 (4.17). ν_{max}; 1721, 1695, 1670, 851, 844 cm^{-1}.

The Reaction of II with Ethyl Acetoacetate. To a solution of 2.24 g of ethyl acetoacetate and 194 mg of sodium in 10 ml of absolute ethanol, 1.4 g of II was added at once with cooling in an ice bath; the mixture was then allowed to stand overnight. The collection of the precipitate and washing with 2 M hydrochloric acid gave 2.20 g of yellow needles of 2-methoxy-5*N*-(4′-ethoxycarbonyl-5′-methyl-1,2,3-triazol-1-yl) tropone (VIII); mp 178 °C from alcohol.

Found: C, 58.30; H, 5.26; N, 14.41%. Calcd for $C_{14}H_{15}O_4N_3$: C, 58.12; H, 5.23; N, 14.53%. ν_{max}; 1721, 1637, 851, 833 cm^{-1}.

The Reaction of II with Acetylacetone. Into a mixture of 250 mg of acetylacetone and 26 mg of sodium in 2.5 ml of absolute ethanol, 200 mg of II were stirred. After the solution had been allowed to stand overnight, the precipitate produced was collected to yield 242 mg of yellow plates, 2-ethoxy-5*N*-(5′-methyl-4′-acetyl-1,2,3-triazol-1-yl)tropone (IX); mp 170 °C.

Found: C, 60.45; H, 5.28; N, 16.20%. Calcd for $C_{13}H_{13}O_3N_3$: C, 60.22; H, 5.50; N, 16.21%. λ_{max}, mμ (log ε); 243 (4.49), 326 (4.15). ν_{max}; 1692, 862, 855 cm^{-1}.

The Reaction of II with Ethyl Benzoylacetate. Two hundred mg of II were added to a solution prepared from 434 mg of ethyl benzoylacetate and 26 mg of sodium in 2 ml of ethanol. After it had stood overnight in a refrigerator, the deposits were separated and crystallized from ethanol to afford 402 mg of colorless crystals of 2-ethoxy-5*N*-(4′-ethoxycarbonyl-5′-phenyl-1,2,3-triazol-1-yl)tropone (X); mp 217 °C.

Found: C, 66.54; H, 5.44; N, 11.84%. Calcd for $C_{20}H_{19}O_4N_3$: C, 65.74; H, 5.24; N, 11.50%. λ_{max}, mμ (log ε); 228 (4.52), 246 (448 sh), 328 (4.12). λ_{max}; 1730, 843, 811, 780, 709 cm^{-1}.

The Reaction of II with Dibenzoylmethane. Two hundred mg of II were added to a solution of 560 mg of dibenzoylmethane dissolved in a sodium ethoxide solution (sodium (35 mg) and absolute ethanol (6 ml)). The orange solution was then concentrated, acidified with 2 M hydrochloric acid, and extracted with benzene to give 400 mg of orange prisms of 2-ethoxy-5*N*-(4′-benzoyl-5′-phenyl-1,2,3-triazol-1-yl)tropone (XI), which were subsequently recrystallized from ethanol; mp 164°C.

17) M. O. Foster and H. M. Judd, *J. Chem. Soc.*, **97**, 259 (1910).
18) All the melting points are uncorrected.

Found: C, 72.65; H, 4.92; N, 10.55%. Calcd for $C_{24}H_{19}O_3N_3$: C, 72.53; H, 4.82; N, 10.57%. λ_{max}, mμ (log ε); 228 (4.46), 252 (4.49), 328 (4.14). ν_{max}; 1618, 1580, 820, 752, 739, 709 cm^{-1}.

The Reaction of 5-Azidotropolone (I) with Malononitrile. An alcoholic solution of 200 mg of I, 180 mg of malononitrile, and 410 mg of triethylamine was stirred for 12 hr. The solvent was then evaporated, and the residue was acidified with 2 M hydrochloric acid to afford 95 mg of a brown powder of 5*N*-(5'-amino-4'-cyano-1,2,3-triazol-1-yl)tropolone (XII), which was recrystallized from DMF; mp 256 °C (dec).

Found: C, 52.24; H, 3.50; N, 30.30%. Calcd for $C_{10}H_7O_2N_5$: C, 52.40; H, 3.08; N, 30.56%. λ_{max}, mμ (log ε); 227 (4.41); 246 (4.20), 346 (3.88).

The Reaction of I with Ethyl Cyanoacetate. Two hundred mg of I, 170 ml of ethyl cyanoacetate, and 270 mg of triethylamine were treated as above. The precipitates given by acidification, when extracted with ethyl acetate from its mother liquid, afforded about 160 mg of I.

The Reaction of 2-(p-Toluenesulfonyloxy)tropone (XIII) with Malononitrile. A suspension of 300 mg of XIII and 204 mg of malononitrile in 2 ml of absolute ethanol was treated with a solution of 100 mg of triethylamine in 2 ml of absolute alcohol. The solution was stirred for 1 hr and then allowed to stand for 7 hr. The precipitates were collected and extracted with hot ethanol. This afforded 69 mg of a brown powder of 5-azido-2-amino-1,3-dicyanoazulene (XV); mp 290°C.

Found: C, 60.97; H, 2.73; N, 36.12%. Calcd for $C_{12}H_6N_6$: C, 61.53; H, 2.58; N, 35.88%. λ_{max}, mμ (log ε); 238 (4.23), 326 (4.45 sh), 336 (4.56), 403 (4.37). ν_{max}; 3350, 3215, 2220, 2110, 872, 787 cm^{-1}.

The non-extractable residue was recrystallized from DMF to afford a yellowish-organge powder of 2-amino-1,3-dicyano-5*N*-(5'-amino-4'-cyano-1,2,3-triazol-1-yl)azulene (XIV); mp 300 °C (dec).

Found: C, 60.36; H, 2.95; N, 36.92%. Calcd for $C_{15}H_8N_8$: C, 59.99; H, 2.69; N, 37.32%. λ_{max}, mμ (log ε); 230 (4.23), 315 (4.27), 238 (4.50), 410 (3.61), 426 (4.80). ν_{max}; 3400, 3280, 2230, 877, 800 cm^{-1}.

The Determination of the Structures of the Condensed Products. *a) The Condensation Reaction of p-Methoxycarbonylphenyl Azide*: To a solution of 150 mg of sodium and 950 mg of ethyl acetoacetate in 2 ml of absolute ethanol, 1.0 g of *p*-methoxycarbonylphenyl azide was added, after which the mixture was cooled in an ice bath. It was allowed to stand for 7 hr, and washed with 2 M hydrochloric acid to afford 1.1 g of colorless plates of 1*N*-*p*-methoxycarbonylphenyl-4-ethoxycarbonyl-5-methyl-1,2,3-triazol (XVII), which was recrystallized from ethanol; mp 174—175 °C.

Found: C, 58.14; H, 5.25; N, 14.64%. Calcd for $C_{14}H_{15}O_4N_3$: C, 58.12; H, 5.23; N, 14.53%. ν_{max}; 2130, 1718, 1285, 852, 841, 765 cm^{-1}.

A solution of 500 mg of XVI, 3 ml of 2 M sodium hydroxide, and 2 ml of ethanol was refluxed for 1 hr, and then acidified with 6 M hydrochloric acid to give 390 mg of colorless, amorphous 4*N*-(4'-carboxyl-5'-methyl-1,2,3-triazol-1-yl)benzoic acid (XVI), which was subsequently recrystallized from ethanol; mp 235°C (dec).

Found: C, 53.88; H, 3.82; N, 16.75%. Calcd for $C_{11}H_9O_4N_3$: C, 53.44; H, 3.67; N, 17.00%. ν_{max}; 2940～2860, 2680～2654, 1685, 859 cm^{-1}.

b) The Rearrangement of VIII: A solution of 0.5 g of VIII in a sodium ethoxide mixture (sodium (87 mg) and absolute ethanol (10 ml)) was refluxed for 16 hr on an oil bath. After the evaporation of the solvent and the addition of water, the solution was heated for 1 hr on a water bath. Then it was acidified with 2 M hydrochloric acid and extracted with ethyl acetate, which had itself been extracted with a sodium bicarbonate solution. It was acidified to afford 200 mg of a colorless powder which can be identified with the XVI given in *a)* by a comparison with their IR spectra and by a mixed-melting-point-test.

The Reaction of XII with Ethyl Cyanoacetate. *a)* To a solution of 200 mg of XII in 200 ml of ethyl acetate in 5 ml DMF, an ethereal diazomethane solution was added until no color change was shown by a ferric chloride test. After it had then been allowed to stand overnight, the solution was concentrated to give 141 mg of a gray powder of 5*N*-(5'-amino-4'-cyano-1,2,3-triazol-1-yl)-2-methoxytropone (XVIII); mp 233 °C (dec).

Found: C, 54.78; H, 3.99; N, 28.31%. Calcd for $C_{11}H_9O_2N_5$: C, 54.32; H, 3.73; N, 28.80%.

b) Into a solution of 100 mg of triethylamine and 65 mg of malononitrile in 2 ml of absolute ethanol, 100 mg XVIII was stirred; the mixture was then allowed to stand for 3 days. The precipitates were collected to afford 143 mg of a gray powder which was found to be identical with IV by a comparison with their IR spectra.

The authors are very much indebted to Professor Tetsuo Nozoe for his kind encouragement and guidance during the course of their work.

The Calculation of Dipole Polarizability and Anisotropy by the CNDO Method

Tomoo MIYAZAKI and Hiroyuki SHINODA

Department of Applied Chemistry, Faculty of Science and Engineering, Waseda University, Nishi-Ohkubo, Shinjuku-ku, Tokyo 160

(Received May 23, 1972)

The dipole polarizabilities and the anisotropies of small linear molecules have been calculated according to a formula in which the frequency of the incident light is taken into account, as derived by the time-dependent perturbation theory. The wave functions and the energies were calculated by the CNDO method, involving the configuration interaction treatment. The effect of the parametrization in the CNDO method on the calculated polarizability and anisotropy has also been discussed. The method has been used to calculate the variations in the anisotropy, the polarizability, α, and its derivatives, $(\partial\alpha/\partial S_i)_0$ and $(\partial^2\alpha/\partial S_i^2)_0$, with the frequency of the incident light, where S_i is the appropriate symmetry coordinate of the molecular vibration.

There have been published several reports in which the polarizability has been investigated theoretically.[1-6] The variational-perturbation method has been applied to calculate the polarizability by several investigators. From the results of this treatment using the LCAO–MO functions of the Roothaan type for the zero-order wave functions, O'Hare and Hurst[1] suggested that the calculated polarizability can be used to determine whether or not the wave functions are appropriate, since the theoretical polarizability is sensitive to the zero-order wave functions. Liebmann and Moskowitz[2] discussed the results of the calculations for the polarizabilities of many compounds by this method. They compared the polarizabilities calculated by the use of different types (Slater- and Gaussian-types) of atomic orbitals with each other. Also, Sadlej[3] calculated the polarizability by the variational-perturbation method, using the complete neglect of differential overlap (CNDO) version, and compared the results of his calculations with those of the non-empirical calculations. He concluded that the CNDO version can be adapted for the calculation of the polarizability.

Davies[4] discussed the theoretical polarizability calculated from the first-order perturbed wave functions in the self-consistent perturbation theory within the framework of the CNDO approximation. From a comparison between the results of calculations in which the 2p orbitals of the hydrogen atom are and are not considered, he concluded that the valence orbital basis set, which is generally used in the LCAO–MO method, was inadequate for the representation of the perturbed wave functions. In the method described above, the perturbing term in the molecular Hamiltonian which arises from the interaction between the molecule and the uniform electric field, **E**, is $H' = -e\sum_i \mathbf{r}_i \cdot \mathbf{E}$, where $\mathbf{r}_i$ is the position vector of the i-th electron.

The finite perturbation theory has been used by Hush and Williams[5,6] to investigate the polarizability and the anisotropy. In this method, the SCF calculation was performed for an appropriate system including an molecule plus a fixed charge on the molecular axis.

Although the polarizability is dependent upon the frequency of the incident light, all the theoretical treatments described above do not take the contribution of the frequency of the incident light into account. In this work, however, an approximate method which is dependent upon the frequency of the incident light has been used to calculate the polarizability of several small molecules. The total wave function used to calculate the polarizability has been obtained by the CNDO method,[7-11] involving the configuration interaction treatment. The dependence of the values of the polarizability and the anisotropy on the frequency of the incident light has been discussed. Moreover, the effect of the parametrization in the CNDO method on the calculated polarizability has been discussed. Furthermore, for example, this approximate method has been used to estimate the dependence of the polarizability derivatives, $(\partial\alpha/\partial S_i)_0$ and $(\partial^2\alpha/\partial S_i^2)_0$, on the frequency of the incident light, where α is the molecular polarizability, and S_i, an appropriate symmetry coordinate.

Methods of Calculation

The Molecular Polarizability. The perturbed wave function (Ψ_a) of the system in the electromagnetic field is represented by the wave functions (Ψ^0's) of the system in the absence of the field:[12]

$$\Psi_a = \Psi_a^0 + \sum_b C_b \Psi_b^0, \tag{1}$$

where, if the energy of the incident light is $\varepsilon(=h\nu)$, the C_b is given by the relation:

$$C_b = \frac{iE_{ba}}{2c\hbar}\mathbf{A}_0^0 \cdot \langle \Psi_b^0 | e\sum_i \mathbf{r}_i | \Psi_a^0 \rangle \left\{ \frac{\exp(i(E_{ba}+\varepsilon)t/\hbar)}{E_{ba}+\varepsilon} + \frac{\exp(i(E_{ba}-\varepsilon)t/\hbar)}{E_{ba}-\varepsilon} \right\} + \text{constant}, \tag{2}$$

1) J. M. O'Hare and R. P. Hurst, *J. Chem. Phys.*, **46**, 2356 (1967).
2) S. P. Liebmann and J. W. Moskowitz, *ibid.*, **54**, 3622 (1971).
3) A. J. Sadlej, *Theor. Chim. Acta*, **21**, 159 (1971).
4) D. W. Davies, *Mol. Phys.*, **17**, 473 (1969).
5) N. S. Hush and M. L. Williams, *Chem. Phys. Lett.*, **5**, 507 (1970).
6) N. S. Hush and M. L. Williams, *ibid.*, **6**, 163 (1970).
7) J. A. Pople, D. P. Santry, and G. A. Segal, *J. Chem. Phys.*, **43**, S129 (1965).
8) J. A. Pople and G. A. Segal, *ibid.*, **43**, S136 (1965).
9) J. A. Pople and G. A. Segal, *ibid.*, **44**, 3289 (1966).
10) J. D. Bene and H. H. Jaffé, *ibid.*, **48**, 1807 (1968).
11) J. D. Bene and H. H. Jaffé, *ibid.*, **48**, 4050 (1968).
12) H. Eyring, J. Walter, and G. E. Kimball, "Quantum Chemistry," John Wiley & Sons, New York (1944), p. 118.

where $E_{ba}=E_b-E_a$ $(=h\nu_{ba})$ and where $\mathbf{A}_0^0$ is the vector relating to the electric field, $\mathbf{E}_0$: $\mathbf{E}_0=\varepsilon/c\hbar\ \mathbf{A}_0^0 \sin \varepsilon/h\ t$.

The dipole moment ($\mathbf{R}_a$) associated with the Ψ_a state as a function of the electric field is:

$$\mathbf{R}_a = \langle\Psi_a^0|e\sum_i \mathbf{r}_i|\Psi_a^0\rangle + \frac{2}{h}\sum_b \frac{\nu_{ba}}{\nu_{ba}^2-\nu^2}\langle\Psi_a^0|e\sum_i \mathbf{r}_i|\Psi_b^0\rangle\langle\Psi_b^0|e\sum_i \mathbf{r}_i|\Psi_a^0\rangle\cdot\boldsymbol{E}_0. \quad (3)$$

The first term on the right-hand side in Eq. (3) is the permanent dipole moment of the system. By averaging the vector quantities over all the orientations of the system with respect to the field, the second term can be rewritten as follows:

$$\frac{2}{3h}\sum_b \frac{\nu_{ba}|\langle\Psi_a^0|e\sum_i \mathbf{r}_i|\Psi_b^0\rangle|^2}{\nu_{ba}^2-\nu^2}\mathbf{E}_0 = \alpha\mathbf{E}_0. \quad (4)$$

Thus, the polarizability, α, can be calculated from the quantum-mechanical expression, Eq. (4).

The Molecular Anisotropy. The molecular anisotropy, κ, which determines the depolarization of light scattered by the molecule, is expressed by the components of the polarizability tensor as follows:

$$\kappa^2 = \{(\alpha-\alpha_1)^2+(\alpha-\alpha_2)^2+(\alpha-\alpha_3)^2\}/6\alpha^2, \quad (5)$$

where α_1, α_2, and α_3 are the principal polarizabilities of the molecule. In the case of linear molecules, Eq. (5) can be simplified as follows:

$$\kappa = (\alpha_{//}-\alpha_\perp)/3\alpha = \Delta\alpha/3\alpha, \quad (6)$$

where $\alpha_{//}=\alpha_1$, $\alpha_\perp=\alpha_2=\alpha_3$.

The Molecular Wave Functions. In this calculation, the molecular wave functions, Ψ^0's, in Eq. (1) are described as the antisymmetrized products of one-electron functions and the excited state, Ψ_b^0, is described as a linear combination of the excited configurations (Φ_{i-k}) obtained by the configuration interaction (CI) treatment. The wave functions and energies of the excited states were improved by these CI treatments, but the improvement of the ground state by considering doubly-excited configurations was abridged to avoid tedious computations.

The one-electron wave functions were determined by means of the CNDO method, that is, the approximate self-consistent molecular orbital method with complete neglect of differential overlap. In an effort to determine the effect of the parametrization in the CNDO method on the theoretical polarizability and anisotropy three different types of calculations were performed.

Method I. The calculation followed the original CNDO/2 method proposed by Pople *et al.*[7-9]

Method II. The calculation was performed according to the modified CNDO method proposed by Bene and Jaffé.[10,11]

Method III. In this method, the calculation was performed under the same approximation as Method II except for the evaluation of the bonding parameter. The distinction in estimating the bonding parameters for the pi-type and for sigma-type interaction was avoided, and the bonding parameter referring to the sigma-type interaction was approximated by the adoption of the method for the pi-type interaction. The numerical values of the parameters are indicated in Table 1.

Table 1. Parameter values (eV)

	Atom	H	C	N	O
β_A^0 [a]	Method I	−9	−21	−25	−31
	Method II	−12	−17	−26	−45
γ_{AA} [b]	Method I[c]	20.40	16.06	19.27	22.48
	Method II[d]	12.85	11.11	12.01	13.00

a) Bonding parameter.
b) One-center electron-repulsion integral.
c) Calculated as a Coulomb repulsion integral over Slater's functions. (Z': H(1s) 1.2, C(2s) 3.25, N(2s) 3.9 and O(2s) 4.55).
d) Calculated as a difference between the ionization potential and electron affinity of 1s for H atom and of 2p for C, N, and O atoms.

In order to obtain the excited states, Ψ_b^0's, required to describe the perturbed wave function by means of Eq. (1), the SCF calculations described above were followed by CI treatment. In the CI treatment, all singly-excited configurations were considered. By the use of the coefficients ($c^{(b)}$'s) of the configurations and the transition moment between the ground state and each excited configuration, the integral in Eq. (4) could be calculated as follows:

$$\langle\Psi_a^0|e\sum_i \mathbf{r}_i|\Psi_b^0\rangle = \sum_i^{occ}\sum_k^{unocc} c_{(i-k)}^{(b)}\langle\Psi_a^0|e\sum_i \mathbf{r}_i|\Phi_{i-k}\rangle. \quad (7)$$

The X-component of the integral on the right-hand side of the above equation is expressed by:

$$\langle\Psi_a^0|e\sum_i X_i|\Phi_{i-k}\rangle = -\sqrt{2}\sum_A\{2.5416X_A\sum_\mu d_{i\mu}^{(A)}d_{k\mu}^{(A)} + 7.3370(d_{i(2s)}^{(A)}d_{k(2p_x)}^{(A)}+d_{i(2p_x)}^{(A)}d_{k(2s)}^{(A)})/Z_A'\} \text{ (Debye)}, \quad (8)$$

where $d_{i\mu}^{(A)}$ is the coefficient of the atomic orbital, χ_μ, on the A atom in the molecular orbital, φ_i; where X_A is the X-component of the position vector (atomic unit) of the atom A, and where Z_A' is the orbital exponent of the A atom. The Y- and Z-components of the integral can be obtained in the same manner by replacing $d_{i(2P_X)}$ in Eq. (8) with $d_{i(2P_Y)}$ and with $d_{i(2P_Z)}$ respectively, and by replacing X_A with Y_A and with Z_A respectively.

The Polarizability Derivatives. The molecular polarizabilities were calculated for the molecule distorted in the manner dictated by the appropriate symmetry coordinate. The desired values were obtained by fitting the calculated polarizabilities to a cubic function with respect to the symmetry coordinate and by taking the first and second derivatives.

Results and Discussion

The calculated polarizabilities are, in Table 2, listed and compared with the theoretical and observed values reported by other investigators. The values calculated by Method I were similar in magnitude to those calculated by Hush[5] and Davies.[4] Generally, they were smaller than the experimental results. The calculated polarizabilities were improved by the use of Methods II and III. From a comparison between the results of different calculations, it has been found that the transition energies and transition moments along the

Table 2. Summary of calculated polarizabilities[a] (Å^3)

Molecule	I[b]	II[b]	III[b]	R1[c]	R2[d]	Obsd[e]
N_2	0.754	1.183	1.281	0.647	0.633	1.77
CO	0.933	1.229	1.368	0.829		1.97
CO_2	1.189	1.823	1.960	0.879		2.63
C_2H_2	1.028	1.727	2.190	0.707		3.49
C_2H_4	1.497	2.137	3.068		1.333	4.22
C_2H_6	1.376	1.355	2.655		1.240	4.47

a) Calculated under the condition that the energy of the incident light was equal to zero.
b) Calculated by Methods I, II, and III in this work.
c) From Ref. 5.
d) From Ref. 4.
e) From Ref. 13.

bond axis vary widely from method to method, while the transition moments perpendicular to the bond axis remain unaltered. Moreover, it seems reasonable to conclude that a direct basic cause of the results for the theoretical polarizabilities being different from those found by different approximate methods is the differences between energy levels which are affected by the bonding parameter in the CNDO calculation.

Table 3. Summary of calculated anisotropies[a]

Molecule	I[b]	II[b]	III[b]	R1[c]	R2[d]	Obsd[e]
N_2	0.472	0.595	0.568	0.391	0.369	0.131
CO	0.236	0.339	0.356	0.145		0.090
CO_2	0.727	0.826	0.754	0.634		0.266
C_2H_2	0.683	0.748	0.697	1.000		0.178
C_2H_4[f]	0.446	0.552	0.420			0.143
C_2H_6	−0.019	−0.071	−0.015		0.008	0.058

a), b), c), d), and e) References to footnotes are the same as those in Table 2.
f) The anisotropy was calculated from Eq. (5).

The calculated anisotropies are summarized in Table 3. Generally, they were larger than the experimental results. However, the order of magnitude in the theoretical values for the molecules was in satisfactory agreement with that obtained from the observed results, such as $CO_2 > C_2H_2 > N_2 > CO > C_2H_6$. The values calculated by Method I were slightly improved as compared to those from Methods II and III. Of course, the values of the $\Delta\alpha$'s showed the same tendencies. However, Method II was adapted for the calculation of the polarizability, as has been stated above. This change in the results can be explained by the facts that the $\alpha_{//}$'s calculated by Method II increased remarkably in comparison with those from Method I, but there was not very much change for the values of $\alpha_{\perp}$'s in these different types of calculations. Thus, an approximate method which provides appropriate values for both the α and $\Delta\alpha$ must be found. Furthermore, the effect of the inner-shell electrons and the consideration of the atomic vacant orbitals, such as the 2p orbital for hydrogen introduced by Davies,[4] remain subjects for future study.

The approximate method for the polarizability calculation in this work is characterized by the introduction of the frequency of the incident light. As an example of the application of this method, variations in the polarizability and anisotropy with the frequency of the incident light were calculated. The results of the calculations are shown in Figs. 1 and 2. These figures show that the calculated values vary with the decrease in the difference between the energy of the incident light and the calculated energy for the first absorption band which is allowed for the electron transition. Furthermore, the polarizability derivatives, $\alpha' = (\partial\alpha/\partial S_i)_0$ and $\alpha'' = (\partial^2\alpha/\partial S_i^2)_0$, with respect to the symmetric stretching coordinate, S_i, were calculated for NH_3 and CO_2 by the use of the wave functions and energies calculated by Method I. The variations in

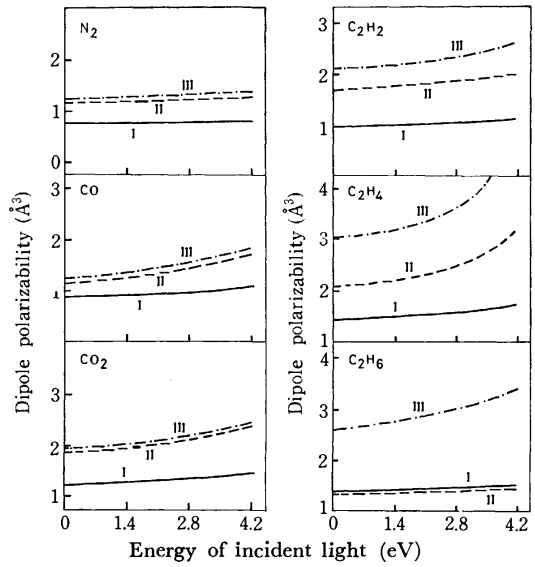

Fig. 1. The variation of the polarizability as a function of the energy of the incident light.
I, II, and III indicate the values calculated by the methods I, II, and III respectively.

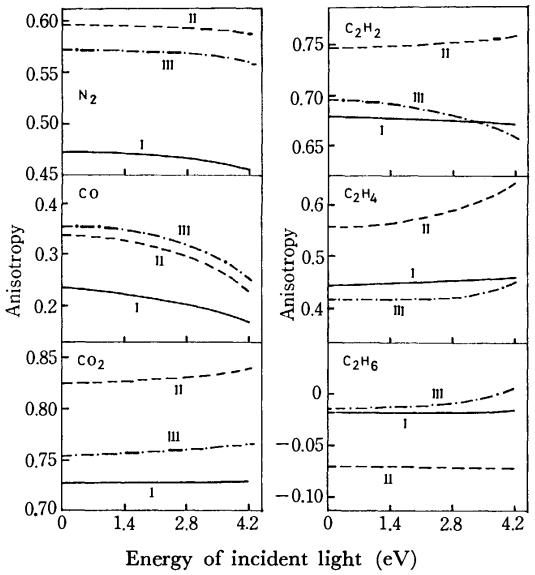

Fig. 2. The variation of the anisotropy as a function of the energy of the incident light.
I, II, and III indicate the values calculated by the methods I, II, and III respectively.

13) N. J. Bridge and A. D. Buckingham, *Proc. Roy. Soc.*, **295**, *A*, 334 (1966).

Table 4. SUMMARY OF POLARIZABILITY DERIVATIVES

Energy of incident light (eV)	CO_2[a,b]		NH_3[a,b]	
	α'(Å²)	α''(Å)	α'(Å²)	α''(Å)
0	1.704	0.829	0.991	0.953
2	1.743	0.883	1.017	0.993
4	1.875	1.082	1.109	1.139
6	2.158	1.600	2.605	2.997
8	2.793	3.211	4.013	6.695
9			7.088	20.563
10	4.820	12.085		
12	34.304	459.015		

a) $\alpha'=\left(\frac{\partial\alpha}{\partial S_i}\right)_0$, and $\alpha''=\left(\frac{\partial^2\alpha}{\partial S_i^2}\right)_0$.

where $S_i=\frac{1}{\sqrt{2}}(\Delta r'_{CO}+\Delta r''_{CO})$ for CO_2,

and $S_i=\frac{1}{\sqrt{3}}(\Delta r'_{NH}+\Delta r''_{NH}+\Delta r'''_{NH})$ for NH_3.

b) Calculated energyies for the first absorption bands were 12.78 eV and 9.98 eV for CO_2 and NH_3 respectively.

the polarizability derivatives with the energy of the incident light were also calculated; they are indicated in Table 4. The α''/α' ratio was calculated as a function with respect to the energy of the incident light; it is shown in Fig. 3. Such a treatment as has been described above can be used for the analysis of the resonance and pre-resonance Raman intensities[14,15] in a manner similar to that used in the infrared region: the dipole-moment derivative, $(\partial\mu/\partial S_i)_0$ and $(\partial^2\mu/\partial S_i^2)_0$, obtained by the CNDO calculation are effective for the theoretical calculation of the infrared absorption intensity of the vibration band.[16–18]

Conclusion

The dipole polarizabilities, α's, and the anisotropies, κ's, of small linear molecules were calculated according to a formula derived from the time-dependent perturbation theory. The method of the calculation in this work is characterized by the introduction of the frequency of the incident light. The calculated polarizabilities were generally smaller than the experimental results. However, the calculated anisotropies and $\Delta\alpha$'s were larger than the observed results. These results of the calculations were discussed on the basis of the values of $\alpha_{//}$ and $\alpha_{\perp}$ calculated with different parametrizations. As an example of the application of this method, the variations in the polarizability and anisotropy with the frequency of the incident light were calculated. Moreover, the polarizability derivatives, $(\partial\alpha/\partial S_i)_0$ and $(\partial^2\alpha/\partial S_i^2)_0$, with respect to the symmetric stretching coordinate, S_i, were calculated for NH_3 and CO_2. Furthermore, the variations in the polarizability derivatives with the energy of the incident light were calculated.

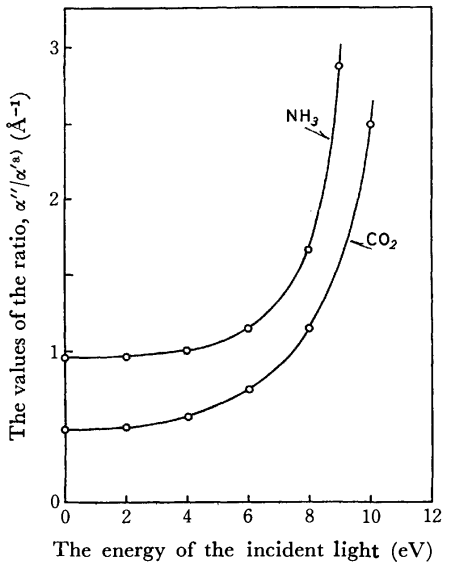

Fig. 3. The variation of the ratio, α''/α',[a] as a function of the energy of the incident light.
a) $\alpha'=(\partial\alpha/\partial S_i)_0$. $\alpha''=(\partial^2\alpha/\partial S_i^2)_0$, where S_i is the symmetry coordinate.

The authors would like to acknowledge the continuing encouragement of Professor K. Higasi. In their calculations, they were helped by the "University Contribution" of UNIVAC Japan, Ltd.

14) W. Hoffmann and H. Moser, *Ber. Bunsenges. Phys. Chem.*, **68**, 129 (1964).
15) H. A. Szymanski, "Raman Spectroscopy," Plenum Press, New York (1967).
16) T. Miyazaki, T. Shigetani, and H. Yamamoto, This Bulletin, **45**, 678 (1972).
17) T. Miyazaki and H. Yamamoto, *ibid.*, **45**, 1669 (1972).
18) I. W. Levin and O. W. Adams, *J. Mol. Spectry.*, **39**, 380 (1971).

Arylation and Vinylation Reactions of Benzo[*b*]furan *via* Organopalladium Intermediates

Akira KASAHARA,* Taeko IZUMI, Minoru YODONO,** Ryu-ichi SAITO, Toru TAKEDA, and Toshiaki SUGAWARA***

Department of Applied Chemistry, Faculty of Engineering, Yamagata University, Yonezawa-shi, Yamagata 992

(Received June 8, 1972)

The Heck reaction of benzo[*b*]furan with arylpalladium chloride leads to the formation of 2-arylbenzo[*b*]-furan derivatives. In the presence of palladium acetate, benzo[*b*]furan reacts in benzene to give 2,2′-bibenzo-[*b*]furyl, accompanied by 2-arylbenzo[*b*]furan. In the phenylation of [2-^{2}H]benzo[*b*]furan with phenylpalladium salts, it was confirmed that no hydride shift takes place in the reaction. In the presence of palladium acetate, benzo[*b*]furan also reacts with olefin to produce benzo[*b*]furyl-substituted olefins, accompanied by a small amount of 2,2′-bibenzo[*b*]furyl, and from the reaction of [β,β-$^2H_2$]styrene and benzo[*b*]furan in the presence of palladium acetate it was confirmed that no hydride shift occurs in the reaction.

It is considered that furan possesses a considerable aromatic character arising from the delocalization of four carbon π-electrons and two paired electrons donated by the oxygen atom. However, furan still has a character which clearly resembles a conjugated diene or enol ether. In order to study whether or not the Heck arylation[1] occurs in the reaction of benzo[*b*]-furan (I) with arylpalladium compounds, the reaction of I with arylmercuric compounds (II) was performed in the presence of palladium salts. This report also contains the results of a study of the reaction of I and olefins in the presence of palladium acetate.

Results and Discussion

In the presence of palladium salts, I was allowed to react with II in polar solvents, such as ethanol. The substitution reaction on the C_2 of I has been observed to lead to the formation of 2-arylbenzo[*b*]furan (III), accompanied by a small amount of biaryl (IV). The reactions carried out are summarized in Table 1. The properties of the products are given in Table 2. Furthermore, in order to study whether or not a hydride shift takes place between the C_2 and C_3 of I in the Heck reaction of I, the reaction of [2-^{2}H]-benzo[*b*]furan (V) with arylpalladium compounds was performed in ethanol at room temperature. The results are summarized in Table II. If the reaction of V with arylpalladium compounds proceeds *via* a hydride shift, the reaction will produce product (III) containing some deuterium on the C_3. However, in the presence of palladium salts, the reactions of V with phenylmercuric

TABLE 1. THE ARYLATION OF BENZO[*b*]FURANS WITH ARYLPALLADIUM COMPOUNDS

Benzo[*b*]furans	Arylating agent	Product	Yield %[a]
Benzo[*b*]furan	Phenylmercuric acetate	2-Phenylbenzo[*b*]furan (III-1)	77
		Biphenyl[b]	7
Benzo[*b*]furan	*p*-Tolylmercuric chloride	2-*p*-Tolylbenzo[*b*]furan (III-2)	79
		Bi-*p*-tolyl[c]	6
Benzo[*b*]furan	*p*-Anisylmercuric chloride	2-*p*-Anisylbenzo[*b*]furan (III-3)	71
		Bi-*p*-anisyl[d]	8
Benzo[*b*]furan	*m*-Nitrophenylmercuric chloride	2-(*m*-Nitrophenyl)benzo[*b*]furan (III-4)	70
		3,3′-Dinitrobiphenyl[e]	5
5-Methylbenzo[*b*]furan	Phenylmercuric acetate	2-Phenyl-5-methylbenzo[*b*]furan (III-5)	75
		Biphenyl[b]	9
5-Methylbenzo[*b*]furan	*p*-Tolylmercuric chloride	2-*p*-Tolyl-5-methylbenzo[*b*]furan (III-6)	72
		Bi-*p*-tolyl[c]	6
5-Methylbenzo[*b*]furan	*p*-Anisylmercuric chloride	2-*p*-Anisyl-5-methylbenzo[*b*]furan (III-7)	66
		Bi-*p*-anisyl[d]	8
5-Methylbenzo[*b*]furan	*m*-Nitrophenylmercuric chloride	2-(*m*-Nitrophenyl)-5-methylbenzo[*b*]furan (III-8)	60
		3,3′-Dinitrobiphenyl	6

a) Yields are based upon the arylating agent.
b) Mp 68—69°C, (lit.[f] mp 69—70°C).
c) Mp 119—120°C, (lit.[f] mp 120°C).
d) Mp 170—171°C, (lit.[f] mp 170—172°C).
e) Mp 201—203°C, (lit.[g] mp 198.5—199.5°C).
f) E. Müller and T. Topel, *Ber.*, **72**, 273 (1939).
g) B. W. Williamson and W. H. Rodebush, *J. Amer. Chem. Soc.*, **63**, 3018 (1941).

* To whom correspondence should be addressed.
** Present address: Mitsubishi Yuka Co., Ltd., Kamisumi-machi, Kashima, Ibaraki.
*** Present address: Mizushima Chemical Co., Ltd., Tsuruoka-shi, Yamagata.

1) R. F. Heck, *J. Amer. Chem. Soc.*, **90**, 5518 (1968); and subsequent papers.

Table 2. Properties and analyses of 2-arylbenzo[*b*]furans (III)

Compound	Mp °C (lit.)	Anal. Found (Calcd) %, C	H	N	IR spectrum (cm^{-1}) and NMR spectrum, ppm (no. of protons).
III-1	120—121 (120—121[a])				
III-2	128—129 (127—129[b])				
III-3	150—151 (151[c])				
III-4	129—130	70.33 (70.28)	3.82 (3.79)	5.86 (5.85)	IR 1530, 1360, 880. NMR δ 7.04 s (1) H on C_3, 7.15—8.14 m (8) aromatic ring protons.
III-5	131—133 (126—129[d])				
III-6	155—156	86.51 (86.44)	6.41 (6.34)		IR 875. NMR δ 2.39 s (3) $-CH_3$, 2.42 s (3) $-CH_3$, 6.88 s (1) H on C_3, 7.15—7.82 m (7) aromatic ring protons.
III-7	172—173 (172[e])				
III-8	157—159	71.29 (71.13)	4.48 (4.37)	5.62 (5.53)	IR 1528, 1355, 882. NMR δ 2.41 s (3) $-CH_3$, 7.04 s (1) H on C_3, 7.17—8.14 m (7) aromatic ring protons

a) P. Yates, *J. Amer. Chem. Soc.*, **74**, 5376 (1952).
b) J. N. Chatterjia and S. K. Roy, *J. Indian Chem.Soc.*, **34**, 98 (1957).
c) M. M. Bokadia, B. R. Brown, and W. Cummings, *J. Chem. Soc.*, **1960**, 3308.
d) F. Wessely and E. Zbiral, *Ann. Chem.*, **605**, 98 (1957).
e) K. K. Thomas and M. M. Bokadia, *J. Indian Chem. Soc.*, **45**, 265 (1968).

Table 3. The reactions of [2-^{2}H]-benzo[*b*]furan (V) with arylmercuric compounds (II)

Arylating agent	Products	Yields (%[a])	D-content of arylbenzo[*b*]furan (III)[b]
Phenylmercuric acetate	III-1	74	0 %[c]
	Biphenyl	6	
p-Tolylmercuric chloride	III-2	76	0 %[c]
	Bi-*p*-tolyl	6	
p-Anisylmercuric chloride	III-3	71	0 %[c]
	Bi-*p*-anisyl		

a) Yields are based upon arylating agent.
b) The deuterium-content of the products was calculated from the mass spectra analyses results.
c) The 60 MHz NMR spectra showed also an absence of *D* in the C_3.

acetate, *p*-tolylmercuric chloride, and *p*-anisylmercuric chloride all result in the formation of III; this indicates that the deuterium content is not at all different from the case of the hydride shift. This clearly shows that no hydride shift occurs in the reaction.

Davidson and Trigg[2] have recently reported that reactions between aryl compounds and palladium salts give arylpalladium complexes, and a biaryl-formation reaction by palladium salts has also been reported.[3] We were interested in whether or not the arylation reaction of I also occurs in the reaction of I, benzene, and palladium acetate, and so the reaction of I with palladium acetate was performed in a solution of acetic acid and benzene for 6 hr. The reactions carried out are summarized in Table 4. Interestingly, in the case of the reaction with benzene, 2,2′-bibenzo[*b*]furyls (VI, homocoupling products) rather than III was formed as the major product, suggesting that the reactivity of I towards palladium acetate is far higher than that of benzene and that I is highly activated by palladium

Table 4. The reactions of benzo[*b*]furans (I) with benzene

Benzo[*b*]furans	Products	Yield %[a]
Benzo[*b*]furan	Biphenyl	4
	III-1	12
	2,2′-Bibenzo[*b*]furyl (VI-1)[b]	68
5-Methylbenzo[*b*]-furan	Biphenyl	5
	III-5	10
	5,5′-Dimethyl-2,2′-bibenzo[*b*]-furyl (VI-2)[c]	70
[2-^{2}H]-Benzo[*b*]-furan	Biphenyl	5
	III-1[d]	11
	VI-1[e]	70

a) Yields are based upon the used benzo[*b*]furans.
b) Mp 194—195°C, (lit.[f] mp 194.5—195.5°C).
c) Mp 217—218°C, IR spectrum: 883 cm^{-1}. NMR spectrum: δ 2.43 s (6) $-CH_3$, 7.01 s (2) furan ring protons, 7.12—7.44 ppm m (6). Found: C, 82.48; H, 5.41%; mol wt 255 (Rast). Calcd for $C_{18}H_{14}O_2$: C, 82.48; H, 5.34%; mol wt 262.
d, e) Deuterium contents of both compounds were 0 % from the mass spectra analyses results and the 60 MHz NMR spectra also showed an absence of D in the furan ring.
f) F. Toda and M. Nakagawa, This Bulletin, **33**, 223 (1960).

2) J. M. Davidson and C. Trigg, *J. Chem. Soc.*, *A*, **1968**, 1324, 1331.
3) R. van Helden and G. Verberg, *Rec. Trav. Chim. Pays-Bas*, **84**, 1263 (1965); J. M. Davidson and C. Trigg, *Chem. Ind.*, **1966**, 457.

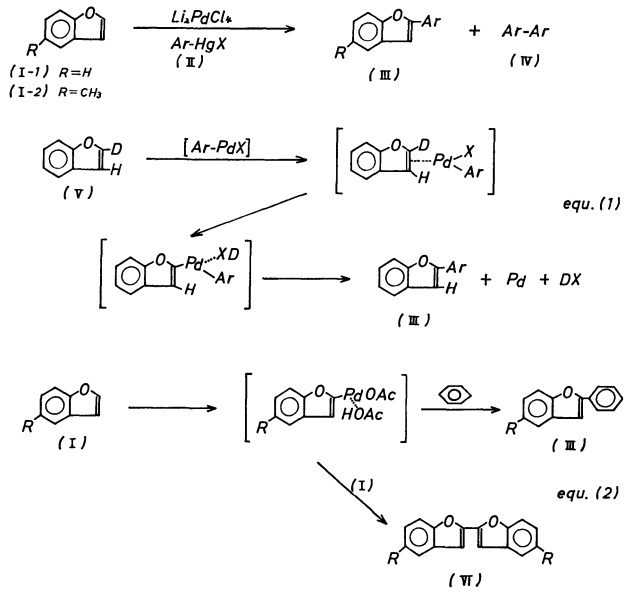

Fig. 1.

salts, thus forming benzo[*b*]furylpalladium salts. The reaction can be explained by Eq. (2) of Fig. 1. Furthermore, the reaction of V and benzene was carried out in the presence of palladium acetate and acetic acid. The deuterium analyses of the products clearly show that no hydride shift occurs in the formation of either VI or III.

On the other hand, Fujiwara *et al.*[4] have described that a reaction mixture of palladium acetate, olefins, benzene derivatives, and acetic acid gives arylation products of olefins. Therefore, in order to investigate the reactivity of I towards olefins, the reaction of I, olefin, and palladium acetate was performed.[5] When a solution of I and olefin in acetic acid was heated at reflux in the presence of palladium acetate, benzo[*b*]furyl-substituted olefin (VII) was obtained as the major product, accompanied by VI. Neither the acetoxylation products of I nor those of olefins were obtained. The results of the reaction are summarized in Table 5. The products were identified by the observation of the IR and NMR spectra (Table 6). For example, the reaction of I-1 with styrene resulted in

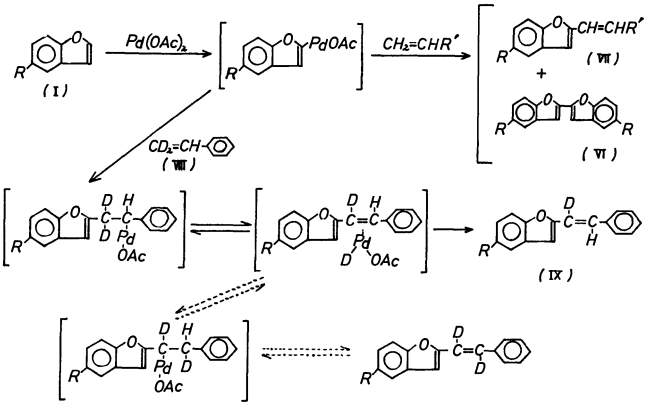

Fig. 2.

TABLE 5. THE REACTIONS OF BENZO[*b*]FURAN (I) WITH OLEFIN

Benzo[*b*]furan	Olefin	Product	Yield %
I–1	Styrene	2-Styrylbenzo[*b*]furan (VII–1)	69
		VI–1	7
I–1	Ethyl acrylate	Ethyl 2-(2-benzo[*b*]furyl)-acrylate (VII–2)	70
		VI–1	5
I–1	Methyl methacrylate	Methyl 2-(2-benzo[*b*]furyl)-methacrylate (VII–3)	53
		VI–1	10
I–1	Ethyl crotonate	Ethyl 2-(2-benzo[*b*]furyl)-crotonate (VII–4)	60
		VI–1	8
I–1	Acrylonitrile	2-(2-Benzo[*b*]furyl)-acrylonitrile (VII–5)	72
		VI–1	8
I–2	Styrene	2-Styryl-5-methylbenzo[*b*]furan (VII–6)	70
		VI–2	6
I–2	Ethyl acrylate	Ethyl 2-(5-methyl-2-benzo[*b*]furyl)-acrylate (VII–7)	67
		VI–2	8
I–2	Methyl methacrylate	Methyl 2-(5-methyl-2-benzo[*b*]furyl)-methacrylate (VII–8)	58
		VI–2	8
I–2	Ethyl crotonate	Ethyl 2-(5-methyl-2-benzo[*b*]furyl)-crotonate (VII–9)	53
		VI–2	9
I–2	Acrylonitrile	2-(5-Methyl-2-benzo[*b*]furyl)-acrylonitrile (VII–10)	62
		VI–2	6
I–2	Methyl vinyl ketone	4-(5-Methyl-2-benzo[*b*]furyl)-3-buten-2-one (VII–11)	67
		VI–2	7
I–2	Acrolein	3-(5-Methyl-2-benzo[*b*]furyl)-2-propenal (VII–12)	55
		VI–2	8

4) Y. Fujiwara, I. Moritani, S. Danno, R. Asano, and S. Teranishi, *J. Amer. Chem. Soc.*, **91**, 7166 (1969); S. Danno, I. Moritani, Y. Fujiwara, and S. Teranishi, *J. Chem. Soc., B*, **1971**, 196.

5) Recently, it has been reported briefly that the reaction of furan and styrene in the presence of palladium acetate resulted in the formation of 2-styrylfuran and 2,5-distyrylfuran: I. Moritani, R. Asano, Y. Fujiwara, and S. Teranishi, Abstracts of Papers Presented at the 26th Annual Meeting of the Chemical Society of Japan (1972), II, p. 1033.

the formation of 2-styrylbenzo[*b*]furan (VII-1), accompanied by a small amount of VI-1. These results indicate that this substitution reaction occurs on the C_2 atom of I and the β-carbon atom of styrene, and also that the reactivity of the benzo[*b*]furylpalladium compounds is far higher toward olefin than toward I. As with Fujiwara's arylation of olefin, it appears that an electron-donating group on olefinic carbon stoms decreases the yields.

Moreover, in order to study whether or not the reaction of I, olefins, and palladium acetate proceeds *via* a hydride shift, the reaction of I with [β,β-$^2H_2$]-styrenes (VIII) was performed in the presence of palladium acetate and acetic acid. If the hydride shift occurs in the reaction of I with VIII, the reaction will produce a mixture of mono- and di-deuterio-derivative of VII. However, the reaction of I with VIII resulted in the formation of monodeuterio-styrylbenzo-[*b*]furans (IX), indicating that the deuterium content is completely different from the case of the hydride shift (D-content=150%). The reaction of V and undeuteriated styrene also produced VII-1, which was free from deuterium. Furthermore, the reaction of V and VIII resulted in the formation of IX. All these results clearly confirmed that no hydride shift takes place in the reaction, and suggested that a loss of hydrido-palladium species from the benzo[*b*]furylpalladium compound-olefin adduct involves the intermediate formation of a hydride-palladium π-complex and is much more likely than the readdition in the reverse direction.

Experimental

Analysis and Materials. All the melting points and boiling points are uncorrected. The infrared spectra were recorded by means of a Hitachi EPI-S IR spectrometer, while the NMR spectra were obtained by a Hitachi H-60 NMR spectrometer at 60 MHz in $CDCl_3$, using tetramethylsilane as the internal standard. Their chemical shifts are recorded as parts per million downfield from tetramethylsilane on the scale, together with the splitting pattern and the relative integrated area: s, singlet; d, doublet; t, triplet; q, quartet; m, multiplet; d-d, double-doublet. The mass spectra were obtained on a Hitachi RMU-6d mass spectrometer, using a direct inlet and an ionization energy of 70 eV.

The palladium acetate was prepared according to the procedure of Wilkinson.[6] The [β,β-$^2H_2$]-styrene (VIII) was prepared from ethyl phenylacetate according to the method described by Schubert and Lamm.[7] The following compounds were synthesized by the methods described in the literature: benzo[*b*]furan[8] (I-1), bp 173—174°C; 5-methylbenzo[*b*]furan[9] (I-2) bp 197—199°C; *p*-tolylmercuric chloride,[10] mp 232—233°C; *p*-anisylmercuric chloride,[11] mp 173—174°C; *m*-nitrophenylmercuric chloride,[12] mp 218—221°C. The phenylmercuric acetate and the starting olefins were of a commercial grade.

Preparation of [2-^2H]-Benzo[b]furan (V). 2-Bromobenzo[*b*]furan was prepared from 2,3-dibromobenzo[*b*]furan in an 80% yield by the method described by Stoermer and Kahlert.[13] 2-Bromobenzo[*b*]furan (4.5 g, 0.179 mol) was reduced with lithium aluminum deuteride (4.5 g, 0.107 mol) in anhydrous tetrahydrofuran to [2-^{2}H]benzo[*b*]furan (V) (bp 173—174°C); 65% yield. NMR spectrum: δ 6.49 (s) H on the C_3; 7.06—7.51 (m) aromatic ring protons. The 60 MHz NMR spectrum showed the absence of H on the C_2, and a mass-spectral analysis indicated that the isotopic purity was 98.5%.

Found: C, 80.78; H, 5.97%. Calcd for C_8H_5DO: C, 80.57; H, 5.90%.

General Procedure for the Arylation of Benzo[b]furans (I). A lithium chloropalladite solution was prepared by stirring 0.84 g (0.02 mol) of anhydrous lithium chloride and 1.77 g (0.01 mol) of anhydrous palladium chloride overnight at room temperature in 100 ml of ethanol. To this lithium chloropalladite solution, a mixture of 0.01 mol of arylmercuric compound (II) and 0.02 mol of I was added, after which the mixture was stirred at room temperature for 12 hr. The products were isolated by filtration to remove a precipitated palladium and by distillation under reduced pressure to remove the solvent. The residue was dissolved in benzene and chromatographed on alumina. The first elution with benzene and recrystallization from ethanol afforded colorless crystals, which were identified as biphenyl derivatives by a mixed-melting-point determination. Further elution with benzene or chloroform and recrystallization from ethanol afforded the respective arylation product (III). The structures of the products were confirmed by a mixed-melting-point determination with an authentic sample and by the observation of the IR and NMR spectra. The results are summarized in Table 1, while the analytical results and the properties of the products are listed in Table 2.

General Procedure for the Arylation of [2-^2H]-Benzo[b]furan (V). In an ethanol (80 ml) solution of lithium chloropalladite (0.01 mol), a mixture of 0.01 mol of an arylmercuric compound (II) and 0.02 mol of V was stirred for 12 hr at room temperature. After the separation of the precipitated palladium, and after the evaporation of the solvent, the residual oil was separated by alumina chromatography. The 2-arylated benzo[*b*]furan thus produced was recrystallized from ethanol. The deuterium-content of the purified products was calculated from a mass-spectra analysis. (see Table 3).

General Procedure for the Reaction of Benzo[b]furans (I) with Benzene. In a solution of dry benzene (100 ml) and acetic acid (40 ml), was dissolved palladium acetate (2.24 g, 0.01 mol) and an equivalent amount of I. The mixture was heated gently under reflux at 80°C with stirring for 6 hr. After the separation of the precipitated palladium, the mixture was poured into water. The organic layer was separated, the aqueous layer was extracted with benzene, and the combined extracts were neutralized, washed, and dried ($MgSO_4$). After the evaporation of the solvent, the residue was dissolved in benzene and chromatographed on alumina. The first elution with benzene afforded colorless crystals which were identified as biphenyl by a mixed-melting-point determination. The second elution with benzene and recrystallization from ethanol afforded the 2-phenylbenzo[*b*]furans (III). Further elution with benzene or chloroform and

6) T. A. Stephenson, S. M. Morehouse, A. R. Powell, J. P. Heffer, and G. Wilkinson, *J. Chem. Soc.*, **1965**, 3632.

7) W. M. Schubert and B. Lamm, *J. Amer. Chem. Soc.*, **88**, 120 (1966).

8) A. W. Burgstahler and L. R. Worden, "Organic Syntheses," Vol. 46, p. 28 (1966).

9) K. von Auwers, *Ann. Chem.*, **408**, 274 (1915).

10) F. C. Whitemore, F. H. Hamilton, and N. Thurman, "Organic Syntheses," Coll. Vol. I, p. 519 (1941).

11) O. Dimroth, *Ber,*. **35**, 2867 (1092).

12) C. Kapproth and F. Westheimer, *J. Amer. Chem. Soc.*, **72**, 4461 (1950).

13) R. Stoermer and B. Kahlert, *Ber.*, **35**, 1636 (1902).

TABLE 6. THE PROPERTIES AND ANALYSES OF 2-BENZO[*b*]FURYL OLEFIN DERIVATIVES (VII)

Compound	Mp °C (lit.)	Anal. Found % (Calcd) C	H	IR spectrum (cm^{-1}) and NMR spectrum (ppm, no. of proton, splitting patterns).
VII-1	121—122	87.29	5.55	IR 960, 875.
		(87.24)	(5.49)	NMR δ 6.62 1 s furan ring proton C_3, 6.89 1 d -CH=C**H**-Ph, 7.12—7.68 10 m aromatic ring protons plus -C**H**=CH-Ph.
VII-2	77—78 (76—77.5[a])			
VII-3	99—100	72.35	5.66	IR 1718, 1640, 880, 810.
		(72.21)	(5.59)	NMR δ 2.14 3 s -CH=C(CH$_3$)-COOMe, 3.82 3 s -COOC**H**$_3$, 6.68 1 s furan ring proton on C_3, 7.20—7.78 5 m aromatic ring protons plus -C**H**=C(CH$_3$)-COOMe
VII-4	97—98	73.08	6.17	IR 1715, 1620, 894, 803
		(73.03)	(6.13)	NMR δ 1.32 3 t -COOCH$_2$C**H**$_3$, 2.53 3 d -C(CH$_3$)=CHCOOEt, 4.21 2 q -COOCC**H**$_2$CH$_3$, 6.62 1 s furan ring proton on C_3, 6.92 1 t -C(CH$_3$)=C**H**-COOEt 7.14—7.60 4 m aromatic ring protons.
VII-5	102—103	78.20	4.24	IR 2220, 1620, 948, 890.
		(78.09)	(4.17)	NMR δ 5.90 1 d -CH=C**H**-CN, 6.61 1 s furan ring proton on C_3, 7.21—7.76 5 m aromatic ring protons plus -C**H**=CH-CN.
		(N 8.31	(8.28))	
VII-6	130—131	87.23	6.11	IR 964, 878.
		(87.15)	(6.02)	NMR δ 2.41 3 s -C**H**$_3$, 6.56 1 s furan ring proton on C_3, 6.86 1 d -CH=C**H**-Ph, 7.08—7.52 9 m aromatic ring protons plus -C**H**=CH-Ph.
VII-7	55—56	73.09	6.16	IR 1723, 1640, 965, 873.
		(73.03)	(6.13)	NMR δ 1.37 3 t -COOCH$_2$C**H**$_3$, 4.28 2 q -COOC**H**$_2$CH$_3$, 6.56 1 d -CH=C**H**-COOEt, 6.62 1 s furan ring proton on C_3, 7.17—7.89 4 m aromatic ring protons plus -C**H**=CH-COOEt
VII-8	97—98	73.14	6.25	IR 1720, 1637, 882, 810.
		(73.03)	(6.13)	NMR δ 2.34 3 d -CH=C(CH$_3$)-COOMe, 2.42 3 s -C**H**$_3$, 3.31 3 s -COOC**H**$_3$, 6.70 1 s furan ring proton on C_3, 7.14—7.56 4 m aromatic ring protons plus -C**H**=C(CH$_3$)-COOMe.
VII-9	95—96	73.82	6.60	IR 1718, 1632, 896, 881.
		(73.75)	(6.65)	NMR δ 1.32 3 t -COOCH$_2$C**H**$_3$, 2.41 3 s -C**H**$_3$, 2.50 3 d -C(C**H**$_3$)=CH-COOEt, 4.26 2 q -COOC**H**$_2$CH$_3$, 6.60 1 s furan ring proton on C_3, 6.84 1 q -C=C**H**-COOEt, 7.16—7.38 3 m aromatic ring protons.
VII-10	79—80	78.77	5.08	IR 2220, 1625, 944, 887.
		(78.67)	(4.95)	NMR δ 2.39 3 s -C**H**$_3$, 5.87 1 d -CH=C**H**-CN, 6.67 1 s furan ring proton on C_3, 7.05—7.49 3 m aromatic ring protons 7.60 1 d -C**H**=CH-CN
		(N 8.84	(8.73))	
VII-11	96—97	78.10	6.13	IR 1680, 1620, 875.
		(77.98)	(6.04)	NMR δ 2.34 3 s -COC**H**$_3$, 2.41 3 s -C**H**$_3$, 6.69 1 s furan ring proton on C_3, 6.84 1 d -CH=C**H**COCH$_3$, 7.15—7.39 4 m aromatic ring proton plus -C**H**=CHCOCH$_3$,
VII-12	99—100	77.52	5.48	IR 2790, 1680, 1620, 960, 870.
				NMR δ 2.42 3 s -C**H**$_3$, 6.63 1 s furan ring proton on C_3, 6.87 1 d-d -CH=C**H**-CHO, 7.21—7.63 4 m aromatic ring proton plus -C**H**=CH-CHO, 9.71 1 d -CH=CH-C**H**O.

a) T. Pan and T.C. Wang, *J. Chinese Chem.Soc. Ser. II*, **8**, 374 (1961).

Table 7. The reaction of bezno[*b*]furan with[β,β-$^2H_2$]-styrene (VIII)

Benzo[*b*]furan	Olefin	Product (yield %)	D-content*)	NMR data (δ, ppm)
I-1	VIII	VI-1 (6)	0%	
		VII-1 (70)	98%[a)]	6.62 1 s furan ring proton on C, 6.89 1 s -CD=C**H**-Ph, 7.14—7.65 9 m aromatic ring protons.
I-2	VIII	VI-2 (6)	0%	
		VII-6 (68)	96%[a)]	2.41 3 s $-CH_3$, 6.58 1 s furan ring proton on C_3, 6.86 1 s -CD=C**H**-Ph, 7.09—7.55 8 m aromatic ring protons.
V	Styrene	VI-1 (7)	0%	
		VII-1 (72)	0%	6.62 1 s furan ring proton on C_3, 6.89 1 d -CH=C**H**-Ph, 7.12—7.68 10 m aromatic ring protons plus -C**H**-CH-Ph.
V	VIII	VI-1 (7)	0%	
		VII-1 (70)	96%[a)]	6.62 1 s furan ring proton on C_3, 6.89 1 s -CD=C**H**-Ph, 7.14—7.65 9 m aromatic ring protons.

*) The deuterium-content of the products was calculated from the mass-spectral analyses results, and on the basis that D-content of product containing one olefinic deuterium is 100%.

a) Neither of the 60 NMR nmr spectra of the products showed also evidence of D in the β-carbon of styryl group.

recrystallization from ethanol afforded colorless crystals which were identified as 2,2′-bibenzo[*b*]furyls (VI). The results are summarized in Table 4.

The Reaction of [2-^2H]-Benzo[b]*furan (V) with Benzene.* In the presence of palladium acetate, the reaction of V, benzene, and acetic acid was carried out by the same procedure as that used in the reaction of I with benzene. The products were purified by chromatography on alumina and recrystallization from ethanol. The results are summarized in Table 4. The isotopic purity of the products was calculated on the basis of a mass-spectral analysis and from the NMR results.

General Procedure for the Reaction of Benzo[b]*furan (I) with Olefins.* A mixture of palladium acetate (10 mmol), olefin (10 mmol), and I (10 mmol) was stirred in acetic acid (100 ml) for 6 hr at reflux. The resulting mixture was filtered to remove palladium metal, and, after the evaporation of the solvent under reduced pressure, the residue was poured into water. The organic layer was extracted with ether, and the ether layer was treated with an aqueous sodium bicarbonate solution, washed with water to free it from acetic acid, and then dried over anhydrous magnesium sulfate. After the evaporation of the solvent, the products were isolated by column chromatography. The first elution with benzene and the subsequent recrystallization from ethanol afforded colorless crystals which were identified as the 2-benzo[*b*]furyl-substituted olefin derivative (VII). Further elution with chloroform and recrystallization from ethanol afforded VI. The structures of the products were confirmed by means of the IR and NMR spectra. The results are summarized in Table 5, while the analytical results and the properties of the products are listed in Table 6.

The reactions of I with VIII, of V with styrene, and of V with VIII proceeded in a manner similar to that described above. The isotopic purity of the products was calculated on the basis of a mass-spectral analysis and from the NMR results. The results are summarized in Table 7.

The authors would like to express their thanks to Professor Yoshio Kitahara of Tohoku University for the measurements of the mass spectra, to Assistant Professor Kaoru Hanaya and Mr. Hideaki Kudo of Yamagata University for the measurements of the NMR spectra, and to the Kawaken Fine Chemical Co., Ltd., for its gift of palladium chloride.

Determination of Catalytic Rate Constants in the Reaction of Lysozyme and Oligosaccharide by Computer Simulation Analysis

Hiroko TADA and Toshiaki KAKITANI*

Department of Physics, Kyoto University, Kyoto 606

**Research Institute for Fundamental Physics, Kyoto University, Kyoto 606*

(Received July 20, 1972)

We have developed Chipman's kinetic study on a reaction of lysozyme and oligosaccharide. That is, we have analyzed how each catalytic rate constant affects the pattern of time-course graphs of oligomer concentrations in the reaction. By fitting computer simulation curves to three experimental time-course graphs, values of the catalytic rate constants for the bond-cleavage, transglycosylation and hydration are determined step by step. Also some binding constants are evaluated.

Recently Chipman formulated a kinetic model for the reaction of lysozyme and oligosaccharides including reaction mechanisms of hydrolysis and transglycosylation.[1] The kinetic equations became much complicated, far from that of Michaelis-Menten type. Numerically solving them by computer, he rather well simulated experimental data[2] of the time-course graphs of oligomer concentrations in the reaction. Performing the least-squares fit to one of the experimental data, he evaluated the rate constant of bond-cleavage and the ratio between the rate constant of transglycosylation and that of hydration as 1.75 sec^{-1} and $2.77\times10^{3}M^{-1}$, respectively. This study is much valuable because a kinetic scheme which includes the transfer reaction is formulated in a simple form, and the value of the rate constant of bond-cleavage is given for the first time. In this paper, we intend to develop his study and determine the values of the rate constants of transglycosylation and hydration which are not determined by him. We do this by analyzing the role of each catalytic rate constant in the pattern of the time-course graph. In the next section, we briefly formulate our kinetic model which differs a little from Chipman's.

Kinetic Model

Lysozyme has six binding sites for the substrate $(GlcNAc\text{-}MurNAc)_n$[3] named A, B, C, D, E, and F, and it cleaves the glycosyl bond locating between the D and E sites of the bound substrate.[4] As MurNAc cannot be bound at the A, C, and E sites, the oligomer is cleaved only between MurNAc and GlcNAc.[5] Therefore, in the kinetic treatment, we can consider the disaccharide GlcNAc-MurNAc as a unit. Then, six species of binding forms are allowed. In Fig. 1 we show our kinetic model. The notation is as follows: D_n is the oligomer $(GlcNAc\text{-}MurNAc)_n$, $C_{n,i}$ the complex of D_n and the enzyme E where the i-th susceptible

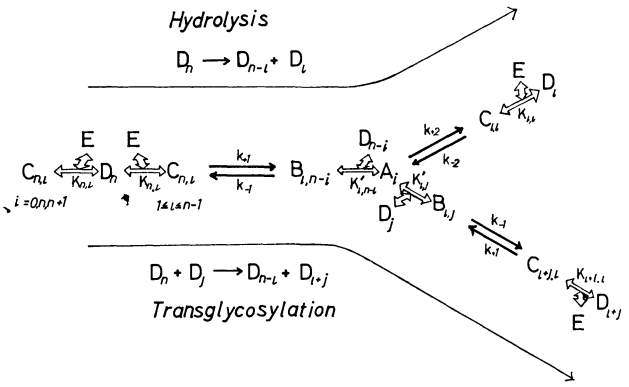

Fig. 1. Kinetic scheme of the lysozyme-catalyzed reaction. The notation is explained in the text.

bond from the non-reducing terminus of the oligosaccharide is at the catalytic site, A_i the "enzyme-carbonium ion intermediate" complex,[4] and $B_{i,n}$ the complex of A_i and D_n in which the non-reducing terminus of D_n is bound at the EF site of A_i. The complexes $C_{n,i}$ for $i=0$, n, $n+1$ are the non-productive ones, and $C_{n,i}$ for $1\leq i\leq n-1$ are the productive ones. Catalytic rate-constants, k_{+1}, k_{-1}, k_{+2}, and k_{-2} are those of bond-cleavage, bond-formation, hydration and its reverse process, respectively. These catalytic rate constants are assumed to be same for both poor and good substrates. The arrow $\overset{\nearrow}{\underset{\searrow}{\Longleftrightarrow}}$ represents a binding process, in which we assume an equilibrium is attained. The binding constant is written beside the arrow. These binding constants are explicitly written as follows:

$$\left.\begin{aligned} &K_{1,0}=K_{EF},\ K_{1,1}=K_{CD},\ K_{1,2}=K_{AB}\\ &K_{n,0}=K_{EF},\ K_{n,1}=K_{C\sim F},\ K_{n,n}=K_{A\sim D},\ K_{n,n+1}=K_{AB}\\ &\qquad\qquad\qquad\qquad\qquad\qquad\qquad\qquad\text{for } n\geq 2\\ &K_{n,i}=K_{A\sim F}\qquad\qquad\text{for } n\geq 3,\ \leq 2i\leq n-1\\ &K'_{n,j}=K_{EF}\qquad\qquad\text{for all } j \text{ and } n. \end{aligned}\right\}\quad(1)$$

This kinetic model is much simplified by considering the following group S_n of the substrates and group I_j of the intermediates within which all species are combined to each other by the binding equilibrium processes:

$$[S_n]=[D_n]+\sum_i[C_{n,i}]+\sum_j[B_{j,n}],\quad(n=1,2,\cdots)\quad(2)$$

$$[I_j]=[A_j]+\sum_n[B_{j,n}].\quad(j=1,2,\cdots)\quad(3)$$

1) D. M. Chipman, *Biochemistry*, **10**, 1714 (1971).

2) D. M. Chipman, J. J. Pollock, and N. Sharon, *J. Biol. Chem.*, **243**, 487 (1968).

3) Abbreviation: GlcNAc, *N*-acetyl-D-glucosamine; MurNAc, *N*-acetyl-muramic acid. All oligosaccharides referred to are linked β-(1→4), with the reducing terminus written to the right. We call $(GlcNAc\text{-}MurNAc)_n$ as $2n$-mer. Particularly those for $n=2,3$, and 4 are named as tetramer, hexamer, and octamer, respectively.

4) D. C. Phillips, *Sci. Amer.*, **215**, 78 (1966).

5) N. Sharon, *Proc. Roy. Soc. Ser. B*,. **167**, 402 (1967).

The kinetic equations for these groups are written as

$$\frac{d[S_1]}{dt} = k_{+2}[A_1] - k_{-1}K_{EF}[D_1]\sum_j[A_j] + k_{+1}K_{C\sim F}[D_2][E] + k_{+1}K_{A\sim F}[E]\sum_{l>2}[D_l], \quad (4)$$

$$\frac{d[S_n]}{dt} = k_{+2}[A_n] - k_{+1}\{K_{C\sim F}+(n-2)K_{A\sim F}\}[D_n][E] - k_{-1}K_{EF}[D_n]\sum_j[A_j] + k_{+1}K_{C\sim F}[D_{n+1}][E] + k_{+1}K_{A\sim F}[E]\sum_{l>n+1}[D_l] + k_{-1}K_{EF}\sum_{m<n}[A_m][D_{n-m}], \quad \text{for } n\geq 2 \quad (5)$$

$$\frac{d[I_j]}{dt} = -k_{+2}[A_j] + k_{+1}K_j'[E]\sum_{l>j}[D_l] - k_{-1}K_{EF}[A_j]\sum_n[D_n], \quad (j=1, 2, \cdots) \quad (6)$$

where

$$[D_n] = [S_n]/(1+K_n[E]+K_{EF}\sum_j[A_j]) \quad (7)$$

$$[A_j] = [I_j]/(1+K_{EF}\sum_n[D_n]) \quad (8)$$

$$[E] = ([E]_0-\sum_j[I_j])/(1+\sum_n K_n[D_n]) \quad (9)$$

$$K_j' = \begin{cases} K_{C\sim F} & \text{for } j=1 \\ K_{A\sim F} & \text{for } j=2, \end{cases} \quad (10)$$

$$K_n = \sum_{i=0}^{n+1}K_{n,i} = \begin{cases} K_{EF}+K_{CD}+K_{AB} & \text{for } n=1 \\ K_{EF}+K_{C\sim F}+(n-2)K_{A\sim F}+K_{A\sim D}+K_{AB}. & \text{for } n\geq 2 \end{cases} \quad (11)$$

In the above $[E]_0$ is the total enzyme concentration.

Here we mension about the difference between our model and Chipman's. Although our model is based on the consideration of the equilibrium at the binding process also for intermediates, Chipman's model is based on the scheme of the two-step enzymic reaction similar to α-chymotrypsin.[6] That is, he neglected, in Fig. 1, all species of B and the complexes C at the exits of the catalytic processes. But this difference is trivial. Indeed, observed quantities of the time-course graphs are the percent radioactivity P_n defined by

$$P_n = 100n[S_n]/\sum_l l[D_l]_0, \quad (12)$$

where $l[D_l]_0$ is the initial substrate concentration of the l-mer measured by GlcNAc-MurNAc unit. Thus, the time-course graph perfectly coincides between both models if our $k_{-1}K_{EF}$ is put equal to Chipman's rate constant of transglycosylation k_T. If either the experiment by which one can detect the species of C or B, or the calculation without the equilibrium-assumption for the binding is made, small difference between the two models will appear.

Numerical Calculation

Experimentally it is shown that k_{-2} is much small compared with all other reaction rate constants.[2] Thus we neglect its process in the numerical calculation. The binding constants $K_{A\sim F}$, $K_{A\sim D}$, and K_{AB} will be equalized with the apparent binding constants experimentally obtained for the hexamer, tetramer, and dimer, respectively. Those values are 3.5×10^4, 2.0×10^3, and 20 M^{-1}, respectively.[7] If we use the additivity-assumption of the binding energy, $K_{C\sim F}$, K_{CD}, and K_{EF} are calculated from the above binding constants as 28, 1.6, and 0.3 M^{-1}, respectively. However, the validity of the additivity-assumption has been proved neither experimentally nor theoretically. Therefore, we treat $K_{C\sim F}$, K_{CD}, and K_{EF} as unknown parameters together with k_{+1}, k_{-1}, and k_{+2}. In the following, we call a reaction, where the $2m$-mer is initially mixed with

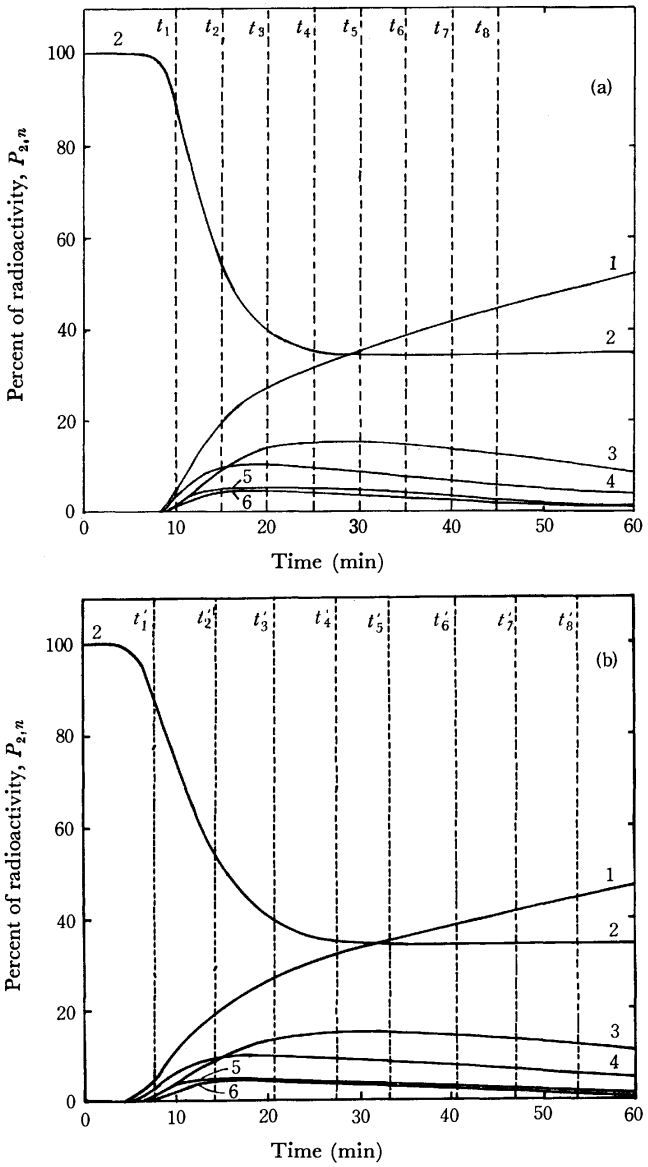

Fig. 2. Comparison of two time-course graphs in the tetramer-reaction between which the value of a is the same but those of the other kinetic constants are not. (a): $k_{+1}=2.0\ sec^{-1}$, $k_{-1}=1.8\times10^3\ sec^{-1}$, $k_{+1}=0.62\ sec^{-1}$, $K_{C\sim F}=2\times10^{-4}M^{-1}$, $K_{CD}=1.6\ M^{-1}$ and $K_{EF}=1.0\ M^{-1}$. (b): $k_{+1}=1.7\ sec^{-1}$, $k_{-1}=3.3\times10^2\ sec^{-1}$. $k_{+2}=0.33\ sec^{-1}$, $K_{C\sim F}=5.0\ M^{-1}$ $K_{CD}=1.6\ M^{-1}$ and $K_{EF}=3.0\ M^{-1}$. The value of a is $3.0\times10^3M^{-1}$ for both (a) and (b). The initial condition is $[D_2]_0=7.5\times10^{-3}M$, $[E]_0=2.1\times10^{-5}M$. The number beside each curve is the value of n.

6) M. L. Bender and F. J. Kézdy, *J. Amer. Chem. Soc.*, **86**, 3704 (1964).

7) D. M. Chipman, V. Grisaro, and N. Sharon, *J. Biol. Chem.*, **242**, 4388 (1967).

lysozyme, as the $2m$-mer reaction. In our numerical calculation, the maximum length of the oligomer is put to be 18-mer. However, for example, in the tetramer-reaction, the largest oligomer given in the experimental curves is $P_{2,6}$. In such a case, we put $P_{2,6}=\sum_{n=6}^{9}P_{2,n}$ in our calculation. For the hexamerand octamer-reactions, we employed the similar procedure.

From the inspection of many time-course graphs with different values of the parameters, we have found the following important properties in this kinetic model. (i) In Fig. 2, we plotted two graphs of the tetramer-reaction, between which the ratio $a=k_{-1}K_{EF}/k_{+2}$ is same but the values of k_{+1}, k_{+2}, $K_{C\sim F}$, and K_{CD} are not same. In Fig. 2(a), we pick up an arbitrary set of times $\{t_i\}$ $(i=1, 2, \cdots, N)$, and obtain $\{P^{a}_{2,n}(t_i)\}$, where $P^{a}_{2,n}(t_i)$ denotes $P_{2,n}$ at time t_i in Fig. 2(a). Then, we find a set of times $\{t_i'\}$ which nicely satisfy the equation

$$P^{b}_{2,n}(t_i') = P^{a}_{2,n}(t_i) \tag{13}$$

for all n in Fig. 2(b) irrespectively of the values of the other parameters. This means that the ratio a is an essential factor which determines the distribution of the oligomer concentrations. This property holds also in the hexamer- and octamer-reactions. In the next section, we shall qualitatively explain this important property of our kinetic model. (ii) The time scale of the reaction is determined mainly by the catalytic rate con stants k_{+1} and k_{+2}. But they do not necessarily change the time scale uniformly. (iii) As shown in Fig. 3, the binding constant $K_{C\sim F}$ plays a role only in the initial stage called "time-lag-region" of the tetramer-reaction and little affects the time-course graphs of the hexamer- and octamer-reactions. This property comes from the fact that the tetramer is a poor substrate although the higher oligomer is a good substrate.[2] (iv) The binding constant K_{EF} affects the time-course graphs only through the form of $k_{-1}K_{EF}$ except when k_{EF} is much larger than K_{AB}. This is easily understood from the fact that K_{EF} enters into the kinetic equations mainly by the form of $k_{-1}K_{EF}$. This property states that we cannot simply determine the value of k_{-1} and K_{EF} independently. (v) The binding constant K_{CD} does not affect our time-course graphs unless K_{CD} is much larger than K_{AB}.

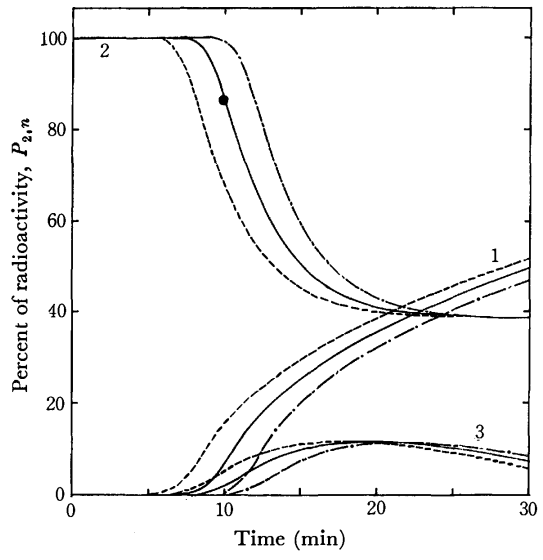

Fig. 3. Time-course graphs of the tetramer-reaction where the value of $K_{C\sim F}$ is varied. ------: $K_{C\sim F}=10^{-5}M^{-1}$, ——: $K_{C\sim F}=10^{-7}M^{-1}$, —·—: $K_{C\sim F}=10^{-9}M^{-1}$. The other parameters are $k_{+1}=3.3$ sec^{-1}, $k_{-1}=9.8\times10^{2}$sec^{-1}, $k_{+2}=0.58$ sec^{-1}, $K_{CD}=1.6$ M^{-1} and $K_{EF}=1.0$ M^{-1}. The initial concentrations of D_2 and E are the same as those in Fig. 2. The black circle is the experimental value of $P_{2,2}$ at 10 min.[2] The number beside each curve is the value of n. Curves of oligomers higher than hexamer are not written in this graph.

Determination of the Ratio $a=k_{-1}K_{EF}/k_{+2}$. In fitting of the theoretical curves to the experiments, we use the experimental values in the early stage of the reaction, because our kinetic model may not be good in the latter stage of the reaction as we discuss later. In the following numerical calculation, we used the times $t_1=10$ min and $t_2=17$ min for the tetramer-reaction, and $t_1=1$ min and $t_2=4$ min for the hexamer- and octamer-reactions.

Using the property (i), we can determine the value of the parameter a by best fitting the theoretical curve to the experimental values $P^{E}_{m.n}(t_1)$ and $P^{E}_{m.n}(t_2)$ for all n in the three reactions, where the superscript E denotes the experiment. We describe below the method of our calculation. First we fix the value of a. Suitably choosing the other parameters, we obtain t_1''s and t_2''s which satisfy the equation

$$P_{m,m}(t_i') = P^{E}_{m,m}(t_i), \qquad (i=1, 2) \tag{14}$$

for the tetramer-, hexamer-, and octamer-reactions, respectively. Then we calculate the following error function:

$$f_{m,i}(a) = \sum\{P_{m,n}(t_i')-P^{E}_{m,n}(t_i)\}^2, \qquad (i=1, 2) \tag{15}$$

Error functions thus obtained depend on a and are plotted in Fig. 4. The sum of these six error functions becomes minimum at $a=1.7\times10^{3}$ M^{-1}. This minimum point is derermined mainly by the three $f_{m,2}$'s. But we should not trust this value so firmly, because the minimum points in error function largely differ from each other. It will be right to say that the value of a is roughly in the region 1.2×10^{3} M$^{-1}<a<4.0\times10^{3}$ M^{-1}.

Determination of k_{+1} *and* k_{+2}. The values of k_{+1} and k_{+2} are not determined uniquely from the fitting procedure to a single kind of reaction, but only a functional relationship between them is obtained. Using the property (ii), we intend to obtain sets of k_{+1} and k_{+2} in each reaction for the fixed value of a. In the tetramer-reaction, the set of k_{+1} and k_{+2} are obtained by the procedure that t_1' and t_2', which are obtained from Eq. (14), may satisfy $t_2'-t_1'=t_2-t_1=7$ min. For the hexamer- and octamer-reactions, they are determined as the average of those which satify $t_1'=t_1=1$ min and $t_2'=t_2=4$ min, respectively. The obtained values k_{+1} and k_{+2} are shown in Fig. 5 for two values of a. Our expectation was that the three curves should cross at a point, which determines the real values of k_{+1} and k_{+2}. Indeed, it is well realized. From this graph, we obtain $k_{+1}=3.3$ sec^{-1} and $k_{+2}=0.58$ sec^{-1} for $a=1.7\times10^{3}$ M^{-1}, and $k_{+1}=2.0$ sec^{-1} and $k_{+2}=0.62$ sec^{-1}

Table 1. Values of the kinetic constants

The free energy of the catalytic rate constant is calculated from the equation $\Delta F^{*}_{x} = -RT \ln (k_x h/\kappa T)$. The cooperative energy E_c is also listed.

Kinetic constants	Ours $a=1.7\times10^{3}M^{-1}$	Ours $a=3.0\times10^{3}M^{-1}$	Chipman's[1] $a=2.77\times10^{3}M^{-1}$
k_{+1} (sec^{-1})	3.3	2.0	1.75
$k_{-1}K_{EF}$ ($M^{-1}sec^{-1}$)	9.8×10^{2}	1.8×10^{3}	Unknown (9.2×10^{4})
k_{+2} (sec^{-1})	0.58	0.62	Unknown (1.0×10^{2})
$K_{C\sim F}$ (M^{-1})	10^{-7}	2×10^{-4}	$\leq 6.3\times10^{-4}$
K_{CD} (M^{-1})	5.7×10^{-8}	1.2×10^{-5}	(0.5)
K_{EF} (M^{-1})	Unknown	Unknown	Unknown
ΔF^{*}_{+1} (kcal/mol)	17.0	17.2	17.4
$\Delta F^{*}_{-1}+\Delta F_{EF}$ (kcal/mol)	13.5	13.1	(10.8)
ΔF^{*}_{+2} (kcal/mol)	18.0	17.9	(14.9)
$\Delta F_{C\sim F}$ (kcal/mol)	9.7	5.1	≥ 4.4
ΔF_{CD} (kcal/mol)	10.0	6.8	(0.4)
E_c (kcal/mol)	11.8	7.2	≥ 6.5

The values in the parentheses are the standard values of Chipman.

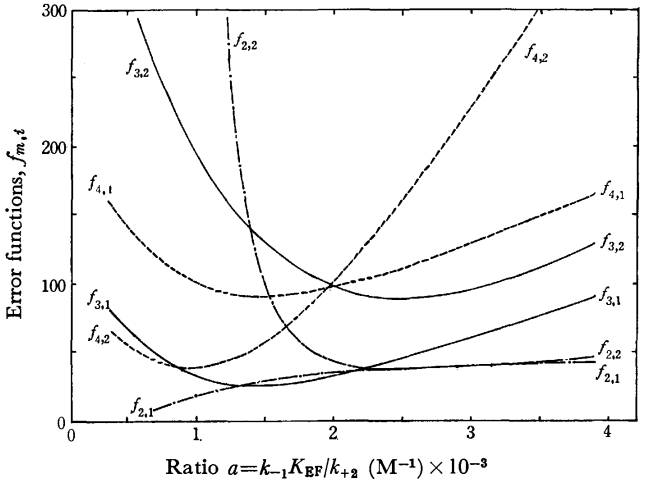

Fig. 4. Graphs of error-functions. -·-·-: tetramer-reaction, ——: hexamer-reaction and ------: octamer-reaction. The intial conditions used for our calculation are as follows: In the tetramer-reaction $[D_2]_0=7.5\times10^{-3}M$ and $[E]_0=2.1\times10^{-5}M$. In the hexamer-reaction $[D_3]_0=2.9\times10^{-4}M$ and $[E]_0=2.0\times10^{-6}M$. In the octamer-reaction $[D_4]_0=2.4\times10^{-4}M$ and $[E]_0=2.0\times10^{-6}M$.

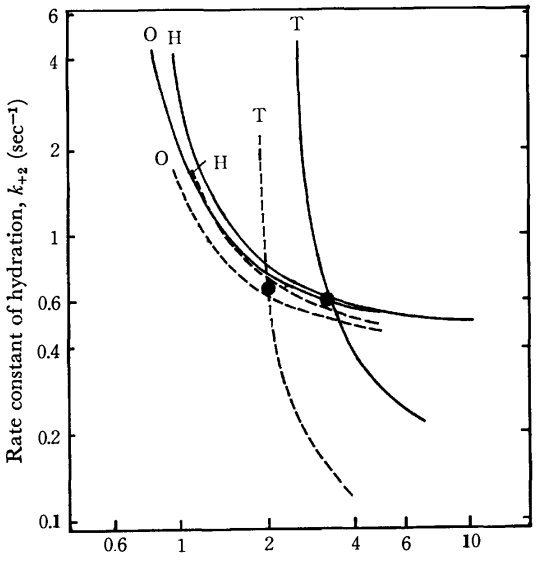

Fig. 5. Graphs of the sets of k_{+1} and k_{+2}. ——: $a=1.7\times10^{3}M^{-1}$ and ------: $a=3.0\times10^{3}M^{-1}$. The letters T, H, and O denote the tetramer–, hexamer– and octamer-reactions, respectively. The black circles are our obtained points through which three curves pass.

for $a=3.0\times10^{3}\ M^{-1}$.

Determination of $K_{C\sim F}$. We use the property (iii). As shown in Fig. 3, we determine the value of $K_{C\sim F}$ in such a way that $P_{2,2}$ may pass $P^{E}_{2,2}(t_1)$, fixing all the other parameters, where $t_1=10$ min. Some theoretical curves for the case of $a=1.7\times10^{3}\ M^{-1}$ are plotted in Fig. 3. From this, we get $K_{C\sim F}=10^{-7}\ M^{-1}$. In the same way, we get $K_{C\sim F}=2\times10^{-4}\ M^{-1}$ for the case of $a=3.0\times10^{3}\ M^{-1}$.

In Table 1, we summarized our results, together with the value of Chipman.[1] The method to get the value of K_{CD} is written in the following section. In Fig. 6, theoretical curves of ours are drawn and compared with the experiment.

Theoretical Analysis and Discussion

At first, we consider the important qualitative characteristics of our kinetic model. The most important one is the property (i), *i.e.*, the distribution of oligomers is almost uniquely determined by the ratio $a=k_{-1}K_{EF}/k_{+2}$. The reduced scheme of the reaction-path of this kinetic model is represented by the groups of the substrates and the intermediates as in Fig. 7, which is called as Path(n,i) henceforth. In the Path(n,i), if the step X(n,i) is rate-determining, the intermediate is rapidly converted to each product through the step Y(i). Then, on a given iteration step, a decrease of ΔC moles in S_n through the Path(n,i) produces the change ΔS_m in S_m. From Eqs. (5) and (6) it is given by

$$\Delta S_m = d_m - d_{i+m} + (\delta_{m,n-i}-\delta_{m,n})\cdot\Delta C, \quad (m=1, 2, \cdots) \qquad (16)$$

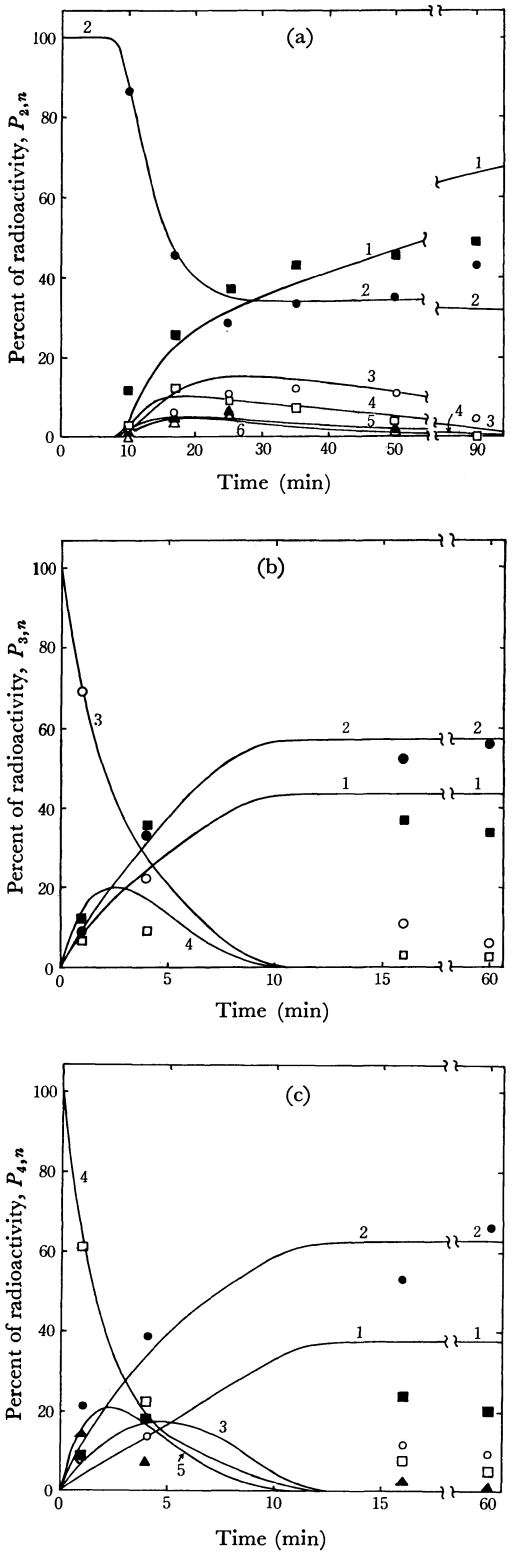

Fig. 6. Theoretical time-course graphs compared with the experiment. (a), (b), and (c) are the graphs of the tetramer-, hexamer- and octamer-reactions. The kinetic constants are as follows: $k_{+1}=2.0\,\mathrm{sec}^{-1}$, $k_{-1}=1.8\times10^{3}\,\mathrm{sec}^{-1}$, $k_{+2}=0.62\,\mathrm{sec}^{-1}$, $K_{C\sim F}=2\times10^{-4}\mathrm{M}^{-1}$, $K_{CD}=1.6\,\mathrm{M}^{-1}$ and $K_{EF}=1.0\,\mathrm{M}^{-1}$. The initial concentrations of the oligomer and the enzyme are same as those in the figure legend of Fig. 4. The experimental points[2] are shown by the following symbols; ■: dimer, ●: tetramer, ○: hexamer, □: octamer, ▲: 10-mer, △: 12-mer. The number beside each curve is the value of n.

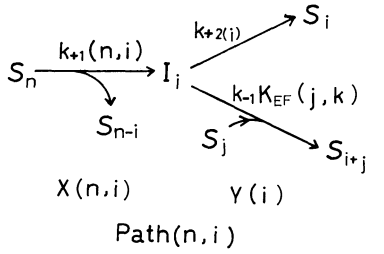

Fig. 7. The reduced scheme of the reaction-path. The step $X(n,i)$ is the process of the bond-cleavage of the $2n$-mer in the productive i-th binding form and the step $Y(i)$ is the process where the carbonium intermediate is converted to an oligomer of different kind depending on the species of the acceptor. The reduced catalytic rate constants in this figure are defined by $k_{+1}(n,i)=k_{+1}K_{n,i}[E]/(1+K_n[E]+K_{EF}\sum_l[A_l])$, $k_{+2}(i)=k_{+2}/(1+K_{EF}\sum_l[D_l])$ and $k_{-1}K_{EF}(i,j)=k_{-1}K_{EF}/\{(1+K_{EF}\sum_l[D_l])(1+K_j[E]+K_{EF}\sum_l[A_l])\}$.

where

$$d_m=\begin{cases}0 & \text{for } m<i\\ \Delta C/(1+a\sum_l[D_l]) & \text{for } m=i\\ \Delta C\cdot a\cdot[D_{m-i}]/(1+a\sum_l[D_l]) & \text{for } m>i\end{cases} \tag{17}$$

and $\delta_{i,j}$ is the Kronecker's delta function. In Eqs. (16) and (17), as $\{[D_l]\}$ are given from the previous step of the iteration procedure, ΔS_m is uniquely determined by a. Since the total reaction is obtained as the sum of this Path(n,i) over n and i, the total change on this iteration step is also uniquely determined by a. The time-course graphs are obtained by accumulating these iteration steps. Thus the pattern of the distribution is uniquely determined by a. When the step $Y(i)$ is rate-determining, the situation is more complicated. Among the groups $\{S_m\}$ $(m=i,\ i+1,\ \cdots)$ directly produced by the step $Y(i)$, the productive complexes $\{C_{m,l}\}$ $(m=i,\ i+1,\ \cdots;\ l=1,\ 2,\ \cdots,\ m-1)$ are immediately converted to $\{S_{m-l}\}$ and $\{I_l\}$ through the steps $\{X(m,l)\}$, and further these products $\{S_{m-l}\}$ pass the same procedure as $\{S_m\}$. Then the changes in S_m and I_m due to a decrease of ΔC moles in I_i through the step $Y(i)$ is obtained, accumulating also the effects of these sequential steps, as follows:

$$\Delta S_m=-d_{i+m}+Z_m\{d_m+d_{m+1}Z_{m+1,m}+\sum_{n>m+1}d_n(Z_{n,m}+\sum_{k=1}^{n-m-1}\sum_{\{n>l_1>l_2>\cdots>l_k>m\}}Z_{n,l_1}Z_{l_1,l_2}\cdots Z_{l_k,m})\} \tag{18}$$

$$\Delta I_m=-\delta_{i,m}\Delta C+\sum_{n>m}d_n[Z_{n,n-m}+(1-\delta_{n,m+1})\times\sum_{k=1}^{n-m-1}Z_{k+m,k}\{Z_{n,k+m}+(1-\delta_{k,n-m-1})\times\sum_{j=1}^{n-k-m-1}\sum_{\{n>l_1>l_2>\cdots>l_j>k+m\}}Z_{n,l_1}Z_{l_1,l_2}\cdots Z_{l_j,k+m}\}], \tag{19}$$

where

$$Z_m=\{1+(K_{EF}+K_{m,m}+K_{m,m+1})[E]+K_{EF}\sum_l[A_l]/(1+K_m[E]+K_{EF}\sum_l[A_l])\}$$

$$Z_{m,j}=K_{m,m-j}[E]/(1+K_m[E]+K_{EF}\sum_l[A_l]) \tag{20}$$

and $\{d_m\}$ are the same as Eq. (17). The sum of $\{n>l_1>l_2>\cdots>l_k>m\}$ denotes to sum up for all the set of l_1, l_2, $\cdots$, l_k satisfying the relation in the parentheses. In Eq. (20), $[E]$ and $\{[A_l]\}$ are given from the previous step of the iteration procedure. Then, also in this case, the distribution of oligomers is uniquely determined by a. When both the steps $X(n,i)$ and $Y(i)$ are rate-determining, the same conclusion may be obtained approximately although the exact explanation is impossible. The other important qualitative characteristic of our model is that; the time scale of the time-course graphs is determined only by the rate constants of the rate-determining steps independently of the other rate constants. When every step is rate-determining, it is dependent on all rate constants. Then, as shown in Fig. 5, the values of k_{+1} and k_{+2} with which the calculated graphs fit to a single time-course graph of the experiment are of the hyperbolic-like relation. These two conclusions are the general qualitative aspects in the endocatenase-catalyzed reaction of oligomers involving the transfer-reaction.

Next we compare our calculation with that of Chipman.[1] Using the method of the least-squares fit to 24 data points of the tetramer-reaction, he obtained the following results: (a) k_{+1} is rate-determining and its value is (1.75 ± 0.17) sec^{-1}, (b) the value of a is $(2.77\pm0.3)\times10^3$ M^{-1}, (c) $k_{-1}K_{EF}$ and k_{+2} are not rate-determining, thus those values are not obtained, and (d) the value of $K_{C\sim F}$ is less than $(6.3\pm12.4)\times10^{-4}$ M^{-1}. His values of a and k_{+1} are rather in agreement with ours. But, his results, (b) and (c), do not seem to be correct judging from our graph of Fig. 5. That is, the tetramer curve in Fig. 5 is almost perpendicular at $k_{+1}\cong1.8$ sec^{-1} and bends to the right as the value of k_{+1} becomes larger than 2.0 sec^{-1}. Thus, k_{+1} is not rate-determining except the perpendicular region of the curve. This means that one cannot determine the values of k_{+1} or k_{+2} but obtain a relation between them from the data of the tetramer-reaction only.[10] In our calculation, we used other two data, *i.e.*, time-course graphs of the hexamer- and octamer-reactions. Finding the cross points among these three curves, we succeeded in determining the values of k_{+1} and k_{+2}. The point corresponding to his standard values lies near the upper-extrapolated tetramer curve, but far above the hexamer and octamer curves in Fig. 5. There may be an argument that the experiments of the hexamer- and octamer-reactions are not so correct.[8] If it is really so, our results will also be corrected. But, our procedure to determine the values of the catalytic rate constants using graphs similar to Fig. 5 is useful whenever other reliable experiments appear. As to the value of $K_{C\sim F}$, our result is consistent with his.

Summarizing the above results and using the value of the free-energy of the hydrolysis of maltose,[9] which is similar to that of MurNAc–GlcNAc, we give in

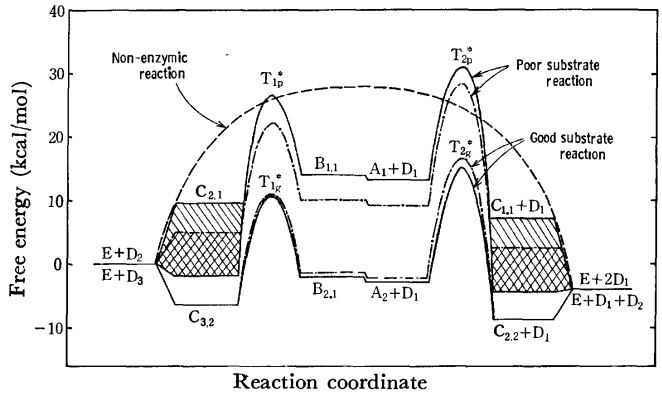

Fig. 8. Free-energy scheme in the lysozyme-catalyzed reaction. The graphs of the tetramer- and hexamer-reactions are written together by fitting the initial energy levels to zero. ——: $a=1.7\times10^3$M^{-1}, -·-·-: $a=3.0\times10^3$M^{-1}. The energy levels of $C_{2,1}$ and $C_{1,1}+D_1$ have uncertainty. The highest levels of them are those obtained from the assumption that the catalytic rate constants are same for both the good and poor substrates. The lowest levels are those obtained from the additivity-assumption of the binding energy. The real energy levels will be between those of the two extreme cases. These graphs are written assuming $K_{EF}=0.3$ M^{-1}. When this value is altered, the energy levels of $B_{1,1}$ and $B_{2,1}$ shift by $-RT\ln(K_{EF}/0.3)$ kcal/mol, keeping all the other energy levels unchanged. T_{1p}^*, T_{2p}^*, T_{1g}^*, T_{2g}^* represent transition states for the poor and good substrates reactions. The energy level of the non-enzymic reaction is also written for comparison.

Fig. 8 a schematic model for the free-energy potential of lysozyme reaction. From the case of the good substrates in Fig. 8, the value of k_{-2} is estimated as about 10^{-4} sec^{-1}, which is much smaller than the other catalytic rate constants as expected. Furthermore, the unknown binding constant K_{CD} is estimated by the difference between the energy height of T_{2p}* from the line $E+2D_1$ and that of T_{2g}* from the line $C_{2,2}+D_1$, as 1.2×10^{-5} M^{-1} and 5.7×10^{-8} M^{-1} for $a=3.0\times10^3$ M^{-1} and 1.7×10^3 M^{-1}, respectively. The non-enzymic case is also drawn in Fig. 8 for comparison, using Piszkiewicz and Bruice's data on the di-*N*-acetylchitobiose.[11] The transition state for the poor substrates has almost the same height as the non-enzymic one, but, for the good substrates, it is largely lowered by as much as 12—13 kcal/mol, which makes the overall rate constant by about 10^9 times larger. This large stabilization of the transition-state is produced by the cooperative binding effect between the AB and C∼F sites. Its cooperative energy is calculated as

$$E_c = -RT\ln(K_{AB}K_{C\sim F}/K_{A\sim F}) - \Delta F_m \qquad (21)$$

where ΔF_m, which is due to the mixing entropy, is about 2.4 kcal/mol. Here, if the additivity-assumption of the binding energy holds, E_c becomes zero. Our value of E_c is 11.8 kcal/mol and 7.2 kcal/mol for $a=1.7\times10^3$ M^{-1} and 3.0×10^3 M^{-1}, respectively. This large value means that the sites A and B play an important role to stabilize the distorted conformation at the D site in the reaction of the good substrates, although the mechanism of it is yet unknown.

8) D. M. Chipman, private communication.

9) R. A. Dedonder, *Ann. Rev. Biochem.*, **30**, 347 (1961).

10) Examining reactions of higher oligosaccharides under low concentration conditions, Chipman seems to have estimated that k_{+2} should be at least of the order of 0.5 sec^{-1}. If it is assumed, his results (b) and (c) are derived.

11) D. Piszkiewicz and T. C. Bruice, *J. Amer. Chem. Soc.*, **90**, 5844 (1968).

It may be also considered, however, that the real reaction of the bond-cleavage of the poor substrates proceeds in the more loosely bound form with less strain (*i.e.* much larger value of $K_{C\sim F}$), and by much smaller value of k_{+1}, maintaining the value of $k_{+1}K_{C\sim F}$ as constant (in the kinetic equations (4)—(9), $K_{C\sim F}$ appears mainly in the form $k_{+1}K_{C\sim F}$). The real energy level of this loosely bound complex may be located somewhere in the hatched region of Fig. 8. Similar consideration may be applied to K_{CD} and k_{-2} for the dimer.

The observable effect of the transglycosylation does not appear until the ratio a becomes so large that the value of $k_{-1}K_{EF}[D]$ becomes comparable to that of k_{+2}. It is reasonable that the order of our obtained value of a is 10^3 M^{-1}, since the substrate concentration is order of 10^{-3}—10^{-4}M in the experiments we used. This result means that the rate constant of the transfer-reaction may be rather large even for the case of other enzyme-catalyzed reactions, in which an effective transfer-reaction had not been detected experimentally. It may be detected, if the suitable initial concentration of the substrate is used, so that the transfer-reaction process becomes comparable to the competitive process.

Recently, using the transient NMR[12] and T-jump method,[13] the forward binding rate constants k_{+b} for GlcNAc, $(GlcNAc)_2$, and $(GlcNAc)_3$ are obtained as 3.5×10^5 $M^{-1}sec^{-1}$, 3.6×10^6 $M^{-1}sec^{-1}$, and 4.44×10^6 $M^{-1}sec^{-1}$, respectively. We find that the binding rate $k_{+b}[D_n][E]$ is not necessarily much larger than the reaction rate $k_{+1}[C_{i,j}]$. Therefore, the equilibrium-assumption about the binding process may not be so good. In the following we shortly examine how our kinetic schemes and simulated time-course graphs are altered if the dynamical process of the binding is effective. The binding constants of the above oligomers are 20—50 M^{-1}, 5×10^3 M^{-1}, and 1.0×10^5 M^{-1}, respectively.[14] Therefore, we find that the binding rate constant does not become large so much as the binding constant does as the oligomer becomes large. This tendency will also apply to the higher oligomers. In addition, binding rate constant of the productive binding may become very small because the D site of the complex must be distorted. From these, it is well expected that the number of the productive complex is much smaller than that calculated from the equilibrium-assumption when considerable numbers of small oligomers coexist. Then, the reaction proceeds much slowly. In the latter stage of the hexamer- and octamer-reactions where dimer and tetramer are considerably produced, the above case might be applied. In the experimental result, this seems to have happened (considerable amounts of the hexamer and octamer remain even at 15 min). In the earlier stage of the reaction, the dynamical binding effect, if exists, might be small.

We think that our kinetic model and treatment based on its qualitative characteristics described in this paper are a useful general method to determine the catalytic rate constants of the endocatenase-catalyzed reaction of oligomer including the transfer-reaction.

The authors wish to express their sincere thanks to Dr. H. Fukutome for valuable discussions and improving this manuscript. They also thank to Prof. D. M. Chipman for the critical comments.

12) B. D. Sykes and C. Parravano, *J. Biol. Chem.*, **244**, 3900 (1969).

13) D. M. Chipman and P. R. Schimmel, *ibid.*, **243**, 3711 (1968).

14) D. M. Chipman and N. Sharon, *Science*, **165**, 454 (1969).

The Reaction of *O,O'*-Diethyl α-Lithiomethylphosphonate with Organic Dihalides

Koichiro OSHIMA, Tamio SHIRAFUJI, Hisashi YAMAMOTO, and Hitosi NOZAKI

Department of Industrial Chemistry, Kyoto University, Yoshida, Kyoto 606

(Received July 28, 1972)

The reactions of the α-lithio derivative of diethyl methylphosphonate with various organic halides are described. The half-reduction of *gem*-dihalocyclopropanes has been achieved with this reagent. The same reagent gives bibenzyl and tetraphenylethane from benzyl bromide and benzhydryl chloride respectively. The deprotonation-metallation process is observed in the reactions of cinnamyl chloride and of *trans*-β-bromostyrene, in which 3-chloro-1,6-diphenyl-1,5-hexadiene and 1,4-diphenyl-3-buten-1-yne are produced respectively.

The half-reduction of olefin-dihalocarbene adducts by organometallic reagents[1] is a useful method for obtaining monohalocyclopropanes, but it has been limited in scope due to competing reactions arising from the intermediary α-halocyclopropylmetal compounds. We have found that the α-lithio derivative of diethyl methylphosphonate appears to be an excellent reagent for the half-reduction of dihalocyclopropanes under mild conditions. This reagent showed promise of largely circumventing the side reactions encountered with other organometallic reagents.

O,O'-Diethyl α-lithiomethylphosphonate (I), prepared simply from *O,O'*-diethyl methylphosphonate and *n*-butyllithium at −78°C,[2] reacted with 1,1-dibromo-2-phenylcyclopropane (IIa) to give the expected 1-bromo-2-phenylcyclopropane (IIIa) as a predominant product

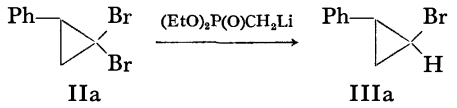

IIa IIIa

(68%). In contrast, the reaction of methylsulfinylcarbanion[3] with the dibromide, IIa, resulted in a polymeric mixture in which the desired bromide, IIIa, was absent. The anion, I, produced 9-bromo-*cis*-bicyclo[6.1.0]nonane (IIIb) from 9,9-dibromo-*cis*-bicyclo[6.1.0]nonane (IIb) in a 66% yield, while with *n*-butyllithium the latter afforded 1,2-cyclononadiene (IV) as the major product.[4]

A variety of *gem*-dihalocyclopropanes have been successfully reduced to the respective monobromides using the phosphonate reagent, as is indicated in Table 1. Most noteworthy is the preferential formation of thermodynamically more stable *trans*- or *exo*-monobromocyclopropanes, which might originate from the *endo-exo* isomerization of the initially-formed halocyclopropyllithium.[5]

TABLE 1. REACTION OF *gem*-DIBROMOCYCLOPROPANES WITH I IN THF

Substrate		Product[a]		
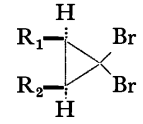	Code	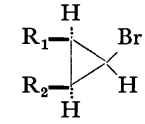	*exo* (*trans*)	*endo* (*cis*)
Code, R_1, R_2		Yield[b] (%)		
IIa, Ph, H	IIIa	68	79	: 21
IIb, $-(CH_2)_6-$	IIIb	66	80	: 20
IIc, $-(CH_2)_4-$	IIIc	82	90	: 10
IId, $-(CH_2)_{10}-$	IIId	65[c]	83	: 17
IIe, $-CH_2-CH=CH_2$	IIIe	75	84	: 16
IIf, *n*-Hexyl, H	IIIf	68	79	: 21

a) Products were identified by IR, NMR, and MS spectra with authentic samples.[1a]
b) Analyzed by glc.
c) Allene was also obtained in 9% yield and was identified by comparison with an authentic sample.

The preparation of the totally reduced cyclopropane derivative was also attained with this reagent. When *ca.* three equivalents of the anion, I, were allowed to react with 1,1-dibromo-2,2-diphenylcyclopropane (V), a mixture of 1-bromo-2,2-diphenylcyclopropane (VI), and 1,1-diphenylcyclopropane (VII) was obtained. The cyclopropane, VII, was obtained as the sole product (62%) when a large excess of the anion, I, was used for this reaction (>6 equiv).

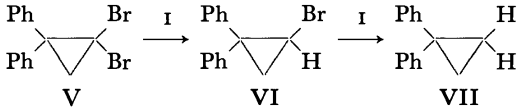

V VI VII

The similarity of the anion, I, to methylsulfinylcarbanion prompted us to examine the reaction of I with other organic halides. Corey and Chaykovski have reported[6] that the treatment of benzyl chloride and benzhydryl chloride with methylsulfinylcarbanion furnished stilbene and tetraphenylethylene respectively.

1) a) T. Shirafuji, K. Oshima, Y. Yamamoto, and H. Nozaki, This Bulletin, **44**, 3161 (1971); b) D. Seyferth, H. Yamazaki, and D. L. Alleston, *J. Org. Chem.*, **28**, 703 (1963); c) D. Seyferth and B. Prokai, *ibid.*, **31**, 1702 (1966); d) T. Ando, H. Yamanaka, F. Namigata, and W. Funasaka, *J. Amer. Chem. Soc.*, **89**, 5719 (1967); e) J. Vilieras and H. Normant, *C. R. Acad. Sci. Paris*, **264**, 593 (1967).

2) E. J. Corey and G. T. Kwiatokowski, *J. Amer. Chem. Soc.*, **88**, 5654 (1966).

3) Methylsulfinylcarbanion is known to be a good reagent for the half-reduction of *gem*-dihalocyclopropanes, see C. L. Osborn, T. C. Shields, B. A. Shoulders, and P. D. Gardner, *Chem. Ind.* (London), **1965**, 766.

4) W. R. Moore and H. R. Ward, *J. Org. Chem.*, **27**, 4179 (1962).

5) G. Köbrich and W. Goyert, *Tetrahedron*, **24**, 4327 (1968); For kinetically controlled semireduction with chromous sulfate, see H. Nozaki, T. Aratani, and R. Noyori, *ibid.*, **23**, 3645 (1967).

6) E. J. Corey and M. Chaykovski, *J. Amer. Chem. Soc.*, **87**, 1345 (1965).

In contrast to these results, the anion, I, gave bibenzyl (VIII) and tetraphenylethane (IX) from benzyl bromide and benzhydryl chloride respectively. We suppose that this novel condensation reaction involves an unstable arylated carbanion, which affords the final product upon reaction with another halide.

Although the above-mentioned reactions are to be ascribed to the dehalogenation-metallation process, the deprotonation-metallation process has also been observed in some cases. Cinnamyl chloride gave 3-chloro-1,6-diphenylhexadiene-1,5 (X), whereas *trans*-β-bromostyrene afforded 1,4-diphenyl-3-buten-1-yne (XI). The latter reaction might involve an intermediary vinylcarbenoid, XII, which reacts with β-bromostyrene to form the methylenecyclopropane, XIII, followed by isomerization to XI through the cumulene derivative, XIV. An alternative pathway might be the direct dimerization of the vinylcarbenoid, XII, to form the cumulene, XIV.[7] The possibility of the formation of

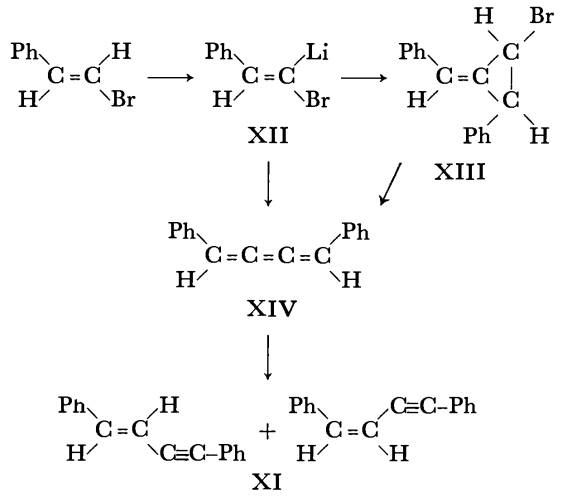

phenylacetylene as an intermediate was excluded by the following experiment. When the solution of I was successively treated with phenylacetylene at −78°C and then with β-bromostyrene, no trace of XI could be detected among the products.

Experimental

All the bps are uncorrected. The microanalyses were performed at the Elemental Analyses Center of Kyoto University and by Mrs. Kiyoko Fujimoto. The NMR spectra were taken with a JEOL C-60H spectrometer and the chemical shifts are reported in δ values relative to the TMS internal standard. The mass spectra were obtained on a Hitachi RMU 6D spectrometer. The glc analyses or separations were performed using a 1 m column of SE-30 (30%) on Chromosorb W and He as the carrier gases.

General Procedure of the Reactions of Organic Halides with O,O'-Diethyl α-Lithiomethylphosphonate (I). In a nitrogen atmosphere, diethyl methylphosphonate was dissolved in freshly-distilled (over LAH) THF so as to give *ca.* a 0.5M solution. The solution was cooled to −78°C on a methanol–dry ice bath, and *n*-butyllithium (1.2 equiv) was added to this solution with stirring. After 15 min, a solution (*ca.* 1M) of organic halide was slowly added at −78°C. The ratio of the bromide to I was taken to be 1: 1.5 unless otherwise stated. The mixture was allowed to stand overnight at room temperature, treated with ice-cold water, and extracted with ether three times. The combined ethereal extracts was concentrated *in vacuo*. The products were separated and identified as usual. The following descriptions refer to cases which are not sufficiently covered by Table 1.

*Reaction of 13,13-Dibromo-*cis*-bicyclo[10.1.0]tridecane (IId).* The dibromide, IId (600 mg, 1.75 mmol), was treated with the anion, I (3.00 mmol), in dry THF (15 ml) at −78°C. A glc analysis of the crude reaction mixture showed the presence of *exo*-IIId (54%), *endo*-IIId (11%), and 1,2-cyclotridecadiene (9%). The bromide, IIId, was separated by preparative glc.

13-Bromo-*cis*-bicyclo[10.1.0]tridecane (IIId): bp 100°C (bath temp.)/0.05 mmHg; IR (neat) 1469, 1447, 1250, 1238, 1225 cm^{-1}; MS *m/e* (relative abundance) 260 (9), 258 (9), 175 (21), 79 (100). The NMR analysis did not reveal the methine proton absorption.

Found: C, 60.5; H, 8.9%. Calcd for $C_{13}H_{23}Br$: C, 60.2; H, 8.9%.

*Reaction of 13,13-Dibromo-*trans*-bicyclo[10.1.0]tridecane (IIg).* The halide, IIg (600 mg, 1.75 mmol), was treated with the anion, I (3.00 mmol), in dry THF (15 ml) at −78°C. The reaction mixture showed the presence of 13-bromo-*trans*-bicyclo[10.1.0]tridecane (IIIg, 72%) and 1,2-cyclotridecadiene (8%) upon glc assay. The bromide, IIIg, was separated by preparative glc.

IIIg: bp 100°C (bath temp.)/0.05 mmHg; IR (neat) 1465, 1443, 1270, 1248, 1237, 1222 cm^{-1}; NMR (CCl_4) δ 0.85 (b, 2), 1.42 (b, 2), 2.72 (q, 1, J_{cis}=7.2 Hz, J_{trans}=3.5 Hz) ppm; MS *m/e* (relative abundance) 260 (12), 258 (12), 179 (10), 135 (18), 109 (31), 95 (100).

Found: C, 60.2; H, 9.1%. Calcd for $C_{13}H_{23}Br$: C, 60.2; H, 8.9%.

Reaction of 7,7-Dibromobicyclo[4.1.0]heptene-3 (IIe). A solution of IIe (850 mg, 3.37 mmol) in THF (2 ml) was added to a solution of I (6.00 mmol) in dry THF (7 ml) at −78°C. The reaction mixture was then worked up as usual. The glc analysis of the resulting oil showed the presence of *exo*-IIIe (63%) and *endo*-IIIe (12%); each component was separated by preparative glc.

exo-7-Bromobicyclo[4.1.0]heptene-3 (*exo*-IIIe): bp 60°C/18 mmHg; IR (neat) 3050, 1655, 1220 cm^{-1}; NMR (CCl_4) δ 5.47 (b, 2), 2.74 (t, 1, J_{trans}=3.1 Hz), 2.37 (b, 4), 1.45 (b, 2) ppm; MS *m/e* (relative abundance) 174 (12), 172 (12), 131 (11), 117 (11), 93 (100).

Found: C, 48.9; H, 5.5%. Calcd for C_7H_9Br: C, 49.2; H, 5.2%.

endo-IIIe: bp 65°C/18 mmHg; IR (neat) 3050, 1668, 1252 cm^{-1}; NMR (CCl_4) δ 3.29 (t, 1, J_{cis}=7.4 Hz) ppm.

Reaction of 1,1-Dibromo-2,2-diphenylcyclopropane (V). The dibromide, V (700 mg, 2.00 mmol), was treated with the anion, I (3.00 mmol), in THF. The glc analysis of the crude reaction mixture showed the presence of 1-bromo-2,2-diphenylcyclopropane (VI, 73%), which was separated by preparative glc.

VI: bp 140°C (bath temp.)/0.05 mmHg; IR (neat) 1252 cm^{-1}; NMR (CCl_4) δ 7.15 (d, 1), 3.56 (t, 1, J=6.5 Hz), 1.73 (d, 2) ppm; MS *m/e* (relative abundance) 274 (3), 272 (3), 194 (41), 193 (100), 115 (100).

When V (350 mg, 1.00 mmol) was treated with I (3.00 mmol), 1,1-diphenylcyclopropane (VII, 40% by glc assay) was obtained in addition to VI (28% by glc assay). When V (60 mg, 0.17 mmol) was treated with I (1.00 mmol), the cyclopropane, VII (62% by glc assay), was obtained as the

7) a) G. Köbrich and W. Drischel, *Tetrahedron*, **22**, 2621 (1966); b) G. Köbrich, H. Heinemann, and W. Zündorf, *ibid.*, **23**, 565 (1967).

sole product.

Reaction of Benzyl Bromide. Benzyl bromide (340 mg, 2.00 mmol) was treated with the anion, I (3.00 mmol), in THF (15 ml) at −78°C. The preparative tlc separation of the crude reaction mixture then gave VIII (127 mg, 70%) as the sole product; it was identical in all respects with an authentic sample.

Reaction of Benzhydryl Chloride. Benzhydryl chloride (200 mg, 1.00 mmol) was treated with the anion, I (1.50 mmol), in THF (7 ml) at −78°C. After the concentration of the dried extracts *in vacuo*, a white solid was obtained. Recrystallization from benzene–hexane (1:1) gave pure IX (125 mg, 75%) as colorless crystals; the IX was identical in all respects with an authentic sample.

Reaction of Cinnamyl Chloride. Cinnamyl chloride (500 mg, 3.30 mmol) was added to a solution of the anion, I (5.00 mmol), in THF (20 ml) at −78°C. The subsequent glc analysis of the reaction mixture showed the presence of 3-chloro-1,6-diphenyl-1,5-diene (X, 71%), which was then separated by preparative glc.

X: bp 160°C (bath temp.)/0.08 mmHg; IR (neat) 1625, 1594, 959, 740, 692 cm^{-1}; NMR (CCl_4) δ 7.13 (b, 10), 6.0 (m, 5), 2.55 (t, 2) ppm; MS *m/e* (relative abundance) 270 (0.51), 268 (0.96), 232 (2.4), 151 (17), 117 (100), 115 (61).

Found: C, 80.3; H, 6.6%. Calcd for $C_{18}H_{17}Cl$: C, 80.4; H, 6.4%.

Reaction of trans-*β-Bromostyrene.* *trans-β*-Bromostyrene (600 mg, 3.30 mmol) was added to a solution of I (4.90 mmol) in THF at −78°C. The usual work up, followed by glc separation, afforded *cis*-XI (79 mg, 39%) and *trans*-XI (15 mg, 8%).

1,4-Diphenyl-*cis*-3-buten-1-yne (*cis*-XI): bp 80°C/0.05 mmHg; IR (neat) 2200, 780 cm^{-1}; NMR (CCl_4) δ 7.73 (m, 2), 7.21 (m, 8), 6.56 and 5.76 (AB q, 1 each, $J_{AB}=15$ Hz); MS *m/e* (relative abundance) 204 (100), 203 (88), 202 (82), 103 (14), 101 (29).

1,4-Diphenyl-*trans*-3-buten-1-yne (*trans*-XI): mp 94—95°C (lit, 95.5—96°C[8]); IR (KBr) 945 cm^{-1}; NMR (CCl_4) δ 7.23 (m, 5), 6.96 and 6.26 (AB q, 1 each, $J_{AB}=12$ Hz) ppm; MS *m/e* (relative abundance) 204 (100), 203 (85), 202 (77), 103 (13), 101 (27).

The authors are grateful to Professor Keiiti Sisido for his generous help and to Dr. Yasusi Yamamoto for his discussions. The financial support from the Ministry of Education, the Japanese Government, and from the Toray Science Foundation is also acknowledged with pleasure.

8) a) H. K. Black, D. H. S. Horn, and B. C. L. Weedon, *J. Chem. Soc.*, **1954**, 1704; b) J. H. Pinckard, B. Wille, and L. Zechmeister, *J. Amer. Chem. Soc.*, **70**, 1938 (1948).

BULLETIN OF THE CHEMICAL SOCIETY OF JAPAN, VOL. 46, 1235—1238 (1973)

Studies on Reactions of the *N*-Phosphonium Salts of Pyridines. I. A New Method for the Activation of Carboxylic Acids *via* the *N*-Phosphonium Salts by Means of the Oxidation of Tri- and Di-esters of Phosphorous Acid in the Presence of Tertiary Amines

Noboru YAMAZAKI and Fukuji HIGASHI

Department of Polymer Science, Tokyo Institute of Technology, Ookayama, Meguro-ku, Tokyo 152

(Received September 8, 1972)

Carboxylic acids were found to be activated by an oxidation mixture prepared from tri- and di-esters of phosphorous acid and mercuric chloride in a pyridine solution; they yielded the corresponding anilides upon treatment with aniline, together with a nearly quantitative yield of metallic mercury. The yield of the anilides was affected by the alkyl groups in the esters and by the tertiary amines. Only a small effect of the steric factor of carboxylic acids upon the reaction was seen in the cases of the diesters, and none at all was observed in the triesters. The reaction was proposed to proceed *via* the *N*-phosphonium salts of pyridines, which were not purely isolated, but which were assumed on the basis of the IR spectra.

Though various methods[1] have been reported for the phosphorylation of alcohols by means of the esters of phosphorous acid, there are few which are effective for the phosphorylation of carboxylic acids.[2] Mukaiyama *et al.*[3] have reported obtaining diethyl acyl phosphates by means of the oxidation of triethyl phosphite and monobromocyanoacetamide in the presence of carboxylic acids. They have also shown that mercuric salts such as mercuric chloride are useful oxidizing agents for the oxidation of phosphorous acid in the course of the preparation of monoalkyl phosphates.[4] In the oxidation of trialkyl phosphite with *N*-chlorosuccinimide, an *N*-phosphonium salt[5] have been suggested to be involved.

1) G. M. Blackburn, "Topics in Phosphorus Chemistry," Vol. 6, Interscience Publishers Inc., New York (1969), p. 187.

2) G. W. Anderson, J. Blodinger, and A. D. Welcher, *J. Amer. Chem. Soc.*, **74**, 5309 (1952).

3) T. Mukaiyama, T. Hata, and O. Mitsunobu, *Yuki Gosei Kagaku Kyokai Shi*, **20**, 969 (1962).

4) T. Obata and T. Mukaiyama, *J. Org. Chem.*, **32**, 1063 (1967).

5) A. K. Tsolis, W. E. McEven, and C. A. Vanderwerf, *Tetrahedron Lett.*, **1964**, 3217.

In a previous paper,[6] we ourselves reported briefly a convenient method for the synthesis of carboxylic amides and esters *via* the *N*-phosphonium salts of pyridine prepared by the oxidation of phosphorous acid and its esters with mercuric chloride in pyridine, and showed that pyridine played an important role in this reaction.

This paper will present the detailed results of the oxidation of various tri- and di-esters of phosphorous acid in tertiary amines, especially in pyridine, resulting in the *N*-phosphonium salts of pyridine, and of the activation of carboxylic acids to give the corresponding amides by means of the salts.

Results and Discussion

Through the studies of this series of reactions, aniline was chosen as the amine component of the amides, because anilides are readily isolated and the yield of the activated carboxylic acids can be estimated almost quantitatively from the amount of the anilides obtained.

When tri- and di-isopropyl esters of phosphorous acid were brought into reaction with mercuric chloride in refluxing pyridine, followed by treatment with an equimolar amount of acetic acid and then with aniline, acetanilide was obtained in 73 and 94% yields respectively, together with a nearly quantitative yield of metallic mercury. In a similar manner, various anilides were successfully synthesized from various phosphites (see Tables 1 and 2). However, no detectable amount of the anilide was obtained when a mixture of acetic acid and aniline was heated in pyridine under reflux in the absence of these phosphorous compounds.

The reaction may be summarized as follows:

$$P(OR)_3 \text{ (or } H\text{-}P(O)(OR)_2) + HgCl_2 \xrightarrow{Py} \text{I (or IV)} + Hg^0$$

$$\xrightarrow{R^1COOH} \text{II (or V)} \xrightarrow{R^2NH_2} R^1CO\text{-}NHR^2 + Py\cdot HCl$$

$$+ O{=}P(OR)_3 \text{ (or } HO\text{-}P(O)(OR)_2)$$

Compounds I, II, IV, and V have been assumed to be the *N*-phosphonium salts of pyridines.[6] The phosphorous compounds may be considered to participate not catalytically but stoichiometrically in this reaction from the fact that the yield of the anilide was reduced with a decrease in the amount of the phosphites in pyridine.

The effect of the alkyl group in the phosphites on this reaction was examined by using various phosphites under identical conditions. From the yield of acetanilide (Table 1), the reactivities of trialkyl phosphites are determined to be in the following order: trimethyl< tri-*n*-butyl≈triethyl<triisopropyl. In the cases of the diesters of phosphorous acid, the order of reactivities was similar to that of the triesters; dimethyl<di-*n*-butyl≈diethyl<diisopropyl. Triphenyl phosphite was not oxidized in this system, whereas diphenyl phosphite gave acetanilide in a 93% yield.

There was expected a side reaction in which alkyl groups of the phosphites were attacked by acids to afford the acid esters. Actually, a small amount of ethyl acetate was detected by the gas-chromatographic analysis of the reaction mixture from acetic acid and the oxidation product (I) of triethyl phosphite, besides a 53% yield of acetanilide. Since a separate experiment gave only a small amount of acetanilide upon the reaction of ethyl acetate with aniline under identical conditions, the amide by the present method was not formed through the reaction of the esters thus obtained with aniline.

The steric requirement of I and IV upon carboxylic acids was not observed in the cases of the triesters, whereas only a small effect was observed in the cases of the diesters, when the carboxylic residues were quite large (see Table 2). These results suggested that the reaction of I and IV with carboxylic acids was a replacement of the chlorine atom by the acyloxy groups instead of an addition of the acyloxy groups to the phosphorus-oxygen double bond in IV, as will be discussed in this paper.

Table 1. The preparation of acetanilide using various phosphites and mercuric chloride in pyridine

Phosphite	Acetanilide, Yield, %
Trimethyl	0
Triethyl	53
Triisopropyl	73
Tri-*n*-butyl	50
Dimethyl	56
Diethyl	77
Diisopropyl	94
Di-*n*-butyl	74
Diphenyl	93

Table 2. The preparation of various anilides using tri- and di-isopropyl phosphites and mercuric chloride in pyridine

Anilides	Triisopropyl phosphite, Yield, %	Diisopropyl phosphite, Yield, %
Acetanilide	73	94
n-Butyranilide	77	98
Isobutyranilide	74	97
Pivalanilide	61	70
Benzanilide	79	78

Tertiary amines influenced the yield of the anilide. Of the amines examined, pyridine was most effective for the reactions of phosphorous acid and its mono- and di-esters. In the case of triisopropyl phosphite, α-picoline among the pyridine derivatives gave the best results; even in 2,6-lutidine acetanilide was obtained in a 59% yield (Table 3). These results indicated that the basicity of the amine was rather more influential than its steric effect on the yield of the anilide. Triethylamine did not yield acetanilide. This may be caused by the instability of the I and/or II obtained from the amine. On the contrary, in the case of diisopropyl phosphite, pyridine gave a better result (a 94% yield of acetanilide) than α-picoline (77% yield).

6) N. Yamazaki and F. Higashi, *Tetrahedron Lett.*, **1972**, 415.

Table 3. The preparation of acetanilide in various tertiary amines using triisopropyl phosphite

Amines	pK_a	Acetanilide[a], Yield, %
Pyridine	5.23	73
α-Picoline	5.97	83
2,6-Lutidine	6.99	59
Triethylamine	10.87	0

a) The reaction was carried out in refluxing pyridine or 115 °C in other pyridines. In the case of triethylamine refluxing acetonitrile was used as solvent.

The difference in the effect between tri- and di-isopropyl phosphites may be caused by the stability and reactivity of I and IV to carboxylic acids and/or amines like aniline.

In order to confirm the proposed mechanism described in a previous paper,[6] we have attempted to isolate the intermediate compounds, I and II, but with only limited success.

The *N*-phosphonium salt of pyridine (I) was separated as an ether-insoluble pale brown syrup from an oxidation mixture of triethyl phosphite. When I or the oxidation mixture, without the separation of I, was treated with carboxylic acids, the *N*-phosphonium salt of pyridine carrying acyloxy groups (II) was obtained. On further treatment of II with aniline, the anilides were obtained in good yields.

The over-all route of the reaction is summarized in Scheme 1:

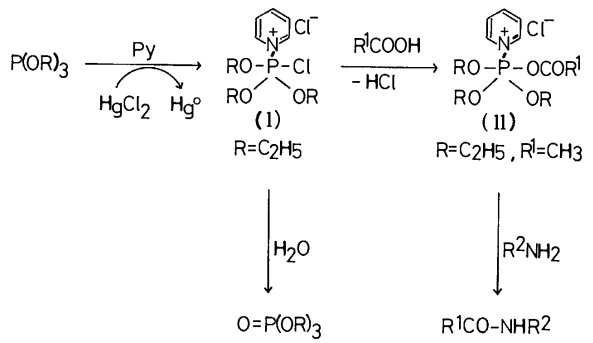

Scheme 1.

These salts, I and II, have not been purely isolated because they were difficult to crystallize and because II was contaminated with pyridine hydrochloride. They were very stable in pyridine and in other aprotic solvents, but unstable in protonic solvents. On the treatment of I with water, triethyl phosphate was obtained in a 45% yield. I could activate alcohols and amines as well as carboxylic acids.[6] II carrying active acyloxy groups gave the corresponding carboxylic amides and esters by aminolysis and alcoholysis respectively.

Generally, trialkyl phosphites are dealkylated when oxidized with halogens. However, the fact that triethyl phosphate was obtained instead of diethyl phosphate when I was treated with water indicated that dealkylation seemed to be exclusive and that the phosphorus compound in I was in the form of a triester.

The IR spectrum of I showed strong absorption bands at 1630 and 1485 cm^{-1} and a weak band at 1580 cm^{-1}. These bands are assumed to be due to $\nu_{C=N^+}$ in the *N*-phosphonium salt of pyridine, judging from the fact that the *N*-phosphoryl pyridines[7] have characteristic bands near 1650 cm^{-1}. Although pyridinium halides and *N*-alkyl-pyridinium halides also have bands[8] around 1630 cm^{-1} which are also attributable to $\nu_{C=N^+}$, the absence of dealkylation on I as has been mentioned above, ruled out the possibility that I was the pyridinium salt. The band at 565 cm^{-1}, which disappeared upon the reaction of acetic acid with I may be due to ν_{P-Cl}.[9]

The UV spectrum of I exhibited the characteristic bands around 260 nm due to a pyridine moiety. The results of the quantitative analysis of chlorine in I by the use of silver nitrate; and of the acid-base titration of I showed that I contained one mole of pyridine and two chlorine atoms.

The proposed chemical structure of I is shown in Scheme 1; it will here be called the *N*-phosphonium salt of pyridine, taking into account its types of reactions, though it might also be named the pyridinium salt.

The band at 1710 cm^{-1} in the IR spectrum of II is due to $\nu_{C=O}$; it is quite similar to that of acetic acid and different from that of diethyl acetyl phosphate[10] at 1780 cm^{-1}. The characteristic bands at 1630, 1580, and 1485 cm^{-1} are due to the $\nu_{C=N^+}$ caused by the *N*-phosphonium salt of a pyridine like I. Though these bands overlapped with those of pyridine hydrochloride, the latter contribution to these bands was not very significant, judging from the weak intensity of the bands at 1535 and 1430 cm^{-1} due to the hydrochloride.

The result of the acid-base titration of II indicated that about equimolar amounts of acetic acid and pyridine were involved in II, assuming that II was contaminated with an equimolar amount of pyridine hydrochloride.

As has been described above, pyridine hydrochloride, which was not observed in I, appeared in this step of the formation of II. This shows that the chlorine atom (or chloride ion) on I may be replaced by the acetoxy group, resulting in II. This explanation is in good agreement with the aforementioned findings on the steric effect of carboxylic acids.

On the basis of these results, II is proposed to be the acyloxy *N*-phosphonium salt of pyridine (Scheme 1). The band due to $\nu_{C=O}$ in II, which was expected to shift to a higher wave number, had a relatively low wave number. This would account for the insufficient migration of electrons on the carbonyl carbon of the acyloxy groups to the phosphorus atom, as has been discussed by Cramer.[10]

In a similar manner, by using the diethyl ester of phosphorous acid, IV and V in Scheme 2 were obtained.

The IR spectrum of IV showed the bands due to $\nu_{C=N^+}$ caused by the *N*-phosphonium salt of pyridine;

7) M. Wakselman and E. Jampel, *Tetrahedron Lett.*, **1970**, 1521.
8) B. Witkop, *Experimentia*, **10**, 420 (1954).
9) R. A. Chittenden and L. C. Thomas, *Spectrochim. Acta*, **21**, 861 (1965).
10) F. Cramer and K. G. Gärtner, *Chem. Ber.*, **91**, 704 (1958).

also those of pyridine hydrochloride were observed. Therefore, in the case of the diester, an intermediate similar to I was formed initially and then it was changed into IVa and IVb by releasing hydrogen chloride in two possible ways. The loss of the chloride anion from pyridinium salt (III) gave IVa, which included a phosphorus-chlorine bond. On the other hand, a phosphorus-oxygen double bond was formed by releasing the chlorine atom on the phosphorus, resulting in IVb. IVa seemed to be more plausible because there was no substantial change in the bands except for the $\nu_{C=O}$ band of acetic acid during the reaction of IV with acetic acid, and it is unlikely that V has the structure corresponding to IVb.

The steric requirement of IV upon carboxylic acids was observed, though it was not very large (see Table 2). This can not be expected from the structure of IVa alone because of the simple replacement of the chlorine atom of IVa by acyloxy groups in the reaction of IVa with the acids, such as was observed on I (Path A in Scheme 2). This fact may be accounted for by the minor participation of IVb, whose reaction with the acids would be a direct attack of the acyloxy anions on the phosphorus atom and would be affected by the steric effect (Path B).

From these results it may be considered that both structures, IVa and its isomer IVb, were involved in this system, and that the former appeared preferably to participate in this reaction.

In the spectrum of V, the bands due to the $\nu_{C=N^+}$ caused by the *N*-phosphonium salt (as in IV) and due to the $\nu_{C=O}$ of the acetoxy group as appeared in II were observed, indicating that V was an *N*-phosphonium salt, like IV (see Scheme 2).

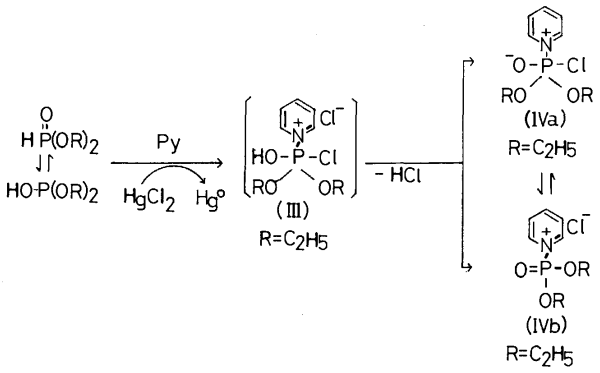

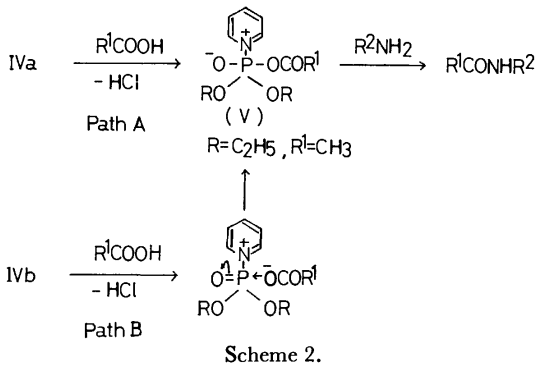

Scheme 2.

Experimental

The infrared spectra were recorded on a Jasco IR-G spectrometer. The syrupy samples were placed between sodium chloride cells or between polyethylene films for low wave numbers (400 to 700 cm^{-1}). The ultraviolet spectrum was taken in ethanol on a Shimadzu RS-27 spectrometer.

The mercuric chloride, tertiary amines, and diphenyl phosphite were obtained from commercial sources. The trialkyl and dialkyl phosphites were prepared according to the literature.[11]

Separation of I and IV. A mixture of equivalent amounts of triethyl phosphite (2.1 g, 12.5 mmol) and mercuric chloride (3.5 g) was refluxed for 1 hr in 20 ml of pyridine. After cooling, the mixture was separated from the liberated metallic mercury and extracted with ether. The separated ether-insoluble syrup (I) was washed with ether to remove the unchanged phosphite and pyridine and was then evaporated under reduced pressure. I was obtained as a pale brown syrup. In the same way, IV was obtained by the reaction of diethyl phosphite (1.8 g, 12.5 mmol) and mercuric chloride (3.5 g) in 20 ml of pyridine.

Separation of II and V. A mixture of equivalent amounts of triethyl phosphite (2.1 g, 12.5 mmol) and mercuric chloride (3.5 g) was refluxed in 20 ml of pyridine. After 1 hr, acetic acid (0.8 g, 12.5 mmol) was added and the mixture was refluxed for an additional hour. By the same procedure as has been described above, II was obtained as a green syrup. Similarly, V was obtained by using diethyl phosphite, mercuric chloride, and acetic acid in pyridine.

Preparation of Anilides using Various Phosphites. The anilides were prepared by the method described in our previous paper.[6] These showed the IR spectra and melting points to be identical with those of authentic samples. Acetanilide was prepared in various tertiary amines in refluxing pyridine or at 115°C in other pyridine derivatives. In the case of triethylamine (4 equiv), the reaction was conducted for 2 hr under reflux in acetonitrile.

11) R. A. McIvor, G. D. MaCarthy, and G. A. Grant, *Can. J. Chem.*, **34**, 1819 (1956); H. McCombie, B. C. Saunders, and G. J. Stacey, *J. Chem. Soc.*, **1954**, 381; A. H. Ford-Moore, and B. J. Perry, "Organic Syntheses," Coll. Vol. 4, p. 955 (1963).

Studies on Reactions of the *N*-Phosphonium Salts of Pyridines. II. A New Method for the Activation of Carboxylic Acids *via* the *N*-Phosphonium Salts by Means of the Oxidation of Phosphorous Acid and Its Monoesters in the Presence of Tertiary Amines

Noboru YAMAZAKI and Fukuji HIGASHI

Department of Polymer Science, Tokyo Institute of Technology, Ookayama, Meguro-ku, Tokyo 152

(Received July 31, 1972)

The oxidation of phosphorous acid and its monoesters with mercuric chloride was carried out in pyridine; they were then treated with carboxylic acids and with aniline. The oxidation reaction was conducted also in the presence of carboxylic acids, after which the mixture was treated with aniline. By both procedures, the corresponding anilides were obtained in good yields. The influence of the steric factors of carboxylic acids, their acidity, and the tertiary amines were observed in the reaction. Phosphorous acid provided a better result than the monoesters. In addition, the chain length of carboxylic acids in the case of the esters influenced the yields of the anilides, which decreased with an increase in the chain length. The structural effect of tertiary amines was studied on pyridine derivatives. The ester residues also affected the yield, and of the esters examined the monophenyl ester was more favorable than the alkyl esters. Other mercuric halides and mercuric acetate were also found effective as oxidizing agents. The reaction was proposed to proceed *via* the *N*-phosphonium salts of pyridines.

In our previous papers,[1,2] we have shown that carboxylic acids could be activated *via* the *N*-phosphonium salt (I) obtained by means of the oxidation of tri- and di-esters of phosphorous acid with mercuric chloride in tertiary amines like pyridine. Salt I is turned into II by the successive reaction with carboxylic acids. Salt II of the acids gives the corresponding amides upon further treatment with amines (Eq. (1)):

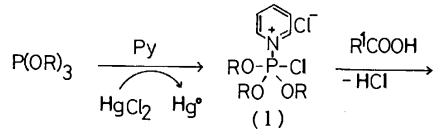

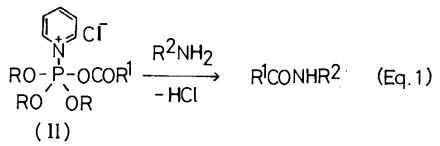

In this paper, we will describe a successful extension of this method to the reaction using phosphorous acid and its monoesters in the place of the tri- and di-esters.

Results and Discussion

The oxidation of phosphorous acid and its monoesters (ammonium salt) with mercuric chloride was carried out in pyridine under reflux in two ways, in the absence and in the presence of carboxylic acids. In Method A, the oxidation was carried out in the absence of the acids in a way similar to those described in previous papers.[1,2] A mixture of equimolar amounts of the ethyl ester and mercuric chloride was refluxed in pyridine for 1 hr and then treated with carboxylic acid for an additional hour of refluxing, followed by further reaction with aniline for 2 hr. The corresponding anilides were obtained in good yields; the yields are listed in Table 1. In Method B, in the presence of carboxylic acids, *e.g.*, when a mixture of equimolar amounts of phosphorous acid or the monoesters, mercuric chloride and acetic acid was refluxed for 1 hr, and then treated with aniline for an additional 2 hr of refluxing, acetanilide was obtained in 92 and 80% yields respectively. In the same way, the anilides of various carboxylic acids were obtained in the yields shown in Tables 1 and 2.

TABLE 1. THE PREPARATION OF VARIOUS ANILIDES USING THE MONOETHYL ESTER OF PHOSPHOROUS ACID AND MERCURIC CHLORIDE IN PYRIDINE

Acid	pK_a	Anilide	Method A	Method B
Acetic	4.77	Acetanilide	92	80
Propionic	4.87	Propionanilide	81	70
n-Butyric	4.82	*n*-Butyranilide	71	59
Isobytyric	4.86	Isobutyranilide	52	40
Benzoic	4.13	Benzanilide	—	39
Phenylacetic	4.31	Phenylacetanilide	—	64
Trifluoroacetic	1.26	Trifluoroacetanilide	—	86

TABLE 2. THE PREPARATION OF VARIOUS ANILIDES USING PHOSPHOROUS ACID AND MERCURIC CHLORIDE IN PYRIDINE (Method B)

Acid	pK_a	Mercuric Salt	Anilide	Yield (%)
Acetic	4.77	$HgCl_2$	Acetanilide	92
Acetic	4.77	$HgBr_2$	Acetanilide	92
Acetic	4.77	HgI_2	Acetanilide	81
Acetic	4.77	$Hg(OAc)_2$	Acetanilide	91
Propionic	4.87	$HgCl_2$	Propionanilide	90
n-Butyric	4.82	$HgCl_2$	*n*-Butyranilide	92
Isobutyric	4.86	$HgCl_2$	Isobutyranilide	79
Pivalic	5.03	$HgCl_2$	Pivalanilide	23
Benzoic	4.13	$HgCl_2$	Benzanilide	44

1) N. Yamazaki and F. Higashi, *Tetrahedron Lett.*, 415 (1972).
2) N. Yamazaki and F. Higashi, Part 1: This Bulletin, **46**, 1235 (1973).

The reaction can be explained in a manner similar to those in previous papers. In the first stage the *N*-phosphonium salt (III) was formed through the oxidation of phosphorous acid and its monoesters with mercuric chloride in pyridine. In this study, however, salt III was unstable in pyridine and was changed into IV by releasing hydrogen chloride. It is conceivable that IV does not contain any chlorine atoms and forms a zwitter-ion structure, since phosphorous acid and its monoesters have more than two hydrogen atoms capable of forming hydrogen chloride. Salt IV is then converted into V by the reaction with carboxylic acid. The aminolysis of V with aniline yielded the amides as is shown in Scheme 1.

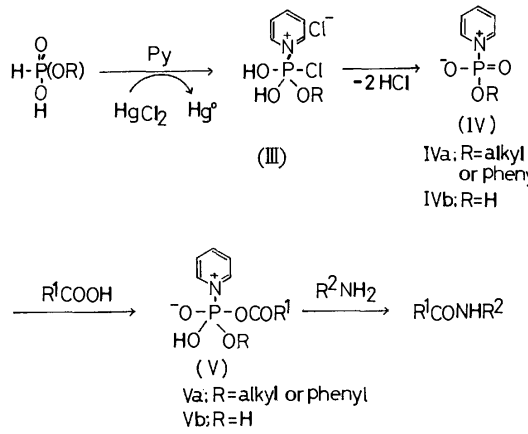

Scheme 1

In order to confirm the proposed mechanism, IV and V were separated through the procedure described in the previous paper and were analyzed by the IR-spectroscopic method, though they were difficult to isolate in pure forms because of contamination with pyridine hydrochloride.

The IR spectra of IVa and IVb showed characteristic absorption bands at 1630 and 1485 cm^{-1}. These bands, which were almost identical with those given by the *N*-phosphonium salts derived from the tri- and di-esters of phosphorous acid, were attributed to the $\nu_{C=N^+}$ in the phosphonium salts of pyridine. Bands due to pyridine hydrochloride were also observed. Since phosphorous acid and its monoesters have two or three hydrogen atoms, they would afford two moles of the hydrochloride. From these results, the structure of IV was proposed, as is shown in Scheme 1.

The characteristic bands appearing at 1630, 1485, and 1710 cm^{-1} in the spectra of Va and Vb were almost identical with those provided by the reaction products from the tri- and di-esters of phosphorous acid and acetic acid. The former two bands were attributed to the $\nu_{C=N^+}$ of the *N*-phosphonium salt, and the latter, to the $\nu_{C=O}$ of the acetoxy group. Therefore, the structure of V was proposed to be the *N*-phosphonium salt carrying the acetoxy group, as is shown in Scheme 1.

In the reaction of the monoethyl ester, it was found that the yield of acetanilide increased from the 80% of Method B to the 92% of Method A. Prolonged heating for an additional hour of aminolysis (from 2 to 3 hr) also improved the yield to 94%. For the improvement of the yield, three explanations are possible: the incomplete oxidation of the ester, the slow nucleophilic reaction with the carboxylate anions, and the insufficient aminolysis of Va. Since the aminolysis with aniline has proceeded almost completely within 2 hr, as will be discussed later, and since metallic mercury was obtained in a nearly quantitative yield within 1 hr under the conditions of Method B, however, insufficient oxidation and aminolysis can be excluded in elucidating the improvement. As a consequence, the rate-determining step in the reactions turned out to be the conversion of IVa to Va by the attack of the carboxylate anions.

On the contrary, these improvements were not observed in the reaction using phosphorous acid. This must be the result of an intramolecular hydrogen bonding in IVb, which will be discussed later in this paper.

The results presented above suggest that the reaction of IV with carboxylic acids to yield V involves a direct nucleophilic attack of the anions on IV. Hence, the reaction might be influenced by the acidity and the steric effect of the acids, and by the electrophilic nature of the phosphorus atom in IV. The electrophilicity would be governed by the electronic nature of the ester residues and by the basicity of the tertiary amines involved in the *N*-phosphonium salt (IV).

The effects of the acidity and the steric factor of carboxylic acids upon the yield of the anilides were studied by using the monoethyl ester (ammonium salt), various carboxylic acids, and mercuric chloride in pyridine (Method B); the results are summarized in Table 1. Sterically hindered carboxylic acids, such as isobutyric and benzoic acids, gave their anilides in yields only about a half of that of acetanilide. The reaction was also influenced by the acidity of the acids. This was evident from the fact that trifluoroacetic acid, with a high pK_a value of 1.26, gave trifluoroacetanilide in 87% yield, although less than a 50% yield would be expected from a consideration of its steric effect alone. Furthermore, the reaction was affected by the chain length of the acids. Among the acids with similar pK_a values, the yields of the corresponding anilides decreased with an increase in the chain length of the acids. For example, acetic, propionic, and *n*-butyric acids, which have their pK_a values in the range of 4.7 to 4.8, gave anilides in 80, 70, and 59% yields respectively. Analogous phenomena were observed in the reaction using the other monoalkyl esters as well (see Table 3).

As has been expected, the reaction would be in-

Table 3. The preparation of anilides using various monoesters of phosphorous acid and mercuric chloride in pyridine (Method B)

Monoester	Anilide, yield, %	
	Acetanilide	*n*-Butyranilide
Methyl	74	54
Ethyl	80	59
Isopropyl	74	59
Phenyl	94	87

fluenced by the electrophilicity of the phosphorus atom in IV, which itself chiefly depends on the electronic character of the ester residues in the monoesters. The effect of the ester residues upon the reaction was studied in terms of the yield of the isolated anilides by using various monoesters (ammonium salt) by Method B (see Table 3). The facts that no effect of the bulkiness of the residues in the alkyl esters was observed, and that the monophenyl ester, inspite of having a more bulky group, gave better results than the monoalkyl esters, indicated that the reaction was not influenced by the bulkiness of the ester residues. In addition, no such substantial decrease in the yields was seen in the monophenyl ester with an increase in the chain length of carboxylic acids as was observed in the monoalkyl esters. These results led us to consider that the presence of electron-attracting groups like the phenyl group decreased the electron density on the phosphorus atom in IVa and facilitated the nucleophilic attack of the carboxylate anions on IVa, not causing a substantial decrease in the yields with an increase in the chain lengths of the acids. On the other hand, the electron-donating groups like the isopropyl group increased the electron density and slowed down the reaction, resulting in a decrease in the yields with an increase in the length.

In the reaction of phosphorous acid, a similar steric effect of the acids upon the yields was observed, though it was not so serious as that observed in the monoesters. The effect of the chain length of the acids was not seen in this case. This might be caused by the intramolecular hydrogen bonding involving in IVb, which facilitates the reaction of IVb with the acids.

In the reaction of IV with carboxylic acids, several differences were observed between IVa (monoesters) and IVb (phosphorous acid). The results of the steric effect, mentioned above, indicated that the nucleophilic attack of carboxylate anions on IVb (R=H) was preferable to that on IVa (R=alkyl or phenyl). As a rule, phenyl and alkyl groups are more electro-positive and electronegative respectively than the hydrogen atom. If the reactivity of IV to the anions is caused by the electron deficiency on the phosphorus atom in IV, which itself depends chiefly on the inductive effect of the ester residues, the relative reactivity of IV might be in the order of IVa (R=phenyl)>IVb (R=H)> IVa (R=alkyl). However, the order obtained in this study was, unexpectedly, IVb (R=H)>IVa (R= phenyl)>IVa (R=alkyl).

This conflict can be explained by considering an intramolecular hydrogen bonding in IVb, as is shown below. Because of this bonding, the phosphorus atom became electron-deficient through the migration of the electrons at the phosphorus-oxygen bond to the oxygen; consequently, the nucleophilic attack of the anions on IVb was facilitated. On the other hand, in the case of the monoesters such a hydrogen bonding was unlikely to be involved in IVa. Therefore, the reactivity of IVa was governed mainly by the inductive effect of the ester residues, since the relative reactivity obtained in this study was IVa (R=phenyl)>IVa (R=alkyl), compatible with the order of the effect.

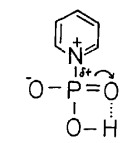

(IVb)

Tertiary amines were expected to play an important role, through the phosphorus-nitrogen bond of IV and V, in affecting the electrophilic nature of the phosphorus atom. Using phosphorous acid, the effect of tertiary amines upon the reaction (the yield of acetanilide) was investigated by varying the substituents in the pyridine nucleus (Table 4). The effects were not in agreement with those obtained by using triesters. In the reaction using the triesters, α-picoline gave a better result than pyridine, and even in 2,6-lutidine acetanilide was obtained in 59% yield. However, in this case pyridine was more favorable than α-picoline, and in 2,6-lutidine the anilide was not formed. The yield in γ-picoline, which was nearly the same as in α-picoline, was worse than that in β-picoline, indicating that the steric effect of the amines was not profound. Though the yield decreased with an increase in the basicity of amine among pyridine derivatives, the effect was inexplicable solely by the basicity, because triethylamine of a high pK_a value in acetonitrile gave acetanilide in 17% yield. The effect of amines appeared to be caused by the stability and reactivity of IV and/or V to carboxylic acids and aniline.

The aminolysis of V with aniline was investigated in reactions using phosphorous acid under various conditions (Table 5). The results showed that the acetoxy group carried by Vb was not so active, and that more than 2 hr of refluxing were required for the complete aminolysis of Vb with aniline. This fact provided additional evidence that V was not in the form of active acetyl phosphates.

Table 4. The preparation of acetanilide in various tertiary amines

Amine	pK_a	Acetanilide, yield, %[a)]
Pyridine	5.23	92
2-Methylpyridine	5.97	64
3-Methylpyridine	5.52	90
4-Methylpyridine	6.02	67
2,6-Dimethylpyridine	6.99	0
Triethylamine	10.87	17[b)]

a) Aminolysis with aniline at 115°C for 2 hr.
b) Under reflux in acetonitrile.

Table 5. The preparation of acetanilide in pyridine under various conditions

Conditions		Acetanilide, yield (%)
Temp., °C	Time, hr[a)]	
80	2	40
90	4	70
Reflux	1	79
Reflux	2	92
Reflux	3	95

a) After aniline was added.

All of the oxidizing agents used in this study, such as mercuric halides and its acetate, were found to be effective for this reaction (see Table 2).

Experimental

The mercuric chloride, tertiary amines, and phosphorous acid were obtained from commercial sources. The monoesters of phosphorous acid were prepared according to the literature.[3]

Separation of IVa (R=Et) and IVb. A mixture of equivalent amounts of the monoethyl ester (ammonium salt) of phosphorous acid (1.60 g, 12.5 mmol) and mercuric chloride (3.5 g) was refluxed for 1 hr in 20 ml of pyridine. After the separation of the liberated metallic mercury and ammonium chloride, IVa was obtained by the procedure described in the previous paper. Similarly, IVb was obtained by the reaction of phosphorous acid (1.03 g, 12.5 mmol) and mercuric chloride (3.5 g) in 20 ml of pyridine.

Separation of Va (R=Et) and Vb. A mixture of equivalent amounts of the monoethyl ester (ammonium salt) of phosphorous acid (1.60 g, 12.5 mmol) or phosphorous acid (1.03 g, 12.5 mmol) and mercuric chloride (3.5 g) was refluxed for 1 hr in 20 ml of pyridine. The reaction mixture was then treated with acetic acid (0.8 g, 12.5 mmol) under reflux for an additional hour. By the aforementioned procedures, Va and Vb were obtained. They were also obtained by the reaction of the monoethyl ester (ammonium salt) or phosphorous acid and mercuric chloride in the presence of acetic acid under reflux for 1 hr in pyridine.

Preparation of Anilides using Phosphorous Acid and Its Monoesters. The anilides were prepared by two methods.

Method A: The oxidation was carried out in the way described above. The reaction mixture was treated with an equivalent carboxylic acid under reflux for 1 hr, and then with a 10% excess of aniline for an additional 2 hr.

Method B: The oxidation was carried out under reflux for 1 hr in the presence of a carboxylic acid, and then treated with aniline for 2 hr under reflux. The product was isolated accoding to the procedure described in a previous paper.[1] The anilides thus obtained showed IR spectra and melting points identical with those of authentic samples.

Preparation of Acetanilide in Various Tertiary Amines. The reactions were carried out by Method B using phosphorous acid in refluxing pyridine or at 115°C in other pyridine derivatives. In the case of triethylamine (4 equiv.), the reaction was conducted in refluxing acetonitrile.

3) P. R. Hammond, *J. Chem. Soc.*, **1962**, 2521.

BULLETIN OF THE CHEMICAL SOCIETY OF JAPAN, VOL. 46, 1242—1246 (1973)

Stereospecific Addition Reaction between Butadiene and Amines

Tadashi NARITA, Nobuyoshi IMAI, and Teiji TSURUTA

Department of Synthetic Chemistry, Faculty of Engineering, The University of Tokyo, Bunkyo-ku, Tokyo 113

(Received August 1, 1972)

The reaction of butadiene with secondary amines initiated by *n*-butyllithium was found to proceed selectively to produce 1-dialkylamino-*cis*-butene-2 under appropriate reaction conditions. For instance, diethylamine produced 1-diethylamino-*cis*-butene-2 in a 98—99% purity. By kinetic and spectroscopic studies, it was concluded that the lithium dialkylamide–dialkylamine (1:2) complex plays an important role in this addition reaction. The second-order rate constants of the reaction are 0.85×10^{-3} l/mol sec for diethylamine and 2.4×10^{-3} l/mol sec for diisobutylamine.

It was previously reported that the reactivity of lithium alkyl was drastically influenced by coupling with lithium 2-alkoxyethoxide.[1-5] Since it seemed worthwhile to examine the influence of lithium 2-alkoxyethoxide upon the reactivity of lithium amide, reactions between butadiene and lithium dialkylamides were studied in the presence of the 2-alkoxyethoxide. Contrary to the case of lithium alkyl, the reactivity of the lithium amide was not significantly influenced by the 2-alkoxyethoxide. However, it was unexpectedly found that lithium dialkylamide was activated in a specific fashion by the stoichiometric quantity of the parent dialkylamine.

This paper will present the results of a study of the reaction of butadiene and dialkylamine initiated by *n*-butyllithium and producing 1-dialkylaminobutene derivatives. A preliminary report of the results was published elsewhere.[6]

Experimental

Most of the experiments were carried out under purified nitrogen to preclude oxygen and atmospheric moisture.

Reagents. Cyclohexane, butadiene, and amines were purified by the usual method. *n*-Butyllithium was prepared from *n*-butyl chloride and lithium metal in purified petroleum ether and was used as a cyclohexane solution.

Synthesis of 1-Dialkylaminobutene Derivatives. The addi-

1) T. Narita, N. Imai, and T. Tsuruta, *Kogyo Kagaku Zasshi*, **72**, 994 (1969).
2) T. Narita, A. Masaki, and T. Tsuruta, *J. Macromol. Sci.-Chem.*, **A4**, 277 (1970).
3) T. Narita, M. Kazato, and T. Tsuruta, *ibid.*, **A4**, 885 (1970).
4) T. Narita and T. Tsuruta, *J. Organometal. Chem.*, **30**, 289 (1971).
5) T. Yamaguchi, T. Narita, and T. Tsuruta, *Polymer J.*, **3**, 573 (1972).
6) N. Imai, T. Narita, and T. Tsuruta, *Tetrahedron Lett.*, **1971**, 3517.

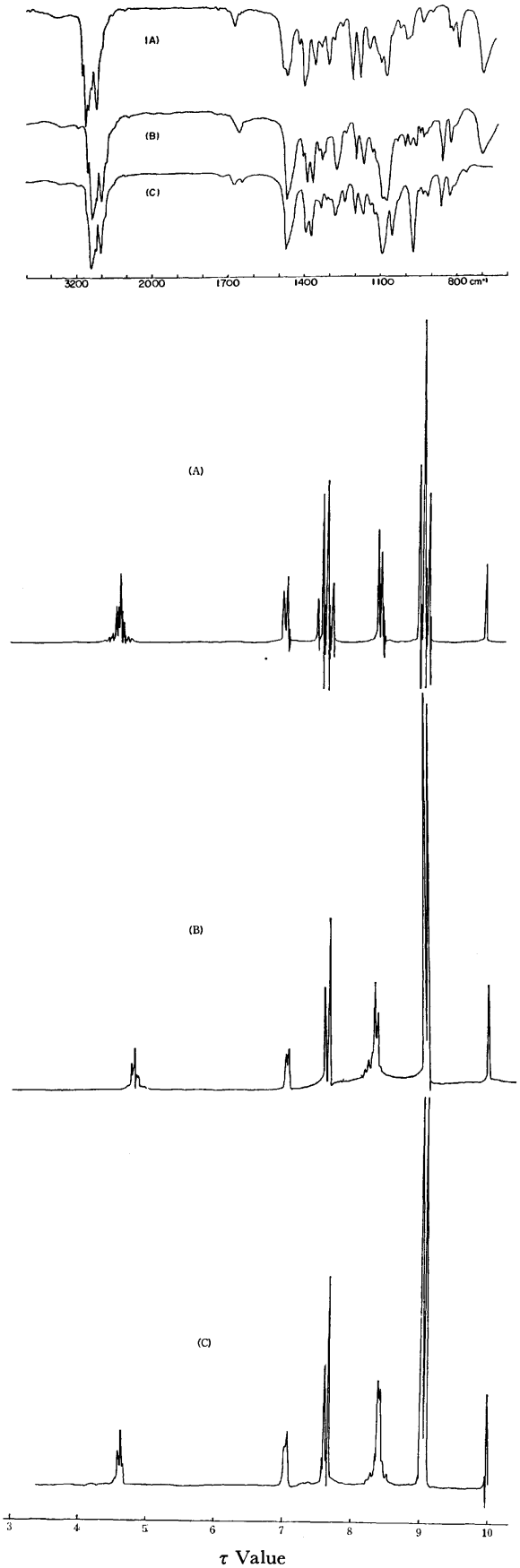

Fig. 1. IR and NMR spectra of (A) 1-diethylamino-*cis*-butene-2, (B) 1-diisobutylamino-*cis*-butene-2, and (C) 1-diisobutylamino-*trans*-butene-2.

tion products of dialkylamine to butadiene were isolated as follows. A 200 ml flask was equipped with a reflux condenser with a dry ice-methanol refrigerant and a KOH drying column. A 100 mmol portion of butadiene vapor was introduced through the KOH column for two hours into a magnetically-stirred cyclohexane solution at 50 °C, into which dialkylamine (100 mmol) and *n*-butyllithium (5 mmol) were added. After the mixture has been stirred another three hours at 50°C, the reaction was stopped by the addition of a small amount of methanol. The products were isolated by fractional distillation and by preparative vapor phase chromatography (vpc). The analyses of the products were performed by NMR, IR, and mass spectrometry. The analytical data are shown in Table 1 and Fig. 1.

Metalation of Amines. A cyclohexane solution of *n*-butyllithium was added to a solution of secondary amine at 0 °C by means of a syringe. After five minutes stirring, an excess of carbon tetrachloride was added in order to decompose the residual *n*-butyllithium; then the mixture was treated with water. *n*-Butane present in the oil layer was analyzed by vpc.

Kinetics of the Addition Reaction. Into a round-bottomed flask equipped with a three-way stop cock, butadiene and cyclohexane were introduced. A solution of the lithium dialkylamide-dialkylamine complex was then added into the flask. The reaction was quenched after various time intervals by sampling a portion of the solution and adding it to an ether solution of methanol. The products were analyzed by vpc.

Results and Discussion

Synthesis of 1-Dialkylaminobutene Derivatives. The results of the addition reaction of dialkylamines to butadiene initiated by a catalytic amount of *n*-butyllithium are summarized in Table 2. The yields of the butenylation products were all about 85% except for the case of diisopropylamine. Higher-molecular-weight compounds than the simple butenylation products were not detected by vpc under these reaction conditions.

Kinetic Studies of the Addition Reaction. The addition reaction of dialkylamine to butadiene in the presence of *n*-butyllithium was assumed to proceed through the following three steps:

$$R_2NH + n\text{-}C_4H_9Li \longrightarrow R_2NLi + n\text{-}C_4H_{10} \quad (1)$$

$$R_2NLi + CH_2{=}CH{-}CH{=}CH_2 \xrightarrow{k_b} R_2NC_4H_6Li \quad (2)$$

$$R_2NC_4H_6Li + R_2NH \xrightarrow{k_t} R_2NC_4H_7 + R_2NLi \quad (3)$$

At first, the metalation of dialkylamine with *n*-butyllithium, Eq. (1), was examined in cyclohexane. After the dialkylamine had been reacted with *n*-butyllithium, the cyclohexane solution was treated with carbon tetrachloride and then with water. The mol of *n*-butane recovered by vpc should be equal to that of the lithium amide formed, since the non-reacting *n*-butyllithium should have been decomposed by CCl_4. The results shown in Table 3 clearly indicate that the reaction of dialkylamine and *n*-butyllithium proceeds stoichiometrically at 0 °C within 5 min to produce lithium dialkylamide.

The dependence of the butadiene concentration on

TABLE 1. ANALYSIS OF PRODUCTS FROM DIALKYLAMINE AND BUTADIENE

Reaction products		NMR spectra (τ value) (a)	(b)(c)	(d)	(e)	(f)	(g)	(h)	Mass spectra M.W.[a]	IR spectra characteristic absorption cm^{-1}
$CH_3CH=CHCH_2N(CH_2CH_3)_2$	*cis*	8.44	4.63	7.06	7.65	9.10			127	690
		3H,d	2H,m	2H,d	4H,q	6H,t			(127.2)	δCH(*cis*-CH=CH–)
	trans	8.39	4.62	7.13	7.66	9.10			127	969
		3H,d	2H,m	2H,d	4H,q	6H,t			(127.2)	δCH(*trans*-CH=CH–)
$CH_3CH=CHCH_2N(CH_2CH_2CH_3)_2$	*cis*	8.41	4.50	6.98	7.71	8.61	9.09		155	690
		3H,d	2H,m	2H,d	4H,t	4H,m	6H,t		(155.3)	δCH(*cis*-CH=CH–)
$CH_3CH=CHCH_2N(CH_2CH_2CH_2CH_3)_2$	*cis*	3H,d	2H,m	2H,d	4H,t	4H,m	4H,m	6H,t	183 (183.3)	690 δCH(*cis*-CH=CH–)
$CH_3CH=CHCH_2N(CH(CH_3)_2)_2$	*cis*	8.44	4.71	7.01	7.07	9.10			155	690
		3H,d	2H,m	2H,d	2H,m	12H,d			(155.3)	δCH(*cis*-CH=CH–)
	trans	8.40	4.65	7.06	7.05	9.10			155	969
		3H,d	2H,m	2H,d	2H,m	12H,d			(155.3)	δCH(*trans*-CH=CH–)
$CH_3CH=CHCH_2N(CH_2CH(CH_3)_2)_2$	*cis*	8.42	4.52	7.03	7.98	8.33	9.08		183	701
		3H,d	2H,m	2H,d	4H,d	2H,m	12H,d		(183.3)	δCH(*cis*-CH=CH–)
	trans	8.33	4.51	7.09	7.99	8.33	9.09		183	968
		3H,d	2H,m	2H,d	4H,d	2H,m	12H,d		(183.3)	δCH(*trans*-CH=CH–)

a) Values in parentheses are the calculated ones.

TABLE 2. ADDITION REACTION PRODUCTS OF DIALKYLAMINE WITH BUTADIENE INITIATED BY *n*-BUTYLLITHIUM[a]

Amine	Total yield (%)	Microstructures of products Vinyl (%)	*trans* (%)	*cis* (%)
Diethylamine	86	1	12	87
Di-*n*-propylamine	86	trace	12	87
Di-*n*-butylamine	75	0	14	86
Diisopropylamine	9	0	45	55
Diisobutylamine	84	0	22	78

a) Dialkylamine 100 mmol, butadiene 100 mmol, *n*-butyllithium 5 mmol, 50 °C.

TABLE 3. REACTION OF DIALKYLAMINE WITH *n*-BUTYLLITHIUM[a]

Amine	Yield of lithium amide (%)
Diethylamine	103
Diisopropylamine	100
Diisobutylamine	99

a) Reaction temp.: 0 °C, reaction time: 5 min.

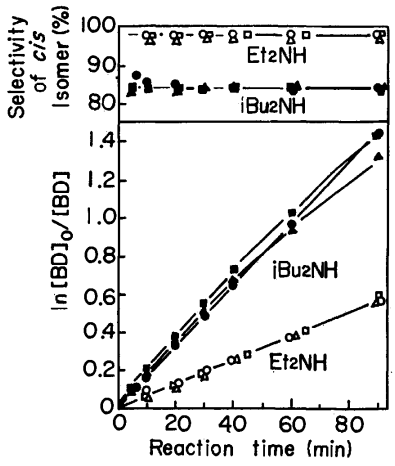

Fig. 2. Dependence of butadiene concentration on addition reaction rate.
[Butadiene]$_0$/[R_2NLi]$_0$ Value, ●○: 1.0, ■□: 2.0, ▲△: 3.0. [R_2NH]$_0$=0.375 M, [R_2NLi]$_0$=0.125 M. Solvent: cyclohexane, reaction temp.: 50 °C

the reaction rate was examined with the ratio of initial concentrations, [R_2NH]$_0$: [R_2NLi]$_0$, being three to one, where R were ethyl and isobutyl. The straight lines in Fig. 2 show that the reaction is in a first-order dependence on the butadiene concentration below the 60% conversion.

The rate, v, of the addition is expressed by Eq. (4):

$$v = k'[\text{butadiene}] \quad (4)$$

The relationship between k' and the initial concentration of lithium dialkylamide at the concentration of [R_2NH]$_0$: [R_2NLi]$_0$=3: 1 is shown in Fig. 3. Pseudo first-order rate constants, k', were found to be proportional to the concentration of lithium dialkylamide

$$k' = k[R_2NLi] \quad (5)$$

where k is the rate constant of the reaction.

The results presented above seem to mean that the rate of the addition reaction varies as the first-order of the concentrations of butadiene and lithium dialkylamide respectively. In the absence of dialkylamine, however, no addition reaction proceeded in cyclohexane, as is shown in Table 4. Addition products were not detected even in such polar solvents as triethylamine or *N,N,N',N'*-tetramethylethylenediamine, which are known to form associated complexes with organolithium compounds. These results suggest that the role of amino-hydrogen is different from that of the usual polar solvents.

In order to get some more information on the species, infrared spectroscopic analyses were carried out with

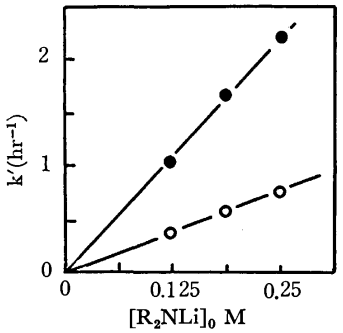

Fig. 3. Relationship between pseudofirst-order rate constant and $[R_2NLi]$. $[R_2NH]_0/[R_2NLi]_0 = 3.0$, $[Butadiene]_0 = 0.250$ M.
Solvent: cyclohexane, reaction temp.: 50 °C
●: diisobutylamine, ○: diethylamine

a mixture of lithium diisobutylamide and diisobutylamine. As is shown in Fig. 4(A), the absorption at 650 cm^{-1} was assignable to the free N–Li stretching frequency, because the characteristic absorptions of C–Li and O–Li were known to appear at 548 and 577 cm^{-1} respectively. The absorption at 650 cm^{-1} decreased as the ratio of the diisobutylamine concentration to the lithium diisobutylamide concentration increased. The absorption disappeared when the ratio exceeded 2.0. At [NH]/[NLi]=2.0 and 3.0 a new peak was observed at 595 cm^{-1}; this peak was detected in the spectrum of neither diisobutylamine nor lithium diisobutylamide. Therefore, this new peak was assigned to a complex of lithium diisobutylamide with diisobutylamine. With the aid of the calibration curve, the concentration of the complex present in the system was calculated from the absorbance of the peak at 650 cm^{-1}. The complex formation of lithium dialkyl-

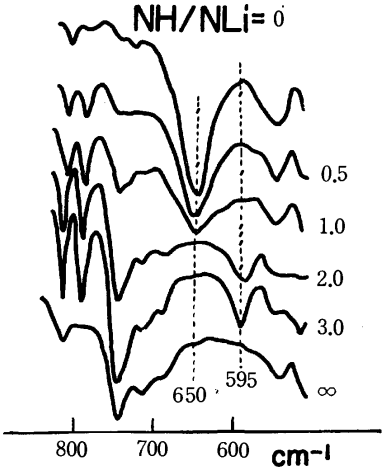

Fig. 4. (A) IR spectra of i-Bu_2NH—i-Bu_2NLi system. $[i\text{-}Bu_2NLi]=0.2$ M, solvent: cyclohexane.

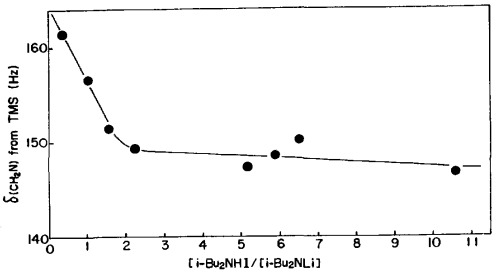

Fig. 4(B). Relation between NMR chemical shift of CH_2N and $[i\text{-}Bu_2NH]/[i\text{-}Bu_2NLi]$ value.
$[i\text{-}Bu_2NLi]=1$ M, solvent: benzene, 60 MHz

amide-dialkylamine (1 : 2) can clearly be seen from the results shown in Table 5.

The formation of the one-to-two complex was also

Table 4. Stereospecific butenylation of R_2NH with butadiene[a)]

R	$\frac{[R_2NH]_0}{[R_2NLi]_0}$	Products yield (%) on butadiene	Microstructure of products		
			Vinyl (%)	*trans* (%)	*cis* (%)
CH_3CH_2	0	0	—	—	—
	3	50	0	2	98
$CH_3CH_2CH_2$	3	47	0	7	93
$CH_3CH_2CH_2CH_2$	3	29	0	5	95
$CH_3\rangle CH$ CH_3	3	0	—	—	—
$CH_3\rangle CHCH_2$ CH_3	0	0	—	—	—
	3	87	0	20	80

a) $[R_2NLi]_0$ 0.25 mol/l. $[Butadiene]_0$ 0.25 mol/l.
Solvent: cyclohexane, reaction temperature: 50 °C, reaction time: 60 min.

Table 5. Analysis of $(i\text{-}C_4H_9)_2$ NLi–$(i\text{-}C_4H_9)_2$NH system with infrared spectra at 650 cm^{-1} band[a)]

Total concentration			$[NLi]_{free}$	$[NLi]_{complex}$	$\frac{[NH]}{[NLi]}$ in complex
$[NH]_0$ mol/l	$[NLi]_0$ mol/l	$\frac{[NH]_0}{[NLi]_0}$			
0	0.20	0	0.20	0	0
0.10	0.20	0.5	0.15	0.05	2.0
0.20	0.20	1.0	0.095	0.105	1.9
0.40	0.20	2.0	0.0	0.20	2.0

a) Solvent: cyclohexane.

suggested by the NMR spectra shown in Fig. 4(B), in which an inflection point was observed at [NH]/[NLi]=2.0. As the proton-exchange reaction between *i*-Bu_2NH and *i*-Bu_2NLi is fast at room temperature, the methylene NMR signals of the complex are observed at the average value of the corresponding signals for its components. Furthermore, an exchange reaction should also be possible between the complex and free *i*-Bu_2NH when more than two times as much of the latter is present as *i*-Bu_2NLi. Another exchange reaction, on the other hand, is operative in the reaction between the complex and free *i*-Bu_2NLi in the region to the left of the inflection point in Fig. 4(B).

The overall scheme of the addition reaction may be drawn as follows:

$$R_2NLi + 2R_2NH \longrightarrow R_2NLi\cdot 2R_2NH \quad (6)$$

$$R_2NLi\cdot 2R_2NH + CH_2{=}CH{-}CH{=}CH_2 \xrightarrow{k_b} R_2NC_4H_6Li\cdot 2R_2NH \quad (7)$$

$$R_2NC_4H_6Li\cdot 2R_2NH + R_2NH \xrightarrow{k_t} R_2NCH_2CH{=}CHCH_3 + R_2NLi\cdot 2R_2NH \quad (8)$$

Since the butenylation, Eq. (7), should be the rate-determining step of the addition reaction, the rate can be expressed as follows:

$$v = k_b[\text{complex}][\text{butadiene}] \quad (9)$$

In the region of $[R_2NH]/[R_2NLi]>2$, the concentration of the complex is controlled by the concentration of lithium amide, so that Eq. (9) can be reduced to Eq. (10):

$$v = k_b[R_2NLi][\text{butadiene}] \quad (10)$$

Equation (10) well explains the results of Fig. 2. On the contrary, in the region of $[R_2NH]/[R_2NLi]\leqq 2$, the concentration of the complex should be controlled by the concentration of dialkylamine, so that Eq. (9) can be reduced to Eq. (11):

$$v = \frac{1}{2}k_b[R_2NH][\text{butadiene}] \quad (11)$$

As a matter of fact, Eq. (11) can be used in the analyses of the addition reaction in the region of $[R_2NH]/[R_2NLi]\leqq 2$, as is shown in Fig. 5.

The rate constants of the reactions calculated from Eq. (9) are summarized in Table 6.

Diisopropylamine did not react with butadiene. No infrared peak assignable to a complex of amine and lithium amide was observed. The steric hindrance of the isopropyl group is presumably the reason for the low reactivity of diisopropylamine.

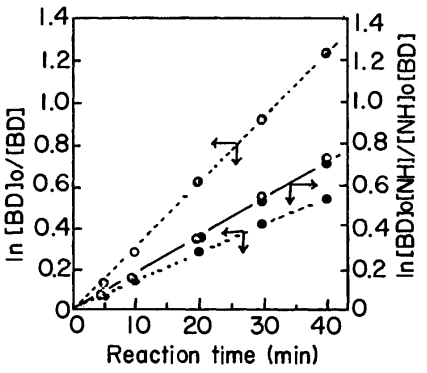

Fig. 5. First and second order analyses of the addition reaction of diisobutylamine with butadiene.
$[i\text{-}Bu_2NLi]_0=[\text{Butadiene}]_0=0.25$ M, solvent: cyclohexane, reaction temp. 50 °C.
$[i\text{-}Bu_2NH]_0/[i\text{-}Bu_2NLi]_0$ value ●: 1.0, ○: 2.0

TABLE 6. RATE CONSTANTS OF THE ADDITION REACTION OF $R_2NLi\cdot 2R_2NH$ WITH BUTADIENE

R	$k\times 10^3$ l/mol sec	*cis* Isomer content (%) 30 min	60 min
CH_3CH_2	0.85	99	99
$CH_3CH_2CH_2$	0.66	94	93
$CH_3CH_2CH_2CH_2$	0.41	96	95
$(CH_3)_2CH$	0	—	—
$(CH_3)_2CHCH_2$	2.4	80	80

The selectivity of the reaction to produce the *cis* isomer decreased when the $[R_2NH]/[R_2NLi]$ value increased (*cf.* Tables 2, 4, and Fig. 2). The selectivity is also affected by the structures of the alkyl groups of dialkylamine, as is shown in Tables 2 and 4. It can safely be concluded that di-*n*-alkylamine produces the *cis* isomer in high purity. Especially, diethylamine gives the *cis* isomer in a 98—99% purity.

Although the structure of the complex has not been clearly elucidated, we wish to propose the following structure on the basis of NMR, IR, and the reactivity of the complex:

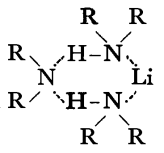

This structure can probably explain the finding that *N,N,N',N'*-tetramethylethylenediamine and triethylamine do not have any positive effects on the reaction of lithium dialkylamide.

Derivatives of Cyclic Disulfides. II.[1] Alkaline Hydrolysis of 1,2-Dithiaacenaphthene *S*-Oxide

Seizo TAMAGAKI, Hiroo HIROTA, and Shigeru OAE

Department of Applied Chemistry, Faculty of Engineering, Osaka City University, Sumiyoshi-ku, Osaka 558

(Received August 24, 1972)

The alkaline hydrolysis of 1,2-Dithiaacenaphthene *S*-oxide has been investigated kinetically, its reactivity being compared with that of its open-chain analog, phenyl benzenethiolsulfinate. The rate was found to be of first order with respect to both hydroxide and the ester. 1,2-Dithiaacenaphthene *S*-oxide was found to be hydrolyzed 10^3 times more slowly than the open-chain analog in an alkaline medium. The reduced reactivity was interpreted on the basis of structural rigidity.

Aromatic five-membered cyclic sulfates and sulfonates are known to be hydrolyzed in alkaline solution 10^6—10^7 times faster than the corresponding open-chain esters,[2] and the main driving force for the remarkable rate enhancement in the hydrolytic reactivities of these five-membered cyclic esters has been believed to be due to the ring strain. The small values of the internal ring angle around the sulfur atom reflect the strain present in these five-membered rings. The hydrolysis of these esters is considered to proceed *via* an intermediate or transition complex which has a structure of approximately trigonal-bipyramid, in which the ring angle around the sulfur atom is close to 90° and the five-membered ring spans apical and equatorial positions. Since the ring angle around the sulfur in the five-membered cyclic esters is close to 90° even in the ground state, the compound can readily assume trigonal-bipyramidal geometry. However, in contrast to the alkaline hydrolysis of five-membered cyclic esters, that of an analogous five-membered cyclic compound containing sulfur-linkage has not been explored despite its inherent importance in biological systems.[3] Thus, we have synthesized 1,2-dithiaacenaphthene *S*-oxide (I) as a model compound, and subjected it to alkaline hydrolysis and compared its reactivity with that of phenyl benzenethiolsulfinate (II).

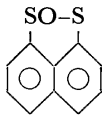

(I)

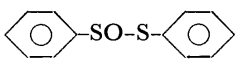

(II)

Although both sulfur atoms are confined rigidly at two peri-positions of naphthalene ring, 1,2-dithiaacenaphthene *S*-oxide is considered to be less strained than the corresponding oxygen-analogs, for the bond length of *S*–*S* linkage is considered to be nearly the same as the non-bonding distance between two peri-positions. However, since the two sulfur atoms in compound (I) are fixed rigidly at peri-positions of naphthalene nucleus, the kinetic behavior of this compound may not be similar to that of the five-membered sulfates or sulfonates.

Results and Discussion

Upon alkaline hydrolysis of I, the product could be separated into two parts; one soluble in ordinary organic solvents such as ether or chloroform, the other insoluble in common organic solvents but very soluble in water. 1,2-Dithiaacenaphthene, *i.e.*, reduced product, was obtained from the organic layer (37%). The latter water-soluble salts were neutralized with hydrochloric acid to afford 1,2-dithiaacenaphthene *S*, *S*-dioxide (8%) and 1,2-dithiaacenaphthene *S*-oxide (23%). A careful analysis of the UV spectra of an alkaline aqueous ethanol solution of 1,2-dithiaacenaphthene *S*-oxide indicates that the characteristic band due to the initial 1,2-dithiaacenaphthene *S*-oxide (247 nm) disappears, and a new band (265 nm) appears as the reaction proceeds. On completion of hydrolysis, the 265 nm band also begins to disappear at a relatively slower rate. The UV spectra and the product analysis suggest that the first stage of the reaction is the formation of a sodium salt of

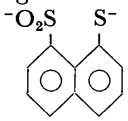

because the attacking site for hydroxide ion in the initial step seems to be the sulfinyl sulfur. The starting material was regenerated in a considerable amount only after neutralization.

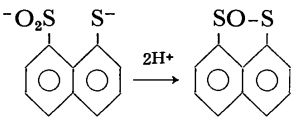

(III) (I)

There are two possible attacking sites for hydroxide in the initial step of the reaction, *i.e.*, the sulfinyl sulfur and the divalent sulfenyl sulfur. According to the HSAB principle,[4] the attack on the sulfinyl sulfur is more favorable than that on the sulfenyl sulfur, since hydroxide ion is a hard base. It is known that in alkaline hydrolysis of aryl arenethiolsulfinate, no hy-

1) Derivatives of Cyclic Disulfides I., S. Tamagaki, and S. Oae, This Bulletin, **45**, 960 (1972).

2) E. T. Kaiser, *Accounts Chem. Res.*, **3**, 145 (1970); P. A. Pristow, J. G. Tillett, and D. W. Wiggins, *J. Chem. Soc., B*, **1968**, 1360; J. G. Tillett and D. W. Wiggins, *J. Org. Chem.*, **35**, 1359 (1970); F. H. Westheimer, *Accounts Chem. Res.*, **1**, 70 (1968).

3) N. Kharasch and C. Y. Meyers, "Organic Sulfur Compound," Vol. 2, Pergamon Press (1966), p. 336.

4) J. O. Edwards and R. G. Pearson, *J. Amer. Chem. Soc.*, **84**, 16 (1962); R. G. Pearson, *ibid.*, **85**, 3533 (1963); *Science*, **151**, 172 (1966).

droxide ion attacks the sulfenyl sulfur in accordance with the HSAB principle.[5] We suggest that the most probable mechanism for this reaction is as follows.

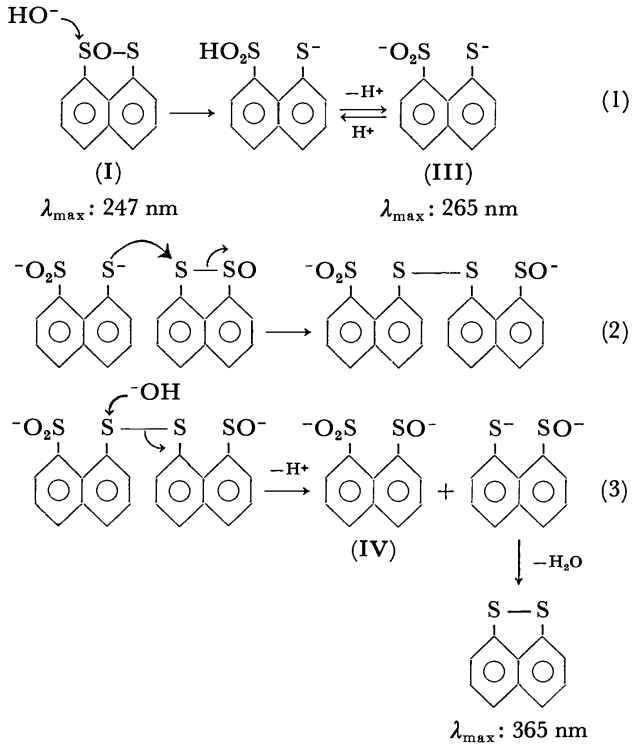

After neutralization

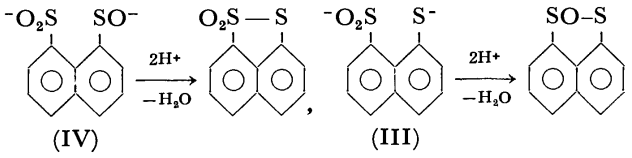

In order to clarify the structural effect on the rate of hydrolysis, we carried out kinetic measurements in a weakly alkaline 60% ethanol–water solvent, keeping the concentration of the ester around 10^{-5} M. Measurements were carried out by observing spectrometrically the disappearance of the chracteristic UV absorption band of 247 nm due to 1,2-dithiaacenaphthene *S*-oxide. The first-order dependence of rate on the initial concentration of the ester was observed. The rate constants are listed in Table 1. The first-order dependence of k_{obs} on the hydroxide ion concentration is also shown in Table 2. The fact that the initial rate was found to be exactly proportional to the initial concentration of both the ester and hydroxide ion indicates that in the first step of the reaction the rate depends only on the concentration of both hydroxide ion and the ester and that the attack of hydroxide ion on sulfinyl sulfur occurs exclusively. We can thus conclude that no subsequent reaction takes place at all in the initial step of the reaction. The initial rate method was found to be approriate for kinetic measurements of the alkaline hydrolysis of 1,2-dithiaacenaphthene *S*-oxide. The second-order constants were easily calculated from the

Table 1. Rate constants for alkaline hydrolysis; dependency of rate on ester concentration[a]

[Ester]$\times 10^5$, M	$-d[OD]/dt \times 10^5$	$k_{OH^-}[OH^-] \times 10^5$, sec^{-1}
2.9	1.9	2.6
4.2	2.5	2.4
5.7	4.0	2.7
8.3	5.8	2.7

a) At 20 °C in 60% EtOH–H_2O $[OH^-]=2.3\times10^{-4}$M

Table 2. Rate constants for alkaline hydrolysis; dependency of rate on OH^- concentration[a]

$[OH^-]\times 10^4$, M	$k_{obsd}\times 10^5$, sec^{-1}	k_{OH^-}, M^{-1} sec^{-1}
1.9	2.4	1.3
1.7	2.3	1.3
0.90	1.1	1.2

a) At 20 °C in 60% EtOH–H_2O $[E]=2.4\times10^{-5}$M

values of k_{obs} by dividing them by the initial concentration of hydroxide ion (Table 3). A kinetic experiment on the alkaline hydrolysis of phenyl benzenethiolsulfinate was also carried out in a pH-controlled buffer solution because the reaction was found to be very fast. The buffer chosen was potassium phosphate monobasic (KH_2PO_4)–sodium phosphate dibasic (Na_2HPO_4) system. The alkaline hydrolysis of 1,2-dithiaacenaphthene *S*-oxide was carried out in a medium of the same ionic strength as in the case of phenyl benzenethiolsulfinate.

In the alkaline hydrolysis of aromatic sulfonates and sulfates, the rates of the five-membered cyclic esters were reported to be 10^6—10^7 times faster than those of the corresponding open-chain analogs.[6]

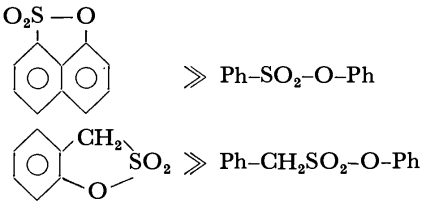

However, five-membered cyclic thiolsulfinate (I) was found to be hydrolyzed 1.5×10^3 times more slowly than the corresponding acylic ester.

The activation energy for the five-membered thiolsulfinate is markedly low, *i.e.*, $\Delta H^{\ddagger}=8.8$ kcal mol^{-1}, while the activation entropy is more negative, *i.e.*, $\Delta S^{\ddagger}=-32$ e.u., than that of phenyl benzenethiolsulfinate. These activation parameters suggest that the markedly small rate of the cyclic thiolsulfinate is mainly caused by the entropy term of free energy of activation. Thus, the surprisingly reduced reactivity of five-membered thiolsulfinate ester as compared with the case of sulfate ester can be rationalized on the basis of the following special nature of 1,2-dithiaacenaphthene skeleton; in 1,2-dithiaacenaphthene *S*-oxide two sulfur atoms are bound rigidly to fit just at the two peri-positions of naphthalene nucleus, *i.e.*, the bond length of *S*–*S* linkage being 2.1 Å according to the atomic radii

5) S. Oae, Y. Yoshikawa, and W. Tagaki, This Bulletin, **42**, 2899 (1969).

6) O. R. Zaborsky and E. T. Kaiser, *J. Amer. Chem. Soc.*, **88**, 3084 (1966); E. T. Kaiser and O. R. Zaborsky, *ibid.*, **89**, 1393 (1967).

Table 3. Alkaline hydrolysis of thiolsulfinate or thiolsulfonate

	k_{OH^-}, $M^{-1}sec^{-1}$	Rel. rate	ΔH^* kcal mol^{-1}	ΔS^* e.u. (30°C)
Ph–SO–S–Ph[a)]	$2.4\times10^3\pm0.2$	1.5×10^3	11.5	−11
SO–S[a)] 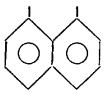	1.6 ± 0.3	1	8.8	−32
Ph–SO_2–S–Ph[b)]	2.4 ± 0.2	1.5	10	−13
SO_2–S 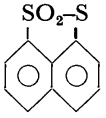	no reaction			

a) In 60% (v/v) EtOH–H_2O at 30°C, μ=0.2.
b) In 60% (v/v) EtOH–H_2O at 45°C.
c) 20, 25, 30, 35°C.

given by Pauling, close to the distance between two peri-positions (2.4 Å). It is evident that the five-membered ring is much less strained than the oxygen analog which is highly strained because of the shorter bond length of S–O linkage (1.8 Å). Therefore the

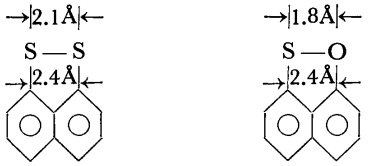

C–S–S angle is supposed to be very close to 90°. This seems to be adequate for the formation of a trigonal bipyramidal transition complex or intermediate of sp^3d configuration in which the ring angle around the sulfur atom is close to 90° and the five-membered ring spans apical and equatorial positions to accomodate the incoming nucleophile, *i.e.*, OH^- ion, giving rise to a lower value of activation enthalpy. The large negative activation entropy of the 1,2-dithiaacenaphthene *S*-oxide as compared with that for the open-chain analog indicates that due to the confinement at the peri-positions the S–S bond cannot be cleaved easily by the attack of the hydroxide ion on the sulfinyl sulfur unless its C–S bond is bent off the normal bond angle of a peri-substituent. A similar rate-retardation should be found in the alkaline hydrolysis of the five-membered cyclic 1,2-dithiaacenaphthene *S*,*S*-dioxide as compared to that of the open-chain benzenethiolsulfonate. The open-chain thiolsulfonate was hydrolyzed overwhelmingly faster than that of the thiosulfonate bearing the naphthalene ring (Table 3).

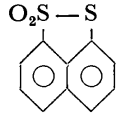

no reaction

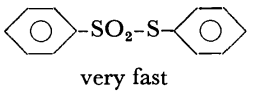

very fast

Experimental

Materials. 1,2-Dithiaacenaphthene was prepared according to the method of Zweig and Hoffmann.[7] 1,2-Dithiaacenaphthene *S*-oxide was obtained by the oxidation of 1,2-dithiaacenaphthene with sodium metaperiodate in dioxane–water or by selective deoxygenation of thiolsulfonate with trimethyl phosphite. The procedure is as follows. 1,2-Dithiaacenaphthene 3.1 g (16.1 mmol) was dissolved in 90 ml of dioxane into which a solution of 6.8 g (30.5 mmol) of sodium metaperiodate in 60 ml of water was added. The resulting solution was kept at room temperature for 12 hr, and then extracted with benzene. The solvent was evaporated and the residue was recrystallized from *n*-hexane–benzene to afford yellow needles, mp 82.5—83.5°C. Another procedure is as follows. Upon refluxing the mixture of 1,2-dithiaacenaphthene *S*,*S*-dioxide 220 mg (1.0 mmol) and trimethyl phosphite 310 mg (2.5 mmol) in 100 ml of benzene for 3 hr, a nearly quantitative amount of 1,2-dithiaacenaphthene *S*-oxide and a trace of 1,2-dithiaacenaphthene were obtained. The reaction mixture was evaporated and the residue was separated by column chromatography. The compound showed an IR stretching band at 1080 cm^{-1} characteristic of the S–O group. UV: max 247 nm (ε: 25700 in 60% EtOH–H_2O) Mass spectrum showed the conversion from *m/e* 206 to *m/e* 178. Found: C, 58.20; H, 2.98%. Calcd for $C_{10}H_6OS_2$: C, 58.27; H, 2.88%. Kinetics: A solution of 1 ml of 1,2-dithiaacenaphthene *S*-oxide (1.2×10^{-3}M) in absolute ethanol was added to a mixture of 29 ml of ethanol and 20 ml of 4.0×10^{-4}M KOH water solution, the latter mixture being kept in a constant temperature bath prior to addition of the ester. An aliquot of the reaction mixture was withdrawn to a UV cell and its optical density near 247 nm was recorded with a Hitachi EPS-3T recording spectrophotometer. Since the reaction was expected to be complicated as illustrated in equations (1)—(3), only the initial rate was used for calculation of the rate constant. The initial slope obtained graphically was found to be proportional to the initial rate of the reaction:

$$-d[ester]/dt = -d(O.D)/dt \times 1/\varepsilon$$
$$= k_{obs}[E_0] = k_{OH}[OH^-][E_0]$$

The plot of the rates against the initial concentration of the ester gave a straight line. (Table 2)

Product. 1,2-Dithiaacenaphthene *S*-oxide (1.84 g, 8.9 mmol) and KOH (0.76 g, 14 mmol) were dissolved in methanol. After being left at room temperature for 12 hr, the solution was evaporated and the residue was extracted with ether and chloroform. Concentration of the extract afforded 1,2-dithiaacenaphthene (583 mg, 37%). The inorganic layer which did not dissolve either in ether or chloroform was neutralized with hydrochloric acid and then extracted with ether and chloroform. After the solvent was removed the residue was separated by column chromatography into 1,2-dithiaacenaphthene *S*-oxide (425 mg, 23%) and 1,2-dithiaacenaphthene *S*,*S*-dioxide (108 mg, 6%).

7) A. Zweig and A. H. Hoffmann, *J. Org. Chem.*, **30**, 3997 (1967).

The Reduction of Triazolium and Tetrazolium Iodides with Sodium Borohydride

Tyuzo Isida, Tetsuo Akiyama, Nobutake Mihara, Sinpei Kozima,* and Keiiti Sisido

Department of Industrial Chemistry, Faculty of Engineering, Kyoto University, Sakyo-ku, Kyoto 606

**Department of Chemistry, College of Liberal Arts and Sciences, Kyoto University, Sakyo-ku, Kyoto 606*

(Received September 12, 1972)

The sodium borohydride reduction of azolium iodides containing two, three, or four nitrogen atoms in the ring was studied. 1,4,5-Trisubstituted tetrazolium iodides gave Δ^2-tetrazolines, whereas 1,3,5-trisubstituted tetrazolium iodide yielded no reduction product. 1,3,4,5-Tetrasubstituted 1,2,4-triazolium iodides and 1,2-disubstituted 1,2,3-triazolium fluorosulfonate were reduced to Δ^2-1,2,4-triazolines and Δ^3-1,2,3-triazoline respectively, but 1,3,4,5-tetrasubstituted 1,2,3-triazolium iodides were not reduced at all. Both pyrazolium and imidazolium salts gave the corresponding azolidines. These results can be explained in terms of the characteristics of sodium borohydride, which reduces selectively the immonium moiety in azolium salts.

The reduction of pyridinium salts and these benzo-derivatives with sodium borohydride has been well-established and utilized as a synthetic tool useful in obtaining hydrogenated heterocycles.[1] With regard to the reduction of azolium salts, thiazolium halides[2,3] and pyrazolium perchlorate[4] give thiazolidines and pyrazolidine respectively in a protic solvent, and benzoisooxazolium[5] and benzoimidazolium salts[6] yield the corresponding benzoazolines. Imidazolium iodides are, however, reduced to ring-cleaved products, *N,N,N'*-trialkylethylene diamines.[7] These confused results prompted us to investigate the unknown behavior of triazolium and tetrazolium salts in the sodium borohydride reduction and to attempt to ascertain the common properties of azolium salts.

In general, azolium salts were treated with excess sodium borohydride in 95% ethanol at room temperature for several hours; the sole products were afforded in good yields when the reduction occurred. The reduction of 1,4,5-trisubstituted tetrazolium iodides (**1**) gave the corresponding Δ^2-tetrazolines (**2**). The analytically-pure Δ^2-tetrazoline (**2a—d**) could be isolated from the ethereal extract of the product without further purification.

The structure of the novel type of Δ^2-tetrazoline was elucidated by means of NMR and elementary analyses. The NMR spectra of **2a—c** displayed a singlet peak at around δ 4.61 ppm associated with the C^5-proton, while that of **2d** showed a quartet at δ 4.15 ppm and a doublet at δ 1.52 ppm assigned to the C^5-proton and the 5-methyl protons respectively. **2a** and **2d** are comparatively unstable to heat and are decomposed completely at 120°C in only a few minutes to give alkyl azides and Schiff's bases, whereas **2b** and **2c** are more stable and are scarcely decomposed at all on heating at 150°C. The formation of Schiff's bases was observed in the mass spectra of these tetrazolines.

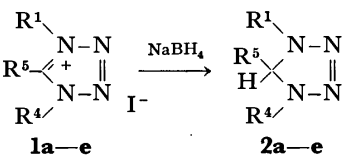

1a—e **2a—e**

	a	**b**	**c**	**d**	**e**
R^1:	CH_3	CH_3	C_2H_5	CH_3	CH_3
R^4:	CH_3	C_2H_5	C_2H_5	C_6H_5	CH_3
R^5:	C_6H_5	C_6H_5	C_6H_5	CH_3	CH_3

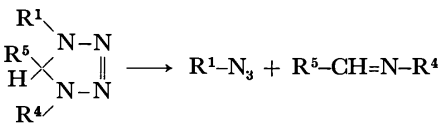

In the reduction of 1,4,5-trimethyltetrazolium iodide (**1e**), the attempted isolation of the product, **2e**, was unsuccessful; however, the formation of **2e** was confirmed by the NMR spectrum of an aqueous solution of the reaction mixture. The spectrum revealed only two kinds of peaks, consisting of a singlet at δ 2.93 ppm and a doublet at δ 1.40 ppm. (A third peak might be hidden behind the absorption peak of water.) The peak at δ 2.93 ppm and the peak at δ 1.40 ppm can be assigned to, respectively, the *N*-methyl and 5-methyl protons of **2e** on the basis of the integral ratio and the chemical shifts, but the 5-methyl protons of the unreacted tetrazolium iodide, **1e**, also have a singlet peak at δ 2.93 ppm. For the further assignment of these peaks a similar reduction of **1e** was attempted in deuterium oxide; the reduced product, **5**, showed only a singlet peak at δ 2.93 ppm. Our previous report has revealed that the rapid hydrogen-deuterium exchange of the 5-methyl protons in 1,4,5-trimethyltetrazolium iodide, **1e**, occurred in a deuterium oxide solution, but no exchange of the 1- and 4-*N*-methyl protons was observed even under strongly basic conditions.[8] Therefore, the singlet peak at δ 2.93 ppm of **5** should be assigned to the 1- and 4-*N*-methyl protons. Similarly, the singlet peak at δ 2.93 ppm of **2e** should be associated not with the 5-methyl protons of the

1) R. E. Lyle and P. S. Anderson, "Advances in Heterocyclic Chemistry," Vol. 6, ed. by A. R. Katritzky and A. J. Boulton, Academic Press, New York and London (1966), p. 45.

2) G. F. Bovicine and D. J. Hennessy, *J. Amer. Chem. Soc.*, **79**, 6325 (1957); H. Hirano, *J. Pharm. Soc. Jap.*, **78**, 1387 (1958).

3) G. M. Clarke and P. Sykes, *J. Chem. Soc., C*, **1967**, 1269, 1141: *Chem. Commun.*, **1965**, 370.

4) A. V. El'tsov and N. M. Omar, *Zh. Org. Khim.*, **4**, 711 (1968): *Chem. Abstr.*, **69**, 2903 (1968).

5) D. S. Kemp, *Tetrahedron*, **23**, 2001 (1967).

6) J. L. Aubagnac, *Bull. Soc. Chim. Fr.*, **1967**, 2184.

7) E. F. Godefroi, *J. Org. Chem.*, **33**, 860 (1968).

8) T. Isida, S. Fujimori, K. Nabika, K. Sisido, and S. Kozima, This Bulletin, **45**, 1246 (1972).

unreacted **1e**, but with the *N*-methyl protons of **2e**. The splitting of the peak of the 5-methyl protons of **2e** into a doublet suggested the presence of a C^5-proton peak hidden behind the absorption peak of water.

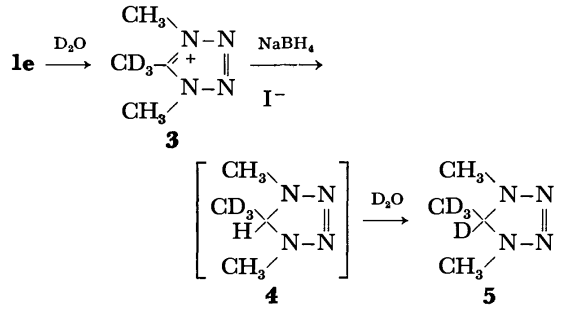

Our previous report[9] has shown that the reaction of 1-methyl-5-phenyltetrazole with methyl iodide gave a mixture of 1,3-dimethyl- and 1,4-dimethyl-5-phenyltetrazolium iodide (**6** and **1a**) at room temperature when the reaction continued for a long time. When a mixture of **1a** and **6**[10] was treated with sodium borohydride, the 1,4-dimethyl salt, **1a**, was reduced to 1,4-dimethyl-Δ^2-tetrazoline, **2a**, but the 1,3-dimethyl salt, **6**, remained unchanged.

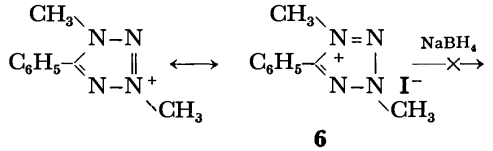

In the reduction of 1,3,4,5-tetrasubstituted 1,2,4-triazolium iodides (**7**),[11] the more electron-deficient 5-carbon atom was attacked by the hydride ion from sodium borohydride. The Δ^2-1,2,4-triazolines (**8**) thus formed showed the presence of the quartet peak of the C^5-proton and the doublet peak assigned to the 5-methyl protons in the NMR spectra.

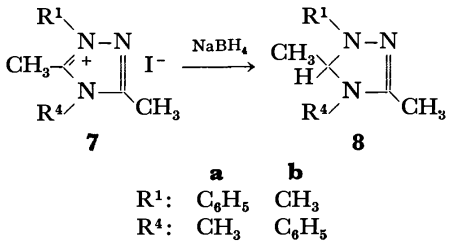

By contrast, the reaction of 4-phenyl- and 4,5-diphenyl-1,3-dimethyl-1,2,3-triazolium iodides (**9**),[12] or 1,3-dimethylbenzotriazolium iodide (**10**)[13] with sodium borohydride gave no reduction product, and each starting iodide was recovered.

1-Methyl-2-phenyl-1,2,3-triazolium fluorosulfonate (**11**)[14] was reduced to the corresponding Δ^3-triazoline (**12**), which was identified by the NMR spectrum and elemental analysis. However, 1,2-dimethylbenzotriazolium iodide (**13**)[13] yielded no reduction product.

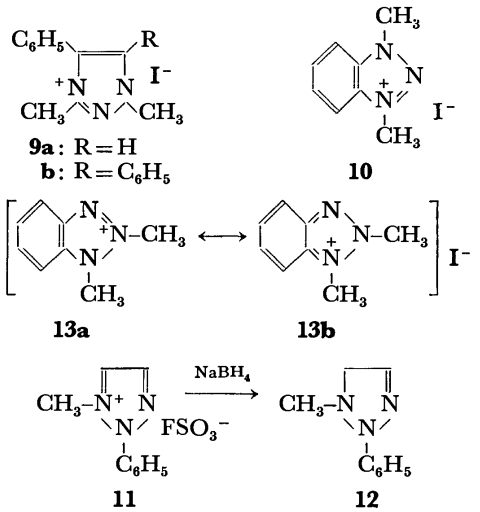

Under conditions similar to those of the above reduction, the treatment of 1,3-dimethyl-4-phenylimidazolium iodide (**14**) gave only one product, 1,3-dimethyl-4-phenyl-imidazolidine (**15**), although Godefroi[7] reported the formation of a ring-cleaved product in the reduction of 1-benzyl-3-alkylimidazolium iodides.

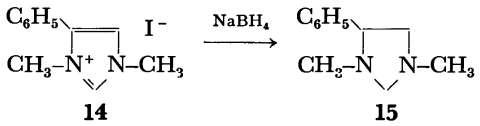

Analogously, the reduction of 1-alkyl-2-methyl-3-phenylpyrazolium iodide (**16**) yielded 1-alkyl-2-methyl-3-phenylpyrazolidine (**17**). This finding is consistent with the finding of El'tsov in the reduction of pyrazolium perchlorate (**16c**).[4]

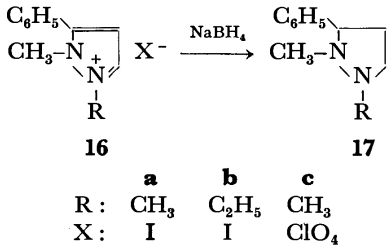

We can summarize the results of the sodium borohydride reduction of azolium iodides as follows. In the case of the tetrazolium iodides, the positions of the substituents at the nitrogen atoms of the tetrazole ring determined whether or not reduction occurred, as is shown by the fact that 1,4,5-trisubstituted tetrazolium iodides (**1**) yielded the partially-reduced Δ^2-tetrazolines, while 1,3,5-trisubstituted tetrazolium iodide (**6**) gave no reduction product. The reduction was more complicated in the cases of triazolium salts and benzotriazolium iodides. 1,2,4-Triazolium iodides (**7**) were

9) T. Isida, S. Kozima, K. Nabika, and K. Sisido, *J. Org. Chem.*, **36**, 3807 (1971).

10) 1,3-Dimethyl-5-phenyltetrazolium iodide (**6**) could not be separated from the salt mixture owing to its thermal instability.

11) G. F. Duffin, J. D. Kendall, and H. R. J. Waddington, *Chem. Ind.* (London), **1954**, 1458.

12) It was prepared by the reaction of 1-methyl-4-phenyl-1,2,3-triazole with methyl iodide. *Cf.* R. H. Wiley and J. Moffat, *J. Amer. Chem. Soc.*, **77**, 1703 (1955).

13) F. Krollpfeiffer, A. Rosenberg, and C. Muhlhausen, *Ann.*, **515**, 113 (1935).

14) M. Begtrup and K. V. Poulson, *Acta Chem. Scand.*, **25**, 2087 (1971): The quarterization of 1-substituted triazole with alkyl iodide gave only 1,3-dialkyltriazolium iodide,[12] and 2-substituted triazole gave no quarternary iodide with alkyl iodide.

readily reduced, and the occurrence of the reduction of 1,2,3-triazolium salts depended on the positions of the substituents at the nitrogen atoms, much as in the case of tetrazolium iodides. Δ^3-1,2,3-Triazoline was derived from 1,2-disubstituted 1,2,3-triazolium salt (**11**), whereas 1,3-disubstituted derivative (**9**) was unchanged. No reduction occurred in two kinds of benzotriazolium iodides (**10** and **13**). Both pyrazolium and imidazolium iodides (**14** and **16**) gave the corresponding diazolidine.

Many investigations of the sodium borohydride reduction of pyridinium salts[15] have revealed the mechanism for the formation of the tetrahydropyridines; Clark and Sykes proposed a similar pathway for the reduction of the thiazolium salts to thiazolidines.[3]

An analogous pathway could be applied to the sodium borohydride reduction of the azolium iodides. All of the azolium salts which can be reduced contain an immonium-ion moiety in the formula of the mesomerism, as is shown by the examples of **1**, **7**, **11**, **14**, and **16**. The other azolium salts (**6** and **9**) which cannot be reduced, by contrast, involve no immonium-ion moiety in the formula. The hydride ion derived from sodium borohydride attacks an electron-deficient carbon of the immonium-ion system in an azolium salt to form an azoline (Reaction a). When there remains an enamine moiety in the structure of a formed azoline, the enamine system re-forms an immonium-ion system with protonation by the protic solvent and is subsequently reduced to azolidine as the final product (Reaction b). The further reduction of both pyrazoline and imidazoline gave the corresponding diazolidines, but neither Δ^2-1,2,4- and Δ^3-1,2,3-triazolines nor Δ^2-tetrazolines could be reduced due to the lack of an enamine moiety in each ring system. The above pathway may be applied to the cases of benzoazolium salts, though the partial reduction product (benzoazoline) was not further reduced, because the C=C

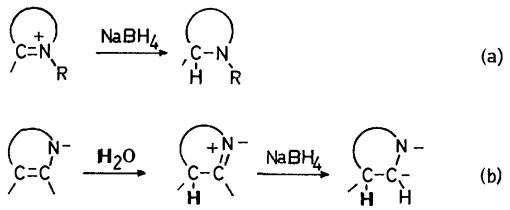

double bond in the benzoazoline is included in the resonance system of the benzene ring and cannot be attacked by sodium borohydride in a protic solvent, much as in the case of dimethylaniline. These examples are typical of the reduction of benzoisooxazolium[5] and benzoimidazolium salts,[6] which gave the corresponding dihydrobenzoazoles. The fruitless reduction of 1,3-disubstituted benzotriazolium iodide (**10**) can be explained by the lack of the immonium-ion moiety in its canonical formula, so that it was not reduced with sodium borohydride and was recovered. One of the canonical formulae (**13b**) of 1,2-disubstituted benzotriazolium iodide (**13**) involves an immonium-ion moiety, but the absence of any reduction of **13** suggests that **13b** may contribute to its resonance in the salt scarcely at all.

15) A. R. Katritzky, *J. Chem. Soc.*, **1955**, 2586; and references in Ref. 1.

Experimental

The melting points were taken on Yanagimoto Seisakusho Micro Melting Point Apparatus, Serial No. 1417. The NMR spectra were obtained on a Japan Electron Optics C-60-H Spectrometer, operating at 60 MHz and with TMS (in $CDCl_3$) or DSS (in D_2O) as the internal reference. The UV spectra were measured in ethanol on a Shimadzu-MPS Spectrophotometer. The elemental analyses were performed by Mrs. K. Fujimoto of this labaratory on a Yanagimoto Autoanalyzer CHN Corder MT-1. The mass spectra were obtained on a Hitachi RMS-4 Mass Spectrometer.

*Reduction of 1,4-Dimethyl-5-phenyltetrazolium Iodide (**1a**) with Sodium Borohydride ($NaBH_4$).* To a solution of 395 mg (1.27 mmol) of **1a**[9] in 10 ml of 95% ethanol at room temperature, we added, portion by portion, 241 mg (6.35 mmol) of $NaBH_4$. After the mixture had ceased foaming, it was heated under reflux for 2 hr (or stirred for 5 hr at room temperature). The solvent was then removed *in vacuo*, and 10 ml of water was added to the residue. The aqueous layer was extracted twice with 20 ml portions of ether; the ether was then evaporated off to dryness *in vacuo* without heating to give 1,4-dimethyl-5-phenyltetrazoline (**2a**) as colorless crystals; 200 mg (89.5%); mp 53.0—53.5°C, NMR ($CDCl_3$) δ 7.46 (s, 5H, 5-phenyl), 4.48 (s, 1H, C^5-proton), 2.86 ppm (s, 6H, *N*-methyl).

Found: C, 61.49; H, 6.82; N, 31.57%. Calcd for $C_9H_{12}N_4$: C, 61.34; H, 6.86; N, 31.80%.

UV (EtOH) λ_{max} 281 nm (ε_{max} 1160).

The heating of **2a** at 120°C for 5 min in a sealed tube gave *N*-benzalmethylamine quantitatively; it was identified by comparison with an authentic sample.[16] The evolved gas was determined to be methyl azide by means of presence in its mass spectrum of a parent ion at *m/e* 57. Similarly, the thermolysis of **2d** gave *N*-ethylideneaniline and methyl azide.

*Reduction of 1-Ethyl-4-methyl-5-phenyltetrazolium Iodide (**1b**).* An analogous treatment of **1b**[9] gave a liquid, **2b**, in a 66.8% yield. Tlc (silica gel) analyses displayed one spot; R_f= 0.50, 9:1 *n*-hexane–ethyl acetate. NMR ($CDCl_3$) δ 7.50 (m, 5H, 5-phenyl), 4.65 (s, 1H, C^5-proton), 3.15 and 1.17 (q and t, 2H and 3H, 1-ethyl), 2.85 ppm (s, 3H, 4-methyl).

Found: C, 63.36; H, 7.36; N, 29.28%. Calcd for $C_{10}H_{14}N_4$: C, 63.13; H, 7.42; N, 29.45%.

*Reduction of 1,4-Diethyl-5-phenyltetrazolium Iodide (**1c**).* An analogous treatment of **1c**[9] gave a liquid, **2c** (R_f=0.56, 9:1 *n*-hexane–ethyl acetate), in a 60.5% yield. NMR ($CDCl_3$) δ 7.45 (m, 5H, 5-phenyl), 4.80 (s, 1H, C^5-proton), 3.11 and 1.13 ppm (q and t, 4H and 6H, *N*-ethyl).

Found: C, 64.27; H, 8.18; N, 27.55%. Calcd for $C_{11}H_{16}N_4$: C, 64.67; H, 7.90; N, 27.43%.

*Preparation of 1,5-Dimethyl-4-phenyltetrazolium Iodide (**1d**).* The reaction of 2 g of 5-methyl-1-phenyltetrazole[17] with an excess of methyl iodide in a sealed glass tube at 100°C for 5 hr gave **1d**;[18] mp 205—206°C.

Found: C, 35.62; H, 3.53; N, 18.68%. Calcd for $C_9H_{11}N_4I$: C, 35.78; H, 3.67; N, 18.55%.

NMR (D_2O) δ 7.80 (s, 5H, 4-phenyl), 4.45 (s, 3H, 1-methyl), 3.00 ppm (s, 3H, 5-methyl).

16) R. B. Moffett, "Organic Syntheses," Vol. 34, 1954, p. 64.

17) E. K. Harvill, R. M. Herbst, E. C. Schreiner, and C. W. Roberts, *J. Org. Chem.*, **15**, 662 (1950).

18) G. F. Duffin, J. D. Kendall, and H. R. J. Waddington, *Chem. Ind.* (London), **1955**, 1355.

*Reduction of 1,5-Dimethyl-4-phenyltetrazolium Iodide (**1d**).* An analogous treatment of **1d** gave a liquid, **2d** (R_f=0.45, 9:1 *n*-hexane–ethyl acetate), in a quantitative yield. NMR ($CDCl_3$) δ 7.35—6.95 (m, 5H, 4-phenyl), 4.15 (q, 1H, C^5-proton), 3.05 (s, 3H, 1-methyl), 1.52 ppm (d, 3H, 5-methyl). UV (EtOH) λ_{max} 304 nm (ε_{max} 3910), 222 nm (2980).

Found: C, 61.57; H, 6.89; N, 31.64%. Calcd for $C_9H_{12}N_4$: C, 61.34; H, 6.86; N, 31.80%.

*Reduction of 1,4,5-Trimethyltetrazolium Iodide (**1e**) in H_2O and D_2O.* The reaction of **1e** with $NaBH_4$ was carried out at room temperature in an NMR tube. After 2 hr, the NMR spectrum showed two kinds of peaks, at δ 2.93 (s) and 1.40 ppm (d); their integral ratio was 2:1.

A solution of **1e** in D_2O was kept at room temperature in an NMR tube. After one week, the singlet at δ 2.93 ppm disappeared. To the above solution we then added $NaBH_4$, and it was kept at room temperature. After 2 hr, the remaining singlet at δ 4.30 ppm disappeared and the singlet at δ 2.93 ppm reappeared.

*Reaction of the Mixture of 1,4-Dimethyl and 1,3-Dimethyl-5-phenyltetrazolium Iodide (**1a** and **6**) with $NaBH_4$ in $CDCl_3$.* A mixture of **1a** and **6**[10] was treated with $NaBH_4$ in $CDCl_3$. After 5 hr, the peak at δ 4.28 ppm disappeared, and instead two peaks, at δ 4.48 and 2.87 ppm (1:6), of **2a** appeared. However, the two peaks at δ 4.75 and 4.52 ppm assigned to the 1- and 3-methyl protons of **6** remained.

*Preparation of 1-Phenyl-3,4,5-trimethyl-1,2,4-triazolium Iodide (**7a**).*[11] We obtained **7a** by heating a solution of 1-phenyl-3,5-dimethyl-1,2,4-triazole in excess methyl iodide in a sealed glass bottle at 100°C for 32 hr. After cooling, the reaction mixture was washed with benzene. The residue was dissolved in minimum acetone, and to the acetone solution we added hexane to precipitate crystals. By the additional precipitation procedure we obtained yellow crystals (mp 169—172°C) in a quantitative yield. NMR ($CDCl_3$) δ 7.67 (m, 5H, *N*-phenyl), 3.84 (s, 3H, 4-methyl), 2.74 (s, 3H, 5-methyl), 2.64 ppm (s, 3H, 3-methyl).[19]

Found: C, 41.96; H, 4.45; N, 12.89%. Calcd for $C_{11}H_{14}N_3I$: C, 41.92; H, 4.48; N, 13.33%.

*Reduction of **7a**.* The treatment of **7a** with $NaBH_4$ gave, in a 70% yield, an unstable liquid whose structure was determined to be 1-phenyl-3,4,5-trimethyl-1,2,4-triazoline (**8a**) by studying its NMR spectrum; δ 7.6—6.8 (m, 5H, 1-phenyl), 4.88 (q, 1H, C^5-proton), 2.73 (s, 3H, 4-methyl), 1.97 (s, 3H, 3-methyl), 1.52 ppm (d, 3H, 5-methyl), and the mass spectrum: a parent ion at *m/e* 189.

*Preparation of 1,3,5-Trimethyl-4-phenyl-1,2,4-triazolium Iodide (**7b**).* The treatment of 3,5-dimethyl-4-phenyl-1,2,4-triazole[20] with excess methyl iodide in a sealed glass bottle at 100°C for 24 hr gave colorless crystals; mp 106—107°C. NMR (D_2O) δ 2.37 (s, 3H, 3-methyl), 2.58 (s, 3H, 5-methyl), 4.07 (s, 3H, 1-methyl), 7.5—8.0 ppm (m, 5H, 4-phenyl).[21]

Found: C, 41.40; H, 4.51; N, 12.99%. Calcd for $C_{11}H_{14}N_3I$: C, 41.92; H, 4.48; N, 13.33%.

*Reduction of **7b**.* Similarly, an unstable liquid (86%) was obtained from **7b**. Its structure was determined to be 1,3,5-trimethyl-4-phenyl-1,2,4-triazoline (**8b**) by studying its NMR spectrum; δ 1.37 (d, 3H, 5-methyl), 1.80 (s, 3H, 3-methyl), 2.72 (s, 3H, 1-methyl), 4.45 (q, 1H, C^5-proton), 7.0—7.5 ppm (m, 5H, 4-phenyl), and the mass spectrum: a parent ion at *m/e* 189.

Attempts at the elemental analysis of **8a** and **8b** were given up because of their instability even at room temperature.

*Reduction of 1-Methyl-2-phenyl-1,2,3-triazolium Fluorosulfonate (**11**).*[14] The reaction of 120 mg (0.463 mmol) of **11** with 30 mg of $NaBH_4$ was also carried out at room temperature in 95% methanol. The conventional treatment of the reaction product gave a viscous liquid (R_f=0.85, 9:1 methylene chloride–ethyl acetate), which was identified as 1-methyl-2-phenyl-1,2,3-triazoline-Δ^3; 69 mg (92.2%); n_{26}^D 1.5738. NMR ($CDCl_3$) δ 2.67 (s, 3H, *N*-methyl), 3.76 (s, 2H, C^5-protons), 6.7—7.5 ppm (m, 6H, C^4-proton and *N*-phenyl).

Found: C, 67.00; H, 6.94; N, 26.06%. Calcd for $C_9H_{11}N_3$: C, 67.05; H, 6.88; N, 26.07%.

*Reduction of 1,3-Dimethyl-4-phenylimidazolium Iodide (**14**).* The treatment of **14** with excess $NaBH_4$ (for 5 hr at room temperature or for 2 hr under reflux) gave a thermally stable liquid. It was distilled at 120°C/20 mmHg (76.9%), and its structure was determined to be 1,3-dimethyl-4-phenylimidazolidine (**15**) by studying its NMR spectrum ($CDCl_3$); δ 7.30 (s, 5H, 4-phenyl), 2.40 (s, 3H, *N*-methyl), 2.20 (s, 3H, *N*-methyl), 2.40—3.90 ppm (m, 5H, ring protons) and the mass spectrum *m/e* 176 (M^+). Its picrate was recrystallized from ethanol; mp 165—167°C.

Found: C, 50.77; H, 4.99; N, 17.31%. Calcd for $C_{17}H_{19}N_5O_7$: C, 50.37; H, 4.72; N, 17.28%.

*Reduction of 1,2-Dimethyl-3-phenylpyrazolium Iodide (**16a**).* By an analogous treatment of **16a**, 1,2-dimethyl-3-phenylpyrazolidine (**17a**) (73.1%) was obtained; bp 140°C/21 mmHg (lit,[22] 80°C/1.2 mmHg); mass spectrum *m/e* 176 (M^+). The recrystallization of its picrate from ethanol gave yellow crystals; mp 178—180°C (lit,[22] 177—179°C).

19) In deuterium oxide solution of **7a**, the rate of H/D exchange reaction of methyl protons at δ 2.74 ppm was faster than that at δ 2.64 ppm, so that the former is assigned to the more electron-deficient 5-methyl protons and the latter is to the 3-methyl protons.

20) R. Meyer, Ger. 579944 (1933): *Chem. Abstr.*, **27**, 4541 (1933).

21) The assignment of the peaks was determined as similarly as **7a**.

22) J. L. Aubagnac, J. Elguero, and R. Jacquier, *Bull. Soc. Chim. Fr.*, **1969**, 3302.

Dehydration in Liquid Sulfur Dioxide. I. Acid Amide and Acid Anhydride Synthesis in an Iodine-Pyridine-Sulfur Dioxide System

Masatomo NOJIMA, Shigeru HASEGAWA, and Niichiro TOKURA

Department of Applied Chemistry, Faculty of Engineering, Osaka University, Suita, Osaka 565

(Received September 25, 1972)

A novel dehydrating reagent consisting of the I_2–pyridine–liq. SO_2 system has been examined in order to obtain acid amides from carboxylic acids and amines in liq. SO_2. Among the amines, aniline gave the most satisfactory results. A fairly good yield was also achieved when the SO_2Cl_2–Py–SO_2 system was used in place of the I_2–Py–SO_2 system. Various amines in the absence of acids in this system gave *N,N'*-disubstituted diaminosulfone derivatives in good yields. Benzoic acid itself in the absence of amines gave benzoic acid anhydride in this system slowly.

Liquid sulfur dioxide has been used as an unique solvent for the carbonium-ion reaction. It is an acidic dipolar aprotic solvent with a considerably small dielectric constant, 12.35 (22°C). The cationic reaction in this solvent is excellently favored. The organic reactions with negative ρ values can be successfully carried out in this solvent with unusual rapidity.[1]

The complex formations between various compounds bearing lone pairs and sulfur dioxide have been studied extensively.[2–5] Amines[2,3] and alcohols[4,5] are known to form 1:1 complexes with sulfur dioxide.

A chemical material called the Karl Fischer reagent,[6,7] consisting of iodine, pyridine, and sulfur dioxide in a 1:10:3 molar ratio, has been widely employed since 1935 for the convenient and quantitative analysis of water content in various substances in which the dehydration reaction of the organic compound is not proceeding.

The present authors have taken up a new liq. SO_2 system, consisting of iodine, pyridine, and sulfur dioxide in 1:3:100 molar ratio, or of sulfuryl chloride, pyridine and sulfur dioxide in the same ratio, in order to develop a new dehydrating reagent for organic chemistry.

Iodine is assumed to be dissociated in this system as:[8]

$$2\text{pyridine} + I_2 \rightleftarrows [\text{Py}\cdot\text{I}\cdot\text{Py}]^+ + I^- \quad (1)$$

Py = pyridine

and water is quantitatively determined as in the following equation:

$$H_2O + I_2 + 3\text{Py} + SO_2 \longrightarrow 2\text{HI}\cdot\text{Py} + SO_3\cdot\text{Py} \quad (2)$$

The dehydrating reaction of the organic compounds seems to proceed through a similar reaction series:

$$\text{RCOOH} + \text{R'NH}_2 + I_2 + 3\text{Py} + SO_2(\text{excess}) \longrightarrow \text{RCONHR'} + 2\text{HI}\cdot\text{Py} + SO_3\cdot\text{Py} \quad (3)$$

Results and Discussion

Amide Synthesis in the I_2–Py–Liq.SO_2 System. Acetic, propionic, and benzoic acids were reacted with several amines such as *n*-propyl amine and aniline. The results are listed in Table 1.

The results indicate that *n*-propyl amine is less reactive than aniline. The reaction might be accounted for by the lesser basicity of aniline as compared to that of *n*-propyl amine, the latter being solvated or complexes with sulfur dioxide to depress the reactivity of the amine greatly.[9]

$$\text{RNH}_2 + SO_2 \overset{K}{\rightleftarrows} \text{RNH}_2\cdot SO_2 \quad (4)$$

$$\text{RCOOH} + \text{R'NH}_2 \longrightarrow \text{RCOO}^-\text{NH}_3^+\text{R'} \xrightarrow[I_2\text{-Py-liq. } SO_2]{-H_2O} \text{RCONHR'} \quad (5)$$

The equilibrium constant, *K*, of the complex formation will be increased as the basicity of RNH_2 becomes larger, and the effective concentration of the amine in the solution will be decreased according to Eq. (4).

Secondly, the reaction of aniline with tetraethyl-

TABLE 1. AMIDE SYNTHESIS IN THE I_2–Py–Liq.SO_2 SYSTEM AT −70°C

Acid	Amine	Product (yield %)	
CH_3COOH	$CH_3CH_2CH_2NH_2$	No reaction	
CH_3COOH	$C_6H_5NH_2$	$CH_3CONHC_6H_5$	(80)
CH_3CH_2COOH	$CH_3CH_2CH_2NH_2$	$CH_3CH_2CONHC_3H_7$	(23)
CH_3CH_2COOH	$C_6H_5NH_2$	$CH_3CH_2CONHC_6H_5$	(36)
C_6H_5COOH	$CH_3CH_2CH_2NH_2$	$C_6H_5CONHC_3H_7$	(49)
C_6H_5COOH	$C_6H_5NH_2$	$C_6H_5CONHC_6H_5$	(85)

1) Recent review: N. Tokura, *Synthesis*, **1971**, 617.
2) a) J. A. Moede and C. Curran, *J. Amer. Chem. Soc.*, **71**, 857 (1949). b) P. A. D. Maine, *J. Chem. Phys.*, **26**, 1036, 1042, 1049 (1957).
3) T. Hata and S. Kinumaki, *Nature*, **203**, 1378 (1964).
4) T. Hata, *Sci. Papers Res. Inst. Non-Aqueous-Soln.*, **10**, 15 (1961).
5) N. Tokura and F. Akiyama, This Bulletin, **39**, 838 (1966).
6) K. Fischer, *Angew .Chem.*, **48**, 394 (1935).
7) E. D. Peters and J. L. Jungnickel, *Anal. Chem.*, **27**, 451 (1955).
8) O. Hassel and H. Hope, *Acta Chem. Scand.*, **15**, 407 (1961).
9) N. Tokura and Y. Kondo, This Bulletin, **36**, 200 (1963).

Table 2. Reaction products of benzoic acid and tetraethyl ammonium benzoate with aniline in the I_2–Py–Liq.SO_2 system

Starting material	Product	
$C_6H_5COOH+C_6H_5NH_2$	$C_6H_5CONHC_6H_5$ (85)	$C_6H_5NHSO_2NHC_6H_5$ (15)
$C_6H_5COON(Et)_4+C_6H_5NH_2$	$C_6H_5CONHC_6H_5$ (18)	$C_6H_5NHSO_2NHC_6H_5$ (24)
	$C_6H_5COOCOC_6H_5$ (14)	

ammonium benzoate in the same system was carried out in order to examine the role of the benzoate ion as the attacking reagent, depicted as follows:

$$C_6H_5COON(Et)_4 \rightleftharpoons C_6H_5COO^- + {}^+N(Et)_4 \quad (6)$$

$$C_6H_5COO^- + SO_2 \rightleftharpoons C_6H_5COO^-\cdot SO_2 \quad (7)$$

$$C_6H_5NH_2 + SO_2 \rightleftharpoons C_6H_5NH_2\cdot SO_2 \quad (8)$$

$$C_6H_5COO^- + {}^+N(Et)_4 + C_6H_5NH_2 + I_2 + Py\text{–}SO_2 \longrightarrow HI\cdot Py + SO_3\cdot Py + I^-N^+(Et)_4 + C_6H_5CONHC_6H_5 \quad (9)$$

However, the possibility of a reaction path through the benzoate anion can be disproved since the distributions of products formed from the two series of reactions are entirely different from each other, as may be seen in Table 2.

The yield of the acid amide is very small in the latter case. Moreover, benzoic acid anhydride was found in the reaction mixture of the reaction between tetraethylammonium benzoate and aniline. These results suggest that the intermediate $(C_6H_5COO)^-$ $(NH_3C_6H_5)^+$ is the most plausible one. The dehydration of benzoic acid itself has been examined in the same system. Benzoic acid is dehydrated to benzoic acid anhydride very gradually, as is shown in Table 3.

Table 3. The dehydration of benzoic acid in the I_2–Py–Liq.SO_2 system

Reaction period	Product (%)
1 hr	No reaction
24 hrs	$C_6H_5COOCOC_6H_5$ (50)
7 days	$C_6H_5COOCOC_6H_5$ (49)

The rate of the acid anhydride formation is very slow compared to that of the formation of the benzanilide; this suggests the path to the acid amide through the reaction of benzoic anhydride and aniline should also be rejected.

The authors also examined the reaction of the amine in this I_2–Py–SO_2 system.

Table 4. Reaction of amines in the I_2–Py–Liq.SO_2 system

Amine	Reaction period	Product	Yield %
Aniline	24	$C_6H_5NHSO_2NHC_6H_5$	50
Aniline+NaOTs	24	$C_6H_5NHSO_2NHC_6H_5$	81
$CH_3CH_2CH_2NH_2$	24	$C_3H_7NHSO_3NHC_3H_7$	10
Aniline	1	$C_6H_5NHSO_2NHC_6H_5$	84
Aniline+NaOTs	1	$C_6H_5NHSO_2NHC_6H_5$	95
Aniline (degassed)	1	$C_6H_5NHSO_2NHC_6H_5$	79

An inspection of Table 4 will show the following point: 1) *n*-Propyl amine gave a much smaller yield of diamino sulfone (10%) than aniline. 2) *N,N'*-Diphenyldiamino sulfone was obtained in a remarkably good yield in the presence of a catalytic amount of sodium toluenesulfonate. 3) Moreover, the yield was decreased when the reaction was prolonged for 24 hr, suggesting that an equilibrium condition will decrease the yield of the diamino sulfone. 4) The degassing of the reaction solution has little effect on the yield of the *N,N'*-diphenyldiamino sulfone. These phenomena suggest that the diamino sulfone formation in the liq. SO_2–I_2–Py system is an iodine-catalyzed dehydrogenation. The mechanism will be discussed further elsewhere.

Lastly, sulfuryl chloride was used in place of iodine in this system. A fair yield was achieved, as is shown in Table 5.

Table 5. Dehydration reaction in the SO_2Cl_2–Py–Liq.SO_2 system

Starting material	Product (yield %)
$C_6H_5COOH+C_6H_5NH_2$	$C_6H_5CONHC_6H_5$ (75)
$CH_3CH_2COOH+C_6H_5NH_2$	$CH_3CH_2CONHC_6H_5$ (27)
$C_6H_5NH_2$	$C_6H_5CHSO_2NHC_6H_5$ (70)

These results are very similar to those for the I_2–Py–liq. SO_2 system, and suggest the following intermediate, $(RCOO)^-(NH_3C_6H_5)^+$, in the reaction course. The overall reaction mechanism may be supposed to be as follows:

$$(RCOO)^-(NH_3C_6H_5)^+ + I^+ + I^- + Py\text{–}SO_2 \longrightarrow RCONHC_6H_5 + 2HI\text{–}Py + SO_3\text{–}Py \quad (10)$$

SO_2Cl_2–Py–liq.SO_2 system:

$$(RCOO)^-(NH_3C_6H_5)^+ + Cl^+ + SO_2Cl^- + Py\text{–}SO_2 \longrightarrow RCONHC_6H_5 + 2HCl\text{–}Py + SO_3\text{–}Py \quad (11)$$

Experimental

Materials. The liquid sulfur dioxide was dried over phosphorus pentoxide and distilled two times. Commercially-sold iodine, benzoic acid, and sodium *p*-toluenesulfonate of a reagent grade were used without further purification. The acetic acid, propionic acid, pyridine, and *n*-propylamine were all purified by the ordinary methods and distilled. A constant middle fraction was collected for use in the preparation.

Preparation of Tetraethylammonium Benzoate. Fowler's method was adopted.[10] Fresh silver oxide was obtained by mixing aqueous silver nitrate and aqueous sodium hydroxide solutions and was washed with water several times. Then silver oxide was added to the aqueous solution of tetraethylammonium iodide. After the removal of the precipitated silver iodide, equivalent moles of benzoic acid were added. By evaporating the water *in vacuo*, tetraethylammonium benzoate was obtained as a white crystal, which was then

10) D. L. Fowler, *J. Amer. Chem. Soc.*, **62**, 1140 (1940).

dried and stored in a dessicator.

IR (KBr) cm^{-1}: 1592, 1550, 1448, 1363, 1160, 990, and 710 cm^{-1}.

The Synthesis of an Amide in the Iodide–PyridineL–iquid SO_2 System. Into 30 ml of liq. SO_2 in a high-pressure glass vessel, 0.015 mol of iodine, 0.045 mol of pyridine, 0.015 mol of a carboxylic acid, and 0.030 mol of an amine were added at −70°C. The reaction mixture was then kept at 30°C for 1 hr. After the reaction, the reaction mixture was chille and poured into an ice-cooled aqueous solution of aboutd 1.5 molar sodium hydroxide and made alkaline. The amide was extracted by ether from the basic reaction mixture. The ethereal solution was washed with a saturated salt solution repeatedly dried over anhydrous sodium sulfate. After the evaporation of the ether, the product was purified by recrystallization and identified as an amide. The residue after the extraction was made acidic again by adding concd hydrochloric acid and was then extracted by ether. From the extract, a small amount of a diamino sulfone was obtained by a similar procedure.

Acetanilide: The reaction of acetic acid (0.9 g) and aniline (2.7 g) gave acetanilide (2.0 g, 80%, recrystallized from benzene). Mp and mixed mp with authentic specimen, 112—114°C;[11] IR (KBr) cm^{-1}: 1658(s), 1597(s), 1560(m), 1439 (m), 1325(m).

N-n-*Propylpropionamide*: The reaction of propionic acid (1.17 g) and *n*-propylamine (1.77 g) gave 0.4 g (27%) of a liquid; bp 64—65°C (0.4 Torr);[12] IR (KBr) cm^{-1}; 3250(m), 1640(s), 1560(s), 1472(s). NMR ($CDCl_3$) τ; 9.1(multiplet), 8.5(sextet), 7.8(quartet), 6.9(quartet), 2.9(singlet).

Propionanilide: The reaction of propionic acid (1.17 g) and aniline (2.70 g) gave 0.8 g (36%) of propionanilide (from benzene). Mass $m/e=149$ (M^+); mp and mixed mp, 104—106°C;[11] IR ($CDCl_3$) cm^{-1}: 1657(s), 1600(s), 1440(s), 745(m), 682(m).

N-n-*Ppropylbenzamide*: The reaction of benzoic acid (1.83 g) and *n*-propylamine (1.77 g) gave 1.2 g of a crystal (49%) (from ethanol–water); mp and mixed mp 83—85°C;[13] IR (KBr) cm^{-1}: 3250(m), 1628(s), 1540(s), 1450(s), 1370(s), NMR ($CDCl_3$) τ: 9.05(t), 8.4(sex), 6.6(q), 2.4(m), 3.15(s).

Benzanilide: The reaction of benzoic acid (1.83 g) and aniline (2.70 g) gave white crystals (from ethanol–water); 2.7 g (85%); mp and mixed mp, 158—161°C;[14] IR (KBr) cm^{-1}: 1650(s), 1530(s), 1439(s), 750(m), 682(m).

The Reaction of an Amine in the Iodide–Pyridine–Liq. SO_2 System. The reaction conditions and the procedure used were the same as those used for the amide synthesis. The molar ratio of the reagents was as follows: amine: iodine: pyridine: liq. $SO_2=2:1:3:100$.

N,N′-*Diphenyldiamino Sulfone*: Aniline (2.70 g) gave crystals (recrystallized from benzene); 3.1 g (84%); mp and mixed mp 111—113.[15] Mass, $m/e=248$ (M^+), 92.64. IR (KBr) cm^{-1}: 3225(m), 1595(m), 1140(m), 930(m), 740(m), 690(m).

N,N′-*Di*-n-*propyldiamino Sulfone*: *n*-Propylamine (1.77 g) gave white crystals (0.3 g, 10%; recrystallized from benzene). Mp and mixed mp 118—120°C.[15] Mass, $m/e=180$ (M^+), 151.58; IR (KBr) cm^{-1}; 3250(m), 1587(m), 1446(m), 1315(s), 1135(s), NMR ($CDCl_3$), τ: 9.0(t), 8.4(sex), 7.0(q), 2.7(s).

The Dehydration Reaction in the SO_2Cl_2–Pyridine–Liq. SO_2 System. We have examined the dehydration reaction of carboxylic acid and amine using sulfuryl chloride instead of iodine. The ratio of the reagents and the reaction conditions were the same as those used in the amide synthesis in the iodine–pyridine–liq. SO_2 system.

The Synthesis of Carboxylic acid Anhydride in the Iodine–pyridine–liq. SO_2 System. The reaction conditions used for the carboxylic acid anhydride synthesis were as follows: carboxylic acid (0.030 mol), iodine (0.015 mol), and pyridine (0.045 mol) were reacted in liq. sulfur dioxide (1.50 mol) for 24 hr at 30°C. The reaction mixture was then treated as has been described in the case of amide synthesis.

Benzoic Anhydride: Benzoic acid (3.66 g) gave 1.2 g of white crystals (yield 49%); mp and mixed mp,[16] 40—42°C. IR (KBr) cm^{-1}; 1785(s), 1720(s), 1600(m), 1450(m), 1210(m), 778(m), 675(s).

The Reaction of Tetraethylammonium Benzoate in the Iodine–Pyridine–Liq.SO_2 System. Into a mixture of pyridine (0.045 mol), iodine (0.015 mol), and aniline (0.030 mol) in liq. SO_2 (1.50 mol), we added 0.015 mol of tetraethylammonium benzoate; the mixture was then reacted for one hour at 30°C. The products were isolated and separated by the usual procedure.

11) E. C. Gilbert, *J. Amer. Chem. Soc.*, **49**, 2297 (1927).
12) S. Goldschmidt, *Ann. Chem.*, **435**, 274 (1923).
13) A. W. Titherley, *J. Chem. Soc.*, **79**, 405 (1901).
14) C. N. Webb, "Organic Syntheses," Coll. Vol. 1, p. 82, (1941).
15) A. Wohl, *Ber.*, **43**, 3295 (1910).
16) H. Adkins and Q. E. Thompson, *J. Amer. Chem. Soc.*, **71**, 2242 (1949).

The Photochemical Reaction of Diphenylacetylene with Enamines[1]

Norioki MIYAMOTO and Hitosi NOZAKI

Department of Industrial Chemistry, Kyoto University, Yoshida, Kyoto 606

(Received September 28, 1972)

The irradiation of a mixture of diphenylacetylene (I) and the enamine of the diethyl ketone (II) or of cyclopentanone (IV) gives two β,γ-unsaturated ketones, III and X respectively, in which the diphenylacetylene moiety is formally inserted into the respective enamine double bond under hydrogen migration. The reaction with the enamine of cyclohexanone (V) affords 2-(1,2-diphenylvinyl)cyclohexanone (XIII) as the major product in addition to the cycloadduct (XV). In each case, the formation of photodimers of I has been observed. The reaction is quenched by the addition of pyrene, is sensitized by triphenylene, and is supposed to proceed by way of a triplet path. The different routes of the enamine reactions can be explained by considering the geometry of the intermediate diradicals.

Little is known about photochemical reactions in which an enamine[2] is attacked by photochemically-excited species. Foote and Wei-Ping reported the oxidative fission of the enamine double bond by singlet oxygen photochemically produced.[3] We ourselves have been interested in the reaction of photoexcited benzophenone with enamines, in which the oxetane formation competes with the hydrogen abstraction at the allylic position,[4] and also in the photoreaction of diphenylacetylene with enaminoesters.[5]

In continuation of previous studies along this line, we have investigated the photoreaction of diphenylacetylene with several types of enamines; the results will be described in this paper.

TABLE 1. PHOTOREACTION OF I WITH ENAMINES IN ETHANOL AND ACETONITRILE

Enamine	solvent	Product (yield[9] in %)
II[6]	EtOH	dimers[7] of I (13), III (10)
	CH_3CN	dimers[7] of I (16), III (18)
IV[6]	EtOH	dimers[7] of I (10), X (15)
	CH_3CN	dimers[7] of I (6.2), X (20)
V[6]	EtOH	dimers[7] of I (10), XIII (11), XV[6] (2.3)
	CH_3CN	dimers[7] of I (15), XIII (15), XV[6] (3.1)

When a benzene or *n*-hexane solution of diphenylacetylene (I) and 3-morpholinopent-2-ene (II)[6] was irradiated, the photodimers of I as described by Büchi *et al.*[7] and Bryce-Smith and Lodge[8] were obtained in a 10% yield.[9] In addition to this, β,γ-unsaturated ketone (III) was isolated as a viscous liquid in a 16% yield[9] upon silica gel-column chromatography (Scheme 1). The assigned structure for III was consistent with the IR, NMR, and UV spectra (see Experimental Section), and the semicarbazone gave correct analyses.

A similar reaction with 1-morpholinocyclopentene (IV) gave a cyclic β,γ-unsaturated ketone (X) as an oil in a 23% yield,[9] along with the photodimers[7] of I (Scheme 2). The structure of X was consistent with the spectroscopic data and was further proven by an alternative chemical method. When X was treated upon activated alumina as has been described by Heap and Whitham,[10] isomerization to an α,β-unsaturated ketone, 2,3-diphenylcyclohept-2-enone (XI), took place readily. The structure of XI was confirmed by the spectra and especially by the NMR, in which the absence of the vinyl-proton signal strongly supported the assigned structure. The precursor of X must be dienamine, IX. The presence of IX in the crude reaction mixture was directly ascertained by observing a characteristic triplet at δ 6.70 ppm (vinyl proton)[11] upon the NMR analysis of the residue obtained by the removal of the unchanged enamine from the irradiation mixture *in vacuo*. It may be noted that the reactions of both II and IV possibly proceed *via* such cyclobutenes as VIII and the dienamines to afford β,γ-unsaturated ketones, III and X, in which the diphenylacetylene moiety has been incorporated formally at the enamine double-bond site under hydrogen migration. Thermal reactions in a similar sense have been recorded exclusively with electronegatively-substituted acetylenes.[12,13] The attempted reaction of I with enamines completely failed to occur thermally in the dark.

When the photochemical reaction of 1-morpholinocyclohexene (V)[6] was effected similarly, a cyclohexanone derivative (XIII) and a minor amount of the adduct (XV) were isolated in 17 and 3.1% yields[9] respectively (Scheme 2).

The structure of XIII was elucidated by studying its

1) A part of this work was presented at the 24th Annual Meeting of the Chemical Society of Japan (1971).

2) For the pertinent references on enamine reactions, see J. Szmuszkovicz, "Advances in Organic Chemistry," Vol. 4, ed. by R. A. Raphael, E. C. Taylor, and H. Wynberg, Interscience, New York, (1963); A. G. Cook, "Enamines," Marcel Dekker, New York, (1969).

3) C. S. Foote and J. Wei-Ping, *Tetrahedron Lett.*, **1968**, 3267.

4) M. Kawanisi, K. Kamogawa, T. Okada, and H. Nozaki, *Tetrahedron*, **24**, 6562 (1968).

5) M. Kawanisi, K. Matsunaga, and N. Miyamoto, This Bulletin, **45**, 1240 (1972).

6) *Y*=morpholino group.

7) G. Büchi, C. W. Perry, and E. W. Robb, *J. Org. Chem.*, **27**, 4106 (1962).

8) D. Bryce-Smith and J. E. Lodge, *J. Chem. Soc.*, **1963**, 695.

9) The yields were based on the I used.

10) N. Heap and G. H. Whitham, *J. Chem. Soc., B*, **1966**, 164.

11) The vinyl proton (triplet) of the IV enamine[6] appeared at δ 4.55 ppm.

12) K. C. Brannock, R. D. Burpitt, V. W. Goodlet, and J. G. Thweat, *J. Org. Chem.*, **28**, 1464 (1963); **29**, 818 (1964).

13) Recently similar reactions have been recorded with respect to the enamine-type double bond of indoles. See R. M. Acheson, J. N. Bridson, and T. M. Cameron, *J. Chem. Soc. Perkin Trans. I*, **1972**, 968.

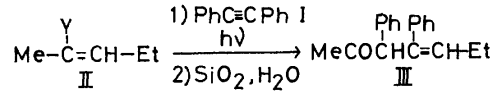

Scheme 1.

spectral data and by elemental analysis as well as by chemical degradation. The oxidation of XIII by Rudloff's method[14] gave 2-benzoylcyclohexanone (XIV), which was identical with the authentic specimen[15] prepared by the benzoylation of the enamine V.

TABLE 2. PHOTOREACTION OF I WITH PIPERIDINOENAMINES IN *n*-HEXANE

Enamine	Product (yield[9] in %)
II[16]	dimers[7] of I (8.2), III (20)
IV[16]	dimers[7] of I (10), X (25)
V[16]	dimers[7] of I (10), XIII (20), XV[16] (2.3)

The structure of the minor product, XV,[6] is mainly based on the spectral evidence. The UV showed the *cis*-stilbene chromophore, and the mass spectrum had eminent peaks at *m/e* 345 (M^+) and 167 (M^+-178). In addition, XV[6] remained unchanged upon chromatographic treatment.

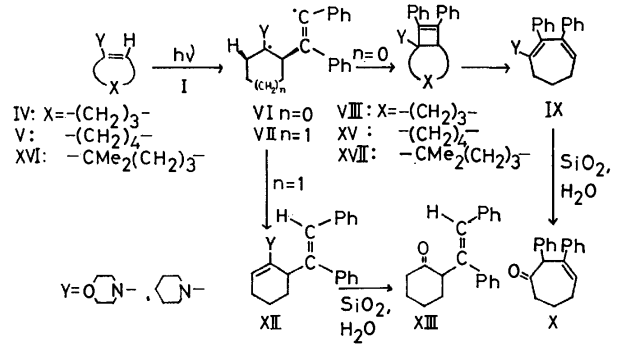

Scheme 2.

The analogous reaction of an enamine[6] of 2,2-dimethylcyclohexanone (XVI) gave only a cycloadduct (XVII)[6] in a 2.0% yield[9] (Scheme 2). The structure was deduced from the spectral data.

Finally, the photoreaction of I with piperidinoenamines[16] of the diethyl ketone, cyclopentanone, and cyclohexanone proceeded much as with the corresponding morpholinoenamines (see Experimental Section).

Discussion

The photodimerization of I has been reported to proceed by way of a triplet path;[7] the same path was also assumed in the 2+2 photoaddition of I on 2,3-dihydropyran.[17] Ample evidence seems to support the idea that the π-π^* triplet pathway of I is important in the addition to enamines. Thus, the addition of pyrene[18] to a mixture of I[19] and enamines resulted in the complete suppression of either the cycloaddition or the dimerization of I.[20] Equimolar concentrations of I and pyrene were used. Since their molar extinction coefficients are approximately equal at the excitation wavelength (log ε=4.1 at 254 nm), the quenching effect of pyrene must be ascribed to the triplet energy transfer rather than to the absorption of the exciting light by itself. Meanwhile, the reaction conducted in a Pyrex vessel under irradiation with light filtered through aqueous 10% $CuSO_4$ was successfully sensitized by triphenylene (E_T=66.6 kcal/mol[18]). The photolysis in the absence of the sensitizer did not occur under the above conditions.

The mechanism of the cycloaddition of I to the IV enamine is considered to be as follows. The electrophilic nature of excited I has been demonstrated in the addition reaction to tetramethylethylene[21] and to 2,3-dihydropyran.[17] When the excited I in the triplet state is added to IV, the cycloadduct thus formed is the bicyclo[3.2.0]hept-6-ene derivative (VIII), which subsequently is isomerized to a cycloheptadiene, IX. The ring-opening of VIII might occur photochemically *via* a disrotatory mode,[22] but the true nature has not yet been determined.[23] The presence of the IX dienamine in the irradiation mixture, as evidenced by NMR spectroscopy, shows that the ring-opening proceeds prior to the hydrolysis upon silica gel.[24]

A priori, the formation of α-substituted cyclohexanone, XIII, may be explained in two ways. The first one is based on the hydrogen abstraction at the allylic position of the V enamine. The efficient abstraction of hydrogen has been observed both with the π-π^* excited state of olefins[25,26] as well as with that of acetylenes, as has been disclosed recently by Roberts *et al.*[27]

This route fails, however, to explain the fact that the reaction of II or of IV does not afford the products of a type such as XIII. Additionally, it should be noted that the hydrogen abstraction of cyclohexanone enamine occurs at the 3 position rather than at 6.[4]

An alternative mechanism (Scheme 2) is based on the facts that the reactive species is in the triplet state and that the reaction occurs independently of the

14) L. Rudloff, *Can. J. Chem.*, **34**, 413 (1965).

15) R. D. Campbell, H. M. Gilow, and G. Stork, *J. Amer. Chem. Soc.*, **84**, 1440 (1963).

16) Y=piperidino group.

17) H. M. Rosenberg and P. Servé, *J. Org. Chem.*, **33**, 1653 (1968).

18) The E_T of pyrene is 48.7 kcal/mol; see W. G. Herkstroeter, A. A. Lamola, and G. S. Hammond, *J. Amer. Chem. Soc.*, **86**, 4537 (1964).

19) The E_T of I has been recorded to be 51 kcal/mol; see M. Beer, *J. Chem. Phys.*, **25**, 745 (1956).

20) Pyrene is an aromatic hydrocarbon useful as a triplet quencher; see A. A. Lamola, "Energy Transfer and Organic Photochemistry," Chap. I, Interscience, New York (1969).

21) O. L. Chapman and W. R. Adams, *J. Amer. Chem. Soc.*, **89**, 4243 (1967).

22) R. B. Woodward and R. Hoffmann, "The Conservation of Orbital Symmetry," Verlag Chemie, Weinheim (1970).

23) J. S. McCanaghy and J. J. Bloomfield, *Tetrahedron Lett.*, **1969**, 3719, 3723: G. R. Branton, H. M. Frey, D. C. Montagne, and I. R. D. Stevens, *Trans. Farady Soc.*, **62**, 659 (1966).

24) Silica gel contains 7% free water physically absorbed; see K. R. Lenge, *Chem. Ind.*, (London) **1968**, 441.

25) K. J. Crowly, *J. Amer. Chem. Soc.*, **85**, 1210 (1963).

26) H. M. Rosenberg and P. Servé, *ibid.*, **91**, 6185 (1969).

27) T. D. Roberts, L. Ardemagni, and H. Shechter, *ibid.*, **91**, 6185 (1969).

solvent polarity. The reaction of I with enamines in ethanol or acetonitrile gave results similar to those in *n*-hexane or benzene (see Experimental Section). We may reasonably assume that the attack of I on V proceeds step by step to give the diradical intermediate VII, first. Subsequent hydrogen abstraction takes place in VII through the six-membered transition state, thus producing an enamine, XII. The hydrogen abstraction caused by vinyl radicals has many precedents in the literature.[28] In sharp contrast, however, the cyclopentyl diradical, VI, gives the recombination product VIII predominantly, as has been stated previously. The difference may be explained as follows. Immediately after the attack of I on the π-bond in enamine, the stilbene moiety presumably occupies an axial position. Hydrogen abstraction takes place easily in such a conformation to give XII, while the less preferred radical recombination in VII forms XV in a far smaller yield. The corresponding intermediate diradical, VI, produced from the five-membered enamine, IV, must be less prone to hydrogen abstraction because of the disfavorable geometry. No hydrogen abstraction is observed, and the radical recombination product is formed exclusively (Scheme 3). The radical recombination was observed also with XVI, which has no removable hydrogen to afford the bicyclic product, XVII.[6]

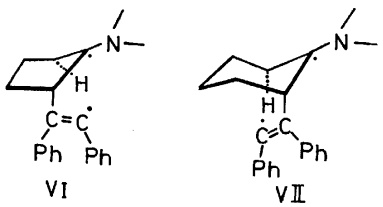

Scheme 3.

Experimental

All the melting points and boiling points are uncorrected. The IR spectra were obtained on a Shimadzu IR-27-G spectrometer in a neat liquid film, unless stated otherwise. The NMR spectra were taken with a JEOL C-60-H spectrometer (60 MHz) with CCl_4 as the solvent, and the chemical shifts are recorded in δ values relative to TMS as the internal standard. The NMR data are given in the order of multiplicity (s=singlet, d=doublet, t=triplet, q=quartet, and m=unresolved multiplet), integration, and assignment. The UV spectra were taken in EtOH on a Hitachi EPS-2 recording spectrophotometer. The MS spectra were obtained with a Hitachi RM-61 spectrometer at 80 eV. The column chromatography was carried out on Mallinckrodt silicic acid (100 mesh). Plates of silica gel G were used for the tlc, and the spots were visualized with iodine vapor.

Irradiation of Diphenylacetylene (I) in the Presence of 3-Morpholinopent-2-ene (II).[6] A solution of I (1.0 g, 5.6 mmol) and II[6] (1.7 g, 11 mmol) in *n*-hexane or benzene (40 ml) was placed in a quartz vessel and irradiated externally by means of 200 W high-pressure mercury arc under a nitrogen atmosphere at room temperature for 48 hr. The progress of the reaction was followed by tlc analyses of aliquots. The reaction mixture was then concentrated *in vacuo*, and the residue was chromatographed over a silica gel-column. Elution with *n*-hexane gave unchanged I (500 mg). Further elution with the same solvent gave 1,2,3-triphenylnaphthalene (the photodimer[7] of I reported by Büchi) (120 mg, 6.1%[9]), which was obtained as colorless crystals; mp 150—152 °C (lit,[7] 151—153 °C), M^+ (356). Later fractions contained a blue crystalline mass, 1,2,3-triphenylazulene (the photodimer[7] of I) (78 mg, 3.8%[9]); mp 216—217 °C (lit,[7] 216—217 °C), M^+ (356). Elution with benzene gave 3,4-diphenylhept-4-en-2-one (III, 220 mg, 16%[9]), which was obtained as a colorless and viscous oil. IR (neat): 3100—3000, 1715, 1600, 700, and 680 cm^{-1}. UV: λ_{max}=245 nm (log ε=4.13). NMR: δ 0.90 (t, 3H, $-CH_2C\underline{H}_3$), 1.55 (d, 3H, $=CH-C\underline{H}_3$), 2.35 (q, 2H, $-C\underline{H}_2CH_3$), 4.65 (s, 1H, $-CPh\underline{H}-$), 5.35 (q, 1H, $=C\underline{H}-CH_3$), and 7.00—7.36 ppm (m, 10H, aromatic). No suitable recrystallization solvent has been found for further purification. Elemental analysis was performed by converting III to its semicarbazone; mp 201—203 °C (benzene–petroleum ether (bp 60—70 °C) (1:1)). (Found: C, 74.5; H, 7.7%. Calcd for $C_{20}H_{23}N_3O$: C, 74.7; H, 7.2%).

Irradiation of I in the Presence of 1-Morpholinocyclopent-1-ene (V).[6] A solution of I (1.0 g, 5.6 mmol) and IV[6] (1.7 g, 11 mmol) in *n*-hexane or benzene (40 ml) was irradiated for 48 hr quite analogously to the above method. The subsequent concentration of the reaction mixture *in vacuo* and elution of the residue adsorbed on a silica gel-column with *n*-hexane gave the unchanged I (430 mg) and the photodimers[7] (160 mg, 7.9%[9]). Elution with benzene gave 2,3-diphenylcyclohept-3-enone (X, 340 mg, 23%[9]), which was obtained as a colorless and viscous oil. IR (neat): 3100—3000, 1705, 1600, 750, and 700 cm^{-1}. UV: λ_{max}=245 nm (log ε=4.18). NMR: δ 1.50—1.90 (m, 2H, CH_2 attached to both sp^3 carbons), 2.20—2.70 (m, 4H, CH_2 adjacent to sp^2 carbons), 6.82 (s, 1H, $-CPh\underline{H}-$), 6.30 (t, 1H, vinyl) and 7.00—7.30 ppm (m, 10H, aromatic). No suitable recrystallization solvent has been found for further purification. Elemental analysis was performed by converting X to its semicarbazone, mp 209—212 °C (benzene–petroleum ether (1:1)). (Found: C, 75.0; H, 6.6%. Calcd for $C_{20}H_{21}N_3O$: C, 75.2; H, 6.6%).

Isomerization of 2,3-Diphenylcyclohept-3-enone (X) to 2,3-Diphenylcyclohept-2-enone (XI). The method was based on the one reported by Whitham[10] in the isomerization of cyclooct-3-enone to cyclooct-2-enone. A benzene solution of 2,3-diphenylcyclohept-3-enone (X, 100 mg, 0.38 mmol) was treated with alumina (5.0 g, Woelm neutral activity I) in a column for 24 hr. Elution with benzene furnished recovered X (20 mg). Further elution with benzene–ether (1:1) afforded 2,3-diphenylcyclohept-2-enone (XI, 65 mg, 65%), which was obtained as white crystals; mp 103—105 °C (*n*-hexane). IR (KBr): 3100—3000, 1680, 1650, 1600, 760, and 700 cm^{-1}. UV: λ_{max}=222 (log ε=4.25), 272 nm (4.10). NMR: δ 1.50—1.90 (m, 4H, CH_2 attached to both sp^3 carbons), 2.20—2.75 (m, 4H, CH_2 adjacent to sp^2 carbons) and 7.00—7.28 ppm (m, 10H, aromatic). (Found: C, 87.3; H, 6.8%. Calcd for $C_{19}H_{18}O$: C, 87.0; H, 6.9%).

Irradiation of I in the Presence of 1-Morpholinocyclohexene (V).[6] A solution of I (1.0 g, 5.6 mmol) and V[6] (1.9 g, 11 mmol) in *n*-hexane or benzene (40 ml) was irradiated for 48 hr in a manner similar to that above. The subsequent concentration of the reaction mixture and elution of the residue adsorbed on a silica gel-column with *n*-hexane gave the unchanged I (390 mg) and the photodimers[7] (98 mg, 4.9%[9]). Elution with benzene afforded 2-(1,2-diphenylvinyl)cyclohexanone (XIII, 231 mg, 15%[9]) as colorless crystals; mp

28) O. Shimamura, "Topics in Stereochemistry," Vol. 4, ed. by E. L. Eliel and N. L. Allinger, Wiley-Interscience, New York (1969), p. 1.

86—87 °C (petroleum ether). IR (KBr): 3050–3000, 1710, 1600, 760, and 700 cm^{-1}. UV: λ_{max}=220 (log ε=4.23), 270 nm (4.11). NMR: δ 1.50—2.06 (m, 6H, β and γ methylenes of the cyclohexanone ring), 2.00—2.50 (m, 2H, $-CH_2-C=O$), 3.30 (t, 1H, methine), 6.30 (s, 1H, vinyl) and 7.00—7.30 ppm (m, 10H, aromatic). (Found: C, 86.4; H, 7.5%. Calcd for $C_{20}H_{20}O$: C, 86.9; H, 7.3%).

Further elution with ether gave 1-morpholino-7,8-diphenylbicyclo[4.2.0]oct-7-ene (XV,[6] 59 mg, 3.1%[9]), which was obtained as colorless crystals; mp 85—86 °C (petroleum ether). IR (KBr): 3100—3000, 1600, 1120, 760, and 700 cm^{-1}. UV: λ_{max}=219 (log ε=4.20), 268 nm (4.10). NMR: δ 1.10—1.80 (m, 4H, CH_2 of the cyclohexane ring), 2.25 (t, 1H, methine), 2.40 (t, 4H, CH_2–N), 3.50 (t, 4H, CH_2–O), and 6.95—7.20 (m, 10H, aromatic). MS: 345 (M^+), 167 (M^+-178). (Found: C, 83.0; H, 8.0%. Calcd for $C_{24}H_{27}NO$: C, 83.0; H, 7.9%).

Oxidative Degradation of 2-(1,2-Diphenylvinyl)cyclohexanone (XVIII) to 2-Benzoylcyclohexanone (XIV). The method was based on that reported by Rudloff.[14] The stock oxidant solution[29] was placed in a flask, and into this was added slowly with stirring XVIII (500 mg, 1.8 mmol) dissolved in *t*-butylalcohol (5.0 ml). The solution was stirred for 3 hr at room temperature, and then the reaction mixture was extracted twice with ether. The combined extracts were washed with brine and then dried (Na_2SO_4). The solvent was evaporated, and the residue was chromatographed over silica gel. Elution with benzene–ether (1: 1) afforded 2-benzoylcyclohexanone (XIV, 240 mg, 65%), which was obtained as colorless crystals; mp 88—89 °C (*n*-hexane–benzene (2: 1)) (lit,[15] 88—89 °C). The authentic sample of XIV was prepared by the benzoylation of the V enamine.[15] The IR spectrum of XIV was superimpossible on that of the authentic specimen.

Irradiation of I in the Presence of 6,6-Dimethyl-1-morpholinocyclohexene (XVI).[6] A solution of I (1.0 g, 5.6 mmol) and XVI[6] (2.1 g, 11 mmol) in *n*-hexane or benzene (40 ml) was irradiated for 48 hr much as above. The subsequent concentration of the reaction mixture and column chromatography afforded 2,2-dimethyl-1-morpholino-7,8-diphenylbicyclo[4.2.0]oct-7-ene (XVII, 41 mg, 2.0%[9]), besides unchanged I (360 mg) and the photodimers[7] (300 mg, 15%[9]). The bicyclic product, XVII,[6] was obtained as colorless crystals; mp 95—96 °C (petroleum ether). IR (neat): 3050—3000, 1600, 1120, 760, and 700 cm^{-1}. NMR: δ 1.12 (s, 6H, CH_3), 1.20—1.80 (m, 6H, CH_2 of the cyclohexane ring), 2.20 (t, 1H, methine), 2.40 (t, 4H, CH_2–N), 3.50 (t, 4H, CH_2–O) and 6.87—7.00 ppm (m, 10H, aromatic). MS: 373 (M^+), 195 (M^+-178). (Found: C, 83.3; H, 8.5%. Calcd for $C_{26}H_{31}NO$: C, 83.6; H, 8.4%).

Quenching Studies in the Presence of Pyrene. A solution of I (300 mg, 1.7 mmol), II[6] (530 mg, 3.4 mmol), and pyrene (200 mg, 1.7 mmol) in *n*-hexane (20 ml) was placed in a quartz vessel and irradiated for 48 hr in a manner similar to that above. Tlc analyses showed that both the photochemical reaction of I with II[6] and the formation of the photodimers[7] of I were completely suppressed. Column chromatography (silica gel) gave totally recovered I (290 mg). The reaction of I with IV[6] or V[6] was similarly quenched by pyrene.

Sensitization by Triphenylene. (a): A solution of I (500 mg, 2.8 mmol), II[6] (870 mg, 5.6 mmol), and triphenylene (640 mg, 2.8 mmol) in benzene (20 ml) was irradiated externally for 48 hr with light filtered through aqueous 10% $CuSO_4$ (200 W high-pressure mercury arc). The subsequent concentration of the reaction mixture *in vacuo* and column chromatography (silica gel-column) afforded the photodimers[7] of I (140 mg, 14%[9]) and III (130 mg, 19%[9]) respectively.

(b): The photoreaction of I (500 mg, 2.8 mmol), IV[6] (860 mg, 5.6 mmol), and triphenylene (640 mg, 2.8 mmol) in benzene (20 ml) afforded the photodimers[7] of I (78 mg, 7.8%[9]) and X (73 mg, 10%[9]) under the same conditions as those described in (*a*).

(c): The photoreaction of I (500 mg, 2.8 mmol), V[6] (946 mg, 5.6 mmol), and triphenylene (640 mg, 2.8 mmol) in benzene (20 ml) afforded the photodimers[7] of I (130 mg, 13%[9]), XIII (130 mg, 17%[9]), and XV[6] (38 mg, 4.1%[9]) under the same conditions as in (*a*). In the absence of triphenylene, the reaction did not occur upon photolysis under the same conditions.

Photoreaction of I with Enamines[6] in Other Solvents. A solution of I (2.8 mmol) and an enamine[6] (5.6 mmol) in a solvent (20 ml) was irradiated in a quartz vessel for 48 hr (200 W high-pressure mercury arc). The results are summarized in Table 1.

Photoreaction of I with Piperidinoenamines.[16] A solution of I (2.8 mmol) and an enamine[16] (5.6 mmol) in *n*-hexane (20 ml) was irradiated for 48 hr much as above. The results are summarized in Table 2.

29) The stock oxidant solution consisted of sodium metaperiodate (20 g, 97 mmol) and potassium permanganate (390 mg, 2.5 mmol) in water (1 l).

Studies on Aminosugars. XXXIII. Syntheses of 4-Azido-2,3,6-tri-*O*-benzyl-4-deoxy- and 6-Azido-2,3,4-tri-*O*-benzyl-6-deoxy-α-D-glucopyranosyl Chloride

Yasushi TAKAGI, Tsutomu TSUCHIYA, and Sumio UMEZAWA

Department of Applied Chemistry, Faculty of Engineering, Keio University, Hiyoshi, Yokohama 222

(Received October 13, 1972)

The titled compounds (**8** and **13**) have been prepared as synthetic intermediates.

As key intermediates for the syntheses of aminoglycosides, the titled compounds have been prepared.

Methyl β-D-galactopyranoside (**1**) was converted into the 2,3,6-tri-*O*-benzoyl derivative (**2**) by means of the procedure of Reist *et al.*[1] utilizing the lower reactivity of C-4 axial hydroxyl group of D-galactose, and after mesylation of the remaining 4-hydroxyl group, the product (**3**) was transformed to methyl 4-azido-2,3,6-tri-*O*-benzoyl-4-deoxy-β-D-glucopyranoside (**4**). After removal of the benzoyl groups, the 4-azido-sugar (**5**) was benzylated to give **6**. Acidic hydrolysis of **6** gave 4-azido-2,3,6-tri-*O*-benzyl-4-deoxy-D-glucose (**7**), unavoidable removal of some of the benzyl groups being accompanied.[2] As for the hydrolysis of methyl glucosides of benzyl sugars, β-anomers generally give higher yields of free sugars than that of α-anomers, as reported by Austin *et al.*[3] The above yield of **7** (48%) was in accord with the above-mentioned view. Treatment of **7** with thionyl chloride gave the desired chloride (**8**). Its NMR spectrum indicated the α-configuration. The chloride was successfully used for the synthesis of 4-amino-4-deoxy-α-D-glucopyranosyl-2-deoxystreptamine.[4]

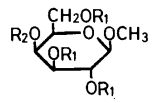

2: R_1=COC_6H_5, R_2=H
3: R_1=COC_6H_5, R_2=SO_2CH_3

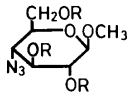

4: R=COC_6H_5
5: R=H
6: R=$CH_2C_6H_5$

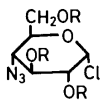

8: R=$CH_2C_6H_5$

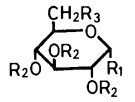

9: R_1=OCH_3, R_2=H, R_3=OTs
10: R_1=OCH_3, R_2=H, R_3=N_3
11: R_1=OCH_3, R_2=$CH_2C_6H_5$, R_3=N_3
13: R_1=Cl, R_2=$CH_2C_6H_5$, R_3=N_3

Methyl 6-azido-6-deoxy-α-D-glucopyranoside (**10**) in a crude state has been prepared by Cramer *et al.*[5] We isolated it in a pure state and converted it into the tri-*O*-benzyl derivative (**11**). Acidic hydrolysis of **11** gave the 6-azido sugar (**12**) in a 37% yield. A similar chlorination as described in the preparation of **8** gave the desired compound (**13**).

The NMR spectrum of **13** indicated the α-configuration. The chloride was useful for the synthesis of 6-amino-6-deoxy-α-D-glucopyranosyl-2-deoxystreptamine.[6]

Experimental

Methyl 2,3,6-Tri-O-benzoyl-β-D-galactopyranoside (2). Mp 146—147 °C, $[\alpha]_D^{21}$ +53.5° (*c* 1, chloroform) (lit,[7] mp 143—144°C, $[\alpha]_D^{18}$ +56.1°).

Methyl 4-Azido-2,3,6-tri-O-benzoyl-β-D-glucopyranoside (4). To a solution of methyl 2,3,6-tri-*O*-benzoyl-4-*O*-mesyl-β-D-galactopyranoside[8] (**3**, 5.05 g) in dry dimethylformamide (DMF) (70 ml), powdered sodium azide (1.75 g) was added and the mixture was stirred at 130—140°C for 4.5 hr. On tlc with benzene–ether (20: 1), the solution showed two spots of R_f 0.6 (**4**, major) and 0.75. Evaporation followed by evaporation with toluene gave a brown residue, which was extracted with chloroform and the extract was washed with water, dried over sodium sulfate and evaporated to give a brown syrup. This was charged on a column of silica gel (150 g) and developed with the solvent system described above. The eluate containing **4** was evaporated to give a pale yellow solid (2.43 g, 53%), which was recrystallized from methanol, mp 124—125°C, $[\alpha]_D^{22}$ +120° (*c* 0.78, chloroform).

Found: C, 63.48; H, 4.78; N, 8.01%. Calcd for $C_{28}H_{25}N_3O_8$: C, 63.27; H, 4.74; N, 7.91%.

Methyl 4-Azido-4-deoxy-β-D-glucopyranoside (5). To a suspension of **4** (1.79 g) in dry methanol (20 ml), 2.4N sodium methylate (0.3 ml) was added and the suspension was stirred at room temperature overnight. The solution, after treatment with Amberlite IR 120 (H form), was evaporated to give a solid, which was washed with ether. Colorless solid obtained (0.70 g, 95%) was recrystallized from ethanol, mp 159.5—161°C, $[\alpha]_D^{22}$ +39° (*c* 0.66, water). NMR (in D_2O): τ 6.44 (3H, s, OCH_3), 5.65 (1H, d, $J_{1,2}$ 7.5 Hz, H-1).

Found: C, 38.63; H, 6.19; N, 19.23%. Calcd for $C_7H_{13}N_3O_5$: C, 38.35; H, 5.98; N, 19.17%.

Methyl 4-Azido-2,3,6-tri-O-benzyl-4-deoxy-β-D-glucopyranoside (6). A solution of **5** (770 mg) in DMF (10 ml) was treated with powdered potassium hydroxide (4.4 g) and benzyl chloride (4.5 g) similarly as described in the preparation of **11**, and chromatographed with benzene–ether (20: 1); colorless solid (1250 mg, 73%) was reprecipitated with benzene–petroleum ether, mp 64—65°C, $[\alpha]_D^{20}$ +80° (*c* 0.82, chloro-

1) E. J. Reist, R. R. Spencer, D. F. Calkins, B. R. Baker, and L. Goodman, *J. Org. Chem.*, **30**, 2312 (1965).
2) C. M. McCloskey, *Adv. Carbohyd. Chem.*, **12**, 137 (1957).
3) P. W. Austin, F. E. Hardy, J. G. Buchanan, and J. Baddiley, *J. Chem. Soc.*, **1965**, 1419.
4) S. Umezawa, Y. Nishimura, and T. Tsuchiya, This Bulletin, **46**, 1263 (1973).
5) F. Cramer, H. Otterbach, and H. Springman, *Chem. Ber.*, **92**, 384 (1959).
6) Y. Nishimura, T. Tsuchiya, and S. Umezawa, This Bulletin, **44**, 2521 (1971).
7) J. S. D. Bacon, D. J. Bell, and H. W. Kosterlitz, *J. Chem. Soc.*, **1939**, 1248.
8) L. N. Owen and P. L. Ragg, *J. Chem. Soc.*, **1966**, 1291.

form). IR (KBr): 2110 cm^{-1} (N_3).

Found: C, 68.93; H, 6.48; N, 8.79%. Calcd for $C_{28}H_{31}N_3O_5$: C, 68.69; H, 6.38; N, 8.58%.

4-Azido-2,3,6-tri-O-*benzyl-4-deoxy*-D-*glucose* (**7**). To a solution of **6** (409 mg) in acetic acid (16 ml), 2N hydrochloric acid (5 ml) was added and the solution was heated at 98°C for 4 hr. On tlc with benzene–ethyl acetate (5: 1), the solution showed four spots of R_f 0.80 (**6**, trace), 0.40 (**7**, major), 0.20, and 0.05. After addition of sodium hydrogen carbonate (1 g), the solvent was evaporated to give a residue. The residue was extracted with chloroform and the extrate was washed with sodium hydrogen carbonate solution and water, dried over sodium sulfate and evaporated to give a syrup. The syrup was charged on a column of silica gel (25 g) and developed with benzene–ethyl acetate (3: 1). The eluate containing **7** was evaporated to give a pale yellow solid (190 mg, 48%), which was recrystallized from benzene–petroleum ether, mp 84—85.5°C, $[\alpha]_D^{20}$ +75° (*c* 0.68, chloroform).

Found: C, 68.48; H, 5.84; N, 9.00%. Calcd for $C_{27}H_{29}N_3O_5$: C, 68.19; H, 6.15; N, 8.84%.

4-Azido-2,3,6-tri-O-*benzyl-4-deoxy*-α-D-*glucopyranosyl Chloride* (**8**). A solution of **7** (2.9 g) in thionyl chloride (90 ml) was allowed to stand at room temperature overnight. The solution was evaporated with toluene *in vacuo* to give a pale yellow syrup. The product was purified by passing a short column of silica gel (24 g) with dry benzene, and the portion (36—108 ml) containing the main product (tlc with benzene, R_f 0.73) was evaporated to give a syrup, 1.98 g (66%), $[\alpha]_D^{18}$ +200° (*c* 3.0, benzene); IR (KBr): 2100 (N_3), 1460, 1365, 740, 700 cm^{-1}; NMR ($CDCl_3$): τ 5.43 (2H, AB q, *J* 12 Hz, $OC\underline{H}_2C_6H_5$), 5.31 (2H, s, $OC\underline{H}_2C_6H_5$), 5.08 (2H, AB q, *J* 12 Hz, $OC\underline{H}_2C_6H_5$), 3.93 (1H, d, *J* 3 Hz, H-1), 2.68 (15H, s, $OCH_2C_6\underline{H}_5$).

Found: C, 65.75; H, 5.76; N, 8.37; Cl, 7.49%. Calcd for $C_{27}H_{28}N_3O_4Cl$: C, 65.65; H, 5.71; N, 8.51; Cl, 7.18%.

Methyl 6-Azido-6-deoxy-α-D-*glucopyranoside* (**10**). To a solution of methyl 6-deoxy-6-*O*-tosyl-α-D-glucopyranoside[5] (**9**) (9.51 g) in dry DMF (130 ml), powdered sodium azide (3.7 g) was added and the mixture was stirred under gentle boiling for 1 hr. Evaporation followed by evaporation with toluene gave a black residue, which was extracted with acetone. The solution, after treatment with charcoal, was evaporated to give a reddish brown syrup. This was charged on a short column of silica gel (40 g) and developed with ethyl acetate. The eluate was evaporated and the residue was dissolved in chloroform. Addition of *n*-hexane gave a thick syrup, 4.41 g (74%), $[\alpha]_D^{22}$ +122° (*c* 1, water); IR: 2100 cm^{-1} (N_3).

Found: C, 38.61; H, 6.03; N, 19.40%. Calcd for $C_7H_{13}N_3O_5$: C, 38.35; H, 5.98; N, 19.17%.

Methyl 6-Azido-2,3,4-tri-O-*benzyl-6-deoxy*-α-D-*glucopyranoside* (**11**). To a solution of **10** (7.41 g) in dry DMF (140 ml), powdered potassium hydroxide (44 g) was added and to the mixture, benzyl chloride (~40 ml) was added at intervals under stirring with occasional cooling. After completion of the reaction (*ca.* 2 hr), the organic layer was separated from an insoluble matter and the latter was washed with chloroform. The combined organic solution was evaporated with toluene to give a residue, which was extracted with chloroform and the extract was evaporated. The residual syrup was heated at 100°C *in vacuo* (~0.1 Torr) to remove volatile materials. The syrup was then dissolved in chloroform and the solution was washed with water, dried over sodium sulfate and evaporated to give a syrup, which was chromatographed on a short column of silica gel (50 g) with benzene–chloroform (1: 1). The eluate containing **11** was evaporated to give a pale-yellow syrup, 12.42 g (75%), $[\alpha]_D^{21}$ +48.2° (*c* 1, chloroform) (lit,[9] +53.1°).

Found: C, 68.73; H, 6.65; N, 8.79%. Calcd for $C_{28}H_{31}N_3O_5$: C, 68.69; H, 6.38; N, 8.58%.

6-Azido-2,3,4-tri-O-*benzyl-6-deoxy*-D-*glucose* (**12**). To a solution of **11** (9.68 g) in acetic acid (160 ml), 3N hydrochloric acid (40 ml) was added and the solution was heated at 90—95°C for 4 hr. On tlc (silica gel) with benzene–ether (10: 1), the solution showed three spots of R_f 0.80 (**11**), 0.35 (**12**, major) and 0, the last spot being strengthened on prolonged reaction. After addition of sodium hydrogen carbonate (8 g), the brown solution was treated with charcoal, and evaporated. The residue was dissolved in chloroform and the solution was washed with water, dried over sodium sulfate and evaporated. The resulting syrup was chromatographed on a column of silica gel (400 g) with benzene–ether (10: 1). The eluate containing **12** was evaporated to give a syrup, which crystallized on scratching, 3.44 g (37%). From the earlier eluate, **11** was recovered (1.80 g). Recrystallization from benzene–petroleum ether gave crystals, mp 78.5—80.5°C, $[\alpha]_D^{21}$ +65° (*c* 1, chloroform), IR (KBr): 3380, 2110 (N_3), 750, 735, 695 cm^{-1}.

Found: C, 68.06; H, 6.36; N, 8.95%. Calcd for $C_{27}H_{29}N_3O_5$: C, 68.19; H, 6.15; N, 8.84%.

6-Azido-2,3,4-tri-O-*benzyl-6-deoxy*-α-D-*glucopyranosyl Chloride* (**13**). A solution of **12** (1.42 g) in thionyl chloride (23 ml) was allowed to stand at 0°C for 2 hr and then at room temperature for 38 hr. On tlc with benzene, the solution gave a single spot at R_f 0.65. The solution was evaporated and then co-evaporated with toluene to give a syrup, which was further purified by column chromatography with silica gel (10 g) and dry benzene to give a pale yellow syrup, 0.95 g (65%), $[\alpha]_D^{24}$ +119° (*c* 0.94, chloroform): IR (liquid film): 2110 (N_3), 730, 695 cm^{-1}; NMR (in $CDCl_3$): τ 3.93 (1H, d, *J* 3.5 Hz, H-1).

Found: C, 65.44; H, 5.60; N, 8.65; Cl, 7.52%. Calcd for $C_{27}H_{28}N_3O_4Cl$: C, 65.65; H, 5.71; N, 8.51; Cl, 7.18%.

9) T. Ueno, N. Kurihara, S. Hashimoto, and M. Nakajima, *Agr. Biol. Chem.*, **31**, 1346 (1967).

Studies on Aminosugars. XXXIV. Synthesis of 4-*O*- and 6-*O*-(4-amino-4-deoxy-α-D-glucopyranosyl)-2-deoxystreptamine[1]

Yoshio NISHIMURA, Tsutomu TSUCHIYA, and Sumio UMEZAWA

Department of Applied Chemistry, Faculty of Engineering, Keio University, Hiyoshi, Yokohama 222

(Received October 13, 1972)

Racemic *O*-isopropylidene derivative of *N,N'*-diethoxycarbonyl-2-deoxystreptamine was glycosidated with 4-azido-2,3,6-tri-*O*-benzyl-4-deoxy-α-D-glucopyranosyl chloride to afford two kinds of position isomers of α-glucoside, which was led to 4-*O*-(4-amino-4-deoxy-α-D-glucopyranosyl)- and 6-*O*-(4-amino-4-deoxy-α-D-glucopyranosyl)-2-deoxystreptamine.

A series of aminosugar glycosides, namely, kanamycin A, B, C, and other related compounds have been synthesized in our laboratories. A group in them is monoglycosyl-2-deoxystreptamines, which are of interest in connection with the investigation of the relationship between chemical structure and antibacterial activity of aminoglycoside antibiotics. 4-*O*- and 6-*O*-α-D-glucopyranosyl-2-deoxystreptamine,[2] 4-*O*-,[3] 5-*O*-[4] and 6-*O*-α-D-glucosaminyl-2-deoxystreptamine,[3] 4-*O*- and 6-*O*-(6-amino-6-deoxy-α-D-glucopyranosyl)-2-deoxy streptamine[5] and 6-*O*-(3-amino-3-deoxy-D-glucosyl)-2-deoxystreptamine[6] have been prepared, and, it has been found that, among them, 4-*O*- and 5-*O*-(2-amino-2-deoxy-α-D-glucopyranosyl)-2-deoxystreptamine[4,7] and 4-*O*-(6-amino-6-deoxy-α-D-glucopyranosyl)-2-deoxystreptamine possess antibacterial activity. As an extension of the work, we describe here the syntheses of 4-amino-4-deoxy-α-D-glucopyranosyl-2-deoxystreptamines (**9**, **10**).

4-Azido-2,3,6-tri-*O*-benzyl-4-deoxy-α-D-glucopyranosyl chloride[8] (**1**) was condensed with a mixture (**2**) of racemic *N,N'*-diethoxycarbonyl-4,5- and 5,6-*O*-isopropylidene-2-deoxystreptamines[2] in dry benzene–dioxane in the presence of mercuric cyanide and Drierite (Chart 1). Separation of the products by column chromatography gave 4-*O*-(4-azido-2,3,6-tri-*O*-benzyl-4-deoxy-α-D-glucopyranosyl)-*N,N'*-diethoxycarbonyl-5,6-*O*-isopropylidene-2-deoxystreptamine (**3**) and 6-*O*-(4-azido-2,3,6-tri-*O*-benzyl-4-deoxy-α-D-glucopyranosyl)-*N,N'*-diethoxycarbonyl-4,5-*O*-isopropylidene-2-deoxy-

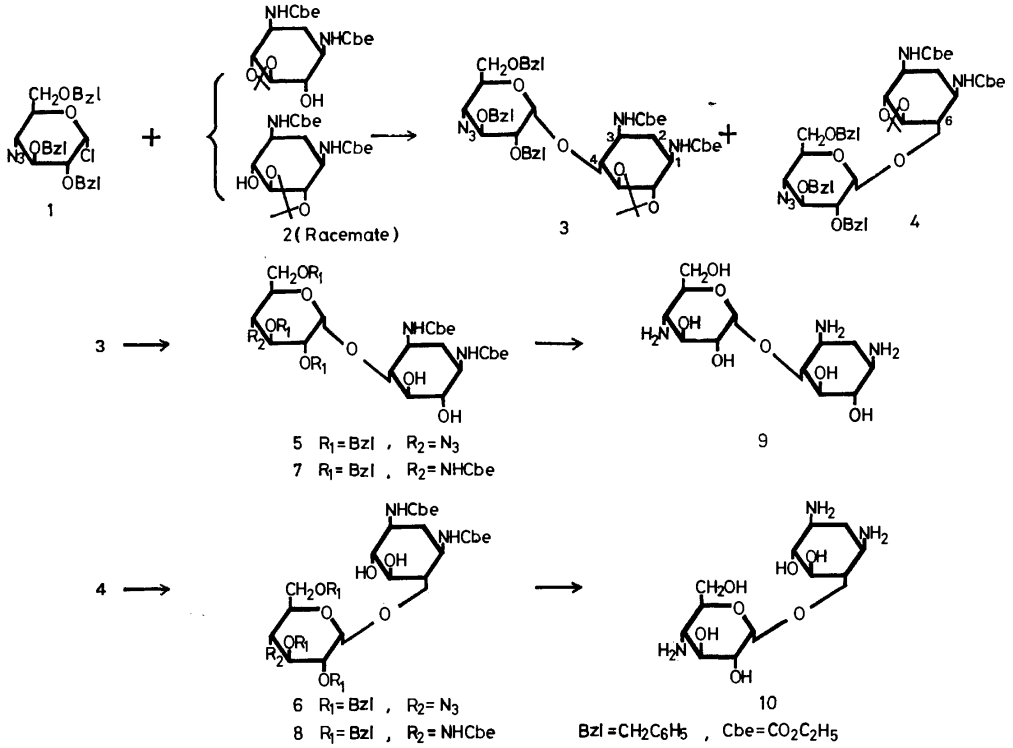

Chart 1.

1) A part of this paper was read at the 26th Annual Meeting of the Chemical Society of Japan, Kanagawa, April, 1972 (See Abstracts of papers of the Meeting Vol. VI, p. 1269).

2) Y. Nishimura, T. Tsuchiya, and S. Umezawa, This Bulletin, **43**, 2960 (1970).

3) S. Umezawa, T. Miyazawa, and T. Tsuchiya, *J. Antibiotics*, **25**, 530 (1972).

4) S. Umezawa, T. Tsuchiya, and H. Fujita, *ibid.*, **19**, 222 (1966).

5) Y. Nishimura, T. Tsuchiya, and S. Umezawa, This Bulletin, **44**, 2521 (1971).

6) S. Koto, K. Tatsuta, E. Kitazawa, and S. Umezawa, *ibid.*, **41**, 2769 (1968).

7) T. Tsuchiya, H. Fujita, and S. Umezawa, *J. Antibiotics*, **17**, 181 (1964).

8) Y. Takagi, T. Tsuchiya, and S. Umezawa, This Bulletin, **46**, 1261 (1970).

streptamine (**4**) in yields of 9.6 and 23%, respectively. Higher yield of 6-*O*-isomer was again here observed.[2,5]

After hydrolysis of **3** and **4** with aqueous acetic acid, the deisopropylidenated products (**5** and **6**) were reduced with Raney nickel and hydrogen to the corresponding amino-derivatives, which were then ethoxycarbonylated to give 4-*O*- and 6-*O*-(2,3,6-tri-*O*-benzyl-4-deoxy-4-ethoxycarbonylamino-α-D-glucopyranosyl)-*N*, *N'*-diethoxycarbonyl-2-deoxystreptamine (**7** and **8**), respectively. Debenzylation of **7** and **8** with palladium black and hydrogen followed by hydrolysis with hot barium hydroxide gave 4-*O*- and 6-*O*-(4-amino-4-deoxy-α-D-glucopyranosyl)-2-deoxystreptamine (**9** and **10**), respectively. Simultaneous reduction of the azido group and debenzylation of **5** and **6** by use of palladium and hydrogen were not adopted by the same reason described in a previous paper.[5]

Respective assignment of 4-*O*- and 6-*O*-glycosidic linkage to **9** and **10** were established by the determination of the values of Δ[M] in tetraminecopper (II) sulfate solutions (TACu).[9] The Δ[M] values of **9** and **10** were +1540° and +165° respectively. The sign and the magnitude of the Δ[M] of **9** indicated that TACu formed complexes between C-1 NH_2 and C-6 OH in 2-deoxystreptamine moiety and between C-3 OH and C-4 NH_2 in the sugar moiety. On the other hand, in **10**, formations of complexes occurred between C-3 NH_2 and C-4 OH in 2-deoxystreptamine moiety and between C-3 OH and C-4 NH_2 in the sugar moiety giving the low Δ[M] value by counteraction of both complexes.

Both compounds, **9** and **10**, showed no antibacterial activity against organisms tested, showing that the position of the amino group in aminoglycosidic deoxystreptamines is one of the important factors in exibiting the antibacterial activity. Other biological activities of **9** and **10** are now under study.

Experimental

The NMR spectra were measured with a Varian A-60D spectrometer. Tetramethylsilane (for the solution other than deuterium oxide) and sodium 4,4-dimethyl-4-silapentane-1-sulfonate (for the solution of deuterium oxide) were used as the internal standards. Thin-layer chromatography (tlc)was carried out on microscope slides coated with silica gel, and the spots were visualized with sulfuric acid. Paper chromatography (ppc) was carried out on Toyo Roshi No. 50 paper.

4-O-(4-Azido-2,3,6-tri-O-benzyl-4-deoxy-α-D-glucopyranosyl)-N, N'-diethoxycarbonyl-5,6-O-isopropylidene-2-deoxystreptamine (3) and 6-O-(4-Azido-2,3,6-tri-O-benzyl-4-deoxy-α-D-glucopyranosyl)-N, N'-diethoxycarbonyl-4,5-O-isopropylidene-2-deoxystreptamine (4). A mixture of **1** (1.99 g, 2 mmol) and freshly prepared Drierite (1.75 g) in anhydrous benzene-dioxane (2:1, 27 ml) was heated at 60°C under stirring for 20 min and to the mixture, **2** (1.11 g, 3.2 mmol) and well dried mercuric cyanide (2.39 g) were added, and the mixture was refluxed for 10 hr under stirring. Mercuric cyanide (2.39 g) was added and the reaction was continued for another 10 hr. The mixture was filtered and the residue was washed with chloroform. The filtrate and the washings combined were evaporated to give a syrup which was dissolved in chloroform. The solution was washed with water, dried over sodium sulfate and evaporated to give a thick syrup (2.89 g). On tlc with chloroform–ethyl acetate (3:1), the syrup showed six spots of R_f 0.97 (starting material, **1**), 0.71, 0.65, 0.57, 0.49, 0.05 (starting material, **2**). The syrup was chromatographed on a column (48×850 mm) of silica gel (Wako Gel, 850 g) with chloroform–ethyl acetate (3:1), and the fractions of 3050—3200 ml and 3260—3490 ml containing the products of R_f 0.57 and R_f 0.49, respectively, were evaporated to give solids, **3** (0.31 g, 9.6% based on **2**) and **4** (0.74 g, 23% based on **2**). **4** was recrystallized from ether to give colorless crystals (0.73 g) but **3** could not be crystallized.

Compound **3**: mp 60—64°C, $[\alpha]_D^{17}$ +76° (*c* 1, chloroform); IR (KBr): 2100 (N_3), 1700 (amide I), 1535 (amide II); NMR ($CDCl_3$): τ 8.78 (6H, t, *J* 7 Hz, $CO_2CH_2C\underline{H}_3$), 8.62 and 8.58 (3H, s, each, isopropylidene), 5.89 (4H, q, *J* 7 Hz, $CO_2C\underline{H}_2CH_3$), 4.85—5.65 (6H, m, $OC\underline{H}_2C_6H_5$), 4.49 (1H, d, *J* ~3 Hz, H-1), 2.65 (15H, s, $OCH_2C_6\underline{H}_5$).

Found: C, 63.01; H, 7.00; N, 8.65%. Calcd for $C_{42}H_{53}N_5O_{11}$: C, 62.75; H, 6.64; N, 8.71%.

Compound **4**: mp 171.5—172.5°C; $[\alpha]_D^{17}$ +82.2° (*c* 1.8, chloroform); IR (KBr): 2100 (N_3), 1690 (amide I), 1535 (amide II); NMR ($CDCl_3$): τ 8.85 and 8.82 (3H, t, each, *J* 7 Hz, $CO_2CH_2C\underline{H}_3$), 8.66 (6H, s, isopropylidene), 5.94 and 5.91 (2H, q, each, *J* 7 Hz, $CO_2C\underline{H}_2CH_3$), 4.9—5.6 (6H, m, $OC\underline{H}_2C_6H_5$), 4.83 (1H, d, *J* ~3 Hz, H-1), 2.68 (15H, s, $OCH_2C_6\underline{H}_5$).

Found: C, 62.54; H, 6.45; N, 9.05%. Calcd for $C_{42}H_{53}N_5O_{11}$: C, 62.75; H, 6.64; N, 8.71%.

4-O-(4-Azido-2,3,6-tri-O-benzyl-4-deoxy-α-D-glucopyranosyl)-N, N'-diethoxycarbonyl-2-deoxystreptamine (5). A solution of **3** (290 mg) in 50% aqueous acetic acid (6.5 ml) was heated at 90°C for 30 min. The solution was poured into water and the resulting precipitate was filtered and washed thoroughly with water. The solid was recrystallized from aqueous acetone (5:1), 230 mg; mp 183—184°C; $[\alpha]_D^{17}$ +122° (*c* 1.5, pyridine); IR (KBr): 3400, 3300, 2100 (N_3), 1690 (amide I), 1540 (amide II); NMR (in pyridine-d_5 containing a small amount of D_2O): τ 8.88 and 8.75 (3H, t, each, *J* 7.3 Hz, $CO_2CH_2C\underline{H}_3$), 5.5—6.5 (15H, skelton protons and $CO_2C\underline{H}_2CH_3$), 4.8—5.6 (6H, m, $OC\underline{H}_2C_6H_5$), 3.80 (1H, d, *J* ~3 Hz, H-1), 2.3—2.9 (15H, m, $OCH_2C_6\underline{H}_5$).

Found: C, 61.02; H, 6.42; N, 8.88%. Calcd for $C_{39}H_{49}N_5O_{11}$: C, 61.33; H, 6.47; N, 9.17%.

6-O-(4-Azido-2,3,6-tri-O-benzyl-4-deoxy-α-D-glucopyranosyl)-N, N'-diethoxycarbonyl-2-deoxystreptamine (6). Compound **4** (720 mg) was treated likewise as described in the preparation of **5**. Crude solid obtained was crystallized from aqueous acetone (5:1), 630 mg (93%); mp 185.5—186°C; $[\alpha]_D^{18}$ +114° (*c* 1.5, pyridine); IR (KBr): 3440, 3300, 2100 (N_3), 1690 (amide I), 1540 (amide II); NMR (in pyridine-d_5 containing a small amount of D_2O): τ 8.88 and 8.85 (3H, t, each, *J* 7.0 Hz, $CO_2CH_2C\underline{H}_3$), 5.6—6.4 (15H, skeleton protons and $CO_2C\underline{H}_2CH_3$), 4.8—5.6 (6H, m, $OC\underline{H}_2C_6H_5$), 4.06 (1H, d, *J* ~3 Hz, H-1), 2.3—2.9 (15H, m, $OCH_2C_6\underline{H}_5$).

Found: C, 61.60; H, 6.48; N, 8.98%. Calcd for $C_{39}H_{49}N_5O_{11}$: C, 61.33; H, 6.47; N, 9.17%.

4-O-(2,3,6-Tri-O-benzyl-4-deoxy-4-ethoxycarbonylamino-α-D-glucopyranosyl)-N,N'-diethoxycarbonyl-2-deoxystreptamine (7). Compound **5** (230 mg) was dissolved in aqueous dioxane (1:15, 3.2 ml) and the solution was hydrogenated with Raney nickel (T-4) and hydrogen under 50 p.s.i. at 42°C for 1 hr. On tlc with benzene–acetone (2:1), **5** (R_f 0.47) disappeared and a product (R_f 0.20) appeared. Filtration and evaporation of the solution gave a syrup (0.22 g), which was dissolved

9) S. Umezawa, T. Tsuchiya, and K. Tatsuta, This Bulletin, **39**, 1235 (1966).

in acetone (3.2 ml). To the solution, water (3.2 ml) was added under vigorous stirring. Anhydrous sodium carbonate (0.15 g) was added to the resulting suspension, and, after agitation for a while, ethoxycarbonyl chloride (0.063 g) was added slowly. Agitation was continued for 30 min. On tlc with the above-mentioned solvent system, the reaction mixture showed a major spot at R_f 0.40. The mixture was evaporated and the residue was dissolved in chloroform. The solution was washed with water, dried over sodium sulfate and evaporated to give a solid (0.23 g). Recrystallization from aqueous ethanol (1:2) gave a colorless solid, 199 mg (84%); mp 142—143°C, $[\alpha]_D^{17}$ +29.8° (*c* 1.4, chloroform); IR (KBr): 3400, 3300, 1695 (amide I), 1540 (amide II); NMR (in $CDCl_3$): τ 8.87, 8.81, and 8.78 (3H, t, each, *J* 7.2 Hz, $CO_2CH_2C\underline{H}_3$), 2.70 (15H, s, $OCH_2C_6\underline{H}_5$).

Found: C, 62.51; H, 7.23; N, 4.94%. Calcd for $C_{42}H_{55}N_3O_{13}$: C, 62.29; H, 6.85; N, 5.19%.

6-O-(2,3,6-Tri-O-benzyl-4-deoxy-4-ethoxycarbonylamino-α-D-glucopyranosyl)-N,N'-diethoxycarbonyl-2-deoxystreptamine (8). Compound **6** (629 mg) was dissolved in aqueous dioxane (1:8, 9 ml) and treated likewise as described above. The chloroform solution obtained after treatment with ethoxycarbonyl chloride was washed with water, dried over sodium sulfate and evaporated to give a residue (0.59 g), which was chromatographed on a column (14×280 mm) of silica gel (Wako Gel, 15 g) with benzene–acetone (2:1). The portion (36—46 ml) containing the major product (R_f 0.40 with benzene–acetone 2:1) was evaporated to give a solid (0.38 g). Recrystallization from aqueous ethanol gave a colorless solid, 315 mg (51%); mp 194—195.5°C, $[\alpha]_D^{17}$ +9.8° (*c* 1.5, chloroform); IR (KBr): 3400, 3300, 1690 (amide I), 1545 (amide II); NMR (in $CDCl_3$): τ 8.87, 8.83, and 8.81 (3H, t, each, *J* 7.0 Hz, $CO_2CH_2C\underline{H}_3$), 2.70 (15H, s, $OCH_2C_6\underline{H}_5$).

Found: C, 62.25; H, 6.73; N, 5.21%. Calcd for $C_{42}H_{55}N_3O_{13}$: C, 62.29; H, 6.85; N, 5.19%.

4-O-(4-Amino-4-deoxy-α-D-glucopyranosyl)-2-deoxystreptamine (9). Compound **7** (200 mg) was dissolved in aqueous dioxane (3:20, 2.3 ml) by heating. A few drops of acetic acid were added and the solution was hydrogenated with freshly prepared palladium black and hydrogen under 50 p.s.i. at 40—45°C for 5 hr. On tlc with benzene–ethanol (4:1), **7** (R_f 0.8) disappeared and a product (R_f 0.2) appeared. Filtration and evaporation of the solution gave a solid (0.13 g), which was dissolved in 1N barium hydroxide (2 ml) and heated at 90°C for 8 hr. On paper chromatography with *n*-butyl-alcohol–pyridine–water–acetic acid (6:4:3:1), the solution showed a ninhydrin positive product ($R_{f\ 2\text{-deoxystreptamine}}$ 0.52). The solution was neutralized with carbon dioxide, and the resulting suspension was boiled for a while. After centrifuging, the upper layer was evaporated. After repeated extraction and evaporation of the residue with boiling water, the final residue was charged on a column (5×44 mm) of Amberlite IRC 50 (NH_4 form) and after washing the column with water, developed with 0.03N ammonia. The portion (70—180 ml) containing **9** was evaporated to give a solid (44 mg). An aqueous solution of the product was acidified with hydrochloric acid to pH 2 and evaporated to give a solid of trihydrochloride dihydrate of **9**, 61.4 mg (53%); $[\alpha]_D^{16}$ +67° (*c* 0.3, water), $[\alpha]_{436}^{16}$ +131° (*c* 0.3, water), $[\alpha]_{436\text{TACu}}^{16}$ +487° (*c* 0.3, TACu), $\Delta[M]_{TACu}^{16}$ +1540°; IR (KBr): 3400, 2920, 1600, 1500, 1100, 1050, 870, 770 cm^{-1}; NMR (in D_2O): τ 8.75 (1H, q, *J* ~13 Hz, H_{ax}-2), 7.87 (1H, double triplets, *J* ~4 Hz and ~13 Hz, H_{eq}-2), 4.67 (1H, d, *J* ~3 Hz, H-1).

Found: C, 30.55; H, 6.59; N, 9.09; Cl, 22.50%. Calcd for $C_{12}H_{25}N_3O_7 \cdot 3HCl \cdot 2H_2O$: C, 30.74; H, 6.88; N, 8.96; Cl, 22.69%.

6-O-(4-Amino-4-deoxy-α-D-glucopyranosyl)-2-deoxystreptamine (10). Compound **8** (0.3 g) was treated similarly as described above. The base (71 mg) obtained was treated with hydrochloric acid to give trihydrochloride dihydrate of **10**, 88.6 mg (51%); $[\alpha]_D^{16}$ +69° (*c* 0.4, water), $[\alpha]_{436}^{16}$ +141° (*c* 0.4, water), $[\alpha]_{436\text{TACu}}^{16}$ +176° (*c* 0.4, TACu), $\Delta[M]_{TACu}^{16}$ +165°; $R_{f\ 2\text{-deoxystreptamine}}$ 0.48 (ppc with the same solvent system described above). The IR spectrum of the hydrochloride was quite similar to that of **9**. NMR (in D_2O): τ 8.74 (1H, q, *J* ~13 Hz, H_{ax}-2), 7.90 (1H, double triplets, *J* ~4 Hz and ~13 Hz, H_{eq}-2), 4.83 (1H, d, *J* ~3 Hz, H-1).

Found: C, 30.65; H, 6.80; N, 9.12; Cl, 22.41%. Calcd for $C_{12}H_{25}N_3O_7 \cdot 3HCl \cdot 2H_2O$: C, 30.74; H, 6.88; N, 8.96; Cl, 22.69%.

The authors wish to thank Dr. Hiroshi Naganawa of Institute of Microbial Chemistry for the measurements of the NMR spectra and Mr. Saburo Nakada for the elemental analysis. The authors also wish to thank Messrs. Toshio Sumida, Ryujiro Namba, and Takayuki Obata for their technical assistances.

Reaction between *p*-Toluenesulfinic Acid and Diphenyldiazomethane[1)]

Michio KOBAYASHI, Hiroshi MINATO, and Hideo FUKUDA

Department of Chemistry, Tokyo Metropolitan University, Fukazawa, Setagaya-ku, Tokyo 158

(Received October 23, 1972)

Reaction between *p*-toluenesulfinic acid and diphenyldiazomethane was investigated in several solvents. Reaction was faster in non-polar solvents and slower in polar solvents. Experiments with $CH_3C_6H_4SO_2D$ showed that protonation of diphenyldiazomethane is the rate-determining step. In non-polar solvents the main product was benzhydryl *p*-tolyl sulfone, whereas in polar solvents benzhydryl *p*-toluenesulfinate was the main product. In ethanol, benzhydryl ethyl ether was also produced. The mechanism of the reaction was discussed.

Although the formation of methyl sulfinates from sulfinic acids and diazomethane is known for a long time,[2)] no reactions of sulfinic acids with other aliphatic diazo compounds have been reported. Since sulfinate anions are ambident, alkylation may give rise to sulfinate esters and sulfones. Ordinary alkylating agents yield sulfones alone,[3)] whereas such powerful alkylating agents as triethyloxonium tetrafluoroborate give ethyl sulfinates as the main products.[4)] Relative yields of esters and sulfones are influenced by the solvent.[5)]

The kinetics and products of the reaction between *p*-toluenesulfinic acid and diphenyldiazomethane has been investigated, and the results are given in this paper.

Results and Discussion

Kinetic Studies. The rate of decrease of diphenyldiazomethane (I) was determined by use of the decrease of the absorption of I at 525 nm. The reaction was of first order in both *p*-toluenesulfinic acid (II) and I. Rates of the reaction were considerably different in various solvents; they were quite large in benzene or dichloromethane and much smaller in dioxane, alcohol or dimethyl sulfoxide. The rate constants in various solvents are shown in Table 1. When the logarithms of the rate constants determined at various temperatures were plotted against $1/T$, good straight lines were obtained. Activation parameters were calculated and are shown in Table 1.

Table 1. Rate constants of the reaction between *p*-toluenesulfinic acid and diphenyldiazomethane in various solvents

Solvent	Temperature (°C)	k (l mol^{-1}sec^{-1})	$\Delta H^{\neq}$ (kcal mol^{-1})	$\Delta S^{\neq}$ (e.u.)
CH_2Cl_2[a)]	20.0	300		
Benzene[a)]	20.0	22		
CH_3CN	20.0	4.9		
Ethanol	20.0	1.6		
Dioxane	34.5	0.419	13.0	−18.1
	30.0	0.321		
	24.8	0.190		
	19.5	0.314		
	20.0[b)]	0.19		
DMSO	35.0	0.103	13.0	−23.6
	30.0	0.0708		
	27.0	0.0570		
	19.0	0.0328		

a) Reaction was rapid, and measurements were not so accurate.
b) By the rate of evolution of nitrogen.

Since the reaction between I and II yields nitrogen quantitatively, the rates of the reaction can be determined from the rates of evolution of nitrogen in the solvents in which the reaction rates are not so great. Although the measurements are not very accurate because of the rapidity of the reaction, the rate constant determined is in fair agreement with the value obtained spectrophotometrically.

The reaction between I and II is a three-step reaction, the first step being probably the rate-determining one.

$$ArSO_2H + Ph_2CN_2 \longrightarrow [Ph_2CHN_2^{\oplus}ArSO_2^{\ominus}] \quad (1)$$

$$[Ph_2CHN_2^{\oplus}ArSO_2^{\ominus}] \longrightarrow [Ph_2CH^{\oplus}ArSO_2^{\ominus}] + N_2 \quad (2)$$

$$[Ph_2CH^{\oplus}ArSO_2^{\ominus}] \longrightarrow Ph_2CHO_2SAr \quad (3)$$

The first step is the protonation of I. Since protonations are usually very rapid, it is doubtful whether or not step (1) is really the rate-determining step. Therefore, $CH_3C_6H_4SO_2D$ was synthesized. When the rate of the reaction between $CH_3C_6H_4SO_2D$ and I was determined in dioxane, measurements were not reproducible because the moisture in air dissolves into the dioxane and the H–D exchange takes place rapidly between $CH_3C_6H_4SO_2D$ and water. The measurements were therefore carried out in dioxane containing 2 vol% of heavy water (or ordinary water). The rates were determined by use of both the absorption at 525 nm and the volume of the nitrogen evolved. Table 2 shows that the rates with the deuterated com-

Table 2. Rates of reaction between Ph_2CN_2 and $C_7H_7SO_2D$ (or $C_7H_7SO_2H$) in dioxane containing 2 vol % D_2O (or H_2O)

Acid	Temp. (°C)	k (l mol^{-1}sec^{-1})	Method[a)]	$\Delta H^{\neq}$ (kcal mol^{-1})	$\Delta S^{\neq}$ (e.u.)
$C_7H_7SO_2D$	29.5	0.148	S	12.8	−18.5
	19.8	0.0666	S		
	15.0	0.0478	S		
	15.0	0.048	V		
$C_7H_7SO_2H$	29.5	0.435	S	14.0	−16.8
	19.5	0.207	S		
	15.0	0.142	S		
	15.0	0.15	V		

a) S=spectrophotometric, V=volumetric.

1) Organic sulfur compounds, Part 39.
2) F. Arndt and A. Scholz, *Ann. Chem.*, **510**, 70 (1934).
3) Houben-Weyl, "Methoden der organischen Chemie," Bd. IX, pp. 231, 333, Georg Thieme Verlag, (1955).
4) M. Kobayashi, This Bulletin, **39**, 1296 (1966); M. Schank, *Ann. Chem.*, **714**, 117 (1968).
5) J. C. Meek and J. S. Fowler, *J. Org. Chem.*, **33**, 3422 (1968).

Table 3. Kinetic isotope effects in the reaction between Ph_2CN_2 and $C_7H_7SO_2H$

Reaction temperature (°C)	29.5	19.8	15.0
k_H/k_D {Spectrophotometrically	2.9	3.1	3.3
k_H/k_D {Volumetrically			3.2

pound are considerably smaller than those with the ordinary sulfinic acid. The kinetic isotope effects (Table 3) were about 3.0. These data show that protonation of I is the rate-determining step; that is, step (2) is faster than step (1). Step (2) proceeds very readily because it yields the resonance-stabilized diphenylmethyl cation.

Rates of reaction in dioxane containing 2 vol% water are greater than those in anhydrous dioxane. This is probably due to the increase of the extent of ionization of II by the addition of water.

Reactions between carboxylic acids and aliphatic diazo compounds have been investigated extensively.[6] The reaction between benzoic acid and diphenyldiazomethane in ethanol is of second order, and k (20°C) is 6.6×10^{-3} $M^{-1}sec^{-1}$, $\Delta H^{\ddagger}=15.6$ kcal mol^{-1}, $\Delta S^{\ddagger}=-15$ e.u.[7] The rates with II shown in Table 1 are far greater than this value. This might be ascribed to the greater dissociation constant of II in comparison with that of benzoic acid.[8] Kinetic isotope effects were observed in the reaction between carboxylic acids and I (with benzoic acid, $k_H/k_D=3.6$ at 35.35°C in ethanol),[9] showing that protonation of I is the rate-determining step. It is of interest that the values of the kinetic isotope effects with carboxylic acids are approximately the same as those with II.

It was reported that the addition of water increased the rates of reaction between carboxylic acids and I in ethanol.[10]

As shown in Table 1, the reaction rates in non-polar solvents are much greater than those in polar solvents. Similar phenomena were observed in the rates of the reactions of carboxylic acids with I.[9]

The greater rates in non-polar solvents can be rationalized as follows. Infrared spectroscopy shows that sulfinic acids exist as dimers or polymers in non-polar solvents or in crystalline state.[11] When such dimeric sulfinic acids react with I, protonation takes place easily, because the sulfinate anion formed is stabilized by association with another sulfinic acid molecule.

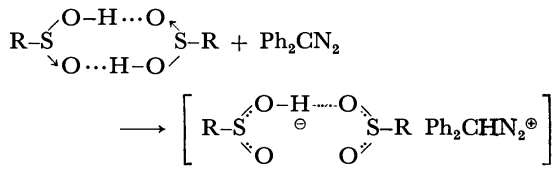

In polar solvents, sulfinic acid molecules lose their dimeric structure and are solvated by solvent molecules. When such solvated molecules are to react with I, the bond between II and a solvent molecule must be cleaved first. This process requires extra energy, and therfore the reaction with I is slower.

Product Studies. In solvents other than alcohols, benzhydryl *p*-toluenesulfinate and benzhydryl *p*-tolyl sulfone were formed in 80—100% yields. The ratio between them varied with the solvent used. Amounts of the products were determined by use of infrared absorptions at 900 and 1140 cm^{-1} (ester) and 1310 cm^{-1} (sulfone) and NMR absorptions. In the reaction in ethanol, benzhydryl ethyl ether was found in addition to the sulfinate and sulfone. The molar ratios of the products in various solvents are shown in Table 4.

Table 4. Molar ratios of the products in various solvents

Solvent	Sulfinate[a]	Sulfone[b]	Ether[c]	Total yield (mol %)
CH_2Cl_2	0	100		80
Benzene	20	80		96
CH_3CN	81	19		100
Ethanol	60	14	26	100
Dioxane	83	17		100
DMSO	100	0		82

a) *p*-$CH_3C_6H_4SO_2CHPh_2$.
b) *p*-$CH_3C_6H_4SO_2CHPh_2$.
c) $C_2H_5OCHPh_2$.

In ethanol, the ratio (Sulfinate+Sulfone)/Ether was nearly constant when the concentrations of I and II were varied in the range $2.4—64.0\times10^{-3}$ M.

In DMSO, only benzhydryl *p*-toluenesulfinate was formed in the earlier period of the reaction, but the sulfinate slowly isomerized to sulfone, and the molar ratio of these two products was about 50:50 after 30 min at room temperature.

Reaction (3) is alkylation of the sulfinate anion by diphenylmethyl cation. Since the reactivity of resonance-stabilized diphenylmethyl cation is much less than that of a simple alkyl cation, not only the sulfinate ester but also the sulfone were formed.

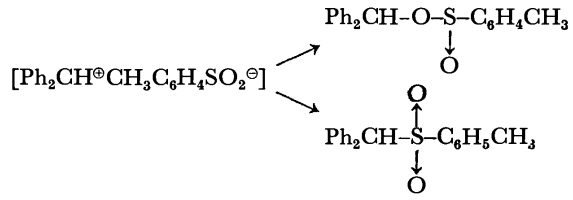

Since sulfones are thermodynamically much more stable than the corresponding sulfinate esters, the above reaction is a kinetically-controlled reaction. In such polar solvents as DMSO, the benzhydryl ester once formed redissociates to an ion pair, which recombines, forming the sulfone. Thermal isomerization of a sulfinate ester to a sulfone has been reported on.[12] It is

6) For reviews. R. A. More O'Ferrall, "Advances in Physical Organic Chemistry," Vol. 5, ed. by V. Gold, Academic Press (1967), p. 331.
7) K. Bowden, A. Buckley, N. B. Chapman, and J. Shorter, *J. Chem. Soc.*, **1964**, 3330.
8) The pK_a value of benzoic acid is 4.6, and that of *p*-toluenesulfinic acid is 1.24 (C. D. Ritchie, J. D. Saltiel, and E. S. Lewis, *J. Amer. Chem. Soc.*, **83**, 4601 (1961)).
9) R. A. More O'Ferrall, W. K. Kwok, and S. I. Miller, *ibid.*, **86**, 5553 (1964).
10) J. D. Roberts, W. Watanabe, and R. E. McMahon, *ibid.*, **73**, 760 (1051).
11) S. Detoni and D. Hadzi, *J. Chem. Soc.*, **1955**, 3163.
12) D. Darwish and E. A. Preston, *Tetrahedron Lett.*, **1964**, 113.

also known that hydrolysis of benzhydryl sulfinate forms the corresponding sulfone as a byproduct.[13]

Table 4 shows that in polar solvents the yields of the sulfinate are greater whereas in non-polar solvents those of the sulfone are greater. This is probably related with the fact that rates of the reaction between I and II are smaller in polar solvents and greater in non-polar solvents. A plausible explanation for this phenomenon is as follows. As described above, sulfinic acids exist as dimers or polymers in non-polar solvents. When such dimeric acid reacts with I, the sulfinate anion formed exists in association with another sulfinic acid molecule. Since the negative charge on this dimer anion is not on a specific oxygen atom, combination of diphenylmethyl cation with the oxygen atom of the dimer anion takes place slowly, and consequently the combination with the sulfur atom takes place relatively rapidly.

In such polar solvents as DMSO and dioxane, sulfinic acid molecules are hydrogen-bonded with solvent molecules and the reaction with I is slow. However, since the sulfinate anions formed are not much solvated, they quickly combine with cations at the negatively charged oxygen atoms, forming the thermodynamically less stable benzhydryl sulfinate as the main product.

In ethanol, benzhydryl ethyl ether was formed in a 26% yield which did not change much when the initial concentrations of I and II were varied. Formation of this ether can be ascribed to the attack of ethanol to the ion pair Ph_2CH^+–$O_2SC_7H_7$ or the solvent-separated ion pair.

When benzoic acid and I were let to react in ethanol, benzhydryl ethyl ether was found in a 45% yield.[10] When 2,4-dinitrophenol and I were let to react in ethanol, benzhydryl ethyl ether was found in a 39% yield.[14] The smaller yield of this ether in the reaction of I and II in ethanol means that the combination of $C_7H_7SO_2^-$ with Ph_2CH^+ is much faster than the combination of ethanol with Ph_2CH^+. This fact suggests that the ion pair Ph_2CH^+–$O_2SC_7H_7$ is tighter than Ph_2CH^+–O_2CR and that the sulfinate anion is more nucleophilic than carboxylate anions.

The reaction between I and II can be expressed in the following scheme.

The life time of the ion pair RSO_2^-–$Ph_2CHN_2^+$ must be very short, and a molecule of nitrogen is quickly lost from the tight ion pair. Probably k_1 is much smaller than k_2, and k_{-1} is also very small in comparison with k_2. The sulfinate and sulfone are formed mainly from the combination of the tight ion pair RSO_2^-–Ph_2CH^+, but part of them must arise from the combination of the solvent-separated ion pair, especially in polar solvents. In ethanol, part of the solvent-separated ion pair reacts with ethanol, forming benzhydryl ethyl ether.

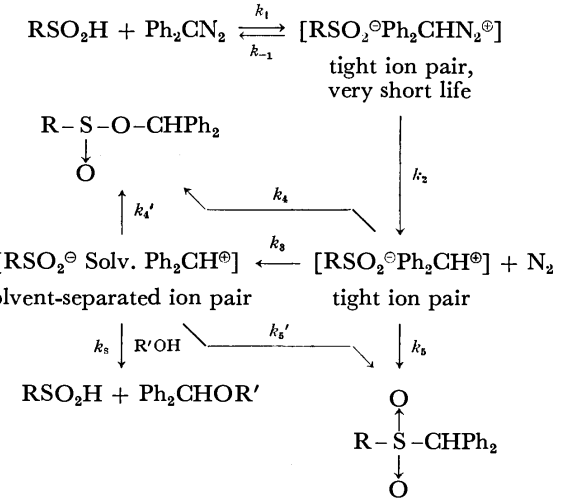

Experimental

Materials. Diphenyldiazomethane, produced by oxidation of benzophenone hydrazone with mercuric oxide, was recrystallized from *n*-hexane; mp 31—32 °C.[15] Benzhydryl *p*-toluenesulfinate was synthesized by condensation of the corresponding acid and alcohol in the presence of dicyclohexylcarbodiimide;[16] mp 79 °C.

Kinetic Measurements. Reaction was followed by the decrease of the absorption of I at 525 nm with a Hitachi EPS-3T spectrophotometer. Neither II nor the reaction products had absorptions in this region. Rates of reaction were also determined volumetrically by use of a gas buret.

Reaction Products. The products of the reaction were separated by recrystallization or column chromatography, and identified by NMR and IR. The ratios of the products in the reaction mixture were determined by use of NMR (δ 3.65, $C_7H_7(SO)OCHPh_2$; δ 4.70, $C_7H_7(SO_2)CHPh_2$; δ 6.3—6.7, $CH_3CH_2OCHPh_2$), and IR (ν_{S-O} 1140 and ν_{C-O} 900 cm^{-1} of sulfinate; ν_{S-O} 1310 cm^{-1} of sulfone). Deuterated solvents (such as dimethyl sulfoxide-d_6) were used whenever necessary for NMR measurements.

13) D. Darwish and R. A. McLaren, *Tetrahedron Lett.* **1962**, 1231. A. H. Bragg, J. C. McFadyen, and J. S. Stevens, *J. Chem. Soc.*, **1958**, 3608.

14) J. D. Roberts, W. Watanabe, and R. E. McMahon, *J. Amer. Chem. Soc.*, **73**, 2521 (1951).

15) E. C. Horning ed., "Organic Syntheses," Coll. Vol. III, p. 351.

16) Y. Miyaji, H. Minato, and M. Kobayashi, This Bulletin, **44**, 862 (1971).

New Agents for *t*-Butyloxycarbonylation and *p*-Methoxybenzyloxycarbonylation of Amino Acids

Takeshi NAGASAWA, Katsumasa KUROIWA, Kouichi NARITA, and Yoshikazu ISOWA*

Research Laboratory for Chemical Fibers, Nitto Boseki Company, Ltd., Fukuyama, Kōriyama, Fukushima
**Sagami Chemical Research Center, Ohnuma, Sagamihara, Kanagawa*

(Received October 30, 1972)

A new method for the preparation of *t*-butyloxycarbonyl amino acids and *p*-methoxybenzyloxycarbonyl amino acids has been devised. The former was obtained in satisfactory yields from amino acids and *t*-butyl *S*-4,6-dimethylpyrimid-2-ylthiocarbonate prepared from *t*-butyl alcohol and (4,6-dimethylpyrimid-2-ylthio)corbonyl chloride in dry pyridine, and the latter was also obtained from amino acids and *p*-methoxybenzyl *S*-4,6-dimethylpyrimid-2-ylthiocarbonate from *p*-methoxybenzyl alcohol and (*S*-4,6-dimethylpyrimid-2-ylthio)carbonyl chloride. These *t*-butyloxycarbonylation and *p*-methoxybenzyloxycarbonylation of amino acids are more convenient than the usual methods.

In recent years the *t*-butyloxycarbonyl (Boc) group[1] has found wide use for protecting the amino moiety of amino acids in peptide synthesis. Its merits are high selectivity and ease of removal by acidolysis (HCl in an inert solvent, or CF_3COOH), and at the same time resistance to hydrogenolysis, alkaline spilitting, hydrazinolysis, as well as absence of appreciable racemization.

The most widely employed reagents for the preparation of Boc-amino acids are Boc-azide,[2] Boc-Cl,[3] and *t*-butyl 2,4,5-trichlorophenyl carbonate,[4] which react with both the free amino acids and their esters in the presence of bases. But these methods suffer from various disadvantages, the strict control of reaction pH required in the case of Boc-azide, unstable property of Boc-Cl, and elaborate purification from 2,4,5-trichlorophenol of Boc-amino acids. A new water soluble agent (4-dimethylamino-1-*t*-butyloxycarbonylpyridinium chloride) for *t*-butyloxycarbonylation of amines was also reported.[5]

We wish to report a new, rapid and tidy method for the preparation of Boc-amino acids. Aminolysis of *t*-butyl *S*-4,6-dimethylpyrimid-2-ylthiocarbonate by the amino moiety of amino acids yields the corresponding Boc-amino acids in good yield; the 2-mercapto-4,6-dimethylpyrimidine liberated being acid soluble is easily separable from the Boc-amino acid, and the aminolysis is carried out at room temperature for 2—24 hr.

The *p*-methoxybenzyloxycarbonyl (Z(OMe))[6] group also has been widely used as a blocking substituent of the amino moiety of amino acids in peptide synthesis.[7] This group allows an easier removal by trifluoroacetic acid. The Z(OMe) group can be introduced with the use of *p*-methoxybenzyl 2,4,5-trichlorophenyl carbonate[8] or *p*-methoxybenzyloxycarbonyl azide.[9] These methods have been used in many cases, but the yields are not satisfactory. In the present investigation, *p*-methoxybenzyl *S*-4,6-dimethylpyrimid-2-ylthiocarbonate was very useful for the preparation of Z(OMe)-amino acids, too.

Results and Discussion

t-Butyl 4,6-Dimethylpyrimidyl-2-thiol Carbonate (IV) and p-Methoxybenzyl 4,6-Dimethylpyrimidyl-2-thiol Carbonate (V). 2-Mercapto-4,6-dimethylpyrimidine hydrochloride (I.HCl) was prepared from acetylacetone, thiourea, and concentrated hydrochloric acid in ethanol in the usual method.[10]

As was clear from the reaction schema shown below, the preparation of sodium 4,6-dimethylpyridine-2-thiolate (II) was described in experimental section in detail.

(4,6-Dimethylpyrimid-2-ylthio)carbonyl chloride(III) was prepared by adding a phosgene to the suspension of II in an inert solvent such as petroleum ether and toluene under cooling (−5——10°C). The resulting product was stable in a water free state at room temperature and solid below about 5°C, but decomposed at a temperature of about 100°C and hence could not be purified by distillation. In the sequent reaction, therefore, III was ordinarily used in a crude form. IV could be prepared readily from *t*-butyl alcohol and III in pyridine at room temperature and V also prepared from *p*-methoxybenzyl alcohol and III in the presence of pyridine in dry ether at room temperature. These reagents (IV and V) were considerably stable, pale yellow crystals and could be stored in a dark and cool place for six months without decomposition.

Boc-Amino Acids and Z(OMe)-Amino Acids. As a guide to model condition for the reaction between

1) B. Bezaz and L. Zervas, *J. Amer. Chem. Soc.*, **83**, 719 (1961). R. Schwyzer, P. Sieber, and H. Kappeler, *Helv. Chim. Acta*, **42**, 2622 (1959).
2) E. Schnabel, *Ann. Chem.*, **702**, 188 (1967).
3) S. Sakakibara, I. Honda, and K. Takada, This Bulletin, **42**, 809 (1969).
4) W. Broadbent, J. S. Morley, and B. E. Stone, *J. Chem. Soc., C*, **1967**, 2632.
5) E. Guibé-Jampel and M. Wakselman, *Chem. Commun.*, **1971**, 267.
6) F. C. Mckay and N. F. Albertson, *J. Amer. Chem. Soc.*, **79**, 4686 (1957).
7) M. Bodansky and M. A. Ondetti, "Peptide Synthesis," John Wiley & Sons, Inc., New York (1966), p. 31. E. Schroder and K. Lubke, "The Peptide," Vol. 1, Academic Press, New York (1965), p. 34.
8) E. Klieger, *Ann. Chem.*, **724**, 204 (1969).
9) F. Weygand and K. Hunger, *Chem. Ber.*, **95**, 1 (1962).
10) R. R. Hunt, J. F. W. McOmie, and E. R. Sayer, *J. Chem. Soc.*, **1959**, 525.

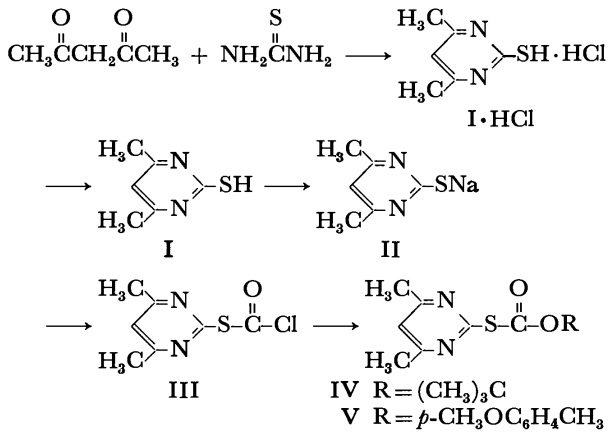

Fig. 1

amino acids and IV, the reaction between leucine and the active ester was first explored.

The effects of bases, solvents, reaction time, and reaction temperature were examined and the following results were found.

With aqueous dioxane as the solvent, the effect of five bases was examined and it was found that all except pyridine promoted the formation of Boc-leucine: the yield of product was greatest using triethylamine (quantitatively), sodium hydroxide (88%) or sodium carbonate (85%) and least using sodium hydrogen

Table 1. Effect of bases in the preparation of Boc-leucine (shown by % yield)[a]

AA/Base[b] (molar ratio)	Base				
	NaOH	$N(C_2H_5)_3$	Na_2CO_3	$NaHCO_3$	C_5H_5N
1.0/1.1	88	83	85	21	trace
1.0/1.5	96	100	—	—	—

a) Reaction condition: Solvent=50% aqueous dioxane; Reaction temperature=30—35°C; Reaction time=10hr
b) AA=amino acid

Table 2. Effect of reaction time and solvents in the preparation of Boc-leucine (shown by % yield)[a]

Base (AA/Base)	Solvent (50% aqueous)	Reaction time (hr)		
		2	5	10
NaOH	Dioxane	80	84	88
(1.0/1.1)	*t*-Butyl alcohol	74	86	86
	DMF[b]	—	86	91
$N(C_2H_5)_3$	Dioxane	—	90	100
(1.0/1.5)	*t*-Butyl alcohol	—	87	97
	DMF	—	99	100

a) Reaction temperature=30—35°C.
b) DMF=dimethylformamide.

Table 3. Effect of reaction temperature in the preparation of Boc-leucine (shown by %yield)[a]

Temperature (°C)	15—20	30—35	40—45
	79	99	92[b]

a) Reaction condition: Solvent=50% aqueous DMF; Base=triethylamine; AA/Base=1.0/1.5; Reaction time=5 hr.
b) Reaction time=2.5 hr.

Table 4. Synthesis of Boc-amino acid derivatives

Amino acid derivative[a]	Yield(%)	Mp (°C) (Solvent)[e]	$[\alpha]_D^{20}$(c, 1)
Ala	99	81—82 (E-P)	−24.0 (AcOH)
Arg(NO_2)	100	123—125 (M-E-PA)	−6.8 (DMF)
Asp	72	116—117 (EA-PA)	−6.4 (MeOH)
Asn	82	175—177 (W)	−7.2 (DMF)
$(Cys)_2$	100	145—146 (EA)	−114.2 (AcOH)
Cys(S-Bzl)	95	66—68 (E-PA)	−43.7 (AcOH)
Glu	100	101—104 (EA-PA)	−15.6 (MeOH)
Gln	61	118—119 (EA-PA)	−2.8 (EtHH)
Gly	92	87—89 (EA-PA)	
His(N^{im}-Bzl)	98	180—182 (Py-EA-PA)	+24.8 (MeOH)
Hyp[b]	81	168—172 (M-E)	−27.9 (AcOH)
Ileu	100	68—71 (PA)	+2.5 (AcOH)
Leu[c]	97	69—74 (Et-W)	−25.0 (AcOH)
Lys[b]	94	132—138 (M-E)	−5.0 (AcOH)
Met[b]	100	134—138 (E-PA)	+15.2 (AcOH)
Phe	92	86—88 (E-PA)	−3.9 (AcOH)
Pro	96	136—137 (EA-PA)	−61.1 (AcOH)
Sar	87	89—90 (EA-PA)	
Ser[d]	85	90—93 (E-PA)	−4.9 (AcOH)
Ser (O-Bzl)	94	55—58 (E-PA)	+22.5 (EtOH)
Thr	90	74—77 (E-PA)	−7.3 (AcOH)
Trp	100	137—139 (EA-PA)	−22.9 (AcOH)
Tyr[b]	99	205—208 (M-E)	+3.8 (AcOH)
Tyr(O-Bzl)	95	109—111 (E-PA)	+16.6 (MeOH)
Val	98	77—79	−6.3 (AcOH)

a) All products were characterized by elementary analyses.
b) Dicyclohexylammonium salt.
c) Monohydrate.
d) Hemihydrate.
e) Abbreviations: E=ether; PA=petroleum ether; M, MeOH=methanol; EA=ethyl acetate; W=water; Py=pyridine; Et, EtOH=ethanol; AcOH=acetic acid; DMF=dimethylformamide.

Table 5. Synthesis of Z(OMe)-amino acid derivatives

Amino acid derivative[a]	Yield (%)	Mp (°C) (Solvent)[c]	$[\alpha]_D^{20}$(*c*, 1)
Ala	95	80—82 (EA–PA)	−12.2 (AcOH)
Arg(NO_2)	97	149—150 (M–E–PA)	−5.3 (MeOH)
Asp	82	125—127 (EA–PA)	+9.7 (AcOH)
Asn	80	160—163 (W)	−5.5 (MeOH)
Cys(S–Bzl)	94	90—92 (EA–PA)	−52.6 (MeOH)
Glu	100	114—116 (EA–PA)	−7.1 (AcOH)
Gln	90	146—147 (W)	−10.0 (MeOH)
Gly	100	96—98 (EA–PA)	
His(N^{Im}–Bzl)	97	203—206 (W)	+6.8 (AcOH)
Ileu	95	63—65 (E–PA)	+8.1 (EtOH)
Leu[b]	99	156—160 (M–E)	−6.9 (MeOH)
Met	99	74—75 (EA–PA)	−23.8 (MeOH)
Phe	93	90—91 (E–PA)	+6.4 (AcOH)
Pro[b]	98	145—148 (M–PA)	−23.7 (MeOH)
Ser	82	98—100 (EA–PA)	+6.7 (AcOH)
Ser(O–Bzl)	80	72—74 (E–PA)	+15.4 (EtOH)
Thr[b]	96	175—177.5 (M–E)	+7.7 (MeOH)
Trp	98	114—116 (EA–PA)	+3.5 (AcOH)
Tyr[b]	94	122—124 (M–E)	+26.7 (MeOH)
Val	99	62—64 (E–PA)	+9.8 (DMF)

a) All products were characterized by elementary analyses.
b) Dicyclohexylammonium salt.
c) Abbreviations: The same as in Table 4.

carbonate (21%) shown in Table 1. Aqueous dioxane and dimethylformamide were rather more superior to other aqueous solvents, and a 10 hr reaction at 30—35°C gave the highest yield of the product shown in Table 2. As shown in Table 3, a five hours reaction gave 79% yield at a temperature of 15—20°C, 99% yield at 30—35°C.

On the bases of these experiences, the standard condition adopted for the reaction between amino acids and IV involved the use of triethylamine and aqueous dioxane or dimethylformamide at 30—35°C or room temperature for overnight. About twenty amino acids were examined and the yields of Boc-amino acids were consistently good as shown in Table 4.

Z(OMe)-amino acids were prepared from V and free amino acids by the same method as described for Boc-amino acids. The products obtained were shown in Table 5.

Experimental

Melting points were all determined in a Yanagimoto electric micromelting point apparatus and are uncorrected, and optical rotations were measured with a JASCO automatic polarimeter DIP-SL. All amino acids were L-configuration in this report.

4,6-Dimethylpyrimidyl-2-thiol Chloroformate (III). A solution of 128 g (3.2 mol) of sodium hydroxide in 600 ml of water was mixed with 420 g (3.0 mol) of I, and the resulting mixture was heated to completely dissolve the I and then allowed to cool. The resulting solution was charged into 15 l of acetone, whereby a sodium salt of I was precipitated. The precipitated sodium salt was recovered by filtration and then dried at 120°C for 24 hr to obtain 462 g (95%). Subsequently, 324 g (2.0 mol) of the above-mentioned sodium salt (II) was added as it was, *i.e.* in the form of solid to 1185 g of petroleum ether, and to the resulting suspension was added to 297 g of phosgene (3.0 mol) at −15——10°C, and the mixture was reacted with stirring at room temperature for 4 hr. After completion of the reaction, excess phosgene was removed by evaporation at 40—50°C while injecting nitrogene into the reaction liquid. Thereafter, the precipitate formed was filtered and then the petroleum ether was removed by evaporation *in vacuo*, to obtain about 365 g of III in crude yield of 90%.

t-*Butyl* S-*4,6-Dimethylpyrimidin-2-ylthiolcarbonate (IV).* Into a solution of 267 g (3.6 mol) of *t*-butyl alcohol in 752 g of pyridine was dropped under stirring and cooling to −5—0°C 364 g (1.9 mol) of the crude III, and the resulting mixture was reacted at 20—25°C for 3 hr. After completion of the reaction, deposited pyridine hydrochloride was separated by filtration, and the filtrate was charged with 2000 ml of water and then extracted 3 times each with 800 ml of petroleum ether. The petoleum ether layer was sufficiently washed with a cold 1N aqueous hydrochloric acid solution, washed twice with a saturated aqueous sodium chloride solution and dried over anhydrous sodium sulfate, and then the petroleum ether was evaporated under reduced pressure, wherby the crystal was obtained. The crystal was washed with a small amount of cold *n*-heptane and then dried to obtain 274—319 g (60—70%) of IV. Mp 50—51°C.

Found: C, 54.88; H, 6.64; N, 11.57; S, 13.29%. Calcd for $C_{11}H_{16}O_2N_2S$: C, 54.98; H, 6.71; N, 11.66; S, 13.34%.

p-*Methoxybenzyl* S-*4,6-Dimethylpyrimidin-2-ylthiolcarbonate (V).* 244 g (2.2 mol) of *p*-methoxybenzyl alcohol and 167 g (2.1 mol) of pyridine were dissolved in 2600 ml of ether. Into the resuting solution was dropped under stirring and cooling to −5—0°C 324 g of the crude III obtained in the above-mentioned procedure, and the resulting mixture was reacted at room temperature for 3 hr. After completion of the reaction, the reaction liquid was once with cold water, twice with a 1N aqueous citric acid solution or a 1N aqueous hydrochloric acid solution cooled to 0°C and a saturated aqueous sodium chloride solution, and dried over anhydrous sodium sulfate and then the ether was evaporated *in vacuo* to obtain 340—388 g (70—80%) of the pale yellow crystal of V. Mp 58—60°C (recrystallized from ether–petroleum ether).

Found: C, 58.98; H, 5.31; N, 9.22; S, 10.48%. Calcd for $C_{15}H_{16}O_3N_2S$: C, 59.19; H, 5.30; N, 9.20; S, 10.54%.

t-*Butyloxycarbonyl Amino Acids and* p-*Methoxybenzyloxycarbonyl Amino Acids (General Method).* 0.10 mol of amino acid

and 0.15 mol (21 ml) of triethylamine were added to 55 ml of water. To the resulting mixture of 0.11 mol of IV or V in 55 ml of dioxane or dimethylformamide, and then the mixture was reacted under stirring at room temperature for several hours. (2—24 hr) After completion of the reaction 150 ml of water was added to the reaction mixture, and unreacted carbonate was extracted twice with 200 ml of ethyl acetate. Subsequently, the aqueous layer was cooled to 0°C and adjusted to pH 2 by addition of a 5N aqueous hydrochloric acid cooled to 0°C, and then extracted once with 150 ml of ethyl acetate and twice with 80 ml of ethyl acetate. Thereafter, the ethyl acetate layers were united together, washed thrice with 100 ml of a 5% aqueous hydrochloric acid cooled to 0°C, and twice with 100 ml of a saturated aqueous sodium chloride solution and dried over anhydrous sodium sulfate (if necessary, using active carbon for decolorization.) and then the ethyl acetate was evaporated *in vacuo*, the resulting solid was recrystallized from the solvent indicated in Tables 4 and 5.

The preparations of Boc-aspagine, Boc-N^{im}-benzylhistidine, Boc-serine, and Boc-threonine were different from the general method in the following parts.

Boc-asparagine. In this procedure, an aqueous layer adjusted to pH 2 was allowed to stand overnight in a cold place (0—5°C) instead of extraction from ethyl acetate, whereby the crystal was deposited. The crystal was recovered by filtration and then washed with cold water to obtain 19.0 g (81.9%) of Boc-asparagine. Mp 175—177°C $[\alpha]_D^{20} = -7.2°$ (*c* 1, DMF).

*Boc-*N^{im}*-benzylhistidine.* This compound was similarly prepared in Boc-asparagine except the following part. In this procedure, pH of an aqueous layer was adjusted to pH 5.4 by acetic acid instead of adjusting pH 2 by a cooled 5N aqueous hydrochloric acid. Yield 33.9 g (98.3%). Mp 180—182°C. $[\alpha]_D^{20} = +24.8°$ (*c* 1, methanol).

Boc-serine. After the aqueous layer was adjusted to pH 2 by addition of a cooled 5N aqueous hydrochloric acid, sodium chloride was added to this mixture. Thereafter, the ethyl acetate layer were united together, washed thrice with 100 ml of a cooled 5% aqueous hydrochloric acid saturated by sodium chloride and dried over anhydrous sodium sulfate and decolorized with active carbon and evaporated *in vacuo* to obtain 17.3 g (84.6%). Mp 90—93°C. $[\alpha]_D^{20} = -4.9°$ (*c* 1, acetic acid).

Boc-threonine was similarly prepared in above described procedure.

BULLETIN OF THE CHEMICAL SOCIETY OF JAPAN, VOL. 46, 1272—1275 (1973)

Quantitative Estimation of the Fehling Reaction of 1-*O*-Protected Uronic Acids

Juji YOSHIMURA, Jun-ichi HASHIMOTO, and Hiroaki ANDO

Laboratory of Chemistry for Natural Products, Faculty of Science, Tokyo Institute of Technology, Ookayama, Meguro-ku, Tokyo

(Received November 8, 1972)

Quantitative estimation of the Fehling reaction of 1-*O*-protected uronic acid derivatives showed that the reducing power of 1-*O*-protected hexofuranuronic acid derivatives corresponds to 23—37% of that of D-glucose. The presumption that the reducing ability might be attributed to the formation of unsaturated *aldehydo*-sugars by removal of the 1-*O*-protecting group through a cupric ion-catalyzed β-elimination was supported by the fact that 2,5-dimethoxy-6-oxo-2,4-hexadienoic acid was formed by alkaline β-elimination of methyl (methyl 2,3,5-tri-*O*-methyl-α-D-glucofuranosid)uronate.

Fehling-negative charactor of *O*-glycosides has been generally recognized in the carbohydrate chemistry for a long time, and only exceptionally, the positive[1-4] or negative[1,4-6] properties of several 1-*O*-protected-D-glucuronic acid derivatives were marked by several researchers. In a previous paper,[7] we have examined qualitatively the Fehling test of nineteen kinds of 1-*O*-protected uronic acid derivatives, and found that hexofuranuronic acids having a hydrogen atom at *C*-5 position were positive, while, pentofuranuronic, hexopyranuronic, and heptofuranuronic acids were negative. The formation of unsaturated aldehydes by removal of the 1-*O*-protecting groups through cupric ion-catalyzed β-elimination was deduced to be responsible for the exposed reducing ability. In this paper, the reducing power was quantitatively estimated and an evidence for the proposed β-elimination was obtained.

Results and Discussion

In addition to the reported thirteen examples,[7] following hexofuranuronic acid derivatives showed again the positive Fehling test: *i.e.*, 5-*O*-acetyl,[4] 5-*O*-tosyl,[8] and 5-bromo-5-deoxy[9] derivatives of 1,2-*O*-isopropyli-

1) W. F. Goebel and F. H. Barber, *J. Biol. Chem.*, **110**, 707 (1935).
2) E. M. Osmann, K. C. Hobbs, and W. E. Walston, *J. Amer. Chem. Soc.*, **73**, 2726 (1951).
3) H. Weidmann, *Ann. Chem.*, **679**, 178 (1964).
4) H. Weidmann, *Monatsch. Chem.*, **96**, 766 (1965).
5) S. Saneyoshi, *Biochem. Z.*, **36**, 22 (1911).
6) F. Smith, *J. Chem. Soc.*, **1944**, 584.
7) H. Ando, K. Ajisaka, J. Hashimoto, and J. Yoshimura, *Nippon Kagaku Kaishi*, 1161 (1972).
8) L. D. Hall, L. Hough, and R. A. Pritchard, *J. Chem. Soc.*, **1961**, 1537.
9) M. Ishidate, M. Kimura, and M. Kawata, *Chem. Pharm. Bull.* (Tokyo), **11**, 1083 (1963).

dene-α-D-glucofuranurono-6,3-lactone; 3,5-di-*O*-methyl,[10] 3,5-di-*O*-acetyl,[11] 5-*O*-acetyl[11] derivatives of methyl 1,2-*O*-isopropylidene-α-D-glucofuranuronate; 1,2-*O*-isopropylidene-α-D-glucofuranuronic acid,[12] its hydrazide (**1**), and 5-*O*-*p*-tosyl amide (**2**); (methyl β-D-glucofuranosid)urono-6,3-lactone (**3**),[12] its 2,5-di-*O*-methyl derivative (**4**),[12] and the α-anomer (**5**)[6] of **4**; methyl (methyl 2,3,5-tri-*O*-methyl-α-D-glucofuranosid)uronate (**6**),[6,13] 3-acetamido-3-deoxy-1,2-*O*-isopropylidene-α-D-allofuranuronic acid (**7**), and 5-bromo-5-deoxy-1,2-*O*-isopropylidene-α-D-idofuranurono-6,3-lactone.[9]

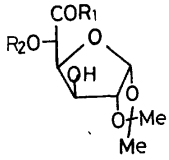

(**1**) R_1=$NHNH_2$; R_2=H
(**2**) R_1=NH_2; R_2=Ts

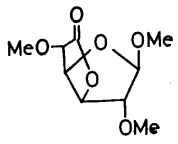

(**4**)

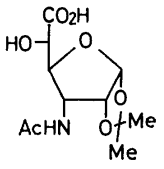

(**7**)

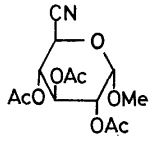

(**8**)

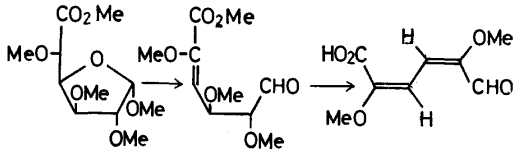

(**6**)

Scheme 1

On the other hand, quantitative estimation of (methyl 2,3,4-tri-*O*-acetyl-α-D-glucopyranosid)urononitrile (**8**), (benzyl 2-acetamido-2-deoxy-α-D-mannopyranosid)-uronic acid,[14] and (benzyl 2-acetamido-2-deoxy-α-D-glucopyranosid)uronamide (**9**),[15] in addition to previously reported Fehling-negative compounds, disclosed that the compound **9**, 1,2: 3,4-di-*O*-isopropylidene-α-D-galactopyranuronic acid (**10**),[16] and methyl (methyl α-D-galactopyranosid)uronate (**11**)[17] have a weak reducing ability.

Among the tested compounds, **1**, **2**, **4**, **7**, and **8** were newly prepared from suitable starting materials, respectively. An attempted esterification of **5** in methanolic hydrogen chloride gave **4** in 46% yield, consisting

10) K. Heyns and W. Bultes, *Chem. Ber.*, **99**, 3477 (1966).
11) M. Ishidate, Z. Tamura, and T. Kinoshita, *Chem. Pharm. Bull.* (Tokyo), **10**, 1258 (1962).
12) L. N. Owens, S. Peat, and W. J. G. Jones, *J. Chem. Soc.*, **1941**, 339; C. L. Mehltretter, B. H. Alexander, R. L. Millies, and C. E. Rist, *J. Amer. Chem. Soc.*, **73**, 2424 (1951).
13) R. E. Reeves, *ibid.*, **62**, 1616 (1940).
14) J. Yoshimura, H. Sakai, N. Oda, and H. Hashimoto, This Bulletin, **45**, 2027 (1972).
15) J. Yoshimura, T. Sato, and H. Ando, *ibid.*, **42**, 2352 (1969).
16) H. M. Sell and K. P. Link, *J. Amer. Chem. Soc.*, **60**, 1813 (1938).
17) J. K. N. Jones and M. Stacey, *J. Chem. Soc.*, **1947**, 1340.

Table 1. Reducing powers for the Fehling solution

Compounds	Oxidation-reduction equivalent
D-Glucose	5.55
Ascorbic acid	5.34
Hydrazine sulfate	3.45
Paraformaldehyde[a]	1.43
D-Glucofuranurono-6,3-lactone	5.95
1,2-*O*-Isopropylidene-[4]	1.37
3	2.04
4	1.40
5	0.46
1,2-*O*-Isopropylidene-α-D-gluco-furanuronamide[12]	1.41
5-Deoxy-, hydrazide[7]	4.86 (1.41)[b]
3,5-Di-*O*-acetyl, nitrile[3]	1.16
1	4.89 (1.44)[b]
6	0.35
(Benzyl β-D-mannofuranosid)urono-6,3-lactone[7]	1.55
(Benzyl β-D-mannofuranosid)uronamide[7]	1.32
Hydrazide[7]	4.25 (0.80)[b]
7	1.27
Pectin[a]	0.97
9	0.43
10	0.40
11	0.50

a) These compounds were treated as the monomers.
b) Values in parentheses present that diminished the reducing power of the hydrazide moiety.

with the fact that the predominant anomer in the Fischer glycosidation of D-glucurono-6,3-lactone was β-form.[2] This anomerization implies the repulsion between C_1- and C_2-methoxy groups and an anomeric effect[18] in the α-furanose ring. The favorable conformation of **4** was deduced to be flattened T^2_3 from the NMR spectrum[19] (*cf.* Experimental section).

Quantitative estimation was carried out by the Bertrand method after refluxing for ten min, and the reducing powers were presented as oxidation-reduction equivalents (Table 1). These values of D-glucose and D-glucurono-6,3-lactone are reasonable compared with those reported.[20] Excepting fully *O*-methylated derivatives (**4** and **6**), all hexofuranuronic acid derivatives showed 23—37% reducing power of that of D-glucose. The facts that D-glucofuranuronic acid derivatives showed almost a constant reducing power and that there is an apparent difference between anomers (**4** and **5**) indicate that the reducing abilities depend on the configuration of the substrates. Lichtmyer and Hudson[21] reported that even enantiomers (D- and L-altrose) showed a different reducing power for the Fehling solution. Therefore, coordination of substrates to L-(+)-tartaric acid–Cu (II) complex will be the

18) J. D. Stevens and H. G. Fletcher, Jr., *J. Org. Chem.*, **33**, 1799 (1968).
19) R. J. Abraham, L. D. Hall, L. Hough, and K. A. McLauchlan, *J. Chem. Soc.*, **1962**, 3699.
20) G. Klein, "Handbuch der Pflanzenanalyse" II. Spezielle Analyse, Wien (1932), p. 786.
21) N. K. Richtmyer and C. S. Hudson, *J. Amer. Chem. Soc.*, **58**, 2540 (1936).

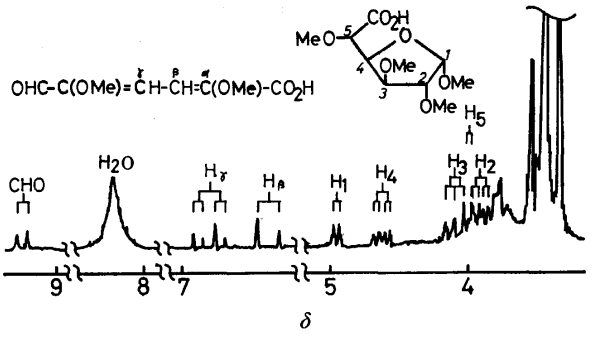

Fig. 1. NMR spectrum of the elimination products of **6** in $CDCl_3$.

first step in this oxidation-reduction, and then proceeds *via* two steps; *i.e.*, oxidation of the resulted complex with oxygen or the complex-catalyzed oxidation of substrate, as was depicted by Singh *et al.*[22]

On the other hand, no substantial change was observed in the NMR spectrum of 1,2-*O*-isopropylidene-α-D-glucofuranurono-6,3-lactone in 0.7M-sodium hydroxide at 55°C for 1 hr,[7] however, it is known that methyl (methyl α-D-glucopyranosid)uronates undergo *t*-butoxide-catalyzed β-elimination to give the corresponding 4-enoses, and the fully *O*-methylated derivative give a higher yield than others.[23] Examination of the product of such a β-elimination of **6** indicated the formation of 2,5-dimethoxy-6-oxo-2,4-hexadienoic acid in UV (λ_{max} 280 nm) and NMR (Fig. 1) spectra. The appearance of aldehyde proton (δ 9.15; d, J= 7.3 Hz) and two olefinic proton signals (δ 6.81; q, J=7.3 and 16 Hz, and δ 6.38; d, J=16 Hz) supported the structure and configuration of the product shown in Scheme 1. A similar examination of methyl 1,2-*O*-isopropylidene-3,5-di-*O*-methyl-α-D-glucofuranuronate showed λ_{max} 295 nm in UV and the appearance of one olefinic proton (δ 6.20; d, J=10.6 Hz) in NMR spectrum, but aldehyde proton signal could not be detected. Thus, it was proved that the β-elimination of hexofuranosiduronic acids gave unsaturated aldehydes, accompanying with liberation of 1-*O*-protecting groups.

On the reason for the weak reducibility of a few hexopyranuronic acids (**9**—**11**), examination of the Fehling test of 4-enoses might give some suggestions, and moreover, it will be worthy to note that the reaction is also stereospecific.

Experimental

All melting points are uncorrected. The solutions were evaporated under diminished pressure at a bath temperature not exceeding 45 °C. Specific rotations were measured in a 0.5-dm tube, with a Carl Zeiss LEP-A1 Polarimeter. The IR spectra were recorded with a Hitachi Model EPI-G2 grating IR spectrophotometer. The NMR spectra were taken in deuteriochloroform with a JNM-4H-100 MHz Spectrometer using tetramethylsilane as an internal standard. Chemical shifts and coupling constants were recorded in δ and Hz units, and frequencies in cm^{-1}.

1,2-O-Isopropylidene-α-D-glucofuranuronohydrazide (1). A solution of 1,2-*O*-isopropylidene-α-D-glucofuranurono-6,3-lactone (5.0 g) in hydrazine (5 ml) was refluxed for 1 hr, and evaporated to give a syrup which was crystallized from ethanol–petroleum ether. Yield, 3.2 g (56%); mp 143—146 °C; $[\alpha]_D^{23}$ −13.0° (*c* 1.08, water). IR: 3400—3300 (OH), 3220—3100 (NH), 1670 and 1520 (CONH), 1615 (NH_2), 1380—1370 (C-CH_3).

Found: C, 43.31; H, 6.17; N, 11.20%. Calcd for $C_9H_{16}N_2O_6$: C, 43.54; H, 6.50; N, 11.29%.

1,2-O-Isopropylidene-5-O-(p-tosyl)-α-D-glucofuranuronamide (2). To a suspended solution of 1,2-*O*-isopropylidene-5-*O*-(*p*-toluenesulfonyl)-α-D-glucofuranurono-6,3-lactone[7] (4.5 g) in methanol (100 ml) was added at −50 °C saturated methanolic ammonia (70 ml), and the resulted solution was kept at this temperature for 1.5 hr, neutralized with 60% acetic acid, evaporated to 15 ml, and then extracted with chloroform. Evaporation of the extracts gave a syrup from which crystals (250 mg, 5%) was obtained by standing the ether solution overnight in a refrigerator. Mp 155—157 °C; $[\alpha]_D^{23}$ +19.4° (*c* 0.99, acetone); IR: 3400 (OH), 3370—3180 (NH_2), 1680 and 1540 ($CONH_2$), 1585, 670, and 760 (benzene).

Found: C, 49.34; H, 5.21; N, 3.49; S, 8.36%. Calcd for $C_{16}H_{21}NO_8S$: C, 49.61; H, 5.47; N, 3.62; S, 8.28%.

(Methyl 2,5-di-O-methyl-β-D-glucofuranosid)urono-6,3-lactone (4). A solution of the α-anomer of **4**[6] (0.3 g) in methanolic hydrogen chloride (5%, 5 ml) was refluxed for 1 hr, and evaporated to give a syrup which was crystallized by standing overnight its methanol solution in a refrigerator. Yield, 46% (139 mg); mp 95.5—97 °C; $[\alpha]_D^{23}$ −19.1° (*c* 1.00, chloroform). IR: 1790 (lactone); NMR: 5.02 (H_1; s, $J_{1,2}\approx 0$), 4.99 (H_4; q, $J_{3,4}$=4.9, $J_{4,5}\approx$6.4), 4.85 (H_3; d, $J_{2,3}\approx 0$), 4.03 (H_5; d), 3.91 (H_2; s), 3.66 (OMe), 4.45 and 4.36 (2×C-CH_3).

Found: C, 49.25; H, 6.49%. Calcd for $C_9H_{14}O_6$: C, 49.54; H, 6.47%.

3-Acetamido-3-deoxy-1,2-O-isopropylidene-α-D-allofuranuronic acid (7). To a suspended solution of 3-acetamido-3-deoxy-1,2-*O*-isopropylidene-α-D-allofuranose[24] (4.8 g, 14 mmol) and platinum-charcoal (10%, 6 g) in water (150 ml) was bubbled oxygen in the rate of 10 ml/sec, under adjusting the pH at 7—7.8 with aqueous sodium bicarbonate (8%). When calculated amount of alkali was consumed, the solution was filtered, and the filtrate was evaporated to give a syrup. A solution of the syrup in acetone–water (1:1 in v/v, 300 ml) was treated four times with IR-120 (30 ml, H-form), and evaporated to give a syrupy product. Yield, 3.65 g (72%); $[\alpha]_D^{23}$ +48.8° (*c* 1.00, methanol); IR: 3350 (OH), 3100 (NH), 1725 (COOH), 1640 and 1550 (NHCO).

Found: C, 47.75; H, 6.40; N, 4.81%. Calcd for $C_{11}H_{17}NO_7$: C, 48.00; H, 6.23; N, 5.09%.

(Methyl 2,3,4-tri-O-acetyl-α-D-glucopyranosid)urononitrile (8). A solution of (methyl 2,3,4-tri-*O*-acetyl-α-D-glucopyranosid)-uronamide[25] (3.32 g, 10 mmol) and *p*-tosyl chloride (5.7 g, 30 mmol) in pyridine (15 ml) was heated at 80 °C for 3 hr, and then poured into ice-water. The precipitate was filtered and recrystallized from methanol. Yield, 70% (2.19 g); mp 156—157 °C; $[\alpha]_D^{23}$ +140° (*c* 0.4, methanol); IR: 1755 (ester).

Found: C, 49.38; H, 5.32; N, 4.37%. Calcd for $C_{13}H_{17}NO_8$: C, 49.52; H, 5.44; N, 4.44%.

This compound was directly obtained from D-glucurono-6,3-lactone in 17% yield, by successive glycosidation, amida-

22) S. V. Singh, O. C. Saxena, and M. P. Singh, *J. Amer. Chem. Soc.*, **92**, 537 (1970).

23) H. Hashimoto, T. Sekiyama, H. Sakai, and J. Yoshimura, This Bulletin, **44**, 235 (1971).

24) H. Ando and J. Yoshimura, *ibid.*, **43**, 2966 (1970).

25) E. Hardegger and D. Spitz, *Helv. Chim. Acta*, **32**, 2165 (1949).

tion, acetylation, and dehydration.

Quantitative Analysis. A mixture of the Fehling solution (A and B, each 25 ml) and sample (20 mg) was boiled for just 10 min, cooled with ice-water, and filtered (Toyoroshi No. 2 filter-paper). Cuprous oxide was dissolved in ferric sulfate solution with boiling, and then the solution was titrated with 0.1M-potassium permanganate. Analysis was repeated two or three times, and blank-test value was reduced from each mean value. Oxidation-reduction equivalent was calculated from the consumed potassium permanganate as follows;

$$\frac{(0.1\text{M-}KMnO_4,\ \text{ml}) \times \text{factor} \times \text{molecular weight}}{(\text{Sample weight, mg})}$$

*Elimination of Methyl (Methyl 2,3,5-tri-*O*-methyl-α-*D*-gluco-furanosid)uronate.* The following sample was used. Bp 63—73 °C/0.017 mmHg (bath temperature, 114—130 °C); $[\alpha]_D^{23}$ +109° (*c* 0.99, chloroform) [lit,[6] +122° (*c* 0.7, water)]; IR: 1740 (ester), 1450—1430 (C–CH_3); NMR: 4.92 (H_1; d, $J_{1,2}$=4.0), 4.52 (H_4; t, $J_{4,5}$=6.3), 4.02 (H_3; t, $J_{3,4}$=6.4), 3.94 (H_5; d), 3.88 (H_2; q, $J_{2,3}$=6.5), 3.77 (CO_2-CH_3), 3.47, 3.45, and 3.41 ($3\times OCH_3$).

A mixed solution of **7** (100 mg) in *t*-butyl alcohol (0.5 ml) and potassium (30 mg) in *t*-butyl alcohol (0.5 ml) was stood for 30 min at room temperature, neutralized with IR-120 (H^+), and evaporated to give a syrup, which was examined with UV and NMR spectrum, as mentioned in the before section.

BULLETIN OF THE CHEMICAL SOCIETY OF JAPAN, VOL. 46, 1275—1278 (1973)

The Reaction of Nitriles with Phosgene. VII.[1] Synthesis of α,β-Unsaturated Isocyanates

Masataka OHOKA, Shozo YANAGIDA, Kenji SUGAHARA, Tetsuo FUJITA, Mitsuo OKAHARA, and Saburo KOMORI

Department of Applied Chemistry, Faculty of Engineering, Osaka University, Yamadakami, Suita, Osaka

(Received December 5, 1972)

The reaction of nitriles with phosgene in the presence of hydrogen chloride was carried out for synthesizing α,β-unsaturated isocyanates. 3-Chloropropionitrile, 2,3-dichloropropionitrile, isobutyronirtile, and 2-chloromethylpropionitrile gave the corresponding α-chloro-α,β-unsaturated isocyanates in moderate yields (27—50%). Propionitrile, *n*-butyronitrile, and 3-phenylpropionitrile gave the corresponding pyrimidines as the major product. 3-Phenylpropionitrile, however, gave the isocyanate as the major product when the amount of benzene as a solvent increased. Reaction pathways to isocyanates and pyrimidines were discussed.

In a previous paper,[1] we reported a new synthesis of styryl isocyanates from arylacetonitriles with phosgene in the presence of hydrogen chloride. We have extended this isocyanate synthesis to variously substituted nitriles to determine its scope and utility for synthesizing α,β-unsaturated isocyanates.

Results and Discussion

Reactions were carried out at 100°C for 5 days in a 80 ml pyrex tube using benzene as a solvent.[2] A mixture of *cis*- and *trans*-α,β-unsaturated isocyanate **2** was formed along with pyrimidine derivative **3** or **4** (Scheme 1). Results are summarized in Table 1.

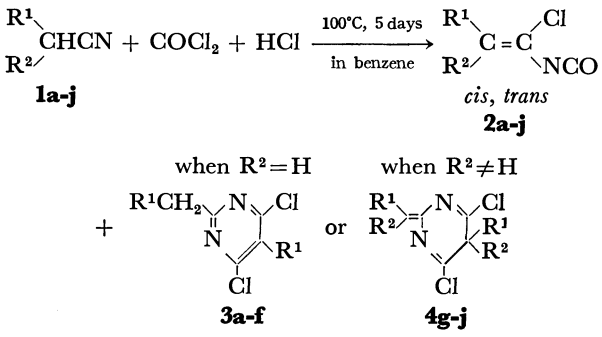

Scheme 1.

1,3-Dichloropropenyl isocyanate (**2e**) and 1,2,3-trichloropropenyl isocyanate (**2g**) were isolated by preparative glpc and were characterized by IR, NMR, and mass spectra and elemental analyses. Other isocyanates were characterized, without isolation, by IR and NMR spectra (Table 2). Their IR spectra showed an isocyanate band at 2255—2260 and a C=C stretching band at 1643—1675 cm^{-1}. Since the isocyanates were usually obtained as a mixture of the starting nitriles and benzene, it was difficult to isolate them by simple distillation. Thus, their yields were determined by NMR spectroscopic methods.

Pyrimidine derivatives **3** and **4** were identified by comparison with authentic samples except for **3c**,[3,4] which was identified by IR, NMR, and mass spectra. We reported that most of these pyrimidines were ob-

1) Part VI: M. Ohoka, S. Yanagida, and S. Komori, *J. Org. Chem.*, **36**, 3542 (1971).

2) Although other aromatic solvents such as toluene and chlorobenzene are preferable for the preparation of isocyanates with high boiling points, such high-boiling solvents are not advantageous for the reaction of a low-boiling nitrile, *e.g.* propionitrile. Thus, benzene was used as the solvent in this investigation.

3) S. Yanagida, T. Fujita, M. Ohoka, R. Kumagai, and S. Komori, This Bulletin, **46**, 299 (1973).

4) Since pyrimidine **4h** is very sensitive to moisture and an analytically pure sample was not obtained,[3] it was identified by its IR spectrum.

Table 1. Synthesis of unsaturated isocyanates[a)]

Run	Nitriles			Yield,[b)] %		Recov.[b)] of nitriles, %
	No	R^1	R^2	Isocyanate	Pyrimidine	
1	**1a**	CH_3	H	13 (**2a**)	50 (**3a**)	12
2	**1b**	C_2H_5	H	8 (**2b**)	38 (**3b**)	
3[c)]	**1c**	i-C_3H_7	H	11 (**2c**)	7 (**3c**)	
4	**1d**	t-C_4H_9	H	trace (**2d**)	0 (**3d**)	92
5	**1e**	$ClCH_2$	H	40 (**2e**)	5 (**3e**)	40
6	**1f**	$C_6H_5CH_2$	H	18 (**2f**)	60 (**3f**)	21
7	**1g**	$ClCH_2$	Cl	27 (**2g**)	5 (**4g**)	52
8	**1h**	CH_3	CH_3	50 (**2h**)	12 (**4h**)	25
9	**1i**	C_2H_5	C_2H_5	14 (**2i**)	trace (**4i**)	81
10	**1j**	$ClCH_2$	CH_3	39 (**2j**)	trace (**4j**)	53
11[d)]	**1f**			31 (**2f**)	14 (**3f**)	51
12[e)]	**1f**			26 (**2f**)	5 (**3f**)	64

a) Reaction conditions are as follows unless otherwise noted. Temperature 100°C, time 5 days, nitrile 35 mmol, HCl 0.5 g (14 mmol), $COCl_2$ 9.5 g (96 mmol), benzene 5 ml.
b) Yields of isocyanates and recoveries of nitriles were determined by NMR.
c) Reaction temperature 150—160 °C, HCl 0.7 g (19 mmol).
d) Benzene 10 ml.
e) Benzene 15 ml.

Table 2. NMR spectra of isocyanates **2**[a)]

Compd	Chemical shift, δ ppm
2a	1.35 (d, 6.8 Hz) and 1.39 (d, 6.8 Hz) (CH_3), 4.93 (q) and 5.11 (q) (H–C=)
2b	4.95 (t, 7.5 Hz) and 5.12 (t, 7.5 Hz) (H–C=)
2c	5.02 (d, 9.9 Hz) and 5.20 (d, 9.0 Hz) (H–C=)
2e	4.08 (d, 8.3 Hz) and 4.12 (d, 8.3 Hz) (total 2 H) (CH_2), 5.46 (t) and 5.66 (t) (total 1 H) (H–C=)
2f	3.55 (d, 7.5 Hz) and 3.38 (d, 7.5 Hz) (total 2 H) (CH_2), 5.33 (t) and 5.53 (t) (total 1 H) (H–C=)
2g	4.35 (s) and 4.38 (s) (CH_2)
2h	1.76 (s) (CH_3)
2j	1.90 (s, 3 H) (CH_3), 4.14 (s, 2 H) (CH_2)
2k	3.55 (d, 2 H, 7.5 Hz) (CH_2), 5.42 (t, 7.5 Hz) and 5.65 (t, 7.5 Hz) (total 1 H) (H–C=)

a) Solvent: **2a**—**c**, benzene; **2e**—**h** and **2j**, CCl_4; **2k**, $CDCl_3$.

tainable in good yields from the reaction of nitrile-HCl 2:2 adducts **5** with phosgene.[3)]

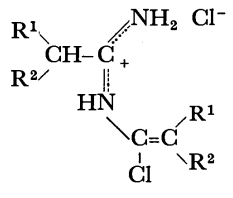

5

3-Chloropropionitrile (**1e**), 2,3-dichloropropionitrile (**1g**), isobutyronitrile (**1h**), and 2-chloromethylpropionitrile (**1j**) gave expected isocyanates in moderate yields (27→50%). However, propionitrile (**1a**), *n*-butyronitrile (**1b**), and 3-phenylpropionitrile (**1f**, run 6) gave expected isocyanates in low yields together with moderate yields (38—60%) of the corresponding pyrimidines. On the other hand, 3-methylbutyronitrile (**1c**), 3,3-dimethylbutyronitrile (**1d**), and 2-ethylbutyronitrile (**1i**) afforded both isocyanates and pyrimidines in very low yields under most recovery of the starting nitriles.

The effect of reaction time and temperature on the yield of isocyanate **2e** was studied (Figs. 1 and 2). As shown in Fig. 1, the yield of **2e** reached a maximum value (*ca.* 40%) after around 5 days, then it gradually decreased and the amount of a resinous substance increased as the reaction time was prolonged. This indicates the existence of equilibria between isocyanate **2e** and starting materials (Scheme 2). The yield of **2e** increased nearly proportionally to temperature giving a maximum value (*ca.* 40%) at around 100°C and then gradually decreased (Fig. 2). Thus, the reaction is optimum at 100°C and for 5 days.

The possible reaction pathways to isocyanates are shown in Scheme 2. The existence of an equilibrium between imidoyl chloride **6** and α-chloroenamine **7** has been proposed by Simchen.[5,6)] In addition, he and his co-workers postulate that the α-chloroenamine rather

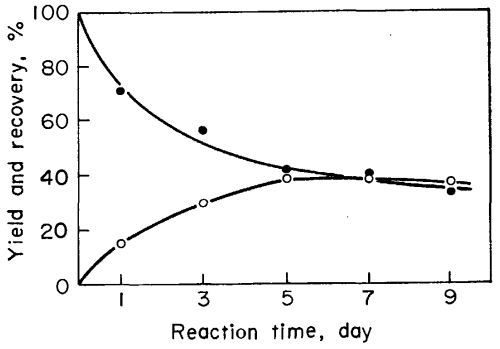

Fig. 1. Effect of reaction time on the yield of isocyanate **2e** and recovery of **1e**: yield of **2e**, ○; recovery of **1e**, ●. Reaction was carried out in 74 ml glass tube. Temperature 100 °C. Amounts of reactants: nitrile **2e** 3.1 g (35 mmol), HCl 0.5 g (14 mmol), $COCl_2$ 9.5 g (96 mmol), benzene 5 ml.

5) G. Simchen and W. Krämer, *Chem. Ber.*, **102**, 3656 (1969).
6) G. Simchen, *ibid.*, **103**, 407 (1970).

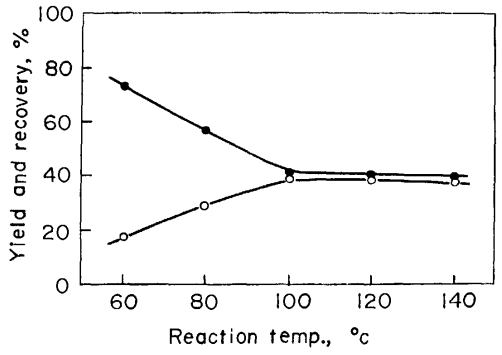

Fig. 2. Effect of reaction temperature on the yield of **2e** and recovery of **1e**: yield of **2e**, ○; recovery of **1e**, ●. Reaction was carried out in 75 ml glass tube. Amounts of reactants are the same as those shown in Fig. 1. Reaction time 5 days.

than the imidoyl chloride is acylated in the intramolecular cyclization of nitriles in the presence of hydrogen chloride.[5-7] However, the phosgenation of benzonitrile *via* imidoyl chloride to *N*-(α-chlorobenzylidene)-carbamoyl chloride **10** was found in our laboratory.[8] Therefore, in our case the phosgenation of both **6** and **7** probably takes place to give carbamoyl chlorides **8** and **9** as intermediates.

$$PhCN + COCl_2 \xrightarrow{HCl} PhC(Cl)=NC(=O)Cl$$

10

The following two paths (a and b) are possible routes to pyrimidines: path a involves a nitrile-HCl 2:2 adduct **5** as an intermediate and path b involves the secondary reactions of isocyanates. The pyrimidine formation *via* path b has been found in the reaction of α-chloro-*p*-nitrostyryl isocyanate with acetonitrile at 60°C in the presence of hydrogen chloride.[1] To clarify the possibility of path b, reactions of isocyanates **2e** and **2f** with some nitriles were carried out.

When **2f** was treated with **1f** in benzene at 100°C for 84 hr in the presence of hydrogen chloride, pyrimidone hydrochloride **11** was obtained in 39% yield along with pyrimidine **3f** (13%). The latter was apparently produced by chlorination of **11** with phosgene formed by the reverse reaction from **2f** (Scheme 2). This clearly indicates that pyrimidines can be formed *via* path b.

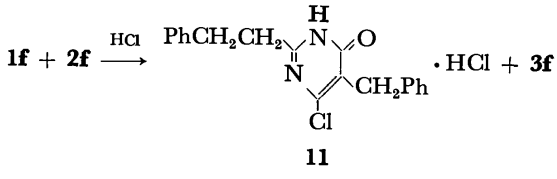

11

On the other hand, the reaction of **2e** with **1e** under similar conditions afforded only pyrimidine **3e** in 13% yield and a trace amount of **2e** was recovered. In addition, the reaction of **2e** with **1a** at 100°C for 3 days in the presence of phosgene and hydrogen chloride did not give **12**, but gave a mixture of **3a** and **3e** (mole ratio 88: 12) and 34% of **2e** was recovered. These facts suggest that the reactivity of isocyanate **2e** toward a nitrile in the presence of hydrogen chloride is lower than that of **2f**.

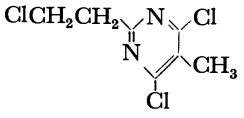

12

Nitrile-HCl 2:2 adducts **5** have been prepared by the reaction of nitriles with hydrogen chloride at 30—60°C using no solvents.[9] To examine whether **5** can also be formed under the reaction conditions or not, the reaction of **1a** with hydrogen chloride was carried out. The reaction at 100°C for 5 days resulted in the recovery of the starting materials. From these facts, pyrimidines are assumed to be formed mainly *via* path b. Since **5** might be formed as a labile intermediate even at 100°C, the pyrimidine formation *via* path a can not be neglected.

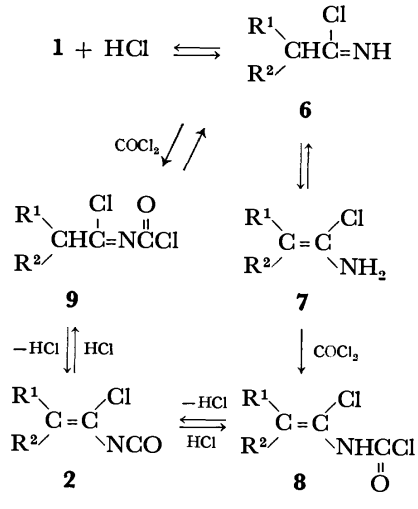

Scheme 2

The yields of isocyanates decreased as the number of β-hydrogens of nitriles decreased by methyl or chlorine substitution (run 3→4, 8→9, 8→10), especially 3,3-dimethylbutyronitrile (**1d**) having no β-hydrogens gave only a trace amount of isocyanate **2d**. This suggests that β-hydrogens stabilize the isocyanates by the hyperconjugation with the C=C bond of the isocyanates and shift the equilibria (Scheme 2) to the side of isocyanates. The stabilization of unsaturated isocyanates by the conjugation with aromatic rings has been observed in the synthesis of styryl isocyanates.[1] Since 2-ethylbutyronitrile (**1i**) has four β-hydrogens, it is expected to give good yield of isocyanate **2i**. However, the yield of **2i** as well as **4i** were low (run 9), indicating that the equilibria shifted to the side of the imidoyl chloride or the starting nitrile. The reason for this shift of the equilibria is not clear at present.

Whereas **1e** gave the isocyanate in good yield, **1a**, **1b**, and **1f** (run 6) gave the corresponding isocyanates in low

7) G. Simchen, *ibid.*, **103**, 389 (1970).

8) S. Yanagida, H. Hayama, M. Yokoe, and S. Komori, *J. Org. Chem.*, **34**, 4125 (1969).

9) S. Yanagida, T. Fujita, M. Ohoka, I. Katagiri, and S. Komori, This Bulletin, **46**, 292 (1973).

yields together with pyrimidines as the major products; this is explained by considering the difference in the reactivity of isocyanates toward nitriles. In the former case only a small amount of **2e** is consumed for the pyrimidine formation *via* path b because of its low reactivity and in the latter cases a considerable amount of the isocyanates is consumed for the pyrimidine formation.

When the amount of benzene as a solvent was increased (run 6→11→12), the yield of pyrimidine **3f** decreased dramatically and that of isocyanate **2f** increased as a result of suppression of path a or b by dilution.

The low yields of pyrimidines in run 7, 8, and 10 are reasonably ascribed to steric hindrance in the formation of **5** (path a) and **13** (path b).

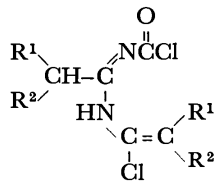

13

As a conclusion, it is essential for obtaining isocyanates exclusively to substitute the nitriles by such substituents that not only stabilize the C=C bond of isocyanates but also suppress both the further reactions of once formed isocyanates and the dimerization of nitriles to **5**, or to dilute the reaction system by a solvent.

Experimental

NMR spectra were obtained using a JNM-G-60 spectrometer (Japan Electron Optics Laboratory Co.) with tetramethylsilane as an internal reference. IR spectra were recorded on a Japan Electronic IR-E spectrophotometer. Mass spectra were recorded on a Hitachi RMU-6E spectrometer. Preparative glpc was carried out with a Yanagimoto G-8 gas chromatograph.

General Procedure. In a 80 ml Pyrex tube was placed 35 mmol of a nitrile and 0.5 g (14 mmol) of anhydrous HCl was dissolved in it; then a solution of 9.5 g (96 mmol) of $COCl_2$ in 5 ml of benzene was added to the mixture. The tube was stoppered, chilled in dry ice–acetone and sealed carefully. It was placed in a 300 ml stainless autoclave containing 70 ml of *n*-hexane and heated at 100°C in an oil bath; *n*-hexane was added to avoid burst of the tube by exerting external pressure. After 5 days the tube was chilled in dry ice–acetone and opened carefully. After $COCl_2$ and HCl were purged, the reaction mixture was distilled at ordinary or under reduced pressure to give a mixture of the objective isocyanate, the starting nitrile, and benzene. The yield of isocyanate and the recovery of nitriles were determined by NMR. Pyrimidines were obtained by distillation or by extraction of the distillation residue of isocyanates with CCl_4.

*Isolation of Pure Isocyanate **2e** and **2g** by Preparative glpc.* Isolation of **2e** and **2g** was carried out using a column (14 mmϕ×150 cm) packed with dioctyl sebacate (7%) on Diasolid L (60—80 mesh) (column temp. 80°C, carrier gas H_2) and a column (14 mmϕ×75 cm) packed with dioctyl sebacate (7%) on Diasolid L (60—80 mesh) (column temp. 100°C, carrier gas H_2), respectively. 1,3-Dichloropropenyl isocyanate (**2e**), IR (liquid film), 2260 (NCO) and 1655 cm^{-1} (C=C); mass spectrum (70 eV) *m/e* (rel. intensity), 151 (17, M^+), 116 (100, M^+–Cl), 88 (8), 63 (38), and 52 (24). (Found: C, 31.62; H, 1.93; N, 9.05%. Calcd for $C_4H_3Cl_2NO$: C, 31.61; H, 1.99; N, 9.23%). 1,2,3-Trichloropropenyl isocyanate (**2g**), IR (liquid film), 2260 (NCO) and 1643 cm^{-1} (C=C); mass spectrum (70 eV) *m/e* (rel. intensity), 185 (23, M^+), 150 (100), 63 (56), and 49 (100). (Found: C, 25.86; H, 1.03; N, 7.79%. Calcd for $C_4H_2Cl_3NO$: C, 25.77; H, 1.03; N, 7.51%).

*4,6-Dichloro-1-isobutyl-5-isopropylpyrimidine (**3c**).* The distillation residue of run 3 was chromatographed on silica gel; *n*-hexane eluted **3c** (colorless liquid), IR (liquid film), 1548, 1500, 1408, 1297, and 800 cm^{-1}; NMR (CCl_4), δ 1.00 (d, 6H, J=6.4 Hz), 1.44 (d, 6H, J=6.8 Hz), 2.05—2.78 (m, 3H), and 3.47 (sep, 1H, J=6.8 Hz); mass spectrum (70 eV) *m/e* (rel. intensity), 246 (15, M^+), 231 (36), 204 (100), and 189 (48).

*Reaction of **2f** with **1f** in the Presence of HCl.* In a 30 ml glass tube was placed a mixture of **2f** (1.1 g, 5.7 mmol) and **1f** (1.4 g, 11 mmol), then anhydrous HCl (0.4 g, 11 mmol) was dissolved in it followed by addition of 2 ml of benzene. The tube was sealed and heated at 100°C for 84 hr. After HCl was purged, the precipitate formed was filtered, washed with a small amount of benzene, and dried *in vacuo* to give tan powder of pyrimid one hydrochloride **11** (0.78 g, 39%), IR (Nujol), 1710 and 1630 cm^{-1}. Its crystallization from EtOH gave colorless fine needles of the free base [6-chloro-5-benzyl-2(2-phenylethyl)-4(3*H*)-pyrimidone], mp 224—225°C, IR (Nujol), 1672 and 1595 cm^{-1}; NMR (CF_3COOH), δ 3.32 (complex, 6H), 4.03 (s, 2H), and 7.24 (m, 10H); mass spectrum (70 eV) *m/e* (rel. intensity), 326 (33, M^++2), 324 (100, M^+), 233 (69), and 91 (71). (Found: C, 70.31; H, 5.31; N, 8.46%. Calcd for $C_{19}H_{17}ClN_2O$: C, 70.26; H, 5.28; N, 8.62%).

The solvent was removed from the filtrate, the residual liquid being distilled under reduced pressure to give 1.1 g of **1f** (contained a trace amount of **2f**). The distillation residue was extracted with CCl_4, the solvent being removed to give **3f** (0.25 g, 13%).

*The Reaction of **2e** with **1e** in the Presence of HCl.* A mixture of **2e** (0.9 g, 5.9 mmol), **1e** (1.1 g, 12 mmol), HCl (0.4 g, 11 mmol), and benzene (2 ml) in a 30 ml glass tube was heated at 100°C for 84 hr. After HCl was purged, the resulting dark precipitate (intractable solid) was filtered off. The solvent was removed from the filtrate and the residual liquid was distilled under reduced pressure to give 0.9 g of **1e** (contained a trace amount of **2e**). The distillation residue was extracted with CCl_4, the solvent being removed under reduced pressure to give a yellow liquid of **3e** (0.2 g, 13%).

*Reaction of **2e** with **1a** in the Presence of $COCl_2$ and HCl.* In a 80 ml Pyrex tube were placed 2.0 g of a mixture of **2e** and **1e** [content of **2e**, 1.8 g (12 mmol)] and 1.3 g (24 mmol) of **1a**, then anhydrous HCl (0.8 g, 23 mmol) was allowed to be absorbed in it followed by addition of a solution of $COCl_2$ (7.2 g, 73 mmol) in 5 ml of benzene. The tube was sealed and heated at 100°C in an oil bath. After 3 days the tube was opened and $COCl_2$ and HCl were purged. The reaction mixture was distilled initially at ordinary pressure to give a mixture of **1a**, **2a**, and benzene, then under reduced pressure to give a mixture of **1e** (0.43 g) and **2e** (0.62 g, 34% recovery). The distillation residue contained 0.98 g of **3a** and 0.17 g of **3e**.

Total Syntheses of Antimycin A_3 and Its Diastereomer

Mitsuhiro KINOSHITA, Shinpei ABURAKI, Masao WADA, and Sumio UMEZAWA

Department of Applied Chemistry, Faculty of Engineering, Keio University, Hiyoshi, Kohoku-ku, Yokohama, Kanagawa

(Received December 18, 1972)

Natural antimycin A_3 (**1A**) and its diastereomer (**1B**) were synthesized. By the syntheses, the correlations between configurations of the enantiomeric 2-butyl-4-hydroxy-3-isovaleryloxypentanoic acids present in the dilactone moieties of **1A** and **1B**, and those of natural (+)blastmycinone (+)**7a** and its enantiomer (−)**7a** were confirmed. The absolute configuration of **1B** was also determined.

In the recent papers we reported the total syntheses of dehexyl-deisovaleryloxy-antimycin A_1[1] as a prototype of antimycin A, and a diastereomeric mixture of antimycin A_3.[2] This paper presents the total syntheses of natural antimycin A_3 (**1A**) and its diastereomer (**1B**) (Fig. 1).

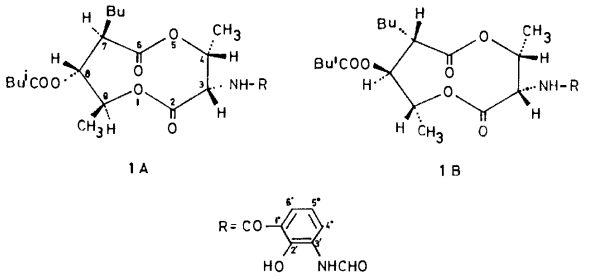

Fig. 1.

The primary structure of antimycin A_3 (blastmycin[3]) which is one of the major components of antimycin A complex was established by van Tamelen, *et al.*,[4] Birch, *et al.*,[5] and Yonehara, *et al.*[6] The absolute configuration for antimycin A_3 was first proposed by Endo and Yonehara[7] in 1967. In their configurational studies, consideration was given to a correlation between the configurations of blastmycin and optically active blastmycinone[6] obtained by saponification of the parent antibiotic and was based on the fact that lithium aluminum hydride reductions of blastmycin and blastmycinone afforded an almostly homogeneous 2-butylpentane-1,3,4-triol,[5] however, the experimental details were not given.

We were interested in the stereochemistry of the unique nine-membered dilactone ring which exists in antimycin A, and in its role playing in biological activity,[8] and attempted to synthesize the natural antimycin A_3 and its diastereomer. After publication of the preliminary report[9] of this paper, we have proposed the revised absolute configuration **1A** of antimycin A_3.[10]

The first important problem in the total synthesis of natural antimycin A_3 was the construction of the nine-membered dilactone ring having the same configuration as that of the natural product. Such a dilactone compound was considered to be obtainable by a lactonization of either type I or III of hydroxyester-acid which is a condensation product of the two kinds of hydroxy acid, *i.e.*, *N*-acyl-L-threonine and 2-butyl-4-hydroxy-3-isovaleryloxypentanoic acid possessing the same configuration as that of the corresponding moiety which exists in the molecule of antimycin A_3.

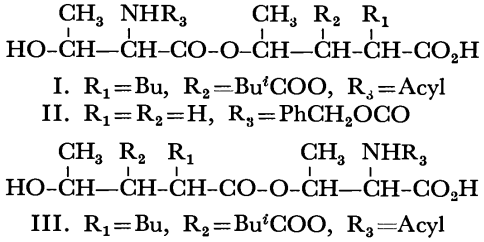

I. R_1=Bu, R_2=Bu^{t}COO, R_3=Acyl
II. R_1=R_2=H, R_3=$PhCH_2OCO$

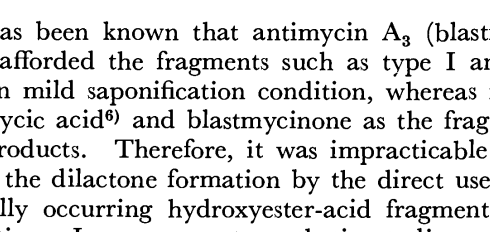

III. R_1=Bu, R_2=Bu^{t}COO, R_3=Acyl

It has been known that antimycin A_3 (blastmycin) never afforded the fragments such as type I and III, even in mild saponification condition, whereas it gave blastmycic acid[6] and blastmycinone as the fragmentation products. Therefore, it was impracticable to examine the dilactone formation by the direct use of the naturally occurring hydroxyester-acid fragment or its derivative. In our recent synthetic studies on antimycins,[1,2] it has already been found that the lactonizations of the synthetic diastereomeric mixtures of the hydroxyester-acid, II and I (R_3=$PhCH_2OCO$), by heating with trifluoroacetic anhydride in benzene afforded the corresponding dilactone compounds in 33 and 6% yields, respectively, only this reagent and reaction condition being effective for these lactonizations. In such a lactonization reaction, the hydroxyester-acids of type I have been considered to be more favorable substrates rather than those of type III, because the absence of free terminal carboxyl group

1) M. Kinoshita and S. Umezawa, This Bulletin, **42**, 854 (1969); *ibid.*, **43**, 897 (1970).
2) M. Kinoshita, M. Wada, and S. Umezawa, *J. Antibiot.* (Tokyo), **22**, 580 (1969).
3) K. Watanabe, T. Tanaka, K. Fukuhara, N. Miyairi, H. Yonehara, and H. Umezawa, *J. Antibiot., Ser. A*, **10**, 39 (1957).
4) E. E. van Tamelen, J. P. Dickie, M. E. Loomans, R. S. Dewey, and F. M. Strong, *J. Amer. Chem. Soc.*, **83**, 1639 (1961).
5) A. J. Birch, D. W. Cameron, Y. Harada, and R. W. Rickard, *J. Chem. Soc.*, **1961**, 889.
6) H. Yonehara and S. Takeuchi, *J. Antibiot., Ser. A*, **11**, 254 (1958).
7) T. Endo and H. Yonehara, Abstracts of Papers, 11th Symposium on The Chemistry of Natural Products (Kyoto), P 269, Sept. 1967.
8) J. S. Reeske, A draft of a review on "Antimycin" which will be published in "Antibiotic," new Ed., by Springer-Verlag Publishers.
9) M. Kinoshita, M. Wada, S. Aburaki, and S. Umezawa, *J. Antibiot.* (Tokyo), **24**, 724 (1971).
10) M. Kinoshita, S. Aburaki, and S. Umezawa, *ibid.*, **25**, 373 (1972).

in the *N*-acyl-L-threonine moiety of I will minimize any danger of the racemization which otherwise as in the case of III, may be caused on the α-carbon atom of the *N*-acylated amino acid unit by the activation of its carboxyl group with trifluoroacetic anhydride at higher temperature, even if α-amino group is protected by an urethan type acyl group such as benzyloxycarbonyl.

The next problem was the synthesis of the natural type of racemic diastereomer of 2-butyl-4-hydroxy-3-isovaleryloxypentanoic acid *t*-butyl ester, which was a useful intermediate for the synthesis of the hydroxy-ester-acids of type I. Of the four racemic diastereomers (**6a**—**6d**) which were prepared by the following synthetic route (Chart 1), the major isomer **6a** was the most promising intermediate, because it could be converted to the natural type (±) blastmycinone **7a**.

The starting material 2-benzyloxypropanal **2** was prepared from methyl 2-benzyloxypropanoate by reduction with diisobutylaluminum hydride.[11] The condensation of this compound with *t*-butyl 2-bromohexanoate **3** was effected smoothly by a modified Reformatsky reaction according to Moriwake[12] using magnesium instead of zinc to yield a mixture of four possible racemic diastereomers of *t*-butyl 4-benzyloxy-2-butyl-3-hydroxypentanoate (**4a**, **4b**, **4c**, and **4d**).

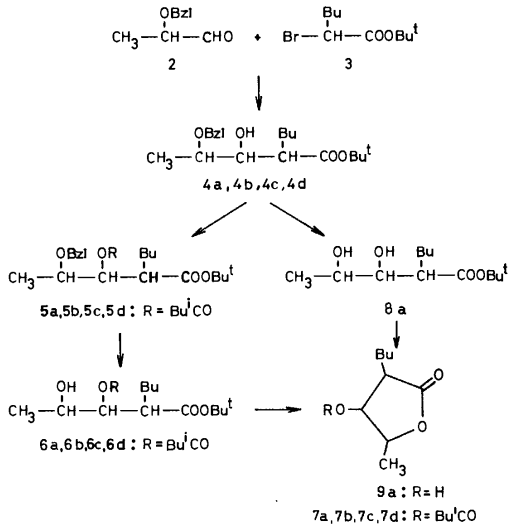

Chart 1.

Preparative isolation of these diastereomers was performed by silica gel column chromatography of the reaction product to give a mixture **4a**+**4b**, **4c**, and **4d** in yields of 43, 12.4, and 6.8% based on **2**, respectively. Repeated column chromatography of fractions containing **4a** and **4b** afforded in a small quantity a homogeneous sample of **4a** and a sample of **4b** contaminated by a trace of **4a**. The samples of **4a** and **4b** showed very similar R_f-values on tlc with several kinds of solvent system, however, their PMR spectra apparently differed in the chemical shifts of *t*-butyl and terminal methyl protons, and this difference was useful for inspection of homogeneity of these diastereomers. Since the preparative separation of **4a** from **4b** by column chromatography was impracticable in this stage, the diastereomeric separation had to be carried over to the next synthetic step.

The mixture **4a**+**4b** obtained above was treated with isovaleric anhydride in pyridine to afford a diastereomeric mixture of *t*-butyl 4-benzyloxy-2-butyl-3-isovaleryloxypentanoate **5a**+**5b**. Column chromatographic separation of the diastereomers was effectively carried out to give **5a** (75%) and **5b** (17%) in homogeneous states, which were identical with the *O*-isovalerylation products derived from the isolated samples of **4a** and **4b**, respectively. These results indicated that the above-mentioned Reformatsky reaction yielded the major diastereomer **4a** with a 56% stereoselectivity.

By the same way other diastereomers, **5c** and **5d** were obtained from **4c** and **4d**, respectively. The four diastereomers, **5a**, **5b**, **5c**, and **5d** were hydrogenolysed over palladium black to afford the corresponding diastereomeric *t*-butyl 2-butyl-4-hydroxy-3-isovaleryloxypentanoates, **6a**, **6b**, **6c**, and **6d**, respectively. In order to determine which diastereomer of the four (**6a**—**6d**) is the objective type of racemic 4-hydroxy-ester, they were converted to the corresponding stable 1,4-lactones, **7a**, **7b**, **7c**, and **7d** by treatment with 5N hydrogen chlorde in dioxane. The resulted structurally homogeneous diastereomeric lactones were readily distinguished by tlc and PMR. From comparison of these lactones with natural antimycin lactone based on tlc, glc, and PMR, it was concluded that the lactone **7a** derived from the major diastereomer **6a** was fortunately the natural type of racemic diastereomer, (±)blastmycinone.

The comparison was first carried out by tlc. The thin-layer chromatogram of natural antimycin lactone obtained from antimycin A complex with a solvent system petroleum ether–diisopropyl ether (7:4) showed a single spot having the same R_f-value as that of **7a**. The comparison by glc was somewhat complicated. The gas chromatogram of **7a** on a polyester succinate column showed a single peak having the same elution time as that of the major peak of natural blastmycinone, which was found in a gas chromatogram of the antimycin lactone. Recently, Yonehara, *et al.*[13] demonstrated by glc that natural blastmycinone is not homogeneous, but it consists of two isomers differing in the structure of the *O*-alkanoyl group. Consequently, our result could confirm that, in the gas chromatogram, the synthetic lactone **7a** shows the same peak with one of the two peaks of so-called blastmycinone and that the peak having longer retention time between the two, corresponds to the blastmycinone possessing isovaleryl group.

The chemical shifts and coupling constants of ring protons, ring methyl and 3-*O*-isovaleryl methyl protons of **7a** were identical with those of natural blastmycinone[14] and antimycin lactone, however, the PMR spectrum in $CDCl_3$ of **7a** showed no doublet at δ 1.15 present in that of the natural lactone. This signal may

11) L. I. Zakharkin, I. M. Khorlina, *Tetrahedron Lett.*, **1962**, 619.
12) T. Moriwake, *J. Org. Chem.*, **31**, 983 (1966).
13) T. Endo and H. Yonehara, *J. Antibiot.* (Tokyo), **23**, 91 (1970).
14) The PMR chart was kindly provided by Prof. H. Yonehara.

be ascribed to the methyl protons of isomeric alkanoyl group in the blastmycinone subcomponent showing the glc peak of shorter retention time. This PMR observation was consisted with the above-mentioned result based on glc. Furthermore, it was confirmed that all the antimycin lactones obtained from antimycin A complex had the same stereochemistry in respect of their lactone rings.

The above stated structural relationship between **7a** and **4a** was also confirmed by an alternative route *via* (±)blastmycinolactol **9a**. Hydrogenolysis of **4a** over palladium black gave *t*-butyl 2-butyl-3,4-dihydroxypentanoate **8a**, which was treated with trifluoroacetic acid. The resulting crystalline hydroxylactone **9a** was *O*-isovalerylated with isovaleric anhydride in pyridine to afford a structurally homogeneous sample of (±)-blastmycinone **7a**. This synthetic route was applied in the syntheses of optically active (+)blastmycinone (+)**7a** and its enantiomer (−)**7a**.

The freshly prepared 4-hydroxyester **6a** was allowed to react with execss amount of *N*-benzyloxycarbonyl-*O*-*t*-butyl-L-threonine in the presence of dicyclohexylcarbodiimide (DCCI) and pyridine at 0°C, to afford a mixture of diastereomeric masked hydroxyester-acids (type I), which was chromatographed on a silica gel column to give optically active homogeneous diastereomers (+)**10A** and (−)**10B** in 29 and 27.7% yields based on **6a**, respectively. It is noteworthy that this step is substantially an optical resolution of the racemic 4-hydroxyester **6a**.

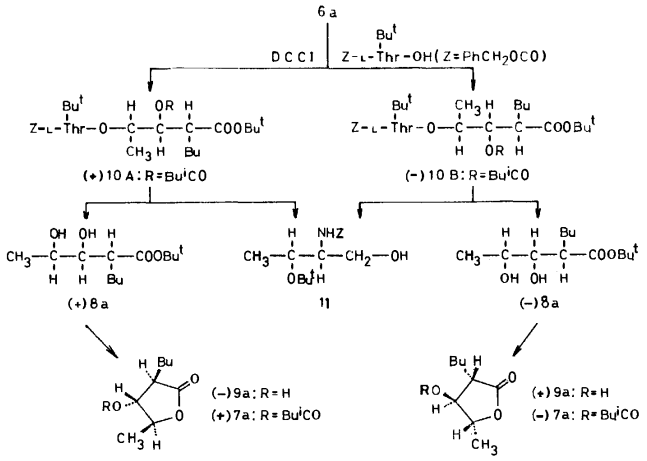

Chart 2.

The configurational assignments of the resolved hydroxyesters present in (+)**10A** and (−)**10B** were undertaken by the following procedure (Chart 2). Selective reduction of (+)**10A** with lithium aluminum hydride at −40°C afforded optically active *t*-butyl (+) 2-butyl-3,4-dihydroxypentanoate (+)**8a** (47.5%) and (−)2-benzyloxycarboxamido-3-*t*-butoxy-1-butanol **11**. De-*t*-butylation of (+)**8a** by the same manner as that of **8a** yielded crystalline (−)blastmycinolactol (−)**9a** with an optical rotation of $[\alpha]_D^{MeOH}$ −18°. Although the rotation of the synthetic specimen was considerably higher than the reported rotation of $[\alpha]_D^{MeOH}$ −5.21° for natural (−)blastmycinolactol[6] obtained from natural (+)blastmycinone, the IR spectrum of (−)**9a** in nujol was very similar to that of natural product.[6] *O*-Isovalerylation of (−)**9a** by the same manner as that of **9a** afforded (+)blastmycinone (+)**7a** with a rotation of $[\alpha]_D^{Chf}$ +10° similar to natural (+)blastmycinone.[6] The PMR spectrum of (+)**7a** was indistinguishable from that of (±)blastmycinone **7a**.

In the same procedure the lithium aluminum hydride reduction of (−)**10B** afforded the enantiomeric dihydroxyester (−)**8a**, from which the corresponding enantiomeric (+)blastmycinolactol (+)**9a** and (−)-blastmycinone (−)**7a** were derived successively.

Recently, we reported in a communication to the editor[10] the absolute configurations of natural (−)-blastmycinolactol and (+)blastmycinone as 2(*R*), 3(*R*), 4(*S*) on the basis of ORD, CD, PMR and through a stereospecific synthesis of the enantiomer (+)**9a** (Chart 2). From these results it was elucidated that (+)**10A** contained an enantiomer of **6a** which had the configuration 2(*R*), 3(*R*), 4(*S*) identical with that of naturally occurring blastmycinone, and that the related racemic diastereomers, **8a**, **6a**, **5a**, and **4a** had a 2,3-*threo*-3,4-*erythro* configuration.

De-*t*-butylation of (+)**10A** with trifluoroacetic acid afforded the desired hydroxyester-acid (type-I, R_3= benzyloxycarbonyl) which was immediately subjected to lactonization. A 0.04M benzene solution of the hydroxyester-acid was heated with about one molar equivalent trifluoroacetic anhydride at 65—70°C for 4 hr. To this mixture additional about one molar trifluoroacetic anhydride was added and was heated at the same temperature for 6 hr. The reaction mixture was immediately evaporated and the residue was chromatographed on a silica gel column to separate fractions containing dilactone compound **12A**. Purification of the crude product by column chromatography afforded **12A** as needles in a 0.8% yield based on (+)**10A**. The compound **12A** was confirmed to be a structurally homogeneous dilactone derivative by elemental analysis, molecular weight determination by mass spectrometry, IR and PMR spectra (Table 1). In this lactonization reaction no other kinds of HBr-ninhydrin positive lactonization product were detected and prolonged heating of the reaction mixture gave rise to a decomposition of **12A** accompanied by rapid formation of some HBr-ninhydrin negative by-products. Attempts to improve the yield of **12A** by use of other kinds of solvent or by changing the quantity of trifluoroacetic anhydride and the reaction temperature were unsuccessful.

On the other hand, the lactonization reaction of the diastereomeric hydroxyester-acid obtained from (−)-

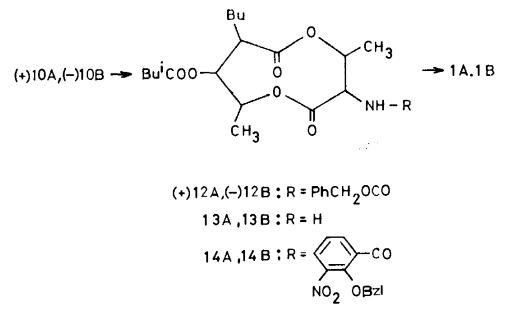

Chart 3.

TABLE 1. PMR-SPECTRA DATA (IN $CDCl_3$). CHEMICAL SHIFTS (δ VALUES) AND COUPLING CONSTANTS (Hz) AT 100 MHz

Compound:	12 A	12 B	14 A	14 B	1 A	Natural antimycin A	1 B
Concentration (*ca.* %)	3	7	3	8	3	3	5
$(C\underline{H}_3)_2CH$	0.96(d)	0.97(d)	0.97(d)	0.97(d)	0.98(d)	0.99(d)	0.99(d)
9-CH_3	1.25(d)[a]	1.30(d)[a]	1.27(d)[a]	1.27(d)[a]	1.29(d)	1.29(d)[a]	1.32(d)[a]
4-CH_3	1.27(d)[a]	1.53(d)[a]	1.09(d)[a]	1.39(d)[a]	1.32(d)	1.32(d)[a]	1.69(d)[a]
H-7	2.46(m)[a]	2.51(m)	2.3—2.6	2.4—2.6	2.54(m)	2.54(m)	2.56(m)
H-9	4.89(dq)[a]	4.75(dq)	4.85(dq)[a]	4.71(dq)	4.96(dq)[a]	4.97(dq)[a]	4.83(dq)
$PhC\underline{H}_2OCO$	5.11(s)	5.11(s)					
H-8	4.8—5.2	5.08(dd)[a]	4.8—5.3	5.16(dd)	5.13(dd)	5.13(dd)[a]	5.14(dd)[a]
H-3	4.8—5.2	4.63(dd)[a]	5.17(dd)	5.11(dd)	5.32(dd)	5.32(dd)[a]	5.13(dd)[a]
$PhC\underline{H}_2Ar$			5.17(s)	5.26(s)			
H-4	5.55(dq)[a]	5.10(dq)[a]	5.55(dq)	4.9—5.4	5.75(dq)	5.75(dq)[a]	5.06(dq)[a]
H-5′			7.35(dd)	7.37(dd)	6.91(dd)	6.90(dd)	6.98(dd)
3-NH	5.48(d)	5.78(d)	8.03(d)	7.9—8.3	7.09(d)	7.10(d)	7.81(d)
H-4′(or H-6′)			7.95(dd)	7.99(dd)	7.25(dd)	7.25(dd)[b]	7.29(dd)
$ArN\underline{H}CHO$					7.97(d)	8.01(d)[b]	7.97(d)
$ArNHC\underline{H}O$					8.50(d)	8.50(d)[b]	8.51(d)
H-6′(or H-4′)			8.25(dd)	8.20(dd)	8.54(dd)	8.54(dd)[b]	8.66(dd)
OH(Ar)					12.55(s)	12.57(s)	12.70(s)
$J_{3,4}$	7.8	6.0	7.6	5.0	7.7	7.7	5.0
J_{4,CH_3}	7.0	6.8	7.0	7.0	7.0	7.0	6.8
$J_{7,8}$		8.8		9.0	*ca.* 9.5	9.5	9.0
$J_{8,9}$		9.8		9.8	*ca.* 10	10.0	9.8
J_{9,CH_3}	6.2	6.2	6.2	6.2	6.2	6.2	6.2
$J_{3,NH}$	*ca.* 8	10.0	7.6	9.0	7.7	7.7	9.0
$J_{4',5'}$ or $J_{5',6'}$			8.0	7.8	8.0	8.0	8.2
$J_{4',6'}$			2.0	2.0	1.6	1.6	1.2

a) Assignment verified by spin decoupling.
b) Splittings were verified by the spectrum of *ca.* 7% solution.

10B was carried out in the condition similar to that described above with exception of the prolonged reaction time (21 hr) to afford a dilactone compound **12B** as needles in a 3.1% yield. Elemental analysis, molecular weight determination, IR and PMR spectra showed **12B** to be a homogeneous diastereomer of **12A**. In this lactonization reaction, no HBr-ninhydrin positive lactones other than **12B** were also detected, however, the formation of two isomeric lactones, (−)**7a** and (−)**7b** as HBr-ninhydrin negative by-products, was found and they were isolated and characterized by tlc, PMR, and optical rotations.

The benzyloxycarbonyl group of **12A** was removed by catalytic hydrogenolysis and the resulting free amino dilactone **13A** was *N*-acylated with *O*-benzyl-3-nitrosalicylic acid *N*-hydroxysuccinimide ester.[1] The product **14A** (65% yield based on **12A**) was then hydrogenolyzed on palladium black and, finally, *N*-formylated with formic acid and DCCI. The final product was isolated by preparative layer chromatography (plc) and purified by recrystallization to afford antimycin A_3 (**1A**) as needles in a 27.3% yield based on **12A**.

The synthetic specimen showed mp 174.0—174.5°C and $[\alpha]_D^{Chf}$ +80°, which were identical with the reported values for the natural antimycin A_3.[15] The mass spectrum of **12A** showed a single molecular ion peak at *m/e* 520. The UV absorptions in methanol and IR absorptions in carbon tetrachloride assignable to lactone carbonyl, formamido and aromatic amido groups were also indistinguishable from those observed in the corresponding spectra of an authentic antimycin A complex.[16] The 100 MHz PMR spectrum of *ca.* 3% deuteriochloroform solution of the synthetic specimen measured in a micro cell was very similar to that of a 3% solution of the authentic sample in a standard cell as shown in Table 1.

Inspection of the 100 MHz PMR spectra in deuteriochloroform and deuteriobenzene of the authentic antimycin A complex revealed that all the antimycin components had the same stereochemistry in respect of their dilactone rings. In view of these points, we came to the conclusion that the synthetic antimycin A_3 had the same ring configuration and conformation as those of natural antimycin A. Through this synthesis of antimycin A_3, it has been confirmed that naturally occurring antimycin A_3 retained in its dilactone structure, the same configuration of (+)blastmycinone derived from the parent antibiotic.

De-*N*-benzyloxycarbonylation of (−)**12B** afforded the free amino dilactone **13B** accompanied by (−)-

15) K. Uzu, H. Kato, K. Kumabe, and H. Harada, *J. Antibiot., Ser. A*, **14**, 205 (1961).

16) The sample of antimycin A complex was generously supplied by the Kyowa Hakko Kogyo Co.: mp 139.0—139.5°C; $[\alpha]_D^{24}$ +80° (*c* 0.4, chloroform); molecular ions of the components at *m/e* (relaitve intensities), 562 (1), 548 (12), 534 (7), 520 (16), 506 (2), and 492 (2).

blastmycinone(−)**7a**, which was considered to be resulted by a spontaneous fragmentation (self-saponification) of **13B**. The reaction product was immediately *N*-acylated to give *N*-(*O*-benzyl-3-nitro) salicyloyl derivative **14B** (24%) and (−)**7a** (24%). The low yield of **14B** may be accounted for by the degradation of **13B** which proceeded parallel to the *N*-acylation reaction.

Preparation of **1B** from **14B** was smoothly carried out by the same procedure as that of **1A** from **14A** to afford the antimycin A_3 diastereomer **1B** with $[\alpha]_D^{Chf}$ −5° as a glassy solid in a 83% yield. The UV spectrum of **1B** was identical with that of **1A**, however, the IR spectrum of **1B** in carbon tetrachloride showed two lactone carbonyl bands at 1758 and 1735 cm^{-1}, instead of single band at 1756 cm^{-1} in that of **1A**. The PMR spectrum of *ca.* 5% deuteriochloroform solution of **1B** considerably differed from that of **1A**, especially, in the chemical shifts of ring protons (H-3, H-4), ring methyl protons (4-CH_3) and aromatic amide proton (3-NH) (Table 1).

The PMR spectra data tabulated in Table 1 indicated that such chracteristic differences between the spectra of **1A** and **1B** were also observed between those of other natural and unnatural types of dilactone derivatives, **12A**—**12B** and **14A**—**14B**. Therefore, this observation shows that the configurations and conformations of both types of dilactone compounds may be closely reflected on their PMR spectra.

We have already proposed the absolute configuration of antimycin A_3 as **1A**[10] based on the abovementioned configurational correlation between antimycin A_3 and natural (+)blastmycinone whose absolute configuration had independently been determined as (+)**7a**. In a similar manner the absolute configuration of the synthetic diastereomer of antimycin A_3 which was correlated to the enantiomeric (−)blastmycinone (−)**7a** should be determined as **1B**.

On paper chromatography with the solvent system water-ethanol-acetone (7:2:1)[17] which was generally used for detection of antimycin A components, both synthetic specimens of antimycin A_3 and its diastereomer showed, on the bioautogram (test organism, *Piricularia orizae*), the single spot corresponding to that of the natural antimycin A_3 in the antimycin complex.

Table 2. MIC(mcg/ml) of synthetic antimycin A_3(**1A**), natural antimycin A complex and synthetic diastereomer (**1B**)

Organisms	1 A	Natural antimycin A	1 B
Candida albicans 3147	12.5	12.5	>25
Candida krusei	50	50	>25
Trichophyton asteroides 429	50	50	>25
Trichophyton mentagrophytes 833	50	50	25
Piricularia oryzae	0.025	0.025	3.12
Pellicularia filamentosa (Sasaki)	25	25	25

Medium: 1% Glucose nutrient agar, 27°C.

Minimal inhibitory concentrations (MIC) of the synthetic specimens **1A** and **1B** and natural antimycin A complex were summarized in Table 2.

Experimental

Melting points were determined on a micro hot stage and are uncorrected unless otherwise noted. UV spectra were taken on a Hitachi Perkin-Elmer UV-VIS spectrometer 139 and IR spectra on a Hitachi IPI-2 spectrometer. PMR spectra were recorded on Varian A-60D and HA-100D spectrometers using TMS as an internal standard. Optical rotations were measured with a Zeiss Photoelectric Precision Polarimeter. Tlc was carried out on WAKOGEL B-5 (Wako Pure Chemical Industries, Ltd.) and silica gel column chromatography on WAKOGEL C-200 which was activated at 110°C for 1 hr. The following solvent systems were used: (A) petroleum ether–diisopropyl ether (IPE) (3:1), (B) hexane–butanone–acetone (20:1:1), (C) hexane–IPE (10:1), (D) benzene–acetone (20:1), (E) benzene–IPE (7:1), (F) petroleum ether–IPE (7:4), (G) benzene–ethyl actate (3:2), (H) petroleum ether–IPE (2:1), (I) benzene–acetone (10:1), (J) ibid. (15:1), (K) hexane–acetone (3:1), (L) hexane–ethyl acetate (3:1), and (M) ibid. (5:3). In general, all concentrations were carried out at reduced pressure below 40°C.

1) Methyl 2-Benzyloxypropanoate. 2-Benzyloxypropanoic acid[18] was treated with methanol and concd H_2SO_4 in a usual manner to obtain the ester in a 82% yield, bp 96—98°C/4.5 Torr, $n_D^{23.7}$ 1.4942.

Found: C, 68.36; H, 7.42%. Calcd for $C_{11}H_{14}O_3$: C, 68.03; H, 7.27%.

2) 2-Benzyloxypropanal (2). A solution of methyl 2-benzyloxypropanoate (7.0 g, 36.1 mmol) in hexane (131 ml) was cooled to −50°C and diisobutylaluminum hydride[19] (6.25 g, 44.0 mmol) was added under dry nitrogen. The solution was ketp at −50°C for 2.5 hr before saturated sodium bisulfite solution (200 ml) was added. The mixture was allowed to warm to room temperature and the layers were separated. The hexane layer was extracted several times with saturated sodium bisulfite solution (total 1.8 l). The combined aqueous layers were washed three times with 200 ml-portions of ether to remove a small amount of 2-benzyloxypropanol and then basified with 4N NaOH to pH 11 with cooling. The separated aldehyde was extracted with ether. The ether extract was washed with saturated NaCl sloution, dried over Na_2SO_4 and evaporated to give 5.21 g (88%) of **2** as a colorless oil; ν_{max}^{liq} 1735 cm^{-1} (CHO).

2,4-Dinitrophenylhydrazone of 2: Mp 112—113°C (methanol)

Found: C, 56.06; H, 4.92; N, 16.09%. Calcd for $C_{16}H_{14}O_5N_4$: C, 55.81; H, 4.68; N, 16.27%.

3) t-Butyl 2-Bromohexanoate (3). 2-Bromohexanoic acid was treated with isobutene and catalytic amount of concd H_2SO_4 in usual way to afford a fraction of **3** boiling at 63—67°C/2.5 Torr in a 77% yield. Analytical sample was obtained by silica gel column chromatography of the product with hexane: bp 73.0—74.5°C (bath temp.)/6 Torr; n_D^{25} 1.4452.

Found: C, 48.01; H, 7.69; Br, 31.86%. Calcd for $C_{10}H_{19}O_2Br$: C, 47.82; H, 7.63; Br, 31.82%.

4) t-Butyl 4-Benzyloxy-2-butyl-3-hydroxypentanoate (4).

(a) Modified Reformatsky Reaction of 2 and 3: Fresh magnesium shavings (1.35 g, 55.5 mmol) were covered with dry

17) W. C. Liu and F. M. Strong, *J. Amer. Chem. Soc.*, **81**, 4387 (1959).

18) L. Feldmann and H. O. L. Fischer, *Arch. Biochem.*, **14**, 117 (1947).

19) A 25% (W/V) solution of diisobutylaluminum hydride in hexane (Mitsuwa's Pure Chemicals) was used.

ether (22 ml) and they were activated by addition of few drops of methyl iodide. When the activation reaction had started, a solution of **2**[20] (5.7 g, 34.8 mmol) and **3** (9.3 g, 37.0 mmol) in dry ether (32 ml) was added under stirring at such a rate that the mixture refluxed gently. After stirring and refluxing for additional 2.5 hr in a water bath, the reaction mixture was cooled with ice-salt bath and decomposed with a mixture of cold 10% H_2SO_4 (54 ml) and crushed ice (15 g). The ether layer was washed with 5% $NaHCO_3$ and saturated NaCl solution and evaporated. The oily residue was dissolved in hexane (140 ml) and the solution was washed with saturated sodium bisulfite solution to remove unchanged **2**. The hexane layer was washed with saturated NaCl solution, dried and evaporated to afford a viscous oil (11.1 g) containing four diastereomers (**4a**, **4b**, **4c**, and **4d**) of title compound **4**.

(b) Preparative Separation of the Diastereomers of 4: The product (11.1 g) obtained in (a) was chromatographed on a silica gel column (2.20 kg, 8.0×79 cm) with the solvent system A to give four main fractions which were evaporated. The fraction 1 (R_f 0.40 A, 1.36 g) was purified by a silica gel column (270 g) with the solvent system B to afford a homogeneous diastereomer **4c** (1.23 g): bp 105—107°C (bath temp.)/0.001 Torr; R_f 0.40 A; $\nu_{max}^{CCl_4}$ (0.01M) 3500 (OH), 1725 and 1705 cm^{-1} (ester); δ ($CDCl_3$) 1.44 (s, Bu^t), 1.26 (d, 4-CH_3, J_{4,CH_3}=5.8 Hz).

Found: C, 71.35; H, 9.44%. Calcd for $C_{20}H_{32}O_4$: C, 71.39; H, 9.59%.

Additional sample of **4c** (0.23 g) was obtained by chromatographic separation of the fraction 2 (vide infra) and total yield of **4c** amounted to 1.46 g (12.4% based on **2**).

The fraction 2 (R_f 0.40 and 0.34 A, 1.14 g) was separated into two fractions by a silica gel column (230 g) with the solvent system A. The first fraction (R_f 0.40 A) gave **4c** (0.23 g) and the second one (R_f 0.34 A) afforded the product (0.77 g) which was shown to be a mixture of diastereomers **4a** and **4b** by inspection of its PMR spectrum, similar to the following fraction 3.

The fraction 3 (R_f 0.34 A) gave the product (4.33 g) which consisted of major diastereomer **4a** contaminated by minor diastereomer **4b**: δ ($CDCl_3$) 1.41 and 1.44 (s, Bu^t), 1.24 and 1.26 (d, 4-CH_3). Microanalysis of a micro distillated sample agreed with the molecular formula $C_{20}H_{32}O_4$ (Found: C, 71.44; H, 9.61%). The total yield of **4a** accompanied by **4b** thus amounted to 5.10 g (43% based on **2**). The content of **4a** in the combined products may be estimated to be *ca.* 83% on the basis of the result of Exp. 5(a).

The fraction 4 (R_f 0.23 A (main spot), 2.03 g) was purified by a silica gel column (400 g) with the solvent system B to give a homogeneous isomer **4d** (0.80 g, 6.8% based on **2**): bp 120—123°C (bath temp.)/0.005 Torr; R_f 0.23 A; $\nu_{max}^{CCl_4}$ (0.01M) 3570, 3470 (OH), 1735 and 1715 cm^{-1} (ester); δ ($CDCl_3$) 1.24 (d, 4-CH_3, J_{4,CH_3}=6.1 Hz) and 1.43 (s, Bu^t).

Found: C, 71.56; H, 9.48%. Calcd for $C_{20}H_{32}O_4$: C, 71.39; H, 9.59%.

(c) Isolation of the Major Diastereomer 4a: The Reformatsky reaction product (15.0 g) was subjected to silica gel column chromatography (1.5 kg, solvent system A) and the eluted fractions showing R_f 0.34 A were inspected by PMR and the fractions containing homogeneous **4a** were collected and evaporated: yield 1.55 g; bp 108—113°C (bath temp.)/0.001 Torr; R_f 0.34 A; $\nu_{max}^{CCl_4}$ (0.01M) 3590 (OH), 1725 and 1710 cm^{-1} (ester); δ($CDCl_3$) 1.24 (d, 4-CH_3, J_{4,CH_3}=6.0 Hz), 1.41 (s, Bu^t), 2.47 (m, H-2), 3.52 (dq, H-4, $J_{3,4}$=4.7 Hz), and 3.89 (dd, H-3, $J_{2,3}$=6.8 Hz).

Found: C, 71.46; H, 9.65%. Calcd for $C_{20}H_{32}O_4$: C, 71.39; H, 9.59%.

(d) Isolation of 4b: Repeated column chromatography (solvent system A) of several fractions which contained the products showing R_f 0.40 and 0.34 A (main spot) in the experiment 4(c) afforded a small amount of the fraction consisting almostly of the isomer **4b**. Although the PMR spectrum of this sample of **4b** revealed that it was still contaminated by a trace of **4a**, the main PMR signals corresponding to **4b** itself was observed therein as followed; δ ($CDCl_3$) 1.26 (d, 4-CH_3, J_{4,CH_3}=6.3 Hz), 1.43 (s, Bu^t), and 3.40—3.80 (m, overlapped 3-H and 4-H).

5) t-Butyl 4-Benzyloxy-2-butyl-3-isovaleryloxypentanoate (5a and 5b). *(a)*: A sample (1.86 g, 5.53 mmol) of the total mixture of **4a** and **4b** obtained in the experiment 4(b) was dissolved in dry pyridine (24 ml) and to this a solution of isovaleric anhydride (2.06 g, 11.0 mmol) in pyridine (12 ml) was added. After standing this mixture for 24 hr at room temperature, an additional isovaleric anhydride (1.03 g in 2 ml of pyridine) was added and kept for 48 hr in the same temperature. The reaction mixture was partitioned between water and ether and the aqueous layer was extracted with ether. The combined organic layers were washed with aqueous 10% citric acid, 5% $NaHCO_3$ and saturated NaCl solutions, successively. The dried ether solution was evaporated and the residue (2.33 g) was chromatographed on a silica gel column (240 g, 3.4×45 cm) with the solvent system C to afford three fractions which were inspected by tlc (system C). The first fraction (R_f 0.43C) gave the homogeneous isomer **5a** (1.42 g, 61.5%) corresponding to **4a**. Additional **5a** (0.31 g) was obtained by column chromatography (silica gel 60 g, solvent system C) of the second fraction (0.40 g) which consisted of **5a** contaminated by a trace of **5b**. Total yield of **5a** was 1.73 g (75%). This sample (190 mg) was again chromatographed on silica gel (19 g) with the solvent system D and the fraction of **5a** (125 mg) was subjected to micro distillation to afford an analytical sample of **5a**: bp 105—119°C (bath temp.)/0.002 Torr; R_f 0.43C; δ($CDCl_3$) 1.21 (d, 4-CH_3, J_{4,CH_3}=6.4 Hz), 1.38 (s, Bu^t), 2.55 (m, H-2), 3.58 (dq, H-4, $J_{3,4}$=4.0 Hz), and 5.44 (dd, H-3, $J_{2,3}$=8.2 Hz).

Found: C, 71.56; H, 9.69%. Calcd for $C_{25}H_{40}O_5$: C, 71.39; H, 9.59%.

The third fraction (R_f 0.37C) gave the diastereomer **5b** (0.39 g, 16.9%) corresponding to **4b** in a homogeneous state. Rechromatography of this sample using the solvent system C followed by micro distillation afforded an analytical sample of **5b**: bp 155—158°C (bath temp.)/0.04 Torr; R_f 0.37C; δ($CDCl_3$) 1.16 (d, 4-CH_3, J_{4,CH_3}=6.3 Hz), 1.42 (s, Bu^t), 3.73 (dq, H-4, $J_{3,4}$=3.2 Hz), and 5.27 (dd, H-3, $J_{2,3}$=9.1 Hz).

Found: C, 71.59; H, 9.70%. Calcd for $C_{25}H_{40}O_5$: C, 71.39; H, 9.59%.

(b): A sample (1.39 g) of **4a** isolated in the experiment 4(c) was *O*-isovalerylated by the same procedure as mentioned above to give a homogeneous sample of **5a** (1.45 g, 84%).

(c): A sample of **4b** in the experiment 4(d) was also *O*-isovalerylated and purified through a silica gel column to afford a homogeneous sample of **5b** in a 83% yield.

6) t-Butyl 4-Benzyloxy-2-butyl-3-isovaleryloxypentanoate (5c and 5d). *O*-Isovalerylations of **4c** and **4d** were performed by the same procedure as described in the experiment 5 to give the corresponding **5c** and **5d** in good yields, respectively. **5c**: bp 140—142°C (bath temp.)/0.01 Torr; δ($CDCl_3$) 1.18 (d, 4-CH_3, J_{4,CH_3}=6.2 Hz), 1.45 (s, Bu^t), 3.73 (dq,

20) The product **2** obtained in Exp. 2 was thoroughly dried under highly reduced pressure (0.001 Torr) at room temperature before use.

H-4, $J_{3,4}$=5.2 Hz), and 5.34 (dd, H-3, $J_{2,3}$=6.5 Hz).

Found: C, 71.57; H, 9.75%. Calcd for $C_{25}H_{40}O_5$: C, 71.39; H, 9.59%.

5d: bp 126—132°C (bath temp.)/0.002 Torr; $\delta(CDCl_3)$ 1.20 (d, 4-CH_3, $J_{4,CH3}$=6.5 Hz), 1.42 (s, Bu^t), 3.73 (dq, H-4, $J_{3,4}$=4.0 Hz), and 5.20 (dd, H-3, $J_{2,3}$=8.5 Hz).

Found: C, 71.10; H, 9.73%. Calcd for $C_{25}H_{40}O_5$: C, 71.39; H, 5.59%.

*7) t-Butyl 2-Butyl-4-hydroxy-3-isovaleryloxypentanoate (**6a**, **6b**, **6c**, and **6d**).* To a solution of **5a** (2.60 g) in methanol (65 ml) was added freshly prepared palladium black (*ca.* 800 mg) and the mixture was vibrated for 1 hr under bubbling with hydrogen. Completion of the hydrogenolysis was confirmed by tlc (solvent system E). The filtered solution was evaporated to give **6a** (1.98 g, 97%) as a colorless oil: ν_{max}^{liq} 3460 (OH) and 1730 cm^{-1} (ester); $\delta(CDCl_3)$ 1.18 (d, 4-CH_3, J_{4,CH_3}=6.5 Hz), 1.45 (s, Bu^t), 3.89 (dq, H-4, $J_{3,4}$=5.0 Hz), and 5.10 (dd, H-3, $J_{2,3}$=7.8 Hz).

By the same procedure, the diastereomers, **6b**, **6c**, and **6d** were also obtained from the corresponding diastereomers, **5b**, **5c**, and **5d** in a yield of 56,[21] 86,[21] and 96%, respectively. The products, **6a**, **6b**, **6c**, and **6d** were immediately used for the subsequent syntheses without further purifications, because their instability for silica gel chromatography or distillation.

*8) 2-Butyl-4-hydroxy-3-isovaleryloxypentanoic Acid-1, 4-Lactone [(±)Blastmycinone] (**7a**).* *(a)*: A sample (41.2 mg) of **6a** was dissolved in 0.08 ml of 5N HCl in dry dioxane and the solution was allowed to stand for 1 hr at room temperature. The reaction mixture was evaporated to afford **7a** (28.8 mg, 90%) as a colorless oil: bp 125—130°C (bath temp.)/8 Torr; R_f 0.66F; glc (polyester succinate on Shimalite 80—100 mesh, 190°C, He gas 125 ml/min) retention time (min) 7.8; $\nu_{max}^{CCl_4}$ 1782 (1,4-lactone) and 1754 cm^{-1} (ester); $\delta(CDCl_3)$ 1.45 (d, 4-CH_3, J_{4,CH_3}=6.5 Hz), 2.69 (m, H-2), 4.37 (dq, H-4, $J_{3,4}$=4.5 Hz), and 4.95 (dd, H-3, $J_{2,3}$=5.8Hz).

Found: C, 65.40; H, 9.16%. Calcd for $C_{14}H_{24}O_4$: C, 65.59; H, 9.44%.

(b): To a solution of (±)blastmycinolactol **9a** (9.7 mg) in dry pyridine (0.76 ml) was added isovaleric anhydride (0.04 ml). The mixture was kept at room temperature for 40 hr. The reaction mixture was partitioned between water and petroleum ether. The aqueous layer was extracted with petroleum ether and the combined organic layers were washed with aqueous 10% citric acid, 5% $NaHCO_3$ and saturated NaCl solution, successively. The dried solution was evaporated and the residue (14 mg) was purified through a silica gel column (2 g) with the solvent system F to give a sample of **7a** (7 mg, 50%), which was identified to the specimen of **7a** obtained in Exp. 8(a) by tlc, glc, and PMR criteria.

*9) Diastereomers, **7b**, **7c**, and **7d** of (±)Blastmycinone **7a**.* Samples of **6b**, **6c**, and **6d** were treated with 5N HCl in dioxane [Exp. 8(a)] to afford the corresponding diastereomeric lactones, **7b**, **7c**, and **7d**, in a yield of 91, 77, and 86%, respectively. The following data were obtained. **7b**: bp 125—130°C (bath temp.)/2.0 Torr; R_f 0.60F; $\nu_{max}^{CCl_4}$ 1798 (lactone) and 1745 cm^{-1} (ester); $\delta(CDCl_3)$ 1.36 (d, 4-CH_3, J_{4,CH_3}=6.5 Hz), 2.65 (m, H-2), 4.28 (dq, H-4, $J_{3,4}$=5.0 Hz), and 5.24 (dd, H-3, $J_{2,3}$=3.0 Hz).

Found: C, 65.76; H, 9.36%. Calcd for $C_{14}H_{24}O_4$: C, 65.59; H, 9.44%.

7c: bp 114—117°C (bath temp.)/2.0 Torr; R_f 0.48F; $\nu_{max}^{CCl_4}$ 1795 (lactone) and 1755 cm^{-1} (ester); $\delta(CDCl_3)$ 1.40 (d, 4-CH_3, J_{4,CH_3}=6.5 Hz), 2.72 (m, H-2), 4.51 (dq, H-4, $J_{3,4}$=0.7 Hz), and 5.20 (dd, H-3, $J_{2,3}$=6.0 Hz).

Found: C, 65.70; H, 9.41%. Calcd for $C_{14}H_{24}O_4$: C, 65.59; H, 9.44%.

7d: bp 135—139°C (bath temp.)/1.0 Torr; mp 38.5—39.0°C; R_f 0.33F; $\nu_{max}^{CCl_4}$ 1795 (lactone) and 1755 cm^{-1} (ester); $\delta(CDCl_3)$ 1.32 (d, 4-CH_3, $J_{4,CH3}$=6.5 Hz), 2.77 (m, H-2), 4.63 (dq, H-4, $J_{3,4}$=3.4 Hz), and 5.68 (dd, H-3, $J_{2,3}$=5.5 Hz).

Found: C, 65.80; H, 9.39%. Calcd for $C_{14}H_{24}O_4$: C, 65.59; H, 9.44%.

*10) 2-Butyl-3,4-dihydroxypentanoic Acid-1,4-Lactone, [(±)-Blastmycinolactol] (**9a**).* A solution of **4a** (23.5 mg) in methanol (3 ml) was stirred with palladium black for 40 min under bubbling with hydrogen. The reaction mixture was filtered and evaporated to give *t*-butyl 2-butyl-3,4-dihydroxypentanoate **8a** (22 mg) as a crystalline solid. The product **8a** was dissolved in trifluoroacetic acid (0.5 ml) and kept for 15 min at room temperature. The solution was evaporated and the syrupy residue was purified by a silica gel column (3 g) with the solvent system G to afford a crystalline product **9a** (12.7 mg, 89%). The product was recrystallized from ethyl acetate–petroleum ether to give a pure sample of **9a** (9.7 mg): mp 49.5—51.0°C; ν_{max}^{KBr} 3440 (OH) and 1735 cm^{-1} (lactone); $\delta(CDCl_3)$ 1.45 (d, 4-CH_3, J_{4,CH_3}=6.2 Hz), 2.58 (m, H-2), 3.84 (dd, H-3, $J_{2,3}$=8.5 Hz), and 4.25 (dq, H-4, $J_{3,4}$=7.0 Hz).

Found: C, 62.51; H, 9.42%. Calcd for $C_9H_{16}O_3$: C, 62.76; H, 9.36%.

*11) Optically Active Diastereomers [(+) **10A** and (−)**10B**] of t-Butyl 4-(N-Benzyloxycarbonyl-O-t-butyl-L-threonyloxy)-2-butyl-3-isovaleryloxypentanoate Derived from **6a**.* A solution of *N*-benzyloxycarbonyl-*O*-*t*-butyl-L-threonine[22] (1.82 g, 5.88 mmol) in dry ether (4.0 ml) was added dropwise during 20 min to a stirred solution of **6a** (1.94 g, 5.88 mmol), DCCI (1.34 g, 6.52 mmol) and dry pyridine (0.5 ml) in dry ether (6 ml) cooled at 0°C. Stirring at 0°C was continued for an additional hour. After standing at 0°C for 41 hr, to the reaction mixture a solution of DCCI (670 mg) in ether (1.8 ml) and dry pyridine (0.25 ml) was added and then a solution of the threonine derivative (910 mg) in ether (2 ml) was dropped under stirring at 0°C. After stirring at 0°C for 8 hr and standing at 0°C for 41 hr, further additions of DCCI (335 mg), dry pyridine (0.13 ml) and a solution of the threonine derivative (460 mg) in ether (2 ml) were undertaken in the same procedure as in the preceding additions and the reaction mixture was kept at 0°C for 24 hr. The precipitate of *N,N'*-dicyclohexylurea (1.67 g) was filtered off and the filtrate was treated with acetic acid (*ca.* 0.2 ml) under stirring at 0°C for 1 hr. An additional urea was removed and the filtrate was washed with 5% $NaHCO_3$, 10% citric acid and saturated NaCl solutions. The dried solution was evaporated to afford an yellow syrup (5.48 g).

The product (5.48 g) was chromatographed on a silica gel column (1.2 kg, 8×43 cm) with the solvent system H to collect three fractions which were concentrated. The first fraction gave a homogeneous sample of (+)**10A** (R_f 0.57H, 995 mg) and an additional sample of (+)**10A** (115 mg) was obtained by column chromatography of the second fraction (273 mg), whose tlc showed the two spots corresponding to (+)**10A** and (−)**10B**. The combined samples of (+)**10A** (1.11 g) was again chromatographed with the solvent system D to afford a pure sample of (+)**10A** (1.06 g, 29%) as a colorless syrup: $[\alpha]_D^{22}$ +10° (*c* 11.4, chloroform); $\delta(CDCl_3)$

21) In the case of the preparations of **6b** and **6c**, unchanged materials had to be removed through a short silica gel column (solvent system E).

22) E. Schröder, *Ann. Chem.*, **670**, 127 (1963).

1.15 (s, OBu^t), 1.19 (d, 4-CH$_3$, J_{4,CH_3}=6.2 Hz), 1.29 (d, 3'-CH$_3$, J=6.8 Hz), 1.48 (s, COOBu^t), 4.0—4.2 (m, H-2', H-3'), 5.05 (dq, H-4, $J_{3,4}$=3.0 Hz), 5.32 (dd, H-3, $J_{2,3}$=9.0 Hz), and 5.60 (d, 2'-NH, $J_{2',NH}$=9.0 Hz).

Found: C, 65.97; H, 9.10; N, 2.35%. Calcd for $C_{34}H_{55}O_9N$: C, 65.67; H, 8.92; N, 2.25%.

The third fraction afforded a sample of the diastereomer (−)**10B** (R_f 0.50H, 978 mg). To this was added an additional sample of (−)**10B** (102 mg) separated by column chromatography of the second fraction above-mentioned and the combined products (1.08 g) were purified by chromatography (solvent system D) to give a pure sample of (−)**10B** (1.01 g, 27.7%) as a colorless syrup: $[\alpha]_D^{22}$ −6° (*c* 10.1, chloroform); δ(CDCl$_3$) 1.13 (s, OBu^t), 1.19 (d, 4-CH$_3$, J_{4,CH_3}=6.5 Hz), 1.27 (d, 3'-CH$_3$, J_{3',CH_3}=6.8 Hz), 1.48 (s, COOBu^t), 4.1—4.3 (m, H-2', H-3'), 5.02 (dq, H-4, $J_{3,4}$=3.0 Hz), 5.30 (dd, H-3, $J_{2,3}$=8.6 Hz), and 5.53 (d, 2'-NH, $J_{2',NH}$=8.7 Hz).

Found: C, 65.90; H, 8.64; N, 2.29%. Calcd for $C_{34}H_{55}O_9N$: C, 65.67; H, 8.92; N, 2.25%.

*12) t-Butyl (+)(2*R*,3*R*,4*S*)-2-Butyl-3,4-dihydroxypentanoate [(+)8a] and Its Enantiomer [(−)8a].* A suspension of LiAlH$_4$ (255 mg, 6.73 mmol) in dry tetrahydrofuran (30 ml) was added in one portion to a stirred solution of (+)**10A** (1.05 g, 1.68 mmol) in dry tetrahydrofuran (30 ml) cooled to −45°C in a dry ice-methanol bath. After stirring at −45—−40°C for 1 hr, ethyl acetate (4 ml) was added to the reaction mixture. The mixture (pH 9) was gradually allowed to warm to 0°C and acidified to pH 2—3 with 2N HCl aqueous under cooling in an ice-bath. The resulting mixture was extracted with ether and ethereal extract was washed with 5% NaHCO$_3$ and saturated NaCl solution. The dried solution was evaporated to afford a colorless oil (1.09 g). This was chromatographed on a silica gel column (210 g, 4×45 cm) with the solvent system I to collect three fractions. From the first fraction the unchanged (+)**10A** (284 mg) was recovered. The second fraction gave (−)2-benzyloxycarboxamido-3-*t*-butyl-1-butanol (**11**) (302 mg): $[\alpha]_D^{20}$ −8° (*c* 2.19, chloroform).

Found: C, 65.04; H, 8.73; N, 4.70%. Calcd for $C_{16}H_{25}O_4N$: C, 65.06; H, 8.53; N, 4.74%.

The third fraction afforded the title compound (+)**8a** (197 mg, 47.5%): mp 48.0—48.5°C; $[\alpha]_D^{23}$ +16° (*c* 2.35, methanol).

Found: C, 63.56; H, 10.74%. Calcd for $C_{13}H_{26}O_4$: C, 63.38; H, 10.64%.

The another title compound (−)**8a** (116 mg, 44.6%) was obtained from (−)**10B** (655 mg) by the same procedure as described for the preparation of the enantiomer (+)**8a**: mp 48.1—48.7°C; $[\alpha]_D^{21}$ −16° (*c* 1.90, methanol).

Found: C, 63.17; H, 10.44%. Calcd for $C_{13}H_{26}O_4$: C, 63.38; H, 10.64%.

*13) (−)(2*R*,3*R*,4*S*)-2-Butyl-3,4-dihydroxypentanoic Acid-1,4-Lactone [(−)Blastmycinolactol][(−)9a] and Its Enantiomer [(+)9a].* By the procedure utilized to obtain **9a** from **8a**, the product (+)**8a** (190 mg) was de-*t*-butylated and lactonized. Purification by chromatography as in the preparation of **9a** followed by recrystallization from ether-petroleum ether afforded (−)**9a** (86.4 mg, 66.5%): mp 50.0—51.0°C; $[\alpha]_D^{22}$ −18° (*c* 1.61, methanol) [lit,[6] mp 49—50°C; $[\alpha]_D^{26}$ −5.27° (*c* 7.8, methanol)].

Found: C, 63.06; H, 9.51%. Calcd for $C_9H_{16}O_3$: C, 62.76; H, 9.36%.

In the same procedure as in the preparation of (−)**9a**, the enantiomer (+)**9a** (80 mg, 70%) was obtained from (−)**8a** (164 mg): mp 50.0—51.0°C; $[\alpha]_D^{23}$ +16° (*c* 1.60, methanol).

Found: C, 62.96; H, 9.56%. Calcd for $C_9H_{16}O_3$: C, 62.76; H, 9.36%.

The PMR spectra (in CDCl$_3$) of (−)**9a** and (+)**9a** were identical with that of (±)blastmycinolactol **9a** and the IR spectra (in nujol) of those were very similar to that[6] of natural product.

*14) (+)(2*R*,3*R*,4*S*)-2-Butyl-4-hydroxy-3-isovaleryloxypentanoic Acid-1,4-Lactone [(+)Blastmycinone][(+)7a] and Its Enantiomer [(−)7a].* The synthetic (−)blastmycinolactol (−)**9a** (23.9 mg) was treated with isovaleric anhydride-pyridin. Work up as described in Exp. 8(b) for the preparation of **7a** gave (+)blastmycinone (+)**7a** (15.3 mg, 42.5%) as a colorless oil: $[\alpha]_D^{23}$ +10° (*c* 1.5, chloroform) [lit,[6] $[\alpha]_D^{25}$ +11.5° (*c* 20.8, chloroform)]. This material was indistinguishable from (±)blastmycinone **7a** by PMR, tlc, and glc criteria.

(−)Blastmycinone (−)**7a** (22.6 mg, 46.5%) was obtained from (+)**9a** (32.4 mg) by the same procedure as described in the preparation of (+)**7a**: $[\alpha]_D^{25}$ −10° (*c* 2.26, chloroform). The PMR spectrum of (−)**7a** was identical with that of (+)**7a**.

*15) (+)(3*S*,4*R*,7*R*,8*R*,9*S*)-3-Benzyloxycarboxamido-7-butyl-4,9-dimethyl-1,5-dioxa-8-isovaleryloxycyclononane-2,6-dione [(+)-12A].* A mixture of (+)**10A** (2.24 g, 3.6 mmol) and trifluoroacetic acid (27 ml) was kept for 10 min at room temperature and then evaporated below 10°C. The residual syrup was coevaporated with ether repeatedly to remove trifluoroacetic acid. The final residue was dried over NaOH for 2 hr under reduced pressure to afford a syrupy de-*t*-butylated product, hydroxyester-acid. The porduct was immediately dissolved in dry benzene (97 ml) and to this was added trifluoroacetic anhydride (0.54 ml, 3.87 mmol). The mixture was heated at 65—70°C in an oil bath and the reaction course was monitored by tlc (solvent system J). After 2—3 hr a faint spot (R_f 0.77 J, HBr-ninhydrin positive) of (+)**12A** and two HBr-ninhydrin negative spots (R_f 0.60, 0.42J) of by-products appeared on tlc. After an additional hour a new HBr-ninhydrin negative spot (R_f 0.95J) appeared and to the reaction mixture was again added trifluoroacetic anhydride (0.54 ml). The heating was further continued for 6 hr, during which the spot of (+)**12A** became more definite, however, rapid formation of the two by-products (R_f 0.60 and 0.95J) was also observed. The reaction mixture was then immediately cooled and evaporated to dryness below 10°C to afford a syrup (2.20 g). As soon as possible the syrup was chromatographed on a silica gel column (300 g, 4.7×50 cm) with the solvent system J to collect fractions containing (+)**12A** (R_f 0.77J). The combined fractions were evaporated. The residual semicrystalline product (*ca.* 25 mg) was again chromatographed on silica gel (2.3 g) with the solvent system F to afford crystals of (+)**12A** (14.2 mg, 0.8%), whose tlc with solvent system K, J, and F showed a single spot. The crystals (14 mg) was recrystallized from ethyl acetate-petroleum ether to give an analytical sample of (+)**12A** (8.2 mg) as long needles: mp 109.0—109.5°C; $[\alpha]_D^{25}$ +70° (*c* 0.5, chloroform); $\nu_{max}^{CCl_4}$ (0.01M) 3440 (NH) and 1756, 1738 cm^{-1} (ester and amide); molecular ion at *m/e* 491.2473 (calcd, 491.2519).

Found: C, 63.65; H, 7.41; N, 2.61%. Calcd for $C_{26}H_{37}O_8N$: C, 63.52; H, 7.59; N, 2.85%.

*16) (−)(3*S*,4*R*,7*S*,8*S*,9*R*)-3-Benzyloxycarboxamido-7-butyl-4,9-dimethyl-1,5-dioxa-8-isovaleryloxycyclononane-2,6-dione [(−)-12B].* By the procedure of the preceding experiment 15, (−)**10B** (1.77 g, 2.84 mmol) was de-*t*-butylated. The product was immediately dissolved in dry benzene (74 ml) and to this was added trifluoroacetic anhydride (0.40 ml, 2.87 mmol). The mixture was heated at 65—70°C. After 30 min a faint spot (R_f 0.60 K, HBr-ninhydrin positive) of

(−)**12B** and a spot (R_f 0.79 K) of blastmycinone were detected on tlc. The heating was continued for 18 hr, during which the two spots became more definite and then trifluoroacetic anhydride (0.40 ml) was again added. After heating for additional 2 hr, the reaction mixture, whose tlc showed the formations of considerable amount of (−)**12B** (R_f 0.60 K) and blastmycinone (R_f 0.77 K) and of additional ninhydrin negative by-product (R_f 0.67 K), was evaporated below 20°C. The resulting syrup was chromatographed on a silica gel column (300 g, 4.5×40 cm) with the solvent system J to collect fractions containing (−)**12B** (R_f 0.77J) and blastmycinone (R_f 0.81J), which were evaporated. The residue (120 mg) was again chromatographed on a silica gel column (12 g, 1.2×25 cm) with the solvent system F to afford the following fractions:

Fraction 1. (−)blastmycinone (−)**7a**; 9.0 mg; $[\alpha]_D^{Chf}$ −9°
Fraction 2. (−)**7a**+(−)**7b** ; 15.2 mg
Fraction 3. (−)**7b** ; 22.3 mg; $[\alpha]_D^{Chf}$ −11°
Fraction 4. (−)**12B** (crystals) ; 43.5 mg (3.1% yield)

The oily products obtained from the fraction 1 and 3 were confirmed to be (−)**7a** and (−)**7b**, respectively, by PMR and optical rotations. The crystals obtained from the fraction 4 showed a single spot on each tlc with the solvent systems, K, J, and F. Recrystallization of the product (43 mg) from petroleum ether gave an analytical sample of (−)**12B** (25.7 mg): mp 87.0—87.5°C; $[\alpha]_D^{25}$ −18° (*c* 1.9, chloroform); $\nu_{max}^{CCl_4}$ (0.01M) 3428 (NH), 1758 and 1738 cm^{-1} (ester and amide); molecular ion at *m/e* 491.2451 (calcd, 491.2519).

Found: C, 63.75; H, 7.57; N, 3.12%. Calcd for $C_{26}H_{37}O_8N$: C, 63.52; H, 7.59; N, 2.85%.

17) Antimycin A_3 (1A). *(a) Amino Dilactone (13A)*: A solution of (+)**12A** (8.1 mg) in methanol (3 ml) was stirred with palladium black for 35 min under bubbling with hydrogen gas. The filtered reduction mixture was evaporated to yield the free amino dilactone **13A** (5.9 mg), whose tlc showed a single sopt detected by ninhydrin and 20% H_2SO_4 reagents.

(b): To a solution of **13A** (5.9 mg) in dry tetrahydrofuran (0.08 ml) was added *O*-benzyl-3-nitrosalicylic acid *N*-hydroxysuccinimide ester (6.2 mg). The mixture was kept for 3 hr at 36°C in an incubator. The reaction mixture (pH 4) was adjusted to pH 6 by addition of triethylamine and again incubated for 25 hr. The resulting solution was evaporated and the residue was chromatographed on silica gel column (0.85 g) with the solvent system L to afford *N*-(*O*-benzyl-3-nitro)salicyloyl derivative **14A** (6.4 mg, 65%) as a yellow glassy solid: $\nu_{max}^{CCl_4}$ (0.01M) 3390 (NH), 1749 (lactone) and 1675, 1603 cm^{-1} (amide).

(c): A solution of **14A** (6.2 mg) in methanol (3 ml) was stirred with palladium black under bubbling with hydrogen gas for 10 min. The filtered solution was evaporated to give a crystalline solid (5 mg). The product was dissolved in tetrahydrofuran (0.06 ml) and to this was added DCCI (4.5 mg) and 98% formic acid (0.8 μl) under ice-cooling. After standing for 4 hr in a refrigerator, the reaction mixture was evaporated and the residue was subjected to plc (one 20×20 cm silica gel plate) with the solvent system M. The strongest fluorescent band which showed the same R_f-value as that of authentic antimycin A complex, was collected and extracted with ether to afford pale orange crystals (4.2 mg). They were recrystallized twice from ether–petroleum ether to give an analytical sample of **1A** (2.3 mg, 27.3% based on (+)**12A**) as colorless needles: mp 174.0—174.5°C (corrected) [lit, 174.5—175°C,[15] 168—169°C,[6] 170.5—171.5°C[17]]; $[\alpha]_D^{24}$ +80° (*c* 0.2, chloroform) [lit, $[\alpha]_D^{26}$ +79.4° (*c* 1, chloroform),[15] $[\alpha]_D^{26}$ +64.3° (*c* 1.0, chloroform)[17]]; λ_{max}^{MeOH} nm (log ε), 225 (4.52) and 320 (3.86); $\nu_{max}^{CCl_4}$ (0.01M) 3420 (NH), 1756 (ester), 1715 (NHCHO), 1644 (ArCONH), 1610 (ArH) and 1531 cm^{-1} (ArCONH); molecular ion at *m/e* 520.2412 (calcd, 520.2421).

Found: C, 59.72; H, 7.15; N, 5.25%. Calcd for $C_{26}H_{36}O_9N_2$: C, 59.99; H, 6.97; N, 5.38%.

18) Diastereomer of 1A (1B). *(a)*: Amino Dilactone (**13B**). By the procedure of Exp. 17(a), (−)**12B** (29 mg) was hydrogenolyzed to afford a reduction product (19.7 mg) whose tlc (solvent L) showed a major ninhydrin positive spot of **13B** and two definite spots of blastmycinone and other ninhydrin positive product.

(b): The reduction product (19.7 mg) was treated with *O*-benzyl-3-nitrosalicylic acid *N*-hydroxysuccinimide ester (22 mg) by the same procedure for **13A**. The concentrated reaction mixture (50 mg) was chromatographed on a silica gel column (5 g) with the solvent system L to collect two fractions. The first fraction gave a colorless oil of (−)**7a** (3.3 mg, *ca.* 24%); $[\alpha]_D^{25}$ −9° (*c* 2.9, chloroform). The PMR spectrum of this ample was identical with that of the specimen of (−)**7a** obtained in Exp. 14. The second fraction afforded *N*-(*O*-benzyl-3-nitro)salicyloyl derivative of **13B** (**14B**) (9.1 mg, *ca.* 24% yield) as a yellow glassy solid: $\nu_{max}^{CCl_4}$ (0.01M) 3410 (NH), 2750 (ester), 1669 and 1602 cm^{-1} (amide).

(c): A sample of **14B** (23.2 mg) was hydrogenolyzed by the procedure of Exp. 17(c) to afford a reduction product whose tlc (solvent system L) showed a single spot by detection with ninhydrin, ethanolic $FeCl_3$ and 20% H_2SO_4 reagents. The product (18 mg) was *N*-formylated with 98% formic acid (2 μl) and DCCI (9.8 mg) in tetrahydrofuran at 0°C. Filtration of urea followed by concentration gave a yellow syrup (21 mg). The syrup was subjected to plc (two 20×20 cm silica gel plates) with the solvent system M to collect the strongest fluorescent bands. The ethereal extract of these bands was evaporated to afford **1B** (15.9 mg, 83% based on **14B**) as a pale yellow syrup. Further purification by plc gave an analytical sample as a colorless glass, whose tlc showed the same R_f-value as that of **1A**: $[\alpha]_D^{21}$ −5° (*c* 1.6, chloroform); λ_{max}^{MeOH} nm (log ε), 225 (4.55) and 320 (3.72); $\nu_{max}^{CCl_4}$ (0.01M) 3420 (NH), 1758 and 1735 (ester), 1714 (NHCHO), 1646 (ArCONH), 1612 (ArH), and 1531 cm^{-1} (ArCONH).

Found: C, 60.29; H, 7.21; N, 5.22%. Calcd for $C_{26}H_{36}O_9N_2$: C, 59.99; H, 6.97; N, 5.38%.

We wish to thank Prof. Hiroshi Yonehara for sample of antimycin lactone and PMR chart of blastmycinone, Prof. Hamao Umezawa for his helpful advice, Dr. Hiroshi Naganawa for the measurement of PMR spectra at 100 MHz, Dr. Masa Hamada for the microbiological tests and to Mr. Saburo Nakada for the elemental analyses.

The Oxidation of 2,3-Dihydro-4*H*-pyran-4-ones[1]

Kikumasa SATO, Seiichi INOUE, and Masao ŌHASHI*

Department of Applied Chemistry, Faculty of Engineering, Yokohama National University, Minami-ku, Yokohama
**Chemical Laboratory, Seimi Chemical Co., Ltd., Chigasaki, Chigasaki-shi, Kanagawa*

(Received June 29, 1972)

The synthesis and oxidation of substituted 2,3-dihydro-4*H*-pyran-4-ones are described. The reaction of crotonoyl chloride with β-ketoester gave dihydro-4*H*-pyran-4-ones (I). Dihydro-γ-pyrone (Ia) is oxidized, hydrolyzed, and subsequently decarboxylated to give 6-methyl maltol (IV).

3-Hydroxy-4*H*-pyran-4-ones, especially 3-hydroxy-2-methyl-4*H*-pyran-4-one, *i.e.*, maltol, have long been known and have been widely used as food flavors. Maltol has been synthesized from kojic acid or pyromeconic acid as the starting material.[2] Recently, these compounds have also been obtained[3] from inaccessible dihydro-γ-pyrones in low yields.

In this investigation, we aimed to get dihydro-γ-pyrones (I) and succeeded in preparing α-diketones by oxidation. We have previously reported on the oxidation of 2-carbethoxy-2-methylcyclopentanone to give 5-carbethoxy-2-hydroxy-5-methylcyclopent-2-en-1-one.[4] These studies have now been extended to dihydro-γ-pyrones (I). I was synthesized directly by the condensation of β-ketoesters with crotonoyl chloride.

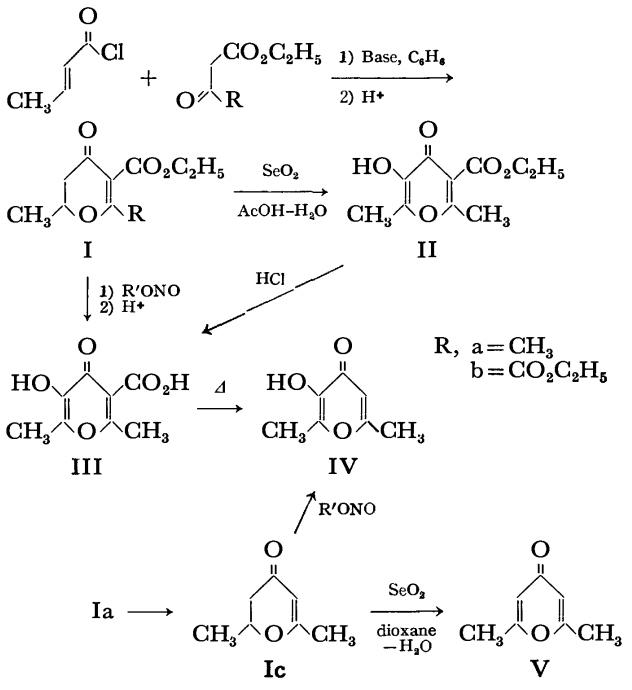

5-Carbethoxy-2,3-dihydro-2,6-dimethyl-4*H*-pyran-4-one (Ia)[5] and 2,3-dihydro-2,6-dimethyl-4*H*-pyran-4-one (Ic)[6] has already been synthesized. 5,6-Dicarbethoxy-2,3-dihydro-2-methyl-4*H*-pyran-4-one (Ib) was obtained by the condensation of sodium ethyl oxalacetate[7] with crotonoyl chloride. The oxidation of Ia with selenium dioxide gave 5-carbethoxy-3-hydroxy-2,6-dimethyl-4*H*-pyran-4-one (II) in a low yield. The hydrolysis of II in hydrochloric acid afforded 5-hydroxy-2,6-dimethyl-4-oxo-4*H*-pyran-3-carboxylic acid (III) in a 75% yield, and subsequent decarboxylation of III in diphenyl ether at 250°C yielded 3-hydroxy-2,6-dimethyl-4*H*-pyran-4-one (IV) in a 30% yield. These compounds, II, III, and IV, had a characteristic odor like maltol and gave an intense violet color with ferric chloride.

However, α-diketone was not isolated from Ib. Dihydro-γ-pyrone (Ic) gave a dehydrogenated compound, 2,6-dimethyl-4*H*-pyran-4-one (V). Furthermore, the nitrosation of Ia followed by acid hydrolysis afforded III. However, Ib gave only a tarry material, and IV was obtained from Ic.

The bromination of Ia with an excess of dioxane dibromide in ether gave 3,3-dibromo-6-dibromomethyl-5-carbethoxy-2,3-dihydro-2-methyl-4*H*-pyran-4-one (VI) in a 72.4% yield. The structure of VI was assigned on the basis of its IR, and NMR spectra and the results of an elemental analysis.

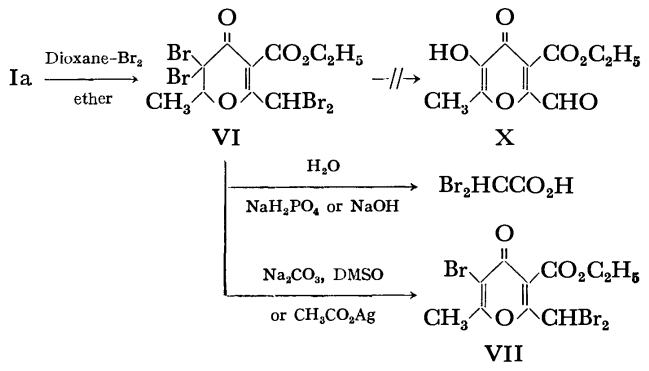

The hydrolysis of VI with sodium biphosphate in dioxane–water at 85°C for 10 hr afforded dibromoacetic acid in an 80% yield. A similar compound was also prepared by the hydrolysis of a dilute sodium hydroxide solution at 0°C for 24 hr. The hydrolysis of 5-carbethoxy-2,3-dihydro-6-methyl-γ-pyrones has been shown to give

1) A part of this paper was presented at the 13th Annual Conference of Terpens and Essential Oils, Kagoshima, October, 1969.

2) M. A. Spielman and M. Freifelder, *J. Amer. Chem. Soc.*, **69**, 2908 (1947); R. L. Miller, B. E. Tate, R. P. Allingham, and H. Rutner, Belg. 625114 (1963); B. E. Tate, U. S. 3171842 (1965).

3) K. Nakanishi, M. Nagao, and K. Okada, *Yakugaku Zasshi* **88**, 1044 (1968), Jap. Pat. 17905 (1967); M. Higuchi *et al.*, Jap. Pat. 21106 (1970); A.A. Schleppnik, U.S. 3474113 (1969); A.A. Schleppnik and M.L. Oftedahl, U. S. 3491122 (1970); *Chem. Abstr.*, **72**, 78880t; A. A. Schleppnik and M. L. Oftedahl, Jap. Pat. 6813 (1970).

4) K. Sato, S. Suzuki, and Y. Kojima, *J. Org. Chem.*, **32**, 339 (1967); K. Sato, Y. Kojima, and H. Sato, *ibid.*, **35**, 2374 (1970).

5) E. Graf and K. C. Liu, *Arch. Pharm.*, **300**, 348 (1967).

6) S. Gelin and R. Gelin, *C. R. Acad. Sci. Paris.*, **264**, 1858 (1967).

7) S. Gelin and R. Gelin, *Bull. Soc. Chim. Fr.*, **1969**, 4091.

3-acetyl-5,6-dihydro-4-hydroxy-α-pyrones, together with δ-acetoxy-β-ketoesters.[5] Similarly, the treatment of aqueous sodium hydroxide with 5-carbethoxy-2-hexyl-2,3-dihydro-6-methyl-4*H*-pyran-4-one (VIII), which has been easily obtained by the condensation of ethyl acetoacetate with 2-nonenoyl chloride, afforded the corresponding α-pyrone (IX) in a 77.9% yield.

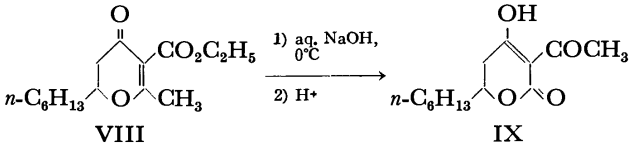

VIII IX

It may be supposed that compound VI is first hydrated to a double bond instead of to its two nucleophilic carbons, and that a subsequent ring cleavage produces dibromoacetic acid. On the other hand, the treatment of VI with equimolar amounts of sodium carbonate in DMSO provided 3-bromo-6-dibromomethyl-5-carbethoxy-2-methyl-4*H*-pyran-4-one (VII) in a 54.6% yield. When silver acetate and VI were refluxed in acetic acid, dehydrobromination also occurred to yield VII. Under various conditions, none of the expected hydrolysis product (X) could be isolated from the reaction mixture.

Accordingly, it may be supposed that the lack of success in introducing the α-carbonyl group into dihydro-γ-pyrones (I) is due to the low stability of the ring, as will be discussed above.

Experimental

All the melting points and boiling points are uncorrected. The infrared spectra were recorded with a Hitachi Model EPI-S2 spectrophotometer, and the ultraviolet spectra, with a Hitachi Model EPS-3T spectrophotometer. The NMR spectra were obtained on a JEOL Model C-60H spectrometer, with tetramethylsilane as the internal reference.

Materials. 5-Carbethoxy-2,3-dihydro-2,6-dimethyl-4*H*-pyran-4-one,[5] 2,3-dihydro-2,6-dimethyl-4*H*-pyran-4-one,[6] sodium ethyl oxalacetate,[7] *n*-butyl nitrite,[8] and crotonoyl chloride[9] were prepared by the method described in the literature. The other chemicals were commercially available and well purified by the usual procedures before use.

*5,6-Dicarbethoxy-2,3-dihydro-2-methyl-4*H*-pyran-4-one (Ib).* To a suspension of sodium ethyl oxalacetate (20 g) (0.095 mol) in 90 ml of dry benzene, 5.3 g (0.05 mol) of crotonoyl chloride diluted with 10 ml of benzene was added, drop by drop, at 15—20 °C for 30 min. The mixture was then refluxed at 70 °C for 1 hr with stirring. After cooling, 50 ml of cold water was added, and the mixture was made slightly acidic with 10% sulfuric acid. The organic layer was separated, and the aqueous layer was extracted with ether. The combined organic layer was washed with water and dried over magnesium sulfate. Fractional distillation under nitrogen gave ethyl oxalacetate and 6.2 g of an oil (bp 150—170 °C/0.7 mmHg). The redistillation of the latter oil gave 4.7 g (36.6%) of pure Ib; bp 142—147 °C/0.3 mmHg; n_D^{20} 1.4872; IR (neat) 1725, 1655 (C=O), 1568 (C=C), 1370, 1300—1030 cm^{-1} (C–O–C); NMR (CCl_4) 1.20 (3H, d, J=8.0), 1.29 (3H, t, J=7.0), 1.36 (3H, t, J=7.0), 2.3—3.1 (2H, m), 4.13 (2H, q, J=7.0), 4.20 (2H, q, J=7.0), 3.9—4.4 (1H, m). Found: C, 56.24; H, 6.66%. Calcd for $C_{12}H_{16}O_6$: C, 56.25; H, 6.29%. 2,4-Dinitrophenylhydrazone; mp 113—115 °C. Found: C, 49.05; H, 4.97%. Calcd for $C_{18}H_{20}N_4O_9$: C, 49.54; H, 4.62%.

*5-Carbethoxy-3-hydroxy-2,6-dimethyl-4*H*-pyran-4-one (II).* To a hot (80 °C) solution of 11.1 g (0.1 mol) of selenium dioxide in 100 ml of acetic acid and 4 ml of water, was added 10 g (0.05 mol) of Ia all at once. The mixture was refluxed with stirring for 24 hr, and then the precipitated selenium was filtered out. The filtrate was concentrated and distilled to give a yellow oil (bp 105—110 °C/0.2 mmHg); when this oil was allowed to stand overnight, it gave a crystalline material together with 4 g of recovered Ia. Filtration, followed by recrystallization from aqueous ethanol, afforded 410 mg (4.0%) of II as colorless needles; mp 155 °C; IR (KBr): 3260 (O–H), 1736, 1665 (C–O), 1605 (C=C), 1225, 1190, 1105 cm^{-1} (C–O–C); UV (EtOH) 222 mμ (ε 13560), 275 mμ (ε 7400); NMR ($CDCl_3$) 1.36 (3H, t, J=7.0), 2.30 (3H, s), 2.40 (3H, s), 4.43 (2H, q, J=7.0), 6.45 (1H, s); Found: C, 56.87; H, 5.94%. Calcd for $C_{10}H_{12}O_5$: C, 56.60; H, 5.70%.

*5-Hydroxy-2,6-dimethyl-4-oxo-4*H*-pyran-3-carboxylic Acid (III).* *a)*: A mixture of 170 mg of II and 3 ml of 6M hydrochloric acid was heated at 100 °C for 2 hr. The cooled mixture was extracted with chloroform and washed with water. The subsequent evaporation of the solvent gave a crude product; this was recrystallized from water to give pure III (112 mg, 75%) as colorless needles; mp 161 °C. IR (KBr): 3300, 3060—2640 (O–H), 1730, 1663 (C=O), 1620, 1570 (C=C) 1220, 1098 cm^{-1} (C–O–C); UV (EtOH), 223 mμ (ε 14000), 279 mμ (ε 6590); NMR ($CDCl_3$) 2.45 (3H, s), 2.86 (3H, s), 6.54 (1H, broad s). Found: C, 52.18; H, 4.72%. Calcd for $C_8H_8O_5$: C, 52.18; H, 4.38%.

b): Dry hydrogen chloride was introduced into a cold, stirred solution of 6.0 g (0.03 mol) of Ia in 40 ml of dry ether at 0 °C for 25 min. Then, 5.0 g (0.05 mol) of *n*-butyl nitrite in 5 ml of ether was added over a period of 30 min at 0—5 °C. The mixture was then heated at 35 °C for 4.5 hr. After cooling, the solvent was removed by distillation and the residue was hydrolyzed with 70 ml of 3M hydrochloric acid by refluxing for 5 hr. The removal of the hydrochloric acid, filtration, and subsequent recrystallization from water provided the product, III (1.0 g, 18.1%), as colorless needles; mp 160—161 °C. The infrared spectrum and the other chemical properties were identified with those of the III presented above.

*3-Hydroxy-2,6-dimethyl-4*H*-pyran-4-one (IV).* *a)*: A solution of 200 mg of III in 4.0 g of diphenyl ether was heated at 250—260 °C for 1 hr. After cooling, the reaction mixture was poured into 0.25M aqueous sodium hydroxide (8 ml) and the aqueous layer was separated. To remove the diphenyl ether, the aqueous layer was extracted with ether and acidified with hydrochloric acid. Extraction with ether, followed by evaporation, gave crude IV; this was recrystallized from water to provide IV (46 mg, 30%) as colorless needles; mp 159—160 °C (lit,[10] mp 162.5 °C). A mixed-melting-point determination with an authentic sample[10] indicated no depression. IR (KBr): 3230 (O–H), 1660 (C=O), 1617, 1580 (C=C), 1215 cm^{-1} (C–O–C); NMR ($CDCl_3$) 2.28 (3H, s), 2.34 (3H, s), 6.25 (1H, s), 7.32 (1H, s). Found: C, 59.97; H, 5.77%. Calcd for $C_7H_8O_3$: C, 60.00; H, 5.75%.

b): To a stirred solution of 1.26 g (0.01 mol) of Ic, 0.8 ml of hydrochloric acid, and 30 ml of ethanol, 3.2 g (0.031 mol)

8) W. A. Noyes, "Organic Syntheses," Coll. Vol. II, p. 546 (1943).

9) R. C. Fuson, R. E. Christ, and G. M. Whitman, *J. Amer. Chem. Soc.*, **58**, 2450 (1936).

10) J. N. Gollie and T. Tickle, *J. Chem. Soc.*, **81**, 1005 (1902).

of *n*-butyl nitrite diluted with 10 ml of ethanol was added at gentle refluxing for 5 min, and then the mixture was kept for 10 hr. The solvent was evaporated and the residue was recrystallized from water to yield 50 mg (3.6%) of IV; mp 159—160 °C.

2,6-Dimethyl-4H-pyran-4-one (V). A mixture of 1.26 g (0.01 mol) of Ic, 1.10 g (0.01 mol) of selenium dioxide, 25 ml of dioxane, and 2.5 ml of water was refluxed with stirring for 40 hr. After cooling the selenium was filtered out and the solvent was removed. The residue was extracted with chloroform, and the subsequent evaporation of the chloroform gave a black oil, which was then sublimed at 150 °C under reduced pressure (15—20 mmHg). The sublimed crystals were recrystallized from chloroform to give 154 mg (12.2%) of V as colorless needles; mp 129—130 °C (lit,[11] mp 132 °C); IR (KBr) 3040 (C–H), 1660 (C=O), 1610, 1590 (C=C), 1396, 1160 (C–O–C), 900 cm^{-1}. The infrared spectrum and the other chemical properties were identical with those of an authentic sample.[11]

3,3-Dibromo-6-dibromomethyl-5-carbethoxy-2,3-dihydro-2-methyl-4H-pyran-4-one (VI). Bromine (39.2 g, 0.248 mol) was stirred into 70 ml of dioxane with cooling over a period of 15 min. The mixture was then diluted with 35 ml of ether, and 7.0 g (0.035 mol) of Ia in 35 ml of ether was dropped in at room temperature over 15 min period. Then the mixture was refluxed for 7 hr and allowed to stand overnight at room temperature. The resulting mixture was poured into ice water. The organic layer was separated, and the aqueous layer was extracted with ether. The combined organic layer was washed with water and dried over magnesium sulfate. The evaporation of the solvent and recrystallization from ethanol afforded colorless plates (13.1 g, 72.4%); mp 88—89 °C IR (KBr): 1710, 1700 (C=O), 1600 cm^{-1} (C=C); NMR (CCl_4) 1.40 (3H, t, J=7.0), 1.95 (3H, d, J=6.0), 4.40 (2H, q, J=7.0), 4.67 (1H, m), 7.05 (1H, s). Found: C, 23.43; H, 2.11%. Calcd for $C_{10}H_{10}Br_4O_4$: C, 23.38; H, 1.96%.

Reaction of VI with Sodium Biphosphate. A mixture of 6.3 g (0.04 mol) of sodium biphosphate, 5.1 g (0.01 mol) of VI, 25 ml of water, and 25 ml of dioxane was stirred at 84—85 °C for 10 hr. After cooling, the organic layer was separated and the aqueous layer was extracted with ether. The combined organic layer was washed with water and dried over magnesium sulfate. After the removal of the ether, the distillation of the residual oil gave 1.8 g (80%) of dibromoacetic acid; bp 110—112 °C/5 mmHg (lit,[12] bp 195—197 °C/250 mmHg). IR (neat): 3020, 2630—2510 (O–H), 1720 (C=O), 910 cm^{-1}; NMR (CCl_4) 5.63 (1H, s), 10.05 (1H, s); mol. wt. 217 (alkali titration), $C_2H_2Br_2O_2$ require 218.

Reaction of VI with Sodium Hydroxide. A mixture of 5.0 g (0.01 mol) of VI, 4.0 g (0.1 mol) of sodium hydroxide, and 100 ml of water was stirred at 0 °C for 24 hr. The resulting mixture was acidified with hydrochloric acid and extracted with ether. After drying, the ether was evaporated and the residual oil was distilled to give 0.8 g (38%) of dibromoacetic acid; bp 90—98 °C/1.0 mmHg.

3-Bromo-6-dibromomethyl-5-carbethoxy-2-methyl-4H-pyran-4-one (VII). *a)*: A mixture of 20.4 g (0.04 mol) of VI and 4.3 g (0.04 mol) of sodium carbonate in 75 ml of DMSO was stirred at 20 °C for 3 hr. The resulting mixture was poured into ice water and extracted with chloroform. After drying, the solvent was evaporated and the residual solid was crystallized from aqueous ethanol to give 9.45 g (54.6%) of VII; mp 149—151 °C. IR (KBr): 1732, 1638 (C=O and C=C), 1395, 1010, 720 cm^{-1}; NMR ($CDCl_3$) 1.36 (3H, t, J=6.8), 2.56 (3H, s), 4.31 (2H, q, J=6.8), 6.59 (1H, s). Found: C, 27.95; H, 2.36%. Calcd for $C_{10}H_9Br_3O_4$: C, 27.74; H, 2.10%.

b): A mixture of 2.6 g (0.005 mol) of VI and 3.3 g (0.02 mol) of silver acetate in 40 ml of acetic acid was refluxed, with stirring, for 4 hr. To the mixture was then added 3 ml of water, after which the hot mixture was refluxed for an additional 2 hr. The subsequent filtration of the silver bromide and evaporation of the solvent gave a crude product. Recrystallization from aqueous ethanol afforded 0.8 g (38%) of VII as fine needles; mp 149—150 °C.

5-Carbethoxy-2-hexyl-2,3-dihydro-6-methyl-4H-pyran-4-one (VIII). A mixture of 5.0 g (0.21 mol) of magnesium turnings, 40 ml of absolute ethanol, 0.5 ml of carbon tetrachloride, and 50 ml of dry benzene was heated under reflux for 3 hr. The solvent was then distilled off, and 100 ml of benzene was added to the magnesium ethoxide. To this suspension, 26 g (0.2 mol) of ethyl acetoacetate was added below 30 °C, and then 36.6 g (0.21 mol) of 2-nonenoyl chloride[13] was slowly added over a period of 30 min at room temperature. The mixture was heated at 70 °C for 20 min with stirring. After cooling, the reaction mixture was acidified with 10% sulfuric acid. The organic layer was separated, and the aqueous layer was extracted with ether. The combined organic layer was washed with water, dried over sodium sulfate, and concentrated. The residue was distilled, thus giving VIII (15.3 g, 57%); bp 137—139 °C/0.3 mmHg, n_D^{20} 1.4825; IR (neat): 1710, 1680 (C=O), 1600 cm^{-1} (C=C); NMR (CCl_4) 0.88 (3H, t, J=7.0), 1.15 (3H, t, J=7.0), 1.30 (10H, broad s), 2.06 (3H, s), 2.28 (2H, d, J=8.2), 4.04 (2H, q, J=7.0), 4.18 (1H, m). Found: C, 66.80; H, 8.95%. Calcd for $C_{15}H_{24}O_4$: C, 67.14; H, 9.01%. 2,4-Dinitrophenylhydrazone; mp 110—113 °C.

3-Acetyl-6-hexyl-5,6-dihydro-4-hydroxy-2H-pyran-2-one (IX). A cold solution of 10.7 g (0.04 mol) of VIII and 3.2 g (0.08 mol) of sodium hydroxide in 160 ml of water was stirred at 0—2 °C for 24 hr. The resulting mixture was acidified with hydrochloric acid, and then the crystalline material was precipitated. Filtration and recrystallization from aqueous ethanol afforded IX (7.5 g, 77.9%) as colorless crystals; mp 69.5—70 °C; IR (KBr): 1690 (C=O), 1565 cm^{-1} (C=C); NMR ($CDCl_3$) 0.88 (3H, t, J=7.0), 1.30 (10H, broad s), 2.53 (3H, s) 2.62 (2H, d, J=1.8), 4.25 (1H, m), 17.4 (1H, s). Found: C, 64.77; H, 8.40%. Calcd for $C_{13}H_{20}O_4$: C, 64.98; H, 8.39%.

The authors wish to express their gratitude Mr. Mitsuo Sato for capable technical assistance in these experiments.

11) F. Feist, *Ann. Chem.*, **257**, 273 (1890).
12) W. H. Perkin, *J. Chem. Soc.*, **65**, 425 (1894).
13) E. Otto and K. Zimmerman, *Ann. Chem.*, **425**, 330 (1921).

The Optical and Electrical Properties of Metal Photo-doped Chalcogenide Glasses

Isamu SHIMIZU, Hiraku SAKUMA, Hiroshi KOKADO, and Eiichi INOUE

Imaging Science and Engineering Laboratory, Tokyo Institute of Technology, O-okayama, Meguro-ku, Tokyo

(Received September 5, 1972)

The optical and electrical properties of the metal photo-doped chalcogenide glasses were studied. The optical absorption of the chalcogenide glasses (*e.g.*, the As–S, As–S–Te, and As–S–Se systems) was increased by the photo-doping of such metals as Ag and Cu in the region of their absorption edges. The electrical conductivity of the glasses also increased with the photo-doping of the metals. The effective band gap obtained from the results of the temperature dependency of the electrical conductivity decreased with the increase in the amount of metal which was photo-doped in the glasses. The results obtained in this study suggest that the metals photo-doped in the chalcogenide glasses behaved as structural modifiers of the glasses, and that the state of density in the gap was increased by the metal photo-doping.

When a binary layer of metal and chalcogenide glass is exposed to light, the metal diffuses into the glass layer. We gave the term "photo-doping"[1] to the phenomenon by analogy with the doping of foreign materials into a crystalline semiconductor. As a result of the metal photo-doping, some drastic changes take place in the optical, electrical, and chemical properties of the chalcogenide glasses. We have succeeded in using the metal-chalcogenide system as a recording process of the optical image.[2] For example, the difference in optical absorption between the metal-doped and undoped areas of the chalcogenide glass layer is sufficiently large to be recorded directly on the system by image-by-image exposure. We obtained a fine relief pattern from the image-by-image exposed layer by taking out the undoped metal with an acid and by etching the undoped chalcogenide glass area with an alkaline solution. This technique is useful in making an optical mask in microfabrication technology. It should be noted that the metal-chalcogenide glass system is suitable for holographic recording.

This paper will report the results on the optical absorption and electrical conductivity of various chalcogenide glasses in which metal is doped by illumination. Judging from the results of our studies undertaken from the standpoint of the band theory, the photo-doped metals in the glass act as structure modifiers of the chalcogenide glass.

Experimental

The materials were prepared by fusing a mixture of appropriate quantities of elements in an evacuated fused quartz tube at 650 °C for 8 hr with occasional agitation. Four compositions of the glasses, $(As_2S_3)_1I_x$, were prepared with $x=$ 0.55, 1.0, 1.5, and 2.0 by heating a mixture of As_2S_3 and iodine in an Ar gas atmosphere.

The binary layer of chalcogenide glass and metal was prepared on a substratum (slide glass) by the successive vacuum evaporation (1×10^{-5} Torr) of the chalcogenide glass and metal (Ag or Cu).

The absorption spectra of the films were measured with a spectrophotometer, Shimadzu MPS-50L. A multi-beam interferometer, Mizojiri Model II, was used to measure the thickness of the layers.

The electrical-conductivity measurements were taken with surface-type cells having Au electrodes 1 mm apart from each other and with a micro-ammeter Takeda Riken TRA-1 (DC apparatus).

Results and Dsicussion

The absorption spectrum of the binary layer represented the sum of the optical absorptions of the metal and chalcogenide glass layers. An area which had been illuminated showed an increase in transmittance in the visible and infra-red regions. This implies that the metal layer was doped into the chalcogenide glass by exposure to light. A typical example of the spectral change in the layer, showing the photo-induced reaction caused between metal and chalcogenide glass, is shown in Fig. 1. The photo-induced reaction took place at the interface of the layers when the incident photons had sufficient energy to excite the electrons of the chalcogenide glass. The tail of the absorption spectrum of the metal photo-doped glass was shifted to a longer wavelength than that of the undoped chalcogenide glass. The disappearance of the metal on the glass was confirmed by observing the decrease in the optical absorption of metal in the infrared region. To

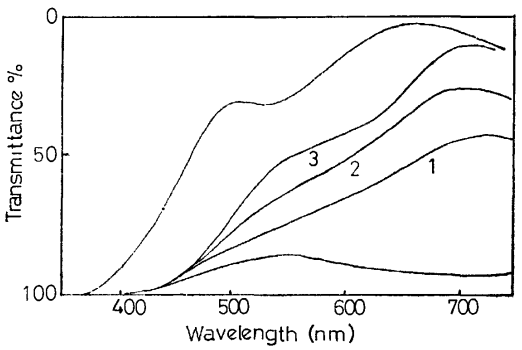

Fig. 1. Spectral transmission as affected by exposure to the light from a mercury lamp (5×10^{-3}W/cm^2) for the indicated time t(sec). The top curve shows the transmission of the chalcogenide glass ($As_{16}S_{80}Te_4$) alone and the bottom curve that of the glass plus a 309 Å Ag layer before irradiation. Curve 1: t=60, 2: t=120, 3: t=300

1) I. Shimizu, H. Sakuma, H. Kokado, and E. Inoue, This Bulletin, **44**, 1173 (1971).

2) H. Sakuma, I. Shimizu, H. Kokado, and E. Inoue, Proceeding of the 3rd conference on solid state devices, Tokyo, 1971, p. 76.

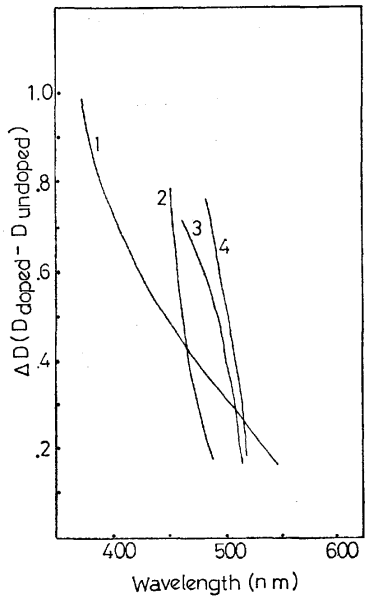

Fig. 2. Difference spectra of Ag(200 Å) photo-doped chalcogenide glasses (As-S system).
Curve 1: $As_{14.8}S_{85.2}$, 2: $As_{43.5}S_{56.5}$, 3: $As_{40}S_{60}$, 4: $As_{21.3}S_{78.7}$
ΔD shows the difference of the optical absorption of the glasses in which Ag of 200 Å in thickness have been photo-doped and the undoped ones.

show the change in the optical absorption of the chalcogenide glass layer caused by the photo-doping of the metal, the difference spectrum was made by plotting the difference in the optical absorption between doped and undoped glasses against the wavelength. Since chalcogenide glass layers (0.5 μm) thicker than the metal layer (200 Å) were used in these measurements, the change in the thickness of the chalcogenide glass layers resulting from the metal photo-doping was negligible. The difference spectral curves of As–S systems in which Ag 200 Å in thickness was photo-doped are shown in Fig. 2. The optical absorption

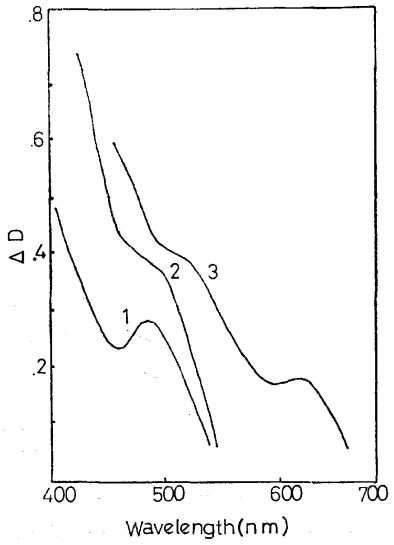

Fig. 3. Difference spectra of the Ag photo-doped chalcogenide glasses (As-S-Te system).
Ag of 100 Å (curve 1) and 200 Å (curve 2) photo-doped in $As_{16}S_{80}Te_4$. Curve 3: Ag (200 Å) photo-doped in $As_{30}S_{50}Te_{20}$

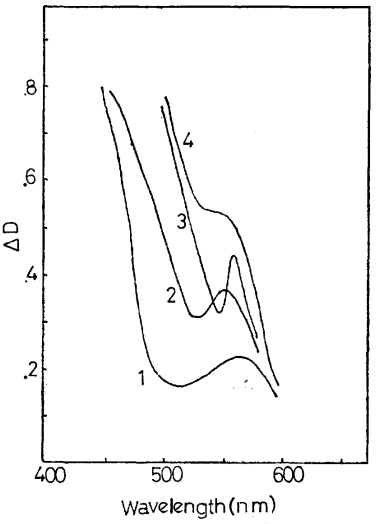

Fig. 4. Difference spectra of Ag (200 Å) photo-doped glasses (As–S–Se) system).
Curve 1: $As_{17.7}S_{70.8}Se_{11.5}$, 2: $As_{30}S_{50}Se_{20}$, 3: $As_{18}S_{40}Se_{42}$, 4: $As_{19}S_{27}Se_{54}$

was increased by metal photo-doping in each glass. Increases in the optical absorption were observed near the absorption tails of the glasses. Since no detectable change in the electron-beam diffraction pattern could be observed in the Ag photo-doped glass layer, it can be assumed that no devitrification was brought about by the Ag photo-doping. The increase in the optical absorption resulting from Ag photo-doping was also observed in other systems, such as As–S–Te and As–S–Se. The difference spectral curves are shown in Figs. 3 and 4. The increase in the optical absorption was in proportion to the amount of Ag which was photo-doped (see Curves 1 and 2 in Fig. 3). In the As–S–Se system, a discrete absorption band (maximum at 565 nm) was observed in the difference spectra, in addition to the increase in the optical absorption which was observed in the absorption tails of the host glasses.

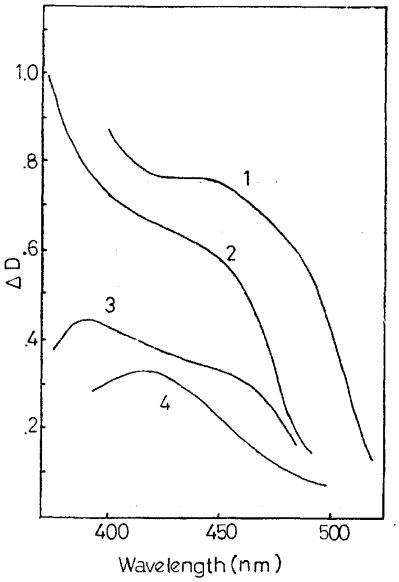

Fig. 5. Difference spectra of Ag (200 Å) photo-doped glasses ($(As_2S_3)_1I_x$).
Curve 1: $x=0$, 2: $x=0.51$, 3: $x=1.0$, 4: $x=1.98$.

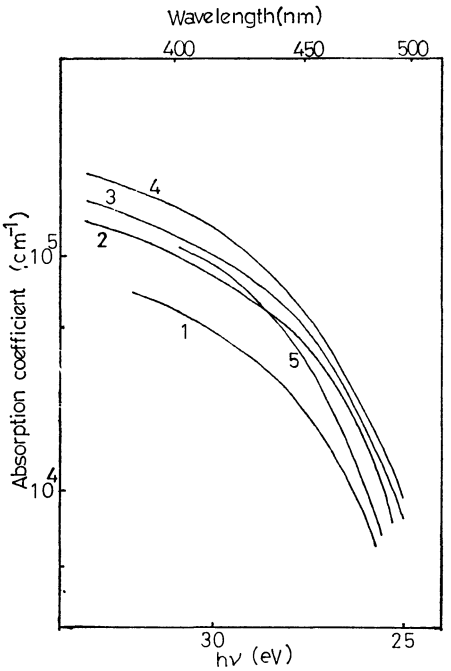

Fig. 6. Absorption spectra of the chalcogenide glasses ($(As_2S_3)_1I_x$).
Curve 1: $x=0$, 2: $x=0.51$, 3: $x=1.0$, 4: $x=1.98$.

The height of the band increased with an increase in the Se content in the glass. In this case, some localized level caused by the interaction between Ag and Se was assumed to be formed in the band gap by Ag photo-doping.

In the glass containing a halogen such as iodine, a charactristic effect on the optical absorption was observed when Ag was doped by illumination. Figure 5, for example, shows the difference spectral curves of the $(As_2S_3)_1I_x$ glass, in which Ag (200 Å in thickness) was photo-doped. A conspicuous increase in the optical absorption was found in the Ag-doped As_2S_3 ($x=0$). On the other hand, the increase in the optical iodine absorption was inhibited by the addition of to the glass. In this case, the tails of the optical absorption of the glasses ($(As_2S_3)_1I_x$) themselves extended to longer wavelengths than those of As_2S_3, as is shown in Fig. 6. From these results, it can be supposed that the photo-doped Ag in the glass is captured by iodine, forming a strong bond such as AgI.

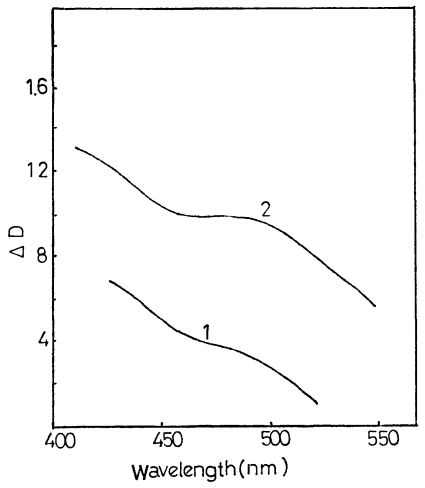

Fig. 7. Difference spectra of the Ag (200 Å) (curve 1) and the Cu (200 Å) (curve 2) photo-doped glass ($(As_2S_3)_1I_{1.98}$)

Figure 7 presents the difference spectral curves of $(As_2S_3)_1I_x$, in which the same amount of Cu as Ag was photo-doped. The increase in the optical absorption caused by the photo-doping of Cu was larger than that of Ag. In the case of Cu photo-doping, the range where the increase in the optical absorption was observed was extended to a longer wavelength than in the case of Ag.

The temperature dependence of the electrical conductivity of chalcogenide glass is generally written as:

$$\sigma = \sigma_0 \exp(\Delta E/kT) \quad (1)$$

where σ and σ_0 are the conductivities and whose ΔE, k, and T denote the activation energy, the Boltzmann factor, and the temperature in an absolute value (K) respectively. This relation tells us that there exists a gap between valence and conduction bands such as in the intrinsic crystalline semiconductors. Since thin film was used for photo-doping in our experiment, the electrical conductivity was measured by means of a surface type cell with Au electrodes 1 mm apart from each other. The current measured with the cell while applying DC voltage (IV) increased with an increase in the magnitude of Ag which had been photo-doped, as is shown in Fig. 8. Besides, the current while applying DC voltage (10 V) against the reciprocal of the absolute temperature was shown as a straight line in the chalcogenide glass ($As_{16}S_{80}Te_4$), in which a corresponding amount of Ag had been photo-doped (see Fig. 9). The ΔE values obtained from the slope of the lines are shown in Table 1. These results imply that the conductivity was increased by the Ag photo-doping, and that, at the same time, "the electrical band gap" ($2\Delta E$) was decreased. These results coincided qualitatively with those of studies of the effect of Ag as a foreign material on the electrical conductivity of chalcogenide glass.[3] In that experiment, the chal-

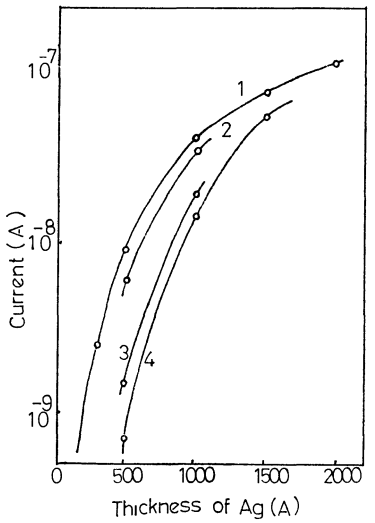

Fig. 8. Current of the Ag photo-doped glasses *vs.* the thickness of the Ag layer which has been doped in the glasses.
Curve 1: $As_{16}S_{80}Te_4$, 2: $As_{40}Se_{60}$, 3: $As_{24}S_{70}Te_6$, 4: $As_{40}S_{60}$

3) R. Andreichin, *J. Non-Crystalline Solids*, **4**, 73 (1970).

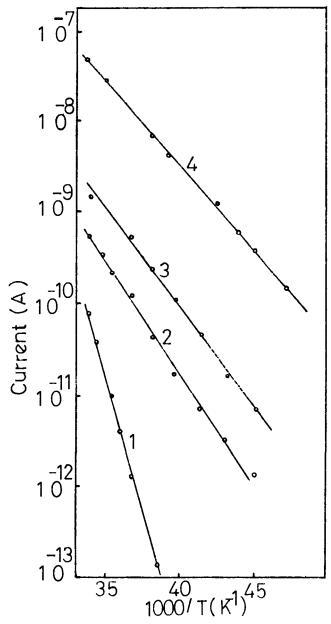

Fig. 9. Current of the Ag photo-doped glass ($As_{16}S_{80}Te_4$) *vs.* reciprocal temperature.
Curve 1: non-doped one, 2: Ag (300 Å), 3: Ag (500 Å), 4: Ag (2000 Å) photo-doped one.

TABLE 1. "ELECTRICAL BAND GAP ($2\Delta E$)" OF THE Ag PHOTO-DOPED CHALCOGENIDE GLASSES

Composition	Photo-doped Ag (Å)	Band gap (eV)
$As_{16}S_{80}Te_4$	0	2.32
	300	0.98
	500	0.88
	2000	0.75
$As_{40}Se_{60}$	0	1.88
	500	0.72
	1000	0.68

cogenide glass containing Ag was prepared by fusing the chalcogenide glass and Ag.

Figure 10 shows the curve obtained by plotting the current against ($1/T$) for the $As_{16}S_{80}Te_4$ layer, in which Cu of a thickness of 500 Å had been photo-doped. The effective gap obtained from the slope was 0.48 eV.

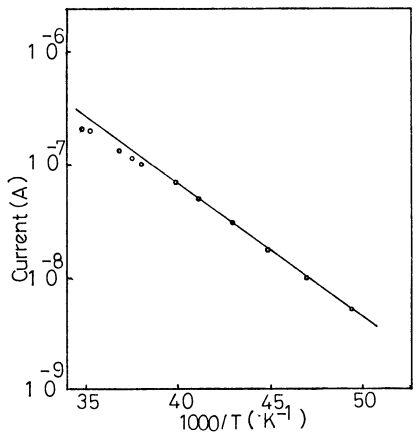

Fig. 10. Current *vs.* reciprocal temperature for the Cu (500 Å) photo-doped glass ($As_{16}S_{80}Te_4$).

This value was smaller than that of the same glass in which Ag of a thickness of 2000 Å had been photo-doped. This result coincided with the results of the effect of the photo-doped Cu on the optical absorption of the chalcogenide glass presented above. This means that Cu is a more effective modifier of the electrical structure of chalcogenide glass than is Ag.

From the theoretical ponit of view, the electrical structure of chalcogenide glass, with which the optical absorption and electrical conductivity mechanism can be elucidated sufficiently, is not clear. It is assumed by Mott[4] that the band structure of the semiconductor is retained, but with some alteration, especially since the curves of the density of the states from tails fall well inside the forbidden gap. Also Fritzsche, Cohen, and Ovshinsky[5] proposed the FCO band model modifying Mott's model to elucidate the optical and electrical properties of chalcogenide glasses.

From the standpoint of the band theory, the role of the metal which was doped into chalcogenide glass by illumination was considered to be a modifier in the band structure of the glass.

As was suggested by the band theory for the crystalline semiconductor, the absorption coefficient (α) in an indirect transition can be written as:

$$\alpha = \text{const}\frac{|M|^2}{h\nu}(h\nu - E_0)^2 \qquad (2)$$

where M is the matrix element of the electrical transition and whose $h\nu$ and E_0 denote the energy of the absorbed photon and the band gap respectively. If M is constant, plotting $(\alpha h\nu)^{1/2}$ against $h\nu$ should result in a straight line. Typical curves showing $(\alpha h\nu)^{1/2}$ versus $h\nu$ for the Ag photo-doped chalcogenide glasses are shown in Fig. 11. When the binary layer is used,

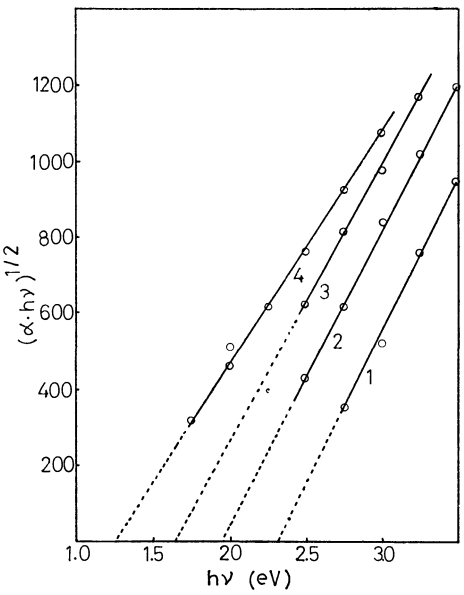

Fig. 11. $(\alpha h\nu)^{1/2}$ *vs.* $h\nu$ for the Ag photo-doped glass ($As_{16}S_{80}Te_4$).
Curve 1: non-doped one, 2: Ag (100 Å), 3: Ag (300 Å), 4: Ag (500A) photo-doped one.

4) N. F. Mott, *Advan. Phys.*, **16**, 49 (1967).
5) M. H. Cohen, H. Fritzsche, and S. R. Ovshinsky, *Phys. Rev. Lett.*, **22**, 1065 (1969).

TABLE 2. "OPTICAL GAP (E_0)" OF THE Ag PHOTO-DOPED CHALCOGENIDE GLASSES

Composition	Photo-doped Ag (Å)	Optical gap (eV)
$As_{16}S_{80}Te_4$	0	2.30
	100	1.95
	300	1.65
	500	1.25
$As_{43.5}S_{56.5}$	0	2.14
	200	1.14
$As_{14.8}S_{85.2}$	0	2.24
	200	1.50
	400	1.25

the photo-induced doping is caused at its interface and the distribution of the photo-doped metal in the glass is not uniform. To improve the uniformity, therefore, the thin layer of the chalcogenide glass (600 Å) was used in this measurement. Except for their tails, the plots all show straight lines. The extrapolation of the linear portions of Fig. 11 intersect with the abscissa at the energy E_0; they are shown in Table 2. This value (E_0) is a convenient fiducial mark for locating the structureless absorption curve; one refers to it as the optical gap. The value for E_0 decreased with the increase in the amount of Ag which was photo-doped in the glass. This shows a tendency similar to the effect of photo-doped metal on the value for $2\Delta E$. However, the value for E_0 does not correspond quantitatively to that for $2\Delta E$ in each sample.

These results also support the idea that the photo-doped metals behave as structure modifiers in covalent noncrystalline semiconductors such as chalcogenide glasses. And resulting from the photo-doping of the metal, the state-density in the band gap increased. It may be supposed that the increases in the optical absorption and the electrical conductivity of the metal photo-doped chalcogenide glass are caused by the increase in the state-density in the gap.

NOTE

BULLETIN OF THE CHEMICAL SOCIETY OF JAPAN, VOL. 46, 1296 (1973)

Electron Transfer Between Tetracyanoethylene and Its Anion Radical

Raymond CHANG and Jeffery PIEHLER

Department of Chemistry, Williams College, Williamstown, Massachusetts, U.S.A.

(Received March 24, 1972)

The rate of homogeneous electron transfer reactions between an organic anion radical and its neutral molecule is usually close to the diffusion-controlled limit; however, such fast reactions can be conveniently studied by the electron spin resonance (ESR) technique.[1] It is now well known that many anion radicals can exist in thermodynamically distinct species called contact ion-pairs, solvent separated ion-pairs, and free ions.[2] For a given radical, the relative concentrations of these species depend on the nature of the metal cation, solvent, and temperature. In solvents of high dielectric constants such as dimethylformamide and hexamethylphosphoramide, these radicals are assumed to be in the free ion form[3] whereas in solvents of low dielectric constants such as 1,2-dimethoxyethane or tetrahydrofuran (THF) they are believed to be predominantly contact ion-pairs.[2] Although a detailed knowledge of the structure of such ion-pairs is often difficult to obtain, their reactivities can be readily compared from the rate measurements on the electron transfer reactions. For example, the second-order rate constants for the transfer reactions between naphthalene and its anion radical in THF with potassium and sodium as counter ions differ by at least a factor of three.[4,5] Presumably, as a result of the proximity of the metal cation in the ion-pair, a sandwich-type of collision complex is formed with the metal ion between two naphthalene molecules.[6] Thus we would expect that the size and charge distribution of the metal ion to have an important influence on the rate of transfer.

We report here the rate measurements on the electron transfer reactions between tetracyanoethylene (TCNE) and its anion radical ($TCNE^-$)

$$TCNE^- + TCNE \rightleftharpoons TCNE + TCNE^-$$

Table 1. SECOND-ORDER RATE CONSTANTS FOR ELECTRON TRANSFER IN THE TCNE–$TCNE^-$ SYSTEM IN THF AT 25 °C

Metal ion	$k \times 10^{-8}$ (M^{-1} sec^{-1})	Activation energy (kcal mol^{-1})
Li	1.8±0.2	2.8±0.2
Na	1.7±0.2	3.1±0.2
K	1.9±0.3	3.1±0.2
Rb	1.8±0.2	2.8±0.2
Cs	2.0±0.4	2.6±0.5

a) Values obtained over the temperature range of 20 °C to −60 °C.

in THF with alkali metals as the counter ion and present indirect evidence on the structure of ion-pair in solution. Table 1 summarizes the second-order rate constants together with the corresponding energies of activation. All the rates were measured in the so-called slow-limit.[1] The most surprising result from Table 1 is that all the rate constants are essentially the same. This implies that the reactivity of the TCNE anion radical is independent of the nature of its counter ion and hence the radical is probably in the free ion form. This is not in accordance with the low dielectric constant of THF (7.4)[7] and the fact that the cyanide functional groups are expected to tightly bind the metal ions. Furthermore, the rate constants here are about an order of magnitude smaller than those for aromatic hydrocarbon free ions. However, the results are at least consistent with the fact that no metal splittings are observed except perhaps in the case of cesium where the ESR lines are somewhat distorted at room temperature, suggesting that there might be a small, unresolved hyperfine interaction due to the cesium nucleus. Linear Arrhenius plots were obtained for all the systems from 20 °C to −60 °C. This suggests that over this temperature range there is only one type of radical anion present and its structure (with the metal ion) is insensitive to the change in dielectric constant of the solvent.

1) R. Chang, *J. Chem. Educ.*, **47**, 563 (1970).
2) N. Hirota, "Radical Ions," ed. by E. T. Kaiser and L. Kevan, Interscience Publishers, New York (1968), p. 35.
3) J. Chandhuri, S. Kume, J. Jagur-Grodzinski, and M. Szwarc, *J. Amer. Chem. Soc.*, **90**, 6421 (1968).
4) R. Chang and C. S. Johnson, Jr., *ibid.*, **88**, 2338 (1966).
5) N. Hirota, R. Carraway, W. Schook, *ibid.*, **90**, 3611 (1968).
6) A. B. Gooch, R. G. Griffin, C. S. Johnson, Jr., and R. Chang, *ibid.*, **93**, 2819 (1971).
7) D. J. Metz and A. Glines, *J. Phys. Chem.*, **71**, 1158 (1967).

Calculation of the Nonradiative Transition Rate for the $^1B_{1u} \rightarrow {}^1B_{2u}$ Transition in Benzene

Noriyuki SHIMAKURA, Yuichi FUJIMURA, and Takeshi NAKAJIMA
Department of Chemistry, Faculty of Science, Tohoku University, Sendai
(Received December 24, 1971)

The nonradiative transition rate for the $^1B_{1u} \rightarrow {}^1B_{2u}$ transition in benzene was calculated taking into account the pseudo-Jahn-Teller distortion in the $^1B_{1u}$ state and using a crude adiabatic approximation. The calculated rate constant is compared with the experimental one reported by Katz *et al.*

In a previous paper,[1] we dealt with a theoretical estimate of the intramolecular nonradiative transition rates for various interstates of benzene as considered from a breakdown of the Born-Oppenheimer approximation. The calculations were carried out on many assumptions which were thought to be justified within statistical limit. Apart from the exact reproduction of experimental data for the nonadiabatic transition rate of $^1B_{1u} \rightarrow {}^1B_{2u}$ transition, there was a significant discrepancy between theory and experiment even in a qualitative sense.

Katz *et al.*[2] have experimentally determined the absorption widths of the $^1E_{1u}$, $^1B_{1u}$, and $^1B_{2u}$ excited states of benzene in solid rare-gas matrices to be about 300, 300, and 0 cm^{-1} respectively. In our calculation, the nonradiative transition rates for $^1E_{1u} \rightarrow {}^1B_{1u}$, $^1B_{2u}$ transitions were predicted to be appreciable, but it turned out that the rate for the $^1B_{1u} \rightarrow {}^1B_{2u}$ transition vanishes.

So far as the $^1B_{1u}$ state is assumed to be of D_{6h} symmetry and expressed by a wavefunction including only singly excited configurations, the transition density between the $^1B_{1u}$ and $^1B_{2u}$ states is exactly zero in π-electron approximation and consequently the nonradiative transition rate vanishes. When the excited states are given in terms of configurations including doubly excited states, the transition density does not vanish. However, the use of wavefunctions including doubly excited configurations as the electronic part of the zeroth-order Born-Oppenheimer vibronic state does not seem to have any significant influence on the nonradiative transition rate.

On the other hand, it is known[3-5] that the $^1B_{1u}$ excited state of benzene is subjected to the pseudo-Jahn-Teller interaction with the $^1E_{1u}$ excited state through vibrations of e_{2g} symmetry, and as a result takes D_{2h} conformations with a quinoidal form or an antiquinoidal. In order to refine the estimation of the nonradiative transition rate for the $^1B_{1u} \rightarrow {}^1B_{2u}$ transition, we should adopt the distorted conformations of D_{2h} symmetry as the zeroth-order Born-Oppenheimer state for the $^1B_{1u}$ state.

Using a simplified, virtual model Sharf and Silbey[6] estimated the line broadening due to interaction between the non-diagonal Born-Oppenheimer states in higher excited electronic states of polyatomic molecules. They used an approximate adiabatic wavefunction for the zeroth-order Born-Oppenheimer vibronic state, and showed that the estimated linewidth obtained with the use of the above wavefunction is of the order of 1 cm^{-1}, whereas experimentally observed linewidths are of several hundred cm^{-1}. Recently they discussed this discrepancy[7] and showed that the vibronic broadening can be properly described through the "crude adiabatic approximation,"[8] whereas the procedure based on the adiabatic wavefunction can be misleading if proper care is not taken. Since both the adiabatic and crude adiabatic Born-Oppenheimer approximations employ complete sets of states, an exact calculation of the nonradiative decay rate could start from either procedure and produce the same, correct result. Nevertheless, since we use the perturbation theory and consider only the lower-order contributions, it is no longer required for the values of the nonradiative transition rate calculated in the crude adiabatic and adiabatic Born-Oppenheimer schemes to be the same or for either scheme to agree with its exact values. It is therefore important to ascertain which scheme would give rise to the smallest higher-order corrections and lead to the fastest convergence. Choice of the zeroth-order wavefunction is related to the problem of which description is more convenient rather than more correct.

In this paper we calculate the nonradiative transition rate for $^1B_{1u} \rightarrow {}^1B_{2u}$, taking into account the pseudo-Jahn-Teller distortion in the $^1B_{1u}$ state and using the crude adiabatic approximation.

Method of Calculation

Let $|s>$ and $\{|l>\}$ denote the optically excited initial Born-Oppenheimer vibronic state and the manifold of isoenergetic Born-Oppenheimer vibronic levels belonging to a lower electronic state, respectively. These vibronic states are the eigenfunctions of a zeroth-order Hamiltonian, H_0, and nonradiative transition is induced by the perturbation term

$$V = H - H_0, \quad (1)$$

1) N. Shimakura, Y. Fujimura, and T. Nakajima, This Bulletin, **45**, 695 (1972).
2) B. Katz, M. Brith, B. Sharf, and J. Jortner, *J. Chem. Phys.*, **52**, 88 (1970).
3) A. D. Liehr, *Z. Naturforsch.*, **13a**, 596 (1960).
4) A. D. Liehr, *J. Phys. Chem.*, **67**, 389 (1963).
5) L. Salem, "The Molecular Orbital Theory of Conjugated Systems," Benjamin, New York (1966).
6) B. Sharf and R. Silbey, *Chem. Phys. Lett.*, **4**, 423 (1969).
7) B. Sharf and R. Silbey, *ibid.*, **4**, 561 (1970).
8) H. C. Longuet-Higgins, *Advan. Spectry.*, **2**, 429 (1961).

where

$$H = T(q) + V(q, Q) + T(Q), \quad (2)$$

$$H_0 = T(q) + V(q, Q_0) + T(Q). \quad (3)$$

$T(q)$ and $T(Q)$ denote the kinetic-energy operator for electronic motion and nuclear motion, respectively, and $V(q, Q)$ is the potential energy operator of the molecular Hamiltonian. Subscript 0 to Q indicates that the corresponding quantity should be evaluated at the ground-state equilibrium nuclear arrangement.

Using resolvent operator R,[9] the exact nonradiative transition rate can be expressed as

$$k_{nr} = \frac{2\pi}{\hbar}\sum_l |\langle s|R|l\rangle|^2 \delta(E_s^0 - E_l^0), \quad (4)$$

where

$$H_0|s\rangle = E_s^0|s\rangle,$$
$$H_0|l\rangle = E_l^0|l\rangle. \quad (5)$$

In the statistical limit, Eq. (4) may be rewritten as[9]

$$k_{nr} = \frac{2\pi}{\hbar}\sum_l |\langle s|V|l\rangle|^2 \delta(E_s^0 - E_l^0) \quad (6)$$

If the most probable path[10] (*vide infra*) can be found for the nonradiative transition, we can represent the nonradiative transition rate by the most dominant term corresponding to the most probable path in the summation in Eq. (6). The nonradiative transition rate from the initial vibronic state $\Psi(^1B_{1u})$ to the final vibronic state $\Psi(^1B_{2u})$, is then written as follows.

$$k_{nr} = \frac{2\pi}{\hbar}|v_{MPP}|^2, \quad (7)$$

where the coupling matrix element v_{MPP} is given by

$$v_{MPP} = \langle \Psi(B_{1u})|\{V(q, Q) - V(q, Q_0)\}|\Psi(B_{2u})\rangle. \quad (8)$$

Let us choose the equilibrium nuclear position for the ground electronic state as an origin and expand the potential energy operator in normal coordinates to the first order. Equation (8) is then rewritten as

$$v_{MPP} = \langle \Psi(B_{1u})|\sum_{i=1}^{3N-6}\{\partial V(q, Q)/\partial Q_i\}_0 Q_i|\Psi(B_{2u})\rangle. \quad (9)$$

Since energy difference between the $^1B_{1u}$ and $^1E_{1u}$ state of benzene is very small, the conventional perturbation scheme for the Herzberg-Teller intensity-borrowing mechanism is not a good approximation in describing the $^1B_{1u}$ state subjected to pseudo-Jahn-Teller interactions with the $^1E_{1u}$ level, and a more refined treatment should be applied. Such calculations for the $^1B_{1u}$ state coupled with the $^1E_{1u}$ state have been carried out by van der Waals *et al.*,[11] who maintained that a single e_{2g} vibration dominates the vibronic mixing. They expanded a proper variational vibronic wavefunction in terms of the crude adiabatic electronic wavefunction, $\Phi^0(=\Phi(q, Q_0))$, which is the electronic wavefunction at the equilibrium configuration in the ground state as in the following.

$$\Psi(B_{1u}) = \eta \prod_{j\neq e_{2g}^c}^{3N-8} \chi''(n, j), \quad (10)$$

$$\eta = \Phi^0(E_{1u}^-)\sum_n L_n\chi''(n, e_{2g}^c) + \Phi^0(B_{1u})\sum_n M_n\chi''(n, e_{2g}^c) + \Phi^0(E_{1u}^+)\sum_n N_n\chi''(n, e_{2g}^c), \quad (11)$$

where the double prime denotes vibrational wavefunctions belonging to the $^1B_{1u}$ state, superscript c to e_{2g} the C–C stretching vibrations, and $\chi''(n, j)$ refers to the harmonic nuclear vibrational function in the jth normal mode in its nth quantum state. L_n, M_n, and N_n are the expansion coefficients to be determined. The summation in Eq. (11) indicates that, to calculate η exactly, we should carry out summation infinitely, but for computational purposes it will have to be truncated. The following points can be inferred from Eqs. (10) and (11). (1) The total wavefunction for the $^1B_{1u}$ state is the product of the vibronic wavefunction which contains only the e_{2g} skeletal stretching mode and the vibrational wavefunction. (2) The vibrational wavefunction is the product of harmonic-oscillator wavefunctions. (3) Only the e_{2g}-type carbon skeleton stretching vibration (e_{2g}^c) is considered since it dominates the vibronic mixing between $^1B_{1u}$ and $^1E_{1u}$ states in benzene. (4) For the $^1B_{1u}$ state we construct a new trial vibronic wavefunction, which is expanded in terms of the crude adiabatic electronic

TABLE 1. FIRST 8 EXPANSION COEFFICIENTS OF L_n AND N_n IN Eq. (11) CORRESPONDING TO THE LOWEST EIGENVALUES[a]

Quantum number of e_{2g} mode	Expansion coefficient L_i and N_k
1	−0.1774786
3	−0.0372783
5	−0.0052206
7	−0.0005606
9	−0.0000491
11	−0.0000036
13	−0.0000002
15	−0.0000000

a) Expansion coefficients vanish if the quantum numbers are even.

TABLE 2. FIRST 8 EXPANSION COEFFICIENTS OF M_n IN Eq. (11) CORRESPONDING TO THE LOWEST EIGENVALUE[a]

Quantum number of e_{2g} mode	Expansion coefficient M_n
0	0.9464586
2	0.1938479
4	0.0282337
6	0.0031885
8	0.0002940
10	0.0000229
12	0.0000015
14	0.0000001

a) Expansion coefficients vanish if the quantum numbers are odd.

9) The off-diagonal components of R contain terms to all orders in perturbation theory.

$$\langle s|R|l\rangle = \langle s|V|l\rangle + \sum_{c\neq s}\frac{\langle s|V|c\rangle\langle c|V|l\rangle}{(E_s - E_c)} + \sum_{c\neq s}\sum_{c'\neq s}\frac{\langle s|V|c\rangle\langle c|V|c'\rangle\langle c'|V|l\rangle}{(E_s - E_c)(E_s - E_{c'})} + \cdots$$

Cf. M. Goldberger and K. Watson, "Collision Theory," Wiley, New York (1964) for more details of the resolvent operator.

10) W. M. Gelbart, K. G. Spears, K. F. Freed, J. Jortner, and S. A. Rice, *Chem. Phys. Lett.*, **6**, 345 (1970).

11) J. H. van der Waals, A. M. D. Berghius, and M. S. De Groot, *Mol. Phys.*, **13**, 301 (1967).

TABLE 3. CALCULATED ELECTRONIC PARTS

Electronic state		Accepting mode (k)	$\langle \Phi^0(f)\|\{\partial V(q, Q)/\partial Q_k\}_0\|\Phi^0(i)\rangle$(eV/Å)
Initial	Final		
$^1B_{1u}$	$^1B_{2u}$	a_{2g}	0
$^1E_{1u}^+ + {}^1E_{1u}^-$	$^1B_{2u}$	e_{2g}	0.3057

wavefunctions of the $^1E_{1u}^+$, $^1B_{1u}$, and $^1E_{1u}^-$ states. The expansion coefficients are further expanded in terms of the vibrational wavefunctions of e_{2g}-type, $\chi(n, e_{2g})$. Some calculated expansion coefficients, L_n, M_n, and N_n, for the vibrational wavefunctions corresponding to the lowest energy are summarized in Tables 1 and 2.

The wavefunction for the $^1B_{2u}$ state is written as follows,

$$\Psi(B_{2u}) = \Phi^0(B_{2u}) \prod_{j\neq 1}^{3N-6} \chi'(n, j) \tag{12}$$

where the prime denotes vibrational wavefunctions belonging to the $^1B_{2u}$ state. Thus we obtain for the coupling matrix element:

$$\begin{aligned} v = {} & \langle \Phi^0(B_{2u})|\{\partial V(q, Q)/\partial Q(e_{2g}^c)\}_0|\Phi^0(E_{1u}^-)\rangle \\ & \times \langle \chi(e_{2g}, n)|Q(e_{2g})|\sum_n L_n \chi(n, e_{2g}^c)\rangle \prod_{j\neq e_{2g}^c}^{3N-8} \langle \chi(n, j)|\chi(0, j)\rangle \\ & + \langle \Phi^0(B_{2u})|\{\partial V(q, Q)/\partial Q(a_{2g})\}_0|\Phi^0(B_{1u})\rangle \\ & \times \langle \chi(n, e_{2g}^c)|\sum_n M_n \chi(n, e_{2g}^c)\rangle \\ & \times \langle \chi(a_{2g}, 1)|Q(a_{2g})|\chi(a_{2g}, 0)\rangle \prod_{j\neq e_{2g}^c, a_{2g}}^{3N-9} \langle \chi(n, j)|\chi(0, j)\rangle \\ & + \langle \Phi^0(B_{2u})|\{\partial V(q, Q)/\partial Q(e_{2g}^c)\}_0|\Phi^0(E_{1u}^+)\rangle \\ & \times \langle \chi(e_{2g}, n)|Q(e_{2g})|\sum_n N_n \chi(n, e_{2g}^c)\rangle \prod_{j\neq e_{2g}^c}^{3N-8} \langle \chi(n, j)|\chi(0, j)\rangle. \end{aligned} \tag{13}$$

Here we have assumed that the vibrational wavefunctions for the $^1B_{1u}$ and $^1B_{2u}$ states are the same as those in the ground state.

We shall now treat the electronic and vibrational parts separately. The electronic parts can be calculated by the same method as that used previously.[1] The values of the calculated electronic parts are summarized in Table 3. Of the electronic parts

$$\langle \Phi^0(B_{2u})|\{\partial V(q, Q)/\partial Q(a_{2g})\}_0|\Phi^0(B_{1u})\rangle,$$

and

$$\langle \Phi^0(B_{2u})|\{\partial V(q, Q)/\partial Q(e_{2g})\}_0|\{\Phi^0(E_{1u}^+) + \Phi(E_{1u}^-)\}\rangle,$$

the former is zero, and the latter appreciable.

We must now decide the mode which accepts the excess energy. It is assumed that the e_{2g}-type C–C stretching vibration (1606 cm^{-1}) is the most probable path for accepting excess energy for the following reason. Equilibrium configuration differs for the ground and excited states of aromatic hydrocarbons only in the totally symmetric normal coordinate. Therefore, only the progression of totally symmetric vibration is observed in absorption and emission spectra of aromatic hydrocarbons. It is known that as the difference in equilibrium configuration and that in vibrational frequency between the initial and final electronic states become larger, the Franck-Condon factor becomes larger at the higher vibrational quantum number of the final states. We assume the vibrational frequencies of each excited electronic state to be the same as those of the ground state. To accept the same excess energy, the oscillator of the high vibrational frequency requires a small vibrational quantum number compared with that of the low vibrational frequency. Thus, the Franck-Condon factor also becomes larger for the higher vibrational frequency of the final state (see Ref. 12 for more details). The difference in the equilibrium configuration between the $^1B_{1u}$ and $^1B_{2u}$ states in benzene is large along the direction of the e_{2g} normal coordinate. In the present model, the nonradiative transition is considered to occur from the $^1B_{1u}$ state subjected to the pseudo-Jahn-Teller interaction with the $^1E_{1u}$ state. Only the e_{2g}-type carbon skeleton stretching vibration is effective in the above interaction and, is thus the most probable accepting mode.

Results and Discussion

The transition densities necessary for calculating the electronic parts of the coupling matrix element are shown in Fig. 1. The calculated nonradiative transition rate constant is given in Table 4 together with

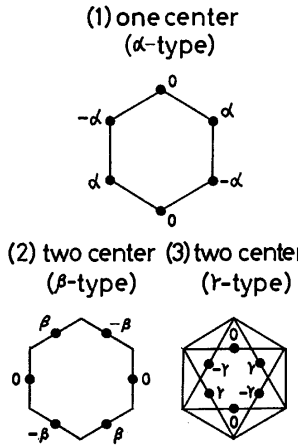

Fig. 1. The electronic energy surface of the lower singlet state of benzene as the function of a_{1g} and e_{2g} normal coordinate displacements.[a]

E_1[b]=4.9 eV E_2[b]=6.2 eV E_3[b]=7.0 eV

a) The same equilibrium points in the $^1E_{1u}$, $^1B_{1u}$, and $^1B_{2u}$ states along totally symmetric C–C stretching coordinate are assumed.

b) D. K. Kearns, *J. Chem. Phys.*, **36**, 1608 (1960).

TABLE 4. NONRADIATIVE TRANSITION RATE CONSTANT

Transition	Calculated rate constant (Calculated half width)	Experimental rate constant (Experimental half width)
$^1B_{1u} \rightarrow {}^1B_{2u}$	3×10^{13} sec^{-1} (150 cm^{-1})	6×10^{13} sec^{-1} (300 cm^{-1})

12) W. Siebrand, *J. Chem. Phys.*, **46**, 440 (1967).

the experimental one, the former being in good agreement with the latter. There may be some cancellations among the various types of error arising from the approximations we employed.

We calculated the nonradiative transition rate from the $^1B_{1u}$ state, which undergoes the pseudo-Jahn-Teller interaction with $^1E_{1u}$ state, to the $^1B_{2u}$ state. We assume that the initial and final states can be expressed by the vibronic wavefunctions with a crude adiabatic wavefunction as an electronic factor. When we use the crude adiabatic wavefunction, the off-equilibrium electronic Hamiltonian is the dominant operator responsible for the line broadening or for the decay of the initial state.

The present calculation shows how the lowest order of the potential energy operator contributes to the nonradiative transition rate in the crude adiabatic approximation.

The procedure should be applied to other cases where the state to be dealt with is very near other states. In such cases, we must take into account the vibronic interaction (the pseudo-Jahn-Teller interaction) between these states, because the interaction between each state is very large.

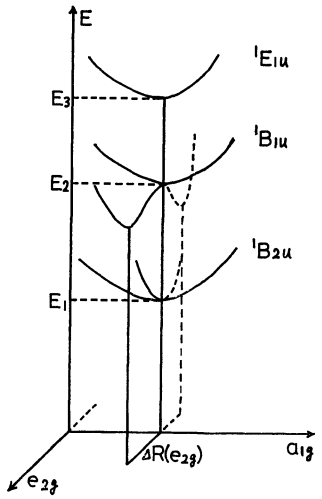

Fig. 2. Calculated transition density between the $^1B_{1u}$ and $(E^+_{1u}+E^-_{1u})$ states.
(1) $\alpha=0$ (2) $\beta=1/3$ (3) $\gamma=0$

The electronic energy surfaces of the $^1E_{1u}$, $^1B_{1u}$, and $^1B_{2u}$ states of benzene as the functions of the a_{1u} and e_{2g} normal coordinate displacements are shown in Fig. 2. The first strong vibrational component in the progressions of the absorption spectrum of the $^1B_{1u}$ state was assigned to $0\text{-}0+\nu_{18}(e_{2g})$.[2] Using these data and the assumed harmonic potential, we estimated the magnitude of difference in equilibrium configuration ΔR (e_{2g}) between the $^1B_{1u}$ and the $^1B_{2u}$ states, arising from the pseudo-Jahn-Teller interaction with the $^1E_{1u}$ state, to be about 0.1 Å.

Fisher and Schneider[13] analyzed the time dependent correlation function about the rate constant and calculated the rate for intersystem crossing from the $^3B_{1u}$ state to the ground state in benzene. They used the saddle point method[14,15] in order to find the most probable path for the intersystem crossing in benzene. They found that 66% (55%) of the energy goes into the C–H (C–D) breathing mode for benzene (deuterobenzene) and the other major energy sinks involve the totally symmetric skeletal breathing mode (990 cm^{-1}), the e_{2g} stretching mode (1584 cm^{-1}) and, to a smaller extent, the out-of-plane vibrations. It is apparent that a certain vibration accepts most of the excess energy. We took into consideration all the possible combinations of the vibrational overlap integrals under the constraint of conservation of the excess electronic energy of the final state.[1] The non-adiabatic Franck-Condon factor was taken as the average value of vibrational coupling matrix elements for computational purposes. We have employed the most probable path method and chosen the e_{2g} C–C stretching vibration as the most probable path. The difference in C–H bond length between the $^1B_{1u}$ and $^1B_{2u}$ states would be small and the C–H normal vibration could not serve as a good accepting mode.[16]

13) S. Fischer and S. Schneider, *Chem. Phys. Lett.*, **10**, 392 (1971).
14) K. F. Freed and J. Jortner, *J. Chem. Phys.*, **52**, 6272 (1970).
15) S. Fischer, *ibid.*, **53**, 3195 (1970).
16) J. P. Byrne, E. F. McCoy, and I. G. Ross, *Aust. J. Chem.*, **18**, 1589 (1965).

The SCF Screened Potential in π-Electron Systems

Toshitaka TERASAKA, Taizo IIJIMA,* Yuichi FUJIMURA, and Takeshi NAKAJIMA
Department of Chemistry, Faculty of Science, Tohoku University, Sendai
(Received May 24, 1972)

The screened potentials in π-electron systems have been calculated using the SCF orbitals and energies, and compared with Little's screened potentials calculated using the Hückel orbitals and energies. The characteristics of the screened potentials in benzenoid and nonbenzenoid aromatic hydrocarbons and in linear polyenes have been studied. It has been found that the use of the screened potential brings about considerable improvements in the triplet excitation energies in particular.

Recently, Gutfreund and Little[1,2] calculated the screened potential in the π-electron system of large conjugated molecules by means of the Random-Phase-Approximation (RPA) method,[3] which is familiar in the field of many-body physics. They have shown that, in the case of a π-electron system, the integral equation for the screened potential becomes a set of linear algebraic equations within the framework of the LCAO approximation. The results of a Hückel calculation are used in the algebraic equations to generate the screened potential, and with this potential an SCF calculation is performed. The excitation energies are calculated using the modified configuration-interaction (CI) method, in which a screened potential different from that used in the ground-state calculation is employed. The main results that they obtained are as follows: First, the qualitative behavior of the screened potential in the π-electron system is notably different from that in a metal or in an electron gas. In the metal and electron gas, the Coulomb potential of a test charge is effectively screened and behaves like $e^{-\lambda r}e^2/r$, where λ is of the order of several angstroms. On the other hand, in the π-electron system, the screened potential at sufficiently large distances exceeds the bare potential (that is, an antiscreening effect). Second, the screened potential shows a position dependence, although the bare potential does not. As a result, the Coulson-Rushbrooke theorem, which states that, in alternant hydrocarbons, the π-electron densities for all the carbon atoms are unity, does not generally hold for the SCF states calculated using the screened potential. Third, both singlet and triplet excitation energies calculated using the modified CI method assuming the screened potential agree more significantly well with the experimental values than do those calculated assuming the bare potential.

In the usual Pariser-Parr-Pople-type SCF calculation, the wavefunctions are determined by the Hartree-Fock potential, and *vice versa*, but the bare potential (consisting of one- and two-center repulsion integrals) is fixed through the SCF process. We wish to propose the following procedure for calculating the screened potential in π-electron systems using the SCF molecular-orbital wavefunctions and energies (this is the main purpose of this paper): at each step of an SCF calculation, let the screened potential be evaluated by the use of the wavefunctions and orbital energies obtained in that step, and then let us proceed to the next step using this screened potential. We call such a screened potential "the SCF screened potential", and the screened potential evaluated using the results of a Hückel calculation, "the Hückel screened potential".

We apply the above procedure to the SCF screened potential in combination with the variable bond-length SCF method,[4] which is known to reproduce well the equilibrium configurations of π-electron systems, to benzenoid and nonbenzenoid aromatic hydrocarbons, and to linear polyenes. We are concerned mainly with the following points: (1) the difference between the Hückel and SCF screened potentials; (2) the variation in the screened potential with respect to the sizes and forms of molecules, and (3) the position-dependence of the screened potential in the above molecules.

Theory

In the RPA method, the integral equation for the screened potential, V, has the following form:[1]

$$V(r_1, r_2, \omega) = V_0(|r_1-r_2|) + \iint dr dr' V_0(|r_1-r|)\pi_0(r, r', \omega)V(r', r_2, \omega), \quad (1)$$

where r_1, r_2, r, and r' are the coordinates of carbon atoms, where V_0 is the bare potential, where ω has the dimension of energy, and where the RPA polarization part, π_0, is given in terms of the single Green function, G_0, as:

$$\pi_0(r, r', \omega) = 2i\int \frac{d\omega'}{2\pi} G_0(r, r', \omega')G_0(r', r, \omega'-\omega). \quad (2)$$

In π-electron systems, the integral Eq. (1) becomes the following set of linear algebraic equations within the framework of the LCAO approximation:

$$V(r_1, r_2, \omega) = V_0(|r_1-r_2|) + \sum_m K(r_1, r_m, \omega)V(r_m, r_2, \omega), \quad (3)$$

where:

$$K(r_1, r_m, \omega) = \sum_n V_0(|r_1-r_n|)\pi_0(r_n, r_m, \omega) = \sum_n V_0(|r_1-r_n|)\sum_{ia} 4\varepsilon_{ia}u_{ia}(r_n)u_{ia}(r_m)/(\omega^2-\varepsilon_{ia})^2, \quad (4)$$

$$\varepsilon_{ia} = \varepsilon_i - \varepsilon_a, \qquad u_{ia}(r_n) = C_{in}C_{an},$$

* Present address: Chisso Co., Ltd., Goi, Chiba.

1) H. Gutfreund and W. A. Little, *Phys. Rev.*, **183**, 68 (1969).
2) H. Gutfreund and W. A. Little, *J. Chem. Phys.*, **50**, 4468 (1969).
3) Leo P. Kadanoff and Gordon Baym, "Quantum Statistical Mechanics," W. A. Benjamin, Inc., New York, (1962).
4) H. Yamaguchi, T. Nakajima, and T. Kunii, *Theoret. Chim. Acta* (Berl.), **12**, 349 (1968).

where ε_i denotes the orbital energy, C_{in}, the atomic-orbital coefficient in a molecular orbital, and the Latin and Greek indices, the unoccupied and occupied orbitals respectively. The screened potential is given in the matrix notation:

$$V(\omega) = [I-K(\omega)]^{-1}V_0, \qquad (5)$$

where I is the unit matrix.

The screened potential in the ground state is calculated using Eq. (5), with $\omega=0$.

Method of Calculation

In this section, we shall briefly outline the following four procedures for use in calculating the screened potentials in the ground states of π-electron systems.

(1) Little's procedure[1] (the Hückel screened potential): The Hückel molecular-orbital wavefunctions and energies are used to evaluate the screened potential, and an SCF calculation is then carried out using this screened potential.

(2) A procedure that combines Procedure (1) with the variable bond-length SCF method:[4] at each step of an SCF calculation, the C–C bond lengths (r) are evaluated from the corresponding bond orders (p) by the use of the relation between r and p, r (Å)$=1.520-0.186p$. Next, the Hückel-type calculation is performed using the core resonance integral which is given by $\beta(r)=(1.397/r)^4\beta(1.397)$.[5] The screened potential is evaluated using the results of the Hückel-type calculation. Using this screened potential, we carry out the next step of the SCF calculation. The process is repeated until self-consistency with respect to the total energy of the ground state is reached.

(3) The screened potential is evaluated at each step of the SCF calculation (the SCF screened potential). Using the molecular orbitals and orbital energies obtained after an iteration of the SCF calculation, we evaluate the screened potential. This screened potential is taken as the potential for the next iterative SCF calculation. The iteration is continued until self-consistency is reached. Notice that, in Procedure (1), the SCF calculation is carried out using a constant Hückel screened potential, while, on the other hand, in Procedure (3), the SCF calculation is carried out using a variable SCF screened potential.

(4) A procedure that combines Procedure (3) with the variable bond-length method. As in the second procedure, at each step of the SCF calculation, the new bond lengths are obtained from the corresponding bond orders. The screened potential is evaluated by means of the bare potential obtained from the new bond lenghts. This screened potential is used in the calculation of the next step. The calculation is repeated until self-consistency is reached.

Results and Discussion

First, let us compare the two kinds of Hückel screened potentials obtained using two different types of bare potentials, the Pariser-Parr (PP) and Mataga-Nishimoto (MN) potentials. In Fig. 1, the two kinds of Hückel screened potentials in benzene are shown, together with both the PP and MN bare potentials. The two kinds of Hückel screened potentials show quite a similar tendency in that, at small distances, the screening is strong and at large distances the anti-screening is appreciable.[6] Although both types of bare one-center potentials have the same value, the two kinds of one-center screened potentials are different from each other, since the one-center screened potential includes the contribution from other positions through the two-center potentials. For the other compounds treated in this paper, we calculate the Hückel and SCF screened potentials using only the MN potential, because the

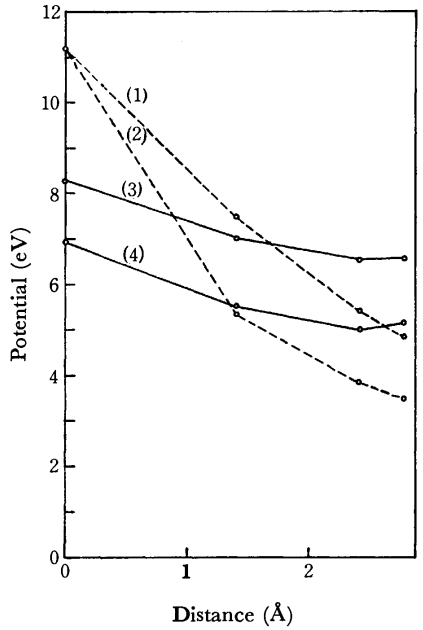

Fig. 1. Two kinds of the Hückel screened potentials in benzene obtained using the Pariser-Parr (PP) and Mataga-Nishimoto (MN) bare potentials; (1) the PP bare potential, (2) the MN bare potential, (3) the PP screened potential, (4) the MN screened potential.

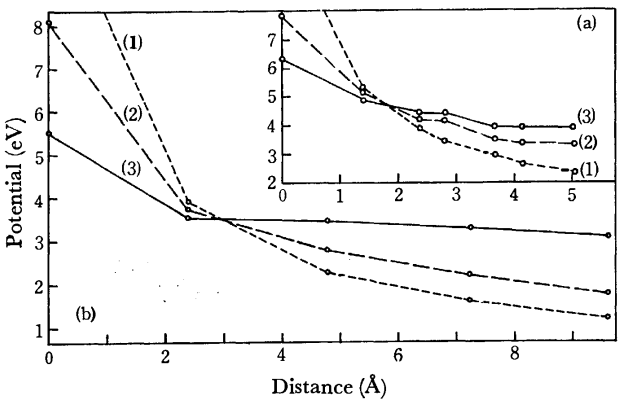

Fig. 2. The Hückel and SCF screened potentials in naphthalene (a) and in the polyene (n=10) (b); (1) the bare potential, (2) the SCF screened potential, (3) the Hückel screened potential.

5) C. Sandrofy, *Bull. Soc. Chim. France*, **1949**, 615.

6) It is considered that the anti-screening appeared in π-electron systems at large distances has to do with the finite size of the system.[1]

screened potentials obtained assuming the PP and MN potentials will probably show a similar qualitative behavior.

Difference between the Hückel and SCF Screened Potentials. The Hückel and SCF screened potentials in naphthalene and the polyene ($C_{10}H_{12}$) are illustrated in Fig. 2. The SCF screened potential shows a tendency similar to the Hückel screened potential, but it is intermediate between the Hückel screened and the bare potentials. That is, the effects of the screening and anti-screening in the SCF screened potential are both weakened. It seems that, in the Hückel screened potential, the effect of the screening and anti-screening of π-electrons tends to be overestimated.

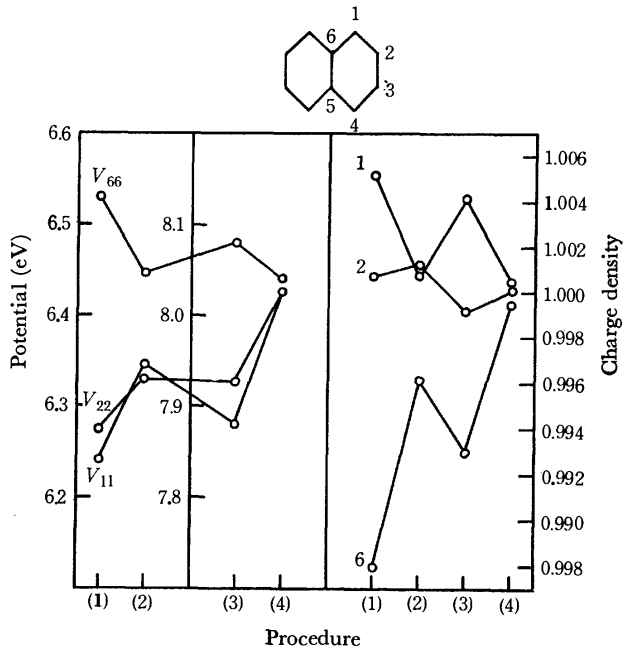

Fig. 3. The one-center screened potentials and charge densities in naphthalene calculated using the four procedures.

Figure 3 presents the one-center screened potentials and the charge densities in naphthalene calculated using the four procedures outlined above. It seems apparent that both the SCF procedure and the variable bond-length method have the effect of making the divergence among the calculated values small, and that this effect is stronger for the variable bond-length method than for the SCF procedure. As Procedure (4) involves both the SCF scheme and the variable bond-length method, the divergence becomes remarkably small. It may also be noted that such an effect appears for both the one-center screened potential and the charge density, and that the degree of breakdown of the Coulson-Rushbrooke theorem becomes appreciably small in the SCF state calculated using Procedure (4). In nonbenzenoid aromatic hydrocarbons and polyenes, there are no such definite effects.

Variation in the Hückel Screened Potential with Respect to the Sizes and Forms of the Molecules. The Hückel screened potentials in benzene, naphthalene, aceazulylene, and aceheptylene are presented in Fig. 4 and compared there with the bare potentials. In Fig. 5,

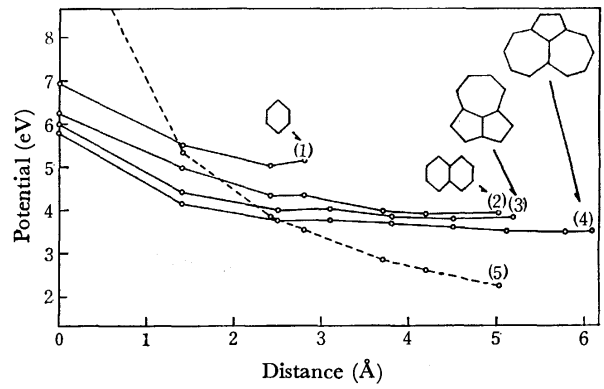

Fig. 4. The Hückel screened potentials; (1) benzene, (2) naphthalene, (3) aceazulylene, (4) aceheptylene, (5) the bare potential.

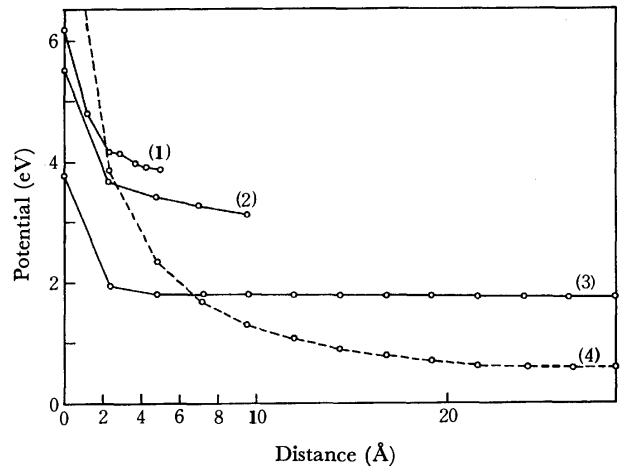

Fig. 5. The Hückel screened potentials in the polyenes ($n=10$ and 30); (1) naphthalene, (2) the polyene ($n=10$), (3) the polyene ($n=30$), (4) the bare potential.

the Hückel screened potentials in linear polyenes (the number of carbon atoms $n=10$ and 30) are shown and compared with the bare and the Hückel screened potentials in naphthalene ($n=10$). Since, in general, the effect of screening is different in various parts of molecules, there is a considerable divergence among the calculated screened potentials, in short ranges in particular; the average values are shown in these figures. From these figures, it will be seen that the screened potential in ring compounds decreases as the n increases, and that, when the n is the same, the screened potential is lower for the chain compound than for the ring compound. It may be stated generally that the larger or longer a molecule is, the stronger the screening in the short range and the weaker the anti-screening in the long range. In long linear polyenes, the Hückel screened potential tends to be constant even at small distances. In such a case, the atomic-orbital coefficients in molecular orbitals obtained from the SCF calculation using the Hückel screened potential tend to be the same as those of the Hückel orbitals.

Position Dependence of the Screened Potential in Polyenes and Benzenoid and Nonbenzenoid Aromatic Hydrocarbons. The carbon atoms in the polyene with $n=10$ are numbered as in Fig. 6. We divide the Hückel screened

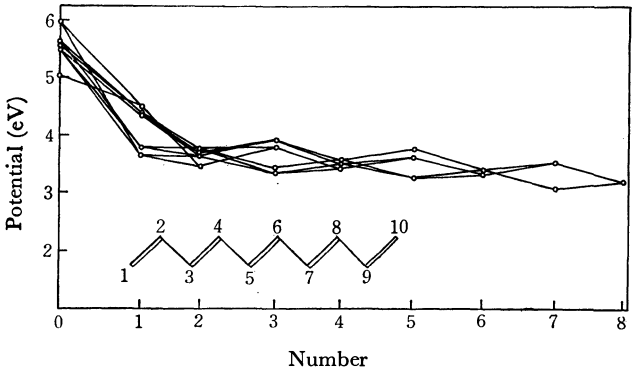

Fig. 6. The Hückel screened potentials in the polyene (n=10) plotted *versus* the number (for the meaning of the number, see the text).

potentials (Procedure (1)) into these groups: V_{11}, V_{12}, V_{13}, ···, $V_{1,10}$; V_{22}, V_{23}, ···, $V_{2,10}$; ···; V_{99}, $V_{9,10}$. In Fig. 6, the screened potentials in each group are plotted *versus* a number that indicates the kind of screened potential, that is, 0: one-center potentials V_{11}, V_{22}, V_{33}, ···; 1: the nearest two-center potentials V_{12}, V_{23}, V_{34}, ···; *etc.* Figure 6 shows that there are two kinds of numbers; that is, at an even number (including 0) one kind of screened potential exists, while at an odd number there exist two kinds of screened potentials in accordance with the strength of the screening.[7] The SCF screened potential (Procedure 3) in the polyene (n=10) presented in Fig. 7 shows a tendency similar to that in the Hückel screened potential.

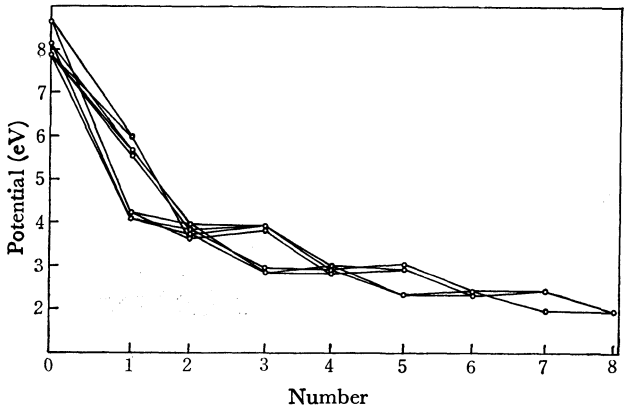

Fig. 7. The SCF screened potentials in the polyene (n=10) plotted *versus* the number (for the meaning of the number, see the text).

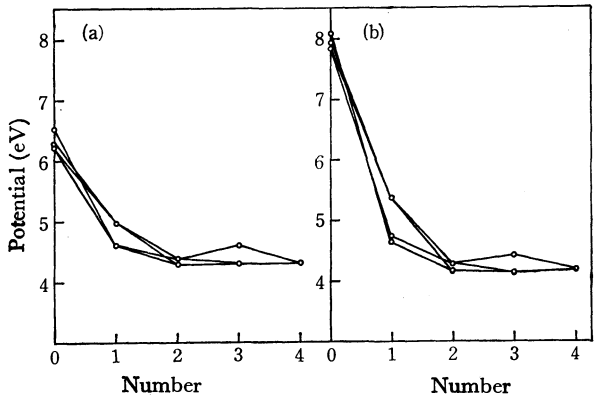

Fig. 8. The Hückel and SCF screened potentials in naphthalene plotted *versus* the number (for the meaning of the number, see the text); (a) the Hückel screened potential, (b) the SCF screened potential.

The results in naphthalene, azulene, aceazulylene, and aceheptylene are shown in Figs. 8—11 respectively. In naphthalene, the 5-membered ring in aceazulylene,

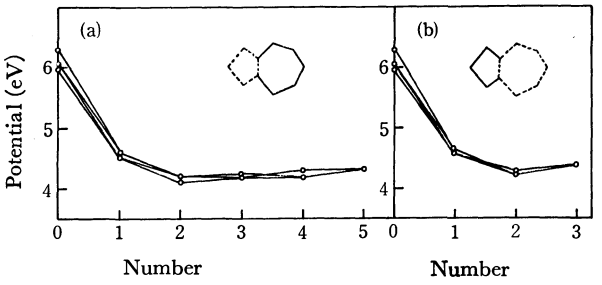

Fig. 9. The Hückel screened potentials in azulene plotted *versus* the number (for the meaning of the number, see the text); (a) the 7-membered ring, (b) the 5-membered ring.

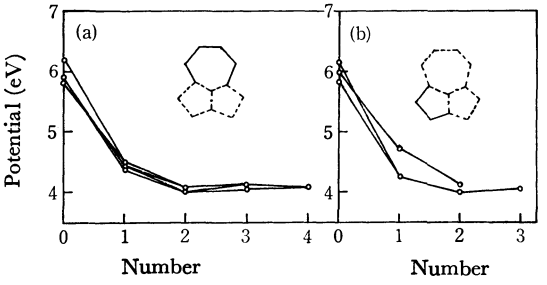

Fig. 10. The Hückel screened potentials in aceazulylene plotted *versus* the number (for the meaning of the number, see the text); (a) the 7-membered ring, (b) the 5-membered ring.

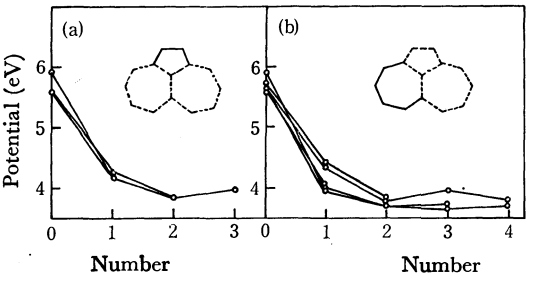

Fig. 11. The Hückel screened potentials in aceheptylene plotted *versus* the number (for the meaning of the number, see the text); (a) the 5-membered ring, (b) the 7-membered ring.

TABLE 1. EXCITATION ENERGIES (IN eV) OF BENZENE

	Symmetry	HSP[a]	BP[b]	Exp.[8]
Singlet	B_{2u}	4.86	4.90	4.89
	B_{1u}	6.08	6.19	6.14
Triplet	B_{1u}	3.69	2.48	3.66
	E_{1u}	4.60	3.99	4.69

a) HSP: the Hückel screened potential.
b) BP: the bare potential.

7) At odd number i, one kind of the screened potentials consists of the potentials between the $2j$-th carbon atoms and the $(2j+i)$-th carbon atoms, and the other consists of the potentials between the $(2j+1)$-th carbon atoms and the $(2j+1+i)$th carbon atoms.

8) D. R. Kearns, *J. Chem. Phys.*, **36**, 1608 (1960).

Table 2. Excitation energies (in eV) of naphthalene

	Symmetry	HSP	Variable			Exp.
			BP	HSP	SCFSP[a]	
Singlet	B_{3u}	4.08	4.18	4.15	4.43	3.97,[9] 4.11[10]
	B_{2u}	4.31	4.68	4.41	4.97	4.51,[9] 4.61[10]
Triplet	B_{2u}	2.44	1.87	2.67	2.88	2.61
	B_{1g}	3.30	2.92	3.40	3.57	

a) SCFSP: the SCF screened potential.

Table 3. Excitation energies (in eV) of aceazulylene

	Symmetry	HSP	Variable		Exp.[a]
			BP[11]	HSP	
Singlet	B_2	1.68	1.73	1.95	1.84
	A_1	2.92	2.91	3.00	2.59, 2.76, 2.94
	B_2	3.64	3.86	3.41	3.19, 3.25, 3.37
	A_1	3.70	3.64	3.69	3.66, 3.79, 3.97
	B_2	4.35	4.79	4.74	4.63
Triplet	B_2	1.90	1.40	1.90	
	A_1	3.20	1.58	2.16	

a) The absorption spectra of dimethyl derivatives.[12]

and the 7-membered ring in aceheptylene, a tendency similar to that in the polyene appears, while in azulene, the 7-membered ring in aceazulylene, and the 5-membered ring in aceheptylene, at each of the numbers the various screened potentials have almost the same value.

We can understand the above characteristics of the screened potential as follows. In the polyene ($n=10$), the screened potentials can be divided into the following two groups according to the numbers:

one group: even numbers (including 0)

0: V_{11}, V_{22}, V_{33}, ⋯

2: V_{13}(), V_{24}(), ⋯

(The number of double bonds $N=1$)

4: V_{15}(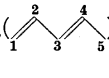), V_{26}(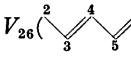), ⋯ ($N=2$)

⋮

the other group: odd numbers

1: V_{12}(), V_{23}(), V_{34}(), ⋯

($N=1$) ($N=0$) ($N=1$)

3: V_{14}(), V_{25}(), V_{36}(), ⋯

($N=2$) ($N=1$) ($N=2$)

⋮

From the above classification of the screened potentials, it may be seen that there are two kinds of screening at the odd numbers in molecules such as polyene in which there exists a strong bond alternation, while there is only one kind of screening at the odd numbers in molecules which do not show a clear bond alternation—for example, benzene and azulene. In naphthalene, there is a fairly clear double-bond fixation, so that the characteristics of the screened potential in Fig. 8 are the same as those of the polyene.

Table 4. Excitation energies (in eV) of aceheptylene

	Symmetry	HSP	Variable		Exp.[a]
			BP[11]	HSP	
Singlet	B_2	1.50	1.52	1.77	1.55
	A_1	2.79	2.89	2.78	2.72
	B_2	3.34	3.47	3.10	3.20
	A_1	3.48	3.82	3.80	3.96, 4.16
	B_2	3.96	4.48	4.27	4.35, 4.56
Triplet	B_2	1.70	1.15	1.57	
	B_2	3.13	1.40	2.01	

a) The absorption spectra of dimethyl derivatives.[12]

Transition Energies of Benzene, Naphthalene, Aceazulylene, and Aceheptylene. Tables 1—4 show the transition energies calculated by using the modified CI method assuming the Hückel screened potential and the SCF screened potential, together with those calculated assuming the bare potential. In these tables, "variable" means that a calculation has been performed in combination with the variable bond-length SCF method. The results agree well with the experimental values. It may be noted that triplet excitation energies calculated using the screened potential are in better agreement with the experimental values than those calculated using the bare potential.

This research was supported in part by a grant from Takeda Sciense Foundation.

9) J. N. Murrell, "The Theory of the Electronic Spectra of Organic Molecules," Methuen, London (1963).

10) American Petroleum Institute, Research Project 44. Ultraviolet Absorption Spectral Data. Carnegie Institute of Thcenology.

11) H. Yamaguchi, T. Terasaka, and T. Nakajima, *Theoret. Chim. Acta* (Berl.), **18**, 255 (1970).

12) K. Hafner and J. Schneider, *Angew. Chem.*, **70**, 702 (1958); *Ann. Chem.*, **624**, 37 (1959); K. Hafner, personal communication to T. Nakajima.

Studies on Fragment Ion Distribution and Reaction by the Use of a Charge Spectrometer. I. Mass Spectra of Methylamine after Charge Exchange with Fast Positive Ions and Their Recombination Energies

Toshio NAGATANI, Kenji YOSIHARA, and Takanobu SHIOKAWA
Department of Chemistry, Faculty of Science, Tohoku University, Sendai 980
(Received June 17, 1972)

Charge exchange reactions with fast positive ions were used to obtain the break down curve and internal energy distribution function of methylamine which differ in several points from those obtained by Sjögren with very slow ions. In the higher region, our results on the population in internal energy distribution function is greater than the previous ones. A valley of the internal energy distribution curve was found in the region 12.0—13.8 eV which is higher than that obtained by Sjögren. The values of RE were reestimated according to recent results.

From our interest in fragment ion distribution and reactivity in nuclear transformations we have studied ion-molecule reactions which might determine the chemical fate of the recoil atom. For direct detection of the reaction paths it was thought that mass spectroscopic methods would be suitable, and a specially designed mass spectrometer, was constructed.[1] This was found useful for studying basic ion-molecule reactions as well as initial charge distributions of decayed atoms.[2]

As regards ion-molecule reactions, typical studies of the ion-molecule reaction initiated by charge exchange have been successfully performed by the use of double mass spectrometers. Lindholm and his co-workers[3] extensively studied the break down curves and internal energy distribution functions of relatively simple gases by means of charge exchange. Valuable information has been obtained on the breaking up of the parent ions and the successive ion-molecule reactions in the reaction chamber. Energy of the incident beam in their work was limited to a low range (900 eV).

In the case of methylamine, Sjögren[4,5] studied the break down curve after the charge exchange reactions with slow ions, and elucidated the internal energy distribution function of the target molecule from the experimental results. It was found that a region with low probability for ionization exists between 11 and 12 eV, and above 15 eV the probability of ionization decreases again. The relation between the electronic structure of the molecule and the break down curve was discussed.

We have studied the dissociation of methylamine with fast ions and compared the results with those by Sjögren who studied it with slow ions. Using fast ions seems to be advantageous as dispersion of energy distribution is much narrow. Interesting findings were obtained on the internal energy distribution function of methylamine.

Experimental

Methylamine as a target molecule was prepared from methylamine hydrochloride (Tokyo Kasei Co.) of guaranteed grade. Methylamine hydrochloride was treated with a saturated solution of potassium hydroxide. Gas of methylamine evolved was dried and vacuum-distilled several times.

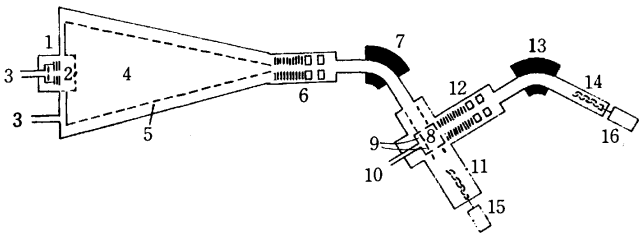

Fig. 1. Schematic diagram of the charge spectrometer.
1. X-ray tube or external ion source 2. Internal ion source 3. Gas inlet 4. Source volume 5. Guide rings 6. Lenses 7. Magnet 8. Reaction chamber 9. Repeller 10. Gas inlet 11. Electron multiplier 12. Lenses 13. Magnet 14. Electron multiplier 15. Recorder 16. Recorder or counter

The mass charge spectrometer is shown in Fig. 1. In place of the X-ray tube an external electron ion source T-2 (Hitachi Co.) may be used, as was the case in this work. Ions generated in an external ion source are introduced into 8 through 7, and impact the neutral atoms or molecules. The produced ions are led into the second analyzing system perpendicular to the incident ion, and detected by 14. Energy of the bombarding electrons in T-2 is 70.0 eV. Positive ions of various gases are produced and selected by the first analyzing system. Details of operation of this assembly have been described previously.[1]

Results and Discussion

The mass spectra of methylamine after charge exchange with 13 kinds of positive ions are shown in Table 1. Acceleration of the incident ions was set at 1850 V. All the values in the table are given when total ionization is normalized to 100. $C_6H_6^+$ was obtained from benzene, C^+ and CO_2^+ from carbon

1) T. Shiokawa, K. Yoshihara, M. Yagi, T. Omori, H. Kaji, M. Hiraga, T. Nagatani, and Y. Takita, *Mass Spectroscopy*, **18**, 1230 (1970).
2) Y. Takita, M. Hiraga, K. Yoshihara, and T. Shiokawa, *Radiochem. Radioanal. Lett.*, **7**, 313 (1971).
3) E. Lindholm, "Ion-Molecule Reactions in Gases," Advances in Chemistry Series 58, American Chem. Soc., Washington, D. C. (1966), p. 1.
4) H. Sjögren, *Arkiv Fysik*, **29**, 565 (1965).
5) H. Sjögren, *ibid.*, **33**, 597 (1966).

Table 1. Mass spectra after charge exchange of methylamine with various positive ions

Primary ion	m/e										
	12	13	14	15	16	26	27	28	29	30	31
He^+	1.0	1.5	3.2	3.6	1.7	2.6	27.5	49.7	2.6	3.3	1.3
C^+			0.4	1.0	0.1		1.3	7.9	3.2	22.1	59.8
Ne^+	1.4	2.6	4.5	4.8	2.9	0.9	14.4	63.9	2.6	1.3	0.2
Cl^+			0.2	1.0	0.2		0.7	10.2	8.4	74.4	4.2
Ar^+	0.2	0.4	1.3	9.5	1.6	0.3	2.0	57.3	7.5	18.2	0.6
Kr^+		0.1	0.5	2.5	0.4	0.1	1.0	21.2	6.0	66.9	1.2
Xe^+			0.2	0.7	0.2		0.3	6.9	8.7	78.9	3.5
Ne^{2+}	1.0	0.9	1.2	1.0	0.7	1.2	2.8	3.9	0.8	11.9	73.0
Ar^{2+}	0.8	1.6	3.3	3.0	2.3	1.3	15.9	41.8	3.1	5.2	21.0
Kr^{2+}	0.2	0.7	2.3	3.7	1.7	0.7	11.4	64.5	4.7	2.4	6.9
Xe^{2+}		0.2	1.0	10.6	1.9	0.2	3.2	60.3	12.2	5.6	2.8
CO_2^+		0.4	1.0	2.4	0.8		1.5	16.2	7.3	64.2	6.1
$C_6H_6^+$							0.4	1.7	1.2	14.7	80.8

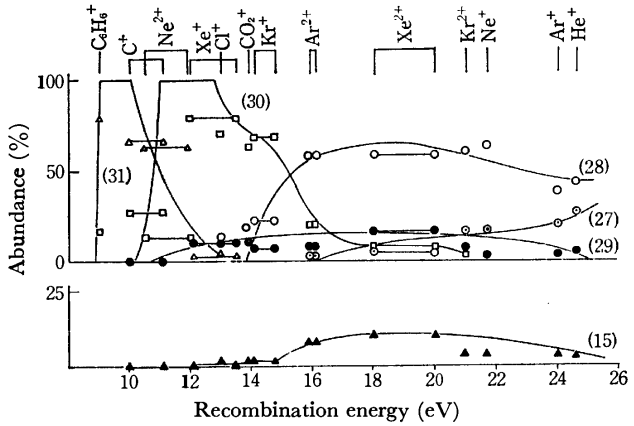

Fig. 2. Breakdown curve of methylamine.

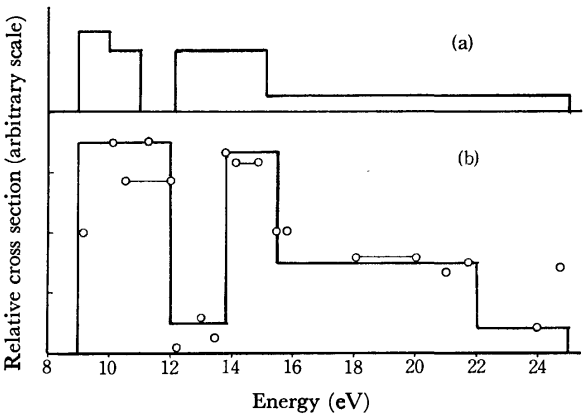

Fig. 3. Internal energy distribution function of methylamine.
(a) Results obtained by Sjögren.[4] (b) Present results.

dioxide, Cl^+ being a fragment ion of trichlorofluoromethane (m/e=35). All the other ions were produced from the corresponding rare gases.

The break down curve of methylamine has been constructed from Table 1 and is shown in Fig. 2. The relation between m/e and chemical formulas is as follows.

(31) $CH_3NH_2^+$	(30) $CH_2NH_2^+$
(29) $CHNH_2^+$	(28) $CHNH^+$
(27) CHN^+	(16) NH_2^+
(15) CH_3^+	(14) CH_2^+, N^+
(13) CH^+	(12) C^+

Figure 3 shows the internal energy distribution function determined by the measurement of a relative cross section to the charge exchange reactions. The shape of the break down curve in Fig. 2 agrees as a whole with that of Sjögren,[4] but our energy distribution function differs somewhat.

Appearance potentials of the major fragment ions from methylamine in Table 1 were determined by experiments in which the target gas was bombarded by ions He^+, Ar^+, and Xe^+ with kinetic energy of 4.0—40.0 eV. Values obtained for the mass peaks are: (31), 9.0; (30), 10.2; (28), 13.6; and (15), 14.4 eV. They are in line fairly good with the values reported.[4,6-10]

Recombination Energies of Bombarding Positive Ions. The recombination energies of positive ions and their abundances are corrected by evaluation of the data in Table 1. They differ somewhat from the published data.[4]

1. He^+ Recombination energy of He^+ was reported to be 24.58 eV. From the break down curve (Fig. 2), however, it seems that there may be a small contribution (5%) of the lower energy level which does not greatly exceed the lowest ionization potential of methylamine. This can be argued from the presence of mass peaks 31 and 30 (Table 1).

2. C^+ Electronic structures, recombination energies and their abundances are reported to be[4]

$2p^2P^0$: 11.26, 10.00, 8.58 eV	74%
$2p^2\,^4P$: 16.58, 12.40 eV	25%

However, the ratio $2p^2P^0$: $2p^2\,^4P$ is concluded to be

6) F. H. Fried, J. L. Franklin, "Electron Impact Phenomena," Academic Press, New York (1957), p. 243.
7) J. E. Collin, *Colloq. Spectros. Intern. 9th.*, (Lyon 1961), **3**, 596 (1962).
8) M. I. Al-Joboury and D. W. Turner, *J. Chem. Soc.* **1963**, 5141.
9) M. I. Al-Joboury and D. W. Turner, *ibid.*, **1964**, 4434.
10) K. Watanabe, *J. Chem. Phys.*, **26**, 542 (1957).

80: 20 from our results.

3. Ne^+ The recombination energies 21.56, 21.66 eV are adopted in this work.

4. Cl^+ The recombination energies of Cl^+ from CCl_3F are reported as follows.[4]

$3p^4\ ^3P$:	13.13, 13.01, 12.96 eV	80%
$3p^4\ ^1D$:	14.45, 14.34 eV	20%
$3p^4\ ^1S$:	16.47, 16.36 eV	0%
$3d^5D$:	15.66, 15.2 eV	0%

The intensity of (15) is extremely small as shown in Table 1. Thus, it is concluded that the level of $3p^4\ ^3P$ is predominant and the effect of the other levels can be neglected.

5. Ar^+ Recombination energies of the ion are 15.76 and 15.94 eV except those of higher levels. These values are adopted in this work.

6. Kr^+ 14.00 and 14.67 eV.

7. Xe^+ 12.13 and 13.44 eV.

8. Ne^{2+} Recombination energy of 10.5—12.0 eV was given when the process $^12s^22p^4 \rightarrow 2s^22p^43x$ occurred. However, the mass peak (28) should be present in almost equal probability with that of (27), and (14) is greater than (15). Therefore, the influence of the level having recombination energy higher than 25 eV is estimated to be about 10%. Probably this is casued by the process $2s^22p^4 \rightarrow 2s^22p^5$.

9. Ar^{2+} Recombination energy of about 9 eV is given for the process $3s^23p^4 \rightarrow 3s^23p^4nx$ which produces (31) by 21%. The remainder is based on the process $3s^23p^4 \rightarrow 3s^23p^5$ (recombination energy: about 24 eV).

10. Kr^{2+} The mass peak 31 of 6.9% is produced by the process $4s^24p^4 \rightarrow 4s^24p^4nx$ with recombination energy of about 9 eV. The remainder is based on the process $4s^24p^4 \rightarrow 4s^24p^5$ (recombination energy: about 21 eV).

11. Xe^{2+} Recombination energy is 18—20 eV (the process $5s^25p^4 \rightarrow 5s^25p^5$ occurs).

12. CO_2^+ In addition to recombination energy of 13.8 eV, the level very near the ionization potential of methylamine contributes about 5%. This increases (13).

13. $C_6H_6^+$ In addition to recombination energy of 9.2 eV, the levels of 10—12 eV are expected to be present. However, these effects are negligibly small and bring no noticeable influence. Absence of the species such as (15) and (14) confirms this argument.

Comparison of Results with Mass Spectra by Electron Impact. When mass spectra are obtained by electron impact, electron energy is usually less than 100 eV. These electrons produce many molecular ions in various excited states, and the average energy of the excited state is considered to be the order of 10 eV. These mass spectra may be computed by taking into consideration the break down curve (Fig. 2) and the internal energy distribution function as in Sjögren's case.[4] Table 2 gives the results calculated with our data, in comparison with the published ones.[4,11–13] Agreement with the observed spectra is satisfactory. However, discrepancy of the fragments produced in the higher energy region is present because population is approximately taken to be zero above 25 eV.

Electronic Structure and Dissociation of Methylamine. The electronic structure of methylamine is shown in Table 3. The data are taken mainly from those of Mulliken[14] and of Turner[15] revised by Sjögren.[5]

In comparison with the results by Sjögren[4] who studied similar phenomena in the low energy region of incident ions, the present results indicate that the [x] electrons are localized on the CH_3 group (IP 15.07 eV after Turner[15]), the [z] electrons on the NH_2 group (IP 16.57 eV after Turner[15]) having large efficiency for charge exchange (Fig. 3). Sjögren has shown only low probabilities for ionization of these groups.

TABLE 2. COMPARISON OF OBSERVED MASS SPECTRA OF METHYLAMINE BY ELECTRON IMPACT WITH THOSE CALCULATED FROM THE DATA OF CHARGE EXCHANGE

m/e	Observed value API[11]	Observed value Collin[12,13]	Calculated value Sjögren[4]	Calculated value This work
(15)	—	5.1	3.6	3.0
(27)	5.7	—	4.4	3.0
(28)	31.4	29.6	27.0	29.4
(29)	5.7	—	5.1	10.0
(30)	35.5	35.1	35.5	31.0
(31)	19.8	19.9	22.0	23.6

TABLE 3. ELECTRONIC STRUCTURE OF METHYLAMINE

Location	$1s^2$ N	$1s^2$ C	$2s^2$ NH_2	$2s^2$ CH_3	z^2 NH_2	x^2 CH_3	y^2 CN	z^2 CH_3	x^2 N
Calculation[a]			27	22	16	14.5	13.5	14.5	11
Photoelectron spectroscopy[b]	421	304	30	24	16.57	15.07	13.94	12.16	9.18

a) According to data of Mulliken[14] (in eV).
b) According to data of Turner[15] revised by Sjögren[5] (in eV).

11) American Petroleum Institute Research Project 44. Catalogue of Mass Spectral Data, Carnegie Institute of Technology, Pittsburgh, 1953, Serial No. 1123.
12) J. Collin, *Bull. Soc. Sci. Liege*, **11**, 446 (1952).
13) J. Collin, *Bull. Soc. Chim. Belg.*, **62**, 441 (1953).
14) R. S. Mulliken, *J. Chem. Phys.*, **3**, 506 (1935).
15) M. I. Al-Joboury and D. W. Turner, *J. Chem. Soc.*, **1964**, 4434.

According to Mulliken, ionization of [y] electrons localized on the CN group is expected to occur at 13.5 eV. If this is the case, a steep rise of CH_3^+ or NH_2^+ will be seen at 13.5 eV in the break down graph. However, such an ionization seems to be suppressed by the weak interaction of the CH_3 and the NH_2 groups in the neighorhood of 13.5 eV (Fig. 2, Table 1). A similar discussion has been given by Sjögren,[4] but our experimental data seem to support this arguement more clearly.

The cause of the difference between our results and Sjögren's has not yet been completely explained. Dynamic treatment would be necessary to solve the problem.

The authors are indebted to Mr. M. Hiraga and Mr. Y. Takita for their kind cooperation throughout this work. They also thank Dr. T. Noda and his staff of Hitachi Co. for construction of the charge spectrometer.

BULLETIN OF THE CHEMICAL SOCIETY OF JAPAN, VOL. 46, 1309—1315 (1973)

Determination of the Intersystem Crossing Probabilities of Acridine in Various Alcohols[1]

Kunihiro TOKUMURA, Koichi KIKUCHI, and Masao KOIZUMI

Department of Chemistry, Faculty of Science, Tohoku University, Aramaki-Aoba, Sendai

(Received June 27, 1972)

Intersystem crossing probabilities ϕ_{ST} of acridine in methanol, ethanol, and 2-propanol were determined by two newly developed methods, relative (r) and absolute (a). The results are as follows. Methanol; 0.27 (r), 0.31 (a). Ethanol; 0.29 (r), 0.33 (a). 2-Propanol; 0.43 (r), 0.45 (a). The above ϕ_{ST} values added to the quantum yield values already obtained of photoreduction occurring at T(n-π^*), *viz.*, $2\phi_R{}^T$ (radical mechanism *via* T(n-π^*), disproportionation of semiquinone being taken into account by a factor of 2) + $\phi_M{}^T$ (molecular mechanism *via* T(n-π^*)), become about the same for the three alcohols. Thus the present data are consistent with our previous data on photoreduction if the intersystem crossing is assumed to occur mainly *via* S*(π-π^*)→T(n-π^*)→T(π-π^*) with the same total ϕ_{ST} for the three alcohols but with T(n-π^*) participating in the reaction in different extent according to the alcohol.

An interesting problem in the photoreduction of acridine is the participation of a higher T(n-π^*) state in the reaction. The possibility was porposed for the first time by Kellmann and Dubois in the photoreduction of acridine in methanol.[2] Vander Donckt and Porter found that only a singlet excited state is involved in the case of 2-propanol.[3] Wilkinson and Dubois also reported a similar result for ethanol.[4] Our results[5] were recently reexamined and corrected to some extent; they show that 53, 33, 31, and 0% of the entire reaction occur at T(n-π^*) in methanol, ethanol, *n*-propanol, and 2-propanol respectively,[6] in agreement with the results of Kellmann, Dubois[2] and Vander Donckt and Porter,[3] but not with those of Wilkinson and Dubois.[4]

The reason for this difference between the four kinds of alcohols is still unknown; determination of the intersystem crossing probabilities ϕ_{ST} in various alcohols might be enlightening. The lowest T(π-π^*) is most likely reached *via* T(n-π^*) since intersystem crossing occurs far more efficiently between n and π states than between π and π,[7] and the level of the former is nearer to the lowest singlet excited state. The ϕ_{ST}-values experimentally obtained are expected to be in the order 2-propanol>ethanol>methanol, if the yields of T(n-π^*) (sum of the yield of T(π-π^*) and the part of T(n-π^*) consumed in reaction) are the same for all the alcohols as is plausible.

Two methods have been newly developed for determining the ϕ_{ST} value. (a) A relative method in which a quantity of fluorescence emitted during a flash is taken as a measure of light absorption, and which is an application of the emission-absorption flash technique.[8] (b) An absolute method in which the quantity of light is measured by means of a K–Fe(III) oxalate actionometer. Knowledge of the yield of triplet state is necessary for both methods.

A necessary condition for the relative method is that the substance under investigation and the reference substance have a common wavelength region for both absorption and fluorescence. Anthracene which satisfies such a condition can be used as a reference for acridine,

1) Photochemistry of Acridines. XX.

2) A. Kellmann and J. T. Dubois, *J. Chem. Phys.*, **42**, 2518 (1965). A. Kellmann, *ibid.*, **63**, 936 (1966).

3) E. Vander Donckt and G. Porter, *ibid.*, **46**, 1173 (1967).

4) F. Wilkinson and J. T. Dubois, *ibid.*, **48**, 2651 (1968).

5) a) M. Koizumi, Y. Ikeda, and T. Iwaoka, *ibid.*, **48**, 1869 (1968). b) M. Koizumi, Y. Ikeda, and H. Yamashita, This Bulletin, **41**, 1056 (1968).

6) M. Hoshino and M. Koizumi, *ibid.*, **45**, 2988 (1972).

7) S. K. Lower and M. A. El-Sayed, *Chem. Rev.*, **1966**, 207 (1966).

8) a) K. Kikuchi, H. Kokubun, and M. Koizumi, This Bulletin, **41**, 1545 (1968); **43**, 2732 (1970). b) *ibid.*, **44**, 1527 (1971).

but the fluorescence intensity of the latter is not strong and there is some difficulty in practice. The principle of the method is as follows. The triplet yield per one flash $[T]_0$ which is given by

$$[T]_0 = \frac{[D_T]_0(\lambda')}{\varepsilon_T(\lambda')d} \quad (1)$$

(where $[D_T]_0(\lambda')$, optical density immediately after a flash, $\varepsilon_T(\lambda')$, molar extinction coefficient at λ') is related to the quantity of light absorption by

$$[T]_0 = \phi_{ST}\int I_{ab}dt \quad (2)$$

in which the integral over the wavelength is omitted for the sake of simplicity. The time integrated fluorescence intensity is written as

$$\int I_F(\lambda)dt = \alpha(\lambda)\phi_F\int I_{ab}dt \quad (3)$$

where ϕ_F is the fluorescence quantum yield and $\alpha(\lambda)$ is a constant depending on the setup of the apparatus and experimental conditions. From Eqs. (1), (2), and (3) we have

$$\phi_{ST}\varepsilon_T(\lambda')d = \alpha(\lambda)\phi_F[D_T]_0(\lambda')\Big/\int I_F(\lambda)dt \quad (4)$$

Since this relation holds both for reference (A) and sample (B), it follows that

$$\frac{\phi_{ST}^B\cdot\varepsilon_T^B(\lambda')}{\phi_{ST}^A\cdot\varepsilon_T^A(\lambda')} = \frac{(\alpha(\lambda)\phi_F)^B}{(\alpha(\lambda)\phi_F)^A}\times\left\{\frac{[D_T]_0(\lambda')^B}{\int I_F^B(\lambda)dt}\Big/\frac{[D_T]_0(\lambda')^A}{\int I_F^A(\lambda)dt}\right\} \quad (5)$$

λ was chosen so that the fluorescence intensities of the two samples could be compared accurately. It is desirable that the fluorescence intensities of the two are nearly equal, that there is no reabsorption at λ and that $dI_F/d\lambda$ is small at λ for both compounds. If ϕ_{ST}^A is known, the experimental determinations of

$$\frac{\varepsilon_T^B(\lambda')}{\varepsilon_T^A(\lambda')}, \frac{(\alpha(\lambda)\phi_F)^B}{(\alpha(\lambda)\phi_F)^A} \text{ and } \left\{\frac{[D_T]_0(\lambda')^B}{\int I_F^B(\lambda)dt}\Big/\frac{[D_T]_0(\lambda')^A}{\int I_F^A(\lambda)dt}\right\}$$

are all that is required to evaluate ϕ_{ST}^B. These are obtained respectively from energy transfer experiments, comparison of fluorescence intensities and the plots of $[D_T]_0(\lambda')$ *vs.* $\int I_F(\lambda)\,dt$.

A direct method is suitable for a substance with weak or no fluorescence. Bowers and Porter developed a somewhat similar method to ours.[9] In order to determine the light absorbed by a sample I_{ab}, they used the relation

$$\frac{I_{ab}}{I_0} = \frac{\int T_f(\nu)[1-T_c(\nu)]d\nu}{\int T_f(\nu)d\nu}$$

where I_0 is the incident light and T_f and T_c are the transmission coefficients of a filter and a sample, respectively. I_{ab} was determined from I_0 and the magnitude of the right term obtained graphically from the transmission profiles of a filter and a sample.

Our method is more experimental in nature. As shown in Fig. 1 an argon lamp specially designed is

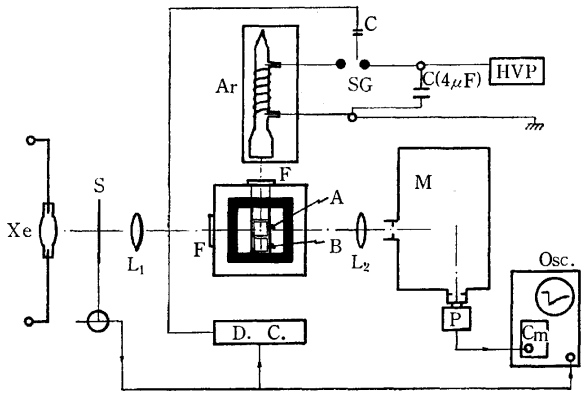

Fig. 1. Diagram of the flash apparatus.
Xe: xenon arc lamp, Ar: argon flash lamp (36 Torr). c: condenser, SG: spark gap, HVP: high voltage pulse, M: grating monochrometer, P: photomultiplier, Osc.: oscilloscope, Cm: comparator, D.C.: delay circuit, A: sample cell, B: actinometer cell, F: filter, L_1,L_2: lens, S: shutter.

placed about 7 cm from a sample cell. The lamp and cell are connected with a cylinder with inner wall painted black. Two cells for sample solution (A) and for actinometer solution (B) (K–Fe(III) oxalate) are placed close to each other. Three sets of measurements are necessary for determining the light quantity absorbed by a sample: a) n_A^0, the number of Fe(II) molecules produced by one flash in B-cell, is determined experimentally when the solvent is in A and the actinometer solution is in B. b) A similar quantity n_A^S is determined when the sample is charged in A and the actinometer solution in B. c) Putting the actinometer solution into A and B, similar quantities m_A in A and n_A^A in B are determined. Thus from (a) and (b), the light absorbed by a sample solution I_{ab}^S is given by

$$\frac{I_{ab}^S}{I_0^1} = \frac{n_A^0-n_A^S}{n_A^0} \quad (6)$$

where I_0^1 is the light intensity close to the inner front side of cell A. Similarly from (a) and (c) we have

$$\frac{I_{ab}^A}{I_0^1} = \frac{n_A^0-n_A^A}{n_A^0} \quad (7)$$

and

$$\frac{m_A}{\phi_{Fe(II)}} = I_{ab}^A\ (\phi_{Fe(II)}, \text{ quantum yield of actinometer}) \quad (8)$$

Hence

$$I_0^1 = \frac{n_A^0}{n_A^0-n_A^A}\times\frac{m_A}{\phi_{Fe(II)}} \quad (9)$$

From Eqs. (6) and (9) we obtain

$$I_{ab}^S = \frac{n_A^0-n_A^S}{n_A^0-n_A^A}\times\frac{m_A}{\phi_{Fe(II)}} \quad (10)$$

The method requires strict constancy in the energy output of the lamp.

Experimental

Substances. Specially purified anthracene was supplied by Prof. S. Kato, Tokyo University. Acridine was purified by the standard method. Proflavine sulfate ($C_{13}H_{11}N_3\cdot$

9) P. G. Bowers and G. Porter, *Proc. Roy. Soc. Ser A*, **296**, 435 (1967). G. Porter and P. G. Bowers, *ibid.*, *Ser .A*, **299**, 348 (1967).

$H_2SO_4 \cdot H_2O$, Tokyo Kasei) was treated with 10N NH_3 aqueous solution and was recrystallized three times from ethanol. Purity of a free base thus obtained was checked by elementary analysis and absorption spectrum. *o*-Phenanthroline (Wako Junyaku) was used without further purification. K-ferrioxalate ($K_3Fe(C_2O_4)_3 \cdot 3H_2O$) was prepared by mixing 300 ml aqueous solution of 1.5 M K-oxalate and 100 ml aqueous solution of 1.5 M $FeCl_3$. A crude sample was purified by recrystallization three times.

Apparatus. An ordinary flash apparatus was used. For the relative method, a xenon arc lamp was used for monitoring the absorption spectra of intermediates. A direct generator was used as a source in most experiments, but was replaced by a lead accumulator when the concentrations of intermediates were very low. The sample cell made of quartz and cylindrical in shape has a 10 cm light path. For the direct method, an argon (36 Torr) flash lamp (Fig. 1) was used. Its time characteristic is shown in Fig. 2 and transmissions of the filters in Fig. 3. All the measurements were made at room temperature.

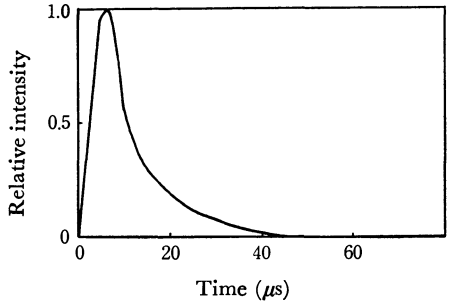

Fig. 2. Time character of the argon lamp.

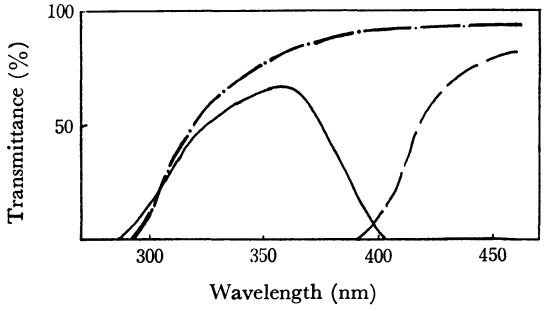

Fig. 3. Character of the filters employed.
—— UVD-2, – – VY-43, —·— alkali glass.

Results

Relative Method. The test was carried out with 9-methyl and 9-phenylanthracene as a sample and anthracene as a reference. The ϕ_{ST} values obtained for ethanol solutions are listed in Table 1 together with the values given in literature. Though the results are found to be satisfactory, the experiments carried out with acridine whose fluorescence is very weak were difficult in contrast to those with great fluorescence intensity. A UVD-2 filter was used for the excitation of anthracene and acridine and VY-43 for the excitation of proflavine.

a) *Determination of the Quantity.*

$$\frac{[D_T]_0^B(\lambda_B') \Big/ \int I_F^B(\lambda)dt}{[D_T]_0^A(\lambda_A') \Big/ \int I_F^A(\lambda)dt}$$

The plots of $[D_T]_0$ *vs.* $\int I_F\, dt$ for anthracene and acridine in methanol, when both quantities were measured at various flash intensities, are shown in Fig. 4. The $[D_T]_0(\lambda')/\int I_F(\lambda)\, dt$ value was evaluated from the slope of the plot. λ was selected in such a way that the ratio of fluorescence intensities I_{An}/I_{Ac} is the smallest. This is also a necessary condition for the accurate determination of $\alpha(\lambda)\phi_F$.

Relative values of $\int I_F(\lambda)\, dt$ were obtained by taking a photograph of oscillogram, tracing it on section paper and measuring the area under the curve. A

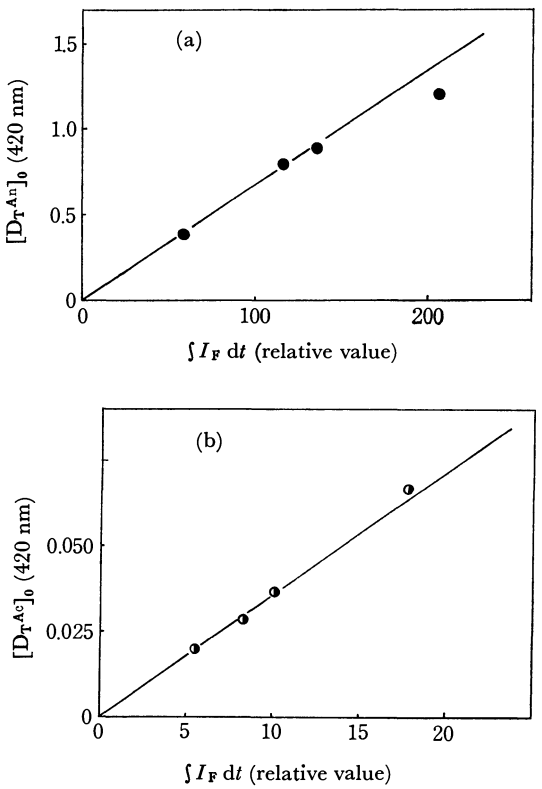

Fig. 4. Plots of $[D_T]_0$ *vs.* $\int I_F dt$ for anthracene (1.6×10^{-5} M) (a) and acridine (8.0×10^{-6} M) (b) in methanol. Absissas; relative values depending upon the experimental conditions, which are set exactly the same for (a) and (b).

Table 1. ϕ_{ST}-Values for ethanol solutions

	ϕ_F	ϕ_{ST}
Anthracene (reference)	0.30[a,b]	0.70[a,b]
9-Methylanthracene	0.35 (0.33[a])	0.67 (0.67[a])
9-Phenylanthracene	0.51 (0.49[a], 0.45[c])	0.50 (0.47[a], 0.51[c])

a) C. A. Parker, "Photoluminescence of Solutions", Elsevier Publishing Co., Amsterdam (1968).
b) C. A. Parker and T. A. Joyce, *Chem. Commun.*, **1966**, 234.
c) A. R. Harrocks, T. Medinger and F. Wilkinson, *Photochem. Photobiol.*, **6**, 21 (1967).

Table 2. ϕ_{ST}-Values and necessary data for their evaluation

Solvent	$\frac{[D_T^{Ac}]_0(420)/\int I_F\,dt}{[D_T^{An}]_0(420)/\int I_F\,dt}$	$\frac{\alpha^{Ac}(\lambda)\,\phi_F^{Ac}}{\alpha^{An}(\lambda)\,\phi_F^{An}}$	$\frac{\varepsilon_T^{Ac}(420)}{\varepsilon_T^{pr}(550)}$	$\frac{\varepsilon_T^{An}(420)}{\varepsilon_T^{Ac}(420)}$	ϕ_{ST}
Methanol	0.532	0.087 (λ=413 nm)	0.74_8	8.7_3	0.27
Ethanol[a)]	0.628	0.092 (λ=413 nm)	0.77_7	7.2_6	0.29
2-Propanol	0.932	0.078 (λ=413 nm)	0.67_9	8.3_9	0.43

a) T-T absorption was measured at 421 nm.

correction was made for the scattered light in the case of acridine. The results are given in Table 2.

b) *Determination of* $(\alpha(\lambda)\phi_F)^B/(\alpha(\lambda)\phi_F)^A$. Solutions were degassed to eliminate the quenching action of oxygen. By adjusting the concentration, excitation was performed at a wavelength at which the absorbance is the same for anthracene and acridine. The fluorescence intensity ratio itself then affords the required quantity. Reabsorption was negligible at the wavelength employed. The results are given in Table 2.

c) *Determination of* $\varepsilon_T^B(\lambda')/\varepsilon_T^A(\lambda')$. An energy transfer method was used to determine the ratio of extinction coefficient. Proflavine was used as an energy donor. This substance has the lowest T-level at 17100 cm^{-1} which is far below the suspected T(n-π^*) level of acridine and significantly higher than the lowest T(π-π^*) of acridine (15840 cm^{-1}) and anthracene.[10] By using a VY-43 filter, proflavine alone can be excited. At moderate concentrations of acridine and anthracene, complete T-energy transfer occurs from donor to acceptor; $[D_T]_0$ of acceptor should then be proportional to $\int I_F\,dt$ of proflavine. The former was measured at 420 nm and the latter at 494 nm. 420 nm is a peak position of T-T absorption of anthracene. The peak of acridine T-T absorption is located at 440 nm but there is an appreciable absorption of proflavine at this wavelength. The plots for anthracene and acridine in methanol are given in Fig. 5. Equally satisfactory plots were obtained also for ethanol and 2-propanol. It was confirmed that the plot of $[D_T]_0$ *vs.* $\int I_F dt$ for the solution containing proflavine alone gives a satisfactory straight line. The results are summarized in Table 2. The ϕ_{ST} values were obtained from the three sets of data.

Absolute Method. The test was carried out with

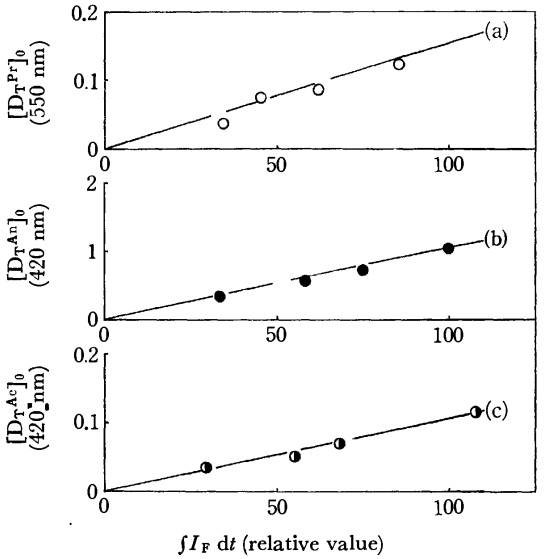

Fig. 5. (a) Plots of $[D_T]_0$ (550 nm) *vs.* $\int I_F dt$ for proflavine in methanol.
(b), (c) Similar plots for (b) anthracene $[D_T^{An}]_0$, (c) acridine $[D_T^{Ac}]_0$ added respectively to the solution of (a) as a T-energy acceptor.

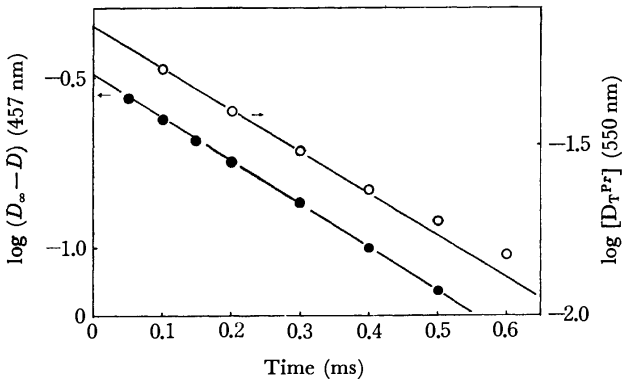

Fig. 6. Decay of triplet (○) and recovery of the ground state (●) for proflavine (1.0×10^{-6} M) in methanol.

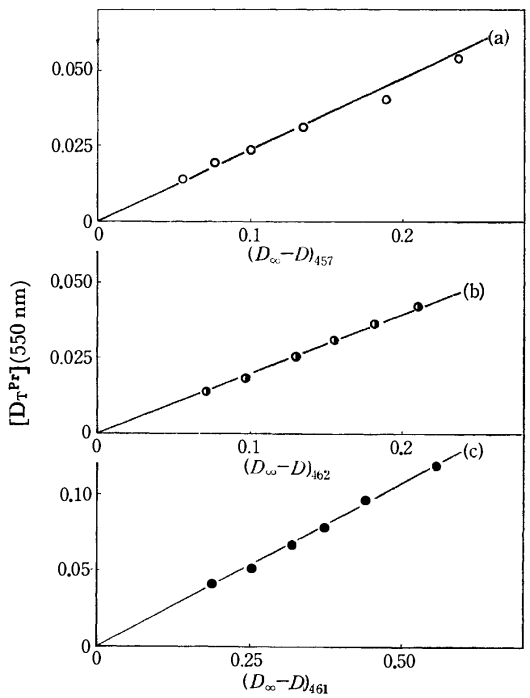

Fig. 7. Relation between $[D_T^{Pr}]$ and $(D_\infty - D)$ values at the same points after flashing.
a) methanol [proflavine]$=1.0\times10^{-6}$ M
b) ethanol [proflavine]$=1.0\times10^{-6}$ M
c) 2-propanol [proflavine]$=1.7\times10^{-6}$ M.

10) C. A. Parker, C. G. Hatchard, and T. A. Joyce, *Nature*, **205**, 1282 (1965).

Table 3. Molar extinction coefficients of T-T absorption of proflavine, anthracene, and acridine

Solvent	$\varepsilon_S^{Pr}(\lambda)$	$\varepsilon_T^{Pr}(550)$	$\varepsilon_T^{An}(\lambda)$	$\varepsilon_T^{Ac}(\lambda)$
Methanol	5.08×10^4 (457)	1.11×10^4	6.57×10^4 (420)	8.23×10^3 (420)
			1.92×10^4 (398)	1.86×10^5 (440)
Ethanol	5.44×10^4 (462)	1.1×10^4 [8b]	4.89×10^4 (420)	8.91×10^3 (424)
			5.20×10^4 (421)	1.85×10^4 (440)
2-Propanol	4.55×10^4 (461)	0.98×10^4	5.68×10^4 (420)	6.67×10^3 (420)
				1.51×10^4 (440)

Table 4. ϕ_{ST}-Values of acridine in methanol, ethanol and 2-propanol obtained by the absolute method

D_{356}	$[Fe(II)]_1$ (M)	$[T]_0$ (M)	$\frac{n_A^0-n_A^A}{n_A^0-n_A^S}$	$\frac{n_A^0-n_A^S}{n_A^0}$	$\frac{m_A}{n_A^0}$	ϕ_{ST}
Methanol						
1.10_8	5.68×10^{-7}	2.20×10^{-7}	1.48	0.676	0.987	0.33_0
1.11_0	8.18×10^{-7}	3.06×10^{-7}	1.50	0.667	1.15	0.32_3
0.54_1	1.05×10^{-6}	2.18×10^{-7}	2.30	0.424	1.19	0.27_4
0.26_6	9.68×10^{-7}	1.30×10^{-7}	4.00	0.250	1.17	0.30_8
						Mean 0.31 ± 0.02
Ethanol						
0.21_3	8.85×10^{-7}	1.06×10^{-7}	4.86	0.206	1.19	0.33_4
0.19_1	8.68×10^{-7}	1.18×10^{-7}	4.29	0.233	1.14	0.33_6
0.19_4	8.71×10^{-7}	1.17×10^{-7}	4.34	0.230	1.15	0.33_4
						Mean 0.33 ± 0.02
2-Propanol						
1.22_1	8.84×10^{-7}	4.77×10^{-7}	1.61	0.621	1.37	0.49_7
0.59_3	1.09×10^{-6}	3.44×10^{-7}	2.18	0.598	1.19	0.41_4
0.66_9	1.06×10^{-6}	4.13×10^{-7}	1.98	0.505	1.20	0.44_6
0.26_2	8.65×10^{-7}	2.05×10^{-7}	3.10	0.322	1.19	0.42_2
						Mean 0.45 ± 0.04

anthracene in 2-propanol. The ϕ_{ST} value obtained was 0.7_6 which agrees fairly well with that in literature.

Determination of $[T]_0$: The optical density and molar extinction coefficient for T-T absorption are required for knowing the triplet concentration. Since $\varepsilon_T^{An}/\varepsilon_T^{Pr}$ and $\varepsilon_T^{Ac}/\varepsilon_T^{Pr}$ are known we need to determine the value of ε_T^{Pr}. Decay of T-T absorption and recovery of the ground state absorption were measured with very dilute solutions of proflavine (1×10^{-6} or 1.17×10^{-6} M). Proflavine has a tendency of dimerization which is especially large in 2-propanol. Hence higher concentrations are undesirable. As shown in Fig. 6, the log $[D_T^{Pr}]$ *vs.* t plot for the former and the log $(D_\infty-D)$ *vs.* t plot for the latter, both methanol solutions, give straight lines with the same slopes. (D_∞ is the optical density when the ground state is recovered completely.) Similar results were obtained for ethanol and 2-propanol solutions.

The $[D_T^{Pr}]$-values are plotted against the $(D_\infty-D)$ values of the corresponding time points in Fig. 7; both values were taken from the results in Fig. 6 and the similar ones. Figure 7 indicates that the ground state proflavine recovers in one to one correspondence as the triplet state decays. ε_T^{Pr} and then ε_T^{Ac} and ε_T^{An} were determined from the slopes and are listed in Table 3.

The yield of triplet state was obtained by extrapolating the decay curve of T-T absorption to the time point of 25 μsec after flashing. The time point was selected taking the time character of the flash lamp (Fig. 2) and the decay rate of the triplet acridine into consideration. n_T, the number of triplet molecules produced, was calculated from the equation

$$n_T = [T]_0 \times \frac{V_1 N}{1000} \qquad (11)$$

where V_1 is the irradiated volume and N is Avogadro's number.

Measurement of the Absorbed Light: Because of low power of the flash, flashing was repeated 30—60 times, for a K-Fe(III) oxalate actinometer to be applicable. The method of measurement was modified to some extent, particularly with respect to coloration. The pH was adjusted to 3.5. Reflection on the cell windows and light scattering were taken into consideration. A correction formula proposed for the case of parallel light was applied,[11] but the correction factors were almost within experimental error.

The quantity of light absorption can be determined by Eq. (10). It is desirable to keep the value of $(n_A^0-n_A^S)/n_A^0$ in the range 0.15—0.20 in order to secure uniform formation of the triplet state. This was not possible experimentally, but the results were satisfactory. It was confirmed that the absorption spectrum of the solution subjected to flashing 30—60 times changed little, indicating that scarcely any reaction occurred.

Optical density of Fe(II)-orthophenanthroline chelate complex at 510 nm D_{510} was measured after being

11) R. E. Hunt and J. L. Hill, *J. Chem. Phys.*, **15**, 111 (1947). M. J. Dignam and D. J. LeRoy, *ibid.*, **26**, 964 (1957). M. A. Davies and P. P. Manning, *J. Amer. Chem. Soc.*, **79**, 5148 (1957).

subjected to flashing 30—60 times. m_A was then evaluated by the following equations.

$$m_A = [Fe(II)]_1 \times \frac{V_2 N}{1000} \quad (12)$$

$$[Fe(II)]_1 = \frac{D_{510}}{\varepsilon_{510} \cdot d} \times \frac{1}{P}$$

where ε_{510} is the molar extinction coefficient of chelate complex, d the light path (1 cm), V_2 a volume of the solution of chelate complex and P the number of flashes.

From Eqs. (10), (11), and (12), ϕ_{ST} can be evaluated by

$$\phi_{ST} = \frac{n_T}{I_{ab}} = \frac{[T]_0}{[Fe(II)]_1} \times \frac{n_A^0 - n_A^A}{n_A^0 - n_A^S} \times \frac{V_1}{V_2}\phi_{Fe(II)} \quad (13)$$

The value of 1.15 was used as $\phi_{Fe(II)}$.[12]

The ϕ_{ST}-values of acridine are listed in Table 4 together with other related quantities. Constancy of the energy output was checked by observing the T-T absorption repeatedly in the course of experiment. This was confirmed by the constancy of m_A/n_A^0 for succeeding experiments. No systematic concentration dependence is observed. Experimental error can not be estimated accurately but might be less than $\pm 10\%$.

Discussion

The ϕ_{ST}-values of acridine obtained by the two methods are listed in Table 5 together with the quantum yields of photoreduction *via* various paths[6] and with other related data. We see that the values obtained by the relative method are systematically a little smaller than those by the absolute method. It is remarkable that the ϕ_{ST}-value in 2-propanol is significantly larger than that in methanol and in ethanol; this is common to the results by the two methods.

It seems reasonable to correlate the large value in 2-propanol with the fact that T(n-π^*) participates in the photoreduction to some extent in ethanol and methanol but not in 2-propanol. ϕ_M^S, ϕ_R^S, ϕ_M^T, and ϕ_R^T in the table are the quantum yields of photoreduction *via* four paths. Subscripts M and R stand for molecular and radical mechanisms, respectively, and superscripts S and T for singlet excited and T(n-π^*) states, respectively. The general scheme of the photoreduction of acridine in alcohols presented by us is as follows.[5,6]

$$A \xrightarrow{h\nu} {}^1A^*$$

$${}^1A^* \longrightarrow A \qquad {}^1A^* \longrightarrow A + h\nu'$$

$${}^1A^* + RCH_2OH \longrightarrow AH\cdot + RCHOH \quad \text{(radical mechanism)}$$

$${}^1A^* + RCH_2OH \longrightarrow AH_2 + RCHO \text{ or } \quad \text{(molecular mechanism)}$$

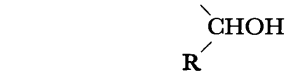

$${}^1A^* \longrightarrow {}^3A(n\text{-}\pi^*)$$

$${}^3A(n\text{-}\pi^*) \longrightarrow {}^3A(\pi\text{-}\pi^*)$$

$${}^3A(n\text{-}\pi^*) + RCH_2OH \longrightarrow AH\cdot + R\dot{C}HOH \quad \text{(radical mechanism)}$$

$${}^3A(n\text{-}\pi^*) + RCH_2OH \longrightarrow AH_2 + RCHO \text{ or } \quad \text{(molecular mechanism)}$$

$$AH\cdot + AH\cdot \longrightarrow AH_2 + A \text{ (disproportionation)} \quad \text{(in methanol and ethanol)}$$

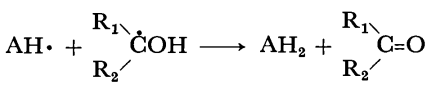

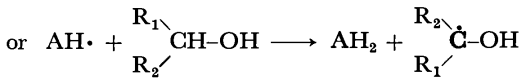

(in 2-propanol)

It is to be noted that the half-reduced radical produced by radical mechanism undergoes disproportionation in methanol and ethanol while in 2-propanol, it is entirely transformed into acridan-type compound.[6,13] The entire quantum yields for the production of T(n-π^*) in methanol and ethanol are then given as the sum $\phi_{ST}+2\phi_R^T+\phi_M^T$. The values are the same for three alcohols within experimental error when one uses the ϕ_{ST} values by the absolute method. It is thus reasonable to consider that the entire quantum yield of the production of T(n-π^*) is about the same for the three alcohols. Thus one can say that the ϕ_{ST} values we obtained and the quantum yields of photoreduction already published are correlated with each other in a consistent way. ϕ_{total} is a fraction of singlet excited state which disappears by reaction, fluorescence and intersystem crossing; the calculation was made in a similar way to the above. Thus $1-\phi_{total}$ is a fraction of eventural

Table 5. Quantum yields of various processes occuring in the excited acridine

Solvent	ϕ_M^S	ϕ_R^S	ϕ_M^T	ϕ_R^T	ϕ_F	ϕ_{ST}	$\phi_{ST}+2\phi_R^T+\phi_M^T$	ϕ_{total}
Methanol	0.027	0.032	0.006	0.063	0.046	r. 0.27	0.42	0.54
						a. 0.31	0.44	0.59
Ethanol	0.043	0.043	0	0.043	0.032	r. 0.29	0.38	0.54
						a. 0.33	0.42	0.58
2-Propanol	0.030	0.058	0	0	0.028	r. 0.43	0.43	0.55
						a. 0.45	0.45	0.57

12) J. G. Calvert and J. N. Pitts, Jr., "Photochemistry," John Wiley & Sons, (1966), p. 784.

13) Y. Miyashita, S. Niizuma, H. Kokubun, and M. Koizumi, This Bulletin, **43**, 3435 (1970).

internal conversion.

Some remarks should be added on the nature of the reactive singlet excited state. Zanker and Prell[14] proposed that S*(n-π^*) instead of S*(π-π^*) is a reactive state for the photoreduction of 9-methylacridine in deaerated ethanol solution. According to their results, the quantum yields for the formation of T(π-π^*) (ϕ_{ST}) and for the photoreduction (ϕ(R)) have about the same temperature dependence with an activation energy of about 800 cal/mol. They concluded that S*(n-π^*) is located above S*(π-π^*) by this amount, both reaction and intersystem crossing occurring mainly at S*(n-π^*). Whitten and Lee also concluded[15] that S*(n-π^*) is a reactive state for the photoreduction of acridine by isopropyl alcohol, toluene, and *p*-methylanisole in some inert solvents. Assuming that reaction occurs only at singlet excited state, they investigated the dependence of ϕ(R) and of the fluorescence of acridine ϕ(F) on the concentration of reducing agents; they found that in most cases fluorescence intensity is scarcely affected by the occurrence of photochemical reaction. We feel, however, that some of their fluorescence intensity data are consistent with the occurrence of quenching on account of the reaction. They inferred that S*(n-π^*) is below S*(π-π^*) in all the cases irrespective of solvent polarity, and S*(π-π^*) attained immediately after the light absorption goes down more or less irreversibly to S*(n-π^*) where reaction and intersystem crossing occur in competition. Conclusions on the relative positions of π-π^* and n-π^* reached by the two groups differ and further studies are necessary to decide which is correct. If the intersystem crossing were to occur only *via* S*(n-π^*)→T(π-π^*), as they both concluded, reaction at T(n-π^*) state would never occur. Our present results, which are consistent with our previous data of the reaction quantum yields, strongly suggest that the intersystem crossing occurs to a significant extent *via* S*(π-π^*)→T(n-π^*)→T(π-π^*) in addition perhaps to the above path. But since the level difference between S*(n-π^*) and S*(π-π^*) is of the order of kT according to Zanker and Prell (although it appears that their values are not so reliable because of the composite nature of ϕ(R) and ϕ_{ST}), it seems more reasonable to consider that both S*(n-π^*) and S*(π-π^*) are mixed with each other to some extent by vibronic interaction. If this is the case, S*(π-π^*) may also participate in the reaction. The temperature dependence of ϕ_{ST} as well as of ϕ(R) would then become more complicated in nature and can not be treated simply by means of the Arrhenius plot. The relative positions would be inverted according to the polarity of solvent, contrary to Whitten and Lee's conclusion.

Although both the nature of the reactive singlet excited state and the process of intersystem crossing require further studies, there is scarcely any doubt that the intersystem crossing occurs for the most part *via* S*(π-π^*)→T(n-π^*)→T(π-π^*).

14) V. Zanker and G. Prell, *Ber. Bunsenges. Phys. Chem.*, **73**, 791 (1969).

15) D. G. Whitten and Y. J. Lee, *J. Amer. Chem. Soc.*, **93**, 961 (1971).

The Determination of the CMC of Surfactants in Some Organic Solvents

Shinya MUTO and Kenjiro MEGURO

Faculty of Science, Science University of Tokyo, Kagurazaka, Shinjuku-ku, Tokyo

(Received June 29, 1972)

Extra absorption spectra appeared when 7,7,8,8-tetracyanoquinodimethane (TCNQ) was solubilized into surfactant organic solvent solutions above the critical micelle concentration (CMC). It was found also that extra absorption spectra appeared when iodine was solubilized into surfactant organic solvent solutions above the CMC. In the former case, the extra absorption spectra are attributed to TCNQ anion radical salts formed between TCNQ and the surfactants. In the latter, the extra absorption spectra are due to charge-transfer interactions of iodine with the surfactants. The intensity of the absorption bands increased with the concentrations of the surfactant. The values of the CMC of the surfactants were determined from this spectral change. The CMC values obtained by the TCNQ solubilization method were larger than those obtained by the iodine solubilization technique. The difference in the CMC between the two methods was interpreted in terms of the difference in solubility and charge-transfer power to the organic solvent between iodine and TCNQ, and the difference in type of electron transition, that is, $n(D)\rightarrow\sigma(A)$ or $n(D)\rightarrow\pi(A)$.

The critical micelle concentrations (CMC's) of oil-soluble surfactants in organic solvents have frequently been determined in the past by three different methods, by the light-scattering method, by the vapour-pressure depression, and by the solubilization technique. As these methods are not easy, a more convenient and simple method is desirable.

In our previous paper,[1] we reported that when TCNQ, a well-known strong electron aceeptor, was solubilized into surfactant aqueous solutions above the CMC, a characteristic color appeared. This phenomenon was applied to the determination of the CMC of various surfactants in aqueous solutions.

Recently, we found that this solubilization is also useful for determining the CMC of oil-soluble surfactants in various organic solvents, for the TCNQ solubilized in surfactant organic solutions above the CMC has characteristic absorption spectra, probably because of the TCNQ anion radical formed by the charge transfer from the surfactant to the TCNQ.

The CMC's of surfactants have also been determined by an iodine-solubilization technique[2] in organic solvents.

In this paper, we will report on the characteristics of the charge-transfer solubilization of TCNQ into surfactant micelle in organic solvents and will compare our results with those of other methods.

Experimental

The surfactants used in this experiment were dodecyl pyridinium iodide and Aerosol OT.

Dodecyl pyridinium iodide (DPI) was synthesized by the usual method[3] in our laborotory; its purity was confirmed by the surface-tension and electroconductance methods.

Aerosol OT (sodium dioctyl sulfosuccinate) was supplied from the Nikko Chemical Co., and this sample was purified as follows. It was dissolved in methanol, and the undissolved material was excluded by means of a fine glass filter and subsequent drying.

TCNQ was synthesized according to a procedure described previously.[4] It was purified by five recrystallizations in acetonitrile. The crystals thus obtained had a rust-colored, flasky form; their purity was confirmed by elementary analysis and by studying the melting point.

Iodine of a G.R. garde was purified by sublimation.

Benzene, cyclohexane, *n*-heptane, and carbon tetrachloride were purified according to the procedure of Kitahara and Kon-no.[5] Chloroform, methyl alcohol, and acetonitrile were purified in the usual way.[6]

For ultraviolet, visible and near-infrared spectra studies, the TCNQ solutions were prepared as follows: a known quantity of the TCNQ was dissolved in a measured volume of various organic solvents (the TCNQ concentartion was about 10^{-4} mol/l), and then this solution was used as the stock solution of the TCNQ (A). The stock solution of the surfactant (B) contained a known concentration of the surfactant well above its CMC. By diluting the B solution with the A solution, a series of concentrations of the surfactant could be obtained, each with the same concentration of TCNQ. This series had to include concentrations above and below the CMC to be determined. All the solutions were prepared at room temperature.

Iodine-surfactant solutions were also prepared in the same manner as the TCNQ-surfactant solutions. In this case, the iodine concentration was kept at 5×10^{-4} mol/l for all the solutions.

The absorption spectra were measured by using a Hitachi Spectrophotometer (Model EPS-2).

Results and Discussion

Interaction between DPI and TCNQ. The absorption spectra of TCNQ solubilized in a chloroform solu-

1) a) S. Muto, K. Deguchi, K. Kobayashi, E. Kaneko, and K. Meguro, *J. Colloid Interface Sci.*, **33**, 475 (1970). b) S. Muto, K. Deguchi, Y. Aono, Y. Shimazaki, and K. Meguro, *ibid.*, **37**, 109 (1971). c) S. Muto, K. Deguchi, Y. Aono, Y. Shimazaki, and K. Meguro, This Bulletin, **44**, 2087 (1971).

2) S. Ross and J. P. Oliver, *J. Phys. Chem.*, **63**, 1671 (1959).

3) K. Meguro and T. Kondo, *Nippon Kagaku Zasshi*, **80**, 818 (1959).

4) D. S. Acker and W. R. Hertler, *J. Amer. Chem. Soc.*, **84**, 3370 (1962).

5) K. Kon-no and A. Kitahara, *J. Colloid Interface Sci.*, **33**, 124 (1970).

6) J. A. Riddick and E. E. Toops, "Organic Solvent," 2nd ed. (Technique of Organic Chemistry Vol. 7), Interscience (1955), pp. 410, 333, 435.

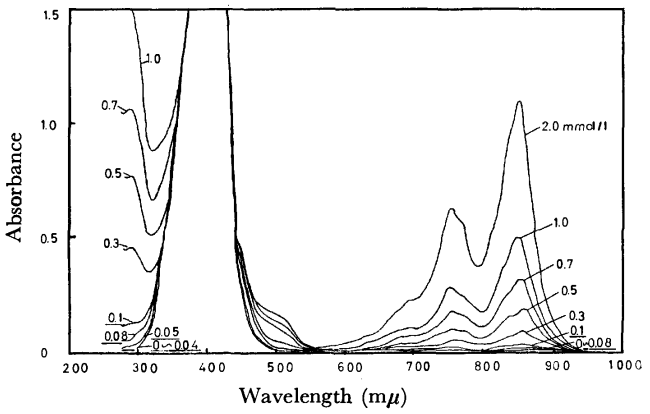

Fig. 1. Visible absorption spectra of TCNQ in DPI chloroform solutions.
TCNQ Concentration: 0.5 mmol/l

tion of DPI are shown in Fig. 1. As is shown in Fig. 1, the spectra at low surfactant concentrations have no appreciable absorption of the TCNQ anion radical (the underlined numbers show the concentration of the surfactant below the CMC). When the concentration reaches a certain value, the spectra change their form rapidly; new bands appear at 480, 680, 750, and 850 mμ, and the optical densities of these absorption bands increase with the concentration of the surfactant. The absorptions at 680, 750, and 850 mμ have already been confirmed as those of the TCNQ anion radical by many authors,[7] but the absorption at 480 mμ does not belong to the anion radical; this absorption band seems to be caused by charge-transfer interaction between the surfactant and the TCNQ. The rapid increase in optical densities at 680, 750, and 850 mμ above some surfactant concentration suggests a rapid increase in the amounts of TCNQ anion radicals in these systems. The reason for the rapid increase in the TCNQ anion radicals is considered to be as follows: it is known that the surfactants make inverted micelles at the CMC in organic solvents. Therefore, at concentrations above the CMC, the surfactant molecules concentrated in the micelle interact with the TCNQ and produce a kind of ionic charge-transfer complex; then the resulting TCNQ anion radicals which have ionic properties are solubilized in the hydrophilic inside of the inverted micelles. From this fact, it was recognized that the surfactant concentration at which the rapid increase in the absorption of the TCNQ anion radical occurred would correspond to the CMC value in organic solvents.

In Fig. 2, the optical density of the spectra of the TCNQ anion solubilized in DPI chloroform solutions is plotted against the surfactant concentrations. The CMC are given by an intercept of the resulting two lines. The CMC's of different surfactants in various organic solvents obtained by this method are summarized in Table 1.

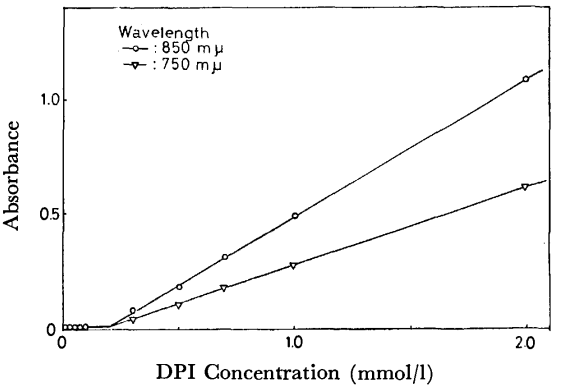

Fig. 2. Relationship between the absorbance and concentration of DPI chloroform solutions.

Table 1. CMC values of surfactants in various organic solvents (TCNQ method, at 20°C)

Surfactant	Solvent	CMC (mmol/l)	Wavelength (mμ)
DPI	Chloroform	0.2	850
	Benzene	0.07	850
	Methanol	—	
Aerosol OT	Chloroform	0.4	850
	Benzene	2.0	850
	Carbontetrachloride	0.6	277
	Methanol	—	

Ralston *et al.*[8] have found that dodecyl ammonium chloride in pure water makes a micelle and exhibits a clear break point in conductance-concentration curve at the CMC, but this break point does not become clear in suitable methyl-alcohol mixtures or in pure methyl alcohol. In these alcohol solutions, the dodecyl ammonium chloride behaves like a normal electrolyte over the entire range of concentration. They explain this fact by assuming a breakdown of the micelle.

This evidence was also confirmed by the spectra change between TCNQ and DPI in methyl alcohol solutions, in which the surfactant can not exist in the micelle form. Figure 3 shows the spectra of TCNQ in a methyl alcohol solution of DPI. The most characteristic feature of the spectra lies in the fact that the optical densities of the absorption peaks at 680, 750,

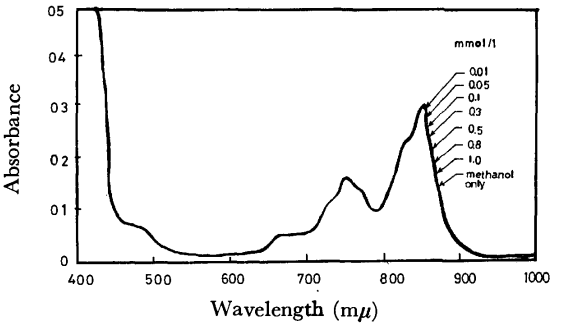

Fig. 3. Absorption spectra of TCNQ in DPI methanol solutions.

7) a) S. R. Melby, R. J. Harder, W. R. Heltler, W. Mahler, R. E. Benson, and W. E. Mochel, *J. Amer. Chem. Soc.*, **84**, 3374 (1962). b) A. Rembaum, A. M. Hermann, F. E. Stewart, and F. Gutmann, *J. Phys. Chem.*, **73**, 513 (1969). c) Y. Iida, This Bulletin, **42**, 71 (1969). d) Y. Iida, *ibid.*, **42**, 637 (1969).

8) a) A. W. Ralston and D. N. Eggenberger, *J. Phys. Chem.*, **52**, 1494 (1948). b) A. W. Ralson and C. W. Hoerr, *J. Amer. Chem. Soc.*, **68**, 851 (1946).

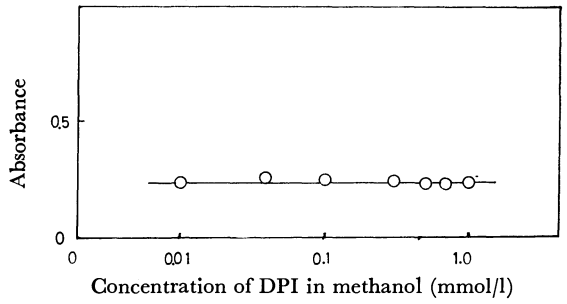

Fig. 4. Relationship between the absorption and concentration of DPI methanol solutions.

and 850 mμ, which are caused by the interaction between the TCNQ and the oxygen atom of methyl alcohol, are not influenced at all by the amounts of DPI. The optical density of TCNQ in DPI methyl alcohol solutions, plotted against the concentrations of DPI, are shown in Fig. 4, which shows more clearly that the optical densities do not change, but keep a constant value with the concentration of DPI. This can be explained by the breakdown of the micelle in the methyl alcohol solution.

Recently, Mukerjee *et al.*[9] found that a new band appeared at 290 mμ in a DPI micellar aqueous solution and a DPI chloroform solution. They reported that this band was due to the formation of a charge-transfer complex between the surfactant micelle and iodine, and also reported that this band could not be observed below the CMC.

We also confirmed that the appearance of the 290 mμ band can be used to as a means of recognizing the micelle formation of DPI in an organic solvent. When DPI was dissolved in chloroform, benzene, and water, a charge-transfer band was observed at 290 mμ. In the DPI methyl alcohol solution, however, the band was not found. This fact confirms that micelle formation does not occur in methyl alcohol solutions.

Interactions between Aerosol OT and TCNQ or Iodine. The absorption spectra of TCNQ solubilized in a chloroform solution of Aerosol OT are shown in Fig. 5. The shape of this absorption spectra is almost the same as that obtained in Fig. 1. This fact is particularly

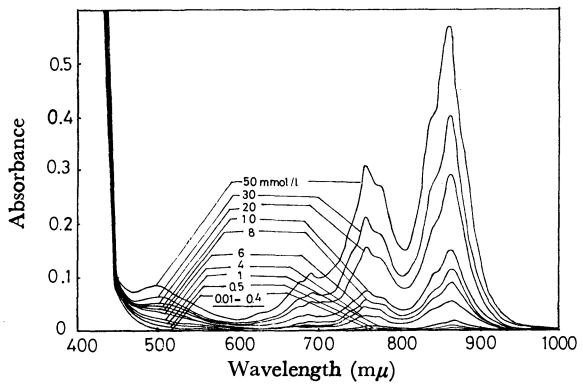

Fig. 5. Visible absorption spectra of TCNQ in Aerosol-OT chloroform solutions.
TCNQ concentration: 0.5 mmol/l

interesting. In this case, no remarkable absorption could be found in the spectra below the CMC, but new bands were observed at 480, 680, 750, and 850 mμ, above the CMC, and the intensities of these bands increased rapidly above the CMC of the surfactant. The surfactant concentration at which the rapid increase in optical densities of the TCNQ anion radical occurred would correspond to the CMC values in organic solvents. Indeed, the CMC value of Aerosol OT in benzene obtained by this method agrees with the data measured by Kon-no and Kitahara[10] (see Table 2). The CMC values of Aerosol OT in different organic solvents are summarized in Table 1.

TABLE 2. COMPARISON OF THE CMC OF AEROSOL OT BENZENE SOLUTION (mmol/l)

Method	Light scattering[a]	Depression of[a] vapour pressure	TCNQ method
CMC	2.8	2.3	2.0

a) K. Kon-no, and A. Kitahara, *Kogyo Kagaku Zasshi*, **68**, 2058(1965).

The data in Table 1 suggest that the micelle formation is influenced by the nature of the solvent; that is, the CMC values increase with the polarity of the solvent (see Table 3). The values in Table 3 agree with the results given by Kitahara and Kon-no.[10]

TABLE 3. THE RELATIONSHIP BETWEEN THE CMC OF SURFACTANTS AND DIELECTRIC CONSTANT OF ORGANIC SOLVENTS (Aerosol OT)

TCNQ method Solvent	Dielectric constant	CMC (mmol/l)
Benzene	2.27	2.0
Carbontetrachloride	2.24	0.6

Iodine method Solvent	Dielectric constant	CMC (mmol/l)
Benzene	2.27	0.9
Carbontetrachloride	2.24	0.3
Cyclohexane	2.01	0.2

Ross *et al.*[2] have described that iodine dissolved in benzene has a band at 490 mμ in its spectrum, but this band decreases upon the addition of a surfactant to this system and a new band appears at 360 mμ, the optical density of which increases with the concentration of the surfactant. They determined the CMC's of many surfactants in nonaqueous media by using the optical density of the iodine spectrum at 360 mμ.

When Aerosol OT was dissolved in various iodine solutions, such as benzene, cyclohexane, chloroform, and carbon tetrachloride, a new iodine band appeared; this band had a slight dependency on the character of the organic solvent. The ordinary band of iodine in an organic solvent, and the new band appearing after the addition of the surfactant, are listed in Table 4. A typical change in the spectrum of iodine in a cyclo-

9) a) A. Ray and P. Mukerjee, *J. Phys. Chem.*, **70**, 2138 (1966). b) P. Mukerjee and A. Ray, *ibid.*, **70**, 2144 (1966).

10) K. Kon-no and A. Kitahara, *Kogyo Kagaku Zasshi*, **68**, 2058 (1965).

TABLE 4. CMC VALUES OF Aerosol OT IN ORGANIC SOLVENTS (IODINE METHOD AT 20 °C)

Surfactant	Solvent	CMC (mmol/l)	New band (wavelength) mμ	Original band (wavelength) mμ
Aerosol OT	Cyclohexane	0.2	386	522
	Chloroform	0.24	272	510
	Benzene	0.9	390	490
	Carbontetrachloride	0.3	280	520

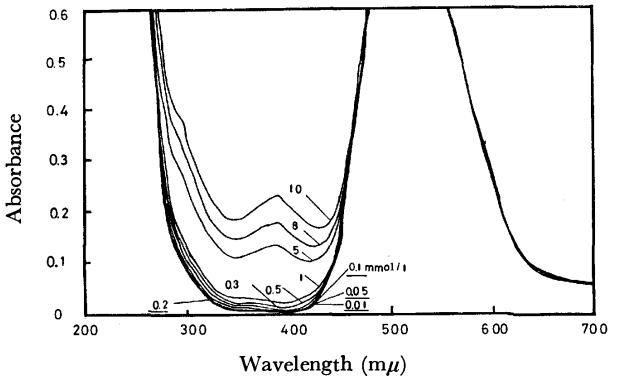

Fig. 6. Visible absorption spectra of I_2 in Aerosol OT cyclohexane solutions.
I_2 concentration: 1 mmol/l

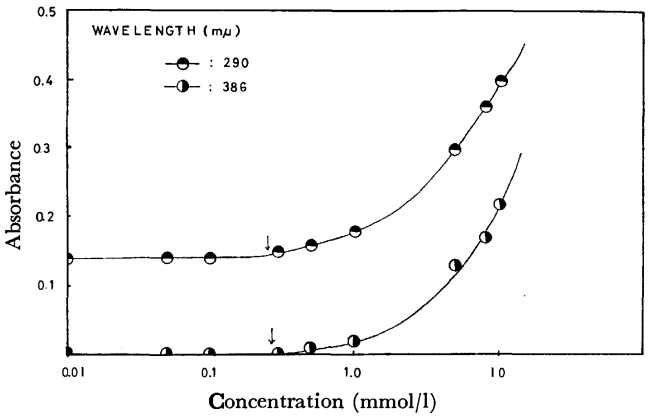

Fig. 7. Relationship between the absorbance and concentration of Aerosol OT cyclohexane solutions.

hexane solution upon the addition of a surfactant is shown in Fig. 6; the figure indicates that a new band appears at 386 mμ and increases in intensity with the concentration of the surfactant. In Fig. 7 the optical density of iodine in Aerosol OT cyclohexane solutions is plotted against the concentrations of Aerosol OT. In this figure, the value of the CMC is given by the change in the slope. The CMC's of several surfactants obtained by this iodine-solubilization technique are summarized in Table 4.

A comparison of the CMC values obtained by the TCNQ solubilization method with those obtained by the iodine method shows that the CMC values estimated by the iodine method are smaller than those obtained by the TCNQ method. At present, although we can not explain exactly why the difference occurs, it may be considered to be that the interaction between the TCNQ and the surfactant is a n(D)→π(A) transition, while the interaction between the iodine and the surfactant is a n(D)→σ(A) transition.

Strong *et al.*[11] have previously reported that the transition energy, ($h\nu_{ct}$), of the n(D)→σ(A) electron transition between a lower alcohol and iodine is about 5 eV.

The $h\nu_{ct}$ value found between Aerosol OT and iodine in cyclohexane and carbon tetrachloride is about 4.6 eV. This value agrees roughly with the value of 5 eV obtained by Strong *et al.* Accordingly, it may be concluded that the transition between Aerosol OT and iodine in cyclohexane and carbon tetrachloride is a n(D)→σ(A) transition.

On the other hand, the interaction between the TCNQ and the nitrogen atom or oxygen atom in the surfactant can be considered to be a n(D)→π(A) transition. From these results, the difference in the CMC between the two methods may originate from the difference in the type of transition between the TCNQ and iodine molecule, and from the difference in solubility to organic solvents.

The ionization potential of organic solvents can be

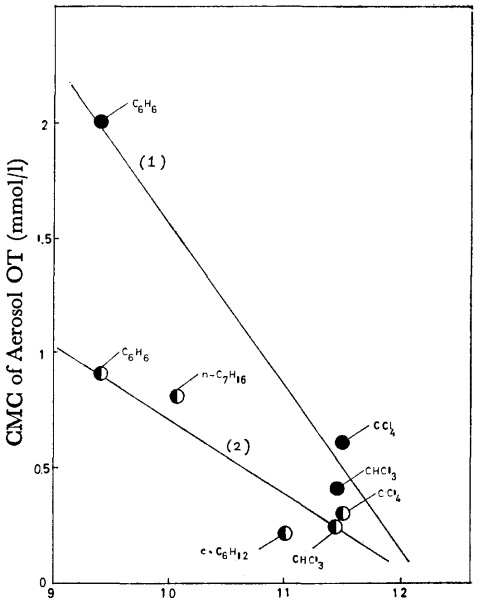

Fig. 8. Relationship between the CMC of Aerosol OT and ionization potential of organic solvents.
●: n–π type ◐: n–σ type

11) R. L. Strong, S. J. Rand, and J. A. Britt, *J. Amer. Chem. Soc.*, **82**, 5053 (1960).

considered to be a measure of the relative donor capacity of organic solvents. The plots of the CMC of Aerosol OT *vs.* the ionization potential of organic solvents are shown in Fig. 8, which suggests that the CMC values obtained by the $n(D)\rightarrow\pi(A)$ transition are larger than those obtained by the $n(D)\rightarrow\sigma(A)$ transition. In Fig. 8, Line (1) is the plot of CMC estimated by the TCNQ method against the ionization potential, while Line (2) is the plot of the CMC estimated by the iodine method against the ionization potential, as the TCNQ method depends on the $n(D)\rightarrow\pi(A)$ transition, and the idoine method, on the $n(D)\rightarrow\sigma(A)$ transition.

The authors wish to thank Dr. Ayao Kitahara for his advice, and the Nikko Chemical Co. for furnishing the samples.

BULLETIN OF THE CHEMICAL SOCIETY OF JAPAN, VOL. 46, 1320—1324 (1973)

Adsorption and Inhibition Effect of Triton X at the Mercury/Solution Interface

Tetsuya OHSAKA, Hajime YAMAMOTO, and Tadashi YOSHIDA

Applied Electrochemical Laboratory, Graduate School of Science and Engineering, Waseda University, Nishi-okubo, Shinjuku-ku, Tokyo 160

(Received July 10, 1972)

The time dependence of differential capacity and that of polarographic current were observed to elucidate the adsorption behavior of Triton X. The adsorption showed a relatively ideal system of the diffusion-controlled type in which semi-infinite linear diffusion was assumed. The results from the two different observations agreed approximately. The Koryta equation was applied to obtain the maximum surface concentration Γ_m of Triton X in the adsorption of the monolayer. $\log \Gamma_m$ decreased linearly with increasing $\log \bar{M}$ (mean molecular weight), the slope being *ca.* -1. In the case of high bulk concentration, the adsorption showed unusual phenomena considered to be caused by the formation of a multi-layer which tended to become marked with the decrease of $\bar{M}$. The inhibition effect of Triton X on reduction current revealed approximately the same tendency regardless of cations Cd^{2+} and Cu^{2+}. Though the dependence of inhibitive action on $\bar{M}$ was relatively small, the degree of inhibition became somewhat small with increasing $\bar{M}$ in contrast to the cases of PVP and PEG. The shape of instantaneous *i vs. t* curve was approximately elucidated by Matsuda's treatment of the system where the limiting current was depressed by diffusion-controlled adsorption. The *i-t* curve revealed that the degree of inhibition scarcely increases until attainment of a certain high coverage when a sharp increase takes place.

The adsorption of water-soluble polymer at the mercury/solution interface is mainly controlled by diffusion. The behavior is approximately explained by means of the Koryta equation,[1] as shown in the cases of polyvinylpyrrolidone (PVP)[2] and polyethyleneglycol (PEG).[3] Triton X (alkylphenoxy polyethoxy ethanols)[4] is often used as a suppressor of the maximum wave in polarography. We examined its interfacial behavior by means of measurements of differential capacity and instantaneous current.

Schmid and Reilley[5] showed instantaneous current *vs.* time curves classified into three extreme cases. The current-time curve depressed by Triton X is a typical example of diffusion-controlled adsorption. Barradas and Kimmerle[6,7] examined the maximum surface concentration Γ_m of Triton X by means of two methods; measurement of suppression of the oxygen maximum wave[6] and that of the potential dependence of interfacial tension.[7] The disagreement between Γ_m's obtained by the two methods seems to result from the formation of a multi-layer. In the present investigation, the formation of a monolayer was considered primarily, the formation of a multi-layer being also taken into account.

Experimental

A DME (dropping mercury electrode) was used as a test electrode. Its drop time was about 12 s for the measurements of differential capacity and instantaneous current, and about 3—4 s for the polarographic measurements. The counter electrode was a cylindrical platinum net with a sufficiently large surface. All potentials were referred to the saturated calomel electrode (SCE).

The differential capacity at the mercury/solution interface was measured with a transformer impedance bridge of 1 kHz whose input was kept less than 10 mV_{P-P}. A series equivalent circuit with resistance and capacitance was used for the bridge measurement.

The instantaneous current *vs.* time curves were determined from the *iR* drop observed with a recorder or an oscilloscope in parallel with 2 kΩ resistance which was connected in series

1) J. Koryta, *Collect. Czech. Chem. Commun.*, **18**, 206 (1953).
2) T. Yoshida, T. Ohsaka, and S. Tanaka, This Bulletin, **45**, 326 (1972).
3) T. Yoshida, T. Ohsaka, and M. Suzuki, *ibid.*, **45**, 3245 (1972).
4) Molecular formula: C_8H_{17}–C$_6$H$_4$–$(OCH_2CH_2)_n$ OH
5) R. W. Schmid and C. N. Reilley, *J. Amer. Chem. Soc.*, **80**, 2087 (1958).
6) R. G. Barradas and F. M. Kimmerle, *J. Electroanal. Chem.*, **11**, 163 (1966).
7) R. G. Barradas and F. M. Kimmerle, *ibid.*, **11**, 128 (1966).

with the DME and the polarization circuit.

Triton X-45, X-100, X-205, and X-405 (Rohm and Haas) were used without further purification, their degrees of polymerization for ethylene oxide groups being 5 ($\bar{M}$=430), 9—10 ($\bar{M}$=600—650), 20 ($\bar{M}$=1100), and 40 ($\bar{M}$=2000), respectively. Solutions were prepared from guaranteed reagent and triply-distilled water. All experiments were conducted in an atmosphere of purified nitrogen at 25°C in 1N sulfuric acid.

Results and Discussion

Dependence of Differential Capacity on Potential (C-E Curves). Figures 1-(a) and (b) show the *C-E* curves of Triton X-45 and X-405 at adsorption time of 5 s. The anodic peaks due to adsorption or desorption were observed at *ca.* 0—0.1 V. No cathodic peak was observed. The adsorption or desorption peaks become large with the increase in bulk concentration. The potential dependence of the peak is seen to some extent except for the case of Triton X-405. Since the differential capacity decreases with the increase of Triton X concentration in a more cathodic potential than an anodic peak, adsorption occurs in this range.

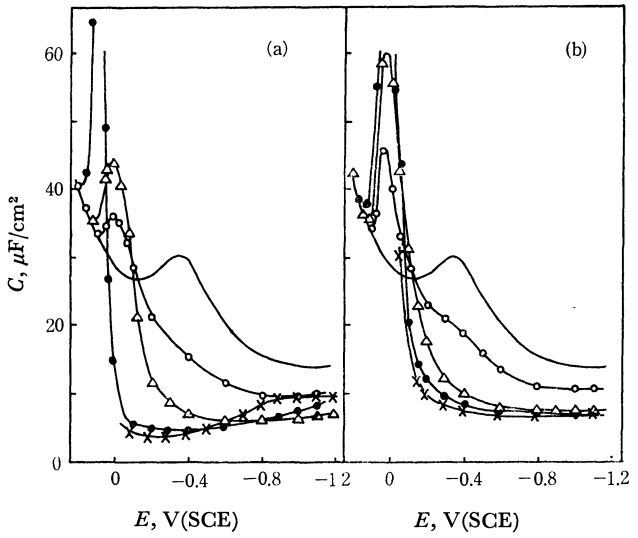

Fig. 1. The differential capacity *vs.* potential curves.
25 °C, adsorption time of 5 s, (a) 1N aqueous sulfuric acid +Triton X-45 (solid line: 0 mg/l, ○: 10 mg/l, △: 20 mg/l, ●: 60 mg/l, ×: 200 mg/l), (b) 1N aqueous sulfuric acid +Triton X-405 (solid line: 0 mg/l, ○: 10 mg/l, △: 20 mg/l, ●: 40 mg/l, ×: 100 mg/l).

In the case of high bulk concentration of Triton X-45, the differential capacity ascends gradually as the potential becomes more cathodic and finally becomes constant independent of potential. The ascent at the cathodic potential can hardly be ascribed to adsorption or desorption but rather to the formation of a multilayer of Triton X as stated by Barradas,[7] since the capacity after the ascent attains a constant value lower than that in the blank solution in a relatively wide range of potential. However, the ascent of differential capacity is scarcely seen in the case of Triton X-405. Since it becomes marked with decreasing $\bar{M}$ in the cathodic potential, it might be more easy for Triton X of low $\bar{M}$ to form the multi-layer.

Dependence of Differential Capacity on Adsorption Time. The differential capacity *vs.* time curve was measured at −0.6 V where the adsorption always attains equilibrium or saturation to form the monolayer. Figures 2-(a) and (b) show the C-$t^{1/2}$ relations of Triton X-45 and X-405, which indicate that the adsorption of Triton X is controlled by diffusion in a relatively low bulk concentration in the same way as in the cases of organic polymers.[2,3]

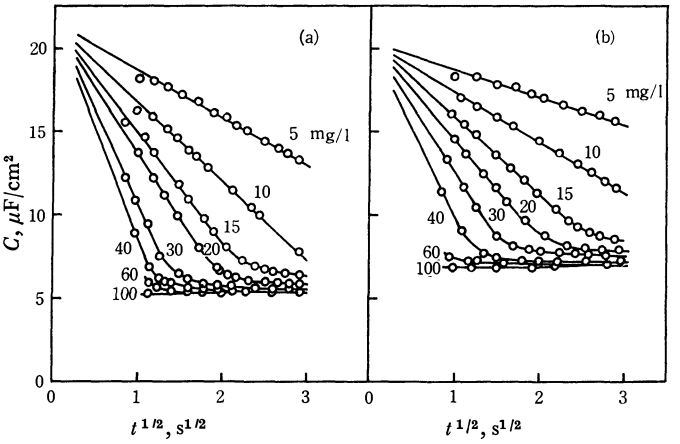

Fig. 2. The differential capacity *vs.* square root of time curves.
25 °C, −0.6 V, (a) 1N sulfuric acid solution+Triton X-45, (b) 1N sulfuric acid solution+Triton X-405.

In the limiting case controlled by linear diffusion, the following relation (1)[8] can be derived from the Koryta equation[1] with the Frumkin parallel condenser model.[9]

$$C = C_0 - 0.736(C_0 - C_s)D^{1/2}\Gamma_m^{-1}at^{1/2} \text{ for } t<t_m \quad (1)$$

where C_0 and C_s are unit area capacities (μF/cm^2) for θ (coverage)=0 and θ=1, a the bulk concentration (mol/cm^3), D the diffusion coefficient (cm^2/sec), t the adsorption time (sec), t_m the time required to attain the saturated adsorption to form the monolayer and Γ_m the maximum surface concentration (mol/cm^2). Equation (1) holds for $t<t_m$. However, when $t\geq t_m$, the differential capacity becomes constant as follows.

$$C = C_s \quad (2)$$

It is seen from Eqs. (1) and (2) that C decreases linearly with $t^{1/2}$ or a when the adsorption is controlled by diffusion ($t<t_m$), while C becomes constant at the saturated adsorption ($t\geq t_m$).

The C-$t^{1/2}$ relation in Fig. 2 consists of two linear portion; one corresponding to that of diffusion-controlled adsorption (C decreases with $t^{1/2}$), and the other to that of saturated adsorption (C is constant). Thus, the results in Fig. 2 are explained by Eqs. (1) and (2). Extrapolation of the two linear portions gives the value of t_m. Though the differential capacity at the adsorption equilibrium somewhat depends on bulk concentration, the initial linear portion was extrapolated

8) P. W. Board, D. Britz, and R. V. Holland, *Electrochim. Acta*, **13**, 1633 (1968).
9) A. N. Frumkin, *Z. Phys.*, **35**, 792 (1926).

to that of C_s for the sake of convenience. The observed C_s may be the value for the multi-layer, but the error due to the selection of C_s is considered to be small because of the small concentration dependence of C at the adsorption equilibrium. It is possible to calculate Γ_m by substituting t_m into the Koryta equation on the assumption of D. Directly obtainable values of $at_m^{1/2}$ ($=\Gamma_m/0.736D^{1/2}$) are also given in Table 1.

Polarograms. The adsorption behavior of surface-active compounds can also be investigated by the inhibition effect on current. Γ_m can be calculated by use of the Koryta equation from the instantaneous current *vs.* time relation (*i-t* curve) where the limiting current is inhibited by diffusion-controlled adsorption.

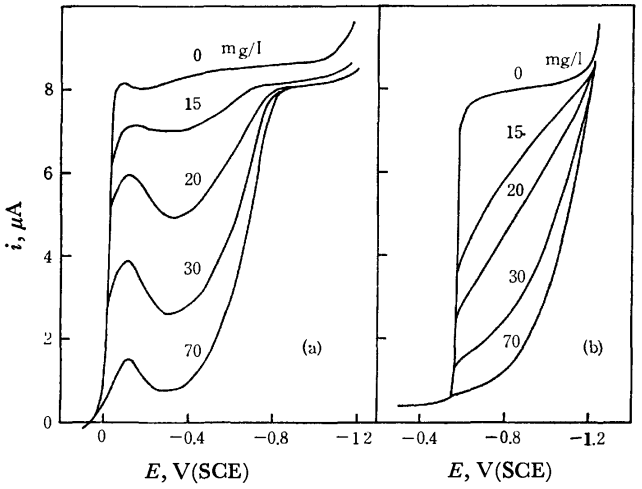

Fig. 3. Polarograms inhibited by Triton X-405.
1N sulfuric acid solution + Triton X-405, (a) depolarizer: 1 mM Cu^{2+}, (b): depolarizer: 1 mM Cd^{2+}.

Figures 3-(a) and (b) give typical examples of the inhibition effect of Triton X-405 on the reduction of Cu^{2+} and Cd^{2+} in 1N sulfuric acid. The reaction is depressed with increasing bulk concentration in both cases. The current peak at *ca.* −0.1 V for Cu^{2+} (Fig. 3-(a)) may be due to the desorption of Triton X-405 since the desorption peak is revealed at *ca.* −0.1 V in the *C-E* curves (*cf.* Fig. 1-(b)). The current begins to increase at *ca.* −0.7 V for Cu^{2+} and at *ca.* −1.0 V for Cd^{2+} (Fig. 3-(b)). The decrease of the inhibition effect can hardly be ascribed to the desorption of inhibitor but rather to the sufficient overpotential in view of the results in Fig. 1.

Instantaneous Current vs. *Time Curves.* The *i-t* relations for the reduction of Cu^{2+} and Cd^{2+} were examined at the potentials of −0.3 and −0.8 V, where the currents are most depressed. Since the *i-t* curves for the inhibition effect of Triton X on cadmium deposition showed a tendency similar to that on copper deposition, the latter is discussed herewith. Figures 4-(a) and (b) show the *i-t* curves of copper deposition inhibited by Triton X-100 and X-405. The initial portion of the *i-t* curve for the process inhibited by Triton X coincides with that for the process with no inhibitor, while the limiting current decreases rapidly at a certain time and finally the reaction is depressed almost completely after full coverage is attained. The time required to attain complete inhibition becomes

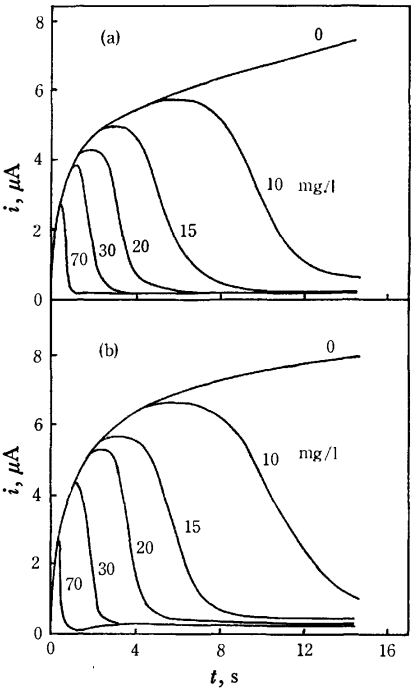

Fig. 4. Instantaneous current *vs.* time curves.
25 °C, −0.3 V, 1 mM Cu^{2+}, (a) 1N sulfuric acid solution + Triton X-100, (b) 1N sulfuric acid solution + Triton X-405.

shorter as the content of Triton X is increased.

The tendency of *i-t* curves for the process inhibited by PVP in 1N sulfuric acid is similar to that in the case of Triton X. However, the *i-t* curves for the process inhibited by PEG[3] show a different tendency, complete inhibition not being attained even at $\theta=1$. The tendency becomes more marked as $\bar{M}$ decreases, that is, the current after attainment of the full coverage depends distinctly on the bulk concentration especially in the case of a relatively low $\bar{M}$ of PEG. Such a tendency can be expected from the behavior of differential capacity which depends on the bulk concentration after attainment of adsorption equilibrium. As seen in Fig. 4, the current after t_m is almost completely inhibited by Triton X in spite of the concentration dependence of differential capacity after attainment of adsorption equilibrium (Fig. 2). Thus, the concentration dependence of C after $t \geq t_m$ may be caused by the formation of a multi-layer.

The time required to attain complete inhibition is given by extrapolating the portion of rapidly decreasing current in *i-t* curve to $i=0$. The t_m values obtained from the relations of $C\text{-}t^{1/2}$ and *i-t* are expressed by t_{mc} and t_{mi}, respectively.

Maximum Surface Concentration of Triton X. The values of $at_{mc}^{1/2}$ and $at_{mi}^{1/2}$ are given in Table 1, since the directly obtainable term in the Koryta equation is $at_m^{1/2}$ which corresponds to the ratio of Γ_m to $D^{1/2}$. The $at_{mc}^{1/2}$ (or $at_{mi}^{1/2}$) value somewhat depends on a, *viz.*, $at_{mc}^{1/2}$ (or $at_{ml}^{1/2}$) becomes somewhat large with a. Such a phenomenon was also observed in the case of PVP[2] and the variation of $at_{mc}^{1/2}$ with a was explained by means of the concentration dependence of diffusion coefficient or the effect of spherical diffusion.

Table 1. Comparison of $at_{mc}^{1/2}$ with $at_{mi}^{1/2}$.

Triton X	$at_{mc}^{1/2}$ a) (mg/l·s$^{1/2}$)	$at_{mi}^{1/2}$ b) (mg/l·s$^{1/2}$)	
		Cu^{2+}	Cd^{2+}
X- 45	35.2	34.8	35.1
X-100	35.4	39.7	42.1
X-205	30.7	37.5	40.6
X-405	43.5	42.5	47.3

a) The mean values of $at_{mc}^{1/2}$ at 5, 10, 15, and 20 mg/l.
b) The mean values of $at_{mi}^{1/2}$ [12] at 10, 20, and 30 mg/l.

The $at_{mc}^{1/2}$ values in Table 1 are the mean values of a at 5, 10, 15, and 20 mg/l, and the $at_{mi}^{1/2}$ values are those at 10, 20, and 30 mg/l. The Γ_m values of Triton X were calculated from the mean values of $at_{cm}^{1/2}$ (or $at_{mi}^{1/2}$) and D[10] assumed by Scholtan's relation[11] ($\bar{M}D^2=10^{-8}$).

Barradas and Kimmerle[6,7] give Γ_m values of Triton X-100 as follows: 22×10^{-10} mol/cm^2 by the interfacial tension measurement[7] and $1.3—1.4\times10^{-10}$ mol/cm^2 by the observation of suppression of polarographic oxygen wave.[6] They have ascribed the disagreement of the results to the formation of a multi-layer, namely, Γ_m by the electrocapillary data corresponds to that of the multi-layer adsorbed perpendicularly with the alkyl end in contact with mercury, while Γ_m by the suppression effect corresponds to that of nearly monolayer which is adsorbed on mercury with planar configuration. The Γ_m values given in Table 2 are considered to be those of the monolayer, since the dependence of differential capacity and that of inhibition upon the diffusion process of adsorbates may be caused mainly by the monolayer formation. From the linear relation of log Γ_m *vs.* log $\bar{M}$ with a slope of *ca.* -1, the configuration of monolayer of Triton X is expected to be flat, which is similar to the cases of PVP[2] and PEG ($\bar{M}\geq600$).[3]

The relation between C_s and thickness of adsorbed layer can be expressed by

$$C_s = \varepsilon/(4\pi\delta) \qquad (3)$$

where ε and δ are the dielectric constant and thickness of the adsorbed layer, respectively. The C_s of Triton X may correspond to that of the multi-layer, since it is relatively low and varies considerably with $\bar{M}$ as compared with the cases of PVP[2] and PEG.[3] The considerable dependence of C_s on $\bar{M}$ is inconsistent with the planar configuration of monolayer at the interface under the assumption of ε=constant. The fact that C_s becomes larger with the increase in $\bar{M}$ is also inconsistent with the configuration of monolayer adsorbed perpendicularly, because C_s should become small with increasing $\bar{M}$ in view of the inverse proportionality between δ and C_s (*cf.* Eq. (3)). Consequently, the configuration of multi-layer adsorbed perpendicularly, assumed by Barradas, is applicable to the results of C_s. It must be taken into account that Triton X of low $\bar{M}$ is apt to form the multi-layer as shown in Fig. 1.

Shape of Instantaneous Current vs. *Time Curve.* Some theoretical approaches to elucidate the polarographic current *vs.* time curve have been given.[1,12,13] The *i-t* curve for the system where the limiting current is inhibited by diffusion-controlled adsorption will be discussed, Weber *et al.*[12] and Kůta and Smoler[13] solved the problem of the inhibition effect on the rate constant of electrode reaction. Matsuda[14] has recently introduced the following theoretical equation for the *i-t*

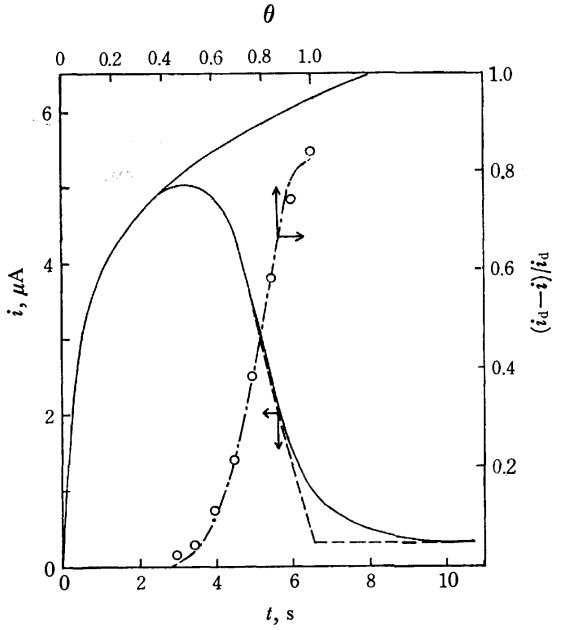

Fig. 5. The time-dependence of instantaneous current inhibited by Triton X, observed or calculated, and the coverage-dependence of inhibition by Triton X.
1N sulfuric acid solution + Triton X-100 of 15 mg/l, 1 mM Cu^{2+}, -0.3 V, *i-t* curves (solid lines: observed curves with and without Triton X, broken line: theoretical curve), $[(i_d-i)/i_d]$-θ curve (circles: observed curve with 15 mg/l Triton X, dashed-dotted line: theoretical curve).

Table 2. Maximum surface concentration and minimum differential capacity of Triton X.

Triton X	Γ_m a)	Γ_m b)	Γ_m c)	C_s
X- 45	1.38×10^{-10}	1.32×10^{-10}	1.33×10^{-10}	5.2
X-100	8.00×10^{-11}	8.96×10^{-11}	9.53×10^{-11}	6.1
X-205	3.62×10^{-11}	4.42×10^{-11}	4.79×10^{-11}	6.5
X-405	2.45×10^{-11}	2.39×10^{-11}	2.66×10^{-11}	6.9

a) Γ_m by means of differential capacity measurenents.
b) Γ_m by means of measurements of the inhibition effect on electrodeposition of copper.
c) Γ_m by means of measurements of the inhibition effect on electrodeposition of cadmium.

10) The values of the diffusion coefficient estimated with $MD^2=10^{-8}$ are 4.84×10^{-6} cm^2/s for Triton X-45, 3.94×10^{-6} for X-100, 3.04×10^{-6} for X-205, and 2.26×10^{-6} for X-405.
11) W. Scholtan, *Makromol. Chem.*, **7**, 209 (1951).
12) J. Weber, J. Koutecky, and J. Koryta, *Z. Electrochem.*, **63**, 583 (1959).
13) J. Kůta and I. Smoler, *ibid.*, **64**, 285 (1960).
14) H. Matsuda, *Rev. Polarog.* (Kyoto), **14**, 87 (1967).

curve assuming that the adsorbed films are perfectly immobile.

$$i = i_d \frac{(1.35\lambda_\infty t^{1/2})^{1.091}}{1+(1.35\lambda_\infty t^{1/2})^{1.091}} \quad (4)$$

where i and i_d are the instantaneous currents with and without adsorbates, respectively, and λ_∞ is given by the following:

$$\lambda_\infty = [\lambda_2+(1-\theta)A/[(1-\theta)\{-\ln(1-\theta)\}]^{1/2}]\theta^{-1}$$

$$\lambda_2 = k_2/D_0^{1/2}, \qquad A = D_0/R_m = K'\theta^z$$

where k_2, D_0, and R_m are respectively the rate constant of forward reaction on the adsorbed surface, the diffusion coefficient of oxidized form of depolarizer and the mean radius of the congregated molecules adsorbed at the interface. K' and z are the arbitrary constants. A typical example in which the limiting current of copper deposition is inhibited by Triton X of 15 mg/l is given in Fig. 5 and shown by the solid line. The theoretical curve whose parameters ($\lambda_2=0.020$, $K'=0.347$, $z=-11.0$, and $t_{mi}=6.5$) are estimated from experimental data is given by the broken line. The shape of i-t curve is well explained by Matsuda's equation except for the region in the neighborhood of $t=t_{mi}$. Figure 5 shows also the inhibition effect by means of $(i_d-i)/i_d$ *vs.* θ relation. The coverage is given by the Koryta equation as $\theta=(t/t_{mi})^{1/2}$. Inhibition is hardly seen at a small coverage and then a sharp rise occurs at a certain coverage. Such a tendency is always revealed by the limiting current which is depressed by diffusion-controlled adsorption. The coverage at which the sharp rise of inhibition occurs may be dependent on the properties of the adsorbates and on the parameter, z, in Eq. (4). The shape of the i-t curve in a relatively ideal system can be explained with Eq. (4). However, further approaches must be made to explain the behavior somewhat deviating from the ideal one, *e.g.*, the i-t curve inhibited by PEG of a relatively low $\bar{M}$.[3]

BULLETIN OF THE CHEMICAL SOCIETY OF JAPAN, VOL. 46, 1324—1329 (1973)

Adsorption of Organic Polymers on Platinum Electrode

Tetsuya OHSAKA, Yasuyuki ABE, and Tadashi YOSHIDA

Applied Electrochemical Laboratory, Graduate School of Science and Engineering, Waseda University, Nishi-okubo, Shinjuku-ku, Tokyo 160

(Received August 14, 1972)

The adsorption behavior of polyvinylpyrrolidone (PVP), polyethyleneglycol (PEG), and alkylphenoxy polyethoxy ethanols (Triton X) on a smooth platinum electrode was investigated by observation of the inhibition effect on the electrosorption of hydrogen and oxygen in the potential range between hydrogen and oxygen evolution. The adsorption of PVP, PEG, and Triton X on platinum always took place within the potential range from −0.20 to 1.25 V *vs.* SCE, the inhibition effect on the electrosorption of hydrogen and oxygen being distinctly shown. The order of inhibition of these adsorbates was Triton X>PVP>PEG. The inhibition effect became larger in most cases with decreasing mean molecular weight of adsorbate. In contrast to the case with a mercury, the adsorbates were oxidized or reduced on the platinum electrode in the adsorption range, the anodic peak due to oxidation being distinctly revealed in the case of PEG.

Many organic polymers are adsorbed so strongly on a DME that the adsorption process is mainly controlled by diffusion.[1-5] The adsorption behaviors of PVP (polyvinylpyrrolidone),[1,6] PEG (polyethyleneglycol),[2,7] and Triton X (alkylphenoxy polyethoxy ethanols)[5,8] investigated at the mercury/solution interface, are explained by means of the Koryta equation,[9] their saturated adsorption being established after diffusion process.

The adsorption of various organic substances on a solid electrode has been investigated by many authors from the viewpoint of corrosion inhibitors and organic additives in electrodeposition, but the adsorption of organic polymers on a solid electrode has been given little attention. We investigated the adsorption of water-soluble polymers on a smooth platinum electrode by observing the inhibition effect on the electrosorption of hydrogen and oxygen.

PVP has high adsorbability due to pyrrolidone radicals containing ketone radical and nitrogen atom. PEG is a polymer of ethylene oxide, extensible and highly crystalline. Triton X is a surface active agent

1) T. Yoshida, T. Ohsaka, and S. Tanaka, This Bulletin, **45**, 326 (1972).

2) T. Yoshida, T. Ohsaka, and M. Suzuki, *ibid.*, **45**, 3245 (1972).

3) P. W. Board, D. Britz, and R. V. Holland, *Electrochim. Acta*, **13**, 1633 (1968).

4) H. Jehring and E. Horn, *Monatsber. Deut. Akad. Wiss. Berlin*, **10**, 295 (1968).

5) T. Ohsaka, H. Yamamoto, and T. Yoshida, This Bulletin, **46**, 1320 (1973).

6) Molecular formula: 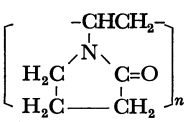

7) Molecular formula: $HO(CH_2CH_2O)_nH$

8) Molecular formula: C_8H_{17}-  -$(OCH_2CH_2)_nOH$

9) J. Koryta, *Collect. Czech. Chem. Commun.*, **18**, 206 (1953).

prepared by the reaction of *t*-octylphenol with ethylene oxide.

Experimental

The test electrodes were a platinum plate (1.870 cm^2), a platinum disk (0.071 cm^2) and platinum wire (0.160 cm^2). The counter electrode was a platinum plate having sufficiently large surface area, and the potentials were determined in reference to the saturated calomel electrode (SCE). Experiments were carried out in 1N sulfuric acid at 30°C in an atmosphere of purified nitrogen. Solutions were prepared with chemical grade reagents and triply-distilled water. PVP (BASF), PEG (Sanyo Chemical Industry), and Triton X (Rohm and Haas) were used without further purification: their mean molecular weight ($\bar{M}$) were 750000, 37000, and 10000 for PVP, 8400, 1000, and 600 for PEG and 2000 (X-405), 1100 (X-205), and 650 (X-100) for Triton X. Potentiostat (Nichia Keiki) and function generator (Nichia Keiki) were used for potential scanning. The test electrode, cleaned with concentrated nitric acid, was pretreated by cyclic scanning at a rate of 10 V/s in 1N sulfuric acid in order to obtain reproducible results. The cyclic scanning curve between −0.20 and 1.25 V was then recorded at a scanning rate of 0.1 V/s by means of a high response X-Y recorder (Toa Electronics). The differential capacity at 1 kHz was determined 5 min after setting the electrode potential by means of a universal bridge (Yokogawa).

Results and Discussion

During the anodic scanning (Fig. 1), adsorbed hydrogen is removed in the potential range −0.2—0.1 V, and an oxygen monolayer is formed in the range 0.55—1.25 V.[10-12] The potential range 0.1—0.55 is the so-called double layer charging region where platinum can be regarded as an ideally polarizable electrode. During the cathodic scanning, the peak at 0.5 V is caused by the reduction of adsorbed oxygen and two peaks between 0.1 and −0.2 V are caused by the electrosorption of hydrogen. The inhibition effect of polymer on the electrosorption can be examined from the decreasing amount of charge of adsorbed hydrogen or oxygen obtained by suitable integration. However, it will be discussed mainly by comparison of the current values at a certain potential, since the content of charge obtained by integrating the region extended over the wide potential range is too complicated due to the oxidation or reduction of adsorbates.

Adsorption of PVP. Figure 1 shows the potentiostatic *i-E* curves inhibited by PVP of $\bar{M}=10000$ whose inhibition effect is the most marked of the three kinds of PVP. During the course of anodic scanning, the two peaks due to the weakly and strongly adsorbed hydrogen become one peak having a constant current independent of the increase of PVP concentration. In the adsorbed oxygen region, the inhibition effect is revealed at the potentials 0.6—1.0, while the anodic current increases in the range 1.0—1.25 V with the addition of PVP. Such an increase may be ascribed

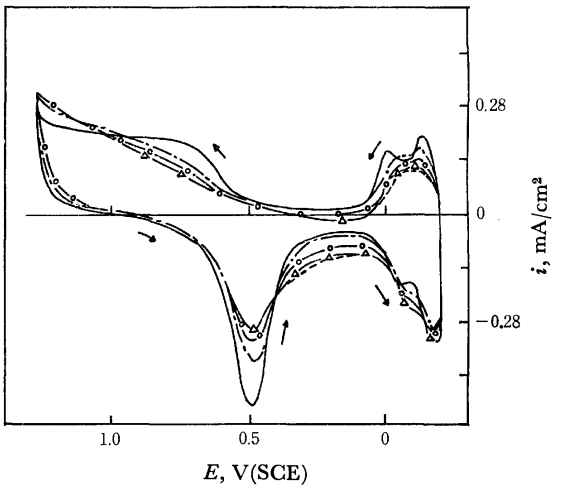

Fig. 1. Potentiostatic *i-E* curves on platinum electrode in the solution of 1N sulfuric acid + PVP, $\bar{M}=10000$.
30 °C, 0.1 V/s, concentration of PVP (—: 0 mg/l PVP, —·—: 10 mg/l, -○-: 50 mg/l, -△-: 150 mg/l, ---: 200 and 300 mg/l).

to either the growth of oxygen layer for the saturated electrosorption at a more positive potential depressed in the range 0.6—1.0 V, or to the oxidation of adsorbed PVP. Since the reduction peak of adsorbed oxygen decreases with increasing PVP concentration (*i.e.*, the amount of adsorbed oxygen decreases with the addition of PVP), the oxidation of PVP may cause the current increase in the anodic range 1.0—1.25 V. During the course of cathodic scanning, the current in the double layer region increases with the addition of PVP. This might result from the reduction of adsorbed PVP since the peak height of cathodic current increases with increasing content of PVP in the adsorbed hydrogen region in spite of the decrease of anodic peak current in this region.

If adsorption or desorption of PVP takes place within the scanning range, the diffusion of adsorbates may influence the adsorption behavior in a similar way to that on a mercury electrode.[1,2,4,5] The dependence of current value on the scanning rate shows a linear relation, which implies that the diffusion of adsorbates has no influence on the adsorption behavior and that PVP always establishes the adsorption equilibrium. Such a dependence of current value is also revealed in the cases of PEG and Triton X.

The anodic peak of the weakly adsorbed hydrogen (P_H) and the cathodic peak of the adsorbed oxygen (P_0) are markedly depressed by the addition of PVP. The dependence of inhibition effect on PVP content is examined in these two regions as shown in Fig. 2. The degree of inhibition is given by $(i_b-i)/i_b$ or $(Q_b-Q)/Q_b$, where i_b or Q_b is the current or charge in solution without adsorbates.

For the oxidation of weakly adsorbed hydrogen (P_H), the degree of inhibition increases sharply until 30 mg/l of PVP and then it increases slowly with increasing PVP concentration (Fig. 2-(a)). The shapes of curves obtained from the peak currents agree approximately with those obtained from the charges. The order of inhibition effect is $\bar{M}=10000>\bar{M}=750000>\bar{M}=37000$

10) M. W. Breiter, *Electrochim. Acta*, **7**, 25 (1962); *Annals New York Acad. Sci.*, **101**, 709 (1963); *J. Phys. Chem.*, **68**, 2249 (1964).
11) F. G. Will, *J. Electrochem. Soc.*, **112**, 451 (1965).
12) H. A. Laitinen and C. G. Enke, *ibid.*, **107**, 773 (1960); K. J. Vetter and J. W. Schultze, *J. Electroanal. Chem.*, **34**, 141 (1972).

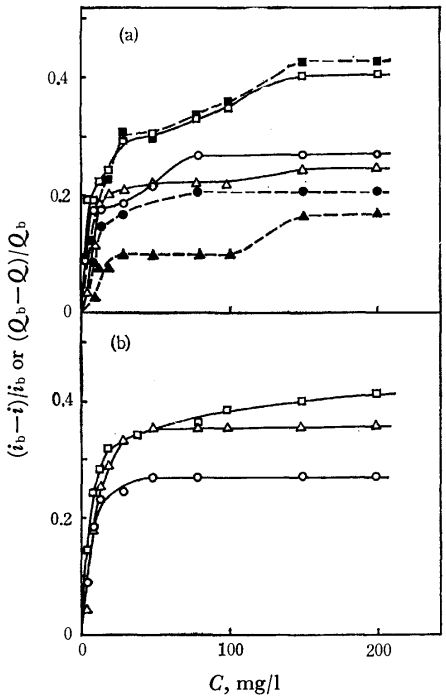

Fig. 2. Concentration dependence of the degree of inhibition on platinum electrode in the solution of 1N sulfuric acid +PVP.
30 °C, 0.1 V/s, solid lines: results from $(i_b-i)/i_b$, broken lines: results from $(Q_b-Q)/Q_b$, (a) the inhibition effect on the anodic peak due to electrosorption of hydrogen, □,■: $\bar{M}$=10000, △,▲: $\bar{M}$=37000, ○,●: M=750000, (b) the inhibition effect on the cathodic peak due to electrosorption of oxygen, □: $\bar{M}$=10000, △: $\bar{M}$=37000, ○: M=750000.

for the bulk concentration greater than 100 mg/l.

For the reduction of adsorbed oxygen (P_0), the degree of inhibition becomes also constant after the sharp increase, and the order of inhibition effect is $\bar{M}$=10000>$\bar{M}$=37000>$\bar{M}$=750000 (Fig. 2-(b)). Since the anodic peak in the adsorbed hydrogen region seems to be influenced by the reduction current of adsorbates, the degree of inhibition obtained from Fig. 2-(a) is somewhat doubtful. The order in Fig. 2-(b) is therefore more reliable than that in Fig. 2-(a). The inhibition effect seems to increase with the decrease in $\bar{M}$.

Adsorption of PEG. Figure 3 shows the adsorption behavior of PEG on a platinum electrode. The anodic peak P_H and the cathodic peak P_0 are depressed by the addition of PEG, while the anodic peak appears at *ca.* 0.7 V (P_{PEG}). The anodic current becomes larger than that in the solution without adsorbates in a range more positive than P_{PEG} and in the double layer charging region. The peak of P_{PEG} may result from the oxidation of adsorbed PEG in view of the depression of P_0 with increasing content of PEG. In a weakly adsorbed hydrogen region the cathodic peak height increases with increasing PEG concentration, which may be ascribed to the reduction of PEG. The degree of inhibition due to the adsorption of PEG can be hardly estimated from these results, as the reduction or oxidation of adsorbed PEG itself overlaps the inhibition effect.

For the purpose of examining the anodic peak at *ca.*

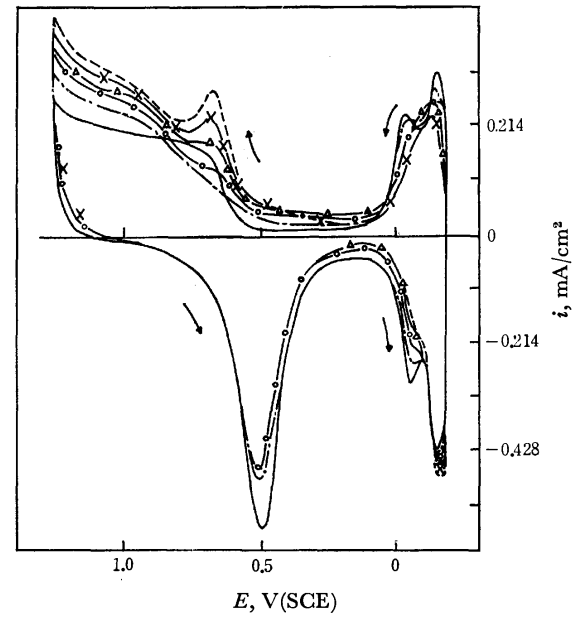

Fig. 3. Potentiostatic *i-E* curves on platinum electrode in the solution of 1N sulfuric acid + PEG, M=1000.
30 °C, 0.1 V/s, concentration of PEG (——: 0 mg/l PEG, -·-: 10 mg/l, -○-: 30 mg/l, -△-: 80 mg/l, -×-: 200 mg/l, ---: 1000 mg/l).

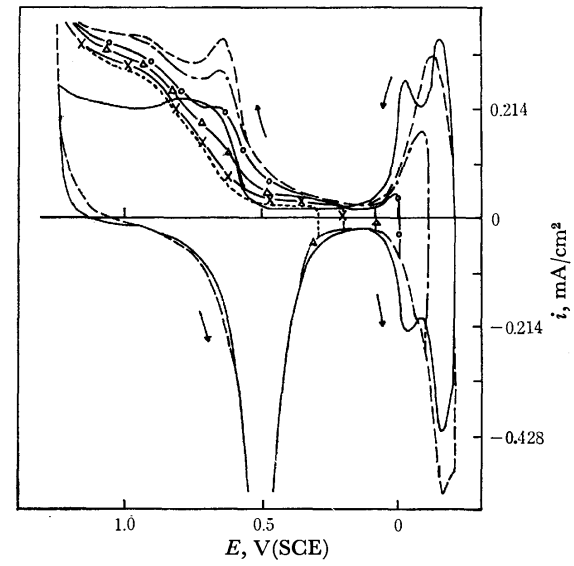

Fig. 4. Potentiostatic *i*—*E* curves on platinum electrode in the solution of 1N sulfuric acid + 1000 mg/l PEG, $\bar{M}$=600.
30 °C, 0.1 V/s, potential ranges (---: −0.2~1.25 V, -·-: −0.1~1.25, -○-: 0.0~1.25, -△-: 0.1~1.25, -×-: 0.2~1.25, ···: 0.3~1.25 V), solid line: *i-E* curve in the solution without adsorbates.

0.7 V (P_{PEG}), the cathodic limit of cyclic scanning was varied as shown in Fig. 4. The current growing at *ca.* 0.7 V begins to appear when the anodic scanning is started from 0.1 V, and a distinct peak is revealed at first by scanning from 0 V. Thus, adsorbates of the reduced type which cause the oxidaiton peak at 0.7 V seem to be produced at a more negative potential than 0.1 V, and the reduced type of adsorbates may increase as the potential becomes negative. It seems that the adsorbed amount of oxidized or reduced type of PEG depends on the electrode potential. However, the

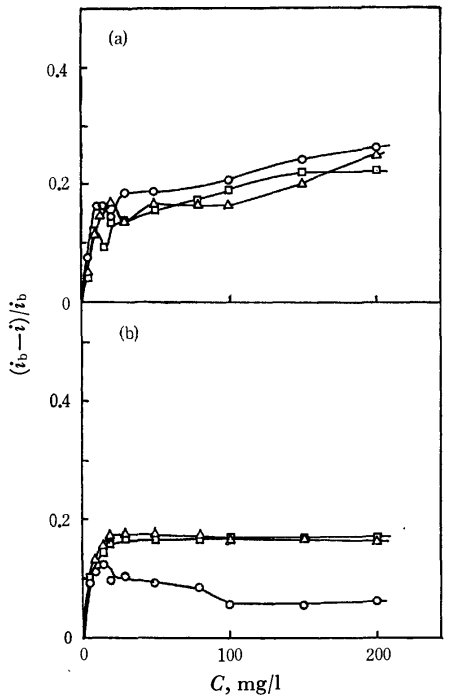

Fig. 5. Concentration dependence of the degree of inhibition on platinum electrode in the solution of 1N sulfuric acid + PEG.
30 °C, 0.1 V/s, (a) the inhibition effect on the anodic peak due to electrosorption of hydrogen, □: $\bar{M}$=600, △: $\bar{M}$=1000, ○: $\bar{M}$=8400, (b) the inhibition effect on the cathodic peak due to electrosorption of oxygen, □: $\bar{M}$=600, △: $\bar{M}$=1000, ○: $\bar{M}$=8400.

total amount of adsorbed PEG is expected to be independent of the potential from the results that the anodic peak at *ca.* 0.7 V (P_{PEG}) is not influenced by scanning after some interruption at −0.2 V and that the peak height increases linearly with the scanning rate.

The degrees of inhibition at P_H and P_0, estimated from the results in Fig. 3, are shown in Fig. 5. The degree of inhibition at P_H increases sharply until a bulk concentration of 10—20 mg/l, which may be influenced to some extent by the reduction of adsorbed PEG (Fig. 5-(a)). It decreases, however, to some extent with increasing PEG concentration just after the steep increase, after which it increases gradually. This may be ascribed to the increase of reduction current of PEG. Thus, the order of degree of inhibition (Fig. 5-(a)) is considered to be unreliable because of the overlapping of the reduction current of PEG and the oxidation current of adsorbed hydrogen.

The degree of inhibition becomes constant (Fig. 5-(b)) for the peak of P_0 at *ca.* 20 mg/l.[13] The order of inhibition is $\bar{M}$=600>$\bar{M}$=1000>$\bar{M}$=8400, namely, the degree of inhibition increases with the decrease of $\bar{M}$.

The peak of P_{PEG}, which may result from the oxidation of PEG, is examined from the concentration dependence of i/i_b at 0.7 V (Fig. 6). In a low concentration range, the value of i/i_b is less than unity and shows a minimum indicating inhibition of the electrosorption of oxygen, but it becomes larger than unity in the concentration range greater than 30—50 mg/l. In the case of PEG of $\bar{M}$=600 and 1000 which reveal P_{PEG}, i/i_b increases with the addition of PEG, while for PEG of $\bar{M}$=8400 which reveals no P_{PEG}, it remains constant in the concentration range greater than 100 mg/l. In the i/i_b plots at 1.0 V (not shown), PEG of $\bar{M}$=600 and 1000 reveal constant i/i_b (*ca.* 1.4) in the range greater than 100 mg/l, while PEG of $\bar{M}$=8400 shows nearly constant values somewhat larger than those of the above. Thus, PEG of high $\bar{M}$ may be more difficult to be oxidized as compared with that of low $\bar{M}$.

The differential capacity at the platinum/solution interface was determined 5 min after setting the electrode potential which was scanned from negative to

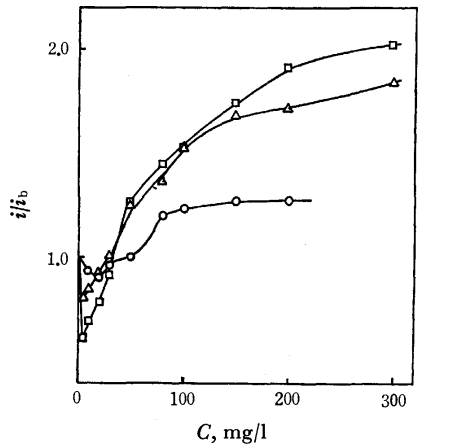

Fig. 6. Concentration dependence of the anodic peak at 0.7 V in the solution of 1N sulfuric acid + PEG.
30 °C, 0.1 V/s, □: solution of 1N sulfuric acid + PEG, $\bar{M}$=600, △: solution of sulfuric acid + PEG, $\bar{M}$=1000, ○: solution of sulfuric acid + PEG, $\bar{M}$=8400.

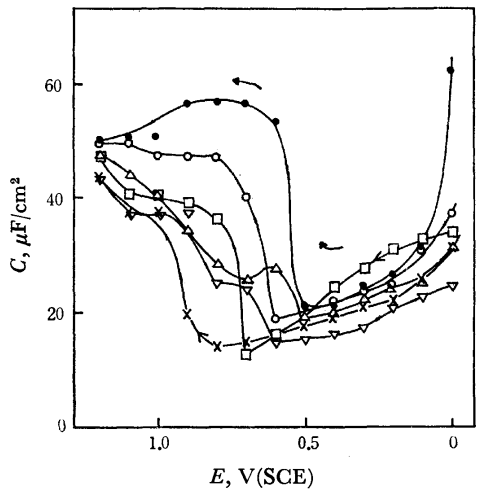

Fig. 7. Potential dependence of differential capacity on platinum electrode in the solution of 1N sulfuric acid + PEG, $\bar{M}$=1000.
30 °C, capacity was determined at 5 min after setting the electrode potential, concentration of PEG, $\bar{M}$=1000 (●: 0 mg/l PEG, ○: 10 mg/l, △: 20 mg/l, □: 50 mg/l, ×: 100 mg/l, ▽: 200 mg/l).

13) In the case of $\bar{M}$=8400, it is peculiar that the degree of inhibition decreases gradually with PEG concentration after the appearance of a peak at *ca.* 20 mg/l. This remains to be explained.

positive (Fig. 7). In the potential range between hydrogen and oxygen evolution, there are three distinct regions for the platinum electrode. In solutions having no adsorbates, the pseudocapacity due to adsorbed hydrogen is revealed between −0.2 and 0.1 V. Hydrogen or oxygen is hardly adsorbed in the so-called double layer region 0.1—0.55 V, while the pseudocapacity due to adsorbed oxygen appears between 0.55 and 1.25 V.

The adsorbed hydrogen and oxygen regions shift to somewhat negative and positive sides, respectively, with the addition of PEG of $\bar{M}$=1000 (Fig. 7). It is certain from the capacity depression that the adsorption of PEG always occurs in these regions. In the adsorbed oxygen region, the capacity depression with increasing content of PEG is complicated. It is too difficult to discuss the capacity behavior in the adsorbed oxygen region from only the results shown in Figs. 3 and 7, though it is doubtless influenced by the oxidation of adsorbed PEG.

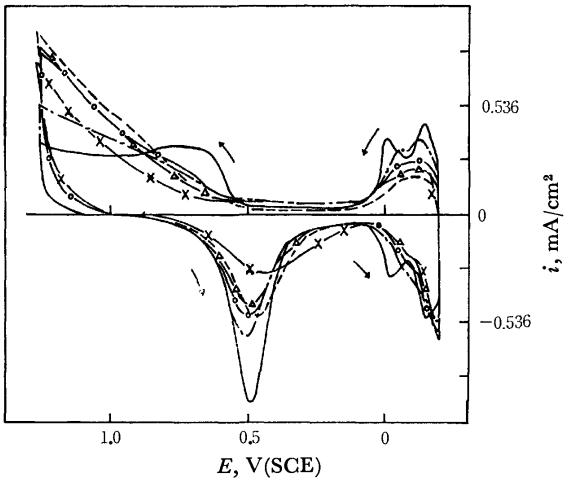

Fig. 8. Potentiostatic i—E curves on platinum electrode in the solution of 1N sulfuric acid + Triton X-205, $\bar{M}$=1100. 30 °C, 0.1 V/s, concentration of Triton X (——: 0 mg/l Triton X, – – –: 30 mg/l, -○-: 100 mg/l, -△-: 200 mg/l, -×-: 400 mg/l, – – –: 1000 mg/l).

Adsorption of Triton X. Figure 8 shows the i-E curves in 1N sulfuric acid containing Triton X of $\bar{M}$=1100. The degree of inhibition at P_H and P_0 and the increase of anodic current in the region $E \geq 0.9$ V are distinctly larger than those for PVP and PEG. The increase of anodic current in the region $E \geq 0.9$ V may be attributed to the oxidation of adsorbed Triton X because the peak of P_0 is depressed by the addition of Triton X. The reduction of oxidized Triton X may occur since the cathodic current increases at the potential of *ca.* 0.4——0.2 V in the cathodic scanning. In the case of Triton X, it is characteristic that the concentration dependence of current is complicated in the potential regions $E \geq 0.9$ V and P_0. Triton X can form micelles,[14] and the above behavior can be ascribed to the formation of multilayer.

Figure 9 shows the relation between the degree of inhibition and the bulk concentration in P_H and P_0

14) R. G. Barradas and F. M. Kimmerle, *J. Electroanal. Chem.*, **11**, 128 (1966).

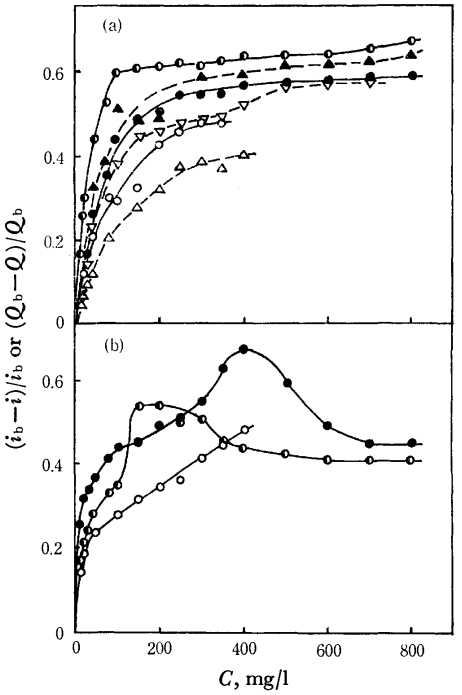

Fig. 9. Concentration dependence of the degree of inhibition on platinum electrode in the solution of 1N sulfuric acid + Triton X.
30 °C, 0.1 V/s, solid lines: results from $(i_b-i)/i_b$, broken lines: results from $(Q_b-Q)/Q_b$, (a) the inhibition effect on the anodic peak due to electrosorption of hydrogen, ◐,▲: X-100, $\bar{M}$=650, ●,▽: X-250, $\bar{M}$=1100, ○,△: X-405, $\bar{M}$=2000. (b) the inhibition effect on the cathodic peak due to the electrosorption of oxygen, ◐: X-100, $\bar{M}$=650, ●: X-205, $\bar{M}$=1100, ○: X-405, $\bar{M}$=2000.

regions. For P_H region, the degree of inhibition increases sharply until 100 mg/l and then becomes nearly constant (Fig. 9-(a)). The order of degree of inhibition is as follows: $\bar{M}$=650 (X-100)>$\bar{M}$=1100 (X-205)>$\bar{M}$=2000 (X-405). For P_0 region, the degree of inhibition *vs.* concentration curve reveals a maximum whose position seems to move to higher concentration range with increasing $\bar{M}$ (Fig. 9-(b)). In general,

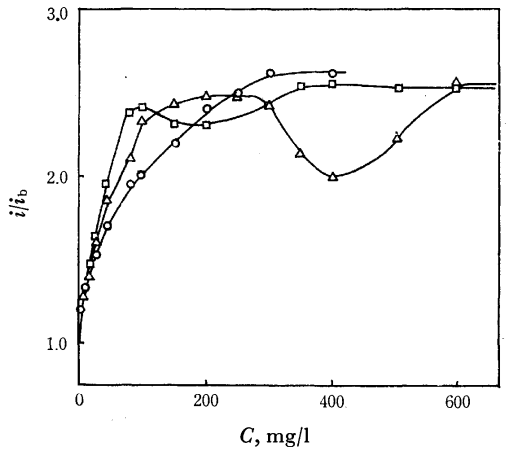

Fig. 10. Concentration dependence of anodic current at 1.2 V in the solution of 1N sulfuric acid + Triton X.
30 °C, 0.1 V/s, □: 1N sulfuric acid + Triton X-100, $\bar{M}$=650, △: 1N sulfuric acid + Triton X-205, $\bar{M}$=1100, ○: 1N sulfuric acid + Triton X-405, $\bar{M}$=2000.

critical micelle concentration (CMC)[15] of Triton X is *ca.* 10^{-2}% or 100 mg/l, and the adsorption of Triton X on mercury electrode shows unusual phenomenon owing to the formation of multilayer.[5,14] The maximum peak in Fig. 9-(b) seems to be related to the formation of multilayer.

Figure 10 shows the concentration dependence of i/i_b at 1.2 V, where the ratio of anodic current (i/i_b) is considered to be approximately proportional to the amount of oxidized Triton X on platinum. After the sharp increase, i/i_b at 1.2 V shows a minimum and then shows a nearly constant value of *ca.* 2.5. The minimum may be ascribed to the formation of a multilayer which prevents Triton X from being oxidized. However, it remains also unknown why the oxidation current increases again with the increase of Triton X content after the appearance of the minimum. It is interesting that the maximum positions in Fig. 9-(b) are nearly in agreement with the minimum positions in Fig. 10.

The inhibition effect of these polymers on the electrosorption of hydrogen or oxygen on platinum is small even in a relatively concentrated solution of adsorbate sufficient to form the monolayer. Such a small inhibition effect upon the process on a platinum electrode may be attributed to the roughness of a solid electrode, where the adsorbed layer of each polymer is considered to be irregular or porous.

Radacanu and Lorenz[16] have examined the process on a solid electrode, which is inhibited by β-naphthoquinoline or dibenzylsulfoxide. The inhibitors are oxidized or reduced by the addition or separation of proton, which may have some connection with hydrogen evolution. Such an analysis might be useful, though the reaction of polymer on platinum is too complicated (*e.g.*, local oxidation or reduction of polymer).

The authors are grateful to Mr. Yasuyuki Konoshima for his kind assistance.

15) CMC: bulk concentration required to form micelle in solution, *cf.*, catalogue of Triton X by Rohm and Haas Co.

16) I. C. Radacanu and W. J. Lorenz, *Electrochim. Acta*, **16**, 995 (1971).

BULLETIN OF THE CHEMICAL SOCIETY OF JAPAN, VOL. 46, 1329—1333 (1973)

Semiconducting Properties of Ln_2CuO_4 (Ln=Rare earths)

Tadao KENJO and Seishi YAJIMA

The Oarai Branch, The Research Institute for Iron, Steel and Other Metals, Tohoku University, Oarai, Ibaraki-ken

(Received July 19, 1972)

The temperature dependence of the resistivity and the thermoelectric power of Ln_2CuO_4 (Ln=rare earths) have been measured. The compounds of Gd, Sm, Nd, and Pr are semiconductive, while La_2CuO_4 shows metallic conductivity. The tetragonal lattice of La_2CuO_4 shrinks in the a axis and expands in the c axis compared to Pr_2CuO_4, in spite of the steady expansion of these lattice parameters for the compounds between Gd and Pr. The thermoelectric power of Ln_2CuO_4, but not La_2CuO_4, is negative, suggesting an electron-conducting or n-type semiconductor. The resistivity of the Ln_2CuO_4 at room temperature increases essentially with an increase in the atomic number of Ln. The plots of the thermoelectric power *vs.* the reciprocal temperature showed a steeper slope for the compounds of the heavier rare earths. The semiconductor-metal transition observed between La_2CuO_4 and Pr_2CuO_4 was explained in relation to the structural change (the shrinkage of the a axis and the expansion of the c axis) as being due to the change in the electron configurations of Cu^{2+}.

In the rare earth oxide–cupric oxide system, two different compounds were found: Ln_2CuO_4 (Ln=La, Pr, Nd, Sm, and Gd)[1] and $Ln_2Cu_2O_5$ (Ln=Tb, Dy, Er, Yb, and Y).[2] Tm, Ho, and Lu were expected to be of the same type as the latter one.[2] The Ln_2CuO_4 compounds are isostructural with tetragonal K_2NiF_4, whose space group is D_{4h}^{17} (I4/mmm).[3]

It should be noted that Ln_2CuO_4 is black.[1] The black color suggests that an appreciable number of electrons in the valence state are excited to a higher energy level by thermal energy as low as room temperature. Therefore, if the higher energy level to which electrons are excited is a conduction band, the conductivity of Ln_2CuO_4 will be in the region of the semiconductor. Further, the crystal structure of Ln_2CuO_4 seems to support the above expectation. In the crystal lattice of Ln_2CuO_4, Cu^{2+} is surrounded by six O^{2-} ions and forms a Cu–O–Cu chain toward the a axis without an interruption by Ln^{3+}. Since 3d-transition metals are thought to make an electron overlapping with O^{2-},[4-6] and since, in fact, the conductivity of

1) R. H. Frushour and K. S. Vorres, AEC Rept. TID-2207 Page E. 1965.

2) O. Schmitz-DuMont and H. Kasper, *Monatsh. Chem.*, **96**, 506 (1965).

3) R. W. G. Wyckoff, "Crystal Structures," Vol. 3, Interscience Publishers, New York, N.Y. (1965), p. 68.

4) C. N. R. Rao and G. V. Subba Rao, *Phys. Stat. Sol.* (a)**1**, 597 (1970).

5) P. M. Raccah and J. B. Goodenough, *J. Appl. Phys.*, **39**, 1209 (1968).

6) J. B. Goodenough, *Phys. Rev.*, **164**, 785 (1967).

many oxides containing 3d-transition metals is in the region of the semiconductor,[4-6] it is very likely that the Cu–O–Cu chain in the Ln_2CuO_4 can be a path for electron transfer.

On the other hand, the role of Ln^{3+} in electrical conduction may not be as important as that of Cu^{2+}, because in the Ln–O bond such an electron overlapping as would contribute to electrical conduction cannot be expected. However, Ln^{3+} may affect the electrical properties and the structure of the compounds indirectly. The configuration of electrons of Cu^{2+}, particularly those of 3d-electrons, are influenced by the ligand field caused mainly by the effective negative charges on the six O^{2-} surrounding Cu^{2+} ions. Since the less electronegative rare earth, or larger rare earth cation, pushes electrons more strongly toward oxygen in the Ln–O bond, the effective negative charges on the O^{2-} of the compounds of less electronegative rare earth can be expected to be greater; in other words, the ligand field at the site of Cu^{2+} is made stronger by replacing Ln with less electronegative Ln. At this time it is difficult to make more detailed predictions of the effect of the ligand-field strength changed by various rare earth cations on the electrical properties of the compounds, but it would be interesting to see if the Ln_2CuO_4 compounds show semiconducting properties and if their electrical conductivity depends upon the size of the rare earth cations.

From the above reason, the compounds of La, Pr, Nd, Sm, and Gd were prepared, and their semiconducting properties investigated.

Experimental

Material and Reagents. Stock solutions of cupric nitrate were prepared by dissolving cupric nitrate of the Kanto Chemical Co., GR grade, into distilled water. Stock solutions of rare earth nitrates were prepared by dissolving each rare earth oxide (99.9% purity; Nippon Yttrium Co., Ltd.) into nitric acid. Both cupric nitrate and rare earth nitrate solutions were standardized against an EDTA standard solution, using XO as the indicator.

Procedure. The Ln_2CuO_4 samples were prepared from gel-like mixed hydroxides. This method is advantageous in giving well-mixed oxide mixtures and denser final specimens than the usual ceramic technique which consists of heating a mixture of the oxides of Cu and Ln. Aliquot portions of cupric nitrate and rare earth nitrate solutions were mixed together, and then a 1 M-NaOH solution was stirred in at 80 °C. The final pH of the solution was adjusted to 11. After the mixture had stood overnight, the mixed precipitates of the hydroxides were filtered and repeatedly washed with distilled water until no sodium ion was detected in the filtrate by the flame test. The gel-like mixtures thus obtained were dried at 120 °C and preheated at 750 °C for 4 hr in air. The samples thus obtained, partially converted to Ln_2CuO_4, were milled, pressed into 15-mmϕ pellets under a pressure of 2.5 t/cm^2, and heated again at 1000 °C for 15 hr in air. Then they were removed from the furnace and cooled in air to room temperature. The mole ratio of Cu to Ln of the samples thus obtained was determined by the following chelatometric titration method. Two aliquot portions were taken from sample solutions obtained by dissolving sample specimens into nitric acid. The total content of Cu^{2+} and Ln^{3+} in the first sample solution was determined using PAN as the indicator. The solution of sodium thiosulfate was added to the second one in order to mask the Cu^{2+}, and then the Ln^{3+} was titrated, using XO as the indicator. The Cu^{2+} content was calculated from the difference between the two titration data. The results of the chemical analysis showed $Ln_2O_3/CuO=1$ within $\pm 0.5\%$ for all the samples obtained. The bulk densities of the specimens obtained were 90—95% of the theoretical values calculated from the X-ray diffraction data. All the samples were found to be single-phase by means of an X-ray diffractometer.

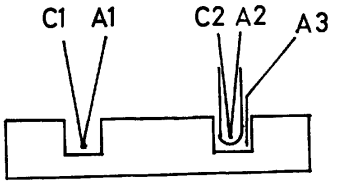

Fig. 1. A device for thermoelectric power measurements. C: chromel wire, A: alumel wire, C2-A2 thermocouple is coated with glass.

For the measurements of the resistivity and of the thermoelectric power, rods 12—13 mm long and 3—4 mm thick were used. The resistivity was measured by the 4-probe method, using Conductive Silver Coating Materials of Du Pont No. 6422 to connect the silver electrode with the oxide specimens. The thermoelectric power was measured using alumel-chromel thermocouples, as is shown in Fig. 1. Two couples of alumel-chromel thermocouples were inserted into two holes cut 8 mm apart in the specimen rods. One of them was coated with glass in order to avoid a short circuit through the rod (C2, A2),[7] and an additional alumel wire was attached to the hole in which the glass-coated thermocouple had been inserted (A3). All the contact between the specimens and the thermocouple wires was made using the Conductive Silver Coating Materials of Du Pont No. 6422. Since this contacting procedure involves heating at 700 °C for 4 hr and subsequent gradual cooling, the sample ends in being annealed. The sample temperature was measured by means of a C1–A1 thermocouple. The temperature difference was taken up from the A1–A2 couple while the C1 was connected with the C2. The potential difference due to the thermoelectric power was measured from the A1–A3 couple. The temperature difference between the two holes was adjusted to be less than 5 °C. All the voltage measurements for resistivity and thermoelectric power were performed by means of a Hitachi QPD_{74} potentiometric 2-pen recorder.

Results

The temperature dependences of the resistivity of various Ln_2CuO_4 are given in Fig. 2. Corrections for the bulk density were made by dividing the raw data by the ratio of the bulk to the theoretical density. These results indicate that the Ln_2CuO_4 (Ln=Gd~Pr) compounds are semiconductive and that La_2CuO_4 compound is metallic. The slopes in these plots are steeper in the higher temperature region than in the lower one except for metallic La_2CuO_4. These plots all seem to fall on identical curves in the high-temperature region.

7) The conductivity of the samples is so high, particularly at the high temperatures, that the temperature difference cannot be measured unless one of the thermocouples is glass-coated.

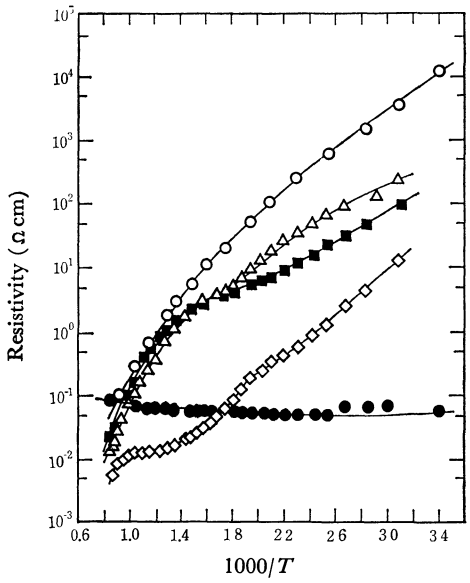

Fig. 2. Temperature dependence of resistivity of various Ln_2CuO_4 compounds.
○: Gd_2CuO_4, △: Nd_2CuO_4, ■: Sm_2CuO_4, ◇: Pr_2CuO_4, ●: La_2CuO_4.

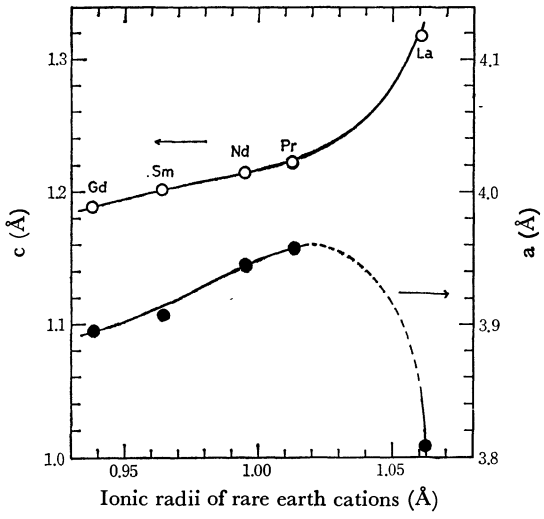

Fig. 3. Lattice parameters of various Ln_2CuO_4 compounds.
○: c axis ●: a axis

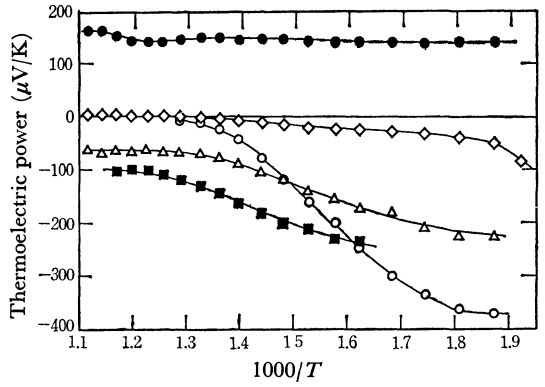

Fig. 4. Temperature dependence of thermoelectric power of various Ln_2CuO_4 compounds.
○: Gd_2CuO_4, △: Nd_2CuO_4, ■: Sm_2CuO_4, ◇: Pr_2CuO_4, ●: La_2CuO_4.

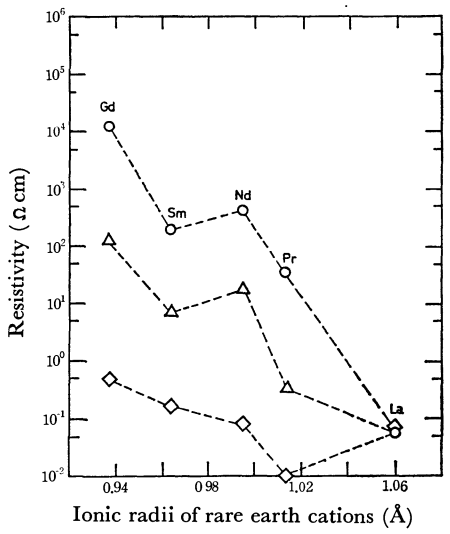

Fig. 5. Relation between resistivity and ionic radii of rare-earth cations of Ln_2CuO_4 compounds.
○: room temperature, △: 200 °C, ◇: 800 °C

The semiconductor-metal transition observed between Pr_2CuO_4 and La_2CuO_4 corresponds to the structural behavior of Ln_2CuO_4 shown in Fig. 3; the parameters of the tetragonal lattice, c and a, increase with an increase in the ionic radii of Ln^{3+} between Gd and Pr, but the c axis of La_2CuO_4 expands more greatly than would be expected from the manner between Pr and Gd and its a axis shrinks by 3.8% against that of Pr_2CuO_4.

As can be seen in Fig. 4, the thermoelectric power, α, in all the Ln_2CuO_4 compounds except for La_2CuO_4 is negative, suggesting an *n*-type semiconductor. The slopes in the α *vs.* $1/T$ plots decrease in this order, Gd<Sm≈Nd<Pr.

Figure 5 shows a dependence of the resistivity on the ionic radii[8] of the rare earth cations of Ln_2CuO_4. At room temperature, the resistivity decreases essentially with an increase in the ionic radii of rare earth cations and at high temperatures it is not so dependent on the ionic radii.

Discussion

The experimental results of this work can be summarized as follows: (1) All the Ln_2CuO_4 compounds except for La_2CuO_4 are semiconductive, while La_2CuO_4 is metallic. (2) The resitsivity, ρ, of Ln_2CuO_4 decreases essentially with an increase in the ionic radii of Ln^{3+}, most markedly at room temperature. The slopes of the log ρ—$1/T$ plots of all the Ln_2CuO_4 except for La_2CuO_4 are steeper at a higher temperature than at a lower, and seem to fall on identical curves at high temperatures. (3) The slope in the plot of the thermoelectric power, α, *vs.* $1/T$ decreases with an increase in the ionic radii of Ln^{3+}. The negative α values of all the Ln_2CuO_4 except for La_2CuO_4 suggest that they are electron conductors. (4) The crystal structure of Ln_2CuO_4 is tetragonal, and the lattice parameters, *c*

8) T. Moeller, "The Chemistry of the Lanthanides," Reinhold Publishing Corporation, New York, N.Y. (1963), p. 21.

and a, of Ln, but not La, increase with an increase in the ionic radii of Ln^{3+}. The axis, a, of La_2CuO_4, however, becomes smaller than that of Pr_2CuO_4 in spite of the fact that the ionic radius of La^{3+} is larger than that of Pr^{3+}, and its c axis expands more greatly than would be expected from the manner in the plots of c *vs.* the ionic radii of Ln^{3+} between Gd and Pr.

At this time it is hard to give a detailed explanation of the temperature dependence of resistivity shown in the summarized results (2), but we believe, as is generally thought for the same behavior of other semiconductors,[9] that the less steep slopes in the lower-temperature region are mainly due to an extrinsic excitation process and that the steeper ones in the higher-temperature region are ascribable to an intrinsic process.

Measurements of the thermoelectric power, as is well known, provide information on carriers.[10] The thermoelectric power, α, is related to the dependence of the number of carriers, n, on the temperature, T, by the following equation:

$$\alpha = d\Delta\phi/dT = (kT/e)(d \log n/dT)$$

where $\Delta\phi$ is the potential difference due to a temperature gradient given on a specimen rod, k is the Boltzmann constant, and e is the electronic charge. When the Maxwell distribution can be applied to $d \log n/dT$, or when:

$$n = N_0 \exp(-E/kT)$$

where E is the activation energy, and N_0, a constant, the following equation can be obtained:

$$\alpha = -E/Te.$$

This indicates that the slope in the plots of α *vs.* $1/T$ corresponds to the activation energy, E.[10]

The negative thermoelectric power (shown in Fig. 4) indicates that the carriers in Ln_2CuO_4 are electrons, supporting the extrinsic excitation procedure described in the previous paragraph, where it was not known whether the carriers were electrons or holes. The donor is most likely Cu^+ formed by a partial decomposition of Cu^{2+} to Cu^+, because Ln_2CuO_4 is decomposed to Cu_2O and Ln_2O_3 at 1000—1200 °C,[11] although no significant amount of Cu(I) was found from the chemical analysis in this study.[12]

A more detailed discussion of the electron configuration of Cu^{2+} is needed to explain the semiconductor-metal transition between Pr_2CuO_4 and La_2CuO_4 and the dependence of the activation energy on the ionic radii of Ln^{3+}. The valence electron configuration of Cu^{2+} is $3d^9$. As is shown in Fig. 6, Cu^{2+} is surrounded by six O^{2-} ions in the Ln_2CuO_4, so that the energy level of the 3d-electrons is split into several energy levels, depending upon the relative positions of the O^{2-} to Cu^{2+}. Now, the c axis is taken as z, and a is

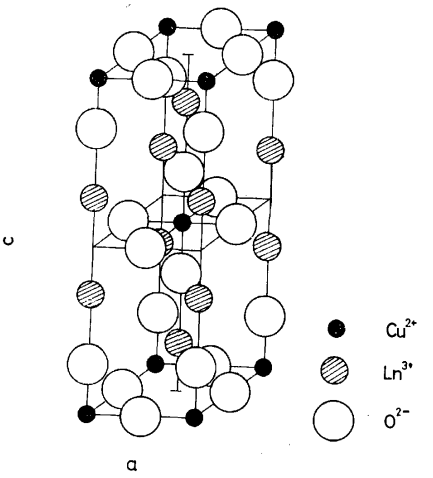

Fig. 6. Crystal structure of Ln_2CuO_4

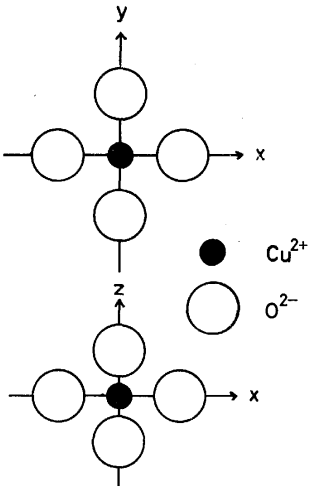

Fig. 7. Octahedron of CuO_6

taken as an x or y coordinate; the O^{2-} are situated on x or y, as is illustated in Fig. 7. The O^{2-} ion on x or y is not equivalent to that on z. It is not known yet which distance is longer, Cu–O on x (or y) or Cu–O on z, but the similar c/a value of K_2CuF_4 (3.066) to that of Gd_2CuO_4 (3.046) suggests that the ratio of $(Cu–O)_x$ to $(Cu–O)_z$ for Gd_2CuO_4 is essentially the same as that of $(Cu–F)_x$ to $(Cu–F)_z$ for K_2CuF_4, $(Cu–F)_x = 2.078$ Å and $(Cu–F)_z = 1.949$ Å.[3] Thus, we made an assumption, but one which is not essential in the following discussion, that $(Cu–O)_x$ is greater than $(Cu–O)_x$. Since the energy level of the 3d-electrons of Cu^{2+} is split in such a way as to minimize the electrostatic energy due to a repulsive force between the electrons on the Cu^{2+} and O^{2-} anions, the most stable 3d-electron configuration of Cu^{2+} probably consists of four levels, as is illustrated in Fig. 8. The energy gaps among these four levels are affected by the ligand-field strength, which depends mainly upon the effective negative charge on O^{2-}. This effective charge on O^{2-} might be influenced by the size of Ln^{3+} in the manner that a more negative charge is provided by the larger (or lighter) rare earth cations, because the larger cations, which come from less electronegative rare earths, may

9) Stephan P. Mitoff, "Progress in Ceramic Science" Vol. 4 edited by J. E. Burke, Pergamon Press (1966), p. 217.

10) Takeo Kawaguchi, "Handotai no Kagaku" Maruzen Co., Ltd., (1971), p. 50.

11) M. Foex, A. Mancheron, and M. Line, *C. R. Acad. Sci. Paris*, **250**, 3027 (1960).

12) The content of the oxygen was obtained from the data of chemical analysis of Cu and Ln, and from the weight of the samples dissolved for the chemical analysis.

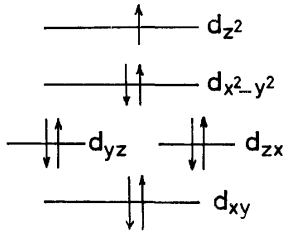

Fig. 8. 3d-electron configurations of Cu^{2+} in Ln_2CuO_4 (Ln=Gd, Sm, Nd, and Pr)

well push electrons more strongly toward oxygen in the Ln–O bond. The greater effective charge, or the greater ligand-field strength, enhances the split energy gap of the 3d-electrons, so that, in the course of replacing the smaller rare earth cation with the larger one, e_g levels rise faster than do the t_{2g} levels, and so that in a rare-earth cation, at last, the e_g levels might be higher than the 4s or 4p level, with a slight structural modification, if necessary.

The trend shown in Figs. 2 and 5, the greater resistivity of the smaller Ln^{3+} compounds, can be explained as being due to: (1) more donors (probably Cu^{+}) in the compounds of the larger rare earth cations and/or (2) the lower activation energy between the donor and the conduction level for the compounds of the larger rare earth cations. The temperature dependence of the resistivity alone (Fig. 2) does not clearly determine which factor predominates, because the slope in the log ρ—$1/T$ plots is not so markedly dependent upon the rare earth of the Ln_2CuO_4 and because the dependence of the mobility on the temperature may not be negligible, particularly for the sintered samples used in this study. The data of thermoelectric power shown in Fig. 4 suggest that the second case is more important; the slope in the plots of α—$1/T$ increases with a decrease in the size of the rare earth cations. The excess electron on the Cu^{+} probably occupies the $3d_{z^2}$, donor level, which rises as the ligand field becomes stronger, so that the energy gap between the donor and the conduction level may be reduced, thus leading to the lower activation energy of the compounds of the larger rare earth cations.

The compound of the largest rare earth cation is La_2CuO_4. The shrinkage of the a axis and the expansion of the c axis compared to Pr_2CuO_4 can be attributed to: (1) the depression of the electron density in the x and y directions instead of the enhancement of that in the z direction and/or (2) a new chemical interaction or bonding between Cu^{2+} and O^{2-} in the x and y directions. Since the metallic conduction of La_2CuO_4 surely suggests a new π-bond formation, because a σ-bond does not contribute to a metallic conduction, the second case described above must hold. The lowest energy level of electrons of Cu^{2+} which can make a π-bond with the 2p-electron of O^{2-} would be 4p, because: (1) the 3d levels except for e_g have already been filled, (2) electrons in the e_g levels are forbidden to make an overlapping with 2p in O^{2-} from the point of view of the symmetry, and (3) the 4s electron in Cu^{2+} can form only a σ-bond with 2p-electrons in O^{2-}. This new electron configuration is reasonable in view of the structural change observed between Pr_2CuO_4 and La_2CuO_4.

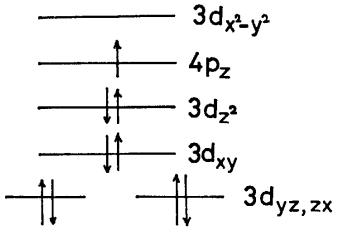

Fig. 9. Electron configuration of Cu^{2+} in La_2CuO_4

The shrinkage of the a axis and the expansion of c axis enhance the electrostatic repulsive force between the O^{2-} anion and the $3d_{x^2-y^2}$ electrons and reduce the same force between the O^{2-} anion and the $3d_{z^2}$ electrons respectively. If the shrinkage of the a axis is great enough, the $3d_{x^2-y^2}$ level would become higher than $4p_z$ as well as $3d_{z^2}$. La_2CuO_4 might be a case of this. If so, the above description leads to a similar electron configuration derived from the π-bond formation. Consequently, the most probable electron configuration is one electron in $4p_z$, two electrons in $3d_{z^2}$, and six electrons in t_{2g}, as is illustrated in Fig. 9. Thus, $4p_z$ electrons in Cu^{2+} form a π-bond with $2p_z$ electrons in O^{2-} over the Cu–O–Cu networks on the c planes, leading to a conduction band three quarters of which is filled with electrons. The conduction band described above also suggested by the magnetic properties of La_2CuO_4; Pauli paramagnetism was observed for La_2CuO_4, suggesting collective electrons rather than localized ones.[6]

Effective Ionic Charges of Several Uniaxial Crystals

Jiro HIRAISHI

National Chemical Laboratory for Industry, Honmachi, Shibuya-ku, Tokyo

(Received August 1, 1972)

A simple equation was derived for obtaining the effective ionic charges of uniaxial crystals on the basis of a rigid ion model by using the optically active lattice vibration frequencies of the TO and LO modes. It was applied to several uniaxial crystals such as wurtzite type (ZnO, ZnS, CdS, and BeO) and rutile type (ZnF_2, TiO_2, SnO_2, and GeO_2) crystals. Lattice vibration frequencies of orthorhombic hydrogen chloride crystal were calculated by means of a point charge model to estimate the effect of the long range Coulomb interaction on the vibrational frequencies of molecular crystals.

It is well-known that large frequency splittings between transverse and longitudinal modes are observed for infrared active lattice vibrations of ionic crystals.[1] The TO–LO splitting arises from long range electrostatic interactions. Kellermann calculated the frequency dispersion curves of the NaCl crystal on the basis of a rigid ion model.[2] The transverse $\omega(\mathrm{T})$ and longitudinal frequencies $\omega(\mathrm{L})$ near the center of the Brillouin zone (wave vector $\boldsymbol{y}\sim 0$) for the crystals of the NaCl type can be calculated from the equations

$$\omega^2(\mathrm{T}) = (1/m_{\mathrm{Na}}+1/m_{\mathrm{Cl}})[\beta-(4\pi/3)(Ze)^2/v_{\mathrm{a}}] \quad (1)$$

$$\omega^2(\mathrm{T}) = (1/m_{\mathrm{Na}}+1/m_{\mathrm{Cl}})[\beta+(8\pi/3)(Ze)^2/v_{\mathrm{a}}] \quad (2)$$

where m_{Na}, m_{Cl}, and v_{a} represent the masses of the Na^+ and Cl^- ions and the volume of the unit cell, respectively, and β the force constant due to the short range interaction. The ionic charges on the Na^+ and Cl^- ions are given by $+Ze$ and $-Ze$, respectively. In the case of the NaCl crystal, the values of Z, β, and $(4\pi/3)(Ze)^2/v_{\mathrm{a}}$ are calculated to be 0.73, 0.34 md/Å, and 0.11 md/Å, respectively, by using the values of $\omega(\mathrm{T})$ (164 cm^{-1}) and $\omega(\mathrm{L})$ (262 cm^{-1}).[1] The result indicates that the long range electrostatic interaction greatly affects the frequency of the lattice vibration of ionic crystals, so that the long range electrostatic interaction should be taken into account in the frequency calculation of the ionic crystals.

Many investigators[3] have calculated the frequencies of the lattice vibrations of ionic crystals on the basis of various models, such as the rigid ion model with effective ionic charges,[4] shell model[5] and deformation dipole model.[6] The calculations for partially ionic crystals, such as SiC, ZnTe, and CdS have also been made.[4,7] In the present work, simple equations were derived to obtain the values of the effective ionic charges of several crystals of wurtzite and rutile types on the basis of the rigid ion model. Usually the effective ionic charges are taken as a parameter to fit the observed frequencies. However, the values of the effective ionic charges can be obtained from the TO–LO splittings, which do not depend on a model of the short range interaction.

For molecular crystals, the lattice vibration frequencies are usually calculated without the long range interaction. The frequencies of the hydrogen chloride crystal was also calculated on the assumption of a point charge on each atom to estimate the amount of TO–LO splittings and the effect of the long range interaction on the lattice vibration frequencies of such a molecular crystal.

Rigid Ion Model and Effective Ionic Charge

In the harmonic approximation, the equation of motion of particles in the crystal is given by

$$\boldsymbol{M}\omega^2\boldsymbol{u} = (\boldsymbol{R}+\boldsymbol{ZCZ})\boldsymbol{u} \quad (3)$$

by the rigid ion model, where the matrices $\boldsymbol{R}$ and $\boldsymbol{C}$ represent the short range and long range electrostatic interactions, respectively. The normal frequencies can be obtained by solving the secular equation

$$|\boldsymbol{M}\omega^2\boldsymbol{I}-\boldsymbol{R}-\boldsymbol{ZCZ}| = 0 \quad (4)$$

The $\boldsymbol{C}$ matrix can be calculated by using Ewald's transformation.[1,2,8] Using the notation of Born and Huang[1] Eq. (3) is written as

$$\begin{aligned}\omega^2\begin{pmatrix}\boldsymbol{y}\\ j\end{pmatrix}w_\alpha\left(k\middle|\begin{matrix}\boldsymbol{y}\\ j\end{matrix}\right) &= \sum_{k'\beta} C^{\mathrm{N}}_{\alpha\beta}\begin{pmatrix}\boldsymbol{y}\\ kk'\end{pmatrix}w_\beta\left(k'\middle|\begin{matrix}\boldsymbol{y}\\ j\end{matrix}\right) - e_k E_\alpha\sqrt{m_k}\\ &+ \sum_{k'\beta}(e_k e_{k'}/m_k)Q_{\alpha\beta}\begin{pmatrix}0\\ kk'\end{pmatrix}w_\beta\left(k\middle|\begin{matrix}\boldsymbol{y}\\ j\end{matrix}\right)\\ &- \sum_{k'\beta}(e_k e_{k'}/\sqrt{m_k m_{k'}})Q_{\alpha\beta}\begin{pmatrix}\boldsymbol{y}\\ kk'\end{pmatrix}w_\beta\left(k'\middle|\begin{matrix}\boldsymbol{y}\\ j\end{matrix}\right)\end{aligned} \quad (5)$$

where the α component of the displacement vector of the k-th particle in the l-th unit cell $u_\alpha(l/k)$ is given by

$$u_\alpha\begin{pmatrix}l\\ k\end{pmatrix} = (1/\sqrt{m_k})w_\alpha(k)\exp\left\{2\pi i\boldsymbol{y}\cdot\boldsymbol{x}\begin{pmatrix}l\\ k\end{pmatrix}-i\omega t\right\} \quad (6)$$

$\boldsymbol{x}(l/k)$ represents the Cartesian coordinate of the particle (l/k). The symlols e_k and m_k represent the ionic charge

1) M. Born and K. Huang, "Dynamical Theory of Crystal Lattices", Oxford University Press, London (1954).

2) E. W. Kellermann, *Phil. Trans. Roy. Soc.*, **238**, 513 (1940).

3) (a) A. D. B. Woods, B. N. Brockhouse, and R. A. Cowley, *Phys. Rev.*, **131**, 1025 (1963). (b) R. A. Cowley, *ibid.*, **134**, A981 (1964). (c) A. M. Karo and J. R. Hardy, *ibid.*, **181**, 1272 (1969). (d) J. G. Traylor, H. G. Smith, R. M. Nicklow, and M. K. Wilkinson, *ibid.*, **B3**, 3457 (1971). (e) S. Ganesan and R. Srinivasan, *Can. J. Phys.*, **40**, 74 (1962).

4) (a) J. F. Vetelino and S. S. Mitra, *Phys. Rev.*, **178**, 1349 (1969). (b) J. F. Vetelino, S. S. Mitra, and K. V. Namjoshi, *ibid.*, **B2**, 967 (1970).

5) (a) B. J. Dick and A. W. Overhauser, *ibid.*, **112**, 90 (1958). (b) J. E. Hanlon and A. W. Lawson, *ibid.*, **113**, 472 (1959).

6) J. R. Hardy, *Phil. Mag.*, **4**, 1278 (1958).

7) M. A. Nusimovici and M. Balkanski, *Phys. Rev.*, **B1**, 595 (1970).

8) R. A. Cowley, *Acta. Crystallogr.*, **15**, 687 (1962).

and mass of particle k, respectively. $C^{N}_{\alpha\beta}(\boldsymbol{y}/_{kk'})$ is a mass-adjusted matrix of R and $Q_{\alpha\beta}(\boldsymbol{y}/_{kk'})$ is a complicated function of k, k' and wave vector $\boldsymbol{y}$, and can be calculated if the crystal structure is known.[9] The macroscopic field

$$E_\alpha = -(4\pi/v_a)(y_\alpha/|\boldsymbol{y}|)\sum_\beta (y_\beta/|\boldsymbol{y}|)\sum_{k'}(e_{k'}/\sqrt{m_{k'}})w_\beta\left(k'\left|\frac{\boldsymbol{y}}{j}\right.\right) \quad (7)$$

is not a regular function of $\boldsymbol{y}$ at $\boldsymbol{y}=0$. Its limiting value depends on the direction by which the point $\boldsymbol{y}=0$ is approached. It gives the TO-LO splittings of the frequencies of the infrared active vibrations.

When the matrices $\boldsymbol{R}$ and $\boldsymbol{C}$ are mass-adjusted, Eq. (4) is written as

$$|\omega^2\boldsymbol{I}-[\boldsymbol{R}+\boldsymbol{ZCZ}]| = 0 \quad (8)$$

where $\boldsymbol{I}$ represents an unit matrix. For a certain infrared active symmetry species at $\boldsymbol{y}\sim 0$, matrix $\boldsymbol{R}$ of the longitudinal mode is exactly the same as that of the transverse mode, while matrices $\boldsymbol{C}$(L) and $\boldsymbol{C}$(T), matrix $\boldsymbol{C}$ of the longitudinal and of the transverse modes, respectively, differ from each other, because of the existence of the macroscopic field. Equation (8) can then be given by

$$|\omega^2(\mathrm{L})\boldsymbol{I}-[\boldsymbol{R}+\boldsymbol{ZC}(\mathrm{L})\boldsymbol{Z}| = 0$$

and

$$|\omega^2(\mathrm{T})\boldsymbol{I}-[\boldsymbol{R}+\boldsymbol{ZC}(\mathrm{T})\boldsymbol{Z}| = 0 \quad (9)$$

We consider the crystals M_nX_m which contain only two different particles such as ZnO and TiO_2. The effective ionic charge on particle M can be written as Ze. The effective charge on particle X is then $-(n/m)Ze$, since the crystal should be electrically neutral. In Eq. (9), $\boldsymbol{Z}$ is a diagonal matrix, the elements of which are effective ionic charges of particles. When matrix $\boldsymbol{C}$ is taken to include the constants e and $-(n/m)e$, we can write matrix $\boldsymbol{ZCZ}$ as $Z^2\boldsymbol{C}$. Thus Eq. (9) becomes

$$\mathrm{Tr}\cdot[\boldsymbol{R}+Z^2\boldsymbol{C}(\mathrm{L})] = \sum_i \omega_i^2(\mathrm{L})$$

and

$$\mathrm{Tr}\cdot[\boldsymbol{R}+Z^2\boldsymbol{C}(\mathrm{T})] = \sum_i \omega_i^2(\mathrm{T}) \quad (10)$$

the value of Z being obtained from the equation

$$Z^2 = [\textstyle\sum_i \omega_i^2(\mathrm{L}) - \sum_i \omega_i^2(\mathrm{T})]/[\mathrm{Tr}\cdot\boldsymbol{C}(\mathrm{L}) - \mathrm{Tr}\cdot\boldsymbol{C}(\mathrm{T})] \quad (11)$$

where Tr. $\boldsymbol{C}$ represents the trace of the matrix $\boldsymbol{C}$.

Effective Ionic Charges of Several Wurtzite and Rutile Type Crystals

We apply Eq. (11) to crystals of wurtzite and rutile type, the transverse and longitudinal frequencies of which are all known.

Wurtzite Type Crystals. The space group of the wurtzite type ZnO crystal is C^4_{6v}-$P_{6_3}mc$ and the unit cell contains two formula units as shown in Fig. 1. At $\boldsymbol{y}\sim 0$, by factor group analysis the lattice vibrations can be classified into $2a_1+2b_1+2e_1+2e_2$. The vibrations of the symmetry species a_1 and e_1 are active in both infrared and Raman spectra, those of e_2 species

9) See the chapter V of Ref. 1.

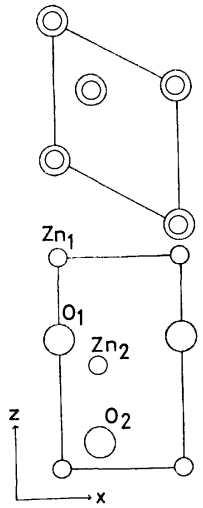

Fig. 1. Crystal structure of ZnO (wurtzite type). The upper figure represents the projection on the ab plane.

Table 1. Cartesian symmetry coordinates for ZnO (zincite)

a_1	$s_1=[z(Zn_1)+z(Zn_2)]/\sqrt{2}$
	$s_2=[z(O_1)+z(O_2)]/\sqrt{2}$
b_1	$s_1=[z(Zn_1)-z(Zn_2)]/\sqrt{2}$
	$s_2=[z(O_1)-z(O_2)]/\sqrt{2}$
e_1	$s_1=[x(Zn_1)+x(Zn_2)]/\sqrt{2}$
	$s_2=[x(O_1)+x(O_2)]/\sqrt{2}$
	$s_1'=[y(Zn_1)+y(Zn_2)]/\sqrt{2}$
	$s_2'=[y(O_1)+y(O_2)]/\sqrt{2}$
e_2	$s_1=[x(Zn_1)-x(Zn_2)]/\sqrt{2}$
	$s_2=[x(O_1)-x(O_2)]/\sqrt{2}$
	$s_1'=[y(Zn_1)-y(Zn_2)]/\sqrt{2}$
	$s_2'=[y(O_1)-y(O_2)]/\sqrt{2}$

are only Raman active, and those of b_1 species are optically inactive. The Cartesian symmetry coordinates are shown in Table 1. The acoustic modes belong to a_1 and e_1 species. When the point $\boldsymbol{y}=0$ is approached by 001 direction, $\boldsymbol{C}(\mathrm{L})a_1$ and $\boldsymbol{C}(\mathrm{T})e_1$ are obtained, where $\boldsymbol{C}(\mathrm{L})a_1$ represents matrix $\boldsymbol{C}$ of the longitudinal mode of a_1 species *etc.* On the other hand, when approached by 100 direction, we can get $\boldsymbol{C}(\mathrm{T})a_1$ and $\boldsymbol{C}(\mathrm{L})e_1$. The $\boldsymbol{C}$ matrices of b_1 and e_2 species are

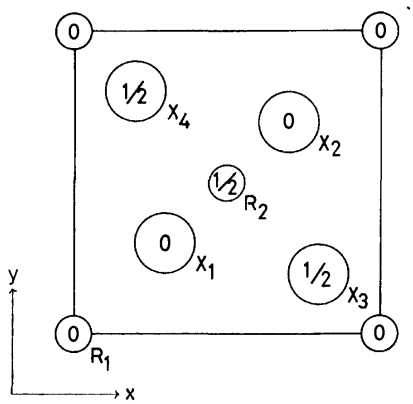

Fig. 2. Crystal structure of rutile type crystals. The figure represents the projection on the ab plane. The numbers in the circles mean the height along c axis.

TABLE 2. EFFECTIVE IONIC CHARGES OF SEVERAL WURTZITE TYPE CRYSTALS

	Symmetry species	Observed frequencies (cm^{-1}) IR	Raman LO	Raman TO	Z	Z_{av}[d]
ZnO	a_1		574[b]	380	1.07	
		(414)[a]				1.05
	e_1		583	407	1.04	
ZnS	a_1		352[b]	274	0.91	
		(274)[c]				0.91
	e_1		352	274	0.91	
CdS	a_1	234[c]	305[b]	228	1.02	
						1.00
	e_1	241	305	235	0.98	
BeO	a_1		1081[b]	678	1.05	
						1.04
	e_1		1097	722	1.03	

a) Ref. 10. b) Ref. 11. c) Ref. 12.
d) The average value of Z obtained from a_1 and e_1 species.

independent of the direction of approach. For certain symmetry species $\mathrm{Tr}\cdot\boldsymbol{C}(\mathrm{L})-\mathrm{Tr}\cdot\boldsymbol{C}(\mathrm{T})$ in Eq. (11) can be calculated by use of the macroscopic field, Eq. (7) and the symmetry coordinates shown in Table 1. The results are

$$\mathrm{Tr}\cdot\boldsymbol{C}(\mathrm{L}) - \mathrm{Tr}\cdot\boldsymbol{C}(\mathrm{T}) = 8\pi(1/m_{\mathrm{Zn}}+1/m_{\mathrm{O}})e^2/v_a \qquad (12)$$

for both a_1 and e_1 species, where the effective ionic charges on Zn and O are $+Ze$ and $-Ze$, respectively. It is not necessary to calculate the complicated function $Q_{\alpha\beta}(\boldsymbol{y}|_{kk'})$. The values of Z obtained from Eqs. (11) and (12) for several wurtzite type crystals are summarized in Table 2.

TABLE 3. CARTESIAN SYMMETRY COORDINATES FOR RUTILE TYPE CRYSTALS

a_{1g}	$s_1=[x(X_1)+y(X_1)-x(X_2)-y(X_2)+x(X_3)-y(X_3)-x(X_4)+y(X_4)]/2\sqrt{2}$
b_{1g}	$s_1=[x(X_1)-y(X_1)-x(X_2)+y(X_2)+x(X_3)+y(X_3)-x(X_4)-y(X_4)]/2\sqrt{2}$
a_{2g}	$s_1=[x(X_1)-y(X_1)-x(X_2)+y(X_2)-x(X_3)-y(X_3)+x(X_4)+y(X_4)]/2\sqrt{2}$
b_{2g}	$s_1=[x(X_1)+y(X_1)-x(X_2)-y(X_2)-x(X_3)+y(X_3)+x(X_4)-y(X_4)]/2\sqrt{2}$
a_{2u}	$s_1=[z(R_1)+z(R_2)]/\sqrt{2}$
	$s_2=[z(X_1)+z(X_2)+z(X_3)+z(X_4)]/2$
b_{2u}	$s_1=[z(R_1)-z(R_2)]/\sqrt{2}$
	$s_2=[z(X_1)+z(X_2)-z(X_3)-z(X_4)]/2$
e_g	$s_1=[z(X_1)-z(X_2)]/\sqrt{2}$
	$s_1'=[z(X_3)-z(X_4)]/\sqrt{2}$
e_u	$s_1=[x(R_1)+y(R_1)]/\sqrt{2}$
	$s_2=[x(R_2)+y(R_2)]/\sqrt{2}$
	$s_3=[x(X_1)+y(X_1)+x(X_2)+y(X_2)]/2$
	$s_4=[x(X_3)+y(X_3)+x(X_4)+y(X_4)]/2$
	$s_1'=[x(R_1)-y(R_1)]/\sqrt{2}$
	$s_2'=[x(R_2)-y(R_2)]/\sqrt{2}$
	$s_3'=[x(X_1)-y(X_1)+x(X_2)-y(X_2)]/2$
	$s_4'=[x(X_3)-y(X_3)+x(X_4)-y(X_4)]/2$

Rutile Type Crystals. The space group of the rutile type crystal RX_2 is $D_{4h}^{14}-P4_2/mnm$ and the unit cell contains two formula units as shown in Fig. 2. At $\boldsymbol{y}\sim 0$, the lattice vibrations are classified by the

TABLE 4. EFFECTIVE IONIC CHARGES OF SEVERAL RUTILE TYPE CRYSTALS

	Symmetry species	Infrared (cm^{-1}) LO	Infrared (cm^{-1}) TO	Z	Z_{av}[f]
TiO_2[a]	a_{2u}	811	167	1.38	
	e_u	806	500		1.35
		458	388	1.31	
		373	183		
SnO_2[b]	a_{2u}	704	465	1.13	
	e_u	757	605		1.13
		368	284	1.13	
		273	243		
GeO_2	a_{2u}[c]	755	455	1.07	
	e_u[c]	815	635		1.08
		470	370	1.08	
		345	300		
	a_{2u}[d]	816	522	1.11	
	e_u[d]	852	709		1.10
		680	652	1.09	
		484	334		
ZnF_2[e]	a_{2u}	488	294	0.80	
	e_u	498	380		0.78
		264	244	0.76	
		227	173		

a) Ref. 13. b) Ref. 15. c) Ref. 16. d) Ref. 17.
e) Ref. 14. f) The average value of Z obtained from species a_1 and e_1.

10) R. J. Collins and D. Kleinman, *J. Phys. Chem. Solids.*, **11**, 190 (1959).
11) C. A. Arguello, D. L. Rousseau, and S. P. S. Porto, *Phys. Rev.*, **181**, 1351 (1969).
12) A. Manabe, A. Mitsuishi, and H. Yoshinaga, *Japanese J. Appl. Phys.*, **6**, 593 (1967).
13) D. M. Eagles, *J. Phys. Chem. Solids*, **25**, 1243 (1964).
14) A. S. Barker, Jr., *Phys. Rev.*, **136**, 1290 (1964).
15) R. Summitt, *J. Appl. Phys.*, **39**, 3762 (1968).
16) D. M. Roessler and W. A. Albers, Jr., *J. Phys. Chem. Solids*, **33**, 293 (1972).
17) A. Kahan, J. W. Goodrum, R. S. Singh, and S. S. Mitra, *J. Appl. Phys.*, **42**, 4444 (1971).

factor group analysis into $a_{1g}+b_{1g}+a_{2g}+2a_{2u}+b_{2g}+2b_{2u}+e_g+4e_u$. The vibrations of the gerade symmetry species except for a_{2g} are Raman active, those of a_{2u} and e_u species infrared active, and those of b_{2u} and a_{2g} species optically inactive. The Cartesian symmetry coordinates are shown in Table 3. The acoustic modes are included in a_{2u} and e_u species. As in the case of wurtzite type crystals, $\mathrm{Tr}\cdot\boldsymbol{C}(\mathrm{L})-\mathrm{Tr}\cdot\boldsymbol{C}(\mathrm{T})$ can be obtained by using the macroscopic field and the symmetry coordinates. The result is given by

$$\mathrm{Tr}\cdot\boldsymbol{C}(\mathrm{L}) - \mathrm{Tr}\cdot\boldsymbol{C}(\mathrm{T}) = 16\pi(2/m_{\mathrm{R}}+1/m_{\mathrm{X}})e^2/v_{\mathrm{a}} \qquad (13)$$

for both a_{2u} and e_u species, where the effective ionic charges on R and X are $+2Ze$ and $-Ze$, respectively. The values of Z obtained from Eqs. (11) and (13) for several rutile type crystals are listed in Table 4. For the crystal GeO_2, two different sets of frequencies were reported.[16,17] Table 4 includes the vlaues of the effective charges on the basis of the two sets.

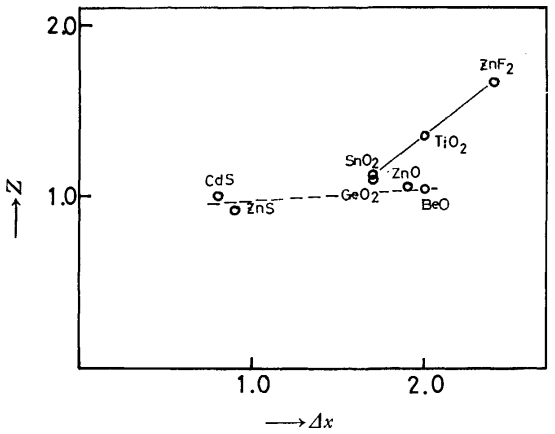

Fig. 3. The relation between the values of the effective ionic charges, Z, and the difference of the Pauling's electronegativity of the positive and negative ions, Δx.

The effective ionic charges on Zn for ZnO, ZnS, and ZnF_2 were found to be 1.05, 0.91, and 1.56 (2×0.78), respectively. The results indicate that the nature of the ionic bonds of oxide and sulfide is more covalent than that of fluoride. Table 4 also shows that the values of Z for the three rutile type oxides increases in the order of $GeO_2<SnO_2<TiO_2$. TiO_2 has a large ionic character, which gives rise to a large TO–LO splitting in the frequencies of a_{2u} species. Figure 3 shows the relation between the values of the effective ionic charges Z and the difference of Pauling's electronegativity[18] of the positive and negative ions $\Delta\chi$. For rutile type crystals a fairly good linear relation is found between Z and $\Delta\chi$. However, for the wurtzite type crystals the values of Z are almost constant.

The values of the effective ionic charges were obtained on the basis of the rigid ion model. However, the ions are not rigid, that is, polarizable. In order to estimate the effect of the polarizable ion, we consider the following two examples, for which the values of the ionic charges were obtained by a model which contained the polarization of ions. For CdS, Nusimovici and Balkanski[7] calculated the phonon frequencies to fit the observed phonon dispersion curves. On the basis of a model which includes valence-bond forces, rigid ion Coulomb forces and electronic and ionic polarization, they gave $1.02e$ as the value of the ionic charge which was very close to the value $1.00e$ in Table 2. Traylor *et al.*[3d] studied the phonon dispersion relation of rutile (TiO_2) and obtained the value $-1.26e$ as Z_0 on the basis of shell model. The value $1.26e$ is also close to the value $1.35e$ given in Table 4.

Orthorhombic Hydrogen Chloride Crystal

In ionic crystals long range interaction is of importance, but in molecular crystals it is usually omitted in the calculation of lattice vibration frequency. We tried to estimate its effect on the lattice vibration frequencies in molecular crystals, and chose orthorhombic hydrogen chloride crystal, since the system is simple and the frequency calculation at $y\sim 0$ was already made by Ito *et al.*[19] on the basis of the force field only due to short range interactions.

The space group of the crystal is C_{2v}^{12}—$Bb2_1m$ and the Bravais cell contains two HCl molecules.[20] Factor group analysis gives the result $4a_1+4b_1+2a_2+2b_2$. The a_1, b_1, and b_2 species contain one acoustic mode each, and can be expected to have different frequencies in transverse and longitudinal modes. The frequencies were calculated by Eq. (4). Matrix $\boldsymbol{R}$ was constructed by the same force field as that adopted by Ito *et al.*[19] Matrix $\boldsymbol{C}$ was set up according to the method of Kellermann[2] on the assumption that the hydrogen atom has an electric charge $+Ze$ and the chlorine atom $-Ze$. The value of Z was determined to be 0.18 from the distance between H and Cl atoms (1.27 Å) and the dipole moment (1.085 D) of the gaseous hydrogen chloride molecule. The distance between D and Cl atoms in the orthorhombic DCl crystal is 1.25 Å,[21] so that the value of Z in the crystal

Table 5. The calculated frequencies for orthorhombic hydrogen chloride crystal (in cm^{-1})

Symmetry species	Calculation 1	Calculation 2	
		TO	LO
a_1	2727	2699	2703
	297	377	401
	97	93	93
b_1	2732	2709	2713
	501	574	593
	109	112	112
a_2	213	303	303
	54	56	56
b_2	215	316	375

a) The values differ slightly from those reported by Ito *et al.*[19], who assumed $F'_{\mathrm{HH}}=-0.1F_{\mathrm{HH}}$. In the present work F'_{HH} was assumed to be zero.

18) L. Pauling, "The Nature of the Chemical Bond," Cornell U. P., Ithaca, N. Y., (1960), 3rd ed.

19) M. Ito, M. Suzuki, and T. Yokoyama, *J. Chem. Phys.*, **50**, 2949 (1969).

20) E. Sándor and R. F. C. Farraw, *Nature*, **215**, 1265 (1967).

21) E. Sándor and R. F. C. Farraw, *ibid.*, **213**, 171 (1967).

can not differ much from the value obtained from gas. The values of the force constants due to the short range interaction were taken to be the same as those by Ito *et al.* The calculated results are shown in Table 5 in which 1 gives the frequencies without long range interaction and 2 those obtained with long range interaction.

As expected the effect of long range interaction in the case of the hydrogen chloride crystal is not so large as that in ionic crystals. The TO–LO splittings of the internal H–Cl stretching vibrations are 4 cm^{-1}. The largest TO–LO splitting of the lattice vibrations is 59 cm^{-1} which was obtained for the librational mode of b_2 species. The vibrational modes of the lowest frequencies of a_1, b_1, and a_2 species are approximately the translational modes of the HCl molecules. It is concluded that their frequencies do not depend on the long range interaction, since the frequencies of calculation 1 and TO and LO frequencies of calculation 2 are about the same. However, for the frequencies of the librational modes, which have the second lowest frequency of all symmetry species, the effect of long range interaction is much larger than that for translational modes.

BULLETIN OF THE CHEMICAL SOCIETY OF JAPAN, VOL. 46, 1338—1342 (1973)

Solubilization Behavior of Mixed Micelles of Anionic and Nonionic Surfactants in Relation to Their Micellar Structures

Fumikatsu Tokiwa and Kaoru Tsujii

Research Laboratories, Kao Soap Company, 2-1-3 Bunka, Sumida-ku, Tokyo 131

(Received August 4, 1972)

The solubilization behavior of mixed micelles of nonionic and anionic surfactants toward a water-insoluble dye, Yellow OB, has been studied. The surfactants examined were a nonionic surfactant, dodecyl polyoxyethylene ether (C_{12}POE), and anionic surfactants with the chemical structure of C_m- 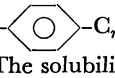 -C_n-SO_3Na, where $m+n=8$ and where m or n is 0, 4, or 8 (and sodium decyl sulfonate for reference). The solubilization greatly depends on the position of the benzene ring in the hydrocarbon chain of the anionic surfactant mixed; in the mixture of C_{12}-POE and C_8- 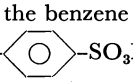 -SO_3Na, the synergistic effect in solubilization is remarkable. The results have been discussed in relation to the structure or compactness of the polyoxyethylene shell of the mixed micelle, and in relation to the interaction of anionic and nonionic surfactants in their mixed micelle, which had previously been observed by NMR measurements.

In general, the solubilizing capacity of a nonionic surfactant of the polyoxyethylene type for water-insoluble matetials is much greater than that of an ionic surfactant with the same hydrocarbon chain length as that of the nonionic surfactant. For example, the solubilizing capacity of dodecyl polyoxyethylene ether (C_{12}POE) for a water-insoluble dye, Yellow OB, is approximately ten times greater than that of sodium dodecyl sulfate.[1] This fact suggests that the polyoxyethylene part in the molecule plays an important role in solubilization, and also that the solubilizing capacity depends greatly on the structure of the polyoxyethylene shell of the micelle.

In previous papers[2,3] studying mixed micelles of C_{12}POE and an anionic surfactant with a benzene ring in the molecule by nuclear magnetic resonance (NMR), it has been shown that, in the mixed micelle, an interaction occurs between the polyoxyethylene part of C_{12}POE and the benzene ring of the anionic surfactant. The extent of the interaction depends also on the position of the benzene ring in the hydrocarbon chain. Such an interaction might be related to the solubilization behavior of the mixed micelles of nonionic and anionic surfactants of these types.

In the present work, the solubilization behavior toward Yellow OB of the following mixed surfactant systems has been studied in order better to understand the interaction of two different surfactants in their mixed micelle and the effect of the structure of the polyoxyethylene shell of the mixed micelle on its solubilization behavior:

System I: C_8- 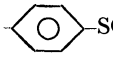 -SO_3Na and C_{12}POE

System II: C_4- 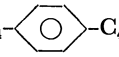 -C_4-SO_3Na and C_{12}POE

System III: 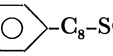 -C_8-SO_3Na and C_{12}POE

System IV: C_{10}-SO_3Na and C_{12}POE

The three anionic surfactants in Systems I, II, and III are different only in the position of the benzene ring in the hydrocarbon chain, and the C_{10}-SO_3Na surfactant in System IV has no benzene ring in the molecule.

1) F. Tokiwa, *J. Phys. Chem.*, **72**, 1214 (1968).
2) F. Tokiwa and K. Tsujii, *J. Phys. Chem.*, **75**, 3560 (1971).
3) F. Tokiwa and K. Tsujii, *J. Colloid Interface Sci.*, **41**, 343 (1972).

Experimental

Materials. The sodium *p*-octylbenzene sulfonate (abbreviated to $C_8\phi S$), sodium δ-(4-butyl phenyl) butyl sulfonate (abbreviated to $C_4\phi C_4S$), and sodium ω-phenyloctyl sulfonate (abbreviated to ϕC_8S) were the same samples as those used in the previous experiments.[2,3] The sodium decyl sulfonate (abbreviated to $C_{10}S$) was prepared by the reaction: $C_8H_{17}CH{=}CH_2+NaHSO_3\rightarrow C_{10}H_{21}SO_3Na$, using *t*-butylperbenzoate as the catalyst. The product obtained, $C_{10}S$, was recrystallized three times from an ethanol-water mixture (95:5). The dodecyl polyoxyethylene ether with 9 oxyethylene units purified by the countercurrent solvent extraction method,[4] was the sample used in a previous work.[2] The polyethylene glycol (abbreviated to PEG), the average molecular weight of which was approximately 400, was of a reagent grade and was purified by ion exchange with Amberlite IR-120 and IRA-410. The Yellow OB (1-*o*-tolyl-azo-2-naphthylamine) was of a reagent grade; it was purified by a procedure previously described.[1]

Solubilization Measurements. The sample solutions were prepared by adding the desired amounts of the anionic surfactant to an aqueous solution of the nonionic surfactant, $C_{12}POE$, of 5×10^{-3} M. Solubilization runs were made in a water bath at 30 ± 0.1 °C for 65 hr to attain equilibrium, the procedure described elsewhere[1] being employed. The Yellow OB described above was used as a solubilizate. The amounts of the solubilized dye were determined by optical-density measurements at a wavelength of 445 mμ by means of a Shimadzu Model AQV-50 spectrophotometer.

The critical micelle concentration (CMC) and the solubilizing capacity of each surfactant were determined from the inflection and slope respectively of the solubilization *vs.* concentration curve.

A similar method was used to determine the solubility of Yellow OB in the mixed solvent of PEG and water at various mixing ratios.

Results and Discussion

Figure 1 shows the solubilization *vs.* concentration curves for Systems I, II, III, and IV, where the amount of Yellow OB, *S*, solubilized by mixed micelles is plotted against the molar concentration of each anionic surfactant, *C*, the concentration of the nonionic surfactant, $C_{12}POE$, being kept constant at 5×10^{-3} M. (On the ordinate, the value of *S* for $C_{12}POE$ alone is displaced to zero.) In System I, a remarkable, synergistic effect in the solubilization of the mixture of $C_8\phi S$ and $C_{12}POE$ is observed. In the other systems, however, their solubilizing capacities in the region of relatively low concentrations are smaller than that of $C_{12}POE$ alone; they depend on the type of anionic surfactant.

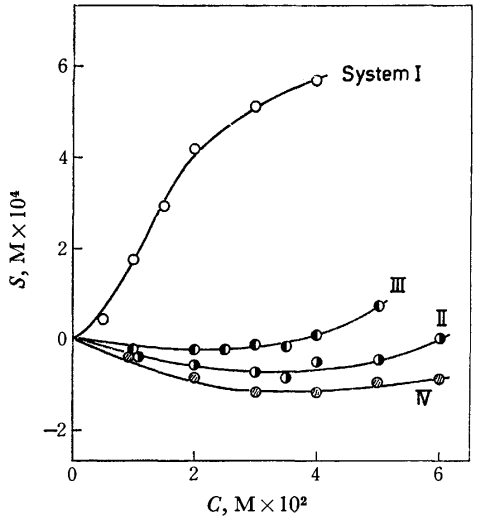

Fig. 1. The curves of the solubilization of Yellow OB *vs.* the concentration of anionic surfactant for Systems I, II, III, and IV at 30 °C, the concentration of $C_{12}POE$ being kept constant at 5×10^{-3} M.

It is known that when two different surfactants are mixed in an aqueous solution, mixed micelles are formed rather than the respective micelles of each surfactant. If we assume that the additivity rule can be applied to the solubilizing capacity, *s*, of these mixed micelles, then the value of *S* can be expressed as:

$$S = (C^t - C^\circ_{1,2})(s_1x_1 + s_2x_2) \quad (1)$$

where the subscripts 1 and 2 refer to anionic and nonionic surfactants respectively; *s*, the solubilizing capacity; *x*, the mole fraction in the micelle phase; $C^\circ_{1,2}$, the CMC of the mixture of the two surfactants, and C^t, the total concentration, *i.e.*, the sum of the concentrations of Surfactants 1 and 2. The $(C^t - C^\circ_{1,2})$ term in Eq. (1) expresses the concentration of surfactants forming mixed micelles. The values of s_1, s_2, and C^t are known, and the values of x_1, x_2, and $C^\circ_{1,2}$ may be estimated as will be shown below.

If we consider a two-component system consisting of both monomer and micelle phases, and assume the system to be ideal, we know that for each component the chemical potentials in the two phases are identical at equilibrium. Under such conditions, the equilibrium between monomers and micelles in a mixed solution of anionic and nonionic surfactants may be expressed[5,6] as:

$$y_1C^\circ_{1,2} = x_1C^\circ_1 \quad (2)$$

and:

$$y_2C^\circ_{1,2} = x_2C^\circ_2 \quad (3)$$

where *x* and *y* are the mole fractions of the surfactants in the micelle and monomer phases respectively, and where C° is the CMC. From Eqs. (2) and (3), the CMC of the mixed surfactants, $C^\circ_{1,2}$, may be written in the form:

$$C^\circ_{1,2} = (C^\circ_1 - C^\circ_2)x_1 + C^\circ_2 \quad (4)$$

as $x_1+x_2=1$ and $y_1+y_2=1$. By definition, on the other hand, the value of x_1 is expressed by:

$$x_1 = \frac{C_1^{\,M}}{C_1^{\,M}+C_2^{\,M}} = \frac{C_1^{\,t}-C_1^{\,m}}{C^t-C^\circ_{1,2}} = \frac{\alpha_1C^t-y_1C^\circ_{1,2}}{C^t-C^\circ_{1,2}} \quad (5)$$

where the superscripts m and M refer to the monomer and the micelle respectively, and where α_1 is the mole fraction of Surfactant 1 in the bulk solution. By combining Eq. (5) with Eqs. (2) and (4), we obtain:

4) K. Nagase and K. Sakaguchi, *Kogyo Kagaku Zasshi*, **64**, 635 (1961).

5) F. Daniels and R. A. Alberty, "Physical Chemistry," John Wiley, New York, N. Y. (1966), p. 145.

6) F. Tokiwa, K. Ohki, and I. Kokubo, This Bulletin, **41**, 2845 (1968).

$$x_1 = \frac{1}{2}\{(1+r)-[(1+r)^2-4r\alpha_1]^{1/2}\}$$

$$r = \frac{C^t}{C_1^\circ - C_2^\circ} \tag{6}$$

The value of $C_{1,2}^\circ$ can also be evaluated by substituting x_1 into Eq. (4). The values of C_1° and C_2° used for these calculations are given in Table 1, together with the values of s_1 and s_2 calculated from the slope of the S *vs.* C curve for each surfactant.

Table 1. Values of C_1° and C_2° (mol/l), and s_1 and s_2 (mol, yellow OB/mol, surfactant) for each system

	$C_1^\circ \times 10^2$	$C_2^\circ \times 10^4$	$s_1 \times 10^3$	$s_2 \times 10$
System I	1.17	1.30	13.0	1.13
System II	2.90	1.30	4.67	1.13
System III	3.45	1.30	8.20	1.13
System IV	4.50	1.30	5.50	1.13

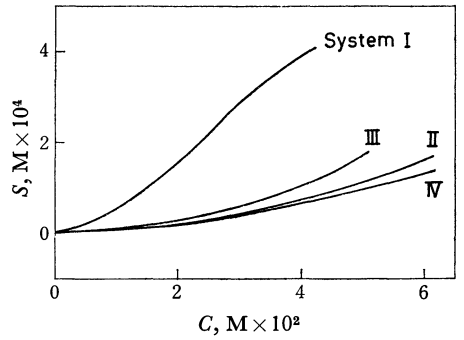

Fig. 2. The solubilization *vs.* concentration curves, calculated by Eq. (1), for Systems I, II, III, and IV.

Using the values of x_1 and x_2 (by definition, $x_2 = 1-x_1$) for Eq. (1), we can draw the S *vs.* C curves of Systems I, II, III, and IV shown in Fig. 1. When these calculated S *vs.* C curves are compared with the observed S *vs.* C curves shown in Fig. 1, we can see that Eq. (1) does not well explain the solubilization behavior of each system; that is, in System I the observed curve is higher than the calculated curve throughout the concentration region examined, and in Systems II, III, and IV the observed curves are lower than the calculated ones. As will be described later, the remarkable, synergistic effect in solubilization observed in System I can be explained in terms of a strong interaction between the benzene ring of $C_8\phi S$ and the polyoxyethylene chain of C_{12}POE in the mixed micelle.[2,3]

The solubilizing capacity of the C_{12}POE micelle toward Yellow OB is probably closely related to the compactness or structure of the polyoxyethylene shell of this micelle. According to previous works,[1,7] sodium dodecylpolyoxyethylene sulfate, which has an ionic head at the terminal of the polyoxyethylene chain, can solubilize the dye much less than C_{12}POE because of less compactness of the polyoxyethylene shell as a result of the electrical repulsion between the charged heads.

7) F. Tokiwa, *J. Phys. Chem.*, **72**, 4331 (1968).

In the present cases, by considerations similar to those indicated above, the polyoxyethylene shell of the C_{12}POE micelle will be made less compact or diluted by mixed micelle formation with an anionic surfactant. This will then result in less solubilization. The compactness of the polyoxyethylene shell consisting of n_2 molecules of C_{12}POE may be written in the form:

$$p = \frac{(M_{POE}/N)n_2}{v_{POE}} \tag{7}$$

where p is the compactness expressed by weight/volume; v_{POE}, the volume of the polyoxyethylene shell of the micelle; M_{POE}, the molecular weight of the polyoxyethylene chain of the C_{12}POE molecule, and N, the Avogadro number. When n_1 molecules of an anionic surfactant are incorporated into this micelle, the volume of the shell will be increased proportionally to n_1. Then, the value of p becomes:

$$p = \frac{(M_{POE}/N)n_2}{v_{POE}+\beta n_1} \tag{8}$$

where β is a constant, *i.e.*, the volume factor of the anionic surfactant molecule added.

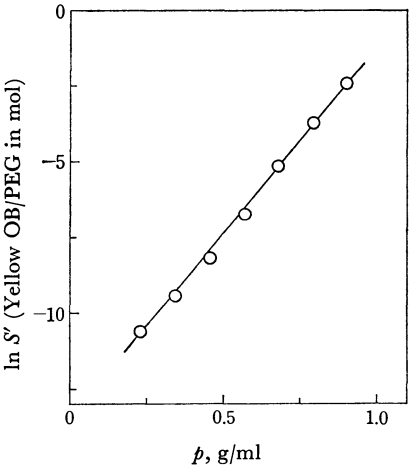

Fig. 3. The solubility of Yellow OB in aqueous PEG solution as a function of the concentration of PEG at 30 °C.

Let us now turn our attention to the solubility of Yellow OB in mixed solvents of PEG and water at different mixing ratios in order to relate p to the solubilizing capacity of mixed micelles. In Fig. 3, the logarithm of the solubility of Yellow OB, S', is plotted against the concentration of PEG, p, in aqueous solution [the value of p corresponds to p in Eq. (8)]. There is a linear relation between ln S' and p; it is given by the equation:

$$\ln S' = Ap + B \tag{9}$$

where A and B are constants. From the slope and intercept of the straight line, the A and B constants may be determined to be 12.2 ml/g and −13.5 respectively.

Here, we regard the polyoxyethylene shell of a mixed micelle as a "small" mixed solvent system consisting of PEG and water. The solubility, S', in Eq. (9), may then be put equal to the solubilizing capacity, S_{dil}^M, of a "diluted" polyoxyethylene shell of the mixed micelle, since the dilution of the polyoxyethylene shell

by an anionic surfactant and the dilution by water are considered to have a similar effect on the solubility of Yellow OB. Then, the compactness, p, of the shell given by Eq. (8) may be related to p in Eq. (9). By combining Eq. (8) with Eq. (9), we obtain:

$$\ln S^{M}_{dil} = A\frac{(M_{POE}/N)n_2}{v_{POE}+\beta n_1} + B$$

$$= A\frac{(M_{POE}/N)}{(v_{POE}/n_2)+\beta(n_1/n_2)} + B \qquad (10)$$

where (n_1/n_2) is the molar ratio of the anionic/nonionic surfactants in the micelle phase and has the relation:

$$n_1/n_2 = x_1/x_2 = x_1/(1-x_1) \qquad (11)$$

The value of (v_{POE}/n_2) is evaluated by inserting the value of S^{M}_{dil} at $x_1/x_2=0$, which may be estimated from the difference between the solubilizing capacities of C_{12}POE and sodium dodecyl sulfonate, into Eq. (10). By using Eq. (10), the S^{M}_{dil} *vs.* (x_1/x_2) curve, for example, at $\beta=15$ Å^3 is drawn in Fig. 4, where β is estimated as will be described later.

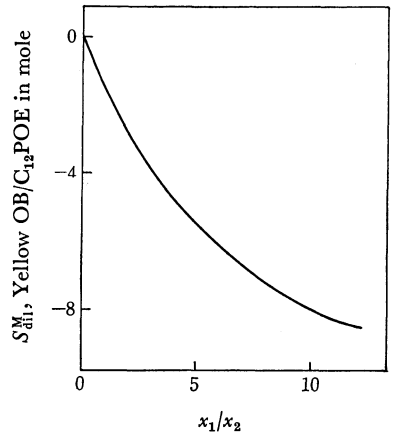

Fig. 4. The solubilizing capacity S^{M}_{dil} of a "diluted" polyoxythylene shell of mixed micelles as a function of x_1/x_2, according to Eq. (10).

From Eq. (6), the variable (x_1/x_2) in Eq. (11) can be given by two variables, C^t and α_1, which are determined in this case only by the concentration, C, of the anionic surfactant. Thus, S^{M}_{dil} can be converted into S_{dil}, which expresses the moles of Yellow OB solubilized per liter of the surfactant solution. In Fig. 5, the S_{dil} *vs.* C relationship at $\beta=15$ Å^3 for System IV is shown.

The constant β in Eq. (10) may be estimated as follows. In System IV, where the anionic surfactant, C_{10}S, has no benzene ring in the molecule, we assume that no interaction occurs between C_{10}S andC_{12}POE. On this assumption, the difference between the value observed (S_{obsd}) and the value calculated (S_{calcd}) by Eq. (1) may be ascribed to the dilution effect of C_{10}S on the polyoxyethylene shell of the C_{12}POE micelle, which can itself be evaluated from Eq. (10). Then, the constant β in Eq. (10) may be estimated by trial and error unitl the $(S_{obsd}-S_{calcd})$ *vs.* C curve overlaps with the S_{dil} *vs.* C curve. When the value of β is chosen as 15 Å^3, we obtain Fig. 5, where the broken line indicates the S_{dil} *vs.* C curve and where the solid line

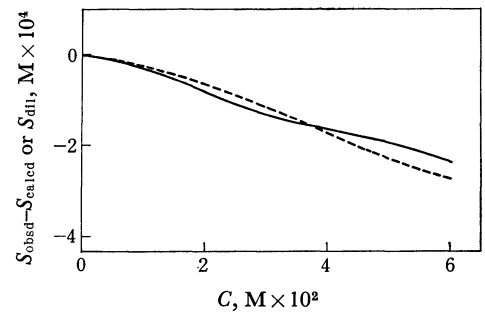

Fig. 5. The $(S_{obsd}-S_{calcd})$ *vs.* C_{calcd} curve (the solid line), and the S_{dil} *vs.* C curve (the broken line) for System IV.

indicates the $(S_{obsd}-S_{calcd})$ *vs.* C curve for System IV. These two curves are in relatively good agreement with each other, showing Eq. (10) to be reasonable although some deviation is seen at high concentrations.

The value of $\beta(=15$ Å$^3)$ seems somewhat smaller than the expected value. However, this can be explained by taking into consideration the facts that the hydrocarbon portion of the anionic surfactant molecule is located in the hydrocarbon core of the mixed micelle, and that only a part of the hydrophilic head can contribute to the dilution of the polyoxyethylene shell of the micelle. For the same reasons, it may be permissible to use the β value of C_{10}S for other anionic surfactants which have different structures of the hydrocarbon part.

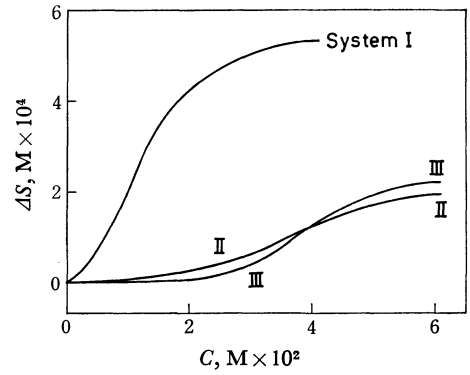

Fig. 6. The synergistic effect, ΔS, in solubilization as a function of C for Systems I, II, and III.

In System I, II, or III, where each anionic surfactant has a benzene ring in the molecule, the difference between the values of S_{obsd} and $(S_{calcd}+S_{dil})$ at a given concentration, C, of the anionic surfactant may be interpreted as a synergistic effect (ΔS) in the solubilization at this C. Figure 6 shows the ΔS *vs.* C curves for Systems I, II, and III; in the calculation of S_{dil}, β is also taken to be 15 Å^3, as has been described above. In System IV, of course, ΔS $(=S_{obsd}-(S_{calcd}+S_{dil})]$ is zero at any C, as has been assumed in the above discussion.

The NMR studies[2,3] of mixed micelles in Systems I, II, and III have shown that the polyoxyethylene chain of C_{12}POE interacts with the benzene ring of the respective anionic surfactant; the extent of the interaction is in order of System I>II>III. The remarkable high values of ΔS seen in System I may

be ascribed to this interaction. On the other hand, the ΔS values in Systems II and III are smaller than the value in System I at all concentrations, and no considerable difference is seen between these two systems. This may be explained by the weaker interaction between the polyoxyethylene chains and the benzene rings in mixed micelles, although the interaction in System II, observed by NMR measurement, is slightly stronger than that in System III.[3)]

The authors wish to express their thanks to Dr. H. Kita for his encouragement in this work, and Dr. Y. Inamoto and Mr. N. Takei for their help in preparing the samples.

BULLETIN OF THE CHEMICAL SOCIETY OF JAPAN, VOL. 46, 1342—1346 (1973)

Interpretation of Photoelectron Spectra of Halomethanes

Shunji KATSUMATA and Katsumi KIMURA

Physical Chemistry Laboratory, Institute of Applied Electricity, Hokkaido University, Sapporo

(Received September 4, 1972)

Theoretical studies of the electronic structure of chloromethanes ($CH_{4-n}Cl_n$, where $n=1\sim4$) were carried out by the CNDO/2 method. The resulting Koopmans' theorem ionization energies were generally in good agreement with the experimental data available, and somewhat different assignments from those previously reported were obtained for the nonbonding orbitals. A "sum rule" was employed for interpreting the photoelectron bands of three series of di- and poly-halomethanes (chloro-, bromo-, and iodo-methanes) in terms of some localized molecular orbitals. Reasonable assignments were derived for the photoelectron spectra of all these halomethanes and the resulting assignments for the chloromethanes were in good accord with those obtained from the CNDO/2 calculation.

The high resolution photoelectron (PE) spectra of all the halomethanes $CH_{4-n}X_n$ ($n=1\sim4$; X=F, Cl, Br, and I) except CI_4 have been reported by Turner *et al.*,[1] Potts *et al.*,[2] and Ragle *et al.*,[3] and interpreted by them in terms of molecular orbital (MO) structures on experimental basis. A theoretical calculation of ionization energy (IE) for chloro- and bromomethanes has been carried out by Dixon *et al.*,[4] with a pseudo one-electron hamiltonian. The PE spectra and electronic structures[1-3] of methyl halides are simple and their outer orbital structures are well understood. For di- and poly-halomethanes, however, the PE spectra are more complicated and some partly conflicting results have been reported for spectral assignment by different workers.[1,2,4] Assignments of the experimental IE's of these compounds to their MO's still seem to remain unresolved, especially for outer electronic structures associated with the nonbonding orbitals of halogen atoms.

Theoretical studies on the electronic structures of fluoromethanes have been carried out with the semi-empirical CNDO/2 method by Davis[5] and Pullen *et al.*,[6] and with the GTO calculation by Brundle *et al.*[7] For other halomethanes, however, no CNDO calculations have been published yet.

We have undertaken a study of a series of chloromethanes using the CNDO/2 method. Furthermore, since Kimura *et al.*[8] recently proposed a sum rule with which the PE spectra of various alkyl monohalides from the methyl to the *n*-butyl can be interpreted in terms of several localized MO's, we employed this method to various polyhalomethanes.

CNDO/2 Calculations of Chloromethanes

The semi-empirical CNDO/2 method treating all the valence electrons in a molecule has been proposed by Pople *et al.*,[9] and extended by Santry and Segal.[10a] to various molecules containing the elements sodium through chlorine. We used this method in calculating IE's of the chloromethanes, taking 1s(H), 2s(C), 2p(C), 3s(Cl), and 3p(Cl) orbitals into account and assuming Koopmans' theorem.

We employed different sets of parameter values for C and H atoms as follows. (1) Values originally used by Pople *et al.*,[9] (2) values given by Del Bene and

1) D. W. Turner, C. Baker, A. G. Baker, and C. R. Brundle. "Molecular Photoelectron Spectroscopy," Wiley-Interscience, New York, 1970.

2) A. W. Potts, H. J. Lempka, D. G. Streets, and W. C. Price, F. R. S., *Phil. Trans. Roy. Soc. Lond.*, **A. 268**, 59 (1970).

3) J. L. Ragle, I. A. Stenhouse, D. C. Frost, and C. A. McDowell, *J. Chem. Phys.*, **53**, 178 (1970).

4) R. N. Dixon, J. N. Murrell, and B. Narayana, *Mol. Phys.*, **20**, 611 (1971).

5) D. W. Davis, *Chem. Phys. Lett.*, **2**, 173 (1968).

6) B. P. Pullen, T. A. Carlson, W. E. Moddeman, G. K. Schweitzer, W. E. Bull, and F. A. Grimm, *J. Chem. Phys.*, **53**, 768 (1970).

7) C. R. Brundle, M. B. Robin, and H. Basch, *ibid.*, **53**, 2196 (1970).

8) K. Kimura, S. Katsumata, Y. Achiba, H. Matsumoto, and S. Nagakura, This Bulletin, **46**, 373 (1973).

9) a) J. A. Pople, D. P. Santry, and G. A. Segal, *J. Chem. Phys.*, **43**, S 129 (1965); b) J. A. Pople and G. A. Segal, *ibid.*, **43**, S 136 (1965); *ibid.*, **44**, 3289 (1966).

10) a) D. P. Santry and G. A. Segal, *ibid.*, **47**, 158 (1967); b) D. P. Santry, *J. Amer. Chem. Soc.*, **90**, 3309 (1968). When his parameter values were used, we employed $\gamma_{Cl}=15.01$ eV reported by H. G. Benson and A. Hudson, *Theoret. Chim. Acta*, **23**, 259 (1971).

Jaffé,[11] and (3) as for (2) except that $\beta_C = -14.0$ eV was used; For Cl atom: (a) values given by Santry and Segal,[10a] (b) values used by Santry,[10b] and (c) as for (a) except that $\beta_{Cl} = -20.0$ eV was used. A value of 14.28 eV was used for γ_{Cl}, evaluated by the approximate formula.[10a] Resonance integrals were approximated by $\beta_{AB} = {}^1/_2 K(\beta_A + \beta_B)$ where K was made to 0.75 when both A and B are Cl atom and 1.0 otherwise, since it has been pointed out by Santry and Segal[10a] that better results can be obtained by introducing such constants for K.

SCF conditions were that the energy of the lowest unoccupied MO and those of the highest and second highest occupied MO's converge within 5×10^{-4} eV. Bond lengths used for CH_3Cl,[12a] CH_2Cl_2,[12b] $CHCl_3$,[12c] and CCl_4[12d] were taken from literature. The calculation was carried out on an electronic computer FACOM 230-60 in Hokkaido University, using a program kindly offered by Dr. M. Tsuda.

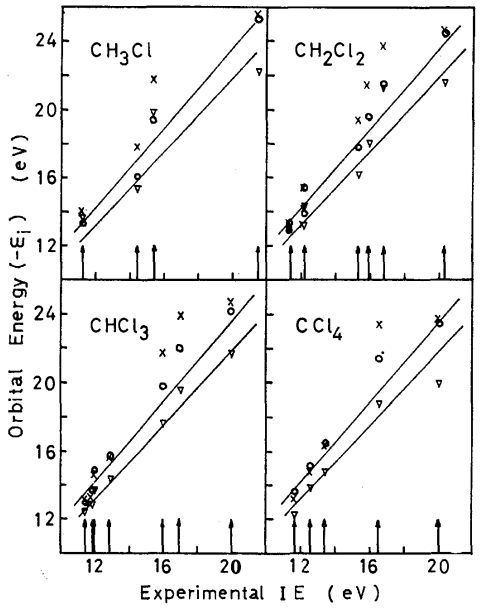

Fig. 1. Plots of the IE's calculated with different sets of parameter values against experimental values. The results obtained with parameter values (3) and (c) are indicated by ○, those of (1) and (a) by X, and those of (2) and (b) by ▽. The positions of experimental IE's are shown with an arrow. Two straight lines with $k=0.85$ (upper) and 0.92 (lower) are shown in each of the chloromethanes.

The IE's calculated with the different sets of parameter values are plotted in Fig. 1 against the corresponding experimental values. Two straight lines with $k=0.85$ and 0.92 are drawn to show a measure for adjusting the theoretical results. It is recognized from theoretical calculations available that the calculated IE's based on Koopmans' theorem are high compared with the experimental ones, so that much better agreement with experiment is obtained if Koopmans' theorem values are empirically reduced by a constant factor[13] or reduced by 4 eV.[14] This was done using a factor of $k=0.85$ or 0.92, as shown in Fig. 1.

Table 1. Comparison of theoretical and experimental results on ionization energies (eV) and orbital assignments

	CNDO/2		Ref. 2 Exptl		Ref. 4
CH_3Cl	11.40 (e)	n(Cl)	11.31 (I_1)	e	e
	13.75 (a_1)	σ(C–Cl)	14.42 (I_2)	a_1	
	16.56 (e)	$\pi(CH_3)$	15.40 (I_3)	e	
	21.59 (a_1)	3s(Cl)	21.5 (I_4)	a_1	
CH_2Cl_2	11.05 (b_1)	n(Cl)	11.40 (I_1,I_2)	b_2,a_2	b_2,b_1
	11.42 (a_1)	n(Cl)			
	11.89 (b_2)	n(Cl)	12.22 (I_3,I_4)	a_1,b_1	a_2,a_1
	13.15 (a_2)	n(Cl)			
	15.22 (b_2)	σ(C–Cl)	15.30 (I_5)	b_2	
	16.74 (a_1)	σ(C–Cl)	15.94 (I_6)	a_1	
	18.37 (b_1)	$\pi(CH_2)$	16.77 (I_7)	b_1	
	20.83 (a_1)	3s(Cl)	20.30 (I_8)	a_1	
$CHCl_3$	11.04 (a_1)	n(Cl)	11.48 (I_1)	a_2	a_2
	11.70 (e′)	n(Cl)	11.91 (I_2)	a_1	e″
	12.71 (a_2)	n(Cl)	12.01 (I_3)	e′	a_1
	13.49 (e″)	n(Cl)	12.85 (I_4)	e″	e′
	16.95 (e′)	σ(C–Cl)	15.99 (I_5)	e′	
	18.80 (a_1)	σ(C–Cl)	16.96 (I_6)	a_1	
	20.55 (a_1)	3s(Cl)	19.80 (I_7)	a_1	
CCl_4	11.63 (t_2)	n(Cl)	11.69 (I_1)	t_1	t_1
	12.93 (t_1)	n(Cl)	12.62 (I_2)	t_2	t_2
	14.11 (e)	n(Cl)	13.44 (I_3)	e	e
	18.27 (t_2)	σ(C–Cl)	16.58 (I_4)	t_2	
	20.10 (a_1)	σ(C–Cl)	20.00 (I_5)	a_1	
	24.39 (t_2)	3s(Cl)			

a) Values of (3) and (c) and a factor of 0.85 for k were used.

The best sets of theoretical results obtained with the values of (3) and (c) are given in Table 1, corresponding to the data indicated by circles in Fig. 1.

Partial and Total sums of Orbital Energies of Halomethanes

In the region below about 17 eV, the PE bands of CH_3X, CH_2X_2, CHX_3, and CX_4 (X=Cl, Br, and I) are considered to be essentially due to ionization of electrons from the localized MO's such as n(X), σ(C–X), $\pi(CH_3)$, and $\pi(CH_2)$. This was supported by the present CNDO/2 calculation for a series of chloromethanes, and in this section we will deal with their IE's from a different standpoint.

If the MO's giving rise to the PE bands in the range 11—17 eV interact very little with inner orbitals such as 2s(C) and ns(X), the total sums of the orbital energies should be almost unchanged considering mutual interactions among the localized MO's. Therefore, we considered that on the basis of Koopmans' theorem the IE's should be interpreted in terms of interactions

11) J. Del Bene and H. H. Jaffé, *J. Chem. Phys.*, **48**, 1807 (1968).
12) a) L. S. Bartell and L. O. Brockway, *ibid.*, **23**, 1860 (1955); b) R. J. Myers and W. D. Gwinn, *ibid.*, **20**, 1420 (1952); c) S. N. Ghosh, R. Trambarulo, and W. Gordy, *ibid.*, **20**, 605 (1952); d) L. S. Bartell, L. O. Brockway, and R. H. Schwendeman, *ibid.*, **23**, 1854 (1955).
13) For instance, see Ref. 7.
14) For instance, see Ref. 5.

TABLE 2. COMPARISON OF CALCULATED AND EXPERIMENTAL SUMS (IN eV)

	Partial sum: e		Partial sum: a_1		Total sum	
	Calcd $[n+\pi]$	Exptl (I_1+I_3)	Calcd $[\sigma]$	Exptl (I_2)	Calcd $[2n+\sigma+2\pi]$	Exptl
CH_3Cl	27.08	27.19[a]	14.42[b]	14.42	68.58	68.80
CH_3Br	26.13	26.18[a]	13.49[b]	13.49	65.75	65.85
CH_3I	25.01	24.93[a]	12.50[b]	12.50	62.52	62.36

	Partial sum: b_1		Partial sum: a_1		Partial sum: a_2		Partial sum: b_2		Total sum	
	Calcd $[n+\pi]$	Exptl (I_1+I_7)	Calcd $[n+\sigma]$	Exptl (I_2+I_6)	Calcd $[n]$	Exptl (I_4)	Calcd $[n+\sigma]$	Exptl (I_3+I_5)	Calcd $[4n+2\sigma+\pi]$	Exptl
CH_2Cl_2	27.08	28.17	27.20	27.34	12.78	12.22	27.20	27.52	94.26	95.25
CH_2Br_2	26.13	26.86	25.32	25.57	11.83	11.28	25.32	25.40	88.60	89.11
CH_2I_2	25.01	24.92	23.21	23.43	10.71	10.56	23.21	22.96	82.14	81.87

	Partial sum: a_1		Partial sum: e′		Partial sum: a_2		Partial sum: e″		Total sum	
	Calcd $[n+\sigma]$	Exptl (I_1+I_6)	Calcd $[n+\sigma]$	Exptl (I_2+I_5)	Calcd $[n]$	Exptl (I_3)	Calcd $[n]$	Exptl (I_4)	Calcd $[6n+3\sigma]$	Exptl
$CHCl_3$	27.20	28.44	27.20	27.90	12.78	12.01	12.78	12.85	119.94	121.95
$CHBr_3$	25.32	26.28	25.32	25.59	11.83	11.28	11.83	11.80	111.45	112.34
CHI_3	23.21	23.75	23.21	22.65	10.71	10.29	10.71	10.50	101.76	100.34

	Partial sum: t_2		Partial sum: t_1		Partial sum: e		Total sum	
	Calcd $[n+\sigma]$	Exptl (I_1+I_4)	Calcd $[n]$	Exptl (I_2)	Calcd $[n]$	Exptl (I_3)	Calcd $[8n+3\sigma]$	Exptl
CCl_4	27.20	28.27	12.78	12.62	12.78	13.44	145.50	149.55
CBr_4	25.32	25.69	11.83	11.17	11.83	12.17	135.11	134.92

a) Values in Ref. 3 were used, numerical values for the Jahn-Teller splittings of the third bands not being reported in Ref. 2.
b) Taken from experimental I_2 values (see also Table 3).

TABLE 3. EMPIRICAL ORBITAL ENERGIES USED FOR THE LOCALIZED MO'S (IN eV), THE NEGATIVE SIGN BEING OMITTED

n(X)[a]:	12.78 (Cl), 11.83_5 (Br), 10.71_5 (I)
σ(C–X)[b]:	14.42 (Cl), 13.49 (Br), 12.50 (I)
$\pi(CH_3)$[c]:	14.3
$\pi(CH_2)$[d]:	14.3

a) Taken from the mean positions of the first PE bands of HX (Ref. 17).
b) Taken from the second IE's of CH_3X (Ref. 2).
c) Obtained from Eq. (1).
d) Assumed to be equal to the value for $\pi(CH_3)$.

among several localized MO's in unperturbed states.

Calculations of the theoretical partial sums are given in Table 2. They were carried out on the basis of the present CNDO/2 assignments by using the formulas given in brackets in which letters n, π, and σ denote parameter values. The parameter values are given in Table 3. Since electrons in the nonbonding orbital of HX and those in the σ(C–X) bonding orbitals of CH_3X are essentially in unperturbed states, the first photoelectron band of HX and the second band of CH_3X are considered to give good standards as unperturbed-state orbital energies. For $\pi(CH_3)$ the orbital energy in its unperturbed state can be estimated by simply considering that the first and third bands of CH_3X arise from the interaction of the $\pi(CH_3)$ and n(X) orbitals. Taking the centers of the Jahn-Teller splittings for the third IE's of CH_3X, we obtained an average value of -14.3 eV for the orbital energy of $n(CH_3)$ from the relation

$$\{-I_1(HX)\}_{av} + \varepsilon^0\{\pi(CH_3)\} = \{-I_1(CH_3X)\}_{av} + \{-I_3(CH_3X)\}_{av} \quad (1)$$

using available IE values. (I_1 values for HX were taken from Ref. 2, and I_1 and I_3 for CH_3X from Ref. 3 since the Jahn-Teller splittings are reported in Ref. 3).

The experimental partial sums (Table 2) were obtained by taking sums over the appropriate I_i's shown in parentheses also on the basis of the CNDO/2 assignments.

The partial sums are taken over the IE's in each symmetry species and the total sums are taken over all under consideration.

In calculating the partial and total sums for bromomethanes and iodomethanes, orbital orderings were assumed to be the same as those of chloromethanes.

Discussion

CNDO/2 Results. From the present calculation it was found that the resulting MO orders are almost independent of the different sets of parameter values with a few exceptions. The best set of calculated IE's is generally in good agreement with the corresponding experimental values (Table 1).

The PE spectrum of CH_3Cl has been reported by several workers,[1-3] the outer electronic structure being interpreted in terms of the orbital structure of $(e)^4(a_1)^2(e)^4$ which was earlier predicted by Mulliken.[15] Our result supports his assignment. Potts *et al.*[2] have observed a PE band at 21.5 eV and ascribed this to a_1(2s, C). However, we found the 21.5 eV band to be ascribed to a_1(3s, Cl) rather than a_1(2s, C). From the resulting wavefunctions it was found that 3pπ(Cl) orbital contributes to the highest occupied MO by 68% with mixing of the $\pi(CH_3)$ orbital, and that the contributions of 3pσ(Cl) and 2p(C) orbitals to the second inner MO are 43 and 46%, respectively. This indicates that the second MO of CH_3Cl is essentially due to σ(C–Cl) bonding.

For CH_2Cl_2, the electronic structure of $(a_2)^2(b_2)^2(a_1)^2(b_1)^2$ was derived for the chlorine nonbonding orbitals (Table 1). The PE spectrum of this compound in the 11—13 eV region consists of two sharp bands (11.40 and 12.22 eV) with nearly equal areas.[2] The spectral appearance indicates that these bands correspond to accidentally degenerate orbitals (in CH_2Br_2 and CH_2I_2 the nonbonding bands have been observed separately[1,2]). The a_2 orbital is strictly nonbonding, being located at the fourth. The order of the nonbonding orbitals obtained here partly differs from that assigned by Potts *et al.*[2] and Dixon *et al.*,[4] while in the inner orbitals the CNDO/2 assignments are in agreement with those proposed by Potts *et al.*[2] However, it is recognized that from a CNDO/2 calculation it is difficult to determine the order of two levels close to each other within about 0.5 eV. It is considered from a symmetry consideration of orbitals that the order of n(a_1) and n(b_2) in CH_2Cl_2 might be reverse and consequentely the assignment by Dixon *et al.*[4] is better.

The nonbonding orbital structure of $CHCl_3$ is expressed by $(e'')^4(a_2)^2(e')^4(a_1)^2$. This orbital assignment differs partly from that reported by other workers.[1,2,4] In CCl_4 the present calculation indicates $(e)^4(t_1)^6(t_2)^6$ for the nonbonding orbital structure, the order of the t_1 and t_2 orbitals being opposite to that reported,[2] and in disagreement with the prediction deduced from the consideration of spin-orbit splittings.[4]

When the parameter values of Santry[10b] are used for Cl, some minor changes occur in the orbital ordering; opposite orders are obtained between the b_1 and b_2 orbitals ascribed to the nonbonding orbitals of CH_2Cl_2 and also between the e′ and a_1 orbitals ascribed to the nonbonding orbitals of $CHCl_3$. It should be mentioned that the resulting MO orderings of the halomethanes depend on the selection of parameter values for Cl atom [(a) and (b)], but independent of those for C and H atoms [(1)—(3)]. The values of (3) and (c) are considerably close to those of (1) and (a) respectively, so that no different orderings occur. In the present work, (3) and (c) were used only for modifying the resulting IE values, giving the better results. From the shape of the spectrum of $CHCl_3$, it is reasonable to consider that the degenerate orbitals are ascribed to the second band rather than the first band. Thus we conclude that, as far as Cl parameter values are concerned, those proposed by Santry and Segal[10a] give better results than those used later by Santry.[10b]

Using the parameter values of (3) and (c), we also calculated total charge densities on the C, H, and Cl atoms of the chloromethanes, and obtained the following values: 4.08 (C), 0.95 (H), and 7.04 (Cl) for CH_3Cl; 3.70 (C), 1.04 (H), and 7.10 (Cl) for CH_2Cl_2; 3.45 (C), 1.11 (H), and 7.14 (Cl) for $CHCl_3$; 3.31 (C) and 7.17 (Cl) for CCl_4.

Partial and Total Orbital-Energy Sums. Good agreements were generally obtained for the total sums in all the halomethanes studied, indicating that the selection of the empirical orbital energies (Table 2) is appropriate. The total sum is independent of orbital assignment in the case of CH_2X_2, whereas in the molecules with the degenerate orbitals it depends on their orbital ordering. The partial sums of course depend always on orbital assignments. We tested various possible assignments and found that the CNDO/2 assignments given in Table 1 are also the best in terms of standard deviations calculated over all the partial sums for each series of CH_2X_2, CHX_3, and CX_4 (where X is Cl, Br, and I) except CI_4 whose PE data are not available.

In calculating the experimental partial sums with an appropriate combination of I_i, in addition to a numerical comparison of experimental and theoretical partial sums the magnitudes of interaction should be also taken into consideration. If there are two nondegenerate localized MO's interacting with each other, the interaction should shift the upper level upwards and the lower level downwards. In CH_2Cl_2, the n and σ levels belonging to a_1 interact with each other to give I_2 (11.40 eV) and I_6 (15.94 eV), causing shifts of 1.38 and 1.52 eV. The n and σ levels belonging to b_2 interact to give I_3 (12.22 eV) and I_6 (15.30 eV), causing shifts of 0.56 and 0.88 eV. Thus, it should be pointed out that the shifts as well as the parameter values we used for n and σ are appropriate. Rigorously speaking, n (or σ) levels in polyhalomethanes should split to some extent to give different orbital energies in different symmetry species because of mutual interactions among equivalent n (or σ). However, there are no remarkable discrepancies between calculated and experimental partial sums when no interactions are considered (Table 2).

If n (or σ) orbitals are split to a large extent by their linear combinations according to orbital symmetry, no good agreement can be obtained between the calculated and experimental partial sums. Taking partial sums over MO's, for instance, in a_1+b_2 and b_1+a_2 in CH_2X_2, better results should be obtained than those in a_1, a_2, b_1, and b_2 separately, where nonbonding

15) R. S. Mulliken, *Phys. Rev.*, **47**, 413 (1935).

orbitals belonging to a_1 and b_2 are symmetric and those belonging to b_1 and a_2 are antisymmetric with respect to the CCl_2 plane. Similar situations also occur in CHX_3 and CX_4. Taking a lower symmetry than the original molecular symmetry, such mutual interactions among n (or σ) can be cancelled in partial sums.

It is interesting to note that the a_2 orbital of CH_2X_2, the a_2 and e'' orbitals of CHX_3, and the t_1 and e orbitals of CX_4 are strictly nonbonding and that the corresponding IE's are in agreement with the n(X) parameter values within about 0.8 eV.

It seems reasonable that the a_2 orbital is completely nonbonding so that its IE is higher than those of other nonbonding orbitals interacting with the σ and π orbitals. The same situation occurs also in CHX_3 and CX_4, *viz.*, the a_2 and e'' orbitals in CHX_3 and the t_1 and e orbitals in CX_4 are lower than other nonbonding orbitals which interact with the σ and π orbitals. The present CNDO/2 calculation supports this view.

It should be mentioned that the sums of the experimental orbital energies can be interpreted in terms of simple model in which only a few localized MO's are taken into account for each of the halomethanes.

Potts *et al.*[2] have also reported PE data for BCl_3, BBr_3, BI_3 as well as their orbital assignments. Applying the sum rule to these compounds, we obtained values of about −125, −115, and −102 eV, respectively, for total sums, considerably close to the total sums obtained for $CHCl_3$, $CHBr_3$, and CHI_3 (−122, −112, and −100 eV, respectively). This indicates that the orbital energy of σ(B–X) is very close to that of σ(C–X) for each halogen.

Finally, let us consider total sums for fluoromethanes. Adopting the assignments proposed by Potts *et al.*,[2] the total experimental sums of CH_3F, CH_2F_2, CHF_3, and CF_4 are −60.72, −78.52, −93.60, and −128.40 eV, respectively,[16] while the corresponding calculated total sums are −60.20, −78.49, −96.46, and −138.10 eV, omitting the σ(C–F) orbital and using an empirical value of −16.05 eV for the nonbonding F orbital which is deduced from the first IE of HF[17] by use of Koopmans' theorem. Thus agreement between the experimental and calculated sums is surprisingly good except for CF_4, where a discrepancy of about 10 eV cannot easily be explained.

Although no unambiguous assignment can be concluded, the sum rule should be very helpful for spectral assignments, especially for analyzing an overlapping band.

16) We used the following values taken from the data of Potts *et al.* (see Ref. 2). CH_3F: 13.04(e), 17.06(e); CH_2F_2: 13.29, 15.25, 15.40, 15.58, 18.97; CHF_3: 14.80, 15.50, 16.16(e), 17.25(e); CF_4: 16.23(t), 17.47(t), 18.50(e).

17) H. J. Lempka, T. R. Passmore, and W. C. Price, *Proc. Roy. Soc.*, *A*, **304**,53 (1968).

BULLETIN OF THE CHEMICAL SOCIETY OF JAPAN, VOL. 46, 1346—1353 (1973)

Chemical Approach to the Radiolysis of Polyphosphate Glass. I. Effects of Sb(III, V), Mo(V, VI) and U(IV, VI) Ions

Yoshimitsu KOBAYASHI and Niro MATSUURA

Department of Pure and Applied Sciences, College of General Education, University of Tokyo, Komaba, Meguro-ku, Tokyo

(Received September 16, 1972)

The yields of radiation-induced electrons and holes trapped in the glass matrix are easily determined by introducing metal ions, such as Sb, Mo, and U ions, into water-soluble $NaPO_3$ polymer glass. Doping 1 mol % of these ions of a lower oxidation state wholly prevents the trapping of holes and results in oxidation to their higher oxidation states. A reaction in the reverse direction also occurs for the same ions of a higher oxidation state, which are converted into a lower one by reduction. This radiation-induced redox reaction has a minimum yield at a dopant composition corresponding to Sb_2O_4 for Sb(III)–Sb(V), Mo_6O_{17} for Mo(V)–Mo(VI), and U_3O_8 for U(IV)–U(VI) redox couples. The largest effective volume among these ions for capturing the holes is for Sb(III). In a high-dose region (10^{20} to 10^{21} eV/g), the yields of the redox products of these ions increase logarithmically with the γ-dose absorbed. This makes it difficult to determine the G-value of the redox products precisely. The approximate values are in an order of magnitude of 0.1 atom per 100 eV absorbed.

The radiation-induced rupture of a chemical bond in a solid polyphosphate glass causes paramagnetic or color centers. The results of a number of authors[1–8] are in agreement with a model which assigns the radia-

1) A. Barkatt, M. Ottolengli, and J. Rabani, *J. Phys. Chem.*, **76**, 203 (1972).
2) A. Treinin; "Radical Ions" Ed. by E. T. Kaiser and L. Kevsn, Interscience Pub. N. Y. (1968), p. 525.
3) T. Feldman, A. Treinin, and V. Voltera; *J. Chem. Phys.*, **42**, 3366 (1965), *ibid.*, **47**, 2754 (1967).
4) Sakka, *Bull. Inst. Chem. Res. Kyoto Univ.*, **48**, 53 (1970).
5) J. C. Stroud, *J. Chem. Phys.*, **43**, 2442 (1965); *ibid.*, **37**, 836 (1962).
6) Y. Nakai, This Bulletin, **38**, 1308 (1965).
7) M. C. R. Symons, S. Subramanian, and H. W. Wardale, *J. Chem. Soc., A*, **1970**, 1239; *ibid.*, 1988 (1970).
8) M. Miura and A. Hasegawa, This Bulletin, **40**, 2553 (1967); *ibid.*, **39**, 1432 (1966).

tion-induced visible colors to holes (electron-deficient centers), each trapped in a network forming a P–O tetrahedron with one or more non-bridging oxygen atoms present in a polyphosphate chain.[2] It is interesting to study from the chemical point of view the nature of these color centers by means of additives introduced into the glass as scavengers of the reactive species produced by radiation.[3–6] A systematic survey was undertaken to find the most adequate additive for estimating the quantitative yields of primary species, holes and electrons. Sodium polyphosphate is a water-soluble glass which is suitable for chemical treatment after exposure to γ-rays.

The change in the optical absorption in irradiated glass was compared with the products in aqueous solution of irradiated glass. Among the dozen additives so far investigated, this paper will treat the redox couples, Mo(V)–Mo(VI), Sb(III)–Sb(V), and U(IV)–U(VI), preferably employed as additives because their visible absorption spectra are separated from the optical absorptions due to holes.

Experimental

Preparation of the Glass. The base glass was prepared by the dehydration of $NaH_2PO_4 \cdot 2H_2O$ to which appropriate amounts of metal oxide, less than 1 mol %, had been admixed. The fusion was carried out in a platinum crucible, principally at 800 °C for 3 hr in air, in order to prepare the Sb(III), Mo(VI), and U(VI) doped glasses. For preparing the U(VI) doped glass, $UO_2(CH_3CO_2)_2 \cdot 2H_2O$ was employed in place of its oxide.[9] The U(IV) and Mo(V) enriched glasses should be melted in the presence of reducing agents under a reducing atmosphere or under vacuum of 10^{-6} Torr. The reducing atmosphere is effected by the use of a graphite crucible surrounded with a pile of graphite rods in an electric furnace or a quartz vessel placed in a vacuum line for vacuum melting.

Optical Measurements. The molten glass was poured into a brass mold with a rectangular form 8.3 mm thick, or it was chilled between two brass plates 2 mm apart. In order to eliminate the difference in the sample thickness and the scattering condition of the sample surface, a small correction was made by the normalization of background absorptions at about 700 nm. The spectra were taken and registered for optical absorption with an EPS-2 Model Hitachi Spectrophotometer, and for ESR spectra, with Japan Electron Optics Lab's JES-2BX model at a microwave frequency of 9400 Mc/s operating with 100 Kc/s field modulation. The molar extinction coefficient was determined by chemical analysis for Mo(V) as $\varepsilon = 17\ M^{-1}\ cm^{-1}$ and for U(IV) as $\varepsilon = 32.1\ M^{-1}\ cm^{-1}$.

Irradiation. The sample was irradiated with a Co^{60} γ-ray source of 3.8×10^{18} eV/g·hr 10 cm from the center in the Institute for Solid State Physics, the University of Tokyo. For the highdose irradiation a Co^{60} source of 1.8×10^{19} eV/g·hr was occasionally used. The irradiations and measurements were performed at room temperature, and the γ-dose calibration was carried out with a Fricke dosimeter, assuming that $G(Fe^{3+}) = 15.5$[10] and that the electron density per unit mass was identical between the glass and Fricke's solution.

Chemical Analysis. The chemical analysis of antimony was made by colorimetry with Folin's reagent for Sb(III) and with Rhodamine B as the reagent for Sb(V).[11] Antimony-doped samples were dissolved in dilute hydrochloric acid (2:1) to prevent the hydrolysis of $HSbCl_6$ to an irreversiblly-aquated form of $HSb(OH)_nCl_{6-n}$.[12,13] Reproducible resulsts were obtained when the dissolution of irradiated samples in hydrochloric acid was effected under the same conditions for a series of runs. The potentiometric titration of Mo(V) with 0.05N $K_2Cr_2O_7$[14] was made after dissolving the irradiated glass in 2N HCl over a water bath for 0.5 hr in order to ensure the decomposition of the polymer phosphate into the monomer. For U(IV), irradiated samples were dissolved in a 5% sulfuric acid solution by bubbling nitrogen gas through the solution to prevent the oxidation of U(IV) to U(VI) due to air oxygen[15] and by keeping the sample solution at about 80 °C during the dissolution in order to effect the complete hydrolysis of polyphosphate. The titration was effected by the addition of excess amounts of a $FeCl_3$ solution by the use of diphenylamine as an indicator. For the titration of the total uranium content, a 5% sulfuric acid solution of the sample glass was passed through a Jone's reductor, after which the resultant U(IV) solution was titrated in the same way.[16]

Results and Discussion

Sb Doped Glass, Effect of Antimony Ions. Upon the γ-irradiation of the polyphosphate glass, an optical absorption due to trapped holes appears with a maxi-

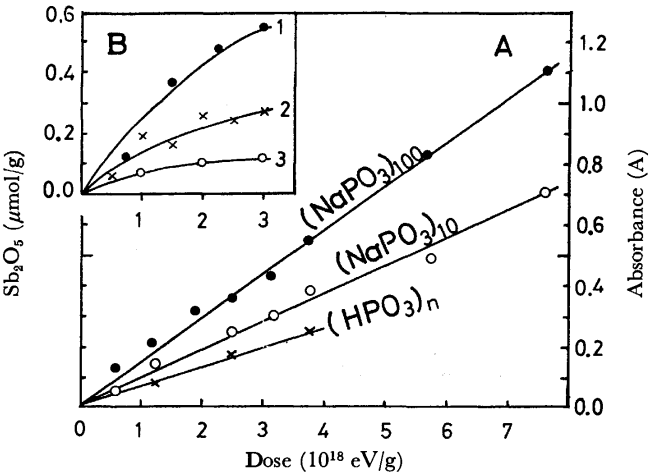

Fig. 1. A: Optical absorption at 510 nm of γ-irradiated polyphosphate glass with optical path 8.3 mm.
B: Yields of antimony (V) oxide, in μmol/gram of $NaPO_3$, from antimony (III) oxide doped glass under γ-ray irradiation. 1: 0.5 mol % of Sb_2O_3 doped, 2: 0.25 mol% of Sb_2O_3 doped and 3: 0.125 mol% of Sb_2O_3 doped. Abscissa the same scale of unit with A.

9) M. Mano and S. Ohashi, This Bulletin, **42**, 3616 (1969).; *ibid.*, **43**, 84 (1970).

10) M. Haissinsky, "La Chimie Nucleaire et ses Applications," Masson, Paris (1957), p.333, N. Miller in "Actions Chimiques et Biologiques des Radiations," Vol. 2, Masson, Paris (1956), p.149.

11) N. Matsuura and M. Kojima, *Japan Analyst*, **6**, 155, 205 (1957).

12) H. M. Neumann, *J. Amer. Chem. Soc.*, **76**, 2611 (1954); C. H. Cheek and H. M. Neumann, *Anal. Chem.*, **27**, 1683 (1955).

13) N. A. Bonner, *J. Amer. Chem. Soc.*, **71**, 3909 (1949).

14) C. E. Cruthamel and C. E. Johnson, *Anal. Chem.*, **26**, 1284 (1954).

15) J. Halpern and J. G. Smith, *Can. J. Chem.*, **34**, 1419 (1956).

16) I. M. Kolthoff and J. J. Lingane, *J. Amer. Chem. Soc.*, **55**, 1871 (1933).

mum peak at 510 nm. Figure 1A shows that the increase in absorbance is proportional to the γ-dose absorbed. The glasses with a mean chain length of phosphate smaller than that of Graham salt have smaller absorptions, and the polyphosphate glass of a chain less than 10 is no more transparent.[17] For Graham salt, with an average chain length of 50 to 100, the optical absorption induced by irradiation is approximately the same, irrespective of the condition used in preparing the sample glass. When the exposure is prolonged beyond a certain limit, 10^{19} eV/g, the change in absorption is no longer linear with the dose, but increases much more slowly.

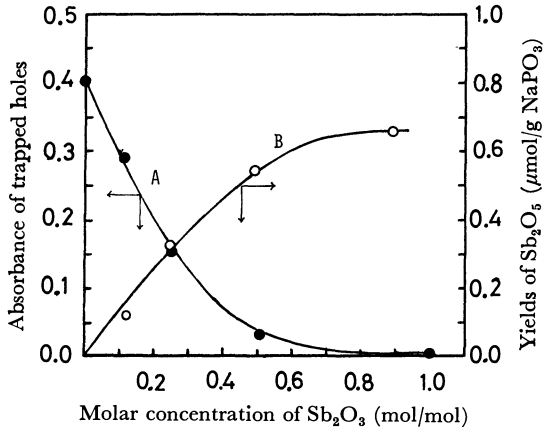

Fig. 2. A: Optical absorbancy at 510 nm due to trapped holes in $NaPO_3$ glass as function of doped Sb_2O_3 molar concentration (Sb_2O_3 mol/$NaPO_3$ mol)
B: Yields of Sb_2O_5 in μmol/g $NaPO_3$ from Sb_2O_3 doped in $NaPO_3$ glass after γ-irradiation of 3×10^{19} eV/g with variation of doped Sb_2O_3 concentration (Sb_2O_3 mol/$NaPO_3$ mol)

Antimony oxide, if one mole % is doped as Sb_2O_3 into polyphosphate glass, entirely suppresses the appearance of the red color due to holes. Pentavalent antimony oxide, Sb_2O_5, is ineffective unless a greater part of the antimony(V) is converted into antimony-(III) by thermal decomposition during the melting of a glass at a temperature higher than 650 °C. The optical absorption at 510 nm decreases exponentially with respect to the concentration of Sb(III). The exponential curve shown in Fig. 2 makes it possible to calculate the effective capture volume of Sb(III) as a hole-formation inhibitor using Stroud's Eq. (1).[5]

$$D_{h^+} = D^{\circ}_{h^+} \cdot \exp(-v \cdot C) \qquad (1)$$

In Eq. (1), D_{h^+} and $D^{\circ}_{h^+}$ are the optical absorbances of the hole in the presence and in the absence of the Sb(III) inhibitor, C, the concentration of Sb(III), and v, the effective volume of the inhibitor against hole formation by radiation. The concentration of Sb_2O_3, C for $D_{h^+}/D^{\circ}_{h^+}=1/e$, is found from Fig. 2 to be 0.125 mol % per one formula weight of $NaPO_3$. The effective capture volume, v, is calculated as 3.8×10^5 Å^3, which is a hundred times as large as the volume occupied by the Sb_2O_3 molecule in the form of Valentinite.[18]

Redox Yields of Sb in Glass. The initial G-values determined for 3×10^{18} eV/g or less are surprisingly large both with respect to the oxidation of Sb(III) to Sb(V) for Sb_2O_3 doped glass and with respect to the reduction of Sb(V) to Sb(III) for Sb_2O_5 doped glass. The curves represented in Figs. 1B and 2B demonstrate an extraordinary high yield of Sb(V), which attains, in the G-value, some ten molecules of Sb_2O_5 per 100 eV of γ-energy absorption. Such a G-value can not be expected from the mechanism of a radiation-induced redox reaction in a solid currently accepted in radiation chemistry.[19] However, in a higher dose region the G-values of Sb(V) formation in Sb(III) doped glass are greatly reduced to an ordinary value of around 0.1. The yields of Sb(III) from Sb(V) in irradiated glass are much more pronounced, attaining a G-value of several hundred in the low-dose region. The Sb(V) content of 1 mol% Sb_2O_5 doped glass prepared at 650 °C for 3 hr showed 90 μmol of Sb_2O_5 per gram of $NaPO_3$ glass before irradiation. This was decreased to 70 μmol/g after irradiation at a dose of 3×10^{18} eV/g. The data obtained are very few and not reliable enough for us to predict the mechanism of the radiation-induced reduction of Sb(V) to Sb(III), because the background content of Sb(III), increased upon thermal treatment before irradiation, surpasses the amount produced by radiation.

Since several oxides, such as Sb_6O_{13} and Sb_2O_4, are known[20] as stable phases in a pure antimony oxide system at a temperature between 650 and 900 °C, these species must be considered in addition to Sb(III) and Sb(V) oxides as major components in a molten glass. Accordingly, the chemical analysis of Sb(III) and Sb(V) was undertaken to see if there was a difference in the average oxidation state of antimony between pure oxide and the same oxide in glass. Figure 3 compares the Sb(III) content in Sb_2O_5 oxide with the same oxide doped into glass be thermal treatment at a temperature from 650 to 800 °C. About a half of the antimony is converted from Sb(V) to Sb(III) for pure oxide in this range of temperature, while the

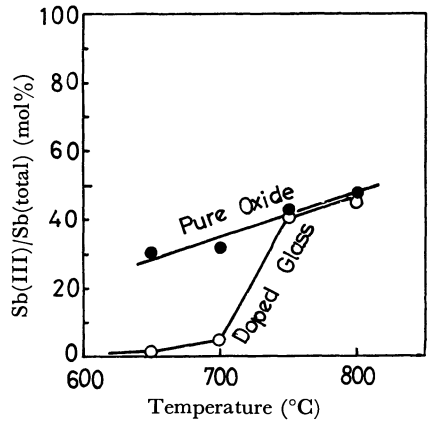

Fig. 3. Variation of Sb(III) content by thermal decomposition in the Sb_2O_5 as pure oxide and the Sb_2O_5 doped in $NaPO_3$ glass in a temperature range 650 to 800 °C.

17) N. Matsuura, T. K. Lin, and Y. Kobayashi, This Bulletin, **43**, 2850 (1970).
18) N. A. Antropov, V. P. Barzakovskii, I. A. Bondari, and U. P. Udalov; "Phase Diagrams of Silicate System" A. N. (1970), p. 203.
19) E. R. Johnson; "Radiation Induced Decomposition of Inorganic Molecular Ions", Gordon & Breach, N. Y. (1970), p. 23.
20) D. I. Stewart, *Can. J. Chem.*, **50**, 690 (1972).

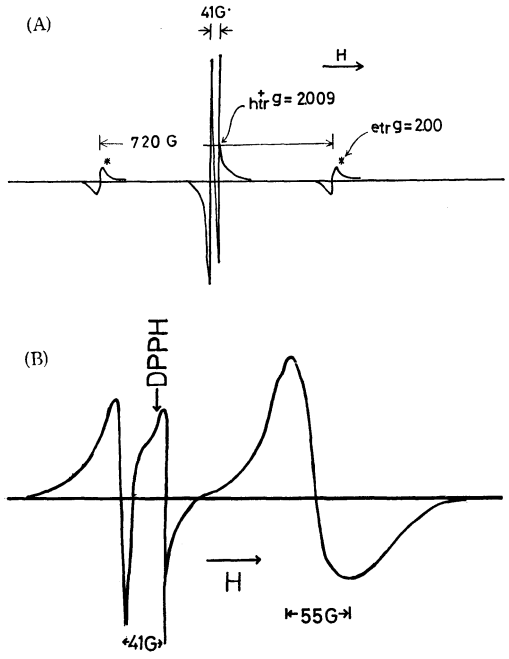

Fig. 6. ESR spectra of γ-irradiated polyphosphate glass. (A) non-doped glass with holes h_{tr} and electrons e^-_{tr}* (identified as PO_3^{2-})[7] (B) Mo(VI)O_3 doped glass with holes h^+_{tr} (right hand doublet) and Mo(V) signal (g=1.917)

the molecular extinction coefficient was determined, by using a sample 8 mm thick between two opposed flat surfaces, to be $\varepsilon=17\ M^{-1}\ cm^{-1}$. The latter spectrum is illustrated in Fig. 5. Figure 6 shows the ESR spectrum of the Mo(V)-containing glass; there is a broad singlet of g=1.917, with 55 Gauss peak-to-peak width which is attributable to the Mo(V) in the glass.[23-25]

Under γ-irradiation, the Mo(VI)-rich glass is red in color and the optical absorption at 510 nm increases with an increase in the absorbed γ-doses. On the contrary, Mo(V)-rich glass, colored bluish-green before irradiation, loses its original color by absorbing radiation energy, but shows no intensity change in the optical absorption at 510 nm due to trapped holes. In Mo(VI)-rich glass, ESR signals of the hole doublet and the Mo(V) singlet appear after irradiation, as is shown in Fig. 6; these two signal intensities grow as the absorbed radiation dose increases. The singlet due to Mo(V) continues to increase after the hole doublet attains saturation. In Mo(V)-enriched glass, no hole signal could be detected up to a sufficiently large γ-dose of 1.5×10^{22} eV/g. Accordingly, dopant molybdenum in the polyphosphate glass is effective for trapping both holes and electrons produced by γ-radiations through Processes (2) and (3):

$$\text{Mo(V)} + h_m = \text{Mo(VI)} \quad (2)$$

$$\text{Mo(VI)} + e_m = \text{Mo(V)} \quad (3)$$

In Eqs. (2) and (3), h_m and e_m are the mobile holes and electrons. Besides the processes postulated by (2) and (3), there must be several other reactions, involving trapping by the glass matrix and the recombination of holes and electrons through a certain recombination center. However, there is no means of detecting the recombination yields or of distinguishing the trapped holes and electrons in the glass matrix from those obtained in the presence of molybdenum.

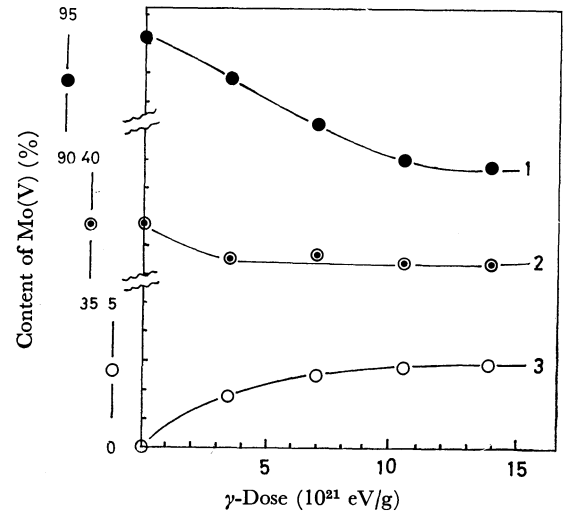

Fig. 7. Variation of Mo(V) content by radiation-effect in polyphosphate glass with total Mo 1 atom % per phosphorus. ●: Mo(V) rich glass (94% Mo^v), ⊙: glass with medium content of Mo(V) (37% Mo^v), ○: Mo(VI) rich glass (Mo^v trace)

Quantitative Estimation of the Dose Effect. The Mo(V) formation through Reaction (3) and the loss of Mo(V) through (2) in the irradiated glass were determined by studying the intensity changes in the optical absorption; the results are shown in Fig. 7. Curve 1 is for Mo(V)-rich glass; its optical density decreases in proportion to the absorbed γ-doses up to the dose of about 1.0×10^{22} eV/g. Beyond this limit, no further decrease of Mo(V) was observed. At the maximum dose of 1.5×10^{22} eV/g, four percent of doped Mo(V) was converted into Mo(VI); the G value calculated from the linear part of the curve is 0.11. Curve 3 is Mo(VI)-rich glass containing no detectable Mo(V), but exhibiting the green color of Mo(V) after irradiation. The radiation-induced formation of Mo-(V) from Mo(VI) is less than 0.03 mol% even at 1.5×10^{22} eV/g. Curve 2 is the intermediate case for the irradiated glass which contains comparative amounts of Mo(V) and Mo(VI). The curve shows little optical absorption change except for that in the very small dose region. Consequently, there must be a stationary condition of redox reaction between Mo(V) and Mo-(VI) at a Mo(V)/Mo(VI) ratio in the proximity of 1 to 2, if one mol % of Mo is present in the glass.

The trapping of holes and the conversion of Mo(VI) to Mo(V) through Reaction (3) are parallel reactions; the rates of the two processes can be followed by measuring the relative intensities of ESR signals for the hole doublet and the Mo(V) singlet. Figure 6B shows the use of these two ESR signals for estimating the relative concentration of trapped holes and Mo(V) in γ-irradiated glass. The observed ratio of trapped

23) K. S. Sechacli and L. Petrakis, *J. Phys. Chem.*, **74**, 4102 (1970).
24) P. R. Edwards and S. Subramanian, and M. C. R. Symons, *Chem. Commun.*, **1968**, 799.
25) R. D. Dowsing and J. F. Gibson, *J. Chem. Soc., A*, **1967**, 655.

Table 1. Trapped holes to Mo(V) concentration ratio, $[h_t^+]/[Mo(V)]$, measured by ESR absorption intensities in γ-irradiated Mo (1 atom %) doped glass

Mo(V) concentration [Mo(V)]/[Mo(total)] %	γ-Dose (10 eV/g) 3.6	7.2	10.8	14.5
Mo(V) enriched (94%)	0	0	0	0
Medium Mo(V) (35—40%)	0.64	1.27	1.11	1.45
Mo(V) poor (Mo(V) absent)	19.3	19.1	19.2	19.3

holes to produced Mo(V), $[h^+]/[Mo(V)]$, is represented in Table 1. For Mo(VI)-rich glass, this ratio is 19.3, independent of the absorbed dose, while the glass containing comparative amounts of Mo(V) and Mo-(VI), but slightly higher in Mo(VI), shows a $[h^+]/[Mo(V)]$ ratio 30 times lower. There is no trapped hole formation in Mo-doped glass if most of the Mo is present in the Mo(V) state. On the basis of these observations it is clear that the trapping of either holes or electrons, and also the transmutation of states from Mo(VI) to Mo(V) and in the reverse direction through Paths (3) and (2) respectively, depend on the Mo(VI)/Mo(V) ratio and on the total content of Mo in the irradiated glass.

Thermal Annealing. By the application of the usual temperature-elevating device of ESR attachment, an attempt was made to study the stability of holes and Mo(V) radicals.[26] There are two ESR signals attributable to the trapped holes and the Mo(V). Upon heating at 200 °C for 15 min the doublet signal due to holes disappears at once. By this thermal treatment the radiation-induced red color of the glass is lost, leaving a faint yellow color behind. Isothermal annealing were made at two fixed temperatures, 110 and 147 °C, by recording the changes in the peak height of the ESR signals every minute. As these isothermal curves are exponential, logarithmic plots of the signal intensity are illustrated in Fig. 8; these plots demonstrate the rapid decay of hole signals along with the invariant intensities of the Mo(V) singlet. Annealing at two temperatures allows us to estimate roughly the activation energy of hole decay. If thermal annealing can be explained only in terms of a recombination of holes with electrons, the decay of trapped holes obeys a bimolecular mechanism, but there is no experimental evidence to prove emission due to recombination during thermal treatment. By means of unimolecular mechanism the activation energy which reflects the average energy required for the escaping of trapped holes from a certain trap depth present in the irradiated polyphophate matrix can be estimated. From the curves in Fig. 8, the value is found to be 0.37 eV. As for the high stability of the Mo(V) produced by irradiation, it can be understood by taking account of the special stability of molybdenum blue oxide, Mo_nO_{3n-1}, as a polymer form which might be present in polyphosphate glass.

26) C. Bettinali and P. Granati, *Z. Phys. Chem. N. F.*, **70**, 24 (1970).

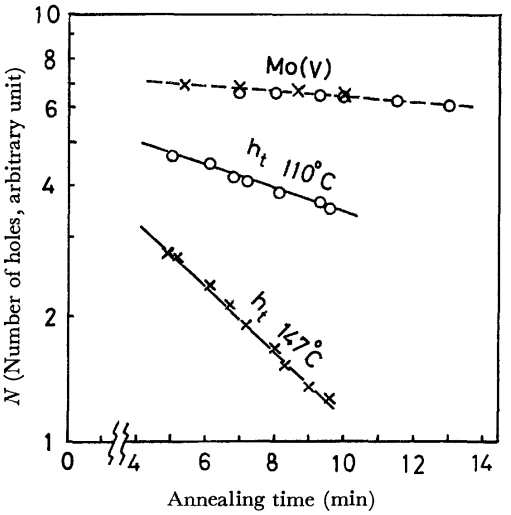

Fig. 8. Isothermal annealing curves of irradiated glass containing Mo(V) by logarithumic plots of the intensity of ESR signal at 110° C and 147 °C

U-Doped Glass, Effect of Uranium. The absorption spectrum of U_3O_8-doped glass before γ-irradiation is shown in Fig. 9. By the chemical analysis of this glass, containing 1.0 atom percent of uranium per phosphorus, the content of U(IV) was found to be 32.4% of the total uranium, while the rest of uranium was U(VI). The UO_3-doped glass prepared by dehydrating a mixture of NaH_2PO_4 and $UO_2(CH_3CO_2)_2$ and by subsequent melting in open air is yellow in color and has no detectable U(IV). The broken curve in Fig. 9 shows a visible absorption due to U(VI) alone observed in the UO_3-doped glass, with a maximum located at 423 nm. By heating uranylacetate in a vacuum at from 800 to 900 °C for a hundred hours, a grey-black oxide was obtained; its U(IV) content was as large as 59% and it had the approximate composition of $UO_{2.4}$. The glass doped with 1 mol% of this oxide is green and has several visible absorption peaks, at 1120, 662, 545, 483, and 423 nm. The last one, 423 nm, may be ascribed to U(VI) and remains little affected by the variation in the U(IV) content in the glass. Table 2 compares the optical absorption at these peaks and the contents of U(IV) measured by chemical analysis[16] in three types of glass samples, with UO_3, U_3O_8, and UO_{2+x} as dopants. The molecular extinction was 32.1 M^{-1} cm^{-1} for U(IV), as determined by the maximum peak at 1120 nm.

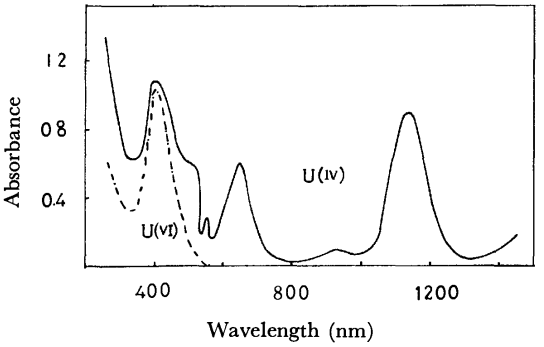

Fig. 9. Optical absorption spectra of U(IV) (full line) and U(VI) (broken line) in polyphosphate glass.

TABLE 2. OPTICAL ABSORPTION AT MAXIMUM PEAKS FOR URANIUM DOPED GLASSES (TOTAL URANIUM CONTENT 1 ATOM % TO P in $NaPO_3$ GLASS)

[U(IV)]/[U(total)] %		Doped oxide UO_{2+x} 55%	U_3O_8 27%	UO_3 0.0
Wavelength λ(nm)	423	0.18 (0.13)[a]	0.21 (0.18)[a]	0.26
	483	0.1	0.05	—
	545	0.1	0.05	—
	662	0.26	0.13	—
	1120	0.38	0.19	—

a) The values in parenthese show the optical densities calculated from U(VI) based on the value of 0.26

The Effect of γ-Radiation on Uranium. Exposure of U_3O_8-doped glass to γ-radiation produced a ESR singlet, with $g=2.6$ and a peak-to-peak width of 762 G, which was bleached by natural aging for one week. This type of ESR signal is shown in Fig. 10, along with the signals due to the holes and electrons trapped as usual found in the glass matrix. A similar type of ESR spectrum reported by Selbin[27] *et al.*, in thorium oxide and other halide compounds closely resembles ours in line shape and peak-to-peak width, but is very different in g-value ($g=1.52$). In $UO_{2.4}$-doped glass as well as in UO_3-doped polyphosphate glass, there were no other signals than holes and electrons trapped in the galss matrix when the glass was irradiated with γ-rays. Although no direct support of the formation of U(V) in the irradiated glass is available as a result of chemical analysis or optical-absorption measurements,[28] this center might be intimately related to the [U(IV)+h_m^+] center. Consequently, a metastable oxidation state of U(V) exists at room temperature only as a transient state from U(IV) to U(VI).

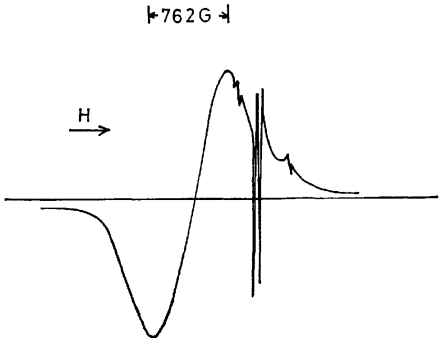

Fig. 10. ESR spectrum of γ-irradiated polyphosphate glass containing uranium(IV) ions, broad line at left with $g=2.6$ assigned to U(V).

Radiation-induced Redox Yields. Conversion between U(IV) and U(VI) and a reaction in the reverse direction in glass under the effect of γ-radiation are shown in Fig. 11. The optical absorption changed at 1120 nm, and the chemical analysis of U(IV)[16,28] was followed by irradiation as a function of the γ-dose. Curve a is

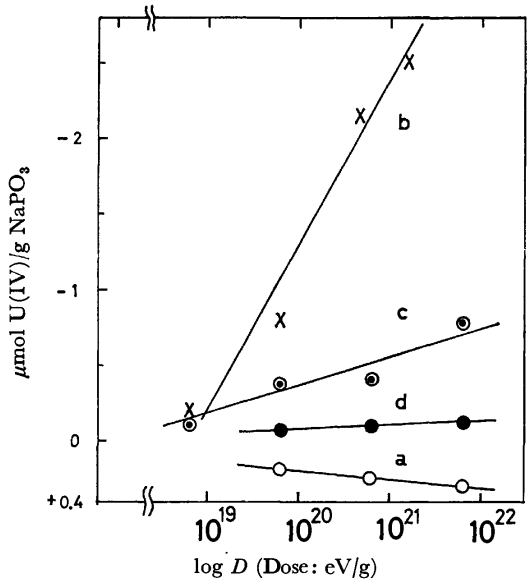

Fig. 11. Variation of U(IV) content as function of absorbed γ-energy in polyphosphate glass a: glass containing U^{VI} 1.00%, b: glass with U^{IV} 0.093%, c: glass with U^{IV} 0.32% 0.32% and U^{VI} 0.201%, and d: glass with U^{IV} 0.32% and U^{VI} 0.64%.

for 1 mol% UO_3 doped glass; it shows that the increase of U(IV) produced by irradiation is so slight as to be measured only by a logarithmic increase in the γ-dose. Curve d is for U_3O_8-doped glass with 0.32 atom % of U(IV) and 0.64 atom % of U(VI); it shows a continuous decrease in U(IV) with an increase in the γ-dose, but at a slower rate than in the case of curve C. At small doses, trapped holes are hard to detect by optical absorption, while ESR doublet signals due to holes begin to appear at a dose of 6×10^{18} eV/g. Curve c is for a glass sample containing 0.60 atom % of U(IV) and 0.20 atom % of U(VI), with an approximate dopant composition of $UO_{2.25}$. This sample glass shows an appreciable decrease in U(IV) content when it is exposed up to 6.4×10^{21} eV/g. These results Curves a, d and c, demonstrate that the exposure of uranium doped glass to γ-radiation causes the conversion of U(IV) to U(VI) or a reverse process, depending on the U(IV)/{U(IV)+U(VI)} ratio in the glass before irradiation. The yields of the converstion in the oxidation state of uranium have a minimum in the glass

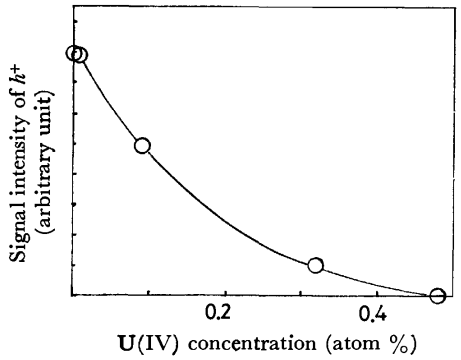

Fig. 12. ESR signal intensity of U(V) produced by γ-irradiation as metastable (U(IV)+h^+_{tr}) center as function of U(IV) concentration in polyphosphate.

27) J. Selbin and J. D. Ortego, *Chem. Rev.*, **69**, 6570m (1969).
28) D. A. Wenz, M. D. Adams, and R. K. Steuhenberg, *Inorg. Chem.*, **3**, 989 (1964).

with a U(IV)/{U(IV)+U(VI)} ratio at approximately 1:2, corresponding to the U_3O_8 composition.

As for the trapped holes thus produced, the intensities of the ESR doublet signals are greatly reduced by an increase in the doped U(IV) content, according to the exponential law shown in Fig. 12. Stroud's equation (1) provides an effective capture volume of U(IV) ions for dry or mobile holes that can be estimated to be 2.58×10^4 Å^3 from the curve in Fig. 12; this indicates a much smaller value than 3.8×10^5 Å^3 in the case of Sb_2O_3 as the dopant. The results in Fig. 12 also demonstrate that 40% of the dopant uranium must be present in the +4 oxidation state for the complete suppression of the trapped holes when 1.0 atom % uranium-doped glass is exposed to γ-radiation with a dose of 6×10^{19} eV/g. The maximum G values for the oxidation of U(IV) to U(VI) were obtained by doping 0.1 atom % of UO_2 oxide in a vacuum; they showed that 93% of uranium present in the +4 oxidation state. They are calculated to be 1.3 at 6×10^{19} eV/g and 0.833 at 6×10^{20} eV/g from the data shown by Curve b in Fig. 11.

Conclusion

For the three systems of redox couples that we have investigated, each has a minimum yields of radiation-induced redox at the concentration corresponding to these compositions; Sb_2O_4 for the Sb(III)–Sb(V) system, Mo_6O_{17} {Mo(V): Mo(VI)=1:2} for the Mo(V)–Mo(VI) system, and U_3O_8 for the U(IV) and U(VI) system, in polyphosphate galss.

The effective capture volumes are 3.8×10^5 Å^3 for U(IV) ions, with respect to the trapping holes. Mo(V) ions take an intermediate value between Sb(III) and U(IV) ions.

Abnormally high radiation yields are observed when antimony oxide is used as the dopant; this is, probably, a particular case of an antimony oxide system whose gas-cleaning action has been used in the glass industry, because of its high oxygen pressure of thermal decomposition.

The approximate G values are 0.9 for 0.57 mol% of Sb_2O_3 and 0.43 mol% of Sb_2O_5, 0.7 for 0.31 mol% of Sb_2O_3 and 0.69 mol% of Sb_2O_5, with respect to the formation of Sb_2O_3 at 1×10^{21} eV/g. The G values of the formation of Mo(V) from Mo(VI) are 0.54 for 0.5 atom % of Mo(VI)-doped glass and 0.18 for 1.0 atom % of U(IV) and a trace of U(VI). They are 1.3 at 6×10^{19} eV/g and 0.833 at 6×10^{20} eV/g. A more sensitive method of analysis of the product is required for a further discussion in detail of the G values, particularly of the initial G values, which are computed in a very-small-dose region.

A kinetic study of the rate of annealing indicates an unimolecular mechanism, providing an activation energy of 0.37 eV for bleaching trapped holes. In the case of Mo, the redox processes between the two oxidation states involve only one electron. In the cases of Sb and U, the difference in oxidation number is two. In these two cases, no conclusive identification of Sb(IV) and U(V) was obtained. However, strong evidence for the formation of an intermediate oxidation state has been presented, and it can be assumed that the redox reactions involved proceed through an one-electron step.

The authors wish to express their thanks to Dr. A. Barkatt, the University of Israel, for his valuable advice.

Dielectric Studies on Isobutyl Halides in the Liquid State

Arati DAS, Alpana GHATAK, and Abul HASAN
Optics Department, Indian Association for the Cultivation of Science, Calcutta-32, India
(Received July 25, 1972)

The activation energies of dielectric relaxation ΔH_τ in three isobutyl halides in the liquid state are found to be almost equal to the mean value of the electrostatic self energies of the *trans* and *gauche* isomers in the corresponding compounds. The energy difference between the two isomers in the liquid state obtained from the dipole moment measurements agree well with those obtained by the spectroscopic method.

From studies of dielectric relaxation of 1,2-dihaloethanes,[1] 1-chloro-2-bromoethane,[2] 1,2-ethane- and 1,2-propane dithiols and 1,2-dichloropropane,[3] it was observed that the activation energy of dielectric relaxation ΔH_τ was almost equal to the electrostatic self energies of polar *gauche* molecules in the liquid state. The electrostatic stabilization energy in all the above liquids was approximately equal to the amount of lowering of the energy difference between the *trans* and *gauche* isomers from the gaseous to the liquid state as pointed out by Wada.[4] These facts indicate that the activation energy ΔH_τ due to intermolecular interactions in these liquids is mainly electrostatic in nature. In order to examine this viewpoint further, the dielectric studies have been extended to the case of three isobutyl halides where the conformers have moderate dipole moments unlike the case of the molecules mentioned above. The results of these investigations are discussed in this paper.

Experimental

Pure samples of 1-chloro-2-methylpropane, 1-bromo-2-methylpropane and 1-iodo-2-methylpropane (Schuchardt, Germany) were distilled under reduced pressure before use. The dielectric permittivities ε' and dielectric losses ε'' of the liquids at different temperatures were measured by Surber's method at 1.62, 3.17 and 3.49 cm microwave regions. The static dielectric constant ε_0 was measured at 1 MHz and the refractive index n was obtained with an Abbe refractometer. The density d was measured with a picnometer and the viscosities η were determined with an Ostwald viscometer. The temperatures in all the experiments were controlled within ± 1°C by a thermostat.

Results

The values of ε_0, ε', ε'', and n^2 at different temperatures for all the liquids are given in Table 1. These data were fitted in Cole-Cole arc plots, some of which

TABLE 2. VALUES OF α, τ, η, ΔH_τ, ΔH_η, AND MEAN ELECTROSTATIC ENERGY $(E_g+E_t)/2$ IN kcal/mol

Temp °C	α	τ psec	η c.poise	Mean E $(E_g/+E_t)/2$	ΔH_τ kcal/mol	ΔH_η kcal/mol
	Isobutyl chloride					
10	0.04	4.88	0.41			
30	0.03	4.35	0.36	0.51	0.40	1.29
50	0.01	3.92	0.32			
	Isobutyl bromide					
10	0.09	6.55	0.57			
30	0.07	5.88	0.49	0.39	0.33	1.32
50	0.04	5.38	0.42			
70	0.01	4.74	0.38			
	Isobutyl iodide					
10	0.11	9.37	0.81			
30	0.10	8.69	0.64	0.3	0.26	1.63
50	0.09	7.77	0.55			

TABLE 1. VALUES OF n^2, ε', ε'', AND ε_0

Temp °C	n_2	$\lambda=1.62$ cm		$\lambda=3.17$ cm		$\lambda=3.49$ cm		ε_0
		ε'	ε''	ε'	ε''	ε'	ε''	
	Isobutyl chloride							
10	1.96	5.80	2.10	6.68	1.40	6.76	1.30	7.19
30	1.94	5.65	1.85	6.35	1.16	6.45	1.05	6.71
50	1.91	5.43	1.61	5.99	0.98	6.04	0.90	6.24
	Isobutyl bromide							
10	2.08	5.30	2.27	6.48	1.78	6.68	1.64	7.53
30	2.05	5.17	2.09	6.22	1.53	6.42	1.34	6.97
50	2.01	5.00	1.90	5.93	1.28	6.09	1.10	6.44
70	1.99	4.96	1.70	5.70	1.10	5.76	0.99	6.04
	Isobutyl iodide							
10	2.24	4.26	1.80	5.35	1.66	5.52	1.59	6.65
30	2.22	4.28	1.72	5.24	1.56	5.37	1.48	6.35
50	2.18	4.30	1.68	5.15	1.38	5.23	1.27	6.02

1) A. Hasan, A. Das, and A. Ghatak, This Bulletin, **44**, 322 (1971).
2) A. Ghatak, A. Das, and A. Hasan, *J. Chem. Phys.*, (in press).
3) A. Hasan, A. Das, and A. Ghatak, *ibid.*, (in press).
4) A. Wada, *ibid.*, **22**, 198 (1954).

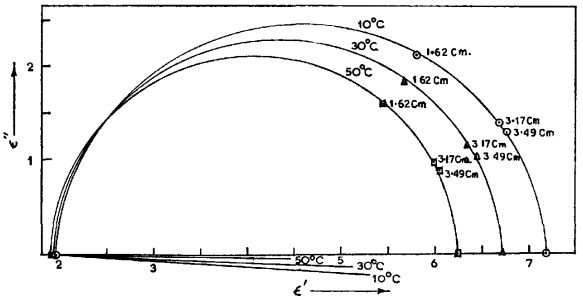

Fig. 1(a). Cole-Cole arc plots of isobutyl chloride at different temperature.

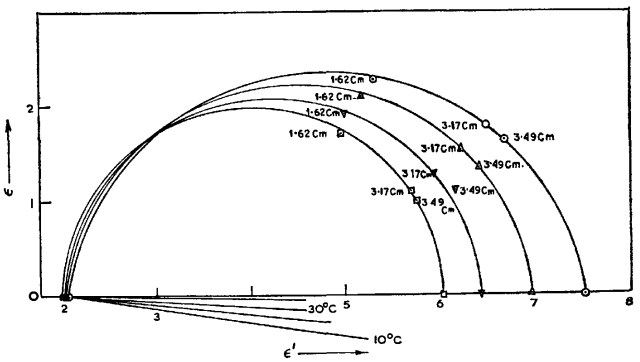

Fig. 1(b). Cole-Cole are plots of isobutyl bromide at different temperature.

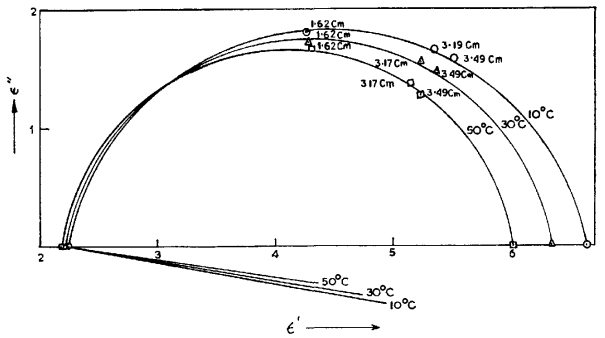

Fig. 1(c). Cole-Cole arc plots of isobutyl iodide at different temperature.

are shown in figures 1 (a, b, c). The most probable relaxation time τ and the distribution parameter α determined from the arc plots are given in Table 2. The activation energies for dielectric relaxation ΔH_τ and for viscous flow ΔH_η were obtained respectively from the straight line plots of log $T\tau$ *vs.* $1/T$ and log η *vs.* $1/T$ (Fig. 2). The values of ΔH_τ and ΔH_η are given in Table 2. The accuracies in the measurements of ε' and ε'' are 2 and 4% respectively.

Discussion

It can be seen from Table 2 that the most probable relaxation time τ of 6.55 psec at 10°C in isobutyl bromide is larger than 4.55 psec in isobutyl chloride but smaller than 9.37 psec in isobutyl iodide at the same temperature. This is consistent with the sizes of the molecules. The relaxation time τ and the distribution parameter α in all the liquids are seen

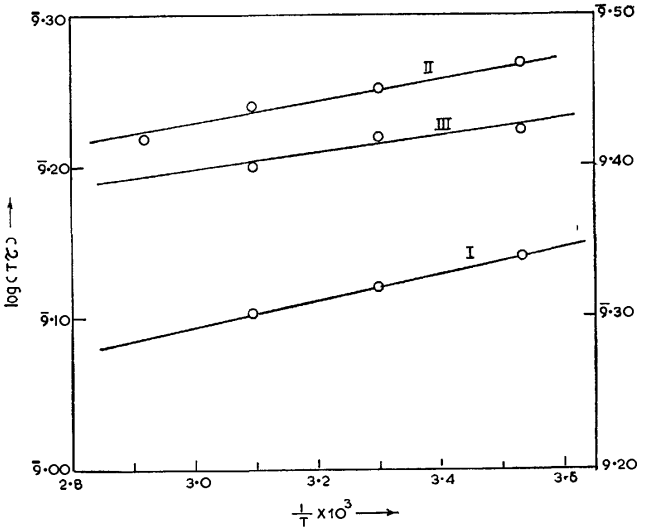

Fig. 2. Plots of log $T\tau$ *vs.* $1/T$.
Curve I: Isobutyl chloride (ordinate left),
Curve II: Isobutyl bromide (ordinate left),
Curve III: Isobutyl iodide (ordinate right).

to decrease with increase of temperature as is generally observed in polar liquids.

The activation energy of dielectric relaxation ΔH_τ is as usual less than the corresponding value for viscous flow ΔH_η in all the liquids. However, while the ΔH_τ-values decrease with increase in size of the molecules, the ΔH_η-values increase in the same order.

Activation Energy and Electrostatic Energy. In the case of some 1,2-disubstituted ethanes[1-3] the dipole activation energy was almost equal to the respective values of electrostatic energy of the polar *gauche* molecules in the liquid state. This is because in all these molecules the dipole moment of *trans* isomer is negligible compared to that of the *gauche* isomer. In the present case, however, in all the isobutyl halides both *trans* and *gauche* isomers have moderately large dipole moments, both contributing to the relaxation process, but as they are almost similar in size the τ-values would be almost the same. Thus it was not possible to analyse the dielectric data in terms of two relaxation processes one due to each, and the activation energy ΔH_τ for the isomers could not be obtained separately. The activation energy obtained experimentally has been taken as the average ΔH_τ of the *trans* and *gauche* isomers.

To correlate the average activation energy with the corresponding values of the electrostatic energy of the two isomers, the dipole moments of the *trans* and *gauche* forms for all the molecules were calculated from their geometrical structures using known bond moments and bond angle values: $\mu_{C-Cl} \approx 1.85$ D,[5] $\mu_{C-Br} \approx 1.7$ D,[5] $\mu_{CH_3} \approx 0.4$ D[6] the carbon valence angle $\approx 110°$ and the azimuthal angle of rotation $\approx 60°$. The value of μ_{C-I} was assumed to be ≈ 1.6 D, a little smaller than that of μ_{C-Br}. The calculated values of μ_g and μ_t are given in Table 3. The values of a^3 (≈ 40 Å^3—

5) J. W. Smith, "Electric Dipole Moments," Butterworths Scientific Publication (1955), p. 292.

6) C. P. Smyth, "Dielectric Behaviour and Structure," McGraw Hill Book Company, Inc., (1955), P. 368.

Table 3. Values of d, m, μ_t, μ_g, and electrostatic energy E_g and E_t in kcal/mol

Temp °C	Density d	Mean moment (m) in D	Dipole moment		Electrostatic energy	
			trans μ_t	*gauche* μ_g	E_{trans}	E_{gauche}
	Isobutyl chloride					
10	0.881	1.92				
30	0.360	1.93	1.60	2.19	0.68	0.36
50	0.316	1.94				
	Isobutyl bromide					
10	1.296	1.91				
30	1.259	1.93				
50	1.230	1.94	1.50	2.01	0.51	0.28
70	1.210	1.95				
	Isobutyl iodide					
10	1.609	1.75				
30	1.580	1.78	1.38	1.90	0.40	0.20
50	1.546	1.81				

50 Å^3) were estimated from a comparison with the molecules of 1,2-dihaloethanes.[7] The electrostatic energies of the *trans* and *gauche* isomers of all the compounds calculated from the relation[7] $E=(\varepsilon-1)/(2\varepsilon+1)\cdot\mu^2/a^3$ are given in Table 3 and their mean values in Table 2. We see that the activation energy in each case is almost equal to the mean value of the electrostatic energies of the *gauche* and *trans* isomers of the respective compounds. This supports the conclusion drawn earlier.[1-3]

Energy Difference between the Isomers in the Liquid State. The energy difference between the isomers in all the liquids were obtained by the method given by Mizushima[7] with the values of the mean moments m of the molecules in the liquid state at different temperatures and the values of μ_g and μ_t calculated as above. The mean moments were calculated by using Onsager's equation[5] from the values of ε_0, d, and n. The energy differences between the two isomers in all the liquids thus obtained are found to agree fairly well with those obtained by spectroscopic studies[8] (Table 4).

Table 4. Energy difference ΔE in kcal/mol

Compound	Liquid (Present work)	Spectroscopic method[8]	
		Liquid	Vapour
Isobutyl chloride	0.39	0.37±0.15	0.23±0.09
Isobutyl bromide	0.20	0.26±0.12	0.3 ±0.03
Isobutyl iodide	0.24	—	—

It may be noted from Table 3 that the electrostatic energies of the *trans* isomer in all the molecules are larger than that of the *gauche* isomer. In the gaseous state also the *trans* isomer is of lower energy in all the compounds. Hence if the electrostatic energy in the liquids was mainly responsible for the intermolecular potential energy, the energy difference between the two isomers in the liquid state would be greater than that of the gaseous state. This is found to be true in the case of isobutyl chloride (Table 4).

The authors are grateful to Dr. S. B. Roy for his guidance and to Professor G. S. Kastha for his continued interest in the work.

7) S. Mizushima, "Structure of Molecule and Internal Rotation," Academic Press Inc., New York (1955), p. 42.

8) E. Wye Jones and W. J. Orville Thomas, *Trans. Faraday Soc.*, **64**, 2911 (1968).

On the MO Perturbation Theory of Molecular Rearrangements

Hiroshi FUJIMOTO, Morio MIYAGI, Shinichi YAMABE, and Kenichi FUKUI
Faculty of Engineering, Kyoto University, Sakyo-ku, Kyoto
(Received September 7, 1972)

The relationship between two simple Hückel MO perturbation treatments of electrocyclic reactions formerly proposed has been examined. The reason why the two different approaches give the same prediction with regard to the favorable paths of the reactions has been established numerically. A calculation of the thermal ring-closing of butadiene has been carried out, including both sigma and pi electrons.

In 1965, Woodward and Hoffmann suggested a selection rule for electrocyclic reaction of conjugated molecules.[1] Various intramolecular reactions as well as intermolecular reactions between two systems have been discussed on the basis of the symmetry properties of the molecular orbitals (MO) of the reactants and the product.[2-18] Since then, several theories for unimolecular reactions have been proposed.[19-24] Some MO and valence-bond (VB) calculations of the favorable course of electrocyclic reactions have also been carried out.[25-29] Among the theoretical approaches to the electrocyclic rearrangements of open conjugated chains, we can find two types of MO perturbation treatments on the level of the simple Hückel approximation.[5] One is to discuss the path of molecular rearrangements by examining the energy change caused by the introduction of a resonance integral between the two termini of a chain, representing the starting of ring-closing by the overlapping of the two terminal atomic orbitals (AO).[5a,b] The other is to apply a partitioning technique to the reaction; thereby, the ring-closing of a conjugated chain can be regarded as if it were an intersystem four-center interaction between the two fragments of a molecule.[5d] The basic idea of the partitioning technique originated from the perturbation theory for the intermolecular interaction of two independent systems has been developed successfully in numerous unimolecular reactions.[5d,f,30] In this paper, we intend first to examine the relationship between these perturbation approaches to molecular rearrangements and then to present some numerical results on the electrocyclic rearrangement of butadiene calculated by use of the extended Hückel MO wave function, in order to observe the behavior of sigma and pi electrons in the reaction.

Simple Hückel MO Perturbation Theory for Unimolecular Rearrangements

Let us first discuss the perturbation theory of the simple Hückel MO method.[31] When the resonance integral between the AO's r and s, represented by β_{rs}, varies by a small amount, $\Delta\beta_{rs}$, that between the

1) R. B. Woodward and R. Hoffmann, *J. Amer. Chem. Soc.*, **87**, 395 (1965).
2) a) R. B. Woodward and R. Hoffmann, *ibid.*, **87**, 2511 (1965). b) R. Hoffmann and R. B. Woodward, *ibid.*, **87**, 2046, 4388, 4389 (1965). c) R. B. Woodward and R. Hoffmann, *Angew. Chem, Int. Ed. Engl.*, **8**, 781 (1969). d) R. Hoffmann and R. B. Woodward, *Accounts Chem. Res.*, **1**, 17 (1969).
3) H. C. Longuet-Higgins and E. W. Abrahamson, *J. Amer. Chem. Soc.*, **87**, 2045 (1965).
4) a) H. E. Zimmerman, *ibid.*, **88**, 1564, 1566 (1966). b) H. E. Zimmerman, *Accounts Chem. Res.*, **4**, 272 (1971).
5) a) K. Fukui, *Tetrahedron Lett.*, **1965**, 2009. b) K. Fukui, This Bulletin, **39**, 498 (1966). c) K. Fukui and H. Fujimoto, *ibid.*, **39**, 2116 (1968). d) K. Fukui and H. Fujimoto, "Mechanisms of Molecular Migrations," Vol. 2, ed. by B. S. Thyagarajan, Interscience, New York (1969), pp. 117—190. e) K. Fukui, "Molecular Orbitals in Chemistry, Physics, and Biology," ed. by P.-O. Löwdin and B. Pullman, Academic Press, New York, N. Y. (1964), pp. 513—537. f) K. Fukui, *Fortschr. Chem. Forsch.*, **15**, 1 (1970).
6) a) L. Salem, *J. Amer. Chem. Soc.*, **90**, 543, 553 (1968). b) A. Devaquet and L. Salem, *ibid.*, **91**, 3793 (1969).
7) a) M. J. S. Dewar, *Tetrahedron, Suppl.* **8**, Part I, 75 (1966). b) M. J. S. Dewar, "Molecular Orbital Theory of Organic Chemistry," McGraw-Hill, New York, N. Y. (1969).
8) W. C. Herndon and L. H. Hall, *Tetrahedron Lett.*, **1967**, 3095.
9) M. J. Goldstein, *J. Amer. Chem. Soc.*, **89**, 6357 (1967).
10) H. E. Simmons and T. Fukunaga, *ibid.*, **89**, 5208 (1967).
11) R. Hoffmann, A. Imamura, and G. D. Zeiss, *ibid.*, **89**, 5215 (1967).
12) F. D. Mango and J. H. Schachtschneider, *ibid.*, **89**, 2484 (1967); **91**, 1030 (1969); **93**, 1123 (1971).
13) G. S. Lewandos and R. Pettit, *Tetrahedron Lett.*, **1971**, 789.
14) S. I. Miller, "Advances in Physical Organic Chemistry," Vol. 6, ed. by V. Gold, Academic Press, New York, N. Y., 1968, pp. 185—232.
15) N. T. Anh, "Les Regles de Woodward-Hoffmann," Edscience, Paris (1970).
16) G. B. Gill, *Quart. Rev.*, **22**, 338 (1968).
17) M. J. Goldstein and R. Hoffmann, *J. Amer. Chem. Soc.*, **93**, 6193 (1971).
18) N. D. Epiotis, *ibid.*, **94**, 1924, 1935, 1941, 1949 (1972).
19) a) C. Trindle and O. Sinanoglu, *ibid.*, **91**, 4054 (1969). b) C. Trindle, *ibid.*, **92**, 3251, 3255 (1970).
20) a) L. Salem, *Chem. Phys. Lett.*, **3**, 99 (1969). b) L. Salem and J. S. Wright, *J. Amer. Chem. Soc.*, **91**, 5947 (1969).
21) R. G. Pearson, *ibid.*, **91**, 1252, 4957 (1969).
22) W. A. Goddard III, *ibid.*, **94**, 793 (1972).
23) K. Fukui and H. Fujimoto, This Bulletin, **40**, 2018 (1967).
24) M. H. Whangbo and I. Lee, *J. Amer. Chem. Soc.*, **93**, 2330 (1971).
25) W. Kutzelnigg, *Tetrahedron Lett.*, **1967**, 4965.
26) a) D. T. Clark and G. Smale, *ibid.*, **1968**, 3673. b) D. T. Clark and G. Smale, *Tetrahedron*, **25**, 13 (1969). c) D. T. Clark and D. R. Armstrong, *Theor. Chim. Acta*, **13**, 365 (1969); **14**, 370 (1969).
27) K. Hsu, R. J. Buenker, and S. D. Peyerimhoff, *J. Amer. Chem. Soc.*, **93**, 2117 (1971).
28) M. J. S. Dewar and S. Kirschner, *ibid.*, **93**, 4290, 4291, 4292 (1971).
29) W. Th. A. M. van der Lugt, and L. J. Oosterhoff, *ibid.*, **91**, 6042 (1969).
30) K. Fukui, *Accounts Chem. Res.*, **4**, 57 (1971).
31) a) K. Fukui, C. Nagata, T. Yonezawa, H. Kato, and K. Morokuma, *J. Chem. Phys.*, **31**, 287 (1959). b) K. Fukui, K. Morokuma, T. Yonezawa, and C. Nagata, This Bulletin, **33**, 963 (1960). c) K. Fukui, A. Imamura, T. Yonezawa, and C. Nagata, *ibid.*, **33**, 1591 (1960).

AO's t and u by an amount of $\Delta\beta_{tu}$, and so on, the change in the electronic energy is given by:

$$\Delta E \cong 4\sum_{i}^{\text{occ}}\sum_{(r,s)} c_r^{(i)}c_s^{(i)}\Delta\beta_{rs} + 2\sum_{i}^{\text{occ}}\sum_{j}^{\text{uno}} \frac{\{\sum_{(r,s)}(c_r^{(i)}c_s^{(j)}+c_r^{(j)}c_s^{(i)})\Delta\beta_{rs}\}^2}{\varepsilon_i-\varepsilon_j} \quad (1)$$

where c_r^i is the coefficient of the AO r in the MO i, where ε_i is its energy, and where $\sum^{\text{occ}}$ and $\sum^{\text{uno}}$ imply the summation over all the occupied and over all the unoccupied MO's respectively. Therefore, in the case of the ring-closing between the two termini r and s of a polyene, the energy change associated with this process is given approximately by:

$$\Delta E \cong 2P_{rs}\gamma\beta_{rs} \quad (2)$$

where P_{rs} is the mobile bond-order between the π AO's at the termini and where $\gamma\beta_{rs}$ is the resonance integral standing for the interaction. Since $\gamma\beta_{rs}$ and the overlap integral, s_{rs}, are opposite in sign, the positive $\gamma\beta_{rs}$ corresponds to the conrotatory, and the negative $\gamma\beta_{rs}$, to the disrotatory, ring-closing (Fig.1).

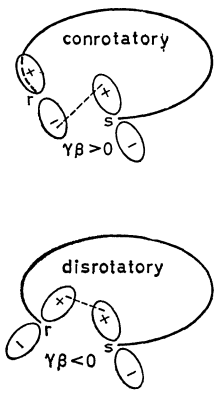

Fig. 1. A schematic representation of conrotatory and disrotatory ring-closing of a polyene.

In the ground-state of butadiene, P_{14} is negative, so the reaction should take place preferentially in such a way as to make $\gamma\beta_{14}$ positive. On the contrary, P_{14} is positive in the first excited-state in favor of the disrotatory ring-closing. The thermal and photochemical ring-closing of hexatriene should take place dominantly in a fashion opposite to that in the case of butadiene, because P_{16} is positive in the ground-state and negative in the first excited-state. In general, P_{rs} is negative in the ground-state and positive in the first excited-state for polyenes with $4n$-electrons, while it is positive in the ground-state and negative in the excited-state for polyenes with $4n+2$ electrons.[5a] The conclusion thus derived from the intramolecular first-order perturbation energy was found to be in excellent agreement with the experimental results and with the results of other theoretical approaches.

When we employ the partitioning technique, we can regard a ring-closing of a conjugated chain as a cyclic interaction between two fragments of a molecule (Fig. 2). The interaction energy between them can be given by (in the ground-state):

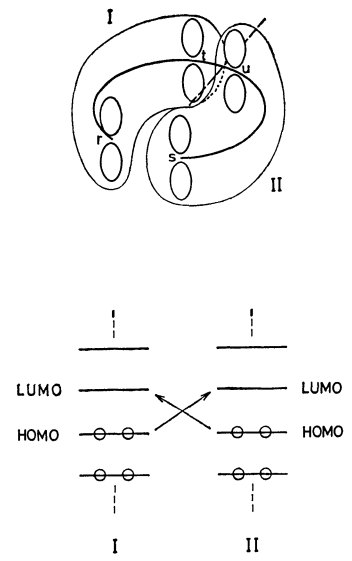

Fig. 2. A schematic representation of partitioning of a polyene into two fragments and the mode of orbital overlap interaction.

$$\Delta E' \cong 2\left(\sum_{i}^{\text{occ}}\sum_{j}^{\text{uno}} - \sum_{i}^{\text{uno}}\sum_{j}^{\text{occ}}\right)\frac{(c_r^{(i)}c_s^{(j)}\gamma\beta + c_t^{(i)}c_u^{(j)}\beta)^2}{\varepsilon_i-\varepsilon_j} \quad (3)$$

if we can assume that the interaction is sufficiently weak as to be called a "perturbation." Equation (3) tells us that the most favorable mode of interaction is determined by the orbital overlap interaction of the occupied MO's of one fragment and the unoccupied MO's of the other fragment. When the highest occupied (HO) MO of one part happens to be degenerate with the lowest unoccupied (LU) MO of the other, the interaction energy can be approximated by:

$$\Delta E' \cong -2|c_r^{(\text{HO})}c_s^{(\text{LU})}\gamma\beta + c_t^{(\text{HO})}c_u^{(\text{LU})}\beta| \quad (4)$$

Even not in such a condition, the interaction between the HOMO of one part and the LUMO of the other part, and the converse, play dominant roles in determining the favorable mode of interaction, in general, because the denominators of these terms in Eq. (3) are obviously smaller than those of the other terms.

When a polyene is partitioned into two odd electron fragments, the interaction energy is given by;

$$\Delta E' \cong -|c_r^{(\text{SO})}c_s^{(\text{SO}')}\gamma\beta + c_t^{(\text{SO})}c_u^{(\text{SO}')}\beta| \quad (5)$$

where SO and SO′ mean the singly-occupied nonbonding MO's of the two fragments.

Let us now consider the thermal ring-closing of butadiene (Fig. 3). When we divide butadiene into two ethylenic parts, the HOMO (S)–LUMO (A) interaction favors the *anti*-mode interaction. Here, S denotes the symmetric MO's with $c_r^{(i)}c_t^{(i)}>0$ and A indicates the antisymmetric MO's with $c_r^{(i)}c_t^{(i)}<0$; we may call the mode of interaction in which β and $\gamma\beta$ possess the same sign "*syn*-interaction," and that in which β and $\gamma\beta$ have different signs, "*anti*-interaction."[5c] The case of division into an allylic part and a single p AO also shows that the interaction should take place preferentially in the *anti*-mode. Accordingly, thermal ring-closing takes place dominantly in a conrotatory fashion.

The interaction between an ethylenic part and a

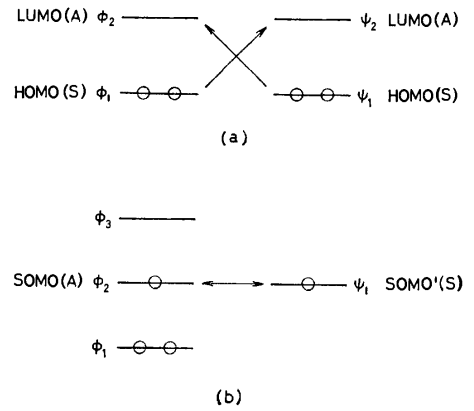

Fig. 3. Orbital overlap interaction in thermal ring-closing of butadiene.
(a) Division into two ethylenic parts
(b) Division into an allylic part and a single p AO

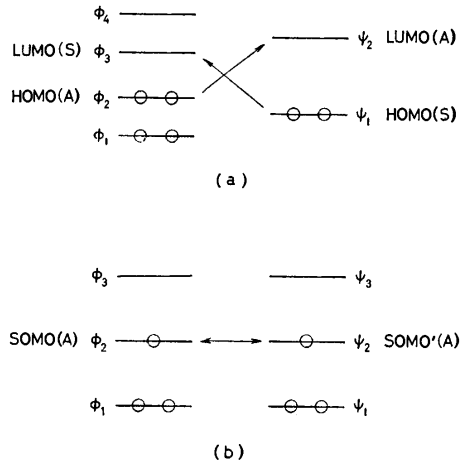

Fig. 4. Orbital overlap interaction in thermal ring-closing of hexatriene.
(a) Division into ethylenic and butadienic part
(b) Division into two allylic parts

butadienic part, and the interaction between two allylic parts, both prefer *syn*-interaction in the ground-state (Fig. 4). Therefore, the ring-closing of hexatriene is liable to occur in a disrotatory manner.

In order to discuss the favorable mode of photochemical reactions, we divide a conjugated chain into two parts, in which one has an excited-electron configuration. In this case, the interaction between SOMO and HOMO and the interaction between SOMO' and LUMO are predominant (Fig. 5).

$$\Delta E' \cong -|(c_r^{(SO)}c_s^{(HO)}\gamma\beta + c_t^{(SO)}c_u^{(HO)}\beta)^2 + (c_r^{(SO')}c_s^{(LU)}\gamma\beta + c_t^{(SO')}c_u^{(LU)}\beta)^2|^{1/2} \quad (6)$$

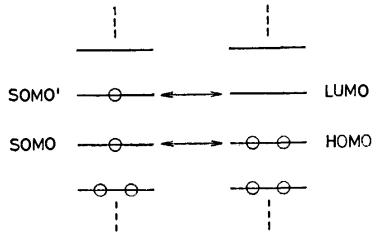

Fig. 5. Mode of orbital overlap interaction in photochemical ring-closing.

Equation (6) corresponds to the case in which SOMO degenerates with HOMO, and SOMO', with LUMO.[5b,32] In some cases, one of the two interaction terms is more important than the other. Consequently, the photochemical ring-closing of butadiene prefers the *syn*-interaction, and that of hexatriene, the *anti*-interaction. In general, the cyclic interaction between two fragments of a polyene with $4n$ electrons takes place preferentially in the *anti*-mode in the ground-state and in the *syn*-mode in the excited-state, while the interaction between two fragments of a polyene possessing $4n+2$ electrons favors the *syn*-mode in the ground-state and the *anti*-mode in the excited-state.[5d]

The Relation between Two Perturbation Approaches

As has been mentioned above, the rule derived from the partitioning analysis of orbital interactions in the thermal and photochemical ring-closing of conjugated chains can give the same prediction as the rule deduced from the intramolecular first-order perturbation. Now, let us discuss the relation between these two approaches to molecular rearrangements by means of some numerical calculations.

Table 1. Division of butadiene MO's into ethylene MO's

	MO's of butadiene[a]			
	φ_1	φ_2	φ_3	φ_4
ϕ_1	0.688	0.688	0.163	−0.163
ϕ_2	0.163	−0.163	−0.688	−0.688
ψ_1	0.688	−0.688	0.163	0.163
ψ_2	0.163	0.163	−0.688	0.688

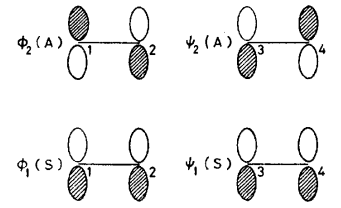

$\phi_t = c_1^{(t)}\chi_1 + c_2^{(t)}\chi_2$ $\quad$ $\psi_j = c_3^{(j)}\chi_3 + c_4^{(j)}\chi_4$

a) MO's of butadiene are numbered in the order of increasing energy.

The four π MO's of butadiene can be expressed by linear combinations of the bonding and antibonding π MO's of two ethylenic fragments (Table 1). It should be noted that the signs of the coefficients depend on how the arbitrary factor, ± 1 is assigned the real MO's of two ethylenic parts. Here and in what follows, we always choose the signs of the MO's so as to make $c_t^{(i)}c_u^{(j)} > 0$, where t and u are the AO's between which the partition of a chain is made, and where i and j denote the MO's of the two fragments. By the use of the coefficients listed in Table 1, the first-order perturbation energy given by Eq. (2) for

32) C. Nagata, A. Imamura, Y. Tagashira, M. Kodama, and N. Fukuda, *J. Theor. Biol.*, **9**, 357 (1965).

the thermal ring-closing of butadiene can be rewritten as:

$$\Delta E = 0.8944\{(c_1^{(1)}c_4^{(2)} + c_1^{(2)}c_4^{(1)})\gamma\beta + (c_2^{(1)}c_3^{(2)} + c_2^{(2)}c_3^{(1)})\beta\} - 0.8944\beta$$

where 0.8944β is the conjugation stabilization of the 2,3-π bond and is common to both the conrotatory and disrotatory processes. The bonding and *anti*-bonding interactions between ϕ_1 and ψ_1 compensate for each other in the simple Hückel MO approximation. Consequently, the energy change associated with the thermal ring-closing can be represented by the interaction of occupied and unoccupied MO pairs, $\phi_1-\psi_2$ and $\psi_1-\phi_2$. Since ϕ_1 and ψ_1 are S MO's and ϕ_2 and ψ_2 are A MO's, the interaction should take place in the *anti*-mode. In the photochemical reaction, the energy change is expressed as:

$$\Delta E = 1.0000\{(c_1^{(1)}c_4^{(1)} + c_1^{(2)}c_4^{(2)})\gamma\beta + (c_2^{(1)}c_3^{(1)} + c_2^{(2)}c_3^{(2)})\beta\} + 0.4472\{(c_1^{(1)}c_4^{(2)} + c_1^{(2)}c_4^{(1)})\gamma\beta + (c_2^{(1)}c_3^{(2)} + c_2^{(2)}c_3^{(1)})\beta\} - 1.4472\beta$$

where 1.4472β is the conjugation energy of the 2,3-π bond in the first excited-state. It can be seen that the interaction between ϕ_1 and ψ_1 and the interaction between ϕ_2 and ψ_2 play dominant roles.

When we divide butadiene into an allylic part and a single p AO, the energy change is given by:

$$\Delta E = 2(0.2236c_1^{(1)} + 0.9487c_1^{(2)} + 0.2236c_1^{(3)})\gamma\beta + 2(0.2236c_3^{(1)} + 0.9487c_3^{(2)} + 0.2236c_3^{(3)})\beta - 1.7888\beta$$

where 1.7888β is the conjugation energy of the 3,4-π bond in the ground-state. We can see that the favorable mode of interaction is governed by the two SOMO's.

Next, let us consider the ring-closing of hexatriene. In case of the division of hexatriene into a butadienic part (ϕ_1, ϕ_2, ϕ_3, ϕ_4) and an ethylenic part (ψ_1, ψ_2), the interaction between ϕ_2 and ψ_2 and the interaction between ϕ_3 and ψ_1 predominate in the thermal ring-closing in favor of the *syn*-interaction, whereas the interaction between ϕ_2 and ψ_1 and the interaction between ϕ_3 and ψ_2 make major contributions to the energy change in the excited-state in favor of the *anti*-interaction (Table 2). The division of hexatriene into two allylic fragments shows the importance of the interaction between two SOMO's in the thermal ring-closing:

Table 2. Contributions of orbital interactions to the energy change in the ring-closing of hexatriene

	Thermal		Photochemical	
	ψ_1(S)	ψ_2(A)	ψ_1(S)	ψ_2(A)
ϕ_1 (S)	0.009	0.352	0.105	0.278
ϕ_2 (A)	−0.004	0.917	0.909	0.447
ϕ_3 (S)	0.917	−0.004	0.447	0.909
ϕ_4 (A)	0.352	0.009	0.278	0.105

ψ: MO's of ethylenic part, ϕ: MO's of butadienic part

$$\Delta E = 0.0692\{(c_1^{(1)}c_6^{(1)} + c_1^{(3)}c_6^{(3)})\gamma\beta + (c_3^{(1)}c_4^{(1)} + c_3^{(3)}c_4^{(3)})\beta\} + 0.3418\{(c_1^{(1)}c_6^{(2)} + c_1^{(3)}c_6^{(2)} + c_1^{(2)}c_6^{(1)} + c_1^{(2)}c_6^{(3)})\gamma\beta + (c_3^{(1)}c_4^{(2)} + c_3^{(3)}c_4^{(2)} + c_3^{(2)}c_4^{(1)} + c_3^{(2)}c_4^{(3)})\beta\} + 0.2418\{(c_1^{(1)}c_6^{(3)} + c_1^{(3)}c_6^{(1)})\gamma\beta + (c_3^{(1)}c_4^{(3)} + c_3^{(3)}c_4^{(1)})\beta\} + 1.8616(c_1^{(2)}c_6^{(2)}\gamma\beta + c_3^{(2)}c_4^{(2)}\beta) - 1.5697\beta$$

The numerical results given above with respect to the thermal and photochemical ring-closing of butadiene and hexatriene have shown that the orbital overlap interaction between HOMO and LUMO (in the case of the partitioning of a polyene into two even electron systems) or between SOMO and SOMO′ (in the case of the partitioning of a polyene into two odd electron systems) plays a dominant role in controlling the stereochemical course of the thermal reaction, while the orbital overlap interaction between HOMO and SOMO and that between LUMO and SOMO′ are important in the photochemical ring-closing. This may be the reason why the partitioning analysis can give the same prediction as that of the first-order perturbation approach; at the same time it suggests that the two approaches to the molecular rearrangements can be equivalent in an approximate sense. The partitioning technique supplies us with the simplest way of discussing the molecular rearrangements in MO terms, regardless of whether any symmetry is retained throughout the reactions or not.

Inclusion of Sigma Electrons

Parr and his collaborators introduced the integral Hellmann-Feynman theorem to calculate the rotation barrier of ethane, obtaining a value of 2.4 kcal/mol; this is in good agreement with the experimental value of 2.9 kcal/mol.[33] Here we will present the results of calculation derived from the application of the theorem, though in a very approximate sense, to the ring-closing of butadiene. Let us consider a state, p, corresponding to a point on the reaction coordinate in the neighborhood of the initial state, i. Then, the energy change by going from i to p is given by;

$$\Delta E = E_p - E_i = \frac{\langle \Psi_i | \Delta H | \Psi_p \rangle}{\langle \Psi_i | \Psi_p \rangle} \qquad (7)$$

$$\Delta H = H_p - H_i$$

where H is the Hamiltonian operator of the system. If we can assume here that the wave function, Ψ_p, is expanded by the wave functions of the state, i:

$$\Psi_p = \Psi_i + \lambda\Psi_i^{(1)} + \lambda^2\Psi_i^{(2)} + \cdots \qquad (8)$$

the energy change can be represented by:

$$\Delta E = \langle \Psi_i | \Delta H | \Psi_i \rangle + \lambda\{\langle \Psi_i | \Delta H | \Psi_i^{(1)} \rangle - \langle \Psi_i | \Delta H | \Psi_i \rangle \langle \Psi_i | \Psi_i^{(1)} \rangle\} + \lambda^2\{\langle \Psi_i | \Delta H | \Psi_i^{(2)} \rangle + \cdots\} + \cdots \qquad (9)$$

The use of the matrix sum rule leads us to the same result as that obtained by Salem.[20] It should be noted that Eq. (7) holds only for the exact wave func-

33) a) H. J. Kim and R. G. Parr, *J. Chem. Phys.*, **41**, 2892 (1964). b) R. W. Wyatt and R. G. Parr, *ibid.*, **43**, s217 (1965).

tion. The concrete forms of $\Psi_i^{(1)}$, $\Psi_i^{(2)}$, $\cdots$, are not necessarily easily obtainable, in general. However, as long as we are concerned with the beginning stage of the reaction, λ is small and the energy change can be measured by taking only the first term, to the roughest approximation:

$$\langle\Psi_i|\Delta H|\Psi_i\rangle = \int\rho_{ii}(1)H'(1)d\tau_1 + \Delta V_{nn} \quad (10)$$

$$\rho_{ii}(1) = N\int\Psi_i^*(1, 2, \cdots, N)\Psi_i(1, 2, \cdots, N)d\tau_2\cdots d\tau_N$$

where ΔV_{nn} is the change in the nuclear repulsion energy and where N is the number of electrons in the system. The change in the Hamiltonian operator due to the change in the relative positions of the nuclei associated with ring-closing is given by:

$$H' = \sum_\mu\sum_k\left(\frac{1}{r_{\mu k}^p} - \frac{1}{r_{\mu k}^i}\right) \quad (11)$$

where μ and k denote the nucleus and the electron respectively, and where

$$r_{\mu k}^i = |\boldsymbol{r}_k - \boldsymbol{r}_\mu|$$
$$r_{\mu k}^p = |\boldsymbol{r}_k - \boldsymbol{r}_\mu'| = |\boldsymbol{r}_k - (\boldsymbol{r}_\mu + \Delta\boldsymbol{R})| = |r_{\mu k}^i - \Delta\boldsymbol{R}| \quad (12)$$

The deformation, $\Delta\boldsymbol{R}$, is given by:

$$\Delta\boldsymbol{R} = \Delta x\cdot\boldsymbol{i} + \Delta y\cdot\boldsymbol{j} + \Delta z\cdot\boldsymbol{k}$$

where $\boldsymbol{i}$, $\boldsymbol{j}$, and $\boldsymbol{k}$ are unit vectors in a three-dimensional space. Thus, we have;

$$\frac{1}{r_{\mu k}^p} - \frac{1}{r_{\mu k}^i} \cong \frac{x-A_x}{(r_{\mu k}^i)^3}\Delta x + \frac{y-A_y}{(r_{\mu k}^i)^3}\Delta y + \frac{z-A_z}{(r_{\mu k}^i)^3}\Delta z \quad (13)$$

where (A_x, A_y, A_z) is the Cartesian coordinate of the nucleus, μ. Consider the rotation of the methylene group about the carbon-carbon axis by an angle of ω (Fig. 6). By this rotation, hydrogen changes its position

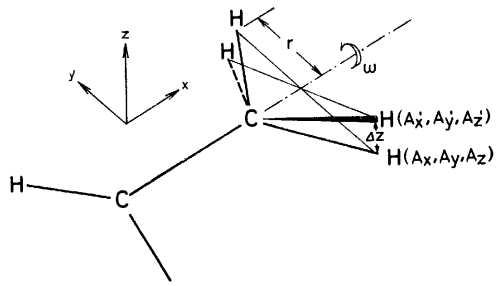

Fig. 6. A schematic representation of the rotation of methylene about carbon-carbon bond axis.

from (A_x, A_y, A_z) to (A_x', A_y', A_z'). Here, we have:

$$A_x' = A_x$$
$$A_y' = A_y + r(1-\cos\omega) \cong A_y + \frac{1}{2}r\omega^2 \quad (13)$$
$$A_z' = A_z + r\sin\omega \cong A_z + r\omega - \frac{1}{6}r\omega^3$$

Since we are concerned with the beginning stage of the reaction, we may disregard the second- and third-order terms with respect to ω. Therefore, we obtain:

$$\Delta x = \Delta y = 0,\ \Delta z = r\omega \quad (15)$$

By the use of the MO wave function for the ground-state, the diagonal element of the first-order density matrix is given by:

$$\rho_{ii}(1) = 2\sum_i^{occ}\phi_i(1)^2 \quad (16)$$

When the MO's ϕ_i are given, as usual, by the linear combinations of AO's, we obtain:

$$\Delta E \cong 2\sum_i^{occ}\sum_\mu\sum_r\sum_s c_r^{(i)}c_s^{(i)}\int\chi_r\frac{z-A_z}{r_{\mu k}^3}\chi_s d\tau\cdot\Delta z + \Delta V_{nn} \quad (17)$$

where χ_r and χ_s are the AO's. It can be seen that Eq. (17) has much the same form as Eq. (2), derived from the simple Hückel MO perturbation. A calculation was made with respect to the thermal ring-closing of butadiene by use of the extended Hückel MO's

Table 3. Energy gradient in the thermal ring-closing of butadiene at $|\omega| = 5°$

	Conrotatory	Disrotatory
ΔE_σ [a]	−4.036	−4.236
ΔE_π [a]	−1.265	−0.772

a) In eV/Bohr-radius unit.

(Table 3).[34] The integrals necessary for the calculation of the energy change were computed by the formula derived by Matsuoka, expanding the Slater AO's into the Gaussian basis set.[35] In the extended Hückel MO approximation, the sum of the energies of doubly-occupied MO's can be a measure of the total energy of the system in the ground-state.[36] Table 3 shows that π electrons favor a conrotatory ring-closing, while σ electrons prefer a disrotatory ring-closing. Furthermore, it is demonstrated that π electrons play a major role in determining the stereochemical course of the electrocyclic rearrangement of butadiene. The results given here are very approximate and can never be a quantitative measure for distinguishing the favorable reaction path. However, this calculation provides us with some information of the energetic aspects of two possible modes of the ring-closing of butadiene, including both the σ and π electrons.

In this paper, we have limited ourselves to the electrocyclic reaction of butadiene and hexatriene in order to accentuate the relation between different perturbation approaches. The methods presented here can be applied, in principle, to any kind of molecular rearrangement.

We are grateful to the Data Processing Center, Kyoto University, for its generous permission to use its FACOM 230-60 computer.

34) R. Hoffmann, *J. Chem. Phys.*, **39**, 1397 (1963); **40**, 2047, 2474, 2480 (1964).
35) O. Matsuoka, *Internat. J. Quant. Chem.*, **5**, 1 (1971).
36) K. Fukui and H. Fujimoto, This Bulletin, **40**, 2787 (1967).

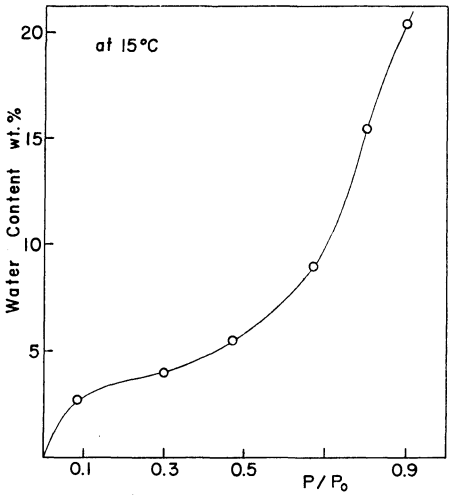

Fig. 2. The water adsorption isotherm of γ-alumina at 15 °C.

Dielectric Measurements. The complex dielectric constant and tan δ were measured using the transformer-bridge method, in the frequencies from 30 Hz to 3 MHz and using the transmission-line method, at 9.72 GHz. The design and the materials of the cell electrodes, the heating and cooling devices, and the measuring procedures employed in this experiment were the same as those in the previous papers.[10,11]

Results and Discussion

Three dielectric anomalies were found to exist in different frequency and temperature ranges on γ-alumina with and without adsorbed water; some of these results at 30 and 300 kHz are shown in Fig. 3. In the figure, three anomalies, I, II and III, are clearly seen at different temperatures. Anomaly II agrees approximately with that found by Ebert[2] and by Dransfeld.[4] These anomalies were dependent on the frequency, the temperature, and the water content.

Anomaly I. Figures 4 and 5 show the frequency effect of ε′ and tan δ at 55 °C, and the Cole-Cole arc

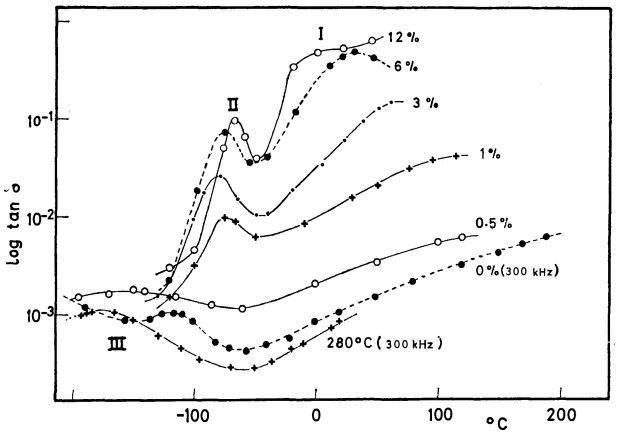

Fig. 3. The relations between temperature and tan δ at 30 kHz and 300 kHz of γ-alumina with various amount of adsorbed water and with heat-treatment, respectively.

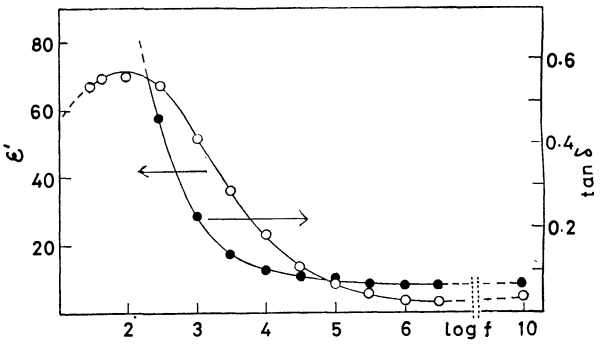

Fig. 4. The ε′ and tan δ *versus* frequency curves of γ-alumina in the range of the dielectric relaxation I containing 3% water at 55 °C.

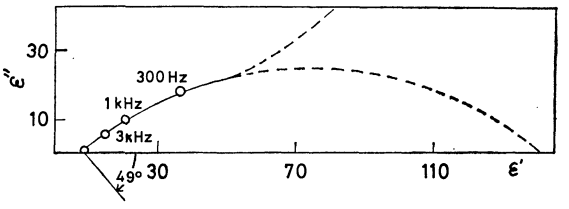

Fig. 5. The Cole-Cole arc of the Relaxation I of γ-alumina containing 3% water at 55 °C.

plot of Anomaly I at 3% water, respectively. These figures show that this anomaly is a dielectric relaxation (Relaxation I), although it seems difficult to tell whether Relaxation I is of the Debye-type or the Wagner-type. It seems clear that Relaxation I has some relation wit the proton in such forms as the ion, the hydroxyl group on the surface, and the adsorbed water, since the relaxation times shift markedly upon the deuterium exchange, as is shown in Fig. 6. The relation between

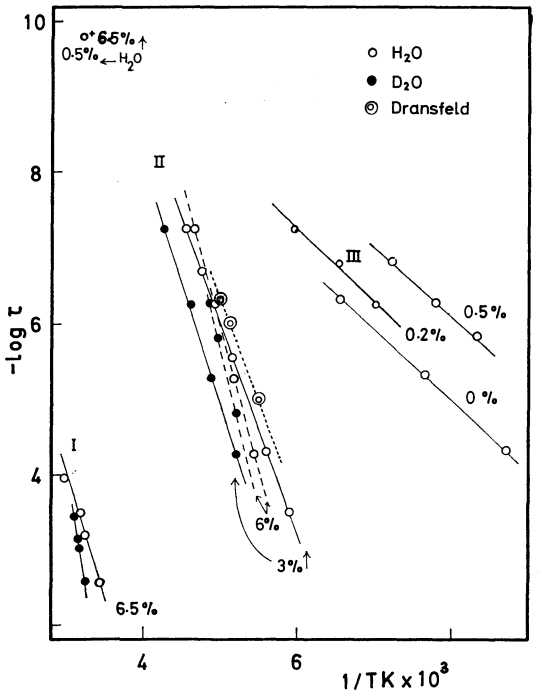

Fig. 6. The relations between logarithm of relaxation times, log τ, of the Relaxations I, II, and III and the reciprocal temperatures on γ-alumina with or without various amount of light and heavy water.

10) S. Kondo and M. Muroya, This Bulletin, **42**, 1165 (1969).
11) S. Kondo and M. Muroya, *Rept. Osaka Electro-Communication Univ.*, **2**, 18 (1966).

TABLE 1. THE ACTIVATION ENERGY, E, AND THE COEFFICIENT, τ_0, OF THE ARRHENIUS EQUATION OF THE RELAXATIONS I, II, AND III OF γ-alumina

Water content (%)	H_2O		D_2O	
	E (kcal/mol)	τ_0 (sec)	E (kcal/mol)	τ_0 (sec)
Relaxation I				
12	11.2±0.5	2×10^{-14}		
6	11.6±0.5	3×10^{-13}	12.2±0.5	1×10^{-14}
3	12.1±0.7	1×10^{-12}		
2	12.4±0.7	1×10^{-12}		
1	11.9±0.7	2×10^{-12}		
Relaxation II				
12	20.6±0.5	4×10^{-27}		
6	17.5±0.5	9×10^{-24}	18.8±0.5	2×10^{-26}
3	13.0±0.5	1×10^{-21}	14.4±0.5	2×10^{-21}
2	14.4±0.5	3×10^{-21}		
1	13.2±0.5	3×10^{-18}		
Relaxation III				
0.5	4.1±1.0	2×10^{-13}		
0.2	4.6±1.0	2×10^{-13}		
0	4.7±1.0	2×10^{-13}		

the relaxation times and the reciprocal temperatures, obtained from the Cole-Cole arc plot, is linear, as is shown in Fig. 6. The activation energy, E, and the coefficient, τ_0, in the Arrhenius expression are shown in Table 1. The values of E do not change with the water content, but those of τ_0 do change appreciably. The magnitude of Relaxation I ($\Delta \tan \delta_{max}$) was estimated from Fig. 7, by subtracting the value of the tan δ maximum from its base line; it is plotted against the water content in Fig. 8. The figure shows that Relaxation I disappears in the neighborhood of 0% water and increases proportionally to the water content up to about the second layer of the adsorbed water (about 6%).

Anomaly II. The relation between the complex dielectric constant and logarithm of frequency, and the Cole-Cole arc plot of Anomaly II at −79 °C, shown in Fig. 3, are given in Figs. 9 and 10 respectively. These curves suggest that this anomaly is a dielectric relaxation of the Maxwell-Wagner type (Relaxation II). The findings by Dransfeld[3] agree approximately

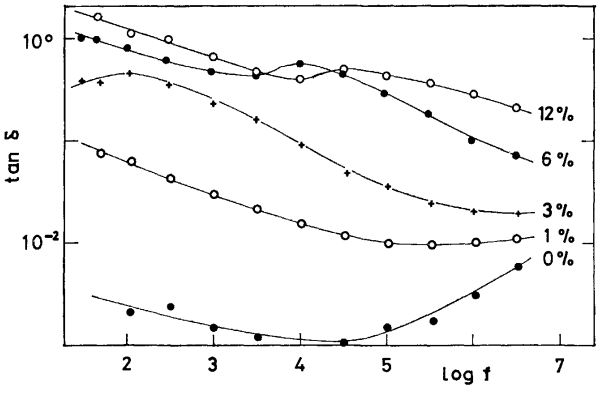

Fig. 7. The curves of frequency versus log tan δ of γ-alumina with various amount of water at 23 °C in the range of Relaxation I.

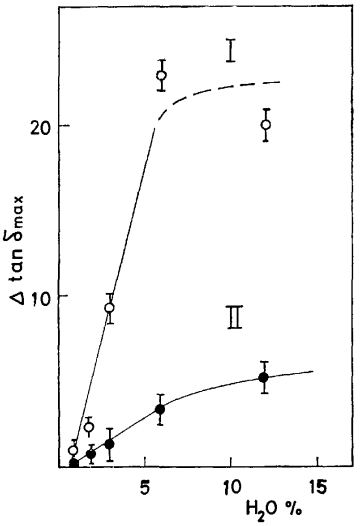

Fig. 8. The relations between the water content and Δ tan δ_{max} which was estimated as the difference of tan δ maxima of the Relaxations I (open circle) and II (full circle) and their baselines.

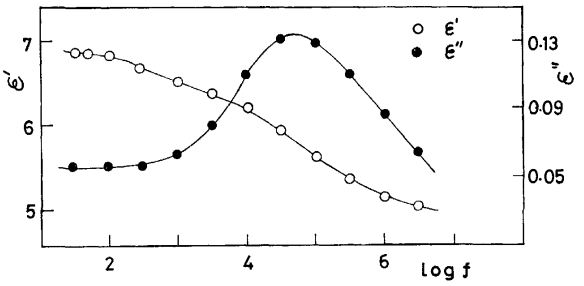

Fig. 9. The relations of ε' and ε'' to the frequency of the Relaxation II of γ-alumina having 3% adsorbed water at −79 °C.

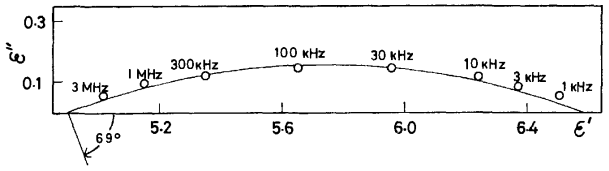

Fig. 10. The Cole-Cole arc of the Relaxation II of γ-alumina containing 3% adsorbed water at −79 °C.

with ours. Since Relaxation II showed a marked frequency shift upon the deuterium exchange, as is shown in Fig. 6, this relaxation seems to be related to either some form of adsorbed water or to some kind of hydroxyl group on the γ-alumina surface. The magnitude of Relaxation II ($\Delta \tan \delta_{max}$) is plotted in Fig. 8 with the same procedure as has been described in the case of Relaxation I. In this figure, Relaxation II behaves similarly to Relaxation I, and both of these relaxations disappear somewhere near 0% water. However, the point of disappearance is not yet known more exactly. The sample heat-treated in the range from 65 to 180 °C, after the saturation of the sample with water at room temperature, contains adsorbed water ranging from 2 to 0% respectively, when we take 180 °C as the desorption temperature. Therefore, it

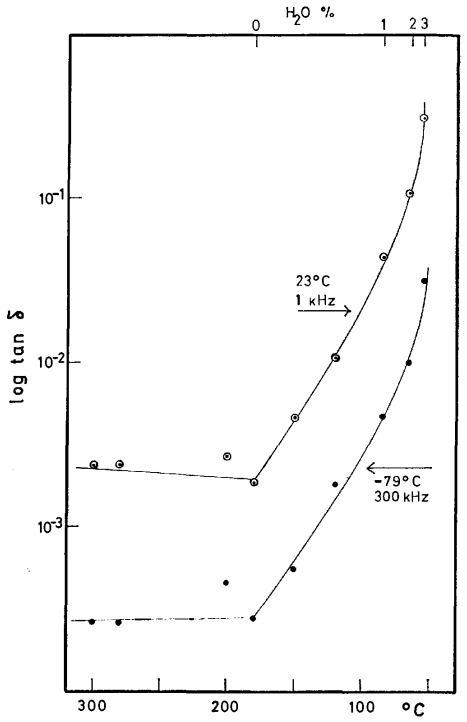

Fig. 11. The relations between tan δ and heat-treatment temperature of γ-alumina at 1 kHz and 300 kHz at 23 °C and −79 °C respectively.

might be possible to see the effect of water content on tan δ more clearly by replacing the horizontal and vertical coordinate axes of Fig. 8 with those of the heat-treatment temperature below and above 180 °C and of tan δ in the range of these dielectric relaxations respectively, as is seen in Fig. 11. The tan δ curves of 1 kHz at 23 °C and 300 kHz at −79 °C in this figure, being situated in the ranges of Relaxations I and II respectively, become constant above 180 °C. This suggests that Relaxations I and II both disappear at about 180 °C; the choice of this temperature as that of the desorption of adsorbed water, as has been mentioned in the previous section, therefore, seems reasonable. Ebert[2] and Dransfeld[3] vaguely attributed this relaxation to the dipole orientation and the proton migration of adsorbed water respectively. Although it may not be simply concluded that Relaxations I and II originate in the adsorbed water on the basis of the present result alone, it might be possible to draw inferences as follows: 1) The dielectric absorption intensity of Relaxation I is larger than that of Relaxation II; hence, Relaxation I might correspond to the larger weight-decrease, as is seen markedly below about 90 °C in Fig. 1. The effect of the adsorbed water for E and the τ_0 of Relaxation I is similar, to some extent, to that of the dielectric relaxation I of silica gel,[10] which was assigned to adsorbed water. Relaxation I might be related to the adsorbed water, being loosely bound to the surface. 2) Relaxation II is smaller than Relaxation I and might correspond to the smaller

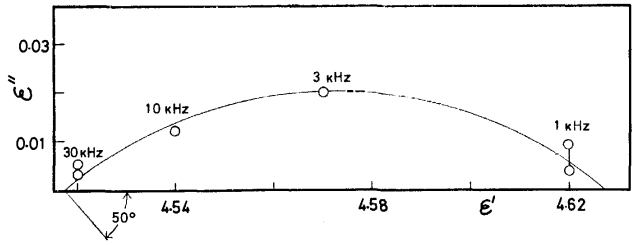

Fig. 12. The Cole-Cole arc of the Relaxation III of γ-alumina at −196 °C.

weight-decrease below about 190 °C in Fig. 1. The effect of adsorbed water for E and τ_0 of this relaxation is somewhat similar to the dielectric relaxation II of silica gel,[9] which was assigned to surface silanol. Relaxation II might thus be related to some kind of surface hydroxyl group which could be dehydrated very easily from the surface of γ-alumina.

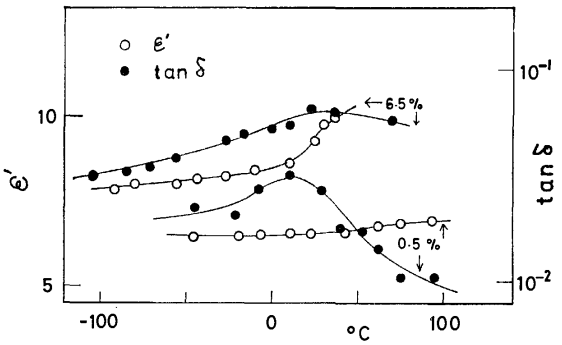

Fig. 13. The relations between tan δ and temperature of γ-alumina with 0.5 and 6.5% water at 9.72 GHz.

Anomaly III. The ε' and ε'' relations of Anomaly III, mentioned in Fig. 3, are plotted at −196 °C in Fig. 12. This relation constitutes the Cole-Cole arc and, therefore, means that Anomaly III is a dielectric relaxation (Relaxation III). The relation between the relaxation times of Relaxation III and the reciprocal temperature plotted in Fig. 6 is linear. Relaxation III becomes observable above the heat-treatment temperature of 120 °C or with a water content of less than 0.5% due to the decrease in the dielectric loss. Relaxation III might thus be related to some kind of hydroxyl group which has a weak interaction with the surroundings, considering the small value of E.

The Dielectric Anomaly at 9.72 GHz. A dielectric anomaly was observed at 9.72 GHz on γ-alumina with various amounts of adsorbed water, as is shown in Fig. 13. This anomaly seems to be a kind of dielectric relaxation according to the temperature effects of ε' and ε'', although the frequency effect could not be measured. We could not ascertain, from the Arrhenius plot in Fig. 6, whether this relaxation belongs to Relaxation II or to III. This relaxation seems, however, to belong to Relaxation II, in view of the similarity of the values of ε' and tan δ.

Ultraviolet Spectra of Hydrazide Solutions and Their Hydrolysis. I. Hydrolysis of Formhydrazide in Acid Solutions

Mitsuo MASHIMA and Fujiko IKEDA

Department of Chemistry, Faculty of Science and Engineering, Saga University, Honjo-machi, Saga

(Received August 19, 1972)

The protonation constant 1.99 of formhydrazide (pK_{BH^+}) has been obtained from measurements of its ultraviolet absorption in dilute sulfuric acid. From the absorption in concentrated sulphuric and perchloric acids, the apparent first-order rate constants of acid-catalyzed hydrolysis have been determined. The reaction mechanism of rate-determining steps has been proposed by means of the plots of Zucker-Hammett and Bunnett.

Ultraviolet absorption spectra and hydrolysis of amides have been of interest to a number of investigators. However, little is known about the ultraviolet spectra and hydrolysis of hydrazides. Edward, Hutchison and Meacock[1] determined the rate constants for the hydrolysis of acethydrazide in aqueous hydrochloric acid. They obtained the first-order rate constants which increase with the increase of acid concentration. For acethydrazide in 0.1N HCl, Lindegren and Niemann[2] determined the apparent ionization constant of $AcNHNH_3^+$ by potentiometric titration and obtained 3.24 for pK_{BH^+}. Recently, the present authors[3] have investigated ultraviolet spectra of some hydrazides in various solvents and have reported on the behavior of a band with maximum at about 190 mμ.

A series of works has been made for examining systematically the spectral change of hydrazides in aqueous solutions by adding electrolytes and non-electrolytes, and for determining the rate constant of the hydrolysis of hydrazides in acid- and alkali-media. The present communication deals with spectroscopical measurements of the protonation constant of formhydrazide and its rate constant of hydrolysis in sulphuric and perchloric acids.

Experimental

Materials and Apparatus. Formhydrazide was synthesized with methylformate and hydrazinehydrate and purified by recrystallization from ether–ethanol mixture: mp 54 °C. Formhydrazidehydrochloride was precipitated from a solution of formhydrazide dissolved in an aqueous hydrochloride by addition of ethanol and the precipitates were washed repeatedly with ethanol: mp 139 °C. Aqueous acid solutions were prepared by dilution of reagent-grade acids with water. They were standardized by titration with standard sodium hydroxide solution. Organic solvents, methanol and dioxane, were of spectrograde.

The ultraviolet solution spectra were measured with a Hitachi EPS-3T Recording Spectrophotometer equipped with a thermostated cell compartment. All the measurements were carried out at 25±0.01 °C.

Rate Measurements. Reactions were followed by recording the change in absorbance A with time. The apparent first-order rate constant k' was calculated graphically from plots of log $(A-A_\infty)$ *vs.* time (min) or by means of a computer program which gives, by adjustment of A_∞, the first-order rate constant which best fits the observed data. In view of the highly dilute reaction solutions, 10^{-3} M (mol/l), used for spectrophotometric examination, no attempt was made to isolate reaction products from the reaction solutions. It is expected that the products are formic acid and hydrazine (or hydrazinium ions). To check the A_∞, the absorption spectra of these materials dissolved in reaction media were examined and compared with those of reaction solutions.

Results and Discussion

Absorption Spectra. The ultraviolet solution spectra of formhydrazide and its hydrochloride are shown in Fig. 1. In water formhydrazide gives a broad absorption band asymmetrically broadened to the low energy side, having probably four component bands with maxima at about 188, 189, 192, and 193 mμ. Such an absorption is characteristic of the hydrazides in water.[3] For formhydrazide this band red-shifts to 203 mμ in methanol and to 212 mμ in dioxane (curves 2 and 3, Fig. 1). It has been tentatively assigned[3] to the $\pi\rightarrow\pi^*$ transition of the carbonyl π-electron system perturbed by the π-electron system of $NHNH_2$ group. If this is the case, the result is not in line with the view that the $\pi\rightarrow\pi^*$ transition band red-shifts by hydrogen bonding in hydroxylic solvents.[4]

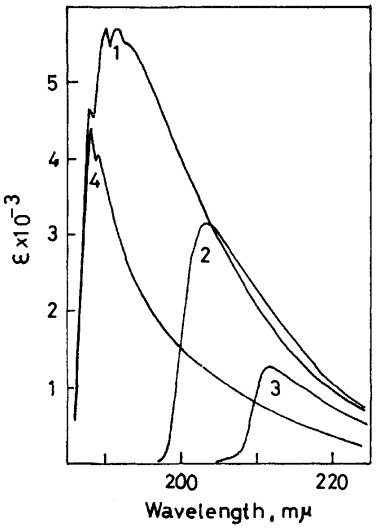

Fig. 1. Ultraviolet spectra of formhydrazide (1, in water; 2, in methanol; 3, in dioxane) and its hydrochloride (4, in water).

1) J. T. Edward, H. P. Hutchison and S. C. R. Meacock, *J. Chem. Soc.*, **1955**, 2520.

2) C. R. Lindegren and C. Niemann, *J. Amer. Chem. Soc.*, **71**, 1504 (1949).

3) M. Mashima and F. Ikeda, *Chem. Lett.*, **1972**, 209.

4) G. C. Pimental and A. L. McClellan, "The Hydrogen Bond," W. H. Freeman and Company, San Francisco (1960), Chap. 4.

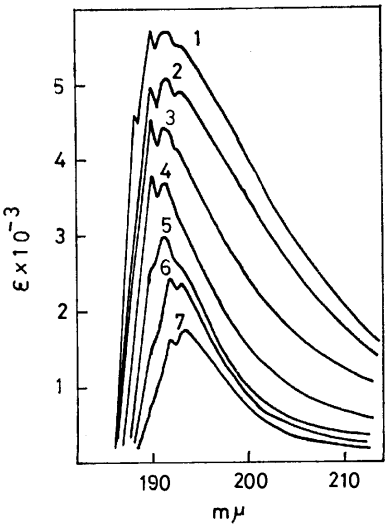

Fig. 2. Spectral changes of formhydrazide in dilute aqueous sulphuric acid.
The acid concentrations are (1) 0, (2) 0.5768×10^{-3}, (3) 0.2884×10^{-2}, (4) 0.1154×10^{-1}, (5) 0.5047×10^{-1}, (6) 0.5678×10^{-1}, (7) 0.1131N.

Formhydrazide hydrochloride in water shows two bands with maxima at 188 and 189 mμ. They are ascribable to electronic transition in formhydrazidinium ion, $HCONHNH_3^+$, which is expected to have two electronic transitions with nearly equal energies.

Spectral Changes in Highly Dilute Sulphuric Acid. Spectral changes in sulphuric acid more dilute than about 0.1N, are shown in Fig. 2. It is seen that the broad band absorbed by formhydrazide in water does not shift but the extinction coefficients are lowered successively with increasing acid concentrations. In such a dilute acid no change in absorbance was observed with time, but a delayed spectral change at about 0.1N (Fig. 3) and a marked change was observed at still higher concentration. The spectral changes with time indicate that the hydrolysis occurs in concentrated acid solutions.

The behavior of two bands absorbed by formhydrazide hydrochloride dissolved in sulphuric acid is shown in Fig. 4. When the concentration of acid is smaller than that of hydrochloride, no change of shape

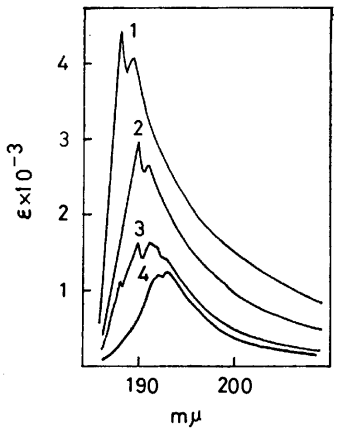

Fig. 4. Ultraviolet spectra $HCONHNH_2$–HCl in aq. H_2SO_4.
(1) 0; (2) 0.1442×10^{-2}; (3) 0.1048×10^{-1}; (4) 0.1442N.

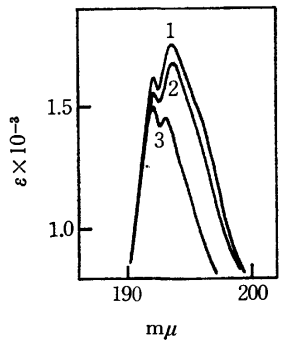

Fig. 3. Spectral change in 0.1132N H_2SO_4.
(1) 14 min (2) 2 hr (3) 17 hr after preparing the solution.

was observed but the two bands red-shift to 190 and 191 mμ, respectively. When the acid concentration exceeds that of hydrochloride, the absorption is similar, in both shape and positions of component peaks, to that of formhydrazide dissolved in water; it indicates that both formhydrazide in water and its hydrochloride in sulphuric acid of an appropriate concentration have the same absorbing species (compare curve 3, Fig. 4 with curve 1, Fig. 1). At still higher acid concentration, *e.g.* about 0.14N, the band is similar in both shape and positions of peaks to those of formhydrazide in about 0.11N of sulphuric acid (compare curve 4, Fig. 4 with curve 7, Fig. 2). Thus, both these solutions seem to have the same absorbing species differing from that contained in the aqueous solution of formhydrazide hydrochloride. The latter would be $HCONHNH_3^+$ or its hydrated species, and the former $HCONHNH_2$ or its hydrated species. From a comparison of 2, 3, and 4 in Fig. 4, it seems that at least two absorbing species are present in the solution giving curve 3. Consequently, in aqueous formhydrazide solution there will be an ionization equilibrium:

$$HCONHNH_3^+ + H_2O \rightleftarrows HCONHNH_2 + H_3O^+,$$

between hydrated molecular species and hydrated ionic species.

Calculation of Thermodynamic Protonation Constant. The ionized species shows the 190 mμ peak which is weakened with the increase of acid concentration (Fig. 2). Therefore, the extinction coefficients at 190 mμ seem to be suitable for calculating the equilibrium constant.

By measuring the extinction coefficient of a base, at any given wavelength, it is possible to calculate the value of pK_{BH^+} for the base from the following equation.[5]

$$pK_{BH^+} = \log\{(\varepsilon-\varepsilon_i)/(\varepsilon_m-\varepsilon)\} + \log(\gamma_i/\gamma_m) - \log a_{H^+}$$

where pK_{BH^+} is the negative logarithm of the thermodynamic dissociation constant for the equilibrium $BH^+ \rightleftarrows B + H^+$, γ_i and γ_m are the activity coefficients of the acid cation BH^+ and the base B, respectively, a_{H^+} is the activity of hydrogen ion; ε_i and ε_m are the extinction coefficients of BH^+ and B, respectively; ε is that due to absorbing species in an appropriate solutions. The values of $\log\gamma_i$ at 25 °C were calculated from the

5) L. A. Flexer, L. P. Hammett, and A. Dingwall, *J. Amer. Chem. Soc.*, **57**, 2103 (1935).

approximate Debye-Hückel equation $\log \gamma_i = -0.510 \times z^2 \times I/(1+1.32 \times I)$, where z is the valency of BH^+ (equal to unity in the present study) and I is the ionic strength of the medium. The values of I were calculated by assuming that in such a dilution as considered here sulphuric acid is almost completely ionized.[6] It was assumed that $\gamma_m = 1$. The values of a_{H^+} were assumed to be equal to those of the mean activity of sulphuric acid, $a_\pm (= m_\pm \gamma_\pm)$, whose values were calculated by using the mean activity coefficients obtained by interpolation from the values in literature.[7] The values of ε_i and ε_m were adjusted by means of a computer program to give the values of pK_{BH^+} which best fit the observed data of ε; the results of calculation are summarized in Table 1. In view of the value of pK_{BH^+} it would appear that formhydrazide is a weaker base than acethydrazide ($pK_{BH^+} = 3.24$).[2] This seems to be in line with the fact that formic acid is a stronger acid than acetic acid.

TABLE 1. VALUES OF pK_{BH^+} AT 25 °C

Molality H_2SO_4	$\log\{(\varepsilon-\varepsilon_i)/(\varepsilon_m-\varepsilon)\}$ [a]	$\log \gamma_i$	$\log a_{H^+}$	pK_{BH^+}
0.2892×10^{-3}	−1.37	−0.01	3.37	1.99
0.7231×10^{-3}	−0.95	−0.02	3.01	2.04
0.1446×10^{-2}	−0.71	−0.03	2.74	2.00
0.2893×10^{-2}	−0.45	−0.04	2.48	1.99
0.4339×10^{-2}	−0.37	−0.05	2.34	1.92
0.5788×10^{-2}	−0.27	−0.06	2.25	1.92
1.443×10^{-2}	+0.19	−0.08	1.94	2.05
				m. 1.99±0.04

a) ε_i and ε_m were assumed to be 5130 and 1450, respectively.

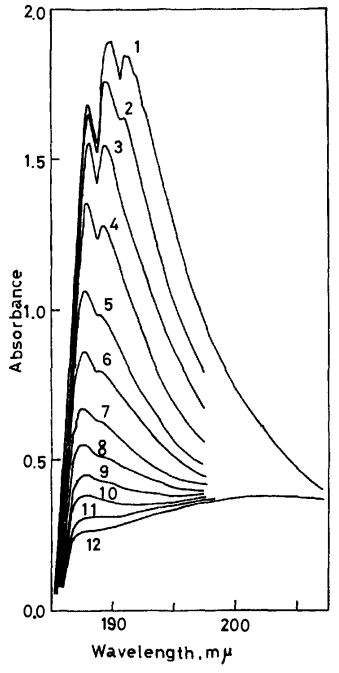

Fig. 5. Spectral changes of $HCONHNH_2$ in 8.51 M H_2SO_4.
(1) 12.0, (2) 13.8, (3) 15.3, (4) 16.8, (5) 18.7, (6) 20.3, (7) 22.3, (8) 24.0, (9) 26.0, (10) 28.0. (11) 33.0, (12) 43.0 min after preparing the solution.

6) T. F. Young and L. A. Blatz, *Chem. Rev.*, **44**, 93 (1949).
7) H. S. Harned and B. B. Owen, "Physical Chemistry of Electrolytic Solutions," 3rd. Ed., Reinhold Pub. Corp., New York (1958), p. 576.

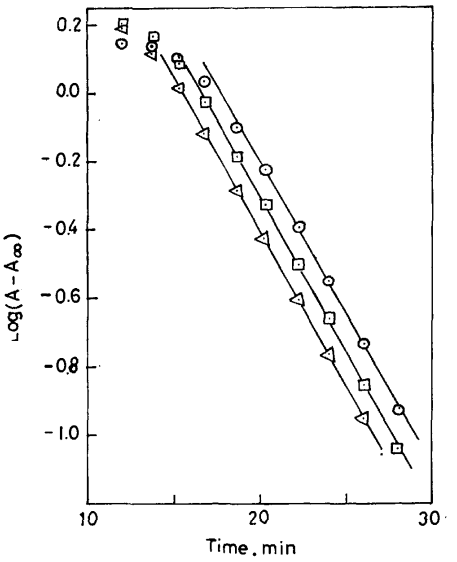

Fig. 6. The $\log (A - A_\infty)$ *vs.* t plots for the hydrolysis of $HCONHNH_2$ in 8.51 M H_2SO_4.
⊙: at 188 mμ, ⊡: at 190 mμ, △: at 191 mμ.

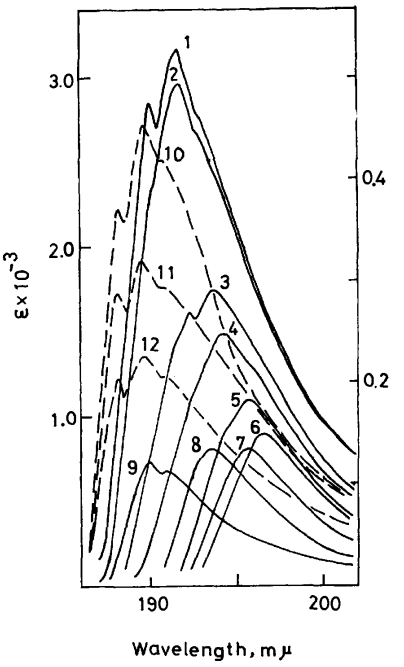

Fig. 7. Spectral changes of $HCONHNH_2$ in aq H_2SO_4 with increasing acid concentration.
(1) 0.01420, (2) 0.02523, (3) 0.05655, (4) 0.1419, (5) 0.5235, (6) 1.627, (7) 2.501, (8) 4.125, (9) 6.593, (10) 7.435, (11) 7.870, (12) 9.360 M.

Hydrolysis in Sulphuric Acid. The change of absorbance with time was observed for the solutions of formhydrazide dissolved in sulphuric acid above about 0.1N. Typical one is shown in Fig. 5 for a reaction solution of formhydrazide (*ca.* 8×10^{-3} M) dissolved in sulphuric acid (*ca.* 8 M). The $\log (A - A_\infty)$ *vs.* t plots at the wavelengths where three peaks are shown primarily by the reaction solution are shown in Fig. 6. The plots give good straight lines having nearly the same slope except for some initial points. The slope therefore definitely gives the apparent first-order rate constant. The presence of points deviating

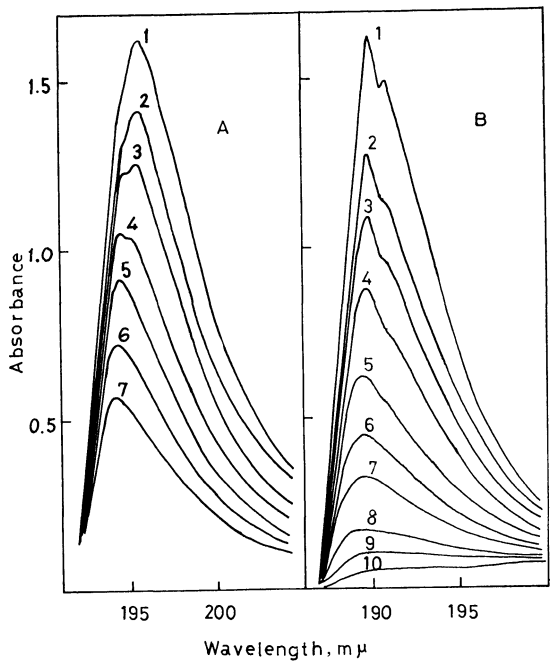

Fig. 8. Spectral changes of $HCONHNH_2$ in aq H_2SO_4.
A; 0.523 M H_2SO_4: (1) 8.25, (2) 22.1, (3) 58.3, (4) 110.6, (5) 155.1, (6) 210.1, (7) 270.1 min; B; 6.59 M H_2SO_4: (1) 9.1, (2) 11.2, (3) 12.5, (4) 14.2, (5) 16.6, (6) 18.9, (7) 21.2, (8) 26.0, (9) 30.6, (10) 42.3 min after preparing the solutions.

from the linear plot indicates that a reaction occurs prior to hydrolysis.

From a comparison of the primary absorption curves of reaction solutions, we see that both the shape of band and the potitions of component peaks change with increasing acid concentration. The initial abosrption curves are given in Fig. 7. In view of the change of the band with time, it is useless to compare the values of extinction coefficient with each other, but the positions of peaks are useful for examining the effects of acidity on the formhydrazide absorption. We give the following comments. (1) At relatively low acidity the absorption band has an intense peak with another rather weak peak (or a shoulder) on the high energy side. This band red-shifts with increasing acid concentration up to about 2 M, and further increasing acid concentration brings about a blue-shift. Moreover, the above main peak disappears prior to hydrolysis and the subpeak is weakened gradually with progress of hydrolysis (Fig. 8A). Thus, it would appear that in this region of acid concentrations the reaction solution contains initially two absorbing species affected by acid media. (2) Another case of typical changes of absorbance with time is shown in Fig. 8B which contains the absorption curves for reaction solutions made up of about 6 M sulphuric acid. The reaction solution shows initially the band with two peaks (the main peak on the high energy side and a subpeak on the low side). A similar band was observed in all the reaction solutions. Therefore, this band may be ascribed to the substrate hydrolyzed immediately. (3) Above about 7 M acid concentration, the reaction solution initially gives a broad absorption band with component peaks at the same positions as those of formhydrazide in water (compare curve 1, Fig. 5 with curve 1, Fig. 1) and increasing acid concentration does not affect the position of component peaks (see dashed cruves in Fig. 7). This indicates that the electronic states of formhydrazide are affected by structures or characters of water molecules in aqueous sulphuric acid. The band, composed of several component bands and observed in sulphuric acid above 7 M, is expected to arise from two absorbing species, one absorbing the band with two peaks at 188 and 189 mμ and the other at 190 and 191 mμ. With the progress of reaction two bands at higher wavelengths, 190 and 191 mμ, disappear first followed by the band at 188 mμ (Fig. 5).

Table 2. First-order rate constant (k') for hydrolysis of formhydrazide

Sulfuric acid		Perchloric acid	
Molarity[a)]	$10^2 \times k'$ (min^{-1})	Molarity	$10^2 \times k'$ (min^{-1})
0.1420	0.145	1.002	0.448
0.2465	0.216	1.861	1.03
0.4068	0.332	2.690	1.84
0.5235	0.4123	3.449	2.45
0.8715	0.785	4.916	3.55
1.140	1.18	5.833	4.08
1.627	1.65	6.783	4.68
2.034	2.31	7.883	5.45
2.551	3.66	8.633	5.88
3.015	5.02	9.009	6.12
3.717	6.88	9.384	6.30
4.125	7.73		
4.766	8.93		
5.746	11.7		
6.592	15.3		
7.435	17.4		
7.870	19.1		
8.510	20.4		
9.360	23.1		

a) Because of the velocity being too high, k' values in concentrations higher than those in the present study could not be determined.

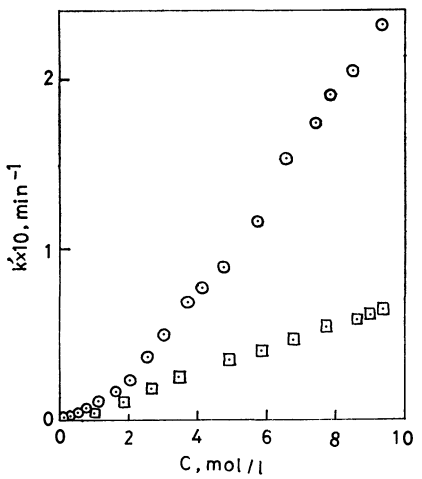

Fig. 9. Dependence of rate constants on acid concentration.
⊙: H_2SO_4, ⊡: $HClO_4$

Rate Constants of Hydrolysis in Sulphuric and Perchloric Acids. The apparent first-order rate constant k' was determined for formhydrazide in sulphuric and perchloric acids. The values of k' are given in Table 2 and the plot of k' *vs.* acid concentration (M) is shown in Fig. 9. The rate constant depends on the acid concentration but not in the same way for both acids. Thus the hydrolysis of formhydrazide seems to be acid catalyzed.

Zucker and Hammett[8] treated quantitavely rate-acidity dependence in acids for the first time. They grouped reactions into two categories, depending on whether the logarithm of the pseudo first-order rate constants were linear either $-H_0$ (negative Hammett's acidity function) or $\log C_{H^+}$ (molar concentration of hydrogen ion), with approximately unit slope. They assumed that reactions of the first type involved rate-determining unimolecular decomposition of protonated substrate (A1 mechanism) and those of the second type

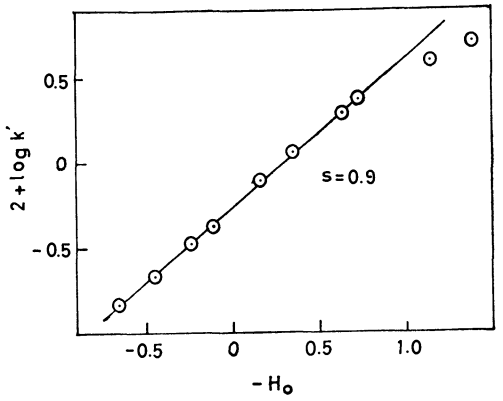

Fig. 10. Log k' *vs.* $-H_0$* plot for the hydrolysis of $HCONHNH_2$ in 0.1—3.0 M H_2SO_4.
* The H_0 values were obtained by interpolation from the values presented in Ref. 9a in the text.

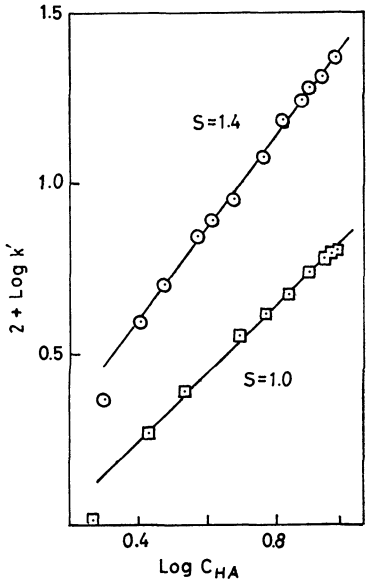

Fig. 11. Log k' *vs.* log M plot for the hydrolysis of $HCONHNH_2$ in moderately concentrated H_2SO_4 and $HClO_4$.
⊙: H_2SO_4, ⊡: $HClO_4$.

8) L. Zucker and L. P. Hammett, *J. Amer. Chem. Soc.*, **61**, 2791 (1939).

involved rate-determining attack on protonated substrate by a water molecule (A2 mechnism).[9]

In a limited range of acid concentrations (0.1—2.0 M), the k' *vs.* $-H_0$ plot (Fig. 10) is straight with a 0.9 slope; at high acid concentration above *ca.* 2 M, the log k' *vs.* log M plot (Fig. 11) is straight with a 1.0 slope (in perchloric acid) and a 1.4 slope (in sulphuric acid). According to the Zucker-Hammett hypothesis, the A1 mechanism seems to be suitable for the rate-determining stage of the hydrolysis of formhydrazide at low acid-concentrations; the A2 mechanism seems to be suitable at high acid-concentrations. However, objection to the Zucker-Hammett hypothesis was discussed theoretically and experimentally by Taft, Deno, and Shell[10] and by later workers.[11]

Bunnett[12] found empirically that, for a large number of reactions, plots of log $k'+H_0$ *vs.* the logarithm of the activity of water (log a_w) in the reaction medium are linear or very nearly linear. The slopes w of these plots vary over a wide range. From a comparison with reactions of known mechanism it was possible to classify reactions into three types according to the magnitude of w values and the role of water in the rate-determining step, as shown in Table 3.

Table 3. Mechanistic interpretation of w (after Bunnett[12])

Range of w value	Role of water in the rate-determining step
−2.5 to 0.0	not involved
+1.2 to +3.3	acts as a nucleophile
>+3.3	acts as a proton transfer agent

For the acid-catalyzed hydrolysis of formhydrazide in concentrated acid solutions, the Bunnett plot is given in Fig. 12 which contains the plot in sulphuric acid above 2.5 M and in perchloric acid above 1.8 M. It is of interest to see that the Zucker-Hammett plot (Fig. 11) gives only a straight line in the range of acid concentration examined in the present study, while the Bunnett plot gives straight lines composed of two parts. According to the Bunnett treatment the w values indicate the following reaction mechanisms of hydrolysis. In moderately strong acid solutions, 2.5—7 M sulphuric acid (w=5.0) and 1.5—6 M perchloric acid (w=5.5), the reaction mechanism contains proton transfer in rate-determining steps. Gillespie[13] has shown on the basis of results of Raman and NMR measurements that perchloric acid dissociates completely up to about 6 M.[14] He compared the H_0 values for these acids

9) For comprehensive treatment, see a) M. A. Paul and F. A. Long, *Chem. Rev.*, **57**, 1 (1957); b) F. A. Long and M. A. Paul, *ibid.*, **57**, 935 (1957).

10) R. W. Taft, N. C. Deno, and P. S. Shell, *Ann. Rev. Phys. Chem.*, **9**, 287 (1958).

11) Contains an extensive bibliography, H. Zollinger, *ibid.*, **13**, 391 (1962).

12) J. F. Bunnett, *J. Amer. Chem. Soc.*, **83**, 4956, 4968, 4973, 4978 (1961).

13) R. J. Gillespie, "Physico Chemical Progresses in Mixed Aqueous Solvents," ed. by F. Franks, Heineman, London (1967), pp.129— 140.

14) See Figs. 7 and 6 in Ref. 13.

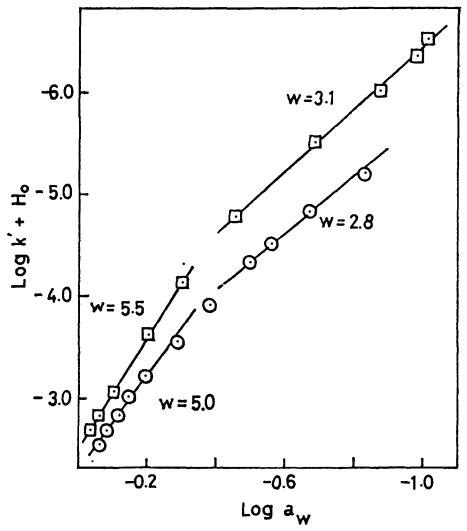

Fig. 12. Log k' + H_0 *vs.* log a_w* plot for the hydrolysis of $HCONHNH_2$. ⊙: H_2SO_4, ⊡: $HClO_4$.
* The a_W values were obtained by interpolation from the values given in Ref. 12 in the text.

at concentrations at which ionization is incomplete, and pointed out that the $HClO_4$ molecule and perhaps also the H_3O^+ ion have a greater proton donating ability in this medium than in H_2SO_4. This is consistent with our results: the rate-determining steps contain proton transfer in the range 1.5—6 M of perchloric acid concentration and the w value in perchloric acid is higher than that in sulphuric acid.

At a still higher acid-concentration than 7 M, water acts as a nucleophile in the slow step. The conclusion depends on the w value of 2.8 for sulphuric acid and of 3.1 for perchloric acid. In this region of acid concentration, both acids would be incompletely ionized. Wyatt[15] interpreted the incomplete ionization of sulphuric acid by postulating that the H_3O^+ ion tends to retain a molecule of hydration. The postulation seems to be consistent with the role of water.

Conclusion

Using a spectrophotometric method, we determined the protonation constant and the apparent first-order rate constant of the acid-catalyzed hydrolysis for formhydrazide.

The number 1.99 has been obtained for pK_{BH^+} of formhydrazide in highly dilute sulphuric acid. Hydrolysis occurs in relatively low dilution (0.1—2.0 M) and involves rate determining unimolecular decomposition of protonated substrate (A1 mechanism), using the Zucker-Hammett, log k' *vs.* $-H_0$ plot. However, in concentrated acid media the Bunnett, log $k'+H_0$ *vs.* log a_w plot is preferable for inspecting the reaction mechanism. Consequently, we have proposed the following mechanism: in the acid media 2—6 M the rate-determining steps contain proton transfer and above about 7 M water acts as a nucleophile.

15) P. A. H. Wyatt, *Disc. Faraday Soc.*, **24**, 162 (1957).

BULLETIN OF THE CHEMICAL SOCIETY OF JAPAN, VOL. 46, 1371—1374 (1973)

Ultraviolet Spectra of Hydrazide Solutions and Their Hydrolysis. II. Hydrolysis of Formhydrazide in Alkaline Solutions

Mitsuo MASHIMA and Fujiko IKEDA

Department of Chemistry, Faculty of Science and Engineering, Saga University, Honjo-machi, Saga

(Received October 7, 1972)

The aparent first-order rate constants of the base catalyzed hydrolysis of formhydrazide have been determined by ultraviolet absorption measurements. Three cases of hydrolysis applicable to three different ranges of NaOH concentrations were recognized. The activation entropies have been calculated from the change of rate constant with temperature. The effects of solvent basicity and temperature on the absorption spectra have also been studied.

Recently, the effects of amide structure, hydroxide ion concentration, temperature, and other variables on the kinetics of base-catalyzed hydrolysis of amides have been studied by a number of investigators.[1] Similar effects on the kinetics of alkaline hydrolysis of hydrazides have not been reported.

The hydrazides are expected to undergo hydrolysis catalyzed by both acid and base. The acidic hydrolysis of formhydrazide has been reported.[2] In the present work we have examined the effects of hydroxide ion concentration and temperature on the kinetics of base-catalyzed hydrolysis of formhydrazide.

Experimental

Materials and apparatus have been described.[2] The alkaline solvents were made by diluting the stock solution of NaOH (reagent grade) immediately before each set of measurements.

1) *Cf., e.g.*, R. H. DeWolfe and R. C. Newcomb, *J. Org. Chem.*, **36**, 3870 (1971).

2) M. Mashima and F. Ikeda, This Bulletin, **46**, 1366 (1973).

Results

Apparent First-Order Rate Constant (k_{obs}). The dependence of k_{obs} upon NaOH concentrations is shown in Table 1 and Fig. 1. The values of k_{obs} increase with increasing NaOH concentration up to a certain value, levelling off near *ca.* 0.5 mol/l, and then decrease gradually.

Table 1. Rate constants of the base-catalyzed hydrolysis of formhydrazide at 25°C

NaOH molarity	$k_{obs}\times10^2$ (min^{-1})	NaOH molarity	$k_{obs}\times10^2$ (min^{-1})
0.101	0.200	0.905	2.24
0.0153	0.282	1.02	2.24
0.0198	0.373	1.36	2.23
0.0253	0.465	1.60	2.16
0.0355	0.691	2.02	2.11
0.0510	1.14	2.51	2.02
0.102	1.27	3.05	1.97
0.130	1.48	3.34	1.94
0.162	1.65	4.05	1.80
0.202	1.87	4.48	1.70
0.250	2.09	5.09	1.65
0.308	2.15	5.51	1.51
0.404	2.26	6.35	1.46
0.510	2.32	8.24	1.05
0.604	2.38	9.16	0.985
0.805	2.27		

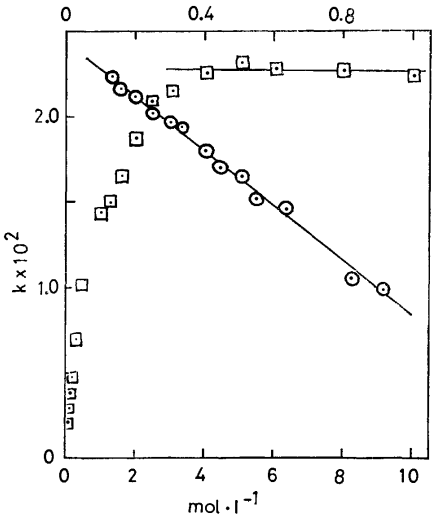

Fig. 1. The plot of k_{obs} *vs.* [NaOH]. ⊡: lower [NaOH] used the upper scale of abscissa, ⊙: higher [NaOH] used the down scale.

Kinetics in Dilute NaOH Solutions. In NaOH solutions (<*ca.* 0.5 mol/l) the reaction scheme is given by the following equations. NH_2NHCHO molecule and OH^- ion combine reversibly to form a complex (1) which decomposes slowly to form products (2).

$$NH_2NHCHO + OH^- \rightleftarrows NH_2NHC^-(OH)OH \quad \text{equil. const. } K \qquad (1)$$

$$NH_2NHC^-(OH)OH \longrightarrow HCOO^- + NH_2NH_2 \quad \text{rate const. } k \qquad (2)$$

Rate laws and K are given by

$$-d[F]/dt = k[A^-] \qquad (3)$$

$$-d[F]/dt = k_{obs}[F] \qquad (4)$$

$$K = \frac{[A^-]}{[A]}\frac{\gamma_{A^-}}{\gamma_A a_{OH^-}}, \qquad (5)$$

where A and A^- stand for NH_2NHCHO and $NH_2NHC^-(OH)OH$, respectively; F=total hydrazide (A+A^-); γ and a are activity coefficient and activity, respectively. The overall rate constant k_{obs} is readily combined with both k and K.

$$1/k_{obs} = 1/k + (1/kK)\times(\gamma_{A^-}/\gamma_A a_{OH^-}) \qquad (6)$$

A plot of $1/k_{obs}$ *vs.* $\gamma_{A^-}/(\gamma_A\times a_{OH^-})$ gives a straight line with a slope $1/kK$ and intercept $1/k$ (Fig. 2). The values of a_{OH^-} were assumed to be equal to those of mean activity ($a_\pm$) of NaOH, calculated by using mean activity coefficient obtained by interpolation from the values of Åkerlöf and Kegeles;[3] the values of γ_{A^-} were calculated from the approximate Debye-Hückel equation $\log\gamma_{A^-} = -0.510\times z^2\times(I)^{1/2}/(1+1.15\times(I)^{1/2})$, where z is the valency of A^- (equal to unity) and I is the ionic strength of aqueous NaOH solutions. A good extrapolation was obtained giving $k=3.03\times10^{-2}$ min^{-1}. With this value the slope gives $K=7.76$. Consequently, the linear plot indicates that in the region of NaOH concentration lower than *ca.* 0.5 mol/l the reaction scheme is given by equations 1 and 2, the rate-determining step being the unimolecular decomposition of the complex (Eq. 2). The true reaction mechanism will be complicated because of the change in hydration in passing from the reactants ($NH_2NHCHO+OH^-$) to the complex and to the resultants.

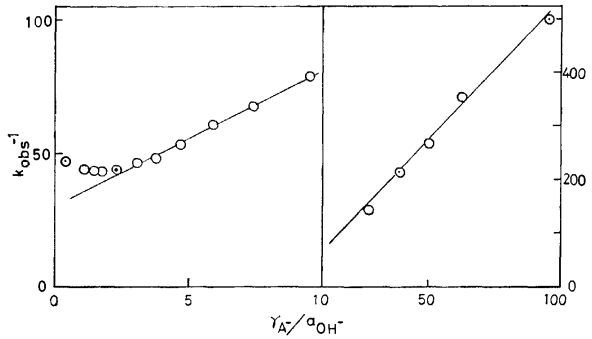

Fig. 2. The $1/k_{obs}$ *vs.* γ_{A^-}/a_{OH^-} plot.

Kinetics in Moderately Concentrated NaOH Solutions. A possible mechanism for the base catalysis is one in which the attacking species is hydroxide ion, the reaction scheme being given by

$$NH_2NHCHO + OH^- \overset{\text{slow}}{\rightleftarrows} HCOO^- + NH_2NH_2 \qquad (7)$$

In this case the overall rate constant k_{obs} can be combined with OH^- concentration by $k_{obs}=k[OH^-]$. As seen from Fig. 1, the plot of k_{obs} *vs.* [OH^-] (taken as equal to the stoichiometric concentration of NaOH) shows that k_{obs} is nearly constant in the narrow range of [NaOH], *ca.* 0.5—1 mol/l. Above *ca.* 1.5 mol/l k_{obs}

3) G. Åkerlöf and G. Kegeles, *J. Amer. Chem. Soc.*, **62**, 620 (1940).

decreases linearly with increasing [NaOH]. Thus, the base-catalyzed hydrolysis would proceed by Eq. (7) in these regions of [NaOH], the changes of hydration numbers being disregarded.

Dependence of Rate Constant on Temperature. Temperature effects were examined at 15, 20, 25, 30, and 35 °C for reaction solutions made with 0.250, 0.582, and 3.34 mol/l [NaOH] (substrate concentrations 1.5—0.6 × 10^{-3} mol/l). These concentrations lie in the three ranges where the hydrolysis proceeds in different ways. The Arrhenius plot, log k_{obs} *vs.* $1/T$ is shown in Fig. 3 and the values of k_{obs} in Table 2. The data give a straight line, the Arrhenius activation energy of 51.3 kcal/mol being obtained from its slope. The entropy of activation, 112 e.u., was calculated for 25 °C by means of the equation given by Bunnett.[4]

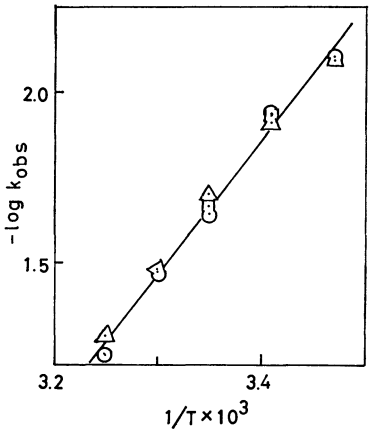

Fig. 3. Arrhenius plot, log k_{obs} *vs.* $1/T$.
⊡: 0.250, ⊙: 0.582, △: 3.34 mol/l.

Table 2. Temperature effects on k_{obs}

Temperature (°C)	$k_{obs} \times 10^2$, min^{-1} NaOH concentration, mol/l		
	3.34	0.582	0.250
15	0.799	0.788	—
20	1.23	1.15	1.16
25	1.94	2.27	2.09
30	3.30	3.35	—
35	5.22	5.93	—

Behavior of Absorption Maxima. The primal absorption maximum of reaction solutions shifts successively to longer wavelengths with increasing NaOH concentration and rising temperature. The temperature effects on λ_{max} is shown in Fig. 4 (the ordinate scale is not available for a comparison of absorption intensity). Figure 5 shows the plot of λ_{max} for a series of [NaOH] against the logarithm of mean activity $a_{\pm}$ of NaOH. At lower NaOH concentration the values of λ_{max} vary linearly with increase in log $a_{\pm}$, but at higher concentration a negative deviation from the line takes place. It is of interest that the change in the value of λ_{max} might be connected with this simple thermodynamic character of solvents.

4) J. F. Bunnett, "Technique of Organic Chemistry," Vol. VIII, Part I, ed. by A. Weissberger, Interscience, New York, N. Y. (1961), p. 201.

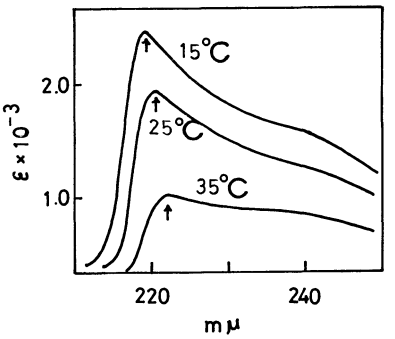

Fig. 4. Temperature effect on absorption of reaction solutions made by 0.582 mol/l NaOH.

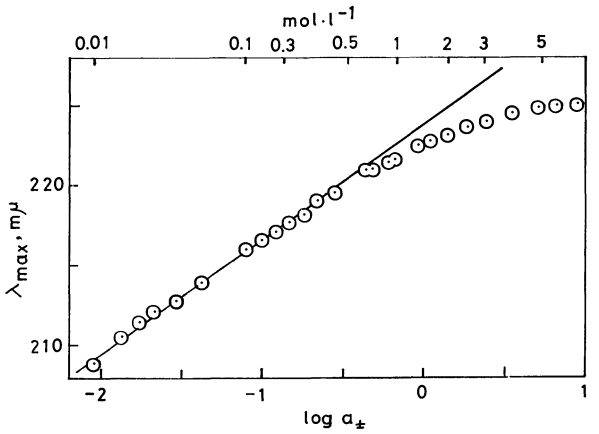

Fig. 5. The plot of λ_{max} *vs.* log $a_{\pm}$.

Discussion

Mechanism of Hydrolysis. The products of alkaline hydrolysis of the hydrazides $RCONHNH_2$ would be carboxyl ions and hydrazine:

$$RCONHNH_2 + OH^- \longrightarrow RCO_2^- + NH_2NH_2. \quad (8)$$

We see that the reaction involves rate-determining unimolecular decomposition of the complex in dilute solutions,

$$S + OH^- \rightleftharpoons SOH^-$$

$$SOH^- \xrightarrow{slow} \neq \longrightarrow \text{products}$$

and the rate-determining nucleophilic attack of OH^- in moderately concentrated solutions,

$$S + OH^- \xrightarrow{slow} \neq \longrightarrow \text{products}.$$

Although the value of activation entropy is based on pseudo-first-order rate constants independent of solvent basicity, the observed medium independence of $\Delta S^{\neq}$ over the range of basicities 0.25—3.34 mol/l would not be expected to lead to such a constancy, provided a mechanism change is involved.

Correlation of k_{obs} with Acidity Function H_-. Yagil and others[5] summarized the formulation of rate expressions of eight types of base-catalyzed reactions, which can be divided into three groups. Our results (Eqs. 1, 2, and 7) belong to the group containing

5) M. Anbar, M. Bostelsky, D. Samuel, and G. Yagil, *J. Amer. Chem. Soc.*, **85**, 2380 (1963).

reactions expected to give a linear plot of $\log k_{obs}$ *vs.* $H_-+\log C_w$,[6] with about unit slope. The plot for our results is shown in Fig. 6 together with the Zucker-Hammett type plot, $\log k_{obs}$ *vs.* H_-. Both plots indicate that, in the range of NaOH concentration shown in Fig. 6, two linear parts can be obtained with slopes (<0.3) deviating greatly from unity, with a boundary point between them.

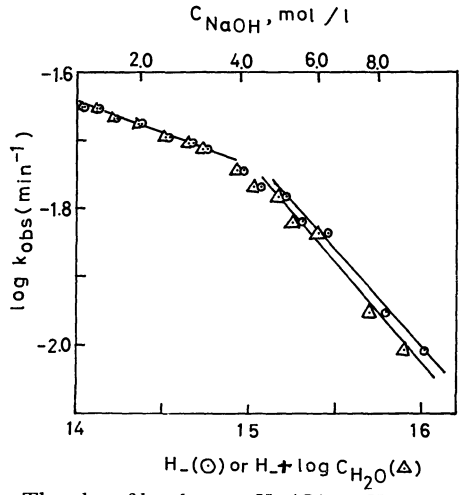

Fig. 6. The plot of $\log k_{obs}$ *vs.* H_- (⊙) or $H_-+\log Cw$ (△).

By analogy with the Bunnett treatment[7] of the acid-catalyzed reactions, $\log k_{obs}-H_-$ was plotted against the logarithm of water activity a_w (Fig. 7) for the hydrolysis in reaction solutions except for ones prepared with very dilute NaOH solutions. Three linear parts were obtained; in dilute NaOH solutions (<*ca.* 0.8 mol/l) with slope 40, in the range *ca.* 1—3 mol/l with 20 and >*ca.* 5 mol/l with 5.6. Assuming that these parts correspond to three types of hydrolysis, one is the rate-determining unimolecular decomposition of the complex $NH_2NHC^-(OH)OH$, and the other two due to the rate-determining nucleophilic attack of OH^- with different values of slope of the plot k_{obs} *vs.* [NaOH], the results being consistent with those given in the preceeding paragraph. As Rochester[8] has pointed out,

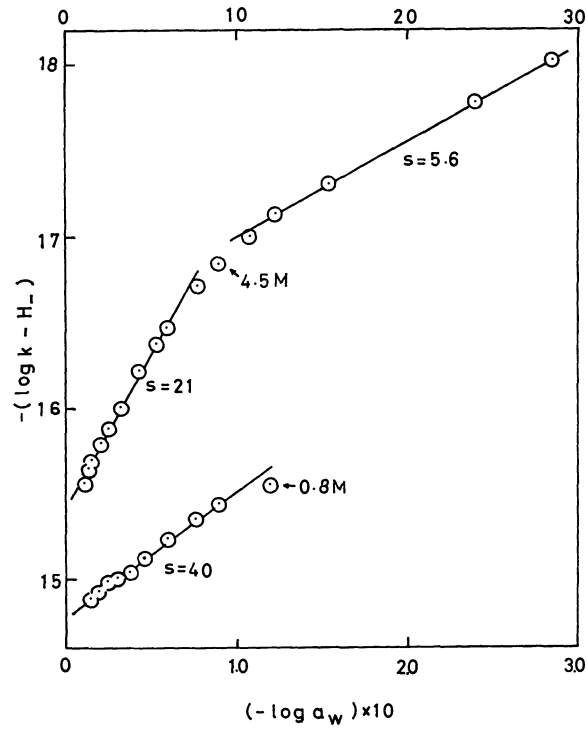

Fig. 7. The plot of $\log k_{obs}-H_-$ *vs.* $\log a_w$. The upper scale of abscissa is used for the upper plots and the lower scale for the lower ones.

the values of slopes of the linear plot, $\log k-H_-$ *vs.* $\log a_w$, would provide useful criteria for the mechanism of reactions in basic media.

Behavior of Absorption Maxima. Smith and Symons[9] ascribed the red-shifts of the first electronic absorption band of solvated iodide ions with temperature rise to an increase in the average radius of the solvent shell. As shown in Fig. 4, the maximum of primary absorption of reaction solutions shifts to longer wavelengths with temperature rise. The effect is ascribable to the change in energy levels of hydrated molecular or ionic species of formhydrazide and to the change of the water shell. It is of interest that there is a linear correlation between λ_{max} and $\log a_\pm$ of NaOH in the range <*ca.* 0.8 mol/l of basicities, where the rate constants have also been combined with $a_\pm$.

6) For C_w denoting the concentration of free water, see G. Yagil and M. Anbar, *J. Amer. Chem. Soc.*, **85**, 2376 (1963).

7) J. F. Bunnett, *ibid.*, **83**, 4956, 4968, 4973, 4978 (1961).

8) C. H. Rochester, "Acidity Functions," Academic Press, London (1970), p. 243.

9) M. Smith and H. C. R. Symons, *Discuss. Faraday Soc.*, **24**, 206 (1957).

The Crystal and Molecular Structure of Piperazinium Terephthalate, $(H_2NC_4H_8NH_2)^{2+}(O_2C\cdot C_6H_4\cdot CO_2)^{2-}$

Setsuo KASHINO, Minoru SASAKI,* and Masao HAISA

Department of Chemistry, Faculty of Science, Okayama University, Tsushima, Okayama 700

(Received November 4, 1972)

Piperazinium terephthalate has been prepared and examined by X-ray analysis. The compound crystallizes in the monoclinic space group $P2_1/c$ with two formula units in a unit cell. The cell dimensions are: $a=9.45$, $b=8.30$, $c=8.33$ Å, and $\beta=117.3°$. The structure was determined by the Patterson method from the data collected with Cu$K\alpha$ radiation on Weissenberg photographs, and refined by the block-diagonal least-squares method with anisotropic temperature factors for non-hydrogen atoms and fixed isotropic ones for hydrogen atoms. The final R value is 0.108 for 941 non-zero reflections. Acid and base moieties occupy the positions of center of symmetry in the cell. Two N^+–H···O^- hydrogen bonds (2.612 and 2.737 Å) link a nitrogen atom of piperazine with two carboxyl oxygens of the acids related by c glide plane to form a three-dimensional hydrogen bond network, in which each oxygen atom accepts one hydrogen bond. The coordination around the nitrogen atom is nearly tetrahedral. The piperazine ring takes a chair form. The twisting angle between the carboxyl group and the benzene ring plane is 17.3°.

During the course of investigation of the structure of the addition compounds of piperidine with benzoic acids,[1] it was found desirable to extend studies to the addition compounds of bifunctional aromatic acids and bifunctional heterocyclic amines. The present paper reports the formation and the crystal and molecular structure of an addition compound of piperazine with terephthalic acid, showing that the compound is piperazinium terephthalate.

Experimental

Piperazinium terephthalate was prepared by dissolving equimolar quantities of terephthalic acid and piperazine in hot water. After the solution had been left to stand at room temperature, colorless prisms separated out. Mp 307 °C (decomp.); IR: antisymmetric $\nu(CO_2^-)$ 1565 cm^{-1}, symmetric $\nu(CO_2^-)$ 1385 cm^{-1}.

Found: C, 57.19; H, 6.56; N, 10.89%. Calcd for $C_{12}H_{16}N_2O_4$: C, 57.13; H, 6.39; N, 11.10%.

Crystals obtained by slow cooling from aqueous solution were monoclinic prisms elongated along the a axis. Cell constants were determined from Weissenberg and oscillation photographs using Cu$K\alpha$ radiation ($\lambda=1.5418$ Å), and calibrated with sodium chloride.

Crystal data: piperazinium terephthalate, $(H_2NC_4H_8NH_2)^{2+}(OOC\cdot C_6H_4\cdot COO)^{2-}$; formula weight=252.3; monoclinic, $a=9.45(2)$, $b=8.30(1)$, $c=8.33(2)$ Å, $\beta=117.3(2)°$, $V=580.4$ Å^3, $D_m=1.44_2$ (by flotation), $D_c=1.443$ g cm^{-3}, $Z=2$.

Linear absorption coefficient for Cu$K\alpha$; $\mu=9.2$ cm^{-1}, $F(000)=268$.

Absent spectra: $h0l$ when l is odd, $0k0$ when k is odd. Space group is $P2_1/c$.

Three different crystals with approximate dimensions $0.3\times0.3\times0.9$, $0.4\times0.3\times0.3$, and $0.3\times0.3\times0.3$ mm were used for a, b, and c axis photographs, respectively. Using Cu$K\alpha$ radiation, multiple-film equi-inclination Weissenberg photographs were taken for the layers from $0kl$ to $7kl$, from $h0l$ to $h5l$, and $hk0$. In all, 941 independent non-zero reflections were observed out of about 1350 possible reflections within the Cu$K\alpha$ sphere. Intensities were estimated by visual comparison with a calibrated intensity scale. After Lorentz, polarization, and spot-shape corrections were made, the intensities of various layers were put on the same relative scale by making use of all the common reflections. The relative values were put on an absolute scale by Wilson's method. No corrections for absorption and extinction effects were made.

Structure Analysis

Since only two molecular units of acid and base moieties were contained in a unit cell of the space

TABLE 1. FINAL ATOMIC PARAMETERS AND ESTIMATED STANDARD DEVIATIONS ($\times10^4$) FOR NON-HYDROGEN ATOMS

The anisotropic temperature factors are defined as $\exp(-B_{11}h^2-B_{22}k^2-B_{33}l^2-B_{12}hk-B_{13}hl-B_{23}kl)$.

Atom	x/a	y/b	z/c	B_{11}	B_{22}	B_{33}	B_{12}	B_{13}	B_{23}
O(1)	6895(4)	6709(4)	768(4)	62(4)	71(5)	58(5)	46(7)	2(8)	3(8)
O(2)	7765(5)	4435(4)	141(4)	117(6)	94(5)	32(5)	71(9)	10(8)	−18(9)
C(1)	7771(5)	5490(5)	1223(5)	28(5)	72(6)	31(6)	3(9)	16(9)	18(11)
C(2)	8928(5)	5238(5)	3179(5)	16(4)	73(6)	39(6)	−8(9)	35(9)	0(10)
C(3)	9347(5)	6513(5)	4414(6)	32(5)	51(6)	54(7)	17(9)	33(10)	11(10)
C(4)	9592(5)	3741(5)	3784(6)	40(5)	62(6)	43(6)	−5(10)	31(10)	−25(11)
C(5)	3480(5)	9221(6)	−614(6)	30(5)	76(7)	72(7)	−23(9)	46(10)	−12(12)
C(6)	4488(5)	9594(6)	1349(6)	55(6)	80(7)	55(7)	−8(10)	81(11)	10(12)
N	6200(4)	9620(5)	1780(4)	35(4)	79(6)	28(5)	13(8)	12(8)	−2(9)

* Present address: Kanebo Co., Ltd., Kanebo-cho, Hofu, Yamaguchi.

1) S. Kashino, Y. Sumida, and M. Haisa, *Acta Crystallogr.*, **B28**, 1374 (1972).

Table 2. Final positional parameters and estimated standard deviations ($\times 10^3$) for hydrogen atoms

Atom	x/a	y/b	z/c	Atom	x/a	y/b	z/c
H (1)	892 (8)	744 (8)	400 (9)	H (5)	430 (8)	1062 (8)	162 (9)
H (2)	928 (8)	277 (8)	290 (9)	H (6)	417 (8)	869 (8)	200 (10)
H (3)	244 (9)	935 (8)	−79 (10)	H (7)	677 (8)	1002 (8)	311 (9)
H (4)	396 (9)	811 (8)	−81 (10)	H (8)	643 (8)	854 (8)	169 (10)

Table 3. Observed and calculated structure factors ($\times 10$)
Unobserved reflections are marked with an asterisk.

group $P2_1/c$, it was most plausible that each of the acid and base moieties should be centrosymmetric and occupy the center of symmetry of the cell. Thus, the center of gravity of the acid moiety was chosen to be (0, 0, 0) and that of the base moiety (1/2, 0, 0), a half of their molecular unit being taken as the asymmetric unit. Orientation of the acid moiety was sought using two-dimensional Patterson projections onto (1 0 0), (0 1 0), and (0 0 1), the (0 1 0) projection being especially suggestive. Approximate positional parameters of all non-hydrogen atoms were then determined by interpretation of the three-dimensional Patterson map. Position of the nitrogen atom was identified by short interatomic distances of about 2.6 Å from the two carboxyl oxygen atoms in the trial structure. The structure was refined by the block-diagonal least-squares method[2] with isotropic temperature factors to an R value of 0.165 and with anisotropic temperature factors to that of 0.125. A difference Fourier synthesis at this stage revealed all eight hydrogen atoms as shown in Fig. 1(b). Further refinement was made with anisotropic temperature factors for the non-hydrogen atoms and with fixed isotropic temperature factors ($B=1.7$ Å^2) for the hydrogen atoms using the following weighting scheme:

$$\sqrt{w} = 0.0, \quad \text{if } F_o < F_{min} \ (=1.0),$$
$$\sqrt{w} = 1.0, \quad \text{if } F_{min} \leq F_o \leq F_{max} \ (=17.0)$$

and

$$\sqrt{w} = F_{max}/F_o, \quad \text{if } F_o > F_{max}.$$

The final R value was 0.108 for 941 non-zero reflections. The final atomic parameters and their estimated standard deviations for non-hydrogen atoms are given in Table 1, and the final positional parameters for hydrogen atoms in Table 2. A composite drawing of the final electron-density map is shown in Fig. 1 along with the difference synthesis map. The observed and calculated structure factors are listed in Table 3.

The atomic scattering factors used were those of Hanson, Herman, Lea, and Skillman.[3] The numerical calculations were performed with the aid of a HITAC 5020E computer of the Computer Center, the University of Tokyo.

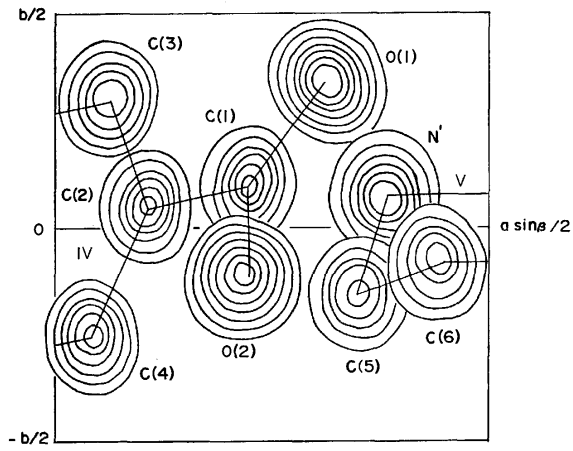

(a)

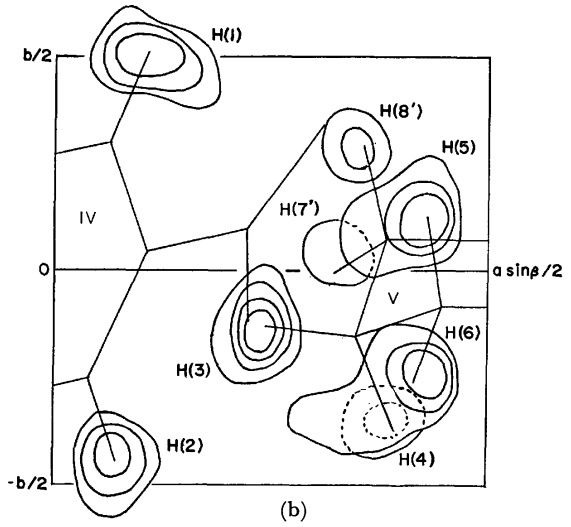

(b)

Fig. 1. (a) Composite drawing of final electron-density map. (b) The difference electron-density map at the stage of $R=0.125$. The contours are at equally spaced intervals on an arbitrary scale. IV and V will be illustrated in Fig. 2.

Results and Discussion

The projections of the crystal structure along the b and a axes are shown in Fig. 2. Two hydrogen bonds of nearly equal length link the nitrogen atom of piperazine with the carboxyl oxygen atoms to form a three-dimensional hydrogen bond network, in which each oxygen atom accepts one hydrogen bond; hydrogen bonds of length 2.737 Å link the acid and base moieties along [1 1 1] and other ones of length 2.616 Å link them along [1 0 2] infinitely. This hydrogen bond scheme explains the high melting point of this compound.

As shown in Fig. 3, the nitrogen atom is nearly tetrahedrally coordinated with the atoms C(6) and C(5') covalently and with the atoms O(1) and O(2') through hydrogen bonds. A difference map (Fig. 1(b)) shows that two hydrogen atoms belong to each nitrogen atom, the N–H bond lengths being determined to be 1.03 and 0.97 Å by the least-squares refinements. It can therefore be concluded that the present compound is composed of piperazinium cation and terephthalate anion, the hydrogen bonds between them being of the type N^+–H···O^-.

Bond angle C(1')–O(2')–N (111.9°) is approximately tetrahedral, but the angle C(1)–O(1)–N (147.0°) deviates considerably from regular tetrahedral angle. Corresponding to the difference, the hydrogen bond length between O(2') and N (2.612 Å) is significantly shorter than that between O(1) and N (2.737 Å). Similar geometries of the hydrogen bond system have been found in the 1: 1 addition compounds of piperidine with p-bromo- and p-chlorobenzoic acids.[1]

Bond lengths and angles of each ion are shown in Fig. 4. The two C–O bond lengths are almost equal to each other (1.251 and 1.255 Å) and shorter than

2) Y. Okaya and T. Ashida, "HBLS IV, The Universal Crystallographic Computing System (I)," The Crystallographic Society of Japan, Tokyo (1967), p. 65.

3) H. H. Hanson, F. Herman, J. D. Lea, and S. Skillman, *Acta Crystallogr.*, **17**, 1040 (1964).

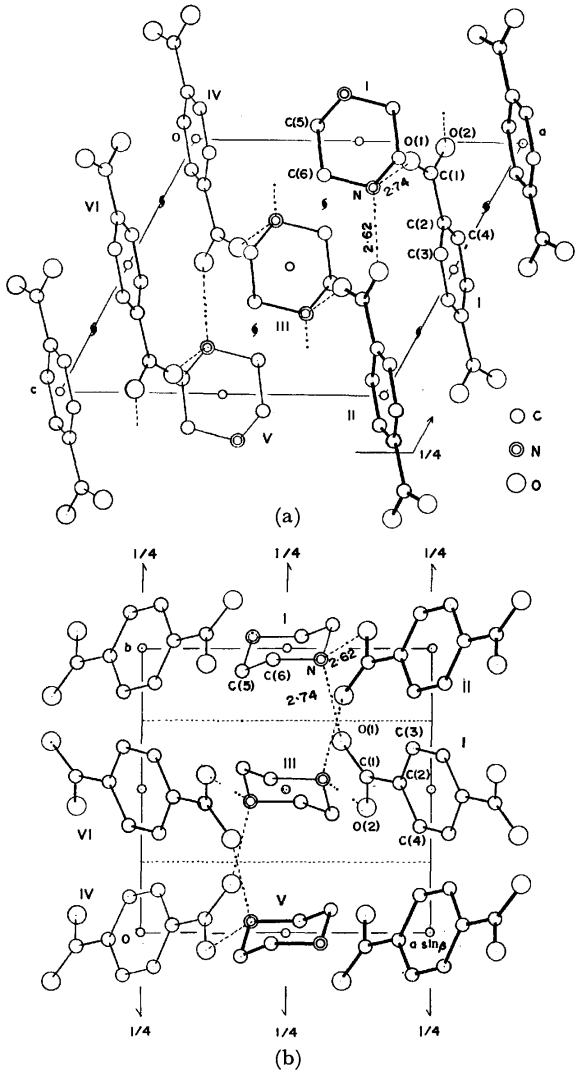

Fig. 2. (a) The projection of the crystal structure along the *b* axis. (b) The projection of the crystal structure along the *a* axis. Hydrogen bonds are shown by broken lines. Key for molecules I: x/a, y/b, z/c (given in Table 1) II: $-x/a+1$, $y/b+1/2$, $-z/c+3/2$ III: (0 −1 −1)II IV: (−1 −1 −1)II V: (0 −1 1)I VI: (−1 0 0)I

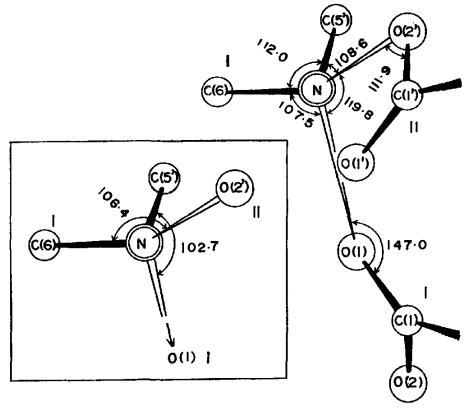

Fig. 3. Molecular geometries around nitrogen atom. Key for molecules is given in Fig. 2. Atoms translated by a center of symmetry in the molecule are shown with prime.

those found in terephthalic acid (1.262 and 1.272 Å),[4] supporting the fact that the acid is ionized. The angles C(2)–C(1)–O(1) and C(2)–C(1)–O(2) differ

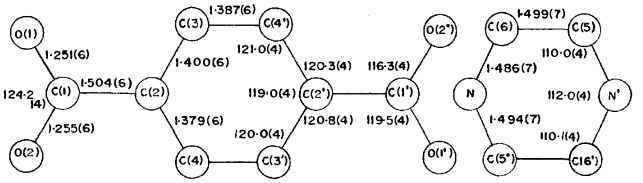

Fig. 4. Bond lengths (Å) and angles (°). The estimated standard deviations are shown in parentheses.

significantly; the former is 119.5° and the latter 116.3°. The mean C–C bond length in the benzene ring is 1.388 Å in agreement with that found in terephthalic acid (1.392 Å).[4] However, a quinonoid character in the benzene ring, which has been found in the terephthalic acid[4] and in terephthalate ion of calcium terephthalate trihydrate,[5] is not appreciable in this compound. The bond length between carboxyl carbon C(1) and aromatic carbon C(2) (1.504 Å) is significantly longer than the corresponding ones in the terephthalic acid (1.483 Å)[4] and in the terephthalate ion of calcium terephthalate trihydrate (1.487 and 1.495 Å).[5] In these two compounds the twisting angle of carboxyl group with respect to the plane of benzene ring are only 5.7—2.2°. In the present compound the angle amounts to 17.3°; distances of atoms C(1), O(1), and O(2) from the benzene ring plane are −0.009, −0.332, and 0.327 Å, respectively. A plausible explanation for the lengthening of the bond between aromatic C and carboxyl C is the diminution of the π-bond character resulting from a large twisting angle. A qualitatively similar relation between the bond length and twisting angle has been found in pyromellitic acid dihydrate.[6]

The molecular geometry of piperazinium ion is

TABLE 4. INTERMOLECULAR DISTANCES WITH THEIR ESTIMATED STANDARD DEVIATIONS GIVEN IN PARENTHESES[a]

From molecule I	To atom	Of molecule	Translation			Distance (Å)
i) Hydrogen bonds						
O (1)	N	I	0	0	0	2.737 (7)
N	O (2′)	II	0	0	0	2.616 (7)
ii) Other distances less than 3.5 Å						
O (1)	C (6)	I	0	0	0	3.485 (7)
O (1)	C (5′)	I	0	0	0	3.394 (8)
O (1)	C (6′)	I	0	0	0	3.482 (7)
C (3)	O (1′)	II	0	0	0	3.348 (8)
C (6)	O (1′)	II	0	0	0	3.495 (9)
N	O (1′)	II	0	0	0	3.268 (9)
O (2)	C (5′)	I	0	−1	0	3.343 (7)
C (6)	O (2′)	II	0	0	0	3.354 (7)
C (5′)	O (2′)	II	0	0	0	3.401 (11)
N	C (1′)	II	0	0	0	3.297 (10)
C (2)	C (6)	II	0	−1	−1	3.466 (9)

a) Key for molecules is given in Fig. 2. Atoms translated by a center of symmetry in the molecule are shown with a prime.

4) M. Bailey and C. J. Brown, *Acta Crystallogr.* **22**, 387 (1967).
5) T. Matsuzaki and Y. Iitaka, *ibid.*, **B28**, 1977 (1972).
6) F. Takusagawa, K. Hirotsu, and A. Shimada, This Bulletin, **44**, 1274 (1971).

identical within the limit of experimental errors with that found by Rérat[7] in piperazine dihydrochloride monohydrate. In the ion one nitrogen atom deviates upward from the plane through four carbon atoms by 0.65 Å and the other must deviate downward by the same distance. Thus the piperazine ring takes a normal chair form. The C–C bond length in the ring (1.499 Å) is in agreement with that found in piperazine hexahydrate (1.491 Å)[8] but significantly shorter than that found in piperazine by gas electron diffraction (1.540 Å).[9] The average C–N bond length is 1.490 Å, which is slightly longer than that observed in the hexahydrate (1.458 Å)[8] and in piperazine (1.467 Å).[9] The C–C–N angles are 110.1 and 111.0°, which are in agreement with those found in the hexahydrate (109.5 and 110.2°), but the C–N–C angle (112.0°) is slightly larger than that found in the hydrate (109.3°).

Intermolecular distances less than 3.5 Å are listed in Table 4. The structure is maintained by closely packed moieties to give a comparatively high density (1.44 g cm^{-3}).

7) C. Rérat, *Acta Crystallogr.*, **13**, 459 (1960).
8) D. Schwarzenbach, *J. Chem. Phys.*, **48**, 4134 (1968).
9) A. Yokozeki and K. Kuchitsu, This Bulletin, **44**, 2352 (1971).

BULLETIN OF THE CHEMICAL SOCIETY OF JAPAN, VOL. 46, 1379—1383 (1973)

ESR of Hot Ions: Ni(I) Complex Ions Produced in Rigid Solutions by γ-Irradiation

Chikara AMANO and Shizuo FUJIWARA

Department of Chemistry, Faculty of Science, The University of Tokyo, Hongo, Bunkyo-ku, Tokyo

(Received November 17, 1972)

Electron spin resonance has been used to study Ni(I) complex ions produced at 77 K through reduction by γ-irradiation of Ni(II) complexes in glassy solvents. The Ni(I) complex ions give axially symmetrical spectra, suggesting that the Ni(I) ions favor tetragonally elongated octahedral form. From the *g*-values it can be shown that the Ni(I)-to-ligand bonding for different ligands increases in covalency in the order: H_2O<edta≪py∼en∼xanthate<phen<dipy≪CN^-. It can also be shown that the metal-to-ligand bonding of the Ni(I) complex ions is less covalent than that of the corresponding Cu(II) complexes. Measurement of the integrated intensity of the ESR spectrum of $[Ni(I)(H_2O)_6]^+$ with reference to a standard sample of $[Cu(II)(H_2O)_6]^{2+}$ shows that at a total dose of 1×10^6 R the yield of the Ni(I) species is $0.21\pm0.04\%$ of the host complex $[Ni(II)(H_2O)_6]^{2+}$. In addition to the anisotropic spectra of the Ni(I) complex ions, isotropic spectra have been observed in several cases, which are probably due to Ni(III) complex ions. Isotropic feature of these spectra may be explained in terms of dynamic Jahn-Teller effect involving the Ni(III) complex ions.

Metal ions of complexes in solids and in rigid solutions are often reduced by X- or γ-irradiation.[1-4] It has also been reported that oxidation of metal ions occurs in some cases.[5] With the gain or loss of an electron these complexes presumably change immediately in configuration of ligands to take structures with fairly long life-time, which give, in some cases, anomalous optical and ESR spectra.[6,7] For example, several Co(II) complex ions produced through reduction of Co(III) complexes by γ-irradiation have been shown to be in the low spin state ($S=1/2$), in contrast to the usual observation of high spin state ($S=3/2$) of Co(II) complexes.[7]

In a preceding paper, an attempt to produce Ni(I) ions in the host lattice by γ-irradiation of Ni(II) complexes has been reported, where it has been shown that only a few Ni(II) complexes give ESR spectra corresponding to Ni(I) state, and that the electronic structure of Ni(I) ions strongly depends on the host lattices.[8]

The present paper concerns with ESR of Ni(I) complex ions in rigid solutions carrying nitrogen and/or sulfur atoms as donating ones. The *g*-values will be used to discuss the nature of the Ni(I)-to-ligand bonding.

Experimental

Nickel(II) chloride hexahydrate was purified by an anion exchange method to remove a trace amount of cobaltous and cupric ions. Several samples with various molar ratios of nickel(II) ions to ligands were prepared. A mixture of ethylene glycol and water (2: 1 v/v) (EG–H_2O) was used as a glassy solvent. A mixture of *ortho*-, *meta*-, and *para*-xylene was also used as a glassy solvent. The systems studied are listed in Table 1. Degassed sample solutions were immersed

1) W. C. Lin, C. A. McDowell, and D. J. Ward, *J. Chem. Phys.*, **49**, 2883 (1968).
2) S. Fujiwara and M. Nakamura, *ibid.*, **52**, 6299 (1970).
3) M. Nakamura and S. Fujiwara, *J. Coord. Chem.*, **1**, 221 (1971).
4) T. Krigas and M. T. Rogers, *J. Chem. Phys.*, **54**, 4769 (1971).
5) T. Krigas and M. T. Rogers, *ibid.*, **55**, 3055 (1971).
6) E. T. Kaisar and L. Kevan (Editors), "Radical Ions," Interscience Publishers, New York (1968).
7) S. Fujiwara, T. Watanabe, and H. Tadano, *J. Coord. Chem.*, **1**, 195 (1971).
8) C. Amano, T. Watanabe, and S. Fujiwara, to be submitted for publication on This Bulletin.

TABLE 1. NICKEL(II)-LIGAND SYSTEMS EXAMINED

Complex	Matrix	Concn of Ni^{2+}(mol/l)	Molar ratios of Ni^{2+} to ligand
Ni(II)–py	EG–H_2O	0.1	1:0, 1:1, 1:2, 1:3, 1:4, 1:5, 1:6, 1:12
Ni(II)–en	EG–H_2O	0.1	1:0, 1:0.5, 1:1, 1:1.5, 1:2, 1:2.5, 1:3, 1:4, 1:6
Ni(II)–dipy	EG–H_2O	0.1	1:0, 1:0.5, 1:1, 1:1.5, 1:2, 1:2.5, 1:3, 1:4, 1:6
Ni(II)–phen	EG–H_2O	0.1	1:0, 1:0.5, 1:1, 1:1.5, 1:2, 1:2.5, 1:3, 1:4, 1:6
Ni(II)–edta	EG–H_2O	0.1	1:0, 1:0.25, 1:0.5, 1:1
Ni(II)–CN^-	EG–H_2O	0.1	1:4
$[Ni(II)(H_2O)_6]Cl_2$	EtOH	0.1	
$[Ni(C_2H_3OS_2)_2]$	Xylene	0.005[a]	
$[Ni(C_3H_5OS_2)_2]$	Xylene	0.01	
$[Ni(C_7H_6O_2N)_2]$	Xylene	0.004[a]	
$[Ni(C_8H_8ON)_2]$	Xylene	0.006[a]	
$[Ni(C_9H_{10}ON)_2]$	Xylene	0.01	
$[Ni(C_{10}H_{12}ON)_2]$	Xylene	0.01	

EG=ethylene glycol, py=pyridine, en=ethylenediamine, dipy=α,α′-dipyridyl, phen=1,10-phenanthroline, $C_2H_3OS_2$=methyl xanthate, $C_3H_5OS_2$=ethyl xanthate, $C_7H_6O_2N$=salicylaldoxime, C_8H_8ON=*N*-methylsalicylaldimine, $C_9H_{10}ON$=*N*-ethylsalicylaldimine, $C_{10}H_{12}ON$=*N*-propylsalicylaldimine.

a) Saturated solution

TABLE 2. ESR PARAMETERS OF NICKEL(I) COMPLEX IONS

Complex ion	Matrix	$g_{//}(\pm 0.002)$	$g_{\perp}(\pm 0.002)$	$k(10^{-4}\,cm^{-1})$	$k'(10^{-4}\,cm^{-1})$
$[Ni(I)(H_2O)_6]^+$	EG–H_2O	2.466	2.076	0.96	0.63
$[Ni(I)(H_2O)_6]^+$	EtOH	2.471	2.078	0.97	0.64
$[Ni(I)(py)(H_2O)_5]^+$	EG–H_2O	2.402	2.073	0.83	0.60
$[Ni(I)(py)_2(H_2O)_4]^+$	EG–H_2O	2.344	2.071	0.72	0.59
$[Ni(I)(py)_3(H_2O)_3]^+$	EG–H_2O	2.316	2.071	0.65	0.59
$[Ni(I)(py)_4(H_2O)_2]^+$	EG–H_2O	2.282	2.068	0.58	0.56
$[Ni(I)(en)(H_2O)_4]^+$	EG–H_2O	2.359	2.072	0.74	0.59
$[Ni(I)(en)_2(H_2O)_2]^+$	EG–H_2O	2.282	2.064	0.58	0.53
$[Ni(I)(phen)(H_2O)_4]^+$	EG–H_2O	2.317	2.076	0.65	0.63
$[Ni(I)(phen)_2(H_2O)_2]^+$	EG–H_2O	2.271	2.078	0.56	0.64
$[Ni(I)(dipy)(H_2O)_4]^+$	EG–H_2O	2.311	2.075	0.64	0.62
$[Ni(I)(dipy)_2(H_2O)_2]^+$	EG–H_2O	2.259	2.074	0.53	0.61
$[Ni(I)(edta)(H_2O)]^{3-}$	EG–H_2O	2.414	2.077	0.86	0.64
$[Ni(I)(CN)_4]^{3-}$	EG–H_2O	2.131	2.030	0.27	0.25
$[Ni(I)(C_2H_3OS_2)_2]^-$	Xylene	2.282	2.076	0.58	0.63
$[Ni(I)(C_3H_5OS_2)_2]^-$	Xylene	2.280	2.074	0.58	0.61
$[Ni(I)(C_7H_6O_2N)_2]^-$	Xylene	2.250[a]		0.52	
$[Ni(I)(C_8H_8ON)_2]^-$	Xylene	2.311[a]		0.64	
$[Ni(I)(C_9H_{10}ON)_2]^-$	Xylene	2.317[a]		0.65	
$[Ni(I)(C_{10}H_{12}ON)_2]^-$	Xylene	2.317[a]		0.65	

a) Rhombic ESR patterns

in liquid nitrogen and given at 77 K a γ-ray dosage of 1×10^6 R from ^{60}Co source with the dose rate of 5×10^4 R/h. ESR spectra were recorded at 77 K on a JEOL 3BSX spectrometer.

The yield of $[Ni(I)(H_2O)_6]^+$ was determined by comparing the integrated ESR intensity of Ni(I) complex ions with that of a standard sample which contained 6.02×10^{16} ions of $[Cu(II)(H_2O)_6]^{2+}$ in EG–H_2O.[9] The samples used in the present experiment contain 6.02×10^{18} ions of $[Ni(II)(H_2O)_6]^{2+}$ and the concentration of $[Ni(II)(H_2O)_6]^{2+}$ is 1.00×10^{-1} mol/l.

9) Since $[Cu(II)(H_2O)_6]^{2+}$ and $[Ni(I)(H_2O)_6]^+$ are almost the same with respect to the anisotropy of the *g*-tensor ($g_{//}=2.400$, $g_{\perp}=2.099$ for Cu(II) and $g_{//}=2.466$, $g_{\perp}=2.076$ for Ni(I)), the ESR transition probability, and hence, the integrated intensity is assumed equal to each other between these two complexes.

Results and Discussion

In all systems examined, the *g*-tensors are nearly axially symmetric. Since ^{61}Ni, only isotope with non-zero nuclear spin, has a very low natural abundance (1.25%), hyperfine structure due to nickel nuclei was not observed. Principal values of the *g*-tensor ($g_{//}$ and $g_{\perp}$) were obtained as usual, and the results are summarized in Table 2.

The yield of $[Ni(I)(H_2O)_6]^+$ was found to be 0.21 ± 0.04% of the amount of the host $[Ni(II)(H_2O)_6]^{2+}$ at a γ-ray dosage of 1×10^6 R.[10]

10) This corresponds to a *G*-value in radiation chemistry of 0.21 ± 0.04.

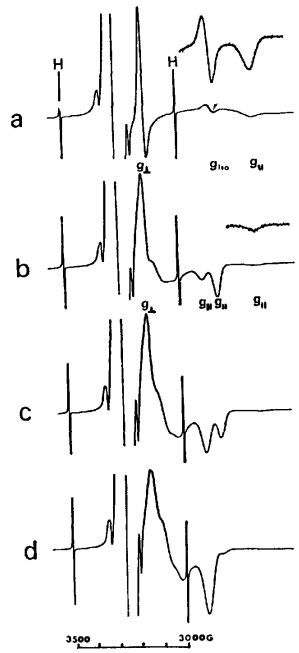

Fig. 1. γ-Irradiated Ni(II)-dipy complexes in rigid ethylene glycol–water solution.
a) Ni^{2+}: dipy=1:0 b) 1:0.5 c) 1:1 d) 1:2

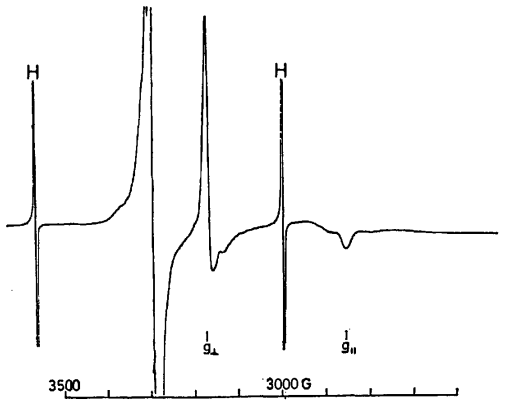

Fig. 2. ESR spectrum of $[Ni(I)\ (ethylxanthate)_2]^-$ produced by γ-irradiation in rigid xylene solution.

The Ni(I) complex ions produced by γ-irradiation are stable at 77 K for several days, but the ESR spectra disappear as soon as the samples are brought to room temperature. ESR spectra due to hydrogen atoms and radicals with unidentified structure are also observed at $g\sim2.0023$ from all samples. All the γ-irradiated samples other than those in rigid xylene solutions show a deep blue color, which is probably due to solvated electrons.

Assignment of ESR Spectra. Experimental results in Table 2 show that $g_{//}>g_{\perp}>g_e$ (=2.0023), and that the $g_{//}$-values are strongly dependent on the kind of ligands. It is also noted that g-shifts ($\Delta g=g_{obs}-2.0023$) are fairly large. The large g-shifts eliminate a possibility that these signals are due to radicals by the solvent and/or ligands. The relation of $g_{//}$, $g_{\perp}$, and g_e for various electron configurations and multiplets predicted by the ligand field theory is summarized in Table 3. High spin state ($S=3/2$) of d^7 electron configuration is eliminated from Table 3, since the observed spectra do not show the nature of high spin state. Complex ions with high spin state should have a spin-lattice relaxation time too short to permit the observation of ESR spectra at 77 K and, even if observed, should have large g-values of 4 or 6 by the contribution of orbital magnetic moment. The g-values in Table 3 have been calculated according to the framework of strong field approximation; cubic field, electron-electron repulsion and tetragonal field are successively applied as perturbations. Actually, we have built multiplet wavefunctions taking electron-electron repulsion into consideration to the first order, which are expressed as the linear combinations of seven electron wavefunctions of determinantal type. For instance, for the wavefunctions belonging to the ground state of ^2E_g we have

$$|^2E_g\ 1/2\ u\rangle = |d_{yz}\overline{d_{yz}}d_{zx}\overline{d_{zx}}d_{xy}\overline{d_{xy}}d_{3z^2-r^2}|$$
$$|^2E_g\ 1/2\ v\rangle = |d_{yz}\overline{d_{yz}}d_{zx}\overline{d_{zx}}d_{xy}\overline{d_{xy}}d_{x^2-y^2}|$$

All the multiplet wavefunctions are the eigenfunctions of spin-operators, S^2 and S_z, and are transformed in similar fashion with the bases of irreducible representations of O_h group. Tetragonal field is taken into account to the first order. Taking spin-orbit interaction ($H_{so}=\sum_{i=1}^{7}\xi(\vec{r}_i)\vec{l}_i\vec{s}_i$) and Zeeman interaction ($H_z=\sum_{i=1}^{7}\beta(\vec{l}_i+2\vec{s}_i)\vec{H}$) as perturbation, the second order energy is calculated within forty functions belonging to the ground and the one electron excited configurations. Although the results in Table 3 are obtained by using a simple crystal field theory, these relations should remain unchanged even if configuration interaction is taken into account in an LCAO MO formalism. As Table 3 shows, case A and case D are consistent with the experimental results. As far as we know, complex ions with the d^7 electron configuration have always been shown to be in the $^2A_{1g}$ state (case C), and a

Table 3. Predicted g-values for four different cases

Case	Config	Multiplet	$g_{//}$	$g_{\perp}$	Order
A	d^9	$^2B_{1g}$	$2+8\zeta/E(^2B_{2g})^{a)}$	$2+2\zeta/E(^2E_g)$	$g_{//}>g_{\perp}>2$
B	d^9	$^2A_{1g}$	2	$2+6\zeta/E(^2E_g)$	$g_{\perp}>g_{//}=2$
C	d^7	$^2A_{1g}$	2	$2+(3+6a_1b_1)\zeta/E(^2E_g{}^a)$ $+(3+6a_2b_2)\zeta/E(^2E_g{}^b)$	$g_{\perp}>g_{//}=2$
D	d^7	$^2B_{1g}$	$2+(4+8a_1b_1)\zeta/E(^2B_{2g}{}^a)^{b,c)}$ $+(4+8a_2b_2)\zeta/E(^2B_{2g}{}^b)$	$2+(1+2a_1b_1)\zeta/E(^2E^a)$ $+(1+2a_2b_2)\zeta/E(^2E_g{}^b)$	$g_{//}>g_{\perp}>2$

a) Energy value when that of the ground multiplet is zero.
b) $a_1=-10B/\{(4B+C+A)^2+100B^2\}^{1/2}$, $b_1=(4B+C+A)/\{(4B+C+A)^2+100B^2\}^{1/2}$, $a_2=-10B/\{(4B+C-A)^2+100B^2\}^{1/2}$, $b_2=(4B+C-A)/\{(4B+C-A)^2+100B^2\}^{1/2}$; $A\equiv(116B^2+8BC+C^2)^{1/2}$.
c) $a_1b_1\sim-0.36$, $a_2b_2\sim0.36$; $B=1115\ cm^{-1}$, $C=5450\ cm^{-1}$ for Ni^{3+}.

Table 4. ESR parameters of copper(II) complexes

Complex ion	Matrix	$g_{//}$	$g_{\perp}$	k	k'	Ref.
$[Cu(II)(H_2O)_6]^{2+}$	Glycerin–H_2O	2.400	2.099	0.60	0.60	a)
$[Cu(II)(py)_4]^{2+}$	H_2O	2.22		0.33		b)
$[Cu(II)(en)(H_2O)_4]^{2+}$	Glycerin–H_2O	2.281	2.058	0.42	0.34	a)
$[Cu(II)(en)_2(H_2O)_2]^{2+}$	Glycerin–H_2O	2.209	2.047	0.31	0.27	a)
$[Cu(II)(phen)_2]^{2+}$	H_2O	2.280		0.42		c)
$[Cu(II)(dipy)_2]^{2+}$	H_2O	2.270		0.40		c)
$[Cu(II)(CN)_4]^{2-}$	MeOH	2.160	2.033	0.24	0.20	d)
$[Cu(II)(C_7H_6O_2N)_2]$	EtOH, $CHCl_3$–Toluene	2.171	2.020	0.25	0.11	e, f)

a) W. S. Lewis, M. Alei, and L. O. Morgan, *J. Chem. Phys.*, **45**, 4003 (1966).
b) K. Wüthrith, *Helv. Chim. Acta*, **49**, 1400 (1966).
c) B. G. Malmström and T. Vänngard, *J. Mol. Biol.*, **2**, 118 (1960).
d) A. Longo and T. Buch, *Inorg. Chem.*, **6**, 556 (1967).
e) A. K. Wiersema and J. J. Windle, *J. Phys. Chem.*, **68**, 2316 (1964).
f) H. R. Gersman and J. D. Swalen, *J. Chem. Phys.*, **36**, 3221 (1961).

d^7 electron configuration in the $^2B_{1g}$ state (case D) has not yet been proved to exist.[11–14] In view of these result, it may be concluded that the observed signals are due to Ni(I) complex ions having the $3d^9$ electron configuration in the $^2B_{1g}$ state (case A).

Structure of Ni(I) Complex Ions. The ESR spectrum shows that $[Ni(I)(H_2O)_6]^+$ has a tetragonally elongated octahedral form, while the host $[Ni(II)(H_2O)_6]^{2+}$ is known to have a regular octahedral form. The lowering of symmetry which is accompanied with the reduction of Ni(II) to Ni(I) is probably due to the Jahn-Teller effect; the ground state of $[Ni(I)(H_2O)_6]^+$ in O_h symmetry would be orbitally degenerate E_g, which is expected to suffer from Jahn-Teller distortion.

Ni(I) Ion-to-ligand Bonding. It has been shown that in a ligand field with D_{4h} symmetry, $g_{//}$ and $g_{\perp}$ for the d^9 electron configuration with $^2B_{1g}$ ground state are given by[15,16]

$$g_{//} = 2.0023 + 8\zeta_0\alpha\beta_1[\alpha\beta_1 - \alpha'\beta_1 S - \alpha'(1-\beta_1^2)^{1/2}T(n)/2]/\Delta E_{xy} \quad (1a)$$

$$g_{\perp} = 2.0023 + 2\zeta_0\alpha\beta[\alpha\beta - \alpha'\beta S - \alpha'(1-\beta^2)^{1/2}T(n)/2^{1/2}]/\Delta E_{xz} \quad (1b)$$

where α and α' are the coefficients for the B_{1g} antibonding orbital, β and $(1-\beta^2)^{1/2}$ are those for E_g, β_1 and $(1-\beta_1^2)^{1/2}$ are for B_{2g}; and ΔE_{xy} and ΔE_{xz} are energy separations between $^2B_{2g}$ and $^2B_{1g}$ and between ^2E_g and $^2B_{1g}$ respectively. Although the Ni(I) complex ions are most probably six-coordinated, Eqs. (1a) and (1b) will be used in the present study by making an assumption that overlap between orbitals of the fifth and sixth ligands and those of the Ni(I) ion is small. Following parameters k and k' represent the degree of delocalization of the 3d electrons of the nickel ion, and may be used as a measure of covalency in the Ni(I) complex ions.[16]

$$k = \alpha\beta_1[\alpha\beta_1 - \alpha'\beta_1 S - \alpha'(1-\beta_1^2)^{1/2}T(n)/2]/\Delta E_{xy} \quad (2a)$$

$$k' = \alpha\beta[\alpha\beta - \alpha'\beta S - \alpha'(1-\beta^2)^{1/2}T(n)/2^{1/2}]/\Delta E_{xz} \quad (2b)$$

It can be seen from Table 2 that the covalency increases in the order: H_2O (0.96) < edta (0.86) ≪ py (0.58) ~ en (0.58) ~ xanthate (0.58) < phen (0.56) < dipy (0.53) ≪ CN^- (0.27). The numbers in parentheses represent parameters k. This order is in agreement with that obtained for Cu(II) complexes (Table 4), well-known spectrochemical series.[17]

In the following the parameter k obtained for the Ni(I) complex ions are compared with those for the corresponding Cu(II) complexes:[18]

$[Ni(I)(H_2O)_6]^+$ (0.96) < $[Cu(II)(H_2O)_6]^{2+}$ (0.60)

$[Ni(I)(en)_2(H_2O)_2]^+$ (0.58) < $[Cu(en)_2(H_2O)_2]^{2+}$ (0.31)

$[Ni(I)(CN)_4]^{3-}$ (0.27) < $[Cu(II)(CN)_4]^{2-}$ (0.24)

In all these cases, the nature of the Ni(I) ion-to-ligand bonding appears to be less covalent than in the case of corresponding Cu(II) ions.

Isotropic Spectra. γ-Irradiated samples containing $[Ni(II)(H_2O)_6]^{2+}$ or $[Ni(II)(edta)(H_2O)]^{2-}$ give additional isotropic spectra. In the cases of $[Ni(II)(en)_3]^{2+}$, $[Ni(II)(phen)_3]^{2+}$ and $[Ni(II)(dipy)_3]^{2+}$ only the isotropic spectra were observed. As in the case of the Ni(I) ions discussed above, the g-shifts are fairly large and are sensitive to the kinds of ligands. These signals

Table 5. ESR parameters of Ni(III) complexes

Complex ion	Matrix	g_{iso} [a] (± 0.01)	H_{msl} [b] (G)
$[Ni(III)(H_2O)_6]^{3+}$	EG–H_2O	2.308	37
$[Ni(III)(H_2O)_6]^{3+}$	EtOH	2.309	35
$[Ni(III)(edta)(H_2O)]^-$	EG–H_2O	2.252	67
$[Ni(III)(en)_3]^{3+}$	EG–H_2O	2.204	47
$[Ni(III)(phen)_3]^{3+}$	EG–H_2O	2.196	45
$[Ni(III)(dipy)_3]^{3+}$	EG–H_2O	2.186	45

a) Isotropic g-value b) Maximum slope line width

11) R. Lacroix, U. Höchli, and K. A. Müller, *Helv. Phys. Acta*, **37**, 627 (1964).
12) S. Geschwind and J. P. Rameika, *J. Appl. Phys.*, **33**, 721 (1961).
13) U. Höchli and K. A. Müller, *Phys. Rev. Lett.*, **12**, 730 (1964), **13**, 565 (1965).
14) U. Höchli, K. A. Müller, and P. Wysling, *Phys. Lett.*, **15**, 5 (1965).
15) A. H. Maki and B. R. McGarvey, *J. Chem. Phys.*, **29**, 31 (1958).
16) D. Kivelson and R. Neiman, *ibid.*, **35**, 149 (1961).
17) B. A. Goodmen and J. B. Raynor, "Electron Spin Resonance of Transition Metal Complexes," *Adv. Trans. Metal. Chem.*, **13**, 135 (1971).
18) In calculation of k and k', ζ_0=605 cm^{-1} (Ni^+) and ζ_0=830 cm^{-1} (Cu^{2+}) were used.[19]
19) T. M. Dunn, *Trans. Faraday Soc.*, **57**, 1441 (1961).

observed at liquid nitrogen temperature disappear irreversibly when the samples are brought to room temperature.

If the isotropic feature of these spectra comes from dynamic Jahn-Teller effect of the Ni(I) complex ions, the g-values should be equal to $(g_{//}+2g_{\perp})/3$. This relation obviously does not hold for $[Ni(I)(H_2O)_6]^+$ and $[Ni(I)(edta)(H_2O)]^{3-}$. Anisotropic g-values, $g_{//}$ and $g_{\perp}$, estimated from this relation are too large for $[Ni(I)(en)_3]^+$, $[Ni(I)(phen)_3]^+$, and $[Ni(I)(dipy)_3]^+$ ($g_{//}\sim 2.4$, $g_{\perp}\sim 2.1$).

Another possibility is that the Ni(II) complexes are oxidized to produce Ni(III). Complex ions with d^7 configuration would have ^2E_g ground state in a strong ligand field with O_h symmetry. Since an orbitally degenerate E state has to be split by the Jahn-Teller effect, complexes with d^7 electron configuration would be lower in symmetry than O_h, and hence give anisotropic g-tensors. In the case of the dynamic Jahn-Teller effect, isotropic g-tensors would be observed. In some d^7 complexes, isotropic g-values have been reported, where the results were interpreted in terms of the dynamic Jahn-Teller effect.[13,14]

The high spin state ($S=3/2$) of d^7 complexes would have a spin-lattice relaxation time too short to permit observation of ESR spectra at 77 K and would not show the g-value of 2 which is observed in the present case.

In view of the above results it may be concluded that a Ni(III) species is produced along with Ni(I) species by γ-irradiation and that the dynamic Jahn-Teller effect is responsible for the isotropic feature of the ESR spectra.

We would like to thank Mr. Shingo Katsura of γ-ray irradiation center for experimental assistance and Dr. Tokuko Watanabe for valuable discussions. We would also like to thank Dr. Yoji Arata for helpful discussions and several remarks in the preparation of this paper.

BULLETIN OF THE CHEMICAL SOCIETY OF JAPAN, VOL. 46, 1383—1388 (1973)

ESR Studies on Radiation-Induced Polymerization of 1,3-Butadiene in Urea Canal Complexes[1)]

Toshio OHMORI,* Takahisa ICHIKAWA,** and Machio IWASAKI

Government Industrial Research Institute, Nagoya, Hirate-machi, Kita-ku, Nagoya

(Received December 28, 1972)

The ESR spectrum of γ-irradiated 1,3-butadiene in urea canal complexes at 77 K consists of 7 lines with a hyperfine splitting of 15 G and is assigned to the monomer radical CH_3–CH=CH–$\dot{C}H_2$ which may be produced by hydrogen addition to the 1,3-butadiene. Upon warming to room temperature the spectrum changes into a 6×2-line spectrum ($a_1=14$ G and $a_2=4$ G), which is attributed to the propagating radical R–$C_\beta H_2$–C_αH=CH–$\dot{C}H_2$ occluded in the urea canals. On cooling back to 77 K, the 6×2-line spectrum is transformed into a 5-line spectrum ($a=14$ G); this spectral change is reversible with temperature and is interpreted in terms of oscillation of the propagating radical around the C_β–C_α bond. On further warming to 400 K, the propagating radical is converted to the "chain" allyl type radical R–CH_2–CH=CH–$\dot{C}$H–CH_2–R′, of which room-temperature spectrum consists of 7×2 lines ($a_1=14$ G and $a_2=4$ G). This radical conversion is explained by hydrogen atom transfer reaction within the propagating radical through the radical chain and/or between the propagating radical and a neighbouring polymer chain. Irradiated 1,3-butadiene-1,1,4,4-d_4 in urea canals is also examined and the results obtained confirm the above-mentioned identifications.

The polymerization of 1,3-butadiene in urea complexes was extensively investigated by White[2)] and the formation of *trans*-1,4-polybutadiene was obtained by irradiation with high energy electron at low temperatures. The initiation of polymer chain growth inside the crystalline lattice[3)] of canal complexes was reported to be quite difficult by other conventional means, *i.e.*, high pressure, heat, ultraviolet rays, and conventional initiators.[4)]

High energy radiation, however, can penetrate into the crystalline lattice of canal complexes. As a result, active species may be produced inside the crystalline lattice. ESR results of irradiated aliphatic monomers

* On leave from Research Laboratory, Japan Synthetic Rubber Co., Ltd.

** Present address: Faculty of Engineering, Hiroshima University, Higashisenda-machi, Hiroshima.

1) Presented at the 21st Annual Meeting of the Chemical Society of Japan, Tokyo, April, 1968.

2) D. M. White, *J. Amer. Chem. Soc.*, **82**, 5678 (1960).

3) The structure of a urea lattice in hydrocarbon-urea complexes was reported to be hexagonal (A. E. Smith, *Acta Crystallogr.*, **5**, 224 (1952)). There are six urea molecules in the unit cell with lattice parameters $a=8.23$ Å and $c=11.0$ Å. Along the c axis the urea molecules form the wall of a canal, of which diameter is 5—6 Å. 1,3-Butadiene molecules are packed in the canal.

4) J. F. Brown, Jr., and D. M. White, *J. Amer. Chem. Soc.*, **82**, 5671 (1960).

(ketones, ethers, and esters) in urea canals[5] have showed that monomer radicals are trapped inside the urea canals. This suggests the possibility that monomer radicals from irradiated 1,3-butadiene-urea complexes may be produced inside the crystalline lattice of the urea complexes. The monomer radicals produced would be expected to initiate the polymerization of 1,3-butadiene.

In our preliminary experiments the irradiation of pure solid 1,3-butadiene did not produce appreciable amounts of polymers, while a 25% conversion to polymer was reported in irradiated 1,3-butadiene-urea complexes.[2] The results indicate that packing of 1,3-butadiene in urea canals is very effective for the polymerization of 1,3-butadiene. One of reasons for this is supposed to be due to the fact that walls formed by the urea molecules can prevent bimolecular termination reactions between growing polymer chains unless two growing polymer chains are both present in an urea canal.

Although the reaction processes of polymerization have been investigated in detail for several solid monomers including 1,3-butadiene by means of ESR,[6] there seems to be no report regarding the nature of active species produced during polymerization in urea canals. In order to elucidate the mechanism of polymerization in urea canals, ESR studies of irradiated 1,3-butadiene-urea complexes have been made at temperatures in the range 77—400 K. The results obtained have indicated that the monomer radical is produced by hydrogen addition to the 1,3-butadiene at 77 K, followed by changing into the propagating radical at elevated temperature. Further warming leads to conversion to the "chain" allyl type radical by intra- and/or intermolecular hydrogen transfer.

Experimental

All the chemicals used for the preparation of the urea canal complexes, with the exception of 1,3-butadiene-1,1,4,4-d_4 (BD-*d*), were obtained from commercial source. The urea was recrystallized several times from water and was dried in a desiccator over anhydrous calcium chloride. The 1,3-butadiene without deuteration (BD-*h*) was distilled *in vacuo* from trap to trap. The BD-*d* was prepared by pyrolysis of the BD-*d*–SO_2 addition compound which was obtained by base-catalyzed deuterium exchange of the BD-*h*–SO_2 addition compound.[7]

The urea canal complexes of BD-*h* or BD-*d* were prepared by the method developed by White[2] with some modifications. A mixture of BD-*h* (60 wt%), urea (40 wt%), and methanol (traces) was sealed in a ESR sample tube and was kept in a low-temperature bath controlled at 218 K for 5 days. This temperature has been reported to be optimum for the formation of BD-*h*–urea complexes.[2]

Irradiation was carried out with a 3-KCi ^{60}Co source at 77 K. The dose rate was 1.5×10^5 R/hr and the total dose was 2×10^6 R. ESR spectra were obtained with a Japan Electron Optics Lab. Co. (JEOL) X-band spectrometer with 100 KHz field modulation at various temperatures. A liquid-nitrogen Dewar was used for measurements at 77 K and a variabletemperature accessory supplied by JEOL was employed form easurements at higher than 90 K.

Polymer products obtained after irradiation of BD-*h*–urea complexes were confirmed to be *trans*-1,4-polybutadiene by comparison of their infrared spectra and intrinsic viscosities with the data reported by White.[2]

Results and Discussion

Monomer Radical. Figure 1a shows the ESR spectrum of BD-*h*–urea complexes which were immediately measured at 77 K after irradiation at 77 K. The spectrum consists of 7 lines with a hyperfine splitting of 15 G. Any significant spectral change in the hyperfine structure did not take place after the sample was heated from 77 to 130 K and was cooled back to 77 K (Fig. 1b). The 7-line spectrum can be ascribed to the allyl type radical (radical I)

$$\overset{\beta}{C}H_3-\overset{\alpha3}{C}H=\overset{\alpha2}{C}H-\dot{\overset{\alpha1}{C}}H_2.$$

R_I

The formation of radical I may be accounted for by hydrogen addition to the conjugated double bond of BD-*h*.

Radical I has an unpaired spin coupling to four α and three β protons. The unpaired spin distribution of radical I is supposed to be approximately similar to that of the allyl radical $CH_2=CH-\dot{C}H_2$. The α-proton

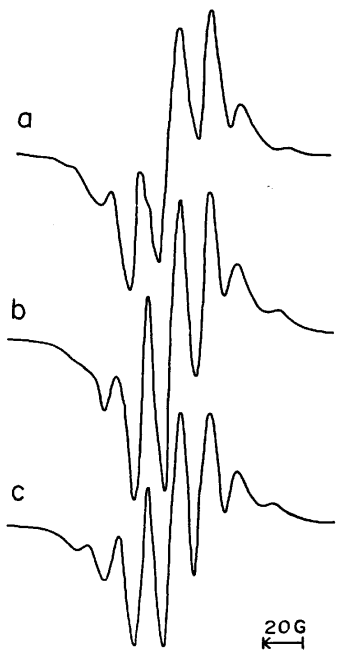

Fig. 1. ESR spectra of 1,3-butadiene-urea complexes irradiated at 77 K, (a) measured at 77 K immediately after irradiation; (b) measured at 77 K after warming to 130 K. (c) Computed spectrum of the monomer radical.

5) O. H. Griffith, *J. Chem. Phys.*, **42**, 2644, 2651 (1965); E. E. Wedum and O. H. Griffith, *Trans. Faraday Soc.*, **62**, 819 (1966).

6) a) Y. Shioji, S. Ohnishi, and I. Nitta, *J. Polymer Sci.*, *A*, **1**, 3373 (1963). b) J. H. O'Donnell, B. McGarvey, and H. Morawetz, *J. Amer. Chem. Soc.*, **86**, 2322 (1964). c) M. J. Bowden and J. H. O'Donnell, *J. Phys. Chem.*, **72**, 1577 (1968). d) Y. Sakai and M. Iwasaki, *J. Polymer Sci.*, *A*,**7**, 1749 (1969). e) T. Shiga, A. Lund, and P. O. Kinell, *Int. J. Radiat. Phys. Chem.*, **3**, 145 (1971).

7) The BD-*h*–urea addition compounds were synthesized by the reaction of BD-*h* and SO_2 under a high pressure (15 kg/cm^2).

coupling constants of radical I, therefore, are assumed to be $a_{\alpha 1}=a_{\alpha 3}=14$ G and $a_{\alpha 2}=4$ G from the values obtained for the allyl radical.[8]

The β-proton coupling constants of radical I can be estimated by the use of the relation[9]

$$a_\beta = 2Q_\beta \cdot \rho_\alpha \cdot \cos^2\theta. \quad (1)$$

In Eq. (1), Q_β is the constant, whose value is assumed to be 29.3 G from Ref. 8, ρ_α is the spin density on the α3-carbon atom, of which value is assumed to be 0.58 from Ref. 8, and θ is the angle between the H–C$_\beta$–C$_{\alpha 3}$ plane and the axis of p_z orbital on the α3-carbon atom. Assuming that the methyl protons of radical I are rapidly rotating, $\cos^2\theta$ in Eq. (1) is averaged out, *i.e.*, $\langle\cos^2\theta\rangle=1/2$. As a result, a_β for the rotating methyl protons is given by the expression

$$a_\beta(CH_3) = Q_\beta \cdot \rho_\alpha. \quad (2)$$

Substitution of the values ($Q_\beta=29.3$ G and $\rho_\alpha=0.58$) into Eq. (2) gives $a_\beta=16$ G. Using these coupling constants estimated and the component lines with Gaussian shape, one obtains the computed spectrum as shown in Fig. 1c. It shows good agreement with the observed spectrum (Fig. 1b).

Maas and Volman[10] have reported the ESR spectrum of radical I produced from 1-buten-3-ol by ultraviolet irradiation; $CH_3-CH(OH)-CH=CH_2 \rightarrow CH_3-CH=CH-\dot{C}H_2+OH$. Its spectrum (7 lines with $a=15$ G) is quite similar to Fig. 1b. An ESR spectrum similar to Fig. 1b has been observed also by Morgan and White[11] in the hydrogen bombardment of BD-*h*; $CH_2=CH-CH=CH_2+H \rightarrow CH_3-CH=CH-\dot{C}H_2$.

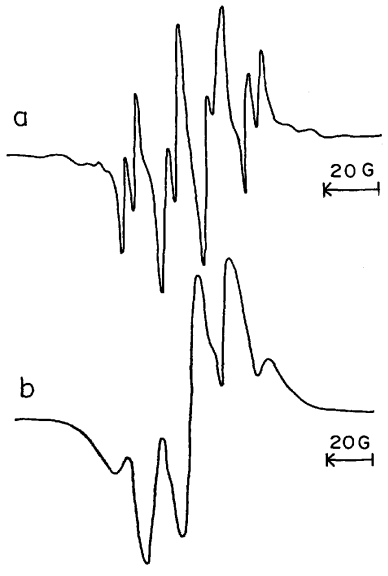

Fig. 2. ESR spectra of irradiated 1,3-butadiene–urea complexes after warming to room temperature. (a) Room-temperature spectrum. (b) 77 K spectrum.

Propagating Radical. Upon warming to room temperature, the 7-line spectrum (Fig. 1b) changed as shown in Fig. 2. The spectrum measured at room temperature (Fig. 2a) is a well resolved spectrum, consisting of 6 lines ($a_1=14$ G) which respectively further split into 2 lines ($a_2=4$ G). On cooling back to 77 K, the 6×2-line spectrum changed into a 5-line spectrum with a hyperfine splitting of 14 G (Fig. 2b). This result indicates the conversion of radical I to another radical species at elevated temperature. When the sample was warmed again to room temperature, the 5-line spectrum reverted to the 6×2-line spectrum. This reversible spectral change may be attributed to a reversible conformation change of the 5-line species with temperature as discussed later.

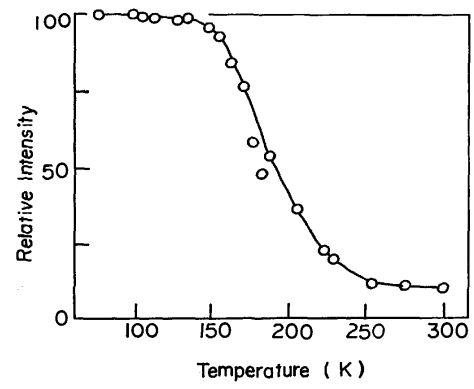

Fig. 3. Decay curve of radicals trapped in irradiated 1,3-butadiene–urea complexes.

Figure 3 shows the decay curve of radicals trapped in urea canals at 77 K. The relative intensity of the ESR signal was recorded after the sample had been annealed for 5 min at each elevated temperature. The radicals began to decay at 140—150 K and stopped decaying at 250—260 K. The radicals surviving after heat treatment up to 300 K were about 10% of the radicals initially trapped at 77 K and were stable at room temperature at least for several days.

Since White[2] has reported that the polymerization of irradiated BD-*h* in urea canals occurs at a low temperature of 195 K, the radical obtained after warming to room temperature is presumably attributable to the propagating radical (radical II) occluded in the urea canals:

$$R_I + n(CH_2=CH-CH=CH_2) \longrightarrow$$

$$R_I-(CH_2-CH=CH-CH_2)_{n-1}-\overset{\beta}{C}H_2-\overset{\alpha 3}{C}H=\overset{\alpha 2}{C}H-\overset{\alpha 1}{\dot{C}}H_2. \quad (3)$$

$$R_{II}$$

As this radical also belongs to the allyl type radical, the unpaired spin distribution is supposed to be similar to that of radical I. The α-proton coupling constants of radical II, therefor, are assumed to be the same as those of radical I, *i.e.*, $a_{\alpha 1}=a_{\alpha 3}=14$ G and $a_{\alpha 2}=4$ G. If both of the two β-coupling constants are 14 G, these five protons ($a_1=14$ G) and one proton ($a_2=4$ G) well account for the 6×2-line spectrum observed at room temperature. The computed spectrum (Fig. 4a) based upon these estimations is in good agreement with the observed spectrum (Fig. 2a).

8) R. W. Fessenden and R. H. Schuler, *J. Chem. Phys.*, **39**, 2147 (1963).

9) C. Heller and H. M. McConnell, *ibid.*, **32**, 1535 (1960); C. Heller, *ibid.*, **36**, 175 (1962).

10) K. A. Mass and D. H. Volman, *Trans. Faraday Soc.*, **60**, 1204 (1964).

11) C. U. Morgan and K. J. White, *J. Amer. Chem. Soc.*, **92**, 3309 (1970).

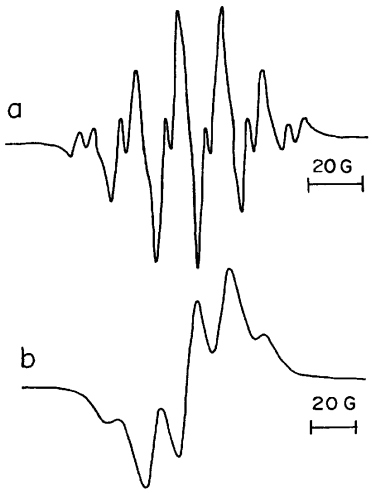

Fig. 4. Computed spectrum of the propagating radical. (a) Room-temperature spectrum. (b) 77 K spectrum.

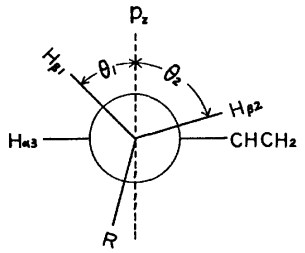

Fig. 5. Conformation of the propagating radical along the direction of the C_β–$C_{\alpha 3}$ bond.

It is well known that the coupling constants of β-methylene protons often exhibit temperature-dependent change[6c,d,12] due to hindered oscillation around the C_β–C_α bonds. At 77 K the motion of a β-methylene group in an aliphatic radical is usually considered to be almost frozen at a fixed conformation. The conformation of radical II at 77 K is depicted in Fig. 5 on the assumption of nonequivalent θ values for the two β protons ($\theta_1 \neq \theta_2$); this leads to nonequivalent β-coupling constants ($a_{\beta 1} \neq a_{\beta 2}$) from Eq. (1). Each of the a_β values can be determined by way of trial and error. When the a_β values were respectively taken to be 19 G ($\theta_1=42°$) and 5 G ($\theta_2=68°$), the appropriate computed spectrum was obtained as shown in Fig. 4b. It is to be noted that the equivalent coupling of 14 G observed at room temperature is nearly equal to the averaged value of 19 and 5 G. This strongly suggests that the two C_β–H bonds undergo rapid exchange or large amplitude oscillation about the two equilibrium positions ($\theta_1=42°$ and $\theta_2=68°$).

This equivalency of the two β-proton couplings may partly contribute to the better resolution of the room-temperature spectrum. However, partial average of α-proton anisotropic couplings due to overall rotation around the molecular chain axis of radical II would be the main cause of the sharper line width of the room-temperature spectrum; such a case has been often

12) S. Ohnishi, S. Sugimoto, and I. Nitta, *J. Chem. Phys.*, **37**, 1283 (1962); M. Kashiwagi and Y. Kurita, *ibid.*, **39**, 3165 (1963); C. Corvaja, *ibid.*, **44**, 1958 (1966).

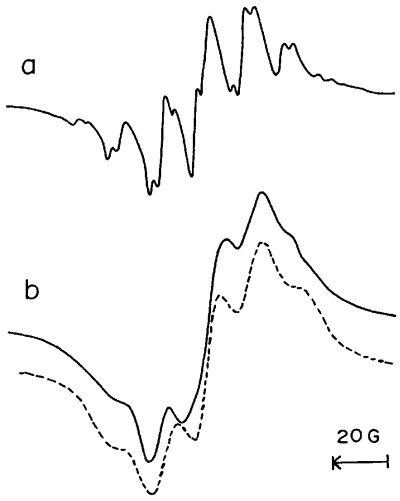

Fig. 6. ESR spectra of irradiated 1,3-butadiene–urea complexes after warming to 400 K. (a) Room-temperature spectrum. (b) 77 K spectrum. Dotted lines indicate the computed spectrum.

reported for radicals trapped in urea canals.[13]

Radical Conversion at 400 K. When the sample was further warmed from 300 K to higher temperatures, radical II began to decay rapidly at 400 K and at the same time changed into another kind of radical. Its spectrum measured at room temperature consists of 7×2 lines ($a_1=14$ G and $a_2=4$ G) as shown in Fig. 6a, while the spectrum at 77 K consists of poorly resolved several lines (Fig. 6b). This spectral change was completly reversible with temperature in the range 77—300 K. The well resolved 7×2-line spectrum is obviously attributable to the interaction of an unpaired spin with six equivalent protons ($a_1=14$ G) and one proton ($a_2=4$ G). This indicates that the radical species is probably an allyl type radical with one more proton ($a=14$ G) than radical II.

At elevated temperature two types of reaction processes may be possible for the conversion of radical II. The one is migration of the unpaired spin site accompanied by intramolecular 1,3 and/or 1,5 hydrogen transfer through the polymer chain of radical II:

$$\sim CH_2\text{-}CH{=}CH\text{-}CH_2\text{-}CH_2\text{-}\dot{C}H\text{-}CH{=}CH_2 \longrightarrow \sim CH_2\text{-}CH{=}CH\text{-}\dot{C}H\text{-}CH_2\text{-}CH_2\text{-}CH{=}CH_2; \quad (4a)$$

$$\sim CH_2\text{-}CH{=}CH\text{-}CH_2\text{-}CH_2\text{-}CH{=}CH\text{-}\dot{C}H_2 \longrightarrow \sim CH_2\text{-}CH{=}CH\text{-}\dot{C}H\text{-}CH_2\text{-}CH{=}CH\text{-}CH_3. \quad (4b)$$

The other is hydrogen abstraction of radical II from a neighbouring polymer chain:[14]

$$R_{II} + \sim CH_2\text{-}CH{=}CH\text{-}CH_2\sim \longrightarrow \sim \overset{\beta 2}{C}H_2\text{-}\overset{\alpha 3}{C}H{=}\overset{\alpha 2}{C}H\text{-}\overset{\alpha 1}{C}H\text{-}\overset{\beta 1}{C}H_2\sim + R_{II}H. \quad (5)$$

R_{III}

All the reaction processes result in the formation of the

13) B. Birrell and O. H. Griffith, *J. Phys. Chem.*, **75**, 3489 (1971).

14) Probably, most of the walls of the urea canals are melted and destroyed by this heat treatment, because remarkable decrease of a cavity Q value which is due to loss of microwave power caused by melting urea molecules is observed for measurement at 400 K. Therefore, the reactions between polymer chains must be taken into consideration.

same "chain" allyl type radical (radical III).

At room temperature all the β-coupling constants of radical III are reasonably expected to become 14 G because of the motion of the β-methylene group as suggested in the case of radical II. The α-proton coupling constants of radical III are supposed to be similar to those of radical II; $a_{\alpha 1}=a_{\alpha 3}=14$ G and $a_{\alpha 2}=4$ G. Consequently, radical III at room temperature has these six equivalent protons ($a_1=14$ G) and one proton ($a_2=4$ G), giving the 7×2-line spectrum.

It is difficult to determine unequivocally the number of component lines from the broad spectrum measured at 77 K. The spectrum, however, agrees closely with the computed spectrum consisting of broad 7 lines ($a=15$ G) with the intensity ratios of 1:6:15:20:15:6:1, as shown in Fig. 6b by dotted lines. This indicates that radical III at 77 K has six equivalent protons with the coupling constants of about 15 G. The 15-G splitting should be due to the protons at the $\alpha 1$, $\alpha 3$, $\beta 1$, and $\beta 2$ positions and a small 4-G splitting expected from the coupling with the $\alpha 2$ proton should be smeared out by the broad line width ($\Delta H=15$ G).

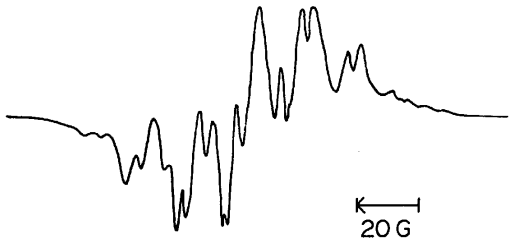

Fig. 7. ESR spectrum of irradiated trans-1,4-polybutadiene–urea complexes measured at room temperature.

It is interesting to note that a 7×2-line spectrum of Fig. 7 which is similar to Fig. 6a is obtained from irradiated *trans*-1,4-polybutadiene–urea complexes.[15] In this case, it seems probable that the radical species is formed by removal of a hydrogen atom from the polymer chain:

$$\sim\!\!\sim CH_2\text{–}CH{=}CH\text{–}CH_2\sim\!\!\sim \longrightarrow$$
$$\sim\!\!\sim CH_2\text{–}CH{=}CH\text{–}\dot{C}H\text{–}CH_2\sim\!\!\sim + H. \quad (6)$$

This results would seem to support the identification of the 7×2-line spectrum of Fig. 6a as radical III.

Recently, Shiga *et al.*[6e] found a 7×2-line spectrum similar to Fig. 6a in an irradiated single crystal of 1,3-butadiene after warming to 143 K and assigned the spectrum to the same species as radical III. The formation of radical III in the crystal was explained by a reaction mechanism similar to (4a) on the assumption of the presence of the propagating radical which was not able to be confirmed. In our case, the conclusive evidence has been obtained for the presence of the propagating radical which is stable even at room temperature. This difference with regard to radical stability might be due to the difference of crystal structure, *i.e.*, the propagating radical in the crystalline lattice of pure 1,3-butadiene might undergo rearrangement to radical III at lower temperature than that in the crystalline lattice of urea canal complexes does.

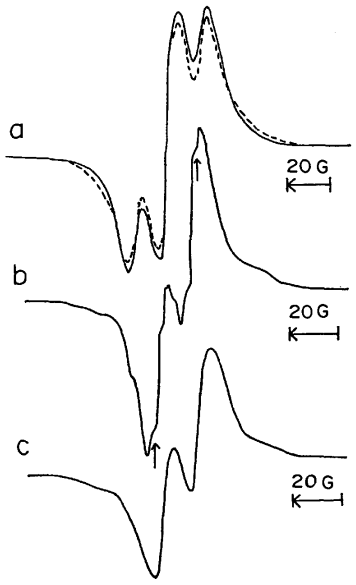

Fig. 8. ESR spectra of irradiated 1,3-butadiene-1,1,4,4-d_4–urea complexes. (a) 77 K spectrum measured immediately after irradiation. Dotted lines indicate the computed spectrum. (b) Room temperature spectrum. Arrows indicate the presence of small splittings. (c) 77 K spectrum after warming.

Radicals from 1,3-Butadiene-1,1,4,4-d_4. Using BD-*d*-urea complexes, a parallel experiment has been made in order to confirm the preceding identifications of the radicals formed in BD-*h*–urea complexes. The ESR spectrum of BD-*d* in urea canals irradiated and measured at 77 K consists of 3 lines with a hyperfine splitting of 15 G (Fig. 8a). There are two possible addition reactions for the formation of the monomer radical, *i.e.*, the hydrogen or deuterium addition to the conjugated double bond of BD-*d*. If the hydrogen addition is the case, the radical to be formed is

$$\overset{\beta}{C}HD_2\text{–}\overset{\alpha 3}{C}H{=}\overset{\alpha 2}{C}H\text{–}\dot{\overset{\alpha 1}{C}}D_2.$$
$$R_{IV}$$

The 3-line spectrum would be interpreted on the assumption; $a_{\alpha 1}{}^{H}=2.2$ G, $a_{\alpha 2}{}^{H}=4.0$ G, $a_{\alpha 3}{}^{H}=14$ G, $a_{\beta}{}^{H}=16.0$ G, and $a_{\beta}{}^{D}=2.5$ G, where the deuteron coupling constants are taken from the relation $a^{D}=0.153\ a^{H}$. The computed spectrum obtained by the use of these coupling constants is shown in Fig. 8a by dotted lines. It shows good agreement with the observed spectrum. Small splittings from the $\alpha 2$ proton and the deuterons are smeared out because of the broad line width ($\Delta H=7$ G).

On the other hand, the deuterium addition would be excluded, because the expected spectrum of the radical $CD_3\text{–}CH{=}CH\text{–}\dot{C}D_2$ consists of 2 lines from the splitting due to the $\alpha 3$ proton. These results suggest that the origin of the hydrogen added may be determined to be either urea or BD-*d* if radicals formed from BD-*d*–urea-d_4 complexes are identified as either $CD_3\text{–}CH{=}CH\text{–}\dot{C}D_2$ or $CD_2H\text{–}CH{=}CH\text{–}\dot{C}D_2$. An attempt to prepare the BD-*d*–urea-d_4 complexes, however, was not successful.

15) The complexes were prepared by storage of irradiated BD-*h*–urea complexes for several months at room temperature. Radicals trapped in the complexes almost disappeared during this storage.

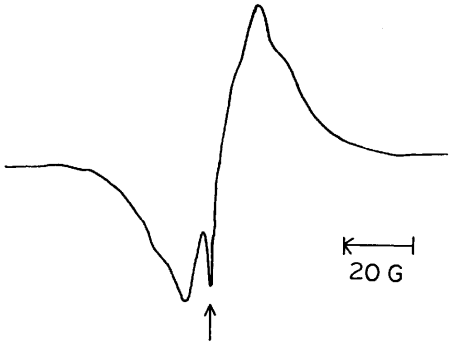

Fig. 9. ESR spectrum of polycrystalline 1,3-butadiene irradiated and measured at 77 K. A peak indicated by an arrow arises from color centers of the quartz sample tube.

It should be noted here that irradiated polycrystalline BD-*h* gives a poorly resolved spectrum at 77 K (Fig. 9) as compared with the spectrum obtained for BD-*h*–urea complexes (Fig. 1a). The formation of several types of radicals with different coupling constants may be the main cause of this poor resolution, as discussed by Shiga *et al.*[6e] Accordingly, the better resolution of Fig. 1a may be due to a selective formation of radical I in the presence of the urea molecules. The probable reaction mechanism explaining the selective radical formation would be proton transfer from the urea molecule to a butadiene anion radical which may be produced by attachment of an ejected electron:

$$(CH_2{=}CH{-}CH{=}CH_2)^- + CO(NH_2)_2 \longrightarrow CH_3{-}CH{=}CH{-}\dot{C}H_2 + CO(NH_2)(NH)^- . \quad (7)$$

Shida and Hamill[16] reported the formation of radical I in an irradiated 1,3-butadiene–methanol system and interpreted the radical formation in terms of a reaction mechanism similar to (7):

$$(CH_2{=}CH{-}CH{=}CH_2)^- + ROH \longrightarrow CH_3{-}CH{=}CH{-}\dot{C}H_2 + RO^- . \quad (8)$$

In an irradiated single crystal of fumaric acid-doped succinic acid, Iwasaki *et al.*[17] recently found the radical formed by the addition of an acidic proton of the host molecule to the fumaric acid-anion radical produced.

When the irradiated BD-*d*–urea complexes were warmed to room temperature and measured at room temperature, the 3-line spectrum at 77 K changed into a 2-line spectrum (a=14 G) with additional small splittings as shown in Fig. 8b. By this heat treatment, the formation of the propagating radical labeled by deuterium is expected from the results obtained for irradiated BD-*h*–urea complexes:

$$CHD_2{-}CH{=}CH{-}\dot{C}D_2 + (CD_2{=}CH{-}CH{=}CD_2)_n \longrightarrow CHD_2{-}CH{=}CH{-}CD_2{-}(CD_2{-}CH{=}CH{-}CD_2)_{n-1} {-}\overset{\beta}{C}D_2{-}\overset{\alpha 3}{C}H{=}\overset{\alpha 2}{C}H{-}\dot{\overset{\alpha 1}{C}}D_2 . \quad (9)$$

R_V

On cooling back to 77 K, the small splittings disappeared, while the 2-line components unchanged (Fig. 8c).

It is evident that the 14-G splitting between the 2-line components should be due to the α3 proton and the small splittings should be due to the α1 deuterons (a=2.2 G), the α2 proton (a=4.0 G), and the β deuterons (a=2.2 G). It is to be noted that the 2-line spectrum of radical V does not show noticiable temperature-dependent changes as compared with the 6×2-line spectrum of radical II. This supports the interpretation that the spectral change of radical II is caused by the temperature dependent β-proton coupligs.

16) T. Shida and W. H. Hamill, *J. Amer. Chem. Soc.*, **88**, 5371 (1966).

17) M. Iwasaki, H. Muto, and K. Toriyama, *J. Chem. Phys.*, **55**, 1894 (1971).

An X-Ray Redetermination of the Crystal Structure of Tin(II) Chloride Dihydrate

Hideko KIRIYAMA, Katsuki KITAHAMA, Osamu NAKAMURA, and Ryôiti KIRIYAMA
The Institute of Scientific and Industrial Research, Osaka University, Yamadakami, Suita, Osaka 565
(Received December 28, 1972)

The crystal structure of tin(II) chloride dihydrate, $SnCl_2 \cdot 2H_2O$ has been redetermined by a single crystal X-ray diffractometer technique. The crystal is monoclinic, space group $P2_1/c$ with $a=9.313$, $b=7.250$, $c=8.970$ Å, $\beta=114°55'$ and $Z=4$. The structure was solved by three-dimensional Patterson and electron density syntheses. An anisotropic least-squares refinement, based on 1695 independent reflections gave an R value of 0.04. The tin(II) atom forms a pyramidal complex with two chlorine atoms and one oxygen atom; the bond lengths in the pyramid are Sn–O, 2.33 and Sn–Cl, 2.50 and 2.56 Å and the bond angles are 86.9, 85.0, and 87.9°. These results support a view that the bonding in dichloroaquotin(II) complex is considerably ionic in character. This crystal consists of double layers of the aquocomplex, $SnCl_2 \cdot (OH_2)$, parallel to (100) with intervening layers of the second water molecules. Both kinds of the water molecules are linked together by hydrogen bonds of 2.74, 2.79, and 2.80 Å into two-dimensional networks. The structure reported previously was found to be in error, although its essential feature was quite similar to the present one.

The crystal structure of $SnCl_2 \cdot 2H_2O$ has been analysed by Kamenar and Grdenić (hereinafter abbreviated as K & G) in 1961.[1] According to their description, the crystal consists of dichloroaquotin(II) complexes and the second water molecules, both of which form alternate layers parallel to the (100) plane and are linked through hydrogen bonds alone. Such an arrangement of the water molecules, especially their hydrogen bonding scheme, strongly suggested the presence of dielectric anomaly similar to those found in copper(II) formate tetrahydrate[2] and also in potassium ferrocyanide trihydrate.[3] Recently, Kiriyama and Kiriyama have found a phase transition at −55 °C from dielectric measurements of this compound and have investigated its mechanism from many approaches such as electric conductivities, thermal analyses, X-ray diffractions, proton and deuteron magnetic resonances (PMR and DMR).[4]

On the basis of these results the phase transition could be ascribed to the ordering of hydrogen atoms within the layer of hydrogen bonded water molecules. However, it was noticed that our PMR and DMR data could not provide consistent locations of the hydrogen atom positions, so far as the crystal structure described by K & G was used. It was therefore thought profitable to redetermine the structure by use of a three-dimentional single crystal X-ray diffractometer, because the previous structure had been derived from incomplete data.

Experimental

Single crystals were prepared from about 18% hydrochloric acid saturated with tin(II) chloride, this being the best condition to obtain large transparent single crystals for NMR and dielectric measurements. The crystal used for the present X-ray work was a monoclinic prism of length 0.50 mm (the c-axis direction) and cross-section 0.08×0.10 mm^2. It was sealed in a Lindeman glass capillary to protect from atmospheric moisture. With the c-axis as the Φ-axis of the instrument, a set of intensity data was collected by use of a Rigaku automatic four-circle diffractometer with Mo$K\alpha$ radiation and the 2θ-ω scan technique. A total of 1695 independent reflections was measured up to a $\sin\theta/\lambda$ limit of 0.72 Å^{-1}. Their intensity data were corrected for polarization and Lorentz effects, but absorption correction was neglected becauce of the small μR value of 0.26.

Unit Cell and Space Group

The systematically absent reflections, $(0k0)$ with k odd and $(h0l)$ with l odd, confirmed the monoclinic space group of $P2_1/c$ originally derived by K & G. The cell dimensions were:

$a=9.313$, $b=7.250$, $c=8.970$Å, $\beta=114°55'$, $V=549.275$Å^3.

The calculated density of 2.707 g cm^{-3}, assuming a unit cell content of four formula units, agreed well with the value of 2.710 g cm^{-3} measured by K & G.

Structure Analysis and Refinement

Fourier syntheses of the three main projections were computed starting from the atomic coordinates given by K & G. The [010] and [001] projections were roughly consistent with their description of structure, while the [100] projection was in quite disagreement. Therefore, three-dimensional Patterson functions were calculated from 1695 reflection data and from this it became evident that all atoms, of course except hydrogens, were located incorrectly. This finding forced us to redetermine the crystal structure of this compound, instead of its refinement.

The tin and chlorine positions could be easily derived from the three-dimensioanl Patterson map, and the oxygen's were located from successive electron density calculations. New parameters thus obtained were used in a block-diagonal least-squares refinement. After four cycles of refinement in which were varied the coordinates, the individual isotropic temperature factors for all non-hydrogen atoms, a scale factor and an over-all temperature factor (a total of 22 parameters), the "discrepancy index" $R=\sum||F_o|-|F_c||/\sum|F_o|$ was

1) B. Kamenar and D. Grdenić, *J. Chem. Soc.*, **1961**, 3954.
2) H. Kiriyama, This Bulletin, **35**, 1199 (1962).
3) S. Waku, H. Hirabayashi, H. Iwasaki, and R. Kiriyama, *J. Phys. Soc. Jap.*, **14**, 973 (1959).
4) H. Kiriyama and R. Kiriyama, *ibid.*, **28**, S 114 (1970).

TABLE 1. ATOMIC COORDINATES WITH THEIR ESTIMATED STANDARD DEVIATIONS

	x/a	y/b	z/c	$B(Å^2)^{a)}$
Sn	0.37441 (5)	0.26178 (6)	0.53584 (5)	2.34 (1)
Cl (1)	0.28643 (22)	0.49226 (25)	0.68748 (22)	2.85 (4)
Cl (2)	0.30612 (20)	0.49997 (24)	0.30501 (20)	2.45 (4)
O (1)	0.10937 (53)	0.17555 (65)	0.41282 (55)	2.41 (12)
O (2)	−0.06738 (58)	0.20658 (71)	0.59835 (62)	2.83 (13)

a) These are values for an isotropic refinement giving the final R-value of 0.068. Temperature factors are in the form of $\exp[-B(\sin\theta/\lambda)^2]$.

TABLE 2. THERMAL PARAMETERS ($\times 10^4$) AND THEIR e.s.d.'s
$T=\exp[-(\beta_{11}h^2+\beta_{22}k^2+\beta_{33}l^2+\beta_{12}hk+\beta_{13}hl+\beta_{23}kl)]$

	β_{11}	β_{22}	β_{33}	β_{12}	β_{13}	β_{23}
Sn	86 (1)	103 (1)	87 (1)	12 (1)	61 (1)	12 (1)
Cl (1)	121 (3)	123 (3)	100 (2)	−5 (5)	105 (4)	−35 (4)
Cl (2)	91 (2)	115 (3)	87 (2)	−5 (4)	60 (4)	42 (4)
O (1)	81 (6)	110 (9)	81 (6)	−30 (12)	55 (10)	−6 (12)
O (2)	92 (7)	120 (9)	112 (8)	26 (13)	65 (12)	0 (14)

reduced to 0.063 for the observed reflections (0.068 including 47 unobserved reflections). At this stage of the refinement the structure obtained was checked by a three-dimensional (F_o-F_c) synthesis, which showed no ripple of more than $8e/Å^3$. Further refinements were computed with five cycles of least-squares calculations, which now included anisotropic temperature factors for tin, chlorine, and oxygen. The other parameters varied were the same as before; the total number was 47. During the last cycle, the shifts in coordinate or thermal parameter values were less than one tenth of the standard deviation for the parameter in question. The R value was now 0.040.

The atomic coordinates and the thermal parameters with their standard deviations obtained from the final anisotropic least squares refinement are listed in Tables 1 and 2. The observed and calculated structure factors are compared in Table 3. The atomic scattering factors used in the above calculations were those for neutral Sn, Cl, and O, respectively, given in International Tables Vol. III. All calculations were performed on the NEAC 2200/500 in the Computer Center Osaka University, using UNICS computer programs, HBLS-LV, RSSFR-5 and RSDA-4.

Description and Discussion of the Structure

The crystal structures projected along [100] and [010] are given in Figs. 1 and 2, respectively. It can be seen that tin(II) chloride dihydrate has a predominant layer-structure parallel to the (100) plane; it is built up from double layers of the dichloroaquotin (II) complex and intervening layers of the second water molecules. Apart from van der Waals forces, these layers are held together by hydrogen bonds. Such a description of the structure appears to be the same as the earlier one. However, the projection along the a axis given in Fig. 1 is largely different from that reported by K & G. It is conceivable that the lack of the [100] projection led the previous work to the erroneous conclusion. Both the structures are compared in Fig. 3, where only the aquocomplex double layers are shown for simplicity.

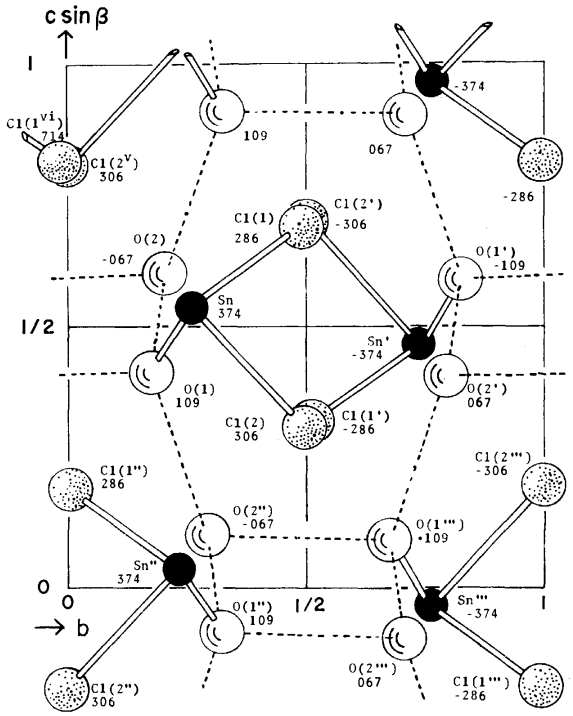

Fig. 1. The crystal structure viewed along the a axis. Hydrogen bonds are indicated by broken lines.

The main interatomic distances and bond angles with the corresponding estimated standard deviations are listed in Table 4, some of them are also shown in Figs. 4 and 5. These values are based on the parameters listed in Table 1. No correction for thermal motions was made.

Structure and Bonding of Dichloroaquotin(II) Complexes

A geometry of the tin(II) coordination is somewhat different from the previous one. The dimensions of the trigonal pyramid, $SnCl_2(OH_2)$ complex, are illus-

TABLE 3. OBSERVED AND CALCULATED STRUCTURE FACTORS FOR $SnCl_2 \cdot 2H_2O$

H	FO	FC	H	FO	FC	H	FO	FC	H	FO	FC	H	FO	FC	H	FO	FC	H	FO	FC	H	FO	FC
K = 0	L = 0		1	32	-32	-10	12	-12	-5	24	23	9	25	24	K = 2	L = 5		2	3	-3	-5	33	33	6	6	6
1	104	-121	2	63	66	-9	3	3	-4	13	-12	10	16	15	-13	1	-1	3	2	-1	-4	8	-7	K = 3	L = 8	
2	74	-72	3	54	-56	-8	17	17	-3	29	-27	11	24	-24	-12	6	6	4	1	0	-3	91	-90	-12	22	-22
3	161	177	4	6	-4	-7	34	-33	-2	13	11	K = 2	L = 1		-11	2	2	K = 2	L = 10		-2	41	37	-11	25	24
4	124	-124	5	31	31	-6	10	-8	-1	16	15	-12	1	0	-10	0	0	-11	5	-5	-1	6	5	-10	7	-7
5	4	2	6	24	-25	-5	48	46	0	18	-18	-11	2	0	-9	5	6	-10	34	35	0	89	-84	-9	16	-17
6	3	-3	K = 0	L = 10		-4	19	-19	1	6	4	-10	10	-11	-8	11	-11	-9	35	-35	1	49	46	-8	42	43
7	33	-33	-12	7	6	-3	33	-31	2	19	19	-9	4	3	-7	2	-1	-8	9	8	2	48	46	-7	39	-39
8	43	43	-11	0	0	-2	76	69	3	10	-10	-8	1	-2	-6	4	-3	-7	21	22	3	19	-18	-6	16	15
9	43	-42	-10	5	-5	-1	45	38	4	0	-1	-7	5	-5	-5	17	-16	-6	19	-18	4	3	3	-5	29	29
10	14	15	-9	27	28	0	74	-69	5	5	5	-6	21	21	-4	17	17	-5	22	22	5	21	20	-4	58	-57
11	20	21	-8	44	-43	1	0	0	6	5	-6	-5	2	0	-3	3	-2	-4	23	-23	6	4	5	-3	52	50
12	32	-31	-7	9	8	2	57	54	7	0	0	-4	10	10	-2	4	-4	-3	13	13	7	24	-24	-2	14	-13
K = 0	L = 2		-6	36	37	3	51	-48	K = 1	L = 8		-3	9	10	-1	18	17	-2	14	14	8	4	2	-1	33	-32
-12	13	-14	-5	73	-74	4	33	-32	-12	25	25	-2	27	-24	0	17	-16	-1	52	-52	9	13	13	0	50	48
-11	37	37	-4	33	32	5	44	43	-11	29	-28	-1	14	15	1	1	-2	0	34	35	K = 3	L = 4		1	41	-40
-10	41	-41	-3	28	27	6	6	-5	-10	6	6	0	16	-13	2	0	0	1	3	0	-12	21	-21	2	6	7
-9	1	0	-2	42	-44	7	22	-22	-9	15	16	1	7	-7	3	8	-8	2	32	-33	-11	7	7	3	17	18
-8	94	93	-1	39	38	8	17	16	-8	53	-53	2	38	34	4	11	10	K = 2	L = 11		-10	25	25	4	30	-31
-7	114	-115	0	0	-2	9	6	6	-7	45	45	3	10	-10	5	0	0	-10	2	1	-9	52	-52	5	22	23
-6	33	33	1	4	-3	10	10	-10	-6	15	-15	4	6	5	6	3	3	-9	1	0	-8	45	45	K = 3	L = 9	
-5	82	81	2	12	13	K = 1	L = 4		-5	31	-31	5	4	5	7	6	7	-8	2	-1	-7	10	-10	-11	0	-1
-4	176	-184	3	21	-22	-13	26	-26	-4	69	68	6	17	-17	8	5	-5	-7	5	5	-6	56	-56	-10	12	12
-3	37	42	K = 0	L = 12		-12	20	20	-3	59	-57	7	0	0	K = 2	L = 6		-6	0	-2	-5	81	82	-9	10	-10
-2	43	-36	-9	26	26	-11	8	-8	-2	16	15	8	7	-7	-13	13	12	-5	3	2	-4	80	-79	-8	4	-4
-1	39	-36	-8	13	-13	-10	27	-27	-1	32	32	9	4	-3	-12	8	7	-4	2	1	-3	12	12	-7	4	1
0	83	94	-7	2	2	-9	62	60	0	58	-59	10	5	5	-11	27	-27	-3	6	-6	-2	65	61	-6	10	-11
1	91	-97	-6	4	5	-8	48	-47	1	48	49	11	3	-1	-10	43	43	-2	3	3	-1	109	-105	-5	5	5
2	145	149	-5	22	-22	-7	24	24	2	8	-7	K = 2	L = 2		-9	26	-26	-1	1	-1	0	94	90	-4	0	-3
3	40	37	-4	20	21	-6	67	67	3	20	-19	-12	33	34	-8	15	-15	0	2	-1	1	10	-9	-3	4	2
4	102	-103	-3	18	-19	-5	106	-106	4	38	39	-11	32	-32	-7	58	58	1	5	5	2	55	-53	-2	16	16
5	110	111	-2	8	-8	-4	98	97	5	24	-24	-10	0	-1	-6	78	-79	K = 3	L = 0		3	88	87	-1	4	-2
6	44	-43	-1	26	27	-3	21	-20	K = 1	L = 9		-9	25	25	-5	22	20	1	96	90	4	51	-50	0	3	3
7	38	-38	K = 1	L = 0		-2	94	-89	-12	5	-5	-8	38	-39	-4	13	13	2	136	-135	5	6	5	1	0	0
8	52	51	1	132	-138	-1	134	134	-11	3	-1	-7	41	41	-3	65	-64	3	85	80	6	32	33	2	4	-3
9	39	-39	2	158	166	0	100	-96	-10	4	4	-6	49	-48	-2	78	73	4	8	-8	7	39	-40	3	0	2
10	9	9	3	107	-101	1	13	13	-9	0	0	-5	34	31	-1	54	-52	5	76	-74	8	22	23	4	9	-10
11	11	12	4	6	6	2	65	63	-8	6	-6	-4	114	111	0	19	19	6	79	77	9	3	-3	K = 3	L = 10	
K = 0	L = 4		5	96	94	3	99	-100	-7	7	6	-3	156	-163	1	75	74	7	48	-47	K = 3	L = 5		-11	22	21
-13	0	0	6	83	-79	4	55	54	-6	8	7	-2	146	145	2	87	-86	8	3	-3	-12	7	-7	-10	18	-17
-12	27	-28	7	63	61	5	15	-15	-5	7	-6	-1	86	79	3	48	49	9	33	33	-11	11	-11	-9	2	-3
-11	36	36	8	5	3	6	40	-40	-4	1	1	0	193	-218	4	23	24	10	33	-32	-10	24	24	-8	25	25
-10	25	-24	9	39	-38	7	46	46	-3	2	-1	1	130	128	5	56	-58	11	19	19	-9	14	-14	-7	32	-32
-9	3	2	10	36	35	8	26	-26	-2	7	-5	2	44	-38	6	33	33	K = 3	L = 1		-8	26	-26	-6	24	23
-8	35	35	11	25	-25	9	6	6	-1	4	3	3	91	-86	7	5	-4	-12	8	8	-7	48	48	-5	3	3
-7	53	-53	12	4	-4	K = 1	L = 5		0	6	-7	4	75	73	K = 2	L = 7		-11	5	-6	-6	6	6	-4	27	-26
-6	100	99	K = 1	L = 1		-13	5	6	1	1	-1	5	61	-60	-13	4	-2	-10	0	0	-5	28	-26	-3	39	40
-5	31	-29	-12	2	2	-12	11	-11	2	9	10	6	27	27	-12	5	5	-9	12	13	-4	30	29	-2	25	-25
-4	75	-73	-11	0	0	-11	1	0	3	3	-3	7	14	15	-11	0	-1	-8	9	-9	-3	23	22	-1	4	-1
-3	123	128	-10	5	-5	-10	19	19	4	0	-2	8	34	-34	-10	3	3	-7	9	9	-2	33	-30	0	27	27
-2	139	-158	-9	1	0	-9	8	-7	K = 1	L = 10		9	37	37	-9	10	10	-6	7	-7	-1	47	-45	1	31	-32
-1	28	-23	-8	4	4	-8	24	-23	-11	21	-22	10	14	-15	-8	6	-6	-5	30	-30	0	26	23	2	15	16
0	66	66	-7	8	-8	-7	25	25	-10	19	20	K = 2	L = 3		-7	3	3	-4	6	6	1	0	0	K = 3	L = 11	
1	123	-129	-6	7	6	-6	14	14	-9	4	0	-12	1	3	-6	2	-2	-3	30	-30	2	51	-50	-10	7	8
2	98	97	-5	9	8	-5	64	-63	-8	30	-30	-11	0	1	-5	9	-9	-2	14	-13	3	34	32	-9	4	-5
3	4	2	-4	5	4	-4	10	9	-7	36	37	-10	7	-7	-4	5	5	-1	24	21	4	22	22	-8	0	0
4	46	-45	-3	39	34	-3	63	61	-6	31	-30	-9	1	2	-3	8	-8	0	33	27	5	25	-25	-7	0	2
5	82	84	-2	23	-21	-2	55	-51	-5	5	-5	-8	12	-13	-2	7	6	1	56	49	6	14	14	-6	4	-3
6	39	-39	-1	32	-26	-1	12	-11	-4	37	36	-7	6	-6	-1	7	7	2	14	-14	7	6	7	-5	6	-7
7	3	-4	0	42	39	0	71	68	-3	45	-44	-6	11	11	0	12	-11	3	21	19	8	10	-9	-4	8	-7
8	25	25	1	50	-42	1	11	-11	-2	27	26	-5	12	-13	1	7	8	4	35	33	K = 3	L = 6		-3	11	11
9	25	-26	2	58	-49	2	33	-31	-1	2	3	-4	20	19	2	4	-4	5	53	-53	-12	22	-23	-2	0	-2
K = 0	L = 6		3	34	31	3	21	20	0	30	-31	-3	13	12	3	10	-10	6	0	-1	-11	20	19	-1	8	-10
-13	13	-13	4	11	11	4	8	8	1	31	32	-2	14	-13	4	5	5	7	21	21	-10	7	7	0	17	18
-12	5	-3	5	21	-20	5	22	-22	2	19	-19	-1	14	13	5	2	-3	8	23	-22	-9	33	-33	K = 4	L = 0	
-11	26	27	6	5	4	6	2	-1	3	1	-1	0	20	-18	6	0	1	9	1	0	-8	54	54	0	179	188
-10	46	-46	7	24	23	7	13	13	K = 1	L = 11		1	1	-1	K = 2	L = 8		10	9	9	-7	38	-36	1	101	-98
-9	27	26	8	8	-7	8	6	-6	-11	3	-1	2	15	13	-12	0	0	11	0	0	-6	14	-13	2	51	-48
-8	6	6	9	13	-14	K = 1	L = 6		-10	2	1	3	9	-9	-11	10	-11	K = 3	L = 2		-5	63	63	3	122	118
-7	52	-50	10	12	12	-13	20	-20	-9	1	0	4	19	18	-10	23	23	-12	11	-11	-4	85	-84	4	73	-70
-6	96	96	11	1	1	-12	25	26	08	7	-8	5	4	4	-9	28	-27	-11	11	-11	-3	40	39	5	16	16
-5	51	-49	K = 1	L = 2		-11	26	-25	-7	8	7	6	7	-7	-8	32	31	-10	31	32	-2	18	16	6	7	7
-4	3	2	-12	14	13	-10	13	-13	-6	6	7	7	6	6	-7	12	11	-9	48	-48	-1	74	-71	7	21	-21
-3	109	115	-11	13	13	-9	40	40	-5	10	-12	8	8	-7	-6	65	-65	-8	24	23	0	73	70	8	30	29
-2	116	-122	-10	33	-34	-8	62	-61	-4	5	5	9	4	-3	-5	78	79	-7	17	16	1	38	-38	9	35	-35
-1	27	27	-9	62	63	-7	44	43	-3	11	11	10	0	0	-4	30	-28	-6	74	-74	2	14	-13	10	10	8
0	30	32	-8	25	-24	-6	23	23	-2	9	-10	K = 2	L = 4		-3	72	-70	-5	96	95	3	50	48	11	16	16
1	87	-91	-7	23	-22	-5	65	-66	-1	6	-6	-13	9	8	-2	80	78	-4	53	-51	4	46	-46	K = 4	L = 1	
2	42	40	-6	89	89	-4	97	97	0	7	8	-12	8	7	-1	41	-40	-3	34	-32	5	23	23	-11	3	-2
3	21	-22	-5	123	-122	-3	55	-53	1	0	0	-11	36	-36	0	16	-16	-2	133	130	6	10	10	-10	12	13
4	3	2	-4	46	44	-2	20	-20	K = 1	L = 12		-10	49	49	1	33	33	-1	125	-121	7	23	-23	-9	4	-4
5	27	27	-3	39	36	-1	84	82	-9	6	-6	-9	19	-18	2	19	-19	0	68	61	K = 3	L = 7		-8	4	5
6	35	-37	-2	145	-152	0	84	-86	-8	9	-9	-8	57	-57	3	25	25	1	59	54	-12	10	10	-7	5	5
7	30	32	-1	147	157	1	50	50	-7	22	23	-7	87	87	4	14	-15	2	105	-99	-11	2	-2	-6	28	-28
8	2	1	0	82	-77	2	21	22	-6	26	-26	-6	76	-75	5	2	-2	3	97	94	-10	11	-10	-5	15	15
K = 0	L = 8		1	61	-57	3	54	-54	-5	10	9	-5	12	-11	K = 2	L = 9		4	39	-37	-9	1	-3	-4	15	-15
-13	22	-22	2	120	118	4	52	53	-4	10	10	-4	81	79	-12	0	0	5	28	-27	-8	14	13	-3	25	-25
-12	15	14	3	131	-132	5	29	-28	-3	25	-26	-3	91	-90	-11	3	-3	6	55	54	-7	14	-13	-2	40	38
-11	18	18	4	43	40	6	14	-14	-2	25	26	-2	112	107	-10	2	3	7	54	-54	-6	19	-20	-1	25	-25
-10	52	-52	5	34	33	7	23	24	-1	8	-8	-1	3	3	-9	0	2	8	16	16	-5	46	45	0	4	2
-9	41	40	6	65	-64	8	26	-27	K = 2	L = 0		0	58	-53	-8	2	-2	9	10	11	-4	2	3	1	15	13
-8	0	-1	7	65	66	K = 1	L = 7		0	105	-97	1	113	113	-7	11	11	10	27	-27	-3	24	-22	2	34	-32
-7	55	-54	8	13	-12	-13	8	-8	1	55	55	2	83	-79	-6	4	-4	K = 3	L = 3		-2	40	38	3	19	19
-6	50	49	9	9	-10	-12	10	10	2	104	-91	3	0	0	-5	6	-4	-12	6	7	-1	5	-4	4	11	-10
-5	22	-22	10	30	30	-11	4	5	3	41	-38	4	36	35	-4	5	6	-11	5	-5	0	24	-22	5	3	-3
-4	20	19	11	23	-24	-10	21	-21	4	150	156	5	65	-64	-3	9	-8	-10	4	-4	1	3	3	6	26	26
-3	19	18	K = 1	L = 3		-9	13	12	5	114	-111	6	40	41	-2	3	2	-9	8	8	2	7	-8	7	10	-9
-2	32	-31	-13	3	-2	-8	22	22	6	16	15	7	12	-12	-1	5	4	-8	8	8	3	0	-1	8	9	9
-1	76	77	-12	0	2	-7	25	-24	7	88	86	8	21	-21	0	2	-2	-7	5	4	4	2	-2	9	7	7
0	44	-46	-11	6	6	-6	6	-5	8	77	-75	9	33	34	1	4	6	-6	13	-13	5	0	1	10	9	-9

Table 3. Continued

H	FO	FC	H	FO	FC	H	FO	FC	H	FO	FC	H	FO	FC	H	FO	FC	H	FO	FC	H	FO	FC
K = 4	L = 2		-3	75	74	-10	5	-5	3	7	6	-6	24	24	-4	15	16	K = 7	L = 3		0	62	62	-5	12	12
-11	29	29	-2	86	-85	-9	5	-6	4	0	0	-5	13	-14	-3	27	-26	-9	6	5	1	41	-41	-4	21	-22
-10	32	-32	-1	28	27	-8	15	16	5	5	-6	-4	8	8	-2	37	37	-8	5	-4	2	22	-22	-3	14	14
-9	2	-2	0	36	36	-7	15	-16	6	12	-12	-3	18	18	-1	35	-35	-7	9	9	3	46	45	-2	5	6
-8	61	62	1	56	-55	-6	12	11	7	11	12	-2	24	-24	0	0	0	-6	19	-19	4	25	-25	-1	11	-10
-7	90	-90	2	34	33	-5	22	22	K = 5	L = 6		-1	35	36	1	33	32	-5	12	11	5	7	8	0	14	15
-6	22	22	3	15	-16	-4	18	-18	-11	14	-14	0	12	-10	2	51	-53	-4	10	11	6	7	7	1	7	-7
-5	63	62	4	1	-1	-3	42	43	-10	7	-5	1	16	-15	3	26	26	-3	50	-50	7	7	-7	K = 9	L = 0	
-4	105	-102	5	17	16	-2	16	-15	-9	30	30	2	38	36	4	17	18	-2	33	34	K = 8	L = 1		1	26	-26
-3	59	59	6	30	-31	-1	34	-33	-8	39	-40	3	30	-29	5	30	-31	-1	9	9	-8	4	4	2	30	31
-2	11	-7	7	22	23	0	41	39	-7	18	19	4	3	1	K = 6	L = 7		0	49	-48	-7	8	9	3	19	-17
-1	21	-20	K = 4	L = 7		1	54	-51	-6	8	8	5	10	10	-10	1	0	1	32	32	-6	16	-18	4	4	-4
0	58	54	-12	5	-6	2	25	-24	-5	43	-43	6	22	-22	-9	13	14	2	6	5	-5	20	22	5	15	15
1	90	-88	-11	0	1	3	24	23	-4	56	55	7	10	10	-8	11	-13	3	13	-13	-4	7	-7	6	19	-20
2	76	71	-10	5	-4	4	17	-16	-3	29	-29	8	6	-6	-7	8	8	4	8	8	-3	20	-21	K = 9	L = 1	
3	12	11	-9	7	-8	5	4	5	-2	5	-4	9	4	-4	-6	3	2	5	2	0	-2	24	25	-6	5	5
4	76	-75	-8	8	10	6	1	0	-1	54	53	K = 6	L = 2		-5	13	-9	6	13	12	-1	25	-27	-5	10	9
5	86	83	-7	14	-14	7	12	11	0	57	-56	-10	2	0	-4	12	12	7	10	-10	0	1	0	-4	21	-23
6	25	-24	-6	6	6	8	7	8	1	26	26	-9	17	17	-3	16	-16	K = 7	L = 4		1	14	14	-3	19	20
7	24	-23	-5	18	17	9	16	-17	2	9	10	-8	15	-15	-2	6	5	-9	24	-25	2	20	-19	-2	8	-9
8	41	41	-4	21	-21	10	11	12	3	39	-40	-7	25	25	-1	7	7	-8	25	26	3	23	23	-1	15	-16
9	29	-30	-3	15	15	K = 5	L = 2		4	33	33	-6	25	-25	0	23	-24	-7	4	1	4	6	-5	0	31	31
10	5	5	-2	2	2	-11	4	5	5	15	-15	-5	10	9	1	15	16	-6	23	-23	5	5	-5	1	20	-20
K = 4	L = 3		-1	15	-15	-10	26	-28	6	7	-5	-4	39	39	2	3	-2	-5	34	35	6	18	19	2	1	-1
-12	6	-6	0	14	14	-9	34	36	K = 5	L = 7		-3	93	-94	3	12	-12	-4	32	-32	7	14	-15	3	13	15
-11	0	-1	1	5	-6	-8	21	-22	-11	8	9	-2	52	50	4	13	13	-3	3	4	K = 8	L = 2		4	16	-16
-10	13	12	2	6	6	-7	17	-16	-10	20	-21	-1	31	31	K = 6	L = 8		-2	22	22	-8	25	26	5	6	5
-9	8	-8	3	7	7	-6	61	61	-9	17	16	0	92	-89	-10	13	12	-1	44	-44	-7	37	-38	K = 9	L = 2	
-8	14	14	4	7	-8	-5	59	-59	-8	14	15	1	78	77	-9	18	-19	0	43	43	-6	10	11	-6	20	22
-7	9	9	5	8	9	-4	31	32	-7	25	-25	2	3	-1	-8	14	14	1	4	-4	-5	27	29	-5	19	-21
-6	13	-13	6	4	-4	-3	26	26	-6	8	8	3	33	-32	-7	3	1	2	27	-27	-4	34	-35	-4	7	9
-5	19	20	K = 4	L = 8		-2	80	-78	-5	2	0	4	42	42	-6	39	-39	3	39	40	-3	26	27	-3	9	10
-4	24	-24	-11	12	13	-1	74	72	-4	11	-10	5	33	-33	-5	46	47	4	27	-27	-2	0	1	-2	20	-21
-3	4	-4	-10	39	-39	0	53	-51	-3	10	-9	6	9	8	-4	16	-9	5	2	-3	-1	8	-7	-1	25	26
-2	21	20	-9	32	32	1	28	-27	-2	8	-9	7	4	5	-3	33	-33	6	15	16	0	17	17	0	14	-15
-1	36	-34	-8	3	3	2	77	75	-1	23	21	8	21	-22	-2	50	51	K = 7	L = 5		1	37	-36	1	6	-5
0	25	23	-7	34	-35	3	71	-69	0	12	-11	K = 6	L = 3		-1	17	-18	-9	6	-6	2	22	21	2	26	27
1	7	4	-6	38	38	4	33	32	1	0	-2	-10	9	-10	0	12	-11	-8	15	-16	3	1	0	3	26	-27
2	28	-27	-5	16	-16	5	26	26	2	27	27	-9	11	11	1	14	15	-7	32	34	4	33	-33	4	9	10
3	15	15	-4	9	7	6	46	-45	3	14	-13	-8	14	-15	2	16	-15	-6	9	-10	5	33	34	K = 9	L = 3	
4	18	-18	-3	4	3	7	36	35	4	3	2	-7	6	-4	3	10	10	-5	13	-13	6	9	-9	-6	9	9
5	2	-4	-2	31	-30	8	12	-12	5	9	9	-6	16	17	K = 6	L = 9		-4	14	15	K = 8	L = 3		-5	13	14
6	9	8	-1	55	54	9	11	-11	K = 5	L = 8		-5	29	-30	-9	0	0	-3	3	-3	-8	7	8	-4	17	-18
7	8	-9	0	34	-33	K = 5	L = 3		-11	17	-17	-4	16	16	-8	8	-8	-2	3	2	-7	5	4	-3	9	9
8	12	12	1	21	-20	-11	11	11	-10	9	8	-3	7	7	-7	15	17	-1	22	-21	-6	12	-12	-2	5	-4
9	3	2	2	55	56	-10	15	-15	-9	14	15	-2	21	-22	-6	8	-7	0	11	11	-5	21	23	-1	3	3
K = 4	L = 4		3	38	-39	-9	3	-2	-8	32	-31	-1	31	31	-5	5	-5	1	13	14	-4	12	-13	0	1	1
-12	20	-20	4	3	-3	-8	20	20	-7	31	31	0	16	-15	-4	16	17	2	37	-37	-3	0	1	1	18	-18
-11	29	30	K = 4	L = 9		-7	37	-38	-6	11	-11	1	5	5	-3	12	-13	3	17	18	-2	17	18	2	28	28
-10	15	-15	-11	8	8	-6	6	5	-5	25	-25	2	22	21	-2	4	3	4	10	11	-1	32	-33	3	6	-7
-9	4	2	-10	4	-3	-5	32	32	-4	39	39	3	24	-24	-1	4	4	5	22	-22	0	14	13	4	18	-19
-8	21	22	-9	8	-8	-4	23	-23	-3	36	-36	4	20	20	0	8	-8	K = 7	L = 6		1	0	0	K = 9	L = 4	
-7	46	-46	-8	4	5	-3	14	15	-2	12	12	5	0	0	1	8	8	-9	16	-17	2	21	-22	-6	9	9
-6	57	58	-7	9	-9	-2	23	23	-1	23	23	6	14	-15	K = 7	L = 0		-8	26	27	3	19	19	-5	25	-27
-5	31	-29	-6	2	2	-1	22	22	0	36	-36	7	11	13	1	32	32	-7	17	-17	4	9	-9	-4	22	23
-4	50	-50	-5	2	1	0	15	-13	1	33	33	8	10	-9	2	56	-55	-6	5	-2	5	0	1	-3	0	-2
-3	100	98	-4	5	-5	1	28	-27	2	7	-6	K = 6	L = 4		3	36	35	-5	34	34	K = 8	L = 4		-2	20	-21
-2	88	-84	-3	14	14	2	45	43	3	17	-18	-10	26	27	4	0	-2	-4	38	-39	-8	7	7	-1	26	28
-1	6	7	-2	11	-11	3	33	-32	4	22	24	-9	11	-11	5	29	-30	-3	16	16	-7	20	-21	0	15	-16
0	62	59	-1	4	-2	4	38	-37	K = 5	L = 9		-8	27	-27	6	41	42	-2	9	9	-6	20	21	1	2	0
1	90	-88	0	9	10	5	42	41	-10	0	-2	-7	53	54	7	18	-18	-1	33	-33	-5	12	-13	2	14	14
2	61	60	1	12	-13	6	14	-14	-9	8	9	-6	31	-31	8	4	-2	0	33	32	-4	16	-17	3	17	-18
3	8	-8	2	6	5	7	14	-15	-8	6	-6	-5	2	0	9	15	17	1	14	-14	-3	40	41	K = 9	L = 5	
4	43	-43	3	3	4	8	17	18	-7	4	3	-4	40	40	K = 7	L = 1		2	5	-4	-2	27	-28	-6	17	19
5	58	58	K = 4	L =10		K = 5	L = 4		-6	14	14	-3	54	-55	-9	9	10	3	24	25	-1	7	8	-5	16	-17
6	29	-28	-10	5	-6	-11	2	-2	-5	15	-15	-2	36	36	-8	17	-17	4	22	-24	0	27	27	-4	1	-2
7	2	-1	-9	20	20	-10	16	-16	-4	5	6	-1	12	-13	-7	10	10	K = 7	L = 7		1	35	-34	-3	28	31
8	21	22	-8	32	-33	-9	31	32	-3	2	-1	0	38	-38	-6	6	-5	-9	4	-5	2	22	23	-2	27	-29
K = 4	L = 5		-7	9	10	-8	37	-37	-2	16	-15	1	55	54	-5	18	-18	-8	10	10	3	5	-4	-1	1	0
-12	8	-9	-6	33	33	-7	12	10	-1	11	11	2	35	-34	-4	23	24	-7	0	1	4	22	-23	0	19	19
-11	2	0	-5	52	-52	-6	32	33	0	10	-12	3	8	7	-3	19	-20	-6	18	-19	5	23	23	1	17	-18
-10	2	2	-4	26	25	-5	65	-65	1	3	-3	4	27	26	-2	2	2	-5	29	29	K = 8	L = 5		K = 9	L = 6	
-9	14	-13	-3	19	20	-4	68	67	2	14	14	5	32	-31	-1	14	14	-4	2	-2	-8	11	13	-5	14	-15
-8	17	18	-2	38	-38	-3	3	-2	K = 5	L =10		6	23	24	0	16	-16	-3	21	-21	-7	0	-4	-4	17	18
-7	3	1	-1	24	24	-2	53	-51	-9	2	1	7	7	-8	1	30	29	-2	29	28	-6	9	-10	-3	12	-13
-6	5	-4	0	6	-4	-1	77	76	-8	16	-17	K = 6	L = 5		2	16	-16	-1	9	-10	-5	18	19	-2	1	-3
-5	24	24	1	5	-4	0	60	-58	-7	29	29	-10	3	-4	3	1	0	0	10	-7	-4	11	-12	-1	16	18
-4	17	-16	K = 4	L =11		1	8	-3	-6	20	-20	-9	12	12	4	34	34	1	10	11	-3	9	10	K =10	L = 0	
-3	7	6	-9	4	3	2	36	34	-5	5	-5	-8	14	-14	5	33	-32	2	11	-12	-2	7	7	0	7	-7
-2	3	3	-8	4	3	3	56	-55	-4	24	24	-7	6	6	6	6	5	3	4	5	-1	14	-15	1	13	13
-1	19	-18	-7	10	-11	4	39	40	-3	32	-32	-6	2	3	7	15	16	K = 7	L = 8		0	20	21	2	9	-8
0	28	27	-6	5	6	5	4	-3	-2	12	13	-5	25	-25	8	19	-20	-8	18	19	1	14	-14	3	4	-5
1	11	-10	-5	1	-1	6	21	-21	-1	5	5	-4	24	24	K = 7	L = 2		-7	19	-20	2	9	-9	K =10	L = 1	
2	4	-4	-4	5	-5	7	31	32	0	17	-17	-3	14	-14	-9	19	-19	-6	8	8	3	15	16	-3	8	10
3	18	19	-3	9	8	8	19	-20	K = 6	L = 0		-2	16	-16	-8	14	14	-5	15	15	4	17	-17	-2	12	-14
4	20	-20	-2	5	-5	K = 5	L = 5		0	26	-25	-1	27	26	-7	6	6	-4	27	-27	K = 8	L = 6		-1	20	21
5	2	0	-1	0	1	-11	7	7	1	46	46	0	21	-21	-6	32	-33	-3	25	25	-8	3	2	0	5	-6
6	0	1	K = 5	L = 0		-10	5	4	2	32	-29	1	6	5	-5	39	40	-2	6	-6	-7	17	-17	1	10	-10
7	10	-10	1	71	-67	-9	3	-2	3	23	-23	2	9	9	-4	29	-30	-1	18	-18	-6	24	25	2	19	20
8	6	5	2	103	100	-8	13	-12	4	68	66	3	12	-11	-3	16	-16	0	23	23	-5	22	-23	K =10	L = 2	
K = 4	L = 6		3	49	-46	-7	2	-1	5	69	-68	4	16	16	-2	55	55	1	18	-18	-4	8	-8	-3	26	-29
-12	4	-3	4	3	-2	-6	21	21	6	0	0	5	5	-6	-1	50	-51	K = 7	L = 9		-3	29	30	-2	15	17
-11	21	21	5	48	46	-5	48	-48	7	45	45	6	2	0	0	23	22	-7	4	5	-2	31	-34	-1	9	10
-10	31	-32	6	57	-56	-4	3	-3	8	42	-42	K = 6	L = 6		1	24	24	-6	10	-10	-1	10	11	0	27	-29
-9	24	24	7	31	29	-3	58	57	9	15	15	-10	22	22	2	46	-46	-5	12	12	0	19	20	1	23	24
-8	8	7	8	2	-1	-2	47	-45	K = 6	L = 1		-9	17	-18	3	35	34	-4	3	-5	1	19	-20	2	1	0
-7	37	-37	9	23	-23	-1	6	6	-10	14	-15	-8	10	-11	4	18	-18	-3	3	-2	2	15	15	K =10	L = 3	
-6	63	63	10	28	28	0	54	53	-9	10	10	-7	32	33	5	12	-12	-2	11	12	K = 8	L = 7		-3	2	2
-5	47	-47	K = 5	L = 1		1	21	-20	-8	2	-2	-6	35	-35	6	27	27	-1	9	-9	-7	15	-15	-2	12	-14
-4	11	-11	-11	4	4	2	2	-1	-7	13	-14	-5	19	19	7	23	-23	K = 8	L = 0		-6	2	1	-1	17	19
																								0	9	-8

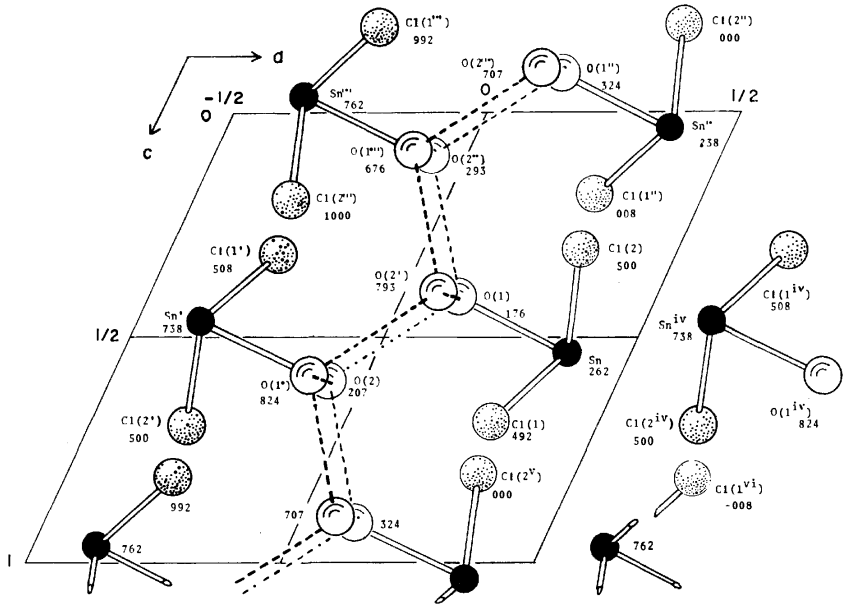

Fig. 2. The crystal structure viewed along the monoclinic *b* axis. Broken lines indicate hydrogen bonds.

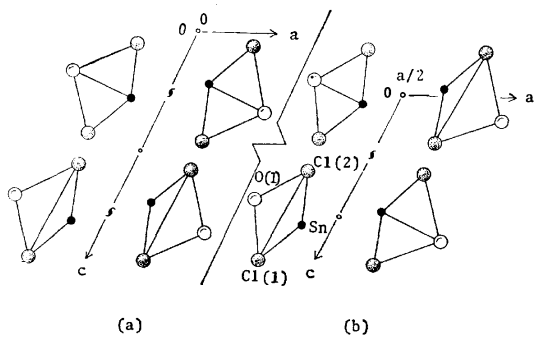

(a) (b)

Fig. 3. Comparison of the earlier structure (a) with the present one (b).

trated in Fig. 4. The tin atom is bonded to two chlorine atoms at distances of 2.50 and 2.56 Å and one oxygen atom at a distance of 2.33 Å; its pyramidal angles are 87.9, 86.9, and 85.0°. Four additional chlorine atoms at distances of 3.21, 3.34, 3.42, and 3.64 Å complete an environment of the tin atom (Table 4(b)). The difference between the two Sn–Cl bond lengths in each pyramid, 0.06 Å, is significantly large, this being thirty times the standard deviation. This might be reasonable if the effects of the lone-pair electrons of a tin atom in the adjacent complex and possibly of the hydrogen bonds are different for two chlorine atoms. The average Sn–Cl distance of 2.53 Å

Table 4. Distances (Å) and angles (°) in $SnCl_2 \cdot 2H_2O$ (Standard deviations in parentheses)

(a)	In the aquocomplex $SnCl_2(OH)_2$			
	Sn–Cl (1)	2.500 (2)	Cl (1)–Sn–Cl (2)	87.85 (8)
	Sn–Cl (2)	2.562 (2)	Cl (1)–Sn–O (1)	84.96 (14)
	Sn–O (1)	2.325 (5)	Cl (2)–Sn–O (1)	86.86 (13)
(b)	On other side of the Sn atom			
	Sn–Cl (1″)	3.416 (3)	Sn–Cl (1^{VI})	3.654 (2)
	Sn–Cl (2^{IV})	3.209 (2)		
	Sn–Cl (2^{V})	3.336 (2)		
(c)	Around the water oxygen atoms			
	O (1)–O (2)	2.800 (9)	O (2′)–O (1‴)–O (2‴)	109.80 (23)
	O (1)–O (2″)	2.736 (6)	O (2″)–O (1‴)–O (2′)	104.98 (20)
	O (1‴)–O (2″)	2.794 (7)	O (2″)–O (1‴)–O (2‴)	89.57 (23)
	Sn‴–O (1‴)–O (2′)	117.56 (25)	O (1)–O (2″)–O (1″)	112.89 (23)
	Sn‴–O (1‴)–O (2″)	112.84 (20)	O (1)–O (2″)–O (1‴)	111.17 (22)
	Sn‴–O (1‴)–O (2‴)	117.95 (20)	O (1″)–O (2″)–O (1‴)	90.43 (23)

Symmetry relations

Atom	x	y	z
Atom′	$-x$	$1.0-y$	$1.0-z$
Atom″	x	$0.5-y$	$z-0.5$
Atom‴	$-x$	$0.5+y$	$0.5-z$
Atom^{IV}	$1.0-x$	$1.0-y$	$1.0-z$
Atom^{V}	x	$0.5-y$	$0.5+z$
Atom^{VI}	$1.0-x$	$y-0.5$	$1.5-z$

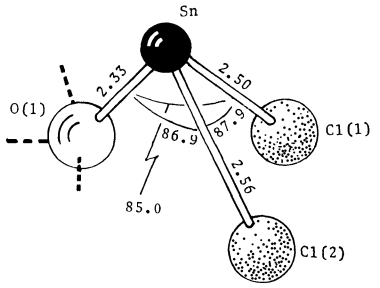

Fig. 4. The geometry of trigonal pyramid, $SnCl_2(OH)_2$ in $SnCl_2 \cdot 2H_2O$.

is close to those of 2.54, 2.54, and 2.63 Å for $K_2SnCl_4 \cdot H_2O$ and also of 2.50, 2.52, and 2.55 Å for $CsSnCl_3$, both of which contain pyramidal trichlorotin(II) complex ions.[5,6]

Molecules of anhydrous tin(II) chloride, $SnCl_2$, in the vapor phase are bent with a bond angle of 95° and with lengths of 2.42 Å.[7] In contrast with these, the tin atom in the crystalline state forms a pyramid with three chlorine atoms at 2.67, 2.78, and 2.78 Å and with Cl–Sn–Cl bond angles 78.0, 79.6, and 79.6°. It is noted here that three additional chlorine atoms at 3.06, 3.18, and 3.28 Å from the tin atom complete the distorted octahedron.[8] The increase in the Sn–Cl bond length of the molecular form must imply an increase in ionic character of this bond. A comparison of these coordinations of the tin atoms with that of $SnCl_2 \cdot 2H_2O$ indicates that an ionicity of the Sn–Cl bond in dichloroaquotin(II) complex molecules is less than that in the anhydrous crystal. This view is supported by ^{119}Sn Mössbauer studies, which have shown that the isomer shifts for the tin(II) atoms in $SnCl_2 \cdot 2H_2O$ and $SnCl_2$ are +(1.30—1.70) and +(2.40—2.50) mm/sec respectively (relative to α-Sn), as compared with a calculated value of +5.6 mm/sec for the hypothetical Sn^{2+} ion.[9]

On the other hand, the Sn–O bond length in the dichloroaquotin(II) complex was found to be 2.32 Å which was larger than the previous value (2.16 Å) given by K & G and also longer than that (2.21 Å) in tin(II) oxide.[10] A recent X-ray work on $KSn(HCOO)_3$ has shown that $Sn(HCOO)_3^-$ ions have again pyramidal configurations with Sn–O distances of 2.14, 2.17, and 2.18 Å and with bond angles of 78.4, 82.9, 83.2°.[11] A comparison of these values suggests that the Sn–O bond in the $SnCl_2(OH_2)$ complex is not essentially covalent, or at least less covalent than those in $KSn(HCOO)_3$ and SnO. However, it must be pointed out that the tin(II) atom in $SnSO_4$ has also a definite pyramidal three coordination with Sn–O bond distances of 2.27, 2.27, 2.25 Å and O–Sn–O angles of 79.0, 77.1, 77.1.[12]

The pyramidal bond angles of 85.0, 86.9, and 87.9° for $SnCl_2 \cdot 2H_2O$ are considerably less than the tetrahedral value required by the sp^3 hybrid configuration, as observed in many tin(II) compounds. Such the pyramidal three coordination of the tin atom can be explained in terms of strong repulsion between lone pair and bond pair from the covalent viewpoint or in terms of an unsymmetrical crystal field distorsion from the electrostatic viewpoint. The experimental values of the bond lengths precisely determined as well as the Mössbauer isomer shift support the idea that the bonding in the dichloroaquotin(II) complex is considerably ionic in character.

Arrangement of the Hydrogen Bonds

Figure 5 shows interatomic distances and bond angles concerning two kinds of the water molecules, one of which, $H_2O(1)$, is coordinated with the tin atom and the other $H_2O(2)$ is not so. Both water oxygen atoms have approximately tetrahedral configurations. These coordinations suggest that one of the lone pairs of oxygen O(1) is specifically directed toward the tin atom and the other is toward a hydrogen bond donor oxygen, namely $H_2O(1)$ is of type H according to the classification by Chidambaram *et al.*[13] Whereas, the water molecule $H_2O(2)$ is probably of type E with the two lone pairs directed toward two hydrogen bond donor oxygens.

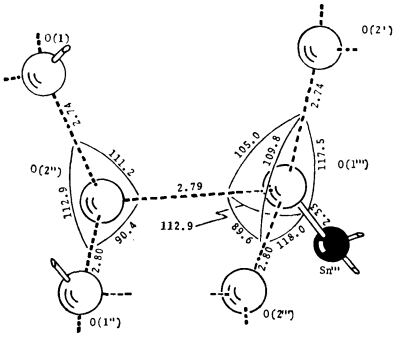

Fig. 5. The coordination of two kinds of water molecules.

The most striking feature of the structure is the arrangement of these water molecules, in particular their hydrogen bonding scheme. Different types of the water molecules are alternately connected by hydrogen bonds and the resulting sheets run parallel to (100) planes throughout the structure (Fig. 2). As mentioned earlier, this compound undergoes the phase transition with sharp peaks of the dielectric constant and the DC conductivity at −55 °C.[4] The remarkable dielectric dispersion observed in the high temperature phase, only when the electric field is applied in the (100) plane, can easily be understood on the basis of the

5) B. Kamenar and D. Grdenić, *J. Inorg. Nucl. Chem.*, **24**, 1039 (1962).
6) F. R. Poulsen and S. E. Rasmussen, *Acta Chem. Scand.*, **24**, 150 (1970).
7) M. W. Lister and L. E. Sutton, *Trans. Faraday Soc.*, **37**, 406 (1941).
8) J. M. van den Berg, *Acta Crystallogr.*, **14**, 1002 (1961).
9) J. D. Donaldson, *Progr. Inorg. Chem.*, **8**, 287 (1967).
10) W. J. Moore and L. Pauling, *J. Amer. Chem. Soc.*, **63**, 1392 (1941).
11) A. Jelen and O. Lindqvist, *Acta Chem. Scand.*, **23**, 3071 (1969).
12) J. D. Donaldson and D. C. Puxley, *Acta Crystallogr.*, **B28**, 864 (1972).
13) R. Chidambaram, A. Sequeira, and S. K. Sikka, *J. Chem. Phys.*, **41**, 3616 (1964).

present structure. Thus, in combination of the NMR results the phase transition can be interpreted in terms of the order-disorder model of the hydrogen atoms within the two-dimentional network of O–H—O hydrogen bonds.

It is interesting to note that there are only three O–H···O hydrogen bonds with distances of 2.736, 2.794, and 2.800 Å and with O··O··O angles near the tetrahedral angle against four available protons of two non-equivalent water molecules. Direct location of these hydrogen atoms was studied by proton and deuteron magnetic resonance and also neutron diffraction experiments.[14,15] These results confirmed our expectation that the hydrogen atom free from the O–H···O bonds should be directed toward one or two chlorine atoms. The further details will be published soon.

As given in Table 2, thermal parameters for all atoms are noticeably large, indicating large thermal motion. Actually this crystal dissolves in its own water of crystallization at about 40 °C.

In passing through the transition and also on deuterium substitution, no significant change in the non-hydrogen atom positions could be detected from the X-ray and the subsequent neutron diffraction works. At the transition point, however, the layer spacing, $a\sin\beta$, of $SnCl_2 \cdot 2H_2O$ did reduce suddenly by an amount of 0.02 Å and the line profiles of all (h00) reflections in the low temperature phase became broader, their half widths being twice the corresponding ones in the high temperature phase.

14) H. Kiriyama, O. Nakamura, and R. Kiriyama, *Acta Crystallogr.*, **A28**, S 240 (1972).
15) H. Kiriyama, O. Nakamura, K. Kitahama, and R. Kiriyama, *ibid.*, **A28**, S 60 (1972).

BULLETIN OF THE CHEMICAL SOCIETY OF JAPAN, VOL. 46, 1395—1399 (1973)

Molecular Structure of Nortricyclene Studied by Gas Electron Diffraction

Robert K. BOHN, Kazumi MIZUNO,* Tsutomu FUKUYAMA,* and Kozo KUCHITSU*

Department of Chemistry and Institute of Materials Science, University of Connecticut, Storrs, Connecticut 06268 U.S.A.

**Department of Chemistry, Faculty of Science, The University of Tokyo, Hongo, Tokyo 113*

(Received January 20, 1973)

The molecular structure of nortricyclene (tricyclo[2.2.1.$0^{2,6}$]heptane) has been studied by gas phase electron diffraction. The average values of the bond distances and their limits of error are: r_g(C–C)$=1.532\pm0.003$ Å and r_g(C–H)$=1.11_4\pm0.01_1$ Å. It is further shown that $r_g(C_3–C_4)=1.55_4\pm0.01_3$ Å, $r_g(C_1–C_2)+r_g(C_2–C_3)=3.04_2\pm0.01_0$ Å, and $\angle C_1–C_7–C_4=96.9\pm0.5°$.

As a part of the structure studies of polycyclic molecules,[1] we have recently determined the structures of norbornane (bicyclo[2.2.1]heptane)[2] and quadricyclene (tetracyclo[2.2.1.$0^{2,6}$.$0^{3,5}$]heptane)[3] by gas electron diffraction. These two compounds have considerably different $C_1–C_7–C_4$ angles, $93.1\pm1.7°$ and $98.5\pm2°$, respectively. Nortricyclene (tricyclo[2.2.1.$0^{2,6}$]heptane), placed between the above molecules, forms a sequence of increasingly strained compounds (Fig. 1); the strain energies are estimated to be about 18, 45, and 100 kcal/mol for norbornane, nortricyclene, and quadricyclene, respectively.[4,5] The solvolytic reactivity of 3-bromonortricyclene is about equal to that of *endo*-3-substituted norbornane and very much less than that of *exo*-3-substituted norbornane.[6]

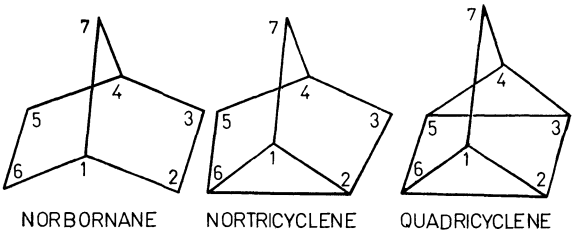

Fig. 1. a) Norbornane, b) Nortricyclene, c) Quadricyclene.

The molecular geometry of nortricyclene was first studied by the visual electron diffraction method by Heilbronner and Schomaker.[7] They determined the average C–C bond distance to be 1.527 Å and showed that the $C_2–C_3$ and $C_3–C_4$ distances have normal values (about 1.54 Å) if the $C_1–C_2$ distance is close to that in cyclopropane (about 1.50 Å). They also estimated the $C_1–C_7–C_4$ angle to be 96.5° with a limit of error of about 2°. One of its derivatives, 4-chloro-

1) K. Kuchitsu, "MTP International Review of Science," Physical Chemistry Series One, Vol. 2 (G. Allen, Ed.), Chapter 6, Medical and Technical Publ. Co., Oxford (1972).

2) A. Yokozeki and K. Kuchitsu, This Bulletin, **44**, 2356 (1971).

3) K. Mizuno, T. Fukuyama, and K. Kuchitsu, *Chem. Lett.*, **1972**, 249.

4) R. B. Turner, P. Goebel, B. J. Mallon, W. von E. Doering, J. F. Coburn, Jr., and M. Pomerantz, *J. Amer. Chem. Soc.*, **90**, 4315 (1968).

5) P. v. R. Schleyer, J. E. Williams, and K. R. Blanchard, *ibid.*, **92**, 2377 (1970).

6) J. D. Roberts, W. Bennett, and R. Armstrong, *ibid.*, **72**, 3329 (1950).

7) E. Heilbronner and V. Schomaker, *Helv. Chim. Acta*, **35**, 1385 (1952).

nortricyclene, has recently been investigated by electron diffraction[8] and by microwave spectroscopy.[9] The present study aims to supply further information on the structure of nortricyclene.

Experimental

A sample of nortricyclene (bp 108—110 °C) with less than 3% impurity, most of which was norbornene, was kindly supplied by Professor I. Tabushi of Kyoto University.[10] Diffraction experiments were carried out at 20 °C with a sample pressure of 30 Torr. Three diffraction photographs taken with 40 kV electrons at a camera length of 107.73± 0.01 mm were analyzed.[11] Diffraction photographs of CO_2 were used for calibration. The molecular intensity curves and the radial distribution curves (Figs. 2, 3) were obtained by standard procedures[12] in the q range from 25 to 120 Å^{-1}.

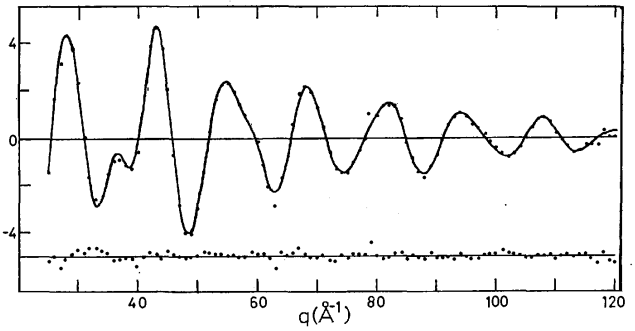

Fig. 2. Experimental molecular intensity for nortricyclene and the residuals (experimental minus best-fit theoretical).

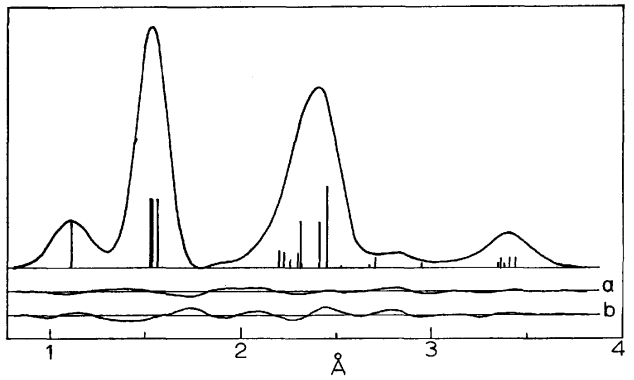

Fig. 3. Experimental radial distribution curve for nortricyclene with an artificial damping factor of exp(−0.00160s^2) and the residuals [(a) experimental minus best-fit theoretical and (b) experimental minus best-fit theoretical with all the C–C bond lengths assumed to be equal].

8) J. F. Chiang, C. F. Wilcox, Jr., and S. H. Bauer, *Tetrahedron*, **25**, 369 (1969).

9) V. W. Laurie, and W. M. Stigliani, *J. Amer. Chem. Soc.*, in press.

10) I. Tabushi, K. Yamamura, and Z. Yoshida, private communication (1972); P. K. Freeman, D. C. George, and V. N. M. Rao, *J. Org. Chem.*, **28**, 3234 (1963).

11) Y. Murata, K. Kuchitsu, and M. Kimura, *Jap. J. Appl. Phys.*, **9**, 591 (1970).

12) Numerical experimental data of the leveled total intensity have been deposited with the Chemical Society of Japan (Document No. 7311).

Analysis

The data were analyzed under the following assumptions:

1) The molecule has C_{3v} symmetry.
2) All C–H bond lengths are equal.
3) Angle H–C–H equals 110°, the angle in norbornane.[2]
4) The H–C_i–H and C–C_i–C angle bisectors (i= 3, 5, 7) are colinear.
5) The methine C–H bonds make equal angles with the adjacent C–C bonds.
6) Vibrational mean square amplitudes and shrinkage corrections (r_a-r_α)[2,13] were calculated from a reasonable set of Urey-Bradley force field parameters (Table 1) and held constant. The calculated values are listed in Table 2.

Table 1. Urey-Bradley force field parameters assumed for nortricyclene[a]

K_{CC}	2.2	H_{CCC}	0.3	$F_{C\cdots C}$	0.2
K_{CH}	4.0	H_{CCH}	0.2	$F_{C\cdots H}$	0.5
		H_{HCH}	0.43	$F_{H\cdots H}$	0.05

a) The units of K and F are md/Å and of H are md. The estimated force constants are taken from Table 1 of Ref. 2 and modified slightly.

Table 2. Calculated mean amplitudes (l_{ij}) and shrinkage corrections (d_{ij}) for nortricyclene[a] (10^{-4}Å)

Atom pair	l_{ij}	d_{ij}	Atom pair	l_{ij}	d_{ij}
C_1–C_2	534	14	$C_7\cdots H_2$	1095	23
C_2–C_3	530	16	$C_1\cdots H_{7a}$	1059	59
C_3–C_4	525	16	$C_4\cdots H_{7a}$	1059	59
C–H	771	131	$C_7\cdots H_4$	1033	27
$C_1\cdots C_4$	586	−1	$C_1\cdots H_4$	947	20
$C_3\cdots C_5$	721	−5	$C_5\cdots H_{7a}$	1016	34
$C_1\cdots C_3$	665	−4	$C_5\cdots H_{7b}$	1537	−23
$H_{7a}\cdots H_{7b}$	1302	120	$C_6\cdots H_{7a}$	1019	30
$C_1\cdots H_2$	1025	56	$C_6\cdots H_{7b}$	1441	−11
$C_3\cdots H_2$	988	60	$C_4\cdots H_2$	929	37

a) The amplitudes and shrinkage corrections[2] (r_a-r_α) calculated for 20 °C.

7) The asymmetry parameter κ for the C–H bond was assumed to be 1.0×10^{-5} Å^3, and the rest of the κ parameters were ignored.[14]

Under the above assumptions the structure is defined by five parameters: the C_1–C_2 (r_1), C_2–C_3 (r_2), C_3–C_4 (r_3) and C–H (average) distances (r_g) and angle C_1–C_7–C_4 (θ defined in the r_a structure[13]). The constraint that all the C–C bond distances were equal was added initially and the average bond distances were determined by a least squares analysis.[15] The best estimates and limits of error were: $r_g(C\text{–}C)_{av}=1.531_8\pm0.002$ Å and $r_g(C\text{–}H)_{av}=1.114\pm0.011$ Å, and the effective C–C

13) K. Kuchitsu and S. J. Cyvin, "Molecular Structures and Vibrations" (S. J. Cyvin, Ed.), Elsevier, Amsterdam (1972), Chapter 12.

14) K. Kuchitsu, This Bulletin, **40**, 505 (1967).

15) Y. Morino, K. Kuchitsu, and Y. Murata, *Acta Crystallogr.*, **18**, 549 (1965).

Table 3. Error matrix[a]

	C_2–C_3	C_3–C_4	C–H_{av}	$\angle C_1$–C_7–C_4	k
C_2–C_3	39	−37	−8	17	−52
C_3–C_4		39	2	−16	54
C–H_{av}			34	−14	22
$\angle C_1$–C_7–C_4				23	−32
k					124

a) Defined in Ref. 16. Units of distances, angle and index of resolution (k) are 10^{-4} Å, 10^{-4} rad. and 10^{-4}, respectively.

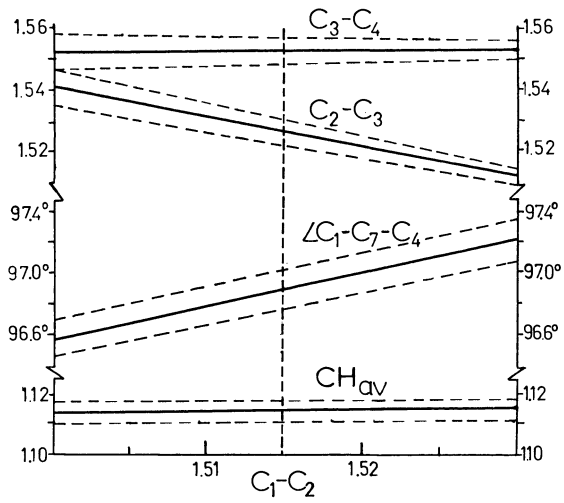

Fig. 4. Correlation of refined parameters with C_1–C_2 in nortricyclene. The vertical dashed line indicates the most probable structure. See text.

mean amplitude was 0.0549±0.003 Å.

Then the constraint of equal C–C distances was released. A series of least squares analyses showed that our experimental data contained information to determine four structural parameters. Thus the r_1 parameter was fixed to several different values, and the rest of the parameters were refined. A typical error matrix[16] is given in Table 3. The most probable estimates of the varied parameters do not depend on the choice of their initial values, but they are not necessarily independent of the choice of r_1. The dependence of the refined parameters on r_1 is shown in Fig. 4 where the value of each parameter bracketed by one standard deviation is plotted against r_1. The r_3 and the C–H_{av} distances are nearly independent of r_1, but the r_2 distance and θ vary linearly with r_1, so that the following equations are found to exist:

$$r_1 + r_2 = 3.04_2 \pm 0.01_0 \text{ Å} \quad (1)$$

$$\theta = 96.8_6 \pm 0.4 + 20(r_1 - 1.515)° \quad (2)$$

The above relations were also confirmed by examination of the weighted sum of squared residuals, $\boldsymbol{V'PV}$, determined for each model. The sum forms a deep valley in the parameter hyperspace along the path defined by Eq. (1). $\boldsymbol{V'PV}$ varies very slowly along that path and forms a shallow minimum at $r_1 \sim 1.51_5$ Å. The parameter values corresponding to this r_1 value are listed in Table 4. The observed intensity and

16) O. Bastiansen, L. Hedberg, and K. Hedberg, *J. Chem. Phys.*, **27**, 1311 (1957).

Table 4. The structure of nortricyclene[a]

	Present study[b]	H.S.[c]
C–C_{av}	$1.531_8 \pm 0.003$ Å	1.527
C_1–C_2	1.515(ass.)$\pm a$[d]	1.50
C_2–C_3	$1.52_7 \pm 0.01_3 \mp 1.1a$	1.54
C_3–C_4	$1.55_4 \pm 0.01_3$	1.54
$\angle C_1$–C_7–C_4	$96.9 \pm 0.4 \pm 20a°$	97±2°
C–H_{av}	$1.11_4 \pm 0.01_1$	1.10
k	$0.95_7 \pm 0.04$	
	Dependent parameters[d]	
$\angle$H–C–H	110°(ass.)	$\angle C_1$–C_2–C_3 107.0°
$\angle C_3$–C_4–C_7	101.5°	$\angle$H–C_1–C_2 122.6°
$\angle C_3$–C_2–(C_1–C_2–C_6)	109.7°	

a) The distances are r_g and the angles are derived from the thermal average (r_a) structure.
b) The errors are 2.5 times a standard deviation derived from a combination of constraint, least squares and scaling errors (See text and Table 5). The values proportional to a indicate the correlation of each parameter with the value of C_1–C_2. The estimated upper limit of a is 0.015 Å.
c) r_a structure. Ref. 7.
d) Dependent parameter values calculated from the structure determined in the present study.

radial distribution curves and those calculated from the best model agree with each other within experimental error (Figs. 2 and 3).

The error limits given in Table 4 contain contributions from several sources: (a) Most of the errors due to constraints 2) through 7) listed above are small compared to the least squares standard errors, as listed in Table 5. They are assumed to be the changes in the refined parameter values caused separately by: (1) allowing the methine C–H distance to be 0.01 Å less than the methylene distance, (2) changing angle H–C–H by 3°, (3) displacing the H–C_i–H angle bisectors by 2° from their respective C–C_i–C angle bisectors toward C_4, (4) bending the methine C–H bond 3° away from the three-fold axis, (5) increasing each vibrational amplitude uniformly by 5%, (6)

Table 5. Errors due to constraints in the structure analysis

Test[a]	C–C_{av}[b]	C–H_{av}[b]	$\angle C_1$–C_7–C_4[c]	k[d]
1	1	1	3	0
2	1	21	2	3
3	0	1	1	0
4	0	4	6	1
5	0	10	6	12
6	2	9	1	0
7	0	5	0	0
σ[e]	7	34	13	10
Scale[f]	6	4	0	0
Total[g]	30	108	40	40

a) Change in the parameters assumed in the least squares analysis. Tests 1 through 7 correspond to those described in text.
b) c) The units are 10^{-4} Å and 10^{-2} degrees, respectively.
d) Index of resolution (10^{-3}).
e) Standard deviation of the least squares analysis.
f) Standard systematic uncertainty in the scale factor.
g) Total estimate of the limit of error.

Table 6. Comparison of related structures

	Norbornane[a] ED[b]	Nortricyclene[a] ED[c]	Quadricyclene ED[d]	4-Chloronortricyclene ED[e]	4-Chloronortricyclene MW[f]
$C-C_{av}$	1.549(3)	1.532(3)	1.529(3)	1.527(3)	1.530
C_1-C_2	1.539(12)	1.51_5 (1_5)	1.51(2)	1.510(16)	1.527
C_2-C_3	1.55_7 (25)	1.52_7 (2_1)	1.56(2)	1.535(10)	1.525
C_1-C_7	1.56_0 (24)		1.54(3)		
C_3-C_4	1.539(12)	1.55_4 (1_4)	1.51(2)	1.537(5)	1.538
$\angle C_1-C_7-C_4$	93.1(17)	96.9(5)	98.5(20)	95.6	96.2
$\angle C_1-C_2-C_3$	103.3	107.0	104.6	107.0	106.6
$\angle(C_1-C_2-C_6)-(C_2-C_3-C_5-C_6)$	106.7	100.9	107.0	102.5	101.8

a) The distances are r_g, and the angles are θ_α defined in Ref. 13. The error limits in parentheses refer to the least significant figure.
b) Ref. 2.
c) The present study.
d) Ref. 3.
e) Ref. 8. The distances are r_a and angles are calculated from those with neglect of shrinkage effects.
f) Ref. 9. The distances and angles are derived from Kraitchman's equation.

diminishing each shrinkage correction by 10% and (7) changing the C–H asymmetry parameter by 30%. (b) The reproducibility of each of the refined parameters among the three plates was less than or equal to the least squares standard deviation. (c) As for the effects of the above assumptions on the separate analysis of the r_2 and r_3 distances, the mean amplitudes of the C–C bonds (5) are the only important source of error. When the three C–C amplitudes were increased uniformly by 5%, the least squares values for the r_2 and r_3 distances were changed by 0.006 Å and −0.007 Å, respectively. (d) An estimated standard error[17] of 0.04% in the scale factor was counted. (e) The square root of the sums of squares of the above errors was multiplied by 2.5 to give the error limit listed after each parameter in Table 4.

With reference to the r_a(C–C) distances in cyclopropane,[18] 1.510±0.002 Å and in 4-chloronortricyclene,[8] 1.510±0.016 Å, r_1 is assumed to be 1.515± a Å, where the upper limit of a is estimated to be 0.015. The second error limit proportional to a, listed separately in Table 4, accounts for the uncertainty in r_1 and the effects of the correlation among the parameters shown in Fig. 4. Thus the final estimates of the r_2 and θ parameters are 1.53±0.02 Å and 96.9± 0.5°, respectively.

It should be mentioned that the above assignment of the radial distribution peak at 2.4 Å is not unique. This peak is mainly composed of the three nonbonded C–C distances: C_1-C_3, C_1-C_4, and C_3-C_5, and an alternative assignment corresponding to θ equal to 105.3°, instead of 96.9°, is also consistent with the electron diffraction data, as Heilbronner and Schomaker pointed out.[7] They noted, however, that the force field consistent with such an equilibrium structure does not compare reasonably with force fields of related molecules. Further evidence that this assingment is hardly acceptable is given by a comparison of this angle with the corresponding angle in 4-chloronortricyclene (Table 6). In the chloro compound the microwave rotational constants[9] allow no ambiguity of this sort, and the C–C assignment in the electron diffraction study[8] is also less ambiguous than in nortricyclene.

Discussion

The nortricyclene structure reported by Heilbronner and Schomaker[7] has been confirmed to be accurate to within their reported limits of error (Table 4). The present study has considerably increased the accuracy of the molecular intensity and of the structural parameters. The average C–C bond length, 1.532±0.003 Å, is nearly equal to the corresponding average value for 4-chloronortricyclene, 1.527±0.003 Å (r_a)[8] or 1.530 Å (r_0).[9] It is considerably shorter than the average bond length in norbornane,[2] 1.549±0.003 Å, but not significantly different from the value in quadricyclene,[3] 1.529±0.003 Å. This reflects the effect of formation of a cyclopropane ring, with its relatively short bonds, in the transformation from norbornane to nortricyclene. In the transformation from nortricyclene to quadricyclene, however, there seem to be balancing effects of formation of a cyclobutane ring, with its relatively long bonds, and that of another cyclopropane ring. The C_3-C_4 bond, 1.55_4 Å, is longer than C_2-C_3, 1.52_7 Å, and appears to be only slightly longer than the value in cyclopentane, 1.546±0.001 Å.[19] The C_2-C_3 bond seems to be similar to the r_s value, 1.522 Å, found in methylcyclopropane.[20] Bond angles determined in the present study agree reasonably well with the corresponding angles in the chloro compound. Angle $C_1-C_7-C_4$ increases regularly among norbornane, nortricyclene and quadricyclene. A more precise deter-

17) K. Kuchitsu, T. Fukuyama, and Y. Morino, *J. Mol. Struct.*, **1**, 463 (1968).
18) O. Bastiansen, F. N. Fritsch, and K. Hedberg, *Acta Crystallogr.*, **17**, 538 (1964).
19) W. J. Adams, H. J. Geise, and L. S. Bartell, *J. Amer. Chem. Soc.*, **92**, 5013 (1970).
20) R. G. Ford and R. A. Beaudet, *J. Chem. Phys.*, **48**, 4671 (1968).

mination of the C–C bond distances must await the availability of rotational constants so that a combined electron diffraction-spectroscopy analysis[1,21] may be carried out.

21) M. Sugié, T. Fukuyama, and K. Kuchitsu, *J. Mol. Struct.* **14**, 333 (1972).

The authors are indebted to Professors Zenichi Yoshida and Iwao Tabushi, and Mr. Kazuo Yamamura for their supply of the sample and for helpful discussions. Robert K. Bohn gratefully acknowledges the financial support of the U. S. National Science Foundation enabling him to take part in the present study at the University of Tokyo.

BULLETIN OF THE CHEMICAL SOCIETY OF JAPAN, VOL. 46, 1399—1407 (1973)

Molecular Vibrations and Force Fields of Alkyl Sulfides. VI. Methyl Ethyl Sulfide and Its Deuterated Compounds, and Diethyl Sulfide

Masaru OHSAKU, Yuji SHIRO,* and Hiromu MURATA

Department of Chemistry, Faculty of Science, Hiroshima University, Higashisenda-machi, Hiroshima
**Shinonome Branch School, Faculty of Education, Hiroshima University, Shinonome-3-chome, Hiroshima*

(Received October 17, 1972)

Deuterated methyl ethyl sulfides, $CD_3SCH_2CH_3$ and $CH_3SCD_2CD_3$, were prepared, and their infrared spectra were recorded in the gaseous, liquid, and solid states. The normal coordinates of methyl ethyl sulfide, its deuterated analogues, and diethyl sulfide have been treated by the use of a modified Urey-Bradley potential field. The conformational analyses of these sulfides were made by the aid of the calculations. In the gaseous and liquid states, two forms (T and G) have been confirmed to exist for $CH_3SCH_2CH_3$, and three forms (TT, TG, and GG), for $CH_3CH_2SCH_2CH_3$. In the solid state, $CH_3SCH_2CH_3$ or $CH_3CH_2SCH_2CH_3$ exists in one form: T or TT. The observed infrared frequencies were compared with the calculated frequencies and were fully assigned.

In our previous papers, we reported the infrared spectra of methyl ethyl sulfide[1] and diethyl sulfide;[2] we postulated two and three conformations for methyl ethyl and diethyl sulfides respectively. However, we could not assign all of the infrared bands observed in the CH_3 rocking, CH_2 deformation, and C–S stretching regions. The purpose of this paper is to make the full assignments of the infrared bands of these sulfides, and to determine the skeletal conformations of methyl ethyl and diethyl sulfides. In order to confirm the vibrational assignments, the normal coordinates have been treated for these molecules. The vibrational analysis has also been extended to deuterated methyl ethyl sulfides: $CD_3SCH_2CH_3$ and $CH_3SCD_2CD_3$.

Vibrational Assignment

Deuterated methyl ethyl sulfides were prepared from CD_3I and CH_3CH_2SH, and from CD_3CD_2Br and CH_3SNa. The method of infrared recording and the instrument used have been described previously.[1] Both samples are contaminated with a very small amount of the normal species. The obtained infrared data are summarized in Tables 1 and 2. The spectra of $CD_3SCH_2CH_3$ are more complicated than those of the normal species. The spectra of $CH_3SCD_2CD_3$ are the most complicated of the three. The observed bands of annealed films are well resolved in both deuterated species. The assignments of the observed bands were made on the basis of the band intensities, band envelopes, and normal coordinates.

Methyl Ethyl Sulfide-d_3. The bands of the methyl group which is bonded to the sulfur atom are shifted directly upon deuteration. The two CD_3 degenerate deformation bands are expected around 1050 cm^{-1}. In this frequency region, we observed fairly complex band peaks. The bands at 1045 and 1040 cm^{-1} in the liquid state are assigned to the CH_3 rocking and the CD_3 degenerate deformation vibrations with reference to the band intensities. The CD_3 symmetrical deformation band is expected around 950 cm^{-1}, while the two CD_3 rocking vibrations are expected around 750 cm^{-1}. We observed some bands in the expected regions and assigned these bands as is shown in Table 1, although the assignments are not straightforward. Below 1400 cm^{-1}, in particular below 800 cm^{-1}, over half of the bands disappear in the solid state. Most of the disappearing bands may be related to the rotational isomerism.

Methyl Ethyl Sulfide-d_5. The ethyl-group vibrations are shifted to a lower frequency region upon deuteration. The other bands except for the C–C stretching band are not so much affected upon deuteration. For this species, the bands observed below 1100 cm^{-1} are very complex. According to the result of the normal-coordinate calculation, each of the normal coordinates can be said to be fairly well coupled with one another—in particular in the CD_3 and CD_2 deforma-

1) M. Ohsaku, Y. Shiro, and H. Murata, This Bulletin, **45**, 954 (1972).
2) M. Ohsaku, Y. Shiro, and H. Murata, *ibid.*, **45**, 956 (1972).

Table 1. Infrared frequencies (cm^{-1}) and assignments of $CD_3SCH_2CH_3$[a]

Gaseous Room temp.	Liquid Room temp.	Solid Annealed	Assignment[b]
2994 2985 vvs 2975	2972 vs	2972 s	ν_{C-H}
2967 sh, s	2965 sh, s	2959 s	ν_{C-H}
		2951 sh, m	—
2947 2942 vvs 2934	2929 vs	2930 m	ν_{C-H}
2925 sh, s 2916 sh, m	2916 sh, s	2918 m	ν_{C-H}
2895 s		2904 w	—
2883 s		2885 vvw	—
2880 s	2875 s	2873 m	ν_{C-H}
2855 m	2855 m	2843 w	—
2844 m	2833 m	2823 vvw	—
2259 2253 s 2240	2235 s	2235 m	ν_{C-D}
	2155 sh, vw	—	—
2147 2140 s 2133	2131 vs	2129 m	ν_{C-D}
2092 w	2090 w	2089 vvw	—
2083 sh, w	2070 w	2074 vvw	—
2020 vw		—	—
2010 vw	2004 w	2004 vvw	—
1464 s	1460 sh, s	1462 s 1455 s	$\delta^d_{CH_3}$
1452 s	1452 vs	1447 m	$\delta^d_{CH_3}$
1443 sh, m	1440 sh, s	—	$\delta^d_{CH_3}$, G
1427 w	1426 s	1432 s	$\delta^b_{CH_2}$
1420 sh, w	1420 sh, m	—	$\delta^b_{CH_2}$, G
1390 1383 w 1377	1377 s	1377 s	$\delta^s_{CH_3}$
	1365 sh, w	—	$\delta^s_{CH_3}$, G
1325 vvw	1320 vvw	—	—
1279 1271 vs 1265	1278 sh, s	1283 s	$\delta^w_{CH_2}$
	1266 vs 1248 sh, m	1269 s 1255 s	$\delta^t_{CH_2}$, $\delta^r_{CH_3}$
1064 m	1063 sh, m	—	$\delta^r_{CH_3}$, G
1056 1053 m 1049	1056 sh, m	1056 w	$\delta^r_{CH_3}$
1045 m	1049 s	1049 vs	$\delta^d_{CD_3}$
1040 sh, w	1045 sh, m	1045 w	$\delta^r_{CH_3}$, $\delta^t_{CH_2}$
1030 sh, w	1040 s	1035 vs	$\delta^d_{CD_3}$
1008 vw	1013 m	1013 w	ν_{C-C}
990 w 985 w	983 m	—	ν_{C-C}, G
977 970 w 965	971 s	966 vs	$\delta^s_{CD_3}$
795 788 w 784	789 s	797 s	$\delta^r_{CH_2}$, $\delta^r_{CH_3}$
777 w 765 sh, w	761 w	—	$\delta^r_{CD_3}$
	750 sh, vw	—	$\delta^r_{CD_3}$, G
726 vvw	724 w	731 m	ν_{C-S}, δ^r_{CD3}
718 vvw	720 sh, vw	721 w	$\delta^r_{CD_3}$
705 vvw	698 vw	—	ν_{C-S}, G
685 vvvw	689 sh, vw	—	—
653 w 646 w	645 sh, w	—	ν_{C-S}, G
641 635 w 632	640 m	640 s 634 w	ν_{C-S}
523 vvw	520 vw	—	—
	360 vvw	—	δ_{skel}, G
	345 vw	348 w	δ_{skel}
	264 vvw	—	δ_{skel}, G
	244 vvw		δ_{skel}

s, strong; m, medium; w, weak; v, very; sh, shoulder.

a) Above 3000, 2800—2300, and 2000—1500 cm^{-1} regions are omitted.

b) ν, stretching; δ^d, degenerate deformation, δ^b, bending; δ^s, symmetrical deformation; δ^w, wagging; δ^t, twisting; δ^r, rocking; δ_{skel}, skeletal deformation (including torsions).

Table 2. Infrared frequencies (cm^{-1}) and assignments of $CH_3SCD_2CD_3$[a]

Gaseous Room temp.	Liquid Room temp.	Solid Annealed	Assignment
3005 s 2998 s	2985 s	2987 w	ν_{C-H}
2988 2980 s 2976	2973 s	2972 m	ν_{C-H}
		2959 sh, vw	—
2936 vs 2924 vs	2917 vs	2917 s	ν_{C-H}
2880 w		2873 vw	—
2872 w 2860 w	2862 m	2864 w	—
2845 w	2838 s	2840 m	—
2240 2233 vs 2226	2228 vs	2232 s	ν_{C-D}
		2222 m	ν_{C-D}
2205 vw	2205 sh, m	2209 vw	—
2195 w		2192 vw	—
2164 w	2174 m	2174 vw	—
2155 w 2145 w	2145 m	2148 w	ν_{C-D}
2130 w	2118 s	2122 w	ν_{C-D}
2089 w		2095 vvw	—
2079 w	2071 s	2071 m	ν_{C-D}
2050 sh, w	2038 w	2038 vvw	—
		2033 vvw	—
1454 s 1448 s	1437 vs	1439 vs	$\delta^d_{CH_3}$
1440 s 1436 s	1427 vs	1428 vs	$\delta^d_{CH_3}$
1425 sh, m	1420 sh, s	—	$\delta^d_{CH_3}$, G
1333 1325 w 1317	1320 m	1327 vw 1320 m	δ^s_{CH3}
	1305 vw	—	—
1220 vvw	1220 vw	—	—

Gaseous Room temp.	Liquid Room temp.	Solid Annealed	Assignment
1151 1141 m 1135	1143 sh, m 1136 m	1141 m 1136 s	ν_{C-C}, $\delta^{d}_{CD_3}$
1070 s	1071 m	1068 vs	$\delta^{d}_{CD_3}$
1063 s	1062 s	1055 vs	$\delta^{d}_{CD_3}$
1057 s	1050 vs	1044 m	$\delta^{b}_{CD_2}$, $\delta^{s}_{CD_3}$
1052 s	1046 sh, s	—	$\delta^{b}_{CD_2}$, $\delta^{s}_{CD_3}$, G
1038 1031 s 1024	1025 vs	1025 vs	$\delta^{w}_{CD_2}$, $\delta^{s}_{CD_3}$
	1013 vvw	1011 vvw	—
988 m 982 s 972 s	978 vs	982 vs	$\delta^{r}_{CH_3}$
	970 sh, w	975 w	$\delta^{r}_{CH_3}$
965 sh, m 957 m 950 sh, w	958 s	962 vs	$\delta^{s}_{CD_3}$, $\delta^{t}_{CD_2}$
893 887 w 883	887 w	893 w	$\delta^{r}_{CD_3}$, ν_{C-C}
	885 vw	—	$\delta^{r}_{CD_3}$, ν_{C-C}, G
		795 vvw	—
785 sh, vw	786 w	786 w	$\delta^{r}_{CD_3}$, $\delta^{t}_{CD_2}$, $\delta^{w}_{CD_2}$
777 w 772 w	770 m	767 m	$\delta^{t}_{CD_2}$, $\delta^{r}_{CD_3}$
765 sh, vw 755 sh, vw	756 w	—	$\delta^{r}_{CD_3}$, $\delta^{r}_{CD_2}$, G
725 vw	725 w	—	ν_{C-S}, G
718 vw 712 vw	716 w	717 s	ν_{C-S}
610 vw	610 w	612 m	ν_{C-S}
577 w 566 w	576 w	—	$\delta^{r}_{CD_2}$, $\delta^{r}_{CD_3}$, G
558 w 555 w	565 m	569 s	$\delta^{r}_{CD_2}$, $\delta^{r}_{CD_3}$
		534 vvw	—
	525 vvw	527 vvw	—
	512 vvw	512 vvw	—
	332 sh, vvw	—	δ_{skel}, G
	321 vw	320 w	δ_{skel}
	235 vvw	—	δ_{skel}, G
	218 vvw		δ_{skel}

a) Above 3010, 2800—2300, and 2000—1500 cm^{-1} regions are omitted.
The other descriptionl are the same to Table 1.

tion regions. However, the bands arising from CH_3 and CD_2CD_3 groups are fairly well separated.

Normal Coordinate Treatment

We made the normal coordinate treatment for four species: $CH_3SCH_2CH_3$, $CD_3SCH_2CH_3$, $CH_3SCD_2CD_3$, and $CH_3CH_2SCH_2CH_3$. The molecular parameters used in the computations were: r(C–H) or r(C–D)=1.09 Å, r(C–S)=1.81 Å, r(C–C)=1.54 Å, and ϕ(CSC)=99°; the other bond angles were assumed to be tetrahedral. The force field used was the Urey-Bradley type potential modified by some interactions. The correction terms were: p, p', p'', n, n', t, g, t', g', t'', g'', and l. The corrections of p, p', n, t, and g have been explained in the first paper of this series.[3] The additional corrections were the bond-interaction constant, p'', between the C–S and C–C bonds; the angle interaction constant, n', between the CCH (or CCD) and HCH (or DCD) angles in the methyl group bonded to the carbon atom; the *trans* and *gauche* coupling constants, t' and g', between the CCH (or CCD) and SCC angles in the methyl group bonded to the carbon atom; the *trans* and *gauche* coupling constants, t'' and g'', between the methylene HCC (or DCC) and methyl CCH (or CCD) angles in the ethyl group, and the angle-interaction constant, l, between the SCH and HCC (or DCC) angles or the CCH (or

Table 3. Modified Urey-Bradley force constants[a] of methyl ethyl and diethyl sulfides

K(C–H)	4.250[b]	CH_3 and CH_2 groups
K(C–S)	1.750[b]	CH_3–S and S–CH_2 bonds
K(C–C)	2.100[c]	CH_2–CH_3 bond
H(HCS)	0.030[b,d]	CH_3 group
H(HCH)	0.370[b,d]	CH_3 group
H(CSC)	0.244[b,d]	CH_3–S–CH_2 and CH_2–S–CH_2 angles
H(SCC)	0.070[c]	S–CH_2–CH_3 angle
H(CCH)	0.210[c]	CH_2 group
H(SCH)	0.170[d]	CH_2 group
H(HCH)	0.350[d]	CH_2 group
H(CCH)	0.186[c]	CH_3 group
F(HCS)	0.763[b,d]	
F(HCH)	0.200[b,d]	
F(CSC)	0.210[b,d]	
F(SCC)	0.700[c]	
F(CCH)	0.470[c]	
F(SCH)	0.390[d]	
F(HCH)	0.200[d]	
F(CCH)	0.540[c]	
κ	0.060[b,d]	CH_3 group
	0.005[d]	CH_2 group
Y	0.054[b,d]	CH_3–S and S–CH_2 bonds
	0.100[c]	CH_2–CH_3 bond
p	−0.115[b,d]	CH_3 and CH_2 groups
p'	−0.100	CH_3–S and S–CH_2 bonds
p''	−0.100	S–CH_2 and CH_2–CH_3 bonds
n	0.033[b,d]	CH_3 group ($\angle$HCS and $\angle$HCH)
n'	0.040	CH_3 group ($\angle$CCH and $\angle$HCH)
t	0.070[b,d]	CH_3 group ($\angle$HCS and $\angle$CSC, *trans*)
g	−0.050[b,d]	CH_3 group ($\angle$HCS and $\angle$CSC, *gauche*)
t'	0.070	CH_3 group ($\angle$CCH and $\angle$SCC, *trans*)
g'	−0.050	CH_3 group ($\angle$CCH and $\angle$SCC, *gauche*)
t''	0.070	CH_3CH_2 group ($\angle$HCC and $\angle$CCH, *trans*)
g''	−0.050	CH_3CH_2 group ($\angle$HCC and $\angle$CCH, *gauche*)
l	0.000	S–CH_2–C

a) Unit of K, H, F, p, p', and p'' is in mdyn/Å; κ, Y, n, n', t, g, t', g', t'', g'', and l is in mdyn·Å; $F'=-0.1F$.
b) From Ref. 3. c) From Ref. 4. d) From Ref. 5.

Table 4. Observed and calculated frequencies (cm^{-1}), and approximate potential energy distribution, PED, (%) of $CH_3SCH_2CH_3$

Obsd[a]	Calcd T	Calcd G	PED
2985_s	2988	2988	$\nu_{C-H}(100)$
2965_s	2987	2987	$\nu_{C-H}(100)$
2957_s	2977	2977	$\nu_{C-H}(100)$
2950_s	2969	2969	$\nu_{C-H}(100)$
2926_s	2963	2963	$\nu_{C-H}(100)$
2915_s	2913	2913	$\nu_{C-H}(100)$
2874_s	2899	2899	$\nu_{C-H}(100)$
2866_s	2878	2878	$\nu_{C-H}(100)$
2855_s			—
2834_s			—
1465_l	1449	1449	$\delta^d_{CH_3}(100)$
1457_l	1448	1448	$\delta^d_{CH_3}(100)$
1448_l	1447	1474	$\delta^d_{CH_3}(100)$
1436_l	1446	1446	$\delta^d_{CH_3}(100)$
1427_l	1427		$\delta^b_{CH_2}(90)$
(1420_l)		1427	$\delta^b_{CH_2}(90)$
1405_s			—
1374_l	1373	1373	$\delta^s_{CH_3}(100)$
1319_l	1320	1320	$\delta^s_{CH_3}(100)$
1305_l			—
(1278_l)		1274	$\delta^w_{CH_2}(95)$
1264_l	1276		$\delta^w_{CH_2}(95)$
1249_l	1260		$\delta^t_{CH_2}(65)$, $\delta^r_{CH_3}(25)$
(1246_l)		1260	$\delta^t_{CH_2}(60)$, $\delta^r_{CH_3}(25)$
(1140_g)			—
1115_l			—
1062_l	1075	1072	T: $\delta^r_{CH_3}(80)$, G: $\delta^r_{CH_3}(85)$
(1045_l)	1046	1050	$\delta^r_{CH_3}(50)$, $\delta^t_{CH_2}(55)$
1008_l			—
995_l	1001		$\nu_{C-C}(60)$, $\delta^r_{CH_3}(35)$
(982_l)		996	$\delta^r_{CH_3}(50)$, $\nu_{C-C}(45)$
968_l	979		$\delta^r_{CH_3}(70)$, $\nu_{C-C}(35)$
(960_l)		977	$\nu_{C-C}(55)$, $\delta^r_{CH_3}(50)$
(955_l)		967	$\delta^r_{CH_3}(100)$
948_l	967		$\delta^r_{CH_3}(100)$
813_s			—
(783_l)		771	$\delta^r_{CH_2}(65)$, $\delta^r_{CH_3}(30)$, $\nu_{C-S}(20)$
758_l	762		$\delta^r_{CH_2}(80)$, $\delta^r_{CH_3}(35)$
726_l	742	731	$\nu_{C-S}(100)$
(676_l)		643	$\nu_{C-S}(100)$
654_l	644		$\nu_{C-S}(100)$
(528_l)			—
(505_l)			—
(363_l)		367	$\delta^b_{SCC}(55)$, $\delta^b_{CSC}(30)$
354_l	348		$\delta^b_{SCC}(60)$, $\delta^b_{CSC}(25)$
(272_l)		272	$\delta^b_{CSC}(35)$, $\tau_{C-C}(35)$, $\delta^b_{SCC}(20)$
238_l	242		$\tau_{C-C}(95)$
220_l	236		$\delta^b_{CSC}(70)$, $\delta^b_{SCC}(25)$
(215_l)		216	$\tau_{C-C}(60)$, $\delta^b_{CSC}(30)$
	175	172	$\tau_{C-S}(95)$
	80	79	$\tau_{C-S}(95)$

a) Figures in parentheses show the bands which disappear in the solid state.
s, solid-, l, liquid-, and g, gaseous-state bands.

Table 5. Observed and calculated frequencies (cm^{-1}), and approximate potential energy distribution, PED, (%) of $CD_3SCH_2CH_3$

Obsd[a]	Calcd T	Calcd G	PED
2972_s	2977	2977	$\nu_{C-H}(100)$
2959_s	2969	2969	$\nu_{C-H}(100)$
2930_s	2963	2963	$\nu_{C-H}(100)$
2918_s	2913	2913	$\nu_{C-H}(100)$
2873_s	2878	2878	$\nu_{C-H}(100)$
2235_s	2211	2211	$\nu_{C-D}(100)$
2235_s	2209	2209	$\nu_{C-D}(100)$
2129_s	2071	2071	$\nu_{C-D}(100)$
1460_l	1449	1449	$\delta^d_{CH_3}(100)$
1452_l	1446		$\delta^d_{CH_3}(100)$
(1440_l)		1446	$\delta^d_{CH_3}(100)$
1426_l	1427		$\delta^b_{CH_2}(90)$
(1420_l)		1427	$\delta^b_{CH_2}(90)$
1377_l	1373		$\delta^s_{CH_3}(100)$
(1365_l)		1373	$\delta^s_{CH_3}(100)$
1278_l	1276	1274	$\delta^w_{CH_2}(95)$
1266_l / 1248_l	1259	1260	T: $\delta^t_{CH_2}(65)$, $\delta^r_{CH_3}(25)$, G: $\delta^t_{CH_2}(60)$, $\delta^r_{CH_3}(25)$
(1063_l)		1073	$\delta^r_{CH_3}(85)$
1056_l	1075		$\delta^r_{CH_3}(80)$
1049_l	1057	1058	$\delta^d_{CD_3}(100)$
1045_l	1046	1049	T: $\delta^r_{CH_3}(50)$, $\delta^t_{CH_2}(55)$, G: $\delta^r_{CH_3}(45)$, $\delta^t_{CH_2}(50)$
1040_l	1055	1055	$\delta^d_{CD_3}(100)$
1013_l	995		$\nu_{C-C}(90)$
(983_l)		987	$\nu_{C-C}(100)$
971_l	975	975	$\delta^s_{CD_3}(100)$
789_l	764	776	T: $\delta^r_{CH_2}(75)$, $\delta^r_{CH_3}(30)$, G: $\delta^r_{CH_2}(50)$, $\delta^r_{CD_3}(25)$, $\delta^r_{CH_3}(25)$
(761_l)	762		$\delta^r_{CD_3}(90)$
(750_l)		754	$\delta^r_{CD_3}(70)$, $\delta^r_{CH_2}(20)$
724_l	727	726	T: $\nu_{C-S}(100)$, G: $\delta^r_{CD_3}(100)$
720_l	724		$\delta^r_{CD_3}(100)$
(698_l)		716	$\nu_{C-S}(100)$
(645_l)		633	$\nu_{C-S}(95)$
640_l	631		$\nu_{C-S}(90)$
(360_l)		358	$\delta^b_{SCC}(60)$, $\delta^b_{CSC}(25)$
345_l	342		$\delta^b_{SCC}(65)$, $\delta^b_{CSC}(20)$
(264_l)		265	$\tau_{C-C}(50)$, $\delta^b_{CSC}(30)$
244_l	241		$\tau_{C-C}(95)$
	218		$\delta^b_{CSC}(75)$, $\delta^b_{SCC}(20)$
		208	$\delta^b_{CSC}(40)$, $\tau_{C-C}(45)$
	128	125	T: $\tau_{C-S}(100)$, G: $\tau_{C-S}(95)$
	77	75	$\tau_{C-S}(95)$

a) See a) of Table 4.

CCD) angles in the methylene group. Most of the force constants used were transferred from or referred to those of related molecules previously reported.[3-5]

3) Y. Shiro, M. Ohsaku, M. Hayashi, and H. Murata, This Bulletin **43**, 609 (1970).
4) M. Hayashi, Y. Shiro, and H. Murata, *ibid.*, **39**, 112 (1966).
5) M. Ohsaku, Y. Shiro, and H. Murata, *ibid.*, **45**, 3035 (1972).

Table 6. Observed and calculated frequencies (cm^{-1}), and approximate potential energy distribution, PED, (%) of $CH_3SCD_2CD_3$

Obsd[a)]	Calcd T	Calcd G	PED
2987_s	2988	2988	$\nu_{C-H}(100)$
2972_s	2987	2987	$\nu_{C-H}(100)$
2917_s	2899	2899	$\nu_{C-H}(100)$
2232_s	2205	2205	$\nu_{C-D}(100)$
2222_s	2201	2201	$\nu_{C-D}(100)$
2148_s	2195	2196	$\nu_{C-D}(100)$
2122_s	2110	2110	$\nu_{C-D}(100)$
2071_s	2058	2058	$\nu_{C-D}(100)$
1437_l	1448	1448	$\delta^d_{CH_3}(100)$
1427_l	1447		$\delta^d_{CH_3}(100)$
(1420_l)		1447	$\delta^d_{CH_3}(100)$
1320_l	1320	1320	$\delta^s_{CH_3}(100)$
1143_l / 1136_l	1104	1096	T: $\nu_{C-C}(70)$, $\delta^d_{CD_3}(40)$, $\delta^w_{CD_2}(25)$
			G: $\nu_{C-C}(70)$, $\delta^d_{CD_3}(50)$, $\delta^w_{CD_2}(20)$
1071_l	1070	1070	$\delta^d_{CD_3}(85)$
1062_l	1069	1069	$\delta^d_{CD_3}(95)$
1050_l	1059		$\delta^b_{CD_2}(55)$, $\delta^s_{CD_3}(45)$
(1046_l)		1057	$\delta^b_{CD_2}(65)$, $\delta^s_{CD_3}(35)$
1025_l	1031	1030	$\delta^w_{CD_2}(40)$, $\delta^s_{CD_3}(50)$
978_l	987	988	$\delta^r_{CH_3}(100)$
970_l	968	967	$\delta^r_{CH_3}(100)$
958_l	945	945	$\delta^s_{CD_3}(60)$, $\delta^t_{CD_2}(40)$
887_l	873		$\delta^r_{CD_3}(45)$, $\nu_{C-C}(25)$
(885_l)		872	$\delta^r_{CD_3}(45)$, $\nu_{C-C}(30)$
786_l	793	797	T: $\delta^r_{CD_3}(45)$, $\delta^w_{CD_2}(30)$
			G: $\delta^t_{CD_2}(45)$, $\delta^r_{CD_3}(25)$, $\nu_{C-S}(20)$
770_l	778		$\delta^t_{CD_2}(80)$, $\delta^r_{CD_3}(25)$
(756_l)		787	$\delta^r_{CD_3}(35)$, $\delta^r_{CD_2}(55)$
(725_l)		726	$\nu_{C-S}(100)$
716_l	739		$\nu_{C-S}(100)$
610_l	599	598	$\nu_{C-S}(90)$
(576_l)		569	$\delta^r_{CD_2}(70)$, $\delta^r_{CD_3}(45)$
565_l	566		$\delta^r_{CD_2}(70)$, $\delta^r_{CD_3}(25)$
(332_l)		335	$\delta^b_{SCC}(50)$, $\delta^b_{CSC}(35)$
321_l	318		$\delta^b_{SCC}(50)$, $\delta^b_{CSC}(35)$
(235_l)		240	$\delta^b_{CSC}(50)$, $\delta^b_{SCC}(30)$
218_l	223		$\delta^b_{CSC}(60)$, $\delta^b_{SCC}(35)$
	184		$\tau_{C-C}(50)$, $\tau_{C-S}(50)$
		171	$\tau_{C-S}(90)$
	166	164	T: $\tau_{C-S}(50)$, $\tau_{C-C}(45)$
			G: $\tau_{C-C}(80)$
	72	71	T: $\tau_{C-S}(100)$
			G: $\tau_{C-S}(95)$

a) See a) of Table 4.

Table 7. Observed and calculated frequencies (cm^{-1}), and approximate potential energy distribution, PED, (%) of $CH_3CH_2SCH_2CH_3$

Obsd[a)]	Calcd TT[b)]	Calcd TG	Calcd GG	PED
2978_s	2977	2977	2977	$\nu_{C-H}(100)$
2978_s	(2976)	2977	2977	$\nu_{C-H}(100)$
2967_s	2969	2969	2969	$\nu_{C-H}(100)$
2967_s	2969	2969	2969	$\nu_{C-H}(100)$
2943_s	(2963)	2963	2963	$\nu_{C-H}(100)$
2936_s	2963	2963	2963	$\nu_{C-H}(100)$
2924_s	2913	2914	2913	$\nu_{C-H}(100)$
2904_s	2913	2913	2913	$\nu_{C-H}(100)$
2873_s	2878	2878	2878	$\nu_{C-H}(100)$
2862_s				—
2853_s	2878	2878	2878	$\nu_{C-H}(100)$
2823_s				—
1478_l	1449	1449	1449	$\delta^d_{CH_3}(100)$
1459_l	1449	1449	1449	$\delta^d_{CH_3}(100)$
1453_l	1446	1446	1446	$\delta^d_{CH_3}(100)$
1449_l	(1446)	1446	1446	$\delta^d_{CH_3}(100)$
1438_l	1428	1427	1427	$\delta^b_{CH_2}(90)$
(1425_l)	1426	1426	1426	$\delta^b_{CH_2}(90)$
1381_l	1373	1373	1373	$\delta^s_{CH_3}(100)$
1373_l	1373	1373	1373	$\delta^s_{CH_3}(100)$
(1294_c)				—
1282_l	1279	1276	1274	TT: $\delta^w_{CH_2}(90)$, TG: $\delta^w_{CH_2}(95)$, GG: $\delta^w_{CH_2}(95)$,
(1272_l)		1274	1273	$\delta^w_{CH_2}(95)$
1258_l	1273			$\delta^w_{CH_2}(90)$
1248_l*	(1258)	1261	1262	TT: $\delta^t_{CH_2}(65)$, $\delta^r_{CH_3}(30)$, TG: $\delta^t_{CH_2}(65)$, $\delta^r_{CH_3}(25)$, GG: $\delta^r_{CH_2}(60)$, $\delta^r_{CH_3}(30)$
1236_l	1261	1260	1259	$\delta^t_{CH_2}(65)$, $\delta^r_{CH_3}(30)$

Table 7. Continued.

Obsd[a]	Calcd			PED
	TT[b]	TG	GG	
1074_I	1079	1076	1074	TT: $\delta^r_{CH_3}(80)$, TG: $\delta^r_{CH_3}(80)$, GG: $\delta^r_{CH_3}(85)$
(1066_c)	1069	1072	1071	$\delta^r_{CH_3}(85)$
1047_I	1049	1051	1051	$\delta^r_{CH_3}(50)$, $\delta^t_{CH_2}(55)$
(1035_c)			1047	$\delta^r_{CH_3}(50)$, $\delta^t_{CH_2}(55)$
1028_I*	(1042)	1045		$\delta^r_{CH_3}(50)$, $\delta^t_{CH_2}(55)$
1005_I				—
992_I	1004	995		TT: $\nu_{C-C}(90)$, TG: $\nu_{C-C}(95)$
983_I	984		987	$\nu_{C-C}(100)$
(981_I)			986	$\nu_{C-C}(100)$
(971_I)		985		$\nu_{C-C}(100)$
(967_I)				—
(958_c)				—
797_c	768			$\delta^r_{CH_2}(80)$, $\delta^r_{CH_3}(35)$
(792_I)			776	$\delta^r_{CH_2}(75)$, $\delta^r_{CH_3}(35)$
(789_I)			765	$\delta^r_{CH_2}(80)$, $\delta^r_{CH_3}(35)$
(782_I)		769		$\delta^r_{CH_2}(80)$, $\delta^r_{CH_3}(35)$
(762_I)	(757)	765		TT: $\delta^r_{CH_2}(85)$, $\delta^r_{CH_3}(30)$, TG: $\delta^r_{CH_2}(80)$, $\delta^r_{CH_3}(35)$
(738_I)				—
(696_I)		667		$\nu_{C-S}(100)$
688_I	669			$\nu_{C-S}(100)$
(656_I)	648		664	$\nu_{C-S}(100)$
(638_I)		638	630	$\nu_{C-S}(100)$
(515_I)				—
(500_I)				—
(475_I)				—
(450_I)				—
(425_I)				—
(390_I)			391	$\delta^b_{CCS}(50)$, $\delta^b_{CSC}(35)$
(384_I)		381		$\delta^b_{CCS}(60)$, $\delta^b_{CSC}(25)$
(376_I)				—
345_I	360			$\delta^b_{CCS}(90)$
337_I	321		335	TT: $\delta^b_{CCS}(40)$, $\delta^b_{CSC}(30)$, GG: $\delta^b_{CCS}(80)$
(306_I)		312		$\delta^b_{CCS}(80)$
(294_I)				—
(260_I)		261		$\tau_{C-C}(70)$
(255_I)			255	$\tau_{C-C}(55)$, $\delta^b_{CCS}(25)$
245_I	239	241	241	$\tau_{C-C}(95)$
	(243)			$\tau_{C-C}(95)$
		190	193	TG: $\delta^b_{CSC}(50)$, $\tau_{C-C}(25)$, GG: $\delta^b_{CSC}(40)$, $\tau_{C-C}(35)$
	175			$\delta^b_{CSC}(60)$, $\delta^b_{CCS}(35)$
			101	$\tau_{C-S}(95)$
	91	95		$\tau_{C-S}(95)$
		75		$\tau_{C-S}(90)$
	(60)		59	TT: $\tau_{C-S}(95)$, GG: $\tau_{C-S}(90)$

* See text. a) c, solution-bands. b) A_2 species in parentheses.
The other notations are the same to Table 4.

The constants of p', p'', n', t', g', t'', g'', and l were assumed to be reasonable in value. It has been supposed that the potential constants are common for all species. The obtained set of the force constants is listed in Table 3. The calculated frequencies of methyl ethyl and diethyl sulfides are summarized in Tables 4—7, together with the observed frequencies.

Molecular Forms. We may suppose two forms, T (C_s) and G (C_1), on methyl ethyl sulfide and three forms, TT (C_{2v}), TG (C_1), and GG (C_2), on diethyl sulfide. Since the GG′ form of diethyl sulfide may have a higher energy than the other forms, we excluded this form from the conformational analysis of diethyl sulfide. The analysis of the molecular forms is made mainly on the bands observed in the CH_2 (or CD_2) rocking, C–S stretching, and skeletal deformation regions. Considering the numbers of the bands which remain in the crystalline films, we may conclude that methyl ethyl and diethyl sulfides exist in one form in the solid state. For methyl ethyl sulfide and the deuterated analogues, the frequencies calculated for the T form correspond well to their solid bands. For

diethyl sulfide, the frequencies calculated for the TT form agreed well with their solid bands. We may, therefore, conclude that the stable forms in the solid state for methyl ethyl and diethyl sulfides are the T and TT forms respectively. The results are in accord with the previous results.[6-9]

In the liquid-state or gaseous-state spectra, we observed more bands than would be expected for one conformation. The bands which disappear in the solid state of methyl ethyl sulfide and its deuterated species correspond well with the frequencies calculated for the G form. For diethyl sulfide, the bands at 1425, 1272, 1066, 971, 782, 762, 696, 638, 384, 306, and at 260 cm^{-1}, which disappear in the solid state, agreed well with the frequencies calculated for the TG form. We still have several bands remaining unassigned in the liquid or gaseous spectra of diethyl sulfide: one band in the CH_3 rocking region, one to three bands in the C–C stretching region, two bands in the CH_2 rocking region, and two to four bands in the skeletal deformation regions. It is unlikely that all of these bands are due to overtones or sum-combinations. Most of these bands correspond well with the frequencies calculated for the GG form. We, therefore, assigned most of these bands to the vibrations of the GG form.

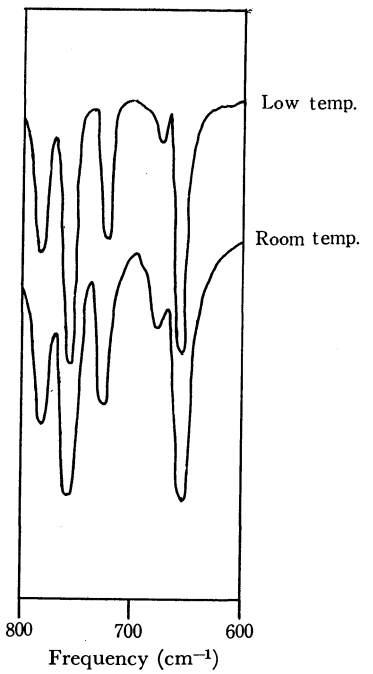

Fig. 1. Infrared spectra of methyl ethyl sulfide in the 800—600 cm^{-1} region observed in the liquid state.

Discussion

Perchard[10] made the vibrational analyses of eight isotopic species of methyl ethyl ether. He concluded that two forms, T and G, exist at room temperature, the former being more stable, and the T form in the solid state, and that the energy difference between the two forms in the liquid state is *ca.* 1.35 kcal/mol. For methyl ethyl sulfide, the intensities of the bands at 783 and 676 cm^{-1} decrease upon cooling, as is shown in Fig. 1. The low-temperature spectrum was recorded at a temperature slightly above its melting point. These bands correspond well to the frequencies calculated for the G form. Thus, the G form is the less stable conformation in the liquid state. The conformations of sulfides correspond well with those of ethers. For methyl isopropyl sulfide,[11] we previously obtained the energy difference of *ca.* 1—1.5 kcal/mol. We suppose that the energy difference for methyl ethyl sulfide is *ca.* 1 kcal/mol.

Recently, Scott and El-Sabban[12] made the normal coordinate treatment for diethyl sulfide, and concluded that the GG form has too much energy to exist as the stable form. Moreover, Snyder and Zerbi[13] and Wieser *et al.*[14] have treated the vibrational spectra and normal coordinates for diethyl ether, and have denied that diethyl ether exists in the GG form with stability. Wieser *et al.* assumed that diethyl ether exists in the TT and TG conformations at room temperature; the TT form is more stable than the TG form by *ca.* 1.1 kcal/mol. They also suggested that the C–H···O intramolecular hydrogen bond stabilizes the TT form. On the other hand, Snyder[15] reported a few of the bands due to the GG conformation for *n*-pentane. He also suggested that the TG form is more stable than the GG form, although there is not so much energy difference between the TG and GG, and TT and TG conformations; the stability is in the order of TT>TG>GG. With reference to the cases of diethyl ether and *n*-pentane, one of the less stable forms of diethyl sulfide may be the TG conformations. As we discussed in the last section, we observed very weak bands which fit the frequencies calculated for the GG form well. Therefore, the existence of the GG form has also been confirmed. The result for *n*-pentane also supports this result. We may now conclude for diethyl sulfide that three conformations of the TT, TG, and GG coexist in the liquid and gaseous states, while only one, namely, the TT form, exists in the solid state.

Figure 2 shows the relations in the observed and calculated frequencies and the frequency shift upon deuteration for the three isotopic methyl ethyl sulfides. The calculated frequencies in general correspond well

6) D. W. Scott, H. L. Finke, J. P. McCullough, M. E. Gross, K. D. Williamson, G. Waddington, and H. M. Huffman, *J. Amer. Chem. Soc.*, **73**, 261 (1951).
7) M. Hayashi, T. Shimanouchi, and S. Mizushima, *J. Chem. Phys.*, **26**, 608 (1957).
8) D. W. Scott, H. L. Finke, W. N. Hubbard, J. P. McCullough, G. D. Oliver, M. E. Gross, C. Katz, K. D. Williamson, G. Waddington, and H. M. Huffman, *J. Amer. Chem. Soc.*, **74**, 4656 (1952).
9) M. Hayashi, *Nippon Kagaku Zasshi*, **77**, 1804 (1956).
10) J. P. Perchard, *Spectrochim. Acta*, **A 26**, 707 (1970).
11) M. Ohsaku, Y. Shiro, and H. Murata, This Bulletin, **45**, 3480 (1972).
12) D. W. Scott and M. Z. El-Sabban, *J. Mol. Spectrosc.*, **30**, 317 (1969).
13) R. G. Snyder and G. Zerbi, *Spectrochim. Acta*, **A 23**, 391 (1967).
14) H. Wieser, W. G. Laidlaw, P. L. Krueger, and H. Fuhrer, *ibid.*, **24A**, 1055 (1968).
15) R. G. Snyder, *J. Chem. Phys.*, **47**, 1316 (1967).

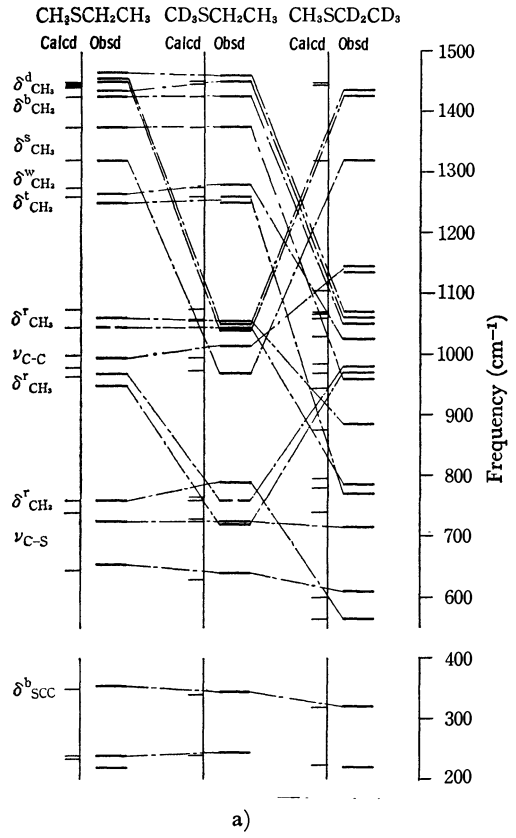

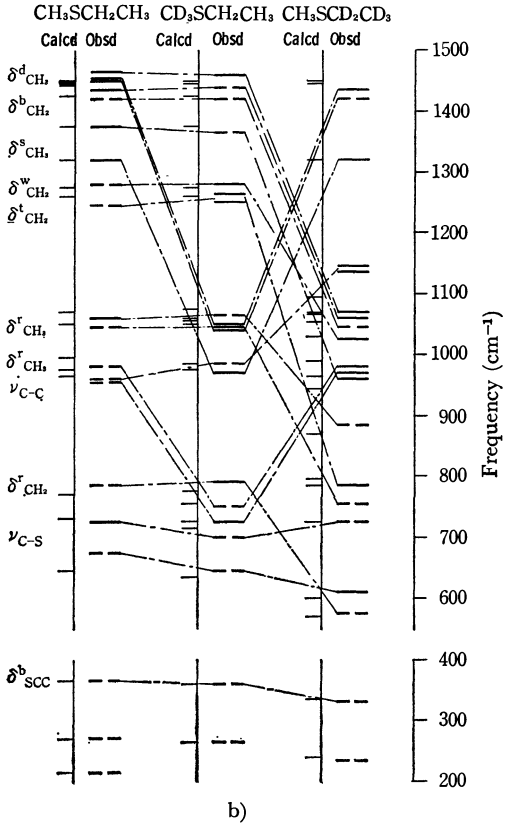

Fig. 2. Comparison of the observed and calculated frequencies (cm^{-1}) among the three isotopic species. Obsd; solid line: the bands appearing in the solid state, broken line: the bands disappearing in the solid state.
a) T form. b) G form.

Table 8. Observed and calculated frequencies (cm^{-1}) of the C–C stretching, C–S stretching, and the SCC bending bands in the T form

	$CH_3SCH_2CH_3$		$CD_3SCH_2CH_3$		$CH_3SCD_2CD_3$	
	Obsd	Calcd	Obsd	Calcd	Obsd	Calcd
ν_{C-C}	995	1001	1013	995	1141[a)]	1104
ν_{C-S}	726	742	724	727	716	739
ν_{C-S}	654	644	640	631	610	599
δ_{SCC}	354	348	345	342	321	318

a) Gaseous-state band.

with the observed ones. The frequency shifts upon deuteration can also be well explained by the calculations. In Table 8 the observed and calculated frequencies for the C–C stretching, C–S stretching, and SCC bending bands for the T form are listed. The observed C–C stretching bands are shifted to a higher frequency region through the $CH_3SCH_2CH_3$, $CD_3SCH_2CH_3$, and $CH_3SCD_2CD_3$ species. The calculated frequencies also show this tendency. On the other hand, the C–S stretching and SCC bending bands are shifted to a lower-frequency region through the above-mentioned species. The calculated frequencies fairly well support the observed tendency. For the G form, the observed frequency shifts upon deuteration are also explained by the normal coordinate treatment. The higher-frequency shift of the C–C stretching band can be understood if we consider that the band is pushed up to a higher frequency region by the CD_3 and CD_2 deformation vibrations.

A_2 Modes of Diethyl Sulfide. For the TT form of diethyl sulfide, the two C–H stretching bands and one each of the CH_3 degenerate deformation, CH_2 twisting, CH_3 rocking, CH_2 rocking, C–C torsion, and the C–S torsional bands belong to the A_2 species. We previously made the assignments of the A_2 modes of dimethyl sulfide[16] by examining the annealed spectra. In the diethyl sulfide, we can expect the distortion of the molecular structure upon crystallization. If the site symmetry of C_{2v} for diethyl sulfides does not remain in the solid state, the former seven bands may appear in the region we recorded.

One of the doublet bands around 2940 cm^{-1} can be assigned to the A_2 mode. The analyses of the annealed bands at 1449, 1442, and 1436 cm^{-1} are very difficult. We may, however, assign one of these bands to the A_2 species. The liquid bands at 1248 and 1028 cm^{-1} persist in the solid state with intensities much weaker than in the liquid state. We can assign these bands to the A_2 twisting and rocking vibrational modes. The frequencies of the observed bands fit the calculated A_2 frequencies well. Among the A_2 modes, the CH_2 rocking, and C–C torsional bands were not observed in the annealed spectra. We now consider that the CH_2 rocking and C–C torsional bands are essentially too weak to appear in the spectrum. Thus, we were able to identify most of the bands belonging to the A_2 species of diethyl sulfide.

16) M. Ohsaku, Y. Shiro, and H. Murata, This Bulletin, **45**, 113 (1972).

Table 9. Characteristic frequencies (cm^{-1}) of the CH_3 and CH_2 deformation regions in the [T] form

	CH_3-SCH_3[a]	CH_3-SCH_2-CH_3	CD_3-SCH_2-CH_3	CH_3-SCD_2-CD_3	$(CH_3$-$CH_2)_2S$
CH_3 deg def	1448	1465	1460	1437	1478
	1432	1457	1452	1427	1459
	1428	1448			1453
	1421	1436			1449
CH_3 sym def	1331	1374	1377	1320	1381
	1303	1319			1373
CH_3 rock	1039	1062	1056	978	1074
	985	1045	1045	970	1066
	952	968			1047
	910	948			1028
CH_2 bend		1427	1426		1438
					1425
CH_2 wag		1264	1278		1282
					1258
CH_2 twist		1249	1266 1248		1248
					1236
CH_2 rock		758	789		797
					762

a) Solid-state bands.

Snyder and Zerbi[13] assigned the bands at 1148 (vw) and 811 cm^{-1} (vw) of diethyl ether to the A_2 species. Also, the bands which may be due to the A_2 modes appear in the C–H stretching and CH_3 degenerate deformation regions in the solid-state spectra. On the other hand, for the species of dimethyl ether, Snyder and Zerbi[13] observed bands which may be due to the A_2 species in the annealed spectra —at 2907 (w) or 2877 (m), 1445 (w), and 1152 cm^{-1} (w)—, although they did not identify them as the A_2 modes. Therefore, it is likely that dimethyl and diethyl ether do not maintain the C_{2v} site symmetry in the solid state either.

CH_3 and CH_2 Deformation Regions. The CH_3 and CH_2 deformation bands of the sulfides in the [T] form are summarized in Table 9. The observed data of dimethyl sulfides are taken from Reference 16. The CH_3 degenerate deformation vibrations appear in the 1480—1420 cm^{-1} region. There are two sorts of symmetrical deformation vibrations, namely, the vibrations of the methyl groups bonded to the sulfur atom (I) and those bonded to the carbon atom (II). The CH_3 symmetrical deformation bands of Case I appear around 1320 cm^{-1}, and the corresponding bands of Case II, around 1380 cm^{-1}. The CH_3 rocking vibrations in the ethyl group are strongly coupled together with the C–C stretching and/or the CH_2 deformation vibrations. In a previous note on methyl ethyl sulfide,[1] we assigned the five bands in the 990—940 cm^{-1} region to the CH_3 rocking vibrations, but we noticed that the bands in the higher-frequency region were not assigned to the sole vibrational mode. It is more reasonable to consider now that the bands at 968 and 962 cm^{-1} in the annealed state of methyl ethyl sulfide are the results of crystal-field splitting. The band at 960 cm^{-1} in the liquid spectrum is assigned to the vibration of the G form. The CH_2 bending vibrations appear in the 1440—1420 cm^{-1} region. The bands assignable to the CH_2 wagging and twisting vibrations appear very close together.

C–S Stretching Region. The C–S stretching bands are shifted to a lower frequency region from dimethyl to diethyl sulfides. This is easily recognized by considering the masses of the groups bonded to the sulfur atom. In a previous note on diethyl sulfide,[2] the band at 738 cm^{-1} in the liquid state was identified as the C–S stretching fundamental. However, this band is too high to assign to the C–S stretching fundamental and too low to assign to the CH_2 rocking fundamental in view of the results on the normal coordinates. At the present time, we cannot reasonably explain this liquid band.

Ionic Mobility of Some Inorganic Ions in Mixed Solvents from Electromigration on Paper

M. M. LAHIRI, B. K. SEAL,* and S. K. MUKHERJEE
Department of Agriculture, University of Calcutta, Calcutta, India
(Received August 24, 1972)

Measurements of ionic mobilities of a number of cations and anions in nonaqueous and mixed solvents were made from electromigration on filter paper, and the apparent advantages of the ionophoretic method over other modern techniques have been explained. The values so obtained have been corrected for (a) electroosmotic and (b) tortuosity (*i.e.*, 'added migration path length') effects, in order to compare them with those in free solution. Considering the combined effect of dielectric constant and viscosity the ionic mobilities obtained by the electrophoretic method are considered to be of correct order of magnitude. The ionic mobilities at constant dielectric constant when plotted against reciprocal of viscosity show a slight deviation from linearity.

A number of direct and indirect methods are available for the determination of ionic mobilities in liquid media under an applied electric field. Of the earlier ones, the methods of Lodge,[1] Whetham,[2] and Hittorf[3] should be mentioned. The most precise one is the moving boundary method, developed by MacInnes,[4] Longsworth,[5] Shedlovsky,[6] and Tiselius.[7]

Whatever the method, the less accurate one of Hittorf or the more precise moving boundary method, they are all time-consuming and require accurate chemical analysis and elaborate techniques. By comparison, the ionophoretic technique lends itself to less complicated equipments which are easy to manipulate. It has also become apparent that it provides fairly accurate values of ionic mobility within a comparatively short time. The promise of paper ionography as an elegant and simple means of measuring ionic mobilities has come to the fore recently. However, a sufficient amount of data is not yet available for the purpose of establishing the potentialities of the technique. Although simple, its degree of reproducibility under varying working conditions has to be accurately ascertained.

Data on ionic mobilities in nonaqueous and mixed media are conspicuous for their paucity. In spite of some inherent difficulties of nonaqueous solutions, ionic mobilities of several alkali metal ions and of a few halide ions have been measured by Gordon and his collaborators[8] in anhydrous methanol and ethanol at 25°C from a combined study of transference number and the equivalent conductivity. Measurement of individual ionic mobilities in formamide ($D=109$) has also been reported.[9] The ionophoretic technique allows more convenient measurements in nonaqueous and/or mixed media, and hence this possibility has been explored to a large extent. Mixed solvents have been preferred because they permit a continuous variation of macroscopic parameters, namely the dielectric constant and the viscosity.

Principle

The factors governing the ionic migration in solution in an electric field can be classified as:

(a) Characteristics related to the particular ion under investigation, namely its charge (sign and magnitude), size, shape, tendency to dissociate, and tendency for complex formation and amphoteric behaviour, if any.

(b) Environmental factors such as electrolyte concentration, ionic strength, dielectric properties, pH, temperature, viscosity, etc.

(c) The uniformity and intensity of the applied field.

In addition, two other important factors often called "barrier effects", influencing the speed of ions are: (i) electroosmotic effect caused by the movement of charged medium, and (ii) tortuosity factor of 'added migration path length' owing to the winding nature of the path created by the fibrous structure of the filter paper. These two factors and consequent corrections according to McDonald and Bermes[10] have been discussed in an earlier communication.[11] McDonald and Bermes have shown that acceptable values of mobility of small as well as macro ions may be obtained after making these two corrections.

As mentioned earlier,[11] four measurements are required for each set of experimental conditions. These include measurement of ionographic mobility,

* Present address: Department of Chemistry, University of Burdwan, Burdwan, West Bengal, India.

1) O. Lodge, "Brit. Assn. Advancement Sci.", **56**, 389—412, Birmingham (1886).

2) W. C. D. Whetham, *Phil. Trans. Roy. Soc.*, **184A**, 337 (1893); *ibid.*, **186A**, 507 (1895).

3) W. Hittorf, *Ann. Phys.*, **89**, 177 (1853); **98**, 1 (1856); **103**, 1 (1858); **106**, 337, 513 (1859).

4) (i) D. A. MacInnes and I. A. Cowperthwaite, *Proc. Nat. Acad. Sci., U.S.A.*, **15**, 18 (1929). (ii) D. A. MacInnes and M. Dole, *J. Amer. Chem. Soc.*, **53**, 1357 (1931).

5) L. G. Longsworth, *J. Amer. Chem. Soc.*, **54**, 2741 (1932).

6) D. A. MacInnes, T. Shedlovsky, and L. G. Longsworth, *J. Amer. Soc.*, **54**, 2758 (1932); *Chem. Rev.*, **13**, 29 (1933).

7) A. Tiselius, *Trans. Faraday Soc.*, **33**, 524 (1937); *Kolloid.-Z.*, **85**, 129 (1938).

8) J. A. Davies, R. L. Kay, and A. R. Gordon, *J. Chem. Phys.*, **19**, 749 (1951); J. R. Graham and A. R. Gordon, *J. Amer. Chem. Soc.*, **79**, 2350 (1957); J. R. Graham, G. S. Kell, and A. R. Gordon, *ibid.*, **79**, 2352 (1957).

9) L. R. Dawson, E. D. Wilhoit, and P. G. Sears, *J. Amer. Chem. Soc.*, **79**, 5906 (1957); L. R. Dawson and C. Berger, *ibid.*, **79**, 4269 (1957); L. R. Dawson, T. M. Newell, and W. J. McCreary, *ibid.*, **76**, 6024 (1954).

10) H. J. McDonald and E. W. Bermes, Jr., *J. Chromatogr*, **4**, 34 (1960).

11) M. M. Lahiri, *J. Indian Chem. Soc.*, **42**, 843 (1965).

and R_D, a modified R_f as in classical chromatography of the migrant and of the electroosmotic indicator.

The general expression:

$$U = \frac{U_E}{R_D^M} \pm \frac{U_{el}}{R_D^{el}}$$

(where U_E denotes the ionographic mobility of the migrant and U_{el} that of the indicator and R_D^M and R_D^{el} denote the R_D values of the migrant and the indicator, respectively) has been utilised for the determination of free solution mobilities of some inorganic ions in mixed solvents. The negative sign is used if the migrant is positively charged, the positive sign if it is charged negatively.

Experimental

In the present communication are included the results for Cu^{2+}, Ni^{2+}, SCN^-, HSO_4^-, $[Fe(CN)_6]^{3-}$ and $[H_2Fe(CN)_6]^{2-}$ ions. HSO_4^- and $[H_2Fe(CN)_6]^{2-}$ actually resulting from the conversion of SO_4^{2-} and $[Fe(CN)_6]^{4-}$ respectively, in the back ground electrolyte having 0.05M acidity. The concentrations used were of the order 10^{-2}M prepared from reagent grade chemicals.

The reagents employed for detecting the ionic species on paper were as follows. Copper and nickel were detected by first spraying the paper with a saturated solution of rubeanic acid in ethanol and then holding the strip over ammonia vapour. Copper gave a dirty green colour and nickel a blue colour. Ferrocyanide and thiocyanate ions on paper were detected by spraying with a dilute solution of ferric chloride. The former gave a deep blue and the latter, a deep red colour. Ferricyanide was detected by spraying the strip with a dilute solution of ferrous sulphate when a blue colour was obtained. Sulphate was detected first by spraying the neutral paper with a 0.05 per cent solution of sodium rhodizonate in water, drying it, and then with a 0.02 per cent aqueous solution of $BaCl_2$, when a colourless spot on a reddish background was obtained. The electroosmotic indicator, glucose (concentration 0.005 g/ml), was detected on paper by spraying the neutral paper strip with an alcoholic solution of aniline oxalate and then heating it to 120°C when a brown spot appeared.

Micropipettes (1 ml capacity, graduated up to 10^{-3} ml) were used to spot a small volume of the substance under investigation on chromatographic paper. The Precision Ionograph (designed by Research Specialties Co., Richmond, California) which utilises the horizontal paper strip in the electrolyte-saturated condition was used with Whatman chromatographic paper No. 1 and the appropriate electrolyte solutions.

The media consisted of solvent mixtures having different dielectric constants. For this purpose, pure and distilled methanol, ethanol, 2-propanol, acetone, dioxane, and ethylene glycol were mixed with water and hydrochloric acid in definite proportions by weight so as to obtain mixtures of known dielectric constants at a particular temperature and of known acidity (0.05M). The "barrier effects" for the above-mentioned ions were evaluated by measureing the R_D values of the migrants and of the electroosmotic indicator in solvent mixtures of different dielectric constants with the help of a locally fabricated Ionograph similar to that proposed by McDonald and Bermes[10] under conditions identical with those above.

To start with an ionographic experiment, two strips (3.8× 57 cm) were simultaneously moistened with the electrolyte from both ends taking care to avoid excess electrolyte and then pressed gently between two dry filter paper sheets in order to make them, as far as possible, uniformly wet. The strips were then placed in position inside the chamber so that they were pulled horizontally taut by pressing gently the graphite electrodes on each end inside the electrolyte vessels. In order that each strip might offer the same resistance towards current flow, which could be observed from the equal length of each strip exposed above the solvent level, the strips were so placed that the mid-point line of each strip just touched the pointed end of a narrow plastic stick on which it rested. Electrolyte was then poured to the same level in each electrode vessel in order to avoid hydrodynamic flow of fluid in the paper, which was independent of electrical potential. A direct current at 200 V was applied for five minutes in order to drain out any excess solvent. The flow of current was then stopped, and to the marked mid-point of each strip, 0.002 ml of a mixture of the solutions of salt and glucose was carefully spotted. The chamber was then made gas-tight virtually by placing a cover and then closing the points of junction of the cover and the top of the base by means of cellophane adhesive tape. The temperature of the chamber was maintained constant at 25°C, thus reducing evaporation of the solvent from the strip to a minimum. A direct current at 200 V was applied for 30 min. The strips were then dried and sprayed with the reagent specific for the particular ion and again dried. The distance of migration of the ion together with the R_D values were utilised for calculation of free solution mobilities.

For ionographic experiments carried out in pure organic media such as formamide, special care was taken to use completely dehydrated copper and nickel salts for preparing solutions in formamide. Anhydrous sulphates of copper and nickel were obtained in the following processes.

(a) Reagent quality $CuSO_4 \cdot 5H_2O$ was heated in an air-oven first at 100°C to obtain the compound of stoichiometric composition $CuSO_4 \cdot H_2O$. This was further heated to 250°C when almost colourless and dehydrated $CuSO_4$ was obtained. The latter sample was finally heated to 360°C to result in anhydrous $CuSO_4$.

(b) Reagent quality $NiSO_4 \cdot 7H_2O$ was heated in an air-oven first at 120°C to obtain a compound having the stoichiometric composition $NiSO_4 \cdot 2H_2O$ which was further heated to 290°C when yellow and anhydrous $NiSO_4$ was obtained.

Anhydrous sulphates of copper and nickel thus obtained were dissolved separately in anhydrous formamide containing HCl upto the acidity of 0.05M and the respective solutions were used in the electromigration experiments in formamide.

Attempts were also made to use, as far as possible, moisture-free formamide which was obtained by lime-distillation under reduced pressure.[12] The boiling point of the moisture-free formamide prepared was 137.5°C under a reduced pressure of 40 mmHg.

Dry hydrogen chloride gas obtained by the action of reagent quality sulphuric acid on analytically pure sodium chloride (previously dried at 120°C overnight) was bubbled into the distilled formamide upto the acidity of 0.05M. Precautions were taken to avoid moisture-contamination as far as possible by keeping the solvent in an all-glass air-tight vessel and reducing the time between the initial preparations and final electromigration experiments.

The purity (particularly with regard to water content) of the sample of formamide was confirmed spectroscopically using IR and NMR techniques. Further information regarding the purity of the sample was obtained from a study

12) L. R. Dawson, T. M. Newell, and W. J. McCreary, *J. Amer. Chem. Soc.*, **76**, 6024 (1954).

of vapour phase chromatography.

IR spectra of (a) formamide, (b) formamide containing HCl upto the acidity of 0.05M (vide experiments) and (c) formamide previously kept under moist atmosphere were studied separately. The spectra of (a) and (b) showed no free water band and intermolecular hydrogen bonded water, and hydrogen bonded-NH group could not be distinguished from the spectra because both absorb practically in the same region. IR spectra of sample (c) suggests that formamide is not highly susceptible to moisture absorption. Moreover, a high resolution NMR spectrum of the sample of formamide taken by a Varian spectrometer (operating frequency 56.445 MHz) showed no line for the water proton even at considerably high gain of the amplifier. A vpc study of the formamide sample further confirmed the absence of water.

Results and Discussion

Details of composition by weight of the different solvent mixtures and the values of their dielectric

Table 1(A). (Room temperature: 25°)

Constituents of the solvent mixture	Composition of the solvent mixture (% by weight)		Dielectric constant of the solvent mixture	Viscosity (100η) cp
	Organic liquid	Water–HCl		
1. Methanol: Water: 0.05M HCl	80	20	40.1	1.007
	40	60	59.6	1.599
	20	80	69.2	1.391
2. Ethanol: Water: 0.05M HCl	70	30	38.0	2.007
	50	50	49.0	2.903
	30	70	61.1	2.084
3. 2-Propanol: Water: 0.05M HCl	60	40	35.3	2.693
	40	60	49.7	3.052
	20	80	64.1	1.908
4. Acetone: Water: 0.05M HCl	50	50	48.2	1.229
	30	70	61.0	1.339
	10	90	73.0	1.09
5. Dioxan: Water: 0.05M HCl	70	30	17.69	1.927
	45	55	38.48	1.518
	20	80	60.79	1.275
6. Ethylene glycol: Water: 0.05M HCl	40	60	66.6	1.46
	20	80	72.8	1.453
	10	90	75.6	1.14
7. Water			78.54	0.8937

Table 1(B). Determination of R_D values in different mixed solvents[a)]

Substances	Methanol: water: HCl dielectric constant.			Ethanol: water: HCl dielectric constant			2-Propanol: water: HCl dielectric constant		
	40.1	59.6	69.2	38.0	49.0	61.1	35.3	49.7	64.1
Cu^{2+}	1.0	1.0	1.0	1.0	1.0	1.0	1.0	1.0	1.0
Ni^{2+}	1.0	1.0	1.0	1.0	1.0	1.0	1.0	1.0	1.0
SCN^-	0.97	0.95	0.90	1.0	1.0	0.92	1.0	1.0	1.0
HSO_4^-	0.67	0.91	0.95	0.84	0.86	0.89	0.88	1.0	1.0
$[Fe(CN)_6]^{3-}$	0.91	1.0	1.0	1.0	1.0	1.0	1.0	1.0	1.0
$[H_2Fe(CN)_6]^{2-}$	0.95	1.0	1.0	1.0	1.0	1.0	1.0	1.0	1.0

Substances	Acetone: water: HCl dielectric constant			Dioxan: water: HCl dielectric constant			Ethylene glycol: water: HCl dielectric constant		
	48.2	61.0	73.0	17.7	38.4	60.8	66.6	72.8	75.6
Cu^{2+}	1.0	1.0	1.0	1.0	1.0	1.0	1.0	1.0	1.0
Ni^{2+}	1.0	1.0	1.0	1.0	1.0	1.0	1.0	1.0	1.0
SCN^-	1.0	1.0	1.0	1.0	0.92	0.92	1.0	0.96	0.94
HSO_4^-	0.92	1.0	1.0	0.85	0.90	0.90	1.0	1.0	1.0
$[Fe(CN)_6]^{3-}$	1.0	1.0	1.0	1.0	1.0	1.0	1.0	1.0	1.0
$[H_2Fe(CN)_6]^{2-}$	1.0	1.0	1.0	1.0	1.0	1.0	1.0	1.0	1.0

a) Since the electrophoretic movement of glucose (used as the electroosmotic indicator) in each of the above-mentioned mixed solvents (Table 2) was zero, determination of R_D value (used as the correction for tortuosity effect of a migrant through the paper) was not done. The electroosmotic effect has been found to be negligible in different nonaqueous solvents[13)]

TABLE 2.
(Experimental conditions: potential gradient=3.508 V/cm; time=30 min; temperature=25°C)

Solvent mixtures with appropriate dielectric constants (D)		Cu^{2+}		Ni^{2+}		SCN^-	
		Distance of migration (mm)	Mobility × 10^4 (computed) (cm^2/Vsec)	Distance of migration (mm)	Mobility × 10^4 (computed) (cm^2/Vsec)	Distance of migration (mm)	Mobility × 10^4 (computed) (cm^2/Vsec)
Methanol: water: 0.05M HCl	40.1	7.5	1.19	8.5	1.35	8.5	1.39
	59.6	11.0	1.74	12.0	1.90	12.5	2.09
	69.2	12.5	1.98	13.5	2.14	14.0	2.46
Ethanol: water: 0.05M HCl	38.0	7.0	1.11	8.0	1.26	7.5	1.19
	49.0	9.0	1.43	10.0	1.58	10.0	1.58
	61.1	11.0	1.74	12.0	1.90	12.0	2.07
2-Propanol: water: 0.05M HCl	35.3	6.0	0.95	7.5	1.19	7.0	1.12
	49.7	8.0	1.26	9.5	1.50	10.5	1.66
	64.1	10.5	1.66	12.0	1.90	13.0	2.06
Acetone: water: 0.05M HCl	48.2	8.5	1.35	10.0	1.58	12.0	1.90
	61.0	10.0	1.58	11.5	1.82	15.0	2.40
	73.0	12.0	1.90	13.5	2.14	18.5	2.93
Dioxane: water: 0.05M HCl	17.69	7.0	1.11	8.0	1.26	7.5	1.19
	38.48	10.0	1.58	11.0	1.74	10.0	1.72
	60.79	13.0	2.06	14.0	2.22	14.0	2.40
Ethylene glycol: water: 0.05M HCl	66.6	7.0	1.11	7.5	1.19	8.0	1.30
	72.8	11.0	1.74	11.0	1.74	14.0	2.30
	75.6	12.5	1.98	13.0	2.06	17.5	2.95

Solvent mixtures with appropriate dielectric constants (D)		HSO_4^-		$[Fe(CN)_6]^{3-}$		$[H_2Fe(CN)_6]^{2-}$	
		Distance of migration (mm)	Mobility × 10^4 (computed) (cm^2/Vsec)	Distance of migration (mm)	Mobility × 10^4 (computed) (cm^2/Vsec)	Distance of migration (mm)	Mobility × 10^4 (computed) (cm^2/Vsec)
Methanol: water: 0.05M HCl	40.1	6.0	1.41	9.5	1.61	5.0	0.84
	59.6	10.5	1.81	15.0	2.38	7.5	1.19
	69.2	12.5	2.09	18.0	2.85	9.0	1.43
Ethanol: water: 0.05M HCl	38.0	5.5	1.04	7.5	1.19	4.0	0.63
	49.0	7.5	1.38	10.0	1.58	5.0	0.79
	61.1	9.5	1.70	12.0	1.90	7.0	1.11
2-Propanol: water: 0.05M HCl	35.3	6.0	1.08	9.0	1.43	4.5	0.71
	49.7	9.0	1.43	13.0	2.06	7.0	1.11
	64.1	11.0	1.74	17.0	2.69	9.0	1.43
Acetone: water: 0.05M HCl	48.2	9.5	1.63	14.0	2.22	8.5	1.35
	61.0	12.0	1.90	17.5	2.77	10.0	1.58
	73.0	14.0	2.22	21.0	3.32	12.0	1.90
Dioxane: water: 0.05M HCl	17.69	6.0	1.11	8.5	1.35	3.5	0.55
	38.48	9.0	1.58	13.0	2.06	6.0	0.95
	60.79	11.5	2.02	18.0	2.85	8.5	1.35
Ethylene glycol: water: 0.05M HCl	66.6	6.0	0.95	7.5	1.19	3.5	0.55
	72.8	10.0	1.58	15.0	2.40	8.0	1.26
	75.6	12.5	1.98	19.0	3.00	11.00	1.74

constants are given in Table 1(A), the R_D values of ions studied in various solvent mixtures in Table 1(B) and the calculated mobilities in Table 2. The ionic mobility varies linearly with the dielectric constant of the medium as shown in Fig. 1. We see that with decreasing dielectric constant of the mixed solvents the ionic mobility gradually decreases. Except for the mixtures containing ethylene glycol, the variations of ionic mobility in the others are more or less similar. The graphs in Fig. 1 when extrapolated to the dielectric constants of the pure organic components give values of the ionic mobilities at a finite concentration (10^{-2}M) and at a particular acidity (0.05M HCl) in these different media. However, verification of these values by direct measurement has not been possible owing to the high resistance in the nonaqueous solvents which as a result evaporate quickly. The ethylene glycol graphs, to be noted, extrapolate to an absurdly negative value.

In each of the mixed media, glucose used as an electroosmotic indicator was found to be practically immobile. This does not mean necessarily that electroosmosis is absent, but under such conditions the ionic

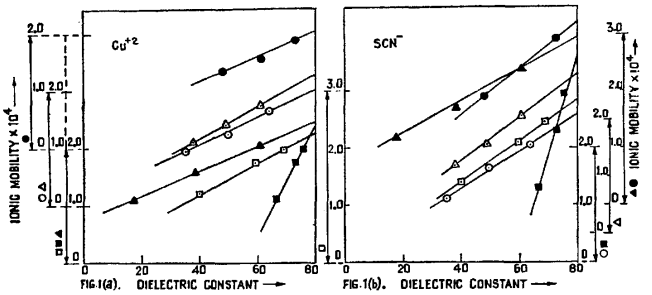

Fig. 1. Ionic mobilily *vs.* dielectric constants.
Solvent mixtures:
1) 2-Propanol: Water: HCl (○)
2) Ethanol: Water: HCl (△)
3) Methanol: Water: HCl (□)
4) Acetone: Water: HCl (●)
5) Dioxan: Water: HCl (▲)
6) Ethylene glycol: Water: HCl (■)

mobilities have to remain uncorrected for this effect. Glucose is therefore unsuitable as an indicator in mixed media, where the magnitude of electroosmotic effect may in reality be very small. Actually Strickler and Mathews[13] found the electroosmotic effect to be negligible in different nonaqueous solvents.

Table 3.

(Experimental conditions: electrolyte medium: formamide-hydrogen chloride mixture (0.05M); (dielectric constant=109.5 and viscosity=0.033 Poise at 25°C); temperature=25°C; potential gradient=3.508 V/cm; time=30 min.)

Migrant	Distance of migration (mm)	R_D value[a]	Computed mobility $\times 10^4$, (cm²/Vsec)	Computed mobility $\times 10^4$ (cm²/Vsec)	
				0.1M HCl	0.1M $HClO_4$
Glucose	0.0	—	—	—	—
Cu^{2+}	2.0	1.0	0.32(0.89)	2.35	—
Ni^{2+}	3.0	1.0	0.48(1.11)	2.61	—
Br^-	8.0	1.0	1.27(1.36)	—	3.61
I^-	8.5	1.0	1.35(1.36)	—	3.61
SCN^-	7.5	1.0	1.19(1.09)	—	2.89
$Cr_2O_7^{2-}$	8.0	0.95	1.33(1.19)	—	3.14
$[Fe(CN)_6]^{3-}$	8.5	1.0	1.35(1.33)	—	3.51

a) Since the electrophoretic movement of glucose (used as the electroosmotic indicator) in the above-mentioned medium was zero, determination of its R_D value was not done. The values in parentheses in the fourth column are the theoretical mobilities.

Of pure organic media, measurements in formamide (D=109) could be successfully made for Cu^{2+}, Ni^{2+}, Br^-, I^-, SCN^-, $Cr_2O_7^{2-}$, $[Fe(CN)_6]^{3-}$ ions in hydrochloric acid. The results are shown in Table 3. Comparing these with the values of ionic mobilities in aqueous media containing HCl and $HClO_4$, it is noted that the ionic mobilities are considerably lower in formamide, particularly for Cu^{2+} and Ni^{2+} ions. The expected increase in ionic mobility in formamide due to its high dielectric constant has apparently not been made due to other factors. One such factor is the viscosity of formamide solutions but it alone cannot explain the decrease observed for Cu^{2+} and Ni^{2+} ions. Even in aqueous mixtures of organic solvents where viscosities are of this order (2-propanol: water–HCl, 40: 60), the ionic mobilities are not so low. One plausible explanation may be as follows: In the aqueous mixtures of organic solvents, the cations remain preferentially hydrated in view of the high polarity and dielectric constant of water and hence the observed mobilities in these mixtures are essentially those of hydrated Cu^{2+} and Ni^{2+} ions. In formamide, the anions remain perhaps unsolvated as in other solvent mixtures and are not therefore much affected, in so far as their mobilities are concerned. This expectation receives support from theoretically computed mobilities[14] which agree fairly well with those observed for these anions in formamide medium. But Cu^{2+} and Ni^{2+} ions are perhaps solvated as usual, and because of the bulkier formamide molecule being attached to these cations thus forming complex basic salts[16] the mobilities are considerably reduced. The solvation of Cu^{2+} and Ni^{2+} ions by formamide is supported by the fact that formamide and its mono- and di-alkyl derivatives and the corresponding compounds derived from acetic acid are known to form complexes with the first group transition elements. Drago *et al.* have actually prepared hexacoordinated complexes of Ni^{2+} and Cr^{3+} ions with the above-mentioned ligands and have studied their spectra and other properties.[17] It is to be noted that care was taken to use completely dehydrated copper and nickel salts for preparing solutions in formamide (vide experiments).

From the graphs in Fig. 1, the mobilities of ions corresponding to any particular value of dielectric constant of the media can be read off. The mobilities corresponding to one such value of D=60 are recorded in Table 4, showing that they are different even though measured, so to say, at the same dielectric constant. Considering the combined effect of viscosity and dielectric constant the ionic mobilities recorded in Tables 2 and 4 are considered to be of correct order of magnitude except in ethylene glycol–water–HCl mixture of dielectric constant 60, where ionic mobilities are absurdly low even a negative value is shown for $[H_2Fe$-

13) A. Strickler and J. H. Mathews, *J. Amer. Chem. Soc.*, **44**, 1647 (1922).

14) The mobilities have been calculated from the quation $U_1 = \eta_{H_2O}/\eta_1 \cdot \varepsilon_1/\varepsilon_{H_2O} U_{H_2O}$ where U_1 is the ionic mobility in mixed medium, η_1 and ε_1 are respectively the viscosity and the dielectric constant of the medium. This expression has been obtained from Walden equation $U = Ze/6\pi\eta r$, assuming that the Stokes ionic radii remain unaltered on changing the medium and the mobility is linearly proportional to the dielectric constant (*cf.* Fig. 1). In calculating the mobilities we have assumed that the mobilities of anions in 0.05M HCl will be close to those in 0.1M $HClO_4$ at the same anion concentration. The mobilities observed of Cu^{2+} and Ni^{2+} ions in 0.05M HCl are 2.37 and 2.93.[15]

15) M. M. Lahiri and S. K. Mukherjee, *J. Indian Chem. Soc.*, **44**, 980 (1967).

16) L. F. Audrieth and J. Kleinberg, "Non-Aqueous Solvents," John Willy & Sons, Inc., New York, Chapman & Hall, Ltd., London, p. 144.

17) R. S. Drago, D. W. Meek, M. D. Joeston, and L. La Roche, *Inorg. Chem.*, **2**, 124 (1963).

TABLE 4(a).
(Dielectric constant=60.)

Solvent system	Viscosity (millipoise)	Fluidity	Isodielectric mobility × 10^4 (cm²/Vsec)					
			Cu^{2+}	Ni^{2+}	SCN^-	HSO_4^-	$[Fe(CN)_6]^{3-}$	$[H_2Fe(CN)_6]^{2-}$
2-Propanol: water: 0.05M HCl	23.00	0.0435	1.55	1.80	1.92	1.63	2.37	1.34
Ethanol: water: 0.05M HCl	21.75	0.0460	1.70	1.87	1.95	1.67	2.00	0.98
Methanol: water: 0.05M HCl	16.00	0.0625	1.74	1.90	2.12	1.85	2.37	2.20
Acetone: water: 0.05M HCl	13.38	0.0747	1.60	1.85	2.35	1.88	2.73	1.60
Dioxane: water: 0.05M HCl	12.88	0.0776	2.05	2.20	2.37	2.00	2.80	1.34
Ethylene glycol: water: 0.05M HCl	12.00	0.0833	0.60	0.62	0.15	0.25	0.00	−0.30

TABLE 4(b).

Solvent system	Dielectric constant	Viscosity cp	Mobility × 10^4 (cm²/Vsec)				
			Cu^{2+}	Ni^{2+}	HSO_4^-	$[Fe(CN)_6]^{3-}$	$[H_2Fe(CN)_6]^{2-}$
Ethylene glycol: water: 0.05MHCl	75.6	1.14	1.98(1.86)	2.06(2.3)	1.98(2.07)	3.0 (2.75)	1.74(1.64)
Ethylene glycol: water: 0.05M HCl	72.8	1.453	1.74(1.46)	1.74(1.8)	1.58(1.62)	2.40(2.16)	1.26(1.29)

a) The values in parentheses are the theoretical mobilities.

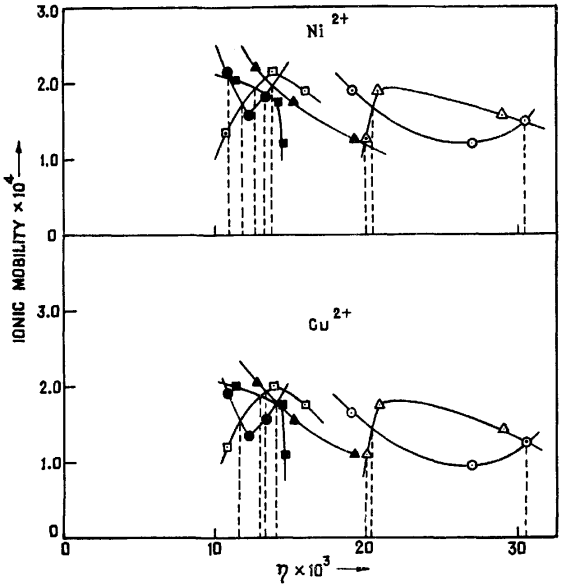

Fig. 2. Ionic mobility *vs.* η.
Solvent mixtures:
1) 2-Propanol: Water: HCl (○)
2) Ethanol: Water: HCl (△)
3) Methanol: Water: HCl (□)
4) Acetone: Water: HCl (●)
5) Dioxan: Water: HCl (▲)
6) Ethylene glycol: Water: HCl (■)

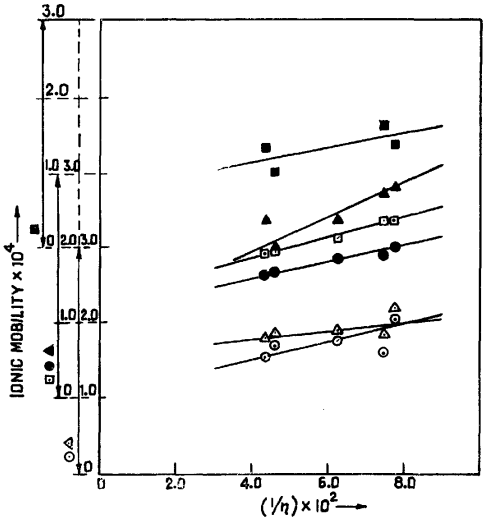

Fig. 3. Ionic mobility *vs.* $1/\eta$.
○: Cu^{2+}, △: Ni^{2+}, □: SCN^-, ●: HSO_4^-, ▲: $[Fe(CN)_6]^{3-}$, ■: $[H_2Fe(CN)_6]^{2-}$.

$(CN)_6]^{2-}$. Consequently the nature of the solvent medium and the ionic size in this medium are both going to influence the measured mobilities.

Viscosity is another factor influencing ionic mobility. The latter has been plotted in Fig. 2 against the viscosity of each of the solvent mixtures, from which it is seen that the curves are more or less smooth. Two and sometimes three or more curves intersect; these points being iso-viscous the corresponding mobilities may be termed iso-viscous mobilities. It is probable that irrespective of the nature of the ion, the curvature of the graphs is characteristic of the particular solvent system. The effect of viscosity under iso-dielectric condition (D=60) is shown by the data given in Table 4. If, however, the ionic mobilities at D=60 are plotted against the fluidity of the media assuming that Stokes ionic radii remain unaltered on changing the medium we have the graphs shown in Fig. 3 which are more linear than those in Fig. 2. The dielectric constants of two ethylene glycol: water: 0.05M HCl sys-

tems are close to that of water. Consequently any effect on ionic mobility in these media will be purely a viscosity effect. Accordingly we calculated the mobilities of ions in these media knowing those in water, on the assumption that the Stokes ionic radii remain unaltered. The agreement between the observed and calculated mobilities is, in view of the assumptions made, considered satisfactory. The results are shown in Table 4(b).

Thanks are due to Dr. (Miss) N. Banerjee of I.I.B.E.M., Calcutta-32, for taking the IR-spectra, to Dr. A. K. Roy of Saha Institute of Nuclear Physics, Calcutta-9, for taking the NMR-spectra, to Dr. U. S. Nandi of the Department of Macromolecules, Indian Association for the Cultivation of Science, Calcutta-32, for according laboratory facilities and to other co-workers of the Department for their kind assistance.

BULLETIN OF THE CHEMICAL SOCIETY OF JAPAN, VOL. 46, 1414—1417 (1973)

Kinetics and Mechanism of the Transformation of Vaterite to Calcite

M. Subba Rao

Department of Inorganic and Physical Chemistry, Indian Institute of Science, Bangalore-12, India

(Received June, 1, 1972)

The transformation of vaterite to calcite was investigated systematically. The transition temperature and the energetics of the transformation were determined from differential thermal curves. The variations of lattice constants and crystallite size, accompanying the transformation were studied by X-ray diffractometry. The kinetics of transformation were investigated in the temperature range 460—490°C. The kinetic data were analysed with the help of three separate solid-state models.

Anhydrous calcium carbonate is known to exist in three crystalline modifications—calcite, aragonite, and vaterite. All the three modifications could be prepared synthetically. Calcite is the stable form of calcium carbonate at ordinary pressure and temperature. Aragonite and vaterite are metastable modifications which transform to calcite on heating. Although the transformation of aragonite to calcite has been studied by several investigators, the only kinetic study on the transformation of anhydrous vaterite to calcite appeared to be the dilatometric investigation of Pruna *et al.*[1] However, there were quite a few investigations of the transformation of vaterite in contact with mother liquor. Here again there was considerable controversy regarding the transformation product. Lucas[2] reported that in the presence of mother liquor, vaterite was transformed to calcite and no aragonite was formed. On the other hand according to Faivre and Wallaeys,[3] both aragonite and calcite were formed by the transformation of nascent vaterite in contact with mother liquor. More recently Bischoff[4] has studied the transformation of vaterite to aragonite in aqueous medium in the presence of magnesium ions.

Owing to the incomplete and often conflicting information existing in the literature regarding the transformation of vaterite, a systematic investigation of the transformation of anhydrous vaterite was carried out. Apart from the kinetics of transformation, the effect of thermal treatment on the cell constants and crystallite sizes was followed from the stage of preparation to well beyond the transformation temperature. The kinetic data were analysed with the help of standard solid state models and the most appropriate model was indicated.

Experimental

Preparation of Vaterite.[5] A solution of 50 g potassium carbonate in 700 ml distilled water and containing 300 ppm sodium hexametaphosphate was heated to 60°C and the solution stirred briskly with a magnetic stirrer. 0.1M calcium chloride solution was added at an average rate of 0.5 ml min^{-1} till 200 ml of the solution were mixed. The crystals of vaterite were filtered off on a sintered glass crucible, washed thoroughly with distilled water and dried by washing with alcohol and ether. The anhydrous vaterite was preserved in a tightly stoppered bottle in a desciccator.

DTA of Vaterite. Differential thermal curves of known weights of vaterite and quartz were obtained on the Shimadzu-Recording DTA apparatus type DT-2A. Ignited alumina was the reference material. The sample and the reference material were uniformly packed into platinum containers which rest on Pt-Pt 10% Rh thermocouples. A heating rate of 12.5°C min^{-1} was employed.

High Temperature Thermostat. The thermostatic unit consisted of a nichrome-wound electrical tubular furnace, placed vertically. Kinetic studies were performed by dropping 20—25 mg of the vaterite sample into 6 mm *i.d.* fused silica tubes situated in the thermostat. The silica tubes rested

1) M. Pruna, R. Faivre, and C. Chaudron, *Bull. Soc. Chim. Fr.*, V, **16**, D205 (1949).

2) G. Lucas, *Bull. Soc. Fr. Mineral. Cristallogr.*, **70**, 185 (1947); *Chem. Abstr.*, **42**, 6708c (1948).

3) R. Faivre and R. Wallaeys, *C. R. Acad. Sci. Paris.*, **231**, 285 (1950).

4) J. L. Bischoff, *Amer. J. Sci.*, **266**, 80 (1968).

5) J. D. C. McConnell, *Mineral Mag.*, **32**, 535 (1960).

in an alloy steel cylindrical block situated midway in the furnace and insulated from the ends of the furnace by means of fire-clay plugs. Temperature was measured by means of a chromel-alumel thermocouple inserted in a fused silica sheath and inserted in a hole at the centre of the alloy steel block. The thermocouple was previously calibrated against melting and fusion points of standard solids. Furnace temperature was monitored by a Tinsley Vernier Potentiometer and controlled by means of a Sunvic energy regulator and variac autotransformer. Recorded temperatures are believed to be accurate to ± 2°C. Experimental runs were terminated by quickly removing the silica tube from the steel block at predetermined time intervals followed by immediate quenching in cold water. The quenched samples were analysed to determine the fractions of calcite and vaterite present in them.

X-Ray Diffraction Technique. X-Ray diffraction photographs of the heat-treated samples were taken using Rich Seifert X-ray unit with filtered copper radiation. 114.6 mm dia. Philips Debye-Scherrer Camera and a cylindrical specimen 0.3 to 0.5 mm dia. were employed. Bragg angles in the range 30—60°θ for the different reflections of vaterite and calcite were measured. The data were subjected to Cohen's[6] least-squares refinement and cell constants were calculated. By measuring the line broadening of the (104) reflection of calcite and (112) reflection of vaterite, the crystalline sizes were calculated using Scherrer[7] equation.

X-Ray powder diffraction photographs of the kinetic samples were taken in a 57.3 mm dia. Philips Debye-Scherrer Camera. Densitometer records of the (104) reflection of calcite and (110), (112), and (114) reflections of vaterite were obtained, employing photovolt transmission density unit and the multiplier photometer model 520-M. In this model full-scale deflection in the most sensitive range corresponds to 0.01 microlumen. The relation[8] between the intensity and fraction of calcite in the mixture was found to be

$$f_c = \frac{I_{104(c)}}{I_{110(v)} + I_{112(v)} + I_{104(c)} + I_{114(v)}} \quad (1)$$

Employing Eq. (1), the fraction of calcite in the kinetic samples was calculated.

Results and Discussion

The differential thermal curve for the sample of vaterite is shown in Fig. 1. The small exothermic peak with the peak temperature of 567°C is attributed to the transformation of vaterite to calcite. The heat of transformation ΔH was calculated by comparison with the peak of $\alpha \rightleftharpoons \beta$ transition in quartz. ΔH was found to be 145 cal mol^{-1}. E_a for the transformation using the method of Borchardt and Daniels[9] was found to be 120 kcal mol^{-1}.

The variation of unit cell volume of calcite and vaterite with temperature is shown in Fig. 3. There is a small contraction in the lattice prior to transformation. The variation of crystallite size with temperatures is represented in Fig. 2. There is a considerable decrease in the crystallite size of vaterite around the transformation temperature.

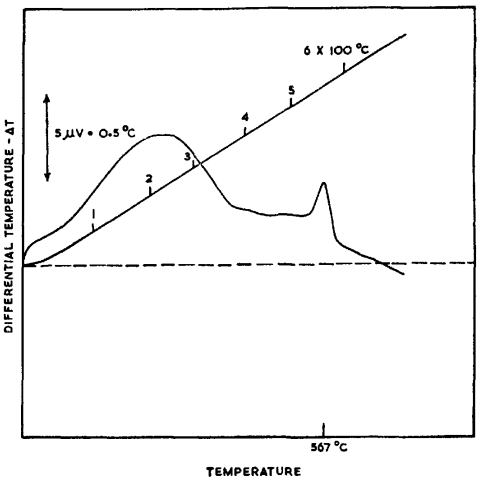

Fig. 1. Differential thermal curve of vaterite.

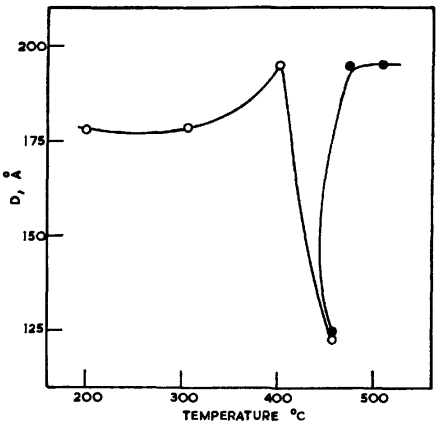

Fig. 2. Variation of the crystallite size of varite-calcite with temperature.

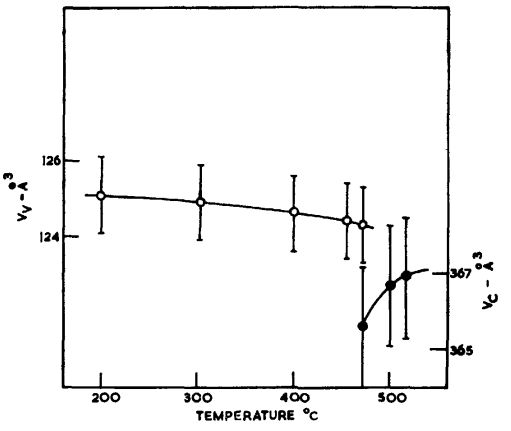

Fig. 3. Variation of lattice constants of vaterite-calcite with temperature.

The experimental results on the transformation rate studies over the temperature range 460—490°C are shown in Figs. 4 and 5. The extent of transformation of vaterite to calcite as a function of time under isothermal conditions is shown in Fig. 4, while in Fig. 5 the conversion of vaterite to calcite as a function of temperature at different times is shown. All the curves in Fig. 5 intersect the temperature axis at 450°C. This can be taken as the point where the rate of trans-

6) M. U. Cohen, *Rev. Sci. Instrum.*, **6**, 68 (1935); **7**, 155 (1936).
7) P. Scherrer, *Göttinger Nachrichten*, **21**, 98 (1918).
8) M. Subba Rao, Ph. D. thesis, submitted to the Indian Institute of Science (1969).
9) H. J. Borchardt and F. Daniels, *J. Amer. Chem. Soc.*, **79**, 41 (1957).

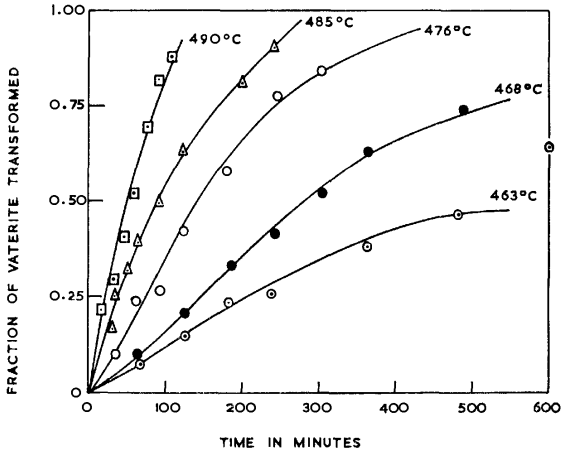

Fig. 4. Conversion of vaterite to calcite as a function of time at different temperatures.

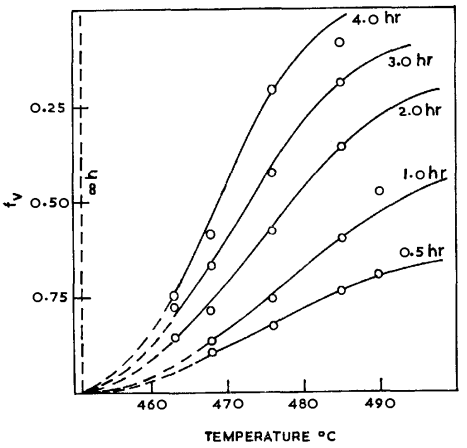

Fig. 5. Conversion of vaterite as a function of temperature for different times.

formation is immeasureably slow, *i.e.*, it takes infinite time.

The transformation curves in Fig. 4, exhibit short acceleratory periods. The kinetic data have been analysed with the help of three models (1) Avrami's[10] equation, (2) Honig's[11] order-disorder theory as applied to diffusionless transitions in solids and (3) Mampel's[12] equation. The relation derived by Avrami[10] includes the interaction between grains of the new phase during transformation. The approximate form of the Avrami rate equation is

$$1 - \alpha = \exp(-kt^n) \qquad (2)$$

where α is the fraction of vaterite transformed to calcite in time 't'. A plot of $\log_{10}\ln(1/1-\alpha)$ against $\log_{10}t$ should give a straight line with 'n' as the slope. Figure 6 shows that the kinetic data on the transformation of vaterite to calcite comply reasonably well with equation (2). The slopes of the lines vary from 1.38 to 1.46 with an average value of 1.42. This value is midway between 4/3 and 3/2. The value of 4/3 gives

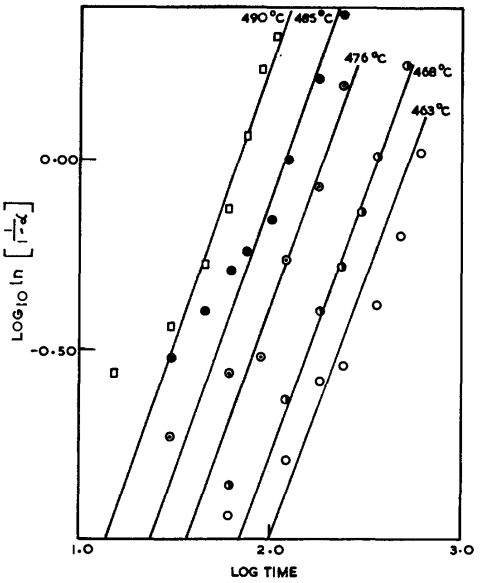

Fig. 6. Avrami plots of the vaterite-calcite transformation data.

a better fit and n is found to be 4/3 in the transformation of aragonite to calcite (communicated to the Indian Journal of Chemistry) which is analogous to the transformation of vaterite to calcite. Hence, the slope is approximated to 4/3 here too. From the slopes of the plots of $-\ln(1-\alpha)^{3/4}$ *vs.* t, a value for the activation energy is extracted and it is found to be 85 kcal mol^{-1}.

In the theory proposed by Honig,[11] a solid undergoing a transformation is represented by the change in the lattice units which transform from an initial state to a final state by two different ways, *i.e.*, a nucleation process and a propagation process. Through application of the methodology of order-disorder theory, Honig[11] has derived the following generalised rate equation.

$$-\frac{1}{k_n}\cdot\frac{d\alpha_0}{dt} = \alpha_0 + \frac{Zk_p}{k_n}\left\{\frac{-1+[1+4(C-1)\alpha_0(1-\alpha_0)]^{1/2}}{2(C-1)}\right\} \qquad (3)$$

In the present transformation α_0 is the fraction of vaterite remaining at time 't', C is a parameter indicating the tendency towards phase aggregation, k_p and k_n are the rate constants for the propagation and nucleation mechanisms respectively. For large values of C the generalised rate equation may be integrated to obtain

$$Zk_p(t-t_0)/(C-1)^{1/2} = \cos^{-1}(2\alpha_0-1) \qquad (3a)$$

Honig has evaluated C as $(1+k_p/k_n)^2$, and thus Eq. (3a) takes on the approximate form

$$Zk_n(t-t_0) = \cos^{-1}(2\alpha_0-1) \qquad (4)$$

where Z is the coordination number of a site in the lattice under consideration and t_0 is an arbitary constant evaluated by curve fitting.

Figure 7 shows that the vaterite→calcite transformation data fit Eq. (4) fairly well. The slope of the lines gives the value of Zk_n. The variation of Zk_n with temperature is shown in Fig. 8.

The value of the exponent in the Avrami's equation (*i.e.*, n=4/3) suggests that the kinetics of the trans-

10) M. Avrami, *J. Chem. Phys.*, **7**, 1103 (1939); **8**, 212 (1940).
11) J. M. Honig in kinetics of high-temperature processes. Kingery (ed.) (John Wiley & Sons, Inc., New York, 1959), Chap, 25.
12) K. L. Mampel, *Z. Phys. Chem.*, **A187**, 43, 235 (1940).

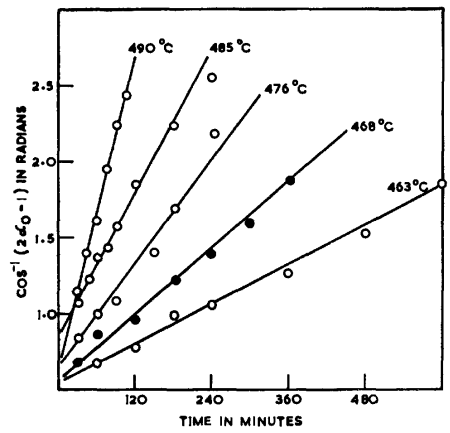

Fig. 7. Order-disorder plots of vaterite-calcite transformation data.

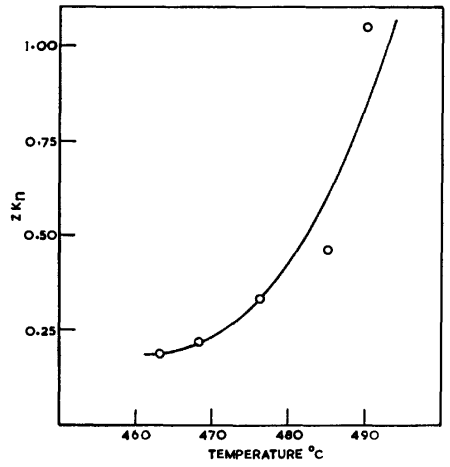

Fig. 8. Variation of Zk_n with temperature.

formation might depend on the interfacial area between the two solids. If the rate of a reaction depends on the area of the interface between the two solids, it can be represented by a 2/3 power law.

The 2/3 power law, *i.e.*, $dx/dt=kx^{2/3}$ can be reduced to the more familiar form

$$1-(1-\alpha)^{1/3} = kt \qquad (5)$$

where α is the fraction transformed in time 't'.

Equation (5) is the familiar contracting volume model, which has been employed to explain the kinetics of thermal decomposition of solids.

Figure 9 shows a few representative plots of the vaterite→calcite transformation data using Eq. (5). Two different linear portions can be recognised on each of the plots. From the slopes of these plots activation energies have been calculated. The values of E_a are 85 kcal mol^{-1} and 95 kcal mol^{-1} respectively for each of the two regions.

Equation (5) is equivalent to one of the limiting forms of Mampels[12] equation. In the Mampel[12] model $k=v/r$ where v is the rate of advance of the interface and r is the radius of the particle.

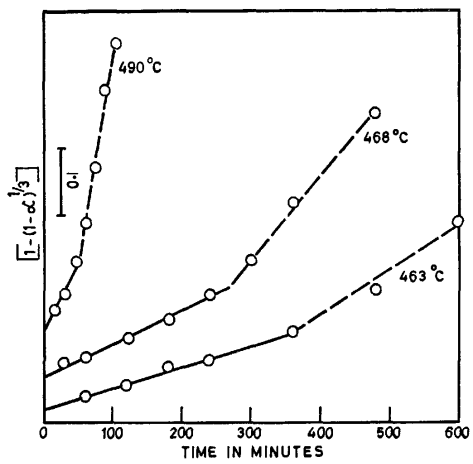

Fig. 9. Plots of $[1-(1-\alpha)^{1/3}]$ *vs.* time for the transformation of vaterite to calcite.

Considering the powder as composed of a large number of isotropic spheres of uniform radius, Mampel derived a general expression for the fraction decomposed, from probability considerations, taking into account the possibility of the overlapping of the zones of decomposition spreading out from neighbouring nuclei. The general expression reduces to simpler forms for three special cases: (i) for small values of t, α is proportional to t^4, (ii) for intermediate periods Eq. (5) gives a close approximation, and (iii) for the final period the reaction tends towards unimolecular law. Mampel has shown that the limits of the three periods are largely determined by the ratio r/v. For very fine powders practically the whole of the reaction follows the unimolecular law. For particles of intermediate size the reaction is represented reasonably well by Eq. (5).

In the present transformation Eq. (5) has been used to explain both the acceleratory and deceleratory kinetics. The slopes of the plots are different for the two regions. There is a break up of particles during the transformation. The particles are probably not reduced to fine powders. It is perhaps this change in the particle size which is responsible for the change in the slope.

Hence, Eq. (5) based on nucleation on the surface and progress of the reaction by interfacial growth is found to explain the complete course of the reaction. Further, in none of the kinetic samples, aragonite phase was detected. In the transformation of anhydrous vaterite to calcite, aragonite is not an intermediate phase.

The author expresses his grateful thanks to Professor A. R. Vasudeva Murthy for suggesting this problem and the advice rendered at different stages of the investigation.

Transmission of Substituent Effects through Oxygen and Sulfur Atoms. I. ^{1}H Chemical Shifts of Ring-substituted Phenyl Vinyl Ethers and Sulfides

Takayuki FUENO, Okitsugu KAJIMOTO, Kunisuke IZAWA, and Mitsuru MASAGO*

Department of Chemistry, Faculty of Engineering Science, Osaka University, Toyonaka, Osaka
**Yoshitomi Pharmaceutical Company, Yoshitomi-cho, Chikujo-gun, Fukuoka*

(Received October 7, 1972)

The proton chemical shifts of the vinyl group in ring-substituted phenyl vinyl ethers (PVE) and sulfides (PVS) were measured and related to the Hammett σ constants. It was found that the ρ value for the *β-trans* proton of PVS, $-0.448\ \tau/\sigma$, is greater in magnitude than that of PVE, $-0.378\ \tau/\sigma$, in contrast to the tendency reported for the methyl hydrogens in anisole and thioanisole. The results can best be explained in terms of the concept of the through-conjugative ($p\pi$-$d\pi$-$p\pi$) behavior of the sulfur atom interposed between two unsaturated groups.

The transmission of substituent effects has been a subject of continuous interest to organic chemists ever since Hammett's proposal of the ρσ relationship.[1] One of the recent problems in this field concerns the role of d-orbitals in transmitting the electronic effects of substituents. Marcus *et al.*[2] summarized numerous reports on the Hammett dependence of ^{1}H chemical shifts in compounds of the XC_6H_4T–H type, in which X is the substituent, and C_6H_4T, the transmitting group. Particular attention was paid to oxygen and sulfur when they form part of T. Thus, by comparing the ρ-values for phenol (T=O) and anisole ($T=OCH_2$) with those for the corresponding sulfur analogs, *i.e.*, thiophenol (T=S) and thioanisole ($T=SCH_2$), they found that the efficiency of oxygen in transmitting the substituent effects is generally greater than that of sulfur. They also discussed the transmission efficiencies of these atoms by citing several experimental results other than ^{1}H chemical shifts and commented that the sulfur atom must show greater efficiency when it acts as an electron acceptor in conjugated systems ("conjugative-acceptor case"). At that time, however, no appropriate and decisive example was available.

The present series of investigations was undertaken in order to look into the mode of the transmission of substituent effects through the sulfur atom both experimentally and theoretically, and thereby to elucidate the mechanism of transmission in relation to the nature of sulfur bondings. In this paper, we will compare the substituent effects on the ^{1}H chemical shifts of vinyl hydrogens in ring-substituted phenyl vinyl ethers (I; Y=O) and sulfides (I; Y=S). These compounds are characterized by the intervention of an oxygen or divalent sulfur atom between two unsaturated moieties,

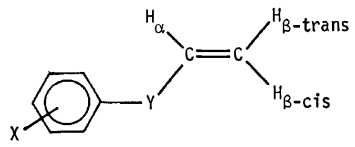

(Y = O,S) I

thus fulfilling Marcus' condition for the "conjugative-acceptor case." For the sake of comparison, the ^{1}H chemical shifts of ring-substituted allylbenzenes and styrenes were also measured.

Experimental

Materials. Ring-substituted phenyl vinyl ethers,[3] phenyl vinyl sulfides,[4] and styrenes[5] were synthesized according to the methods given in the literature. Ring-substituted allylbenzenes were prepared from allyl bromide and the corresponding bromobenzenes through Grignard coupling; the boiling points (°C/mmHg) of the products were: *p*-CH_3O 83/9.5, *p*-CH_3 75/23.5, *m*-CH_3 60/10, H 156—157/760, *p*-Cl 82/15.5 and *m*-Cl 83/25.

NMR Measurements. The NMR spectra were recorded on a JNM 4H-100 spectrometer (JEOL) operating at a frequency of 100 MHz. All the compounds were examined at room temperature as 10% (by volume) solutions in CCl_4. The chemical shifts did not vary significantly with concentration, and they were accurate to within ±0.05 Hz. TMS was used as the internal standard.

Assignment of Signals. The NMR signals for the ethylenic α, *β-cis*, and *β-trans* protons of phenyl vinyl ethers and sulfides appear as three quartets. They were assigned to the relevant protons on the basis of the well-known differences in the coupling constants, J_{gem}, J_{trans}, and J_{cis}. The chemical shifts were determined as the mean value of each set of quartet peaks. The ABX system analysis was also carried out by computer calculations; this confirmed the results. In the case of allylbenzenes, the singals of the ethylenic protons were split into three sets of twelve peaks. The complicated signals were analyzed by computer calculations for a 5-spin system.

Results

Table 1 summarizes the H–H coupling, J (Fig. 1), for phenyl vinyl sulfide (PVS), phenyl vinyl ether (PVE), allylbenzene (ABz), and styrene (St). The values of J are not sensitive to ring-substitution within the limits of experimental error.

The chemical shifts, τ, observed for the vinyl protons are listed in Table 2. It can be seen that the τ-values

1) L. P. Hammett, "Physical Organic Chemistry," McGraw-Hill, New York, N. Y. (1940), Chapter 7.
2) S. H. Marcus, W. F. Reynold, and S. I. Miller, *J. Org. Chem.*, **31**, 1872 (1966).
3) S. M. McElvain and B. Fajardo-Pinzon, *J. Amer. Chem. Soc.*, **67**, 650 (1945).
4) H. Meerwein, *Chem. Ber.*, **90**, 841 (1957).
5) W. S. Emerson, *Chem. Rev.*, **49**, 347 (1949).

Table 1. Coupling constants for some compounds (in Hz)

	J_{gem}	J_{trans}	J_{cis}	$J_{\alpha\text{-}CH_2}$	J_{allyl}
	−1.5	13.8	6.0		
	0	16.4	9.4		
	1.9	17.4	9.6	6.6	−1.6
	1.1	17.5	10.7		

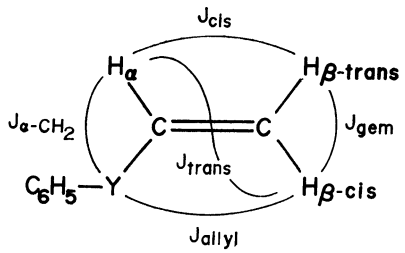

Fig. 1. Couplings between side-chain protons in $C_6H_5YCH=CH_2$.

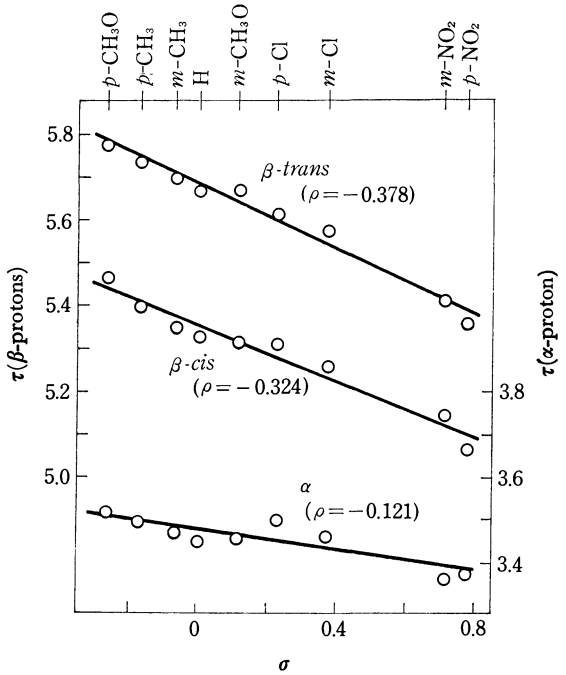

Fig. 2. Hammett plots of the ^{1}H chemical shifts for the ethylenic protons of phenyl vinyl ethers.

tend to decrease with the increase in the electron-accepting ability of the substituents.

In Fig. 2, the chemical shifts of the *β-trans*, *β-cis*, and α protons of PVE derivatives are plotted against the Hammett σ constans of the substituents. Least-squares fits of the plots to the linear relationships, $\tau_X-\tau_H=\rho\sigma$, resulted in the sensitivity constants, ρ, of −0.378, −0.324, and −0.121 τ/σ for the *β-trans*, *β-cis*, and α protons, respectively. The plots of the *β-trans* protons were found to be better correlated with σ than those of the remaining two types of protons.

The proton chemical shifts of the PVS, ABz, and St derivatives were examined likewise. The results are given in Table 2, where the correlation coefficients, *r*, and standard deviations, *s*, are listed together with the ρ-values. The α protons of ABz and St derivatives were hardly correlated with σ. The ρ-values for both the *β-trans* and *β-cis* protons were found to decrease in magnitude in the order: PVS>PVE>St>ABz. In Fig. 3, the Hammett plots of the *β-trans* protons for the four types of compounds are shown.

Recently, Yamada, Tsuno, and Yukawa[6] succeeded in improving the Hammett-type correlation for the chemical shifts of *m*-substituted aromatic side-chain protons by introducing correction terms for the ring-current diminution by substitution and for the substituent magnetic anisotropy. These corrections do not appear to be important in our *β-trans* protons, probably because they are situated relatively distant from the substituents. Thus, the ρ-values for the *β-trans* protons may be used as a basis for discussing the relative effi-

Table 2. Chemical shifts of aliphatic protons in ring-substituted phenyl vinyl ethers, phenyl vinyl sulfides, allybenzenes and styrenes (in τ)

Substituent X	PVE (–O–)			PVS (–S–)			ABz (–CH_2–)			St (–None–)			σ
	α	β_c	β_t	α	β_c	β_t	α	β_c	β_t	α	β_c	β_t	
p-CH_3O	3.513	5.467	5.775	3.627	5.015	4.868	4.118	5.030	5.030	3.430	4.501	4.966	−0.268
p-CH_3	3.491	5.397	5.736	3.605	4.883	4.818	4.113	5.021	5.024	3.406	4.412	4.905	−0.170
m-CH_3	3.468	5.351	5.701	3.549	4.767	4.744	4.110	5.010	5.013	3.400	4.373	4.868	−0.069
H	3.447	5.326	5.670	3.559	4.774	4.747	4.093	5.000	5.001	3.358	4.352	4.842	0
m-CH_3O	3.454[a]	5.317	5.671	—	—	—	4.105	4.995	4.985	3.394[a]	4.367	4.846	0.115
p-Cl	3.498	5.303	5.617	3.583	4.728	4.680	4.130	4.934	4.985	3.401	4.363	4.806	0.227
m-Cl	3.456	5.255	5.576	3.542	4.622	4.611	4.119	4.959	4.945	3.403	4.316	4.764	0.373
m-NO_2	3.366	5.145	5.414	—	—	—	—	—	—	3.284	4.152	4.602	0.710
p-NO_2	3.374	5.067	5.360	3.458	4.377	4.370	—	—	—	—	—	—	0.778
ρ	−0.121	−0.324	−0.378	−0.134	−0.539	−0.448	—	−0.137	−0.126	—	−0.290	−0.335	
r	0.875	0.979	0.988	0.891	0.962	0.987	—	0.895	0.972	—	0.936	0.980	
s	0.025	0.025	0.022	0.031	0.058	0.032	—	0.031	0.014	—	0.045	0.027	

a) Overlappings of α-proton peaks with those of phenyl protons introduced some uncertainty into the obtained values.

6) H. Yamada, Y. Tsuno, and Y. Yukawa, This Bulletin, **43**, 1459 (1970).

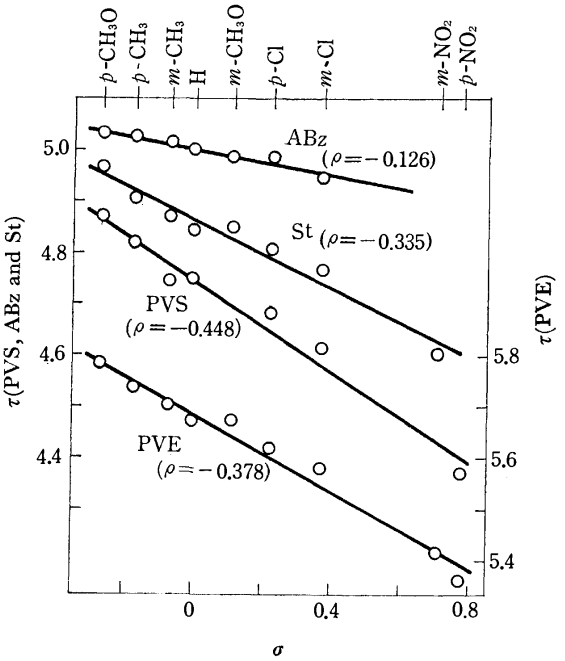

Fig. 3. Hammett plots of the *β-trans* ^{1}H chemical shifts for phenyl vinyl ethers (PVE), phenyl vinyl sulfides (PVS), allylbenzenes (ABz) and styrenes (St).

ciencies of oxygen, sulfur, and carbon atoms in transmitting the effects of ring substituents to the side chains.

Discussion

(A) Electronic Behavior of Oxygen and Sulfur. The proton chemical shifts and coupling constants of several alkyl vinyl sulfides have recently been reported by Ceccarilli and Chiellini.[7] Comparing their results with those for oxygen analogs,[8] they suggested that the decreased shielding of the terminal vinyl protons in the sulfides is due to the electron-accepting conjugation of the sulfur atom. The lower-field shifts of the *β-trans* protons of phenyl vinyl sulfides relative to the ethers (Table 2) can be interpreted in a similar manner.

The chemical shift of a proton bonded to a carbon atom is thought to depend largely on the total electron density at that carbon atom. This view has recently been supported theoretically.[9] With these points in mind, we may discuss the electronic behavior of the intervening atom or group, Y, in $C_6H_5YCH{=}CH_2$ and $C_6H_5YCH_3$.

The chemical shifts of the side-chain protons in the two types of compounds, where Y is O, S, and CH_2, are compared in Table 3. We see that the τ-values of the β-hydrogens in $C_6H_5YCH{=}CH_2$ decrease in the order: PVE>ABz>PVS, *i.e.* O>CH_2>S. The order changes into CH_2>S>O for the methyl hydrogens in $C_6H_5YCH_3$. Since the electron density of the β-carbon in the vinyl compounds is controlled mainly by the electron-donating or -accepting character of Y through the π-bond, the O>CH_2>S order should be taken to reflect the order of the π-electron-donating ability of these atoms or group. In the same manner, it should be the effect of Y through the σ-bond that determines the electron density of the methyl carbon in $C_6H_5YCH_3$. The observed order of chemical shifts, CH_2>S>O, suggests that the electron-accepting character of Y through the σ-bond increases in the CH_2>S>O order. Therefore, it can be said that oxygen behaves as a π-doner-σ-acceptor, while divalent sulfur acts as a π,σ-acceptor, provided allylbenzene is taken as the standard.

Table 3. Comparisons of the proton chemical shifts

Compound	Proton	Chemical shifts (τ) –O–	–S–	$-CH_3-$
$C_6H_5YCH_3$	methyl	6.34[2]	7.58[2]	8.80[10]
$C_6H_5YCH{=}CH_2$	α	3.45	3.56	4.09
	β-cis	5.33	4.77	5.00
	β-trans	5.67	4.75	5.00

(B) Transmission Efficiency. The ρ-values for the methyl proton in $XC_6H_4YCH_3$ and the *β-trans* protons in $XC_6H_4YCH{=}CH_2$ are summarized in Table 4. Toluene, in which no atom is interposed between the phenyl ring and the methyl group, has a ρ value of -0.214 τ/σ. When a CH_2 group intervenes, ρ decreases in magnitude to -0.113,[10] about one half the value for toluene. When the CH_2 group is replaced by an oxygen atom, the efficiency of transmission increases to -0.270,[11] which exceeds in magnitude the corresponding value for toluene. That is to say, the electronic effect is transmitted with amplification under the influence of the oxygen atom. On the contrary, the sulfur atom has no such effect. The ρ value of thioanisole is only -0.115,[2] nearly equal to that of ethylbenzene. This indicates that, in $XC_6H_4YCH_3$, sulfur is a less efficient transmitter of substituent effects than oxygen.

In $XC_6H_4YCH{=}CH_2$, the transmission efficiency attenuates on going from styrene (-0.335) to allylbenzene (-0.126) and is amplified by the insertion of oxygen

Table 4. ρ-Values for the chemical shifts of terminal protons

Compound	Proton	ρ (τ/σ) –O–	–S–	$-CH_2-$	–None–
$X-C_6H_4Y-CH_3$	methyl	-0.270[11]	-0.115[2]	-0.113[10]	-0.214[2]
$X-C_6H_4Y-CH{=}CH_2$	*β-trans*	-0.378	-0.448	-0.126	-0.335

7) G. Ceccarilli and E. Chiellini, *Org. Magn. Resonance*, **2**, 409 (1970).
8) H. Yuki, K. Hatada, and M. Takeshita, *J. Polymer. Sci., A-1*, **7**, 667 (1969).
9) O. Kajimoto and T. Fueno, *Chem. Lett.*, **1972**, 103.
10) K. L. Williamson, N. C. Jacobs, and K. T. Soucy, *J. Amer. Chem. Soc.*, **86**, 4021 (1964).
11) C. Heathcock, *Can. J. Chem.*, **40**, 1865 (1962).

(−0.378), in just the same manner as in $XC_6H_4YCH_3$. One surprising exception is the enhancement of the transmission efficiency of sulfur; the ρ value (−0.448) of PVS is not only greater than that of styrene but exceeds the value for PVE. This finding can be deemed as the first clear example of a case which supports Marcus' conjecture regarding an enhanced transmission efficiency of sulfur relative to oxygen.[2)]

Comparing the transmission efficiencies of sulfur and oxygen, Marcus *et al.*[2)] only mentioned that sulfur must be favored over oxygen in situations where the d-orbitals of sulfur can participate in conjugation. In our opinion, however, this reasoning is still rather ambiguous.

According to Price and Oae,[12)] the sulfur atom shows three unique conjugative contributions in addition to the usual electron-donating conjugation common to oxygen and sulfur. Of the three contributions, the electron-accepting and electron-sharing pπ-dπ conjugations play important roles in stabilizing the anionic and radical intermediates. The remaining one is expected to be important when the sulfur atom is placed between two unsaturated groups. This contribution is often referred to as the "through-conjugative" contribution.

As the system examined here has two unsaturated groups directly bonded to the sulfur atom, it seems reasonable to attribute the cause of the enhanced transmission to the through-conjugative contribution of the sulfur atom. That is, the transmission of substituent effects is considered to be enhanced by the contribution of the following canonical structure involving a pπ-dπ-pπ conjugation:

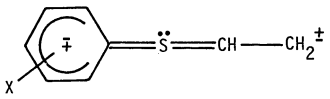

II

In connection with the above argument, recent experimental results by Oae and Yano[13)] are of particular interest. They examined the E2-type elimination reaction of β-arylthioethyl chloride kinetically and found that the ρ value for this reaction, 1.98, was greater than that of the oxygen analog, 1.33. As the intermediate suggested for this reaction (III) has a structure similar to that of PVS, it is probable that the "through-conjugative" contribution of the sulfur atom shows up in the transition state. In addition, the reported ratio of reaction constants between sulfur and oxygen derivatives ($\rho_s/\rho_o=1.49$) is a little greater than that observed

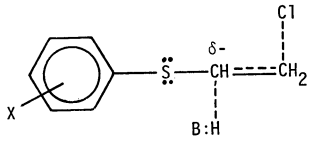

III

in our PMR measurements ($\rho_s/\rho_o=1.19$). This suggests that the ρ_s/ρ_o ratio increases with an increase in the anionic character of the system considered.

In conclusion, the sulfur atom behaves as a strong transmitter of substituent effects when interposed between two unsaturated groups. This can be interpreted in terms of the "through-conjugation" of the sulfur atom.

The authors are grateful to Mr. Y. Terawaki of this Faculty for his measurements of the proton magnetic resonance spectra and to Professor T. Otsu of Osaka City University for supplying the *p*-nitrophenyl vinyl sulfide.

12) C. C. Price and S. Oae, "Sulfur Bonding," Ronald Press, N. Y. (1962).
13) S. Oae and Y. Yano, *Tetrahedron*, **24**, 5721 (1968).

Transmission of Substituent Effects through Oxygen and Sulfur Atoms. II. ^{13}C Chemical Shifts of Ring-Substituted Phenyl Vinyl Ethers and Sulfides

Okitsugu KAJIMOTO, Masaru KOBAYASHI, and Takayuki FUENO

Department of Chemistry, Faculty of Engineering Science, Osaka University, Toyonaka, Osaka 560

(Received October 7, 1972)

The ^{13}C chemical shifts of ring-substituted phenyl vinyl ethers and sulfides were measured and discussed in relation to the change in electron distribution caused by the ring-substitution. The Hammett plots of the shifts for the terminal carbon confirm the greater transmission efficiency of sulfur atom. An "inverse" substituent effect was found for the α-carbon of both compounds. This suggests that the bond-polarization plays an important role in the transmission of electronic effect.

In the preceding paper,[1] transmission of substituent effects through oxygen and divalent sulfur has been investigated for proton-magnetic-resonance (PMR) chemical shifts. The usual Hammett ρσ treatment revealed that divalent sulfur atom, when interposed between two conjugated systems, behaves as a more efficient transmitter of the electronic effect than oxygen atom. It was then suggested that the d-orbital of sulfur may play an important role in the transmission of substituent effect by an additional resonance contribution termed "through-conjugation."

Critically speaking, however, some uncertainty attaches to the investigation of substituent effect based on PMR substituent chemical shifts. Proton chemical shifts do not reflect a unique physical quantity of molecules. They are affected by several factors such as the diamagnetic as well as paramagnetic shielding by electrons of the hydrogen atom in question and the adjacent atom.[2] On the other hand, ^{13}C chemical shifts can be definitely related to the electron density of the carbon atom of interest. Therefore, measurements of the ^{13}C substituent chemical shifts enable us to estimate directly the electronic effects of substituents on the electron densities of various carbon atom in molecules.

In this paper, we compare the ^{13}C chemical shifts of substituted phenyl vinyl ethers and sulfides. The substituent effects on the terminal carbon were found to be in line with the results of PMR studies.[1] Further, the substituent dependence of the chemical shifts of other carbon atoms offered an interesting information on the mechanism of the transmission of electronic effects.

Experimental

The ^{13}C NMR spectra (neat) were taken at 26°C on a JEOL C-60HL spectrometer equipped with a 15.09 MHz RF unit. The signal-to-noise ratio of the spectra was enhanced by the ^{13}C–H noise decoupling. The chemical shift measurements were carried out by a nuclear resonance single side-band technique; they were accurate to within ±0.2 ppm. CS_2 was used as an external standard; higher-field shifts were represented by positive δ values.

Results

Assignments were based on the additivity rule[3] and on the splitting of peaks on partial decoupling. There are some uncertainties in the assignment of the peaks spaced within 1 ppm. All the peaks assigned are listed in Tables 1 and 2.

The ^{13}C chemical shifts δ of the α and β carbons were found to be linearly correlated with Hammett σ values, as shown in Figs. 2 and 3, respectively. The ρ values, defined by $\delta_X-\delta_H=\rho\sigma$, are listed in Table 3, together with correlation coefficients r and standard deviations s. It is noteworthy (1) that, with both the α- and β-carbons, PVS has the ρ values greater in

TABLE 1. ^{13}C CHEMICAL SHIFTS FOR RING-SUBSTITUTED PHENYL VINYL ETHERS (ppm from CS_2)

Substituent	Aromatic carbon[a]						Vinyl carbon[a]		Substituent carbon
	1	2	3	4	5	6	α	β	
p-CH_3O	42.5	74.6	78.4	37.5	78.4	74.6	43.6	99.5	137.7
p-CH_3	38.3	76.1	62.8	60.8	62.8	76.1	44.5	98.8	172.1
m-CH_3	34.6	75.2	53.7	69.1	63.7	79.0	45.0	98.2	171.3
H	36.5	76.1	63.4	69.9	63.4	76.1	45.2	97.8	—
m-CH_3O	35.3	89.7	32.3	84.3	63.0	84.2	45.3	97.7	138.0
p-Cl	37.6	74.6	63.3	64.8	63.3	74.6	45.3	96.8	—
m-Cl	35.8	75.5	58.0	69.7	62.6	77.8	46.0	96.3	—

a) The numberings of the carbons are as follows:

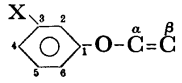

1) T. Fueno, O. Kajimoto, K. Izawa, and M. Masago, This Bulletin, **46**, 1418 (1973).

2) O. Kajimoto and T. Fueno, *Chem. Lett.*, **1972**, 103.

3) P. C. Lauterbur, *J. Amer. Chem. Soc.*, **83**, 1846 (1961).

TABLE 2. ^{13}C CHEMICAL SHIFTS FOR RING-SUBSTITUTED PHENYL VINYL SULFIDES (ppm from CS_2)

Substituent	Aromatic carbon[a]						Vinyl carbon[a]		Substituent carbon
	1	2	3	4	5	6	α	β	
p-CH_3O	69.1	58.8	77.8	33.5	77.8	58.8	58.8	80.1	137.6
p-CH_3	62.5	61.7	63.0	56.0	63.0	61.7	60.0	79.0	171.5
m-CH_3	58.6	61.8	54.2	65.3	63.8	64.9	60.5	77.9	171.2
H	58.5	62.6	63.8	66.0	63.8	66.0	61.2	77.4	—
p-Cl	59.8	61.5	63.6	59.6	63.6	61.5	61.5	76.5	—
m-Cl	55.7	63.6	57.9	65.9	62.7	65.3	62.2	75.3	—

a) For the numberings, see Table 1.

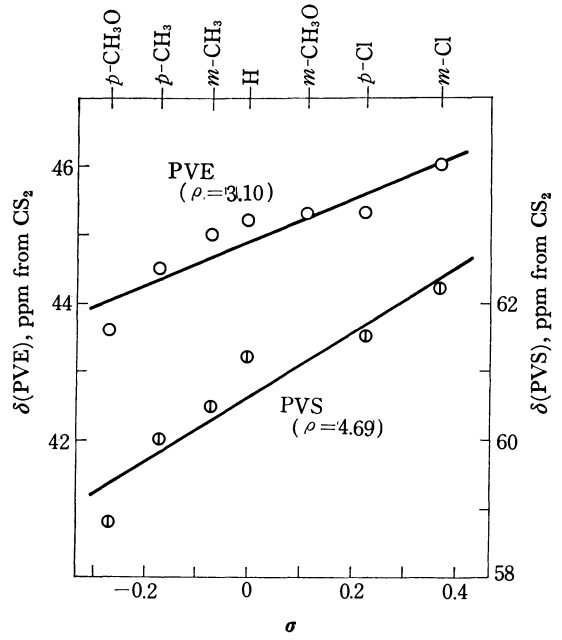

Fig. 1. Hammett plots of the ^{13}C chemical shifts for the α-carbons of phenyl vinyl ethers (PVE) and phenyl vinyl sulfides (PVS).

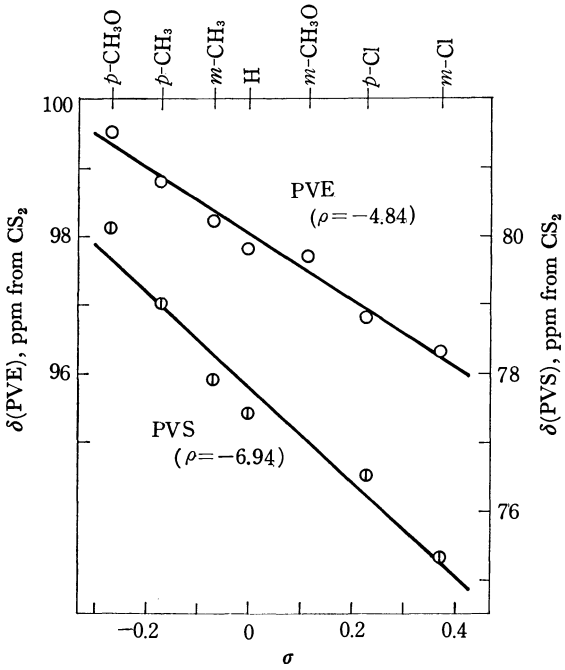

Fig. 2. Hammett plots of the ^{13}C chemical shifts for the β-carbons of phenyl vinyl ethers (PVE) and phenyl vinyl sulfides (PVS).

TABLE 3. SENSITIVITY CONSTANTS ρ FOR THE ^{13}C CHEMICAL SHIFTS OF PHENYL VINYL ETHERS AND SULFIDES (ppm/σ)

	α-Carbon		β-Carbon	
	-O-	-S-	-O-	-S-
ρ[a]	3.10	4.69	−4.84	−6.94
r	0.921	0.944	0.987	0.980
s	0.59	0.82	0.35	0.70

a) $\delta_X-\delta_H=\rho\sigma_X$.

magnitude than those of PVE and (2) that, for both PVE and PVS, the ρ values for β-carbons are positive while those for α-carbons, negative.

Discussion

Electron Distributions in PVE and PVS. There have been several treatments of the relation between ^{13}C chemical shift and the electron density of the carbon atom. Spiesecke and Schneider[4] measured the ^{13}C chemical shifts δ for $C_5H_5^-$, C_6H_6, $C_7H_7^+$, and $C_8H_8^{++}$ and proposed the empirical relation

$$\delta = 160(q_\pi - 1) \text{ ppm} \quad (1)$$

where q_π is the π-electron density of the carbon atom in question. Karplus and Pople[5] justified the above equation on the basis of π-molecular orbital calculations.

Recently, Tokuhiro and Fraenkel[6] calculated the ^{13}C chemical shifts of nitrogen heterocycles using the Karplus-Pople equation coupled with all-valence-shell-electron SCF-MO's. They found that, even though the observed shifts are roughly linear with the π-charge, the linearity is considerably improved when δ is plotted against the total electronic charge. Using the CNDO wave functions of Bene and Jaffé,[7] they obtained the equation;

$$\delta = 155(q_{\pi+\sigma} - 4) \text{ ppm} \quad (2)$$

where $q_{\pi+\sigma}$ is the total electron density on the carbon atom of interest. Bloor and Breen[8] also obtained linearity between δ and *total charge* using CNDO/2 MO's.

In reality, however, many approximations are invoked for the derivation of Pople's equation from the

4) H. Spiesecke and W. G. Schneider, *Tetrahedron Lett.*, **1961**, 468.
5) M. Karplus and J. A. Pople, *J. Chem. Phys.*, **38**, 2803 (1963).
6) T. Tokuhiro and G. Fraenkel, *J. Amer. Chem. Soc.*, **91**, 5005 (1969).
7) J. D. Bene and H. H. Jaffé, *J. Chem. Phys.*, **48**, 1807 (1968).
8) J. E. Bloor and D. L. Breen, *J. Phys. Chem.*, **72**, 716 (1968).

formal expression of Ramsey. Therefore, one should be careful in applying the above linear relationship to carbon nuclei of much different environment. In such cases, chemical shifts may be largely affected by factors other than electron density. For the compounds treated in this paper, however, all the carbon nuclei are situated in so similar a condition that it would be reasonable to assume a roughly linear relationship. In what follows, therefore, we will consider the ^{13}C chemical shift as a measure of the electron density on carbon atom.

Table 4. Side chain ^{13}C chemical shifts (ppm from CS_2)

Compound	Carbon	Chemical shifts		
		-O-	-S-	$-CH_2-$
$C_6H_5-Y-CH_3$	methyl	138.8[a]	177.0	179.4[b]
$C_6H_5-Y-CH=CH_2$	α	45.2	61.2	55.6
	β	97.8	77.4	77.6

a) Ref. 10.
b) G. B. Savitsky and K. Namikawa, *J. Chem. Phys.*, **67**, 2430 (1963).

Table 4 summarizes the side-chain ^{13}C chemical shifts of anisole, PVE and their sulfur analogs. The methyl carbon of anisole shows a shift considerably lower than that of thioanisole. This implies that oxygen attracts electron through σ-bond more strongly than does sulfur. On the other hand, the ethylenic β-carbon of PVE is observed at δ about 20 ppm higher than that of PVS. This reflects a strong π-donating character of oxygen. These results confirm the validity of our conclusion which was previously drawn on the basis of ^1H chemical shifts of the same compounds.

Illustrated below are the ^{13}C chemical shifts of the various carbons of PVE and PVS with respect to benzene. Because of the parallelism between δ and electron density, these shifts may be regarded as representing the electron distribution over the molecules. Positive values correspond to excess electron.

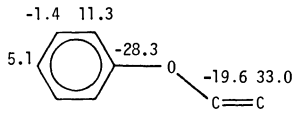

I

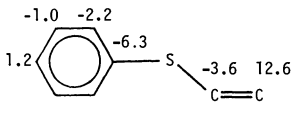

II

It is seen that the presence of oxygen atom increases the electron densities of the β carbon of the vinyl moiety as well as the *ortho* and *para* carbons of the benzene ring. The tendency is in accord with the prediction which can be made on the basis of classical canonical structures.

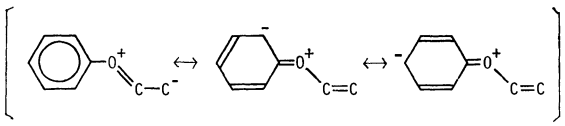

III

On the other hand, the charge distribution is rather uniform in PVS. This can also be rationalized by considering the canonical forms in which the sulfur atom acts as a π-electron accepter.

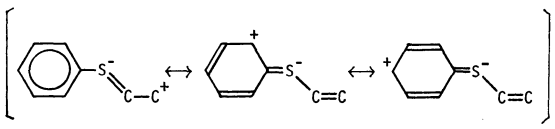

IV

Participation of such structures in resonance should neutralize the charge alternation caused by III, resulting in a flat distribution of electrons.

Substituent Effects on the Chemical Shifts of α and β Carbons. The Hammett-type substituent effects on ^{13}C chemical shifts were first reported by Spiesecke and Schneider[9] for monosubstituted benzenes. Later on, Dhami and Stothers[10] measured the ^{13}C chemical shifts of ring-substituted styrenes, anisoles, acetophenones, and methyl benzoates. Side-chain ^{13}C chemical shifts of these compounds, however, did not show clear dependence on Hammett's σ except for the β-carbon of styrenes. Our present work provides additional examples of fairly good Hammett dependence of ^{13}C chemical shifts. Moreover, it gives us interesting informations concerning the transmission of electronic effects.

First, we compare the magnitudes of ρ between PVE and PVS. Thus, the ρ values for PVS are about 1.5 times greater than thoes of PVE with both the α and β carbons, indicating an enhanced transmission of substituent effects through sulfur atom. As has been described previously, this is considered to have been caused mainly by the through-conjugative participation of sulfur d-orbitals in π-conjuagtion. The presence of $p\pi$-orbitals in both sides of sulfur atom is the essential condition for it. The concept can best be represented pictorially by the structure

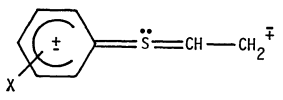

V

Next, the signs of ρ enable us to deduce the mechanism of transmission. For the β-carbons of both PVE and PVS, the observed peaks tend to show lower-field shifts with the increase in the σ-value of substituent groups. This means that the electron density on carbon atom decreases as the electron-withdrawing ability of substituents increases. For the α-carbon, however, the chemical shift shows an "inverse" dependence on substituents; an electron-withdrawing substituent increases the electron density on the α-carbon.

One explanation for these facts may be given in terms of bond polarization. It is not unreasonable to consider that the substituent effects are transmitted by successive polarization of –CH=CH– units.

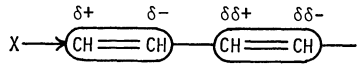

In the *p*-CH_3O derivatives for instance, the increments in the ^{13}C chemical shifts caused by the ring substitu-

9) H. Spiesecke and W. G. Schneider, *J. Chem. Phys.*, **35**, 731 (1961).
10) K. S. Dhami and J. B. Stothers, *Can. J. Chem.*, **43**, 479 (1965); *ibid.*, **43**, 510 (1965); *ibid.*, **44**, 2855 (1966); *ibid.*, **45**, 233 (1967).

tion are as follows:

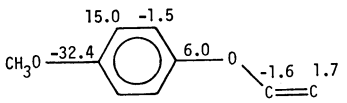

Successive bond polarization can clearly be seen.

Thus, the direction of substituent effect on the α-carbon should be the reverse of that on the β-carbon. Validity of this concept has already been proved for the case of *trans*-1-substituted-1,3-butadienes by comparing the observed ^{13}C chemical shifts with the electron distribution calculated by the CNDO/2 method.[11] Similar theoretical treatments of PVE and PVS will be given in a subsequent paper.

In conclusion, sulfur atom transmits the electronic effect of substituents more efficiently than oxygen atom, primarily through its pπ-dπ-pπ conjugation. Substituent effects on the ^{13}C chemical shifts of the α and β carbons of a vinyl group are opposite in direction, indicating polarization of the vinyl π-bond.

The authors are indebted to Mr. H. Okuda, this Faculty, for the ^{13}C NMR measurements.

11) O. Kajimoto and T. Fueno, *Tetrahedron Lett.*, **1972**, 3329.

BULLETIN OF THE CHEMICAL SOCIETY OF JAPAN, VOL. 46, 1425—1428 (1973)

Transmission of Substituent Effects through Oxygen and Sulfur Atoms. III. The Ionization Equilibrium Constants of Ring-substituted *cis*-β-Phenoxyacrylic Acids

Okitsugu KAJIMOTO, Masaru KOBAYASHI, and Takayuki FUENO

Department of Chemistry, Faculty of Engineering Science, Osaka University, Toyonaka, Osaka 560

(Received October 7, 1972)

cis-β-Phenoxyacrylic acid and several of its ring-substituted derivatives were prepared, and their ionization constants were determined in 50% ethanol–water at 25 °C. The Hammett ρ value for the ionization of these acids, 0.439, is smaller than that reported for *cis*-β-phenylthioacrylic acids, 0.531. The greater efficiency of the sulfur atom in transmitting the substituent effects is explainable in terms of the "through-conjugation" of the sulfur atom in the thioacrylate anions formed.

In the preceding two papers,[1,2] we treated the effects of substituents on the ^1H and ^{13}C chemical shifts of phenyl vinyl ether and sulfide. It was found that the sulfur atom behaves as a more efficient transmitter of substituent effects than does oxygen when it is interposed between two unsaturated groups. This finding offered strong evidence for the presence of a "through-conjugation" in sulfur bondings.[3] In this paper we will examine the ρ values for acid ionization, since ionization equilibria are fundamental to Hammett's ρσ relationship.

Hogeveen[4] reported the ionization constants of *cis*-β-phenylthioacrylic acids (I, abbreviated as *cis*-β-PSA hereafter).[5] For the purpose of comparison, we prepared *cis*-β-phenoxyacrylic acid (II, abbreviated as *cis*-β-POA) and its *p*-CH_3O, *m*-CH_3O, *p*-CH_3, *m*-CH_3, *p*-Cl, and *m*-Cl derivatives, and measured their ionization constants, K_a. The ρ-value for *cis*-β-PSA was found to be greater than that for *cis*-β-POA.

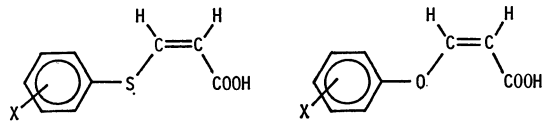

I II

Experimental

Synthesis of cis-β-*Phenoxyacrylic Acids.* The *cis*-β-phenoxyacrylic acids were prepared by the direct *trans* addition of a substituted phenol to propiolic acid in aqueous potassium hydroxide.

$$XC_6H_4OH + HC{\equiv}CCOOH \xrightarrow{OH^-} II$$

The procedure for preparation was analogous to that used for the base-catalyzed addition of thiophenol to propiolic acid.[6] A substituted phenol (0.1 mol) was dissolved in 60 ml of 4N potassium hydroxide, and then the solution was heated to 60—70°C under stirring. After 0.1 mol of propiolic acid had been added, the mixture was stirred for 2—3 hr at 70—80 °C and then cooled. On acidifying the solution with hydrochloric acid, a sol layer was separated out. The liquid layer, together with the sol layer, was subjected to extraction with ether. A 5% aqueous potassium hydroxide was added to the extract, and the aqueous layer was carefully neutralized, and then separated from the ethereal layer. The subsequent acidification of the aqueous layer with hydrochloric acid gave a solid product. It was isolated by filtration and recrystallized from ligroin. The products were identified by elemental analysis and by NMR spectral measurements (Table 1).

In preparing *cis*-β-POA, we at first followed Gottesman's method:[7]

1) T. Fueno, O. Kajimoto, K. Izawa, and M. Masago, This Bulletin, **46**, 1418 (1973).

2) O. Kajimoto, M. Kobayashi, and T. Fueno, *ibid.*, **46**, 1422 (1973).

3) C. C. Price and S. Oae, "Sulfur Bonding," Ronald Press, New York, N. Y. (1962).

4) H. Hogeveen, *Rec. Trav. Chim.*, **83**, 813 (1964); H. Hogeveen, G. Maccagnani, and F. Taddei, *ibid.*, **83**, 937 (1964).

5) In this paper we refer to the ethylenic carbon atoms at the positions α and β with respect to the –COOH group as the α and β carbons, respectively. Therefore, care must be taken when one compares the properties of these carbon atoms with those of the α and β carbons in phenyl vinyl ether or thioether.

6) F. Montanari and A. Negrini, *Gazz. Chim. Ital.*, **87**, 1073 (1957).

7) E. Gottesman, *Ber.*, **66**, 1168 (1933).

TABLE 1. MELTING POINTS, ELEMENTAL ANALYSIS DATA AND PROTON CHEMICAL SHIFTS OF *cis*-β-PHENOXYACRYLIC ACIDS

Substituent	Mp	Calcd %		Found %		Chem. shift (τ)		$J_{\alpha\beta}$
	°C	C	H	C	H	α	β	cps
p-CH_3O	125	61.85	5.19	62.12	5.16	4.865	3.101	7.0
p-CH_3	118	67.41	5.66	67.49	5.66	4.843	3.059	7.1
m-CH_3	83	67.41	5.66	67.44	5.74	4.826	3.025	7.0
H	79	65.85	4.91	66.20	4.74	4.811	3.039	7.2
	(127)	(65.85)	(4.91)	(65.71)	(4.85)	(4.46)	(2.09)	(12.5)[a]
m-CH_3O	89	61.85	5.19	61.79	5.23	4.800	3.014	7.2
p-Cl	132	54.43	3.55	54.20	3.43	4.780	3.089	6.8
m-Cl	116	54.43	3.55	54.63	3.47	4.765	3.065	7.0

a) The figures in parentheses are for *trans*-β-phnoxyacrylic acid.

$$C_6H_5ONa + HC{\equiv}CCOOEt \xrightarrow[H_2O]{OH^-} \text{II}$$

He reported that the product had a mp of 129 °C and concluded it to be a *cis*-acid. Our NMR measurement, however, revealed that it was a *trans* isomer. For the *p*-Cl derivative, also, a mixture of *cis* and *trans* isomers was formed. No doubt, his identification was erroneous.

Determination of the Ionization Constants. The pK_a values were determined potentiometrically with a Hitachi-Horiba Model F-5 pH meter at 25±0.5 °C by the ordinary method.[8] A 25 ml portion of 0.01N acid in aqueous ethanol (50% by volume) was titrated with a 0.1N potassium hydroxide solution under a nitrogen flow. The pK_a values were then calculated by the following equation:

$$pK_a = pH + \log \frac{[HA]-[H^+]}{[A^-]+[H^+]}$$

where [HA] is the concentration of acid, $[A^-]$ is the stoichiometric concentration of ionized acid, which can be regarded as equal to the concentration of KOH added, and $[H^+]$ is the hydrogen-ion concentration as determined from the measured pH, which can be neglected when the pH is above 5.

In practice, the pK_a of each acid was determined as an average value of eight data measured in the pH range of 4.7—6.3. The scatters of the measured data from the average value did not exceed ±0.02.

NMR Measurements. The details were described in a previous paper.[1] Samples, 10% in $CDCl_3$, were examined at room temperature. The experimental errors were no greater than ±0.5 Hz.

IR Measurements. The IR spectra of β-POA's were recorded on a Hitachi Perkin-Elmer 225 spectrometer as 5×10^{-3} mol/l CCl_4 solutions in a 1 cm quartz cell. On the dilution of the solution, the associated OH stretching peak of *cis*-β-POA did not change in its intensity relative to the free OH peak. Evidently this peak originates from intramolecular hydrogen bonding.

Results

The apparent ionization constants of substituted *cis*-β-POA measured by the above method are given in Table 2, together with those of *cis*-β-PSA reported by Hogeveen.[4] The Hammett relationship was found to hold, as is shown in Fig. 1. The least-squares fit gave ρ=0.439, with the correlation coefficient of 0.974. The ρ value is smaller than that of 0.531 which was reported by Hogeveen for *cis*-β-PSA.

The chemical shifts of the α-proton of *cis*-β-POA are plotted against the Hammett σ-values in Fig. 2; this

TABLE 2. IONIZATION CONSTANTS (pK_a) OF *cis*-β-PHENOXYACRYLIC AND *cis*-β-PHENYLTHIOACRYLIC ACIDS

Substituent	*cis*-β-POA	*cis*-β-PSA[4]
p-CH_3O	6.09	6.01
p-CH_3	6.08	5.98
m-CH_3	6.05	—
H	6.02	5.93
	(5.86)[a]	(5.78)[a]
m-CH_3O	5.98	—
p-Cl	5.91	5.76
m-Cl	5.81	—
m-NO_2	—	5.55
p-NO_2	—	5.44

a) The pK_a values for the *trans* acids.

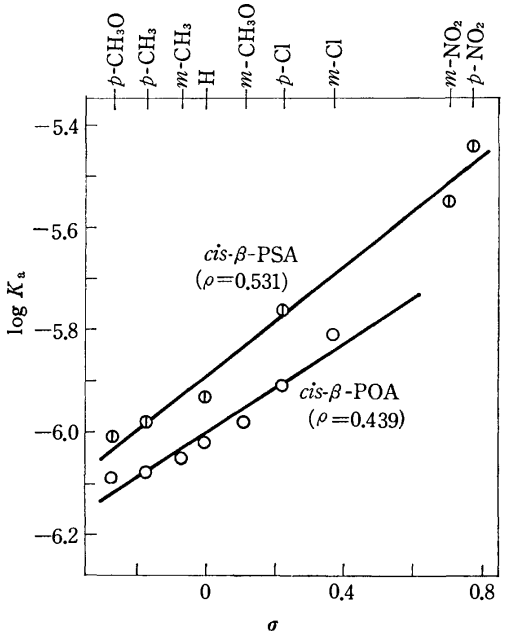

Fig. 1. Hammett plots of ionization equilibrium constants for *cis*-β-phenoxyacrylic acids (*cis*-β-POA) and *cis*-β-phenylthioacrylic acids (*cis*-β-PSA).

8) A. Albert and E. P. Serjeant, "Ionization Constants of Acids and Bases. A Laboratory Manual," Methuen and Co. Ltd. (1962).

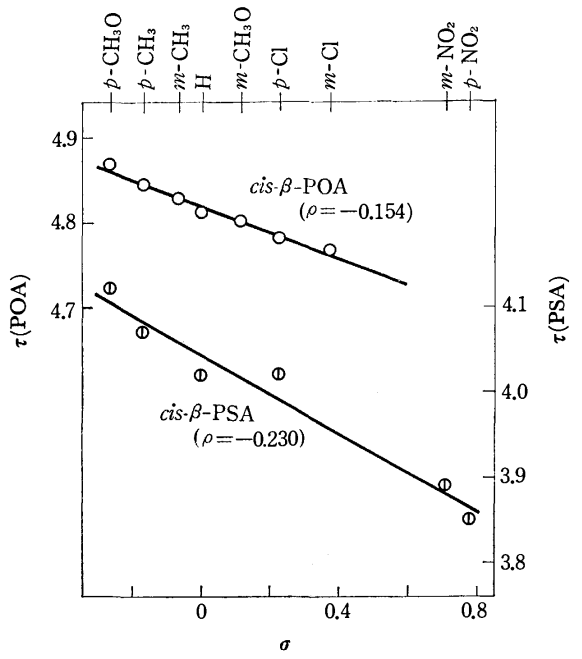

Fig. 2. Hammett plots of the α-proton chemical shifts of *cis*-β-phenoxyacrylic acids (*cis*-β-POA) and *cis*-β-phenylthioacrylic acids (*cis*-β-PSA).

plot gives the ρ value of $-0.154\ \tau/\sigma$. The corresponding value for *cis*-β-PSA[4] was found to be −0.230.

Discussion

(A) Transmission of Substituent Effects. We will compare the relative efficiencies of oxygen and sulfur atoms in transmitting the electronic effects of substituents on the ionization constants of $XC_6H_4YCH_2COOH$ and $XC_6H_4YCH{=}CHCOOH$.

Behaghel and Rollmann[9] measured the ionization constants of $C_6H_5OCH_2COOH$, $C_6H_5SCH_2COOH$, $C_6H_5SeCH_2COOH$, and some of their derivatives. However, recent measurements of pK_a by Pasto *et al.*[10] for substituted phenylthioacetic acids have revealed that the data obtained by those workers are not reliable. Hence, we have evaluated the ρ value on the basis of the pK_a data reported by the latter workers. Fortunately, the ionization constants of phenoxyacetic acids have also been extensively examined in aqueous solution by Hayes and Branch.[11] For the sake of fair comparisons, we selected the CH_3O, CH_3, H, Cl, and NO_2 derivatives and evaluated the ρ-values with respect to only these substituents. The results are summarized in Table 3.

Phenoxyacetic acids show a slightly larger ρ value (0.312) than phenylthioacetic acids (0.296)—*i.e.*, O>S. Conversely, with the acrylic type of acids, the result is O<S, as has already been described. Thus, there is an enhanced transmission by the sulfur atom interposed between two unsaturated groups. This fact reinforces the validity of the concept of the "through-conjugative" behavior of the sulfur atom.[1,2] The conjugation is considered to be involved more favorably in the anions formed than in the undissociated acids.

Table 3. ρ-Values and the related quantities for the ionization equilibria

	$X-C_6H_4-Y-CH_2COOH$		$X-C_6H_4-Y-CH=CHCOOH$(*cis*)	
	O[11]	S[10]	O	S[4]
ρ	0.312	0.296	0.439	0.531
r	0.985	0.980	0.974	0.991
s	0.021	0.021	0.046	0.035
n[a]	9	8	7	6
pK_a(X=H)	3.17	3.53	6.02	5.93

a) The number of substituents.

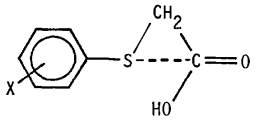

III

A comparison of the ρ values of the acetic acid derivative gives us additional information of interest. For ^1H chemical shifts, the ρ value varied by a factor of 2 on going from aniosles (−0.270) to thioanisoles (−0.115).[1] In acid dissociation, the diminution in the ρ value is very small. This distinction can be understood by considering the nonbonding interaction[12] between the sulfur atom and the carbonyl group in phenylthioacetic acids III. That is, the acids are provided with two routes for the transmission of the substituent effects, one through σ-bonds and the other through direct nonbonding interaction. The dependence of pK_a on the substituents can thus become greater than would be expected simply from the inefficient transmission through the σ-bonds alone.

The ^1H chemical shifts observed for *cis*-β-POA deserve special attention. The shifts of the α-proton in the *cis*-acids were found to conform to the Hammett relationship, with ρ=−0.154. The ρ value obtained is smaller in magnitude than that for the sulfur analogs, −0.230. These results are in line with our previous observations with phenyl vinyl ethers and sulfides.[1,5]

(B) Relative Acid Strengths of Unsubstituted Acids. The pK_a values of the unsubstituted acids of interest are listed at the bottom of Table 3. Phenoxyacetic acid is more acidic than phenylthioacetic acid, whereas *cis*-phenoxyacrylic acid is a weaker acid than its sulfur

9) O. Behaghel and M. Rollmann, *J. Prakt. Chem.*, **114**, 287 (1926).

10) D. J. Pasto, D. McMillan, and T. Murphy, *J. Org. Chem.*, **30**, 2688 (1965).

11) N. V. Hayes and G. E. K. Branch, *J. Amer. Chem. Soc.*, **65**, 1555 (1943).

12) Such an interaction has also been proposed by Oae and Yano.[13] They investigated the effect of ring-substituents on the E2 elimination of 3-phenylthio-propyl chlorides and their oxygen analogs. Rate of elimination for the phenylthio derivatives showed Hammett type dependence with the reaction constant of 0.37, while, for oxygen analogs, no noticeable substituent dependence could be found. From this fact, they suggested that the nonbonding interaction may be operative between sulfur atom and terminal two carbons at the transition state.

13) S. Oae and Y. Yano, 23th Annual Meeting of the Chemical Society of Japan (1970); Preprint III, p. 1374.

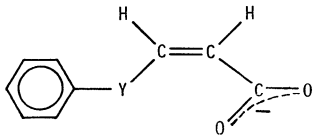

IV

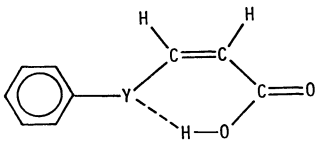

V

analog. This contrast may be explained by considering the anionic form of these acids. With β-phenylthioacrylic acid, the anion, IV, is much stabilized by the electron-accepting conjugation of the sulfur atom. As the acid dissociation equilibria are controlled by the stability of the resulting anion, the thioacrylic acid may well show a greater acidity than its oxygen analog. By contrast, in the case of saturated acids, no such conjugation can occur, resulting in the greater acidity of the oxygen-containing acid because of the greater electronegativity of the oxygen atom.

In addition, the acidity of *trans*-β-POA is greater than that of its *cis* isomer, contrary to the case of cinnamic acids.[14] Such a trend has already been pointed out for β-PSA by Hogeveen, but he gave no explanation.[4] It might be explained in terms of hydrogen-bonded six-membered ring in the *cis*-acids. The hydrogen bonding in V should prevent the ionization, thus decreasing its acidity. This is not the case for *trans*-acid.

The IR measurements of *cis*- and *trans*-β-POA confirm the above interpretation. *cis*-β-POA shows two peaks, at 3543 and 3483 cm^{-1}; the former corresponds to free OH stretching, while the latter corresponds to the intramolecular associated OH stretching.[15,16] By contrast, the *trans* isomer gives only one peak of free OH, at 3546 cm^{-1}. For β-PSA, we have no data, but the situation is probably the same as in β-POA. In fact, a report is available which shows that the electron-donating ability of ethereal sulfur is nearly the same as, or a little greater than, that of oxygen in the hydrogen bonding.[17]

14) J. F. J. Dippy and J. E. Page, *J. Chem. Soc.*, **1938**, 357.

15) M. Ōki and M. Hirota, This Bulletin, **33**, 119 (1960).

16) M. Davies and D. M. F. Griffiths, *J. Chem. Soc.*, **1955**, 132.

17) B. B. Wayland and R. S. Drago, *J. Amer. Chem. Soc.*, **86**, 5240 (1964).

BULLETIN OF THE CHEMICAL SOCIETY OF JAPAN, VOL. 46, 1428—1432 (1973)

Bond Orbital Calculations on the Methane and Silane Molecules

Susumu KOHDA and Shigeyoshi KATAGIRI

Department of Chemistry, Faculty of Science, Hirosaki University, Hirosaki 036

(Received September 14, 1972)

The non-empirical calculations of CH_4 and SiH_4 are carried out by the bond orbital (BO) and McWeeny and Ohno (MBO) methods. The lowest total energies obtained in these calculations are −40.1621 and −290.1809 a.u. for CH_4 and SiH_4 respectively. The ordinary SC–LCAO–MO calculations are also made for the sake of comparison using the same parameters. The results are compared with the similar calculations of H_2O and NH_3, we can thus see that the BO and MBO calculations show almost the same features as in H_2O and NH_3.

With various approximations and different basis sets, many theoretical calculations have been done for a number of polyatomic molecules. The more complicated the molecular wave functions become, the less lucid the chemical intuition or pictorial image for the chemical bonds, lone pairs, and inner shells becomes. Hurley, Lennard-Jones, and Pople,[1] and Parr and Parks[2] gave satisfactory discussions of the separated-electron-pair method in which electrons in a molecule are classified into groups for the chemical bonds, lone pairs, and inner shells, and in which the total wave function is written as an anti-symmetrized product of the localized two-electron functions, one for each group. McWeeny and Ohno[3] have carried out the non-empirical calculations of the water molecule using such a concept. They proposed a method of constructing the electron-pair functions from orbitals with pair nonorthogonality which were not given by the former authors explicitly. They obtained a fairly good total energy as compared with the ordinary SC–LCAO–MO results. Tsuchida and Ohno[4] made a similar calculation of NH_3, and concluded that the general features were almost the same for H_2O and for NH_3.

In this investigation, we carried out the non-empirical calculations of CH_4 and SiH_4 using the SC–LCAO–MO, BO, and McWeeny and Ohno methods (They utilized

1) A. C. Hurley, J. E. Lennard-Jones, and J. A. Pople, *Proc. Roy. Soc. Ser. A.*, **220**, 446 (1953).

2) J. M. Parks and R. G. Parr, *J. Chem. Phys.*, **28**, 335 (1958).

3) R. McWeeny and K. Ohno, *Proc. Roy. Soc. Ser. A*, **255**, 367 (1960).

4) A. Tsuchida and K. Ohno, *J. Chem. Phys.*, **39**, 600 (1963).

the term "modified electron-pair method." Here we will call it the "modified bond orbital method," MBO). The MBO approximation is an extension of BO. We will describe these methods briefly in the following sections.

The CH_4 and SiH_4 molecules differ from H_2O and NH_3 in the point that the former molecules have no lone pair. In SiH_4, furthermore, the valence orbital quantum number is higher than in the others by one. Therefore, it seemed that it would be interesting to see, in the BO and MBO methods, whether or not the frozen-core approximation is as adequate in the CH_4 and SiH_4 molecules as in H_2O and NH_3.[3,4]

The basis sets used throughout this paper are the minimal Slater-type AO's. The orbital exponents have the following values, which were obtained from Slater's rules except for the hydrogen 1s AO's:

$$\delta_{1s}(C)=5.7,\ \delta_{2s}(C)=\delta_{2p}(C)=1.625 \text{ and } \delta_{1s}(H)=1.2$$

for CH_4, and:

$$\delta_{1s}(Si)=13.7,\ \delta_{2s}(Si)=\delta_{2p}(Si)=4.925,$$
$$\delta_{3s}(Si)=\delta_{3p}(Si)=1.383 \text{ and } \delta_{1s}(H)=1.2$$

for SiH_4. The molecular geometry is assumed to be tetrahedral for both molecules. The bond distances are fixed to be 2.05 a.u.[14] and 2.796 a.u.[5] for the C–H and Si–H bonds respectively.

SC-LCAO-MO Calculation

The CH_4 molecule has been studied by many authors using semi-empirical and non-empirical methods.[6–15] For the SiH_4 molecule, however, there have not been many studies.[16–18] Among others, Boers and Lipscomb[19] recently reported SC–LCAO–MO calculations with and without Si 3d AO's. The sets of orbital exponents and bond distances in our calculations are different from theirs. We made ordinary SC–LCAO–MO calculations[20] in order to compare them with the BO and MBO calculations.

Table 1. CH_4

1) Orbital energy and MO				
ε (a.u.)	H	1s	2s	2p
−11.2713 ($1a_1$)	−0.0058	0.9953	0.0279	0
−0.9366 ($2a_1$)	0.1587	−0.2016	0.6626	0
−0.5455 ($1t_2$)	0.2840	0	0	0.5957
−0.5455 ($1t_2$)	0.2840	0	0	0.5957
−0.5455 ($1t_2$)	0.2840	0	0	0.5957
2) Atomic population				
Orbital	H	1s	2s	2p
Population	0.865	1.996	1.271	1.091
3) Total energy			−40.1130 a.u.	

The results of the calculations on CH_4 and SiH_4 are shown in Tables 1 and 2, along with the atomic populations[21] and total energy, which are in reasonable agreement with the values of Palke and Lipscomb[13] and of Boers and Lipscomb.[19]

BO Calculation

Methane. Here we transformed the original non-orthogonal basis set:

$$a = (1s, 2s, 2p_x, 2p_y, 2p_z, H_1, H_2, H_3, H_4) \quad (3)$$

where H_i is the 1s AO of the ith hydrogen atom, into the orthonormalized basis:

Table 2. SiH_4

1) Orbital energy and MO						
ε (a.u.)	H	1s	2s	3s	2p	3p
−68.648 ($1a_1$)	0.001	0.995	0.016	−0.003	0	0
−6.001 ($2a_1$)	−0.009	−0.343	1.047	0.050	0	0
−4.110 ($1t_2$)	0.011	0	0	0	0.989	0.066
−4.110 ($1t_2$)	0.011	0	0	0	0.989	0.066
−4.110 ($1t_2$)	0.011	0	0	0	0.989	0.066
−0.738 ($3a_1$)	0.188	0.054	−0.192	0.648	0	0
−0.510 ($2t_2$)	0.296	0	0	0	−0.145	0.537
−0.510 ($2t_2$)	0.296	0	0	0	−0.145	0.537
−0.510 ($2t_2$)	0.296	0	0	0	−0.145	0.537
2) Atomic population						
Orbital	H	1s	2s	3s	2p	3p
Population	0.967	2.000	1.997	1.254	1.987	0.973
3) Total energy				−290.1690 a.u.		

5) D. R. J. Boyd, *ibid.*, **23**, 922 (1955).
6) J. A. Pople and G. A. Seagel, *ibid.*, **43**, S136 (1965).
7) R. Hoffman, *ibid.*, **39**, 1397 (1963).
8) S. Katagiri and C. Sandorfy, *Theoret. Chim. Acta*, **4**, 203 (1966).
9) A. F. Saturno and G. Parr, *J. Chem. Phys.*, **33**, 22 (1960).
10) R. K. Nesbet, *ibid.*, **32**, 1114 (1960).
11) M. Kelessinger and R. McWeeny, *ibid.*, **37**, 601 (1962).
12) J. J. Sinai, *ibid.*, **39**, 1575 (1963).
13) W. E. Palke and W. N. Lipscomb, *J. Amer. Chem. Soc.*, **88**, 2384 (1966).
14) R. M. Pitzer, *J. Chem. Phys.*, **46**, 4871 (1967).
15) G. P. Arrighiri, C. Guidotti, M. Maestro, R. Moccia, and O. Salvetti, *ibid.*, **49**, 2224 (1968).
16) C. Carter, *Proc. Roy. Soc. Ser. A*, **235**, 321 (1956).
17) R. Moccia, *J. Chem. Phys.*, **40**, 2164 (1964).
18) D. B. Cook and P. Palmieri, *Chem. Phys. Lett.*, **3**, 219 (1969).
19) F. P. Boer and W. N. Lipscomb, *J. Chem. Phys.*, **50**, 989 (1969).
20) C. C. J. Roothaan, *Rev. Mod. Phys.*, **23**, 69 (1951).
21) R. S. Mulliken, *J. Chem. Phys.*, **23**, 1833, 1841, 2238, 2343 (1955).

$$\boldsymbol{b} = (1s, b_1, h_1, b_2, h_2, b_3, h_3, b_4, h_4) \quad (4)$$

by the procedure of McWeeny and Ohno.[3] That is, all the valence orbitals were Schmidt-orthogonalized to the carbon inner shell (1s), the carbon 2s′ and 2p orbitals were tetrahedrally hybridized, and finally all the obtained orbitals were orthonormalized according to Lowdin's method. The result is expressed by the matrix form as:

$$\boldsymbol{b} = \boldsymbol{a}\boldsymbol{V} \quad (5)$$

where $\boldsymbol{V}$ is the (9×9) transformation matrix. The orthonormalized orbitals, b_i and h_i, were used to construct the bond orbitals (BO's). As the b_i points to the ith H atom, the ith BO is defined by:

$$B_i = \sqrt{1-\lambda^2}\, b_i + \lambda h_i \quad (6)$$

where λ is a variational parameter. We constructed the ground-state wave function from these BO's as follows:

$$\Psi = \det|1s\bar{1}sB_1\bar{B}_1B_2\bar{B}_2B_3\bar{B}_3B_4\bar{B}_4|, \quad (7)$$

the orbitals without and with a bar in the Slater determinant accomodate electrons with α and β spins respectively.

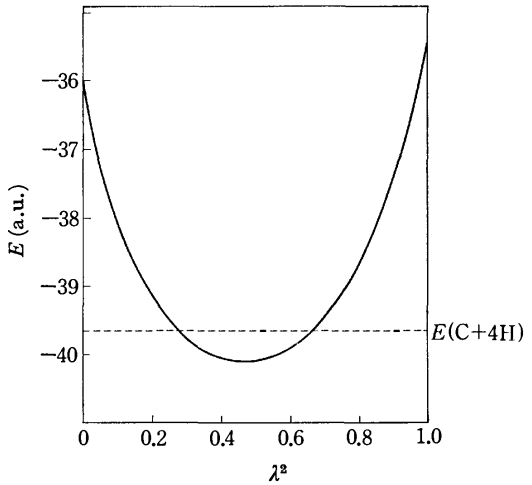

Fig. 1. The total energy of CH_4 as a function of λ^2. The dotted line is the energy of four atoms (E. Clementi, *J. Chem. Phys.*, **40**, 1944 (1964)).

The total energy is expressed as a function of the parameter, λ^2, the calculated results are shown in Fig. 1. The variational parameter which makes the total energy minimum is found to be $\lambda^2=0.46$. This value is very close to those for H_2O ($\lambda^2=0.43$) and NH_3 ($\lambda^2=0.42$). The minimum value, −40.1074 a.u., of the total energy is only slightly higher than the SC–LCAO–MO result, −40.1130 a.u., presented in the previous section.

Silane. The valence orbitals of the Si atom are the 3s and 3p AO's, and we assume that the 2s and 2p AO's also form the inner shells. The basis set, $\boldsymbol{a}$, is transformed into the orthonormalized basis set, $\boldsymbol{b}$, in the same manner as in CH_4:

$$\boldsymbol{a} = (1s, 2s, 3s, 2p_x, 2p_y, 2p_z, 3p_x, 3p_y, 3p_z, H_1, H_2, H_3, H_4) \quad (8)$$

$$\boldsymbol{b} = (1s, 2s, 2p_x, 2p_y, 2p_z, b_1, h_1, b_2, h_2, b_3, h_3, b_4, h_4) \quad (9)$$

$$= \boldsymbol{a}\boldsymbol{V} \quad (10)$$

where $\boldsymbol{V}$ is the (13×13) transformation matrix. The ground-state wave function is expressed as:

$$\Psi = \det|(K^2)(L^8)B_1\bar{B}_1B_2\bar{B}_2B_3\bar{B}_3B_4\bar{B}_4| \quad (11)$$

where (K^2) and (L^8) indicate $(1s\bar{1}s)$ and $(2s\bar{2}s2p_x\bar{2}p_x2p_y\bar{2}p_y2p_z\bar{2}p_z)$ respectively, and where B_i are the BO's defined in Eq. (6).

In Fig. 2 the total energy is given as a function of λ^2. We find the minimal energy to be −290.1267 a.u. when λ^2 is 0.48; this value is not very different from that of CH_4. The total energy is, however, considerably higher than that of the SC–LCAO–MO result, −290.1690 a.u.

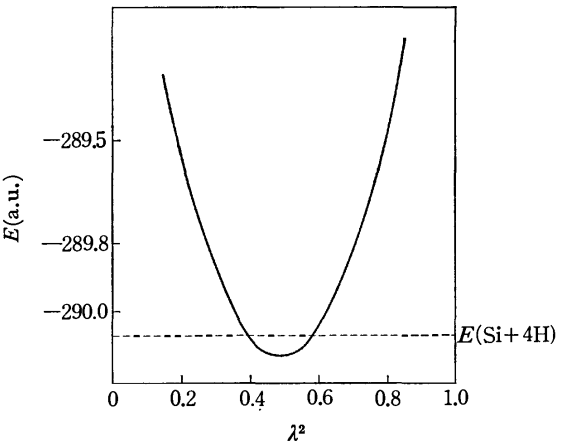

Fig. 2. The total energy of SiH_4 as a function of λ^2. The dotted line is the energy of four atoms (E. Clementi, *J. Chem. Phys.*, **40**, 1944 (1964)).

MBO Calculation

By using the orthonormalized orbitals, b_i and h_i, obtained in the previous section, two BO's, B_i and $\tilde{B}_i$, are defined as follows:

$$B_i = \sqrt{1-\lambda^2}\, b_i + \lambda h_i \quad (12)$$

$$\tilde{B}_i = \sqrt{1-\mu^2}\, b_i + \mu h_i, \quad (13)$$

from which we construct the electron-pair function of the ith bond as Eq. (14):

$$(B_i\tilde{B}_i) = N[\det|B_i\bar{\tilde{B}}_i| + \det|\tilde{B}_i\bar{B}_i|] \quad (14)$$

where N is a normalization constant. The total wave functions of the ground state are given by Eqs. (15) and (16) for CH_4 and SiH_4 respectively:

$$\Psi_m = \det|(K^2)(B_1\tilde{B}_1)(B_2\tilde{B}_2)(B_3\tilde{B}_3)(B_4\tilde{B}_4)| \quad (15)$$

$$\Psi_s = \det|(K^2)(L^8)(B_1\tilde{B}_1)(B_2\tilde{B}_2)(B_3\tilde{B}_3)(B_4\tilde{B}_4)|. \quad (16)$$

Equation (14) reflects the concept of the "different orbitals for different spins"; and the total energy expressions for CH_4 and SiH_4 become a little more complicated because of the overlap between B_i and $\tilde{B}_i$, which is given as $\sqrt{(1-\lambda^2)(1-\mu^2)}+\lambda\mu$.

The dependence of the total energy on the parameters, λ^2 and μ^2, is shown in Figs. 3 and 4 for each molecule. The best pairs of the parameters, λ^2 and μ^2, are 0.74 and 0.19, and 0.78 and 0.20, which give the total energies of −40.1621 and −290.1809 a.u. for CH_4 and SiH_4 respectively. The lowering of the

total energy from the SC-LCAO-MO result is bigger in CH_4 than in SiH_4. However, the lowering from the BO calculation is about the same for both molecules.

In Table 3 the results are summarized, along with the results of other calculations for the sake of comparison.

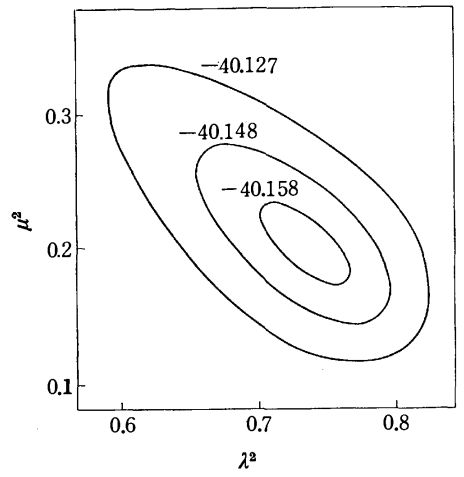

Fig. 3. The contour map of the total energy of CH_4 (in a.u.).

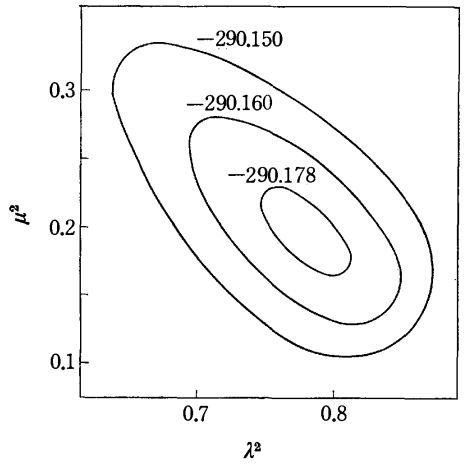

Fig. 4. The contour map of the total energy of SiH_4 (in a.u.).

Table 3. Total energy for CH_4 and SiH_4 (in a.u.)

	CH_4	SiH_4
SC-LCAO-MO (Present)	−40.1130	−290.1690
SC-LCAO-MO	−40.1140[a]	−290.4250[b]
OC-SCF-MO[d]	−39.8660[c]	−290.1024[c]
BO Appro.	−40.1074 (λ^2=0.46)	−290.1267 (λ^2=0.48)
MBO Appro.	−40.1621 (λ^2=0.74, μ^2=0.19)	−290.1809 λ^2=0.78, μ^2=0.20)
Experiment	−40.522	−292.141

a) Ref. 13.
b) Ref. 19 (The best atom orbital exponents were used for the Si atom).
c) Ref. 17.
d) One-Center Basis Set SCF-MO's.

Discussion

Tsuchida and Ohno[4] discussed the degree of localization for the two basic AO's of NH_3, which correspond to the basic AO's given in Eqs. (3) and (4) for CH_4 in our calculations. They calculated the self-Coulomb integral $(\chi\chi|\chi\chi)$[23] as the measure of the localization for the atomic orbital, χ. In our orthonormalized and original AO's, the self-Coulomb integrals are:

$$(hh|hh) = 0.8432 \text{ a.u.}$$
$$(HH|HH) = 0.7500 \text{ a.u.}$$

for CH_4, and:

$$(hh|hh) = 0.8722 \text{ a.u.}$$
$$(HH|HH) = 0.7500 \text{ a.u.}$$

for SiH_4. We can see that the orthonormalized AO's are more localized than the original AO's in both molecules.

In the MO theory, as is well known, a wave function given by a single Slater determinant is invariant with respect to the unitary transformation among the doubly-filled MO's. Moreover, we can construct, from the MO's in Tables 1 and 2, the equivalent orbitals,[24-27] ψ_i, which may be considered as localized orbitals along the ith C–H or Si–H bond. For example, ψ_2 of SiH_4 may be expressed as follows:

$$\psi_2 = \frac{1}{2}(3a_1+2t_{2,x}+2t_{2,y}+2t_{2,z}),$$

where other MO's are assumed to form purely the inner shells of the Si atom, not entering into the chemical bond, and are neglected. Rewritten in terms of original AO's, the equivalent orbital is:

$$\psi_2 = 0.027(1s) - 0.096(2s) + 0.324(3s) - 0.073(2p) + 0.268(3p) + 0.864(H_2) - 0.163(H_1+H_3+H_4).$$

Comparing the above equivalent orbital with the corresponding bond orbital, B_2, at the optimum parameter:

$$B_2 = 0.021(1s) - 0.079(2s) + 0.301(3s) - 0.055(2p) + 0.287(3p) + 0.521(H_2) - 0.034(H_1+H_3+H_4),$$

we can see that the two orbitals, ψ_2 and B_2, are very similar; this is the same in the case of the CH_4 molecule. It is notable that we can get such similar orbital by entirely different approaches. Such a similarity of the two orbitals has already been shown in NH_3.[4]

The BO calculation gives a higher total energy than does the SC-LCAO-MO calculation, but the MBO calculation gives a lower one in both molecules if the same basis set is used. In SiH_4, as is shown in Eq. (9), the 2s and 2p AO's are fixed as inner shells and are not allowed to take part in the binding. The gross atomic populations of the 2s and 2p AO's resulting from the SC-LCAO-MO calculation are smaller than

22) P. O. Lowdin, *J. Chem. Phys.* **18**, 365 (1950).
23) G. G. Hall, *Rep. Progr. Phys.*, **22**, 1 (1959).
24) J. E. Lennard-Jones, *Proc. Roy. Soc. Ser. A.* **198**, 1, 14 (1949).
25) G. G. Hall and J. E. Lennard-Jones, *ibid.*, **202**, 155 (1950).
26) J. E. Lennard-Jones and J. A. Pople, *ibid.*, **202**, 166 (1950).
27) G. G. Hall, *ibid.*, **202**, 336 (1950). About the localized orbitals, see also K. Ruedenberg, *Rev. Mod. Phys.*, **34**, 326 (1962) and C. Edmiston and K. Ruedenberg, *ibid.*, **35**, 457 (1963).

2. This seems to be the reason why the energy lowering from the SC–LCAO–MO results by the MBO method is smaller in SiH_4. In the MBO calculation we take into account the electron correlation between the different spins, α and β, to some extent. However, no such consideration is taken into account in the BO calculation. The optimum values of λ^2 and μ^2 are considerably different from that of λ^2 in the BO for both the molecules. This is also clearly reflected in the B_i and $\tilde{B}_i$ orbitals, given in Eqs. (12) and (13). These orbitals for SiH_4 are as follows:

$$B_2 = 0.014(1s) - 0.064(2s) + 0.035(3s) - 0.031(2p) + 0.087(3p) + 0.901(H_2) - 0.022(H_1+H_3+H_4),$$

$$\tilde{B}_2 = 0.025(1s) + 0.087(2s) + 0.527(3s) - 0.073(2p) + 0.452(3p) + 0.110(H_2) - 0.052(H_1+H_3+H_4).$$

The energy lowering from the BO approximation should be regarded as resulting from this intrabond correlation.

To summarize briefly, we can obtain, without self-consistent iterative calculations, total energies comparable to or slightly better than the SC–LCAO–MO results. And the optimum polarization parameters, in the BO method, take about the same value in CH_4, SiH_4, NH_3, and H_2O. It may be considered that the above obtained values are useful as the optimum polarization parameters for the covalent X–H bond of other molecules.

We are now preparing the application of the BO method to the excited states of CH_4.[28]

The authors wish to express their hearty thanks to Professor K. Ohno for his valuable discussions.

The molecular integrals were calculated on the HITAC 5020E Computer at the University of Tokyo Computer Centre, using the library program written by Professor H. Taketa. The authors are very grateful to him for his helpful communications about the use of the program (Y4/TC/AD05; Molecular Integral over CGTO).

The rest of the calculations were carried out on the NEAC 2200 Model 700 Computer at the Tohoku University Computer Center and on the HIPAC 103 Computer at Hirosaki University.

28) The anti-bonding BO's are defined as $A_i=\lambda b_i-\sqrt{1-\lambda^2}\,h_i$

BULLETIN OF THE CHEMICAL SOCIETY OF JAPAN, VOL. 46, 1432—1437 (1973)

A Method of Correction of the Angular Resolution for Determination of Absolute Total Cross Sections Using Molecular Beams

Isao KUSUNOKI*

Department of Chemistry, Faculty of Science, Kyoto University, Sakyo-ku, Kyoto 606

(Received May 25, 1972)

A general method is given for the correction of angular resolution for the case in which primary beams have a monochromatic velocity and the target gases in the scattering chamber have Maxwellian distribution. In the center-of-mass system the differential cross section for small angles are expressed by three analytical formulas. An apparent differential cross section in the laboratory system is given by averaging contributing differential cross sections in the center-of-mass system. For correction of the angular resolution, the detection probability R is defined for rectangular beams and detector. Using the apparent differential cross section with R-function and beam profile, we can determine the correction factor $\Delta Q_{\mathrm{eff}}(v_{\mathrm{i}})/Q_{\mathrm{eff}}(v_{\mathrm{i}})$. The expression of angular resolution has been applied to previous experimental data.

In a previous study for the determination of absolute total cross sections using molecular beams,[1] sources of error were pointed out and corrected. However, Busch's correction[2] used for the angular resolution of the beam apparatus is not complete, because the formula is only applicable to the case $v_{\mathrm{i}} \gg v_{\mathrm{kw}}$ (*i.e.*, the velocity of the primary beam is much greater than the most probable velocity of the target gases). This is not always the case for experiments in thermal energy range. A general method applicable for slow primary beams is discussed in this paper. For the sake of simplicity, it is assumed that the primary beams have a monochromatic velocity and the target gases in the scattering chamber have Maxwellian distribution.

1. Differential Cross Section in the Center-of-mass System

In the thermal energy range, the total scattering cross section and the differential cross section for small angles are mainly determined by the van der Waals force. The van der Waals potential is given by

$$V(r) = -C/r^{s}. \tag{1}$$

The van der Waals constant C is related to the absolute total cross section Q by the Schiff-Landau-Lifshitz approximation as follows.

$$Q = p(s)\left[\frac{C}{\hbar g}\right]^{2/(s-1)}, \tag{2}$$

* Present address: Reseach Institute for Scientific Measurements, Tohoku University, Sanjo, Sendai 980.

1) I. Kusunoki, This Bulletin, **44**, 2067 (1971).

2) F. Busch, *Z. Phys.*, **193**, 412 (1966).

where

$$p(s) = \frac{\pi^2[2f(s)]^{2/(s-1)}}{\sin\left(\frac{\pi}{2}-1\right)\Gamma\left(\frac{2}{s}-1\right)}.$$

In this case the differential cross section in the classical theory is given by[3]

$$\sigma_c(\theta) = \frac{(s-1)^{2/s}}{s}\left(\frac{2f(s)C}{\mu g^2}\right)^{2/s}\theta^{-2(s+1)/s}, \quad (3)$$

where

$$f(s) = \frac{\sqrt{\pi}\,\Gamma\left(\frac{s-1}{2}\right)}{2\Gamma\left(\frac{s}{2}\right)},$$

μ is the reduced mass, and g the relative velocity. According to Mason *et al.*,[4] this formula is only applicable above the critical angle,

$$\theta_c \approx \left[\frac{\pi^2\hbar^2}{2\mu}\right]^{s/2s-2}[(s-1)f(s)C]^{-1/(s-1)}E^{-(s-2)/(2s-2)}, \quad (5)$$

where

$$E = \frac{1}{2}\mu g^2. \quad (6)$$

For $s=6$ the angle corresponds to

$$\theta_c \simeq 4.445\theta^*. \quad (6)$$

where

$$\theta^* = \frac{1}{k}\sqrt{\frac{\pi}{Q}} \quad (7)$$

and $k=\mu g/\hbar$.

The differential cross section for very small angle can be approximated by a semi-classical theory; Mason *et al.* put it into the following compact exponential form.

$$\sigma_s(\theta) = \left[\frac{kQ}{4\pi}\right]^2\left[1+\tan^2\left(\frac{\pi}{s-1}\right)\right]\exp\left[-\frac{g(s)k^2Q\theta^2}{8\pi}\right], \quad (8)$$

where

$$g(s) = \left[\Gamma\left(\frac{2}{s-1}\right)\right]^2\left[2\pi\Gamma\left(\frac{4}{s-1}\right)\right]^{-1}\tan\left(\frac{2\pi}{s-1}\right), \; s>5 \quad (9)$$

However, Eq. (8) is only applicable for angles such as

$$\theta < [\pi^2 g(s)/2]^{-1/2}\theta_c. \quad (10)$$

For $s=6$ this is reduced to $\theta<0.31\theta_c(=1.38\theta^*)$.

From the above discussion the differential cross sections for the angular range $\theta_c>\theta>0.31\theta_c$ cannot be obtained. But in Busch's paper both Eqs. (3) and (8) are used to express the differential cross section over the whole small angular range, connecting the two equations at the larger one ($2.817\theta^*$) of the angles where they intersect. It seems that the differential cross section is overestimated in the angular range $2.817\theta^*>\theta>1.38\theta^*$. (See Fig. 1). We have used a modified classical cross section given by Mason *et al.* in the angles smaller than θ_c:

$$\sigma_m(\theta) = \sigma_c(\theta)[1+(2kb\theta)^{-2}+\cdots]$$
$$\simeq \sigma_c(\theta)\left[1+\frac{\pi}{2k^2\theta^2Q}\right]. \quad (11)$$

3) E. W. Kennard, "Kinetic Theory of Gases," McGraw-Hill Book Company, Inc., New York (1938).

4) E. A. Mason, J. T. Vanderslice, and C. J. G. Raw, *J. Chem. Phys.*, **40**, 2153 (1964).

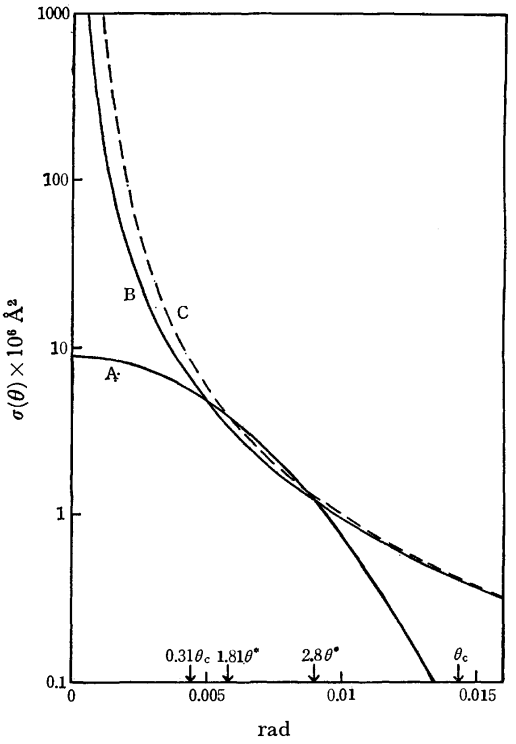

Fig. 1. Differential cross section for K–Ar at g=800 m/s. Curve A is the small-angle quantum result according to Eq. (8), Curve B is the classical result according to Eq. (5), and Curve C (dashed curve) the almost classical result according to Eq. (11).

To connect Eqs. (11) and (8) smoothly, the angles of the cross points of the two equations were estimated by a computer under the experimental conditions given previously.[1] The inner angle of the cross points was always obtained near $\theta=1.81\theta^*$. The differential cross sections for small-angle scattering are then expressed by the following three formulas.

$$\begin{aligned} &\theta > 4.445\theta^* && \sigma(\theta) = \sigma_c(\theta) \\ &4.445\theta^* > \theta > 1.81\theta^* && \sigma(\theta) = \sigma_m(\theta) \\ &1.81\theta^* > \theta && \sigma(\theta) = \sigma_s(\theta). \end{aligned} \quad (12)$$

By the use of these differential cross sections, the curve of $\sigma(\theta)$ turns out to be smoothen as shown in Fig. 1.

2. Differential Cross Section in the Laboratory System

For the correction of the angular resolution in the laboratory (LAB) system, it is necessary to convert the differential cross sections from the center-of-mass (c.m.) system into the LAB system. Figure 2 shows the geometrical relationship for the transformation. The notations in Fig. 2 are as follows.

$\boldsymbol{v}_i$, the velocity vector of the beam particle before the collision in the LAB system.

$\boldsymbol{v}_k$, the velocity vector of the target particle before the collision in the LAB system.

$\boldsymbol{u}_i$, the velocity vector of the beam particle before the collision in the c.m. system.

(Primed quantities such as $\boldsymbol{v}_i'$, $\boldsymbol{v}_k'$, and $\boldsymbol{u}_i'$ designate "after the collision".)

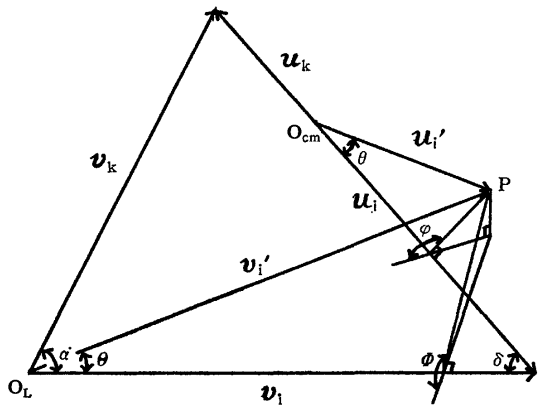

Fig. 2. The definition of quantities for the transformation from the center-of-mass system to the laboratory system.

g, the relative velocity vector before the collision.
α, the angle between v_i and v_k.
δ, the angle between g and v_i.
θ, the deflection angle of the beam particle in the c.m. system.
Θ, the deflection angle of the beam particle in the LAB system.
φ, the azimuthal angle of the vector of u_i' in the c.m. system.
Φ, the azimuthal angle of the vector of v_i' in the LAB system.

The magnitude of the relative velocity is then given by

$$g = \sqrt{v_l^2+v_k^2-2v_lv_k\cos\alpha}, \tag{13}$$

and the angle δ by

$$\delta = \sin^{-1}\frac{v_k\sin\alpha}{\sqrt{v_l^2+v_k^2-2v_lv_k\cos\alpha}}. \tag{14}$$

Therefore, both values of g and δ are determined by a set of (v_i, v_k, α).

For elastic collisions it is evident that a small angle in the c.m. system is transformed into a small angle in the LAB system. According to Helbing,[5] the transformation formulas between the c.m. system and the LAB system can be approximated for small deflection angles as follows.

$$\Theta = \theta\left(\frac{\mu g}{m_iv_i}\right)(1-\sin^2\delta\cos^2\varphi)^{1/2}, \tag{15}$$

$$\tan\Phi = \tan|\varphi|/\cos\delta, \quad \varphi \gtrless 0 \rightleftarrows \Phi \gtrless 0 \tag{16}$$

$$\frac{d\omega}{d\Omega} = \left(\frac{m_iv_l}{\mu g}\right)^2|\cos\delta|^{-1}. \tag{17}$$

The differential cross section in the LAB system can then be given by

$$\sigma(\Theta, \Phi) = \sigma(\theta, \varphi)\frac{d\omega}{d\Omega}, \tag{18}$$

where θ is determined by a set of $(v_i, m_i, v_k, m_k, \alpha, \varphi, \Theta)$. The total cross section $Q(g)$ in Eqs. (8) and (11) is related to $Q(v_i)$ by Eq. (2):

$$Q(g) = Q(v_i)\left(\frac{v_l}{g}\right)^{2/s-1}. \tag{19}$$

If the target gas follows the Maxwellian distribution $f(v_k)$ and isotropic spatial distribution, the particles scattered into a laboratory angle Θ are originated from those scattered at various angles in the c.m. system. In such a case, the apparent differential cross section for small-angle scattering in the LAB system is given by

$$\sigma_{ap}(v_i, \Theta) = \frac{1}{4\pi}\int_0^\pi\int_0^\infty\int_0^{2\pi}\sigma(\theta)\frac{d\omega}{d\Omega}f(v_k)\sin\alpha d\varphi dv_k d\alpha. \tag{20}$$

If the apparent differential cross section multiplied by $2\pi\sin\Theta$ is integrated from 0 to π, the effective total cross section averaged by the thermal motion of the target gas will be obtained:

$$Q_{eff}(v_l) = 2\pi\int_0^\pi\sigma_{ap}(v_l, \Theta)\sin\Theta d\Theta \tag{21}$$

3. Correction of the Angular Resolution

Beam apparatus always have finite angular resolution for detection of scattering events. If the cross section of the beam is a very small circle and that of the detector a circle of finite radius, the apparatus will have a constant resolving power γ at a distance from a scattering point to the detector. In this case, the correction value of the total cross section for the beam deflected into small angles is given by

$$\Delta Q_{eff}(v_l) = 2\pi\int_0^\gamma\sigma_{ap}(v_i, \Theta)\sin\Theta d\Theta. \tag{22}$$

In general, however, cross sections of the beam and the detector are narrow rectangles.[1] In such a case, the angular resolving power is not constant, but depends on the position in the plane of the detector and the scattering point in the scattering region. Let us consider the dependence of resolution on the position of a beam particle in a scattering plane and on the position of detection of the particle. (See Fig. 3.)

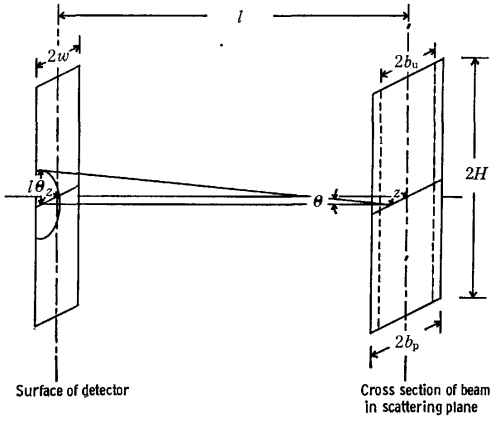

Fig. 3. Geometrical parameters for the correction of angular resolution.

It is assumed herewith that the width of the beam is much smaller than its height, the intensity distribution in the beam is uniform along its height and the detector has infinite length. The intensity distribution along its width is determined by the geometrical relationship of the beam apparatus. The widths of the umbra and penumbra in the trapezoidal profile are given by

$$2b_u = \left\{w_c-(w_s-w_c)\frac{l_{cd}}{l_{sc}}\right\}, \tag{23}$$

5) R. Helbing, *J. Chem. Phys.*, **48**, 472 (1968).

and

$$2b_p = \left\{w_c + (w_s + w_c)\frac{l_{cd}}{l_{sc}}\right\}, \tag{24}$$

respectively, where w_c and w_s are the widths of the collimating slit and source slit, respectively, l_{cd} is the distance from the collimating slit to the detector, and l_{sc} is the distance from the source slit to the collimating slit. If the central line of the beam along its height coincides with that of the detector, the intensity of the unscattered primary beam depends on the horizontal distance z from the vertical central line, and is given by

$$\begin{aligned} &z < b_u && i_0(z) = i_m, \\ &b_u < z < b_p && i_0(z) = \frac{b_p - z}{b_p - b_u} i_m, \\ &b_p < z && i_0(z) = 0, \end{aligned} \tag{25}$$

where i_m is the intensity per unit width in the umbra. The intensity of the unscattered beam measured by the detector is then given by

$$I_0 = \int_{-w}^{w} i_0(z)\mathrm{d}z, \tag{26}$$

where $2w$ is the width of the detector.

Consider a particle scattered from a point at a distance l from the plane of the detector and at a distance z from the vertical central line of the beam (Fig. 3). If the trajectories of the incident particles at the scattering plane are sufficiently parallel to each other, a part of the beam scattered through an angle Θ and falling on the detector is given by

$$2\pi n i(z) R(z, l, \Theta)\sigma_{ap}(\Theta) \sin\Theta \mathrm{d}\Theta, \tag{27}$$

where n is the density of the scattering gas, $i(z)$ is the beam intensity at the scattering point, and $R(z,l,\Theta)$ is the portion of the circumference of the circular cone of the scattered beam intercepted by the detector. When the radius of the base of the circular cone at the detector is r, we have $\Theta \equiv \tan^{-1} r/l \simeq r/l$ for small angle scattering. Thus the R-function is given by the following expressions.

for $z \geq w$

$$\begin{aligned} &z - w \geq l\Theta && R(z, l, \Theta) = 0, \\ &z + w \geq l\Theta \geq z - w && R(z, l, \Theta) = \frac{1}{\pi}\cos^{-1}\left(\frac{z-w}{l\Theta}\right), \\ &l\Theta \geq z + w && \\ & && R(z, l, \Theta) = \frac{1}{\pi}\left\{\cos^{-1}\left(\frac{z-w}{l\Theta}\right) - \cos^{-1}\left(\frac{z+w}{l\Theta}\right)\right\}, \\ &l\Theta \gg z + w && R(z, l, \Theta) \longrightarrow \frac{2w}{\pi l\Theta}, \end{aligned} \tag{28}$$

for $z < w$

$$\begin{aligned} &l\Theta \leq w - z && R(z, l, \Theta) = 1, \\ &z + w \geq l\Theta > w - z && \\ & && R(z, l, \Theta) = 1 - \frac{1}{\pi}\cos^{-1}\left(\frac{w-z}{l\Theta}\right), \\ &l\Theta > w + z && \\ & && R(z, l, \Theta) = 1 - \frac{1}{\pi}\cos^{-1}\left(\frac{w-z}{l\Theta}\right) \\ & && \quad - \frac{1}{\pi}\cos^{-1}\left(\frac{w+z}{l\Theta}\right), \\ &l\Theta \gg w + z && R(z, l, \Theta) \longrightarrow \frac{2w}{\pi l\Theta}. \end{aligned} \tag{29}$$

for special case of $z = 0$

$$\begin{aligned} &l\Theta \leq w && R(l, \Theta) = 1, \\ &l\Theta > w && R(l, \Theta) = 1 - \frac{2}{\pi}\cos^{-1}\left(\frac{w}{l\Theta}\right), \\ &l\Theta \gg w && R(l, \Theta) \longrightarrow \frac{2w}{\pi l\Theta}. \end{aligned} \tag{30}$$

The parameter z takes values smaller than b_p. Thus when Θ is much larger than b_p/l and w/l, the R-function can be approximated by $2w/\pi l\Theta$ which is independent of z.

If the width of the beam is much smaller than that of the detector, the correction of the effective total cross section is given by

$$\begin{aligned} \Delta Q_{eff}(v_i) &= 2\pi\int_0^{\pi} R(\Theta)\sigma_{ap}(v_i, \Theta)\sin\Theta \mathrm{d}\Theta \\ &\simeq 2\pi\int_0^{\Theta'} \sigma_{ap}(v_i, \Theta)\Theta \mathrm{d}\Theta \\ &\quad + 2\pi\int_{\Theta'}^{3\Theta'} \sigma_{ap}(v_i, \Theta)\Theta \sin^{-1}\frac{w}{l\Theta}\mathrm{d}\Theta \\ &\quad + 4w/l\int_{3\Theta'}^{\pi} \sigma_{ap}(v_i, \Theta)\mathrm{d}\Theta, \end{aligned} \tag{31}$$

where $\Theta' = w/l$. However, it is not appropriate to give an absolute value for the correction of the total cross section. It is better to use the ratio $\Delta Q_{eff}(v_i)/Q_{eff}(v_i)$. Thus, the correction factor for the above case is given by

$$\frac{\Delta Q_{eff}(v_i)}{Q_{eff}(v_i)} = \frac{\int_0^{\pi} R(\Theta)\sigma_{ap}(v_i, \Theta)\sin\Theta \mathrm{d}\Theta}{\int_0^{\pi}\sigma_{ap}(v_i, \Theta)\sin\Theta \mathrm{d}\Theta}. \tag{32}$$

If the width of the beam is larger than that of the detector, a part of the beam does not contribute to I_0 but some atoms in that part are scattered into the detector. In this case, the correction factor at constant l is given by

$$\frac{\Delta Q_{eff}(v_i)}{Q_{eff}(v_i)} = \frac{\int_0^{b_p}\int_0^{\pi} i(z)R(z, \Theta)\sigma_{ap}(v_i, \Theta)\sin\Theta \mathrm{d}\Theta \mathrm{d}z}{\int_0^{w}\int_0^{\pi} i(z)\sigma_{ap}(v_i, \Theta)\sin\Theta \mathrm{d}\Theta \mathrm{d}z}. \tag{33}$$

If the values of b_p/l and w/l are smaller than the critical angle Θ^* which corresponds to θ^*, the R-functions which contribute mostly to the correction value are independent of z. Thus, Eq. (33) is approximated by

$$\frac{\Delta Q_{eff}(v_i)}{Q_{eff}(v_i)} \simeq F \times \frac{\int_0^{\pi}\bar{R}(\Theta)\sigma_{ap}(\Theta)\sin\Theta \mathrm{d}\Theta}{\int_0^{\pi}\sigma_{ap}(\Theta)\sin\Theta \mathrm{d}\Theta}, \tag{34}$$

where

$$F = \frac{\int_0^{b_p} i_0(z)\mathrm{d}z}{\int_0^{w} i_0(z)\mathrm{d}z}, \tag{35}$$

and

$$\bar{R}(\Theta) = \frac{\int_0^{b_p} i_0(z)R(z, \Theta)\mathrm{d}z}{\int_0^{b_p} i_0(z)\mathrm{d}z}. \tag{36}$$

The value of F is obtained from the geometrical relation between the beam profile and the detector width, and

the value of the $\bar{R}$-function can be easily calculated by a computer.

The more complete correction formula for the angular resolution is

$$\frac{\Delta Q_{\mathrm{eff}}(v_1)}{Q_{\mathrm{eff}}(v_1)} = \frac{\int_{l_{cd}-L}^{l_{cd}}\int_{-b_p}^{b_p}\int_0^{\pi} i_0(z)e^{-nQ(l_{cd}-l)}R(z,l,\Theta)\sigma_{ap}(v_1,\Theta)\sin\Theta d\Theta dz dl}{\int_{l_{cd}-L}^{l_{cd}}\int_{-\mathrm{Min}(b_p,w)}^{\mathrm{Min}(b_p,w)}\int_0^{\pi} i_0(z)e^{-nQ(l_{cd}-l)}\sigma_{ap}(v_1,\Theta)\sin\Theta d\Theta dz dl}, \quad (37)$$

where L is the effective length of the scattering chamber. However, if l_{cd} is much greater than L, Eq. (33) can be used as a satisfactory correction for angular resolution.

4. Application

Equation (34) has been applied to the previous experimental data.[1] The $\bar{R}$-function expressed by Eq. (36) was calculated by a computer for $b_p=0.049$ mm, $b_u=0.02$ mm, $w=0.0175$ mm, and $l=85$ mm. The $\bar{R}$-function has an asymptote at $\Theta \gg 2w/l$ as shown in Fig. 4. In order to obtain the apparent differential cross sections, Eq. (20) was also calculated by a computer by means of the Monte Carlo method. In this calculation the van der Waals constants obtained in the previous paper were used.[1] In Fig. 5 the apparent differential cross sections multiplied by $2\pi \sin\Theta$ are shown for the several different beam velocities in K–Ar system. Shaded areas show the correction parts of the total cross sections given by

$$2\pi\int_0^{\pi}\bar{R}(\Theta)\sigma_{ap}(\Theta)\sin\Theta d\Theta \quad (38)$$

In Eq. (34), F is the ratio of the beam profile to that covered by the detector, and the denominator is equal to the effective total cross sections obtained by the experiment. Values of Eq. (34) were estimated for the various primary beam velocities and are shown in Fig. 6 together with the values calculated by Busch's formulas,[6] the latter being a little larger. It should be noted that our correction factors do not vary as $v_1^{4/5}$ as is predicted by Busch, and for K–Ar system the

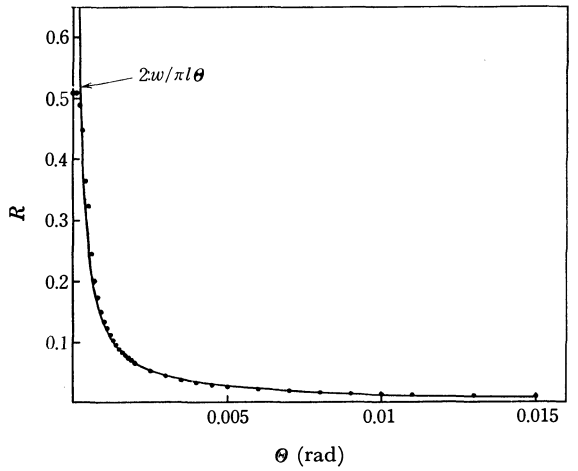

Fig. 4. Plot of $R(\Theta)$ calculated for the previous experimental parameters.

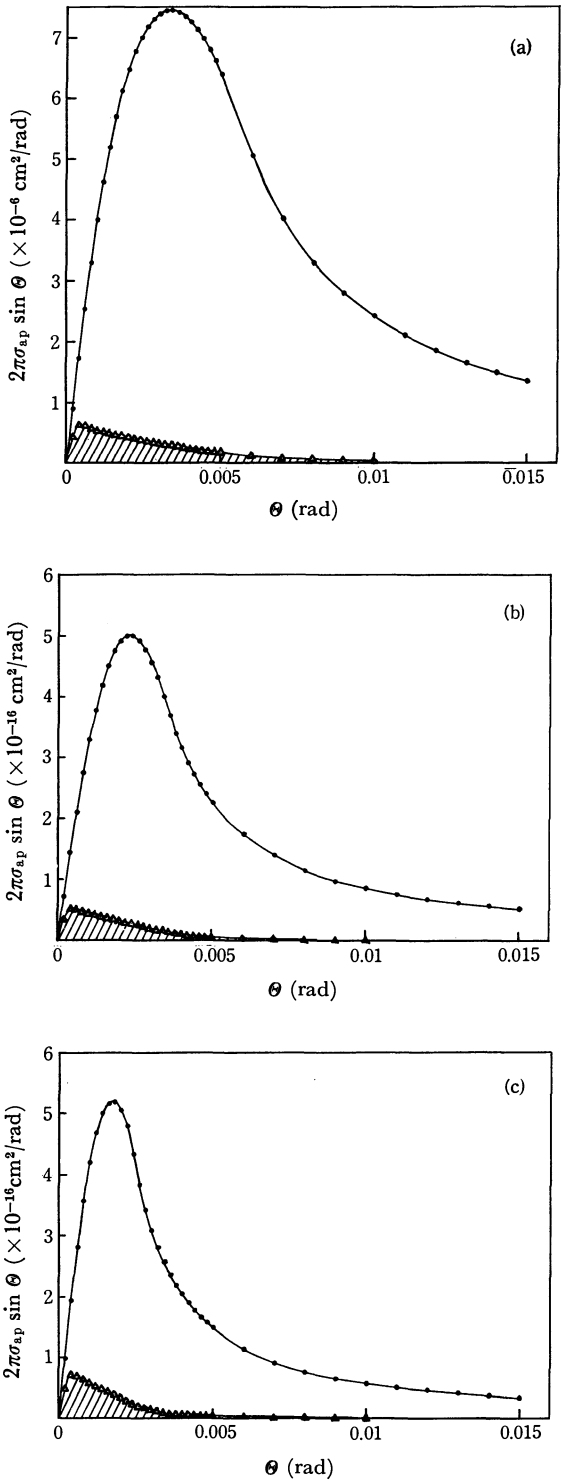

Fig. 5. Differential cross sections at small angles in the laboratory system.
K–Ar system. (a) $v_1=400$ m/s, (b) $v_1=720$ m/s, (c) $v_1=1100$ m/s.
Shaded areas show the parts deflected into the detector.

values become larger in low velocity range. It shows that Busch's approximation can not be applied to a

6) Busch gave different formulas for the correction of the angular resolution in Ref. 2 and in *Z. Phys.*, **199**, 518 (1967). The values calculated by the formula in Ref. 2 are smaller than in the other paper.

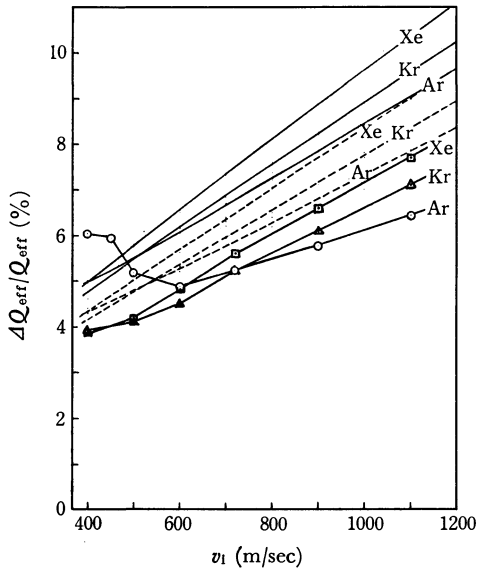

Fig. 6. Plots of $\Delta Q_{eff}(v_i)/Q_{eff}(v_i)$ for K–Ar, K–Kr, and K–Xe systems. Curves were obtained from Busch's formulas;

$$\frac{\Delta Q}{Q} = 0.0765\sqrt{Qk_i^2}\gamma\left(1+\frac{0.368}{x^2}\right) \text{ for the solid curve,}$$

$$\frac{\Delta Q}{Q} = 0.0665\sqrt{Qk_i^2}\gamma\left(1+\frac{0.376}{x^2}\right) \text{ for the dashed curve.}$$

case under usual experimental conditions in the thermal energy range.

In the above calculation to estimate correction ratio the van der Waals constants given in the previous paper were used. The correction applied there was not as good as here. However, the correction ratio varies only slightly with the change of constant value. For example, ten percent change of the value of C in K–Ar system results in five percent change of $\Delta Q_{eff}/Q_{eff}$ at $v_i = 720$ m/sec. Therefore, the values of the absolute effective total cross section estimated by the present method were hardly affected by the applied values of C. Therefore, if we start with a reasonable value of C, the estimated C will be almost similar to the initial one.

To reestimate the previous experimental data, the effective total cross sections have been corrected for the angular resolution using the values in Fig. 6 at first. Following the procedure, the effective total cross sections have been corrected by the thermal motion of the target gases, and the absolute total cross sections Q_w were obtained. The van der Waals constants reestimated from these Q_w are

$$C_{K-Ar} = 231\times10^{-60}\ \text{erg}\cdot\text{cm}^6$$

$$C_{K-Kr} = 337\times10^{-60}\ \text{erg}\cdot\text{cm}^6$$

$$C_{K-Xe} = 515\times10^{-60}\ \text{erg}\cdot\text{cm}^6$$

These values are a little smaller than the previous values. However, the conclusions in the previous paper have not been affected by the present procedure.

The author would like to thank Professor Kumasaburo Kodera for his valuable advice. The FACOM 230-60 computer system of Kyoto University was used for the calculation.

BULLETIN OF THE CHEMICAL SOCIETY OF JAPAN, VOL. 46, 1437—1441 (1973)

A Study on Restricted Rotation in 1-Acylpyrroles[1)]

Taku MATSUO, Hideto SHOSENJI,* and Reiji MIYAMOTO**

Department of Organic Synthesis, Faculty of Engineering, Kyushu University, Hakozaki, Fukuoka 812

(Received July 4, 1972)

Restricted rotation of the *N*-acyl group in 1-acylpyrroles was studied by means of NMR spectroscopy. The free energy of activation ($\Delta F_c^{\ddagger}$) for 1-formylpyrrole is 14.1 kcal/mol, which is less than that for DMF by 6.8 kcal/mol. The value of $\Delta F_c^{\ddagger}$ decreases in the order 1-formyl-, 1-acetyl-, and 1-benzoyl-pyrrole in exactly the same manner as is found in the series of *N,N*-dimethylamides with the corresponding acyl group: the difference in $\Delta F_c^{\ddagger}$ between a pair of compounds with the same acyl group in the two series remains constant (*ca.* 6 kcal/mol). The $\Delta F_c^{\ddagger}$-value for 3,4-dimethyl-1-acetylpyrrole is larger than that for 1-acetylpyrrole by 1 kcal/mol. In this particular case, the entropy of activation was found to be responsible for the difference in barrier height.

Restricted rotation about the C–N bond in 1-acylpyrroles was studied by two groups.[2)] The origin of restricted rotation has been suggested to be the partial double bond character of the C–N bond between the pyrryl and carbonyl groups as in the case of dimethylformamide and its analogues. Since the ionization potential of pyrrole (8.97 eV) is close to that of dimethylamine (8.93 eV),[3)] the significance of the ionic structure (I) may be as great as that in the case of dimethylformamide.

* Present address: Department of Synthetic Chemistry, Faculty of Engineering, Kumamoto University, Kurokami-cho, Kumamoto.

** Present address: Institute of Service Engineering, Mitsui Polychemicals Co. Ltd., Ichihara-shi, Chiba.

1) Contribution No. 258 from the Department of Organic Synthesis, Faculty of Engineering, Kyushu University.

2) a) T. Matsuo and H. Shosenji, *Chem. Commun.*, **1969**, 501. b) K.-I. Dahlqvist and S. Forsén, *J. Phys. Chem.*, **73**, 4142 (1969).

3) a) I. Omura, H. Baba, and K. Higashi, *J. Phys. Soc., Jap.*, **10**. 317 (1955). b) J. Collin, *Can. J. Chem.*, **37**, 1053 (1959).

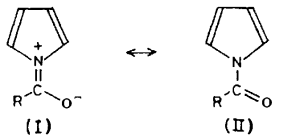

(I) (II)

A study of the electronic spectra of 1-acylpyrroles has also revealed that the π electron system of the carbonyl group strongly interacts with that of the pyrryl group.[4] Hence, the suggested origin of the barrier to the internal rotation is a very reasonable explanation. In order to study the nature of the barrier further in detail, the temperature dependence of the NMR spectra of a series of 1-acylpyrroles was investigated.

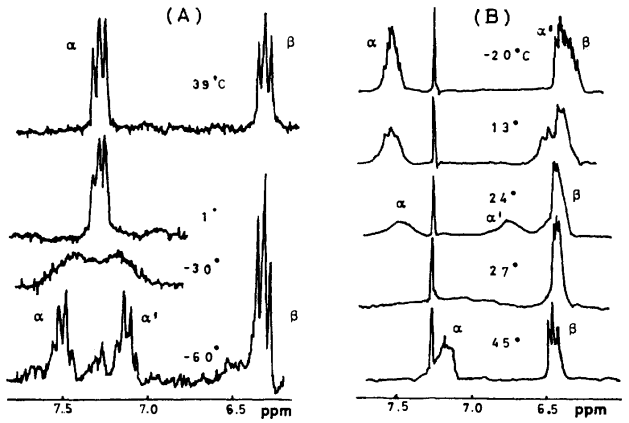

Fig. 1. The temperature dependence of the ring proton signals of 1-acetylpyrrole (A) and 1-pentachlorobenzoylpyrrole (B).

Results and Discussion

NMR spectra of most 1-acylpyrroles are temperature dependent. Two examples are shown in Fig. 1. At low temperature, the signals due to the protons at the 2- and 5-positions split into two peaks which indicate that the two methine protons are under nonequivalent electromagnetic environments. The nonequivalence is ascribed to the fact that the rotation of the carbonyl group about the C–N bond is restricted. Since the spin systems of most of the 1-acylpyrroles under investigation are rather complex, an accurate value for the rate of rotation at various temperatures can be obtained only through a complete line-shape analysis including the effects of spin-spin couplings. It is known, however, that the free energy of activation ($\Delta F_c^{\ddagger}$) at the coalescence temperature (T_c) can be obtained with reasonable accuracy by the use of an approximate method based on Gutowsky and Holm's equation and absolute rate theory:

$$\Delta F_c^{\ddagger} = R \cdot T_c \ln (k \cdot T_c \cdot \tau_c / h) \quad (1)$$

where

$$\tau_c = \sqrt{2}/(\pi \delta \nu_0) \quad (2)$$

The values of $\Delta F_c^{\ddagger}$ thus obtained are practically good enough to be used for comparing the barrier heights between various amides.[5] The results are summarized in Table 1. The barrier to the internal rotation decreases in the order 1-formyl-, 1-acetyl-, and 1-benzoylpyrrole. The same trend is also observed with *N,N*-dimethylamides, when the acyl group is changed in the order formyl, acetyl, and benzoyl group.[5] In order to examine the relationship between these two series of compounds, the barriers to the restricted rotation in *N,N*-dimethylamides are compared with those for 1-acylpyrroles with the corresponding acyl group (Table 2).[6] The difference in $\Delta F_c^{\ddagger}$ between a pair of compounds with the same acyl group in the two series is defined as $\delta\Delta$. We should notice that the $\delta\Delta$-values are nearly the same among the investigated three acyl groups.

Table 1. Spectral data for the restricted rotations of 1-acylpyrroles

Compound	$\delta\nu_0$ [a]	T_c [b]	$\Delta F_c^{\ddagger}$ [c]
1-Formylpyrrole	21.0	5	14.1
1-Acetylpyrrole	22.9	−28	12.5
3,4-Dimethyl-1-acetylpyrrole	24.7	−5	13.5
1-Benzoylpyrrole		<-70	
3,4-Dimethyl-1-benzoylpyrrole	38[d]	−56	11[e]
1-(2′,4′,6′-trimethylbenzoyl)pyrrole	73	65	16.5
1-Pentachlorobenzoylpyrrole	67	27	14.6

a) Peak separation (Hz) at the temperature where the rate of rotation is slow enough in NMR time scale. The errors are within 0.5 Hz unless specified.
b) Coalescence temperature in °C.
c) Free energy of activation in kcal/mol for the restricted rotation. Accuracies are estimated to be 0.1 kcal/mol.
d) The error is less than 2 Hz.
e) The error is less than 0.2 kcal/mol.

Table 2. Difference in barrier heights between *N,N*-dimethylamides and 1-acylpyrroles

Barrier	*N,N*-Dimethylformamide	*N,N*-Dimethylacetamide	*N,N*-Dimethylbenzamide
$\Delta F_c^{\ddagger}$ [a]	20.9	18.1	16.0
$\delta\Delta$ [b]	6.8	5.6	6[c]

a) The free energy of activation (kcal/mol) for *N,N*-dimethylamides as summarized by Stewart and Siddall[5].
b) The difference in $\Delta F_c^{\ddagger}$ between *N,N*-dimethylamides and 1-acylpyrroles with the corresponding acyl group.
c) The barrier in 1-benzoylpyrrole is estimated to be 10 kcal/mol as described in Footnote 6.

4) T. Matsuo and H. Shosenji, This Bulletin, **45**, 1349 (1972).
5) W. E. Stewart and T. H. Siddall, III, *Chem. Rev.*, **70**, 517 (1970).

6) The barrier for 1-benzoylpyrrole itself could not be obtained, since the coalescence temperature was below −70°C which was the lowest limit accessible in the present experiment. The approximate barrier height, however, may be estimated as follows. Assuming that the $\delta\nu_0$ value for 1-benzoylpyrrole is equal to that for 3,4-dimethyl-1-benzoylpyrrole, and that T_c is −75 °C, the barrier height is calculated to be 10 kcal/mol, which may be taken to be an approximate value for the upper limit of $\Delta F_c^{\ddagger}$ for 1-benzoylpyrrole. On the basis of the $\Delta F_c^{\ddagger}$ value for 3,4-dimethyl-1-benzoylpyrrole (11 kcal/mol), we can also estimate $\Delta F_c^{\ddagger}$ for 1-benzoylpyrrole to be approximately 10 kcal/mol, provided that the effect of the methyl groups on the 3- and 4-positions is assumed to lower the barrier by 1 kcal/mol as in the case of 1-acetylpyrrole and 3,4-dimethyl-1-acetylpyrrole.

The barrier to the internal rotation is mainly determined by two factors: the electronic state of the molecule as represented by its double bond character, and the steric hindrance during the rotation. The relative importance of these two factors is expected to vary considerably depending on the nature of the substituent on the amide group. Let us first consider the case of 1-formylpyrrole and *N,N*-dimethylformamide. By the use of molecular models, it is easily understood that no steric strain is expected during the internal rotation around the C–N bond. The barrier height in this case should therefore be determined by purely electronic factors alone. The difference in $\Delta F_c^{\neq}$, 6.8 kcal/mol, is thus taken to represent the fact that the double bond character of the C–N bond in 1-formylpyrrole is less than that in *N,N*-dimethylformamide.

In the case of 1-acetylpyrrole, a completely planar configuration can not be assumed because the presence of steric strain is indicated by the molecular model. The plane of the acetyl group should be twisted with respect to that of the pyrryl group in the ground state. In other words, the valley of the potential energy curve for 1-acetylpyrrole should be shallower than that for 1-formylpyrrole. Thus, the decrease in the rotational barrier in 1-acetylpyrrole is ascribed to the decrease in the double bond character due to the presence of steric strain in the ground state as in the case of *N,N*-dimethylacetamide.[5] In addition, it is also understood that the effect of the pyrryl group is very close to that of the *N,N*-dimethylamino group, since the decrease in $\Delta F_c^{\neq}$ on going from 1-formylpyrrole to 1-acetylpyrrole is almost the same as the difference in the rotational barrier between *N,N*-dimethylformamide and *N,N*-dimethylacetamide.

The case of 1-benzoylpyrrole is an example where both electronic and steric factors are equally important. In analogy to the case of *N,N*-dimethylbenzamide,[5] the contribution of cross conjugation between the phenyl and carbonyl groups as represented by III is expected to be effective in reducing the barrier height in 1-benzoylpyrrole. In addition, we can not disregard the

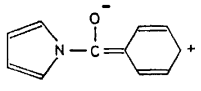

(III)

fact that 1-benzoylpyrrole is not expected to take a completely planar configuration because of the large steric hindrance between the phenyl and the pyrryl groups. As a consequence, the C–N bond is expected to be slightly twisted already in the ground state so that its double bond character is reduced. This might be another reason for the barrier height in 1-benzoylpyrrole being so much lower than that in 1-formylpyrrole.

The steric factors become extremely important in the case of 1-(2′,4′,6′-trimethylbenzoyl)pyrrole and 1-pentachlorobenzoylpyrrole. The steric hindrance due to the substituents at the *ortho* positions forces the carbonyl group to take an almost perpendicular position with respect to the plane of the phenyl group. The pyrryl group, on the other hand, seems to remain coplanar

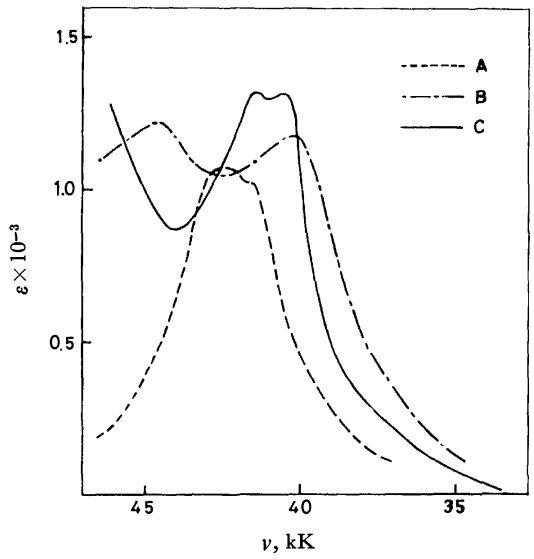

Fig. 2. Electronic absorption spectra of 1-acetylpyrrole (A), 1-benzoylpyrrole (B), and 1-(2′,4′,6′-trimethylbenzoyl)-pyrrole (C) in *n*-hexane.

with the carbonyl group. This is strongly supported by the fact that the electronic spectra of 1-(2′,4′,6′-trimethylbenzoyl)pyrrole is found to be close to that of 1-acetylpyrrole than that of 1-benzoylpyrrole (Fig. 2). In correspondence with this, the barrier heights in 1-(2′,4′,6′-trimethylbenzoyl)pyrrole and 1-pentachlorobenzoylpyrrole are surprisingly large as compared with that in 1-benzoylpyrrole (Table 1). Due to the above steric factors, the contribution of cross conjugation as represented by III is considered to be negligible in the electronic structures of 1-(2′,4′,6′-trimethylbenzoyl)pyrrole and 1-pentachlorobenzoylpyrrole. As a consequence, the double bond character of the C–N bond in 1-benzoylpyrrole is expected to increase on the introduction of substituents at both *ortho* positions. In other words, the valley of the potential energy curve for the restricted rotation becomes deeper than in the case without substituents. The present results are in agreement with this expectation. However, we should further notice that the barrier in 1-(2′,4′,6′-trimethylbenzoyl)pyrrole exceeds that in 1-formylpyrrole by more than 2 kcal/mol. This is unlikely to be explained by the change in the electronic factor alone. On the other hand, it is easily understood from the molecular model that the internal rotation of the pyrryl group with respect to the carbonyl group is strongly hindered in the transition state by the presence of substituents at the *ortho* positions. In other words, the top of the potential energy curve for the restricted rotation of the C–N bond in 1-(2′,4′,6′-trimethylbenzoyl)pyrrole is considered to be appreciably raised by the steric hindrance due to the two methyl groups. This steric hindrance may be mainly responsible for the extraordinary large $\Delta F_c^{\neq}$-value for 1-(2′,4′,6′-trimethylbenzoyl)pyrrole. The data for 1-pentachlorobenzoylpyrrole may be analogously explained as due to the combined influence of the two different effects of the substituents at the *ortho* position: the increase in the double bond character of the C–N bond in its

ground state and the presence of large steric hindrance to the internal rotation in the transition state. The slightly lower barrier height in 1-pentachlorobenzoylpyrrole, in comparison with that in 1-(2′,4′,6′-trimethylbenzoyl)pyrrole, can be correlated with the fact that the van der Waals radius of chlorine atom (1.8 Å) is less than that for the methyl group (2.0 Å). Exactly the same type of *ortho*-substituent effects as described above have also been known in the study of internal rotation of *N,N*-dimethylbenzamide.[7] The difference in $\Delta F_c^{\ddagger}$ between 1-(2′,4′,6′-trimethylbenzoyl)pyrrole and *N,N*-dimethyl-2,4,6-trimethylbenzamide (6.0 kcal/mol) is not far from the corresponding difference between 1-formylpyrrole and *N,N*-dimethylformamide (6.8 kcal/mol). On the basis of this result together with the data in Table 2, it is concluded that the double bond character of the C–N bond in 1-acylpyrrole is invariably less than that in the corresponding *N,N*-dimethylamide by an almost constant amount irrespective of the nature of the acyl group.

If an electron-donating group is substituted on the pyrryl group, the significance of the ionic structure (I) increases and the barrier height will be raised as long as the steric factors are not affected by the substitution. In expectation of these effects, the restricted rotation of 3,4-dimethyl-1-acylpyrroles was further investigated in detail. On the introduction of methyl groups at the 3- and 4-positions of 1-acylpyrrole, $\Delta F_c^{\ddagger}$ is found to increase by 1 kcal/mol in comparison with the case without the methyl groups (Table 1). Analogously, the barrier to the internal rotation in 1-benzoylpyrrole is clearly raised by the introduction of methyl groups at the 3- and 4-positions of the pyrryl group.[6] These effects of the methyl groups on the 3- and 4-positions of the pyrryl group are surprisingly large, if we recall the fact that the difference in $\Delta F_c^{\ddagger}$ between 1-acylpyrroles and *N,N*-dimethylamide is no more than 6 kcal/mol. In order to clarify the methyl substitution effect on the barrier height in detail, the temperature dependence of the proton signals of 3,4-dimethyl-1-acetylpyrrole was studied by the use of total line-shape analysis. The ring proton signals of this compound should be analyzed as a part of a ABX_3Y_3 system in principle. No one has analyzed the NMR spectra of such a complex system under chemical exchange. On the other hand, the method of analysis for AB spin system with chemical exchange between A and B has been well established.[8] Thus the present data were analyzed by the use of the line shape comparison method for the AB spin system with a slight modification. The signals for the ring protons at the 2- and 5-positions were calculated at first by the use of Heidbergs' line shape equation for the AB spin system.[8] The contribution of the methyl protons at the 3- and 4-positions was then taken into consideration by assuming that each ring proton signal was split into a quartet

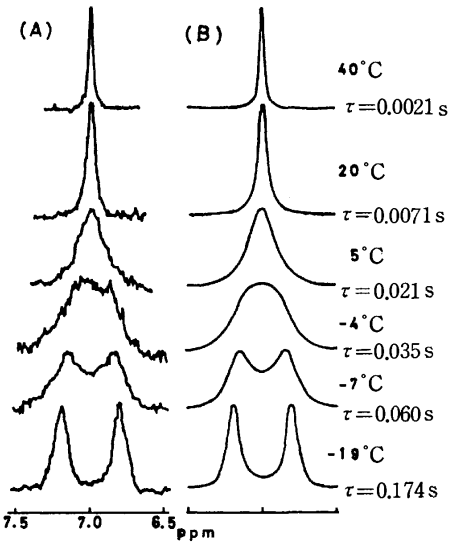

Fig. 3. The temperature dependence of the ring proton signals of 3,4-dimethyl-1-acetylpyrrole.
(A), The observed spectra; (B), The theoretical spectra.

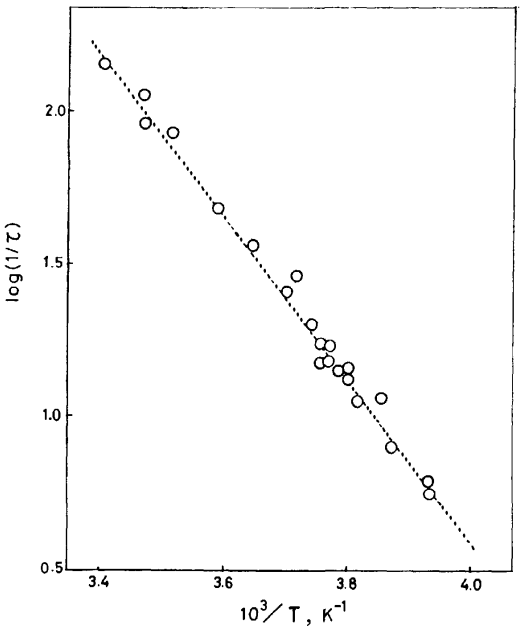

Fig. 4. An Arrhenius plot of the rate of the restricted rotation in 3,4-dimethyl-1-acetylpyrrole.

Table 3. Activation parameters for the restricted rotation of 3,4-dimethyl-1-acetylpyrrole and 1-acetylpyrrole[a]

Compound	E_a	$\Delta F^{\ddagger}_{298K}$	$\Delta H^{\ddagger}$	$\Delta S^{\ddagger}$
3,4-Dimethyl-1-acetylpyrrole	12.2±0.9	14.3±0.9	11.7±0.9	−8.7±3.7
1-Acetylpyrrole	12.6±0.1	12.1±0.1	12.0±0.1	−0.6±0.6

a) The values for 1-acetylpyrroles are those given by Dahlqvist and Forsén[2b]. They are given in kcal/mol except for the case of $\Delta S^{\ddagger}$ which is expressed in e.u.

7) A. Mannschreck, A. Mattheus, and G. Rissman, *J. Mol. Spectrosc.*, **23**, 15 (1967).

8) J. Heidberg, J. A. Weil, G. A. Janusonis, and J. K. Andersen, *J. Amer. Chem. Soc.*, **41**, 1033 (1964).

BULLETIN OF THE CHEMICAL SOCIETY OF JAPAN, VOL. 46, 1441—1450 (1973)

The Crystal and Molecular Structure of 4,10b-Methano-8*H*-benzo[*ab*]cyclodecen-8-one

Ryosuke YAHASHI,* Hirotaka SHIMANOUCHI, and Yoshio SASADA

Laboratory of Chemistry for Natural Products, Tokyo Institute of Technology, Ookayama, Meguro-ku, Tokyo 152

(Received August 24, 1972)

4,10b-Methano-8*H*-benzo[*ab*]cyclodecen-8-one ($C_{14}H_{10}O$), a stable derivative of so-called 1,6-methano[10]-annulene, forms reddish orange crystals of the space group Pbca, with eight molecules in a unit cell with dimensions of $a=16.567$, $b=14.090$, and $c=8.418$ Å. The structure was solved by the symbolic addition method and refined by the block-diagonal least-squares method. The final R factor was 0.080 for the 1386 independent observed reflections. The lengths of the peripheral bonds of the [10]annulene nucleus do not exhibit any apparent alternation. The peripheral eight atoms are approximately coplanar. The C–O distance (1.236 Å) is longer than those in quinones and tropones, and it is consistent with the large dipole moment and high basicity of the present molecule.

Contrary to the prediction by Hückel's(4n+2)rule, so-called [10]annulene does not show aromaticity. This is because [10]annulene is not likely to take a stable planar conformation.[1] The bridged analogs (I) of the [10]annulene,[2-4] however, are aromatic, and the X-ray analyses of several derivatives have indicated that the [10]annulene nucleus has the structural characteristics of the aromatic compound. Recently, 4,10b-methano-8*H*-benzo[*ab*]cyclodecen-8-one (II),[5b] a derivative of 1,6-methano[10]annulene (Ia), has been synthesized by Murata *et al.*[5a] Although it was anticipated that the condensed six-membered ring would result in a strain in the molecule, the aromatic character is retained in the ten-membered ring of II; for instance, a diamagnetic ring current has been observed.[5]

* Present address: Research Laboratories, Kyowa Hakko Kogyo, Machida, Tokyo 194.

1) S. Masamune, K. Hojo, K. Hojo, G. Biogam, and D. L. Rabenstein, *J. Amer. Chem. Soc.*, **93**, 4966 (1971).

2) E. Vogel, "Aromaticity," Special publication No. 21, The Chemical Society, London (1967) p. 113.

3) F. Sondheimer and A. Shani, *J. Amer. Chem. Soc.*, **86**, 3168

4) E. Vogel, W. Pretzer, and W. A. Böll, *Tetrahedron Lett.*, **1965**, 3613.

5) a) I. Murata, T. Nakazawa, and T. Tatsuoka, *ibid.*, **1971**, 1789. b) In reference 5a this compound was called 1*H*-cyclohexa[4,5,6-*de*]methano[10]annulen-1-one.

II can also be regarded as a bridged analog of phenalenone (III), which is a highly polarized ketone.[6] It is interesting that II is more polar than III.[5a]

The present work has been undertaken in order to examine the effect of the condensed ring on the aromaticity of the [10]annulene system and to ascertain the structural basis of the highly-polarized nature of II.

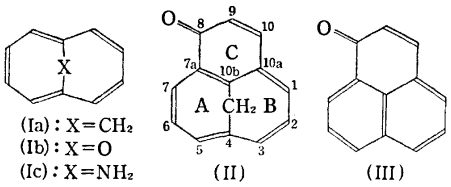

Experimental

Crystals of **II**, kindly supplied by Professor **I.** Murata, were recrystallized from the ether–petroleum ether mixture. They were reddish-orange mass crystals. The unit-cell dimensions were determined from zero-layer Weissenberg photographs about the *b* and *c* axes. Spacings of about 40 reflections, calibrated with superimposed aluminum powder lines, were subjected to the least-squares treatment. The density of the crystals was measured by the flotation method. Since the systematic absences of reflections are *hk*0 for *h* odd, *h*0*l* for *l* odd, and 0*kl* for *k* odd, the space group was determined to be Pbca. The crystal data of II are summarized in Table 1.

TABLE 1. CRYSTAL DATA

Formula	$C_{14}H_{10}O$
MW	194.2
Crystal system	Orthorhombic
Space group	Pbca
a	16.567±0.004 Å
b	14.090±0.003 Å
c	8.418±0.002 Å
Volume of a unit cell	1965.0 Å^3
Density calculated	1.312 g·cm^{-3}
Density measured	1.316 g·cm^{-3}
F(000)	816
μ(Cu*K*α)	6.51 cm^{-1}
Number of molecules per unit cell	8

The reflections were recorded, using Cu*K*α radiation, on equi-inclination multiple-film Weissenberg photographs for 0—10 layers around the *b* axis and 0—6 layers around *c*. The dimensions of the crystals used were 0.35×0.2×0.7 mm and 0.6×0.2×1.3 mm for the *b* and *c* axis rotations respectively.

The intensities were first estimated by visual comparison with a standard scale prepared with the same crystal. Since then a TV-densitometer has become available, and it has been proved that the TV-densitometer method is more accurate and time-saving than the visual method.[7] Therefore, the intensities were remeasured by means of the TV-densitometer.

The intensity data of 2019 independent reflections (90.0% within the Cu*K*α sphere) were collected; 632 of them were

TABLE 2. FINAL ATOMIC COORDINATES AND TEMPERATURE FACTORS AND THEIR STANDARD DEVIATIONS
All quantities are multiplied by 10^4 except temperature factors of hydrogen atoms. E.s.d.'s are in parentheses. The anisotropic temperature factors are expressed in the form of exp $\{-(B_{11}h^2+B_{22}k^2+B_{33}l^2+B_{12}hk+B_{13}hl+B_{23}kl)\}$.

	x/*a*	*y*/*b*	*z*/*c*	*B*(Å^2)	B_{11}	B_{22}	B_{33}	B_{12}	B_{13}	B_{23}
O(1)	−0716(2)	0963(2)	2269(4)		464(12)	1464(30)	3183(68)	−745(32)	−948(48)	1357(76)
C(1)	−0256(2)	1440(3)	3103(4)		289(12)	1065(31)	1882(66)	−143(32)	80(46)	1104(76)
C(2)	−0365(2)	2451(3)	3380(5)		396(14)	1065(31)	2258(75)	619(39)	410(55)	842(85)
C(3)	0158(2)	2983(3)	4181(4)		663(20)	792(27)	1782(68)	794(39)	651(61)	421(71)
C(4)	0875(2)	2562(3)	4887(4)		467(14)	567(19)	1375(50)	168(31)	399(45)	55(54)
C(5)	0915(2)	1563(2)	4885(4)		263(10)	537(18)	1253(48)	53(23)	370(36)	285(49)
C(6)	0483(2)	1010(2)	3811(4)		291(11)	582(20)	1601(55)	−148(25)	94(40)	507(55)
C(7)	0777(2)	0141(2)	3269(5)		591(19)	487(21)	2094(69)	−304(32)	−286(62)	119(61)
C(8)	1592(3)	−0127(3)	3215(5)		718(22)	468(21)	2270(75)	233(35)	195(72)	−163(65)
C(9)	2243(2)	0397(3)	3724(5)		462(16)	665(24)	2076(70)	539(32)	329(54)	323(67)
C(10)	2188(2)	1122(3)	4837(4)		292(11)	704(22)	1722(59)	175(26)	−3(43)	492(62)
C(11)	2658(2)	1953(3)	4875(4)		338(13)	1007(29)	1744(63)	−178(34)	−78(49)	264(74)
C(12)	2376(2)	2805(3)	5304(5)		601(19)	903(31)	1880(69)	−585(39)	−213(62)	2(76)
C(13)	1545(3)	3114(3)	5316(4)		881(24)	538(22)	1466(60)	−148(37)	183(67)	−309(60)
C(14)	1486(2)	1093(2)	5979(4)		335(12)	617(21)	1378(52)	3(26)	131(41)	429(54)
H(1)	−0781(23)	2756(29)	2908(49)	6.7(1.2)						
H(2)	0065(22)	3750(26)	4344(41)	4.7(0.9)						
H(3)	0387(22)	−0260(28)	2683(50)	6.2(1.1)						
H(4)	1708(21)	−0718(24)	2642(44)	4.6(0.9)						
H(5)	2738(24)	0280(29)	3052(47)	6.6(1.2)						
H(6)	3241(25)	1914(30)	4501(53)	7.8(1.3)						
H(7)	2787(27)	3348(32)	5615(55)	9.2(1.5)						
H(8)	1426(24)	3834(30)	5535(49)	6.7(1.2)						
H(9)	1577(18)	1473(21)	7028(34)	2.5(0.7)						
H(10)	1327(20)	0410(24)	6360(41)	4.2(0.9)						

6) S. Hunig and E. Wolff, *Chimia*, **22**, 33 (1968).

7) H. Shimanouchi, K. Ibata, and Y. Sasada, (1972) Unpublished work.

TABLE 3. OBSERVED AND CALCULATED STRUCTURE FACTORS ($\times 5$).

H	FO	FC	H	FO	FC	H	FO	FC	H	FO	FC	H	FO	FC	H	FO	FC	H	FO	FC	H	FO	FC	H	FO	FC
K,L= 0	0		2	56	-52	18	0	-4	2	28	-27	10	22	24	4	82	78	12	26	-31	13	71	69	K,L= 8	3		5	51	-51
2	208	178	4	0	-6	19	19	23	3	70	71	11	23	-25	5	241	-231	13	21	17	14	36	37	0	70	-70	6	0	-8
4	343	333	6	79	78	20	0	-1	4	18	-16	K,L= 16		1	6	97	-99	14	40	-43	15	61	61	1	28	27	7	18	15
6	388	-372	8	32	-24	K,L= 4		1	5	45	-42	0	0	6	7	34	-32	15	0	-13	16	17	-3	2	28	-28	8	0	-1
8	54	-49	10	76	-75	0	160	-160	6	27	-28	1	25	-22	8	29	25	16	0	12	17	14	-13	3	121	123	9	14	14
10	200	-205	12	0	-2	1	257	253	7	23	-16	2	0	-12	9	0	-10	17	13	-16	18	37	-41	4	32	33	10	0	-3
12	107	106	14	51	55	2	131	-126	8	31	-26	3	17	14	10	0	1	K,L= 10		2	19	0	-1	5	0	7	11	0	0
14	61	73	16	23	23	3	27	28	9	89	88	4	0	11	11	41	-38	0	23	14	20	7	-7	6	18	-26	12	0	4
16	162	-163	K,L= 11		0	4	127	-118	10	0	3	5	0	8	12	72	74	1	0	-3	K,L= 3		3	7	0	10	K,L= 15		3
18	27	-23	2	29	-24	5	55	57	11	73	82	6	0	13	13	28	24	2	84	-79	1	34	53	8	15	-17	1	0	1
20	16	-21	4	32	27	6	181	176	12	21	-21	7	22	-21	14	28	-28	3	91	88	2	102	101	9	22	20	2	0	2
K,L= 1		0	6	120	-116	7	162	151	13	19	15	8	0	7	15	86	91	4	117	117	3	102	-99	10	25	-22	3	19	-17
2	514	-539	8	82	-76	8	80	79	14	0	9	K,L= 17		1	16	43	46	5	81	87	4	79	74	11	0	-8	4	21	16
4	196	180	10	88	-89	9	118	112	15	24	-23	1	0	7	17	20	25	6	108	106	5	172	-161	12	42	-44	5	0	0
6	224	216	12	29	34	10	0	-8	16	0	12	2	0	3	18	33	-35	7	86	86	6	0	-14	13	60	65	6	27	29
8	143	132	14	20	20	11	0	4	17	0	10	3	0	0	19	0	13	8	54	59	7	142	-135	14	43	-49	7	14	7
10	38	39	16	0	-2	12	0	-6	18	13	7	4	0	0	20	12	-15	9	25	20	8	0	3	15	0	3	8	0	-6
12	52	48	K,L= 12		0	13	56	-55	K,L= 10		1	5	20	-21	K,L= 5		2	10	56	-56	9	28	25	16	0	6	9	11	8
14	56	-59	0	0	15	14	38	-42	0	25	-11	K,L= 0		2	1	41	46	11	40	36	10	56	-57	17	12	3	10	0	10
16	26	-19	2	87	89	15	0	17	1	21	20	0	492	514	2	25	25	12	72	-70	11	107	105	18	9	10	K,L= 16		3
18	58	57	4	104	-103	16	24	-28	2	0	-12	1	185	189	3	40	-35	13	18	17	12	0	5	K,L= 9		3	0	0	4
K,L= 2	0		6	43	-39	17	0	-9	3	20	-7	2	599	-635	4	18	16	14	0	-2	13	43	45	1	95	92	K,L= 0		4
0	328	-357	8	69	-76	18	16	-22	4	42	-44	3	41	46	5	23	24	15	19	-16	14	0	-1	2	19	17	0	235	228
2	178	-185	10	0	8	19	0	16	5	26	-26	4	131	130	6	16	-13	K,L= 11		2	15	26	25	3	20	-8	1	172	-177
4	324	-326	12	24	20	20	0	6	6	67	66	5	352	329	7	63	-61	1	0	3	16	0	0	4	57	-61	2	177	-176
6	59	53	14	22	-26	K,L= 5		1	7	52	50	6	203	-193	8	0	-14	2	0	15	17	23	-25	5	91	-92	3	21	18
8	223	-215	K,L= 13		0	1	245	241	8	33	23	7	41	-41	9	0	17	3	70	70	18	0	-7	6	64	-71	4	78	-76
10	45	-35	2	40	-48	2	312	-313	9	0	14	8	263	259	10	25	27	4	101	103	19	19	21	7	9	-16	5	237	221
12	49	-46	4	59	-61	3	113	-114	10	27	-25	9	196	-184	11	32	-38	5	0	9	K,L= 4		5	8	28	22	6	315	-301
14	115	109	6	0	-12	4	0	-14	11	0	15	10	64	64	12	42	39	6	22	-16	0	27	28	9	48	-49	7	80	78
16	35	33	8	27	24	5	250	234	12	0	17	11	59	-60	13	29	31	7	64	-62	1	74	-66	10	0	-6	8	0	7
18	46	51	10	29	27	6	68	56	13	39	-41	12	50	56	14	31	33	8	50	-50	2	120	-114	11	42	44	9	54	56
20	0	-2	12	0	1	7	23	11	14	0	6	13	56	-55	15	0	-2	9	27	27	3	99	-93	12	0	-11	10	114	108
K,L= 3		0	14	12	18	8	45	42	15	25	27	14	0	11	16	24	21	10	38	-44	4	168	-165	13	0	1	11	173	165
2	49	-51	K,L= 14		0	9	74	75	16	0	11	15	0	-14	17	0	8	11	19	12	5	252	-245	14	24	24	12	118	122
4	201	206	0	62	-62	10	116	110	17	0	-9	16	62	-63	18	14	-14	12	33	35	6	47	-49	15	16	-19	13	57	60
6	195	-181	2	0	13	11	143	-141	K,L= 11		1	17	17	-16	19	0	6	13	0	-10	7	36	35	16	17	18	14	20	14
8	90	-81	4	0	8	12	57	58	1	0	-8	18	25	18	K,L= 6		2	14	0	9	8	31	-31	17	11	-10	15	0	11
10	204	-208	6	0	9	13	63	68	2	39	-43	19	31	39	0	0	3	15	21	22	9	22	20	K,L= 18		3	16	28	-30
12	95	98	8	17	18	14	60	-62	3	26	-22	20	19	22	1	89	92	K,L= 12		2	10	35	-38	0	25	21	17	17	-4
14	38	37	10	25	29	15	45	-48	4	0	-16	K,L= 1		2	2	54	67	0	33	-29	11	0	8	1	20	-12	18	14	-23
16	68	73	12	33	40	16	56	-62	5	28	25	1	387	400	3	18	17	1	0	13	12	49	47	2	31	25	19	0	-3
18	54	64	K,L= 15		0	17	0	11	6	0	-1	2	624	-668	4	18	-15	2	40	39	13	0	-2	3	0	-9	K,L= 1		4
20	18	15	2	33	33	18	0	-16	7	0	4	3	532	536	5	79	-70	3	39	42	14	28	29	4	31	-28	1	43	-39
K,L= 4		0	4	42	-46	19	0	3	8	40	-42	4	333	-326	6	30	-27	4	51	-54	15	22	8	5	50	-48	2	111	-98
0	53	54	6	0	-6	20	0	-9	9	0	10	5	166	162	7	0	0	5	35	-37	16	0	6	6	41	39	3	89	75
2	108	-117	8	46	42	K,L= 6		1	10	0	17	6	112	-108	8	32	-35	6	31	-30	17	0	9	7	58	61	4	21	-21
4	75	74	10	0	18	0	56	53	11	25	-28	7	67	-63	9	17	12	7	0	0	18	7	-14	8	0	16	5	68	-58
6	76	-76	K,L= 1		1	1	180	-178	12	0	-17	8	51	40	10	22	-11	8	0	-11	19	0	4	9	33	36	6	50	47
8	54	46	1	361	-366	2	226	229	13	0	7	9	38	31	11	0	-6	9	31	-29	K,L= 5		3	10	18	10	7	67	-61
10	0	15	2	144	-131	3	109	-107	14	0	8	10	20	23	12	0	-5	10	35	34	1	143	150	11	21	-3	8	89	83
12	67	70	3	217	202	4	20	18	15	17	-16	11	0	-10	13	31	31	11	36	-39	2	46	48	12	25	26	9	25	20
14	51	-49	4	166	158	5	53	51	16	0	6	12	32	-29	14	0	-9	12	0	13	3	214	-206	13	24	-25	10	17	15
16	39	36	5	0	0	6	55	59	K,L= 12		1	13	80	-77	15	36	41	13	0	-6	4	240	232	14	0	11	11	75	78
18	0	-4	6	52	-46	7	68	-58	0	0	-7	14	93	-91	16	0	5	14	0	-5	5	66	64	15	0	-14	12	75	-70
20	0	-4	7	158	150	8	22	-1	1	37	40	15	35	-36	17	0	2	15	0	-4	6	165	151	16	0	0	13	16	24
K,L= 5		0	8	59	56	9	32	-33	2	20	-20	16	51	-52	18	0	3	K,L= 13		2	7	133	-133	K,L= 11		3	14	36	-41
2	125	115	9	19	-12	10	37	39	3	28	-26	17	0	-18	19	0	-14	1	20	19	8	30	-27	1	28	24	15	47	49
4	21	-15	10	0	3	11	0	11	4	0	-4	18	37	38	K,L= 7		2	2	38	-44	9	39	40	2	0	0	16	14	-17
6	73	-62	11	66	61	12	0	13	5	65	68	19	0	-13	1	46	-39	3	27	29	10	0	-9	3	33	-34	17	16	12
8	152	155	12	39	31	13	0	7	6	55	56	20	0	12	2	98	91	4	0	0	11	55	-55	4	15	-18	18	32	33
10	40	-35	13	41	-41	14	0	-25	7	0	-13	K,L= 2		2	3	73	-69	5	0	-16	12	26	26	5	0	-8	19	11	11
12	0	0	14	0	2	15	33	-36	8	37	40	0	711	-861	4	78	81	6	20	20	13	91	94	6	24	8	K,L= 2		4
14	34	-33	15	27	23	16	0	-4	9	0	2	1	405	410	5	0	-11	7	64	-64	14	0	-7	7	23	19	0	321	-326
16	21	-16	16	48	49	17	27	29	10	27	-25	2	145	155	6	109	109	K,L= 14		2	15	25	-23	8	0	0	1	105	-106
18	50	-52	17	33	41	18	22	-24	11	0	-5	3	68	68	7	0	-8	0	44	-49	16	0	-2	9	33	-34	2	205	207
K,L= 6		0	18	0	19	19	16	19	12	0	0	4	42	38	8	135	-127	1	0	0	17	19	14	10	38	37	3	237	-234
0	0	-9	19	20	-24	K,L= 7		1	13	30	-37	5	222	216	9	56	56	2	0	5	18	17	20	11	13	9	4	46	38
2	122	-125	20	0	3	1	233	-233	14	0	-20	6	234	231	10	0	3	3	20	20	19	12	-11	12	0	9	5	104	-100
4	111	-115	K,L= 2		1	2	94	-93	15	0	-4	7	87	85	11	0	15	4	19	23	K,L= 6		3	13	0	7	6	195	189
6	128	124	0	466	-492	3	61	51	K,L= 13		1	8	30	-25	12	58	-59	5	54	-52	0	116	-120	14	26	33	7	108	-104
8	64	64	1	422	425	4	44	-42	1	20	-27	9	33	30	13	68	68	6	0	-10	1	143	-136	15	0	0	8	30	-26
10	88	87	2	298	-295	5	24	-23	2	25	-21	10	22	16	14	24	22	K,L= 15		2	2	158	149	K,L= 12		3	9	0	2
12	52	55	3	11	7	6	0	9	3	0	-4	11	37	-36	15	21	18	1	0	14	3	29	23	0	0	-4	10	23	24
14	0	-15	4	235	-220	7	41	39	4	0	5	12	148	-150	16	18	12	2	20	17	4	54	57	1	0	6	11	0	8
16	44	-45	5	206	202	8	27	25	5	0	21	13	21	-23	17	11	-12	K,L= 1		3	5	88	-92	2	0	-5	12	62	-60
18	0	-17	6	289	284	9	79	-74	6	30	33	14	22	-21	18	17	12	1	262	267	6	25	24	3	84	-87	13	23	-16
K,L= 7		0	7	143	-135	10	79	82	7	0	-18	15	0	0	K,L= 8		2	2	69	-72	7	51	49	4	23	-19	14	0	-6
2	17	-1	8	167	158	11	31	-33	8	0	-6	16	0	10	0	105	-115	3	97	-92	8	22	-22	5	10	-18	15	31	-32
4	142	-139	9	88	-76	12	34	36	9	0	18	17	30	-36	1	0	4	4	172	-162	9	38	33	6	10	-10	16	24	24
6	0	-29	10	25	28	13	67	-73	10	22	24	18	0	13	2	24	-10	5	78	79	10	43	45	7	35	-36	17	0	-4
8	24	18	11	52	-51	14	28	17	11	30	-37	19	0	0	3	35	33	6	201	-189	11	52	-51	8	24	17	18	0	-3
10	39	30	12	0	21	15	44	47	12	0	-12	20	0	2	4	0	-5	7	89	79	12	33	-29	9	20	16	19	0	5
12	70	-66	13	66	-67	16	0	-5	13	0	6	K,L= 3		2	5	49	-52	8	126	113	13	0	-13	10	0	-2	K,L= 3		4
14	0	-20	14	12	2	17	22	16	14	0	-18	1	126	-136	6	75	-76	9	85	-74	14	25	-25	11	0	0	1	26	33
16	31	-30	15	32	39	18	0	2	K,L= 14		1	2	82	-80	7	24	-22	10	0	7	15	54	-60	12	26	29	2	248	253
18	25	-30	16	0	1	19	16	20	0	0	-17	3	20	10	8	0	-19	11	53	-56	16	19	22	13	12	6	3	28	-24
K,L= 8		0	17	57	-62	K,L= 8		1	1	0	-8	4	70	64	9	89	-97	12	35	36	17	0	4	14	7	3	4	201	188
0	223	215	18	0	4	0	0	5	2	34	-42	5	39	41	10	34	37	13	29	23	18	14	14	15	6	-2	5	23	19
2	146	135	19	22	-14	1	47	38	3	48	56	6	106	-101	11	35	-34	14	0	8	19	0	-20	K,L= 13		3	6	60	55
4	90	-86	20	22	28	2	22	23	4	17	-10	7	204	-194	12	20	-14	15	33	-32	K,L= 7		3	1	0	-7	7	112	-104
6	47	-45	K,L= 3		1	3	22	12	5	0	-4	8	39	41	13	24	-17	16	23	18	1	44	48	2	0	3	8	58	59
8	63	-71	1	102	-107	4	62	-58	6	28	32	9	57	62	14	22	24	17	0	1	2	21	23	3	0	15	9	26	-27
10	21	18	2	411	-397	5	53	54	7	23	25	10	26	-15	15	16	-8	18	15	-13	3	39	37	4	0	-13	10	43	-44
12	20	15	3	158	148	6	28	-31	8	23	28	11	38	-40	16	0	11	19	17	-13	4	26	-22	5	0	5	11	59	-56
14	0	14	4	76	-74	7	120	-120	9	18	-23	12	78	78	17	0	-6	K,L= 2		3	5	23	25	6	0	10	12	38	-37
16	42	-54	5	215	-207	8	66	-68	10	0	-1	13	0	-12	18	17	15	0	58	55	6	0	3	7	0	-7	13	0	-9
18	26	-31	6	121	-120	9	73	-73	11	0	13	14	0	-3	K,L= 9		2	1	19	32	7	84	79	8	24	-23	14	7	8
K,L= 9		0	7	59	-54	10	62	-66	12	0	9	15	21	-23	1	47	49	2	236	236	8	20	-12	9	0	-5	15	21	-17
2	17	-17	8	67	-62	11	0	6	K,L= 15		1	16	24	-15	2	22	-14	3	94	-92	9	74	-71	10	0	-3	16	14	2
4	53	-55	9	22	-23	12	0	-12	1	26	33	17	36	40	3	0	-3	4	91	-79	10	18	-17	11	18	5	17	21	26
6	25	19	10	0	-5	13	57	62	2	0	-10	18	18	-14	4	49	-46	5	95	92	11	35	29	12	10	-9	18	18	-14
8	251	246	11	56	58	14	0	-12	3	0	-7	19	0	4	5	0	2	6	84	72	12	55	-55	13	11	-13	K,L= 4		4
10	86	87	12	0	2	15	0	19	4	0	10	20	16	-18	6	0	-4	7	89	-83	13	0	-17	K,L= 14		3	0	78	-75
12	58	58	13	67	-69	16	26	28	5	25	24	K,L= 4		2	7	70	-69	8	22	18	14	21	-19	0	0	-7	1	104	-105
14	0	-17	14	76	-78	17	0	5	6	26	26	0	64	-53	8	55	50	9	30	-28	15	35	40	1	0	7	2	19	-1
16	0	-3	15	0	6	18	12	17	7	0	-7	1	187	192	9	27	19	10	14	12	16	23	-22	2	19	-19	3	27	30
K,L= 10		0	16	32	-36	K,L= 9		1	8	0	0	2	119	118	10	29	-24	11	113	108	17	18	-21	3	0	5	4	49	-50
0	156	147	17	51	-56	1	0	-17	9	0	2	3	18	-13	11	33	-13	12	51	50	18	0	2	4	0	-8	5	41	-39

Table 3. Continued

H	FO	FC	H	FO	FC	H	FO	FC	H	FO	FC	H	FO	FC	H	FO	FC	H	FO	FC	H	FO	FC	H	FO	FC
6	27	27	0	24	-23	3	44	-40	16	11	-11	K,L=	0	6	15	19	19	1	14	-19	10	0	12	2	0	-6	K,L=	2	9
7	22	8	1	71	-66	4	61	62	K,L=	8	5	0	229	217	16	11	-14	2	14	-11	11	0	-12	3	46	-47	0	68	-70
8	27	28	2	104	-102	5	80	82	0	36	40	1	26	-11	K,L=	6	6	3	13	-10	12	0	-2	4	0	19	1	49	52
9	0	10	3	66	-73	6	61	59	1	23	17	2	51	-49	0	83	82	4	25	-26	13	0	-5	5	24	19	2	28	27
10	96	-94	4	73	76	7	112	-114	2	47	-50	3	70	67	1	19	-8	5	0	0	14	0	13	6	49	-47	3	19	19
11	19	-5	5	27	27	8	23	6	3	78	79	4	22	18	2	18	-11	6	10	-3	K,L=	7	7	7	0	7	4	0	8
12	17	10	6	17	5	9	124	-127	4	55	53	5	26	-24	3	17	-6	7	9	-9	1	0	8	8	21	-20	5	22	20
13	34	-34	7	21	-21	10	22	-19	5	0	-2	6	131	-133	4	58	-56	8	26	29	2	33	-33	9	20	17	6	0	11
14	38	-35	8	29	30	11	19	11	6	41	-38	7	38	-36	5	29	30	K,L=	14	6	3	36	37	10	35	-41	7	0	2
15	23	-21	9	7	0	12	51	-50	7	23	-24	8	16	-11	6	16	7	0	9	3	4	25	-23	11	0	-13	8	0	-5
16	31	34	10	13	-17	13	18	11	8	20	10	9	77	-76	7	19	-19	1	9	1	5	0	25	12	19	18	9	0	9
17	15	2	11	32	33	14	33	-36	9	24	-23	10	32	25	8	0	1	2	9	0	6	0	10	13	27	36	10	0	7
18	11	-6	12	22	-24	15	19	19	10	21	12	11	26	-28	9	16	9	3	11	8	7	24	24	K,L=	4	8	11	0	-7
19	0	-10	13	16	-14	16	15	10	11	25	-28	12	18	14	10	18	-6	4	10	-11	8	0	20	0	37	-37	K,L=	3	9
K,L=	5	4	14	15	11	17	0	0	12	0	0	13	0	1	11	17	-12	5	0	-2	9	18	-25	1	28	-31	1	33	32
1	26	23	15	18	-22	18	5	6	13	16	13	14	26	-31	12	35	38	K,L=	1	7	10	29	35	2	0	0	2	37	43
2	27	24	K,L=	11	4	K,L=	3	5	14	17	15	15	33	46	13	17	10	1	47	-46	11	0	-12	3	27	24	3	23	-20
3	18	-17	1	0	2	1	39	32	15	13	-10	16	43	-55	14	18	20	2	82	-79	12	0	14	4	0	22	4	0	9
4	50	-53	2	82	82	2	109	106	16	0	-4	17	13	20	15	19	-25	3	0	-8	13	0	-13	5	0	6	5	0	-20
5	31	27	3	47	40	3	125	127	K,L=	9	5	K,L=	1	6	16	0	-7	4	32	32	K,L=	8	7	6	0	4	6	0	0
6	15	15	4	92	84	4	46	-47	1	27	28	1	11	-4	K,L=	7	6	5	0	0	0	0	12	7	0	0	7	0	-5
7	64	64	5	50	48	5	39	34	2	53	46	2	61	-53	1	0	-1	6	51	50	1	25	25	8	23	23	8	0	25
8	75	-73	6	0	5	6	0	8	3	0	2	3	41	34	2	19	-17	7	68	68	2	65	-72	9	35	-39	9	0	-11
9	18	1	7	37	36	7	24	-24	4	50	50	4	19	-15	3	79	88	8	0	13	3	29	30	10	0	13	10	0	2
10	0	13	8	8	-5	8	19	-15	5	60	-63	5	45	-39	4	14	-5	9	0	-11	4	0	14	11	0	-12	K,L=	4	9
11	0	5	9	7	10	9	82	80	6	0	-12	6	70	69	5	36	-40	10	40	42	5	0	0	12	0	1	0	23	23
12	30	-28	10	18	-14	10	22	-17	7	0	2	7	16	-1	6	32	31	11	0	2	6	29	30	13	0	-6	1	0	-8
13	20	8	11	0	-10	11	38	42	8	30	29	8	148	146	7	19	-9	12	0	20	7	29	-33	K,L=	5	8	2	0	-3
14	19	10	12	16	15	12	30	-31	9	29	-30	9	18	9	8	48	-47	13	0	-7	8	33	37	1	16	18	3	0	-4
15	8	6	13	27	-29	13	32	-35	10	35	-36	10	87	86	9	38	-43	14	27	-29	9	25	-26	2	0	4	4	0	1
16	15	-9	14	20	25	14	26	26	11	0	3	11	45	44	10	19	14	15	0	0	10	0	-12	3	28	14	5	0	-9
17	0	-1	K,L=	12	4	15	20	-18	12	24	24	12	19	-7	11	18	14	16	0	-31	11	0	-7	4	0	6	6	0	0
18	0	2	0	30	30	16	0	8	13	16	-12	13	21	-4	12	15	10	K,L=	2	7	12	0	-2	5	0	2	7	0	7
K,L=	6	4	1	8	-6	17	25	-28	14	0	7	14	12	-14	13	41	-46	0	103	-104	13	9	6	6	0	-1	8	0	11
0	34	35	2	19	11	18	0	-5	15	12	-12	15	22	5	14	20	21	1	41	48	K,L=	9	7	7	0	-10	9	13	0
1	44	-44	3	11	-12	K,L=	4	5	K,L=	10	5	16	12	-12	15	9	9	2	36	35	1	0	14	8	0	11	10	0	1
2	25	24	4	38	-37	0	102	96	0	0	1	17	29	-39	K,L=	8	6	3	0	-8	2	28	-27	9	19	-15	K,L=	5	9
3	23	-18	5	11	3	1	51	-53	1	31	-29	K,L=	2	6	0	51	54	4	0	1	3	0	-5	10	0	8	1	29	30
4	10	-8	6	0	-13	2	108	-103	2	9	7	0	71	-69	1	47	52	5	72	70	4	33	38	11	0	-13	2	0	9
5	38	40	7	0	-6	3	27	24	3	33	-31	1	30	34	2	37	35	6	32	-37	5	27	-29	12	16	19	3	0	-5
6	51	51	8	0	5	4	0	3	4	0	-10	2	15	11	3	16	8	7	0	-8	6	0	1	K,L=	6	8	4	0	-1
7	0	-7	9	0	0	5	25	-16	5	0	-11	3	0	-1	4	17	16	8	35	-37	7	0	3	0	38	-44	5	0	9
8	24	28	10	23	25	6	34	-33	6	21	-9	4	15	-6	5	38	-45	9	0	5	8	0	8	1	0	-3	6	0	1
9	35	40	11	9	3	7	37	39	7	14	-7	5	56	-57	6	18	-12	10	0	3	9	0	8	2	27	-27	7	0	-2
10	52	-54	12	23	24	8	0	8	8	23	-18	6	83	81	7	18	-13	11	40	42	10	0	-14	3	0	5	8	0	-4
11	0	11	13	12	-9	9	28	-24	9	23	-22	7	0	4	8	18	-15	12	21	-17	11	0	12	4	0	-6	9	0	-7
12	33	-26	K,L=	13	4	10	29	-34	10	18	15	8	22	-18	9	18	-12	13	24	23	12	0	18	5	35	40	K,L=	6	9
13	14	9	1	0	-10	11	0	0	11	0	-2	9	25	19	10	26	31	14	14	-22	K,L=	10	7	6	0	-3	0	15	-21
14	28	-36	2	0	-8	12	13	12	12	16	-2	10	26	18	11	27	-28	15	0	15	0	22	-6	7	0	-9	1	0	-4
15	0	-1	3	22	-17	13	26	-27	13	17	-14	11	29	-26	12	12	6	K,L=	3	7	1	0	9	8	0	17	2	0	6
16	14	-18	4	0	5	14	12	7	14	15	18	12	12	-4	13	11	-4	1	0	24	2	0	-4	9	0	-13	3	22	-25
17	18	17	5	0	8	15	15	-12	15	0	-4	13	0	1	14	9	-5	2	0	14	3	0	-18	10	0	14	4	28	-31
18	0	5	6	21	19	16	0	-3	K,L=	11	5	14	28	33	15	6	24	3	29	24	4	0	-15	11	0	-9	5	0	3
K,L=	7	4	7	0	-6	17	16	11	1	27	27	15	15	-8	K,L=	9	6	4	43	-45	5	0	5	12	0	1	6	0	-15
1	17	3	8	0	7	18	0	10	2	23	18	16	15	22	1	65	61	5	0	-25	6	0	13	K,L=	7	8	7	0	-2
2	55	-59	9	7	-2	K,L=	5	5	3	21	21	17	7	2	2	29	-28	6	28	-29	7	0	14	1	29	-31	8	17	-18
3	18	13	10	0	-2	1	134	-142	4	31	39	K,L=	3	6	3	18	3	7	0	0	8	0	-8	2	0	13	K,L=	8	9
4	55	-50	11	0	-9	2	24	-21	5	20	12	1	37	-30	4	30	-31	8	29	-26	9	17	9	3	37	43	0	18	21
5	30	21	K,L=	14	4	3	56	-56	6	0	14	2	24	22	5	22	-21	9	0	7	10	0	3	4	0	21	1	0	-2
6	77	80	0	16	12	4	40	-43	7	0	14	3	57	-53	6	0	-1	10	0	-3	11	0	8	5	0	-11	2	0	0
7	90	93	1	0	-7	5	63	62	8	0	9	4	27	-21	7	15	-7	11	28	36	K,L=	0	8	6	25	25	3	0	0
8	122	-121	2	0	-1	6	0	14	9	17	-19	5	48	52	8	54	58	12	0	-20	0	68	69	7	22	-14	4	14	18
9	14	-14	3	0	5	7	56	-57	10	16	-12	6	86	-87	9	23	-25	13	0	-8	1	29	27	8	0	8	5	0	-9
10	79	76	4	0	12	8	35	-35	11	18	-18	7	68	67	10	14	10	14	13	14	2	49	-46	9	0	1	6	9	13
11	19	-14	5	22	-22	9	115	115	12	12	-3	8	28	26	11	15	5	15	0	-4	3	0	10	10	0	2	7	9	-18
12	0	-1	6	0	1	10	23	20	13	0	-2	9	53	53	12	13	1	K,L=	4	7	4	0	-5	11	17	18	K,L=	0	10
13	26	-26	7	0	1	11	24	-20	K,L=	12	5	10	34	-35	13	16	15	0	109	106	5	0	-15	K,L=	8	8	0	52	55
14	27	29	8	0	0	12	23	17	0	0	-5	11	18	7	14	10	-23	1	0	-13	6	89	-90	0	0	6	1	0	13
15	22	-19	9	11	11	13	0	4	1	9	-9	12	13	-6	K,L=	10	6	2	0	-6	7	31	-32	1	38	35	2	0	7
16	0	-7	10	26	-28	14	19	21	2	26	28	13	16	15	0	54	-58	3	28	-25	8	0	2	2	0	11	3	0	12
17	17	-22	K,L=	15	4	15	26	-30	3	20	-27	14	16	-1	1	15	11	4	33	35	9	34	-41	3	0	22	4	0	-11
K,L=	8	4	1	0	0	16	0	11	4	21	14	15	17	-19	2	74	-76	5	0	-16	10	21	18	4	0	-7	5	36	44
0	25	-18	2	0	2	17	15	12	5	54	59	16	9	7	3	41	-46	6	11	-3	11	0	-13	5	20	-23	K,L=	1	10
1	20	-17	3	27	-27	K,L=	6	5	6	25	-26	17	16	-20	4	18	14	7	0	10	12	0	13	6	0	-3	1	0	-2
2	18	12	4	0	6	0	23	23	7	20	-17	K,L=	4	6	5	0	-1	8	0	17	13	15	-7	7	0	5	2	27	-27
3	13	12	5	8	6	1	42	-40	8	0	-7	0	125	128	6	11	-1	9	0	-3	14	0	6	8	0	-10	3	0	-1
4	27	30	6	0	8	2	49	47	9	0	-4	1	46	-48	7	17	-14	10	0	-21	K,L=	1	8	9	13	-2	4	0	-16
5	37	31	7	30	34	3	61	58	10	0	3	2	30	26	8	14	-3	11	0	1	1	0	19	10	7	7	5	23	-26
6	78	-77	8	0	-2	4	19	14	11	22	23	3	81	81	9	12	15	12	0	14	2	56	-55	K,L=	9	8	6	0	13
7	25	26	K,L=	16	4	5	19	12	12	8	-5	4	74	-69	10	18	-11	13	23	-27	3	0	3	1	29	31	7	19	-26
8	0	5	0	19	19	6	60	-55	K,L=	13	5	5	17	14	11	13	9	14	0	-5	4	40	-41	2	23	-28	K,L=	2	10
9	0	3	1	5	-4	7	63	65	1	35	-37	6	30	-29	12	12	-8	15	0	-12	5	40	-41	3	0	-2	0	0	-13
10	64	68	2	0	-2	8	35	-34	2	16	9	7	63	62	13	0	2	K,L=	5	7	6	0	-5	4	0	6	1	0	5
11	22	22	3	11	-4	9	57	62	3	25	25	8	37	-38	K,L=	11	6	1	0	-9	7	33	-30	5	0	-1	2	0	-5
12	19	18	4	9	6	10	38	39	4	17	-20	9	24	24	1	23	-20	2	32	-27	8	0	16	6	0	-5	3	22	-25
13	21	-13	K,L=	1	5	11	0	1	5	15	8	10	60	-63	2	39	38	3	0	-15	9	0	-18	7	0	-9	4	0	1
14	0	10	1	22	-26	12	0	-2	6	17	-19	11	24	25	3	0	0	4	0	-20	10	0	5	8	0	9	5	0	-5
15	13	-7	2	91	81	13	14	13	7	16	-8	12	30	27	4	13	3	5	0	-4	11	0	10	K,L=	10	8	6	0	19
16	0	-4	3	34	-25	14	22	23	8	0	8	13	20	21	5	0	3	6	0	-6	12	0	-14	0	0	-15	K,L=	3	10
17	0	-12	4	69	65	15	10	-6	9	14	13	14	0	2	6	36	-38	7	54	-49	13	0	3	1	0	3	1	16	16
K,L=	9	4	5	14	-4	16	15	-13	10	15	-17	15	16	-19	7	18	19	8	29	-29	14	0	-8	2	0	4	2	0	-8
1	46	-46	6	49	51	17	14	21	K,L=	14	5	16	14	1	8	0	4	9	0	1	K,L=	2	8	3	0	-23	3	0	-4
2	46	-45	7	0	-9	K,L=	7	5	0	15	19	17	9	3	9	0	2	10	20	21	0	27	-30	4	30	30	4	19	22
3	112	-119	8	19	-15	1	95	-94	1	0	-3	K,L=	5	6	10	14	-16	11	26	-26	1	31	36	5	0	-7	5	22	23
4	88	-90	9	53	-54	2	25	23	2	0	10	1	42	-44	11	11	-2	12	0	-8	2	0	5	6	0	13	6	0	4
5	21	-23	10	34	-27	3	46	43	3	17	16	2	19	7	K,L=	12	6	13	0	8	3	0	-9	7	0	3	K,L=	4	10
6	21	-20	11	87	-82	4	46	-47	4	0	-9	3	19	-17	0	52	56	14	0	8	4	47	45	K,L=	1	9	0	27	-30
7	26	24	12	31	-30	5	33	39	5	0	-6	4	24	-20	1	22	22	K,L=	6	7	5	0	-5	1	0	-10	1	19	-19
8	23	14	13	0	12	6	0	-9	6	0	-2	5	36	-36	2	46	48	0	22	-22	6	32	36	2	32	-28	2	0	0
9	20	-8	14	0	1	7	68	66	7	14	-13	6	19	-8	3	0	0	1	0	7	7	27	29	3	0	8	3	0	-6
10	22	17	15	0	21	8	0	-8	8	13	-15	7	21	18	4	24	-22	2	0	-23	8	0	-4	4	0	2	4	0	-3
11	17	1	16	0	-1	9	9	-7	K,L=	15	5	8	15	-7	5	22	19	3	0	-18	9	32	39	5	0	-6	5	12	-11
12	11	-11	17	31	34	10	20	-16	1	22	-22	9	23	-22	6	0	0	4	26	-24	10	0	-16	6	24	-24			
13	33	33	18	13	5	11	0	3	2	13	-10	10	16	4	7	0	-3	5	0	2	11	0	9	7	0	0			
14	18	-20	K,L=	2	5	12	19	-16	3	0	-1	11	23	24	8	0	-5	6	0	19	12	29	-38	8	0	-7			
15	7	-2	0	77	-78	13	29	-31	4	0	2	12	11	1	9	11	-8	7	0	1	13	0	3	9	0	-6			
16	0	7	1	0	9	14	7	-9	5	0	-5	13	17	-10	10	14	15	8	0	13	K,L=	3	8	10	20	-21			
K,L=	10	4	2	98	94	15	33	42	6	0	0	14	0	3	K,L=	13	6	9	15	17	1	0	14	11	0	15			

found to have zero intensity. Lorentz and polarization corrections were made as usual, but the absorption correction was omitted. The intensities of elongated reflections on upper-layer photographs were corrected for spot size by a method proposed by Takenaka.[8]

Structure Determination and Refinement

In the earlier stage of the structure determination, visual data were used. The symbolic addition procedure was used for sign-determination. As a starting set, the signs of the following strong reflections were chosen;

h	k	l	$\|E\|$	sign
8	1	6	3.26	+
9	5	5	2.78	+
15	4	2	2.77	+
13	7	6	2.65	A
4	11	4	2.55	B

where A and B were symbols.

Using the triple-product sign relationships, the signs of 160 reflections out of 275 with $|E| \geq 1.5$ were determined in terms of A and B. From a further investigation of the list of the triple-product sign relations, it seemed most probable that A is — and B is +. The *E*-map computed with these signs clearly showed all fifteen non-hydrogen atoms.

The structure factors were calculated using these fifteen atoms, the *R* factor being 0.425 for the observed reflections. A Fourier refinement and the block-diagonal least-squares refinement were carried out successively. Four cycles of calculations using isotropic temperature factors reduced the *R* factor to 0.231. Anisotropic temperature factors were then introduced, and the *R* factor dropped to 0.155. At this stage, the coordinates of the hydrogen atoms were given by assuming a suitable geometry. The strongest reflection, 022, was excluded because it seemed to suffer from secondary extinction. The *R* factor decreased to 0.135 after four cycles; the isotropic hydrogen atoms were also shifted. Since the intensity data measured by means of the TV-densitometer became available at this stage, they were used for further refinement. After six cycles, the *R* factor was reduced to 0.080 for the observed reflections, excluding the 022 reflection. When this was included, $R=0.081$.

The atomic scattering factors were taken from the International Tables for X-ray Crystallography.[9] The final coordinates and temperature factors are given in Table 2. The observed and calculated structure factors are listed in Table 3.

The thermal ellipsoids of atoms are shown in Fig. 1. It seems that the entire molecule undergoes a rigid-body libration around the center of gravity. Then, the thermal motion of the molecule was analysed, assuming that all atoms form a rigid body.[10]

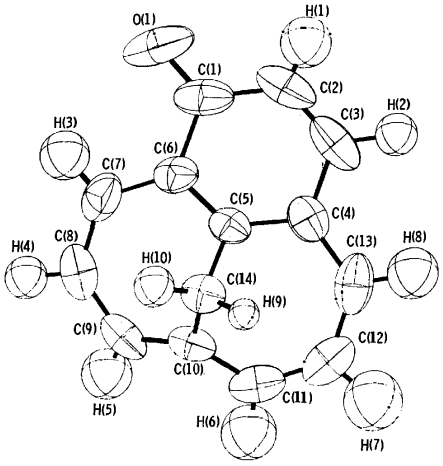

Fig. 1. Thermal ellipsoid of the molecule at the 50% probability level, viewed along the normal to its mean plane.

Table 4. Rigid-body thermal motion

(a) Principal axes of the molecule relative to the crystal axes (a, b, c)

Moment of inertia (Atomic weight·Å²)		Direction cosines of eigen vectors l	m	n
1	434.0	0.922	0.114	0.370
2	665.5	0.215	−0.945	−0.246
3	1024.7	−0.322	−0.307	0.896

(b) Rigid-body vibration tensors

$$\mathbf{T} = \begin{pmatrix} 0.0047 & -0.0068 & 0.0035 \\ & 0.0450 & -0.0010 \\ & & 0.0341 \end{pmatrix}$$

$$\sigma(\mathbf{T}) = \begin{pmatrix} 0.0029 & 0.0026 & 0.0031 \\ & 0.0033 & 0.0034 \\ & & 0.0054 \end{pmatrix} \text{ in Å}^2$$

$$\boldsymbol{\omega} = \begin{pmatrix} 17.74 & 0.50 & 2.66 \\ & 14.43 & 4.24 \\ & & 34.92 \end{pmatrix}$$

$$\sigma(\boldsymbol{\omega}) = \begin{pmatrix} 4.24 & 2.15 & 2.62 \\ & 2.78 & 2.11 \\ & & 1.91 \end{pmatrix} \text{ in deg}^2$$

(c) Principal axes of the **T** and $\boldsymbol{\omega}$ tensors relative to the crystal axes

	R.m.s. amplitude	Direction cosines of eigen vectors l	m	n
T	0.181 Å	−0.644	−0.215	0.735
	0.197	−0.623	0.705	−0.339
	0.229	0.445	0.676	0.558
$\boldsymbol{\omega}$	3.7 deg	0.281	−0.866	−0.414
	4.2	−0.950	−0.189	−0.249
	6.0	−0.137	−0.463	0.876

The anisotropic temperature factors, B_{ij}, were transformed to U tensors referred to the three principal axes of the moment of inertia of the molecule, the origin of the coordinate system being at the center of gravity (Table 4(a)). The translation and libration tensors, **T** and $\boldsymbol{\omega}$, of the rigid molecule were derived from U's. Since the agreement between the U's observed and those calculated from **T** and $\boldsymbol{\omega}$ was good (Table 5), the rigid-body model was justified.

The positions of the electron-density peaks are shifted

8) A. Takenaka, to be published.

9) "International Tables for X-ray Crystallography," Vol. III. Birmingham, Kynoch Press, (1962).

10) D. W. J. Cruickshank, *Acta Crystallogr.*, **9**, 754 (1956).

TABLE 5. OBSERVED AND CALCULATED U_{ij}'s IN Å^2

Atom		U_{11}	U_{22}	U_{33}	U_{12}	U_{13}	U_{23}
O (1)	Obsd	0.044	0.182	0.101	0.013	0.004	−0.038
	Calcd	0.049	0.163	0.086	0.014	−0.003	−0.016
C (1)	Obsd	0.048	0.120	0.047	−0.016	0.011	−0.014
	Calcd	0.045	0.101	0.057	−0.009	0.003	−0.008
C (2)	Obsd	0.079	0.098	0.066	−0.051	0.005	0.003
	Calcd	0.069	0.097	0.068	−0.042	0.004	−0.007
C (3)	Obsd	0.115	0.064	0.057	−0.044	−0.008	0.010
	Calcd	0.096	0.057	0.065	−0.032	0.002	−0.002
C (4)	Obsd	0.075	0.052	0.045	−0.009	0.002	0.006
	Calcd	0.071	0.045	0.047	−0.004	0.001	0.000
C (5)	Obsd	0.048	0.054	0.033	−0.010	0.010	0.001
	Calcd	0.047	0.047	0.034	−0.007	0.003	−0.000
C (6)	Obsd	0.045	0.068	0.044	−0.002	0.010	−0.012
	Calcd	0.048	0.057	0.041	−0.001	0.004	−0.004
C (7)	Obsd	0.070	0.062	0.074	0.020	−0.003	−0.018
	Calcd	0.086	0.053	0.059	0.012	−0.002	−0.004
C (8)	Obsd	0.104	0.043	0.082	−0.004	−0.004	−0.002
	Calcd	0.121	0.047	0.072	−0.016	−0.001	0.004
C (9)	Obsd	0.081	0.058	0.067	−0.034	0.001	0.002
	Calcd	0.094	0.073	0.067	−0.042	0.007	0.004
C (10)	Obsd	0.047	0.072	0.054	−0.020	0.002	−0.005
	Calcd	0.052	0.084	0.054	−0.024	0.004	−0.005
C (11)	Obsd	0.046	0.105	0.060	−0.001	0.005	0.003
	Calcd	0.046	0.131	0.068	−0.006	0.009	−0.012
C (12)	Obsd	0.069	0.104	0.069	0.031	0.000	−0.005
	Calcd	0.066	0.121	0.076	0.032	0.002	−0.016
C (13)	Obsd	0.114	0.056	0.060	0.024	−0.013	0.002
	Calcd	0.093	0.066	0.068	0.025	−0.004	−0.007
C (14)	Obsd	0.052	0.066	0.041	−0.008	0.004	−0.005
	Calcd	0.053	0.067	0.041	−0.010	−0.003	−0.005

by the molecular libration. Therefore, the bond lengths and angles were corrected for this effect using the eigen values and vectors of ω (Table 4(b) and 4(c)).

The computations were done on a HITAC 5020E computer at the University of Tokyo and on a HITAC 8500 computer at Tokyo Institute of Technology. The programs in the Universal Crystallographic Computation Program System[11] were used with some modifications. Three programs, TLSU for the determination of the cell dimensions, TDRW for the data reduction, and DEAM for plotting the thermal ellipsoid, all written by Takenaka, were used.

Results and Discussion

Molecular Geometry. The bond lengths and angles are illustrated in Fig. 2. The lengths corrected for thermal motion are listed in Table 6. Since these corrections are fairly small, the following discussion is based on the uncorrected values. The corrected bond

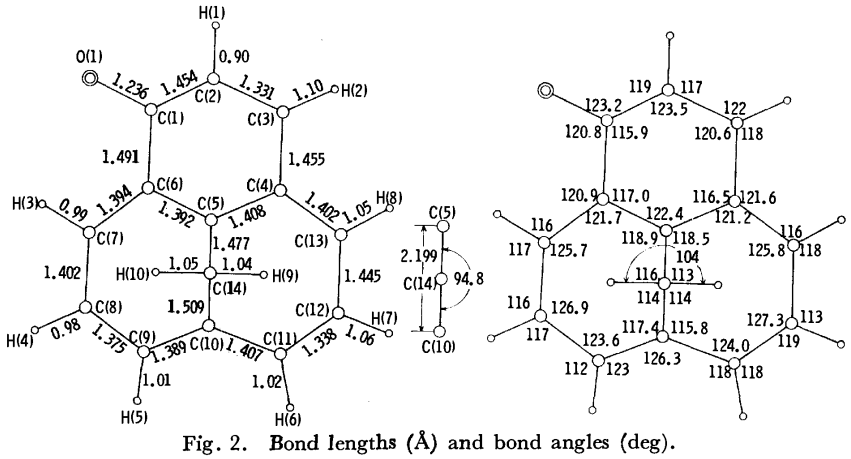

Fig. 2. Bond lengths (Å) and bond angles (deg).

11) "Universal Crystallographic Computation Program System," ed. by T. Sakurai, Published by Crystallographic Society of Japan, (1967).

TABLE 6. BOND LENGTHS (Å) AND BOND ANGLES (deg) E.s.d.'s are in parentheses.

		Corrected for thermal motions		
O(1)–C(1)	1.236 (5)	1.237	C(2)–H(1)	0.90 (4)
C(1)–C(2)	1.454 (6)	1.459	C(3)–H(2)	1.10 (4)
C(2)–C(3)	1.331 (6)	1.335	C(7)–H(3)	0.99 (4)
C(3)–C(4)	1.455 (5)	1.459	C(8)–H(4)	0.98 (4)
C(4)–C(5)	1.408 (5)	1.416	C(9)–H(5)	1.01 (4)
C(5)–C(6)	1.392 (4)	1.401	C(11)–H(6)	1.02 (5)
C(6)–C(1)	1.491 (5)	1.495	C(12)–H(7)	1.06 (5)
C(6)–C(7)	1.394 (5)	1.399	C(13)–H(8)	1.05 (4)
C(7)–C(8)	1.402 (6)	1.407	C(14)–H(9)	1.04 (3)
C(8)–C(9)	1.375 (6)	1.380	C(14)–H(10)	1.05 (4)
C(9)–C(10)	1.389 (5)	1.395		
C(10)–C(11)	1.407 (5)	1.411		
C(11)–C(12)	1.338 (6)	1.342		
C(12)–C(13)	1.445 (6)	1.449		
C(13)–C(4)	1.402 (6)	1.406		
C(5)–C(14)	1.477 (4)	1.484		
C(10)–C(14)	1.509 (5)	1.515		

O(1)–C(1)–C(2)	123.2 (4)	C(1)–C(2)–H(1)	119 (3)
O(1)–C(1)–C(6)	120.8 (4)	C(3)–C(2)–H(1)	117 (3)
C(6)–C(1)–C(2)	115.9 (4)	C(2)–C(3)–H(2)	122 (2)
C(1)–C(2)–C(3)	123.5 (4)	C(4)–C(3)–H(2)	118 (2)
C(2)–C(3)–C(4)	120.6 (4)	C(6)–C(7)–H(3)	116 (2)
C(3)–C(4)–C(5)	116.5 (3)	C(8)–C(7)–H(3)	117 (2)
C(3)–C(4)–C(13)	121.6 (4)	C(7)–C(8)–H(4)	116 (2)
C(13)–C(4)–C(5)	121.2 (3)	C(9)–C(8)–H(4)	117 (2)
C(4)–C(5)–C(6)	122.4 (3)	C(8)–C(9)–H(5)	112 (2)
C(4)–C(5)–C(14)	118.5 (3)	C(10)–C(9)–H(5)	123 (2)
C(6)–C(5)–C(14)	118.9 (3)	C(10)–C(11)–H(6)	118 (3)
C(5)–C(6)–C(1)	117.0 (3)	C(12)–C(11)–H(6)	118 (3)
C(5)–C(6)–C(7)	121.7 (3)	C(11)–C(12)–H(7)	119 (3)
C(1)–C(6)–C(7)	120.9 (3)	C(13)–C(12)–H(7)	113 (3)
C(6)–C(7)–C(8)	125.7 (4)	C(12)–C(13)–H(8)	118 (2)
C(7)–C(8)–C(9)	126.9 (4)	C(4)–C(13)–H(8)	116 (2)
C(8)–C(9)–C(10)	123.6 (4)	C(5)–C(14)–H(9)	113 (2)
C(9)–C(10)–C(11)	126.3 (4)	C(10)–C(14)–H(9)	114 (2)
C(9)–C(10)–C(14)	117.4 (3)	C(5)–C(14)–H(10)	116 (2)
C(11)–C(10)–C(14)	115.8 (3)	C(10)–C(14)–H(10)	114 (2)
C(10)–C(11)–C(12)	124.0 (4)	H(9)–C(14)–H(10)	104 (3)
C(11)–C(12)–C(13)	127.3 (4)		
C(12)–C(13)–C(4)	125.8 (4)		
C(5)–C(14)–C(10)	94.8 (3)		

angles are not listed; the maximum correction is 0.2°.

The lengths of the peripheral bonds of the [10]-annulene nucleus do not exhibit any apparent alternation, and all the C–C bond lengths except for C(11)–C(12) and C(12)–C(13) are quite close to that in benzene (1.392±0.004 Å).[12]

The eight atoms, C(4), C(6), C(7), C(8), C(9), C(11), C(12), and C(13), are approximately coplanar; the displacements of these atoms from their mean plane are given in Table 7. Similar characteristics are found in 1,6-methano-cyclodecapentaene-2-carboxylic acid (IV);[13] the root-mean-square deviations of the

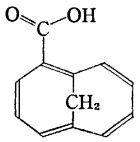

(IV)

eight atoms are 0.025 Å for the present compound and 0.034 Å for IV.[13] It seems that the planarity of the nucleus and, therefore, the aromaticity are not affected by the condensation of the six-membered ring(C). The torsion angles of the bonds, C(4)–C(5), C(5)–C(6), C(9)–C(10), and C(10)–C(11), which inevitably have large values in the [10]annulene nucleus, as is shown in Fig. 3(a), are also nearly equal to the corresponding angles in IV.[13]

In the methylene bridge, the C(10)–C(14) bond

12) L. E. Sutton, "Tables of Interatomic Distances and Configurations in Molecules and Ions. Supplement." Special publication No. 18, The Chemical Society, London (1965).

13) M. Dabler and J. D. Dunitz, *Helv. Chim. Acta*, **48**, 1429 (1965).

TABLE 7. LEAST-SQUARES PLANES

The equations of the planes are expressed in the form $Ax+By+Cz+D=0$.

Plane	A	B	C	D
1	0.0918	0.3616	−0.9278	2.365
2	0.5053	0.1950	−0.8406	2.016
3	0.0890	0.3866	−0.9180	2.327
4	0.0892	0.3157	−0.9447	2.616
5	0.1821	0.6712	−0.7186	1.203
6	−0.0046	0.0143	−0.9999	4.076
7	0.7355	0.0604	−0.6749	1.500
8	−0.6022	0.4724	−0.6437	4.009
9	−0.2699	−0.8913	−0.3644	3.871
10	0.5093	0.1929	−0.8387	2.012

Deviations of atoms from the planes in Å

1		2		3		4	
*C- 4	−0.014	*C- 1	0.002	*C- 6	0.004	*C- 4	−0.001
*C- 6	−0.023	*C- 2	−0.008	*C- 7	−0.008	*C-11	0.001
*C- 7	0.002	*C- 3	0.009	*C- 8	0.008	*C-12	−0.003
*C- 8	0.032	*C- 4	−0.005	*C- 9	−0.004	*C-13	0.002
*C- 9	−0.000	*C- 6	0.002	C- 4	0.075	C- 5	−0.438
*C-11	−0.043	C- 5	−0.245	C- 5	−0.461	C- 6	0.107
*C-12	0.013	C- 7	0.392	C-10	−0.477	C- 7	0.194
*C-13	0.035	C-13	0.403	C-11	0.016	C- 8	0.239
C- 5	−0.514	C-14	−0.670	C-12	0.107	C- 9	0.163
C-10	−0.508	O- 1	0.075	C-13	0.143	C-10	−0.408
C-14	−1.522			C-14	−1.479	C-14	−1.433
5		7		8		10	
*C- 5	0.002	*C- 4	0.009	*C- 9	0.019	*C- 1	−0.004
*C- 6	−0.002	*C- 5	−0.026	*C-10	−0.048	*C- 3	0.004
*C- 9	0.002	*C- 6	0.011	*C-11	0.016	*C- 4	−0.004
*C-10	−0.002	*C-14	0.008	*C-14	0.014	*C- 6	0.004
		C- 1	−0.452	C- 8	0.595	C- 2	−0.017
		C- 3	−0.428	C-12	0.632	C- 5	−0.240
6		C- 7	0.602			C- 7	0.397
*C- 4	0.008	C-13	0.627	9		C-13	0.408
*C- 5	−0.011			*C- 5	0.000	C-14	−0.658
*C-10	0.011			*C-10	0.000	O- 1	0.067
*C-11	−0.008			*C-14	−0.000		

(* Asterisks indicate atoms included in the plane calculations.)

Dihedral angles between the planes

1 ∧ 2	26.3°	3 ∧ 4	175.7°	5 ∧ 6	136.7°	7 ∧ 8	91.2°
3 ∧ 5	20.7°	4 ∧ 6	18.4°	5 ∧ 9	67.3°	6 ∧ 9	69.3°

length (1.509 Å) is in good agreement with the typical value for the C(sp^3)–C(sp^2) bond (1.505±0.005 Å),[12] while the C(5)–C(14) length (1.477 Å) is significantly shorter. The C(4)–C(5)–C(6) angle is smaller than C(9)–C(10)–C(11). This is consistent with the C–C-length difference in the bridge. These changes may reasonably be interpreted as a result of the strain by the ring (C). The same explanation may also apply to the significant decrease in the internal angles at C(7) and C(13) in comparison with those in IV.[13]

The C(5)–C(14)–C(10) angle (94.8°) is significantly smaller than the corresponding angles in 1,6-methanocyclodecapentaene-2-carboxylic acid (IV) (99.6°)[13] and 11,11-difluoro-1,6-methano-[10]annulene (101°),[14] and is larger than that in tricarbonyl-1,6-methanocyclodecapentaenechromium (92.4°).[15]

The spatial approaches of the bridged methylene protons to the [10]annulene nucleus are shown in Fig. 4.

The C(1)–O(1) bond distance (1.236 Å) is significantly longer than the C=O double-bond lengths in quinones (1.222 Å in *p*-benzoquinone,[16] 1.223 Å in 2,5-dimethyl-*p*-benzoquinone,[17] 1.224 Å in 2,2-di(1,4-naphthoquinone)[18]) and in tropones (1.228 Å in 4,5-benzotropone,[19] 1.227 Å in 2,7-dimethyl-4,5-benzotropone,[20] 1.225 Å in 5,7-dibromo-2,3-benzotropone,[21] 1.227 Å in 5-chloro-2,3-benzotropone[21]). The elonga-

14) C. M. Gramaccioli and M. Simonetta, *Acta Crystallogr.*, **B27**, 2231 (1971).

15) P. E. Baikie and O. S. Mills, *J. Chem. Soc., A*, **1969**, 328.

16) J. Trotter, *Acta Crystallogr.*, **13**, 86 (1960).

17) F. L. Hirshfeld and D. Rabinovich, *ibid.*, **23**, 989 (1967).

18) H. L. Ammon, M. Sundaralingam, and J. M. Stewart, *ibid.*, **B25**, 336 (1969).

19) K. Ibata, H. Shimanouchi, and Y. Sasada, to be published.

20) K. Ibata, H. Shimanouchi, and Y. Sasada, *Chemistry Lett.*, **1973**, 269.

21) K. Ibata, T. Hata, H. Shimanouchi, and Y. Sasada, *Chem. Commun.*, **1972**, 339.

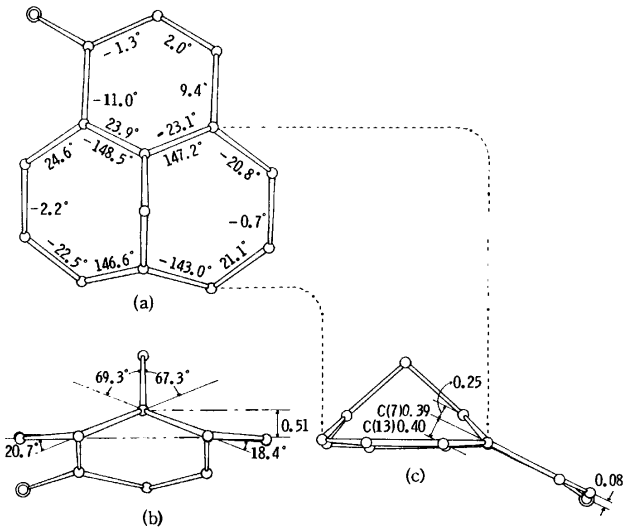

Fig. 3. (a) The molecule viewed along the normal to the mean plane 1 in Table 7. The torsion angles of the bonds are shown. (b) The molecule viewed along C(10)–C(5). 0.51Å is a deviation of C(5) and C(10) from the mean plane 1 in Table 7. (c) The molecule viewed along the normal to the plane 9 in Table 7. 0.25 Å, 0.08 Å, 0.39 Å, and 0.40 Å are the deviations of C(5), O(1), C(7), and C(13), respectively from the plane 2 in Table 7.

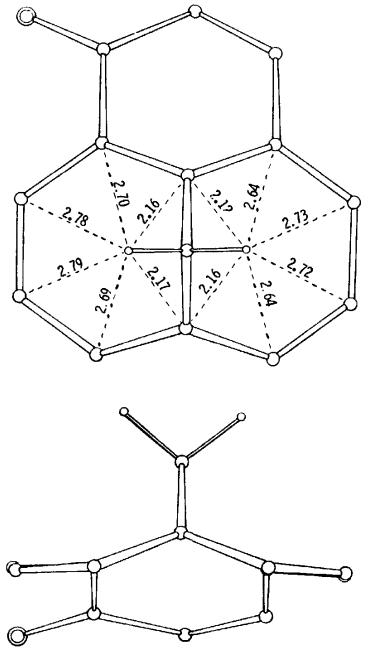

Fig. 4. The spatial approaches (Å) of the bridged methylene protons to the [10]annulene nucleus.

tion of the C=O bond is consistent with the low carbonyl stretching frequency (1605 cm^{-1}).[5] This observation suggests the highly polarized nature of the C=O bond in the present compound, which explains the large dipole moment (4.36 D)[5] and the high basicity (pK_b= −2.6).[5]

The C(1)–C(6) bond (1.491 Å) is slightly longer than the typical C(sp^2)–C(sp^2) single bond,[22] suggesting that its double-bond nature is negligibly small. On the other hand, the C(1)–C(2) and C(3)–C(4) bond lengths are almost equal to one another and are significantly shorter than C(1)–C(6). This may indicate the resonance interaction of the carbonyl group with the [10]annulene nucleus through C(1)–C(2)–C(3)–C(4), not through the C(1)–C(6) bond. This interaction may perturb the π-electron system of the [10]annulene nucleus so as to result in the longer C(12)–C(13) and shorter C(11)–C(12) bonds. It is interesting that the effect of the carbonyl group emerges in the most distant portion of the molecule. This explains well the large dipole moment of the present molecule.

The C(2)–C(3) length (1.331 Å) seems not to favor the above hypothesis, since it is as short as the C=C distance in ethylene.[23] Cruickshank suggests, however, that the ethylene distance might not be used as the standard value for double bonds in a different environment.[24] A possible explanation for the shortening is that the polarization of the C=O group may lead to an increase in the p character in the C(1)–C(2) bond and to a concomitant increase in the s component in the C(2)–C(3), which reduces the length.[25] This reasoning is supported by the values of the C(6)–C(1)–C(2) angle (115.9°) and C(1)–C(2)–C(3) (123.5°). It should be added that, although a contraction of the internal angles at the carbonyl carbons has been observed, the present angle is the smallest among the various quinones.[16–18]

In the six-membered ring (C), five atoms, C(1), C(2), C(3), C(4), and C(6), are coplanar within the limits of error (Plane 2 in Table 7), while only the C(5) atom deviates (by 0.25 Å) (Fig. 3(c)). The mutual displacements of C(5) and C(7) from Plane 2 result in the twist of the C(1)–C(6) bond. If this bond were of double-bond character, it should cause a displacement of C(2) from the reference plane to form a slight boat conformation, as has been reported for the case of the benzene ring in 8,16-oxido-*cis*[2,2]metacyclophane-1,9-diene (V).[26] This is not the case; the C(2)

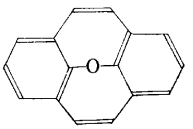

(V)

atom does not deviate significantly; this is consistent with the view of the bond nature of C(1)–C(6) presented above.

The three-dimensional feature of the molecule is shown in Fig. 3. The dihedral angle between Plane 7 and Plane 8 is 91.2°, and the non-bonded distance between C(5) and C(10) is 2.199 Å. The overlap integral, *S*, between the 2p-orbitals of C(5) and C(10) is estimated using the tables by Mulliken, Rieke,

22) M. J. S. Dewar and H. N. Schmeising. *Tetrahedron*, **11**, 96 (1960).

23) L. S. Bartell and R. A. Bonham, *J. Chem. Phys.*, **31**, 400 (1959).

24) D. W. J. Cruickshank, *Tetrahedron*, **17**, 155 (1962).

25) H. L. Ammon, M. R. Smith, and E. Kelso, *Acta Crystallogr.*, **B28**, 246 (1972).

26) A. W. Hanson and K. Huml, *ibid.*, **B25**, 2310 (1969).

Orloff, and Orloff,[27] where the 2p-orbitals are assumed to be normal to the above planes. The calculated value of 0.142 for $S_{5,10}$ is twice as large as the $S_{1,6}$ of 0.072 reported for the cycloheptatriene ring of thujic acid.[28] In connection with this, the conformation of the seven-membered ring(A) has been examined. As may be seen in Fig. 3(b), the ring is in a boat conformation, with angles of 67.3 and 20.7° between Plane 5 and Plane 9, and between Plane 5 and Plane 3, respectively. These values lie between the corresponding values in the norcaradiene structure (VI) (71.9 and

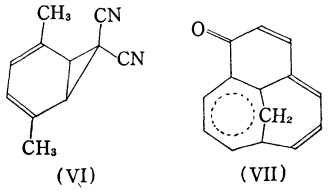

(VI) (VII)

4.2°)[29] and those in the cycloheptatriene structure in thujic acid (47.9 and 24.4°).[28] This suggests some contribution from the (VII) structure to the ground-state structure of the molecule.

Crystal Structure. The packing diagram of the crystal viewed along the *c* axis is shown in Fig. 5. The shortest C···C, O···H, and H···H contacts are 3.468, 2.47, and 2.32 Å respectively. The packing appears to be fairly efficient, but there are no abnormally short intermolecular contacts. Therefore, the distortions of the molecule, which do exist, may be ascribed to intramolecular rather than to intermolecular effects. The molecules are so arranged that the large dipole moments cancel each other out by means of the center of symmetry.

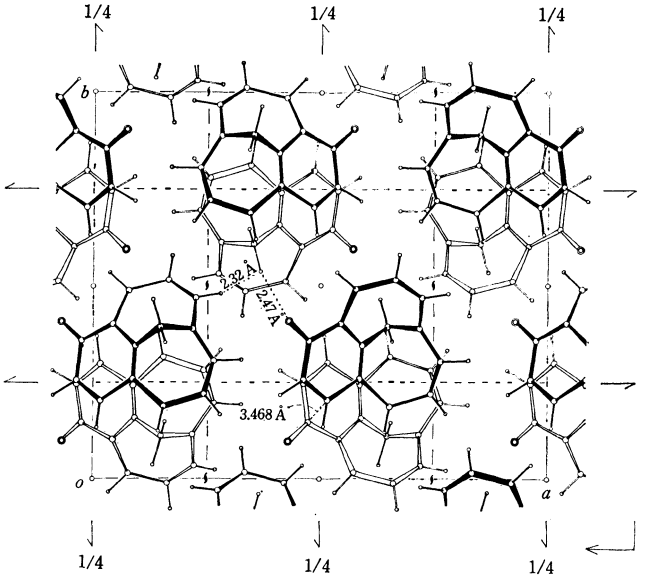

Fig. 5. The crystal structure projected along the *c* axis with some short intermolecular contacts (Å).

The authors are grateful to Professor Ichiro Murata of Osaka University for supplying the sample and to Dr. Kenzo Hirayama of Research Laboratories, Fuji Photo Film Co. for advice on the nomenclature of the compound.

27) R. S. Mulliken, C. A. Rieke, D. Orloff, and H. Orloff, *J. Chem. Phys.*, **17**, 1248 (1949).
28) R. E. Davis and A. Tulinsky, *J. Amer. Chem. Soc.*, **88**, 4583 (1966).
29) C. J. Fritchie, Jr., *Acta Crystallogr.*, **20**, 27 (1960).

BULLETIN OF THE CHEMICAL SOCIETY OF JAPAN, VOL. 46, 1450—1454 (1973)

Studies on the Fragment Ion Distribution and Their Reactions by the Use of a Charge Spectrometer. II. The Charge Exchange Reactions in Methanol with Fast Positive Ions

Toshio NAGATANI, Kenji YOSHIHARA, and Takanobu SHIOKAWA

Department of Chemistry, Faculty of Science, Tohoku University, Aoba, Aramaki, Sendai

(Received August 28, 1972)

Distribution of fragment ions after bombardment of a methanol molecule with various positive ions has been studied by the use of a double mass spectrometer. It was found that the internal energy distribution function has fine structures. The appearance potentials of the fragment ions were re-estimated. From the results the mass spectra of methanol by electron impact were interpreted fairly accurately. The successive ion-molecule reactions after the charge exchange were studied by increasing pressure in the reaction chamber. The behaviors of the metastable ions were also investigated.

Friedman *et al.*[1] studied electron impact of methanol with a mass spectrometer, and observed unimolecular decomposition of the molecular ions of the excited states. They tried to interpret their results by the theory of the rate processes.[2] Their results showed a discrepancy from the theoretical values, which seems to result from the inaccuracy of the internal energy distribution function they used.

1) L. Friedman, F. A. Long, and M. Wolfsberg, *J. Chem. Phys.*, **27**, 613 (1957).

2) H. M. Rosenstock, M. B. Wahlenstein, A. L. Wahrhaftig, and H. Eyring, *Proc. Nat. Acad. Sci. U. S.*, **38**, 667 (1952).

Wilmenius and Lindholm[3] also studied dissociation of methanol by impact of slow positive ions and tried to interpret the results by means of an internal energy distribution function. Their results showed no essential change from those of Friedman *et al.* in which a flat distribution 10.9(ionization potential)—18.1 eV was assumed. It is not appropriate to assume such a simple distribution if a more precise consideration is adopted.

The authors studied the break down curve and the internal energy distribution function of methanol by impact of fast positive ions by means of a double mass spectrometer. This study is an extention of the previous work on methylamine[4,5] which is of an isoelectric structure with methanol. A more accurate interpretation of mass spectra by electron impact has been made by improvement of the internal energy distribution function.

Successive ion-molecule reactions in the reaction chamber have been studied by increasing pressure of the neutral molecules. The behaviors of metastable ions were traced.

Experimental

Details of the apparatus[6a] have been described.[6b] Methanol of a reagent grade was purified by repeated distillation. The gases used for the positive ion sources were almost the same as in the previous work.[6b]

The mass spectra of methanol after charge exchange with fast positive ions (1850 eV) are shown in Table 1. The recombination energies are not always considered to be the same as those for the experiment of methylamine. Evaluation of the recombination energy is as follows.

(1) He^+. 24.58 eV.

(2) Ne^+. 21.56 and 21.66 eV.

(3) Cl^+. This ion is of *m/e* ratio 35, produced by electron bombardment of CCl_3F. As the contribution from $3p^4\ ^1S$ and $3d\ ^5D$ is very small, ions with *m/e* ratios (32) and (31) are produced predominantly. The ion with the ratio (15) is obtained through the contribution of $3p^4\ ^1D$ by 5.4%.

(4) Ar^+. 15.76 and 15.94 eV.
The minor peak which is present near peak (27) comes from the metastable transition $CH_2OH^+ \rightarrow CHO^+$. This is not a collision induced dissociation reaction but a unimolecular decomposition.

(5) Kr^+. 14.00 and 14.67 eV.
Contribution from the high energy levels is negligibly small.

(6) Xe^+. Mainly 12.13 and 13.44 eV.
About 5% contibution is derived from the higher energy levels.

(7) Ne^{2+}. Besides the recombination energies of 10.5—12.0 eV, recombination of $2s^22p^4 \rightarrow 2s2p^5$ can contribute to the charge exchange. The latter is about 10% in methylamine,[4] while it is as large as about 30% in methanol. The absolute value of this energy is higher than 25 eV which is the upper limit of the energy we considered, since the relation (13)>(14)>(15) holds among the abundances of the ions (Table 1, Fig. 1). Contribution of this recombination energy in the higher region will give a small error in estimation of the cross section of charge exchange.

(8) Ar^{2+}. A mass peak (32) of 5.6% is given by the process $3s^23p^4\ ^3P$ or ^1D to $3s3p^6$ which has a recombination energy of 11.5—12.5 or 13—14 eV. Peak (31) is produced by 8.0% due to the same process. Contribution from the

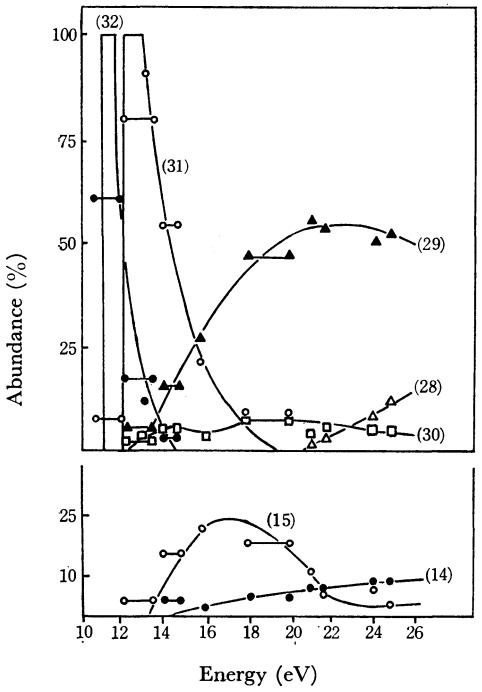

Fig. 1. Breakdown curve of methanol.

Table 1. Mass spectra after charge exchange of methanol with various positive ions (in %)

Primary Ion	*m/e* (12)	(13)	(14)	(15)	(16)	(17)	(27)	(28)	(29)	(30)	(31)	(32)
He^+	4.1	6.6	9.4	2.7	1.4	2.7		10.0	53.3	3.8	4.7	1.0
Ne^+	3.6	6.3	9.7	4.4	1.2	3.3		6.3	56.4	4.5	3.0	0.6
Cl^+	0.1	0.6	1.6	5.4		0.4		0.7	9.4	3.8	64.6	12.7
Ar^+	0.6	1.6	4.2	29.2	0.6	1.0	0.4	1.3	35.0	2.7	24.8	1.9
Kr^+	0.2	0.8	3.1	15.7	0.1	0.6		0.6	15.9	4.9	54.4	3.7
Xe^+	0.1	0.6	2.0	2.4		0.2		0.2	7.7	3.8	66.3	16.3
Ne^{2+}	6.3	7.4	3.6	1.4	3.7	3.4		8.0	10.7	1.1	6.5	47.9
Ar^{2+}	2.1	4.1	8.5	6.1	0.9	3.2		7.6	49.7	3.6	8.0	5.6
Kr^{2+}	1.9	4.2	9.8	9.9	0.7	4.9		5.5	53.6	5.1	3.7	0.7
Xe^{2+}	0.4	1.3	5.3	17.9	0.2	0.9		1.7	55.9	6.8	8.8	0.6

3) P. Wilmenius and E. Lindholm, *Arkiv Fysik*, **21**, 97 (1962).
4) T. Nagatani, K. Yoshihara, and T. Shiokawa, This Bulletin, **46**, 1306 (1973).
5) T. Nagatani, K. Yoshihara, and T. Shiokawa, to be published.
6) a) This can be used also for the study of the ion-molecule reaction as a tandem mass spectrometer. b) T. Shiokawa, K. Yoshihara, M. Yagi, T. Omori, H. Kaji, M. Hiraga, T. Nagatani, and Y. Takita, *Mass Spectrosc.*, **18**, 1230 (1970).

process $3s^23p^4 \rightarrow 3s^23p^4$ nx can be neglected. When the breakdown curve is drawn, the fragment ions such as (29), (28), and (14) produced by the charge exchange of recombination energy 24.0 eV should be corrected by about 15%.

(9) Kr^{2+}. 21.0 eV.

(10) Xe^{2+}. 18—20 eV.

Breakdown Curve and Energy Distribution Function. The breakdown curve determined from the fragment distribution (Table 1) and the recombination energies of the ions is shown in Fig. 1. The internal energy distribution function of methanol obtained from the measured values of the cross section for the charge exchange reactions is shown in Fig. 2.

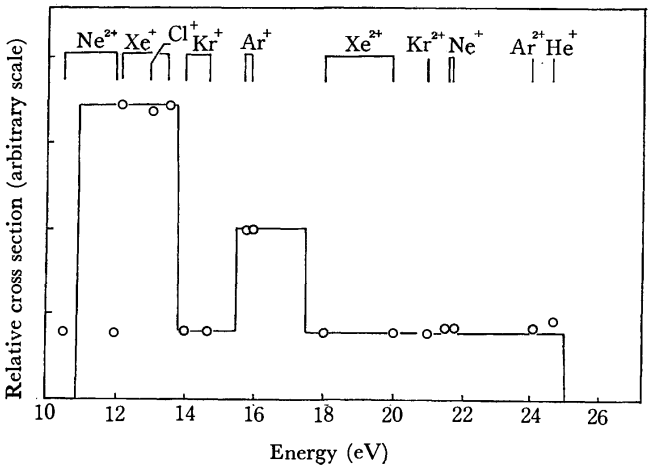

Fig. 2. Internal energy distribution function of methanol.

The behaviors of the seven dominant fragment ions (Fig. 1) are in line with the results of Wilmenius and Lindholm[3] but the appearance potentials are not always the same as those of Friedman *et al.* Potentials will be considered as follows.

(32) CH_3OH^+: 10.9 eV.

(31) CH_2OH^+: 12.0 eV.

These values are slightly lower than those of Friedman *et al.*,[1] but in good accrodance with those of Wilmenius and Lindholm.[3]

(30) $CHOH^+$: Formation of this ion starts from 12.3 eV, and it increases and then decreases, showing the second increase at about 16 eV. This indicates that there are two processes in the formation of the ion of *m/e* (30). The precursor ions corresponding to these processes are the ion of *m/e* (32) and (31).

(29) CHO^+: 13.1 eV.

Wilmenius and Lindholm[3] adopted the value of 14.2 eV. However, we have good evidence that the energy is lying at 13.1 eV from the experiment using the source volume as a cascade type double mass spectrometer.[7]

(28) CO^+. It was difficult to decide the appearance potential accurately. As shown in Table 1, a small quantity of the ion with *m/e* already appeared in the lower energy region (this might be due to contamination of N_2^+), but it is obvious that the value of the appearance potential is beyond 20.0 eV (Fig. 1). In this work we adopted 20.0 eV. The value supports the view that the formation of species (28) is due to the dissociation (32)→(28)+4H.[1]

(15) CH_3^+: 13.3 eV.

This is slightly lower than the value 14.0 eV previously reported.[1,2,8] In the experiment using a charge spectrometer as a cascade-type double mass spectrometer[7] it was determined to be 13.3 eV. This value is best responsible to the trend of the break down curve in the present study.

(14) CH_2^+: 14.2 eV.

The internal energy distribution function has a valley as in the case of methylamine[4] in the range 14.0—15.5 eV (Fig. 2). The ionization potential of (y) electron localized in CO has been reported to be 13.1 eV[3] or 14.64 eV.[9] Thus, the valley shows the presence of interaction which suppresses the formation of CH_3^+ and/or OH^+ by breaking of the C–O bond after the ionization of the (y) electrons. Up to now, the energy distribution function of methanol was assumed to be rectangular while that for methylamine[4,10] and for acetylene[11] were reported to possess valleys. The fact that a valley can be seen also in methanol suggests the presence of the interaction between the CH_3 and OH groups, although it is weaker than in the case of methylamine and acetylene.

Discussion

Comparison of the Present Data with Those of Mass Spectra by Electron Impact. The integrated value taken from the breakdown curve is expected to agree with the mass spectra by electron impact regardless of the contribution of high energy excitation of the molecules. Usually mass spectra obtained by electron bombardment is considered to satisfy these conditions, because the bombarding electrons used for ionization have kinetic energy less than 100 eV. The mass spectra are shown in Table 2. Results for ions of energy higher than 20 eV tend to disagree (Table 2, see (28)). This is because the contribution of ions with energies beyond 25 eV has been neglected in the energy distribution curve (Fig. 2). Except for this the agreement is quite satisfactory.

Reactions of Excited Ions. As in the case of methylamine the reactions of excited ions produced by charge exchange were investigated as a function of increasing gas pressure. The results for Cl^+ as a source material of the charge exchange are shown in Fig. 3. The experiments using He^+, Ne^+, Ar^+, Kr^+, Xe^+, Ne^{2+},

Table 2. Comparison of mass spectra by electron impact with those calculated from the results of charge exchange (in %)

m/e	Electron impact		Calculated from charge exchange
	Friedman[1]	Cummings[12]	
14	1.5	2.1	2.9
15	8.5	12.4	10.5
28	5.5	2.1	1.2
29	19.5	26.2	27.3
30	2.6	3.1	4.2
31	37.2	34.5	33.6
32	25.2	19.7	20.6

7) T. Nagatani, K. Yoshihara, and T. Shiokawa, *Mass Spectrosc.*, **20**, 97 (1972).

8) F. P. Lossing, K. U. Ingold, and I. H. S. Henderson, *J. Chem. Phys.*, **22**, 1489 (1954).

9) H. Sjögren, *Arkiv Fysik*, **33**, 597 (1966).

10) H. Sjögren, *ibid.*, **29**, 565 (1965).

11) E. Lindholm, I. Szabo, and P. Wilmenius, *ibid.*, **25**, 417 (1963).

12) C. S. Cummings and W. Bleakney, *Phys. Rev.*, **58**, 787 (1940).

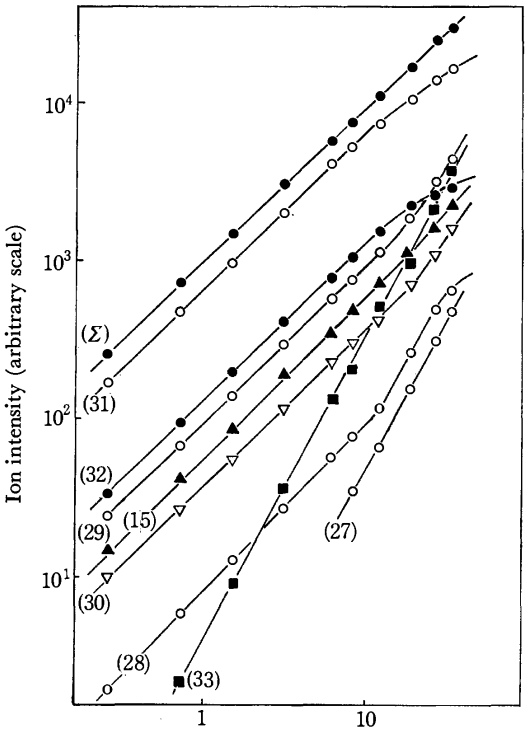

Fig. 3. Pressure dependence of the fragment ion intensity in methanol bombarded by Cl^+.

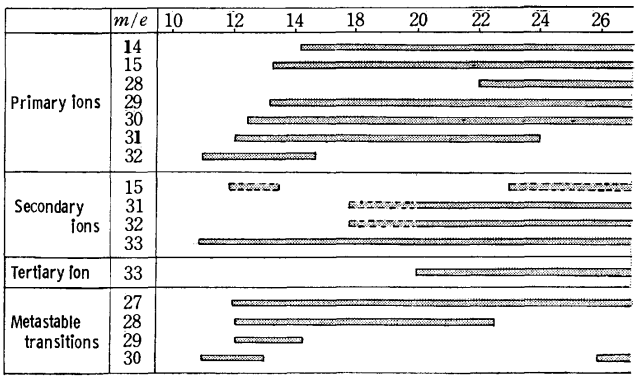

Fig. 4. Occurrence of various ions and its relation to the energy range.

Ar^{2+}, Kr^{2+}, and Xe^{2+} have also been carried out in the same way.[13] From the results we can analyze the relation between the appearance of ions and their energy range as shown in Fig. 4. Some interesting aspects in four energy regions are discussed.

(i) 10.9—12.0 eV: The parent ion is predominantly produced for the primary process. A secondary ion (33) is produced by proton transfer or hydrogen atom transfer between the parent ion and the methanol molecule. Metastable transition can be explained by elimination of a hydrogen atom from the parent ion (32) at the moment of collision with the methanol molecules.

13) T. Nagatani, Thesis Tohoku Univ., (1970).

(ii) 12.0—15.0 eV: (31) is the principal fragment ion for the primary process although (32) contributes to some extent. Its regeneration can be observed as a secondary process for methylamine. In the case of methanol, however, such a process cannot be observed. It was revealed[7] that the charge transfer cross section for methanol is very small in this region compared to the total ionization cross section. This supports the view that there is no secondary process producing (31) except for the formation of (33).

Metastable transition is caused by elimination of a hydrogen atom or molecule from (31) or (30). A possibility of the presence of the isomers $CH_2{=}O^+H$ and $C^+H_2{-}OH$ could be detected in this case.

(iii) 15.0—18.0 eV: Main primary ions are (31), (29), and (15). (33) is again produced in this region as a secondary product, but the mechanism of its formation is not clear.

(iv) 18.0—25.0 eV: (29) is predominant, various secondary and tertiary ions being also observed. Proton transfer, charge transfer and hydride ion transfer between (29) and methanol produce the ions (33), (32), and (31), respectively.

With regard to metastable transition, the metastable peak (27) is observed according to the process

$$(29) + CH_3OH \longrightarrow (28) + H + CH_3OH$$

This causes an apprarent peak at (27). We also see the presence of the metastable peak (30) above 24 eV. This species may be produced by the dissociation of the ion (32) through its regeneration reaction on collision between ions (29) or (28) and methanol molecules. It was revealed that (32) easily dissociated above 24 eV.[7]

Table 3. Ion-molecule reactions in methanol

Energy	Process	Mass peak
10.9—12.0 eV	H^+ transfer:	
	$CH_3OH^+ + CH_3OH \longrightarrow CH_3OH_2^+$	(33)
	H transfer:	
	$CH_3OH^+ + CH_3OH \longrightarrow CH_3OH_2^+$	(33)
	Metastable transition:	
	$CH_3OH^+ \xrightarrow{-H} CH_2OH^+$	(30)
12.1—15.0 eV	H^+ transfer:	
	$CH_2OH^+ + CH_3OH \longrightarrow CH_3OH_2^+$	(33)
	Metastable transition:	
	$CH_2OH^+ \xrightarrow{-H} CHOH^+$	(29)
	$CH_2OH \xrightarrow{-2H} CHO^+$	(27)
	$CHOH \xrightarrow{-H} CHO^+$	(28)
18.0—25.0 eV	H^+ transfer:	
	$CHO^+ + CH_3OH \longrightarrow CH_3OH_2^+$	(33)
	Electron transfer:	
	$CHO^+ + CH_3OH \longrightarrow CH_3OH^+$	(32)
	H^- transfer:	
	$CHO^+ + CH_3OH \longrightarrow CH_2OH^+$	(31)
	Metastable transition:	
	$CHO^+ \xrightarrow{-H} CO^+$	(27)

The C–O bond rupture leads to the formation of ions (15) *etc.* There is only a weak interaction between the CH_3 group and the OH group, which makes breaking of the bond easy.

The ion-molecule reactions in methanol are summarized in Table 3.

Kotoyori *et al.*[14] studied the reactions of methanol with accelerated rare gas ions and discussed the formation of the final chemical species. They concluded that charge exchange reactions are not important in determination of the final chemical products.

The authors thank Mr. M. Hiraga for his kind cooperation throughout this work.

14) T. Kotoyori, M. Takahashi, and A. Ichinose, This Bulletin, **44**, 2893 (1971).

BULLETIN OF THE CHEMICAL SOCIETY OF JAPAN, VOL. 46, 1454—1456 (1973)

Derivatographic Studies on Transition Metal Complexes. X.[1] Thermal Octahedral-to-Square Planar Transformation of Ni(*NN*-deen)$_2$X$_2$·*n*H$_2$O in Solid Phase[2]

Ryokichi TSUCHIYA, Seiji JOBA, Akira UEHARA, and Eishin KYUNO
Department of Chemistry, Faculty of Science, Kanazawa University, Kanazawa

(Received June 22, 1972)

Thermal reactions of the complexes [Ni(H$_2$O)$_2$(*NN*-deen)$_2$]X$_2$·*n*H$_2$O (*NN*-deen is *N,N*-diethylethylenediamine and X is Cl or Br) were investigated. It was found by derivatography and spectral and magnetic measurements that the bromide undergoes transformation from octahedral to square planar structure by "deaquation" upon heating, whereas the chloride turned to the dichloro complex by thermal "deaquation-anation" losing the coordinated water and drawing chloride ion into the coordination sphere with retention of octahedral structure around the central metal. No such transformation could be found in the corresponding iodide and nitrate, since only diamagnetic complexes, [Ni(*NN*-deen)$_2$]X$_2$ (X is I or NO$_3$), and no paramagentic complexes were obtained.

When a nickel(II) atom is surrounded by the same six ligands forming a regular octahedral configuration, it forms a blue type complex with magnetic moment 3.1—3.2 B.M. due to two unpaired electrons in 3d orbital with a small orbital contribution.[3] The red, brown and yellow nickel(II) complexes show a diamagnetic behavior due to the lower energy of the triplet ground state relative to the singlet state,[4,5] taking a planar structure in a strong field with coordination number 4. Some green and blue nickel(II) complexes are known,[3] which take a tetrahedral structure with coordination number 4 having two unpaired 3d electrons.

Since the three types of nickel(II) complexes give characteristic electronic spectra as regards symmetry,[6,7] the structure of the complexes and their thermal reaction products can be assigned by observing the spectra and other physical properties.

It is of interest to investigate the structural transformation of nickel(II) complexes upon heating. Structural transformations after complete dehydration of nickel(II) complexes containing *C,C'*-substituted ethylenediamine are known.[8,9] Nickel(II) complexes containing ethylenediamine itself[3] or its *N*-alkyl-substituted products[6] as diamine such as Ni(diamine)$_2$X$_2$·*n*H$_2$O or Ni(diamine)$_2$X$_2$, are known. However, no detailed studies on the structural change upon heating have been made.

Studies on the thermal structural transformation of some metal complexes have been carried out recently by means of derivatography.[1,10-12] The present work was undertaken to find whether or not the nickel(II) complexes with *N,N*-diethylethylenediamine undergo structural transformation from octahedral to square planar in the solid phase depending upon the kind of counter anions.

Experimental

Preparation of Complexes. *N,N*-Diethylethylenediamine was of commercial reagent grade and used without purification. Complexes Ni(*NN*-deen)$_2$Cl$_2$·2H$_2$O, Ni(*NN*-deen)$_2$Br$_2$·3H$_2$O, Ni(*NN*-deen)$_2$I$_2$ and Ni(*NN*-deen)$_2$(NO$_3$)$_2$ were prepared by the known method,[6] their chemical formulas being identified by elemental analysis and spectral measurement.

1) Part IX in this series; See R. Tsuchiya, S. Nakagawa, A. Uehara, and E. Kyuno, This Bulletin, **46**, 169 (1973).
2) Presented at the 24th Annual Meeting of the Chemical Society of Japan, Osaka, April, 1971.
3) R. S. Nyholm, *Chem. Rev.*, **53**, 263 (1953).
4) G. Maki, *J. Chem. Phys.*, **28**, 651 (1958); **29**, 162, 1129 (1958).
5) C. J. Ballhausen and A. D. Liehr, *J. Amer. Chem. Soc.*, **81**, 538 (1959).
6) D.M.L. Goodgame and L.M. Venanzi, *J. Chem. Soc.*, **1963**, 616, 5909.
7) C. Furlani and G. Sartori, *J. Inorg. Nucl. Chem.*, **8**, 126 (1958).
8) I. Lifschitz, J. G. Bos, and K. M. Dijkema, *Z. Anorg. Allg. Chem.*, **242**, 97 (1939).
9) I. Lifschitz and J. G. Bos, *Rec. Trav. Chim.*, **59**, 407 (1940).
10) R. Tsuchiya, K. Murai, A. Uehara, and E. Kyuno, This Bulletin, **43**, 1383 (1970).
11) R. Tsuchiya, Y. Nakata, and E. Kyuno, *ibid.*, **44**, 705 (1971).
12) R. Tsuchiya, M. Suzuki, and E. Kyuno, *ibid.*, **44**, 709 (1971).

Derivatographic Measurements. The derivatograms were obtained with a MOM Derivatograph Typ-OD-102.[13] 0.5 g of finely powdered sample (100—200 mesh inch^{-1}) was used in each run. Measurements were carried out under a constant flow of nitrogen stream with a heating rate of 1 °C min^{-1} unless otherwise stated.

Spectral Measurements. Visible and UV spectra in the solid state were measured by the diffuse reflectance method with a Hitachi EPU-2A spectrophotometer equipped with a standard Hitachi reflection attachment. IR spectra were obtained with JASCO-IR-E and IR-F infrared spectrophotometers.

Magnetic Measurements. The effective magnetic moments were evaluated from the magnetic susceptibilities measured by the Gouy method at room temperature. Hg[Co(NCS)$_4$] was used as reference material. Susceptibilities of the complexes were corrected by applying Pascal's constants of the elements involved.

Results and Discussion

Derivatography. The derivatograms of Ni(*NN*-deen)$_2$Cl$_2$·2H$_2$O and Ni(*NN*-deen)$_2$Br$_2$·3H$_2$O are shown in Fig. 1. The former shows a loss of two moles of water upon heating at 80—110 °C in the TG curve, an endothermic peak appearing in the DTA curve. It seems that the anhydrous complex Ni(*NN*-deen)$_2$Cl$_2$ is produced.

The bromide complex loses one mole of water at 30—65 °C and two moles at 70—110 °C, giving two endothermic peaks in the corresponding dehydration temperature ranges in the DTA. The anhydrous complex Ni(*NN*-deen)$_2$Br$_2$ seems to be formed.

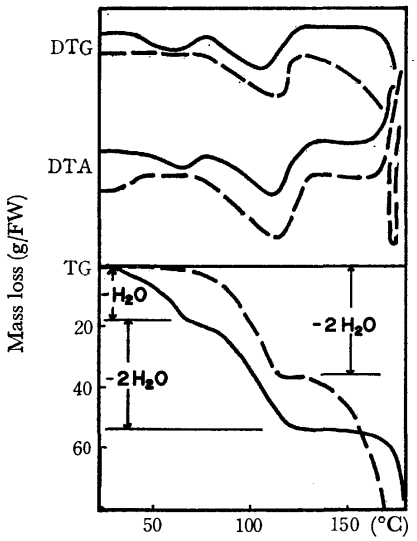

Fig. 1. Derivatograms of Ni(*NN*-deen)$_2$Cl$_2$·2H$_2$O(----) and Ni(*NN*-deen)$_2$Br$_2$·3H$_2$O (——).

Absorption Spectra. The visible absorption spectra of the complexes Ni(*NN*-deen)$_2$X$_2$·nH$_2$O measured in solid state by the diffuse reflectance method are shown in Fig. 2, together with those of the anhydrous complexes Ni(*NN*-deen)$_2$X$_2$ (X is Cl or Br), obtained by heating the corresponding hydrated complexes at 110 °C.

13) F. Paulik, J. Paulik, and L. Erdey, *Talanta*, **13**, 1405 (1966).

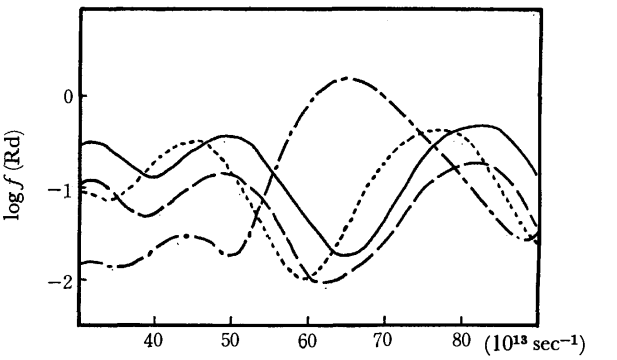

Fig. 2. Electronic spectra of Ni(*NN*-deen)$_2$Cl$_2$·2H$_2$O (——), Ni(*NN*-deen)$_2$Br$_2$·3H$_2$O (——) and those after heating them at 110 °C (----) and at 110 °C (————).

We see from Fig. 2 that the hydrated complexes Ni(*NN*-deen)$_2$X$_2$·nH$_2$O both give three absorption bands at 30, 49, and 80×10^{13} sec^{-1}, which can be assigned to the electron transitions taking place in the Oh symmetry complexes of d^8 metal,[6,7] $^3A_{2g}\rightarrow{}^3T_{2g}$, $^3A_{2g}\rightarrow{}^3T_{1g}$ (F) and $^3A_{2g}\rightarrow{}^3T_{1g}$ (P), respectively, irrespective of the kind of counter ions such as Cl$^-$ or Br$^-$.

The absorption spectra of the anhydrous complexes Ni(*NN*-deen)$_2$X$_2$, where X is I or NO$_3$, are given in Fig. 3. They show that the anhydrous complexes Ni(*NN*-deen)$_2$X$_2$ both give a relatively strong absorption band at 64—65$\times10^{13}$ sec^{-1}, characteristic of the square planar structure in nickel(II) complexes and probably assignable to the transition $^1A_{1g}\rightarrow{}^1A_{2g}$.

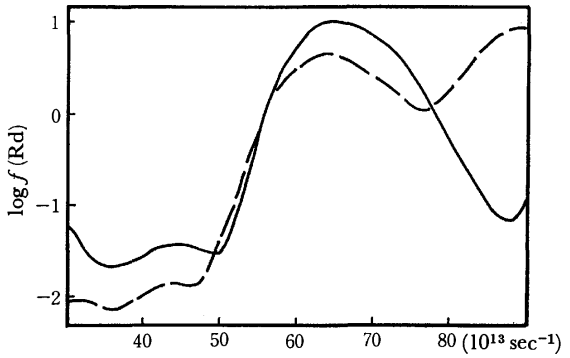

Fig. 3. Electronic spectra of Ni(*NN*-deen)$_2$I$_2$ (——) and Ni(*NN*-deen)$_2$(NO$_3$)$_2$ (——).

We see that the spectrum of the anhydrous chloride obtained upon heating is analogous to that of the mother hydrated chloride except for a slight shift of maximum peak to the longer wavelength region (Fig. 2), whereas the spectrum of the anhydrous bromide is analogous to that of the anhydrous iodide and nitrate (Fig. 3). The results suggest that the hydrated chloride turns to the dichloro complex through deaquation-anation upon heating with retention of the octahedral coordination, while the bromide is converted into the square planar coordination as the result of dehydration alone. Thus, the hydrated chloride and bromide are both diaquo octahedral complexes and their thermal reactions can be assumed to proceed as follows.

$$[Ni(H_2O)_2(NN\text{-deen})_2]Cl_2 \longrightarrow [NiCl_2(NN\text{-deen})_2] + 2H_2O$$

$$[Ni(H_2O)_2(NN\text{-deen})_2]Br_2\cdot H_2O \longrightarrow [Ni(NN\text{-deen})_2]Br_2 + 3H_2O$$

From the similarity of spectra of the anhydrous complex bromide (Fig. 2) and of the iodide and nitrate (Fig. 3), the complex iodide and nitrate can be represented by $[Ni(NN\text{-deen})_2]I_2$ and $[Ni(NN\text{-deen})_2](NO_3)_2$, respectively.

IR Spectra. Infrared and far-infrared absorption spectra were measured in order to see whether the anions in the complexes are coordinated and to obtain configurational information. The IR spectra of the diaquo complexes exhibit an absorption peak assigned to the stretching vibration, ν_{OH}, at *ca.* 3200 cm^{-1} and that for the bending vibration, δ_{OH}, at *ca.* 1600 cm^{-1}, the patterns of the chloride and bromide being the same. This supports the results given by electronic absorption measurement and derivatography where the diaquo complex chloride and bromide are represented by $[Ni(H_2O)_2(NN\text{-deen})_2]Cl_2$ and $[Ni(H_2O)_2(NN\text{-deen})_2]Br_2\cdot H_2O$ respectively.

The IR spectra of the anhydrous complex chloride and bromide obtained by heating the corresponding diaquo complexes are shown in Fig. 4, together with those of the iodide and nitrate. The absorption peaks of the OH group in the former two complexes are quenched as a result of dehydration, and the patterns of the bromide, iodide, and nitrate are approximately analogous to each other but differ from that of the chloride. These results confirm the chemical formulas $[Ni(NN\text{-deen})_2]Br_2$, $[Ni(NN\text{-deen})_2]I_2$, $[Ni(NN\text{-deen})_2](NO_3)_2$, and $[NiCl_2(NN\text{-deen})_2]$ for the bromide, iodide, nitrate, and chloride, respectively, in which the former three have a square planar structure and the last one has an octahedral structure with chloride ions in coordination.

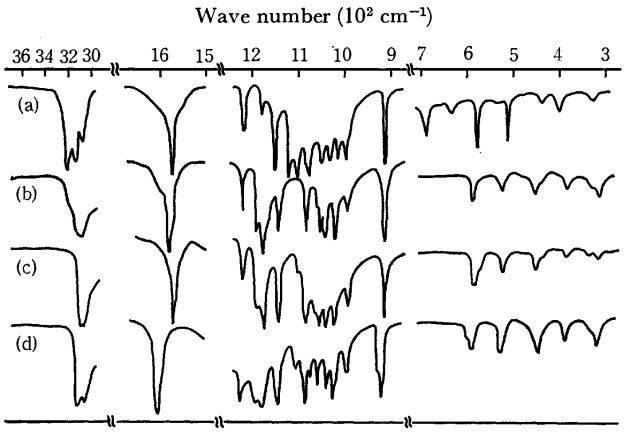

Fig. 4. IR and Far-IR spectra of (a) $Ni(NN\text{-deen})_2Cl_2$, (b) $Ni(NN\text{-deen})_2Br_2$, (c) $Ni(NN\text{-deen})_2I_2$, and (d) $Ni(NN\text{-deen})_2(NO_3)_2$.

Magnetic Susceptibility Measurement. The values of the effective magnetic moments of the complexes are summarized in Table 1 together with their colors. The fact that the diaquobis(diamine) complex chloride and bromide, including the dichloro complex formed by heating the former, show paramagnetism and the anhydrous iodide and nitrate diamagnetism confirms the respective structures predicted by spectral measurements. It was found that the hydrated diaquo complex bromide lost paramagnetism remarkably upon heating (Table 1).

Table 1. Magnetic moments and colors of the complexes

Complex	Color	Magnetic moment μ_{eff} (B.M.)
$[Ni(H_2O)_2(NN\text{-deen})_2]Cl_2$	blue	3.21 (28 °C)
$[Ni(H_2O)_2(NN\text{-deen})_2]Br_2\cdot H_2O$	blue	3.30 (20 °C)
$[Ni(NN\text{-deen})_2]I_2$	orange	diamag.
$[Ni(NN\text{-deen})_2](NO_3)_2$	orange	diamag.
$[NiCl_2(NN\text{-deen})_2]$	green	3.19 (20 °C)
$[Ni(NN\text{-deen})_2]Br_2$	orange yellow	0.9 (20 °C)

It is concluded that the diaquo complex bromide undergoes structural transformation from octahedral to square planar configuration by way of thermal deaquation in a solid phase, whereas the diaquo complex chloride undergoes no structural transformation but a thermal deaquation-anation reaction, forming the dichloro complex simultaneously (Fig. 5).

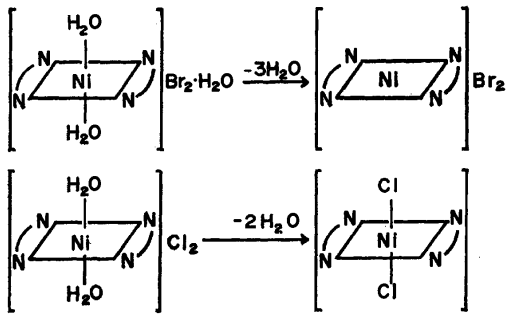

Fig. 5. Thermal reaction schemes of $[Ni(H_2O)_2(NN\text{-deen})_2]Br_2\cdot H_2O$ and $[Ni(H_2O)_2(NN\text{-deen})_2]Cl_2$.

Alkoxy and Phenoxy Bridged Dimeric Copper(II) Complexes with Salicylaldimine Ligands

J. O. MINERS and E. SINN*

Chemistry Department, Victoria University of Wellington, P.O. Box 196, Wellington, New Zealand

(Received December 13, 1971)

The tridentate Schiff base *N*-3-hydroxy-*n*-propylsalicylaldimine can be coordinated with copper(II) to form three kinds of dimeric oxy-bridged antiferromagnetic complexes (metal: ligand ratio—1: 1), as well as the normal monomeric complex. In one of the dimeric complexes pairs of copper atoms are bridged by pairs of the deprotonated alcoholic oxygens of the ligands. The others have an extra ligand X (X=–Cl, $-ONO_2$) per copper atom, the metals are bridged by phenolic oxygens, the alcoholic hydroxyls are not deprotonated, but are either coordinated (if X=Cl) to five-coordinated copper atoms in discrete dimer molecules, or participate in intermolecular hydrogen bonding linking individual dimeric molecules in which the copper atoms are four-coordinated. In the presence of pyridine, ammonia, or mild inorganic base, a rearrangement reaction can be induced, resulting in conversion of the phenolic-bridged (five-coordinated copper) dimer into the related alcoholic-bridged (four-coordinated copper) dimer. This behaviour is not followed by *N*-hydroxyethylsalicylaldimine which appears to form only one kind of copper complex [Cu(Lig)X] (X=–Cl, $-ONO_2$); in which the metal atoms are essentially planar and do not take part in strong antiferromagnetic interactions.

Yamada *et al.*[1a] and Kato *et al.*[1b] found that 3-hydroxy-*n*-propylsalicylaldimine can be used to form dimeric copper(II) complexes. Two possible structures were recognised for these complexes, I and II, of which I was preferred by the latter authors.[1b]

Contemporary and subsequent work on salicylaldimines without alcoholic side-chains showed that binuclear and trinuclear complexes can be formed very readily using the ability of phenolic oxygens to become three-coordinated.[2] Bidentate salicylaldimines were used to form dimers, III(a),[3] III(b),[4] and tetradentate salicylaldimines to form bi- and tri-nuclear metal complexes IV[5] and V.[6] The structures were assigned on the basis of synthetic, magnetic, ultraviolet-visible and infrared data. In particular a shift of about 20 cm^{-1} in the infrared absorption near 1540 cm^{-1} tentatively assigned to the phenolic C–O stretch,[3,4] was found to be characteristic of the formation of complexes III—V from monomeric complexes. This infrared shift can be taken as characteristic of bridging *via* the phenolic oxygens of salicylaldimines, and if bridging occurs without involving the phenolic oxygens, as in structure I, no such shift is expected.

Single crystal X-ray studies have since confirmed these structures for two binuclear copper(II) complexes of type III,[7] and three of type IV,[7,8] and two mixed metal complexes of type V, one with metal atoms (Cu–Na–Cu) in a flattened isosceles triangular array[9] and one with the metals (Cu–Mn–Cu) in a straight line.[10] A complex of type III, but with the substituent R-groups 3-hydroxy-*n*-propyl, has also been subjected to X-ray study, and found to have phenolic oxygen bridged structure, with the alcoholic hydroxyl groups coordinated to the copper atoms VI.[11]

These results appear to indicate a preference for bridging *via* phenolic oxygens in polynuclear salicylaldimines, even if alocholic oxygens are available in the ligand. However, the nonexistence of alcoholic oxygen bridges does not necessarily follow. It is now of interest to determine whether such bridging occurs, and, if it does, under what conditions. We report here an investigation of dimeric complexes with -R-OH substituted salicylaldimines, where R=$-CH_2-CH_2-$ and $-CH_2-CH_2-CH_2-$.

Regardless of whether alocholic or phenolic oxygen bridging is preferred in complex I (or II), this complex is closely related to complex VI. Complex VI, $[CuC_{10}H_{11}NO_2 \cdot HCl]_2$ may be regarded as a hydrochloride addition compound of complex I (or II) $[CuC_{10}H_{11}NO_2]_2$, and it should therefore be possible to find conditions for the conversion of the less stable of the two complexes to the more stable, and perhaps also for the reverse reaction. This aspect is also investigated.

Experimental

The parent monomeric complexes were prepared in the standard way[12] by warming the copper(II) complex of the salicylaldehyde or 5-chlorosalicylaldehyde with the appro-

* Present address: Chemistry Department, University of Virginia, Charlottesville, Va. 22901 U.S.A.

1) (a) S. Yamada, Y. Kuge, and K. Yamanouchi, *Inorg. Chim. Acta*, **1**, 139 (1967). (b) M. Kato, Y. Muto, H. B. Jonassen, K, Imai, and A. Harano, This Bulletin, **41**, 1864 (1968).

2) E. Sinn and C. M. Harris, *Coord. Chem. Rev.*, **4**, 391 (1969).

3) S. J. Gruber, C. M. Harris, and E. Sinn, *Inorg. Nucl. Chem. Lett.*, **3**, 495 (1967); C. M. Harris, J. M. James, P. J. Milham, and E. Sinn, *Inorg. Chim. Acta*, **3**, 81 (1969); R. B. Coles, C. M. Harris, and E. Sinn, *Inorg. Chem.*, **8**, 2607 (1969).

4) J. O. Miners and E. Sinn, *Synth. Inorg. Metal-Org. Chem.*, **2**, 231 (1972); J. O. Miners, E. Sinn, R. B. Coles, and C. M. Harris, *J. Chem. Soc. Dalton*, **1972**, 1149.

5) S. J. Gruber, C. M. Harris, and E. Sinn, *Inorg. Chem.*, **7**, 268 (1968).

6) S. J. Gruber, C. M. Harris, and E. Sinn, *Inorg. Nucl. Chem. Lett.*, **4**, 107 (1968); *J. Chem. Phys.*, **49**, 2183 (1968); *J. Inorg. Nucl. Chem.*, **30**, 1805 (1968).

7) E. Sinn and W. T. Robinson, *Chem. Commun.*, **1972**, 359.

8) C. A. Bear, J. M. Waters, and T. N. Waters, *Chem. Commun.*, **1971**, 703.

9) G. H. W. Milburn, M. R. Truter, and B. L. Vickery, *ibid.*, **1968**, 1188.

10) N. C. Stephenson, private communication.

11) J. A. Bertrand, J. A. Kelly, and J. L. Breece, *Inorg. Chim. Acta*, **3**, 247 (1969).

12) R. H. Holm, G. W. Everett, Jr., and A. Chakravorty, *Progr. Inorg. Chem.*, **7**, 83 (1966).

Table 1. Microanalytical data

Complex	Empirical formula	Calcd (%)			Found (%)		
		C	H	N	C	H	N
[Cu(EtOH·ClSal)NO_3]	$CuClC_9H_9N_2O_5$	33.4	2.8	8.6	33.5	2.9	8.2
[Cu(EtOH·ClSal)Cl]	$CuCl_2C_9H_9NO_5$	36.3	3.0	4.7	36.1	3.0	4.5
[Cu(EtOH·Sal)NO_3]	$CuC_9H_{10}N_2O_5$	37.3	3.5	9.7	37.0	3.5	9.5
[Cu(EtOH·Sal)Cl]	$CuClC_9H_{10}NO_5$	41.1	4.0	5.3	41.0	4.3	5.2
[Cu(3-PrOH·Sal)NO_3]$_2$	$Cu_2C_{20}H_{24}N_4O_{10}$	39.5	4.0	9.2	39.5	4.0	9.2
[Cu(3-PrOH·Sal)Cl]$_2$	$Cu_2C_{20}H_{24}N_2O_4Cl_2$	43.3	4.4	5.1	43.4	4.5	5.0
[Cu(3-PrO·Sal)]$_2$	$Cu_2C_{20}H_{22}N_2O_4$	49.9	4.6		50.0	4.6	

priate amine, and recrystallising from chloroform–ethanol. Cu(PrOH·Sal)$_2$ formed as an oil, and a solid was obtained only after standing.

The copper chloride or nitrate adducts were prepared by the standard method for complexes of type III,[3,4] *viz.* by the reaction of the appropriate copper(II) salicylaldimine complex with copper(II) chloride or copper(II) nitrate in methanol.

For brevity, we denote 3-hydroxy-*n*-propylsalicylaldimine and 2-hydroxyethyl-5-chlorosalicylaldimine as 3-PrOH·Sal and EtOH·ClSal respectively. Deprotonation of the alcoholic hydroxyl group is indicated by omission of "H" from the abbreviation.

Analytical data are listed in Table 1.

Infrared Spectra. IR spectra were determined on nujol and hexachlorobutadiene mulls of the compounds. Both a Unicam SP200 and a Perkin-Elmer 221 spectrophotometer were used to obtain the spectra. The spectrum of a polystyrene film was recorded on the same chart as a reference to allow accurate measurements of the bands.

Electronic Spectra. Electronic spectra were determined on the solid compounds using a Unicam SP200 spectrophotometer.

Electron Spin Resonance Measurements. ESR measurements were made on a Varian V4502-15 ESR spectrometer at the Physics and Engineering Laboratory of the D.S.I.R., Wellington. We are grateful to Mr. M. Collins for access to this apparatus.

Magnetic Susceptibility Measurements.[14] Magnetic susceptibility measurements were made as previously described,[3,5] in the range 100—400°K on a cryostat-controlled Gouy balance apparatus. The agreement of the observed magnetic susceptibility values, per gram atom of copper, χ_M (corrected for diamagnetism using Pascal's constants[13] with the Bleaney-Bowers Eq. (1) was tested where appropriate, and the value of the singlet-triplet separation, $-2J$, and of the Landé splitting factor, g, obtained from the best fit.[2-5,14]

$$\chi_M = \frac{Ng^2\beta^2}{3kT}\left(1+\frac{1}{3}e^{-2J/kT}\right)^{-1} + N\alpha \qquad (1)$$

Here the symbols have their usual meanings. $N\alpha$ was assumed to have the value 6×10^{-5} c.g.s.e.m.u.[2-5,14,15] Where Eq. (1) was not satisfied, the data was compared with Eq. (2) for trinuclear complexes,[16] as well as models for infinite lattice interactions

$$\chi_M = \frac{Ng^2\beta^2}{12kT}\cdot(e^{-A+B}+e^{-A-B}+10e^{A})/$$
$$(e^{-A+B}+e^{-A-B}+2e^{A}) + N\alpha \qquad (2)$$

where $A=(J_{12}+J_{23}+J_{13})/kT$, $B=(J_{12}^2+J_{23}^2+J_{13}^2-J_{12}J_{23}-J_{12}J_{13}-J_{23}J_{13})^{1/2}/kT$ and the J_{ij} are the exchange integrals between the three pairs of copper atoms.

Magnetic moments (in Bohr Magnetons) were calculated using the relation

$$\mu_{eff} = \sqrt{8.0(\chi_M - N\alpha)T}$$

In the absence of magnetic exchange interactions, g may be estimated from the relation $\mu_{eff}=g\sqrt{S(S+1)}$.

X-Ray Powder Diffraction Patterns. X-Ray diffraction paterns were recorded using a powder diffractometer with a Phillips Wide Range Goniometer PW1050/25.

Density Measurements. Densities were measured at 20°C by suspending crystals in solutions of equal density. The suspending solutions comprised acetone–carbon tetrachloride–bromoform mixtures and their densities were measured with a set of hydrometers calibrated to 0.0005 g cm^{-3}. The observed crystal densities are considered accurate and reproducible to $\pm$0.005 g cm^{-3}.

Results and Discussion

Magnetic Properties. Kato *et al.*[1] prepared complexes I (or II) [Cu(3-PrO·Sal)]$_2$ with four different ring substituents X, but found the properties to be so similar within the series that the complex with X=H can be taken as a representative compound when making comparisons with compounds belonging to different groups. In fact, variation of the ring substituent X in [Cu(3-PrO·Sal)]$_2$ has rather less effect on the properties than similar variation of X in complexes of type III[2,5-7] or IV.[2-6,17] This suggests that [Cu(3-PrO·Sal)]$_2$ may belong to a different category than III and IV, in agreement with the postulate for structure I for the complex.[1b]

Table 2 lists the magnetic properties of the various complexes with 3-PrOH·Sal, EtOH·Sal, and EtOH·ClSal. The complexes with 3-PrOH·Sal behave as binuclear antiferromagnets and Fig. 1 compares the experimental data with those calculated from Eq. (1). The values of J and g required to fit the data are listed in Table 3. The data indicate a much stronger interaction in [Cu(3-PrO·Sal)]$_2$ than in any of the others, again suggesting that complexes of the types [Cu·

13) P. W. Selwood, "Magnetochemistry," Interscience, N. Y., (1956).
14) B. Bleaney and K. D. Bowers, *Proc. Roy. Soc., Ser. A*, **214**, 451 (1952); B. N. Figgis and R. L. Martin, *J. Chem. Soc.*, **1956**, 3837.
15) B. N. Figgis and J. Lewis, *Progr. Inorg. Chem.*, **6**, 72 (1964).
16) E. Sinn, *Inorg. Nucl. Chem. Lett.*, **5**, 193 (1969).
17) C.M. Harris, S. Kokot, and E. Sinn, *Austral. J. Chem.*, **25**, 45 (1972).

Table 2. Magnetic data for dimeric copper(II) complexes

Temperature T in K; χ_M in c.g.s.e.m.u.; μ_{eff} in B.M.

[Cu(3-PrOH·Sal)NO_3]$_2$												
T	114.0	143.0	175.0	204.5	233.0	308.5	345.5					
$10^6\chi_M$	290	456	602	668	732	755	735					
μ_{eff}	0.47	0.58	0.87	1.01	1.11	1.31	1.36					
[Cu(3-PrOH·Sal)Cl]$_2$												
T	138.0	166.5	191.5	227.0	264.0	286.0	306.5	348.5	387.5			
$10^6\chi_M$	144	211	239	340	420	465	492	522	530			
μ_{eff}	0.30	0.46	0.53	0.72	0.87	0.96	1.03	1.13	1.20			
[Cu(3-PrO·Sal)]$_2$[a]												
T	288	303										
$10^6\chi_M$	91	101										
μ_{eff}	0.27	0.31										
[Cu(EtOH·ClSal)NO_3]												
T	79.0	102.0	116.5	127.5	147.5	168.0	193.0	212.5	234.0	260.8	283.5	345.5
$10^6\chi_M$	2549	2277	1955	1806	1670	1534	1398	1299	1261	1175	1113	977
μ_{eff}	1.25	1.34	1.32	1.33	1.37	1.40	1.43	1.45	1.49	1.52	1.54	1.59
[Cu(EtOH·ClSal)Cl]												
T	77.0	114.0	136.0	181.0	214.0	247.0	272.5	302.0	348.0	381.5		
$10^6\chi_M$	4963	3437	2931	2280	1901	1600	1434	1288	1162	1065		
μ_{eff}	1.74	1.77	1.78	1.81	1.80	1.77	1.76	1.76	1.79	1.80		
[Cu(EtOH·Sal)NO_3]												
T	86.0	103.0	123.5	141.5	164.5	184.0	201.1	219.5	296.0	320.5		
$10^6\chi_M$	4101	3642	2961	2665	2354	2132	1927	1829	1459	1402		
μ_{eff}	1.66	1.71	1.69	1.71	1.73	1.74	1.73	1.76	1.82	1.85		
[Cu(EtOH·Sal)Cl]												
T	118.3	150.2	191.2	246.6	309.4							
$10^6\chi_M$	3380	2602	2119	1630	1338							
μ_{eff}	1.79	1.77	1.80	1.79	1.82							

a) Calc. from data in Ref. 1

Table 3. Values of $-2J$ and g for the complexes

	Susceptibility[a]		ESR		
	$-2J$	g	$g_{//}$ ($\pm$0.01)	$g_\perp$ ($\pm$0.004)	$\langle g \rangle$
[Cu(EtOH·ClSal)NO_3]	(b)	(b)			
[Cu(EtOH·ClSal)Cl]	$<$10	2.06	2.28	2.018	2.11$\pm$0.01
[Cu(EtOH·Sal)NO_3]	$<$30	(b)			
[Cu(EtOH·Sal)Cl]	$<$10	2.06			
[Cu(3-PrOH·Sal)NO_3]$_2$	320	2.08	2.29	2.037	2.12$\pm$0.01
[Cu(3-PrOH·Sal)Cl]$_2$	470	2.09	2.31	2.048	2.14$\pm$0.01
[Cu(3-PrO·Sal)]$_2$	1020[c]	2.10	—	—	2.05$\pm$0.03[d]

a) Accuracy of J is expected to be better than 3%; accuracy of g should be about 4% when estimated from Eq. (1).
b) Not evaluated (see text).
c) Accuracy is expected to be low due to very low paramagnetism.
d) Accuracy low owing to very small population of the triplet state, which results in very poor signal to noise ratio.

LigH]$_2$ and [Cu·Lig·X]$_2$ fall into two separate categories where LigH=3-PrOH·Sal.

The relative accuracy of experimental points on the χ *vs.* T curves is much greater than their absolute accuracy, and therefore the accuracy of J values obtained by comparison with Eq. (1) is expected to be high while the accuracy of the g values is expected to be low. ESR measurements were made at room temperature and at 77 K to obtain accurate g values. The values of g were estimated from the ESR spectra in the normal way.[18] (Table 3).

The magnetic properties of the complexes [Cu(EtOH·ClSal)X] differ markedly from their 3-PrOH·Sal analogues. When X=Cl, the complex shows no significant interactions and when X=ONO_2, antiferromagnetic interactions are observed, but the magnetic properties are more consistent with Eq. (2) than Eq. (1). However, we do not consider the data to be sufficiently characteristic to make a positive assignment of structure, at this stage. Measurements down to liquid helium temperatures are desirable, and X-ray

18) K. Kneubuhl, *J. Chem. Phys.*, **33**, 1074 (1960); G. Burns, *J. Appl. Phys.*, **32**, 2048 (1961); H. R. Gersmann and J. D. Swalen, *J. Chem. Phys.*, **36**, 3221 (1962); J. A. Weil and H. G. Hecht, *ibid.*, **38**, 281 (1963); A. A. Tomlinson and B. J. Hathaway, *J. Chem. Soc. A*, **1968**, 2578.

Table 4. Electronic spectra (18000—8000 cm^{-1} region), selected infrared bands, melting points (°C), and densities ($g \cdot cm^{-1}$)

	λ	1540[a] region	3000 region	$-ONO_2$ region	Mp	Density
$[Cu(EtOH \cdot Sal)NO_3]$	15000	1550 (7)	3300	1286 1022 810	dec	1.79
$[Cu(EtOH \cdot Sal)Cl]$	14300	1548 (5)	3200	—	187	1.73
$[Cu(EtOH \cdot ClSal)NO_3]$	15300	1544 (8)	3350	1490sh 1289s 1019m 800m	dec	1.82
$[Cu(EtOH \cdot ClSal)Cl]$	14200	1535 (−1)	3150	—	189	1.79
$[Cu(3\text{-}PrOH \cdot Sal)NO_3]_2$	14800	1558 (18)	2880	1277s 1026s 814m	dec	1.76
$[Cu(3\text{-}PrOH \cdot Sal)Cl]_2$	13400sh 11400s	1562 (22)	3380	—	166	1.70
$[Cu(3\text{-}PrO \cdot Sal)]_2$	17600	1578 (−2)	—	—	280	1.67

s=strong; m=medium; sh=shoulder.

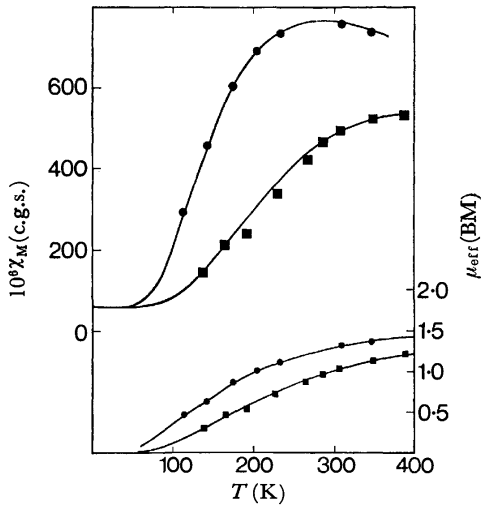

Fig. 1. Experimental and calculated (Eq. (1)) magnetic properties for $[Cu(PrOH \cdot Sal)NO_3]_2$ and $[Cu(PrOH \cdot Sal)Cl]_2$.

crystallographic studies will be undertaken to clarify the situation.

Spectra. The electronic spectra of the complexes, listed in Table 3, indicate a four-coordinated environment[5,19] about copper, for all the complexes except $[Cu(3\text{-}PrOH \cdot Sal)Cl]_2$, VI, which is known to be five-coordinated, with a trigonal bipyramid configuration. The spectrum of complex VI is similar to those[20] of known[21] distorted bipyramidal complexes such as [Cu(tren)NCS]SCN and $[Cu(bipy)_2I]I$. The most noteworthy feature of the spectra is the difference between the complexes $[Cu(3\text{-}PrOH \cdot Sal)X]_2$ (X=Cl, NO_3). It appears that when X is changed from Cl to NO_3, the structure changes from VI to a four-coordinate arrangement. This behaviour is not paralleled by the analogous complexes with EtOH·ClSal.

The spectra of the four-coordinated complexes suggest a copper environment that is closer to planar than tetrahedral. The shift of 500 cm^{-1} from $[Cu(EtOH \cdot ClSal)NO_3]$ to $[Cu(3\text{-}PrOH \cdot Sal)NO_3]_2$ suggests a slightly greater distortion from planarity in the latter complex,[6,19] since the ligand field strengths of EtOH·ClSal and 3-PrOH·Sal should be fairly close in magnitude. The other differences between the absorption maxima of the four-coordinate complexes are expected to arise from differences in ligand field strengths (X= Cl, NO_3, or no ligand) as well as the differences in the relative distortions from planarity.

Infrared Spectra. The formation of a phenolic oxygen bridge between two metal atoms is considered to result in a shift (~20 cm^{-1}) to higher energies of the salicylaldimine phenolic C–O stretching frequency near 1540 cm^{-1}. This is therefore a most important band for structural assignments and is listed for each complex in Table 4. The expected shift is observed in all the complexes with 3-PrOH·Sal except $[Cu(3\text{-}PrO \cdot Sal)]_2$, indicating absence of phenolic oxygen bridging, and hence structure I for this complex, but structures of types III and VI for the other complexes. Of the complexes with EtOH·Sal and EtOH·ClSal, only $[Cu(EtOH \cdot ClSal)NO_3]$ exhibits a small shift in this region, indicating weak phenolic oxygen bridges for this complex and no significant phenolic bridging for the other complexes.

The infrared absorptions due to the nitrato group in $[Cu(EtOH \cdot ClSal)NO_3]_2$ and $[Cu(3\text{-}PrOH \cdot Sal)NO_3]_2$ confirm that the nitrate is coordinated rather than ionic, but add no new information, since infrared spectra cannot distinguish between mono- and bidentate nitrate coordination.[22] It is therefore necessary to invoke the structural assignment from visible spectra

19) L. Sacconi and M. Ciampolini, *J. Chem. Soc.*, **1964**, 276; A. von Kiss, G. Bacskai, and P. Coskan, *J. Prakt. Chem.*, **160**, 1 (1942); J. Ferguson, *J. Chem. Phys.*, **34**, 2206 (1961); R. L. Belford and T. S. Piper, *Mol. Phys.*, **5**, 251 (1962); R. H. Holm, *J. Amer. Chem. Soc.*, **82**, 5632 (1960); J. Lewis and R. A. Walton, *J. Chem. Soc. A*, **1966**, 1559.

20) R. C. Slate, A. A. Tomlinson, B. J. Hathaway, and D. E. Billing, *J. Chem. Soc. A*, **1968**, 61.

21) P. C. Jain and E. C. Lingafelter, *J. Amer. Chem. Soc.*, **89**, 724 (1967); G. A. Barclay, B. F. Hoskins, and C. H. Kennard, *J. Chem. Soc.*, **1963**, **5691**.

22) K. Nakamoto "Infrared Spectra of Inorganic and Coordination Compounds," Wiley, N. Y. (1963).

to determine monodentate nitrato coordination. Such coordination appears to be necessary in order to make up the required coordination number in each case. (In the special case where the alcoholic oxygens are involved in hydrogen bonding they are unlikely to be available for coordination to copper). These nitrato complexes are similar to the nitrato complexes of type III with Cl replaced by monodentate ONO_2.[4] In all these complexes, infrared absorptions at 790—813, 1005—1022, 1280—1286, 1488—1495 cm^{-1}, typical of coordinated nitrate,[22,23] were observed only in the nitrato complexes, but not in the analogous chloro derivatives (III or VI), nor in the parent monomeric Schiff base complexes.[4]

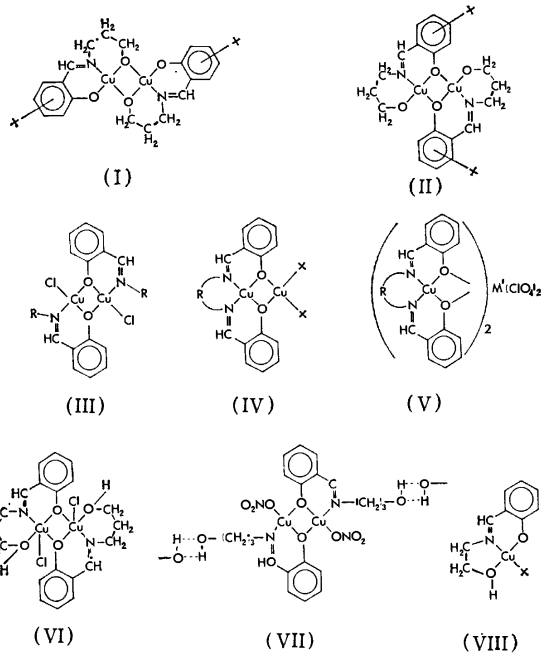

The O–H stretching region, 2800—3500 cm^{-1}, was examined to determine the bonding of the OH group (Table 4). As expected, $[Cu(3\text{-}PrO\cdot Sal)]_2$ has no bands in this region. Complex VI, which has the OH group coordinated to the metal, has a high energy band in this region. Similar bands occur in all but one of the remaining complexes, suggesting similar coordination of the OH groups. The significant exception is $[Cu(3\text{-}PrOH\cdot Sal)NO_3]_2$ which has a lower energy band, in keeping with a structure involving hydrogen bonding to the hydroxyalkyl group. This postulate is supported by the observation of extensive intermolecular hydrogen bonding in the X-ray study of $[Cu(EtOH\cdot Sal)_2]$[24] while the analogous complex $[Cu(EtOH\cdot ClSal)]_2$ has its OH band at 3100 cm^{-1}. Thus the most likely structure for the complex $[Cu(3\text{-}PrOH\cdot Sal)NO_3]_2$ is VII. The infrared evidence is not conclusive for the complexes involving EtOH·Sal and EtOH·ClSal since some of the bands are weak and broad, but when the other evidence is taken into account, the most likely structure for these complexes is VIII. Cross-linking *via* intermolecular Cu–O or hydrogen bonds, or both, between individual molecules of type VIII seems probable, especially in the complex $[Cu(EtOH\cdot ClSal)NO_3]$ and to a lesser extent $[Cu(EtOH\cdot Sal)NO_3]$. The former complex should perhaps be formulated as $[Cu(EtOH\cdot ClSal)NO_3]_n$ but, as discussed above, n may not be reliably evaluated at this stage. Fortunately, these complexes readily form large (green) crystals, so that single crystal X-ray studies should be accessible.

Rearrangement Reactions. To test the possibility of the interconversion reaction (3),

$$[Cu(3\text{-}PrO\cdot Sal)]_2 + HX \rightleftharpoons [Cu(3\text{-}PrOH\cdot Sal)X]_2 \quad (3)$$

complex I, $[Cu(3\text{-}PrO\cdot Sal)]_2$ was treated with HCl in methanol, and deep brown crystals which separated from the mixture were shown to be identical with complex VI $[Cu(3\text{-}PrOH\cdot Sal)Cl]_2$, having identical infrared spectra and X-ray diffraction patterns, and the same melting points, densities and optical spectra. The reverse conversion was effected by boiling VI in the base pyridine. Dark red crystals which separated on cooling were shown by the same techniques to be identical with I. In each case the reaction appeared to be complete in a few minutes. The procedure was repeated with the nitrato analogue, VII, and a period of days was required for a smaller yield of the product. This slower reaction is not surprising in view of the different structures VI and VII proposed for the chloro and nitrato complexes: the former could undergo internal rearrangement more readily than the latter. The mechanism of these reactions is under further investigation.

It has not been found possible to prepare the complex analagous to I using EtO·Sal in place of 3-PrO·Sal.[1,25] It appears that dimeric analogues to VI using EtOH·Sal in place of 3-PrOH·Sal are not readily formed either.

Conclusion

The main structures I, VI, and VII, occur in copper(II) complexes with *N*-3-hydroxy-*n*-propylsalicylaldimine, and direct chemical interconversion between them is possible. When the hydroxypropyl group is shortened to hydroxyethyl, only one structure, VIII, seems likely, with some degree of molecular aggregation.

$$CuL_2 + CuX_2 \longrightarrow 2[CuLX]$$

In the 3-PrOH·Sal complexes, if the alcoholic oxygen is not deprotonated, bridging occurs easily *via* the phenolic oxygens to form binuclear complexes. The alcoholic oxygen may be coordinated as in VI, but need not be, and may participate in intermolecular hydrogen bonding (VII) instead. When the alcoholic oxygen is deprotonated and coordinated, bridging *via* this oxygen (I) is preferred.

23) B. M. Gatehouse, R. S. Nyholm, and S. E. Livingstone, *J. Chem. Soc.*, **1957**, 4222.

24) E. R. Bokyo, D. Hall, M. Kinloch, and T. N. Waters, *Acta Crystallogr.*, **21**, 614 (1966).

25) A. Nakahara, H. Yamamoto, and H. Matsumoto, This Bulletin, **37**, 1137 (1964).

Binuclear Metal Complexes. VI.[1] Syntheses and Properties of Binuclear Copper(II) Complexes of 2,6-Bis[*N*-(β-dialkylaminoethyl)iminomethyl]-4-methylphenol[2]

Hisashi Okawa, Tadashi Tokii,* Yasuomi Nonaka, Yoneichiro Muto,* and Sigeo Kida

Department of Chemistry, Faculty of Science, Kyushu University, Hakozaki, Fukuoka 812

**Department of Chemistry, Saga University, Saga*

(Received September 18, 1972)

A new series of binuclear copper(II) complexes, $[Fsal(=NenNR_2)_2Cu_2X]^{2+}$ (R=Me and Et, X=Cl, Br, and OH), were synthesized, where $Fsal(=NenNR_2)_2$ indicates the Schiff base prepared from 2,6-diformyl-4-methylphenol and *N,N*-dialkylethylenediamine (alkyl=methyl(Me) and ethyl(Et)). Two copper(II) ions are connected with the phenolic oxygen and X. The complexes obtained were characterized by elemental analyses, infrared and visible spectra, molar conductivities in methanol, ESR spectra and magnetic susceptibilities. It was found that the stability of the complexes decreases in the order X=OH≫Br>Cl. It was concluded from cryomagnetic measurements that the effect of the bridging group X on spin-coupling decreases in the order OH≫Br>Cl.

It is known that 2,6-diformyl-4-methylphenol and its Schiff base derivatives[3-7] form a novel class of binuclear copper(II) complexes, in which two copper(II) ions are bridged with two different groups. We suggested that there is a relationship between the simply coordinating and bridging groups concerning the stability of the binuclear copper(II) complexes.[5] In order to find the relationship it is necessary to synthesize many binuclear copper(II) complexes with a variety of coordinating and bridging groups. We attempted the preparation of some binuclear copper(II) complexes of the Schiff bases 2,6-bis[*N*-(β-dialkylaminoethyl)iminomethyl]-4-methylphenol made from 2,6-diformyl-4-methylphenol and *N,N*-dialkylethylenediamine (alkyl=methyl and ethyl).

We synthesized six binuclear copper(II) complexes of the type $[Fsal(=NenNR_2)_2Cu_2X]^{2+}$, where $Fsal(=NenNR_2)_2$ denotes the Schiff bases and X the second bridging group (phenolic oxygen will be called the first bridging group). The structures and properties of the complexes were studied by elemental analyses, IR and visible spectra, molar conductivities in methanol, ESR spectra and magnetic susceptibilities, magnetic exchange interaction also being examined. Since only the second bridging group in the complexes is variable, we can estimate its effect on the spin-coupling between the two copper(II) ions.

Experimental

Syntheses. The synthetic method for 2,6-diformyl-4-methylphenol was described elsewhere.[4]

[Fsal(=NenNMe$_2$)$_2$Cu$_2$Cl]Cl$_2$: 2,6-Diformyl-4-methylphenol (330 mg) and anhydrous copper(II) chloride (538 mg) were dissolved in absolute methanol (30 ml). To the solution was added a solution of *N,N*-dimethylethylenediamine (352 mg) in absolute methanol (5 ml). The reaction mixture was warmed and concentrated to 15 ml to give green needles. They were recrystallized from anhydrous methanol–benzene.

Found: C, 38.08; H, 5.22; N, 10.59; Cl, 19.64%. Calcd for $C_{17}H_{27}N_4OCl_3Cu_2$: C, 38.03; H, 5.07; N, 10.44; Cl, 19.81%.

[Fsal(=NenNMe$_2$)$_2$Cu$_2$Br]Br$_2$: To a solution of 2,6-diformyl-4-methylphenol (330 mg) and anhydrous copper(II) bromide (894 mg) in methanol (30 ml) was added a methanolic solution (5 ml) of *N,N*-dimethylethylenediamine (352 mg). After the reaction mixture was boiled and concentrated to 20 ml, dark green needles were obtained. They were filtered and washed with a small amount of cold absolute methanol.

Found: C, 30.52; H, 4.22; N, 8.36; Br, 35.37%. Calcd for $C_{17}H_{27}N_4OBr_3Cu_2$: C, 30.47; H, 4.06; N, 8.36; Br, 35.77%.

[Fsal(=NenNMe$_2$)$_2$Cu$_2$OH](ClO$_4$)$_2$: 2,6-Diformyl-4-methylphenol (330 mg), *N,N*-dimethylethylenediamine (352 mg) and copper(II) perchlorate hexahydrate (1482 mg) were mixed in methanol (30 ml). The reaction mixture was concentrated to 15 ml and diluted with water (15 ml) to give greenish blue prisms. They were recrystallized from water to give blue prisms.

Found: C, 31.74; H, 4.58; N, 8.69; Cu, 19.51%. Calcd for $C_{17}H_{28}N_4O_{10}Cl_2Cu_2$: C, 31.59; H, 4.37; N, 8.67; Cu, 19.66%.

[Fsal(=NenNEt$_2$)$_2$Cu$_2$Cl]Cl$_2$: This compound was prepared by a method similar to that for $[Fsal(=NenNMe_2)_2Cu_2Cl]Cl_2$. Recrystallization was carried out from anhydrous methanol–ethanol.

Found: C, 42.51; H, 6.01; N, 9.13; Cl, 18.12%. Calcd for $C_{21}H_{35}N_4OCl_3Cu_2$: C, 42.54; H, 5.95; N, 9.45; Cl, 17.94%.

[Fsal(=NenNEt$_2$)$_2$Cu$_2$Br]Br$_2$: This complex was synthesized by treating 2,6-diformyl-4-methylphenol (330 mg), anhydrous copper(II) bromide (894 mg) and *N,N*-diethylethylenediamine (464 mg) in ethanol. Violet prisms separated were collected and washed with a small amount of ethanol.

Found: C, 32.92; H, 4.83; N, 7.19; Br, 31.62%. Calcd for $C_{21}H_{35}N_4OBr_3Cu_2 \cdot 2H_2O$: C, 33.09; H, 5.1[illegible]; N [illegible].35; Br, 31.44%.

An anhydrous complex was obtained when the dihydrate was recrystallized from absolute methanol three times and then heated at 110 °C under reduced pressure.

[Fsal(=NenNEt$_2$)$_2$Cu$_2$OH](ClO$_4$)$_2$: The synthetic method for this complex is nearly the same as that for $[Fsal(=NenNMe_2)_2Cu_2OH](ClO_4)_2$. The violet needles separated were collected and recrystallized three times from water.

1) Part V: H. Okawa, M. Honda, and S. Kida, *Chem. Lett.*, **1972**, 1027.

2) This work was presented at the 21th Symposium of Coordination Chemistry, Nagoya, November 18, 1971.

3) H. Okawa, This Bulletin, **43**, 3019 (1970).

4) H. Okawa and S. Kida, *ibid.*, **44**, 1172 (1971).

5) H. Okawa, S. Kida, Y. Muto, and T. Tokii, *ibid.*, **45**, 2480 (1972).

6) R. Robson, *Inorg. Nucl. Chem. Lett.*, **6**, 125 (1970).

7) B. F. Hoskins, R. Robson, and H. Schaap, *ibid.*, **8**, 21 (1972).

Found: C, 35.95; H, 5.23; N, 7.81%. Calcd for $C_{21}H_{36}N_4O_{10}Cl_2Cu_2$: C, 35.90; H, 5.17; N, 7.98%.

Measurements. Infrared spectra were measured with a Hitachi EPI-S2 spectrophotometer in the region 4000—650 cm^{-1} on a KBr disk. Electronic spectra on solids and in solutions (methanol, water and pyridine) were determined with a Hitachi EPS-3T recording spectrophotometer. ESR spectra (X-band) were measured on powder and in solutions with a JES-ME-3 spectrometer at various temperatures. Magnetic susceptibilities were determined by the Gouy method in the range from liquid nitrogen to room temperature. The apparatus for the measurements was described elsewhere.[5] Effective magnetic moments μ_{eff} were calculated by the equation

$$\mu_{eff} = 2.83\sqrt{(\chi_A - N\alpha)T},$$

where χ_A is the atomic susceptibility corrected by use of Pascal's constants[8,9] for diamagnetism and $N\alpha$ the temperature independent paramagnetism of copper(II) ion. Molar conductivities of the complexes were determined in an absolute methanol solution (*ca.* 10^{-3} mol) at 25 °C.

Results and Discussion

Some IR absorption bands of the complexes are given in Table 1. Very sharp peaks at 3510 cm^{-1} in $[Fsal(=NenNMe_2)_2Cu_2OH](ClO_4)_2$ and $[Fsal(=NenNEt_2)_2Cu_2OH](ClO_4)_2$ are assigned to the O–H stretching vibration. Two peaks in the region 1650—1635 cm^{-1} may be assigned to the C=N stretching vibrations. The skeletal vibration[10] observed at 1555—1560 cm^{-1} supports the binuclear structure bridged with a phenolic oxygen.[11] Two strong bands near 1320 and 1080 cm^{-1} are tentatively assigned to the C–O and =C–N stretching vibrations, respectively.[10] Two OH-bridged complexes show a broad, strong band due to perchlorate ion[12] in the region 1120—1060 cm^{-1}.

Molar conductivities of the complexes in absolute methanol are given in Table 1. All complexes were found to be 1:2 electrolytes. The mass spectrum of $[Fsal(=NenNEt_2)_2Cu_2Cl]Cl_2$ exhibits two peaks at m/e= 521 and 523, attributable to the $[Fsal(=NenNEt_2)_2Cu_2Cl]^+$ ion. Thus two peaks at m/e=458 and 460 and two peaks at m/e=359 and 360 may be assigned to the $Fsal(=NenNEt_2)_2CuCl^+$ and $Fsal(=NenNEt_2)_2^+$ ions respectively. We concluded that the complexes possess the binuclear structure shown in Fig. 1.

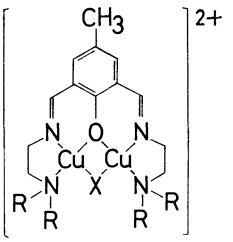

R=CH_3 and C_2H_5 X=Cl, Br, and OH

Fig. 1. Structure of $[Fsal(=NenNR_2)_2Cu_2X]^{2+}$.

The d-d bands of the complexes are given in Table 2. As was expected from spectrochemical series, the reflection spectra of the OH-bridged complexes have a d-d band at higher energy than those of the corresponding halogen-bridged complexes. However, the energy difference in d-d band (2.1—5.5 kK) between the OH-bridged and the halogen-bridged complexes is markedly larger than that in the case of the glycine-Schiff base complexes (0.9—1.0 kK).[5] This indicates

Table 1. IR absorption bands and molar conductivity

$[Fsal(=NenNR_2)_2Cu_2X]^{2+}$		IR (cm^{-1})							Molar conductivity (Ω^{-1} cm^2 mol^{-1})
R	X	O–H	C=N		skeletal	C–O	=C–N	ClO_4^-	
CH_3	Cl		1650	1634	1556	1322	1080		181
CH_3	Br		1650	1635	1558	1318	1080		173
CH_3	OH	3510	1650	1635	1556	1332		1120—1060	220
C_2H_5	Cl		1650	1634	1555	1328	1082		179
C_2H_5	Br		1653	1640	1560	1325	1080		199
C_2H_5	OH	3510	1650	1640	1567	1323		1120—1070	216

Table 2. Ligand field bands (mμ).

$[Fsal(=NenNR_2)_2Cu_2X]^{2+}$		Powder		Solution (ε)		
R	X			MeOH	H_2O	py
CH_3	Cl	700	500_{sh}	680(109)		
CH_3	Br	730	500_{sh}	690(125)		
CH_3	OH	610		630(99)	630(90)	650(110)
C_2H_5	Cl	770	510_{sh}	690(120)		
C_2H_5	Br	790	500_{sh}	680(127)		
C_2H_5	OH	550		625(115)	610(111)	665(138)

sh: shoulder

8) G. Foex, G. J. Gorter, and L. J. Smits, "Constantes Selectionnees, Diamagnetisme et Paramagnetisme, Relaxation Paramagnetique," Masson & Cie, Paris (1957), p. 222.
9) P. W. Selwood, "Magnetochemistry," Interscience Publishers, New York (1956), pp. 78, 91.
10) H. Okawa, and S. Kida, This Bulletin, **45**, 1759 (1972).
11) E. Sinn and C. M. Harris, *Coord. Chem. Rev.*, **4**, 391 (1969).
12) B. J. Hathaway and A. E. Underhill, *J. Chem. Soc.*, **1961**, 3091.

that the OH- and the halogen-bridged complexes possess a molecular structure differing from each other in solid states, depending on the counter ions. Since no appreciable coordination is expected for perchlorate ion, the coordination around the copper(II) ion in the OH-bridged complexes may be practically planar. In this case a larger steric requirement of the ethyl group compared with the methyl group will exclude the fifth coordination in the apical position. The coordination bonds in tetragonal plane in $[Fsal(=NenNEt_2)_2Cu_2OH](ClO_4)_2$ are therefore much strengthened and its solid spectrum has a band at higher energy than $[Fsal(=NenNMe_2)_2Cu_2OH](ClO_4)_2$. On the other hand the halogeno ion in $[Fsal(=NenNR_2)_2Cu_2X]X_2$ (X=Cl and Br) will coordinate to the copper(II) ion to form a five-coordination. Such a tetragonal-pyramidal structure was found for similar binuclear copper(II) complexes.[13] In the five-coordinate complexes the ethyl group will make a larger internal strain compared with the methyl group. In fact, $[Fsal(=NenNEt_2)_2Cu_2X]X_2$ has a d-d band at lower energy than the corresponding $[Fsal(=NenNMe_2)_2Cu_2X]X_2$ (X=Cl and Br).

All the above complexes appear to take a five- or six-coordinate structure in methanol with the solvent molecule in an apical position. However, the six-coordination seems impossible judging from the steric hindrance between the R and methanol molecules. The OH-bridged complexes have a d-d band at a lower energy in methanol than in a solid state. This suggests that the coordination around copper(II) is tetragonal-pyramidal in methanol. The halogeno-bridged complexes possess a d-d band at higher energy in methanol than in a solid state. This implies that a halogeno atom in the fifth coordination position was replaced by a solvent molecule in methanol.

Both the OH-bridged complexes may keep the same structure in water, in methanol and in pyridine. The halogeno-bridged complexes are only stable in absolute methanol and easily decomposed in water and in pyridine. The Br-bridged complexes seem to be more stable than the corresponding Cl-bridged complexes, since $[Fsal(=NenNR_2)_2Cu_2Cl]Cl_2$ was partly decomposed after long exposure to air. Thus the relative stability of the complexes increases in the order X=OH$\gg$Br$>$Cl. This is the reverse of that found for the series of binuclear copper(II) complexes derived from 2,6-diformyl-4-methylphenol and glycine.[5]

The powder ESR spectra of the $[Fsal(=NenNMe_2)_2Cu_2X]^{2+}$ complexes (X=Cl, Br, and OH) are given in Fig. 2. Each spectrum is very similar to the corresponding spectrum of the $[Fsal(=NenNEt_2)_2Cu_2X]^{2+}$ complexes. The Cl-bridged complex showed a broad band (*ca.* 6000 gauss width) centered around 3500 gauss. Similar broad spectra was observed for dichloro-μ-chloro-μ-(2,6-diformyl-4-methylphenolato)dicopper(II)[3] and for the binuclear copper(II) complexes of the Schiff bases derived from 2,6-diformyl-4-methylphenol and α-amino acids.[5] The spectrum of the Br-bridged complex was also broad. The signal observed at 1700 gauss may be assigned to the $\Delta M_s=2$ transition. A signal at 3200 gauss may be due to the presence of a trace of impurity of mononuclear species. The spectrum of the OH-bridged complex showed two signals at 6000 and 1600 gauss, tentatively assigned to the $\Delta M_s=1$ and the $\Delta M_s=2$ transitions respectively. The ESR spectra of the complexes in methanol and of the OH-bridged complexes in water and in pyridine showed no signal except for a weak band at 3200 gauss due to paramagnetic impurity.

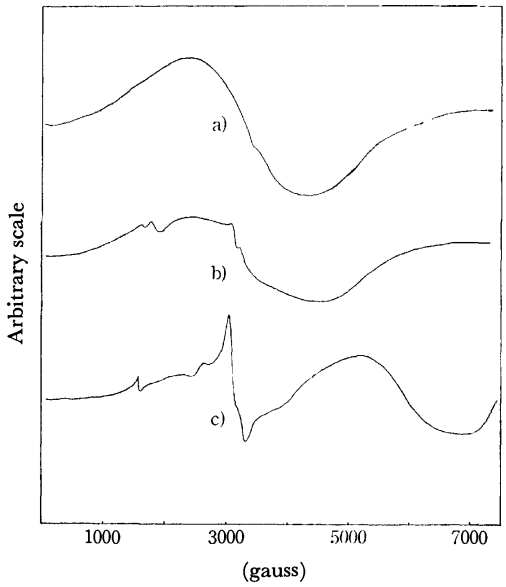

Fig. 2. ESR spectra of $[Fsal(=NenNMe_2)_2Cu_2X]Y_2$.
a) X=Cl, Y=Cl; b) X=Br, Y=Br;
c) X=OH, Y=ClO_4.

The ESR spectrum of $[Fsal(=NenNEt_2)_2Cu_2OH](ClO_4)_2$ was measured at various temperatures. The results are given in Fig. 3. Intensities of the signals at 5500 and 1600 gauss decrease with the lowering of temperature; the signal at 5500 gauss practically disappeared at 133 K. It is clear that an antiferro-

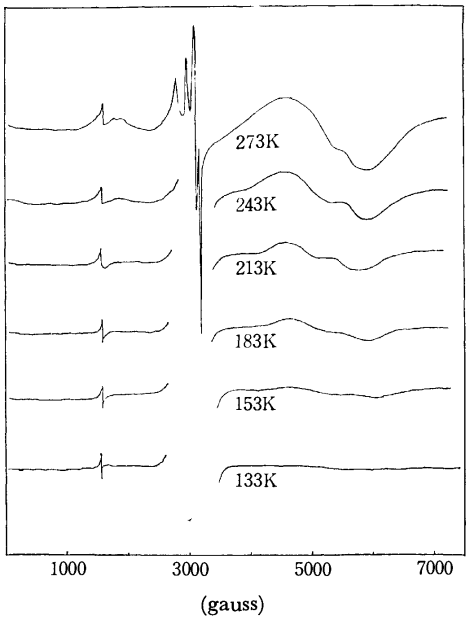

Fig. 3. ESR spectra of $[Fsal(=NenNEt_2)_2Cu_2OH](ClO_4)_2$ at various temperatures.

13) N. F. Pilkington and R. Robson, *Austral. J. Chem.*, **23**, 2225 (1970).

magnetic exchange interaction occurs between the two copper(II) ions.

All the complexes showed demagnetisation by spin-pairing in line with the results of the ESR data. Magnetic susceptibilities were measured over a temperature range 70—300 K. Experimental data can be explained on the basis of the Bleaney-Bowers equation[14]

$$\chi_A = \frac{Ng^2\beta^2}{3kT}\left[1+\frac{1}{3}\exp(-2J/kT)\right]^{-1} + N\alpha,$$

where the symbols have their usual meanings. The $-2J$, g, and $N\alpha$ values were determined by the best fit of the χ_A value to the Bleaney-Bowers equation (Fig. 4). The values are given in Table 3. The $-2J$ value, which is the energy separation between the singlet and triplet states, indicates the degree of the spin-exchange interaction between the copper(II) ions.

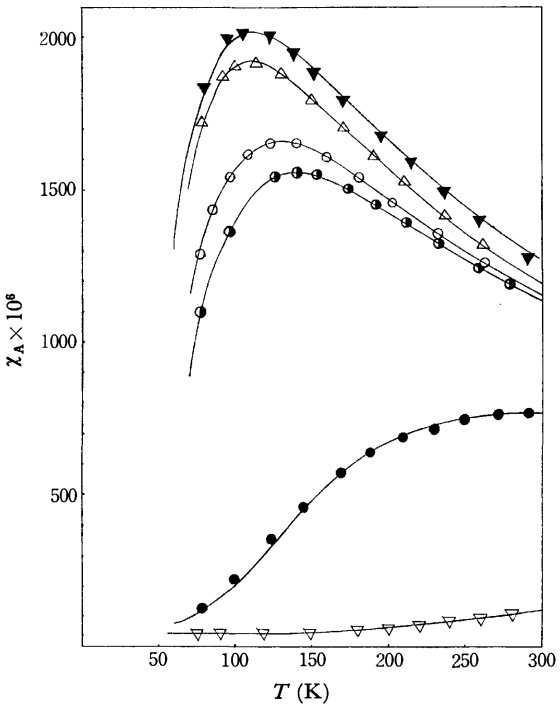

Fig. 4. Variation of molar susceptibilities with temperature of complexes; (○) R=Me X=Cl, (◑) R=Me X=Br, (●) R=Me X=OH, (△) R=Et X=Cl, (▼) R=Et X=Br, and (▽) R=Et X=OH.

Table 3. Values of $-2J(cm^{-1})$, g, $N\alpha$ (c.g.s., e.m.u.) and μ_{eff} (B.M.)

R	X	$-2J$	g	$N\alpha\times10^6$	μ_{eff}(K)
CH_3	Cl	143	2.10	45	1.61(299.3)
CH_3	Br	155	2.10	60	1.61(301.1)
CH_3	OH	330	2.11	60	1.29(291.8)
C_2H_5	Cl	123	2.10	40	1.66(302.6)
C_2H_5	Br	125	2.16	60	1.68(291.6)
C_2H_5	OH	865	2.15	46	0.49(303.4)

14) B. Bleaney and K. D. Bowers, *Proc. Roy. Soc., Ser. A*, **214**, 451 (1952).

The spin-exchange interaction may be caused by a super exchange mechanism rather than direct overlapping of 3d-orbitals, since the distance between two metal ions is about 2.9 Å for the complex of a structure similar to the present complexes.[7] The halogen-bridged complexes were found to have nearly the same molecular structure, their powder X-ray diffraction spectra being practically the same. If we suppose as a first approximation that the degree of the spin-exchange through the first bridging group is the same throughout the series of complexes, then the $-2J$ value reflects the effect of the second bridging group on spin-pairing between the copper(II) ions. The results given in Table 3 indicate that the bromide bridge is more effective in spin-coupling than the chloride bridge in both series of complexes. This is in line with the results obtained for the copper(II) halides[15] and the cobalt(II) complexes.[16] On the other hand, the two OH-bridged complexes have much larger $-2J$ values than the others. It is well-known[15] that oxygen-bridges are generally more effective than halogeno-bridges in spin-coupling. It may be said that the effect of the second bridging group on the antiferromagnetic exchange interaction increases in the order X=OH$\gg$Br$>$Cl.

It is interesting to consider the correlation between the d-d band and the $-2J$ value of the complexes. It is clear that $[Fsal(=NenNEt_2)_2Cu_2OH](ClO_4)_2$ has a d-d band at higher energy and a larger $-2J$ value than $[Fsal(=NenNMe_2)_2Cu_2OH](ClO_4)_2$. In the halogeno-bridged complexes, $[Fsal(=NenNMe_2)_2Cu_2X]X_2$ (X=Cl and Br) always shows a d-d band at higher energy and a larger $-2J$ value than the corresponding $[Fsal(=NenNEt_2)_2Cu_2X]X_2$. This implies that the more planar the configuration around the copper(II) ion the larger the magnetic exchange between the copper(II) ions. This trend in the d-d band and $-2J$ value has been found by Muto *et al.*[17] and Kato *et al.*[18] for the binuclear copper(II) complexes of pyridine-*N*-oxides and *N*-aryl-salicylaldimines. The binuclear copper(II) complex prepared from pyridine-*N*-oxide and copper(II) bromide has a magnetic moment 0.29 B.M., which is smaller than 0.63 B.M. for the complex made from copper(II) chloride. It was recently demonstrated by X-ray analysis[19] that these magnetic moments are explained in terms of the planarities of the complexes.

15) M. Kato, H. B. Jonassen, and J. C. Fanning, *Chem. Rev.*, **64**, 99 (1964).

16) A. B. P. Lever, L. K. Thompson, and W. M. Reiff, *Inorg. Chem.*, **11**, 104 (1972).

17) Y. Muto, M. Kato, H. B. Jonassen, and L. C. Cusachs, This Bulletin, **42**, 417 (1969).

18) M. Kato, Y. Muto, H. B. Janassen, K. Imai, K. Katsuki, and S. Ikegami, *ibid.*, 2555 (1969).

19) J. E. Whinnery and W. H. Watson, *J. Coord. Chem.*, **1**, 207 (1972).

Transference of Water to the Nitrobenzene Phase for the Extraction of Tris(1,10-phenanthroline)iron (II) and Tris(2,2′-bipyridine)iron(II) Chelate Salts

Yuroku YAMAMOTO, Tsunehiko TARUMOTO, and Takao TARUI

Department of Chemistry, Faculty of Science, Hiroshima University, Higashisenda-machi, Hiroshima 730

(Received October 2, 1972)

The amount of water transferred to the nitrobenzene phase was determined for the extraction of ion pairs of tris(1,10-phenanthroline)iron(II) and tris(2,2′-bipyridine) iron(II) with halide and pseudohalide anions. For both chelate systems the smaller the anion, the greater the amount of water transported, very similar results being obtained for a common anion. The results were discussed in relation to water of crystallization, extractability and temperature effect.

During the course of studies on the solvent extraction mechanism of tris(1,10-phenanthroline)iron(II) and tris(2,2′-bipyridine)iron(II) chelate ion pairs, our attention was drawn to the problem of how ion pairs are hydrated. We showed[1] that a small amount of water in nitrobenzene greatly affects the heats of solution of the chelate salts.

In order to investigate the role of water in solvent extraction, the amount of water transported by the ion pairs was determined. Similar studies were carried out by varying chelate cations.[2] However, no effects of anions were observed. We observed a very clear trend depending on the counter anions. Similar results were obtained between both chelate salts with a common counter anion. A part of the work has been reported.[3]

Experimental

Materials. Crystals of $Fe(phen)_3(ClO_4)_2$, $Fe(phen)_3(SCN)_2$, $Fe(phen)_3I_2$, $Fe(phen)_3Br_2$, $Fe(bipy)_3(ClO_4)_2$, $Fe(bipy)_3(SCN)_2$, $Fe(bipy)_3I_2$, and $Fe(bipy)_3Br_2$ were prepared as follows. In 400 ml of water, 0.01 mol of Mohr's salt and 0.03 mol of 1,10-phenanthroline or 2,2′-bipyridine were dissolved. To the resulting dark red solution was added 30 ml of saturated solution of sodium salt of a corresponding anion and the solution was condensed to an appropriate volume on a water bath at about 80 °C. The solution was cooled to room temperature and the crystalline precipitate was separated by filtration. Crystals thus obtained were recrystallized twice from water and air-dried. The purity was confirmed by analysis at the Center for Chemical Analysis of Kyoto University. The analytical results are shown in Table 1.

Nitrobenzene of analytical reagent grade was successively washed with sulfuric acid, sodium hydroxide and distilled water, and was then distilled under reduced pressure.

Apparatus. A Karl Fischer automatic titrator, MK-SS of Kyoto Electronics Co., Ltd. was used for determination of the water content. The concentration of the chelate salts was determined with a spectrophotometer, Hitachi 139.

Procedure. In a glass bottle, 100 ml of nitrobenzene was mixed with 50 ml of water for 4 days under stirring with a magnetic stirrer at 25±0.1 °C and the water content in nitrobenzene was occasionally checked by Karl Fischer titration. It was found that stirring for 24 hr was sufficient for the water content in nitrobenzene to become constant. A certain amount of a chelate salt was then added to this mixed solvent and the solution was stirred for 3 hr. Distribution of the chelate salt between water and nitrobenzene was found to be complete after 10 min stirring from measurement of the absorbance of both phases (510 nm for aqueous phase and 516 nm for organic phase). For an aliquot of the nitrobenzene extract, the water content was determined by titration. The concentration of the chelate salt was determined from the absorbance at 516 nm with the aid of a calibration curve prepared beforehand.

Results and Discussion

The water content at 25 °C was plotted against the concentration of $Fe(phen)_3I_2$ as in Fig. 1. The lines

TABLE 1. RESULTS OF ANALYSIS OF $FeL_3X_2 \cdot nH_2O$

X	L	n[a]	C %		H %		N %	
			Calcd	Found	Calcd	Found	Calcd	Found
ClO_4	phen	1	53.16	53.94	3.23	3.26	10.33	10.59
	bipy	0	49.82	49.69	3.34	3.38	11.62	11.63
SCN	phen	2	60.95	61.17	3.78	3.96	14.97	14.90
	bipy	3	55.33	55.06	4.35	4.37	16.13	16.03
I	phen	2	48.78	48.73	3.18	3.16	9.48	9.76
	bipy	5	41.50	41.70	3.95	3.95	9.68	9.64
Br	phen	6	50.02	49.55	4.21	4.16	9.73	9.70
	bipy	5	46.54	46.22	4.43	4.56	10.85	10.85

a) Round numbers were allotted so that experimental values of elements most closely fit the calculated ones.

1) Y. Yamamoto and T. Tarumoto, *Anal. Lett.*, **3**, 537 (1970).
2) S. Burchett and C. E. Meloan, *Separ. Sci.*, **3**, 119 (1968); D. R. Gere and C. E. Meloan, *ibid.*, **3**, 298 (1968).
3) Y. Yamamoto, T. Tarumoto, and T. Tarui, *Chem. Lett.*, **1972**, 459.

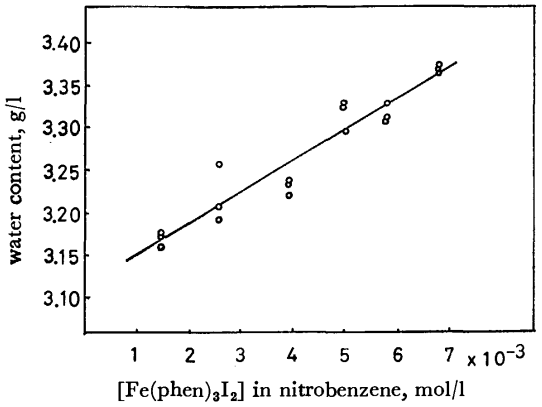

Fig. 1. Water content *vs.* the concentration of the chelate salt in nitrobenzene, 25 °C.

were drawn by means of the least-squares method. The water content increases linearly as the chelate salt concentration increases. This holds for all the other chelate salts. The concentration ranges tested were: (1) phenanthroline series, for perchlorate $1.8—5.2\times10^{-2}$, for thiocyanate $0.89—7.4\times10^{-3}$, for iodide $1.5—6.8\times10^{-3}$ and for bromide $1.4—2.4\times10^{-4}$ mol/l, (2) bipyridine series for perchlorate $3.6\times10^{-3}—3.8\times10^{-2}$, for thiocyanate $7.2\times10^{-4}—6.0\times10^{-3}$ for iodide $1.4—6.8\times10^{-3}$ and for bromide $7.2\times10^{-5}—4.8\times10^{-4}$ mol/l in the nitrobenzene phase.

The water content in nitrobenzene in the absence of chelate salts was 2.57 g/kg and the cross sections of the plots, water content *vs.* chelate salt concentration agreed with this within experimental error. Thus the number of water molecules transported by the chelate salts was calculated from the slope of the plots. The results are shown in Table 2 where they are also compared with the number of water of crystallization obtained from TGA measurements and elemental analyses.

Very similar results were obtained for the two series. Bipyridine-bromide salt shows a somewhat lower value than that of the corresponding phenanthroline salt because the concentration of $Fe(bipy)_3Br_2$ in the aqueous phase is much higher than that of $Fe(phen)_3Br_2$. For the phenanthroline series, there is a consistency between the number of transported water and that of water of crystallization. Also for the bipyridine series similar results were obtained between the transferred water and the water of crystallization except for iodide. The consistency for the former series might be fortuitous,

Table 2. Water transferred and the water of crystallization with FeL_3X_2 (in mol/mol of the chelate salt)

L	X	Temp (°C)	Water transferred	Water of crystallization	
				TGA	Analysis
phen	ClO_4	25	0.64±0.04	1	1
		20	0.56±0.02		
	SCN	25	1.9 ±0.1	1.5	2
		20	1.9 ±0.1		
	I	25	2.1 ±0.2	2	2
		20	1.6 ±0.1		
	Br	25	5.5 ±0.8	6	6
		20	—		
bipy	ClO_4	25	0.72±0.02	0	0
		20	0.58±0.01		
	I	25	2.1 ±0.2	5	5
		20	1.6 ±0.1		
	Br	25	3.6 ±1.9	5	5
		20	—		

there being no reason why the crystalline state should be similar to the ions in solution. However, it can be concluded that water is transported exclusively by the anions and the chelate cations take no part in the transference. The chlorides did not offer any useful information because of their extremely low extractability.

Temperature effect was also studied by carrying out the same procedure at 20 °C. Lower values were obtained as shown in Table 2. The solubility of water in nitrobenzene was also found to decrease as the temperature is lowered (2.57 g/kg at 25 °C and 2.16 g/kg at 20 °C). This suggests that the water transported by the chelate salts is in equilibrium with the dissolved water in nitrobenzene.

The ability of the anions to carry water into the nitrobenzene phase seems to be related to the tendency of their hydration; the smaller the anions, the greater the amount of water transported. This may cause the lower extractability of the ion pairs with smaller counter anions.[4] However, it is difficult to conclude from our results whether the transferred water in nitrobenzene exists hydrated to the anions or it is dispersed in the organic phase.

4) Y. Yamamoto, T. Tarumoto, and E. Iwamoto, *ibid.*, **1972**, 255.

Cadmium and Silver Sulfide-impregnated Silicone Rubber Membranes as Selective Electrodes for Cadmium Ions

Hiroshi HIRATA and Kenji DATE

Wireless Research Laboratory, Matsushita Electric Industrial Co., Ltd., Kadoma, Osaka 571

(Received September 12, 1972)

Silicone rubber membranes impregnated with mixtures of cadmium sulfide and silver sulfide were developed as selective electrodes for cadmium ions in a solution. Both co-precipitated and sintered mixtures could be used as the active materials for the electrode membrane, but here the membrane which contained a mixture in which cadmium sulfide had been added to silver sulfide after they had been precipitated individually did not show the satisfactory response characteristics. The Nernstian slope was obtained in the activity range from 10^{-1} to 10^{-5} M Cd^{2+}, while the analytical range was from 10^{-1} to 10^{-6} M. These potentials did not change at pH values from 2.5 to 7.5. Among common ions, silver, copper(II), mercury(II), iron(III), sulfide, and iodide ions interfered seriously. About 10—100 times as many lead and bromide ions and more than 1000 times as many alkali metals, alkaline earth metals, zinc, aluminum, nickel, manganese(II), cobalt, nitrate, and perchlorate ions were tolerated in coexistence with cadmium ions.

Many attempts have recently been made to obtain the precipitate-impregnated membranes as selective electrodes.[1] Pungor[2] developed silver salt-impregnated silicone rubber membrane electrodes for chloride, bromide, iodide, sulfide, and silver ions.

As for ion-selective electrodes for cations other than silver ions, various kinds of precipitate-impregnated membranes were made. These membrane electrodes, however, proved unsatisfactory for potentiometric measurements, either because they did not give the desired response or because they had no selectivity toward particular ions in a solution.

Copper(I) sulfide-impregnated silicone rubber membrane electrodes have been developed for copper(II) ions in our laboratory.[3] The internal electrode and internal solution have been eliminated by attaching the membrane to the surface of a metal directly. Lead sulfide-impregnated silicone rubber membrane electrodes for lead ions have also been described in a previous paper,[4] in which an investigation of the soaking effect of the membrane before the measurement has been presented.

On the other hand, a cadmium ion-selective compressed membrane electrode, the membrane of which comprised an intimate mixture of silver sulfide and cadmium sulfide, has been developed by Frant and Ross.[1] Subsequently, a cadmium ion-selective ceramic membrane electrode has been prepared by applying a hot-pressing method; this membrane contains cadmium sulfide, silver sulfide, and copper(I) sulfide.[5]

The present paper will describe the development of selective electrodes for cadmium ions using cadmium and silver sulfide-impregnated silicone rubber membranes, which have the same construction as has been described in the previous papers. It will also discuss the incorporation effect of silver sulfide.

Experimental

Apparatus and Reagents. An Orion Model 801 digital pH/mV meter was used to make the potentiometric measurements. A Horiba Seisakusho 2530-05T saturated calomel electrode was used as the reference electrode. The silicone rubber was obtained from the Shin-Etsu Chemical Co., and all the reagents were Nakarai Chemical reagent-grade materials and were used without further purification.

Preparation of Cadmium and Silver Sulfide-impregnated Silicone Rubber Membrane Electrodes. The preparation of the active materials can be divided roughly into the following two methods; the co-precipitation method, which consists of bubbling hydrogen sulfide through an aqueous solution containing cadmium and silver nitrates in order to precipitate a mixture of silver and cadmium sulfides at room temperature, and the sintering method, which consists of the sintering of the mixture of cadmium and silver sulfides at 300—500 °C for 3 hr in a stream of hydrogen sulfide at 50—100 ml min^{-1}. The silver sulfide for the sintered mixture was prepared by the direct reaction of silver metal powder and sulfur in a nitrogen gas stream, as has previously been described.[6] The cadmium sulfide was made by bubbling hydrogen sulfide through an aqueous solution of cadmium nitrate at room temperature.

The sulfide-mixture thus sintered was ground to a particle size of less than 10 μm. The powdered mixture of cadmium and silver sulfides was then mixed with 25 w/w% of silicone rubber. A platinum plate (1 mm thick) or wire (1 mm in diameter) which was directly connected with a leading wire was coated with the mixture to a thickness of about 0.5 mm. After being polymerized, the membrane was held in a plastic holder filled with epoxy resin.

The membrane electrode was then soaked in a 10^{-2} M aqueous solution of cadmium nitrate at 25 °C for a week.

Measurement of Potentials The potentials developed by the membrane electrode in the test solution were measured with a saturated calomel electrode as the reference electrode at 25±0.1 °C. The slope of the straight line of E *vs.* log $a_{Cd^{2+}}$ and the concentration range for the obedience to Nernst's law were investigated in order to evaluate the validity of the electrode membrane.

Magnetic stirring was employed at a constant rate to insure good reproducibility. Between measurements, the

1) R. A. Durst (Ed.), "Ion-Selective Electrodes," N. B. S. Spec. Publ. 348, U. S. Printing Office, Washington, (1970).
2) E. Pungor, *Anal. Chem.*, **39**, A28 (1967).
3) H. Hirata and K. Date, *Talanta*, **17**, 883 (1970).
4) H. Hirata and K. Date, *Anal. Chem.*, **43**, 279 (1971).
5) H. Hirata and K. Higashiyama, *Z. Anal. Chem.*, **257**, 104 (1971).
6) H. Hirata and K. Higashiyama, *Anal. Chim. Acta*, **54**, 415 (1971).

electrode pair was rinsed several times with distilled water. The outer chamber of the double-junction reference electrode was drained and filled daily prior to the measurements of the potentials with 0.1 M of potassium nitrate solution.

No potential changes were observed on filling. Standard solutions containing 10^{-4} M or less of Cd^{+2} should be prepared whenever their potentials are measured. Otherwise, deviations from the Nernst law may arise through the adsorption of the solution on the wall of a beaker and the contamination of the solution.

Results and Discussion

The copper(II) sulfide-impregnated silicone rubber membrane selectively responded to cupric ions,[3] although copper(II) sulfide was a crystal with a high-electron conductivity.[7] However, the copper(II) sulfide-compressed membrane did not respond to cupric ions unless silver sulfide was added. Lead sulfide is also a semiconducting polar crystal with a high-electron conductivity at room temperature.[8] Nevertheless, the lead sulfide-impregnated silicone rubber membrane electrode responded to lead ions and showed a good selectivity, as has been described in a previous paper.[4] However, a pure lead sulfide sintered or compressed membrane, in which no trace of silver could be detected by emission spectroscopy, proved inert to lead ions in a solution. On the basis of the above results, the differentiation in the behavior of heterogeneous and homogeneous membrane electrodes seems to involve not only mechanical but also electrochemical problems.

The pure cadmium sulfide used was an insulator at room temperature, so that the cadmium sulfide-impregnated silicone rubber membrane electrode provided no meaningful response as an ion-selective electrode for cadmium ions. When the pure cadmium sulfide was sintered in a nitrogen gas stream including a slight amount of oxygen, pulverized, and impregnated in silicone rubber, the membrane thus obtained could act as a semiconductor. Its conductivity is supposed to be induced by the presence of a slight excess of cadmium produced by oxidation of cadmium sulfide. The potentials produced by the electrode membrane were unsteady and sensitive to the presence of static charges and visible light. This electrode membrane could not provide the Nernstian slope at all.

In the case of cadmium sulfide mixed with a metal sulfide other than silver sulfide, such as a cadmium sulfide-cuprous sulfide system, the sintered mixture-impregnated silicone rubber membrane electrode did not exhibit any effective response toward cadmium ions, although the membrane had semiconductive characteristics because of the conductivity of cuprous sulfide.

When cadmium sulfide was incorporated with silver sulfide in the silicone rubber membrane, the electrode fabricated from the membrane showed sensitive and stable potentials toward cadmium ions. Figure 1 shows the relationship between the potentials and the activities

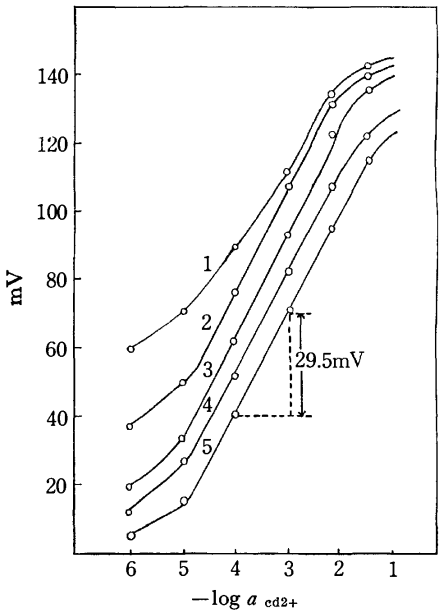

Fig. 1. Relationship between electrode potential and activity of cadmium ion. Weight ratio of CdS to Ag_2S. 1. 80 to 20, 2. 60 to 40, 3. 20 to 80, 4. 10 to 90, 5. 5 to 95.

of cadmium ions by the silicone rubber membrane electrodes containing a mixture of cadmium sulfide and silver sulfide prepared by the precipitation method.

Only the membranes containing an intimate and uniform mixture of silver sulfide and cadmium sulfide obtained by the co-precipitation method showed very satisfactory potential changes in relation to the concentration of cadmium ions. However, sufficient potential changes were not observed with the membrane containing a mixture of cadmium and silver sulfides which had been separately precipitated. The differentiation of the structure of the two mixtures has, however, not yet been clarified enough.

The co-precipitate-impregnated membrane electrode yielded a linear response toward cadmium ions over a concentration range of 10^{-1}—10^{-5} M cadmium nitrate, with an observed slope of 29.5 mV per log Cd^{2+} unit at 25 °C; this is in good agreement with the Nernst law. The analytical concentration range by this electrode was 10^{-1}—10^{-6} M. However, the best membrane of the impregnated silicone rubber electrode is less sensitive than the compressed or sintered membrane electrodes.[5] In general, the response characteristics, such as the sensitivity and response rate, of a precipitate-impregnated silicone rubber membrane electrode seems to be inferior to those of a precipitate-compressed or a precipitate-sintered membrane electrode.

As for the composition of the active materials, more than 60 w/w % of cadmium sulfide and less than 40 w/w % of silver sulfide could not provide sufficient potential changes or high response rates to the changes in the cadmium ion concentration.

When the mixture of cadmium sulfide and silver sulfide obtained by the sintering method was used as an active material, the silicone rubber membrane showed almost the same response characteristics as the co-precipitate-impregnated one. However, the sufficient

7) H. Devaux and J. Cayrel, *C. R. Acad. Sci. Paris*, **198**, 1339 (1934).

8) R. L. Petritz and W. W. Scanlon, *Phys. Rev.*, **97**, 1620 (1955).

potential changes were not observed with the membrane containing the mixture of cadmium and silver sulfides which had been separately prepared by the reaction of the corresponding metal and sulfur.

The response time of the measuring cell was a few sec for 10^{-2} M Cd^{+2} and about ten min for a 10^{-6} M solution. The membrane had to be soaked in a 10^{-2} M cadmium nitrate solution for more than 5 days after its preparation. However, once the membrane was soaked, the potentials were stable and steady even if the membrane was exposed to air for more than two weeks.

When the fraction of the silicone rubber in the membrane was more than 50% by weight, the potentials were unsteady and unstable, so that it could not be measured. When it was decreased to less than 50%, the time required for soaking in the solution of cadmium nitrate decreased and the potentials became more stable; potential properties similar to those shown in Fig. 1 were thus obtained. However, the lower the fraction of silicone rubber in the membrane, the lower the adhesive force.

Effect of Temperature. The co-precipitate- or the sintered mixture-impregnated silicone rubber membrane electrodes are affected by changes in the temperature. The single potential of a reference electrode changes slowly with the temperature because of changes in the solubility equilibrium on which the electrode potential depends. The potential of the silicone rubber membrane electrode for cadmium ions also varies with the temperature, as is indicated by the Nernst factor, 2.303 $RT/2F$, within the limits of experimental error. The electrodes could be safely used at temperatures between 0 and 60 °C.

Influence of pH. The desirable pH of a solution was adjusted with newly-prepared buffer solutions. Figure 2 shows the influence of pH on the potentials of cadmium ion-selective silicone rubber membrane electrodes in 10^{-2} and 10^{-4} M Cd^{+2} solutions.

The potentials did not change between pH 2.5 to 7.5. They decreased sharply, however, when the pH increased above 7.5, for the precipitation of $Cd(OH)_2$ occurred. Of course, the pH at which the precipitation begins depends on the concentration of cadmium ions. The resulting curves in Fig. 2 also show that the measurable pH-range is independent of the presence of silicone rubber. The cadmium sulfide content in the membrane did not affect the range of pH, either.

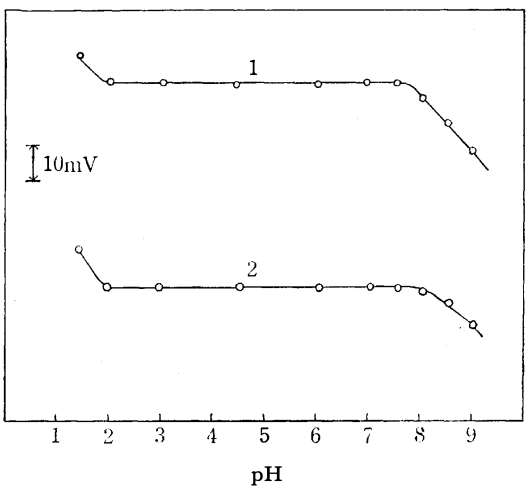

Fig. 2. Influence of pH. 1. 10^{-2} M Cd^{2+}, 2. 10^{-4} M Cd^{2+}

Dynamic Response Rate. When an ion-selective membrane electrode is used for the concentration control of a reaction process or as an indicator electrode in the potentiometric titration, the dynamic response characteristics are very important factors. The cadmium ion-selective precipitate-impregnated silicone rubber membrane electrode was evaluated by exposing the electrode to a rapid change in cadmium-ion concentration (exactly twofold) and recording the e.m.f. *vs.* time function. Some typical response curves are represented in Fig. 3. In the observed concentration range, the co-precipitate-impregnated electrode was found to establish the equilibrium reading rather rapidly after the applied concentration was changed. The sintered mixture-impregnated membrane electrode could equilibrate more quickly than the co-precipitate-impregnated one.

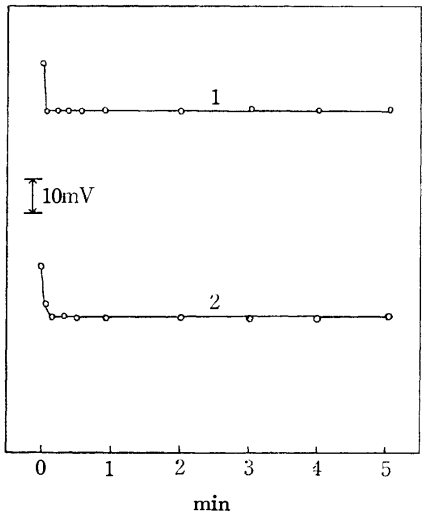

Fig. 3. Dynamic response rate.
1. 10^{-2} M—5×10^{-3} M, 2. 10^{-4} M—5×10^{-5} M

All of the curves thus obtained were smooth and of an identical shape; the e.m.f. values expected on the basis of the calibration curves were attained in all cases. The response rate of the electrode used depends on the stirring method, the efficiency of the solution mixing, and the cleanliness of the membrane surface, but is independent of the initial ion concentration over the entire range studied.

However, when the impregnated silicone rubber membrane contained a mixture in which cadmium sulfide had been added to silver sulfide after they had been precipitated individually, the electrode fabricated from this membrane did not show a fast dynamic response rate.

Selectivity. No electrode is entirely selective toward a particular ion in a solution, and the presence of the other ions may seriously impair electrode performance. It is, therefore, important to be aware of such interferences. An approximate selectivity con-

stant can be derived experimentally from the ratio of ionic concentrations where the interfering ions cause a deviation from the expected theoretical slope, 2.303 $RT/2F$. Tests of the effects of several ions on the membrane electrodes were made in solutions containing 10^{-4} M of cadmium ions. The concentration ratios of common ions to cadmium ions were varied from 1 to 1000. Among common ions, silver, copper(II), mercury(II), iron(III), sulfide, and iodide ions interfered seriously. About 10—100 times as many lead and bromide ions and more than 1000 times as many alkali metals, alkaline earth metals, zinc, aluminum, nickel, manganese(II), cobalt, nitrate, and perchlorate ions were tolerated in coexistence with cadmium ions.

The numerical selectivity ratios of the electrode for cadmium ions with respect to these common ions were not evaluated, but in view of these findings it is clear that this electrode is well suited for the selective analytical measurement of cadmium ion activity in a wide variety of practical systems.

The authors wish to thank Dr. S. Kisaka, Dr. K. Sugihara, and Dr. S. Mori for their encouragement during this work.

BULLETIN OF THE CHEMICAL SOCIETY OF JAPAN, VOL. 46, 1471—1479 (1973)

Electronic Spectra of High-Spin Iron(III) Tetraphenylporphins

Hiroshi KOBAYASHI, Yasuo YANAGAWA, Hisajiro OSADA,
Shuji MINAMI, and Masayuki SHIMIZU

Department of Chemistry, Tokyo Institute of Technology, Ookayama, Meguro-ku, Tokyo 152

(Received September 16, 1972)

Characterization of the electronic absorption spectra of high-spin iron(III) porphyrins was carried out on the basis of observation and theoretical calculation for tetraphenylporphinatoiron(III) and -manganese(III) complexes.

Electronic absorption spectra of the iron(III) porphyrins have not been wholly understood, although experimental correlations between the electronic structure and spectra have been studied mainly for analysis of their behaviors in the biological processes. Many physico-chemical studies have been carried out on the ferri-hemoproteins occurring in nature such as methemoglobin, catalase, peroxidase, and cytochromes.[1] We present in this paper a characterization of the electronic absorption spectra of high-spin iron(III) porphyrins on the basis of observation and theoretical calculation for tetraphenylporphinatoiron(III) and -manganese(III) complexes.

Experimental

Synthesis of the Metal-free Base of Tetraphenylporphin. $\alpha,\beta,\gamma,\delta$-Tetraphenylporphin (TPP) was synthesized from pyrrole and benzaldehyde by the method of Adler *et al.*[2] Methods developed by Rothermund and by others[3] were also used in preliminary experiments. TPP was precipitated from chloroform elute of the product by adding excess methanol. The crystals thus obtained were recrystallized from chloroform-methanol mixture. Chromatographic purification was repeated on activated alumina columns using chloroform as solvent and also eluent. After the eluate was concentrated, excess methanol was added. Purple needle crystals thus obtained were identified by elemental analysis.

Found: C, 86.02; H, 5.18; N, 8.94%. Calcd for $C_{44}H_{30}N_4$: C, 85.97; H, 4.92; N, 9.11%.

The electronic absorption spectrum of the product dissolved in benzene was in excellent agreement with reported spectra.[4-6]

Syntheses of Tetraphenylporphinatoiron(III) Complexes. The methods of Rothermund and Menotti[7] and Dorough *et al.*[8] were employed with some modification. About 500 mg of the metal-free base and 300 mg sodium chloride were dissolved in 50 ml chloroform. A saturated solution of ferrous acetate in acetic acid, prepared just before use by dissolving iron powder in 150 ml glacial acetic acid while still warm, was added to a chloroform solution of TPP. The mixture was refluxed for 3 hr and then most of the chloroform and acetic acid was distilled off. When the solution was concentrated up to 50 ml, TPPFe(III)Cl was precipitated by adding methanol. The crystals thus obtained were repeatedly recrystallized from the mixed solvent chloroform-methanol. The recrystallized blue violet needle crystals were identified

1) See, for example, J. E. Falk, "Porphyrins and Metalloporphyrins," Elsevier Publishing Co., Amsterdam (1964); J. E. Falk, R. Lemberg and R. K. Morton, "Haematin Enzymes," Pergamon Press, Oxford (1961); B. Chance, R. W. Estabrook and T. Yonetani, "Hemes and Hemoproteins," Academic Press, New York (1966).

2) A. D. Adler, F. R. Longo, J. D. Finarelli, J. Goldmacher, J. Assour and L. Korsakoff, *J. Org. Chem.*, **32**, 476 (1967).

3) P. Rothermund, *J. Amer. Chem. Soc.*, **59**, 2010 (1935); P. Rothermund and A. R. Menotti, *ibid.*, **63**, 267 (1941); S. Aronoff and M. Calvin, *J. Org. Chem.*, **8**, 205 (1934); R. H. Ball, G. D. Dorough and, M. Calvin, *J. Amer. Chem. Soc.*, **68**, 2278 (1946).

4) D. W. Thomas and A. E. Martell, *J. Amer. Chem. Soc.*, **78**, 1335, 1338 (1956).

5) G. M. Badger, R. A. Jones, and R. L. Laslett, *Austral. J. Chem.*, **17**, 1028 (1964).

6) J. Mullins, A. D. Adler, and R. Hochstrasser, *J. Chem. Phys.*, **43**, 2548 (1965).

7) P. Rothermund and A. R. Menotti, *J. Amer. Chem. Soc.*, **70**, 1808 (1948).

8) G. P. Dorough, J. R. Miller, and F. M. Huennekens, *ibid.*, **73**, 4315 (1951).

TABLE 1. ELEMENTAL ANALYSES

TPPFe(III)X	Found (%)				Calcd (%)			
	C	H	N	Fe	C	H	N	Fe
$C_{44}H_{28}N_4FeBr$	71.27	3.89	7.51	7.32	70.61	3.77	7.49	7.46
$C_{44}H_{28}N_4FeI$	68.19	3.70	7.36	7.15	66.44	3.55	7.04	7.02
$C_{44}H_{28}N_4FeSCN$	73.39	3.86	9.36	7.72	74.38	3.88	9.64	7.69
$C_{44}H_{28}N_4FeOCOCH_3$	75.13	4.23	7.47	7.70	75.93	4.39	7.70	7.68

by elemental analysis.

Found: C, 74.81; H, 4.11; N, 7.76; Fe, 7.82%. Calcd for $C_{44}H_{28}N_4FeCl$: C, 75.07; H, 4.01; N, 7.96; Fe, 7.93%. Iron was determined by colorimetry using phenanthroline.

TPPFe(III)Br, TPPFe(III)I, TPPFe(III)SCN, and TPPFe(III)$OCOCH_3$ were synthesized and purified by similar methods to those for TPPFe(III)Cl. The products were identified by elemental analyses (Table 1).

Synthesis of Tetraphenylporphinatomanganese(III) Chloride. TPPMn(III)$Cl\cdot H_2O$ was prepared by the method of Rothermund and Menotti.[7] The metal-free base and manganese(II) acetate were refluxed in a mixed solvent chloroform-acetic acid. Recrystallization from mixed solvent dry chloroform-ligroin gave green crystals. The absorption spectrum of the complex dissolved in pyridine was in good agreement with that in the literature.[9]

Found: C, 74.85; H, 4.30; N, 8.18; Mn, 7.67%. Calcd for $C_{44}H_{28}N_4MnCl\cdot H_2O$: C, 73.28; H, 4.19; N, 7.77; Mn, 7.62%.

Manganese was determined by colorimetry after it had been oxidized to permanganate.

Measurements of Absorption Spectra and Magnetic Circular Dichroism. Electronic absorption spectra were recorded on a Shimadzu recording spectrophotometer Model MPS-50 and a Beckman DU spectrophotometer using quartz cells of 0.1 and 1.0 cm light path. Solvents were benzene, methanol and pyridine purified by fractional distillations using a 1.5 m wire packed column and dried by the usual procedures.[10]

The absorption spectra of powder samples were measured by the opal glass method.[11] Instead of an opal glass plate, we placed a sheet of tracing paper smeared with the solid sample in front of the window of an end-on type photomultiplier in the Shimadzu spectrophotometer. The absorption spectra thus obtained were better than those observed by the original opal glass method.

Circular dichroism under an external magnetic field (MCD) was measured by a JASCO automatic recording spectropolarimeter Model ORD/UV-5 with CD attachment and an electromagnet.[12] The magnetic field was set at 10000 Gauss.

Magnetic Susceptibility. Magnetic susceptibilities of the complexes were measured at room temperature by means of the Gouy method. After calibrating for the diamagnetic term by the usual method,[13] the magnetic moment of complexes was evaluated. The magnetic moment in solution was also determined by the same method.

TABLE 2. MAGNETIC MOMENTS OF IRON(III)- AND MANGANESE (III) TETRAPHENYLPORPHINS

Complex	Magnetic moment (Bohr magneton)	Number of unpaired electrons	Spin state
TPPFe(III)Cl	5.88	5	$S=5/2$
TPPFe(III)Br	6.08	5	$S=5/2$
TPPFe(III)I	5.71	5	$S=5/2$
TPPFe(III)SCN	5.75	5	$S=5/2$
TPPFe(III)$OCOCH_3$	6.03	5	$S=5/2$
TPPFe(III)Cl in chloroform	5.6	5	$S=5/2$
TPPMn(III)$Cl\cdot H_2O$	4.98	4	$S=2$

Results and Discussion

Iron(III) porphins with an ionic axial ligand such as Cl^-, Br^-, I^-, SCN^-, CH_3COO^- are in the high-spin state $S=5/2$. The spin state of TPPFe(III)X was identified by magnetic susceptibility measurements. The results are summarized in Table 2. These high-spin TPPFe(III)X complexes with different axial ligands actually gave the same absorption spectrum in shape and position. A typical absorption spectrum of TPPFe(III)X ($S=5/2$) in benzene is shown in Fig. 1. The spectrum has a more complicated profile as compared with the typical absorption spectra obtained for the lowest (π, π^*) transitions of the square planar metal porphins. Figure 1 also shows characteristic

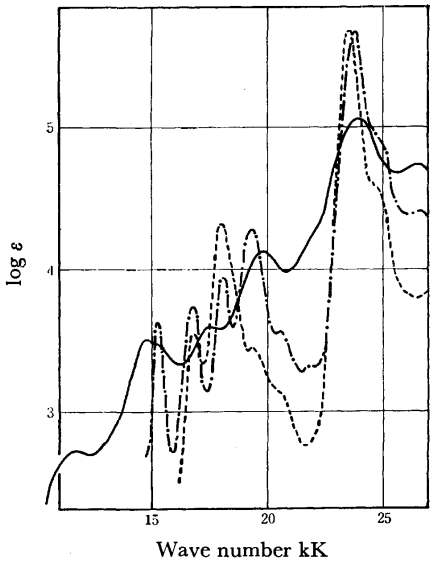

Fig. 1. Absorption spectra of TPPFe(III)Cl, TPPZn(II) and the metal free base in benzene.
——: TPPFe(III)Cl - - -: TPPZn(II)
-·-·-: $TPPH_2$

9) L. J. Boucher, *ibid.*, **92**, 2725 (1970).
10) J. A. Riddick and E. E. Troops, "Organic Solvents, Techniques of Organic Chemistry," Vol. 7, ed. by A. Weissberger, Interscience Publishers, New York (1955).
11) K. Shibata, "Methods of Biochemical Analysis," Vol. 7, ed. by D. Glick, Intersciences Publishers, New York (1959), p. 77.
12) H. Kobayashi, M. Shimizu, and I. Fujita, This Bulletin, **43**, 2335 (1970).
13) B. N. Figgis and J. Lewis, "Modern Coordination Chemistry," ed. by J. Lewis and R. G. Wilkins, Interscience Publishers, New York (1960), p. 415.

absorption spectra of the metal-free porphin (D_{2h}) and square planar metal porphins (D_{4h}).

The general feature of the absorption spectrum of TPPFe(III)X is in good agreement with that of a characteristic absorption spectrum of the high-spin species of ferri-hemoproteins. George, Beetlestone and Griffith separated high- and low-spin spectral types for the ferri-hemoproteins by combining spectroscopic and magnetic data,[14] and showed that in the case of ferri-hemoproteins, the iron(III) porphyrin is in an equilibrium between two spin states $S=5/2$ and $S=1/2$. They were able to get limiting spectra from the mixture spectra of two spin states. Although the existence of negative absorption regions shows some deficiency in their assumptions, the overall results seem to be sound.

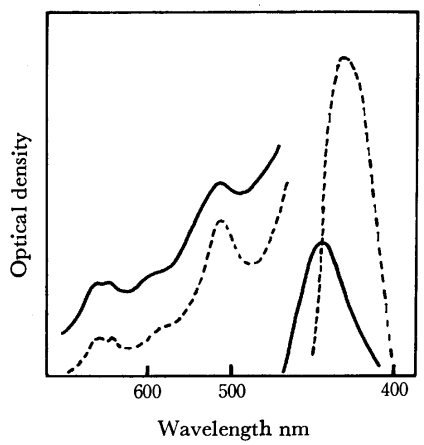

Fig. 2. Absorption spectrum of TPPFe(III)Cl in the solid state.
——: powder ---: benzene solution

The magnetic susceptibility measurement of TPPFe(III)Cl in chloroform solution indicates that the spin state found in the solid state is well preserved in chloroform solution. Chloroform was used instead of benzene because of the higher solubility of porphin. The absorption spectrum of TPPFe(III)Cl in chloroform was coincident with that of the benzene solution. In contrast, the solid state absorption spectrum of TPPFe(III)Cl obtained by the modified opal glass method was in good agreement with that of the benzene solution except for a red shift of the Soret band in the solid state which might be due to an exciton coupling between the strong Soret oscillators packed in a molecular crystal (Fig. 2). The spin state of the complex TPPFe(III)Cl does not change upon dissolution. Thus such a complicated spectrum as shown in Fig. 1 should be assigned to the absorption spectrum characteristic of high-spin iron(III) porphin.

The lowest excitations in a typical D_{4h} metal porphin are assigned to the lowest (π, π^*) transitions approximately described by a 50-50 admixture of the transitions $(3a_2)\rightarrow(4e)$ and $(1a_1)\rightarrow(4e)$, where $(3a_2)$ and $(1a_1)$ are the highest occupied orbitals and (4e) the degenerate lowest vacant orbitals. A configuration interaction between these two excited configurations

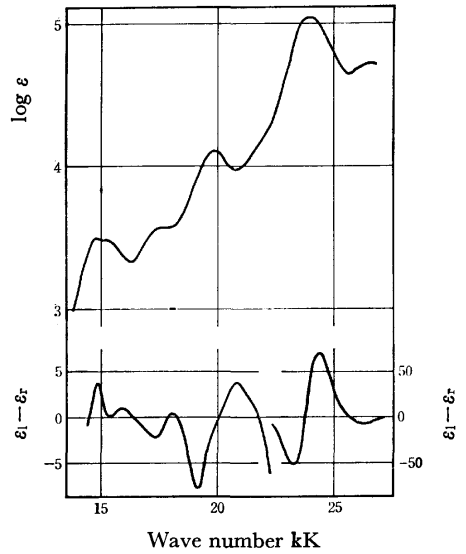

Fig. 3. MCD spectrum of TPPFe(III)Cl in benzene.
Upper: absorption spectrum Lower: MCD spectrum

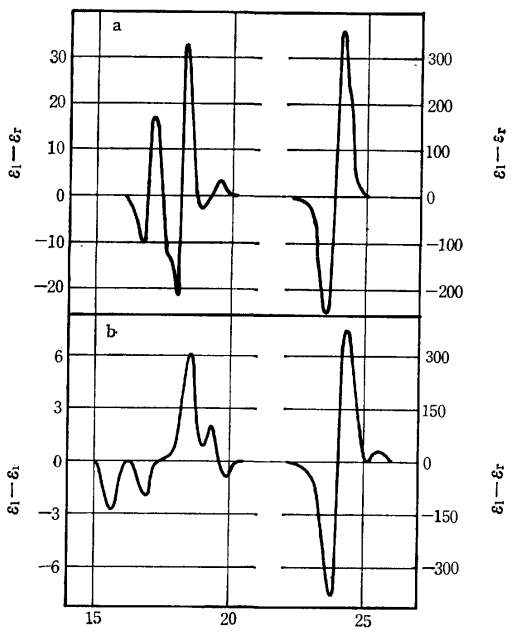

Fig. 4. MCD spectra of TPPZn(II) and the metal free base in benzene.
a: TPPZn(II), b: $TPPH_2$

gives rise to the lowest transition of forbidden character and the second lowest transition of allowed character, the former being Q transition and the latter B transition (or Soret transition). This is a four-orbital description of the lowest (π, π^*) transition in porphin.[15] The lowest electronic excitations of TPPZn(II), in which only a very small π interaction between metal and porphin is present, are well described by the four-orbital model.[16,17] However, the model can not ex-

14) P. George, J. Beetlestone, and J. S. Griffith, "Haematin Enzymes," ed. by J. E. Falk, R. Lemberg, and R. K. Morton, Pergamon Press, Oxford (1961), p. 105.

15) M. Gouterman, *J. Chem. Phys.*, **30**, 1139 (1959).
16) H. Kobayashi, *ibid.*, **30**, 1362 (1959).
17) C. Weiss, H. Kobayashi, and M. Gouterman, *J. Mol. Spectrosc.*, **16**, 415 (1965).

plain the lowest excitations of high-spin TPPFe(III)X complexes. A similarity in the visible absorption spectra of high-spin iron(III) porphin and the metal-free base has been pointed out.[18] However, these two porphins show quite different MCD spectra as shown in Figs. 3 and 4. The visible and near-ultraviolet absorption spectra of the metal-free base are described as the lowest (π, π^*) transitions. Thus the splitting of the visible Q band was, in principle, well reproduced by a Pariser-Parr-Pople molecular orbital calculation.[17]

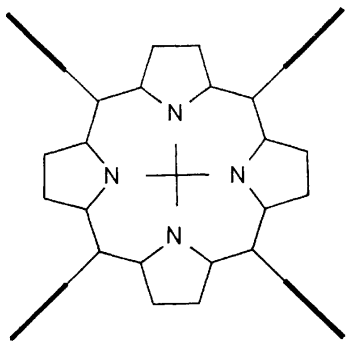

Fig. 5. Molecular geometry of metal tetraphenylporphin. Phenyl groups are actually perpendicular to the molecular plane of porphin.

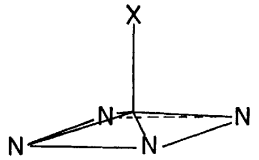

Fig. 6, The coordination sphere of iron(III) ion in TPPFe(III)X. Iron ion is slightly out of the porphin plane.

Tetraphenylporphin has a planar structure as shown in Fig. 5. The central iron is displaced out-of-plane from the nitrogen atoms by 0.4 Å as found by X-ray crystallographical studies on various metal porphyrins including metal tetraphenylporphins.[19,19a] The structure of the coordination sphere of iron(III) ion in TPPFe(III)X is schematically shown in Fig. 6. A simple argument in terms of the angular-overlap model predicts the ordering of d orbitals in a planar ligand field of porphin:[20]

$$\varepsilon(x^2-y^2) = \Delta,\ \varepsilon(z^2) = \Delta/3,\ \varepsilon(xy) = \varepsilon(yz) = \varepsilon(zx) = 0,$$

where Δ is the ligand field splitting parameter. Since a mixing between z^2 and s orbitals is crucial in a planar environment, $\varepsilon(z^2)$ is much lower than that predicted from the angular-overlap model and is, in fact, close to zero. The energy difference $\varepsilon(x^2-y^2)-\varepsilon(z^2)$ varies with the axial ligand field and can be parametrized as $x\Delta$. The energy of the possible ground configurations of TPPFe(III)X is approximately given as follows:

$$\begin{aligned}
&{}^6A_1\ [(xy)(yz)(zx)(z^2)(x^2-y^2)] && (2-x)\Delta - 35B,\\
&{}^4A_2\ [(xy)^2(yz)(zx)(z^2)] && (1-x)\Delta - B,\\
&{}^2E\ \ [(xy)^2(zx)^2(yz)] && \\
&\quad\ [(xy)^2(yz)^2(zx)] && 20B,
\end{aligned}$$

where B is Racah's electrostatic interaction parameter (assumed $C=4B$). The energy diagram of the ground configuration is given in Fig. 7. The value of Δ in porphin has been evaluated 25—31B by an extended Hückel molecular orbital calculation.[21] The value was consistent with the observations on tetraphenylporphinatoiron(II) complexes.[20] As Fig. 7 shows, the

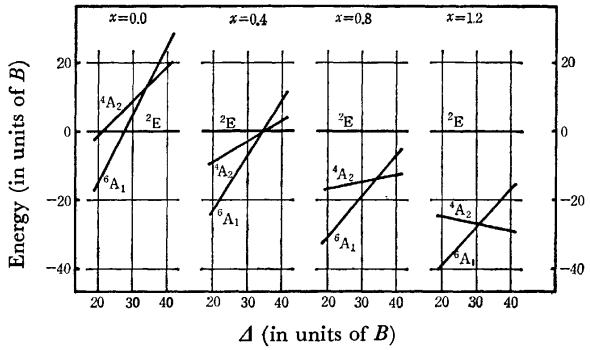

Fig. 7. Energy diagrams of the ground state of iron(III) ion in TPPFe(III)X. Δ is the ligand field splitting parameter in units of B and $x\Delta(\varepsilon(x^2-y^2)-\varepsilon(z^2))$, the axial ligand field parameter.

most stable ground configuration for Δ=25—31B is ^{6}A if the axial ligand field is not so strong. Since the axial ligand field of the complexes studied is as weak as x=0.4—1.0, the ground configuration is ^{6}A and all the five d orbitals are singly occupied. Thus the spin-allowed excited states should be sextet. The charge-transfer excitations of an electron in the highest filled porphin π orbitals to the half-filled d_{zx} and d_{yz} orbitals (dπ orbitals) give rise to degenerate excited states of E symmetry. Since iron dπ orbitals and the lowest vacant orbitals 4e of porphin are of the same centrosymmetry, an electronic delocalization between these orbitals appreciably occurs when they are energetically close. Thus the lowest excited sextets of E symmetry should be described by a superposition of the antisymmetric product wavefunctions ^{6}E[^{3}E($1a_1\rightarrow 4e$)·^{6}A], ^{6}E[^{3}E($3a_2\rightarrow 4e$)·^{6}A], ^{6}E[^{1}E($1a_1\rightarrow 4e$)·^{6}A], ^{6}E[^{1}E($3a_2\rightarrow 4e$)·^{6}A], ^{6}E[^{2}A$_1$($1a_1$)·^{5}E(dπ)], and ^{6}E[^{2}A$_2$($3a_2$)·^{5}E(dπ)],

18) W. Scheler, G. Schoffa, and H. Jung, *Biochem. Z.*, **329**, 232 (1957); W. Scheler, *ibid.*, **332**, 344, 542 (1960).

19) J. L. Hoard, G. H. Cohen, and M. D. Glick, *J. Amer. Chem. Soc.*, **89**, 1992 (1967).

19a) J. L. Hoard, M. J. Hamor, T. A. Hamor, and W. S. Caughey, *J. Amer. Chem. Soc.*, **87**, 2312 (1965); D. F. Koenig, *Acta Crystallogr.*, **18**, 663 (1965); J. L. Hoard, "Hemes and Hemoproteins," ed. by B. Chance, R. W. Estabrook, and T. Yonetani, Academic Press, New York (1966), p. 9; D. M. Collins, R. Countryman, and J. L. Hoard, *J. Amer. Chem. Soc.*, **94**, 2006 (1972); L. J. Radonovich, A. Bloom, and J. L. Hoard, *J. Amer. Chem. Soc.*, **94**, 2073 (1972); A. B. Hoffman, D. M. Collins, V. W. Day, E. B. Fleischer, T. S. Srivastava, and J. L. Hoard, *ibid.*, **94**, 3620 (1972); J. C. Kendrew, *Science*, **139**, 1259 (1963); M. F. Perutz, *ibid.*, **140**, 863 (1963); M. F. Perutz, H. Muirhead, J. M. Cox, and L. C. G. Goaman, *Nature*, **219**, 131 (1968).

20) H. Kobayashi, and Y. Yanagawa, This Bulletin, **45**, 450 (1972).

21) M. Zerner, M. Gouterman, and H. Kobayashi, *Theoret. Chim. Acta*, **6**, 363 (1966).

where $^3E(1a_1\rightarrow 4e)$, $^3E(3a_2\rightarrow 4e)$, $^1E(1a_1\rightarrow 4e)$, and $^1E(3a_2\rightarrow 4e)$ denote the wavefunctions of the lowest porphin-localized triplet and singlet excited states, respectively, ^6A denotes the ground iron(III) sextet state, and $^6E[^2A_1(1a_1)\cdot{}^5E(d\pi)]$ and $^6E[^2A_2(3a_2)\cdot{}^5E(d\pi)]$ the excited state arising from the "porphin to iron(III) ion" charge-transfers $1a_1\rightarrow d\pi$ and $3a_2\rightarrow d\pi$, respectively. Delocalization between the orbitals $d\pi$ and 4e connects two states that differ by a single orbital, as in $^6E[^{1,3}E(1a_1\rightarrow 4e)\cdot{}^6A]$ and $^6E[^2A_1(1a_1)\cdot{}^5E(d\pi)]$, $^6E[^{1,3}E(3a_2\rightarrow 4e)\cdot{}^6A]$ and $^6E[^2A_2(3a_2)\cdot{}^5E(d\pi)]$.

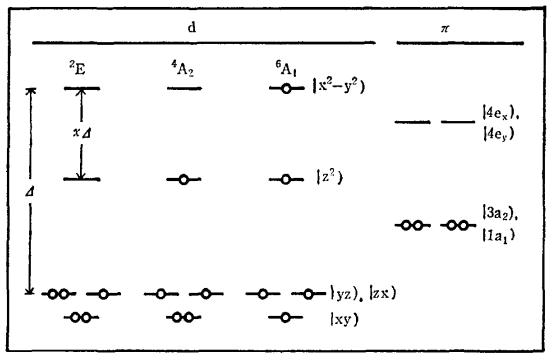

Fig. 8. Energy levels of the top filled and the lowest vacant orbitals (schematic).

The energies of the charge-transfers from $1a_1$, $3a_2$ to $d\pi$ are not as low as expected from the orbital energy diagrams shown in Fig. 8, since the charge-transfer needs an extra work done for a change of the electrostatic potential term. When an electron makes a transfer from the conjugation circuit of porphin with radius R to the central iron(III) ion, the extra work done against a change in the electrostatic potential is approximately given e^2/R assuming a neutral charge distribution in the ground state. The radius R of the main conjugation circuit of porphin is estimated to be 3.3 Å from the X-ray data. Thus e^2/R is evaluated to be 4.4 eV.[19]

The energies of the lowest excitations localized in porphin are given as follows. For the transition $1a_1\rightarrow 4e$,

$$\varepsilon(4e)-\varepsilon(1a_1)-(a_1a_1|ee)+\binom{2}{0}(a_1e|a_1e)$$

and for the transition $3a_2\rightarrow 4e$,

$$\varepsilon(4e)-\varepsilon(3a_2)-(a_2a_2|ee)+\binom{2}{0}(a_2e|a_2e)$$

where ε denotes molecular orbital energy, $(a_1a_1|ee)$ and $(a_1a_1|ee)$ denote the Coulomb integrals over the molecular orbitals, $1a_1$, $3a_2$, and 4e, $(a_1e|a_1e)$ and $(a_2e|a_2e)$, the exchange integrals, and the upper integer of $\binom{2}{0}$ denotes the coefficient for the singlet and the lower one for the triplet. Gouterman has pointed out an accidental degeneracy of the top filled orbitals on the basis of the observed substituent effects of the singlet-singlet absorption spectra of porphins.[15] Strictly speaking, it is an accidental degeneracy of the lowest excited singlet configurations rather than one of the top filled orbitals:

$$\begin{aligned}&\varepsilon(4e)-\varepsilon(1a_1)-(a_1a_1|ee)+2(a_1e|a_1e)\\&\fallingdotseq\varepsilon(4e)-\varepsilon(3a_2)-(a_2a_2|ee)+2(a_2e|a_2e).\end{aligned}$$

Experimental evidences show that the excited singlet configuration $(1a_1)(4e)$ is slightly lower than the excited singlet configuration $(3a_2)(4e)$. The energies of these configurations are given by $(E+2K)\pm(E'+2K')$, where $E\equiv\varepsilon(4e)-\{\varepsilon(3a_2)+\varepsilon(1a_1)\}/2-\{(a_2a_2|ee)+(a_1a_1|ee)\}/2$, $E'\equiv\{\varepsilon(1a_1)-\varepsilon(3a_2)\}/2+\{(a_1a_1|ee)-(a_2a_2|ee)\}/2$, $K\equiv\{(a_2e|a_2e)+(a_1e|a_1e)\}/2$, and $K'\equiv\{(a_2e|a_2e)-(a_1e|a_1e)\}/2$. The energies of the lowest excited singlets are given by $(E+2K)\pm\sqrt{(E'+2K')^2+(2K'')^2}$, where $2K''$ denotes configuration interaction matrix $2(a_1e|a_2e)$. Gouterman's finding that $E'+2K'\fallingdotseq 0$ does not necessarily imply an accidental degeneracy of the lowest triplets. The energies of the lowest triplets are given by $E\pm E'\fallingdotseq E\mp 2K'$. As experimental evidences show, $E'+2K'\equiv\varepsilon$ is small but positive. Thus the triplet $(3a_2)(4e)$ is lower than the triplet $(1a_1)(4e)$ when $2K'>\varepsilon$, but higher when $2K'<\varepsilon$. A Pariser-Parr-Pople SCMO calculation has revealed that $\varepsilon\fallingdotseq 0$, $2K'>\varepsilon$ and $\varepsilon(1a_1)\fallingdotseq\varepsilon(3a_2)$. Thus the lowest triplet is much likely to be $(3a_2)(4e)$, although it was recently assigned to the triplet $(1a_1)(4e)$ because of no nitrogen hyperfine structure being observed in the ESR spectrum of the lowest triplet of zinc(II) porphin.[22] The orbital $(1a_1)$, in fact, lacks populations on the central nitrogens, whereas the orbital (4e) has populations on the nitrogens as well as $(3a_2)$. No further evidences to support the lowest triplet $(1a_1)(4e)$ have been presented.

A circular box is described by a radial coordinate r and angular coordinate θ. Orbitals are written $|\pm k)=f(r)\exp(\pm ik\theta)$, where k denotes orbital angular momentum. The orbital pair $(3a_2\pm i1a_1)/\sqrt{2}$ can be identified with the degenerate pair of circular box orbitals $|\pm 4)=f(r)\exp(\pm 4i\theta)$, and the lowest empty 4e orbitals $|\pm 5)=f(r)\exp(\pm 5i\theta)$.[23] In the ground state, a pair of orbitals which has z components of angular momentum $\lambda_z=\pm 4$ and angular momentum $\lambda=4$ is filled with four electrons; the ground configuration is denoted $(4)^4$ and has zero angular momentum $\Lambda_z=0$. The first excited configurations arise by exciting a $\lambda=4$ electron to an orbital with $\lambda=5$, and are denoted $(4)^35$. The configurations give rise to degenerate pairs of excited states with $\Lambda_z=\pm 1$ and $\Lambda_z=\pm 9$.

A degenerate $d\pi$ orbital pair, zx and yz, causes a charge-transfer interaction with the porphin π molecular orbitals of E symmetry. The orbital pair can be rewritten $|\pm 1)=(zx\pm iyz)/\sqrt{2}$, where ± 1 denotes the z components of angular momentum $\lambda=1$. A one-electron term connecting the orbitals $|\pm 1)$ and $|\pm 5)$, $(\pm 1|h^{\mathrm{eff}}|\pm 5)\equiv\beta$, gives rise to a delocalization of the porphin π electrons toward the half-filled iron(III) $d\pi$ orbitals.

The electrons in the orbitals with $\lambda=1$, $\lambda=4$, and $\lambda=5$ are assumed to move in a one-electron effective core field set up by the nuclei and the remaining electrons and to interact with one another by the two-

22) I. Y. Chan, W. G. van Dorp, T. J. Schaafsma, and J. H. van der Waals, *Mol. Phys.*, **22**, 741 (1971).
23) M. Gouterman, *J. Chem. Phys.*, **33**, 1523 (1960).

TABLE 3. GROUND AND EXCITED SEXTETS OF HIGH-SPIN IRON(III) PORPHIN

State	Configuration	Λ_z	$2S+1$	Energy
^6A	$\varepsilon\theta\zeta(+1)(-1)(+4)^2(-4)^2$	0	6	0
$^6E_{CT}$	$\varepsilon\theta\zeta(+1)^2(-1)(+4)^2(-4)$	+5	6	E_{CT}
	$\varepsilon\theta\zeta(+1)(-1)^2(+4)(-4)^2$	−5	6	E_{CT}
$^6E_{CT}$	$\varepsilon\theta\zeta(+1)^2(-1)(+4)(-4)^2$	−3	6	E_{CT}
	$\varepsilon\theta\zeta(+1)(-1)^2(+4)^2(-4)$	+3	6	E_{CT}
^6E_T	$\varepsilon\theta\zeta(+1)(-1)(+4)^2(-4)(+5)$	+9	6	E
	$\varepsilon\theta\zeta(+1)(-1)(+4)(-4)^2(-5)$	−9	6	E
^6E_T	$\varepsilon\theta\zeta(+1)(-1)(+4)(-4)^2(+5)$	+1	6	E
	$\varepsilon\theta\zeta(+1)(-1)(+4)^2(-4)(-5)$	−1	6	E
^6E_Q	$\varepsilon\theta\zeta(+1)(-1)(+4)^2(-4)(+5)$	+9	6	$E+2K_9$
	$\varepsilon\theta\zeta(+1)(-1)(+4)(-4)^2(-5)$	−9	6	$E+2K_9$
^6E_B	$\varepsilon\theta\zeta(+1)(-1)(+4)(-4)^2(+5)$	+1	6	$E+2K_1$
	$\varepsilon\theta\zeta(+1)(-1)(+4)_2(-4)(-5)$	−1	6	$E+2K_1$

Mixing terms for high-spin iron(III) porphin

	$^6E_{CT}$	$^6E_{CT}$	^6E_T	^6E_T	^6E_Q	^6E_B
$^6E_{CT}$	E_{CT}	ε''	$\sqrt{\frac{70}{10}}\beta$	0	$\sqrt{\frac{2}{2}}\beta$	0
$^6E_{CT}$		E_{CT}	0	$\sqrt{\frac{70}{10}}\beta$	0	$\sqrt{\frac{2}{2}}\beta$
^6E_T			E	ε'	0	0
^6E_T				E	0	0
^6E_Q					$E+2K_9$	ε
^6E_B						$E+2K_1$

Mixing terms for high-spin manganese(III) porphin

	$^5E_{CT}$	$^5E_{CT}$	^5E_T	^5E_T	^5E_Q	^5E_B
$^5E_{CT}$	E_{CT}	ε''	$\sqrt{\frac{3}{2}}$	0	$\sqrt{\frac{2}{2}}\beta$	0
$^5E_{CT}$		E_{CT}	0	$\sqrt{\frac{3}{2}}\beta$	0	$\sqrt{\frac{2}{2}}\beta$
^5E_T			E	ε'	0	0
^5E_T				E	0	0
^5E_Q					$E+2K_9$	ε
^5E_B						$E+2K_1$

electron term e^2/r_{ij}. Wavefunctions are taken as Slater determinants which are eigenfunctions of total spin sextet. In Table 3 are given the sextet states arising from the configurations $\varepsilon\theta\zeta(1)^2(4)^4$, $\varepsilon\theta\zeta(1)^3(4)^3$, and $\varepsilon\theta\zeta(1)^2(4)^3(5)$, ε denoting iron x^2-y^2 orbital, θ, z^2 orbital and ζ, xy orbital, respectively. Slater determinants are then taken as follows:

$$|+5\rangle \equiv |\varepsilon\theta\zeta+1-1+4+\bar{4}-4+\bar{1}|$$

$$|-3\rangle \equiv |\varepsilon\theta\zeta+1-1+4+\bar{1}-4-\bar{4}|$$

$$\begin{aligned}|+9a\rangle \equiv [&5\{|\varepsilon\theta\zeta+1-1+4+\bar{4}-4+\bar{5}|\\ &+|\varepsilon\theta\zeta+1-1+4+\bar{4}-\bar{4}+5|\}\\ &-2\{|\varepsilon\theta\zeta+1-\bar{1}+4+\bar{4}-4+5|\\ &+|\varepsilon\theta\bar{\zeta}+1-1+4+\bar{4}-4+5|\\ &+|\varepsilon\bar{\theta}\zeta+1-1+4+\bar{4}-4+5|\\ &+|\bar{\varepsilon}\theta\zeta+1-1+4+\bar{4}-4+5|\}]/\sqrt{70}\end{aligned}$$

$$\begin{aligned}|+1a\rangle \equiv [&5\{|\varepsilon\theta\zeta+1-1+4+\bar{5}-4-\bar{4}|\\ &+|\varepsilon\theta\zeta+1-1+\bar{4}+5-4-\bar{4}|\}\\ &-2\{|\varepsilon\theta\zeta+1-\bar{1}+4+5-4-\bar{4}|\\ &+|\varepsilon\theta\zeta+\bar{1}-1+4+5-4-\bar{4}|\\ &+|\varepsilon\theta\bar{\zeta}+1-1+4+5-4-\bar{4}|\\ &+|\varepsilon\bar{\theta}\zeta+1-1+4+5-4-\bar{4}|\\ &+|\bar{\varepsilon}\theta\zeta+1-1+4+5-4-\bar{4}|\}]/\sqrt{70}\end{aligned}$$

$$\begin{aligned}|+9b\rangle \equiv \{&|\varepsilon\theta\zeta+1-1+4+\bar{4}-4+\bar{5}|\\ &-|\varepsilon\theta\zeta+1-1+4+\bar{4}-\bar{4}+5|\}/\sqrt{2}\end{aligned}$$

$$\begin{aligned}|+1b\rangle \equiv \{&|\varepsilon\theta\zeta+1-1+4+\bar{5}-4-\bar{4}|\\ &-|\varepsilon\theta\zeta+1-1+\bar{4}+5-4-\bar{4}|\}/\sqrt{2},\end{aligned}$$

where no bar implies spin α, a bar implies spin β and the molecular orbitals are denoted by their λ_z values.

The energies of the excited sextets including porphin triplets (^6E_T, $|\pm 9a\rangle$ and ^6E_T, $|\pm 1a\rangle$), porphin Q and B singlets (^6E_Q, $|\pm 9b\rangle$ and ^6E_B, $|\pm 1b\rangle$), and "porphin to high-spin iron(III)" charge-transfer states ($^6E_{CT}$, $|\pm 5\rangle$ and $^6E_{CT}$, $|\mp 3\rangle$) are given in Table 3 in terms of energy parameters E, E_{CT}, K_1, and K_9, where $K_1 \equiv K+K''$ and $K_9 \equiv K-K''$. The mixing terms are also given in Table 3 in terms of delocalization parameter β and off-diagonal corrections for the circular box model. As stated before, we have $\varepsilon \equiv E'+2K'$ and $\varepsilon' \equiv E'$. An off-diagonal term between the charge-transfer states

$$\varepsilon'' \equiv \{\varepsilon(1a_1)-\varepsilon(3a_2)\}/2 + \{(a_1a_1|d\pi d\pi)-(a_2a_2|d\pi d\pi)\}/2$$

is introduced. Coulomb repulsions $(a_1a_1|d\pi d\pi)$ and $(a_2a_2|d\pi d\pi)$, however, are less sensitive to the angular nodal character of the wave functions involved and do not differ much from other. Thus ε'' should be rather small.

To reproduce the transition energies and the intensity ratio of Q and B bands of TPPCo(II), it has been assumed that

$$E = 14810\ \text{cm}^{-1},\ K_1 = 4600\ \text{cm}^{-1},\ K_9 = 2530\ \text{cm}^{-1}$$

and $\varepsilon = \varepsilon' = \pm 1480\ \text{cm}^{-1}$.[24] Since a change in E was expected for tervalent central metal ion, the parameters were readjusted to give a better description of the spectrum of TPPCo(III)Cl complex:

$$E = 13070\ \text{cm}^{-1},\ K_1 = 4600\ \text{cm}^{-1},\ K_9 = 2730\ \text{cm}^{-1}$$

and $\varepsilon = \varepsilon' = \pm 1340\ \text{cm}^{-1}$. From the coefficients on nitrogens of the molecular orbital 4e[17] and a value of resonance integral assumed by Hanazaki and Nagakura for a calculation of tris(bipyridine)iron(II) complex,[25] β was obtained as $-3000\ \text{cm}^{-1}$. The lowest excited sextets were calculated for a variety of E_{CT} and ε's. They are shown as a function of E_{CT} in Fig. 9. The lowest excitations of high-spin TPPFe(III)X complex (Fig. 10) are well reproduced $E_{CT} = 12500\ \text{cm}^{-1}$. Contributions of the composite excited states to each of the lowest excited states are given in Table 4, together with the effective numbers of the transferred charge in the excited states. The MCD spectrum of TPPFe(III)-Cl in benzene (Fig. 3) shows a normal A-term dispersion in each absorption band. This reveals that each of the lowest excited states is degenerate and has a characteristic orbital angular momentum. The value

24) H. Kobayashi, T. Hara, and Y. Kaizu, This Bulletin, **45**, 2148 (1972).

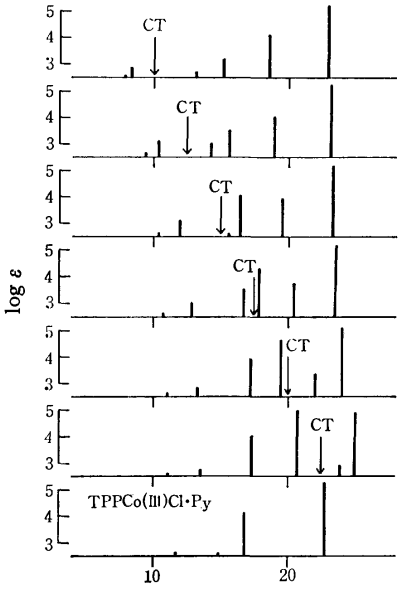

Fig. 9. The lowest excited sextets of TPPFe(III)X calculated as a function of E_{CT}. CT implies the assumed E_{CT}.

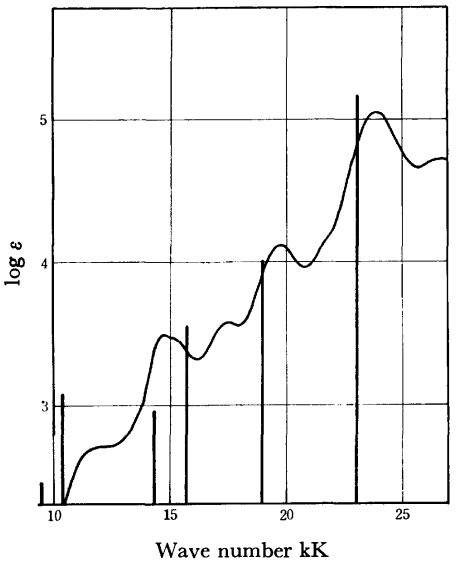

Fig. 10. The calculated lowest excitations of TPPFe(III)X. The assumed parameter values are $E=13070$ cm^{-1}, $E_{CT}=12500$ cm^{-1}, $K_1=4600$ cm^{-1}, $K_9=2730$ cm^{-1}, $\beta=-3000$ cm^{-1}, $\varepsilon=1340$ cm^{-1}, $\varepsilon'=-1340$ cm^{-1}, and $\varepsilon''=0$ cm^{-1}.

Table 4. Calculated compositions of the excited sextet states of high-spin iron(III) porphin

	a^{6}E	b^{6}E	c^{6}E	d^{6}E	e^{6}E	f^{6}E
Excitation energy (cm^{-1})	9410	10400	14300	15700	19000	23100
log ε	2.43	3.08	2.97	3.55	4.01	5.16
$^6E_{CT}$ ($A_z=\pm5$)	0.5017	−0.5681	−0.4875	0.2481	−0.3502	−0.0616
$^6E_{CT}$ ($A_z=\mp3$)	0.4505	0.6024	−0.4921	−0.3713	0.1246	−0.1967
^6E_T ($A_z=\pm9$)	0.5274	−0.3336	0.5286	−0.5497	0.1699	0.0090
^6E_T ($A_z=\pm1$)	0.5017	0.3981	0.4313	0.6270	−0.0916	0.0478
^6E_T ($A_z=\pm9$)	0.1074	−0.1690	−0.2139	0.2725	0.8665	0.2983
^6E_S ($A_z=\pm1$)	0.0631	0.1267	−0.0949	−0.1763	−0.2715	0.9307
A_z ($\hbar$)	±3.51	±1.96	±3.58	±3.71	±7.67	±1.57
Number of the transferred charge	0.455	0.686	0.480	0.199	0.138	0.042

The assumed parameter values are $E=13070$ cm^{-1}, $E_{CT}=12500$ cm^{-1}, $K_1=4600$ cm^{-1}, $K_9=2730$ cm^{-1}, $\beta=-3000$ cm^{-1}, $\varepsilon=1340$ cm^{-1}, $\varepsilon'=-1340$ cm^{-1}, and $\varepsilon''=0$ cm^{-1}.

of the orbital angular momentum in porphin excited state calculated by the circular box model (Table 4) is just an index of the orbital angular momentum but can predict a correct sign of A-term dispersion.[24] However, the molecular orbital calculations in a rather sophisticated form have given a wrong sign of A-term dispersion in the B band.[26]

Contributions of the "porphin to metal" charge-transfer excited states depend upon dπ electron affinity of the π electron-accepting metal ion. The electron affinity is estimated by application of the method of Griffith[27] using atomic spectroscopic data.[28] Differences between the dπ electron affinities of high-spin manganese(III), high-spin iron(III) and low-spin iron(III) are evaluated as shown in Table 5. The order of the electron affinity is low-spin Fe(III)>high-spin Fe(III)>high-spin Mn(III). Since σ-donation of the porphin nitrogens neutralizes the positive charge of the central metal ion, the electron affinity should be corrected for the electroneutralization effect.[29] The correction must be sizable, however, the ordering obtained above is still applicable to the metal ion in complex. A higher tendency of reduction is expected for a molecular environment to stabilize the low-spin iron(III) porphin, but the "porphin to iron" charge-

25) I. Hanazaki and S. Nagakura, *Inorg. Chem.*, **8**, 648 (1969).
26) A. J. McHugh, M. Gouterman, and C. Weiss, Jr., *Theoret. Chim. Acta*, **24**, 346 (1972).
27) J. S. Griffith, "The Theory of Transition-Metal Ions," Cambridge University Press (1961), p. 100.
28) C. E. Moore, "Atomic Energy Levels," Vol. 2, National Bureau of Standards, Washington (1952).
29) I. Fujita, T. Yazaki, Y. Torii, and H. Kobayashi, This Bulletin, **45**, 2156 (1972).

TABLE 5. dπ ELECTRON AFFINITY

Species	Configuration energy		Electron affinity (E_a)		ΔE_a
Mn(III)	Mn(III) d^4	$-4U+6A-21B$	$-\phi'+2B+6C$	constant -29.31 eV	
high-spin	Mn(II) d^5	$-5U+10A-19B+6C$			
					1.33 eV
Fe(III)	Fe(III) d^5	$-5U+10A-35B$	$-\phi+7C$	constant -30.64 eV	
high-spin	Fe(II) d^6	$-6U+15A-35B+7C$			
					2.27_5 eV
Fe(III)	Fe(III) d^5	$-5U+10A-20B+10C$	$-\phi-10B+5C$	constant -32.91_5 eV	
low-spin	Fe(II) d^6	$-6U+15A-30B+15C$			

Electron attaching process

Mn(III) high-spin
Mn(III) [d^4: $(xy)(yz)(zx)(z^2)$]+e → Mn(II)[d^5: $(xy)(yz)^2(zx)(z^2)$]

Fe(III) high-spin
Fe(III)[d^5: $(xy)(yz)(zx)(z^2)(x^2-y^2)$]+e → Fe(II)[$d^6$: $(xy)(yz)^2(zx)(z^2)(x^2-y^2)$]

Fe(III) low-spin
Fe(III)[d^5: $(xy)^2(yz)(zx)^2$]+e → Fe(II)[d^6: $(xy)^2(yz)^2(zx)^2$]

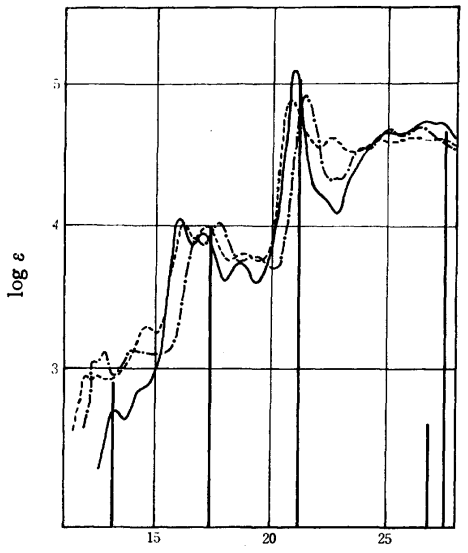

Fig. 11. Absorption spectra of TPPMn(III)Cl·H_2O.
——: benzene solution – – –: pyridine solution
–·–·–: methanol solution
Vertical lines imply calculated spectra.

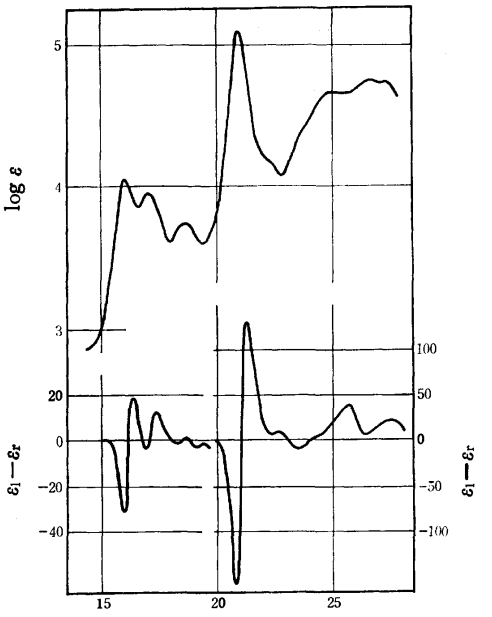

Fig. 12. MCD spectrum of TPPMn(III)Cl·H_2O in benzene.
Upper: absorption spectrum Lower: MCD spectrum

transfer excited states are too low to cause an appreciable interaction with the porphin (π, π^*) excited states. In fact, a spectrum assigned to the low-spin iron(III) porphyrin by George *et al.*[14] does not differ much from the (π, π^*) spectrum of typical metal porphyrin.

The charge-transfer states in high-spin manganese(III) porphin must be as high as the porphin B state. In fact, a remarkable splitting of the B band is observed (Fig. 11). The charge-transfer excited states slightly higher than B state push down the B state and grant an intensity to the porphin singlet-triplet excitations by similar configuration interactions as in the case of high-spin iron(III) porphin. The energy matrices are given in Table 3. The absorption spectrum of TPPMn(III)Cl·H_2O was well reproduced (Fig. 11) by a calculation assuming $E_{CT}=25000$ cm^{-1}, $\beta=-4000$ cm^{-1}. The MCD spectrum of TPPMn(III)Cl·H_2O in benzene is shown in Fig. 12. A normal A-term MCD dispersion with $A/D=1$ was observed in the 21000 cm^{-1} band. Boucher also obtained a similar MCD spectrum of protoporphin IX dimethylester manganese(III) chloride in chloroform.[9] Such spectrum has been observed in the B band of typical metal porphins. Mixing of the "porphin to manganese(III)" charge-transfer excitations gives rise to a remarkable spectral shift and a redistribution of spectral intensity, but the 21000 cm^{-1} transition is still predominantly made of B excitation (Table 6). The value of β in high-spin manganese(III) was assumed to be slightly higher than that of high-spin iron(III) so as to reproduce the observation. The iron(III) in TPPFe(III)Cl is pentacoordinate and is out-of-plane from the coordinating nitrogens according to X-ray studies, whereas the manganese(III) in TPPMn(III)Cl·H_2O is

TABLE 6. CALCLUATED COMPOSITIONS OF THE EXCITED QUINTET STATES OF HIGH-SPIN MANGANESE(III) PORPHIN

	a^5E	b^5E	c^5E	d^5E	e^5E	f^5E
Excitation energy (cm^{-1})	10800	13200	17400	21200	26800	27500
log	2.00	2.89	3.98	5.02	2.61	4.66
${}^5E_{CT}$ ($\Lambda_z=\pm5$)	0.1797	0.2265	0.2327	0.1547	0.8961	0.1882
${}^5E_{CT}$ ($\Lambda_z=\pm3$)	0.1734	−0.2188	−0.0523	0.4417	−0.2151	0.8228
${}^5E_T$ ($\Lambda_z=\pm9$)	0.6860	0.6514	−0.2212	−0.0358	−0.2329	−0.0271
${}^5E_T$ ($\Lambda_z=\pm1$)	0.6799	−0.6691	0.1107	−0.1835	0.0768	−0.1954
${}^5E_S$ ($\Lambda_z=\pm9$)	0.0598	0.1439	0.8975	0.2536	−0.2976	−0.1316
${}^5E_S$ ($\Lambda_z=\pm1$)	0.0359	−0.0899	−0.2764	0.8251	0.0459	−0.4810
Λ_z ($\hbar$)	±4.80	±4.57	±8.04	±0.68	±5.18	∓1.42
Number of the transferred charge	0.062	0.099	0.057	0.220	0.849	0.713

The assumed parameter values are $E=13070\ cm^{-1}$, $E=25000\ cm^{-1}$, $K_1=4600\ cm^{-1}$, $K_\theta=2730\ cm^{-1}$, $\beta=-4000\ cm^{-1}$, $\varepsilon=1340\ cm^{-1}$, $\varepsilon'=-1340\ cm^{-1}$, and $\varepsilon''=0\ cm^{-1}$.

hexacoordinate and must be in the nitrogen plane. Thus the conjugation between the central ion and porphin is increased in TPPMn(III)Cl·H_2O.

Since metal dπ and the lowest vacant π orbitals 4e are of the same symmetry, an electron delocalization between them occurs appreciably when they are energetically close to each other. The delocalization effect grants the charge-transfer excitation an intensity of the allowed B excitation, although the pure charge-transfer excitation, in principle, is forbidden. In the case of open-shell configurations such as in high-spin iron(III) and high-spin manganese(III), the charge-transfer state causes a connection not only with singlet but also with triplet (π, π^*) states, making the singlet-triplet (π, π^*) excitations partially allowed. Thus the complex spectra of high-spin iron(III)- and manganese(III) porphyrins are assigned to the excited states arising from the configuration interactions of porphyrin excited triplet and singlet (π, π^*) states and "porphyrin to metal" charge-transfer excited states.

Our sincere thanks are due to Dr. Kiyoko Yamamoto for her advice concerning the preparation of tetraphenylporphin, and also to Dr. Kazuo Shibata for his suggestion on the opal glass method. One of the authors (H. K.) wishes to thank Profs. M. Kotani, W. S. Caughey, and M. P. Gouterman for their helpful discussions.

Identification of Normal Paraffins and Olefins from Thermal Decomposition Products of Polyethylene

Takeaki A. IIDA, Kenichi HONDA, and Hiroshi NOZAKI
Institute of Industrial Science, University of Tokyo, Roppongi, Minato-ku, Tokyo 106
(Received August 25, 1972)

Straight-chain components of the high boiling fractions of thermal decomposition products of low-density polyethylene were obtained through urea adduct formation, and analyzed by chromatographic separation methods. They were found to be a mixture of approximately 60 wt% of paraffins (C_{10} to C_{30}), 35 wt% of terminal olefins (C_{10} to C_{26}), and 5 wt% of nonterminal olefins (C_{10} to C_{26}) with predominantly 2-alkenes. A silica gel–silver nitrate mixture was found to be useful for chromatographic separation of hydrocarbon components.

Thermal decomposition products of polyethylene are a complex mixture of saturated and unsaturated hydrocarbons. It is important to know the types of these compounds as well as to determine the structures of individual hydrocarbons, not only for elucidation of the mechanism of thermal decomposition of polyethylene, but also for regeneration of polyethylene as an industrial raw materials.

Thermal decomposition products of polyethylene have been determined by many investigators. Kambe and Shibasaki[1] analyzed the thermal decomposition products of polyethylene by gas chromatography and identified several paraffins and olefins with carbon numbers from C_5 to C_9. Tsuchiya and Sumi[2] made a comprehensive analysis of the volatile thermal decomposition products by gas chromatography. They discussed the mechanism of the decomposition by assuming intramolecular transfer of free radicals. The result was valuable for identification of the thermal decomposition products consisting of low boiling fractions of hydrocarbons from C_1 to C_6. Madorsky[3] determined thermal decomposition products of polyethylene by mass spectrometry. Moiseev[4] used gas chromatography for the separation of decomposition products of low boiling fractions, and explained the formation of volatile thermal decomposition products by assuming intramolecular transfer of radicals or isomerization. However, high boiling fractions which constitute a major portion of decomposition products have not been so extensively investigated. The present work deals with the identification of straight-chain hydrocarbons of thermal decomposition products of low-density polyethylene obtained through urea adduct formation. Emphasis was placed on the separation and identification of an olefin mixture.

Experimental

Materials used. Commercial low-density polyethylene was used; its properties are given in Table 1.

Thermal Decomposition. The apparatus is illustrated in Fig. 1. A universal-joint Pyrex Claisen-flask containing 10 g of sample was prepared. Nitrogen gas was introduced into the flask in order to prevent the oxidation of polyethylene and decomposition products. The sample was decomposed for 120 min at 420°C. The high boiling fractions, which constitute 75 wt% of thermal decomposition products, were collected in a flask (5, Fig. 1), heated with a water bath at 80 °C. The mixture of saturated and olefinic hydrocarbons was used as a starting material.

TABLE 1. PROPERTIES OF LOW-DENSITY POLYETHYLENE

Appearance: white, translucent, solid
Density: 0.923 g/cm^3
Softening point: 97°C
Crystalline melting point: 102°C
Molecular weight: about 56000

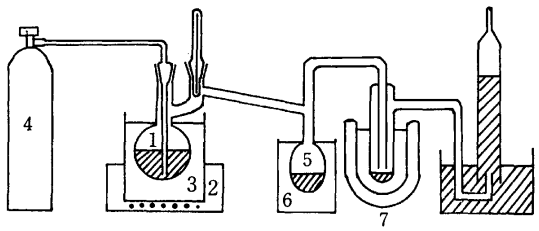

Fig. 1. Apparatus for the thermal decomposition of polyethylene.
1 Polyethylene sample, 2 Electric furnace, 3 KNO_3–$NaNO_2$–$NaNO_3$ salt bath, 4 N_2 gas, 5 High boiling fraction, 6 Water bath, 7 Liquid nitrogen trap.

Analysis. *(1) Reagents*: Silica gel impregnated with silver nitrate for elution column chromatography was prepared by thoroughly mixing 40 grams of silica gel (Wakogel, C-100) and 8 g of 50% aqueous silver nitrate, followed by drying in the dark at 120 °C for 4 hr.[5] Thin-layer plates of silica gel–silver nitrate were prepared by spraying the usual 250-micron layer of silica gel (Wakogel, B-10) with 20% aqueous silver nitrate, followed by reactivation at 110°C for 10—15 min. A *n*-hexane–benzene mixture (20 to 1) was used as a developing solvent system. Spots were detected by spraying 60% sulfuric acid and heating at 100 to 150°C.

(2) Apparatus: For gas-liquid chromatography (glc) on a preparative scale, a Beckman Megachrom instrument with 2 m columns in parallel was used. The column packing was 7% methyl silicone polymer (SE-30) coated on 40- to 60-mesh Microsorb F. The temperature range was 193—203 °C. For analytical glc, a Shimadzu Model GC-4APE1 instrument was used in conjunction with a hydrogen flame detector. Dual column, 4 mm in diameter and 2 m in length packed with

1) H. Kambe and Y. Shibasaki, *J. Soc. Polym. Sci. Jap.*, **20**, 641 (1963).
2) Y. Tsuchiya and K. Sumi, *J. Polym. Sci., A-1*, **6**, 415 (1968).
3) S. L. Madorsky, "Thermal Degradation of Organic Polymers," Interscience, N. Y. p. 93 (1964).
4) V. D. Moiseev, *Soviet Plastics*, (*English Transl. Dec.* 1963), *Dec.*, 6 (1964).
5) H. Wagner, J. D. Goetschel, and P. Lesch, *Helv. Chim. Acta*, **46**, 2986 (1963).

1.5% OV-17 on silanized Shimalite W, were generally used with a temperature program of 4 °C per minute. Nitrogen was used as carrier gas. Infrared spectra were obtained by Hitach-Perkin Elmer Model 210 Spectrophotometers.

(3) Procedure: The thermal decomposition product of the high boiling fraction was resolved into straight-chain and branched-chain hydrocarbons through a urea complex formation technique. The infrared spectra of these straight-chain hydrocarbons were first obtained. Analytical glc of this sample was obtained with the use of OV-17 column. Tlc as well as elution column chromatography (silica gel–silver nitrate) were carried out to separate paraffin, terminal olefin and nonterminal olefins. The amounts of paraffin, terminal olefin and nonterminal olefin were determined by direct weighing of the concentrates. Each peak separated by the analytical glc and consisting of hydrocarbon of the same carbon number was fractionated by preparative scale glc with the use of SE-30 column. The double bond distribution in nonterminal olefin was estimated by ozonolysis of the fractioned hydrocarbon followed by glc analysis of the derived carboxylic acid methyl esters.

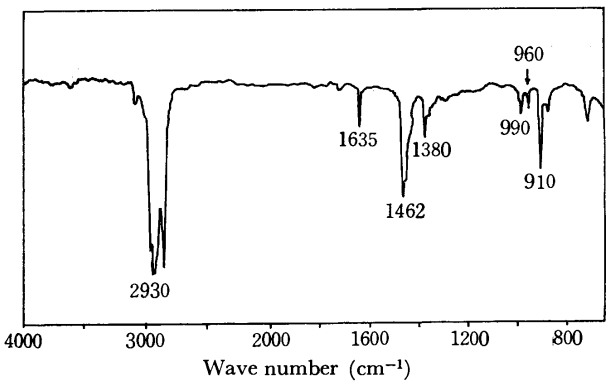

Fig. 2. Infrared spectrum of straight-chain paraffin and olefin from the thermal decomposition products of polyethylene.

Results and Discussion

The yield of urea adduct formation of straight-chain paraffin and olefin mixture was about 25 wt% of the high boiling fractions. Infrared spectra of the straight-chain hydrocarbons are shown in Fig. 2. The spectra at 2930 and 1462 cm^{-1} correspond to stretching band and deformation band of C–H bond, respectively. Methyls are observed at 1380 cm^{-1}, terminal olefins at 910 and 990 cm^{-1} (deformation bands) and 1635 cm^{-1} (stretching band) and nonterminal olefin (*trans*) at 960 cm^{-1} (deformation band). Thus, it can be said that the hydrocarbon mixture consists of paraffins, terminal olefins and nonterminal olefins. Analytical glc of the straight-chain paraffin and olefin mixture added with authentic specimens of *n*-paraffins of $C_{16}H_{34}$, $C_{20}H_{42}$, $C_{26}H_{54}$ is shown in Fig. 3. We see that carbon numbers are distributed from C_{10} to C_{30} through a maximum at around C_{16}. It is also noted that each peak from C_{11} to C_{26} shows two resolved peaks. Since there is the possibility of separation of olefin and paraffin of the same carbon numbers on the glc of OV-17 column, the two peaks probably represent olefin and paraffin of the same carbon numbers.

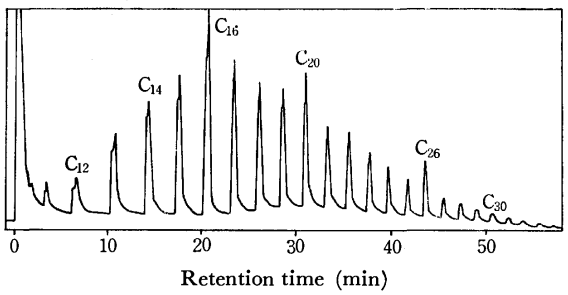

Fig. 3. Gas chromatogram of straight-chain hydrocarbons from the decomposition products of polyethylene.

Paraffin, terminal olefin and nonterminal olefins were completely separated from each other on tlc as well as by elution column chromatography. Among olefins, the terminal one was most strongly adsorbed; the more the double bond goes toward the center of the chain, the less it is adsorbed. Tlc (silica gel–silver nitrate) showed three spots, assigned by infrared spectra to be paraffin, nonterminal olefin, and terminal olefin in this order. The amounts of paraffin, terminal olefin and nonterminal olefin separated by elution column chromatography using silica gel–silver nitrate are given in Table 2.

Table 2. Amounts of paraffin, nonterminal olefin, and terminal olefin separated by elution column chromatography

Sample No.	Paraffin (wt%)	Nonterminal olefin (wt%)	Terminal olefin (wt%)	Tar (wt%)
1	62.7	5.7	30.6	1.0
2	65.1	5.5	28.2	1.1
3	52.6	5.6	40.9	1.0
4	56.7	5.2	37.2	0.9

Figure 4 shows the analytical glc of the normal paraffin concentrate separated by elution column chromatography (silica gel–silver nitrate) with *n*-$C_{16}H_{34}$ added as an authentic specimen. In this case the peak on C_{16} is not resolved. On the other hand, as shown in Fig. 5, the analytical glc of the terminal olefin concentrate with *n*-$C_{16}H_{34}$ added shows two resolved peaks on the C_{16} peak. It was found by the retention time of *n*-$C_{16}H_{34}$ that peak A corresponds to terminal olefin and peak B to paraffin of *n*-$C_{16}H_{34}$. It was also confirmed that nonterminal olefin and terminal olefin were not separated from each other

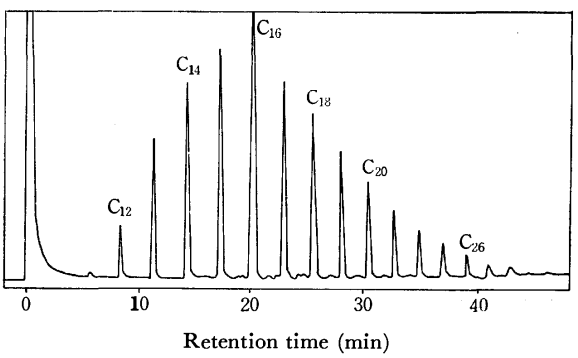

Fig. 4. Gas chromatogram of straight-chain paraffins from the thermal decomposition products of polyethylene.

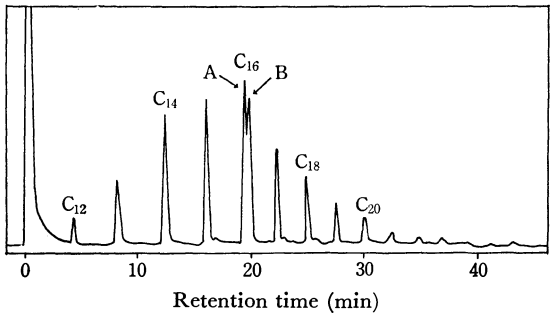

Fig. 5. Gas chromatogram of straight-chain terminal olefins from the thermal decomposition products of polyethylene.

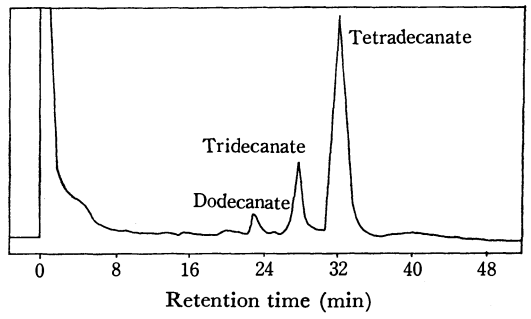

Fig. 6. Gas chromatogram of carboxylic acid methyl esters obtained from straight-chain C_{16} nonterminal olefins.

on the glc of OV-17 column. It is therefore considered that two resolved peaks correspond to olefin and paraffin of the same carbon numbers, respectively.

In order to determine the double bond distribution in nonterminal olefins, the ozonolysis of C_{16} nonterminal olefin concentrate fractionated by preparative scale glc was carried out and glc analysis of the derived carboxylic acid methyl esters was followed. The result is shown in Fig. 6. A noticeable fact about the straight-chain olefinic components is that double bond distribution is strongly favored toward the end of the chain. This supports the mechanism of the decomposition reaction on the assumption of intramolecular transfer of free radicals from the end of the chain to the center as proposed by Tsuchiya and Sumi.[2]

Many usages of this decomposition product are considered, a prospective one being the production of biodegradable detergents from terminal olefins.[6]

The authors wish to express their appreciation to Professor S. Makishima for valuable discussions and Dr. A. Tahara and Dr. T. Iida for suggestions and the measurements of glc. They also thank Mr. T. Kiuchi for help in the experiments.

6) C. L. Furrow, *Ind. Eng. Chem.*, **7**, 26 (1968); C. J. Norton, *J. Org. Chem.*, **33**, 4158 (1968).

BULLETIN OF THE CHEMICAL SOCIETY OF JAPAN, VOL. 46, 1482—1488 (1973)

Asymmetric Hydrogenation of C=O Double Bond with Modified Raney Nickel. XXVII. Asymmetric Hydrogenation of Acetylacetone*

Tadashi TANABE**

Division of Organic Chemistry, Institute for Protein Research, Osaka University, Osaka

(Received April 14, 1972)

The asymmetric (enantioselective) hydrogenation process of acetylacetone (AA), which is a highly enolized compound, was studied by the use of catalysts modified with D-tartaric acid, and L-glutamic acid. AA corroded the Raney nickel catalyst during the hydrogenation. The modification protected the catalyst from corrosion, and the protective effects by the amino acids were greater than that by the hydroxy acid. The modification with tartaric acid increased the hydrogenation velocity of AA, but the amino acid hardly affected the hydrogenation velocity. The glutamic acid on the catalyst surface reacted with AA to form a Schiff base during the hydrogenation. The hydrogenation proceeded mainly by means of a two-step process *via* 2-pentanol-4-on. The modifying pH and temperature affected the asymmetric activity of the catalyst. In the first step of the hydrogenation, the catalyst modified with D-tartaric acid showed a high asymmetric activity, but the one modified with L-glutamic acid exhibited a low asymmetric activity as a result of the Schiff base formation. In the second step, the modification with D-tartaric acid promoted the formation of racemic 2,4-pentanediol (II), and the L-glutamic acid increased the production of *meso* II.

The asymmetric (enantioselective) hydrogenations of methyl acetoacetate with asymmetrically-modified Raney nickel catalysts have been extensively studied in our laboratory.[1] The relation between the asymmetric activity in the hydrogenation of methyl acetoacetate (MAA) and the structure of the modifying reagent has been clarified, and the interaction of MAA and the modifying reagents has been discussed.

* A part of this study was presented at the 24th Annual Meeting of the Chemistry Society of Japan, Osaka, 1971.

** Present address: Department of Medical Chemistry, Faculty of Medicine, Kyoto University, Sakyo-ku, Kyoto.

1) Y. Izumi, *Angew. Chem. Int. Ed. Engl.*, **10**, 871 (1971).

In the course of the investigation, β-diketone and β-keto ester were found to be favorable substrates for the asymmetric hydrogenation.[2] As the β-diketone or the β-keto ester is a highly enolized compound, the favorable character of these compounds might be related to their enolization. β-Diketone and β-keto ester have also been characterized as strong chelating reagents. Accordingly, their characters should be studied from the viewpoint of their chelation during the hydrogenation process. In the present work, the hydrogenation mechanism of acetylacetone (AA), which is a strong chelating reagent, and the contribution of the chelation of the substrate on the catalyst surface have been investigated.

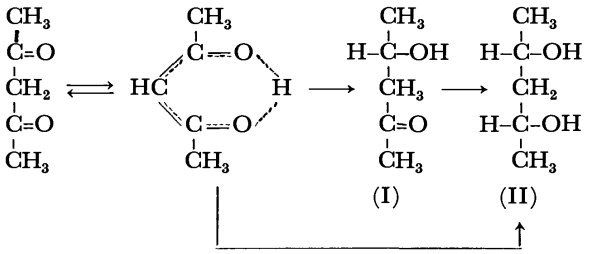

Scheme 1.

If two carbonyl groups are adsorbed planarly and are hydrogenated in a single step on the catalyst surface, the hydrogenation product thus formed 2,4-pentanediol (II), may be expected to be the *meso* isomer, as is shown in Scheme 1. However, if the reaction proceeds by a successive two-step process, 2-pentanol-4-on (I) should be produced as the intermediate and the final hydrogenation product might be a mixture of racemic and *meso* 2,4-pentanediol. The asymmetric hydrogenation of AA could occur only by means of the latter mechanism. As it seemed that the modification might change the hydrogenation mechanism, the asymmetric hydrogenation of AA was studied using catalysts modified with L-glutamic acid and D-tartaric acid, and unmodified ones.

Experimental

Preparation of the Modified Raney Nickel Catalyst.[3] One gram of Raney nickel alloy (Ni: Al=4: 6) was developed with 14 ml of a 20% sodium hydroxide solution, and the mixture was kept for 1 hr at 100 °C. After the removal of the sodium hydroxide solution by decantation, the catalyst was washed with 300 ml of water. One hundred and fifty milliliters of a 1—2% modifying solution, which had been adjusted to the specified pH and temperature, was then added to the catalyst, and the mixture was allowed to stand at the specified temperature for 1.5 hr. After the modifying solution had then been removed by decantation, the catalyst was washed once with water and twice with methanol.

Asymmetric Hydrogenation of the Substrate and Hydrogenation Velocity. Ten millimiters of the substrate was hydrogenated with a modified Raney nickel catalyst prepared from 1.0 g of the alloy in a glass vessel placed in a 0.1 *l* shaking autoclave. The hydrogenation temperature and the initial pressure were 65±3 °C and 100 kg/cm² respectively. When the calculated amount of hydrogen was consumed, the hydrogenation was stopped and the product was distilled. The hydrogenation rate was calculated from the readings of the gauge at intervals of fifteen or twenty minutes.

a) 2-Pentanol-4-on. The fraction with 70—90 °C/20 mmHg was collected and treated with basic cupric carbonate at 60 °C for 3 hr. After the removal of the cupric carbonate and the precipitated cupric acetylacetonate by filtration, the liquid was distilled under reduced pressure and fractionated into two main fractions, 73—77 and 107—109 °C/22 mmHg. The fraction with a bp of 73—77 °C/21 mmHg was collected and redistilled through a McMahon column (10 cm) packed with stainless wire-netting (3 mm, 100 mesh) (bp 75—76 °C/21 mmHg), while the fraction with a bp of 107—109 °C/22 mmHg was left for 2,4-pentanediol.

b) 2,4-Pentanediol. The fraction with a bp of 107—109 °C/22 mmHg was collected.

Measurement of the Corroded Nickel from the Catalyst. Ten milliliters of acetylacetone was hydrogenated with 0.4 g of the modified catalyst, and the reaction was stopped at the point when the one mole of hydrogen has been consumed. The catalyst was removed by filtration, and the catalyst was washed with methanol. The filtrate and the washings were combined, and the solution was concentrated to dryness under reduced pressure. Twenty-five milliliters of nitric acid (d=1.48) and 25 ml of water were then added to the residue, and the mixture was kept 24 hr at 90 °C. The resulting solution was concentrated to dryness under reduced pressure. After the addition of 25 ml of water, the solution was concentrated to dryness; a 25 ml portion of a 14% aqueous ammonium solution was added to the residue, and the insoluble material was removed by filtration. Dimethylglyoxime saturated in conc. aqueous ammonia was added to the filtrate until no further nickel dimethylglyoxime was precipitated. The reaction mixture was allowed to stand for 1 hr at room temperature, and then the nickel dimethylglyoxime was collected using a glass filter, washed with 50 ml of conc. aqueous ammonia, dried at 60 °C for 4 hr in a vacuum desiccator, and weighed.[4]

Preparation of Schiff Base of Acetylacetone and Disodium Glutamate.[5] Six grams of L-glutamic acid was dissolved in a mixture of 4 g of sodium hydroxide, 15 ml of acetylacetone, 10 ml of water, and 100 ml of methanol. The solution was then concentrated to dryness, and the residue was recrystallized from methanol. Yield, 8 g. Found: C, 43.96; H, 4.93; N, 4.94%. Calcd for $C_{10}H_{13}O_5N \cdot Na_2$: C, 43.96; H, 4.80; N, 5.13%. $[\alpha]_D^{20}$ +70.4° (*c* 4, water).

Measurement of the Optical Rotation of the Product. The optical rotations of 2,4-pentanediol and 2-pentanol-4-on were measured in a 1 dm tube without dilution. The absolute configurations of (−)-2,4-pentanediol and (−)-2-pentanol-4-on were identified as R, and their specific rotations were calculated to be −47 and −18°.[6]

Measurement of the Components in a Reaction Mixture. Ten milliliters of acetylacetone (0.1 mol) was hydrogenated with 0.4 g of a modified Raney nickel catalyst; at the point when the calculated atoms of hydrogen had been taken up, the reaction was stopped. The contents of acetylacetone, 2,4-pentanediol, and 2-pentanol-4-on were estimated by gas-liquid chromatography. Conditions: column, 1.5% NPGS

2) Y. Izumi, M. Imaida, T. Harada, T. Tanabe, S. Yajima, and T. Ninomiya, This Bulletin, **42**, 241 (1969).

3) Y. Izumi, T. Harada, T. Tanabe, and K. Okuda, *ibid.*, **44**, 1418 (1971).

4) O. Z. Brunk, *Angew. Chem.*, **19**, 1793 (1906).

5) E. Dane, F. Dress, P. Konra, and T. Dockner, *Angew. Chem. Int. Ed. Engl.*, **1**, 658 (1962).

6) T. Tanabe, This Bulletin, to be published.

on Chromosorb W, 3-m glass column, temp. 95 °C.

Ratios of Racemic and meso *2,4-Pentanediols in the Reaction Mixture.* The ratios of racemic and *meso* 2,4-pentanediols were estimated from the gas-liquid chromatograms of the benzylidene derivatives.[6] Since the deviations of the ratios of the racemic and *meso* diols after and before distillation were within a few percent, the error by distillation can be disregarded.

Results and Discussion

The Protective Effect of the Modification Against the Corrosion of Nickel by Acetylacetone (AA). Acetylacetone is known as a strong corrosive reagent of metals, and the corrosion of the nickel catalyst with AA was found in the course of the study of the asymmetric hydrogenation with the modified Raney nickel catalyst.

TABLE 1. EFFECT OF MODIFICATION ON ELUTION OF NICKEL FROM CATALYST

No	Modifying reagent	Modifying condition		Eluted nickel from catalyst (%)[a]
		pH	temp. °C	
1	—	—	—	30
2	D-Tartaric acid	2.0	0	9
3	D-Tartaric aicd	5.0	0	7
4	D-Tartaric acid	10.0	0	23
5	D-Tartaric aicd	5.0	100	16
6	D-Tartaric aicd	10.0	100	24
7	L-Glutamic acid	5.0	0	2
8	L-Glutamic acid	5.0	100	7
9	L-Histidine	7.9	0	3
10[b]	—	—	—	0
11[c]	—	—	—	76

a) 400 mg of catalyst and 10 ml of acetylacetone were used.
b) Two moles of hydrogen was adsorbed.
c) Shaked for the same hours as in No. 1 under no hydrogen at 65 °C.

In order to study the interaction between the substrate and the nickel of the catalyst, the amount of the corroded nickel half-way through the hydrogenation of AA was determined according to the method of Brunk.[4] The results are shown in Table 1. Also in Table 1 are listed the amounts of the corroded nickel from the unmodified catalyst the half-way through and after the completion of the hydrogenation.

As may be seen in Table 1, the unmodified catalyst was more strongly corroded than the modified catalysts and as much as 30% of the nickel was dissolved. The modified catalysts, however, were corroded increasingly in the order of those modified with histidine, glutamic acid, and tartaric acid. The order was the reverse of that of the stabilities of the nickel chelates of these modifying reagents.

The results suggest that the modifying reagents inhibit the formation of the nickel chelate of AA and protect the catalyst surface from corrosion by AA. The nickel chelate was not detected in the reaction mixture at the completion of the hydrogenation. This fact shows that the nickel chelate once formed in the reaction system is hydrogenated to 2,4-pentanediol and nickel metal. The same observation has also been made previously in the hydrogenations of the nickel chelate of β-ketocarbonyl compounds with a modified Raney nickel catalyst.[7]

The results presented above suggest that AA is hydrogenated with an unmodified catalyst in a way very similar to that of the nickel chelate. In the hydrogenation with a modified catalyst, however, AA is hydrogenated without forming a complete chelate by the action of the modifying reagent.

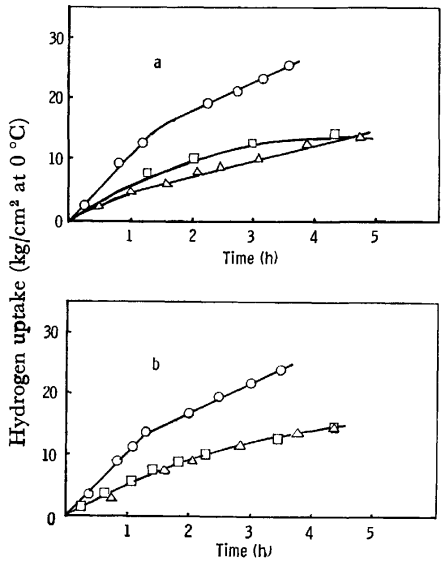

Fig. 1. Hydrogenation uptake rate in hydrogenation of acetylacetone and methyl acetoacetate.
10 ml of acetylacetone or methyl acetoacetate was hydrogenated with 400 mg of catalyst. a: acetylacetone; b: methyl acetoacetate.
-□- unmodified; -○- modified with D-tartaric acid at pH 5.0, 0 °C; -△- modified with L-glutamic acid at pH 5.0, 0 °C.

The Effect of the Modification on the Hydrogenation Velocity. The changes in the hydrogen uptake during the initial 5 hr in the hydrogenations of AA and MAA with the catalyst modified with D-tartaric acid, and with L-glutamic acid are shown in Fig. 1. in comparison with those hydrogenated with an unmodified catalyst.

In the cases of both AA and MAA, the catalyst modified with tartaric acid had about twice the hydrogenation activity of the catalyst modified with glutamic acid and the unmodified catalyst. The hydrogenation activity of the catalyst modified with glutamic acid was slightly weaker than that of the unmodified catalyst in the hydrogenation of AA. Moreover, in the hydrogenation of MAA, the two catalysts had similar activities.

These facts seem to show that the modification does not inhibit the absorption of the substrate and that tartaric acid and glutamic acid on the catalyst surface

7) T. Tanabe, T. Ninomiya, and Y. Izumi, This Bulletin, **43**, 2276 (1970).

may contribute to the enantiotopic selection *via* different mechanisms.

The Change in the Reaction Component Attended by the Progress of Hydrogenation. The hydrogenation of AA into 2,4-pentanediol (II) can be considered to take place *via* two processes: a one-step process by which II is produced directly from AA, and a two-step process by which II is produced *via* 2-pentanol-4-on (I). In order to clarify the effect of the modification on the hydrogenation process of AA, the changes in the components in the hydrogenation systems were studied during the progress of hydrogenation. The amounts of AA, I, and II were determined by gas-liquid chromatography; the results are shown in Fig. 2.

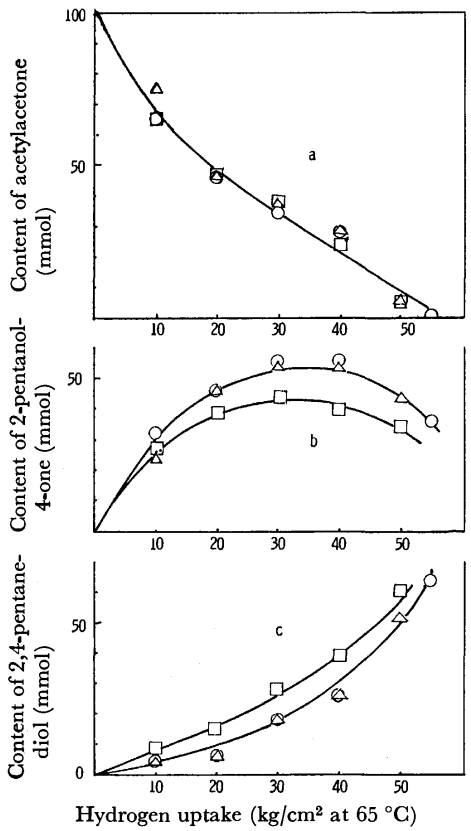

Fig. 2. Effects of modification on contents of acetylacetone, 2-pentanol-4-on and 2,4-pentanediol.
a: acetylacetone; b: 2-pentanol-4-on; c: 2,4-pentanediol.
-□- unmodified; -○- modified with D-tartaric acid; -△- modified with L-glutamic acid. The catalyst was modified at pH 5.0, 0 °C.

As may be seen in Fig. 2, the initial consumptions of AA ($-dAA/d\not{p}$) by both modified and unmodified catalysts are 87 mmol/kg·cm^{-2}·g-cat. and no effects of the modifications are observed. The initial formation of I by the unmodified and modified catalysts were about 70 and 80 mmol/kg·cm^{-2}·g-cat. respectively. Accordingly, more than eighty percent of AA was converted to II by the two-step process with the unmodified catalyst, and the modification improves the two-step process of hydrogenation. These facts show that the hydrogenation of AA with a Raney nickel catalyst mainly proceeds by the two-step process.

The Effect of the Modifying pH *on the Asymmetric Activity of the Catalyst.* In the hydrogenation of AA, the effect of the modifying pH on the asymmetric activities of the catalysts modified with D-tartaric acid and L-glutamic acid were investigated; the results are shown in Figs. 3 and 4. The asymmetric activities of the catalysts are represented by the optical rotation of 2,4-pentanediol. Also, the components of racemic 2,4-pentanediol in the hydrogenation products are shown in the figures. Upon modification with D-tartaric acid, the maximum asymmetric activity was observed at pH 10. The ratio of the DL-compound to the *meso*-compound was not affected by the modifying pH of the catalyst.

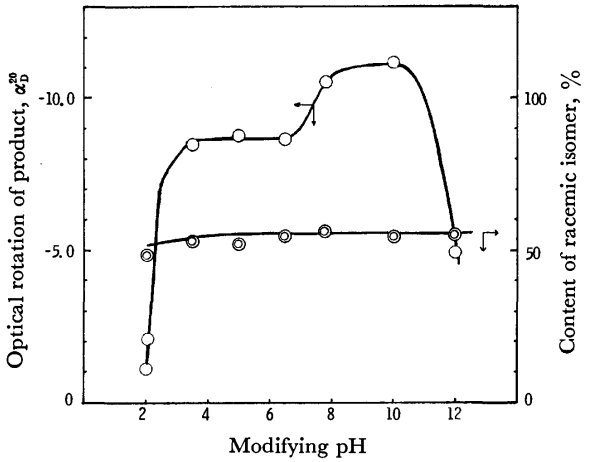

Fig. 3. Effect of modifying pH on asymmetric hydrogenation of acetylacetone on modification with D-tartaric acid at 0 °C and content of racemic 2,4-pentanediol.

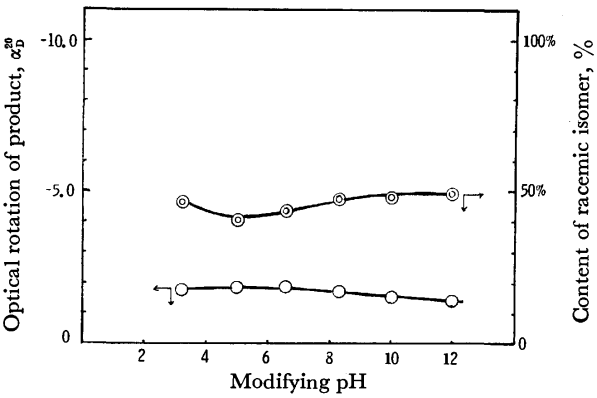

Fig. 4. Effect of modifying pH on asymmetric hydrogenation of acetylacetone using Raney nickel catalyst modified with L-glutamic acid at 0 °C and component of racemic 2,4-pentanediol.

The effect of the modifying pH was found to be closely related to the result obtained in the study of the adsorption of AA on the evaporated nickel film by Ninomiya of our research group.[8] That is, AA adsorbs in different states on the evaporated nickel films pretreated with tartaric acid at pH 2, 5, and 9. The optimum modifying pH for the asymmetric activity of the catalyst at pH 8—10 and a shoulder at pH 3—6 seem to correspond to the two different adsorption

8) T. Ninomiya, *ibid.*, **45**, 2551 (1972).

spectra of AA at pH 5 and 9.

Upon modification with L-glutamic acid, the asymmetric activity of the catalyst and the content of the racemic isomer were not influenced by the modifying pH. The asymmetric activity of the catalyst was found to be much less than that of the one modified with tartaric acid. The results show that the asymmetric hydrogenation of AA with the catalyst modified with glutamic acid proceeds under a different mode of interaction between the modifying reagent and the substrate from that of the catalyst modified with tartaric acid.

The Effect of the Modifying Temperature on the Asymmetric Activity of the Catalyst. The effect of the modifying temperature on the asymmetric activity of the catalyst was studied; the results are shown in Table 2.

TABLE 2. EFFECT OF MODIFYING TEMPERATURE

Modifying reagent	Modifying condition		Optical rotation of 2,4-pentanediol, α_D^{20}
	Temp. (°C)	pH	
D-Tartaric acid	0	5.0	−8.78
D-Tartaric aicd	100	5.0	−17.39
D-Tartaric acid	0	10.0	−12.15
D-Tartaric acid	100	10.0	−12.96
L-Glutamic acid	0	5.0	−1.88
L-Glutamic acid	100	5.0	−1.26

Upon modification with D-tartaric acid, the asymmetric activity of the catalyst modified at pH 5.0 was increased by the increase in the modifying temperature, while the catalyst modified at pH 10 was not affected by the modifying temperature. The asymmetric activity of the catalyst modified with L-glutamic acid at pH 5.0 decreased with the increase in the modifying temperature. These results show that the two acids on the catalyst surface affect the asymmetric hydrogenation in different manners.

The Asymmetric Activity of the Recovered Catalyst Modified with Glutamic Acid. As AA can react with an amino acid and produce the Schiff base,[5] there is a possibility that the glutamic acid on the catalyst surface changes into the Schiff base during the hydrogenation of AA.

In order to make clear this possibility, the recovered catalyst once used in the hydrogenation of AA was subjected again to the hydrogenation of MAA; the results are compared with the asymmetric activities of the catalysts modified with the Schiff base of L-glutamic acid and acetylacetone in Table 3. In the hydrogenation of MAA, the catalyst once used for the hydrogenation of AA did not show the original asymmetric activity of the catalyst modified with L-glutamic acid.

These facts show that the amino group of glutamic acid on the catalyst surface reacts with AA and forms the Schiff base during the hydrogenation, as is shown in Scheme 2:

$$\mathrm{R\text{-}NH_2 + AA \longrightarrow R\text{-}N{=}C(CH_3)\text{-}CH_2\text{-}COCH_3 \longrightarrow R\text{-}N\text{-}C(CH_3){=}CH\text{-}CO\text{-}CH_3}\ (\mathrm{H})$$

Scheme 2.

The Effect of the Corrosion of Nickel on the Asymmetric Activity of the Catalyst. As has already been described, a part of the catalyst turned out to be the nickel-AA chelate and the chelate is hydrogenated to 2,4-pentanediol and nickel at the completion of the hydrogenation. Therefore, the asymmetric activities of the catalysts may be expected to vary with the change in the surface structure. In order to study the alterations of the asymmetric activities of the catalysts during the hydrogenation of AA, the optical rotations of 2,4-pentanediol produced at the middle and completed stages of hydrogenation were measured; the results are shown in Table 4.

The asymmetric activity of catalyst modified with tartaric acid at 0 °C slightly decreased, while that of the one modified at 100 °C did not change, during the hydrogenation. The asymmetric activities of the catalysts modified with glutamic acid rather increased with the progress of the hydrogenation.

The Asymmetric Hydrogenation of AA to I with the Modified Raney Nickel Catalyst. As the hydrogenation of AA was found to proceed by the successive hydrogenation mechanism, it was obvious that AA undergoes the

TABLE 3. ASYMMETRIC ACTIVITIES OF RECOVERED CATALYST AND THE CATALYST MODIFIED WITH THE SCHIFF BASE OF L-GLUTAMIC ACID AND ACETYLACETONE

Substrate	Catalyst	Product	Optical rotation, α_D^{20}
Acetylacetone	L-Glutamic acid pH 5.0, 0 °C	2,4-Pentanediol	−1.88
Methyl acetoacetate	Recovered catalyst of No. 1	Methyl 3-hydroxybutyrate	−1.55
Methyl acetoacetate	L-Glutamic acid pH 5.0, 0 °C	Methyl 3-hydroxybutyrate	−4.98[a]
Acetylacetone	Na_2 L-Glu.-AA Schiff base Methanol soln. 0 °C	2,4-Pentanediol	−1.43
Acetylacetone	L-Glutamic acid pH 10.0, 0 °C	2,4-Pentanediol	−1.50

a) T. Tanabe, K. Okuda, and Y. Izumi, to be published in This Bulletin.

Table 4. Optical rotations of 2,4-pentanediol at the middle and last stages

Modifying reagent	Modifying condition			Optical rotation, α_D^{20}
	pH	Temp., °C		
D-Tartaric acid	5.0	0	a	−10.60
			b	−8.78
D-Tartaric acid	5.0	100	a	−18.25
			b	−17.39
L-Glutamic acid	5.0	0	a	−1.01
			b	−1.88
L-Glutamic acid	5.0	100	a	−0.13
			b	−1.26

a) About one mole of hydrogen was absorbed.
b) Two moles of hydrogen was absorbed.

Table 5. Asymmetric hydrogenation of AA to I with modified catalyst

Modifying conditions	Optical rotation of 2-pentanol-4-on, α_D^{20} (P%)
D-Tartaric acid pH 5.0, 0 °C	−6.02 (33)
D-Tartaric acid pH 5.0, 100 °C	−10.44 (57)
L-Glutamic acid pH 5.0, 0 °C	−0.44 (2.4)
L-Glutamic acid pH 5.0, 100 °C	−0.20 (1.1)

stereospecific hydrogenation in, two steps, AA to I and I to II. In order to determine the asymmetric yields of the products in the step of AA to I, I was isolated from the reaction mixture at the point of an hydrogen uptake of one mole; the optical rotations and asymmetric yields of the products obtained are shown in Table 5.

Table 6. Effect of asymmetric center of I on hydrogenation of I to II with unmodified catalyst

Optical purity of substrate, 2-pentanol-4-on	Optical yield of product, 2,4-pentanediol	Content of racemic diol
57%	28%	50%
2.4%	1.2%	50%

As may be seen in the table, the asymmetric yields (P%) of the hydrogenation with the catalysts modified with D-tartaric acid at 0 and 100 °C were 33 and 56% respectively. These asymmetric yields are quite similar to those in the hydrogenation of MAA, the keto-enol equilibrium of which shifts more to the keto form than does that of AA. Low asymmetric yields (2.4 and 1.1%) were observed with the catalyst modified with L-glutamic acid. The results with D-tartaric acid suggest that the keto-enol equilibrium does not affect the asymmetric yield of the product. The results obtained in the hydrogenation of AA with the catalyst modified with glutamic acid can not be compared with the asymmetric yields in the hydrogenation of MAA because of the Schiff base formation of glutamic acid with AA.

The Diastereoselectivity[1] *of the Unmodified Catalyst in the Hydrogenations of I to II.* Because of the possibility of the diastereoselective hydrogenation of I under the influence of the asymmetric center of I, partially optically-active I was hydrogenated with the unmodified catalyst; the optical purities of the products are shown in Table 6.

As the optical purities of II are half of those of I, and as the racemic isomers of II are 50%, it is obvious that the second asymmetric center at the 4-position is produced without any influence of the already existing asymmetric center at the 2-position. In other words, the unmodified catalyst showed no diastereoselectivity to I.

The Enantioselectivity and the Diastereoselectivity of the Modified Catalyst in the Hydrogenation of I to II. In order to determine the enantioselectivities and the diastereoselectivities of the catalysts modified with L-glutamic acid and D-tartaric acid, pratially optically-active I was hydrogenated with catalysts modified under the same conditions as those used for the preparation of partially optically-active I. The proportions of racemic and *meso* isomers were determined by the gas-liquid chromatography of their optical purities of the products.

Also in Table 7, the conversion rates of 2*R*-I (or 2*S*-I) to 2*R*, 4*R*- and 2*R*, 4*S*-II (or 2*S*, 4*R*- and 2*S*, 4*S*-II), K_{RR} and K_{RS} (or K_{SR} and K_{SS}) are shown; the ratios of the conversion rate, K_{RR}/K_{RS} (or K_{SR}/K_{SS}) are calculated from these results.

The K_{RR}/K_{RS} and K_{SR}/K_{SS} ratios of the catalyst modified with D-tartaric acid at 0 °C (100 °C) were 1.3 (1.8) and 1.0 (1.2) respectively. These facts show that the carbonyl groups of both *R*-I and *S*-I were hydrogenated to the alcohol with a 4*R*-configuration independently of the asymmetric center of I. That is, the hydrogenation was enantioselective rather than diastereoselective.

On the other hand, in the hydrogenation with the catalyst modified with L-glutamic acid at 0 °C (100 °C), the K_{RR}/K_{RS} and K_{SR}/K_{SS} ratios were 0.75 (0.67) and 1.7 (1.8) respectively. The results indicate that the carbonyl group at the 4-position of I with the 2*R*- or 2*S*-configuration is reduced to the alcohol with the 4*S*- or 4*R*-configuration respectively rather than with a 4*R*- or 4*S*-configuration. That is, new asymmetric centers which have absolute configurations, the reverse of those of I are produced by the catalyst modified

TABLE 7. STEREOSPECIFIC HYDROGENATION OF I TO II WITH MODIFIED RANEY NICKEL CATALYST

Modifying reagent (Temp. °C)	Content of Opt. isomer of I (%)	Ratio	Content of Opt. isomer of II (%)	Obs. Opt. yield (*RR-SS*)	Content of racemic diol (*RR*+*SS*)	Content of *meso* diol (*RS*+*SR*)
D-Tartaric acid (0)	*R*-(66)	$K_{RR}/K_{RS}=1.3$	*RR*(37) *RS*(29)	20%	54%	45%
	S-(34)	$K_{SR}/K_{SS}=1.0$	*SR*(17) *SS*(17)			
D-Tartaric acid (100)	*R*-(78)	$K_{RR}/K_{RS}=1.8$	*RR*(50) *RS*(28)	40%	60%	40%
	S-(22)	$K_{SR}/K_{SS}=1.2$	*SR*(12) *SS*(10)			
L-Glutamic acid (0)	*R*-(51)	$K_{RR}/K_{RS}=0.75$	*RR*(22) *RS*(29)	4%	40%	60%
	S-(49)	$K_{SR}/K_{SS}=1.7$	*SR*(31) *SS*(18)			
L-Glutamic acid (100)	*R*-(50)	$K_{RR}/K_{RS}=0.67$	*RR*(20) *RS*(30)	2%	38%	62%
	S-(50)	$K_{SR}/K_{SS}=1.8$	*SR*(32) *SS*(18)			

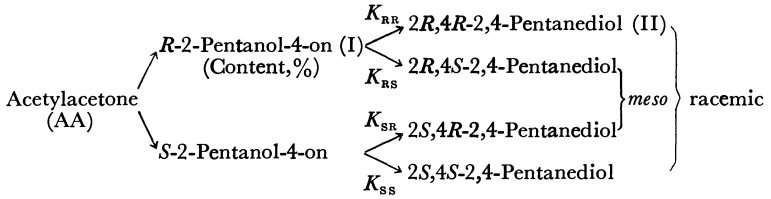

with glutamic acid. That is the catalyst modified with glutamic acid has a stronger diastereoselectivity than enantioselectivity.

Furthermore, both the catalysts modified with tartaric acid and glutamic acid increased in enantioselectivity and in diastereoselectivity respectively with the increase in the modifying temperature. These facts seem to suggest that the changes in the asymmetric activities of the catalyst with the modifying temperature are not caused by the change in the intrinsic adsorption mode of the modifying reagent. It can also be concluded that asymmetric hydrogenations with the catalysts modified with tartaric acid and with glutamic acid proceed *via* different mechanisms.

Conclusion

When AA was hydrogenated with the catalyst modified with tartaric acid, the effective asymmetric hydrogenations were performed at the step of AA to I in a very similar asymmetric yield, as in MAA, which has a keto-enol equilibrium constant different from that of AA. This fact indicates that the apparent keto-enol equilibrium of the substrate is not an important factor in the enantioselection of the substrate. At the step of I to II, the catalysts modified with tartaric acid and with glutamic acid showed enantioselectivity and diastereoselectivity respectively. The unmodified catalyst has neither enantioselectivity nor diastereoselectivity.

AA usually strongly corrodes the Raney nickel catalyst during the hydrogenation, but the modification protected the catalyst from the corrosion by AA. The hydrogenation velocity, however, was not decreased by the modification. Evidence which suggests a difference in the hydrogenation mechanisms in the catalysts modified with tartaric acid and glutamic acid were found in the hydrogenation velocities of AA, in asymmetric activities of AA to I and I to II, and in the modifying pH and temperature dependencies of the asymmetric activities of the catalysts. The glutamic acid on the catalyst surface reacted with AA and became the Schiff base derivative during the hydrogenation.

The auther wishes to express his thanks to Professor Yoshiharu Izumi for his continuous guidance and help, and also to Miss Kiku Koike and Mrs. Nobuko Okuhara for making the elemental analyses.

Peptide Synthesis *via* *N*-Acylated Aziridinone.[1] II. The Reaction of *N*-Acylated Aziridinone and Its Use in Peptide Synthesis

Muneji MIYOSHI

Department of Synthetic Chemistry, Research Laboratory of Applied Biochemistry, Tanabe Seiyaku Co., Ltd., Kashima-cho, Higashiyodogawa-ku, Osaka 532

(Received July 21, 1972)

Optically active *N*-acylated aziridinone, which was synthesized by the dehydration of the corresponding L-acylamino acid, was treated with various nucleophiles, such as alcohol, amine, and water. The ring fission of the aziridinone took place exclusively at the carbonyl-nitrogen bond to give L-acylamino acid derivatives. The reaction was used successfully in the peptide synthesis, using an amino acid ester as a nucleophile. A retention of the optical activity was observed throughout the reaction.

Interest in aziridinone chemistry has increased since Baumgarten[2] first proved the existence of *N*-*t*-butyl-3-phenylaziridinone by spectral studies in 1961. Recently, a number of data on the physical and chemical properties of the aziridinone have been accumulated, and work on it is still in progress.

The aziridinone chemistry reported[3-8] thus far may be summarized as follows.

All of the aziridinones synthesized to date have the *N*-substituent, which is an electron-donating and a sterically bulky alkyl group. Among them, *N*-*t*-butyl and *N*-adamantyl-aziridinones were isolated in the pure form.

Among the substituents at *C*-3, the bulky alkyl group generally increases the stability of the ring, while the aryl group decreases the stability of the aziridinone under otherwise identical conditions. *C*-3 disubstituted aziridinones are more stable than *C*-3 monosubstituted ones under the same conditions. In general, the *N*-*t*-alkyl-aziridinones isolated and investigated are very reactive with nucleophiles to give the corresponding adducts by the fission of the three-membered ring. Depending on the nucleophiles, a high selectivity is observed in the type of ring opening. For example, reactions with proton-containing nucleophiles, such as water, alcohols, amines, and ethyl glycinate, lead exclusively to amides because of the fission at the alkyl-nitrogen bond. On the other hand, reactions with aprotic nucleophiles, such as sodium methoxide and potassium *t*-butoxide, give amino acid derivatives as the only product, corresponding to a ring-opening at the carbonyl-nitrogen bond.

In the previous paper,[9] the author reported a new method of synthesizing the optically-active *N*-acylated aziridinones, which have a hydrogen atom on the asymmetric carbon at *C*-3, from the corresponding L-acylamino acids. The present paper will describe the reactivity of the new *N*-acylated aziridinones and an approach to the peptide synthesis by the use of these compounds.

Results and Discussion

Reactions of 3-Benzyl-1-benzyloxycarbonylaziridin-2-one (I) with Various Nucleophiles. The 3-benzyl-1-benzyloxycarbonylaziridine-2-one (I) was synthesized by the dehydration of benzyloxycarbonyl-L-phenylalanine (Z-Phe), as had been described in detail previously.[9]

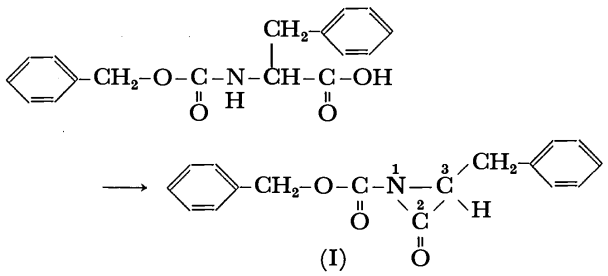

(I)

The crystals of I were dissolved in anhydrous tetrahydrofuran (THF), and all of the reactions with nucleophiles were carried out at −10——0 °C over a period of one hour under stirring. The nucleophiles used in this study were water, *t*-butyl alcohol, potassium *t*-butoxide, aniline, and benzylamine. The results are summarized

1) A part of this study has been reported in a preliminary communication. This Bulletin, **43**, 3321 (1970). Also presented at the 8th Symposium on Peptide Chemistry, Osaka, Nov. 1970, and at the 24th Annual Meeting of the Chemical Society of Japan, Osaka, April, 1971.

2) H. E. Baumgarten, R. L. Zey, and U. Krolls, *J. Amer. Chem. Soc.*, **83**, 4469 (1961).

3) H. E. Baumgarten, *ibid.*, **84**, 4975 (1962); H. E. Baumgarten and J. F. Fureholzer, *ibid.*, **85**, 3303 (1963); H. E. Baumgarten, R. D. Clark, and S. L. Endres, *Tetrahedron Lett.*, **1967**, 5033.

4) J. C. Sheehan and I. Lengyel, *J. Amer. Chem. Soc.*, **86**, 1356 (1964); J. C. Sheehan and I. Lengyel, *J. Org. Chem.*, **31**, 4244 (1966); J. C. Sheehan and J. Beeson, *J. Amer. Chem. Soc.*, **89**, 362, 366 (1967); J. C. Sheehan and M. M. Nafissi-V, *ibid.*, **91**, 1176 (1969).

5) I. Lengyel and D. B. Uliss, *Chem. Commun.*, **1968**, 1621; I. Lengyel and J. C. Sheehan, *Angew. Chem.*, **80**, 27, (1968).

6) K. Bott, *Angew. Chem.*, **79**, 943 (1967); K. Bott, *Tetrahedron Lett.*, **1968**, 3323; K, Boot. *Chem. Ber.*, **103**, 3850 (1970); K. Bott, *Ann. Chem.*, **755**, 58 (1972).

7) E. R. Talaty, A. E. Dupuy, Jr., and A. E. Cancienne, Jr., *J. Heterocycl. Chem.*, **4**, 657 (1967); E. R. Talaty and A. E. Dupuy, Jr., *Chem. Commun.*, **1968**, 790; E. R. Talay, A' E. Dupuy, Jr., and T. H. Golson, *ibid.*, **1969**, 49; E. R. Talay and C. M. Utermoehlen, *ibid.*, **1970**, 473; E. R. Talay, C. M. Utermoehlen, and L. H. Stekoll, *Synthesis*, **1971**, 543; E. R. Talay, and C. M. Utermoehlen, *Tetrahedron Lett.*, **1970**, 3321; E. R. Talaty, A. E. Dupuy, Jr., C. K. Johnson, T. P. Pirotte, W. A. Fletcher, and R. E. Thosmpson, *ibid.*, **1970**, 4435.

8) A. H. J. Wang, I. C. Paul, E. R. Talaty, and A. E. Dupuy, Jr., *Chem. Commun.*, **1972**, 43.

9) Part I. This Bulletin, **46**, 212 (1973).

Table 1. Reaction of I with nucleophiles

No.	Nucleophile	Product	Yield (%)	Mp (°C)	$[\alpha]_D^{20}$ (*c* 1)
1	*t*-BuOH	Z–Phe–OBu^t	83.3	81—82	−6.0(EtOH)
2	*t*-BuOK	Z–Phe–OBu^t	56.8	81—82	−6.0(EtOH)
3	NH_2⟨⟩	Z–Phe–NH⟨⟩	84.6	164—166	+30.0(THF)
4	NH_2CH_2⟨⟩	Z–Phe–$NHCH_2$⟨⟩	85.3	157—158	−12.0(THF)
5	H_2O	$(Z\text{–Phe})_2O$	47.2	144—146	+14.6(Dioxane)
6	H_2/Pd	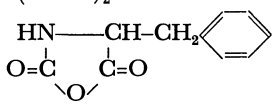	78.5	96—98	−110.4(THF)

in Table 1.

It is interesting to note that all of the products obtained are amino acid derivatives, corresponding to the fission of the carbonyl-nitrogen bond on the ring. The exclusive selectivity of this ring fission is observed even when *t*-butyl alcohol is used as a proton-containing nucleophile. The same product of benzyloxycarbonyl-L-phenylalanine *t*-butyl ester (Z–Phe–OBu^t) is also obtained by the use of potassium *t*-butoxide, which is an aprotic nucleophile.

The fact that the ring fission always takes place at the carbonyl-nitrogen bond, no matter what the species of the attacking nucleophiles, may be attributed to the lower electron density on the ring of I compared with that of *N*-*t*-alkyl-aziridinone.

As an urethan carbonyl group affects lone-pair electrons of the nitrogen atom so as to decrease the electron density, the protonation ability of the nitrogen atom on the ring as a Lewis-base would be diminished. Therefore, a nucleophile would selectively attack the carbonyl carbon, even if a proton donor were present in the reaction media. Further, the effect of the *N*,*N*-diacyl group should also be taken into consideration. The possibility of the selective ring fission at the carbonyl-nitrogen bond would be greatly increased because of the sensitive reactivity of the *N*-substituted diacyl group. The results of an MO calculation also support the above explanation of the observed ring fission; these data will be summarized later.

It is also interesting to note that the reaction of I with water leads to the formation of an intermolecular anhydride of Z–Phe (5), while catalytic hydrogenation over palladium-black in ether gives the corresponding intramolecular anhydride (6); the so-called "*N*-carboxy-α-amino acid anhydride" (NCA).

Wieland and Bernhard[10] reported that Z-amino acid reacted with phosgene ($COCl_2$) at 0 °C in the presence of tertiary amine to form the same intermolecular anhydride (5). In this study, I was directly treated with water to form Z–Phe in the first step; the formation of the anhydride (5) would occur *via* an intermolecular attack by the ionized carboxyl anion of the Z–Phe on the carbonyl carbon of the other molecule of the aziridinone.

On the contrary, hydrogenolysis takes place at the benzyl-oxygen bond to form toluene and a carbamic

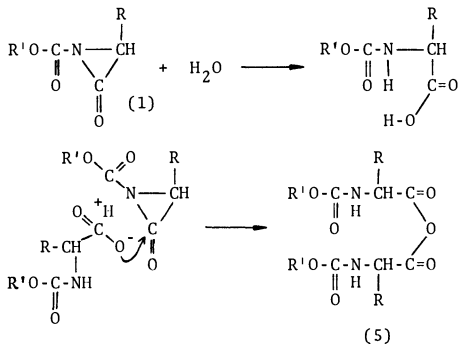

(5)

acid residue, when catalytic hydrogenation is carried out in anhydrous ether. Therefore, the fast intramolecular attack by the carboxyl group on the adjacent carbonyl carbon in the same molecule must then take place before the decarboxylation of the carbamic acid occurs.

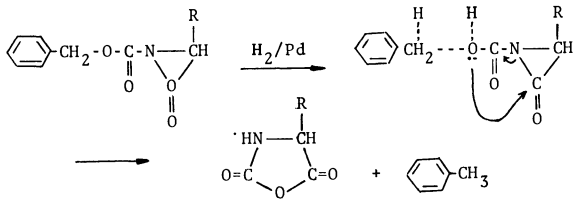

(6)

The proposed mechanism is partially similar to that of the NCA formation reaction commonly employed. In this case, the intramolecular attack by the carboxyl group of the carbamic acid on the activated carbonyl group in the same molecule takes place under anhydrous conditions at 40—60 °C.

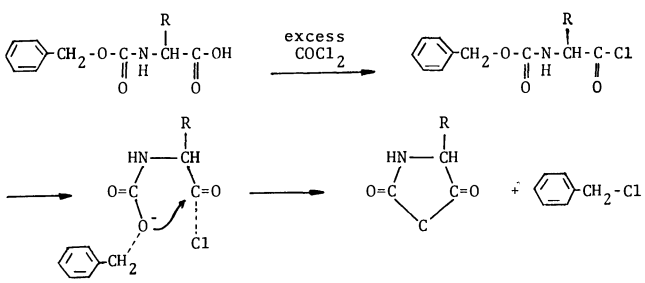

It should also be noted that the retention of the full optical activity is observed in every reaction. This observation suggests two significant facts. The first is that I has a full optical activity and that racemization does not occur during the ring-formation reaction. The

10) T. Wieland and H. Bernhard, *Ann. Chem.*, **572**, 190 (1951).

Table 2. Reaction of *N*-acylated aziridinones derived from acyl amino acid

No.	Acyl amino acid	Nucleophile	Product	Yield (%)	Mp (°C)	$[\alpha]_D^{20}$ (*c* 1)
7	Z–Val	MeOH	Z–Val–OMe	81.9	54—55	−18.9(MeOH)
8	Z–Ala	H_2O	$(Z\text{–}Ala)_2O$	45.2	120—122	−11.0(THF)
9	Z–Val	H_2O	$(Z\text{–}Val)_2O$	45.6	96—98	+10.7(THF)
10	Br–Z–Phe	H_2O	$(Br\text{–}Z\text{–}Phe)_2O$	51.1	147—148.5	+2.0(THF)
11	Cl–Z–Phe	H_2O	$(Cl\text{–}Z\text{–}Phe)_2O$	47.8	149—150	−3.0(THF)
12	Tos–Phe	MeOH	Tos–Phe–OMe	52.5	91—93	+3.1(MeOH)

second is that the ring-opening reaction of I with various nucleophiles also proceeds without racemization.

Reaction of N-*Acylated Aziridinone with Nucleophiles.* From the subsequent study, it was found that the isolation of I synthesized is not always necessary for the sake of the successive reaction with nucleophiles; the reaction was performed directly by the use of the I without isolation before use. Thus, the reaction procedure may not only be simplified but may also be applied to other *N*-acylated aziridinones which are not isolated in the crystalline form. The results are summarized in Table 2.

Reaction of N-*Acylated Aziridinones with Amino Acid Derivatives.* The crystal of I was dissolved in chloroform, and into this solution was added a solution

Table 3. Reaction of *N*-acylated aziridinones with amino acid derivatives

No	Z–AA	Nucleophile	Product
13	Z–Phe[a]	H–Gly–OEt	Z–Phe–Gly–OEt
14	Z–Ala	H–Gly–OEt	Z–Ala–Gly–OEt
15	Z–Val	H–Gly–OEt	Z–Val–Gly–OEt
16	Z–Leu	H–Gly–OEt	Z–Leu–Gly–OEt
17	Z–Ile	H–Gly–OEt	Z–Ile–Gly–OEt
18	Z–Met	H–Gly–OEt	Z–Met–Gly–OEt
19	Z–(Ph)Gly	H–Gly–OEt	Z–(Ph)Gly–Gly–OEt
20	Z–Phe	H–Ile–OEt	Z–Phe–Ile–OEt
21	Z–Phe	H–Val(Me)–OMe[b]	Z–Phe–Val(Me)–OMe
22	Z–Phe	H–Ile–OH	Z–Phe–Ile–OH
23	Z–Phe	H–Val–OH	Z–Phe–Val–OH
24	Z–Phe	H–Ile–Gly–OMe	Z–Phe–Ile–Gly–OMe
25	Z–Thr	H–Phe–OMe	Z–Thr–Phe–OMe
26	Z–Trp	H–Met–OMe	Z–Trp–Met–OMe
27	Z–Azp(Bzl)	H–Phe–OMe	Z–Azp(Bzl)–Phe–OMe
28	Z–Lys(Tos)	H–Gly–OEt	Z–Lys(Tos)–Gly–OEt
29	Tos–Phe	H–Gly–OEt	Tos–Phe–Gly–OEt

No	Yield (%)	Mp (°C)	$[\alpha]_D^{20}$ (*c* 1)	Lit.[18,19]	Found (%)			Calcd (%)		
					C	H	N	C	H	N
13	83.8	109—111	−16.8[c]	−17[c]	65.63	6.37	7.38	65.61	6.29	7.29
14	71.1	99—101	−22.2[c]	−18	58.54	6.49	9.10	58.43	6.54	9.09
15	81.7	162—164	−27.0[c]	−31[d]	60.58	7.17	8.41	60.70	7.19	8.33
16	63.8	102—104	−25.5[c]	−27[c]	61.92	7.37	8.17	61.70	7.48	8.00
17	64.5	155—156	−25.6[c]	−24[d]	61.47	7.28	7.83	61.70	7.48	8.00
18	68.0	92—93	−15.5[c]	−20[f]	55.30	6.53	7.43	55.43	6.56	7.61
19	55.6	142—144	+32.5[c]		65.28	6.18	7.59	64.85	5.99	7.56
20	62.5	98—99	−10.0[d]	−10[c]	67.72	7.23	6.29	68.16	7.32	6.36
21	81.0	79—81	−70.0[d]		67.78	6.93	6.60	67.58	7.09	6.57
22	48.5	122—124	+5.1[e]		65.38	7.08	6.95	66.97	6.84	6.79
23	38.8	411—143	−3.4[e]		66.13	6.55	7:04	66.31	6.58	7.03
24	71.8	188—189	−31.0[d]	−30[d]	64.74	6.94	8.53	64.85	6.49	8.73
25	55.8	103—105	+6.1[f]		63.87	6.32	6.60	64.06	5.87	6.79
26	77.9	137—138	−24.0[d]		61.90	6.16	8.89	62.10	6.05	8.69
27	72.4	114—116	−14.8[f]	−15[f]	67.01	5.68	5.52	67.17	5.83	5.40
28	66.7	151—152	−4.8[g]	−4.7	56.98	6.42	8.21	57.79	6.49	8.09
29	49.4	105—107	+27.9[c]		59.34	5.97	7.00	59.40	5.98	6.93

a) Crystal of (I) was used. b) *N*-Methyl valine methyl ester, reacted overnight. c) In EtOH. d) In MeOH. e) In THF. f) In DMF. g) In $CHCl_3$.

of ethyl glycinate at −10——20 °C under stirring for one hr. The reaction proceeded selectively to form an optically-active peptide by the fission of the carbonyl-nitrogen bond, as had been expected.

An amino acid ester hydrochloride dissolved in chloroform ($CHCl_3$) was neutralized with an equivalent triethylamine (TEA) and used for further experiments without removal of triethylamine hydrochloride (TEA–HCl) formed in the solution.

Various 3-substituted-1-benzyloxycarbonyl-aziridin-2-ones were prepared from the corresponding benzyloxycarbonyl-L-amino acid (Z–AA) in the same manner as had been described earlier.[9] Into the reaction mixture of the aziridinone was directly added a solution of amino acid ester at −10——20 °C under stirring; the reaction was then allowed to continue for one hr.

Prior to the reaction, a functional group in the side chain of Z–AA was protected by a protecting group commonly used in peptide chemistry. It was found that the reaction also proceeded selectively by the fission of the carbonyl-nitrogen bond to form an optically-active peptide. The results are summarized in Table 3.

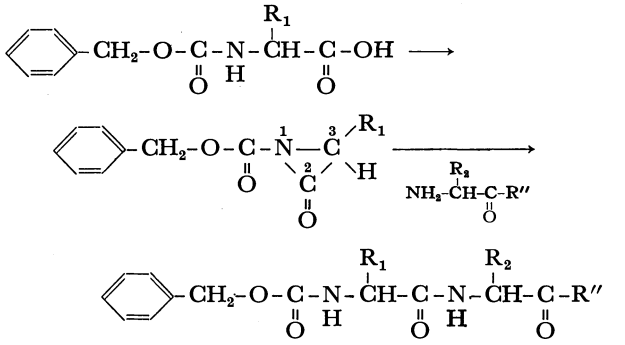

When free amino acid was used as a nucleophile, it was dissolved in 2 N sodium hydroxide and the coupling reaction was carried out in an aqueous solvent system. In this case, free amino acid would react with either of the aziridinone and the anhydride resulting from the decomposition of the aziridinone by the excess water, as is shown in the next scheme.

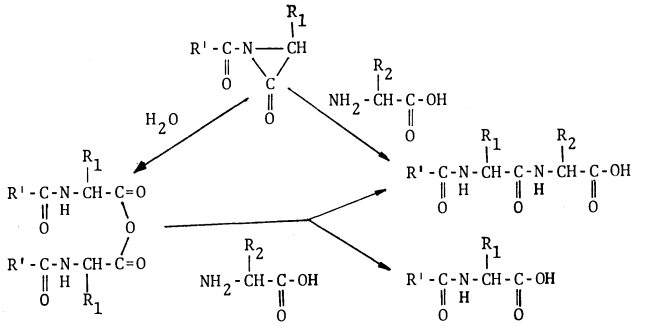

The substituent at *C*-3 in the 3-substituted-1-benzyloxycarbonyl-aziridin-2-one corresponds to the side chain (R_1) of amino acid. As is shown in Table 3, no distinct difference in the yields of the peptides was observed among the reaction of ethyl glycinate with the aziridinones derived from alanine, valine, leucine, and isoleucine. In fact, each of the reactions seems to proceed with little difference in the tlc. The variety of the yields observed in the reactions seems rather to be caused by the experimental conditions.

In most conventional peptide coupling methods, however, it is well known that the yield of a desired peptide is still unsatisfactory with an amino acid containing a bulky alkyl side chain. It should be noted that, in this coupling method, the bulkiness of the side chain (R_1) of amino acid does not have any substantial effect on the yields of the peptides.

As has been mentioned earlier, a bulky alkyl group at *C*-3 in the *N*-*t*-alkyl-aziridinone generally increases the stability of the ring under otherwise identical conditions. In the formation of the aziridinone, the bulkiness of R_1 would bring about a good result by diminishing the decomposition of the extremely reactive ring. Such a contribution of the bulky R_1 to the formation of the ring would offset its lower reactivity in the subsequent ring opening reaction with an amino acid ester due to the steric effect of R_1.

The corresponding aziridinone derived from benzyloxycarbonyl-glycine (Z–Gly, R_1=H) was, however, too unstable to be isolated. The product resulting from the subsequent reaction with ethyl glycinate could not be identified, though Wieland and Heinke[11] reported that *N*,*N*′-dibenzyloxycarbonyl-glycylglycine was obtained from the reaction of Z–Gly with ethyl glycinate by the use of their "phosphorus oxychloride method."

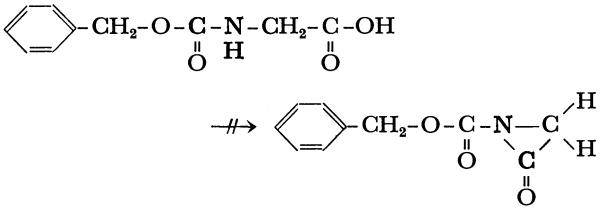

In the case of an imino acid such as proline, the *N*-substituted-aziridinone cannot be formed and the coupling method in the present study can not be used.

A Characteristic of the New Peptide Coupling Method. A peptide coupling is generally carried out by two consecutive procedures; first introducing an electron-withdrawing group to the carboxyl group of acyl amino acid in order to activate the carbonyl carbon, and then, reacting it with the amino group of the other amino acid and peptide, as is shown in the next scheme:

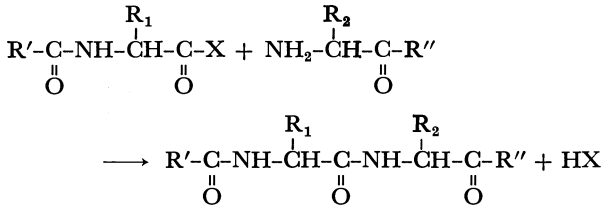

An activating group (X) should be eliminated before the nucleophilic substitution by an amino group to the carbonyl carbon is accomplished. The HX formed subsequently in the reaction media must be removed in order for the reaction to proceed completely. The reactivity is influenced by the ease of the elimination of the activating group (X), and the reaction proceeds *via* either an elimination reaction mechanism or a substitution reaction mechanism, depending on the

11) T. Wieland and B. Heinke, *Ann. Chem.*, **599**, 70 (1956).

Table 4. Electron densities at HOMO and LUMO

	HOMO				LUMO			
	A		B		A		B	
	N_1	O_4	N_1	O_4	C_2	C_3	C_2	C_3
S	0	0	0	0.0013	0	0.0001	0.0002	0.0002
Px	0	0	0.2465	0.0093	0.0001	0.0001	0.0010	0.0034
Py	0	0	0.0333	0.1255	0.0002	0.0001	0.0004	0.0017
Pz	0.0008	0	0.1102	0.0035	1.2701	0.0097	1.9694	0.0087
Total	0.0008	0	0.3900	0.1396	1.2704	0.0100	1.9710	0.0140

reaction conditions.

On the contrary, the *N*-acylated aziridinone does not involve any leaving group in the molecule. The acylated nitrogen atom, which is a member of the skeleton of amino acid itself, plays an effective role as a kind of electron-withdrawing group. Thus, the activation of the carbonyl-carbon depends largely upon the lower electron density on the ring as well as upon the extremely strained structure of the hetero three-membered ring, and the peptide coupling proceeds *via* a ring-opening addition reaction mechanism.

The retention of the full optical activity observed in the resulting peptides is caused by the following factors:

1) The reaction proceeds *via* a ring-opening addition reaction mechanism and no leaving group is eliminated during the reaction.

2) The addition reaction takes place rapidly at −10——20 °C within an hour because of the reactivity of the aziridinone.

3) No bases other than the amino acid ester itself are present in the reaction media, and no base-catalyzed abstraction of a proton on the asymmetric carbon takes place during the coupling reaction.

Thus, the new coupling method *via* *N*-acylated aziridinone will serve as a useful technique for peptide synthesis.

MO Calculation. An MO calculation of two types of aziridinone was carried out by the extended Hückel method[12–14] in order to find a clue to the explanation of the experimental results in the nucleophilic ring-opening reaction of *N*-acylated aziridinone.

1-Benzyloxycarbonyl-3-methyl-aziridinone (**A**) and 1-*t*-butyl-3-methyl-aziridinone (**B**) were chosen as the models of the *N*-acylated- and *N*-*t*-alkyl-aziridinones respectively.

For the input data of the bond length and the bond angles of the aziridinone ring, the X-ray analysis data of 1,3-diadamantyl-aziridinone reported by Wang *et al.*[8] were used; that is, the configuration at the nitrogen is pyramidal (the nitrogen atom lying 0.534 Å from the plane defined by its three substituents), and the adamantyl groups are *trans* to each other.

The calculated bond populations and atomic populations are shown in Scheme 1.

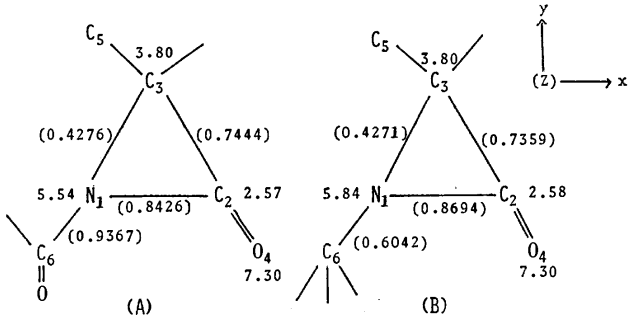

Scheme 1. Bond populations and atomic populations of the Aziridinone (A) and (B).
(A): 1-carbobenzoxy-3-methyl-aziridinone
(B): 1-*t*-butyl-3-methyl-aziridinone

A remarkable difference between (**A**) and (**B**) was observed, especially in the populations of N_1. The bond population of N_1–C_2 in (**A**) was smaller than that in (**B**) (0.8426; 0.8694) because of the increased interaction of N_1–C_6 (0.9367; 0.6042). A less atomic population of N_1 (5.54; 5.84) was also obtained, showing that the total electron density on the ring of (**A**) was much reduced compared to that of (**B**).

The AO populations of N_1 show that the decrease in the total charge of N_1 in (**A**) is mainly governed by the charge on the *Px*-orbital, corresponding to the reduced contribution of the N_1–C_2 bond.

AO Populations of N_1

Orbital	*S*	*Px*	*Py*	*Pz*	Total
(**A**)	1.4161	1.1460	1.3623	1.6252	5.5496
(**B**)	1.4975	1.3185	1.3979	1.6294	5.8433

In the nucleophilic ring opening reaction of the aziridinone, the position of the ring fission depends largely upon the nature of the attacking nucleophile as well as on the electronic structure of the ring, in which both HOMO and LUMO play a significant role.

The calculated electron densities at HOMO are shown in Table 4.

In the case of (**A**), the lone pairs scarcely exist on either N_1 or O_4. Under such circumstances, protonation does not occur even when a proton donor is present in the reaction system.

On the contrary, both N_1 and O_4 in (**B**) have enough lone pairs at HOMO to protonate if a proton donor is

12) R. Hoffmann, *J. Chem. Phys.*, **39**, 1397 (1963); R. S. Mulliken, *ibid.*, **23**, 1833 (1955); R. S. Mulliken, *ibid.*, **23**, 1841 (1955).

13) T. Yonezawa, K. Shimizu, *Yuki Gosei Kagaku Kyokai Shi*, **26**, 719 (1968).

14) The resonance integrals (H_{rs}) were evaluated by the Mulliken approximation, where S_{rs} represents the overlap integral between AOs

$$H_{rs} = \frac{1.75}{2}(H_{rr}+H_{ss})\cdot S_{rs}$$

MO: molecular orbital AO: atomic orbital HOMO: highest occupied MO LUMO: lowest unoccupied MO.

present. It is noted that, in the electron density of N_1 in (**B**), the contribution of the *Px*-orbital is the largest, showing that the lone pair of N_1 at HOMO would partially delocalize with the carbonyl oxygen (O_4).

The electron densities at LUMO in Table 4 clearly show that the interaction of an attacking nucleophile with C_2 is the largest and that the addition of a nucleophile takes place selectively at the C_2 position if a proton donor is absent. In spite of the decisive difference on the total electron density between C_2 and C_3 in (**B**), the AO electron densities of both *Px*- and *Py*-orbitals of C_3 at LUMO are greater than those of C_2. The possibility of the nucleophilic attack on C_3 in (**B**) seems, accordingly, to be greater than that in (**A**) if an attacking nucleophile comes from near the direction of the *x* or *y*-axis.

On the other hand, in a proton-containing reaction system, the protonation of (**B**) will occur, prior to the attack of the nucleophile, at the position of either N_1 or O_4, since both of them have a reactive lone pair at HOMO.

In this case, the reaction may proceed in a different way, as has been reported previously.[3-7]

Although more quantitative claculations will be required to discuss further in detail, the calculated data presented above may reasonably explain the experimental results observed in the present study.

Experimental

The melting points are uncorrected. Thin layer chromatography (tlc) was performed with silica gel G (Merck), and the spots were detected by ninhydrin on heating at 100 °C after developing in the buffer solution ($CHCl_3$: AcOEt: AcOH, 85: 15: 3). The IR spectra were obtained using a Shimadzu IR-27G apparatus. The NMR spectra were recorded at 60 MHz in $CDCl_3$ with TMS as the internal standard using a Hitachi R-20A apparatus. The optical rotations were measured with a Yanagimoto OR-100 apparatus. THF, ether, and petroleum ether used throughout this experiment were dried over sodium metal wire after distillation. The $COCl_2$ gas was absorbed on dry ether to prepare the $COCl_2$–ether solution and was stored in a refrigerator. The TEA was purified by distillation before use.

Benzyloxycarbonyl-L-phenylalanine t-*Butyl Ester (1) and (2).* (a) Crystals of 3-benzyl-1-benzyloxycarbonylaziridin-2-one (1) (2.81 g, 0.01 mol) were dissolved in 30 ml of THF. Into this solution 15 ml of *t*-butanol was added with stirring at −10 °C. Subsequently, a 3 ml portion of pyridine was added to the reaction mixture. A ninhydrin positive spot at R_f 0.9 on tlc decreased, and at R_f 0.8 a new spot appeared; the latter detected by HBr/ninhydrin (hydrobromic acid must be sprayed over the plate prior to the detection by ninhydrin). After 1 hr, ethyl acetate (100 ml) was added to the reaction mixture, which was then washed with 5% sodium bicarbonate, 1M hydrochloric acid, and water successively, and dried over magnesium sulfate. The organic layer was evaporated under reduced pressure, and the residue was crystallized with ethyl acetate and petroleum ether. Recrystallization from the same solvents afforded 2.96 g (83.3%). Mp 81—82 °C, $[\alpha]_D^{20}$ −6.0° (*c* 1, EtOH). IR: $\nu_{C=O}$ 1745, 1695 cm^{-1}; ν_{NH} 3380 cm^{-1}. Found: C, 71.29; H, 6.80; N. 3.77%. Calcd for $C_{21}H_{25}NO_4$: C, 70.90; H, 7.09; N, 3.94%. Lit,[15] $[\alpha]_D^{20}$ −4.4° (*c* 2, EtOH).

(b) Freshly-prepared potassium *t*-butoxide (15 g, containing excess *t*-butanol) suspended in 50 ml of THF was stirred into a solution of I (2.81 g, 0.01 mol) in 30 ml of THF at −10 °C, and the reaction was allowed to continue for 1 hr at −10—0 °C. Then, ethyl acetate (150 ml) was added to the reaction mixture, and it was worked up in the same manner as had been described above. The crystals, 2.02 g (56.8%), were identified with those afforded in (a).

Benzyloxycarbonyl-L-phenylalanine Anilide (3). Into a solution of I (2.81 g, 0.01 mol) in THF (30 ml), 10 ml of aniline was added with stirring at −10 °C. After 1 hr, ethyl acetate (100 ml) was added; the reaction mixture was then washed with 1M hydrochloric acid, 5% sodium bicarbonate and water successively, and dried over magnesium sulfate. Evaporation *in vacuo* gave the product, which was subsequently recrystallized from ethyl acetate and petroleum ether. Yield, 3.16 g (84.6%), mp 164—166 °C, $[\alpha]_D^{20}$ +30.0° (*c* 1, THF). IR: $\nu_{C=O}$ 1690, 1655, 1540 cm^{-1}; ν_{NH} 3300 cm^{-1}. Found: C, 73.65; H, 5.92; N, 7.53%. Calcd for $C_{23}H_{22}N_2O_3$: C, 73.78; H, 5.92; N, 7.48%.

Benzyloxycarbonyl-L-phenylalanine Benzylamide (4). Into a solution of I (2.81 g, 0.01 mol) in THF (30 ml), 10 ml of benzylamine was added with stirring at −10 °C; stirring was then continued for 1 hr at −10—0 °C. After ethyl acetate (100 ml) had then been added, the reaction mixture was worked up in the way described in (3). Recrystallization from ethyl acetate gave 3.31 g (85.3%). Mp 157—158 °C, $[\alpha]_D^{20}$ −12.0° (*c* 1, DMF). IR: $\nu_{C=O}$ 1685, 1645, 1540 cm^{-1}; ν_{NH} 3300 cm^{-1}. Found: C, 74.40; H, 6.21; N, 7.34%. Calcd for $C_{24}H_{24}N_2O_3$: C, 74.20; H, 6.23; N, 7.21%.

Benzyloxycarbonyl-L-phenylalanine Anhydride (5). I (2.81 g, 0.01 mol) was dissolved in a mixture of THF (20 ml) and ethyl acetate (50 ml) at −10 °C; then 10 ml of water was stirred and the reaction temperature was allowed to rise to −5—0 °C over a 30 min period. The tlc showed two spots of R_f 0.7 and R_f 0.5 (Z–Phe) which were detected by HBr/ninhydrin respectively. The reaction mixture was washed twice with ice-cold 2% sodium bicarbonate and dried over magnesium sulfate. Evaporation *in vacuo* gave the product, which was subsequently recrystallized from ethyl acetate. 1.37 g (47.2%), mp 144—146 °C, $[\alpha]_D^{20}$ +14.6° (*c* 1, dioxane). IR: $\nu_{C=O}$ 1830, 1755, 1695 cm^{-1}; ν_{NH} 3300 cm^{-1}. Found: C, 70.15; H, 5.66; N, 4.76%. Calcd for $C_{34}H_{32}N_2O_7$: C, 70.33; H, 5.56; N, 4.83%. Lit,[16] mp 139—140 °C, $[\alpha]_D^{20}$ +19.7° (*c* 1, CH_2Cl_2).

4-Benzyl-2,5-oxazolidinedione (6). I (2.81 g, 0.01 mol) was dissolved in 100 ml of ether at 0 °C. After adding 1 g of 5% palladium-charcoal to the solution, catalytic hydrogenation was carried out under bubbling hydrogen gas at room temperature over a period of 30 min. Tlc showed a new spot at R_f 0.8, which was detected by ninhydrin. After the filtration of the catalyst, the ether was evaporated under reduced pressure on an ice bath. To the residue ether and petroleum ether were added; the solution was then stored in a refrigerator. Recrystallization from the same solvents yielded 1.50 g (78.5%); mp 96—98 °C (decomp.). $[\alpha]_D^{20}$ −110.4° (*c* 1, THF). IR: $\nu_{C=O}$ 1855, 1760 cm^{-1}; ν_{HN} 3250 cm^{-1}. NMR ($CDCl_3$, δ): 7.25 (m, 5H), 6.37 (bs, 1H), 4.54 (q, 1H), 3.10 (dd, 2H). Found: C, 63.51; H, 4.80; N, 7.20%. Calcd for $C_{10}H_9NO_3$: C, 62.82; H, 4.75; N, 7.33%.

Benzyloxycarbonyl-L-valine Methyl Ester (7). To a solution of benzyloxycarbonyl-L-valine (25.1 g, 0.1 mol) in 200 ml of THF, $COCl_2$–ether solution (50 ml, containing 0.1 mol of

15) G. W. Anderson and F. M. Callahan, *J. Amer. Chem. Soc.*, **82**, 3359 (1960).

16) E. Wünsch and G. Wendlberger, *Chem. Ber.*, **100**, 160 (1967).

$COCl_2$) was added at −20 °C. TEA (14 ml, 0.1 mol) in 30 ml of ether was then stirred drop by drop to the solution over a period of 30 min at −20 °C. After 30 min, TEA (14 ml, 0.1 mol) in 30 ml of ether was added, drop by drop, to the reaction mixture again. After an additional 30 min of stirring at −20 °C, 100 ml of methanol was added to the reaction mixture; the reaction temperature was then allowed to rise to −5——10 °C with stirring for 1 hr. Ethyl acetate (500 ml) was added to the reaction mixture, it was washed with 5% sodium bicarbonate, 1 N hydrochloric acid, and water successively, and the organic layer was dried over magnesium sulfate. The evaporation to the solvent under reduced pressure afforded the product, which was subsequently recrystallized from ethyl acetate and petroleum ether. 21.7 g (81.9%). Mp 54—56 °C, $[\alpha]_D^{20}$ −18.9° (*c* 1, MeOH). IR: $\nu_{C=O}$ 1745, 1690 cm^{-1}; ν_{NH} 3350 cm^{-1}. Found: C, 63.59; H, 7.46; N, 5.47%. Calcd for $C_{14}H_{19}NO_4$: C, 63.38; H, 7.22; N, 5.28%. Lit,[17] mp 56—57 °C, $[\alpha]_D$ −16.0° (*c* 3.1, EtOH).

General Procedure for the Anhydrides (8—11). Benzyloxycarbonyl-L-amino acid or *p*-halogeno-benzyloxycarbonyl-L-amino acid (0.1 mol) was dissolved in 200—300 ml of THF. To the solution, $COCl_2$–ether (50 ml, containing 0.1 mol of $COCl_2$) was added at −20——30 °C. TEA (14 ml, 0.1 mol) in 30 ml of ether was stirred, drop by drop, into the solution during 30 min at the same temperature. After 30 min, TEA (14 ml, 0.1 mol) in 30 ml of ether was added again in the same way as above. After an additional 30 mins' stirring, 600 ml of ethyl acetate was added; the reaction mixture was then washed with 100 ml of ice-cold water. The washing of the organic layer with ice-cold water was repeated several times. Then the organic layer was washed twice more with ice-cold 2% sodium bicarbonate, and it was dried over magnesium sulfate. The evaporation of the solvent *in vacuo* gave the product, which was recrystallized from ethyl acetate and petroleum ether. IR: $\nu_{C=O}$ 1830—1810; 1760—1750, 1700—1685 cm^{-1}; ν_{NH} 3350—3300 cm^{-1}.

Benzyloxycarbonyl-L-alanine Anhydride (8). Mp 120—122 °C, $[\alpha]_D^{20}$ −11.0° (*c* 1, THF). Found: C, 60.41; H, 5.71; N, 6.29%. Calcd for $C_{22}H_{24}N_2O_7$: C, 61.67; H, 5.65; N, 6.54%.

Benzyloxycarbonyl-L-valine Anhydride (9). Mp 96—98 °C, $[\alpha]_D^{20}$ +10.7° (*c* 1, THF). Found: C, 64.53; H, 6.64; N, 5.78%. Calcd for $C_{26}H_{32}N_2O_7$: C, 64.45; H, 6.66; N, 5.78%.

p-*Bromo-benzyloxycarbonyl-L-phenylalanine Anhydride (10).* Mp 147—148.5 °C, $[\alpha]_D^{20}$ +2.0° (*c* 1, THF). Found: C, 55.30; H, 4.09; N, 3.79; Br, 21.64%. Calcd for $C_{34}H_{30}N_2O_7Br_2$: C, 54.57; H, 4.08; N, 3.68; Br, 20.29%.

p-*Chloro-benzyloxycarbonyl-L-phenylalanine Anhydride (11).* Mp 149—150 °C, $[\alpha]_D^{20}$ −3.0° (*c* 1, THF). Found: C, 62.67; H, 4.95; N, 4.30; Cl, 10.73%. Calcd for $C_{34}H_{30}N_2O_7Cl_2$: C, 62.72; H, 4.60; N, 4.33; Cl, 10.25%.

p-*Toluenesulfonyl-L-phenylalanine Methyl Ester (12).* To a solution of *p*-toluenesulfonyl-L-phenylalanine (31.9 g, 0.1 mol) in 300 ml of THF, $COCl_2$–ether solution (50 ml, containing 0.1 mol of $COCl_2$) was added at −20 °C. TEA (14 ml, 0.1 mol) in 30 ml of ether was then added, drop by drop, to the solution at −20——30 °C. After 30 min, TEA (14 ml, 0.1 mol) in 30 ml of ether was added, drop by drop, to the reaction mixture again, and it was worked up in the same manner as had been described in (7). 17.5 g (52.5%). Mp 91—93 °C, $[\alpha]_D^{20}$ +3.1° (*c* 1, MeOH). IR: $\nu_{C=O}$ 1730 cm^{-1}; ν_{NH} 3270 cm^{-1}. Found: C, 60.89; H, 5.79; N, 4.36%. Calcd for $C_{17}H_{19}NO_4S$: C, 61.25; H, 5.75; N, 4.20%.

Benzyloxycarbonyl-L-phenylalanyl-glycine Ethyl Ester (13). To a solution of ethyl glycinate hydrochloride (1.4 g, 0.01 mol) in 30 ml of $CHCl_3$, TEA (1.4 ml, 0.01 mol) was added for neutralization. Crystals of I (2.81 g, 0.01 mol) were dissolved in 20 ml of THF at −10 °C. Into this solution of I, the $CHCl_3$ solution of ethyl glycinate was added at −10——20 °C; the reaction was then allowed to continue for 1 hr with stirring at the same temperature. After adding 40 ml of $CHCl_3$ to the reaction mixture, it was washed with 5% sodium bicarbonate, 1 N hydrochloric acid and water successively, and dried over magnesium sulfate. The evaporation of the solvent under reduced pressure afforded the product, which was recrystallized from ethyl acetate and petroleum ether. Yield, 3.22 g (83.8%), mp 109—111 °C, $[\alpha]_D^{20}$ −16.8° (*c* 1, EtOH). IR: $\nu_{C=O}$ 1760, 1695, 1655, 1540 cm^{-1}; ν_{NH} 3300 cm^{-1}.

General Procedure of the Reaction of 3-Substituted-1-benzyloxycarbonylaziridin-2-one with Amino Acid Ester. L-Amino acid ester hydrochloride (0.05 mol) was dissolved in 150—200 ml of $CHCl_3$, which was then neutralized with TEA (7 ml, 0.05 mol) at 0 °C. To a solution of benzyloxycarbonyl-L-amino acid (0.05 mol) in 100—200 ml of THF, a $COCl_2$–ether solution (25 ml, containing 0.05 mol of $COCl_2$) was added at −20——30 °C. TEA (7 ml, 0.05 mol) in 15 ml of ether was stirred, drop by drop, into the solution over a period of 30 min at −20——30 °C. After 30 min, TEA (7 ml, 0.05 mol) in 15 ml of ether was added again to the reaction mixture in the same way. After an additional 30 min, into the reaction mixture, a $CHCl_3$ solution of the L-amino acid ester was then added at −20 °C; the reaction proceeded for 1 hr at −10——20 °C. A 400 ml portion of $CHCl_3$ was then added to the reaction mixture; it was washd with 5% sodium bicaronate, 1 N hydrochloric acid, and water successively, and dried over magnesium sulfate. The organic layer was evaporated under reduced pressure, then the crude product was crystallized with an appropriate solvent system.

Among the compounds listed in Table 3, there are some exceptions. In the case of Z–Phe–Val(Me)–OMe (21), considerable amounts of the *N*-methyl valine methyl ester still remained in the reaction mixture after 1 hr; they were detected by ninhydrin on tlc. The reaction was continued ovrenight with stirring at 0——10 °C. In the case of Z–Phe–Ile–Gly–OMe (24), the dipeptide ester was reacted with the aziridinone; the reaction proceeded in the same manner as had been described in the other cases of amino acid esters.

General Procedure of the Reaction of 3-Substituted-1-benzyloxycarbonylaziridin-2-one with Free Amino Acid. To a solution of benzyloxycarbonyl-L-amino acid (0.05 mol) in THF (200 ml), $COCl_2$–ether (25 ml, containing 0.05 mol of $COCl_2$) was added at −20——30 °C. TEA (7 ml, 0.05 mol) in ether (15 ml) was then stirred, drop by drop, into the solution over a 30 min period at the same temperature. After 30 min, TEA (7 ml, 0.05 mol) in ether (15 ml) was again added to the reaction mixture in the same manner as above. After 30 min, to the reaction mixture, a solution of L-amino acid (0.05 mol) in 2M sodium hydroxide was added at −10 °C; the reaction was then continued overnight with stirring at 0——5 °C. After adding ethyl acetate (600 ml), the reaction mixture was washed with 1 N hydrochloric acid and water, and then dried over magnesium sulfate. Evaporation *in vacuo* gave a mixture of Z-dipeptide and Z-amino acid. Crystallization was repeated with an appropriate solvent system.

---

17) M. A. Nyman and R. M. Herbst, *J. Org. Chem.*, **15**, 108 (1950).

18) G. R. Pettit, "Synthetic Peptides," Vol. I and II. Van Nostrand Reinhold Company, New York. (1970 and 1971).

19) J. P. Greenstein and M. Winitz, "Chemistry of the Amino Acids" Vol. 2, John Wiley & Sons Inc., New York (1971).

p-*Toluenesulfonyl*-L-*phenylalanyl-glycine Ethyl Ester (29)*. To a solution of *p*-toluenesulfonyl-L-phenylalanine (31.9 g, 0.1 mol) in THF (200 ml), a $COCl_2$–ether solution (50 ml, containing 0.1 mol of $COCl_2$) was added at −20 °C. TEA (14 ml, 0.1 mol) in ether (30 ml) was added, drop by drop, to the solution at −20——30 °C. After 30 min, TEA (14 ml, 0.1 mol) in ether (30 ml) was again added to the reaction mixture in the same way as above. Ethyl glycinate hydrochloride (14 g, 0.1 mol) dissolved in $CHCl_3$ (300 ml) was neutralized with TEA (14 ml, 0.1 mol); then the $CHCl_3$ solution was stirred into the reaction mixture at −20 °C. The reaction was allowed to continue overnight at 0—10 °C. 600 ml of $CHCl_3$ was added to the reaction mixture, which was then worked up in the same manner as had been described as the General Procedure. Recrystallization from ethyl acetate afforded 19.9 g (49.4%).

The author wishes to express his hearty gratitude to Professor Tetsuo Shiba of Osaka University for his valuable advice. Acknowledgement is made to Dr. T. Takayanagi and Dr. I. Chibata of Tanabe Seiyaku Co., Ltd., for their encouragement. Thanks are extended to Mr. H. Tamura for his assistance in the experimental work.

BULLETIN OF THE CHEMICAL SOCIETY OF JAPAN, VOL. 46, 1496—1498 (1973)

A Kinetic Study on the Decomposition of Benzyl *N*-(Hydroxymethyl)carbamate in Alkaline Solution[1]

Shigeya TAKEUCHI

Department of Chemistry, Faculty of Education, Toyama University, Gofuku, Toyama

(Received August 11, 1972)

The decomposition of benzyl *N*-hydroxymethylcarbamate (*N*-BHMC) by potassium hydroxide was carried out in a mixed solvent dioxane–water. The following rate equation was obtained. $R_0=k[N\text{-BHMC}]_0[\text{KOH}]_0$, where $[N\text{-BHMC}]_0$ and $[\text{KOH}]_0$ denote the initial concentrations of *N*-BHMC and potassium hydroxide, respectively. The equation is analogous to that of Ugelstadt[2] obtained for the hydrolytic decomposition of *N*-hydroxymethylbenzamide. Thus the reaction was assumed to proceed *via* the three steps:

1) $C_6H_5CH_2OCONHCH_2OH + OH^- \rightleftharpoons C_6H_5CH_2OCONHCH_2O^- + H_2O$
2) $C_6H_5CH_2OCONHCH_2O^- \rightleftharpoons C_6H_5CH_2OCONH^- + CH_2O$
3) $C_6H_5CH_2OCONH^- + H_2O \rightleftharpoons C_6H_5CH_2OCONH_2 + OH^-$

We studied the reaction of benzyl carbamate (BC) with formaldehyde (F) in an aqueous dioxane solution using potassium hydroxide as a catalyst.[3] It was found that the rate equation is given by

$$R_0' = k'[\text{BC}]_0[\text{KOH}]_0[\text{F}]_0^{1 \text{ or } 0}$$

and the reaction order of formaldehyde changes from 1 to 0 with its concentration.

The following rate equation was obtained for the rate of decomposition of benzyl *N*-hydroxymethylcarbamate (*N*-BHMC) by potassium hydroxide.

$$R_0 = k[N\text{-BHMC}]_0[\text{KOH}]_0$$

where $[N\text{-BHMC}]_0$ and $[\text{KOH}]_0$ denote the initial concentrations of *N*-BHMC and potassium hydroxide, respectively.

The mechanism for decomposition of *N*-BHMC might be the same as Ugelstadt's in the reaction of the hydrolytic decomposition of *N*-hydroxymethylbenzamide.

Experimental

Materials. Benzyl carbamate was prepared by the method of Kraft[4] and recrystallized from toluene. Commercial toluene was used without further purification. Commercial dioxane was distilled at 101 °C.

Preparation of N-BHMC. To 15.1 g (0.1 mol) of benzyl carbamate in a 300 ml three-necked flask equipped with a stirrer, thermometer and condenser were added 12.2 g (0.15 mol) of 37% formaldehyde and 100 ml of water. The reaction mixture was stirred for 30 min at 60 °C at pH 8.6. Subsequently, the mixture was dissolved in 30 ml of methanol and cooled in a refrigerator. The solid separated was recrystallized from toluene to give *N*-BHMC as white needles; 10.2 g (5.6%), mp 86.5—87.5 °C. A test with a Tollens reagent was positive. IR (cm^{-1}); 3330 (ν(NH), ν(OH)), 1690 (ν(C=O)), 1520 (ν(CN)+δ(NH)). NMR (ppm); 7.94 (1H, –NH–), 7.39 (5H, $-C_6H_5$), 5.5—5.7 (1H, –OH), 5.1 (2H, $-CH_2-$), 4.4—4.64 (2H, $-N-CH_2O-$).

Found: C, 59.22; H, 6.38; N, 7.81%. Calcd for $C_8H_9NO_2$: C, 59.35; H, 6.59; N, 7.69%.

Measurement of the Rate of Decomposition. The rate was derived by measurement of the quantity of formaldehyde formed from the hydrolytic decomposition of *N*-BHMC.

A mixture of fixed amount of *N*-BHMC and 35 ml of dioxane was placed in a 50 ml volumetric flask and kept at constant temperature. After 20—30 min, a fixed amount of an aqueous solution of potassium hydroxide and then water were added up to the marked line, the time when the potassium hydroxide was added being taken as the starting time. 5 ml of the reaction mixture was then taken out at intervals. The concentration of the formaldehyde caused by the decomposition of *N*-BHMC was estimated by the KCN–

1) The preceding paper: S. Takeuchi, M. Kinoshita, K. Kō, and M. Imoto, *Makromol. Chem.*, **157**, 63 (1972).
2) J. Ugelstadt, *Bull. Soc. Chim. Fr.*, **1955**, 138.
3) S. Takeuchi, M. Kinoshita, K. Kō, and M. Imoto, *Kogyo Kagaku Zasshi*, **72**, 1362 (1969).

$Hg(NO_3)_2$ method.[5]

Results and Discussion

Reaction Order of N-*BHMC in the Hydrolytic Decomposition.* With the concentration of potassium hydroxide kept at 8.55×10^{-4} mol/l, the concentration of *N*-BHMC varied from 0.01 to 0.08 mol/l. A linear relationship was obtained between $\log a/(a-x)\times10^{-3}$ and t, where the initial concentrations of *N*-BHMC and formaldehyde resulting from the reaction were given as a and x. Figure 1 shows the relationship between $\log a/(a-x)\times10^{-3}$ and t.

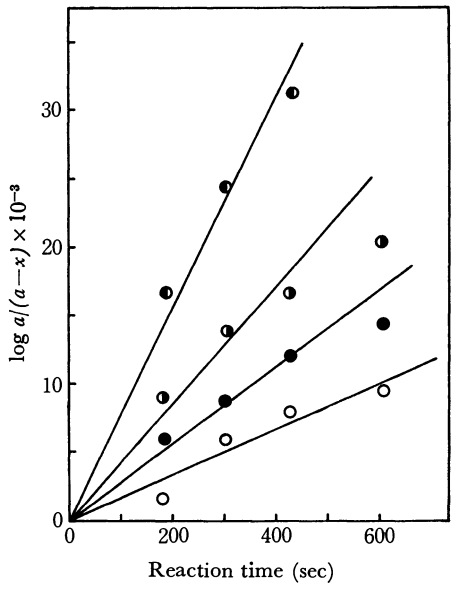

Fig. 1. The relationship between $\log a/(a-x)$ and t.
a=initial concentrations of *N*-BHMC.
x=consumption of *N*-BHMC.
N-BHMC in mol/l: -○- 0.01; -●- 0.02; -◑- 0.04; -◐- 0.08.

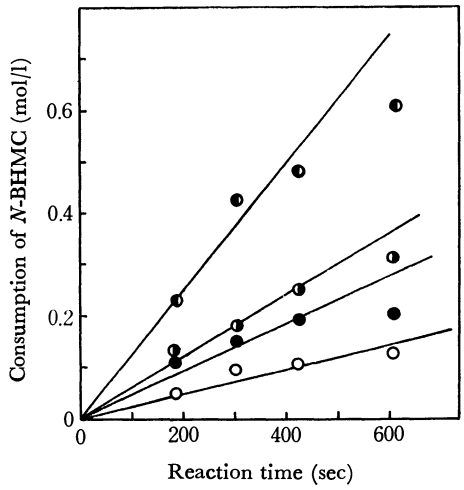

Fig. 2. The consumption of *N*-BHMC *vs.* reaction time at 35 °C.
The reaction conditions were as follows:
N-BHMC 0.04 mol/l. KOH 2.57—12.82×10^{-4} mol/l.

4) W. M. Kraft, *J. Amer. Chem. Soc.*, **70**, 3569 (1948).
5) J. I. de Jonge and J. de Jonge, *Rec. Trav. Chim. Pays-Bas*, **72**, 356 (1953).

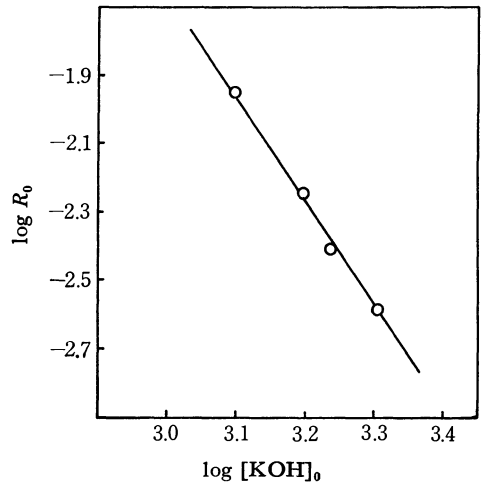

Fig. 3. The relationship between the rate and the concentration of KOH.

The reaction order of *N*-BHMC on the formation of formaldehyde is concluded to be 1.

Reaction Order of Potassium Hydroxide. With the concentration of *N*-BHMC kept at 0.04 mol/l, the concentration of potassium hydroxide varied from 2.57 to 12.82×10^{-4} mol/l. The rate of formation of formaldehyde increased linearly with progress of the reaction (Fig. 2), and the reaction order in potassium hydroxide was determined to be 1 from the slope of the straight line (Fig. 3).

From these results, the rate equation can be represented as follows.

$$R_0 = k[N\text{-BHMC}]_0[\text{KOH}]_0$$

Activation Energy of the Reaction. The activation energy of reaction of decomposition of *N*-BHMC in the presence of potassium hydroxide was calculated to be 14.4 kcal/mol at 30, 35, 40, 45, and 50 °C (Fig. 4). The value was higher than that of the reaction of formation of *N*-BHMC from benzyl carbamate and formaldehyde (13.8 kcal/mol). The activation entropy was calculated to be −22.24 e.u.

The Reaction Mechanism. Benzyl carbamate and

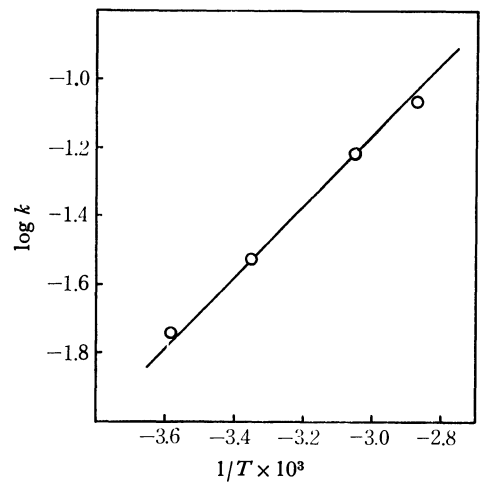

Fig. 4. The relationship between $\log k$ and T.

formaldehyde were proved to be obtained from the reaction of decomposition of *N*-BHMC.

$$C_6H_5CH_2OCONHCH_2OH \xrightarrow{OH^-} C_6H_5CH_2OCONH_2 + CH_2O$$

The reaction might proceed *via* the three steps which Ugelstadt showed in the reaction of decomposition of *N*-hydroxymethylbenzamide.

(1) $C_6H_5CH_2OCONHCH_2OH + OH^- \underset{k_{-1}}{\overset{k_1}{\rightleftharpoons}} C_6H_5CH_2OCONHCH_2O^- + H_2O$

(2) $C_6H_5CH_2OCONHCH_2O^- \underset{k_{-2}}{\overset{k_2}{\rightleftharpoons}} C_6H_5CH_2OCONH^- + CH_2O$

(3) $C_6H_5CH_2OCONH^- + H_2O \rightleftharpoons C_6H_5CH_2OCONH_2 + OH^-$

Reactions (1) and (3) are supposed to reach equilibria rapidly. The rate of decomposition is given by

$$R_0 = k_2[C_6H_5CH_2OCONHCH_2O^-] \quad \text{(a)}$$

From the steady state method we obtain

$$\frac{d[N\text{-BHMC}^-]}{dt} = k_1[N\text{-BHMC}][OH^-] - k_{-1}[N\text{-BHMC}^-] - k_2[N\text{-BHMC}^-] = 0$$

Thus

$$[N\text{-BHMC}^-] = \frac{k_1[N\text{-BHMC}][OH^-]}{k_{-1}+k_2} \quad \text{(b)}$$

From Eqs. (a) and (b) we get

$$R_0 = \frac{d[F]}{dt} = k_2[N\text{-BHMC}^-] = \frac{k_2k_1[N\text{-BHMC}][OH^-]}{k_{-1}+k_2} = \frac{k_2k_1}{k_{-1}+k_2}[N\text{-BHMC}][OH^-] = k[N\text{-BHMC}][OH^-]$$

The author wishes to express his thanks to Prof. Minoru Imoto, Kansai University, for his guidance,to Prof. Masayoshi Kinoshita, Osaka City University, for suggestions and encouragement, and to Dr. Eisaku Ninagawa, for valuable discussions.

BULLETIN OF THE CHEMICAL SOCIETY OF JAPAN, VOL. 46, 1498—1501 (1973)

The Reactions of 2-Hydroxybenzophenones with Lead Tetraacetate and Manganic Acetate

Kazu KUROSAWA, Yasuko SASAKI,* and Mikio IKEDA**

Department of Chemistry, Faculty of Science, Kumamoto University, Kurokami-2-39-1, Kumamoto

(Received August 11, 1972)

2-Hydroxy-4-methoxy- and 2-hydroxy-4,4′-dimethoxybenzophenones were oxidized to dimeric compounds with lead tetraacetate and with manganic acetate. 2-Hydroxy-2′,4,4′-trimethoxy- and 2-hydroxy-3′,4,4′-trimethoxybenzophenones were oxidized to substituted xanthones. The structures of the products were determined by NMR and mass spectra, and were confirmed by syntheses.

In the reaction of phenolic compounds with lead tetraacetate, it was demonstrated that oxidative cyclization took place in 2′-hydroxychalcones[1,2] and in the Schiff base from *o*-aminophenols,[3] giving rise to aurones and benzoxazols respectively. We investigated the reactions of 2-hydroxybenzophenones with lead tetraacetate and with manganic acetate in the hope that they could be oxidized to xanthones; it was found that trisubstituted 2-hydroxybenzophenones did give xanthones and that mono- and di-substituted 2-hydroxybenzophenones give dimeric products.

When 2-hydroxy-4-methoxybenzophenone (Ia) and 2-hydroxy-4,4′-dimethoxybenzophenone (Ib) were treated with lead tetraacetate and with manganic acetate respectively, several products (II, III, IV, and VI) were isolated after separation by column chromatography and preparative tlc. They are listed in Table 1.

Product (IIb) has a higher melting point (232—234 °C), and its mass spectrum showed the molecular ion at *m/e* 514, corresponding to a molecular formula of $C_{30}H_{28}O_8$. This indicates that IIb is a dimeric compound. The IR and UV spectra of IIb were very similar to those of Ia and Ib (Table 2). The NMR spectra (60 MHz) of IIa, IIb, their acetates (Ac-IIa and Ac-IIb), and a methyl ether (Me-IIb) showed two singlets in the aromatic region, indicating the presence of *para*-related protons. This reveals that the newly-formed bond is located at the C_5-position in IIb. The chemical shifts of the protons and other protons on phenyl and *p*-methoxyphenyl groups were well correlated in these compounds (Table 3). These spectral data showed that IIb is 5,5′-bis(*p*-methoxybenzoyl)-4,4′-dihydroxy-2,2′-dimethoxybiphenyl. The structure of IIa was also determined to be 5,5′-dibenzoyl-4,4′-dihydroxy-2,2′-dimethoxybiphenyl.

The IIIb product, $C_{15}H_{14}O_5$ (mp 164—165 °C), was obtained only when lead tetraacetate was used in the

* Present address: Department of Applied Science, Faculty of Engineering, Kyushu University, Fukuoka.

** Present address: Taiho Kogyo Co., Ltd., Izumi-cho, Totsuka-ku, Yokohama.

1) K. Kurosawa, This Bulletin, **42**, 1456 (1969).
2) K. Kurosawa and J. Higuchi, *ibid.*, **45**, 1132 (1972).
3) F. F. Stephens and J. D. Bower, *J. Chem. Soc.*, **1949**, 2971.

Table 1. Reaction of 2-hydroxybenzophenones with $Pb(OAc)_4$ and $Mn(OAc)_3$ in AcOH

Compound	Reagent	Reaction conditions			Recovery of I (%)	Product (%)				
		Molar ratio	Time(hr)	Temp. (°C)						
Ia[4]	$Mn(OAc)_3$	1 : 4	5	100	Ia(40)	IIa(7)		IVa(10)		VIa(16)
Ia	$Pb(OAc)_4$	1 : 2	5	100	Ia(15)	IIa(15)	IIIa(3.3)			VIa(36)
Ib[5]	$Mn(OAc)_3$	1 : 4	5	100	Ib(18)	IIb(11)		IVb(3.7)		VIb(18)
Ib	$Pb(OAc)_4$	1 : 2	5	100	Ib(6)	IIb(21)	IIIb(1)			VIb(32)
Ic	$Mn(OAc)_3$	1 : 4	$4\frac{2}{3}$	100	Ic(4)				Vc(24)[6]	VIc(10)[7]
Ic	$Pb(OAc)_4$	1 : 2	3	100	Ic(12)				Vc(2)	VIc(14)
Id	$Mn(OAc)_3$	1 : 4	5	100					Vd(42)	VId(9)[8]
Id	$Pb(OAc)_4$	1 : 2	5	100					Vd(30)	VId(10)

Table 2. IR and UV spectral data for benzophenones, biphenyls and xanthones

Compound	Mp (°C)	νOH	νCO (cm^{-1})	$\nu OCOCH_3$	λ_{max} (nm) (ε)			
Ia	64	3000	1620			244(10700)	290(15000)	329(9600)
Ib	117—118	3000	1620				294(16700)	332(13600)
Ic	104—105	3000	1620		233(15000)		285(16000)	333(12700)
Id	135—136	3000	1623		237(17200)		290(15100)	336(16000)
Ie	136—137[b]	3100	1615		240(s)(8760)	253(s)(6750)	288(11400)	344(11400)
If	147—148	3100	1620		233(s)(15600)	249(s)(13100)	288(13100)	365(11500)
IIIa	182—183	3565	1640			255(15200)	292(9900)	370(7700)
IIIb	164—165	3565	1639			256(10600)	296(13100)	370(8350)
IIa	199—200	3000	1620			254(31300)	289(24600)	345(12500)
IIb	232—234	3000	1620		226(30200)	260(35000)	296(36800)	350(20000)
Ac-IIa	219—220		1655	1762		254(40000)	284(s)(23100)	
Ac-IIb	190—191		1648	1760		256(s)(27200)	292(41700)	
Me-IIb	190—191		1649			259(31800)	288(41200)	
IVa	217—218		1670			251(37100)	285(18500)	331(10300)
			1630					
			1618					
IVb	207—208		1680			244(30600)	292(34800)	331(18100)
			1665					
			1640					
			1620					
Vc	182—183		1648		243(44100)	269(10800)	313(23900)	320(26200)
Vd	216—217		1643		246(35300)	267(11400)	313(20600)	342(s)(10300)

reaction; it was isolated from the mother liquor of IIb. The IR spectrum of IIIb was quite similar to those of IIa and IIb except that an absorption due to a hydroxyl group appeared at 3565 cm^{-1}. Its NMR spectrum showed two singlets in the aromatic region, again indicating the presence of *para*-related protons: the rest of the spectrum was very close to that of IIb. Thus, the structure of IIIb was determined to be 2-(*p*-methoxy) benzoyl-5-methoxyhydroquinone; this was finally confirmed by synthesis. The reaction of 2-methoxyhydroquinone[9] and anisic acid, with boron-trifluoride as a catalyst, gave IIIb. IIIa was also prepared in a similar way.

The IVb product, $C_{30}H_{24}O_9$ (analysis and mass spectrum) (mp 207—208 °C), showed complicated carbonyl absorptions (1620—1680 cm^{-1}) in the IR spectrum, indicating the presence of quinone carbonyls. The NMR spectrum of IVb (60 MHz) exhibited four methoxy groups (at δ 3.76, 3.85, 3.88, and 3.91), three protons (at δ 6.02 (s), 6.40 (s), and 7.38 (s)), two *para*-substituted phenyl groups (at δ 6.83 (d, 2H), 7.78 (d, 2H), 7.00 (d, 2H), and 7.52 (d, 2H)), and a proton at a lower field corresponding to a hydroxyl proton. These spectral data showed that a bond formation took place at the phenyl group having the hydroxyl group. This leads to two possible structures; *p*-quinone (IVb) and *o*-quinone (IVb'). Considering that the singlet appeared at δ 6.02, the *p*-quinone structure (IVb) is favored; IVb' must be oxidized further to a symmetrical biquinone which was not found in the reaction mixture. The IVb was determined to be 3-(4'-hydroxy-2'-methoxy-5'-*p*-methoxybenzoyl) phenyl-2-methoxy-5-(*p*-methoxy)benzoylbenzoquinone. Similarly, the structure of IVa was also determined to be 5-benzoyl-3-

4) B. Konig and St. v. Kostanecki, *Chem. Ber.*, **39**, 4028 (1906).
5) P. C. Johnson and A. Robertson, *J. Chem. Soc.*, **1950**, 2381.
6) R. K. Grover, G. D. Shah, and R. C. Shah, *ibid.*, **1955**, 3982.
7) "Beilsteins Handbuch der Organischen Chemie," Vol. 10, 379.
8) *ibid.*, Vol. 10, 388.
9) N. L. Drake, H. C. Harris, and C. B. Jaeger, Jr., *J. Amer. Chem. Soc.*, **70**, 168 (1948).

TABLE 3. NMR SPECTRAL DATA FOR BENZOPHENONES AND BIPHENYLS(δ VALUE AT 60 MHz)

Compound	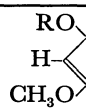		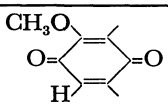	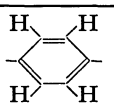		Ph	CH_3O	$OCOCH_3$	OH
IIa	6.52(2)	7.39(2)				7.2—7.3(10)	3.82 (6)		
IIb	6.52(2)	7.46(2)		7.64(4)	6.90(4)		3.85(12)		
Me-IIb	6.55(2)	7.28(2)		7.79(4)	6.86(4)		3.78 (6)		
							3.83(12)		
Ac-IIa	6.64(2)	7.48(2)				7.3—7.9(10)	3.84 (6)	2.04(6)	
Ac-IIb	6.73(2)	7.42(2)		7.75(4)	6.88(4)		3.83 (6)	2.08(6)	
							3.86 (6)		
IIIa	6.58(1)	7.13(1)				7.4—7.8 (5)	3.96 (3)		5.25(1)
IIIb	6.53(1)	7.14(1)		7.66(2)	6.96(2)		3.88 (3)		5.26(1)
							3.96 (3)		
IVa	6.41(1)	7.33(1)	6.02(1)			7.1—8.1(10)	3.69 (3)		
							3.83 (3)		
IVb	6.40(1)	7.38(1)	6.02(1)	7.52(2)	7.00(2)		3.76 (3)		
				7.78(2)	6.83(2)		3.85 (3)		
							3.88 (3)		
							3.91 (3)		

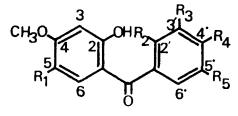

Ia $R_1=R_2=R_3=R_4=R_5=H$
Ib $R_1=R_2=R_3=R_5=H$. $R_4=OCH_3$
Ic $R_1=R_3=R_5=H$. $R_2=R_4=OCH_3$
Id $R_1=R_2=R_3=H$. $R_4=R_5=OCH_3$
Ie $R_1=R_3=R_5=H$. $R_2=OH$. $R_4=OCH_3$
If $R_1=R_3=H$. $R_2=OH$. $R_4=R_5=OCH_3$
IIIa $R_1=OH$. $R_2=R_3=R_4=R_5=H$
IIIb $R_1=OH$. $R_2=R_3=R_5=H$. $R_4=OCH_3$

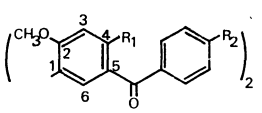

IIa $R_2=H$. $R_1=OH$
IIb $R_1=OH$. $R_2=OCH_3$
Ac-IIa $R_2=H$. $R_1=OAc$
Ac-IIb $R_1=OAc$. $R_2=OCH_3$
Me-IIb $R_1=R_2=OCH_3$

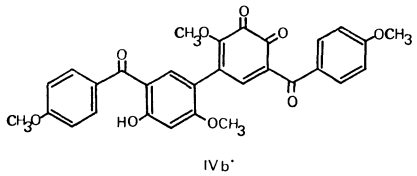

IVb

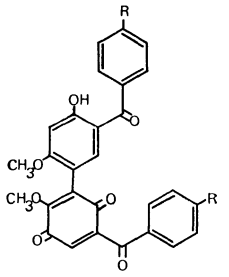

IVa R = H
IVb R = OCH_3

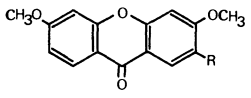

Vc R = H
Vd R = OCH_3

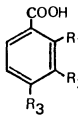

VIa $R_1=R_2=R_3=H$
VIb $R_1=R_2=H$. $R_3=OCH_3$
VIc $R_2=H$. $R_1=R_3=OCH_3$
VId $R_1=H$. $R_2=R_3=OCH_3$

(5'-benzoyl-4'-hydroxy-2'-methoxy)phenyl-2-methoxybenzoquinone. Benzoic acid (VIa) and anisic acid (VIb) were obtained from the reaction mixtures of Ia and Ib respectively, and were identified with authentic samples by studying their IR spectra.

When 2-hydroxy-2',4,4'-trimethoxybenzophenone (Ic) and 2-hydroxy-3',4,4'-trimethoxybenzophenone (Id) were oxidized with lead tetraacetate or with manganic acetate, Vc and Vd respectively were obtained as the products. The mass spectrum of Vc showed the molecular ion at *m/e* 256, corresponding to a molecular formula of $C_{15}H_{12}O_4$; this indicated that an intramolecular coupling between the hydroxyl group and the C_2'-position in Ic took place and that the methanol was removed from Ic. Vc was found to be 3,6-dimethoxyxanthone; it was identical with that prepared from Ie.[6] The structure of Vd was similarly determined to be 2,3,6-trimethoxyxanthone. This was also identified by independent synthesis from If.

2,4-Dimethoxybenzoic acid (VIc) and 3,4-dimethoxybenzoic acid (VId) were isolated from reaction mixtures of Ic and Id respectively. They were identified with authentic samples by a comparison by their IR spectra and also by the vpc of their methyl esters. Thus, the reaction takes place as expected in the cases of Ic and Id, but the reaction with Ia and Ib are not so simple.

The formation of the dimeric products (IIa, IIb, IVa, and IVb) may suggest a free radical mechanism,[10-12] but an ionic mechanism cannot be ruled out, for a phenoxylium cation has been known to convert to a dimeric product with phenol:[13]

$$ArOH + ArO^+ \longrightarrow \text{dimeric product} + H^+$$

Both paths are equally probable, and no conclusive evidence to differentiate these two paths in the present situation is available at this time.

Although only four of the benzophenones were examined so far, this reaction was shown to be an useful method in synthesizing xanthones from 2-hydroxybenzophenones.

Experimental

NMR spectra were recorded for deuteriochloroform solutions with a Hitachi NMR spectrometer model R-20B with

10) M. A. DaRooge and L. R. Mohoney, *J. Org. Chem.*, **32**, 1 (1967).
11) A. Onopchenko and J. G. D. Schulz, *ibid.*, **37**, 2564 (1972).
12) M. J. S. Dewar and T. Nakaya, *J. Amer. Chem. Soc.*, **90**, 7134 (1968).
13) D. G. Hewitt, *J. Chem. Soc., C*, **1971**, 1750.

Table 4. Analyses of new compounds

Compound	Molecular formula	Found		Calcd	
		C%	H%	C%	H%
Ic	$C_{16}H_{16}O_5$	66.72	5.65	66.66	5.59
Id	$C_{16}H_{16}O_5$	66.54	5.65	66.66	5.59
If	$C_{16}H_{16}O_6$	63.33	5.43	63.15	5.30
IIa	$C_{28}H_{22}O_6$	74.02	5.01	74.00	4.88
IIb	$C_{30}H_{26}O_8$	69.81	5.07	70.03	5.09
Ac-IIa	$C_{32}H_{28}O_8$	71.42	4.96	71.10	5.22
Ac-IIb	$C_{34}H_{30}O_{10}$	68.35	5.06	68.22	5.05
Me-IIb	$C_{32}H_{30}O_8$	70.68	5.57	70.83	5.57
IIIa	$C_{14}H_{12}O_4$	68.75	5.15	68.84	4.95
IIIb	$C_{15}H_{14}O_5 \cdot \frac{1}{6}C_6H_6$	67.01	5.29	66.89	5.26
IVa	$C_{28}H_{20}O_7$	72.51	4.38	71.79	4.30
IVb	$C_{30}H_{24}O_9$	68.42	4.57	68.18	4.58
Vd	$C_{16}H_{14}O_5$	67.05	5.08	67.12	4.93

tetramethylsilane as an internal standard; IR spectra were recorded for chloroform solutions with a JASCO DS 403G grating spectrometer; UV spectra were obtained for methanol solutions with a Hitachi EPS-3T spectrophotometer; mass spectra were recorded with a Hitachi mass spectrometer, RMU-6L; vpc were recorded with a Shimadzu GC-1C using polyethyleneglycol-succinate at 200 °C. Preparative and analytical tlc were carried out with Wakogel B10. Melting points were determined with a Yanagimoto micro-melting-point apparatus and uncorrected.

Materials. Lead tetraacetate and manganic acetate were prepared according to the references.[14,15]

2-Hydroxybenzophenones. 2-Hydroxybenzophenones (Ib, Ic, and Id) were prepared from 3-methoxyphenol and corresponding benzoic acids with boron trifluoride as catalyst and purified by recrystallization from ethanol. Ia was obtained from partial methylation of 2,4-dihydroxybenzophenone[4] which was prepared by the reaction of resorcinol and benzoic acid. If was prepared by the reaction of 3,4-dimethoxyphenol[16] (500 mg) and 2-hydroxy-4-methoxybenzoic acid[17] (450 mg) with phosphorus oxychloride (3.5 ml) and fused zinc chloride (1.5 g) heating at 65—70 °C for 1 hr and separated on silica gel (20 g) eluting with benzene, followed by recrystallization from ethanol. IIIa and IIIb were prepared by the reaction of 2-methoxyhydroquinone[9] (10 mmol), and benzoic acid (10 mmol) and anisic acid (10 mmol), respectively, with boron trifluoride etherate (20 ml), heating at 100 °C for 30—45 min. This gave IIa (5%) and IIIb (26%), respectively.

Reaction of Lead Tetraacetate with 2-Hydroxybenzophenones (Ia—d). 2-Hydroxybenzophenone (10 mmol) and lead tetraacetate (20 mmol) were dissolved in acetic acid (100 ml) and heated at 100 °C for 5 hr. After removal of the acetic acid, the resulting viscous liquid was treated with 2N sulfuric acid and then extracted with chloroform (100 ml). The chloroform layer was washed with aqueous sodium bicarbonate and saturated sodium chloride solution. The chloroform solution was evaporated and the residue was separated on silica gel (100 g). The column was eluted with benzene and then chloroform. From benzene fraction, II, III, and V were obtained after recrystallization from benzene or ethanol. The chloroform fraction was concentrated and again separated on tlc effected with chloroform, but this failed to give any crystalline compound. After acidification of the sodium bicarbonate solution, VI was obtained.

Reaction of Manganic Acetate with 2-Hydroxybenzophenones (Ia—d). 2-Hydroxybenzophenone (10 mmol) and manganic acetate (40 mmol) was dissolved into acetic acid (100 ml) containing acetic anhydride (1.0 ml). The mixture was heated at 100 °C until the colour of the manganic acetate disappeared. It usually took 5 hr. After removal of the acetic acid and acetic anhydride, the remaining viscous liquid was treated with 2N sulfuric acid (100 ml) and then extracted with chloroform. Working up in the same way as in the above, products II, IV, V, and VI were obtained.

Acetylation of II. IIa (100 mg) and IIb (100 mg), respectively, were treated with acetic anhydride (0.5 ml) in pyridine (1 ml) at room temperature overnight. The reaction mixture was poured into iced water and the precipitates were collected. After recrystallization from ethanol Ac-IIa (89 mg, 75%) and Ac-IIb (106 mg, 91%) were obtained.

Methylation of IIb. IIb (50 mg) was treated with dimethylsulfate (128 mg) in acetone (10 ml) containing anhydrous potassium carbonate (283 mg) under reflux for 4 hr. After removal of the acetone, the residue was triturated with water and the precipitates were collected. The crude product was recrystallized from ethanol to give a methyl ether (Me-IIb) (42 mg, 80%).

2,3,6-Trimethoxyxanthone (Vd). 2,2′-Dihydroxy-4,4′,5-trimethoxybenzophenone (If) (100 mg) was heated in water in a sieled tube at 230—240 °C for an hr. The crude product was collected and recrystallized from a mixture of chloroform and ethanol. This gave Vd (64 mg, 68%).

Authors wish to thank Dr. Shinzaburo Hishida and the staff of Hitachi Co., Ltd. at Katsuta for measuring NMR and mass spectra.

14) L. F. Audrieth, "Inorganic Syntheses" Vol. 3, McGraw-Hill, New York (1950), p. 47.
15) P. J. Andrulis, Jr., M. J. S. Dewar, R. Dietz, and R. L. Hunt, *J. Amer. Chem., Soc.* **88**, 5473 (1966).
16) R. I. Meltzer and J. Doczi, *ibid.*, **72**, 4986 (1950).
17) St. v. Kostanecki and J. Tambor, *Chem. Ber.*, **28**, 2309 (1895).

Chemistry of Mixed Transition-metal Complexes. V.[1] The Preparation of Several Mixed Transition-metal Complexes with Two μ-Diphenylphosphido Groups

Katsutoshi YASUFUKU and Hiroshi YAMAZAKI
The Institute of Physical and Chemical Research, Wako-shi, Saitama

(Received August 21, 1972)

Several mixed transition-metal complexes with two μ-diphenylphosphido groups as bridging ligands were prepared from bis(diphenylphosphine)metal complexes and diiodometal complexes by means of the action of amine or a Grignard reagent.

Homometallic dinuclear complexes with two μ-phosphido groups have been studied extensively,[2] but few of the heterometallic dinuclear complexes are known. Only one patent claim of $(CO)_nM\text{-}(\mu\text{-}PR_2)_2\text{-}M'(CO)_m$ [M=Cr, Mo, W (n=4), M'=Fe (m=3), R=Ph; M=Cr, M'=Mo (n= m=4), R=CH_3,] has been reported.[3] In the previous papers[4,5] of this series, we reported the preparation of mixed transition-metal complexes with one μ-diphenylphosphido group from the diphenylphosphinemetal complexes and the halogenometal complexes by dehydrohalogenation with amines. Now, we wish to report the preparation of several mixed transition-metal complexes with two μ-diphenylphosphido groups from bis(diphenylphosphine)metal complexes and diiodometal complexes; this is as an extension of the previous work.

Results and Discussion

The treatment of an equimolar mixture of carbonyl-π-cyclopentadienyldiiodocobalt (I) and tricarbonyl-bis-(diphenylphosphine)iron (II) with excess diethylamine in methylene chloride at room temperature gave π-cyclopentadienylcobalt-bis(μ-diphenylphosphido)tricarbonyliron (III) as brown crystals. The mass spectrum shows the molecular ion at m/e 634 and ions corresponding to the successive losses of three carbonyls. The IR spectrum (in benzene) shows $\nu_{C\equiv O}$ at 2000s and 1945s cm^{-1} and indicates that the carbonyls are all of the terminal type.

$$\underset{\text{I}}{\pi\text{-}C_5H_5Co(CO)I_2} + \underset{\text{II}}{(HPh_2P)_2Fe(CO)_3} \xrightarrow{Et_2NH} \underset{\text{III}}{\pi\text{-}C_5H_5Co(\mu\text{-}PPh_2)_2Fe(CO)_3}$$

A similar treatment of a mixture of I or tetracarbonyl-diiodoiron (IV) with tetracarbonyl-bis(diphenylphosphine)molybdenum[6] failed to give the desired mixed-metal complexes, although the tetracarbonyl-molybdenum-bis(μ-diphenylphosphido)tricarbonyliron had been prepared by the reaction of tetracarbonyl-diphenylphosphineiron with pentacarbonyl-chlorodiphenylphosphinemolybdenum.[3]

It is known that bis(triphenylphosphine)-π-cyclopentadienyl-cobalt and -rhodium, π-$C_5H_5M(PPh_3)_2$ (M=Co, Rh), can readily be prepared by the treatment of triphenylphosphine-π-cyclopentadienyl-diiodo-cobalt and -rhodium with isorpopylmagnesium bromide in the presence of triphenylphosphine.[7] We also attempted to prepare new bis(diphenylphosphine)metal complexes of the π-$C_5H_5M(PPh_2H)_2$ type according to this procedure. The treatment of I, π-cyclopentadienyl-diiodo-rhodium (V), or -iridium (VI) with an equimolar amount of diphenylphosphine afforded monodiphenylphosphine complexes of the π-$C_5H_5M(PPh_2H)I_2$ type (VII, M=Co; VIII, M=Rh; IX, M=Ir). The treatment of I or V with two molar equivalents of diphenylphosphine, or the treatment of VII or VIII with one molar equivalent of diphenylphosphine, gave bis-diphenylphosphine complexes of the π-$C_5H_5M(PPh_2H)_2I_2$ type (X, M=Co; XI, M=Rh). No corresponding iridium complex was obtained. The compounds thus obtained are summarized in Table 1. All the compounds are very stable in air. The solubility of the bis-diphenylphosphine complexes is lower than that of the corresponding mono-diphenylphosphine complexes, probably because of the influence of the partial ionic character.

Though attempts to isolate the π-$C_5H_5M(PPh_2H)_2$ complexes were not successful, several new mixed transition-metal complexes with two μ-diphenylphosphido groups were obtained by the reaction of the bis-diphenylphosphine complexes, X and XI, with isopropylmagnesium bromide in the presence of some diiodometal complexes. Thus, the treatment of X with excess isopropylmagnesium bromide in the presence of an equimolar amount of IV gave III in a yield comparable with that of the amine method described above. The use of isopropylmagnesium bromide instead of the amine in the reaction of I with II also afforded III. This suggests that the Grignard reagent may act not only as a reducing agent, but also as a base, though no

1) Part IV in this series: K. Yasufuku and H. Yamazaki, *J. Organometal. Chem.*, **38**, 367 (1972).
2) J. P. Candlin, K. A. Taylor, and D. J. Thompson, "Reactions of Transition-metal Complexes," Elsevier, Amsterdam, (1968), p. 375.
3) Neth. Appl., 6,611,373 (1967); *Chem. Abstr.*, **67**, 54266.
4) K. Yasufuku and H. Yamazaki, This Bulletin, **43**, 1588 (1970).
5) K. Yasufuku and H. Yamazaki, *J. Organometal. Chem.*, **28**, 415 (1971).
6) J. G. Smith and D. T. Thompson, *J. Chem. Soc.*, *A*, **1967**, 1694.
7) H. Yamazaki and N. Hagihara, This Bulletin, **44**, 2260 (1971).

Table 1. The diphenylphosphine complexes

Compound	Color	Yield (%)	Mp (°C)	Analyses (%) Found (Calcd) C	H	I	NMR (τ)[a] π-C_5H_5	P–H	IR (cm^{-1})[c] ν_{P-H}
VII	black	73	165—166	36.22 (36.20)	3.14 (2.86)	45.62 (45.00)	4.78 (s)	2.50 (d, J=417 Hz)	
VIII	brown	77	225—228	33.68 (33.58)	2.90 (2.65)	41.94 (41.74)	4.41 (d, J=2 Hz)	2.30 (d, J=425 Hz)	
IX	red	91	242—246	29.41 (29.28)	2.57 (2.31)	36.31 (36.40)	4.43 (d, J=1.5 Hz)	1.66 (d, J=430 Hz)	
X	black	91	157—163	45.97 (46.43)	3.87 (3.63)	34.19 (33.83)	4.30 (s)	2.08[b] (d, J=416 Hz)	2250
XI	red	84	168—172	43.96 (43.86)	3.63 (3.43)	32.25 (31.96)	4.01 (t, J=1 Hz)	2.10[b] (d, J=428 Hz)	2270

a) Measured in $CDCl_3$.
b) Intensity of the doublet was about one half of expected one.
c) Measured in C_6H_6. No P–H stretching absorptions were observed in the cases of VII, VIII, and IX.

Table 2. The bis-μ-diphenylphosphido complexes

Compound	Color	Yield (%)	Decomp. Temp. (°C)	Found (Calcd) C	H	NMR[a] (τ) π-C_5H_5
III	dark brown	17	210	60.96 (60.60)	3.93 (3.97)	5.06 (s)
XII	red	18	260	56.96 (56.12)	3.77 (3.57)	4.54 (s)
XIII	black	25	250	61.59 (61.65)	4.60 (4.57)	4.72 (s) 5.37 (s)
XIV	black	44	300	66.28 (66.03)	5.00 (4.89)	5.32 (s)
XV	red	29	300	58.23 (57.81)	4.53 (4.28)	4.80 (s)
XVI[b]	yellow	1	310	—	—	4.86 (s)

a) Measured in $CDCl_3$. Protons of PPh_2 appeared in 2.0—3.3 τ as multiplet.
b) No elemental analysis was carried out because of the failure to obtained enough amount.

exact mechanism is clear from these observations only. Tricarbonyliron-bis(μ-diphenylphosphido)-π-cyclopentadienylrhodium (XII) was prepared from XI and IV by a similar treatment. The mass spectrum of XII showed a pattern similar to that of III.

π-$C_5H_5M(PPh_2H)_2I_2$ + $I_2Fe(CO)_4$
X (M=Co), XI (M=Rh) IV

$\xrightarrow{i\text{-PrMgBr}}$ π-C_5H_5M(–P(Ph)–)$_2$–$Fe(CO)_3$

III (M=Co)
XII (M=Rh)

The similar treatment of XI with I afforded π-cyclopentadienylcobalt-bis(μ-diphenylphosphido)-π-cyclopentadienylrhodium (XIII).

π-$C_5H_5Rh(PPh_2H)_2I_2$ + π-$C_5H_5Co(CO)I_2$
XI I

$\xrightarrow{i\text{-PrMgBr}}$ π-C_5H_5Rh(–P(Ph)–)$_2$–Co-π-C_5H_5

III

The homometallic bis-μ-diphenylphosphido complexes of cobalt (XIV) and of rhodium (XV) were obtained by the treatment of the mono-diphenylphosphine complexes, VII and VIII respectively, with isopropylmagnesium bromide. The iridium analogue (XVI) was also obtained from IX, though the yield was very low. The cobalt complex (XIV) is already known,[8] but the other two complexes are new ones. All the compounds are stable in air, and in their mass spectra the parent ion peak is the strongest in every case.

π-$C_5H_5M(PPh_2H)I_2$ $\xrightarrow{i\text{-PrMgBr}}$ π-C_5H_5M(–P(Ph)–)$_2$–M-π-C_5H_5

VII (M=Co), VIII (M=Rh), XI (M=Ir)

XIV (M=Co)
XV (M=Rh)
XVI (M=Ir)

The reaction of an equimolar mixture of the monodiphenylphosphine complexes of cobalt (VII) and rhodium (VIII) with isopropylmagnesium bromide afforded a mixture of XIII, XIV, and XV as the product. A similar treatment of a mixture of the

8) R. G. Hayter, *Inorg. Chem.*, **2**, 103 (1963).

mono-diphenylphosphine complexes of rhodium (VIII) and iridium (IX) gave only a mixture of XV and XVI. The failure to detect a mixed metal complex of rhodium and iridium is probably the result of differences in the reactivities of the mono-diphenylphosphine complexes and/or the stabilities of the reaction intermediates.

The data for the bis(μ-diphenylphosphido)metal complexes prepared are collected in Table 2.

Experimental

The preparations were carried out under an atmosphere of nitrogen. The diphenylphosphine was prepared as has been described in a previous paper,[5] while the tricarbonyl-bis-(diphenylphosphine)iron was prepared by the method of Thompson.[6] The carbonyl-π-cyclopentadienyl-diiodo-cobalt (I),[9] π-cyclopentadienyl-diiodo-rhodium (V),[10] and -iridium (VI)[11] were prepared according to the known procedures. The melting points were determined using a Yanaco micro-melting-point apparatus. The spectra were measured with a Perkin-Elmer grating infrared spectrophotometer, Type 521, a JEOL nuclear magnetic resonance spectrometer, Type C-60, and a JEOL mass spectrometer, Type 1S, at 75 eV.

Preparation of Diphenylphosphine Complexes. To a solution of I (2.0 g, 4.9 mmol) in CH_2Cl_2 (50 ml) was added diphenylphosphine (1.0 g, 5.4 mmol) under magnetic stirring. After the evolution of gas had ceased, the solution was concentrated. The subsequent addition of hexane gave black crystals of VII (2.3 g). For analytical purposes, the compound was purified by chromatography on a silica-gel column (Wakogel C-200).

In the case of the preparation of the rhodium and iridium analogues (VIII and IX), the reactions were continued until all of the almost-insoluble V and VI disappeared.

For the preparation of the bis-diphenylphosphine complexes (X and XI), two molar equivalents of diphenylphosphine to V or VI were employed.

The results are summarized in Table 1.

Preparation of π-$C_5H_5M(\mu$-$PPh_2)_2Fe(CO)_3$ (III, M=Co; XII, M=Rh). *Method (a)*: I (0.10 g, 0.25 mmol) and II (0.12 g, 0.23 mmol) were stirred in THF (12 ml) with diethylamine (0.3 ml) at room temperature for two days. The reaction mixture was then evaporated under reduced pressure, and the residue dissolved in benzene was chromatographed on a silica-gel column. From the brown fraction eluted with a hexane–benzene mixture (1/1), dark brown crystals of III (0.024 g) were obtained.

Method (b): To a solution of X (0.23 g, 0.31 mmol) and IV (0.15 g, 0.35 mmol) in THF (20 ml) and benzene (10 ml) was added isopropylmagnesium bromide (5 ml) in ether (5 ml). The reaction mixture was hydrolyzed with aqueous ammonium chloride, and the organic layer was dried with sodium sulfate. After concentration, the residue was chromatographed on a silica-gel column and eluted by a benzene–hexane mixture (1/1). From the brown eluate, dark brown crystals of III (0.033 g) were obtained.

By the same procedure, the rhodium-iron complex, XII (0.039 g), was obtained from XI (0.24 g, 0.30 mmol) and IV (0.13 g, 0.31 mmol).

Mcthod (c): I (0.10 g, 0.25 mmol) and II (0.12 g, 0.23 mmol) were treated in THF (10 ml) and benzene (5 ml) with isopropylmagnesium bromide (2 mmol) in ether (2 ml) at 0 °C for 5 hr. A procedure similar to that used in the (b) method gave III (0.018 g).

Preparation of π-$C_5H_5Co(\mu$-$PPh_2)_2Rh$ π-C_5H_5 (XIII). To a solution of XI (0.26 g, 0.33 mmol) and I (0.41 g, 0.10 mmol) in THF (15 ml) and benzene (30 ml) was added lsopropylmagnesium bromide (6 mmol) in ether (6 ml) at 0 °C. After several minutes, the reaction mixture was hydrolyzed with aqueous ammonium chloride and the organic layer was dried with sodium sulfate. After concentration, the residue was chromatographed on an alumina column and eluted by a benzene–hexane mixture (1/1). From the brown eluate, black crystals of XIII (0.054 g) were obtained.

Preparation of π-$C_5H_5M(\mu$-$PPh_2)_2M$ π-C_5H_5, (XIV, M=Co; XV, M=Rh; XVI, M=Ir). A solution of VII (0.56 g, 1.0 mmol) in benzene (20 ml) was treated, drop by drop with isopropylmagnesium bromide (5 mmol) in ether (5 ml) at 0 °C. By a procedure similar to that presented above, black crystals of XIV (0.14 g) were obtained. Similarly, XV and XVI were prepared. All of the bis-μ-phosphido complexes thus prepared are summarized in Table 2.

9) R. B. King, "Organometallic Syntheses," Vol. 1, Academic Press, New York, N. Y. (1965), p. 118.

10) A. Kasahara, T. Izumi, and K. Tanaka, This Bulletin, **40**, 699 (1967).

11) H. Yamazaki, *ibid.*, **44**, 582 (1971).

Arylation of Olefin with Iodobenzene Catalyzed by Palladium

Kunio MORI, Tsutomu MIZOROKI, and Atsumu OZAKI

Research Laboratory of Resources Utilization, Tokyo Institute of Technology, Ookayama, Meguro-ku, Tokyo 152

(Received October 4, 1972)

Arylation of propylene, ethylene, styrene, and methyl acrylate with iodobenzene was found to be catalyzed by metallic palladium in methanol to give methylstyrene, styrene, *t*-stilbene, and methyl cinnamate, respectively. Their yields and selectivities increased significantly by the addition of excess potassium acetate as an acceptor of hydriodic acid formed. The course of catalytic reaction is discussed in terms of the oxidative addition of iodobenzene to a palladium complex of low oxidation state.

Oxidative addition of organic halides to metal complexes of low oxidation state is well-known a method of σ-organometallic complexes. Before such an addition is made to a catalytic reaction, it should be considered whether the metal complex of low oxidation state specified as a catalyst is regenerated during the course of reaction. In the carbonylation of phenyl halide catalyzed by bis(triphenylphosphine)carbonylchlororhodium(I) in benzene,[1] benzoyl and halogen ligands are reductively eliminated from $C_6H_5CORh(PPh_3)_2(CO)(Cl)(X)$ to give benzoyl halide and $Rh(PPh_3)_2(CO)Cl$, with the result that the rhodium(I) complex works well as the catalyst. Nickel tetracarbonyl is also labile for oxidative addition of organic halides such as phenyl and allyl halides to give acyl nickel carbonyls.[2,3] In this case, however, these nickel complexes decompose into nickel(II) halide to give α-diketones or esters, their formation depending on the solvent used. Accordingly, nickel carbonyl seems to have no catalytic activity for the carbonylation of organic halide except under enforced reaction conditions. It was shown[4] that the carbonylation rate of phenyl halide with nickel carbonyl in methanol increased significantly by the addition of potassium acetate as an acceptor of hydrohalogenic acid formed. It was considered that the acid strongly inhibited the coordination of carbon monoxide to regenerate a nickel carbonyl of low oxidation state. The same effect of potassium acetate is also observed in the palladium black-catalyzed carbonylation of phenyl halide[5] in spite of the fact that metallic palladium has a higher oxidation potential than nickel. These results led us to investigate the effect of potassium acetate on other kinds of catalytic reactions to see whether the inhibition by proton is observed only in carbonylation. It was found that palladium black is highly active and selective for the catalytic arylation of olefin with iodobenzene in the presence of potassium acetate.[6] The present paper deals with the palladium catalyzed arylation of propylene, ethylene, styrene, and methyl cinnamate with phenyl halide to give the corresponding styrene derivatives.

Experimental

A given amount of palladium catalyst ($PdCl_2$ or Pd-black) and a methanol solution (30—35 ml) of phenyl halides and potassium acetate were placed in a titanium-alloy autoclave (100 ml) equipped with a magnetic stirrer (when liquid olefin was used, it was also dissolved in the methanol solution). The autoclave was purged thoroughly with nitrogen and gaseous olefin was then introduced. In the case of liquid olefin, nitrogen gas was charged up to 10 kg/cm^2. The autoclave was heated up to the desired temperature by an electric furnace within 20 min. and the temperature was kept constant for 2—3 hr. It was then cooled rapidly to room temperature with water and gaseous materials were discharged. The products were taken out from the autoclave by using a sufficient amount of methanol or acetone, and they were separated from palladium black before their amounts were quantitatively determined by gas chromatography, using a suitable substance as an internal standard. A DC-550 columun was used for the determination of styrene, α-, β-methylstyrene, methyl cinnamate, and phenyl halides, and a SE-30 columun for 1,1-diphenylethylene and *t*-stilbene with hydrogen as a carrier gas. All materials were commerical products, their purity being checked by gas chromatography before use.

Results

The effect of potassium acetate (pK_a of CH_3COOH= 4.7) on the arylation of ethylene with iodobenzene catalyzed by palladium dichloride in methanol was examined. The results are shown in Table 1. The yield of styrene increased with increase in the amount of potassium acetate, no residual iodobenzene being detected when the amount (mole) of potassium acetate added exceeded that of iodobenzene used. Most of the palladium dichloride was reduced to metallic palladium after the reaction. Pyridine (pK_a of $C_5H_5NH^+$=5.4) and sodium benzoate (pK_a of C_6H_5COOH=4.2) showed a similar effect on the arylation of ethylene. No catalytic arylation, however, was observed with potassium trichloroacetate (pK_a of CCl_3COOH=0.7). Palladium black also catalyzed the arylation with high activity as shown in Table 1. There is hardly any difference between palladium dichloride and palladium black in catalytic activity. The effect of acetic acid as a solvent was examined, since hydriodic acid formed by arylation gives potassium iodide and acetic acid during the reaction when potassium acetate is present in the reaction

1) J. Tsuji, and K. Ohno, *J. Amer. Chem. Soc.*, **88**, 3452 (1966); *Tetrahedron Lett.*, **1966**, 4713.
2) N. L. Bauld, *ibid.*, **1963**, 1841.
3) F. Guerrieri, and G. P. Chiusoli, *J. Organometal. Chem.*, **15**, 209 (1968).
4) M. Nakayama and T. Mizoroki, This Bulletin, **42**, 1124 (1969); *ibid.*, **44**, 508 (1971).
5) T. Mizoroki, unpublished result.
6) T. Mizoroki, K. Mori, and A. Ozaki, This Bulletin, **44**, 581, (1971).

Table 1. Effect of potassium acetate

Catalyst	C_6H_5I (mmol)		AcOK (mmol)	Styrene (mmol)	Conversion[a] (%)
$PdCl_2$ (0.5 mmol)	50		0	trace	—
	50		15	13	26
	50		30	24	48
	50		60	37	74
	50	(Py)	60	19	36
	50	(CCl_3COOK)	60	trace	—
Pd-black (1 mmol)	30		0	3.3	11
	30		12	9.3	31
	30		20	16	53
	30		30	21	70
	30		40	27	90
	30		50	26	88

CH_3OH, 30 ml; $P_{C_2H_4}$, 8—10 kg/cm²; Temperature 120—125 °C; Time, 3 hr.
a) Based on C_6H_5I employed.

medium. The addition of acetic acid as the solvent considerably decreased the yield of styrene (Table 2).

The effects of the amount of palladium black and palladium dichloride on the conversion of iodobenzene were examined at 75 °C, 100 °C, and 125 °C. The degrees of conversion of iodobenzene are plotted against the amount of palladium catalyst in Fig. 1. The conversion at 100 °C becomes nearly constant when the amount of palladium black and palladium dichloride exceeds 0.5 and 2.5 mmol, respectively. Palladium black seems to be more active than palladium dichloride. It is to be noted that a large amount of palladium dichloride gives nearly the same conversion as that obtained from palladium black. The selectivity of styrene formation is 60—90% (Table 1). Even under a higher pressure of ethylene, the selectivity is less than 90%, *t*-stilbene and 1,1-diphenylethylene being always detected. It was found that styrene is also arylated with iodobenzene to give quantitatively *t*-stilbene and 1,1-diphenylethylene (Table 3). This is why the selectivity of styrene from ethylene and iodobenzene is always less than 90%. The results of arylation of propylene, ethylene, styrene, and methyl acrylate are summarized in Table 4. These olefins give almost quantitatively methylstyrene, styrene, *t*-stilbene, and methyl cinnamate, respectively. Propylene gives a considerable amount of α-methylstyrene as well as β-methylstyrene, while methyl acrylate gives exclusively methyl cinnamate. Reactivity of phenyl halide decreases in the order $C_6H_5I > C_6H_5Br \gg C_6H_5Cl$, whereas the arylation of ethylene or propylene with a bromobenzene derivative (Table 5) shows that the reactivity of bromobenzene derivatives decreases in the order *p*-chlorobromobenzene > bromobenzene ≥ *p*-bromotoluene > *p*-bromoanisole. On the other hand, the yields of arylation product with bro-

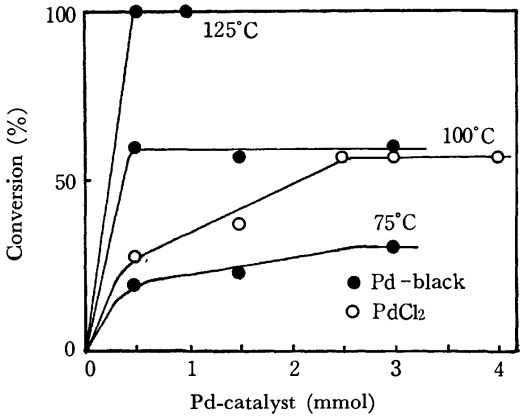

Fig. 1. Effect of the amount of Pd-cat.
C_6H_5I, 30 mmol; AcOK, 50 mmol; CH_3OH, 30 ml; $P_{C_2H_4}$, 10 kg/cm²; Time, 2 hr.

Table 2. Effect of acetic acid as solvent

Solvent (ml)		Conversion (%)	Selectivity[a] (%)
CH_3OH	AcOH		
0	30	47	57
10	20	70	62
20	10	95	73
30	0	100	87

C_6H_5I, 30 mmol; AcOK, 50 mmol; Pd-black, 1 mmol; $P_{C_2H_4}$, 10 kg/cm²; Temperature 125°C; Time, 3 hr
a) Based on C_6H_5I consumed.

Table 3. Selectivity of arylation product

Olefin		C_6H_5I (mmol)	Arylation product			Conversion (%)	Selectivity (%)
C_2H_4 (kg/cm²)	Styrene (mmol)		Styrene (mmol)	*t*-Stilbene (mmol)	1,1-Diphenylethylene (mmol)		
5		10	8.4			100	84
10		10	8.2			100	82
20		10	8.8			100	88
10		20	17			100	85
10		40	31			100	78
	10	10		7.3	1.4	87	100
	20	10		7.9	1.5	94	100
	30	10		9.0	1.0	100	100

Pd-black, 1 mmol; AcOK, 50 mmol; CH_3OH, 30 ml; Time, 3 hr; Temperature 125°C.

Table 4. Arylation of substituted olefin

	C_6H_5I (mmol)	AcOK (mmol)	Olefin	Conversion (%)	Arylation product (mmol)		Selectivity (%)	Isomer distribution α/β
1	30	48	C_3H_6 3.5 kg/cm² a)	100	$C_6H_5C(CH_3)=CH_2$	8.1	27	2.7
					$C_6H_5CH=CHCH_3$	22	73	
2	50	60	C_2H_4 8.0 kg/cm² a)	100	$C_6H_5CH=CH_2$	37	74	—
3	50	60	C_6H_5-CH=CH_2 100 mmol	100	$(C_6H_5)_2C=CH_2$	45	10	7.5
					t-$C_6H_6CH=CHC_6H_5$	6	90	
4	30	48	$CH_2=CH(COOCH_3)$ 6.0 mmol	100	$C_6H_6CH=CHCOOCH_3$	29	—	>50
					$C_6H_6C(COOCH_3)=CH_2$	—	97	

a) Introduced at room temperature.

Table 5. Reactivity of bromobenzene derivatives

p-Br-C_6H_4-X	Conversion (%)a) With C_2H_4 (10 kg/cm²)	With C_3H_6 (3.5 kg/cm²)
X=OCH_3	0	—
CH_3	6.7	—
H	6.7	6.7
Cl	10	13

p-Br-C_6H_5-X, 30 mmol; AcOK, 40 mmol; CH_3OH, 30 ml; Pd-black, 1 mmol; Temperature 125°C; Time 3 hr.
a) Calculated from the amount of *p*-Br-C_6H_5-X consumed.

mobenzene indicate that the reactivity of olefins decreases approximately in the order propylene>ethylene>styrene>methyl acrylate, where no arylation of methyl acrylate with bromobenzene is observed. Addition of triphenylphosphine slightly increased the yield of methylstyrene from propylene and bromobenzene. However, no effect was observed in the isomer distribution of methylstyrene. Triphenylphosphine reacted with iodobenzene to give tetraphenylphosphonium iodide almost quantitatively under the same reaction condition (calcd for $(C_6H_5)_4PI$: H, 4.17%; C, 60.37%; I, 27.23%. Found: H, 4.3%; C, 61.8 %; I, 27.2%).

Discussion

It was reported that ethylene or styrene is arylated with benzene in the presence of palladium(II) diacetate ($C_6H_6+C_6H_5CH=CH_2+Pd(AcO)_2 \rightarrow$ t-$C_6H_5CH=CH$-$C_6H_5+Pd+2AcOH$).[7] The arylation, however, consumes a stoichiometric amount of palladium(II) diacetate, which is reduced to metallic palladium. The arylation is not catalytic with respect to palladium with no simultaneous reoxidation of metallic palladium. Heck found that σ-phenylpalladium(II) acetate prepared from phenylmercuric acetate and palladium diacetate reacts with olefin under mild condition to give styrene derivatives:[8]

$$C_6H_5Hg(AcO) + Pd(AcO)_2 \rightarrow (C_6H_5)Pd(AcO) + Hg(AcO)_2$$

$$C_6H_5Pd(AcO) + CH_2=CH_2 \rightarrow C_6H_5CH=CH_2 + Pd + AcOH$$

In this case, the palladium(II) compound is also reduced into metallic palladium, arylation taking place stoichiometrically. However, arylation of olefin with iodobenzene is effectively catalyzed by metallic palladium, its catalytic efficiency being significantly large.

Palladium(II) dichloride is easily reduced to metallic palladium in a boiling methanol solution. Thus, most of the palladium(II) dichloride we used should be present as metallic palladium during the course of arylation. This may be why practically no difference is observed between palladium dichloride and metallic palladium in their catalytic activities (Table 1). The reaction rate must be determined by some interaction of phenyl halides with palladium catalyst, since their reactivity decreases in the order $C_6H_5I>C_6H_5Br\gg C_6H_5Cl$, which is parallel with the strength of bond energy between carbon and halogen atom. The question is whether the arylation is catalyzed by palladium black suspended in the methanol solution, or by palladium complex dissolved in it. If the suspended palladium black catalyzes the arylation of ethylene, the yield of styrene should increase with the amount of palladium catalyst, since the surface area of palladium black contacting iodobenzene must increase with the amount of palladium black. The yield of styrene, however, does not increase (Fig. 1). This suggests that an active species of the catalyst is some palladium complex dissolved in the methanol solution. Accordingly, the highest rate of arylation of olefin would be obtained with a saturated solution of the palladium complex. Palladium complexes are slightly soluble

7) Y. Fujiwara, I. Moritani, S. Danno, R. Asano, and S. Teranishi, *J. Amer. Chem. Soc.*, **91**, 7166 (1969).

8) R. F. Heck, *ibid.*, **91**, 6707 (1969).

in methanol, with the result that the conversion of iodobenzene does not increase with the increase in the amount of palladium catalyst (Fig. 1).

Another point to be considered is what kind of palladium complex is supplied from the palladium black suspended during the course of reaction. If the complex were present in the form of palladium(II) compound, arylation with benzene would be expected. This was examined by the arylation of styrene with benzene in the presence of iodobenzene, using a relatively large amount of palladium black. The total amount of arylation product (*t*-stilbene and 1,1-diphenylethylene) is almost equal to that of iodobenzene consumed (Table 6). This supports the view that palladium black supplies no palladium(II) compound which is active for the arylation of styrene with benzene. It can thus be postulated that the oxidation state of the active palladium complex is low, probably zero, in the solution.

Table 6. Reaction of C_6H_5I with styrene in C_6H_6

Time (hr)	Consumed C_6H_5I (mmol)	Arylation product		Selectivity (%)
		t-Stilbene (mmol)	1,1-Diphenyl ethylene (mmol)	
3	1.8	1.6	0.26	100
8	3.2	2.7	0.26	93

C_6H_5I, 10 mmol; C_6H_6, 30 ml; Styrene, 26 mmol; AcOH, 5 ml; AcONa, 15 mmol; Pd-black, 5 mmol; Temperature 125 °C.

a) Based on the amount of C_6H_5I consumed

Taking into account the well-known oxidative addition of phenyl halide to low valent palladium complexes to give σ-aryl palladium(II) halide,[9] the following reaction scheme can be proposed;

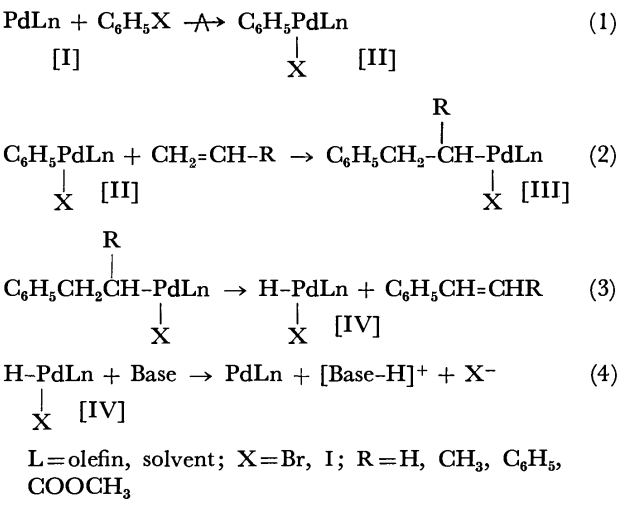

Phenyl halide is oxidatively added to low valent palladium complex [I] to give σ-phenyl palladium complex[II], to which the olefin is inserted, followed by elimination of β-hydrogen to give [IV] and arylation product. Paths (2) and (3) have been investigated in detail.[8] Arylation with iodobenzene is significantly enhanced in a basic medium. This is in line with the fact that the yield of styrene considerably decreased in acetic acid solvent (Table 2). Such a basic medium should be favorable for paths (3) and (4) to regenerate the low valent palladium complex[10] and also for preventing the decomposition of σ-complex[II]. A stoichiometric reaction of styrene with bis(triphenylphosphine)σ-phenyl(iodo)palladium(II) was examined in methanol at its reflux temperature for the effect of potassium acetate on the reaction paths analogous to (2) and (3). No arylation of styrene was observed even in the presence of a large amount of potassium acetate, probably because triphenylphosphine inhibited the coordination of styrene to the palladium complex. The role of potassium acetate remains unclarified.

9) P. Fitton, M. P. Johnson, and J. E. McKeon, *Chem. Commun.*, **1968**, 6; K. Kudo, M. Hidai, T. Maruyama, and Y. Uchida, *bid.*, **1970**, 1701.

10) L. F. Hines and J. K. Stille, *J. Amer. Chem. Soc.*, **94**, 485 (1972); T. Hosokawa and P. Maitlis, *ibid.*, **94**, 3239 (1972).

Syntheses of Some Cyanine Dyes of Bunte Salt Type

Masashi YAMAMOTO, Shigeo NAKAMURA, Kunio YOSHIMURA,
Masuo YUGE, Shiro MOROSAWA, and Akira YOKOO

Department of Chemistry, Faculty of Science, Okayama University, Tsushima, Okayama 700

(Received October 18, 1972)

In order to investigate the photosensitivity of compounds such as photosensitizing dyes of Bunte salt type which have not been synthesized yet, the following compounds were prepared: 1,1′-di-(2-potassiumsulfothioethyl)-4,4′-tricarbocyanine acetate (VI), 1,1′-di-(2-potassiumsulfothioethyl)-2,2′-tricarbocyanine acetate (VII), 6,6′-dimethyl-3,3′-di-(2-potassiumsulfothioethyl)dithiacarbocyanine acetate (VIII), and 3-(2-bromoethyl)-3′-(sulfothioethyl)-5,6,5′,6′-tetramethoxydithiacarbocyanine (XII).

Three kinds of substituted 1-(2-bromoethyl)quinolinium bromide(II) (4-methyl (a), 2-methyl- (b), and 6-ethoxy-2-methyl- (c)) were subjected to reaction with sodium thiosulfate to yield the corresponding thiosulfates (IIIa, b, and c), respectively. Similarly, four kinds of substituted 4-(2-bromoethyl)benzothiazolium bromides (IV) (2-methyl- (a), 2,6-dimethyl-, (b), 6-methoxy-2-methyl- (c), and 2,5-dimethyl- (d)) gave the corresponding thiosulfates (Va, b, c, and d).

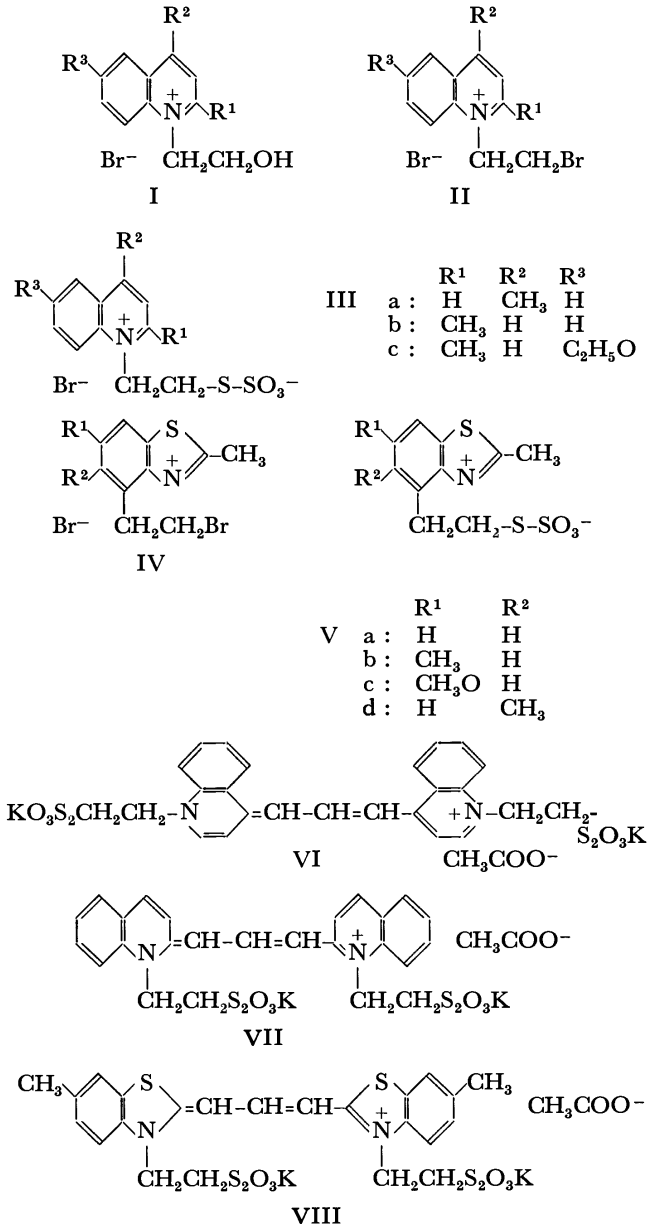

Fig. 1.

IIIa, IIIb and Vb yielded the corresponding cyanine dyes (VI, VII and VIII) in low yields on being heated[1] with aniline and ethyl orthoformate, followed by heating with acetic anhydride and potassium acetate. IIIa, IIIb, and Va gave their thiosulfates (IX, X and XI) by heating with aniline and ethyl orthoformate. In order to introduce a thiosulfate group into the carbocyanine dye, 3,3′-di-(2-bromoethyl)-5,6,5′,6′-tetramethoxydithiacarbocyanine bromide (XIV) was derived from the corresponding hydroxyethyl compound (XIII). However, it was found that only one bromoethyl group in XIV was converted into the sulfothioethyl group with sodium thiosulfate.

An attempt to obtain 1,1′-di-(2-potassiumsulfothioethyl)-2,4′-tricarbocyanine acetate by heating a mixture of IX and IIIb in the presence of acetic anhydride and potassium acetate gave a powder, which had an absorption maximum in the visible region, λ(MeOH)[2]

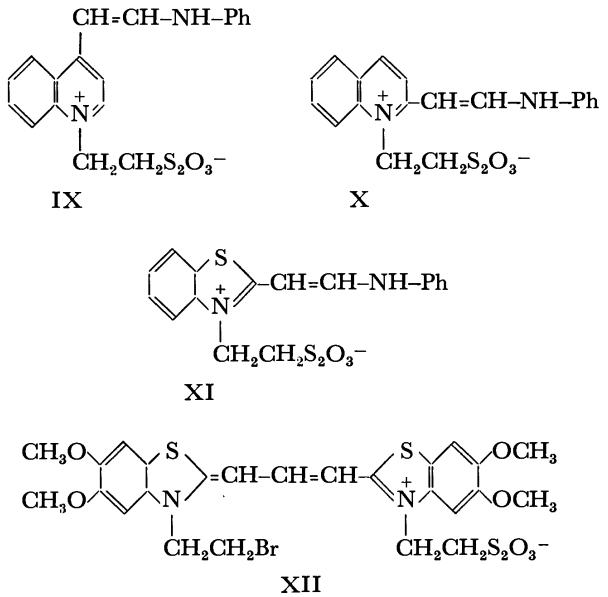

Fig. 2.

1) T. Ogata, *Rikwagaku Kenkyu-jo Iho*, **13**, 501, 549 (1934).
2) Indicated in nm.

673—674 (ν(KBr)[3] 1209 and 1025). Reaction of IIIa with 1-(2-hydroxyethyl)-4-(phenylaminoethenyl)quinolinium bromide, expected to form 1-(2-hydroxyethyl)-1'-(2-potassiumsulfothioethyl)-4,4'-tricarbocyanine acetate, gave a powder possessing an absorption maximum in the visible region, λ(MeOH) 728 (ν(KBr) 1232, 1195, and 1021). An attempt to prepare 3,3'-di-(2-potassiumsulfothioethyl)dithiacarbocyanine acetate as in the formation of VIII yielded a crystal which showed an absorption maximum in the visible region, λ(EtOH) 556—557 (ν (KBr) 1221—1208 and 1024).

Experimental[4]

1-(2-Bromoethyl)-4-methylquinolinium Bromide (IIa). A mixture of 10.0 g of 1-(2-hydroxyethyl)-4-methylquinolinium bromide (I) and 8.0 g of phosphorus tribromide was heated at 110 °C for 10 min. The reaction mixture was triturated repeatedly with ether, and the solid was recrystallized from ethanol to give 11.4 g of colorless crystals, mp 205 °C (decomp.).

S-[2-(4-Methylquinolinium-1-yl)ethyl]thiosulfate (IIIa). A mixture of 10.0 g of IIa and 8.0 g of sodium thiosulfate in 120 ml of water was heated on a water bath for 2.5 hr and then kept in a refrigerator. The crystals fromed were collected, washed with 30 ml of ethanol and finally recrystallized from water to yield 8.4 g of colorless crystals, mp 216—218 °C (decomp.), ν(KBr) 1230, 1215, and 1027.

Found: C, 50.73; H, 4.48; N, 4.81%. Calcd for $C_{12}H_{13}NO_3S_2$: C, 50.87; H, 4.59; N, 4.95%.

S-[2-(2-Methylquinolinium-1-yl)ethyl]thiosulfate (IIIb). A mixture of 10.6 g of IIb and 8.1 g of sodium thiosulfate in 130 ml of water was heated on a water bath for 1 hr. After being left to stand at room temperature, the crystals deposited were recrystallized from water to give 7.9 g of colorless crystals, mp 227—228 °C (decomp.). ν(KBr) 1247, 1233, 1224, 1208, and 1022.

Found: C, 50.97; H, 4.47; N, 4.76%. Calcd for $C_{12}H_{13}NO_3S_2$: C, 50.87; H, 4.59; N, 4.95%.

S-[2-(6-Ethoxy-2-methylquinolinium-1-yl)ethyl]thiosulfate (IIIc). A mixture of 5.0 g of IIc and 3.4 g of sodium thiosulfate in 30 ml of water was heated on a water bath for 1 hr, and then kept in a refrigerator. The resulting crystals were recrystallized from water to give 1.5 g of colorless crystals, mp 223 °C (decomp.). ν(KBr) 1234—1217 and 1022.

Found: C, 51.51; H, 5.59; N, 3.90%. Calcd for $C_{14}H_{17}NO_4S_2$: C, 51.34; H, 5.20; N, 4.28%.

S-[2-(2-Methylbenzothiazolium-3-yl)ethyl]thiosulfate (Va). A mixture of 5.6 g of IVa and 4.1 g of sodium thiosulfate in 20 ml of water was heated at 80—90 °C for 10 min. The crystals formed on standing were collected and recrystallized from water to give 2.9 g of colorless crystals, mp 191—193 °C (decomp.). ν(KBr) 1240, 1228, 1221, 1208, 1193, and 1023.

Found: C, 41.28; H, 3.37; N, 4.61%. Calcd for $C_{10}H_{11}NO_3S_3$: C, 41.50; H, 3.80; N, 4.84%.

S-[2-(2,6-Dimethylbenzothiazolium-3-yl)ethyl]thiosulfate (Vb). A mixture of 7.0 g of IVb and 5.0 g of sodium thiosulfate in 10 ml of water was treated as for Va. Yield, 3.9 g of colorless crystals, mp 203—204°C (decomp.), ν(KBr) 1246, 1230, 1209, 1021, and 1011.

Found: C, 43.12; H, 4.22; N, 4.37%. Calcd for $C_{11}H_{13}NO_3S_3$: C, 43.54; H, 4.29; N, 4.62%.

S-[2-(6-Methoxy-2-methylbenzothiazolium-3-yl)ethyl]thiosulfate (Vc). A mixture of 7.3 g of IVc and 5.0 g of sodium thiosulfate in 10 ml of water was treated as for Va. Yield, 4.6 g of colorless crystals, mp 206—207 °C (decomp.). ν(KBr) 1245, 1220, 1204, and 1016.

Found (dried at 130°C, 3 hr): C, 40.84; H, 4.08; N, 4.44%. Calcd for $C_{11}H_{13}NO_4S_3$: C, 41.35; H, 4.07; N, 4.39%.

S-[2-(2,5-Dimethylbenzothiazolium-3-yl)ethyl]thiosulfate (Vd). A mixture of 7.0 g of IVd and 5.0 g of sodium thiosulfate in 10 ml of water was treated as for Va. Yield, 4.0 g of colorless crystals, mp 192—194 °C (decomp.). ν(KBr) 1237, 1220 (shoulder), 1213, and 1020.

Found (dried at 120°C, 3 hr): C, 42.63; H, 4.04; N, 4.41%. Calcd for $C_{11}H_{13}NO_3S_3$: C, 43.54; H, 4.29; N, 4.62%.

1,1'-Di-(2-potassiumsulfothioethyl)-4,4'-tricarbocyanine Acetate (VI). A mixture of 1.3 g of finely-powdered IIIa, 0.80 g of aniline and 0.35 g of ethyl orthoformate was heated at 88 °C under stirring for 20 min. 3.0 g of acetic anhydride and 1.5 g of potassium acetate were added to the mixture, which was then heated at 110—120 °C for 10 min. The reaction mixture was triturated three times with ether, methanol, and water successively, and then finally with 50 ml of hot water. The residue was then extracted three times by refluxing with a 500 ml-portion of methanol each time. The combined methanolic solution was concentrated to 300 ml, passed through a column (cellulose powder) maintained at 50—55 °C, and then eluted with 2 l of hot methanol. A blue-colored fraction of the eluate was concentrated to 50 ml and set aside to yield 30 mg of crystals, mp 241—242 °C (decomp.). Soluble with difficulty in water and most organic solvents. λ (MeOH) 728 (ε 2.05×10^5). ν (KBr) 1234, 1200, and 1028—1019.

Found: C, 45.36; H, 4.39; N, 3.75%. Calcd for $C_{27}H_{26}K_2N_2O_8S_4$: C, 45.46; H, 3.68; N, 3.93%.

1,1'-Di-(2-potassiumsulfothioethyl)-2,2'-tricarbocyanine Acetate (VII). A mixture of 0.50 g of finely-powdered IIIb, 0.40 g of aniline and 0.25 g of ethyl orthoformate was heated at 120 °C for 9 min under stirring. To this were added 0.80 g of acetic anhydride and 0.80 g of potassium acetate, and the mixture was heated at 140 °C for 9 min. The reaction mixture was successively triturated and decanted with ether, ethanol, and water. The residue was refluxed twice with a 500 ml-portion of methanol, transferred to a Soxhlet apparatus and further extracted with methanol to give 140 mg of crystals, mp 236—237 °C (decomp.). Soluble with difficulty in water and most organic solvents. λ (MeOH) 625 (ε 1.51×10^5). ν (KBr) 1236, 1214, and 1027.

Found: C, 45.08; H, 3.42; N, 3.96%. Calcd for $C_{27}H_{26}K_2N_2O_8S_4$: C, 45.46; H, 3.68; N, 3.93%.

6,6'-Dimethyl-3,3'-di-(2-potassiumsulfothioethyl)dithiacarbocyanine Acetate (VIII). A mixture of 0.60 g of Vb, 0.20 g of aniline and 0.30 g of ethyl orthoformate was heated at 100°C for 5—10 min. To this were added 0.20 g of acetic anhydride and 0.27 g of potassium acetate, and heating was continued for 5—10 min at 160 °C. The reaction mixture was successively triturated with hot ethanol and hot water, and the residue was extracted three times with a 100 ml-portion of hot methanol each time. The combined methanolic solution was passed through a column (cellulose powder) maintained hot, and eluted with hot methanol. A red-colored fraction of the eluate was again passed through

3) Indicated in cm^{-1}.

4) IR peaks appearing only in the regions 1200—1230 (strong) and 1020 (strong) and considered to be characteristic of the thiosulfate group of Bunte salt are given.

the column. The red fraction of the eluate gave 45 mg of crystals on concentration, mp 223—225 °C (decomp.). Soluble with difficulty in water and most organic solvents. λ (MeOH–H_2O (19 : 1)) 570 (ε 2.6×10^4). ν (KBr) 1240—1203, and 1027.

Found: C, 39.78; H, 3.68; N, 3.89%. Calcd for $C_{25}H_{26}K_2N_2O_8S_6$: C, 39.86; H, 3.46; N, 3.72%.

S-[*2-(4-Phenylaminoethenylquinolinium-1-yl)ethyl*]*thiosulfate (IX).* A mixture of 1.15 g of IIIa, 0.60 g of aniline and 0.70 g of ethyl orthoformate was heated at 123 °C for 10 min under stirring. The reaction mixture was triturated successively with ether, ethanol, and hot water. The residue was recrystallized from DMF–DMSO (1 : 1) to give 1.25 g of crystals, mp 252—253 °C (decomp.). λ (MeOH) 492. ν (KBr) 1227, 1220, and 1014.

Found (dried at 120 °C, 3 hr): C, 58.40; H, 5.03; N, 7.27%. Calcd for $C_{19}H_{18}N_2O_3S_2$: C, 59.05; H, 4.67; N, 7.25%.

S-[*2-(2-Phenylaminoethenylquinolinium-1-yl)ethyl*]*thiosulfate (X).* A mixture of 0.28 g of IIIb, 0.30 g of aniline and 0.40 g of ethyl orthoformate was heated at 120 °C for 15 min under stirring. The reaction mixture was triturated successively with ether, ethanol, and hot water. The residue was dissolved in methanol, and the solution was passed through a column (cellulose powder). Concentration of a yellow-colored fraction of the eluate yielded crystals, which were recrystallized from methanol. Yield, 80 mg, mp 240—241 °C (decomp.). λ (MeOH) 451. ν (KBr) 1245, 1235, 1227, 1024 (shoulder), and 1019.

Found: C, 57.10; H, 5.12; N, 6.49%. Calcd for $C_{19}H_{18}N_2O_3S_2\cdot CH_3OH$: C, 57.39; H, 5.30; N, 6.69%.

S-[*2-(2-Phenylaminoethenylbenzothiazolium-3-yl)ethyl*]*thiosulfate (XI).* A mixture of 3.7 g of Va, 1.0 g of aniline and 0.80 g of ethyl orthoformate was heated at 100 °C for 10 min under stirring. The reaction mixture was triturated with ethanol and decanted. The residue was dissolved in methanol and passed through a column (cellulose powder). Concentration of a yellow-colored fraction of the eluate gave crystals, which were then recrystallized from methanol. Yield, 1.4 g, mp 250—252 °C. λ (MeOH) 420. ν (KBr) 1244, 1232, 1203, and 1022.

3,3'-Di-(2-hydroxyethyl)-5,6,5',6'-tetramethoxydithiacarbocyanine Bromide (XIII). A mixture of 2.0 g of 3-(2-hydroxyethyl)-5,6-dimethoxy-2-methylbenzothiazolium bromide, 0.60 g of anilline, and 0.90 g of ethyl orthoformate was heated at 115 °C for 7 min under stirring. To this were added 1.8 g potassium acetate and 0.70 g of acetic acid, and heating was continued at 160 °C for 7 min. The reaction mixture was triturated successively with ether, ethanol, and water. Recryatallization of the residue from methanol–ether gave crude crystals, which were dissolved in methanol. The methanolic solution was passed through a column (cellulose powder), and eluted with methanol. The crystals from the eluate on concentration were similarly treated twice. Yield, 1.6 g, mp 259—260 °C. λ (MeOH) 605.

Found: C, 50.65; H, 4.99; N, 4.69%. Calcd for $C_{25}H_{29}BrN_2O_6S_2$: C, 50.25; H, 4.86; N, 4.69%.

3,3'-Di-(2-bromoethyl)-5,6,5',6'-tetramethoxydithiacarbocyanine Bromide (XIV). A mixture of 0.50 g of XIII and 3.8 g phosphorus tribromide was kept at room temperature for 5 hr. The reaction mixture was triturated with benzene, and the residue was recrystallized from methanol–ether (1 : 1). The crystals formed were dissolved in methanol, treated chromatographically as for XIII, and finally recrystallized from methanol. Yield, 0.43 g, mp 226—228 °C. λ (MeOH) 605.

Found: C, 41.12; H, 3.69; N, 3.75%. Calcd for $C_{25}H_{27}Br_3N_2O_4S_2$: C, 41.50; H, 3.74; N, 3.87%.

3-(2-Bromoethyl)-3'-sulfothioethyl-5,6,5',6'-tetramethoxydithiacarbocyanine (XII). A mixture of 1.0 g of XIV and 0.90 g of sodium thiosulfate in 300 ml of methanol was heated under reflux for 20 hr. The reaction mixture was carefully concentrated by distilling methanol until XII began to crystallize (otherwise, excess sodium thiosulfate deposited.) The crystals, after recrystallization once from methanol–ether, were dissolved in methanol, passed through a column (cellulose powder), and eluted with DMF. The crystals obtained from the eluate were finally recrystallized from methanol. Yield, 0.70 g, mp 213—215 °C, λ (MeOH) 610 ε 6.24×10^4). ν (KBr) 1270—1223 and 1025.

Found: C, 41.25; H, 4.41; N, 4.07; S, 16.55%. Calcd for $C_{25}H_{27}BrN_2O_7S_4\cdot3H_2O$: C, 41.14; H, 4.53; N, 3.84; S, 17.59%. Found (dried at 145 °C, 7 hr): C, 44.17; H, 4.57; N, 4.06%. Calcd for $C_{25}H_{27}BrN_2O_7S_4$: C, 44.43; H, 4.00; N, 4.15%.

The authors are indebted to the Japanese Research Institute for Photosensitizing Dyes Co., Ltd. for the donation of the starting materials, quinolines and thiazoles.

Formation of Sulfur Ylids by Catalytic Action of Dialkoxy Disulfides[1]

Haruo MATSUYAMA, Hiroshi MINATO, and Michio KOBAYASHI
Department of Chemistry, Tokyo Metropolitan University, Fukazawa, Setagaya, Tokyo

(Received November 30, 1972)

In the presence of a catalytic amount of a dialkoxy disulfide, dimethyl diazomalonate spontaneously reacted with a dialkyl sulfide in the absence of light at room temperature, and the corresponding sulfonium ylid was formed. The kinetics and products of this reaction were investigated, and its mechanism was discussed.

Very little has been published on the chemistry of dialkoxy disulfides, which can be prepared from sulfur monochloride and alcohols. In our laboratories various reactions of these interesting compounds have been studied, and the mechanisms of their reactions with Lewis acids have been described in a recent publication.[2]

In an attempt to study the reaction between diisopropoxy disulfide and bis(methoxycarbonyl)carbene, the disulfide was mixed with dimethyl diazomalonate in dimethyl sulfide at room temperature. Surprisingly, an ylid was formed in the absence of light at room temperature.

The formation of an ylid from dimethyl diazomalonate and dimethyl sulfide was reported by Ando *et al.*[3] They stated that the diazomalonate decomposed and yielded the corresponding carbene only when the diazo compound was irradiated with a UV light or heated near 110 °C in the presence of a copper catalyst.

$$N_2C(CO_2CH_3)_2 + CH_3SCH_3 \xrightarrow[10\text{—}15\,^\circ\text{C},\ 30\ \text{hr}]{i\text{-PrOSSOPr-}i} CH_3\overset{\oplus}{S}(\overset{\ominus}{C}(CO_2CH_3)_2)CH_3 + N_2$$

The formation of sulfur ylids by catalytic action of dialkoxy disulfides was studied, and the results are described in this paper.

Results and Discussion

When dimethyl diazomalonate (IIa) was dissolved in a dialkyl sulfide (I) in the presence of a catalytic amount of diisopropoxy disulfide (IIIa) at room temperature, nitrogen gas was evolved and the corresponding ylid was formed in a good yield. Table 1 summarized the results of the reactions with several sulfides.

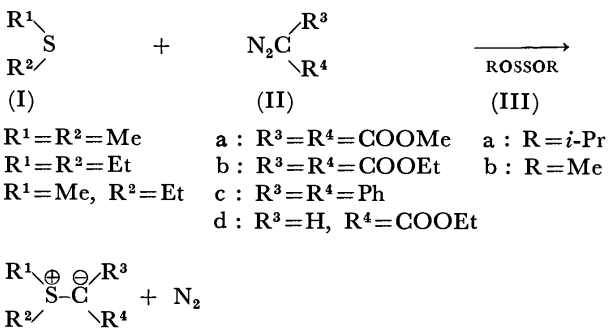

(I) (II) (III)

a : $R^1=R^2=Me$ a : $R^3=R^4=COOMe$ a : R = *i*-Pr
b : $R^1=R^2=Et$ b : $R^3=R^4=COOEt$ b : R = Me
c : $R^1=Me$, $R^2=Et$ c : $R^3=R^4=Ph$
d : $R^3=H$, $R^4=COOEt$

1) Organic Sulfur Compounds. Part XL.
2) M. Kobayashi, H. Minato, and K. Shimada, *Int. J. Sulfur Chem.*, **A**, **1**, 105 (1971).

Table 1. Formation of ylids from dimethyl diazomalonate and sulfides in the presence of diisopropoxy disulfide[a]

R^1–S–R^2	Temp. (°C)	Ylid (%)	N_2 (%)
$R^1=R^2=Me$	17	80	96
	20	75	90
	20[b]	67	100
$R^1=R^2=Et$	17	78	90
	20	67	84
	20[b]	76	92
$R^1=Me$, $R^2=Et$	20	72	75
$R^1=R^2=Me$	(hν)[c]	88	
	($CuSO_4$, 110 °C)[c]	75	

a) A mixture consists of a sulfide 30 mmol, $N_2C(CO_2Me)_2$ 5 mmol, and *i*-PrOSSOPr-*i* 1 mmol.
b) Dark reaction (covered with aluminum foil).
c) Reference 3); in the absence of diisopropoxy disulfide.

In the absence of III, no reaction was observed between I and II. No reaction was observed between II and III either. Reaction took place only when the three components are present. III is simply a catalyst and remains unchanged. The diazo compounds decompose smoothly at room temperature without irradiation of UV light. Visible light cannot be the cause for the reaction, since the decomposition proceeded equally well when the reaction flask was completely covered and shielded from light.

When the rates of evolution of nitrogen from a mixture of I, IIa and IIIa were determined, they were of first order in IIa at least until about 50% decomposition. The half life of IIa at 20 °C was about 4 hr, and the first order rate constant k_1 was 3.84×10^{-5} sec.$^{-1}$

Table 2. Comparison of the sulfides possessing catalytic activity on the reaction between dimethyl diazomalonate and dimethyl sulfide[a]

Catalytic sulfides[b]	Temp. (°C)	10^5k_1 (sec^{-1})	$\tau_{1/2}$ (hr)	Ylid (%)	N_2 (%)
MeOSSOMe	20	4.5	4.7	71	81
EtOSSOEt	20	8.1	2.6	68	96
i-PrOSSOPr-*i*	20	5.1	4.0	75	90
EtOSOEt	20	6.4	5.0	66	93
NC–SS–CN	25		*ca.* 3 days	50	

a) A mixture consists of Me_2S 30 mmol, $N_2C(CO_2Me)_2$ 5 mmol, and a catalytic sulfide, 1 mmol.
b) Found to be inactive: MeSSMe, $Et_2NSSNEt_2$, BzSSBz, ClSSCl.

In an attempt to determine what is responsible for the catalytic activity of III, other compounds possessing similar catalytic activity were sought for. As Table 2 shows, dialkyl sulfoxylates, ROSOR, and thiocyanogen, NC–SS–CN, were found to be effective, whereas dimethyl disulfide, diethylamino disulfide, benzoyl disulfide and sulfur monochloride were inactive.

Since the electronegativity of sulfur is 2.5 and that of oxygen is 3.5,[4] the electron density on the sulfur atoms of III must be smaller due to the presence of the electron-withdrawing oxygen atoms. The electron density on the sulfur atoms of dialkyl sulfoxylates and thiocyanogen must be small due to the presence of the electron-withdrawing alkoxy and cyano groups.

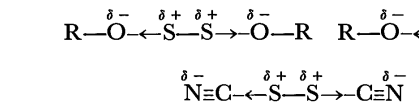

Therefore, the divalent sulfur atom containing a small positive charge due to electron-withdrawing substituents is probably responsible for the catalytic formation of ylids from I and II.

Various diazo compounds were examined as to their reactivity, and the results are summarized in Table 3. In mixtures with Ib and IIIa, dimethyl and diethyl diazomalonates decomposed smoothly at room temperature, yielding an ylid and nitrogen. Ethyl diazoacetate, diphenyldiazomethane and ethyl azidoformate decomposed very slowly (about 10% decomposition in 4 days). Three diazo compounds containing an acetyl group did not decompose at all.

Table 3. Comparison of the reactivities of diazo compounds with diethyl sulfide in the presence of diisopropoxy disulfide at 20 °C[a]

Diazo compounds[b]	10^5k_1 (sec^{-1})	$\tau_{1/2}$ (hr)	Ylid (%)	N_2 (%)
$N_2C(COOMe)_2$	3.8	4.3	67	84
$N_2C(COOEt)_2$	0.7	27.5	45	57

a) A mixture consists of Et_2S 30 mmol, R_2CN_2 5 mmol, and *i*-PrOSSOPr-*i* 1 mmol.
b) No Reaction: $N_2C(COMe)_2$, $N_2C(COMe)(COOMe)$, $N_2C(COMe)(COOEt)$. Very slow decomposition (ca 10%/4 day): $N_2CHCOOEt$, N_2CPh_2, N_3CO_2Et.

Table 4. Comparison of the reactivities of sulfides with dimethyl diazomalonate in the presence of diisopropoxy disulfide[a]

Sulfides[b]	Temp. (°C)	10^5k_1 (sec^{-1})	Rel. React.	$\tau_{1/2}$ (hr)
MeSMe	17	4.0	5	5.2
EtSEt	17	3.2	4	5.9
	17	0.80	1	24
MeSEt	20	0.66	0.8	29

a) A mixture consists of a sulfide 30 mmol, $N_2C(COOMe)_2$ 5 mmol, and *i*-PrOSSOPr-*i*, 1 mmol.
b) No reaction: PhSMe, PhSEt, Dimethyl sulfoxide. Slow reaction: *n*-BuSMe (ylid 66% in 10 days at 20 °C).

Then, various dialkyl sulfides were examined as to their reactivity, and the results are summarized in Table 4. In mixtures with IIa and IIIa, methyl phenyl sulfide, ethyl phenyl sulfide and dimethyl sulfoxide did not react at all, and *n*-butyl methyl sulfide reacted very slowly (the yield of ylid was 66% after 10 days at 20°C). These findings suggest that an electron-rich sulfide is reactive, and the reaction is slow with a bulky alkyl group.

The pseudo first order rate constants determined from the rates of nitrogen evolution show that dimethyl sulfide and diethyl sulfide react with IIa quite rapidly, whereas ethyl methyl sulfide and tetrahydrothiophene react slowly. Thus, the electronic and steric effects in this reaction are rather complex, and not straightfoward.

When Ia, IIa and IIIb were mixed in an NMR tube, and the changes of the concentrations of the reactants were observed, it was found that the decrease of IIa corresponded to the formation of the ylid, whereas IIIb remained unchanged. The results are shown in Fig. 1. It is clear that III is not a reactant, but a catalyst. However, the increase in the concentration of III resulted in the increase in the rate of nitrogen evolution. An induction period of about 10 min was observed, during which nitrogen was not evolved.

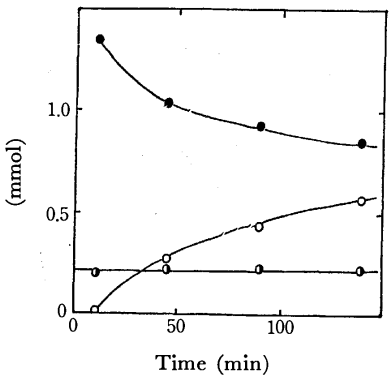

Fig. 1. Changes of amounts of the reactants and products in an NMR Tube at 35 °C.
(The initial mixture consists of Ia 2.42, IIa 1.35, IIIb 0.20, and CH_3NO_2 1.85 mmol)
●: $N_2C(CO_2Me)_2$, ○: $Me_2\overset{\oplus}{S}-\overset{\ominus}{C}(CO_2Me)_2$, ◑: MeOSSOMe

The experiments described so far used excess I as the solvent. When the mixture was diluted with such polar solvents as nitromethane and acetonitrile, the decomposition of IIa became slower. When *n*-hexane was used as the solvent, IIa did not decompose.

The rates of the decomposition of IIa in a mixture with Ib and IIIa were determined at various temperatures, and it was found that the rates were in the order of $k_{20°}>k_{17°}>k_{30°}$. It is clear that above a certain temperature this reaction becomes slower.

As for the mechanism of this reaction, the following two pathways seem possible. Scheme 1 involves the formation of a complex between II and III, and the complex is supposed to react with I.

3) W. Ando, T. Yagihara, S. Tozune, S. Nakaido, and T. Migita, *Tetrahedron Lett.*, **1969**, 1979.
4) L. Pauling, "Nature of the Chemical Bond," Cornell Univ. Press, Ithaca (1960), p. 88.

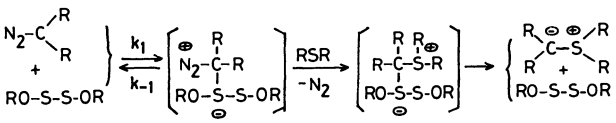

Scheme 1.

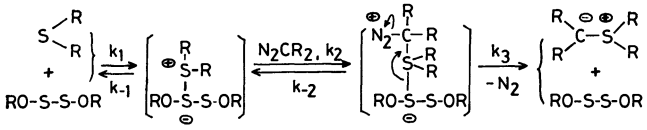

Scheme 2.

Scheme 2 involves the formation of a complex between I and III, and the complex is supposed to react with II.

Attempts were made in order to detect the presence of complexes in the mixtures of I, II, and III. The UV spectrum of a mixture of IIa and III did not show any sign of interaction between them. The UV spectra of the mixtures of Ia and III, or Ib and III showed no sign either.

However, when tetrahydrothiophene was mixed with IIIb, the mixture turned orange yellow. If IIa was added to this colored mixture, the corresponding ylid was formed and IIIb was recovered unchanged. If IIa was not added and the mixture was allowed to stand at room temperature for more than ten minutes, sulfur precipitated, and the products of decomposition of IIIb were found.

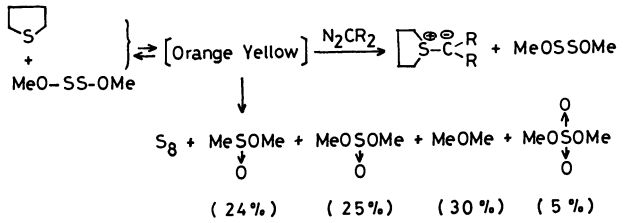

The five products shown above are the compounds found as the products of the decomposition of IIIb when the latter was mixed with triethyloxonium tetrafluoroborate.[2] As the species present in the orange yellow mixture, the following structure seems probable.

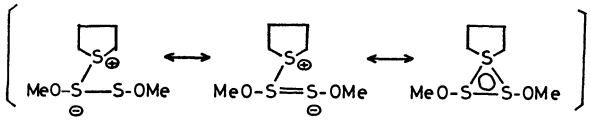

In our previous paper dealing with the reaction between IIIb and $Et_3O^+BF_4^-$, evidence was presented indicating the presence of the following intermediate.

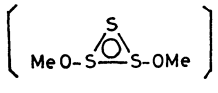

Scheme 2 is favored on the basis of the findings that IIIb and tetrahydrothiophene form the orange yellow complex which readily react with IIa, forming the ylid and nitrogen. Thus, the data described in this paper suggest that the reactions among I, II and III are represented by Scheme 2.

Experimental

Materials. Dimethyl sulfide, tetrahydrothiophene, dimethyl disulfide and dimethyl sulfoxide were of reagent grade and used without further purification. Other sulfides were prepared from the corresponding sodium mercaptides and alkyl halides.[5] Dimethoxy disulfide, diethoxy disulfide and diisopropoxy disulfide were synthesized by the method of Thompson.[6] Diethyl sulfoxylate was prepared from the reaction between diethoxy disulfide and sodium ethoxide by the method of Meusen.[7] Thiocyanogen[8] and benzoyl disulfide[9] were prepared by the methods described in the literature. Sulfur monochloride was freshly distilled, and used immediately. Diethylamino disulfide was synthesized by adding sulfur monochloride (0.1 mol) to a dichloromethane solution of diethylamine (0.4 mol) at 0 °C; bp 115 °C/6 mmHg. Dimethyl diazomalonate, diethyl diazomalonate, acetyldiazoacetone, methyl acetodiazoacetate and ethyl acetodiazoacetate were prepared by transdiazotization of corresponding carbonyl compounds with tosyl azide.[10] Ethyl diazoacetate,[11] diphenyldiazomethane (mp 31—32 °C; lit,[12] 29—33 °C) and ethyl azidoformate[13] were prepared according to the methods described in the literature.

Kinetics and Products. A 50 ml flask containing a mixture of 30 mmol of I, 5 mmol of II and 1 mmol of III was placed in a constant-temperature bath, and the amount of nitrogen evolved was determined by use of a gas buret. After the evolution of nitrogen ceased, a small amount of *n*-hexane was added to the mixture, and the ylid crystals formed were filtered and weighed. The melting points, IR and NMR spectra of the ylids obtained were identical with those reported in the literature.[14]

Reaction in an NMR Tube. A mixture of Ia (2.42 mmol), IIa (1.35 mmol) and IIIb (0.20 mmol) containing nitromethane (1.85 mmol) as the internal standard was placed in an NMR tube at 35 °C, and decreases of $(C\underline{H}_3)_2S$ (δ, 2.01 ppm) and $N_2C(CO_2C\underline{H}_3)_2$ (3.75 ppm) absorptions and increases of $(C\underline{H}_3)_2\overset{\oplus}{S}-\overset{\ominus}{C}(CO_2CH_3)_2$ (2.82 ppm) absorption were determined on the basis of the absorption of CH_3NO_2 (4.33 ppm).

Reaction between Dimethoxy Disulfide and Tetrahydrothiophene in an NMR Tube. When dimethoxy disulfide (3.2 mmol)

5) A. I. Vogel, *J. Chem. Soc.*, **1948**, 1822.
6) Q. E. Thompson, M. M. Crutchfield, M. W. Dietrich, and E. Pierron, *J. Org. Chem.*, **30**, 2692 (1965).
7) A. Meusen, *Ber.*, **69**, 937 (1936).
8) L. F. Fieser and M. Fieser, "Reagents for Organic Syntheses," Vol. 1, John Wiley, New York (1967), p. 1152.
9) "Organic Syntheses," Coll. Vol. 3, p. 116.
10) M. Rosenberg, P. Yates, J. Hendrickson, and W. Wolf, *Tetrahedron Lett.*, **1964**, 2285.
11) "Organic Syntheses," Coll. Vol. 3, p. 392.
12) "Organic Syntheses," Coll. Vol. 3, p. 351: J. B. Miller, *J. Org. Chem.*, **24**, 560 (1959).
13) R. S. Berry, D. Cornell, and W. Lwowski, *J. Amer. Chem. Soc.*, **85**, 1199 (1963).
14) W. Ando, T. Yagihara, S. Tozune, I. Imai, J. Suzuki, T. Toyama, S. Nakaido, and T. Migita, *J. Org. Chem.*, **37**, 1721 (1972).

and tetrahydrothiophene (3.0 mmol) were mixed at room temperature, the mixture turned orange yellow in a few minutes, and sulfur precipitated in about ten minutes. After 40 minutes, nitromethane was added as the internal standard, and the products were analyzed by means of their NMR absorptions. Reactants; $(CH_3OS)_2$, δ, 3.65 ppm, $(CH_2CH_2)_2S$, multiplets at 1.93 and 2.82 ppm: Products; $CH_3SO_2\underline{CH}_3$ (3.70 ppm, 0.48 mmol), $(CH_3O)_2SO$ (3.55 ppm, 0.50 mmol), $(CH_3O)_2SO_2$ (3.90 ppm, 0.10 mmol) and $(CH_3)_2O$ (3.20 ppm, 0.60 mmol).

BULLETIN OF THE CHEMICAL SOCIETY OF JAPAN, VOL. 46, 1515—1519 (1973)

Branched-Chain Sugars. II. On the Configuration of Branched-Chain Sugars from Methyl 2-*O*-Benzoyl-4,6-*O*-benzylidene-α-D-ribo-hexopyranosid-3-ulose

Juji YOSHIMURA, Ken-ichi SATO, Kazuhiko KOBAYASHI, and Chung-gi SHIN*

Laboratory of Chemistry for Natural Products, Faculty of Science, Tokyo Institute of Technology, Ookayama, Meguro-ku, Tokyo

**Laboratory of Organic Chemistry, Kanagawa University, Kanagawa-ku, Yokohama*

(Received November 30, 1972)

Stereoselectivities in diazomethane and nitromethane reaction of methyl 2-*O*-benzoyl-4,6-*O*-benzylidene-α-D-ribo-hexopyranosid-3-ulose were examined. Reduction of the epoxidation product (**2**) gave an epimeric 3-*C*-methyl derivative in contrast with that obtained by the Grignard reaction. Comparison of NMR spectra of the corresponding di-*O*-acetate of the both epimers proved that **2** has the gluco-configuration. Ring-opening of the epoxide with alkali, methanolic ammonia, and acid gave the corresponding 3-*C*-hydroxymethyl, 3-*C*-aminomethyl (**17**), and de-*O*-benzylidenated product, respectively. Hydrogenation of the 3-*C*-nitromethyl derivative (**21**) obtained by nitromethane condensation, in the presence of Raney nickel, accompanied with benzoyl-migration to give 3-*C*-benzamidomethyl derivative (**22**). De-benzoylation of **22** with methanolic potassium hydroxide gave 3-*C*-aminomethyl derivative (**26**) and an orthoester-type compound. Comparison of **26** with **17** and their derivatives indicated that **21** has the allo-configuration. The both configurations were also supported by the optical rotation of 3-*C*-benzamidomethyl derivatives in cuprammonium solution.

In the previous paper,[1] we reported that the nitromethane and the Reformatsky reaction of 1,2 : 5,6-di-*O*-isopropylidene-α-D-ribo-hexofuranos-3-ulose gave D-allo-type branched-chain sugars, while the diazomethane reaction afforded D-gluco-type product, indicating that the reagent attacked the carbonyl group from the more hindered site. The stereoselectivity of the latter stimulated us to examine with a pyranosid-3-ulose, and nitromethane and diazomethane reaction of methyl 2-*O*-benzoyl-4,6-*O*-benzylidene-α-D-ribo-hexopyranosid-3-ulose (**1**)[2] were examined in this report.

Results

Diazomethane Condensation. Diazomethane condensation of **1** in benzene–ethanol gave a sirupy spiro-epoxide (**2**) in 77% yield. In order to determine the configuration, **2** was hydrogenated with lithium aluminium hydride to the 3-*C*-methyl derivative (**3**), which was successively converted into the corresponding 2-*O*-acetate (**4**) and 2,3-di-*O*-acetate (**5**) by base- and acid-catalyzed acetylation, respectively. On the other hand, a 3-*C*-methyl derivative (**6**) obtained by the Grignard reaction, of which the configuration was assigned to be of allo-type,[2,3] was also converted into 2-*O*-acetate (**7**) and 2,3-di-*O*-acetate (**8**). Comparison of **3** with **6** and their derivatives showed that they are 3-epimers to each other, and the chemical shifts of *tert*-acetoxy protons in **5** (δ 1.95) and **8** (δ 2.05) indicated an equatorial and axial one, respectively.[4] Thus, the configuration of **2** was confirmed to be of D-gluco-type.

The epoxide-ring of **2** resisted, to some extent, to alkaline opening than the corresponding furanose derivative,[1] and alkali treatment of **2** at room temperature gave de-*O*-benzoylated epoxide (**9**), which was further converted to the 2-*O*-acetate (**10**). Treatment of **9** with refluxing aqueous potassium hydroxide for 10 hr gave a water-soluble 3-*C*-hydroxymethyl derivative (**11**), which was then acetylated to 2,3-di-*O*-acetate (**12**). Acetonation of **11** gave 3,3′-*O*-isopropylidene derivative (**13**), of which the position of the isopropylidene group was determined from the fact that **13** gave the mono-*O*-acetate (**14**) by base-catalyzed acetylation. The epoxide-ring opening was also performed by refluxing **2** with 80% acetic acid, accompanying with hydrolysis of the benzylidene group, to give methyl 2-*O*-benzoyl-3-*C*-hydroxymethyl-α-D-glucopyranoside (**15**), which was confirmed by conversion into the corresponding tetra-*O*-acetate (**16**). Moreover, treatment of **9** with ethanolic ammonia in a sealed tube at 90 °C for 3 hr gave 3-*C*-aminomethyl derivative (**17**), which was then converted into the corresponding *N*-benzoyl derivative (**18**), its di-*O*-acetate (**19**), and *N*,*O*-triacetate (**20**), respectively.

1) J. Yoshimura, K. Kobayashi, K. Sato, and M. Funabashi, This Bulletin, **45**, 1806 (1972).

2) F. A. Carey and K. O. Hodgson, *Carbohyd. Res.*, **12**, 463 (1970).

3) G. B. Howarth, W. A. Szarek, and J. K. N. Jones, *Canad. J. Chem.*, **46**, 3691 (1968).

4) F. W. Lichtenthaler and P. Emig, *Tetrahedron Lett.*, **1967**, 577.

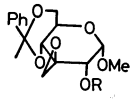

(2) R=Bz (3) $R_1=R_2=H$ (6) $R_1=R_2=H$
(9) R=H (4) R_1=Ac, $R_2=H$ (7) R_1=Ac, $R_2=H$
(10) R=Ac (5) $R_1=R_2$=Ac (8) $R_1=R_2$=Ac

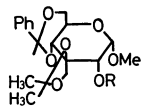

(13) R=H
(14) R=Ac

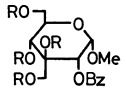

(15) R=H
(16) R=Ac

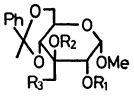

(11) $R_1=R_2=H$, $R_3=OH$
(12) R_1=Ac, $R_2=H$, $R_3=OAc$
(17) $R_1=R_2=H$, $R_3=NH_2$
(18) $R_1=R_2=H$, R_3=NHBz
(19) $R_1=R_2$=Ac, R_3=NHBz
(20) $R_1=R_2$=Ac, R_3=NHAc

Nitromethane Condensation. Reaction of **1** with nitromethane in tetrahydrofuran in the presence of sodium methoxide gave a 3-*C*-nitromethyl derivative (**21**) in 80% yield. Hydrogenation of **21** in the presence of Raney nickel accompanied with the migration of 2-*O*-benzoyl group to give 3-*C*-benzamidomethyl derivative (**22**). Base- and acid-catalyzed acetylation of **22** gave the corresponding 2-*O*-acetate (**23**) and 2,3-di-*O*-acetate (**24**), respectively. Debenzoylation of **22** with methanolic potassium hydroxide gave 3-*C*-aminomethyl derivative (**26**), an orthoester-type product (**25**), and **22**. Comparison of **22** with **18**, **24** with **19**, and **26** with **17** indicated them to be 3-epimers to each other. Furthermore, the positive rotational change ($[M]_{436}^{\text{Cupra A}}$ +1670°) of **22** in cuprammonium solution[5] and negative change ($[M]_{436}^{\text{Cupra A}}$ −635°) of **18** indicated D-allo and D-gluco-configuration, respectively. Thus, the configuration of **21** was proved to be of D-allo-type.

Compound **25**, having still two phenyl groups in the NMR and analytical data, showed no absorptions of amino and oxazolidine groups in IR spectrum, and changes to **22** by standing in a moist state. Attempted acetylation of **25** in dry pyridine gave quantitatively 3-*C*-acetamidomethyl-2-*O*-acetyl derivative (**27**) which was also obtained by acetylation of **26**. From these facts, **25** was deduced to be methyl 3-*C*-aminomethyl-4,6-*O*-benzylidene-2,3,*N*-benzylidine-α-D-allopyranoside. Formation of **25** will be explained by the nucleophillic attack of hydroxyl anions at C_2- and C_3-positions on the sterically favorable carbonyl function of benzamido group to give the thermodynamically controlled product. Conversion of **25** into **27** might occur through hydrolysis of acyloxonium ion formed by cleavage of the orthoamide bond by *N*-acetylation.[6]

5) R. E. Reeves, *Adv. Carbohyd. Chem.*, **6**, 131 (1951).

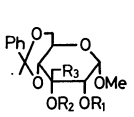

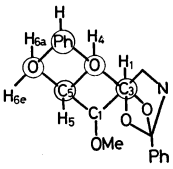

(21) R_1=Bz, $R_2=H$, $R_3=NO_2$ (25)
(22) $R_1=R_2=H$, R_3=NHBz
(23) R_1=Ac, $R_2=H$, R_3=NHBz
(24) $R_1=R_2$=Ac, R_3=NHBz
(26) $R_1=R_2=H$, $R_3=NH_2$
(27) R_1=Ac, $R_2=H$, R_3=NHAc

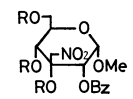

(28) R=H
(29) R=Ac

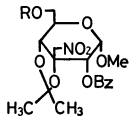

(30) R=H
(31) R=Ac

On the other hand, partial hydrogenation of **21** in the presence of palladium-charcoal or hydrolysis with 0.1 N-sulfuric acid gave methyl 2-*O*-benzoyl-3-*C*-nitromethyl-α-D-allo-pyranoside (**28**), which was then converted into the tri-*O*-acetate (**29**) by acid-catalyzed acetylation. Acetonation of **28** gave an isopropylidene derivative (**30**), which was converted to mono-*O*-acetate (**31**). The structure of **30** was deduced to be 3,4-*O*-isopropylidene derivative from the chemical shift of C–CH_3 protons (δ 1.47 and 1.49).[7]

Discussion

On the stereoselectivities in nucleophilic addition to methyl 4,6-*O*-benzylidene-α-D-ribo-hexopyranosid-3-uloses, following facts are known. Reduction[8] of 2-*O*-tosyl derivative; reduction,[8] the Grignard[9] and dimethyloxosulfonium methylide[10] reaction of the corresponding 2-acetamido-2-deoxy derivative; and the Grignard[11] and the oxosulfonium ylide[12] reaction of 2-deoxy derivative gave D-allo-type products, while the reaction of acetonitrile with the 2-deoxy derivative in liquid ammonia gave D-gluco-type product.[13] These results indicate that nucleophiles in the former reactions attacked the carbonyl group from the less hindered site, and in the latter from the hindered site (Fig. 1). Thus, nitromethane condensation mentioned here is classified into the former type, though it generally gives various mixture of diastereomers,

6) H. Bredereck, G. Simchen, and S. Rebsdat, *Chem. Ber.*, **101**, 1872 (1968).
7) N. Bagget, K. W. Buch, A. B. Foster, R. Jefferis, B. H. Rees, and J. M. Webber, *J. Chem. Soc.*, **1965**, 3382.
8) B. R. Baker and D. H. Buss, *J. Org. Chem.*, **30**, 2304, 2308 (1965).
9) B. R. Baker and D. H. Buss, *ibid.*, **31**, 217 (1966).
10) J. H. Jordaan and S. Smedley, *Carbohyd. Res.*, **16**, 177 (1971).
11) B. Flaharty, W. G. Overend, and N. R. Williams, *J. Chem. Soc. C*, **1966**, 398.
12) R. D. King, W. G. Overend, J. Wells, and N. R. Williams, *Chem. Commum.*, **1967**, 726.
13) A. Rosenthal and G. Schöllnhammer, *Carbohyd. Res.*, **15**, 421 (1970).

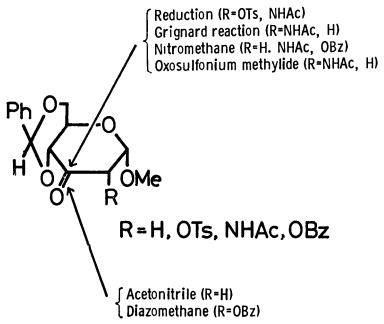

Fig. 1.

depending on the condition used.[14]

On the other hand, stereoselectivity of diazomethane addition is usually complicated by the formation of ring-expanded product depending on the solvent used. For an example, Flaherty *et al.*[15] obtained 30% of the ring-expanded product and a small amount of normal epoxide of D-gluco-type by the reaction with methyl 4,6-*O*-benzylidene-2-deoxy-α-D-erythro-hexopyranosid-3-ulose in methanol. However, 1,2-*O*-isopropylidene-α-D-furanos-3-uloses gave the normal spiro-epoxides which are resulted by attacking the reagent from the inside of the V-shaped *cis*-fused five-membered ring.[1,16] Reaction of methyl α-D-pyranosid-2-uloses in ether–alcohol, having two oxygens at the both vicinal carbon, gave a mixture of diastereomers,[17] however, one which has the epoxide carbon in the site of C_1-methoxy group was predominant. Inch *et al.*[18] examined the steric influence of *C*-alkyl group vicinal to the carbonyl group by the reaction with 4,6-*O*-benzylidene-3-deoxy-3-*C*-ethyl-α-D-arabino- and -ribo-hexo-pyranosid-2-ulose, and showed that *C*-ethyl group in reverse side to C_1-methoxy group enhanced the formation of the predominant product mentioned above, and that in the same side hindered it to afford another epimer predominantly. They discussed on the conformation of zwitterionic intermediates for explanation of the configuration of ring-expanded products.

However, accumulated data mentioned here indicate that the stereoselectivity might be controlled at first by attractive interactions between vicinal or neighboring hydroxyl oxygens and diazomethylene cation of zwitterionic intermediates, and therefore, the polarity of solvents play an important role. The complemental stereoselectivities of the Grignard and diazomethane reaction mentioned by us and by Horwitz *et al.*[16] support this deduction. Thus, the steric position of C_1-methoxy oxygen for the carbonyl group might control the configuration of the product in this experiment.

14) G. J. Lourens, *Tetrahedron Lett.*, **1969**, 3733; A. Rosenthal and K. S. Ong, *ibid.*, **1969** 3981; S. W. Gunner, R. D. King, W. G. Overend, and N. R. Williams, *J. Chem. Soc., C*, **1970**, 1954; A. Rosenthal, K. S. Ong, and D. Baker, *Carbohyd. Res.*, **13**, 113 (1970).

15) B. Flaherty, W. G. Overend, and N. R. Williams, *Chem. Comm.*, **1966** 434.

16) S. Naher, W. G. Overend, and N. R. Williams, *Chem. Ind.* (London), **1967**, 2114; J. P. Horwitz, N. Mody, and R. Gasser, *J. Org. Chem.*, **35**, 2335 (1970).

17) W. G. Overend and N. R. Williams, *J. Chem. Soc., C*, **1968**, 3446; R. J. Ferrier, W. G. Overend, G. A. Rafferty, H. M. Wall, and N. R. Williams, *ibid.*, **1968**, 1091.

18) T. D. Inch, G. J. Lewis, R. P. Pell, and N. R. Williams, *Chem. Commun.*, **1970**, 1549.

Experimental

All melting points are uncorrected. The solutions were evaporated under diminished pressure at a bath temperature not exceeding 45 °C. Specific rotations were measured in a 0.5-dm tube, with a Carl Zeiss LEP-Al Polarimeter. The IR spectra were recorded with a Hitachi Model EPI-G2 grating IR spectrophotometer. The NMR spectra were taken in deuteriochloroform, with a JNM-4H-100 MHz Spectrometer using tetramethylsilane as an internal standard. Chemical shifts and coupling constants were recorded in δ and Hz units, and frequencies in cm^{-1}.

*Methyl 3,3′-Anhydro-2-O-benzoyl-4,6-O-benzylidene-3-C-(hydroxymethyl)-α-D-glucopyranoside (**2**).* To a suspended solution of **1** (4 g, 10.4 mmol) in benzene (150 ml)–ethanol (50 ml) was added dropwise a solution of diazomethane (20 mmol) in ether (50 ml) at 0 °C. With proceeding the reaction, the mixture turned to homogeneous. After standing at 0 °C for 3 hr and at room temperature for 28 hr, the solution was evaporated, and the resulted sirup was fractionated through Kiesel-gel (70—325 mesh, Merck Co.), by eluating with benzene–methanol (15 : 1). From the first fraction, the spiro-epoxide was obtain as a sirup in 77.3% (3.2 g) yield. $[\alpha]_D^{23}$ +113° (*c* 1.06, $CHCl_3$); IR: 1720 (ester), 1590 and 710 (Ph); NMR: *ca.* 7.30 and 7.95 (2× Ph, m), 5.51 (PhCH=), 5.41 (H_1; d, $J_{1,2}$=3.7), 5.10 (H_2; d), 4.35 (H_5; sex, $J_{4,5}$=13.5), 3.97 (H_{6e}; t, $J_{6a,6e}$ =10, $J_{5,6e}$= 10), *ca.* 3.91 (H_4; d), *ca.* 3.90 (H_{6a}; t, $J_{5,6a}$=10), 3.40 (OMe), 3.20 (epoxy-CH_2; s).

Found: C, 65.77; H, 6.10%. Calcd for $C_{22}H_{22}O_7$; C, 66.32; H, 5.57%.

*Methyl 4,6-O-Benzylidene-3-C-methyl-α-D-glucopyranoside (**3**).* To a solution of **9** (800 mg, 2.64 mmol) in ether (30 ml) was added lithium aluminium hydride (0.2 g, 53 mmol), and the mixture was refluxed for 7 hr. The excess $LiAlH_4$ was carefully decomposed with water, and the water layer was extracted with ether. The combined ether extract was washed with water, dried with anhydrous magnesium sulfate, and evaporated to give a colorless sirup. The sirup was crystallized and recrystallized from chloroform–*n*-hexane. Yield, 86% (690 mg). A similar treatment of **2** gave the same compound in 79% yield. Mp 80—82 °C; $[\alpha]_D^{23}$ +91.0° (*c* 1.25, $CHCl_3$); IR: 3523 and 3250 (OH); NMR; 1.40 (C–CH_3; s).

Found: C, 60.84; H, 7.16%. Calcd for $C_{15}H_{20}O_6$: C, 60.80; H, 6.80%.

2-*O*-Acetyl and 2,3-di-*O*-acetyl derivatives of **3** was prepared as follows.

*a) 2-O-Acetate (**4**):* Acetylation of **3** with acetic anhydride in pyridine gave sirupy acetate in a quantitative yield. $[\alpha]_D^{23}$ +72.5° (*c* 1.44, $CHCl_3$); IR: 3450 (OH), 1740 (ester); NMR: 2.50 (OH; s), 2.10 (OAc), 1.45 (C–CH_3).

Found: C, 59.94; H, 6.60%. Calcd for $C_{17}H_{22}O_7$: C, 60.34; H, 6.55%.

*b) 2,3-Di-O-acetate (**5**):* A solution of **3** (100 mg) and *p*-toluenesulfonic acid (20 mg) in acetic anhydride (3 ml) was stirred at room temperature for 1.5 hr, poured into ice-water, and the resulted solution was extracted with chloroform. The extracts were washed with sodium bicarbonate

and then water, dried, and evaporated to give a crystals which was recrystallized from ethanol–*n*-hexane. Yield, 91% (105 mg); mp 156—157°C; $[\alpha]_D^{23}$ +15.4° (*c* 0.95; $CHCl_3$); IR: 1740 (ester); NMR: *ca.* 7.37 (Ph; m), 5.89 (H_2; d, $J_{1,2}$= 4.2), 5.55 (PhCH=), 4.87 (H_1; d), 4.85 (H_4; d, $J_{4,5}$=7.5), 4.30 (H_5; sex, $J_{5,6a}=J_{5,6e}$=7.5), 3.97—3.65 (H_{6a} and H_{6e}; m), 3.40 (OMe), 2.14 (*sec*-OAc), 1.95 (*tert*-OAc), 1.62 (C–CH_3).

Found: C, 60.18; H, 6.45%. Calcd for $C_{19}H_{24}O_8$: C, 59.99; H, 6.36%.

*2-O-Acetyl and 2,3-Di-O-acetyl Derivatives of Methyl 4,6-O-benzylidene-3-C-methyl-α-D-allopyranoside (**6**).* *a) 2-O-Acetate (**7**)*: This compound was obtained from **6**[2,3] by the usual method in a quantitative yield. Mp 95—96 °C; $[\alpha]_D^{23}$ +69.8° (*c* 1.2, $CHCl_3$). IR: 3475 (OH), 1730 (OAc); NMR: 2.16 (OAc), 1.28 (C–CH_3).

Found: C, 60.66; H, 6.72%. Calcd for $C_{17}H_{22}O_7$: C, 60.34; H, 6.55%.

*b) 2,3-Di-O-acetate (**8**)*: Acid-catalyzed acetylation of **6** gave **8** in a quantitative yield, which was recrystallized from ether–*n*-hexane. Mp 97—98°C; $[\alpha]_D^{23}$ +53.5° (*c* 1.03, $CHCl_3$); IR: 1740 (OAc); NMR: *ca.* 7.35 (Ph; m), 5.51 (PhCH=), 4.90 (H_1; d, $J_{1,2}$=4.2), 4.71 (H_2; d), 4.40—3.55 (H_4, H_5, H_{6a} and H_{6e}; m), 3.40 (OMe), 2.16 (*sec*-OAc), 2.05 (*tert*-OAc), 1.78 (C–CH_3).

Found: C, 60.41; H, 6.52%. Calcd for $C_{19}H_{24}O_8$: C, 59.99; H, 6.36%.

*Methyl 3,3′-Anhydro-4,6-O-benzylidene-3-C-(hydroxymethyl)-α-D-glucopyranoside (**9**).* A solution of **2** (1.0 g, 2.51 mmol) and potassium hydroxide (0.5 g) in acetone (20 ml)–water (10 ml) was stirred for 1.5 hr, until **2** has disappeared on tlc. Evaporation of acetone caused deposition of needles, which was gathered after further addition of water (15 ml). These crystals (0.67 g) contain crystalline water detectable in IR (3200, 3450, 3530 cm^{-1}) and NMR spectra. Recrystallization from ethanol–acetone gave needles in 81.5% (0.62 g) yield. Mp 179—180 °C; $[\alpha]_D^{23}$ +111 ° (*c* 1.06, $CHCl_3$); IR: 3320 (OH).

Found: C, 60.01; H, 5.83%. Calcd for $C_{15}H_{18}O_6 \cdot 1/3H_2O$: C, 59.98; H, 5.60%.

Usual acetylation of **9** gave the sirupy *2-O-acetate* (**10**) in a quantitative yield. $[\alpha]_D^{23}$ +96.0° (*c* 1.04, $CHCl_3$); IR; 1750 (OAc); NMR: 7.26 (Ph; m), 5.45 (PhCH=), 5.15 (H_1; d, $J_{1,2}$=3.7), 4.92 (H_2; d), 4.40—3.65 (H_4, H_5, H_{6a} and H_{6e}; m), 3.35 (OMe), 3.07 and 2.98 (epoxy-CH_2; ABq, $J_{a,b}$=5), 2.05 (OAc).

Found: C, 60.75; H, 6.09%. Calcd for $C_{17}H_{20}O_7$: C, 60.71; H, 5.99%.

*Methyl 3-Acetoxymethyl-2-O-acetyl-4,6-O-benzylidene-α-D-glucopyranoside (**12**).* A suspended solution of **9** (2.0 g) and potassium hydroxide (1.5 g) in water (75 ml) was refluxed for 10 hr to make the solution homogeneous, and then extracted with *n*-butanol, after neutralization of the cooled solution with 2N-hydrochloric acid. The extracts was washed with a small amount of water, evaporated to give a sirup (**11**) (1.7 g, 80%); $[\alpha]_D^{23}$ +77.8° (*c* 1.44, $CHCl_3$).

Found: C, 57.67; H, 6.81%. Calcd for $C_{15}H_{20}O_7$: C, 57.68; H, 6.46%.

Acetylation of **11** by the usual method give the sirupy *di-O-acetate* (**12**) in a quantitative yield. $[\alpha]_D^{23}$ +53.6° (*c* 1.14, $CHCl_3$); IR: 3450 (OH), 1735 (OAc); NMR: 7.32 (Ph; m), 5.41 (PhCH=), 5.10 and 4.27 ($C_3'H_2$; ABq, J= 12.5), 4.96 (H_1; d, $J_{1,2}$=3.7), 4.83 (H_2; d), 4.27 (H_5; m), 4.05—3.55 (H_4, H_{6a} and H_{6e}; m), 3.37 (OMe), 2.12 (*sec*-OAc), 1.78 (OAc).

Found: C, 57.46; H, 6.35%. Calcd for $C_{19}H_{24}O_9$: C, 57.57; H, 6.10%.

*Methyl 4,6-O-Benzylidene-3,3′-O-isopropylidene-α-D-glucopyranoside (**13**).* A suspended solution of **11** (200 mg, 0.64 mmol), anhydrous cupric sulfate (0.5 g) in acetone (20 ml) containing one drop of conc. sulfuric acid was stirred for 24 hr at room temperature, neutralized with barium carbonate, filtered through active carbon, and the filtrate was evaporated to give a sirup (210 mg). Crystallization of the sirup from ethanol–water gave needles in 53% (120 mg) mg) yield. Mp 133—134 °C; $[\alpha]_D^{23}$ +55.0° (*c* 1.18, $CHCl_3$); IR: 3500 (OH).

Found: C, 61.35; H, 7.00%. Calcd for $C_{18}H_{24}O_7$: C, 61.35; H, 6.86%.

Acetylation of **13** by the usual method gave the sirupy 2-O-*acetate* (**14**) in a good yield. $[\alpha]_D^{23}$+49.8° (*c* 1.31, $CHCl_3$); IR: 1750 (OAc), 1370 and 1380 (C–CH_3); NMR: *ca.* 7.40 (Ph; m), 5.60 (PhCH=), 5.03 (H_1; d, $J_{1,2}$=3.7), 4.89 (H_2; d), 4.40 and 4.25 ($C_3'H_2$; ABq, J=9.7), 4.45—4.20 (H_5; m), 3.90—3.60 (H_4, H_{6a} and H_{6e}; m), 3.38 (OMe), 2.16 (OAc), 1.49 and 1.36 (2×C–CH_3).

Found: C, 60.85; H, 7.09%. Calcd for $C_{20}H_{26}O_8$: C, 60.90; H, 6.64%.

*Methyl 3-C-Acetoxymethyl-3,4,6-tri-O-acetyl-2-O-benzoyl-α-D-glucopyranoside (**16**).* A solution of **2** (300 mg, 0.753 mmol) in acetic acid (80%, 60 ml) was refluxed for 18 hr, and evaporated to give a sirup. *n*-Butanol solution (150 ml) of the sirup was washed with saturated sodium bicarbonate and then a small amount of water, decolorized, and evaporated to give a sirup (**15**) in 73% (180 mg) yield. $[\alpha]_D^{23}$ +112° (c 1.10, $CHCl_3$).

Found: C, 54.34; H, 6.11%. Calcd for $C_{15}H_{20}O_8$: C, 54.87; H, 6.14%.

Acid-catalyzed acetylation of **15** (120 mg) gave **16** in a quantitative yield, which was recrystallized from ether–*n*-hexane. Mp 84—86°C; $[\alpha]_D^{23}$ +109° (*c* 1.01, $CHCl_3$); NMR: *ca.* 8.13 and 7.55 (Ph; m), 6.24 (H_1; d, $J_{1,2}$=3.75), 5.92 (H_4; d, $J_{4,5}$=10.0), 5.03 (H_2; d), 5.02 and 4.85 ($C_3'H_2$: ABq, J=10.5), 4.48—4.02 (H_5, H_{6a} and H_{6e}; m), 3.42 (OMe), 2.10, 2.08, 2.00, and 1.92 (4×OAc).

Found: C, 55.63; H, 5.72%. Calcd for $C_{23}H_{28}O_{12}$: C, 55.62; H, 5.69%.

*Methyl 4,6-O-Benzylidene-3-C-aminomethyl-α-D-glucopyranoside (**17**).* A solution of **9** (1.0 g, 3.3 mmol) in saturated ethanolic ammonia (25 ml) was heated for 3 hr in a sealed tube at 80—90°C, and evaporated to give needles, which was recrystallized from ethanol. Yield, 78% (0.8 g); mp 158—159 °C; $[\alpha]_D^{23}$ +92.0° (*c* 1.07, $CHCl_3$). IR: 3390 and 3350 (OH), 3300 (NH_2).

Found: C, 57.87; H, 6.87; N, 4.45%. Calcd for $C_{15}H_{21}NO_6$: C, 57.86; H, 6.80; N, 4.50%.

Acyl derivatives (**18**, **19**, and **20**) of **17** was obtained as follows.

*a) N-Benzoyl Derivatives (**18**)*: To a solution of **17** (300 mg, 0.965 mmol) in methanol (20 ml) was added benzoic anhydride (225 mg, 1.0 mmol) and the resulted solution was refluxed for 5 hr, evaporated to give a sirup which was crystallized from ether. Yield, 67.5% (260 mg); mp 154—155°C; $[\alpha]_D^{23}$+12.0° (*c* 1.05, $CHCl_3$). IR: *ca.* 3400 (NH and OH), 1640 (amide).

Found: C, 63.60; H, 6.20; N, 3.67%. Calcd for $C_{22}H_{25} \cdot NO_7$: C, 63.60; H, 6.07; N, 3.37%.

*b) 2,3-Di-O-acetyl-N-benzoyl Derivative (**19**)*: Acid-catalyzed acetylation of **18** gave the corresponding sirupy di-*O*-acetate in a quantitative yield. $[\alpha]_D^{23}$ −40.8° (*c* 1.48, $CHCl_3$).

Found: C, 62.44; H, 5.96; N, 2.77%. Calcd for C_{26}-

$H_{29}NO_9$: C, 62.51; H, 5.85; N, 2.80%.

*c) N,O-Triacetate (**20**)*: Acid-catalyzed acetylation of **17** (100 mg, 0.329 mmol) gave the *N,O*-triacetate in 97% (136 mg) yield. Mp 180—181°C; $[\alpha]_D^{23}$ −19.6° (*c* 1.36, $CHCl_3$). IR: 3300 (NH), 1750 and 1730 (OAc), 1640 and 1555 (amide); NMR: 7.42 (Ph; s), 6.45 (NH), 5.94 (H_1; d, $J_{1,2}$=4.7), 5.50 (PhCH=), 5.10 (H_4; d, $J_{4,5}$=10.0), 4.84 (H_2; d), 4.42—3.80 (H_5, $H_6{}^a$ and H_6 ; m), 3.87 and 3.68 ($C_3{}'H_2$; ABq, J=9.5), 3.39 (OMe), 2.13 (*sec*-OAc), 1.97 (NAc), 1.77 (*tert*-OAc).

Found: C, 57.62; H, 6.24; N, 3.30%. Calcd for $C_{21}H_{27}NO_9$: C, 57.66; H, 6.22; N, 3.20%.

*Methyl 2-O-Benzoyl-4,6-O-benzylidene-3-C-nitromethyl-α-D-allopyranoside (**21**)*. To a solution of nitromethane (30 ml) in tetrahydrofuran (30 ml) were added successively sodium methoxide (Na; 0.4 g, 174 mmol) and **1** (6 g, 156 mmol) with stirring, the resulted solution was stirred for 3 hr at room temperature, neutralized with acetic acid (60%), extracted with chloroform. The extract was washed with water, and evaporated to give needles which was recrystallized from acetone–ethanol. Yield, 80.5% (5.6 g); mp 169—170°C; $[\alpha]_D^{23}$ +73.8° (*c* 1.0, acetone). IR: 3440 (OH), 1720 (OBz), 1543 (NO_2); NMR: *ca.* 8.08 and 7.46 (Ph; m), 5.58 (PhCH=), 5.22 (H_1; d, $J_{1,2}$=4.3), 5.20 (H_2; d), 4.75 and 4.70 ($C_3{}'H_2$; ABq, J=12.0), 4.41 (H_{6e}; q), 4.25 (OH), 4.22 (H_5; sex, $J_{5,6a}$=9.0, $J_{5,6e}$=4.5), 3.81 (H_{6a}; t, $J_{6a,6e}$=9.0), 3.74 (H_4; d, $J_{4,5}$=9.5), 3.43 (OMe).

Found: C, 59.60; H, 5.40; N, 2.91%. Calcd for $C_{22}H_{23}NO_9$: C, 59.32; H, 5.21; N, 3.14%.

*Methyl 4,6-O-Benzylidene-3-C-benzamidomethyl-α-D-allo-pyranoside (**22**)*. A solution of **21** (4 g, 9 mmol) in methanol (100 ml) was hydrogenated in an autoclave in the presence of Raney nickel at 30 atm, 70 °C for 6 hr, filtered in hot state, and evaporated to give prisms which were recrystallized from ethanol. Yield, 2.4 g (65%); mp 234—235°C; $[\alpha]_D^{23}$ −19.3° (*c* 1.0, acetone).

Found: C, 64.04; H, 5.84; N, 3.40%. Calcd for $C_{22}H_{25}NO_7$: C, 63.60; H, 6.07; N, 3.37%.

Acetyl derivatives of **22** was synthesized as follows;

*a) 2-O-Acetate (**23**)*: Acetylation of **22** by the usual method and recrystallization of the product from ethanol–*n*-hexane gave 23 in 77% yield. Mp 214—215°C; $[\alpha]_D^{23}$ +44.4° (*c* 0.96, $CHCl_3$). IR: 3490 (OH), 3430 (NH), 1720 (OAc), 1642 and 1515 (amide); NMR: 7.70—7.30 (2×Ph; m), 7.00 (NH), 4.90 (H_1; d, $J_{1,2}$=4.0), 4.86 (H_2; d), 4.35 (H_{6e}; q, $J_{5,6e}$=9.5), 4.10 and 3.35 (C_3H_2; ABq. J=13.5), *ca.* 4.02 (H_5; m), 3.58 (H_4; d, $J_{4,5}$=9.5), 3.24 (H_{6a}; q, $J_{6a,6e}$=9.3), 2.13 (OAc).

Found: C, 62.96; H, 5.87; N, 3.09%. Calcd for $C_{24}H_{27}NO_8$: C, 63.01; H, 5.95; N, 3.06%.

*b) 2,3-Di-O-acetate (**24**)*: Acid-catalyzed acetylation of **22**, and recrystallization of the product from ethanol–*n*-hexane gave **25** in 83% yield. Mp 175—176°C; $[\alpha]_D^{23}$+23.1° (*c* 1.05, $CHCl_3$).

Found: C, 62.43; H, 5.84; N, 2.83%. Calcd for $C_{26}H_{29}NO_9$: C, 62.51; H, 5.85; N, 2.80%.

*De-N-benzoylation of **22***. A suspended solution of **22** (3.0 g) in methanolic potassium hydroxide (6 g in 15 ml) was refluxed for 5 hr, the precipitate (sodium benzoate) was filtered off, and the filtrate was poured into water. The resulted solution was extracted with chloroform, and the extract was washed with water, and evaporated to give crystals which were recrystallized from acetone. Yield, 0.9 g (36%). The structure of this crystal was determined to be methyl 4,6-*O*-benzylidene-2,3,*N*-benzylidine-3-*C*-(hydroxymethyl)-α-D-allopyranoside (**25**). Mp 194—197°C (dec.); $[\alpha]_D^{23}$ +64.2° (*c* 1.0, EtOH); IR: 1600 (Ph), 1525 (C–N), and 1380.

Found: C, 61.03; H, 6.35; N, 3.20%. Calcd for $C_{22}H_{23}NO_6\cdot 2H_2O$: C, 60.96; H, 6.28; N, 3.23%.

On the other hand, the water layer was extracted with *n*-butanol, after neutralization with 4N hydrochloric acid. Evaporation of *n*-butanol extracts gave de-*O*-benzoylated free amine **26** (24.0%, 0.6 g) and **22** (23.3%, 0.7 g) by fractional crystallization from methanol. Mp 205—210°C (dec.); $[\alpha]_D^{23}$ +79.4° (*c* 1.0, H_2O); IR: 3350 (OH), 3120 and 3050 (NH_2).

Found: C, 51.85; H, 6.27; N, 3.80%. Calcd for $C_{15}H_{21}NO_6\cdot 2H_2O$: C, 51.86; H, 7.25; N, 4.03%.

Base-catalyzed acetylation of **25** and **26** gave the corresponding 3-C-*acetamidomethyl*-2-O-*acetyl derivative* (**27**) in a quantitative yield. Mp 168°C; $[\alpha]_D^{23}$+39.7° (*c* 0.92, $CHCl_3$); IR: 3430 (OH), 3360 (NH), 1720 (ester), 1650 and 1530 (amide).

Found: C, 57.65; H, 6.11; N, 3.43%. Calcd for $C_{19}H_{25}NO_8$: C, 57.71; H, 6.37; N, 3.54%.

*Methyl 2-O-Benzoyl-3-C-nitromethyl-α-D-allopyranoside (**28**)*. To a solution of **21** (3.0 g) in acetone (20 ml) was added portionwise 0.2 N sulfuric acid (15 ml) at 40 °C, maintained at the temperature for 3 hr, neutralized with sodium bicarbonate, and concentrated. The residue was extracted with ethanol, and the ethanol solution was evaporated to give a sirup which was recrystallized from methanol–water. Yield, 87% (2.1 g); mp 152—154°C; $[\alpha]_D^{23}$ +92.5° (*c* 1.0, ethanol). IR: 3410 and 3510 (OH), 1720 (OBz), 1540 (NO_2).

Found: C, 50.83; H, 5.03; N, 4.04%. Calcd for $C_{15}H_{19}NO_9$: C, 50.42; H, 5.36; N, 3.92%.

This compound was also prepared by partial hydrogenation of **22** in the presence of palladium-charcoal in 53% yield, and it was converted into sirupy tri-*O*-acetate (**29**) by acid-catalyzed acetylation in 90% yield. $[\alpha]_D^{23}$ +91.5° (*c* 1.25, $CHCl_3$); IR: 1720 and 1760 (ester), 1550 (NO_2).

Found: C, 52.97; H, 5.55; N, 2.87%. Calcd for $C_{21}H_{25}NO_{12}$: C, 52.17; H, 5.21; N, 2.90%.

*Methyl 2-O-Benzoyl-3,4-O-isopropylidene-3-C-nitromethyl-α-D-allopyranoside (**30**)*. A suspended solution of **28** (1 g), and anhydrous cupric sulfate (2 g) in acetone (50 ml) containing one drop of sulfuric acid was stirred for 3 days at room temperature, neutralized with barium carbonate, filtered, and the filtrate was evaporated to give a sirupy product. The sirup was fractionated through a Kiesel gel 60 (Merck) column with benzene–methanol effluent (15 : 1) to give **28** (0.25 g) and **30** (0.67 g, 58%) which was crystallized from ethanol–*n*-hexane. Mp 138—139°C.

Found: C, 54.18; G, 5.57; N, 3.83%. Calcd for $C_{18}H_{23}NO_9$: C, 54.40; H, 5.83; N, 3.53%.

Acid-catalyzed acetylation of **30** gave *6*-O-*acetate* (**31**) in a quantitative yield, which was recrystallized from ethanol–*n*-hexane. Mp 143—143.5°C; IR: 1720 (ester), 1560 (NO_2), 1370 (CCH_3); NMR: 8.07—4.51 (Ph; m), 5.87 (H_1; d, $J_{1.2}$=5.1), 4.99 (H_2; d), 4.64 (C_3H_2; s), 4.58—5.10 (H_4, H_5, and $H_{6a,b}$; m), 3.40 (OMe), 2.10 (OAc), 1.40 and 1.29 (2×CCH_3).

Found: C, 54.44; H, 5.77; N, 3.11%. Calcd for $C_{20}H_{25}NO_{10}$: C, 54.66; H, 5.74; N, 3.19%.

The authors are grateful to Mr. Hitoshi Matsumoto for NMR measurements, and members of the Laboratory of Organic Analysis for elemental analysis.

Optically Active Triptycenes. VI.[1] Optical Resolution of 2,5-Dihydroxy-8-methoxycarbonyltriptycene and Absolute Configuration of 2,5-Dimethoxy-8-methoxycarbonyltriptycene

Yasumi SHIMIZU, Taketoshi NAITO, Fumio OGURA, and Masazumi NAKAGAWA

Department of Chemistry, Faculty of Science, Osaka University, Toyonaka, Osaka 560

(Received December 1, 1972)

After several unsuccessful attempts, optical resolution of 2,5-dihydroxy-8-methoxycarbonyltriptycene could be attained by means of bis-camphanate derivative. The absolute configuration of (+)-2,5-dimethoxy-8-methoxycarbonyltriptycene derived from (+)-2,5-dihydroxy-8-methoxycarbonyltriptycene was determined as 1*R*,6*S* by chemical correlation with (+)-2,5-dimethoxy-7-dimethylaminotriptycene hydrobromide whose absolute configuration had been proved to be 1*R*,6*S* by the X-ray structure analysis using the Bijvoet method.

Optically active triptycene derivatives can be regarded as ideally suited model compounds for the study of rotatory properties in view of their rigid and definite molecular structure. As reported in previous papers, 2,5,7- and 2,5,8-trisubstituted triptycene derivatives have been synthesized and one of the former compounds has been resolved into enantiomers[2] which could be transformed in a number of optically active 2,5,7-trisubstituted triptycenes bearing various kinds of substituent groups.[3] We have also reported the synthesis and absolute configuration of optically active 2,7-disubstituted triptycenes[4] and the analysis of their CD spectra.[5]

The direction of long-axis polarized transition moment in 7-substituted benzene ring in 2,5,7-trisubstituted triptycenes is parallel to the three-fold symmetry axis of triptycene skeleton, whereas the direction of the transition moment in 8-substituted nucleus in 2,5,8-trisubstituted derivatives should deviate from the parallel direction.[6] Therefore, it seemed to be of considerable interest to compare the optical rotatory properties of 2,5,8-trisubstituted triptycenes with those of 2,5,7-trisubstituted analogues. The present paper deals with the optical resolution of 2,5-dihydroxy-8-methoxycarbonyltriptycene and determination of the absolute configuration of its dimethyl ether derivative by chemical means.

Optical Resolution. The optical resolution of 2,5-disubstituted-8-carboxytriptycenes using the carboxyl group (R_2) as a handle was encountered by serious difficulty. Since the difficulty seemed to be ascribable to the remote position of R_2 from the asymmetric center, 2,5-dihydroxy-8-carboxytriptycene was converted into 2,5-diacyloxy-8-carboxytriptycenes (IIIa–d) bearing various acyl groups with increasing steric requirement to increase the interaction with resolving agent attached to carboxyl group at 8-position. All

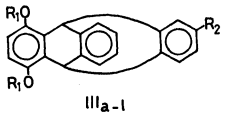

IIIa-l

a : R_1=$COCH_3$, R_2=COOH;
b : R_1=$COCH(CH_3)_2$, R_2=COOH
c : R_1=$COC(CH_3)_3$, R_2=COOH
d : R_1=$CO(CH_2)_2COOH$, R_2=COOH
e : R_1=$COCH_2$–M, R_2=$COOCH_3$
f : R_1=$CONHCH(\alpha\text{-Naph})CH_3$, R_2=$COOCH_3$
g : R_1=Camph, R_2=$COOCH_3$
h : R_1=H, R_2=$COOCH_3$
i : R_1=CH_3, R_2=$COOCH_3$
j : R_1=CH_3, R_2=COOH
k : R_1=$COCH_3$ R_2=COO–Chol
l : R_1=$COCH(CH_3)_2$, R_2=COO–Chol

M=*l*-menthoxy, α-Naph=α-naphthyl, Chol=cholesteryl, Camph=(−)-camphanoyl

attempts to resolve IIIa–b with optically active amines and alkaloids gave fruitless results. Partial resolution was observed in the case of IIId. However, complete resolution could not be achieved owing to a gradual decomposition of IIId during the course of fractional recrystallization. Considering the presence of carboxyl groups in acyloxy substituents in IIId, the introduction of acid phthalate groups into 2- and 5-positions was attempted. But bis-acid phthalate derivative could not be obtained in pure form. The attempts of resolution *via* menthoxyacetate (IIIe) or urethane (IIIf) gave unsatisfactory results. The alkaloid salts of IIIj and cholesteryl derivatives (IIIk and IIIl) could be obtained in good crystalline states. However, no optical resolution could be attained with these derivatives.

Considering these fruitless results, we decided to use camphanic acid as resolving agent[7] which has a reacting site at a proximity of its own asymmetric center. The synthesis of 2,5-dihydroxy-8-methoxycarbonyltriptycene (IIIh) was performed by the reported method[2] with modification. The Diels-Alder reaction of *p*-benzoquinone with 2-methoxycarbonylanthracene was carried out in dioxane in place of benzene resulting in a much higher yield of the adduct (II, 65%). The adduct (II) could be separated in a high melting and low melting stereoisomers by recrystal-

1) For Part V of this series, see Ref. 4b.

2) A. Sonoda, F. Ogura, and M. Nakagawa, This Bulletin, **35**, 853 (1962).

3) a) F. Ogura and M. Nakagawa, *ibid.*, **38**, 155 (1965); b) F. Ogura, Y. Sakata, and M. Nakagawa, *ibid.*, **45**, 3646 (1972); c) F. Ogura and M. Nakagaws, *ibid.*, **46**, 651 (1973).

4) a) M. Kuritani, Y. Sakata, F. Ogura, and M. Nakagawa, *Chimia*, **26**, 470 (1972); b) M. Kuritani, Y. Sakata, F. Ogura, and M. Nakagawa, This Bulletin, **46**, 605 (1973).

5) J. Tanaka, F. Ogura, M. Kuritani, and M. Nakagawa, *Chimia*, **26**, 471 (1972).

6) J. R. Platt, *J. Chem. Phys.*, **19**, 263 (1951); J. Petruska, *ibid.*, **34**, 1111 (1961).

7) *Cf.*, H. Gerlach, *Helv. Chim. Acta*, **51**, 1587 (1968).

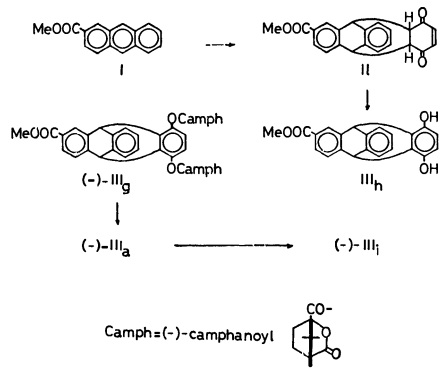

Scheme 1. Optical resolution of 2,5-dihydroxy-8-methoxycarbonyltriptycene (IIIh).

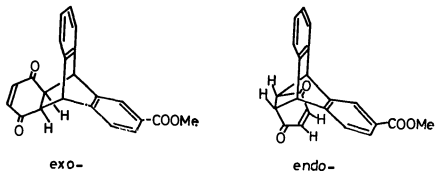

lization from methanol which could be assigned to *exo*- and *endo*-isomers, respectively, on the basis of NMR spectral evidence. As illustrated in Fig. 1, *endo*-isomer exhibits poorly resolved signal of olefinic protons at τ 3.62, whereas the olefinic protons of *exo*-isomer gave a sharp singlet at τ 3.63. The splitting of signal of *endo*-isomer can be reasonably attributed to the anisotropy of methoxycarbonyl group situated in a relatively proximate position. Treatment of a mixture of *endo*- and *exo*-isomers (II) in benzene with hydrogen chloride yielded 2,5-dihydroxy-8-methoxycarbonyltriptycene (IIIh).

(−)-Camphanic acid chloride was prepared from (+)-camphor *via* (+)-camphoric acid, (−)-camphoric anhydride and (−)-monobromocamphoric anhydride.[8]

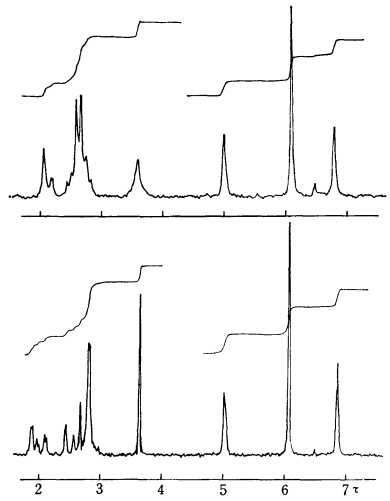

Fig. 1. NMR spectra of *endo*- (top) and *exo*-adducts (bottom) (II).

8) O. Aschan, *Acta Soc. Sci. fenn.*, **21**, 1 (1895); *Chem. Zentr.*, **1895II**, 967.

The reaction of acid chloride with IIIh in pyridine afforded bis-camphanate (IIIg) in a high yield (82—97%). Bis-camphanate (IIIg) was repeatedly recrystallized from methanol (4—7 times) to give crystals with a constant specific rotation. The resolved bis-camphanate (IIIg) was dissolved in methanol saturated with hydrogen chloride and the mixture was refluxed to convert IIIg into (−)-IIIh and methyl camphanate. Chromatography of the reaction product on silica gel afforded (−)-IIIh in a quantitative yield. (−)-2,5-Dimethoxy-8-methoxycarbonyltriptycene (IIIi) was obtained from (−)-IIIh on treatment with dimethyl sulfate.

Absolute Configuration. The reaction of allyl chloride with crude phenol (VI) obtained by hydrolysis of the diazonium salt of (+)-2,5-dimethoxy-7-aminotriptycene (IV)[3b] afforded (+)-allyl ether (VII).

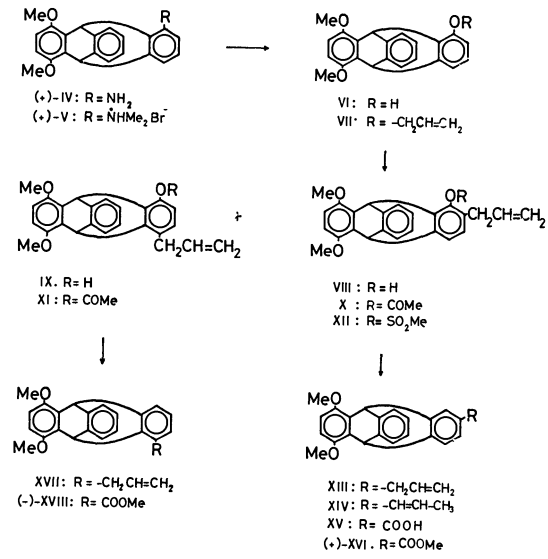

Scheme 2. Chemical correlation of 2,5,7-trisubstituted triptycene with 2,5,8-trisubstituted triptycene.

The Claisen rearrangement of (+)-VII in boiling diethylaniline gave rearranged products (VIII and IX) in an almost quantitative yield. Separation of VIII and IX could be attained by chromatography on silica gel. Although the purification of the allylic phenols (VIII and IX) were found to be difficult, the IR spectrum of IX in Nujol exhibits a sharp absorption at 3400 cm^{-1} due to stretching vibration of OH group, on the other hand, the spectrum of VIII shows a broad absorption at 3300—3350 cm^{-1}. Broadening of the band to higher wave number can be presumably attributed to an increased crowding by the presence of vicinal allyl group. Acetylation of VIII and IX yielded pure X and XI, respectively. The NMR spectra of X and XI provide further support for the assigned structures. The bridgehead protons of XI exhibit signals at τ 4.10 and 3.88. On the other hand, those of X give signals at τ 4.20 and 4.15. The signal at τ 3.88 in XI can be assigned to bridgehead proton at C-6 which suffers the deshielding effect of acetoxyl group at C-7. The fact that the bridgehead protons of X resonate at nearly the same field (τ 4.20

and 4.15) indicates a decrease of deshielding effect of acetoxyl group due to a twisting by a steric interference with the vicinal allyl substituent.

Crude methanesulfonate (XII) obtained from VIII and methanesulfonyl chloride was treated with sodium in liquid ammonia[9] to give XIII. Allylic rearrangement of XIII with potassium hydroxide in diethylene glycol yielded propenyl derivative (XIV). 2,5-Dimethoxy-8-carboxytriptycene (XV) obtained by permanganate oxidation of XIV was converted into (+)-methyl ester (XVI). The NMR spectrum of XVI was found to be identical with that of (−)-IIIi obtained by the optical resolution of (±)-IIIh. The melting points [(+)-XVI: mp 255.8—256.1 °C; (−)-IIIi: mp 256.1—256.8 °C] and optical rotations [(+)-XVI: $[\alpha]_D^{16}$+11.3°, $[\alpha]_{500}^{16}$+19.7° (*c* 0.531, dioxane); (−)-IIIi: $[\alpha]_D^{20}$−10.3°, $[\alpha]_{500}^{16}$−20.5° (*c* 0.291, dioxane)] indicate clearly that (+)-XVI is the antipode of (−)-IIIi. Because the absolute configuration of (+)-V derived from (+)-IV has been determined as 1*R*, 6*S* by the Bijvoet method of X-ray structure analysis,[10] the chemical correlation of (+)-XVI with (+)-IV clearly demonstrates 1*R*,6*S* absolute configuration of (+)-XVI, *i.e.*, 1*R*,6*S* absolute configuration of (−)-IIIi.

A mixture of VIII and IX obtained by the Claisen rearrangement of (+)-VII was converted into a mixture of propenyl derivatives (XIV and XVII) according to the method used for VIII. Permanganate oxidation of the mixture XIV and XVII followed by esterification afforded (+)-XVI and (−)-XVIII. The NMR spectrum of (−)-XVIII is identical with that of (+)-2,5-dimethoxy-7-methoxycarbonyltriptycene (XIX).[3b]. The specific rotations of (−)-XVIII and (+)-XIX indicate that the former is the enantiomer of the latter [(−)-XVIII: $[\alpha]_D^{20}$−23.2°; (+)-XIX: $[\alpha]_D^{25}$+25.5° (*c* 0.7475, dioxane)]. Because it is evident that (−)-XVIII is derived from *para*-Claisen rearrangement product (IX), and (+)-IV, the parent compound of (+)-XVI and (−)-XVIII, has been prepared from (+)-XVIII,[3b] the formation of (−)-XVIII from (+)-IV provides an interesting instance of conversion of absolute configuration of triptycene derivative by the transfer of a substituent group from 7- to 10-position.

Experimental

The melting points were measured on Mettler FP2 apparatus and Shimadzu Kohfler micro hot stage, and uncorrected. Purified and anhydrous solvents were used, unless otherwise stated. The IR spectra were obtained on Hitachi EPI-2 or JACSO DS-301 spectrometer. The electronic spectra were measured with Hitachi EPS-3T spectrophotometer. The NMR spectra in deuteriochloroform were taken with Varian A-60 spectrometer using TMS as an internal standard and given in τ-values. The rotations and CD spectra were obtained on Yanagimoto ORD-185 and JASCO J-20 spectropolarimeters, respectively. The shoulder and inflection are denoted with an asterisk. Only the main peaks of IR and NMR spectra were recorded.

Preparation of Adduct (II). To a hot solution of 2-methoxycarbonylanthracene (I, 10.0 g, 0.042 mol) in dioxane (120 ml) was added in one portion a solution of *p*-benzoquinone (10.0 g, 0.093 mol) in the same solvent (50 ml). After being stirred for 7 hr, the mixture was concentrated under reduced pressure and the quinone remained was removed by steam distillation. The residue was extracted with benzene and crystalline solid (13.7 g) obtained by working up the benzene extract was recrystallized twice from methanol to give a mixture of *endo*- and *exo*-II as yellow crystals (9.5 g, 65%). Repeated recrystallization of the mixture from methanol afforded *exo*-II (less soluble) and *endo*-II (more soluble).

exo-II, mp 188—189 °C (sintered at 170 °C), IR (KBr disk): $\nu_{C=O}$ 1717, 1677 cm^{-1}, NMR: 6.87 (s, 2H, bridge), 6.07 (s, 3H, $-CO_2CH_3$), 5.02 (s, 2H, bridgehead), 3.63 (s, 2H, olefinic), 1.88—2.81 (m, 7H, aromatic), UV: $\lambda_{max}^{dioxane}$ (ε) 240* (15,600), 247* (13,600), 251* (12,300), 257* (9,010), 262* (6,490), 269* (3,110), 275* (2,180), 284* (1,390), 360* (71.5), 378 (76.3), 400* (55.7), 420* (22.5) nm.

Found: C, 76.30; H, 4.73%. Calcd for $C_{22}H_{16}O_4$: C, 76.73; H, 4.68%.

endo-II, mp 149—157 °C (sintered at 148 °C), IR (KBr disk): $\nu_{C=O}$ 1725, 1675 cm^{-1}, NMR: 6.81 (s, 2H, bridge), 6.11 (s, 3H, $-CO_2CH_3$), 5.01 (s, 2H, bridgehead), 3.62 (broad s, 2H, olefinic), 2.07—2.83 (m, 7H, aromatic), UV: $\lambda_{max}^{dioxane}$ (ε) 238.5 (16,200), 243.5 (15,500), 249 (16,000), 255 (15,100), 261 (9.170), 271* (2,710), 284* (1,380), 360* (69.1), 377 (78.8), 395* (63.8), 410* (18.0) nm.

Found: C, 76.18; H, 4.76%. Calcd for $C_{22}H_{16}O_4$: C, 76.73; H, 4.68%.

2,5-Dihydroxy-8-methoxycarbonyltriptycene (IIIh). Hydrogen chloride was introduced to a solution of a mixture of *endo*- and *exo*-II (20.0 g, 0.058 mol) in benzene (400 ml). After the mixture was allowed to stand for 4 hr at room temperature, the reaction mixture containing colorless fine crystals was concentrated under reduced pressure. The residue was recrystallized from benzene to yield IIIh, colorless crystals, mp 159—162 °C, 17.1 g (85%), IR (Nujol mull): ν_{OH} 3270, $\nu_{C=O}$ 1690 cm^{-1}.

Found: C, 76.56; H, 5.06%. Calcd for $C_{22}H_{16}O_4$: C, 76.73; H, 4.68%.

IIIh was also obtained in a 60.8% yield by refluxing a mixture of 2,5-dihydroxy-8-carboxytriptycene[2] (14.5 g), methanol (73 ml) and sulfuric acid (4.4 ml) for 8 hr.

2,5-Bis(camphanoyl)-8-methoxycarbonyltriptycene (IIIg). A solution of IIIh (15.0 g, 0.0436 mol), camphanoyl chloride[8] (20.8 g, 0.0960 mol) in pyridine (330 ml) was allowed to stand overnight at room temperature. The mixture was poured onto ice-water (2 l) and extracted with benzene. The extract was washed successively with 1 M hydrochloric acid, water, 1% aqueous sodium hydrogen carbonate and water, and dried. Concentration of the extract afforded colorless crystals, mp 141—188°C, 21.1 g (81.8%), IR (Nujol mull): 1795, 1730 cm^{-1}.

The crystals decomposed on an attempted chromatography on silica gel.

A portion of the bis-camphanate (2.7 g) was repeatedly recrystallized from methanol (4—7 times) to obtain bis-camphanate with constant specific rotation, mp 195.9—198.2 °C (the mp gradually increased to 240 °C and again decreased to the constant value during the course of recrystallization), IR (Nujol mull) 1800, 1730 cm^{-1}, $[\alpha]_{390}^{15}$

9) H. W. Thompson, *J. Org. Chem.*, **33**, 621 (1968).

10) N. Sakabe, K. Sakabe, K. Ozeki-Minakata, and J. Tanaka, presented at the 9th International Congress of Crystallography (1972); *Acta Crystallogr.*, **B28**, 3441 (1972).

$-20.4°$ (c 0.588, dioxane).

Found: C, 71.25; H, 5.73%. Calcd for $C_{42}H_{40}O_{10}$: C, 71.58; H, 5.72%.

Optically pure bis-camphanate was also obtained when a solution of the crude bis-camphanate (2.7 g) in dichloromethane (10 ml) was mixed with hot methanol (500 ml) and the mixture was concentrated to one-half of its original volume.

(−)-2,5-Dihydroxy-8-methoxycarbonyltriptycene (IIIh). To a mixture of optically pure bis-camphanate (IIIg, 2.05 g) in methanol (140 ml) was introduced hydrogen chloride for 40 min under ice-cooling, and the mixture was refluxed for 5 hr to give a colorless homogeneous solution. After one-half of the methanol had been removed under reduced pressure at room temperature, the reaction mixture was poured into a saturated sodium chloride solution (300 ml) and extracted with ether. The extract, after being washed with a saturated aqueous sodium chloride, was concentrated under reduced pressure. Crude crystals (1.96 g) thus obtained were chromatographed on silica gel (Merck, 250 g). Elution with benzene–ether (9 : 1) afforded methyl camphanate (1.04 g). Crude (−)-IIIh (1.13 g) obtained by elution with benzene–ether (7.5 : 2.5) was recrystallized from a small amount of benzene to give pure (−)-IIIh, colorless crystals, 0.90 g (90%), $[\alpha]_{589}^{20}$ −9.71° (c 0.258, ethanol).

(−)-2,5-Dimethoxy-8-methoxycarbonyltriptycene (IIIi). A solution of (−)-IIIh (37.0 mg, 0.107 mmol) in acetone (30 ml) was refluxed for 6 hr under stirring with dimethyl sulfate (112 mg) in the presence of anhydrous potassium carbonate (200 mg). The reaction mixture was worked up by the usual way to give crude (−)-IIIi which was dissolved in benzene and passed through a short column of alumina. Crystals obtained from the filtrate were recrystallized from methanol to give pure (−)-IIIi, mp 256.1—256.8 °C (racemate, mp 248—249 °C), $[\alpha]_D^{20}$ −10.3° (c 0.291, dioxane), UV: λ_{max}^{EtOH} (ε) 303* (4.030), 292 (6,480), 285* (5,830), 267 (7,870), 226 (35,700), 203.5 (52,800) nm, CD: λ_{max}^{EtOH} ($\Delta\varepsilon$) 320 (+0.3), 299.2 (−3.11), 289.8 (+1.80), 280.5 (−0.29), 268.0 (+9.41), 261.5 (+4.99), 243.5 (+20.9), 229.0 (−44.9), 218.6 (+31.9), 208.4 (−35.5) nm.

Found: C, 77.35; H, 5.49%. Calcd for $C_{24}H_{20}O_4$: C, 77.40; H, 5.41%.

2,5-Dimethoxy-7-allyloxytriptycene (VII). (+)-2,5-dimethoxy-7-aminotriptycene[3b] (IV, 6.95 g, 21.1 mmol) was dissolved in hot acetic acid (307 ml) and a solution of sodium nitrite (0.49 g, 21.3 mmol) in water (42 ml) and acetic acid (100 ml) were added at 12—14 °C over a period of 1 hr. After the mixture being stirred for 30 min at the same temperature, the solution of diazonium salt was added dropwise over a 40-min period to boiling 3 M sulfuric acid under vigorous stirring, and stirring was continued for further 30 min under reflux. Precipitate obtained on cooling the reaction mixture was washed with water to give crude (+)-VI, 6.44 g (92%). A mixture of the crude (+)-VI (6.34 g, 19.2 mmol), acetone (340 ml), potassium carbonate (8.4 g), allyl chloride (4.0 g) and a small amount of sodium iodide was refluxed for 19 hr under stirring. Further amount of allyl chloride (2.0 g) was added during the period of reflux. Insoluble material was removed by filtration and the filtrate was concentrated under reduced pressure. The residue was extracted with benzene. The extract, after washing and drying, was evaporated under reduced pressure to give crude (+)-VII (7.3 g). The crude (+)-VII was chromatographed on alumina. Crystals obtained from benzene-eluate were recrystallized from the same solvent to yield pure (+)-VII, mp 255.0—256.0 °C, 4.57 g (59.3% based on (+)-IV), (racemate, mp 229.5—231.0 °C).

Found: C, 80.94, H, 6.07%. Calcd for $C_{25}H_{22}O_3$: C, 81.05; H, 5.99%.

(+)-2,5-Dimethoxy-7-hydroxy-8-allyltriptycene (VIII) and (−)-2,5-Dimethoxy-7-hydroxy-10-allyltriptycene (IX). A solution of (+)-VII (4.25 g, 11.5 mmol) in diethylaniline (450 ml) was refluxed for 6 hr under nitrogen atmosphere. The reaction mixture was acidified with 8 M hydrochloric acid under ice-cooling and then mixed with water (2.5 l), and extracted with benzene. The extract, after being washed and dried, was evaporated to give an amorphous solid (4.27 g). The solid dissolved in benzene was chromatographed on silica gel (Merck). Elution with benzene afforded (+)-VIII 3.37 g (79.3%), IR (Nujol mull): 3300—3550 (broad), 715 cm^{-1}, and (−)-IX, 0.82 g (19.3%), IR (Nujol mull): 3400 (sharp), 735, 725 cm^{-1} was obtained from benzene–ether eluate (8 : 2).

(+)-2,5-Dimethoxy-7-acetoxy-8-allyltriptycene (X). The product obtained by the acetylation of (+)-VIII (223 mg, 0.602 mmol) with acetic anhydride (7 ml) and sodium acetate (0.1 g) by the usual way was dissolved in benzene and chromatographed on silica gel. The crystals obtained from benzene-eluate were recrystallized twice from ethanol, mp 166.8—169.0 °C, 137.0 mg (55%) (racemate, mp 167.0—168.0°C), IR (Nujol mull): $\nu_{C=O}$, 1770, 1760*, $\nu_{C=C(allyl)}$, 1645 cm^{-1}, $[\alpha]_D^{20}$ +13.0° (c 0.276, dioxane), NMR: 7.57 (s, CH_3CO–), 6.25 (s, CH_3O–), 4.20, 4.15 (bridgehead), 3.57 (aromatic H(3), H(4)).

Found: C, 78.18; H, 5.95%. Calcd for $C_{27}H_{24}O_4$: C, 78.62; H, 5.86%.

(−)-2,5-Dimethoxy-7-acetoxy-10-allyltriptycene (XI). According to the procedure for (+)-X, (−)-IX was converted into (−)-XI, mp 223.0—223.7 °C (from ethanol), 0.58 g (61%), IR (Nujol mull): $\nu_{C=O}$, 1770, $\nu_{C=C(allyl)}$, 1645 cm^{-1}, $[\alpha]_D^{20}$ −5.6° (c 0.252, dioxane),, NMR: 7.60 (CH_3CO–), 6.25 (CH_3O–), 4.10, 3.88 (bridgehead), 3.55 (aromatic, H(3), H(4)), 3.28 (aromatic, H(8), H(9), AB-quartet, J_{AB}= 8 Hz).

Found: C, 78.25; H, 5.77%. Calcd for $C_{27}H_{24}O_4$: C, 78.62; H, 5.86%.

(+)-2,5-Dimethoxy-8-allyltriptycene (XIII). Methanesulfonyl chloride (2.0 g) was added to a solution of (+)-VIII (3.37 g, 9.09 mmol) in pyridine (30 ml). After being kept at room temperature overnight, the reaction mixture was poured onto ice-water, acidified with 3 M hydrochloric acid and extracted with benzene. After being washed and dried, the solvent was removed under reduced pressure, yielding crude (+)-XII, 3.95 g (97%) as an amorphous solid, IR (Nujol mull): 1360 cm^{-1} (racemate, 1350 cm^{-1}). A solution of crude (+)-XII, 3.89 g (8.67 mmol) in tetrahydrofuran (150 ml) was added to liquid ammonia. Sodium, 0.51 g (22.3 mg-atom) was added to the stirred solution. After being stirred for 10 min, ammonium chloride (5 g) was added to the reaction mixture, and allowed to stand overnight at room temperature. Volatile material was removed under reduced pressure and the residue was extracted with benzene. The extract, after washing and drying, was concentrated to give crude amorphous (+)-XIII, 3.17 g which was chromatographed on silica gel (Merck). Elution with carbon tetrachloride–benzene (3 : 7) afforded crude (+)-XIII, 1.40 g (48%). Recovered (+)-VIII, 1.40 g (42%) was obtained from ether–benzene (1 : 9) eluate which was converted into (+)-XII and reduced with sodium in liquid ammonia. This procedure was repeated twice to give (+)-XIII (total 2.66 g, 83.9%) and recovered (+)-VIII (0.18 g, 5.4%).

(+)-2,5-Dimethoxy-8-propenyltriptycene (XIV). A mixture of (+)-XIII (2.68 g, 7.57 mmol), diethylene glycol (27 ml) and finely powdered potassium hydroxide (3.0 g) was heated to 190—220 °C for 1.5 hr. Crystals deposited were washed successively with a small amount of diethylene glycol and water to yield (+)-XIV, colorless needles, 2.45 g (91.5%). Second crop of crystals obtained from the mother liquor were recrystallized from ethanol, yielding pure (+)-XIV, 0.16 g (total yield 2.61 g, 97.6%), mp 226.2—231.0 °C, NMR: 8.21 (d, J=5 Hz, CH_3 of propenyl), 4.17 (s, bridgehead).

Found: C, 84.63; H, 6.25%. Calcd for $C_{25}H_{22}O_2$: C, 84.71; H, 6.26%.

(+)-2,5-Dimethoxy-8-methoxycarbonyltriptycene (XVI). Potassium permanganate (5.24 g) was added to a solution of (+)-XIV (2.20 g, 6.21 mmol) in acetone (920 ml) and the mixture was stirred at room temperature overnight. Excess permanganate was reduced by sodium hydrogen sulfite and manganese dioxide was removed by filtration. The residue obtained by evaporation of the solvent was mixed with 3M hydrochloric acid and extracted with benzene. The extract, after being washed and dried, was concentrated to yield crude (+)-XV (2.44 g). A mixture of the crude (+)-XV, (2.41 g), methanol (150 ml) and concentrated sulfuric acid (5 ml) was refluxed for 8 hr and the reaction mixture was worked up by the usual way to yield crude amorphous (+)-XVI (2.66 g) which was chromatographed on alumina. Crystals obtained from benzene-eluate were recrystallized from methanol, yielding pure (+)-XVI, mp 255.8—256.1 °C, 0.803 g (34.8% based on XIV), $[\alpha]_D^{16}$ +11.7° (c 0.531, dioxane). (racemate, mp 248—249 °C, sintered at 237 °C).

The NMR spectrum of (+)-XVI was found to be identical with that of (−)-2,5-dimethoxy-8-methoxycarbonyltriptycene (IIIi).

Found: C, 77.39; H, 5.37%. Calcd for $C_{24}H_{20}O_4$: C, 77.40; H, 5.41%.

(−)-2,5-Dimethoxy-7-methoxycarbonyltriptycene (XVIII). A mixture of VIII and IX, product of the Claisen rearrangement of (+)-VII, was converted into a mixture of propenyl derivatives (XIV and XVII) according to the procedure used in the transformation of (+)-VIII into (+)-XIV. Permanganate oxidation followed by esterification of the mixture of XIV and XVII afforded a mixture of (+)-XVI and (−)-XVIII which was repeatedly chromatographed on alumina using carbon tetrachloride–benzene (1 : 4) as an eluant. Crystals obtained from initial eluate were recrystallized from methanol to give (−)-XVIII, mp 267.4—268.0 °C $[\alpha]_D^{20}$ −23.2° (c 0.198, dioxane). (−)-XVIII gave an identical NMR spectrum with that of (+)-2,5-dimethoxy-7-methoxycarbonyltriptycene prepared by a different route.[3b]

Found: C, 76.80; H, 5.33%. Calcd for $C_{24}H_{20}O_4$: C, 77.40; H, 5.41%.

Preparation of 2,5-Diacyloxy-8-carboxytriptycenes (IIIa—d). Crude 2,5-dihydroxy-8-carboxytriptycene[2] was heated with a large excess of corresponding acid anhydride or acid chloride in the absence or presence of solvent. The reaction mixture was treated with water and the acid formed from excess of reagent was removed. Crude materials were purified by recrystallization. The structures were confirmed by elemental analyses, IR and NMR spectroscopy. Reaction conditions, melting points, solvent of recrystallization and yields are summarized in Table 1.

2,5-Bis(1-menthoxyacetoxy)-8-methoxycarbonyltriptycene (IIIe). To an ice-cooled solution of IIIh (2.10 g, 6.10 mmol) in pyridine (10 ml) was added *l*-menthoxyacetyl chloride (3.12 g, 13.4 mmol) over a 10-min period under nitrogen atmosphere. The mixture was stirred for 80 min under ice-cooling and then for 17 hr at 33 °C. The neutral portion of the reaction product dissolved in benzene was passed through a column of silica gel (30 g) and eluted successively with benzene–ligroin and benzene. Crude IIIe (2.25 g, 50.6%) obtained from the eluates was recrystallized 3 times from methanol–methyl acetate to give pure IIIe, mp 177.5—181 °C, $[\alpha]_D^{25}$ −53.1° (methanol). IIIe gave unsatisfactory result of hydrogen analysis.

Found: C, 74.96; H, 6.87%. Calcd for $C_{46}H_{56}O_8$: C, 74.97; H, 7.66%.

2,5-Dimethoxy-8-carboxytriptycene (IIIj). A mixture of IIIi (0.67 g), acetic acid (44 ml) and 3M sulfuric acid (11 ml) was refluxed for 12 hr. Colorless crystals (0.575 g, 88.7%) deposited on cooling the reaction mixture, after being washed with water and dried, were recrystallized from methanol and then sublimed *in vacuo* to give pure IIIj. IIIj showed double melting points, mp 140—150 °C, mp 280.2—283.5 °C.

Found: C, 76.86; H. 5.03%. Calcd for $C_{23}H_{18}O_7$: C, 77.08; H, 5.06%.

Preparation of 8-Cholesteryloxycarbonyltriptycene Derivatives (IIIk and IIIl). IIIa and IIIb in tetrahydrofuran were converted into corresponding acid chloride by the reaction with thionyl chloride according to the usual way. A mixture of the acid chloride, cholesterol and pyridine was heated. The reaction product dissolved in benzene was chromatographed on alumina. IIIk and IIIl were obtained from benzene eluate. Their IR and NMR spectra were found to be consistent with the assigned structures. They gave satisfactory data of elemental analyses. Reaction conditions and physical properties are summarized in Table 2.

TABLE 1. 2,5-DIACYLOXY-8-CARBOXYTRIPTYCENE (IIIa—d)

Product	Dihydroxy compound (g)	Acylating agent (g)	Solvent (ml)	Reaction time (hr)	Reaction temp. (°C)	Yield (g)	Yield (%)	Mp (°C)	Solvent of recryst.
IIIa[2]	2.1	acetic anhydride (40 ml) + sodium acetate 16.3	none	4	100	1.9	49.5	235—237	acetic acid
IIIb	0.92	isobutyric anhydride 9	none	1.5	100	0.95	72.2	137—145	benzene
IIIc	3.49	trimethylacetyl chloride 7.2	pyridine 6	3.0	reflux	1.26	23.7	253—255	methanol
IIId	4.0	succinic anhydride	pyridine 100	7.5	75	5.25	81.5	167—172.5	ethyl acetate

Table 2. 8-Cholesteryloxycarbonyltriptycene derivatives (IIIk and IIIl)

Product	Triptycene (g)	Cholesterol (g)	Solvent (ml)	Reaction temp. (°C)	Reaction time (hr)	Mp (°C)	$[\alpha]_D$ in dioxane	Solvent of recryst.
IIIk	1.00	1.10	20	85	3.5	212—216	+6.18° (*c* 0.648)	ethanol
IIIl	1.10	0.92	5	75	5.0	196—201	+11.2° (*c* 0.807)	methanol–methyl acetate

(+)-2,5-Bis(1-α-naphthylethylcarbamoyl)-8-methoxycarbonyltriptycene (IIIf). To a boiling solution of IIIh (1.00 g, 2.91 mmol) in toluene (80 ml) was added a solution (−)-1-α-naphthylethyl isocyanate (1.20 g, 6.11 mmol) in the same solvent (20 ml). After several drops of triethylamine had been added, the mixture was refluxed for 5 hr under stirring. Crude IIIf (2.13 g, IR: ν_{NH} 3300, $\nu_{C=O}$ 1720 cm^{-1}) obtained by evaporating the solvent under reduced pressure was recrystallized 6 times from carbon tetrachloride to give pure IIIf, 39.7 mg, mp 140—144 °C, $[\alpha]_D^{24}$ +12.9° (*c* 1.07, benzene). IIIf (25 mg) thus obtained was dissolved in a mixture of acetic acid (10 ml) and concentrated hydrochloric acid (10 ml) and the mixture was refluxed for 4 hr. 2,5-Dihydroxy-8-carboxytriptycene formed showed no optical activity.

BULLETIN OF THE CHEMICAL SOCIETY OF JAPAN, VOL. 46, 1525—1528 (1973)

Aminosugars. XXI. Conformation of Cyclic Imido Groups Attached to the Glucopyranose-ring[1]

Masaharu IWAKAWA and Juji YOSHIMURA

Laboratory of Chemistry for Natural Products, Faculty of Science, Tokyo Institute of Technology, Ookayama, Meguro-ku, Tokyo

(Received December 18, 1972)

Conformation of cyclic imido groups at different positions on *O*-acetylated-D-glucopyranose-ring was examined from the anisotropic effect of the carbonyls on vicinal ring-protons. The imide-plane at β-C_1, C_3 were deduced to be slightly inclined counter-clockwise, from the right angle to the mean plane of the pyranose ring, and that at α-C_2 and C_4 clockwise. 3-Deoxy-1,2 ; 5,6-di-*O*-isopropylidene-3-phthalimido-α-D-gluco- and -allofuranose were also examined.

Conformations of lactol-rings of monosaccharides[2] and their derivatives[3] in solution have been widely analyzed by NMR, however, those of substituents have been scarcely studied. In the course of synthetic studies of this series, we have noticed in NMR spectra of some phthalimido and succinimido derivatives that some vicinal ring protons showed a remarkable shift to lower fields, reflecting the steric direction of the magnetic anisotropy of the imide-carbonyl groups. This paper deals with the conformation of the cyclic imide-ring attached to various positions of the D-glucopyranose-ring in terms of comparison of the chemical shift of ring protons with that of the corresponding acetamido derivative.

Results and Discussion

Acetylated 2-deoxy-2-phthalimido-α- (**1**)[4,5] and -β-D-glucopyranose (**2**)[6], and 2-deoxy-2-succinimido-α- (**3**)[7] and -β-D-glucopyranose (**4**)[7,8] have been generally synthesized by the imidation method of tetra-*O*-acetyl-2-amino-2-deoxy-α- and -β-D-glucose[4,6,7,8] or by simulutaneous acetylation and imidation of mono-*N*-acylated derivative.[5] Benzyl 3,4,6-tri-*O*-acetyl-2-deoxy-2-phthalimido-α-D-glucopyranoside (**5**) and ethyl 3-*O*-acetyl-4,6-*O*-benzylidene-2-deoxy-2-phthalimido-α-D-glucopyranoside (**6**), 1-*N*-phthalyl 2,3-di-*O*-acetyl-4,6-*O*-benzylidene-β-D-glucopyranosylamine (**7**), methyl 2-*O*-acetyl-4,6-*O*-benzylidene-3-deoxy-3-phthalimido-α-D-glucopyranose (**8**), and methyl 2,3,6-tri-*O*-acetyl-4-deoxy-4-phthalimido-β-D-glucopyranoside (**9**) were newly prepared by the latter method from suitable starting materials. 3-Deoxy-1,2;5,6-di-*O*-isopropylidene-3-phthalimido-α-D-allofuranose (**10**) and -α-D-glucofuranose (**11**) were synthesized by the former method from the corresponding aminosugars.

All NMR spectra of new compounds and other cyclic imide derivatives, except that of **1**[5], were measured at 100 MHz, and analyzed with double resonance techniques. To estimate the deshielding effect of imide-carbonyl groups, NMR spectra of the corres-

1) Part XX. This Bulletin, **45**, 2027 (1972).
2) S. J. Angel, *Angew. Chem.*, **81**, 172 (1969).
3) L. D. Hall, *Advan. Carbohyd. Chem.*, **19**, 51 (1964).
4) S. Akiya and T. Osawa, *Chem. Pharm. Soc. Jap.*, **8**, 583 (1960).
5) S. Hirano, *Carbohyd. Res.*, **16**, 229 (1971).
6) S. Akiya and T. Osawa, *Yakugaku Zasshi*, **77**, 726 (1957).
7) S. Akiya and T. Osawa, *Chem. Pharm. Soc. Jap.*, **8**, 588 (1960).
8) B. R. Baker, J. P. Joseph, R. E. Schaub, and J. H. Williams *J. Org. Chem.*, **19**, 1786 (1954).

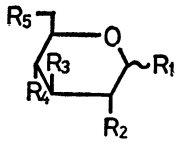

	R_1	R_2	R_3	R_4	R_5
1:	α-OAc	–N=Phth	OAc	OAc	OAc
2:	β-OAc	–N=Phth	OAc	OAc	OAc
3:	α-OAc	–N=Suc	OAc	OAc	OAc
4:	β-OAc	–N=Suc	OAc	OAc	OAc
5:	α-OAc	$-N(Ac)_2$	OAc	OAc	OAc
6:	β-OAc	$-N(Ac)_2$	OAc	OAc	OAc
7:	α-OBzl	–N=Phth	OAc	OAc	OAc
8:	α-OEt	–N=Phth	OAc	4,6-*O*–Ben	
9:	β-N=Phth	OAc	OAc	4,6-*O*–Ben	
10:	α-OMe	OAc	–N=Phth	4,6-*O*–Ben	
13:	β-OMe	OAc	OAc	–N=Phth	OAc

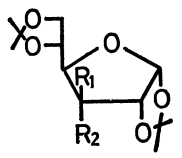

	R_1	R_2
11:	H	–N=Phth
12:	–N=Phth	H

Phth: Phthalyl, Suc: Succinyl, Ben: Benzylidene

TABLE 1. $\Delta\delta$ VALUE OF RING PROTONS BETWEEN THE CYCLIC IMIDO AND ACETAMIDO DERIVATIVE OF D-GLUCOPYRANOSES

Compounds		$\Delta\delta$ value			
No.	Substituents	H_1	H_2	H_3	H_1+H_3
1	2-Phthalimido-α	−0.09	−0.27	−1.36	−1.45
2	2-Phthalimido-β	−0.74	−0.04	−0.70	−1.44
3	2-Succinimido-α	+0.07	−0.05	−1.24	−1.17
4	2-Succinimido-β	−0.67	+0.16	−0.53	−1.20
5	Benzyl 2-phthalimido-α	−0.03	−0.16	−1.42	−1.45
6	Ethyl 4,6-*O*-Ben-2-phthalimido-α	−0.08	−0.22	−1.35	−1.43
7	1-Phthalimido-β	−0.17	−0.86		
12	2-Acetylacetamido-α	−0.05	−0.20	−0.91	−0.96
13	2-Acetylacetamido-β	−0.83	−0.54	−0.72	−1.55
		H_2	H_3	H_4	H_2+H_4
8	Methyl 4,6-*O*-Ben-3-phthalimido-α	−0.53			
10	1,2; 5,6-Di-*O*-Ip-3-phthalimodo-α-D-allofura.	−0.10	−0.23	*ca.* −1.3	*ca.* −1.4
11	1,2; 5,6-Di-*O*-Ip-3-phthalimido-α-D-glucofura.	−0.38	−0.52	−0.22	−0.60
		H_3	H_4	H_5	H_3+H_5
9	4-Phthalimido-β	−0.64	+0.34	−0.89	−1.53

Ip: Isopropylidene Ben: Benzylidene

ponding acetamido derivatives were taken in the same conditions, except that of **1**—**4**[9] and **8**.[10] The corresponding acetamido derivatives of **6**, **7**, and **9** were newly prepared. The chemical shift differences ($\Delta\delta$ values) of vicinal ring protons between cyclic imido and acetamido derivatives were summarized in Table 1, together with that of 1,3,4,6-tetra-*O*-acetyl-2-(*N*-acetylacetamido)-2-deoxy-α- (**12**) and -β-D-glucopyranose (**13**) reported by Inch *et al.*[9]

Comparison of $\Delta\delta$ values of **12** (α-anomer) and **13** (β-anomer) showed that only H_3 proton was shifted remarkably (0.91 ppm) in the case of **12**, while both H_1 and H_3 protons were substantially deshielded (0.83 and 0.72 ppm) in the case of **13**. The similar tendency was also observed in the case of phthalimido (**1**, **2**) and succinimido (**3**, **4**) derivatives, however, deshielding of H_3 proton in α-anomers (**1**, **3**) was further enhanced from 0.33 to 0.45 ppm compared with **12**. The steric direction of magnetic anisotropy of acetylacetamide-carbonyl groups in **12** and **13** might be, to some extent, controlled by the steric compression, and that in **1**—**4** are to be fixed by chemical bonding. Inch et al explained the difference in $\Delta\delta_{H_3}$ of **12** and **13** by the additional deshielding effect of axial C_1-acetoxy group, however, this enhancement must be attributed to the difference of the steric direction of magnetic anisotropy between non-fixed and fixed imide-carbonyl groups, in which the cyclic imide plane is inclined toward H_3 proton by the repulsion of axial C_1-acetoxy group, as was shown in Fig. 1. These deductions were supported by the fact that the deshielding effect on H_3-proton in **5** (1.42 ppm) and **6** (1.35 ppm) are still

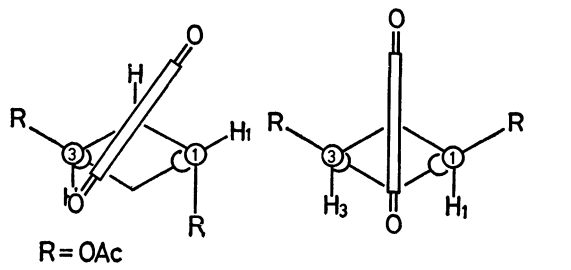

(**1**) (**2**)

H_3	H_1	H_3	H_1
−1.0 ppm	−0.02 ppm	−0.18 ppm	−0.18 ppm

Fig. 1. Conformation of 2-phthalimido group of **1** and **2**.

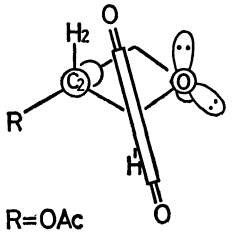

(**7**)

Fig. 2. Conformation of 1-phthalimido group of **7**.

9) T. D. Inch, J. R. Plimmer, and H. G. Flecher, Jr., *J. Org. Chem.* **31**, 1825 (1966).
10) R. D. Guthrie and L. F. Johnson, *J. Chem. Soc.*, **1961**, 4166.

large. Difference in these values may indicate that the benzyloxy group is bulkier than the ethoxy group.

It is interesting that the sum of $\Delta\delta$ value of H_1 and H_3 protons is almost constant in 2-phthalimido derivatives (**1**, **2**, **5**, **6**), regardless of the configuration of anomeric carbon, the smaller sum in succinimido and acetylacetamido derivatives might be attributed to the absence of the anisotropy of benzene ring, and the randomness of the conformation of carbonyl groups, respectively.

On the other hand, Booth[11] showed that the plane of phthalimide in *trans*-4-(*t*-butyl)-1-phthalimidocyclohexane ring is at right angle to the mean plane of the cyclohexane ring in the preferred conformation and that the vicinal axial protons resonate at about 0.7 ppm lower magnetic field than the vicinal equatorial protons by the deshielding effect of the magnetic anisotropy of the phthalimide-carbonyl group. The difference of $\Delta\delta$ value of H_1-proton in α- and β-anomers are consistent with that of cyclohexane derivative. X-ray analysis of phthalimido-cyclohexane[12] and phthalimide itself[13] showed the co-planerity of three bonds of nitrogen and the conformation offered by Booth.[11] An attempted estimation of deshielding effect of an imide-carbonyl group on the vicinal protons from theoretically calculated values of long-range shielding[14] indicated that the values in the α-anomers and the general tendency in β-anomers consisted with that of measured. Consequently, the phthalimide-plane in **1** is inclined clockwise about 30—35°.

The $\Delta\delta$ value of H_2-proton in **7** is a little bit larger than that of H_3 in **2**, indicating an electrostatic repulsion between the carbonyl group and lone paired electrons of the lactol-oxygen (Fig. 2). In contrary, a smaller $\Delta\delta$ value of H_2 in **8** than that of H_1 and H_3 in **2** indicates a little counterclockwise inclination of the phthalimide ring, though $\Delta\delta$ value of H_4 could not be estimated. In the case of 4-phthalimido derivative (**9**), larger $\Delta\delta$ value of H_5 than that of H_3 indicates that C_5-acetoxymethyl is bulkier than C_3-acetoxy group.

In case of 3-deoxy-1,2-*O*-isopropylidene-3-phthalimido-α-D-furanoses in which C_2 and C_3 atoms are displaced in opposite side from the plane of the other ring atoms, the remarkable shift of H_5 in **10** indicates that the phthalimide ring is inclined clockwise about 30°, in order to decrease the steric hindrance with endomethyl of 1,2-*O*-isopropylidene group and the repulsion with C_2-oxygen, while the phthalimido group in **11** seems to be free from such hindrances.

Thus, the steric direction of anisotropy of cyclic imido group is diagnostic for the steric compression and electrostatic effect of environment.

Experimental

Melting points were determined with Yanaco micro melting point apparatus and not corrected. Optical rotations were measured with a Carl Zeiss LEP-Al Polarimeter, in a 0.5-dm tube. NMR spectra were taken with JEOL 4H-100 NMR spectrometer in 10% deuteriochloroform solution containing tetramethylsilane as an internal reference. Chemical shifts and coupling constants were given in δ and Hz units, respectively.

General Synthesis of Cyclic Imido Derivatives: a) Free aminosugars were treated with phthalic anhydride or succinic anhydride in appropriate quantity of methanol, and after standing overnight the corresponding monoacylated compounds were obtained as precipitates or as a sirup by evaporation of the solution. The products were dried over phosphorous pentoxide and then treated with acetic anhydride (2 equimolar amounts) in pyridine solution. After standing 1 day at room temperature the mixture was poured into ice-water, and precipitates appeared (**6**) were filtrated and recrystallized from suitable solvents. When a sirup deposited, it was extracted with chloroform, and the sirup obtained from the extracts were purified chromatographically, using a column or preparative thin layer of silicagel (**5**, **7**, **8**, **9**).

b) A solution of aminosugar (1 mmol) and phthalic anhydride (1.1 mmol) in pyridine (1 ml) was kept overnight at room temperature, and then acetic anhydride (2 mmol) was added. After 24 hr, the mixture was poured into ice-water, the sirup deposited was extracted with chloroform and treated in the usual manner. The product was chromatographed on silica gel column (**10**, **11**).

*Benzyl 3,4,6-tri-O-acetyl-2-deoxy-2-phthalimido-α-D-glucopyranoside (**5**)* was prepared from benzyl 2-amino-2-deoxy-α-D-glucopyranoside hydrochloride.[15] A sirup was obtained in 24% yield. $[\alpha]_D^{23}=+173°$ (*c* 1.69, $CHCl_3$); NMR: 1.85, 2.03, and 2.10 (3×Ac), 3.80—4.35 (H_5, H_6, and $H_{6'}$; m), 4.45 and 4.72 ($-CH_2-$; ABq, $J_{AB}=11.75$), 4.52 (H_2; q, $J_{1,2}=3.75$, $J_{2,3}=11.25$), 5.00 (H_1; d), 5.08 (H_4; t, $J_{3,4}=J_{4,5}=10.0$), 6.70 (H_3; q), 7.10 (Ph; s), 7.80 (Ph; m).

Found: C, 61.20; H, 5.19; N, 2.80%. Calcd for $C_{27}H_{27}NO_{10}$: C, 61.71; H, 5.18; N, 2.67%.

*Ethyl 3-O-acetyl-4,6-O-benzylidene-2-deoxy-2-phthalimido-α-D-glucopyranoside (**6**)* was obtained in 26% yield from ethyl 2-acetamido-2-deoxy-α-D-glucopyranoside[16] by benzylidenation, de-*N*-acetylation, and phthalimidation. $[\alpha]_D^{23}=+125°$ (*c* 0.88, $CHCl_3$); NMR: 1.10 (CH_3; t, $J=7.0$), 1.90 (OAc), 3.2—4.4 ($-CH_2-$; H_4, H_5, H_6 and $H_{6'}$), 4.55 (H_2; q, $J_{1,2}=3.75$, $J_{2,3}=11.25$), 4.93 (H_1; d), 5.52 (-CH=; s), 6.70 (H_3; q, $J_{3,4}=10.0$), 7.3—7.9 (2×Ph; m).

Found: C, 64.23; H, 5.39; N, 3.00%. Calcd for $C_{25}H_{25}NO_8$: C, 64.39; H, 5.49; N, 2.92%.

The corresponding acetamide derivative was prepared by the treatment with acetic anhydride in pyridine in 54% yield. Mp. 181.5—182°C (EtOH); $[\alpha]_D^{20}=+44.6°$ (*c* 1.09, $CHCl_3$); NMR: 1.25 (CH_3; t, $J=7.0$), 1.98 (OAc), 2.08 (NAc), 3.4—4.1 (H_4, H_5, H_6, $H_{6'}$, and $-CH_2-$), 4.33 (H_2: sextet, $J_{1,2}=3.75$, $J_{2,3}=J_{H_3,NH}=10.0$), 4.85 (H_1; d), 5.35 (H_3; t, $J_{3,4}=10.0$), 5.55 (-CH=; s), 5.90 (NH; d), 7.40 (Ph; m).

Found: C, 60.03; H, 6.62; N, 3.65%. Calcd for $C_{19}H_{25}NO_7$: C, 60.14; H, 6.64; N, 3.69%.

*1-N-Phthalimido-2,3-di-O-acetyl-4,6-O-benzylidene-β-D-glucopyranosylamine (**7**)* was prepared from 4,6-*O*-benzylidene-β-D-glucopyranosylamine[17] in 93% yield, and recrystallized from ethyl acetate. Mp. 238.5—240°C; $[\alpha]_D^{23}=-37.0°$

11) H. Booth, *Prog. NMR Spectrosc.*, **5**, 308 (1969).
12) P. Groth, *Acta Chem. Scand.*, **23**, 1076 (1969).
13) E. Matzat, *Acta Crystallogr., B*, **28**, 415 (1972).
14) L. M. Jackman and S. Sternhell, "Applications of Nuclear Magnetic Resonance Spectroscopy in Organic Chemistry", 2nd. Ed., Pergamon Press (1969).
15) J. Yoshimura, M. Fujimori, Y. Sugiyama, and H. Ando, This Bulletin, **44**, 3131 (1971).
16) J. Yoshimura, H. Ando, Y. Takahashi, H. Ono, and T. Sato, *Nippon Kagaku Zasshi*, **85**, 142 (1964).
17) C. Contsogeorgopoulos and L. Zervas, *J. Amer. Chem. Soc.*, **83**, 1885 (1961).

(c 1.01, $CHCl_3$); NMR: 1.90 and 2.05 (2×OAc), 3.6—4.4 (H_4, H_5, H_6, and H_6'; m), 5.47 (H_3; t, $J_{2,3}=J_{3,4}=9.0$) 5.49 (H_1; d, $J_{1,2}=9.0$), 5.04 (-CH=; s), 6.18 (H_2; t), 7.5—7.9 (2×Ph; m).

Found: C, 61.84; H, 4.81; N, 2.86%. Calcd for $C_{25}H_{23}NO_9$: C, 62.36; H, 4.81; N, 2.86%.

The corresponding *N*-acetamido derivative was prepared in the usual manner in 91% yield. Mp. 228—229°C; $[\alpha]_D^{23}=-20.9°$ (c 0.99, $CHCl_3$); NMR: 1.95—2.05 (2×OAc and NAc), 3.6—4.4 (H_4, H_5, H_6, and H_6), 4.90 (H_3; t, $J_{2,3}=J_{3,4}=10.0$), 5.32 (H_1; d, and H_2; t, $J_{1,2}=J_{2,3}=J_{N,H}=10.0$), 5.45 (-CH=; s), 6.17 (NH), 7.34 (Ph; m).

Found: C, 57.39; H, 5.79; N, 3.54%. Calcd for $C_{19}H_{23}NO_8$: C, 58.01; H, 5.89; N, 3.59%.

*Methyl 4,6-O-benzylidene-3-deoxy-3-phthalimido-α-D-glucopyranoside (**8**)* was prepared from methyl 3-amino-3-deoxy-4,6-*O*-benzylidene-α-D-glucopyranoside.[10] Mp. 225—230°C; $[\alpha]_D^{23}=+8.4°$ (c 0.71, $CHCl_3$); NMR: 1.93 (OAc), 3.45 (OCH_3), *ca.* 3.6—4.1 (H_6 and H_6'), 4.30 (H_5; m), 4.58 (H_4; t, $J_{3,4}=J_{4,5}=10.0$), 4.90 (H_3; t, $J_{2,3}=10.0$), 5.02 (H_1; d, $J_{1,2}=3.0$), 5.48 (-CH=; s), 5.60 (H_2; q).

Found: C, 62.98; H, 5.15; N, 2.99%. Calcd for $C_{24}H_{23}NO_8$: C, 63.57; H, 5.11; N, 3.09%.

*Methyl 2,3,6-tri-O-acetyl-4-deoxy-4-phthalimido-β-D-glucopyranoside (**9**)* was prepared in 30% yield from sirupy methyl 4-amino-4-deoxy-β-D-glucopyranoside, which was synthesized as follows. The crystals[18] (mp 80—90°C) obtained by glycosidation of D-galactose in methanol containing 1% of hydrogen chloride was treated as described in the literature[19] to give a sirupy product in 11% over all yield. Mp. 180—180.5°C; $[\alpha]_D^{23}=-87.1°$ (c 1.02, $CHCl_3$); NMR: 1.82, 1.95, 2.03 (3×OAc), 3.53 (OCH_3), 4.06 and 4.28 (H_6 and H_6'; d, ABq, $J_{6,6'}=12.5$, $J_{5,6'}=J_{5,6}=3.1$), 4.44 (H_4; t, $J_{4,5}=10.0$, $J_{3,4}=9.1$), 4.58 (H_1; d, $J_{1,2}=8.1$), 4.57 (H_5; sextet), 5.05 (H_2; q, $J_{2,3}=9.0$), 5.79 (H_3; t), 7.80 (Ph; m).

Found: C, 56.00; H, 5.24; N, 3.09%. Calcd for $C_{21}H_{23}NO_{10}$: C, 56.12; H, 5.16; N, 3.12%.

The corresponding acetamido derivative was prepared in the usual manner in 48% yield. Mp. 200—200.5°C; $[\alpha]_D^{23}=+13.8°$ (c 1.0, $CHCl_3$); NMR: 1.90, 2.02, 2.07 (3×OAc and NAc), 3.48 (OCH_3), 3.68 (H_5; sextet, $J_{5,6}=J_{5,6'}=3.75$, $J_{4,5}=9.5$), 4.10 (H_4; t, $J_{3,4}=9.5$), 4.23 (H_6 and H_6'; d), 4.42 (H_1; d, $J_{1,2}=7.5$), 4.95 (H_2; q, $J_{2,3}=9.5$), 5.15 (H_3; t).

Found: C, 49.87; H, 6.35; N, 3.95%. Calcd for $C_{15}H_{23}NO_9$: C, 49.86; H, 6.42; N, 3.88%.

*3-Deoxy-3-phthalimido-1,2;5,6-di-O-isopropylidene-α-D-allofuranose (**10**)* was prepared from 3-amino-3-deoxy-1,2;5,6-di-*O*-isopropylidene-α-D-allofuranose[20] in 67% yield. Recrystallization from ethanol gave a bulk solid. Mp. 131—132°C; $[\alpha]_D^{23}=+159°$ (c 1.04, $CHCl_3$); NMR: 1.28 and 1.60 (4×CH_3), *ca.* 3.8—4.3 (H_5, H_6, and H_6'; m), 4.48 (H_3; q, $J_{3,4}=10.0$, $J_{2,3}=5.0$), 4.73 (H_2; t, $J_{1,2}=4.5$), 5.52 (H_4; q, $J_{4,5}=5.0$), 5.88 (H_1; d), 7.25 (Ph; m).

Found: C, 61.81; H, 5.91; N, 3.56%. Calcd for $C_{20}H_{23}NO_7$: C, 61.69; H, 5.95; N, 3.60%.

*3-Deoxy-3-phthalimido-1,2;5,6-di-O-isopropylidene-α-D-glucofuranose (**11**)* was prepared from 3-amino-3-deoxy-1,2;5,6-di-*O*-isopropylidene-α-D-glucofuranose[21] in 86% yield. $[\alpha]_D^{23}=+32.7°$ (c 1.09, $CHCl_3$); NMR: 1.08, 1.33, 1.55 (4×CH_3), 3.7—4.0 (H_5, H_6, and H_6'), 4.42 (H_4; q, $J_{3,4}=5.25$, $J_{4,5}=7.50$), 4.92 (H_3; d), 4.95 (H_2; d, $J_{1,2}=3.75$), 6.31 (H_1; d), 7.82 (Ph; m).

Found: C, 62.13; H, 6.15; N, 3.56%. Calcd for $C_{20}H_{23}NO_7$: C, 61.69; H, 5.95; N, 3.60%.

NMR Data of Known Compounds. 1,3,4,6-Tetra-*O*-acetyl-2-deoxy-2-phthalimido-β-D-glucopyranoside (**2**)[6,8]; 1.38, 1.99, 2.04, 2.11 (4×OAc), *ca.* 3.9—4.45 (H_5, H_6, and $H_{6'}$), 4.48 (H_2; q, $J_{1,2}=8.75$, $J_{2,3}=10.5$), 5.21 (H_4; t, $J_{3,4}=J_{4,5}=9.5$), 5.90 (H_3; q), 6.51 (H_1; d), 7.81 (Ph; m).

1,3,4,6-Tetra-*O*-acetyl-2-deoxy-2-succinimido-α-D-glucopyranoside (**3**)[7]; 1.95; 2.02, 2.04, and 2.08 (4×OAc), 2.64 ($-CH_2CH_2-$; s), *ca.* 3.8—4.4 (H_5, H_6 and H_6), 4.51 (H_2; q, $J_{1,2}=3.75$, $J_{2,3}=11.25$), 5.07 (H_4; t, $J_{3,4}=J_{4,5}=9.5$), 6.13 (H_1; d), 6.44 (H_3; q).

1,3,4,6-Tetra-*O*-acetyl-2-deoxy-2-succinimido-β-D-glucopyranoside (**4**)[7]; 1.93, 2.00, 2.02, and 2.06 (4×OAc), 2.63 ($-CH_2CH_2-$; s), 3.94 (H_5; m), *ca.* 4.0—4.4 (H_6 and H_6), 4.28 (H_2; t), 5.13 (H_4; t, $J_{3,4}=J_{4,5}=9.0$), 5.73 (H_3; t, $J_{2,3}=10.0$), 6.44 (H_1; d).

Benzyl 2-acetamido-3,4,6-tri-*O*-acetyl-2-deoxy-α-D-glucopyranoside (**5**)[22]; (-NH proton was diminished by shaking with deuterium oxide), 1.92, 2.05, 2.13 (3×OAc, NAc), 3.8—4.25 (H_5, H_6, and H_6'), 4.36 (H_2; q, $J_{1,2}=3.75$, $J_{2,3}=7.5$), 4.51 and 4.72 ($-CH_2-$; ABq, $J_{AB}=11.5$), 4.97 (H_1; d), 5.13 (H_4; t, $J_{3,4}=J_{4,5}=9.5$), 5.28 (H_3; q), 7.48 (Ph).

3-Acetamido-3-deoxy-1,2;5,6-di-*O*-isopropylidene-α-D-allofuranose (**10**)[23]; 1.35, 1.45, 1.58 (4×CH_3), 2.02 (NAc), 3.8—4.32 (H_4, H_5, H_6, and H_6'). (H_3 was assigned to 4.25 by irradiating at H_2) *ca.* 4.2 (H_4), 4.62 (H_2; q, $J_{1,2}=3.75$, $J_{2,3}=4.75$), 5.84 (H_1; d), 6.07 (NH; d, $J=8.0$).

3-Acetamido-3-deoxy-1,2;5,6-di-*O*-isopropylidene-α-D-glucofuranose (**11**)[24]; 1.29, 1.34, 1.42, 1.50 (4×CH_3), 2.00 (NAc), 3.86 (H_6; q, $J_{6,6'}=8.50$), 4.10 (H_6'; q, $J_{4,5}=J_{5,6}=J_{5,6'}=6.25$), 4.20 ($H_4$; q, $J_{3,4}=3.50$), 4.31 (H_5; q), 4.40 (H_3; q, $J_{H_3-NH}=7.0$), 4.57 (H_2; d, $J_{1,2}=3.75$), 5.85 (H_1; d), 6.78 (NH; d).

The authors are indebted to Mr. K. Fukukawa and H. Matsumoto for NMR measurements, Mr. Y. Ogura for his help for a part of experiments, and members of Laboratory of Organic Analysis for microelemental analysis.

18) J. K. Dale and C. S. Hudson, *J. Amer. Chem. Soc.*, **52**, 2534 (1930).
19) E. J. Reist, R. R. Spencer, D. F. Calkins, B. R. Baker, and L. Goodman, *J. Org. Chem.*, **30**, 2312 (1965).
20) M. L. Wolfrom, F. Shafizadeh, and R. K. Armstrong, *J. Amer. Chem. Soc.*, **80**, 4885 (1958).
21) W. Meyer, *Angew. Chem. Int. Ed. Engl.*, 5, 967 (1966).
22) J. Yoshimura, M. Funabashi, S. Ishige, and T. Sato, This Bulletin, **39**, 1760 (1966).
23) B. Coxon and L. Hough, *J. Chem. Soc.*, **1961**, 1643.
24) D. T. Williams and J. K. Jones, *Can. J. Chem.*, **45**, 7 (1967).

Photochemical Reaction of 1,2-Naphthoquinone and Its Derivatives with Xanthene[1]

Kazuhiro MARUYAMA and Akio TAKUWA*

Department of Chemistry, Faculty of Science, Kyoto University, Kyoto 606

**Department of Chemistry, Faculty of Literature and Science, Shimane University, Matsue*

(Received December 27, 1972)

In contrast to other *o*-quinones, photochemical reaction of 1,2-naphthoquinone with xanthene gave a 1 : 1 adduct in which xanthene moiety is attached to position C_4, *i.e.*, 1,4-dihydro-2-hydroxy-4-xanthyl-1-ketonaphthalene (**2a**). The analogous photo-adducts, **2b**, **2c**, and **2d**, were obtained by the photochemical reaction of 3-chloro-1,2-naphthoquinone, 3-bromo-1,2-naphthoquinone, and 6-bromo-1,2-naphthoquinone with xanthene, respectively. The dynamic aspect of these reactions was also examined using the CIDNP technique and the reaction mechanism was discussed.

When *o*-quinones are irradiated in solution in the presence of hydrogen donors, "1,2-adduct" or "1,4-adduct"[2] is generally obtained corresponding to nature of the solvent used.[3] For example, Rubin[4] has shown that phenanthraquinone was irradiated in alkyl benzenes to give "1,2-adduct" and in ethers to give "1,4-adduct," respectively. Thus, the photochemical reactions of *o*-quinones, especially of phenanthraquinone, with hydrogen donors have been extensively investigated. However, the photochemical reaction of 1,2-naphthoquinone has not yet been described presumably from the view of its instability. However, it has been reported that the photochemical reactions of 1,2-naphthoquinone derivatives with aromatic aldehyde and stilbene[5] gave "1,4-adduct" and dioxin, respectively. Photochemical reaction of 1,2-naphthoquinone, 3-chloro-1,2-naphthoquinone, 3-bromo-1,2-naphthoquinone, and 6-bromo-1,2-naphthoquinone with xanthene as hydrogen donor were investigated in this work.

Results and Discussion

Reaction Products and Structure Determination. Equimolar 1,2-naphthoquinone and xanthene dissolved in benzene was irradiated in the usual glass tube for five hours. Photo-adduct precipitated is unstable in polar solvent or to a prolonged irradiation, it decomposes gradually to 1,2-naphthoquinone, its quinhydrone, 9,9′-bixanthyl, and some tarry matters. The structure of the photo-adduct was confirmed by the followings: the mild oxidation of the adduct, **2a**, with potassium permanganate gave phthalic acid and xanthone. The IR spectrum of **2a** exhibited the presence of both of intramoleculary hydrogen bonded hydroxyl group (3375 cm^{-1}) and chelated carbonyl (1640 cm^{-1}) group. The peaks at *m/e* 340, 181, 159, and 131 found in the mass spectrum of **2a** were interpreted in the term of scheme 1.

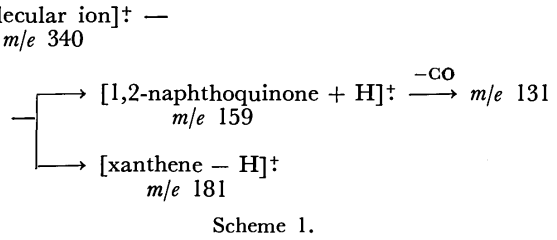

Scheme 1.

Elemental analysis and these results described above indicate that **2a** is a 1 : 1 adduct of 1,2-naphthoquinone and xanthene. The NMR spectrum of **2a** is shown in Fig. 1 and Table 1. The assignment of corresponding protons in Table 1 were confirmed by the followings. The signal at δ : 1.55 disappeared on addition of deutrium oxide in the sample, therefore it is due to hydroxyl proton (H_α). When the signal at δ : 3.93 (quartet) was irradiated by the spin decoupling technique, the doublet signals at δ : 4.54 and 5.76 changed to singlet, respectively. The signal at δ : 4.54 could not be observed with the photo-adduct which was obtained by the photochemical reaction of 1,2-naphthoquinone with xanthene-9-d_2, and at the same time the signal at δ : 3.93 changed to doublet. These results indicate that H_γ coupled with H_β and H_δ, respectively and thus H_δ is assigned to methine proton of xanthene moiety in the photo-adduct. Analogous photo-adducts having similar structure (**2b**, **2c**, and **2d**) were obtained by the photochemical reaction of 3-chloro-1,2-naphthoquinone, 3-bromo-1,2-naphthoquinone, and

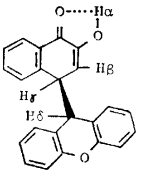

2a

1) A part of this work was reported by K. Maruyama and A. Takuwa, *Chem. Lett.*, **1972** 135.

2) In general, photo-adducts of *o*-quinone with RH having the next structures; $-\overset{OH}{\overset{|}{\underset{R}{\underset{|}{C_1}}}}-\overset{O}{\overset{\|}{C_2}}-$ and $-\overset{OH}{\overset{|}{C_1}}=\overset{OR}{\overset{|}{C_2}}-$, are used to call "1,2-adduct" and "1,4-adduct", respectively.

3) A. Schönberg, G. O. Schneck, and O. A. Neumüller, "Preparative Organic Photochemistry", Springer-Verlag, New York, Inc. (1968).

4) M. B. Rubin, *J. Org. Chem.*, **28**, 1949 (1963). M. B. Rubin and P. Zwitkowits, *ibid.*, **29**, 2362 (1964).

5) A. Schönberg, N. Latif, P. Moubasher, and A. Sina, *J. Chem. Soc.*, **1951**, 1364. A. Schönberg, W. I. Awad, and G. A. Mousa, *J. Amer. Chem. Soc.*, **77**, 3850 (1955). A, Mustafa, A. H. E. Narash, A. K. E. Mansour, and S. M. A. E. Omran, *ibid.*, **78**, 4306 (1956).

TABLE 1. NMR DATA OF **2a**—**2d** IN $CDCl_3$ (δ-VALUES FROM TMS)

	H_α	H_β	H_γ	H_δ	Aromatic-H	Coupling constant (Hz)
2a	1.55 b	5.76 d	3.93 q	4.54 d	5.50—7.95 m	J=4.5, J=3.8
2b	1.62 b	—	4.15 d	4.96 d	6.15—7.93 m	J=3.5
2c	1.61 b	—	4.11 d	4.85 d	5.98—7.80 m	J=3.6
2d	1.61 b	5.78 d	4.03 q	4.62 d	5.95—8.00 m	J=4.4, J=3.6

b=broad, d=doublet, q=quartet, m=multiplet
Assignments of protons correspond to the structural formula of **2a**.

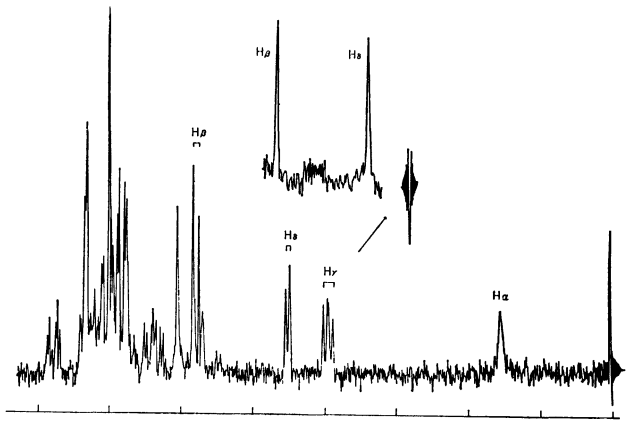

Fig. 1. NMR spectrum of **2a** in $CDCl_3$.

6-bromo-1,2-naphthoquinone with xanthene. The NMR spectra of these photo-adducts are summarized in Table 1.

Reaction Mechanism and CIDNP. 1,2-Naphthoquinones have a maximum absorption band owing to n–π^* transition at 520—527 nm (ε, 66—162) in chloroform.[6] 1,2-Naphthoquinone and its halogeno derivatives in benzene are excited *via* n–π^* to their photochemically active triplet states. The excited species abstract hydrogen from xanthene and simultaneously radical pair may be formed in solvent cage. The resulting radical pair is to be coupled to produce the photo-adduct. When the radical pair couples to give such a photo-adduct, the proton at the nearest-neighbor to the coupling center may give rise to the polarized PMR signals.[7] In the examination of the photochemical reaction of 1,2-naphthoquinone with xanthene in benzene by CIDNP technique, we could

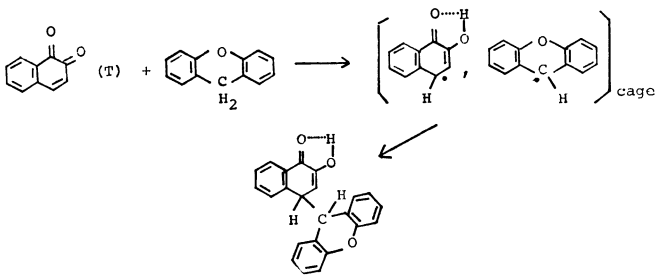

Scheme 2.

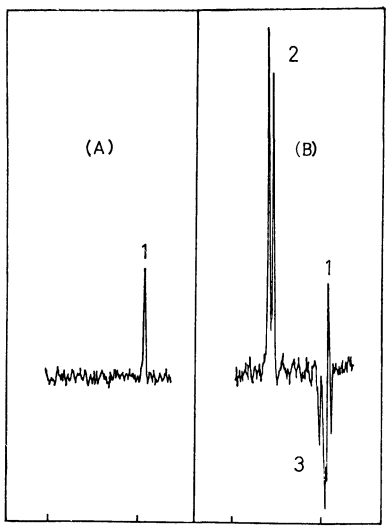

Fig. 2. Polarized PMR spectrum observed in the reaction of 1,2-naphthoquinone with xanthene in benzene solution.
A) Before irradiation. Signal 1: methylene protons of xanthene.
B) During the cource of irradiation. Signal 1: methylene protons of xanthene. Signal 2: absorption polarized signals, which correspond to the methine proton (H_δ) of xanthene rest in photo-adduct, **2a**. Signal 3: emission polarized signals, which correspond to the 4-position proton (H_γ) of quinone rest in photo-adduct, **2a**.

recognize the strongly polarized PMR signals only at δ : 4.34 (doublet, enhanced absorption), and δ : 3.93 (quartet, enhanced emission) signals. (Fig. 2). The CIDNP signals of photochemical reaction of 3-chloro-1,2-naphthoquinone with xanthene are shown in Fig. 3. Photochemical reaction of 6-bromo-1,2-naphthoquinone and 3-bromo-1,2-naphthoquinone with xanthene revealed the analogous polarized PMR signals in Figs. 2 and 3, respectively. The chemical shifts of these polarized PMR signals coincided with the δ-values of H_γ and H_δ in photo-adducts (**2a**–**2d**) as shown in Table 1. These phenomena indicate that the C_4-position of semiquinone radical coupled with xanthyl radical to give adduct. "1,2-Adduct" or "1,4-adduct" was not produced even in the course of reaction. If it was produced, a singlet polarized PMR signal (due to methine proton of xanthene moiety) should be observed as an instance of photochemical reaction of phenanthraquinone with xanthene.[8] The CIDNP

6) R. W. A. Oliver, R. M. Rashman, and A. W. Somerville, *Tetrahedron*, **24**, 4067 (1968).

7) For example, K. Maruyama, H. Shindo, T. Otsuki, and T. Maruyama, This Bulletin, **44**, 2756 (1971), and other papers cited in this paper.

8) K. Maruyama, T. Maruyama, and H. Shindo, This Bulletin, **44**, 585 (1971); **44**, 2000 (1971); **44**, 2789 (1971); **44**, 2885 (1971).

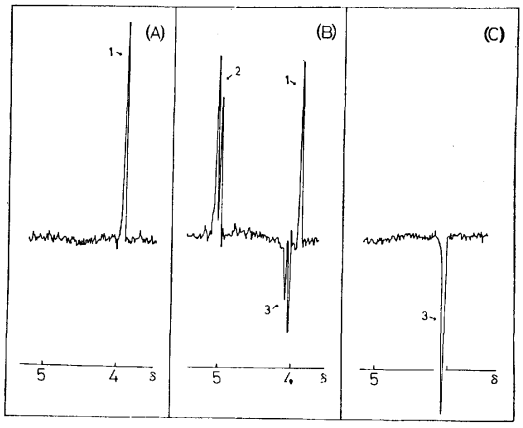

Fig. 3. Polarized PMR spectrum observed in the reaction of 3-chloro-1,2-naphthoquinone with xanthene in benzene solution.
A) Before irradiation. Signal 1: methylene protons of xanthene.
B) During the course of irradiation. Signal 1: methylene protons of xanthene. Signal 2: absorption polarized signals, which correspond to the methine proton (H_δ) of xanthene rest in photo-adduct, **2b**. Signal 3: emission polarized signals, which correspond to the 4-position proton (H_γ) of quinone rest in photo-adduct, **2b**.
C) Enhanced emission signal observed during irradiation in the reaction of 3-chloro-1,2-naphthoquinone with xanthene-9-d_2. Signal 3 due to the 4-position proton of the quinone rest in photo-adduct.

signal of the photochemical reaction of 3-chloro-1,2-naphthoquinone with xanthene-9-d_2 is shown in Fig. 3-C. The doublet enhanced absorption signals (due to the methine proton of xanthene moiety) in Fig. 3-B could not be observed and singlet enhanced emission signal was only observed corresponding to the doublet enhanced emission signal in Fig. 3-B. Therefore, the doublet enhanced absorption signals and enhanced emission signal in Fig. 3-B correspond to the proton of quinone moiety and the methine proton of xanthene moiety, respectively.

Experimental

Materials. 1,2-Naphthoquinone (mp 121—122 °C) was prepared by the oxidation of 1-amino-2-naphthol hydrochloride with ferric chloride.[9] 6-Bromo-1,2-naphthoquinone (mp 156 °C) was prepared by the oxidation of 6-bromo-2-naphthol with Fremy's salt.[6] 3-Chloro-1,2-naphthoquinone (mp 171 °C)[10] and 3-bromo-1,2-naphthoquinone (mp 164 °C)[11] were prepared by the chlorination and bromination of 1,2-naphthoquinone, respectively. Xanthene-9-d_2 was prepared by the reduction of xanthone with lithium aluminium deuteride.[12] Xanthene commercially available was further purified by recrystallization.

Spectra. Infrared spectra were taken with Jasco IR-G and Hitachi 215 infrared spectrometers with KBr disc. NMR spectra were observed with a JEOL C-60 HL spectrometer in $CDCl_3$(saturated) as a solvent and TMS as an internal indicater.

Photochemical Reaction. A typical photochemical reaction was accomplished as the following: 1,2-Naphthoquinones (0.5 mmol) and xanthene (0.5 mmol) dissolved or suspended in benzene was irradiated in ordinary glass tube by 300 W high-pressure mercury arc lamp through 5—10 cm thick water layer at 0—5 °C. Yield was nearly 50—60% in all cases.

Analyses of Photochemical Products. 1,4-Dihydro-2-hydroxy-4-xanthyl-1-ketonaphthalene (**2a**): A suspension of 1,2-naphthoquinone and xanthene in benzene was irradiated for 5 hr. A white needles deposited was collected and recrystallized from benzene–petroleum at ordinary temperature; White needles, mp 121—123 °C (dec.); IR, ν_{OH}: 3375, $\nu_{C=O}$: 1640 cm^{-1}). Elemental analysis, Found, C: 81.31, H: 4.81%. Calcd for $C_{23}H_{16}O_3$, C: 81.16, H: 4.74%. Oxidation of **2a** with potassium permanganate in acetone–water solution gave phthalic acid, mp 190—190.5 °C and xanthone, mp 173 °C, undepressed on admixture with an authentic specimen.

*1,4-Dihydro-2-hydroxy-3-chloro-4-xanthyl-1-ketonaphthalene (**2b**).* Irradiation of the benzene solution of 3-chloro-1,2-naphthoquinone and xanthene was for 4 hr. The characteristic orange-red color of the quinone faded to pale yellow. Removal of the benzene under reduced pressure left a yellowish brown solid mass. It was washed with petroleum ether and then small amount of benzene, and recrystallized from benzene–petroleum ether, pale yellow leaves, mp 157—158 °C (dec.); ν_{OH}: 3375 cm^{-1}, $\nu_{C=O}$: 1665 (w), 1640(vs) cm^{-1}, Found; C: 73,63, H: 3.86%, Calcd for $C_{23}H_{15}ClO_3$, C: 73.70, H: 4.03%.

*1,4-Dihydro-2-hydroxy-3-bromo-4-xanthyl-1-ketonaphthalene (**2c**)* Separation and purification were the analogous work-up described above, pale yellow prism, mp 143—144 °C (dec.); ν_{OH}: 3375 cm^{-1}, $\nu_{C=O}$: 1665 (w), 1640 (vs) cm^{-1}; Found, C: 65.85, H: 3.54%, Calcd for, $C_{23}H_{15}BrO_3$, C: 65.81, H: 3.61%.

*1,2-Dihydro-2-hydroxy-4-xanthyl-6-bromo-1-ketonaphthalene (**2d**).* Irradiation of the benzene solution of 6-bromo-1,2-naphthoquinone and xanthene was for 2 hr. The characteristic reddish brown color of the quinone faded to almost colorless. Benzene was removed under reduced pressure, and the resulting brown solid was washed with petroleum ether and then with benzene containing 50% petroleum ether, and recrystallized from benzene–petroleum ether; white needles, mp 130—131 °C (dec.); ν_{OH}: 3375 cm^{-1}, $\nu_{C=O}$: 1640 cm^{-1}; Found, C: 65.71, H: 3.54%, Calcd for $C_{23}H_{15}BrO_3$, C: 65.89, H: 3.61%.

CIDNP Examination. Investigation of these photochemical reactions by CIDNP technique was performed using JEOL C-60 HL spectrometer, equipped with the modified NMR probe for the photo-irradiation. The detailed method used was described in this Bulletin by K. Maruyama *et al.*[7]

9) A. H. Blatt, "Organic Syntheses" Coll. Vol. 2, p. 430 (1948).
10) T. Zincke, *Ber.*, **19**, 2497 (1886).
11) T. Zincke, *ibid.*, **19**, 2495 (1886).
12) A. Mustafa and M. K. Hilmy, *J. Chem. Soc.*, **1952**, 1345.

Studies on Nitro Sugars. III.[1] The Synthesis of 3-Nitrohexofuranose Derivatives

Tetsuyoshi TAKAMOTO, Yoh-ichi YOKOTA, Rokuro SUDOH, and Toshio NAKAGAWA*

Department of Chemistry, Tokyo Institute of Technology, O-okayama, Meguro-ku, Tokyo 152

**Department of Chemistry, Yokohama City University, Mutsuura-cho, Kanazawa-ku, Yokohama 236*

(Received July 31, 1972)

The oxidation of 1,2;5,6-di-*O*-isopropylidene-3-oximino-α-D-*ribo*-hexofuranose (**1**) with trifluoroperacetic acid at a low temperature afforded, in a 75% yield, the corresponding 3-nitro-allofuranose (**3**), but at a high temperature it gave at least three nitro compounds, *i.e.*, **3**, 3-deoxy-1,2-*O*-isopropylidene-3-nitro-α-D-allofuranose (**6**) and 3,6-anhydro-3-nitro-α-D-glucofuranose (**8**). **6** was converted to 5,6-di-*O*-acetate (**7**) and confirmed by comparison with the 3-epimer (**11**), which was prepared by the acetonation of 3-deoxy-3-nitro-D-glucose, partial hydrolysis and acetylation. The structure of **8** was instrumentally determined and supported by the fragmentation pathways in its mass spectrometry. The formation of **8** was assumed to proceed through nitronic acid (**5**) as an intermediate.

In our studies of nitro sugars for synthesizing some kinds of carbohydrate derivatives,[2,3] *e. g.*, branched sugars,[4] epoxides,[4] polyamino sugars,[5] and 2′-nucleosides,[6] a new method of synthesizing nitro sugars, particularly 2- and 3-nitro sugars, in an entirely different way had been required as a matter of course. Recently, we have presented[7] a novel route to nitro sugars with the following reaction sequence: >CH–OH⟶>C=O⟶>C=NOH⟶>CH–NO_2; in this route we used trifluoroperacetic acid oxidation[8] for the final step, and thus synthesized some 3-deoxy-3-nitro-α-D-pento- and hexo-furanose in excellent yields. Thie new method seems to promise a wide application, being capable of introducing a nitro group into a desired position of a furanose ring as well as of a pyranose one.[9]

In connection with the examination of this method, we now describe the oxidation of 3-oximino-hexofuranose derivative, the isolation of two by-products and the determination of their structures.

Results and Discussion

When 1,2;5,6-di-*O*-isopropylidene-3-oximino-α-D-*ribo*-hexofuranose (**1**)[10] was treated below 5 °C with trifluoroperacetic acid in the presence of dibasic sodium phosphate in acetonitrile, the corresponding 3-deoxy-3-nitroallo-furanose (**3**), $\nu_{as\ NO_2}$ 1560 cm^{-1}, was easily prepared in a 75% yield.[7] The *allo*-configuration of **3** was assigned on the basis of the coupling constant, $J_{2.3}$ (4.5 Hz)[11] and a chemical identification; the catalytic reduction of **3**, followed by *N*-acetylation, gave, in an 86% yield, 3-acetamido-3-deoxy-1,2; 5,6-di-*O*-isopropylidene-α-D-allofuranose (**4**), which was characterized by comparison with an authentic sample.[12]

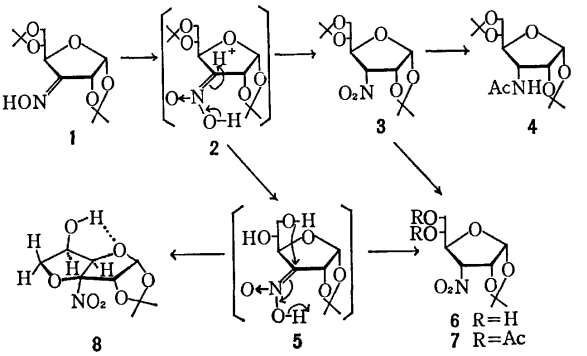

Scheme 1.

On the tlc of the reaction mixture, at least two by-products were detected. Under refluxing conditions, in contrast to the case with a low temperature, compound **3** was not detected, but the amounts of the by-products increased. The two by-products, 3-deoxy-1,2-*O*-isopropylidene-3-nitro-α-D-allofuranose (**6**) and 3,6-anhydro-1,2-*O*-isopropylidene-3-nitro-α-D-glucofuranose (**8**), were isolated by column chromatography, with benzene–acetone (20 : 1) as the eluent.

The structural and configurational assignments of these products rest on chemical as well as on spectroscopic evidence. The former was converted to the corresponding 5,6-di-*O*-acetate (**7**), which showed that $J_{2.3}$=3.5 Hz[11] can be assigned to the *allo*-configuration, when compared with the *gluco*-isomer (**11**), which has not coupling constant between H-2 and H-3 (see Fig. 2). The latter, $C_9H_{13}NO_7$, was unchanged by periodate oxidation and recovered. In the IR spectra, $\nu_{as\ NO_2}$ band at 1550 cm^{-1} (KBr disc) and a weak intramolecular hydrogen bond between the hydroxyl group and the ring-oxygen atom at 3555 cm^{-1} in the 0.15—0.004 mol/l concentration range in chloroform

1) Part II, *Carbohyd. Res.*, in press.

2) F. W. Lichtenthaler, *Angew. Chem.*, **76**, 84 (1964); *Newer Methods of Preparative Org. Chem.*, **4**, 155 (1968); *Fortschr. Chem. Forsch.*, **14**, 556 (1970).

3) H. H. Baer, *Advan. Carbohyd. Chem. Biochem.*, **24**, 67 (1969).

4) T. Sakakibara, S. Kumazawa, and T. Nakagawa, This Bulletin, **43**, 2655 (1970).

5) T. Nakagawa, Y. Sato, T. Takamoto, F. W. Lichtenthaler, and N. Majer, *ibid.*, **43**, 3866 (1970).

6) T. Nakagawa, T. Sakakibara, and S. Kumazawa, *Tetrahedron Lett.*, 1970, 1645.

7) T. Takamoto, R. Sudoh and T. Nakagawa, *ibid.*, **1971**, 2053.

8) W. D. Emmons and A. S. Pagano, *J. Amer. Chem. Soc.*, **77**, 4557 (1955).

9) T. Takamoto, Doctor Dissertation, Tokyo Institute of Technology, January 1972.

10) K. Onodera, S. Hirano and N. Kashimura, *Carbohyd. Res.*, **6**, 276 (1968).

11) R. J. Abraham, L. D. Hall, L. Hough, and K. A. Mclauchlan, *Chem. Ind.* (London), **1962**, 213; *J. Chem. Soc.*, **1962**, 3699.

Table 1. The NMR data of 3-nitro-hexofuranose derivatives (TMS as an internal standard in $CDCl_3$)

Compound	Chemical shift of ring protons (τ)							Other protons (τ)	Coupling constant (Hz)						
	H-1	H-2	H-3	H-4	H-5	H-6	H-6′		J_{12}	J_{23}	J_{34}	J_{45}	J_{56}	$J_{56'}$	$J_{66'}$
3	4.09 d	4.95 q	5.1—5.3 m			5.7—6.2 m		8.45, 8.60, 8.65, 8.67 CH_3>C<CH_3	4	4.5	?	?	?	?	?
7	4.12 d	?	4.71 q	4.85—5.1 m		5.51 q	5.94 q	8.44, 8.64 CH_3>C<CH_3; 7.94, 7.97 OAc	3	3.5	7	?	3	4.5	12
8	3.94 d	5.22 d	—	4.61 d	5.42 q	5.80 q	5.95 q	8.42, 8.61 CH_3>C<CH_3; 7.53 OH	4	—	—	5	5	5	10
9	3.92 d	5.02 d	4.92 d	5.66 q		5.8—6.2 m		8.47, 8.56, 8.64, 8.68 CH_3>C<CH_3	4	0	4	8	?	?	?
11	3.90 d	5.00 d	4.93 d	5.34 q	5.09 o	5.43 q	5.89 q	8.48, 8.64 CH_3>C<CH_3; 7.94 OAc	3	0	4	8	3	4	12

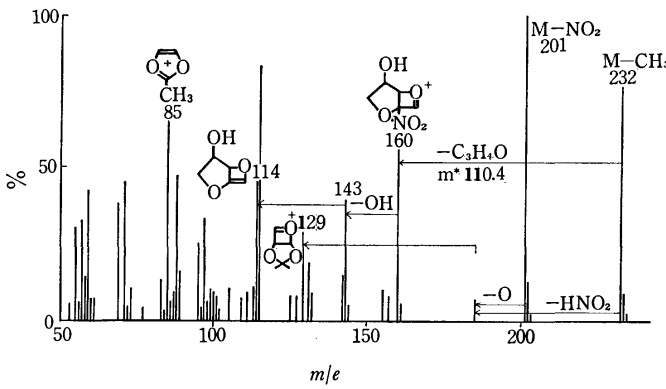

Fig. 1. Mass spectrum of 3,6-anhydro-1,2-*O*-isopropylidene-3-nitro-α-D-glucofuranose (**8**).

are observed. In the NMR spectrum, as is shown in Table 1, two methyl protons of the *O*-isopropylidene group, one hydroxyl proton, and six ring-proton signals of the sugar skeleton are observed. The NMR data suggest the absence of the ring proton at the C-3 position. Furthermore, the mass spectrum provides two significant pieces of information regarding the structure; the M–CH_3 ion peak at *m/e* 232, which is characteristic[13] of *O*-isopropylidene derivatives, and the M–NO_2 peak at *m/e* 201, which means a specific structure since no split of $-NO_2$ at the first step was observed[14] in the mass spectra of ten new nitro sugars which have a secondary nitro group besides nitroolefin and **8**. Consequently, the 3,6-anhydro structure of **8** was found to agree with all these data; it was also supported by the fragmentation pathways, as is shown in Fig. 1.

As is shown in Table 2, the formation of **3**, **6**, and **8** was obviously dependent on the temperature and on the ratio of trifluoroperacetic acid and dibasic sodium phosphate used as a buffer. In this reaction, as is shown in Scheme 1, the intermediary nitronic acid (**2**) may be normally converted to **3** through prototropy from the upper side of the furanose ring under mild conditions. In the presence of a smaller amount of the buffer and/or under an elevated temperature, however, **3** should be hydrolyzed to afford **6**. On the other hand, the 3,6-anhydro derivative **8** may be formed through the intermediate (**5**) which is derived from **2** by partial hydrolysis with trifluoroacetic acid under

Table 2. Reaction conditions and yields on oxidation of **1**

Mole ratio to **1**		Temperature °C	Time (hr)	Yield (%)[a]		
CF_3CO_3H	Na_2HPO_4			**3**	**6**	**8**
2.1	14	5	2	75	trace	trace
3.3	14	5	2	62	2	2
1.05	1.25	20	2	9	38	14
2.1	2.5	20	2	10	30	11
2.1	5.6	55	1	19	5	20
2.1	5.6	reflux	0.5	trace	13	15
2.1	14	reflux	0.5	1	15	18

a) As a separated product by column chromatography.

12) B. Coxon and L. Hough, *J. Chem. Soc.*, **1961**, 1643.
13) N. K. Kochetkov and O. S. Chizhov, *Advan. Carbohyd. Chem.*, **21**, 39 (1966).
14) T. Takamoto, R. Sudoh, and T. Nakagawa, unpublished data.

severe conditions; that is, an oxygen atom at the C–6 position of **5** attacks the cationic C–3 carbon atom to form oxidatively the 3,6-anhydro structure because of the presence of the peracid. However, the conversion of **5** to **6** through prototropy may also be possible. Under acidic conditions, nitronic acids are generally accessible to protonation, followed by a nucleophilic attack such as that of a hydroxide and bromide ion to afford nitroso compounds.[15] However, the formation of **8**, with a nitro group, can not be interpreted by a similar mechanism. Therefore, the removal of a hydride ion from the nitronic acid with the assistance of the peracid may enhance the cationic character of the C–3 carbon atom, thus making the hydroxyl oxygen atom at C–6 attack it nucleophilically.

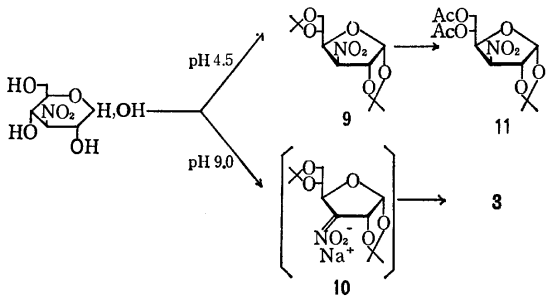

Scheme 2.

In order to discuss NMR-spectrometrically a 3-nitrohexofuranose series, the synthesis of the *gluco*-isomer by the usual acetonation[16] was examined. However, it failed in the case of the usual neutralization, which is performed in an alkaline medium. The acetonation[17] of 3-deoxy-3-nitro-D-glucose in acetone using zinc chloride and phosphoric acid, followed by neutralization at pH 9, afforded **3** in a 15% yield, whereas at pH 4.5 3-deoxy-1,2; 5,6-di-*O*-isopropylidene-3-nitro-α-D-glucofuranose (**9**) was obtained in an 18% yield. Through the intermediary of aci-salt (**10**), **3** might be formed. The partial hydrolysis of **9**, followed by acetylation with acetic anhydride and boron trifluoride, afforded, in a 34% yield, 5,6-di-*O*-acetyl-3-deoxy-1,2-*O*-isopropylidene-3-nitro-α-D-glucofuranose (**11**), which was confirmed by the coupling constant, $J_{2,3}=0$, in the NMR spectrum (Fig. 2).

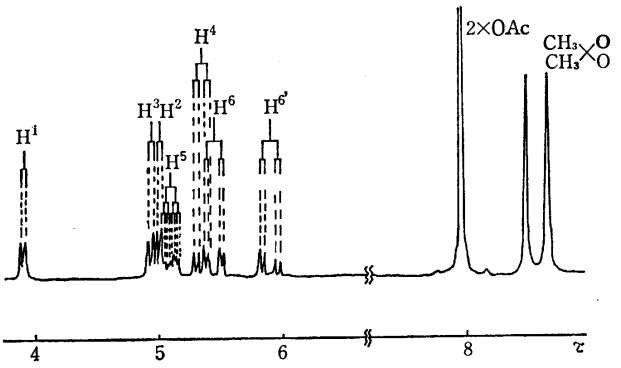

Fig. 2. 100 MHz NMR spectrum of 5,6-di-*O*-acetyl-3-deoxy-1,2-*O*-isopropylidene-3-nitro-α-D-glucofuranose (**11**).

Experimental

General. All the melting points were determined in capillaries and are uncorrected. The specific rotations were measured with a Carl Zeiss photoelectric polarimeter. The NMR spectra were recorded at 100 MHz with a JNM-4H-100 (JEOL) spectrometer in chloroform-*d*, using tetramethylsilane as the internal standard. The column chromatography was carried out on silica gel (100 mesh, Mallinckrodt, St. Louis). The tlc's were performed on silica gel (Wakogel B-5, Japan), with a solvent system of (A) benzene–acetone (30 : 1) or (B) benzene–methanol (19 : 1). All the evaporation were performed *in vacuo*.

*3-Dexoy-1,2;5,6-di-O-isopropylidene-3-nitro-α-D-allofuranose (**3**).* Into a solution of trifluoroperacetic acid in acetonitrile, prepared by mixing successively 90% hydrogen peroxide (289 mg, 7.64 mmol), trifluoroacetic anhydride (1.93 g, 9.2 mmol), acetonitrile (8 ml), dibasic sodium phosphate (7.3 g, 51.4 mmol), and urea (0.05 g), 1,2;5,6-di-*O*-isopropylidene-3-oximino-α-D-*ribo*-hexofuranose (**1**)[10] (1 g, 3.66 mmol) was slowly stirred below 5 °C. After 2 hr, the mixture was evaporated below 40 °C and extracted with chloroform (4× 20 ml); the extract was washed with water three times and evaporated. The resulting crystals were recrystallized from chloroform/petroleum ether to give 0.8 g (75%), showing a mp of 112—113 °C, $[\alpha]_D^{20}$ +106° (*c* 1, $CHCl_3$), IR(KBr): 1560 cm^{-1} (ν_{NO_2}) and tlc (solvent A): R_f 0.37.

Found: C, 50.01; H, 6.61; N, 4.81%. Calcd for $C_{12}H_{19}NO_7$: C, 49.82; H, 6.62; N, 4.84%.

*3-Acetamido-3-deoxy-1,2;5,6-di-O-isopropylidene-α-D-allofuranose (**4**).* Into a suspension of prehydrogenated 10% Pd–C (0.5 g) in methanol containing 1 M acetic acid (1.6 ml), **3** (0.45 g) was stirred in an atmosphere of hydrogen at 1 atm. After 24 hr, the reaction mixture, absorbing 138 ml of hydrogen (theoretical: 110 ml), was filtered and evaporated; then the residue was dissolved in methanol (10 ml) and acetylated with acetic anhydride (0.3 ml) at room temperature. After 1 hr, the mixture was evaporated until it became odorless. The remaining crystals were recrystallized from ethanol/petroleum ether to give 0.4 g (86%); mp 126—127 °C; $[\alpha]_D^{20}$ +73° (*c* 1, $CHCl_3$). The other data agreed completely with the authentic sample.

*5,6-Di-O-acetyl-3-deoxy-1,2-O-isopropylidene-3-nitro-α-D-allofuranose (**7**).* Into a mixture of 90% hydrogen peroxide (79.4 mg, 2.1 mmol), trifluoroacetic anhydride (525 mg, 2.5 mmol), acetonitrile (3 ml), dibasic sodium phophate (355 mg, 2.5 mmol) and urea (10 mg), **1** (273 mg, 1 mmol) was stirred at room temperature. The reaction mixture was evaporated below 40 °C and chromatographed on a silica-gel column (10×2.7 cm) with chloroform. The eluate was collected in 50-ml portions. Fractions No. 5—8 were combined and evaporated. The remaining sirup was treated with acetic anhydride (160 mg) in pyridine (4 ml) at room temperature. After the reaction mixture had stood for 1.5 hr, its evaporation gave crude crystals which were subsequently recrystallized from ether–petroleum ether. Yield, 75 mg (23%); mp 106—107 °C; $[\alpha]_D^{20}$ +110° (*c* 0.9, $CHCl_3$);

15) A. T. Nielsen, "The Chemistry of the Nitro and Nitroso Group," Part 1, ed. by H. Feuer, Interscience Publishers, New York (1966) p. 384.

16) O. T. Schmidt, "Methods in Carbohydrate Chemistry," Vol. II, ed. by R. L. Whistler and M. L. Wolform, Academic Press, New York (1963) p. 318.

17) In a recent paper, Kovář and Bear reported another method because of unsatisfactory results in the usual manner. J. Kovář H. H. Baer, *Can. J. Chem.*, **49**, 3203 (1971).

IR(KBr): 1740 ($\nu_{C=O}$), 1560 cm^{-1} (ν_{NO_2}); tlc (solvent A): R_f 0.18.

Found: C, 46.78; H, 5.61; N, 4.08%. Calcd for $C_{13}H_{19}NO_9$: C, 46.85; H, 5.75; N, 4.20%.

*3,6-Anhydro-1,2-O-isopropylidene-3-nitro-α-D-glucofuranose (**8**).* Into a mixture of 90% hydrogen peroxide (289 mg, 7.64 mmol), trifluoroacetic anhydride (1.93 g, 9.2 mmol), acetonitrile (2 ml), dibasic sodium phosphate (2.93 g, 20.6 mmol), and urea (73 mg), **1** (1 g, 3.66 mmol) was stirred. The mixture was heated at 55 °C for 1 hr and then evaporated. The mixture was put on a silica-gel column (7.2×3.0 cm) with benzene. After the elution of 150 ml of benzene, **8** was eluted with benzene–acetone (19 : 1) and recrystallized from chloroform–petroleum ether. Yield, 146 mg (16%); mp 140—141 °C; $[\alpha]_D^{20}$ +58° (*c* 1, $CHCl_3$); IR(KBr): 1550 cm^{-1} (ν_{NO_2}); tlc (solvent B): R_f 0.52.

Found: C, 43.78; H, 5.10; N, 5.43%. Calcd for $C_9H_{13}NO_7$: C, 43.73; H, 5.30; N, 5.67%.

Acetonation of 3-Deoxy-3-notro-D-glucose. A mixture of 3-deoxy-3-nitro-D-glucose (200 mg), acetone (8 ml), zinc chloride (290 mg), and 85% phosphoric acid (250 mg) was stirred at room temperature for 24 hr. The reaction mixture was then slowly stirred into a diluted sodium carbonate solution, with the pH kept at 9.0 or 4.5. Chromatography on a silica-gel column with benzene, followed by recrystallization, afforded **3** (40 mg, 15%) or **9** (49 mg, 18%). **9**: mp 61—62 °C; $[\alpha]_D^{20}$ +7.3° (*c* 1, $CHCl_3$); IR(KBr): 1550 cm^{-1} (NO_2); tlc (solvent A): R_f 0.37.

Found: C, 49.96; H, 6.50; N, 4.83%. Calcd for $C_{12}H_{19}NO_7$: C, 49.82; H, 6.62; N, 4.84%.

*5,6-Di-O-acetyl-3-deoxy-1,2-O-isopropylidene-3-nitro-α-D-glucofuranose (**11**).* Into a solution of **9** (200 mg) in acetone (15 ml), 0.8% sulfuric acid (15 ml) was stirred. After 21 hr, the solution was completely neutralized with barium carbonate and filtered. The filtrate was evaporated and acetylated with acetic anhydride (0.5 ml) and boron trifluoride etherate (2 drops). Then the reaction mixture was evaporated and chromatographed with benzene. The fraction containing **11** was easily detected by tlc. The recrystallization of the residue from ether–petroleum ether afforded crystalline **11** (69 mg, 34%); mp 79—80 °C; $[\alpha]_D^{20}$ +17° (*c* 1.1, $CHCl_3$); IR(KBr): 1740 (C=O), 1550 cm^{-1} (NO_2); tlc (solvent A): R_f 0.18.

Found: C, 46.59; H, 5.76; N, 4.04%. Calcd for $C_{13}H_{19}NO_9$: C, 46.85; H, 5.75; N, 4.20%.

The authors wish to thank Mitsubishi Gas Chemical Co., Inc., for the gift of 90% hydrogen peroxide and Mr. Hitoshi Matsumoto for recording the NMR spectra.

BULLETIN OF THE CHEMICAL SOCIETY OF JAPAN, VOL. 46, 1535—1539 (1973)

The Acid-catalyzed Isomerization of α-Ylangene and α-Ylangene Epoxide

Yoshimoto OHTA and Yoshio HIROSE

The Institute of Food Chemistry, Dojimanaka, Kita-ku, Osaka 530

(Received August 17, 1972)

Upon treatment with dilute mineral acid, α-ylangene afforded two alcohols with amorphane carbon skeletons, 10β-hydroxyamorpha-4-ene (**16**) and 10α-hydroxyamorpha-4-ene (**17**). The carbonic acid-induced isomerization of α-ylangene epoxide yielded 3α-hydroxy-α-amorphene (**19**), 3α-hydroxy-δ-amorphene (**20**), and 3α,10α-dihydroxyamorpha-4-ene (**21**). The structures of these compounds were strictly determined, and the revised structure **16** of δ-cadinol proposed by Lin was shown to conflict with the results of the isomerization of α-ylangene and with the previously-reported conversion of α-copaene into δ-cadinol (**10**) and T-muurolol (**11**) under similar conditions.

As has been reported in a previous communication, some tricyclic sesquiterpene hydrocarbons containing a cyclopropane or a cyclobutane ring adjacent to a double bond in their molecule, such as α-cubebene (**1**), α-copaene (**2**), and α-ylangene (**3**), were easily isomerized by dilute mineral acid to give hydrocarbons and alcohols of the cadalene type.[1] Cadina-4,6(1)-diene (**4**), δ-cadinene (**5**), cadina-1,4-diene (**6**), cubenol (**7**), and epi-cubenol (**8**) were obtained from α-cubebene, and α-muurolene (**9**), δ-cadinene, δ-cadinol (**10**), and T-muurolol (**11**) from α-copaene. α-Ylangene afforded α-amorphene (**12**) and δ-amorphene (**13**), together with a small amount of oxygenated compounds of an unestablished structure.

Recently, Ohloff and his co-workers[2] performed the proton-induced isomerization of α-copaene epoxide in aqueous carbonic acid and reported the formation of three products, including (−)-3β-hydroxy-T-muurolol, which had previously been isolated from *Taiwania Cryptomerioides* by Lin.[3] These acid-catalyzed reactions are helpful in correlating these closely-resembling sesquiterpenoids of the cadalene type. In this paper, we wish to report the structure determination of compounds obtained from α-ylangene and α-ylangene epoxide by dilute-acid treatments.

Isomerization of α-Ylangene. α-Ylangene **3** was allowed to react with 0.1 N-sulfuric acid in aqueous acetone under reflux for three hours. Two sesquiterpene hydrocarbons, α-amorphene **12** and δ-amorphene **13**, were then isolated as the major components of the product (90%) in a ratio of 2 : 1, together with three oxygen-containing compounds (**15**—**17**) in a total amount less than 10% of the product. None of these

1) Y. Ohta, K. Ohara, and Y. Hirose, *Tetrahedron Lett.*, **1968**, 4181.

2) G. Ohloff and M. Pawlak, *Helv. Chim. Acta*, **53**, 245 (1970).

3) Y. H. Kuo, Y. S. Cheng, and Y. T. Lin, *Tetrahedron Lett.*, **1969**, 2375.

polar compounds isolated were identical with any material previously reported.

Compound (**15**) is an oil exhibiting the molecular ion at *m/e* 222 ($C_{15}H_{26}O$) and the base peak at *m/e* 161 in its mass spectrum. In its IR spectrum, no absorption maxima due to a hydroxyl or a carbonyl group or a double bond are observed, while the four strong bands in the region between 1145—1050 cm^{-1} suggest the presence of oxide linkage. Signals assignable to an isopropyl group at 0.86 and 0.88 (each 3H, doublets) and two methyl groups on the carbon-bearing ether-oxygen atom at 0.99 and 1.08 ppm were observed in its NMR spectrum. These spectral data led us to conclude that the structure of this oxide as **15**.

Compound (**16**) showed a molecular ion at *m/e* 222 ($C_{15}H_{26}O$) and an absorption maximum due to a hydroxyl group at 3650 cm^{-1}. Its NMR spectrum exhibited the signals attributable to an isopropyl group (0.88 and 0.96, two doublets), a methyl group on a carbon-bearing hydroxyl group (1.19), and an olefinic methyl group and a proton (1.68 and 5.47 ppm). On dehydration with thionyl chloride in pyridine, it afforded two hydrocarbons in a ratio of 1 : 1.5, which were confirmed to be α-amorphene **12** and δ-amorphene **13** respectively by comparing their IR spectra and retention times in glc with those of the authentic samples. These chemical and spectral proofs support the idea that this compound is an amorphene-type alcohol carrying the hydroxyl group at C-10 and the trisubstituted double bond at C-4, as is shown by its structure **16**.

Compound (**17**) also showed a molecular ion at *m/e* 222 ($C_{15}H_{26}O$) and a hydroxyl absorption band at 3300 cm^{-1}. Its NMR spectrum closely resembled that of **16**; 0.90 and 0.96 (an isopropyl group), 1.22 (a methyl group on a carbon-carrying hydroxyl group), 1.64 (3H) and 5.34 ppm (1H) (a trisubstituted double bond). The dehydration of this alcohol with thionyl chloride in pyridine furnished one major and two minor hydrocarbons; the main product (above 90%) was identified as α-amorphene, while the others were identified as γ-(**14**) and δ-amorphene. Thus, Compound **17** is probably an epimeric isomer of **16** in view of the configuration of the hydroxyl group at C-10. The configurations of the hydroxyl groups of these alcohols, **16** and **17**, may be supposed to be β-axial and α-equatorial respectively on the basis of the results of their dehydration reactions. It is generally accepted that the *trans*-antiparallel elimination of the water molecule from an alcohol occurs by means of the action of thionyl chloride in pyridine, and, in our case, one of the epimeric isomers carrying the α-equatorial hydroxyl group at C-10 can be expected to give α-amorphene as the main dehydration product, since only the β-hydrogen atom at C-9 is *trans*-antiparallel toward the hydroxyl group in the amorpha-4-ene skeleton. Thus, the **17** alcohol is determined to be 10α-hydroxy-amorpha-4-ene. In contrast, the configuration of the hydroxyl group of the **16** alcohol, which afforded α- and δ-amorphene in a comparable ratio, was reasonably decided to be β-axial, since the α-hydrogen atoms on both C-1 and C-9 satisfied this condition.

Isomerization of α-Ylangene Epoxide. The reaction of α-ylangene with monoperphthalic acid in the presence of anhydrous sodium carbonate afforded α-ylangene epoxide (**18**) in a good yield. On treatment with aqueous carbonic acid in the same way as has been reported by Ohloff,[2] the epoxide yielded two monoalcohols (**19**, **20**) and a diol (**21**). The diol was crystallized from the reaction-product mixture, while the others were purified by chromatography on a silica-gel column.

Compound **19** showed a molecular ion at *m/e* 220 ($C_{15}H_{24}O$) and its absorption maximum at 3350 cm^{-1}. In its NMR spectrum, the signals assignable to the following groupings are observed: an isopropyl group (0.92 and 0.95), two olefinic methyls (1.72) and protons (5.3 and 5.45), and a secondary hydroxyl proton (4.00 ppm, multiplet, $W_{1/2h}$ 21 Hz). The oxidation of **19** with manganese dioxide furnished an unsaturated ketone (**22**), $\nu_{C=O}$ 1670 cm^{-1}, which was chromatographically and spectroscopically identical with the authentic material obtained from α-amorphene by *tert*-butyl chromate oxidation.[4] Therefore, the secondary hydroxyl group was located at C-3 of the α-amorphene skeleton, and the structure of this alcohol was concluded to be 3-hydroxy-α-amorphene **19**.

Another mono-ol **20**, $C_{15}H_{24}O$ (M^+ 220), ν_{OH} 3350 cm^{-1}, exhibited the following NMR signals: 0.92 (6H, doublet, an isopropyl group), 1.62 and 1.70 (two olefinic methyls), 5.46 (an olefinic proton), and 4.10 ppm (1H, multiplet, $W_{1/2h}$ 20 Hz, a secondary hydroxyl proton). On the basis of these spectral data and the mechanism of this epoxide-cleavage reaction,[2] the structure of this alcohol was established as **20** except for the stereochemistry of the hydroxyl group at C-3.

The last compound obtained from the epoxide, needle crystals (mp 136 °C), showed a molecular ion at *m/e* 238 ($C_{15}H_{26}O_2$) in its mass spectrum. The spectral data showed the signals for an isopropyl group (0.92, 6H, doublet, 1380 and 1385 cm^{-1}), a trisubstituted double bond (3H at 1.71 and 1H at 5.36, 1660 and 840 cm^{-1}), a tertiary methyl group on a carbon-bearing hydroxyl group (singlet at 1.13), and a secondary hydroxyl group (1H multiplet at 4.18 ppm, $W_{1/2h}$ 19 Hz, 3400 cm^{-1}). On acetylation with acetic anhydride in pyridine at room temperature, it afforded a hydroxy acetate in an excellent yield (ν_{max} 3350, 1740 cm^{-1}). The secondary hydroxyl group was placed at the allylic position C-3, since it gave, on oxidation with manganese dioxide, an α,β-unsaturated hydroxy ketone (**23**), ν_{max} 3500, 1640 cm^{-1}; downfield-shifted olefinic methyl (1.77 ppm) and proton (6.55 ppm). Furthermore, the reduction of the monoacetate of **21** with calcium in liquid ammonia[5] yielded a sole product which was identical in all respects with the **17** obtained from α-ylangene directly.

All of the allylic hydroxyl groups of **19**, **20**, and **21** can be expected to have the same configuration and

4) Y. Ohta and Y. Hirose, *Tetrahedron Lett.*, **1969**, 1601.
5) K. Takeda, K. Sakurai and H. Ishii, *Tetrahedron*, **27**, 6049 (1971).

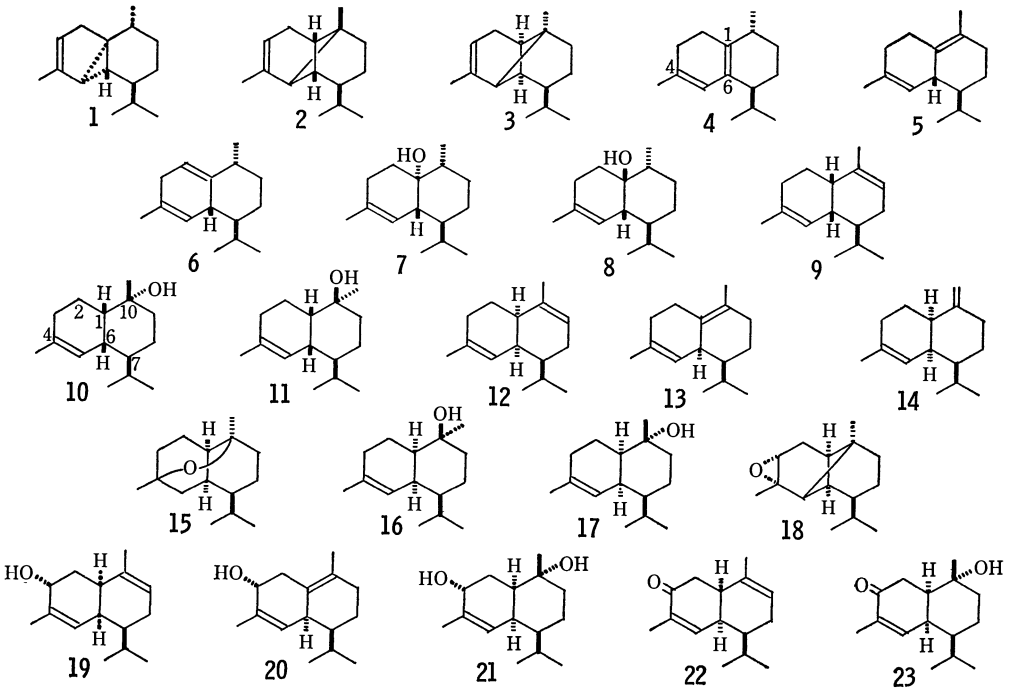

Fig.

can be decided as α-equatorial, since the observed $W_{1/2h}$ values of the secondary hydroxyl protons of these compounds are 21, 20, and 19 Hz respectively; the corresponding protons in the two tetrahydro derivatives obtained from **19** by catalytic hydrogenation also exhibited signals with $W_{1/2h}$ values of 21 and 25 Hz respectively in their NMR spectra. The stereochemistry of the tertiary hydroxyl group at C-10 of the diol **21** was reasonably decided to be α-equatorial on the basis of the reaction mechanism[2] and the successful conversion of **21** into **17**.

No compounds of the amorphane carbon skeleton with an oxygen functional group have yet been isolated from natural sources, but it is highly probable that some of them will be found in nature considering the stability and the biogenetical accessibility of such compounds.

Recently, Lin and his co-workers proposed a revised structure **16** for δ-cadinol that has an amorphane carbon skeleton.[6] However, this revised structure conflicts with the results that the acid-catalyzed isomerization of α-copaene afforded δ-cadinol and T-muurolol,[1] and that the dehydration of δ-cadinol yielded α- and γ-muurolene and δ-cadinene[6,7] 10β-Hydroxyamorpha-4-ene **16**, obtained from α-ylangene in our experiment, has a structure corresponding to their revised δ-cadinol, but it shows no identity with δ-cadinol in any other respect. Accordingly, we wish to propose again the previous structure **10** for δ-cadinol.

6) Y. T. Lin, Y. S. Cheng, and Y. H. Kuo, *ibid.*, **27**, 5337 (1971).

7) The dehydration of δ-cadinol with thionyl chloride in pyridine was carried out in our laboratory, too; α-muurolene (80%), γ-muurolene (15%), and δ-cadinene (5%) were identified as the dehydration products.

8) J. Pliva, M. Horak, V. Herout, and F. Šorm, "Die Terpene. I. Sesquiterpene," Akademie Verlarg, Berlin, (1960), S221.

Experimental

The melting points are uncorrected. The NMR spectra were taken on a Hitachi model R-20B NMR spectrometer (60 MHz), using TMS as the internal standard, and the chemical shifts are given in δ-values. The mass spectra were measured on a Hitachi RMU-6 mass spectrometer at 80 eV. The optical rotations were measured on a Perkin-Elmer model 141 polarimeter. The IR spectra were recorded on a Hitachi model EPI-G2 spectrophotometer. A Hitachi F6-D gas chromatograph fitted with a HB-2000 capillary column (0.25 mm × 45 m) was used for the analytical glc, and a Varian model 90-P gas chromatograph, for preparative purposes.

Isomerization of α-Ylangene. α-Ylangene was obtained from essential oil of the fruit of *Schisandra chinensis* as the main component of the oil. The oil was fractionally distilled under reduced pressure, and the fraction (bp 93—94 °C/9 mmHg) was chromatographed over neutral alumina (Merck, Grade II-III), using *n*-hexane as the solvent, to remove the oxygenated compounds. The hydrocarbon fraction thus obtained was further chromatographed over silica gel impregnated with 15% of silver nitrate, using *n*-hexane as the solvent, to give pure α-ylangene, which was identified by an IR spectrum comparison[8], $[\alpha]_D$ +55.6° (in chloroform). A solution of α-ylangene(3.5 g) in 2 l of 70% aqueous acetone containing 0.1 N sulfuric acid was heated under reflux for 3 hr. After cooling, the reaction mixture was neutralized with a 10% sodium bicarbonate solution, the solvent was then evaporated off to about a half volume under reduced pressure. The residue was extracted with ether, and the organic layer was washed with water and dried over anhydrous sodium sulfate. The product (3.0 g) was subjected to chromatographic separation on neutral alumina, and a hydrocarbon fraction (2.7 g) eluted with *n*-hexane and a fraction of oxygenated compounds (0.24 g) eluted with a 10% ether-*n*-hexane mixture were obtained. The hydrocarbon fraction was shown to consist of three compounds in

a ratio of 10 : 60 : 30 by analytical glc; the mixture was subjected to glc separation (Carbowax 20 M, 3/8″×20 ft column at 180 °C) to give α-ylangene, α-amorphene ($[\alpha]_D$ −127.6°, in chloroform) and, δ-amorphene ($[\alpha]_D$ +16.1° in chloroform) in order. The fraction of the polar compounds was shown to contain three compounds, (**15**), (**16**), and (**17**), in a ratio of 2 : 2.5 : 3, when purified by preparative glc (SE-30, 3/8″×10 ft column at 190 °C), they showed the following physical data. *Oxide (**15**)*; liquid, MS: *m/e* 222 (M^+, $C_{15}H_{26}O$, 72%) and 161 (base peak); IR: 1370, 1360, 1240, 1140, 1080, 1060, 1050, 1010, 1000, 985, and 970 cm^{-1}; NMR (CCl_4): 0.86 and 0.88 (each 3H, two doublets, J=6.0 Hz, $-CH(C\underline{H}_3)_2$), 0.99 and 1.08 (each 3H, singlet, $-O-\overset{|}{C}-C\underline{H}_3$). *10α-Hydroxyamorpha-4-ene (**16**)*; Oil, $[\alpha]_D$ −3.4°(*c*, 0.3 in chloroform), MS: *m/e* 222 (M^+, $C_{15}H_{26}O$), 189, 161(100%), 121, 120, 119, and 105; IR: 3650, 1660, 1390, 1080, 920, 865 and 780 cm^{-1}; NMR ($CDCl_3$): 0.88 and 0.96 (each 3H, two doublets, J=6.0 Hz, $-CH(C\underline{H}_3)_2$), 1.19 (3H, singlet, $HO-\overset{|}{C}-C\underline{H}_3$), 1.68 (3H, broad singlet, $-\overset{|}{C}=\overset{|}{C}-C\underline{H}_3$) and 5.47 (1H, broad singlet, $-\overset{|}{C}=\overset{|}{C}-\underline{H}$). *10β-Hydroxyamorpha-4-ene (**17**)*; mp 42 °C (recrystallized from petroleum ether), $[\alpha]_D$ −8.7° (*c* 0.5, chloroform), MS: *m/e* 222 (M^+, $C_{15}H_{26}O$), 204, 189, 164, 161, 121, and 95 (100%); IR: 3300, 1670, 1385, 1380, 1370, 1120, 1000, 940, 860, and 825 cm^{-1}; NMR ($CDCl_3$); 0.90 and 0.96 (each 3H, two doublets, J=6.0 Hz, $-CH(C\underline{H}_3)_2$), 1.22(3H, singlet, $HO-\overset{|}{C}-C\underline{H}_3$), 1.64 (3H, broad singlet, $-\overset{|}{C}=\overset{|}{C}-C\underline{H}_3$) and 5.34 (1H, broad singlet, $-\overset{|}{C}=\overset{|}{C}-\underline{H}$).

*Dehydration of 10β-Hydroxyamorpha-4-ene (**17**).* The alcohol **17** (7 mg) was dissolved in pyridine (1 ml) and treated with 30 mg of thionyl chloride at 0 °C for 15 min. The reaction mixture was poured into 30 ml of an ice-cold 10% sodium bicarbonate aqueous solution and extracted with 50% ether–*n*-hexane. The organic layer was washed with water and dried over anhydrous sodium sulfate. The subsequent evaporation of the solvent gave 5 mg of an oily product which was subjected to glc separation; the α-amorphene (60%) and δ-amorphene (40%) thus obtained were identified by comparing their IR spectra with those of authentic samples.

*Dehydration of 10α-Hydroxyamorpha-4-ene (**16**).* A solution of 15 mg of **16** in 1 ml of pyridine was treated with thionyl chloride (75 mg) at 0 °C for 20 min. The subsequent usual work-up of the reaction mixture afforded 10 mg of a hydrocarbon mixture; after glc separation, α-amorphene (above 90%), γ-amorphene, and δ-amorphene were identified by comparing their IR spectra and R_t in glc with those of authentic samples.

Epoxidation of α-Ylangene. Into a solution of α-ylangene (5.0 g) in dichloromethane (100 ml) suspended in anhydrous sodium carbonate (3.9 g), and 8.4% ether solution of monoperphthalic acid (4.9 g) was stirred, drop by drop, at 0° C over a 15 min period. The reaction mixture was stirred at 4 °C for 18 hr. The precipitate was then filtered off using a glass filter, and the filtrate was washed with water and dried over anhydrous potassium carbonate. The oily product thus obtained (4.8 g) was subjected to column chromatographic purification over neutral alumina, using dichloromethane as the solvent, to give 4.5 g of α-ylangene epoxide **18**, which showed the following spectral data: prominent peaks at *m/e* 220 (M^+, $C_{15}H_{24}O$), 177 and 107 (100%) in its mass spectrum; absorption bands at 1380, 1375, 1370, 1095, 1060, 1020, 900, 840, 830, 820, and 720 cm^{-1} in its IR spectrum; NMR signals (CCl_4) at 0.86 (6H, doublet, J=5.4 Hz, $-CH(C\underline{H}_3)_2$), 0.88 (3H, singlet, $-\overset{|}{C}-C\underline{H}_3$), 1.29 (3H, singlet, $-\overset{|}{C}(\overset{O}{\diagdown\diagup})\overset{|}{C}-C\underline{H}_3$), 2.10 (1H, singlet, $\underline{H}C-\overset{|}{C}(\overset{O}{\diagdown\diagup})\overset{|}{C}-$), and 2.86 (1H, broad peak, $-\overset{|}{C}(\overset{O}{\diagdown\diagup})\overset{|}{C}-\underline{H}$).

Isomerization of α-Ylangene Epoxide. α-Ylangene epoxide (2.0 g) was added to a solution of dry ice (4 g) dissolved in 80 ml of freshly-distilled water. The mixture was shaken vigorously using a mechanical shaker for 20 hr at room temperature. The subsequent extraction of the reaction mixture with 300 ml of ether, drying over anhydrous sodium sulfate, and evaporation of the solvent afforded 1.8 g of a viscous oil which was stored, after the addition of 10 ml of an ether–*n*-hexane mixture (1 : 2), in a refrigerator overnight to deposit needle crystals of the diol **20**. The crystals (310 mg) were then filtered off and recrystallized from 50% ether in *n*-hexane; mp 136.0—136.5 °C, $[\alpha]_D$ +32.6° (*c* 0.3, chloroform), IR: 3400, 1660, 1415, 1385, 1380, 1120, 1040, 1025, 950, 905, and 840 cm^{-1}; MS; *m/e* 238 (M^+, $C_{15}H_{26}O_2$), 220, 202, 177 and 159 (100%); NMR ($CDCl_3$): 0.87 and 0.93 (each 3H, two doublets, J=6.0 Hz, $-CH(C\underline{H}_3)_2$, 1.13 (3H, singlet, $HO-\overset{|}{C}-C\underline{H}_3$), 1.71 (3H, broad singlet, $-\overset{|}{C}=\overset{|}{C}-C\underline{H}_3$), 4.18 (1H, broad peak, $W_{1/2h}$ 19 Hz, $HO-\overset{|}{C}-\underline{H}$) and 5.36 (1H, broad singlet, $-\overset{|}{C}=\overset{|}{C}-\underline{H}$). Found: C, 75.84; H, 10.88%. Calcd for $C_{15}H_{26}O_2$: C, 75.58; H, 11.00%.

The mother liquor was subjected to column chromatography over silica gel; 3α-hydroxy-δ-amorphene **20** (400 mg) and 3α-hydroxy-α-amorphene **19** (1.0 g) were then obtained by elution with 20% ether in *n*-hexane. *3α-Hydroxy δ-amorphene (**20**)*, oil, $[\alpha]_D$ +61.7° (*c*, 0.5 in chloroform), showed the following spectral data: IR: 3350, 1660, 1385, 1370, 1040 and 840 cm^{-1}; NMR ($CDCl_3$): 0.92 (6H, doublet, J=6.0 Hz, $-CH(C\underline{H}_3)_2$), 1.62 (3H, broad singlet, $-\overset{|}{C}=\overset{|}{C}-C\underline{H}_3$), 1.70 (3H, doublet, J=2.5 Hz, $-\overset{|}{C}=\overset{|}{C}-C\underline{H}_3$), 4.10 (1H, multiplet, $W_{1/2h}$ 20 Hz, $HO-\overset{|}{C}-\underline{H}$), and 5.46 (1H, broad singlet, $-\overset{|}{C}=\overset{|}{C}-\underline{H}$). *3α-Hydroxy-α-amorphene (**19**)*, oil $[\alpha]_D$ −69.9° (*c*, 1.4 in chloroform), showed the following spectral data: IR: 3350, 1660, 1385, 1370, 1050, 1015, 850, 830, and 785 cm^{-1}; NMR ($CDCl_3$): 0.92 and 0.95 (each 3H, two doublets, J=6.0 Hz, $-CH(C\underline{H}_3)_2$), 1.72 (6H, finely-split multiplet, two olefinic methyl groups), 4.00 (1H, broad peak, $W_{1/2h}$ 21 Hz, $HO-\overset{|}{C}-\underline{H}$), 5.3 (1H, broad singlet, $-\overset{|}{C}=\overset{|}{C}-\underline{H}$), and 5.4 (1H, broad peak, $-\overset{|}{C}=\overset{|}{C}-\underline{H}$).

*Oxidation of 3α-Hydroxy-α-amorphene (**19**).* To a solution of **19** (300 mg) in 50 ml of dichloromethane, manganese dioxide (3 g) was added; the mixture was then sitrred for 3.5 hr at room temperature. The subsequent filtration of the reagent and evaporation of the solvent gave 250 mg of an oily product. A pure sample obtained by glc separation (Carbowax 20 M, 3/8″×5 ft column at 180 °C) showed IR bands at 1670, 1380, 1370, 1110, 1095, 940, 900, and 825 cm^{-1}. This α,β-unsaturated ketone was identified with the authentic α-amorphene-3-one **22** obtained from α-amorphene by *tert*-butyl chromate oxidation by comparing their IR spectra, R_f on tlc and R_t in glc.

*Oxidation of the Diol (**21**).* Manganese dioxide (350 mg) was added to a solution of the diol **21** (50 mg) in dichloromethane (10 ml), the mixture was then stirred for 3 hr at room temperature. The usual work-up of the reaction mixture afforded crystals of α,β-unsaturated hydroxy ketone

23 (45 mg), which were then recrystallized from *n*-hexane; mp 129.5—130.5 °C; IR: 3500, 1640, 1408, 1375, 1365, 1110, 940, and 900 cm^{-1}; NMR ($CDCl_3$): 0.95 and 1.03 (each 3H, two doublets, J=6.0 Hz, $-CH(C\underline{H}_3)_2$), 1.00 (3H, singlet, $HO-\overset{|}{C}-C\underline{H}_3$), 1.77(3H, broad singlet, $-CO-\overset{|}{C}=\overset{|}{C}-C\underline{H}_3$), and 6.55 (1H, broad singlet, $\underline{H}C=\overset{|}{C}-\overset{|}{C}=O$).

*Acetylation of the Diol (**21**).* The diol **21** (145 mg) was treated with dry pyridine (5 ml) and acetic anhydride (1 ml) at room temperature for 5.5 hr. The reaction mixture was poured into a dilute sodium bicarbonate solution and extracted with ether. The organic layer was washed with water, dried over anhydrous sodium sulfate, and evaporated to give crude mono acetate (140 mg), which was then recrystallized from *n*-hexane; mp 117—118 °C, IR: 3275, 1740, 1250, 1125 and 1015 cm^{-1}; NMR ($CDCl_3$): 0.95 and 0.90 (each 3H, two doublets), $-CH(C\underline{H}_3)_2$), 1.19 (3H, singlet, $HO-\overset{|}{C}-C\underline{H}_3$), 1.62 (3H, broad peak, $-\overset{|}{C}=\overset{|}{C}-C\underline{H}_3$), 2.05 (3H, singlet, $C\underline{H}_3COO-$), 5.45 (1H, multiplet, $AcO-\overset{|}{C}-\underline{H}$), and 5.60 (1H, broad singlet, $-\overset{|}{C}=\overset{|}{C}-\underline{H}$). Found: C, 72.75; H, 10.02%. Calcd for $C_{17}H_{28}O_3$: C, 72.82; H, 10.06%.

Reduction of the Diol Monoacetate. A solution of the monoacetate (85 mg) in toluene (3 ml) was stirred, drop by drop over a 15 min period, into a solution of calcium (0.8 g) in liquid ammonia (40 ml) at −70 °C. After the subsequent addition of ammonium chloride (3 g) to the mixture, the ammonia was evaporated. Water (150 ml) was added to the residue, and the residue was extracted with ether; the extract was washed with water dried over anhydrous sodium sulfate. The crude product was shown by tlc to contain almost a sole component, which was purified by glc separation (SE-30, 3/8″×10 ft column at 190 °C). The IR and NMR spectra, R_t in glc and R_f on tlc, of this reduction product were shown to be identical with those of 10α-hydroxyamorpha-4-ene **17**.

BULLETIN OF THE CHEMICAL SOCIETY OF JAPAN, VOL. 46, 1539—1545 (1973)

Intramolecular Participation of Sulfide Linkage in the Reactivity of Carbene and Diazoalkanes. I. Alkylcarbenes and Diazoalkanes Bearing Alkylthio, Arylthio, and Allylthio Groups on α-Carbon

Iwao Ojima and Kiyosi Kondo

Sagami Chemical Research Center, Nishi-Onuma, Sagamihara 229

(Received October 4, 1972)

α-Alkyl- and α-arylthioalkylcarbenes were thermally or photochemically generated from the corresponding ketones according to a modification of the Bamford-Stevens method. The carbenes thus generated were found to form labile episulfonium ylides, which then rearranged to vinyl sulfides. The episulfonium ylides were trapped with diethyl maleate and dimethyl fumarate. An α-allylthioalkylcarbene was generated by the photolysis of α-allylthioacetophenone tosylhydrazone in the presence of sodium methoxide at −70 °C; this afforded α-allylthiostyrene exclusively. A smooth thio-Claisen rearrangement of the resulting α-allylthiostyrene was also observed. 3-Thiabicyclo[3.1.0]hexane was obtained when α-allylthioacetophenone tosylhydrazone was decomposed thermally at 150 °C, or photochemically at 10 °C in the presence of bases. The mechanisms of these new reactions are also discussed.

The formation of ylides by an intermolecular electrophilic addition of carbenes to the lone pair of hetero atoms is a well-known reaction.[1] This behavior of carbenes led us to postulate that a carbene carbon is transformed into an ylide carbon by the intramolecular participation of the sulfur atom when a sulfide linkage is present in the same molecule. Although an ordinary carbene is electrophilic and can be added to electron-deficient olefins only with great difficulty,[2] the carbene of this type would act as a nucleophilic reagent, similar to the Wanzlick's carbenes[3] and cycloheptatrienylidene.[4] In addition, the above-mentioned intramolecular reaction of carbenes may afford small, hitherto unknown ring ylides, which are difficult to prepare by the usual salt methods.[5] In this respect, we have already reported, in preliminary form, evidence for the intervention of the thietanonium ylide generated from the carbene bearing sulfide linkage on the γ-position.[6,7] We have now investigated the reactions of alkyl carbenes bearing alkylthio, arylthio, and allythio groups on α-carbon. This paper will present a full account of our research into this subject.

1) G. Wittig and M. Schlosser, *Tetrahedron*, **18**, 1023 (1962); W. E. Parham and R. Koncos, *J. Amer. Chem. Soc.*, **83**, 4034 (1961); W. E. Parham and S. H. Groen, *J. Org. Chem.*, **29**, 2214 (1964); W. Ando, T. Yagihara, S. Tozune, and T. Migita, *J. Amer. Chem. Soc.*, **91**, 2786 (1969); V. Franzen and L. Finketcher, *Ann. Chem.*, **617**, 1(1958); J. Dieckmann, *J. Org. Chem.*, **28**, 2933 (1963); M. Saunders and R. W. Murray, *Tetrahedron*, **6**, 88 (1959); H, Nozaki, R. Noyori, and K. Sisido, *ibid.*, **20**, 1125 (1964).

2) W. Kirmse, "Carbene Chemistry," Academic Press, New York, 1964,

3) For example, H. W. Wanzlick and E. Schikora, *Angew. Chem.*, **72**, 494 (1960); H. W. Wanzlick and H. J. Kleiner, *Chem. Ber.*, **96**, 3024 (1963).

4) W. M. Jones and C. L. Ennis, *J. Amer. Chem. Soc.*, **91**, 6391 (1969).

5) A. W. Johnson, "Ylid Chemistry," Academic Press (New York), 1966, pp 310—314.

6) K. Kondo and I. Ojima, *Chem. Commun.*, **1972**, 62.

7) K. Kondo and I. Ojima, *Chem. Lett.*, **1972**, 119,

Results and Discussion

Reactions of α-Alkylthio- and α-Arylthio-alkylcarbenes. In 1967, Kirmse and Buschhoff reported the effects of ether linkage on the β-position,[8] and Robson and Shechter reported those of oxygen, nitrogen, and sulfur on the β-position,[9] in view of the neighboring effects of hetero atoms on carbenes. The effects of hetero atoms on the β-position may be summarized as follows: i) An alkoxy group on the β-position promoted markedly a rearrangement of a methyl on the α-carbon to the carbene carbon. The rate of the rearrangement of the alkoxy group is faster than that of hydrogen in the case of bis(α-alkoxy)alkylcarbene. ii) The rearrangement of an arylthio group on the α-carbon of the carbene is quite effective as compared with those of an alkoxy and alkylamino groups. In the latter communication, they observed an exclusive 1,2-shift of arylthio group to the electron-deficient center and interpreted the reaction as a concerted process through an ylide-like transition state. However, a possibility of the existence of an intermediate ylide still remains. Therefore, the reaction was reinvestigated in detail in the hope of obtaining evidence for the intervention of episulfonium ylide.

Carbenes were generated by the thermal or photochemical decomposition of sodium salts of the tosylhydrazones(**1a—d**), in accordance with the Bamford-Stevens method.[10] The results of the thermal decomposition in diglyme at 150 °C and of photolysis using a high-pressure Hg lamp in monoglyme at 10 °C are listed in Table 1, while the supposed reaction paths are described in Scheme 1.

As for the configuration of the olefin **2** produced by the 1,2-hydride shift, it is noteworthy that the ratios of the thermodynamically-unstable *cis*-isomer were

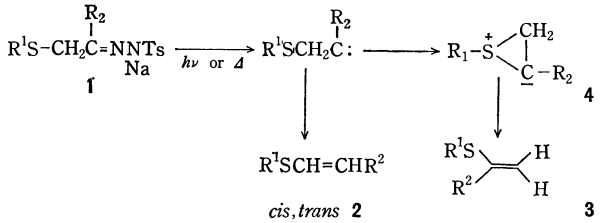

Scheme 1.

Table 1. Products ratios[a] in the decomposition of tosylhydrazones **1a—d**

	R^1	R^2	Photolysis		Thermolysis	
			2	**3**	**2**	**3**
a	Ph	Ph	1	99	10	90
b	Et	Ph	30	70	14	86
c	*t*-Bu	Ph	22	78	15	85
d	Ph	Me	0	100	40	60

a) Products ratio was calculated from vpc peak area using a column packed with 20% SE-30 at 150—200 °C.

8) W. Kirmse and M. Buschhoff, *Chem. Ber.*, **100**, 1491 (1967).
9) J. H. Robson and H. Shechter, *J. Amer. Chem. Soc.*, **89**, 7112 (1967).
10) W. R. Bamford and T. S. Stevens, *J. Chem. Soc.*, **1952**, 4735.

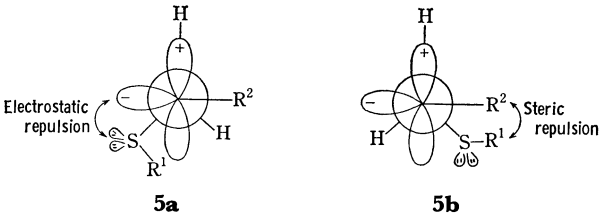

Scheme 2.

predominant in all cases examined: $R^1=R^2=$Ph, *cis*/*trans*=98/2; $R^1=$Et, $R^2=$Ph, *cis*/*trans*=66/34 and $R^1=t$-Bu, $R^2=$Ph, *cis*/*trans*=69/31. The results can reasonably be explained by considering the conformations of the singlet carbenes. It has generally been accepted that the hydrogen migration occurs in the singlet state.[11] Scheme 2 depicts the Newman projection of the singlet carbene.

The *trans*-olefin will be produced from the **5a** conformation and the *cis*-olefin, from **5b**. From the steric point of view, **5a** is expected to be more stable than **5b**. However, from the electronic point of view **5a** is less stable, because of the electrostatic repulsion between the lone pair of the sp^2-hybridized carbene and those of the sulfur atom. The preferential formation of the *cis*-isomers means that the electrostatic repulsion is the dominant factor in determining the conformations of these carbenes. Similar results were observed by Kirmse and Buschhoff in the case of α-alkoxyalkylcarbenes,[8] and by Yamamoto and Moritani in the case of α-carbethoxyalkylcarbenes.[12] As for the olefin, **3**, produced by the rearrangement of the alkylthio or arythio group, the probability of the rearrangement is considerably affected both by the substituent on the carbene carbon and that on the sulfur atom. That is, the ratio of the migration *vs.* the hydride shift seems to be determined by the stability of the hypothetical episulfonium ylide. In general, a phenyl group on ylide carbon delocalizes the negative charge by means of a resonance effect. On the contrary, a methyl group on the same carbon destabilizes the ylide by its inductive effect. In the case of thermolysis, the ratio of the olefin **3** to the olefin **2** was reduced remarkably from 10/90 to 40/60, as the substituent on the ylide carbon was changed from phenyl to methyl; this behavior might reflect the thermal stability of the intermediate episulfonium ylide. In sharp contrast with this, the phenyl substituent on sulfur plays a key role in determining the ratio of the olefin **3** to the olefin **2** when the carbene is produced by photolysis. Though we have no persuasive explanation for the phenomena, the result is probably due to the inherent difference between the two types of carbenes, *i. e.*, thermally- and photochemically-generated carbenes.

All attempts to trap these carbenes by cyclohexene were in vain. Furthermore, no reaction could be observed with such electron-rich olefins as morpholinocyclohexene and dihydropyran. However, these

11) I. Moritani, Y. Yamamoto, and S. Murahashi, *Tetrahedron Lett.*, **1968**, 5755, 5967.
12) Y. Yamamoto and I. Moritani, *Tetrahedron*, **26**, 1235 (1970).

Table 2. Reactions of the Ylides **4** with electron-deficient olefins

6	R^1	R^2	X	Olefin	Yield(%)	NMR (τ) Ring proton	NMR (τ) Methylene
a	Ph	Ph	COOEt	*cis*	72	7.45(1H), 7.10(1H)	6.54(2H, AB)
b	Ph	Me	COOEt	*cis*	67	7.83(2H)	6.82(2H, AB)
c	Ph	Me	COOEt	*trans*	61	7.81(2H)	6.84(2H, AB)

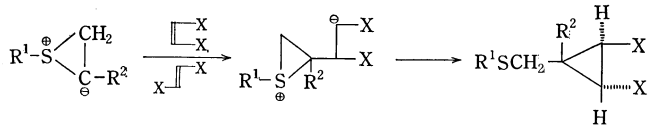

4 **7** **6**

Scheme 3.

carbenes were found to react with electron-deficient olefins, *e. g.*, α, β-unsaturated carboxylic esters, to produce cyclopropanes in good yields.

The configuration of the obtained cyclopropanes was found to be *trans* about the substituent, **X**, irrespective of the configurations of the starting olefins. The configuration was determined on the basis of its NMR spectrum, in which the methylene protons adjacent to the sulfur atom displayed an AB quartet caused by asymmetric vicinal carbon. The results are summarized in Table 2. Consequently, as is shown in Scheme 3, the reaction should proceed in a two-step mechanism *via* betain, **7**. It might be said that the expected transformation of carbene to ylide was successfully realized by its nucleophilic addition to electron-deficient olefins. However, much as in the case of cycloheptatrienylidene[4] the possibility of the formation of cyclopropane *via* pyrazoline can not be rigorously excluded, because the diazoalkane is knwon to be the precursor of the carbene in the decomposition of tosylhydrazones by the Bamford-Stevens procedure.[10,13,23] To clarify this possibility, the tosylhydrazone **8** which has a structure quite analogous with **1d** except for the absence of sulfide linkage in the same molecule, was reacted under the same conditions in the presence of diethyl maleate.

The cyclopropane **9**, which is considered to be formed through the 1,3-cycloaddition of the diazoalkane

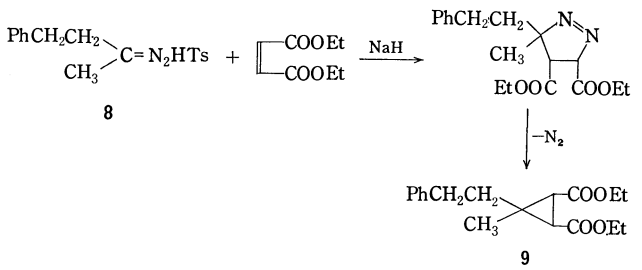

8 **9**

Scheme 4.

to the olefin, was obtained in only a 15% yield. This result indicates that a part of the cyclopropane **6** might be produced by the 1,3-cycloaddition route. However, the major path should be the ylide process. These results suggest that the reaction might become a useful synthetic device for the formation of cyclopropanes which can not be obtained by the usual carbene process.

Intramolecular Reactions of α-Allylthioalkylcarbene. The reaction of the α-allylthioalkylcarbene obtained from the sodium salt of α-allylthioacetophenone tosylhydrazone (**1e**) was investigated. In sharp contrast with that observed at 10 °C (*vide infra*), the photochemically-produced carbene showed a characteristic behavior.

At least three types of reactions leading to the final products are possible for this carbene, as is shown in Scheme 5: The 1,2-hydride shift to the olefin **11**, the 1,2-migration of the allylthio group through the intermediate ylide, **14**, and the [2,3]sigmatropic rearrangement[6] of the ylide **14**. A careful examination of the photolysate by NMR indicated that the carbene was transformed into a mixture of allyl 1-phenylvinyl sulfide, **10** (89%), and allyl 2-phenylvinyl sulfide, **11** (11%), in an almost quantitative yield. The ratio of *cis*-**11** to *trans*-**11** was found to be 79 : 21, which is again in good agreement with the results observed in the cases of alkylthio- and arylthio-alkylcarbenes. The allyl vinyl sulfide, **10**, obtained was thermally unstable. Thus, the structure was determined by measuring the NMR spectrum of the photolysate at −23 °C. The spectrum clearly demonstrated that the predominant component in the photolysate was the olefin **10**. In this case, the episulfonium ylide, **14**, can also be assumed to be an intermediate in the reaction.

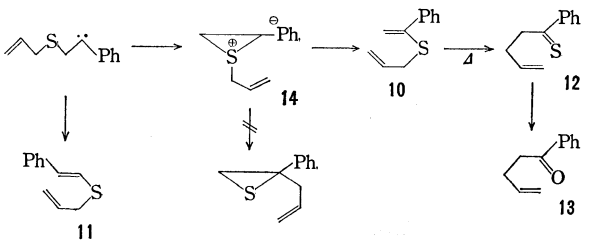

14 **10** **12** **11** **13**

Scheme 5.

When the photolysate was kept in the dark at room temperature for a few hours, an intensive violet color spread over the solution and its NMR spectrum became completely different from that of **10**. This compound was stable under a nitrogen atmosphere, and its electronic spectrum displayed an absorption maximum at 560 nm which was almost the same as that of thioaceto-

13) D. G. Farnum, *J. Org. Chem.*, **28**, 870 (1963).
14) J. Fabian, H. Viola, and R. Mayer, *Tetrahedron*, **23**, 4323 (1967).
23) J. W. Powell and M. C. Whiting, *ibid.*, **7**, 305 (1959).

Table 3. NMR Spectral data for the olefinic protons of **2**, **3**, **10** and **11** (τ, CCl_4)

R^1	R^2	R^1S, H^b / R^2, H^a	R^1S–CH^a=CH^b–R^2 *cis*	*trans*
Ph	Ph	4.82, s, (H^b) 4.48, s, (H^a)	3.61, ABq J_{ab}= 11Hz	3.33, ABq J_{ab}= 17Hz
Et	Ph	4.93, s, (H^b) 4.67, s, (H^a)	3.84, ABq J_{ab}= 11Hz	3.57, ABq J_{ab}= 17Hz
t-Bu	Ph	4.40, d, (H^b) 4.33, d, (H^a) J_{ab}= 1Hz	3.71, ABq J_{ab}= 12Hz	3.36, ABq J_{ab}= 16Hz
Ph	Me	5.23, s, (H^b) 5.00, s, (H^a)	4.40—3.80, m	
Allyl	Ph	4.80, s, (H^b) 4.53, s, (H^a)	3.69, ABq J_{ab}= 11Hz	3.41, ABp J_{ab}= 16Hz

phenone and which could be assigned to the n–π^* transition of the thio-carbonyl function. On the basis of these spectra, this compound was assigned to thioketone, **12**. Chemical evidence for the thioketone, **12**, was also obtained; the violet color of the thioketone, **12**, gradually disappeared under atmospheric conditions. The products were separated and purified by column chromatography on silica, and the ketone, **13**, and sulfide, **11**, were finally isolated. The structure of the ketone, **13**, was determined by studying its NMR, IR, and mass spectra. Although the thio-Claisen rearrangements were observed in many systems,[15] that of a simple allyl vinyl sulfide system has not yet been reported. A recent report by Corey and Shulman[16] described how their attempted thermal thio-Claisen rearrangement of R_2C=$CHSCH_2CH$=CH_2 at 160—180 °C was unsuccessful, and how mercuric oxide was found to be an effective catalyst to promote the rearrangement and produce aldehyde directly. In our system, however, the thio-Claisen rearrangement occurs quite smoothly at room temperature without the aid of any catalyst. The substituent on the vinyl group seems to have a decisive effect on the ease of this rearrangement. That is, though two allyl vinyl sulfides were obtained in our system, only one, *i. e.*, the sulfide **10**, underwent thio-Claisen rearrangement, while the other, *i. e.*, the sulfide **11**, was recovered unchanged. The ease must be due partly to the stability of the product.

Intramolecular 1,3-Cycloaddition of α-Allylthioalkyldiazoalkane. α-Allylthioacetophenone tosylhydrazone (**1e**) was thermally decomposed in diglyme in the presence of sodium methoxide at 150 °C. The distillation of the reaction mixture under reduced pressure or the purification of the product by column chromatography afforded 1-phenyl-3-thiabicyclo[3.1.0]-hexane (**16**) as the sole isolable product in a 68.5% yield; no olefins caused by the carbenic process could be detected in the product. The photodecomposition of the sodium salts of tosylhydrazone, **1e**, in monoglyme at 10 °C also afforded 3-thiabicyclo[3.1.0]-hexane **16** in an 87.5% yield. The carbenic process of this α-allylthio system was observed only when the photolysis was carried out at −70 °C. Thus, the cycloaddition must involve a thermal process at some stage of the consecutive reactions. The formation of 3-thiabicyclo[3.1.0]hexane, **16**, can be explained by assuming an intramolecular cycloaddition of the diazoalkane to the double bond of the allylthio group to afford the bicyclic pyrazoline and the subsequent elimination of a molecular nitrogen, as is shown in Scheme 6.

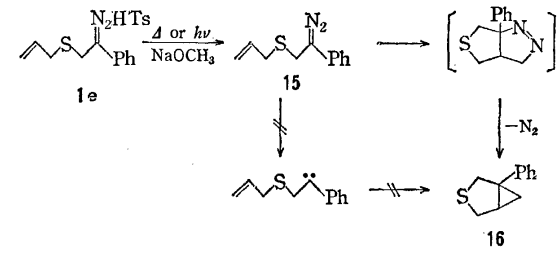

Scheme 6.

A similar behavior was also observed when a β-allylthioalkyldiazoalkane was generated by the thermal decomposition of the corresponding tosylhydrazone. In the latter case, we could actually isolate the bicyclic pyrazoline.[17] The first step of the thermolysis is known to be the formation of the diazo compounds.[23] As far as we know, there has been no report on the formation of the diazo compounds from the corresponding sodium salts of tosylhydrazones under photolytic conditions. We could, however, actually observe a characteristic red color of the compounds during the initial stage of the photolyses of **1a**∼**1e**. Thus, the intramolecular 1,3-cycloaddition of the transient diazo function to the allyl moiety seems to be a quite effective process, even at 10 °C. The reason for the ease of this cycloaddition might be its intramolecular nature. The high performance of the reaction may open a novel synthetic route to thiabicyclic systems.

Experimental

Measurements. The melting points and boiling points were uncorrected. The infrared spectra were recorded on a Hitachi-Perkin-Elmer Model 337 Infracord or a Hitachi EPI-G3 spectrophotometer, using samples as neat liquid, KBr disks, or Nujol mulls. The nuclear magnetic resonance spectra were obtained by the use of a Varian HA-100 or Hitachi R20-B spectrometer, using TMS as the internal standard. The mass spectra were measured with the use of a Hitachi RMU-6E spectrometer at 70 eV. Analytical gas chromatography (vpc) was carried out on a Hitachi K-53 equipped with a flame-ionization detecter using a 1 m×3 mm column packed with 20% SE-30 or 10% QF-1 on chromosorb W. Photolyses were carried out with the use of a 450-W high-pressure mercury lamp (Ushio Electric Inc.).

*Materials. α-Phenylthioacetophenone Tosylhydrazone (**1a**):* Benzenethiol (13.8 g, 0.125 mol) was added to a solution of

15) For example, D. J. W. Schuijl, and L. Brandsma, *Rec. Trav. Chim. Pays-Bas*, **87**, 957 (1968); H. Kwart and T. J. George, *Chem. Commun.*, **1970**, 433.

16) E. J. Corey and J. I. Schulman, *J. Amer. Chem. Soc.*, **92**, 5522 (1970).

17) K. Kondo and I. Ojima, *Chem. Commun.*, **1972**, 63.

200 ml of absolute ethanol and 2.88 g of sodium (0.125 g-atom). To this solution, 25 g of α-bromoacetophenone (0.125 mol) in 100 ml of ethanol was added slowly, and then the mixture was gradually heated to reflux for 2 hr. After the reaction mixture had been cooled to room temperature, the precipitated sodium bromide was filtered off and the filtrate was concentrated. The residue was dissolved in chloroform, washed with water, and dried over anhydrous magnesium sulfate. After the solvent had been removed, the oily product was cooled with dry ice to afford yellow crystals. The product was recrystallized from ethanol; 15.7 g (55%) of pure α-phenylthioacetophenone were thus obtained. Mp 52 °C (lit,[18] 53—54 °C).

A mixture of 12 g (0.65 mol) of tosylhydrazide and 11.4 g (0.05 mol) of α-phenylthioacetophenone in 100 ml of ethanol was heated for half an hour under reflux. Then, the solution was cooled with dry ice; white needles of the tosylhydrazone, **1a**, were thus precipitated (16.8 g, 85%). Mp 105—106 °C. Found: C, 63.72; H, 4.93; N, 6.98; S, 16.13%. Calcd for $C_{21}H_{20}N_2O_2S_2$: C, 63.51; H, 5.08; N, 7.06; S, 16.17%.

In a similar manner, α-ethylthioacetophenone tosylhydrazone (**1b**) and α-*t*-butylthioacetophenone tosylhydrazone (**1c**) were prepared. α-Ethylthioacetophenone: bp 120 °C/1.5 mmHg (lit,[19], 106 °C/0.3 mmHg). Tosylhydrazone **1b**: Colorless needles, mp 126—127 °C. Found: C, 58.43; H, 5.69; N, 8.05; S, 18.41%. Calcd for $C_{17}H_{20}N_2O_2S_2$: C, 58.59; H, 5.78; N, 8.04; S, 18.40%. α-*t*-Butylthioacetophenone: bp 124 °C/2.5 mmHg. Tosylhydrazone **1c**: Colorless needles, mp 175—176 °C. Found: C, 60.44; H, 6.27; N, 7.27; S, 17.10%. Calcd for $C_{19}H_{24}N_2O_2S_2$: C, 60.61; H, 6.42; N, 7.44; S, 17.03%.

*α-Phenylthioacetone Tosylhydrazone (**1d**)*: α-Phenylthioacetone was prepared from 20 g (0.182 mol) of benzenethiol, 4.2 g (0.182 g-atom) of sodium, and 25 g (0.183 mol) of bromoacetone in 150 ml of absolute ethanol in a manner similar to that used in the case of α-phenylthioacetophenone; 17.5 g (57%) of the ketone were thus obtained. Bp 100—102 °C/1.0 mmHg (lit,[20] 160—165 °C/22 mmHg). The tosylhydrazone of α-phenylthioacetone was prepared from 16.7 g (0.1 mol) of the ketone and 20 g (0.107 mol) of tosylhydrazide in the presence of a few drops of concentrated sulfuric acid in 150 ml of ethanol at room temperature (29.1 g, 87%). mp 148—149 °C. Found: C, 57.36; H, 5.15; N, 8.29; S, 19.17%. Calcd for $C_{16}H_{18}N_2O_2S_2$: C, 57.46; H, 5.42; N, 8.38; S, 19.17%.

*Thermal Decomposition of the Tosylhydrazones, **1a-d***: A typical procedure will be described for the thermal decomposition of α-phenylthioacetophenone tosylhydrazone (**1a**).

The tosylhydrazone **1a** (396 mg, 1.0 mmol) was dissolved in 50 ml of diglyme, and then a 60-mg portion (*ca.* 1.2 mmol) of sodium hydride (50% suspension in mineral oil) was stirred in. After the evolution of hydrogen had ceased, the reaction flask was immersed into an oil bath which was maintained at 180 °C. The reaction mixture was heated under reflux for a few minutes; during this time the evolution of nitrogen was observed. After the precipitated sodium *p*-toluenesulfinate had been filtered off, the reaction mixture was concentrated under reduced pressure, dissolved in chloroform, washed with water, and then dried over anhydrous magnesium sulfate. The products were determined by studying the NMR spectrum, which was measured after the crude products had been distilled under reduced pressure. The yields and products ratios were calculated by comparing the vpc peak area of the crude products with that of pure samples, which had been prepared from benzenethiol and phenylacetylene,[21] and by analysing the integration of the NMR spectrum of the crude products. The total yield (**2a**+**3a**) was 44.5%.

In a similar manner, other tosylhydrazones (**1b—d**) were decomposed; olefins (**2** and **3**) were thus obtained in similar yields and were detected by means of the vpc and/or NMR spectra. Authentic samples were prepared from ethanethiol and phenylacetylene,[21] 2-methyl-2-propanethiol and phenylacetylene, and benzenethiol and allen.[22] The NMR spectral data for the olefinic protons of these vinyl sulfides are listed in Table 3.

*Photolyses of the Tosylhydrazones, **1a—d***: A typical procedure will be described for the photolysis of α-phenylthioacetophenone tosylhydrazone (**1a**).

The tosylhydrazone, **1a** (396 mg, 1.0 mmol), was dissolved in 20 ml of monoglyme, and then 60 mg (*ca.* 0.12 mmol) of sodium hydride in mineral oil was added to a pyrex cell. After the initial evolution of hydrogen had ceased, the reaction mixture was bubbled with dry nitrogen gas and then irradiated externally with a 450-W high-pressure Hg lamp for several hours. After the irradiation, the reaction mixture was concentrated, dissolved in chloroform, washed with water, and dried over anhydrous magnesium sulfate. The products were detected by NMR and vpc, as has been described above. The total yield (**2a**+**3a**) was 82%.

Similarly, other tosylhydrazones were photolysed; olefins (**2** and **3**) were thus obtained in similar yields.

*Thermal Decompositions of the Tosylhydrazones (**1a**, **1d**, and **8**) in the Presence of Electron-deficient Olefins.* A typical procedure will be described for the thermolysis of α-phenylthioacetone tosylhydrazone (**1d**) in the presence of diethyl maleate.

α-Phenylthioacetone tosylhydrazone (**1d**) (1.00 g, 3.0 mmol) was dissolved in 50 ml of diglyme, and then a 180-mg portion (ca. 3.6 mmol) of sodium hydride in mineral oil was added. After the evolution of hydrogen had been completed, a 2.6-g portion (15.1 mmol) of diethyl maleate was added. Then, the reaction flask was immersed into an oil bath, the temperature of which was maintained at 180°C with stirring. After the evolution of nitrogen had ceased, the reaction mixture was refluxed for an hour. The sodium *p*-toluenesulfinate thus precipitated was filtered off using a glass filter, and the filtrate was distilled to remove the solvent and unreacted diethyl maleate. The residue was dissolved in chloroform, washed with water, and dried over anhydrous magnesium sulfate. The solution was concentrated and chromatographed on silica (WAKO C-200). The cyclopropane **6b** (664 mg, 67%) was eluted by benzene.

In a similar manner, the cyclopropanes **6a**, **6c**, and **9** were obtained in 72, 61, and 15% yields, respectively. The yields of the cyclopropanes, as calculated from the vpc peak areas, were about ten percent higher than those obtained from chromatographic separations. 1-Phenyl-1-phenylthiomethyl-2,3-dicarboethoxycyclopropane (**6a**): NMR (CCl_4, TMS): τ 9.05 (H^a: t, J_{ac}=7Hz, 3H), 8.70 (H^b: t, J_{bd}= 7 Hz, 3H), 7.32 (H^f, H^g; AB_q, J_{fg}=6 Hz, 2H), 6.54 (H^e:

18) W. J. Kenny, J. A. Walsh, and D. A. Davenport, *J. Amer. Chem. Soc.*, **83**, 4019 (1961).

19) V. Prelog, V. Hahn, H. Bauchli, and H. C. Beyerman, *Helv. Chim. Acta*, **27**, 1209 (1944).

20) J. E. Banfield, W. Davies, N. W. Gamble, and S. Middleton, *J. Chem. Soc.*, **1956**, 4791.

21) A. A. Oswald, K. Griesbaum, B. E. Hudson, Jr., and J. M. Bregman, *J. Amer. Chem. Soc.*, **86**, 2877 (1964).

22) W. H. Mueller and K. Griesbaum, *J. Org. Chem.*, **32**, 856 (1967).

AB_q, $J_{ee}=12$ Hz, 2H), 6.23 (H^c: quartet, $J_{ac}=7$ Hz, 2H), 5.88 (H^a: quartet, $J_{bd}=7$ Hz, 2H), 2.98 (H^h: broad s, 5H) and 2.82 (H^i: broad s, 5H).

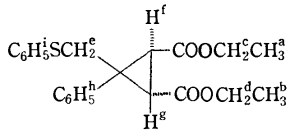

IR (neat): 1730 ($\nu_{C=O}$) and 1180 cm^{-1} (ν_{C-O}) Mass: 384 M^+. Found: C, 68.31; H, 6.28; S, 8.44%. Calcd for $C_{22}H_{24}O_4S$: C, 68.72; H, 6.29; S, 8.34%.

1-Methyl-1-phenylthiomethyl-2,3-dicarboethoxycyclopropane (**6b**): NMR (CCl_4, TMS): τ 8.74 (H^a, H^b: t, $J_{ac}=J_{bd}=7$ Hz, 6H), 7.83 (H^g, H^h: s, 2H), 6.82 (H^f; AB_q, $J_{ff}=13$ Hz, 2H), 5.95 (H^c, H^d: quartet, $J_{ac}=J_{bd}=7$ Hz, 4H) and 2.5—3.0 (H^i; m, 5H).

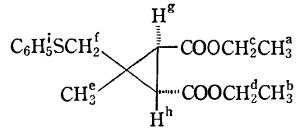

IR (neat): 1720 ($\nu_{C=O}$), and 1160 cm^{-1} (ν_{C-O}). Mass: 322 M^+. Found: C, 63.01; H, 6.75; S, 10.15%. Calcd for $C_{17}H_{22}O_4S$: C, 63.33; H, 6.88; S, 9.94%.

1-Methyl-1-phenylthiomethyl-2,3-dimethoxycyclopropane (**6c**): NMR (CCl_4, TMS): τ 8.62 (H^c: s, 3H), 7.81 (H^e, H^f: s, 2H), 6.84 (H^d: AB_q, $J_{dd}=12$ Hz, 2H), 6.42 (H^a: s, 3H), 6.39 (H^b: s, 3H), and 2.5—3.0 (H^g: m, 5H).

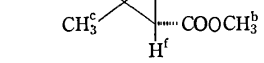

IR (neat): 1730 ($\nu_{C=O}$) and 1165 cm^{-1} (ν_{C-O}). Mass: 294 M^+. Found: C, 61.28; H, 5.88; S, 10.78%. Calcd for $C_{15}H_{18}O_4S$: C, 61.20; H, 6.16; S, 10.89%.

1-Methyl-1-(2-phenylethyl)-2,3-dicarboethoxycyclopropane (**9**): NMR (CCl_4, TMS): τ 8.72 (H^a, H^b: t, $J_{ac}=J_{bd}=7$ Hz, 6H), 8.65 (H^e: s, 3H), 8.3—8.0 (H^f: m, 2H), 7.88 (H^h, H^i: s, 2H), 7.70—7.25 (H^g: m, 2H), 5.93 (H^c, H^d: quartet, $J_{ac}=J_{bd}=7$ Hz, 4H) and 3.05—2.80 (H^j: m, 5H).

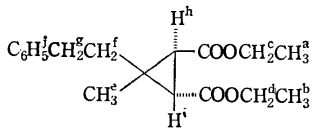

IR (neat): 1730 ($\nu_{C=O}$) and 1170 cm^{-1} (ν_{C-O}) Mass: 304 M^+. Found: C, 71.05; H, 8.10%. Calcd for $C_{18}H_{24}O_4$: C, 71.03; H, 7.95%.

*α-Allylthioacetophenone Tosylhydrazone (**1e**).* To 150 ml of absolute ethanol, a 1.55-g portion (0.068 g-atom) of sodium was added. After the evolution of hydrogen had ceased, a 5.0-g portion (0.068 mol) of allylmercaptan was added to the solution, and the mixture was stirred for an hour. Into the solution we then stirred a solution of 13.5 g (0.068 mol) of bromoacetophenone in 100 ml of absolute ethanol; then, the reaction mixture was gradually heated to reflux over a 1-hr period. The sodium bromide thus precipitated was filtered off, and the filtrate was concentrated. The residue was dissolved in chloroform, washed with water, dried over anhydrous magnesium sulfate, and distilled. Yield, 61%. $PhCOCH_2SCH_2CH_2{=}CH_2$: bp 102—104 °C/0.2 mmHg, IR (neat): 1690 ($\nu_{C=O}$) 985 and 920 cm^{-1} $\left(\delta\ \begin{matrix}H\\H\end{matrix}\!\!>C=C<\!\!H\right)$.

The tosylhydrazone, **1e**, was prepared from 3.78 g (0.0207 mol) of α-allylthioacetophenone and 3.66 g (0.0207 mol) of tosylhydrazide in 95% ethanol in the presence of a drop of concentrated sulfuric acid. Tosylhydrazone **1e**: Colorless prisms, mp 106—107 °C, Found: C, 59.55; H, 5.79; N, 7.67; S, 17.84%. Calcd for $C_{18}H_{20}N_2O_2S_2$: C, 59.97; H, 5.59; N, 7.77; S, 17.79%.

*Photolysis of α-Allylthioacetophenone Tosylhydrazone (**1e**) in the Presence of Sodium Methoxide at Low Temperatures.* The tosylhydrazone **1e** (360 mg, 1.0 mmol) was dissolved in 30 ml of monoglyme in the photolysis vessel, and a 60-mg portion (1.1 mmol) of sodium methoxide was added. The solution was bubbled with nitrogen, and then stirred with a magnetic stirrer for an hour and irradiated. The temperature of the dry ice-ethanol solution was kept constant at −70 °C during the irradiation. The solution was irradiated for about 2.5 hr until the pink-color of the diazo compound had disappeared; then, the precipitated sodium *p*-toluenesulfinate was filtered off rapidly. The cool filtrate was concentrated under a vacuum; the residue was dissolved in cold ether and was washed with ice water as quickly as possible and the organic layer was dried over anhydrous magnesium sulfate in a dry ice box. The solution was then again concentrated by the use of a vacuum pump; the residue was dissolved in deuterochloroform including tetramethylsilane and poured into a NMR sample tube under a stream of nitrogen, after which the tube was closed. The NMR sample was stored in a dry ice–ethanol solution, and the NMR spectrum was measured at −23 °C. The predominant product was found to be 1-phenylvinyl allyl sulfide (**10**). **10**: NMR ($CDCl_3$, TMS, −23°C): τ 6.71 (H^c: d, $J_{bc}=7$ Hz, 2H), 5.10—4.85 (H^a: m, 2H), 4.80 (H^e: s, 1H), 4.54 (H^d; s, 1H), 4.40—3.90 (H^b: m, 1H), and 2.80—2.30 (H^f: m, 5H).

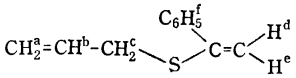

The structures of the minor products, *cis*- and *trans*-2-phenylvinyl allyl sulfides, were determined by studying their nmr and mass spectra. The pure sample was obtained by chromatography on silica, employing *n*-hexane as the eluent. **11**: NMR (CCl_4, TMS, *cis*, *trans* mixture): τ 6.69 (H^c: d, $J=7$ Hz, 2H), 5.00—4.70 (H^a: ,m 2H), 4.40—3.90 (H^b: m, 1H),

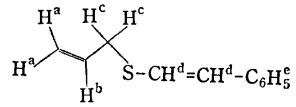

3.80 (*cis*-H^d; AB_q, $J=11$ Hz) (2H)
3.51 (*trans*-H_d: AB_q, $J=15$ Hz)
and 2.90—2.50 (H^e: m, 5H) mass: $m/e=176$ M^+, 135 M^+-41, base peak, 91 $C_7H_7^+$, and 77 Ph^+. When the sample which had been subjected to the NMR measurement was left at room temperature for half an hour, a violet color spread over the solution. The NMR spectrum was again measured at room temperature. The spectrum showed the disappearance of the olefin **10** and the production of new species which showed a benzoyl-type spectrum. The electronic spectrum of the sample showed an absorption maximum at 560 nm in the visible region; such an absorption maximum is characteristic of thiophenones. On the basis of these spectra, the new

species which was produced thermally was assigned to buten-3-yl phenyl thioketone (**12**). When the sample was left under atmospheric conditions at room temperature overnight, the violet color completely faded. The precipitated, white solid, which was probably sulfur, was filtered off, and the filtrate was chromatographed on silica. Buten-3-yl phenyl ketone (**13**) was eluted with benzene. The NMR spectrum of the ketone, **13**, closely resembled that of the thioketone, **10**.

10: NMR ($CDCl_3$, TMS): τ 7.44 (H^c: quartet, $J=7$ Hz, 2H), 6.70—6.50 (H^d: m, 2H), 5.20—4.70 (H^a: m, 2H), 4.35—3.85 (H^b: m, 1H), 2.85—2.35 and 2.10—1.90 (H^e: m, 5H).

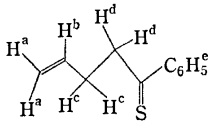

Although the absorption assigned to $CH_2{}^d$ was considered to be a triplet, it appeared as a multiplet. Therefore, a decoupling technique was employed to ascertain the assignments of $CH_2{}^c$ and $CH_2{}^d$. No unusual coupling could, however, be observed. That is, the absorption peak assigned to $CH_2{}^c$ appeared as a doublet ($J=6$ Hz) when $CH_2{}^d$ was irradiated, and the peak assigned to $CH_2{}^d$ appeared as a singlet when $CH_2{}^c$ was irradiated. Consequently, it is unclear why the peak assigned to $CH_2{}^d$ did not appear as a triplet.

13: NMR (CCl_4, TMS): τ 7.58 (H_c: quartet, $J=7$ Hz, 2H), 7.04 (H^d: t, $J=7$ Hz, 2H), 5.20—4.85 (H^a: m, 2H), 4.40—3.90 (H^b: m, 1H), and 2.90—2,50, 2.20—2.00 (H^e: m, 5H).

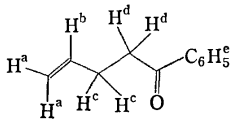

IR (neat): 1680 ($\nu_{C=O}$), 1635 (ν_{C-O}) and 970, 910 cm^{-1} $\left(\delta \begin{matrix} H \\ \end{matrix}\!\!>\!\!=\!\!<\!\!\begin{matrix} H \\ H \end{matrix}\right)$.

Mass: 160 M^+, 105 $PhCO^+$, base peak, and 77 Ph^+.

*The Thermal Decomposition and Photolysis of α-Allylthioacetophenone Tosylhydrazone (**1e**).* The tosylhydrazone, **1e** (360 mg, 1.0 mmol), and 60 mg (1.1 mmol) of sodium methoxide were dissolved in 40 ml of monoglyme in the photolysis vessel and stirred. The solution was bubbled with a dry nitrogen stream, and the vessel was closed. Photolysis was carried out using a 450-W high-pressure Hg lamp for 3 hr, after which the vessel was cooled by a water stream during irradiation. The sodium *p*-toluenesulfinate thus precipitated was filtered off, and the residue was concentrated and chromatographed on silica. 1-Phenyl-3-thiabicyclo[3.1.0]hexane (**16**) (87.5%) was eluted, with benzene as the sole product.

The thermal decomposition of the tosylhydrazone **1e** was carried out in a manner similar to that used in the case of the decomposition of the **1a-d** tosylhydrazones, though sodium methoxide was used instead of sodium hydride. The vacuum distillation of the reaction mixture afforded 3-thiabicyclo [3.1.0]hexane(**16**) in a 68.5% yield.

The yields were calculated by comparing the vpc peak area of the crude product with that of pure samples.

16: NMR (CCl_4, TMS): τ 9.17 ($H_A{}^a$: quartet, $J_{ab}=8$ Hz, 1H), 8.49 ($H_B{}^a$: t, $J_{ab}=4$ Hz, $J_{aa}=1$ H, 6 Hz), 8.23 (H^b: quintet, $J_{ab}=8$ Hz, 4 Hz, $J_{bc}=4$ Hz, 0 Hz, 1H), 7.14 ($H_A{}^c$: d, $J_{cc}=11$ Hz, $J_{bc}=0$ Hz, 1H), 6.90 (H^d: AB_q, $J_{dd}=11$ Hz, 2H), 6.79 ($H_B{}^c$: quartet, $J_{bc}=4$ Hz, $J_{cc}=11$ Hz, 1H), and 3.00—2.70 (H : m, 5H).

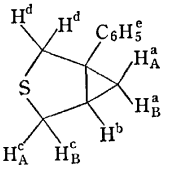

Mass: 176 M^+ base peak, 143 M^+–SH, 135 M^+-41  , 128 M^+-48, 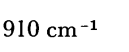 , 91 C_7H_7, and 77 Ph^+. Found: C, 74.98; H, 6.74; S, 18.23%. Calcd for $C_{11}H_{12}S$: C, 74.95; H, 6.86; S, 18.19%.

Circular Dichroism Studies of Ring-conformational and rotational Equilibria in 2-Isopropenylcyclohexanones[1]

Satoru WATANABE

Department of Chemistry, Faculty of Science, Hiroshima University, Higashisenda-machi, Hiroshima

(Received September 16, 1972)

The temperature-dependent circular dichroism of optically active β,γ-unsaturated ketones, (2*S*, 5*R*)-(−)-2-isopropenyl-2,5-dimethylcyclohexanone (**2**) and (2*S*, 5*R*)-(−)-2-isopropenyl-5-methylcyclohexanone (**3**), and of the corresponding saturated ketones, (2*S*, 5*R*)-(−)-2-isopropyl-2,5-dimethylcyclohexanone (**1**), has been measured at the n→π^* transition in order to determine the relative disposition between the carbonyl group and the ethylenic bond of the isopropenyl group of the β,γ-unsaturated ketones. The compound (**2**) exhibited the sign of a Cotton effect opposite to that of the corresponding saturated compound (**1**), and the circular dichroism of the compound (**3**) behaved quite differently from menthone (**4**). The result has been discussed mainly in terms of the geometry of the carbonyl group and the ethylenic bond of the isopropenyl group. Thus, it has been concluded that the preferred conformations of the compounds (**1**), (**2**), and (**3**), are **1A**, **2A-III**, and **3A-I** respectively.

Circular dichroism (CD) measurements at various temperatures have been found to be very useful in studying the conformational analysis of a flexible α,β-unsaturated carbonyl compound, because of the peculiar sensitivity of this method to subtle conformational alteration.[3-5] The long-wavelength β,γ-unsaturated carbonyl transition has been previously pointed out[6,7] to take on some of the aspects usually characteristic of the transitions of dissymmetric chromophores; the amplitude of Cotton effect curves in β,γ-unsaturated ketones is known[6,7] to be critically dependent on the relative disposition between the carbonyl group and the ethylenic bond. This concept has now been applied to the conformational analysis of β,γ-unsaturated carbonyl compounds in a situation where the free rotation may occur. This paper will deal with the relative disposition between the carbonyl chromophore and the ethylenic bond of β,γ-unsaturated ketones, (2*S*, 5*R*)-(−)-2-isopropenyl-2,5-dimethylcyclohexanone (**2**) and (2*S*, 5*R*)-(−)-2-isopropenyl-5-methylcyclohexanone (**3**), as studied by means of the temperature-dependent circular dichroism at the n→π^* transition and in comparison with the circular dichroism of the corresponding saturated ketones, (2*S*, 5*R*)-(−)-2-isopropyl-2,5-dimethylcyclohexanone (**1**) and (2*S*, 5*R*)-(−)-2-isopropyl-5-methylcyclohexanone (**4**).[8]

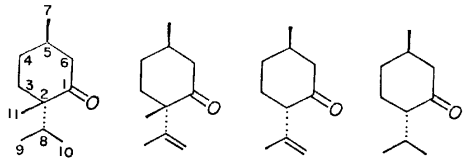

1 **2** **3** **4**

Results and Discussion

The CD curves of (2*S*, 5*R*)-(−)-2-isopropyl-2,5-dimethylcyclohexanone (**1**) in selected solvents showed only a positive Cotton effect. However, a decrease in the rotational strength was observed upon changing the solvent from a nonpolar to a polar one. The methylmenthone (**1**) may exist in two interconvertible chair conformations, **1A**⇌**1B**. According to the octant rule, the conformer **1A** should exhibit a positive Cotton effect, and the conformer **1B**, a negative one. Therefore, the positively-rotating conformer **1A** with an equatorial isopropyl group is preferential in the nonpolar solvents. The temperature-dependent CD curves of the compound (**1**) in the MI (Fig. 1) and the EPA solvents both exhibited only a positive Cotton effect with the increase in the rotational strength upon a lowering of the temperature from 25 to −186 °C. The increase in the positive sign is attributable mainly

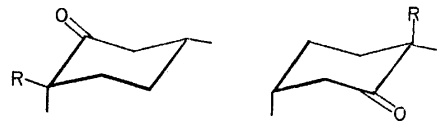

1A: R=Isopropyl **1B**: R=Isopropyl
2A: R= Isopropenyl **2B**: R=Isopropenyl

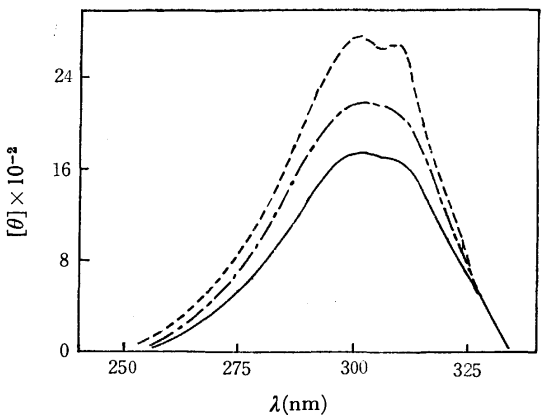

Fig. 1. CD curves of (2*S*, 5*R*)-(−)-2-isopropyl-2,5-dimethylcyclohexanone (**1**) in the MI solvent: —— at +25 °C, ———— at −74 °C, and --- at −186 °C.

1) This paper had been read at the 24th Annual Meeting of the Chemical Society of Japan, Osaka, April, 1971 and forms Part XXI[2] in the Hiroshima University series of "Stereochemical Studies of Monoterpene Compounds,"

2) Paper XX, T. Hirata, This Bulletin, **45**, 3458 (1972).

3) G. Snatzke and E. Schwinum, *Tetrahedron*, **22**, 761 (1966).

4) T. Suga, K. Imamura, and T. Shishibori, This Bulletin, **45**, 545 (1972).

5) T. Suga and K. Imamura, *ibid.*, **45**, 2060 (1972).

6) A. Moscowitz, K. Mislow, M. A. W. Glass, and C. Djerassi, *J. Amer. Chem. Soc.*, **84**, 1945 (1962).

7) K. Mislow and J. G. Berger, *ibid.*, **84**, 1956 (1962).

8) K. M. Wellman, P. H. A. Laur, W. S. Briggs, A. Moscowitz, and C. Djerassi, *ibid.*, **87**, 66 (1965).

to the contribution of the ring conformation, and also partly to the rotational preferred conformation of the isopropyl group.[9] In that case, the isopropyl group contributes to the rotational strength only when the compound (**1**) takes the conformer **1A**. Therefore, this positive increase implies that the positively-rotating conformer, **1A**, is more stable than the conformer **1B** in respect to the energetic and steric requirements. Thus, the compound (**1**) exclusively exists in the conformer **1A**, frozen out, at −186 °C.

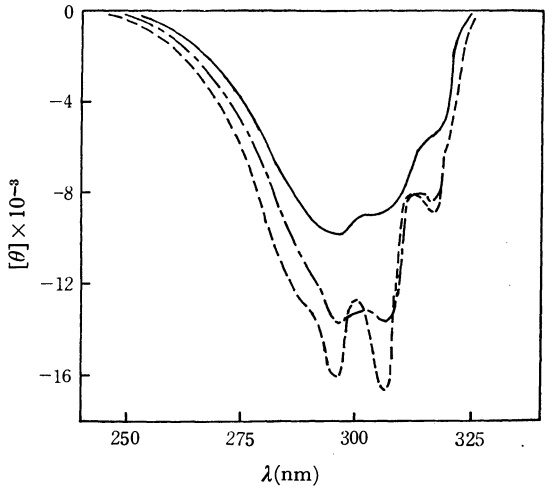

Fig. 2. CD curves of (2*S*, 5*R*)-(−)-2-isopropenyl-2,5-dimethylcyclohexanone (**2**) in the MI solvent: —— at +25 °C, — — — at −74 °C, and --- at −186 °C.

The CD curves of (2*S*, 5*R*)-(−)-2-isopropenyl-2,5-dimethylcyclohexanone (**2**) in various solvents exhibited only a negative Cotton effect with an increase in the rotational strength upon changing the solvent from a polar to a nonpolar one, in contrast with the case of the corresponding saturated compound (**1**). The CD curves in the MI solvent are illustrated in Fig. 2. The methylisopulegone (**2**) may exist in two interconvertible chair conformations, **2A**⇌**2B**, as well as the corresponding saturated compound (**1**). The conformer **2B** should exhibit a negative Cotton effect. If the free rotation of the isopropenyl group of the conformer **2A** is assumed not to contribute to the sign of a Cotton effect, the conformer **2A** may exhibit a positive Cotton effect. Therefore, the negative sign of a Cotton effect observed may be caused by the conformer **2B**. As has been mentioned above, however, the most preferred conformation of the methylmenthone (**1**) is the conformer **1A** with the equatorial isopropyl group at lower temperatures. The replacement of the isopropyl group with the slightly less bulky isopropenyl one is considered not to induce the inversion of the alkylated cyclohexane skeleton. Accordingly, the most preferred conformation for the compound (**2**) should be the conformer **2A** with the equatorial isopropenyl group at lower temperatures. The negative Cotton effect observed for the compound (**2**) should, consequently, be attributable to the relative disposition between the carbonyl group and the ethylenic bond of the isopropenyl group in the conformer **2A**, as has been pointed out previously.[6,7] The sign and the rotational strength of the Cotton effect of β,γ-unsaturated ketones are critically dependent on the array of double bonds.

The possible preferred conformations of the isopropenyl group in the conformer **2A** by the Newman projection with the corresponding octant projection, as viewed from C-8 to C-2, may be represented as is shown in Chart 1, judging from the conformation of 1-butene[10] and the energy barrier of *n*-butane.[11] The maximum interaction between the 9-methyl group and the 3-methylene or the 11-methyl group may be approximated by a butane function with a maximum value of 6.0 kcal/mol. The signs of a Cotton effect shown were predicted by an examination of the model[12] for each conformation in Chart 1. The conformers **2A-I** and **2A-II** should exhibit a positive Cotton effect and the conformer, **2A-III**, a negative one. The strong negative sign of the compound (**2**) at −186 °C was thus attributed to the conformer **2A-III**. Therefore, the conformer **2A-III** in the chair form is preferential at lower temperatures and in nonpolar solvents.

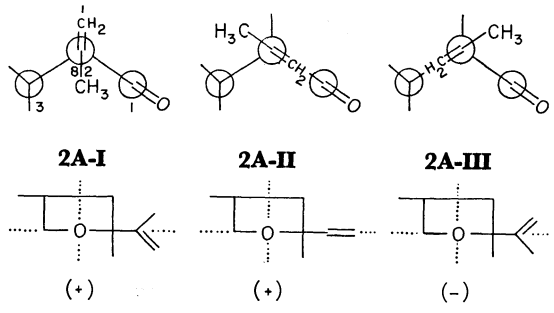

Chart 1. Possible preferred conformations, octant projections of the ethylenic bond in the conformation **2A** as viewed from C-8 to C-2, and the predicted signs of a Cotton effect.

The CD curves of both compound (**2**) and compound (**1**) in decalin showed a decrease in the rotational strength with the change of the temperature from −74 to +150 °C, although the signs are opposite. This implies that the positively-rotating conformer, **1A**, decreased with an increasing population of the unstable conformer, **1B**, when the temperature was raised. The negatively-rotating conformer, **2B**, like the compound (**1**), will increase at higher temperatures, exhibiting an augmentation of the negative CD curves. However, the opposite situations observed in the CD cruves of the compound (**2**) and the compound (**1**) seem to indicate that the contribution of a Cotton effect caused by the free rotation of the isopropenyl group in the conformer **2A** overcomes the contribution of a Cotton effect of the increasing conformer, **2B**.

The CD curves of isopulegone, (2*S*, 5*R*)-(−)-2-isopropenyl-5-methylcyclohexanone (**3**), showed only a

9) K. M. Wellman, W. S. Briggs, and C. Djerassi, *J. Amer. Chem. Soc.*, **87**, 73 (1965).

10) A. A. Bother-By, C. Naar-Colin, and H. Gunther, *ibid.*, **84**, 2748 (1962).

11) K. Ito, *ibid.*, **75**, 3430 (1953).

12) Examined by "Dreiding Stereomodels," W. Buchi Manufacture of Glass Apparatus Flawil, Switzerland.

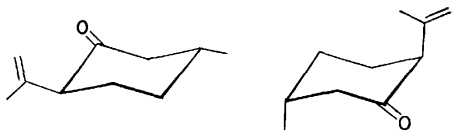

3A 3B

negative Cotton effect with an increase in the rotational strength in a nonpolar solvent, such as carbon tetrachloride, over that in a polar one. The ketone (**3**) may exist in two interconvertible chair conformations, **3A** and **3B**. The negative Cotton effect should be attributed to the conformer **3B** and/or to the conformer **3A-I** shown in Chart 2, in the same way as has been discussed in connection with the compound (**2**). The observation of a strong negative Cotton effect for the compound (**3**) in nonpolar solvents obviously indicates that the compound is composed of the conformer **3A-I** and the conformer **3B** in a conformational equilibrium, **3A**⇌**3B**, since, even if the isopropyl group of (−)-menthone (**4**) is replaced by the slightly less bulky isopropenyl group, the populations of the unstable diaxial conformer with a strong negative Cotton effect will probably comprise at least 3%, in a manner similar to that in the case of the parent compound, (−)-menthone (**4**).[8]

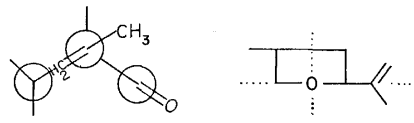

3A-1 (−)

Chart 2. The preferred conformation, the octant projection of the ethylenic bond in the conformation **3A** as viewed from C-8 to C-2, and the predicted sign of a Cotton effect.

This interpretation is further supported by the variable temperature circular dichroism. Upon the lowering of the temperature from +25 to −186 °C, the CD curves of the compound (**3**) exhibited a negative Cotton effect with the increase in the rotational strength in the EPA solvent (Fig. 3), but with the decrease in the MI solvent (Fig. 4). The decrease in the rotational strength of a neagtive Cotton effect in the nonpolar solvent was interpreted as an indication of the increase in the energetically more stable, diequatorial conformer, **3A**, at the sacrifice of the diaxial conformer, **3B**, with the stronger rotational strength, upon the lowering of the temperature. This result is further supported by high-temperature CD curves in decalin. At higher temperatures, the CD curves exhibited an increase in the negative sign, implying the augmentaion of the unstable diaxial conformer, **3B**, with the strong rotational strength, analogously to the case of (−)-menthone (**4**).[8] On the other hand, the increase in the rotational strength of the negative sign in the EPA solvent at lower temperatures implies the preference of the conformer **3A** at room temperature and the increase in the population of the conformer **3A-I** upon the lowering of the temperature. Thus, it seems likely that the most preferred conformation of the compound (**3**) is **3A-I**.

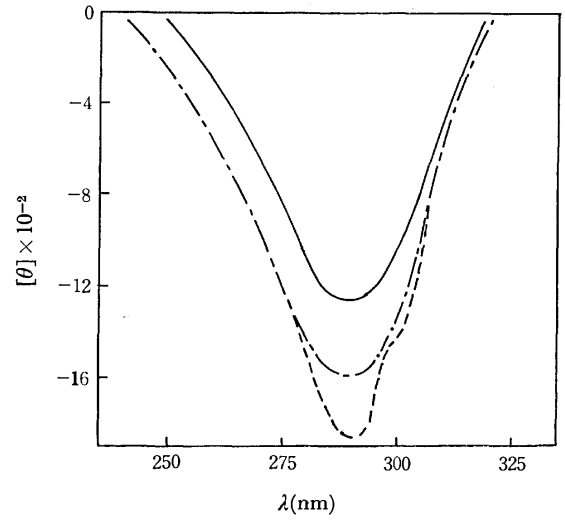

Fig. 3. CD cruves of (2*S*, 5*R*)-(−)-2-isopropenyl-5-methylcyclohexanone (**3**) in the EPA solvent: —— at +25 °C, ——— at −74 °C, and ---- at −186 °C.

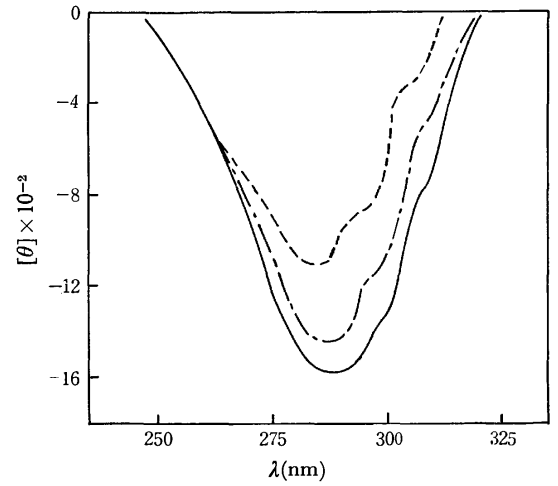

Fig. 4. CD curves of (2*S*, 5*R*)-(−)-2-isopropenyl-5-methylcyclohexanone (**3**) in the MI solvent: —— at +25 °C, ——— at −74 °C, and ---- at −186 °C.

The absolute value of the rotational strength of the β,γ-unsaturated ketones was four to five times that of the corresponding saturated compounds. It is likely that the array between the carbonyl group and the ethylenic bond in the conformer **2A-III** and **3A-I** contributes to the increase in their molecular ellipticity by several times, as compared with the corresponding saturated compounds.

Experimental

Measurements. The CD curves were obtained by means of a Japan Spectroscopic Co., Ltd., automatically-recording spectropolarimeter, Model ORD/UV-5, equipped with a circular dichroism attachment, using a variable-temperature CD cell. The EPA solvent was composed of ether–isopentane–ethanol in the ratio of 5:5:2 by volume. The MI solvent was composed of methylcyclohexane–isopentane of the ratio of 1:3 by volume. The NMR, IR, and UV spectra, although not shown below completly, exactly supported the structure

of the compounds on which the CD curves were measured. Gas-chromatographic analyses were made at 100—150 °C, using a Hitachi Perkin-Elmer F6-D gas chromatograph with a flame ionization-type detector and a 3 mm×1 m column packed with 10%-polyethylene glycol-6000 on Celite.

(2S, 5R)-(−)-2-Isopropyl-2,5-dimethylcyclohexanone (1). The catalytic hydrogenation of methylisopulegone (**2**) (200 mg) (described later) in methanol on 10% palladium-charcoal gave the compound (**1**) (150 mg) with the following properties: bp 176 °C, n_D^{25} 1.4543, $[\alpha]_D^{25}$ −7.3° (MeOH, *c* 0.1636); 99.7% pure by analytical glc; NMR (CCl_4) 0.72—1.00 ppm (m, 12H, $-CH_3$); ν_{max}^{liq} 1700 (C=O), 1378, and 1392 cm^{-1} (isopropyl group); λ_{max}^{MeOH} 291 nm (ε 38.0); CD (max) in MeOH (*c* 0.164): $[\theta]_{308}^{+25°}$ +932, in dioxane (*c* 0.189): $[\theta]_{308}^{+25°}$ +1467, in isooctane (*c* 0.192): $[\theta]_{311}^{+25°}$ +1530, in CCl_4 (*c* 0.163): $[\theta]_{311}^{+25°}$ +1973, in decalin (*c* 0.184): $[\theta]_{300}^{-74°}$ +1452, and $[\theta]_{310}^{-74°}$ +1531, $[\theta]_{300}^{+25°}$ +1333, $[\theta]_{305}^{+74°}$ +935, $[\theta]_{305}^{+150°}$ +606, in EPA (*c* 0.131): $[\theta]_{300}^{+25°}$ +1379 and $[\theta]_{310}^{+25°}$ +1352, $[\theta]_{300}^{-74°}$ +2023 and $[\theta]_{310}^{-74°}$ +2071, $[\theta]_{299}^{-190°}$ +3698 and $[\theta]_{308}^{-190°}$ +3742.

(2S, 5R)-(−)-2-Isopropenyl-2,5-dimethylcyclohexanone (2). This compound was synthesized by the methylation of (+)-pulegone (bp 81—82 °C/5 mmHg, n_D^{25} 1.4843, d_4^{25} 0.9303, $[\alpha]_D^{25}$ +23.0° (neat)) following the method in the literature.[13] It was found to be 99.5% pure by analytical glc and showed the following physical properties: bp 69—70 °C/8 mmHg, n_D^{25} 1.4682, d_4^{25} 0.9231, $[\alpha]_D^{25}$ −139.2° (neat); the semicarbazone derivative, mp 201—202 °C; NMR (CCl_4) 0.96 ppm (d, *J*=6.0 Hz, 3H, $CH-CH_3$), 1.10 (s, 3H, $-CH_3$), 1.68 (s, 3H, $=C-CH_3$), 4.76 and 4.88 (m, 2H, $=CH_2$); ν_{max}^{liq} 3075, 1640, 890 ($C=CH_2$), 1706 cm^{-1} (C=O); λ_{max}^{MeOH} 294 nm (ε 51.6); CD (max) in MeOH (*c* 0.135): $[\theta]_{296}^{+25°}$ −6411, in dioxane (*c* 0.175): $[\theta]_{295}^{+25°}$ −6642, in isooctane (*c* 0.042): $[\theta]_{298}^{+25°}$ −9782, in CCl_4 (*c* 0.095): $[\theta]_{300}^{+25°}$ −10841, in decalin (*c* 0.062): $[\theta]_{307}^{-74°}$ −14300, $[\theta]_{297}^{+25°}$ −12016, $[\theta]_{298}^{+74°}$ −10598, $[\theta]_{300}^{+150°}$ −8487, in EPA (*c* 0.063): $[\theta]_{298}^{+25°}$ −8765, $[\theta]_{301}^{-74°}$ −9794 and $[\theta]_{308}^{-74°}$ −10406, $[\theta]_{297}^{-190°}$ −13416 and $[\theta]_{305}^{-190°}$ −14522.

(2S, 5R)-(−)-2-Isopropenyl-5-methylcyclohexanone (3). The oxidation of (−)-isopulegol (bp 93.0 °C/10 mmHg, n_D^{25} 1.4676, d_4^{25} 0.9052, $[\alpha]_D^{25}$ −22.3° (neat)) with a chromium trioxide-pyridine complex afforded the compound (**3**): bp 86 °C/10 mmHg, n_D^{25} 1.4670, d_4^{25} 0.9252, $[\alpha]_D^{25}$ +7.9° (neat); 94% pure by analytical glc; NMR (CCl_4) 1.40 ppm (d, *J*=4.0 Hz, 3H, $CH-C\underline{H}_3$), 1.70 (s, 3H, $=C-CH_3$), 4.63 and 4.79 (m, 2H, $=CH_2$); ν_{max}^{liq} 3050, 1649, 890 ($C=CH_2$), 1712 cm^{-1} (C=O); λ_{max}^{MeOH} 297 nm (ε 29.7); CD (max) in MeOH (*c* 0.166): $[\theta]_{288}^{+25°}$ −1104, in dioxane (*c* 0.185): $[\theta]_{294}^{+25°}$ −1598, in isooctane (*c* 0.166): $[\theta]_{294}^{+25°}$ −1510, in CCl_4 (*c* 0.125): $[\theta]_{295}^{+25°}$ −1685, in decalin (*c* 0.185): $[\theta]_{293}^{-74°}$ −1510, $[\theta]_{294}^{+25°}$ −1518, $[\theta]_{294}^{+74°}$ −1598, $[\theta]_{296}^{+150°}$ −1635.

The author wishes to thank Dr. Takayuki Suga of Hiroshima University for his guidance and encouragement, and the Takasago Perfumery Co. for its gifts of pulegone and isopulegol.

13) T. Suga and S. Watanabe, This Bulletin, **45**, 340 (1972).

NOTES

BULLETIN OF THE CHEMICAL SOCIETY OF JAPAN, VOL. 46, 1550—1551 (1973)

Asymmetric Hydrogenation of C=O Double Bond with Modified Raney Nickel. XXVI. Asymmetric Hydrogenation of β-Keto Esters

Tadashi TANABE* and Yoshiharu IZUMI

Division of Organic Chemistry, Institute for Protein Research, Osaka University, Suita, Osaka 565

(Received March 9, 1972)

It was found that the Raney nickel catalyst modified with the α-amino or α-hydroxy acid catalyzed the hydrogenations of β-keto esters to the corresponding β-hydroxyesters in good asymmetric yields, and that the alkoxy moiety of the ester of acetoacetic acid influenced the asymmetric yields.[1] For the elucidation of the enantiotopic selection[2] mechanism of the modified Raney nickel catalyst, the effect of the bulk of the acyl group on the asymmetric yield of the product has been studied with various methyl acylacetates.

Experimental

Preparation of the Substrate. The methyl acylacetates were prepared by the ester-interchange of the ethyl acylacetates with sodium methoxide in methanol. The ethyl acylacetates were synthesized by the decomposition of the acylated malonic esters, which had been prepared from magnesium malonate and acyl chloride by the method of Riegel *et al.*[3] Ethyl oxalacetate was prepared by the condensation of ethyl acetate and ethyl oxalate with sodium.[4]

Optical Resolution of DL-*3-Hydroxy*-n-*valeric Acid.* One hundred grams of ethyl propionylacetate[2] was reduced with 2.4 g of a Raney nickel catalyst[1]; the product was hydrolyzed with a slightly excess 50% sodium hydroxide solution and acidified with concd hydrochloric acid equivalent to the alkali used. After concentration *in vacuo*, the acid was extracted with acetone and the acetone was removed by distillation under reduced pressure. Seventy grams of the acid was thus obtained.

Quinine monohydrate (152 g) in 1 l of water was neutralized with 50 g of DL-3-hydroxy-*n*-valeric acid at 100°C. Then the solution was cooled to room temperature. The quinine salts were collected by filtration and recrystallized once from water. Yield, 90 g; mp 112°C.

Found: C, 65.33; H, 8.19; N, 5.91%. Calcd for $C_{25}H_{36}O_6N_2$: C, 65.19; H, 7.88; N, 6.08%.

$[\alpha]_D^{20}$ −119° (*c* 1, ethanol).

Ninety grams of the quinine salt was suspended in 1.5 l of water and decomposed with 90 ml of a 10% sodium hydroxide solution. The mixture was then let stand overnight, after which the quinine was removed by filtration. The solution was washed with 150 ml of chloroform five times, neutralized with N hydrochloric acid, and concentrated to dryness. The sodium salt was extracted with ethanol, and the ethanol solution was cooled to room temperature. The sodium salts were filtered off and dried in a vacuum desiccator at 60°C. Yield, 26 g; mp 116 °C. $[\alpha]_D^{20}$ +8.48° (*c* 4, water).

Found: C, 41.65; H, 6.95%. Calcd for $C_5H_9O_3Na \cdot 1/4H_2O$: C, 41.52; H, 6.62%.

Preparation of Methyl L$_8$[5]-*(+)-3-Hydroxy*-n-*valerate.* Five grams of the sodium salt was dissolved in 50 ml of water; the solution was then acidified with 3.2 ml of concd hydrochloric acid and concentrated to dryness under reduced pressure. The acid was extracted with 100 ml of ether and esterified with diazomethane.[6] After the removal of the ether, the ester was distilled under reduced pressure. Yield, 3.6 g; bp 81°C/17 mmHg.

Found: C, 53.80; H, 9.33%. Calcd for $C_6H_{12}O_3$: C, 54.53; H, 9.15%.

α_D^{20} +18.60 (without dilution).

Preparation of the Modified Raney Nickel Catalyst and Measurement of the Asymmetric Activity of the Catalyst. The procedures for the preparation of the modified Raney nickel catalyst and the measurement of the asymmetric activity were the same as have been described in a previous paper.[7]

Results and Discussion

In order to elucidate the effect of the bulk of the acyl group of the β-keto ester on the asymmetric activity of the catalyst, various methyl acylacetates and diethyl oxalacetate were hydrogenated with catalysts modified with L-glutamic acid and D-tartaric acid. The acyl groups used were propionyl, *n*-butyryl, isobutyryl, and octanoyl groups. The results are compared in Table 1 with those of the hydrogenation of methyl acetoacetate.

With the catalysts modified by D-tartaric acid, and by L-glutamic acid, the methyl acylacetates were hydrogenated to the products of the levorotatory optical rotation.[8]

Upon modification with tartaric acid, the asymmetric yield was higher in methyl propionylacetate than in methyl acetoacetate and a product with a large op-

* Present adress: Kyoto University, Faculty of Medicine, Sakyo-ku, Kyoto.

1) Y. Izumi, M. Imaida, T. Harada, T. Tanabe, S. Yajima, and T. Ninomiya, This Bulletin, **42**, 241 (1969).

2) The definition was proposed in *Angew. Chem., Int. Ed. Engl.*, **10**, 871 (1971).

3) B. Riegel and W. M. Lilienfeld, *J. Amer. Chem. Soc.*, **67**, 1273 (1945).

4) W. Wislicenus, *Ann.*, **246**, 315 (1888).

5) P. A. Levene and H. L. Haller, *J. Biol. Chem.*, **76**, 415 (1928).

6) H. Pechman, *Ber.*, **27**, 1888 (1894).

7) Y. Izumi, T. Harada, T. Tanabe, and K. Okuda, This Bulletin, **44**, 1418 (1971).

8) The optical rotations of the methyl esters of optically-active 3-hydroxycaproic acid, 3-hydroxy-4-methyl-*n*-valeric acid, and 3-hydroxycapric acid have not been obtained successfully. However, the optical rotations of optically-pure methyl 3-hydroxybutyrate and methyl 3-hydroxy-*n*-valerate were 23.8 and 18.6° respectively and the elongation of the carbon chain in the 3-hydroxy-*n*-aliphatic acid seems to be accompanied by a decrease in the optical rotation.

Table 1. Relation between asymmetric yield and bulk of acyl group of β-keto ester

$R\text{-}CO\text{-}CH_2\text{-}COOCH_3$

Substrate R in $RCOCH_2COOCH_3$	Modifying[b] reagent	Optical rotation of product, α_D^{20}	Asymmetric yield P %
CH_3-	L-Glutamic acid	−5.03	21[a]
CH_3CH_2-	L-Glutamic acid	−3.13	17
$CH_3(CH_2)_2$-	L-Glutamic acid	−1.29	—
$(CH_3)_2CH$-	L-Glutamic acid	−4.06	—
$CH_3(CH_2)_6$-	L-Glutamic acid	−0.28	—
CH_3-	D-Tartaric acid	−7.73	33[a]
CH_3CH_2-	D-Tartaric acid	−10.19	55
$CH_3(CH_2)_2$-	D-Tartaric acid	−4.23	—
$(CH_3)_2CH$-	D-Tartaric acid	−15.95	—
$CH_3(CH_2)_6$-	D-Tartaric acid	−0.61	—
CH_3CH_2-	D-Tartaric acid[c]	−12.25	66
C_2H_5OCO-[d]	D-Tartaric acid	0	0

a) Part XXV of this series: T. Tanabe, K. Okuda, and Y. Izumi, to be reported in this Bulletin.
b) Modifying condition: pH 5.0, 0 °C.
c) Modified at pH 5.0, 100 °C.
d) Diethyl oxalacetate.

tical rotation was obtained in the hydrogenation of methyl isobutyrylacetate. These facts suggest that the bulk of the acyl group contributed to the enantiotopic selection of the substrate by D-tartaric acid on the catalyst surface. Upon modification at 100°C, a higher asymmetric yield (66%) was obtained in the hydrogenation of methyl propionylacetate.

The catalyst modified with L-glutamic acid was found to have a different asymmetric activity than the one modified with D-tartaric acid. Though the asymmetric directions of the products were levorotatory, it seemed that the asymmetric yields of the products were not much affected by the bulk of the acyl group. Accordingly, a high asymmetric yield would not be obtained by the modification of the acyl group of the methyl acylacetate.

Diethyl oxalacetate was not asymmetrically hydrogenated with the catalyst modified with tartaric acid, as may be seen in Table 1. This result suggests that the smaller defference in the groups around the carbonyl group to be reduced may result in the difficulty of the enantiotopic selection by the modifying reagent.

The results presented above show that the sorts of the substituents and the steric requirement around the carbonyl group of the substrate are very important for the enantiotopic selection by the modifying reagent, especially in the asymmetric hydrogenation by the catalyst modified with tartaric acid.

The authors wish to express their thanks to Miss Kiku Koike and Mrs. Nobuko Okuhara for their elemental analyses and to the Kawaken Fine Chemicals Co., Ltd., Tokyo for the supply of Raney nickel.

BULLETIN OF THE CHEMICAL SOCIETY OF JAPAN, VOL. 46, 1551—1552 (1973)

Viscosity *B* Coefficients for Some Alkyl Sulfates in Aqueous Solutions

Kunio TAMAKI, Yōko ŌHARA, and Yoshio ISOMURA

Department of Chemistry, Yokohama City University, Kanazawa-ku, Yokohama 236

(Received May 29, 1972)

In the previous paper,[1] the change in the partial molal heat capacity of a homologous series of sodium alkyl sulfates has been discussed in terms of the change in water structure for the dissolution of the solutes into water. This paper will drscribe our experimental findings on the viscosity of sodium alkyl sulfates in aqueous solutions.

Experimental

The viscosities were measured in Ubbelohde-type viscosimeters with flow times for water at 25 °C of about 800 s in a constant-temperature bath controlled to ±0.01 °C of the specified temperature. It was found that the kinetic energy correction was negligible in this work. The densities were measured in Ostwald pycnometers. The relative viscosities were calculated in the usual manner, using the data on the flow time and the density. The sodium alkyl sulfates used were the same samples as those described in the previous paper.[1]

1) K. Tamaki, Y. Isomura, and Y. Ōhara, This Bulletin, **45**, 2939 (1972).

Results and Discussion

The viscosity of an aqueous solution of electrolytes, η, can be represented by the Jones-Dole equation:[2]

$$\eta/\eta_0 = 1 + AC^{1/2} + BC \quad (1)$$

where η_0 is the viscosity of water, C is the concentration (molality), A is the constant related to the ion-ion interaction, and B is the viscosity B coefficient. Equation (1) is thus converted to:

$$(\eta/\eta_0 - 1)/C^{1/2} = A + BC^{1/2} \quad (2)$$

When the left-hand side of Eq. (2) is plotted against $C^{1/2}$, the viscosity B coefficient is obtained as the slope of a linear line. For example, Fig. 1 shows the results of the plotting of Eq. (2) at 25 °C. The values of the viscosity B coefficient thus obtained are summarized in Table 1. The estimated error in the B values is ±0.005. The constant, A, was theoretically interpreted by Falkenhagen and can be calculat-

2) G. Jones and M. Dole, *J. Amer. Chem. Soc.*, **51**, 1950 (1929).

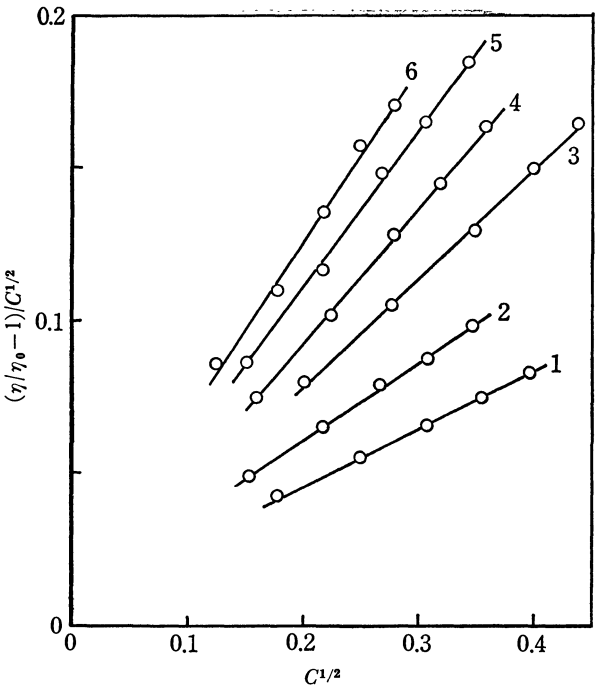

Fig. 1. $(\eta/\eta_0-1)/C^{1/2}$ *vs.* $C^{1/2}$ plot at 25 °C. 1, methyl; 2, ethyl; 3, propyl; 4, butyl; 5, pentyl; 6, hexyl.

Table 1. Viscosity *B* coefficient for sodium alkyl sulfates at several temperatures

Compound	10 °C	25 °C	35 °C	45 °C	50 °C
Methyl	—	0.188	0.190	—	0.200
Ethyl	0.263	0.265	—	—	0.270
Propyl	—	0.348	0.340	0.327	—
Butyl	—	0.423	—	—	—
Pentyl	—	0.504	0.457	—	—
Hexyl	—	0.582	—	—	—

ed using the data of the limiting equivalent conductivity of the salt, cation, and anion.[3] In this work, the electrical conductivities were measured with a Yokogawa BVZ-13A audio-frequency bridge using a frequency of 1000 Hz. In general, the calculated values of *A* were found to be in good agreement with those obtained from the semi-empirical Eq. (2).

The *B* values for the homologous sodium alkyl sulfates increase linearly with the number of carbon atoms in the alkyl chains at 25 °C. The average increment per methylene group is 0.079. Similar relations have been observed for homologous alkylammonium bromides[4] and for homologous amino acids, $NH_3^+(CH_2)_xCOO^-$.[5] The increments per methylene group were 0.080 at 25 °C for the alkylammonium bromides[4] and 0.084 at 25 °C for the amino acids.[5] The contribution permethylene group to the viscosity *B* coefficient is considered to be about 0.080 at 25 °C.

As far as we are aware, there has been no report of a negative *B* coefficient for organic electrolytes in water.[4-8] This suggests the water-structure-making effect for all organic electrolytes, if we adopt the view of Gurney,[9] the *B* coefficient being interpreted in terms of a specific ion-solvent interaction. However, the viscosity *B* coefficient consists of the contribution from the ion-solvent interaction plus the contribution from the size of the ion (Einstein effect).[10] Large molecular ions such as organic ions may be expected to have a large viscosity increment arising from the Einstein effect.[10] With regard to the temperature dependence of the *B* values, this Einstein effect will remain fairly constant and better criteria for structure influences will be obtained.[10] Kay *et al.*[6] reported an increase in the viscosity *B* coefficient with the temperature for a structure-breaking ion such as tetramethylammonium salt and a decrease for a structure-making salt, such as tetrapropyl- and tetrabutylammonium salts. A similar relation has been reported for the homologous amino acids.[5] It may be seen in Table 1 that the methyl salt, a structure-breaking solute,[1] shows a slight increase in *B* value with the increase in the temperature between 25 and 50 °C, and that the ethyl salt, a borderline solute,[1] is rather insensitive to the temperature between 10 and 50 °C. On the other hand, for propyl salt, which is classified as a structure-making solute,[1] the *B* value decreases slightly with the temperature between 25 and 45 °C. A more remarkable decrease was found in the range of 25—35 °C for pentyl salt, which is an excellent structure-making solute.[1] On comparing these facts with those given in the previous paper,[1] it may be concluded for the homologous sodium alkyl sulfates that there is a close relationship between the temperature dependence of the viscosity *B* coefficient and the change in the partial molal heat capacity.[1]

The *B* values listed in Table 1 are naturally made up of the sum of the contributions from both sodium and alkyl sulfate ions. Fortunately, the B values of the sodium ion is practically constant between 15 and 42.5 °C.[10] Therefore, the temperature dependence of the viscosity *B* coefficient of the sodium salts discussed above conveniently reflects the nature of the alkyl sulfate anions.

3) H. S. Harnd and B. B. Owen, "The Physical Chemistry of Electrolytic Solutions," 3rd ed, Reinhold, New York (1958), p. 240.

4) J. E. Desnoyers, M. Arel and P-A. Leduc, *Can. J. Chem.* **47**, 547 (1969).

5) W. Devine and B. M. Lowe, *J. Chem. Soc., A*, **1971**, 2113.

6) R. L. Kay, T. Vituccio, C. Zawoyski, and D. F. Evans, *J. Phys. Chem.*, **70**, 2336 (1966).

7) C. T. Robertson and H. J. V. Tyrell, *J. Chem. Soc., A*, **1969**, 1938.

8) B. M. Lowe and H. M. Rendall, *Trans. Faraday Soc.*, **67**, 2318 (1971).

9) R. W. Gurney, "Ionic Processes in Solution," McGraw-Hill, New York (1953), p. 159.

10) R. H. Stokes and R. Mills, "Viscosity of Electrolytes and Related Properties," Pergamon, Oxford (1965), p. 39.

BULLETIN OF THE CHEMICAL SOCIETY OF JAPAN, VOL. 46, 1553—1554 (1973)

Synthesis of Bis(2,4,5-trimethylphenyl)-, Bis(2,4,6-trimethylphenyl)-, and Bis(3,4,5-trimethylphenyl)tetramethyloctadecanonaene

Toshio HAMASAKI*, Kiyoshi CHIN**, Nobuhisa OKUKADO, and Masaru YAMAGUCHI

Department of Chemistry, Faculty of Science, Kyushu University, Higashi-ku, Fukuoka 812

(Received September 12, 1972)

Three isomeric aromatic carotenoid hydrocarbons (I, II, and III) were synthesized, in order to compare them with unidentified minor carotenoid hydrocarbons present in a sea sponge "*Reniera japonica*", known to produce three aromatic carotenoids (IV, V, and VI) as the major constituents of its coloring matter.[1] None of these synthetic products have so far been proved to be identical with those from a natural source.

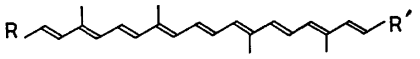

I R=R'=2,4,5-$(CH_3)_3C_6H_2$-
II R=R'=2,4,6-$(CH_3)_3C_6H_2$-
III R=R'=3,4,5-$(CH_3)_3C_6H_2$-
IV (isorenieratene) R=R'=2,3,6-$(CH_3)_3C_6H_2$-
V (renieratene) R=2,3,6-$(CH_3)_3C_6H_2$-, R'=2,3,4-$(CH_3)_3C_6H_2$-
VI (renierapurpurin) R=R'=2,3,4-$(CH_3)_3C_6H_2$-

Synthesis was carried out according to the conventional $C_{10}+C_{20}+C_{10}$ route,[2] where crocetin dialdehyde was condensed with an appropriate trimethylbenzilidenetriphenylphosphorane.

The highest λ_{max} of the synthetic and natural aromatic pigments are listed in Table 1 in the order of decreasing wavelength. Variations of λ_{max} can be satisfactorily explained in terms of non-planarity between benzene ring and polyene chain, caused by 2- and 6-standing methyl groups and the buttressing effect of 3-standing methyl groups on benzene rings.

TABLE 1. THE HIGHEST λ_{max} OF AROMATIC CAROTENOIDS

Compound	III	I	VI	V	II	IV
λ_{max} (benzene, mμ)	491	490	486	477	471	466

The pigments were adsorbed on alumina (Merck, neutral; Grade II: from benzene solution) in the following sequence of decreasing adsorbability: III, VI, I, V, II, IV.

Experimental

Materials. 2,4,5-, 2,4,6-, and 3,4,5-Trimethylbenzyl alcohol were prepared by lithium aluminium hydride reduction of the corresponding methyl trimethylbenzoates. The recrystallized alcohols melted at 83—83.5°C (lit, 83—83.5°C[3]), 86.5—87°C (lit, 87—88°C[4]) and 74—75°C (lit, 78°C[5]), respectively.

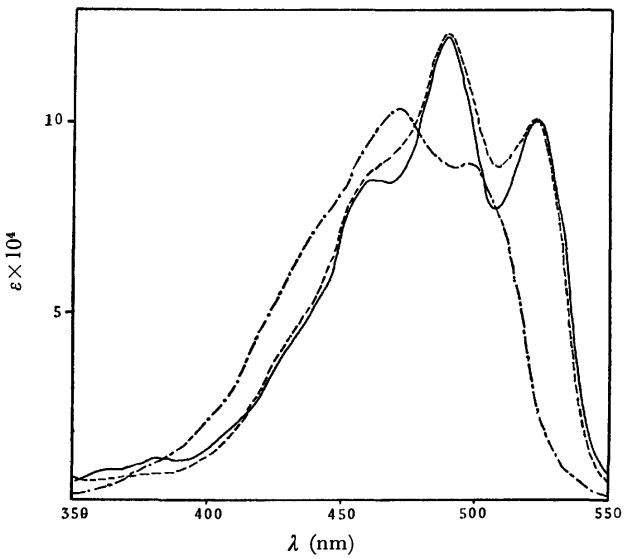

Fig. 1. Absorption curves of I (----), II (—·—·), and III (——) (benzene).

(Trimethylbenzyl)triphenylphosphonium Bromides. These were prepared from the corresponding alcohols in a similar way to that described by Cooper *et al.* on analogous phosphonium bromides.[6] (2,4,5-Trimethylbenzyl)triphenylphosphonium bromide: colorless prisms, mp 204—205°C (Found: C, 70.79; H, 6.32. Calcd for $C_{28}H_{28}BrP$: C, 70.74; H, 5.94%). 2,4,6-Trimethylbenzyl analogue: colorless needles, mp 243—245 °C (Found: C, 69.70; H, 6.15%). 3,4,5-Trimethylbenzyl analogue: colorless plates, mp 250—252 °C (Found: C, 70.20; H, 6.29%).

1,18-Bis(2,4,5-trimethylphenyl)-3,7,12,16-tetramethyloctadecanonaene (I). An ethereal solution of phenyllithium (0.8 M, 0.4 ml) was added to a stirred suspension of (2,4,5-trimethylbenzyl)triphenylphosphonium bromide (121 mg) in ether (4 ml). After stirring for one hour, two drops of methylene chloride were added to destroy excess base. A solution of crocetindial[7] (25 mg) in methylene chloride (1 ml) was then added, and the mixture was stirred under reflux for four hours. The mixture was diluted with methanol (50 ml), and kept at 0 °C overnight. The precipitate was washed with boiling methanol several times and recrystal-

* Present address: Yoshitomi Lab., Research Dept., Yoshitomi Pharmaceutical Industries, Ltd., Yoshitomi, Chikujo-gun, Fukuoka Pref.

** Present address: Research Institute of Industrial Science, Kyushu University, Higashi-ku, Fukuoka.

1) M. Yamaguchi, This Bulletin, **30**, 111, 979 (1957); **31**, 51, 739 (1958); **33**, 1560 (1960).

2) H. Mayer and O. Isler "Carotenoids," ed. by O. Isler, H. Gutmann, and U. Solms, Birkhäuser, Basel, (1971) p. 496.

3) R. D. Lake and B. B. Corson, *J. Org. Chem.*, **24**, 1823 (1959).

4) J. J. Bost, R. E. Kepner, and A. D. Webb, *ibid.*, **22**, 51 (1957).

5) H. Krömer, *Ber.*, **24**, 2407 (1891).

6) R. D. G. Cooper, J. B. Davis, and B. C. L. Weedon, *J. Chem. Soc.*, **1963**, 5637.

7) O. Isler, H. Gutmann, H. Lindlar, M. Montavon, R. Rüegg, G. Ryser, and P. Zeller, *Helv. Chim. Acta*, **39**, 463 (1956).

lized from a mixture of chloroform and ethanol giving I as purple plates, 18.6 mg, m. p. 208—210°C (evacuated capillary). ν_{max} (KBr disk); 3020, 2990, 2930, 2875, 1565, 1502, 1460, 1446, 1398, 1368, 1320, 1267, 1196, 1180, 1025, 1003, 964, 875, 845, 825, and 690 cm^{-1}. UV spectrum; Fig. 1.

1,18-Bis(2,4,6-trimethylphenyl)-3,7,12,16-tetramethyloctadecanonaene (II). This was prepared in a similar way to that for (I). Purple red plates, 10 mg, mp 199—200°C. ν_{max} 3020, 2990, 2910, 2860, 1608, 1560, 1475, 1443, 1395, 1376, 1365, 1030, 1006, 967, 854, 825, 805 and 726 cm^{-1}. UV spectrum; Fig. 1.

1,18-Bis(3,4,5-trimethylphenyl)-3,7,12,16-tetramethyloctadecanonaene (III). This was prepared in a similar way to that for (I). Purple plates, 10 mg, mp 215—216°C. ν_{max}; 3020, 2920, 2860, 1600, 1555, 1480, 1440, 1390, 1365, 1295, 1155, 1030, 1006, 960, 873, 838, 828, 765, and 705 cm^{-1}. UV spectrum; Fig. 1.

BULLETIN OF THE CHEMICAL SOCIETY OF JAPAN, VOL. 46, 1554—1556 (1973)

Interaction Parameters of Poly(*o*-chlorostyrene)-Solvent Systems

Kunihiko GEKKO and Kimiyoshi MATSUMURA*

Department of Food Science and Technology, Faculty of Agriculture, Nagoya University, Nagoya 464

** Department of Chemistry, Aichi Kyoiku University, Kariya 448*

(Received August 14, 1972)

The thermodynamic properties of a polymer-solvent mixture have generally been analysed using the equation introduced by Flory and Huggins:[1,2]

$$\ln a_1 = \ln (1-v_2) + v_2 + \chi v_2^2 \quad (1)$$

where a_1, v_2, and χ represent the activity of the solvent, the volume fraction of the polymer, and the interaction parameter between the polymer and the solvent respectively. It has been indicated, on the basis of both experimental and theoretical studies,[3-7] that the χ value depends on the polymer concentration. However, we do not have enough systematic investigations[8-10] to be able to understand the characteristic behavior of χ in relation to such physical quantities of the polymer and the solvent as the dipole moment. In this paper, we will discuss the effects of the concentration and the dipole moment on the interaction parameters of poly(*o*-chlorostyrene)-solvent systems by means of isopiestic vapor-pressure measurements.

Experimental

Materials. Atactic poly(*o*-chlorostyrene)(PoCS) was prepared and fractionated following the method reported in the previous paper.[11] The average molecular weight of the polymer used in this experiment was determined to be 60.7×10^4 by measuring the intrinsic viscosity of toluene solutions at 25°C.[12] The density of this material was 1.268 and 1.255 g/ml at 25 and 40°C respectively. To clarify the dipole-moment effect of the solvent on χ, we used benzene and methyl ethyl ketone (MEK) as solvents; they have almost identical molar volumes and cohesive energy densities. These solvents were purified by the conventional purification method.

Methods. The apparatus and procedures for measuring the equilibrium vapor sorption were similar to those used in a previous paper.[6] The volume fraction of the polymer at equilibrium was calculated from the experimentally-determined weight fraction by assuming that the solvent volume and the polymer volume are additive on mixing. The activity, a_1, of the solvent was obtained from $a_1 = P_1/P_1^0$, where P_1^0 and P_1 are the vapor pressure of the pure solvent and of the solvent on the polymer solution respectively at a given temperature.

Results and Discussion

The sorption isotherms of benzene and MEK for PoCS are shown in Fig. 1, in which the data for polystyrene(PS)–benzene[13] and PS–MEK[14] systems are also shown as references. It is clear that benzene more easily comes into contact with both polymers, PoCS and PS, than MEK does. This is consistent with the fact that MEK becomes a theta solvent for PoCS at 25 °C, though benzene is a good solvent.[12] From the values of v_2 and P_1/P_1^0, we calculated the Flory-Huggins interaction parameter, χ, using Eq. (1). The values thus obtained are listed in Table 1 and are plotted against v_2 in Fig. 2. In general, the concentration dependence of χ has been expressed by a series of v_2 by Huggins:[7]

$$\chi = A + Bv_2 + Cv_2^2 + \cdots\cdots \quad (2)$$

where A, B, C, *etc.* are constant values independent

1) P. J. Flory, *J. Chem. Phys.*, **10**, 51 (1942).
2) M. L. Huggins, *Ann. N. Y. Acad. Sci.*, **43**, 1 (1942).
3) W. R. Krigbaum and D. O. Geymer, *J. Amer. Chem. Soc.*, **81**, 1859 (1959).
4) C. H. Baker, W. B. Brown, G. Gee, J. S. Rowlisnos, D. Stubley, and R. E. Yeadon, *Polymer*, **3**, 215 (1962).
5) C. Booth, G. Gee, G. Holden, and G. R. Williamson, *Polymer*, **5**, 343 (1964).
6) H. Ochiai, K. Gekko, and H. Yamamura, *J. Polym. Sci.*, **9**, 1629 (1971).
7) M. L. Huggins, *J. Amer. Chem. Soc.*, **86**, 3535 (1964).
8) H. Yamakawa, S. A. Rice, R. Corneliussen, and L. Kotin, *J. Chem. Phys.*, **38**, 1759 (1963).
9) R. Corneliussen, S. A. Rice, and H. Yamakawa, *ibid.*, **38**, 1768 (1963).
10) H. Daoust and A. Hade, *Polymer*, **9**, 47 (1968).
11) K. Matsumura, *Makromol. Chem.*, **124**, 204 (1969).
12) K. Matsumura, *Polym. J.*, **1**, 322 (1970).
13) E. C. Baughan, *Trans. Faraday Soc.*, **44**, 495 (1948).
14) C. E. H. Bawn, R. F. J. Freeman, and A. R. Kamaliddin, *ibid.*, **46**, 677 (1950).

Table 1. The variation of P_1/P_1^0 and χ with v_2 for PoCS–benzene and PoCS–MEK systems

Benzene						MEK		
25 °C			40 °C			25 °C		
P_1/P_1^0	v_2	χ	P_1/P_1^0	v_2	χ	P_1/P_1^0	v_2	χ
0.9747	0.414	0.55	0.8419	0.660	0.57	0.8899	0.711	0.82
0.6928	0.784	0.62	0.7880	0.730	0.64	0.8222	0.768	0.84
0.5830	0.830	0.58	0.6384	0.801	0.57	0.6745	0.845	0.88
0.3566	0.915	0.62	0.4714	0.883	0.65	0.4646	0.916	0.95
0.2400	0.947	0.63	0.1159	0.978	0.69	0.4631	0.925	1.04
0.1607	0.965	0.60				0.2415	0.968	1.13

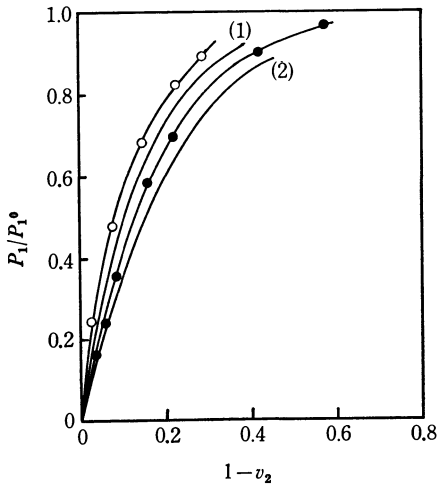

Fig. 1. The sorption isotherms of benzene (-●-) and MEK (-○-) for PoCS at 25 °C. The line (1) and (2) represent the data for PS–MEK system at 25 °C[14] and PS–benzene system at 20 °C[13], respectively.

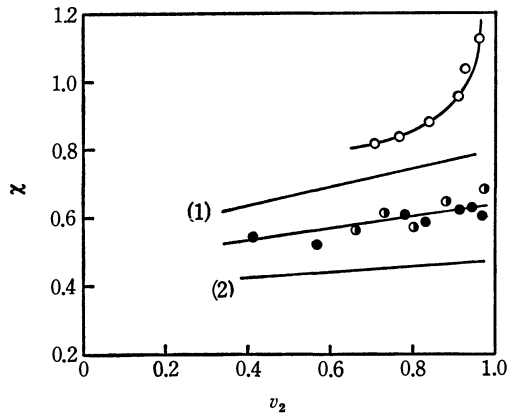

Fig. 2. The concentration dependence of χ for PoCS–benzene (-●-, 25 °C; -◑-, 40 °C) and PoCS–MEK (-○-, 25 °C) systems. The lines (1) and (2) represent the data for PS–MEK system at 25 °C[14] and for PS–benzene system at 20 °C[13], respectively.

of the concentration. In the system of PoCS–benzene, there exists a linear relation with a small positive slope between v_2 and χ, similar to the case in the PS–benzene solution. The effect of the temperature on χ for this system could not be ascertained in this experiment, which may suggest that there is almost no heat of mixing. On the other hand, in the PoCS–MEK system there is remarkable concentration dependence of χ, requiring the third and the higher terms on the right-hand side of Eq. (2), and the χ values are considerably larger than those of the PoCS–benzene system.

Now, it is considered that χ depends on the enthalpy factors, such as the cohesive energy and the interaction energy due to the dipole moment or the hydrogen bonding between the solvent and polymer molecules, and also on the entropy factors, such as the size and shape of the polymer and solvent molecules. The molar volume of MEK is 89.6 ml/mol, which is close to that of benzene, 89.3 ml/mol at 25°C. Further the solubility parameters of benzene and MEK are 9.15 and 9.22 $(cal/ml)^{1/2}$ respectively. Judging from these data, there seems to be almost no difference in the solvent power between the two solvents. Accordingly, the characteristic difference in χ between the systems of PoCS–benzene and PoCS–MEK is probably due to such factors as the molecular shapes, the hydrogen-bonding abilities, and the dipole moments of the solvents; the dipole moment of benzene is zero, and that of MEK is 2.75 Debye (D). We may consider that the effect of the hydrogen bond is not so predominant for this characteristic behavior of PoCS–MEK system, by analogy with the results for the vapor-pressure behavior of the polypropylene–MEK and natural rubber–MEK systems.[5]

According to Yamakawa *et al.*,[8] the thermodynamic interaction parameter, χ, is the sum of the χ^* which arises from the non-polar interaction and the χ_p which arises from the polar interaction; that is, $\chi=\chi^*+\chi_p$. For the concentration dependence of χ_p, the following conclusion was also obtained by them:

(a) χ_p increases with an increase in the concentration when the dipole moment of the solvent (μ_1) is greater than that of the polymer segment(μ_2)

(b) $\chi_p=0$ when $\mu_1=\mu_2$

(c) χ_p decreases with an increase in the concentration when $\mu_1<\mu_2$. It was also found that the polarizabilities of the solvent and the polymer segment affect χ_p to a smaller extent than the dipole moments do.[8] Furthermore, χ^* may usually be considered as a slowly decreasing function of the concentration from both the theoretical and experimental points of view.[8,15,16] In analyzing the results we obtained on the basis of the above theoretical conclusion, we take

15) M. Fixman, *J. Chem. Phys.*, **35**, 889 (1961).

16) P. J. Flory, "Principles of Polymer Chemistry," Cornell University Press, Ithaca, New York (1953), p. 515.

0.36D for the μ_2 of PS[17] and assume that the μ_2 of PoCS is the same as the dipole moment of *o*-chlorotoluene, 1.43D, since no value has been reported for the μ_2 of PoCS.

The remarkable increase in χ with the polymer concentration for the PoCS–MEK system where $\mu_1 > \mu_2$ suggests that, for this system, the contribution of χ_p to the total χ is significant in comparison with that of χ^*, as much as in the PS–MEK system. That is, the continuum model of concentrated solutions by Yamakawa *et al.*[8] is considered to be valid for the PoCS–MEK system also. On the other hand, the χ values for the systems of PoCS–benzene and PS–benzene increased slowly with the concentration, as is shown in Fig. 2, though they should decrease with the concentration judging from the fact that $\mu_1 < \mu_2$, if the continuum model is valid for these systems. This discrepancy of the continuum model for the PoCS–benzene system may be due to the orientation of the benzene rings of the polymer and the solvent, since such an orientation has been found in the case of the PS-benzene system.[18]

17) W. R. Krigbaum and A. Roig, *J. Chem. Phys.*, **31**, 544 (1959).

18) H. Tompa, *J. Polym. Sci.*, **8**, 51 (1952); K. Sato and A. Nishioka, *J. Polym, Sci., A-2* **10**, 489 (1972).

BULLETIN OF THE CHEMICAL SOCIETY OF JAPAN, VOL. 46, 1556—1558 (1973)

Laser-induced Chemical Reactions. VI. On the Formation Processes of Acetylene

Ko Taki

Faculty of Industrial Hygiene, Kitasato University, Sagamihara-shi, Kanagawa 228

Pil Hyon Kim and Susumu Namba

The Institute of Physical and Chemical Research, Wako-shi, Saitama 351

(Received August 18, 1972)

The reactions of the carbon vapor produced by various methods[1-9] with hydrocarbons have been extensively studied. In previous papers,[10,11] the present authors have described the reactions of carbon vapor produced by the irradiation of a focused laser beam with hydrogen and low-molecular-weight hydrocarbons.

It has been assumed that, in the reaction of the carbon vapor produced by the laser irradiation with hydrocarbons, C_2 species play the main role in the product-forming step. Acetylene is the main product. The formation of acetylene has been considered to consist of hydrogen abstraction by C_2 species. However, there have been some doubts as to the product-forming processes, because acetylene may also be formed by the thermal decomposition of the reactant on the heated target surface or by the decomposition caused by the collision of the vaporized species with the reactant (collisional decomposition). The evidence for this is that when the laser beam was irradiated on a nickel metal target in ethane,[12,13] some decomposed fragmented hydrocarbons (mainly acetylene) were produced. In this case, the fraction of the thermal decomposition is considered to be small as compared with the collisional decomposition, because when the power density of the irradiated beam was lowered so as not to vaporize the target material, the acetylene yield decreased remarkably.

In this paper, by using a ^{14}C-enriched carbon target and a hydrocarbon reactant, or by using a graphite target and ^{14}C-labeled ethane as the reactant, the details of the formation processes of acetylene were investigated.

Experimental

Preparation of the ^{14}C-enriched Carbon Target. The ^{14}C-enriched carbon target was prepared by the thermal decomposition of ^{14}C-labeled acetylene at 1000°C in a quartz tube, as is shown in Fig. 1. The carbon film deposited on the quartz plate was used as the target. In a preliminary experiment, the target did not give gas chromatographically any other gaseous products except carbon monoxide[14] upon laser irradiation in a vacuum.

Preparation of the ^{14}C-labeled Ethane. The ^{14}C-labeled ethane was prepared by the reduction of ^{14}C-labeled acetylene by using PtO_2 and H_2 in a closed system, and it was purified gas chromatographically using a silica gel column.

Laser Irradiation. The laser-irradiation apparatus and experimental procedures were described previously.[10,11] The carbon target in a 7-ml cell filled with ethane or ethylene was irradiated by a focused laser beam. The output energy

1) M. Marshall, C. Mackay, and R. Wolfgang, *J. Amer. Chem. Soc.*, **86**, 4741 (1964).
2) H. J. Ache and A. P. Wolf, *ibid.*, **88**, 888 (1966).,
3) K. D. Bayes, *ibid.*, **84**, 4077 (1962).
4) P. S. Skell and R. R. Engel, *ibid.*, **88**, 4883 (1966).
5) P. S. Skell, L. D. Wescott, Jr., J. P. Golstein, and R. R. Engel, *ibid.*, **85**, 1023 (1963).
6) P. S. Skell and R. F. Harris, *ibid.*, **88**, 5933 (1966).
7) G. J. Pontrell, *J. Chem. Phys.*, **43**, 2571 (1965).
8) J. A. Howe, *ibid.*, **39**, 1362 (1963).
9) J. E. Mentall and R. W. Nickolls, *ibid.*, **46**, 2881 (1967).
10) K. Taki, P. H. Kim, and S. Namba, This Bulletin, **42**, 823 (1969).
11) K. Taki, P. H. Kim, and S. Namba, *ibid.*, **42**, 2377 (1969).
12) K. Taki, P. H. Kim, and S. Namba, *ibid.*, **45**, 2052 (1972).
13) K. Taki, P. H. Kim, and S. Namba, to be published.
14) Carbon monoxide was produced by the heating of carbon in quartz tube at about 1000 °C.[15]
15) P. Gouverneur, M. A. Schreuders, and P. N. Degens, *Anal. Chim. Acta*, **5**, 293 (1951).

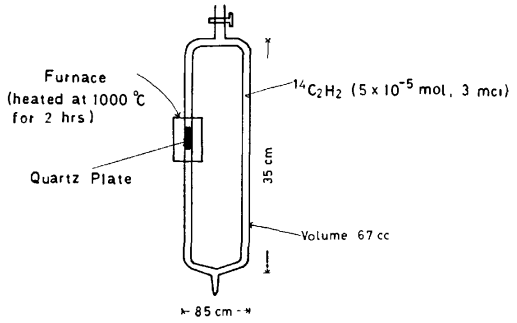

Fig. 1. Preparation of ^{14}C-enriched carbon target.

and pulse duration of the ruby laser were about 3 J and 0.5 ms respectively.

Analysis and Measurement of Radioactivity. The analysis of the products and the measurement of the radioactivity were performed on a radio-gaschromatograph. In the reaction of the ^{14}C-labeled ethane with carbon vapor from the graphite target, the specific activity was calculated from both the radioactivity and the product yield. In the reaction of ethane or ethylene with radioactive carbon vapor from the ^{14}C-enriched carbon target, the radioactivity was enough to be detected by one-pulse laser irradiation, but the product yield was too small to be determined[16] by radio-gaschromatography. In this case, the total activity was measured by adding a carrier.

Results and Discussion

When the laser beam was irradiated on nonradioactive graphite in ^{14}C-labeled ethane, the main product was acetylene, as has been described previously; the radioactivity was also found in acetylene, as is shown in Table 1. The radioactivity of acetylene indicates that the formation process of acetylene is due not only to the abstraction by C_2, but also to the decomposition of ethane.

On the other hand, when the laser beam was irradiated on the ^{14}C-enriched carbon film in ethane, radioactivity was found in the acetylene produced, but not in the ethylene produced. The above results indicate that ethylene is produced by the decomposition of ethane.

Table 1. Specific activity in the reaction of carbon vapor with ^{14}C-labeled ethane

Specific activity (μCi/mol)		Specific activity ratio of ethane to acetylene (α/β)	K_1/K_2 ($\alpha/\beta-1$)
Ethane (Substrate)	Acetylene (Product)		
1.95	0.92	1.6—2.1	0.6—1.1
0.94	0.60		

Ethane pressure: 400—700 Torr.

When the laser beam was irradiated on the ^{14}C-enriched carbon film in ethylene, the radioactivity of the acetylene produced was about twice that of the C_4-compounds produced, but the yield of acetylene was about six times that of the C_4-compounds, as is shown in Table 2. The data show that the formation of acetylene is due to the decomposition of ethylene, also.

When radioactive ethane is used as the reactant, by assuming the C_2 species to be the reaction species, the main formation processes of acetylene may be estimated as follows:

$$C_2H_6^* + C_2 \xrightarrow{K_1} C_2H_2 + \text{other hydrocarbons} \quad \text{abstraction.} \tag{1}$$

$$C_2H_6^* + C_2 \xrightarrow{K_2} C_2H_2^* + \text{other hydrocarbons} \quad \text{decomposition.} \tag{2}$$

$$C_2H_6 + C_2 \xrightarrow{K_3} C_2H_2 + \text{other hydrocarbons} \quad \text{abstraction.} \tag{3}$$

$$C_2H_6 + C_2 \xrightarrow{K_4} C_2H_2 + \text{other hydrocarbons} \quad \text{decomposition.} \tag{4}$$

$C_2H_6^*$ and $C_2H_2^*$ indicate radioactive ethane and acetylene. Reactions (2) and (4) show the collisional decomposition of ethane. The ratio of the amount of the active material to that of the nonactive one is derived from the specific activity, and the value of $C_2H_6^*/C_2H_6=\alpha$ and $C_2H_2^*/C_2H_2=\beta$ are extremely small. The ratio of the product yield can be derived as follows:

$$\frac{C_2H_2}{C_2H_2^*} = \frac{K_1[C_2][C_2H_6^*]+K_3[C_2][C_2H_6]+K_4[C_2][C_2H_6]}{K_2[C_2][C_2H_6^*]} = \frac{1}{\beta} \tag{5}$$

Since the two rates of abstraction reactions, (1) and (3), and also the two rates of decomposition reactions, (2), and (4), are equal,

$$K_1 = K_3 \text{ and } K_2 = K_4 \tag{6}$$

Then,

Table 2. Activity in the reaction of ^{14}C-enriched carbon vapor with ethylene

Total activity of products (cps)			Activity ratio of C_4-compounds to acetylene (γ)	Yield ratio of acetylene to C_4-compounds (δ)	K_9/K_{10} ($1/(\gamma\delta-2)$)
C_4-compounds		Acetylene			
Diacetylene	Vinylacetylene				
4500	680	8550	0.46—0.61	—6	0.6—1.3
3130	420	7730			

Ethylene pressure: 600—700 Torr.

16) The product yield was determined by the flame ionization detector.

$$\frac{K_1}{K_2} = \left(\frac{\alpha}{\beta} - 1\right)\frac{1}{\alpha+1} \approx \frac{\alpha}{\beta} - 1 \quad (7)$$

The ratio of the rate constant of the abstraction to that of the decomposition was calculated from the experimental data; the value thus obtained was from 0.6 to 1.1 under those experimental conditions.

Similar results are also obtained in the reaction of the carbon vapor from the ^{14}C-enriched carbon target with ethylene. In this case, the following schemes are assumed:

$$C_2H_4 + C_2^* \xrightarrow{K_8} C_4^*\text{-compounds} \quad (8)$$
addition.[17]

$$C_2H_4 + C_2^* \xrightarrow{K_9} C_2H_2^* + C_2H_2 \quad (9)$$
abstraction.

$$C_2H_4 + C_2^* \xrightarrow{K_{10}} C_2H_2 + \text{other hydrocarbons} \quad (10)$$
decomposition.

17) If the nonradioactive C_4-compounds are produced partly by the thermal decomposition of two molecules of ethylene, the value K_9/K_{10} becomes smaller than $1/(\gamma\delta-2)$ by the similar calculation. The result may not be conflicted with the conclusion of this paper.

Reactions (8), (9), and (10) are also applicable to nonactive C_2 species. The ratio of the total activity of C_4-compounds to that of acetylene shows the ratio of the rate constant of K_8 to K_9 ($K_8/K_9=\gamma$). The ratio of the acetylene yield to the C_4-compound yield can be derived as follows:

$$\frac{\text{Acetylene}}{C_4\text{-compounds}} = \frac{2K_9 + K_{10}}{K_8} = \delta \quad (11)$$

Therefore,

$$\frac{K_9}{K_{10}} = \frac{1}{\gamma\delta - 2} \quad (12)$$

The ratio of the rate constant of the abstraction to that of the decomposition was calculated to be from 0.6 to 1.3 under those experimental conditions. This is in agreement with the result obtained in the reaction of carbon vapor with ^{14}C-labeled ethane.

From the above results, it may be concluded that the formation processes of acetylene are due to the collisional decomposition of the reactant with the vapor produced by the laser irradiation, as well as to the abstraction by C_2 species.

The authors wish to acknowledge the help of Dr. M. Matsui in the measurement of radioactivity using radio-gaschromatography.

BULLETIN OF THE CHEMICAL SOCIETY OF JAPAN, VOL. 46, 1558—1560 (1973)

Photoelectron Spectra of Tetrahydropyran, 1,3-Dioxane, and 1,4-Dioxane

Tsunetoshi KOBAYASHI and Saburo NAGAKURA

The Institute for Solid State Physics, The University of Tokyo, Roppongi, Minato, Tokyo 106

(Received September 12, 1972)

Photoelectron spectroscopy is useful for the study of electronic structures of molecules, in particular of occupied orbital energies of molecules. In this paper, we study the photoelectron spectra of such cyclic ethers as tetrahydropyran, 1,3-dioxane, and 1,4-dioxane, special attention being paid upon the interaction between oxygen lone pair orbitals in dioxanes which contain two oxygen atoms.

Experimental

Materials. Tetrahydropyran, 1,3-dioxane, and 1,4-dioxane were purified in usual ways and their purities were checked with gas chromatograms and NMR spectra.

Measurements. Photoelectron spectra (PES) were measured with a JASCO Model PE-1 photoelectron spectrometer by using the 584 Å helium resonance line as a light source.

Theoretical

The CNDO/2[1] calculation was carried out for the cyclic ethers under consideration by a FACOM 270—30 computer at the Institute of Physical and Chemical Research. The geometrical structure of 1,4-dioxane necessary for the calculation was taken from Ref. 2, and those of tetrahydropyran and 1,3-dioxane were properly assumed on the basis of the appropriate data given in Ref. 2. These compounds take a chair form at room temperature.[2-4]

Results and Discussion

PES of these cyclic ethers are shown in Fig. 1, and the vertical ionization potentials (Ip_v's) obtained from PES are summarized in Table 1. The observed orbital energies, ε_{obs}, estimated by Koopmans' theorem,[5] $\varepsilon_{obs}=-Ip_v$, are shown in Fig. 2a. In Fig. 2b, the orbital energies calculated by the CNDO/2 method, ε_{calc}'s, are shown for the purpose of comparison.

1) J. A. Pople and G. A. Segal, *J. Chem. Phys.*, **44**, 3289 (1966).

2) "Tables of Interatomic Distances and Configuration in Molecules and Ions," Special Publication No. 11, ed. by L. E. Sutton, The Chemical Society, London (1958); *ibid.*, No. 18 (1965).

3) V. M. Rao and R. Kewley, *Can. J. Chem.*, **47**, 1289 (1969).

4) H. M. Pickett and H. L. Strauss, *J. Amer. Chem. Soc.*, **92**, 7281 (1970).

5) T. Koopmans, *Physica*, **1**, 104 (1934).

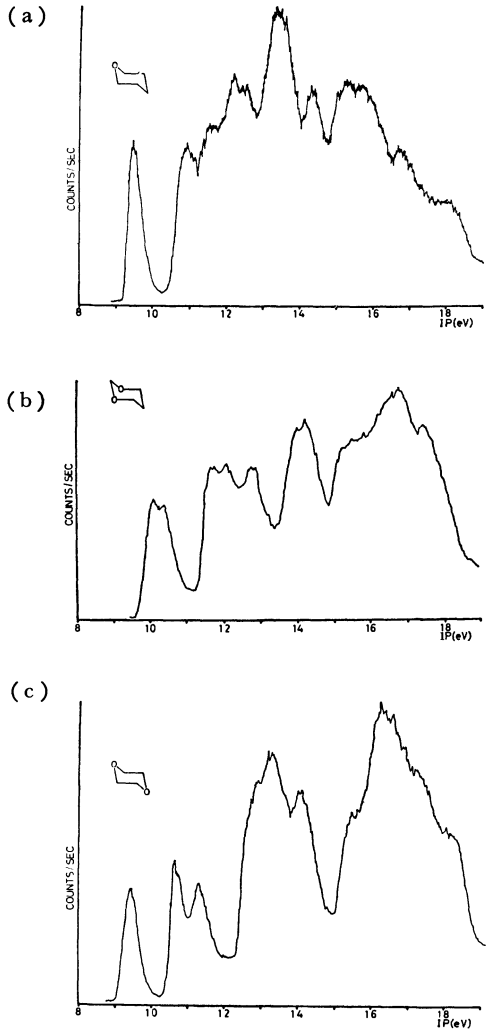

Fig. 1. Photoelectron spectra of (a) tetrahydropyran, (b) 1,3-dioxane, and (c) 1,4-dioxane.

TABLE 1. OBSERVED VERTICAL IONIZATION POTENTIALS (Ip_v's) OF TETRAHYDROPYRAN, 1,3-DIOXANE, AND 1,4-DIOXANE IN eV

PES band	Tetrahydropyran	1,3-Dioxane	1,4-Dioxane
1	9.48 a'	10.12 a''	9.41 a_g
2	10.90 a'	10.38 a'	10.60 a_g
3	11.57 a''	11.66 a'	11.27 b_g
4	12.19	12.07	12.86
5	12.53	12.80	13.26
6	13.30 (broad)	14.00	13.60
7	14.28	14.17	14.06
8	15.23 (broad)	15.21 (broad)	15.40 (broad)

Concerning the first Ip's of these compounds, the relative height of the calculated molecular orbitals reproduces quite well the observed tendency as clearly seen in Fig. 2. Therefore, we may assign the first Ip's of these compounds to the highest occupied orbitals given by the CNDO/2 calculations. That is to say, the first Ip's of tetrahydropyran, 1,3-dioxane,

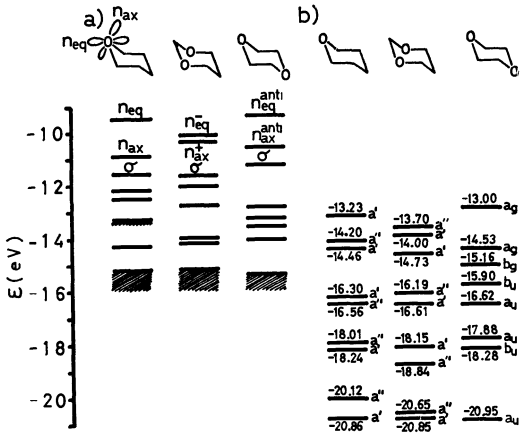

Fig. 2. Orbital energy diagrams.
a) The observed orbital energy diagram obtained on the assumption, $\varepsilon = -Ip_v$ (Koopmans' theorem).
b) The orbital energy diagram obtained by the CNDO/2 calculation.

and 1,4-dioxane may be ascribed to the equatorial type lone pair (n_{eq}) orbital of the oxygen atom, to the antibonding combination of the two n_{eq} orbitals of the two oxygen atoms (n_{eq}^-), and the antiparallel type combination of the two n_{eq} orbitals of the two oxygen atoms (n_{eq}^{anti}), respectively.

Cradock and Whiteford[6] assigned the first (10.04 eV), second (11.91 eV), and third (13.43 eV) bands of methyl ether to $b_1(n)$, $a_1(n)$, and $b_2(\sigma)$ from the analogy with the assignment on the water molecule.[7] The splitting between the two n orbitals is 1.87 eV for methyl ether. The corresponding three bands appear at 9.61, 11.08 (adiabatic) and 11.92 eV (adiabatic) for ethyl ether,[8] the splitting between the two n orbitals being 1.47 eV (adiabatic). These three bands correspond well in their positions to the lower energy three bands of tetrahydropyran at 9.48, 10.90, and 11.57 eV. This seems to mean that the second band of tetrahydropyran may be related with the non-bonding orbital.[9] According to this assignment, the splitting between the n_{eq} and n_{ax} orbitals is 1.42 eV.

The CNDO/2 calculation shows that the orbitals of 1,3-dioxane are ordered from the top as follows: n_{eq}^-, n_{ax}^+, σ, n_{ax}^-, σ, n_{eq}^+. The second highest occupied MO, n_{ax}^+, is represented by the bonding type combination of the two n_{ax} orbitals of the two oxygen atoms. The calculated energy difference between the n_{eq}^- and n_{ax}^+ orbitals (0.30 eV) corresponds well to the observed difference between the first and second bands (0.26 eV). This may support the assignment of the

6) S. Cradock and R. A. Whiteford, *J. Chem. Soc., Faraday Trans.* 2, **68**, 281 (1972).
7) J. Dewiche, P. Natalis, and J. E. Collin, *Int. J. Mass Spec. Ion. Phys.*, **5**, 443 (1970).
8) M. I. Al-Joboury and D. W. Turner, *J. Chem. Soc.*, **1964**, 4434.
9) This assignment is reverse to the prediction from the CNDO/2 calculation. Since the observed splitting between the second and third orbitals is rather small for tetrahydropyran (0.67 eV), their orders may be difficult to be determined by the CNDO/2 calculation.

second band. According to the above-mentioned order of the orbitals, the observed fourth and sixth bands of 1,3-dioxane may tentatively be assigned to the n_{ax}^- and n_{eq}^+ orbitals, respectively, and the splittings between the n_{ax}^+, and n_{ax}^- orbitals and between the n_{eq}^- and n_{eq}^+ orbitals amount to 1.69 and 3.88 eV, respectively. The two n_{eq} orbitals of 1,3-dioxane may interact through space rather than through bond[10] because the overlap integral between them is not small, while the two n_{ax} orbitals may interact through bond rather than through space.

According to the CNDO/2 calculation shown in Fig. 2, the occupied MO's of 1,4-dioxane decrease their energies in the following order: $n_{eq}^{anti} > n_{ax}^{anti} > \sigma > n_{ax}^{para} > \sigma > \sigma > n_{eq}^{para}$. Here n_{ax}^{para} and n_{eq}^{para} mean the parallel type combinations of the two n_{ax} orbitals and of the two n_{eq} orbitals, respectively. According to this tentative assignment, the splittings between the n_{ax}^{anti} and n_{ax}^{para} orbitals and between the n_{eq}^{anti} and n_{eq}^{para} orbitals may become 2.26 eV and 4.65 eV, respectively. In 1,4-dioxane the interactions between the two n_{ax} orbitals as well as between the two n_{eq} orbitals may occur through bond rather than through space.

Recently Sweigart and Turner[11] reported the PES of these compounds and discussed the interaction between nonbonding orbitals belonging to two different oxygen atoms of each molecule. In their study, however, they did not make any theoretical calculation and did not consider the presence of the two types (equatorial and axial) of nonbonding orbitals on each oxygen atom of these compounds.

10) R. Hoffmann, A. Imamura, and W. J. Hehre, *J. Amer. Chem. Soc.*, **90**, 1499 (1968).

11) D. A. Sweigart and D. W. Turner, *ibid.*, **94**, 5599 (1972).

BULLETIN OF THE CHEMICAL SOCIETY OF JAPAN, VOL. 46, 1560—1562 (1973)

Microwave Spectrum and Centrifugal Distortion Effects of Thionyl Fluoride

Ichiro YAMAGUCHI, Osamu OHASHI, Hirotaka TAKAHASHI, Takeshi SAKAIZUMI, and Masao ONDA

Department of Chemistry, Faculty of Science and Technology, Sophia University, Tokyo 102

(Received September 14, 1972)

Ferguson analysed the microwave spectrum of thionyl fluoride and obtained the structure and dipole moment of the molecule.[1] Assignment of the spectral lines was so made that the low J R-branch lines fit the frequencies calculated from the rigid molecular model. The reported frequencies, however, do not coincide with the calculated values in a high J range. The larger the J value, the greater the deviation; *e. g.*, for the line $12_{93} \leftarrow 12_{94}$ the deviation is as large as 11.44 MHz. The centrifugal distortion effect is expected to account for the deviation. In this paper we report on several series of Q-branches newly observed for the normal species $^{32}S^{16}O^{19}F_2$, and the analyses of the spectrum taking into account the centrifugal distortion effect.

Thionyl fluoride was synthesized by the reaction of thionyl chloride with antimony(III) fluoride.[2] Conventional microwave spectrometers were used with 100 kHz Stark modulation. The sample pressure was 0.01—0.015 mmHg and the spectrum was observed at dry ice and room temperatures. The frequency range observed was 8.0—36.0 GHz.

The observed transition frequencies are given in Table 1. Spectral analysis was made on the basis of Watson's formula for the centrifugal distortion effect.[3] Thionyl fluoride molecule has C_s symmetry. It may therefore be inappropriate to account for the observed deviations by considering the first order perturbation terms only. However, it can be seen from the table that the deviation of observed frequencies from the calculated ones obtained by the least squares fit with Watson's formula is very small throughout, and the higher order terms were therefore neglected.

The transition frequencies calculated from the rigid rotor model with the rotational constants given by Ferguson were the first reference to the assignment of the observed lines. However, deviations of the observed frequencies were apparent from the rigid rotor model frequencies. It was worthwhile to divide the lines into several series, each having a specific set of K_{-1} and K_{+1} (Table 1). The observed frequencies in a series, when appropriately assigned, showed a regular variation of the deviation with changing J value, which greatly helped in obtaining the final assignment. The assigned lines were used for the least squares fit of transition frequency. This process was continued until most of the observed frequencies coincide with the calculated ones, the centrifugal corrections also being shown in Table 1.

The effective rotational constants and centrifugal distortion coefficients thus obtained are shown in Table 2, together with the rotational constants given by Ferguson.

In our assignments of many spectral lines, taking into account the centrifugal distortion effect, we found some misassignments made by Ferguson. Examples are given in Fig. 1, where the spectra (a) observed, (b) calculated for a model with centrifugal distortion

1) R. C. Ferguson, *J. Amer. Chem. Soc.*, **76**, 850 (1954).
2) H. Booth and F. C. Mericola, *ibid.*, **62**, 640 (1940).
3) J. K. G. Watson, *J. Chem. Phys.*, **45**, 1360 (1966).

Table 1. Observed transition frequencies and centrifugal distortion effect (in MHz)

Transition	ν_{obsd}[a]	$\nu_{obsd}-\nu_{calcd}$	Centrifugal[b] correction
* $1_{10} \leftarrow 0_{00}$	16971.72	0.00	−0.04
* $2_{11} \leftarrow 1_{01}$	33685.48	0.04	−0.40
* $2_{20} \leftarrow 1_{10}$	33957.30	−0.01	−0.30
* $2_{21} \leftarrow 1_{11}$	34201.06	−0.04	−0.13
* $2_{11} \leftarrow 1_{10}$	30023.61	0.02	−0.45
* $3_{03} \leftarrow 2_{02}$	33254.98	−0.39	−0.26
* $3_{13} \leftarrow 2_{12}$	33242.12	0.39	−0.29
$J_{J-1,1} \leftarrow J_{J-1,2}$			
$2_{11} \leftarrow 2_{12}$	10211.78	−0.10	−0.40
$3_{21} \leftarrow 3_{22}$	9833.88	−0.10	−0.81
$4_{31} \leftarrow 4_{32}$	9336.83	0.00	−1.26
$5_{41} \leftarrow 5_{42}$	8727.72	0.04	−1.69
$6_{51} \leftarrow 6_{52}$	8017.63	0.09	−2.00
$J_{J,1} \leftarrow J_{J-2,2}$			
$2_{21} \leftarrow 2_{02}$	10999.56	0.04	0.06
$3_{31} \leftarrow 3_{12}$	11450.76	0.09	0.04
$4_{41} \leftarrow 4_{22}$	12120.18	0.05	−0.06
$5_{51} \leftarrow 5_{32}$	13059.21	0.04	−0.42
$6_{61} \leftarrow 6_{42}$	14319.88	−0.01	−1.33
$7_{71} \leftarrow 7_{52}$	15945.86	−0.02	−3.26
$8_{81} \leftarrow 8_{62}$	17964.68	−0.01	−6.82
$9_{91} \leftarrow 9_{72}$	20384.98	−0.07	−12.70
$10_{10,1} \leftarrow 10_{82}$	23198.52	0.01	−21.68
$11_{11,1} \leftarrow 11_{92}$	26382.98	−0.07	−34.57
$12_{12,1} \leftarrow 12_{10,2}$	29906.00	−0.05	−52.18
$13_{13,1} \leftarrow 13_{11,2}$	33726.06	0.05	−75.28
$J_{J-2,2} \leftarrow J_{J-2,3}$			
$3_{12} \leftarrow 3_{13}$	17602.39	−0.18	−0.57
* $4_{22} \leftarrow 4_{23}$	17501.15	−0.10	−1.27
* $5_{32} \leftarrow 5_{33}$	17305.39	−0.10	−2.18
* $6_{42} \leftarrow 6_{43}$	16980.32	−0.10	−3.23
$7_{52} \leftarrow 7_{53}$	16498.74	−0.02	−4.27
$8_{62} \leftarrow 8_{63}$	15846.78	0.00	−5.15
$9_{72} \leftarrow 9_{73}$	15025.59	−0.12	−5.66
$10_{82} \leftarrow 10_{83}$	14049.12	0.00	−5.66
$11_{92} \leftarrow 11_{93}$	12938.99	0.02	−5.02
$12_{10,2} \leftarrow 12_{10,3}$	11722.67	0.03	−3.64
$13_{11,2} \leftarrow 13_{11,3}$	10431.60	−0.01	−1.49
$14_{12,2} \leftarrow 14_{12,3}$	9101.33	0.05	1.40
$J_{J-1,2} \leftarrow J_{J-3,3}$			
$3_{22} \leftarrow 3_{03}$	17673.53	0.18	−0.41
$4_{32} \leftarrow 4_{13}$	17713.75	0.20	−0.83
$5_{42} \leftarrow 5_{23}$	17798.06	0.08	−1.29
$6_{52} \leftarrow 6_{33}$	17952.08	0.08	−1.76
$J_{J-3,3} \leftarrow J_{J-3,4}$			
* $7_{43} \leftarrow 7_{44}$	24553.88	−0.09	−4.61
$8_{53} \leftarrow 8_{54}$	24419.44	−0.16	−6.28
$9_{63} \leftarrow 9_{64}$	24205.04	−0.09	−8.11
$10_{73} \leftarrow 10_{74}$	23879.74	0.13	−9.98
$11_{83} \leftarrow 11_{84}$	23409.74	0.02	−11.68
$12_{93} \leftarrow 12_{94}$	22765.10	−0.02	−12.88
$13_{10,3} \leftarrow 13_{10,4}$	21924.72	0.03	−13.23
$14_{11,3} \leftarrow 14_{11,4}$	20881.38	−0.02	−12.42

Table 1. continued.

Transition	ν_{obsd}[a]	$\nu_{obsd}-\nu_{calcd}$	Centrifugal[b] correction
$J_{J-2,3} \leftarrow J_{J-4,4}$			
$7_{53} \leftarrow 7_{34}$	24656.04	0.11	−4.11
$8_{63} \leftarrow 8_{44}$	24642.56	0.11	−5.32
$9_{73} \leftarrow 9_{54}$	24645.68	0.06	−6.52
$10_{83} \leftarrow 10_{64}$	24682.38	−0.04	−7.69

* Transitions observed by Ferguson.

a) Experimental uncertainty in frequency measurement; ±0.05 MHz.

b) ν(calcd for rigid model)−ν(calcd for model with centrifugal distortion effect).

Table 2. Effective rotational constants, asymmetry parameter, and centrifugal distortion constants

Best fit values

A =8614.73±0.05 MHz	d_J =−0.135 MHz
B =8357.03±0.05 MHz	d_{JK} = 5.602 MHz
C =4952.94±0.05 MHz	d_K =−2.30 MHz
κ = 0.859250	d_{WJ} = 1.72×10^{-5}
	d_{WK} = -6.55×10^{-4}

Corresponding values given by Ferguson[1]

A =8614.75±0.10 MHz
B =8356.98±0.10 MHz
C =4952.96±0.10 MHz
κ = 0.859213

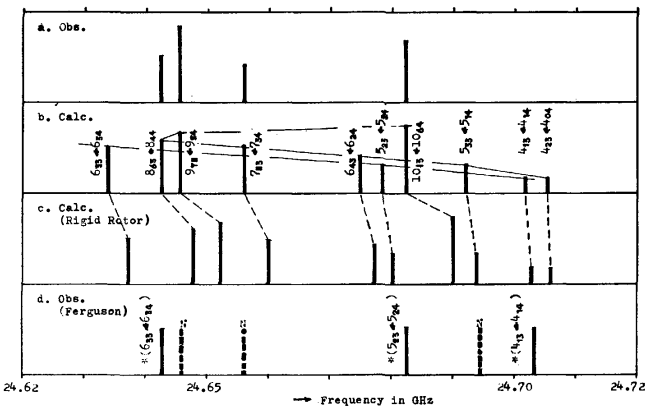

Fig. 1. Observed and calculated spectra in a range of 24.6 −24.7 GHz. a. observed, b. calculated (centrifugal distortion model), c. calculated (rigid rotor model), d. observed by Ferguson.

* Assignment made by Ferguson.

N. Not assigned lines appeared in "Microwave Spectral Table", National Bureau of Standards Monograph 70, Vol. IV (1968), p. 340.

effect, (c) calculated for rigid model, and (d) observed by Ferguson are arranged in order for the region 24.6—24.7 GHz. In this region, two series of spectral lines with different sets of K_{-1} and K_{+1} overlap each other.

It is shown that, even for transitions with relatively small J values, analysis without considering the cen-

trifugal distortion effect leads to making misassignments for molecules such as thionyl halides.[4] Clear and unequivocal assignments are given in Fig. 1.

The authors are greatly indebted to Dr. C. Matsumura, the Government Chemical Research Institute, for use of the spectrometer and computer.

4) Cf. e. g., J. Burie, J. -L. Destombes, A. Dubrulle, and G. Journel, *C. R. Acad. Sci. Paris Ser. B*, **267**, 48 (1968); G. Journel, A. Dubrulle, J. -L, Destombes, and C. Marliere, *ibid.*, **271** 331 (1970).

Note added in proof. A paper by Lucas and Smith (*J. Mol. Spectrosc.*, **43**, 327 (1972)) appeared after this article had been accepted. They analysed the microwave spectrum of thionyl fluoride and obtained centrifugal distortion constants up to sextic ones. Their quartic constants, when transformed into Watson's type constants, differ from ours. It has been confirmed, however, that the constants converge to our values, if the transformed quartic constants are inserted into the least squares fit procedure we adopted (up to the quartic terms) as the initial data for iterations.

BULLETIN OF THE CHEMICAL SOCIETY OF JAPAN, VOL. 46, 1562—1563 (1973)

Studies on the Interaction between Long Chain Alcohols and Alkyl Sulfates. III. Magnetic Properties of Intermolecular Complexes

Yoshikiyo MOROI, Kinshi MOTOMURA, and Ryohei MATUURA
Department of Chemistry, Faculty of Science, Kyushu University, Fukuoka 812

(Received October 19, 1972)

In previous papers, reports were given on the formation of intermolecular complexes between long chain alcohols and metal alkyl sulfates.[1,2] Magnetic properties were examined for the complexes, formed between dodecyl alcohol and dodecyl sulfate, $M(DS)_2$, of divalent metal cations such as Mn^{2+}, Co^{2+}, Ni^{2+}, and Cu^{2+} by measuring the electron spin resonance (ESR) and magnetic susceptibility. It is expected that the difference in magnetic property between complex L and complex H, formed above and below the melting point of dodecyl alcohol (25 °C), respectively,[2] can be found by these methods.

Experimental

The apparatus for ESR measurement was a JEOL JES-ME-3X spectrometer of variable-temperature type. Molar ratio of alcohol to sulfate was 6.

Magnetic susceptibilities were measured by Gouy's method. Because of stickiness of the complex it was mixed with NaCl powder (90% wt.) and used as the sample. The specific susceptibility was calculated by Wiedemann's additivity law[3] from the value of the mixed sample:

$$\chi = \chi_1 P_1 + \chi_2 P_2 \cdots\cdots \chi_n P_n \qquad (1)$$

where χ is susceptibility of the mixture; χ_n and P_n are susceptibility and weight fraction for the components, respectively. The value of χ_{NaCl} used was -0.515×10^{-6} e.m.u.[4] In order to examine applicability of this dilution method the magnetic susceptibilities of $CuSO_4\cdot5H_2O$ and $M(DS)_2\cdot nH_2O$ were also measured using not only sodium chloride but also naphthalene as a dispersion medium. Since color of the mixture of $CuSO_4\cdot5H_2O$ with NaCl changes with time, the susceptibility was measured just after mixing. Reproducibility was checked by repeating measurement twice for each mixed sample. The result was satisfactory.

Results and Discussion

It is difficult to discuss the electronic state of metals except copper with the results of ESR measurement, since they are in a state of high spin. Thus, only the

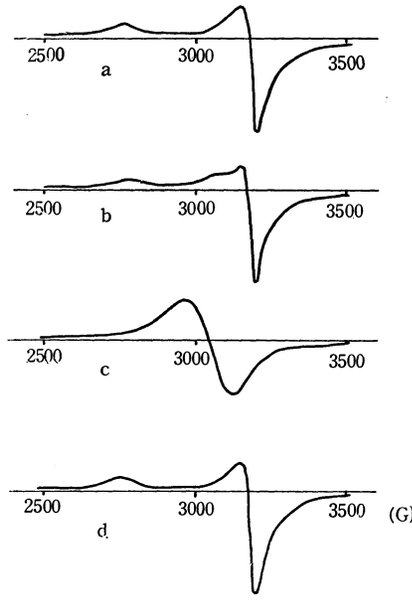

Fig. 1. ESR spectra of complex L, complex H and $Cu(DS)_2\cdot4H_2O$.
a: complex L (−10°C), b: complex H (28°C),
c: $Cu(DS)_2$ dissolved in DOH (50°C),
d: $Cu(DS)_2\cdot4H_2O$ (28°C)

1) Y. Moroi, K. Motomura, and R. Matuura, This Bulletin, **44**, 2078 (1971).
2) Y. Moroi, K. Motomura, and R. Matuura, *ibid.* **45**, 2697 (1972).
3) P. W. Selwood, "Magnetochemistry," Interscience Publishers, Inc., N. Y. (1956), p. 107.
4) The Chemical Society of Japan, "Kagaku Benran", Maruzen Co., Ltd. (1966), p. 1081.

complex of copper was examined by ESR at various temperatures. The results are shown in Fig. 1. The ESR spectra show hardly any difference between complexes L, H, and $Cu(DS)_2 \cdot 4H_2O$ (a, b, d in Fig. 1). It is evident that the four ligands around the copper atom form a typical square-planar structure. The isotropic pattern at a higher temperature (c in Fig. 1) indicates the dissolution of the complex into DOH.

Table 1. Magnetic susceptibilities and magnetic moments

Sample	Temp. (°C)	$\chi \times 10^6$ (emu)	μ_{eff} (B.M.)
$CuSO_4 \cdot 5H_2O$	25	6.2	1.9
$CuSO_4 \cdot 5H_2O$	25	6.2	1.9
$CuSO_4 \cdot 5H_2O$ (*)	25	5.8	1.9
$Mn(DS)_2 \cdot 6H_2O$	25	19	5.6
$Mn(DS)_2 \cdot 6H_2O$	25	18	5.5
$Mn(DS)_2 \cdot 4DOH$ (L)	20	9.8	5.7
$Mn(DS)_2 \cdot 6DOH$ (H)	35	6.7	5.3
$Co(DS)_2 \cdot 6H_2O$	25	12	4.5
$Co(DS)_2 \cdot 4DOH$ (L)	20	3.0	5.7
$Co(DS)_2 \cdot 6DOH$ (H)	35	4.0	4.2
$Ni(DS)_2 \cdot 6H_2O$	25	5.5	3.0
$Ni(DS)_2 \cdot 4DOH$ (L)	20	6.3	4.6
$Ni(DS)_2 \cdot 6DOH$ (H)	35	1.9	2.6
$Cu(DS)_2 \cdot 4H_2O$	25	1.7	1.6
$Cu(DS)_2 \cdot 4H_2O$ (*)	25	2.3	1.9
$Cu(DS)_2 \cdot 4DOH$ (L)	20	2.0	(2.5)
$Cu(DS)_2 \cdot 6DOH$ (H)	35	1.3	2.1

(*): the dispersing agent is naphthalene.

It is concluded that the alcohol molecules enter the region of metal dodecyl sulfate and form the intermolecular complex with it, the chemical structure around the metal being scarcely changed.

The results of specific susceptibility and magnetic moment are given in Table 1. Since the main object is to detect the difference in chemical state between the complex H and complex L, effective magnetic moment μ_{eff} was calculated by the following equation neglecting diamagnetic term.

$$\mu_{eff} = \sqrt{\frac{3k\chi T}{N\beta^2}} \quad \text{(B.M.)} \qquad (2)$$

where k is Boltzmann's constant, T absolute temperature, N Avogadro's number and β the Bohr magneton. From the fairly good reproducibility of the results of $CuSO_4 \cdot 5H_2O$ and $Mn(DS)_2 \cdot 6H_2O$, it is evident that a difference exists between the values of μ_{eff} of complexes H and L, which means that they are in different chemical states. Metals except manganese in complex H are more similar in chemical state to those in $M(DS)_2 \cdot nH_2O$ than those in complex L. For manganese, there was little difference in the chemical state between $Mn(DS)_2 \cdot 6H_2O$, $Mn(DS)_2 \cdot 4DOH$ and $Mn(DS)_2 \cdot 6DOH$.

We might conclude that a long chain alcohol infiltrates into the crystal of a metal alkyl sulfate to form a intermolecular complex with the hydroxyl group of the alcohol intermediating. The intermolecular energy was found to be similar in order to that of hydrogen bonding, namely 7—8 kcal/mol-alcohol.[1,2]

The authors wish to express their thanks to Dr. T. Isobe for his kind help and discussion.

BULLETIN OF THE CHEMICAL SOCIETY OF JAPAN, VOL. 46, 1563—1564 (1973)

Synthesis of a Nucleotide Analog Preparation of 7-(2′-Acetoxypropyl)theophylline 3′-Phosphate

Toru SEITA, Kiyoshi YAMAUCHI, Masayoshi KINOSHITA, and Minoru IMOTO*

Department of Applied Chemistry, Faculty of Engineering, Osaka City University, Sumiyoshi-ku, Osaka 558

** Department of Applied Chemistry, Kansai University, Suita, Osaka 565*

(Received August 11, 1972)

Phosphorylation of the nucleoside analog 9-(2′,3′-dihydroxypropyl)adenine and its polycondensation using *N,N′*-dicyclohexylcarbodiimide as a dehydrating agent gave an oligomer of the nucleotide analog, oligo-3-(9-adenyl)-2-hydroxypropyl phosphate.[1] The polynucleotide analog containing adenine showed a significant hypochromic effect mixed with denaturated RNA or DNA.[2] This shows that the polynucleotide analog retains its polynucleotide-like behaviors such as hypochromicity after the substitution of ribose with 2′,3′-propanediol.

The position of phosphorylation, primary or secondary, is of interest as regards the preparation of such nucleotide analogs.

We have studied the preparation of a nucleotide analog, 7-(2′-acetoxypropyl)theophylline 3′-phosphate.

Tritylation[3] of 7-(2′,3′-dihydroxypropyl)theophylline (I) was carried out with trityl chloride in refluxing dry pyridine. 7-(3′-Trityloxy-2′-hydroxypropyl)-theophylline (II) was obtained in 42% yield and showed a new infrared absorption at 870 cm^{-1} corresponding to the trityl group. Compound (II) gave

1) T. Seita, K. Yamauchi, M. Kinoshita, and M. Imoto, This Bulletin, **45**, 926 (1972).

2) T. Seita, K. Yamauchi, M. Kinoshita, and M. Imoto, *Makromol. Chem.*, **154**, 255 (1972).

3) P. A. Lerene and R. S. Tipson, *J. Biol. Chem.*, **121**, 131 (1937).

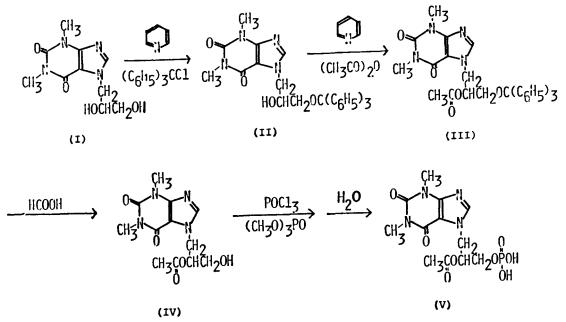

Scheme 1.

7-(2′-acetoxy-3′-trityloxypropyl)theophylline (III) by the reaction with acetic anhydride in pyridine. The infrared spectrum showed a strong absorption at 1730 cm^{-1} corresponding to the carbonyl group. The trityl group was then removed by treatment with 98% formic acid at room temperature, to give 7-(2′-acetoxy-3′-hydroxypropyl)theophylline (IV). Phosphorylation of IV with phosphorus oxychloride in trimethyl phosphate yielded 7-(2′-acetoxypropyl)theophylline 3′-phosphate (V).

When the reaction of free 7-(2′,3′-dihydroxypropyl)-theophylline (I) with phosphorus oxychloride was carried out in trimethyl phosphate,[4] compound (VI) was obtained in 41% yield. This was further treated with Ac_2O to afford VII.

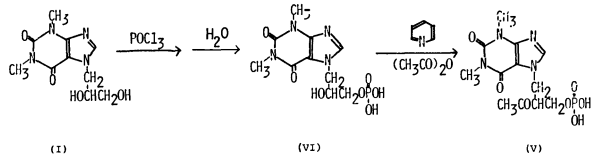

Scheme 2.

The infrared and ultraviolet spectra, melting point, R_f value and elementary analytical values of compound (VII) agree well with those of V. This suggests that VI is 7-(2′-hydroxypropyl)theophylline 3′-phosphate, propanediol derivatives containing nucleoside bases such as I being phosphorylated selectively at the primary hydroxyl group, by means of phosphorus oxychloride.

Experimental

Infrared absorption spectra were taken on a Jasco Model IR-G Spectrometer, and ultraviolet absorption spectra on a Hitachi Spectrometer Model EPS-3T. Paper chromatography was carried out by ascending technique using Whatman No. 3 paper. All melting points are uncorrected.

7-(2′-Hydroxy-3′-trityloxypropyl)theophylline (II). To a refluxing solution of 7-(2′-,3′-dihydroxypropyl)theophylline (I) (20 g; 79 mmol) in dry pyridine (300 ml) was added dropwise a solution of trityl chloride (23 g; 83 mmole) in dry pyridine (150 ml). The addition was completed in 7 hr and then the mixture was allowed to stand at room temperature. The mixture was poured into 2 l of ice-water with continuous stirring. Solid material was collected by filtration and recrystallized from ethanol to give colorless needles; mp 175—176 °C. Yield, 16.2 g (42%). Found: C, 69.87; H, 5.41; N, 11.01%. Calcd for $C_{29}H_{28}N_4O_4$: C, 70.14; H, 5.64; N, 11.29%.

7-(2′-Acetoxy-3′-trityloxypropyl)theophylline (III). Compound (II) (14.85 g; 30 mmol) was added to a mixture of acetic anhydride (70 ml) and dry pyridine (100 ml) and stirred for 20 hr at room temperature. The reaction mixture was poured into 0.5 l of ice-water with rapid stirring. Solid material was collected by filtration and recrystallized from ethanol to give III as colorless needles; mp 137—138 °C. Yield, 8.72 g (55%). Found: C, 69.49; H, 5.59; N, 9.72%. Calcd for $C_{31}H_{30}N_4O_5$: C, 69.13; H, 5.61; N, 10.40%.

7-(2′-Acetoxy-3′-hydroxypropyl)theophylline (IV). Compound (III) (8.7 g; 16.7 mmol) was dissolved in 98% formic acid (70 ml). The solution was kept at room temperature for 40 hr. The precipitate was filtered off and the filtrate was concentrated under reduced pressure. The residue was recrystallized from ethanol to give colorless needles; mp 129—131 °C. Yield, 0.72 g (15%). Found: C, 48.98; H, 5.42; N, 18.48%. Calcd for $C_{12}H_{16}N_4O_5$: C, 48.68; H, 5.44; N, 18.91%.

7-(2′-Acetoxypropyl)theophylline 3′-Phosphate (V). To a solution of compound (IV) (0.7 g; 2.37 mmol) in trimethyl phosphate (8 ml) was added phosphorus oxychloride (0.4 g; 2.6 mmol) at 0 °C followed by stirring for 8 hr. Water was then added and stirring was continued for 40 min. After evaporation of water at a temperature below 50 °C, a mixture of ethanol and ether (3 : 7) was added. White precipitate was chromatographed on silica gel (Mallinckrodt). Elution with *n*-propanol–concd NH_4OH–water (6 : 2 : 2) gave 0.22 g of (V). Recrystallization from ethanol gave 0.2 g (22%) of (V) as colorless needles; mp 137—138 °C. Found: C, 38.79; H, 4.56; N, 14.37%. Calcd for $C_{12}H_{17}N_4O_8P$: C, 38.30; H, 4.56; N, 14.89%.

$\lambda_{max}^{H_2O}$ 274 mμ (ε=8000); 264 mμ (ε=8600), 255 mμ (ε=7800). R_f=0.45 (solvent; *n*-propanol–concd NH_4OH–H_2O 6 : 2 : 2).

Acetylation of Compound (VI). Compound (VI) (1.0 g; 3 mmol) was allowed to react with acetic anhydride (15 ml) in dry pyridine (20 ml) and the mixture was stirred for 20 hr. at room temperature. The solid product was collected by filtration and recrystallized from acetic anhydride–pyridine (4 : 6). The product was compound (V). Yield, 0.42 g (37%).

4) a) M. Yoshikawa, T. Kato, and T. Takenishi, *Tetrahedron Lett.*, **1967**, 5065. b) M. Yoshikawa, T. Kato, and T. Takenishi, This Bulletin, **42**, 3505 (1969).

BULLETIN OF THE CHEMICAL SOCIETY OF JAPAN, VOL. 46, 1565 (1973)

The Isolation of *trans*-Chrysanthenyl Acetate and Chrysanthenone from the Essential Oil of *Chrysanthemum shiwogiku*

Akihiko MATSUO, Yasuto UCHIO, Mitsuru NAKAYAMA, and Shûichi HAYASHI

Department of Chemistry, Faculty of Science, Hiroshima University, Higashisenda, Hiroshima 730

(Received September 12, 1972)

In the course of our chemosystematic investigation of *Crysanthemum* species native in Japan, the essential oil of *Chrysanthemum shiwogiku* Kitam. (Japanese name, Shiogiku; chromosomes, 2n=72) was examined, (+)-*trans*-chrysanthenyl acetate being isolated as the major component (23.2%). Furthermore, seven monoterpenoids containing (+)-chrysanthenone (2.1%) were isolated, and the occurrence of a trace of *trans*-chrysanthenol was confirmed gas chromatographically. Although (+)-chrysanthenone[1] and (−)-*cis*-chrysanthenyl acetate[2] have been previously isolated from other plants of the same *Chrysanthemum*, and (−)-*trans*-chrysanthenol has been synthesized from (−)-α-pinene by Joulain and Rouessac[3] immediately after the present investigation was carried out, (+)-*trans*-chrysanthenyl acetate has not yet been synthesized, nor has it been isolated in nature.

Experimental

The essential oil ($[\alpha]_D$ −11.7°, n_D 1.4830, d_4 0.9395) was obtained by the steam-distillation of stalks and leaves of the plants collected beside the sea at Maruyama in Muroto City in a 0.06% yield of the fresh plants. It was subjected to fractional distillation at reduced pressure and then to silica gel elution chromatography with a mixed solvent of hexane and ethyl acetate (4 : 1) in order to isolate each component.

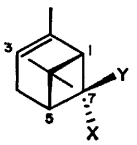

(I) X=OAc, Y=H

(II) X=OH, Y=H

(III) X,Y=O

Chart

Results and Discussion

(+)-trans-*Chrysanthenyl Acetate (I).* The main component ($[\alpha]_D$ +32.0°, 1.75% in $CHCl_3$; n_D 1.4666) has $C_{12}H_{18}O_2$ (M^+ 194). The IR and NMR spectra exhibited a geminal dimethyl (ν_{max}^{liq} 1375 and 1360 cm^{-1}; $\delta_{ppm}^{CCl_4}$ 0.88 and 1.25, each 3H, s), a trisubstituted double bond containing a methyl group (ν 795 cm^{-1}; δ 1.57, 3H, q, J=2.0 Hz and 5.30, 1H, m), and a methine proton (δ 4.87, 1H, t, J=6.0 Hz) bearing an acetoxy residue (ν 1740, 1248, and 1035 cm^{-1}; δ 1.88, 3H, s). Since the NMR spectrum closely resembled that of α-pinene[4] except for the singlet at δ 1.88 and the triplet at δ 4.87, the compound could be characterized as the acetate of a hydroxyl derivative of α-pinene. When this acetate was treated with lithium aluminium hydride in dry ether, it underwent reduction and was converted into a secondary alcohol (II) ($C_{10}H_{16}O$; $[\alpha]_D$ −55.0°, 1.04% in $CHCl_3$; 3.5-DNB, mp 112—113°C; ν_{max}^{liq} 3450, 1085 and 795 cm^{-1}), whose NMR spectrum ($\delta_{ppm}^{CCl_4}$ 0.87 and 1.22, each 3H, s; 1.68, 3H, q, J=2.0 Hz; 4.20, 1H, t, J=6.0 Hz; 5.51, 1H, m) was in a good agreement with that of the (−)-*trans*-chrysanthenol (II) synthesized lately from (−)-α-pinene.[3] Especially, the coupling constant (t, J=6.0 Hz) of the C_7-methine proton signal showed the alcohol to be of the *trans*-form. The secondary alcohol (II) was further oxidized with a Conforth reagent in pyridine to give a unique four-membered ring ketone (III), ($[\alpha]_D$ +63.8°, 0.26% in $CHCl_3$; ν_{max}^{liq} 1780, 1380, 1370, 790, and 740 cm^{-1}; $\delta_{ppm}^{CCl_4}$ 1.20 and 1.23, each 3H, s; 1.73, 3H, q, J=2.0 Hz; 5.31, 1H, m), whose IR and NMR spectra coincided with those of (+)-chrysanthenone.[5] Therefore, it was concluded that the original compound was the (+)-*trans*-chrysanthenyl acetate.

(+)-Chrysanthenone (III) and trans-*Chrysanthenol (II).* A ketone ($[\alpha]_D$ +30.0°, 0.30% in isooctane) was isolated through silica gel elution chromatography: its IR and NMR spectra coincided with those of the chrysanthenone obtained from the chrysanthenyl acetate as described above. In the gas chromatography of the essential oil, a small peak corresponding to *trans*-chrysanthenol was detected by the use of SE-30 and PEG-6000 columns, but further identification was not attempted.

Other Constituents. From the essential oil, α-pinene (0.8%), camphene (2.3%), sabinene (1.0%), *p*-cymene (12.7%), camphor (10.9%), borneol (5.5%), bornyl acetate (2.8%), α-copaene (0.3%), β-elemene (1.4%), β-caryophyllene (2.9%), ε-cadinene (5.7%), and caryophyllene oxide (1.3%), in addition to the above α-pinene derivatives, (+)-*trans*-chrysanthenyl acetate (23.3%), *trans*-chrysanthenol (trace) and (+)-chrysanthenone (2.1%), were isolated and identified by IR, NMR, and mass spectrometries.

The authors are indebted to Professor Ryûso Tanaka, Department of Botany, Hiroshima University, for collecting and identifying the plant material.

1) A. R. Penfold, E. R. Ramage and J. L. Simonsen, *J. Chem. Soc.*, **1939**, 1496; E. P. Blanchard, *Chem. Ind.*, **1958**, 293; M. Kotake and H. Nonaka, *Ann. Chem.*, **607**, 153 (1957).

2) J. T. Pinhey and I. A. Southwell, *Aust. J. Chem.*, **34**, 1311 (1971).

3) D. Joulain and F. Rouessac, *Chem. Commun.*, **1972**, 314.

4) Varian Associates, "Nuclear Magnetic Resonance Spectra Catalog," Vol. 1, Varian Associates, Palo Alto, Cal., (1962). p. 272.

5) The IR and NMR spectra were kindly supplied by Dr. H. Chikamatsu, Osaka University and Dr. J. T. Pinhey, Sydney University.

BULLETIN OF THE CHEMICAL SOCIETY OF JAPAN, VOL. 46, 1566—1567 (1973)

The Selective Hydrogenation of the Knoevenagel Condensates of Acetylacetone with Aldehydes Catalyzed by Raney Nickel as a Route to 3-Substituted 2,4-Pentanediones[1]

Kaku UEHARA, Mitsuo ITO, and Makoto TANAKA

Department of Applied Chemistry, Faculty of Engineering, University of Osaka Prefecture, Sakai-shi, Osaka 591

(Received October 30, 1972)

In an earlier communication,[2] it has been reported briefly that the Knoevenagel condensate of acetylacetone with butyraldehyde or propionaldehyde was hydrogenated with Raney nickel to give 3-butyl- or 3-propyl-2,4-pentanedione. In this paper, the hydrogenation of some other Knoevenagel condensates of acetylacetone with aldehydes will be described in more detail as a new general route to 3-substituted 2,4-pentanediones.

In the presence of piperidine, acetylacetone reacted with butyraldehyde, propionaldehyde, crotonaldehyde, acetaldehyde, benzaldehyde, and furfural to give the Knoevenagel condensates **1**, **2**, **3**, **4**, **5**, and **6** respectively.

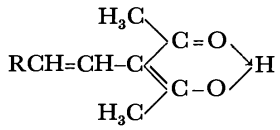

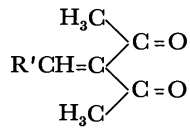

1: R=CH_3CH_2–, **2**: R=CH_3–, **3**: R′=CH_3CH=CH–

4: R′=CH_3–, **5**: R′= 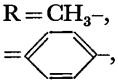 , **6**: R′= 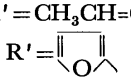

1 and **2** exist predominantly in the enol form and give green crystalline copper(II) chelates. On the other hand, **3** to **6** have no labile hydrogen to form the enol, and therefore give no crystalline copper(II) chelate.

These condensates, **1** to **6**, were hydrogenated with Raney nickel to give 3-butyl-2,4-pentanedione (**7**), 3-propyl-2,4-pentanedione (**8**), 3-ethyl-2,4-pentanedione (**9**), 3-benzyl-2,4-pentanedione (**10**), 3-furfuryl-2,4-pentanedione (**11**), and 3-tetrahydrofurfuryl-2,4-pentanedione (**12**). These diketones are effective chelating agents and give gray crystalline copper(II) chelates. The data o the hydrogenation of **1** to **6** are shown in Table 1.

Table 1. The hydrogenation of Knoevenagel condensates

Knoevenagel condensate		Raney nickel (g)	Temp. (°C)	Time (min)	Product		Yield (%)
No.	(g)				No.	(g)	
1	20	1	70	60	**7**	17.1	86
2	20	2	70	60	**8**	16.8	83
3	15	1.5	70	455	**7**	13.2	88
4	5.5	0.3	70	150	**9**	4.0	72
5	16	1	70	150	**10**	14.1	88
6	12	1	50	30	**11**	8.6	72
6	12	1	70	70	**12**	9.0	84

In the hydrogenation of **6** at 50 °C, it was possible to interrupt the reaction to obtain **11**. The present method seems to be a general route to 3-substituted 2,4-pentanedions.

At the temperature of 100 or 120°C, a low-boiling fraction, such as 2-heptanone, benzylacetone, or tetrahydrofurfurylacetone, was produced as a by-product by the deacylation of the corresponding diketones. These monoketones remained without further hydrogenation to alcohols even at the temperature of 120 °C. This fact suggests that β-diketone modifies the hydrogenation activity of the Raney nickel in the manner described by Izumi *et al.*[3]

By the addition of **7**, the rate of the hydrogenation of 2-heptanone was decreased, resulting in a decrease in the yield of 2-heptanol. In the hydrogenation of 4-hepten-2-one, it was found that the hydrogen uptake occurred in two stages, and that the rate of the first stage was little affected by the addition of **7**. When the reaction was interrupted after the absorption of one mole equivalent of hydrogen, only 2-heptanone was formed. The additive, **7**, was recovered unchanged after the hydrogenation.

These results suggest that the activity of Raney nickel is decreased only for the carbonyl group and that, therefore, the selectivity for the C=C double bond is increased in the presence of 3-substituted 2,4-pentanedione. The modifying action of the β-diketone probably had a favorable effect on the selective hydrogenation of the Knoevenagel condensates of acetylacetone with aldehydes to 3-substituted 2,4-pentanedione.

Experimental

All the boiling points are uncorrected. The acetylacetone, aldehydes, and piperidine were of a reagent grade and were obtained from commercial sources. The Raney nickel used in this work was of the W-1 type, prepared by the ordinary method.[4] A stirring-type autoclave with a void of 100 ml was used as the reaction vessel.

Knoevenagel Condensates of Acetylacetone with Aldehydes. An equimolar mixture of acetylacetone and an aldehyde was placed in a 200-ml flask equipped with a stopper. After cooling, 0.4 mol%[5] of piperidine was added, drop by drop,

1) Paper XVII in a series of "Catalytic Behavior of Metal Chelate Compounds."

2) K. Uehara, T. Matsumura, T. Nishi, F. Tamura, and N. Murata, *Kogyo Kagaku Zasshi*, **69**, 2027 (1966).

3) H. Fukawa, Y. Izumi, S. Komatsu, and S. Akabori, This Bulletin, **35**, 1703 (1962).

4) L. W. Covert and H. Adkins, *J. Amer. Chem. Soc.*, **54**, 4116 (1932).

5) The large exess of piperidine resulted in an appreciable decrease in the yield of Knoevenagel condensates.

and the mixture was kept at 0 °C for 7 hr. The reaction mixture was then subjected to fractional distillation. 3-(1-Butenyl)-2,4-pentanedione (**1**); bp 92—95 °C/16 mmHg (lit,[6] bp 83—85.5 °C/9 mmHg), n_D^{19} 1.4839, yield, 60%. 3-(1-Propenyl)-2,4-pentanedione (**2**); bp 81—84 °C/14 mmHg, n_D^{25} 1.4845, yield, 56.8%. Found: C, 68.74; H, 8.90%, Calcd for $C_8H_{12}O_2$: C, 68.54; H, 8.90%. 3-(2-Butenylidene)-2,4-pentanedione (**3**); bp 117—120 °C/20 mmHg, n_D^{25} 1.5175, d_4^{25} 1.0120, yield, 54%. 3-Ethylidene-2,4-pentanedione (**4**); bp 90—95 °C/20 mmHg, n_D^{25} 1.4652 (lit,[7] bp 44—45°C/0.04 mmHg, n_D^{25} 1.4608), yield, 7.6%. 3-Benzylidene-2,4-pentanedione (**5**); bp 142—143 °C/4 mmHg, n_D^{25} 1.5180, yield, 44%. 3-Furfurylidene-2,4-pentanedione (**6**); bp 120—124 °C/2 mmHg (lit,[8] bp 128—129 °C/4 mmHg), n_D^{30} 1.5872.

Hydrogenation of the Knoevenagel Condensates. Each condensate, from **1** to **6**, was dissolved in 5 ml of ethanol and then hydrogenated in an atmosphere of hydrogen under an initial pressure of 100 kg/cm² at 50 to 120 °C with Raney nickel. After the theoretical amount of hydrogen had been taken up, the reaction mixture was subjected to fractional distillation. The following products were thus obtained: 3-Butyl-2,4-pentanedione (**7**); bp 99—103 °C/14 mmHg, n_D^{29} 1.4428 (lit,[9] bp 98—102 °C/16—17 mmHg, n_D^{25} 1.4442). 3-Propyl-2,4-pentanedione (**8**); bp 93—96 °C/21 mmHg (lit,[10] bp 75—77 °C/12 mmHg), n_D^{25} 1.4420. 3-Ethyl-2,4-pentanedione (**9**); bp 80—83 °C/25 mmHg, n_D^{17} 1.4399 (lit,[11] bp 80—81 °C/21 mmHg). 3-Benzyl-2,4-pentanedione (**10**); bp 90—94 °C/1 mmHg, n_D^{25} 1.5265(lit, [12] bp 115—118 °C/4 mmHg, n_D^{25} 1.5236). 3-Furfuryl-2,4-pentanedione (**11**); bp 107—108 °C/4 mmHg, n_D^{16} 1.4963; IR spectrum: 1720 (C=O), 1680 (C=C), 1600 (enol), 1070 cm⁻¹ (C–O–C). Mass spectrum: *m/e* 180 (parent peak), *m/e* 137 $(P\text{–}COCH_3)^+$, *m/e* 81 . 3-Tetrahydrofurfuryl-2,4-pentanedione (**12**); bp 109—112 °C/2 mmHg, n_D^{17} 1.4676, IR spectrum: 1720 (C=O), 1600 (enol), 1070 cm⁻¹ (C–O–C). Mass spectrum: *m/e* 184 (Parent peak), *m/e* 141 $(P\text{–}COCH_3)^+$, *m/e* 85 , *m/e* 71 .

The IR spectra of the hydrogenated products from **7** to **10** were identical with those of the authentic samples which had been prepared by the reaction of sodium acetylacetonate with alkyl halides.[13,14]

*Copper(II) Chelate from **7** to **12**.* The copper(II) chelates from **7** to **12** were prepared by mixing an aqueous solution of cupric acetate and an ethanol solution of the hydrogenated products from **7** to **12**. They were then recrystallized from benzene–ligroin. The microanalyses were as follows: **7**, Found: C, 57.51; H, 8.24%. Calcd for $C_{18}H_{30}O_4Cu$: C, 57.80; H, 8.03%. **8**, Found: C, 55.05; H, 7.77%, Calcd for $C_{16}H_{26}O_4Cu$: C, 55.55; H, 7.58%. **9**, Found: C, 52.84; H, 7.10%, Calcd for $C_{14}H_{22}O_4Cu$: C, 52.90; H, 6.98%. **10**, Found: C, 65.04; H, 5.93%, Calcd for $C_{24}H_{26}O_4Cu$: C, 65.21; H, 5.93%. **11**, Found: C, 56.72; H, 5.25%, Calcd for $C_{20}H_{22}O_6Cu$: C, 56.92; H, 5.25%. **12**, Found: C, 55.29; H, 6.90%, Calcd for $C_{20}H_{30}O_6Cu$: C, 55.86; H, 7.03%.

Hydrogenation of 2-Heptanone or 4-Hepten-2-one. 2-Heptanone was a commercial G.R.-grade sample. 4-Hepten-2-one was prepared by the deacylation of **1** in the presence of its copper(II) chelate in methanol.[15] They were hydrogenated with 100 kg/cm² hydrogen with Raney nickel in the presence of **7** at 70 °C. In the course of the reaction, the hydrogen-uptake was followed manometrically. The fractional distillation of the reaction mixture gave 2-heptanol (bp 74—75 °C/23 mmHg) and/or 2-heptanone (bp 54—55 °C/17 mmHg).

6) G. B. Payne, *J. Org. Chem.*, **24**, 1830 (1959).
7) B. D. Wilson, *ibid.*, **28**, 314 (1963).
8) H. Midorikawa, This Bulletin, **27**, 213 (1954).
9) D. F. Martin, W. C. Fernelius, and M. Shamma, *J. Amer. Chem. Soc.*, **81**, 130 (1959).
10) T. Shono, M. Tanaka, Y. Murotani, and K. Shinra, *Nippon Kagaku Zasshi*, **88**, 1068 (1967).
11) C. R. Hauser and J. T. Adams, *J. Amer. Chem. Soc.*, **66**, 345 (1944).
12) Y. Murakami and K. Nakamura, This Bulletin, **39**, 901 (1966).
13) G. T. Morgan and A. E. Rawson, *J. Soc. Chem. Ind.*, **44**, 462 (1925); *Chem. Abstr.*, **20**, 192 (1926).
14) G. T. Morgan, *J. Chem. Soc.*, **1925**, 797.
15) K. Uehara, S. Shionoiri, M. Tanaka and N. Murata, This Bulletin, **45**, 1570 (1972).

BULLETIN OF THE CHEMICAL SOCIETY OF JAPAN, VOL. 46, 1568—1569 (1973)

The Ring-Opening Reactivities of Three-Membered Cyclic Compounds. I. The Ring-Opening Reactions of Three-Membered Cyclic Compounds by Hydrogen Chloride

Hiroshi KAKIUCHI and Takao IIJIMA

Department of Applied Chemistry, Faculty of Engineering, Yokohama National University, Ooka, Minami-ku, Yokohama 233

(Received March 14, 1972)

There have been many reports about the relative reactivities of cyclic ethers in cationic copolymerizations,[1-3] and these reactivities have been evaluated as linear combinations of the basicity of the ring and the ring strain[2] or the radical dissociation energy of the broken bond.[3]

There have, however, been few reports discussing how the changes in the heteroatoms of the rings influence the reactivities of heterocyclic compounds.[4,5] In this paper, the ring-opening reactions of three-membered cyclic compounds by hydrogen chloride will be studied in toluene in order to discuss their relative reactivities. As three-membered rings, methyl cyclopropane (MCP), propylene oxide (PO), propylenimine (PI), and propylene sulfide (PS) will be used.

Results and Discussion

Ring-opening reactions of MCP were carried out at 40 °C and 60 °C. In these reactions, isobutyl chloride, **1a**, could not be observed; only *sec*-butyl chloride, **1b**, could be detected by gas chromatography. The ring-opening reaction rate was so slow that the kinetic study was difficult.

TABLE 1. RATE CONSTANTS FOR THE RING-OPENING REACTIONS BY HCl

Reaction temp. (°C)[a]	PO 10^2k_2 (l/mol s)	PI 10^2k_2 (l/mol s)	PS 10^4k_2 (l/mol s)
40			4.83 4.81 5.02
30	10.1 10.3	4.49 5.29	3.14 3.04 3.06
20	3.62 4.05	3.23 3.80	2.00 2.09 1.91
10	2.77 2.59	2.52 2.21	1.53
0	1.46 1.48 1.34	1.52 1.70	

a) ±0.1°C

The ring-opening reactions of three-membered heterocyclic compound by HCl obey second-order kinetics, depending on the first order both in the heterocyclic compound concentration and in the HCl concentration. The kinetic results are shown in Table 1. According to the Eyring equations, the activation parameters were calculated; they are shown in Table 2. In these reaction systems, two kinds of reaction products were produced:

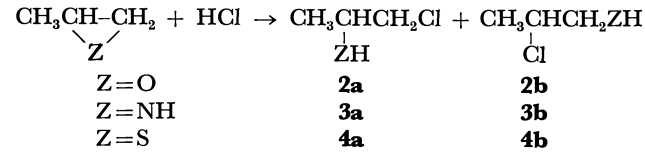

The ring-opening reaction products of PO were separated into their components, **2a** and **2b**, by gas chromatography, and each of them was analyzed by NMR spectroscopy. In the gas chromatogram, two peaks of the reaction products were observed with retention times 8.7 and 11.4 min, respectively. The chemical shift of the methyl protons of the former is 8.70 τ, and that of those of the latter, 8.50 τ. Considering the difference between the shielding effect due to a substituent in the β-position to methyl protons, the former is **2a**, and the latter, **2b**.[6]

Two kinds of aminopropanols in the PI–HCl reaction system were analyzed by NMR(D_2O) spectroscopy. The methyl-proton spectra of two kinds of reaction products were separated into 1.35 and 1.55 ppm, respectively; the lower-field absorption in the signals was assigned to the abnormal product, **3b**.

In the ring-opening reaction of PS, two kinds of chloropropanethiols were analyzed by both gas chromatography and NMR(C_6H_6) spectroscopy according to the modified method of Schwarz.[7]

The results of product analyses (Table 2) show that the ring-opening reactions of three-membered heterocyclic compounds proceed *via* an S_N2-type mechanism and that the normal products, **2a**, **3a**, and **4a**, are produced in larger amounts.[5,8] The reaction rate decreases in the following order: PO, PI, PS, and MCP. The order of the reactivity corresponds to neither that of the basicity[9] nor that of the ring strain[10]

1) S. Iwatsuki, Y. Takikawa, M. Yamashita, and Y. Ishii; *Kogyo Kagaku Zasshi*, **67**, 142 (1964).
2) S. Aoki, K. Fujikawa, T. Otsu, and M. Imoto, *J. Polym. Sci. Part A-1*, **6**, 2585 (1968).
3) T. Kagiya, Y. Sumida, and T. Inoue, *Polymer J.*, **1**, 312 (1970).
4) N. S. Isaacs, *Can. J. Chem.*, **44**, 395 (1966).
5) N. S. Isaacs and K. Neelakantan, *ibid.*, **46**, 1043 (1968).
6) J. W. Emsley and L. H. Sutcliff, "High Resolution Nuclear Resonance Spectroscopy," Vol. 2, Pergamon Press, Oxford (1966). p. 676.
7) N. V. Schwarz, *J. Org. Chem.*, **33**, 2896 (1968).
8) P. A. Gembitskii, N. M. Loim, and D. S. Zhuk, *Russ. Chem. Revs.*, **35**, 105 (1966).
9) E. Lippert and H. Prigge, *Ann. Chem.*, **659**, 81 (1962).

Table 2. The activation parameters and the product ratios in the ring-opening reaction of three-membered cyclic compounds by HCl

	MCP	PO	PI	PS
$\Delta H^{\neq}$(kcal/mol)[a]	—	9.5±0.5	5.5±0.3	6.7±0.3
$\Delta S^{\neq}$(e.u.)[a]		−32.0±1.9	−46.3±1.0	−51.8±0.9
Product ratio[b] (a : b)	0 : 100	67 : 33	86 : 14	62 : 38
Ring strain[c] (kcal/mol)	27.43	27.28	26.87	19.78
Association const[d] with phenol K (l/mol)	?	5.95	139	1.081

a) At 30 °C, b) At room temp., c) Ref. 10, d) At 20 °C. See ref. 9. That of PI was calculated from the average value of ethylene imine and 2,2-dimethylethylene imine.

(Table 2). In the protonic acid system, the ring-opening reaction is that of the conjugate acid by the anion, as follows:

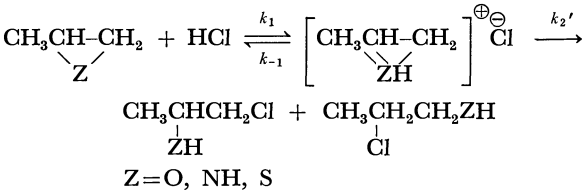

Z=O, NH, S

The apparent rate constant, k_2, can, then, be expressed as the product of the equilibrium constant, $K(=k_1/k_{-1})$, and the rate constant of the elementary reaction, k_2'. The former is related to the basicity of the ring, while the latter is influenced by the ring strain of the conjugate acid. However, it is difficult to find the dependence of the ring-opening reactivity on either the ring strain or the basicity of the ring, because the relation between the ring strain of the three-membered ring and that of its conjugate acid is unknown and the equilibrium constant can not be determined.

The details of the reactions of MCP in other protonic acid systems will be reported in the near future.

Experimental

Reagents. Methyl cyclopropane was prepared by the method of Demjanoff[11] and was dried over phosphorus pentoxide. Propylene oxide was a commercial product; it was dried over calcium hydride and then distilled; bp 35.0 °C. Propyleneimine was prepared by the method of Wenker,[12] dried over sodium metal, and distilled; bp 64.0—66.0 °C. Propylene sulfide was prepared by the method of Bordwell *et al*,[13] dried over anhydrous sodium carbonate, and distilled; bp 72.0—75.0 °C. All three-membered cyclic compounds were distilled just before use. Toluene was purified by the usual method, and the anhydrous HCl solution in toluene was prepared by the method of Manson.[14]

Kinetic Measurements. The reaction was carried out in toluene under dry nitrogen in a 200 ml four-necked flask equipped with a thermometer, a stirrer, and a cooler. The gas chromatographic conditions in the MCP–HCl reaction were: internal standard, carbon tetrachloride; column materials, 25 wt% tricresyl phosphate 75 cm×3 mm; column temp., 40 °C; carrier gas, He 50 ml/min. The rate constants for the reaction of PO with HCl were measured in the following manner. At desired time intervals, a constant volume of the reaction mixture was withdrawn and poured into a constant volume of a potassium hydroxide methanol solution (M/10). The conversion of PO was calculated from the amount of the remaining potassium hydroxide, which was determined with a benzoic acid methanol solution (M/25), using phenolphthalein as the indicator. The reaction rate of PO was too fast to determine the conversion of PO by gas chromatography. Kinetic measurements of the reaction of PI with HCl were carried out in the same manner as those of the PO–HCl reaction system except that initial mole ratio, HCl/PI, was controlled at 2. The true residual values of HCl were calculated as twice the apparent values of HCl, because two kinds of aminopropanols act as bases in the back titration. The influence of PI should be negligible, for PI is a weak and it consumes only HCl 1×10^{-5} mol/PI 0.01 mol. The rate constants for the reaction of PS with HCl were measured by determining the residual PS under the following gas chromatographic conditions: internal standard, chlorobenzene; column material, 25 wt% tricresyl phosphate 75 cm×3 mm; column temp., 120 °C; carrier gas, He 50 ml/min. In this reaction, the residual HCl could not be determined because the reaction products, chloropropanethiols, act as acids.

Product Analyses. *sec*-Butyl chloride was prepared as an authentic sample from *sec*-butyl alcohol. The gas chromatographic conditions in the PO–HCl reaction system were: column material, carbowax 1500 300 cm×3 mm; column temp., 80 °C; carrier gas, He 50 ml/min. 2-Chloro-*n*-propylamine hydrochloride was prepared as an authentic sample from 1-amino-2-propanol hydrochloride; mp 186.0—187.0 °C(lit,[15] 187—190 °C). 2-Chloropropane-1-thiol, **4b**, was prepared by the method of Davis *et al.*;[16] it contained about 10% of the isomer, **4a**.

10) A. S. Pell and G. Pilcher, *Trans. Faraday Soc.*, **61**, 71 (1965).
11) N. Demjanoff, *Ber.*, **28**, 21 (1895).
12) H. Wenker, *J. Amer. Chem. Soc.*, **57**, 2328 (1935).
13) F. G. Bordwell and H. W. Anderson, *ibid.*, **75**, 4959 (1953).
14) R. N. Manson, "Inorganic Syntheses," Vol. 1, p. 147 (1939).
15) L. Smith and B. Platon, *Ber.*, **55B**, 3141 (1922).
16) W. Davis and W. E. Savige, *J. Chem. Soc.*, **1950**, 317.

BULLETIN OF THE CHEMICAL SOCIETY OF JAPAN, VOL. 46, 1570—1571 (1973)

4-(1,2-Diacetoxyethyl)pyridine and Its Chemical Properties

Toshiyuki FURUYAMA, Koichi MORI, Ichiro NAGOYA, Kazuo TAMURA, and Masatsugu YOSHINO

Technical Research Laboratory, Asahi Chemical Industry Co., Ltd., Nakadai, Itabashi-ku, Tokyo 174

(Received November 28, 1972)

A new compound 4-(1,2-diacetoxyethyl)pyridine was synthesized from reaction of (4-pyridyl)-1,2-ethanediol (I) with acetic anhydride. It was converted into α-acetoxy-4-vinylpyridine (II) (yield, 85%) on being heated in acetic anhydride. The compound shows a characteristic NMR spectrum with respect to its methylene splitting, indicating that the two protons on methylene are not chemically equivalent.

Haas *et al.*[1] treated (I) with acetic anhydride and obtained α-acetoxy-4-vinylpyridine. They stated that the formation of 4-(1,2-diacetoxyethyl)pyridine (III) was unlikely since the deacetylation of the analogous compound, 2-(1,2-diacetoxyethyl)pyridine, seldom affords α-acetoxy-2-vinylpyridine. Their proposed mechanism which involves an intermediate compound of a half acylated diol is shown.

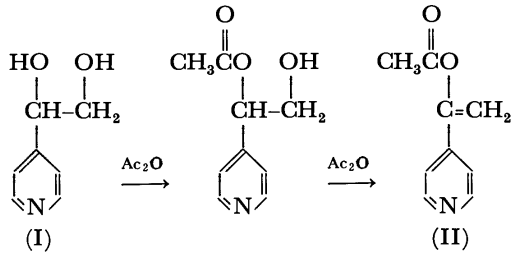

Scheme (1)

Having succeeded in synthesizing α-acetoxy-4-vinylpyridine (II) from 4-(1,2-diacetoxyethyl)pyridine in an 85% yield, we propose a mechanism which involves the formation of (III) as follows.

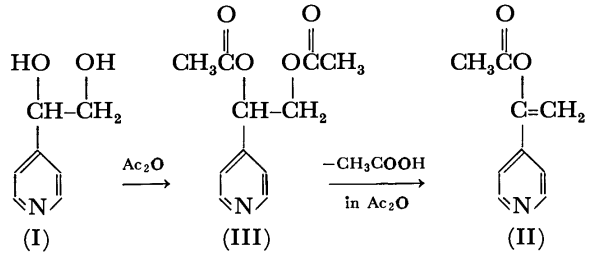

Scheme (2)

Results and Discussion

The formation of III from I is fast and the yield is quantitative. 4-(1,2-Diacetoxyethyl)pyridine, bp. 112 °C/0.28 mmHg, mp. 46.5 °C (DSC method) and $n_D^{25.5}$ 1.4908, can be distilled from the reaction solution by the removal of the acetic acid formed and excess acetic anhydride just after I is dissolved into acetic anhydride. In this case the molar ratio of I to acetic anhydride is 1 : 7.5. The reaction (exothermic) was carried out at inner temperature of *ca.* 40 °C for 30 min under occasional water cooling.

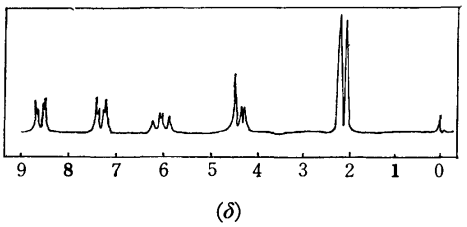

Fig. 1. 60 MHz NMR spectrum 4-(1,2-diacetoxyethyl)pyridine in $CDCl_3$.

The NMR spectrum of III at 60 MHz in deuterochloroform at room temperature is shown in Fig. 1. The methylene peaks ($H_{(c)}$, 4.33 δ; $H_{(d)}$, 4.37 δ) appear as three peaks ($|J_{(c)(e)}|$, 7 cps; $|J_{(d)(e)}|$, 4.5 cps; $|J_{gem}|$, 12 cps), and the methine peaks ($H_{(e)}$, 6.03 δ) were four peaks.

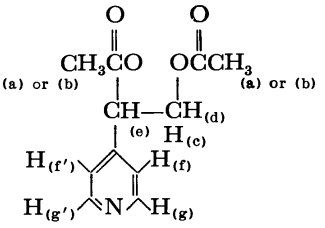

This indicates that the methylene protons are not chemically equivalent. A similar example of aspartic acid in D_2O, was reported by Silverstein and Bassler,[2] where methylene protons adjacent to the asymmetric carbon appear as a triplet. However, the possibility that 4-(1,2-diacetoxyethyl)-pyridine takes a specific conformation cannot be ruled out, since the deacetylation of 4-(1,2-diacetoxyethyl)pyridine *via* a six membered transition state easily takes place to form α-acetoxy-4-vinylpyridine (scheme (3)).

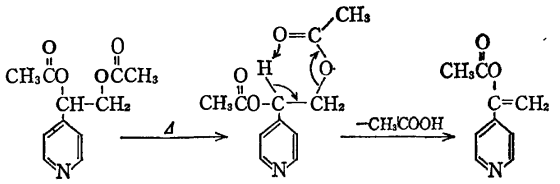

Scheme 3.

A kinetic study for the deacetylation reaction of III was carried out in acetic anhydride at 130 °C (Fig. 2). The deacetylation obeys a first order reaction.

1) H. C. Haas, H. S. Kolesinski, and N. W. Schuler, *J. Polym. Sci., B*, **3**, 879 (1965).

2) R. M. Silverstein and G. C. Bassler, "Spectrometric Identification of Organic Compounds," Japanese Ed. translated by S. Araki and Y. Mashiko, Tokyo Kagakudojin, Tokyo (1969), p. 135.

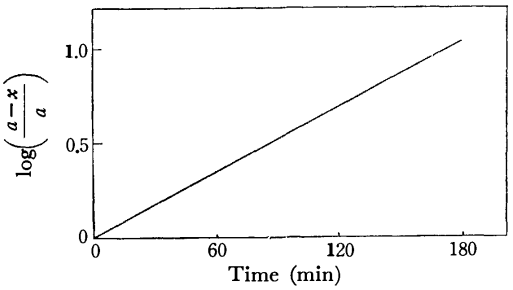

Fig. 2. The deacetylation reaction of 4-(1,2-diacetoxyethyl)-pyridine at 130°C.
a: initial 4-(1,2-diacetoxyethyl)pyridine (mol)
x: product formed (mol)

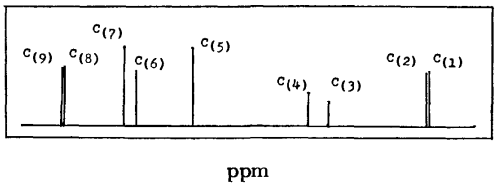

Fig. 3. Carbon-13 NMR spectrum of 4-(1,2-diacetoxyethyl)-pyridine in D_2O.

The yield of deacetylation is as high as 50%, according to the Haas method[1] or the improved Haas method,[3] in contrast to the present method (85% yield) which involves III as an intermediate compound.

A carbon-13 NMR spectrum of III proves the formation of 4-(1,2-diacetoxyethyl)pyridine (Fig. 3).

α-Acetoxy-4-vinylpyridine which was synthesized by the present method can be crystallized with mp of 12.6 °C, and be polymerized with both γ-rays and radical initiators.[4]

3) T. Furuyama, K. Mori, and R. Wakasa, This Bulletin, **45**, 1924 (1972).
4) T. Furuyama, K. Mori, and R. Wakasa, *J. Polym. Sci.*, *A*-1, **9**, 3411 (1971).
5) E. Breitmaier, G. Jung, and W. Voelter, *Angew. Chem. Intern. Ed.*, **10**, 673 (1971).

Experimental

4-(1,2-Diacetoxyethyl)pyridine. To 10 g (0.07 mol) of pyridyl)-1,2-ethanediol was added 55 g (0.54 mol) acetic anhydride. The reaction started exothermally, pasty (4-pyridyl)-1,2-ethanediol being gradually dissolved. The system was maintained at approximately 40 °C for 30 min by occasional water cooling. Acetic acid and the excess acetic anhydride were removed under reduced pressure. The subsequent vacuum distillation gave 4-(1,2-diacetoxyethyl)pyridine in a quantitative yield: bp. 112°C/0.28 mmHg. mp. 45.6°C (DSC method). $n_D^{25.5}$ 1.4908. Found: C, 59.2; H, 5.9; N, 6.3%. Calcd for $C_{11}H_{13}O_4N$: C, 59.2; H, 5.9; N, 6.3%.

Deacetylation. A mixture of 10 g (0.045 mol) of 4-(1,2-diacetoxyethyl)pyridine and 35 g (0.343 mol) of acetic anhydride was maintained at 130°C for 6 hr in thermobath. The subsequent fractional distillation under reduced pressure gave α-acetoxy-4-vinylpyridine, yield 85%, mp 12.6°C. The results for bp and elemental analysis for C, H, and N are the same as described previously.[3] Kinetic study was carried out by taking small portion of the reaction mixture and measuring the decreasing methylene protons with a 60 MHz NMR instrument.

Carbon-13 NMR Spectrum. This was measured with JEOL 100 MHz spectrometer (JNM-PET-100) in heavy water at room temperature by the pulse Fourier transform NMR method.[5]

Carbon-13 NMR: $C_{(1)}$ or $C_{(2)}$, ppm 20.9 or 21.1; $C_{(3)}$ 66.2; $C_{(4)}$, 73.3; $C_{(5)}$, 122.6; $C_{(6)}$, 147.2; $C_{(7)}$, 149.9; $C_{(8)}$ or $C_{(9)}$ 173.3 or 173.9 (TMS reference).

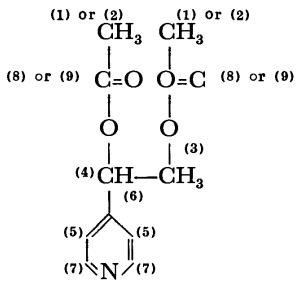

BULLETIN OF THE CHEMICAL SOCIETY OF JAPAN, VOL. 46, 1572—1573 (1973)

Synthesis of Some Substituted Nucleoside Analogs

Toru SEITA, Masayoshi KINOSHITA, and Minoru IMOTO*

Depatment of Applied Chemistry, Osaka City University, Sumiyoshi-ku, Osaka 558

**Department of Applied Chemitry, Kansai University, Suita, Osaka 565*

(Received December, 1972)

Polymers which contain nucleic acid bases in their main chain or in side groups present many interesting problems with respect to their physicochemical properties. But the water-insolubility of polymers was often encountered and was unsuitable for the study of physicochemical properties. This problem was solved by the introduction of phosphoric ester group into the main chain of polymer.[1-2] The authors have synthesized, further, water-soluble polymers particularly paying attention to the new structural analogs of nucleic acid.[3] Takemoto *et al.* reported on the derivatives of nucleic acid bases.[4]

In this paper we describe the synthesis of 5-substituted uracil. The oligomers and polymers obtained from compounds of these types may provide a mean of studying chemotherapeutic applications. One of the most interesting utilization may be the incorporation of 5-halouracils into polymer, especially of the most important anti-cancer material, 5-fluorouracil.

Bromination of 1-(2′,3′-dihydroxypropyl)-uracil was carried out using bromine in mixture of 0.5 M nitric acid and *p*-dioxane to give 1-(2′,3′-dihydroxypropyl)-5-bromouracil (**1**). When 1-(2′,3′-dihydroxypropyl)-uracil was refluxed with iodine under similar condition described above, the 1-(2′,3′-dihydroxypropyl)-5-iodouracil (**2**) was formed in good yield. The position of substitution of bromine or iodine atom was confirmed by ultraviolet absorption. The ultraviolet absorption spectra of **1** and **2** are shifted toward longer wavelength than that of 1-(2′,3′-dihydroxypropyl)-uracil. The position of halogen atom was also checked by the absence of absorption peak at τ 4.2 corresponding to H-5 of uracil ring.

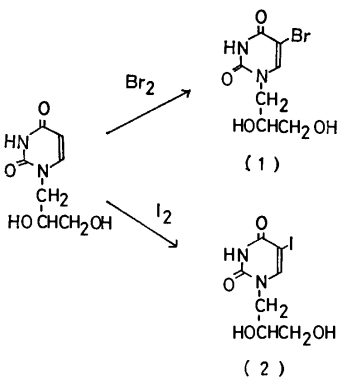

Scheme 1.

Thymine was treated with glycidol in DMF containing a trace of anhydrous potassium carbonate at 60—70 °C. Chromatography of reaction mixture on silica gel using benzene–ethanol as solvent gave the 1-(2′,3′-dihydroxypropyl)-5-methyluracil (**3**). Also the reaction of 5-fluorouracil with equimolar glycidol was carried out under similar condition to give 1-(2′,3′-dihydroxypropyl)-5-fluorouracil (**4**).

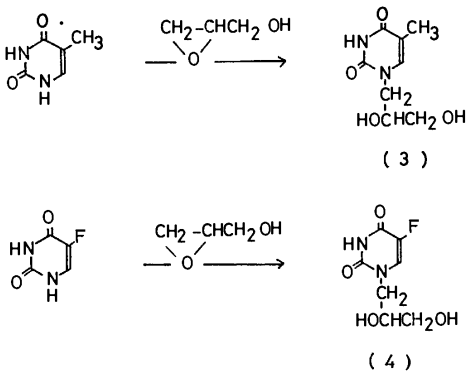

Scheme 2.

Experimental

The IR spectra were run on a JASCO Model IR-G Spectrometer. The UV spectra were measured by a Hitachi Recording Spectrometer Model ESP-3T. The NMR spectra were recorded with a Hitachi-Perkin-Elmer apparatus, Model R-20.

1-(2′,3′-Dihydroxypropyl)-5-bromouracil (1). A solution of 1-(2′,3′-dihydroxypropyl)-uracil (1.86 g, 10 mmol) dissolved in a mixture of 0.5 M nitric acid (20 ml) and *p*-dioxane (80 ml) was added to a solution of bromine (2.4 g, 15 mmol) in 20 ml of carbon tetrachloride, and the solution was stirred at room temperature for 3 hr. The reaction mixture was evaporated under reduced pressure to dryness. The oil residue is dissolved in ethanol, and the solution was evaporated to dryness. The obtained precipitate was recrystallized from ethanol to give **1** (2.5 g, (85%)) as colorless needles.

Mp 202—204°C, UV: $\lambda_{max}^{H_2O}$ 211 mμ (ε=9800), 283 mμ (ε=9100), IR: 3300 (OH), 1700, 1650 (bromouracil ring) and 1090, 1030 (primary and secondary alcohol C–O); NMR (DMSO-d_6) τ −1.15 (br s, 1, N_3–H), 2.0 (s, 1, C_6–H), 5.5 (br s, 2, $C_{2',3'}$-OH), 5.8—6.5 (m, 3, $C_{2',3'}$–H), 6.65 (br s, 2, C_1, –H); Found: C, 31.69; H, 3.48; N, 10.49%. Calcd for $C_7H_9N_2O_4Br$: C, 31.71; H, 3.42; N, 10.56%.

1-(2′,3′-Dihydroxypropyl)-5-iodouracil (2). Into a solu-

1) T. Seita, K. Yamauchi, M. Kinoshita, and M. Imoto, This Bulletin, **45**, 926 (1972).

2) T. Seita, K. Yamauchi, M. Kinoshita, and M. Imoto, *Makromol. Chem.*, **154**, 255 (1972).

3) T. Seita, K. Yamauchi, M. Kinoshita, and M. Imoto *ibid.*, **154**, 263 (1972).

4) a) K. Kondo, M. Miyata, and K. Takemoto, This Bulletin, **44**, 2554 (1971). b) N. Ueda. T. Kawabata and K. Takemoto, *J. Heterocyclic Chem.*, **8**, 827 (1971).

tion of 1-(2′,3′-dihydroxypropyl)-uracil (0.86 g, 10 mmol) in a mixture of 0.5 M nitric acid (20 ml) and *p*-dioxane (80 ml), iodine (5.1 g, 20 mmol) was added and the solution was refluxed for 3 hr. After allowing to cool to room temperature, the solvent was evaporated under reduced pressure. The residue was recrystallized from ethanol to give **2** (2.18 g, (80%)) as colorless needles.

Mp. 196—198°C, UV: $\lambda_{max}^{H_2O}$ 219 mμ (ε=12000), 292 mμ (ε=9800), IR; 3350 (OH), 1690, 1660 (iodouracil ring) and 1090, 1020 (primary and secondary alcohol C–O); NMR (DMSO-d_6) τ −1.15 (br s, 1, N_3–H), 1.9 (s, 1, C_6–H), 5.6 (br s, 2, $C_{2',3'}$–OH), 5.9—6.4 (m, 3, $C_{2',3'}$–H), 6.5 (br s, 2, $C_{1'}$–H); Found: C, 26.86; H, 2.90; N, 8.62%. Calcd for $C_7H_9N_2O_4I$: C, 26.93; H, 2.90; N, 8.97%.

*1-(2′,3′-Dihydroxypropyl)-5-methyluracil (**3**).* Thymine (1.25 g, 10 mmol) and glycidol (0.74 g, 10 mmole) in DMF (50 ml) containing a trace amount of anhydrous potassium carbonate was stirred at 60—65°C for 8 hr. The solvent was evaporated to dryness under reduced pressure. The residue was chromatographed over silica gel using a mixture of benzene and ethanol (4 : 1) as solvent. The obtained product was recrystallized from benzene–ethanol (7 : 1) to give the compound **3** (0.8 g, (40%)) as colorless needles.

Mp. 145—146°C, UV: $\lambda_{max}^{H_2O}$ 210 mμ (ε=13500), 273 mμ (ε=12000), IR: 3500 (OH), 1660 (thymine ring) and 1090, 1040 (primary and secondary alcohol C–O); NMR (DMSO-d_6) τ −1.15 (br s, 1, N_3–H), 8.2 (s, 3, N_5–CH_3), 2.8 (s, 1, C_6–H), 5.6 (br s, 2, $C_{2',3'}$–OH), 5.9—6.5 (m, 3, $C_{2',3'}$–H), 6.6 (br s, 2, $C_{1'}$–H); Found: C, 47.81; H, 5.89; N, 13.87%. Calcd for $C_8H_{12}N_2O_4$: C, 48.02; H, 6.04; N, 13.99%.

*1-(2′,3′-Dihydroxypropyl)-5-fluorouracil (**4**).* 5-Fluorouracil (1.29 g, 10 mmol) and glycidol (0.74 g, 10 mmol) was reacted in the way described in the case of **3**. The obtained product was recrystallized from a mixture of benzene–ethanol (9 : 1) to give the compound **4** (0.76 g, (38%)) as colorless needles.

Mp. 147—149°C; UV $\lambda_{max}^{H_2O}$ 210 mμ (ε=9800), 275 mμ (ε=9000), IR: 3350 (OH), 1720, 1650 (fluorouracil ring) and 1070, 1020 (primary and secondary alcohol C–O); NMR (DMSO-d_6) τ −1.18 (br s, 1, N_3–H), 2.2 (d, 1, C_6–H), 5.2 (br s, 2, $C_{2',3'}$–OH), 6.0—6.6 (m, 3, $C_{2',3'}$–H), 6.7 (br s, 2, $C_{1'}$–H); Found: C, 41.42; H, 4.51; N, 13.76%. Calcd for $C_7H_9N_2O_4F$: C, 41.18; H, 4.44; N, 13.72%.

BULLETIN OF THE CHEMICAL SOCIETY OF JAPAN, VOL. 46, 1573—1575 (1973)

Bildung von 1,4-Bis(2,2′-biphenylylen)-1,3-butadien[1)]

Masahiro MINABE und Kazuo SUZUKI

Abteilung für Chemische Industrie der Universität Utsunomiya, Ishii-cho, Utsunomiya 321-31

(Eingegangen am 27. Juni 1972)

Bekanntlich wird bei der Michaelschen Reaktion von 9,9′-Bifluorenyliden (**5**) mit Fluoren (**1a**) in Äthanol in Gegenwart von Natrium-äthylat als Katalysator neben 9,9′:9′,9″-Terfluorenyl, Schmp 293° (zers) (**8b**) auch 1,4-Bis(2,2′-biphenylylen)-1,3-butadien (**6a**)[2)] in kleiner Menge gebildet.[3)] 1,4-Bis(4,4′-dibrom-2,2′-biphenylylen)-1,3-butadien sowie 1-(4,4′-Dibrom-2,2′-biphenylylen)-4-(2,2′-biphenylylen)-1,3-butadien sind bereits als Nebenprodukte der Reaktion von 2,7,2′,7′-Tetrabrom-9,9′-bifluorenyliden mit **1a** erhalten worden.[4)] Ferner ist bekannt, dass durch Erhitzung unter Rückfluss von Fluorens in Gegenwart einer Base in Äthanol unter Durchleitung von Sauerstoff entsprechende 1,3-Butadiene gebildet werden.[5)]

Nachdem die Michaelsche Reaktion von **5** mit **1a** wiederholt worden war und die Produkte überprüft worden waren, wurde festgestellt, dass 9,9′:9′,9″-Terfluorenyl, Schmp 257° (zers) (**8a**), **8b**, **6a**, 9-Äthylidenfluoren (**3**),[6)] Fluorenon (**2a**), und 1,6-Bis(2,2′-biphenylylen)-1,3,5-hexatrien (**7**)[7)] isoliert wurden.

Falls auf einem ähnlichen Weg wie Stahrfoss[5a)] in Gegenwart von Kaliumhydroxyd **1a** in Äthanol aufgelöst und bei Durchleitung von Sauerstoff unter Rückfluss erhitzt wurde, wurden **6a**, **7**, **2a**, **3**, und **1a** erzeugt, während jedoch nur **1a** zurückgeblieben war, wenn dieselbe Reaction in Stickstoff-Atmosphäre ausgeführt oder Äthanol statt Methanol eingesetzt wurde.

In einem anderen Fall wurde durch die Reaktion von **1a** mit Acetaldehyd in Stickstoff-Atmosphäre in Gegenwart einer Base in Methanol **3** in kleiner Menge isoliert.[8)] Da jedoch **6a** nicht durch die Einwirkung von Lösungsmitteln ausser Äthanol (z. B. Methanol und Pyridin) gebildet wird, ist anzunehmen, dass das Reaktionsprodukt **3** von **1a** mit Äthanol ein Zwischenprodukt bei der Bildung von **6a** sein dürfte. Also sollte ein Teil des Äthanols als Lösungsmittel infolge der Gegenwart von Sauerstoff[9)] und Base zu Acetaldehyd oxydiert und weiter durch die Kondensation

1) Studien in der Fluoren Reihe. XXIX. XXVIII Mitt.: M. Minabe und K. Suzuki, Dieses Bulletin, **45**, 3196 (1972).

2) J. M. Edinger und A. R. Day, *J. Org. Chem.*, **36**, 240 (1971).

3) L. A. Pinck und G. E. Hilbert, *J. Amer. Chem. Soc.*, **68**, 2014 (1946).

4) K. Suzuki, M. Minabe, M. Fujimoto, und N. Nohara, Dieses Bulletin, **42**, 1609 (1969).

5) a) M. K. Stahrfoss, *Bull. Soc. Chim. Fr.*, (4), **29**, 142 (1921). b) Nach irgendeinem der obigen beiden Verfahren wurden verschiedene 1,3-Butadiene erhalten. Für Fluor-Deriv.: M. Minabe, A. Tanaka, M. Wakui, und K. Suzuki, Dieses Bulletin, **44**, 1614 (1971). Für Chlor-Deriv.: M. Minabe und K. Suzuki, Unveröffentlicht. Für Brom-Deriv.: K. Suzuki, *Nippon Kagaku Zasshi*, **72**, 825 (1951); **75**, 711, 793 (1954); K. Suzuki und S. Kajigaeshi, *Yuki Gosei Kagaku Kyokai Shi*, **16**, 82, 304 (1958). Für Jod-Deriv.: M. Minabe und K. Suzuki, Dieses Bulletin, **45**, 3196 (1972).

6) K. L. Schoen und E. I. Becker, *J. Amer. Chem. Soc.*, **77**, 6030 (1955).

7) H. Fischer und H. Fischer, *Chem. Ber.*, **99**, 658 (1966).

8) R. F. Schultz und C. F. Smullin, *J. Amer. Chem. Soc.*, **62**, 2904 (1940).

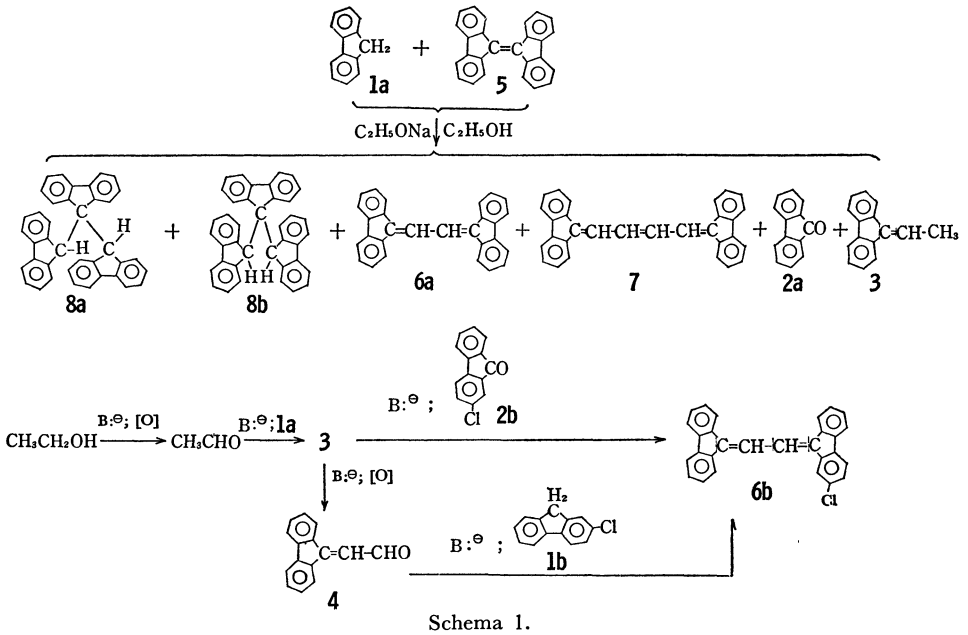

Schema 1.

mit **1a** zu **3** geführt werden.

Durch Erhitzung unter Rückfluss von **3** und 2-Chlorfluorenon (**2b**) in Methanol–Kali–Lösung in Stickstoff-Atmosphäre wird 1-(4-Chlor-2,2′-biphenylylen)-4-(2,2′-biphenylylen)-1,3-butadien (**6b**) in einer Ausbeute von 17% erhalten, während dieselbe jedoch nicht durch die Reaktion mit 2-Chlorfluoren (**1b**) beobachtet worden ist.

Dieses Experiment ergab, dass als ein Bildungsweg von **6a** die Kondensation von **2a** mit **3** in Betracht gezogen wird. Es ist jedoch anzunehmen, dass infolge der Existenz von Sauerstoff in dem Reaktionssystem unter den Bedingungen der Michaelschen Reaktion **3** oxydiert wurde und so sich dessen Oxydationsprodukt an der Bildung von **6a** beteiligt hatte. In der Tat wurde zwar durch die Erhitzung unter Rückfluss von der Lösung **3** in Methanol in Gegenwart von Kaliumhydroxyd in Stickstoff-Atmosphäre nur **3** wiedergewonnen, jedoch entstand **7** in kleiner Menge durch die Reaktion mit **3** bei Durchleitung von Sauerstoff.

Durch die Reaktion von β-(9-Fluorenyliden)acetaldehyd (**4**),[10] welches aus **3** über β-(9-Fluorenyliden)-äthanol[11] in 2-stufiger Oxydation synthetisiert ist, wurde neben **1b** **6b** in einer Ausbeute von 77% erhalten; und durch Reaktion von **3** mit **4** wurde entsprechendes Kondensationsprodukt **7** isoliert.

Aus den obigen Ergebnissen lässt sich schliessen, dass die Bildung von 1,3-Butadienen nach dem dargestellten Schema abläuft. Ein Teil des Äthanols wurde zu Acetaldehyd oxydiert und dann durch Kondensation mit Fluorens zu 9-Äthylidenfluorens übergeführt. Durch die Reaktion von diesem 9-Äthylidenfluorens mit Fluorens wurden entsprechende 1,3-Butadiene gebildet, und durch die Oxydation von diesen 9-Äthylidenfluorens wurde entsprechendes Aldehyd gebildet, welches durch die Kondensation mit Fluorenons schliesslich 1,3-Butadiene gebildet hatte. Es ist jedoch nicht klar, welche von beiden Reaktionen unter den experimentallen Bedingungen der Michaelschen Reaktion zuerst abläuft.

Beschreibung der Versuche

Die Schmelzpunkte sind unkorrigiert. Sämtliche IR Spektren wurden nach der KBr-Methode gemessen. Zur Messung der NMR-Spektren war JEOL-60HL (Japan Electron Optics Lab. Co., Ltd.) (TMS als innerer Standard) in CCl_4 massgebend.

Michaelsche Additionsreaktion von ***5*** *mit* ***1a***: Eine Mischung von **5** (3.28 g, 10 mMol), **1a** (1.99 g, 12 mMol), Natriumäthylat (5.0 g), und absolutem Äthanol (50 ml) wurde in einem Bombenrohr bei 97—100 °C 11 Std erhitzt. Die nach Abkühlung auf Raumtemperatur abgeschiedenen Kristalle wurden filtriert und aus Pyridin, Benzol, und Essigsäureäthylester umkristallisiert und **8a** (2.1 g, 43%), Schmp 254—256 °C (zers), **8b** (0.30 g, 6%), Schmp 292—293 °C (zers), **6a** (0.08 g, 2%) in rotgelblichen Nadelkristallen, Schmp 365 °C (zers) (Lit.[2] Schmp 381 °C), und **7** in geringer Menge, in rötlichen Nadelkristallen, Schmp 330 °C (zers) (Lit.[12] Schmp 331.5—333°C), erhalten.

Der nach dem Zusatz von Wasser in die Äthanol-Mutterlauge abgeschiedene Niederschlag wurde der nach Trocknung über Benzol-Aluminiumoxyd chromatographiert, wobei aus den Fraktionen **3** (0.02 g, 1%), Schmp 102—104 °C (Pikrät, Schmp 155—156 °C), und **1a** (0.09 g, 5%), Schmp 112—114 °C, erhalten wurden. Aus dem gelblichen Adsorptionsband wurde mit Äthanol **2a** (0.1 g, 2%), Schmp 83—85°C, eluiert.

Reaktion von ***1a***. *1) Einwirkung von Sauerstoff in Äthanol*: Die Lösung von **1a** (8.3 g, 50 mMol) und Kaliumhydroxyd (5.0 g) in Äthanol (100 ml) wurde unter Durchlei-

9) Im allgemeinen wird die Michaelsche Additionsreaktion dieser Art bei Vorhandensein von Luft vorgenommen.

10) E. D. Bergmann, H. W.-Feilchenfeld, und N. Mandel, *Vietnamica Chim. Acta*, **1966**, 129; *Chem. Abstr.*, **72**, 3278 (1970).

11) R. Kuhn und U. Breyer, *Ann. Chem.*, **661**, 173 (1963).

12) E. F. Magoon und L. Zechmeister, *J. Amer. Chem. Soc.*, **77**, 5642 (1955).

tung von Säuerstoff 10 Std unter Rückfluss erhitzt, wobei die abgeschiedenen Rot-Kristalle aus Pyridin umkristallisiert wurden, so dass **6a** (0.21 g, 2.4%) und **7** (0.01 g, 0.1%) erhalten wurden. Bei der Behandlung der Äthanol-Mutterlauge in der gleichen Weise wie oben konnten **2a** (0.17 g, 1.8%), **3** (1.19 g, 12.4%), und **1a** (6.68 g, 80.5%) isoliert werden.

2) Reaktion mit Acetaldehyd: In die Mischung von Kaliumhydroxyd (5.0 g) und **1a** (8.3 g) in Methanol (130 ml) wurde Methanol-Lösung (10 ml) mit Acetaldehyd (2.5 g) unter säuerstoff-frei getrocknetem Stickstoff 20 Min lang getropft. Weiter wurde ein langer Rückflusskühler mit Eiswasser zugefügt und 40 Min unter mildem Rückfluss erwärmt, wonach durch Sublimation und Umkristallisation **3** (0.016 g, 0.2%) und **1a** (6.96 g, 84%) isoliert wurden.

*Reaktion von **3**.* *1)* Die Lösung von **3** (3.84 g, 20 mMol) in Methanol (150 ml) mit Kaliumhydroxyd (5.0 g) wurde unter Durchleitung von Sauerstoff 10 Std unter Rückfluss erhitzt, woraus ein abgeschiedenes rotes Produkt nach der Umkristallisation aus Pyridin **7** (0.17 g, 5%) lieferte. Aus der Methanol-Mutterlauge liessen sich nach der üblichen Aufbereitung **2a** (0.10 g, 3%) und **3** (2.58 g, 67%) gewinnen.

*2) Reaktion mit **2b***: Die Lösung von Methanol (150 ml) mit Kaliumhydroxyd (5.0 g) wurde nach dem Zusatz von **3** (1.92 g, 10 mMol) und **2b** (2.15 g, 10 mMol) in Stickstoff-Atmosphäre 10 Std unter Rückfluss erhitzt. Der abgeschiedene Niederschlag wurde abgesaugt und aus Pyridin umkristallisiert, wobei **6b** (0.63 g, 17%), Schmp 370—372 °C (zers), erhalten wurde. Gef: C, 86.43; H, 4.18%. Ber für $C_{28}H_{17}Cl$: C, 86.48; H, 4.41%.

Aus der Methanol-Mutterlauge wurden **3** (1.57 g, 82%) und **2b** (1.72 g, 80%) gewonnen.

*Oxydation von **3** mit Selendioxyd*: **3** (10.0 g) und Selendioxyd (3.2 g) wurden in verfeinerter Essigsäure (160 ml) 1 Std unter Rückfluss erhitzt. Dann wurde das von Selen befreite Filtrat mit Wasser verdünnt und mit Benzol extrahiert, dann wurde die Benzolschicht über Aluminium-oxyd chromatographiert, wobei aus dem rötlichen Aluminiumoxyd-Adsorptionsband β-(9-Fluorenyliden)äthanol (1.3 g, 12%), Schmp 146—147 °C in einem farblosen Nadelkristall, erhalten wurde. Mass: m/e 208 (M^+). IR: 3205 cm^{-1} (–OH).

Das weitere Acetyl-Derivat wurde durch Einwirkung von Essigsäureanhydrid in wasserfreiem Benzol erhalten. Nach der Umkristallisation aus Äthanol wurden farblose Nadelkristalle, Schmp 97—98 °C, gebildet. Gef: C, 81.58; H, 5.64%. Ber für $C_{17}H_{14}O_2$: C, 81.72; H, 5.79%. Mass: m/e 250 (M^+). IR: 1735 cm^{-1} (>C=O). NMR: δ 2.05 (s, 3H), 5.16 (d, 2H), 6.53 (t, 1H), und 7.03—7.68 ppm (m, 8H).

Oxydation von β-(9-Fluorenyliden)äthanol mit Mangandioxyd: Eine Probe von 0.9 g wurde in Benzol (250 ml) gelöst und durch eine Säule (etwa 4 cm) mit Mangandioxyd (15 g) (E. Merck, zur Synthesis) laufen lassen. Nach Trennung und Reinigung durch Chromatography über Aluminiumoxyd und Umkristallisation wurden **4** (0.33 g, 37%), Schmp 116.5—117.5 °C, in einem gelblichen Nadelkristall und **2a** (0.1 g, 10%) isoliert. IR von **4**: 1656 cm^{-1} (–CHO).

2,4-Dinitrophenylhydrazon von **4**, rötliche Nadeln vom Schmp 324—326 °C (zers). Gef: C, 65.12; H, 3.53; N, 14.60%. Ber für $C_{21}H_{14}N_4O_4$: C, 65.28; H, 3.65; N, 14.50%.

*Reaktion von **4** mit **1b***: Die Lösung von **4** (206 mg, 1 mMol) und **1b** (200.5 mg, 1 mMol) in Methanol (15 ml) mit Kaliumhydroxyd (500 mg) wurde in Stickstoff-Atmosphäre 40 Min unter Rückfluss erhitzt, wobei nach der Umkristallisation von abgeschiedenen Kristallen aus Pyridin **6b** (300.9 mg, 77%) erhalten wurde. Ferner wurde aus der Methanol-Mutterlauge **4** (3.0 mg, 1%) zurückgewonnen.

*Reaktion von **4** mit **3***: Bei der Reaktion von **4** mit **3** (192 mg, 1 mMol) anstelle von **1b** bei der obigen Reaktion wurden **7** (189.9 mg, 50%), **3** (69.6 mg, 36%), und **4** (3.1 mg, 1%) isoliert.

BULLETIN OF THE CHEMICAL SOCIETY OF JAPAN, VOL. 46, 1575—1576 (1973)

The NQR Spectrum and Structure of Hexachloropentafulvene[1)]

Israel AGRANAT,[2a)] Michael HAYEK,[2b)] and David GILL[2b,c)]

The Hebrew University of Jerusalem, Jerusalem, Israel

(Received July 10, 1972)

Pure nuclear quadrupole resonance (NQR) studies on molecular crystals have been applied to the determination of distribution of molecular electrons.[3-6)] Recently, West and his co-workers have successfully applied NQR spectroscopy to the study of the perchlorocarbon series.[7-9)] The validity of this method depends on correct assignments of the wealth of resonance (obtained experimentally) to the different chlorine atoms present in the molecule under study. We wish to report the ^{35}Cl NQR spectra of hexachloropentafulvene (I)[10,11)] and 3,4-bis(dichloromethylene)-1,2-dichlorocyclobutene (II)[12)] and their analyses in

1) Fulvenes and Thermochromic Ethylenes. Part 76.

2) (a) Department of Organic Chemistry, to whom enquiries should be addressed. (b) Department of Physics. (c) Present address: Scientific Research Laboratory, Ford Motor Company, Dearborn, Michigan 48121, USA.

3) T. P. Das and E. L. Hahn, "Nuclear Quadrupole Resonance Spectroscopy," Suppl. **1** in "Solid State Physics, Advances in Research and Applications," F. Seitz and D. Turnbull, Eds., Academic Press, New York, N.Y. (1958), p. 119.

4) H. O. Hooper and P. J. Bray, *J. Chem. Phys.*, **33**, 334 (1960).

5) G. Semin and E. I. Fedin in "The Mössbauer Effect and Its Applications in Chemistry," V. I. Gol'danskii, Ed., Consultants Bureau, New York, N.Y. (1964). pp, 68—119.

6) E. A. C. Lucken, "Nuclear Quadrupole Coupling Constants," Academic Press, New York, N.Y. (1969).

7) A. Roedig, R. Helm, R. West, and R. M. Smith, *Tetrahedron Lett.*, **1969**, 2137.

8) R. M. Smith and R. West, *ibid.*, **1969**, 2141.

9) R. M. Smith and R. West, *J. Org. Chem.*, **35**, 2681 (1970).

10) K. Dinbergs, Ph. D. Thesis, Purdue University, 1955; *Diss. Abstr.*, **16**, 1063 (1956).

11) E. T. McBee, E. P. Wesseler, D. L. Crain, R. Hurnaus, and T. Hodgins, *J. Org. Chem.*, **37**, 683 (1972).

12) A. Fujino, Y. Nagata, and T. Sakan, This Bulletin, **37**, 295 (1965).

terms of the dipolar and spatial structures of these nonbenzenoid cyclic conjugated chlorocarbons.[13,14]

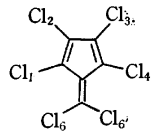

I

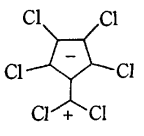

Ia

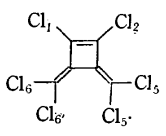

II

The spectrum of I consists of the following six frequencies: 36.783, 37.163, 37.805, 38.086, 38.179, and 38.303 MHz. They fall into two groups, A and B, centered at 37.0 MHz (2 lines) and 38.1 MHz (4 lines), respectively. The large frequency separation between the two groups of lines (>1 MHz) indicates the presence of at least two types of chlorine atoms. The splitting within each group may still be attributed to solid-state intermolecular forces.[5,6,15] In order to draw any conclusions from the NQR spectrum pertaining to the dipolar character or to the spatial structure of I, a correct assignment of the resonances of the NQR spectrum is necessary. Out of the various possible alternatives, one point emerges clearly: the frequencies of Cl_2 and Cl_3 are represented by group A and not by Group B. This assignment is based on the analysis of the NQR spectra of a series of 1,2,3,4-tetrachlorofulvenes and related substances, which indicate that the ^{35}Cl resonance of Cl_2 and Cl_3 appears consistently in the 36.5 MHz region, and is not affected by the substituents at the exocyclic (6,6′) positions.[16] Thus group B should be assigned to Cl_1, Cl_4, Cl_6, and Cl_6'. The alternative assignment suggested by Hashimoto and Mano[17] which attributed group A to Cl_6 and Cl_6' and group B to Cl_1, Cl_2, Cl_3, and Cl_4 does not seem to be justified. They claimed that their assignment was supported by the contribution of the dipolar, "aromatic" structure Ia to the ground state of I. The experimental dipole moment of I in (cyclohexane) solution (1.00D),[18] *does not* indicate any substantial contribution of Ia in the ground state. In any event, the extent of such a contribution cannot account for a decrease in the resonance frequencies of Cl_6 and Cl_6'. Moreover, such a contribution should cause not only a decrease in the electron density of the p_π orbitals of Cl_6 and Cl_6', but also an increase in the respective electron densities of Cl_1, Cl_2, Cl_3, and Cl_4. As shown above, there is no evidence of a shift to higher frequencies of Cl_2 and Cl_3 which should have accompanied such an increase. We conclude that the NQR spectrum of I does not reveal the presence of a contribution of Ia.

The most striking feature in the NQR spectrum of I is the shift to higher frequencies (38.1 MHz region) of the two chlorine atoms "*ortho*" to the "fulvenic" double bond, Cl_1 and Cl_4. The shift is even greater than the one observed in the ^{35}Cl NQR spectrum of octachloropentafulvalene (37.7 MHz region) and interpreted as due to noncovalent intramolecular interactions of the bucking C–Cl groups.[19] This shift (in I) could be explained in terms of the strong perturbations of the electrons of Cl_1 and in the C_1–Cl_1 bond produced by the C_6–Cl_6 dipole.[20] The spatial relationship between Cl_1 and Cl_6 resembles somewhat the *peri*-relationship of the chlorine atoms in positions 1 and 8 in the naphthalene nucleus. Accordingly, an analogy may be drawn from the ^{35}Cl NQR spectrum of 1,2,3,6,7,8-hexachloronaphthalene, in which the resonance representing Cl_1 and Cl_8 appears at *ca.* 38.2 MHz (77 K).[21]

In contrast to I, the ^{35}Cl NQR spectrum of its pseudoalternant isomer II (3 lines at 36.358, 37.835, and 37.971 MHz) was not irregular. For II, Hashimoto and Mano reported six lines falling into two groups centered at *ca.* 36.4 MHz (two lines) and 38.0 MHz (four lines).[17] In particular, the 36.4 MHz resonance due to the chlorine atoms attached directly to the cyclobutene ring (Cl_1 and Cl_2) appears in the normal region for such chlorine atoms. The absorption is thus not shifted to higher frequencies by the electrostatic field of the C_6–Cl_6 and C_5–Cl_5 dipoles. The absence of such an effect (relative to the respective effect observed in I) may be explained by the different geometry of the molecule imposed by the cyclobutene ring. Consequently, the distances between the C_6–Cl_6 dipole and Cl_1 (and the C_1–Cl_1 bond) are larger and their relative orientation is different from that in I.

On the basis of the NQR spectrum of I we predict a small distance between Cl_1 and Cl_6.

We are greatly indebted to Dr. K. Mano of the Research Institute for Atomic Energy, Osaka City University, Sumiyoshiku, Osaka, Japan, for conveying to us his results prior to publication.

13) The measurements were taken using a regenerative detector at 80 K, and were observed on the oscilloscope screen with a signal-to-noise ratio of 10: 1, the error being ~0.001 MHz.

14) D. Gill, M. Hayek, Y. Alon, and A. Simievic, *Rev. Sci. Instr.*, **38**, 1583 (1967).

15) E. A. C. Lucken, *Tetrahedron Suppl.*, 2, **19**, 123 (1963).

16) I. Agranat, D. Gill, M. Hayek, R. M. J. Loewenstein, and E. D. Bergmann, Abstracts of Papers, International Symposium on the Chemistry of Nonbenzenoid Aromatic Compounds (ISNA), Sendai, Japan, August 1970, p. 199.

17) M. Hashimoto and K. Mano, This Bulletin, **45**, 706 (1972).

18) I. Agranat, H. Weiler-Feilchenfeld, and R. M. J. Loewenstein, *Chem. Commun.*, **1970**, 1153.

19) I. Agranat, D. Gill, M. Hayek, and R. M. J. Loewenstein, *J. Chem. Phys.*, **51**, 2756 (1969).

20) E. Scrocco in "Advances Chemical Physics", Vol. V, I. Prigogine, Ed., Interscience Publishers, New York, N. Y., 1963, p. 319.

21) I. P. Biryukov, M. G. Voronkov, and I. A. Safin, "Tables of Nuclear Quadrupole Resonance Frequencies," Israel Program for Scientific Translations, Jerusalem (1969), p. 59.

BULLETIN OF THE CHEMICAL SOCIETY OF JAPAN, VOL. 46, 1577—1578 (1973)

Electronic Properties of the Neutral Radicals from Phenothiazines

Mamoru KAMIYA, Takehiro MITSUI, and Yukio AKAHORI
Shizuoka College of Pharmacy, Oshika, Shizuoka 420

(Received June 15, 1972)

In the course of numerous studies of phenothiazine radicals, it has been found by the ESR method that a neutral phenothiazinyl radical is produced from phenothiazine by photochemical and chemical oxidations.[1-4] However, little attention has been paid to the substituted radicals or to the electronic spectrum of the non-substituted radical itself. In this note we shall discuss the assignment of the electronic spectra of the phenothiazinyl radicals, with reference to the ESR spectra and the effect of air-contact upon the radical decay, and with the aid of a theoretical calculation of the electronic spectra.

Experimental and Calculation

1-Methylphenothiazine and 1-methoxyphenothiazine were prepared by the thionation of the corresponding diarylamines.[5] The compounds used were purified by repeated sublimations under a high vacuum. Two different methods, that is, the chemical method of Tsujino[4] and the photochemical method of Shine and Mach,[1] were used for the radical formation because such by-products as the phenothiazine nitroxide radical and phenothiazine dimers, which would be less destroyed by air-contact than the phenothiazinyl radical, are likely to be produced by these methods. The solvent used in the chemical oxidation was prepared by mixing equimolar amounts of spectro-grade dimethyl sulfoxide and acetic anhydride. The radical solutions were prepared by dissolving materials in degassed solvents. The solutions were filtered by means of a glass filter and directly led to a UV cell or an ESR tube. All of these procedures were performed in a vacuum line. The electronic absorption spectra were recorded with a Hitachi EPS-2 spectrophotometer using a 10 mm cell. The ESR spectra were obtained with a Nippon-Denshi JES-3BS-X spectrometer with 100 KHz modulation.

The calculations of the electronic spectra of phenothiazinyl radicals were performed by means of the open-shell SCF method[6] with limited CI. The two-center Coulomb integrals were evaluated by means of the Nishimoto-Mataga formula, and the core-resonance integrals by means of the variable β-core method. The CI calculations were done including 24 singly-excited configurations composed of $(i\rightarrow k)_\alpha$, $(i\rightarrow k)_\beta$, $(i\rightarrow m)$, and $(m\rightarrow k)$, where φ_m=half-occupied orbital; $i=m$-3, m-2, m-1, and $k=m+1$, $m+2$, $m+3$; the notations of $(i\rightarrow k)_\alpha$ and $(i\rightarrow k)_\beta$ were taken from Ref. 7.

Results and Discussion

As is shown in Fig. 1, new absorption maxima appear at 462 and 615 nm upon the chemical oxidation of phenothiazine. The longer-wavelength band has a shoulder near 645 nm. The λ_{nm}^{max} values for 1-methylphenothiazine were 464 and 610 nm. The absorption curve changes in the wavelength region shorter than 400 nm had to be excluded on account of the largely overshadowing absorption of the parent molecules. These solutions exhibited the strong ESR spectra due to the corresponding neutral radicals. The ESR spectrum of the 1-methylsubstituted radical shown in Fig. 2 is reported for the first time here. Though not completely resolved, the spectrum could be analyzed with $a^N=7.0$—7.2, $a_{3,7}^H=3.5$, $a_9^H=2.2$—2.5, and $a_{2,8}^H=0.7$—0.9 gauss. These values are not very different from the values for the non-substituted radicals.[2,4] On the other hand, only a weak absorption with λ_{nm}^{max} ~470 nm appeared upon the chemical oxidation of 1-methoxyphenothiazine, and a weak ESR signal was observed only after the temperature had been lowered to −30°C.

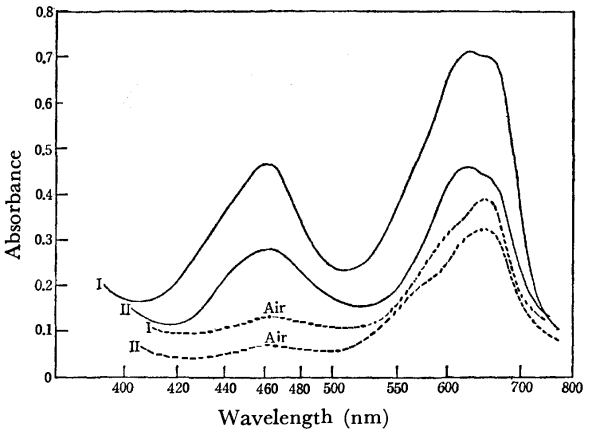

Fig. 1. The electronic spectra observed at the formation of phenothiazinyl radicals in a degassed DMSO+Ac_2O solution. (I) non-substituted and (II) 1-methyl-substituted phenothiazines.

After the exposure of the solutions to air, the absorbance of the longer-wavelength peak showed considerable values even when no ESR spectrum of the radicals could be detected clearly. At this stage, the location of the λ_{nm}^{max} of the longer-wavelength band shifted to 640—645 nm, just in the region where a shoulder had been observed in the initial spectrum. The solutions which were exposed to air until the ESR spectrum could not be detected were submitted to thin-layer chromatography using petroleum ether–ether (2 : 1) as the developing solvent. The 1,10′- and 3,10′-dimers of phenothiazine were detected by

1) H. J. Shine and E. E. Mach, *J. Org. Chem.*, **30**, 2130 (1965).
2) B. C. Gilbert, P. Hanson, R. O. C. Norman and B. T. Sutcliffe, *Chem. Commun.*, **1966**, 161.
3) C. Jackson and N. K. D. Patel, *Tetrahedron Lett.*, **1967**, 2255.
4) Y. Tsujino, *ibid.*, **1968**, 4111.
5) S. P. Massie and P. K. Kadaba, *J. Org. Chem.*, **21**, 347 (1956).
6) H. C. Longuet-Higgins and J. A. Pople, *Proc. Phys. Soc. Ser. A*, **68**, 591 (1955).
7) A. Ishitani and S. Nagakura, *Theoret. Chim. Acta*, **4**, 236 (1966).
8) Y. Tsujino, *Nippon Kagaku Zasshi*, **90**, 304 (1969).

Table 1. Observed and calculated results of electronic spectra

a) Phenothiazinyl Radical

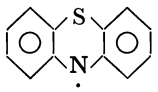

ΔE_{obsd} (eV)	Without CI		With CI	
	ΔE_{calcd} (eV)	f_{calcd}	ΔE_{calcd} (eV)	f_{calcd}
~2.02	2.31	0.09	1.59	0.11
2.69—2.70	2.72	0.52	1.90	0.01
	2.88	0.07	2.21	0.05
			2.28	0.04
			2.49	0.08
			2.87	0.27

b) 1-Methyl-phenothiazinyl Radical

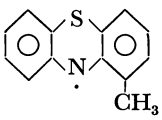

	Without CI		With CI	
	ΔE_{calcd} (eV)	f_{calcd}	ΔE_{calcd} (eV)	f_{calcd}
~2.03	2.28	0.12	1.32	0.06
2.68—2.69	2.72	0.45	1.34	0.05
	3.89	0.09	1.89	0.01
			2.43	0.10
			2.63	0.15
			2.78	0.41

*) Parametrizations are as follows:

		C	N	S	H_3
The valence-state I_p and E_A in eV:	I_p	11.16	14.12	23.59	10.256
	E_A	0.03	1.78	10.54	0.93

The core-resonance integrals (β_{rs}) in eV:

$\beta_{C-C}=-0.51\,P_{C-C}-1.84$, $\beta_{C-N}=-0.53\,P_{C-N}-2.02$, $\beta_{C-S}=-0.33\,P_{C-S}-1.80$, $\beta_{C-H_3}=-4.111$.

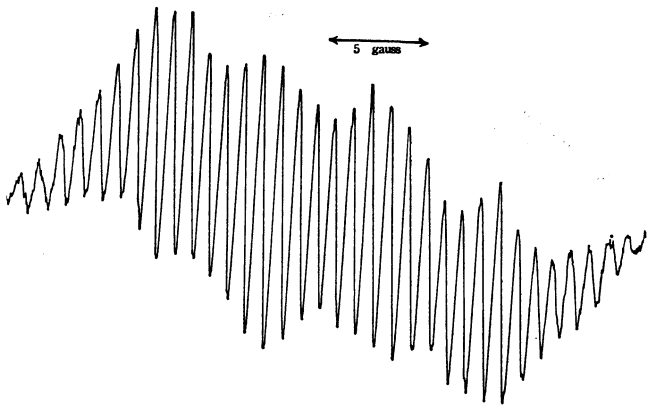

Fig. 2. The ESR spectrum of 1-methylphenothiazinyl radical produced in DMSO+AC_2O at room temperature.

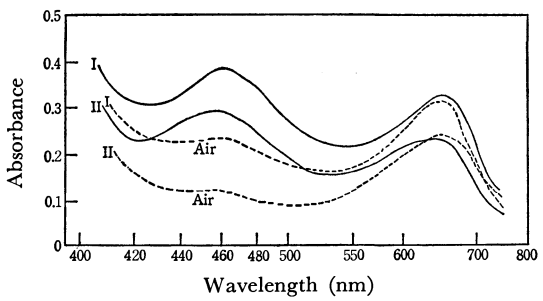

Fig. 3. The electronic spectra observed at the formation of phenothiazinyl radicals in a photoirradiated ethanol solution. (I) non-substituted and (II) 1-methyl-substituted phenothiazines.

means of the spots with R_f=0.8—0.9 and 0.4—0.5 respectively, in accordance with the findings of Tsujino.[8] The 3,10'-dimer of 1-methylphenothiazine was also detected with the spot, R_f=0.3—0.4. The spots, R_f=0.0—0.2, which are probably related to the polymerized by-products, were also found in the two systems. These results serve to correlate the 640—645 nm absorption with the radical-decay products.

In the photochemical oxidations, the λ_{nm}^{max} values of the new absorption maxima are 459 and 650 nm for the phenothiazine solution, and 462 and 653 nm for the 1-methylphenothiazine solution. When these solutions were exposed to air until the ESR signal could not be detected, the longer-wavelength bands alone retained considerable values of absorbance. According to the results of the adopted method of irradiation using an Ushio XS-501A xenon lamp, the changes in the absorption spectrum of the 1-methoxyphenothiazine solution took place very slowly, to the extent that a weak absorption maximum around 650 nm was found after 15 hr's irradiation.

The calculated data of the electronic spectra indicate the existence of weak transitions below 2 eV which might be masked by the strong absorptions of the radical-decay products. This trend appears to be promoted remarkably by the CI calculation. The calculated data both with and without CI suggest that moderately intense transitions of the neutral radicals exist in the region of the shorter-wavelength bands which are observed upon the radical formations.

The authors wish to thank Mr. Takeshi Akiyama for his co-operation in making the spectroscopic measurements. Thanks are also due to Dr. Michiya Itoh of the University of Tokyo and Dr. Fumihiko Hirota of Shizuoka University for useful guidance and discussion.

BULLETIN OF THE CHEMICAL SOCIETY OF JAPAN, VOL. 46, 1579—1580 (1973)

2,2-Dimethyl[7](2,6)pyridinophane and the Flipping of Its Heptamethylene Chain

Shinsaku FUJITA, Kazuo IMAMURA, and Hitosi NOZAKI

Department of Industrial Chemistry, Kyoto University, Sakyo-ku, Kyoto 606

(Received October 20, 1972)

The NMR spectra of heterophanes give useful information on the stereochemistry of the polymethylene chains incorporated.[1-8] The present report will deal with two 2,2-dimethyl derivatives of [7](2,6)pyridinophane (I).

The methylation of [7](2,6)pyridinophan-1-one (II) with potassium *t*-butoxide and methyl iodide gave 2,2-dimethyl[7](2,6)pyridinophan-1-one (III), the Huang Minlon reduction of which then afforded 2,2-dimethyl-[7](2,6)pyridinophane (IV).

At room temperature, the NMR spectrum of IV (Fig. 1) showed the singlet signal of 1-methylene at δ 2.58 and the singlet signal of *gem*-dimethyl at δ 0.84. The two-proton multiplet centered at δ 0.01 was assigned to the C-4 protons by analogy with [7]-(2,6)pyridinophane (I) itself.[5] In the most reasonable crown-type conformation (V) for IV, one proton (H_x) on C-4 was forced into the π-cloud and should be subject to anisotropic shielding due to the pyridine ring. At low temperatures (−87.5 °C and −111 °C), the two methyl groups, finding themselves in different environments, showed two broad singlets, at δ 1.04 and δ 0.56 respectively (Fig. 1). The AB spin system of 1-methylene showed an average singlet peak at room temperature, but a typical AB quartet at low temperatures. The C-4 protons were also found to exhibit a one-proton signal at δ −1.44.

These facts indicated that the conformation of IV was frozen to the extreme conformer (V) at low temperatures. The estimated energy barriers ($\Delta G_c^{\ddagger}$) for the conformational change (V⇄V′) are shown in Table 1, as well as the coalescence temperature (T_c). The NMR spectra of the ketone (III) was also temperature-dependent. The signal of the methyl groups appeared as a singlet (δ 1.21) at room temperature, broadened at the coalescence temperature (−61.0 °C) and then reappeared as two broad singlets (δ 1.26 and δ 1.06) at −94.0 °C). The estimated $\Delta G^{\ddagger}_c$ value is shown in Table 1.

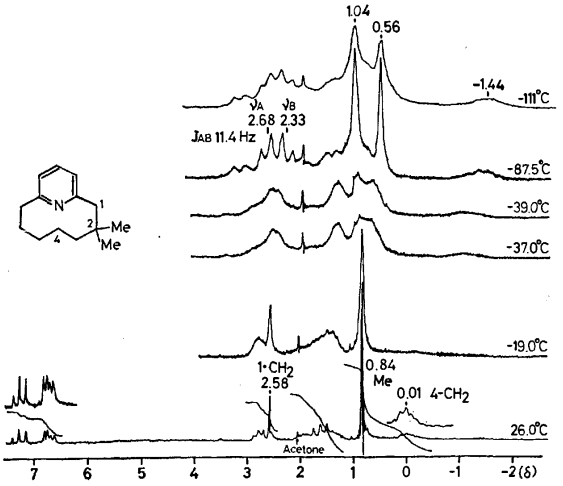

Fig. 1. The Dynamic NMR Spectra of IV (60 MHz in $CFCl_3$, TMS Internal Standard)

I R=H, X=H_2
II R=H, X=O
III R=Me, X=O
IV R=Me, X=H_2

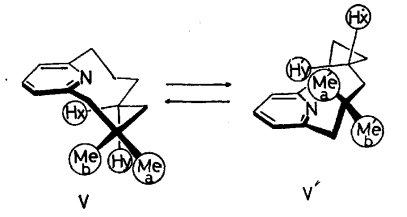

Experimental

2,2-Dimethyl[7](2,6)pyridinophan-1-one (III). A solution of [7](2,6)pyridinophan-1-one (II) (567 mg, 3.0 mmol)[5] in *t*-butyl alcohol (5 ml) was added to a solution (10 ml) of potassium *t*-butoxide (from 4.0 g of potassium). The mixture was heated under reflux for 1 hr. After cooling, methyl iodide (10 ml) was added in one portion, and then the mixture was heated at reflux for 19 hr. The reaction mixture was poured into water and extracted with ether. The combined ethereal extracts were dried over sodium sulfate and concentrated *in vacuo*. The concentrate was methylated once more with potassium *t*-butoxide (from 3.0 g of potassium) and methyl iodide (10 ml). The crude product was distilled, giving III as a colorless oil (441 mg, 68%); bp 77 °C/0.07 mmHg. IR (neat): 3075, 2960, 2927, 2875, 1679, 1590, 1574, 1474, 1458, 1440, 1379, 1354, 1322, 1298, 1245, 1208, 1147, 1070, 1020, 999, 911, 863, 819, 775, 752, 739, 664 cm^{-1}. MS *m/e* (relative abundance): 217 (37), 202 (11), 200 (11), 189 (20), 188 (10), 174 (16), 163 (15), 161 (10), 160 (14), 147 (10), 146 (18), 133 (12), 132 (11), 121 (12), 120 (12), 107 (30), 106 (64), 94 (10), 93 (100), 92 (10), 91 (11), 77 (11), 65 (17), 41 (26). UV $\lambda_{max}^{n\text{-hexane}}$ (log ε): 234.5 nm (3.79), 272 nm (3.50).

1) S. Fujita, T. Kawaguti, and H. Nozaki, This Bulletin, **43**, 2596 (1970).
2) S. Fujita, T. Kawaguti, and H. Nozaki, *Tetrahedron Lett.*, **1971**, 1119.
3) H. Nozaki, T. Koyama, T. Mori and R. Noyori, *ibid.*, **1968**, 2181; *Tetrahedron*, **25**, 5357 (1969).
4) S. Fujita and H. Nozaki, *Yuki Gosei Kagaku Kyokai Shi*, **30**, 679 (1972).
5) a) S. Fujita and H. Nozaki, This Bulletin, **44**, 2827 (1971). b) H. Nozaki, S. Fujita, and T. Mori, *ibid.*, **42**, 1163 (1969).
6) S. Fujita, K. Imamura, and H. Nozaki, *ibid.*, **45**, 1881 (1972).
7) S. Fujita, S. Hirano, and H. Nozaki, *Tetrahedron Lett.*, **1972**, 403.
8) S. Fujita, Y. Hayashi, and H. Nozaki, *ibid.*, **1972**, 1645.

Table 1. The energy barriers of the flipping of the heptamethylene chains[a)]

Compound	Signal	T_c (°C)	$\Delta\nu$ (Hz)	J_{AB} (Hz)	k_c (sec^{-1})	$\Delta G^{\neq}{}_c$[b)] (kcal/mol)
IV	*gem*-dimethyl	−37.0	28.8[c)]	—	64.1[d)]	11.8
	1-methylene	−39.0	18.1[c)]	11.4[c)]	45.9[e)]	11.8
	C-4 protons	−19.0	174[c,f)]	—	387[d)]	11.9
I[g)]	C-4 protons	−75.5	194[h,f)]	—	432[d)]	9.0
III	gem-dimethyl	−61.0	12.0[i)]	—	26.7[d)]	10.8

a) The dynamic NMR spectra were determined on a JEOL C-60-H spectrometer at 60 MHz, using $CFCl_3$ as the solvent and tetramethylsilane as the internal standard. See Fig. 1. b) $\Delta G^{\neq}{}_c = 2.303RT_c(10.319 - \log k_c + \log T_c)$ (Ref. 9).
c) Determined at −111 °C. d) $k_c = \pi\Delta\nu/\sqrt{2}$ (Ref. 9). e) $k_c = \pi\sqrt{\Delta\nu^2 + 6J_{AB}{}^2}/\sqrt{2}$ (Ref. 9).
f) As the signal of the low-field counterpart of the C-4 protons was concealed behind those of other methylenes, the $\Delta\nu$ value was estimated on the basis of the average chemical shift at room temperature and of the high-field shift at a low temperature.
g) Reported in Ref. 5. h) Determined at −111 °C. i) Determined at −94.0 °C.

Found: C, 77.5; H, 8.7; N, 6.2%. Calcd for $C_{14}H_{19}NO$: C, 77.4; H, 8.8; N, 6.5%.

2,2-Dimethyl[7](2,6)pyridinophane (IV). To a solution of potassium hydroxide (127 mg, 2.3 mmol) in triethylene glycol (5 ml), were added the ketone (III) (160 mg, 0.74 mmol) and hydrazine hydrate (80%, 0.5 ml). The mixture was heated under nitrogen at a reflux temperature for 2 hr. An additional portion of hydrazine hydrate (0.1 ml) was added during this period. The bath temperature was raised to 230 °C, and the excess hydrazine and water were distilled off over a 3-hr period. After the solution had been cooled, water was added to the mixture and the product was extracted with *n*-hexane. The combined extracts were dried over sodium sulfate. Concentration and distillation afforded the 2,2-dimethyl derivative (IV) (50 mg, 33%); bp 49°C/0.2 mmHg. IR (neat): 3070, 2955, 2930, 2870, 1590, 1579, 1459, 1383, 1362, 1325, 1239, 1138, 1086, 994, 862, 810, 798, 755, 747, 729, 710 cm^{-1}. MS *m/e* (relative abundance): 203 (38), 202 (17), 188 (34), 161 (13), 160 (18), 149 (15), 147 (44), 146 (18), 134 (11), 121 (23), 120 (80), 108 (10), 107 (100), 106 (19), 77 (14), 41 (18). UV $\lambda_{max}^{n\text{-hexane}}$ 214 (3.94), 269.5 (3.34).

Found: C, 82.6; H, 10.5; N, 6.8%. Calcd for $C_{14}H_{21}N$: C, 82.7; H, 10.4; N, 6.9%.

9) a) G. Binsch, "Topics in Stereochemistry," Vol. 3, ed. by E. L. Eliel and N. L. Allinger, Interscience Publishers, New York (1968), pp. 97—192. b) I. C. Calder and P. J. Garratt, *J. Chem. Soc., B*, **1967**, 660.

A Temperature-jump Study of the Kinetics of the Complex Formation of Iron(III) with *m*-Nitrophenol

Kiyoshi TAMURA

Department of Chemistry, Defense Academy, Yokosuka 239

(Received December 7, 1972)

By a new method here proposed, an expression of the relaxation time has been obtained for the formation of the monocomplex of iron(III) with a univalent anionic ligand. The method enables us to express the rate equation in a manner analogous to the second-order reaction, and to calculate the relaxation time with less mathematical labor. The validity of the treatment has been confirmed by applying it to the analysis of the complex formation reaction of iron(III) with *m*-nitrophenol. The kinetic measurement was performed with the temperature-jump method in an acidic aqueous solution at 25 °C and at an ionic strength of 0.10. Over the acidity range studied ($0.005 \leqq [H^+] \leqq 0.026$ M), the complex formation occurs significantly *via* one path: $FeOH^{2+} + m\text{-}NO_2C_6H_4OH \rightleftharpoons m\text{-}NO_2C_6H_4OFe^{2+} + H_2O$. The forward and backward rate constants obtained are $5.9 \times 10^2\ M^{-1}\ s^{-1}$ and $1.8 \times 10^2\ s^{-1}$ respectively. These results have been confirmed by examining the earlier kinetic data on similar reactions.

The reactions of iron(III) complexes in aqueous solutions have been the object of much recent interest[1-3] because of the apparent dependence of the formation rates of the complexes on the basicity of the entering ligand; no such dependence is shown by the bivalent transition or by most alkaline earth metal ions, where the rate-determining step is considered to be the removal of a water molecule from the inner coordination sphere of the cation. The apparent ligand specificity has been almost entirely removed by the general reaction mechanism proposed by Seewald and Sutin[4] and later developed by Cavasino and his co-workers.[5] Also, kinetic studies[4-10] have shown that the reaction mechanism interprets well the rates of the formation of iron(III) complexes with anionic ligands of a wide range of basicity.

Recently, Osugi, *et al.*[11] studied the complex formation of iron(III) with *p*-nitrophenol, which is an anionic ligand of a very high basicity. Soon after, Cavasino and Dio[12] also investigated similar reactions with some monosubstituted phenols. However, there was some inconformity concerning the reaction paths reported by these authors, and little kinetic information has been given elsewhere on complex formation with such ligands of a very high basicity.

The reactions of iron(III) with high-basicity ligands may be important as an extreme example of the reaction mechanism, and so more detailed investigations are required. In the present investigation, the complex formation of iron(III) was studied, with *m*-nitrophenol as the ligand. The kinetic measurement was carried out by the temperature-jump relaxation method. The present author has also proposed a new method of analysis for calculating the relaxation time with less mathematical labor; this method was elucidated in the course of this investigation.

Experimental

Materials. All of the chemicals used were of a reagent grade. Each sample solution was prepared by mixing appropriate ammounts of solutions of 0.05 M $Fe(NO_3)_3$, 0.1 M $m\text{-}NO_2C_6H_4OH$, and 0.1 M $HClO_4$, by then adjusting the ionic strength to 0.10 by the addition of KNO_3, and finally by diluting to a definite volume. The content of iron(III) in the ferric nitrate solution was determined by complexometric titration with disodium EDTA,[13] and the concentration of the acid solution was standardized with sodium hydroxide.

Temperature-jump Apparatus. The temperature-jump apparatus was a modification of those described by Hammes and Fasella[14] and by Kresheck *et al.*[15] It was operated by a single-beam optical system. A schematic diagram and the construction of the observation cell are shown in Figs. 1 and 2 respectively. The cell is constructed from an acrylresin disk 2 cm thick, through the center of which a hole 1 cm square has been bored. The solution chamber consists of the hole and the gold-coated walls of the brass electrodes, and accommodates 2 cm^3 of the solution. Two quartz windows enable optical observation through the solution, with a path of 1 cm. The temperature of the solution is controlled within ± 0.2 °C by circulating thermostated ethanol through the hollow electrodes.

A 0.4 μF condenser bank charged to 16 kV was discharged through the cell by means of an air gap. The temperature jump of the solution was 5 ± 0.5 °C, as determined by the change in the absorbance (at 550 mμ) of a phenolphthalein

1) M. Eigen, "Advances in the Chemistry of the Coordination Compounds," ed. by S. Kirschner, The Macmillan Co., New York, N. Y. (1961), p. 371.
2) H. Wendt and H. Strehlow, *Z. Elektrochem.*, **66**, 228 (1962).
3) F. P. Cavasino and M. Eigen, *Ric. Sci. Rend.*, *A*, **4**, 509 (1964).
4) D. Seewald and N. Sutin, *Inorg. Chem.*, **2**, 643 (1963).
5) F. Accascina, F. P. Cavasino, and S. D'Alessandro, *J. Phys. Chem.*, **71**, 2474 (1967).
6) F. P. Cavasino, *ibid.*, **72**, 1378 (1968).
7) F. L. Baker and W. MacF. Smith, *Can. J. Chem.*, **48**, 3100 (1970).
8) T. Yasunaga and S. Harada, This Bulletin, **42**, 2165 (1969).
9) F. Accascina, F. P. Cavasino, and E. Di Dio, *Trans. Faraday Soc.*, **65**, 489 (1969).
10) A. D. Gilmour and A. McAuley, *J. Chem. Soc.*, *A*, **1969**, 2345.
11) J. Osugi, H. Nakatani, and T. Fujii, *Nippon Kagaku Zasshi*, **90**, 529 (1969).
12) F. P. Cavasino and E. Di Dio, *J. Chem. Soc.*, *A*, **1970**, 1151.
13) F. J. Welcher, "The Analytical Uses of Ethylenediamine Tetraacetic Acid," D. Van Nostrand Co., Inc., Princeton, N. J. (1958), p. 225.
14) G. G. Hammes and P. Fasella, *J. Amer. Chem. Soc.*, **84**, 4644 (1962).
15) G. C. Kresheck, E. Hamori, G. Davenport, and H. A. Scheraga, *ibid.*, **88**, 246 (1966).

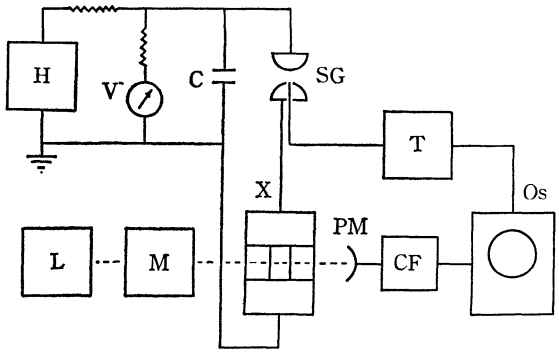

Fig. 1. Schematic diagram of the temperature-jump apparatus.
(L) light source; (M) monochromator; (X) observation cell; (PM) photomultiplier; (CF) cathode follower; (Os) oscilloscope; (H) high voltage generator; (V) vacuum-tube voltmeter; (C) condenser; (SG) spark gap; (T) trigger-pulse generator.

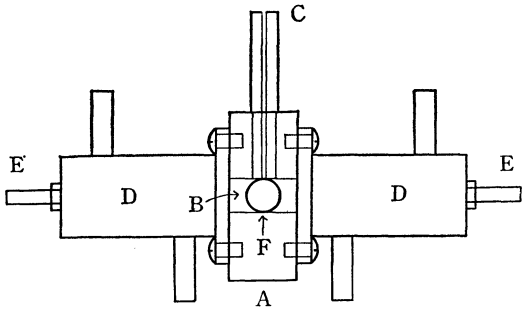

Fig. 2. Construction of the observation cell.
(A) acryl-resin cell; (B) solution space; (C) acryl-resin stopper with an orrifice to exhaust thermal pressure; (D) hollow brass electrodes (gold-coated at the solution sides) with outlets for circulating thermostated liquid; (E) leads to the discharging circuit; (F) quartz windows.
The direction of the observation light beam is perpendicular to the plane of the diagram.

solution. The indicator solution used contained 6×10^{-8} M phenolphthalein and 0.02 M glycine; the pH and the ionic strength were 9.5 and 0.10 (with KNO_3) respectively. The relaxation time of the heating period was 40 μs at this ionic strength.

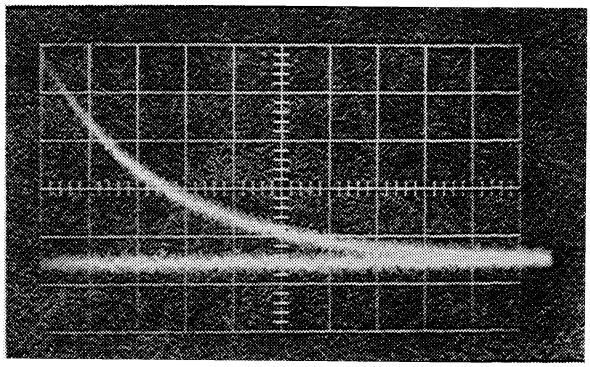

Fig. 3. An oscillograph of the temperature-jump relaxation experiment for iron(III) with *m*-nitrophenol. The data for this system are given in the last raw of Table 1. The sweep rate is 2 ms per division. The upper curve shows the relaxation effect corresponding to an increase in absorbance. The lower straight-line is the following trace of this curve after the intermittent time of 20 ms, showing an attainment of the transient equilibrium.

Results

The temperature-jump measurement was carried out at the wavelength of 508 mμ, where the *m*-NO_2-$C_6H_4OFe^{2+}$ ion exhibits the maximum absorbance.[16] All the solutions cited in Table 1 showed a single relaxation effect in the time range of 2×10^{-4}—0.05 s; this effect may be associated with the complex formation reaction. A second, smaller effect was also observed in the time range longer than this; the relaxation time was very roughly estimated not to be smaller than 0.4 s. The second relaxation effect did not interfere with the evaluation of the relaxation time related to the complexation. Blank solutions containing only ferric nitrate or *m*-nitrophenol at the same conditions of concentration, ionic strength, and pH had not shown any evidence of relaxation effect in the same time ranges. Moreover, there was no discernible kinetic difference between the sample solutions after several hours had elapsed and a few months had, after preparation. A representative relaxation effect of the complex formation is shown in Fig. 3.

TABLE 1. KINETIC DATA FOR THE REACTION OF IRON(III) WITH *m*-NITROPHENOL AT $\mu=0.10$ AND 25 °C

$[Fe(III)]_0$ (10^{-3} M)	$[HA]_0$ (10^{-2} M)	$[HClO_4]_0$ (10^{-3} M)	$[H^+]$ (10^{-3} M)	τ^{-1} (s^{-1})	k_f ($M^{-1}s^{-1}$)	$k_f/(1-\alpha)$ ($M^{-1}s^{-1}$)
1.98	4.81	4.16	5.02	205	229	626
0.992	4.81	5.94	6.30	188	183	582
2.98	3.20	7.13	8.18	179	147	562
9.98	5.00	5.94	9.43	213	153	652
4.96	1.20	8.32	9.76	163	120	523
4.99	5.00	11.9	12.9	197	113	617
9.92	3.20	11.9	14.5	188	98.6	593
9.98	5.00	17.8	19.9	193	77.1	608
9.92	1.20	17.8	19.9	168	68.5	540
4.96	3.20	23.8	24.7	174	58.4	558
9.98	5.00	23.8	26.1	189	59.9	601
						Av. 587±64

The subscript (0) for bracket indicates total stoichiometric concentration.

16) Z. L. Ernst and F. G. Herring, *Trans. Faraday Soc.*, **61**, 454 (1965).

The reciprocal relaxation time (τ^{-1}) was evaluated by the plot of the logarithm of the oscilloscope amplitude *vs.* the time. Here, the least-squares method was employed to obtain the most probable value. All the relaxation times quoted in Table 1 are means of at least five runs; the maximum error is about ±10%.

The pH of each solution was measured at 25±0.5 °C with a Hitachi-Horiba pH meter, Model F-7SS, calibrated with standard buffer solutions. The equilibrium hydrogen-ion concentrations were calculated from the measured pH values by using the activity coefficient (0.825)[17]; they are also shown in Table 1. The hydrogen-ion concentration thus obtained agreed within ±3% with that which was evaluated from the stoichiometric concentration of perchloric acid by taking into account the reaction equilibria, (3), (4), and (5).

Discussion

Potentiometric[18] and spectrophotometric[19–23] studies have shown that the following equilibria exist in an aqueous acid solution containing ferric ions with m-nitrophenol:

$$HA \rightleftharpoons A^- + H^+ \qquad K_H \qquad (1)$$

$$Fe^{3+} + A^- \rightleftharpoons FeA^{2+} \qquad K_c \qquad (2)$$

$$Fe^{3+} + HA \rightleftharpoons FeA^{2+} + H^+ \qquad K_b \qquad (3)$$

$$Fe^{3+} + H_2O \rightleftharpoons FeOH^{2+} + H^+ \qquad K_{OH} \qquad (4)$$

$$2\,FeOH^{2+} \rightleftharpoons Fe_2(OH)_2^{4+} \qquad K_d \qquad (5)$$

where HA indicates m-$NO_2C_6H_4OH$ and where K_H, K_c, K_b ($=K_HK_c$), K_{OH}, and K_d are the equilibrium constants for the corresponding reactions. Here, the presence of $Fe(OH)_2^+$ may be ignored.[24,25] Reaction (5) occurs so slowly that it may contribute little to the complex formation kinetics; for the present conditions, the reported rate constants[26,27] give $\tau \geqq 0.4$ s, which corresponds with the second relaxation time observed.

With these hypotheses, the overall mechanism for the formation of the FeA^{2+} complex may be expressed in a general form:[5,6,9]

$$\begin{array}{ccc} Fe^{3+} + A^- + H^+ & \underset{k_{-1}}{\overset{k_1}{\rightleftharpoons}} & \\ \Big\downarrow\uparrow K_H & & \\ Fe^{3+} + HA & \underset{k_{-2}}{\overset{k_2}{\rightleftharpoons}} & FeA^{2+} + H^+ \\ \Big\downarrow\uparrow K_{OH} & & \Big\downarrow\uparrow K_x \\ FeOH^{2+} + HA + H^+ & \underset{k_{-3}}{\overset{k_3}{\rightleftharpoons}} & Fe(OH)A^+ + 2\,H^+ \\ \Big\downarrow\uparrow K_H & & \\ FeOH^{2+} + A^- + 2\,H^+ & \underset{k_{-4}}{\overset{k_4}{\rightleftharpoons}} & \end{array} \qquad (6)$$

where the water molecule was omitted from the reactions for the sake of simplicity. The protolytic reactions (vertical steps) occur rapidly relative to the complex formation reactions, and are considered to be in equilibria throughout the course of the complex formation. Hence, only one relaxation time, associated with slower metal-complex formation reactions, can be obtained from the reaction scheme; the solution has already been given by Cavasino and his co-workers.[5,6,9] However, the present author will present here a different method of analysis, one which simplifies the rate equation and which makes it possible to calculate the relaxation time with less mathematical labor.

We notice the rapid protolytic reactions and express the overall free metal ions, free ligands, and metal-complexes by M, L, and ML, respectively, defining their concentrations as follows:

$$[M] \equiv [Fe^{3+}] + [FeOH^{2+}] \qquad (7)$$

$$[L] \equiv [A^-] + [HA] \qquad (8)$$

$$[ML] \equiv [FeA^{2+}] + [Fe(OH)A^+] \qquad (9)$$

with these conditions and definitions:

$$\alpha \equiv \frac{[Fe^{3+}]}{[M]} = \frac{[H^+]}{K_{OH}+[H^+]} \qquad (10)$$

$$\beta \equiv \frac{[A^-]}{[L]} = \frac{K_H}{K_H+[H^+]} \qquad (11)$$

$$\gamma \equiv \frac{[FeA^{2+}]}{[ML]} = \frac{[H^+]}{K_x+[H^+]} \qquad (12)$$

where K_x is the equilibrium constant of the hydrolysis of FeA^{2+}. Then, the rate equation is given by:

$$\frac{d[ML]}{dt} = k_f[M][L] - k_b[ML] = k_f\left([M][L] - \frac{[ML]}{K}\right) \qquad (13)$$

where:

$$k_f = k_1\alpha\beta + k_2\alpha(1-\beta) + k_3(1-\alpha)(1-\beta) + k_4(1-\alpha)\beta \qquad (14)$$

$$k_b = k_{-1}\gamma + k_{-2}\gamma[H^+] + k_{-3}(1-\gamma)[H^+] + k_{-4}(1-\gamma) \qquad (15)$$

$$K = \frac{k_f}{k_b} = K_c\left(\frac{\alpha\beta}{\gamma}\right) \qquad (16)$$

Here, k_f and k_b may be called the (apparent) overall forward and backward rate constants respectively.

By expanding Eq. (13) in the vicinity of the equilibrium concentrations and by using conservation relations:

$$\Delta[M] = \Delta[L] = -\Delta[ML] \qquad (17)$$

we obtain:

$$\frac{d\Delta[ML]}{dt} = -k_f\left([M]+[L]+\frac{1}{K}-\frac{[ML]}{K^2}\frac{\Delta K}{\Delta[ML]}\right)\Delta[ML] \qquad (18)$$

17) R. P. Frankenthal, "Handbook of Analytical Chemistry," 1st Ed., ed. by L. Meites, McGraw-Hill Book Co., Inc., London (1963), p. 1-6.
18) K. E. Jabalpurwala and R. M. Milburn, *J. Amer. Chem. Soc.*, **88**, 3224 (1966).
19) R. M. Milburn, *ibid.*, **77**, 2064 (1955).
20) R. M. Milburn, *ibid.*, **89**, 54 (1967).
21) A. G. Desai and R. M. Milburn, *ibid.*, **91**, 1958 (1969).
22) R. M. Milburn and W. C. Vosburgh, *ibid.*, **77**, 1352 (1955).
23) R. M. Milburn, *ibid.*, **79**, 537 (1957).
24) A. B. Lamb and A. G. Jacques, *ibid.*, **60**, 1215 (1938).
25) P. Hemmes, L. D. Rich, D. L. Cole, and E. M. Eyring, *J. Phys. Chem.*, **75**, 929 (1971).
26) H. Wendt, *Z. Elektrochem.*, **66**, 235 (1962).
27) H. Wendt, *Inorg. Chem.*, **8**, 1527 (1969).

where the symbol Δ indicates the deviation from the equilibrium value. From Eq. (18), the relaxation time, τ, is given by:

$$\frac{1}{\tau} = k_f B \tag{19}$$

where:

$$B = [M] + [L] + \frac{1}{K} + \phi \tag{20}$$

and:

$$\phi \equiv -\frac{[ML]}{K^2}\frac{\Delta K}{\Delta[ML]} = \frac{(\alpha-\beta-\gamma+1)^2[M][L]}{[H^+]+\alpha(1-\alpha)[M]+\beta(1-\beta)[L]+\gamma(1-\gamma)[ML]} \tag{21}$$

The term ϕ results from the fact that K is a function of $[H^+]$, which varies rapidly following the slower complex formation reactions. The last form of Eq. (21) can readily be obtained from Eqs. (16), (10), (11), and (12) by using the condition of electroneutrality together with Eq. (17); here, the contribution of $[OH^-]$ has been ignored in the calculations. All the quantities in Eqs. (19), (20), and (21) are expressed by the equilibrium values, and the K defined in Eq. (16) reduces to the apparent equilibrium constant, or to what is called the "apparent stability constant": $K=[ML]/[M][L]$.

The evaluation of B from Eqs. (20) and (21) requires the values of [M], [L], [ML], α, β, and γ. In the present case, the hydrolysis constant, K_x, could, unfortunately, not be found in the literature. However, that of $FeSCN^{2+}$ has been reported to be $K_x=6.5\times10^{-5}$ at $\mu=1.2$ and 25 °C.[28] Moreover, the second hydrolysis constant of the ferric ion[24,25] may be regarded as the hydrolysis constant of the $FeOH^{2+}$ complex: $K_x=(0.8\text{—}2)\times10^{-5}$ at $\mu\approx0$ and 25 °C. As these complexes give similar K_x values in spite of the large difference between the basicities of the thiocyanate and hydroxide ions (*i.e.*, $pK_H=1$ and 16), the same order of magnitude may be assigned to the K_x value for the monocomplex of iron(III) with the univalent anionic ligand. Therefore, in the acidity range ($[H^+]=0.005\text{—}0.026$ M) of the present work, the condition of $K_x \ll [H^+]$, which is equivalent to that of $[Fe(OH)A^+] \ll [FeA^{2+}]$, may be satisfied, and we obtain $\gamma=1$ and $[ML]=[FeA^{2+}]$ by means of Eq. (12). This corresponds to the steady-state assumption for the concentration of $Fe(OH)A^+$ usually adopted.[5-12] Under the present acidity conditions, the concentration of the free phenolate ion, A^-, is much lower than that of the acid ligand, HA, as $pK_H=8$ for *m*-nitrophenol; $\beta\approx[A^-]/[HA]$ is in the range $10^{-6}\text{—}10^{-7}$. Therefore, we need only the $[Fe^{3+}]$, $[FeOH^{2+}]$, [HA], and $[FeA^{2+}]$ concentrations to evaluate B. These equilibrium concentrations were obtained from the total stoichiometric concentrations of iron(III) and *m*-nitrophenol, from the equilibrium hydrogen-ion concentration, in Table 1, and from the equilibrium constant, K_b, K_{OH}, and K_d.

Milburn and his co-workers[18-21] reported several values of K_b in the course of their potentiometric[18] and spectrophotometric[19-21] studies. Desai and Milburn[21] obtained, most recently, by their careful spectrophotometric measurements: $K_b=0.94\times10^{-2}$ at $\mu=0.10$ and 25 °C. As the somewhat larger values reported earlier[18-20] left moderately large uncertainties in the absolute values,[21] this value was adopted as the most reliable value available at present. The values of K_{OH} and K_d at $\mu=0.10$ and 25 °C were obtained from Milburn and Vosburgh's measurements[22]: $K_{OH}=2.89\times10^{-3}$ and $K_d=1.7\times10^2$.

The overall forward rate constant, k_f, was calculated by means of Eq. (19), using the $1/\tau$ value in Table 1 and the value of B. The results are also shown in Table 1. As could be expected from Eq. (14), the k_f value depends only on the hydrogen-ion concentration; it decreases with an increase in the hydrogen-ion concentration. From the present condition, $\beta\approx10^{-6}\text{—}10^{-7}$, together with the k_f value in Table 1, it seems that we may safely ignore the first and fourth terms in Eq. (14); if these terms contribute significantly to k_f, the k_1 and k_4 values should be greater than $10^6\ M^{-1}\ s^{-1}$, values such as have not been observed for other univalent anionic ligands.[4,5,8,9] Ignoring β with respect to 1 in the second and third terms in Eq. (14) and dividing by $(1-\alpha)$, we obtain:

$$\frac{k_f}{1-\alpha} = \frac{k_2[H^+]}{K_{OH}} + k_3 \tag{22}$$

As is shown in the last column of Table 1, the value of $k_f/(1-\alpha)$ is practically independent of the hydrogen-ion concentration; the deviations from the mean value are almost within the limits of the experimental errors in τ (*ca.* $\pm10\%$). Therefore, the first term of Eq. (22) may be ignored, and the k_3 value is determined to be $(5.9\pm0.6)\times10^2\ M^{-1}\ s^{-1}$.

By inserting the approximate relations $k_f=k_3(1-\alpha)$, $\gamma=1$, and $\beta=K_H/[H^+]$ into Eq. (16), and by using the equilibrium relations of $K_HK_c=K_b$ and $k_3/k_{-3}=K_xK_b/K_{OH}$, we obtain:

$$k_b = \frac{k_3 K_{OH}}{K_b} = k_{-3} K_x \tag{23}$$

The last form of Eq. (23) corresponds to the third term of Eq. (15). From the second form of Eq. (23), the k_b value was obtained as $(1.8\pm0.2)\times10^2\ s^{-1}$.

From the above results, the following reaction path may be said to contribute mainly to the rate of the complex formation:

$$FeOH^{2+} + HA \underset{k_{-3}}{\overset{k_3}{\rightleftharpoons}} Fe(OH)A^+ + H^+ \underset{K_x}{\rightleftharpoons} FeA^{2+} + H_2O \tag{24}$$

where the forward and backward rate constants correspond to k_3 and k_b respectively.

For the monocomplex formation of iron(III) with substituted phenols, earlier kinetic studies have been made by Osugi *et al.*[11] and by Cavasino and Dio[12] with temperature-jump measurements at $\mu=0.10$ and at 25 °C. With *p*-nitrophenol as the ligand, the former

28) M. W. Lister and D. E. Rivington, *Can. J. Chem.*, **33**, 1572 (1955).

authors[11] obtained the same reaction path as (24), showing a considerable contribution of the reaction path involving the rate constant, k_2. On the other hand, the latter authors[12] found the sole effective reaction path to be (24), with some monosubstituted phenols. The above authors[11,12] reported k_3 values over the range of $(1.1—3.2)\times10^3$ M^{-1} s^{-1}; these values are two times or more larger than the present value. However, the k_3 values of the above authors[11,12] may require some corrections, for they used in their calculations Milburn[20] or Ernst and Herring[12] K_b values, which are, except for the case of (unsubstituted) phenol, somewhat larger than those of Desai and Milburn,[21] whose value was adopted in this study as the most recent and reliable value. According to Cavasino and Dio's approximation,[12] the k_3 value is almost proportionally affected by the K_b value used: $k_3 \approx K_b/(K_{OH}\tau)$.

The kinetic data of the above authors[11,12] were then re-examined by using Desai and Milburn's K_b values and by using the present method of calculation. All the data examined, including that of Osugi *et al.*, did not show any significant contribution of the rate constant, k_2, to the complex formation rates. The value, $k_2=32$ M^{-1} s^{-1}, reported by Osugi *et al.*[11] may result mainly from their method of estimation, which overweighes the data in the low-acidity region. The above results confirm again the present conclusion of the sole reaction path (24). The k_3 values in Table 2 are those

Table 2. Kinetic data for the formation of iron(III) monocomplexes with substituted phenols at $\mu=0.10$ and 25 °C

Substituent group	$10^{-2}k_3$[a] (M^{-1} s^{-1})	10^2K_b[c]	pK_H[c]	Ref.[f]
m-CH_3	16[b]	1.00[d]	9.88[e]	C-D
H	15	0.92	9.80	C-D
p-Cl	6.6	0.60	9.16	C-D
m-Cl	13	1.26	8.80	C-D
o-Cl	3.5	0.69	8.25	C-D
m-NO_2	8.0	0.94	8.12	C-D
m-NO_2	5.9	0.94	8.12	T
p-NO_2	8.2	1.39	6.89	C-D
p-NO_2	9.1	1.39	6.89	O-N-F

a) Value estimated by the present author, unless otherwise noted.
b) Original value.[12]
c) Desai and Milburn's value,[21] unless otherwise noted.
d) Ernst and Herring's value.[12]
e) Biggs and Robioson's value.[12]
f) C-D: Cavasino and Dio[12] T: Present author O-N-F: Osugi, Nakatani, and Fujii.[11]

estimated by the present author, except that for m-cresol, which is the original value.[12] The K_b values used for the calculation and the pK_H values for the ligand are also shown in the same table. As has been expected, the k_3 values re-estimated are all smaller than the original ones, except for the case of phenol, which gives the same value as the original one.[12] These values conform well with the present author's value.

We notice further that the k_3 values in Table 2 lie in a comparatively narrow range, $(3.5—16)\times10^2$ M^{-1} s^{-1}, in spite of the different nature and position of the substituent groups in the aromatic ring and the different basicity of the entering ligand ($pK_H=7—10$). As has been pointed out by Cavasino and Dio,[12] this suggests that the first step of reaction path (24) may proceed through the S_N1 mechanism, which involves the loss of a water molecule in the rate-determining step. However, the k_3 values in Table 2 are somewhat smaller than those reported in the earlier kinetic studies[4,5,9,10] for the corresponding reactions with HN_3,[4,5] HF,[4,5] CH_3CO_2H,[9] $ClCH_2CO_2H$,[9] $C_2H_5CO_2H$,[9] and $C_6H_5CH(OH)CO_2H$[10]: $k_3=(2.56—7.4)\times10^3$ M^{-1} s^{-1} at 20—25 °C and at $\mu=0.1—1.0$. A full explanation must await further investigations.

As is shown in Eqs. (7)—(21), the present method of analysis is mathematically simpler and more suggestive than the treatments of the previous investigators.[3,5,6,8,9,11,12] However, except for the different definitions of k_f and B, the present expression of the relaxation time, Eq. (19), is essentially equivalent to that of Cavasino and his co-workers[5,6,9] (with $\gamma=1$), and also to that of Osugi *et al.*[11] (with $\gamma=1$ and $\beta=0$). The apparent forward rate constant (usually designated as k_f or k_{obs}) differs from author to author, simply because they select different reactions as representative in the reaction scheme. Cavasino and his co-workers[5,9] took the reaction involving Fe^{3+} with A^- as representative; the k_{obs} used by them corresponds to the $k_f/\alpha\beta$ in the present expression, which exhibits a much higher order of magnitude with such ligands of a very high basicity as phenols.[12] Osugi *et al.*[11] selected the reaction of Fe^{3+} with HA as representative; the k_f used by them is equivalent to the k_f/α (with $\beta=0$) in the present study.

The k_f defined by Eq. (14) has a more general form, without taking any definite reaction as representative, and may give the value of the moderate magnitude with a ligand of a wide range of basicity. From the reasons above, the present author considered it appropriate as an (apparent) overall forward rate constant of complexation. A similar treatment has been given by Hammes and Schimmel,[29,30] but they ignored the term corresponding to ϕ in Eq. (20) and so their expression may be applicable only to strongly buffered reaction systems.[30] The present treatment may be easily extended to the analysis of more complicated reactions, such as protonated complex formation reactions.

Through this investigation, the present author considered that the validity of the present method of analysis may be well confirmed, and also that the functioning of the newly built temperature-jump apparatus was satisfactory.

29) G. G. Hammes and P. R. Schimmel, *J. Phys. Chem.*, **70**, 2319 (1966).
30) G. G. Hammes and P. R. Schimmel, *ibid.*, **71**, 917 (1967).

The Adiabatic Compressibility of Nonelectrolyte Aqueous Solutions in Relation to the Structures of Water and Solutions. II.

Harumi ENDO

Department of Applied Physics, Defense Academy, Yokosuka 239

(Received September 16, 1972)

From the temperature dependency of the adiabatic compressibility in aqueous systems of nonelectrolytes, established by ultrasonic measurements, it is concluded that structural units to be termed "liquid clathrate hydrates" do exist for various systems, the concentration of the zero temperature coefficient of adiabatic compressibility representing the composition-mole-ratio, r_c^β(water/solute), for these hydrates. Hydrates with r_c^β= 7.2/3 (for methanol, formamide, and urea) and 17 (for acetone and ethanol) correspond to the solid clathrate hydrates of Structures I and II respectively, while those with r_c^β=24, 28, 32, *etc*, can be explained on the basis of appropriate assumptions.

In the previous paper,[1] the sound velocity (V) and density (ρ) in aqueous solutions of urea (U), dimethylurea (DMU), thiourea (TU), acetamide (AA), acetone (A), and dimethylformamide (DMF) were measured, and the adiabatic compressibility (β) of solutions was calculated at various concentrations (μ: mole fraction) by means of the relation: $\beta = 1/(\rho \cdot V^2)$. In that paper, it was found that, for each system, the V–μ curves and β–μ curves for various temperatures have a common intersection at the fixed concentrations of μ_c^V and μ_c^β respectively, the sound velocity (V_c) and adiabatic compressibility (β_c) of a solution at these concentrations being independent of the temperature over a certain range (ΔT_c^V and ΔT_c^β respectively). In the cases of aqueous solutions of A and ethanol (Et), the mole ratio r_c^V=(water/solute) at μ_c^β was equal to the number of water molecules in the framework of the solid clathrate hydrate (Structure II type). Therefore, we assumed that the structure of this type also exists in solutions, and named this structure "liquid clathrate hydrate". From these results, it may be expected that, for solutions other than A and Et, the value of r_c^β also corresponds to the number of water molecules of a liquid clathrate hydrate of another type characteristic of the respective solutes.

In the present study, the adiabatic compressibility of aqueous solutions of diethylurea (DEU), formamide (F), dimethylacetamide (DMAA), and diethylacetamide (DEAA) will be determined over the temperature range from 20 to 50 °C, and over that of hexamethylenetetramine (HMT) from 22 to 50 °C, by measuring the densities and the sound velocities of the solutions.

As in the previous paper,[1] the parameters, V_c, β_c, ΔT_c^V, ΔT_c^β, μ_c^V, and μ_c^β, are determined for these systems in order to examine their relation with the liquid structure. Two other parameters, v_c^V (volume fraction for 20 °C at μ_c^V) and v_c^β (volume fraction for 20 °C at μ_c^β), are introduced. On the basis of a model of the liquid clathrate hydrate, the properties and the dissolved states of a solute in water are discussed by means of the β_c—r_c^β relationships for various systems.

Experimental

Materials. The DEU and HMT were purified by the recrystallization of reagent-grade products from absolute alcohol. To purify F, DMAA, and DEAA, the reagent-grade products are distilled twice under reduced pressure before use.

Apparatus. A crystal-controlled ultrasonic interferometer operating at a frequency of 5 MHz is used to measure the standing waves. The measuring cell containing a solution is immersed in an oil bath, the temperature of which is kept constant within ±0.1 °C.

Results

In Figs. 1—5, the sound velocity is plotted against the mole fraction for aqueous solutions of DEU, F, DMAA, and DEAA respectively over the temperature range of ΔT=20—50 °C and HMT over the range of ΔT=22—50 °C. All of the V–μ curves (Figs. 1—5) within a certain temperature range (ΔT_c^V) have a common intersection at a fixed concentration (μ_c^V). Although this temperature range (ΔT_c^V) is usually narrow (*ca.* 15—20 °C), this intersection is clearly discernible. The values of V_c, ΔT_c^V, and μ_c^V for the various aqueous systems here investigated are summarized in Table 1, together with the previous results[1] and a few data found in the literature.[2-6]

Figures 6—10 show the β–μ curves for aqueous solutions of DEU, F, DMAA, and DEAA respectively over the observed temperature range from 20 to 50 °C and HMT over the range of ΔT=22—50 °C. The β–μ curves for a certain temperature range also intersect at a common point. The numerical values of μ_c^β are slightly different from those of μ_c^V, while the temperature range, ΔT_c^β, is nearly the same as ΔT_c^V. The β_c, ΔT_c^β, and μ_c^β values at the converging point in the β–μ curves are summarized in Table 2. Table 2 also contains the data of the previous study[1] and those taken from other authors.[2-6]

In Fig. 11, V_c is plotted against the mole ratio r_c^V=(water/solute) at μ_c^V for various solutes. This plot shows that r_c^V shifts to a higher value with an increase in the molecular weight of solutes, but no clear

1) H. Endo, This Bulletin, **46**, 1106 (1973).
2) K. Raghunath, Ph. D. Thesis, Univ. of Sri Venkateswara, Tirupati, 1968.
3) N. Takenaka and K. Arakawa, 15th Meeting of the Onpa no Bussei to Kagaku Toron Kai, (1970), Preprints p. 64.
4) F. Hirata and K. Arakawa, *ibid.*, 15th, p. 67.
5) N. Takenaka and K. Arakawa, *ibid.*, 16th, 1971, p. 25.
6) N. Kiyohara, N. Takenaka, and K. Arakawa, *ibid.*, 16th 1971, p. 16.

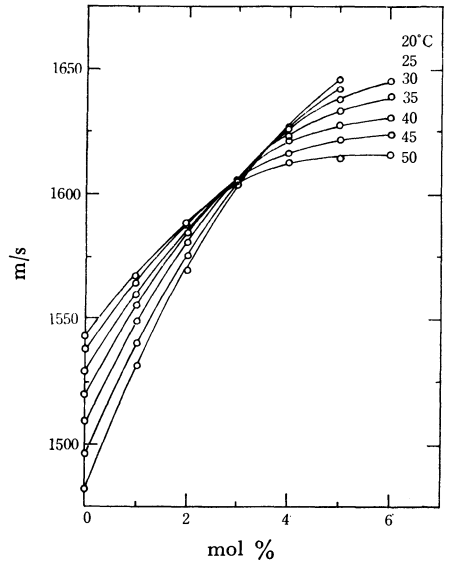

Fig. 1. Sound velocity *vs.* concentration of DEU aqueous solutions.

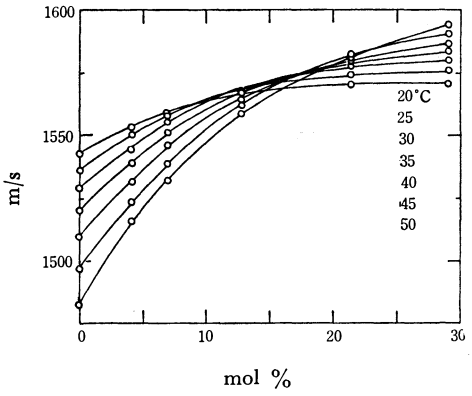

Fig. 2. Sound velocity *vs.* concentration of F aqueous solutions.

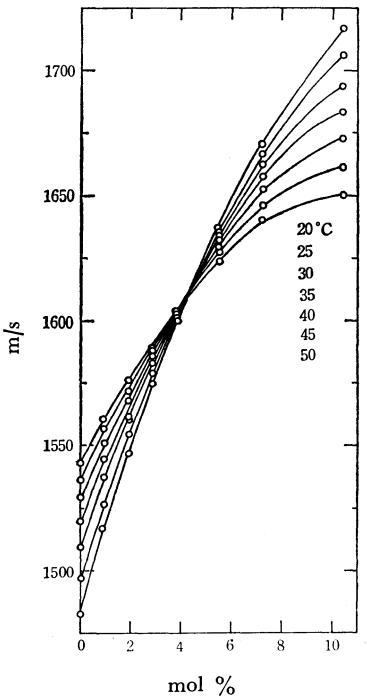

Fig. 3. Sound velocity *vs.* concentration of DMAA aqueous solutions.

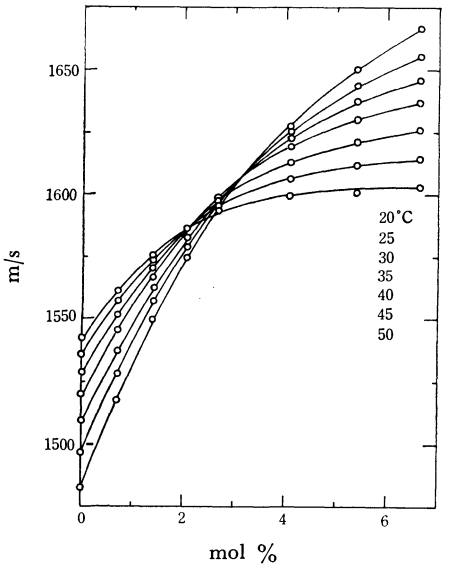

Fig. 4. Sound velocty *vs.* concentration of DEAA aqueous solutions.

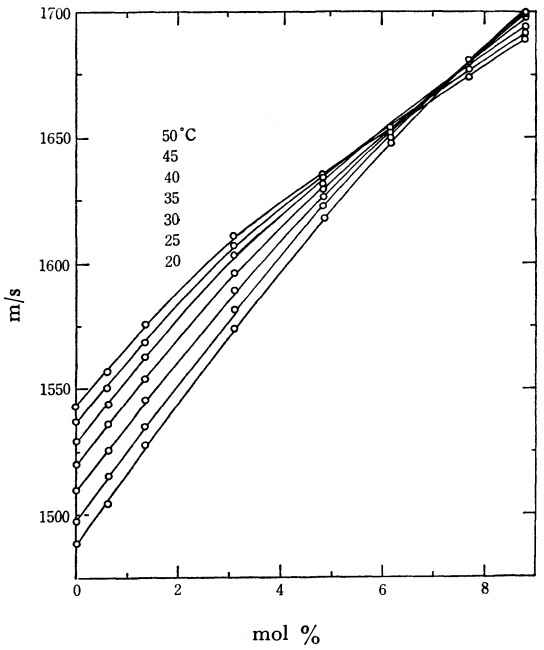

Fig. 5. Sound velocity *vs.* concentration of HMT aqueous solutions.

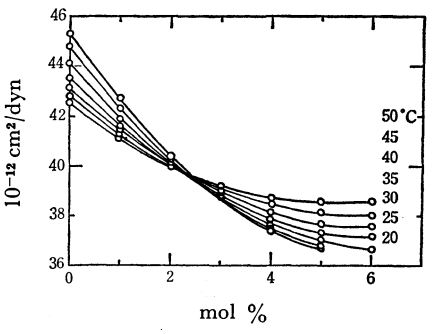

Fig. 6. Adiabatic compressibility of DEU aqueous solutions.

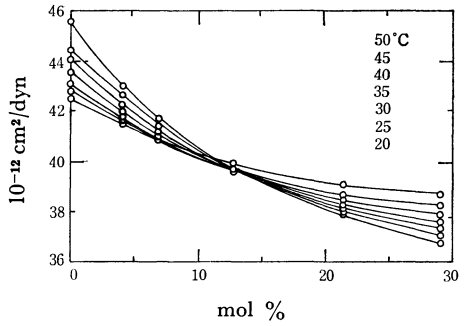

Fig. 7. Adiabatic compressibility *vs.* concentration of F aqueous solutions.

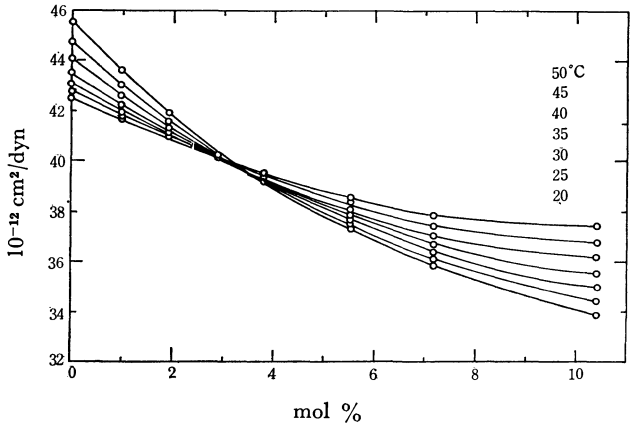

Fig. 8. Adiabatic compressibility *vs.* concentration of DMAA aqueous solutions.

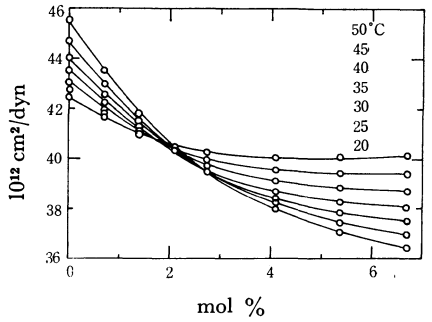

Fig. 9. Adiabatic compressibility *vs.* concentration of DEAA aqueous solutions.

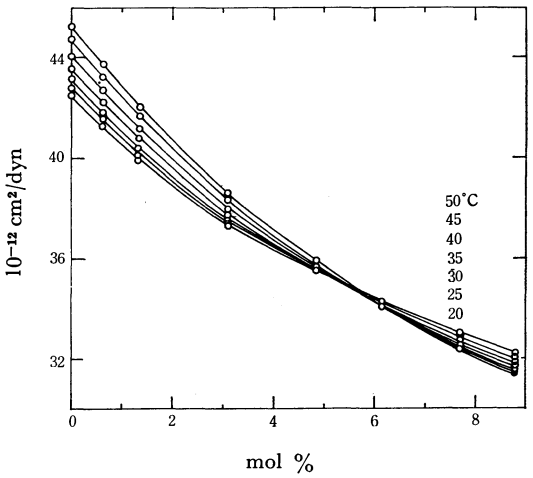

Fig. 10. Adiabatic compressibility *vs.* concentration of HMT aqueous solutions.

Table 1. Data concerning sound velocity

	V_c m/s	μ_c^V mol%	r_c^V	v_c^V vol%	ΔT_c^V °C
U	1688	18.0	4.5	35.6	20—40
DMU	1641	6.5	14.3	22.9	20—35
TU	1628	8.8	10.3	22.5	50—60
AA	1615	11.2	7.9	26.3	20—35
A	1573	6.2	15.1	21.2	20—30
DMF	1591	4.7	20.3	17.5	20—50
Me	1574	13.5	6.3	25.9	20—30
Et	1605	6.8	13.7	19.1	20—40
Pr	1580	5.2	18.2	18.5	0—20
Mo	1565	3.7	26.1	15.6	20—60
DEU	1620	3.6	26.8	18.7	20—30
F	1575	17.3	4.8	31.5	25—40
DMAA	1620	4.6	21.5	20.0	20—35
DEAA	1610	3.3	29.7	19.1	20—35
HMT	1681	7.8	12.0	32.8	22—35
D[2]	1574	5.4	17.4	21.2	30—40
G[2]	1690	12.0	7.3	35.5	30—50
DGDE[3] TEAC[4]	1610			20	10—30
DGDM[5]	1610			18	10—30
DMSO[6]	1605	6.0	15.7	20	25—45

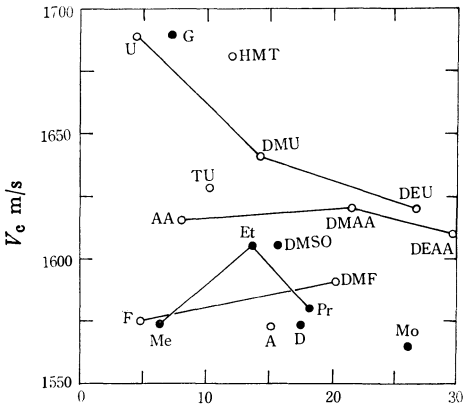

Fig. 11. V_c *vs.* r_c^V for various solutes.
○: present study, ●: others, ——: homolog series.

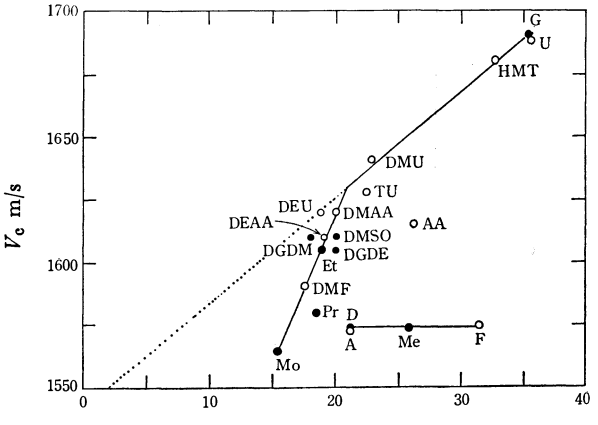

Fig. 12. V_c *vs.* v_c^V (vol % at 20 °C) for various solutes.

Table 2. Data concerning adiabatic compressiblity

	$\beta_c \times 10^{-12}$ cm²/dyn	μ_c^β mol%	r_c^β	v_c^β vol%	ΔT_c^β °C
U	34.8	11.8	7.4	25.2	20—50
DMU	37.5	5.2	18.2	19.0	20—40
TU	38.7	4.0	24.0	11.1	50—60
AA	39.0	8.0	11.5	19.7	20—35
A	41.6	5.6	16.8	19.4	20—30
DMF	39.9	4.2	22.8	15.8	20—40
Me	42.1	10.5	8.5	20.8	20—40
Et	40.7	5.5	17.2	15.8	20—30
Pr	41.7	4.1	23.4	15.1	10—30
Mo					
DEU	38.3	3.3	29.8	17.2	20—30
F	39.5	12.8	6.8	24.4	25—40
DMAA	39.5	3.5	27.6	15.7	20—40
DEAA	39.6	2.7	36.0	16.3	20—35
HMT	34.0	6.3	15.0	27.9	22—35
D[2]	40.7	4.0	24.0	16.4	30—40
G[2]	36.2	6.0	15.8	20.4	30—50
DGDE[3]					
TEAC[4]	34	3	32.6	19.9	20—35
DGDM[5]					
DMSO[6]	39.5	4	24	14	25—35

relationship is found between V_c and r_c^V, even among the items of the homolog series.

In Fig. 12, V_c is plotted against the volume fraction (v_c^V) at 20°C at μ_c^V. According to this plot, however, the points for AA, A, Me (methanol), and F markedly deviate from the plotted curve, the latter three having nearly the same sound velocity. Each of them, other than A, is the lowest-molecular-weight substance in the homolog.

It is possible that the smooth curve can be subdivided into two straight lines meeting at (1630 m/s, 21.0 vol %). One group consists of the U-homolog series, HMT, and G, for which:

$$V_c = 403\, v_c^V + 1547 \text{ (m/s)} \quad (v_c^V \text{ in volume fraction})$$

while the other consists of the F-, AA-, and alcohol-homolog series, except for the lowest-molecular-weight substances in each homolog, for which:

$$V_c = 1143\, v_c^V + 1390 \text{ (m/s)}$$

In Fig. 13, β_c is plotted against r_c^β for various solutes. According to this plot, the homolog series may be classified into two groups. The first group is that of the AA-homolog series, for which an approximately linear relationship between β_c and r_c^β holds:

$$\beta_c = (0.0225\, r_c^\beta + 38.7) \times 10^{-12} \text{ (cm²/dyn)}$$

The second group is that of another homolog series, for which the β_c—r_c^β curves are not linear.

In Fig. 14, β_c is plotted against v_c^β, the volume fraction at 20 °C at μ_c^β, instead of at r_c^β. According to this plot, in a manner similar to that in the case of V_c—v_c^V plot, the solutes studied fall on a smooth curve independent of the sort of solute. Here also, as in the case of the V_c—v_c^V plot, the points for AA, A, Me and F deviate from a smooth curve, these solutes,

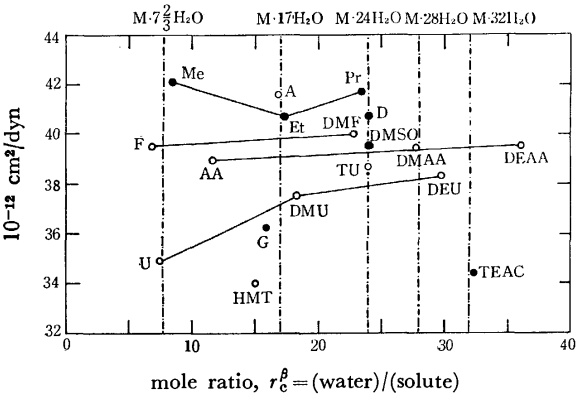

Fig. 13. β_c *vs.* r_c^β for various solutes.
○: present study, ●: others, ——: homolog series.

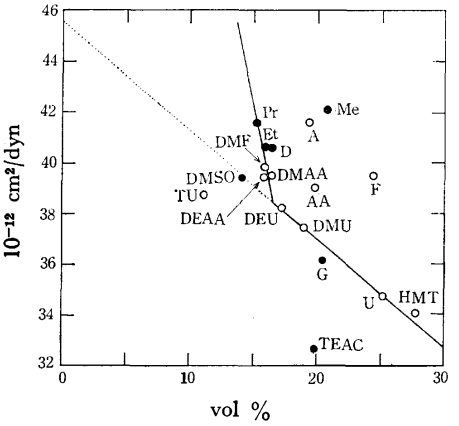

Fig. 14. β_c *vs.* v_c^β (vol % at 20°C) for various solutes.
○: present study, ●: otheres.

other than A, being the lowest-molecular-weight substances in each homolog. The plots in Fig. 14 may be divided into three groups. The first group is the U-homolog series, HMT, dimethyl sulfoxide (DMSO), glycerin (G), *etc.* The second group is the F-, AA-, and alcohol-homolog series, except the lowest-molecular-weight substances in each homolog, and dioxane (D). The third group is the remaining substances (the lowest-molecular-weight substance in each homolog and A).

In the first group, a plot of β_c against v_c^β gives a straight line:

$$\beta_c = (45.6 - 42.7\, v_c^\beta) \times 10^{-12} \text{ (cm²/dyn)} \quad (1)$$

where 45.6×10^{-12} cm²/dyn is the compressibility of water at 20 °C. The second group corresponds to the following equation:

$$\beta_c = (77.5 - 236.7\, v_c^\beta) \times 10^{-12} \text{ (cm²/dyn)} \quad (2)$$

Here, the range of v_c^β is given by $(0.135 \leqq v_c^\beta \leqq 0.165)$. The two straight lines (1) and (2) meet at a point of (38.5×10^{-12} cm²/dyn, 16.5 vol%). In the third group, however, no such relationship exists between β_c and v_c^β.

Discussion and Considerations

The X-ray diffraction studies of liquid water suggest that the water has long-range ordered structure.

The framework of the structure in liquid water consists of a hexagonal ice-I structure with numerous cavities, which can accommodate another species of water, the non-hydrogen-bonded water.

The compressibility (β) of liquid water consists of two parts:

$$\beta = \beta_\infty + \beta_{st} \tag{3}$$

where β_∞ is the instantaneous compressibility due to the compression of the molecules and the intermolecular distance, and where β_{st} is the structural compressibility due to the breakdown of intermolecular bonds accompanying the destruction of the open structure. Therefore, the temperature derivatives of β in aqueous solution are given by:

$$\frac{d\beta}{dT} = \frac{d\beta_\infty}{dT} + \frac{d\beta_{st}}{dT} \tag{4}$$

It may be assumed that Eq. (3) is also applicable to nonelectrolyte aqueous solutions. Also, it may be assumed that the number of clusters of water molecules does not change appreciably up to μ_c^β, the solute molecules being all accommodated in water-clusters. The instantaneous compressibility, β_∞, consists of two parts, one due to the instantaneous compression of clusters and the other due to the compression of the intercluster distance. The former does not change appreciably because the elasticity of the cluster is mainly caused by the framework, the cavity-site water molecules, and the solute molecules adopted in water-clusters not contributing to the elasticity. Also, the latter does not change up to μ_c^β, because the number of clusters does not change up to μ_c^β: there are no free solute molecules, either. Therefore, it may be concluded that β_∞ is quite constant and that $d\beta_\infty/dT = 0$ up to μ_c^β. This solution model, accommodating all the solute molecules in water-clusters up to a certain concentration, is presumably consistent also with the partial molal volume data. It has been reported that the value of the partial molal volume of water in ethanol solution[7] is independent of the concentration up to about 10-mol% Et, nearly corresponding to our, μ_c^β, while the partial molal volume of Et diminishes up to this concentration, and then increases again. For higher concentrations, $\mu > \mu_c^\beta$, it may be assumed that the increase in the number of solute molecules accompanies the increase in the number of clusters, this decreasing β_{st} and increasing β_∞. On the basis of this model we obtain Table 3 showing the temperature derivatives of β_∞ and β_{st} for various concentration ranges. In the aqueous solutions at μ_c^β within ΔT_c^β, it can be seen from Figs. 6—10 that $d\beta/dT = 0$. As it is assumed that $d\beta_\infty/dT = 0$ for $\mu \leqq \mu_c^\beta$, it follows that $d\beta_{st}/dT = 0$ at $\mu = \mu_c^\beta$. It follows that $d\beta_{st}/dT = 0$ for $\mu > \mu_c^\beta$ also, because $\beta_{st} \fallingdotseq 0$ for this concentration range, according to our model. Therefore, it may be concluded that the structure of a solution at the crossing concentration for the β–μ curves consists of repeat-units with a mole ratio of r_c^β, which may be termed "liquid clathrate hydrate". The repeat-unit, presumably being a caga-like structure, may be similar to the solid clathrate hydrate known for a few solutes.

TABLE 3. THE CONCENTRATION DEPENDENCE OF TEMPERATURE DERIVATIVES OF ADIABATIC COMPRESSIBILITY IN AQUEOUS SOLUTIONS

Concentration	Model		Experimental
	$\frac{d\beta_\infty}{dT}$	$\frac{d\beta_{st}}{dT}$	$\frac{d\beta}{dT} = \frac{d\beta_\infty}{dT} + \frac{d\beta_{st}}{dT}$
$\mu < \mu_c^\beta$	0	<0	<0
$\mu = \mu_c^\beta$	0	0	0
$\mu > \mu_c^\beta$	>0	0	>0

In Fig. 13, β_c is plotted against r_c^β for all the substances listed in Table 2. As can be seen in Fig. 13, most of the solutes fall nearly on parallel (dotted) straight lines $r_c^\beta = \text{const.}$ Some of these mole ratios correspond to those known in solid clathrate hydrates: we can assume the existence of liquid clathrate hydrates with the same structure, while other can be be explained on the basis of some simplified assumptions.

There are two sorts of hydrates which are known as Structures I and II respectively. Structure I includes hydrates of small molecules, such as Cl_2, SO_2, and ethylene oxide. Structure II for hydrates has been found in larger hydrating molecules, such as A, Et, and tetrahydrofuran. The unit cell of Structure I, containing 46 water molecules, consists of a close packing of two dodecahedra, consists of 20 water molecules and with a radius of 5.2 Å, and six tetradecahedra, consisting of 24 water molecules and with a radius of 5.9 Å.

If the guest molecules, M, occupy only the larger cavity, the ideal stoichiometrical composition will be $6M \cdot 46H_2O$, *i. e.*, $r_c^\beta = 7.2/3$. When the tetradecahedra containing a solute are freely floating in the liquid water in the isolated state, without composing a solid clathrate hydrate of the Structure-I type, the composition of this polyhedra is $M \cdot 24H_2O$, *i. e.*, $r_c^\beta = 24$. In the Structure II solid clathrate hydrate, the unit cell containing 136 water molecules consists of 16 dodecahedra with a radius of 4.8 Å, and 8 hexadecahedra with a radius of 6.9 Å. Here, the hexadecahedra consist of 28 water molecules. If only the larger cavity is occupied by a guest molecule, the ideal stoichiometrical composition in Type II will be $8M \cdot 136H_2O$, *i. e.*, $r_c^\beta = 17$. When the hexadecahedra containing a solute are freely floating in solution, the composition of this polyhedra is $M \cdot 28H_2O$, *i. e.*, $r_c^\beta = 28$. As can be seen in Fig. 13, $r_c^\beta = 20$ is absent in $\beta_c^\beta - r_c^\beta$ curves for various solutes. From these results, it can be concluded that the dodecahedra with a radius of 4.8—5.2 Å are too small to accommodate a solute in their cavity.

It should be noted that among the many quaternary ammonium salts, only tetrabutyl- and tetraamylammonium salts form solid clathrate hydrates, while no solid clathrate hydrate is known for tetraethylammonium chloride (TEAC). As may be seen from Ref.

7) A. G. Mitchell and W. F. Wynne-Jones, *Disscus. Faraday Soc.*, **15**, 161 (1953).

4, TEAC has a converging point in the β–μ curves. Here, the value of r_c^β is found to be 32.6. This r_c^β, 32, presumably corresponding to that of the octadecahedra. Therefore, it may be concluded that TEAC also forms a liquid clathrate hydrate in liquid water in a manner similar to that in the cases of other nonelectrolyte solutes.

It may be noticed in Fig. 13 that a larger solute molecule exhibits a lower compressibility, β_c, for the same r_c^β, *i. e.*, for the same liquid clathrate structure. This is to be expected, because cavities accommodating larger solute molecules are more "rigid" when the polyhedra are crushed by acoustic pressure; this may correspond to the so-called "rigidity" of icebergs around a solute molecule (*e. g.*, tetraalkylammonium salts[8]).

It is known that, in some cases,[9,10] the framework-structure of water in solid clathrate hydrates may be replaced by solute molecules. Therefore, it seems reasonable to assume that the framework-structure of water in aqueous solutions may also be replaced by a solute molecule in some cases. It may be seen in Eqs. (1) and (2) that the coefficient of v_c^β in the latter is remarkably larger than that in the former. This presumably indicates that the latter group of molecules (such as the F-, AA, and alcohol-homolog series, except for the lowest-molecular-weight substances in each homolog) fill up the cavity only, while the former group (such as the U-homolog series, DMSO, and TU) also collaborates as constitutive parts in forming the framework.

The author wishes to thank Prof. T. Sasaki of the Tokyo Metropolitan University for his helpful discussions and generous support of this research and also Prof. O. Nomoto of the Defense Academy for valuable suggestions and discussions.

8) E. Wicke, *Angew. Chem., Int. Ed.*, **5**, 106 (1966).
9) D. Glew, *Nature*, **201**, 922 (1964).
10) T. Mark and R. McMullan, *J. Chem. Phys.*, **42**, 2732 (1965).

BULLETIN OF THE CHEMICAL SOCIETY OF JAPAN, VOL. 46, 1591—1596 (1973)

Mössbauer Study of the Thermal Decomposition Products of $SrFeO_4$

Toshio ICHIDA*

Institute for Chemical Research, Kyoto University, Uji, Kyoto 611

(Received December 11, 1972)

The thermal decomposition products of $SrFeO_4$ were studied by ^{57}Fe-Mössbauer-effect and X-ray-diffraction measurements. Below 300 °C in air, an amorphous Fe^{3+} product was formed. The Fe^{4+} or Fe^{5+} state was not observed in the process. A single-phase product with a perovskite structure was obtained in air at temperatures above 400 °C. The products obtained between 400 and 650 °C showed cubic symmetry, but above 700 °C they showed tetragonal distortion. Two kinds of Fe^{3+}-ion sites were detected in the tetragonal $SrFeO_x$ compounds. All the products obtained under the oxygen pressures from 50 to 500 atm and at temperatures from 300 to 900 °C showed cubic symmetry. The Fe^{3+}/Fe^{4+} ratio in those products was determined from the relative intensities of the Mössbauer absorptions.

Regarding the abnormal valence states of iron, several works have been reported. As examples of hexavalent iron compounds, K_2FeO_4, $SrFeO_4$, and $BaFeO_4$ are known[1-3] and their magnetic properties have been investigated.[4-6] It is well known that tetravalent iron, Fe^{4+}, is formed easily in alkaline-earth orthoferrate, $RFeO_x$ (R=Ca, Sr, Ba; $2.5<x\leqq3.0$).[7-17]

The present author and his associates have prepared pure samples of the three hexavalent iron compounds and investigated their magnetic properties.[5,6] The decomposition products of K_2FeO_4 and $BaFeO_4$ have also been investigated. In the case of K_2FeO_4, no intermediate valence state was observed between the hexavalent and trivalent states.[18] By the decomposition of

* On leave from Kawasaki Steel Corporation.
Present address: Research Laboratories, Kawasaki Steel Corporation, 1, Kawasaki-cho, Chiba 280.

1) H. J. Hrostowski and A. B. Scott, *J. Chem. Phys.*, **18**, 105 (1950).
2) G. W. Thompson, L. T. Ockerman, and J. M. Schreyer, *J. Amer. Chem. Soc.*, **73**, 1379 (1951).
3) V. R. Scholder, H. V. Bunsen, F. Kindervater, and W. Zeiss, *Z. Anorg. Allg. Chem.*, **282**, 268 (1955).
4) G. K. Wertheim and R. H. Herber, *J. Chem. Phys.*, **36**, 2497 (1962).
5) T. Shinjo, T. Ichida, and T. Takada, *J. Phys. Soc. Jap.*, **26**, 1547 (1969).
6) T. Shinjo, T. Ichida, and T. Takada, *ibid.*, **29**, 111 (1970).
7) H. Watanabe, *ibid.*, **12**, 515 (1957).
8) G. Shirane, D. E. Cox, and S. L. Ruby, *Phys. Rev.*, **125**, 1158 (1962).
9) P. K. Gallagher, J. B. MacChesney, and D. N. E. Buchanan, *J. Chem. Phys.*, **41**, 2429 (1964).
10) J. B. MacChesney, R. C. Sherwood, and J. F. Potter, *ibid.*, **43**, 1907 (1965).
11) P. K. Gallagher, J. B. MacChesney, and D. N. E. Buchanan, *ibid.*, **43**, 516 (1965).
12) J. B. MacChesney, J. F. Potter, R. C. Sherwood, and H. J. Williams, *J. Chem. Phys.*, **43**, 3317 (1965).
13) T. R. Clevenger, Jr., *J. Amer. Ceram. Soc.*, **46**, 207 (1963).
14) U. Shimony and J. M. Kundsen, *Phys. Rev.*, **144**, 361 (1966).
15) J. B. MacChesney, J. J. Jetzt, J. F. Potter, H. J. Williams, and R. C. Sherwood, *J. Amer. Ceram. Soc.*, **49**, 644 (1966).
16) S. Mori, *J. Phys. Soc. Jap.*, **28**, 44 (1970).
17) F. Kanamaru, H. Miyamoto, Y. Mimura, M. Koizumi, N. Shimada, S. Kume, and S. Shin, *Mater. Res. Bull.*, **5**, 257 (1970).
18) T. Ichida, This Bulletin, **46**, 79 (1973).

$BaFeO_4$ in the low temperature range, two new phases were found with the composition of $BaFeO_x$ ($2.5<x<3.0$).[19] As for the decomposition of $SrFeO_4$, there has been no detailed report except for a brief paper by Scholder *et al.*, which reported that a perovskite, $SrFeO_3$, was formed by heating $SrFeO_4$ in an oxygen atmosphere at about 700 °C.[20] As will be reported in this paper, perovskite-type $SrFeO_x$ compounds with various oxygen deficiencies were obtained by heating $SrFeO_4$ under different conditions.

There have been several reports concerning the perovskite-type $SrFeO_x$ system. All of the $SrFeO_x$ samples used in the previous works were prepared by the ordinary ceramic method; α-Fe_2O_3 and strontium carbonate or strontium formate were treated under various oxygen pressures and temperatures. Watanabe[7] measured the magnetic susceptibility and electrical conductivity of $SrFeO_x$ compounds containing Fe^{4+} ions, and suggested the combined effect of the double exchange and the usual exchange interactions in these compounds. The Mössbauer-effect of the $SrFeO_x$ ($2.5<x<3.0$) compounds was measured by Shirane *et al.*[8] They found that the isomer shift of the tetravalent-state iron in $SrFeO_{2.86}$ was about 0.0 mm/s relative to that of pure iron. MacChesney *et al.*[9,10] prepared $SrFeO_x$ ($2.5<x\leqq3.0$) compounds by equilibrating $SrFeO_{2.50}$ at oxygen pressures ranging from 0.2 to 855 atm. They also studied the crystallographic and magnetic properties of $SrFeO_x$ ($2.5\leqq x\leqq3.0$) compounds by means of X-ray-diffraction, Mössbauer-effect, susceptibility, and resistivity measurements.

The present work was undertaken in order to investigate equilibrium phases in a lower temperature range for the $SrFeO_x$ system. As a starting material, the hexavalent iron compound, $SrFeO_4$, has a definite merit; the equilibrium state is attained more rapidly in fine particles of the decomposition products than in those of the other starting materials thus far used. X-ray-diffraction and Mössbauer-effect measurements were carried out in order to examine each of the products. The ratios of Fe^{3+} ans Fe^{4+} ions in the perovskite-type products were estimated by the curve resolutions of the Mössbauer spectra.

Experimental

Using a pure sample of K_2FeO_4 obtained by a previously-reported procedure,[18] $SrFeO_4$ was prepared according to the method of Scholder *et al.*[3]

To a mixed solution of strontium hydroxide and strontium acetate, a 0.5% potassium hydroxide solution containing K_2FeO_4 was added. The filtered precipitate of $SrFeO_4$ was stored in a desiccator after having been washed with chilled alcohol and acetone successively. In the preparation of $SrFeO_4$, the distilled water, from which the carbon dioxide had been expelled, was used in order to prevent the formation of strontium carbonate. All of the reactions were carried out at about 0 °C in order to avoid the reduction of Fe^{6+} ions. By the X-ray-diffraction technique, the sample was confirmed to be a single phase of $SrFeO_4$. The particle shape of $SrFeO_4$, observed by means of an electron microscope, was granular, with a diameter of 2—4 μ. The measurements of the magnetization and the Mössbauer-effect were carried out at 80 K in order to be sure of the absence of any ferromagnetic impurity and any iron ion other than the Fe^{6+} ions.[6]

This pure sample of $SrFeO_4$ was then heated under the oxygen pressures from 0.2 to 500 atm. For the heating in air or in an oxygen atmosphere, the sample was spread thinly on a boat made of porcelain or platinum; it was heated then below 1200 °C for 50 hr and cooled rapidly to room temperature. For some of the samples, the heating period was prolonged to 1500 hr, but no difference was observed in the experimental results of the X-ray-diffraction and Mössbauer-effect measurements. For the heating under high oxygen pressures, the sample was placed in a test tube of silica or gold; this test tube was put in a cone-seal hydrothermal reaction vessel made of Stellite. These samples were quenched to cold water with the reactor after being kept at temperatures below 900 °C for 50 hr under oxygen pressures of less than 500 atm.

The phase identification of the products obtained was accomplished by X-ray-diffraction techniques. In the measurements of the lattice parameters of cubic or tetragonal $SrFeO_x$ compounds, the (200) reflections were used. The Mössbauer-effect measurements were carried out using an apparatus consisting of an Elron driving unit, AME-20, and a Northern Scientific Co. 1024-channel pulse-height analyzer, NS-600. The temperature of the absorber was varied between 4.2 and 293 K. The gamma-ray source, ^{57}Co embedded in Cu metal, was always kept at room temperature. The calibration of the velocity scale was made by using pure Fe and α-Fe_2O_3 as standard absorbers. The isomer shift is expressed relative to pure Fe metal. The ratios of the Fe^{3+} and Fe^{4+} ions, and the isomer shifts and quadrupole splittings of the products were estimated from the ^{57}Fe Mössbauer spectra by using a Curve Resolver-310 (Du Pont Co.).

Results and Discussion

X-Ray-diffraction Measurements. Strontium fer-

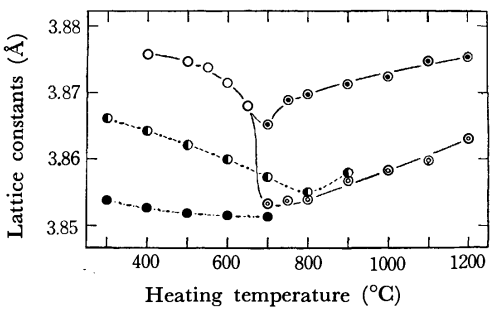

Fig. 1. Lattice parameters of the perovskite-type $SrFeO_x$ ($2.5<x<3.0$) products obtained by heating $SrFeO_4$ at various conditions. The abscissa shows the heating temperature.
○: a_0 of a cubic $SrFeO_x$ phase obtained in air.
◎: a_0 of a tetragonal $SrFeO_x$ phase obtained in air.
⊙: c_0 of a tetragonal $SrFeO_x$ phase obtained in air.
◐: a_0 of a cubic $SrFeO_x$ phase obtained under the oxygen pressures of 50 atm.
●: a_0 of a cubic $SrFeO_x$ phase obtained under the oxygen pressures of 500 atm.

19) T. Ichida, *J. Solid State Chem.*, **7**, No. 3 (1973) to be published.
20) V. R. Scholder, F. Kindervater, and W. Zeiss, *Z. Anorg. Allg. Chem.*, **283**, 338 (1956).

rate, $SrFeO_4$, began to decompose abruptly at about 70 °C in air. The products formed below 300 °C in air showed no X-ray-diffraction peak. The products obtained by heating $SrFeO_4$ in air or in an oxygen atmosphere at temperatures from 400 to 650 °C consisted of a single phase of a cubic perovskite structure, while those formed above 700 °C were a single phase of a tetragonal perovskite structure. The products obtained under the oxygen pressures from 50 to 500 atm and at temperatures from 300 to 900 °C were a single phase of a cubic perovskite structure.

The lattice constants were measured using the (200) reflections; the results are depicted in Fig. 1. It has been known in the $SrFeO_x$ ($2.5<x\leqq3.0$) system with the perovskite structure that the lattice constants decreased with an increase in the Fe^{4+}-ion concentration, for the Fe^{4+} ion has a smaller ionic radius than the Fe^{3+} ion. According to Clevenger,[13] the ionic radii of the Fe^{3+} and Fe^{4+} ions are 0.67 Å and 0.59 Å respectively.

Mössbauer-effect Measurements. The Mössbauer spectrum, measured at room temperature, of the decomposition products obtained by heating $SrFeO_4$ for 4 hr at 160 °C in air consisted of a narrow single-line absorption at −0.86 mm/s and a broad symmetric doublet. The narrow single-line absorption is characteristic of the Fe^{6+} state. This absorption disappeared when the amorphous product was heated at 160 °C for more than 10 days. The Mössbauer spectra of the amorphous decomposition product measured at room temperature and at 4.2 K are shown in Fig. 2. At room temperature, a broad symmetric doublet was observed. The isomer shift and quadrupole splitting of the doublet were +0.35±0.02 mm/s and 0.57±0.02 mm/s respectively. A set of six broad absorptions with the internal magnetic field of 480±5 kOe appeared at 4.2 K. These Mössbauer parameters are characteristic of the Fe^{3+} state. All of the iron ions in the amorphous product were trivalent. No intermediate valence state, the Fe^{5+} or Fe^{4+} ion, was detected in any decomposition product in this work. Judging from the Mössbauer spectra and from the fact that no X-ray diffraction peak was observed, it seems that the product consists of ultrafine particles which show superparamagnetism at room temperature. The broad line-width is caused by the inhomogeneity of the crystallographic circumstances of the iron ions. These results observed in the thermal decomposition process of $SrFeO_4$ are very similar with those found in the case of K_2FeO_4.[18]

The Mössbauer absorption spectra of the products with a cubic perovskite structure obtained by heating $SrFeO_4$ below 600 °C in air are shown in Fig. 3 (spectra measured at room temperature) and in Fig. 4 (at 4.2 K). The results show that most of the iron ions in the cubic perovskite phase obtained at lower temperatures were in trivalent state and that the Fe^{4+}-ion concentration increased gradually with the increase in the heating temperature up to 600 °C. Besides, it was found that, in these products with a cubic perovskite structure, there was only one kind of species for each of the Fe^{3+} and Fe^{4+} ions. In Fig. 3, the results of the curve resolutions obtained by fitting the paramagnetic Mössbauer spectra with Lorentzian curves using a Curve Resolver-310 (Du Pont Co.) are represented by broken lines. The paramagnetic spectrum of the Fe^{3+} ions was composed of a symmetric doublet with an isomer shift of +0.22±0.02 mm/s, and with a quadrupole splitting of 0.63± 0.02 mm/s, while that of the Fe^{4+} ions was composed of a singlet with an isomer shift of +0.07±0.02 mm/s.

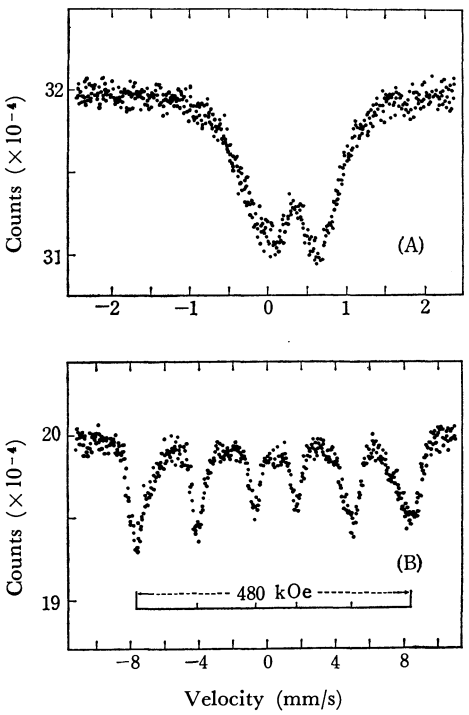

Fig. 2. ^{57}Fe Mössbauer absorption spectra at 293 K(A) and 4.2 K(B) of an amorphous product obtained by heating $SrFeO_4$ at 160 °C in air for 10 days.

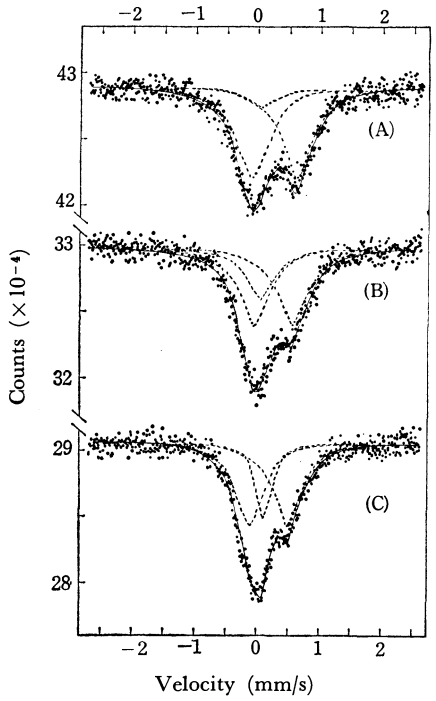

Fig. 3. ^{57}Fe Mössbauer absorption spectra at 293 K of cubic perovskite $SrFeO_x$ compounds obtained by heating $SrFeO_4$ in air at 400 °C(A), 500 °C(B), and 600 °C(C).

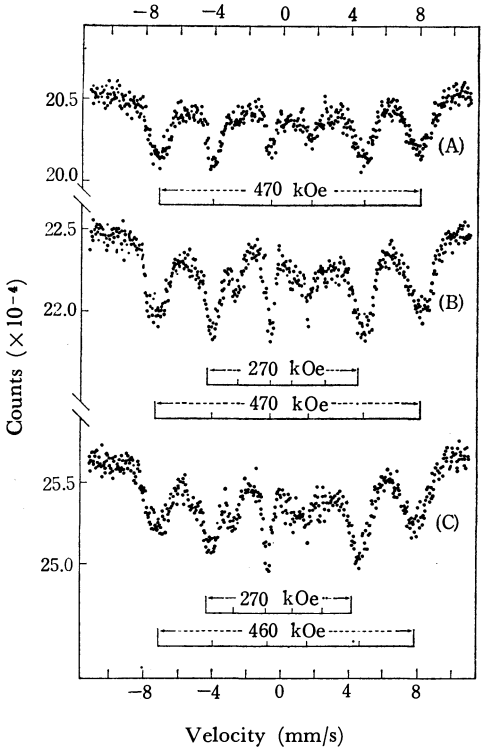

Fig. 4. ^{57}Fe Mössbauer absorption spectra at 4.2 K of cubic perovskite $SrFeO_x$ compounds obtained by heating $SrFeO_4$ in air at 400 °C(A), 500 °C(B), and 600 °C(C).

The Mössbauer spectra of the products with a tetragonally distorted perovskite structure, obtained by heating at 800 °C and 1200 °C in air, are shown in Fig. 5 (spectra measured at room temperature) and in Fig. 6 (at 4.2 K). In contrast to the cubic samples (Fig. 3), two extra absorptions appeared at about +1.0 mm/s and −0.3 mm/s in the spectrum of a tetragonal sample obtained by heating at 800 °C in air. The relative intensities of these two outer-most absorptions increased with the increase in the heating temperature. This spectrum should be interpreted as having two kinds of Fe^{3+} sites in the tetragonal phase. This interpretation is supported by the results in a magnetically-ordered state. In Fig. 5, the results of the curve resolutions are represented by broken lines. The paramagnetic Mössbauer spectra of tetragonal $SrFeO_x$ samples were composed of three kinds of absorptions: (1) a singlet of Fe^{4+} with an isomer shift of +0.07±0.02 mm/s, (2) an Fe^{3+}-I doublet of Fe^{3+} with an isomer shift and a quadrupole splitting of +0.19±0.02 mm/s and 0.63±0.02 mm/s respectively, and (3) an Fe^{3+}-II doublet of Fe^{3+} with an isomer shift and a quadrupole splitting of +0.38±0.02 mm/s and 1.25±0.02 mm/s respectively. Fe^{3+}-I is similar to those in the cubic perovskite phase (Fig. 3).

The Mössbauer spectra of tetragonally-distorted samples measured at 4.2 K (Fig. 6) were very complex. In the spectrum of the tetragonal perovskite sample obtained at 800 °C in air (Fig. 6), two kinds of magnetically-split Fe^{3+} absorptions were observed; one had an internal magnetic field of 500 kOe and a negligibly small quadrupole interaction, and the other,

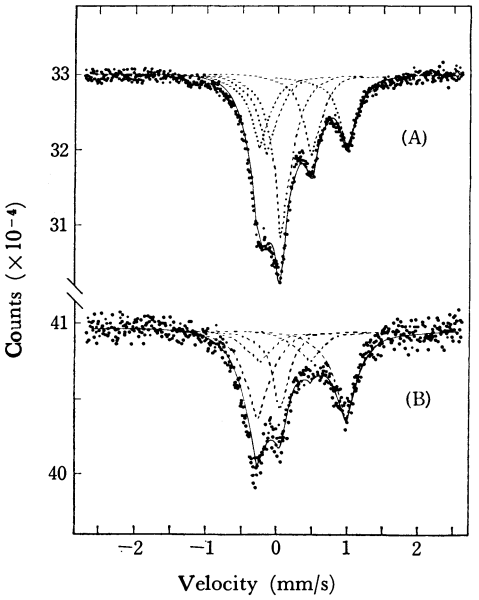

Fig. 5. ^{57}Fe Mössbauer absorption spectra at 293 K of tetragonal perovskite $SrFeO_x$ compounds obtained by heating $SrFeO_4$ in air at 800 °C(A) and 1200 °C(B).

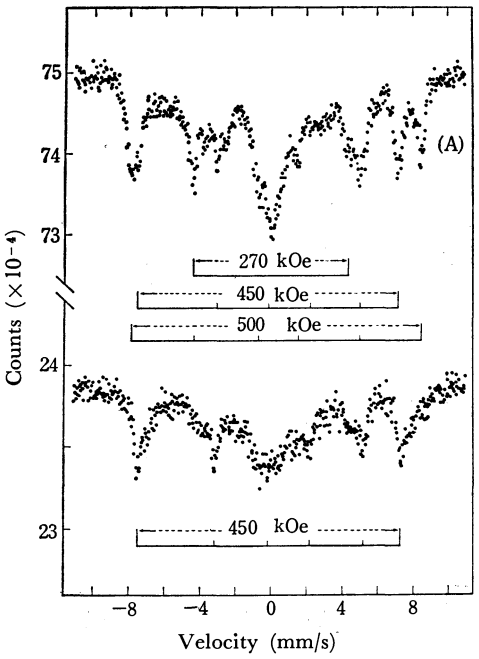

Fig. 6. ^{57}Fe Mössbauer absorption spectra at 4.2 K of tetragonal perovskite $SrFeO_x$ compounds obtained by heating $SrFeO_4$ in air at 800 °C(A) and 1200 °C(B).

an internal magnetic field of 450 kOe and a large quadrupole interaction (S_1—S_2; −2.30±0.05 mm/s). The absorption due to Fe^{4+} ions showed an internal magnetic field of 270 kOe, which was consistent with the data on Fe^{4+} ions in the cubic perovskite phase with a large oxygen deficiency (Fig. 4). The spectra of the tetragonally-distorted $SrFeO_x$ samples showed that a considerable part of both the Fe^{3+} and Fe^{4+} ions was in a paramagnetic state even at 4.2 K (see Fig. 6). It was obvious that the relative intensity of the Fe^{3+}-II increased with the increase in the heating temperature from 800 to 1200 °C. The Mössbauer

spectrum measured at 4.2 K on the tetragonal $SrFeO_x$ sample obtained at 1200 °C in air consisted mainly of magnetically-ordered Fe^{3+}-II absorptions and a paramagnetic absorption. The relative intensities of the Fe^{4+} absorptions and Fe^{3+}-I was small.

The X-ray results show that a sample has a cubic structure if the heating temperature is lower than 700 °C. In the Mössbauer results, however, the Fe^{3+}-II doublet appeared in a sample heated at 650 °C as a result of local distortion.

As is shown in Fig. 1, the perovskite-type products obtained by heating $SrFeO_4$ below 900 °C and at oxygen pressures from 50 to 500 atm showed no tetragonal distortion. The lattice constants of the products obtained under the oxygen pressures of 500 atm were near 3.850 Å, which had previously been reported as the value for the non-defective cubic perovskite, $SrFeO_3$.[10] The product obtained at 700 °C and at oxygen pressures of 500 atm showed the smallest lattice constant, therefore; it was supposed that it had the largest Fe^{4+} concentration among the samples obtained in this work. The Mössbauer spectra of the sample are shown in Fig. 7. The results of the curve resolutions on the paramagnetic spectrum are represented there by broken lines.

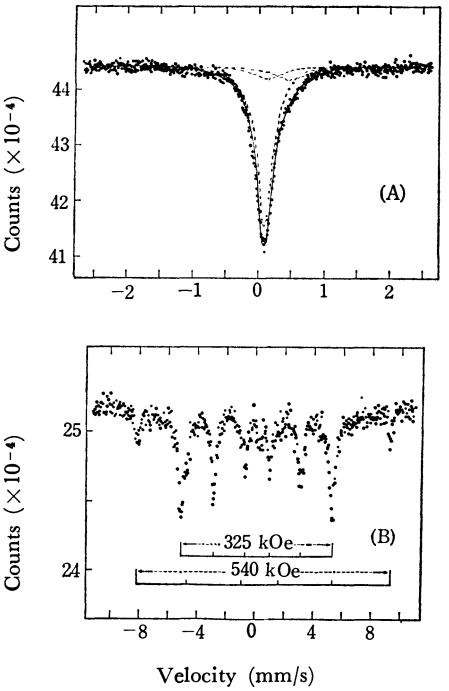

Fig. 7. ^{57}Fe Mössbauer absorption spectra at 293 K(A) and 4.2 K(B) of a cubic perovskite $SrFeO_x$ compound obtained by heating $SrFeO_4$ at 700 °C and the oxygen pressures of 500 atm.

The relative intensity of Fe^{3+}/Fe^{4+} was estimated by measuring the areas of the Mössbauer absorption spectra. Consequently, it was confirmed that the relative intensity does not change with the temperature. The oxygen contents in the $SrFeO_x$ products formed under various conditions were determined by using the ratio of the Fe^{3+} and Fe^{4+} ions thus obtained. The results are shown in Fig. 8. Isobaric curves for

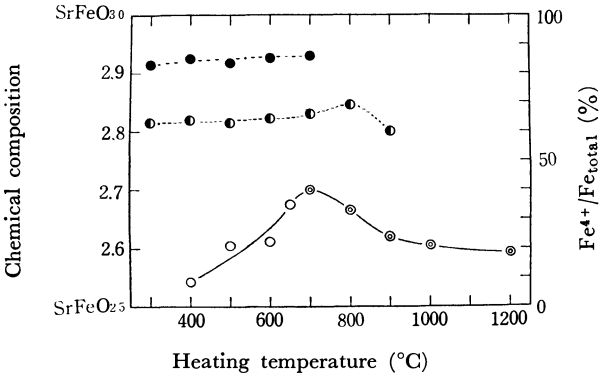

Fig. 8. Relation among the oxygen concentrations and heating conditions in the perovskite-type $SrFeO_x$ ($2.5<x<3.0$) compounds obtained by heating $SrFeO_4$. The abscissa shows the heating temperature.
○: a cubic $SrFeO_x$ phase obtained in air.
◎: a tetragonal $SrFeO_x$ phase obtained in air.
◐: a cubic $SrFeO_x$ phase obtained under the oxygen pressures of 50 atm.
●: a cubic $SrFeO_x$ phase obtained under the oxygen pressures of 500 atm.

0.2, 50, and 500 atm oxygen pressures are drawn to show the variation in the total composition with the temperature and the pressure.

Comparison with Previously-reported Results. It has been reported, for the $SrFeO_x$ ($2.5<x\leqq3.0$) system, that the cubic perovskite structure was no longer stable when the concentration of Fe^{3+} ion exceeded 30%.[10] Then a tetragonal distortion occurred. When the concentration of Fe^{3+} was more than 70%, the other phase, $SrFeO_{2.50}$, with a dicalcium ferrite structure, became more stable than the perovskite. On the other hand, in the present work, a cubic perovskite $SrFeO_x$ product with a Fe^{3+}-ion concentration of about 90% was obtained when $SrFeO_4$ was heated in air below 650 °C. The tetragonal perovskites obtained above 700 °C in air included Fe^{3+} ions in a concentration of 60—80%. Such a disagreement with the previous data may be due to the difference in the starting material.

In the case of $BaTiO_3$, which has the same perovskite structure, it has been reported that the crystal system of the compound is affected by the particle size.[21,22] Barium titanate, $BaTiO_3$, is transformed from a cubic to a tetragonal system below the Néel temperature (393 K). Ern[21] reported that fine particles (200 Å) of barium titanate obtained by a wet method show a cubic perovskite structure with $a_0=4.035$ Å even at room temperature. Nishimoto *et al.*[22] also prepared fine particles (≧500 Å) of barium titanate by the thermal decomposition of barium titanyl oxalate tetrahydrate, $BaTiO(C_2O_4)_2\cdot4H_2O$, at temperatures from 600 to 1100 °C; they found that the tetragonality decreased with a decrease in the particle size. In the present case of $SrFeO_x$ compounds obtained by heating $SrFeO_4$ at low temperatures, the cubic structure with a high oxygen deficiency

21) V. Ern, *J. Amer. Ceram. Soc.*, **46**, 295 (1963).
22) K. Nishimoto, Y. Goto, N. Nakanishi, and S. Kachi, *Funtai oyobi Funmatsu Yakin*, (Kyoto), **14**, 221 (1967).

seems to be stabilized when the particle size is small.

Another characteristic of the Mössbauer spectra observed on the tetragonal $SrFeO_x$ (Fig. 6) was the existence of a paramagnetic component even at 4.2 K. Gallagher *et al.*[9] have also observed very similar spectra on oxygen-deficient $SrFeO_x$. Since the linewidth of their X-ray peaks was very narrow, it is not possible that these samples consist of ultra-fine particles which show superparamagnetism even at 4.2 K. At the present stage, no likely interpretation can be proposed, but the oxygen vacancies with high concentrations should play an important role in determining the magnetic properties. There remain some unsolved problems with regard to the complicated magnetic structure of $SrFeO_x$ ($2.5<x<3.0$) compounds.

The author would like to express his hearty thanks to Professor Toshio Takada for his guidance during the course of this work. The author also wishes to thank Professor Yoshichika Bando, Dr. Teruya Shinjo, Dr. Masao Kiyama and Dr. Koji Kosuge for their continuous guidance and helpful discussions. Thanks are also due to Dr. Mitsuo Imai and Dr. Koji Sanbongi of the Research Laboratories, Kawasaki Steel Corporation for their warm encouragement. He also wishes to thank the Kawasaki Steel Corporation for giving him an opportunity to study at Kyoto University.

BULLETIN OF THE CHEMICAL SOCIETY OF JAPAN, VOL. 46, 1596—1602 (1973)

Apparent Molal Volumes of Some Organic Electrolytes in a Dilute Aqueous Solution at 5, 25, and 45 °C

Masao SAKURAI

Department of Polymer Science, Faculty of Science, Hokkaido University, Sapporo 060

(Received December 11, 1972)

The apparent molal volumes, ϕ_v, of five series of homologous organic salts of the $H(CH_2)_nCOONa$ (n=0—6), $(CH_2)_n(COONa)_2$ (n=0,2,3,4,6,8), $H(CH_2)_nNH_3Cl$ (n=0,2,6), $(CH_2)_n(NH_3Cl)_2$ (n=2,3,6), and $H(CH_2)_nSO_3Na$ (n=1,2) types in a dilute aqueous solution have been measured by means of a float method as a function of the concentration and the temperature. The coefficients of the deviation of ϕ_v from the Debye-Hückel limiting law, b_v, are negative for most organic electrolytes. The large positive b_v values observed for the sodium oxalate and sodium succinate solutions at 5 °C have been attributed to ion-pair formation. The partial molal expansibility of organic ions has been evaluated and interpreted on the basis of the multilayer hydration model proposed by Frank and Wen. The estimation of volume increments per CH_2 group suggests that the influences of ammonium ions on the hydrophobic hydration around CH_2 groups differ significantly from those of carboxylate ions. The volume change accompanying the substitution of a terminal hydrogen atom with an ionic group has been calculated, and discussed in connection with the overlapping effect of electrostriction in bolaform electrolytes.

Our previous short communication[1] has pointed out that the volumetric behavior of polyelectrolytes in an aqueous solution appears to be complicated by the fact that the interactions between ionic groups or hydrophobic groups on a polymer chain do not disappear even at an infinite dilution. In order to elucidate the complicated behavior of the polyelectrolytes, reliable volumetric information on various organic salts must be established.

It is well known that the concentration and temperature dependence of the apparent molal volumes, ϕ_v, of tetraalkylammonium halides (n-R_4NX) in water are abnormal compared to the case of simple electrolytes.[2-7] For example, the concentration dependence of the ϕ_v of n-Bu_4NBr exhibits both a maximum and a minimum, and the limiting partial molal volumes of the R_4NX do not go through a maximum when plotted against the temperature. This anomalous volumetric behavior of the R_4NX has been interpreted in terms of the enhancement or stabilization of the hydrogen-bonded structure of water in the vicinity of the nonpolar hydrocarbon portion of the R_4N^+ ions (hydrophobic hydration).

In the studies of the R_4NX solutions, the electrostriction of water molecules by the R_4N^+ ions has been considered to be almost negligible, since the central charges are completely masked by the large hydrocarbon groups. For more common organic electrolytes, there have been some careful examinations of the concentration dependence of ϕ_v at 25 °C in the cases of mono-, di-, and trisubstituted aliphatic ammonium salts,[8-10] cyclic ammonium

1) M. Sakurai, T. Nakajima, T. Komatsu, and T. Nakagawa, *Chem. Lett.*, **1972**, 355.
2) W.-Y. Wen and S. Saito, *J. Phys. Chem.*, **68**, 2639 (1964); *ibid.*, **69**, 3569 (1965).
3) B. E. Conway, R. E. Verrall, and J. E. Desnoyers, *Trans. Faraday Soc.*, **62**, 2738 (1966).
4) F. Franks and H. T. Smith, *ibid.*, **63**, 2586 (1967).
5) F. J. Millero and W. Drost-Hansen, *J. Phys. Chem.*, **72**, 1758 (1968).
6) G. Gopal and M. A. Siddiqi, *ibid.*, **72**, 1814 (1968).
7) F. J. Millero, *Chem. Rev.*, **71**, 147 (1971); "Structure and Transport Processes in Water and Aqueous Solutions," ed. by R. A. Horne, Wiley-Interscience, New York, N. Y. (1971), Chapter 13.
8) J. E. Desnoyers and M. Arel, *Can. J. Chem.*, **45**, 359 (1967).
9) R. E. Verrall and B. E. Conway, *J. Phys. Chem.*, **70**, 3961 (1966).
10) L. H. Laliberté and B. E. Conway, *ibid.*, **74**, 4116 (1970).

salts,[11] sodium carboxylates,[12] and sodium alkylsulfates.[13,14]

This report will describe the results of precision-density measurements of the dilute aqueous solutions of several organic salts of the 1-1 and 2-1 (bolaform) types at 5, 25, and 45° C. The apparent molal volumes and the partial molal expansibilities have been calculated from these density data.

Experimental

Materials. The *n*-alkylamine hydrochlorides and sodium salts of formic, acetic, and propionic acids were reagent grade materials and were recrystallized from ethanol, acetone, or water. The dihydrochlorides of ethylenediamine, trimethylenediamine, and hexamethylenediamine were precipitated from ethanol solutions of the amines by the addition of an equivalent amount of hydrochloric acid, and were then washed with ethanol and acetone. All the other salts were prepared by the neutralization of the corresponding carboxylic acids or alkylsulfonic acids with sodium hydroxide, and were purified by crystallization from water-ethanol or water-acetone mixtures. Each salt was dried under a vacuum for at least 3 days before use. Deionized water was distilled using an quartz still.

Procedure. The solution densities were evaluated to six decimal places by means of a float method similar to that described by Desnoyers and Arel.[8] The float, with a volume of about 200 ml, was suspended to the pan of a Mettler balance (Model H20T) by a thin nylon thread (0.11 mm dia.). The volume of the float was calculated by weighing it in air and in pure water at a constant temperature. The temperature inside the cell was controlled to ±0.001 °C by circulating water from a well-insulated bath. The densities of pure water were taken as 0.999992, 0.997075, and 0.990244 g/ml at 5, 25, and 45 °C respectively.[15] The water was degassed to prevent the formation of bubbles on the float during the experiment. The effect of the surface tension at the nylon-solution interface was neglected. The reproducibility of the density measurements was found to be better than 2×10^{-6} g/ml.

The solutions were prepared by adding weighed amounts of the concentrated stock solutions into a cell containing a known amount of pure water. Only for sodium oxalate was dry solid salt added because of its low solubility in water.

The apparent molal volumes were calculated from the density measurements using this equation:

$$\phi_v = \frac{1000(d_0-d)}{mdd_0} + \frac{M}{d} \qquad (1)$$

where d_0 is the density of water; d, that of the solution; M, the molecular weight of the salt, and m, its molality.

Results

The concentration dependence of the apparent molal volumes of the electrolytes can be fitted to the equation of Redlich and Meyer:[16]

$$\phi_v = \phi_v^\circ + S_v\sqrt{c} + b_v c \qquad (2)$$

where ϕ_v° is the limiting apparent molal volume; S_v, the theoretical limiting slope; b_v, an empirical constant determined from the experimental results, and c, the molar concentration converted from the known density. The limiting slope can be derived from the Debye-Hückel limiting law; hence, it depends on the temperature, the physical properties of the solvent, and the valence factor of the electrolytes. The values of S_v for 1-1 and 2-1 electrolytes at 5, 25, and 45 °C were calculated from the table in Ref. 16.

A few typical examples of the plots of $\phi_v - S_v\sqrt{c}$ *vs.* c are shown in Figs. 1 and 2. From these figures, the values of the ϕ_v° (equal to the limiting partial molal volume, $\bar{V}^\circ$) and the b_v slope were calculated for all the electrolytes studied. The results are given in Table 1. The $\bar{V}^\circ$ values of sodium formate, sodium acetate, and sodium butyrate at 25°C are in good agreement with the data reported by King.[12]

Discussion

Deviations from the Limiting Law. As is shown in Table 1, most of the b_v values are more or less negative, like those of simple electrolytes, except at lower temperatures. The negative deviation from the limiting law is expected if the equation for the concentration dependence of ϕ_v is derived from the extended Debye-Hückel law, including the ion-size parameter, a (Owen-Brinkley equation).[7] The extremely large negative b_v values observed for bolaform electrolytes may be accounted for qualitatively by this equation. Since the increase in the chain length is equivalent to the increase in a, very nega-

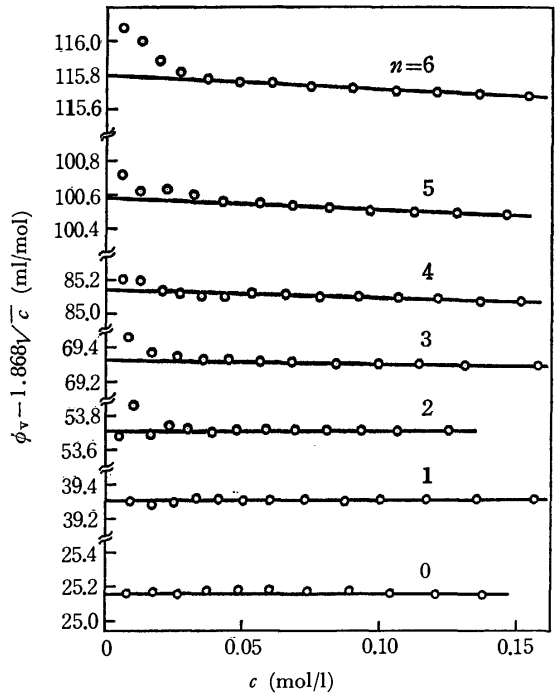

Fig. 1. Apparent molal volumes of sodium carboxylates, $H(CH_2)_nCOONa$, in water at 25 °C.

11) S. Cabani, G. Conti, L. Lepori, and G. Leva, *ibid.*, **76**, 1343 (1972).
12) E. J. King, *ibid.*, **73**, 1220 (1969).
13) F. Franks and H. T. Smith, *ibid.*, **68**, 3581 (1964).
14) F. Franks, M. J. Quickenden, R. R. Ravenhill, and H. T. Smith, *ibid.*, **72**, 2668 (1968).
15) G. S. Kell, *J. Chem. Eng. Data*, **12**, 66 (1967).
16) O. Redlich and D. M. Meyer, *Chem. Rev.*, **64**, 221 (1964).

Table 1. Values of $\overline{V}^\circ$ ($=\phi_V^\circ$) and b_V at 5, 25, and 45 °C

n	$\overline{V}^\circ$ (ml/mol)			b_V (1 ml/mol²)		
	5° C	25 °C	45 °C	5 °C	25 °C	45 °C
			$H(CH_2)_nCOONa$			
0	22.53	25.15	26.20	0.6	0.0	−1.1
1		39.31			0.0	
2	51.19	53.71	55.15	0.8	0.0	−1.0
3		69.32			−0.2	
4		85.14			−0.4	
5		100.58			−0.7	
6	111.55	115.80	119.48	−0.3	−0.8	−0.7
			$(CH_2)_n(COONa)_2$			
0	22.56	28.08	30.08	5.6	−2.2	−6.5
2	48.85	54.10	55.82	1.7	−3.5	−7.1
3		69.98			−4.0	
4		86.24			−5.6	
6		117.61			−4.4	
8		148.91			−4.2	
			$H(CH_2)_nNH_3Cl$			
0	34.51	35.78	36.03	0.4	−0.5	−1.0
2	70.13	71.23	71.86	−0.7	−0.8	−1.3
6	132.55	135.26	137.50	−3.1	−2.8	−2.3
			$(CH_2)_n(NH_3Cl)_2$			
2	76.95	80.10	80.72	−1.1	−5.5	−8.2
3		99.58			−5.1	
6		152.04			−9.4	
			$H(CH_2)_nSO_3Na$			
1		53.88			0.0	
2	68.66	71.56	73.14	0.7	−0.1	−1.5

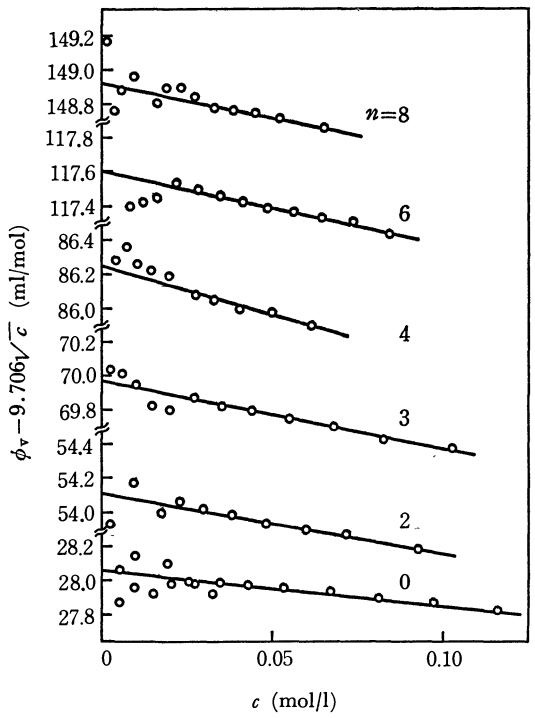

Fig. 2. Apparent molal volumes of sodium dicarboxylates, $(CH_2)_n(COONa)_2$, in water at 25 °C.

tive b_V values should be observed for larger bolaform electrolytes.

However, the Owen-Brinkley equation cannot give a reasonable interpretation of the positive b_V values observed for some electrolytes at 5°C, or of the change in b_V values with the increase in the chain length in the case of the 1-1 type homologous series, in which the a values are all the same.[8,17] From these points of view, the study of the b_V as a function of the size, the charge, and the temperature is assumed to provide useful information about ion-ion interactions.

The b_V values observed for 1-1 electrolytes become more negative with the increase in the number of CH_2 groups; this is analogous to the results obtained for n-alkylamine hydrobromides by Desnoyers and Arel.[8]

In aqueous solutions, as is well recognized, hydrophobic solutes enhance or stabilize the hydrogen-bonded structure of water in the vicinity of the nonpolar groups. Such a nonpolar group-water interaction is sometimes called "hydrophobic hydration" to distinguish it from normal hydration. Experimental evidence has confirmed a net contraction in volume when hydrophobic hydration takes place, although there has been no general agreement on the exact nature of the structure of water in this hydration layer.[18] At present it seems most reasonable to interpret the volumetric behavior of nonpolar solutes

17) J. E. Desnoyers, M. Arel, and P. A. Leduc, *Can. J. Chem.* **47**, 547 (1969).
18) E. Wicke, *Angew. Chem., Int. Ed.*, **5**, 106 (1966).

in water in terms of the formation of "quasi-clathrate cages."[2,4]

As the concentration increases, the overlap of these cage systems results in a more efficient contraction in volume as a result of the co-operative stabilization of the hydrogen-bonded structure. Consequently, larger negative b_v values should be observed for the 1–1 organic salts with larger hydrocarbon portions.

Millero has pointed out that an examination of the temperature dependence of b_v can reveal the nature of the ion-ion interactions.[19,20] Table 1 shows that the effects of the temperature on the b_v are similar to the cases of more common electrolytes such as NaCl, in that $\partial b_v/\partial T$ is negative for all the organic salts except for the *n*-hexylamine hydrochloride solution, in which $\partial b_v/\partial T$ is positive as in *n*-Bu_4NBr. The latter behavior may be interpreted on the basis of the assumption that the volume contraction caused by the overlap of the hydrophobic hydration with the increase in concentration is more pronounced at lower temperatures, since the hydrogen-bonded structure of water is stabilized at low temperatures.

For the bolaform electrolytes, the $\partial b_v/\partial T$ values are much more negative. In contrast with the effect of hydrophobic hydration, the negative contribution of the electrostriction to the ϕ_v is more pronounced at higher temperatures, according to the Drude-Nernst equation.[7] Therefore, the negative $\partial b_v/\partial T$ value can be interpreted in terms of the overlap of the highly-electrostricted regions caused by charges in the like sign of the divalent bolaform ions.

It is noteworthy that the b_v values for sodium oxalate and sodium succinate are large and positive at 5°C. The positive b_v value has been interpreted in terms of the cation-anion interactions[21] or the ion-pair formation.[19] The ion-pair formation may be regarded as the limiting case of the cation-anion attraction. Thus, one can predict an ion-pairing in aqueous solutions of the bolaform electrolytes such as sodium oxalate at very low temperatures.

Partial Molal Volumes and Expansibilities of Ions. The study of the limiting partial molal volume, $\overline{V}^\circ$, and the limiting partial molal expansibility, $\overline{E}^\circ = \partial\overline{V}^\circ/\partial T$, may be a useful tool for elucidating ion-water interactions. It has been well established that the $\overline{V}^\circ$ of an electrolyte is equal to the sum of its ionic components: $\overline{V}^\circ = \overline{V}^\circ(\text{cation}) + \overline{V}^\circ(\text{anion})$.[21] Many workers have attempted to determine the individual ionic volume by means of various methods, and many different values of the partial molal volume of a proton, $\overline{V}^\circ(H^+)$, have been reported.[7]

In the present analysis, we have utilized the equation for the temperature dependence of the $\overline{V}^\circ(H^+)$ proposed by Millero:[7]

$$\overline{V}^\circ(H^+) = -5.1 - 0.008\,T - 1.7 \times 10^{-4}T^2 \qquad (3)$$

Table 2. Values of $\overline{V}^\circ$ (ion) at 5, 25, and 45 °C, and $\overline{E}^\circ$ (ion) at 15 and 35 °C

n	$\overline{V}^\circ$(ion) (ml/mol)			$\overline{E}^\circ$(ion) (ml/mol deg)	
	5 °C	25 °C	45 °C	15 °C	35 °C
H^+	−5.1	−5.4	−5.8	−0.015	−0.020
Cl^-	21.8	23.2	24.2	0.070	0.050
Na^+	−7.6	−6.6	−6.6	0.050	0.000
			$H(CH_2)_nCOO^-$		
0	30.1	31.8	32.8	0.085	0.050
2	58.8	60.3	61.8	0.075	0.075
6	119.2	122.4	126.1	0.160	0.185
			$-OOC(CH_2)_nCOO^-$		
0	37.8	41.3	43.3	0.175	0.100
2	64.1	67.3	69.0	0.160	0.085
			$H(CH_2)_nNH_3^+$		
0	12.7	12.6	11.8	−0.005	−0.040
2	48.3	48.0	47.7	−0.015	−0.015
6	110.8	112.1	113.3	0.015	0.060
			$^+H_3N(CH_2)_nNH_3^+$		
2	33.4	33.7	32.3	0.015	−0.070
			$H(CH_2)_nSO_3^-$		
2	76.3	78.2	79.7	0.095	0.075

By using this equation and the additivity principle, one can calculate the values of $\overline{V}^\circ(Cl^-)$ and $\overline{V}^\circ(Na^+)$ from the $\overline{V}^\circ$ data for HCl[22] and NaCl,[19] and hence those of the $\overline{V}^\circ$(ion) for the organic ions from our $\overline{V}^\circ$ data. The results are given in Table 2, together with the $\overline{E}^\circ$(ion) values at 15 and 35 °C.

The $\overline{V}^\circ$(ion) and $\overline{E}^\circ$(ion) can be divided into four major components on the basis of the multilayer hydration model proposed by Frank and Wen:[23]

$$\overline{V}^\circ(\text{ion}) = \overline{V}^\circ(\text{cryst}) + \overline{V}^\circ(\text{elect}) + \overline{V}^\circ(\text{disord}) + \overline{V}^\circ(\text{str}) \qquad (4)$$

$$\overline{E}^\circ(\text{iron}) = \overline{E}^\circ(\text{cryst}) + \overline{E}^\circ(\text{elect}) + \overline{E}^\circ(\text{disord}) + \overline{E}^\circ(\text{str}) \qquad (5)$$

where (cryst) means the crystal partial molal component; (elect), the contribution of the electrostrictional effect; (disord), that of the disordered or void space-packing effect, and (str), that of hydrophobic hydration. A detailed discussion of the natures of these components has been given by Millero.[7]

Table 2 shows that the $\overline{E}^\circ$(ion) values for the alkylammonium ions are much smaller than those for the carboxylate ions with the same hydrocarbon chains. As has been mentioned above, the volume decrease due to the electrostriction is, as a first approximation, more pronounced at higher temperature. Therefore, this finding may be attributed to the larger contribution of the $\overline{E}^\circ$(elect) for the NH_3^+ group than for the COO^- group, because of a low charge density on the

19) F. J. Millero, *J. Phys. Chem.*, **74**, 356 (1970).
20) F. J. Millero, *J. Chem. Eng. Data*, **15**, 562 (1970); *ibid.*, **16**, 229 (1971).
21) J. E. Desnoyers, M. Arel, G. Perron, and C. Jolicoeur, *J. Phys. Chem.*, **73**, 3346 (1969).
22) G. Akerlöf and J. W. Teare, *J. Amer. Chem. Soc.*, **60**, 1226 (1938).
23) H. S. Frank and W.-Y. Wen, *Discuss. Faraday Soc.*, **24**, 133 (1957).

COO^- group due to electron delocalization.[12] This also appears to fit well the findings on the volume changes for ionization reactions reported by Kauzmann *et al*; the volume decrease accompanying the ionization of carboxylic acids is only one half that of alkylamines.[24] It should, however, be noted that there remains some uncertainty as to the above conclusion because of an ambiguity in the determination of the absolute $\overline{V}^\circ(H^+)$ values.

It is of interest to examine the temperature dependence of the $\overline{E}^\circ$(ion) in connection with the hydrocarbon-chain length. Table 2 apparently shows that the $\partial\overline{E}^\circ(\text{ion})/\partial T$ value is negative for the $n=0$ compounds, nearly zero for $n=2$, and positive for $n=6$ in the series of both *n*-alkylammonium ions and carboxylate ions. The positive temperature dependence of the $\overline{E}^\circ$, which has been found for R_4NX or hydrophobic nonelectrolytes, implies that the $\overline{V}^\circ$-temperature plot does not go through a maximum; in this it is unlike the simple inorganic ions. This behavior can be ascribed to the effect of the hydrophobic hydration around the long hydrocarbon chains, since the hydrogen-bonded structure of water is sensitive to the temperature and, hence, the negative contribution of $\overline{V}^\circ$(str) to the $\overline{V}^\circ$(ion) should become less important as the temperature is increased. A similar discussion has been made by Hepler in relation to the pressure dependence of the partial molal heat capacity.[25]

The finding that the hydrophobic hydration predominantly contributes to the ion-water interactions for the ions with $n>2$ is consistent with the findings on the heat of transfer from H_2O to D_2O for sodium carboxylates reported by Snell and Greyson[26] and on that for *n*-alkylamine hydrobromides reported by Desnoyers *et al.*[27]

Particular attention should be given to the fact that the $\overline{E}^\circ$(ion) values of the ammonium ion and the ethylammonium ion are negative, while $\overline{E}^\circ(Na^+)$ is positive. At least the tendency that $\overline{E}^\circ(Na^+)>\overline{E}^\circ(NH_4^+)$ or $\overline{E}^\circ(EtNH_3^+)$ is not affected by any choice of the $\overline{V}^\circ(H^+)$ values. Millero *et al.*[5] have accounted for the low $\overline{E}^\circ$ of the NH_4Cl in terms of the ability of NH_4^+ to form an "icelike" structure. Their proposal, however, could not interpret the negative $\partial\overline{E}^\circ(NH_4^+)/\partial T$ value. Although we have no clear explanation of this finding at present, it might be correlated with the unknown nature of the $\overline{V}^\circ$(disord) or $\overline{E}^\circ$(disord) terms for organic ions. Furthermore, it should be kept in mind that the last three components in Eqs. (4) and (5) are inseparable from each other as a result of their overlapping or competing effects, as will be described in the following section.

Partial Molal Volume of a CH_2 Group. The difference in the $\overline{V}^\circ$ for the successive homologous salts is taken as the contribution of a methylene group, $\overline{V}^\circ(CH_2)$, to the limiting partial molal volume of the organic ion in water. This quantity may be affected by the changes in the overlapping or competing effects between $\overline{V}^\circ$(elect), $\overline{V}^\circ$(disord), and $\overline{V}^\circ$(str). The $\overline{V}^\circ(CH_2)$ values are shown in Fig. 3 as a function of the chain length, and are compared with similar data obtained for other homologous organic salts.[3,8,11]

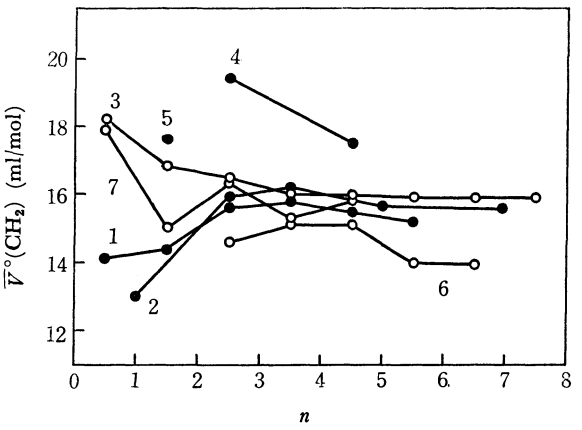

Fig. 3. The values of $\overline{V}^\circ(CH_2)$ as a function of chain length, calculated from the $\overline{V}^\circ$ data of homologous salts. 1: $H(CH_2)_nCOONa$, 2: $(CH_2)_n(COONa)_2$, 3: $H(CH_2)_nNH_3Br$,[8] 4: $(CH_2)_n(NH_3Cl)_2$, 5: $H(CH_2)_nSO_3Na$, 6: $(CH_2)_nNH_2Cl$,[11] 7: $[H(CH_2)_n]_4NBr$.[3,8]

It appears that the values of $\overline{V}^\circ(CH_2)$ approach about 16 ml/mol at 25 °C as the chain length increases. This value is quite similar to those obtained for sodium alkyl sulfates[14] and alcohols.[28] The methylene groups far apart from ionic groups may promote the structure of water in their vicinity without any disturbance by the ionic groups. Therefore, it can be stated that the partial molal volume of a CH_2 group in water is about 16 ml/mol at 25 °C when such a "normal" hydrophobic hydration takes place.

On the other hand, the deviations of the $\overline{V}^\circ(CH_2)$ values from the value of 16 ml/mol can be predicted for the electrolytes with shorter hydrocarbon chains as a result of the influences of the ionic groups. As Fig. 3 clearly shows, in fact, positive deviations are found for ammonium salts and sulfonates, and negative deviations for carboxylates. These results suggest that the influence of the COO^- group on the hydrophobic hydration surrounding CH_2 groups is significantly different from that of the NH_3^+ or SO_3^- groups.

For cyclic ammonium salts,[11] the $\overline{V}^\circ(CH_2)$ values deviate from the 16 ml/mol value even for longer-chain salts; this may indicate that the partial molal volume of a CH_2 group in a cyclic structure differs from that in an open chain.

It should be noted that the $\overline{V}^\circ$ values of the R_4NBr series increase in a peculiar manner with the increase in the alkyl-chain length. This implies that one cannot obtain a linear relation between the $\overline{V}^\circ$ and

24) W. Kauzmann, A. Bodanszky, and J. Rasper, *J. Amer. Chem. Soc.*, **84**, 1777 (1962).
25) L. G. Hepler, *Can. J. Chem.*, **47**, 4613 (1969).
26) H. Snell and J. Greyson, *J. Phys. Chem.*, **74**, 2148 (1970).
27) J. E. Desnoyers, R. Francescon, P. Picker, and C. Jolicoeur, *Can. J. Chem.*, **49**, 3460 (1971).
28) T. Nakajima, to be published.

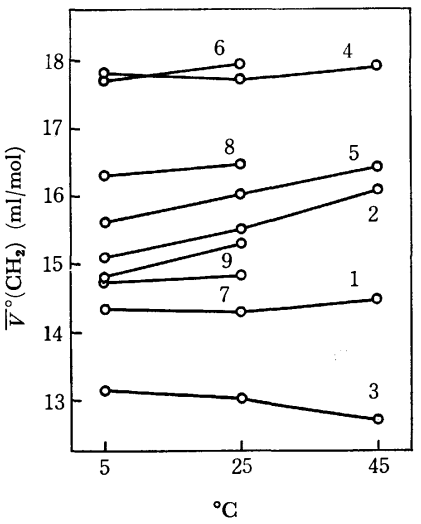

Fig. 4. Temperature dependence of the $\overline{V}°(CH_2)$ evaluated from the difference in the $\overline{V}°$ values of the salts with $n=$ 0, 2 and 6; 1: $H(CH_2)_nCOONa$; (2−0), 2: $H(CH_2)_n$-$COONa$; (6−2), 3: $(CH_2)_n(COONa)_2$; (2−0), 4: $H(CH_2)_nNH_3Cl$; (2−0), 5: $H(CH_2)_nNH_3Cl$; (6−2), 6: $[H(CH_2)_n]_4NBr$; (1−0),[4,8] 7: $[H(CH_2)_n]_4NBr$; (2−1),[4] 8: $[H(CH_2)_n]_4NBr$; (3−2),[4] 9: $[H(CH_2)_n]_4NBr$; (4−3).[4]

the molecular weights of cations, though such a relationship was assumed by Conway *et al.*[3] in order to determine the ionic partial molal volume of the Br^- ion.

The effect of the temperature on the $\overline{V}°(CH_2)$ value is shown in Fig. 4, together with the data for R_4NBr series.[4] The mean values of $\overline{V}°(CH_2)$, evaluated from the difference in the $\overline{V}°$ values of ethylamine and *n*-hexylamine hydrochloride, $\Delta\overline{V}°(n=6-2)$, are in excellent agreement with the values calculated for alcohols[28] at all the temperatures studied. Therefore, these values may reflect the effect of "normal" hydrophobic hydration at all temperatures. The partial molal volume of a CH_2 group far apart from the ionic group for the sodium carboxylates is apparently smaller than that for the *n*-alkylamine hydrochlorides at all temperatures. In both series, however, the temperature dependence of the $\overline{V}°(CH_2)$ is almost linear or slightly concave upward.

The mean values of $\overline{V}°(CH_2)$ evaluated from $\Delta\overline{V}°$ $(n=2-0)$ for both series exhibit less temperature dependence, while their absolute values differ greatly. Furthermore, the temperature dependence of the $\overline{V}°(CH_2)$ calculated from the $\overline{V}°$ values of sodium oxalate and succinate is obviously negative. Such a negative temperature dependence may be attributed to the strong influences of electrostriction on the $\overline{V}°$, as was discussed in the preceding section.

It should be noticed that we were unable to find any distinct difference in the temperature dependences of the $\overline{V}°(CH_2)$ values between carboxylate ions and *n*-alkylammonium ions. On the other hand, the $\overline{V}°$ (CH_2) values are considerably different in their dependences on the chain length. A similar situation is found in the results for the R_4NBr solutions (Fig. 4). If the marked difference in the $\overline{V}°(CH_2)$ behavior were caused by any structural change of water, it would also cause a difference in the temperature dependence of the $\overline{V}°(CH_2)$ value between carboxylate ions and *n*-alkylammonium ions. The experimental results, however, do not coincide with this prediction. Therefore, it may be concluded that the volume change caused by the overlapping or competing effects between $\overline{V}°$(elect), $\overline{V}°$(disord), and $\overline{V}°$(str) is insensitive to the temperature. An alternative explanation is that the $\overline{V}°$(ion) in Eq. (4) involves another additional component, whose nature is less temperature-sensitive. In this connection we wish to call attention to a calculation for the volume change on the mixing of hard spheres of different sizes.[29]

Volume Change for the Substitution with an Ionic Group. It is of interest to evaluate the volume change for the substitution of a terminal hydrogen atom on a hydrocarbon chain with an ionic group as follows:

$$H(CH_2)_nH \xrightarrow{\Delta\overline{V}_1°} H(CH_2)_nCOO^-$$

$$H(CH_2)_nCOO^- \xrightarrow{\Delta\overline{V}_2°} {}^-OOC(CH_2)_nCOO^-$$

Table 3. $\overline{V}°$ of hydrocarbons, $H(CH_2)_nH$, in water at 25 °C

n	1	2	3	4	5	6
$\overline{V}°$ (ml/mol)	37.3[a]	51.2[a]	66.8[a]	82.7[b]	98.6[b]	114.5[b]

a) Ref. 30.
b) These values were evaluated by the addition of $\overline{V}°(CH_2)=15.9$ ml/mol[8,28] to the $\overline{V}°$ value of propane.

Table 4. The volume changes for the substitution of H atom with ionic groups at 25 °C

n	$\Delta\overline{V}_1°$(ml/mol)	$\Delta\overline{V}_2°$(ml/mol)
	$H(CH_2)_nH \rightarrow H(CH_2)_nCOO^- \rightarrow {}^-OOC(CH_2)_nCOO^-$	
1	18.6	—
2	9.1	7.0
3	9.1	7.3
4	9.0	7.7
5	8.6	—
6	7.9	8.4
	$H(CH_2)_nH \rightarrow H(CH_2)_nNH_3^+ \rightarrow {}^+H_3N(CH_2)_nNH_3^+$	
1	−6.6[a]	—
2	−3.2	−14.3
3	−2.7[a]	−10.9
4	−2.6[a]	—
5	−2.5[a]	—
6	−2.4	−6.5

a) These values were calculated from the $\overline{V}°$ data of Desnoyers and Arel[8] for *n*-alkylamine hydrobromides assuming that $\overline{V}°(Br^-)-\overline{V}°(Cl^-)=6.9$ ml/mol[21] at 25 °C.

29) P. Assarsson and F. R. Eirich, *J. Phys. Chem.*, **72**, 2710 (1968).

$$H(CH_2)_nH \xrightarrow{\Delta\bar{V}_1^\circ} H(CH_2)_nNH_3^+$$
$$\xrightarrow{\Delta\bar{V}_2^\circ} {}^+H_3N(CH_2)_nNH_3^+$$

The partial molal volumes of methane, ethane and propane in water were taken from the data by Masterton;[30] they are listed in Table 3.

The results are given in Table 4. As the number of methylene groups is increased, the $\Delta\bar{V}_1^\circ$ values decrease for the carboxylate ions, whereas the opposite order was observed for the alkylammonium ions. This finding might be correlated with the difference in the $\bar{V}^\circ(CH_2)$ observed for these two homologous series.

30) W. L. Masterton, *J. Chem. Phys.*, **22**, 1830 (1954).

It is noteworthy that the $\Delta\bar{V}_2^\circ$ values are much more negative than the $\Delta\bar{V}_1^\circ$ values in the case of substitution with the NH_3^+ group. This behavior may be interpreted in terms of the "reinforcing effect on the electrostriction,,[24] as a result of the overlap of the electrostricted regions around the two NH_3^+ groups on the bolaform ion. It seems that the reinforcing effects caused by the diammonium ions are more remarkable than in the case of the dicarboxylate ions.

The author wishes to thank Professor Tsurutaro Nakagawa, Professor Tsuyoshi Komatsu, and Mr. Toshio Nakajima for their helpful advice. The present work has been supported in part by a Grant for Scientific Research from the Ministry of Education.

BULLETIN OF THE CHEMICAL SOCIETY OF JAPAN, VOL. 46, 1602—1609 (1973)

Excited States and Intermediates in the Photochemistry of Chromium(III) Complexes Studied by Flash Method

Takeshi OHNO and Shunji KATO

Institute of Chemistry, College of General Education, Osaka University, Toyonaka, Osaka 560

(Received September 19, 1972)

Photoreactions of $K_3[Cr^{III}(NCS)_6]$ and $NH_4[Cr^{III}(NCS)_4(NH_3)_2]$ were investigated by means of a flash technique. At low temperature (−87 °C), the lowest excited doublet states (^2E_g) of the complexes were easily observed on d–d excitation in acetone, the yields decreasing rapidly with rising temperature. In methanol–ethyleneglycol–water, ^2E_g states of both complexes were easily observed at dry-ice temperature, but not at −46 °C. Thus, the lowest excited quartet state ($^4T_{2g}$), the precursor of ^2E_g state, should rapidly undergo photolysis at room temperature before being converted into the ^2E_g state. The rate of thermal degradation of $^4T_{2g}$ state including chemical reactions was calculated to be *ca.* 10^{10} s^{-1} at room temperature. The decay rate of ^2E_g state was estimated to be *ca.* 10^5 s^{-1} at room temperature. In the presence of organic compounds having carbonyl group, a strong and sharp absorption band near the UV region was observed at room temperature. Irradiation of UV light produced $(NCS)_2^-$ radical for both complexes.

It is well-known that ligands in some chromium(III) complexes in solution are replaced by solvent molecules on photo-excitation.[1] In such a reaction, it is important to make certain which excited state of the complex ion is reactive. It is possible to estimate the reactivities of the excited states from their electronic configurations. Chromium-ligand bonds might be elongated in the excited quartet states with an electronic configuration of $(t_2)^2(e)$ in view of a strong field approximation. However, the bond length in the excited doublet state with the configuration $(t_2)^2(\bar{t}_2)$, may be similar to that in the ground state. In principle, the broad absorption band and the large separation between the 0–0 bands of the absorption and emission spectra show a deformation of structure in the excited state. Thus, it is inferred that the excited quartet states differ to a great extent from the ground state in conformation, but not the excited doublet state. It is reasonable that the larger the deformation of the excited state, the easier for a solvent molecule to make a new bond with the central metal ion of the complex. On the other hand, ^2E_g with a long natural lifetime (10^{-1}∼10^{-3} s) will be more favorable for reaction than the short living $^4T_{2g}$ (10^{-9}∼10^{-10} s).[2,3]

Many reports have appeared dealing with reaction states. Some of them support the view that the doublet state takes part in the reaction. The quantum yields of the photochemical reactions of chromium (III) complexes such as $[Cr^{III}(NH_3)_6]^{3+}$, $[Cr^{III}(NCS)_4(NH_3)_2]^-$, $[Cr^{III}(urea)_6]^{3+}$, and $[Cr^{III}(NCS)_6]^{3-}$ are known to be independent of the excitation wavelength.[4-6] This suggests that the lowest excited states are the reacting species.

1) A. W. Adamson, W. L. Waltz, E. Zinato, D. W. Watts, P. D. Fleischauer, and R. D. Lindholm, *Chem. Rev.*, **68**, 542 (1968).

2) K. K. Chatterjee and L. S. Forster, *Spectrochim. Acta*, **20**, 1603 (1964).

3) H. L. Schläfer, H. Gausmann, and H. Witzke, *J. Chem. Phys.*, **46**, 1423 (1967).

4) M. R. Edelson and R. A. Plane, *J. Phys. Chem.*, **63**, 327 (1959).

5) M. R. Edelson and R. A. Plane, *Inorg. Chem.*, **3**, 231 (1964).

6) E. E. Weger and A. W. Adamson, *J. Amer. Chem. Soc.*, **88**, 394 (1966).

Plane[5] and Schläfer[7] supposed that the reacting species was the lowest excited doublet state (^2E_g). This inference seemed to be supported by the fact that the yield of the phosphorescence (0.23) at low temperature[2] was close to that of the aquation reaction (0.28) at room temperature for $K_3[Cr^{III}(NCS)_6]$.

Some others support the view that the quartet states are also reactive. In the case of *cis*-$[Cr^{III}(en)_2(OH)_2]^+$, the quantum yield ratio of *cis-trans* isomerization to aquation was dependent on the excitation wavelength (the ratio was 1.5 on excitation to the first excited quartet state $^4T_{2g}$, and 2.8 to the second excited quartet state $^4T_{1g}$, and 9.6 to ^2E_g at 25 °C[8]). In the case of $[Cr^{III}(NCS)(NH_3)_5]^{2+}$, the quantum yield on direct excitation to ^2E_g is not larger than that to $^4T_{2g}$ and $^4T_{1g}$ states.[9] Chen and Porter[10] and Longford *et al.*[11] proposed the participation of $^4T_{2g}$ state as well as ^2E_g state in the photoreactions of Chromium(III) complexes. They stated that photolysis was less effectively quenched by iodide, hydroxyl and $[Cr^{III}(CN)_6]^{3-}$ than phosphorescence was.

The reacting states in the photolysis of chromium complexes remains still unclarified. We tried to solve the problem by means of the technique of flash photolysis. Phosphorescent states (^2E_g) of some chromium complexes such as $K_3[Cr^{III}(NCS)_6]$ and $NH_4[Cr^{III}(NCS)_4(NH_3)_2]$ were observed by the flash method in a rigid solvent (EPA) at −196 °C.[12] Transient intermediates such ^2E_g state were investigated in a wide temperature range for the purpose of clarifying the mechanism of the photochemical reactions.

Experimental

Apparatus and Procedure. Flash experiments at low temperature were carried out with a flash apparatus.[12] A quartz cell was placed in a Dewar filled with methanol which was cooled with dry ice or liquid nitrogen. Temperature was measured with a copper-constantan thermojunction inserted in the sample solution.

For flash experiments at room temperature, the following flash apparatus was used. Two lamps were placed 5 cm apart in parallel. The sample cell was made of a glass tube, 100 mm long and 10 mm in inner diameter with silica windows at the end. It was located between the two lamps.

Some glass filters (Toshiba) and solution filters were set between the sample cell and the flash lamps. Their transmittances are shown in Fig. 1.

The outputs of a photomultiplier, 1P-28 (Hamamatsu TV.) were recorded with a Hitachi synchroscope V-116. Transient absorption spectra were composed from the oscillographic data of the absorption change observed at various wave numbers. The absorption change in near IR rigion was photographed on Sakura infra-red film. Number of photons absorbed by a chromium complex was measured with a Reineck salt actinometer.[6]

Materials. $K_3[Cr^{III}(NCS)_6]4H_2O$, $NH_4[Cr^{III}(NCS)_4(NH_3)_2]3/2H_2O$, and $[Co^{III}(NCS)(NH_3)_5]SO_4\cdot 2H_2O$, were prepared by the methods reported by Dakin,[13] Roesler,[14] and Werner,[15] respectively.

Potassium iodide was recrystallized three times from water. Ferric nitrate of G. R. grade was used without further purification. Acrylamide of high purity was supplied by Prof. H. Takemura of Nara Women's University. Ethanol was refluxed with silver nitrate, dried over calcium oxide and distilled. Other solvents (G. R. grade) such as methanol, ethyleneglycol, ethylacetate, dimethylformamide, acetophenone, and acetonitril were used without further purification.

Results

General Aspects. The absorption spectrum of $K_3[Cr^{III}(NCS)_6]$ in acetone at room temperature is shown in Fig. 1. Two weak absorption bands in visible region have been assigned to d-d transitions ($^4A_{2g}\rightarrow{}^4T_{2g}$: 17.8 kK, $^4A_{2g}\rightarrow{}^4T_{1g}$: 24.2 kK) and a strong absorption in near UV region to ligand excitation.[16]

When a 2.0×10^{-3} M acetone solution of $K_3[Cr^{III}(NCS)_6]$ was flashed with visible light (filter-24) below −30 °C, the transient spectrum observed agreed with that in EPA solution at −196 °C (Fig. 2). Hence, it is safe to regard it as the ^2E_g state of $K_3[Cr^{III}(NCS)_6]$. With temperature rise, the production of ^2E_g became smaller and could not be detected at 0 °C. A sharp band appeared near the UV region (28.2 kK) above −30 °C. At room temperature, only this band was prominent. The intermediate showing it is denoted by "X".

A flashing on the acetone solution with no filter

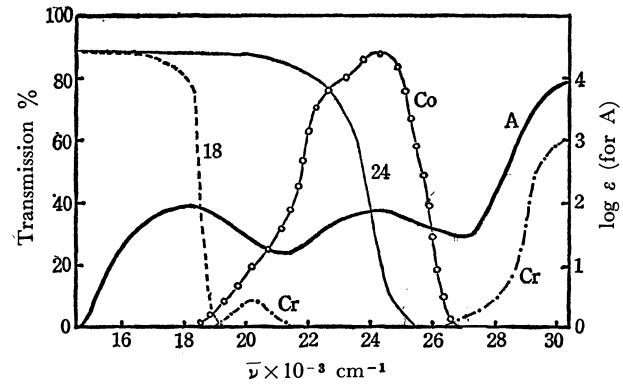

Fig. 1. Absorption spectrum of $K_3[Cr^{III}(NCS)_6]$ and transmission spectra of various filters.
A: $K_3[Cr^{III}(NCS)_6]$ in acetone,
Cr: solution filter of chromium alum aqueous solution,
Co: solution filter of $K_2[Co^{II}(NCS)_4]$ tertiarybutylalcohol solution,
18: glass filter, Toshiba V-O52,
24: glass filter, Toshiba V-Y42.

7) H. J. Schläfer, *Z. Physik. Chem.* (Frankfurt), **11**, 65 (1957).
8) A. W. Adamson, "Mechanisms of Inorganic Reactions", Advances in Chemistry Series, No 49, American Chemical Society, Washington, D. C., 1965.
9) R. D. Lindholm, E. Zinato, and A. W. Adamson, *J. Phys. Chem.*, **71**, 3713 (1967).
10) S. Chen and G. B. Porter, *Chem. Phys. Lett.*, **6**, 41 (1970).
11) C. H. Langford and L. Tipping, *Can. J. Chem.*, **50**, 887 (1972). N. A. P. Kane-Maguire and C. H. Longford, *J. Amer. Chem. Soc.*, **94**, 2125 (1972).
12) T. Ohno and S. Kato, This Bulletin, **43**, 8 (1970).
13) H. D. Dakin, "Organic Syntheses" Vol. 15, p. 74 (1935).
14) J. Roesler, *Ann.* **141**, 185 (1867).
15) A. Werner and A. Muller, *Z. Anorg. Chem.*, **22**, 102 (1900).
16) C. K. Jørgensen, "Absorption Spectra and Chemical Bonding in Complexes", Pergamon Press, Ltd., London (1962), p. 116.

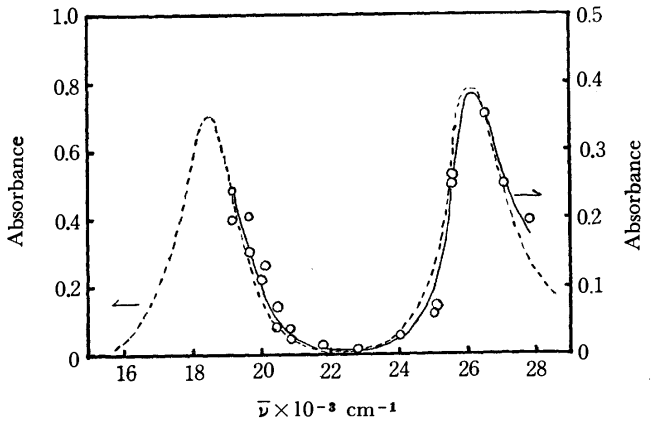

Fig. 2. Transient absorption spectra for $K_3[Cr^{III}(NCS)_6]$ 30 μs after flashing at low temperature.
-O-: 2×10^{-3} M acetone solution of $K_3[Cr^{III}(NCS)_6]$ at -61 ± 5 °C, 200J flash with filter-18,
·····: 10^{-3} M EPA solution of $K_3[Cr^{III}(NCS)_6]$ at -196 °C, 100J flash with filter-24.

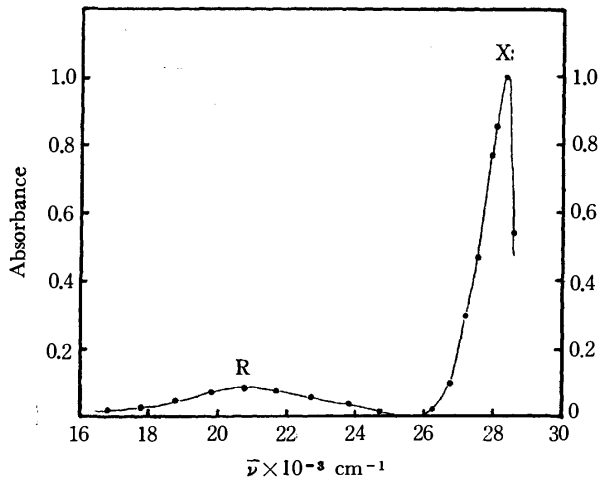

Fig. 3. Transient absorption spectrum when a 10^{-3} M acetone solution of $K_3[Cr^{III}(NCS)_6]$ in a glass cell with 200J flash at room temperature.

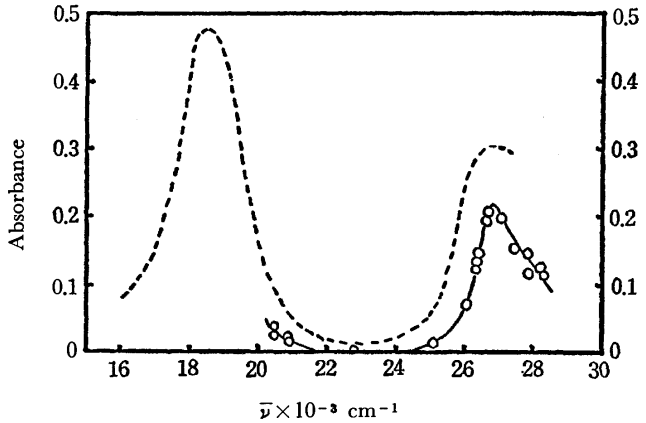

Fig. 4. Transient absorption spectra for $NH_4[Cr^{III}(NCS)_4(NH_3)_2]$ 30 μs after flashing at low temperature.
-O-: 5×10^{-3} M acetone solution of the complex at -61 ± 5 °C, 200J flash with filter-18,
·····: 10^{-3} M of the complex in polymethylmethacrylate at -196 °C 100J flash with filter-24.

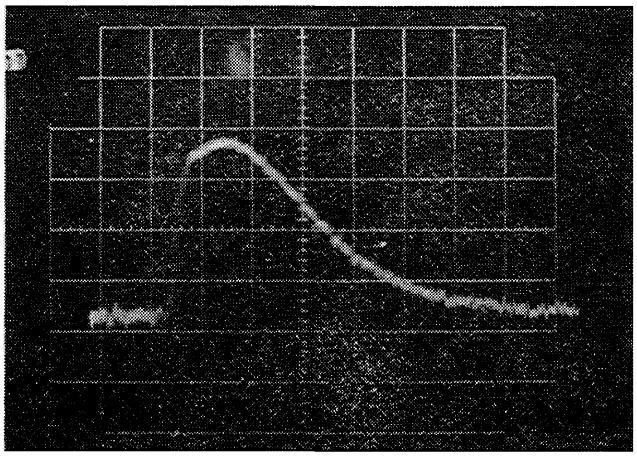

Fig. 5. A typical oscilogram of a transient absorption, observed at 26.3 kK, when a 10^{-3} M acetone solution of $K_3[Cr^{III}(NCS)_6]$ was flashed with filter-24 at -78°C. One large division is 10 μs.

produced transiently a broad band in addition to the sharp band of X at room temperature (Fig. 3). The broad absorption spectrum in visible region is due to a third intermediate denoted by "R". R vanished several milliseconds after flashing, while X survived a few seconds after the disappearance of R.

A single flash with filter-24 on $K_3[Cr^{III}(NCS)_6]$ at room temperature produced 4×10^{-5} M of free thiocyanate ion which was analyzed as ferric thiocyanate.

As in the case of $NH_4[Cr^{III}(NCS)_4(NH_3)_2]$, three intermediates were detected depending on experimental conditions. As shown in Fig. 4, a transient absorption observed at -61 ± 5 °C can be assigned to ^2E_g state referring to the absorption spectrum of ^2E_g state at -196 °C in polymethylmethacrylate. With rise in temperature the yield of ^2E_g state decreased, R and X becoming observable. The absorption maximum and the decay rate of X for $NH_4[Cr^{III}(NCS)_4(NH_3)_2]$ were similar to those of X for $K_3[Cr^{III}(NCS)_6]$.

In the case of other solvents, the behaviors of three

Table 1. Relation between intermediates and excitation conditions in acetone

Complexes	Excited states directly produced	Temp. °C	Intermediates
$K_3[Cr^{III}(NCS)_6]$	LE[a], $^4T_{1g}$, $^4T_{2g}$	25	X, R
	LE	25	R
	$^4T_{1g}$, $^4T_{2g}$	25	X
	$^4T_{1g}$	25	X
	$^4T_{2g}$	25	X
	$^4T_{1g}$, $^4T_{2g}$	-87	^2E_g
	$^4T_{1g}$, $^4T_{2g}$	-196[b]	^2E_g
$NH_4[Cr^{III}(NCS)_4(NH_3)_2]$	LE, $^4T_{1g}$, $^4T_{2g}$	25	X, R
	$^4T_{1g}$, $^4T_{2g}$	25	X
	$^4T_{1g}$, $^4T_{2g}$	-87	^2E_g
	$^4T_{1g}$, $^4T_{2g}$	-196[c]	^2E_g

a) LE denotes an excited state localized in ligand.
b) The solvent used was EPA.[12]
c) Methylmethacrylate dissolving the chromium complex was polymerized.

intermediates were very similar to those in acetone except that X was not observed in methanol, ethanol, and water.

Observed intermediates under various experimental conditions are listed in Table 1. The excitation in d-d band (to $^4T_{2g}$ and $^4T_{1g}$) produces ^2E_g state below −10 °C and X above −30 °C, the excitation in the ligand band (UV) produces R in acetone.

^2E_g State. When a 10^{-3}M acetone solution of $K_3[Cr^{III}(NCS)_6]$ was flashed at −78 °C, absorbance of the ^2E_g state reached maximum at 10 μs and then decreased rapidly (Fig. 5).

The decay was of first order and the rate constant did not vary in the range from −87 °C to −10 °C. Hence the initial absorbances due to ^2E_g produced by flashing were obtained in high accuracy by analysis of the decay curves. The absorbance was 3.0 at 27 kK for a 1.0×10^{-3} M acetone solution of $K_3[Cr^{III}(NCS)_6]$ at −78 °C, and decreased to 0.66 at −46 °C. In order to avoid experimental errors due to smaller absorbance at higher temperature, more concentrated acetone solution (4.0×10^{-3} M) of $K_3[Cr^{III}(NCS)_6]$ was examined above −54 °C. The values 2.0 at −46 °C and 0.23 at −9 °C were obtained as the initial absorbances of ^2E_g. At 0 °C, production of the ^2E_g state could not be detected even during the course of flash illumination with more concentrated solutions. The effect of temperature upon production is shown in Fig. 6.

The ordinate gives the quantum yield calculated on the conventional assumption that yield is unity −87 °C. Thus, the calculated yields are the largest possible values.

In the case of $NH_4[Cr^{III}(NCS)_4(NH_3)_2]$ in acetone, similar behaviors were observed. The lifetime was constant from −87 °C to −18 °C, making the measurement of the relative yield accurate. The quantum yields are calculated also on the assumption that yield is unity at −87 °C. The temperature dependence of the quantum yield is shown in Fig. 7.

In the cases of ethanol and ethanol–ethyleneglycol (1 : 1) solutions of $K_3[Cr^{III}(NCS)_6]$, temperature dependence of the yield of the ^2E_g state was similar to that in acetone solution. Absorbance could still be detected at −30°C for 5.0×10^{-3} M ethanol–ethyl-

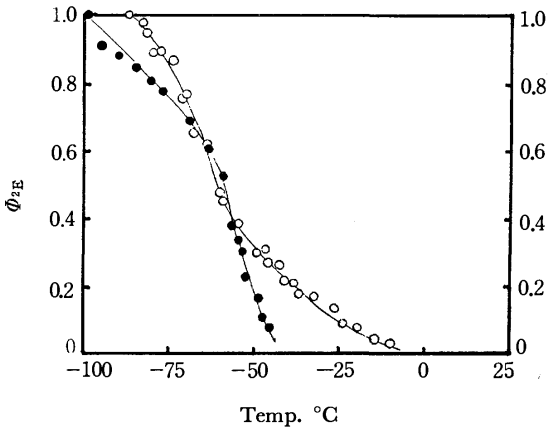

Fig. 6. Effects of temperature upon the yields of ^2E_g state of $K_3[Cr^{III}(NCS)_6]$, when flashed with filter-24.
○: 1—4×10^{-3} M in acetone,
●: 1—4×10^{-3} M in the mixed solvent.

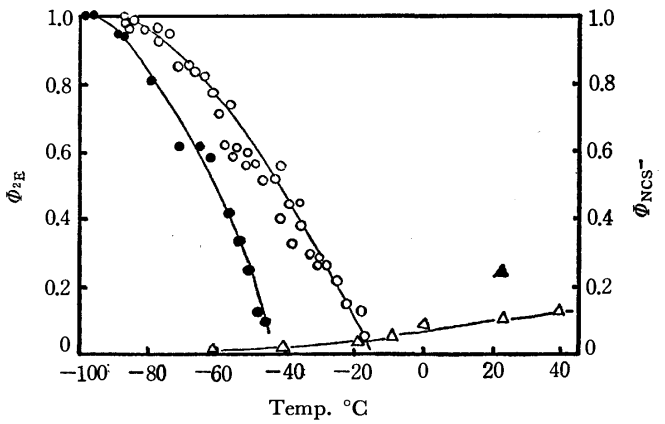

Fig. 7. Effects of temperature upon the yields of ^2E_g state and chemical reactions of $NH_4[Cr^{III}(NCS)_4(NH_3)_2]$, when flashed with filter-24.
○: the yield of ^2E_g in acetone,
△: the yield for free SCN^- in acetone,
●: the yield of ^2E_g in methanol-ethyleneglycol-water,
▲: the yield for free SCN^- in methanol-ethyleneglycol-water.

Table 2. Production and lifetime of ^2E_g state under various conditions

Complex	Concentration M	Temperature °C	Solvent	Absorption 10 μs after flashing	Lifetime μs
$K_3[Cr^{III}(NCS)_6]$	1×10^{-3}	−87	acetone	3.1	20
	1×10^{-3}	−60	acetone	1.0	20
	4×10^{-3}	−54	acetone	2.5	20
	4×10^{-3}	−9	acetone	0.23	20
	1×10^{-3}	−100	mixed[a)]	1.9	2500
	4×10^{-3}	−56	mixed	1.3	21
	1×10^{-3}	−196	EPA	—	10000
$NH_4[Cr^{III}(NCS)_4(NH_3)_2]$	2×10^{-3}	−87	acetone	2.8	20
	5×10^{-3}	−18	acetone	0.49	20
	1×10^{-3}	−100	mixed[a)]	2.2	300
	4×10^{-3}	−62	mixed	1.1	19
	1×10^{-3}	−196	polymer	—	310

a) The "mixed" indicates a mixture of methanol, ethyleneglycol, and water (2 : 2 : 3).

eneglycol (1 : 1) solution of $K_3[Cr^{III}(NCS)_6]$.

For methanol-ethyleneglycol-water solutions (2 : 2 : 3) of $K_3[Cr^{III}(NCS)_6]$ and $NH_4[Cr^{III}(NCS)_4(NH_3)_2]$, transient absorption was easily observed at −100 °C. However, it weakened rapidly with temperature rise, and could not be observed at all above −45 °C. Changes of yields with temperature are shown in Figs. 6 and 7. The accuracy is less satisfactory than in the case of the acetone solution, as the lifetime of the ^2E_g state greatly changes in the range from −100 °C to −50 °C. The absorbances in various conditions are shown in Table 2.

The quantum yield Φ_E is formulated as follows.

$$\Phi_E = \frac{k_i}{k_i + k_d} \tag{1}$$

where k_i and k_d are rate constants of intersystem crossing and thermal deactivation of $^4T_{2g}$ state (precursor of ^2E_g state), respectively. Eq. (1) is rewritten as follows.

$$\ln\left(\frac{1}{\Phi_E} - 1\right) = \ln\frac{k_d}{k_i} \tag{2}$$

$$= \ln\frac{A_d}{A_i} - \frac{E_d - E_i}{RT} \tag{3}$$

where suffixes d and i denote the thermal deactivation process and the intersystem crossing process, respectively, A and E the frequency factor and the activation energy, respectively. When the temperature dependence of quantum yield (Fig. 6) is analyzed by means of Eq. (3), a linear relation with a break at −62 °C is obtained for both complexes in methanol-ethyleneglycol-water (Fig. 8).

The decay processes are of first order with respect to the concentration of the ^2E_g state, and the rate constants are the same for all complexes examined, 5.0×10^{-4} s^{-1} in acetone, independent of temperature and concentration (Fig. 9). On the other hand, in methanol-ethyleneglycol-water solvent, the decay rates are dependent on temperature as shown in Table 2 and Fig. 10. The apparent activation energy of the deactivation process of the ^2E_g state was obtained to be 11 kcal/mol in a temperature region higher than −70 °C for both complexes.

Intermediate X. Intermediate X observed in acetone solutions of $K_3[Cr^{III}(NCS)_6]$ and $NH_4[Cr^{III}(NCS)_4(NH_3)_2]$ on d-d excitation at room temperature, has a sharp absorption band near the UV region. Similar spectra were observed in ethylacetate, dimethylformamide, acetophenone and polymethylmethacrylate, but not in ethanol, methanol, aceto-

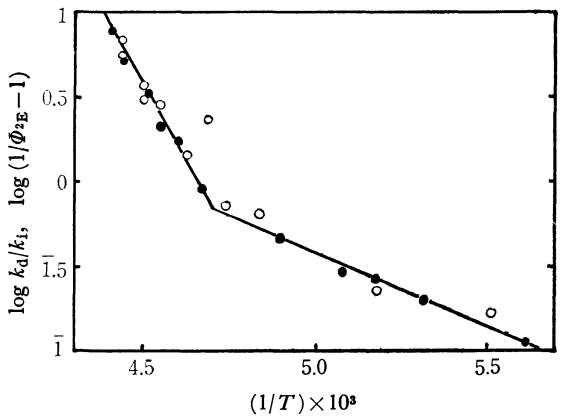

Fig. 8. Eq. (III) as a function of reciprocal of temperature for methanol-ethyleneglycol-water solutions of the complexes.
○: 1—4×10^{-3} M of $K_3[Cr^{III}(NCS)_6]$,
●: 2—5×10^{-3} M of $NH_4[Cr^{III}(NCS)_4(NH_3)_2]$.

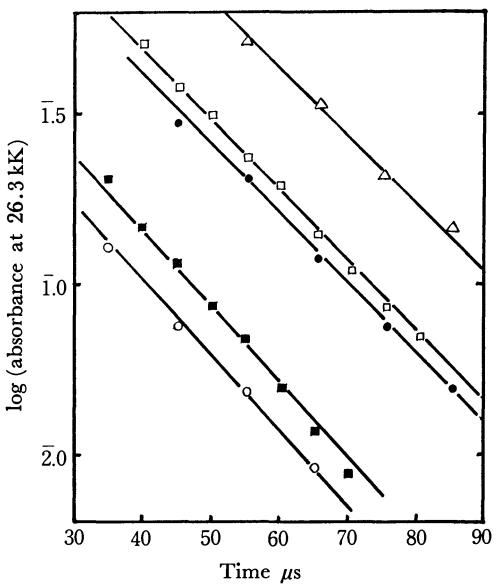

Fig. 9. First order decay of ^2E_g state formed by flashing $K_3[Cr^{III}(NCS)_6]$ in acetone.
△: 4×10^{-3} M at −59 °C,
●: 4×10^{-3} M at −32 °C,
○: 4×10^{-3} M at −14 °C,
□: 1×10^{-3} M at −69 °C,
■: 1×10^{-3} M at −46 °C.

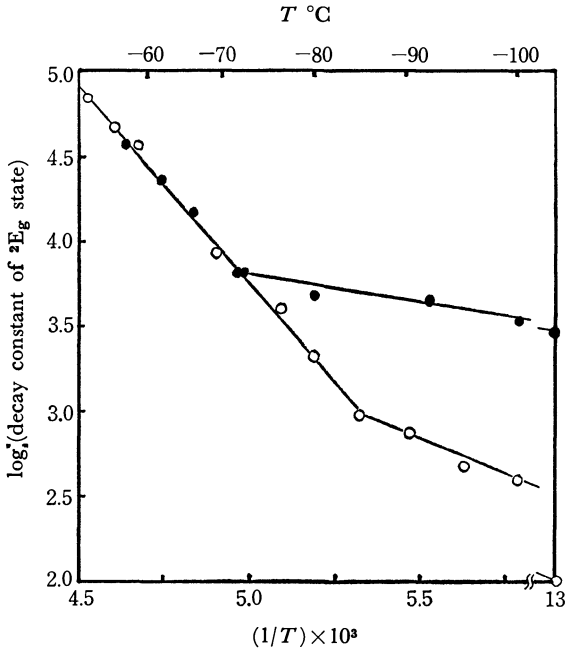

Fig. 10. Effects of temperature on the decay constants of ^2E_g states formed by flashing the complex in methanol-ethyleneglycol-water.
○: $K_3[Cr^{III}(NCS)_6]$,
●: $NH_4[Cr^{III}(NCS)_4(NH_3)_2]$.

Table 3. Behavior of intermediate X at room temperature

Complex	Solvent	Abs. max. kK	Decay constant s^{-1}
$K_3[Cr^{III}(NCS)_6]$	acetone	28.2	0.24
$NH_4[Cr^{III}(NCS)_4(NH_3)_2]$	acetone	28.6	0.06
$K_3[Cr^{III}(NCS)_6]$	DMF[a]	26.6	8.6×10^4
$NH_4[Cr^{III}(NCS)_4(NH_3)_2]$	DMF[a]	26.8	7.8×10^4
$K_3[Cr^{III}(NCS)_6]$	polymer[b]	27.2	0.2
$NH_4[Cr^{III}(NCS)_4(NH_3)_2]$	polymer[b]	27.4	0.2

a) DMF: dimethylformamide.
b) Methylmethacrylate dissolving the chromium complex was polymerized.

Table 4. Production and rate constant of decay process of intermediate X at room temperature

Solvent		Production	Decay constant s^{-1}
Acetone %	Ethanol %		
100	0	0.600	0.25
97.5	2.5	0.511	1.3
95.0	5.0	0.450	2.1
90.0	10.0	0.447	2.9
85.0	15.0	0.477	3.4
10.0	90.0	0.170	8.1
0	100	0	—

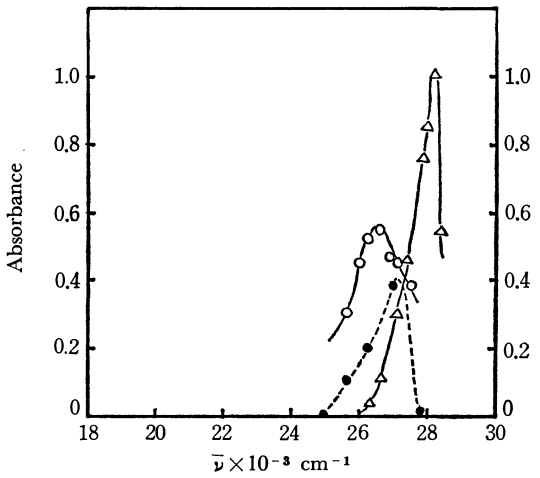

Fig. 11. Transient absorption spectra of various X-intermediates produced by flashing various solutions of $K_3[Cr^{III}(NCS)_6]$ at room temperature.
△: 1×10^{-3} M in acetone,
●: 1×10^{-3} M in polymethylmethacrylate,
○: 4×10^{-3} M in dimethylformamide.

nitril, and water on d-d excitation. It is worth noticing that all solvents in which the intermediate appeared have a carbonyl group, and that the wave number of the absorption maxima does not depend upon the species of the complex but upon the solvent as shown in Table 3 and Fig. 11.

Decay of the intermediate, regarded as of first order process, also depends on the solvent (Table 3). It is very slow except the case of dimethylformamide. Characteristics such as yields, absorption maxima and decay constants differ with solvent. Thus, X is assumed to be a reaction product between solvent and photoproduct of the complex. For the sake of confirmation the behavior of X was studied in mixed solvents of acetone and ethanol (Table 4). Its production and lifetime gradually decrease with increasing fraction of ethanol, but is observable even in 90% ethanol solution.

Intermediate R. When 1.0×10^{-3} M acetone solution of $K_3[Cr^{III}(NCS)_6]$ was irradiated with UV light, a transient species intermediate R with absorption maximum at 21.5 kK was observed. This was also produced from both complexes in other solvents such as ethanol, methanol, and water. A single flash irradiation through UV filter made an absorbance of 0.15 at absorption maximum, and finally gave 180 μM of free thiocyanate ion. The absorption spectrum due to R was also observed in aqueous solution of $[Co^{III}(NCS)(NH_3)_5]SO_4$ on irradiation of full light. Cobalt(III) was reduced to cobalt(II) during the course of photodecomposition of the complex. It is reasonable that NCS^- coordinating to cobalt is oxidized to thiocyanate radical, accompanied by the reduction of cobalt(III), since thiocyanate ion has the highest reducing potential in the system.

To clarify the character of R, potassium iodide or acrylamide was added as a radical scavenger. Decay of R in all the cases examined was of first order process with respect to R. Addition of the scavenger to an aqueous solution of $K_3[Cr^{III}(NCS)_6]$, reduced the lifetime under aerobic conditions. The decay constant observed (k_{obs}) is given by

$$k_{obs} = k_o + k_S[S] \quad (4)$$

where k_o denotes the decay constant in the absence of scavenger and k_S the second order rate constant of the reaction between R and a scavenger, and [S] the concentration of the scavenger. From the dependence of decay constants on the concentration of scavenger (Fig. 12), the value of k_S are evaluated as shown in Table 5.

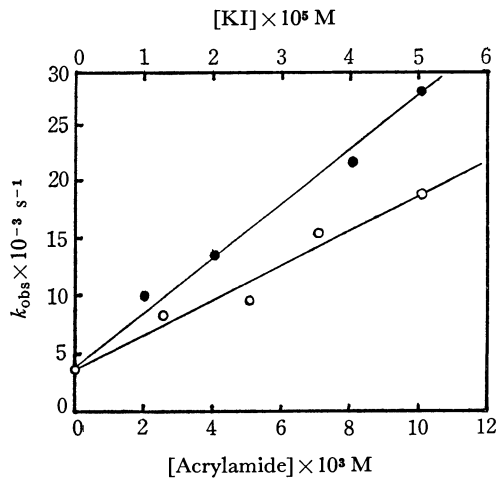

Fig. 12. Relationships between decay constants of R-intermediate and the concentration of potassium iodide and acrylamide added.
○: acrylamide (the bottom scale),
●: potassium iodide (the upper scale).

TABLE 5. REACTION RATE CONSTANTS k_o AND k_S OF $(NCS)_2^-$ AT ROOM TEMPERATURE

	k_o s^{-1}		k_S $M^{-1}s^{-1}$
$K_3[Cr^{III}(NCS)_6]$	2.8×10^3	KI	5.0×10^8
$[Co^{III}(NCS)(NH_3)_5]SO_4$	2.3×10^3	Acrylamide	1.6×10^6

Discussion

Changes of the quantum yields and the lifetimes of ^2E_g states from -100 °C to -10 °C give information on the behaviors of both $^4T_{2g}$ and ^2E_g states. The values of the quantum yields of the ^2E_g state (Table 6) were calculated on the assumption that the quantum yields were unity at -87 °C in acetone and -100 °C in the methanol-etyleneglycol-water. They fall less than 0.1 at -25 °C. The quantum yield at room temperature was extrapolated to be the order of 10^{-3}. However, the quantum yields of decomposition of the complexes are 0.12—0.34 at room temperature. It is worth noticing that they are much higher than the extrapolated yields at room temperature. The quantum yield of decomposition increased but the yields of ^2E_g state decreased with rising temperature (Fig. 7). Thus, it is concluded that the decomposition of the complexes in the $^4T_{2g}$ state competes with the intersystem crossing to the ^2E_g state and that $^4T_{2g}$ decomposes rapidly before being converted into ^2E_g state at room temperature.

The low quantum yield (<0.1) at -25 °C, means that the rate constant of the thermal deactivation (k_d) of $^4T_{2g}$ is at least ten times as large as that of the intersystem crossing (k_i) according to Eq. (1). Because of the fall of Φ_E with temperature, k_d may be much larger at room temperature. The rate constant of the fluorescence process (k_f, the reciprocal of the natural lifetime) is calculated to be about 10^5 s^{-1} using Einstein's equation of spontaneous transition probability.[17] For all complexes examined, no fluorescence has been detected even at -196 °C. Therefore, k_i may be 10^4 times as large as k_f on the ground that fluorometers can detect fluorescence with a quantum yield of 10^{-4}. Accordingly, k_d is estimated to be larger than 10^{10} s^{-1} at room temperature.

On the other hand, the rate constant of phosphorescence process (the reciprocal of natural lifetime) is obtained to be $10\sim10^3$ s^{-1} by Einstein's equation. The observed lifetime of ^2E_g state indicated that the rate constant of thermal deactivation for both complexes was 5.0×10^4 s^{-1} at -9 °C——-87 °C in acetone and at about -50 °C in the mixed solvent. It is surprising that the change of lifetime with temperature was largely dependent on the solvents and not on the complexes. It is inferred that a strong interaction of the fluid solvent with ^2E_g probably causes its degradation to the ground state or $^4A_{2g}$.

Comparing the rate constants (10^{10} s^{-1}) of the thermal deactivation of the $^4T_{2g}$ and ^2E_g states (10^5 s^{-1}, it is concluded that the former is influenced by solvent molecules more strongly. It should be pointed out that the temperature dependence of Φ_E does not change with the species of the complexes but with solvent. This shows that the deactivation processes of the $^4T_{2g}$ state consist in the interaction of the solvent molecules, which lead to chemical change in part. It is plausible that long metal-ligand bonds in the $^4T_{2g}$ state induce the interaction of the central metal with solvent which results in bimolecular reaction. A bimolecular reaction is also suggested by the fact that $NH_4[Cr^{III}(NCS)_4(NH_3)_2]$ was almost non-reactive at -70 °C (Fig. 7). If a hexa-coordinated complex is dissociated in its excited state and decomposes monomolecularly on irradiation, the yield of photochemical reaction will be independent of temperature. $Cr^0(CO)_6$ is such a case, decomposing photochemically to five coordinated complex with high efficiency even at -196 °C.[18]

TABLE 6. QUANTUM YIELDS OF THE DECOMPOSITION OF COMPLEXES AND ^2E_g STATE FORMATION

Complex	Solvent	Decomposition	^2E_g formation
$K_3[Cr^{III}(NCS)_6]$	acetone	0.12 (23°C)	0.03 (−9°C)
	mixed		0.07 (−45°C)
	water	0.26 (23°C) [a]	
$NH_4[Cr^{III}(NCS)_4(NH_3)_2]$	acetone	0.13 (41°C)	0.10 (−18°C)
	mixed	0.25 (23°C) [b]	0.10 (−46°C)
	water	0.34 (40°C) [a]	

a) E. E. Wegner and A. W. Adamson, *J. Amer. Chem. Soc.*, **88**, 394 (1966).
b) A. W. Adamson, *J. Phys. Chem.*, **71**, 798 (1967).

It is difficult to say whether the second excited state, $^4T_{1g}$, reacts in its lifetime or not. It is generally believed that the second excited states of aromatic molecules have too short a lifetime (10^{-12} s) to react or fluoresce with a few exception.[19] The situation is assumed to be the same for the $^4T_{1g}$ state of chromium complexes, though, if predissociative, it will decompose in one vibration. From this point of view, one can not deny the view that the chemical reaction would take place during the course of lifetime.

The complexes decomposed at higher temperature. Intermediate X appeared in solvents having carbonyl group such as acetone, but not in ethanol, methanol, acetonitrile, and water. If X were produced in the monomolecular decomposition of the complexes also in ethanol and water but not detected because of the rapid quenching of the solvents, a small amount of ethanol would effectively shorten the lifetime of X. Actually, however, X has a long lifetime of 0.12 s even in 90% ethanol solution. It is not reasonable to consider that X decays too rapidly to be detected in pure ethanol when it has a long lifetime of 0.12 s in 90% ethanol solution. When acetone was added to ethanol by 10%, appreciable amount of X was produced.

17) J. G. Calvert and J. M. Pitts, Jr., "Photochemistry," John Wiley and Sons, Inc., New York (1967), p. 173.
18) W. Strohmeier and K. Gerlach, *Chem. Ber.*, **94**, 398 (1961).
19) M. Beerand and H. C. Longuet-Higgins, *J. Chem. Phys.*, **23**, 1390 (1955).

It is thus concluded that acetone is required as a reactant to produce X. Data were not sufficient to identify X, but we might guess that the species produced by a reaction between acetone and the complexes on irradiation, is probably either $[Cr^{III}(NCS)_5(CH_3)_2CO]^{2-}$ or $(NCS)^- \cdot (CH_3)_2CO$. The latter, a molecular complex between thiocyanate ion and acetone, is more probable from the fact that ketones form molecular complexes with sodium iodide, lithium iodide, or sodium hydrogensulfide which are similar to thiocyanate salts in chemical aspect. $[Cr^{III}(NCS)_5(CH_3)_2CO]^{2-}$ cannot be considered to have such a short lifetime as observed.

The absorption spectrum of R agrees with that of the transient species found by Adams *et al.*[20] Baxendale and Scott found[21] the same spectrum in the radiolysis of pottassium thiocyanate aqueous solution and attributed it to $(NCS)_2^-$ on the basis of its kinetical dependence on potassium thiocyanate concentration, but no evidence was given to show it to be a radical. It is concluded that R is a radical because it reacts very fast with radical scavengers such as potassium iodide and acrylamide. Formation of acrylamide radical in a reaction between R and acrylamide was confirmed by the fact that the polymerization of acrylamide solution containing $[Co^{III}(NCS)(NH_3)_5](NCS)_2$ is initiated by illumination.[22]

20) G. E. Adams, J. W. Boag, and B. D. Michael, *Trans. Faraday Soc.*, **61**, 1674 (1965).
21) J. H. Baxendale and S. A. Scott, *Chem. Commun.*, **1967**, 699.
22) H. Takemura, private communication.

Chromium(II) could not be detected in the photoreactions of $K_3[Cr^{III}(NCS)_6]$ and $NH_4[Cr^{III}(NCS)_4(NH_3)_2]$ in deaerated solution. Another transient species with very short lifetime (a few μs) was observed in deaerated ethanol solution of the complex, which has a broad absorption spectrum with maximum at 13.6 kK. Since the maximum and lifetime of the transient absorption are similar to those of solvated electron,[23] the following reaction seems to take place,

$$[Cr^{III}(NCS)_6]^{3-} + h\nu \rightarrow [Cr^{III}(NCS)_4]^- + (NCS)_2^- + e_{solv} \quad (5)$$

Summary

Excitation to the d–d excited state $^4T_{2g}$ of $K_3[Cr^{III}(NCS)_6]$ and $NH_4[Cr^{III}(NCS)_4(NH_3)_2]$, is followed by both nonradiative transition to the ^2E_g and the release of one of the ligands (thiocyanate ion). With temperature rise, the release of thiocyanate ion becomes faster and the freshly released thiocyanate ion forms an adduct with carbonyl compound such as acetone and ethylacetate, which decomposes slowly. Irradiation of UV light to the complexes produces a thiocyanate ion radical $(NCS)_2^-$.

Financial support from Fuji Photo Film Co., LTD. is gratefully acknowledged.

23) L. M. Dorfman and M. S. Matheson, "Progress in Reaction Kinetics," Vol. 3, Pergamon Press, Oxford (1965), p. 284.

BULLETIN OF THE CHEMICAL SOCIETY OF JAPAN, VOL. 46, 1609—1616 (1973)

Charge-transfer and Proton-transfer in the Formation of Molecular Complexes. VI.[1] 3,3′,5,5′-Tetranitrobiphenyl-4,4′-diol Complexes with Aromatic Amines

Gunzi SAITO and Yoshio MATSUNAGA

Department of Chemistry, Faculty of Science, Hokkaido University, Sapporo 060

(Received October 20, 1972)

The 3,3′,5,5′-tetranitrobiphenyl-4,4′-diol complexes with twenty-eight aromatic monoamines were prepared and characterized on the basis of their compositions and vibrational and electronic spectra. Many amines were found to form yellow-colored complexes with a 1 : 1 composition and orange- or red-colored complexes with a mole ratio of 2 : 1 or higher. The former complexes appeared to be salts formed by means of the proton-transfer from the diol to the amine molecule, while the latter appeared to be complexes of a new type where charge-transfer and proton-transfer interactions simultaneously operate. The deep coloration of the latter complexes was interpreted in terms of a charge-transfer interaction between the anion derived from the diol and the second monoamine molecule. Furthermore, the complexes with ten aromatic diamines were examined. The 1 : 1 *o*-dianisidine complex was of particular interest in that it is either of the charge-transfer type or of the proton-transfer type, depending upon the preparative conditions.

Recently, we showed that, as is established on the basis of the vibrational and electronic spectra, the orange-colored α-naphthylamine-picric acid (2 : 1) complex previously prepared by Kofler consists of the picrate ion, the protonated amine, and the α-naphthylamine molecule.[2,3] The deep coloration of this complex was attributed to the charge-transfer interaction between the picrate ion and the naphthylamine molecule. For brevity, such a complex will be denoted as

1) Part V: Y. Matsunaga, This Bulletin, **46**, 998 (1973).

2) A. Kofler, *Z. Elektrochem.*, **50**, 200 (1944).

3) Y. Matsunaga and G. Saito, This Bulletin, **45**, 963 (1972).

a complex of the CPT type because of the simultaneous operation of charge-transfer (CT) and proton-transfer (PT) interactions between the component molecules.

With the hope of extending the scope of complexes of the CPT type, we then examined the picric acid complexes with benzidine and its five derivatives.[4] We suggested three possible cases of complexes of the CPT type in these combinations and found examples for two of them. In the 1 : 1 complexes with *o*-tolidine, *o*-dianisidine, and *N,N,N′,N′*-tetramethylbenzidine, a part of the diamine molecule was found to act as a proton-acceptor, while the other part acted as an electron donor. This case may be schematically shown as follows:

$$H_2N\text{-}\phi\text{-}\phi\text{-}NH_3^+\cdots\cdots{}^-O\text{-}Pi$$
$$\vdots$$
$$H_2N\text{-}\phi\text{-}\phi\text{-}NH_3^+ \qquad \text{(I)}.$$

Secondly, the black-colored complex with benzidine of a 2 : 1 composition was also found to be of the CPT type. The mode of interaction in this case may be analogous to that in the above-mentioned naphthylamine complex and may be shown by:

$$H_2N\text{-}\phi\text{-}\phi\text{-}NH_3^+\cdots\cdots{}^-O\text{-}Pi$$
$$\vdots$$
$$H_2N\text{-}\phi\text{-}\phi\text{-}NH_2 \qquad \text{(II)}.$$

The last case is expected to be found among complexes of a 1 : 2 composition, where one of the picric acids is a proton donor and where the other is an electron acceptor. The constitution may be described by the following formula:

$$H_2N\text{-}\phi\text{-}\phi\text{-}NH_3^+\cdots\cdots{}^-O\text{-}Pi$$
$$\vdots$$
$$PiOH \qquad \text{(III)}.$$

Unfortunately, no example of the complex represented by this formula could be found among the picric acid complexes. As has been demonstrated with the picric acid and 2,4-dinitrophenol complexes with aromatic monoamines,[5,6] a delicate balance between the pK_a value of picric acid and the first and second pK_a values of the diamine must be achieved to produce such a complex.

Many aromatic monoamines are available and can cover a wider range of pK_a values than can benzidine and its derivatives; therefore, the chance of finding complexes of the CPT type represented by:

$$HO\text{-}\phi\text{-}\phi\text{-}O^-\cdots\cdots H_3N^+\text{-}Ar$$
$$\vdots$$
$$H_2N\text{-}Ar \qquad \text{(IV)}$$

may be much better than that of finding complexes represented by (III). 3,3′,5,5′-Tetranitrobiphenyl-4,4′-diol, hereafter abbreviated as TNBP, seemed to be the best choice for this purpose. The pK_a value in methanol has been determined by Hart and Detroit to be 4.90±0.06.[7] As Schwarzenbach and Rudin have shown that the pK_a values of *o*- and *p*-nitrophenols measured in 49% ethanol, are smaller by as much as 2 than those measured in 95% ethanol,[8] we may predict that TNBP is a weaker acid than picric acid (pK_a= 0.42 in water), but is a stronger acid than 2,6-dinitrophenol (pK_a=3.71 in water).[9,10] As for the electron-acceptor strength, TNBP is as strong as picric acid and *s*-trinitrobenzene, as will be described in the following section.

Experimental

Materials. The TNBP was prepared, starting from benzidine, by the procedure of Kunze[11] or that of Borsche and Scholten.[12] Recrystallization from glacial acetic acid gave fine, yellow-colored needles. In the former procedure, biphenyl-4,4′-diol was isolated as an intermediate by the method given by Hirsch.[13] The complexes were precipitated by mixing various amounts of the component compounds separately dissolved in hot benzene. Their compositions were determined by elementary analysis.

Measurements. The vibrational spectra of the solid samples were recorded as hexachloro-1,3-butadiene mulls on a JASCO IR-G infrared spectrophotometer, and the electronic spectra, on a Beckman DK-2A spectroreflectometer.

Results and Discussion

Electron-acceptor Strength of TNBP. In order to estimate the electron-acceptor strength of TNBP, the energies of the CT absorption maxima in the TNBP complexes with a series of electron donors were compared with those in the corresponding complexes of picric acid, *s*-trinitrobenzene, and *p*-chloranil. The absorptions were mostly measured in solids, but some were also measured in chloroform. The values obtained are listed in Table 1. Here, the electron donors are arranged in terms of the energy of the CT absorption maximum observed with the *p*-chloranil complex in chloroform. The energy values in the complexes of three nitro compounds with a given electron donor are close to each other; therefore, the electron-acceptor strength of TNBP appears to be comparable with those of picric acid and *s*-trinitrobenzene. The plot of the energies of the CT absorption maxima in the complexes of TNBP (Y) against those in the corresponding *p*-chloranil complexes (X) is covered by this equation:

$$Y = X + (4.1\pm1.0) \qquad (1)$$

The solid TNBP complexes with pyrene, anthracene, perylene, phenothiazine, and benzo[*c*]- and dibenzo-[*c,h*]-phenothiazines were found by elementary analysis to be of a 1 : 1 composition. The compositions of the amine complexes in Table 1 will be discussed in the following sections.

Spectra of TNBP and Its Salts. The diffuse reflectance spectrum of TNBP shows an absorption maxi-

4) G. Saito and Y. Matsunaga, This Bulletin., **46**, 714 (1973).
5) G. Saito and Y. Matsunaga, *ibid.*, **44**, 3328 (1971).
6) N. Inoue and Y. Matsunaga, *ibid.*, **45**, 3478 (1972).
7) H. Hart and W. J. Detroit, *J. Amer. Chem. Soc.*, **74**, 5214 (1952).
8) G. Schwarzenbach and E. Rudin, *Helv. Chim. Acta*, **22**, 360 (1939).
9) H. v. Halban and M. Seiler, *ibid.*, **21**, 385 (1938).
10) G. Kortüm and H. Wilski, *Z. Phys. Chem. N. F.*, **2**, 256 (1954).
11) E. Kunze, *Ber.*, **21**, 3331 (1888).
12) W. Borsche and B. G. B. Scholten, *ibid.*, **50**, 608 (1917).
13) R. Hirsch, *ibid.*, **22**, 335 (1889).

Table 1. Energies of CT absorption maxima in the complexes of TNBP, picric acid, *s*-trinitrobenzene, and *p*-chloranil (in kK).
The values in parentheses are those in the solid complexes.

Donor	TNBP	Picric acid	*s*-Trinitrobenzene	*p*-Chloranil
Hexamethylbenzene	23.1		25.3[a]	19.3
4,4′-Dimethoxybiphenyl	21.1			17.7
Pyrene	(20—21)		22.2 (22.5)[b]	16.2
N,*N*-Dimethylamino-*p*-benzaldehyde	(20—21)	*	(23.0)	16.0
Anthracene	(20)	(20)	(21.8)[b]	15.6
Diphenylamine	(19—20)		21.7[c]	15.3
3,3′-Dichloro-*o*-tolidine	(18.4)	*	21.3 (19.5)	14.3
3,3′-Dibromo-*o*-tolidine	(20.6)	(18.0)	20.4 (18.2)	14.1
Phenyl-α-naphthylamine	(18.8)	21.0	21.0	14.1
o-Dianisidine	(16.5)	*	(17.3)	13.4
Perylene	(18)	(18)	(20.4)[b]	13.2
Phenothiazine	(17.3)	(17.1)	19.1 (16.7)	12.3
Benzo[*c*]-phenothiazine	16.0 (16.6)	18.2 (14.7)	17.9 (15.7)	12.3
Dibenzo[*c*,*h*]phenothiazine	14.0 (15.4)	17.3 (14.1)	17.4 (18.2)	10.8

* Only the complexes of the PT type are available.
a) Taken from Ref. 14 (The solvent is carbon tetrachloride).
b) Taken from Ref. 15.
c) Taken from Ref. 16.

mum at 26.3 kK. In chloroform, the maximum is shifted to 27.6 kK. This value is a little lower than that of 28.2 kK observed in methanol by Hart and Detroit.[7] These authors located the absorption maximum of the monovalent anion at 22.4 kK when examining the spectral change upon the addition of sodium methoxide. The disodium salt was isolated as a bright red powder. The absorption maximum is located at 21.6 kK in the solid salt and at 22.0 kK when dissolved in acetone. In the vibrational spectra of the solid TNBP and the disodium salt, a band at about 3100 cm^{-1} assignable to the CH stretching is the only sharp one observed in the region from 2000 to 4000 cm^{-1}.

The Monoamine Complexes. The solid complexes were isolated; the twenty-eight aromatic monoamines are arranged in the order of decreasing pK_a value in Table 2.[17] An interesting result of the present study is the observation that the nine primary amines out of sixteen with pK_a values higher than 2.71 form yellow complexes of a 1 : 1 composition and also orange or red complexes of a 2 : 1 composition. Regardless of the composition, all of them show a vibrational pattern characteristic of phenolates of primary amines.

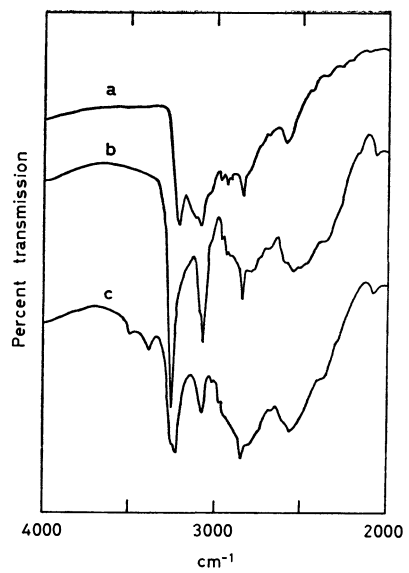

Fig. 1. Vibrational spectra; (a) *p*-anisidine-picric acid, (b) *p*-anisidine-TNBP (1:1), (c) *p*-anisidine-TNBP (2:1).

In other words, the spectra in the region from 2000 to 4000 cm^{-1} more or less resemble those of the corresponding picric acid complexes, which are known to be of the PT type. For example, the vibrational spectra of the 1 : 1 *p*-anisidine complex is compared with that of the picric acid complex in Fig. 1. Moreover, the similarity between the spectrum of the 1 : 1 complex and that of the 2 : 1 complex must be noted. Thus,

14) G. Briegleb and J. Czekalla, *Z. Elektrochem.*, **59**, 184 (1955).
15) M. S. J. Dewar and A. R. Lepley, *J. Amer. Chem. Soc.*, **83**, 4560 (1962).
16) A. Bier, *Rec. Trav. Chim.*, **75**, 866 (1956).
17) D. D. Perrin, "Dissociation Constants of Organic Bases in Aqueous Solution," Butterworths, London (1965), pp. 58—91.

TABLE 2. TNBP COMPLEXES WITH AROMATIC MONOAMINES

Amine	pK_a	Color	Mole ratio	Elementary analysis			
				Found		Calcd	
				C%	H%	C%	H%
N,N-Diethyl-*m*-toluidine	7.12	Red	2 : 1	57.74	5.55	58.96	5.78
		Red	3 : 1	63.55	6.76	63.16	6.67
N,N-Diethylaniline	6.61	Orange	1 : 1	51.14	3.92	51.26	4.08
		Dark orange	5 : 3	56.04	5.04	56.00	5.05
N,N-Dimethyl-*o*-toluidine	6.11	Orange	1 : 1	50.22	3.76	50.30	3.79
p-Anisidine	5.34	Yellow	1 : 1	46.39	3.05	46.63	3.07
		Yellow	2 : 3	44.76	2.83	44.64	2.68
		Brown	2 : 1	50.95	3.99	50.98	3.92
N,N-Dimethyl-*m*-toluidine	5.34	Orange	1 : 1	50.34	3.92	50.30	3.79
		Dark orange	5 : 2	59.08	5.35	58.85	5.47
p-Phenetidine	5.20	Bright yellow	1 : 1	47.33	3.44	47.71	3.38
		Russet	2 : 1	52.60	4.36	52.50	4.38
N,N-Dimethylaniline	5.15	Bright russet	1 : 1	49.56	3.54	49.28	3.49
p-Toluidine	5.09	Bright yellow	1 : 1	48.31	3.14	48.20	3.17
		Dark russet	2 : 1	53.97	4.30	53.79	4.14
2,4-Dimethylaniline	4.90	Bright yellow	1 : 1	48.16	3.15	48.20	3.17
		Brown	2 : 1	53.60	4.16	53.79	4.14
N-Methylaniline	4.85	Bright yellow	1 : 2	44.38	2.42	44.34	2.50
m-Toluidine	4.68	Bright yellow	1 : 1	48.16	3.15	48.20	3.17
		Dark russet	2 : 1	53.60	4.16	53.79	4.14
Aniline	4.59	Bright yellow	1 : 1	46.15	2.76	47.06	2.83
		Dark russet	2 : 1	52.24	3.62	52.17	3.62
o-Anisidine	4.52	Yellow	1 : 1	46.81	3.19	46.63	3.07
		Reddish orange	5 : 2	52.64	4.21	52.56	4.23
		Red	5 : 1	57.24	5.16	57.49	5.20
o-Phenetidine	4.43	Yellow	3 : 2	49.92	3.72	50.31	3.94
		Yellowish orange	2 : 1	52.41	4.35	52.50	4.38
o-Toluidine	4.39	Bright yellow	1 : 1	48.33	3.35	48.20	3.17
		Orange red	2 : 1	53.71	4.18	53.79	4.14
m-Anisidine	4.20	Yellow	1 : 1	46.62	3.09	46.63	3.07
		Brownish yellow	2 : 1	51.27	4.05	50.98	3.92
β-Naphthylamine	4.16	Light orange	1 : 1	51.82	2.97	51.87	2.95
p-Chloroaniline	3.99	Bright yellow	1 : 1	44.07 (Cl 7.06	2.50	43.77 7.19)	2.43
		Orange	5 : 1	50.20	3.79	50.22	3.59
α-Naphthylamine	3.92	Orange	2 : 1	57.72	3.67	58.90	3.68
m-Chloroaniline	3.33	Yellow	1 : 1	(Cl 7.15		7.19)	
		Orange	2 : 1	46.19	2.92	46.38	2.90
3-Nitro-4-methylaniline	2.96	Bright yellow	1 : 1	44.34	2.79	43.68	2.68
o-Chloroaniline	2.71	Orange	2 : 1	46.38	2.91	46.38	2.90
o-Iodoaniline	2.60	Red	1 : 1	36.96	2.15	36.92	2.05
o-Bromoaniline	2.55	Dull yellow	4 : 1	41.08 (Br 30.58	2.88	40.99 30.36)	2.85
m-Nitroaniline	2.46	Yellow	3 : 2	43.82	2.63	43.98	2.62
		Orange	2 : 1	45.03	2.80	44.86	2.80
N,N-Dimethylamino-*p*-benzaldehyde	1.62	Red	1 : 1	49.19	3.29	48.93	3.30
Diphenylamine	0.79	Black	1 : 1	53.85	3.30	53.83	3.18
Phenyl-*α*-naphthylamine	?	Jet black	1 : 2	50.71	2.81	50.47	2.63

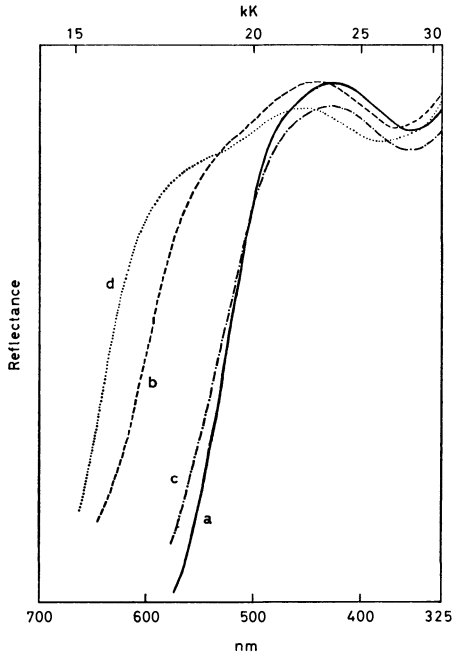

Fig. 2. Reflectance spectra; (a) *p*-anisidine-TNBP (1:1), (b) *p*-anisidine-TNBP (2:1), (c) aniline-TNBP (1:1), (d) aniline-TNBP (2:1).

the presence of PT from TNBP to the amine molecule in both the 1 : 1 and 2 : 1 complexes seems to be certain. In addition, the presence of two weak bands at 3380 and 3480 cm^{-1} in the spectrum of the 2 : 1 complex clearly indicates that the second amine is not protonated.

In general, the 1 : 1 complex exhibits a broad absorption band with a maximum at about 23.1—24.6 kK, which may be attributed to the TNBP monovalent anion. On the other hand, an additional absorption appears in most of the 2 : 1 complexes as a shoulder located on the lower-energy side of the main band. Obviously the deep coloration of the 2 : 1 complex is due to the appearance of this low-energy band. Fig. 2 presents the reflectance spectra of the 1 : 1 and 2 : 1 *p*-anisidine complexes. The absorption maximum appearing at 23.5 kK (425 nm) in the 1 : 1 complex is shifted a little towards the lower-energy side by combination with the second amine molecule. Furthermore, a new absorption can be seen in the region from 500 to 650 nm. The shoulder is located around 19 kK (525 nm). By analogy with the case of picric acid,[3,18] we may assume that the electron-acceptor strength of TNBP is not much affected by the dissociation. The location of the above-mentioned shoulder is fairly close to the energy value given by Eq. (1) with $X=16.2$. This result is strikingly different from the observation made for complexes represented by (I) and also from what would be expected for the complexes represented by (III). We established in a previous paper that the electron-donor strength of the monoprotonated diamine cation is essentially determined by that of the unprotonated half. The present result leads to the conclusion that the 2 : 1 *p*-anisidine complex is of the CPT type represented by Formula (IV). Although the vibrational bands to be assigned to the neutral amines are hardly detectable in the other eight 2 : 1 complexes, the fact that these amines are weaker bases than *p*-anisidine leaves little doubt as to the absence of PT in the second amine molecules. These complexes are probably of the same nature, judging from the deep coloration or the appearance of a new absorption on the lower-energy side of the main band; see the other example presented in Fig. 2. The deeply colored 2 : 1 complexes of *o*-phenetidine, *o*-chloroaniline, and α-naphthylamine with the characteristic vibrational pattern of phenolates of primary amines may also be of the same CPT type. On the other hand, the 2 : 3 complex of *p*-anisidine and the 3 : 2 complex of *o*-phenetidine are both yellow. Their vibrational spectra indicate the presence of PT. No additional electronic absorption band to be assigned to the CT interaction can be detected in them.

Upon heating, the 2 : 1 complex easily loses one molecule of the amine. However, further heating results in decomposition. These processes can be well demonstrated by the vibrational spectra. For example, the spectrum of the 2 : 1 *p*-toluidine complex turns into that of the 1 : 1 complex when it is heated to about 160 °C. This change is accompanied, of course, by the loss of the low-energy absorption band characteristic of the 2 : 1 compoex. After heating to 220 °C, the vibrational pattern differs substantially from that of TNBP. Thus, the amine participating in the CT interaction with the TNBP anion is much more easily removable than the one acting as a proton acceptor.

o-Anisidine was found to form complexes of 5 : 2 and 5 : 1 compositions in addition to that of a 1 : 1 composition. The coexistence of NH_2 and NH_3^+ groups is proved by their vibrational spectra (see Fig. 3). The intensities of the bands due to the NH_2 group are rather weak; therefore, we may explain the earlier observation that the corresponding bands are hardly observable in most of the 2 : 1 complexes of the CPT type. The shift of the strong absorption band at 23.8

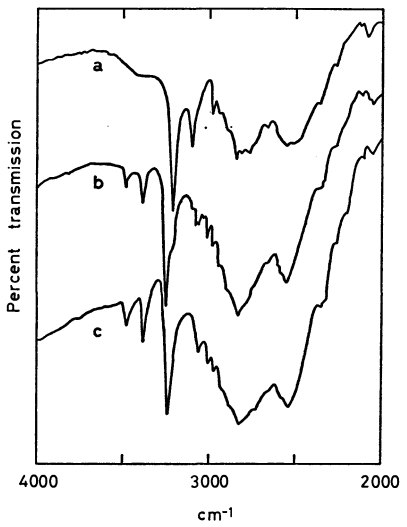

Fig. 3. Vibrational spectra of *o*-anisidine-TNBP; (a) the 1:1 complex, (b) the 5:2 complex, (c) the 5:1 complex.

18) G. Saito and Y. Matsunaga, This Bulletin, **45**, 2214 (1972).

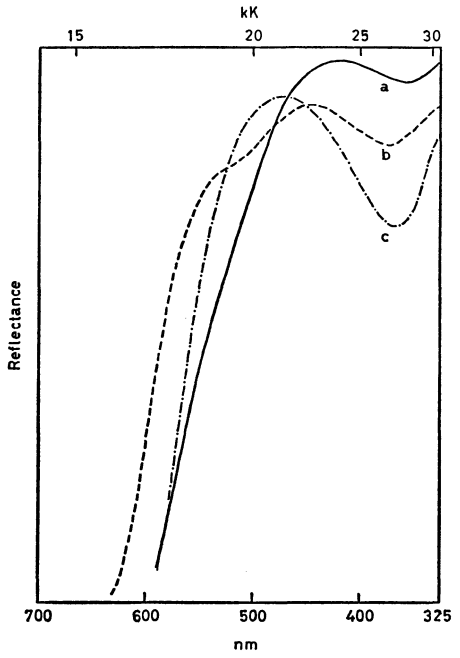

Fig. 4. Reflectance spectra; (a) *o*-anisidine-TNBP (1:1), (b) *o*-anisidine-TNBP (5:2), (c) *N,N*-diethyl-*m*-toluidine-TNBP (3:1).

kK in the 1 : 1 complex by about 1 kK towards the lower-energy side in the 5 : 2 complex and the appearance of a low-energy absorption in the latter complex may be seen in Fig. 4. In view of the magnitude of the pK_a value of the amine, and also the location of the band arising from the proton-donor component, TNBP may be supposed to be in the form of the monovalent anion; however, it is not clear how many anisidine molecules are involved in the CT interaction. The spectroscopic examination of the 5 : 1 *p*-chloroaniline complex showed that this complex can be classified into the same group as the above-mentioned *o*-anisidine complexes.

Of the amines with pK_a values below 2.60, some complexes are of the CT type and some are of the CPT type. No PT interaction was detected in the complexes of the following four bases: *o*-iodoaniline, *N,N*-dimethylamino-*p*-benzaldehyde, diphenylamine, and phenyl-α-naphthylamine. The pK_a value of the last mentioned is not known. As we may see in Table 2, naphthylamines are weaker bases than aniline; therefore, this amine is undoubtedly weaker than diphenylamine, and so the weakest among the amines employed. By contrast, the vibrational spectra of complexes of *o*-bromoaniline and *m*-nitroaniline, which have pK_a values slightly lower than that of *o*-iodoaniline, indicate the occurrence of PT in the complex formation. This irregularity reflects the fact that *o*-iodoaniline is the strongest electron donor among these three; $X=18.6$ for *o*-iodoaniline, compared with the values of 20.0 and 22.7 for *o*-bromoaniline and *m*-nitroaniline respectively. In accordance with the assumption made earlier, these observations suggest that the first pK_a value of TNBP in water is close to the pK_a values of these amines: 2.46—2.60. Although both diphenylamine and phenyl-α-naphthylamine have been known to form 1 : 2 complexes with *s*-trinitrobenzene,[19] the compositions of the TNBP complexes differ from each other, reflecting the size of the component molecules.

Now let us turn our attention to the complexes of *N*-substituted anilines, which are the strongest proton acceptors among the amines examined. They form deeply colored 1 : 1 complexes with TNBP, despite the occurrence of PT, as is indicated by their vibrational spectra. For example, the russet 1 : 1 *N,N*-dimethylaniline complex exhibits the vibrational pattern characteristic of phenolates of tertiary amines, with bands located in the region from 2250 to 2750 cm^{-1}.[20] A strong absorption located at 22.0 kK is observed in the electronic spectrum. The deep coloration must be wholly attributed to the breadth of this band. Besides the 1 : 1 complex, these amines give 5 : 3, 5 : 2, 2 : 1, and/or 3 : 1 complexes. Their color is deeper than that of the 1 : 1 complexes. In the case of the complexes of *N,N*-diethyl-*m*-toluidine, the strongest proton acceptor studied here, red powders with 2 : 1 and 3 : 1 compositions were obtained. Their electronic spectra are similar to each other and show a strong absorption at 21.3 kK (see Fig. 4). If the complexes are of the CPT type, the CT band can be predicted to appear at about 17 kK, according to Eq. (1). Nonetheless, we cannot see any indication of the presence of such a band. As the location of a strong absorption band is a little lower than that in complexes of the CPT type, and as the amine has a high pK_a value, the TNBP in this complex may be in the form of a divalent anion. If so, the second pK_a value of TNBP must be as high as the range covered by these amines. Thus, the difference between the first and second pK_a of the biphenyldiol is appreciably larger than that found for benzidine. This may be the reason why we can easily find complexes of the CPT type represented by (IV), but not those of the type represented by (III). *N*-Methylaniline, the only *N*-monosubstituted aniline used in this work, gives samples containing more amine than 1 : 2. Such preparations easily lose the amine even at room temperature; therefore, we could isolate no other stoichiometric complex.

The Diamine Complexes. The complexes prepared are listed in Table 3. They may be classified into two groups, those of the PT type and those of the CT type. *o*-Dianisidine can form complexes of both the PT and CT types.

The 1 : 1 complexes with *o*-tolidine, *p*-phenylenediamine, 1,5-diaminonaphthalene, and 1,6-diaminopyrene clearly exhibit the vibrational bands characteristic of the NH_3^+ group, but not those characteristic of the NH_2 group. On the other hand, the appearance of the electronic absorption band in the range from 22.5 to 23.6 kK may be accounted for by proposing that the 1 : 1 complex is composed of the TNBP monovalent anion and the monoprotonated diamine cation. The reason why the vibrational bands due to NH_2 group are not detectable remains unknown; however, we have

19) J. J. Sudborough and S. H. Beard, *J. Chem. Soc.*, **97**, 773 (1910).
20) R. P. Mariella, M. J. Gruber, and J. W. Elder, *J. Org. Chem.*, **26**, 3217 (1961).

TABLE 3. TNBP COMPLEXES WITH AROMATIC DIAMINES

Amine	Color	Mole ratio	Elementary analysis			
			Found		Calcd.	
			C%	H%	C%	H%
p-Phenylenediamine	Orange	1 : 1	45.39	2.92	45.57	2.95
Diaminodurene	Orange	3 : 2	52.23	4.40	52.92	4.91
1,5-Diaminonaphthalene	Orange	1 : 1	50.55	3.18	50.38	3.05
1,6-Diaminopyrene	Dark orange	1 : 1	55.57	3.11	56.19	3.01
Benzidine	Orange	3 : 2	55.05	3.56	56.07	3.74
N,N,N',N'-Tetramethylbenzidine	Light red	1 : 2	50.70	3.68	49.38	3.29
o-Tolidine	Light red	1 : 1	54.03	3.84	53.98	3.81
o-Dianisidine	Yellowish orange	1 : 1	50.95	3.60	51.15	3.61
	Black	1 : 1	51.34	3.67	51.15	3.61
3,3'-Dichloro-*o*-tolidine	Jet black	1 : 1	48.56	3.09	48.22	3.09
3,3'-Dibromo-*o*-tolidine	Brown	1 : 1	42.61	2.67	42.39	2.72

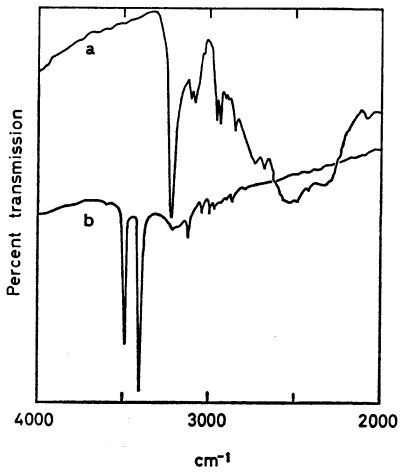

Fig. 5. Vibrational spectra of *o*-dianisidine-TNBP (1:1) complex; (a) the yellow form, (b) the black form.

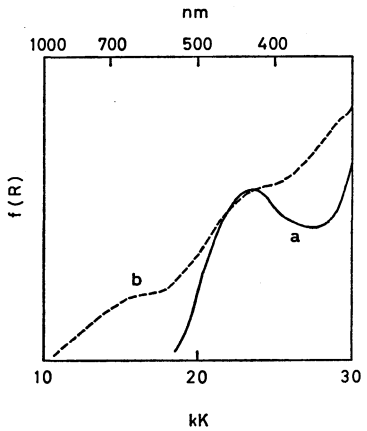

Fig. 6. Diffuse reflection spectra of *o*-dianisidine-TNBP (1:1) complex; (a) the yellow form, (b) the black form.

encountered the same problem in the 2 : 1 monoamine complexes. The yellowish-orange form of the *o*-dianisidine complex is another member of this group. As is shown in Fig. 5, the protonation of the diamine is firmly established by the broad vibrational bands appearing below 3000 cm^{-1}. The electronic absorption band arising from the proton-donor component is located at 23.5 kK; see Curve a, plotted using the Kubelka-Munk function, in Fig. 6. On the basis of a comparison between the pK_a values of benzidine, 4.95 and 3.85, and that of aniline, 4.59, the second pK_a value of *o*-dianisidine is expected to be below 4. Consequently, the possibility that two protons are transferred from the TNBP to the *o*-dianisidine molecule may be eliminated. If this complex is of the CPT type, the electronic spectrum may be similar to that of the 5 : 2 *o*-anisidine complex, shown in Fig. 4, as the electron-donor strength of the monoprotonated *o*-dianisidine may be anticipated to be close to that of *o*-anisidine. No absorption ascribable to the CT interaction between the TNBP monovalent anion and the monoprotonated diamine cation was observed in the *o*-dianisidine complex. This conclusion also applies to the 1 : 1 diamine complexes discussed above.

The coexistence of NH_2 and NH_3^+ groups in the 3 : 2 complexes with benzidine and diaminodurene is evidenced by the vibrational spectra, which are in accordance with a high ratio of the NH_2 group to NH_3^+ group. Nevertheless, no CT absorption band can be found in them. Tetramethylbenzidine combines with TNBP in a mole ratio of 1 : 2. As this diamine is a strong base, the constitution may be expressed by $[(CH_3)_2NH\text{-}\phi\text{-}\phi\text{-}NH(CH_3)_2]^{2+}(HO\text{-}\phi\text{-}\phi\text{-}O^-)_2$. The location of a strong electronic absorption at 22.8 kK seems not to be inconsistent with this expression.

A further result of importance in this study is that *o*-dianisidine can form not only a PT complex, but also a CT complex, with TNBP. On the mixing of benzene solutions containing equimolar amounts of the component compounds, a yellow complex was precipitated, while a small amount of fine, black needles appeared together with the yellow precipitate when the solutions were diluted and when a large excess of the diamine was employed. The black needles were separated from the mixture with tweezers. Surprisingly, the mole ratio of the diamine to TNBP was found to be identical in these two specimens. The black form exhibits vibrational bands assignable to the NH_2 group at 3395 and 3490 cm^{-1} and an electronic absorption assignable

to the CT interaction at 16.6 kK (see Figs. 5 and 6). The shoulder appearing at about 23 kK suggests that our black specimen is slightly contaminated with the yellow form. The band maximum located at 28.5 kK may be attributed to the TNBP molecule. The transitions from the black form to the yellow one, and *vice versa*, have so far not been observed. 3,3′-Dihalo-*o*-tolidines are the weakest bases among the diamines employed. The 1 : 1 complexes with TNBP are of the CT type. The energies of the CT absorption bands in these complexes are given in Table 1.

BULLETIN OF THE CHEMICAL SOCIETY OF JAPAN, VOL. 46, 1616—1619 (1973)

Infrared Study of Carbon Dioxide Adsorbed on Magnesium and Calcium Oxides

Yasuo FUKUDA and Kozo TANABE

Department of Chemistry, Faculty of Science, Hokkaido University, Sapporo 060

(Received August 14, 1972)

The infrared absorption spectra of CO_2 adsorbed on MgO and CaO were measured in the wide region 700—4000 cm^{-1} at various amounts of adsorbed CO_2 and temperatures of adsorption and desorption. It has been found that both uni- and bidentate carbonates are formed on MgO when a small amount of CO_2 is adsorbed and that unidentate carbonates predominate as the amount of adsorbed CO_2 is increased. On the other hand, only unidentate species were formed on CaO at room temperature independently of the amount of adsorbed CO_2, but bidentate species were also formed on CaO when the temperature of adsorption was high. The unidentate carbonates formed on both MgO and CaO at room temperature partially changed to bidentate carbonates upon evacuation at higher temperatures. The correlation between $\Delta\nu=|\nu_1-\nu_5|$ and the partial charge on oxygen atoms of various oxides, which corresponds to basic strength on the surface, was examined.

Calcium and magnesium oxides were reported recently to catalyze the esterification of benzaldehyde,[1] the dehydrochlorination of chlorinated ethanes,[2] the decomposition of diacetone alcohol[3] and the isomerization of olefins such as 1-butene,[4] limonene *etc.*[5] It has been pointed out that their catalytic activities are entirely due to the surface basic properties[1-5] and depended largely on the amount of adsorbed carbon dioxide.[3,4] Therefore, it is desirable to study the adsorption of acidic carbon dioxide on the basic oxides in order to characterize the basic properties.

Infrared studies of adsorbed CO_2 have been made for various oxides such as NiO,[6] TiO_2,[7] ZnO,[8] BeO[9] and MgO[10,11] but not for CaO. As for MgO, the formation of bidentate carbonate and carbonate ion was reported by Gregg and Ramsay[10] and that of bi- and unidentate carbonates by Evans and Whateley.[11] However, since the former authors did not observe the spectra in the low frequency region below 1200 cm^{-1}, while the latter ones did not study the spectral change with the amount of adsorbed CO_2, we attempted to observe the spectra in the region of 4000—700 cm^{-1} by varying greatly the amounts of adsorbed CO_2 and by changing the temperature of desorption to make clearer the behavior of adsorbed species. The spectra of CO_2 adsorbed on CaO were observed similarly to those for MgO. It is the purpose of the present work to distinguish the difference in adsorbed species of CO_2 between MgO and CaO and to study the correlation of basic properties of the oxides with the observed spectral data.

Experimental

Thin discs of calcium hydroxide (guaranteed reagent of Kanto Chemical Co.) and basic magnesium carbonate (guaranteed reagent of E. Merck Co.) prepared by pressing at 120 kg/cm^2 were mounted on a Nichrome wire holder placed in the heating zone of an infrared cell and decomposed to their oxides by evacuating at 700 °C for 3 hr. The calcined discs were moved into the optical path with a magnet and evacuated to about 4×10^{-6} mmHg at room temperature. The cell (66.8 ml of a dead space) was constructed of quartz and had cemented sodium chloride windows.

The amounts of CO_2 (99.99% purity) dosed into the cell were determined volumetrically. The spectra of adsorbed CO_2 were observed 30 min after CO_2 was introduced. Since no absorption band for free CO_2 (2350 cm^{-1}) was observed in any experiment, all the CO_2 dosed were regarded as adsorbed on the oxides. Desorption of CO_2 was carried out by evacuating samples at temperatures of 25—700 °C for 30 min.

All the measurements of infrared spectra were carried out at room temperature with a Hitachi model 215 infrared spectrophotometer.

1) K. Saito and K. Tanabe, *Shokubai* (Tokyo), **11**, (25th Symp. Catalysis, Preprints of Papers), 206 (1969).
2) J. Take, N. Kikuchi, and Y. Yoneda, *J. Catal.*, **21**, 164 (1971).
3) K. Yoneuchi, S. Okazaki, Y. Fukuda, and K. Tanabe, *Nippon Kagaku Zasshi*, **92**, 815 (1971); Y. Fukuda, K. Tanabe, and S. Okazaki, *ibid.*, 513 (1972).
4) K. Tanabe, N. Yoshii, and H. Hattori, *Chem. Commun.*, **1971**, 464.
5) M. Albeck, C. Rav-acha, E. Gil-av, and O. Schächter, *J. Catal.*, **22**, 219 (1971).
6) R. P. Eischens and W. A. Pliskin "Advances in Catalysis," Vol. IX, Academic Press Inc., New York (1957), p. 662.
7) D. J. C. Yates, *J. Phys. Chem.*, **65**, 746 (1961).
8) J. H. Tayler and C. H. Amberg, *Can. J. Chem.*, **39**, 535 (1961). S. Matsushita and T. Nakata, *J. Chem. Phys.*, **36**, 665 (1962).
9) W. I. Stuart and T. L. Whateley, *Trans. Faraday Soc.*, **61**, 2763 (1965).
10) S. J. Gregg and J. D. Ramsay, *J. Chem. Soc., A*, 2784 (1970).
11) J. V. Evans and T. L. Whateley, *Trans. Faraday Soc.*, **63**, 2769 (1967).

The weights of the samples determined after a series of IR spectral measurements were 10.0 and 20.8 mg for MgO in Fig. 1 and CaO in Fig. 3, respectively. The surface areas measured by nitrogen adsorption were 52 and 158 m^2/g, respectively, for CaO and MgO evacuated at 700 °C for 3 hr.

Results and Discussion

Both calcium and magnesium oxides heat-treated at 700 °C *in vacuo* for 3 hr showed infrared absorption bands at 840—1100 cm^{-1} (a broad band at 1000 cm^{-1} and a weak one at 840 cm^{-1} on MgO; a weak band at 1100 cm^{-1} and a broad one at 1060 cm^{-1} on CaO) which are due to the oxides themselves but no bands for OH and CO_2 which are possible impurities in the oxides. Both samples on which CO_2 was adsorbed showed no bands above 1700 cm^{-1}.

Adsorption of CO_2 on MgO at Room Temperature. Figure 1 shows the spectral changes caused by varying the amounts of CO_2 adsorbed on MgO. The stronger bands at 1670, 1315, 1000 and 850 cm^{-1} and the broad or weak bands at 1550, 1410 and 1050 cm^{-1} were observed in spectrum (2) of Fig. 1, where 0.23×10^{-3} mmol of CO_2 was adsorbed. In spectrum (3) of Fig. 1 where the adsorbed amount of CO_2 was increased, new bands appeared at 1630, 1280, 950 and 830 cm^{-1} and all the bands increased in intensity in spectrum (4). In spectra (5) and (6), the intensity of the bands at 1550, 1410, 1050 and 860 cm^{-1} increased, while the intensity of the other bands decreased.

On the basis of the analysis by Fujita *et al.*,[12] Evans and Whateley[11] considered that the splitting of the carbonate ion asymmetric stretching band (ν_3) is about 100 and 300 cm^{-1} for unidentate and bidentate carbonate, respectively, as shown below.[13] And they reported that the bands at 1665, 1325, 1005 and 850 cm^{-1} observed for CO_2 adsorbed on MgO could be assigned

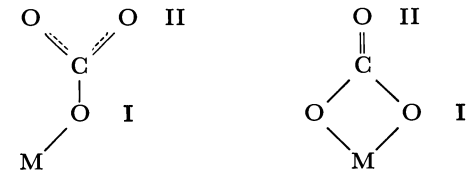

unidentate complex bidentate complex

to the bidentate carbonate complex and those at 1510, 1390, 1035 and 865 cm^{-1} to the unidentate carbonate complex. They attributed the strong bands at 1625 and 1275 cm^{-1} to bidentate carbonate or bridging carbonate because of the large splitting of the two bands. However, if bridging carbonate is of the type $\begin{matrix}-O\\-O\end{matrix}\!\!>\!C{=}O$, the band should appear at 1750 cm^{-1}.[14] Therefore, the bands at 1625 and 1275 cm^{-1} are believed due to bidentate carbonate. From these results, the bands at 1670, 1315, 1000 and 850 cm^{-1} and those at 1630, 1280, 950 and 830 cm^{-1} are assigned to bidentate carbonate. The bands at 1550, 1410, 1050 and 860 cm^{-1} can be assigned to the unidentate carbonate complex.

It is concluded from these observations that both uni- and bidentate carbonates are formed on MgO when a small amount of CO_2 is adsorbed and that unidentate carbonate is predominantly formed when there is a large amount of adsorbed CO_2.

Desorption of CO_2 from MgO. The changes in the spectra of a sample, which had CO_2 adsorbed at room temperature, produced by evacuation at 25—700 °C for 30 min are shown in Fig. 2. In spectra (1)

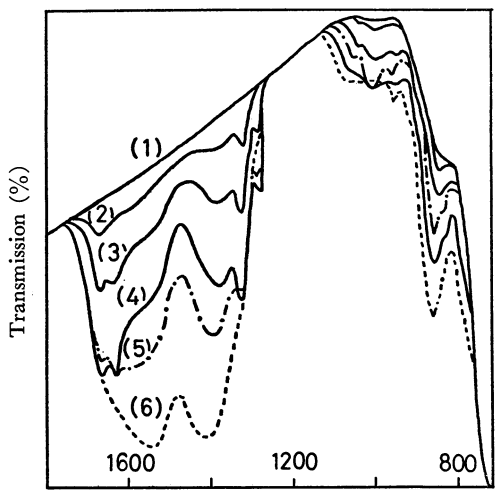

Fig. 1. Spectral changes for CO_2 adsorbed on MgO at room temperature for various adsorbed amounts; (1); 0 mmol (background), (2); 0.23×10^{-3} mmol ($\theta=0.02$), (3); 0.69×10^{-3} mmol ($\theta=0.06$), (4); 2.2×10^{-3} mmol ($\theta=0.16$), (5); 2.9×10^{-3} mmol ($\theta=0.25$), (6); 5.2×10^{-3} mmol ($\theta=0.38$).

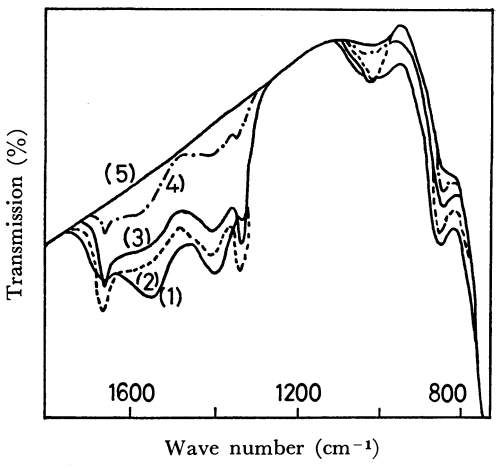

Fig. 2. Spectral changes due to CO_2 desorption from MgO at various evacuation temperatures; (1); room temp, (2); 240 °C; (3); 300 °C; (4); 400 °C (5); 700 °C.

12) J. Fujita, A. Martell, and K. Nakamoto, *J. Chem. Phys.*, **36**, 339 (1962).

13) Evans and Whateley[11] assumed that $\Delta\nu=|\nu_1-\nu_5|$ is a splitting of the carbonate ion asymmetric stretching band (ν_3), where ν_1 represents $\nu(C-O_{II})+\nu(C-O_I)$, $\nu(C-O_{II})$ and ν_5 does $\nu(C-O_{II})$, $\nu(C-O_I)+\delta(O_ICO_{II})$ for uni- and bidentate carbonate complexes, respectively.[12] However, Fujita *et al.*[12] say that it is impossible to determine which of three C–O stretching vibrations is due to the splitting of ν_3. Therefore, $\Delta\nu$ was used instead of the splitting of ν_3 in the present work.

14) L. H. Little, "Infra-Red Spectra of Adsorbed Species," Academic Press, London and New York (1965).

where the sample was evacuated at room temperature, broad bands appeared at 1550, 1410 and 1050—1000 cm^{-1} with weak bands at 1670, 1330 (shoulder) and 845 cm^{-1}. These bands were not changed by evacuation at 100 °C. By elevating evacuation temperature to 240 °C (spectra (2)), the spectra were changed greatly. The bands at 1550 and 1410 cm^{-1} decreased in intensity, while those at 1670 and 1330 cm^{-1} increased. The bands at 1050—1000 cm^{-1} became sharp at 1030 cm^{-1} and the band at 845 cm^{-1} shifted to 855 cm^{-1}. All bands decreased greatly in intensity on evacuation at 400 °C and the bands at 1800—1100 cm^{-1} disappeared at 700 °C.

The spectral changes caused by CO_2 desorption indicate that some unidentate carbonate is converted to bidentate carbonate by evacuation at 240 °C and both carbonates disappear at 700 °C.

Adsorption of CO_2 on CaO at Room Temperature. The absorption spectra of CO_2 adsorbed on CaO are shown in Fig. 3. Five bands were observed at 1520, 1490, 1415, 1060 and 860 cm^{-1} when 2.8×10^{-4} mmol of CO_2 was adsorbed. With an increase in the amount of adsorbed CO_2, the intensities of these bands increased and those at 1520 and 1490 cm^{-1} became a broad band at 1510 cm^{-1}. When the amount of adsorbed CO_2 was increased to more than 8.2×10^{-3} mmol, a band appeared at 2350 cm^{-1} and it disappeared upon evacuation at room temperature. Since the band at 2350 cm^{-1} is assigned to gaseous CO_2 and 8.2×10^{-3} mmol of dosed CO_2 corresponds to $\theta=0.96$ (calculated by assuming that the cross-section area of CO_2 is 19.5 Å^2), the five bands are attributed to the surface species. Because the value of $\Delta\nu$ is about 100 cm^{-1}, these bands may be assigned to a unidentate carbonate complex and the bands at 1520—1490, 1415, 1060 and 860 cm^{-1} to $\nu(C\text{-}O_{II})$, $\nu(C\text{-}O_{II})+\nu(C\text{-}O_{I})$, $\nu(C\text{-}O_{I})+\nu(C\text{-}O_{II})$ and π vibrations, respectively. Thus, the adsorbed species of CO_2 on CaO is different from that on MgO and only unidentate carbonate independent of the amount of adsorbed CO_2 is formed.

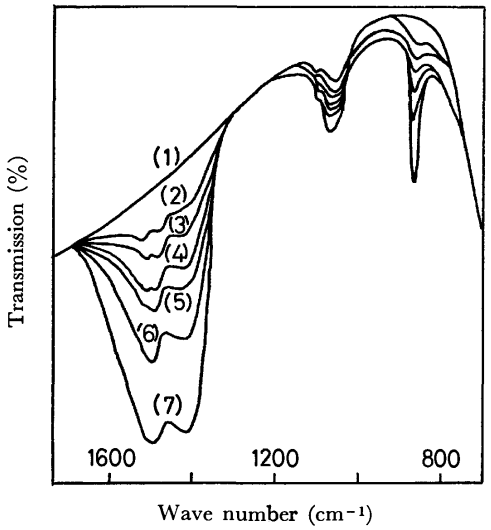

Fig. 3. Spectral changes for CO_2 adsorbed on CaO at room temperature at various adsorbed amounts; (1); 0 mmol (background) (2); 2.8×10^{-4} mmol ($\theta=0.03$), (3); 5.6×10^{-4} mmol ($\theta=0.06$), (4); 9.3×10^{-4} mmol ($\theta=0.10$), (5); 1.2×10^{-3} mmol ($\theta=0.13$), (6); 2.4×10^{-3} mmol ($\theta=0.26$), (7); 5.0×10^{-3} mmol ($\theta=0.55$).

Desorption of CO_2 from CaO. The spectral changes produced by CO_2 adsorbed on CaO at room temperature and evacuated at 310—700 °C are shown in Table 1. Many bands were observed when the sample was evacuated at 210—370 °C and new bands appeared upon evacuation at 110 and 210 °C.

On the basis of the observed characteristic features of the spectral changes upon CO_2 desorption, the bands other than unidentate species bands are classified into the following two groups; one (B_1) include bands at 1635, 1290—1302 and 980 cm^{-1} and the other (B_2) include bands at 1550—1570, 1308—1315, 1050 and 850 cm^{-1}. Since the value of $\Delta\nu$ is about 300 cm^{-1} in both the groups, they are assigned as bidentate carbonate complexes.

The behavior of CO_2 adsorbed on CaO is shown below,

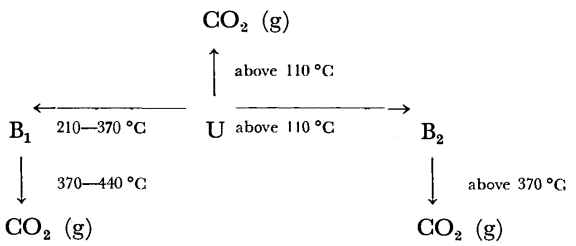

where U is the unidentate carbonate complex.

Table 1. Changes of the bands upon evacuation at various temperatures

Evac. temp. °C	25	110	210	310	370	460
		B_2 1570(A), 1308(A)	B_2 1570(I), 1308(I)	B_2 1550(I), 1315	B_2 1550(D), 1315(D)	B_2 1550, 1315, 1050, 850
			B_1 1635(A), 1290(A), 970(A)	B_1 1635(I), 1302, 980	B_1 1635(D), 1302(D), 980(D)	
	U 1500, 1420, 1060, 860	U 1500(D), 1420(D), 1060, 860	U 1500(D), 1420(D), 1060, 860	U 1500(D), 1420(D), 1050, 850	U 1500(D), 1420(D), 1050(D), 850(D)	

U: Unidentate carbonate, B_1, B_2; Bidentate carbonate, (I); Increase in intensity of the band, (D); Decrease in intensity of the band, (A); New band appeared by evacuation.

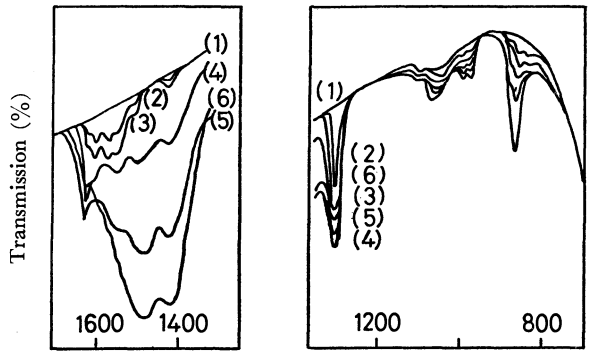

Fig. 4. Spectral changes for CO_2 adsorbed on CaO at 350 °C for various adsorbed amount; (1); 0 mmol (background), (2); 0.23×10^{-3} mmol, (3); 0.46×10^{-3} mmol, (4); 0.69×10^{-3} mmol, (5); 2.2×10^{-3} mmol, (6); 2.5×10^{-3} mmol.

Adsorption of CO_2 on CaO at 350 °C. Figure 4 shows the spectral changes produced by varying the amount of CO_2 which was adsorbed on CaO at 350 °C.

In the case of a small amount of adsorbed CO_2, the bands at 1635—1550 and 1308—1302 cm^{-1} were stronger than those around 1500 and 1430 cm^{-1} and the latter increased with increasing amount of adsorbed CO_2. Judging from the value of $\Delta\nu$, the former bands can be assigned to a bidentate carbonate complex and the latter to a unidentate carbonate complex, though it is difficult to assign all bands observed.

Correlation of $\Delta\nu=|\nu_1-\nu_5|$ with the Partial Charge δ_0 on Oxygen of Metal Oxides. It was reported that the active sites of MgO and CaO for decomposition of diacetone alcohol are basic sites (O^{2-} ions) and the activity is related to the partial charge on oxygen or the basic strength of the oxides.[15] Since CO_2 is bonded to surface oxygen to form uni- or bidentate carbonates, $\Delta\nu$ is also expected to be related to δ_0. In the case of bidentate carbonate, the values of $\Delta\nu$ are known to be 420 cm^{-1} for BeO[9] and were found to be 350 and 240 cm^{-1} for MgO and CaO, respectively. The values of δ_0 for BeO, MgO and CaO are known to be −0.35, −0.50 and −0.57 respectively.[16] Therefore, a correlation between $\Delta\nu$ and δ_0 seems to exist in the case of alkaline earth metal oxides. However, the correlation does not hold in the cases of TiO_2[7] and ThO_2.[17] This seems to indicate that the magnitude of $\Delta\nu$ does not depend only on δ_0, since CO_2 needs to bond not only to surface oxygen, but also to surface metal for the formation of bidentate carbonate.

In the case of unidentate carbonate, the values of $\Delta\nu$ are known to be 150—190 cm^{-1} for ZnO[8], TiO_2[7] and ThO_2[17] and were found to be 140 and 70 cm^{-1} for MgO and CaO respectively. Since δ_0 values for these oxides are −0.27∼−0.29, −0.50 and −0.57 respectively, there exists a fairly good correlation. However, more data for $\Delta\nu$ with oxides will be needed for a full discussion of this correlation.

15) Y. Fukuda and K. Tanabe, *Shokubai* (Tokyo), **14**, (31st Symp. Catalysis, Preprints of Papers), 129 (1972).
16) R. T. Sanderson, *Inorg. Chem.*, **3**, 925 (1964).
17) P. Pichat, J. Véron, B. Claudel, and M. V. Mathieu, *J. Chim. Phys.*, **63**, 1026 (1966).

BULLETIN OF THE CHEMICAL SOCIETY OF JAPAN, VOL. 46, 1619—1623 (1973)

Initiation Step of Methane Pyrolysis. Further Studies on Initiation Step of Methane Pyrolysis

Takayuki YANO

Institute of Space and Aeronautical Science, University of Tokyo, Meguro-ku, Tokyo 153

(Received October 7, 1971)

The pyrolysis of diluted mixture of equimolar CH_4 and CD_4 were performed in a shock tube between ~1500 K and ~1600 K, and pyrolysis products were quantitatively determined. A small amount of oxygen contaminating the sample gases had no influence on the results. The isotope exchange reactions in the equimolar lean mixture of H_2 and D_2 were also performed under the same conditions of methane pyrolysis. The results explained that the isotope exchange reaction between H_2 and D_2 had no influence on the hydrogen isotopic distribution produced by the CH_4–CD_4 pyrolysis. From the hydrogen isotopic distribution of the products of CH_4–CD_4 pyrolysis, methyl radical mechanism was confirmed as the initiation step of methane pyrolysis.

In the previous paper,[1] it was concluded that the initiation step of the methane pyrolysis was

$$CH_4 \longrightarrow CH_3 + H \qquad (1)$$

but not be

$$CH_4 \longrightarrow CH_2 + H_2. \qquad (2)$$

This conclusion was derived from the predominant yield of HD molecule produced by the pyrolysis of an equimolar mixture of CH_4 and CD_4. If there is any side-reaction, however, and if it affects the isotopic distribution among hydrogen, the above-mentioned conclusion would become uncertain. It is desirable, therefore, to study the effects of the side-reactions on the hydrogen isotopic distribution. The following three exchange reactions, that is, (i) the reaction between reactant molecules, CH_4 and CD_4; (ii) the reaction between reactant methane and product hydrogen; and (iii) the reaction between product hydrogen

1) T. Yano and K. Kuratani, This Bulletin, **41**, 799 (1968).

molecules are examined. The effect of the small amounts of oxygen should be also taken into account, since Meyerson and Watt[2] have proved that the small amounts of oxygen accelerate the decomposition rate of hydrogen molecules significantly. If the considerable amounts of hydrogen atoms were formed by this reaction, the predominant yield of species HD would be obtained.

The exchange reaction between CH_4 and CD_4 behind a reflected shock wave was studied by Burcat and Lifshitz[3] in the temperature range from 1340 to 1745 K. When their rate equation is applied to the typical experimental runs reported in the previous paper, the extent of the exchange between CH_4 and CD_4 is calculated to be $(CD_3H)/(CD_4)=0.1$, *i.e.*, only 10% each of CH_4 and CD_4 may be converted to CH_3D and CD_3H, respectively. Then, if CH_3D and CD_3H are initially formed and then pyrolysis occurs, hydrogen molecules would be formed as follows by the methylene mechanism,

$$0.90\ CH_4 \rightarrow CH_2 + H_2$$

$$0.10\ CH_3D \rightarrow CH_2 + HD \text{ or } CHD + H_2 \text{ in equal amount}$$

$$0.10\ CD_3H \rightarrow CD_2 + HD \text{ or } CHD + D_2 \text{ in equal amount}$$

$$0.90\ CD_4 \rightarrow CD_2 + D_2 \qquad (3)$$

and the ratio of $(H_2) : (HD) : (D_2)$ would be 0.95 : 0.10 : 0.95. This clearly shows that the amount of HD produced by this scheme is much less than that obtained by the CH_4–CD_4 pyrolysis experiment. The effect of this side-reaction, (i), may be ignored.

The effect of the second reaction (ii) can be estimated by the results of Watt *et al.*[4] and the isotopic distribution ratio by the methylene mechanism proves

$$(H_2) : (HD) : (D_2) = 1.0 : 0.28 : 1.0. \qquad (4)$$

Therefore, the effect of the second side-reaction may also be neglected.

As to the third side-reaction, (iii), circumstances are rather complicated. According to the rate law of Bauer,[5] an appreciable amount of HD is formed by the H_2–D_2 exchange reaction and it will be quite difficult to decide whether the initiation step of the methane pyrolysis will be eq. (1) or eq. (2). Later, however, Lifshitz[6] corrected the Bauer's result and when Lifshitz's result is adopted for the calculation the amount of HD is smaller than the value calculated from the Bauer's rate expression. The amount of HD calculated would be further small, if the H_2–D_2 exchange reaction occurs through the bimolecular process and the phenomenological expression given by Bauer can be used. Only a little influence on our previous conclusion is expected. These discrepancies are mainly due to the difference of the reaction order with respect to hydrogen. Accordingly, to know the effect of the third side-reaction to the methane pyrolysis, it is desirable to reinvestigate the exchange reaction of hydrogen molecules itself in the same low concentration as actually observed in the methane pyrolysis.

Experimental

High quality hydrogen (99.9999%), deuterium (99.5%) obtained from Takachiho Co. and high quality argon (99.999 %) supplied by Tomoe Co. were used without further purification.

For the study of the isotopic exchange between hydrogens, 1% of H_2 and 1% of D_2 were mixed with 98% of argon and after being kept over night, this mixture was further diluted tenfold by argon gas. The latter mixture was shock heated.

For the study of the effect of the trace amounts of oxygen on the methane pyrolysis, 99.5% perdeuteromethane (CD_4) from Matheson Co., pure methane (99.5%) and high quality argon were used.

Oxygen contents in CH_4 and CD_4 were analyzed by gas chromatography and were found to be 0.5% and 50 ppm, respectively. The gas chromatographic system was built into a vacuum line to avoid air contamination. For the removal of a small amount of oxygen from methanes, impure methane was passed through a freshly reduced copper column at 160 °C. By this process, the oxygen content in the original CD_4 and CH_4 was reduced from 5000 to 50 and from 50 to 7 ppm, respectively. The oxygen content in the high quality argon gas, was also analyzed in a similar manner after being passed through the copper column at 160 °C, and it was confirmed to be less than 1 ppm. Then, two gas mixtures of 6% each of CH_4 and CD_4 in high quality argon gas were prepared. In the mixture A, purified CH_4 and CD_4 were diluted in argon and in the mixture B, unpurified CH_4 and CD_4 were used. Consequently the oxygen levels of mixture A and B were about 3 and 300 ppm, respectively.

In addition to the careful preparation of sample gases, the contamination during the storage and the gas handling was also examined. Gas mixtures were kept for at least 15 hours in a gas holder to accomplish complete mixing. Then, a part of the sample gas was analyzed by gas chromatography before shock heating and it was confirmed that the oxygen contamination during the storage was negligible. The gas leak of the driven section of the shock tube, however, was about 6×10^{-5}Torr/min and the air contamination from this was to be estimated. High quality argon was introduced into the driven section to the level of 65 Torr and was kept for two days. After that, the gas was analyzed by gas chromatography. Oxygen contamination was about 300 ppm after 48 hr at the total pressure of 65 Torr. That is, about 0.5 ppm of oxygen was mixed into the sample gas since it took 5 min to handle the sample gas in the driven section before shock firing.

The shock tube used in this study was the same that Tsuda and Kuratani[7] used, but the volume of a damp tank of driver gas was changed from 20 l to 80 l to decrease the amount of driver gas mixing into the sample gas after reaction. As soon as the shock was fired and the reaction was over, the reaction mixture behind the reflected shock wave was withdrawn into an evacuated vessel and its composition was determined by the gas chromatograph Shimadzu GC-1C. Isotopic hydrogen molecules were separated by an alumina column coated with $MnCl_2$ of 2 m length at 77 K. After the separation of H_2, HD and D_2, the gas flow, using He

2) A. L. Meyerson and W. S. Watt, *J. Chem. Phys.*, **49**, 425 (1968).
3) A. Burcat and A. Lifshitz, *ibid.*, **52**, 3613 (1970).
4) W. S. Watt, P. Borrell, D. Lewis and S. H. Bauer, *ibid.*, **45**, 444 (1966).
5) S. H. Bauer and E. Occa, *ibid.*, **45**, 434 (1966).
6) A. Burcat and A. Lifshitz, *ibid.*, **47**, 3079 (1967).
7) M. Tsuda and K. Kuratani, This Bulletin, **41** 53 (1968).

as a carrier gas, was introduced into the heated column of CuO to oxidize these components to water vapors and was detected by a cathetometer. The analysis of the hydrocarbons were also made by the gas chromaotgraphy with a charcoal column of 1 m length and a hydrogen flame ionization detector.

Results

H_2–D_2 Exchange Reaction. Reaction times behind the reflected shock wave were assumed to be the same as the residence time observed by a pressure transducer at an end plate and were nearly 1 ms. The temperature range was 1135~1940 K. Reaction rates observed, $\Delta(\mathrm{HD})/\Delta t$, are compared with those calculated by Bauer's rate law in Table 1. It is obvious that the isotope exchange rate is about one hundredth of the rate calculated from the equation obtained by Bauer at high concentration of hydrogen molecules and that the reaction orders with respect to H_2 and D_2, given by Bauer, is not accurate at least at the low concentration ranges of hydrogen. For the accurate estimation of the partial reaction order with respect to H_2 and D_2, it is necessary to study in the concentration range as wide as possible. Bauer carried out the study in a relatively high concentration, while the present work was studied in a relatively low concentration, and when two experiments are combined, the sum of the partial orders can be estimated more accurately.

Since the argon concentration in above two experiments is alike, the difference of the reaction rate due to the argon concentration may be ignored. Therefore, the empirical power-rate expression was deduced to

$$\Delta(\mathrm{HD})/\Delta t = k(\mathrm{H_2})^y(\mathrm{D_2})^x \qquad (5)$$

in which k includes the contribution of argon. When the mixtures were restricted to the equimolar ones, the sum of the partial reaction orders, or $n=x+y$, and the activation energy, E, could be determined by the least-squares method (Fig. 1). From the figure, the values of E and n were determined to be 41.2 kcal/mol and 1.80 respectively.

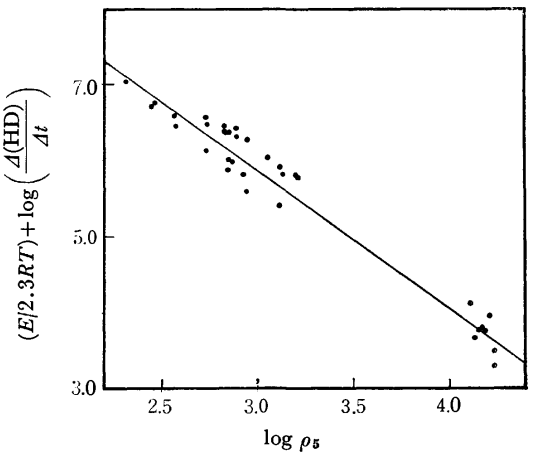

Fig. 1. The determination of reaction order n by the relation derived from Eq. (5) with E=41.2 kcal/mol at the least standard deviation. (n=1.80 from the slope)
ρ_5: The total density of sample gas mixture behind the reflected shock wave.
Bauer: ●, Yano: ◐

CH_4–CD_4 Pyrolysis. *Mixture A*: Reaction times behind the reflected shock wave were about 1 ms and the temperature range was 1501~1678 K. For all of the experimental runs, (H_2) : (HD) : (D_2) ratios were examined and for some, hydrocarbons were also analyzed as shown in Table 2. The average ratios $(HD)/(H_2)$ and $(D_2)/(H_2)$ were 1.56±0.05 and 0.50±0.05, respectively. These values are slightly different from those in the previous paper[1] (1.7 and 0.6 respectively). Because of the improved separation between gas chromatographic peaks, the ratios obtained in the present work are more accurate than those in the previous paper.

Mixture B: Temperature range was 1470~1608 K. The average ratios $(HD)/(H_2)$ and $(D_2)/(H_2)$ were

Table 1. Observed H_2-D_2 exchange reaction rate and the one calculated by Bauer's equation

T_5K	ρ_5 ×10³	τ ms	$(\rho_5)_{HD}$ ×10⁶	$(HD)/(H_2)$	$\Delta(HD)/\Delta t$ Obsd ×10³	$\Delta(HD)/\Delta t$ Calcd ×10¹
1135	2.83	0.964	nil	—	—	0.001
1183	2.73	1.00	nil	—	—	0.003
1255	3.04	0.828	0.008	0.0025	0.0971	0.101
1395	3.84	0.934	3.30	0.092	3.53	0.891
1417	3.07	0.861	0.928	0.029	1.07	0.711
1497	3.24	0.952	4.10	0.14	4.31	1.91
1540	3.18	0.861	8.41	0.29	9.77	2.61
1555	3.43	0.783	6.24	0.21	7.97	3.61
1556	3.62	0.843	5.03	0.15	5.97	3.81
1610	3.44	0.813	10.21	0.36	12.5	5.91
1670	2.67	1.08	18.1	0.79	16.61	6.91

ρ_5: Total density of the sample gas behind a reflected shock wave, expressed in mol/l.
$(\rho_5)_{HD}$: ρ_5 multiplied by mole fraction of product HD.

8) The contribution from argon to the rate was taken into account, as proposed by Bauer, the values of E and n were calculated to be 41.2 kcal/mol and 1.84, respectively.

TABLE 2. PRODUCTS DISTRIBUTION OF METHANE PYROLYSIS
(Product yields are represented in mol% of sample gas)

	Mixt. A					Mixt. B					
T_5K	1501	1517	1519	1578	1600	1470	1530	1532	1552	1580	1608
Run	1	3	4	2	5	6	7	9	10	8	11
H_2 %	0.0056	0.0052	0.0077	0.0279	0.0416	0.0029	0.0175	0.0155	0.0227	0.0368	0.0670
HD %	0.0088	0.0100	0.0115	0.0403	0.0580	0.0058	0.0265	0.0236	0.0336	0.0549	0.1070
D_2 %	0.0026	0.0030	0.0030	0.0135	0.0167	0.0007	0.0105	0.0090	0.0113	0.0202	0.0416
ΣH %	0.0170	0.0182	0.0222	0.0817	0.1163	0.0094	0.0545	0.0481	0.0676	0.1119	0.2156
C_2H_6 %	0.0078	0.0106	0.0112	0.0230	0.0228	— a)	— a)	0.0197	0.0233	0.0282	0.0337
C_2H_4 %	0.0017	0.0035	0.0041	0.0179	0.0240	— a)	— a)	0.0107	0.0148	0.0218	0.0427
C_2H_2 %	nil	0.0002	0.0002	0.0025	0.0029	— a)	— a)	0.0001	0.0004	0.0011	0.0036
$\Sigma' C_2$ %	0.0112	0.0182	0.0200	0.0663	0.0795	—	—	0.041	0.053	0.075	0.13
HD/H_2	1.57	1.92	1.49	1.44	1.39	1.97	1.51	1.52	1.48	1.49	1.63
D_2/H_2	0.46	0.58	0.39	0.48	0.40	0.24	0.60	0.58	0.50	0.55	0.64
$\Sigma C_2/\Sigma H$	0.56	0.79	0.70	0.53	0.43						

a) Not studied.

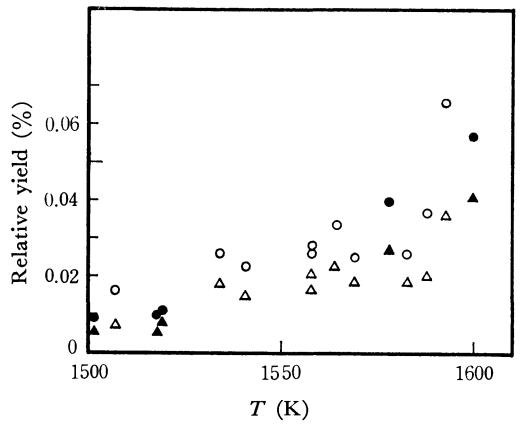

Fig. 2. The effect of oxygen on the relative yields of products at various temperature.
Mixture A ●: (HD) ▲: (H_2)
Mixture B ○: (HD) △: (H_2)

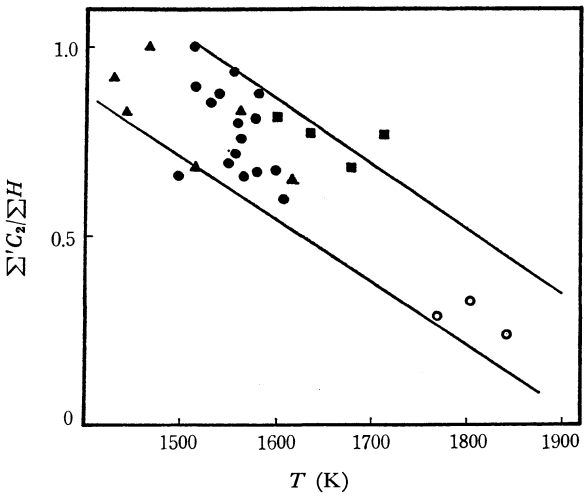

Fig. 3. The temperature dependence of $\Sigma' C_2/\Sigma H$.
Yano ●: CH_4-CD_4-Ar(6—6—88%) $\tau = 1$ ms
○: CH_4-Ar(12—88%) $\tau = 1$ ms
Skinner ▲: CH_4-Ar(12—88%) $\tau = 1$ ms
■: CH_4-Ar(12—88%) $\tau = 10$ ms

found to be 1.53±0.05 and 0.60±0.05, respectively (see Table 2, Mixt. B). These values are in good agreement with those obtained for the mixture A. As shown in Fig. 2, the effect of the trace amounts of oxygen (less than 300 ppm) is negligible. This conclusion is consistent with the calculation[9] after Meyerson.

As described in the previous paper, methane is converted into ethane in the early reaction stage and the latter is further transformed into ethylene, acetylene and higher hydrocarbons. When the products of the methane pyrolysis are assumed to be only C_2 hydrocarbons, the total hydrogen produced by the pyrolysis, ΣH ($=(H_2)+(HD)+(D_2)$), should be equivalent to the sum $\Sigma' C_2 (=(C_2H_6)+2(C_2H_4)+3(C_2H_2))$. ΣH is, however, always larger than $\Sigma' C_2$ in both the present and the previous works, and the ratio $\Sigma' C_2/\Sigma H$ decreases as the temperature increases as shown in Fig. 3. In order to confirm this, product analysis was made for three runs shock heated at higher temperature with a mixture of 12% CH_4 in argon. From Table 3, it is clear that at higher temperatures the ratio $\Sigma' C_2/\Sigma H$ decreased remarkably. This inclination may be explained by the formation of higher hydrocarbons during the pyrolysis of methane. Actually, a small amount of propylene was detected in the experimental runs 8 and 11 (see Table 2, Mixt. B).

9) Even if hydrogen molecules are produced by the methane pyrolysis *via* methylene mechanism and dissociated into hydrogen atoms, at the rate given by Meyerson and Watt under the presence of 1000 ppm oxygen, and if H and D atoms from this process may be converted into HD molecules by the abstraction reaction with CH_4 and CD_4, *i. e.*,

$$\left.\begin{array}{l} H+CD_4 \rightarrow HD+CD_3 \\ D+CH_4 \rightarrow HD+CH_3 \end{array}\right\} \quad k_1 = 1.5\times10^{11}\exp(-14000/RT) \ (\mathrm{mol^{-1}\cdot l\cdot s^{-1}}) \qquad (A),$$

the amount of HD molecules obtained through these processes will be only 1.4% of total hydrogen molecules initially produced. The reactions

$$\left.\begin{array}{l} H+D_2 \rightarrow HD+D \\ D+H_2 \rightarrow HD+H \end{array}\right\} \quad k_2 = 5\times10^{10}\exp(-7500/RT) \ (\mathrm{mol^{-1}\cdot l\cdot s^{-1}}) \qquad (B)$$

are ignored since the processes (A) are faster than (B).

This small value with respect to HD molecules, obtained on above assumptions, contradicts with the experimental results.

Table 3. $\sum'C_2/H_2$ at relatively high temperature in CH_4 (12% in Ar) pyrolysis

	C_2H_6 %	C_2H_4 %	C_2H_2 %	$\sum'C_2$ %	H_2 %	$\sum'C_2/H_2$	T_5K
Run 1	0.0135	0.0700	0.0775	0.386	1.9	0.203	1848
Run 2	0.0286	0.1439	0.0955	0.603	2.11	0.286	1770
Run 3	0.0300	0.1512	0.1026	0.640	1.99	0.325	1805

Discussion

The yield of HD molecules in products has great significance in judging the validity of a methyl mechanism, proposed by Skinner,[10] compared with a methylene mechanism by Kevorkian.[11] In the previous paper, the formation of only C_2 hydrocarbons was taken into consideration, and the product hydrogen was divided into two parts, the primary and the secondary hydrogen. That is, the primary hydrogen was produced from the process

$$2\,CH_4 \longrightarrow C_2H_6 + H_2, \tag{6}$$

and the secondary one was produced from the dehydrogenation process,

$$C_2H_6 \longrightarrow C_2H_4 + H_2$$
$$\longrightarrow C_2H_2 + H_2. \tag{7}$$

Then, the formation of one mole of ethane corresponded to one mole of the primary hydrogen. And one mole of ethylene in the products corresponded to one mole each of the primary and the secondary hydrogens. In the similar way, the formation of one mole acetylene is equivalent to one mole primary and two moles secondary hydrogens. According to a methylene mechanism, small amount of HD would be formed in the primary process, while in the secondary process HD would be appreciably formed. Yet, the previous experimental results have been inconsistent with methylene mechanism as far as only C_2 hydrocarbons are concerned, even if the equilibrium distribution of hydrogen isotopes among the secondary hydrogens is assumed.

As shown in Fig. 3, however, the formation of considerable amounts of higher hydrocarbons is revealed. Therefore, the contribution from the higher hydrocarbons must be considered in addition to C_2 hydrocarbons, and the problem should be discussed more precisely. The ratio of the primary hydrogen to total hydrogen $\sum H$, A, is now expressed,

$$A = (\sum C_2 + \sum F_n(C_n))/\sum H \qquad (n \gtrsim 3) \tag{8}$$

where $\sum C_2$ gives the sum of C_2 hydrocarbons, *i.e.*, $\sum C_2 = (C_2H_6) + (C_2H_4) + (C_2H_2)$, and $F_n(C_n)$ means the sum of the primary hydrogen corresponding to C_n hydrocarbons. When the concentration of the hydrocarbon C_nH_m is expressed by C_n,

$$F_n(C_n) = n \cdot C_n/2. \tag{9}$$

To simplify the notation, A is divided into two parts, A' and A'', or

$$A = (\sum C_2 + \sum nC_n/2)\sum H = \sum C_2/\sum H + \sum nC_n/2\sum H$$
$$= A' + A''. \tag{10}$$

A' can be directly obtained from experimental data but A'' cannot because nC_n is unknown. The minimum value of A'', however, can be estimated from the extreme case where the n-carbons skeleton is taking the place of C_n-hydrocarbons. That is, all of the hydrogen atoms, attached to the carbon atom of the reactant methane molecule, are converted into hydrogen molecules. When $g(C_n)$ gives the amount of the total hydrogen released through the formation of C_n-skeleton, following two equations are obtained,

$$g_n(C_n) = 2n \cdot C_n \tag{11}$$

$$\sum_{n \geq 3} g_n(C_n) = \sum H - \sum' C_2. \tag{12}$$

Since $\sum'C_2$ has a value between $0.60\sum H$ and $0.92\sum H$ (Table 2), $\sum nC_n$ comes between $0.20\sum H$ and $0.04\sum H$, therefore, the minimum value of A'' is given by,

$$A'' = \sum nC_n/2\sum H = 0.1 \sim 0.02. \tag{13}$$

The value of A' has proved to be between 0.43 and 0.79 (see Table 2, Mixt. A) and so, A is estimated to be between 0.53 and 0.81.[12] Therefore, from this A and eq. (4), $(H_2)_{prim}$ and the upper limit of $(HD)_{prim}$ are expected to be,

$$(H_2)_{prim} = (1.0/2.28)(\sum H)_{prim} = (1.0/2.28)(\sum H)A \tag{14}$$

$$(HD)_{prim} = (0.28/2.28)(\sum H)_{prim} = (0.28/2.28)(\sum H)A. \tag{15}$$

while, the isotopic distribution in the secondary hydrogen is assumed to be in equilibrium state. The amount of $(H_2)_{sec}$ and $(HD)_{sec}$ are given as,

$$(H_2)_{sec} = (1-A)(\sum H)/4 \tag{16}$$

$$(HD)_{sce} = (1-A)(\sum H)(2/4). \tag{17}$$

The ratio of HD to H_2 is now expressed as,

$$(HD)/(H_2) = \{(HD)_{prim} + (HD)_{sec}\}/\{(H_2)_{prim} + (H_2)_{sec}\}$$
$$= \{4(0.28/2.28)A + 2(1-A)\}/\{4(1.0/2.28)A + (1-A)\}$$
$$= 0.86 \sim 0.48. \tag{18}$$

Thus, even if the most favorable cases for the methylene mechanism are assumed, it cannot explain the observed high ratio of 1.53 for $(HD)/(H_2)$.

Since no carbon-soot was detected but actually propylene and also other hydrocarbons are expected, the value of calculated A'' should be higher and the ratio $(HD)/(H_2)$ should be lower than those calculated above for carbon skeletons.

The author wishes to thank Professor Kenji Kuratani for his helpful discussions and encouragement.

10) G. B. Skinner and R. A. Ruehrwein, *J. Phys. Chem.*, **63**, 1736 (1959).

11) V. Kevorkian, G. E. Hearth and M. Boudart, *ibid.*, **64**, 964 (1960).

12) There is a positive correlation between $\sum'C_2/\sum H$ and $\sum C_2/\sum H$ in the present experimental conditions. That is, A' values of 0.43 and 0.79 correspond to $\sum'C_2/\sum H$ values of 0.69 and 0.92, respectively. So, the range of A value is 0.53~0.81.

An Investigation of a Surface Reaction between Pyrrhotite and the Hydrogen–Hydrogen Sulfide Mixture

Masayuki KATSUMOTO, Kazuo FUEKI, and Takashi MUKAIBO

Department of Industrial Chemistry, Faculty of Engineering, The University of Tokyo, Hongo, Bunkyo-ku, Tokyo 113

(Received August 31, 1972)

The isotopic exchange between H_2S and D_2 has been studied in the temperature range from 480 °C to 551 °C on a pyrrhotite specimen. The isotopic exchange reaction proceeded *via* these steps:

$$H_2S + D_2 = D_2S + H_2$$
$$H_2 + D_2 = 2\,HD$$

From the analysis of the kinetic data, the rate constant of the sulfurization of $Fe_{1-x}S$ by "hydrogen sulfide,"[1] k_i, and that of reduction by "hydrogen,"[1] k_i', were determined. It was found that k_i is inversely proportional to the sulfur activity of $Fe_{1-x}S$, a_S, and that k_i' is independent of it. It was found that the rate equation for the sulfurization of $Fe_{1-x}S$ in the "hydrogen"–"hydrogen sulfide" gas mixture could be expressed in the form of $v = kP_{\text{"}H_2S\text{"}}a_S^{-1} - k'P_{\text{"}H_2\text{"}}$.[1] A possible mechanism of the reaction at the surface of $Fe_{1-x}S$ is discussed.

For the elucidation of the mechanism of the gas-solid interface reaction, it is necessary to determine the reaction rate as a function of the activity of chemical species in a solid as well as the partial pressure of the reactant gases. Such a study was first carried out by Kobayashi and Wagner[2] for the reduction of silver sulfide by "hydrogen." Several methods have been developed on the same basis of the theory proposed by them and have been applied to oxide and sulfide systems.[3–7]

The present work aims to study the reaction at the interface between β-$Fe_{1-x}S$ and a "hydrogen"–"hydrogen sulfide" gas mixture by using the isotopic exchange method.

Experimental

$Fe_{1-x}S$ Specimen. An iron specimen was taken from a Ferrovac E sheet (0.05 mm thick). After being polished with 1000-emery paper and cleaned by petroleum ether, it was sulfurized in a gas mixture of hydrogen sulfide and hydrogen at 580 °C. As the $Fe_{1-x}S$ was fragile, it could not be used in the form of "foil" through many runs. Therefore, it was crushed lightly and the powder larger than 170 mesh was used as a sample. The surface area was 133.3 $cm^2\,g^{-1}$.

Isotopic Exchange Method. The apparatus, the method of the purification of gases, and the experimental procedure were essentially the same as in the isotopic exchange experiment on Cu_2S.[7] As the pyrrhotite sample was a powder, a Pyrex glass reaction vessel with a G3 filter (Fig. 1) was used, and the temperature was measured at a position near the sulfide sample.

The isotopic exchange was carried out after the chemical equilibrium had been reached between the sulfide and the "hydrogen"–"hydrogen sulfide" gas mixture. Therefore, a_S, the sulfur activity of the solid, defined as the pressure ratio of "hydrogen sulfide" to "hydrogen," was kept constant throughout the isotopic exchange run, irrespective of the change in the concentration of isotopic species.

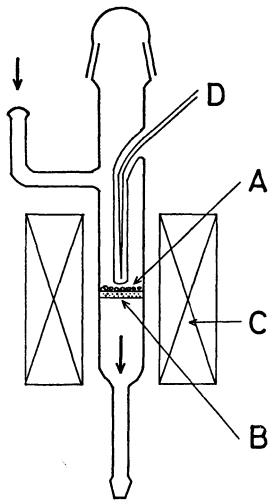

Fig. 1. Reaction vessel for the isotopic exchange experiment.
A $Fe_{1-x}S$ specimen B G3 filter
C furnace D Thermocouple

A blank test showed that, in the absence of $Fe_{1-x}S$, no exchange occurred below 528 °C, whereas a little exchange did occur at 551 °C. No deposition of sulfur occurred at the cold portions of reaction vessel over all the temperature and gas composition ranges studied.

Results and Discussion

Isotopic Exchange Reaction. Figures 2–4 give the change in x_{H_2}, x_{HD}, and x_{D_2}, the mole fractions of H_2, HD, and D_2 respectively, at different sulfur activities.

The following two mechanisms are possible for the formation of H_2 and HD. In the first mechanism, H and D atoms are formed by the dissociation of H_2S and D_2 *via* (1a) and (1b):

$$H_2S \rightleftharpoons HS(ad) + H(ad) \quad (1a)$$
$$D_2 \rightleftharpoons 2\,D(ad) \quad (1b)$$

where H(ad), D(ad), and HS(ad) represent H, D,

1) Terms such as "hydrogen" and "hydrogen sulfide" are used in a generic sense, irrespective of the isotopic species. The chemical symbols "H_2S" and "H_2" are employed for the chemical species of "hydrogen sulfide" and "hydrogen" respectively.

2) H. Kobayashi and C. Wagner, *J. Chem. Phys.*, **26**, 1609 (1957).
3) H. J. Grabke, *Ber. Bunsenges. Phys. Chem.*, **69**. 48 (1965).
4) S. Stotz, *ibid.*, **70**, 37 (1966).
5) S. Kurihara, K. Fueki, T. Mukaibo, and Y. Wada, This Bulletin, **43**, 2761 (1970).
6) M. Takeda, K. Fueki, and T. Mukaibo, *Denki Kagaku*, **35**, 283 (1967).
7) K. Fueki, H. Inaba, and T. Mukaibo, This Bulletin, **43**, 23 (1970).

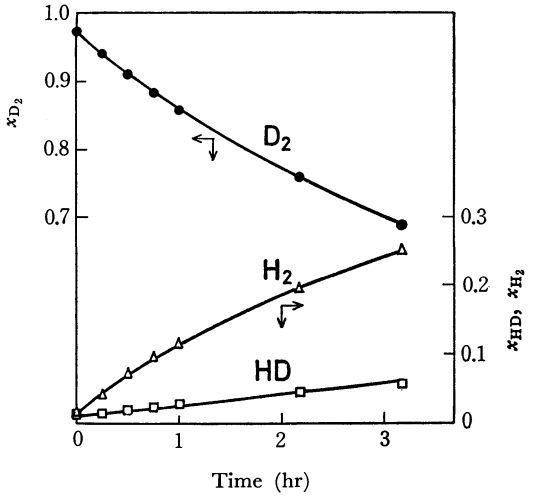

Fig. 2. Change in x_{D_2}, x_{HD} and, x_{H_2} with time. (551 °C, $P^o_{H_2S}=123.6$ mmHg, $P^o_{D_2}=30.9$ mmHg, $a_S=4$).

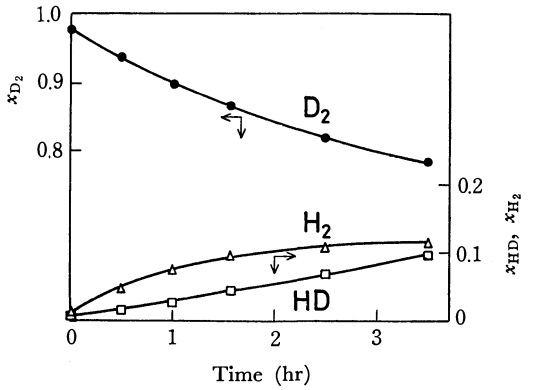

Fig. 3. Change in x_{D_2}, x_{HD}, and x_{H_2} with time. (551 °C, $P^o_{H_2S}=17.6$ mmHg, $P^o_{D_2}=70.4$ mmHg, $a_S=1/4$).

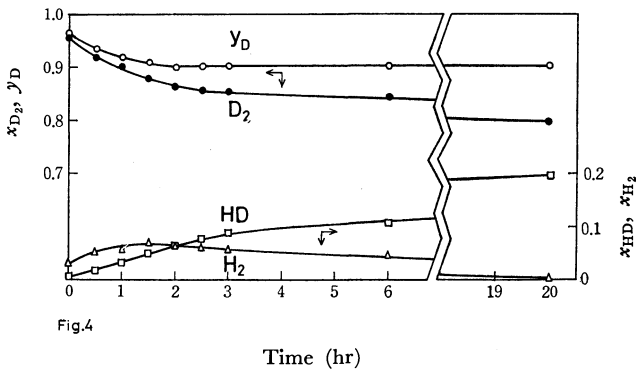

Fig. 4. Change in y_D, x_{D_2}, x_{HD}, and x_{H_2} with time. (551 °C, $P^o_{H_2S}=12.5$ mmHg, $P^o_{D_2}=125$ mmHg, $a_S=1/10$).

and HS adsorbed on the surface of $Fe_{1-x}S$. Then, H_2 and HD are formed by these reactions:

$$D(ad) + H(ad) \rightleftharpoons HD \quad (1c)$$

$$H(ad) + H(ad) \rightleftharpoons H_2 \quad (1d)$$

In the second mechanism, H_2S is directly converted to H_2, giving a sulfur atom to the lattice site on $Fe_{1-x}S$

$$H_2S \rightleftharpoons H_2 + S(lattice) \quad (2a)$$

The (2a) reaction is characterized as the redox reaction or as the two atom-direct exchange reaction. Then, H_2 and D_2 react to form HD:

$$H_2 + D_2 \rightleftharpoons 2\,HD \quad (2b)$$

As may be seen from Figs. 2—4, the rate of HD formation was smaller than that of H_2 in the initial period, and the formation of HD became remarkable only after the concentration of H_2 became high. These facts suggest that the (2a) and (2b) mechanisms are more predominant than (1a)—(1d). The second mechanism may also be confirmed as follows.

Let us define y_D, the fraction of D in "hydrogen," by:

$$y_D = x_{D_2} + \frac{1}{2}x_{HD} \quad (3a)$$

and y_H, the fraction of H in "hydrogen," by:

$$y_H = x_{H_2} + \frac{1}{2}x_{HD} \quad (3b)$$

At $a_s=1/10$, y_D decreases with time during the initial period, but it reaches a constant value at the time corresponding to the maximum of x_{H_2}; thereafter it remains unchanged, while x_{H_2}, x_{HD}, and x_{D_2} are still changing. When the value of a_s is 1/10, the ratio of H to D is also 1/10. Thus, after the isotopic equilibrium is attained between "hydrogen" and "hydrogen sulfide," the ratio of y_H to y_D is 1/10; *i.e.*, y_D is 0.909. Figure 4 shows that the constant value of y_D is equal to 0.909 within the limits of experimental error. The results clearly show that the H to D ratio attains equilibrium at the time x_{H_2} reaches its maximum and that, thereafter, only relative changes of x_{H_2}, x_{HD}, and x_{D_2} occur. That is, these results mean that H_2 and HD are formed by the mechanisms of (2a)—(2b) and not by (1a)—(1d).

At the beginning of the reaction, only H_2S and D_2 exist in the gas phase of the reaction system. Because the exchange reaction proceeds *via* (2a) and (2b), the amount of H in "hydrogen" at any time represents the amount of H transported from "hydrogen sulfide" to "hydrogen" *via* (2a). Similarly, the amount of D in "hydrogen sulfide" represents the amount of D transported from "hydrogen" to "hydrogen sulfide" *via* (2a). Accordingly, the change in the amount of D in "hydrogen" with time is given by this equation:

$$\frac{1}{A}\frac{dn_D}{dt} = \frac{RT}{V}(k_i n_D' - k_i' n_D) \quad (4)$$

where A is the surface area of $Fe_{1-x}S$, where k_i and k_i' are the rate constant of sulfurization and reduction respectively (mol atm^{-1} cm^{-2} hr^{-1}), and where V is the volume of the reaction system. n_D and n_D' are defined as follows:

$$n_D = n_{D_2} + \frac{1}{2}n_{HD} = n_{\text{"}H_2\text{"}}y_D \quad (5)$$

$$n_D' = n_{D_2S} + \frac{1}{2}n_{HDS} = n_{\text{"}H_2S\text{"}}y_D' \quad (6)$$

where n_{D_2}, n_{HD}, n_{D_2S}, and n_{HDS} represent the number of moles of D_2, HD, D_2S, and HDS respectively. $n_{\text{"}H_2\text{"}}$ and $n_{\text{"}H_2S\text{"}}$ are the number of moles of "hydrogen" and "hydrogen sulfide" respectively. y_D' is defined in the same manner as in the case of (3a) for "hydrogen sulfide."

At the beginning of the reaction:

$$n_D + n_D' = n_D^\circ = n_{\text{"H}_2\text{"}} x_{D_2}^\circ = n_{\text{"H}_2\text{"}} y_D^\circ \quad (7)$$

The insertion of Eq. (7) into Eq. (4) yields:

$$\frac{dn_D}{dt} = \frac{ART}{V}[k_i n_D^\circ - (k_i + k_i')n_D] \quad (8)$$

After the isotopic equilibrium between "hydrogen" and "hydrogen sulfide" has been attained, $dn_D/dt=0$ and $n_D=n_D^e$; *i.e.*,

$$\frac{dn_D}{dt} = \frac{ART}{V}[k_i n_D^\circ - (k_i + k_i')n_D^e] = 0 \quad (9)$$

Accordingly,

$$\frac{n_D^e}{n_D^\circ} = \frac{k_i}{k_i + k_i'} \quad (10)$$

By integrating Eq. (8) and using Eq. (10), we obtain:

$$-\log\frac{n_D - n_D^e}{n_D^\circ - n_D^e} = \frac{ART}{2.303\,V}(k_i + k_i')t \quad (11)$$

By replacing n_D, n_D°, and n_D^e by y_D, y_D°, and y_D^e respectively, Eq. (11) can be rewritten as:

$$-\log\frac{y_D - y_D^e}{y_D^\circ - y_D^e} = \frac{ART}{2.303\,V}(k_i + k_i')t \quad (12)$$

Figures 5—7 show the plot of $\log\{(y_D - y_D^e)/(y_D^\circ - y_D^e)\}$ *vs.* t for the data given in Figs. 2—4 respectively. The plots are linear irrespective of the HD formation. If we denote the slope of the plot of $-\log\{(y_D - y_D^e)/(y_D^\circ - y_D^e)\}$ against t by α, k_i and k_i' can be represented by the following equations:

$$k_i = \frac{2.303\,V}{ART}\alpha\frac{y_D^e}{y_D^\circ} \quad (13)$$

$$k_i' = \frac{2.303\,V}{ART}\alpha\left(1 - \frac{y_D^e}{y_D^\circ}\right) \quad (14)$$

The k_i and k_i' calculated by Eqs. (13) and (14) using α were independent of the total pressure.

Figure 8 gives the plots log k_i and log k_i' against log a_s. Both plots are linear at 551 °C and 480 °C. The slopes of log k_i *vs.* log a_s are −1.00 for 551 °C and −0.97 for 480 °C. The slopes of log k_i' *vs.* log a_s are 0.00 and 0.03 respectively.

The Arrhenius plot of k_i at $a_s=1$ is given in Fig. 9. The activation energy determined from the slope is 26.8 kcal mol^{-1}.

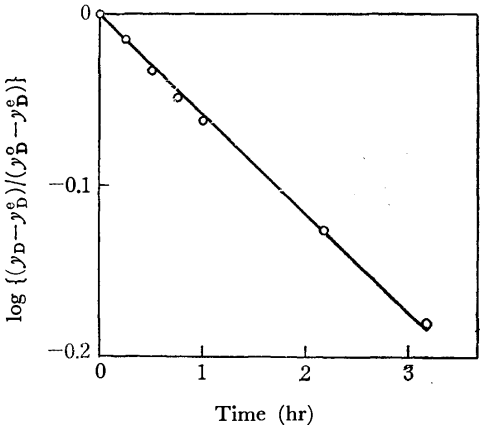

Fig. 5. Plot of log $\{(y_D - y_D^e)/(y_D^\circ - y_D^e)\}$ *vs.* t for the data given in Fig. 2.

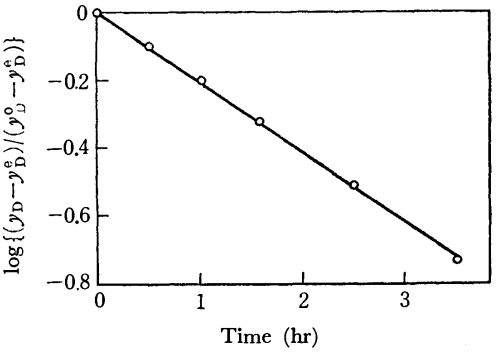

Fig. 6. Plot of log $\{(y_D - y_D^e)/(y_D^\circ - y_D^e)\}$ *vs.* t for the data given in Fig. 3.

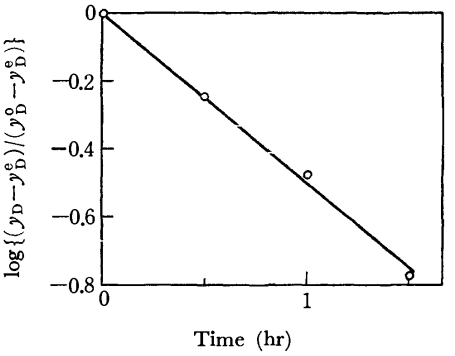

Fig. 7. Plot of log $\{(y_D - y_D^e)/(y_D^\circ - y_D^e)\}$ *vs.* t for the data given in Fig. 4.

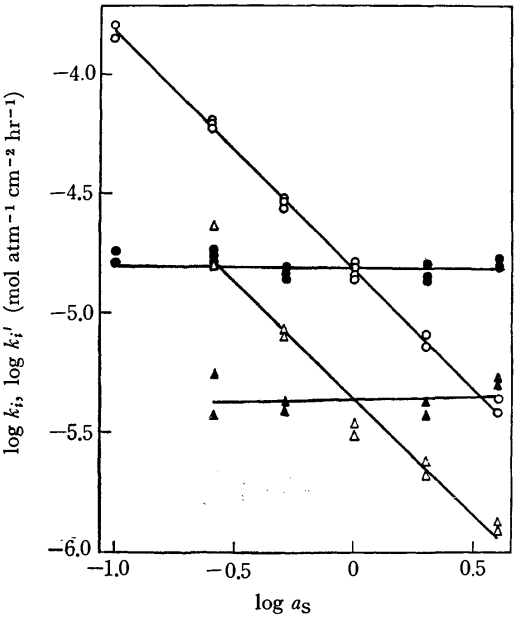

Fig. 8. Plot of log k_i and log k_i' against log a_S.
○ k_i ● k_i' } 551 °C △ k_i ▲ k_i' } 480 °C

Reaction Mechanism of Sulfurization. From the results of this study, the rate of redox reaction proceeding *via* (2a) can be expressed by this equation:

$$v = k_i P_{\text{"H}_2\text{S"}} - k_i' P_{\text{"H}_2\text{"}} = k P_{\text{"H}_2\text{S"}} a_S^{-1} - k' P_{\text{"H}_2\text{"}} \quad (15)$$

where k and k' are constants.

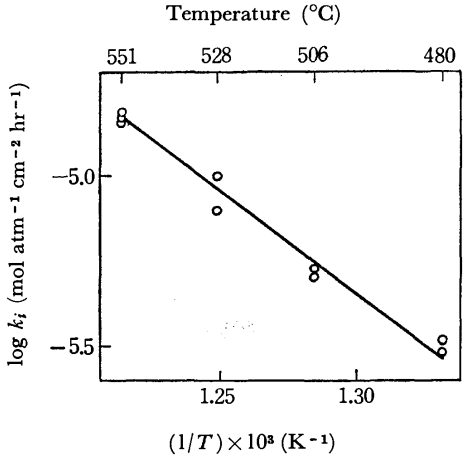

Fig. 9. Arrhenius plot for k_i at $a_S=1$.

Kobayashi and Wagner considered that e^-, S, S^-, and S^{2-} are reactants in Ag_2S and proposed the following three mechanisms for the reduction of Ag_2S by "hydrogen":

$$\text{"}H_2\text{"} + S \rightleftharpoons \text{"}H_2S\text{"} \quad (16A)$$

$$\text{"}H_2\text{"} + S^- \rightleftharpoons \text{"}H_2S\text{"} + e^- \quad (16B)$$

$$\text{"}H_2\text{"} + S^{2-} \rightleftharpoons \text{"}H_2S\text{"} + 2\,e^- \quad (16C)$$

where S, S^-, and S^{2-} are sulfur atom, mono-, and divalent sulfur ions respectively and where e^- is an electron. They showed that the rate equations for (16A) to (16C) can be expressed in a general formula:

$$v = k'P_{\text{"}H_2\text{"}}a_S^{m-} - kP_{\text{"}H_2S\text{"}}a_e^m \quad (17)$$

where m is integers characteristic of the reaction mechanism.

Let us first discuss the mechanism of the redox reaction on the pyrrhotite surface by the Kobayashi-Wagner mechanism.

Pyrrhotite is known as a semiconductor below the Néel temperature. However, the temperature coefficient of the conductivity is negative in the temperature range of this study, *i. e.*, above the Néel temperature[8–10], and the conductivity is independent of a_s.[10] As the conductivity is $\sim10^3$ mho-cm, we can conclude that β-$Fe_{1-x}S$ is a compound of metallic conduction. The metallic conduction is due to a half-filled narrow d-band. If the ratio of S to Fe changes, the number of electrons in the d-band also changes. However, we can expect that the Fermi level of electron will not be influenced because the density of the state of the narrow d-band is very high. Accordingly, we can assume that the activity of the electron, a_e, is nearly constant over the whole experimental range of a_s, *i. e.*,

$$a_e \cong \text{const.} \quad (18)$$

Among e^-, S, S^-, and S^{2-}, the following equilibrium relationships exist:

$$S^- \rightleftharpoons S + e^- \quad (19A)$$

$$S^{2-} \rightleftharpoons S + 2\,e^- \quad (19B)$$

i. e.

$$a_S{}^- \propto a_S \quad (20A)$$

$$a_S{}^{2-} \propto a_S \quad (20B)$$

Therefore, for mechanisms (16A) to (16C), the rate equation of the sulfurization reaction of the pyrrhotite should be expressed in this form:

$$v = kP_{\text{"}H_2S\text{"}} - k'P_{\text{"}H_2\text{"}}a_S \quad (21)$$

This dependence of the reaction rate on a_s does not agree with the results observed in this study.

Next, les us consider the Fe atom as a reactant in sulfide. In this case, the reaction mechanism is:

$$\text{"}H_2S\text{"} + \text{Fe(sulfide)} \rightleftharpoons \text{"}H_2\text{"} + FeS \quad (22)$$

and the rate equation is:

$$v = kP_{\text{"}H_2S\text{"}}a_{Fe} - k'P_{\text{"}H_2\text{"}}a_{FeS} \quad (23)$$

Since the activity of $Fe_{1-x}S$ is nearly constant, irrespective of nonstoichiometry,[11]

$$a_{Fe} = \text{const}\cdot a_S{}^{-1} \quad (24)$$

The insertion of Eq. (24) into Eq. (23) yields:

$$v = kP_{\text{"}H_2S\text{"}}a_S{}^{-1} - k'P_{\text{"}H_2\text{"}} \quad (25)$$

Therefore, it may be concluded that Eq. (22) is a possible mechanism for the redox reaction on the pyrrhotite surface.

Summary

(1) The isotopic exchange between H_2S and D_2 on $Fe_{1-x}S$ was investigated as a function of the temperature and of a_s, the sulfur activity of $Fe_{1-x}S$.

(2) It was found that the isotopic exchange reaction proceeds *via*:

$$H_2S + D_2 \rightleftharpoons D_2S + H_2$$

$$H_2 + D_2 \rightleftharpoons 2\,HD$$

(3) The rate equation for the sulfurization of $Fe_{1-x}S$ in the "hydrogen"-"hydrogen sulfide" gas mixture was

$$v = kP_{\text{"}H_2S\text{"}}a_S{}^{-1} - k'P_{\text{"}H_2\text{"}}$$

The activation energy was 26.8 kcal mol^{-1}.

(4) The reaction mechanism of redox reaction was discussed.

The authors wish to express their thanks to Dr. Masahiko Tsuchiya and Dr. Ju Kumanotani of the Faculty of Engineering, the University of Tokyo, for their help in carrying out the mass-spectroscopic analysis.

8) S. Fujime, M. Murakami, and E. Hirahara, *J. Phys. Soc. Jap.*, **16**, 183 (1961).

9) M. Murakami, *ibid.*, **16**, 187 (1961).

10) H. I. Kaplan and W. L. Worrell, "Chem. Extended Defects Non-Metal. Solids, Proc. Inst. Advan. Study 1969" (pub. 1970) ed. by Leroy Eyring. North-Holland Publ. Co., Amsterdam, Neth. p. 561.

11) K. Niwa and T. Wada, *Met. Soc. Conf.*, **8**, 945 (1961).

Studies on Fragment Ion Distribution and Reactions by the Use of a Charge Spectrometer. III. Reactivities of the Excited Ions from Methylamine after Charge Exchange with Positive Ions

Toshio NAGATANI, Kenji YOSHIHARA, and Takanobu SHIOKAWA

Department of Chemistry, Faculty of Science, Tohoku University, Aoba, Aramaki, Sendai 980

(Received July 31, 1972)

The behavior of the excited ions produced by positive ion impact in methylamine has been studied in the reaction chamber of a double mass spectrometer at elevated pressure. The ion-molecule reactions have been discussed for three energy regions. Metastable transitions taking place in the reaction chamber and in the Giese lens have also been studied in the corresponding regions.

Ordinary mass spectrometry deals with cases in which molecular ions or their fragment ions initially produced in the ionization chamber collide with sample gases and form secondary or tertiary products when gas pressure is enhanced. Studies have been carried out on these phenomena using electron impact but only a few have been made using positive ion impact.[1,2,3]

Positive ions accelerated to the order of kilo electron volt are extremely useful for charge exchange reactions with neutral molecules.[4] If the reaction chamber is filled with methylamine, the fragment ions from the excited molecular ions after charge exchange with the positive ions react with methylamine having kinetic energy given by the repeller voltage.

This paper deals with the reaction of the ionic species which are pulled in the second optical system and various processes of ion-molecule reactions in the reaction chamber of the charge spectrometers. Flying ions in the Giese lens system have shown characteristic features because the lens is long and located in a position neighboring the reaction chamber of high pressure. The behavior of the excited ions in particular has been investigated.

Experimental

The charge spectrometer was described in detail.[5] It consists of a double mass spectrometer having a large source volume for the study of charge distribution. Two sets of mass analyzers are connected perpendicular to each other and there is a reaction chamber in the crossing. A Hitachi T-2 ion source was used. The pressure of the reaction chamber could not be measured directly since distribution of gas density was not at all uniform. However, relative values of pressure in the reaction chamber could be expressed by reading the McLeod gauge of the gas-inlet system which leads gases through an orifice (0.300 ml/s).

All the gases used were of high purity or purified several times before use when necessary. Other details were reported previously.[4]

An example of the relationship between gas pressure and the intensities of various ionic species after charge exchange is shown in Fig. 1. Methylamine molecules were subjected to the impact of Xe^+ ions. The pressure given in the abscissa is that of methylamine in the gas reservoir of the sample inlet system. The repeller field was set at a sufficient strength 15.0 V/cm) expected to protect it from the phenomena of an unsuitable reaction order as pointed out by Hamill for CD_4.[6] Fig. 1 shows satisfactory results for determination of the reaction order, the gradient of the straight line representing the reaction order. In the low pressure region all the ions except that of m/e=32(abbreviated as (32), see Table 2) have the gradient of unity. This indicates that they are primary fragment ions after charge exchange with Xe^+. On the other hand, (32) is observed when the pressure in the reaction chamber increases, and its gradient differs from that of others showing the value of 2. It is obvious that (32) is the secondary product of an initially formed ion with methylamine.

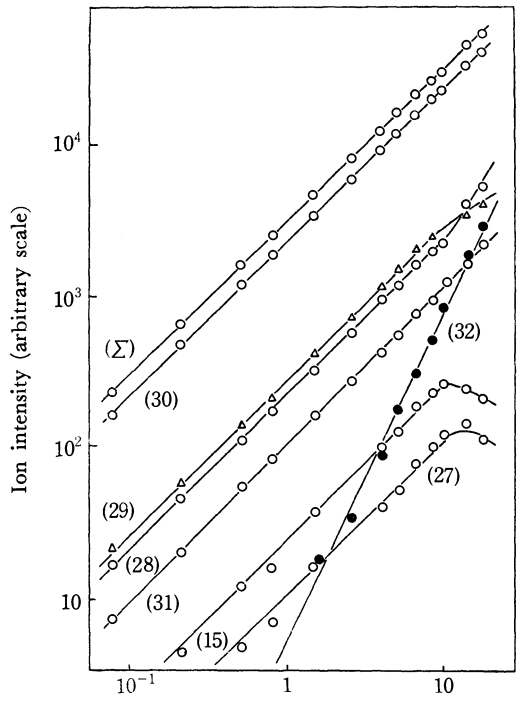

Fig. 1. Pressure dependence of the fragment ion distribution in methylamine bombarded with Xe^+.

1) I. Szabo, *Arkiv Fysik*, **33**, 57 (1967).
2) I. Szabo, *ibid.*, **35**, 339 (1968).
3) G. Sahlström and I. Szabo, *ibid.*, **38**, 145 (1968).
4) T. Nagatani, K. Yoshihara, and T. Shiokawa, This Bulletin **46**, 1306 (1973).
5) T. Shiokawa, K. Yoshihara, M. Yagi, T. Omori, H. Kaji, M. Hiraga, T. Nagatani, and Y. Takita, *Mass Spectroscopy*, **18**, 1230 (1970).
6) N. Boelrijk and W. H. Hamill, *J. Amer. Chem. Soc.*, **84**, 730 (1962).

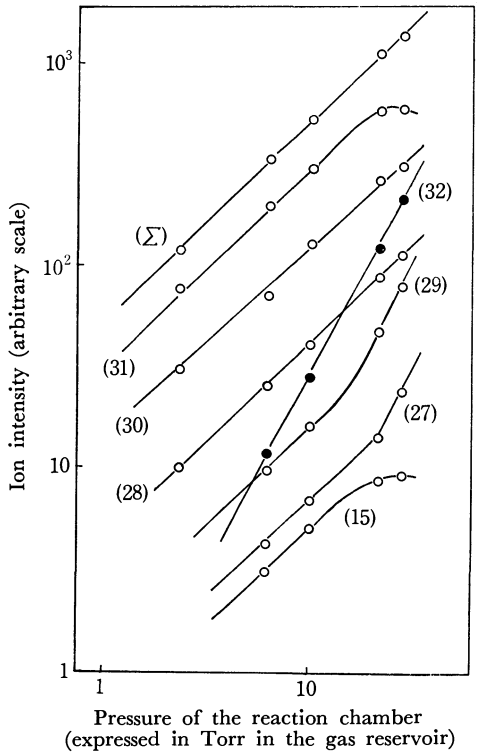

Fig. 2. Pressure dependence of the fragment ion distribution in methylamine bombarded with C^+.

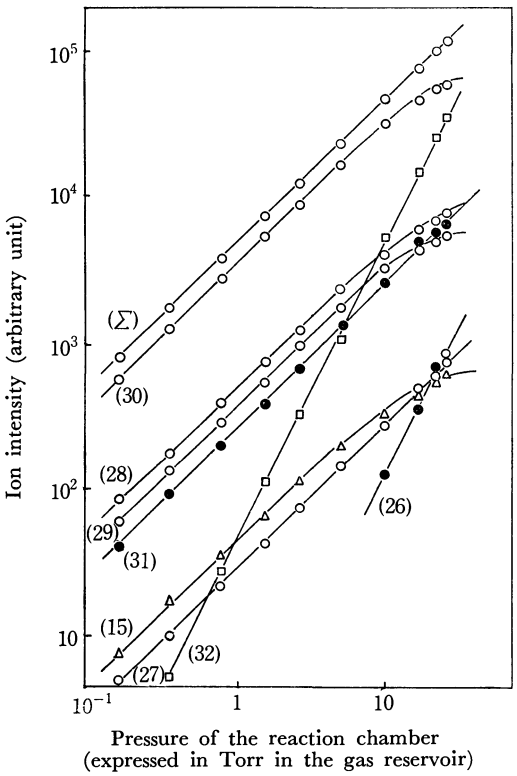

Fig. 3. Pressure dependence of the fragment ion distribution in methylamine bombarded with Cl^+.

Results and Discussion

Impact of methylamine with various positive ions has been performed in the reaction chamber at elevated pressure. The results with C^+, Cl^+ and Xe^{++} are shown in Figs. 2–4. Similar experiments using benzene, Ne^{++}, Xe^+, CO_2^+, Kr^+, Ar^+, Kr^{++}, Ne^+, Ar^{++} and He^+ have been described.[7] Detailed features depend on the energy received by the charge exchange. The break down curve should be taken into consideration.[4] The relation between the appearance of certain ions and their energy region is indicated graphically (Fig. 5).

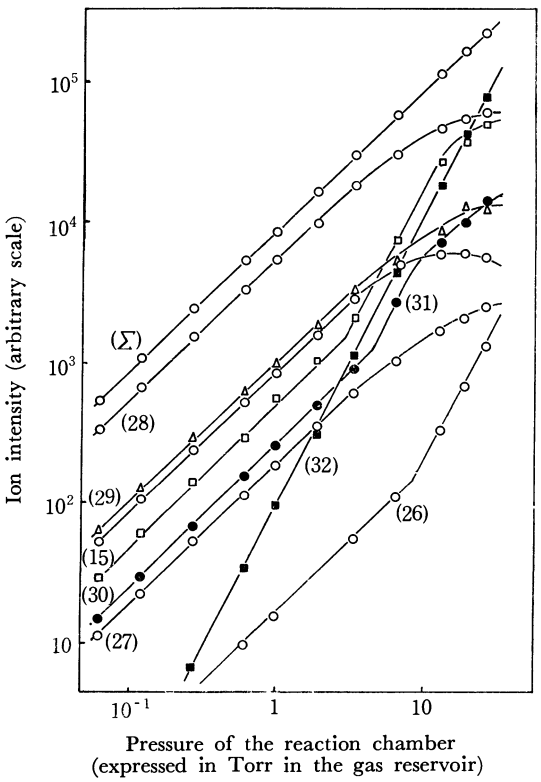

Fig. 4. Pressure dependence of the fragment ion distribution in methylamine bombarded with Xe^{++}.

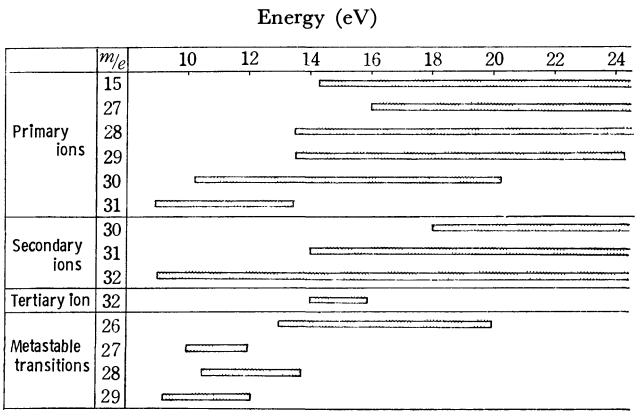

Fig. 5. Occurrence of various ions and its relation to the energy range.

The metastable transitions are considered to correspond to those shown in Table 1. These transitions take place during passage through the accelerating system before entering the magnetic field. The resolving power of this apparatus is about 50 for 1 mm slit width, and the peaks due to the metastable transi-

7) T. Nagatani, Thesis, Tohoku Univ., 1971.

TABLE 1. METASTABLE TRANSITION IN POSITIVE ION IMPACT OF METHYLAMINE

M_1	M_2	M*	M_1	M_2	M*
31	30	29.03	29	27	25.14
31	29	27.13	28	27	26.04
30	29	28.03	28	26	24.14
30	28	26.13	27	26	25.04
29	28	27.03			

M* observed m/e ratio which can be calculated theoretically.[8]

tions may overlap with the ordinary ions. In the higher pressure region (Figs. 1-4), however, the behavior of the metastable ions seems to differ from that of the other ions.

The relation between excitation energy of methylamine molecule ion and the behavior of ionic species can be treated according to classification of the energy regions into three parts. Dominant ionic species are (31), (30) and (28).

i) 9.0—12.0 eV

Ion (31) collides with the parent molecule to give (32) through transfer of a hydrogen atom or a proton. A part of (31) releases a hydrogen atom or molecule to produce (30) or (29) during the flying path in the Giese lenses of 126 mm length. These species will be observed as the peaks of (29) or (27). This process is collision-induced dissociation as was reported by Melton and Well.[9]

ii) 12.1—14.7 eV

The products of ion-molecule reactions in this region are (32) and (31). (31) may be given by charge exchange or hydrogen atom transfer.[10]

The recombination energy of (30) is expected to be not so far from 13 eV, and charge exchange may be important in this case.

Metastable peaks of (28) and (26) are observed after release of a hydrogen atom or molecule from the most abundant ion (30).

A set of isomers $CH_2{=}N^+H_2$ and $C^+H_2{-}NH_2$ might exist for the mass peak (30).[11] Probably the former is formed in the low energy region not much above 9.0 eV which is the ionization potential of nonbonding nitrogen orbital [za']. The latter will be formed in the higher energy region. It is plausible that these isomers in the reaction chamber show different behavior at elevated pressure, though detection of the difference is difficult. The meatstable peak (28) is observed in the low energy region and (26) in the higher energy region (Fig. 5). It is not clear whether this difference is due to the different behavior of the isomers or to the difference of the excited states of the produced ion (30). It seems that the latter is more important for determining the number of hydrogen atoms eliminated from the ion, since this is possible for the other cases.

iii) 15.8—25.0 eV.

The fragment ion (28) is present most abundantly. This reacts with methylamine to produce three kinds of secondary ions (32), (31) or (30) through the processes of proton transfer.

The secondary ion (30) after the change exchange with Xe^{++} seems to be highly excited, being raised up to 2.8 eV above its appearance potential. This is rarely observed in usual molecules. Metastable transition in this energy region is observed not in the initially produced ions but in the secondary ions. No collision-induced dissociation takes place in the case of (28).

As the recombination energy of (28) is considered to be appreciably high, He^+ in the cascade-type mass spectrometer was used as the monitor of the collision induced reactions. It was shown that the maximum probability for the charge exchange was observed in acceleration of 100—200 eV. The ion flying through the Giese lenses will attain this acceleration energy

TABLE 2. CLASSIFICATION OF ION-MOLECULE REACTIONS IN METHYLAMINE AFTER CHARGE EXCHANGE WITH POSITIVE IONS

Energy range	Process	Mass Peak
9.0—12.0 eV	H transfer:	
	$CH_3NH_2^+ + CH_3NH_2 \rightarrow CH_3NH_3^+$	(32)
	H^+ transfer:	
	$CH_3NH_2^+ + CH_3NH_2 \rightarrow CH_3NH_3^+$	(32)
	Metastable transition:	
	$CH_3NH_2^+ \xrightarrow{-H} CH_2NH_2^+$	(29)
	$CH_3NH_2^+ \xrightarrow{-2H} CHNH_2^+$	(27)
12.1—14.0 eV	H^+ transfer:	
	$CH_2NH_2^+ + CH_3NH_2 \rightarrow CH_3NH_3^+$	(32)
	Electron transfer:	
	$CH_2NH_2^+ + CH_3NH_2 \rightarrow CH_3NH_2^+$	(31)
	H transfer:	
	$CH_2NH_2^+ + CH_3NH_2 \rightarrow CH_3NH_2^+$	(31)
	Metastable transition:	
	$CH_2NH_2^+ \xrightarrow{-H} CHNH_2^+$	(28)
	$CH_2NH_2^+ \xrightarrow{-2H} CHNH^+$	(26)
15.8—25.0 eV	H^+ transfer:	
	$CHNH^+ + CH_3NH_2 \rightarrow CH_3NH_3^+$	(32)
	Electron transfer:	
	$CHNH^+ + CH_3NH_2 \rightarrow CH_3NH_2^+$	(31)
	H^- transfer:	
	$CHNH^+ + CH_3NH_2 \rightarrow CH_2NH_2^+$	(30)
	Metastable transition:	
	$CH_2NH_2^+ \xrightarrow{-2H} CHNH^+$	(26)

8) J. H. Beyon and A. E. Fontaine, "Modern Aspect of Mass Spectrometry," ed. by R. I. Reed, Plenum Press, New York (1968), p. 113.

9) C. E. Melton and C. F. Well, *J. Chem. Phys.*, **27**, 1132 (1957).

10) When xenon ions of low recombination energy were bombarded to methylamine molecules filled in the source volume, it was indicated that more than 50% of total ionization is due to charge exchange above 12 eV.

11) H. Sjögren, *Arkiv Fysik*, **29**, 565 (1965).

very easily.

In the whole energy range from the ionization potential of methylamine to 25 eV, contributions from (15) and (29) are quite low.

The rate constant of the ion-molecule reaction $CH_3NH_2^+ + CH_3NH_2 \rightarrow CH_3NH_3^+ + CH_2NH_2(CH_3NH)$ is given as 0.6×10^{-9} cm^3 molecule^{-1} sec^{-1} by Jones and Harrison,[12] who carried out experiments by electron impact. In this study, however, this type of reaction can be neglected because in the energy region of the secondary product (30) there is no primary ion of (31) as shown in Fig. 5.

The ion- molecule reactions of various ionic species are classified in Table 2.

The authors' thanks are due to Mr. M. Hiraga and Mr. Y. Takita for their kind cooperation throughout this work.

12) E. G. Jones and A. G. Harrison, *Can. J. Chem.*, **45**, 3119 (1967).

BULLETIN OF THE CHEMICAL SOCIETY OF JAPAN, VOL. 46, 1631—1638 (1973)

Studies of the Surface of Rutile Single Crystals by Means of Electrical Conductivity

Toru IWAKI

Department of Chemistry, Faculty of Science, Hiroshima University, Higashisenda-machi, Hiroshima 730

(Received October 6, 1972)

The surface properties of rutile single crystals were studied by the measurement of the d.c. electrical conductivity. Upon successive thermal treatments *in vacuo* from 25 to 550 °C, the electrical conductivity on the (110) plane increased remarkable, while the activation energy decreased. The addition of oxygen decreased the conductivity according to the oxidation temperature, whereas the reduction by hydrogen above 300 °C increased the conductivity greatly. The number of carriers was also determined from the measurement of the Hall effect. These results, by reference to those of the photoconductivity, were interpreted in terms of the change in the energy band structure near the surface associated with the defect centers on the surface.

It is well known that titanium dioxide, though it is an insulator in the stoichiometric composition, becames an *n*-type semiconductor as a result of the removal of oxygen atoms when treated at a high temperature *in vacuo* or in a reducing gas, such as hydrogen or carbon monoxide.[1] The reduction process may bring about a remarkable change in the structure and properties of the surface and also in the bulk, since oxygen atoms are removed from the surface and also from the bulk through the surface region. A number of studies of reduced titanium dioxide have been made by means of measurements of the electrical conductivities,[2] photoelectronic properties,[3-5] dielectric properties,[6] and diffusion of foreign atoms[7,8] in order to clarify the electronic structure in the bulk, but few have taken into account the properties of the surface.[9,10] So far, the heat of immersion in water and the adsorption of water vapor on the surface were examined for the powder specimen with an anatase modification; it has been found that these phenomena are considerably affected by a departure from the stoichiometric composition.[10] The purpose of the present study is to examine the surface of a single crystal with a rutile modification by the measurement of the electrical conductivity along with the photoconductivity.

The crystal structure of rutile is tetragonal; a titanium ion is located in the center of eight oxygen ions, and an oxygen ion is surrounded by three titanium ions on the (110) plane, which is a cleavage plane. The bond length between a titanium ion and an oxygen ion is longer by 0.044 Å in the (110) direction than in the other two directions.[11] In this study, the electrical conductivity was measured mostly along the c-axis on the (110) plane. Since the value of the conductivity differs to some extent from one specimen to another, the conductivity was measured for a definite specimen treated successively in the following manner: outgassing from room temperature to an elevated temperature, oxidation with oxygen, and then reduction with hydrogen. As a result, it was clarified that the surface

1) F. A. Grant, *Rev. Modern Phys.*, **31**, 646 (1959).

2) a) R. G. Breckenridge and W. R. Hosler, *Phys. Rev.*, **91**, 793 (1953). b) L. E. Hollander and P. L. Castro, *ibid.*, **119**, 1882 (1960). c) R. R. Hasiguti, K. Minami, and H. Yonemitsu, *J. Phys. Soc. Jap.*, **16**, 2223 (1961). d) V. N. Bogomolov and V. P. Zhuze, *Fiz. Tverd. Tela*, **5**, 3285 (1963). e) G. A. Acket and J. Volger, *Phys. Lett.*, **8**, 244 (1964). f) J. H. Becker and W. R. Hosler, *Phys. Rev.*, **137**, 1872 (1965).

3) a) D. C. Cronemeyer, *ibid.*, **87**, 876 (1952). b) D. C. Cronemeyer, *ibid.*, **113**, 1222 (1959).

4) O. W. Johnson, W. O. Ohlsen, and P. I. Kingsbury, Jr., *ibid.*, **175**, 1102 (1968).

5) A. K. Ghosh, F. G. Wakim, and R. R. Addiss, Jr., *ibid.*, **184**, 979 (1969).

6) L. A. K. Dominik and R. K. MacCrone, *ibid.*, **163**, 756 (1967).

7) O. W. Johnson, *ibid.*, **136**, 284 (1964).

8) V. I. Barbanel' and V. N. Bogomolov, *Fiz. Tverd. Tela*, **11**, 2671 (1969).

9) T. J. Gray, C. C. McCain, and N. G. Masse, *J. Phys. Chem.*, **63**, 472 (1959).

10) T. Iwaki and M. Miura, This Bulletin, **44**, 1754 (1971).

11) R. W. G. Wyckoff, "Crystal Structures," Vol. 1, John Wiley & Sons, New York, N. Y. (1963), p. 251.

conductivity varied remarkably with the treatment. Further, the surface properties of a rutile single crystal were examined by means of measurements of the Hall effect and the photoconductivity.

Experimental

Material. A single crystal of rutile grown by the Verneuil method was obtained from the Nakazumi Crystal Co., Ltd. According to the spectroscopic analysis, its purity was above 99.99%; the main impurity was sodium, the amount of which was less than 0.005%.[12] The (110) plane was obtained by cleaving the crystal at a high temperature and was polished smoothly with α-corundum 0.1~0.2 μ in diameter. The dimensions of the crystal were 10×10×2 mm³. The specimen was treated with a chromic acid mixture, washed thoroughly with distilled water, and then dried at room temperature.

Electrode. As an electrode for the measurement of the electrical conductivity, gold was evaporated onto the (110) plane held at 100 °C. Various types of electrodes as is illustrated in Fig. 1 were used. As to Type I in the figure,

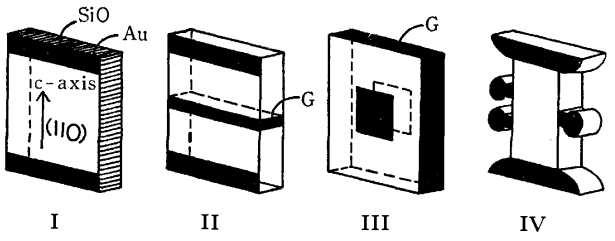

Fig. 1. Schematic drawing of four types of electrodes on the (110) planes of rutile single crystals.

all sides of the crystal were coated with evaporated SiO film in order to bring these surfaces to an insulator. Types II and III have guard-ring electrodes mounted to surround the surface in two ways. When the guard ring is grounded, the current which flows only in the bulk can be obtained since the surface current is intercepted by the guard ring, while both currents can be obtained when the guard ring is not grounded. Type IV, which was used for the measurement of the Hall effect, was formed by means of an ultrasonic cutter. The conductivity was measured parallel to the c-axis except for the case of Type III. Besides gold, several electrode materials such as In, Ti, and Ag, were evaporated on the surface of Type I in order to examine the contact between rutile and gold; further, the voltage-current character was examined at 25 °C under several treatments.

Treatments. A rutile single crystal connected with electrodes was placed in a quartz cell; in this the crystal was thermally treated as will be described below. Both the dark conductivity and the photoconductivity were measured below room temperature in the same cell after each treatment. The treatment of the sample was as follows: evacuation was carried out at 10^{-5} Torr at temperatures from 25 to 300 °C for 3 hr and above 400 °C for 1 hr, oxygen was added at temperatures varying between 25 and 500 °C for several minutes under a pressure of 20~50 Torr, followed by evacuation at 25 °C, and then hydrogen was added under the same conditions as in the case of oxygen, followed by evacuation at the temperature at which the hydrogen has been introduced. A liquid-nitrogen trap was used to protect the specimen from contamination by organic substances.[10]

Measurements. The electrical conductivity was measured at temperatures between −196 and 25 °C after helium gas had been introduced into the cell at 25 °C. A dry cell of about 1.5 V was used as the electric source. The electric current was measured with an Ohkura Electric Co. Model Am 5001 high-impedance microvoltammeter. The Hall e.m.f. was obtained in a three-electrode system under a magnetic field of about 4600 gauss. The photoconductivity was measured at −196 and 25 °C in the wavelength range between 350 and 600 mμ by using a tungsten lamp as the light source and interference filters. The intensity of the illuminating light was calibrated by means of a chemical actinometer using potassium ferrioxalate[13] and Rhodamine B.[14] The absorption spectrum was measured at −133 °C. and at room temperature over the wavelength range from 0.22 to 2.5 μ.

Results and Discussion

Contact between Rutile and Gold. When a metal and a semiconductor are brought into contact, a contact potential is formed by the difference between the work functions of these two materials. It was found that the electrical conductivity for the same specimen showed almost the same value regardless of the kind of electrode materials, such as In, Ti, Ag, and Au. The relationship between the electric current and the applied voltage indicated the Ohm law, as is shown in Fig. 2. From the above results, the Schottky barrier, which is generally seen in Si, GaAs, *etc.*[15], may not be formed in this contact. The measurement by the four-contact method, however, indicated a slight contact resistance at a low temperature when the specimen was evacuated above 300 °C.

According to the value of the electron affinity of rutile reported recently,[16] it is probable that the accumulation layer is formed near the surface by the contact with gold,[17] as is illustrated in Fig. 3, where the Fermi level of rutile is located below the conduction band, judging from the *n*-type semiconductor. The

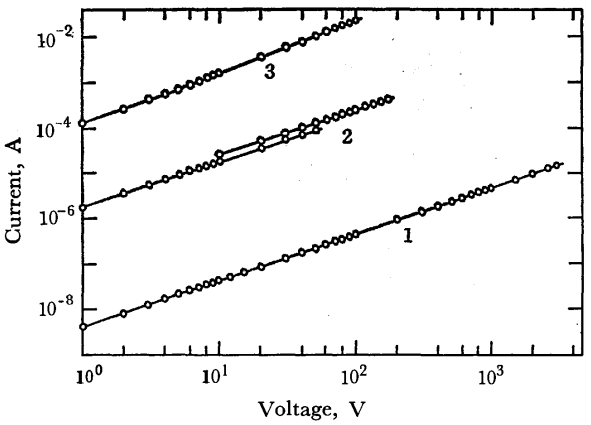

Fig. 2. Voltage-current characteristics for the contact between gold and rutile treated *in vacuo* at several temperatures; (1) 25 °C, (2) 300 °C, and (3) 500 °C.

12) Y. Nakazumi, *Seramikkusu*, **3**, 731 (1968).
13) C. G. Hatchard and C. A. Parker., *Proc. Roy. Soc.* (London), **235**, 518 (1956).
14) G. Wever and F. W. J. Teale, *Trans. Faraday Soc.*, **53**, 646 (1957).

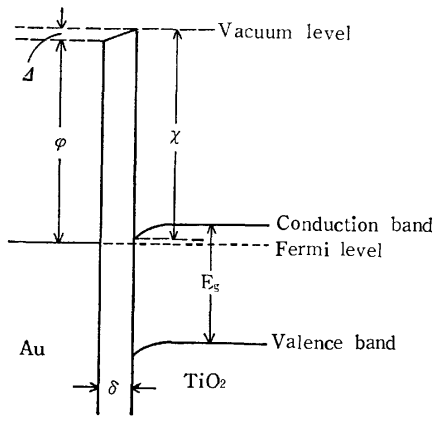

Fig. 3. Energy level diagram for gold and rutile in electrical equilibrium.
E_g: Band gap of rutile, 3.03 eV.
φ: Work function of gold, 5.32±0.1 eV.
x: Electron affinity of rutile, 5.56 eV.
Δ: Potential across interfacial layer.
δ: Thickness of interfacial layer.

energy level of the surface which is treated under various conditions may differ from that in the bulk because of the presence of impurities, lattice defects, and adsorbed gases, though the former may be identical with the latter if the surface is in an idealized state.

Changes in the Electrical Conductivity with Various Treatments. The changes in the electrical conductivity of the rutile treated successively at temperatures from 25 to 550 °C *in vacuo* are shown in Fig. 4(a) as a function of the reciprocal absolute temperature. The value of conductivity, σ, is expressed by the unit of mho/cm and also by that of mho; the latter unit is introduced on the basis of two-dimensional conductivity. It is clear from the figure that the conductivity increased remarkably with the outgassing temperature. A linear relation between log σ and $1/T$ was obtained over a considerably wide temperature range. The electrical conductivity can be expressed as $\sigma=\sigma_0 \exp(-\varepsilon/kT)$; ε is the activation energy for the electrical conductivity and is nearly equal to $E_d/2$ in this temperature range, where E_d is the donor level measured from the bottom of the conduction band, as will be discussed later. When the outgassing temperature increased from 25 to 550 °C, the conductivity at 25 °C, $\sigma_{25°C}$, increased by 10^5, while ε decreased from 0.25 to 0.10 eV. The oxidation at 500 °C lowered the value of $\sigma_{25°C}$ as low as below 10^{-13}. Not even evacuation at 500 °C restored the conductivity above 10^{-13}, but the introduction of hydrogen above 300 °C did. The reduction with hydrogen at 500 °C increased the conductivity remarkably and changed the sign of the temperature coefficient at around −25 °C, as can be seen in Fig. 4(b). On the other hand, when oxygen was added at a high temperature, σ decreased and ε increased. Moreover, when hydrogen was added at a high temperature after the oxidation, σ increased and ε

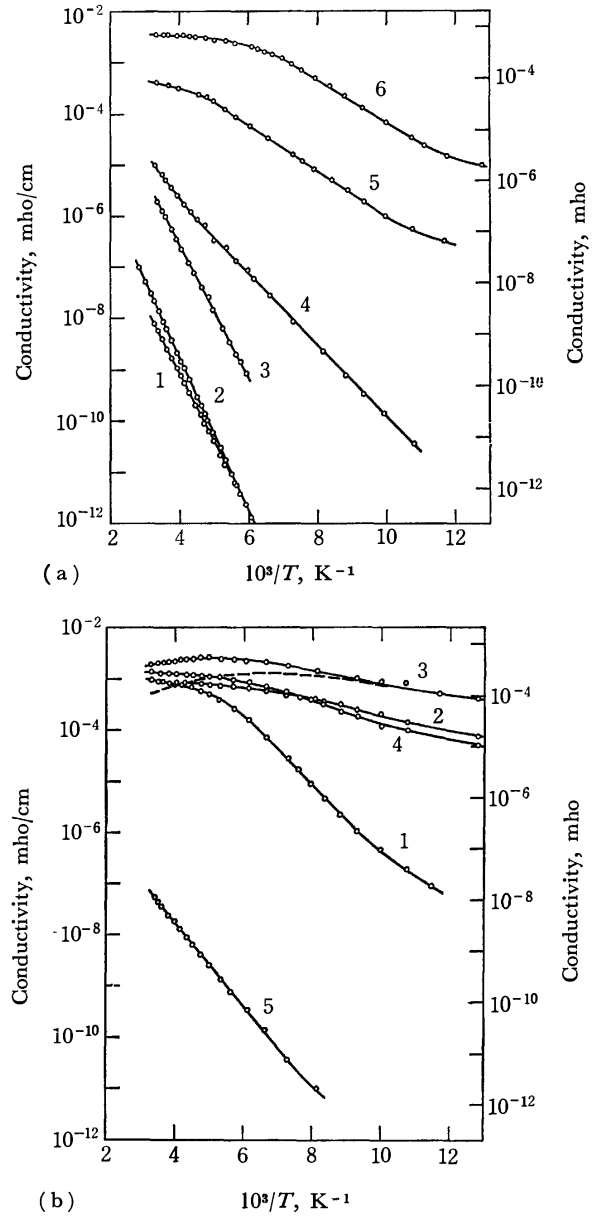

Fig. 4. Electrical conductivity of rutile treated under various conditions as a function of reciprocal absolute temperature.
(a) Successive evacuation at the following temperatures: (1) 25 °C, (2) 100 °C, (3) 200 °C, (4) 300 °C, (5) 400 °C, and (6) 550 °C.
(b) Successive introduction of oxygen or hydrogen as follows: (1) hydrogen, at 500 °C for 2 min after oxidation at 500 °C, (2) hydrogen, at 500 °C for 5 min, (3) hydrogen, at 500 °C for 5 min, (4) oxygen, at 25 °C for 2 min, and (5) oxygen, at 500 °C for 2 min.

decreased. This behavior observed by means of the reduction and oxidation cycle were reversible on the same sample, illustrating "Meyer's rule" that the larger the concentration of electrons, the lower the the activation energy becames.[18] The addition of oxygen at room temperature after the reduction also decreased the conductivity, which is represented by Curve 4 in Fig. 4(b). The decrement of the conductivity by the adsorption of oxygen is indicated by the dotted line in the figure. These results may indicate

15) A. M. Cowley and S. M. Sze, *J. Appl. Phys.*, **36**, 3212 (1965).
16) O. W. Johnson and J. W. DeFord, *ibid.*, **43**, 807 (1972).
17) J. C. Riviére, "Solid State Surface Science," Vol. 1, ed. by M. Green, Marcel Dekker, New York, N. Y. (1969), p. 179.
18) W. Meyer and F. Neldel, *Physik. Z.*, **38**, 1014 (1937).

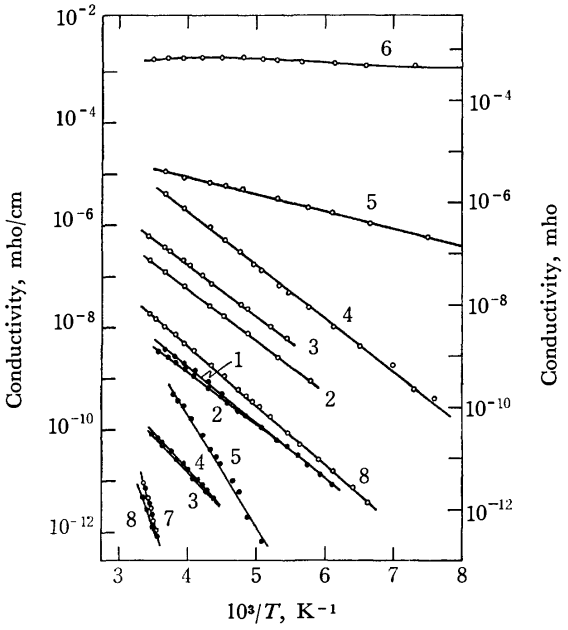

Fig. 5. Electrical conductivity of rutile with a guard ring treated under various conditions as a function of reciprocal absolute temperature. Successive treatments *in vacuo* and introduction of oxygen or hydrogen for 2 min at the following temperatures: (1) 25 °C, (2) 100 °C, (3) 200 °C, (4) 300 °C, (5) 500 °C, (6) hydrogen, 500 °C, after oxidation at 500 °C, (7) oxygen, 500 °C, and (8) hydrogen, 300 °C. In Figs. 5 and 6, open circle indicates that a guard ring was not grounded and closed one shows that it was grounded.

the effect of the adsorbed oxygen on the conductivity and the existence of the surface conductivity of the reduced rutile.

Contribution of Bulk Conductivity. The conductivity for the sample with a guard ring may clarify the problem of whether the remarkable variations in the electrical conductivity with pretreatments, as described above, occur predominantly on the surface region or in the bulk. The results for Type II presented in Fig. 1 are shown in Fig. 5. The closed circle given in the figure means that the guard ring was grounded, representing a bulk conductivity. The conductivity values obtained for the bulk were extremely small, though they differed to some extent according to the treatment. The conductivity with the guard ring not grounded shows a tendency similar to that in the case of Type I. The effect of the bulk on the conductivity seems negligibly small in the temperature range examined except for the case of the oxidation at high temperatures; the oxidation at high temperature makes the surface contribution extremely small.

The results of the conductivity in the case of Type III are shown in Fig. 6. When the specimen was evacuated at 100 and 200 °C, the bulk conductance became lower than 10^{-13} A/V. The bulk conductance increased after evacuation above 300 °C and increased significantly at 650 °C, though it is much smaller than the contribution of the surface. The oxidation at 500 °C after evacuation at 650 °C reduced the conductance extremely, as in the cases of Types I and II. Figure 6(b) demonstrates the dependence of the conductance

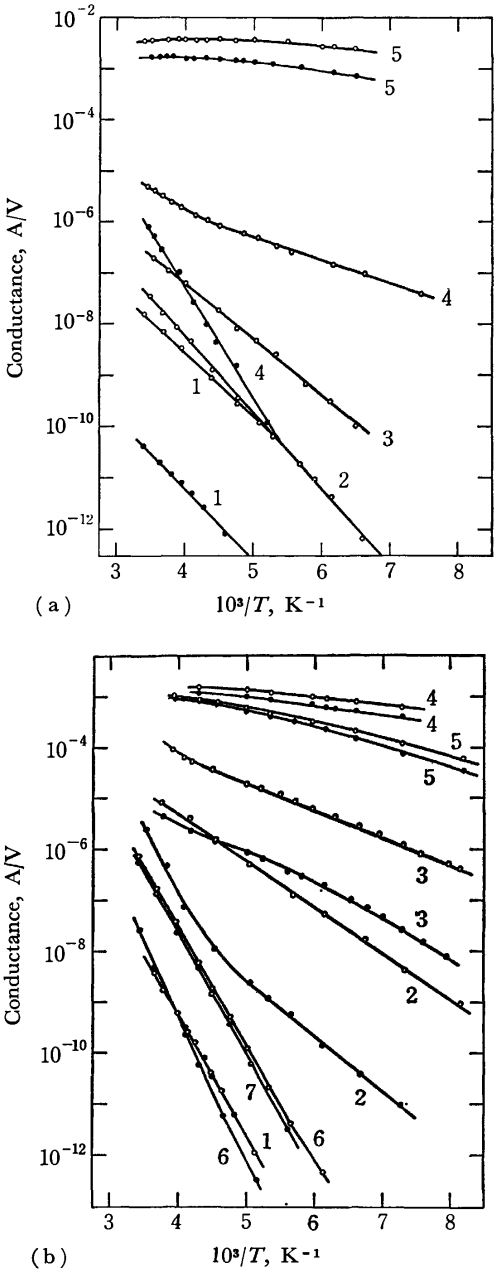

Fig. 6. Electric conductance of rutile with a guard ring under various treatments as a function of reciprocal absolute temperature.
(a) Successive evacuation at the following temperatures: (1) 25 °C, (2) 100 °C, (3) 200 °C, (4) 300 °C, and (5) 650 °C, (b) Successive introduction of oxygen or hydrogen for 2 min at the following temperatures: (1) hydrogen, 200 °C. after oxidation at 500 °C, (2) hydrogen, 300 °C, (3) hydrogen, 400 °C, (4) hydrogen, 500 °C, (5) oxygen, 100 °C, (6) oxygen, 400 °C, and (7) evacuation at 500 °C.

on the reduced state of rutile, which was treated by the reduction with hydrogen at temperatures between 200 and 500 °C. After the oxidation at 500 °C, outgassing at a high temperature did not recover the conductance, but the reduction by hydrogen did.

Surface State of Rutile. An idealized model of the (110) plane of rutile is illustrated in Fig. 7. The following three kinds of oxygen ions are present on the surface: A, above the titanium ion, B, between the titanium ions, and C, on the same plane as the

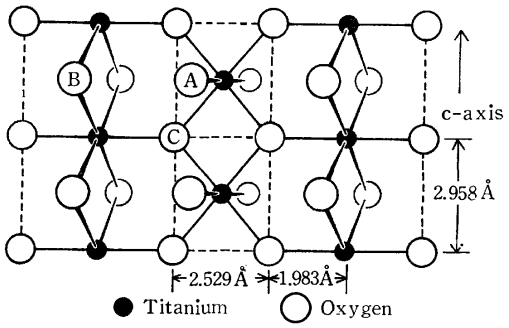

Fig. 7. Atomic model for the (110) plane of the surface of rutile.

titanium ions on the surface. Some of these oxygen ions can be excluded from the surface by virtue of the law of electric neutrality. The removal of the A oxygen is most probable because it is situated remotest from the plane composed of titanium ions. In general, the real surface of titanium dioxide is covered with hydroxyl groups which combine with titanium ions.[19] When titanium dioxide is evacuated at a high temperature, an oxo-structure similar to B in the figure is formed as a result of the condensation of these hydroxyl groups. As the surface oxo-structures thus produced are distorted,[10] these sites are considered to act as donors.

On the other hand, defect centers such as oxygen vacancies rather than interstitial titanium ions are produced by the removal of oxygen atoms when rutile is kept at high temperatures below 700 °C *in vacuo*[20] or in hydrogen.[21,22] The removal of one oxygen atom produces two electrons which reside in the oxygen vacancy or neighboring titanium ions of the lattice and which also serve as donors. Since the surface conductivity increased as the reduction proceeded, oxygen atoms, for example, B and C in the figure, may be removed from the surface. From the viewpoint of the band structure, the crystal imperfections on the surface create the energy level within the forbidden gap. This level is generally called the "surface state". When the donors in the surface state, such as the oxygen vacancy and Ti^{3+}, release the electrons to the conduction band at a moderate temperature, the surface is positively charged; the electrostatic potential for electrons bends down near the surface, in analogy with the scheme shown in Fig. 3. Therefore, as the accumulation layer is formed, the probability of the transition of the electron from the donor level to the conduction band becomes large and the concentration of the carrier electrons in the conduction band near the surface region may increase.

When oxygen molecules are admitted to the specimen at a high temperature after reduction, some are incorporated in the crystal lattice as O^{2-}, while the others adsorb as O^- and O_2^- on the surface. The incorporated oxygen may not be the defect center, but the anion radicals may form the surface state by drawing electrons from the conduction band and the donor level. As the surface is charged negatively, the surface potential bends upward to near the surface, resulting in the formation of the depletion layer.

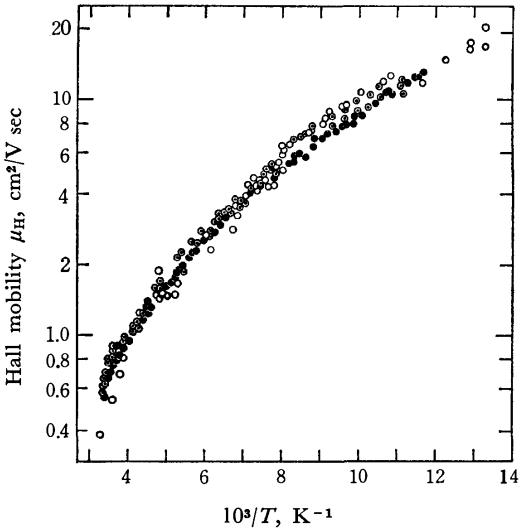

Fig. 8. Hall mobility of rutile treated under several conditions as a function of reciprocal absolute temperature. Treatments; ○: evacuation at 500 °C, ●: reduction by hydrogen at 450 °C for 2 min, and ⊙: reduction by hydrogen at 500 °C for 7 hr. The electrical conductivities at 25 °C, $\sigma_{25°C}$, of the specimens treated above are 1.6×10^{-3}, 3.5×10^{-3}, and 1.5×10^{-1} mho/cm, respectively.

Hall Mobility. The Hall e.m.f. was measured at temperatures between −196 and 25 °C for a specimen reduced under several conditions. The Hall mobility, μ_H, is given as the product of the Hall coefficient and the conductivity. The results are shown in Fig. 8. The value changed over the range from 0.4 to 20 cm²/V s, and the following relation was obtained in this temperature range: $\mu_H \propto T^{-5/2}$. In general, when carrier electrons in a semiconductor are scattered by the thermal vibration of the crystal lattice, the mobility can be expressed as follows: $\mu \propto T^{-3/2} m^{*(-5/2)}$, where m^* is the effective mass of an electron.[23] Since the oxygen ion in rutile is considerably polarizable,[24] lattice scattering by the optical mode of vibration as well as by the acoustical mode must be taken into account in a manner similar to that in the case of the mobility of hole carriers in Si or Ge.[25] The estimated value of m^* has been reported to be $10\sim30\ m$,[26] where m is the mass of a free electron. Yahia has suggested that the large effective mass at room temperature is due to a small polaron mass.[27] The low mobility may arise from the large effective mass. It should be noted that the mobility is not influenced even by the reduction with hydrogen for a long time, though the reduction may produce the defect centers

19) T. Iwaki, M. Komuro, and M. Miura, This Bulletin, **45**, 2343 (1972).
20) V. I. Barbanel', V. N. Bogomolov, S. A. Borodin, and S. I. Budarina, *Fiz. Tverd. Tela*, **11**, 534 (1969).
21) R. D. Shannon, *J. Appl. Phys.*, **35**, 3414 (1964).
22) T. R. Sandin and P. H. Keesom, *Phys. Rev.*, **177**, 1370 (1969).
23) J. Bardeen and W. Shockley, *ibid.*, **80**, 72 (1950).
24) E. Yamaka and K. Narita, *Phys. Lett.*, **23**, 645 (1966).
25) J. M. Ziman, "Electrons and Phonons," Oxford University Press, London (1960), p. 440.
26) H. P. R. Frederikse, *J. Appl. Phys. Suppl.*, **32**, 2211 (1961).
27) J. Yahia, *Phys. Lett.*, **23**, 425 (1966).

Table 1. Donor level, donor concentration, and Fermi level of rutile

Treatment (°C)	E_{d_b} (eV)	E_{d_s} (eV)	n_s[a] 230 °C (cm^{-2})	n_s[a] 400 °C (cm^{-2})	ζ_b[b] −196 °C (eV)	ζ_b[b] 25 °C (eV)	ζ_s[b] −196 °C (eV)	ζ_s[b] 25 °C (eV)
25	0.66	0.67	2×10^{12}	8×10^{13}	0.38—0.29	0.54—0.59	0.33—0.35	0.36—0.41
100	0.68	0.70	5×10^{12}	4×10^{13}	0.39—0.40	0.56—0.40	0.35—0.36	0.38—0.41
200	0.58	0.59	4×10^{13}	3×10^{14}	0.33—0.34	0.48—0.51	0.29—0.34	0.30—0.33
300	0.34	0.35	2.5×10^{14}	8×10^{14}	0.21	0.35—0.37	0.17	0.17—0.18
400	0.21	0.21	1.2×10^{15}	1.8×10^{15}	0.14	0.27—0.28	0.10	0.09—0.10
500	0.19	0.20	1.1×10^{16}	1.4×10^{16}	0.13	0.24	0.08	0.06
H_2(500)	0.07	0.07	9×10^{15}	1.2×10^{16}	0.07	0.18	0.02	0.00
O_2(500)	0.35	0.38	4×10^{12}	1.4×10^{13}	0.24	0.42—0.43	0.20	0.24

a) n_b is larger by 5 times than n_s.

b) Fermi levels ζ_b and ζ_s are estimated respectively from the following relations:

$$\zeta_b = \frac{1}{2}E_{d_b} - \frac{1}{2}kT\log\frac{2N_d}{N_0(T)(m^*/m)^{3/2}} \text{ and } \zeta_s = \frac{1}{2}E_{d_s} - \frac{1}{2}kT\log\frac{N_d}{4(m^*/m)[N_0(T)/2]^{2/3}}.$$

in bulk to a considerable extent. This implies that the mobility of the carrier electron in rutile is not affected by the lattice defect on the surface or in the bulk. Therefore, this may be due to a small mean free path of the carrier electrons compared with the scattering cross-section of such lattice defects as oxygen vacancies. When the mobility, μ, is known, the concentration of carrier electrons, n, can be estimated from the relation: $\sigma = en\mu$, where e is the electronic charge. When the Hall mobility is presumed to be equal to the true mobility and also to be independent of the treatments, it is revealed that the variation in the conductivity with the treatments *in vacuo* at temperatures between room temperature and 300 °C is caused mainly by the variation in the concentration of carriers, and that the reversion of the temperature coefficient of the conductivity for the case of the reduction by hydrogen as indicated in Fig. 4(b) is to be ascribed to a decrease in the mobility with an increase in the temperature. If the donor level is composed of a single level, the two-dimensional concentration of carrier electrons, n_s, and the three-dimensional one, n_b, in the temperature range studied can be given, respectively, by:

$$n_S = (m^*/m)^{1/2}N_{d_s}^{1/2}[N_0(T)/2]^{1/3}\exp(-E_{d_s}/2kT),$$

$$n_b = (m^*/m)^{3/4}[N_{d_b}N_0(T)/2]^{1/2}\exp(-E_{d_b}/2kT),$$

where:

$$N_0(T) = 2(2\pi mkT/h^2)^{3/2};$$

N_{d_s} and N_{d_b} are the two-dimensional and three-dimensional concentrations of donors respectively, and E_{d_s} and E_{d_b} are the two-dimensional and three-dimensional donor levels respectively. The values of N_{d_s} and E_{d_s} are obtained from the intercept and the slope of the relation between $n_s/T^{1/2}$ and $1/T$ respectively, and N_{d_b} and E_{d_b}, from those between $n_b/T^{3/4}$ and $1/T$. However, the donor concentration obtained from the intercept is overestimated, as has been revealed in ZnO.[28] As the donor centers were not completely exhausted at room temperature, the concentrations of the donor at 230 °C and 400 °C were estimated by the extrapolation of the relation between n and $1/T$ to these two temperatures, because an intrinsic conductivity of rutile occurred above 600 °C.[3a] The results are listed in Table 1. From the crystal structure of rutile, the number of titanium ions was calculated to be $3.2\times10^{22}/cm^3$. On the assumption that all the oxygen atoms were removed from the surface of the (110) plane, the amount of the released electrons was calculated to be $4.36\times10^{15}/cm^2$. It is clear from the table that the electrical conduction for the specimen evacuated at 500 °C occurs not only on the top layer of the surface, but also considerably beneath the surface. The table also contains the Fermi levels, whose values were calculated by estimating m^* to be 25 m.

Photoconductivity. The typical spectral responses of the photoconductivity of the rutile measured at room temperature and −196 °C are shown in Fig. 9. The maxima in the photoconductivity curves occurred at

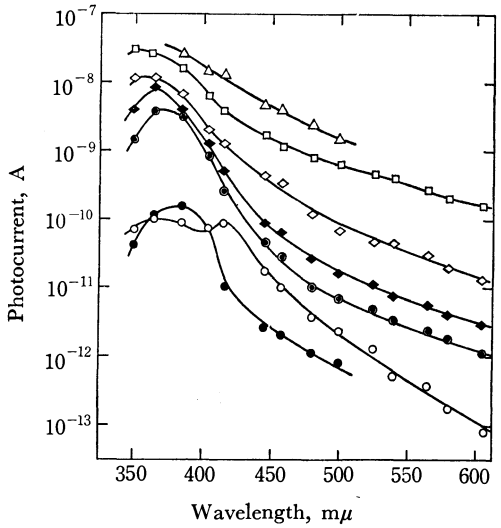

Fig. 9. Spectral responses of photoconductivity of rutile treated under several conditions at 25 and −196 °C. Treatment; ⊙: evacuation at 300 °C, −196 °C, ◇: evacuation at 400 °C, 25 °C, ◆: evacuation at 400 °C, −196 °C, □: evacuation at 500 °C, 25 °C, △: reduction by hydrogen at 500 °C for 2 min, 25°C, ○: oxidation at 500 °C for 2 min, 25 °C, and ●: oxidation at 500 °C for 2 min, −196 °C.

28) S. E. Harrison, *Phys. Rev.*, **93**, 52 (1954).

the wavelengths between 350 and 400 mμ, which are near the fundamental absorption edge, as may be seen in Fig. 11. The photoconductivity increased as the out-gassing temperature rose from 300 to 500 °C. In particular, the photoconductivity in the wavelength region longer than the absorption edge increased when the rutile was reduced by hydrogen. This finding suggests that the large number of donors near the conduction band contribute to the photocurrent at the long wavelength. The rather sharper peak in the curve at −196 °C than that at room temperature may come from the more distinct band width of the forbidden gap, since most of the electrons are present in donor centers rather than in a conduction band at a low temperature. When the rutile was oxidized at 500 °C, a new maximum appeared at 415 mμ in the photoconductivity spectra at room temperature. This peak has also been observed for highly-oxidized rutile.[5,29] It may be presumed from the results of the conductivity measurements that donor levels are hardly present below the conduction band at the surface because of the formation of the depletion layer near the surface because of the presence of O^- or O_2^-. Therefore, this peak may be attributable to excitation from a level, such as O_2^- or O^-, near the valence band on the surface to the conduction band.

It is clear from Fig. 9 that the photocurrent of the rutile increases with an increase in the conductivity, *i.e.*, the dark current. The relationship between the photocurrent at 405 mμ and the dark current at room temperature is shown in Fig. 10. This implies that the population of electrons in the donor level on the surface may increase, since the accumulation layer becomes remarkable with a rise in the Fermi level on the surface. The photocurrents of both the specimen treated with hydrogen and that treated with oxygen decayed slowly when the illuminating light was cut off; This may be due to the existence of traps in the specimen treated with hydrogen and to the photodesorption of the adsorbed oxygen molecules from the specimen treated with oxygen.

Absorption Spectra. The absorption spectra of the rutile did not change upon the thermal treatment *in vacuo*, as is shown in Fig. 11. This finding is similar to that of Cronemeyer.[3a] The absorption edge shifted from 420 to 410 mμ as the temperature decreased from

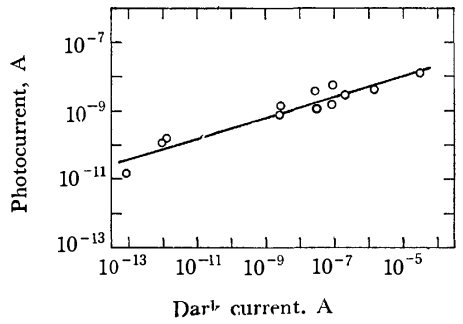

Fig. 10. Relation between the photocurrent at 405 mμ and the dark current at 25 °C.

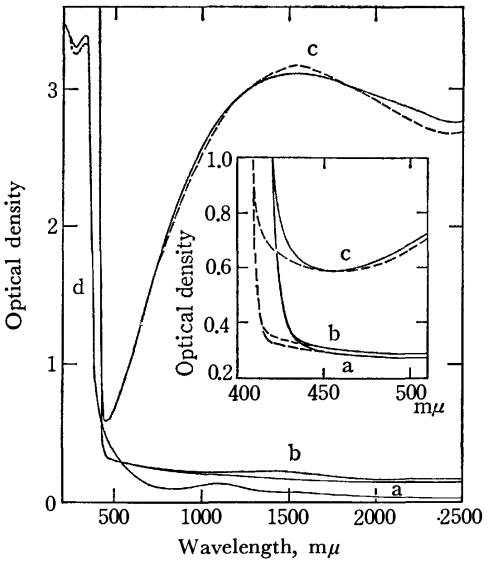

Fig. 11. Optical densities of a rutile single crystal and thin film treated under several conditions. Single crystal: (a) oxidation at 450 °C for 3 min, (b) reduction at 500 °C for 10 min, and (c) reduction at 500 °C for 3 hr. Thin film prepared by the oxidation of the evaporated film of titanium at 1100 °C: (d) oxidation and reduction at 500 °C. Full lines show the optical density measured at 25 °C and dotted lines at −133 °C.

room temperature to −133 °C. A broad absorption centered at 1.5 μ appeared upon the reduction with hydrogen and increased extremely remarkably with the reduction time, though the absorption edge did not change entirely. The absorption spectrum of a thin film of rutile showed maxima at 330 mμ and a slight peak at 1.1 μ. These peaks did not change with the temperature. The optical density near the band gap was not changed by the reduction, whereas the photoconductivity changed markedly.

It is clear from the results of the electrical conductivity and the photoconductivity that the electronic state near the surface of the rutile single crystal is changed remarkably by the contact with oxygen or hydrogen for a short time, while the electronic state in bulk is also changed. It has been considered that hydrogen atoms can diffuse into the bulk of rutile and act as donors.[7,30] However, the evacuation at a high temperature may remove the hydrogen atoms as in the case of ZnO.[31] The reversible change in the electrical conduction by the reduction-oxidation cycle indicates that oxygen atoms may be removed easily from the surface or bind to the surface even under the mild conditions studied. The change in the activation energy with the concentration of donors may be considered to depend on the position of the Fermi level in relation to the conduction band on the surface in addition to the effect of the interactions between donors.[3b] As oxygen atoms can not be removed below 300 °C, the increase in the electrical conductivity and

29) K. Mizushima and S. Iida, *J. Phys. Soc. Jap.*, **31**, 950 (1971).

30) G. J. Hill, *J. Phys. D*, **1**, 1151 (1968).

31) G. Heiland, E. Mollow, and F. Stöckmann, "Solid State Physics," Vol. 8, ed. by F. Seitz and D. Turnball, Academic Press, New York, N. Y. (1959), p. 191.

photoconductivity when rutile is evacuated below that temperature suggests that the active oxo-structure produced by the condensation of hydroxyl groups on the surface can act as donors in the electrical conduction on the surface.

The author wishes to express his appreciation to Professor Masaji Miura for suggesting this investigation as well as for his continuous encouragement during the course of this work. Thanks are also due to Professor Hiroo Inokuchi of the University of Tokyo for valuable suggestions and discussions.

BULLETIN OF THE CHEMICAL SOCIETY OF JAPAN, VOL. 46, 1638— 1640(1973)

The Properties of Water in Macromolecular Gels. VI. The Relationship between the Rheological Properties and the States of Water in Macromolecular Gels

Masuo AIZAWA,* Shuichi SUZUKI,* Teruo SUZUKI,** and Hiroshi TOYAMA**

*Research Laboratory of Resources Utilization, Tokyo Institute of Technology, Meguro-ku, Tokyo 152

**Japan Electron Optics Laboratory Co., Ltd., Akishima, Tokyo 196

(Received July 20, 1972)

The relationship between the rheological properties and the states of water in macromolecular gels is investigated by both the rheological and nuclear magnetic resonance methods. In accordance with the stress-strain curve, macromolecular gels are shown to be classifiable into: (1) an agarose type of gel which shows great gel strength and brittleness at breaking; (2) a κ-carrageenan type of gel showing great gel strength, but ductility at breaking, and (3) a λ-carrageenan type of gel, which has very little gel strength and is pasty. The dependence of the NMR line-width of water in gels on the polymer concentration and on the temperature reveals that the motional state of water in gels is restricted in this order: the agarose type of gel > the κ-carrageenan type of gel > the λ-carrageenan type of gel. These results show that the state of water is closely related with the rheological properties of macromolecular gels.

The states of water existing in polysaccharide gels, such as agarose-, κ- and λ-carrageenan-, and curdlan-type polysaccharide gels, have previously been studied by the electrochemical method,[1,2] by means of nuclear magnetic reasonance,[3,4] and by the dilatometric method.[5] These studies have revealed that so-called free water is a mixture of at least two different states of water; one is comparable with ordinary water except that it is prevented from flowing out, and the other is less mobile than ordinary water, but more mobile than so-called bound water.

On the other hand, various rheological types of gel can be found in polysaccharide gels. Agarose gels, for instance, exhibit brittleness, while k-carrageenan gels show ductility. It has not been clarified yet, however, what affects these rheological properties of macromolecular gels. This investigation was carried out with the aim of clarifying how to correlate the states of water to the rheological properties of macromolecular gels.

The states of water existing in gels are quite difficult to survey by means of spectroscopic measurements because of their poor transparency. Nuclear magnetic resonance (NMR) methods may be more suitable for such investigations, for the motional states of water can be estimated through the NMR line-width of the proton signal. Agarose-, κ- and λ-carrageenan-, and curdlan-type polysaccharide gels were measured for the NMR line-width of their water, and the line-widths were compared with their rheological properties.

Experimental

Samples. Agarose-, κ-carrageenan-, λ-carrageenan-, and curdlan-type polysaccharide gels prepared at the required water contents were used as the samples. Curdlan-type polysaccharide is a bacterial gel-forming β-1,3-glucan obtained from the culture filtrate of a mutant strain (NTK-U, IFO 13140) of *Alcaligenes faecalis var. myxogenes*, strain 10C3K.[6]

Gel Strength and Elasticity Measurement. The stress-strain curves for gels were obtained at 25 °C by the use of a gel-strength tester. The water contents of gels were measured before and after the mechanical test.

NMR Spectra. The proton NMR spectra were obtained using a JNM-C-60HL high-resolution NMR spectrometer, as has been described previously.[3] The sample was sealed in a standard sample tube (5 mm ϕ O.D.). The temperature was measured by means of a copper constantan thermocouple near the sample tube.

Results

Rheological Properties of Various Polysaccharide Gels. Gel strength is known as a gel property. It is not sufficient, however, as a basis for profiling the rheologi-

1) J. Mizuguchi, M. Takahashi, and M. Aizawa, *Nippon Kagaku Zasshi*, **91**, 723 (1970).

2) J. Mizuguchi, M. Takahashi, and M. Aizawa, *ibid.*, **91**, 961 (1970).

3) M. Aizawa, J. Mizuguchi, S. Suzuki, S. Hayashi, T. Suzuki, N. Mitomo, and H. Toyama, This Bulletin, **45**, 3031 (1972).

4) M. Aizawa, S. Suzuki, T. Suzuki, and H. Toyama, *ibid.*, (in press).

5) M. Aizawa and S. Suzuki, *ibid.*, **44**, 2967 (1971).

6) T. Harada, A. Misaki, and H. Saito, *Arch. Biochem. Biophys.*, **124**, 292 (1968).

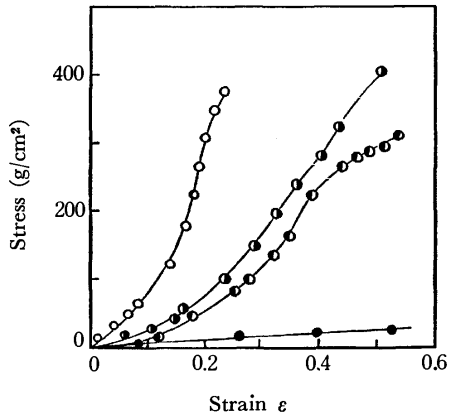

Fig. 1. Stress-strain curves of agarose (—○—), curdlan-type polysaccharide (—◑—), κ-carrangeenan (—◐—) and λ-carrageenan (—●—) gels containing 2% of polysaccharide.

cal properties of gels, because it shows only the maximum at the breaking point. A stress-strain curve may be convenient as a basis for classifying the rheological properties of the various polysaccharide gels.

The stress-strain curves at 25 °C are shown in Fig. 1 for agarose-, κ-carrageenan-, λ-carrageenan-, and curdlan-type polysaccharide gels. The polysaccharide content of each is 2%. The strain is indicated as ε in the abscissa, showing the ratio of the contraction to the length of the gel which is free from stress.

In the range of low stress, the stress correlates linearly with the strain. The gradients of the stress-strain curves, *i. e.*, the elastic moduli, increase in the following order: λ-carrageenan<κ-carrageenan and curdlan-type polysaccharide<agarose. The end points of the curves show the stress at the breaking point, the so-called gel strength. The λ-carrageenan gel has very little gel strength. The other three kinds of gels exhibit comparable gel strengths.

The stress-strain curve of agarose gel has an inflection point at $\varepsilon=0.2$, following the abrupt rise between this inflection point and the breaking point. Thus, this type of gel shows brittleness. κ-Carrageenan gel gives an inflection point in the stress-strain curve around $\varepsilon=0.4$, and the slope of the line in the range from this inflection point to the breaking point is moderate compared to that of the agarose gel. The curdlan-type polysaccharide gel resembles the κ-carrageenan gels in its rheological properties.

On the other hand, the λ-carrageenan gel markedly contracts when subjected to even a slight stress, showing paste-like properties. Therefore, the polysaccharide gels investigated can be classified as follows:

(1) The agarose type of gel, which shows great gel strength and brittleness at breaking.

(2) The κ-carrageenan type of gel, which shows great gel strength and ductility at breaking, and

(3) The λ-carrageenan type of gel, which shows very little gel strength and paste-like properties.

NMR Line-width of Water in Gels. The polysaccharide gels can be classified into three groups according to the rheological properties mentioned above. As the NMR line-width is known to be related to the spin-spin relaxation time, T_2 which indicates the motional states of nuclear spin, and is known to become narrow when the nucleus is in a vigorous motional state,[7] the NMR line-width of water was investigated for these three types of polysaccharide gel.

For agarose-, κ- and λ-carrageenan-, and curdlan-type polysaccharide gels, the NMR line-width of water is illustrated at various concentrations in Fig. 2. The line-width is indicated in Hz units as the half-width of the maximum peak height. The line-width widens with the increase in the polysaccharide concentration for each gel. The concentration dependence of the line-width is most prominent for agarose gels, as is shown in Fig. 2. In contrast, the line-width changes only slightly with the increase in the λ-carrageenan concentration. The concentration dependences of the line-width of water in κ-carrageenan and curdlan-type polysaccharide gels lie between those agarose and λ-carrageenan gels. These results indicate that water is more restricted in the agarose type of gel than in the κ-carrageenan and λ-carrageenan types of gel.

Temperature Dependence of the NMR Line-width of Water in Gels. The temperature dependence of the NMR line-width of water can offer effective information concerning the states of water in gels. The temperature dependence of the line-width below 0 °C is shown in Fig. 3 for agarose, κ-carrageenan, and curdlan-type polysaccharide gels containing 92% of water by weight. The line-width increases with the temperature decrease, this shows the restriction of the motional state of water. Most water existing in gels changes in phase from a liquid into a solid at 0 °C, this accompanies the drastic change of the line-width. As the line-width of water in the solid state, frozen water, is too wide to be detected by a high-resolution NMR spectrometer, the NMR signal of water frozen at 0 °C may be eliminated below 0 °C. Therefore, the NMR line-width shown in Fig. 3 has been determined by studying the water molecules which remains unfrozen even in this temperature range. In Fig. 3, an anomalous temperature dependence of the line-width is found in the temperature range from 0 to −20 °C. This anomalous temperature depen-

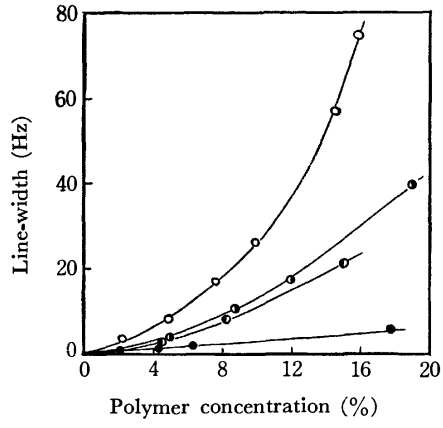

Fig. 2. NMR line-width of water in agarose (—○—), curdlan-type polysaccharide (—◑—), κ-carrageenan (—◐—) and λ-carrageenan (—●—) gels.

7) H. S. Gutowsky and G. E. Pake, *J. Chem. Phys.*, **18**, 162 (1950).

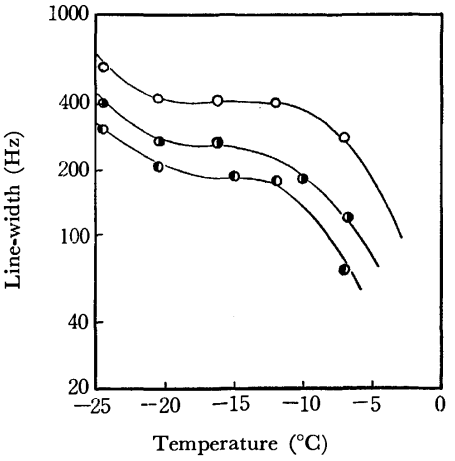

Fig. 3. Temperature dependence of NMR line-width of water in agarose (—○—), curdlan-type polysaccharide (—◑—) and κ-carrageenan (—◐—) gels containing 92% of water.

dence may be caused by the phase-transition of water which remains unfrozen below 0 °C.

Moreover, water in an agarose gel exhibits a wider line-width in this temperature range than the other two kinds of polysaccharide gel. This indicates that the motional state of water which remains unfrozen below 0 °C is restricted more extremely in an agarose gel than in the other two kinds of gel. The restriction of the motional state of water which remains unfrozen below 0 °C is in the order: agarose>curdlan-type polysaccharide>κ-carrageenan gels. This restriction order quite agrees with the results derived from the polymer-concentration dependence of the NMR line-width.

Generally, the NMR line-width gets narrower with an increase in the temperature (motional narrowing). On the contrary, the line-width of water existing in polysaccharide gels was found to become wider with the increase in the temperature above 0 °C, as has been reported previously.[4] Such an anomalous temperature dependence of the line-width can be expected to be closely related to the rheological properties of polysaccharide gels.

The temperature effects on the NMR line-width of water are presented in Fig. 4 for agarose-, κ-carrageenan-, λ-carrageenan-, and curdlan-type polysaccharide gels containing 92, 91, and 92% of water respectively. In Fig. 4, the line-width of water in an agarose gel is shown to increase with the increase in temperature up to approximately 35 °C, and then to decrease above this temperature. The anomalous temperature effect is the most prominent in the agarose gel. Water involved in the curdlan-type polysaccharide and κ-carrageenan gels increases the line-width, with a slight inclination, with the increase in the temperature, giving no maxima. This anomalous effect is not so marked, but is rather, negligible in a λ-carrageenan gel. The magnitude of the anomalous temperature effect on the line-width decreases in this order: agarose>curdlan-type polysaccharide and κ-carrageenan>λ-carrageenan gels.

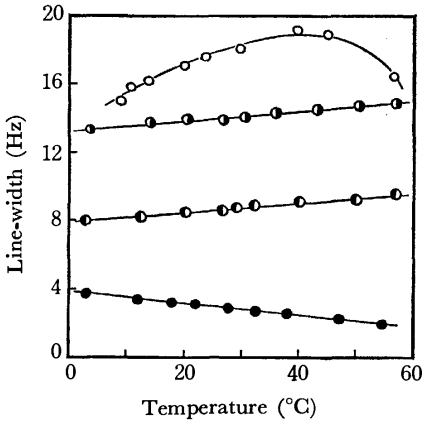

Fig. 4. Anomalous temperature dependence of NMR line-width of water in agarose (—○—), curdlan-type polysaccharide (—◑—), κ-carrageenan (—◐—) and λ-carrageenan (—●—) gels containing 92, 92, 91 and 92% of water respectively.

Discussion

The nuclear magnetic resonance properties of water in polysaccharide gels may be summarized as follows:

(1) For agarose gels, the line-width of water depends markedly on the polysaccharide concentration of the gel, the anomalous temperature effect on the line-width is the most prominent, and the line-width is wider than in the other gels at the same concentration and the same temperature.

(2) The line-width of water in λ-carrageenan gels is not so dependent on the polymer concentration, and the anomalous temperature effect on the line-width is rather negligible.

(3) The properties of the water involved in curdlan-type polysaccharide and κ-carrageenan gels are intermediate between those of the above two types of polysaccharide gels. As was shown in the previous papers,[3,4] these properties reflect the motional state of water in gels. These results indicate that the motional state of water is restricted in this order: agarose>curdlan-type polysaccharide and κ-carrageenan>λ-carrageenan gels.

The above order corresponds reasonably well to that of the rheological classification. In other words, the water involved in the rheologically-strong gels is extremely restricted or immobilized. Therefore, a close relationship between the rheological properties of gels and the states of water existing in it was revealed.

Summary

The nuclear magnetic resonance properties of water showed that the restriction effect on the motional state of water was the most marked in agarose gels among the polysaccharide gels surveyed, and that it was loosened in this order: agarose>curdlan-type polysaccharide, κ-carrageenan>λ-carrageenan gels. On the other hand, the polysaccharide gels were revealed to be classifiable into three groups according to their rheological properties: (1) the agarose type of gel, (2) the κ-carrageenan type of gel, and (3) the λ-carrageenan type of gel. A close relationship between the motional state of water and the rheological properties was found on the basis of the above results.

The 2288 Å Photolysis of Hydrogen Iodide in the Presence of Ethylene and Propylene

Yasuhisa SANO and Shin SATO

Department of Applied Physics, Tokyo Institute of Technology, Ookayama, Meguro-ku, Tokyo 152

(Received August 15, 1972)

The photolysis of hydrogen iodide at 2288 Å has been investigated in the presence of ethylene or propylene. The combinations studied were DI–C_2H_4, HI–C_2D_4, and DI–C_3H_6. In all combinations, the formation of a large amount of HD was observed; this may be attributed to the reaction of hot hydrogen atoms. The pressure dependence of the relative yields of HD and total hydrogen suggested that, of the two possible hot hydrogen atom reactions with ethylene, the abstraction reaction,

$$D^* + C_2H_4 \longrightarrow C_2H_3 + HD \quad (2)$$

does not occur, while the substitution reaction,

$$D^* + C_2H_4 \longrightarrow C_2H_3D + H \quad (3)$$

is the important process. In the case of propylene, however, the abstraction of H by D* is important for the formation of HD. The measured ratios of C_2H_3D/HD in the DI–C_2H_4 system and of C_2D_3H/HD in the HI–C_2D_4 system were consistent with the above conclusion. Reaction (3) is probably not a real substitution reaction, but a combination of the addition reaction of a hydrogen atom to ethylene and the rapid decomposition of the excited ethyl radical produced.

When hydrogen iodide is photolyzed at 2288 Å, hot hydrogen atoms are produced.[1,2] The excess translational energy amounts to 2.3 eV if the iodine atoms produced are in their ground state ($^2P_{3/2}$). According to the estimation of Compton and Martin,[2] about 20% of total iodine atoms are produced in the first excited state ($^2P_{1/2}$) in the 2288 Å photolysis of hydrogen iodide. In this case, the excess energy of hydrogen atoms is reduced to 1.4 eV.

In a previous communication,[3] we have suggested that the deuterium atoms produced in the photolysis of deuterium iodide at 2288 Å undergo the following reaction:

$$D^* + C_2H_4 \longrightarrow C_2H_3D + H$$

The present paper will report the details of this experiment, and also the results with different combinations, HI–C_2D_4 and DI–C_3H_6.

Experimental

Materials. The deuterium iodide was synthesized by heating a mixture of deuterium (Takachiho Chemical Co.) and iodine (Koso Chemical Co.) on platinized asbestos in a Pyrex tube at 400 °C for two days. The DI thus produced was distilled three times from a bath at 200 K to that at 77 K, with the rejection of the head and tail fractions. The DI gas thus synthesized was stored in a bulb covered with Al-foil. During the storage, the HI content gradually increased, probably because of a proton-exchange reaction between DI and water in glass or in grease. The HI content was estimated from the H_2 : HD : D_2 ratio obtained in the photolysis of DI. Since the extinction coefficient of HI at 2288 Å is a little larger than that of DI,[4] the HI content will be overestimated. The initial content of HI was less than 5%. When the content reached 15%, the reactant gas was renewed.

The hydrogen iodide was prepared by dropping hydriodic acid (Yanagishima Pharmaceutical Co.) on phosphorus pentoxide (Kishida Chemical Co.) cooled at 0 °C in a flow of nitrogen gas.

The C_2H_4, C_3H_6 (Takachiho Chemical Co.) and C_2D_4 (Merck Sharp & Dohme Co.) were used after bulb-to-bulb distillations. Mass spectrometric analysis showed that C_2D_4 contained 4% C_2D_3H.

Apparatus and Procedure. Home-made cadmium resonance lamps[5] were used for irradiation. When, of the two resonance lines, the 2288 Å line was cut off with the Toshiba UV-D 25 filter, the reaction products were very few. Therefore, all the measurements were carried out without a filter. The contribution of the 3261 Å resonance line to the reaction must be less than a few percent, because the extinction coefficient of hydrogen iodide at 2288 Å is about 200 $l \cdot mol^{-1} \cdot cm^{-1}$ and that at 3261 Å is a hundred times smaller.[6]

Before irradiation, all the faces of the quartz reaction vessel, 5 cm long and 5 cm in diameter, were heated with a torch under a vacuum to remove any deposit; however, the complete removal of iodine could not be achieved. All the experiments were done at room temperature. Immediately before and after the run with hydrocarbons, the photolysis of DI or HI without hydrocarbons was made in order to estimate the intensity of the light and in order to obtain the HI content when DI was used as a reactant. If the two measurements, before and after the run with hydrocarbons, did not agree within the limits of experimental error, this series of measurements was discarded.

The amounts of the products were measured volumetrically with a Toepler pump, and their analyses were made by mass spectrometry. Before the analysis of the H_2 : HD : D_2 ratio, it was determined that no significant isotope exchange was induced during the mass-spectrometric analysis. When the amount of C_2H_3D or C_2D_3H in ethylene was estimated, the correction for the ^{13}C natural abundance was applied to the data. Because of the presence of a large amount of C_2H_4 or C_2D_4, the estimated values of C_2H_3D

1) R. J. Carter, W. H. Hamill, and R. R. Williams, Jr., *J. Amer. Chem. Soc.*, **77**, 6457 (1955).
2) L. E. Compton and R. M. Martin, *J. Phys. Chem.*, **73**, 3474 (1969).
3) Y. Sano and S. Sato, This Bulletin, **44**, 3213 (1971).
4) J. R. Bates, J. O. Halford, and L. C. Anderson, *J. Chem. Phys.*, **3**, 415 (1935).
5) S. Tsunashima and S. Sato, This Bulletin, **41**, 284 (1968).
6) R. M. Martin and J. E. Willard, *J. Chem. Phys.*, **40**, 2999 (1964).

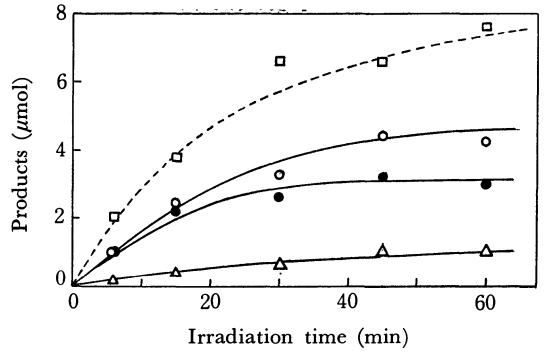

Fig. 1. The irradiation time dependence of the products in the 2288 Å photolysis of DI in the presence of C_2H_4.
□: C_2H_3D, ○: HD, ●: D_2, △: H_2

and C_2D_3H are not accurate, the error probably being ±50%.

Results

DI-C_2H_4. Figure 1 shows the time dependence of the products, D_2, HD, H_2, and C_2H_3D, from the photolysis of DI-C_2H_4 mixture. The DI gas used here contained 15% HI. The initial pressure of deuterium iodide was 5 Torr, and the initial $[C_2H_4]_i/[DI]_i$ ratio was 0.85. Since the contamination of HI could not be avoided, the following procedure was applied to the experimental results as correction. In the first place, the ratios of $x=[HD]_0/[D_2]_0$ and $y=[H_2]_0/[D_2]_0$ were calculated. Here, the suffix 0 denotes the absence of C_2H_4. Then the following correction was applied to the data:

$$[HD]_{corr} = [HD]_e - [D_2]_e x$$

$$[H_2]_{corr} = [H_2]_e - [D_2]_e y$$

Here, the suffix e denotes the presence of C_2H_4, while the suffix corr denotes the corrected values. The $[H_2]_{corr}$ values thus obtained were always very close to zero.

Figure 2 shows the relative yields of D_2+HD, D_2, and HD as a function of the initial ratio of C_2H_4 to DI. Here, the initial pressure of DI was kept at 5 Torr and the pressure of C_2H_4 was changed. The conversion of DI was less than 20%. The yield of D_2 in the photolysis of DI was taken as unity. The correction described above has already been applied. Table 1 shows the $[C_2H_3D]/[HD]$ ratio, which was

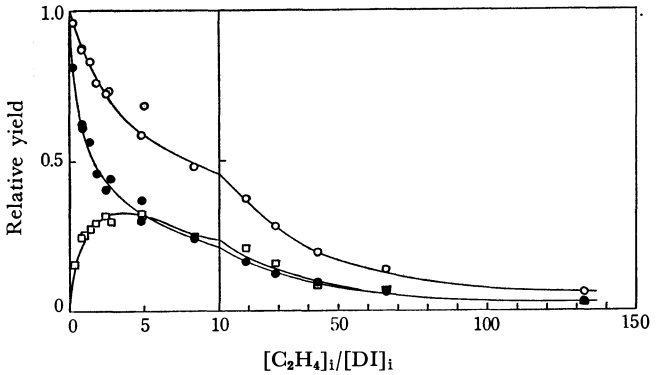

Fig. 2. The relative yields of D_2+HD (○), D_2 (●), and HD (□) as a function of the initial $[C_2H_4]_i/[DI]_i$ ratio.

Table 1. The $[C_2H_3D]/[HD]$ ratio as a function of the $[C_2H_4]_i/[DI]_i$ ratio. (The initial pressure of DI is 5 Torr. Irradiation time is 6 min.)

$[C_2H_4]_i/[DI]_i$	$[C_2H_3D]/[HD]$
0.27	1.5
0.84	1.5
1.40	2.4
1.88	1.5
2.51	1.8
8.35	2.0

obtained in the same series of data measurement as is shown in Fig. 2. At $[C_2H_4]_i/[DI]_i$ ratios higher than 10, the $[C_2H_3D]/[HD]$ ratios could not be measured because of a large amount of C_2H_4. In spite of the careful inspection of the mass spectrograms, no products other than C_2H_3D, such as acetylene or ethane, could be observed.

HI-C_2D_4. The relative yields of H_2+HD, H_2, and HD are shown in Fig. 3 as a function of the $[C_2D_4]/[HI]_i$ ratio. In this case, no correction except the contribution of 4% C_2D_3H in C_2D_4 to the observed yields was necessary. Table 2 shows the $[C_2D_3H]_i/[HD]_i$ ratio as a function of the $[C_2D_4]_i/[HI]_i$ ratio. Several measurements were made in the presence of the saturated vapor pressure of iodine, which was intentionally introduced in the system. Practically no difference between the data obtained in the presence and in the absence of iodine was observed. The

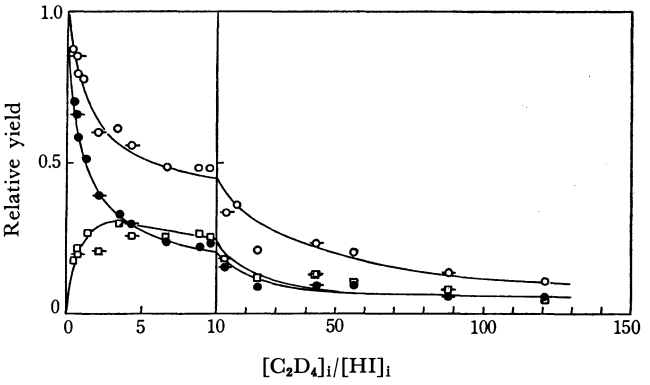

Fig. 3. The relative yields of H_2+HD (○), H_2 (●), and HD (□) as a function of the initial $[C_2D_4]_i/[HI]_i$ ratio. The bar means the presence of the iodine intentionally introduced.

Table 2. The $[C_2D_3H]/[HD]$ ratio as a function of the $[C_2D_4]_i/[HI]_i$ ratio. (The initial pressure of HI is 5 Torr. Iodine vapor was intentionally introduced.)

$[C_2D_4]_i/[HI]_i$	Irradiation time (min)	$[C_2D_3H]/[HD]$
0.41	6	0.7
0.74	6	1.3
1.24	6	0.9
3.39	6	1.0
0.71	16	0.8
2.09	16	2.0
4.27	16	1.9

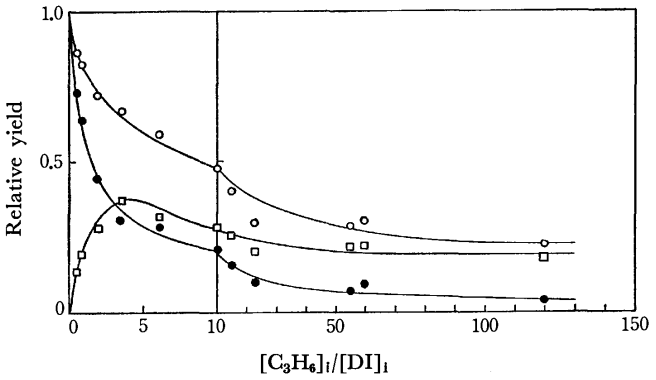

Fig. 4. The relative yields of D_2+HD (○), D_2 (●), and HD (□) as a function of the initial $[C_3H_6]_i/[DI]_i$ ratio.

$[C_2D_3H]/HD]$ ratios obtained in this series of experiments are also shown in Table 2.

DI-C_3H_6. Propylene was also used as a counterpart in the photolysis of DI. Figure 4 shows the relative yields of D_2+HD, D_2, and HD as a function of the $[C_3H_6]_i/[DI]_i$ ratio. A correction similar to that to the DI-C_2H_4 system has already been applied. Obviously the curves for D_2+HD, D_2, and HD are very similar to those obtained with C_2H_4; however, the [HD] values do not approach zero, but level off at about 0.2. The mass-spectrometric analysis for the formation of C_3H_5D could not be carried out because the attempt to separate propylene from deuterium iodide was not successful.

Discussion

It is well known that the reaction of thermal hydrogen atoms with ethylene or propylene leads almost exclusively to the formation of the ethyl or isopropyl radical. According to the estimation of Jennings and Cvetanović,[7] the k_a/k_b ratios are zero for ethylene and 0.045 for propylene.

$$H + RH \longrightarrow H_2 + R \qquad a$$

$$H + RH \longrightarrow RH_2 \qquad b$$

Woolley and Cvetanović reinvestigated these ratios and reported zero for ethylene and 0.082 for propylene. Therefore, the formation of a large amount of HD observed in the present experiment may be considered to be evidence for a hot hydrogen atom reaction. However, the reaction of the (a) type is not necessarily the only mechanism for the formation of HD. Another possible mechanism is the following substitution reaction:

$$D^* + RH \longrightarrow H + RD$$

followed by:

$$H + DI \longrightarrow HD + I$$

Such a substitution reaction has been observed with recoil tritium atoms from a nuclear reaction.[8] Which type of reaction is responsible for the formation of HD is one of the main concerns in this paper.

As Figs. 2 and 3 show, the formation of HD in the system containing ethylene approaches zero with the increase in the ratio of ethylene to hydrogen iodide. This result suggests that the hot hydrogen atom does not abstract a hydrogen atom from ethylene in the first collision. If it does, a certain fraction of HD should remain even at the higher $[C_2H_4]_i/[DI_i]$ ratios, because the $[DI]_i$ was kept at a constant value, 5 Torr. In the system containing propylene, on the other hand, the HD formation levels off at a constant value with the increase in propylene, as is shown in Fig. 4.

In order to discuss these reactions, the following reaction scheme was considered:

$$DI + h\nu \rightarrow D^* + I \qquad (0)$$

$$D^* + DI \rightarrow D_2 + I \qquad (1)$$

$$D^* + RH \rightarrow HD + R \qquad (2)$$

$$D^* + RH \rightarrow H + RD \qquad (3)$$

$$D^* + RH \rightarrow D + RH \qquad (4)$$

$$D^* + I_2 \rightarrow DI + I \qquad (5)$$

$$D + DI \rightarrow D_2 + I \qquad (6)$$

$$D + RH \rightarrow RHD \qquad (7)$$

$$D + RH \rightarrow HD + R \qquad (8)$$

$$D + I_2 \rightarrow DI + I \qquad (9)$$

$$H + DI \rightarrow HD + I \qquad (10)$$

$$H + RH \rightarrow RH_2 \qquad (11)$$

$$H + RH \rightarrow H_2 + R \qquad (12)$$

$$H + I_2 \rightarrow HI + I \qquad (13)$$

$$R + DI \rightarrow RD + I \qquad (14)$$

$$R + RH \rightarrow R_2H \qquad (15)$$

$$R + I_2 \rightarrow RI + I \qquad (16)$$

$$I + I + M \rightarrow I_2 + M \qquad (17)$$

For the discussion of the HI–C_2D_4 system, H and D in the scheme should be exchanged. In this reaction scheme, the moderation of D* atoms by DI and I_2 was not included, because the heavy molecules, such as DI and I_2, would not be effective moderators for hot hydrogen atoms. Table 3 summarizes the average fraction of energy lost per collision, assuming an elastic head-on collision. According to the estimation of Martin and Willard,[6] the average fractions of energy lost per collision in the systems of H*+C_2D_6 and of D*+C_2H_6 are, respectively, 0.19 and 0.51, values which are 1.5 and 2 times that of the energy lost per elastic head-on collision. Ob-

Table 3. Average fraction (f) of the energy lost per elastic head-on collision

Reactants	f
H* + HI	0.03
D* + DI	0.06
H* + C_2D_4	0.12
D* + C_2H_4	0.25

7) K. R. Jennings and R. J. Cvetanović, *J. Chem. Phys.*, **35**, 1233 (1961); G. R. Woolley and R. J. Cvetanović, *ibid.*, **50**, 4705 (1969).

8) J. W. Root, W. Breckenridge, and F. S. Rowland, *ibid.*, **43**, 3694 (1965).

viously, even in the case of 2.3 eV D* in C_2H_4, several collisions are necessary for the complete thermalization. In the present treatment, however, it has been assumed that only one collision is effective enough to thermalize the hot hydrogen atom; otherwise, the kinetic treatment cannot easily be carried out.

When the conversion is not large, the steady-state-treatment on the reasonable assumptions that $k_3 \gg k_8$ and that $k_1[DI] \gg k_5[I_2]$ gives the following relationship: Here, ϕ denotes the relative yield of $[D_2]+[HD]$, and β stands for the following ratio:

$$\frac{1-\beta}{1-\phi} = 1 + \frac{k_2}{k_3+k_4} + \frac{k_1}{k_3+k_4}\frac{[DI]}{[RH]} \qquad \text{(I)}$$

$$\beta^{-1} = 1 + \frac{k_7[RH]}{k_6[DI]} + \frac{k_9[I_2]}{k_6[DI]}$$

$$= 1 + \frac{k_{11}[RH]}{k_{10}[DI]} + \frac{k_{13}[I_2]}{k_{10}[DI]} \qquad \text{(II)}$$

The equality between the second equation and the third in Eq. (II) is acceptable, because Reactions (6), (7), and (9) are the reactions of deuterium atoms DI, RH, and I_2 respectively, while Reactions (10), (11), and (13) are those of hydrogen atoms with DI, RH, and I_2 respectively.

Since Reactions (10), (11), and (13) are those of thermal hydrogen atoms, the specific rates are rather accurately known. According to the measurements of Penzhorn and Darwent,[9,10] the ratio of k's for the reactions of thermal hydrogen atoms with I_2 and HI is expressed by $4.96 \exp(640/RT)$, and $k(H+C_2H_4)/k(H+HI)$ is equal to $0.30 \exp(-845/RT)$. Cvetanović and Doyle reported $k(H+C_3H_6)/k(H+C_2H_4) = 1.53$ at 20 °C.[11] For the present calculations, the following values were used: 0.0738 for k_7/k_6 of ethylene, 0.113 for k_7/k_6 of propylene, and 14.3 for k_9/k_6. As has been described in the results for the system of HI–C_2D_4, the intentionally-introduced iodine did not affect the formation of H_2 and HD. Judging from this result and from the difficulty in completely removing iodine in the reaction vessel, it may be said that all the reactions reported here take place in the presence of iodine vapor. Therefore, the following calculations were carried out on the assumption that the iodine pressure in the reaction vessel was 0.195 Torr, the saturated vapor pressure of iodine at 20 °C.[12]

Figure 5 shows the plots of the left-hand side of Eq. (I) as a function of the [Deuterium iodide]/[Olefin] ratio. From these linear relationships, the values listed in Table 4 were obtained. It may be noticed here that the value of k_2 is very small in the case of ethylene.

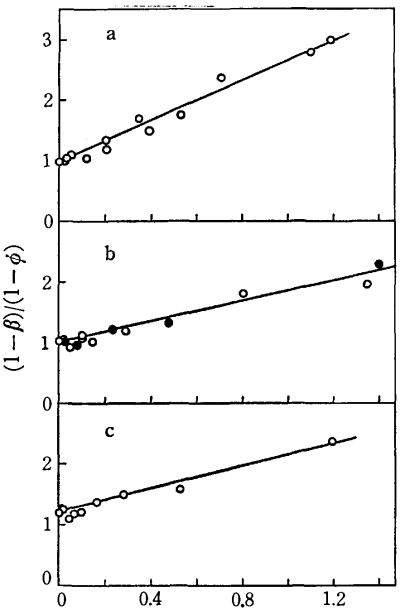

Fig. 5. The plots for Eq. (I).
a: $[DI]_i/[C_2H_4]_i$, b: $[HI]_i/[C_2D_4]_i$, c: $[DI]_i/[C_3H_6]_i$

TABLE 4. THE CALCULATED VALUES OF THE RATIOS OF k's

System	$k_2/(k_3+k_4)$	$k_1/(k_3+k_4)$	
C_2H_4–DI	0.0	1.6	$k_1 \gg k_2$
C_2D_4–HI	0.0	0.85	
C_3H_6–DI	0.2	1.0	$k_1 = 5k_2$

The steady-state treatment based on the reaction scheme proposed above also gives this relation:

$$\frac{\phi_D}{\phi_{HD}} = \frac{\beta k_4}{k_2+\beta k_3} + \frac{k_1}{k_2+\beta k_3}\frac{[DI]_i}{[C_2H_4]_i} \qquad \text{(III)}$$

In the system of DI–C_2H_4, the value of k_2 may be taken to be zero; then, the plots of ϕ_{H_2}/ϕ_{HD} as a function of $[DI]_i/\beta[C_2H_4]_i$ should give a straight line. Similarly, in the HI–C_2D_4 system the ϕ_{H_2}/ϕ_{HD} ratio should be linearly dependent on the $[HI]_i/\beta[C_2D_4]_i$ ratio. The results are shown in Fig. 6. The slopes and the intercepts of the straight lines give $k_4/k_3 \sim 0.7$ and $k_1/k_3 \sim 1.0$ for both systems. However, these values should not be taken too seriously, because in them errors from various sources are accumulated. Therefore, the only thing we can say is that all the values of k_1, k_3, and k_4 are in the same order.

Consequently, we can conclude from the above two analyses that the k_2 is much smaller than the k_3 in the system with ethylene and that the k_2 is more than 20% of the k_3 in the system with propylene.

In the experiments on the DI–C_2H_4 and HI–C_2D_4 systems, we measured the amounts of C_2H_3D and C_2D_3H produced. The ratios of $[C_2H_3D]/[HD]$ and $[C_2D_3H]/[HD]$ are listed in Tables 1 and 2. Although the data are very scattered, they may be enough to show that the ratios are between 1.0 and 2.0.

Since we know that thermal hydrogen atoms are about 10 times more reactive to hydrogen iodide than

9) R. D. Penzhorn and B. deB. Darwent, *J. Phys. Chem.*, **72**, 1639 (1968).
10) R. D. Penzhorn and B. deB. Darwent, *J. Chem. Phys.*, **55**, 1508 (1971).
11) R. J. Cvetanović and L. C. Doyle, *ibid.*, **50**, 4705 (1969).
12) L. J. Gillespie and L. H. D. Fraser, *J. Amer. Chem. Soc.*, **58**, 2260 (1936).

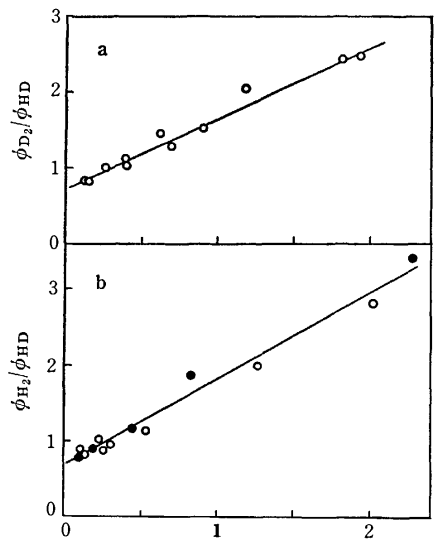

Fig. 6. The plots for Eq. (III).
a: $[DI]_i/\beta[C_2H_4]_i$, b: $[HI]_i/\beta[C_2D_4]_i$

to olefins, and since the C_2D_3H and C_2H_3D values were measured in the Olefin/Hydrogen Iodide ratio range of 0.4~8, we can derive the following relationship by using the steady-state treatment:

$$\frac{[RD]}{[HD]} = \frac{k_2+(1+\gamma)k_3}{k_3+(1+\gamma)k_2} \qquad (IV)$$

Here, γ stands for the following ratio:

$$\gamma = \frac{k_{13}[I_2]}{k_{10}[DI]} = \frac{k_{16}[I_2]}{k_{14}[DI]} \qquad (V)$$

The equality between the second term and the third in Eq. (V) may be admitted for the same reason as in the case of Eq. (II). At the temperature of 20 °C, the k_{13}/k_{10} ratio is equal to 14.3, as has already been stated. Therefore, the value of γ for the present experiment is calculated to be $0.6(=14.4\times0.195/5.0)$. In the above discussion, the inequality $k_2 \ll k_3$ has been derived in the DI–C_2H_4 and HI–C_2D_4 systems. The substitution of this relation into Eq. (IV) leads to the conclusion that the [RD]/[HD] ratio should be 1.6. This value is not inconsistent with the observed values.

In the discussion of the reactions of tritium atoms from a nuclear reaction with saturated hydrocarbons, Wolfgang indicated that the threshold energy of the substitution reaction is higher than that of the abstraction reaction.[13] If this rule is applicable to ethylene, the present conclusion, $k_2 \ll k_3$, is obviously inconsistent with the statement of Wolfgang. However, according to the paper presented by Turner and Cvetanović,[14] when D atoms produced by the mercury-photosensitized decomposition of n-C_4D_{10} add to C_2H_4, the isotopic exchange occurs, but it does not occur when H atoms add to C_2D_4. Comparing these results with ours, we believe that the substitution reaction observed in the present experiment occurs through the rapid decomposition of excited ethyl radicals produced, the internal energy of which is much higher than that of the ethyl radicals discussed by Turner and Cvetanović.

If the Kassel equation, $k=(1-\varepsilon_0/\varepsilon)^{s-1}$, is applicable to the unimolecular decomposition of ethyl radicals, the lifetime may be calculated to be in the order of 10^{-11} s by using the following values: $A=10^{13.6}$, $\varepsilon_0=40.7$ kcal mol^{-1},[15] $\varepsilon=40.7+50$, and $s=8$. This lifetime is obviously too short to be affected by the pressure used in the present experiment.

13) R. Wolfgang, "Progress in Reaction Kinetics," vol. 3, edited by G. Porter, Pergamon Press, (1965) p. 97.
14) A. H. Turner and R. J. Cvetanović, *Can. J. Chem.*, **37**, 1075 (1959).
15) H. E. O'Neal and S. W. Benson, "Kinetic Data on Gas Phase Unimolecular Reactions" NSRDS-NBS 21, U.S. Department of Commerce, N.B.S. (1970).

Laser Photolysis Studies on the Ionization of *N*-Vinylcarbazole and *N*-Ethylcarbazole in the Presence and Absence of Electron Acceptors[1)]

Yoshio TANIGUCHI, Yasuzo NISHINA, and Noboru MATAGA*

Department of Chemistry, Faculty of Engineering Science, Osaka University, Toyonaka, Osaka 565

(Received November 22, 1972)

Formation of solvated ion radicals in the *N*-vinylcarbazole (VCZ)-and *N*-ethylcarbazole (ECZ)-electron acceptor systems in polar solvents has been studied by means of laser photolysis, transient photoconductivity and transient absorption measurements. Ion radical formation due to the encounter collision between an excited VCZ or ECZ and electron acceptor was confirmed directly. In the absence of electron acceptor, formation of cation radicals of carbazoles due to biphotonic process was observed in polar solvents. The $S_n \leftarrow S_1$ spectra of these molecules were observed both in polar and nonpolar solvents.

It was postulated that the photopolymerization of VCZ in the presence of electron acceptors is initiated by cation radicals formed by the electron transfer from VCZ molecules to acceptors in the excited state.[2)] However, no direct experimental evidence has been given on the mechanism of cation radical formation.

We have shown the ion radical formation due to the encounter collision between an excited pyrene and *N*,*N*-dimethylaniline (DMA) and also between an excited anthracene and DMA in moderately and strongly polar solvents by means of laser photolysis, transient photoconductivity and absorption measurements.[3,4)] We carried out analogous studies on VCZ, using 1,2,4,5-tetracyanobenzene (TCNB) and tetracyanoethylene (TCNE) as electron acceptors, and confirmed the formation of solvated cation radicals of VCZ and anion radicals of the acceptor due to the encounter collision between the excited VCZ and the ground state acceptor.

We also studied the photoionization of VCZ in polar solvents in the absence of the electron acceptor, since photopolymerization of VCZ can even thus be observed. The formation of VCZ cation radicals was found to be due to a biphotonic absorption process. $S_n \leftarrow S_1$ spectra of VCZ might be important for the elucidation of its excited state electronic structure.

We examined ECZ in detail for the purpose of comparison and obtained similar results to those of VCZ.

Experimental

The same Q-switched ruby laser as described previously[3,5)] was used. The ion radicals produced were observed by measurement of the transient photocurrent and the transient absorption spectra induced by laser excitation, the methods for these measurements being the same as before. For examining the effect of exciting light intensity on the photocurrent, the intensity of the laser pulse was reduced by using neutral filters composed of wire gauzes. Relative values of the exciting intensity were monitored by measuring the intensity of light partially reflected by means of a beam splitter with a photomultiplier. The absolute value was determined by a ballistic thermopile TRG model 100 (Hadron). Measurements of fluorescence decay times were carried out by using a nitrogen gas laser.

TCNB was the same sample as used before and recrystallized from ethanol several times before use. TCNB was purified by repeated recrystallization from monochlorobenzene and sublimation in a vacuum. Solvents were Merck spectrograde and used without purification. Concentrations of VCZ and ECZ in solutions for the measurements were *ca.* 1.0×10^{-3} M, where the optical density of the solution at 347 nm was *ca.* unity. Concentrations of the electron acceptors in solutions for the laser photolysis were *ca.* 1.0×10^{-2} M. All solutions were deaerated by repeated freeze-pump-thaw cycles.

Results and Discussion

A. Formation and Annihilation Mechanisms of VCZ and ECZ Cation Radicals under the Presence of Electron Acceptors. The transient photocurrents of VCZ–TCNB–acetonitrile and ECZ–TCNE–methylene chloride systems are shown in Figs. 1 and 2, respectively. We see that the dissociated and solvated ion radicals are produced by excitation with 347 nm laser pulse, and vanish due to bimolecular recombination reaction. In a more concentrated solution, there arises a charge transfer (CT) absorption band near 570 nm due to complex formation. However, in the present case, the interaction of VCZ with TCNB in the ground state can be ignored, since no CT absorption is observed. The ion radicals (Figs. 1 and 2) might be formed by the encounter collision between excited carbazoles and

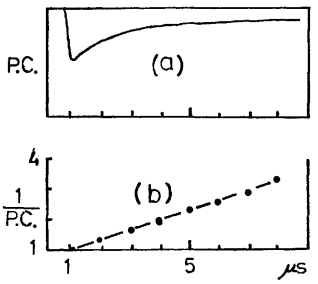

Fig. 1. Transient photocurrent of the VCZ-TCNB-acetonitrile system.
(a) The decay curve of photocurrents.
(b) The reciprocal of the photocurrent *vs.* time relation.

* To whom correspondence should be addressed.

1) A preliminary report was published in *Chem. Lett.*, **1972**. 221.

2) *Cf. e.g*, S. Tazuke, *Yuki Gosei Kagaku*, **27**, 15 (1969). *Adv. Polymer Sci.*, **6**, 321 (1969).

3) Y. Taniguchi, Y. Nishina, and N. Mataga, This Bulletin, **45**, 764 (1972).

4) Y. Taniguchi and N. Mataga, *Chem. Phys. Lett.*, **13**, 596 (1972).

5) H. Masuhara, N. Shimada, N. Tsujino, and N. Mataga, This Bulletin, **44**, 3310 (1971).

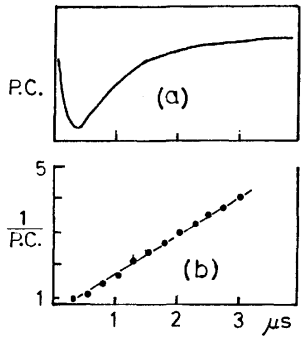

Fig. 2. Transient photocurrent of the ECZ-TCNE-methylene chloride system.
(a) The decay curve of photocurrent.
(b) The reciprocal of the photocurrent *vs.* time relation.

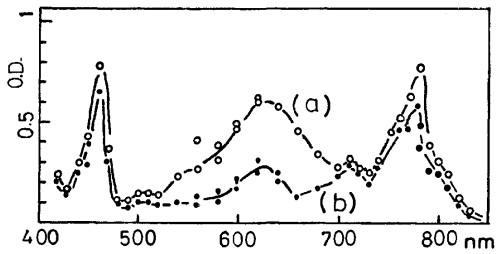

Fig. 3. Transient absorption spectra of VCZ-TCNB-acetonitrile system. The delay time from the laser pulse, (a) 0, (b) 200 ns.

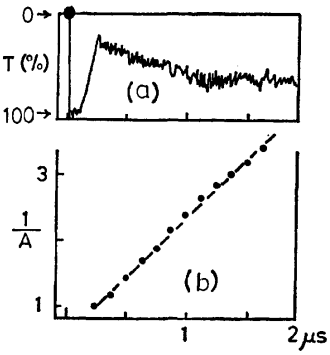

Fig. 4. The decay process of the absorption at 780 nm.
(a) The observed decay curve of the absorbance.
(b) The reciprocal of the absorbance *vs.* time relation.

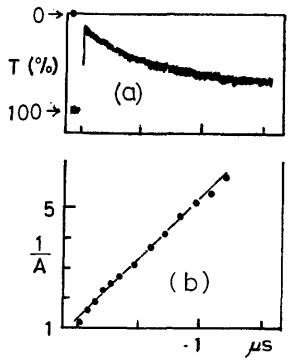

Fig. 5. The decay process of the absorption at 460 nm.
(a) The observed decay curve of the absorbance.
(b) The reciprocal of the absorbance *vs.* time relation.

acceptors. We examined the effect of the addition of acceptors on the fluorescence decay time and yield of VCZ in acetonitrile solution. The results can be reproduced by the simple Stern-Volmer equation, $\tau/\tau_0=1/(1+\tau_0 k[A])$, from which k values were evaluated to be $1.5\times10^{10}\,M^{-1}\,s^{-1}$ for VCZ–TCNB system and $1.3\times10^{10}\,M^{-1}s^{-1}$ for VCZ–TCNE system. These values of the rate constant of the quenching reaction indicate that the excited VCZ molecules make diffusion-controlled encounter collision with acceptor molecules. Analogous results were obtained by fluorescence yield measurements.

The ion radical formation can be confirmed also by transient absorption measurements. The transient absorption spectra of VCZ–TCNB–acetonitrile system are shown in Fig. 3. The decay of the optical absorption at 780 nm and the reciprocal of the absorbance *vs.* time relation are shown, respectively, in Figs. 4a and 4b, and the decay process at 460 nm in Figs. 5a and 5b. The absorbance *vs.* time relation at *ca.* 710 nm is similar to that at 780 nm. The decay curve of the absorption at *ca.* 620 nm consists of two components. The short lived component of the absorption at 540—680 nm may be ascribed to the transition from the lowest excited singlet (S_1) to the higher excited singlet (S_n) state of VCZ. The decay of the long lived component is the same as that at 780 nm. The transient absorption bands at 780, 710 and 620 nm with a rather long life may be ascribed to the VCZ cation radical since they are similar to those of the VCZ cation radical obtained by radiolysis at low temperatures.[7] The absorption band at *ca.* 460 nm can be ascribed to the TCNB anion radical. The results show that the ion radicals formed by the electron transfer from the excited VCZ to TCNB decay due to the bimolecular recombination reaction.

The photoionization of VCZ in the presence of TCNB was also examined for the tetrahydrofurane (THF) solution, the results being shown in Figs. 6 and 7. They are similar to those in the case of acetonitrile solution, except that the amount of produced ions is considerably smaller. We observed both dissociated ion radical

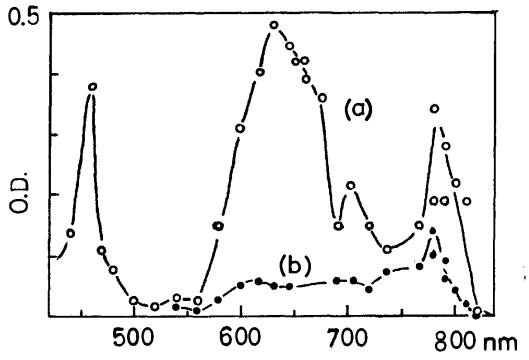

Fig. 6. Transient absorption spectra of VCZ-TCNB-THF system. The delay time from the laser pulse, (a) 0, (b) 500 ns.

6) N. Nakashima, N. Mataga, F. Ushio, and C. Yamanaka, *Z. Phys. Chem., N. F.*, **79**, 150 (1972).
7) Y. Shirota, K. Kawai, N. Yamamoto, K. Tada, T. Shida, H. Mikawa, and H. Tsubomura, This Bulletin, **45**, 2683 (1972).

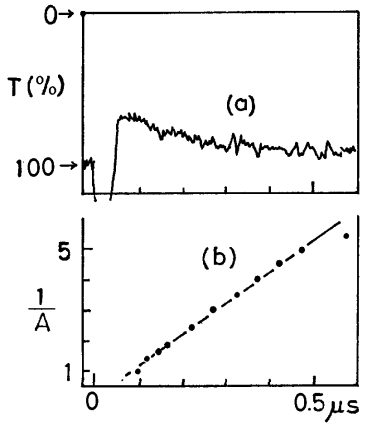

Fig. 7. The decay process of the absorption at 765 nm. The same system as in Fig. 6.
(a) The observed decay curve of the absorbance.
(b) The reciprocal of the absorbance *vs.* time relation.

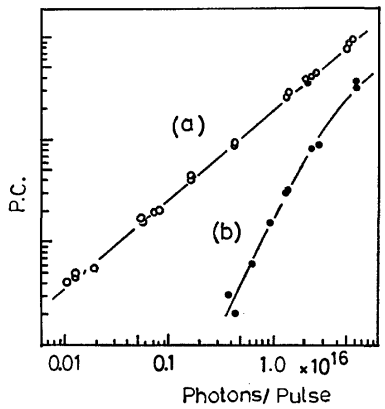

Fig. 8. The effect of the exciting light intensity on the peak photocurrent.
(a) VCZ-TCNB-acetonitrile system.
(b) VCZ-acetonitrile system.

formation and fluorescent exciplex formation in the case of pyrene–*N*,*N*-dimethylaniline–THF system, but no fluorescent exciplex formation was observed in the present case. This was the same also in the case of ECZ–TCNB system.

It is possible that ionization of VCZ or ECZ due to double photon absorption occurs since the exciting light pulse we used is fairly strong. For the sake of confirmation we investigated the effect of exciting light intensity on the peak photocurrent, the results of which are given in Fig. 8. We see that the ionization is a one-photon process in the case of the VCZ–TCNB–acetonitrile system.

We can conclude that the photoionization process of the VCZ–acceptor system is the encounter collision between the excited VCZ and the acceptor molecule followed by one electron transfer from the excited VCZ to the acceptor leading to the dissociation into ions.

The results might be of some interest for the elucidation of the CT photopolymerization mechanisms. Only a very small part of the dissociated ion radicals which have escaped deactivation due to recombination might initiate the polymerization.

B. Photoionization of VCZ and ECZ in the Absence of Electron Acceptors. In the photoionization of VCZ and ECZ in polar solvents in the absence of electron acceptors, the formation of their cation radicals was confirmed by transient absorption and transient photoconductivity measurements. The decay process of the absorption of VCZ cation radical in acetonitrile solution is shown in Fig. 9 and the transient absorption spectra of ECZ–methanol system in Fig. 10.

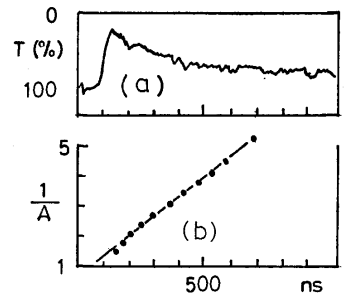

Fig. 9. The decay process of the absorption at 720 nm in the case of VCZ-acetonitrile system.
(a) The observed decay curve of the absorbance.
(b) The reciprocal of the absorbance *vs.* time relation.

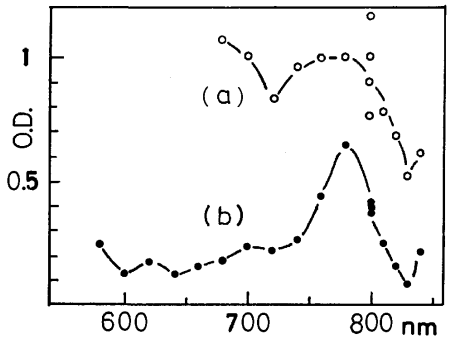

Fig. 10. Transient absorption spectra of ECZ-methanol system. The delay time from the laser pulse. (a) 0, (b) 100 ns.

The photocurrent in two-component system is similar to that of three-component systems, but in the former it is due to solvated cation radicals and solvated electrons.

We have confirmed that ionization is mainly due to the double photon process. The result in the case of VCZ–acetonitrile two-component system is shown in Fig. 8.

C. $S_n \leftarrow S_1$ Absorption Spectra of VCZ and ECZ. In order to examine the $S_n \leftarrow S_1$ transitions of VCZ and

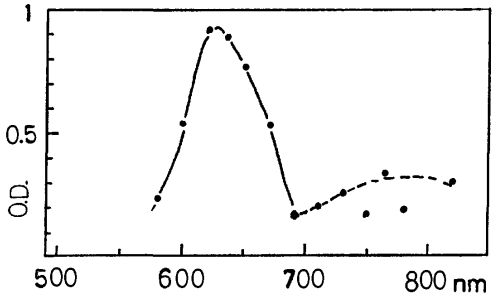

Fig. 11. Transient absorption spectra of VCZ-*n*-hexane system immediately after the excitation.

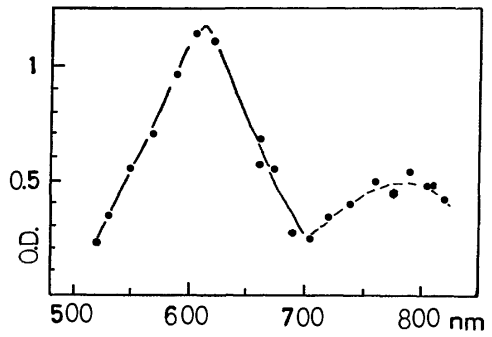

Fig. 12. Transient absorption spectra of ECZ-*n*-hexane system immediately after the excitation.

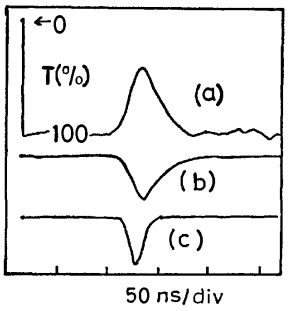

Fig. 13. The rise and decay curves of the transient absorption and fluorescence of VCZ-*n*-hexane system.
(a) Absorption at 620 nm.
(b) Fluorescence at 370 nm.
(c) Exciting laser pulse.

ECZ in detail, we carried out the laser photolysis and transient absorption measurements in n-hexane solution of these molecules, in order to avoid the formation of ion radicals.

The transient absorption spectra of VCZ-*n*-hexane and ECZ-*n*-hexane systems are shown in Figs. 11 and 12, respectively. The rise and decay curves of the transient absorption and the fluorescence of VCZ-*n*-hexane system are shown in Fig. 13. We can conclude that the observed transient absorption spectra are due to the $S_n \leftarrow S_1$ transitions, since the decay process of absorption is approximately the same as that of the fluorescence.

It might be of interest to note that the 620 nm band in the $S_n \leftarrow S_1$ spectra is similar to the absorption band of biphenyl anion. According to theoretical calculations on the electronic structures of carbazole[8,9] and VCZ[9], a considerable amount of charge transfer from nitrogen to the biphenyl part occurs in the S_1 state. Thus, the structure of these molecules in the equilibrium S_1 state might be highly polar where the biphenyl part is negatively charged, giving rise to $S_n \leftarrow S_1$ spectra similar to the absorption band of biphenyl anion. On the other hand, the wavelengths of the absorption bands in the $S_n \leftarrow S_1$ spectra are similar to those in the absorption spectra of cation radicals of VCZ and ECZ. Similarity of the $S_n \leftarrow S_1$ spectra of a molecule to those of its cation radical may be understood at least qualitatively on the basis of simple MO theory.

The authors wish to express their thanks to Dr. S. Tazuke, Kyoto University (presently at Tokyo Institute of Technology), for the VCZ and ECZ samples and for valuable discussions. They are indebted to Dr. K. Nishimoto, Osaka City University, for showing them his unpublished results of MO calculation.

8) N. Mataga, Y. Torihashi, and K. Ezumi, *Theoret. Chim. Acta*, **2**, 158 (1964).
9) K. Nishimoto, Private communication.

A Kinetic Study of the Mutarotation of D-Xylose by the Polarographic Method[1]

Tokuji IKEDA and Mitsugi SENDA

Department of Agricultural Chemistry, Faculty of Agriculture, Kyoto University, Sakyo-ku, Kyoto 606

(Received September 2, 1972)

The polarographic behavior of D-xylose in several buffer solutions was investigated. The rate constants, k_1, k_2, k_{-1}, and k_{-2}, of the mutarotation of α-D-xylose, assumed as $\alpha \underset{k_{-1}}{\overset{k_1}{\rightleftharpoons}} \gamma \underset{k_2}{\overset{k_{-2}}{\rightleftharpoons}} \beta$, were calculated by the use of Wiesner's method, but with a modified equation for the polarographic current. The overall mutarotation rate constant, k_o, which is defined by $k_o=(k_1k_{-2}+k_{-1}k_2)/(k_{-1}+k_{-2})$, was also determined. The rate constants, k_o, k_1, and k_2, were analyzed as a linear function of the buffer concentration. It was revealed that the catalytic effects of the buffer salts were mainly due to their basic components for all the buffer salts investigated. The Brönsted plots of k_1 and k_2 for all the basic components gave straight lines with the same slope of 0.42. The rate constants for several amines deviated from the slope; this deviation was ascribed to the steric hindrance caused by their large molecular sizes.

The mutarotation of reducing sugar in an aqueous solution is catalyzed by the use of acids and bases.[2-4] The measurements of the mutarotation velocity are usually made by polarimetry, NMR and other such methods, but the results are in most cases interpreted in terms of the mutarotation rate constant, k_o, defined by $k_o=k_\alpha+k_\beta$, where the reaction mechanism is assumed to be as in Eq. (1):

$$\alpha\text{-pyranose} \underset{k_\beta}{\overset{k_\alpha}{\rightleftharpoons}} \beta\text{-pyranose} \tag{1}$$

Los, Simpson, and Wiesner[5] have shown that, by the use of the polarographic method, four individual rate constants, k_1, k_2, k_{-1} and k_{-2}, of the mutarotation assumed as in Eq. (2):

$$\alpha\text{-pyranose} \underset{k_{-1}}{\overset{k_1}{\rightleftharpoons}} \gamma\text{-form} \underset{k_2}{\overset{k_{-2}}{\rightleftharpoons}} \beta\text{-pyranose} \tag{2}$$

can be determined; here, the intermediate γ-form is assumed to be an electroactive free aldehyde form, and the polarographic current produced by a monosaccharide, such as D-glucose, is controlled by the kinetics of the formation of the γ-form from α- and β-pyranose. Experimental study of the isotope exchange of D-glucose C-1-^{18}O also supports the idea that the formation of the aldehydrol form is negligible in mutarotation kinetics.[2]

In this study, the individual rate constants of the base-catalyzed mutarotation of α-D-xylose are determined by the polarographic method; this method is based on Wiesner's assumption, but with a modified equation for the polarographic current. The results are discussed in view of the base-catalyzed reaction.

Expression for The Polarographic Current of D-*Xylose.* According to Los, Simpson, and Wiesner, the polarographic kinetic current, i_k, of monosaccharide when it is present in two forms, *e. g.*, α- and β-pyranose at the concentrations of C_α and C_β, is given by:

$$\bar{i}_k = nF\bar{q}(D/(k_{-1}+k_{-2}))^{1/2}(k_1C_\alpha+k_2C_\beta) \tag{3}$$

where n denotes the number of electrons consumed in the electrolysis per molecule; F, the Faraday; $\bar{q}$, the mean electrode surface area, and D, the diffusion coefficient of the monosaccharide. Eq. (3) was first derived by assuming a reaction layer on the electrode surface, the thickness of which was given by:

$$\mu = (D/(k_{-1}+k_{-2}))^{1/2} \tag{4}$$

We ourselves have previously shown[6] that Eq. (3) can be derived by a rigorous mathematical procedure on the following assumption:

$$\tau(k_{-1}+k_1) \gg 1 \qquad \tau(k_{-2}+k_2) \gg 1, \tag{5}$$

τ being the drop time, and

$$K_\alpha = k_{-1}/k_1 \gg 1 \qquad K_\beta = k_{-2}/k_2 \gg 1, \tag{6}$$

while k_1/k_2 is not extremely different from unity. This is actually the case with D-glucose.[5] A similar argument has also been advanced by Paldus and Koutecký.[7]

As will be demonstrated later in this study, however, the rate constants for D-xylose are not so large as Eq. (5) predicts. Accordingly, a modified equation has to be used in analyzing the polarograpnic current of D-xylose.

By a close investigation of the rigorous mathematical solution for the polarographic kinetic current reported by Koutecký and Brdička,[8] and by assuming the reaction layer given by Eq. (4), we may derive a modified equation of the polarographic current:

$$\bar{i}_l = \bar{i}_k + \bar{i}_{corr} \tag{7}$$

with:

$$\bar{i}_{corr} = \frac{\bar{i}_d}{K_\alpha+K_\beta} \times \frac{1-\exp(-\tau(k_{-1}+k_{-2}))}{\tau(k_{-1}+k_{-2})} \times \frac{1.13}{1.13+(\tau(k_{-1}+k_{-2}))^{1/2}} \tag{8}$$

1) Presented at 17th. Ann. Symp. Polarography, Fukuoka, Oct. 16—18, 1971.

2) W. Pigman and H. S. Isbell, "Advances in Carbohydrate Chemistry," Vol. 23, ed. by M. L. Wolfrom, and R. S. Tipson, Academic Press. London (1968), p. 11.

3) H. S. Isbell and W. Pigman, "Advances in Carbohydrate Chemistry and Biochemistry," Vol. 24, ed. by M. L. Wolfrom, and R. S. Tipson, Academic Press. London. (1969), p. 13.

4) B. Capon, *Chem. Rev.*, **69**, 407 (1969).

5) J. M. Los, L. B. Simpson, and K. Wiesner, *J. Amer. Chem. Soc.*, **78**, 1564 (1956).

6) M. Senda, *Rev. Polarogr.* (Kyoto), **6**, 95 (1958).

7) J. Paldus and J. Koutecký, *Collect. Czech. Chem. Commun.*, **23**, 376 (1958).

8) J. Koutecký and R. Brdička, *ibid.*, 12, 337 (1947).

and:

$$\bar{i}_d = \kappa(C_\alpha + C_\beta) \qquad \kappa\text{: Ilković constant,} \tag{9}$$

under the following conditions:

$$(\tau(k_{-1}+k_{-2}))^{1/2}/(K_\alpha + K_\beta) \ll 1 \tag{10}$$

and:

$$K_\alpha \gg 1, \qquad K_\beta \gg 1 \tag{11}$$

In these equations, $\bar{i}_k$ is defined by Eq. (3), $\bar{i}_{corr}$ is the correction term, and $\bar{i}_d$ is the diffusion current given by the Ilkovič equation, with the total bulk concentration of monosaccharide, being $C_\alpha + C_\beta$. Some details of the derivation of Eq. (7) are given in the Appendix.

As the mutarotation takes place in the bulk of the solution, the concentrations of α- and β-pyranose, C_α, and C_β, change with the time. For example, if we dissolve α-D-xylose in a solution at time $t=0$, C_α decreases with the time, whereas C_β increases with the time, in accordance with the following equation:[5]

$$C_\alpha = (C_\alpha)_{t\to\infty}(1 + K\exp(-k_o t)) \tag{12}$$

$$C_\beta = (C_\beta)_{t\to\infty}(1 - \exp(-k_o t)) \tag{13}$$

where:

$$k_o = (k_1 k_{-2} + k_{-1}k_2)/(k_{-1}+k_{-2}), \tag{14}$$

$$K = (C_\beta/C_\alpha)_{t\to\infty} = (C_\beta)_{t\to\infty}/(C_\alpha)_{t\to\infty} = K_\beta/K_\alpha, \tag{15}$$

and:

$$C_\alpha + C_\beta = C_{total} = (C_\alpha)_{t=0}, \tag{16}$$

where the concentration of the intermediate γ-form is assumed to be negligibly small. That is, the polarographic current, which is given by Eq. (7) or Eq. (3), changes with the time. The combination of Eqs. (12) to (16) with Eq. (7) to analyze the polarographic current, that was recorded as a function of the time, makes it possible to compute the four rate constants, k_1, k_{-2}, k_{-1}, and k_2, in Eq. (2).

Experimental

Materials. The α-D-xylose was recrystallized from an aqueous solution;[10] $[\alpha]_D^{25} = +96$, mp 146 °C, mutarotation rate const. $k_o = 1.30 \times 10^{-3}\ s^{-1}$ in water at 25±0.5 °C. All the other chemicals used were of a reagent grade. The solutions were prepared with bidistilled water. The buffer components were NaH_2PO_4–Na_2HPO_4, NH_3–NH_4Cl, Trys(hydroxymethyl)amino methane (TRIS), Tris(hydroxymethyl)methyl glycine (TRICINE), and N,N-bis(2-hydroxyethyl)glycine (BICINE). Potassium chloride was used to adjust the ionic strength to the desired values (usually 0.5).

Equipment. A Yanagimoto polaro-recorder type PA-103 was used for all the polarographic measurements. A Yanagimoto controlled-potential electrolyzer, type VE-3, was used for controlled-potential electrolysis, while the polarimetric measurements were carried out with a Yanagimoto polarimeter, type OR-20. The pH values were measured with a Hitachi Horiba M-5 pH meter.

An electrolysis cell (20 ml in capacity) was used; it was connected with a saturated calomel electrode (SCE) by means of an agar-gelatin bridge containing potassium chloride. All the experiments were carried out in a water thermostat controlled at 25±0.05 °C.

Method. A supporting electrolyte solution (15 ml) of the desired composition was freed of oxygen by passing a nitrogen stream through the solution. First, the residual current was recorded by means of the polarograph. Second, after the potential of the dropping mercury electrode has been set at −1.75 V *vs.* SCE, a weighed amount of α-D-xylose was dissolved in the deoxygenated electrolyte solution; the passing of the nitrogen stream through the solution was continued for about 30 seconds to complete the dissolution of the α-D-xylose. Then, the current intensity at −1.75 V *vs.* SCE was recorded as a function of the time. The recording of the current was continued until the current intensity reached a constant value. The nitrogen stream was passed over the solution during the measurement. Finally, after the mutarotation eqilibrium had been reached, a whole polarographic wave of the D-xylose was recorded. The current intensity was corrected for the residual current.

Results

General Polarographic Behavior of D-Xylose. The polarographic behavior of an equilibrated mixture of D-xylose was studied. At pH values lower than 9.5, no appreciable change in the polarogram of equilibrated solution of D-xylose was observed, at least not within two hours, at 25 °C. No appreciable change in specific rotation was observed, either. These results suggest that no hydrolysis, carbonyl amino reaction, or any complicated reaction of D-xylose occurs under the conditions used in the present experiment.

A few examples of the experimental results on the dependence of the limiting current, $\bar{i}_l$, on the height of the mercury reservior, h, are shown in Table 1. The limiting current was inclined to increase slightly with an increase in the height of the mercury reservior. An analysis of the current-time (i-t) curve for single drop has shown that the slope of the log i *vs.* log t plot is 1.8/3, which is slightly smaller than the theoretical value, 2/3, which is expected for a purely kinetic current defined by Eq. (3). These results support

Table 1. Dependence of the limiting current $\bar{i}_l$ on the height of mercury reservior h

The concentration of D-xylose 0.066 M, Temp. 25 °C

h (cm)	$\bar{i}_l$ (cm)[a]		
	Phosphate buff. 0.05 M, pH 6.99	TRIS buff. 0.05 M, pH 8.04	TRIS buff. 0.20 M, pH 8.04
62.4	2.3_6	4.4_0	4.8_1
72.4	2.4_7	4.5_2	5.0_1
82.4	2.4_5	4.6_0	5.0_2
c.f. $\bar{i}_l/\bar{i}_d$[b]	2.96×10^{-3}	5.67×10^{-3}	6.28×10^{-3}

a) Current sens. 0.4 μA/cm.
b) i_d: Hypothetical diffusion current of D-xylose.

9) Recently Nishihara and Matsuda have carried out more rigorous mathematical analysis of the problem by use of an electronic computer (Presented at 17th. Ann. Symp. Polarography, Fukuoka, Oct. 16—18, 1971). Preliminary examination showed that the errors resulted by use of Eqs. (7) to (9) did not exceed 8% for $(k\tau)^{1/2}<2$, under the condition (10) and (11).

10) K. Anno and N. Seno, "Jikken Kagaku Koza", Vol. 23, ed. by S. Akabori and S. Funahashi, (in Japanese) Maruzen, Tokyo, (1957), p. 336.

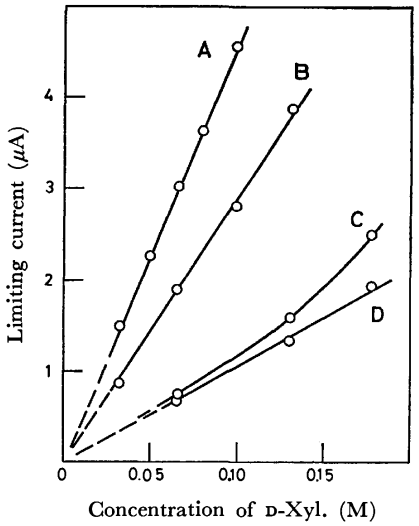

Fig. 1. Relationships between limiting current and the concentration of D-xylose. 25 °C, A: Ammonia buff. 0.100 M pH 8.79, B: TRIS buff. 0.020 M, pH 8.25, C: Phosphate buff. 0.005 M, pH 6.99, D: Phosphate buff. 0.070 M, pH 6.12.

the idea that the correction term, i_{corr}, in Eq. (7) should not be neglected in interpreting the kinetic current produced by D-xylose.

The limiting current is proportional to the D-xylose concentration in various supporting electrolyte solutions, as is shown by Curves A, B, and D in Fig. 1, but at a very low concentration of the buffer component a deviation from the linearity was observed, as is exemplified by Curve C in Fig. 1. Table 2 and Fig. 2 show the effects of the buffer concentration and the pH on the limiting current. In a basic solution, the limiting current increased exponentially with the pH. In an ammonia buffer solution with a pH of about 9, the limiting current decreased with a decrease in the concentration of the buffer component. On the contrary, in the phosphate buffer solution, the limiting current first decreased with a decrease in the concentration of the buffer component, but at a lower concentration (0.005 M) it began to increase and finally reached an unusually large value in an unbuffered solution. This last result might be explained by the autocatalytic effect of the hydroxy anion produced in company with the electro-reduction of D-xylose at the electrode surface. A simlar phenomenon has been reported by Brdička and his coworker[11-13] for the electro-reduction of formaldehyde at the dropping mercury electrode in an unbuffered solution.

A controlled potential electrolysis of D-xylose was carried out at the mercury-pool cathode in an ammonia buffer solution with a pH of 9.5. After about nine hours of electrolysis at −1.8 V *vs.* SCE, the kinetic wave of D-xylose disappeared almost completely (Fig. 3). During the electrolysis, the generation of

11) R. Brdička, *Collect. Czech. Chem. Commun.*, **20**, 387 (1955).
12) R. Brdička, *Z. Electrochem.*, **59**, 787 (1955).
13) R. Brdička and L. Němec, *Rev. Polarogr.* (Kyoto), **11**, 5 (1963).

TABLE 2. THE LIMITING CURRENT WITH VARIOUS BUFFER CONCENTRATIONS

Ammonia buff. pH 9.40 D-Xyl. 0.040 M	i_l (μA)	Phosphate buff. pH 6.99 D-Xyl. 0.066 M	i_l (μA)
0.533 M	4.01	0.100 M	1.06
0.268	3.44	0.050	0.92
0.133	3.03	0.010	0.68
0.067	2.78	0.005	0.67
0.033	2.68	0.001	1.22
		none	9.68

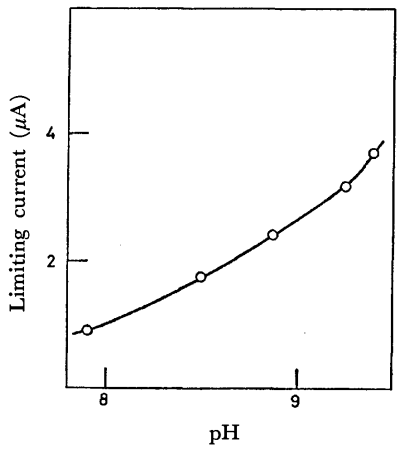

Fig. 2. The dependence of the limiting current on pH. D-xylose: 0.04 M, Ammonia buff.: 0.50 M, 25 °C.

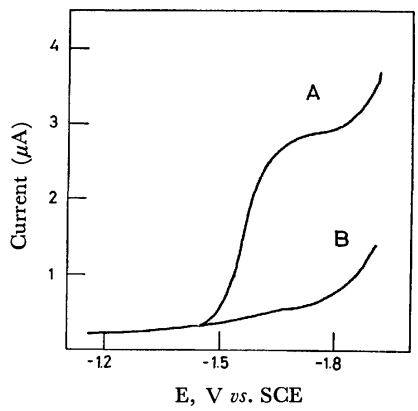

Fig. 3. Controlled potential electrolysis of D-xylose at mercury cathode −1.8 V *vs.* SCE. Ammonia buff.: 1.0 M, pH 9.5, 25 °C. A: 0.05 M D-xylose, B: After about nine hours of electrolysis.

bubbles was observed on the mercury-cathode surface. This may be attributed to the evolution of hydrogen, which occurs parallel with the reduction of D-xylose. The electrolyzed solution was paper-chromatographed,[14] and the spot of D-xylitol was identified on the chromatogram. Provided that the number of electrons consumed per molecule of D-xylose is 2, calculation showed that about two thirds of the total electricity was consumed by the reduction of the D-xylose and one third, by the reduction of the hydrogen

14) Ref. 10) p. 392.

Table 3. Buffer solutions
The concentration of D-xylose 0.132—0.066 M
Temp. 25 °C, Ionic strength 0.5

Buffer	Base Component	pK_A	Concentration (mol/l)	pH
Phosphate	HPO_4^{2-}	7.2	0.03—0.10	6.12—6.99
TRICINE	$(CH_2OH)_3-CNH-OOCCH_2$	8.1	0.02—0.20	7.88—8.42
TRIS	$(CH_2OH)_3-CNH_2$	8.2	0.02—0.20	8.04—8.42
BICINE	$(C_2H_4OH)_2-N-OOCCH_2$	8.3	0.02—0.15	8.10—8.92
Ammonia	NH_3	9.2	0.05—0.50	8.16—8.59

Table 4. The overall and individual rate constants in various buffer solutions

	Phosphate 0.05 M pH 6.99	TRICINE 0.10 M pH 8.22	TRIS 0.10 M pH 8.27	BICINE 0.10 M pH 8.29	Ammonia 0.10 M pH 8.59
k_o s^{-1}	9.1×10^{-3}	5.3×10^{-3}	6.5×10^{-3}	3.4×10^{-3}	8.7×10^{-3}
k_1 s^{-1}	16.2×10^{-3}	8.1×10^{-3}	9.9×10^{-3}	4.5×10^{-3}	15.9×10^{-3}
k_2 s^{-1}	5.0×10^{-3}	3.2×10^{-3}	3.8×10^{-3}	2.2×10^{-3}	4.7×10^{-3}
k_{-1} s^{-1}	15.2	0.9	1.3	0.4	2.1
k_{-2} s^{-1}	8.6	0.7	0.9	0.4	1.1
$K_\alpha+K_\beta$	2.7×10^3	3.3×10^2	3.7×10^2	2.7×10^2	3.7×10^2

ion, in the controlled-potential electrolysis on the mercury-pool electrode at −1.8 V.

Determination of Mutarotation Rate-Constants of α-D-Xylose. The composition and pH's of the buffer solution in which the mutarotation rate-constants were determined are summarized in Table 3. These conditions have been selected to avoid complexities arising from too high a basisity or too low a buffer concentration, as has been described above. Too high a concentration of buffer components resulted in an increase in the final ascending of the base current and made accurate measurement of the limiting current difficult.

The experimental results were analyzed by the use of the theoretical equations given above, and the individual rate constants, k_1, k_2, k_{-1}, and k_{-2}, were computed. In applying Eqs. (7), (8) and (4), a successive approximation method was employed. The computation was carried out by the use of an electronic computer, FACOM 230—60 (Kyoto University). The diffusion coefficient, D, was assumed to be 6.58×10^{-6} $cm^2\,s^{-1}$,[15] and the equilibrium constant, K (defined by Eq. (15)), to be 1.873.[2]

Examples of the four individual rate constants, k_1, k_2, k_{-1}, and k_{-2}, and the overall rate-constant, k_o, defined by Eqs. (2) and (14), are shown in Table 4. In general, the backword or ring-closing rate constants, k_{-1} and k_{-2}, could be determined with only a poor precision. Accordingly, a detailed analysis of the rate constants was made with the forward or ring-opening rate constants, k_1 and k_2, and the overall rate constant, k_o.

15) L. Friedman and P. G. Carpenter, *J. Amer. Chem. Soc.*, **61**, 1745 (1939).

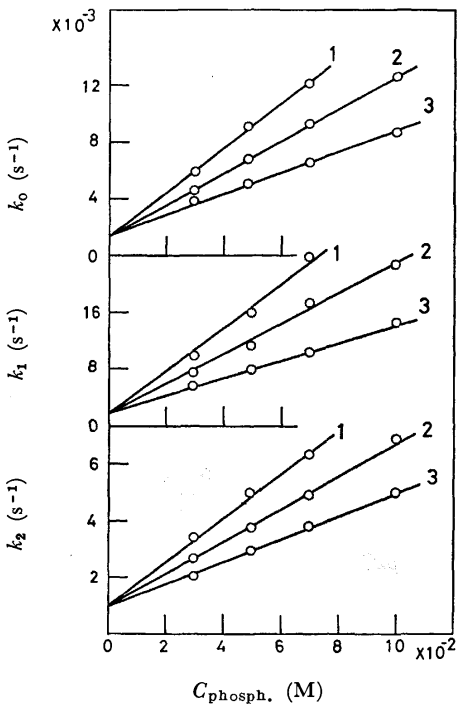

Fig. 4. The rate constants as a function of the concentration of phosphate buffer, $C_{phosph.}$ 25 °C, 1: pH 6.99, 2: pH 6.59, 3: pH 6.12.

At a constant pH, the rate constants, k_o, k_1, and k_2, increased linearly to the buffer concentration. Some representative results are shown in Fig. 4 and Fig. 5.

Generally, the rate constant of a catalyzed reaction can be expressed as follows:[3]

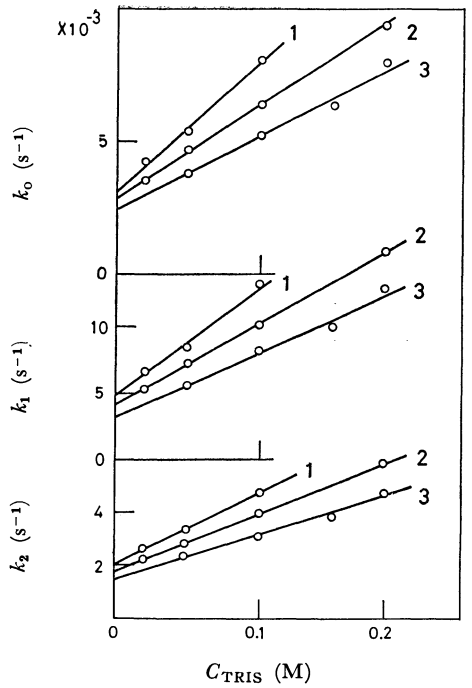

Fig. 5. The rate constants as a function of the concentration of TRIS buffer, C_{TRIS}. 25 °C, 1: pH 8.42, 2: pH 8.27, 3: pH 8.04.

$$k_i = k_{i,w} + k_{i,OH}(OH^-) + k_{i,A}(A) + k_{i,B}(B) \quad (17)$$
$$i=0,\ 1 \text{ and } 2$$

where $k_{i,w}$ represents the catalytic constant of the solvent molecule (water in our case), where $k_{i,OH}$, $k_{i,A}$, and $k_{i,B}$, represent the catalytic coefficients of the catalysts indicated by the subscripts, and where the symbols in brackets represent the concentrations (activities) of the catalysts, OH^-, A, and B, being the hydroxyl ion, acid, and the base of buffer components. In this expression, the concentration of the hydrogen ion is neglected because the measurements were made in neutral or basic solutions. The contribution of the D-xylose anion is also neglected. The significance of this approximation will be discussed later.

When the rate constant is plotted against the sum of the concentrations of the buffer components, $C_{buff}=(A)+(B)$, at a given pH, a straight line is obtained; the slope of this line is $(k_{i,A}M+k_{i,B})/(1+M)$, M being $(A)/(B)$, and the intercept on the k_i-axis is $k_{i,w}+k_{i,OH}(OH^-)$. A plot of this intercept against (OH^-) will give a straight line, from which $k_{i,OH}$ (slope) and $k_{i,w}$ (intercept) can be obtained. Fig. 4 shows a plot of k_i *vs.* C_{buff} for phosphate buffer solutions of pH 6.12, 6.59, and 6.99. Three straight lines with different slopes are obtained, but their intercepts on the k_i-axis coincide within the limits of experimental error. These results suggest that $k_{i,OH}(OH^-)$ is negligible in comparison with $k_{i,w}$ in such neutral solutions. Fig. 5 shows the same plot for the TRIS buffer; straight lines with different slopes and different intercepts on the k_i-axis are given for each solution at a given pH. Similar results were obtained for all the other basic buffers. The intercept values thus obtained from the k_i *vs.* C_{buff} curves are plotted against (OH^-) in Fig. 6. In accordance with theoretical

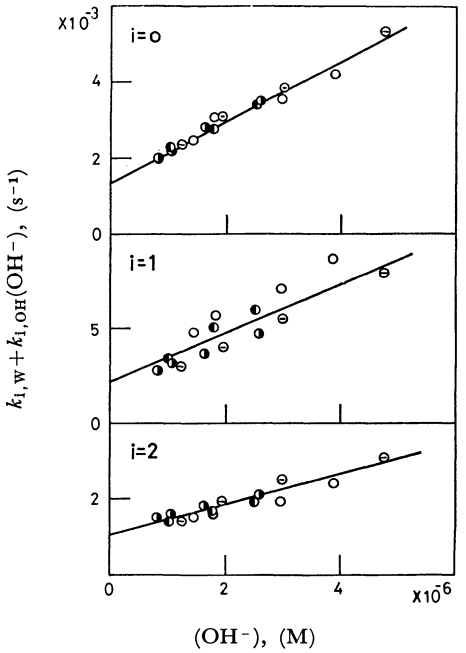

Fig. 6. The plot of $k_{i,w}-k_{i,OH}(OH^-)$ against the concentration of hydroxy ion, (OH^-).
○: NH_3, ◐: TRIS, ◑: TRICINE, ⊖: BICINE

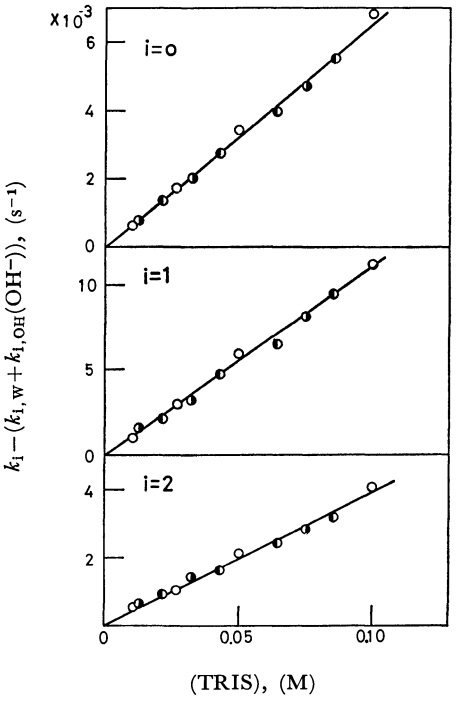

Fig. 7. The plot of $k_i-(k_{i,w}+k_{i,OH}(OH^-))$ against the concentration of the base conponent of TRIS buffer. (TRIS).
○: $M=1$, ◑: $M=4/6$, ◐: $M=6/4$.

considerations, all the data are distributed along the regression line, from which $k_{i,w}$ and $k_{i,OH}$ for overall as well as individual reaction rates are determined. The $k_{i,w}$ value obtained in this way is in good agreement with those obtained from the intercepts in Fig. 4 (*e. g.* $k_{o,w}=1.3\times10^{-3}$ s^{-1} from Fig. 6 and $k_{o,w}=1.4\times10^{-3}$ s^{-1} from Fig. 4).

Figure 7 shows a plot of $k_i-(k_{i,w}+k_{i,OH}(OH^-))$ against (B) for the TRIS buffer. A straight line with

a slope of $k_{i,B}+M\times K_{i,A}$ can be expected from each for a given M. As may be seen from the figure, however, all the points lie on a single straight line, irrespective of the M values. This suggests that $k_{i,B}\gg M\times k_{i,A}$ *i. e.*, that $k_{i,A}$ is negligibly small compared with $k_{i,B}$ for the buffer components examined. Similar results were obtained for all the other basic buffers examined.

Discussion

The values of the catalytic rate coefficients are summarized in Table 5. The coefficients, $k_{i,B}$'s, for B=TRIS, TRICINE, and BICINE are those for the base components of the amine buffers. The water molecule is both an acid and a base, but for the mutarotation of D-glucose in a neutral solution, the basic catalytic function is supposed to predominate over the acid one.[3] For the mutarotation of D-xylose, the same argument is justified on the basis of the Brönsted plot (Fig. 8). The HPO_4^{2-} and $H_2PO_4^-$ ions are also bifunctional, but in a neutral buffer solution the former ion functions as a base, and the latter, as an acid. Accordingly, their catalytic activities, as observed in a neutral solution, should in the first place be basic for HPO_4^{2-} and acidic for $H_2PO_4^-$. It may be seen in Table 5 that, except for the rate coefficients for $H_2PO_4^-$, the rate coefficients, $k_{i,B}$, for the $\alpha\rightarrow\gamma$ reaction are always larger than the $k_{2,B}$ for $\beta\rightarrow\gamma$, where B is a base catalyst. In Fig. 8, log $k_{i,B}$ and log $k_{2,B}$ are plotted against the pK_A value of the base catalyst, B. The rate coefficients for the water molecule, assumed to be a base catalyst, were calculated by means of $k_{i,w}/55.6$ M and plotted against pK_A= $-\log 55.6$.[3] The rate coefficients for H_2O, HPO_4^{2-}, NH_3 and OH^- are on a straight line with a slope of 0.42. The value of this slope seems reasonable in view of the value, 0.40 or 0.34, observed for the overall mutarotation rate constants of D-glucose.[3] The rate coefficients for the base components of TRIS, TRICINE, and BICINE are smaller than the theoretical values expected from the Brönsted plot and their pK's, and become smaller with an increase in their molecular size. These results should be attributed to the steric hindrance effect in the catalytic mutarotation reaction.[16,17] Smith[18] and Los and Simpson[19,20] have pointed out that the catalytic effect caused by sugar anion can generally not be neglected. According to these authors, the rate coefficient for (OH^-) in Eq. (17) should be rewritten as:

$$k_{i,OH} = k'_{i,OH} + k_{i,xyl}(xyl)K_{xyl}/K_w$$

where k'_{OH} and $k_{i,xyl}$ are the true rate coefficients for OH^- and the xylosate anion respectively, where (xyl) is the concentration of D-xylose where $K_{xyl}(=10^{-12.3})$[21] is the dissosiation constant of the Xylose⇌Xylosate Anion+H^+ reaction, and where K_w is the ionic product of water. Appling the Brönsted rule (Fig. 8) to D-xylose, we obtain $k_{i,xyl}\sim 30$ s^{-1} l/mol. In our experiments, (xyl) was 0.06 M, so that $k_{i,xyl}$ (xyl) $K_{xyl}/K_w\sim$ 90 s^{-1} l/mol, which is approximately 8% or less of $k_{i,OH}$. Accordingly, the effect by the xylosate anion may be considered to be of secondary significance in our case. In reality, no appreciable experimental indication was given of the significant contribution of the xylosate anion to catalysis, such as a nonlinear dependence of the polarographic current on (xyl).

The equilibrium constants of the γ-form to the α- and β-pyranose forms, $K_\alpha+K_\beta$, are given in Table 4. These values were found to change slightly with the change in the buffer concentration; for example, $K_\alpha+K_\beta$ for the TRIS buffer changed 4.5×10^2 to 2.5×10^2 with the change in the buffer concentration from 0.20 to 0.02 M, while $K_\alpha+K_\beta$ for the phosphate buffer changed from 4.2×10^3 to 2.1×10^3 with the change in the buffer concentration from 0.10 to 0.03 M. A similar downward trend of $K_\alpha+K_\beta$ with a decrease in the buffer concentration was also reported by previous authors.[5] The relatively large difference between the $K_\alpha+K_\beta$ values obtained from the phosphate buffer and the amine buffers should also be noted. These results suggest a further complicated structure of the intermediate form in the reaction mechanism of the mutarotation of monosaccharide. Further studies on the mechanism of mutarotation for monosaccharide are now in progress in this laboratory and will be

Table 5. The overall and the forward rate coefficients of the mutarotation of D-xylose
(Temp. 25 °C)

	o	i 1	i 2
$k_{i,w}$ (s^{-1})	1.4×10^{-3} a)	2.4×10^{-3}	1.0×10^{-3}
$k_{i,H_2PO_4^-}$ (s^{-1} l mol^{-1})	0.2×10^{-2}	0.3×10^{-2}	1.7×10^{-2}
$k_{i,HPO_4^{2-}}$ (s^{-1} l mol^{-1})	2.1×10^{-1}	4.1×10^{-1}	1.0×10^{-1}
$k_{i,TRICINE}$ (s^{-1} l mol^{-1})	4.2×10^{-2}	7.7×10^{-2}	2.4×10^{-2}
$k_{i,TRIS}$ (s^{-1} l mol^{-1})	6.7×10^{-2}	1.1×10^{-1}	4.2×10^{-2}
$k_{i,BICINE}$ (s^{-1} l mol^{-1})	1.0×10^{-2}	2.0×10^{-2}	7.5×10^{-3}
k_{i,NH_3} (s^{-1} l mol^{-1})	4.7×10^{-1}	7.6×10^{-1}	2.5×10^{-1}
$k_{i,OH}$ (s^{-1} l mol^{-1})	8.0×10^2	1.2×10^3	4.0×10^2

a) $1.3\times10^{-3}s^{-1}$ was obtained by polarimetry.

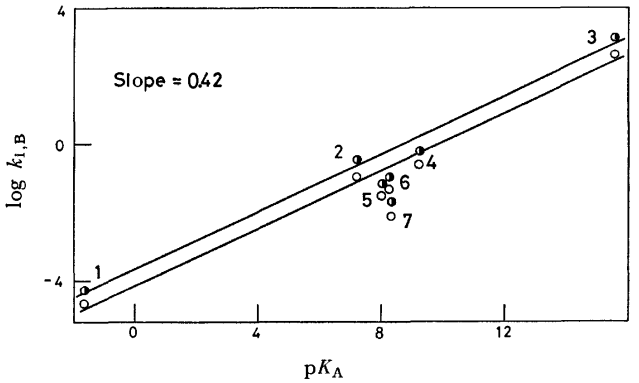

Fig. 8. Brönsted plot for the mutarotation of D-xylose.
◑: k_1, ○: k_2, 1: H_2O, 2: HPO_4^{2-} 3: OH^-, 4: NH_3, 5: TRICINE, 6: TRIS, 7: BICINE.

16) P. P. Rony, *J. Amer. Chem. Soc.*, **91**, 4244 (1969).
17) H. Huang, Adrian N. H. Yeo, and L. H. L. Chiba, *J. Chem. Soc., B* **1969**, 836.
18) G. F. Smith, *ibid.*, **1936**, 1824.
19) L. M. Los and L. B. Simpson, *Rec. Trav. Chim. Pays-Bas.*, **73**, 941 (1954).
20) J. M. Los and L. B. Simpson, *ibid.*, **75**, 267 (1956).
21) J. J. Christensen, J. H. Rytting, and R. M. Izett, *J. Chem. Soc., B* **1970**, 1646.

presented in another paper.[22]

This research was aided in part by a Scientific Reserch Grant from the Ministry of Education, to which the authors' thanks are due.

Appendix

The expression for the instantaneous limiting current, $i(t)$, of an electrode reaction with a preceding chemical reaction;

$$\underset{\text{(chem)}}{A} \underset{k_b}{\overset{k_f}{\rightleftharpoons}} \underset{\text{(el.)}}{Ox} \xrightarrow{ne} Red, \qquad (1')$$

at a stantionary plane electrode has been given by:[8]

$$\frac{i(t)}{nFq} = \frac{D^{1/2}C^*}{\pi^{1/2}(K^2-1)}\left[\frac{K\exp(-lt)-1}{t^{1/2}} + \frac{K^2(\pi k_f)^{1/2}}{(K-1)^{1/2}} \times \exp\left(\frac{k_f t}{K-1}\right)\left\{\operatorname{erf}\left(K\left(\frac{k_f t}{K-1}\right)^{1/2}\right) - \operatorname{erf}\left(\left(\frac{k_f t}{K-1}\right)^{1/2}\right)\right\}\right], \qquad (2')$$

where n indicates the number of electrons involved in the electrode reaction; q, the electrode surface area; D, the diffusion coefficient of the depolarizer; C^*, the sum of the concentrations of A and Ox; $K=k_b/k_f$, and $l=k_f+k_b$.

When $K \gg 1$ and when lt is in the order of unity or less, so that $(k_f t/K)^{1/2} \simeq (lt)^{1/2}/K$, $K\exp(-lt) \gg 1$, $\operatorname{erfc}((lt)^{1/2}/K) \simeq 1$, and $\exp(lt/K^2) \simeq 1$, Eq. (2') may be reduced in a good approximation to:

$$\frac{i(t)}{nFq} = \frac{D^{1/2}C^* l^{1/2}}{K} + \frac{D^{1/2}C^*}{K(\pi t)^{1/2}} \times \exp(-lt) \times \{1-(\pi lt)^{1/2}\exp(lt)\operatorname{erfc}((lt)^{1/2})\} \qquad (3')$$

Accordingly, the mean limiting current, $\bar{i}_l$, at the dropping mercury electrode is given by:

$$\bar{i}_l = \frac{1}{\tau}\int_0^\tau nFq\frac{D^{1/2}C^* l^{1/2}}{K}dt + \frac{1}{\tau}\int_0^\tau nFq\frac{D^{1/2}C^*}{K(\pi t)^{1/2}} \times \exp(-lt)\{1-(\pi lt)^{1/2}\exp(lt)\operatorname{erfc}((lt)^{1/2})\}dt \qquad (4')$$

22) In course of preparation.

The second term on the right-hand side of Eq. (4') could be given in the first approximation for a smaller value of $l\tau$ by:

$$g_2(\tau) = \frac{1-\exp(-l\tau)}{l\tau}\left[\frac{1}{\tau}\int_0^\tau nFq\frac{D^{1/2}C^*}{K(\pi t)^{1/2}}dt - \frac{1}{\tau}\int_0^\tau nFq\frac{D^{1/2}C^*}{K}l^{1/2}\exp(lt)\operatorname{erfc}((lt)^{1/2})dt\right] \qquad (5')$$

Furthermore, according to Matsuda[23] or Koutecký,[24] the second term in the brackets on the right-hand side of Eq. (5') should be replaced by $(\bar{i}_d/K)/(1+1.13(l\tau)^{-1/2})$ for the case of the dropping mercury electrode. In conclusion, the mean limiting current, $\bar{i}_l$, at the dropping mercury electrode may be given by:

$$\bar{i}_l = 0.81\frac{(l\tau)^{1/2}}{K}\bar{i}_d + \frac{\bar{i}_d}{K} \times \frac{1-\exp(-l\tau)}{l\tau} \times \left(1-\frac{1}{1+1.13(l\tau)^{-1/2}}\right) \qquad (6')$$

where $\bar{i}_d$ is the diffusion current given by the Ilkovič equation with the total bulk concentration, C^*.

If we proceed with the reaction scheme (2), $K_\alpha+K_\beta$ and $k_{-1}+k_{-2}$ should be substituted for K and l respectively.[6] we thus obtain Eq. (7'):

$$\bar{i}_l = 0.81\frac{(\tau(k_{-1}+k_{-2}))^{1/2}}{K_\alpha+K_\beta}\bar{i}_d + \frac{\bar{i}_d}{K_\alpha+K_\beta} \times \frac{1-\exp(-\tau(k_{-1}+k_{-2}))}{\tau(k_{-1}+k_{-2})} \times \left(1-\frac{1}{1+1.13(\tau(k_{-1}+k_{-2}))^{-1/2}}\right) \qquad (7')$$

The first term on the right-hand side of Eq. (7') corresponds to $\bar{i}_k$ in Eq. (7), and the second term, to $\bar{i}_{corr}$. It can easily be seen that $\bar{i}_l$ is reduced to $\bar{i}_k$ when $(k_{-1}+k_{-2}) \gg 1$, whereas $\bar{i}_l$ is reduced to $\bar{i}_d/(K_\alpha+K_\beta)$ when $\tau(k_{-1}+k_{-2})$ becomes zero.[9]

23) H. Matsuda and Y. Ayabe, This Bulletin, **28**, 422 (1955).
24) J. Weber and J. Koutecký, *Collect. Czech. Chem. Commun.*, **20**, 980 (1955).

Ultrasonic Absorption in Aqueous Solutions of Octylamine. Kinetic Investigation of Proton Transfer Reaction

Sadakatsu NISHIKAWA, Tatsuya YASUNAGA, and Nobuhide TATSUMOTO

Department of Chemistry, Faculty of Science, Hiroshima University, Higashisenda-machi, Hiroshima 730

(Received December 7, 1972)

The ultrasonic absorption in the mesomorphic state of octylamine water system was characterized by double relaxations. One in the lower frequency range has been explained by the structural relaxation theory of the two state model. In order to clarify the mechanism of the relaxation in the higher frequency range, the ultrasonic absorption in a relatively dilute aqueous solution was measured. The mechanism of the absorption was attributed to hydrolysis from the concentration dependence of the relaxation time. The rate constant k_f for the proton transfer reaction, the equilibrium constant $K=k_b/k_f$, and the standard volume change ΔV resulting from the reaction were determined to be 1.0×10^{10} M^{-1} sec^{-1}, 7.6×10^{-3} M, and 32 cc mol^{-1} respectively.

A large amount of data has been accumulated on the equilibrium properties of aqueous solutions of amines. However, the knowledge of their dynamic properties in the solutions is limited. An ultrasonic absorption method has provided the very useful informations on dynamic properties in the liquid phase. In recent years, the ultrasonic absorptions in aqueous solutions of various amines have been measured and some mechanism associated with the excess absorptions have been proposed.[1-10]

The ultrasonic absorption in the mesomorphic state of octylamine water system is characterized by double relaxations. One in the lower frequency range was explained by the structural relaxation theory of the two state model. The explanation of the other in the higher frequency range remains unclarified.

The purpose of the present investigation is to report the results of the ultrasonic absorption measurement in the relatively dilute aqueous solutions of octylamine, to elucidate the mechanism and to clarify the relation between the excess absorption in the higher frequency range in the mesomorphic state and that in the relatively dilute solutions of octylamine.

In addition, an octylamine water system is one of lyotropic liquid crystals related very closely to biological systems.[11] Clarification of its dynamic properties, therefore, is of interest for understanding the biochemical reactions.

Experimental

The octylamine was of guaranteed grade and purified by distillation. The purity was verified to be higher than 99.9% by the gas chromatography. Deionized and distilled water was used as a solvent. Measurements of ultrasonic absorptions were carried out at odd harmonic frequencies of 0.5, 5, and 20 MHz X-cut quartz transducers by the pulse technique.[12] The frequency range was 2.5—220 MHz. The ultrasonic absorption measurement cell was air-tight and dry nitrogen gas was passed over the solution. The sing-around method was employed at 1.92 MHz to measure the sound velocity. Two kinds of picnometers were used for the measurement of density. The pH values of the solutions were measured by a Hitachi-Horiba Type F-5 pH meter. The temperature range of the ultrasonic absorption measurement was 12—36 °C and the concentration range 0.501—4.76 M.

Results

In general, the sound absorption caused by several relaxation processes is given by

$$\alpha/f^2 = \sum_j \frac{A_j}{1+(f/f_{rj})^2} + B \qquad (1)$$

where f_{rj} is the relaxation frequency for the jth process and A_j and B are constants.

Representative ultrasonic absorption spectra at 3.79

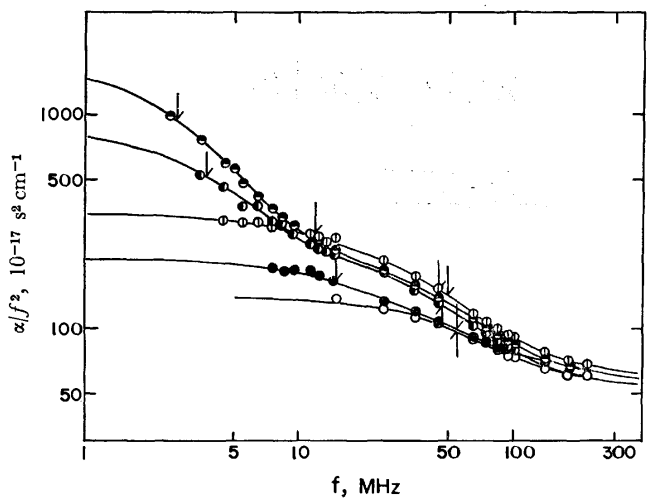

Fig. 1. Representative ultrasonic absorption spectra of the aqueous solution of octylamine at 3.79 M.
The arrows show the relaxation frequency:
◔, 12 °C; ◐, 22 °C; ◕, 30 °C; ●, 35 °C; ○, 36 °C.

1) M. Eigen and L. de Maeyer, "Technique of Organic Chemistry," Vol. VIII, part 2, A Weissberger, Jr., Ed., John Wiley and Sons, Inc., New York N. Y., (1961).
2) G. Maass, Ph. D. Theses, Univ. of Göttingen (1962).
3) M. Eigen, G. Maass, and G. Schwarz, *Z. Phys. Chem.*, **74**, 319 (1971).
4) M. M. Emara, G. Atkinson, and E. Baumgartner, *J. Phys. Chem.* **76**, 334 (1972).
5) H. Inoue, *J. Sci, Hiroshima Univ. Ser. A-II*, **34**, 17 (1970).
6) S. Nishikawa, T. Nakamoto, and T. Yasunaga, This Bulletin **46**, 324 (1973).
7) J. F. McKellar and J. H. Andreae, *Nature*, **195**, 865 (1962).
8) R. N. Barfield and W. G. Schneider, *J. Chem. Phys.*, **31**, 488 (1959).
9) J. H. Andreae, P. D. Edmonds, and J. F. McKellar, *Acustica*, **15**, 74 (1965).
10) S. Nishikawa and T. Yasunaga, This Bulletin, **46**, 1098 (1973).
11) J. L. F. Fergason and G. H. Brown, *J. Amer. Oil. Chem. Soc.*, **45**, 120 (1968).
12) N. Tatsumoto, *J. Chem. Phys.*, **47**, 4561 (1967).

Table 1. Relaxation parameters and density for aqueous solutions of octylamine at 20 °C

M	pH	ρ (g cm^{-3})	c (10^3 m sec^{-1})	f_r (MHz)		A (10^{-17} sec^2 cm^{-1})		B
			In the isotropic state					
0.501	11.47	0.9821	1.475	17.5		100		48.3
0.531	11.47	0.9818	1.474	18		121		46.1
0.782	11.53	0.9736	1.469	19		141		50.7
0.843	11.58	0.9715	1.470	20		130		55.3
0.978	11.74	0.9676	1.464	22		142		51.8
1.300	11.93	0.9597	1.456	27		146		56.5
			In the mesomorphic state					
				f_{r1}	f_{r2}	A_1	A_2	
3.10	—	0.9028	1.447	7	40	231	137	54.2
3.79	—	0.8782	1.456	6	50	346	138	57.6
4.76	—	0.9586	1.459	6	60	518	127	51.8

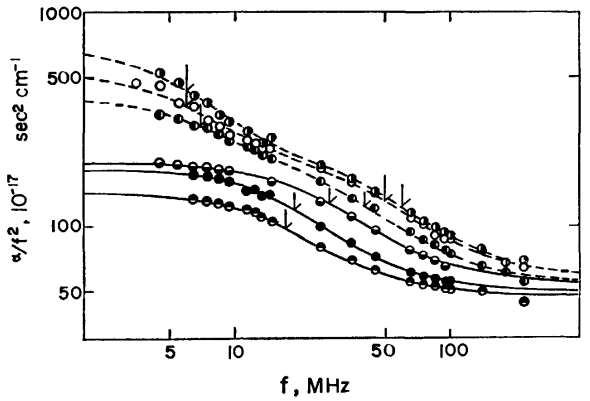

Fig. 2. Ultrasonic absorption in the aqueous solution of octylamine at various concentrations at 20 °C:
◑, 4.76 M; ○, 3.79 M; ◐, 3.10 M; ◒, 1.30 M; ●, 0.782 M; ◓, 0.501 M.

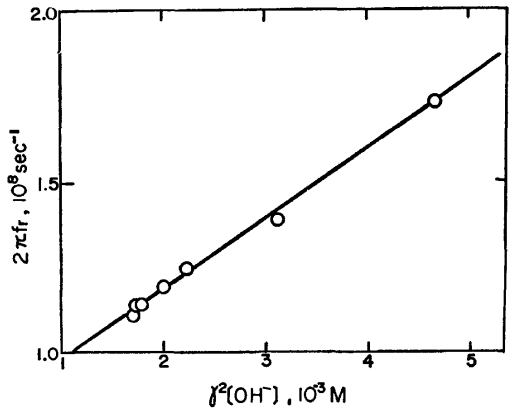

Fig. 3. The plots of $2\pi f_r$ *vs.* concentration at 20 °C. The straight line is a least-squares fit of the experimental points.

M (0.15 mol fraction of octylamine) at various temperatures are shown in Fig. 1. These spectra except one at 36 °C are characterized by double relaxations which correspond to the case of $j=1, 2$ in Eq. (1). The spectrum at 36 °C is described by the single relaxation equation which is the case $j=1$ in Eq. (1). The mesomorphic state of the octylamine water system is transformed to the isotropic one by heating. Since the transition temperature from mesomorphic to isotropic state is 35 °C at 3.79 M, the spectrum at 36 °C is that in the isotropic state. The excess absorption in the lower frequency range decreases abruptly as soon as the phase changes into the isotropic state, but that in the higher frequency range remains even in the isotropic state. The ultrasonic absorption spectra at various concentrations at 20 °C are shown in Fig. 2. The dashed lines are the spectra in the mesomorphic state, characterized by double relaxations. The solid lines are those for the relatively dilute solutions in the isotropic state, characterized by single relaxation. The values of relaxation frequency f_{rj} and constants A_j and B were determined so as to obtain the best fit of the data to Eq. (1). The values are listed in Table 1 together with the observed values of the sound velocity and density.

If the mechanism of the excess absorption in the relatively dilute solutions is attributed to the perturbation of the equilibrium[1-6]

$$R\text{-}NH_3^+ + OH^- \underset{k_b}{\overset{k_f}{\rightleftharpoons}} R\text{-}NH_2 + H_2O \qquad (2)$$

where k_f and k_b are forward and backward rate constants respectively, the relation between the relaxation frequency and the rate constants is given by

$$1/\tau = 2\pi f_r = k_f([R\text{-}NH_3^+]+[OH^-])\Pi\gamma_i + k_b \qquad (3)$$

where τ is relaxation time and γ_i an activity coefficient of species i. If the activity coefficient and concentration of $R\text{-}NH_3^+$ ion are equal to those of OH^- ion respectively at each concentration, Eq. (3) can be written as

$$1/\tau = 2\pi f_r = 2k_f\gamma^2[OH^-] + k_b \qquad (4)$$

where γ is the mean activity coefficient. The activity coefficients were calculated by the Davies equation[13]

$$-\log\gamma = 0.5\left[\frac{\sqrt{I}}{1+\sqrt{I}} - 0.3I\right] \qquad (5)$$

where I is the ionic strength. Figure 3 shows the plots of $2\pi f_r$ *vs.* $\gamma^2[OH^-]$. The forward and backward rate constants were determined from the slope and inter-

13) C. W. Davies, "Ion Association," Butter Worths, London (1962).

Table 2. Rate and equilibrium constants and standard volume change at 20°C

System	k_f (M^{-1} sec^{-1})	k_b (sec^{-1})	K (M)	ΔV (cc mol^{-1})	Reference
$NH_4^+ + OH^- \rightleftarrows NH_3 + H_2O$	3.6×10^{10}	6.0×10^{5}	1.7×10^{-5}	26.8	(2) (3)
$CH_3NH_3^+ + OH^- \rightleftarrows CH_3NH_2 + H_2O$	3.7×10^{10}	1.6×10^{7}	4.2×10^{-4}	26.1	(2) (3)
$(C_2H_5)NH_3^+ + OH^- \rightleftarrows (C_2H_5)NH_2 + H_2O$	3.2×10^{10}	1.4×10^{7}	4.7×10^{-4}	24.3	(2) (3)
$(C_3H_7)NH_3^+ + OH^- \rightleftarrows (C_3H_7)NH_2 + H_2O$	3.0×10^{10}	1.2×10^{7}	4.0×10^{-4}	24.0	(2)
$(C_4H_9)NH_3^+ + OH^- \rightleftarrows (C_4H_9)NH_2 + H_2O$	4.1×10^{10}	1.1×10^{8}	2.5×10^{-3}	32	(6)
$(C_8H_{17})NH_3^+ + OH^- \rightleftarrows (C_8H_{17})NH_2 + H_2O$	1.0×10^{10}	7.6×10^{7}	7.6×10^{-3}	32	this work

cept, respectively, by the least-mean-squares method. The standard volume change ΔV resulting from the reaction could be determined as follows. The excess absorption per wavelength shows a maximum at a frequency $f=f_r$ and is given by

$$(\alpha\lambda)_{max} = \frac{1}{2}Af_r c \tag{6}$$

where $(\alpha\lambda)_{max}$ is the maximum excess absorption per wavelength and c the velocity of sound. For a chemical process of the type represented by Eq. (2), the maximum excess absorption per wavelength is given by

$$(\alpha\lambda)_{max} = \frac{1}{2}\pi\rho c^2V^2RT\Gamma_c\left\{\left(\frac{\beta\Delta H}{C_pRT}\right)-\left(\frac{\Delta V}{VRT}\right)\right\}^2 \tag{7}$$

$$\Gamma_c = \left(\frac{1}{[OH^-]}+\frac{1}{[R\text{-}NH_3^+]}+\frac{1}{[R\text{-}NH_2]}\right)^{-1} \tag{8}$$

where ρ is density, V the molar volume, R the gas constant, β the thermal expansion coefficient, C_p the specific heat at constant pressure, and T the absolute temperature. In the case of a relatively dilute solution of amine, the first term in the bracket of Eq. (7) is negligibly small compared with the second term. The standard volume change resulting from the hydrolysis of octylamine was calculated by means of Eqs. (6) and (7). The values of rate constants, equilibrium constant, and standard volume change are listed in Table 2 together with those for other monoamines.

Since the aqueous solution of octylamine is separated into two phases below 0.5 M at 20 °C, measurements were impossible below 0.5 M.

Discussion

The excess absorption mechanism in the mesomorphic state in the higher frequency range can not be interpreted quantitatively since the ionic concentration in that state is not determined accurately. However, excess absorption is observed even in the isotropic state as is seen in Fig. 1 and the relaxation frequencies seem to increase continuously with concentration as is seen in Fig. 2. The mechanism of the excess absorption in the mesomorphic state is therefore regarded to be identical with that in the relatively dilute solution. The linearity of the plots of $2\pi f_r$ *vs.* $\gamma^2[OH^-]$ in Fig. 3 indicates that the cause of the excess absorption is attributed to the perturbation of the equilibrium given by Eq. (2). The value of the rate constant k_f obtained is pertinent to the proton transfer reaction, since it is, in general, of the order 10^{10}—10^{11} M^{-1} s^{-1}. However, the equilibrium constant determined by the

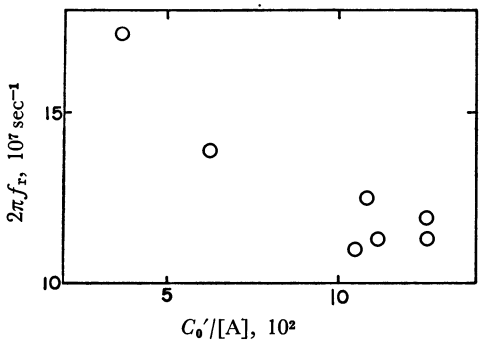

Fig. 4. The plots of $2\pi f_r$ *vs.* C_0'/[A] at 20 °C.

relation $K=k_b/k_f$ does not agree with the value reported 4.5×10^{-4} M at 25 °C[14] which was obtained in various dilutions of alcohol such as to permit satisfactory extrapolation to pure water in a concentration less than 0.016 M because of the limited solubility of octylamine in water. Since our investigation was carried out in concentrations higher than 0.5 M, a comparison of the results may not be suitable.

The process of hydrolysis of amine[3] is not so simple as that expressed by Eq. (2). It proceeds through a complex formation by hydrogen bonding as follows

$$R\text{-}NH_3^+ + OH^- \underset{k_{21}}{\overset{k_{12}}{\rightleftharpoons}} R\text{-}NH_3^+\cdots$$

$$OH^- \underset{k_{32}}{\overset{k_{23}}{\rightleftharpoons}} R\text{-}NH_2 + H_2O \tag{9}$$

Under the conditions[3] of $k_{23}\gg k_{21}$, the rate constants in Eq. (2) are expressed as follows

$$k_f = k_{12}, \quad k_b = k_{21}\frac{k_{32}}{k_{23}} \tag{10}$$

Consequently, the collision frequency of reaction partners, $R\text{-}NH_3^+$ and OH^- ions, might affect the magnitude of the rate constant k_f. The octylamine molecule consists of a long hydrophobic chain and a small hydrophilic group, *viz.*, the reaction site might be so small compared with the size of the molecule. Therefore, the effective collision frequency for the reaction might decrease. As is seen in Table 2, the rate constant k_f for octylamine is small compared with those for other monoamines.[2,3]

The excess absorption mechanism attributed to the perturbation of the equilibrium expressed as $nA \underset{k_2}{\overset{k_1}{\rightleftharpoons}} A_n$

14) C. W. Hoerr, M. R. McCorkle, and A. W. Rals, *J. Amer. Chem. Soc.*, **65**, 328 (1943).

by McKellar and Andreae[7] should be reconsidered. The relation between relaxation time and concentration for this mechanism is derived as follows.

$$1/\tau = 2\pi f_r = -k_2(n-1) + nk_2C_0'/[A] \quad (11)$$

where n is the aggregation number, [A] the concentration of monomer, k_2 the rate constant and $C_0' = [A]+n[A_n]$. If the cause of the excess absorption were attributed to the association-dissociation reaction, the plots of $2\pi f_r$ *vs.* $C_0'/[A]$ should be a straight line with a positive slope and a negative intercept according to Eq. (11). However, the results do not obey Eq. (11), *viz.*, the plots of $2\pi f_r$ *vs.* $C_0'/[A]$ seems to have a negative slope and positive intercept as is shown in Fig. 4. The mechanism due to the aggregation reaction might, therefore, be ruled out as that of the excess absorption.

BULLETIN OF THE CHEMICAL SOCIETY OF JAPAN, VOL. 46, 1660—1663 (1973)

Dielectric Behavior of the Packing Bed of Alumina Granules with Adsorbed Water

Kaoru UMEYA and Takashi KANNO

Department of Chemical Engineering, Faculty of Engineering, Tohoku University, Aramaki-Aoba, Sendai 980

(Received December 16, 1971)

Dielectric behavior of the packing bed of alumina granules with various amounts of adsorbed water were determined in the frequency range 30 Hz—3 MHz. The dielectric relaxations characterized by a distribution in relaxation time were attributed to interfacial polarizations due to the adsorbed ions accumulated around the non-conductive points (*i.e.*, discontinuous points on conducting paths consisting of water films adsorbed on alumina granules). Some of the adsorbed ions were carried away to the electrodes through the points of contact between the water films adsorbed on granules adjacent to each other (*i.e.*, continuous conducting paths), giving rise to d.c. conductance and electrode polarization. When insulating sheets were inserted between the electrodes and surfaces of the packing bed, both the d.c. conductance and electrode polarization disappeared and another dielectric relaxation was observed. This was attributed to the interfacial polarization due to the ions accumulated at the interfaces between insulating sheets and water adsorbed on alumina granules.

Dielectric studies of water adsorbed on inorganic oxides have been made.[1,2] In order to study the mechanism of adsorption of water vapor and the nature of the adsorbed water, dielectric isotherms have frequently been determined for several frequencies.[3,4] With increasing amounts of adsorbate, contribution of adsorbed ions becomes significant and dielectric relaxations due to the interfacial polarizations are observed if measurements are made over a wide frequency range.[5-7] However, their mechanism has not been discussed in detail.

In the present study we discuss the mechanism of dielectric relaxations observed for the packing bed of alumina granules with adsorbed water. Since such a system is an assembly of individual granules, the dielectric properties as well as electrical conductance are affected by packing conditions of alumina granules. The results also change with the conditions of the contact of the specimen with electrode, since electrical conduction can be prevented if the contact is incomplete. For the sake of confirmation measurements were also made on a system in which electrical conduction was prevented by inserting polyethylene sheets (0.07 mm in thickness) between the electrodes and surfaces of the packing bed. The dependence of dielectric properties upon particle size was also studied.

Experimental

Alumina granules, spherical particles of porous alumina granules containing 10% silica "Neobead D" supplied from Mizusawa Chemical Engineering Co., Ltd. were used. Their specific surface area is 300 m^2/g. True density and packing density are 3.10 and 0.5—0.6 g/cm^3, respectively. Granules of two different particle size, *i.e.*, about 0.3 mm and 1.0 mm in diameter, were used.

A Type TR-1B Transformer Bridge from Ando Electric Company was employed for measurements of capacitance and conductance over the frequency range 30 Hz—3 MHz.

Results and Discussion

Dielectric Constant and Dielectric Loss. Dielectric constant ε' and dielectric loss ε'' measured on the packing bed of alumina granules with adsorbed water are plotted against frequency in Fig. 1, and compared with those of the specimen with insulating sheets inserted between the electrodes and surfaces of the packing bed. The dielectric loss of the specimen without insulators was obtained by subtracting the d.c. conductance.

In the lower frequency range the dielectric constant

1) R. L. McIntosh, "Dielectric Behavior of Physically Adsorbed Gases", Marcel Dekker, Inc., New York (1966).
2) S. S. Dukhin, "Surface and Colloid Science," Vol. 3, ed. by E. Matijevic, Wiley-Interscience, New York (1971), p. 83.
3) M. G. Baldwin and J. C. Morrow, *J. Chem. Phys.*, **36**, 1591 (1962).
4) N. K. Nair and J. M. Thorp, *Trans. Faraday Soc.*, **61**, 962, 975 (1965).
5) P. G. Hall and G. K. Kouvarellis, *ibid.*, **64**, 1940 (1968).
6) S. M. Nelson, H. H. Huang, and L. E. Sutton, *ibid.*, **65**, 225 (1969).
7) E. McCafferty, V. Pravdic, and A. C. Zettlemoyer, *ibid.*, **66**, 1720 (1970).

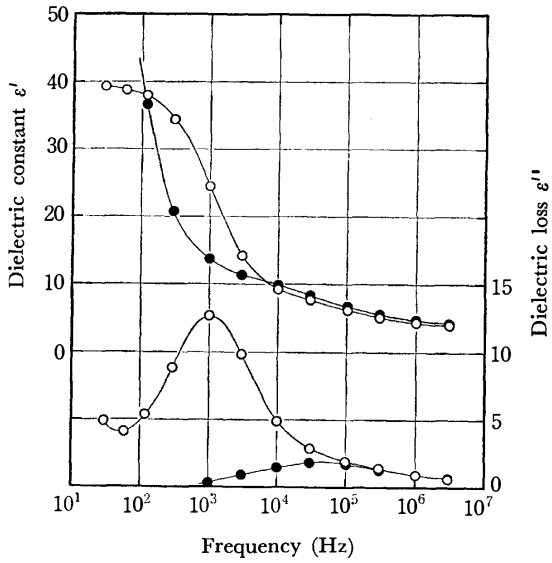

Fig. 1. Frequency dependence of dielectric constant and dielectric loss at 30 °C. Amount of water adsorbed: 200 mg/g. Particle diameter: 0.3 mm.
○: measured with insulating sheets.
●: measured without insulating sheets.

of the specimen with no insulating sheets increased rapidly with decreasing frequency. This can be attributed to the electrode polarization which arises from the electrolytic polarization of ions on electrode surfaces. In the same frequency range the dielectric constant of the specimen with insulating sheets had a tendency to reach a plateau with decreasing frequency accompanied by a distinct peak in the dielectric loss curve. This can be attributed to the dielectric relaxation due to the interfacial polarization which arises from the ions accumulated at the interfaces between insulating sheets and water adsorbed on alumina granules.

In a higher frequency range the dielectric constants of both specimens decreased gradually with increasing frequency. The dielectric dispersion can be attributed to the interfacial polarizations which arise from the adsorbed ions within the packing bed of alumina granules. A well-defined peak in the dielectric loss curve was observed for the specimen without insulating sheets, whereas in the case of that with insulators no distinct peak was found. It can be seen, however, that the dielectric loss curve of the specimen with insulating sheets almost coincides with that of the specimen without insulators in frequency range above 100 kHz.

Complex Plane Plots of ε' and ε''. The complex plane plots of ε' and ε'' measured on the specimen without insulators gave a circular-arc as shown in Fig. 2. Thus the complex dielectric constant of the packing bed of alumina granules with adsorbed water is represented approximately by the following equation:[8,9]

$$\varepsilon^* = \varepsilon_h + \frac{\varepsilon_l - \varepsilon_h}{1+(i\omega\tau)^\beta} + \frac{\kappa_1}{i\omega\varepsilon_v} \qquad (1)$$

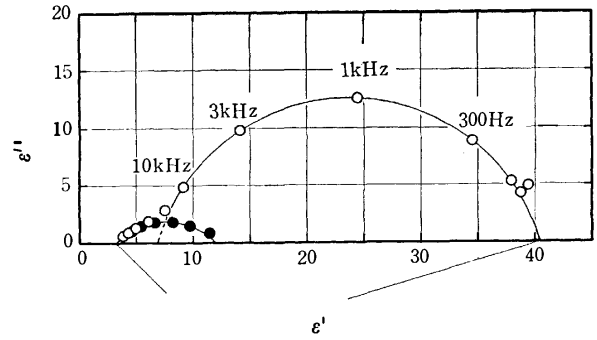

Fig. 2. Complex plane plots of ε' and ε''. Amount of water adsorbed: 200 mg/g. Particle diameter: 0.3 mm.
○: measured with insulating sheets.
●: measured without insulating sheets.

where ε_h and ε_l are the limiting dielectric constants at high and low frequencies, respectively; κ_1 is the limiting conductivity at low frequency (*i.e.*, d.c. conductivity) subtracted in calculating the dielectric loss; $\omega(=2\pi f)$ measuring angular frequency, $\tau(=1/2\pi f_0)$ mean relaxation time, f and f_0 measuring frequency and relaxation frequency for which the dielectric loss is a maximum, respectively; β parameter for the distribution of relaxation times, and $\varepsilon_v=8.8541\times10^{-14}$ F/cm and $i=\sqrt{-1}$.

In the case of the specimen with insulating sheets a large circular-arc corresponding to the relaxation in low frequencies was observed. Several plots in the high frequency range deviate from the ciruclar-arc and lie on that of the specimen without insulators. The tail appearing on the circular-arc reveals the presence of another dielectric relaxation in the high frequency range, which seems to be the same relaxation as that of the specimen without insulators. The complex dielectric constant of the specimen with insulating sheets, therefore, can be expressed by the following equation:

$$\varepsilon^* = \varepsilon_h + \frac{\varepsilon_l - \varepsilon_h}{1+(i\omega\tau_1)^\beta} + \frac{\varepsilon_l - \varepsilon_i}{1+(i\omega\tau_2)^\alpha} \qquad (2)$$

where ε_h, ε_l and ε_i denote the values of limiting dielectric constants at high and low frequencies and at an intermediate plateau, respectively; τ_1 and τ_2 are the mean relaxation times of polarizations at high and low frequencies, respectively; β and α are parameters for the distribution of relaxation time of individual polarization.

Since the relaxations in high and low frequencies overlapped partially, no distinct corresponding circular-arcs were observed. The circular-arc in low frequencies (Fig. 2) might not represent the one corresponding to the relaxation in low frequencies precisely, but involves a part of relaxation in high frequencies.

The dielectric relaxations overlapping each other were separated into two individual ones. The circular-arc corresponding to the relaxation at high frequencies was first drawn with respect to that of the specimen without insulators (broken line, Fig. 3). From this the numerical values of the first and second terms of the right side in Eq. (2) were determined. The dielectric constants and dielectric losses calculated by

8) T. Hanai, "Emulsion Science," ed. by P. Sherman, Academic Press, London and New York (1968), p. 354.
9) K. S. Cole and R. H. Cole, *J. Chem. Phys.*, **9**, 314 (1941).

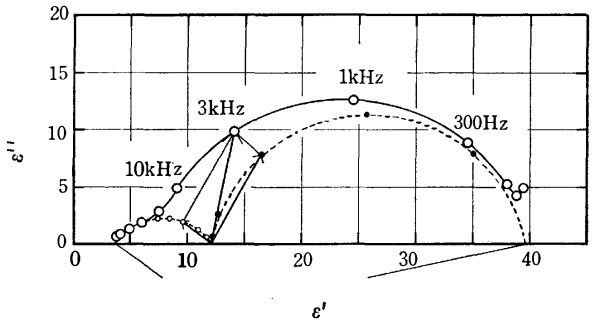

Fig. 3. Complex plane plots of ε' and ε'' separated into two individual circular-arcs (broken curve).

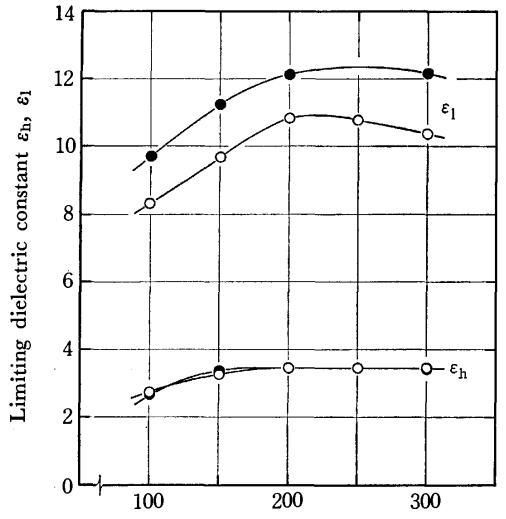

Fig. 4. Limiting dielectric constants ε_h, ε_l as a function of amount of adsorbed water. Particle diameter: 1.0(○), 0.3(●) mm.

use of this equation are plotted with open circles.

The dielectric constants of the relaxation in low frequencies can be obtained by adding the values equal to the dielectric decrements due to relaxation in high frequencies to those observed. The dielectric loss of relaxation in low frequencies can also be obtained by subtracting the values due to relaxation in high frequencies from those observed. The complex plane plots obtained by use of these values are shown by a broken line with full circles. These procedures can also be expressed in vector form (Fig. 3).

A similar behavior to that mentioned above was observed in different amounts of adsorbed water for both the specimens with and without insulating sheets.

For the specimen without insulators, dielectric measurements were also carried out on granules of about 1.0 mm in diameter. The experimental values of the parameters in Eq. (1) will be discussed in detail.

Limiting Dielectric Constants: The limiting dielectric constants at high and low frequencies ε_h and ε_l, respectively, are plotted against the amounts of adsorbed water in Fig. 4. The values of ε_h and ε_l increased first with increasing amount of adsorbed water, but for higher water content, the value of ε_l decreased with the increase of the amount of adsorbed water, and that of ε_h remained almost constant.

Murphy and Lowry proposed a mechanism of dielectric polarization for "Interstitial Conducting Systems."[10] The electrical conduction of moistened dielectrics takes place through interstitial conducting paths of water film containing ions in a certain concentration. The ions near the surface are adsorbed so strongly that they cannot be detached under the effect of an external field but can be displaced along the surface, giving rise to polarization.

Miles and Robertson,[11] and Schwarz[12] extended the Wagner theory[13] to a dispersed system of spherical particles with electrical double layer.

However, these theories cannot interpret the decrease of the values of ε_l observed in a large amount of adsorbed water. The dielectric relaxations observed in this study might be attributed to the interfacial polarization which arises from the ions accumulated around the non-conductive gaps between water films adsorbed on the granules adjacent to each other, *i.e.*, discontinuous points on conducting paths. At a higher water content these gaps are bridged with water films and the ions accumulated may be carried away to the electrode through the points of contact, giving rise to d.c. conductance and electrode polarization. Thus in higher water contents the values of ε_l decrease with increasing amount of adsorbed water.

The values of ε_l also change with particle size as shown in Fig. 4. This may be interpreted by the difference in number of non-conductive points. The packing bed of small granules may be expected to have a large number of non-conductive points, resulting in an increase in the value of ε_l.

The values of ε_h corresponding to polarization due to the ions strongly adsorbed were not affected by particle size. This is understandable since the specific surface area of the granules do not change with the difference in particle size as they have a porous structure.

Mean Relaxation Frequency: The mean relaxation frequency f_0 is plotted in Fig. 5 as a function of the

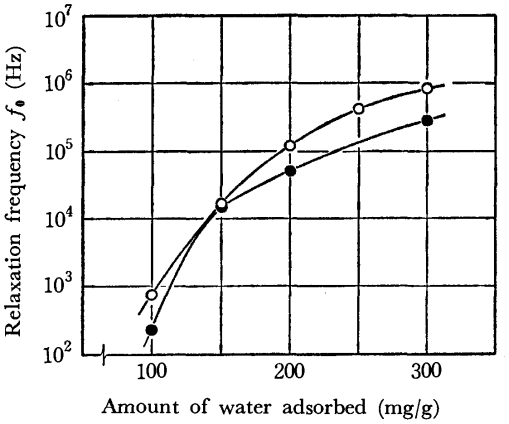

Fig. 5. Mean relaxation frequency f_0 as a function of amount of adsorbed water. Paticle diameter: 1.0(○), 0.3(●) mm.

10) E. L. Murphy and H. H. Lowry, *J. Phys. Chem.*, **34**, 598 (1930).
11) J. B. Miles and H. R. Robertson, *Phys. Rev.*, **40**, 583 (1932).
12) G. Schwarz, *J. Phys. Chem.*, **66**, 2636 (1962).
13) K. W. Wagner, *Arch. Elektrotech.*, **2**, 371 (1914).

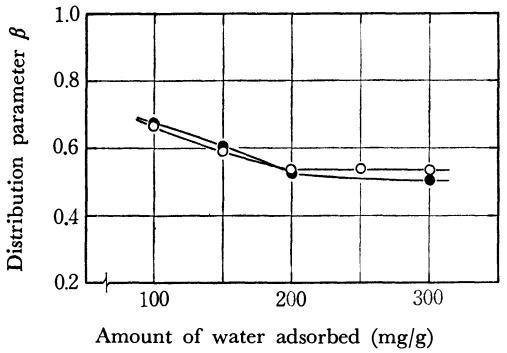

Fig. 6. Distribution parameter β as a function of amount of adsorbed water. Particle diameter: 1.0(○), 0.3(●) mm.

amount of water adsorbed. The increase in the value of f_0 with increasing adsorbate can be attributed to the formation of weakly adsorbed layers. The decrease in the rate of increase of f_0 in a higher water content can be attributed to the saturation or decrease in the polarization described above.

The mean relaxation frequency increases with the increase of particle size. This can be interpreted in terms of the difference in geometrical surface area as well as the difference in number of non-conductive points. As the particle size increases geometrical surface area decreases, and the effect of surface becomes smaller for the same water content.

Distribution Parameter: The distribution parameter β is plotted in Fig. 6 as a function of the amount of adsorbate. Decrease in the value of β at low water content can be interpreted in terms of the increase in polarization with a small relaxation time. For water content above 200 mg/g the value of β remained almost constant irrespective of the amount of adsorbate. This is attributed to the saturation or decrease in polarization. The value of β was not affected by particle size (Fig. 6).

Table 1. Values of ε_h, ε_l, ε_l, f_{01}, f_{02}, β and α in various amounts of water adsorbed on alumina

Amount adsorbed (mg/g)	ε_h	ε_l	ε_l	f_{01} (kHz)	f_{02} (kHz)	β	α
100	2.9	10.1	—	0.56	—	0.733	—
200	3.6	12.1	39.8	16.8	1.1	0.628	0.872
300	3.5	11.5	38.7	224	8.5	0.600	0.922

The results observed for the specimen with insulating sheets are shown in Table 1.

The limiting dielectric constants ε_h and ε_l, the mean relaxation frequency f_{01} and the distribution parameter β for the specimen with insulating sheets were almost coincident with those of the specimen without insulators. The limiting dielectric constant at low frequency ε_l and the mean relaxation frequency f_{02} can be explained by means of the Maxwell theory of a stratified model.[8] The distribution in relaxation time can be attributed to the heterogeneity in limiting conductivity at low frequency κ_l observed for the specimen without insulators.

BULLETIN OF THE CHEMICAL SOCIETY OF JAPAN, VOL. 46, 1663—1667 (1973)

Kinetics of the Reaction at the Silver–Silver Sulfide Interface

Junichiro MIZUSAKI, Kazuo FUEKI, and Takashi MUKAIBO

Department of Industrial Chemistry, Faculty of Engineering, The University of Tokyo, Hongo, Bunkyo-ku, Tokyo 113

(Received August 30, 1972)

The reaction rate at the Ag/Ag_2S interface was determined as a function of silver activity of Ag_2S in the temperature range 215—400 °C. The silver activity of Ag_2S at the interface was measured electrochemically by means of an Ag/AgI electrode. The reaction rate was measured by the direct sulfurization method (Wagner's pellet method) and by Rickert's method using $Ag/AgI/Ag_2S/Pt$ cell. The rates obtained by the two methods were in good agreement. It was found that this is a first-order reaction with respect to the activity of sulfur in Ag_2S and that the rate equation is given by

$$v = 1.0 \times 10^4 \{\exp(-18000/RT)\} a_S \text{ eqv cm}^{-2}\text{ s}^{-1} \quad \text{(i)}$$

The following reaction mechanism prevails at the interface.

$$2Ag(Ag) + S(Ag_2S) \longrightarrow 2Ag^+(Ag_2S) + S^{2-}(Ag_2S) \quad \text{(ii)}$$

Solid state reactions such as oxidation or sulfurization of metals or formation of spinels involve a solid–solid interface reaction as an elementary process. Because of the fact that the rate of reaction at a solid–solid interface is much higher than that of diffusion in a solid phase, the solid–solid interface reaction has not been studied kinetically yet. However, a few systems have been found recently in which the solid–solid interface reaction has an effect on the overall reaction rate.

Rickert and his co-workers showed that the sulfurization of silver is a mixed controlled reaction of three elementary processes, *i.e.*, reaction at the Ag/Ag_2S interface, diffusion in Ag_2S, and reaction at the $Ag_2S/S(g)$ interface. They tried to measure the reaction rate at the Ag/Ag_2S interface quantitatively by the coulometric titration method.[1-3] Schmalzried and his collaborators studied the formation of spinels,

1) H. Rickert, *Z. Phys. Chem., N. F.*, **23**, 355 (1960).
2) H. Rickert and C. D. O'Briain, *ibid.*, **31**, 71 (1962).
3) H. Rickert and K. H. Tostmann, *Werkstoffe und Korrosion* **21**, 965 (1970).

such as $ZnAl_2O_4$, from their constituent oxides, and discussed the influence of the reactions at the ZnO/$ZnAl_2O_4$ and $ZnAl_2O_4/Al_2O_3$ boundaries on the overall reaction rate.[4,5] Leute and Kalb investigated the interdiffusion for the system (Hg, Cd)Te/(Hg, Cd)Se, and discussed the influence of the interface reaction in the initial stage.[6] In these investigations, however, no quantitative treatment was performed.

The present study was undertaken to investigate the reaction at the Ag/Ag_2S interface kinetically.

Experimental

In order to obtain the reaction rate as a function of the silver activity of silver sulfide at the solid-solid interface, the direct sulfurization method (Wagner's pellet method[1,7]) and Rickert's coulometric titration method[2] were used.

Direct Sulfurization Method. A schematic diagram of the experimental arrangement is shown in Fig. 1. The sulfurization rate of silver by liquid sulfur was determined from the growth rate of the sulfide layer. The silver activity of silver sulfide at the interface was measured electrochemically with an Ag/AgI electrode. The rate equation was determined from the sulfurization rate and silver activity at the interface.

The essential part of the apparatus for the direct sulfurization method is shown in Fig. 2. A silver cylinder (10 mm in diameter) with a small hole (1.5 mm in diameter) along its axis was fabricated from a silver rod (99.9% pure). The surface in contact with the Ag_2S pellet was polished with No. 1000 emery papers and 0.3 μ alumina polishing powder. A compact silver sulfide rod (10 mm in diameter) prepared by direct sulfurization of the silver rod was sliced into pellets about 0.5 mm in thickness. The pellets were also polished to attain good contact with the silver cylinder. Sulfur of reagent grade was purified several times by distillation.

The Ag/AgI electrode consisting of a silver wire (0.2 mm in diameter) and silver iodide of reagent grade was assembled in a small alumina tube of 1.2 mm in outer diameter. The electrode was placed in the hole of the silver cylinder with its upper edge in contact with the Ag_2S pellet near the Ag/Ag_2S interface. A pyrex tube, with inner diameter 6—8 mm was used to press the Ag_2S pellet and to hold liquid sulfur in it. In order to assure good contact between the cylinder and the Ag_2S pellet, a pressure of about 3 kg/cm^2 was applied by a spring or weight through the pyrex tube.

An electric furnace was constructed by winding nichrome wires around the pyrex tube in order to follow the growth of Ag_2S layer continuously from the outside by means of a cathetometer. The reaction temperature was controlled by an electric controller within ± 1 °C. Measurements were performed in purified nitrogen atmosphere.

Coulometric Titration Method. The coulometric titration method was originated by Rickert and O'Briain.[2] The principle is schematically shown in Fig. 3. When a potential difference is given between Ag(II) and Ag_2S, silver is removed from Ag_2S to Ag(II) in the form of Ag^+ ions and electrons. Namely, Ag^+ ions are transported through the AgI pellet since silver iodide is a pure ionic conductor, and electrons are removed from Ag_2S to Ag(II) through a Pt wire. The rate of silver removal can thus be measured as an electric current by means of an ammeter A. As silver

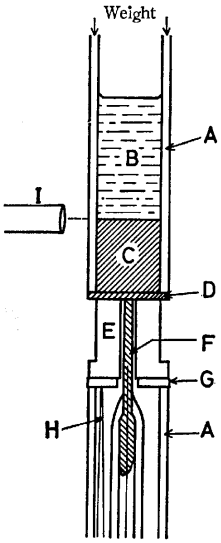

Fig. 2. Apparatus for direct sulfurization method.
(A) Pyrex tube (B) Liquid sulfur
(C) Ag_2S formed (D) Ag_2S pellet
(E) Ag cylinder (F) Ag/AgI electrode
(G) Pt electrode (H) Thermocouple
(I) Cathetometer

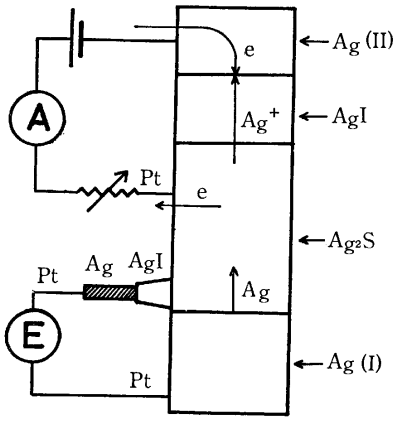

Fig. 3. Schematic diagram of coulometric titration method.

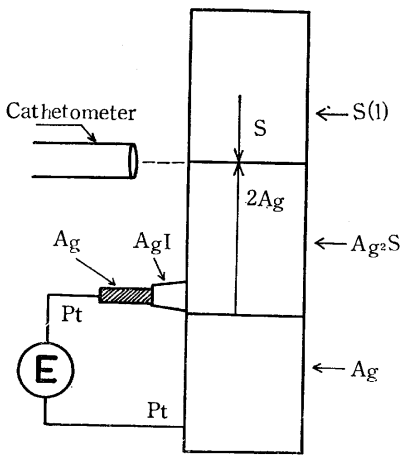

Fig. 1. Schematic diagram of direct sulfurization method.

4) H. Schmalzried, *Ber. Dtsch. Keram. Ges.*, **42**, 11 (1965).
5) C. A. Duckwitz and H. Schmalzried, *Z. Phys. Chem., N. F.*, **76**, 173 (1971).
6) V. Leute and A. Kalb, *J. Phys. Chem. Solids*, **33**, 417 (1972).
7) C. Wagner, *Z. Phys. Chem., B*, **21**, 25 (1933).

is removed from Ag_2S to Ag(II), an equivalent amount of silver goes into the Ag_2S pellet across the Ag(I)/Ag_2S interface. When a steady state is established, the rate of reaction at the Ag(I)/Ag_2S interface is equal to that of removal of silver from the Ag_2S pellet. The silver activity of silver sulfide is measured electrochemically by means of an Ag/AgI electrode. An Ag_2S pellet of about 2 mm in thickness was used. The AgI pellet was prepared by pressing silver iodide powder of reagent grade in a die under the pressure of 7 t/cm^2. The pellet was 10 mm in diameter and about 7 mm in thickness. The electric furnace and other experimental apparatus were almost the same as those used in the direct sulfurization method.

Results

Direct Sulfurization Method. A typical result is shown in Fig. 4. E(mV) is the potential drop at the Ag/Ag_2S interface and x(mm) the thickness of the silver sulfide layer formed. The reaction rate v(eqv cm^{-2} s^{-1}) was calculated by the graphical differentiation of x-time curves. The silver activity of Ag_2S, a_{Ag}, is related to E as follows:

$$\log a_{Ag} = -\frac{EF}{2.3RT} \quad (1)$$

where F is the Faraday constant. The activity of metallic silver is taken as unity.

The plots of $\log v$ *vs.* $\log a_{Ag}$ were obtained at 250, 300, 340, and 400 °C by the direct sulfurization method.

Coulometric titration method. Fig. 5 shows the time dependence of E when silver was removed from Ag_2S to Ag(II) at constant currents. The reaction rate v(eqv cm^{-2} s^{-1}) was calculated from the electric current and the area of the Ag/Ag_2S interface. We see that the steady state was attained in a short time when the reaction rate was high.

The plots of $\log v$ *vs.* $\log a_{Ag}$ are given by open circles and solid lines in Fig. 6. Circles show the experimental average values. Empirical solid lines were calculated by the method of least-squares, bars showing the standard deviation from the solid line. The slope of the line is -1.9 ± 0.3, -2.1 ± 0.3, -2.3 ± 0.3, and -2.2 ± 0.6 for the temperatures 215, 250, 300, and 350 °C, respectively. Because of the difficulty in attaining a reproducible good contact between silver and silver sulfide, scattering of the experimental values could not be noticeably reduced.

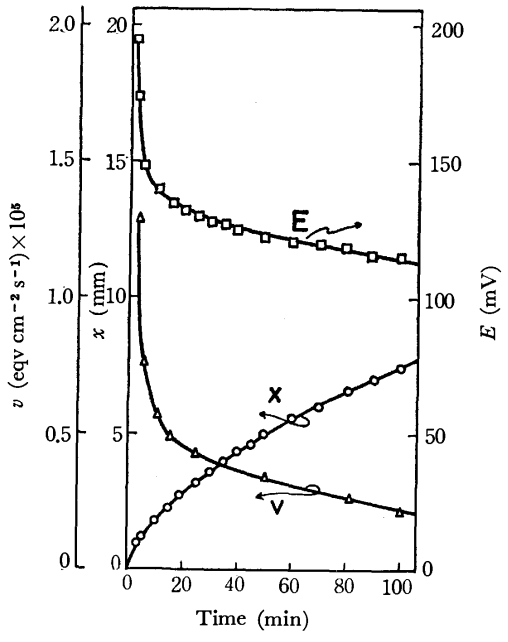

Fig. 4. Change of E, v, and x with time at 300 °C; direct sulfurization method.

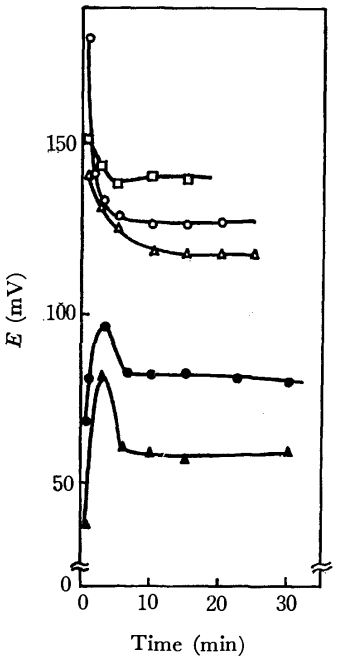

Fig. 5. Change of E with time at 300 °C; coulometric titration method.
□: 4.0×10^{-6} eqv cm^{-2} s^{-1} ○: 2.0×10^{-6} eqv cm^{-2} s^{-1}
△: 1.0×10^{-6} eqv cm^{-2} s^{-1} ●: 2.0×10^{-7} eqv cm^{-2} s^{-1}
▲: 1.0×10^{-7} eqv cm^{-2} s^{-1}

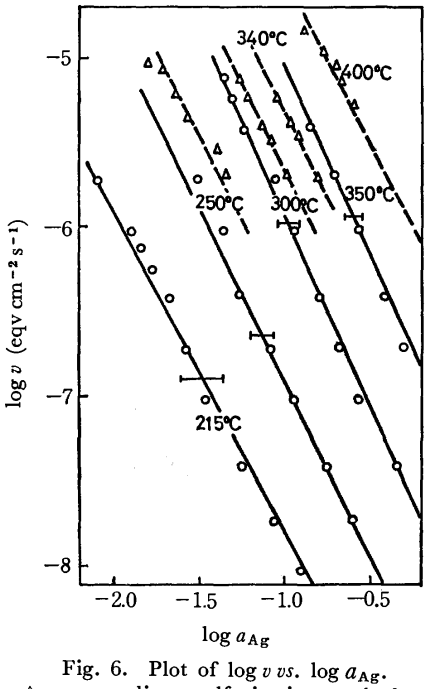

Fig. 6. Plot of $\log v$ *vs.* $\log a_{Ag}$.
△, ----; direct sulfurization method.
○, ——; coulometric titration method.

The results obtained by both methods are in fairly good agreement (Fig. 6).

Rickert and his co-workers showed that the relation between log v *vs.* log a_{Ag} is not linear at 220 and 300 °C, but we found a linear relation.

Discussion

Mechanism. Kobayashi and Wagner[8] studied the reduction of Ag_2S by H_2 at 300 °C and obtained the rate of reduction at the gas-solid interface as a function of a_S. They proposed three mechanisms wherein S, S^-, S^{2-}, and electrons are reactants in solid phase. If the same reactants take part in the reaction between silver and Ag_2S, the transfer of silver atom from metal sulfide would proceed by the most predominant of the following three mechanisms.

$$2Ag(I) + S(II) \rightarrow Ag_2S(II) \qquad (2.A)$$

$$2Ag(I) + S^-(II) \rightarrow Ag_2S(II) + e^-(II) \qquad (2.B)$$

$$2Ag(I) + S^{2-}(II) \rightarrow Ag_2S(II) + 2e^-(II) \qquad (2.C)$$

where (I) denotes the metal phase, (II) the sulfide phase, and e^- is electron.

The corresponding rate equations for these mechanisms are

$$v_A = K_A[a_{Ag}(I)]^2 a_S - K_A' a_{Ag_2S} \qquad (3.A)$$

$$v_B = K_B[a_{Ag}(I)]^2 a_{S^-} - K_B' a_{Ag_2S} a_{e^-} \qquad (3.B)$$

$$v_C = K_C[a_{Ag}(I)]^2 a_{S^{2-}} - K_C' a_{Ag_2S}(a_{e^-})^2 \qquad (3.C)$$

Since the reaction proceeds under the condition far from equilibrium in our case the reverse reactions can be neglected.

The silver activity of metal phase is unity and thus the rate equations (3.A)—(3.C) are rewritten as

$$v_A = k_A a_S \qquad (4.A)$$

$$v_B = k_B a_{S^-} \qquad (4.B)$$

$$v_C = k_C a_{S^{2-}} \qquad (4.C)$$

According to Wagner[9], a_{Ag_2S} and a_{Ag} of α-Ag_2S are constant irrespective of nonstoichiometry of the sulfide, *viz.*,

$$a_{Ag_2S} = \text{const} \qquad (5)$$

$$a_{Ag^+} = \text{const} \qquad (6)$$

Assuming the chemical equilibria between species in α-Ag_2S, we obtain

$$Ag = Ag^+ + e^-$$

$$a_{Ag^+} a_{e^-} = K_1 a_{Ag} \qquad (7)$$

$$S^{2-} = S + 2e^-$$

$$a_S (a_{e^-})^2 = K_2 a_{S^{2-}} \qquad (8)$$

$$S^- = S + e^-$$

$$a_S a_{e^-} = K_3 a_{S^-} \qquad (9)$$

$$2Ag + S = Ag_2S$$

$$a_{Ag_2S} = K_4 (a_{Ag})^2 a_S \qquad (10)$$

Where K_1, K_2, K_3, and K_4 are equilibrium constants.

From Eqs. (5)—(10), we get

$$a_S \propto (a_{Ag})^{-2} \qquad (11)$$

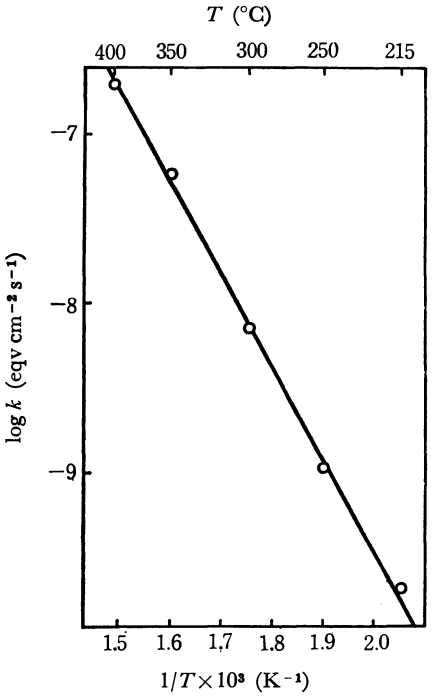

Fig. 7. Arrhenius plot of k.

$$a_{S^-} \propto (a_{Ag})^{-1} \qquad (12)$$

$$a_{S^{2-}} \propto (a_{Ag})^0 \qquad (13)$$

Thus, Eqs. (4.A)—(4.C) are expressed in the form

$$v = k(a_{Ag})^n \qquad (14)$$

where $n=-2$ for mechanism (A), $n=-1$ for mechanism (B) and $n=0$ for mechanism (C).

We found that n varies from −1.9 to −2.3. Thus, it is concluded that n is −2 and that mechanism (A) prevails for the reaction at the Ag/Ag_2S interface.

Rate Constants. The logarithms of the rate constants for each temperature can be obtained from extrapolation of the lines (Fig. 6) to the ordinate $\log a_{Ag} = 0$. Figure 7 shows the Arrhenius plot of k, which is expressed by

$$k = 251 \exp(-25000/RT) \quad \text{eqv cm}^{-2}\,\text{s}^{-1} \qquad (15)$$

Therefore the rate equation is

$$v = 251\{\exp(-25000/RT)\,(a_{Ag})^{-2}\}\text{eqv cm}^{-2}\,\text{s}^{-1} \qquad (16)$$

If the activities of sulfur of Ag_2S under reaction and in equilibrium with Ag are expressed in terms of a_S and a_S^0, respectively, we have

$$a_S (a_{Ag})^2 = a_S^0 \qquad (17)$$

Hence

$$(a_{Ag})^{-2} = \frac{a_S}{a_S^0} \qquad (18)$$

Substituting (18) into (16) we have

$$v = 251\{\exp(-25000/RT)\}(a_S/a_S^0)\ \text{eqv cm}^{-2}\,\text{s}^{-1} \qquad (19)$$

According to Kiukkola and Wagner[10] the standard free energy of formation of Ag_2S, ΔG^0, is

$$\Delta G^0 = -7.04 - 0.00735\,T \quad \text{kcal/mol} \qquad (20)$$

ΔG^0 is related to a_S^0 as follows.

$$\Delta G^0 = RT \ln a_S^0 \quad \text{kcal/mol} \qquad (21)$$

8) H. Kobayashi and C. Wagner, *J. Chem. Phys.*, **26**, 1609 (1957).
9) C. Wagner, *ibid.*, **21**, 1819 (1953).
10) K. Kiukkola and C. Wagner, *J. Electrochem. Soc.*, **104**, 379 (1957).

Eq. (19) can be written as

$$v = 1.00 \times 10^4 \{\exp(-18000/RT)\} a_S \text{ eqv cm}^{-2}\text{ s}^{-1} \quad (22)$$

Summary

(I) The solid-solid interface reaction between silver and silver-sulfide was investigated kinetically by the direct sulfurization and coulometic titration methods.

(2) The reaction rate was determined as a function of a_S, silver activity of silver-sulfide, at 215—400 °C.

The rate quation is

$$v = 1.00 \times 10^4 \{\exp(18000/RT) a_S\} \text{ eqv cm}^{-2}\text{ s}^{-1}$$

(3) The reaction mechanism was discussed on Kobayashi-Wagner's theory. The following mechanism was found to be predominant.

$$2Ag(Ag) + S(Ag_2S) \rightarrow 2Ag^+(Ag_2S) + S^{2-}(Ag_2S)$$

BULLETIN OF THE CHEMICAL SOCIETY OF JAPAN, VOL. 46, 1667—1669 (1973)

Chemical Analysis of Mixtures of Metals by a Logarithmic Extrapolation Method

Yukio NAGAOSA and Tatsuo YONEKUBO

Faculty of Engineering, Fukui University, Bunkyo, Fukui 910

(Received March 8, 1972)

Decomposition of the ternary molybdophosphoric acid of titanium(IV), vanadium(V), zirconium(IV) and niobium(V) by complexing agents such as oxalate, citrate or tartrate was found from a kinetic study to be of first-order with respect to each metal ion. The half lives and activation energies of decomposition were also examined. From the results chemical analysis of mixtures of the metals was studied by a logarithmic extrapolation method, utilizing the difference in decomposition rate. Metals in binary systems such as Zr–Nb, V–Zr, Nb–V, Ti–V and Ti–Nb could be determined simultaneously within a relative error of ±5%. Determination of 0.01∼0.2 mg of vanadium was carried out in the presence of titanium (0.1 mg), zirconium (0.5 mg), niobium (0.5 mg) and other diverse ions. Iron(III), aluminum, germanium(IV) and iodide interfered with the determination.

Spectrophotometric determination of titanium(IV), vanadium(V), zirconium(IV) and niobium(V) utilizing their chelate compounds, ternary heteropoly acids and peroxy compounds has been widely used.[1–5] The heteropoly acid method is sensitive in the determination of each metal, but can not be applied to mixtures of these metals because of their mutual interference.

For the chemical analysis of mixtures of these metals, the authors reported on a simultaneous determination of titanium(IV) and vanadium (V), based on the different rate of decomposition of each ternary molybdophosphoric acid in hydrochloric acid solution, without tedious separation procedure.[6] However, the method has the disadvantage that zirconium(IV) and niobium(V) should not be present since they form a precipitate.

The logarithmic extrapolation method has also been used for the analysis of mixtures of two components because of its simplicity and convenience.[7–10] Tanaka *et al.* used this method in the analysis of mixtures of some heavy metals, utilizing different rates of ligand substitution reactions.[11]

A method has been proposed for the simultaneous determination of two of the metal ions, titanium(IV), vanadium(V), zirconium(IV) and niobium(V) by the logarithmic extrapolation technique. This method is based on the different rates of decomposition of the ternary molybdophosphate of metal ions by complexing agents such as citrate, oxalate or tartrate. The kinetics of decomposition was examined by spectrophotometry, and a mixture of the four metal ions was analyzed in the presence of diverse ions.

General Considerations

The logarithmic extrapolation method[12–14] has been applied. After the faster reacting component(A) has reacted completely, the amount of the slower reacting component(B) at the initial time is determined by extrapolating the first-order plots to zero time, the amount of the former at the initial time being estimated by extrapolating logarithm of the difference between the

1) E. B. Sandell, "Colorimetric Determination of Traces of Metals," 3rd Ed., Interscience Publishers, New York (1959).
2) A. K. Babko, *Talanta*, **15**, 721 (1968).
3) R. M. Veitsmann, *Zavodsk. Lab.*, **25**, 408 (1959).
4) M. Jean, *Anal. Chim. Acta*, **31**, 24 (1964).
5) Y. Nagaosa, R. Seto, M. Satake, and T. Yonekubo, *Nippon Kagaku Zasshi*, **92**, 1216 (1971).
6) Y. Nagaosa, T. Yonekubo, M. Satake, and R. Seto, *Bunseki Kagaku*, **21**, 215 (1972).
7) C. N. Reilly, "Advances in Analytical Chemistry and Instrumentation," Vol. 2, Interscience Publishers, New York (1963).
8) K. B. Yatsimirskii, "Kinetic Methods of Analysis," Pergamon Press, Oxford (1966).
9) H. B. Mark, Jr. and G. A. Rechnitz, "Kinetics in Analytical Chemistry," Interscience Publishers, New York (1968).
10) J. G. Hanna and S. Siggia, *J. Pharm. Sci.*, **55**, 541 (1960).
11) M. Tanaka, S. Funahashi, and K. Shirai, *Anal. Chim. Acta*, **39**, 437 (1967).
12) L. C. King and M. Fefer, *Anal. Chem.*, **29**, 1057 (1957).
13) P. D. Bartlett and M. S. Swain, *J. Amer. Chem. Soc.*, **77**, 2801 (1955).
14) B. E. Salzman and N. Gilbert, *Anal. Chem.*, **31**, 1914 (1959).

total absorbance and the absorbance due to B to zero time. The procedure is as follows.

Logarithm of the net absorbance, log E_t, is plotted against time, E_t being obtained by subtracting the blank absorbance from that of the sample solution containing A and B. With the lapse of time diagram (I) gives first a curve, then a straight line when the ratio of rate constants for A and B is large enough. The straight line in (I) is extrapolated (line II) to zero time, to give an intercept of log $E_{B,0}$, logarithm of the absorbance due to initial B. Next, logarithm of the difference in absorbance, obtained by subtracting the absorbance in (II) from that in (I), is plotted against time. The intercept at zero time is log $E_{A,0}$, logarithm of the absorbance due to initial A (diagram III). The concentrations of A and B are calculated from $E_{A,0}$, and $E_{B.0}$ with the aid of calibration curves.

Experimental

Reagent. All the chemicals were of analytical reagent grade. Water was deionized and distilled. The solutions prepared were 0.1 M potassium dihydrogen phosphate, 0.2 M sodium molybdate dihydrate, 0.1 mg metal ion per ml (Ti, V, Zr and Nb) and 0.25 M complexing agent solution (ammonium oxalate monohydrate, sodium citrate dihydrate and sodium tartrate dihydrate).

Apparatus. Spectrophotometric measurements were made on a Hitachi Recorder QPD$_{53}$ and a spectrophotometer Model 139, with 1 cm and 5.3 cm quartz cells. A pH meter, Toa Electronics Ltd., Model HA-5A was used.

Experimental Procedure. One ml phosphate solution was added to 10 ml molybdate solution in a 100 ml beaker, to which was then added a sample solution containing metal ions. The solution was diluted to *ca.* 40 ml with water, the pH being adjusted to 1.5 with 0.5 M sulfuric acid, and made up to 50 ml with water. The mixture was set aside for 2 hr and then 40 ml of the solution was transferred to a 50 ml cell. To this was added 10 ml of complexing agent solution, and the change in transmittance of the solution was recorded at 400 nm as a function of time. A blank solution containing phosphate and molybdate was treated in the same manner. All the experiments were carried out at 20±0.2 °C unless otherwise mentioned.

Results and Discussion

Molar Extinction Coefficients. The absorption spectra of the ternary molybdophosphoric acids and the reagent blank give peaks in the ultraviolet range.[15] Hence, all the absorbances were measured at 400 nm where the absorbance of the reagent blank was considerably low. The molar extinction coefficients of the ternary molybdophosphoric acids were kinetically determined. Figure 1 shows plots of log E_t *vs.* time t, which correspond to the decomposition of ternary molybdophosphoric acids by the complexing agent in 1 cm cells. The linear plots show that the decomposition follows the first-order rate law under the given conditions. The molar extinction coefficients of each ternary molybdophosphoric acid were estimated from the extrapolated intercept to time zero (log E_0). They

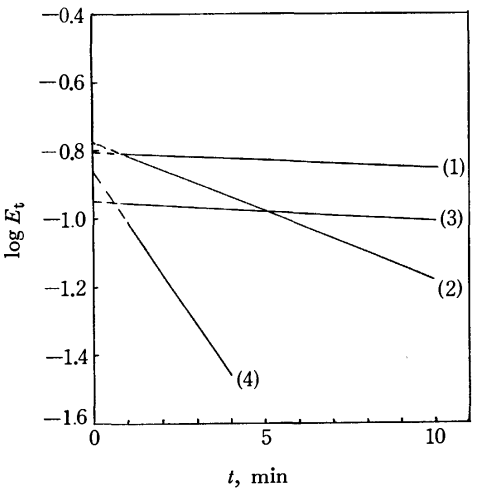

Fig. 1. Determination of E_0 for each metal.
(1) Ti(IV) 0.24 mg/50 ml (0.05 M citrate)
(2) V(V) 0.16 mg/50 ml (0.05 M citrate)
(3) Zr(IV) 0.40 mg/50 ml (0.50 M citrate)
(4) Nb(V) 0.40 mg/50 ml (0.05 M tartrate)
Cell length: 1 cm, temperature: 20 °C

were 1.57×10^3, 2.67×10^3, 1.28×10^3 and 1.52×10^3 for molybdotitanophosphoric, molybdovanadophosphoric, molybdozirconophosphoric and molybdoniobiophosphoric acid, respectively. Beer's law holds up to the concentration of 1 mg/50 ml of each metal at 400 nm.

On the other hand, the absorbance of the reagent blank was approximately 1.0 at 400 nm under the given conditions, but it decreased after the addition of a complexing agent to the solution and finally reached a constant value of 0.01 after 1 min. It is clear that molybdophosphoric acid itself decomposes completely within 1 min.

Half Life. In order to predict the possibility of the simultaneous determination of these metals in their binary mixtures, it is necessary to know the half life of the decomposition of each ternary molybdophosphoric acid by the complexing agent. It can be obtained from the plot of log E_t *vs.* t required for the decomposition. The results are given in Table 1. The half lives decreased in the order V>Ti>Zr>Nb for oxalate system and Ti>Zr>V>Nb for citrate or tartrate system. The following conclusions can be drawn: (1) Of these metals vanadium gives the longest half life for the oxalate system, in good accordance with the previous results,[6,16] where molybdo-

TABLE 1. VALUES OF HALF LIFE
Concentration of complexing agent: 0.05 M, wavelength: 400 nm, cell length: 5.3 cm, temperature: 20 °C

Metal	Half life (min)		
	Oxalate	Citrate	Tartrate
Ti[a]	1.50	70.0	66.0
V[a]	9.60	9.60	11.6
Zr[b]	0.83	49.0	20.0
Nb[b]	0.80	0.27	2.0

a) 0.08 mg taken b) 0.4 mg taken

15) K. Murata, Y. Yokoyama, and S. Ikeda, *Anal. Chim. Acta*, **48**, 349 (1969).

16) P. Pakalns, *ibid.*, **50**, 103 (1970).

Table 2. Values of the Arrhenius activation energy (E_A)
Concentration of complexing agent: 0.05 M, wavelength: 400 nm, cell length: 5.3 cm

Metal	E_A kcal mol^{-1}		
	Oxalate	Citrate	Tartrate
Ti[a)]	4.4	17.5	14.9
V[a)]	16.3	15.4	17.9
Zr[b)]	17.0	16.9	15.8
Nb[b)]	7.5	13.9	14.4

a) 0.08 mg taken b) 0.4 mg taken

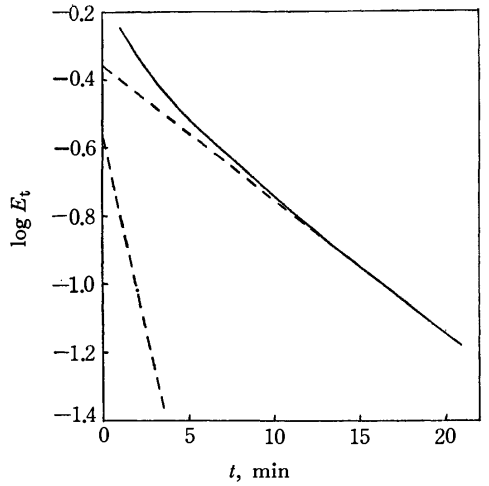

Fig. 2. Decomposition curve of mixture of Zr(0.5 mg) and Nb(0.5 mg) with tartrate.
Solid line: experimental data, dashed line: extrapolated data, tartrate: 0.05 M, cell length: 5.3 cm, temperature: 20 °C.

vanadophosphoric acid is the most inert in aqueous solution. (2) For citrate and tartrate systems, the half lives of quadrivalent metal ions (Ti,Zr) are longer than those of quinquevalent metal ions (V, Nb).

Activation Energy. Influence of temperature on the decomposition rate was examined at 15, 20, 25, and 30 °C. Straight Arrhenius plots gave the activation energies summarized in Table 2. They indicate that the activation energies for decomposition by oxalate are 4.4 kcal mol^{-1} and 7.5 kcal mol^{-1} for molybdotitanophosphoric and molybdoniobiophosphoric acids, respectively, and 13.9～17.9 kcal mol^{-1} for the other decomposition systems.

Simultaneous Determination of Two Metal Ions. In order to carry out the extrapolation method successfully, the ratio of the decomposition rate constants of the ternary molybdophosphoric acids in the mixture, k_A/k_B, should be greater than 4 for the case in which the ratio of initial concentration of two metals $[A]_0/[B]_0$ is equal to unity.[9] Pairs of metals in which the differential kinetic determination seems possible were chosen from Table 1, and simultaneous determination of the metal ions was examined. The result for a mixture of zirconium and niobium is given in Fig. 2. From plots of log E_t *vs.* t, the concentrations of zirconium and niobium were determined from the intercepts obtained by extrapolation (Table 3). Synthetic samples of Zr–Nb, V–Zr, Nb–V, Ti–V, and Ti–Nb have been successfully analyzed within a relative error of ±5%.

Table 3. Analysis of binary mixtures
Concentration of complexing agent: 0.05 M, wavelength: 400 nm, cell length: 5.3 cm, temperature: 20 °C

Mixture	Taken(mg)		Found(mg)		Complexing agent used
Zr–V	0.500	0.100	0.500	0.100	Oxalate
Nb–V	0.500	0.100	0.481	0.100	Oxalate
Nb–V	0.500	0.050	0.480	0.049	Oxalate
Ti–V	0.100	0.100	0.097	0.099	Oxalate
Ti–V	0.200	0.050	0.198	0.049	Oxalate
Ti–Nb	0.100	0.500	0.099	0.488	Tartrate
Zr–Nb	0.500	0.500	0.498	0.501	Tartrate
Zr–Nb	0.100	0.500	0.099	0.505	Tartrate
Ti–Zr[a)]	0.200	0.500	0.203	0.365	Tartrate
Ti–Zr[a)]	0.100	0.100	0.101	0.083	Tartrate

a) Temperature 25 °C

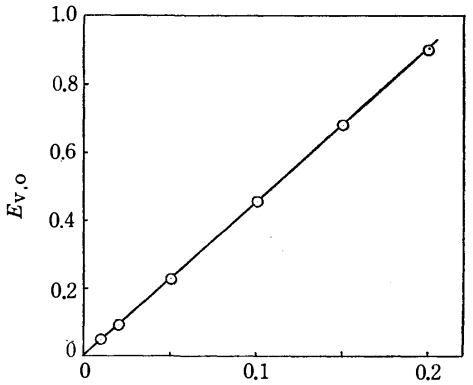

Fig. 3. Determination of V in the presence of Ti(0.1 mg), Zr(0.5 mg) and Nb(0.5 mg).
Oxalate: 0.05 M, cell length: 5.3 cm, temperature: 20 °C.

An attempt was made to analyze a mixture of titanium and zirconium using tartrate at 25 °C. Titanium was determined in the mixture but not zirconium (Table 3).

Determination of Vanadium in the Presence of Titanium, Zirconium and Niobium. We see from Table 1 that vanadium can be determined in the presence of titanium, zirconium and niobium by using oxalate as complexing agent, since the half life of molybdovanadophosphoric acid is more than six times greater than those of the other metals. Analysis of 0.01～0.2 mg of vanadium in the presence of titanium (0.1 mg), zirconium(0.5 mg) and niobium(0.5 mg) was examined at 20 °C. The plot of absorbance $E_{V,O}$, *vs.* the amount of vanadium gives a straight line (Fig. 3). The present method can be applied to the determination of vanadium in the presence of the other three metals.

Diverse Ions. The effect of diverse ions on the determination of 0.1 mg of vanadium was examined in the presence of titanium (0.1 mg), zirconium (0.5 mg) and niobium (0.5 mg). Five mg of Co(II), Ni(II), Mn(II), Cu(II), Cr(VI) and 0.1 mg of Si(IV), As(V) and W(VI) gave no interference, but 0.05 mg of Ge(IV) and 5 mg of iodide interfered with determination. Iron(III) and aluminum should not be present because of the formation of precipitate, and calcium for that of its oxalate.

Potential-step Anodic Stripping Voltammetry

Masahiro KOMATSU

Government Industrial Research Institute, Kyushu, Tosu, Saga 841

(Received August 7, 1972)

The application of anodic potential-step stripping voltammetry for the determination of metal ion was investigated. From the dependence of stripping current ($i_{a,d}$) on electrode radius, the rotational speed of the stirring rod in electrodeposition and electrodeposition time for Cd(II) in 1 M KCl, the diffusion-controlled process could be theoretically predicted. The calibration curves of Cd(II), Mn(II), Ni(II), Zn(II), and Sb(III) were found to be linear in the range 0.01—0.1 ppm, and those of Tl(I), Cu(II), Pb(II), Sn(II), Bi(III), and In(III) in the range 0.02—0.2 ppm, by analysis at time $t=1.25$ sec on current-time curves. The ratio $i_{a,d}/i_{a,p}$ increased in the order $n=3<2<1$, where $i_{a,d}$ is the anodic diffusion current obtained by the potential-step method, and $i_{a,p}$ the anodic peak current obtained by the linearly varying potential method. The ratio of irreversible electron transfer reaction differed from that of the reversible one. The coefficient of variation in the measurement of peak heights was ±3% for 0.1 ppm or 0.2 ppm of metal ion.

Anodic stripping voltammetry has been found to be a very sensitive means for the determination of trace metal ions.[1] The metal ion to be determined is first electrodeposited on a stationary electrode and then stripped from this electrode by reoxidation of mercury amalgam. In the latter process, many reoxidation methods such as linearly varying potential method,[2] a.c. polarography,[3] square wave polarography,[4] constant current electrolysis,[5,6] coulostatic method,[7] and pulse polarography[8] have been employed. Mamantov *et al.* used the potential-step method to reoxidize mercury amalgam and applied it for the determination of cadmium ion.[5] Anodic potential-step stripping voltammetry was applied for the determination of the diffusion coefficient of metal atom in a hanging mercury drop electrode by analyzing the anodic current-time curve.[9,10] However, no papers dealing with the determination of metal ion have appeared except for that of Mamantov *et al.* It appeared to be worthwhile to investigate the applicability of anodic potential-step stripping voltammetry to the determination of metal ions and to compare the result with that of anodic stripping voltammetry under lineraly varying potential.

Experimental

Reagents. Standard solution of metal ions were prepared by dissolving metal salts of analytical reagent grade, and were standardized by complexometric titration with EDTA, except for tin(II) which was standardized gravimetrically.[11] Nitrates were used for Tl(I), Pb(II), Ni(II), and Zn(II), and chlorides for others.

Potassium chloride was purified by extracting heavy metals with dithizone–chloroform system, being recrystallized twice and heated at 300 °C in an electric furnace for 3 hr.

All the other reagents were of reagent grade and used without purification. Water was deionized on a mixed-bed ion-exchange resin and then distilled from alkaline permanganate solution.

Apparatus. The instrument for anodic stripping voltammetry with potential-step was set up with an automatic potential controller(Type AP-1, Shimadzu Co., Ltd.) for electrodepositing process and a potentiostat(Type PS-2, Shimadzu Co., Ltd.) for reoxidizing process from mercury amalgams. Switching from electrodepositing potential to reoxidizing potential was done by a mercury-relay(Type MC-1, NEC Co., Ltd.). The load resistance was adjusted with a precision variable resistor(Type 2786, Yokogawa Elec. Work, Ltd.) inserted in series with the load resistor of the potentiostat. *IR* drop across the variable resistor was applied to the recorder input for measuring cell current. A preliminary test showed that the *IR* drop was linearly proportional to the load resistance from 0 to 3000 Ω and from 0 to 10000 Ω. Current-time curves were recorded on a recorder(Type D-5SN, Rikendenshi Co., Ltd.) with 480 mm/min chart speed, a full-scale sensitivity of 10 mV and a nominal full scale response time of 0.4 sec. For anodic stripping voltammetry at linearly varying potential, a conventional polarograph(Type p-8, Yanagimoto Co., Ltd.) with a 1 V/1.1 min sweep rate and 180 mm/min chart speed was used.

A balanced head stationary hanging mercury drop electrode (HMDE)[12] and a saturated calomel electrode with KNO_3 agar-bridge were arranged with a beaker type electrolysis cell (*ca.* 100 ml). The characteristics of HMDE used were: $t=4.25$ min, $m=3.6$ mg/min. The electrode surface area was 0.028 cm², unless otherwise stated. The characteristics of another HMDE used for examining the relation between anodic diffusion current and the electrode radius were: $t=22.25$ min, $m=1.1$ mg/min.

All the experiments were carried out at room temperature.

Procedure. The method followed standard anodic stripping procedure.[13] A 50 ml solution containing the desired amount of metal and supporting electrolyte was transferred into the electrolysis cell. High purity nitrogen gas was passed through the solution for at least 15 min to remove oxygen. The solution was stirred with 360 rpm (driven by a synchronous rotating motor, unless otherwise

1) E. Barendrecht, "Electroanalytical Chemistry," Vol. 2, ed. by A. J. Bard, Marcell Dekker, New York (1967), p. 53.
2) J. G. Nikelly and W. D. Cooke, *Anal. Chem.*, **29**, 933 (1957).
3) W. L. Underkofler and I. Shain, *ibid.*, **37**, 218 (1965).
4) G. C. Barker, *Anal. Chim. Acta*, **18**, 118 (1958).
5) G. Mamantov, P. Papoff, and P. Delahay, *J. Amer. Chem. Soc.*, **79**, 4034 (1957).
6) A. R. Niebst and A. J. Bard, *J. Electroanal. Chem.*, **6**, 332 (1963).
7) P. Delahay, *Anal. Chem.*, **34**, 1662 (1962).
8) G. D. Christian, *J. Electroanal. Chem.*, **23**, 1 (1969).
9) B. K. Hovespian and I. Shain, *ibid.*, **12**, 397 (1966).
10) W. G. Stevens and I. Shain, *J. Phys. Chem.*, **70**, 2276 (1966).
11) R. A. Day, Jr. and A. L. Underwood, "Quantitave Analysis," Prentice-Hall, New York (1958), p. 278.
12) Y. Yamazaki, *Rev. Polarog.* (Kyoto), **13**, 26 (1965).
13) I. Shain, "Treatise on Analytical Chemistry," ed. by Koltoff and Elving, Part 1, Sec. D-2, Chap. 50, Interscience, New York (1963).

Table 1. Comparison between anodic stripping voltammetry by the potential-step method and linearly varying potential method

Metal ion	Concen (ppm)	Supporting electrolyte	Deposition potential V *vs.* SCE	Reoxidation potential V *vs.* SCE	$i_{a,d}$ (μA)	$i_{a,p}$ (μA)	$i_{a,d}/i_{a,p}$	$E_{a,p}-E_{a,p}$
Tl(I)	0.2	1 M KCl	−0.70	−0.40	−0.80	−0.67	1.20	59
Cu(II)	0.2	1 M KCl	−0.45	−0.05	−1.04	−0.88	1.20	59
Cd(II)	0.1	1 M KCl	−0.95	−0.55	−0.95	−0.99	0.96	29
Pb(II)	0.2	1 M KCl	−0.60	−0.35	−0.97	−1.03	0.96	29
Sn(II)	0.2	1 M HCl	−0.80	−0.30	−0.74	−0.77	0.95	29
Zn(II)	0.2	1 M KCl	−1.20	−0.95	−2.78	−2.78	1.00	33
Zn(II)	0.2	0.5 M NH_3 +1 M NH_4Cl	−1.40	−0.60	−3.80	−1.90	2.00	106
Mn(II)	0.1	1 M KCl	−1.65	−1.10	−1.58	−0.46	3.46	166
Ni(II)	0.1	1 M KSCN	−0.80	−0.30	−0.65	−0.38	1.70	76
In(III)	0.2	1 M KCl +0.1 M HCl	−0.60	−0.35	−0.68	−0.96	0.71	19
Bi(III)	0.2	1 M H_2SO_4	−0.15	+0.10	−1.28	−1.76	0.72	19
Sb(III)	0.1	1 M H_2SO_4 +0.01 M KSCN	−0.25	−0.02	−0.88	−1.08	0.81	20

stated). During the course of the experiment, the solution was kept under nitrogen atmosphere. The deposition and reoxidation potentials of each metal ion are given in Table 1.

After deposition for 5 min, stirring was stopped for 30 sec, the chart was driven to record the current-time curve and the potential was switched from electrodeposition potential to reoxidation potential by a mercury-relay.

Results and Discussion

Typical anodic current-time curves for Zn(II), Cd(II), Pb(II), Cu(II), and supporting electrolyte are shown in Fig. 1. Their residual currents which result from charging of the electrical double layer suddenly rise to a maximum and then decay to zero. Anodic current at constant potential electrolysis under the diffusion-controlled condition($i_{a,d}$) is given by[10]

$$i_{a,d} = nFAD_RC_R^* [-1/\sqrt{\pi D_R t} + 1/r_0 - (2/\sqrt{\pi D_R t}) \sum_{n=1}^{\infty} \exp - (n^2 r_0^2/D_R t)] \quad (1)$$

where C_R^* is the initial uniform concentration of deposited metal in the spherical mercury drop electrode, D_R the diffusion coefficient, t the time elapsed from beginning of stripping electrolysis, n the number of electron involved in the electron transfer reaction, r_0 the electrode radius, and A the area of electrode surface. The following semi-empirical equation for the electrodeposition process indicates that the limiting cathodic current i_c for an HMDE is a function of the radius of mercury drop r_0, the diffusion coefficient D_0(cm²/sec), the bulk concentration of the metal ion O to be determined C_o^*(mM), the rpm of the stirring rod U and constant k[1]:

$$i_c = (4\pi r_0 nFD_oC_o^* + knr_0^2D_o^{2/3}C_o^*U^{1/2}) \ \mu A \quad (2)$$

where the first term in the right hand side is the value

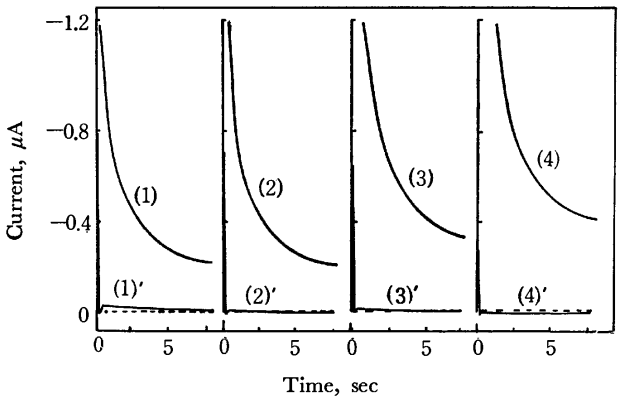

Fig. 1. Typical anodic stripping curves of Cu(II), Pb(II), Cd(II), Cu(II), and KCl.
(1) Cu(II), 0.1 ppm; (1)' 1 M KCl
(2) Pb(II), 0.1 ppm; (2)' 1 M KCl
(3) Cd(II), 0.1 ppm; (3)' 1 M KCl
(4) Zn(II), 0.1 ppm; (4)' 1 M KCl
Electrodeposition time for all metal ions, 5 min and for KCl, zero time.

of i_c at $U=0$. This can be neglected if the rotational speed is high.[14] The concentration of the reductant C_R^* is expressed as follows by means of cathodic current i_c and electrodeposition time τ.[15]

$$C_R^* = \frac{3i_c\tau}{4\pi nFr_0^3} \quad (3)$$

Since the third term in the right hand side of equation (1) is small when t is less than about 30 sec,[10] anodic diffusion current ($i_{a,d}$) is expressed as follows from equations (1), (2) and (3).

$$i_{a,d} = 4\pi knFD_R\tau D_o^{2/3}C_o^*U^{1/2}\left(\frac{-1}{\sqrt{\pi D_R t}}r_0+1\right) \quad (4)$$

The dependence of $i_{a,d}$ upon r_0, $U^{1/2}$ and τ was examined for Cd(II) in 1 M KCl, Mamantov *et al.* having reported that its electrode reaction was dif-

14) R. Neeb and I. Kiehnast, *Z. Anal. Chem.*, **266**, 153 (1967).

15) I. Shain and J. Lewinson, *Anal. Chem.*, **33**, 187 (1961).

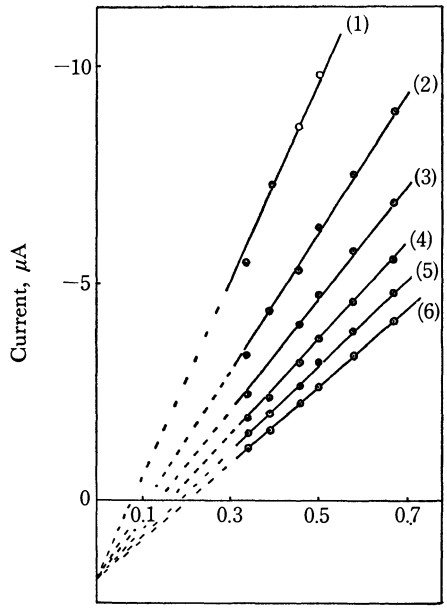

Fig. 2. Relation between anodic diffusion current and the radius of stationary mercury drop electrode.
(1) $t=1.25$ sec, (2) 2.50 sec, (3) 3.75 sec, (4) 5.0 sec, (5) 6.25 sec, (6) 7.50 sec.
Cd(II), 1 ppm in 1 M KCl; electrodeposition potential, −0.95 V *vs.* SCE; reoxidation potential −0.55 V *vs.* SCE; electrodeposition time, 5 min.

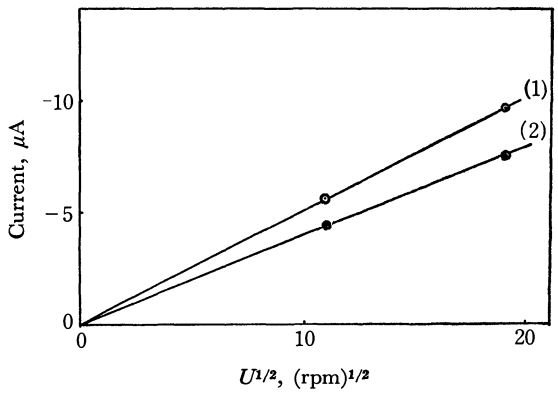

Fig. 3. Relation between anodic diffusion current and square root of speed of stirring rod.
Cd(II), 1 ppm in 1 M KCl; Electrode surface area, (1) 0.028 cm^2; (2) 0.018 cm^2; $t=1.25$ sec; Other conditions as in Fig. 2.

fusion-controlled. The relation between $i_{a,d}$ and r_0 is shown in Fig. 2. The various radii of the stationary mercury drop electrode were obtained by changing mercury run-off time. The $i_{a,d}$ for all the fixed times of the current-time curve after the start of reoxidation was linearly proportional to r_0. When extrapolated to zero radius, each line intersected at the same point. Since the spherical diffusion process is divergent, spherical correction acts to reduce the current below the value expected for a plane electrode. As a result, the $i_{a,d}$ *vs.* r_0 and also $i_{a,d}$ *vs.* $1/\sqrt{t}$ plots(Figs. 5 and 6) were extrapolated to a positive value. The relation between $i_{a,d}$ and $U^{1/2}$ is shown in Fig. 3. The $i_{a,d}$ was measured at two rotational speeds (rpm 360 and

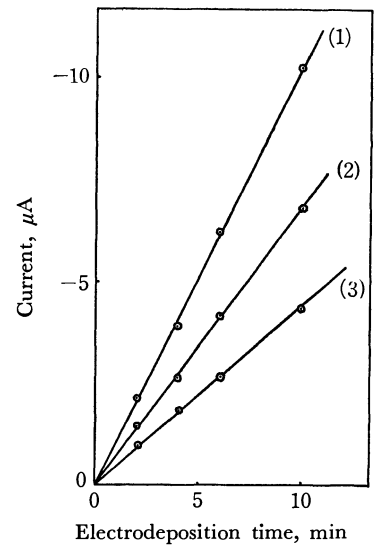

Fig. 4. Relation between anodic diffusion current and electrodeposition time.
(1) $t=1.25$ sec, (2) 2.50 sec, (3) 3.75 sec.
Cd(II), 1 ppm in 1 M KCl; Other conditions as in Fig. 2.

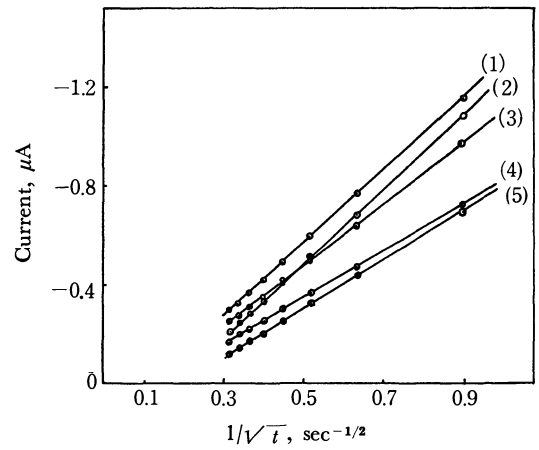

Fig. 5. Relation between i_a and $1/\sqrt{t}$.
Concentration of each metal ion, 0.1 ppm; electrodeposition time, 5 min; electrodeposition potential and reoxidation potential are given in Table 1.
(1) Zn(II) in 1 M KCl, (2) Mn(II), (3) Sb(III), (4) Cd II), (5) Ni(II).

120), and was found to be linearly proportional to $U^{1/2}$ for two different electrode surfaces. The $i_{a,d}$ *vs.* $U^{1/2}$ plots for both surfaces pass through the origin. The relation between $i_{a,d}$ and τ is shown in Fig. 4, The $i_{a,d}$ at the fixed time of the current-time curves is linearly proportional to τ from 1 to 10 min. All these lines pass through the origin.

If the electrode reaction is diffusion-controlled, the $i_{a,d}$ *vs.* $1/\sqrt{t}$ plot should be linear. $i_{a,d}$ was plotted against $1/\sqrt{t}$ over the time interval 1.25—10 sec after the start of reoxidation for all the metals used. All the resulting curves are linear and their electrode reactions found to be diffusion-controlled. The results are shown in Figs. 5 and 6. Although Ni(II) can easily form intermetallic compounds, the current-time curve of Ni(II) decayed with $t^{-1/2}$ at 0.1 ppm

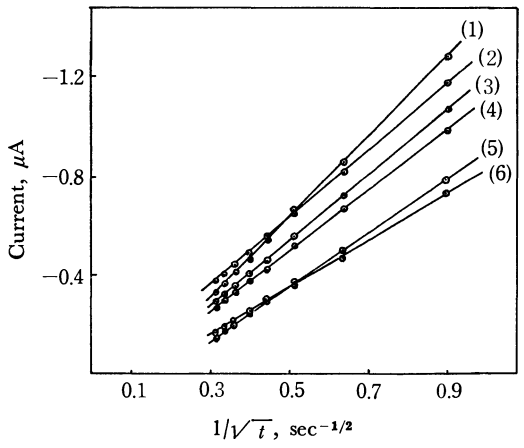

Fig. 6. Relation between i_a and $1/\sqrt{t}$.
Concentration of each metal ion, 0.2 ppm; electrodeposition time, 5 min; electrodeposition potential and reoxidation potential are given in Table 1.
(1) Bi(III), (2) Cu(II), (3) Pb(II), (4) In(III), (5) Sn(II), (6) Tl(I).

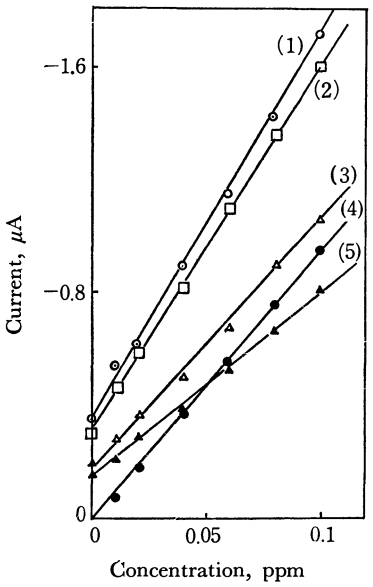

Fig. 7. Calibration curves of metal ions.
(1) Zn(II) in 1 M KCl, (2) Mn(II), (3) Sb(III), (4) Cd(II), (5) Ni(II).
Electrodeposition potential, reoxidation potential and supporting electrolytes are given in Table 1.

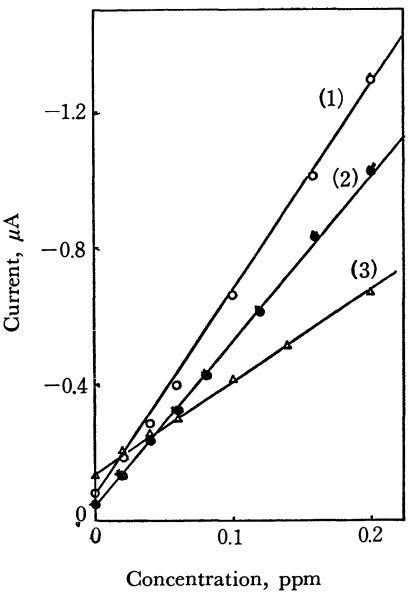

Fig. 8. Calibration curves of metal ions.
(1) Bi(III), (2) In(III), (3) Tl(I).
Electrodeposition potential, reoxidation potential and supporting electrolytes are given in Table 1.

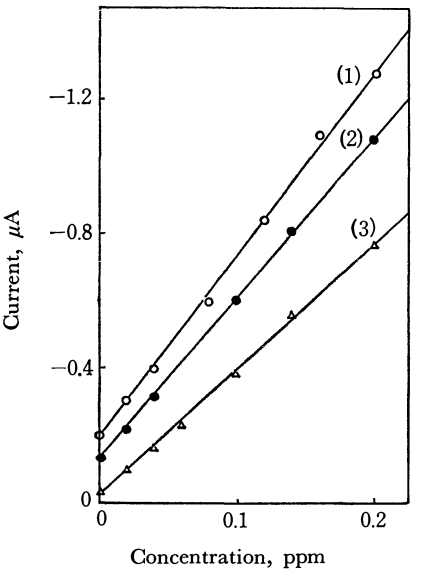

Fig. 9. Calibration curves of metal ions.
(1) Cu(I), (2) Pb(II), (3) Sn(II).
Electrodeposition potential, reoxidation potential and supporting electrolytes are given in Table 1.

concentration, showing that the electrode reaction is diffusion-controlled. Calibration curves are shown in Figs. 7, 8 and 9. 5 min was chosen as electrodeposition time for all the metal ions. The reoxidation potential was chosen to have a positive value to make anodic diffusion current independent of potential. The $i_{a,d}$ was measured at $t=1.25$ sec on the current-time curve. The value at zero concentration for each metal ion was due to impurities in the supporting electrolyte. Straight lines were obtained from 0.01 to 0.1 ppm for Cd(II), Mn(II), Ni(II), Zn(II), and Sb(III), and from 0.02 to 0.2 ppm for Tl(I), Cu(II), Pb(II), Sn(II), In(III), and Bi(III). It is of interest that even 0.01 ppm Mn(II) was determined by this method. 0.1 ppm Mn(VII) at most was determined by colorimetric determination[16] and 0.05 ppm Mn(III) by square wave polarography.[17]

As anodic diffusion current decreases with $1/\sqrt{t}$, it will be possible to determine a wide range of concentration of the metal ion from a current-time curve. According to Mamantov's suggestion,[5] concentration below 10^{-7} M of metal ion could be determined, if the current at a shorter time than $t=1.25$ sec has been measured.

Anodic diffusion current($i_{a,d}$) obtained by the potential-step reoxidation method were compared with

16) JIS K 0102 (1971).
17) T. Fujinaga and K. Hagiwara, *Bunseki Kagaku*, **11**, 442 (1962).

anodic current($i_{a,p}$) obtained by the linearly varying potential method. The results, including the potential difference between anodic peak potential ($E_{a,p}$) and anodic half-peak potential($E_{a,p/2}$) are given in Table 1. In the case of Cu(II), the electrodeposition potential and reoxidation potential correspond to Cu(0)→Cu(I) or one electron reoxidation.[18]

The ratio $i_{a,d}/i_{a,p}$ of reversible electron transfer reaction in which $E_{a,p}-E_{a,p/2}$ is $58/n$, increases in the order $n=3<2<1$.

Although the ratios can be varied by changing the sweep rate, the order $n=3<2<1$ will not change. This is because $i_{a,d}$ is in direct proportion to n, and $i_{a,p}$ is in direct proportion to $n^{3/2}$ under the diffusion-controlled condition.[19]

The ratio $i_{a,d}/i_{a,p}$ of Ni(II), Mn(II), and Zn(II) is larger than that of reversible two electron transfer reaction, and the ratio of Zn(II) in 1 M KCl differs from that in 0.5 M NH_3+1 M NH_4Cl. This is because $i_{a,p}$ is affected by α which may have a different value depending on the kind of supporting electrolytes.[20,21] The $i_{a,d}$ value of irreversible electron transfer reaction is considered to be close to the value of the reversible electron transfer reaction, since the reoxidation potential was chosen so as to be far more anodic than the anodic half-wave potential in this experiment.[22] This is why the ratio $i_{a,d}/i_{a,p}$ of Sb(III) differs from the other reversible three electron transfer reactions. Jacobsen and Rojahn reported that Sb(III) was not a strictly reversible process in 1 M H_2SO_4+0.01 M KSCN.[23]

The value $i_{a,d}/i_{a,p}$ indicates that anodic stripping voltammetry with potential-step method is more sensitive than linearly varying potential method for metal ions of which electron transfer reaction is irreversible. However, it has the disavantage of being more difficult to render analysis of certain ion mixtures with proximate anodic peak potentials or adverse relative concentration.

Acknowledgement

The author wishes to express his gratitude to Dr. H. Kakiyama for his encouragement throughout this work.

18) I. M. Kolthoff and J. J. Lingane, "Polarography," Interscience, New York (1953), p. 494.
19) P. Delahay, "New Instrumental method in Electrochemistry," Interscience, New York (1964), p. 118.
20) H. Matsuda and Y. Ayabe, *Z. Electrochem.*, **54**, 494 (1955).
21) R. S. Nicholson and I. Shain, *Anal. Chem.*, **36**, 706 (1964).
22) Ref. 19, p. 79.
23) E. Jacobsen and T. Rojahn, *Anal. Chim. Acta*, **54**, 261 (1971).

BULLETIN OF THE CHEMICAL SOCIETY OF JAPAN, VOL. 46, 1674—1676 (1973)

Potentiometric Studies of Cadmium- and Zinc-Halide Complexes in Acetonitrile

Makoto AIHARA and Seizo MISUMI

Inorganic Chemistry Laboratory, Faculty of Science, Kyushu University, Fukuoka 812

(Received December 18, 1972)

The overall formation constants of cadmium- and zinc-halide complexes in acetonitrile were determined by potentiometric titration using a saturated metal amalgam indicator electrode. The effect of ion-pair formation was taken into consideration to elucidate the free halide ion concentration in the experiments. The values of log β_3 and log β_4 for cadmium-halide complex were found to be: I^-, 22.4 and 26.5; Br^-, 25.3 and 29.8; Cl^-, 29.2 and 34.0. The values for zinc-chloride complex were 20.1 and 23.4.

Cadmium-, zinc- and manganese(II)-iodide complexes were studied polarographically in acetonitrile and the overall formation constants of these complexes were evaluated.[1] The formation of some halide complexes in non-aqueous solvents was studied potentiometrically by a number of investigators, too.[2-4] As acetonitrile has the donor number of 14.1, many ligand-exchange reactions have been studied in this solvent.[5]

In this work, cadmium-, and zinc-halide complexes have been studied potentiometrically in acetonitrile. The overall formation constants of the halide complexes were determined and the free halide ion concentration was corrected for the effect of ion-pairing. The data obtained were compared with those previously reported by polarography.

Experimental

Materials. Tetraethylammonium halides (Et_4NX) were prepared, purified several times and dried at 60 °C *in vacuo*. Other reagents were prepared as described previously.[1]

Apparatus. Potentials were measured by YOKOGAWA 2802 digital voltmeter with a manual impedance converter. The cell for potentiometric titration had a stopper of silicone rubber which had openings for a microburet tip, nitrogen inlet and outlet tubes and an SCE.[1] The SCE was isolated from the solution by a bridge of 0.1 M Et_4NClO_4 in acetonitrile with ultrafine sintered-glass membranes. The indicator electrode was a saturated metal amalgam,

1) S. Misumi and M. Aihara, *Talanta*, **19**, 549 (1972).
2) S. E. Manahan and R. T. Iwamoto, *Inorg. Chem.*, **4**, 1409 (1965).
3) N. I. Kotsaf and V. M. Samoilenko, *Russ. J. Inorg. Chem.*, **14**, 1431 (1969).
4) J. K. Senne and B. Kratochvil, *Anal. Chem.*, **43**, 79 (1971).
5) V. Gutmann, "Coordination Chemistry in Non-aqueous Solutions," Springer-Verlag, Wien (1968).

prepared by warming pure piece of reagent grade metal with thrice-distilled mercury under a stream of nitrogen.

Procedure. Potentiometric titration curve was obtained by the titration of 0.50 mM metal(II) ion with 0.05 M Et_4NX in acetonitrile. The titrant contained the same concentration of metal(II) ion as that in the cell. The concentration of Et_4N^+ was kept constant (0.1 M) for each solution of metal(II) ion and Et_4NX.

Et_4NClO_4[6] and Et_4NCl[7] were assumed to be completely dissociated in acetonitrile and the K_a values of the association constants used were 4.7 for Et_4NBr[6] and 5 for Et_4NI.[8]

The solution in the cell was deaerated by nitrogen gas presaturated with acetonitrile. All the potential measurements were made at 25.0±0.1 °C.

Results and Discussion

The potentiometric titration curves for cadmium-halide system are shown in Fig. 1. ΔE is the potential difference between cell potentials when halide is present and when it is absent. C_X and C_M are the total concentrations of halide and of metal(II), respectively. Each titration curve has an inflection point at $C_X/C_M=3$. Inflection at $C_X/C_M=4$ becomes larger in the order of iodide, bromide and chloride. The formation of CdX_3^- and CdX_4^{2-} (X=I, Br and Cl) was found to occur in acetonitrile.

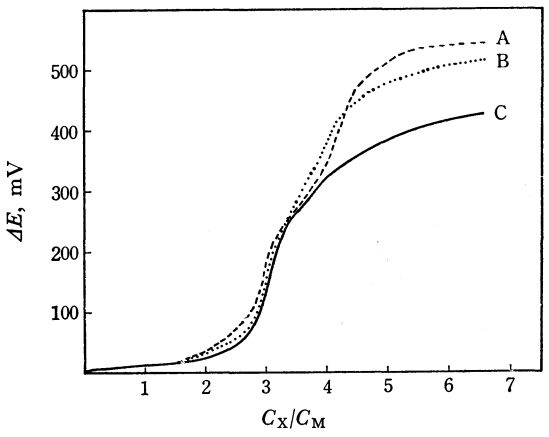

Fig. 1. Potentiometric titration curves for the titration of 0.5 mM Cd(II) with 0.05 M Et_4NCl (curve A), Et_4NBr (curve B) and Et_4NI (curve C).

The formation constants for cadmium- and zinc-halide complexes could not be calculated by Leden's method[9] because of the large inflection of titration curve but were determined in the following way.

In acetonitrile, the concentration of halide ion must be corrected for ion-pair formation. The total concentrations of metal(II) ion and halide are given by Eqs. (1) and (2).

$$C_M = [M^{2+}] + \sum_1^p [MX_p^{2-p}] \quad (1)$$

$$C_X = [X^-] + [Et_4NX] + \sum_1^p p[MX_p^{2-p}]$$

$$= [X^-] + K_a[Et_4N^+]_t[X^-] + \sum_1^p p[MX_p^{2-p}] \quad (2)$$

The total concentration of Et_4N^+, $[Et_4N^+]_t$ was kept to be 0.1 M by addition of the appropriate amount of Et_4NClO_4.

Assuming that the concentration of MX^+ and MX_2 to be negligible at $C_X/C_M \geq 3$, Eqs. (3) and (4) are derived from Eqs. (1) and (2).

$$YK_4[X^-]^2 + (Y+Y'K_4)[X^-] - Y'' = 0 \quad (3)$$

$$[MX_4^{2-}] = Y'' - Y[X^-] \quad (4)$$

where $Y=1+0.1K_a$, $Y'=4C_M-C_X-4[M^{2+}]$, $Y''=3[M^{2+}]+C_X-3C_M$ and $K_4=[MX_4^{2-}]/[MX_3^-][X^-]$

The potential shift (ΔE) by addition of halide is given by Eq. (5)

$$\Delta E = \frac{0.0591}{2} \log \frac{C_M}{[M^{2+}]} \quad (5)$$

and the overall formation constant β_4 is

$$\beta_4 = \frac{[MX_4^{2-}]}{[M^{2+}][X^-]^4} \quad (6)$$

A series of values was assumed for K_4 and corresponding values of β_4 were calculated by using Eqs. (3), (4), (5), and (6). The resulting values of log β_4 were plotted against the assumed value of log K_4. The different lines obtained from different points on the titration curve intersect at one point. For example, there can be seen the intersection point as shown in Fig. 2 for cadmium-iodide system. The value of β_3 was calculated from β_4 and K_4.

The plots for the other systems also intersect at one point.

The values of the formation constants for metal(II)-halide systems obtained by potentiometry and polarography[1] are summarized in Table 1.

The agreement between the values of the formation constant obtained for tetraiodocadmium(II) ion by potentiometry and by polarography is quite satisfactory.

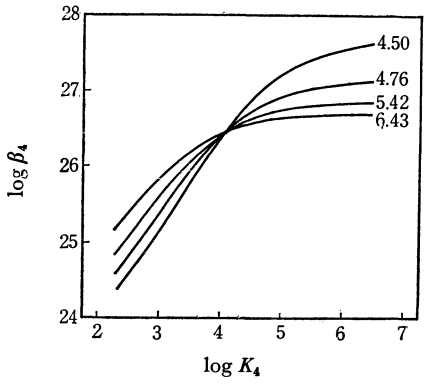

Fig. 2. Graphical solution of the formation constants (β_4 and K_4) for cadmium-iodide system.
Numbers on curves indicate mole ratio, C_I/C_{Cd}.

6) G. A. Forcier and J. W. Olver, *Electrochim. Acta*, **14**, 135 (1969).
7) I. Y. Ahmed and C. D. Schmulbach, *J. Phys. Chem.*, **71**, 2358 (1967).
8) D. F. Evans, C. Zawoyski, and R. L. Kay, *ibid.*, **69**, 3878 (1965).
9) I. Leden, *Z. Phys. Chem.* (Leipzig), **A 188**, 160 (1941).

Table 1. Logarithms of the overall formation constants β_n for cadmium- and zinc-halide systems

System	β_n	Potentiometric data	Polarographic data
Cd(II)-I^-	β_3	22.4	
	β_4	26.5	26.2
-Br^-	β_3	25.3	
	β_4	29.8	29
-Cl^-	β_3	29.2	
	β_4	34.0	
Zn(II)-I^-	β_4		18.4
-Cl^-	β_3	20.1	
	β_4	23.4	

In the case of the cadmium-bromide system, β_3 and β_4 were obtained by potentiometry, whereas only a crude value of β_4 was obtained by polarography. The stability of metal-chloride complex in acetonitrile follows the natural order of stability, that is, Ni(II)< Cu(II)>Zn(II).[2,10]

10) I. V. Nelson and R. T. Iwamoto, *J. Electroanal. Chem.*, **6**, 234 (1963).

These data indicate increasing stability of tri- and tetra-halogeno complexes in the order I<Br<Cl.

The values of β_4 obtained for cadmium- and zinc-halide systems in acetonitrile (donor number,[5] DN= 14.1) were compared with those in other solvents such as dimethyl sulfoxide (DN=29.8), methanol (DN= 33.8) and formamide (DN=39.1).

In the cadmium-chloride system, the stability (log β_4) decreases in the order acetonitrile (34.0)≫methanol (6.1)[11]>formamide (5.5).[12] In the zinc-chloride system, the value of log β_4 is larger in acetonitrile (23.5) than that in dimethyl sulfoxide (16.25).[13] The stability for other systems decreases with increasing donor number of the solvent, too.

Thus, a solvent of low donor number such as acetonitrile was confirmed to be effective for the formation of halide complexes.

The authors are grateful to the Ministry of Education for financial support given for this work.

11) Ya. I. Tur'yan and B. P. Zhantalai, *Zh. Neorg. Khim*, **5**, 1748 (1960).

12) H-S Hsiung, *Thesis*, Univ. Cincinnati, *Univ. Microfilms* 60-6444, *Diss. Abstr.*, **21**, 3629 (1960).

13) K. H. Pool, *J. Polarog. Soc.*, **13**, 23 (1967).

BULLETIN OF THE CHEMICAL SOCIETY OF JAPAN, VOL. 46, 1676—1680 (1973)

The Internal Friction of Glasses Containing Alkali under an Electric Field

Hiroyasu SAKAMURA and Minoru IMAOKA

Institute of Industrial Science, The University of Tokyo, Roppongi, Minato-ku, Tokyo 106

(Received May 31, 1972)

The change of the internal friction of sodium silicate and sodium borate glasses under an electric field was studied by means of a torsion pendulum technique. It was found that the internal friction increased under an electric field and that the increase was related to the numbers of vibration, the strength of the electric field, and the Na_2O content. The increase in internal friction in the glasses with a high Na_2O content was large because of the electrolysis of the glasses, which resulted in the removal of sodium ions. It was proposed that the internal friction increased because the removal of sodium ions was promoted by torsional oscillation under an electric field and that the deformation of the network took place around holes which were left behind by the removal of the sodium ions.

In an experiment with a glass containing alkali, an internal friction peak caused by the diffusion of sodium ions has been observed near room temperature over a period of the order of seconds.[1,2] When an alternating voltage is applied to a glass containing alkali, an electric loss with an activation energy and relaxation time almost the same as those of the internal friction has been observed.[3] In this case, alkali ions under electric stress move back and forth through the network structure of a glass. When an electric field is applied to a glass, an absorption current appears first, and then a constant current flows. The former causes polarization in a glass. The latter is due to ionic conduction. Alkali ions move to the cathode side under an electric field, some of them, however, stop within the network. Though alkali ions are forced to move within a glass by external force, their movement is controlled by the glass network structures. It is interesting to study the combined effect of electric and mechanical forces on glasses.

In Copley's experiment, an electric field was applied between the center and the surface of a glass bar sample and electrolysis was carried out for a constant time at 250 °C.[4] We are, however, interested in the polarization phenomenon, so we measured the internal friction by applying an electric field between the two ends of a glass bar sample.

Experimental

The apparatus used in this work is almost the same as Forry's except that a torsion pendulum is hung by means

1) J. V. Fitzgerald, *J. Amer. Ceram. Soc.*, **34**, 339 (1951).
2) L. C. Hoffman and W. A. Weyl, *Glass Ind.*, **38**, 81 (1957).
3) H. E. Taylor, *J. Soc. Glass Technol.*, **41**, 350 (1957); **43**, 124 (1959).
4) G. J. Copley, *J. Amer. Ceram. Soc.*, **51**, 667 (1968).

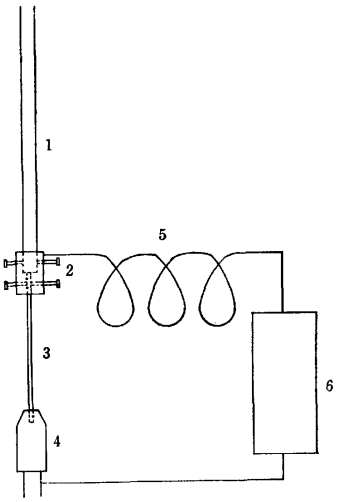

Fig. 1. Schema of a sample holder.
1: Pyrex tube, 2: Connector, 3: Sample, 4: Chuck, 5: Copper wire, 6: Voltage generator.

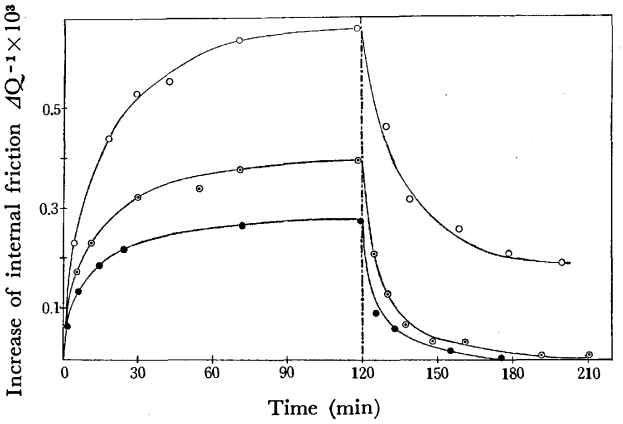

Fig. 2. Increase and decrease of internal friction as a function of time for the system SiO_2-Na_2O glasses under an electric field (3000 V/cm) and those after the removal of electric field. Period is 0.4 Hz and temperature 18± 0.1 °C.
○: Na_2O 40 mol%, ⊙: Na_2O 35 mol%,
●: Na_2O 30 mol%

of a nylon string.[5-7] The influence from the twist of the string was minimized by using a long string (45 cm). Other advantages of hanging it with a nylon string are that the tension to a sample becomes smaller and the frequency of vibration can be easily varied as much as tenfold for the same sample.

The chuck holding a sample was insulated from metal parts by means of a Pyrex tube, as is shown in Fig. 1, lest an unnecessary vibration should be raised by coulombic force. A sample was connected with such thin copper wire lead (0.075 mm in diameter) that it affected nothing.

The glasses used were systems of SiO_2-Na_2O and B_2O_3-Na_2O. Each sample was about 1.5 mm in diameter and 30 mm in length. Since these glasses are hygroscopic and are apt to cause surface conduction, a drying box with silca gel was used, keeping the humidity low (below 10%).

Hot water within a plastic vessel was used instead of an electric furnace to raise the temperature. Below 0 °C, even a very little moisture was frozen, electrified, and stuck on the surface of a sample, so the temperature range was limited to from 0 to 40 °C.

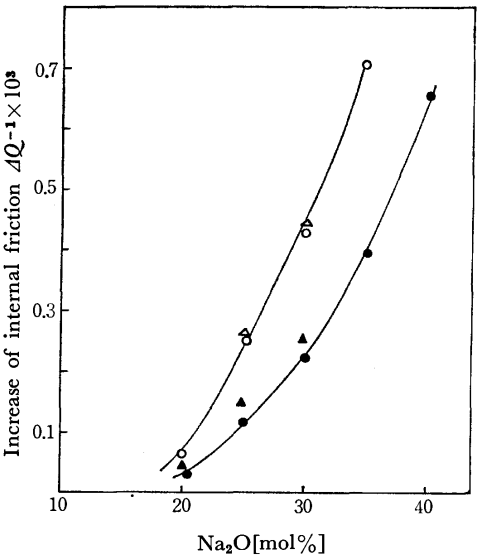

Fig. 3. ΔQ^{-1} value versus Na_2O content after an electric field (3000 V/cm) was applied for two hours. Period is 0.4 Hz and temperature 18±0 1 °C. Relative humidity is above 50% in atmosphere and below 10% in a drying box.
●: Silicate glasses in a drying box
○: Silicate glasses in atmosphere
▲: Borate glasses in a drying box
△: Borate glasses in atmosphere

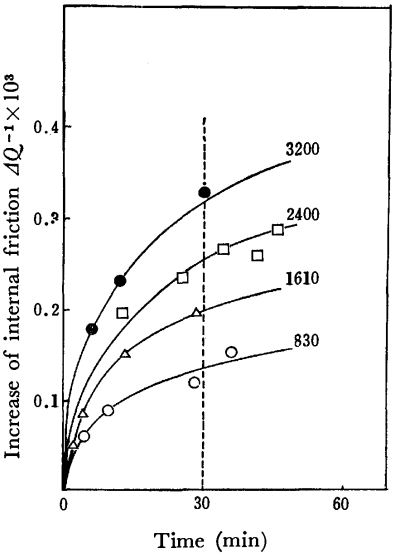

Fig. 4. Increase of internal friction as a function of electric field strength for 0.35 Na_2O+0.65 SiO_2 glasses
Period is 0.4 Hz.
○: 830 V/cm, △: 1610 V/cm, □: 2400 V/cm,
●: 3200 V/cm.

Results

The internal friction at a constant temperature and a constant voltage under continuous torsional oscillation increased gradually with the time finally reaching a constant value, as is shown in Fig. 2. ΔQ^{-1} is the difference between the internal friction under

5) K. E. Forry, *ibid.*, **40**, 90 (1957).
6) J. V. Fitzgerald, *ibid.*, **34**, 314 (1951).
7) G. J. Copley, *Phys. Chem. Glasses*, **8**, 38 (1967).

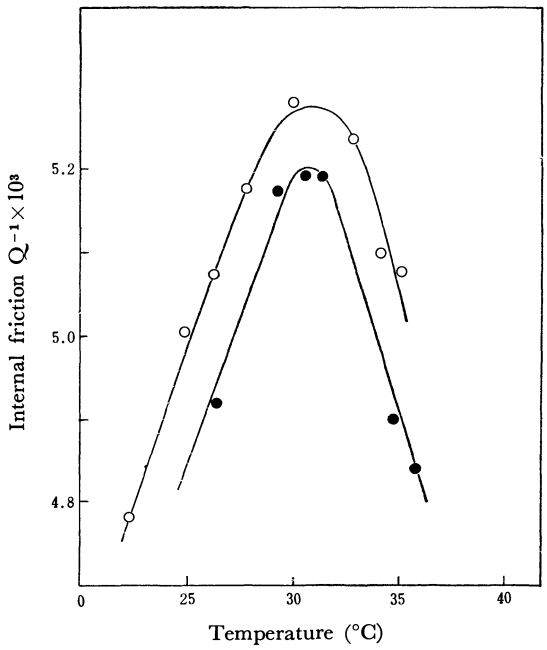

Fig. 5. Influence of electric field on the peak of internal friction for a 0.25 Na_2O+0.75 B_2O_3 glass at 0.4 Hz.
○: under an electric field (2700 V/cm)
●: after removal of an electric field

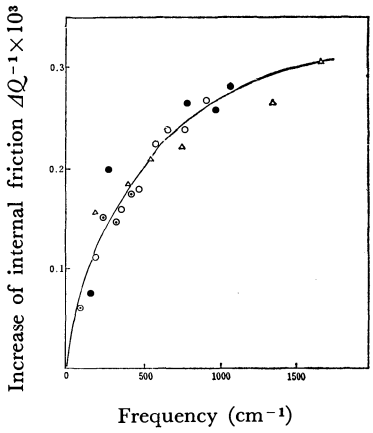

Fig. 6. Relationship between the increase of internal friction and numbers of vibration for a 0.35 Na_2O+0.65 SiO_2 glass at 18 °C. Electric field applied is 2700 V/cm.
○: 0.14 Hz, ⊙: 0.17 Hz, ●: 0.41 Hz, △: 0.69 Hz.

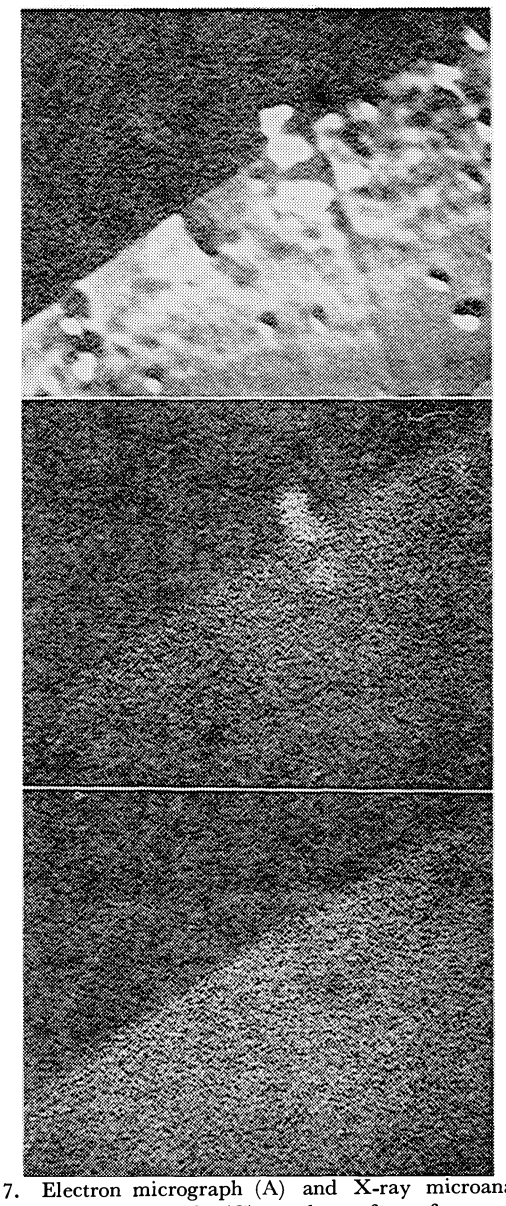

Fig. 7. Electron micrograph (A) and X-ray microanalysis by NaK_α (B) and Si-k_α (C) on the surface of a cut-edge of a 0.40 Na_2O+0.60 SiO_2 glass bar sample near cathode after an electric field was applied for a while. In B some sodium product can be seen at the edge of the surface but in C it can not be seen. Magnification is 1080.

the electric field and that without the electric field. When it reached a constant value, the electric field was removed. The ΔQ^{-1} value decreased gradually and approached zero under continuous torsional oscillation. The internal friction under an electric field was found to increase as the concentration of the sodium ion in a glass increased. The change in internal friction for the 0.4 Na_2O+0.6 SiO_2 glass was especially large, and the ΔQ^{-1} value did not return to zero after the removal of the electric field. This indicates that some irreversible change occurred in the sample.

Figure 3 shows the change in the internal friction versus the Na_2O content. There was little difference between the curves for the SiO_2–Na_2O and B_2O_3–Na_2O systems. Their curves were nearly parabolical. The internal friction, as measured in a drying box, was generally smaller than that in an ordinary room. The increase in internal friction was in proportion to the strength of the electric field. For instance, the ΔQ^{-1} values after the electric field was applied for 30 minutes were found to be proportional to the electric field in the range from 8×10^2 to 32×10^2 V/cm, as is shown in Fig. 4. The electric field had little influence on the peak position, but the background became higher than that obtained without an electric field, as is shown in Fig. 5.

When the ΔQ^{-1} values for various periods were plotted as a function of the numbers of vibration, it was found that the period had no influence, but that the numbers of vibration did influence the change in internal friction, as is shown in Fig. 6.

When a 0.4 Na_2O+0.6 SiO_2 glass was measured, a part of the sample near the chuck on the cathode clouded and then cracked before long. This is pro-

bably because of the presence of product obtained through electrolysis (see Fig. 7). This seems to be the reason why the curve of the internal friction for the 0.4 Na_2O+0.6 SiO_2 glass (Fig. 2) did not return to zero after the removal of the electric field.

Discussion

The curves in Fig. 2 were normalized at their saturated values, as is shown in Fig. 8. Among these curves for the increasing internal friction (solid lines), Curve 3 is quite different from Curves 1 and 2. The difference is caused by electrolysis. In the cases shown by Curves 1 and 2, very little electrolysis occurs, so their internal friction returns to the orginal value after the removal of the electric field. The returning curves 1 and 2, after the removal of an electric field (broken lines), are different from the increasing curves 1 and 2 (solid lines). During this experiment, torsional oscillation was always applied to a sample. If torsional oscillation is not applied under an electric field, the values of the internal friction will scarcely alter at all. The increase in internal friction will occur only when torsional oscillation and an electric field are applied to a sample simultaneously. When an electric field is removed after the internal friction reaches a saturated value, the internal friction decreases rapidly even without torsional oscillation. This suggests that sodium ions which have been raised to a higher potential energy level return to their original lower potential level by thermal vibration. This is one of the causes of the difference between a solid line and a broken line.

The increase in internal friction was scarcely observed in the glass with a low Na_2O content, below 15 mol%, but in the glass of Na_2O above 20 mol% it increased considerably with the Na_2O content, as is shown in Fig. 3. In the glasses of the SiO_2–Na_2O systems, the background of internal friction is large in a glass with a low Na_2O content (below 100 °C) and is large in one with a high content (over 100 °C).[5] It may be supposed that the background below 100 °C is affected by the deformation of the porous frame structure of SiO_2 while over 100 °C it is affected by the increase in the flexibility of the Si–O network due to sodium ions. The background in the temperature range of this experiment seems to be affected mostly by the deformation of the porous frame structure of SiO_2 and very little by the flexibility of the Si–O network. In a higher-Na_2O-content glass, the three-dimensional network structure is destroyed and the background becomes lower. When an Na_2O-containing glass is subjected to torsional oscillation under an electric field, the network structure is apt to be deformed around holes which are left behind by the removal of sodium ions. Thus, the internal friction must increase. The network structure will deform more easily near continuous holes than near an isolated hole. Such continuous holes can be made more in higher-Na_2O-content glasses. Moreover, electrolysis is also apt to occur. This is the reason why the increase in internal friction is high in the glass with a high Na_2O content and very low in the glass with a Na_2O content of less than 15 mol%.

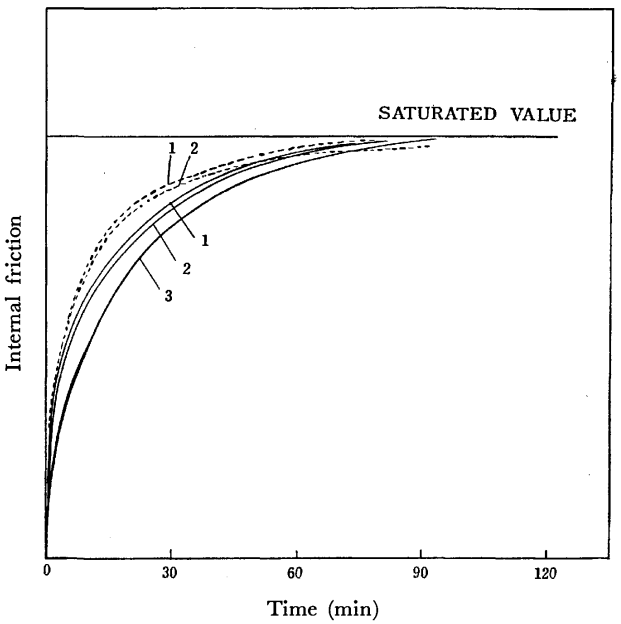

Fig. 8. Variation of internal friction with time. Each saturated value in Fig. 2 is normalized.
1: Na_2O 30 mol%, 2: Na_2O 35 mol%,
3: Na_2O 40 mol%
——: under electric field
----: after the removal of electric field

The results can almost all be explained in terms of Copley's proposal that the increase in background is characteristic of a more open, loosely-bound structure because of the removal of a certain number of sodium ions.[4] The internal friction was found to increase with the strength of the electric field. This means that the number of holes which are left behind by the removal of the sodium ions is proportional to the strength of the electric field, so that the background of internal friction rises in proportion to the number of holes. The characteristic of the increase in the background is, however, related to the network structure of glass composition. From the facts that the increase in background shows saturation with time and that it does not change with the period of torsional oscillation, but with the number of vibrations, a mechanism in which some of the sodium ions moving under an electric field are trapped somewhere in the network structure when the network is deformed can be proposed. As soon as an electric field is applied, some holes are produced by polarization, and hence the background increases, yet sodium ions are supposed to move from a hole to a hole which has nonbridging oxygen ions. When sodium ions are trapped somewhere in the network structure, the number of holes seems to increase. These sodium ions cannot slip easily from the traps without torsional oscillation after an electric field is removed. They can, however, slip gradually because of thermal vibration.

According to Copley's experiment, the peak position of the internal friction caused by sodium ions shifts slightly,[4] but we did not observe such a change. In Copley's experiment, the surface concentration of

the sodium ions changed by electrolysis. In our experiment, the change in the concentration of the sodium ions is caused by polarization and electrolysis occurs only near the cathode in the axial direction of a sample. Therefore, there is probably no influence on the peak position.

BULLETIN OF THE CHEMICAL SOCIETY OF JAPAN, VOL. 46, 1680—1686 (1973)

The Hydrolysis of Ferric Complexes. Magnetic and Spectrophotometric Studies of Aqueous Solutions of Ferric Salts

Masao KIYAMA and Toshio TAKADA

Institute for Chemical Research, Kyoto University, Kyoto 611

(Received December 3, 1971)

Ferric chloro, ferric aquo, and ferric sulfato complexes in acidic solutions have been hydrolyzed at temperatures below 70 °C to form polynuclear complexes of iron(III). Magnetic and spectrophotometric studies have then been carried out in order to clarify the nature of the polynuclear complexes. From these studies, their empirical formulas are presumed to be $Fe_2(OH)_2Cl_2O$, $Fe_2(OH)_3(NO_3)_3$, $Fe_2(OH)_3(SO_4)_{3/2}$, and $Fe_3(OH)_2(SO_4)_{7/2}$. The iron ions in these polynuclear complexes are in a high spin state, as are those in the ferric complexes, iron oxides, and oxyhydrates. It is proposed that, in all these polynuclear complexes except $Fe_3(OH)_2(SO_4)_{7/2}$, edge-shared octahedral dimer units are antiferromagnetically linked with one another by hydroxy or oxo bridging. When the hydrolysis temperature is raised, these polynuclear complexes are further hydrolyzed to form precipitates. The complexes of $Fe_2(OH)_2Cl_2O$, $Fe_2(OH)_3(SO_4)_{3/2}$, and $Fe_3(OH)_2(SO_4)_{7/2}$ give β-FeOOH, α-FeOOH, and $RFe_3(OH)_6(SO_4)_2$ (R=Na, K or NH_4) respectively, whereas the complex of $Fe_2(OH)_3(NO_3)_3$ gives α-FeOOH or α-Fe_2O_3, depending on the temperature.

When ferric salt solutions are heated or made alkaline, the ferric ions in them are hydrolyzed to form precipitates of various iron compounds. It is known that a ferric chloride solution gives β-FeOOH,[1-3] whereas a ferric nitrate solution gives α-FeOOH or α-Fe_2O_3, or a mixture of them, depending on the hydrolysis temperature.[4,5] Also, a ferric sulfate solution gives α-FeOOH or a basic sulfate, or a mixture of them, depending on the pH.[6] We consider that what kind of precipitate is formed by hydrolysis is closely connected with the nature of the ferric complexes present in the solutions just before the formation of precipitates.

The ferric complexes which are present as monomers in strongly acidic solutions of ferric salts have so far been studied by means of X-ray diffraction,[7,8] spectrophotometry,[9-13] magnetic measurement,[14-16] potentiometry,[17] *etc.* Among these methods the spectrophotometry in the region of electronic absorption has been used particularly for the study of Cl^-, SO_4^{2-}, and OH^- ligands. The electronic absorption curves of acidic solutions of ferric salts have been studied by many investigators. It has been clarified by these studies that such ferric complexes as chloro, sulfato, hydroxo, and aquo complexes are present in the strongly acidic solutions, depending on the kind and concentration of the anions in them. By decreasing the acidity of the solutions, polynuclear complexes of iron(III) are formed.

The polynuclear complexes formed in solutions of ferric perchlorate and ferric nitrate have also been studied by several investigators. From a potentiometric study, Hedstrom first proposed that the polynuclear complex formed by the hydrolysis of a diluted ferric perchlorate solution was a dimer.[17] The pH dependence of the magnetic susceptibilities and the optical absorption spectra of similar solutions was studied by Mulay and Selwood, who proposed that a diamagnetic dimer was formed by the hydrolysis of the same.[18] Also, Zvyagintsev and Loppato reported that a tetramer was formed by the hydrolysis of ferric nitrate.[19] The polynuclear complex in a ferric nitrate solution was studied in detail by Spiro *et al.* using various methods. Spiro *et al.* observed that the poly-

1) W. O. Milligan and H. B. Weiser, *J. Amer. Chem. Soc.*, **57**, 238 (1935).
2) A. L. MacKay, *Mineral. Mag.*, **32**, 545 (1960).
3) R. H. H. Wolf, M. Wrisscher, and J. Siparo-Zulijevic, *Kolloid-Z. Z. Polymere*, **215**, 57 (1967).
4) K. Wefers, *Ber. D. K. G.*, **43**, 677 (1966).
5) I. Kataoka, *Nihon Dojo Hiryo Gakkai Shi*, **29**, 9 (1959).
6) T. V. Arden, *J. Chem. Soc.*, **1951**, 350.
7) C. L. Standley and R.F. Kruh, *J. Chem. Phys.* **34**, 1450 (1961).
8) M. D. Lind, *ibid.*, **46**, 2010 (1967).
9) A. V. Kiss, J. Abrham, and I. Hegedus, *Z. Anorg. Allg. Chem.*, **244**, 98 (1940).
10) E. Rabinowitch and W. H. Stockmayer, *J. Amer. Chem. Soc.*, **64**, 335 (1942).
11) G. A. Gamlen and D. O. Jordan, *J. Chem. Soc.*, **1953**, 1435.
12) M. Ishibashi, T. Shigematsu, Y. Yamamoto, M. Tabuchi, and T. Kitagawa, This Bulletin, **30**, 433 (1957).
13) R. A. Whiteker and N. Davidson, *J. Amer. Chem. Soc.*, **75**, 3081 (1953).
14) I. Dezsi, V. D. Gorobchenko, I. I. Lukashevich, and A. Vertes, *Chem. Phys. Lett.*, **2**, 665 (1968).
15) A. Bose, *Proc. Ind. Acad. Sci., A*, **1**, 754 (1934).
16) S. Broersma, *J. Chem. Phys.*, **26**, 1405 (1957).
17) B. O. A. Hedstrom, *Arkiv Kemi*, **6**, 1 (1953).
18) L. N. Mulay and P. W. Selword, *J. Amer. Chem. Soc.*, **77**, 2693 (1955).
19) O. E. Zvyagintsev and Yu. S. Lopatto, *Russian J. Inorg. Chem.*, **6**, 439 (1961).

nuclear complex consisted of a great number of iron ions.[20] Further, the structure of this complex was discussed by Schugar *et al.*, who pointed out that it was not a diamagnetic complex, but a paramagnetic one with a spin angular moment of $S=1$ per iron, and presumed that it was composed of many aquo dimers, $Fe=(OH)_2=Fe$.[21]

In order to discuss the mechanism of precipitation in solutions of different ferric salts, further investigations of the nature of complexes present in the solutions are needed. In this paper, the possible structure and the chemical composition of the polynuclear complexes will be discussed on the basis of the spectrophotometric and magnetic data.

Experimental

Sample Solution. Chemical reagents of an analytica grade were used in the present experiments. Desired quantities of ferric chloride, ferric nitrate, and ferric sulfate were dissolved in 1.00 N hydrochloric acid, nitric acid, and sulfuric acid solutions respectively. To each of these strongly acidic solutions of ferric salts, alkali solutions were added in various ratios below the chemical equivalent. By this addition, a precipitate was formed. However, it disappeared on agitation. The resultant acidic solutions were diluted with distilled water to desired concentrations of the ferric ion and stored in polyethylene bottles. The magnetic susceptibilities and the absorption spectra of these acidic solutions, which contained no visible precipitates, were then measured.

Apparatus. The measurements of the optical absorption spectra were carried out using a Shimadzu spectrometer, Model QR-50. The optical path in its sample container was selected from among 0.003, 0.010, and 1.0 cm by the use of quartz spacers of different sizes according to the concentration of the ferric ion and the frequency of the light. The absorbance value was obtained at intervals of 0.5 mμ. The extinction coefficient was calculated using Lambert-Beer's formula.

The magnetic susceptibilities of the solutions were measured as follows. A schematic illustration of the magnetic balance used is shown in Fig. 1. Each solution was introduced into a double cylindrical vessel (A) 2.5 cm in external diam., 1.8 cm in internal diam., and 40 cm in length, which was placed between the pole pieces of a magnet (B). A cylindrical quartz rod (C) with a cross-sectional area of 0.48 cm^2 and a length of 20 cm was hung in the vessel by means of a platinum wire from one arm of a chemical balance (D). The lower end of the rod was brought to the center between the pole pieces.

The repulsion force, F, of the lower end of the rod was measured by the chemical balance in the magnetic field range 0.2—13.5 kOe. The magnetic susceptibility, K, per unit of volume of the solution was calculated as follows:

$$2F/(H_A^2-H_B^2)A = K - K_0$$

where H_A is the strength of the magnetic field at the lower end of the rod; H_B, that at the upper end (negligibly small); K_0, the magnetic susceptibility per unit of volume of the rod, and A, the cross sectional area of the rod. The magnetic susceptibility of the rod was calibrated with a standard solution of $NiCl_2$ and was found to be

$$-0.395\times10^{-6}/cm^2(-0.878\times10^{-6}/g).$$

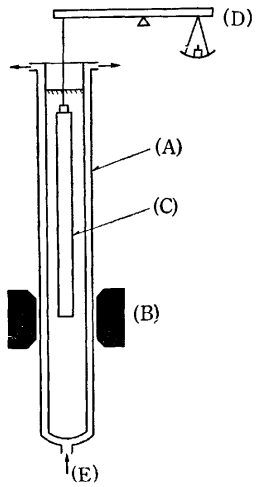

Fig. 1. Schematic illustration of vessel and magnetic balance used.
(A) Double cylindrical vessel, (B) Magnet, (C) Quartz rod, (D) Chemical balance, (E) Temperature-controlled water

The density of the solution was measured by using a density bottle, while the magnetic susceptibility per g-atom of the ferric ion in the solution was calculated making corrections for the diamagnetic elements in the solution. The magnetic moment, μ_{eff}, was calculated by the usual formula, $\mu_{eff}=2.84\sqrt{X_{Fe}\times T}$, where T is the absolute temperature. The pH was measured using a Horiba electrode pH meter.

Results

Spectrophotometric Data. Figures 2, 3, and 4 show the absorption curves of acidic solutions containing 0.3 N-ferric salt, 0.5 N-acid, and alkali in different concentrations from 0 to 0.7 N. There are absorption bands with peaks at 90 and 130×10^{13} Hz for the chloride, at 120×10^{13} Hz for the nitrate, and at 100 and 130×10^{13} Hz for the sulfate. When the acidity was decreased, the colors of these solutions (yellow for the chloride, light blue for the nitrate, and orange yellow for the sulfate) changed to reddish brown and these absorption bands broadened as may be seen in these figures. In order to find the relation between the frequencies of the peaks of absorption bands and the experimental conditions, optical measurements of acidic solutions with different concentrations of ferric salt, acid, and alkali were carried out in the frequency range from 70 to 140×10^{13} Hz at different temperatures. The results are given in Tables 1, 2, and 3.

Magnetic Data. Magnetic measurements of the same solutions were made in the range from 0.2 to 13.5 kOe at different temperatures. Their susceptibilities did not show any magnetic-field dependence at a given temperature. The magnetic moments, μ_{eff}, calculated from the magnetic data are given in the right-hand columns of Tables 1, 2, and 3.

In the above experiments, the pH values of the so-

20) T. G. Spiro, S. E. Allerton, J. Renner, A. Terzis, R. Bills, and P. Saltman, *J. Amer. Chem. Soc.*, **88**, 2721 (1966).
21) H. Schugar, C. Walling, R. B. Jones, and H. B. Gray, *ibid.*, **89**, 3712 (1967).

Fig. 2. Absorption curves of solutions containing 0.1 M-$FeCl_3$, 0.5 M HCl and nM NaOH at 25 °C: ---- n=0; ----- n=0.5; ---- n=0.6; —— n=0.7.

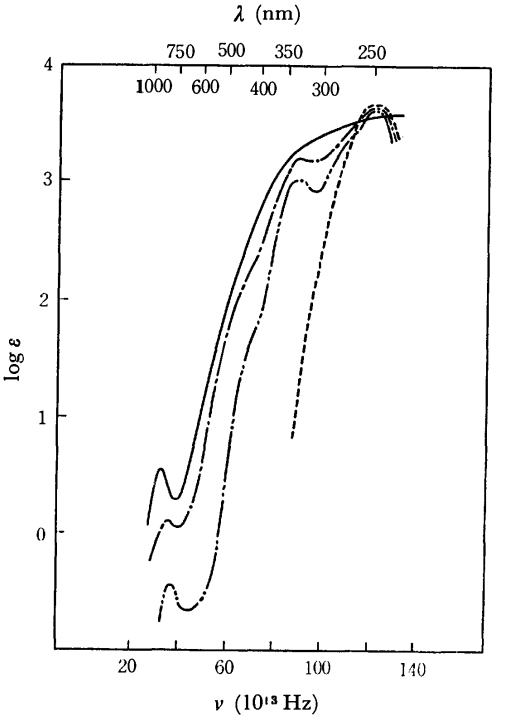

Fig. 3. Absorption curves of solutions containing 0.1 M $Fe(NO_3)_3$, 0.5 M HNO_3 and nM NaOH at 25 °C: ---- n=0; ----- n=0.5; ---- n=0.6; —— n=0.7.

lutions with no excess acid decreased with the time and the time dependence of the pH became smaller upon a decrease in the temperature. In order to obtain the susceptibility at different acidities, magnetic measurements of the solutions 0.1 g-iron atom/l at 17 °C were made at 13.5 kOe. The experimental results are summarized in Table 4.

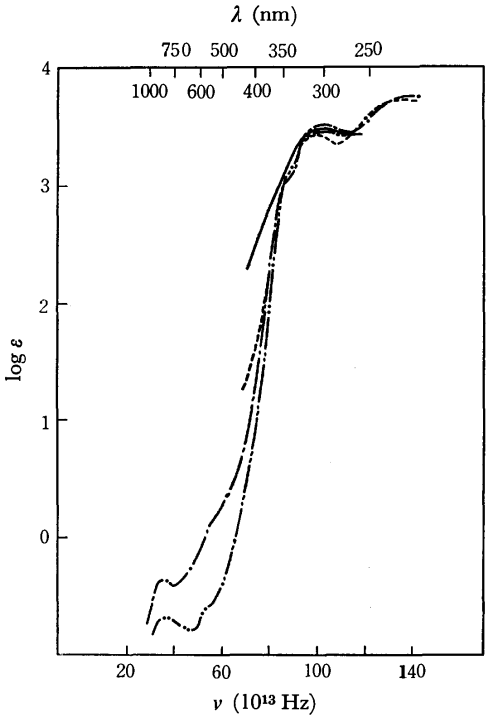

Fig. 4. Absorption curves of solutions containing 0.05 M $Fe_2(SO_4)_3$, 0.25 M H_2SO_4 and nM NaOH at 25 °C: ---- n=0; ----- n=0.5; ---- n=0.6; —— n=0.7.

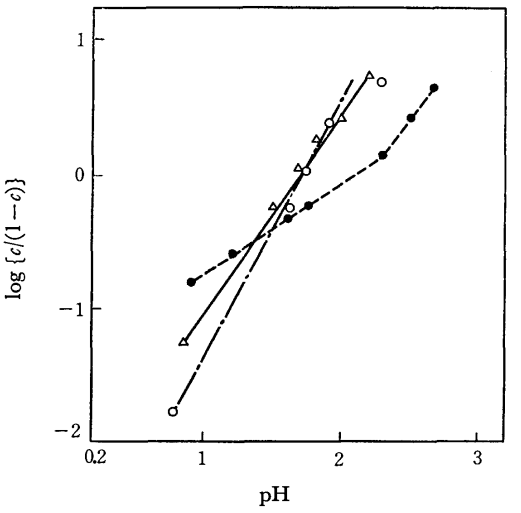

Fig. 5. Fraction of iron ions hydrolyzed in ferric salt solutions (0.1 g-iron atom/l) at various pH at 17 °C. The fraction is given by log $\{c/(1-c)\}$, where c is the concentration of iron ions present as polynuclear complexes: ○=chloride, △=nitrate, ●=sulfate.

Discussion

In strongly acidic solutions of ferric chloride, ferric sulfate, and ferric nitrate, ferric chloro, ferric sulfato, and ferric aquo complexes are formed respectively. These ferric complexes strongly absorb the light of frequencies in the ultraviolet region, the frequencies of the peaks of their absorption bands depending on the kind of ligands in them. Table 5 gives the frequencies and wavelengths of their peaks in the ultraviolet region.

Tables 1—3 indicate that the ferric complexes in

Table 1. Spectrophotometric data and magnetic moments of iron ions in chloride solution
(a=NH_4OH, b=NaOH used as alkali)

Composition (mol/l)			Temp. (°C)	ν (10^{13}/s)	log·ε	ν (10^{13}/s)	log ε	μ_{eff} (BM)
$FeCl_3$	HCl	Alkali						
0.01	0.5	0	30	90	3.0	132	3.7	5.8
0.01	0.5	0	50	90	3.1	134	3.7	5.8
0.01	0.5	0	70	90	3.2	134	3.7	5.8
0.01	0.5	0.45 a	30	90	3.0	136	3.7	5.8
0.01	0.5	0.45 a	60	90	3.2	136	3.7	5.8
0.01	0.5	0.51 a	30	92	3.3	136	3.7	4.4
0.01	0.5	0.52 a	30	105	3.4	136	3.7	
0.10	0.5	0	30	90	3.27	134	3.82	5.93
0.10	0.5	0	60	89	3.38			5.99
0.10	0.5	0.50 b	30	90	3.31	134	3.76	5.4
0.10	0.5	0.50 b	60	89	3.38			5.5
0.10	0.5	0.70 b	30	102	3.43	139	3.73	4.4

Table 2. Spectrophotometric data and magnetic moments of iron ions in nitrate solutions
(a=NH_4OH, b=NaOH used as alkali)

Composition (mol/l)			Temp. (°C)	ν (10^{13} Hz)	log ε	ν (10^{13} Hz)	log ε	μ_{eff} (BM)
$Fe(NO_3)_3$	HNO_3	Alkali						
0.004	0.022	0	35	120	3.46			5.8
0.004	0.022	0	70	102	3.10			5.8
0.004	0.022	0.008 a	35	103	3.16			
0.004	0.022	0.008 a	50	100	3.42			
0.004	0.022	0.008 a	70	100	3.42			
0.05	0.50	0	21	125	3.68			5.7
0.05	0.50	0	60	125	3.64			5.6
0.05	0.50	0.50 b	19	125	3.65	91	3.01	5.2
0.05	0.50	0.50 b	60	126	3.64	91	3.12	4.9
0.05	0.50	0.60 b	19	125	3.55	91	3.07	5.0
0.05	0.50	0.60 b	60	127	3.61			4.8
0.10	0.50	0.50 b	19	90	3.02			5.2
0.10	0.50	0.50 b	60	90	3.12			5.1
0.10	0.50	0.60 b	19	90	3.16			4.9

Table 3. Spectrophotometric data and magnetic moments of iron ions in sulfate solutions
(a=NH_4OH, b=$(NH_4)_2SO_4$, c=LiOH, d=CH_3COONa used as alkali or additive)

Composition (mol/l)			Temp. (°C)	ν (10^{13} Hz)	log ε	ν (10^{13} Hz)	log ε	μ_{eff} (BM)
$Fe_2(SO_4)_3$	H_2SO_4	Other						
0.005	0.025	0	27	135	3.5	98	3.2	5.8
0.005	0.025	0.05 a	27	137	3.5	101	3.3	5.0
0.005	0.025	0.06 a	27	138	3.8	104	3.5	4.5
0.025	0.25	0	20	135	3.73	100	3.42	5.6
0.025	0.25	0.5 b	20	137	3.73	101	3.52	5.6
0.025	0.25	1.0 b	20	101	3.55			5.6
0.025	0.25	2.0 b	20	101	3.60			5.5
0.025	0.25	0.5 c	20	137	3.78	100	3.51	5.4
0.025	0.25	0.6 c	20	139	3.77	101	3.51	5.1
0.025	0.25	0.5 d	20	100	3.49			5.2
0.025	0.25	0.5 d	60	99	3.09			5.0
0.025	0.25	1.0 d	20	89	3.19			3.1
0.025	0.25	1.0 d	60	89	3.1			3.4
0.025	0.25	2.0 d	20	89	3.24			3.1
0.025	0.25	2.0 d	60	89	3.3			3.5
0.050	0.25	0	30	137	3.72	100	3.47	5.7
0.050	0.25	0.5 c	30	138	3.74	101	3.47	5.4
0.050	0.25	0.6 c	30	139	3.75	103	3.50	5.1
0.050	0.25	0.7 c	30	109	3.50			4.1
0.050	0.25	0.5 d	20	97	3.45			5.2
0.050	0.25	2.0 d	20	89	3.2	121	3.3	3.1
0.050	0.25	2.0 d	60	89	3.3			3.6

TABLE 4. MAGNETIC DATA OF SOLUTIONS OF FERRIC CHLORIDE, NITRATE AND SULFATE AT 17 °C

Composition (mol/l)			pH	Sp. gr.	$-F$ (mg)	$-K$ ($\times 10^6$)	X_{Fe} ($\times 10^2$)	μ_{eff}
Ferric salt	Acid	Alkali						
$FeCl_3$	HCl	NaOH						
0.10	0.50	0	0.5	1.021	66.5	0.731	1.41	5.96
		0.10	0.52	1.022	65.5	0.690	1.38	5.90
		0.20	0.57	1.026	65.5	0.690	1.38	5.90
		0·40	0.93	1.030	65.0	0.677	1.37	5.88
		0.50	1.64	1.032	54.0	0.414	1.11	5.30
		0.60	1.73	1.033	49.0	0.294	0.99	5.00
		0.70	1.90	1.035	42.7	0.144	0.84	4.62
		0.75	2.29	1.036	38.5	0.044	0.75	4.34
$Fe(NO_3)_3$	HNO_3	NaOH						
0.10	0.50	0	0.58	1.035	65.2	0.682	1.38	5.90
		0.10	0.63	1.038	66.0	0.702	1.39	5.91
		0.20	0.70	1.040	64.5	0.665	1.36	5.85
		0.40	0.86	1.043	63.0	0.630	1.33	5.78
		0.50	1.49	1.047	53.5	0.402	1.10	5.26
		0.60	1.69	1.048	48.5	0.282	0.98	4.98
		0.70	1.83	1.049	44.7	0.192	0.89	4.74
		0.75	2.00	1.050	42.3	0.134	0.83	4.58
		0.77	2.20	1.053	39.2	0.056	0.76	4.36
$Fe_2(SO)_4$	H_2SO_4	LiOH						
0.05	0.25	0	0.78	1.035	64.3	0.662	1.365	5.85
		0.10	0.80	1.039	63.2	0.634	1.28	5.69
		0.20	0.89	1.040	62.5	0.618	1.27	5.64
		0.40	1.18	1.047	61.0	0.582	1.22	5.53
		0.50	1.58	1.050	58.2	0.514	1.15	5.38
		0.55	1.73	1.050	56.5	0.453	1.10	5.24
		0.60	2.31	1.051	49.0	0.296	0.95	4.87
		0.65	2.42	1.051	43.5	0.163	0.83	4.56
		0.70	2.62	1.053	40.5	0.093	0.76	4.35

TABLE 5. FREQUENCIES (ν IN 10^{13} Hz) AND WAVE LENGTHS (λ IN mμ) OF ABSORPTION BANDS OF VARIOUS FERRIC COMPLEXES

Complex	ν	λ	ν	λ	ν	λ	Ref.
$[Fe(H_2O)_6]^{3+}$	111	270	125	240			10, 11, 18
$[FeOH]^{2+}$	125	240					18
$[Fe_2(OH)]_2^{4+}$	89	335					18
$[FeCl]^{2+}$	88	340	122	245			11
$[FeCl_2]^{+}$	88	340	122	245			11
$[FeCl_3]$	75	400	88	340	120	250	11
$[FeCl_4]^{-}$	83	360	96	310	120	250	11
$[FeSO_4]^{+}$	99	303					13
$[Fe(SO_4)_2]^{-}$	100	300					13

the strongly acidic solutions are paramagnetic in a high spin state, and that the frequencies of the peaks are determined by the kind and concentration of the anions in the solutions. Regardless of the concentration of ferric ions and the temperature, peaks appear at 89—90 $\times 10^{13}$ Hz, 120—125 $\times 10^{13}$ Hz, and 98—100 $\times 10^{13}$ Hz for strongly acidic solutions of ferric chloride, ferric nitrate, and ferric sulfate respectively. These peaks are due to ferric chloro, ferric aquo, and ferric sulfato complexes respectively. The strongly acidic solutions of ferric chloride and ferric sulfate show peaks (though not sharp) in the region of 132—137 $\times 10^{13}$ Hz, too. They are considered to be due to ferric chloro and ferric sulfato complexes respectively.

As the acidity of the strongly acidic solutions is decreased, the absorption bands become broad and obscure, as may be seen in Figs. 2, 3, and 4. This broadening may be due to the fact that a polynuclear complex containing a great number of ferric ions is formed in each solution and that its concentration increases with a decrease in the acidity, so that light in the ultraviolet region is strongly scattered. Also, the increase in the concentration of the polynuclear complex causes the magnetic susceptibility, X, of the ferric ions to decrease. The decrease in X may be due to the fact that the polynuclear complex contains antiferromagnetic couplings, though the ferric ions in the polynuclear complex as well as those in the strongly acidic solutions are in a high-spin state, as will be described later.

It is known that all the ferric ions present in crystals of α-FeOOH, β-FeOOH, and α-Fe_2O_3 are in a high spin state (S=5/2, five unpaired spins per iron) and are bound to O^{2-} and/or OH^- ions at angles of 90°

and either 120° or 180°.[22-25] When the bond angle between these ferric ions is between 120° and 180°, the spins can align themselves to each other by means of a superexchange interaction whose strength depends on the distance and angle between them. This bridging, called an antiferro magnetic coupling, causes the X value to decrease. Because both the iron ions in the ferric complexes and those in the final products of hydrolysis are in a high spin state, it is reasonable to consider that the iron ions in the polynuclear complexes, intermediates, are not in a low spin state, but in a high spin one, and that the polynuclear complexes must have antiferromagnetic couplings, causing the decrease in the X value.

It is known that upon a decrease in the acidity, the X decreases to a certain value. According to Mulay and Selwood's magnetic data, X of the ferric ions in a 0.04 M $Fe(ClO_4)_3$ solution at 16 °C decreased to 6.3 and 6.2×10^{-3} per g-iron atom when the pH was increased to 1.9 and 2.45 respectively.[18] Schuger et al. also reported that, in a 0.195 M $Fe(ClO_4)_3$ solution at 25 °C, X decreased to about 6.9×10^{-3} per g-iron atom.[21] It is supposed that when the solution reaches a state where a further decrease in its acidity causes hardly any decrease in X, most of the ferric complexes in it have been hydrolyzed to form a polynuclear complex.

The usual formula for the hydrolysis of the ferric ion is written as follows:

$$Fe^{3+} + nH_2O = Fe(OH)_n^{3-n} + nH^+$$

Let c represent the wt fraction of ferric ions as a polynuclear complex, $Fe(OH)_n^{3-n}$; X_{Fe}, the susceptibility/g-atom of the total ferric ions present at different acidities; X_T, that/g-atom of ferric ions present as a ferric complex, Fe^{3+}; and X_P, that/g atom of ferric ions present as the polynuclear complex. Assuming that $X_{Fe}=cX_P+(1-c)X_T$ and that X_P is independent of acidity, it is given as:

$$c = (X_T-X_{Fe})/(X_T-X_P)$$

In the present experiment, unfortunately, the X value independent of the acidity could not be obtained (the magnetic measurements were not made for the solutions with higher pH values than the values shown in Table 4, as the presence of a precipitate was observed). From the X_{Fe} values in Table 4, the c values at different acidities are calculated for the solutions at 17 °C using the $X_P=6.2\times10^{-3}$ obtained by Mulay and Selwood.[18] The c values thus obtained are plotted against the pH in Fig. 5. As may be seen in the figure, the points for the chloride and the nitrate are on straight lines, while those for the sulfate on a curved line. These lines have different slopes and intercepts. Since $\log K=\log(Fe(OH)_n^{3-n})\times(H^+)^n/(Fe^{3+})$ in the hydrolysis formula, the slope(n) and intercept ($\log K$) represent the OH^- (or $2O^{2-}$)/Fe^{3+} ratio in each polynuclear complex and its formation constant respectively. The n and $\log K$ values obtained are given in Table 6.

Table 6. Slopes (n) and intercepts ($\log K$) for each ferric salt solution in Fig. 5

Chloride		Nitrate		Sulfate			
n	$\log K$	n	$\log K$	n	$\log K$	n	$\log K$
2.2	−3.7	1.4	−2.5	0.7	−1.4	1.4	−3.0

It is supposed that the X_P value depends on the particle size and the structure of the polynuclear complex which are affected by the kind of ferric complex. Spiro *et al.* reported that the particle size of the polynuclear complex in the nitrate is nearly independent of the degree of hydrolysis of the aquo ferric complex.[20] The nature of the polynuclear complexes formed by the hydrolysis of the aquo ferric complex has been widely studied, but that of the polynuclear ones formed by the hydrolysis of other ferric complexes, such as the chloro ferric complexes, has not yet been sufficiently studied.

We believe that the X_P value of the polynuclear complex formed in the ferric chloride solution is not less than 3.4×10^{-3}, which is the room-temperature molar susceptibility of the final product, β-FeOOH, of the hydrolysis of the ferric chloro complexes. The c values for the chloride are also calculated using $X_P=3.4\times10^{-3}$. The n and pK values for the chloride obtained by the graphical method are 2 and 3.7 respectively.

These n values suggest that the polynuclear complex formed by the hydrolysis of the aquo ferric complex in the nitrate contains $[Fe_2(OH)_3]^{3+}$ cations. In the sulfate, a polynuclear complex containing $[Fe_2(OH)_3]^{3+}$ or one containing $[Fe_3(OH)_2]^{7+}$, or a mixture of them, is formed, depending on the pH. The polynuclear one formed in the chloride contains $[Fe(OH)_2]^+$ cations.

It is impossible to determine from the n values whether the ligand is OH^- or O^{2-}. Tables 2 and 3 show that when the acidity of ferric nitrate solutions is decreased, absorption peaks appear at 90—91 $\times10^{13}$ Hz, and that when a ferric sulfate solution is added to excess sodium acetate, a peak appears at 89×10^{13} Hz. It was found by Schugar *et al.* that a dimeric complex, $[Fe(pic)_2OH]_2$(pic=picolinic radical), contains a dihydroxo-bridged structural unit, $Fe_2(OH)_2$.[26] Also, Anderegg pointed out that $[Fe(pic)_2OH]_2$ and polynuclear complexes formed by the hydrolysis of a ferric aquo complex must have a similar bridging structure, because they exhibit similar electronic spectral bands at 87.5 and 89×10^{13} Hz respectively.[27] It is evident that the dihydroxo-bridged structural units exist in the polynuclear complexes containing $Fe_2(OH)_3$ cations. Where edge-shared octahedral dimers, $[Fe_2(OH)_2(H_2O)_8]^{4+}$, are weakly bound by water molecules to form a polynuclear complex, the decrease in the X value may, however, be slight at room temperature, since magnetic superexchange

22) Y. Bando *et al.*, *J. Phys. Soc. Jap.*, **20**, 2086 (1955).
23) T. Takada *et al.*, *ibid.*, **19**, 1744 (1964).
24) T. Shinjo, *ibid.*, **21**, 917 (1966).
25) D. L. Keszthelyi, D. Kulgawczuk, B. Mcinar, and N. A. Eissa, *Phys. Status Solidi.*, **22** 617 (1967).
26) H. J. Schugar, G. R. Rossmann, and H. B. Gray, *J. Amer. Chem. Soc.* **91**, 4564 (1969).
27) von G. Anderegg, *Helv. Chim. Acta*, **43**, 1530 (1960).

interaction is weak. We propose that the edge-shared octahedral dimers are antiferromagnetically bound together by monohydroxo-bridging to give a zigzag polynuclear cation of a structure such as is shown below:

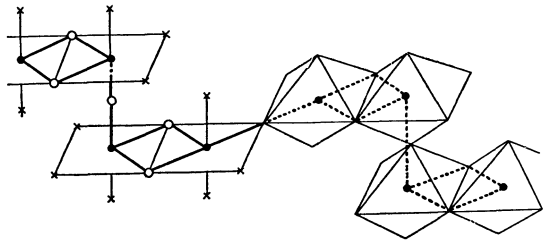

where ●, O, and × are Fe^{3+}, OH^-, and H_2O respectively.

The ferric chloride solutions show absorption peaks at 90×10^{13} Hz regardless of the presence of polynuclear complexes. Therefore, it is impossible to determine from the spectroscopic data whether or not the polynuclear complex in the chloride contains the dimers. However, from the crystal structure and magnetic properties of the β-FeOOH formed by the hydrolysis of ferric chloride,[2,25] it can be presumed that the edge-shared octahedral dimers are antiferromagnetically bound together by oxo-bridging to give a ring-like polynuclear cation of a structure such as is shown below:

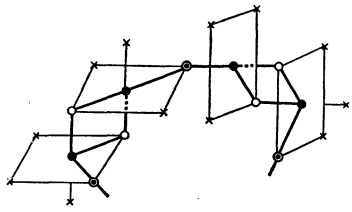

where ●, O, ⊙, and × are Fe^{3+}, OH^-, O^{2-}, and H_2O respectively.

The polynuclear complexes may be composed of the polynuclear cations and the acid ions, NO_3^-, $SO^2{}_4^-$, and Cl^-; they would thus be enabled to keep their electric neutrality. Among these anions, SO_4^{2-} and Cl^- are probably bound to the ferric ions as ligands in these complexes. The reactions by which the polynuclear complexes are formed may be roughly expressed by the following formulas, where the H_2O ligands are omitted:

$$2Fe(NO_3)_3 + 3H_2O = Fe_2(OH)_3(NO_3)_3 + 3HNO_3$$

$$Fe_2(SO_4)_3 + 3H_2O = Fe_2(OH)_3(SO_4)_{3/2} + (3/2)H_2SO_4$$

$$(3/2)Fe_2(SO_4)_3 + 2H_2O = Fe_3(OH)_2(SO_4)_{7/2} + H_2SO_4$$

$$2FeCl_3 + 4H_2O = Fe_2(OH)_2Cl_2O + 4HCl$$

On heating, these polynuclear complexes are further hydrolyzed. The $Fe_2(OH)_3(SO_4)_{3/2}$ and $Fe_2(OH)_3(NO_3)_3$ complexes form the precipitate of α-FeOOH, and the $Fe_2(OH)_2Cl_2O$ complex forms the precipitate of β-FeOOH. When Na^+, K^+, or NH_4^+ ion exists in the acidic solution of ferric sulfate, (Na, K or NH_4)-$Fe_3(OH)_6(SO_4)_2$ is formed as a crystalline precipitate of the basic sulfate.

When the temperature is raised, α-Fe_2O_3 is formed. Also, the formation temperature differs with the kind of polynuclear complex. For example, α-Fe_2O_3 began to be formed at about 60 °C in the ferric nitrate solution, and at about 90 °C in the sulfate and chloride solutions. Which is formed, α-Fe_2O_3 or FeOOH (α or β), may be determined by the change in the structures of the polynuclear complexes. It may also be supposed that the temperature at which the structural change begins is lower for the $Fe_2(OH)_3(NO_3)_3$ complex than for the others. The temperature dependence of the magnetic susceptibility of the ferric ions in acidic solutions of ferric nitrate, ferric chloride, and ferric sulfate was investigated by Bose at temperatures between room temperature and the boiling point.[15] His data suggest that the structure of the ferric ion in the nitrate solution varies with the temperature, since among these three kinds of ferric ions, the ferric ion in the nitrate solution has a magnetic transition point at about 343 K (70 °C) on the $1/X$ *vs.* temperature (K) curve.

Our proposal on the compositions and structures of the polynuclear complexes can well explain the experimental results obtained by many workers. It also gives a fundamental understanding of their nature. In order to clarify the mechanism of precipitation in ferric salt solutions, it will be necessary to determine precisely the compositions and structures of the polynuclear complexes present in them.

One of us (M. K.) is indebted to Professor Yuroku Yamamoto, Hiroshima University, for suggesting this problem and to Mr. Yoshihiro Onoda for his assistance in the experiments. Thanks are also due to Drs. Toshiro Tsuji, Yoshichika Bando and Teruya Shinjo for their valuable discussions.

Isomerism of the Metal Complexes Containing Multidentate Ligands. III. Geometric and Optical Isomers of the Tris(2-methyl-1,2-propanediamine)cobalt(III) Ion[1]

Masaaki KOJIMA, Yuzo YOSHIKAWA, and Kazuo YAMASAKI

Department of Chemistry, Faculty of Science, Nagoya University, Chikusa-ku, Nagoya 464

(Received December 11, 1972)

The tris(2-methyl-1,2-propanediamine)cobalt(III) complex was prepared, and four possible isomers, geometrical and optical, were isolated by column chromatography on SP-Sephadex. Their configurations were assigned on the basis of the formation ratio and electronic, infrared, circular dichroism and PMR spectra: they were later confirmed by X-ray analysis.

For a tris(diamine) complex with a symmetrical bidentate ligand like ethylenediamine, only a pair of optical isomers are formed, whereas for a complex with an unsymmetrical bidentate ligand geometrical isomers can be expected in addition to optical isomers. In 1968 MacDermott[2] separated *mer* and *facial* isomers of Λ-[Co(*l*-pn)$_3$]$^{3+}$* as the chloride and bromide by the gradual evaporation of their aqueous solutions, and found that the physical properties were similar for these two isomers. More recently, Crossing and Snow[3] tried to study the *mer* isomer by X-ray structure analysis, but they failed to find good crystals for their purpose.

With unsymmetrical 2-methyl-1,2-propanediamine (*iso*-butylenediamine, abbreviated as ibn) as the ligand, the isolation and characterization of four isomers, geometrical and optical, of the tris(ibn)cobalt(III) complex will be described in this paper (*cf.* Fig. 1).

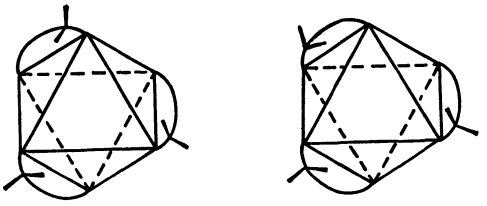

Λ(*facial*) Λ(*mer*)

Fig. 1. Geometric isomers of Λ-[Co(ibn)$_3$]$^{3+}$.

Experimental

Measurements. All the measurements were done in the same way as in the previous papers.[1]

Ligand. The *iso*-butylenediamine was obtained from the Aldrich Chem. Co., U.S.A., and was used without further purification.

Preparation of the Complex. To 3.8 g (10 mmol) of [CoBr(NH$_3$)$_5$]Br$_2$ suspended in 50 ml of water, 3 g (34 mmol) of the ligand was added. After 0.5 g of active charcoal had been added, the mixture was stirred for several days at room temperature; the brown solution thus obtained was directly subjected to column chromatography on SP-Sephadex after the removal of the charcoal.

Chromatographic Separation of the Isomers. A column chromatographic method on ion-exchange Sephadex developed by us[4] was used to separate and, at the same time, resolve the isomers. The SP-Sephadex C-25 used was a product of Pharmacia, Sweden, which has sulfopropyl groups as the cation-exchange group. An SP-Sephadex column of ϕ2.7 cm × 130 cm was prepared; on the top of the adsorbent layer, the same SP-Sephadex, saturated in advance with the prepared complex solution, was poured so as to make a layer about 5 mm thick. As the eluent we used a 0.15 M sodium (+)$_{589}$-tartrate solution with an elution velocity of 0.4—0.5 ml per minute. Under these conditions, 7—10 days were required for the complete elution of the complex, which produced three separate bands, I, II, and III (Fig. 2). The effluent was separated into fractions of 15 ml each, and the absorbance of each fraction at 475 nm (cell thickness, 1 cm) was plotted against the volume ratio of the effluent (V) *versus* the bed volume of the column (V_t=750 ml). The isomers corresponding to the fastest and

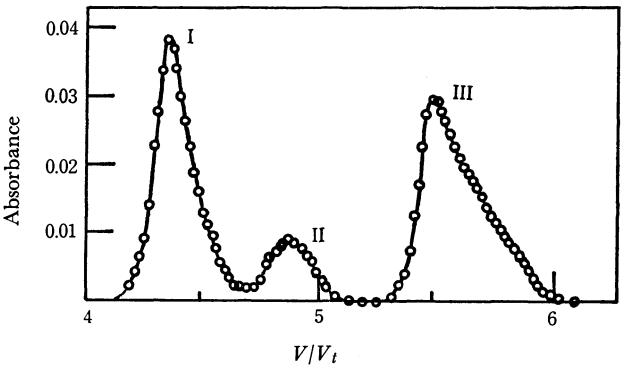

Fig. 2. Elution curve.
Eluent: 0.15 M sodium (+)$_{589}$-tartrate solution.

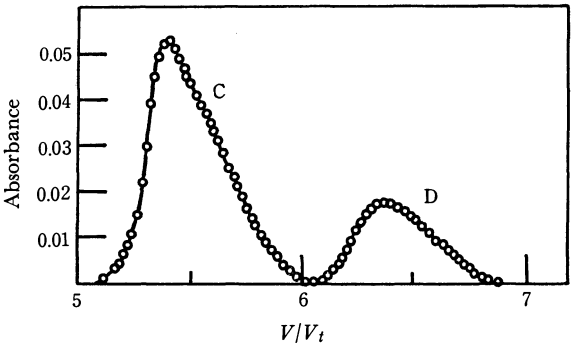

Fig. 3. Elution curve of the fractions corresponding to the peak III of Fig. 2.
Eluent: 0.3 M sodium (+)$_{589}$-tartratoantimonate(III).

* *l*-pn denotes (−)$_{589}$-propylenediamine.

1) A part of the present investigation was presented at the 14th ICCC, Toronto, Canada, June, 1972. Parts I and II were published in This Bulletin, **45**, 179, 3451 (1972).

2) T. E. MacDermott, *Inorg. Chim. Acta*, **2**, 81, (1968).

3) P. F. Crossing and M. R. Snow, *J. Chem. Soc., Dalton*, **1972**, 295.

4) Y. Yoshikawa and K. Yamasaki, *Inorg. Nucl. Chem. Lett.*, **6**, 523 (1970).

Table 1. Chemical compositions of the isomers

Complex	Elemental analyses (Calcd. value)			
	Co (%)	C (%)	H (%)	N (%)
A: $[Co(ibn)_3]Cl_3 \cdot 4H_2O$	11.84 (11.74)	28.71 (28.72)	8.53 (8.84)	16.87 (16.75)
B: $[Co(ibn)_3]Cl_3 \cdot 3H_2O$	12.11 (12.18)	30.08 (29.79)	7.84 (8.75)	17.15 (17.37)
C: $[Co(ibn)_3]Cl_3 \cdot 4H_2O$	11.85	29.06	8.35	17.03
D: $[Co(ibn)_3]Cl_3 \cdot 3H_2O$	11.84	29.76	8.02	17.04

middle peaks, I and II, were named A and B respectively. All these fractions were optically active, the signs of both I and II being plus, and that of the slowest III being minus for the Na-D line; their area ratio was 3 : 1 : 4. As the III peak had a small shoulder and seemed to be a mixture of isomers, the fractions corresponding to the III peak were diluted 4—5 times with water; then they were again adsorbed on SP-Sephadex, this time a 0.3 M sodium $(+)_{589}$-tartratoantimonate(III) being used as the eluent. The elution curve showed two peaks; these isomers were named C and D respectively (Fig. 3). Thus, the area ratio of the four peaks corresponding to the A, B, C, and D isomers was 3 : 1 : 3 : 1; no further separation was possible, not even by repeated chromatography.

Purification of the Isomers. The isomers separated as the tartrates and tartratoantimonates(III) were converted into chlorides by adsorption on SP-Sephadex, followed by elution by a 1 M sodium chloride solution. These chlorides were precipitated as hexacyanocobaltates; they were then again converted into chlorides by the anion-exchange resin, as has been described before.[1] The four isomers have the chemical compositions shown in Table 1.

Effects of Eluents on the Separation Order of the Isomers. As we have described above, these four isomers were eluted by sodium $(+)_{589}$-tartrate in the order of A, B, and (C+D); the subsequent separation of the last mixture into C and D was accomplished by sodium $(+)_{589}$-tartratoantimonate(III). If sodium $(+)_{589}$-tartratoantimonate(III) was used first, the order of separation was A, C, and (B+D), and the last mixture was further separated by sodium $(+)_{589}$-tartrate. Thus, sodium $(+)_{589}$-tartratoantimonate(III) is effective in separating geometric isomers, whereas sodium $(+)_{589}$-tartrate is effective in separating optical isomers. Sodium $(+)_{589}$-tartratoarsenate(III) was prepared and tested for separation with the same results as for sodium $(+)_{589}$-tartratoantimonate(III).

Results and Discussion

Absorption (AB) and Circular Dichroism (CD) Spectra. In Fig. 4 the AB and CD spectra of the B isomer are shown, while Tables 2 and 3 list their data. The maximum of the octahedral $^1T_{1g} \leftarrow {}^1A_{1g}$ absorption (480 nm) is at a longer wavelength than the $[Co(en)_3]^{3+}$ (467 nm) and Λ-$[Co(l\text{-pn})_3]^{3+}$ (467 nm) ions; the shift may be due to the two methyl groups of the ligand, since one of them is forced to be in the axial position regardless of the chelate-ring conformation(δ or λ). The CD band corresponding to the first absorption band is at 494 nm ($\Delta\varepsilon$=3.00), which splits into two at 503 nm ($\Delta\varepsilon$=2.16) and 450 nm ($\Delta\varepsilon$=−1.08) upon the addition of sodium phosphate, the presence of the

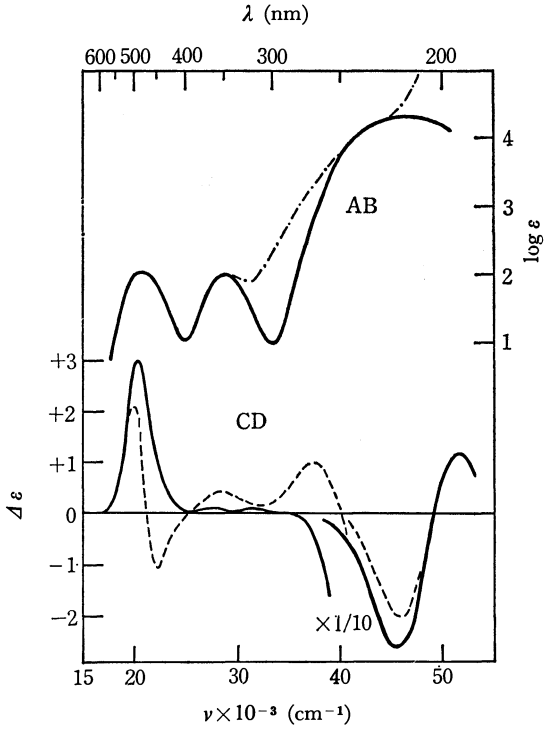

Fig. 4. AB and CD spectra of the isomer B; —— in water, —·— and ---- in 0.2 M Na_3PO_4 solution.

Table 2. Absorption spectra (in cm^{-1})

Complex	First Band $^1A_{1g} \rightarrow {}^1T_{1g}$	Second Band $^1A_{1g} \rightarrow {}^1T_{2g}$	CT Band $N(\sigma) \rightarrow e_g(\sigma^*)$
A(Λ-*mer*)	20800 (108)	28800 (101)	46300 (20400)
B(Λ-*facial*)	20800 (110)	28800 (102)	46500 (20400)
C(Δ-*mer*)	20800 (107)	28800 (100)	46500 (21400)
D(Δ-*facial*)	20800 (112)	28800 (106)	46500 (20400)

CT: Charge transfer
Molar extinction coefficients (ε) are given in parentheses.

Table 3. Circular dichroism spectra (in cm^{-1})

Complex	First band	Second band	CT band
A(Λ-*mer*)	20200 (+2.80)	27500 (+0.18) 30600 (+0.12)	45100 (−27) 51600 (+ 9)
B(Λ-*facial*)	20200 (+3.00)	27600 (+0.12) 30800 (+0.09)	45300 (−26) 51800 (+12)
C(Δ-*mer*)	20200 (−2.79)	27500 (−0.18) 30300 (−0.12)	45100 (+29) 51800 (−11)
D(Δ-*facial*)	20200 (−2.99)	27400 (−0.12) 30300 (−0.08)	45300 (+26) 52400 (−12)

$\Delta\varepsilon$ values are given in parentheses.

Table 4. Some characteristic IR bands of the isomers A and B (in cm^{-1})

A(*Λ-mer*)	1300(m)	1268(m)	1098(sh)	—	890(m)	814(m)
B(*Λ-facial*)	1313(m)	1258(m)	—	1050(w)	897(m)	829(m)

m: medium, w: weak, sh: shoulder

A_2 component being disclosed (Fig. 4). At the same time, a new CD band appears at 266 nm ($\Delta\varepsilon=0.98$) which corresponds to the charge-transfer absorption due to ion-pair formation. This CD band is characteristic of the *lel* conformation, and has never been observed for an *ob* conformation like *Δ*-$[Co(d\text{-pn})_3]^{3+}$ ion.[5] The CD spectrum of the A isomer is almost the same as that of B (Table 3). The C and D isomers show almost the identical CD spectra, with the sign opposite to that of the B isomer. The AB and CD spectral data of the four isomers are listed in Tables 2 and 3 respectively.

Infrared Spectrum. The infrared spectrum of the A isomer is slightly different from that of B in shape and position, but it is difficult to assign their configurations on the basis of the infrared spectrum alone. Some characteristic bands are listed in Table 4.

PMR Spectrum. As the *facial* isomer has a threefold axis and three equivalent chelate rings, two PMR signals due to the equatorial and axial methyl groups are expected to appear in the methyl region. On the other hand, the *mer* isomer, which has neither equivalent chelate rings nor an axis of rotation, should show more complicated methyl signals, consisting of up to six peaks. Figure 5 shows the signals observed for the A and B isomers. For the B isomer, only two peaks ($\tau=8.48$, 8.73 ppm) are found, with the area ratio 1 : 1. The peak in the higher field is attributed to the axial methyl group, since the axial proton of the methylene group was found to show signals in a higher field than the equatorial one as a result of the larger shielding by the central metal for $[M(en)_3]^{3+}$ and $[M(l\text{-pn})_3]^{3+}$, where M is Ru(II), Rh(III), Co(III), or Pt(IV).[6] The complicated signals observed for the A isomer at 60 MHz were resolved into five peaks ($\tau=8.44$, 8.58, 8.68, 8.74, 8.77 ppm) at 100 MHz, with the intensity ratio of 1 : 2 : 1 : 1 : 1 suggesting that the A isomer was the *mer* isomer (Fig. 5). MacDermott[2] reported that no difference was observed for two geometrical isomers of *Δ*-$[Co(l\text{-pn})_3]^{3+}$ at 60 MHz, but recently Sudmeier *et al.*[7] have measured the 251 MHz PMR spectrum by the Co-59 decoupling technique and have found a fine structure

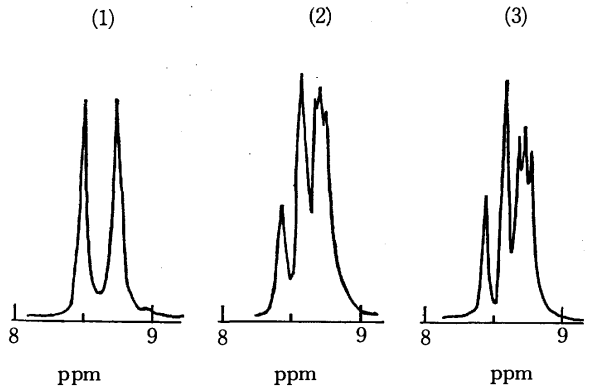

Fig. 5. PMR spectra of (1) the isomer B (60 MHz), (2) the isomer A (60 MHz) and (3) the isomer A (100 MHz) in DMSO-d_6 with TMS as an internal reference.

attributable to nonequivalent propylenediamine rings arising from the presence of geometrical isomers.

Assignment of the Structures. The configurations of the isomers isolated were assigned by means of the formation ratio and the CD and PMR spectra. The relationship between the absolute configuration and the CD spectrum of the tris(diamine)cobalt(III) complexes has been well established[8]; the complex which shows a major positive CD band in the region of the octahedral $^1T_{1g}\leftarrow{}^1A_{1g}$ absorption has the *Λ* configuration in terms of the IUPAC nomenclature. Further, the statistical formation ratio of the *mer* isomer to the *facial* isomer should be 3 : 1 under equilibrium conditions. Thus, the formation ratio, 3 : 1, actually found for the A and B isomers, both of which show a major positive CD band in the first absorption region, indicates that the A isomer is *Λ-mer* and B isomer *Λ-facial*. Similarly, the C and D isomers were identified as *Δ-mer* and *Δ-facial* respectively. The PMR spectral results support these assignments, too. The structure and the absolute configuration of the D isomer was determined by X-ray analysis[9] to be *Δ-facial* with three *lel* chelate rings, confirming the structures proposed above.

A part of the expenses was met by a Grant-in-Aid of the Ministry of Education.

5) S. F. Mason and B. J. Norman, *J. Chem. Soc., A*, **1966**, 307.
6) J. K. Beattie and L. H. Novak, *J. Amer. Chem. Soc.*, **93**, 620 (1971).
7) J. L. Sudmeier, G. L. Blackmer, C. H. Bradley, and F. A. L. Anet, *ibid.*, **94**, 757 (1972).
8) A. J. McCaffery and S. F. Mason, *Mol. Phys.*, **6**, 359 (1963).
9) Private communication of Professor Y. Saito, University of Tokyo. A detailed report will be published in *Acta Crystallogr.*

Determination of Arsenic(III) by Anodic Stripping Method Using Co-deposition with Copper

Takeshi KUWABARA, Shigetaka SUZUKI, and Shun ARAKI

Department of Industrial Chemistry, Faculty of Engineering, Tokyo Metropolitan University, Setagaya-ku, Tokyo 158

(Received June 10, 1972)

The determination of arsenic(III) by anodic stripping using co-deposition with copper was worked out. A 0.24 M hydrochloric acid containing arsenic(III) and copper(II) was electrolyzed with a rotating platinum electrode (rpm=800) at a constant current. The deposit on the electrode was stripped by linear potential sweep method in 4 M hydrochloric acid. The stripping voltammogram was recorded in the span voltage −0.2—+1.2 volt *vs.* SCE. The stripping voltammogram showed two peaks, at zero volt and 0.5 volt *vs.* SCE. The area of the second peak was proportional to the concentration of arsenic. Linear dynamic range was 1—20 microgram per milliliter. The method was rapid and simple, the time required for analysis being about 35 minutes (electrolysis temperature, 25 °C). X-ray and electron diffractions indicate that the second peak in the stripping voltammogram results from the dissolution of Cu_3As.

Stripping voltammetry was developed to increase the sensitivity of electroanalytical methods. Anodic stripping voltammetry consists of a preliminary concentration or deposition process and a dissolution or stripping (anodic oxidation) process. The deposition step is carried out for a definite time under reproducible conditions, and the stripping process mostly by means of voltammetric scanning. This method has been applied only to elements such as copper or silver, which are easily deposited alone on a working electrode.[1]

However, it is known that some elements such as arsenic and tellurium, which are hardly deposited alone on a working electrode, have been easily co-deposited with copper on a solid electrode. Some electrogravimetric analyses utilizing co-deposition of two elements have been reported.[2-6]

We have developed anodic stripping voltammetry for arsenic using co-deposition with copper. Arsenic(III) and copper were first deposited cathodically on a rotating platinum electrode, and the deposit was stripped in another electrolytic cell. The resulting stripping voltammogram showed two peaks. Arsenic was determined from the area of the second peak. Electrolysis conditions both in the stripping and deposition steps were studied, composition of the deposit being also investigated.

Experimental

Apparatus. The apparatus is shown schematically in Fig. 1. A Yanagimoto polarograph Model PA-101 was used as the source of scanning voltage and the recorder in the stripping step. A Yanagimoto controlled potential electrolyzer Model VE-3 was used as the source of constant current. A rotating platinum electrode(RPE) with surface area 0.35 cm^2 was used as a working electrode. The counter electrode was a platinum plate in the deposition step and a saturated calomel electrode (SCE) in the stripping step.

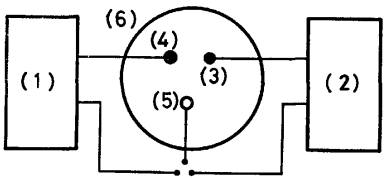

Fig. 1. Schematic diagram of anodic stripping apparatus. (1) Polarograph; (2) Galvano-stat; (3) Platinum plate electrode; (4) SCE; (5) RPE; (6) Electrolytic cell with sintered glass membrane

Reagents. Standard solution of copper: Pure copper (0.6406 g of four nine purity) was dissolved into concentrated nitric acid (7 ml). After evaporation of the solution to dryness, the residue was dissolved in 10 ml of concentrated hydrochloric acid and then the total volume was made up to 1 l. The concentration of copper was 1.008×10^{-2} M, or 0.6406 mg per ml.

Stadard solution of arsenic: A weighed amount of pure arsenic(III) oxide (0.6605 g) was dissolved in 100 ml of sodium hydroxide solution (0.46%) and acidified with concentrated hydrochloric acid. The total volume was then made up to 500 ml. One ml of this solution contained 1.000 mg of arsenic.

Deionized water was used throughout the experiment. All other reagents were of guaranteed grade.

Results

Stripping Voltammogram of Arsenic. A hydrochloric acid solution of arsenic(III) and copper(II) was electrolyzed with a RPE at a constant current of 100 mA for 30 minutes. The RPE was used as a cathode and a platinum plate as a counter electrode. The deposit on the RPE was stripped in a fresh hydrochloric acid solution by linear potential sweep method, the stripping voltammogram (SV-gram) being recorded. The range of span voltage was −0.2—+1.0 volt *vs.* SCE. The resulting voltammogram is shown in Fig. 2, curve 3, and the SV-gram obtained in the same way in the absence of arsenic, curve 2. No peak appeared in the absence of copper.

Thus, the first peak at 0 volt resulting from stripping of copper and the second peak at +0.5 volt *vs.* SCE indicate the presence of arsenic.

Experimental Conditions in the Stripping Step. The SV-gram showed two peaks resulting from dissolu-

1) E. Barendrecht, "Electroanalytical Chemistry," Vol. 2, ed., A. J. Bard, Dekker, New York (1967).
2) S. Torrance, *Analyst*, **63**, 104 (1938).
3) G. Norwitz, *Z. Anal. Chem.*, **131**, 410 (1950).
4) G. Norwitz, *Anal. Chim. Acta*, **5**, 109 (1951).
5) H. Terrey and J. Thabit, *J. Chem. Soc.*, **1957**, 3064.
6) H. Terrey and J. Thabit, *ibid.*, **1958**, 1303.

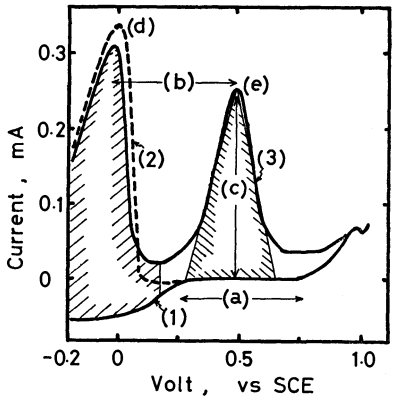

Fig. 2. Anodic stripping voltammogram of arsenic co-deposited with copper.
Deposition: Electrolyte (at 25 °C), Curve 1, 2.4×10^{-1} M HCl; Curve 2, 4×10^{-4} M copper in 2.4×10^{-1} M HCl; curve 3, 1.3×10^{-4} M arsenic, 2×10^{-4} M copper in 2.4×10^{-1} M HCl.
Current, 150 mA; Time, 30 min.
Stripping: Scan rate, 0.21 V/min; Span volt. range, $-0.2-+1.2$ V (*vs.* SCE). Electrolyte, 4 M HCl
(a) Zero current range of "background" ($|i|<2\,\mu$A); (b) Distance between two peaks; (c) Peak height of the second peak; (d) First peak; (e) Second peak.

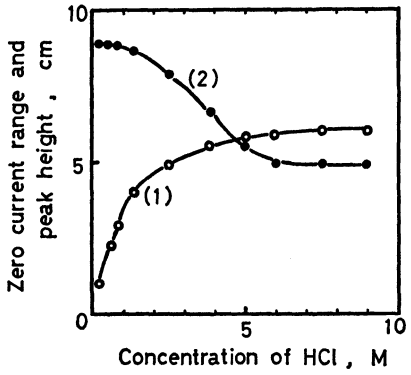

Fig. 3. Effects of concentration of HCl in the stripping step.
Curve 1, Distance of two peaks. Curve 2, Zero current range of background in the stripping step.
Deposition: Electrolyte, 1×10^{-3} M copper, 6.7×10^{-4} M arsenic in 4.8×10^{-1} M HCl at 25 °C Current, 25 mA; time, 5 min
Stripping conditions: Same as Fig. 2.

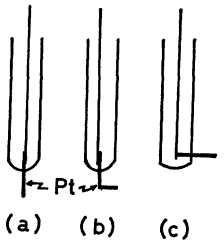

Fig. 4. Types of the rotating platinum electrodes.

tion of copper and arsenic. The supporting electrolyte in which two peaks appear in good separation and sensitivity should be chosen. After deposition was over, stripping was carried out in various supporting

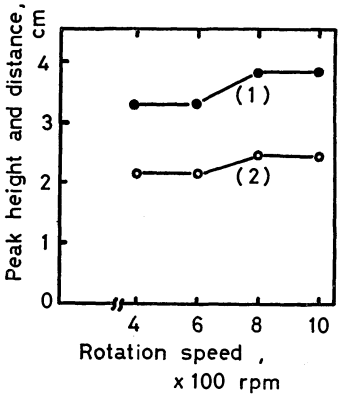

Fig. 5. Effect of the rotation speed of RPE.
Curve 1, Distance between two peaks. Curve 2, Peak height of the second peak.
Experimental conditions: Same as Fig. 3.

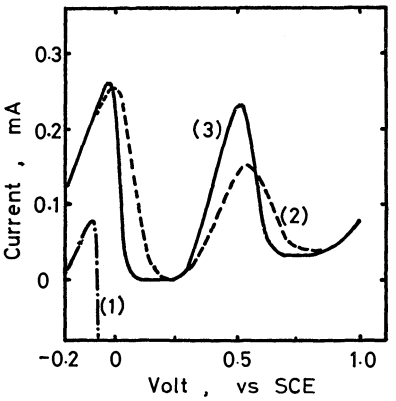

Fig. 6. SV-gram obtained in the cell with or without a membrane.
Curve 1. Cell: without a membrane; Electrolyte: deposition and stripping steps, 0.25 M HCl
Curve 2. Cell: with a membrane; Electrolyte: deposition and stripping steps, 0.25 M HCl
Curve 3. Cell: with a membrane; Electrolyte; deposition step, 0.25 M HCl stripping step, 0.5 M HCl

electrolytes such as sodium sulfate, sodium chloride, perchloric acid and hydrochloric acid, the best SV-gram being obtained in hydrochloric acid solution.

The effect of concentration of hydrochloric acid on the SV-gram was examined under definite conditions in the deposition step. The results are shown in Fig. 3. We see that 3—4 M hydrochloric acid is preferable as regards the extent of the zero current range of the background (Fig. 2) and separation of two peaks in the SV-gram. Subsequent stripping was therefore carried out in 4 M hydrochloric acid.

The rotating platinum electrodes used are shown in Fig. 4. They were rotated at a constant speed by a synchronous motor. Type (a) was preferable to any other electrode because turbulence produced by rotation was less and the current more steady and reproducible. The current depends on the rate of rotation, which also affects reproducibility: the precision deteriorates if the rate of rotation is either too high or low. The rpm 800—1000 was preferable (Fig. 5). The rpm 800 was employed. The RPE was pre-

treated electrolytically in nitric acid solution by a controlled current of 400 mA. Its polarity was reversed every 5 minutes so that the electrode was in turn the anode, cathode and anode.

The electrolytic deposition was carried out from 0.25 M hydrochloric acid solution of arsenic and copper in a cell without a membrane. After deposition, the deposit was stripped in the same electrolyte. The stripping voltammogram is shown in Fig. 6, curve 1. The curve shows that a reduction current restricted by an oxidant was too large to obtain a SV-gram. The oxidant should be dissolved chlorine generated at the counter electrode during the course of deposition and diffused to the surface of the RPE. Curve 2 was obtained in a cell with a sintered glass membrane by stripping into the same electrolyte as that used in the deposition step. It is seen that the cell should have the membrane to prevent interfering electrode reaction.

Curve 3 was obtained by using 0.25 M HCl as the electrolyte in the deposition step and 0.5 M HCl in the stripping. The cell used had a membrane. The difference between curves 2 and 3 was accounted for by the change of the concentration of HCl in the stripping step. Two peaks appearing in the curve 3 were sharper than those in curve 2. Sharpness of the peak indicates the reversibility of the electrode process. Sharpness changed with the concentration of HCl. The stripping reaction seems to occur accompanied by the formation of a chloro-complex ion.

Experimental Conditions in the Deposition Step. Supporting electrolytes such as sodium sulfate, sodium chloride, perchloric acid and hydrochloric acid were used in the deposition step and the deposit was stripped under definite conditions. Hydrochloric acid was found to be the most suitable electrolyte. Under optimum conditions in the stripping step, the effect of concentration of hydrochloric acid was examined in the deposition bath containing definite amounts of arsenic and copper. Effects of concentration of the acid on the height of the second peak are shown in Fig. 7.

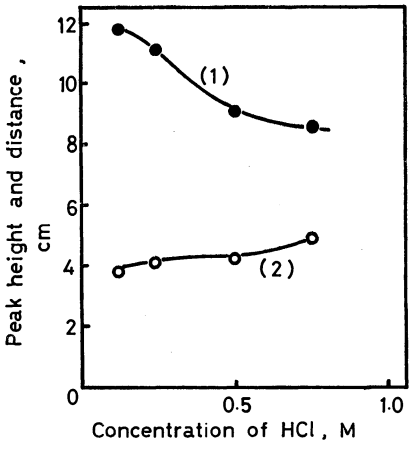

Fig. 7. Effect of concentration of HCl in the deposition step.
Curve 1, peak height; Curve 2, distance between two peaks; Experimental conditions: Same as Fig. 3.

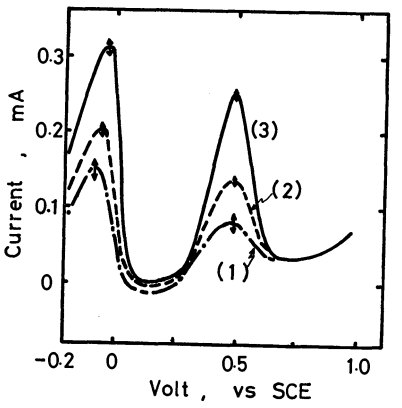

Fig. 8. Effects of deposition current density on peak height.
Curve 1, 0.057 A/cm²; Curve 2, 0.143 A/cm²; Curve 3, 0.286 A/cm². Arrows show ranges of experimental results.

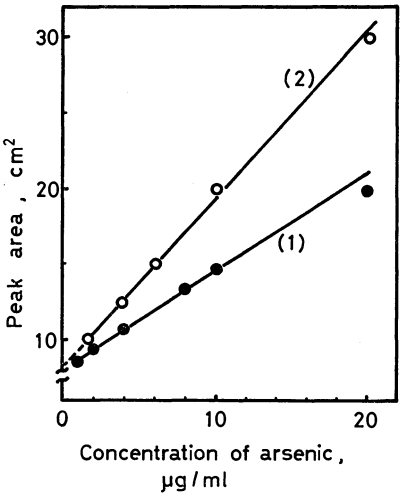

Fig. 9. Analytical curves.
Deposition: Electrolyte, 0.24 M HCl, 2×10^{-4} M Copper; Current, (1) 100 mA, (2) 150 mA
Other experimental conditions: Same as Fig. 2.

Taking into account the height of the second peak and distance between two peaks, 0.2—0.25 M hydrochloric acid solution was found to be preferable for the electrolyte in the deposition step. Hydrochloric acid of 0.24 M was employed. As regards the reproducibility of peak height, the optimum deposition current should be greater than 50 mA (current density 0.14 A/cm²). The results are shown in Fig. 8. The reproducibility deteriorated when the deposition current exceeded 150 mA. It seems that the current density 0.24—0.4 A/cm² is suitable. Current densities 0.28 and 0.42 A/cm² (100 and 150 mA, respectively) were employed.

The potential of a working electrode (RPE) was about −1.0 V *vs.* SCE at 100 mA of the deposition current.

Analytical Results. The second peak in SV-gram resulted from the presence of arsenic. A set of 0.24 M hydrochloric acid solutions containing arsenic in concentrations from 10^{-5} M to 2.6×10^{-4} M with copper (2×10^{-4} M) were prepared. Arsenic was co-deposited with copper on RPE at the constant current of 100 or 150 mA for 30 minutes. After

deposition, the deposit was stripped into 4 M hydrochloric acid by the linear potential sweep method and the SV-gram was recorded. The areas of the second peaks were calculated through the method of height times width at half height, taking zero current as the the base line (Fig. 2), and were found to be proportional to the amounts of arsenic (Fig. 9). Two analytical curves were obtained for two different deposition current densities. Arsenic was determined in the range $(1—20)\times10^{-6}$ g/ml with a relative deviation less than 10%. Analytical curves did not pass through the zero point because of the capacity current and the graphical method used for measuring the peak areas.

Discussion

Composition of the Deposit. Since it was difficult to obtain the X-ray diffraction pattern of the deposited film on the RPE directly, a platinum sheet (17 mm × 17 mm) was employed as the working electrode instead and the deposition process was carried out with different cathodic current densities, *viz.*, 0.10, 0.16, and 0.28 A/cm². The diffraction pattern was obtained with X-ray of CuK_α. It is thought that the phase structure of the deposited film is influenced not only by the cathodic potential but also the rate of cathodic reaction, but that no difference in diffraction pattern is observed with the change of current density. Thus, deposition was carried out with the current density 0.28 A/cm² for 25 hr in different solutions as follows:

(1) 2×10^{-4} M copper, 2.67×10^{-4} M arsenic (As, 2.02×10^{-5} g/ml), 0.24 M HCl

(2) 2×10^{-4} M copper, 2.67×10^{-5} M arsenic 0.24 M HCl

However, no difference in diffraction pattern was observed also in this case. Distances between planes, "*d*" values and their relative intensities were calculated from the diffraction patterns. On being compared with data from the ASTM powder data file, the results were found to indicate the presence of Cu_3As and/or Cu_2As in the deposit.

Electron diffraction pattern of the deposit showed that composition of copper arsenide in the deposit was Cu_3As, which was also the most stable in the phase diagram of Cu-As alloys.[7]

Electrode Reaction in the Stripping Step. The deposit on the RPE was first stripped at the constant potential of +0.25 volt *vs.* SCE into 4 M hydrochloric acid. The potential was satisfactory to complete the first anodic oxidation. The copper dissolved in electrolyte was determined by the spectrophotometric method with zinc dibenzyldithiocarbamate.[8] The number of coulombs in the electrode reaction were calculated from total amounts of copper dissolved and the areas under the first peaks.

Table 1. Amounts of copper in the first peak

Amounts of Cu, by colorimetry W, (μg)	Peak area (cm²)	Numbers of coulombs, Q (mC)	Valency, n[a]
36.0	39.0	56.2	1.03
35.2	37.8	54.5	1.02
32.8	36.1	52.0	1.04
39.6	42.4	61.0	1.01
39.6	41.5	59.8	1.00

a) $n=QM/WF$, M: atomic weight of copper, F: Faraday constant.
Deposition: Electrolyte, 1.07×10^{-4} M arsenic in 2×10^{-4} M copper and 0.24 M HCl; Total volume, 10 ml; Current, 10 mA; Time, 28—30 min
Stripping: Scan rate, 0.21 V/min; Span volt. range, −0.2—+1.2 V *vs.* SCE

Table 2. Amounts of copper in the second peak

Amounts of Cu, by colorimetry W_1 (μg)	Peak area (cm²)	Amounts of Cu as Cu (II) by coulometry W_2 (μg)	W_2/W_1 (%)
21.8	30.2	14.3	65.5
21.0	30.0	14.2	67.6
17.8	24.8	11.8	66.3
11.8	17.0	8.1	68.5
10.8	16.3	7.7	71.0

Deposition: Electrolyte, 2.67×10^{-4} M arsenic in 2×10^{-4} M copper and 0.24 M HCl; Total volume, 10 ml; Current, 150 mA; Time, 25—32 min
Stripping: Conditions same as Table 1.

It was thought that the electrode reaction was oxidation of copper to univalent state(Table 1).

The deposit was thus stripped at the constant potential +0.75 volt *vs.* SCE into a new stripping bath of 4 M hydrochloric acid. This potential corresponded to that of completion of the second anodic oxidation. The total amount of copper dissolved into the electrolyte was determined by the spectrophotometric method and compared with the value calculated from the areas of the second peaks.

Copper was also found in the electrolyte in which the second anodic oxidation occurred, and aresnic was also detected in the electrolyte by Gutzeit's method (Table 2). The number of coulombs under the second peak was equal to two-thirds of the values calculated from oxidizing copper to copper(II) ion and did not coincide with them. The peak potential of the second peak deviated greatly from the half-wave potential in the polarography of arsenic (−0.45, or −0.88 volt) or of copper(II) (+0.03 volt *vs.* SCE) in 1 M HCl. It is considered that the second peak in the SV-gram resulted from dissolution of Cu_3As. The mechanism of the electrode reaction of the second anodic oxidation is not clarified.

Effects of Diverse Ions. The deposition of copper and arsenic was carried out in the presence of several ions by the same procedure employed in the determination of arsenic.

7) Hansen, "Constitution of Binary Alloys," 2nd Ed., McGraw-Hill, New York (1958).

8) T. Mukoyama and T. Hasebe, *Bunseki Kagaku*, **20**, 1033 (1971).

Sodium and calcium ions did not interfere in the deposition. We thought that barium would interfere in the deposition with formation of a stable alloy with copper, but no interference was observed. Zinc and nickel, however, had an effect on the area of the second peak in SV-gram.

No effects of foreign anions such as sulfate, nitrate and perchlorate ions were observed.

The authors thank Dr. Y. Tanabe for helpful discussions and suggestions in analysing X-ray and electron diffraction patterns.

BULLETIN OF THE CHEMICAL SOCIETY OF JAPAN, VOL. 46, 1694—1698 (1973)

The Analytical Application of Sulfur Analogues of β-Diketones. II. The Separation of Mercury(II), Cobalt(II), and Zinc(II) as Their STTA (1,1,1-Trifluoro-4-(2-thienyl)-4-mercaptobut-3-en-2-one) Complexes by Extraction Chromatography

Takaharu HONJO and Toshiyasu KIBA

Department of Chemistry, Faculty of Science, Kanazawa University, Kanazawa, Ishikawa 920

(Received November 10, 1972)

The behavior of trace amounts of mercury(II), cobalt(II), and zinc(II) in liquid-liquid extraction have been investigated with 1,1,1-trifluoro-4-(2-thienyl)-4-mercaptobut-3-en-2-one in cyclohexane, and the results applied to the separation of the three metals as their STTA complexes by extraction chromatography. A chromatographic column in which 10^{-3} M STTA in cyclohexane supported on Kel-F(poly-trifluorochloroethylene) powder was the stationary phase has been employed throughout this work. After the metal ions had been retained on the column by passing a sample solution of pH 5.5—6.0 through the column, the zinc(II) was eluted with an aqueous solution of pH 5.0 and then the mercury(II) was eluted with 1M hydrochloric acid. Last of all, since the cobalt had been caught so tightly on the column that it could not be removed even with concentrated hydrochloric acid, acetone was poured down the column in order to wash down all the organic phase together with the cobalt. The relation between the extraction chromatography and the liquid-liquid extraction in batches has been discussed with regard to the metal-STTA system under the same conditions.

In recent years, extraction chromatography has received increasing interest as a powerful technique in the separation of various metal ions.[1] In this chromatography, the stationary phase is an organic extractant held on an inert support, while the mobile phase is a sample solution itself or an aqueous solution adjusted to an adequate condition. By this attractive method, it is possible to separate effectively inorganic compounds despite their low separability; further, it is a means of clarifying the extraction mechanism of the separation process. Because the extraction and back-extraction may recur many times throughout the chromatographic process, the separation of the difficultly-separable compounds can be achieved. The process is closely related to the ordinary batch extraction, so the optimum conditions for the chromatographic separation may be predicted from the distribution ratio (of the compound) given by the liquid-liquid extraction of the same system.

In extraction chromatography, the extraction systems involving ion association have been frequently applied, but the chelate extraction systems only rarely. For example, dithizone, TTA (thenoyltrifluoroacetone), and α-hydroxyoxime have been used in the extraction chromatography of several metal ions: In,[2,3] Zn,[4,5] and Hg,[6] by dithizone, some radio isotopes,[7] by dithizone; Fe–Co,[8] by dithizone; alkaline earth,[9] by TTA; alkali metals,[10] by TTA; Am–Ce–La,[11] by TTA and Cu,[12] by α-hydroxyoxime.

In this investigation, the behavior of trace amounts of mercury(II), cobalt(II), and zinc(II) in solvent extraction with STTA in cyclohexane has been examined in detail; in consequence, the separation of these metals has been achieved by extraction chromatography under the optimum conditions established by the present authors.

Experimental

Apparatus. A glass chromatographic column used was of 1 cm in diameter and 20 cm in length, with a coarse glass frit and a stopcock on the bottom and a separation funnel as an eluent reservoir on the top. The effluent was collected in fractions by means of a Toyo Kagaku Sangyo fraction collector, Model E–E, holding 200 tubes. The scintil-

1) E. Cerrai and G. Ghersini, "Reversed-Phase Extraction Chromatography in Inorganic Chemistry," "Advances in Chromatagraphy," Vol. 9, Marcel Dekker Inc., New York (1970), p. 3.
2) T. B. Pierce and P. F. Peck, *Analyst*, **86**, 580 (1961).
3) D. Mapper and J. R. Fryer, *ibid.*, **87**, 297 (1962).
4) T. B. Pierce and P. F. Peck, *ibid.*, **87**, 369 (1962).
5) F. Sebesta, *J. Radioanal. Chem.*, **6**, 41 (1970).
6) T. B. Pierce and P. F. Peck, *Anal. Chim. Acta*, **26**, 557 (1962).
7) F. Sebesta, *ibid.*, **7**, 41 (1971).
8) V. Spevackova and M. Krivanek, *Radiochem. Radioanal. Lett.*, **3**, 63 (1970).
9) I. Akaza, This Bulletin, **39**, 980 (1966).
10) D. A. Li, *J. Chromatogr.*, **26**, 342 (1967).
11) N. Cvjeticanin, *ibid.*, **34**, 520 (1968).
12) J. S. Fritz, D. R. Beuerman, and J. J. Richard, *Talanta*, **18**, 1095 (1971).

lation counter, the pH meter, the shaking machine, and the spectrophotometer were ordinary ones.

Materials. The Daiflon-300 (trade name of polytrifluorochloroethylene) moulding powder, which is non-inflammable, exceptionally stable, and resistant to temperature as well as to chemicals, was purchased from Daikin Kogyo KK. The material was dried at 80 °C, stored in a silica gel desiccator, and then ground with a mixing grinder; the particles were then collected between 42 to 80 mesh by sieving them through screens. The STTA was synthesized by a modification by the present authors of the method reported by Berg and Reed.[13] The chlorides of such radioisotopes as ^{60}Co, ^{203}Hg, and ^{65}Zn were purchased from the Radiochemical Centre, Amersham, England, and from the New England Nuclear Corp., U.S.A. The cyclohexane was purified by distillation. All the other reagents were reagent-grade materials and were used without further purification.

Extraction. Extraction was carried out for a buffered solution containing a radioactive tracer (in a concentration of a few ppm); the solution was made to have 0.1 M acetic acid (in the acidic region) or 0.1 M boric acid (in the basic region), and its pH was adjusted to an appropriate value with a 0.1—1 M hydrochloric acid or a 0.1—1 M sodium hydroxide solution. Five or ten milliliters of this solution and an equal volume of 10^{-3} M STTA in cyclohexane were put in a 30-ml glass-stoppered centrifuge tube and shaken by means of a shaking machine (300 rpm in an amplitude of 4 cm) for 2—60 min at room temperature (25—29 °C). After centrifugation, an 3-ml aliquot of each phase was pipetted out into a test tube (14 mm in diameter), and the radioactivity was counted with the NaI(Tl) scintillation counter. The pH of the aqueous phase after the extraction was again measured.

Back Extraction. A 5-ml aliquot of an organic phase which had been prepared by the standard extraction procedure was shaken with a 5-ml portion of an aqueous solution adjusted to the desired pH for 2—60 min at room temperature.[14] The distribution was determined as in the case of the extraction.

Preparation of the Column and the Procedure in Extraction Chromatography. To 5 g of Kel-F powder of 42—80 mesh, a 20-ml portion of a solution containing 10^{-3} M STTA in cyclohexane was added; the mixture was then stirred in a small 100-ml beaker until it became homogeneous. Then, a 10-ml portion of distilled water adjusted to the desired pH and pre-equilibriated with a small portion of the 10^{-3} M STTA cyclohexane solution was added, and finally the mixture was allowed to stand for an hour.

After the excess of STTA-cyclohexane solution had been taken off by decantation, the mixture was poured into a column which had been filled with an eluting solution; the voids were eliminated by gently pressing the column with a glass rod. During the course of this manipulation, the stop cock was opened a little to make the eluting solution flow through the column spontaneously. Then, the stop cock was closed and the column was again filled with the eluting solution. These procedures were repeated so as to prevent the loss of the cyclohexane solution. The chromatographic column bed thus prepared (20 cm in height) was washed with 200 ml of pre-equilibrated water coming from the reservoir fitted at the top of the tube in order to eliminate the excess organic solution. Two milliliters of a solution containing a trace amount of radioisotopes were then poured onto the column, the metals were retained on the column by passing through an aqueous solution of pH 5.5—6.0 at a flow rate of 0.2 ml/min, and then the metals were released from the column by passing through at 0.5 ml/min, the eluting solution adjusted to the desired condition. The effluent was collected in 5-ml fractions by means of the automatic fraction collector, and the chromatographic behavior of the metals was examined by counting the radioactivity of each fraction.

Theoretical

Solvent Extraction. In the extraction system of divalent metal(M^{2+})–HR(STTA)–diluent(cyclohexane), the net distribution ratio of a metal, D, and that of the back-extraction, D^*, are generally described as follows:

$$D = \frac{(MR_2)_0}{\sum_{m=0}(MR_m^{(2-m)+}) + \sum_{i=0}(M(OH)_i^{(2-i)+}) + \sum_{j=0}(MX_j^{(2-j)+})} \quad (1)$$

$$D^* = 1/D \quad (2)$$

where ( ) and ( )$_0$ designate the concentration of chemical species in the aqueous phase and in the organic phase respectively, and where $M(OH)_i^{(2-i)+}$ and $MX_j^{(2-j)+}$ indicate the metal hydroxocomplexes and the water-soluble complexes formed with a masking agent, etc. The percentage of extraction, $\%E$, and the percentage of back-extraction, $\%E_{Back}$ were calculated by means of the following equations:

$$\%E = \frac{D}{(V/V_0)+D} \cdot 100 \quad (3)$$

$$\%E_{Back} = 100 - \%E \quad (4)$$

where V and V_0 are the volumes of the aqueous and the organic phase respectively.

Extraction Chromatography. The partition on the column, based on the theory of Martin and Synge,[15] seems to correspond to the counter-current system consisting of a series of plates. It has been demonstrated that the distribution ratio of metals in the extraction chromatography, D**, can be related by the following equation[15,16]:

$$D^{**} = \frac{V_m - V^*}{V_0^*} \quad (5)$$

where V_m is the volume of the eluate to the maximum of the eluted metal concentration, where V^* is the volume of the mobile phase, and where V_0^* is that of the stationary phase. In extraction chromatography, the extraction and the back-extraction of metals between the organic phase and the aqueous phase should be repeated many times; the $\%E$ and the $\%E_{Back}$ of metals in the column can be expressed by the following equation:

$$\%E = \frac{D^{**}}{(V^*/V_0^*)+D^{**}} \cdot 100 = \left(1 - \frac{V^*}{V_m}\right) \cdot 100 \quad (6)$$

If the extraction equilibrium is ideal and is attained

13) T. Honjo and T. Kiba, This Bulletin, **45**, 185 (1972).
14) T. Honjo, T. Kiba, and S. Yashima, IUPAC International Congress on Analytical Chemistry, Kyoto, April, 1972, p. 405.
15) A. J. P. Martin and R. L. M. Synge, *Biochem. J.*, **35**, 1358 (1941).
16) H. B. F. Dixon, *J. Chromatogr.*, **7**, 467 (1962).

rapidly at any interval under certain extraction conditions, it may be established that $D=1/D^*=D^{**}$ and that $\%E=100-\%E_{Back}$ between the solvent extraction and the extraction chromatography.

Results and Discussion

The symbols in all the figures, A→O and O→A respectively, denote the extraction and the back-extraction of chemical species.

Distribution of STTA. The STTA in cyclohexane showed its absorption maximum at 365 nm and a molar absorption coefficient of 1.90×10^4.[13] The absorption spectra of STTA in cyclohexane and in an aqueous phase after the shaking of 10 ml of the 10^{-3} M STTA cyclohexane solution with 10 ml of an aqueous solution of pH 6.0 are shown in Fig. 1. The content of STTA in the aqueous solution was estimated by conventional spectrophotometry to be

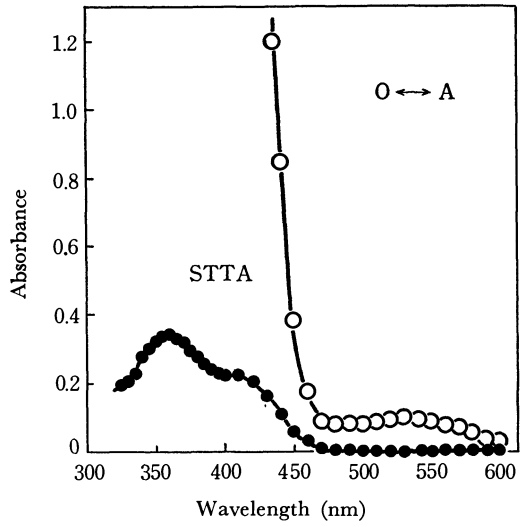

Fig. 1. Absorption spectra of STTA in the aqueous and the organic phase.
Organic phase: 10 ml of 10^{-3} M STTA in cyclohexane.
Aqueous phase: 10 ml of aqueous solution of pH 6.0.
Shaking time: 30 min.
—●— Aqueous phase, —○— Organic phase

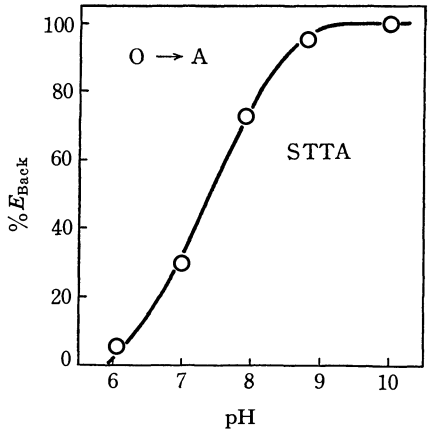

Fig. 2. Dependence on pH of the back-extraction of STTA.
Organic phase: 10 ml of 10^{-3} M STTA in cyclohexane.
Aqueous phase: 10 ml of aqueous solution of various pH.
Shaking time: 30—60 min.

3×10^{-5} M. The percentage of the back-extraction of STTA in cyclohexane as a function of the pH is shown in Fig. 2. The STTA was found to transfer itself partially into an aqueous solution from the cyclohexane phase at pH 6.0 and completely above pH 9.5. In the column extraction, an aqueous solution containing the metal ion to be extracted is always in contact with the fresh organic solvent on the column; the STTA in the organic phase will gradually dissolve in the aqueous phase and will be taken away from the extraction systems. Therefore, the eluting solutions should be pre-equilibrated with the STTA cyclohexane solution. The STTA was stable in both the aqueous and the organic phases for at least 10 hours under the present experimental conditions.

Liquid-liquid Extraction of Mercury(II), Cobalt(II), and Zinc(II). The extraction and the back-extraction of trace amounts of mercury(II), cobalt(II), and zinc(II) by 10^{-3} M STTA in cyclohexane were carried out; the results are shown in Fig. 3 as a function of the pH of the aqueous phase. It is enough to keep the concentration of 10^{-3} M STTA in cyclohexane to achieve the quantitative extraction of trace amounts of these metal ions in the acidic regions.[13,14] The extraction curves, show that the quantitative extractions of these metals are attained above pH 1.0 (Hg), pH 4.5 (Co), and pH 6.0 (Zn) respectively. The back-extractions of Hg and Zn from the organic phase were complete below pH 0 (1 M HCl) and pH 3.5 respectively, while that of Co is impossible in any pH region as has been described in the preceding paper.[13] The curves of the extraction and back-extraction of Hg and Zn obtained in the present extraction system were identical, indicating that the extraction equilib-

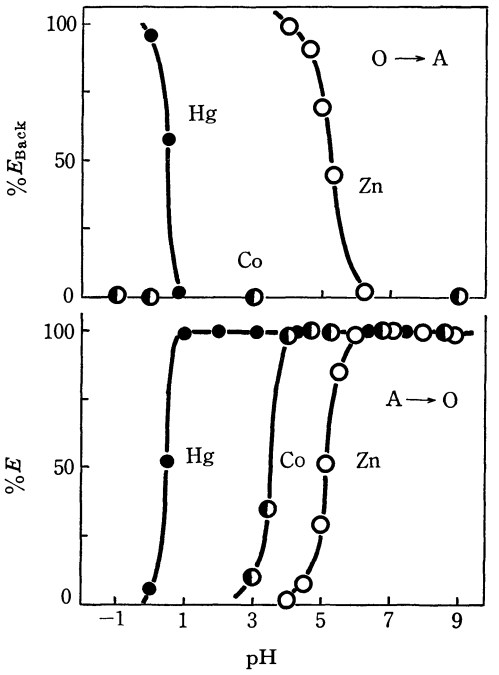

Fig. 3. Extraction and back extraction behavior of mercury(II), cobalt(II), and zinc(II)-STTA complexes as a function of pH.
Metal: —●— Hg(II), —◐— Co(II), —○— Zn(II)
Shaking time: 15 min.

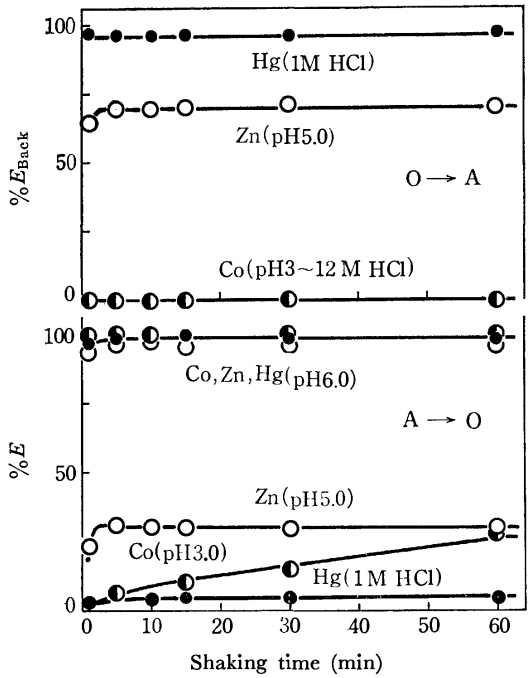

Fig. 4. Extraction and back-extraction behavior of mercury(II), cobalt(II), and zinc(II)-STTA complexes as a function of shaking time.
Metal: —●— Hg(II), —◐— Co(II), —○— Zn(II)

rium is reached within 30 minutes. The extraction and the back-extraction curves in Fig. 4 also demonstrate that the time required to reach the equilibrium is within 5 minutes in the extraction of the STTA chelates of Hg and Zn. The extraction of Co is quite rapid at pH 6.0, while it is quite show at pH 3.0, as can be seen in Fig. 4. The optimum pH for the extraction of Co into the STTA–cyclohexane seems to be above pH 5.5. However, the back-extraction of cobalt did not occur at all with any hydrochloric acid solution.[13] The extraction of cobalt(II) seemed to be accompanied by a transformation of the $Co(STTA)_2$ into an inert complex such as $Co(STTA)_3$.[14] The ratio of the volume of the stationary phase to the mobile phase in the extraction chromatography was 2.6 : 1, so the effect of the volume of the aqueous and organic phases in batch extraction was studied. When the volume of the aqueous phase was kept at 5 ml, when that of the volume of the organic phase of 10^{-3} M STTA in cyclohexane was varied from 5 ml to 15 ml, and when the $\%E$ and the $\%E_{Back}$ of metals were measured after every extraction, almost the same results were obtained in each case, as Figs. 3 and 4 show.

The Volume of the Stationary Phase. The volume of the stationary phase was determined by the following three methods: 1) In an Erlenmyer flask fitted with a glass stopper, 20 ml of a cyclohexane solution, 10 ml of distilled water, and 5 g of Kel–F powder were mixed together for a few minutes, and then the mixture was allowed to stand for one hour at room temperature. The unadsorbed solvent was subsequently drained through a small glass filter into a measuring cylinder placed in a slightly evacuated vessel. The difference between the volume of the cyclohexane solution initially taken and that measured in the cylinder showed the volume of the solvent adsorbed on the Kel–F. 2) Twelve milliliters of a cyclohexane solution, 10 ml of an eluting solution, and 5 g of Kel–F were put in a vessel with a stopper; the mixture was mixed well until it became homogeneous, and then it was allowed to stand for one hour. The slurry was then poured into the column tube and gently packed with a glass rod so as to be homogeneous. The column was then washed with 200 ml of the eluting solution at the flow rate of 2—3 ml/min, after which the excess of the solvent on the column was brought down into a receiver and the volume of the released solvent was measured by means of a measuring cylinder. The difference between the volume of the organic solvent initially taken and that of the released showed the volume of the stationary phase in ml. 3) The organic solution remaining on the column was completely taken out by passing 50 ml of acetone through the column, followed by washing with 100—150 ml of the eluting solution. All of the effluent was collected in a 250 ml flask fitted with a glass stopper, and shaken by hand so as to separate the two phases clearly. The volume of this organic phase seems to be the volume of the stationary phase of the column. The average of the values determined by the three methods was 9.3 ml for the stationary phase.

The Volume of the Mobile Phase. The space volume of the mobile phase of the column was determined by the elution of a ^{60}Co tracer in 0.1 M hydrochloric acid. The column bed was prepared in a glass tube as has been described above, and the eluting solution was drained until the liquid surface came just to the top of the column bed. One drop of a 0.1 M HCl solution containing ^{60}Co in a tracer quantity was placed at the top of the column bed, and the solution was eluted with the 0.1 M hydrochloric acid solution at the flow rate of 0.12 ml/min. Each five-drop portion (0.3 ml) of the effluent was collected in a test tube, and its radioactivity was counted by means of a NaI(Tl) scintillation counter. The volume of the eluting solution to the maximum peak of the elution curve of ^{60}Co appears to indicate the volume of

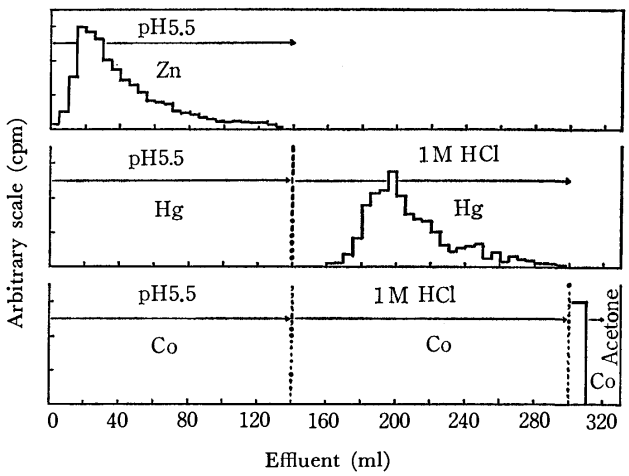

Fig. 5. Individual elution behavior of a trace amount of mercury(II), cobalt(II), and zinc(II) on a 10^{-3} M STTA–cyclohexane-Kel-F column.

the mobile phase in the column. The mean value of the mobile phase, as determined by the present method was 3.6 ml.

Chromatographic Behavior of Mercury(II), Cobalt(II), and Zinc(II). The chromatographic behavior of each metal ion was examined by loading 2 ml of a test solution containing only its radioactive tracer after it had been adjusted to pH 5.5. The results are shown in Fig. 5, in which Zn(II) is found to be completely eluted with 140 ml of the eluting solution of pH 5.5, while Hg(II) and Co(II) did not appear in the effluent under these conditions. When the eluting solution of 1 M HCl was passed through the column, Hg(II) was released in 160—300 ml of the effluent, while all of the cobalt was strongly held in the stationary phase as it was. The cobalt was not eluted even with a concentrated HCl solution, as could have been predicted from the extraction behavior. Therefore, the cobalt was finally washed down as metal chelates in cyclohexane by passing acetone through the column.

Mutual Separation of Mercury(II), Cobalt(II), and Zinc(II) from a Mixed Solution. Taking advantage of the results of the chromatographic behavior of an individual ion, the separation of the three metal ions from the mixed solution was carried out; the elution scheme is shown in Fig. 6. The cobalt was retained entirely on the column, while the zinc(II) was completely eluted with an aqueous solution of pH 5.0, and the mercury(II), with a 1 M HCl solution. Last of all, the cobalt was collected as metal chelates in the cyclohexane solution by passing acetone through the column. The average recovery for the three metal ions was 99.9%.

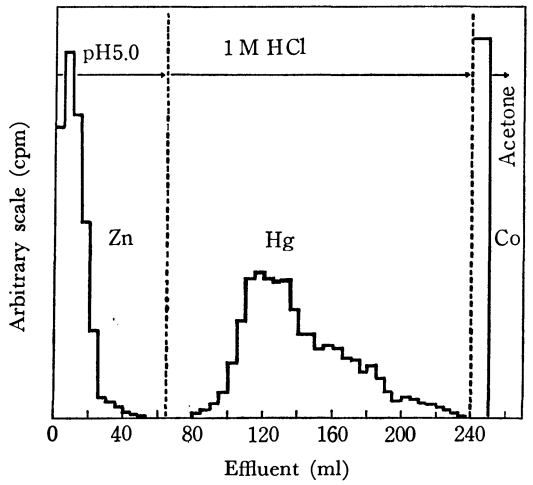

Fig. 6. Mutual separation of a trace amount of mercury(II), cobalt(II), and zinc(II) from the mixed solution on a 10^{-3} M STTA-cyclohexane-Kel-F column.

TABLE 1. $\%E$ AND $\%E_{Back}$ OF MERCURY(II), COBALT(II), AND ZINC(II) OBTAINED FROM THE EXTRACTION AND ELUTION CURVES

Metal	Acidity	Liquid-liquid extraction			Extraction chromatography
		$\%E$	$\%E_{Back}$		$\%E$
			Found	Calc.	
Zn	pH 5.5	85.0	26.0	15.0	79.4
Hg	1 M HCl	4.5	96.2	95.5	93.7
Co	12 M HCl	0.0	not back extracted		not eluted

The Relation of the Extraction Chromatography to the Liquid-liquid Extraction. The precentage of extraction ($\%E$) and the percentage of back-extraction ($\%E_{Back}$), as obtained from the liquid-liquid extraction and the extraction chromatography of the metals, are given in Table 1. The $\%E$ of zinc(II) which was obtained by means of liquid-liquid extraction differs somewhat from the value estimated by means of extraction chromatography, while that of mercury(II) is quite different in the two methods. Moreover, the $\%E_{Back}$ of Zn(II) and Hg(II) deviated a little from the theoretical values. These facts indicate that the ideal extraction equilibrium was not strictly established in either the batch or column extraction of the metal-STTA-cyclohexane system. A similar henomenon has been observed in alkali earth metal-TTA-MIBK systems.[9] This apparent discrepancy may be caused by the differences in the contact times of the two phases and/or by the time-lag in the complex formation in the extraction and the back-extraction processes.

Trinuclear Intermediates Isolated in the Reactions of Bis(acetylacetonato)-nickel(II) with Dry Hydrogen Bromide

Kiyoshi Isobe, Kenichiro Noda,* Yukio Nakamura, and Shinichi Kawaguchi
Department of Chemistry, Faculty of Science, Osaka City University, Sumiyoshi-ku, Osaka 558
(Received September 25, 1972)

The reactions of bis(acetylacetonato)nickel(II) with restricted amounts of dry hydrogen bromide have been performed in appropriate mixtures of dichloromethane and petroleum ether at room temperature or lower in order to isolate the intermediary products, $Ni_3Br(acac)_5$, $Ni_3Br_2(acac)_4$, and $Ni_3Br_4(acac)_2$. The essentially octahedral trinuclear structure of $Ni_3Br(acac)_5$ was established on the basis of elemental analysis, by molecular-weight and magnetic-moment determinations, and by studying the electronic and IR spectra. $Ni_3Br_2(acac)_4$ and $Ni_3Br_4(acac)_2$ were characterized less satisfactorily because of their lower solubilities. The reactions of these mixed complexes with pyridine have also been examined; a new complex $NiBr(acac)(py)_3$ was thus obtained in addition to the known compound, $Ni(acac)_2(py)_2$.

As an extension of our studies of the reactions of various metal acetylacetonate complexes with bromine,[1-6] we have examined the reaction between bis(acetylacetonato)nickel(II) and bromine in dichloromethane.[7] Bis(acetylacetonato)cobalt(II) is known to exist as a tetrameric molecule in crystals[8] and to be trimeric in non-coordinating solvents.[9,10] Oligomeric mixed cobalt(II) complexes containing bridging acetylacetonate anions, such as $Co_3(acac)_6(H_2O)$,[11] $Co_2(acac)_4(py)$,[10] and $Co_2(acac)_4L_2$, where L is water,[12] pyridine,[10] or cyclohexylamine,[13] have also been reported. In a reaction of bis(acetylacetonato)-cobalt(II) with an equimolar amount of bromine in dichloromethane at 0 °C, a dimeric mixed complex, $Co_2Br_2(acac)_2$, was isolated,[6] but no other tetrameric or trimeric intermediary compound has yet been identified.

The trimeric nature of anhydrous bis(acetylacetonato)nickel(II) has also been well established for crystals[14] and in non-donor solvents,[15] The relative stabilities of the trimeric structure of $M(acac)_2$ in non-coordinating solvents are considered to be in the following order:[16] Ni(II)>Co(II)>Mn(II)>Zn(II). Thus, the reaction of bis(acetylacetonato)nickel(II) with bromine was expected to afford some trinuclear intermediary products preserving the bridging acetylacetonate anions. In fact, novel mixed complexes, $Ni_3Br_2(acac)_4$ and $Ni_3Br_4(acac)_2$, were obtained by the reactions of $Ni_3(acac)_6$ with restricted amounts of bromine in dichloromethane.[7] In such reactions monobromoacetylacetone is also produced; it is neither volatile nor stable, and gives some trouble in the purification of intermediates. To avoid this difficulty, hydrogen bromide was employed in place of bromine. Acetylacetone is produced instead, but the general pattern of the reaction is the same as with bromine.[2,3]

In the reaction of bis(acetylacetonato)nickel(II) with dry hydrogen bromide in dichloromethane, another trinuclear intermediary product, $Ni_3Br(acac)_5$, was obtained.[17] This paper will report in detail on the isolation and characterization of these three trinuclear complexes.

Experimental

Materials. Bis(acetylacetonato)diaquonickel(II) prepared by the method of Charles and Pawlikowski[18] was recrystallized three times from methanol, and then dehydrated to anhydrous $Ni_3(acac)_6$ by heating it at 100 °C *in vacuo* for 4 hr (Found: Ni, 23.45; C, 45.63; H, 5.55%). Dichloromethane was purified and dried by the standard method.[19] Hydrogen bromide was generated by a reaction between tetraline and bromine, and was dissolved in purified dichloromethane.[2] Petroleum ether was distilled over metallic sodium, and a fraction distilled at 40—50 °C was used. For optical measurements, the petroleum ether was purified according to the method of Tonberg and Johnston.[20] Pyridine was freshly distilled before use.

Reactions of Bis(acetylacetonato)nickel(II) with Dry Hydrogen Bromide. Bis(acetylacetonato)nickel(II) was dissolved in a mixture of dichloromethane and petroleum ether in

* Present address: The Osaka Municipal Technical Research Institute, Kita-ku, Osaka.

1) Y. Nakamura and S. Kawaguchi, This Bulletin, **38**, 954 (1965).
2) T. Ogura, Y. Kojima, Y. Nakamura, and S. Kawaguchi, *ibid.*, **38**, 1468 (1965).
3) Y. Nakamura and S. Kawaguchi, *ibid.*, **40**, 1179 (1967).
4) Y. Nakamura, M. Hirata, and S. Kawaguchi, *ibid.*, **40**, 2572 (1967).
5) Y. Nakamura, M. Gotani, and S. Kawaguchi, *ibid.*, **45**, 457 (1972).
6) Y. Nakamura, N. Kanehisa, and S. Kawaguchi, *ibid.*, **45**, 485 (1972).
7) Y. Nakamura, K. Noda, and S. Kawaguchi, Abstracts of the 14th Symposium on the Metal Coordination Compounds, Fukuoka, Nov. 1964, p. 126.
8) F. A. Cotton and R. C. Elder, *Inorg. Chem.*, **4**, 1145 (1965).
9) D. P. Graddon, *Nature*, **195**, 891 (1962).
10) J. P. Fackler, Jr., *Inorg. Chem.*, **2**, 266 (1963).
11) F. A. Cotton and R. Eiss, *J. Amer. Chem. Soc.*, **90**, 38 (1968).
12) F. A. Cotton and R. C. Elder, *Inorg. Chem.*, **5**, 423 (1966).
13) J. A. Bertrand and A. R. Kalyanaraman, *Inorg. Chim. Acta*, **5**, 167 (1971).
14) G. J. Bullen, R. Mason, and P. Pauling, *Inorg. Chem.*, **4**, 456 (1965).
15) a) D. P. Graddon and E. C. Watton, *Nature*, **190**, 906 (1961); b) F. A. Cotton and J. P. Fackler, Jr., *J. Amer. Chem Soc.*, **83**, 2818 (1961).
16) D. P. Graddon and G. M. Mockler, *Aust. J. Chem.*, **17**, 1119 (1964).
17) K. Isobe, Y. Nakamura, and S. Kawaguchi, *Inorg. Nucl. Chem. Lett.*, **7**, 927 (1971).
18) R. G. Charles and M. A. Pawlikowski, *J. Phys. Chem.*, **62**, 440 (1958).
19) J. A. Riddick and W. B. Bunger, "Organic Solvents," 3rd. ed., Wiley-Interscience, New York (1970), p. 770.
20) Ref. 19), p. 594.

a three-necked flask equipped with a burette, a glass tube containing phosphorus pentoxide, and another glass tube connected to filtration equipment by means of polyethylene tubing. With vigorous magnetic stirring, a dichloromethane solution of hydrogen bromide (*ca.* 0.1 M) was gradually added from the burette. The precipitate thus formed was transferred *via* the polyethylene tubing to a vacuum filtration apparatus set up in a desiccator containing phosphorus pentoxide. When no precipitate was separated, the solvent was evaporated to some extent to obtain a precipitate.

If enough amount of hydrogen bromide is used, the ultimate product of the reaction is nickel(II) bromide (Found: Ni, 26.60; Br, 72.67%. Yield: 99%). However, when a restricted amount of hydrogen bromide is employed, three kinds of intermediary products are obtained, depending on the reactants' mole ratio. In each case, a mixed solvent containing appropriate portions of dichloromethane and petroleum ether was used to discriminate a desired intermediary product from other species.

Bromopentakis(acetylacetonato)trinickel(II), $Ni_3Br(acac)_5$. Two grams (2.6 mmol) of $Ni_3(acac)_6$ were dissolved in 200 ml of a mixture of dichloromethane and petroleum ether (1 : 10 by volume). Into this solution vigorously stirred, we then added, drop by drop, 26 ml of a dichloromethane solution of hydrogen bromide (2.6 mmol) from the burette. The solution was green throughout the reaction, showing no remarkable change. The solvent was evaporated up to about one fifth in volume, thus producing a green precipitate. Found: Ni, 23.21; Br, 10.24; C, 40.01; H, 4.86%. Calcd for $C_{25}H_{35}O_{10}BrNi_3$: Ni, 23.41; Br, 10.63; C, 39.91; H, 4.66%. Yield: 80%.

The $Ni_3(acac)_6$ reactant is highly soluble in dichloromethane and does not precipitate even when a solution of the same concentration as above is concentrated to one twentieth in volume. The possibility that the above reaction product may be a mixture of unreacted $Ni_3(acac)_6$ and some product can thus be rejected.

Dibromotetrakis(acetylacetonato)trinickel(II), $Ni_3Br_2(acac)_4$. (1) Two grams (2.6 mmol) of $Ni_3(acac)_6$ was dissolved in 100 ml of a mixture of dichloromethane and petroleum ether (2 : 15 by volume), and was then kept at $-5\sim-10$ °C by cooling with ice and salt. To this solution we then gradually added a 0.1 M solution of hydrogen bromide (5.2 mmol) in dichloromethane. After about 1.5 times as many moles of hydrogen bromide had been added, a yellow-green hygroscopic precipitate began to separate out. Found: Ni, 23.39; Br, 20.65; C, 32.05; H, 4.21%. Calcd for $C_{20}H_{28}O_8Br_2Ni_3$: Ni, 24.05; Br, 21.82; C, 32.77; H, 3.82%. Yield: 85%.

(2) Alternatively, 1.5 g (2 mmol) of $Ni_3Br(acac)_5$ was allowed to react with an equimolar amount of hydrogen bromide in dichloromethane–petroleum ether (1 : 1 by volume) at $-5\sim-10$ °C. A yellow green precipitate began to appear at about the middle of the overall reaction. The analytical data and infrared spectra of this product coincide completely with those of the specimen prepared in (1). Found: Ni, 23.00; Br, 20.90; C, 32.66; H, 4.38%. Yield: 92%.

Tetrabromobis(acetylacetonato)trinickel(II), $Ni_3Br_4(acac)_2$. (1) Two grams (2.6 mmol) of $Ni_3(acac)_6$ were dissolved in 40 ml of a mixture (1 : 3 by volume) of dichloromethane and petroleum ether. To this solution we then added a dichloromethane solution of four times as many moles of hydrogen bromide with cooling at $-5\sim-10$ °C. A very hygroscopic yellow powder precipitated; this powder turned brownish yellow on drying. Found: Ni, 25.45; Br, 50.21; C, 14.77; H, 2.20%. Calcd for $C_{10}H_{14}O_4Br_4Ni_3$: Ni, 25.37; Br, 48.91; C, 17.29; H, 2.01%. Yield: 95%.

(2) In 100 ml of a mixed solvent (7 : 3 by volume) of dichloromethane and petroleum ether, 1.5 g (2 mmol) of $Ni_3Br(acac)_5$ were allowed to react with three times as many moles of hydrogen bromide at $-5\sim-10$ °C. When about half the hydrogen bromide had been added, a yellow precipitate began to appear. Found: Ni, 24.41; Br, 49.10%. Yield: 93%.

The analytical data for $Ni_3Br_2(acac)_4$ and $Ni_3Br_4(acac)_2$ are very poor due to their very hygroscopic characters.

The Reaction of Bromopentakis(acetylacetonato)trinickel(II) with Pyridine. One gram (1.33 mmol) of $Ni_3Br(acac)_5$ was dissolved in 30 ml of dichloromethane. To this solution we then added, drop by drop, 15 ml of a dichloromethane solution containing 9.31 mmol of pyridine. The reaction mixture was kept standing for a week in a desiccator equipped with a glass tube containing calcium chloride. The solvent was thus vaporized almost to dryness. Two kinds of crystals resulted. Blue-violet crystals were dissolved in benzene, but other blue crystals remained insoluble and gave the following analysis. Found: Ni, 12.74; Br, 17.10; C, 50.98; H, 4.90; N, 8.66%. Calcd for $NiBr(acac)(py)_3=C_{20}H_{22}O_2N_3BrNi$: Ni, 12.36; Br, 16.82; C, 50.52; H, 4.63; N, 8.84%. Yield: 90% on the basis of Eq. (11), which will be shown in the Results and Discussion section. The benzene solution was evaporated to dryness, and the residue was recrystallized from methanol to give blue-violet crystals. Found: Ni, 14.46; C, 57.59; H, 5.85; N, 7.02%. Calcd for $Ni(acac)_2(py)_2=C_{20}H_{24}O_4N_2Ni$: Ni, 14.14; C, 57.81; H, 5.78; N, 6.74%. Yield of crystals: 60% on the basis of Eq. (11).

The Reaction of Dibromotetrakis(acetylacetonato)trinickel(II) with Pyridine. A dichloromethane solution (20 ml) of pyridine (5.44 mmol) was added, drop by drop, to a suspension of $Ni_3Br_2(acac)_4$ (0.5 g, 0.68 mmol) in dichloromethane (30 ml). The complex was dissolved gradually with an increase in the amount of pyridine added. The blue solution was kept standing for two days in an evacuated desiccator. The residue was extracted with benzene, and the remaining blue crystals were identified by the IR assay as $NiBr(acac)(py)_3$. Yield: 20% on the basis of Eq. (12). To the benzene extract, petroleum ether was added to separate an impure, pale green precipitate; the filtrate was evaporated to give blue violet crystals which were identified by the IR assay as $Ni(acac)_2(py)_2$. Yield: 65% on the basis of Eq. (12).

The Reaction of Tetrabromobis(acetylacetonato)trinickel(II) with Pyridine. A dichloromethane solution of excess pyridine was added to a dichloromethane suspension of $Ni_3Br_4(acac)_2$. A blue solution was concentrated by evaporation to give pale blue-green crystals. Found: Ni, 10.90; Br, 30.10; C, 44.34; H, 3.86; N, 10.32%. Calcd for $NiBr_2(py)_4=C_{20}H_{20}N_4Br_2Ni$: Ni, 10.98; Br, 29.88; C, 44.91; H, 3.77; N, 10.47%. Yield: 82% on the basis of Eq. (13). The filtrate was evaporated to dryness, and the residue was recrystallized from methanol to give blue-violet crystals of $Ni(acac)_2(py)_2$. Yield: 40% on the basis of Eq. (13).

Analysis and Measurements. All the solid samples were subjected to elemental analysis after drying *in vacuo* at room temperature. Nickel and bromine were determined gravimetrically as bis(dimethylglyoximato)nickel(II) and silver bromide respectively. To determine the concentration of hydrogen bromide in dichloromethane, an aqueous solution of sodium hydroxide was added to an aliquot of the hydrogen bromide solution, and the excess alkali was titrated with 0.1 N sulfuric acid, using phenolphthalein as an indicator.

The visible and ultraviolet absorption spectra were measured by means of a Hitachi EPS-3T autorecording spectro-

photometer. The molar absorption coefficients of trinuclear complexes are expressed on the basis of the gram-atom of nickel(II). The infrared spectra were taken in Nujol on JASCO IR-E (4000—700 cm^{-1}), Hitachi EPI-L (700—200 cm^{-1}), and FIS-3 (400—30 cm^{-1}) infrared spectrophotometers.

The magnetic susceptibility was measured at room temperature by the Gouy method by means of an automatically-recording magnetic balance (Shimadzu Seisakusho Co., Ltd.). Hexaamminechromium(III) chloride and mercury-(II) tetraisothiocyanatocobaltate(II) were used as the reference compounds.

The molecular weight was determined cryoscopically in benzene by means of an apparatus manufactured by Knauer, Germany. Tris(acetylacetonato)aluminium was used as the reference.

Results and Discussion

When six times as many moles of dry hydrogen bromide were allowed to react with $Ni_3(acac)_6$ in dichloromethane, anhydrous nickel(II) bromide precipitated in a 99% yield. The UV spectrum of the filtrate showed that six times as many moles of acetylacetone were produced in this reaction, certifying the following stoichiometry.

$$Ni_3(acac)_6 + 6HBr = 3NiBr_2 + 6acacH \quad (1)$$

Here, acacH stands for an acetylacetone molecule.

The overall reaction (1) must proceed *via* several consecutive steps, and it depends on the relative rates of these elementary steps whether or not some intermediary products can be isolated and characterized. Fortunately, the trinuclear framework of $Ni_3(acac)_6$ was strong enough, and the differences among the rates of the consecutive reaction steps were large enough, for three kinds of intermediary products to be isolated in satisfactory yields and purities. The reactions producing these mixed complexes may be represented by the following equations:

$$Ni_3(acac)_6 + HBr = Ni_3Br(acac)_5 + acacH \quad (2)$$

$$Ni_3Br(acac)_5 + HBr = Ni_3Br_2(acac)_4 + acacH \quad (3)$$

$$Ni_3Br_2(acac)_4 + 2HBr = Ni_3Br_4(acac)_2 + 2acacH \quad (4)$$

In principle, two more intermediates, $Ni_3Br_3(acac)_3$ and $Ni_3Br_5(acac)$, may be expected to be involved in the course of the conversion of $Ni_3(acac)_6$ to nickel(II) bromide. However, even the tribromo-intermediate could not be obtained. The reason for this is not clear, but $Ni_3Br_3(acac)_3$ might be especially unstable compared to $Ni_3Br_2(acac)_4$ and $Ni_3Br_4(acac)_2$.

The three isolated mixed complexes show a very remarkable trend in their properties. For instance, they show intermediate colors between the green of $Ni_3(acac)_6$ and the orange of nickel(II) bromide. $Ni_3Br(acac)_5$ is quite soluble in dichloromethane, but $Ni_3Br_2(acac)_4$ is much less soluble and $Ni_3Br_4(acac)_2$ is insoluble in the same solvent. The hygroscopic character is remarkably enhanced with an increase in the content of bromine.

Properties of $Ni_3Br(acac)_5$. As is shown in Table 1, the molecular weight determined cryoscopically in benzene indicates that this is a trinuclear complex. The ultraviolet absorption spectrum in Fig. 1 and the visible absorption spectrum in Fig. 2 also support the trinuclear and essentially octahedral structure of this compound. The ultraviolet spectra of bis(acetylacetonato)nickel(II) in dry dichloromethane have recently been reinvestigated in detail;[21] the more intense absorption band at 265 nm has been attributed to the trinuclear molecule, while the low-energy band at 300 nm has been attributed to the mononuclear dihydrated species. The high-energy band of Curve 2

Table 1. Molecular weights of $Ni_3(acac)_6$ and $Ni_3Br(acac)_5$ determined cryoscopically in benzene

Concn, M	$Ni_3(acac)_6$	Concn, M	$Ni_3Br(acac)_5$
0.0991	780	0.0792	750
0.0496	728	0.0396	717
0.0248	764	0.0198	747
Average	757	Average	738
Theoretical	771	Theoretical	752

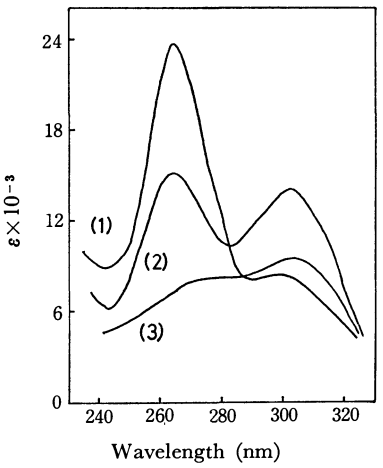

Fig. 1. The ultraviolet absorption spectra of $Ni_3(acac)_6$ (curve 1), $Ni_3Br(acac)_5$ (curve 2), and $Ni_3Br_2(acac)_4$ (curve 3) in dichloromethane.

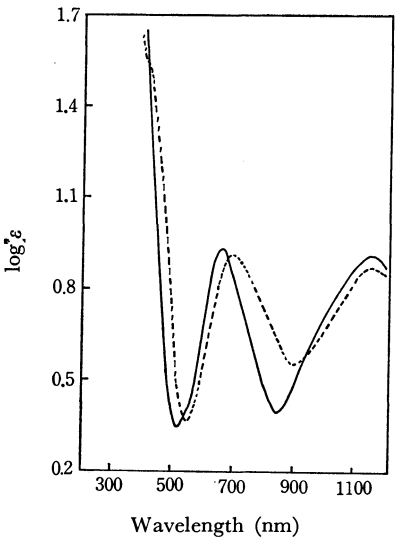

Fig. 2. The visible absorption spectra of $Ni_3(acac)_6$ (——) and $Ni_3Br(acac)_5$ (----) in dichloromethane.

in Fig. 1 indicates the existence of the trinuclear framework in $Ni_3Br(acac)_5$.

The visible absorption spectrum of $Ni_3(acac)_6$ in dichloromethane shows two maxima, at 1150 (ε=8.2) and 660 nm (ε=8.5), closely resembling the pattern in cyclohexane reported by Cotton and Fackler.[15b] The spectrum of $Ni_3Br(acac)_5$ also has two maxima, at 1140 (ε=7.4) and 695 nm (ε=8.2), revealing the essentially octahedral environment of the nickel(II) ion in this compound. The observed effective magnetic moment of 3.51 B.M. also indicates the high-spin state of the nickel(II) ion.

In order for $Ni_3Br(acac)_5$ to exist as a discrete trinuclear molecule, one of the three nickel ions must assume a pentacoordinate structure. In other words, it seems probable that one of the non-bridging acetylacetonate groups in $Ni_3(acac)_6$ was displaced by a bromide anion. The shoulder observed at 405 nm (Fig. 2) might reflect the five-coordinate nickel(II).[22] In fact, the shoulder disappeared on the addition of equimolar pyridine to the solution of $Ni_3Br(acac)_5$, presumably because of the completion of the totally octahedral structure.

As is shown in Fig. 3, the infrared spectrum of $Ni_3Br(acac)_5$ is much more complicated than that of $Ni_3(acac)_6$, suggesting the poorer symmetry of the former compound. Such a spectral feature also supports the above structural consideration.

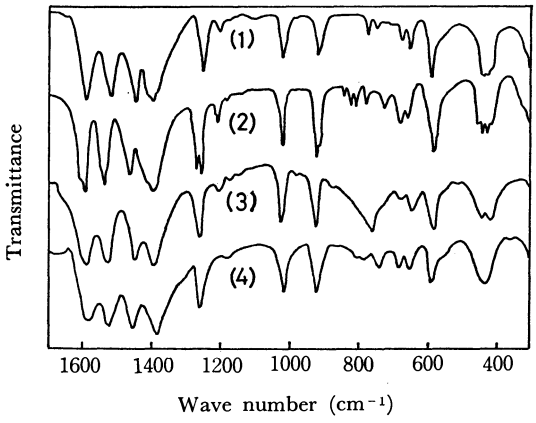

Fig. 3. The infrared absorption spectra in Nujol mull of $Ni_3(acac)_6$ (curve 1), $Ni_3Br(acac)_5$ (curve 2), $Ni_3Br_2(acac)_4$ (curve 3), and $Ni_3Br_4(acac)_2$ (curve 4).

$Ni_3Br_2(acac)_4$ and $Ni_3Br_4(acac)_2$. The lower solubilities of these dibromo and tetrabromo complexes in the appropriate solvents prevented the molecular-weight determination. The ultraviolet spectrum of $Ni_3Br_2(acac)_4$ (Curve 3 in Fig. 1) has a broad band at 260—280 nm, indicating the maintenance of the trinuclear framework.

In a previous paper,[21] the peak-height ratio of the high-energy to low-energy bands for bis(acetylacetonato)nickel(II) was found to decrease with an increase in the water content of dichloromethane due to the depolymerization equilibrium:

$$Ni_3(acac)_6 + 6H_2O \rightleftharpoons 3Ni(acac)_2(H_2O)_2 \quad (5)$$

Although the three spectra in Fig. 1 were taken in dichloromethane of almost same water content (*ca.* 4.5×10^{-3} M), the low-energy band grows at the expense of the high-energy band as the bromine content of the mixed complex increases. A depolymerization equilibrium similar to (5) might be more favorable for $Ni_3Br(acac)_5$ than for $Ni_3(acac)_6$, and more favorable for $Ni_3Br_2(acac)_4$ than for $Ni_3Br(acac)_5$.

The effective magnetic moment of $Ni_3Br_2(acac)_4$ (3.38 B.M.) is appreciably lower than that, 3.51 B.M., for $Ni_3Br(acac)_5$; it is rather near to that, 3.37 B.M., for $Ni_3(acac)_6$. In the previous section it was presumed that a non-bridging acetylacetonate ligand was displaced by the attack of hydrogen bromide (Eq. (2)). If this presumption be extended to the second step of the reaction (Eq. (3)), another non-bridging acetylacetonate group will be displaced, as is illustrated by Eq. (6).

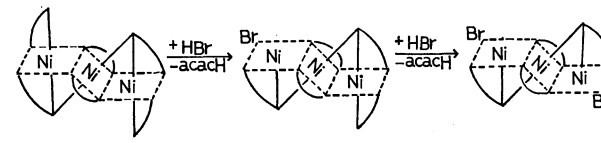

(6)

In order for $Ni_3Br_2(acac)_4$ to retain the trinuclear structure, both terminal nickel(II) ions must be in the five-coordinate environment. Of course, it is not at all clear whether a square-pyramidal or a trigonal-bipyramidal structure is preferred. The infrared spectrum of $Ni_3Br_2(acac)_4$ (Curve 3 in Fig. 3) is much simpler than that of $Ni_3Br(acac)_5$ and rather resembles that of $Ni_3(acac)_6$, indicating that the symmetry of $Ni_3Br_2(acac)_4$ is higher than that of $Ni_3Br(acac)_5$. It is very unfortunate that the visible absorption spectrum of $Ni_3Br_2(acac)_4$, which might exhibit the characteristic feature of the five-coordinate nickel(II), can not be observed because of its low solubility.

The tetrabromo-complex $Ni_3Br_4(acac)_2$ is more hygroscopic than $Ni_3Br_2(acac)_4$, and its low solubility in nondonor solvents prevented satisfactory characterization. The infrared spectrum of $Ni_3Br_4(acac)_2$ (Curve 4 in Fig. 3) is rather simple, resembling that of $Ni_3(acac)_6$. In order to retain the trinuclear structure, all three nickel(II) ions in $Ni_3Br_4(acac)_2$ must be in the four-coordinate environment. The observed paramagnetism (μ_{eff}=3.33 B.M.) clearly shows the square-planar arrangement to be impossible. Thus a tetrahedral structure such as the following may be imagined:

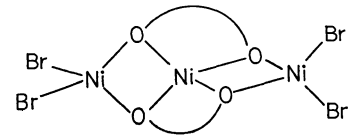

Adduct Formations. A methanolic solution of bis(acetylacetonato)nickel(II) shows an absorption maximum at 295 nm, accompanied by a shoulder on the longer-wavelength side. Cotton and Fackler[15b] presumed that the solute is entirely present as the sol-

21) K. Isobe, Y. Nakamura, and S. Kawaguchi, This Bulletin, **46**, 166 (1973).

22) L. Sacconi, "Transition Metal Chemistry," Vol. 4, ed. by R. L. Ccrlin, Marcel Dekker, Inc. N. Y. (1968), p. 199.

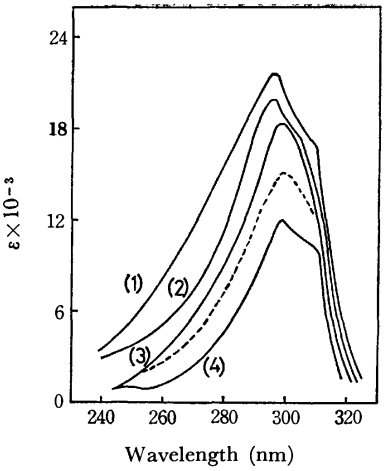

Fig. 4. The ultraviolet absorption spectra in methanol of $Ni_3(acac)_6$ (curve 1, λ_{max}=295 nm, ε=21710), $Ni_3Br(acac)_5$ (curve 2, λ_{max}=295 nm, ε=19818), $Ni_3Br_2(acac)_4$ (curve 3, λ_{max}=299 nm, ε=18560), and $Ni_3Br_4(acac)_2$ (curve 4, λ_{max}=299 nm, ε=11952). A dashed curve is a spectrum calculated for a presumed species $NiBr(acac)(CH_3OH)_3$ (λ_{max}=300 nm, ε=15885).

vated species, $Ni(acac)_2 \cdot 2CH_3OH$, which was recently prepared by the reaction of $Ni_3(acac)_6$ with methanol in petroleum ether.[21]

Fig. 4 shows the ultraviolet absorption spectra of bis(acetylacetonato)nickel(II) and of three bromo-complexes derived therefrom. All these spectra show quite a striking resemblance to each other except that the apparent molar extinction coefficient decreases with the decrease in the acetylacetonate anions involved. These spectral features clearly indicate that the trinuclear mixed complexes are also depolymerized in such a coordinating solvent, just as $Ni_3(acac)_6$ is. In analogy with Eq. (5), these reactions might be represented by the following equations:

$$Ni_3(acac)_6 + 6CH_3OH = 3Ni(acac)_2(CH_3OH)_2 \quad (7)$$

$$Ni_3Br(acac)_5 + 7CH_3OH = 2Ni(acac)_2(CH_3OH)_2 + NiBr(acac)(CH_3OH)_3 \quad (8)$$

$$Ni_3Br_2(acac)_4 + 8CH_3OH = Ni(acac)_2(CH_3OH)_2 + 2NiBr(acac)(CH_3OH)_3 \quad (9)$$

$$Ni_3Br_4(acac)_2 + 10CH_3OH = Ni(acac)_2(CH_3OH)_2 + 2NiBr_2(CH_3OH)_4 \quad (10)$$

The presumed complex, $NiBr(acac)(CH_3OH)_3$, has not yet been isolated, but its spectrum can be calculated from Curves 1 and 2 or from Curves 1 and 3 in Fig. 4. These two calculated spectra are very close to each other; an averaged curve is drawn in Fig. 4.

In order to study such depolymerization (adduct formation) reactions more precisely, the reactions of these trinuclear complexes with pyridine were examined in dichloromethane. As has been described in the Experimental section, addition products reconciled with the following equations were obtained in satisfactory yields:

$$Ni_3Br(acac)_5 + 7py = 2Ni(acac)_2(py)_2 + NiBr(acac)(py)_3 \quad (11)$$

$$Ni_3Br_2(acac)_4 + 8py = Ni(acac)_2(py)_2 + 2NiBr(acac)(py)_3 \quad (12)$$

$$Ni_3Br_4(acac)_2 + 10py = Ni(acac)_2(py)_2 + 2NiBr_2(py)_4 \quad (13)$$

The fact that $Ni_3Br(acac)_5$ gave $NiBr(acac)(py)_3$ in the reaction with pyridine supports the assumption that $Ni_3Br(acac)_5$ contains a five-coordinate nickel(II). Furthermore, the fact that $Ni_3Br_2(acac)_4$ also produced $NiBr(acac)(py)_3$ and not $NiBr_2(py)_4$ clearly indicates that the two bromine atoms are linked to different nickel atoms in $Ni_3Br_2(acac)_4$ in accordance with the formula in Eq. (6).

Bis(acetylacetonato)bis(pyridine)nickel(II) was identified by elemental analysis and by comparing the IR and electronic spectra with those in the literature.[23,24] Dibromotetrakis(pyridine)nickel(II) is also a known compound; it was identified by elemental analysis and studying its IR spectrum.[25] On the contrary, bromo(acetylacetonato)tris(pyridine)nickel(II) $NiBr(acac)(py)_3$ is a new compound. In Fig. 5, the infrared spectrum in the 100—700 cm^{-1} region is compared with that of $Ni(acac)_2(py)_2$. A combination band at 574 cm^{-1} which was previously assigned to ν(Ni–O) and ring vibrations in $Ni(acac)_2(py)_2$[24] is replaced by two peaks, at 571 and 557 cm^{-1}, in $NiBr(acac)(py)_3$, indicating weaker Ni–O bonding and poorer symmetry in the latter complex. The ν(Ni–O)+ν(CR) at 438 cm^{-1} in the former complex is also shifted to 433 cm^{-1} in the latter; a similar feature is also observed in the 200—300 cm^{-1} region. Three strong peaks are observed at 262, 247, and 235 cm^{-1} for $NiBr(acac)(py)_3$ instead of the ν (Ni–O) and ν(Ni–N) bands at 272 and 250 cm^{-1} in $Ni(acac)_2(py)_2$. It is not certain whether or not one of the three peaks in the former complex should be assigned to the ν(Ni–Br) vibration, although no other strong peak attributable to ν (Ni–Br) is noticed.

Supplemental Discussion. Fackler[26] prepared

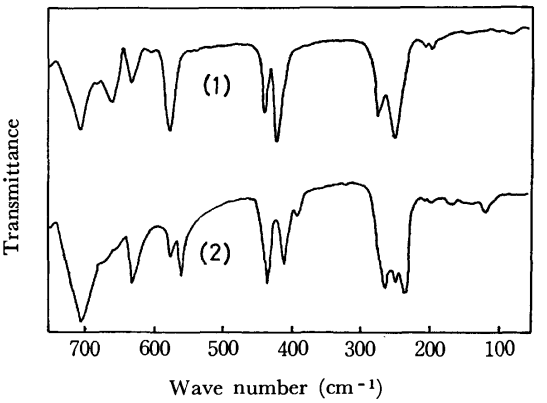

Fig. 5. The infrared spectra in Nujol mull of $Ni(acac)_2(py)_2$ (curve 1) and $NiBr(acac)(py)_3$ (curve 2).

23) J. T. Hashagen and J. P. Fackler, Jr., *J. Amer. Chem. Soc.*, **87**, 2821 (1965).
24) K. Nakamoto, C. Udovich, and J. Takemoto, *ibid.*, **92**, 3973 (1970).
25) R. J. H. Clark and C. S. Williams, *Inorg. Chem.*, **4**, 350 (1965).
26) J. P. Fackler, Jr., *J. Amer. Chem. Soc.*, **84**, 24 (1962).

tetrakis(acetylacetonato)pyridinedinickel(II) $Ni_2(acac)_4py$ by the reaction of $Ni_3(acac)_6$ with a restricted amount of pyridine in benzene. Bertrand *et al.* synthesized $Ni(acac)(OCH_3)(CH_3OH)$ by the reaction of $Ni_3(acac)_6$ with equimolar potassium hydroxide in refluxing methanol. This compound is tetrameric in chloroform and is isostructural with $[Co(acac)(OCH_3)(CH_3OH)]_4$, which takes a cubane-type structure.[27] However, no derivative retaining the trinuclear framework of $Ni_3(acac)_6$ has yet been reported except $Ni_3OH(acest)_5$ which was obtained by Hay and Hook[28] in the reaction between the aqueous nickel(II) ion and ethyl acetoacetate (acestH) in the presence of potassium hydroxide or ammonia. The trinuclear octahedral structure of this compound was established by the cryoscopic and spectral measurements in benzene; an OH-bridged structure was presumed on the basis of the very sharp OH stretching band at 3587 cm^{-1} and the preliminary NMR data in benzene. $Ni_3Br(acac)_5$ prepared in the present study might have a structure similar to that of this ester complex, but the possibility of a bromide-bridging contrary to the proposed structure in Eq. (6) can not be denied. The conclusive description of the molecular structures of these trinuclear mixed complexes must await X-ray studies.

We are indebted to Dr. Hanako Kobayashi of Kyoto University for her help in the magnetic measurements and also to Mr. J. Gohda for the elemental analyses. Financial aid by the Ministry of Education and the kind supply of acetylacetone by the Daicel Co., Ltd., are also acknowledged.

27) J. A. Bertrand, A. P. Ginsberg, R. I. Kaplan, C. E. Kirkwood, R. L. Martin, and R. C. Sherwood, *Inorg. Chem.*, **10**, 240 (1971).

28) R. W. Hay and G. E. R. Hook, *Aust. J. Chem.*, **17**, 601 (1964).

BULLETIN OF THE CHEMICAL SOCIETY OF JAPAN, VOL. 46, 1704—1705 (1973)

Stability Constants of Lanthanoid(III) Complexes with 7-Bromo-8-hydroxy-5-quinolinesulfonic Acid

Gurcharan Singh MANKU
Hans Raj College, Delhi-110007, India

(Received September 21, 1971)

Stability constants of the tervalent yttrium and lanthanoid complexes with 7-bromo-8-hydroxy-5-quinolinesulfonic acid have been determined in aqueous medium containing 0.100 M sodium perchlorate at 25±1 °C by means of pH-titration. The trends in the order of the stability constants of these complexes are also discussed.

The metal complexes of 8-quinolinol have been extensively investigated, but those of 7-bromo-8-hydroxy-5-quinolinesulfonic acid do not appear to have been investigated in detail. This is especially the case with complexes with the tervalent lanthanoid ions. The present communication describes the results of pH-titration for the determination of stoichiometric stability constants K of the tervalent yttrium and the lanthanoid complexes with 7-bromo-8-hydroxy-5-quinolinesulfonic acid in aqueous solutions containing 0.100 M sodium perchlorate at 25° (±1°)C. The results indicate a stepwise formation of 1:1, 1:2, and 1:3 metal : ligand complexes. The $\log K_3$ values could not be determined with an accuracy better than ±0.8 because of the precipitate formation around $\bar{n}=1.9$—2.2.

Experimental

7-Bromo-8-hydroxy-5-quinolinesulfonic Acid was prepared from 8-quinolinol.[1] *Lanthanoid(III) perchlorate* solutions were prepared by dissolving 84—100 mg of the oxides (Johnson, Matthey & Co. Ltd., Specpure grade) in 5 ml of warm 0.84 M perchloric acid, and diluting the solutions to 100 ml with water. The concentration of perchloric acid in the metal solutions was determined by Gran's titrimetric method.[2] A 0.50 M sodium perchlorate (B.D.H.) solution was used to keep the concentration of the perchlorate ions at 0.100 M in the final solutions used for titration. *Sodium hydroxide* solution, free from carbonate, was prepared from sodium hydroxide pellets (B.D.H.) and standardized against potassium hydrogen phthalate.

Titration Procedure. The following solutions were prepared for the titration of a set of metal — ligand concentrations:

(1) 5.00 ml of E molar perchloric acid, 4.00 ml of 0.50 M sodium perchlorate, and 11.00 ml water,

(2) 5.00 ml of E molar perchloric acid, 4.00 ml of 0.50 molar sodium perchlorate, 1.00 ml of water, and 10.00 ml of T_L molar 7-bromo-8-hydroxy-5-quinolinesulfonic acid,

(3) 5.00 ml of T_M molar metal solution (prepared in E' molar perchloric acid) adjusted to E molar acid concentration (using sodium hydroxide or perchloric acid), (4.00—10 E') ml of 0.50 molar sodium perchlorate (10 E' ml of 0.50 molar sodium perchlorate solution compensating the perchlorate ions present in metal solutions, *i.e.*, for 5.00 ml of E' molar perchloric acid; E' was in the range 0.0437—0.0213 M for different metal solutions), (1.00+10 E') ml of water and 10.00 ml of T_L molar 7-bromo-8-hydroxy-5-quinolinesulfonic acid.

The value of E was kept at 1.00×10^{-3} M. Solution (1), (2), or (3) was then titrated against 1 M molar sodium hydroxide,

1) R. G. W. Hollingshead, "Oxine and Its Derivatives," Butterworths Scientific Publications (1959), Vol. 3.

2) G. Gran, *Analyst*, **77**, 661 (1962).

and the equilibrium pH of the solution at each addition of alkali was recorded. Each titration was repeated till the equilibrium pH of the solutions after each addition of alkali was found to be within 0.02 pH units. Titration of solution (3) was, however, discontinued at the appearance of opalescence in solution.

Calculations

The plots of $\bar{n}$, the ligand number, *vs.* pL, L being the equilibrium concentration of the ligand, for a metal complex were calculated from the results of titration using equations similar to those proposed by Irving and Rossotti:[3]

$$\bar{n}_h = \left(yT_L + \frac{(V_1-V_2)(N+E)}{V^0+V_1}\right)/T_L \quad (1)$$

$$\bar{n} = \frac{(V_3-V_2)(N+E+(y-\bar{n}_h)T_L)}{(V^0+V_2)\bar{n}_h T_M} \quad (2)$$

and

$$pL = -\log L = \log \frac{\sum_0^J \beta_j^H (H^+)^j}{T_L - \bar{n}T_M} \times \frac{V^0+V_3}{V^0} \quad (3)$$

where the symbols have their usual meanings.[3]

As the formation function for mononuclear complexes can be given by

$$\bar{n} = \frac{K_1L+2K_1K_2L^2+3K_1K_2K_3L^3}{1+K_1L+K_1K_2L^2+K_1K_2K_3L^3} \quad (4)$$

the corresponding stability constants K_n were calculated from the experimental points from the linear plots of the equations

$$\frac{\bar{n}}{1-\bar{n}}\cdot\frac{1}{L} = K_1 + \frac{2-\bar{n}}{1-\bar{n}}\cdot K_1K_2L \quad (5)$$

and

$$\left(\frac{\bar{n}}{2-\bar{n}}\cdot\frac{1}{L} + \frac{\bar{n}-1}{2-\bar{n}}\cdot K_1\right)\frac{1}{L} = K_1K_2 + \frac{3-\bar{n}}{2-\bar{n}}\cdot K_1K_2K_3L. \quad (6)$$

Results and Discussion

Assuming the ligand to be the bivalent anion of the unionized molecule (obtained by the ionization of the sulfonic acid and the hydroxyl groups), the *proton association constants* for the ligand were determined to be $\log K_1^H = 7.32 \pm 0.03$, $\log K_2^H = 4.38 \pm 0.03$, and $\log K_3^H$ less than 2 in aqueous solutions containing 0.100 M sodium perchlorate at 25 °C. The stability constants for yttrium(III) and lanthanoid(III) complexes with 7-bromo-8-hydroxy-5-quinolinesulfonic acid are given in Table 1.

We see that for the lanthanoid(III) complexes, $\log K$ increases regularly with the atomic number of the lanthanoid from lanthanum to europium, the values for gadolinium complexes being lower than those for the europium complexes, a trend established for the lanthanoid complexes.[4] In case of heavy lanthanoid complexes, however, two trends are observed:

(1) $\log K_1$ increases regularly from gadolinium to ytterbium,

(2) $\log K_2$ increases from gadolinium to holmium and then drops for the next members of the series.

The first trend is very common for the lanthanoid complexes. The less common second trend is also observed. This might be due to the steric factors involved in the introduction of the second ligand molecule to the 1 : 1 complex.

The $\log K$ values for lutetium complexes are lower than those for ytterbium complexes, probably due to the same factors as responsible for the gadolinium-break.

As a result of their observations on the stability constants of the lanthanoid and yttrium complexes with a common ligand, Yoneda *et al.*[5] concluded that the $\log K$ for yttrium complex is comparable to that for light lanthanoid complexes in case of monodentate ligands, but of the heavy lanthanoid complexes for multidentate ligands forming chelate structure. As expected for the present ligand, the stability constants for yttrium(III) complexes are among those of the heavy lanthanoid complexes.

Table 1. Stoichiometric stability constants of 7-bromo-8-hydroxy-5-quinolinesulfonate complexes at 25°C and at μ=0.100 M ($NaClO_4$)

Lanthanoid(III) ion	$\log K_1$[a]	$\log K_2$[b]	$\log K_3$[c]
La	4.68	4.03	3.4
Ce	4.81	4.19	3.6
Pr	4.97	4.30	3.9
Nd	5.09	4.43	4.0
Eu	5.43	4.70	4.3
Sm	5.30	4.57	4.2
Gd	5.21	4.64	4.0
Tb	5.32	4.77	4.1
Dy	5.45	4.85	4.1
Ho	5.59	4.89	4.1
Er	5.69	4.81	4.0
Tm	5.82	4.73	3.9
Yb	5.93	4.64	3.8
Lu	5.82	4.50[d]	
Y	5.50	4.86	4.2

a) ±0.04 b) ±0.08 c) ±0.8 d) ±0.15

3) H. M. Irving and H. S. Rossotti, *J. Chem. Soc.*, **1954**, 2904.

4) T. Moeller, D. F. Martin, L. C. Thompson, R. Ferrus, G. R. Fiestel, and W. J. Randall, *Chem. Rev.*, **65**, 1 (1965).

5) H. Yoneda, G. R. Choppin, J. L. Bear, and A. J. Graffeo, *Inorg. Chem.*, **4**, 244 (1965) and references therein.

The Atomic Absorption Spectrophotometric Determination of Arsenic and Selenium in Premixed Inert Gas(Entrained Air)-Hydrogen Flames with a "Multi-flame" Burner

Taketoshi NAKAHARA, Hirohito NISHINO, Makoto MUNEMORI*, and Sôichirô MUSHA

Department of Applied Chemistry, College of Engineering, University of Osaka Prefecture, Mozu-umemachi, Sakai 591

** Laboratory of Environmental Chemistry, College of Engineering, University of Osaka Prefecture, Mozu-umemachi, Sakai 591*

(Received August 21, 1972)

The determination of arsenic and selenium by atomic absorption spectrophotometry was established in premixed inert gas(entrained air)-hydrogen flames using a "multi-flame" burner. Arsenic and selenium electrodeless discharge lamps were used as the sources of radiation. The optimum operating conditions for the atomic absorption measurements for arsenic and selenium at 193.7 and 196.1 nm respectively were investigated. Under the optimum conditions, the sensitivities for 1% absorption were 0.17 and 0.15 ppm for arsenic and selenium respectively. Many other elements and acids interfered with the determination of arsenic and selenium in these low-temperature flames. Most of the interferences were found to be completely eliminated, in appearance, by adding a large amount (2000 ppm) of tin(II) chloride to the sample solutions. Furthermore, a gas-sampling technique for arsenic was studied in order to improve the arsenic sensitivity and in order to eliminate the interferences from other elements. The present method was applied to the determination of arsenic in sulfide ores and steels with satisfactory results.

There are two major difficulties in the determination of arsenic and selenium by atomic absorption spectrophotometry; the first is the high flame background absorption and the noise levels obtained at the resonance lines of these elements below 200 nm, and the second is the relatively low intensity and poor stability shown by many arsenic and selenium hollow-cathode lamps. By using a hollow-cathode lamp and an air-acetylene flame, the sensitivities have been reported to be 1.0 ppm for arsenic[1-3] at 193.7 nm and to be 1.0 ppm for selenium[1-4] at 196.1 nm. Later, the present authors[5] have described the determination of selenium in sulfur and obtained the sensitivity of 0.4 ppm for 1% absorption in an air-hydrogen flame with a total-consumption nebulizer-burner.

Several attempts have been made to overcome the difficulties due to the absorptions of arsenic- and selenium-radiations by the atmosphere, by optical components, and by flame gases. Arsenic and selenium may be atomized efficiently in argon-hydrogen flame[2] and nitrogen-hydrogen flame[6] burning with entrained air. These flames exhibit greater transparencies below 200 nm than do conventional air-hydrogen or air-acetylene flames, resulting in improved signal-to-noise ratios. However, the determination of arsenic and selenium in these cool flames may suffer from interferences from various foreign elements. Kirkbright and Ranson[7] have used the slightly fuel-rich nitrous oxide-acetylene flame to remove the interferences from foregin elements. Ando *et al.*[6] have employed long-path-length Vycor cells with a nitrogen(entrained air)-hydrogen flame to determine arsenic; they thus obtained the sensitivity of 0.006 ppm for 1% absorption. Massmann[8] has used an electrically-heated graphite cell in the argon atmosphere to show the possibility of determining arsenic down to 0.1 ppm. The use of electrodeless discharge lamps as an alternative to hollow-cathode lamps in atomic absorption spectrophotometry has been reported.[3,9-13] Potentially these line sources have the advantage of having a higher output intensity and a narrower emission line free from self-absorption or self-reversal; therefore, they may allow operation at low amplifier-gain and spectral-bandpass settings.

In this investigation, the determination of arsenic and selenium in premixed inert gas (entrained air)-hydrogen flames with a "multi-flame" burner[14] has been established by using arsenic and selenium electrodeless discharge lamps as sources of radiation. The performance characteristics of the electrodeless discharge lamps, the interferences, and their elimination in the determination of both elements have been studied in detail. Furthermore, a gas-sampling technique[15] for arsenic has been studied in order to improve the sensitivity and eliminate the interferences. The present method has then been applied to the determination of arsenic in several sulfide ores and steels.

Experimental

Apparatus. A Nippon Jarrell-Ash Model AA-1 atomic absorption/flame emission spectrophotometer fitted with a HTV R—106 photomultiplier was used on a single-pass

1) W. Slavin and S. Sprague, *At. Absorption Newslett.*, **3**, 1 (1964).
2) H. L. Kahn and J. E. Schallis, *ibid.*, **7**, 5 (1968).
3) G. F. Kirkbright, M. Sargent, and T. S. West, *ibid.*, **8**, 34 (1969).
4) C. S. Rann and A. N. Hambly, *Anal. Chim. Acta*, **32**, 346 (1965).
5) T. Nakahara, M. Munemori, and S. Musha, *ibid.*, **50**, 51 (1970).
6) A. Ando, M. Suzuki, K. Fuwa, and B. L. Vallee, *Anal. Chem.*, **41**, 1974 (1969).
7) G. F. Kirkbright and L. Ranson, *ibid.*, **43**, 1238 (1971).
8) H. Massmann, *Z. Anal. Chem.*, **225**, 203 (1967).
9) A. S. Bazhov, *Zavod. Lab.*, **33**, 1096 (1967).
10) R. M. Dagnall, K. C. Thompson, and T. S. West, *At. Absorption Newslett.*, **6**, 117 (1967).
11) R. M. Dagnall and T. S. West, *Appl. Opt.*, **7**, 1287 (1968).
12) K. E. Zacha, M. P. Bratzel, J. D. Winefordner, and J. M. Mansfield, *Anal. Chem.*, **40**, 1733 (1968).
13) O. Menis and T. C. Rains, *ibid.*, **41**, 952 (1969).
14) T. Nakahara, H. Date, M. Munemori, and S. Musha, This Bulletin, **46**, 637 (1973).
15) W. Holak, *Anal. Chem.*, **41**, 1712 (1969).

system. A "multi-flame" burner[14] constructed in the authors' laboratory in conjuction with a Techtron nebulizer-chamber was also used.

The line sources employed were arsenic and selenium electrodeless discharge lamps (EMI Electronics, Ltd., Great Britain), which were operated in a 3/4-wave resonant cavity, Model 211 L, at 2450 MHz with a "Microtron 200" power generator (Electro-Medical Supplies, Ltd., Great Britain) coupled with a reflected power meter. The discharge was initiated with a "Tesla" high-frequency vacuum tester.

The hydrogen, argon and nitrogen flow rates were controlled by means of needle valves and were measured on calibrated flow meters.

Reagents. A standard arsenic solution (1000 ppm) was prepared by dissolving 1.386 g of arsenious oxide of an analytical-reagent grade with 2 g of sodium hydroxide and 20 ml of distilled water, by neutralizing with hydrochloric acid, and by then diluting the solution to 1000 ml with distilled water.

A stardard selenium solution (1000 ppm) was prepared by dissolving 1.000 g of high-purity selenium metal in 5 ml of nitric acid and by then diluting the solution to 1000 ml with distilled water.

Diluted solutions of arsenic and selenium were prepared from the stock solutions as required.

All the acids and inorganic salts used were of either an analytical-reagent grade or the highest quality available.

Results and Discussion

Wavelengths and Flame Conditions. The relative intensities and sensitivities of the arsenic and selenium lines radiated from the electrodeless discharge lamps indicated that the arsenic 189.0-nm line was the most sensitive, but when we take the noise levels into consideration the arsenic 193.7-nm line was the most useful, while the selenium 196.1-nm line was the most sensitive and useful.

The effect of the flame composition and the flame height on the arsenic and selenium atomic absorptions was studied in premixed inert gas(entrained air)-hydrogen flames. The flame composition and the flame height had remarkable effects on the arsenic and selenium atomic absorptions in these flames. The optimum flame conditions obtained for arsenic and selenium are shown in Table 1.

Table 1. Optimum flame conditions for arsenic and selenium

	Arsenic	Selenium
Argon (entrained air)-hydrogen flame		
Hydrogen flow rate (l/min)	9.4	7.2
Argon flow rate (l/min)	4.5	4.5
Argon pressure (kg/cm²)	1.5	1.5
Sample aspiration rate (ml/min)	8.9	8.9
Flame height above burner head (mm)	4.0	2.0
Nitrogen (entrained air)-hydrogen flame		
Hydrogen flow rate (l/min)	9.4	6.5
Nitrogen flow rate (l/min)	5.0	5.0
Nitrogen pressure (kg/cm²)	1.5	1.5
Sample aspiration rate (ml/min)	9.0	9.0
Flame height above burner head (mm)	5.0	3.0

Optimization of Some Experimental Parameters in the Operation of Microwave-excited Electrodeless Discharge Lamps. Many workers have used microwave-excited electrodeless discharge lamps in atomic absorption and atomic fluorescence spectrophotometry, and have described their advantages and limitations.[11-13,16-18] Since the performance characteristics of the electrodeless discharge lamps are not always identical, it appeared necessary to establish the optimum operating conditions of each electrodeless discharge lamp employed. The efficiency with which the electrodeless discharge lamps were operated was found to depend to a large extent on the proper choice of resonant cavity. The electrodeless discharge lamps employed in this study were not discharged in a 3/4-wave resonant cavity Model 210 L (Electro-Medical Supplies, Ltd.) under any circumstance.

Although it had been expected[19] that tuning was dependent on the discharge characteristics and, consequently, dependent upon the microwave power applied, a change in the tuning characteristics with a variation in the microwave power is generally impossible to detect. Consequently, apart from occasional checks, the cavity was tuned to give as low a reflected power as possible. A reflected-power meter may be used to facilitate the tuning of the cavity and to ensure that the reflected power is not so high that the mag-

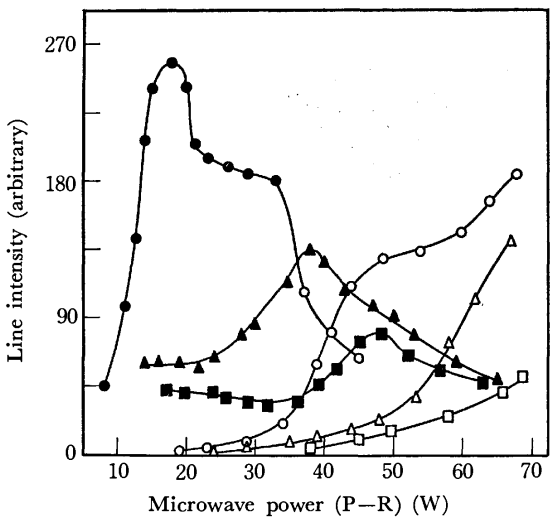

Fig. 1. Effect of microwave power on line intensities of arsenic and selenium.
At the 193.7 nm arsenic line
—●— Without cooling
—▲— With cooling (nitrogen flow rate : 2 l/min)
—■— With cooling (nitrogen flow rate : 3 l/min)
At the 196.1 nm selenium line
—○— Without cooling
—△— With cooling (nitrogen flow rate : 3 l/min)
—□— With cooling (nitrogen flow rate : 6 l/min)

16) J. M. Mansfield, M. P. Bratzel, H. O. Norgordon, K. E. Zacha, D. O. Knapp, and J. D. Winefordner, *Spectrochim. Acta*, **23B**, 389 (1968).
17) C. H. Corliss, W. R. Borzmann, and F. O. Westfall, *J. Opt. Soc. Amer.*, **43**, 398 (1953).
18) D. C. Cooke, R. M. Dagnall, and T. S. West, *Anal. Chim. Acta*, **54**, 381 (1971).
19) F. C. Fehsenfeld, K. M. Evenson, and H. P. Broida, *Rev. Sci. Instr.*, **36**, 294 (1965).

netron may be damaged. Provided that powers not higher than about 75 W are used, there is little possibility of damage being caused, and visual tuning to maximum lamp intensity is quite satisfactory.

The effect of microwave power (the power indicated on the microwave generator minus the reflected power (P–R) was taken) on the resonance-line intensity was examined for arsenic and selenium electrodeless discharge lamps. The results obtained are shown in Fig. 1. The cooling of electrodeless discharge lamps has been recommended by some workers.[20,21] As is shown in Fig. 1, a decrease in the line intensity was observed with both electrodeless discharge lamps when they were cooled with nitrogen. Furthermore, the maximum in the intensity of the 193.7-nm arsenic line shifted from a lower to a higher microwave power with an increase in the nitrogen flow rate. Although the line intensities were decreased with an increase in the nitrogen flow rate, the cooling produced an increased stability and considerably shorter warming-up periods by means of improved insulation from draughts. However, it was necessary for the flow rate of cooling nitrogen to be accurately regulated; otherwise, the cooling rather resulted in poor stability. In this study, the nitrogen from a cylinder was used as the cooling gas after drying with anhydrous calcium chloride instead of dry air, because a small pressure variation in an air compressor remarkably affected the line intensity with both elelectrodeless discharge lamps employed.

Then, the effect of the microwave power (P–R) on the atomic absorption signals of arsenic and selenium was examined. The absorbance variations obtained in the microwave power range from 8 to 70 W with and without the use of nitrogen cooling are shown in Fig. 2. The arsenic atomic absorption was remarkably increased with a decrease in the microwave power, while no or little variation with microwave power was observed for selenium. As is shown in Fig. 2, the nitrogen cooling produced an increase in the atomic absorption signals. However, a nitrogen flow rate of more than 2.0 l/min gave a constant absorbance for either arsenic or selenium. This phenomenon is presumably due to the fact that there is little or no self-absorption and/or self-reversal effects so long as the microwave power is small. Particularly for arsenic, this may be the case. A self-reversal effect has been noticed with some microwave-excited electrodeless discharge lamps,[22] but this may be readily overcome by using a slightly reduced operating microwave power and/or by cooling the lamp, as has been described above.

Thus, the optimization of the microwave power and the nitrogen cooling was important to the atomic absorption signal rather than the line intensity. The short-term stability of the lamps employed was similar, virtually better than 5% and often 2%, and the drift rate was less than 2% per hour for both arsenic and selenium lamps.

The optimum operating conditions for the atomic absorptions of arsenic and selenium may be summarized as follows. The microwave power(P–R) values were 8 and 20 W for arsenic and selenium respectively. The flow rate of nitrogen as a cooling gas was 2.0 l/min; it was accurately controlled with a needle valve and measured on a calibrated flow meter.

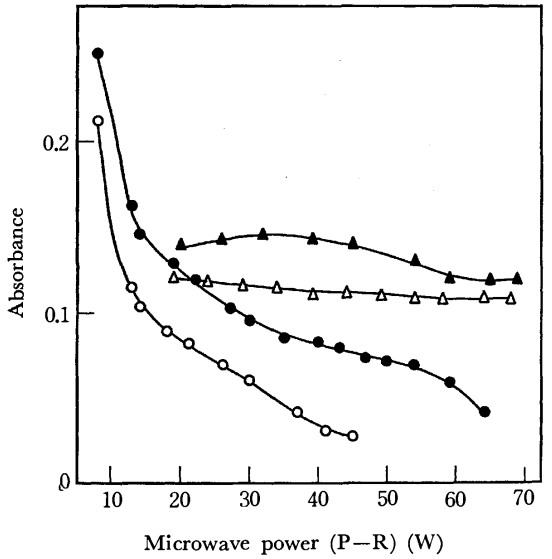

Fig. 2. Effect of microwave power on the determination of arsenic and selenium.
At the 193.7 nm arsenic line
—●— With cooling, —○— Without cooling
At the 196.1 nm selenium line
—▲— With cooling, —△— Without cooling

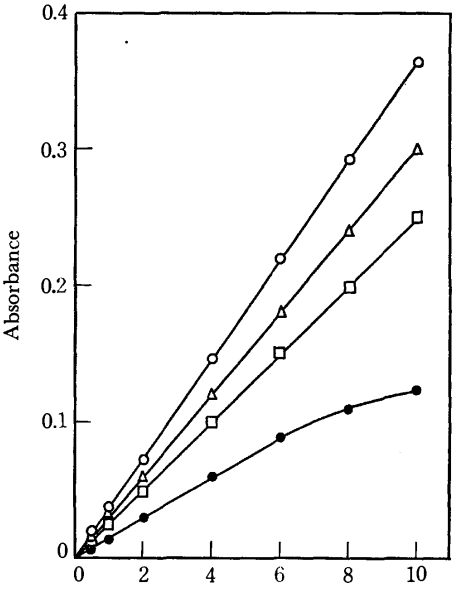

Fig. 3. Calibration graphs for arsenic and selenium in argon (entrained air)-hydrogen flame.
—○— At 189.0 nm arsenic line (microwave power : 8 W)
—△— At 196.1 nm selenium line (microwave power : 20 W)
—□— At 193.7 nm arsenic line (microwave power : 8 W)
—●— At 193.7 nm arsenic line (microwave power : 19 W)

20) R. F. Browner, R. M. Dagnall, and T. S. West, *Anal. Chim. Acta*, **46**, 207 (1969).
21) R. M. Dagnall, G. F. Kirkbright, and T. S. West, *ibid.*, **47**, 407 (1969).
22) R. M. Dagnall, K. C. Thompson, and T. S. West, *Talanta*, **14**, 1151 (1967).

Calibration Graphs for Arsenic and Selenium. The calibration graphs for arsenic and selenium in the argon(entrained air)-hydrogen flame under the optimum experimental conditions described above were linear in the range of 0—10 ppm, as is shown in Fig. 3, with a precision of the mean relative standard deviation of about 3%, but the graph obtained at the 193.7-nm arsenic line with the higher microwave power (19 W) was bent slightly towards the concentration axis from 6 to 10 ppm. This bending is presumably due to self-absorption and/or self-reversal effects at a higher microwave power. The sensitivities (ppm for 1% absorption) over the linear ranges were found to be 0.17 and 0.15 ppm at the 193.7-nm arsenic line and the 196.1-nm selenium line respectively. No appreciable difference in the sensitivities between the argon(entrained air)-hydrogen flame and the nitrogen (entrained air)-hydrogen flame was observed.

Effects of Acids on the Atomic Absorptions of Arsenic and Selenium. The effects of the acids generally used for the dissolution of various practical samples in the determination of arsenic and selenium were examined in both the flames. The acids were hydrochloric, nitric, perchloric, phosphoric, and sulfuric acids. The concentrations of arsenic and selenium were 10 and 15 ppm respectively, and the concentration range of the acids was 0–3.0 N. The results obtained for arsenic in the argon(entrained air)-hydrogen flame are shown in Fig. 4. Similar results for selenium were obtained in both the flames. Hydrochloric, nitric, and perchloric acids had little effect on the atomic absorptions of arsenic and selenium, while sulfuric acid caused either an enhancement or depression, depending on its concentration. Phosphoric acid caused a depressing interference, independent of its concentration. The present authors have reported previously that hydrochloric, nitric, perchloric, and phosphoric acids, unlike sulfuric acid, had no effect on the selenium atomic absorption at the 196.1-nm line in the hotter air-hydrogen flame with a total-consumption nebulizer-burner.[5]

It was noted that the solutions containing nitric, perchloric, phosphoric, and sulfuric acids in the absence of both arsenic and selenium gave background absorptions at 193.7 and 196.1 nm in the inert gas(entrained air)-hydrogen flames under the optimum contions for the arsenic and selenium atomic absorptions. These background absorptions were not linear with respect to their concentrations. The background absorbances at 193.7 nm were found to be 0.101, 0.053, 0.026, and 0.019 in the argon(entrained air)-hydrogen flame for sulfuric, phosphoric, perchloric, and nitric acids respectively at a 3.0-N concentration level, and to be 0.107, 0.050, 0.021, and 0.011 in the nitrogen (entrained air)-hydrogen flame for sulfuric, phosphoric, nitric, and perchloric acids respectively at the same concentration level. The results shown in Fig. 4 have been corrected for the background absorptions at each concentration of the acids. The background absorption seems to be ascribable to the molecular absorption, the light scattering, and/or the variation in the refractive index within the flame caused by vaporization of concentrated solutions.[5]

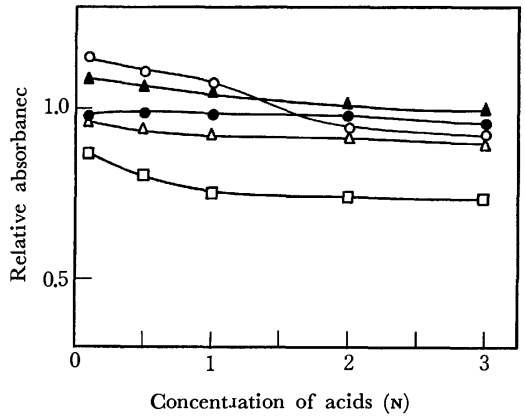

Fig. 4. Effect of acids on the determination of arsenic in argon (entrained air)-hydrogen flame.
Concentration of arsenic : 10 ppm
—○— Sulfuric acid, —▲— Perchloric acid,
—●— Hydrochloric acid, —△— Nitric acid,
—□— Phosphoric acid

Effects of Foreign Elements on the Determination of Arsenic and Selenium. The effects of various foreign elements on the determination of arsenic and selenium have been studied in an air-hydrogen,[5] an air-acetylene flame,[23] and a nitrogen-shielded air-acetylene flame.[3] The present authors have established that the determination of tin[24] and bismuth[25] in premixed inert gas(entrained air)-hydrogen flames suffer from interference from foreign elements because of the inability of the cool flames to vaporize or atomize the other elements present in the sample solutions. The interference effects of various other elements on the atomic absorptions of arsenic and selenium were studied in inert gas(entrained air)-hydrogen flames under the optimum conditions established above. The atomic absorptions were recorded in the presence of a 20-fold weight excess of diverse elements for 10 and 5 ppm of arsenic and selenium respectively. The results obtained in the argon(entrained air)-hydrogen flame are shown in Table 2. It can be seen from Table 2 that many elements produce depressing interferences with the determination of arsenic and selenium. The depressing interferences due to antimony, cadmium, manganese, selenium, and bismuth in the determination of arsenic, and those due to barium, lead, mercury, and zinc in the determination of selenium, were completely overcome by using a slightly acidic solution (0.2–0.5 N in hydrochloric acid). These interferences may also be overcome by using a hotter flame, such as a nitrous oxide-acetylene flame.[7]

However, further investigations of the depressing interferences indicated that most of the depressing interferences with the arsenic and selenium atomic absorptions were eliminated, in appearance, by adding a great amount (2000 ppm) of tin to the sample solutions, as is shown in Table 3. Although the

23) C. L. Chakrabarti, *Anal. Chim. Acta*, **42**, 379 (1968).
24) T. Nakahara, M. Munemori, and S. Musha, *ibid.*, **62**, 267 (1972).
25) T. Nakahara, M. Munemori, and S. Musha, This Bulletin, **46**, 1166 (1973).

TABLE 2. EFFECT OF VARIOUS OTHER ELEMENTS ON THE DETERMINATION OF ARSENIC AND SELENIUM

Element[g]	Relative absorbance		Element[g]	Relative absorbance	
	Arsenic[h]	Selenium[i]		Arsenic[h]	Selenium[i]
None	1.00	1.00	Mn[a]	0.82	0.33
Ag[a]	0.98	1.04	Mo[f]	0.86	0.84
Al[b]	0.92	0.25	Na[b]	1.00	1.01
As[c]	—	0.96	Ni[e]	0.29	0.64
Au[b]	1.00	0.89	Pb[a]	0.98	0.42
B[d]	0.85	1.04	Pd[b]	0.35	0.32
Ba[b]	1.00	0.54	Pt[b]	0.98	0.90
Be[e]	0.85	0.91	Rb[b]	1.02	1.00
Bi[a]	0.97	0.99	Sb[b]	1.01	1.00
Ca[a]	0.94	0.74	Se[c]	0.92	—
Ce[e]	0.94	0.74	Si[c]	0.22	0.21
Co[b]	0.76	0.72	Sn[b]	1.06	1.07
Cr[b]	0.79	0.53	Sr[a]	0.85	0.67
Cs[b]	1.03	0.99	Te[c]	1.05	1.03
Cu[e]	1.05	0.92	Th[a]	0.53	0.31
Fe[b]	0.88	0.92	Ti[b]	1.05	0.96
Hg[b]	0.89	0.87	Tl[a]	0.99	1.00
In[b]	1.01	0.98	V[f]	1.02	1.03
K[b]	1.01	1.00	W[c]	1.03	1.02
La[b]	0.93	0.81	Y[a]	0.37	0.00
Li[b]	1.04	0.89	Zn[a]	0.86	0.97
Mg[b]	0.99	0.88	Zr[a]	0.80	0.53

a) Added as nitrate. b) Added as chloride. c) Added as sodium arsenite, selenite, silicate, tellurite or tungstate, respectively. d) Added as boric acid. e) Added as sulfate. f) Added as ammonium molybdate or vanadate, respectively. g) The concentration of the elements added, 200 ppm for arsenic and 100 ppm for selenium. h) The concentration of arsenic was 10 ppm. i) The concentration of selenium was 5 ppm.

TABLE 3. EFFECT OF TIN ON THE DEPRESSING INTERFERENCES WITH THE DETERMINATION OF ARSENIC IN AN ARGON (ENTRAINED AIR)-HYDROGEN FLAME

Element[a]	Relative absorbance for arsenic[b]				
	Tin added (ppm)				
	0	2000	5000	10000	2000
Al	0.84	1.04	1.03	1.05	1.00
B	0.80	1.00	1.00	1.06	1.05
Ca	0.86	1.03	0.98	0.97	0.98
Co	0.88	0.93	0.95	0.94	0.95
Cr	0.87	0.99	1.00	1.03	1.06
Fe	0.79	1.05	1.04	1.03	1.05
Mo	0.78	0.99	0.98	1.01	1.00
Ni	0.48	1.02	0.99	0.98	1.03
Si	0.67	0.95	0.96	0.94	0.95
V	0.88	1.01	0.99	0.99	1.00
Zr	0.73	0.96	0.98	0.98	0.95

a) The concentration of the elements added was 1200 ppm.
b) The concentration of arsenic was 10 ppm.

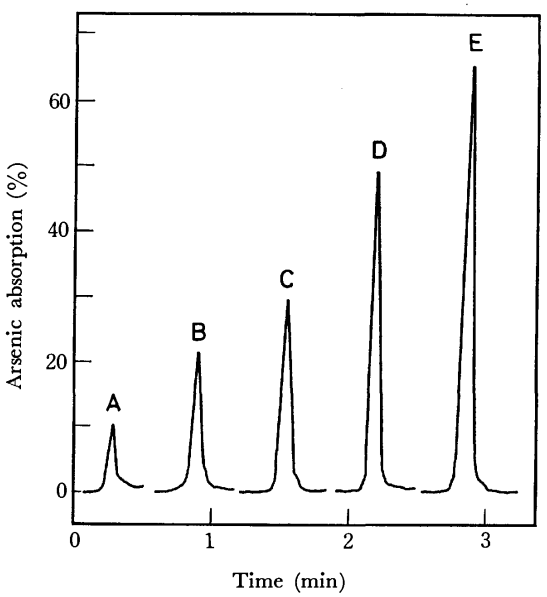

Fig. 5. Arsenic atomic absorption signals by gas-sampling technique.
Flame: Argon (entrained air)-hydrogen flame
A: Reagent blank B: 0.05 μg of arsenic
C: 0.1 μg of arsenic D: 0.2 μg of arsenic
E: 0.4 μg of arsenic

mechanism of the elimination of the depressing interferences in the presence of tin has not been explained satisfactorily, the present method could be applied to the determination of arsenic or selenium in some practical samples with satisfactory results.

Gas-sampling Technique for the Determination of Arsenic. Arsenic often needs to be determined in trace amounts, and an improvement in the sensitivity of the atomic absorption spectrophotometric method would be desirable. This can be achieved if arsenic is generated from the sample solution, col-

lected in a cold trap with, for example, liquid nitrogen, and then passed into the burner of an atomic absorption spectrophotometer; the atomic absorption signal is recorded as a function of the time. Holak[15] has reported this gas-sampling technique for arsenic determination by atomic absorption spectrophotometry, and obtained the detection limit of 0.04 μg of arsenic.

This gas-sampling technique was applied to the present method. Examples of response signals are shown in Fig. 5. A preliminary study indicated that the sensitivity for 1% absorption was 0.004 μg (4 ng) in quantities or 0.13 ppb in concentration, and Beer's law was established as holding between the absorbance and the amount of arsenic.

The main advantage of the gas-sampling technique is its suitability for trace analysis. The element is isolated from the matrix elements, and the total quantity is used to produce a sharp absorption signal. In addition, interferences often associated with solutions, such as those with high concentrations, and light scattering, as well as chemical interferences, are virtually eliminated.

Determination of Arsenic in Sulfide Ores and Steels. Based on the above-mentioned observations, the following procedures for the determination of arsenic in sulfide ores and steels were developed.

A 0.5-g ore sample was weighed and dissolved in 25 ml of diluted *aqua regia* by gentle heating on a hot plate. After the solution had then been cooled, the insoluble solids (sulfur and silicate) were filtered off with a filter paper. The filtrate was transferred to a 100-ml volumetric flask and diluted to volume with distilled water. Determinations were made by the standard addition method, and also by the calibration graph method. In either case the arsenic atomic absorptions were measured at 193.7 nm in the presence of 2000-ppm tin (as stannous chloride) as a suppressor of the interferences from other elements under the above-mentioned optimum operating conditions. The results of the determination of arsenic in sulfide ores by atomic absorption spectrophotometry are shown in Table 4.

Table 4. Results of the determination of arsenic in sulfide ores by atomic absorption spectrophotometry

Sample	Arsenic content (%)			
	$Ar-H_2$[a]		N_2-H_2[b]	
A mine ore (Cu conc.)	0.29_2[c]	0.28_4[d]	0.28_3[c]	0.29_1[d]
	0.31_7[c]	0.28_9[d]	0.29_2[c]	0.28_3[d]
	0.27_9[c]	0.29_3[d]	0.28_2[c]	0.29_5[d]
B mine ore (S conc.)	0.45_1[c]	0.44_5[d]	0.45_9[c]	0.45_2[d]
	0.46_3[c]	0.44_9[d]	0.44_8[c]	0.45_6[d]
	0.45_5[c]	0.46_1[d]	0.45_0[c]	0.45_4[d]

a) Argon (entrained air)-hydrogen flame.
b) Nitrogen (entrained air)-hydrogen flame.
c) Determined by standard addition method.
d) Determined by calibration graph method.

Table 5. Results of the determination of arsenic by atomic absorption spectrophotometry in conjunction with a gas-sampling technique

Sample	Arsenic content (%)	
	Cert. value	Atomic absorption method
GK-9 Stainless steel[a]	0.012	0.011_8[b]
GK-10 Cast iron[a]	0.029	0.028_5[b]

a) Supplied by Kansai Bunseki Kenkyukai.
b) An average of 5 determinations.

A 0.1-g steel sample was weighed and dissolved in 10 ml of *aqua regia* by heating on a hot plate. After evaporation to dryness, the residue was dissolved in 10 ml of hydrochloric acid by gentle heating on a hot plate. The solution was transferred to a 100-ml volumetric flask and diluted to volume with distilled water. The resultant solution was employed as the sample solution. The determination of arsenic was followed below. A 5-ml portion of the sample solution was transferred into a 300-ml Erlenmeyer flask, and 0.5 ml of a 35% stannous chloride solution, 40 ml of 6 N hydrochloric acid, and 5 ml of a 20% potassium iodide solution were added. After about 10 min, 5 g of sandy zinc metal were added and the arsine generated was collected with a U-tube filled with glass beads in liquid nitrogen. The U-tube was removed from the liquid nitrogen and allowed to come to room temperature. The arsenic atomic absorption signals were measured at 193.7 nm in the argon(entrained air)-hydrogen flame. The results are shown in Table 5.

We would like to thank the Ministry of Education for its Scientific Research Grant to one of us (M. M.).

Peroxo-, Oxo-, and catena-Oxo-Manganese Complexes with *N,N'*-Ethylenebis(salicylideneimine) Analogues[1]

Takayuki MATSUSHITA, Tatsuo YARINO*, Isao MASUDA, Toshiyuki SHONO, and Koichiro SHINRA

Department of Applied Chemistry, Faculty of Engineering, Osaka University, Yamada-kami, Suita, Osaka 565

(Received May 29, 1972)

By the reaction of Mn^{II}(salen) (salen=*N,N'*-ethylenebis(salicylideneiminato) dianion) and its analogues with molecular oxygen in organic solvents, three types of complexes including as structural units the Mn^{III}–O_2–Mn^{III}, –(–Mn^{IV}–O–)–$_n$, and Mn^{IV}=O bonds respectively, have been obtained, and characterized by means of their electronic and infrared spectra, by thermogravimetric analysis, and in terms of their magnetic properties. The lower magnetic moments for [Mn^{III}(salen)]$_2O_2$ and –[–Mn^{IV}(salen)–O–]–$_n$ than those expected have been interpreted in terms of antiferromagnetic interactions. The oxo complex was found to give the catena-oxo complex quantitatively in a DMF, DMSO, or Py solution. The effects of the oxygen partial pressure and the nature of the substituent in the organic part on the complex formation were investigated. A lower partial pressure of oxygen has the advantage of yielding the μ-peroxo complex in a higher yield. A discussion of the reaction mechanism is also included.

The Mn^{II}(salen)[2] was first reported by Tsumaki[3] to react with oxygen to yield Mn^{III}(salen)OH, for which Lewis *et al.*[4] later proposed a polymeric structure including unitary Mn^{III}(salen)–O–Mn^{III}(salen)·H_2O on the basis of the magnetic property. Recently, Johnson *et al.*[5] have reported that Mn^{II}(salpr)[2] takes up molecular oxygen in a benzene solution. In the present study, three types of complexes involving Mn^{III}-O_2-Mn^{III}, –(–Mn^{IV}–O–)–$_n$, and Mn^{IV}=O bonds respectively are shown to be obtainable upon reacting the Mn^{II}(salen) and its analogues with molecular oxygen in organic solvents.

Experimental

Manganese(II) Complexes. The preparation of Mn^{II}(salen) and Mn^{II}(3-MeO-salen)·H_2O[2] was carried out in a nitrogen atmosphere according to a modification of the procedure of the literature.[4] Mn^{II}(5-NO_2-salen)[2] was obtained by allowing the pyridine adduct, Mn^{II}(5-NO_2-salen)·2Py, which had been prepared by the reaction of 5-NO_2-salenH_2 with $MnCl_2$·$4H_2O$ in a *ca.* 50% aqueous pyridine solution, to stand *in vacuo* at 90—100 °C for 12 hours. The compounds were confirmed by elemental analyses.

Peroxo-, Oxo-, and catena-Oxo-Manganese Complexes. *μ-Peroxo-bis-*NN'*-ethylenebis(salicylideneiminato)manganese(III)*, [*Mn^{III}(salen)*]$_2O_2$: Mn^{II}(salen) (2.0 g) was dissolved in DMSO (150 ml) in a nitrogen atmosphere, and then the solution was kept in oxygen (1 atm) at room temperature for about 12 hours. Two grams of precipitates were thus separated. The precipitates were extracted with CH_2Cl_2 (1 l), and then the solvent was evaporated to *ca.* 50 ml to leave reddish-brown crystals. They were separated by filtration and then dried *in vacuo* at 50 °C for 6 hours. Yield: 0.2 g. When the solution of Mn^{II}(salen) was kept in a nitrogen atmosphere which contained about 2.0 vol% of oxygen, the crystals of the μ-peroxo complex could be obtained in a *ca.* 90% yield. The μ-peroxo complex is soluble in CH_2Cl_2 (*ca.* 0.4 g/l) and is slightly souble in DMSO and DMF.

*Oxo-*N,N'*-ethylenebis(3-methoxy-salicylideneiminato) manganese (IV) Methanol Adduct, O=Mn^{IV}(3-MeO-salen)·2MeOH*: Mn^{II}(3-MeO-salen)·H_2O (2.0 g) was suspended in absolute MeOH (200 ml), and then oxygen gas was bubbled through the mixture while it was being stirred for *ca.* 20 hours. The solution turned greenish-brown, and dark-green, crystalline needles were separated. The crystals were filtered and dried *in vacuo*. Further crystals were obtained by concentrating the filtrate. Yield: 1.4 g. The complex was recrystallized from methanol.

*Poly, catena-oxo-*N,N'*-ethylenebis(salicylideneiminato)manganese-(IV), –[–Mn^{IV}(salen)–O–]–$_n$*: Mn^{II}(salen) (1.0 g) was dissolved in Py (100 ml) under a nitrogen atmosphere, and then the solution was allowed to stand for about 20 hours in dry oxygen (1 atm). The brown precipitates thus separated were centrifuged, washed with MeOH, and then dried *in vacuo*. Yield: 0.95 g.

*Poly, catena-oxo-*N,N'*-ethylenebis(3-methoxy-salicylideneiminato)-manganese(IV), –[–Mn^{IV}(3-MeO-salen)–O–]–$_n$*: The complex was obtained from Mn^{II}(3-MeO-salen)·H_2O in the way described above. Yield: 93%.

*Poly, catena-oxo-*N,N'*-ethylenebis(5-nitro-salicylideneiminato)-manganese(IV) Dimethylformamide Adduct, –[–Mn^{IV}(5-NO_2-salen)–O–]–$_n$(DMF)$_n$*: The complex was prepared by a similar reaction of Mn^{II}(5-NO_2-salen) in a DMF solution. Yield: 90%.

These catena-oxo complexes are amorphous, and they are insoluble in water and in common organic solvents.

Measurements. The oxygen uptake was measured by using a Warburg manometer. The infrared spectra were obtained in Nujol mulls using a JASCO IR-L spectrophotometer in the 400—4000 cm^{-1} region, and a Hitachi EPI-L spectrophotometer in the 200—700 cm^{-1} region. The electronic spectra were recorded on a Hitachi EPS-3 spectrophotometer. The magnetic susceptibility was measured for a powder sample by the Faraday method, using a torsion balance[6] over the temperature range from 77 to 293 K,

* Present address: Teijin Co., Matsuyama Factory, Kita-yoshida, Matsuyama.

1) Preliminary communication; T. Yarino, T. Matsushita, I. Masuda, and K. Shinra, *Chem. Commun.*, **1970**, 1317.

2) The following abbreviations are used; salenH_2; *N,N'*-ethylenebis(salicylideneimine), 3-MeO-salenH_2; *N,N'*-ethylenebis-(3-methoxy-salicylideneimine), 5-NO_2-salenH_2; *N,N'*-ethylenebis-(5-nitro-salicylideneimine), salprH_2; *N,N'*-1,3-propanebis(salicylideneimine), DMF; *N,N'*-dimethylformamide, DMSO; dimethylsulfoxide, Py; pyridine, MeOH; methanol.

3) T. Tsumaki, *Nippon Kagaku Zasshi*, **55**, 1245 (1934).

4) J. Lewis, F. E. Mabbs, and H. Weigold, *J. Chem. Soc. A*, **1968**, 1699.

5) G. L. Johnson, and W. D. Beveridge, *Inorg. Nucl. Chem. Lett.*, **3**, 323 (1967).

6) T. Mori, C. Miyake, and T. Sano, *Trans. JIM*, **4**, 158 (1963).

Table 1. Analytical data

	Complex[2]	Calcd %				Found %			
		C	H	N	Mn	C	H	N	Mn
I	$[Mn^{III}(salen)]_2O_2$	57.00	4.19	8.31	16.29	56.00	4.04	8.13	16.60
II	$-[-Mn^{IV}(salen)-O-]-_n$	57.00	4.19	8.31	16.29	56.12	4.04	8.26	16.47
III	$-[-Mn^{IV}(3\text{-MeO-salen})-O-]-_n$	54.41	4.57	7.05	13.76	53.50	4.65	6.84	13.63
IV	$-[-Mn^{IV}(5\text{-}NO_2\text{-salen})-O-]-_n\cdot(DMF)_n$	45.60	3.84	14.00	10.98	45.39	3.77	13.77	10.89
V	$O{=}Mn^{IV}(3\text{-MeO-salen})\cdot 2MeOH$	51.85	5.63	6.04	11.85	51.75	5.93	5.76	12.13

and by the Gouy method at room temperature. The equipment was calibrated using a standard nickel chloride solution. Thermogravimetric and differential thermal analyses were carried out using a Rigaku Denki DG-CIH Thermoflex, at a heating rate of 5 °C/min or 2.5 °C/min, and under a nitrogen stream.

Results and Discussion

As is shown in Table 1, the analytical data of the aerial oxidation products of Mn^{II}(X-salen) are in fair agreement with the Mn(X-salen)O formula. The data of the manometric measurements shown in Table 2 indicate that the Mn^{II}(X-salen) uptake oxygen in a Mn : O_2 molar ratio of 1 : 0.5 is consistent with the above results. However, as will be discussed below, these products can be classified into three types of complexes, including Mn^{III}–O_2–Mn^{III}, $-(-Mn^{IV}-O-)-_n$, and $Mn^{IV}{=}O$ bonds respectively, on the basis of their physicochemical data.

Table 2. Oxygen uptake of Mn^{II} (X-salen)[a]

Complex	Solvent	Molar ratio: O_2/complex	Time:[b] min.
Mn^{II}(salen)	DMSO	0.53	30
	DMF	0.46	5
	MeOH	0.30	1440
Mn^{II}(3-MeO-salen)·H_2O	DMSO	0.48	40
	MeOH	0.40	1200
Mn^{II}(5-NO_2-salen)·2Py	DMF	0.40	2160

a) Measurements were carried out at 20 °C.
b) The time needed for attaining equilibrium.

Solubility. Complex I (*cf.* Table 1) is slightly soluble in such organic solvents as CH_2Cl_2, DMF and DMSO, while Complexes II and III are insoluble in these solvents. Complex IV is soluble in DMSO, but sparingly so. It should be noted that Complex V is soluble in MeOH without decomposition, whereas in a Py, DMF, DMSO, or CH_2Cl_2 solution it is converted to an insoluble complex, III, in an almost quantitative yield.

Thermogravimetric Analyses. Complexes II, III, and IV show a similar pattern in the TGA curves (Fig. 1), decreasing in weight in the 200—225 °C range and with subsequent decomposition. These weight losses correspond to that caused by the release of 0.5 mole of oxygen per manganese atom.

Though Complex I shows a similar weight loss at 198 °C which is thought to be caused by the liberation of 0.5 mole of oxygen per manganese atom (observed, 4.6%; calcd, 5.3%), no other remarkable decomposition is, in this case, observed to occur until *ca.* 250 °C. It should be noticed that, upon heating at about 200 °C for 1 hour *in vacuo*, the complex was converted to the Mn^{II}(salen) in an 85% yield.

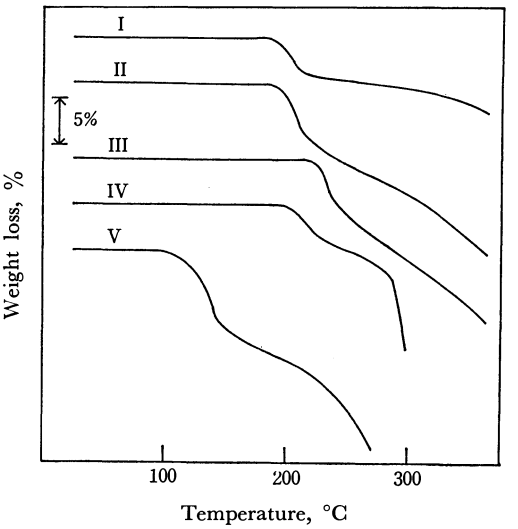

Fig. 1. TGA curves.
I: $[Mn^{III}(salen)]_2O_2$, II: $-[-Mn^{IV}(salen)-O-]-_n$, III: $-[-Mn^{IV}(3\text{-MeO-salen})-O-]-_n$, IV: $-[-Mn^{IV}(5\text{-}NO_2\text{-salen})-O-]-_n$, V: $O{=}Mn^{IV}(3\text{-MeO-salen})\cdot 2MeOH$.

Complex V decreases in weight corresponding to the release of two moles of MeOH per manganese atom between 70 and 140 °C, and then it decomposes.

Magnetic Properties. Lewis *et al.*[4] have reported that polymeric $[Mn(salen)-O-Mn(salen)]\cdot H_2O$ shows a room-temperature magnetic moment of 2.03—1.92 B.M., and that there exists a large antiferromagnetic interaction with $J=-90\ cm^{-1}$ for a binuclear cluster ($S=2$, $g=2.00$, and $N\alpha=0$ or $S=1$, $g=2.05$, and $N\alpha=0$). Complex I in the present work shows 1.96 B.M. (Table 3) at room temperature, a value which is considerably lower than those (4.96—4.98 B.M.) found for the Mn^{III}(salen)X-type complexes where X is Br^- or I^-.[7] Moreover, a significant deviation from the Curie-Weiss law is observed over the temperature range from 77 to 296 K (Fig. 2). Below *ca.* 130 K, the data fit fairly well a curve calculated by assuming a binuclear cluster, Mn–O_2–Mn, with $J=-85\ cm^{-1}$, $S=1$, $g=2.00$, and $N\alpha=O$. However, at higher temperatures they deviate from the curve and fit, rather, one calculated for $J=-90\ cm^{-1}$, $S=2$, $g=2.00$, and $N\alpha=0$. These magnetic data can

7) C. P. Probhakaran, and C. C. Patel, *J. Inorg. Nucl. Chem.*, **31**, 3319 (1969).

TABLE 3. MAGNETIC MOMENTS, AND CHARACTERISTIC IR BANDS

	Complex	μ_{eff}, B.M.[a]	IR bands, cm^{-1}
	Mn^{II}(salen)	5.28(5.27)[b]	
	Mn^{II}(3-MeO-salen)·H_2O	5.92	
I	$[Mn^{III}(salen)]_2O_2$	1.96	645, 631
II	-[-Mn^{IV}(salen)-O-]-$_n$	1.99	662, 602
III	-[-Mn^{IV}(3-MeO-salen)-O-]-$_n$	1.58	655, 609
V	O=Mn^{IV}(3-MeO-salen)·2MeOH	3.81	840

a) At 296 K
b) Taken from Ref. 4.

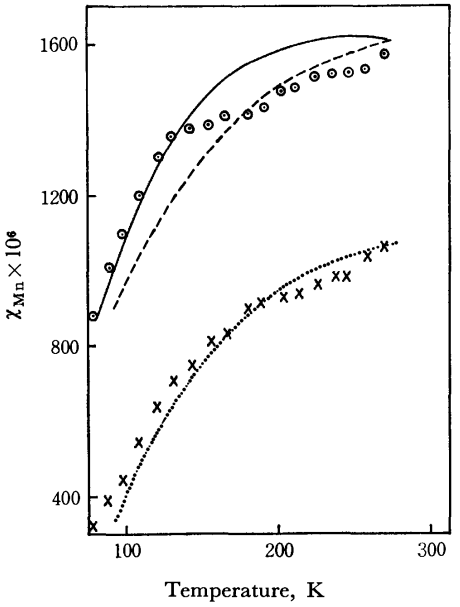

Fig. 2. Magnetic susceptibilities.
⊙: Experimental results for $[Mn^{III}(salen)]_2O_2$.
——: calculated for a binuclear cluster $S=1$, $J=-85$ cm^{-1}, $g=2.00$, $N\alpha=0$. ---: calculated for a binuclear cluster $S=2$, $J=-90$ cm^{-1}, $g=2.00$, $N\alpha=0$.
×: Experimental results for -[-Mn^{IV}(3-MeO-salen)-O-]-$_n$.
·····: calculated for a binuclear cluster $S=3/2$, $J=-125$ cm^{-1}, $g=2.00$, $N\alpha=0$.

be understood by taking into consideration the thermal equilibrium between spin-free and spin-paired configurations in the complex. As for Complexes II and III, their room-temperature magnetic moments are lower than that (3.75 B.M.) of the spin-only value expected for the octahedral Mn(IV) complexes. Moreover, the magnetic susceptibilities deviate from the Curie-Weiss law (Fig. 2); this deviation is probably caused by antiferromagnetic interaction between manganese atoms bridged by the oxygen atom. Kubo *et al.*[8] have reported that the magnetic susceptibilities of ammonium pentafluoromanganate(III), which has a linear chain structure, fit the curve calculated for a one-dimensional array of Ising spins $S=2$ above 80 K, assuming a "reduced" spin magnetic moment. The data for Complexes II and III do not fit the curve calculated assuming Ising spins $S=3/2$. As is shown in Fig. 2, the data fit, rather, the curve calculated by

8) S. Emori, M. Inoue, M. Kishita, and M. Kubo, *Inorg. Chem.*, **8**, 1385 (1969).

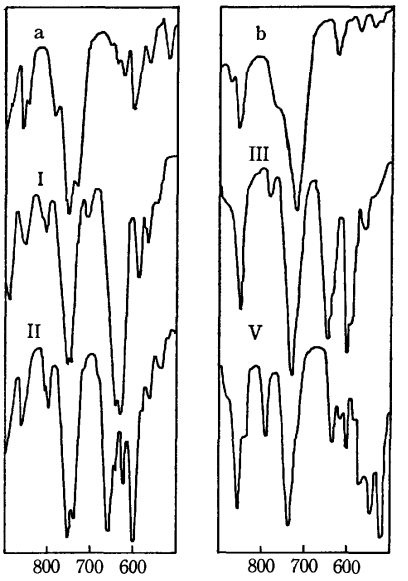

Fig. 3. IR spectra (in Nujol mulls).
a: Mn^{II}(salen), I: $[Mn^{III}(salen)]_2O_2$, II: -[-Mn^{IV}(salen)-O-]-$_n$, b: Mn^{II}(3-MeO-salen)·H_2O, III: -[-Mn^{IV}(3-MeO-salen)-O-]-$_n$, V: O=Mn^{IV}(3-MeO-salen)·2MeOH.

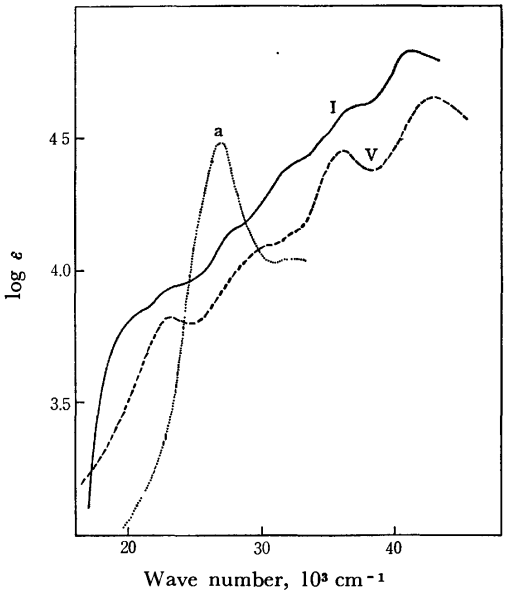

Fig. 4. Electronic spectra.
a: Mn^{II}(salen) in pyridine, I: $[Mn^{III}(salen)]_2O_2$ in dichloromethane, V: O=Mn^{IV}(3-MeO-salen)·2MeOH in methanol.

assuming a binuclear cluster including Mn–O–Mn bonding with $S=3/2$. Moreover, $J=-95$ cm^{-1} and -125 cm^{-1} are proposed Complexes II and III respectively. As for Complex V, the room-temperature magnetic moment, 3.81 B.M., is consistent with that expected for a high-spin Mn(IV). In this case, the magnetic susceptibilities fit the Curie-Weiss law well.

Infrared Spectra. Complexes I–IV show IR spectral frequencies which are comparable with those of the corresponding Mn^{II}(X-salen) in the 700—4000 cm^{-1} region. On the other hand, as is shown in Fig. 3 and Table 3, the spectra of the complexes in the 600—700 cm^{-1} region are characterized by two intense

absorption bands. The μ-oxo, $[Fe(salen)]_2O$,[4] and μ-peroxo, $[\{Co(NH_3)_5\}O_2](NO_3)_4$, including a metal-oxygen bond, show similar bands at 820 and 560 cm^{-1} respectively. In the case of Complex V, a new band is observed at 840 cm^{-1}. In view of the fact that the $[O=Mn(salen)]_2O_2$ complex, which is considered to involve both Mn=O and Mn–O_2–Mn bonds, shows the characteristic band at 884 cm^{-1} referred to the Mn=O, and those at 640 and 623 cm^{-1} referred to Mn–O bonds,[9] it is likely to ascribe the above bands in the 600—700 cm^{-1} to the Mn–O bond, and the band at 840 cm^{-1}, to the Mn=O bond.

Electronic Spectra. The electronic absorption spectra of the Mn^{II}(salen) and Complexes I and V in solution are represented in Fig. 4. The absorption bands appearing in the wave-number region higher than 25 kK are thought to be associated mainly with the ligand transitions. As may be seen in Fig. 4, the Mn^{II}(salen) shows no intense absorption band in the visible region. Information concerning the structure of the oxygenated complexes may be obtained by inspecting the visible spectral features. It has been reported that the spin-free manganese(III) complexes with an octahedral configuration give rise to a d–d transition band ($^5E_g \rightarrow {}^5T_{2g}$) with log ε=2.5 around 20 kK.[10] On the other hand, the spin-free penta-coordinate Mn^{III}(salen)X, where X is Br^- or I^-, shows two absorption bands, around 20 kK with log ε=3.0 and around 25 kK with log ε=3.5; these have been described by Prabhakaran *et al.*[7] as a d–d transition and a charge-transfer band respectively. As can be seen in Fig. 4, the spectral pattern of Complex I with two absorption bands at *ca.* 20.0 and *ca.* 23.2 kK resembles that of the penta-coordinate manganese(III)-complexes. Thus, as for Complex I, the visible and the IR spectral properties, as well as the thermal property, which indicates a reversible release of oxygen, led us to conclude that Complex I includes a μ-peroxo bond and that the structure can be depicted as is shown in Fig. 5-(a). As has been mentioned, the magnetic moment, 1.96 B.M., of Complex I (*cf.* Table 3), lower than that expected for the penta-coordinate manganese(III)-complexes with a square-pyramidal structure, can be explained in terms of an antiferromagnetic exchange which may be caused by the formation of a binuclear structure through the μ-peroxo bond. The magnetic moment, 3.81 B.M., of Complex V (*cf.* Table 3) agrees with the assumption that the complex includes a spin-free Mn(IV). The visible electronic spectrum of Complex V, unlike that of Complex I, shows only one peak, at 23.2 kK. This spectral feature is not inconsistent with those of such spin-free, octahedral manganese(IV) complexes as $[MnF_6]^{2-}$ and $[MnCl_6]^{2-}$, which show absorption maxima at 21.8 and 17.9 kK respectively.[11] On the basis of these facts, a proposed structure for Complex V is shown in Fig. 5-(c). The insolubility of Complexes II, III, and IV did not allow measurements of the electronic spectra in solution. However, the magnetic properties and the IR spectral data, as well as the fact that they are obtained from the oxo complexes, led us to propose the structure for the complexes shown in Fig. 5-(b).

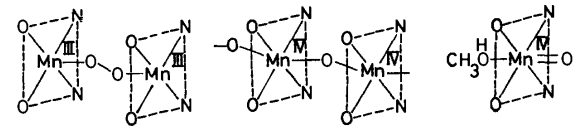

(a) (b) (c)

Fig. 5. Schematic structures proposed for the complexes.

Effects of Oxygen Partial Pressure, Solvent, and Substituent on the Oxidation Reaction. As has been discussed above, three types of complexes containing a μ-peroxo-, catena-oxo-, or oxo-bond were isolated in the reactions of the Mn^{II}(X-salen) with oxygen in organic solvents. In this section we will consider the effects of the oxygen partial pressure and of the nature of the solvents and substituents, X, on the complex formation.

As has been descrived in the Experimental part, the Mn^{II}(salen) yielded, upon reaction with oxygen in a DMSO solution, the μ-peroxo complex as a precipitate plus precipitates of the catena-oxo complex. As can be seen in Table 4, the amount of the μ-peroxo complex of the above precipitates increases with a decrease in the partial pressure of oxygen applied in the reaction system; it increases up to 86% when oxygen diluted to 1.7 vol% by mixing with nitrogen is used. It can be noticed that, in Py and DMF solutions, the reaction using dilute oxygen gave the μ-peroxo complex, although the reaction using pure oxygen only afforded the catena-oxo complex.

Table 4. The effects of oxygen partial pressure and solvents on the formation of $[Mn^{III}(salen)]_2O_2$ and $-[-Mn^{IV}(salen)-O-]-_n$[a]

P_{O_2} (vol%)[b]	Yield[c]		
	DMSO	DMF	Py
1.7	86	82	21
10	—	50	—
20	—	16	0
100	10	0	0

a) The reactions were carried out using Mn^{II}(salen) (1 g) and solvent (50 ml), at room temperature for 15 hr.. $[Mn^{III}(salen)]_2O_2$ was separated as soluble part by extraction with CH_2Cl_2.

b) Represented in volume % of O_2 in mixed $O_2 + N_2$ at atmospheric pressure and room temperature.

c) Corresponds to $\frac{[Mn^{III}(salen)]_2O_2}{[Mn^{III}(salen)]_2O_2 + -[-Mn^{IV}(salen)-O-]-_n} \times 100$ in gram.

The above results (*cf.* Table 4) suggest that the formation of the μ-peroxo complex is favored in the solvents in the following order; Py<DMF<DMSO, and that it is also favored when oxygen with a lower partial pressure is reacted.

As for the Mn^{II}(3-MeO-salen)·H_2O and Mn^{II}(5-NO_2-salen)·2Py complexes, the corresponding μ-peroxo complex could not be obtained even if the reac-

9) M. Tamaki, I. Masuda, and K. Shinra, *Chem. Lett.*, **1972** 165.

10) R. Dingle, *Acta Chem. Scand.*, **20**, 33 (1966).

11) A. B. P. Lever, "Inorganic Electronic Spectroscopy," Elsevier Publishing Co., (1963), p. 283.

tion was carried out in a DMSO solution using dilute oxygen of 1.7 vol%. The oxo complex, O=Mn^{IV}(3-MeO-salen)·2MeOH, was successfully isolated only for the 3-MeO-substituted complex in a MeOH solution. Further, it is of importance that, in a DMF, DMSO, or Py solution, the oxo complex is transformed to the insoluble catena-oxo complex,–[–Mn^{IV}(3-MeO-salen)–O–]$_n$, almost quantitatively, indicating that the reaction forming the catena-oxo complex proceeds *via* the oxo complex. The low solubility of the catena-oxo and μ-peroxo complexes did not allow kinetical measurements. However, in view of the results obtained in the present study, it can be interpreted by assuming that the reactions proceed as follows:

$$S\text{–}(Mn^{II})\text{–}S + O_2 \xrightarrow{k_1} S\text{–}(Mn^{III})\text{–}O_2 + S \quad (1)$$

$$S\text{–}(Mn^{III})\text{–}O_2 + O_2\text{–}(Mn^{III})\text{–}S \xrightarrow{k_2} 2S\text{–}(Mn^{III})\text{–}O\cdot + O_2 \quad (2)$$

$$S\text{–}(Mn^{III})\text{–}O\cdot \longrightarrow S\text{–}(Mn^{IV})\text{=}O \quad (2\text{-}1)$$

$$n[S\text{–}(Mn^{IV})\text{=}O] \longrightarrow \text{–}[\text{–}(Mn^{IV})\text{–}O\text{–}]_n\text{–} + n\cdot S \quad (2\text{-}2)$$

$$S\text{–}(Mn^{III})\text{–}O_2 + S\text{–}(Mn^{II})\text{–}S \xrightarrow{k_3} S\text{–}(Mn^{III})\text{–}O_2\text{–}(Mn^{III})\text{–}S \quad (3)$$

((Mn) represents a parent complex, Mn^{II}(X–salen).)

As is illustrated in Fig. 4, the Mn^{II}(salen) shows an electronic absorption maximum at 27.0 kK (log ε=4.5); this maximum is shifted to a lower frequency with the solvents in the order of MeOH (28.7 kK)< DMF (27.7 kK)<DMSO (27.6 kK)<Py (27.0 kK). Similar spectral behavior is observed for the substituted Mn^{II}(X-salen). These results seem to indicate that the complexes are coordinated with the solvent in solutions. In fact, an adduct with a solvent, *e.g.*, Mn^{II}(5-NO_2-salen)·2Py, is isolated. Hence, the reaction of the manganese (II) complexes with oxygen could be initiated by replacing a coordinated solvent molecule with oxygen, thus forming an intermediate superoxo complex, as is shown in Equation (1). When assuming that the unstable superoxo complex thus formed undergoes reactions to yield both oxo- and μ-peroxo complexes, following Equations (2), and (3) respectively, the reaction rate in respect to the superoxo complex can be given as:

$$d[S\text{–}(Mn^{III})\text{–}O_2]/dt = k_1[O_2][S\text{–}(Mn^{II})\text{–}S] - k_2[S\text{–}(Mn^{III})\text{–}O_2]^2 - k_3[S\text{–}(Mn^{II})\text{–}S][S\text{–}(Mn^{III})\text{–}O_2] \quad (4)$$

where k_1, k_2, and k_3 are the rate constants in Reactions (1), (2), and (3) respectively.[12] Reactions (2—1) and (2—2) are thought to follow Reaction (2) very rapidly in DMF, DMSO, and Py solutions. In view of the fact that the catena-oxo, and μ-peroxo complexes were separated out of the reaction system as precipitates, the concentration of the superoxo complex involved in solution must remain approximately constant during the reaction; that is,

$$d[S\text{–}(Mn^{III})\text{–}O_2]/dt \fallingdotseq 0 \quad (5)$$

Thus, the ratio of the yield of the catena-oxo complex to the μ-peroxo complex can qualitatively be described as:[12]

$$\frac{\text{catena-oxo complex}}{\mu\text{-peroxo complex}} \propto \frac{k_1k_2}{k_3^2}\cdot\frac{[O_2]}{[S\text{–}(Mn^{II})\text{–}S]} \quad (6)$$

proportional to the ratio of $[O_2]$ to $[S\text{–}(Mn^{II})\text{–}S]$. This relation can explain the experimental finding (*cf.* Table 4) that the yield of the catena-oxo complex decreases with a decrease in the oxygen concentration.

In a solvent such as Py, which tends to coordinate with a stronger affinity toward the central manganese ion, it is not unreasonable to expect a smaller k_1 than in another solvent. Hence, the higher yield of the catena-oxo complex by the reaction in the Py solution implies smaller k_3 and k_1 values. The failure to obtain the μ-peroxo compound of the Mn^{II}(3-MeO-salen)·H_2O may be attributed mainly to a larger k_1 caused by the electron-donating MeO group, which weakens the bonding of the central manganese ion with the solvent. The fact that the Mn^{II}(5-NO_2-salen)·2Py yielded the catena-oxo complex, even in the DMSO solution, can be explained in terms of a stronger bonding with the solvent due to the electron-withdrawing NO_2 group.

The authors wish to thank Associate Professor C. Miyake for the use of equipment for magnetic susceptibility measurements by means of the Faraday method.

12) From Eqs. (4) and (5), concentration of superoxo complex is given as follows,

$$[S\text{-}(Mn^{III})\text{-}O_2] = \frac{[S\text{-}(Mn^{II})\text{-}S]}{2k_2} \times(-k_3+\sqrt{k_3^2+4k_1k_2[O_2]/[S\text{-}(Mn^{II})\text{-}S]}). \quad (i)$$

And, the rate equation respect to catena-oxo-, and μ-peroxo-complexes are given by Eqs. (ii) and (iii), respectively:

$$d[\text{-}(\text{-}(Mn^{IV})\text{-}O\text{-})_n\text{-}]/dt = (1/n)\cdot d[S\text{-}(Mn^{III})\text{-}O\cdot]/dt = (k_2/n)\cdot[S\text{-}(Mn^{III})\text{-}O_2]^2 \quad (ii)$$

$$d[S\text{-}(Mn^{III})\text{-}O_2\text{-}(Mn^{III})\text{-}S]/dt = k_3[S\text{-}(Mn^{III})\text{-}O_2][S\text{-}(Mn^{II})\text{-}S] \quad (iii)$$

Then, from the Eqs. (i), (ii) and (iii) the ratio of reaction rate for catena-oxo complex to that for μ-peroxo complex is derived as,

$$\frac{d[\text{-}(\text{-}(Mn^{IV})\text{-}O\text{-})_n\text{-}]/dt}{d[S\text{-}(Mn^{III})\text{-}O_2\text{-}(Mn^{III})\text{-}S]/dt} = \frac{k_2[S\text{-}(Mn^{III})\text{-}O_2]}{nk_3[S\text{-}(Mn^{II})\text{-}S]} = (1/2n)\left(-1+\sqrt{1+(4k_1k_2/k_3^2)\frac{[O_2]}{[S\text{-}(Mn^{II})\text{-}S]}}\right) \quad (iv)$$

Eq. (iv) can be qualitatively transformed as shown by Eq. (6).

Pyrolysis-Gas Chromatographic Studies of Ionically-chlorinated Poly-α-methylstyrenes

Tadaoki OKUMOTO* and Tsugio TAKEUCHI**

* *Engineering Department, Nagoya Rubber Co., Ltd., Haruhi-mura, Nishikasugai-gun, Aichi 452*

** *Department of Synthetic Chemistry, Faculty of Engineering, Nagoya University, Chikusa-ku, Nagoya 464*

(Received October 7, 1972)

The microstructure of ionically-chlorinated poly-α-methylstyrene with or without a catalyst and the distribution of chlorine in the aromatic nucleus of the polymers were studied by means of pyrolysis-gas chromatography. The degradation products, such as α-methylstyrene, *p*-chloro-α-methylstyrene, and 3,4-dichloro-α-methylstyrene, gave good information about substitution reactions on the aromatic nucleus in original poly-α-methylstyrene. The differences between two series of ionically-chlorinated poly-α-methylstyrene were also discussed on the basis of yield of α-methylstyrene and *p*-chloro-α-methylstyrene.

Chlorinated polystyrenes and poly-α-methylstyrenes have been synthesized by both ionic and radical mechanisms. The chlorination of polystyrene has been the subject of a number of investigations.[1-4] However, only one study of the chlorinated poly-α-methylstyrene (CPMS) has been reported.[4]

Jenkins *et al.*[1] have examined the radically-chlorinated polystyrene by the use of an IR spectrometer, etc. They reported the determination of the change in the infrared spectrum, the glass transition temperatures, and the molecular weight of the polymers.

In our previous work[2] we have studied the distribution of chlorine atoms as a function of the degree of chlorination in the chlorinated polystyrene formed by radical chlorination by means of pyrolysis-gas chromatography(PGC).

Teyssie *et al.*[3] have investigated the structure of ionically-chlorinated polystyrene by both chemical and infrared spectrometric analyses and concluded that the chlorine is preferentially oriented in the para, and secondarily in the ortho, position, and that, with the further introduction of chlorine, 3,4-, 2,5- and, to a lesser extent, 2,4-dichloro-substituted phenyl groups are formed.

Bachman *et al.*[4] elucidated the depolymerization of ionically-chlorinated polystyrene and poly-α-methylstyrene and identified halogenated styrene and α-methylstyrenes, such as *p*-chlorostyrene, 3,4-dichlorostyrene and 3,4-dichloro-α-methylstyrene, after the fractional distillation of the depolymerized mixture.

In the present work, we have studied a pyrolysis-gas chromatographic method for elucidating the microstructure of ionically-chlorinated poly-α-methylstyrene, especially the distribution of chlorine in the aromatic nucleus of the polymers.

Experimental

Materials. The poly-α-methylstyrene was dissolved in chloroform and then purified. Chlorine gas was introduced into the polymer solution with constant stirring. Two series of ionically-chlorinated poly-α-methylstyrenes were prepared by the following methods of chlorination. The first method was a catalytic method where CPMS was synthesized by the chlorination of poly-α-methylstyrene in the iron powder, which acted as a catalyst in the dark. The second method was a direct method, where poly-α-methylstyrene was chlorinated in the absence of a catalyst. The samples were purified by the same procedure as that described in our previous work.[2] The polymers formed by the catalytic and direct methods will be abbreviated as "CPMS–Cat" and "CPMS–Direct" respectively. The chlorine content of the chlorinated polymers was chemically determined.

The degree of chlorination (DC) of the samples is defined as the number of chlorine atoms contained per monomer unit in the polymer as follows:

$$DC = \frac{118.19 \times Cl\ wt\%}{3545 - 34.4 \times Cl\ wt\%}$$

Pyrolysis-Gas Chromatographic Conditions. The pyrolysis of the polymer was carried out by means of a furnace-type pyrolyzer (Hitachi Model KP-1) which was directly attached to the inlet port of a gas chromatograph equipped with dual flame-ionization detectors. At the optimum pyrolysis temperature, 550 °C, reproducible and characteristic pyrograms were obtained.

The gas-chromatographic conditions were the same as those described in our previous work.[2] Separation columns (3 mm i. d. × 2 m) packed with Diasolid L (80—100 mesh) and coated with PEG-6000 (10 wt% to the support) were used at programmed temperatures ranging from 100 to 210°C at a rate of 5 °C/min. The peaks on the pyrograms were identified by the use of PGC–MS and Hitachi–RMS-4 apparatuses and by means of the retention data of the pure substances.

Infrared Spectrometry. The infrared absorbance curves were obtained on Hitachi Model EPI-S_2 spectrometer. The various chlorinated poly-α-methylstyrene samples were examined by the KBr disc method.

Results and Discussion

In the following discussion, α-methylstyrene, *p*-chloro-α-methylstyrene, and 3,4-dichloro-α-methylstyrene are briefly denoted by MS, *p*-CMS, and 3,4-CMS respectively.

Figure 1 shows typical pyrograms of poly-α-methylstyrene and CPMS–Cat at the pyrolysis temperature of 550 °C. Raw poly-α-methylstyrene yields, nearly quantitatively, the α-methylstyrene monomer, while, with the rise in the degree of chlorination, chlorinated

1) R. K. Jenkins, N. R. Byrd, and J. L. Lister, *J. Appl. Polym. Sci.*, **12**, 2059 (1968).

2) S. Tsuge, H. Ito and T. Takeuchi, This Bulletin, **43**, 3341 (1970).

3) Ph. Teyssie, M. C. Wilde, and G. Smets, *J. Polym. Sci.*, **16**, 429 (1955).

4) G. B. Bachman, H. Hellman, K. R. Robinson, R. W. Finholt, E. J. Kahlar, L. J. Filar, L. L. Levis, and D. D. Micucci, *J. Org. Chem.*, **12**, 108 (1947).

Table 1. Realtive yields of pyrolysis products in CPMS–Cat (mol%)

Sample (No.)	Chlorine content (wt%)	Degree of chlorination (DC)[a)]	α-methyl-styrene	*p*-chloro-α-methylstyrene	3,4-dichloro-α-methylstyrene
1	3.5	0.12	92.8	7.2	—
2	8.6	0.31	76.0	18.0	6.0
3	12.5	0.47	65.5	25.4	9.1
4	17.5	0.70	48.3	38.2	13.5
5	22.4	0.95	35.6	48.1	16.3
6	24.0	1.04	23.3	55.1	21.6
7	26.3	1.18	16.8	59.5	23.7
8	28.9	1.34	11.2	62.7	26.1
9	29.4	1.37	9.3	66.4	24.3
10	31.8	1.53	5.4	68.9	25.7

a) Calculated from the chemical analysis.

Table 2. Relative yields of pyrolysis products in CPMS–direct (mol%)

Sample (No.)	Chlorine content (wt%)	Degree of chlorination (DC)[a)]	α-methyl-styrene	*p*-chloro-α-methylstyrene	3,4-dichloro-α-methylstyrene
1	6.2	0.22	87.0	10.6	2.4
2	12.9	0.49	67.4	23.7	8.9
3	17.8	0.71	47.8	38.2	14.0
4	20.4	0.85	39.4	43.4	17.2
5	23.3	1.03	33.4	47.6	18.7
6	26.1	1.17	29.4	49.4	21.2
7	29.4	1.37	23.2	53.8	23.0
8	34.8	1.75	19.2	52.2	28.6

a) Calculated from the chemical analysis.

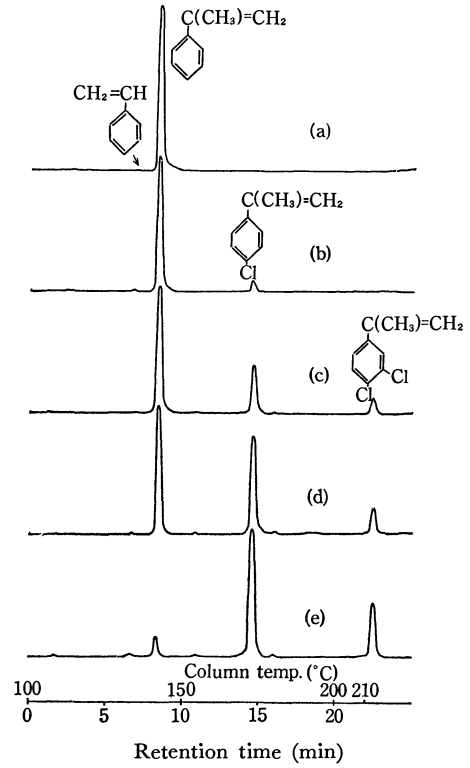

Fig. 1. Typical pyrograms of CPMS-Cat at 550 °C.
(a): PMS,, (b)—(d): CPMS; (b): DC=0.12, (c): DC=0.47, (d): DC=0.95, (e): DC=1.53

poly-α-methylstyrene yields two kinds of chlorine-substituted α-methylstyrene, such as *p*-CMS and 3,4-CMS. The relative yields of α-methylstyrene derivatives from the CPMS-Cat and -Direct methods are summarized in Tables I and II, where a small amount of styrene is added to the yield of α-methylstyrene. These values are calculated from the relative peak areas appearing on the pyrograms, considering the relative sensitivities of compounds for the flame-ionization detectors.

Figure 2 shows the relationships between the DC and the yields of the degradation products of the ionically CPMS-Cat and -Direct methods. The two series of CPMS differ generally from one another, especially in the yields of MS and *p*-CMS, as is shown in Fig. 2. It is apparent from the above observations that a chlorination reaction is taking place, mainly on the aromatic nucleus. The chlorine is nearly oriented in the para position and with the further introduction of chlorine, 3,4-dichloro-substituted phenyl group is formed.

Figure 3 shows the infrared spectrum of chlorinated poly-α-methylstyrene with various DC. The disappearance of the absorption bands at 700, 750, and 1030 cm^{-1} is indicative of chlorine substitution on the aromatic nucleus. On the other hand, sharp bands of 825 and 1010 cm^{-1} which are related to the position of the substitution in the nucleus appear on the spectrum with the rise in DC. These results are in

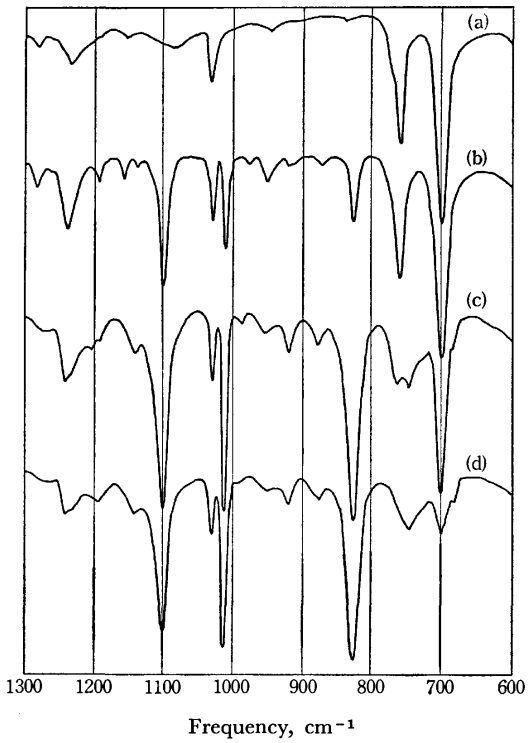

Fig. 3. Infrared spectra of CPMS-Cat.
(a): PMS, (b)—(d): CPMS; (b): DC=0.47, (C): DC=1.18, (d): DC=1.53

fairly good agreement with those of polystyrene reported by Teyssie et al.[3]

At a small degree of chlorination with or without a catalyst, only the yield of *p*-CMS through monochloro-substituted α-methyl styrene appeared on the pyrograms, while the yield of isomers did not appear. This is different from the case with chlorinated polystyrene. This is mainly due to the steric hindrance of methyl group in the polymer. This is also supported by the fact the yield of dichloro-substituted α-methylstyrene is almost 3,4-CMS.

The ionic chlorination of poly-α-methylstyrene mainly proceeds by means of the direct substitution of the aromatic nucleus under these conditions. At the beginning of chlorination, a substitution reaction takes place in nearly the para position. The second chlorine atom is preferentially directed into the phenyl ring

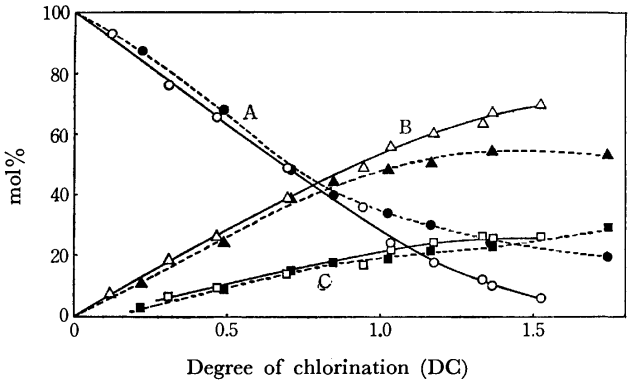

Fig. 2. Relationships between the degree of chlorination (DC) and relative yields of the degradation products of CPMS.
—— Solid line: CPMS-Cat
---- Broken line: CPMS-Direct
A: α-methylstyrene, B: *p*-chloro-α-methylstyrene
C: 3,4-dichloro-α-methylstyrene.

in the 3 positions for the para chloro-α-methyl styrene unit before all the phenyl ring is substituted. It is also thus apparent that the formation of *p*-CMS is locally competitive with the formation of 3,4-CMS.

Consequently, *p*-CMS is formed by the following mechanisms;

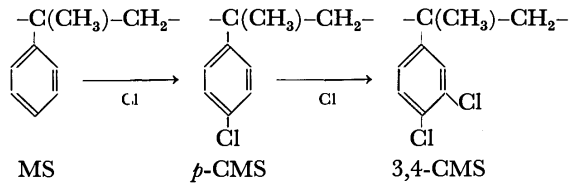

The two series of CPMS differ from one another, especially in the yields of α-methylstyrene and *p*-chloro-α-methylstyrene, as is illustrated in Fig. 2.

No appreciable differences are observed between the two series of CPMS with respect to the yields of dichloro-α-methylstyrene. However, the yields of MS and *p*-CMS change in different ways as a function of DC. The ratio of *p*-CMS to 3,4-CMS of CPMS-Cat is also larger than that of CPMS-Direct. These results suggest that the distribution of the chlorine introduced to the phenyl ring of CPMS-Cat is more homogeneous than that of CPMS-Direct.

The Hydrolysis of Y^{3+}, La^{3+}, Gd^{3+}, and Er^{3+} Ions in an Aqueous Solution Containing 3 M (Li)ClO_4 as an Ionic Medium

Toshihiko AMAYA*, Hidetake KAKIHANA, and Masunobu MAEDA**

Research Laboratory of Nuclear Reactor, Tokyo Institute of Technology, O-okayama, Meguro, Tokyo 152

***Department of Electrochemistry, Tokyo Institute of Technology, O-okayama, Meguro, Tokyo 152*

(Received December 8, 1972)

The hydrolysis equilibria of Y^{3+}, La^{3+}, Gd^{3+}, and Er^{3+} ions have been studied at 25 °C in 3 M (Li)ClO_4 by measuring the hydrogen-ion concentration with a glass electrode. All the test solutions containing hydrolyzed species prepared by the addition of alkali were acidified by means of constant-current coulometry. The data, which indicate a slight hydrolysis of the relevant ions, can be explained by assuming the formation of the following complexes: $Y(OH)_2^{+}$, $\log \beta_{2,1} = -17.0 \pm 0.1$; $Y_2(OH)_2^{4+}$, $\log \beta_{2,2} = -14.04 \pm 0.01$; $LaOH^{2+}$, $\log \beta_{1,1} = -10.04 \pm 0.01$; $GdOH^{2+}$, $\log \beta_{1,1} = -8.20 \pm 0.01$; $Er(OH)_2^{+}$, $\log \beta_{2,1} = -17.4 \pm 0.1$; $Er_2(OH)_2^{4+}$, $\log \beta_{2,2} = -13.72 \pm 0.01$.

So far, very few quantitative investigations have been made of the hydrolysis of rare-earth ions.[1]

In 1946 Moeller[2] measured the acidity of a series of rare-earth sulfate solutions at 25 °C by the use of a glass electrode and found that only a small part of the rare-earth ions were transformed to hydrolysis species of $LnOH^{2+}$ before precipitation started.

Wheelwright, Spedding, and Schwarzenbach[3] titrated a 0.01 M $LaCl_3$ solution with NaOH using a glass electrode and reported the formation of $LaOH^{2+}$ with $\log \beta_{1,1} = -8.4$ (at 20 °C).

Tobias and Garrett[4] studied the hydrolysis equilibria of Nd^{3+} and Pr^{3+} ions at 25 °C and found that a very small part of the metal ions could be present as hydrolysis products in solution. They found $NdOH^{2+}$ and $PrOH^{2+}$ to have the same stability constant of $\log \beta_{1,1} = -8.5$.

In 1961 Biedermann and Ciavatta[5] investigated the hydrolysis of the La^{3+} ion by measuring the concentration of the hydrogen ion with a glass electrode. They explained the results in the $\log h$ range from −6.5 to −8.1 by assuming the formation of $LaOH^{2+}$, La_2OH^{5+}, and $La_5(OH)_9^{6+}$ (or $La_6(OH)_{10}^{8+}$), the corresponding stability constants being $\log \beta_{1,1} = -10.1$, $\log \beta_{1,2} = -9.9_5$, and $\log \beta_{9,5} = -71.4_5$ (or $\log \beta_{10,6} = -78.7_5$) (at 25 °C).

Biedermann and Newman[6] investigated the hydrolytic reaction of the Ce^{3+} ion and reported that only the $Ce_3(OH)_5^{4+}$ species with $\log \beta_{5,3} = -35.7_5$ was formed.

In 1964 Biedermann and Ciavatta[7] studied the hydrolysis equilibria of the Y^{3+} ion by the application of constant-current coulometry. Their data, which indicated that, at most 3% of the Y^{3+} ions were transformed to the hydrolysis species, without the formation of any precipitate, were explained by assuming the formation of a dimer, $Y_2(OH)_2^{4+}$, with $\log \beta_{2,2} = -14.30$ as the main species. As minor species they found the YOH^{2+} and $Y_3(OH)_5^{4+}$, the stability constants of which were $\beta_{1,1} = -9.1$ and $\log \beta_{5,3} = -33.8$.

From the previous investigations described above, it has been found that the hydrolytic reactions of rare-earth ions become measurable at $\log h \leq -5$, and that not more than a small percentage of the metal ions can be transformed to hydrolysis products without the formation of a precipitate.

In the present work, therefore, we made an effort to keep contamination with protolytic impurities to a minimum when preparing test solutions containing hydrolyzed species, and employed the "back titration" method with a constant current coulometer, which had been found to be suitable for the study of a slightly buffered solution.[7,8]

The present study will deal with the hydrolytic reactions of Y^{3+}, La^{3+}, Gd^{3+}, and Er^{3+} ions in 3 M (Li)ClO_4.

Symbols

h	concentration of the free hydrogen ion.
H	analytical excess of hydrogen ions $= [ClO_4^-] - 3B - [Li^+]$.
B	total concentration of metal ions.
b	concentration of the free metal ion.
z	average number of hydrogen ions set free per metal ion.
p	number of OH groups bound to hydrolyzed species.
q	number of metal present in hydrolyzed species.
$\beta_{p,q}$	equilibrium constant of the following reaction: $qLn^{3+} + pH_2O = Ln_q(OH)_p^{(3q-p)+} + pH^+$
(p, q)	Complex, $Ln_q(OH)_p^{(3q-p)+}$
E	emf (mV).
Ln^{3+}	rare-earth ion.

Experimental

Reagents and Analysis. The lanthanum perchlorate solution was prepared from lanthanum oxide of a 99.99%

* Present address: NGK Insulators Co., Mizuho, Nagoya.

1) a) L. G. Sillén and A. E. Martell, "Stability Constants of Metal-Ion Complexes", The Chemical Society, London (1964). b) L. G. Sillén and A. E. Martell, "Stability Constants of Metal-Ion Complexes, Supplement No. 1", The Chemical Society, London (1971).

2) T. Moeller, *J. Phys. Chem.*, **50**, 242 (1946).

3) E. J. Wheelwright, F. H. Spedding, and G. Schwarzenbach, *J. Amer. Chem. Soc.*, **75**, 4196 (1953).

4) R. S. Tobias and A. B. Garrett, *ibid.*, **80**, 3532 (1958).

5) G. Biedermann and L. Ciavatta, *Acta Chem. Scand.*, **15**, 1347 (1961).

6) G. Biedermann and L. Newman, *Arkiv Kemi*, **22**, 303 (1964).

7) G. Biedermann and L. Ciavatta, *ibid.*, **22**, 352 (1964).

8) G. Biedermann and L. Ciavatta, *Acta Chem. Scand.*, **16**, 2221 (1962).

purity supplied by the Shin-estu Chemical Co. The oxide, which had been ignited at around 900 °C, was dissolved in a slight excess of hot perchloric acid, and the lanthanum perchlorate was recrystallized twice from water. In the stock solution thus prepared, no chloride, sulfate, or ferric ions could be detected. The La(III) content of the stock solution was determined by the precipitation of the La^{3+} ion as the oxalate and by ignition to the oxide. The total perchlorate concentration in the stock solution was determined by neutralization after passing a definite amount of the solution through a column of the cation exchange resin, Dowex 50W-12, of the H^+ form.

The other rare-earth perchlorate solutions were prepared and analyzed by the same procedures as those used for the $La(ClO_4)_3$ solution.

The lithium perchlorate was prepared by the method described by Biedermann and Ciavatta.[5]

Apparatus. The titration cell consisted of two Wilhelm-type half-cells[9] for emf measurements and for constant-current coulometry.

Glass electrodes of the Beckman type No. 40498 were employed.

The pH meter used was a Radiometer PHM-4C pH-meter (Copenhagen).

A Coulometric Analyzer (Leeds & Northrup Co., Philadelphia) was used as the constant-current power source.

Preparation of Test Solutions. The hydrolyzed test solutions of rare-earth ions were prepared by the following two methods. (1) For the system of the Y^{3+} ion, a slightly acidic yttrium perchlorate solution was electrolyzed to reduce the H^+ ions by constant-current coulometry to the point where the value of Z was around 0.015; this was found to be the highest value to be reached without precipitation. For the electrolysis, the same circuit as Ciavatta's[10] was used. In the test solution thus prepared, no colloidal precipitate could be detected nephelometrically.

(2) For the systems of La^{3+}, Gd^{3+}, and Er^{3+} ions, the test solutions were prepared as follows.

We started with a slightly acidic rare-earth perchlorate solution ($\log h \leqq -3$) which had been freed from CO_2 by passing purified nitrogen gas through. The solution was electrolyzed to reduce H^+ ions by using a d.c. power supply until precipitates appeared. Equilibration was made at 25 °C by stirring the mixture for about two days with a Teflon-covered bar; then, the precipitates were removed through G4 glass filters. These procedures were carried out under an atmosphere of nitrogen gas. In each case, the filtered solution was carefully examined for turbidity, but no suspended particle could be detected. No indication of slow precipitation was found in an aliquot of the filtered solution which was occasionally tested for turbidity over half a year's time.

Emf Measurements. The general composition of a test solution can be written as:
B M Ln^{3+}, H M H^+, $(3-3B-H)$ M Li^+, 3 M ClO_4^-, where H, the analytical hydrogen ion concentration is often negative.

The test solution was titrated by means of constant-current coulometry, a coulometric circuit similar to Ciavatta's[10] being used.

The potentiometric measurements were made by the use of this cell:

GE | test solution | Ref (A)

where GE denotes a glass electrode, and Ref, the reference half-cell | 3 M $LiClO_4$ | 2.99 M $LiClO_4$ + 0.01 M $AgClO_4$ | Ag-ClAg. The emf of the cell(A) at 25 °C can be described as;

$$E = E_0 + 59.15 \log h \quad (1)$$

where E_0 is a constant into which the term of the activity coefficient of the hydrogen ion and that of the liquid-junction potential are incorporated.

All the emf measurements were performed at 25.00±0.01 °C in a parrafin oil thermostat in a room thermostated at 25±1 °C.

Results and Discussion

The values of $Z(\log h)_B$ for each metal ion, which form the basis of the following calculations, are graphically shown in Fig. 1.

The experimental data were treated by graphical methods to determine the compositions of the hydrolysis species and the corresponding approximate stability constants; then, computer calculations were made to find the most probable values of the stability constants.

If the formation of a series of reaction products with the general composition of $Ln_q(OH)_p^{(3q-p)+}$ is assumed, the concentration of the hydrogen ion set free by hydrolysis, BZ, is given by the general form:

$$BZ = \sum_p \sum_q p\beta_{p,q}[Ln^{3+}]^q[H^+]^{-p} = \sum_p \sum_q p\beta_{p,q} b^q h^{-p} \quad (2)$$

Since the maximal value of Z never exceeds 0.02 in the solutions studied, we may simplify, without introducing any appreciable error, the preliminary calculations by using this approximation:

$$[Ln^{3+}] = b \simeq B \quad (3)$$

By substituting this relation into Eq. (2) and by rearranging, we obtain:

$$Zh = \sum_p pK_p h^{-(p-1)} \quad (4)$$

where:

$$K_p = \sum_q \beta_{p,q} B^{q-1} \quad (5)$$

Primary information on the compositions of the hydrolysis species and the corresponding stability constants was obtained by the use of Eqs. (4) and (5).

For the system of the Y^{3+} ion, the plots of Zh against h^{-1} gave a set of straight lines with various slopes and with a zero intercept. This indicates that p is equal to 2. In order to determine the values of q, the values of the $(K_2 = 2\sum_q \beta_{2,q} B^{q-1})$ slope were plotted against B. The plot closely approximated a straight line; this establishes that q is equal to 1 and 2 at $p=2$. Thus, the hydrolysis species formed are $Y(OH)_2^+$ and $Y_2(OH)_2^{4+}$. Their stability constants were estimated from the intercept and slope of the straight line according to Eq. (5).

For the system of the La^{3+} ion, the plots of Zh *vs.* h^{-1} showed a horizontal line independent of B; this indicates that p and q are equal to 1. The hydrolysis species formed is $LaOH^{2+}$. The stability constant was estimated from the intercept.

For the system of the Gd^{3+} ion, the plots of Zh *vs.* h^{-1} gave the same results as that for the system of the La^{3+} ion: p and q are equal to 1. The hydrolysis

9) W. Forsling, S. Hietanen, and L. G. Sillén, *ibid.*, **6**, 901 (1952).
10) L. Ciavatta, *Arkiv Kemi*, **20**, 417 (1962).

values for $\beta_{p,q}$ they obtained were log $\beta_{1,1}=-10.0\pm0.1$, $\beta_{1,2}=-9.9_5\pm0.1$, and log $\beta_{9,5}=-71.4_5\pm0.1$ (or log $\beta_{10,6}=-78.7_5\pm0.1$). The stability constants for the (1,1) species obtained by us was the same as that obtained by Biedermann and Ciavatta. None of the (1,2) and (9,5) (or (10.6)) complexes they found were detected in the present work.

The authors are indebted to Dr. Hitoshi Ohtaki for his valuable discussions.

BULLETIN OF THE CHEMICAL SOCIETY OF JAPAN, VOL. 46, 1723—1726 (1973)

Cobalt(II) Complexes of Diethylenetriamine-*N,N',N''*-triacetic Acid

Toshio KAWATO, Hajime KANATOMI, and Ichiro MURASE

Laboratory of Chemistry, College of General Education, Kyushu University, Ropponmatsu, Fukuoka 810

(Received November 28, 1972)

Cobalt(II) complexes of diethylenetriamine-*N,N',N''*-triacetic acid (DTTA) were prepared. From spectrophotometric and magnetic data, diaquo-DTTA-Co(II) was found to have an octahedral arrangement in which the *N,N'*-diacetate moiety and two water molecules are in the coordination sphere, and the terminal amino acid residue dangles outside. On heating the diaquo-complex, thermal rearrangement occurred with loss of water and the complex took a tetrahedral configuration. This was confirmed by its electronic spectrum and magnetic moment. The tetrahedral complex turned to another octahedral complex with absorption of water, the configuration of which seemed to differ from the original as judged by spectral difference. Cobalt(II) complexes of ethylenediamine-*N,N'*-diacetic acid (EDDA) were also prepared and investigated for the sake of comparison.

Diethylenetriaminepentaacetic acid(DTPA) is well-known as a potentially octadentate chelating ligand to form stable complexes with a number of metal ions. Many geometrical isomers are possible for Co(III) complexes of hexacoordination. Recently several Co(III)–DTPA complexes were isolated, the structure of the nitro complex being elucidated by means of PMR spectroscopy.[1] The terminal iminodiacetate group was found to be dangling and free from the coordination sphere. On the other hand, Co(III) complexes of diethylenetriamine-*N*-acetic acid and diethylenetriamine-*N'*-acetic acid were isolated as dinitro, dichloro and other derivatives, and their configurations were discussed on the bases of electronic spectra.[2] All the donor groups in these ligands were found to coordinate to the Co(III) ion.

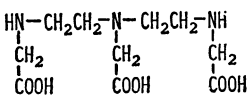

DTTA

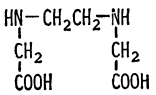

EDDA

It is of interest to study the donor function of hexadentate diethylenetriamine-*N,N',N''*-triacetic acid (DTTA) with Co(III) ion. We therefore examined the reaction of DTTA with Co(II) ion to obtain a Co(II) complex which might be converted into a Co(III) complex by oxidation. Eventually, it was found that the Co(II) complex was fairly stable against oxidation and isolated as red-pink crystals. It was also found that the red-pink complex shows thermochromism at elevated temperature to blue-violet with loss of water, turning pink at room temperature in moist air. This paper deals with the structure determination of the Co(II) complexes by means of infrared and visible absorption spectra, magnetic moment, differential thermal analysis and thermogravimetric analysis, and the mechanism of thermochromism in terms of structure change. Co(II) and Co(III) complexes of ethylenediamine-*N,N'*-diacetic acid(EDDA) were also investigated for the sake of comparison.

Experimental

The infrared spectra were determined in potassium bromide disks with a Hitachi EPI-S2 spectrophotometer, while the electronic spectra were measured with a Hitachi EPS-3T spectrophotometer. Measurements of the magnetic moment were carried out at room temperature by the Gouy-method. The DTA curve was recorded under nitrogen stream with a Rigakudenki Thermoflex 8001 with a 5 mg sample on an aluminium cell at a heating rate of 10 °C/min using alumina as a reference.

Diethylenetriamine-N,N',N''-*triacetic Acid (DTTA).* The synthetic route of DTTA is shown in scheme. The terminal amino groups of diethylenetriamine-*N'*-acetic acid[2] were reacted with two equivalent bromomalonic acid in alkaline solution and the product was decarboxylated in dilute hydrochloric acid to give DTTA hydrochloride. It was thus confirmed that an acetic acid group attaches to each nitrogen atom of the diethylenetriamine molecule.

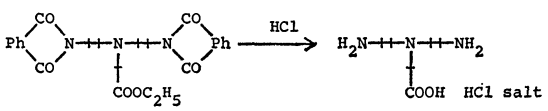

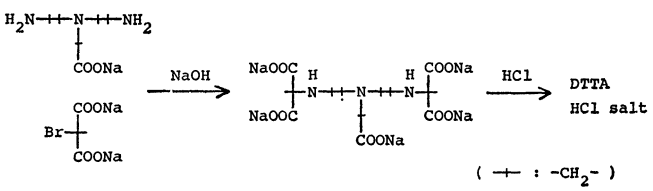

1) B. B. Smith and R. H. Betts, *J. Amer. Chem. Soc.*, **91**, 7749 (1969).

2) P. W. Schneider and J. P. Collman, *Inorg. Chem.*, **7**, 2010 (1968).

A mixture of 25.6 g (0.014 mol) of bromomalonic acid and 19 g (0.071 mol) of diethylenetriamine-*N'*-acetic acid trihydrochloride in 80 ml of water was carefully neutralized with 20% aqueous sodium hydoxide below 15 °C using phenolphthalein as an indicator. The solution was then heated at about 75 °C for an hour, being maintained its pink color by the dropwise addition of sodium hydroxide. After being heated at 85 °C for another hour, the solution was concentrated to 80 ml in a vacuum, the pH being brought to 2 with hydrochloric acid. The acidic solution containing diethylenetriamine-*N'*-acetic-*N,N''*-dimalonic acid was refluxed for 30 min until termination of the evolution of CO_2 and evaporated almost to dryness in a vacuum. The residue was extracted with ethanol containing a small amount of hydrochloric acid, the ethanol solution being evaporated to dryness in a vacuum. The product assumed to be DTTA trihydrochloride was a very hygroscopic glassy material. Since an attempt at crystallization failed, it was used directly for the preparation of the Co(II) complexes.

Diaquo-DTTA-Co(II): Red-pink Complex. To a solution of 5.4 g (0.014 mol) of DTTA trihydrochloride in 20 ml of water was added 3.33 g (0.014 mol) of cobalt(II) chloride hexahydrate in a minimum amount of water. The mixture was carefully neutralized at pH 7 with 20% aqueous sodium hydroxide. After filtration to remove a trace of violet precipitate, the filtrate was concentrated to 15 ml in a vacuum at 60 °C. On standing for a week, a red-pink crystalline powder was obtained, which was collected by filtration and washed with water and dried over calcium chloride at room temperature: yield 2 g. The complex could be recrystallized from boiling water. It was pure enough without further purification.

Found: C, 29.75; H, 5.95; N, 10.51%. Calcd for $[Co(dtta)(H_2O)_2]2H_2O$[3]: C, 29.56; H, 6.20; N, 10.34%.

The reaction conducted under nitrogen gave the same complex indicating that no oxidation took place in the air.

Thermochromisms. On being heated at 150 °C in an open vessel, the red-pink DTTA-Co(II) turned blue-violet, turned pink on cooling to room temperature. When the blue-violet complex was kept in a dry atmosphere, no color change took place even at room temperature.

Blue-violet complex, Found: C, 35.83; H, 5.00; N, 12.64%. Calcd for [Co(dtta)]: C, 35.94; H, 5.13; N, 12.57%.

Pink complex, Found: C, 29.48; H, 6.16; N, 10.44%. Calcd for $[Co(dtta)(H_2O)_2]2H_2O$: C, 29.56; H, 6.20; N, 10.34%.

*Ethylenediamine-*N,N'*-diacetic Acid (EDDA).* Although this compound is well-known, only one method of preparation has been reported with no mention of the yield.[4] We have prepared the hydrochloride in a different way with a fairly good yield.

To a suspension of 26.6 g of ethylenediamine dihydrochloride in 200 ml of ether was added with vigorous stirring 19.6 g of sodium cyanide in 30 ml of water at 2—5 °C. After standing for 10 min, 36 g of formalin (37%) was added dropwise over a period of 30 min at a temperature below 10 °C. The reaction mixture was further stirred for 2 hr at room temperature and 200 ml of methanol was added and chilled to 5 °C. The resulting sodium chloride was filtered and hydrogen chloride was saturated to the filtrate at 10 °C. The resulting precipitate was filtered and washed with methanol. Thus 40 g of ethylenediamine-*N,N'*-diacetonitrile dihydrochloride containing a small amount of sodium chloride was obtained.

3) (dtta) represents a dianion of DTTA.

To 700 ml of concentrated hydrochloric acid was added portionwise 40 g of freshly prepared dinitrile at 0—5 °C, and the mixture was stirred for 20 hr at room temperature and then diluted with 700 ml of water. The solution was boiled for 2 hr and concentrated in a vacuum until crystals began to deposit. The mixture was diluted with 150 ml of methanol and kept in a refrigerator overnight. The product was filtered and washed with methanol : yield 28 g. Recrystallization was carried out from dilute methanol containing a small amount of hydrochloric acid.

Found: C, 28.86; H, 5.73; N, 11.38%. Calcd for $C_6H_{12}N_2O_4 2HCl$: C, 28.93; H, 5.67; N, 11.25%.

Diaquo-EDDA-Co(II). The procedure was the same as in the preparation of diaquo-DTTA-Co(II) except that 3.5 g (0.014 mol) of EDDA dihydrochloride was reacted in place of DTTA trihydrochloride and the reaction and separation were carried out under nitrogen. The complex was obtained as pink crystals in a yield of 2 g which was then dried over calcium chloride and stored in a nitrogen atmosphere.

Found: C, 25.93; H, 5.35; N, 10.26%. Calcd for $[Co(edda)(H_2O)_2]1/2H_2O$[5]: C, 25.90; H, 5.45; N, 10.07%.

Aquo-hydroxo-EDDA-Co(III). Diaquo-EDDA-Co(II) was dissolved in water and air was bubbled through the solution at room temperature. Oxidation occurred within a few minutes and the solution turned to violet. It was concentrated to a small volume and kept standing in a refrigerator for a week to give violet needles. The sample was dried over calcium chloride in a vacuum.

Found: C, 26.51; H, 5.26; N, 10.19%. Calcd for $[Co(edda)(OH)(H_2O)]$: C, 26.88; H, 4.89; N, 10.45%.

Results and Discussion

DTTA is a tribasic acid and can behave as a hexadentate ligand with N_3O_3 arrangement. The Co(II) complexes obtained were neutral carrying no counter cation. Thus the possibility of hexacoordination with trinegative ligand species can be excluded. The infrared spectrum of red-pink DTTA-Co(II) is shown in Fig. 1. In the carbonyl stretching region, it exhibits two absorptions at 1585 cm^{-1} and 1645 cm^{-1} indicating the presence of two kinds of carboxylic acid groups. Since the stretching vibration of the free carboxylic acid groups is seen at 1740 cm^{-1} in

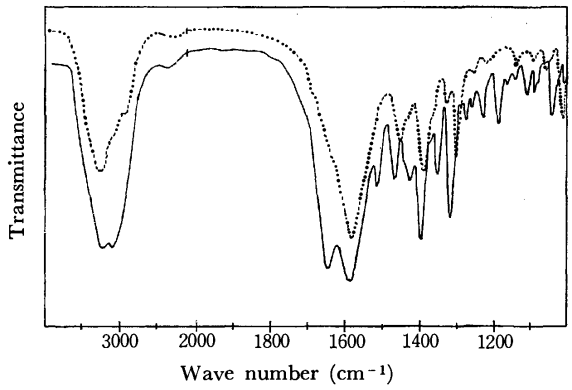

Fig. 1. IR spectra of diaquo-DTTA-Co(II) (——) and diaquo-EDDA-Co(II) (----).

4) M. Mori, M. Shibata, E. Kyuno and F. Maruyama, This Bulletin, **35**, 75 (1962).

5) (edda) represents a dianion of EDDA.

DTTA trihydrochloride and EDDA dihydrochloride, no such unionized groups are present in the complex. Thus the two absorptions can be assumed to be due to coordinated and uncoordinated but ionized carboxylate vibrations. The stretching mode of the coordinated carboxylate in a similar ligand can be seen in EDDA-Co(II) in which the two acetate groups undoubtedly coordinate to the metal ion. Diaquo-EDDA-Co(II) was sensitive against air-oxidation, though the infrared spectrum obtained under careful operation showed a single sharp peak at 1585 cm^{-1} which is attributed to COO-Co(II) stretching vibration (Fig. 1). Assuming that EDDA moiety in DTTA molecule coordinates to the Co(II) ion, the absorption at 1585 cm^{-1} in DTTA-Co(II) can be assigned to the coordinated carboxylate as well as that in EDDA-Co(II). The one at 1645 cm^{-1} seems to be due to the remaining carboxylate which exists as a dipolar ion with the α-amino group dangling outside the coordination sphere. This is supported by the fact that the area ratio of the absorption bands in the coordinated and uncoordinated carboxylate is approximately 2 : 1. In other words, DTTA coordinates to the Co(II) ion as a tetradentate ligand of linear O-N-N-O type and the remaining amino acid residue exists as a zwitter ion in crystals.

Since the red-pink complex shows a magnetic moment of μ_{effect}=4.96 B. M. which is normal for a high-spin octahedral Co(II) complex, the remaining two positions of the coordination sphere are occupied by water molecules, the presence of which was suggested from the elemental and thermal analyses. The charts of differential thermal analysis (DTA) and thermogravimetric analysis (TGA) of the red-pink complex are given in Fig. 2. The weight loss of 18% up to 150 °C corresponds very closely to four moles of water (calcd: 17.7%), which probably consists of two moles of coordinated and two moles of lattice water. However, no difference is observed between the curves of the two kinds of water. The DTA curve indicates two endothermic peaks at 133 °C and around 155 °C. The large peak at 133 °C is due to the elimination of water as judged from the TGA curve. The other broad peak may be due to some phase transition in the crystalline structure.

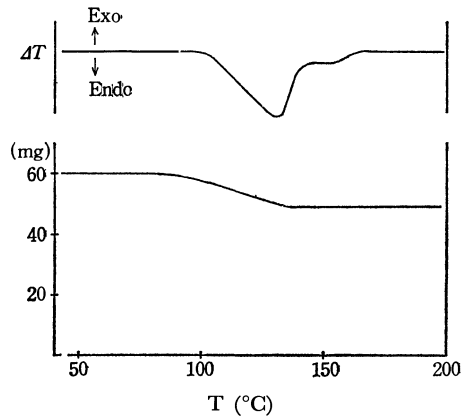

Fig. 2. DTA and TGA curves for diaquo-DTTA-Co(II).

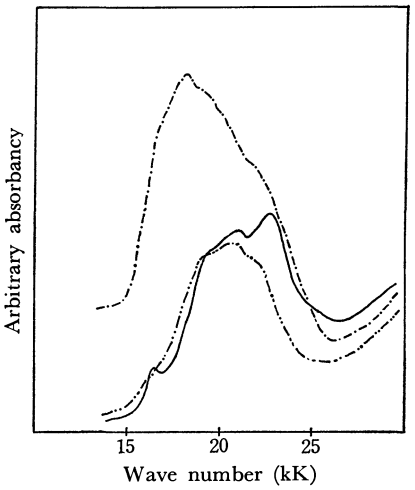

Fig. 3. Reflectance spectra of DTTA-Co(II) complexes: ——: red pink diaquo-DTTA-Co(II); —·—: blue violet anhydrous DTTA-Co(II); —··—: pink diaquo-DTTA-Co(II).

The blue-violet complex obtained by heating the red-pink one at 150 °C carries no water and shows a magnetic moment of μ_{effect}=4.66 B. M. Because of its high hygroscopicity, no well-defined infrared spectrum could be obtained. The broad absorption around 1590—1650 cm^{-1} suggests the presence of two kinds of carboxylate groups like those in diaquo-DTTA-Co(II). The electronic spectrum in solid exhibits d-d transition as a broad band around 18 kK (Fig. 3). This implies a high spin tetrahedral configuration of low symmetry for the complex, where O-N-N-O coordination occurs around the Co(II) ion and the terminal iminoacetate group dangles like that in diaquo-DTTA-Co(II).

When the blue-violet complex was allowed to come in contact with moist air, the color turned pink with absorption of four moles of water. The pink complex was rather sensitive against air-oxidation. The mag-

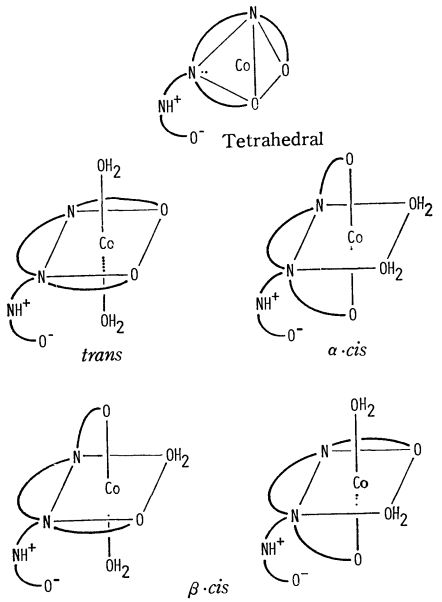

Fig. 4. Tetrahedral and possible four octahedral arrangements of DTTA-Co(II) complexes.

netic moment was slightly lower at μ_{effect}=4.83 B.M. decreasing gradually on standing in the air. The infrared spectral pattern was superimposable with that of the red-pink complex. An octahedral configuration is therefore reasonable for the pink complex in the same sense as in the red-pink one. On the other hand, the electronic spectrum of the former differs from that of the latter (Fig. 3).

In diaquo-DTTA-Co(II) in which the terminal iminoacetate group dangles, four stereoisomers are possible (Fig. 4). The difference in the electronic spectrum may be due to the fact that the red-pink and pink complexes are stereoisomers of this type. Exact assignment of their configurations, however, is impossible at present.

In diaquo-EDDA-Co(II), the EDDA anion coordinates as a tetradentate ligand. An octahedral configuration is provided, since its spectral pattern is similar to that of diaquo-DTTA-Co(II) (Fig. 5). However, the magnetic moment varied in each sample around an average value of μ_{effect}=4.4 B.M. which is lower than that for ordinary octahedral Co(II) complexes. This is due to a contamination by a Co(III) complex formed by inevitable air-oxidation during the course of measurements.

The pink coloration of diaquo-EDDA-Co(II) turned violet on heating at 150 °C in the absence of oxygen, returning to pink in a moist atmosphere at room temperature. In contact with air, the latter pink complex turned very quickly to deep violet. The thermochromism from pink to violet was probably due to dehydration. However, an extremely high sensitivity of the violet complex against air-oxidation and moisture made it impossible to confirm it. A tetrahedral configuration is suggested for the violet complex from the electronic spectrum in solid (Fig. 5). It exhibits a d–d transition band having a typical strong absorption at 19.1 kK.

The deep violet one caused by air-oxidation is undoubtedly a Co(III) complex. Elemental analysis indicates formula [Co(edda)(OH)(H_2O)]. This is supported by taking the formation condition into consideration, since no inorganic anion besides a hydroxide ion was present in the solution from which the crystals were obtained. The infrared spectrum shows a carboxylate stretching vibration due to COO–Co(III) at 1650 cm^{-1}. An octahedral configuration is seen in its electronic spectrum in solid which exhibits a typical d–d transition pattern having an absorption maxima at 18.7 kK and 26.3 kK (Fig. 5). Co(III) complexes of EDDA were investigated by several authors[6] and their stereochemistry has already been established. However, the geometry of the hydroxide ion and the water molecule in the octahedral arrangement is not clear in the present complex.

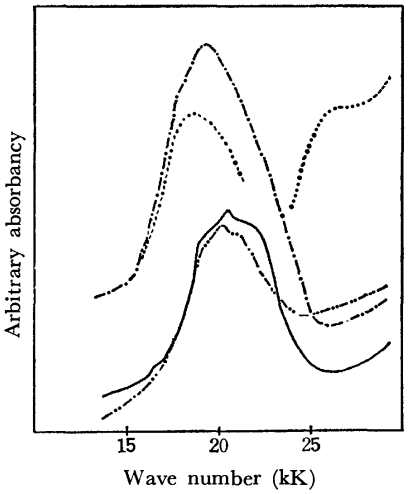

Fig. 5. Reflectance spectra of EDDA-Co(II) and EDDA-Co(III) complexes; ——: pink diaquo-EDDA-Co(II); —·—: violet anhydrous EDDA-Co(II); —··—: pink EDDA-Co(II) from violet one by aquation; ----: violet EDDA-Co(III).

6) J. I. Legg and D. W. Cooke, *Inorg. Chem.*, **4**, 1576 (1965); J. I. Legg, D. W. Cooke, and B. E. Douglas, *ibid.*, **6**, 700 (1967); J. L. Sudmeier and G. Occupati, *ibid.*, **7**, 2524 (1968); C. W. Van Saun and B. E. Douglas, *ibid.*, **8**, 115 (1969); P. F. Coleman, J. I. Legg, and J. Steele, *ibid.*, **9**, 937 (1970); K. Kuroda and K. Watanabe, This Bulletin, **44**, 1034 (1971); K. Kuroda, *Chem. Lett.*, **1972**, 197, 719.

Studies on Nitro Carboxylic Acids. III. The Reaction of α-Nitroolefins with Triethyl or Diethyl Phosphite[1]

Chung-gi SHIN, Yasuchika YONEZAWA, Katsuhiro KATAYAMA,[2] and Juji YOSHIMURA*

Laboratory of Organic Chemistry, Faculty of Engineering, Kanagawa University, Rokkakubashi, Kanagawa-ku, Yokohama 221

** Laboratory of Chemistry for Natural Products, Faculty of Science, Tokyo Institute of Technology, Ookayama, Meguro-ku, Tokyo 152*

(Received July 4, 1972)

The reaction of α-nitroolefins with triethyl or diethyl phosphite was studied and structural assignment of the products was made by spectroscopic analyses. Ethyl α,β-unsaturated α-nitrocarboxylates (IV) and 1-nitroalkenes (V) reacted with triethyl phosphite to afford ethyl β-diethoxyphosphinyl-α,β-unsaturated-carboxylates (IX) and 2-diethoxyphosphinyl-1-alkenes (X), respectively. Compound (IV) reacted with diethyl phosphite to give ethyl β-diethoxyphosphinyl-α-nitrocarboxylates (VI). The geometrical isomerism in IX and the reaction mechanism were discussed.

Numerous reports have appeared on the deoxygenation and intramolecular cyclization reaction of aromatic nitro and nitroso compounds with tervalent organophosphorus reagents,[3-7] but little attention has been paid to that of aliphatic nitro compounds with the above reagents.[3]

The reaction of ethyl α,β-unsaturated α-nitrocarboxylates (IV)[8,9] with triethyl phosphite gives ethyl β-diethoxyphosphinyl-α,β-unsaturated-carboxylates (IX). Only two kinds of vinylphosphonates (IXa and IXb) have recently been prepared by nucleophilic substitution of the corresponding activated vinyl halides with triethyl phosphite, as useful intermediates (Arbuzov reaction).[10,11]

In the present paper, detailed studies on the reaction of α-nitro-olefins (IV and V) with triethyl or diethyl phosphite and on the structural assignment of products are described.

Results and Discussion

Reactions of α-Nitroolefins with Triethyl Phosphite. When a benzene solution of IV and triethyl phosphite was refluxed for about 3 hr, evolution of a gaseous substance was observed. This was trapped and identified by gas chromatography to be ethyl nitrite. Fractional distillation of the reaction mixture gave ethyl β-diethoxyphosphinyl-α,β-unsaturated-carboxylates (IX) as a colorless oil in good yield.

Similar reaction of ethyl 3-hydroxy (Id)-, 3-acetoxy (IId)- and 3-methoxy-2-nitrohexanoates (IIId) with triethyl phosphite also gave IXd and ethyl nitrite, together with a small amount of water, acetic acid and methanol, respectively. It is well-known that hydroxy, acetoxy and methoxy groups in the 3-position of 2-nitrocarboxylic esters are easily eliminated in the persence of base to afford the corresponding nitroolefins.[1,8,12,13] The reaction might thus be preceded by the elimination of the substituents in the presence of triethyl phosphite as Lewis base. In the cases of Id and IIId, the yield of IXd decreased a great deal.

Under similar experimental conditions, 1-nitroalkenes (V) also reacted with triethyl phosphite to afford 2-diethoxyphosphinyl-1-alkenes (X) as a colorless oil in good yield. The results are summarized in Table 1, 2, 3, and 4.

Structural Assignment of IX and X. The streeochemical assignment of IX and X was made on the basis of independent preparation from vinyl halides and triethyl phosphite,[11] elementary and spectroscopic analyses. NMR spectra of IX (Table 2) showed two kinds of vinyl hydrogen signals, one with smaller coupling constants ($J_{P,H}$=23.5—28.4 Hz) appearing in the lower magnetic field and the other in higher field with larger coupling constants ($J_{P,H}$=43.5—46.3 Hz) and were assigned to *cis* and *trans* isomers,[14] respectively.

Similarly, two vinyl hydrogen signals of *cis* and *trans* to the phosphorus atom appeared in lower and higher magnetic fields with smaller ($J_{P,H}$=22.5—23.8 Hz) and larger ($J_{P,H}$=46.3—50.0 Hz) coupling constants, respectively. The composition of *cis* and *trans* isomers in IX was evaluated from the intensity of the vinyl proton signals to be approximately 7/3.

The infrared spectra of IX showed a waek band of carbon-carbon double bond in the region 1615—1630 cm^{-1} and two strong bands of P=O and P-O-C groups at 1250 and 1020—1025 cm^{-1}, respectively (Table 2). The absorption pattern of X is essentially the same

1) Part II of this series: C. Shin, Y. Yonezawa, H. Narukawa, K. Nanjo, and, J. Yoshimura, This Bulletin, **45**, 3595 (1972). A part of this work was presented at the 25th Annual Meeting of the Chemical Society of Japan, Tokyo, 13 October, 1971.

2) Present adress: Tōkō Kagaku Co., Ltd., Itabashi-ku, Tokyo.

3) J. I. G. Cadogan, *Quart. Rev.*, **22**, 222 (1968).

4) T. Kametani, T. Yamanaka, and K. Ogasawara, *Chem. Commun*, **1963**, 786.

5) P. H. Scott, C. P. Smith, E. Kober, and J. W. Churchill, *Tetrahedron Lett.*, **1970**, 1153.

6) R. J. Sundberg, B. P. Das, and R. H. Smith, *J. Amer. Chem. Soc.*, **91**, 658 (1969).

7) R. J. Sundberg, R. H. Smith, and J. E. Bloor, *ibid.*, **91**, 3392 (1969).

8) C. Shin, Y. Yonezawa, and J. Yoshimura, This Bulletin, **44**, 3488 (1971).

9) C. Shin, M. Masaki, and M. Ohta, *ibid.*, **43**, 3219 (1970).

10) G. Pattenden and B. J. Walker, *J. Chem. Soc., C*, **1969**, 531.

11) V. A. Kukuhtin, Yu. Yu. Samitov, and K. M. Kirillova, *Izv. Akad. Nauk SSSR, Ser. Khim.*, **1962** (2), 356; *Chem. Abstr.*, **67**, 21361s (1967).

12) K. Yamagishi and Y. Ishibiki, *Nippon Kagaku Zasshi*, **81**, 971 (1960).

13) S. Umezawa and S. Zen, This Bulletin, **36**, 1143 (1963).

14) A. M. Aguiar and D. Daigle, *J. Org. Chem.*, **30**, 2826, 3527 (1965).

TABLE 1. PHYSICAL CONSTANTS, YIELDS, AND ELEMENTARY ANALYSES OF IX

Compound	Bp °C/mmHg	Yield (%)	Formula	Found (Calcd) C%	Found (Calcd) H%
IXb	118—121/2	72.4	$C_{10}H_{19}O_5P$	47.89(48.00)	7.62(7.60)
IXc	121—123/1.5	67.2	$C_{11}H_{21}O_5P$	49.78(50.00)	8.19(7.90)
IXd	117—122/1	77.3	$C_{12}H_{23}O_5P$	51.59(51.79)	8.03(8.27)
IXe	119—122/1.5	62.8	$C_{12}H_{23}O_5P$	51.56(51.79)	8.66(8.27)
IXf	150—152/0.5	65.6	$C_{15}H_{20}O_5P$	57.61(57.69)	6.79(6.73)

TABLE 2. NMR[a] AND IR[b] SPECTRA OF IX

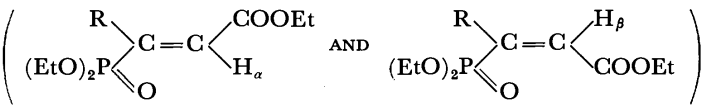

Compound	*cis*-H_α (τ)		*trans*-H_β (τ)		J_{PH} (Hz) *cis*	J_{PH} (Hz) *trans*	COOEt (s)[c]	C=C (w)[d]	P=O (s)	P–O–C (s)	ratio *cis*	ratio *trans*
IXb	3.39	3.63	3.51	3.95	24.5	44.5	1723	1634	1250	1020	7	3
IXc	3.43	3.67	3.56	4.02	25.0	46.3	1725	1630	1250	1025	6	4
IXd	3.19	3.45	3.34	3.80	25.0	45.8	1727	1628	1250	1025	7	3
IXe	3.46	3.71	3.53	3.99	28.4	46.3	1722	1620	1250	1020	7	3
IXf	3.18	3.42	3.30	3.73	23.5	43.5	1730	1615	1250	1020	7	3

a; 100 MHz, in CCl_4. b; cm^{-1}, in NaCl. c; s=strong. d; w=weak.

TABLE 3. PHYSICAL CONSTANTS, YIELDS, AND ELEMENTARY ANALYSES OF X

Compound	Bp °C/mmHg	Yield (%)	Formula	Found (Calcd) C%	Found (Calcd) H%
Xc	65—67/4	71	$C_8H_{17}O_3P$	50.28(50.00)	9.01(8.85)
Xd	77—80/2	47	$C_9H_{19}O_3P$	52.38(52.42)	9.13(9.22)
Xe	70—73/3	65	$C_9H_{19}O_3P$	52.31(52.42)	9.29(9.22)
Xf	120—125/0.35	31	$C_{12}H_{17}O_3P$	60.21(60.00)	6.98(7.09)

TABLE 4. NMR[a] AND IR[b] SPECTRA OF X

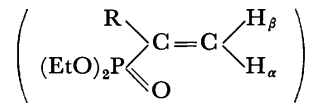

Compound	*cis*-H_α (τ)		*trans*-H_β (τ)		J_{PH} (Hz) *cis*	J_{PH} (Hz) *trans*	C=C (w)[c]	P=O (s)[d]	P–O–C (s)[d]
Xc	3.89	4.10	4.00	4.50	22.5	49.0	1630	1245	1023
Xd	3.88	4.11	4.04	4.53	23.8	50.0	1640	1250	1030
Xe	3.85	4.08	3.94	4.45	23.0	48.0	1630	1240	1020
Xf	3.56	3.78	3.62	4.09	22.5	46.3	1680	1250	1025

a; 100 MHz, in $CDCl_3$. b; cm^{-1}, in NaCl. c; w=weak. d; s=strong.

as that of IX except for the lack of ethoxycarbonyl band (Table 4).

Reaction of α-Nitroolefins with Diethyl Phosphite. In contrast to triethyl phosphite, diethyl phosphite can add to the olefinic bond of IV easily. When a mixture of IV and the phosphite was heated at 100 °C for 2 hr, the expected ethyl α-nitro-β-diethoxyphosphinylcarboxylates (VI) were obtained in about 50% yield. Compounds (VI) keep the nitro group, which showed stretching bands at *ca* 1565 and 1370 cm^{-1} in the infrared spectra. The disappearance of the stretching band of carbon-carbon double bond in the region 1640—1665 cm^{-1} and the appearance of P=O and P–O–C groups at 1250 and *ca* 1020 cm^{-1} seem to support the formation of VI.

Reaction Mechanism. From the results, it is postulated that the triethyl phosphite attacked nucleophilically on the β-position of the nitro-olefins (aci-form; VII) and cyclized to afford five-membered intermediates, 3-ethoxycarbonyl-Δ^2-1,2,5-oxazaphospholine-2-oxide derivatives (VIII), and the subsequent concerted reaction in VIII occurred to give IX and X together with ethyl nitrite (Scheme 1). In fact, in the case of isopropyl derivative (VIIIe, R′=COOEt), an unstable intermediate was obtained under mild conditions and decomposed to IXe and ethyl nitrite during the course of redistillation.

On the other hand, diethyl phosphite added nucleophilically to β-position of the nitroolefins (nitro-form; IV) affords VI.

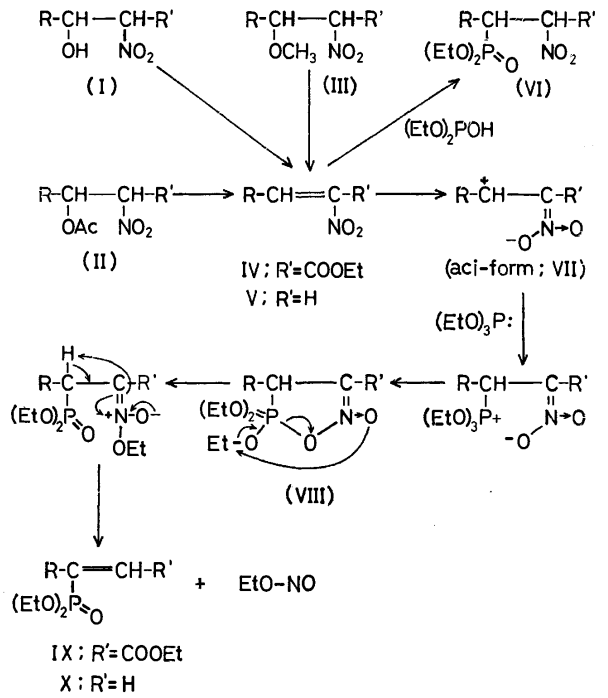

a; R=H, b; R=CH_3, c; R=C_2H_5, d; R=n-C_3H_7, e; R=i-C_3H_7, f; R=C_6H_5

Scheme 1.

Experimental

All boiling points are uncorrected. The IR spectra were recorded on a Hitachi EPI-S2 spectrometer. The NMR spectra were measured with a JNM-4H-100 spectrometer (Japan Electron Optics Laboratory Co., Ltd.) at 100 MHz.

Materials. Ethyl α,β-unsaturated α-nitrocarboxylates were prepared by the reaction of ethyl α,β-unsaturated carboxylates with fuming nitric acid.[9] Ethyl α-nitrocinnamate was prepared according to the method of Dornow and Menzel.[15]

Reactions of IV with Triethyl Phosphite. A solution of IV (0.05 mol) in dry benzene (40 ml) was added dropwise, with stirring, to triethyl phosphite (0.05 mol) at a temperature below −5 °C. After being stirred for 3 hr at this temperature, the mixture was allowed to warm to room temperature, when stirring was continued for 1 hr. When the mixture was refluxed for about 3 hr, evolution of gaseous substance was observed. This was trapped in a U-tube fitted at the top of a condenser and cooled below −20 °C, and identified to be ethyl nitrite by gas chromatography. After concentration of the reaction solution, the residual oil was distilled under reduced pressure to afford a colorless oil, which was identified as ethyl β-diethoxyphosphinyl-α,β-unsaturated-carboxylates (IX). The results are summarized in Tables 1 and 2.

Reaction of IVe with Triethyl Phosphite below 30 °C. Ethyl 4-methyl-2-nitro-2-pentenoate (IVe; 5 g) was added dropwise, with stirring, to triethyl phosphite (10 g) at a temperature below −20 °C. After stirring for 2 hr, the mixture was allowed to warm slowly to room temperature and stirring was continued for 2 days at 30 °C. After concentration of the reaction mixture, the residual viscous oil was carefully distilled in a vacuum to afford 3-ethoxycarbonyl-4-isopropyl-Δ^2-1,2,5-oxazaphospholine-2-oxide (VIIIe) as yellow viscous oil (3.9 g, 41.5%), bp 95—105 °C/0.001 mmHg. IR (KBr disk): 1730 (-COOEt), 1625 (-C=N-), 1240 (-P-O-), and 1030 (P-O-C-) cm^{-1}.

Found: N, 4.14%. Calcd for $C_{14}H_{28}NO_7P$: N, 3.87%.

When a solution of VIIIe (2.8 g) in dry benzene (30 ml) was refluxed for 3 hr and the reaction solution was concentrated, residual oil was obtained accompanied by liberation of ethyl nitrite. The oil was distilled under reduced pressure to afford a colorless oil, which was identified as ethyl 3-diethoxyphosphinyl-4-methyl-2-pentenoate (IXe; 1.9 g, 74 %).

Reactions of V with Triethyl Phosphite. 1-Nitro-1-alkene (0.05 mol) was added dropwise, with stirring, to triethyl phosphite (0.07 mol) maintained below 15 °C. After stirring for 1 hr, the mixture was allowed to stand at 40 °C for about 2 hr when liberation of ethyl nitrite ceased. Concentration of the reaction mixture afforded residual oil, which was identified as 2-diethoxyphosphinyl-1-alkene (X). The results are summarized in Tables 3 and 4.

Reactions of Id-IIId with Triethyl Phosphite. Ethyl 3-acetoxy-2-nitrohexanoate[13] (IId; 0.03 mol) was added dropwise, with stirring, to a solution of triethyl phosphite (0.03 mol) in dry benzene (20 ml) cooled below 15 °C. After being stirred for 30 minutes at room temperature, the solution was refluxed for 1 hr. After concentration of the reaction solution, the residual oil was distilled under reduced pressure to afford a colorless oil, which was identified as ethyl 3-diethoxyphosphinyl-2-hexenoate (IXb). Yield 68.3%.

An analogous treatment of ethyl 3-hydroxy-2-nitrohexanoate (Id)[13] and ethyl 3-methoxy-2-nitrohexanoate (IIId)[9] with triethyl phosphite under reflux for 6 hr also afforded IXd, in 38.5 and 23.5% yields, respectively.

Reactions of IV with Diethyl Phosphite. Diethyl phosphite (0.03 mol) was added dropwise, with stirring, to ethyl 2-nitropentenoate (IVc; 0.03 mol) at room temperature, and the mixture was heated at 100 °C for 2 hr when it changed to brown. After concentration of the reaction mixture, the residual oil was distilled under reduced pressure to afford a colorless oil (68%, bp 130—135 °C/0.75 mmHg), which was identified as ethyl 3-diethoxyphosphinyl-2-nitropentanoate (VIc). IR(KBr disk): 1750 (-COOEt), 1565 and 1370 (-NO_2), 1250 (P=O), and 1020 (P-O-C) cm^{-1}. NMR ($CDCl_3$): 4.40—4.75 τ (double doublets, J=7.0 Hz) and 4.58 τ(doublet, J_{P-C-CH}=16.2 Hz).

Found: C, 42.84; H, 6.91; N. 4.33%. Calcd for $C_{11}H_{22}NO_7P$: C, 42.85; H, 7.07; N, 4.50%.

An analogous treatment of ethyl 2-nitrobutenoate (IVb) with diethyl phosphite also afforded ethyl 3-diethoxyphosphinyl-2-nitrobutanoate (VIb). Yield 41%, bp 126—128 °C/0.8 mmHg. IR: 1755 (-COOEt), 1565 and 1370 (-NO_2), 1250 (P=O), and 1020 (P-O-C) cm^{-1}. NMR: 4.60—4.73 τ(double doublets, J=6.8 Hz) and 4.66 τ(doublet, J_{P-C-CH}=12.5 Hz).

Found: C, 40.32; H, 6.83; N, 4.32%. Calcd for $C_{10}H_{20}NO_7P$: C, 40.40; H, 6.73; N, 4.71.%

15) A. Dornow and H. Menzel, *Ann. Chem.*, **588**, 40 (1959).

Solvolysis of Organic Phosphates. VIII. γ-Elimination in the Spontaneous Hydrolysis of 2-Chloro-3-pyridylmethyl Phosphate[1]

Yukito MURAKAMI, Junzo SUNAMOTO, and Naomi KANAMOTO

Department of Organic Synthesis, Faculty of Engineering, Kyushu University, Hakozaki, Higashi-ku, Fukuoka 812

(Received July 17, 1972)

2-Chloro-3-pyridylmethyl phosphate was hydrolyzed in aqueous media. All runs were carried out in a pH range 1—3 where the reactive species are essentially of neutral and monoanion forms. The main reaction product was 3-hydroxymethyl-2-pyridone, the reaction following an apparent first-order kinetics with respect to both pyridone formation and liberation of inorganic phosphate. The hydrolytic elimination of the 2-chlorine atom was catalyzed to a great extent by the phosphate group. The dephosphorylation was effected by the presence of the 2-chlorine atom as well. The hydrolysis of the neutral phosphate species, which is in general inert to hydrolysis, was much accelerated in the present hydrolysis. A plausible mechanism was presented in terms of the concerted elimination of both 2-chlorine atom and phosphate moiety by their mutual catalytic participation. Besides the main reaction process, a normal hydrolysis affording 2-chloro-3-pyridylmethanol was also detected to proceed to a minor extent.

In a series of studies on the hydrolysis of organic phosphates, we have shown some distinct types of neighboring group participation in dephosphorylation processes. Both pyridinium and quinolinium groups were observed to play an intramolecular general acid catalysis in the hydrolysis of 2-pyridylalkyl phosphates[2,3] and 8-quinolyl phosphate,[4] respectively, in their zwitterion forms. A neighboring hydroxyl group acted as a remarkable acid catalyst in the hydrolysis of 3-hydroxy-2-pyridylmethyl phosphate.[5]

The phosphate group occasionally provides a proximity effect on the elimination of another functional group in the molecule. The hydrolytic elimination of β-chlorine in 2,2,2-trichloroethanol was almost inhibited by the presence of a phosphate group, as apparent in the solvolysis study of 2,2,2-trichloroethyl phosphate.[6] This study on the hydrolysis mechanism of 2-chloro-3-pyridylmethyl phosphate provides another type of proximity effect caused by the participation of both γ-chlorine atom and phosphate. These groups located mutually in the neighboring space showed marked catalytic effects in their hydrolytic elimination.

Experimental

Materials. Details of synthesis and purification procedures for 2-chloro-3-pyridylmethyl phosphate are described elsewhere.[7] UV (in 0.02 M-perchloric acid at room temperature): 266 nm (ε 3100) and 273 nm (ε 2800). NMR (0.71 M in DMSO-d_6, TMS as internal reference): δ 5.03 (2H, d, $J_{CH_2-^{31}P}$=8.0 Hz, -C$\underline{H_2}$-), 6.61 (2H, s, -O$\underline{H}$), 7.54 (1H, q, J_{4-5}=7.5 Hz and J_{5-6}=5.0 Hz, H-5), 8.02 (1H, q, J_{4-6}=2.0 Hz, H-4), and 8.46 (1H, q, H-6).

2-Chloro-3-pyridylmethanol was prepared by LAH reduction of methyl 2-chloronicotinate.[7] UV (in 0.02 M-perchloric acid at room temperature): 266 nm (ε 4700) and 273 nm (ε 4400). NMR (0.40 M in DMSO, TMS as internal reference): δ 4.57 (2H, d, J_{CH_2-OH}=4.5 Hz, -C$\underline{H_2}$-), 5.49 (1H, t, -O$\underline{H}$), 7.43 (1H, q, J_{4-5}=7.5 Hz and J_{5-6}=4.5 Hz, H-5), 7.95 (1H, q, J_{4-6}=2.0 Hz, H-4), and 8.19 (1H, broad d, H-6).

3-Hydroxymethyl-2-pyridone was synthesized through diazotization of 2-amino-3-hydroxymethylpyridine followed by hydrolysis.[7] UV (in 0.02 M-perchloric acid at room temperature): 228 nm (ε 5300) and 297 nm (ε 5140). IR (0.2 M in 0.1 M-deuteroperchloric acid): 1640 cm^{-1} (C=O). NMR (0.40 M in DMSO, TMS as internal reference): δ 4.28 (2H, broad s, -C$\underline{H_2}$-), 4.91 (1H, broad s, -O$\underline{H}$), 6.17 (1H, t, J_{4-5}=J_{5-6}=6.5 Hz, H-5), 7.22 (1H, broad q, J_{4-6}=1.5 Hz, H-4), and 7.38 (1H, broad d, H-6).

Acid Dissociation Constants. The acid dissociation constants of the phosphate were obtained by the usual potentiometric titration.[2] The values found for pK_{H_2A} and pK_{HA} were 1.8 and 6.3 at 80 °C, and 2.17 and 5.97 at 25 °C, respectively, an ionic strength being maintained at 0.10 with potassium nitrate. The neutralization equivalence was 106.68 and 108.90 (calcd. 111.77) at 80 and 25 °C, respectively. The values of acid dissociation constants at elevated temperature were not sufficiently reproducible, especially for pK_{H_2A}. This was most likely caused by a trace hydrolysis of the phosphate during the course of titration to give off hydrochloric acid.

Product Analyses. The chromatographic solvent used was a mixture of *n*-propanol, concentrated aqueous ammonia, and water (6 : 3 : 1 by vol.). An acid molybdate spray reagent[8] was used for detection of phosphorus-containing spots. Paper chromatography and tlc were carried out with Toyo Roshi No. 50 filter paper and Tokyo Kasei spot film (silica gel), respectively, in combination with the above solvent and developing reagent. The R_f-values found for inorganic phosphate and 2-chloro-3-pyridylmethyl phosphate were ≈0.0 and 0.34, respectively, by paper chromatography, and 0.0 and 0.45 by tlc.

(i) A 2.02×10^{-3} M aqueous solution of 2-chrolo-3-pyridylmethyl phosphate was hydrolyzed in a sealed pyrex tube for 10.5 hr at 90 °C and pH 1.0 with an ionic strength of 0.10 ($HClO_4$). At the end the conversion was 30.0%, calculated from the determination of liberated inorganic phosphate. UV spectrum of the resulting hydrolyzate indicated the formation of 2-chloro-3-pyridylmethanol and 3-hydroxymethyl-2-pyridone (Fig. 1). No other organic phosphorus compounds besides the starting phosphate were

1) Contribution No. 278 from this Department.
2) Y. Murakami and M. Takagi, *J. Amer. Chem. Soc.*, **91**, 5130 (1969).
3) Y. Murakami, J. Sunamoto, and N. Kanamoto, This Bulletin, **46**, 871 (1973).
4) Y. Murakami and J. Sunamoto, *ibid.*, **44**, 1939 (1971).
5) Y. Murakami, J. Sunamoto, and H. Ishizu, *ibid.*, **45**, 590 (1972).
6) Y. Murakami, J. Sunamoto, and N. Kanamoto, *Chem. Lett.*, **1972**, 699.
7) Y. Murakami, J. Sunamoto, S. Kinuwaki, and H. Honda, This Bulletin, in press.
8) E. Karl-Kroupa, *Anal. Chem.*, **28**, 1091 (1956).

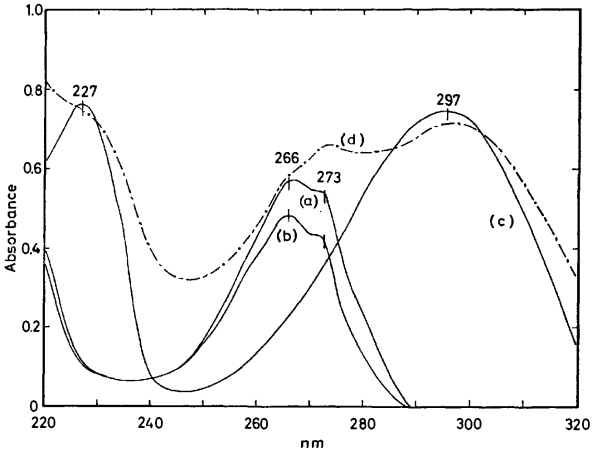

Fig. 1. Ultraviolet absorption spectra in 0.02 M-perchloric acid: (a) 2-chloro-3-pyridylmethyl phosphate, 1.58×10^{-4} M; (b) 2-chloro-3-pyridylmethanol, 1.26×10^{-4} M; (c) 3-hydroxymethyl-2-pyridone, 1.44×10^{-4} M; (d) the hydrolyzate of 2-chloro-3-pyridylmethyl phosphate, the initial phosphate solution of 0.103 M was treated at 90 °C and $-\log[H^+]=1.0$ for 23 hr and diluted 5/3 times for measurement.

detected by means of paper and thin layer chromatographic techniques. (ii) A 0.103 M 2-chloro-3-pyridylmethyl phosphate solution in 0.1 M-deuteroperchloric acid was placed in a sealed Pyrex tube and allowed to stand for 23 hr at 90 °C. White precipitates formed were removed by filtration and the filtrate was subjected to IR measurement. The absorption band attributable to the carbonyl stretching mode was weak but observable at 1640 cm^{-1}. The white precipitates formed was identified as 3-hydroxymethyl-2-pyridone by tlc with the use of UV light for detection, R_f 0.65. A 0.196 M solution of 2-chloro-3-pyridylmethanol in 0.1 M-deuteroperchloric acid was treated under the same conditions. However, significant transformation of this alcohol was not detected by any analytical method. (iii) 2-Chloro-3-pyridylmethyl phosphate (47.32 mg) was dissolved in DMSO-d_6 (0.30 ml) containing 10 μl of deuterium oxide, placed in a sealed Pyrex tube and kept at 95 °C for 21 hr. The reaction was followed by NMR with TMS as an internal reference. A doublet signal of the methylene protons in the starting phosphate gradually decreased, whereas a singlet signal assignable to the methylene protons of 2-chloro-3-pyridylmethanol increased in intensity. Another signal due to the methylene protons appeared at 4.28 ppm and increased markedly in intensity with the progress of reaction. This signal was assigned to the methylene protons in 3-hydroxymethyl-2-pyridone with the aid of an authentic sample. No other methylene signal of a doublet nature was detected throughout the reaction. After 4 hr of the reaction period, a white crystalline mass (the pyridone) started to precipitate. The yield of the pyridone was approximately 90% at the end of the reaction.

Kinetic Procedures. The experimental and analytical procedures were essentially the same as those employed for the hydrolysis studies of 2-pyrdidylalkyl phosphates at higher temperature.[3] All runs were carried out in aqueous media at 90.0±0.1 °C with an ionic strength of 0.10 ($HClO_4$–$NaClO_4$) over the $-\log[H^+]$ range 1.0—3.0, where the phosphate exists in three forms, cation, neutral, and monoanion. The pH-deviation did not exceed ±0.02 during the course of reaction. The hydrolytic decomposition of the phosphate was followed by determination of the liberated inorganic phosphate.[2-5] The formation of 3-hydroxymethyl-2-pyridone was measured spectrophotometrically at 297 nm.

Results and Discussion

Acid Dissociation Process. The second acid dissociation constant found for the present phosphate ($pK_{H_2A}\approx2$) was comparatively smaller than those for the other pyridylalkyl phosphates (pK_{H_2A} 4-5).[2-6] Brown and McDaniel obtained spectrophotometrically the pK_a-values of chloropyridines in aqueous system at 25 °C; 0.72 for the 2-isomer and 2.84 for the 3-isomer.[9] The pK_a-values for dissociation of a pyridinium proton in pyridine[10] and 3-pyridylmethyl phosphate[11] are 5.45 and 4.86 at 25 °C, respectively. The phosphorylated hydroxymethyl group apparently tends to act as an electron-withdrawing substituent to some extent. Thus, the pK_a-value for dissociation of a pyridinium proton in the present phosphate should be less than that for 2-chloropyridine. The most plausible acid dissociation process is presented in Scheme 1. An intramolecular hydrogen bonding of

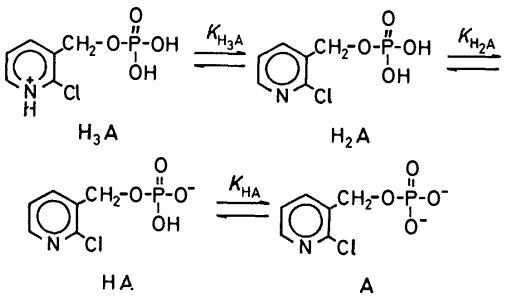

Scheme 1.

the phosphate moiety with the chlorine atom may cause the trapping of the phosphate proton, and consequently the pK_{H_2A}-value may become a little larger than that of ordinary alkyl phosphates.

Reaction Mechanisms. We may conclude from product analyses that 2-chloro-3-pyridylmethyl phosphate undergoes hydrolytic decomposition to afford 3-hydroxymethyl-2-pyridone as the major product

Table 1. Apparent first-order rate constants for the spontaneous hydrolysis of 2-chloro-3-pyridylmethyl phosphate; obtained from the analysis of inorganic phosphate at 90.0±0.1°C and $\mu=0.10$

$-\log[H^+]$	$10^5\times k_{P_i}$, sec^{-1}	$-\log[H^+]$	$10^5\times k_{P_i}$, sec^{-1}
1.01	0.85	1.92	0.72
1.14	0.83	2.15	0.68
1.83	0.73	2.26	0.59
1.91	0.70	2.82	0.57

9) H. C. Brown and D. H. McDaniel, *J. Amer. Chem. Soc.*, **77**, 3753 (1955).
10) J. Bjerrum, G. Schwarzenbach, and L. G. Sillén, "Stability Constants. Part I. Organic Ligands," The Chemical Society, London (1957).
11) Y. Murakami, M. Takagi, and H. Nishi, This Bulletin, **39**, 1197 (1966).

along with a small amount of 2-chloro-3-pyridylmethanol. The apparent first-order rate constants obtained from analysis of the liberated inorganic phosphate are listed in Table 1. A good first-order kinetics was also established for the pyridone formation. The rate constants obtained by both methods were almost comparable: for example, $k_{Pi}=1.02\times10^{-5}$ sec^{-1} for the liberation of inorganic phosphate and $k'=0.93\times10^{-5}$ sec^{-1} for the formation of the pyridone at 90.7±0.1 °C and $-\log[H^+]=1.0$ with an ionic strength of 0.10 ($HClO_4$). The difference between these two rate constants is significant since the presence of a small amount of 2-chloro-3-pyridylmethanol, the normal hydrolysis product, was no doubt detected by NMR. Thus, the whole reaction scheme consists of two competitive reactions as shown in Scheme 2. One may provide two possible mechanisms for the pyridone formation process; consecutive (Scheme 3) and concerted bimolecular (Scheme 4). Although other organic phosphates besides the starting one could not be detected in the course of hydrolysis reaction, we would not completely eliminate the possible formation of 2-hydroxy-3-pyridylmethyl phosphate (I or its keto-isomer, 1,2-dihydro-2-oxo-3-pyridylmethyl phosphate, II) as a labile intermediate in the pathway to the pyridone formation.

The neighboring acidic phosphate moiety seems to promote the elimination of the γ-chlorine atom through

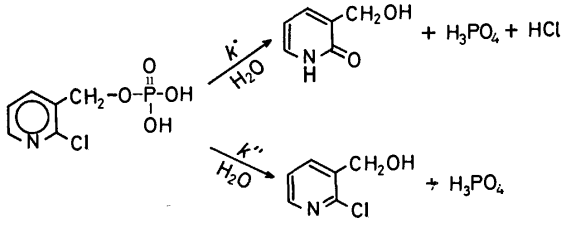

Scheme 2.

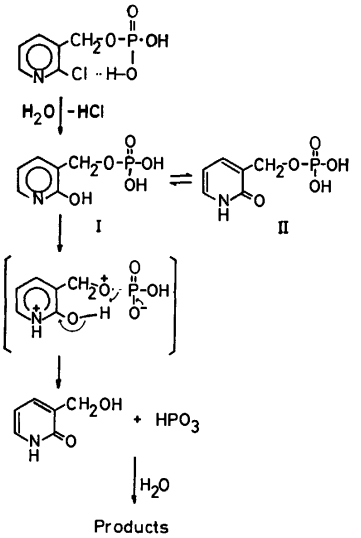

Scheme 3. (A consecutive reaction mechanism).

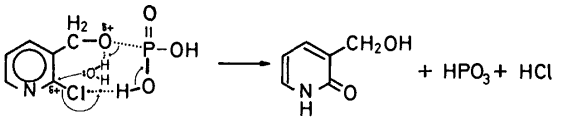

Scheme 4. (A concerted bimolecular mechanism).

the intramolecular Cl···H···O hydrogen bonding. Examination by the Dreiding-type model (Fig. 2) shows that the chlorine atom and the phosphate hydroxyl group can be favorably oriented in space to form a linear hydrogen bonding with the preferential orbital direction.

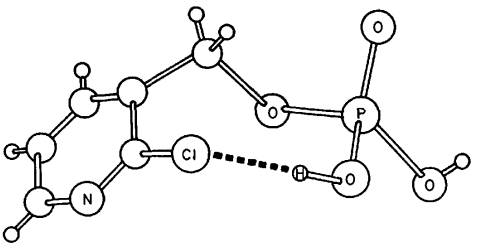

Fig. 2. Stereoview of the molecular configuration and the geometry for intramolecular hydrogen bonding between the chlorine atom and the phosphate moiety in 2-chloro-3-pyridylmethyl dihydrogen phosphate.

Using pK_a-values evaluated at 80 °C for each ionic species of the present phosphate[12] and the observed rate constants listed in Table 1, we calculated the apparent specific rate constants for the hydrolysis according to the usual computation procedures;[2-5] $k_{H_2A}=1.0\times10^{-5}$ and $k_{HA}=0.5\times10^{-5}$ sec^{-1} at 90 °C. It is well-known that the neutral alkyl dihydrogen phosphates are in general very inert to hydrolysis.[13,14] The hydrolysis rate constants for the neutral species of methyl and ethyl phosphates, for example, are 0.5×10^{-6} [13] and 0.7×10^{-6} sec^{-1} [14] at 100 °C, respectively. The hydrolysis reaction of the present neutral phosphate species, mainly giving rise to pyridone formation, was apparently much accelerated relative to the hydrolysis of those alkyl phosphates. The profound rate enhancement for the neutral phosphate hydrolysis can not be explained only by the usual electronic effect brought about by the 2-chloropyridyl group, but can be attributed to direct participation of the chlorine atom at the dephosphorylation site.

In conclusion, 2-chloro-3-pyridylmethyl phosphate was hydrolyzed primarily to afford the pyridone by the mutual participation of the chlorine atom and the phosphate group (Scheme 4).

12) The pK_{H_3A}-value for dissociation of the pyridinium proton was estimated to be 0.7 in reference to the value for 2-chloropyridine.[9] Care was taken to minimize the possible error in each specific rate constant caused by this estimation.

13) C. A. Bunton, D. R. Llewellyn, K. G. Oldham, and C. A. Vernon, *J. Chem. Soc.*, **1958**, 3574.

14) L. Kugel and M. Halmann, *J. Org. Chem.*, **32**, 642 (1967).

Methylene Analogs of Cyclobutenedione. VI.[1] Interconversion between 3,4-Dimethylcyclobut-3-ene-1,2-dione and 3,4-Dimethylenecyclobutane-1,2-dione

Fumio Toda and Nobuhiro Ooi

Department of Industrial Chemistry, Faculty of Engineering, Ehime University, Matsuyama 790

(Received July 10, 1972)

Treatment of 3,4-bis(diphenylmethyl)cyclobut-3-ene-1,2-dione (I) with bromine in ROH (R=H, Me, Et, and *i*-Pr) afforded 3,4-bis(diphenylmethylene)cyclobutane-1,2-dione (IV) and 3-diphenylmethyl-4-alkoxydiphenylmethylcyclobut-3-ene-1,2-dione (III) in various ratios depending on the steric bulkiness of R of ROH. Acidification of a solution of III in KOH–MeOH, in which III exists in the form of enolate anion (VIII), afforded III and IV in various ratios depending on the steric nature of the substituent R. Bromination of IV in 99% acetic acid afforded 3,4-bis(hydroxydiphenylmethyl)cyclobut-3-ene-1,2-dione (XI). Although the bromination of XI with phosphorus tribromide afforded IV, that with bromine afforded the 2,5-dihydrofuran derivative (XVII). The reaction of I with *o*-phenylenediamine to afford azamethylenecyclobutane derivatives XXV and XXVI is described.

The ring-hydrogen of 3-phenylcyclobut-3-ene-1,2-dione reacts with halogen to afford 4-halo-3-phenylcyclobut-3-ene-1,2-dione.[2-4] However, no reaction of hydrogen on the carbon bound to the cyclobutenedione ring has yet been reported. We have studied the reaction of 3,4-bis(diphenylmethyl)cyclobut-3-ene-1,2-dione (I) with electrophile and found that interconversion between I and 3,4-bis(diphenylmethylene)cyclobutane-1,2-dione (IV) occurs easily.

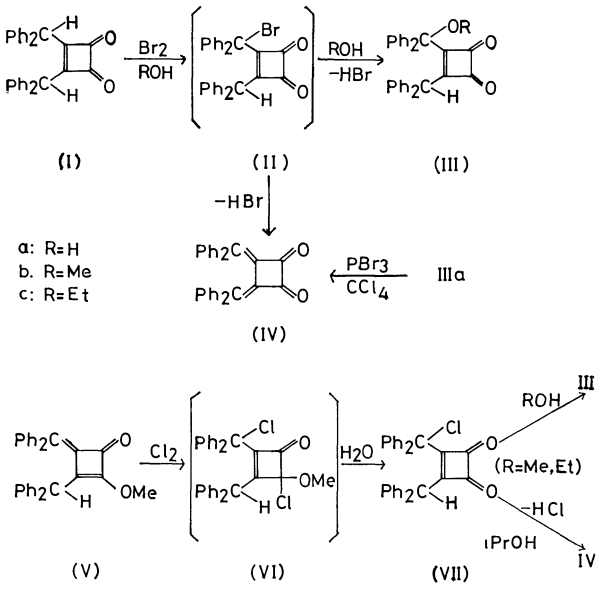

Scheme 1.

The reaction of I with bromine in 10% aqueous acetonitrile afforded 3-diphenylmethyl-4-hydroxydiphenylmethylcyclobut-3-ene-1,2-dione (IIIa) in a 45% yield. In methanol, 3-diphenylmethyl-4-methoxydiphenylmethylcyclobut-3-ene-1,2-dione (IIIb) was obtained in a 53% yield. On the other hand, the reaction of I with bromine in ethanol afforded 3-diphenylmethyl-4-ethoxydiphenylmethylcyclobut-3-ene-1,2-dione (IIIc) and IV in 39 and 13% yields, respectively, but that in 2-propanol afforded IV as the sole product (47% yield).

The reactions can be interpreted by assuming 3-diphenylmethyl-4-bromodiphenylmethylcyclobut-3-ene-1,2-dione (II) to be an intermediate. It is understandable that substitution of bromine of II with hydroxylic or alkoxylic nucleophile to afford III is in competition with the elimination of hydrogen bromide from II to afford IV (Scheme 1). The intermediacy of II is likely, since the bromination of IIIa with phosphorus tribromide in carbon tetrachloride afforded IV in a 52% yield. In order to confirm the intermediacy of II, preparation of its chloro-analog (VI) was attempted. Bubbling of chlorine through a solution of 2-methoxy-3-diphenylmethyl-4-diphenylmethylenecyclobut-2-en-1-one (V)[5] in ether afforded an oil. This was identified to be 3-diphenylmethyl-4-chlorodiphenylmethylcyclobut-3-ene-1,2-dione (VII) by means of IR and UV spectra, though the oil was too unstable for further purification. The strong IR absorption bands of VII, 1785 (νC=O) and 1640 cm^{-1} (νC=C), are charactaristic of cyclobutenedione derivatives as shown by I, III, and X. A possible reaction mechanism for the formation of VII is the hydrolysis of VI initially produced by the 1,4-addition of chlorine to V, since it has been established that α-halo-α-alkoxycyclobutanone is easily hydrolyzed into cyclobutenedione.[5] The reaction of VII with methanol and ethanol at room temperature afforded IIIb and IIIc in 64 and 59% yields, respectively. The reaction of VII with 2-propanol afforded IV in a 32% yield. It is thus reasonable to assume that II is an intermediate of the reaction of I with ROH in the presence of bromine. The reason for the difference between the reaction of VII with ethanol to afford IIIc and that of I with ethanol in the presence of bromine to afforded IIIc and IV is not clear.

UV spectra of IIIa, IIIb, and IIIc in 5% KOH–MeOH, 324 (18900), 323 (16000), and 323 nm (ε, 4700), respectively, were comparable with the spectrum of I in the same solvent, 330 nm (ε, 21700).[6]

1) Part V: F. Toda and J. Fujita, This Bulletin, **45**, 1928 (1972).

2) M. P. Cava and M. J. Mithchell, "Cyclobutadiene and Related Compounds," Academic Press, New York and London (1967), p. 128.

3) E. J. Smutny and J. D. Roberts, *J. Amer. Chem. Soc.*, **77**. 3420 (1955).

4) E. J. Smutny, M. E. Caserio, and J. D. Roberts, *ibid.*, **82**, 1793 (1960).

5) F. Toda and Y. Takehira, This Bulletin, **45**, 1816 (1972).

6) F. Toda and N. Ooi, This Bulletin, **45**, 1820 (1972).

Since it has been established that I dissolved in KOH–MeOH in the form of enolate anion (IX), the enolate form of III is considered to be VIII. The wavelength of the absorption band of VIII is slightly smaller than that of IX. The greater the sterical bulkiness of R in VIII, the smaller the molecular extinction coefficient ε. This suggests that the steric crowding between alkoxydiphenylmethyl and diphenylmethylene moieties increases the transition energy but decreases the probability of the electronic excitation of VIII.

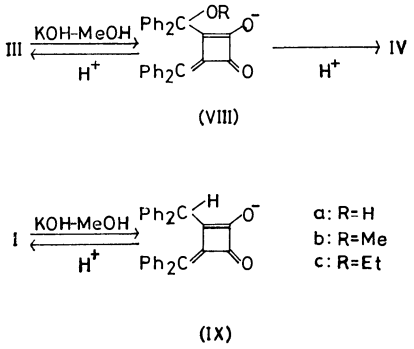

Scheme 2.

Acidification of IX affords I quantitatively,[6] but that of VIII was found to afford III and IV (Table 1). Major products obtained by the acidification of VIIIa and VIIIb were IIIa and IV, respectively. It seems possible that the ketonization of VIII leading to IV is predominant when R is relatively bulky. However, the ketonization of VIIIc afforded IIIc predominantly. A possible interpretation for the anomaly is that the ethoxy and enolate anion groups in IIIc are prevented from being arranged on an effective coplane for elimination.

Table 1. Yields (%) and products obtained by the ketonization of VIII

Enolate anion	Products (%)	
VIIIa	IIIa (60)	IV (5)
VIIIb	IIIb (25)	IV (56)
VIIIc	IIIc (83)	IV (8)

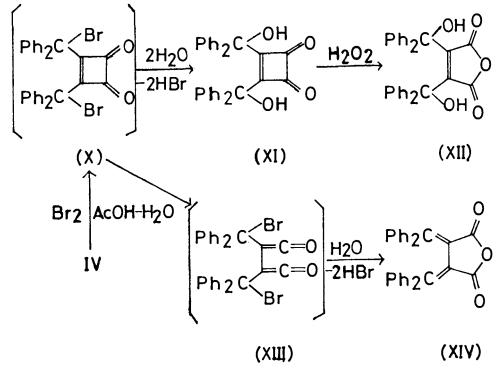

Scheme 3.

We reported that the reaction of IV with water in carbon tetrachloride in the presence of bromine affords 3,4-bis(diphenylmethylene)succinic anhydride (XIV) *via* the cyclobutenedione derivative (X) and the bisketene (XIII) successively[1] (Scheme 3). By means of a similar reaction in a protic solvent, one can expect the isolation of a stable cyclobutenedione derivative produced by the substitution of one or two bromines of X with nucleophile, instead of the conversion of X into XIII. The reaction of IV with bromine in 99% acetic acid afforded 3,4-bis(hydroxydiphenylmethyl)cyclobut-3-ene-1,2-dione (XI) and XIV in 55 and 6% yields, respectively. The formation of XI can be explained by the reaction of water and X initially produced by the 1,4-addition of bromine to IV. The production of X as an intermediate is supported by the isolation of XIV, though in a low yield (Scheme 3). The intermediacy of X was also confirmed by the reaction of XI with phosphorus tribromide in carbon tetrachloride to afford IV in a 43% yield. The reaction also gives structural evidence for XI. The structure of XI was further identified by its oxidation with hydrogen peroxide[2] to afford 3,4-bis(hydroxydiphenylmethyl)maleic anhydride (XII).

In order to prepare 3,4-bis(methoxydiphenylmethyl)-cyclobut-3-ene-1,2-dione, XI was made to react with methanol in the presence of bromine. However, 2,2,5,5-tetraphenyl-3-bromo-4-methoxalyl-2,5-dihydrofuran (XVII) was isolated in a 45% yield. The structure of XVII was identified by means of spectral data, and by its conversion into the known compound (XIX). Decarboxylation of 2,2,5,5-tetraphenyl-3-bromo-4-carboxy-2,5-dihydrofuran (XVIII), obtained by base-catalyzed hydrolysis followed by decarbonylation of XVII, afforded 2,2,5,5-tetraphenyl-3-bromo-2,5-dihydrofuran (XIX). The spectral data of XIX were

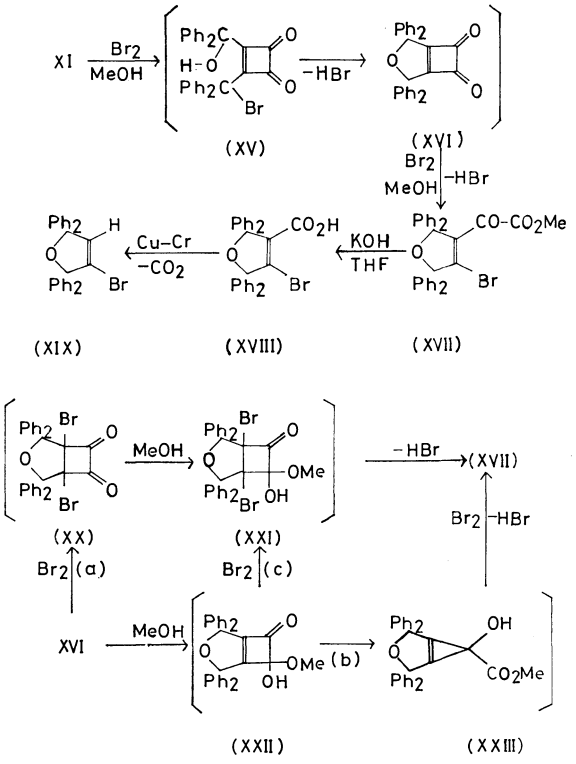

Scheme 4.

identical with those of an authentic sample.[7]

The reaction mechanism for the production of XVII can be explained by the intramolecular cyclization of XV into XVI followed by ring-opening, as shown in Scheme 4. The formation of the bicyclic intermediate (XVI) would precede the ring-opening of the cyclobutene-dione system, since the cyclobutenedione system was stable under the reaction conditions, as can be seen in the reaction of I with bromine in methanol to afford IIIb predominantly but not ring-opened product. The highly strained cyclobutenedione system of XVI would undergo ring-cleavage even under the acidic conditions of hydrogen bromide generated during the course of reaction, whereas the cyclobutenediones I and III were stable under such conditions (Scheme 2).

For the KOH-catalyzed ring-cleavage of phenylcyclobutenedione to afford benzylidenepyruvic acid, two mechanisms have been postulated, (a) addition-elimination[2,8] and (b) cyclopropenol mechanism.[2,9] However, (a) is unlikely since the addition of bromine to the double bond of cyclobutenedione system does not occur,[3,4] while (b) is also unlikely because of the highly strained nature of the bicyclic cyclopropene intermediate (XXIII). Another mechanism (c) can be applied to the present ring-cleavage of XVI. Since it is the ring-opening of XXI produced by the addition of bromine to XXII it might be considered the most probable mechanism.

Previous attempts to prepare the quinoxaline derivative having a fused cyclobutadiene ring, *i. e.*, 3,8-diazanaphtho[*b*]cyclobutadiene, have failed.[2,3,4,10] The reaction of I with *o*-phenylenediamine was carried out, with the expectation of obtaining the quinoxaline derivative of I. Contrary to expectation, the reaction afforded complex (XXV) and diazatrimethylenecyclobutane derivative (XXVI) in 15 and 17% yields, respectively. Their structures were identified by means of IR, UV, and NMR spectral data. The complex nature of XXV was confirmed by its acid-catalyzed reaction to afford XXVI in a 85% yield. Two protonation sites, β- and δ-carbon, are available for the protonation of dienamine.[11] The protonation on the β-carbon of XXV can afford XXVI. However, that on the δ-carbon of XXV which should produce the quinoxaline derivative of I, was not observed. The NMR spectrum of XXVI showed two AB-type doublets at 4.62 and 5.85 τ. Since the NMR spectrum of XXVI-d prepared by the reaction of XXV with DCl in D_2O showed one methine proton signal at 5.87 τ as a singlet, the structure of XXVI produced by the protonation on the β-carbon of XXV is determined.

The MS spectrum of the complex (XXV) showed the ion peak of each component at *m/e* 486 and 108, in addition to the parent ion peak at *m/e* 594. The fragmentation pattern of the azadimethylenecyclobutene component of XXV was similar to that of XXVI. In both cases, fragment ion peaks, *m/e* 319 (M^+-Ph_2CH), *m/e* 152 (M^+-2Ph_2CH) and an intense peak at *m/e* 167 (Ph_2CH) were observed.

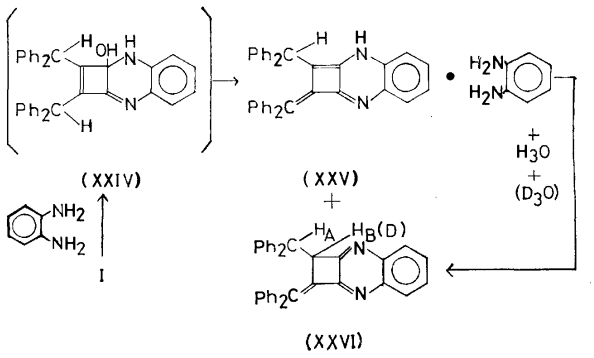

Scheme 5.

Experimental

All the melting points were uncorrected. IR and NMR spectra were measured in Nujol mull and $CDCl_3$ respectively, unless otherwise stated. Mass spectra were measured with an ionization energy of 70 eV.

Reactions of I with ROH in the Presence of Bromine. With H_2O: A solution of I[6] (0.30 g) and bromine (0.66 g) in 10% aqueous acetonitrile (10 ml) was heated under reflux for 3 hr. The cooled reaction mixture was diluted with benzene (100 ml), and washed successively with aqueous sodium thiosulfate and water, and dried over anhydrous sodium sulfate. The crude product remaining after evaporation of benzene was recrystallized from methanol to afford IIIa (0.14 g, 45%) as colorless prisms, mp 140—141 °C. IR: 1780 and 1765 (C=O) and 1570 cm^{-1} (C=C); λ_{max}^{EtOH}: 258 sh (10400), 265 sh (8900), 275 sh nm (ε, 7000); NMR: 2.3—3.1 (m, Ph, 20 H), 4.39 (s, CH, 1H), and 6.80 τ (s, OH, 1H).

Found: C, 83.42; H, 5.08%. Calcd for $C_{30}H_{22}O_3$: C, 83.70; H, 5.15%.

With MeOH: A solution of I (0.30 g) and bromine (0.66 g) in methanol (30 ml) was heated under reflux for 1 hr. The crude crystals remaining after the evaporation of methanol were recrystallized from methanol to afford IIIb (0.17 g, 53%) as colorless needles, mp 127—128 °C. IR: 1775 (C=O) and 1570 cm^{-1} (C=O); λ_{max}^{EtOH}: 259 sh (10500), 265 sh (9200), and 274 sh nm (ε, 7700); NMR (CCl_4): 2.5—3.0 (d, Ph, 20 H), 3.95 (s, CH, 1H), and 6.97 τ (s, OCH_3, 3H).

Found: C, 84.01; H, 5.46%. Calcd for $C_{31}H_{24}O_3$: C, 83.76; H, 5.44%.

With EtOH: A solution of I (0.30 g) and bromine (0.66 g) in ethanol (30 ml) was heated under reflux for 1 hr. Recrystallization from ethanol of the crude product obtained by evaporation of ethanol afforded a mixture of two crystalline forms, colorless and green crystals, which were separated mechanically. Recrystallization of the colorless crystals from ethanol afforded IIIc (0.13 g, 39%), mp 155—156 °C. IR: 1780 (C=O) and 1580 cm^{-1} (C=C); λ_{max}^{EtOH}: 260 sh (10300), 266 sh (9200), and 273 sh nm (ε, 7800); NMR (CCl_4): 2.4—3.1 (m, Ph, 20H), 3.91 (s, CH, 1H), 6.86 (q, J=7 Hz, CH_2, 2H), and 8.76 τ (t, J=7 Hz, CH_3, 3H).

Found: C, 84.09; H, 5.62%. Calcd for $C_{32}H_{26}O_3$: C, 83.82; H, 5.72%.

Recrystallization of the green crystals from acetonitrile

7) H. Tani and F. Toda, This Bulletin, **37**, 470 (1964).
8) A. T. Blomquist and E. A. LaLancette, *J. Amer. Chem. Soc.*, **84**, 220 (1962).
9) L. Skattbøl and J. D. Roberts, *ibid.*, **80**, 4085 (1958).
10) W. Ried and A. H. Schmidt, *Ann.*, **742**, 116 (1970).
11) G. H. Alt, "Enamines: Synthesis, Structure, and Reaction," ed. by A. G. Cook, Marcel Dekker, New York and London (1969), p. 118.

afforded IV (0.04 g, 13%) as green prisms, mp 206—207 °C (lit,[12] mp 206—207 °C).

With i-PrOH: A solution of I (0.30 g) and bromine (0.66 g) in 2-propanol (20 ml) was heated under reflux for 1 hr. The crude crystals separated out by the cooling of the reaction mixture were recrystallized from acetonitrile to afford IV (0.14 g, 47%) as green prisms, mp 206—207 °C.

The Reaction of IIIa with Phosphorus Tribromide. To a solution of IIIa (0.05 g) in carbon tetrachloride (3 ml) was added phosphorus tribromide (0.06 ml) at 0 °C, and the mixture was then stirred at 0 °C for 15 min. The crude product which crystallized out was recrystallized from acetonitrile to afford IV (0.025 g, 52%) as green prisms, mp 206—207 °C.

Synthesis of 3-Chlorodiphenylmethyl-4-diphenylmethylcyclobutene-1,2-dione (VII). Chlorine was bubbled through a solution of V[5] (0.30 g) in ether (20 ml) at room temperature for 5 min. The ethereal solution was washed successively with aqueous sodium thiosulfate and water, and dried over anhydrous sodium sulfate. Evaporation of the solvent afforded VII (0.30 g, 95%) as pale green oil. IR (liquid film): 1785 (C=O) and 1640 cm^{-1} (C=C); λ_{max}^{EtOH}: 243 sh (5700), 259 sh (3700), 266 sh (3300), and 273 sh nm (ε, 2900).

No satisfactory analytical data were obtained since the oil was too unstable for purification.

Reaction of VII with ROH. *With MeOH*: A solution of VII (0.30 g) in methanol (5 ml) was stirred at room temperature for 24 hr. The crude crystals separated out were recrystallized from methanol to afford IIIb (0.19 g, 64%) as colorless needles, mp 127—128 °C.

With EtOH: Treatment of VII (0.30 g) in ethanol (5 ml) by the same method as that employed for the reaction of of VII with methanol afforded IIIc, 0.18 g (59%) as colorless needles, after recrystallization from methanol, mp 155—156 °C.

With i-PrOH: Treatment of VII (0.30 g) in 2-propanol (5 ml) by the same method as that employed for the reaction of VII with methanol afforded IV, 0.09 g (32%) as green prisms, mp 206—207 °C, after recrystallization from acetonitrile.

Ketonization of The Enolate Anion VIII. To a solution of IIIa (0.1 g) in 10% methanolic potassium hydroxide (3 ml), was added concd hydrochloric acid (0.5 ml). The crude product separated out was washed with water. Recrystallization from methanol afforded a mixture of two crystalline forms, colorless needles and green prisms, which were separated mechanically. Recrystallization of the former from methanol afforded IIIa (0.06 g, 60%), mp 140—141 °C, while that of the latter from acetonitrile afforded IV (0.005 g, 5%), mp 206—207 °C.

The same treatment of IIIb and IIIc as that employed for IIIa afforded IV and the corresponding ketonization product (III), respectively, in the yields given in Table 1.

Reaction of IV with Bromine in Aqueous Acetic Acid. A mixture of IV (1.0 g), bromine (2.2 g) and 1% aqueous acetic acid (100 ml) was stirred at 70—75 °C for 1.5 hr. The reaction mixture was concentrated to dryness, and the residue was taken up in benzene (100 ml). The benzene solution was washed successively with aqueous sodium thiosulfate and water, and dried over anhydrous sodium sulfate. After removal of benzene, the residue was recrystallized from methanol to afford a mixture of two crystalline forms, colorless and red rhombs, which were separated mechanically. Recrystallization of the former from methanol afforded XI (0.6 g, 55%), mp 179—180 °C. IR: 3480 and 3360 (OH), 1810 and 1785 (C=O), and 1570 cm^{-1}.

Recrystallization of the latter from ethyl acetate afforded XIV (0.065 g, 6%), mp 230 °C (lit,[12] mp 230 °C).

Reaction of XI with Phosphorus Tribromide. To a solution of XI (0.1 g) in carbon tetrachloride (5 ml) was added phosphorus tribromide (0.12 ml) at 0 °C, and the mixture was then stirred at 0 °C for 15 min. Recrystallization from acetonitrile of the crude crystals which separated out afforded IV (0.04 g, 43%) as green prisms, mp 206—207 °C.

Oxidation of XI with Hydrogen Peroxide. A mixture of XI (0.15 g), 30% aqueous hydrogen peroxide (3 ml), and acetic acid (60 ml) was stirred at room temperature for 3 days. The crude crystals which separated out by the addition of water to the reaction mixture were washed with water. Recrystallization from methanol afforded XII (0.08 g, 51%) as colorless prisms, mp 205—206 °C. IR: 3480 and 3320 (OH), 1835 and 1770 (C=O), and 1590 cm^{-1} (C=C); λ_{max}^{EtOH}: 212 (24500), 255 (6700), and 285 sh nm (ε, 3500); NMR: 2.5—3.0 (m, Ph, 20 H) and 4.80 τ (s, OH, 2H).

Found: C, 78.06; H, 4.69%. Calcd for $C_{30}H_{22}O_5$: C, 77.91; H, 4.80%.

Reaction of IV with Bromine in Methanol. A solution of IV (0.11 g) and bromine (0.22 g) in methanol (10 ml) was heated under reflux for 45 min. The crude crystals formed by cooling the reaction mixture were recrystallized from acetone to afford XVII (0.06 g, 45%) as colorless prisms, mp 190—191 °C. IR: 1740 and 1690 (C=O), 1620 (C=C), 1235 (ester), and 1015 cm^{-1} (ether); $\lambda_{max}^{CHCl_3}$: 266 (8000) and 275 sh nm (ε, 7500); NMR: 2.6—2.9 (m, Ph, 20 H) and 6.20 τ (s, CO_2CH_3, 3H); MS: m/e 538 (M^+).

Found: C, 69.29; H, 4.15%. Calcd for $C_{31}H_{23}O_4Br$: C, 69.01; H, 4.26%.

Hydrolysis and Decarbonylation of XVII. A mixture of XVII (0.22 g), potassium hydroxide (0.42 g), tetrahydrofuran (8 ml) and acetone (7 ml) was heated under reflux for 7 hr. To the residue remaining after evaporation of the solvent of the reaction mixture to dryness was added dil hydrochloric acid and the crystalline solid obtained was washed with water. Recrystallization of the dried crude product from tetrahydrofuran–cyclohexane afforded XVIII (0.12 g, 61%), mp 278—279 °C. IR: 3000—2500 (CO_2H), 1690 (C=O), and 1600 cm^{-1} (C=C); λ_{max}^{EtOH} 238 sh (12400), 258 sh (5200), 264 sh (3500) and 268 sh nm (ε, 2400).

Found: C, 70.35; H, 3.94%. Calcd for $C_{29}H_{21}O_3Br$: C, 70.02; H, 4.22%.

Decarboxylation of XVIII. A mixture of XVIII (0.15 g), quinoline (5 ml), and a catalytic amount of copper chromite was heated under reflux for 4 hr. The cooled reaction mixture was diluted with ether (100 ml), and the ether solution was washed successively with dil hydrochloric acid and water, and dried over anhydrous sodium sulfate. The crude crystals obtained by evaporation of ether were recrystallized from methanol to afford XIX (0.08 g, 59%), mp 175 °C (lit,[7] mp 175 °C).

Reaction of I with o-Phenylenediamine. A mixture of I (1.00 g) and *o*-phenylenediamine (0.26 g) was allowed to remain at 130 °C for 40 min. The crude crystals obtained by the addition of methanol (1 ml) to the cooled reaction mixture were fractionated into two crystalline forms, pale yellow and yellow, by fractional recrystallization from tetrahydrofuran. Recrystallization of the former, relatively insoluble in tetrahydrofuran, from tetrahydrofuran–chloroform afforded XXV (0.22 g, 15%) as pale yellow prisms, mp 204—207 °C. IR: 3300 (NH) and 1610 cm^{-1} (C=N); $\lambda_{max}^{CHCl_3}$: 304 nm (ε, 5800); MS: *m/e* (rel intensity) 594 (4), 486 (23), 319 (9), 236 (18), 167 (100), 152 (8), and 108 (11).

Found: C, 84.75; H, 5.72; N, 9.39%. Calcd for

12) F. Toda and K. Akagi, *Tetrahedron*, **27**, 2801 (1971).

$C_{42}H_{34}N_4$: C, 84.85; H, 5.72; N, 9.43%.

Recrystallization of the latter, relatively soluble in tetrahydrofuran, from acetone afforded XXVI (0.2 g, 17%), mp 172—173 °C. IR: 1640 cm^{-1} (C=N); $\lambda_{max}^{CHCl_3}$: 275 (16800) and 385 nm (ε, 19000); NMR: 1.8—3.1 (m, Ph, 24H), 4.62 (d, J=2.5 Hz, H_B, 1H), and 5.85 τ (d, J=2.5 Hz, H_A, 1H); MS: *m/e* (rel intensity) 486 (34), 319 (10), 167 (100), and 152 (7).

Found: C, 88.67; H, 5.28%. Calcd for $C_{36}H_{26}N_2$: C, 88.86; H, 5.38%.

Reaction of XXV with Hydrochloric Acid. A suspension of XXV (0.1 g) in methanol (5 ml)–concd hydrochloric acid (0.6 ml) was stirred at room temperature for 30 min. The crude product obtained by concentration of the reaction mixture to dryness was suspended in water and then collected by filtration. The recrystallization of the dried crude product from acetone afforded XXVI (0.07 g, 85%), mp 172—173 °C. IR spectral data were identical with those of an authentic sample. Treatment of XXV (0.1 g) in methanol-d (2 ml)–concd deuteriochloric acid (0.6 ml) by the same method as that employed above, afforded XXVI-d (0.07 g, 85%). NMR: 1.8—3.1 (m, Ph, 24H) and 5.87 τ (s, H_A, 1H).

BULLETIN OF THE CHEMICAL SOCIETY OF JAPAN, VOL. 46, 1737—1740 (1973)

Methylene Analogs of Cyclobutenedione. VII.[1] Photolysis of 2,3-Bis(diphenylmethylene)cyclobutanone and Its Derivatives

Fumio TODA, Hisao NAKAOKA, Kentaro YUWANE, and Eishiro TODO

Department of Industrial Chemistry, Faculty of Engineering, Ehime University, Matsuyama 790

(Received July 29, 1972)

Photolysis of 2,2-dimethoxy-3,4-bis(diphenylmethylene)cyclobutanone (I), 2,3-bis(diphenylmethylene)cyclobutanone (XIV), and 3,4-bis(diphenylmethylene)cyclobutanedione (XXV) in methanol was investigated. Photolysis of I afforded tricyclic compound(II) and dimethyl cyclobutanedicarboxylate (III) in 48 and 35% yields, respectively. Photolysis of XIV and XXV afforded the dihydronaphthalene derivatives (XIX) (88% yield) and XXIV (72% yield), respectively. The mechanisms of these reactions were also studied.

Two types of reaction for the photolysis of the four-membered ketones in alcohol, *viz.*, photo ring-expansion of cyclobutanone to tetrahydrofuran derivative *via* oxacarbene intermediate (1)[2-8] and the photo ring-cleavage of cyclobutenone to ester *via* ketene intermediate (2),[9-11] have been reported. However, no

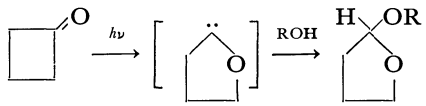

(1)

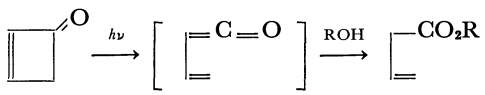

(2)

photolysis of 2,3-dimethylenecyclobutanone derivative has yet been reported, although 2,4-dimethylenecyclobutanone has been shown to be inert to the photolysis in alcohol.[8] We have studied the photolysis of 2,3-bis(diphenylmethylene)cyclobutanone derivatives, I, XIV, and XXV in methanol, in order to confirm which type of reaction is appropriate. The photochemical reaction between the two over-crowded diphenylmethylene moieties of the cyclobutanones is also of interest.

Photolysis of I[12] in methanol under nitrogen at room temperature afforded methanol-insoluble colorless needles ($C_{32}H_{26}O_3$) and methanol-soluble colorless prisms ($C_{32}H_{28}O_4$). The former was identified to be II by means of spectral data and chemical reactions. The IR spectrum of II showed all the three oxygen atoms to be of ether linkage. The NMR spectrum showed the presence of the two magnetically nonequivalent methoxy group, in addition to one quite deshielded (3.95 τ) methine proton, and nineteen aromatic protons. However, the UV spectrum of II in ethanol, 294 nm (ε, 7900), differed from that of 1,4-diphenylbuta-1,3-diene in benzene, 334 nm (ε,

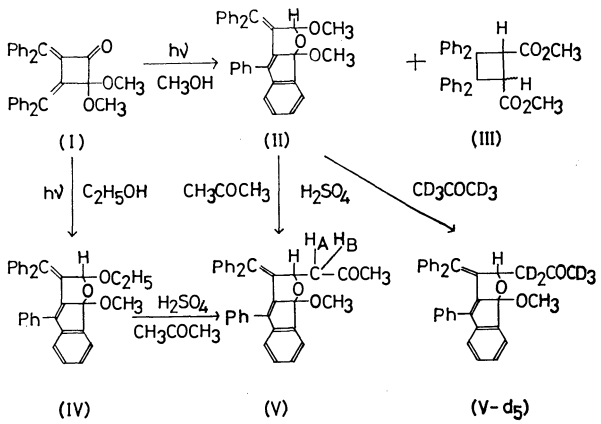

Scheme 1.

1) Part VI: F. Toda and N. Ooi, This Bulletin, **46**, 1733 (1973).
2) H. U. Hostettler, *Helv. Chim. Acta*, **49**, 2417 (1966).
3) G. Quinkert, G. Cimbollek, and G. Buhr, *Tetrahedron Lett.*, **1966**, 4573.
4) R. F. C. Brown and R. K. Solly, *ibid.*, **1966**, 169.
5) H. A. Staab and J. Ipaktschi, *ibid.*, **1966**, 583.
6) H. A. Staab and J. Ipaktschi, *Chem. Ber.*, **101**, 1457 (1968).
7) J. G. Pacifici and C. Diebert, *J. Amer. Chem. Soc.*, **91**, 4595 (1969).
8) D. R. Morton, E. Lee-Ruff, R. M. Southam, and N. J. Turro, *ibid.*, **92**, 4349 (1970).
9) J. D. Roberts and F. B. Mallory, *ibid.*, **83**, 393 (1961).
10) J. E. Baldwin and M. C. McDaniel, *ibid.*, **89**, 1537 (1967).
11) J. E. Baldwin and M. C. McDaniel, *ibid.*, **90**, 6118 (1968).
12) F. Toda and K. Akagi, *Tetrahedron*, **27**, 2801 (1971).

40000).[13] The difference is attributable to the non-coplanarity of II, since studies on a molecular model of II show that the indene and the diphenylmethylene chromophores are prevented from being arranged on a coplane.

In order to distinguish the two methoxy groups of II, II was allowed to react with acetone in the presence of concd sulfuric acid to afford the substitution reaction product (V). The NMR spectrum of V showed the methine proton signal as a quartet centered at 4.12 τ, and the methylene proton signal at 7.6—7.9 τ as a multiplet, in addition to the methoxy methyl and the acetyl methyl proton signals as a singlet at 6.99 and 8.10 τ, respectively. The multiplicity of the methine and methylene proton signals is probably due to the spin-spin coupling between the methine proton and the two magnetically nonequivalent methylene protons (H_A and H_B). The nonequivalency of the two methylene protons is probably due to an asymmetric effect. Direct evidence for the coupling was obtained by using V-d_5 which was prepared by the reaction of II and acetone-d_6. In the NMR spectrum of V-d_5, a methine proton signal appeared at 4.20 τ as a singlet in addition to a singlet signal of methoxy at 7.02 τ.

In order to determine the origin of the two methoxy groups of II, the photolysis of I in ethanol was carried out, and the ring-expanded product (IV) was obtained. The structure of IV was identified by its reaction with acetone to afford V. The magnetic nonequivalency of the two methylene protons of the ethoxy of IV is also probably due to an asymmetric effect. The production of IV in the above photolysis shows that the methoxy on the bridge-head and the other methoxy of II were derived from I and methanol, respectively. This was further supported by the photolysis of I-d_6 in methanol to afford II-d_3 (Scheme 2). The acid-catalyzed reaction of II-d_3 with acetone afforded V-d_3. The structures of II-d_3 and V-d_3 were determined by means of the spectral data.

The photolysis of I to afford II corresponds to the type of reaction (1). The reaction might then proceed *via* an oxacarbene intermediate. Depending on whether or not the dihydrofuran-ring formation precedes the indene-ring formation, two reaction paths (a) and (b), and thereafter the oxacarbene intermediates, VI and XI, are applicable (Scheme 2). However, we could obtain no further evidence to distinguish the path.

The structure of the methanol-soluble compound accompanying II in the photolysis of I was identified by spectral data to be the cyclobutane derivative (III). The NMR data indicating that all the aromatic protons appear at a relatively higher field, 2.7—3.6 τ, agree with the structure of III, in which four phenyls are shielded each other. However, the geometry of the two carbomethoxy group could not be determined. The MS spectrum of III showed a fragment ion peak at *m/e* 238 which is just half of the mass of its parent ion. The data show that III undergoes ring-cleavage easily in the manner of (x) but not (y) (Scheme 2).

Formation of III can be interpreted by the photo ring-cleavage of XII initially produced by the photo ring-closure of I, to afford the ketene intermediate (XIII) and finally III. This type of photo reaction is analogous to (2). The conversion of XIII into III would proceed by the addition of methanol and water to the ketene and dimethoxyethylene moieties, respectively, followed by the elimination of methanol. Since II and III were obtained in 35 and 48% yields, respectively, when the photolysis of I was carried out in 95%

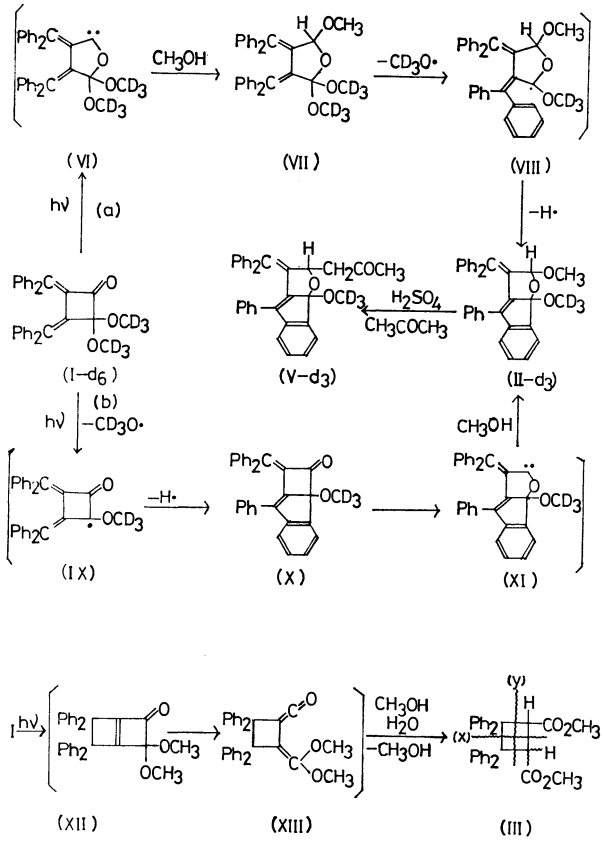

Scheme 2.

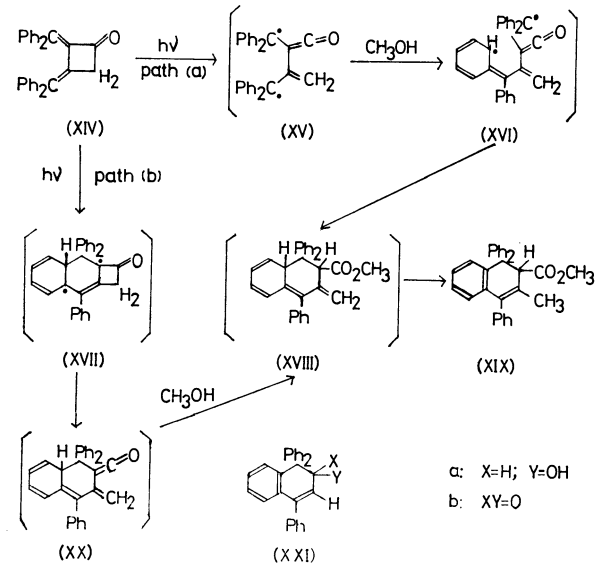

Scheme 3.

13) K. W. Hausser, R. Kuhn, and A. Smakula, *Z. Phys. Chem.*, **B29**, 384 (1935).

methanol, it is clear that water is essential for the formation of III.

In order to clarify the special role of the methoxy group of I in its photolysis, the photolysis of XIV[12] was carried out, under the same conditions as those employed for I, and afforded the dihydronaphthalene derivative (XIX) as the sole product (85% yield). Its structure was identified by means of spectral data. The UV spectrum of XIX, 285 nm (ε, 6900), was comparable to that of the analogous compound (XXIa),[14] 288 nm (ε, 6000).

Two possible reaction paths (a) and (b) can be written for the formation of XIX (Scheme 3). The choice of path depends on whether the ring-cleavage of the cyclobutanone-ring or the reaction between the two diphenylmethylene moieties occurs initially.

Although it is difficult to define the real mechanistic pathway, it is clear that the photo reaction of XIV proceeds *via* a pathway analogous to (2). From a comparison of the photolysis of I to afford II with that of XIV to afford XIX, the special role of the methoxy group of I in its photolysis is clear. (b) is therefore the more plausible path of the photolysis of I to afford II (Scheme 2).

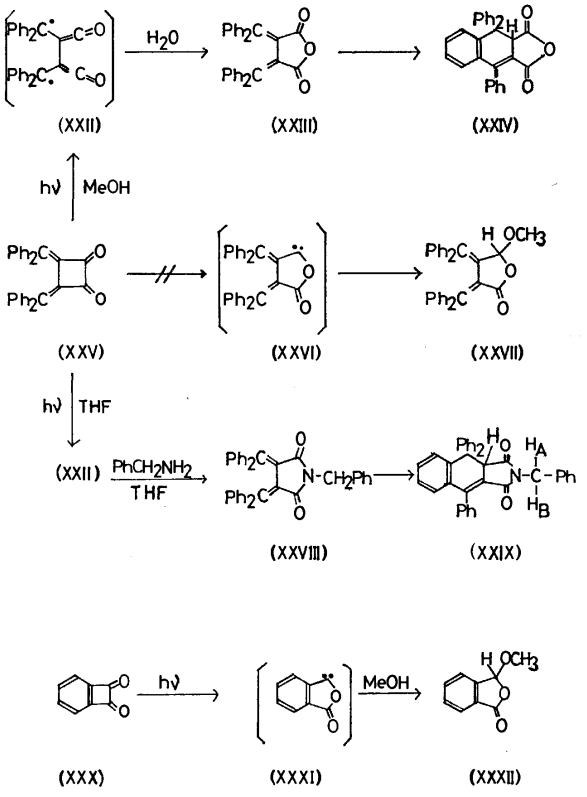

Scheme 4.

The photolysis of the diketone (XXV)[12] is of interest as regards the photolysis of benzocyclobutenedione (XXX) to afford the benzolactone (XXXII), the product of the type of reaction (1). The photolysis of XXV in 99% methanol afforded the acid anhydride (XXIV) in a 72% yield, but no detectable amount of lactone (XXVII). The structure of XXIV was identified by means of spectral data. The UV spectral bands of XXIV in chloroform, 242 (14000) and 315 nm (ε, 14000), were comparable to those of XXIb in ethanol, 240 sh (8100) and 316 nm (ε, 8900).[14] Since the photolysis of XXIII[12] under the same conditions as employed for XXV afforded XXIV in a 82% yield, XXIII is a probable intermediate of the photolysis of XXV. A possible precursor of XXIII is the bisketene (XXII) which is produced by ring-cleavage of XXV of type (2). The reaction of the bisketene (XXII) with water to afford the acid anhydride (XXIII) is reasonable, since the reaction of XXV with water in the presence of bromine to afford XXIII *via* XXII has been postulated,[15] and the photochemical reaction of XXV with benzylamine in dry tetrahydrofuran afforded XXIX *via* XXVIII. The intermediacy of XXVIII in the latter photolysis was defined by a separate photolysis of XXVIII prepared according to a modified procedure to afford XXIX.

The structure of XXIX was identified by means of spectral data. The magnetic nonequivalence of the two methylene protons of XXIX (H_A and H_B) gives further structural evidence for XXIX which has asymmetric center.

Experimental

All the melting points were uncorrected. Photolysis was carried out at room temperature under nitrogen atmosphere, with a 100-W high-pressure mercury lamp (Riko Kagaku Sangyo Co.). IR, UV, and NMR spectra were measured in Nujol mull, EtOH, and $CDCl_3$ respectively, unless otherwise stated. Mass spectra were measured with an ionization energy of 70 eV.

Photolysis of I in Methanol. A suspension of finely-powdered I (1.09 g) in 99% methanol (100 ml) was irradiated under stirring for 17 hr. The crude product precipitated was collected by filtration, and recrystallized from ethyl acetate to afford II as colorless needles; 0.52 g (48%); mp 180—181 °C. IR: 1120, 1010, and 990 cm^{-1} (C-O-C); λ_{max}: 237 (20200) and 294 nm (ε, 7900); NMR: 1.85—2.00 (m, Ph, 1H), 2.2—2.9 (m, Ph, 18 H), 3.95 (s, CH, 1H), 6.85 (s, OCH_3, 3H), and 7.03 τ (s, OCH_3, 3H); MS: *m/e* (rel intensity) 458.1917 (M^+ 458.1882, 2), 427 (40), 426 (100), 411 (90), 381 (15), 367 (20), and 278 (20).

Found: C, 84.01; H, 5.65%. Calcd for $C_{32}H_{26}O_3$: C, 83.82; H, 5.72%.

Concentration of the mother liquor remaining after the separation of crude II by filtration afforded crude crystals. Their recrystallization from ethyl acetate afforded III as colorless prisms; 0.38 g (35%); mp 172—174 °C. IR: 1740 and 1725 (C=O), and 1230 cm^{-1} (ester); λ_{max}: 262 (1100), 269 (1100), and 275 nm (ε, 700); NMR: 2.7—3.6 (m, Ph, 20 H), 5.03 (s, CH, 2H), and 6.63 τ (s, CO_2CH_3, 6H); MS: *m/e* (rel intensity) 238.0982 ($M^+/2$ 238.0992, 100), 237 (22), 207 (53), 179 (30), and 178 (25).

Found: C, 80.71; H, 5.73%; mol wt (benzene), 471. Calcd for $C_{32}H_{28}O_4$: C, 80.64; H, 5.92%; mol wt, 476.

When the photolysis of I was carried out in 95% methanol, II and III were obtained in 35 and 48% yields, respectively.

Photolysis of I in Ethanol. A suspension of finely-powdered I (1.0 g) in 99% ethanol (100 ml) was irradiated

14) F. Toda and K. Akagi, *Tetrahedron*, **27**, 3795 (1969).

15) F. Toda and J. Fujita, This Bulletin, **45**, 1928 (1972).

under stirring for 17 hr. The crude product precipitated was recrystallized from ethyl acetate to afford IV as colorless needles 0.68 g (68%); mp 176—177 °C. IR: 1110, 1010, and 995 cm^{-1} (C–O–C); NMR: 1.95—2.00 (m, Ph, 1H), 2.2—2.9 (m, Ph, 18H), 3.86 (s, CH, 1H), 6.2—6.9 (m, OCH_2CH_3, 2H), and 7.02 (s, OCH_3, 3H), and 9.21 τ (t, OCH_2CH_3, 3H).

Found: C, 84.10; H, 5.83%. Calcd for $C_{33}H_{28}O_3$: C, 83.87; H, 5.97%.

Photolysis of I-d_6 in Methanol. A suspension of finely-powdered I-d_6 (0.45 g), prepared from XXV and methanol-d_4 in 99% methanol (50 ml) was irradiated under stirring for 17 hr.[12] The crude product precipitated was recrystallized from ethyl acetate to afford I-d_3; 0.2 g (45%). IR: 2080 cm^{-1} (OCD_3) and 1110, 1005, and 990 cm^{-1} (C–O–C); NMR: 1.85—2.00 (m, Ph, 1H), 2.2—2.9 (m, Ph, 18H), 3.92 (s, CH, 1H), and 6.82 τ (s, OCH_3, 3H).

Acid-catalyzed Reactions of II, IV, and I-d_3 with Acetone. A solution of II (0.2 g) and three drops of concd sulfuric acid in acetone (10 ml) was heated under reflux for 20 min. The crude crystals obtained by the evaporation of the solvent to dryness were washed with water, dried and recrystallized from ethyl acetate to afford V as colorless needles; 0.15 g (71%); mp 243—244 °C. IR: 1720 (C=O), and 1060 and 995 cm^{-1}(C–O–C); λ_{max} ($CHCl_3$): 249 (28100) and 297 nm (ε, 10200); NMR: 1.8—2.0 (m, Ph, 1H), 2.2—2.9 (m, Ph, 18H), 4.12 (q, CH, 1H), 6.99 (s, OCH_3, 3H), 7.6—7.9 (m, CH_2, 2H), and 8.10 τ (s, $COCH_3$, 3H).

Found: C, 84.27; H, 5.54%. Calcd for $C_{34}H_{28}O_3$: C, 84.27; H, 5.82%.

The same treatment of IV with acetone as for II afforded V in a 65% yield.

The same treatment of II with acetone-d_6 as for II afforded V-d_5 in a 70% yield. IR: 1715 (C=O) and 1065 cm^{-1} (C–O–C); NMR: 1.85—2.05 (m, Ph, 1H), 2.3—3.0 (m, Ph, 18 H), 4.20 (s, CH, 1H), and 7.02 τ (s, OCH_3, 3H).

The same treatment of II-d_3 with acetone as for II afforded V-d_3 in a 50% yield. IR: 1720 (C=O) and 1060 cm^{-1} (C–O–C); NMR: 1.8—2.0 (m, Ph, 1H), 2.2—2.9 (m, Ph, 18H), 4.10 (q, CH, 1H), 7.5—7.8 (m, CH_2, 2H), and 8.11 τ (s, $COCH_3$, 3H).

Photolysis of XIV in Methanol. A suspension of finely-powdered XIV (1.03 g) in 99% methanol (100 ml) was irradiated under stirring for 17 hr. The crude crystals obtained by the evaporation of the solvent to dryness were recrystallized from ethyl acetate to afford XIX as colorless needles; 0.91 g (88%); mp 146—147 °C. IR: 1700 and 1720 (C=O), and 1225 cm^{-1} (ester); λ_{max}: 228 (18600) and 285 nm (ε, 6900); NMR: 2.5—3.1 (m, Ph, 18H), 3.25—3.45 (m, Ph, 1H), 6.03 (s, CH, 1H), 6.62 (s, CO_2CH_3, 3H), and 8.26 τ (s, CH_3 3H); MS: *m/e* (rel intensity) 430.1938 (M^+, 430.1932, 100), 398 (7), 371 (57), 356 (18), 293 (32), 279 (14), 278 (14), and 215 (13).

Found: C, 86.33; H, 5.88%. Calcd for $C_{31}H_{26}O_2$: C, 86.48; H, 6.09%.

Photolysis of XXV in Methanol. A suspension of finely-powdered XXV (1.0 g) in 99% methanol (100 ml) was irradiated under stirring for 17 hr. The crude crystals remaining after the evaporation of solvent were recrystallized from ethyl acetate to afford XXIV as colorless prisms; 0.73 g (72%); mp 225—226 °C. IR: 1760 and 1820 cm^{-1} (C=O); λ_{max}($CHCl_3$): 315 (12200) and 340 sh nm (ε, 7400); NMR: 2.5—3.2 (m, Ph, 18H), 3.2—3.4 (m, Ph, 1H), and 4.91 τ (s, CH, 1H); MS: *m/e* (rel intensity) 428.1437 (M^+ 428.1412, 100), 384 (98), 355 (56), 350 (86), 330 (98), 307 (75), 279 (98), and 278 (98).

Found: C, 84.36; H, 4.81%. Calcd for $C_{30}H_{20}O_3$: C, 84.09; H, 4.71%.

Photolysis of XXIII in Methanol. A suspension of finely-powdered XXIII (1.0 g) in 99% methanol (100 ml) was irradiated under stirring for 2 hr. The crude crystals remaining after the evaporation of solvent to dryness were recrystallized from ethyl acetate to afford XXIV; 0.82 g (82%). The IR spectral data were identical with those of an authentic sample prepared by the photolysis of XXV in methanol.

Photo Reaction of XXV with Benzylamine in Tetrahydrofuran. A solution of XXV (1.26 g) and benzylamine (3.2 g) in dry tetrahydrofuran (150 ml) was irradiated under stirring for 17hr. The residue remaining after the evaporation of the solvent was taken up in ether. The ether solution was washed successively with dil hydrochloric acid and water, and dried over sodium sulfate. The crude product obtained by the evaporation of solvent was chromatographed on alumina with carbon tetrachloride as a solvent. The elution with benzene afforded XXIX as colorless plates; 0.18 g (11%); mp 221—222.5 °C. IR: 1760 and 1690 (C=O), 1630 (C=C), and 1430 cm^{-1} (CH_2); λ_{max}($CHCl_3$): 310 (16800) and 340 sh nm (ε, 8800). NMR: 2.9—3.0 (m, Ph, 24H), 5.22 (s, CH, 1H), and 5.41 τ (q, CH_2, 2H); MS: *m/e* (rel intensity) 517.2015 (M^+ 517.2041, 100), 440 (28), 439 (55), 384 (17), 356 (65), and 307 (38).

Found: C, 85.54; H, 5.27%. Calcd for $C_{37}H_{27}O_2N$: C, 85.85; H, 5.26%.

Preparation of XXVIII. A mixture of XXV (3.9 g), bromine (2 g), benzylamine (10 g) and dry carbon tetrachloride (300 ml) was stirred at room temperature for 30 min. After removal of the amine salt formed as a result of filtration, the filtrate was evaporated to dryness to afford crude crystals. Recrystallization of the crude crystals from acetone afforded XXVIII as yellow plates; 2.2 g (45%); mp 227—228 °C. IR: 1750 and 1690 (C=O), and 1430 cm^{-1} (CH_2); λ_{max}: 252 (29000), 309 (21800), and 400 nm (ε, 11100). NMR: 2.4—3.2(m, Ph, 25H) and 5.31 τ (s, CH_2, 2H); MS: *m/e* (rel intensity) 517.2059 (M^+ 517.2041, 81), 384 (100), 356 (36), and 307 (36).

Found: C, 85.65; H, 5.32%. Calcd for $C_{37}H_{27}O_2N$: C, 85.85; H, 5.26%.

Photolysis of XXVIII in Tetrahydrofuran. A solution of XXVIII (1.12 g) in dry tetrahydrofuran (100 ml) was irradiated for 7 hr. The crude crystals obtained by the evaporation of solvent was recrystallized from ethyl acetate to afford XXIX as colorless plates; 0.50 g (45%). The IR spectral data were identical with those of an authentic sample prepared by the photo reaction of XXV with benzylamine.

Oxygen-18 Scrambling Reaction of Aroyl Alkyl Carbonates

Shigeru Oae, Yuzuru Uchida,[1] Ken Fujimori, and Seizi Kozuka

Department of Applied Chemistry, Faculty of Engineering, Osaka City University, Sugimoto-cho, Sumiyoshi-ku, Osaka 558

(Received August 9, 1972)

Specifically ^{18}O-labeled *p*-substituted benzoyl cyclohexyl carbonates (**1**) were prepared and heated at 45, 70 and 75 °C, and novel stepwise oxygen scrambling was found to take place in **1**. On being heated at 45 °C, the carbonic carbonyl oxygen atom and the oxygen atom sandwiched between the two carbonyl carbon atoms of **1** were found to scramble. The ^{18}O-scrambling among the above two and carboxylic carbonyl oxygen atoms of **1** was found to take place at 70 or 75 °C. A good first order kinetic dependence was observed for the first step of the scrambling at 45 °C but no substituent effect. An intramolecular mechanism involving two steps of equilibration is proposed.

We reported on the basis of ^{18}O-tracer studies of the decomposition of several diacyl peroxides[2] that the carboxy-inversion is the major pathway for the decomposition of *sec*- and *tert*-alkylformyl peroxides, while ^{18}O-scrambling is observed not only in the original peroxide but also in the intermediate of the decomposition, *i.e.*, acyl alkyl carbonates. We extended our ^{18}O-tracer study to the ^{18}O-scrambling of the aroyl alkyl carbonates,[3] specifically ^{18}O-labeled benzoyl l-apocamphyl carbonate being employed, and an intramolecular oxygen scrambling reaction was found. Although a zwitterion mechanism (scheme 1) has been suggested for the ^{18}O-scrambling, another intramolecular mechanism, *viz.*, an ion pair pathway is possible (scheme 2).[3] Kinetic determinations of the ^{18}O-scrambling with ^{18}O-labled substituted benzoyl l-apocamphyl carbonates are considered to be very helpful for making choice of the two mechanisms. We have studied the reactions of *p*-substituted benzoyl alkyl carbonates having a cyclohexyl group as the alkyl moiety instead of the l-apocamphyl group, and found an interesting stepwise scrambling of ^{18}O in these compounds. A discussion on detailed mechanism of the ^{18}O-scrambling reaction of the aroyl alkyl carbonates is given.

Zwitterion mechanism

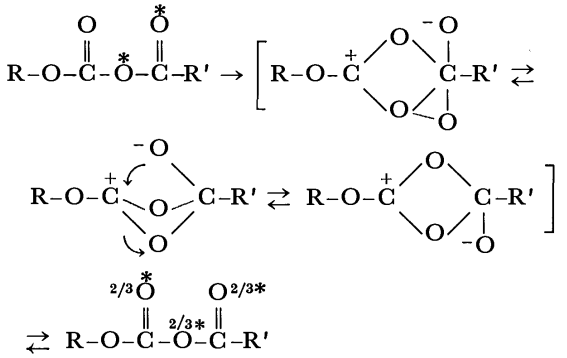

Scheme 1.

Ion pair mechanism

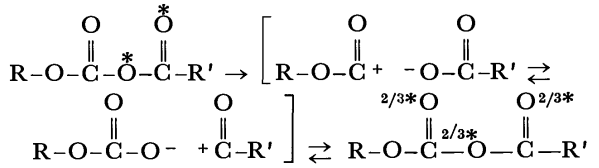

Scheme 2.

Results and Discussion

p-Substituted benzoyl cyclohexyl carbonates (**1**) specifically ^{18}O-labeled in γ- and δ-oxygen atoms were prepared as usual by the reaction of cyclohexyl chloroformate with the ^{18}O-labeled *p*-substituted benzoic acids in the presence of triethylamine in ethereal solution as in the following.[4]

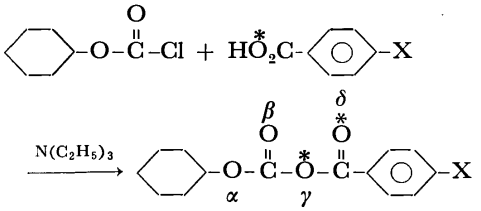

(1)

1a X=CN, **b** X=H, **c** X=CH_3

The aroyl carbonates (**1**) thus prepared were dissolved in CCl_4 (0.04 M) and heated at 45 °C for 24 hr, at 70 °C for 12 hr or at 75 °C for 24 hr. The aroyl alkyl carbonate was recovered quantitatively without decomposition. ^{18}O-Distribution in the recovered carbonate (**1**) was analyzed according to the following cleavage reactions.[3,5]

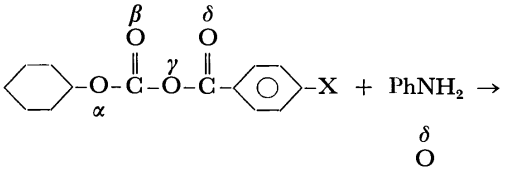

(2)

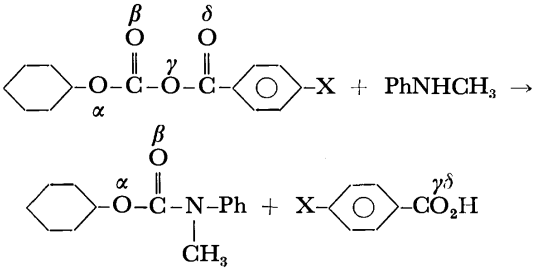

(3)

1) Present address: Department of Applied Chemistry, Osaka Institute of Technology, Asahi-ku, Osaka, Japan.

2) a) T. Kashiwagi, S. Kozuka, and S. Oae, *Tetrahedron*, **26**, 3619 (1970). b) S. Oae, K. Fujimori, and Y. Uchida, *ibid.*, **28**, 5321 (1972).

3) S. Oae, K. Fujimori, and S. Kozuka, *ibid.*, **28**, 5327 (1972).

4) a) C. J. Michejda and D. S. Tarbell, *J. Amer. Chem. Soc.*, **84**, 4113 (1962). b) C. J. Michejda and D. S. Tarbell, *J. Org. Chem.*, **29**, 1168 (1964).

5) N. A. Leister and D. S. Tarbell, *J. Org. Chem.*, **23**, 1152 (1958).

Table 1. ^{18}O-Distribution in the aroyl alkyl carbonates

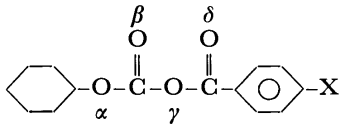

Aroyl alkyl carbonate	From starting material			^{18}O-Content (Excess atom %)[a] From recovered meterial			^{18}O-Distribution in oxygen atom (%)[b]			Reaction conditions	
	Carbamate	Acid	Anilide	Carbamate	Acid	Anilide	β[c]	γ[d]	δ[e]	Temp (°C)	Time (hr)
1a	0.00	0.84	0.81[f]	0.18	0.66	0.81[f]	21	29	50	45	24
1b	—	1.39	1.38	0.33	1.07	1.34	24	28	49	45	24
1c	0.00	1.04	1.02	0.24	0.80	0.99	23	27	49	45	25
1a	0.00	0.94	0.92	0.29	0.66	0.73	31	31	40	70	12
1b	—	1.39	1.38	0.44	0.97	1.03	32	32	37	70	12
1c	0.00	1.04	1.02	0.34	0.72	0.76	33	32	37	70	12
1a	—	0.87	0.85	0.29	0.59	0.57[g]	33	34	34	75	24

a) Estimated error ± 0.005 (excess atom %). b) Based on the total amount of ^{18}O. c) Calculated from the ^{18}O-content of the carbamate. d) Estimated from the ^{18}O-content of the acid and the anilide. e) Calculated from the ^{18}O-content of the anilide. f) Carbon dioxide obtained from reaction (2) contained 0.46 excess atom % of ^{18}O. g) Carbon dioxide obtained from the reaction with aniline contained 0.57 excess atom % of ^{18}O.

The ^{18}O-analytical data and percentages of ^{18}O-distributions are summarized in Table 1. There was no ^{18}O-scrambling during the preparation of the aroyl alkyl carbonates and the α-oxygen atom remained without scrambling even after being heated at 75 °C for 24 hr. We see that nearly all the original ^{18}O-label was retained in the δ-oxygen atom after heating at 45 °C for 24 hr, while scrambling was found between β- and γ-oxygen atoms. In addition, the δ-oxygen atom participates in the oxygen scrambling reaction on heating at 70 °C for 12 hr. These results suggest a stepwise ^{18}O-scrambling for the carbonates.

An intermolecular chain process (4)—(7) for the mechanism of ^{18}O-scrambling was ruled out on the basis of the ^{18}O-content of benzoic anhydride obtained from the reaction of ^{18}O-labeled benzoyl 1-apocamphyl carbonate with unlabeled benzoic acid.[3]

Intermolecular mechanism

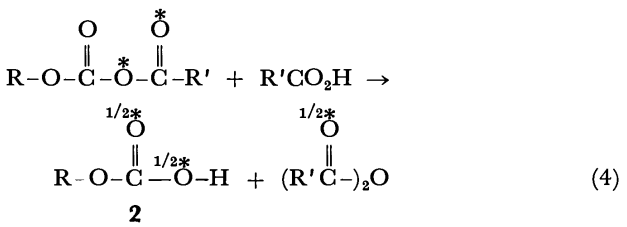

(4)

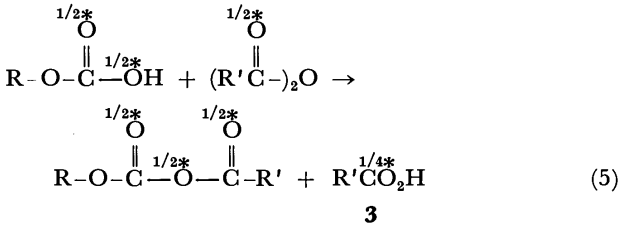

(5)

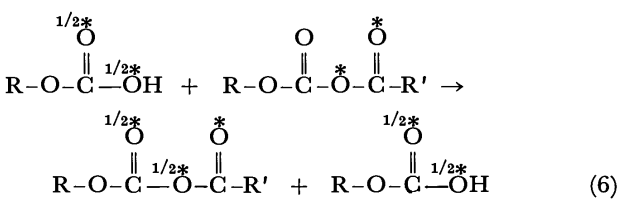

(6)

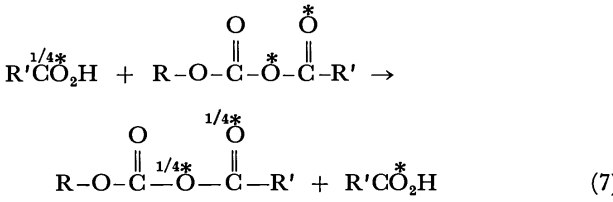

(7)

The intermolecular mechanism can be ruled out also in the present studies involving the following crossover experiments. If the reaction proceeds with the alkyl carbonic acid (**2**) as the chain carrier (5—6), ^{18}O would be incorporated into the recovered **1a** by the crossover experiment of unlabeled **1a** and labeled **1b**. On the other hand, if the carboxylic acid (**3**) is the chain carrier as shown in (4) and (7), labeled *p*-toluic acid would be expected in the reaction of labeled **1c** with unlabeled *p*-toluic acid. An equimolar amount of unlabeled **1a** was heated with ^{18}O-labeled **1b** in the γ- and δ-oxygen atoms at 45 °C for 48 hr in CCl_4. Although a complete ^{18}O-scrambling of β- and γ-oxygen atoms was found, no excess of ^{18}O was found in the *p*-cyanobenzoic acid obtained by the treatment of the recovered **1a** with *N*-methylaniline (3). The reaction of **1c** with an equimolar amount of unlabeled *p*-toluic acid was carried out at 70 °C for 12 hr in CCl_4. *p*-Toluic acid was recovered quantitatively, no excess ^{18}O being found in the recovered acid. The results show that the mode of oxygen scrambling reaction of aroyl alkyl carbonates is quite different from that of carboxylic anhydrides.[6] Another possible ^{18}O-scrambling mechanism of the β- and γ-oxygen atoms is one involving ionic dissociation in solvent cage in view of the stepwise nature of the reaction as shown below.

If this is the case, a large negative ρ value would be expected in the kinetics of the ^{18}O-scrambling for substituted benzoyl derivatives.

The rate of scrambling between β- and γ-oxygen atoms at 45 °C can be obtained by measuring the decreasing amount of ^{18}O in the carboxylic acids ob-

6) L. Ponticorvo and D. Rittenberg, *J. Amer. Chem. Soc.*, **76**, 1705 (1954).

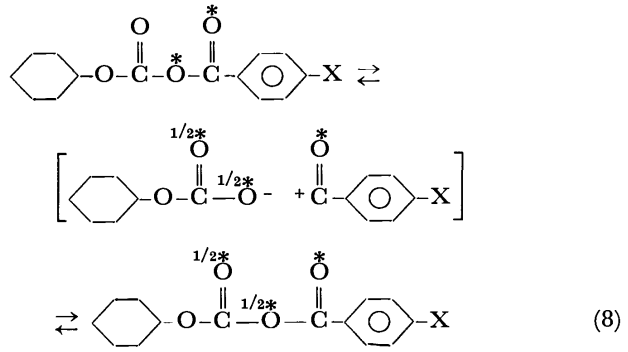

(8)

tained by treatment of the recovered carbonate with *N*-methylaniline (3). Good first-order rate constants of the ^{18}O-scrambling of β- and γ-oxygen atoms were observed: $2.42\pm0.05\times10^{-5}$ sec^{-1} (**1a**); $2.85\pm0.28\times10^{-5}$ sec^{-1} (**1b**); $2.74\pm0.02\times10^{-5}$ sec^{-1} (**1c**). Since there is no substituent effect, the ion pair mechanism (8) can be ruled out. A mechanism involving homolytic cleavage of the C–O bond is also unlikely since the aroyl alkyl carbonates did not decompose at all under the reaction conditions.

The only conceivable intramolecular mechanism to rationalize the observations is an intramolecular pathway involving nucleophilic attack of carbonic oxygen (β) on the carboxylic carbon as shown below.[3]

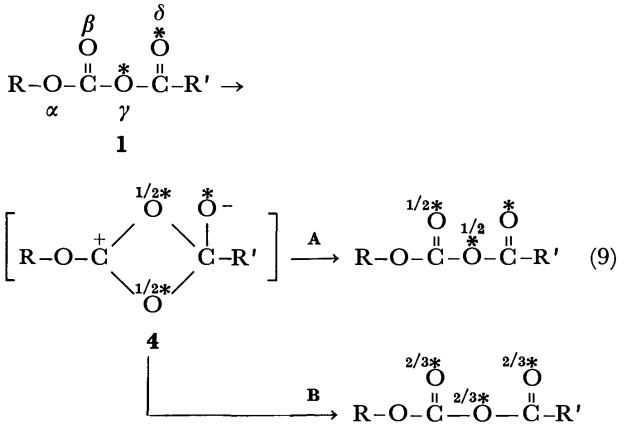

1

4

According to this mechanism, the nucleophilic attack of the β-oxygen on the carbon gives rise to the formation of an intermediate (**4**), which allows only the exchange of the β- and γ-oxygen atoms at the lower temperature (path **A**). In this process, the electron withdrawing group at the para position of the phenyl group would decrease the electron density at benzylic position of **1** and enhance the nucleophilic attack of β-oxygen atom on the carboxylic carbon atom. The structure of intermediate (**4**) is visualized as a resonance hybrid (**4'**) somewhere between the following five extremers.[7]

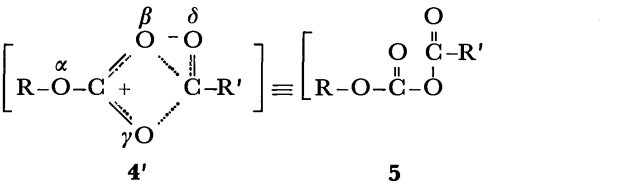

4' **5**

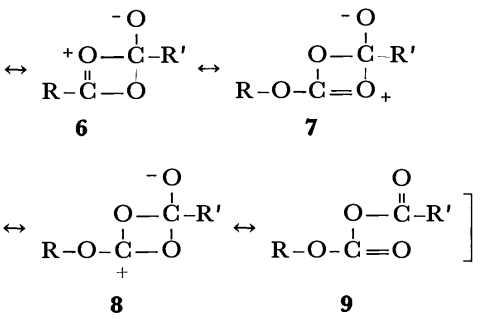

6 **7** **8** **9**

The rate of oxygen scrambling between β- and γ-oxygen atoms would therefore be determined by the stability of **4**, in which the substituent on R' which stabllizes positive charge on β- and γ-oxygen atoms instabilizes the negative charge on δ-oxygen atom. Since β-, γ- and δ-oxygen atoms are situated in the same position with respect to R', the opposite substituent effect would be canceled as a whole. The other possible explanation of no substituent effect of first step of oxygen scrambling is that polar canonical forms **6**, **7** and **8** hardly contribute to the structure of **4**, with respect to oxygen scrambling of acetyl peroxide (1, 3 sigmatropy) as suggested by Goldstein and Judson.[8]

The new oxygen scrambling in **1** can be regarded as an intramolecular 1, 3 acyl migration as shown by

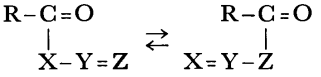

(10)

Several examples of reaction (10) are summarized in Table 2. Curtin and Miller observed the small positive ρ-value, 0.6—0.7 and proposed a similar mechanism for the *O*- to *N*-acyl migration as in the following[7]

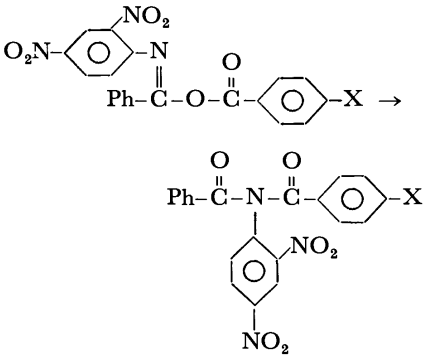

(11)

At higher temperatures, the δ-oxygen atom in the intermediate (**4**) attacks the carbonic carbon (Scheme 1) either *via* the concerted bond formation and breaking process or *via* formation of an alternative intermediate (**5**). The three oxygen atoms of the carbonates **1** (β, γ and δ) thus scramble completely (path **B**).

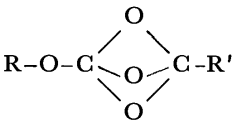

5

7) D. Y. Curtin and L. L. Miller, *ibid.*, **89**, 637 (1967).

8) M. J. Goldstein and H. A. Judson, *ibid.*, **92**, 4119 (1970).

Table 2. Survey of some 1,3 acyl migrations

R-C=O / X-Y=Z			R-C=O / X=Y-Z	
X	Z	Y	Example	Ref.
O	O	C	Aroyl alkyl carbonates	This work, 2b
N	N	C	*N*-Acylamidines	9
N	N	N	*N*-Acyltriazenes	10
N	O	C	Isoimides	7
N	O	N	*N*-Nitrosoamides	11
S	N	C	*S*-Acylisothioureas	12

Experimental

Preparation of Cyclohexyl Chloroformate. To 45 g of phosgene cooled in an ice-bath was added 25 g of cyclohexanol, and the reaction mixture was allowed to stand overnight at room temperature. Excess phosgene was removed and cyclohexyl chloroformate was distilled under reduced pressure (90—91 °C/31 mmHg, 86%).

Preparation of ^{18}O-Labeled p-*Cyanobenzoyl Cyclohexyl Carbonate (**1a**).* In a flask equipped with a stirrer and a dropping funnel were placed 300 ml of dry ether, 10 g of ^{18}O-labeled *p*-cyanobenzoic acid and 6.8 g of triethylamine. The mixture was cooled to 0 °C with an ice-bath, 11.0 g of cyclohexyl chloroformate in 30 ml of dry ether being then added dropwise over a period of 1 hr. Stirring was continued for 4 hr. The amine hydrochloride was filtered off, and the filtrate was washed with dil HCl, dil aqueous $NaHCO_3$ and water and dried over Na_2SO_4. Evaporation of the solvent left 15.0 g of colorless crystals. Recrystallization from CCl_4–petroleum ether gave 12.6 g of **1a**, mp 54.5—55.0 °C. IR: 5.59 and 5.76 μ ($\nu_{C=O}$). Found: C, 66.08; H, 5.55; N, 5.03%. Calcd for $C_{15}H_{15}NO_4$: C, 65.92; H, 5.53; N, 5.13%.

*^{18}O-Labeled Benzoyl Cyclohexyl Carbonate (**1b**) and p-Toluyl Cyclohexyl Carbonate (**1c**)* were prepared from ^{18}O-labeled benzoic acid and *p*-toluic acid in the same way as for **1a** in 67 and 91% yields, respectively. **1b**: mp 21.0—21.5 °C resrystallized from pet. ether. IR: 5.59 and 5.76 μ ($\nu_{C=O}$). Found: C, 68.00; H, 6.32. Calcd for $C_{14}H_{16}O_4$: C, 67.73; H, 6.50% **1c**: mp 25.5—26.5 °C, IR: 5.59 and 5.76 μ ($\nu_{C=O}$). Found: C, 68.90; H, 6.76%. Calcd for $C_{15}H_{18}O_4$: C, 68.68; H, 6.92%.

^{18}O-Scrambling in the Aroyl Alkyl Carbonates. A typical run is as follows: A solution of 2.73 g of **1a** in 1 l CCl_4 was warmed at 45 °C for 24 hr. The solvent was removed under reduced pressure at room temperature and the residue was used for the following cleavage reaction, the products being subjected to ^{18}O-analysis.[2)]

Reaction of Aroyl Alkyl Carbonates with Aniline. In a typical run, 0.40 g of aniline was added 10 ml CCl_4 solution of 0.82 g of **1a** at room temperature and the mixture was allowed to stand for 1.5 hr. *p*-Cyanobenzanilide was collected by filtration and recrystallized from chloroform, mp 180—180.5 °C, and subjected to ^{18}O-analysis. The filtrate was diluted with 30 ml of ether and washed with dil HCl, dil $NaHCO_3$ and water, and dried over Na_2SO_4. Solvent was removed and the residue was chromatographed through an activated alumina column with benzene and ether as eluents. A fraction which came out in the latter was identified as cyclohexanol and subjected to ^{18}O-analysis. In order to collect carbon dioxide, the reaction was carried out as follows: The aroyl alkyl carbonate (**1**) (0.30 g) and 5 ml of CCl_4 were placed in a flask with two necks, one equipped with a bent tube charged with 0.2 g of aniline and the other connected to a vacuum line. After evacuation of the flask with cooling in a dry ice-acetone bath, it was warmed up to room temperature and aniline was added by turning the bent tube. The carbon dioxide evolved was collected in a trap cooled with liquid N_2, sublimed three times in the vacuum line and then subjected to ^{18}O-analysis.

Reaction of Aroyl Alkyl Carbonates with N-*Methylaniline.* In a typical run, 0.4 g of *N*-methylaniline was added to a solution of 0.82 g of **1a** in 10 ml CCl_4 at room temperature. The reaction was allowed to continue for 1.5 hr. Solid material was collected by filtration, recrystallized from chloroform, identified as *p*-cyanobenzoic acid, mp 219.0—219.5 °C, and subjected to ^{18}O-analysis. The filtrate was washed with dil HCl dil aqueous $NaHCO_3$ and water, then dried over Na_2SO_4. CCl_4 was removed by distillation, and the residue was chromatographed on silica gel column with benzene as an eluent. The early fraction was distilled under reduced pressure (bp 135—136 °C/3 mmHg), identified as cyclohexyl *N*-methyl-*N*-phenyl carbamate with the authentic sample and subjected to ^{18}O-analysis.

Preparation of Cyclohexyl N-*Methyl*-N-*Phenyl Carbamate.* To a mixture of 6.0 g of *N*-methylaniline and 5.0 g of triethylamine in 40 ml of dry ether was added 8.2 g of cyclohexyl chloroformate in 10 ml dry ether with stirring at 0 °C. Stirring was continued for 1 hr. Amine hydrochloride was filtrated off and the filtrate was washed with dil HCl, dil $NaHCO_3$ and water, then dried over Na_2SO_4. The ether was removed by distillation and the residue was distilled under reduced pressure to yield 8.8 g of cyclohexyl *N*-methyl-*N*-phenyl carbamate, bp 135—136 °C/3 mmHg. Found: C, 71.88; H, 8.28; N, 5.72%. Calcd for $C_{14}H_{19}O_2N$: C, 72.02; H, 8.21; N, 6.00%.

*Reaction of ^{18}O-Labeled **1c** with* p-*Toluic Aicd.* A solution of 1.31 g of **1c**, labeled with 1.04 excess atom % of ^{18}O at γ- and δ-oxygen atoms, and 0.66 g of unlabeled *p*-toluic acid in 125 ml CCl_4 was heated at 70 °C for 12 hr. After heating the free acid was extracted with aqueous $NaHCO_3$. The water layer was acidified with HCl and extracted with ether. The etheral solution was washed with water and dried over Na_2SO_4. The ether was evaporated to give 0.66 g *p*-toluic acid which was recrystallized from benzene, mp 179.0—179.5 °C and subjected to ^{18}O-analysis.

*Crossover Experiment between Unlabeled **1a** and Labeled **1b**.* A mixture of 1.36 g of unlabeled **1a** and 1.20 g of labeled **1b** (1.39 excess atom % in the γ- and δ-oxygen atom) in 250 ml of CCl_4 was heated at 45 °C for 48 hr. The solvent was removed under reduced pressure at room temperature. **1a** (0.7 g) was recovered by the fractional recrystallization of the residue from CCl_4–pet. ether. **1a** recovered was treated with *N*-methylaniline (**3**) to yield 0.17 g of *p*-cyanobenzoic acid which was subjected to ^{18}O-analysis (0.00 excess atom %).

Preparation of ^{18}O-Labeled p-*Cyanobenzoic Acid.* In a flask equipped with a stirrer and a dropping funnel were placed 33 g of *p*-cyanobenzoyl chloride, 40 g of triethylamine and 300 ml of dry dioxane to which was added dropwise

9) H. L. Wheeler, T. B. Johnson, and D. F. McFarland, *J. Amer. Chem. Soc.*, **25**, 790 (1903).

10) a) M. O. Forsten and C. S. Garland, *J. Chem. Soc.*, **95**, 2051 (1909). b) J. D. Druliner, Ph. D. Thesis. University of Illinois, 1966.

11) K. B. Wiberg, T. M. Shryne and R. R. Kintner, *J. Amer. Chem. Soc.*, **79**, 3160 (1957).

12) R. F. Pratt and T. C. Bruice, *ibid.*, **94**, 2823 (1972).

4.0 g of ^{18}O-enriched water (1.5 atom%) in 10 ml of dry dioxane. Stirring was continued for 2 hr. The reaction mixture was filtered and the precipitate was washed with 100 ml of dioxane. The filtrate and washing solution were combined and the solvent was removed by distillation. The residue was dissolved in 300 ml of water and acidified with HCl. The precipitate was filtered, washed with water and dried. The acid was recrystallized from chloroform–acetone, mp 217.0—218.0 °C.

Kinetics of ^{18}O-Scrambling in the Aroyl Alkyl Carbonates. Kinetics of ^{18}O-scrambling between β- and γ-oxygen atoms were followed by measurement of the decreasing amount of ^{18}O in *p*-substiutted benzoic acids formed by cleavage reaction (3). The aroyl alkyl carbonates were heated at 45 °C in CCl_4 (0.04 mol/l).

^{18}O-Analysis was carried out in the same way as reported previously.[2)]

We wish to thank Professor S. Okazaki for the supply of ^{18}O-water which made this work possible.

BULLETIN OF THE CHEMICAL SOCIETY OF JAPAN, VOL. 46, 1745—1751 (1973)

Mechanism of Oxygen Exchange Reaction of Diaryl and Alkyl Aryl Sulfoxides in Sulfuric Acid*

Norio KUNIEDA and Shigeru OAE

Department of Applied Chemistry, Faculty of Engineering, Osaka City University, Sugimoto-cho, Sumiyoshi-ku, Osaka 558

(Received August 21, 1972)

The mechanistic investigations of the concurrent oxygen exchange and racemization reactions of ^{18}O-labeled and optically active methyl *p*-tolyl sulfoxide (I) and phenyl *p*-tolyl sulfoxide (II) in sulfuric acid of various concentrations have been carried out by the determination of detailed kinetics. The kinetic data were analyzed in the lights of k_{ex}/k_{rac} values, activation parameters, correlations between the rates and acidity functions, solvent isotope effects, polar effects of substituents, etc.. A gradual change of mechanism of the reaction from an S_N2 type process to a predominant A-1 like one (in above 95% sulfuric acid) with the increase of the concentration of sulfuric acid was observed. All these observations suggest that the A-1 like reaction takes place through a cation radical ($-\overset{+\cdot}{S}-$) or a dication ($-\overset{++}{S}-$) intermediate at higher concentrations of sulfuric acid, while the S_N2 type reaction that involves a water molecule as nucleophile in the rate-limiting step is the predominant path in less concentrated sulfuric acid.

The concurrent oxygen exchange and racemization reactions of optically active and ^{18}O-labeled (*on sulfoxide oxygen*) sulfoxides are advantageous to study the nature of nucleophilic substitution on the trivalent sulfur atom, which is one of the important subject in organic sulfur chemistry, and have attracted considerable attentions in recent years. Several studies have been reported on the acid-catalyzed oxygen exchange and racemization reactions of sulfoxides.[1-7] Among these, the concurrent oxygen exchange and racemization reactions of diaryl sulfoxides in concentrated sulfuric acid is the most extensitvely studied, since it was the first example discovered.[8-10] When ^{18}O-labeled and optically active sulfoxides are dissolved in a concentrated sulfuric acid, one observes the concurrent oxygen exchange and racemization of the sulfoxide.

However, in order to clarify the over-all feature of these reactions, in which the mode of the reaction displays a gradual change with the change of the concentration of sulfuric acid, more detailed kinetic investigations are desirable especially since it has recently been shown that the sulfoxides do not behave as Hammett bases.[19,20,31]

We now have investigated the oxygen exchange and racemization reactions of methyl *p*-tolyl sulfoxide (I) as well as phenyl *p*-tolyl sulfoxide (II) much more in detail in sulfuric acids of various concentrations. And a reinvestigation of our previous results[9,10] has also been carried out.

Results and Discussion

Careful kinetic experiments have been conducted mainly on the rates of concurrent oxygen exchange and racemization reactions of methyl *p*-tolyl sulfoxide (I), 1.08 *atom*%-^{18}O $[\alpha]_D^{23}+146°$ (Acetone), and phenyl *p*-tolyl sulfoxide (II), 1.12 *atom*%-^{18}O $[\alpha]_D^{20}+27.6°$ (EtOH), in sulfuric acid of various concentrations ranging from 52.4% to 94.8% at several temperatures. These results are listed in Table 1.

When the reaction proceeds through the A-1 type

* Oxygen Exchange Reaction of Sulfoxides in Sulfuric Acid. Part VII (Sulfoxides 47).

1) a) K. Mislow, T. Simmons, J. T. Mellilo, and A. L. Ternay, Jr., *J. Amer. Chem. Soc.*, **86**, 1452 (1964). b) K. Mislow, *Record of Chemical Progress*, **28**, 217 (1967).
2) H. Yoshida, T. Numata, and S. Oae, This Bulletin, **44**, 2875 (1971).
3) G. Modena, U. Quintily, and G. Scorrano, *J. Amer. Chem. Soc.*, **94**, 202 (1972).
4) S. Oae, M. Yokoyama, and M. Kise, This Bulletin, **41**, 1221 (1968).
5) N. Kunieda and S. Oae, *ibid.*, **41**, 1025 (1968).
6) a) S. Oae, N. Kunieda, and W. Tagaki, *Chem. & Ind.*, **1965**, 1790. b) N. Kunieda, K. Sakai, and S. Oae, This Bulletin, **42**, 1090 (1969).
7) M. Kise and S. Oae, *ibid.*, **43**, 1804, 1416, 1426 (1970).
8) S. Oae, T. Kitao, Y. Kitaoka, and S. Kawamura, *ibid.*, **38**, 546 (1965).
9) S. Oae and N. Kunieda, *ibid.*, **41**, 696 (1968).
10) N. Kunieda and S. Oae, *ibid.*, **42**, 1324 (1969).

TABLE 1. RATE CONSTANTS FOR THE OXYGEN EXCHANGE AND RACEMIZATION REACTIONS OF p-CH_3-C_6H_4-SO-R IN SULFURIC ACID

R;	H_2SO_4 (wt%)	Temp. (°C)	10^4k_{rac} (s^{-1})	10^4k_{ex} (s^{-1})	10^4k_1 (s^{-1})[e]	Method[b]
CH_3[a]	94.8[c]	5	11.2 ±0.5	9.63 ±0.12		A
	94.2	12.5	24.5 ±0.1		24.5	B
	94.2	10	17.8 ±0.2		17.8	B
	94.2	5	9.61 ±0.21		9.61	B
	93.8	20	38.9 ±1.2		38.9	B
	93.8	15	21.5 ±0.3		21.5	B
	93.8	10	11.8 ±0.2		11.8	B
	93.8	5	6.37 ±0.23		6.37	B
	93.1	12.5	17.7 ±0.07		17.7	B
	92.7[c]	30	81.7 ±1.5	57.2 ±2.2		A
	91.9	12.5	14.0 ±0.8		14.0	B
	89.8	12.5	7.72 ±0.73		7.72	B
	89.5	30	40.3 ±1.5		40.3	B
	83.5	30	8.50 ±0.10		8.52	B
	80.2	30	3.55 ±0.11		3.56	B
	74.6	30	1.19 ±0.06		1.20	B
	68.8	30	0.440±0.010		0.456	B
	64.7	30	0.266±0.002		0.285	B
	64.7	40	0.703±0.015		0.753	B
	64.7	47	1.20 ±0.02		1.29	B
	58.5	30	0.145±0.05		0.170	B
	58.5[c]	30	0.263±0.022	0.126±0.010		A
	55.0	30	0.105±0.003		0.135	B
	52.4	30	0.074±0.001		0.104	B
C_6H_5[d]	95.9	5	4.20	4.07	4.20	A
	95.5	5	3.32	3.22	3.32	A
	91.0	5	0.891	0.705	0.891	A
	86.9	30	2.91	1.89	2.91	A
	83.4	30	1.39	0.900	1.40	A
	80.5	30	0.880	0.458	0.884	A
	75.4	60	6.95	3.40	7.06	A

a) Sulfoxide=0.03 mol/l. b) Method of the rate measurement; see Experimental section. c) Sulfoxide=0.1 mol/l. d) Data of our previous experiment.[10] e) The pK_{SH^+} values used here are, for phenyl p-tolyl sulfoxide (−2.39), for methyl p-tolyl sulfoxide (−2.22), the values of Landini *et al.*.[31]

TABLE 2. k_{ex}/k_{rac} VALUES OF (+) p-CH_3-C_6H_4-SO-R-^{18}O IN SULFURIC ACID AT 30°C

R;	H_2SO_4 (wt%)	k_{ex}/k_{rac}[c]
CH_3	94.8[b]	0.86
	92.7	0.70
	58.5	0.48
C_6H_5	95.5[b]	0.97
	91.0[b]	0.75
	86.9	0.65
	83.5	0.64
	75.4	0.49[a]

a) Average value of three runs of kinetics at 40, 50 and 60°C. b) At 5°C. c) These rate constants are of pseudo-first-order rate.

TABLE 3. ACTIVATION PARAMETERS OF RACEMIZATION REACTION OF (+) p-$CH_3C_6H_4SO$-R IN SULFURIC ACID

R;	H_2SO_4 (wt%)	E_a (kcal/mol)[a]	$\Delta S^{\neq}$ (e. u.)[a]
CH_3	94.2	20.2	−1.17
	93.8	19.8	−5.94
	64.7	17.1	−25.1
C_6H_5[a]	95.5	24.0	+9.86[b]
	90.8	18.5	−10.8
	85.6	17.5	−17.5
	75.4	18.6	−18.9

a) These values are based on pseudo first-order rate constants. b) This is smaller than that reported in the previous report.[10]

route, each cleavage of S–O bond in the rate limiting step which results in oxygen exchange will cause racemization, and $k_{exchange}$ (k_{ex}) is equal to $k_{racemization}$ (k_{rac}), since it passes through a symmetrical intermediate such as $-\overset{+\cdot}{S}-$ or $-\overset{++}{S}-$. While, when the reaction proceeds through the S_N2 type route, the k_{ex}/k_{rac} value becomes 0.5.

The k_{ex}/k_{rac} values for I in 94.8% acid and for II in 95.5% acid were found to be 0.86 and 0.97, respectively. While the values for I in 58.5% acid and in 75.4% acid were 0.48 and 0.49, respectively. Thus the predominant path of the reaction in the less con-

centrated acid is an S_N2 type. And the k_{ex}/k_{rac} value increases gradually with the increase of the acid concentration. However, the values change drastically in above *ca.* 93% acid.

The energies and entropies of activation, E_a and $\Delta S^{\neq}$, obtained in sulfuric acid of several concentrations are listed in Table 3. The E_a value increases significantly while $\Delta S^{\neq}$ value changes from the large negative value to a small negative or positive one with the increase of the acid concentration. In the highly concentrated acid region, the $\Delta S^{\neq}$ values of I and II are −1.77 e.u. (in 94.2% acid) and +9.86 e.u. (in 95.5% acid), respectively. While in a less concentrated acid, the $\Delta S^{\neq}$ values are −25.1 e.u. (in 64.7% acid) for I and −18.9 e.u. (in 75.4% acid) for II, respectively. These values are typical for S_N2 type reactions.[11] The drastic change of the $\Delta S^{\neq}$ value is also observed in the higher concentrated acid region above ca. 93—95%.

In these concentrated sulfuric acids, the sulfoxides are considered to be protonated[13] almost completely (Eq. 2). Therefore, the rate can be expressed as a function of the concentration of the protonated sulfoxide, [S⁺–OH], (Eq. 3,4).

$$\mathrm{R{-}\underset{\underset{\mathrm{O}}{\downarrow}}{S}{-}R' + H^+ \overset{K_{SH^+}}{\rightleftharpoons} R{-}\overset{+}{S}{-}\underset{\underset{\mathrm{OH}}{|}}{R'}} \qquad (2)$$

$$\text{Rate} = k_1[\mathrm{S^+{-}OH}] \qquad (3)$$

$$k_1 = k_{obs}(h_0^m + K_{SH^+})/h_0^m \qquad (4)$$

where, K_{SH^+} and h_0^m[16] are the thermodynamic ionization constant of the sulfoxides and the acidity function fitted for the sulfoxide-bases, respectively.

In order to solve the rate equation, the accurate pK_{SH^+} values of the sulfoxides are necessary. The p*Ka* values of several sulfoxides have been determined.[17–20] However, it has known that the sulfoxides do not behave as Hammett bases, since the gradient of log [SH⁺]/[S] *vs.* H_0 for the sulfoxides were found to be smaller than unity.[19,20] For example, the average gradient for substituted diphenyl sulfoxides was found to be 0.59.[20b,c] The H_0 scale is based on substituted aniline indicators.[21] Therefore, an acidity function which is strictly appropriate to study especially the ionization behaviors of sulfoxides is most desirable, like the H_A for amide bases,[22,23] and H_0 for benzophenone bases.[24] However, it is difficult to determine the peculiar acidity function just fitted for sulfoxide-bases, and hence it has not been worked out. Yates and McClelland[26] have introduced the H_S function as the ester-base acidity function. And the H_S was obtained by the following empirical relationships, $\log [SH^+]/[S] = -H_s + pK_{SH^+}$; $\log [SH^+]/[S] = -mH_0 +$ const.; $H_S = mH_0$, where m is the slope of plot of the ionization ratio for acetates *vs.* the available H_0 scale. Here, we also undertook the same treatment for the sulfoxide-base. From the average gradient of log [SH⁺]/[S] vs H_0 measured by UV and NMR, mentioned above, we have chosen to use m=0.60 and 0.6 H_0 instead of H_0 in this study.[27] Recently, Landini *et al.*[31,33] have found that the H_A function developed by Yates *et al.*[22] satisfactorily represents the protonation behaviors of the sulfoxides. The H_A is about 0.65 H_0 (between 50 and 80% acid), which also corresponds closely to the approximation, $m=0.6$, for the value of sulfoxide-bases mentioned above. Then the rate constants, k_1, of both the oxygen exchange and racemization reactions were calculated by the eq. 4 using h_A and $h_0^{0.6}$ and the pK_{SH^+} values, where $h_0^{0.6}$ was used to conduct the kinetic data in higher than 80% acid.

The rate constants, k_1, obtained are listed in Table 1, which also increase with the increase of the acid concentration. The acid dependencies of the rates are collected in Table 4. At first, diagrams correlating the logarithmus of the rates of racemization of both I and II against H_A(or $0.6H_0$) were made. At highly concentrated acid regions, log k_1 was found to be in a

11) For example, the $\Delta S^{\neq}$ value for the racemization reaction of II with acetic anhydride which is a typical S_N2 type process was found to be −28.6 e. u.[12]

12) S. Oae and M. Kise, *Tetrahedron Lett.*, **1967**, 1409.

13) It has been shown by Gillespie and Passerini[14] and Oae *et al.*[15] through the cryoscopic measurement that the sulfoxides ionize in the concentrated sulfuric acid in the following manner (eq. 1).

$$\mathrm{R{-}\underset{\underset{\mathrm{O}}{\downarrow}}{S}{-}R' + H_2SO_4 \rightleftharpoons R{-}\overset{+}{S}{-}\underset{\underset{\mathrm{OH}}{|}}{R'} + HSO_4^+} \qquad (1)$$

14) R. J. Gillespie and R. C. Passerini, *J. Chem. Soc.*, **1956**, 3850.

15) S. Oae, T. Kitao, and Y. Kitaoka, This Bulletin, **38**, 543 (1965).

16) This symbol is one given by Yates in his paper.[25]

17) P. Nylen, *Z. Anorg. Allgem. Chem.*, **246**, 227 (1941).

18) K. K. Andersen, W. H. Edmonds, J. B. Biasotti, and R. A. Strecker, *J. Org. Chem.*, **31**, 2859 (1966).

19) a) P. Haake and R. D. Cook, *Tetrahedron Lett.*, **1968**, 427. b) P. Haake, R. D. Cook, and G. H. Hurst, *J. Amer. Chem. Soc.*, **89**, 2650 (1967).

20) a) S. Oae, K. Sakai, and N. Kunieda, This Bulletin, **42**, 1966 (1969). b) N. Kunieda and S. Oae, unpublished data. c) Haake and Cook also reported the similar small slopes for phenyl methyl sulfoxide (0.62) and dimethyl sulfoxide (0.61) in the pK_{SH^+} determinations by NMR chemical shift measurements of methyl group in sulfuric acid,[19]

21) L. P. Hammett, "Physical Organic Chemistry", McGraw-Hill Book Co. Inc., New York, N. Y., 1970, Chap. 9.

22) K. Yates, J. B. Stevens, and A. R. Katritzky, *Can. J. Chem.*, **42**, 1957 (1964).

23) K. Yates and J. B. Stevens, *ibid.*, **43**, 529 (1965).

24) T. G. Bonner and J. Phillips, *J. Chem. Soc.* (B), **1966**, 650.

25) K. Yates, *Accounts Chem. Res.*, **4**, 136 (1971).

26) K. Yates and R. A. McClelland, *J. Amer. Chem. Soc.*, **89**, 2686 (1967).

27) The H_0 values used here are the data reevaluated more recently by Johnson *et al.*[30] The measurements of ionization ratio of sulfoxides by us[20] and Haake and Cook[19] refer to H_0 scales compiled by Long and Paul[28] and Jorgenson and Hartter,[29] which will not be strictly correct when the Johnson *et al.* values are used. However, since the difference of the two H_0 scales is at most 0.2 H_0 at all acid range, it may be parmitted to use these values of ionization ratios.

28) M. A. Paul and F. A. Long, *Chem. Revs.*, **57**, 1 (1957).

29) M. J. Jorgenson and D. R. Hartter, *J. Amer. Chem. Soc.*, **85**, 878 (1963).

30) C. D. Johnson, A. R. Katritzky, and S. A. Shapiro, *ibid.*, **91**, 6654 (1969).

31) D. Landini, G. Modena, G. Scorrano, and F. Taddei, *ibid.*, **91**, 6704 (1969).

32) J. F. Bunnett and F. P. Olsen, *Can. J. Chem.*, **44**, 1899 (1966).

33) D. Landini, G. Modena, F. Montanari, and G. Scorrano, *J. Amer. Chem. Soc.*, **92**, 7168 (1970).

TABLE 4. CORRELATION BETWEEN ACIDITY FUNCTIONS AND RATE CONSTANTS OF RACEMIZATION OF p-CH_3-C_6H_4SOR IN SULFURIC ACID

R;	H_2SO_4 (wt%)[a]	log k_1 *vs.* H_A ($0.6H_0$)	log $k_{obs}+H_0$ *vs.* log a_{H_2O}	log $k_{obs}+H_A$ ($0.6H_0$) *vs.* log a_{H_2O}	log k_1+H_0 *vs.* $H_0+\log[H^+]$
CH_3	52.4—68.8	0.583	1.86(0.999)	0.388(0.988)	0.770(0.999)
	89.8—94.2	1.18(0.997)[b]	0.328(0.985)	−0.116[c]	0.336(0.986)
C_6H_4	64.7—74.4	0.750	1.44(0.999)	0.317(0.949)	0.701(0.991)
	93.3—96.3	1.44(0.990)	0.133[c]	−0.272(0.866)	0.300(0.880)

a) Range of sulfuric acid concentration. b) Correlation coefficient.
c) It's correlation showed as low value because the slope is very low.

linear relationship with $0.6H_0$. The slopes for I at above 89.8% acid and for II at above 93.3% acid were 1.18 and 1.44, respectively. This means that the reaction proceeds through a predominant A-1 type route, according to the Zucker-Hammett hypothesis.[34] As the concentration of acid decreases, the plot of log k_1 *vs.* acidity functions start to deviate markedly from the linear slopes to lower ones.

The Bunnett w-values,[35] at the range of less concentrated acid for I(below 68.8%) and for II(below 74.4%) are 1.86 and 1.44, respectively. Whereas, at sulfuric acids of above 89.9% for I and above 93.3% for II, the w-values are 0.328 and 0.133, respectively. Though the values are little larger than zero and cannot be classified strictly into the class $w \leqq 0$ of the criterion, the values seem to indicate that the reaction proceeds through a nearly A-1 type route in which water does not participate in the rate limiting step. According to the modified Bunnett hydration parameter treatment[23,25,36] using H_A or $0.6H_0$ for H_X, the slopes (r), at the highly concentrated acid region, show smaller values than zero (*i. e.* for I; −0.116 (above 89.8%), for II; −0.272 (above 93.3%)), and at the less concentrated acid region, however, the slopes show small positive values. However, the equation, log k_{obs}−log h_A (or $h_0^{0.6}$)/[$K_{SH^+}+h_A$ (or $h_0^{0.6}$)]$=r \log a_{H_2O}+$ const., gives a large negative r values at all range of the plot both for I and II, even at the less concentrated acid region.

The plot[32] of (log $k_{obs}+H_0$) against ($H_0+\log[H^+]$) also gave a linear slope at the less concentrated acid range. The ϕ values for I and II are 0.770 and 0.701, respectively. On the other hand, at the range of concentrated acid, the slopes for I, and II were larger than that expected from a typical A-1 mechanism. The plot of ($\log k_1+H_0$) *vs.* ($H_0+\log[H^+]$) showed a similar slope.[37] These results seem to indicate that the S_N2 type reaction takes place competitively in no small portion, even in the high acid region above 85%. The plot of $\log k_{obs}-\log h_0^m/(K_{SH^+}+h_0^m)$ *vs.* ($H_0+\log[H^+]$), where h_0^m is h_A or $h_0^{0.6}$, showed high negative ϕ values for both I and II at all ranges of the acid concentration, even including less concentrated acids. Similar large negative ϕ values have been observed, for instance, in the reduction of sulfoxides by halide ion(−1.2∼−1.6)[33] and Wallach rearrangement(−1.8∼−0.4),[38] which have been believed to involve two protons in the rate limiting step.

It would be difficult to apply the Bunnett[35] and the Bunnett and Olsen[32] criteria to analyze directly the reaction at the high acid region.

TABLE 5. EFFECT OF DEUTERIOSULFURIC ACID ON THE RACEMIZATION RATE OF I AND II

Sulfoxide	Sulfuric acid (mol/l)	Temp. (°C)	$\times 10^4$ s^{-1} [a]		k_H/k_D
			$k_{H_2SO_4}$	$k_{D_2SO_4}$	
I	17.48	10	18.6	13.9	1.34
	17.09	10	10.8	8.71	1.24
	14.61	25	3.10	2.60	1.19
	11.40	45	2.43	2.57	0.946
	10.27	30	0.306	0.322	0.950
	10.27	45	1.48	1.59	0.931
II	17.68	10	7.00	6.93	1.01
	13.02	45	1.97	1.78	1.11

a) Pseudo first order rate constants using Method B. These values are average ones for three or four measurements.

Table 5 summarizes the values of the ratio of the rate, k_H/k_D, *i. e.* the ratio of the rates of the racemization of I and II in D_2SO_4–D_2O media to those in ordinary H_2SO_4–H_2O media. The solvent isotope effect observed is not very large. As described earlier, in both highly and moderately concentrated sulfuric acids, the sulfoxides are considered to be protonated almost completely. Therefore, if the reaction proceeds through an A-1 type route, the isotope effect would be found only in the step of unimolecular S–O bond cleavage of the protonated sulfoxides, and its k_H/k_D value at the concentrated acid regions should be close to unity. In the case of II, the value is indeed 1.01 at the acid of 17.68 mol/l. However, the value of I was found to be a larger than one, *i.e.* 1.34, in the acid of similar concentration, *i.e.* 17.48 mol/l. This means that, in the case of I, an S_N2 type reaction involving the nucleophilic attack of water on the protonated sulfoxide takes place to substantial extent even at the high concentrated acid region, and hence the solvent

34) M. A. Paul and F. A. Long, *Chem. Revs.*, **57**, 935 (1957); L. Zucker and L. P. Hammett, *J. Amer. Chem. Soc.*, **61**, 2791 (1939).
35) J. F. Bunnett, *ibid.*, **82**, 499 (1960); **83**, 4956 (1961); **83**, 4968 (1961); **83**, 4973 (1961); **83**, 4978 (1961).
36) K. Yates and J. C. Riordan, *Can. J. Chem.*, **43**, 2328 (1965).
37) Landini *et al.* applied the same treatment using k_1 into a study of the reduction of sulfoxides by halide ion in aqueous perchloric acid, and they gave the ϕ values in the range from −0.12 to +0.06.[33]
38) E. Buncel and B. T. Lawton, *Can. J. Chem.*, **43**, 862 (1965).

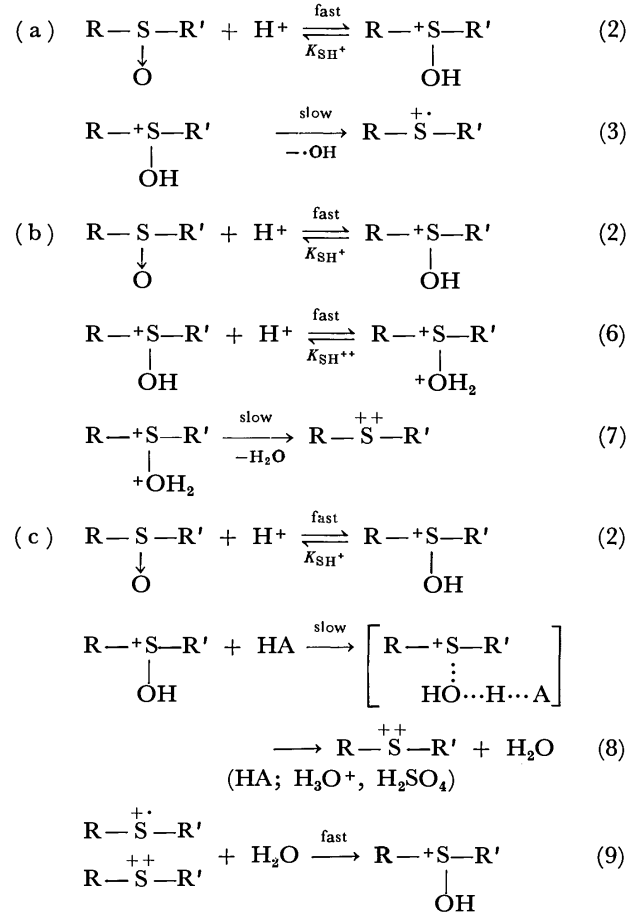

Scheme 1. A-1 like mechanism.

isotope effect due to the difference of the nucleophilicities between D_2O and H_2O would appear. As the acid concentration decreases, the k_H/k_D value of I also decreases gradually, and at 10.27 mol/l, the isotope effect is reversed, *i.e.* $k_H/k_D=0.931$. Thus it is clear that the initial protonation equilibrium controls the isotope effect, because in the less concentrated acids the protonation would not be complete.

There are a few concievable pathways for the A-1 type S–O bond cleavage that fit to these observations, as shown in Scheme 1.

The several ESR studies of the sulfur containing aromatic compounds have been done.[39] Shine *et al.*[40] revealed that noticeable ESR signals of the corresponding cation radical were observed from 96% sulfuric acid solutions of *p,p'*-disubstituted diphenyl sulfoxides. Recently, we have also found the ESR signals from 96.3% sulfuric acid solutions of *p,p'*-ditolyl sulfoxide and II,[9] though the signal from II has no hyperfine structure. These ESR results suggest that the route (a) involving the homolytic cleavage to form an incipient cation radical intermediate is the most likely possibility, in the case of diaryl sulfoxides. The polar effects of *p*-substituents on the oxygen exchange reaction rates are very small in comparison with that of the typical S_N1 type reactions (see Table 6). This rather small polar effect also seems to favor the route (a). While the 96% sulfuric acid solution of I is colorless,[41] and no noticeable ESR signal was detected for I from the 96% acid solution. It is dubious, therefore, that I undergoes the reaction depicted by route (a), in the acid below 96% concentration.

Table 6. Rate constants of ^{18}O-exchange of *p*-X-$C_6H_4S^{18}O$-C_6H_5[a] in 95.3% sulfuric acid at 5°C

X;	$10^4 k_{ex}$ (sec^{-1})[b]
CH_3	2.92±0.20
H	1.15±0.08
Cl	1.53±0.05
NO_2	1.13±0.03

a) Sulfoxide=0.12 mol/l, by Method A.
b) These values are much the same as those of our previous work.[9]

The pathways (b) and (c), including the dication intermediate, must also be included among the A-1 type reactions. For the unimolecular S–O bond cleavage, the second protonation or a second proton transfer from acid media to the mono-protonated sulfoxide is considered to be neccessary, since, OH group being a poor leaving group, the S^+–OH should pick up one more proton before the heterolytic cleavage of S–O bond. Route (b) begins with a rapid protonation equilibrium (Eq. 2) and followed by a second protonation (Eq. 7) again on the oxygen. Then the rate-limiting step becomes the loss of a water molecule from the diprotonated sulfoxide. This dication intermediate is similar to the carbonium ion in the acid catalyzed oxygen exchange reaction of alcohols.[42]

If the reaction proceeds through the overall two-proton process, the rate is expressed by the use of the H_+ function.[43] The kinetic analyses with the H_+ function also permit the reaction in the concentrated acid to follow the route (b). Though we can find no value of H_+ available for this treatment, the parallelism has been found between H_+ and H_0 in the sulfuric acid media,[43-44] and hence H_A or $0.6H_0$ could be substituted for H_+ in this instance,[45] even though

39) U. Schmidt, K. Kabitze and K. Markau, *Angew. Chem.*, **72**, 708 (1960); U. Schmidt, *ibid.*, **76**, 629 (1964); H. J. Shine, "The Formation of Cations and Cation Radicals from Aromatic Sulfides and Sulfoxides," in "Organosulfur Chemistry," ed by M. J. Janssen, Intra-Science (1967), Chap. 6. and the references cited therin.

40) H. J. Shine, M. Rahman, H. Seeger and G.-S. Wu, *J. Org. Chem.*, **32**, 1901 (1967).

41) The color of the solution of I at nearly 100% acid is orange.

42) The references cited in; D. Samuel and B. L. Silver, "Oxygen Isotope Exchange Reactions of Organic Compounds", Vol. 3, in "Advances in Physical Organic Chemistry", ed. by V. Gold, Academic Press, New York, N. Y. (1965), Chap. 3.

43) T. G. Bonner and J. C. Lockhart, *J. Chem. Soc.*, **1957**, 364; J. C. D. Brand, W. C. Horning, and M. B. Thornley, *ibid.*, **1952**, 1374; P. Veteśnik, J. Bielavský, and M. Večeřa, *Collect. Czeck. Chem. Commun.*, **33**, 1687 (1968).

44) M. Isaks and H. H. Jaffé, *J. Amer. Chem. Soc.*, **86**, 2210 (1964).

45) This approximation has been reported to be applied satisfactorily for the mechanistic interpretation of the reactions involving the two protonation equilibrium such as hydrolysis of 4-dimethoxymethylpyridinium ion[46] and Wallach rearrangement.[38]

46) M. W. Fuller and W. M. Schubert, *J. Amer. Chem. Soc.*, **85**, 108 (1963).

Table 7. Rates of racemization of sulfoxides *p*-Tolyl-SO-R

R;	64.7% H_2SO_4[a] 10^4k (s^{-1})	96.7% H_2SO_4[b] 10^4k (s^{-1})	HCl[c] 10^5k (s^{-1})	HCl[d] 10^6k (s^{-1})
CH_3	4.20 ±0.40(3.53)	7.58 ±0.25(3.18)	3700(463)	
C_2H_5	2.30 ±0.15(1.93)		957(120)	
Phenyl	1.19 ±0.03(1.00)	2.38 ±0.10(1.00)	8.00(1.00)	27.6(1.00)
o-Tolyl	0.557±0.018(0.468)		4.53(0.566)	
Mesityl		0.268±0.013(0.113)	0.042(0.0052)	0.125(0.0045)

a) Sulfoxide=0.16 mol/l, at 30 °C. b) Sulfoxide=0.1 mol/l, at 0 °C.
c) In a 1 : 2 v/v mixture of 12 M aqueous HCl and dioxane at 25 °C (Ref. 1).
d) In 3.93 M-HCl in 80% dioxane-water, at 25 °C (Ref. 2). e) The relative rates are given in parentheses.

an error may be introduced.

Meanwhile, in the strong acid above *ca.* 93%, all acid species in the medium must take the form of either H_3O^+ or H_2SO_4. Then the route (c) including the general acid catalyzed removal of water would be conceivable. However, according to this mechanism, since it includes a proton transfer from the acid medium to the mono-protonated sulfoxide, a large isotope effect, $k_H/k_D>1$, must be expected. Actually, the isotope effect observed in the racemization of I in 17.68 mol/l is nearly one, as shown in Table 5. So this route (c) can be excluded.

All these results seem to suggest that sulfoxide I undergoes much less the A-1 reaction than II, and the legitimate A-1 type reaction takes place with I

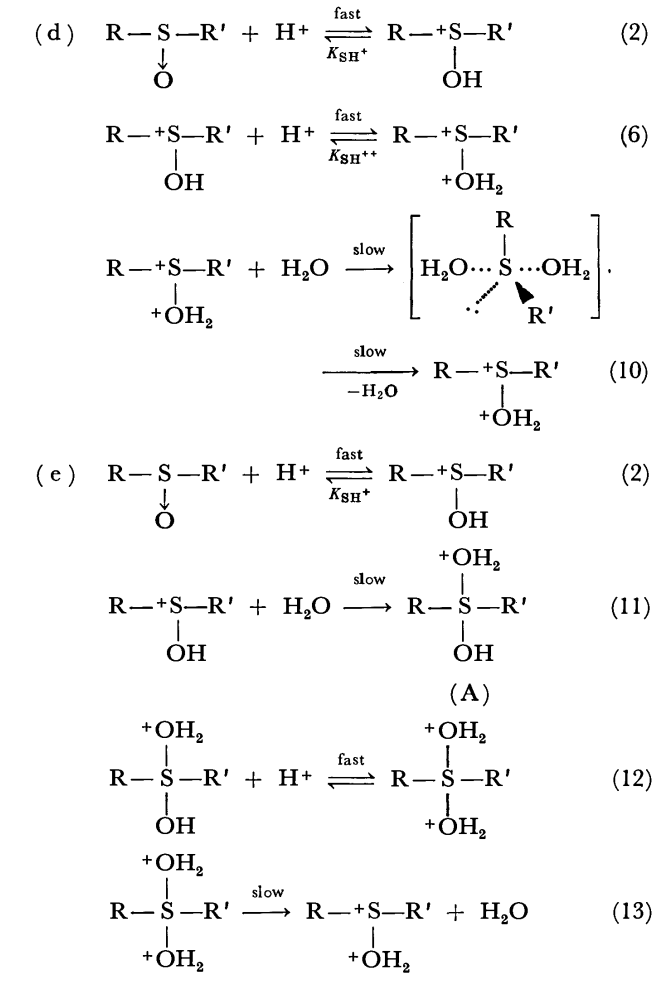

Scheme 2. S_N2-like mechanism.

only in an extremely concentrated sulfuric acid close to 100%. This may be attributed to the higher stability of the monoprotonated sulfoxide I and the less stability of the intermediate such as cation radical or dication derived from I.

The following two alternative routes (d) and (e) (in Scheme II) may be postulated for the S_N2 type reaction.

There are differences between the two routes (d and e) in the second protonation step and in the degree of bonding of both entering and leaving groups on sulfur atom at the transition state. The reaction *via* route (d) includes the rate-limiting displacement of water molecules on the sulfur atom. And the every displacements cause the "Walden Inversion" at the sulfur atom, since both entering and leaving water molecules assume axial-axial positions at the trigonal bipyramidal transition.[47] The scheme *via* route (e) begins with the first equilibrium of mono-protonation, followed by the slow nucleophilic attack of water to form intermediate (A), and the subsequent fast second protonation to (A). The racemization may take place in the step 11 or 12 or both, and the oxygen exchange takes place at the step 13. Up to now, many reactions including tetracovalent pentacoordinate sulfur intermediates have been investigated. The acid catalyzed reduction of sulfoxides by halide ion[33,48] and recemization reaction of sulfoxides in aqueous hydrochloric acid[1,2] have been known to form a halohydrine intermediate ($R_1R_2S(OH)X$), and in these reactions, large steric effects on the rates by bulky substituents attacked to the central sulfur atom have been found owing to the tightness of the intermediate. If the title reaction would take place through the route (e), a similarly large steric effect must be expected. The steric effects observed in the racemizations of *p*-tolyl alkyl and *p*-tolyl aryl sulfoxides in 64.7% sulfuric acid were studied. However, as shown in Table 7, the steric effect is not so large and almost the same as that in 96.7% sulfuric acid. Thus, the route (e) including the intervention of a tight intermediate seems unlikely.

The rate constants, k_1, of the oxygen exchange of several *p*-substituted diphenyl and methyl phenyl sulfoxides were measured in the less concentrated acid.

47) S. Oae, *Quart. Rept. Sulfur Chem.*, **5**, 53 (1970).
48) J. H. Krueger, *Inorg. Chem.*, **5**, 132 (1966); D. Landini, F. Montanari, G. Modena, and G. Scorrano, *Chem. Commun.*, **1968**, 86; R. A. Strecker and K. K. Andersen, *J. Org. Chem.*, **33**, 2234 (1968).

Table 8. Rate constants of ^{18}O-exchange of substituted sulfoxides R_1-$S^{18}O$-C_6H_4-R_2

R_1;	R_2;	H_2SO_4 (wt%)	10^4k_{obs} (s^{-1})	10^4k_1 (s^{-1})[c]
Phenyl[a]	*p*-CH_3	75.4	1.45	1.54
Phenyl	H	75.4	1.85	2.08
Phenyl	*p*-Cl	75.4	1.98	2.30
Phenyl	*p*-NO_2	75.4	2.43	
CH_3[b]	*p*-CH_3	64.7	0.202	0.216
CH_3	H	64.7	0.238	0.257
CH_3	*p*-Cl	64.7	0.241	0.270

a) Sulfoxide=0.1 mol/l, at 50°C,[10] Method A.
b) Sulfoxide=0.1 mol/l, at 30°C, Method A.
c) k_1 was calculated using the pK_{BH^+} values established by Landini *et al.*[31] (for methyl phenyl sulfoxides), and by us (for diphenyl sulfoxides).

One finds in Table 8 that the polar effects of *p*-substituents on k_1 are not large. When log k_1 values obtained were plotted against σ^+, a good straight line was obtained (for diphenyl sulfoxides $\rho=0.412$, and for methyl phenyl sulfoxides $\rho=0.250$). However, the small positive values of ρ seems only to point out that the nucleophilic substitution of the protonated sulfoxide by water is the slow rate-limiting step of the reaction at a less concentrated sulfuric acid.

Experimental

Materials. *Optically Active Sulfoxides* were prepared from (−)menthyl (−) *p*-toluenesulfinate [mp 107—7.5 °C, $[\alpha]_D$ −200.4° ($c=1.85$, $l=0.5$ acetone)(lit,[49] mp 106—7 °C, $[\alpha]_D^{25}$ −199.2° (acetone)] and the corresponding aryl or alkyl Grignard's reagent according to the method developed by Andersen.[50] The mp or bp and specific rotations of sulfoxides obtained are as follows. *p*-Tolyl-SO-R; (R; mp or bp, specific rotation ($l=0.5$), (lit)[51]). CH_3; 74 °C, $[\alpha]_D^{23}$ +146.0° ($c=1.80$, acetone), (73—74.5 °C, $[\alpha]_D$ +145.5° (acetone)), C_2H_5; 95—97 °C/0.5 mmHg, $[\alpha]_D^{25}$ +184° ($c=1.3$, acetone), (123—126 °C/1.5 mmHg, $[\alpha]_D^{25}$ +186°(acetone)), C_6H_5; 92 °C, $[\alpha]_D^{20}$ +27.6°($c=1.53$, EtOH), (92—93 °C, $[\alpha]_D$ +27°(EtOH)), *o*-CH_3-C_6H_4; 78—78.5 °C, $[\alpha]_D^{20}$ −90.5°($c=1.21$, acetone), (77.8—78.5 °C, $[\alpha]_D$ −89.1° (acetone)), Mesityl; 107—107.5 °C, $[\alpha]_D^{22}$ −265.5° ($c=1.53$, EtOH), (107—107.5 °C, $[\alpha]_D$ −259° (EtOH)).

^{18}O-Labeled Sulfoxides were prepared by the bromine-oxidation of the corresponding sulfides in the presence of ^{18}O-enriched water(1.62 *atom*%-^{18}O) in acetic acid by the similar procedure described in our previous paper.[52] A sulfide (1 mol) was dissolved in a mixture of ^{18}O-enriched water(2—5 mol, 1.62 *atom*%-^{18}O), pyridine(5 mol) and acetic acid, and the solution was cooled under 0 °C, and then acetic acid solution of bromine (1 mol) was added dropwise over a period of 1 hr. After stirring for 1 hr, the mixture was poured into a large amount of ice-water, and the aqueous solution was neutralized with sodium bicarbonate. The resulted sulfoxide was extracted with chloroform, and the extract was washed with 10% aqueous solution of sodium thiosulfate and water, respectively, and dried. Finally, chloroform was distilled off and the crude ^{18}O-labeled sulfoxide was purified by distillation or recrystallization. Their mp or bp and *atom*%-^{18}O are as follows. $C_6H_5SOC_6H_4$-R; (R; mp or bp(lit)[53], *atom*%-^{18}O), *p*-CH_3; 71.5—72 °C (71 °C), 1.12, H; 70—71 °C(71 °C), 0.852, *p*-Cl; 45—46 °C (45—46 °C), 1.23, *p*-NO_2; 107 °C (106—107 °C), 0.996(This oxide was prepared using 3.50 *atom*%-$H_2^{18}O$). $CH_3SOC_6H_4$-R; (R; mp or bp(lit), *atom*%-^{18}O), *p*-CH_3; 42—43 °C (42—43 °C),[53] 1.08, H; 84 °C/0.25 mmHg(85 °C/0.5 mmHg),[54] 0.997, *p*-Cl; 46—48 °C(47—48 °C),[53] 0.983.

Kinetic Procedures. The rate of oxygen exchange and racemization were measured by the following two methods using YANAGIMOTO OR-10 TYPE polarimeter and HITACHI RMU-6E TYPE mass-spectrometer.

Method A(for both oxygen exchange and racemization). An ^{18}O-labeled or an optically active sulfoxide of a set mol was dissolved in sulfuric acid at a preset temperature. Aliquot portion(5 ml) of the solution was taken up from time to time for 5—7 times, and was quenched with 100 ml of ice-water. The sulfoxide recovered was then extracted with carbon tetrachloride or chloroform and the extract was washed with water, 10% aqueous solution of sodium carbonate and water, respectively, and dried over anhydrous sodium sulfate, and the solvent was then distilled off. The sulfoxide resulted was dried and subjected to both ^{18}O-analysis or specific rotation measurement. The ^{18}O-atom% was calculated from the mass peak heights 44 and 46 of carbon dioxide according to the method described by Samuel.[55] The rate constant for oxygen exchange were calculated from the equation, $\log \beta_0-\beta/\beta_t-\beta=kt/2.303$, where β_0 and β_t are atom% of ^{18}O at time 0 and t, respectively, and β is the atom% of ^{18}O of natural CO_2. The pseudo-first-order rate constant for the racemization was calculated from the equation, $\log \alpha_0'/\alpha_t'=kt/2.303$, where α_0' and α_t' are the specific rotation, $[\alpha]_D$, at time 0 and t, respectively.

Method B (for racemization): In the square shape cell (5 cm) was placed a sulfuric acid solution containing an optically active sulfoxide of a set mol, the rate was measured directly by checking the rotation, α, of polarimeter which was set at a desired temperature with a constant temperature bath connected. The pseudo-first-order rate constants were evaluated by the following equation, $\log \alpha_0/\alpha_t=kt/2.303$, where α_0 and α_t are the rotatory power at time 0 and t, respectively.

Sulfuric Acid. The concentration(wt%) of sulfuric acid medium was determined by titration with a standard alkali solution. The H_0 values of the media were obtained by interpolation from a graph of the data of Johnson *et al.*[30] D_2SO_4–D_2O solutions were prepared from MERCK D_2SO_4 (*min.* 99%-*d*) by dilution with D_2O (*min.* 99.75%-*d*). The concentration of acid was determined by titration of a weighed sample with a standard alkali solution. The molarity of the acid was calculated from the specific gravity. The specific gravities of ordinary acids used here are the values in the established table,[56] and these of deuterio acid media were newly determined by weight-method. The activity of water, $\log a_{H_2O}$, of the acid media was the value interpolated from the table of Giauque *et al.*[57]

49) H. F. Herbrandson, R. T. Dickerson, Jr., and J. Winstein, *J. Amer. Chem. Soc.*, **78**, 2576 (1956).
50) K. K. Andersen, *Tetrahedron Lett.*, **1962**, 93.
51) K. Mislow, M. M. Green, P. Laur, J. T. Melillo, T. Simmons, and A. L. Ternay, Jr., *J. Amer. Chem. Soc.*, **87**, 1958 (1965).
52) S. Oae, Y. Ohnishi, S. Kozuka, and W. Tagaki, This Bulletin, **39**, 364 (1966).
53) A. Cerniani and G. Modena, *Gazz. Chim. Ital.*, **89**, 834 (1959).
54) K. K. Andersen, *J. Org. Chem.*, **29**, 1953 (1965).
55) D. Samuel, "Methodology by Oxygen Isotope," in "Oxygenease," Chap. 2, ed by O. Hayaishi, Academic Press, New York, N. Y., (1962).
56) "Kagaku Binran", ed by Chem. Soc. Japan. Maruzen, Japan (1966), p. 439.
57) W. F. Giauque, E. W. Hornung, J. E. Kunzler, and T. R. Rubin, *J. Amer. Chem. Soc.*, **82**, 62 (1960).

Preparation, Polymerization, and Copolymerization of *N*-Vinyl Phthalimidine[1)]

Kenichi MURATA

Government Industrial Research Institute, Osaka, Midorigaoka, Ikeda, Osaka 563

(Received August 30, 1972)

The preparation, polymerization, and copolymerization of *N*-vinyl phthalimidine were investigated. The monomer was prepared by the dehydrochlorination of *N*-(β-chloroethyl) phthalimidine. Polymerization was carried out in the presence of radical or cationic initiators in bulk and in solution. It was found that polymerizability with cationic initiators was larger than that with radical ones. The resulting polymers had a softening point in the range of 160—180 °C, the reduced viscosities being small. Copolymerization with acrylonitrile and styrene was carried out in dimethylformamide and benzene by radical initiators. The monomer reactivity ratios and Alfrey-Price Q and e values calculated from the copolymerization data of the monomer (M_1) and styrene (M_2) were $r_1=0.05$, $r_2=7.4$, $Q_1=0.30$, and $e_1=-1.80$. Values for *N*-vinyl pyrrolidone (M_1) were likewise determined for the sake of comparison, and found to be $r_1=0.02$, $r_2=12.0$, $Q_1=0.22$, and $e_1=-1.99$.

The polymerization and copolymerization of *N*-vinyl imides such as *N*-vinyl phthalimide and *N*-vinyl succinimide by radical process have been reported by many workers. In previous papers,[2-4)] the author reported on the polymerization and graft-copolymerization by γ-ray radiation, and the copolymerization by radical initiators.

N-Vinyl phthalimidine has been synthesized by Ooki,[5)] and Kato and Yoshida,[6)] but its polymerization and copolymerization have hardly been discussed at all.

In this paper the author reports a new preparative method of *N*-vinyl phthalimidine, and its polymerization and copolymerization.

Experimental

N-Vinyl Phthalimidine. The monomer was prepared *via* the dehydrochlorination of *N*-(β-chloroethyl) phthalimidine obtained after the condensation of monoethanolamine with phthalide and the following chlorination.

N-(β-Hydroxyethyl) Phthalimidine: To 16.0 g (0.26 mol) of monoethanolamine was added 35.0 g (0.26 mol) of phthalide, and the mixture was heated at 190—200 °C for about 6 hr to remove the water formed by condensation reaction. The amount of water removed was approximately 4 ml. The reaction product crystallized completely at room temperature. Recrystallization from benzene yielded 41.4 g (90%) of *N*-(β-hydroxyethyl) phthalimidine as colorless plates with a melting point of 119—120 °C (lit. mp 113—114 °C[6)]).

Found: C, 67.48; H, 6.06; N, 7.81%; mol wt (Rast), 181. Calcd for $C_{10}H_{11}NO_2$: C, 67.78; H, 6.26; N, 7.91%; mol wt, 177.2.

N-(β-Chloroethyl) Phthalimidine: To a solution containing 23.0 g (0.13 mol) of *N*-(β-hydroxyethyl) phthalimidine in 100 ml of benzene was added, drop by drop, 18.0 g (0.15 mol) of thionyl chloride with stirring at 5—10 °C for 30 min. After addition was completed, stirring was continued for 6 hr at room temperature. The solvent and volatile parts were removed as much as possible under reduced pressure, and the remaining part then began to crystallize. The crude crystals were also dissolved in a small amount of fresh benzene and the solution was poured into a large amount of petroleum benzine (bp 50—90 °C) to obtain 24.2 g (95%) of the crystals with a melting point of 78—82 °C. Recrystallization from petroleum benzine gave *N*-(β-chloroethyl) phthalimidine as colorless plates, mp 81—82 °C.

Found: C, 61.89; H, 5.06; N, 7.29%; mol wt (Rast), 199. Calcd for $C_{10}H_{10}NOCl$: C, 61.39; H, 5.15; N, 7.16%; mol wt, 195.7.

N-Vinyl Phthalimidine: To a solution containing 19.6 g (0.10 mol) of *N*-(β-chloroethyl) phthalimidine in 150 ml of benzene was added 10 g (0.18 mol) of potassium hydroxide pellets. The mixture was refluxed for 15 hr, while the liberated water was collected in a receiver. The reaction product was filtered to remove potassium chloride. The filtrate was concentrated under reduced pressure, and the remaining part then began to crystallize. Recrystallization from petroleum benzine gave 11.0 g (69%) of *N*-vinyl phthalimidine as colorless needles with a melting point of 66—67 °C (lit. mp 66—67 °C,[5)] mp 66.5 °C[6)]); its infrared absorption bands were at 1680 (phthalimidine carbonyl), 1610 (benzene ring), 1630, 1420, 975, 935 (vinyl), and 730 cm^{-1} (*o*-disubstituted benzene) (Fig. 1).

The ultraviolet absorption maxima in ethanol were: 228.5 (ε, 10900), 236 (8390), 276 (10000), and 280 nm (9860).

Found: C, 75.52; H, 5.52; N, 8.83%; mol wt (Rast), 164. Calcd for $C_{10}H_9NO$: C, 75.45; H, 5.70; N, 8.80%; mol wt, 159.2.

Other Materials. Commercial vinyl monomers such as acrylonitrile, styrene, and *N*-vinyl pyrrolidone were purified in the usual manners prior to use. Commercial initiators, azobisisobutylonitrile, benzoyl peroxide, boron trifluoride etherate, and stannic chloride were purified by reprecipitation, recrystallization, and distillation. Solvents, benzene and dimethylformamide were also purified according to the usual methods.

Polymerization Procedure. For polymerization and copolymerization in the presence of initiator, the required amounts of monomers, initiator, and solvent were weighed into a glass ampule, sealed under nitrogen atmosphere except for the cationic polymerization. In the radiation-induced polymerization, the ampule was irradiated by a cobalt-60 source for a given time.

After polymerization, the contents in the ampule were poured into a large amount of diethylether and methanol to precipitate the homopolymer and copolymer, respectively. The resulting polymers were filtered, washed with diethylether or methanol, dried under reduced pressure and weighed.

Elemental Analyses. The copolymers were purified by repeated precipitations. The copolymer compositions were determined by carbon and nitrogen analyses with a Yanagimoto C. H. N. Corder, Model MT-1.

1) Paper presented at the 20th Annual Meeting of the Society of Polymer Science, Japan, Tokyo, May 25, 1971.
2) K. Murata, *J. Polym. Sci., A-1*, **5**, 2942 (1967).
3) K. Murata, This Bulletin, **40**, 2187 (1967).
4) K. Murata and A. Terada, This Bulletin, **39**, 2494 (1966).
5) S. Ooki, *Yakugaku Zasshi*, **70**, 102 (1950).
6) K. Kato and M. Yoshida, *Nippon Kagaku Zasshi*, **87**, 1100 (1966).

Viscosity Measurement. The reduced viscosity of the resulting polymer was determined at 30±0.01 °C as a 0.50% solution in dimethylformamide with an Ostwald viscometer.

Infrared Absorption Spectra. The infrared absorption spectra were obtained with a JASCO Infrared spectrophotometer, Model IR-G.

Results and Discussion

Preparation of N-*Vinyl Phthalimidine.* *N*-Vinyl phthalimidine was prepared by the olefin decomposition of the corresponding quaternary ammonium hydroxide by Ooki[5] for the first time with only a 43% yield. Kato and Yoshida[6] obtained the same monomer by the pyrolysis of *N*-(β-acetoxyethyl) phthalimidine, but the method when traced by the author gave a very poor yield.

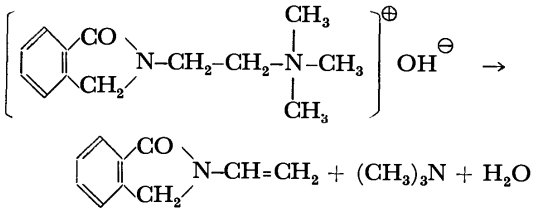

A new method was worked out to improve the yield. The monomer was prepared by the dehydrochlorination of *N*-(β-chloroethyl) phthalimidine.

The chlorination reaction of *N*-(β-hydroxyethyl) phthalimidine with thionyl chloride in benzene afforded *N*-(β-chloroethyl) phthalimidine as colorless plates with a 119—120 °C melting point in a good yield. The dehydrochlorination reaction of the

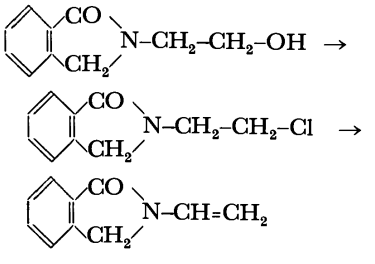

chloride was carried out by the use of potassium hydroxide pellets in benzene to give *N*-vinyl phthalimidine as colorless needles with a melting point of 66—67 °C in a 69% yield. The infrared absorption spectrum was shown in Fig. 1.

Polymerization of N-*Vinyl Phthalimidine.* This was carried out in bulk or solution state. Initiators such as azobisisobutyronitrile (AIBN), benzoyl peroxide (BPO), boron trifluoride etherate, and stannic chloride, and also γ-rays from a cobalt-60 source were used. The results are shown in Table 1. We see that the polymerizability by AIBN is larger than that by BPO, the tendency being observed also in the polymerization of *N*-vinyl pyrrolidone. The *N*-vinyl phthalimidine was similarly polymerized by irradiation of γ-rays. Polymerization in the presence of cationic initiators was carried out more effectively compared with that in the presence of radical ones. This is because Alfrey-Price *e* value for *N*-vinyl phthalimidine is large and negative (Table 4).

The resulting polymer is a transparent resin having a 160—180 °C softening point, and soluble in benzene and insoluble in water in contrast to *N*-vinyl pyrrolidone polymer. The reduced viscosities of all the polymers were small, particularly in the polymers obtained by cationic polymerization.

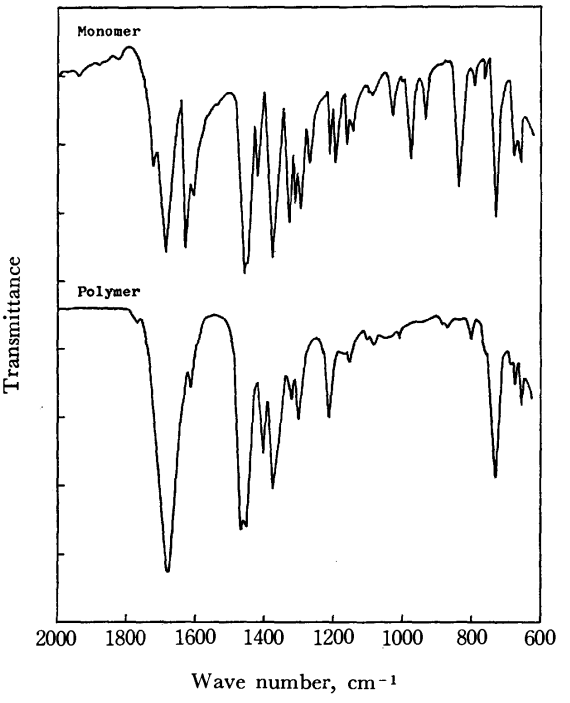

Fig. 1. Infrared absorption spectra of *N*-vinyl phthalimidine and its polymer in Nujol paste.

The infrared absorption spectrum of this *N*-vinyl phthalimidine polymer is shown in Fig. 1, no absorption bands (1630, 975, and 933 cm^{-1}) due to vinyl group in the original monomer being found.

Copolymerization of N-*Vinyl Phthalimidine.* The results of the copolymerization of *N*-vinyl phthalimidine with acrylonitrile and styrene by the use of BPO in dimethylformamide at 60 °C are shown in Table 2, together with those of *N*-vinyl pyrrolidone for comparison. The analytical data show that the *N*-vinyl phthalimidine can polymerize with the vinyl monomers, but *N*-vinyl phthalimidine is less reactive to enter the copolymer with styrene than that with acrylonitrile. The tendency was also observed in the copolymerization of *N*-vinyl pyrrolidone.

In an attempt to determine the monomer reactivity ratios for the system of *N*-vinyl phthalimidine and styrene, copolymerizations in dimethylformamide and in benzene were carried out statically at 60 °C. The monomer ratio in the initial stage was varied, while BPO or AIBN was used as the radical source at a concentration of 1.0 mol% in each case. All the procedures were carried out in less than 10% conversion to determine the initial stage of each copolymerization.

The results of copolymerization by BPO in dimethylformamide are given in Table 3. M_1 and M_2 denote the molar concentrations of *N*-vinyl phthalimidine and styrene, respectively, at the initial feeding, and m_1 and m_2 the molar fractions of the monomers

TABLE 1. POLYMERIZATION OF *N*-VINYL PHTHALIMIDINE[a)]

Initiator	mol%	Benzene ml	Temperature °C	Time hr	Yield %	Reduced viscosity dl/g
AIBN	1.0	0	70	1.0	28.2	—
AIBN	1.0	0	70	3.0	60.3	0.14
AIBN	1.0	1.00	60	24.0	23.8	—
BPO	0.66	0	70	24.0	6.5	—
BPO	3.0	1.00	70	45.0	16.1	0.05
γ-Ray	2.5×10^5 R/hr	1.00	25	42.0	29.7	0.07
γ-Ray	2.5×10^5 R/hr	1.00	25	96.0	63.4	—
BF_3Et_2O	2.0	1.00	20	0.33	74.0	0.03
BF_3Et_2O	8.0	1.00	20	0.17	87.1	0.03
$SnCl_4$	2.0	1.00	20	0.17	36.1	0.03

a) Cationic polymerization was carried out in air.

TABLE 2. COPOLYMERIZATIONS OF *N*-VINYL PHTHALIMIDINE (VPH) AND *N*-VINYL PYRROLIDONE (VPY) WITH ACRYLONITRILE (AN) AND STYRENE (St) BY BENZOYL PEROXIDE[a)]

Monomer (M_1)	10^{-4} mol	Comonomer	10^{-4} mol	BPO mg	Time hr	Yield %	Nitrogen %	m_1 in copolymer mol%
VPH	25	AN	75	5	1.3	6.8	14.75 14.75	40
VPH	22	AN	66	10	3.0	28.2	14.81 14.86	39
VPH	22	St	34	10	26.0	19.3	1.28 1.37	10
VPY	32	AN	66	5	1.0	22.0	18.13 18.20	42
VPY	32	St	34	10	26.0	17.3	1.23 1.22	9

a) Solvent, dimethylformamide 1.00 ml; temperature, 60 °C.

TABLE 3. COPOLYMERIZATION OF *N*-VINYL PHTHALIMIDINE (M_1) WITH STYRENE (M_2) BY BENZOYL PEROXIDE[a)]

Monomers M_1	10^{-4} mol M_2	Polymn. rate %/hr	Carbon %	Nitrogen %	Mol% from C% m_1	Mol% from C% m_2	mol% from N% m_1	mol% from N% m_2
5	45	3.1_0	92.13 92.05	0.27 0.30	0.5	99.5	2.6	97.4
10	40	2.3_8	91.68 91.55	0.59 0.58	2.3	97.7	4.5	95.5
15	35	1.8_2	91.25 90.98	0.84 0.84	4.3	95.7	6.5	93.5
20	30	1.6_7	90.38 90.37	1.10 1.13	7.4	92.6	8.7	91.3
25	25	1.1_9	89.01 89.03	1.41 1.45	13.3	86.7	11.3	88.7
30	20	0.7_7	87.92 88.19	1.76 1.87	17.7	82.3	14.6	85.4
35	15	0.4_2	86.19 87.11	2.27 2.29	24.5	75.5	18.6	81.4

a) Initiator, BPO 1.0 mol%; solvent, dimethylformamide 0.50 ml; temperature, 60 °C.

in the resulting copolymers calculated from the carbon and nitrogen analyses. According to the curve fitting method with use of all the average values of respective m_1 and m_2, the following was obtained.

$$r_1=0.05$$
and $$r_2=7.4.$$

The results of copolymerization by AIBN in benzene were close to those obtained above.

The copolymerization of *N*-vinyl pyrrolidone–styrene system was similarly carried out in the presence of BPO in dimethylformamide. The monomer reactivity ratios were calculated in the same way and found to be

$$r_1=0.02$$
and $$r_2=12.0.$$

Bork and Coleman[7] have dealt with the copoly-

7) J. F. Bork and L. E. Coleman, *J. Polym. Sci.*, **43**, 413 (1960).

Table 4. Alfrey-Price Q and e values of *N*-vinyl lactams and *N*-vinyl imides

Monomer	Q	e
N-Vinyl phthalimidine	0.30	−1.80
N-Vinyl pyrrolidone	0.22	−1.99
N-Vinyl phthalimide	0.09	−0.13
N-Vinyl succinimide	0.06	−0.17

merization of the same system by AIBN in benzene at 50 °C, their results being $r_1=0.045$ and $r_2=15.7$. These are close to the values obtained herewith.

In the copolymerizations of *N*-vinyl phthalimidine and *N*-vinyl pyrrolidone with styrene, it was also found that the rates of copolymerization decreased in proportion to the increase in the initial feedings of *N*-vinyl phthalimidine and *N*-vinyl pyrrolidone.

The Q and e Parameters. The Q and e parameters for these monomers were calculated according to the Alfrey-Price scheme[8] by using the values, r_1 and r_2, and $Q=1.0$ and $e=-0.8$ for styrene. The calculated Q and e values and those of *N*-vinyl imides[3] of related type are shown in Table 4. The respective pairs of the Q and e parameters of *N*-vinyl phthalimidine and *N*-vinyl pyrrolidone are very similar to each other. This indicates that the effects of the two substituents on the radical polymerization of such monomers closely resemble each other.

The e values of *N*-vinyl phthalimidine and *N*-vinyl pyrrolidone are much more negative than those of *N*-vinyl phthalimide and *N*-vinyl succinimide. This may be explained by the electron-attractive power (mesomeric effect) of carbonyl group in these monomers.

8) T. Alfrey and C. C. Price, *J. Polym. Sci.*, **2**, 101 (1974).

BULLETIN OF THE CHEMICAL SOCIETY OF JAPAN, VOL. 46, 1755—1759 (1973)

The Synthesis of 4-Chloro-3-benzoyl-2-azetinone Derivatives and Their Conversion into *N*-Benzoyl-2,4-azetidinedione Derivatives

Kiyotada Matsui and Masatoshi Motoi

Department of Industrial Chemistry, Faculty of Technology, Kanazawa University, Kodatsuno, Kanazawa 921

(Received September 14, 1972)

The treatment of ethyl α-cyanophenylacetate with benzoyl chloride in the presence of 2 equivalents of aluminum chloride in nitrobenzene afforded 4-chloro-3-benzoyl-3-phenyl- (6% yield) and 4-chloro-3-benzoyl-3-(*p*-benzoylphenyl)-2-azetinone (28%) at 50 °C. The same treatment of ethyl α-cyanopropionate afforded 4-chloro-3-benzoyl-3-methyl-2-azetinone (37%). The hydrolytic splitting of the chlorine atoms from the first two azetinones resulted in the formation of *N*-benzoyl-2,4-azetidinedione derivatives (36 and 20% respectively), whereas from the last we obtained *N*-benzoyl-α-carboxypropionamide (18%). These azetinone derivatives, when warmed with sodium methoxide in methanol, were converted into α-benzoyl α-cyano esters. The treatment of α-benzoyl α-cyano esters with aluminum chloride also afforded the azetinone derivatives in low yields.

Earlier studies of the aluminum chloride-catalyzed acylation[1] of active methylene compounds with acid chlorides were extended to the use of α-cyano esters as substrates. Thus, it was found that 4-chloro-3-benzoyl-2-azetinone derivatives could be formed from α-benzoylated α-cyano esters. The reconversion of the azetinone derivatives to the latter esters and their transannular, hydrolytic rearrangement to *N*-benzoyl-2,4-azetidinedione derivatives (*N*-benzoylmalonimides) were encountered.

When ethyl cyanoacetate was treated with benzoyl chloride in the presence of aluminum chloride in nitrobenzene at 55 °C, ethyl benzoylcyanoacetate was obtained as the main product. According to our previously-proposed mechanism,[1] the acylation can be explained in terms of an intramolecular condensation reaction which proceeds by means of the elimination of aluminum chloride from the coordination complex between acyl chloride and dichloroaluminum enolate as is shown in Scheme 1.

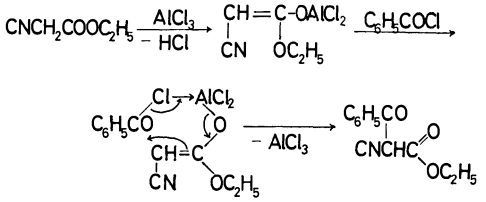

Scheme 1.

The benzoylation of ethyl α-cyanophenylacetate afforded a substance (Ia) in the presence of one equivalent of aluminum chloride at 50 °C, but the use of a larger amount of the condensing agent led to the formation of another substance (Ia′) besides Ia, while the benzoylation of ethyl α-cyanopropionate afforded only one product (Ib). The IR spectra of Ia, Ia′, and Ib are comparable to each other, none showing any band due to the cyano group. Their molecular formulas indicate that the α-benzoylated cyano ester is converted into Ia or Ib by losing its ethoxyl group and gaining a chlorine atom, and that Ia′ is a benzoylated

1) T. Nojiri and K. Matsui, *Nippon Kagaku Zasshi*, **87**, 880 (1966); T. Nojiri, I. Hashimoto, M. Motoi, and K. Matsui, This Bulletin, **42**, 3359 (1969); K. Matsui, M. Motoi, and T. Nojiri, *ibid.*, **46**, 562 (1973).

product from the Ia. Thus, each of the structures seems to have a 4-chloro-3-benzoyl-2-azetinone ring. The reaction seems to be a novel case of the Ritter reaction[2] known as the nucleophilic addition of a nitrile to a carbonium ion in the presence of sulfuric acid. By analogy with the mechanism proposed for the aluminum chloride-catalyzed transacylation[3] between β-diketones and esters, the mechanism for the present reaction can be depicted as in Scheme 2.

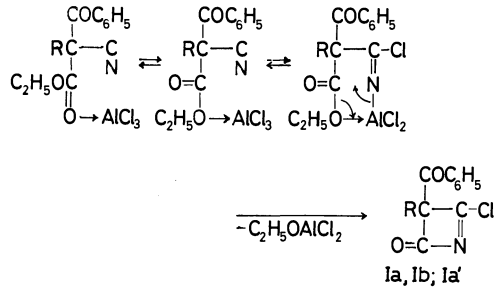

a: R=C_6H_5; b: R=CH_3; a′: R=*p*-$C_6H_5COC_6H_4$

Scheme 2.

The formation of Ia′ can be ascribed to the Friedel-Crafts benzoylation at the *para* position of the phenyl group of Ia, because the hydrolysis of Ia′ gives *p*-benzoylated compounds, as will be described in the Experimental section. The facile formation of the four-membered ring from the α-substituted, but not from the unsubstituted cyanoacetic ester, seems to be ascribable to a deviation from the normal valence angle by the introduction of a benzoyl group into the α position of the ester.

The treatment of 4-chloro-3-benzoyl-3-phenyl- (Ia), 4-chloro-3-benzoyl-3-(*p*-benzoylphenyl)- (Ia′), and 4-chloro-3-benzoyl-3-methyl-2-azetinone (Ib) with sodium methoxide in methanol gave their respective products, all of which show the IR spectra characteristic of α-benzoyl α-cyano esters, but the treatment of ethyl α-benzoyl-α-cyanophenylacetate and -α-cyanopropionate with aluminum chloride in nitrobenzene gave Ia and Ia′, and Ib, respectively, in low yields. These findings support the assigned structures. The formation of this Ia′ suggests that free benzoyl chloride is liberated from the reactants during the reaction because of the reversibility[1] of the aluminum chloride-catalyzed acylation with acyl chlorides. The formation of α-benzoyl α-cyano ester by ring-opening can be explained in terms of the 1,4 attack of sodium methoxide on the 4-chloro-2-azetinone ring, as is illustrated in Scheme 3.

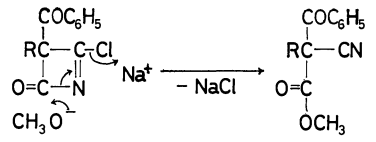

Scheme 3.

The hydrolytic splitting of the chlorine atom from Ia with glacial acetic acid containing a few drops of concentrated hydrochloric acid resulted in small amounts of *N*-benzoylphenylacetamide (IVa) and another substance (IIa), together with the unaltered Ia (47%), without giving a detectable amount of benzoic acid. The product IIa, with the composition of the expected 3-benzoyl-3-phenyl-2,4-azetidinedione, melts at 228.5—229.5 °C and is soluble in an aqueous sodium bicarbonate solution. In this solution, the IIa is partly converted into IVa on standing at room temperature, but remains unchanged to a certain extent. Obviously, the benzoyl group migrates from the carbon to the nitrogen atom.

The IR spectrum of Ia is somewhat similar to that of IIa, as will be described in the Experimental section. In the frequency region higher than 1200 cm^{-1}, however, a comparison of the two spectra shows that the absorption bands for Ia at 1745 cm^{-1} and at 1238 and 1217 cm^{-1}, which may be due to ClC=N and Ar-CO-C respectively, are replaced by the bands at 1660 and 1629 cm^{-1}, and at 1426, 1402, and 1276 cm^{-1}, which may be assigned mainly to NC=O and N≡C_3 respectively, in IIa, which has no absorption due to N-H. Thus, the benzoyl group in IIa must be situated on the nitrogen atom; hence, IIa may be characterized as *N*-benzoyl-3-phenyl-2,4-azetidinedione. A similar acidic hydrolysis of Ia′ provided a chlorine-free substance (IIa′) (mp 228—230 °C), which was characterized as *N*-benzoyl-3-(*p*-benzoylphenyl)-2,4-azetidinedione by its IR spectrum, which is similar to that of IIa. Moreover, under more drastic conditions, Ia′ as well as Ia was hydrolyzed to give benzamide derived from the rearranged products.

A solution of Ia in methanol containing sodium carbonate, on standing at room temperature, also afforded a small amount of IIa, a trace of IVa, and an oil which was soluble in an aqueous sodium hydroxide solution but not in a sodium bicarbonate solution. This oil reacted to give an unidentified 2,4-dinitrophenylhydrazone which was not formed from Ia, and it was converted into desoxybenzoin (Va) and benzil upon treatment with sodium nitrite and sulfuric acid. The formation of such a hydrazone or ketones suggests that, in an alkaline medium, a part of either Ia or intermediate 3-benzoyl-3-phenyl-2,4-azetidinedione can be hydrolyzed with ring-opening prior to the rearrangement, as is shown in Scheme 4.

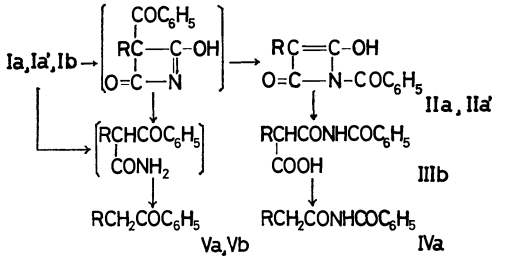

Scheme 4.

The rearrangement, being independent of the acidities of media, seems to proceed intramolecularly through both resonance-stabilized anions from the 3-benzoyl-

2) L. I. Krimen and D. J. Cota, "Organic Reactions," Vol. 17, p. 213 (1969).

3) K. Matsui and M. Motoi, This Bulletin, **46**, 565 (1973).

and *N*-benzoyl-azetidinedione derivatives. Accordingly, the transannular migration of the benzoyl group can be considered as being due to the relative unstability of the former anion which has a quaternary carbon atom linked to the three carbonyl groups. For this electrophilic rearrangement, the transition state shown in Scheme 5 may be passed through.

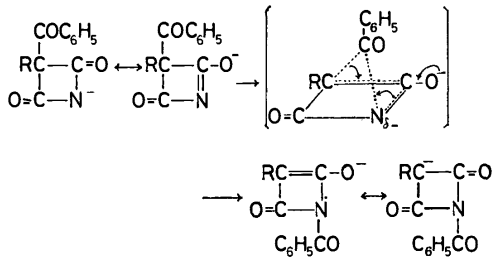

Sceheme 5

Ib, under conditions similar to those in the above acidic hydrolysis of Ia, was converted into *N*-benzoyl-α-carboxypropionamide (IIIb) (18%), benzoic acid, and a mixture, giving the unaltered Ib (75%). The acidic hydrolysis of the mixture gave a slight amount of propiophenone (Vb). It can be seen that Ib undergoes the same rearrangement and subsequent ring-opening to give IIIb; it is also subject to some acid cleavage.

Further work is required on the general preparation of *N*-acyl-2,4-azetidinediones.

Experimental

Materials. Commercial ethyl cyanoacetate was distilled at 206—207 °C before use. The ethyl α-cyanopropionate[4] and ethyl α-cyanophenylacetate[5] were prepared according to the literature, boiling at 86.4—87 °C/17 mmHg and at 125—127 °C/3.5 mmHg respectively. IR of the latter: 2250, 1747, 1240, 1028 cm^{-1}. Ethyl α-benzoyl-α-cyanophenylacetate was prepared from ethyl α-cyanophenylacetate by a modification of the method described in the literature[6]; bp 135—136 °C/0.03 mmHg. Found: C, 73.48; H, 5.13; N, 4.71%. Calcd for $C_{18}H_{15}NO_3$: C, 73.7; H, 5.17; N, 4.78%. IR: 2264, 1763—1749, 1696, 1218—1184, 1005 cm^{-1}. Ethyl α-benzoyl-α-cyanopropionate was also prepared as above; bp 116—117 °C/0.4 mmHg. Found: C, 67.54; H, 5.63; N, 5.94%. Calcd for $C_{13}H_{13}NO_3$: C, 67.51; H, 5.68; N, 6.06%. IR: 2207, 1752, 1709, 1259—1229, 1014 cm^{-1}.

General Procedure for Preparing Crude Ethyl Benzoylcyanoacetate and 4-Chloro-3-benzoyl-2-azetinone Derivatives. To a cold solution of aluminum chloride in dry nitrobenzene (10 ml), which was placed in a 50-ml flask equipped with a calcium chloride tube, we added the cyano ester (15 mmol) and then benzoyl chloride (4.2 g, 30 mmol) with cooling. The mixture was kept, with occasional swirling, in a thermostat. The reaction mixture was then stirred into a mixture of crushed ice and hydrochloric acid, after which the mixture was shaken with ether. The upper layer was washed with water to remove the aluminum chloride, and then shaken occasionally with a sodium bicarbonate solution until the Beilstein test for benzoyl chloride showed negligible results. The upper layer was then concentrated and steam-distilled *in vacuo* to leave a crude crystalline product.

a) Ethyl Benzoylcyanoacetate: The crude product obtained from ethyl cyanoacetate (1.7 g) by using aluminum chloride (4 g, 30 mmol) at 55 °C for 20 hr was found to consist of slight amounts of dibenzoyl- and tribenzoyl-methane by the use of the procedures described in our previous papers.[1] The aqueous sodium bicarbonate extract, after having been acidified with hydrochloric acid, was shaken with ethyl acetate. The upper layer was shaken with an aqueous copper acetate solution, and then the resulting product was filtered from copper benzoate. The upper layer of the filtrate was dried over sodium sulfate and concentrated to give a copper complex (mp 231—233 °C, ethanol), which was usually decomposed to give ethyl benzoylcyanoacetate. The aqueous solution containing aluminum chloride, after standing for a week, was extracted with ether. The evaporation of the ether extract gave an oil which was subsequently crystallized from ethanol to give ethyl benzoylcyanoacetate; mp 39—40 °C, (Found: N, 6.16%). The total yield was 41%.

b) 4-Chloro-3-benzoyl-3-phenyl-2-azetinone, Ia: The crude product obtained from ethyl α-cyanophenylacetate (2.84 g) by using aluminum chloride (15 mmol) at 50 °C for 48 hr was dissolved in a slight amount of benzene; then the solution was transferred onto a column packed with silica gel (60—200 mesh). Ia, eluted with benzene–petroleum ether (1 : 1), was recrystallized from ethanol as colorless needles (0.65 g, 15%), mp 184—185 °C. Found: C, 67.33; H, 3.56; Cl, 12.91; N, 4.91%. Calcd for $C_{16}H_{10}ClNO_2$: C, 67.73; H, 3.56; Cl, 12.49; N, 4.94%. MS: M^+=283, 285 (intensity ratio, 3 : 1). IR(KBr): 1745(s), 1707(sh), 1601(sh), 1592(s), 1567(s), 1547(s), 1491(m), 1446(m), 1350(s), 1314(w), 1238(s), 1217(m), 1176(w), 1043(m), 1020(m) cm^{-1}.

c) 4-Chloro-3-benzoyl-3-(p-benzoylphenyl)-2-azetinone, Ia': The crude product from the same treatment with 30 mmol of aluminum chloride was chromatographed successively with benzene–petroleum ether (1 : 1) and benzene–ether (3 : 1), giving 0.26 g (6%) of Ia and 1.64 g (28%) of Ia' respectively. The latter, on recrystallization from ethanol, melts at 164.5—165 °C. Found: C, 71.30; H, 3.68; Cl, 8.89; N, 3.64%. Calcd for $C_{23}H_{14}ClNO_3$: C, 71.23; H, 3.64; Cl, 9.14; N, 3.61%. MS: M^+=387, 389 (3 : 1). IR(KBr): 1754(s), 1704(sh), 1669(s), 1598(s), 1570(s), 1535(s), 1502(m), 1447(m), 1355(s), 1315(m), 1279(s), 1239(s), 1227(m), 1175(w), 1041(m), 1020(w) cm^{-1}.

d) 4-Chloro-3-benzoyl-3-methyl-2-azetinone, Ib: The crude product obtained from ethyl α-cyanopropionate (1.9 g) by using 30 mmol of aluminum chloride at 50 °C for 48 hr was recrystallized from ethanol to give Ib(1.22 g, 37%), mp 123—124 °C (ethanol). It decomposes, with the formation of benzoic acid, over a long period in air. Found: C, 60.22; H, 3.74; Cl, 16.06; N, 6.36%. Calcd for $C_{11}H_8ClNO_2$: C, 59.64; H, 3.61; Cl, 16.03; N, 6.32%. MS: M^+=221, 223 (3 : 1). IR(KBr): 1750(s), 1707(sh), 1603(s), 1575(m), 1554(s), 1489(w), 1448(m), 1387(m), 1349(m), 1313(w), 1247(m), 1223(m), 1050(m), 1015(w) cm^{-1}.

Ia and Ia', or Ib from the α-Benzoyl α-Cyano Ester. When ethyl α-benzoyl-α-cyanophenylacetate (2.9 g, 10 mmol) in a nitrobenzene solution (10 ml) of aluminum chloride (1.6 g, 12 mmol) was kept at 50 °C for 22 hr (as in the case of *c*) above), Ia and Ia' were obtained from the reaction mixture in trace and 7-mg amounts respectively. The yields were

4) N. Zelinsky, *Ber.*, **21**, 162 (1888).
5) E. C. Horning and A. F. Finelli, "Organic Syntheses," Coll. Vol. IV, p. 461 (1963).
6) A. Haller, *C. R. Acad. Sci. Paris*, **105**, 169 (1887).

increased to 0.5 mg and 12 mg respectively when the amount of aluminum chloride and the reaction temperature were decreased to 5 mmol and to 40 °C respectively. Under the former conditions, 70 mg of Ib were obtained from 2.3 g (10 mmol) of ethyl α-benzoyl-α-cyanopropionate. These azetinones were identified by the mixed-melting-point method.

α-Benzoyl α-Cyano Ester from Ia, Ia', or Ib. A benzene solution (2 ml) of Ia (2 mmol) was added to a sodium methoxide solution made from sodium (0.002 g atom) and methanol (3 ml). After 1 hr, the mixture was warmed at 40 °C for 1 hr. The cooled reaction mixture was acidified with an aqueous acetic acid and then shaken with ether. The ether layer, after having been washed with a sodium bicarbonate solution, was dried and concentrated; then the remaining oil was placed in a column packed with silica gel. Benzene–ether (14 : 1) was used as the eluent. The fractions, each showing a single spot on tlc, were collected. The resulting product was concentrated to leave an oil. The IR spectra for the oils from Ia and Ib were similar to those of ethyl α-benzoyl-α-cyanophenylacetate and -α-cyanopropionate respectively. In the same way, the IR spectrum of the oil from Ia' was found to be similar to that for Ia, so it seems to be due to methyl α-benzoyl-α-cyano-*p*-benzoylphenylacetate. No search for compounds with a methoxyl group in the products was made because of the small amounts involved.

Hydrolysis of Ia. a): Two drops of concd hydrochloric acid were added to a solution of Ia (0.3 g) in benzene (1 ml) and glacial acetic acid (5 ml); then the solution was warmed at 50—51 °C for 2 hr. The cooled reaction mixture was diluted with water and then shaken with ether–benzene (5 : 1). The upper layer, freed from acetic acid by washing with water, was shaken with a saturated sodium bicarbonate solution. The upper layer was then dried and evaporated to leave a crystalline mass, which was subsequently recrystallized from ethanol to give Ia (0.14 g). The lower layer, after the removal of the ether dissolved, was acidified to precipitate crude *N*-benzoyl-3-phenyl-2,4-azetidinedione (IIa) (0.1 g, 36%, mp 226—228 °C), which was collected by filtration. The crude IIa in ether was washed with an aqueous solution of a slight amount of sodium bicarbonate; then it was dried and concentrated by passing a stream of dry air, giving colorless crystals; mp 228.5—229.5 °C. Found: C, 72.67; H, 4.19; N, 5.42%. Calcd for $C_{16}H_{11}NO_3$: C, 72.44; H, 4.19; N, 5.28%. IR(KBr): 1710(sh), 1660(s), 1629(m), 1612(m), 1579(m), 1552(s), 1496(w), 1448(m), 1426(s), 1402(s), 1352(s), 1309(m), 1276(s), 1115(m) cm^{-1}.

The filtrate separated from the above crude IIa was extracted with ether. The resulting extract was dried and concentrated to give colorless crystals (20 mg, 8%), which were subsequently recrystallized from ether to give *N*-benzoylphenylacetamide; mp 138.5—139.5 °C. This melting point was undepressed on admixture with a synthesized sample melting at 139—140 °C (lit.[7] 129—130 °C). Found: N, 5.8%. IR(KBr): 3287, 1732, 1686, 1605 cm^{-1}.

b): A solution of Ia (50 mg) in benzene (1 ml) and ethanol (10 ml) was added to a mixture of an aqueous solution (4 ml) of sodium carbonate (35 mg) and methanol (30 ml). The resulting solution was stirred with a magnetic stirrer at room temperature for 6 hr. The reaction mixture was then steam-distilled *in vacuo* to remove the organic solvent. The residue was separated as above into an oil, IIa (7 mg), and *N*-benzoylphenylacetamide (a trace). The oil, containing a small amount of Ia, gave a 2,4-dinitrophenylhydrazone. The isolated products were identified by mixed-melting-point method.

c): A solution of Ia (100 mg) in benzene (2 ml) and ethanol (20 ml) was added to a warm mixture of methanol (40 ml) and an aqueous solution (5 ml) of sodium carbonate (100 mg). The resulting solution was warmed at 60—65 °C for 8 hr. The reaction mixture, after the removal of the organic solvent, was shaken with ether. The lower layer, on acidification, gave phenylacetic acid (mp 79—80 °C (water)) and benzoic acid (mp 119—120 °C). The upper layer, after extraction with a sodium hydroxide solution, was evaporated to give benzamide (mp 129—130 °C (ether)). The alkaline extract, after acidification, was reextracted with ether. The evaporation of the ether extract gave an oil. An excess amount of sodium nitrite powder was added in small portions to a solution of this oil in 80% sulfuric acid over a 12-hr period with occasional heating up to 50—60 °C; then the reaction mixture was diluted with warm water. The ether extract from the sulfuric acid solution was concentrated and then steam distilled. The residue was alkalized with a sodium hydroxide solution and then extracted with ether. An oil obtained from the ether extract gave a 2,4-dinitrophenylhydrazone melting at <195 °C (ethanol). A similar treatment of the above distillate led to crystals melting at <185 °C. The first and last melting points were undepressed on admixture with the 2,4-dinitrophenylhydrazone of benzil (mp 200—202 °C) and that of desoxybenzoin (mp 203—204 °C) respectively.

Acid Hydrolysis of Ia'. a): Ia', when treated as has been described in the case of the hydrolysis of Ia, *a)*, was converted into *N*-benzoyl-3-(*p*-benzoylphenyl)-2,4-azetidinedione (20%); mp 228—230 °C (tetrahydrofuran). Found: C, 74.82; H, 4.03; N, 3.55%. Calcd for $C_{23}H_{15}NO_4$: C, 74.78; H, 4.10; N, 3.79%. IR(KBr): 1705(sh), 1662(sh), 1652(s), 1630(m), 1605(m), 1580(m), 1563(s), 1495(w), 1447(w), 1425(s), 1400(s), 1353(s), 1314(s), 1280(s), 1262(m), 1173(m), 1115(m) cm^{-1}.

b): To a solution of Ia' (100 mg) in glacial acetic acid (2 ml), we added one drop each of concd sulfuric acid and water; then the solution was refluxed for 0.5 hr. The reaction mixture was subsequently diluted with water, neutralized with sodium bicarbonate, and then shaken with ether. The evaporation of the upper layer left crystals, which were then triturated with water. The water-insoluble crystals were recrystallized from ether–methanol to give *p*-benzoylphenylacetamide; mp 140—141 °C (lit.[8] 136—137 °C). Found: C, 75.34; H, 5.66; N, 5.70%. From the aqueous solution, benzamide was separated; it was then crystallized from ether–petroleum ether; mp 127—128 °C. The above lower layer was acidified and then extracted with ether. The ether extract, freed from acetic acid, was evaporated to give crystals, which were then triturated with water. The water-insoluble crystals were recrystallized from benzene to give *p*-benzoylphenylacetic acid; mp 113—114 °C (lit.[8] 112—114 °C). Found: C, 75.18; H, 5.15%. From the aqueous solution, benzoic acid was isolated. The benzoic acid and benzamide were identified by the mixed-melting-point method.

Acid Hydrolysis of Ib. Six drops of concd hydrochloric acid were added to a solution of Ib (2 g) in benzene (5 ml) and glacial acetic acid (30 ml); then the solution

7) H. L. Wheeler, T. B. Johnson, and D. F. McFarland, *J. Amer. Chem., Soc.* **25**, 787 (1903).

8) R. P. Zelinski, B. W. Turnquest, and E. C. Martin, *ibid.*, **73**, 5521 (1951).

was warmed at 65—66 °C for 0.5 hr. The reaction mixture was separated as in the case of the hydrolysis of Ia, *a)*. The unaltered Ib weighed 1.5 g. The sodium bicarbonate extract, after acidification, was extracted with ether. The ether extract was evaporated to give a crystalline mass, which was triturated with ether–petroleum ether (1 : 4); then the insoluble crystals were collected by filtration. From the filtrate, benzoic acid was obtained. The organic solvent-insoluble crystals were treated with a sodium bicarbonate solution; then the product was filtered from an insoluble substance. The filtrate on acidification gave crystals. A solution of these crystals in ether was concentrated by passing dry air to give *N*-benzoyl-α-carboxypropionamide (0.36 g, 18%) in the form of colorless needles, which melted at 129 °C with decomposition. Found: C, 59.71; H, 5.04; N, 6.20%. Calcd for $C_{11}H_{11}NO_4$: C, 59.72; H, 5.01; N, 6.33%. IR (KBr): 3400—3370, 3306, 1712, 1682, 1602 cm^{-1}. The thermal decomposition of this carboxy amide gave *N*-benzoylpropionamide. It was crystallized from petroleum ether (mp 98—98.5 °C), giving no depression on admixture with a synthesized sample (lit.[9] mp 98 °C). IR(KBr): 3295, 1713, 1683, 1602 cm^{-1}.

The mother liquor from the crystallization of the above carboxy amide, the sodium bicarbonate-insoluble substance, and the aqueous acidic filtrates were combined; then the mixture, after the addition of a few mls of concd hydrochloric acid, was steam-distilled. The distillate gave 2,4-dinitrophenylhydrazone of propiophenone. It was recrystallized from ethanol (mp 197—199 °C), giving no depression on admixture with an authentic sample melting at 199—200 °C.

The present authors wish to express their thanks to Professor Hiroshi Suda and to Miss Michiko Araki of this faculty for their elemental analyses.

9) H. L. Wheeler, P. T. Walden, and H. F. Metcalf, *ibid.*, **20**, 64 (1898).

BULLETIN OF THE CHEMICAL SOCIETY OF JAPAN, VOL. 46, 1759—1762 (1973)

The Nucleophilic Photo-substitution Reaction of Anthraquinone Derivatives. I. The Photo-amination of Sodium 1-Amino-4-bromoanthraquinone-2-sulfonate

Haruo INOUE, Mitsuhiko HIDA, Tran Dinh TUONG*,** and Takashi MURATA*

Department of Industrial Chemistry, Faculty of Engineering, Tokyo Metropolitan University, Setagaya-ku, Tokyo 158

**Department of Synthetic Chemistry, Faculty of Engineering, The University of Tokyo, Hongo, Tokyo 113*

(Received September 20, 1972)

The photo-amination reaction of sodium 1-amino-4-bromoanthraquinone-2-sulfonate (I) was studied. The experimental results may be summarized as follows: 1) The photo-reaction is evoked by the absorption of light corresponding to the first absorption band (490 nm) of (I); 2) no dark reaction is observed: 3) aromatic amines appeared not to photo-react with (I); 4) the larger the polarity of the solvents used, the greater the yield of the product; 5) in the absence of oxygen, the photo-reaction was stopped. The possible reaction schemes were discussed.

The photochemistry of anthraquinone derivatives has attracted much attention in relation to the photo-tendering effects of vat dyes, and many studies concerning photo-reduction and photo-annelation have been reported.[1] However, the photo-substitution reactions of anthraquinones have rarely been reported on. Only two examples have been reported: the photolysis of 3-nitroalizarin in aerated methanol to give 4-methoxy-3-nitroalizarin, and the photolysis of anthraquinone-2-sulfonic acid in oxygen-free water to give hydroxyanthraquinones.[2,3] We ourselves have previously found that sodium 1-amino-4-bromoanthraquinone-2-sulfonate (bromamine acid) is photo-aminated to produce sodium 1,4-diaminoanthraquinone-2-sulfonate.[4] In this paper, details of the photo-amination will be reported and the most probable mechanism of the reaction will be discussed.

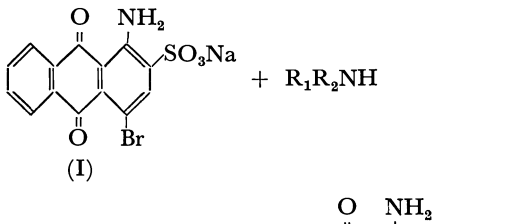

(I)

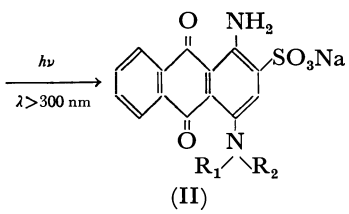

(II)

$R_1R_2NH \sim NH_3$, CH_3NH_2, $C_2H_5NH_2$, n-$C_3H_7NH_2$, n-$C_4H_9NH_2$, CH_2-$(CH_2)_4$-NH.

Experimental

Materials. The sodium 1-amino-4-bromoanthraquinone-2-sulfonate(bromamine acid) was purified by repeated salting out and by subsequent recrystalization from 1 : 1 ethanol-water. The sodium 1,4-diaminoanthraquinone-2-sulfonate was prepared by the hydrolysis of sodium 1-amino-

** Present address: Institute of Industrial Science, The University of Tokyo, Tokyo.

1) J. M. Bruce, *Quart. Rev.*, **21**, 405 (1967).

2) H. C. Van Beek and P. P. Heertjes, *J. Chem. Soc.*, **1962**, 83.

3) A. D. Broadbent, *Chem. Commun.*, **1967**, 382.

4) H. Inoue, T. D. Tuong, M. Hida, and T. Murata, *J. Chem. Soc., D*, **1971**, 1347.

TABLE 1. λ_{max} OF PHOTO-AMINATED PRODUCTS IN 4 : 1 2-PROPANOL-WATER

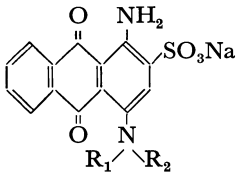

	$-NH_3$	$-NHCH_2$	$-NHC_2H_5$	$-NHC_3H_7$	$-NHC_4H_9$	$-N-(CH_2)_4-CH_2$
λ_{max} (nm)	565	588	587	586	587	605
	607	634	633	632	633	

4(N-benzenesulfonyl)-aminoanthraquinone-2-sulfonate. The other authentic samples of sodium 1-amino-4-alkylamino-anthraquinone-2-sulfonate were prepared in an autoclave by an Ullmann condensation reaction from bromamine acid and the corresponding alkylamine in the presence of cupric sulfate as the catalyst.

Solvents. Water was passed through ion-exchange resin columns (specific resistance: 10^6 ohm/cm). The methanol was purified by repeated fractional distillations. The 1-propanol and tertiary butanol were refluxed over lime and fractionally distilled. The ethanol was distilled with 5 ml of concd sulfuric acid and 20 ml of water per liter; then it was refluxed with silver nitrate and potassium hydroxide, and finally fractionally distilled. The acetonitrile was refluxed with sodium carbonate and potassium permanganate, and then distilled. It was subsequently refluxed with phosphorus pentoxide, fractionally distilled, and finally distilled over potassium carbonate. The extra-pure reagent of dioxane (Tokyo Kasei Co.) was used without further purification.

Measurements. A Shimadzu recording spectrophoto meter, model MPS 50, was used for the measurements of the visible absorption spectra.

Isolation of the Product. After the irradiation of light, the solvent was distilled from the reaction system at 30 °C under reduced pressure; the blue-colored product was separated by the method of cellulose-column chromatography with a developing solution of water.

Results and Discussion

Photo-reaction of I with Various Amines. A solution of 0.990×10^{-4} mol/l of bromamine acid and 4.37×10^{-2} mol/l of ammonia in an aerated 4 : 1 2-propanol-water mixture was irradiated at 30 °C by means of a water-jacketed 500 W high-pressure mercury lamp filtered with a glass which allows a radiation of $\lambda>300$ nm. The color of the solution turned from red to blue upon the irradiation. The visible absorption spectrum of the reaction system is shown in Fig. 1. As the reaction proceeded, the absorption intensity at 490 nm(λ_{max}) decreased with the increase in the intensities at 565 nm(λ_{max}) and 607 nm(λ_{max}), and the isosbestic points were at 382 nm and 525 nm. The newly-appeared absorption bands of 565 nm(λ_{max}) and 607 nm(λ_{max}) agreed with those of the authentic sodium 1,4-diaminoanthraquinone-2-sulfonate(II). Hence, this result suggested that the photo-reaction of bromamine acid(I) with ammonia gives only sodium 1,4-diaminoanthraquinone-2-sulfonate(II). The IR spectrum of the blue product and the paper chromatogram also supported this suggestion. Similar photo-aminations of bromamine acid(I) by alkylamines such as methylamine, ethylamine, *n*-propylamine, *n*-butylamine, and the piperidine were also observed. The wavelengths of the maximum absorption in the visible region of products in 4 : 1 2-propanol-water are compared in Table 1. In the case of piperidine, the reaction proceeds rather fast as compared with the case of other alkylamines. As is shown in Fig. 2, when the irradia-

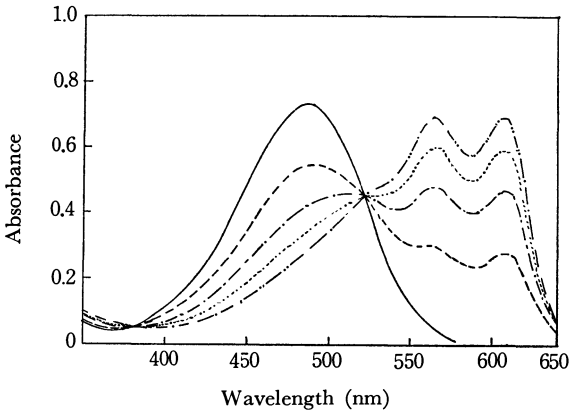

Fig. 1. Visible absorption spectra of the reaction system [I]~0.990×10^{-4} mol/l, [NH_3]~4.37×10^{-2} mol/l in 4 : 1 2-PrOH-H_2O.
——: 0 hr, ----: 2 hr, —·—: 4 hr, ·····: 6 hr, —··—: 8 hr.

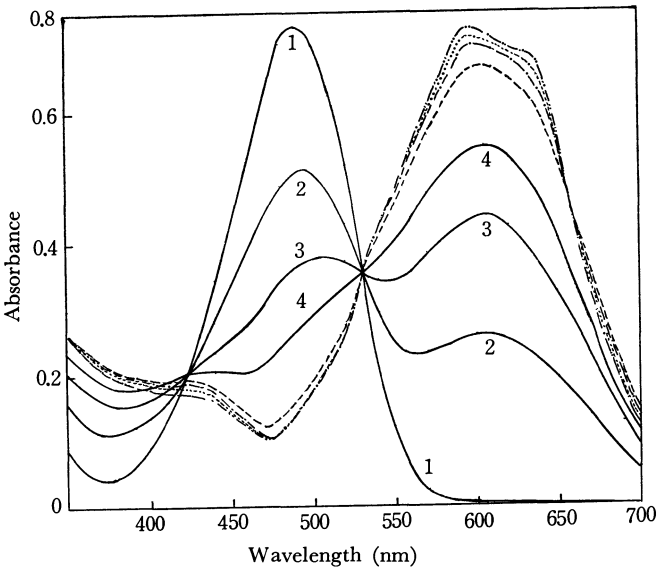

Fig. 2. Visible absorption spectra of the reaction system [I]~0.990×10^{-4} mol/l. [Piperidine]~5.00×10^{-2} mol/l in 4 : 1 2-PrOH-H_2O.
1: 0 min, 2: 20 min, 3: 40 min, 4: 60 min,
----: 2 hr, —·—: 4 hr, ----: 6 hr, —··—: 8 hr.

tion was carried out for more than 1 hr, the isosbestic point at 423 nm in the early stage of reaction disappeared and new two isosbestic points appeared in the neighbourhoods of 350 nm and 660 nm. Moreover, the broad absorption band of 605 nm(λ_{max}) split into two peaks; it resembles that in the spectrum of the reaction products of other alkylamines. These facts seem to indicate that bromamine acid may be photo-aminated by piperidine to produce sodium 1-amino-4-piperidinoanthraquinone-2-sulfonate, followed by the ring opening of the piperidine ring. When aromatic amines such as aniline and diphenylamine were used, the substitution reaction did not occur and (I) remained unchanged.

Photo-reaction of I with the Hydroxyl Ion. A solution of 0.990×10^{-4} mol/l of bromamine acid and 4.84×10^{-2} mol/l of sodium hydroxide in an aerated 4 : 1 2-propanol–water mixture was irradiated under the same conditions as have been given above. The absorption intensity of the first band(λ_{max}=490 nm) of bromamine acid decreased, and a new absorption band at 612 nm initially appeared and then decreased with the irradiation; that is, the photo-decomposition of bromamine acid by the hydroxyl ion takes place exclusively. Nothing about the new absorption band at 612 nm was made clear. However, this band seems likely to be caused by either of two possible intermediates. One is a photo-reduced intermediate, since the new absorption band has a tendency to disappear upon the bubbling in of air. The other is sodium 1-amino-4-hydroxyanthraquinone-2-sulfonate, which may be considered to be once produced and then soon decomposed, since it has an absorption peak at 612 nm in an alkaline solution.

Photolysis of I. A solution of 0.990×10^{-4} mol/l of bromamine acid in a 4 : 1 2-propanol–water mixture was irradiated under the same conditions as in the case of the reaction with ammonia. After 8 hrs' irradiation, no change was observed in the absorption spectrum of the reaction system; that is, bromamine acid remained unchanged in the absence of amines or hydroxyl ion.

Effect of the Solvent. The photo-substitution reactions of bromamine acid (I) with ammonia were carried out in various solvents. As is shown in Fig. 3, the yields of the aminated product decreased in the following order: 4 : 1 CH_3CN–H_2O>4 : 1 2-PrOH–H_2O>4 : 1 EtOH–H_2O>4 : 1 MeOH–H_2O>4 : 1 1-PrOH–H_2O>4 : 1 *t*-BuOH–H_2O>4 : 1 Dioxane–H_2O>H_2O; that is, bromamine acid is more reactive in polar solvents, such as acetonitrile and alcohols, than in less polar solvents, such as dioxane, except in the case of water. This seems to imply the existence of a polar intermediate, which may be stabilized by the polar solvents.

Effect of the Wavelength of Irradiation. When the substance was irradiated with light including the UV region (λ<300 nm), the photo-amination reaction did not take place and the photo-decomposition of bromamine acid predominated. When the irradiating light was λ>420 nm, including only the region of the first absorption band (λ_{max}=490 nm), the substitution reaction proceeded as well as in the case of the radiation of λ>300 nm. Moreover, no dark reaction was observed under the same conditions in the case of any amine. From these results it may be concluded that the amination of bromamine acid by ammonia is induced by the absorption of light corresponding to the first absorption band of bromamine acid.

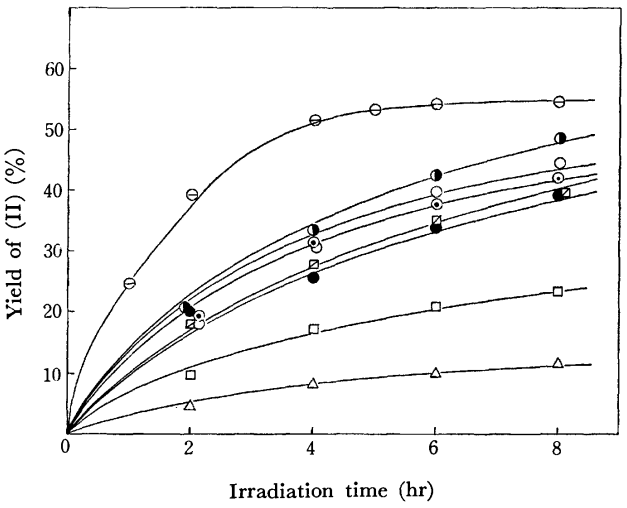

Fig. 3. Effect of the solvents on the yield of (II) [I]~0.990×10^{-4} mol/l, [NH_3]~4.37×10^{-2} mol/l.
⊖: 4 : 1 CH_3CN–H_2O, ◑: 4 : 1 2-PrOH–H_2O,
○: 4 : 1 EtOH–H_2O, ⊙: 4 : 1 MeOH–H_2O,
▨: 4 : 1 1-PrOH–H_2O, ●: 4 : 1 *t*-BuOH–H_2O,
□: 4 : 1 Dioxane–H_2O, △: H_2O.

Photo-reaction of 1-Bromoanthraquinone with Ammonia. A solution of 1-bromoanthraquinone (1.0×10^{-4} mol/l) and ammonia (4.37×10^{-2} mol/l) in a 4 : 1 2-propanol–water mixture was irradiated in the way described above. No change was observed in the near UV and visible absorption spectra of the reaction system, and it was concluded that 1-bromoanthraquinone was not photoaminated by ammonia. This eliminates the possibility that the photo-induced cleavage of the C–Br bond may take place in the early stage of the photo-amination of bromamine acid.[5] This is also supported by the fact that no debrominated product such as sodium 1-aminoanthraquinone-2-sulfonate was detected in the photo-amination reaction of bromamine acid.

Effect of Oxygen. The reaction almost stopped under nitrogen. This suggests that dissolved oxygen has an important role in the photo-amination of bromamine acid. As has been mentioned above, the photo-reduction of quinones is well known, and the photo-amination may be considered to proceed through the intermediates which may be produced by several photo-

5) Several examples of the photo-cleavage reactions of α-substituted aliphatic ketones, induced by the polarization of the C=O group in the excited n–π* state, are known to be;

$$-\overset{\overset{O}{\|}}{C}-\overset{\overset{X}{|}}{C}- \xrightarrow{h\nu} -\overset{\overset{O}{\|}}{C}-\overset{\overset{\pm}{|}}{C}- + \overset{\pm}{X} \quad (\pm\sim+,\ -,\ \text{or.})$$

where X is an electronegative species such as a halogen atom. (cf., for example, O. Jeger, K. Schaffner, and H. Wehrli, *Pure Appl. Chem.*, **9**, 555 (1964); J. A. Barltrop and A. Thomson, *J. Chem. Soc., C*, **1968**, 155; J. Hill, *Chem. Commun.*, **1966**, 260.)

reduction processes;[1,6,7]

a) $AQ^* + R\text{-}H \rightarrow AQH\cdot, AQH_2, AQ^{\cdot-}$

b) $AQ^* + OH^- \rightarrow AQ^{\cdot-}$

c) $AQ^* + R_1R_2\ddot{N}H \rightarrow [AQ^{\cdot-} \cdots\cdots R_1R_2\overset{+\cdot}{N}H] \downarrow AQ^{\cdot-}, AQH\cdot$

However, in the presence of oxygen it is well known that these intermediates are immediately oxidized and that the quinone is regenerated.[8,9] In the case of sodium anthraquinone-2-sulfonate, Bridge and Reed observed that the concentrations of the intermediate semiquinone radical and the radical anion decrease with the increase in the oxygene concentration.[10] Therefore, if the photo-amination proceeds through these intermediates, the reaction is expected to be enhanced under nitrogen and retarded under air. However, the experimental results were contrary to the above expectation. Therefore, it seems that this scheme is also invalid. Further, Cooper and Talbot observed that both oxygen and metal ions, such as Fe^{3+}, have oxidizing power for intermediate radicals which are generated from quinones by photo-reduction.[11] According to their report, the photo-reaction of bromamine acid with ammonia in a 4 : 1 2-propanol–water mixture was carried out under nitrogen in the presence of Fe^{3+} (about 10^{-2} mol/l of ferric chloride or potassium ferricyanide) in place of the molecular oxygen. If the photo-amination reaction proceeds through the process of oxidation by the molecular oxygen of intermediate radicals generated in the photo-reduction of the anthraquinone nucleus, the reaction may be expected to take place upon the addition of Fe^{3+} as an oxidizing agent under nitrogen. However, no reaction was observed. These results suggest that molecular oxygen does not act as a simple oxidizing agent, but plays a more complicated role in the photo-amination reaction. The following other possible photochemical schemes including interactions with oxygen were also considered:

i) the photo-amination through the interaction of bromamine acid with singlet oxygen, which may be produced by the sensitizing effect of the triplet state of bromamine acid;

ii) the photo-amination through the interaction of excited bromamine acid with ground-state oxygen to form some complex as below:[12]

$$AQBr^* + O_2 \longrightarrow [AQBr^{\oplus} \cdots\cdots O_2^{\ominus}]$$

$$\swarrow \qquad \searrow^{R_1R_2NH}$$

$$AQBr + O_2 \qquad \text{Amination}$$

etc.

It seems very difficult to deduce the mechanism of the photo-amination reaction of bromamine acid from only the above experimental results. A detailed kinetic study of the reaction will be reported in the near future.

6) In the study of the photo-reduction of 2-piperidinoanthraquinone, Phllips and his co-workers reported that, in a high concentration of the hydroxyl ion, the electron transfer from the hydroxyl ion to the excited 2-piperidinoanthraquinone can take place. (G. O. Phillips, A. K. Davies, and J. F. McKeller, *J. Chem. Soc.*, D, **1970**, 519).

7) S. G. Cohen and A. D. Litt, *Tetrahedron Lett.*, **1970**, 837.

8) J. L. Bolland and H. R. Cooper, *Nature*, **172**, 413 (1953).

9) *Idem*, *Proc. Roy. Soc.*, *Ser.*, *A*, **225**, 405 (1954).

10) N. K. Bridge and M. Reed, *Trans. Faraday Soc.*, **56**, 1796 (1960).

11) H. R. Cooper and Miss B. M. Talbot, *ibid.*, **61**, 506 (1965).

12) In the study of photo-fading of xanthene dyes complex formation between excited dye and ground state oxygen has been reported as,

$$D^*(T) + O_2 \longrightarrow [\overset{\oplus}{D}\cdots\overset{\ominus}{O_2}]$$

Y. Usui and M. Koizumi, This Bulletin, **40**, 440 (1967).

BULLETIN OF THE CHEMICAL SOCIETY OF JAPAN, VOL. 46, 1762—1764 (1973)

Poly(vinyl alcohol) with Pending 5-Substituted Uracils

Toru SEITA, Masayoshi KINOSHITA, and Minoru IMOTO*

Department of Applied Chemistry, Faculty of Engineering, Osaka City University, Osaka 558
**Department of Applied Chemistry, Faculty of Engineering, Kansai University, Osaka 564*

(Received September 27, 1972)

5-Chloro-, bromo-, iodo-, *N*-ethylamino-, and *N,N'*-diethylamino-1-[(2'-dihydrogenphosphato)-ethyl]-uracil were synthesized from 1-(2'-hydroxyethyl)-uracil through the combination of halogenation, phosphorylation, and subsequent amination. These compounds were coupled with poly(vinyl alcohol) using *N,N'*-dicyclohexylcarbodiimide as a dehydrating agent to give polymers having 5-substituted uracils as pending groups.

In previous papers we have reported on the syntheses of oligonucleotide analogues from *N*-(2'-hydroxy-3'-dihydrogenphosphato)-propyl derivative of nucleic-acid bases.[1,2] These oligomers were very soluble in water and showed significant hypochromic effect, a typical spectroscopic behavior of natural polynucleotides. As another polymer we prepared poly(vinyl alcohol) having nucleic-acid bases as pending groups by the condensation of *N*-(2'-hydroxyethyl) derivatives of nucleic-acid bases with poly(vinyl al-

1) T. Seita, K. Yamauchi, M. Kinoshita, and M. Imoto, This Bulletin, **45**, 926 (1972).

2) T. Seita, K. Yamauchi, M. Kinoshita, and M. Imoto, *Makromol. Chem.*, **154**, 255 (1972).

cohol). The polymers obtained were also hygroscopic and very soluble in water and showed the same hypochromic effect.[3] The excellent solubility makes it possible to use these polymers for biological systems as polymeric drugs. A most interesting utilization might be found in the incorporation of 5-halo-uracils, especially the important anti-cancer material 5-fluoro-uracil, into polymers.

This paper deals with the syntheses of 5-substituted 1-[(2′-dihydrogenphosphato)-ethyl]-uracils and their coupling with poly(vinyl alcohol).

1-(2′-Hydroxyethyl)-uracil (I) was readily converted into 1-(2′-hydroxyethyl)-5-iodouracil (III) in good yield by refluxing with iodine in 1,4-dioxane and 0.5 M nitric acid. Reaction of compound (III) with phosphorus oxychloride in trimethyl phosphate and subsequent hydrolysis gave 1-[(2′-dihydrogenphosphato)-ethyl]-5-iodouracil (IV). Compound (IV) was also obtained by refluxing 1-[(2′-dihydrogenphosphato)ethyl]-uracil (II) with iodine in 1,4-dioxane and 0.5 M nitric acid. Bromination of (I) was carried out using the system bromine, carbon tetrachloride and 0.5 M nitric acid at room temperature. 1-[(2′-Dihydrogenphosphato)-ethyl]-5-bromouracil (V) was easily prepared by both the reactions a) of 1-(2′-hydroxyethyl)-5-bromouracil with phosphorus oxychloride and b) of the compound (II) with bromine. *N*-Ethylamino and *N,N*-diethylamino groups were introduced into uracil by the reaction of compound (V) with ethylamine and diethylamine, respectively. These reaction paths are shown in Scheme 1.

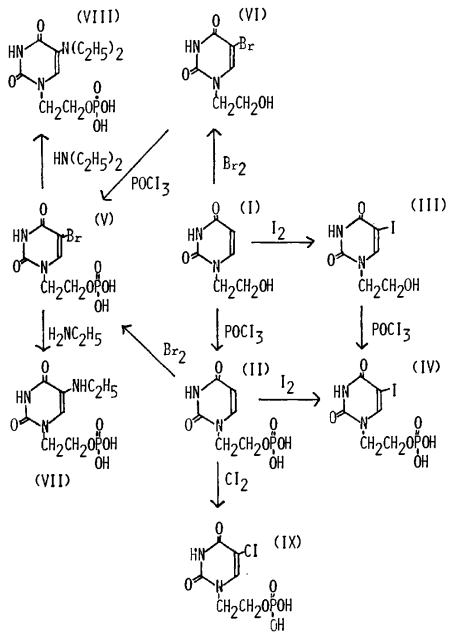

Scheme 1

As shown in Scheme 2, the condensation reaction of 5-substituted-1-[(2′-dihydrogenphosphato)-ethyl]-uracils with poly(vinyl alcohol) was carried out using *N,N′*-dicyclohexylcarbodiimide (DCC) as a dehydrating agent in refluxing dimethylformamide (DMF)-water mixture (9 : 1).

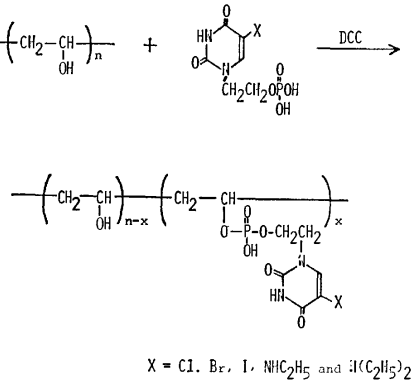

Scheme 2

The results of incorporation are given in Table 1. Nitrogen analysis showed that about half of the original hydroxy groups of poly(vinyl alcohol) was occupied by the uracil derivatives. The white powdery polymers obtained were very soluble in water and showed typical infrared absorptions at 1300—1000 cm^{-1} due to phosphoric ester. Ultraviolet absorptions were identical with those of the starting uracil derivatives.

Table 1. Condensation of 5-Substituted-1-[(2′-dihydrogenphosphato)-ethyl]-uracil (5-X-1-MOU) with PVA

X	Reaction time (hr)	Yield %	Content of 5-X-1-MOU (mol%)	UV Spectra $\lambda_{max}^{H_2O}$ (nm)
Cl	25	68	58	213, 280
Br	24	62	48	212, 282
I	20	58	42	217, 291
NHC_2H_5	25	60	52	213, 284
$N(C_2H_5)_2$	25	42	39	212, 282

Experimental

The melting points are uncorrected. The infrared (IR) spectra were obtained on a JASCO Model IR-G Spectrometer. The ultraviolet (UV) spectra were measured with a Hitachi Recording Spectrometer Model EPS-3T. Paper chromatography was carried out by the ascending technique using Toyo Roshi No 50 paper. Solvents for chromatography were a mixture of *n*-propanol, concd NH_4OH and water (6 : 2 : 2) (solvent A), and a mixture of concd NH_4OH, ethanol and water (10 : 15 : 2) (solvent B).

Poly(vinyl alcohol) used as stem polymer had a degree of polymerization of 300.

1-(2′-Hydroxyethyl)-5-iodouracil (III). Iodine 2.58 g (20 mmol) was added to a solution of 1-(2′-hydroxyethyl)-uracil (I) 1.7 g (10.9 mmol) in 0.5 M nitric acid (12 ml) and 1,4-dioxane (48 ml). The solution was heated at 100 °C for 4 hr. After the reaction mixture was allowed to cool to room temperature, the solvents were evaporated under reduced pressure. The residue was recrystallized from ethanol to give colorless prism crystals. Yield 85%; mp 197—200 °C; R_f of tlc 0.88 (solvent B); $\lambda_{max}^{H_2O}$, 217 mμ (ε=10440), 290 mμ (ε=8156); IR, 3350 (s), 1710(s), 1670(s), 1450(m), 1440(w), 1350(s), 1250(m), 1130(w), 1050(m),

3) T. Seita, K. Yamauchi, M. Kinoshita, and M. Imoto, *ibid.*, **154**, 263 (1972).

1010(s), 900(w), 600(s) cm^{-1}; Found: C, 25.54; H, 2.51; N, 9.89%. Calcd for $C_6H_7O_3N_2I$: C, 25.58; H, 2.44; N, 9.93%.

1-(2'-Hydroxyethyl)-5-bromouracil (VI). Bromine 1.2 g (15 mmol) dissolved in 8 ml of carbon tetrachloride was added to a solution of (I) 1.5 g (9.6 mmol) in a mixture of 0.5 M nitric acid (8 ml) and 1,4-dioxane (32 ml), and the solution was stirred at room temperature for 5 hr. The solvent were evaporated to dryness under reduced pressure. The residue was recrystallized from ethanol to give colorless needle crystals. Yield 87%; mp 209—211 °C; R_f of tlc 0.86 (solvent B); $\lambda_{max}^{H_2O}$, 212 mμ (ε=9251), 281 mμ (ε=8980); IR, 3350(s), 1710(s), 1670(s), 1450(m), 1340(s), 1230(w), 1050(s), 930(m), 880(w), 860(m), 750(s) cm^{-1}; Found: C, 30.51; H, 3.04; N, 11.81%. Calcd for $C_6H_7O_3N_2Br$: C, 30.64; H, 3.01; N, 11.92%.

1-[2'-Dihydrogenphosphato)-ethyl]-5-iodouracil (IV). a) 2.4 g of iodine (18.9 mmol) was added to a solution of 1.2 g of 1-[2'-dihydrogenphosphato)-ethyl]-uracil (II) (5.09 mmol) in 0.5 M nitric acid (10 ml) and 1,4-dioxane (40 ml). The procedure was similar to that for (III). Colorless powdery crystals were obtained by recrystallization from a minimal amount of absolute ethanol. Yield 69%.

b) 0.46 g of phosphorus oxychloride (3 mmol) was added at 0 °C to a suspension of 0.7 g of (III) (2.48 mmol) in trimethyl phosphate (7 ml). After stirring for 6 hr, water (3 ml) was added and stirring was continued for 1 hr. The water added was removed under reduced pressure below 50 °C, and the residue was poured into ethanol–ether mixture. The white precipitate was recrystallized from a minimal amount of absolute ethanol to give colorless powdery crystals. mp 216—217 °C; R_f of paper chromatography 0.25 (solvent A); $\lambda_{max}^{H_2O}$, 217 mμ (ε=10655), 290 mμ (ε=8196); IR, 3000(s), 1700(s), 1650(s), 1470(m), 1430(w), 1240(m), 1060(w), 1040(s), 980(s), 850(w), 660(w), 620(m) cm^{-1}; Found: C, 20.31; H, 2.21, N, 8.18%. Calcd for $C_6H_9N_2O_6PI$: C, 19.90; H, 2.23; N, 7.74%.

1-[(2'-Dihydrogenphosphato)-ethyl]-5-bromouracil (V). a) 0.5 g of (II) (2.1 mmol) was dissolved in a hot mixture of 0.5 M nitric acid (4 ml) and 1.4-dioxane (16 ml). A solution of 0.48 g of bromine (6 mmol) in carbon tetrachloride (4 ml) was added to the above solution at room temperature. After being kept at room temperature overnight, the solvents were evaporated under reduced pressure. The residue was recrystallized from ethanol–ether mixture to give colorless needle crystals. Yield 68%.

b) 0.4 g of phosphorus oxychloride (3 mmol) was added to a suspension of 0.5 g of (VI) (2.13 mmol) in trimethyl phosphate (5 ml) and treated as the synthesis of (IV)-b). Colorless needle crystals were obtained by recrystallization from ether–ethanol mixture. mp 236—237 °C; R_f of paper chromatography 0.33 (solvent A); $\lambda_{max}^{H_2O}$, 212 mμ (ε=8414), 281 mμ (ε=8090); IR, 3000(s), 1700(s), 1650(s), 1470(m), 1430(w), 1350(w), 1040(s), 980(s), 650(w), 620(m), 530(m) cm^{-1}; Found: C, 23.39; H, 2.49; N, 9.28%. Calcd for $C_6H_9N_2O_6PBr$: C, 22.88; H, 2.56; N, 8.89%.

1-[(1'-Dihydrogenphosphato)-ethyl]-5-chlorouracil (IX). 5.35 g of chlorine (7.5 mmol) dissolved in carbon tetrachloride (10 ml) was added to a solution of 1.0 g of (II) (4.2 mmol) in acetic acid (60 ml) and the solution was kept at room temperature for 1 hr. The solution was then concentrated to half the volume and refluxed for 30 min. The solvents were evaporated to dryness under reduced pressure. The residue was recrystallized from the ether–ethanol mixture to give colorless crystals. Yield 90%, mp 212—214 °C, $\lambda_{max}^{H_2O}$, 213 mμ (ε=12000), 280 mμ (ε=9800); IR, 3050(m), 1690(s), 1640(s), 1460(m), 1420(m), 1060(w), 1030(s), 980(m), 660(w), 520(m) cm^{-1}; Found: C, 26.19; H, 2.89; N, 9.92; Cl, 12.34%. Calcd for $C_6H_8N_2O_6PCl$: C, 26.64; H, 2.98; N, 10.35; Cl, 13.10%.

1-[(2'-Dihydrogenphosphato)-ethyl]-5-(N-ethylamino)-uracil (VII). A solution of 0.35 g of (V) (1.0 mmol) in 50% ethylamine (10 ml) was stirred for 24 hr at room temperature. The reaction mixture was evaporated to dryness under reduced pressure. Colorless plate crystals were obtained by recrystallization from ethanol–water mixture. Yield 58%, mp 214—216 °C, R_f of paper chromatography 0.27 (solvent A), $\lambda_{max}^{H_2O}$, 212 mμ (ε=7090), 281 mμ (ε=6986): IR 3150(s), 1710(s), 1610(m), 1440(s), 1380(w), 1340(s), 1240(m), 1010 (s), 780(m), 640(w) cm^{-1}; Found: C, 27.84; H, 5.48; N, 16.07%. Calcd for $C_8H_{14}N_3O_6P$: C, 28.25; H, 5.53; N, 16.47%.

1-[(2'-Dihydrogenphosphato)-ethyl]-5-(N,N-diethylamino)-uracil (VIII). A solution of 0.35 g of (V) (1.0 mmol) in 50% diethylamine (12 ml) was refluxed for 5 hr and then treated as in the synthesis of (VI). Yield 53%, mp 235—236 °C, R_f of paper chromatography 0.22 (solvent A), $\lambda_{max}^{H_2O}$, 212 mμ (ε=9064), 281 mμ (ε=8953); IR, 2540(s), 1680(s), 1610(m), 1500(w), 1420(m), 1340(s), 1230(s), 1150(m), 1030(s), 890(s), 640(w) cm^{-1}; Found: C, 38.51; H, 5.79; N, 13.24%. Calcd for $C_{10}H_{18}N_3O_6P$: C, 39.10; H, 5.90; N, 13.68%.

Condensation of 5-Substituted 1-[(2'-Dihydrogenphosphato)-ethyl]-uracils with Poly(vinyl alcohol). 5-Substituted 1-[(2'-dihydrogenphosphato)-ethyl]-uracil (7.7 mmol) and PVA (0.22 g) were dissolved in boiling water. To the solution was added DMF (12 ml) and the water was then evaporated to substitute the solvent for DMF. DDC (30 g) was added to the DMF solution and the mixture was refluxed for 25—25 hr. After cooling the reaction mixture was poured into a large amount of water and allowed to stand at room temperature overnight. The mixture was filtered and the filtrate was evaporated under reduced pressure to obtain a white polymer as residue. The polymer obtained was purified by column chromatography with Sephadex G-25 eluted with water.

N-Halogen Compounds of Cyanamide Derivatives. I[1] Rearrangement of *N*-Alkylhaloamidines

Toshio FUCHIGAMI, Eiichi ICHIKAWA, and Keijiro ODO

Faculty of Engineering, Tokyo Institute of Technology, Ookayama, Meguro-ku, Tokyo 152

(Received October 13, 1972)

The reactions of *N*-chloroamidines with various dehydrochlorinating reagents were studied. *N*-Alkyl-*N'*-chloroamidines were treated with sodium alkoxide, sodium hydroxide, and silver oxide to form *O*-alkylisoureas, ureas, and carbodiimides, respectively. However, *N*-chloro-*N'*,*N'*-dialkylamidines did not afford corresponding products. The mechanisms for the rearrangements are discussed.

N-Haloamidines are unique in reactivity and useful as transient intermediates. A few reports on *N*-haloamidines have appeared, among which the synthesis of thiadiazoles by Goerdeler[2] and that of benzimidazoles by Grenda[3] are notable. However, no systematic examination of *N*-haloamidines has been made.

The present investigation was undertaken to prepare *N*-alkyl-*N'*-chlorobenzamidines and study their reactivity. We have attempted to prepare various *N*-chloroamidines and to reveal their chemical behavior with various kinds of dehydrochlorinating reagents and the relationship between their structure and reactivity.

Results and Discussion

Preparation of Amidines. *N*-Methyl-*N'*-phenylbenzamidine[4] was prepared from *N*-phenylbenzimidoylchloride and methylamine. The other amidine hydrochlorides were prepared from the corresponding iminoethers and amines by Pinner's method.[5]

Chlorination of Amidines. *N*-Chloroamidines were prepared from amidine hydrochlorides and sodium hypochlorite in water at −5—5 °C. Most of the *N*-chloroamidines were solids with low melting points, their active chlorine contents determined iodometrically being in good agreement with the corresponding calculated values. No effects of substituents were observed on the yield in chlorination except for *N*,*N*-pentamethylenebenzamidine.

Structure of N-*Alkyl*-N'-*chloroamidines.* The most possible structure of *N*-chloroamidine is (**K**) in consideration of the kinetic study of *N*-chlorination,[6] NMR spectra of *N*-haloamidines[7] and substitution reactions with thiocyanate or cyanide ion.[2,8]

$$\mathrm{R{-}\overset{\overset{\mathrm{NCl}}{\|}}{C}{-}NHR'} \qquad (\mathbf{K})$$

Reaction of N-*Chloroamidines with Alkaline Reagents. Reaction of* N-*Chloroamidines with Sodium Alkoxides*: Methoxide was mainly employed but other alkoxides such as ethoxide, isopropoxide, and *t*-butoxide were also tested in certain cases.

When *N*-alkylhaloamidine (**2**∼**5**) was treated with sodium alkoxide in alcohol at 60 °C (under reflux in case of sodium methoxide in methanol), an oily material was obtained. A larger part of the material was identified as a mixture of *N*-alkyl-*N'*-phenyl-*O*-alkylisourea (**A1**∼**7**) (main product) and benzoate (**B**). Products (**A6,7**) were isolated as their picrates but the others (**A1**∼**5**) were identified by means of preparative gas chromatography since they coud not be separated by distillation *in vacuo*. The yields of **A** and **B** were determined using glc. **5** gave a small amount of a by-product, cyaphenine (**C**).

An active chlorine did not disappear even when **7** was treated with such a strong base as sodium *t*-butoxide. The Neber rearrangement[9] was expected in the treatment of **10** which has an α-methylene group with sodium *t*-butoxide, but no product due to such a rearrangement was formed.

Structures of new compound (**A1**∼**7**) were established by the following examinations.

a) Acid hydrolysis: **A1**∼**7** were converted into the corresponding ureas.

b) Elemental analysis of their free bases or picrates.

c) Comparison of the IR spectra and glc retention times with those of authentic samples prepared by the reactions of carbodiimides and alcohols.

The boiling points of authentic samples (**A1**∼**5**) are shown in Table 4.

Reaction of N-*Chloroamidines with Sodium Hydroxide in a* 50% *Aqueous Methanolic Solution*: An aqueous solution of amidine hydrochloride was treated with sodium hypochlorite to form *N*-chloroamidine, which was refluxed with sodium hydroxide in aqueous methanol, yielding colorless crystalline solid and an oily material. The former was identified as *N*-alkyl-*N'*-arylurea (**D**) by comparison of its melting point and IR spectrum with those of the authentic sample. A larger part of the latter was identified as *N*-alkyl-*N'*-phenyl-*O*-alkylisourea (**A**) on the basis of IR spectrum and glc retention time.

In an aqueous methanolic solution, most *N*-chloroamidines gave **A**, while in the absence of methanol, they afforded **D** instead.

1 gave no **D** but sodium phenyl cyanamide (**F**), which was converted further into phenylurea by acid hydrolysis.

In the case of *N*,*N*-disubstituted amidines (**7**—**10**), no rearrangement took place and the products of hydrolysis (**E**) were obtained.

1) Part LXXXIV of "Studies of Cyanamide Derivatives"
2) J. Goerdeler, *Chem. Ber.*, **87**, 57 (1954).
3) V. J. Grenda, R. E. Jones, G. Gale, and M. Sletzinger, *J. Org. Chem.*, **30**, 259 (1965).
4) C. Gerhart, *Ann.*, **108**, 219 (1858).
5) A. Pinner, "Organic Syntheses," Coll. I, p. 5 (1956).
6) E. W. C. M. Thomm and M. Wayman, *Can. J. Chem.*, **47**, 3289 (1969).
7) A. Heesing and G. Maleck, *Tetrahedron Lett.*, 1967, 3851.
8) J. Goerdeler and D. Loevenich, *Chem. Ber.*, **86**, 890 (1953).
9) C. O'Bren, *Chem. Rev.*, **64**, 81 (1964).

Table 1. Preparation of amidines

Amidine	Yield %	Mp °C	Anal (Calcd) (%) C	H	N
Ph–C(=NH·HCl)–NH_2	89	78— 82 (74— 82)[5]			
Ph–C(=NH·HCl)–NHMe	100	225 (223)[13]			
Ph–C(=NH·HCl)–NHEt	81	162—164 (161)[10]			
Ph–C(=NH·HCl)–NH*iso*Pr	92	232—233	60.34 (60.28)	7.72 (7.59)	14.09 (14.06)
Ph–C(=NH·HCl)–NHBzl	89	230—232 (222—225)[11]			
Ph–C(=NH·HCl)–NMe_2	100	258—260 (255—256)[12]			
Ph–C(=NH·HCl)–N⟨ring⟩	95	215 (204—207)[9]			
p-$CH_3C_6H_4$–C(=NH·HCl)–NHMe	88	209—211	58.61 (58.54)	7.11 (7.10)	15.13 (15.17)
$PhCH_2$–C(=NH·HCl)–NMe_2	100	213—215	60.23 (60.45)	7.86 (7.61)	14.12 (14.10)
Ph–C(=N–Ph)–NHMe	93	132—133 (134)[4]			

Table 2. Preparation of *N*-Chloroamidines

N-Chloroamidine No		Yield %	Mp °C	Appearance	Cl Anal[a] (Calcd%)
1	Ph–C(=NCl)–NH_2	92	74	colorless needles	22.84 (22.93)
2	Ph–C(=NCl)–NHMe	91	69.5—70	colorless needles	21.01 (21.02)
3	Ph–C(=NCl)–NHEt	96	—	light yellowish liquid	19.63 (19.41)
4	Ph–C(=NCl)–NH*iso*Pr	87	49—49.5	colorless needles	17.94 (18.03)
5	Ph–C(=NCl)–NHBzl	70	54.5—55	colorless needles	14.24 (14.49)
6	*p*-$CH_3C_6H_4$–C(=NCl)–NHMe	85	98—99	colorless needles	19.30 (19.41)
7	Ph–C(=NCl)–NMe_2	87	—	light yellowlish liquid	18.86 (19.41)
8	Ph–C(=NCl)–N⟨ring⟩	32	83	colorless needles	15.92 (15.92)
9	Ph–C(=N–Ph)–NClMe	90	61—61.5	yellowish plates	14.05 (14.49)
10	$PhCH_2$–C(=NCl)–NMe_2	87	61	colorless granular form	17.97 (18.03)

The solids were recrystallized from ether-petroleum ether.
a) The active chlorine contents were iodometrically determined.

10) W. Lossen and M. Kobbert, *Ann.*, **265**, 158 (1891).
11) A. W. Hofmann and S. Gabriel, *Ber.*, **25**, 1585 (1892).
12) F. L. Pyman, *J. Chem. Soc.*, **123**, 3370 (1923).

Table 3. Reaction of *N*-chloroamidines with sodium alkoxide

$$R^1\text{–}\underset{\underset{NCl}{\|}}{C}\text{–}NR^2R^3 \xrightarrow[\text{in } R^4OH]{R^4ONa} R^1N{=}\underset{\underset{OR^4}{|}}{C}\text{–}NR^2R^3 + R^1COOR^4$$

(A) (B)

No	*N*-Chloroamidine R^1	R^2	R^3	Alkoxide R^4	R. Time (hr)	Products (%)[a] (A)	(B)	(C)[b]
2	Ph	H	Me	Me	3.0	46	15	—
				Et	0.7	45	22	—
				iso-Pr	0.2	44	5	—
3	Ph	H	Et	Me	1.0	41	22	—
4	Ph	H	*iso*-Pr	Me	1.5	18	29	—
5	Ph	H	Bzl	Me	2.5	33	3	1
				Et	1.5	47	4	1
7	Ph	Me	Me	Me	30.0[c]	—	—	—
				Et	11.0[c]	—	—	—
10	$PhCH_2$	Me	Me	*t*-Bu	2.0[d]	—	—	—

a) gas chromatography column: Silicone H. V., column temp.: 140°C, carrier gas: H_2 20 ml/min.
b) 2,4,6-triphenyl-*s*-triazine. c) Active chlorine did not disappear. d) The product could not be isolated.

Table 4. Analytical data of *O*-alkylisourea (A)

$$R^1N{=}\underset{\underset{OR^4}{|}}{C}\text{–}NR^2R^3 \quad (R^1{=}Ph)$$

(A) $(R^2{=}H)$

	O-Alkylisourea R^3	R^4	Free base Bp[a] (°C/mmHg)	Anal (Calcd) (%) C	H	N	Picrate Mp (°C)	Anal (Calcd) (%) C	H	N
A1	Me	Me	135—196/31	65.89 (65.83)	7.52 (7.37)	17.01 (17.06)	—	—	—	—
A2	Me	Et	110/32	67.31 (67.39)	7.81 (7.92)	15.60 (15.72)	124—125	47.27 (47.18)	4.30 (4.21)	17.26 (17.19)
A3	Me	*iso*-Pr	110—120/19	68.48 (68.72)	8.39 (8.39)	14.60 (14.52)	142—143 (decmp)	48.54 (48.46)	4.37 (4.55)	16.61 (16.62)
A4	Et	Me	87—88/23	66.66 (67.39)	8.10 (7.92)	15.84 (15.72)	—	—	—	—
A5	*iso*-Pr	Me	57—60/ 2	68.89 (68.72)	8.47 (8.39)	14.12 (14.52)	—	—	—	—
A6	Bzl	Me	—	—	—	—	148—149	53.76 (53.73)	4.12 (4.18)	14.90 (14.92)
A7	Bzl	Et	—	—	—	—	88— 92	52.70 (52.73)	4.55 (4.63)	13.93 (13.97)[b]

a) Boiling point of authentic sample. b) Monohydrate.

Table 5. Reaction of *N*-chloroamidines with sodium hydroxide (part 1)

$$R^1\text{–}\underset{\underset{NCl}{\|}}{C}\text{–}NHR^2 \xrightarrow[\text{in 50\% aq. MeOH}]{NaOH} R^1N{=}\underset{\underset{OMe}{|}}{C}\text{–}NHR^2 + R^1COOMe + R^1NHC\underset{\underset{O}{\|}}{}NHR^2$$

(A) (B) (D)

No	*N*-Chloroamidine (R^1)	(R^2)	Solvent	R. Time (hr)	Products (Yield %) (A)	(B)	(D)	(E)[a]	(F)[b]
1	Ph	H	50% aq. MeOH	10.0	—	—	—	65	9[c]
2	Ph	Me	50% aq. MeOH	2.5	3	—	23	—	—
			50% aq. Dioxane	10.0	—	—	24	—	—
3	Ph	Et	50% aq. MeOH	2.5	35	7	—	—	—
			H_2O	4.0	—	—	31	—	—
4	Ph	*iso*-Pr	50% aq. MeOH	3.0	18	6	—	—	—
5	Ph	Bzl	50% aq. MeOH	6.0	3	3	10	4	—
6	*p*-$CH_3C_6H_4$	Me	H_2O	12.0	—	—	17	—	—

a) R^1CONH_2. b) $R^1\underset{\underset{Na}{|}}{N}\text{–}C{\equiv}N$. c) Yield of phenylurea.

Table 6. Reaction of *N*-chloroamidines with sodium hydroxide (Part 2)

N-Chloroamidine $\xrightarrow[\text{in 50 \%aq. MeOH}]{\text{NaOH}}$ R^1CONH_2 (**E**)

N-Chloroamidine No	(R^1)	R. Time (hr.)	Product (**E**) (yield %)
7	Ph	3.0	31
8	Ph	6.0	42
9	Ph	3.0	—[a]
10	Bzl	2.0	19

a) The structure has not been established yet. The same product can be obtained from alkaline hydrolysis of *N*-methyl-*N'*-phenylbenzamidine.

Mechanisms of Rearrangement. The basicity of alkoxide ions was found to have large effects on the rates of dehydrochlorination. The reactivity of alkoxide ions was found to be in the order *iso*-$PrO^{\ominus}$> $EtO^{\ominus}$> $MeO^{\ominus}$.

In the reactions of *N*-chloroamidines having no hydrogen on the nitrogen atom with sodium alkoxide in alcohol or sodium hydroxide in an aqueous alcohol, the active chlorine did not disappear and no rearrangement took place. (Tables 3 and 6).

This rearrangement may be initiated by removal of a proton from the NH group with an alkoxide ion or hydroxide ion. The loss of a chloride ion from the resulting anion and the migration of the aryl group to a nitrogen atom probably take place simultaneously to form a carbodiimide as an intermediate. The carbodiimide thus produced may react with water or alcohol to give urea or *O*-alkylisourea (Scheme 1), and by-products esters of benzoic acid and cyaphenine may be formed (Scheme 2).

Reaction of N-*Chloroamidines with Silver Oxide.* *N*-Alkyl-*N'*-chloroamidines were mixed with silver oxide in ligroin and then refluxed. This gave rise to rearrangement, giving carbodiimides (**G**). Their infrared spectra showed a characteristic carbodiimide absorption at 2150 cm^{-1} and agreed completely with those of authentic samples. When these carbodiimides were refluxed in dilute hydrochloric acid, the corresponding ureas were obtained.

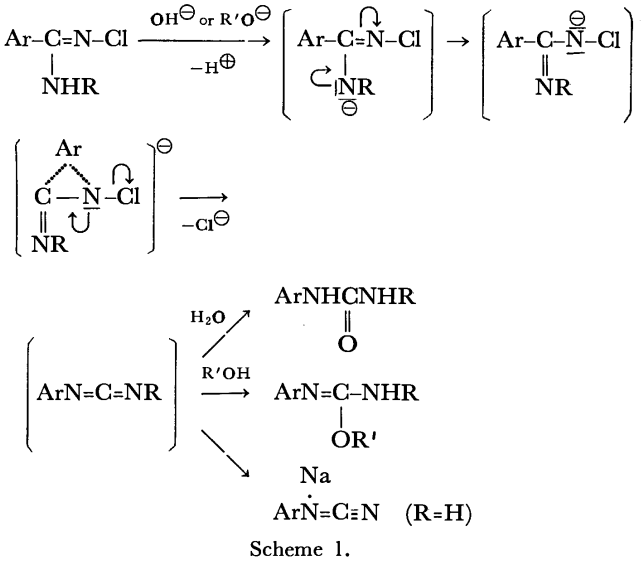

Scheme 1.

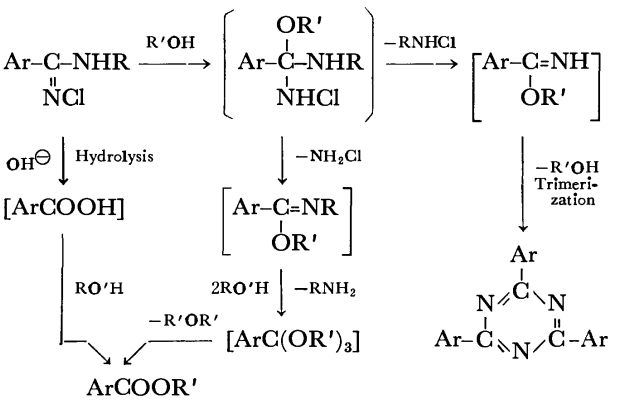

Scheme 2.

N-Methyl-*N'*-chloroamidine (**2**) gave no carbodiimide at all, but *N*-chlorobenzamidine (**1**) gave silver phenylcyanamide, which was converted into phenylurea by acid hydrolysis.

The rearrangement may proceed via a nitrenium cation (**L**) to form carbodiimide or cyanamide. The same mechanism was suggested by Haruki *et al.*[13]

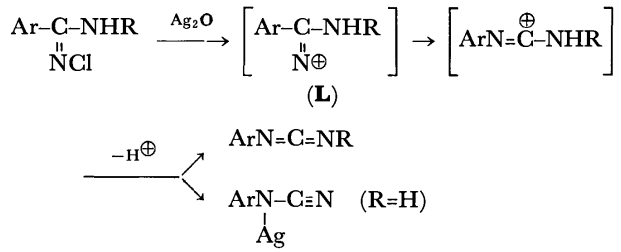

Scheme 3.

Experimental

Amidines. *N*-Methyl-*N'*-phenylbenzamidine was prepared from *N*-phenylbenzimidoyl chloride in ethereal solution and aqueous methylamine.[4] The other amidine hydrochlorides were prepared from the corresponding iminoethers and amines in water or ethanol by Pinner's method.[5]

N-*Chloroamidines.* As a typical experiment the preparation of *N*-chloro-*N'*-methylbenzamidine (**2**) is given. To a stirred solution of *N*-methylbenzamidine hydrochloride[14] (3.14 g, 0.02 mol) in water–ether (20 ml–40 ml) was gradually added 0.024 mol of sodium hypochlorite, the temperature being kept below 5 °C. After about 5 min of continued stirring, the ether layer was separated and residual *N*-chloroamidine was extracted twice with 10 ml portions of ether. The combined ether extracts were dried (Na_2SO_4) for 2 hr, filtered, and evaporated under reduced pressure at room temperature. The yield of **2** was 3.06 g (91%), mp 69 °C. Recrystallization from ether–petroleum ether gave a pure product, mp 69.5—70 °C.

The other *N*-chloroamidines were prepared as above.

Reaction of N-*Chloroamidines with Sodium Alkoxide.* *Reaction of* ***5*** *with Sodium Methoxide in Methanol*: To a stirred so-

13) E. Haruki, T. Inaike, and E. Imoto, This Bulletin, **41**, 1361 (1968).

14) H. L. Wheeler, *J. Amer. Chem. Soc.*, **20**, 489 (1898).

TABLE 7. FORMATION OF CARBODIIMIDES FROM *N*-CHLOROAMIDINES

$$Ph\text{-}\underset{\underset{NCl}{\|}}{C}\text{-}NHR \xrightarrow[\text{in Ligroin}]{Ag_2O} PhN{=}C{=}NR \quad (\mathbf{G})$$

R	R. Time (hr)	Product	Bp (°C/mmHg) (Ref.)	Yield %	Anal (Calcd) (%) C	H	N
H	2.0	(**H**)[a]	—	10[b]	—	—	—
Me	0.3	dark tarry oil	—	—	—	—	—
Et	0.3	(**G**)	38—42/4	28	—	—	19.07 (19.16)
Isopr	0.3	(**G**)	75—80/2 (111—112/14)[15]	35	74.09 (74.94)	7.40 (7.55)	17.18 (17.48)
Bzl	0.3	(**G**)[c]	—	33[b]	—	—	—

a) PhN(Ag)-C≡N. b) Yield of the corresponding urea. c) This could not be distilled because of a by-product.

lution of sodium methoxide prepared from sodium (0.28 g, 0.012 mol) and 25 ml of absolute methanol was added 2.45 g of *N*-benzyl-*N'*-chlorobenzamidine (**5**).

The mixture was then refluxed for 2.5 hr when sodium chloride precipitated. The solvent was removed by distillation under reduced pressure and the residue was mixed with water (10 ml). The upper oily layer was extracted once with a 20 ml portion and twice with 10 ml portions of ether. After the combined ethereal extracts were dried (Na_2SO_4), filtered and concentrated under reduced pressure, colorless needle crystals of 2,4,6-triphenyl-*s*-triazine (**C**) and a yellowish oily material were obtained. **C** was separated by filtration and recrystallized from benzene, mp 230—235 °C. The yield was 0.04 g (1%). (Found: C, 81.53; H, 4.89; N, 13.58%. Calcd for $C_{21}H_{15}N_3$: C, 81.53; H, 4.85; N, 13.58%).

To an ethereal solution of the filtrate containing a yellowish oily material was added a saturated ethereal solution of picric acid. The picrate of *N*-benzyl-*N'*-phenyl-*O*-methylisourea (**A6**) precipitated was collected by filtration and recrystallized from methanol, mp 148—149 °C. The yield was 33%.

A small part of the above filtrate was subjected to glc analysis and methyl benzoate was detected.

Reaction of **2** *with Sodium Ethoxide in Ethanol*: A mixture of **2** (4.22 g, 0.025 mol) and sodium ethoxide prepared from sodium (0.69 g, 0.03 g atom) and 25 ml of absolute ethanol was stirred at 60 °C for 0.7 hr. After working up the mixture as described above, the oily material was distilled under reduced pressure to give a fraction, bp 80—88 °C/3—40 mmHg (2.86 g). The fraction was subjected to glc analysis. *N*-Methyl-*N'*-phenyl-*O*-ethylisourea (**A2**) and ethyl benzoate were isolated by preparative gas chromatography (Silicone H. V.).

The authentic sample of **A2** was prepared according to the method of Forman *et al.*[14]

Reactions with the other *N*-chloroamidines were carried out similarly. The products are given in Table 3.

Reaction of N-*Chloroamidines with Sodium Hydroxide. Reaction of* **2** *with Sodium Hydroxide in 50% Aqueous Methanol*: To a stirred solution of *N*-methylbenzamidine hydrochloride (1.71 g, 0.01 mol) in 12 ml of water was added sodium hypochlorite (0.012 mol) at −5—5 °C to yield a suspension of the intermediate *N*-chloro compound (**2**). After about 5 min of stirring, an aqueous methanolic solution (water-methanol, 5 ml—25 ml) of sodium hydroxide (0.48 g, 0.012 mol) was added and the mixture was refluxed for 2.5 hr. When the reaction mixture was evaporated under reduced pressure and methanol was almost removed, crystals precipitated and were washed with ether to yield *N*-methyl-*N'*-phenylurea, mp 149 °C (0.34 g, 23%). Recrystallization from aqueous methanol gave a pure product, which showed no depression of its melting point (149—150 °C) upon a mixed-melting-point determination with an authentic sample. The washings and ethereal extracts from the reaction mixture were combined, dried (Na_2SO_4) and filtered. **A1** was detected by glc.

Reaction of **2** *with Sodium Hydroxide in 50% Aqueous Dioxane*: **2** obtained from *N*-methylbenzamidine hydrochloride (1.71 g, 0.01 mol) according to the same procedure as above was refluxed in 50% aqueous dioxane (50 ml) for 10 hr. When the reaction mixture was evaporated under reduced pressure and dioxane was almost removed, crystals precipitated. *N*-methyl-*N'*-phenylurea, mp 149 °C (0.36 g, 24%).

Reaction of **3** *with Sodium Hydroxide in* 50% *Aqueous Methanol*: Yellowish oily material was similarly obtained from *N*-chloro-*N'*-ethylbenzamidine (**3**) (0.01 mol). The yields of *N*-ethyl-*N'*-phenyl-*O*-methylisourea (**A4**, 35%) and methyl benzoate (7%) were determined using glc.

Reaction of **1** *with Sodium Hydroxide in 50% Aqueous Methanol*: **1** similarly obtained from benzamidine hydrochloride (3.85 g, 0.02 mol) was refluxed for 10 hr. When methanol was almost removed by evaporation under reduced pressure from reaction mixture, colorless leaflets (benzamide, 2.12 g, 65%) precipitated and were separated by filtration. The filtrate was evaporated and the residue extracted with hot ethanol (29 ml). The extract was concentrated to give the residual solid (sodium phenylcyanamide, **F**). Its infrared spectrum showed characteristic absorption of the cyano group at 2200 cm^{-1}. The residue was refluxed in 2 N hydrochloric acid (6 ml) for 40 min. After cooling and addition of aqueous sodium hydroxide solution to make the reaction mixture neutral, phenylurea was separated. (0.24 g, 9%, mp 146—148 °C).

The other *N*-chloroamidines were treated with sodium hydroxide by a similar method.

Reaction of N-*Chloroamidines with Silver Oxide. Reaction of* **4** *with Silver Oxide*: A suspension of **4** (11.80 g, 0.06 mol) and silver oxide (30 g, 0.13 mol) in anhydrous ligroin (60 ml) was heated under reflux for 0.3 hr. The insoluble matter was separated by filtration and the filtrate was distilled under reduced pressure to give a fraction with a bp of 75—80 °C/2 mmHg (3.37 g, 35%), which was identified

14) S. E. Forman, C. A. Erickson, and H. Adelman, *J. Org. Chem.*, **28**, 2653 (1963).
15) I. G. Hinton and R. F. Webb, *J. Chem. Soc.*, **1961**, 5051.

as *N*-isopropyl-*N'*-phenylcarbodiimide by comparison of its infrared spectrum with that of an authentic sample prepared by the treatment of *N*-isopropyl-*N'*-phenylthiourea with HgO. The distillate was refluxed in 1 N hydrochloric acid for 0.25 hr. After cooling and addition of aqueous sodium hydroxide solution to make the reaction mixture neutral, solid *N*-isopropyl-*N'*-phenylurea was obtained.

Reaction of ***1*** *with Silver Oxide*: A suspension of **1** (3.09 g, 0.02 mol) and silver oxide (10 g, 0.043 mol) in anhydrous ligroin (50 ml) was refluxed for 2 hr. The insoluble matter separated by filtration showed characteristic absorption of the cyano group at 2200 cm^{-1} in its infrared spectrum. The solid refluxed in 6 N hydrochloric acid and the insoluble matter was separated by filtration. After cooling, colorless plates were precipitated, which were identified as phenylurea, mp 147 °C, 0.26 g, 10%.

BULLETIN OF THE CHEMICAL SOCIETY OF JAPAN, VOL. 46, 1770—1772 (1973)

Studies of Azo Colors. XI.[1] The Diazo-coupling Reaction of Pyrroles

Kazuo MITSUMURA, Yōji HASHIDA, Shizen SEKIGUCHI, and Kohji MATSUI

Department of Synthetic Chemistry, Faculty of Engineering, Gunma University, Tenjincho, Kiryu, Gunma 376

(Received October 18, 1972)

Kinetic studies have been made of the coupling reaction of several diazonium salts with pyrrole, *N*-methylpyrrole, and *N*-ethoxycarbonylpyrrole. In the case of pyrrole, it was found, from the dependence of the apparent rate constant on the pH values, that the undissociated pyrrole reacted with diazonium salts in the pH range from 4.7 to 8.2, whereas in the pH region higher than 10.0 the reactive species was the conjugate base of pyrrole. The reactivity of the pyrrole anion was higher by a factor of 8 powers of ten than that of the undissociated pyrrole. The effects of the substituents of diazonium salts on the reaction rates were also investigated. The ρ-values (4.3—4.6) obtained in the Hammett plots were practically the same as those of diazo-coupling reactions which involve ordinary aromatic amines as coupling components.

Normally, diazo-coupling reactions take place between diazonium salts and substituted aromatic hydrocarbons, especially phenols and aromatic amines. The mechanisms and the structural effects of these reactions have been studied kinetically.[2]

Heterocyclic compounds, such as pyrrole,[3,4] indole,[5] imidazole,[6] and indazole,[7] have also long been known to react with diazonium salts to form azo compounds. Although the kinetic studies of some of these reactions have been carried out,[8,9] no detailed information on their mechanism and reactivity has yet been reported. In this paper, we wish to report the kinetics of the reactions of pyrroles with diazonium salts.

Results and Discussion

Brown and his co-workers[8] investigated the kinetics of the reaction of imidazole with diazonium salts. They found that the reaction of the diazonium ion with the imidazole anion formed by the ionization of the N–H bond was the rate-determining step. On the other hand, in the reaction of indole with diazonium salts, Binks and his co-worker[9] suggested that the undissociated indole was the reactive species.

Pyrrole is known to react with a diazonium salt, preferentially at the 2-position in a neutral solution, to form a monoazo compound, and to form a 2,5-bisazo compound in an alkaline solution.[3] However, it was confirmed by thin-layer chromatography that only a monoazo compound was obtained under our kinetic conditions, as will be described below.

Kinetic experiments have been carried out on the reactions of diazonium salts with 50 to 100 as many pyrroles in an aqueous buffer solution; the apparent rate constants (k') were calculated from Eq. (1), where E_t and E_∞ are the optical densities of the azo-compound at time t and at infinity respectively.

$$k't = \ln \frac{E_\infty}{E_\infty - E_t} \quad (1)$$

In each kinetic run, an increase in the optical density of the azo-compound obeyed good pseudo-first-order kinetics. The reactions also showed a first-order dependence on the concentration of pyrrole. The dependences of the rate constants (k') on the pH values are listed in Tables 1, 2, and 3. In the pH range treated in Tables 1, 2, and 3, the diazonium salts are considered to exist practically as diazonium ions.[10] In the case of pyrrole, it has become apparent that the rate constant increases with increases in the pH values in the alkaline region. For example, in the reaction of pyrrole with *p*-methoxybenzenediazonium salt (Table 1) or benzenediazonium salt (Table 2), the reaction rate is independent of the pH values in

1) Part X: Y. Hashida, M. Tanaka, and K. Matsui, submitted, this Bulletin.

2) H. Zollinger, "Azo and Diazo Chemistry," Interscience Publishers, New York, N.Y. (1961), p. 221; L. P. Hammett, "Physical Organic Chemistry," 2nd ed., McGraw-Hill Book Co., New York, N.Y. (1961), p. 171.

3) O. Fisher and E. Hepp, *Ber.*, **19**, 2251 (1886).

4) A. Treibs and G. Fritz, *Ann. Chem.*, **611**, 162 (1958).

5) W. Madelung and O. Wilhelmi, *Ber.*, **57**, 234 (1924).

6) R. G. Fargher and F. L. Pyman, *J. Chem. Soc.*, **115**, 217 (1919).

7) E. Bamberger, *Ann. Chem.*, **305**, 298 (1899).

8) R. D. Brown, H. C. Duffin, J. C. Maynard, and J. H. Ridd, *J. Chem. Soc.*, **1953**, 3937.

9) J. H. Binks and H. J. Ridd, *ibid.*, **1957**, 2398.

10) E. S. Lewis and H. Shur, *Chem. Ber.*, **91**, 2350 (1958).

Table 1. Dependence of the rate constant (k') for the reaction of pyrrole with *p*-methoxybenzenediazonium salt on pH at 20°C (Pyrrole 4×10^{-3} mol/l; Diazonium salt 4×10^{-5} mol/l)

pH	4.69	6.01	5.89	6.31	7.11	7.49
k' (min^{-1})	0.0491	0.0472	0.0548	0.0570	0.0642	0.0617
k_2 ($l\,mol^{-1}\,min^{-1}$)	1.23×10^{1}	1.18×10^{1}	1.38×10^{1}	1.43×10^{1}	1.61×10^{1}	1.54×10^{1}

pH	8.21	8.97	9.27	9.38	10.07	10.30	10.51	10.90
k' (min^{-1})	0.0672	0.118	0.172	0.201	0.532	0.861	1.33	3.48
k_2 ($l\,mol^{-1}\,min^{-1}$)	1.68×10^{1}	—	—	—	—	3.49×10^{9} (2.47×10^{-10}) a)	3.33×10^{9} (4.00×10^{-10})	3.55×10^{9} (9.84×10^{-10})

a) Values in parentheses are the concentration of pyrrole anion under experimental conditions.

Table 2. Dependence of the rate constant (k') for the reaction of pyrrole with benzenediazonium salt on pH at 20°C (Pyrrole 4×10^{-3} mol/l; Diazonium salt 4×10^{-5} mol/l)

pH	5.01	6.31	7.11	8.21	9.27	10.30
k' (min^{-1})	1.32	1.48	1.63	1.80	3.51	20.8

Table 3. Dependence of the rate constant (k') for the reaction of *N*-methylpyrrole with *p*-methylbenzenediazonium salt on pH at 20°C (Pyrrole 4×10^{-3} mol/l; Diazonium salt 4×10^{-5} mol/l)

pH	5.10	5.79	6.30	6.30	8.13	10.13
k' (min^{-1})	0.741	0.778	0.944	0.970	1.04	1.26

the pH range from 4.7 to 8.2; there is a slight dependence of k' on the pH values in the same range, which will be discussed later. However, the rate constant increased considerably when the pH value rose above 9.0.

The pK_a values of the pyrrole cation and pyrrole have been known to be 0.4[11] and 17.55[12] respectively. Therefore, pyrrole does not substantially dissociate in the pH range from 4.7 to 8.2. Thus, the fact that the reaction rate is independent of the pH may be explained by assuming that the undissociated pyrrole reacts with the diazonium salts (Eq. 2):

$$pH < 8.2 \qquad v = k_2(Ar\text{-}\overset{+}{N}_2)\left(\text{C}_4\text{H}_4\text{NH}\right) \qquad (2)$$

On the other hand, the reactive species is likely to be the pyrrole anion in an alkaline solution (Eq. 3), because the slope of the line between the log k' and pH values is close to unity in the pH region above pH 10.0. Furthermore, the observation that the reaction rates of *N*-methylpyrrole are essentially independent of the pH values, even in the alkaline region, supports the view mentioned above.

$$pH > 10.0 \qquad v = k_2(Ar\text{-}\overset{+}{N}_2)\left(\text{C}_4\text{H}_4\text{N}^-\right) \qquad (3)$$

Therefore, the second-order rate constants (k_2) were obtained according to Eq. (2) or (3) by dividing the first-order rate constants (k') by the undissociated pyrrole concentration or by the pyrrole anion concentration respectively. The results for the reaction of pyrrole with *p*-methoxybenzenediazonium salt are given in Table 1.

Table 4. Base catalyses in the reactions of substituted benzenediazonium salt with pyrroles at 20°C (Pyrrole 4×10^{-3}; Diazonium salt 4×10^{-5})

Pyrroles	Substituents	pH	Pyridine concn. (mol/l)	k' (min^{-1})
Pyrrole	*p*-OCH_3	6.3	0.0	0.0570
			0.1	0.0672
			0.2	0.0749
			0.4	0.0890
			0.6	0.104
Pyrrole	H	10.6	0.0	1.48
			0.1	1.72
			0.2	1.78
			0.4	2.00
			0.6	2.16
N-Methylpyrrole	*p*-CH_3	6.3	0.0	0.944
			0.1	1.03
			0.2	1.13
			0.4	1.30
			0.6	1.49

As can be seen from Table 1, the second-order rate constants (k_2) thus obtained are independent of the pH values of the medium, even in the alkaline region, suggesting that the application of Eq. (3) is reasonable. The pyrrole anion reacted faster by a factor of some 8 powers of ten than the undissociated pyrrole. The difference between the reactivities of these two species is similar to that observed between the reactivities of the naphthol and the naphtholate ion.[13] The reactivity of the pyrrole anion is greater by a factor of 5 orders than that of the naphtholate ion.[1]

It has been well known that some diazo-coupling reactions are accelerated by a base such as pyridine,[2] which acts as a proton acceptor from the intermediate of the substitution reaction. In order to confirm the base catalysis in the present study, the rate constants in the presence of the base (pyridine) have been measured. The results are given in Table 4. From these results, it can be seen that the reactions of pyrrole (pH 6.3), the pyrrole anion (pH 10.6), and *N*-methyl-

11) L. A. Paquette, "Principles of Modern Heterocyclic Chemistry," W. A. Benjamin, Inc., New York, N.Y. (1968), p. 105.
12) G. Yagil, *Tetrahedron*, **23**, 2855 (1967).
13) H. Kropáčová, J. Panchartek, V. Stěrba, and K. Valter, *Collect. Chech. Chem. Commun.*, **35**, 3287 (1970).
14) H. Zollinger, *Helv. Chim. Acta*, **38**, 1623 (1955).

Table 5. Rate constants (k_2) for the reactions of pyrroles with substituted benzenediazonium salt at pH 6.3 (20°C)

Pyrrole	Substituent	k_2 ($l\,mol^{-1}\,min^{-1}$)
Pyrrole	*p*-OCH_3	1.43×10^1
	p-CH_3	6.65×10^1
	m-CH_3	1.77×10^2
	H	3.70×10^2
	m-OCH	8.85×10^2
N-Methylpyrrole	*p*-OCH_3	5.08×10^1
	p-CH_3	2.36×10^2
	m-CH_3	5.85×10^2
	H	1.03×10^3
	m-OCH_3	2.46×10^3
N-ethoxycarbonylpyrrole	*p*-CH_3	4.79
	m-CH_3	1.61×10^1
	H	2.92×10^1
	m-OCH_3	9.15×10^1
	p-Cl	3.58×10^2

pyrrole were slightly catalyzed by the base. As has been described previously, in our experiments the rate measurements were performed in buffer solutions; the buffer reagent may be assumed to act also as a base in these cases. Therefore, the slight dependence of k' on the pH values in the pH range from 4.7 to 8.2 may be ascribed to the difference in the catalytic actions of buffer solutions.

In the cases of pyrrole, *N*-methylpyrrole, and *N*-ethoxycarbonylpyrrole, the influence of substituents in the diazonium salts on the rate constants was also investigated (Table 5). The results may be expressed by the following Hammett equations*[20]:

Pyrrole	$\log k_2 = 4.63\sigma + 2.51$	$r=0.992$
N-Methylpyrrole	$\log k_2 = 4.28\sigma + 2.99$	$r=0.986$
N-Ethoxycarbonylpyrrole	$\log k_2 = 4.64\sigma + 1.48$	$r=0.985$

It can be seen from these results that the influence of the *N*-substituents in pyrrole on the reaction constant is small and that these ρ-values are similar to those in the coupling reactions of diazonium salts with ordinary aromatic amines, such as *N*,*N*-dimethylaniline (ρ; 4.34)[15] and 1-naphthylamine (ρ; 4.94).[15]

Experimental

Materials. The *N*-ethoxycarbonylpyrrole was prepared according to the method of Ciamician[16] from ethyl chloroformate and potassium salt of pyrrole. The commercial pyrrole, *N*-methylpyrrole, and aromatic amines used as diazo components were purified by distillation or by recrystallization prior to use. Their purities were checked by means of their physical constants and by gas-liquid chromatography.

Kinetic Measurements. The procedure was essentially the same as that described in an earlier paper.[17] The kinetic measurements were carried out in aqueous buffer solutions at 20 °C and at a constant ionic strength (0.04). Kinetic measurements in the presence of pyridine were carried out at a constant pH (6.3 or 10.3) according to the procedure of Zollinger *et al.*[8]

15) Y. Hashida, M. Tanaka, and K. Matsui, Abstract of the 25st Annual Meeting of the Chemical Society of Japan (1971), Reprint, p. 254.
16) G. L. Ciamician and M. Dannstedt, *Ber.*, **15**, 2579 (1882).
17) Y. Hashida, K. Nakajima, S. Sekiguchi, and K. Matsui, *Kogyo Kagaku Zasshi*, **72**, 1132 (1969).
18) H. Zollinger, *Helv. Chim. Acta*, **38**, 1597 (1955).
19) D. H. McDaniel and H. C. Brown, *J. Org. Chem.*, **23**, 420 (1958).
20) Substituent constants were taken from Ref. 19).

BULLETIN OF THE CHEMICAL SOCIETY OF JAPAN, VOL. 46, 1772—1776 (1973)

Phenanthro[4,5-*bcd*]furan Derivatives. I. A Synthesis of 5-Hydroxy-1-methoxyphenanthro[4,5-*bcd*]furan

Takahachi SHIMIZU, Takaaki HORAGUCHI, and Akio WATANABE

Department of Chemistry, Faculty of Science, Niigata University, Igarashi, Niigata 950–21

(Received October, 11, 1972)

5-Hydroxy-1-methoxyphenanthro[4,5-*bcd*]furan(I;R=MeO) was synthesized by dehydrogenation with 20% palladium on charcoal from 5,6,7,7a,8,9-hexahydro-1-methoxy-5-oxophenanthro[4,5-*bcd*]furan(XVII), which had itself been prepared *via* a naphthofuran derivative (XVI) starting from 5,8-dimethoxy-1-tetralone (VII).

Morphine gives a variety of non-nitrogenous degradation products,[1] including morphenol (I;R=H), which has not yet been synthesized. Burger and Avakian[2] failed to cyclize the acid (II;R=H, n=1) to a phenanthrol derivative (III; R=H); similarly, the acid (II; R=MeO, n=2) was converted to the indenone (IV)[3] rather than to a phenahthro[4,5-*bcd*]-furan. Dendy *et al.*[4] succeeded in cyclizing it with a partially hydroaromatic precursor (V; R=MeO) into the ketone (VI), but the yield was too poor for them to continue the project further. They ascribed these difficulties of cyclization to a strain in the fused-

1) E. Mosettig and E. Meitzner, *J. Amer. Chem. Soc.*, **56**, 2738 (1934).
2) A. Burger and S. Avakian, *ibid.*, **62**, 226 (1940).
3) H. Gilman and L. C. Cheney, *ibid.*, **61**, 4149 (1938).
4) A. V. Dendy, J. H. P. Tyman, and W. B. Wahlley, *J. Chem. Soc.*, **1963**, 4040.

ring system.

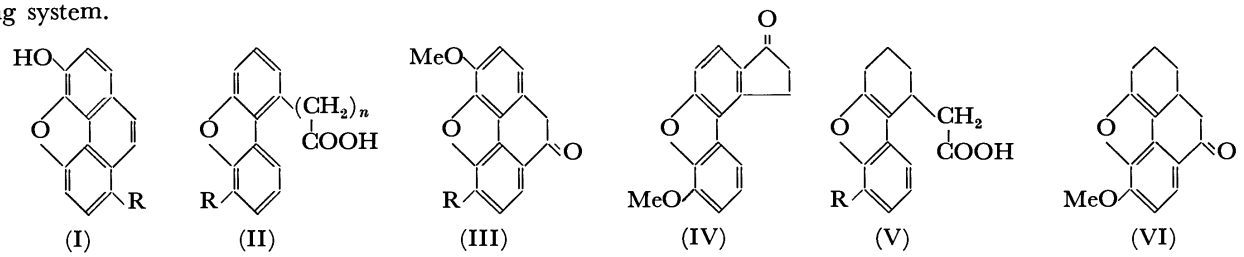

An approach to the synthesis of morphenol, not from a dibenzofuran, but from the naphtho[1,8-*bc*]furan derivative (XVI), was planned. In this paper, the results of a model experiment will be reported, this experiment led to a successful synthesis of a kind of methoxymorphenol, 5-hydroxy-1-methoxyphenanthro-[4,5-*bcd*]furan(I; R=MeO).

Results and Discussion

The naphtho[1,8-*bc*]furan derivative (XVI) was prepared from 5,8-dimethoxy-1-tetralone (VII) *via* a series of intermediate, as is shown in scheme 1.

5,8-Dimethoxy-1-tetralone (VII) was prepared starting from 3-(2,5-dimethoxybenzoyl)propionic acid (*cf.* the Experimental section). VII was formylated[5] to give VIII, with ethyl formate on the methylene group adjacent to the carbonyl group, becasue the methylene was not expected to be active enough to react with methyl acrylate because of the electronic effect of two methoxy groups on the benzene ring.[6] The addition reaction of VIII with methyl acrylate was performed in a refluxing methanol solution containing a small amount of triethylamine; this gave X in a good yield rather than IX. The propionic acid derivative (XI) was prepared from X by saponification. The heating of XI with pyridinium chloride[7] afforded a dihydric phenol derivative (XII). XII showed a absorption due to OH stretching at 3400 cm^{-1} in the infrared absorption spectrum and reacted with ferric chloride.

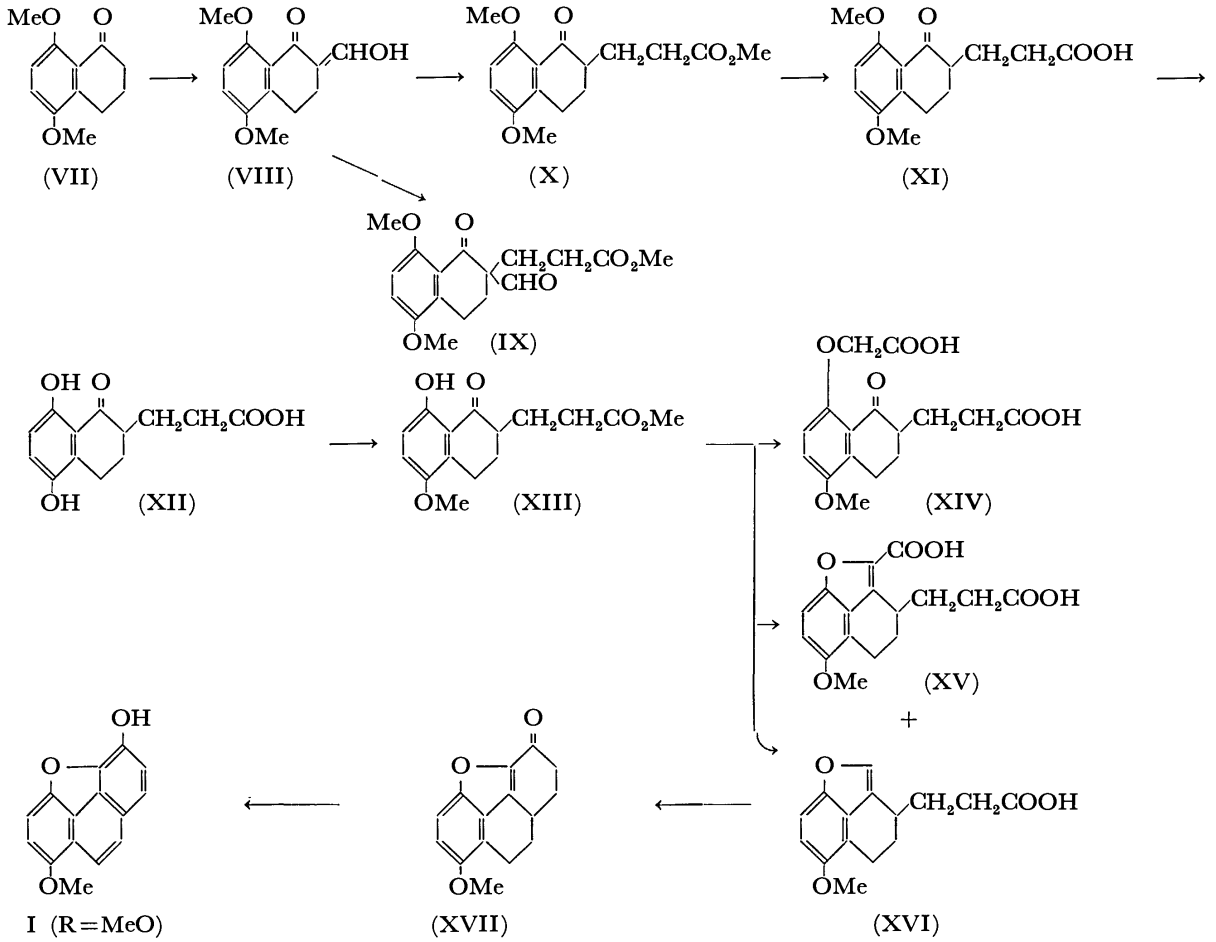

Scheme 1.

5) R. B. Turner, D. E. Nettleton, J. R. and R. F. Ferebee, *J. Amer. Chem. Soc.*, **76**, 5923 (1956).

6) R. E. Juday, *ibid.*, **75**, 4071 (1953).

7) M. S. Newman and R. L. Childers, *J. Org. Chem.*, **32**, 62 (1967).

The reaction mixture changed in color from blue to brown in time. The reaction of XII with dimethyl sulfate afforded a good yield of a monohydric phenol, which then reacted with ferric chloride to result in a blue color. In spite of the color reaction, XIII did not manifest any OH stretching absorption in the infrared absorption spectrum above 3000 cm^{-1}; such a phenomenon is, though, often observed for *O*-acyl phenols.[8]

Let us turn now to a consideration of the building of the strained fused-ring; our first effort involved the transformation of XIII into the naphtho[1,8-*bc*]furan derivative (XVI). The reaction of the tetralone (XIII) with a mixture of ethyl bromoacetate and potassium carbonate in acetone at 100 °C, followed by saponification, afforded the dicarboxylic acid (XIV), which was then heated with a mixture of acetic anhydride and sodium acetate in the expectation that the naphthofuran would be formed. However, no evolution of carbon dioxide was observed, indicating no reaction, that these was not even under the above reaction conditions.

In the course of further studies of the formation of a furan ring, a convenient method for the direct synthesis of naphtho[1,8-*bc*]furan from 8-hydroxy-1-tetralone was discovered by accident: the heating of the tetralone in ethyl bromoacetate at 170 °C, followed by saponification, gave two crystalline products, 3-(4,5-dihydro-6-methoxy-3*H*-naphtho[1,8-*bc*]fur-3-yl)propionic acid (XVI) and 3-(2-carboxy-4,5-dihydro-6-methoxy-3*H*-naphtho[1,8-*bc*]fur-3-yl)propionic acid (XV), but XIV was not detected. The structures of XV and XVI were discussed on the basis of their spectral properties and subsequent transformations. The infrared spectrum for XV shows a conjugated-carbonyl band at 1693 cm^{-1} in addition to an unconjugated-carbonyl band at 1710 cm^{-1}. XV was transformed into XVI by heating with a mixture of quinoline and copper. The ultraviolet spectrum of XVI shows λ_{max}^{EtOH} 253 nm (ε 9300) and 292 nm (ε 3600), similar to those of the benzofurans, and the nuclear magnetic resonance absorption spectrum shows a sharp singlet at τ 2.43 which might be ascribed to a methine hydrogen on the furan ring. The acid (XVI), when heated at 90 °C in polyphosphoric acid, was transformed into the expected ketone (XVII) in a good yield; this substance showed an absorption band due to a conjugated-carbonyl group at 1660 cm^{-1} in the infrared absorption spectrum.

For aromatization[9] of XVII to the phenol I (R=MeO), palladium on charcoal was used as the catalyst; the yield was 20%. The resulting phenol decomposes at 187—191 °C and gives an intense blue fluorescence in an alkaline solution, much like morphenol I (R=H). The structure of I (R=MeO) was established on the basis of its spectral properties. The nuclear magnetic absorption spectrum showed the existence of a methoxyl group at τ 5.49 (s), two equivalently-situated hydrogens on the phenanthrene ring at τ 2.13 (s), four hydrogens on the phenanthrene ring at τ 2.23—2.82 (oct), and a hydroxyl group at τ 0.59 (s); moreover, the band at τ 2.23—2.82 (oct) could be explained as an assembly of two kinds of AB-type resonances. The ultraviolet absorption spectrum of I (R=MeO) is very similar to that of morphenol methyl ether.[10] The infrared absorption spectrum of I (R=MeO) posseses bands corresponding to three kinds of two adjacent hydrogens on the phenanthrene ring at 800 and 826 cm^{-1}—one of the three expected absorptions is overlapped with one of the two residual absorptions—and a broad band corresponding to the hydroxyl group at 3250 cm^{-1}.

This phenolic compound is believed to be the never-before-synthesized phenanthro[4,5-*bcd*]furan. The ketone (XVII) must be as strained as the ketone (VI) prepared by Dendy *et al.*,[4] since the two ketones are very similar to each other in fused-ring structure. From this point of view, it is surprising that we unexpectedly obtained good yields in two cyclizations, from XIII to a mixture of XV and XVI, and from XVI to XVII. However, that the latter cyclization proceeded under mild reaction conditions suggests that the strain was dominantly introduced in the former cyclization, in which a drastic reaction condition was required to give a lower yield. This suggestion is surported by the experiments of Royer *et al.*[11]

Experimental

All the melting point are uncorrected. The chromatography was performed over silica gel (WAKOGEL C-200, Wako Pure Chemical Industries, Ltd.). The polyphosphoric acid was prepared from 85% phosphoric acid (470 g) and phosphorus pentoxide (516 g) by heating at 160—165 °C for 5 hr. Unless otherwise stated, sodium sulfate was employed as the drying agent. The infrared spectra were determined with a JASCO Model DS 402 G infrared spectrophotometer. The ultraviolet spectra were determined with a Shimadzu Model MR-31 spectrophotometer. The nuclear magnetic resonance spectra were determined at 100 MHz with a JEOL Model 4H-100 NMR spectrometer, using tetramethylsilane as the internal standard. Their chemical shifts are presented in terms of the τ value.

4-(2,5-Dimethoxyphenyl)butyric Acid. In a vessel for reduction we placed a solution of 3-(2,5-dimethoxybenzoyl)-propionic acid (40 g) in acetic acid (120 ml), a solution of palladium chloride (0.25 g) in 0.1 M hydrochloric acid (32 ml), and active charcoal (12.0 g). The hydrogenation[12] was carried out at room temperature and at atmospheric pressure until the hydrogen uptake had ceased. The catalyst was then filtered out, and the filtrate was evaporated under

8) "Documentation of Molecular Spectroscopy" (D.M.S.), Butterworth and Co. (Publishers) Ltd., Lomdon, No. 5522, 6755, 9300; L. J. Bellamy, "The infrared Spectra of Complex Molecules," 2nd ed., John Wiley & Sons, Inc., New York, (1958), pp. 103-104.

9) R. B. Turner, D. E. Nettleton, *J. Amer. Chem. Soc.*, **76**, 5923 (1956); E. Mosettig and H. M. Duvoll, *ibid.*, **59**, 367 (1937).

10) H. Rapoport, A. D. Batchs, and J. E. Gordon, *ibid.*, **80**, 5767 (1958).

11) R. Royer, E. Bisagni, and G. Menichi, *Bull. Soc. Chim. Fr.*, **1964** (9), 2112; *Chem. Abstr.*, **62**, 1618h (1965). They obtained 2-acetyl{or 2-(*p*-methoxybenzoyl)}-6-methoxy-4,5-dihydro-3*H*-naphtho[1,8-*bc*]furan by condensation of 8-hydroxy-5-methoxy-1-tetralone with chloromethyl methyl (or *p*-methoxyphenyl) ketone; however, the yields are poor (2.5% or 17%, respectively).

12) S. Mitsuo, H. Saito, and H. Mamuro, *Nippon Kagaku Zasshi*, **81**, 292 (1960); *Chem. Abstr.*, **59**, 437f (1962).

reduced pressure to leave a viscous oil. Trituration with ice-cold water, followed by the washing of the resulting crystals with water, gave a crude solid in a 76.5% yield (57.5 g). Recrystallization from 30% aqueous ethanol afforded the pure 4-(2,5-dimethoxyphenyl)butyric acid as colorless plates; mp 66—68 °C. The mixed melting point with an authentic sample[11] did not depressed.

5,8-Dimethoxy-1-tetralone (VII). A mixture of γ-(2,5-dimethoxyphenyl)butyric acid (25 g) and polyphosphoric acid (325 g) was stirred at 50 °C for 8.5 hr. The resulting yellow mixture was diluted with ice-cold water and extracted with ether. The ether was washed with 1M aqueous potassium carbonate and with water, and then dried. After the removal of the solvent the extract was crystallized from *n*-hexane–ether to give 13.4 g (58.2%) of VII as colorless needles; mp 62—63 °C (lit,[11] mp 61 °C).

Found: C, 69.82; H, 6.74%. Calcd for $C_{12}H_{14}O_3$: C, 69.90; H, 6.84%.

2-Hydroxymethylidene-5,8-dimethoxy-1-tetralone (VIII). In a 500-ml flask equipped with a stirrer and a dropping funnel we placed sodium methylate powder (from 6.6 g of sodium metal and 70 ml of absolute methanol) and benzene (200 ml). Into the suspension ethyl formate (36 ml) was stirred over a 5-min period under cooling in ice-cold water; the stirring was then continued for 1 more hr. The tetralone (VII, 15 g) in benzene (120 ml) was added, drop by drop, over 50-min period, during which the reaction temperature was kept below room temperature. The ice-bath was then removed, and the stirring was continued for an additional 2.5 hr. The reaction mixture was then acidified with 2 M hydrochloric acid (150 ml) to give crystals of VIII. Recrystallization from 60% ethanol afforded 13.7 g of the pure VIII as colorless needles; mp 85—86 °C. IR(KBr): 3270 cm^{-1} (OH), 1263 cm^{-1}(C=O). NMR($CDCl_3$): τ 1.67 (OH).

Found: C, 66.61; H, 6.08%. Calcd for $C_{13}H_{14}O_4$: C, 66.74; H, 6.03%.

Methyl 3-(1,2,3,4-Tetrahydro-5,8-dimethoxy-1-oxo-2-naphthyl)-propionate (X). To 20.0 g of VIII we added 12.0 g of methyl acrylate, 27.0 g of triethylamine, and 80% methanol (80 ml), after which the mixture was refluxed for 7.5 hr. The reaction mixture was then extracted with ether. To remove the triethylamine and the acidic compounds, the ether (800 ml) was washed with five 100-ml portions of 0.5 M hydrochloric acid and then with four 50-ml portions of 2 M aqueous patossium carbonate, and washed with water. The ether, after drying, was evaporated to an oil, which was warmed on a steambath under reduced pressure to remove the unreacted methyl acrylate. Crystallization from methanol gave 14.3 g (57.2%) of X as colorless needles; mp 64—65 °C. IR(KBr): 1737 ($COOCH_3$), 1692 cm^{-1} (C=O). NMR (CCl_4): τ 6.45 ($COOCH_3$, s).

Found: C, 65.88; H, 6.91%. Calcd for $C_{16}H_{20}O_5$: C, 65.75; H, 6.81%.

3-(1,2,3,4-Tetrahydro-5,8-dimethoxy-1-oxo-2-naphthyl)propionic Acid (XI). Into a saturated alcoholic solution of X (20 g) we stirred, drop by drop, 3 M aqueous potassium hydroxide until the last few drops no longer induced instantaneous milky turbidity. After standing for 30 min, the reaction mixture was diluted with water and acidified with 6 M hydrochloric acid to give precipitates of XI. Recrystallization from 60% ethanol afforded 15.8 g (83.0%) of the pure XI as colorless needles; mp 139—140.5 °C. IR (KBr): 1716 (COOH), 1685 cm^{-1} (C=O).

Found: C, 64.76; H, 6.55%. Calcd for $C_{15}H_{18}O_5$: C, 64.74; H, 6.47%.

3-(1,2,3,4-Tetrahydro-5,8-dihydroxy-1-oxo-2-naphthyl)propionic Acid (XII). A mixture of XI (10.0 g) and pyridinium chloride (45 g) was heated at 220 °C (bath temp.) for 2.5 hr. The reaction mixture was dissolved in 2 M aqueous sodium hydroxide and filtered. The filtrate was acidified with 6 M hydrochloric acid and then extracted with ether. The ether was washed with three 80-ml portions of 1 M hydrochloric acid to remove the pyridine; then it was further washed with water and dried. The ether was evaporated to yellow crystals. Recrystallization from 25% ethanol gave 7.8 g (86.8%) of XII as yellow needles; mp 125—126 °C. IR(KBr): 3390 (OH), 1722 (COOH), 1625 cm^{-1}(C=O).

Found: C, 62.02; H, 5.70%. Calcd for $C_{13}H_{14}O_5$: C, 62.40; H, 5.60%.

Methyl 3-(1,2,3,4-Tetrahydro-8-hydroxy-5-methoxy-1-oxo-2-naphthyl)propionate (XIII). A mixture of XII (10.0 g), dimethyl sulfate (18.5 g), potassium carbonate (22.5 g) and acetone (33.5 g) was heated under reflux for 2 hr. The reaction mixture was refluxed with water (150 ml) for 15 min and then extracted with ether. The ether extract was washed with water, dried, and evaporated to a yellow solid. Recrystallization from methanol gave 8.5 g (76.3%) of XIII as yellow needles; mp 66.5—67.5 °C. IR(KBr): 1728 ($COOCH_3$), 1638 cm^{-1} (C=O).

Found: C, 64.75; H, 6.11%. Calcd for $C_{15}H_{18}O_5$: C, 64.74; H, 6.47%.

3-(1,2,3,4-Tetrahydro-8-carboxymethoxy-5-methoxy-1-oxo-2-naphthyl)propionic Acid (XIV). A mixture of XIII (1.0 g), ethyl bromoacetate (3.1 g), potassium carbonate (3.4 g), and methyl ethyl ketone (50 ml) was heated under reflux for 3 hr; ethyl bromoacetate (2.0 g) was then added to the mixture, and the refluxing was continued for an additional 3 hr. The reaction mixture was filtered and thoroughly washed with hot acetone, and then the filtrate and washings were combined and evaporated to dryness. The residue was treated much as has been described in connection with the preparation of XI to give 150 mg of XIV (13% based on XIII) as colorless prisms; mp 179—185 °C (decomp.). IR(KBr): 1780 (OCH_2COOH), 1705 (COOH), 1659 cm^{-1} (C=O).

Found: C, 59.39; H, 5.70%. Calcd for $C_{16}H_{18}O_7$: C: 59.70; H, 5.59%.

3-(2-Carboxy-4,5-dihydro-6-methoxy-3H-naphtho[1,8-bc]fur-3-yl)propionic Acid (XV) and 3-(4,5-Dihydro-6-methoxy-3H-naphtho[1,8-bc]fur-3-yl)propionic Acid (XVI). A mixture of XIII (2.0 g), ethyl bromoacetate (6.2 g), potassium carbonate (2.3 g), and methyl ethyl ketone (2.2 g) was heated at 170 °C (bath temp.) for 3 hr; ethyl bromoacetate (2.0 g) was then added to the mixture, and the refluxing was continued for an additional 3 hr. The dark brown and almost dry reaction mixture thus obtained was extracted with hot acetone, and the acetone was evaporated. The residue was hydrolyzed much as has been described in connection with the preparation of XI, and the resulting alkaline solution was acidified with 6 M hydrochloric acid and extracted with ether. The ether was washed with water, dried, and evaporated to dryness. The solid mass was separated into two moieties, one of which is insoluble in benzene. The benzene-insoluble moiety was crystallized from tetrahydrofuran–benzene to give 0.95 g (43.5%) of XV as colorless needles; mp 195—196 °C. IR (KBr): 1710, 1693 cm^{-1} (COOH).

Found: C, 63.11; H, 5.43%. Calcd for $C_{16}H_{16}O_6$: C, 63.16; H, 5.26%.

The other moiety in benzene was chromatographed over silica gel and eluted with benzene–ether (97 : 3). A yellow fraction was collected, and the solvent was evaporated. The residue was crystallized from benzene–*n*-hexane to give 0.1 g (8.8%) of XVI as colorless needles; mp 123—124 °C. IR (KBr): 1705 cm^{-1} (COOH). NMR(CD_3COCD_3): τ 2.43

(H on the furan ring. UV: λ_{max}^{EtOH} 253 (ε 9300), 292 (ε 3600), 302 nm (ε 3200).

Found: C, 68.88; H, 6.10%. Calcd for $C_{15}H_{16}O_4$: C, 69.21; H, 6.15%.

Decarboxylation of XV. A mixture of 8.0 g of quinoline, 0.6 g of XV, and 0.6 g of copper powder was heated at 150 °C for 1.5 hr, during which carbon dioxide was evolved, and then at 155 °C for 10 more min. The mixture was acidified with 1 M hydrochloric acid and extracted with ether. The ether extract (500 ml) was washed four 50-ml portions of 2 M hydrochloric acid, and with water, and then dried, after which the ether was evaporated. The residue in benzene was chromatographed over silica gel and eluted with benzene–ether (93 : 7). An orange fraction was collected, and the solvent was evaporated. The residue was crystallized from benzene–*n*-hexane to give 0.23 g (44.9%) of XVI as colorless needles; mp 123—124 °C.

*5,6,7,7a,8,9-Hexahydro-1-methoxy-5-oxophenanthro[4,5-*bcd*]furan (XVII).* A mixture of 0.4 g of XVI and 36.5 g of polyphosphoric acid was stirred at 80 °C for 3.5 hr. The violet reaction mixture was poured onto ice and extracted with ether. The ether (500 ml) was washed with water, with four 70-ml portions of 1 M aqueous potassium carbonate, and with water, and then dried. The ether was evaporated to give crystals. Recrystallization from ethanol gave 0.25 g (67.1%) of XVII as colorless needles; mp 170—170.5 °C. IR(KBr): 1660 cm^{-1}(C=O).

Found: C, 74.03; H, 5.83%. Calcd for $C_{15}H_{14}O_3$: C, 74.37; H, 5.79%.

*5-Hydroxy-1-methoxyphenanthro[4,5-*bcd*]furan (*I: *R=MeO).* A mixture of 0.1 g of XVII, 0.2 g of 20% palladium on charcoal, and 2.0 g of α-methylnaphthalene was heated at 240 °C for 30 hr in a nitrogen atmosphere. The catalyst was then filtered out and washed with ether. The filtrate and washings were combined, and the ether was extracted with five 50-ml portions of 1 M potassium hydroxide. The alkaline solution was washed with two 30-ml portions of carbon tetrachloride and acidified with 6 M hydrochloric acid, and the resulting precipitates were extracted with ether. The ether extract was washed with water and dried, and the ether was evaporated. The residue was dissolved in benzene containing a little ether, chromatographed over silica gel, and eluted with benzene–ether (9 : 1). A yellow fraction was collected, and the solvent was evaporated to give crystals. Recrystallization from benzene gave 0.02 g (20.3%) of I (R=MeO) as colorless needles; mp 187—191 °C (decomp.). IR(KBr): 3240 (OH), 825, 800 cm^{-1} (2H). NMR(CD_3COCD_3): τ 4.59 (MeO, s), 2.82, 2.73, 2.31, 2.23 (q, 2H), 2.58, 2.53, 2.49, 2.44 (q, 2H), 2.13 (2H), 0.59 (OH). UV: λ_{max}^{EtOH} 242 (ε 56300), 265 (ε 23500), 313 (ε 11300), 327 (ε 15700), 351 (ε 8120), 370 nm (ε 14700).

Found: C, 75.45; H, 4.29%. Calcd for $C_{15}H_{10}O_3$: C, 75.76; H, 4.26%.

The authors wish to thank Prof. N. Fudaka for his interest and encouragement, Mr. Y. Takahashi for the elemental analyses, and Mr. H. Saisu for infrared analyses.

BULLETIN OF THE CHEMICAL SOCIETY OF JAPAN, VOL. 46, 1776—1779 (1973)

The Palladium-catalyzed Arylation of 4-Chromanone Enol Esters. A New Synthesis of Isoflavanones

Ryu-ichi SAITO, Taeko IZUMI, and Akira KASAHARA*

Department of Applied Chemistry, Faculty of Engineering, Yamagata University, Yonezawa-shi, Yamagata 992

(Received October 31, 1972)

Heck's reaction of 4-chromanone enol esters with arylpalladium compounds in acetic acid afforded isoflavanones in a high yield. The structural elucidation of these products was accomplished by spectral inspections.

Isoflavanones (I) have been synthesized by the hydrogenation of the corresponding isoflavones,[1-4] by the oxidation of isoflavanes,[5] by the reduction of 3-hydroxyisoflavanones with zinc in aqueous acetic acid,[6] and by the action of methylene diiodide on *o*-hydroxydeoxybenzoin.[7] Recently, Heck[8] has reported that arylpalladium compounds, generated *in situ* from arylmercury compounds (II) and palladium salts, reacted with ketone enol esters to form α-arylketones as the major products. In this report we wish to report

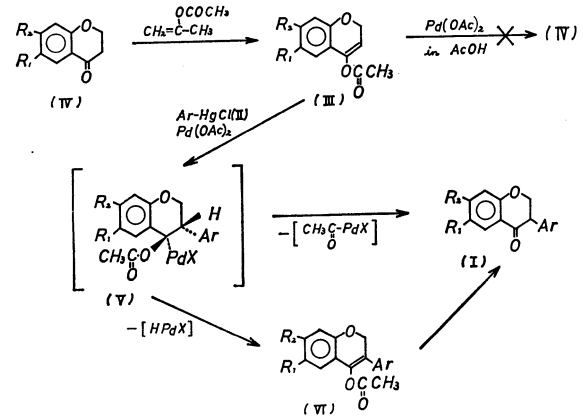

Fig. 1

* To whom communications should be addressed.

1) E. L. Anderson and G. F. Marrian, *J. Biol. Chem.*, **127**, 649 (1939).

2) N. Narasimhachari and T. R. Seshadri, *Proc. Indian Acad. Sci., Sect. A*, **35**, 202 (1952).

3) F. E. King and K. G. Neill, *J. Chem. Soc.*, **1952**, 4752.

4) N. Inoue, *Nippon Kagaku Zasshi*, **79**, 112 (1958).

5) A. McGookin, A. Robertson, and W. B. Whalley, *J. Chem. Soc.*, **1940**, 787; A. Robertson, C. W. Suckling, and W. B. Whalley, *ibid.*, **1949**, 1576.

6) N. Inoue, *Nippon Kagaku Zasshi*, **79**, 218 (1958).

7) S. K. Aggarwal, S. K. Grover, and T. R. Seshadri, *Indian J. Chem.*, **7**, 1059 (1969).

8) R. F. Heck. *J. Amer. Chem. Soc.*, **90**, 5535 (1968).

Table 1. Arylation reaction of 4-chromanone enol acetates (III)

4-Chromanone enol acetate	Arylating agent	Product	Yield %
IIIa	IIa	Isoflavanone (Ia)	75
IIIa	IIb	4'-Methylisoflavanone (Ib)	70
IIIa	IIc	4'-Methoxyisoflavanone (Ic)	75
IIIa	IId	3'-Nitroisoflavanone (Id)	65
IIIa	IIe	4'-Phenylisoflavanone (Ie)	60
IIIa	IIf	4'-Chloroisoflavanone (If)	60
IIIb	IIa	6-Methoxyisoflavanone (Ig)	68
IIIb	IIb	6-Methoxy-4'-methylisoflavanone (Ih)	72
IIIb	IIc	6,4'-Dimethoxyisoflavanone (Ii)	70
IIIb	IId	6-Methoxy-3'-nitroisoflavanone (Ij)	70
IIIb	IIe	6-Methoxy-4'-phenylisoflavanone (Ik)	65
IIIb	IIf	6-Methoxy-4'-chloroisoflavanone (Il)	68
IIIc	IIa	7-Methoxyisoflavanone (Im)	60
IIIc	IIb	7-Methoxy-4'-methylisoflavanone (In)	65
IIIc	IIc	7,4'-Dimethoxyisoflavanone (Io)	70
IIIc	IId	7-Methoxy-3'-nitroisoflavanone (Ip)	70
IIIc	IIe	7-Methoxy-4'-phenylisoflavanone (Iq)	65
IIIc	IIf	7-Methoxy-4'-chloroisoflavanone (Ir)	70

the application of this new reaction to 4-chromanone enol esters (III); this method gave I in a high yield.

III was obtained in 80—90% yields by the reaction of 4-chromanones (IV) with isopropenyl acetate at reflux. In the presence of palladium acetate, III was treated with II in acetic acid at room temperature to produce I. For example, the reaction of 4-chromanone enol acetate (IIIa) with phenylmercuric acetate (IIa) resulted in the formation of isoflavanone (Ia) (yield=75%), which was identified by a comparison of its NMR and IR spectra with those of an authentic sample.[4] Similarly, 6-methoxy- and 7-methoxy-isoflavanone (Ig and Im) were synthesized from 6-methoxy- and 7-methoxy-4-chromanone enol acetate (IIIb and IIIc) respectively. The reactions carried out are summarized in Table 1.

Recent studies of the Heck reaction have shown that the reaction usually gives products consistent with a *cis* addition of the arylpalladium compounds to olefin, followed by a *cis* palladium hydride elimination and readdition.[9] In the reaction of III with arylpalladium compounds, the sterically-preferred direction of addition appears to be to add the aryl group to the least-substituted carbon atom (C_3) of the double bond. In the initially-formed adduct (V), the *trans* elimination of palladium with a neighboring hydride produces an arylated enol ester (VI), while the elimination of palladium with an acyl group produces a carbonyl compound (I). Previously it was suggested that, in the phenylation of enol esters, the elimination of palladium with an acyl group in the adduct appears to be produce the carbonyl compounds,[8] but Heck[10] has recently shown that the cupric chloride used as a co-catalyst is responsible for the formation of phenylacetaldehyde in the phenylation of vinyl acetate and that presumably the elimination of palladium with an acyl group does not occur. However, in the arylation reaction of III without using cupric chloride as a co-catalyst, the reaction mixtures produced little, if any, VI, affording only I. Moreover, since the enol ester, IIIa, can not be changed to the IVa ketone in an acetic acid solution of palladium acetate, it is clear that the I does not all come from the hydrolysis of VI and that the elimination of palladium with an acyl group produces I.

Experimental

All the melting points and boiling points are uncorrected. The IR spectra were taken with a Hitachi model 215 grating spectrometer. The NMR spectra were recorded on a Hitachi model H-60 spectrometer, operating at 60 MHz in a $CDCl_3$ solution; the chemical shifts were given in ppm from the TMS internal standard. The NMR signals in a singlet are designated as s; in a doublet, as d; in a triplet, as t, and in a multiplet, as m.

Materials. The palladium acetate was prepared according to the procedure of Wilkinson.[11] The following compounds were synthesized by the methods described in the literature: 4-chromanone (IVa), bp 120—122 °C/9 mmHg (lit,[12] bp 127—128 °C/13 mmHg); 6-methoxy-4-chromanone (IVb), mp 48—49 °C (lit,[13] mp 49 °C); 7-methoxy-4-chromanone (IVc), mp 52—53 °C (lit,[14] mp 52—54 °C); *p*-tolylmercuric chloride (IIb), mp 232—233 °C (lit,[15] mp 233 °C); *p*-anisylmercuric chloride (IIc), mp 173—174 °C (lit,[16] mp 173—174 °C); *m*-nitrophenylmercuric chloride

9) R. F. Heck, *ibid.*, **91**, 6767 (1969); *ibid.*, **93**, 6896 (1971); P. M. Henry and G. A. Ward, *ibid.*, **94**, 673 (1972).
10) P. M. Maitlis, "The Organic Chemistry of Palladium", Vol. II, Academic Press, New York, 1971, p. 13, footnote,
11) T. A. Stepheson, S. M. Morehouse, A. R. Powell, J. P. Heffer, and G. Wilkinson, *J. Chem. Soc.*, **1965**, 3632.
12) F. Arndt and G. Kallner, *Ber.*, **57**, 202 (1924).
13) P. Pfeiffer, H. Oberlin, and E. Konermann, *ibid.*, **58**, 1947 (1925).
14) P. Pfeiffer and J. Oberlin, *ibid.*, **57**, 212 (1924).
15) F. C. Whitemore, F. H. Hamilton, and N. Thurman, "Organic Syntheses," Coll. Vol. I, 519 (1941).
16) O. Dimorth, *Ber.*, **35**, 2853 (1902).

TABLE 2. ANALYSES AND PROPERTIES OF ISOFLAVANONES (I)

Compound	Mp °C (lit)	Found (%) C	Found (%) H	Calcd (%) C	Calcd (%) H	IR and NMR spectra
Ia	76—77 (77[a])					
Ib	83—84	80.52	5.81	80.64	5.92	IR 1683, 800, and 760 cm^{-1}. NMR δ 2.36 (s 3H, CH_3–), 3.94 (t 1H, J=6.0 Hz, proton on C_3), 4.65 (d 2H, J=6.0 Hz, protons on C_2), and 6.89—7.98 ppm (m 8H, aromatic ring protons).
Ic	98—99	75.43	5.38	75.57	5.55	IR 1685, 810, and 740 cm^{-1}. NMR δ 3.80 (s 3H, CH_3O–), 3.94 (t 1H, J=6.6 Hz, proton on C_3), 4.65 (d 2H, J=6.6 Hz, protons on C_2), and 6.77—7.97 ppm (m 8H, aromatic protons).
Id	139—140	66.85 (N=5.06)	4.01	66.91 (N=5.20)	4.12	IR 16.85, 1532, 1350, 810, and 730 cm^{-1}. NMR δ 4.11 (t 1H, J=7.2 Hz, proton on C_3), 4.72 (d 2H, J=7.2 Hz, protons on C_2), and 6.93—8.13 ppm (m 8H, aromatic ring protons).
Ie	170—171	83.83	5.19	83.98	5.37	IR 1685, 810, 740, and 690 cm^{-1}. NMR δ 4.01 (t 1H, J=6.6 Hz, proton on C_3), 4.70 (d 2H, J=6.6 Hz, protons on C_2), and 6.90—7.98 ppm (m 13H, aromatic ring protons).
If	111—112 (111[b])					
Ig	107—108 (108[a])					
Ih	84—85	75.95	5.89	76.10	6.01	IR 1680, 820, 800, and 720 cm^{-1}. NMR δ 2.35 (s 3H, CH_3–), 3.81 (s 3H, CH_3O–), 3.92 (t 1H, J=6.6 Hz, proton on C_3), 4.62 (d 2H, J=6.6 Hz, protons on C_2), and 6.97—7.37 ppm (m 7H, aromatic ring protons).
Ii	51—53	71.69	5.62	71.82	5.67	IR 1680, 820, 755, and 725 cm^{-1}. NMR δ 3.79 (s 6H, CH_3O–), 3.88 (t 1H, J=6.6 Hz, proton on C_3), 4.59 (d 2H, J=6.6 Hz, protons on C_2), and 6.77—7.38 ppm (m 7H, aromatic ring protons).
Ij	119—120	64.07 (N=4.52)	4.30	64.21 (N=4.68)	4.38	IR 1680, 1527, 1345, 860, and 808 cm^{-1}. NMR δ 3.80 (s 3H, CH_3O–), 3.89 (t 1H, J=6.0 Hz, proton on C_3), 4.68 (d 2H, J=6.0 Hz, protons on C_2), and 6.79—7.38 ppm (m 7H, aromatic ring protons).
Ik	122—123	79.85	5.37	79.98	5.49	IR 1680, 820, 750, 720, and 690 cm^{-1}. NMR δ 3.78 (s 3H, CH_3O–), 3.89 (t 1H, J=6.6 Hz, proton on C_3), 4.68 (d 2H, J=6.0 Hz, protons on C_2), and 6.79—7.45 ppm (m 12H, aromatic ring protons).
Il	100—101	65.36	4.41	66.55	4.53	IR 1680, 820, and 740 cm^{-1}. NMR δ 3.78 (s 3H, CH_3O–), 3.89 (t 1H, J=6.6 Hz, proton on C_3), 4.68 (d 2H, J=6.6 Hz, protons on C_2), and 6.79—7.38 ppm (m 7H aromatic ring protons).
Im	92—93 (93[a])					
In	122—123	76.03	5.90	76.10	6.01	IR 1683, 820, 805, and 720 cm^{-1}. NMR δ 2.34 (s 3H, CH_3–), 3.82 (s 3H, CH_3O–), 3.87 (t 1H, J=6.6 Hz, proton on C_3), 4.64 (d 2H, J=6.6 Hz, protons on C_2), and 6.64—7.92 ppm (m 7H, aromatic ring protons).
Io	128—129 (126,[c,d] 128—129[e])					
Ip	130—131	64.12 (N=4.60)	4.26	64.21 (N=4.68)	4.38	IR 16.80, 1529, 1345, 860, and 800 cm^{-1}. NMR δ 3.79 (s 3H, CH_3O–), 3.89 (t 1H, J=6.6 Hz, proton on C_3), 4.66 (d 2H, J=6.6 Hz, protons on C_2), and 6.48—7.87 ppm (m 7H, aromatic ring protons).

Table 2. (continued)

Compound	Mp °C (lit)	Found (%) C	Found (%) H	Calcd (%) C	Calcd (%) H	IR and NMR spectra
Iq	187—188	79.94	5.37	79.98	5.49	IR 1680, 817, 750, 720, and 690 cm^{-1}. NMR δ 3.82 (s 3H, CH_3O–), 3.93 (t 1H, J=6.0 Hz, proton on C_3), 4.66 (d 2H, J=6.0 Hz, protons on C_2), and 6.44—7.91 ppm (m 12H, aromatic ring protons).
Ir	141—142	66.48	4.47	66.55	4.53	IR 1680, 820, and 738 cm^{-1}. NMR δ 3.83 (s 3H, CH_3O–), 3.88 (t 1H, J=6.6 Hz, proton on C_3), 4.68 (d 2H, J=6.6 Hz, protons on C_2), and 6.41—7.92 ppm (m 7H, aromatic ring protons).

a) N. Inoue, *Nippon Kagaku Zasshi*, **79**, 112, 218 (1958).
b) R. W. J. Carney, W. L. Benge, J. Wojikunski, A. A. Rezi, L. Dorfman, and G. D. Stevens, *J. Med. Chem.*, **9**, 516 (1966).
c) E. L. Anderson and G. F. Marrian, *J. Biol. Chem.*, **127**, 649 (1935).
d) R. B. Bradbury and D. E. White, *J. Chem. Soc.*, **1943**, 871.
e) N. Inoue, *Nippon Kagaku Zasshi*, **79**, 215 (1958).

(IId), mp 218—220 °C (lit,[17] mp 218—221 °C); *p*-phenylphenylmercuric chloride (IIe), mp>360 °C (lit,[18] mp> 360 °C); and *p*-chlorophenylmercuric chloride (IIf); mp 223—225 °C (lit,[19] mp 225 °C). The phenylmercuric acetate (IIa) and isopropenyl acetate were of a commercial grade. The acetic acid was dried over phosphorus pentoxide and distilled before use.

Preparation of 4-Chromanone Enol Acetates (III). A mixture of 4.0 g of IV, 16 ml of isopropenyl acetate, and 0.4 g of *p*-toluene sulfonic acid was refluxed for 36 hr under nitrogen. After 200 ml of benzene was added to the reaction mixture, the benzene solution was washed successively with water, dilute aqueous sodium bicarbonate, and water. The benzene extracts were dried over anhydrous magnesium sulfate and evaporated to dryness *in vacuo*. The residue was distilled under reduced pressure to give enol acetates (III) (yield, 80—90%). The following compounds were prepared in this manner.

4-Chromanone Enol Acetate (IIIa, $R_1=R_2=H$). Bp 150—152 °C/13 mmHg. IR spectrum: 1760, 1210, and 743 cm^{-1}. NMR spectrum: δ 2.33 (s, 3H, CH_3COO–), 4.87 (d, 2H, J=4.2 Hz, protons on C_2), 5.46 (t, 1H, J=4.2 Hz, olefinic proton on C_3), and 6.81—7.83 *ppm* (m, 4H, aromatic ring protons).

Found: C, 69.61; H, 5.38%. Calcd for $C_{11}H_{10}O_3$: C. 69.46; H, 5.30%.

6-Methoxy-4-chromanone Enol Acetate (IIIb, $R_1=-OCH_3$, $R_2=H$). Bp 162—164 °C/7 mmHg. IR spectrum: 1765, 1210, 900, and 802 cm^{-1}. NMR spectrum: δ 2.15 (s, 3H, CH_3COO–), 3.69 (s, 3H, CH_3O–), 4.82 (d 2H, J= 4.8 Hz, protons on C_2), 5.29 (t, 1H, J=4.8 Hz, olefinic proton on C_3), and 6.96—7.38 ppm (m, 3H, aromatic ring protons).

Found: C, 65.57; H, 5.60%. Calcd for $C_{12}H_{12}O_4$: C, 65.44; H, 5.49%.

7-Methoxy-4-chromanone Enol Acetate (IIIc, $R_1=H$, $R_2=CH_3O$–). Bp 159—161 °C/6 mmHg. IR spectrum: 1760, 1208, 900, and 800 cm^{-1}. NMR spectrum: δ 2.18 (s, 3H, CH_3COO–), 3.67 (s, 3H, CH_3O–), 4.84 (d, 2H, J= 4.6 Hz, protons on C_2), 5.36 (t, 1H, J=4.6 Hz, olefinic proton on C_3), and 6.88—7.64 ppm (m, 3H, aromatic ring protons).

Found: C, 65.48; H, 5.58%. Calcd for $C_{12}H_{12}O_4$: C, 65.44; H, 5.49%.

General Procedures for the Arylation of III. A mixture of 10 mmol of III, 10 mmol of II, and 10 mmol of palladium acetate was stirred overnight in 80 ml of acetic acid at room temperature. After the resulting mixture has been filtered to remove the precipitated palladium metal, the filtrate was evaporated to dryness *in vacuo* to remove the acetic acid. The residue was poured into water and was extracted with chloroform. The chloroform solution was treated with dilute aqueous sodium bicarbonate, washed with water to free it from acetic acid, and then dried over anhydrous magnesium sulfate. After the evaporation of the solvent, the products were isolated by column chromatography on alumina with benzene and by crystallization from alcohol. The identities of the products formed were proved by mixed-melting-point determinations or by comparisons of the IR or NMR spectra with those of authentic samples. The analytical results and properties of the products are listed in Table 2.

The authers would like to express their thanks to Associate Professor Kaoru Hanaya and Mr. Hideaki Kudo of Yamagata University for the measurements of NMR spectra, and to the Kawaken Fine Chemical Co., Ltd., for a gift of palladium.

17) C. Kapproth and F. Westheimer, *J. Amer. Chem. Soc.*, **72**, 4461 (1950).
18) R. F. Heck, *ibid.*, **90**, 5518 (1968).
19) M. E. Hanke, *ibid.*, **45**, 1321 (1923).

One-Electron Reduction of Carbonium Ions. III. The Effect of Added Anions on the Rate of Reduction of the Tropylium Ion with Cr(II)[1]

Kunio Okamoto, Koichi Komatsu, Susumu Tsukada, and Osamu Murai

Department of Hydrocarbon Chemistry, Faculty of Engineering, Kyoto University, Sakyo-ku, Kyoto 606

(Received October 30, 1972)

The one-electron reduction of tropylium fluoroborate with Cr(II) was carried out in aqueous solution containing various anions (Cl^-, Br^-, SO_4^{2-}, HSO_4^-, BF_4^- and ClO_4^-) which were added as proton acids or as sodium salts, and the reaction rate at 25 °C was measured by the use of the flow method. It was found that Cl^-, Br^-, and SO_4^{2-} exhibit the characteristic rate-accelerating effect, whereas BF_4^- and ClO_4^- show a slight rate-retarding effect. From the extrapolation of the anion concentration to zero, it was indicated that this reaction can proceed even in the absence of added anions. From these findings, together with the results of chemical and spectrophotometrical analyses of the Cr(III) species, it was concluded that the reduction of the tropylium ion with Cr(II) proceeds through an electron-transfer step where the anion (Cl^-, Br^-, or SO_4^{2-}) or the water molecule acts as a weakly interacting electron-transfer bridge. This mechanism is essentially analogous to the "inner-sphere mechanism" known in the field of inorganic metal complex chemistry.

In the preceding paper,[2] we have reported on the reactivities of the cycloheptatrienyl and triphenylmethyl cations with a series of metallic powders and of the low-valent metallic ions, and demonstrated that the spectra of the reduction product yields may be regarded as a measure of the reducibility of the respective carbonium ions. As an extension of this work, a more quantitative investigation of the reducibility by the use of kinetic measurements seems of interest. Among the various reductants examined in the previous work, Cr(II) was found to be a satisfactory reagent, especially for kinetic measurements, since the one-electron reduction with Cr(II) proceeds quite readily without forming any by-product, as has already been reported in the case of some carbonium ions.[2,3] Prior to the kinetic study with respect to the reducibility of various stable carbonium ions, it seems necessary to clarify the mechanistic characteristics of this reaction by the use of a single representative carbonium ion, *e.g.*, the cycloheptatrienyl cation (the tropylium ion).

In the field of inorganic chemistry, the mechanisms for the reduction of several transition-metal complexes with Cr(II) are well established and are, in general, classified into "inner-sphere" and "outer-sphere" mechanisms depending upon whether or not an electron-transfer bridge between the reductant and the oxidant exists.[4]

On the other hand, for organic compounds, Cr(II) is known to be a potent and versatile reducing agent and has been used in the reduction of carbonium ions,[2,3] organic halides,[3c,5] olefins,[6] and carbonyl compounds.[6a] Among these reactions, the reduction of organic halides was interpreted as proceeding through reaction sequences analogous to the inner-sphere mechanism mentioned above, with the halide ion acting as an electron-transfer bridge between the organic moiety and Cr(II):[5a-d,g]

$$RX + Cr^{2+} \rightarrow [R\cdots X\cdots Cr]^{2+} \rightarrow R\cdot + CrX^{2+} \qquad (1)$$

It is currently accepted that the produced radical species is rapidly captured by the second chromous ion to furnish an organochromic complexes, which subsequently dimerizes with an unchanged halide or undergoes protonolysis to give a monomeric hydrocarbon.[3c,5c,e] There is also an exceptional case in which the first-formed radical abstracts the hydrogen atom before the formation of the organometallic complex.[5g]

In contrast to the reduction of organic halides, the chromous-ion reduction of carbonium ions usually gives rise to only dimers of the corresponding radicals,[2,3] but no kinetic investigation of this reaction has been reported. We chose the tropylium ion as a representative of stable carbonium ions and successfully measured the reduction rate with Cr(II) in an aqueous solution by the use of flow method; some findings of the effect of various added anions upon the reduction rate were obtained. The Cr(III) species produced under the various conditions were also analyzed chemically and spectrophotometrically. From the results obtained by these experiments, we wish to clarify the mechanism and scope of the reaction in this paper.

Results

Kinetic Measurements of the Reaction of the Tropylium Ion with Cr(II). As has already been reported,[2,3d] the tropylium ion reacts with Cr(II) quite rapidly

1) Presented at the 22nd Annual Meeting of the Chemical Society of Japan, Tokyo, April, 1969.

2) Part II: K. Okamoto, K. Komatsu, and H. Shingu, This Bulletin, **42**, 3249 (1969).

3) a) J. B. Conant and H. B. Cutter, *J. Amer. Chem. Soc.*, **48**, 1016 (1926), and the references cited therein; b) J. B. Conant and N. W. Bigelow, *ibid.*, **53**, 676 (1931); c) L. H. Slaugh and J. H. Raley, *Tetrahedron*, **20**, 1005 (1964); d) W. T. Bowie and M. Feldman, *J. Phys. Chem.*, **71**, 3696 (1967).

4) a) H. Taube, *Advan. Inorg. Chem. Radiochem.*, **1**, 1 (1959); b) J. Halpern, *Quart. Rev.*, **15**, 207 (1961); c) F. Basolo and P. G. Pearson, "Mechanism of Inorganic Reactions," 2nd ed., John Wiley & Sons, New York, N. Y. (1967), Chap. 6.

5) a) F. A. L. Anet and E. Le Blanc, *J. Amer. Chem. Soc.*, **79**, 2649 (1957); b) C. E. Castro, *ibid.*, **83**, 3262 (1961); c) C. E. Castro and W. C. Kray, *ibid.*, **85**, 2768 (1963); d) J. K. Kochi and D. D. Davis, *ibid.*, **86**, 5264 (1964), and the references cited therein; e) J. K. Kochi and D. Buchanan, *ibid.*, **87**, 853 (1965); f) R. P. A. Sneeden and H. P. Throndsen, *Chem. Commun.*, **1965**, 509; g) D. H. R. Barton, N. K. Basu, R. H. Hesse, F. S. Morehouse, and M. M. Pechert, *J. Amer. Chem. Soc.*, **88**, 3016 (1966), and the references cited therein.

6) a) K. D. Kopple, *ibid.*, **84**, 1586 (1962); b) C. E. Castro, R. D. Stephens and S. Mojé, *ibid.*, **88**, 4964 (1966).

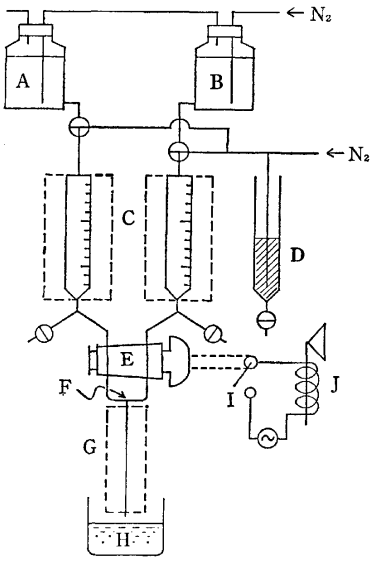

Fig. 1. A schematic diagram of "flow method" apparatus for the kinetic measurements.
A: the tropylium ion, B: Cr(II), C: water-jacketed burette, D: Hg, E: main stopcock, F: mixing chamber, G: water-jacketed reaction tube, H: "stop solution," I: knife switch connected to E, J: buzzer.

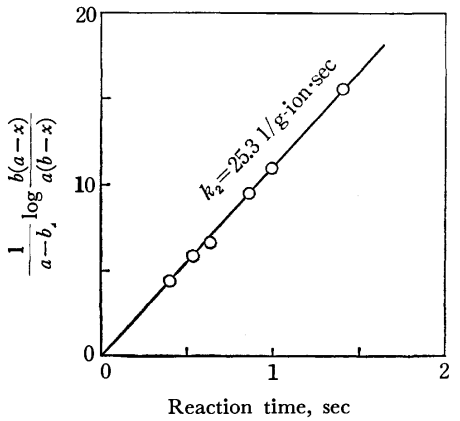

Fig. 2. The rate of the reaction of the tropylium ion with Cr(II) in 0.2 N HCl at 25 °C.
$[C_7H_7^+]_0=0.81\times10^{-2}$ g-ion/l
$[Cr(II)]_0=1.8\times10^{-2}$ g-ion/l

and quantitatively to give the dimer, bitropyl. The kinetic measurement of this reaction was made at 25 °C by the use of the apparatus depicted in Fig. 1. The aqueous acid solutions of the tropylium ion and of Cr(II) were mixed in a T-shaped mixing chamber and then allowed to react while flowing down through a reaction tube. The reaction time was 0.2—1.5 sec, depending on the length of the tube. After the quenching of the reaction by the use of the instantaneous oxidation of the unchanged Cr(II) with an aqueous solution of $CuSO_4$,[7] bitropyl was extract-

Table 1. The rate constants for the reaction of the tropylium ion with Cr(II) in aqueous acid solutions at 25°C

Solvent Acid,	N	Initial concentration $C_7H_7^+$ 10^{-2} g-ion/l	Initial concentration Cr(II) 10^{-2} g-ion/l	k_2 l/g-ion·sec
HCl	0.2	0.81	1.8	25.3
	1.7	0.71	1.6	63.2
	2.9	0.67	1.9	76.6
	2.9	1.8	3.0	74.1
	2.9	2.0	3.7	73.8
	4.4	0.65	1.0	83.0
HBr	0.2	0.85	1.6	24.6
	2.9	0.85	1.1	70.3
	2.9	0.68	1.7	68.0
H_2SO_4	0.05	0.99	3.2	24.9
	0.1	1.0	3.1	27.1
	0.6	1.2	2.1	22.6
	1.0	0.85	2.7	18.8
	1.8	0.81	2.9	14.3
HBF_4	0.2	2.0	4.0	8.6
	2.9	1.7	27	3.3
$HClO_4$	0.2	2.1	5.2	7.6
	1.2	2.4	5.4	4.3
	2.9	1.7	17	1.4

Table 2. The rate constants for the reaction of the tropylium ion with Cr(II) in the presence of anions added as sodium salts in aqueous acid solutions (0.2 N) at 25°C

Acid (0.2 N)	Added anion	g-ion/l	Initial concentration C_7H^+ 10^{-2} g-ion/l	Initial concentration Cr(II) 10^{-2} g-ion/l	k_2 l/g-ion·sec
HCl	Cl^-	0.0	0.81	1.8	25.3
		1.0	0.84	2.7	60.2
		2.5	0.56	1.4	84.0
		4.0	0.58	1.0	87.4
HBr	Br^-	0.0	0.85	1.6	24.6
		1.0	0.68	2.2	50.6
		1.8	0.93	1.7	65.1
		1.9	0.66	1.4	65.8
		3.4	0.57	1.3	65.8
		4.0	0.93	1.7	65.9
H_2SO_4	SO_4^{2-}	0.0	1.0	3.1	27.1
		0.3	0.92	1.9	45.5
		1.0	0.92	2.0	58.0
		1.6	0.82	2.1	64.4
H_2SO_4	HSO_4^-	0.3	0.90	1.9	33.8
		1.0	0.90	1.8	35.0
		2.0	0.93	1.8	32.9
		3.5	0.88	2.2	26.0
HBF_4	BF_4^-	0.0	2.0	4.0	8.6
		1.0	1.9	4.5	6.4
		2.5	2.2	4.4	3.5
		4.5	1.8	5.4	1.4
$HClO_4$	ClO_4^-	0.0	2.1	5.2	7.6
		2.8	2.5	3.5	2.1

7) It was ascertained that Cu(II) has no interaction with unchanged tropylium ion under these conditions; see the Experimental section. The reactions of Cu(II) with the tropyl radical, such as the one reported by Kochi and Rust (J. K. Kochi and F. F. Rust, *J. Amer. Chem. Soc.* **83**, 2017 (1961)), seem to be negligible, if present at all, because the coupling reaction of the tropyl radical is supposed to be so fast ($k_2\sim2\times10^7$ M^{-1} sec^{-1} (22 °C); M. L. Morrell and G. Vincow, *J. Amer. Chem. Soc.*, **91**, 6389 (1969)) that, at this stage of the reaction, the steady-state concentration of the radical must be negligibly small compared with the concentration of the tropylium ion or bitropyl.

ed with *n*-hexane and determined by ultraviolet spectroscopy. The initial concentrations of both the reagents were set so that the concentration of Cr(II) would be 1.5 to 3.0 fold greater than that of the tropylium ion. The results for the various reaction times were treated according to the ordinary second-order rate equation (first-order for each reagent) to give a good straight line through the point of origin, as is shown in Fig. 2. The reaction conditions and the graphically-obtained values of the second-order rate constants are listed in Tables 1 and 2.

In a representative run, the unchanged tropylium ion was determined from the ultraviolet spectrum of the aqueous layer, and the material balance was found to be >97.5%. The product, bitropyl, was characterized on the basis of its infrared spectrum, the purity being ascertained by thin-layer chromatography.

The Effect of Added Anions on the Reduction Rate. In order to obtain information on the mechanism operating, especially at the electron-transfer step, the reaction of the tropylium ion with Cr(II) was carried out in aqueous acid solutions containing various anions (Cl^-, Br^-, SO_4^{2-}, HSO_4^-, BF_4^-, and ClO_4^-), which were added as proton acids or as sodium salts; the effects of the concentrations and of the nature of the anions upon the rate of the reaction were then examined. Among the results shown in Tables 1 and 2 and in Figs. 3 and 4, the following are noteworthy: (a) Cl^-, Br^-, and SO_4^{2-} have the characteristic effect of increasing the rate of the reaction; (b) this rate-increasing effect approaches its maximum as the concentration of the anion is increased; (c) on the contrary, BF_4^- and ClO_4^- show only a slight rate-retarding effect; (d) the extrapolation of the concentration of each anion leads to the same intercept where $k_2=9$ (l/g.ion.sec) at 25 °C; (e) H_2SO_4 and HSO_4^- seemingly exhibit a rate-accelerating effect at lower concentrations and a rate-retarding effect at higher concentrations. Among these findings, the observation (d) clearly indicates that the presence of halide ions is not essential for the reduction of the tropylium ion, as has been reported in the cases of the triphenylmethyl and diphenylmethyl cations.[3c] This result is in sharp contrast to the observation made by Castro[6b] that the 1,1-diphenylethyl cation can not be reduced by Cr(II) unless the chloride ion is added. The characteristic effect shown by H_2SO_4 and HSO_4^- as described in (e) seems to be attributable to the equilibrium composition[8] of H_2SO_4, HSO_4^-, and SO_4^{2-} in an aqueous solution; at lower concentrations, the SO_4^{2-} ion, which is predominant as a result of the nearly complete dissociation of H_2SO_4 or HSO_4^-, exerts a rate-accelerating effect, whereas at higher concentrations, undissociated H_2SO_4 and HSO_4^- seem to retard the reaction.

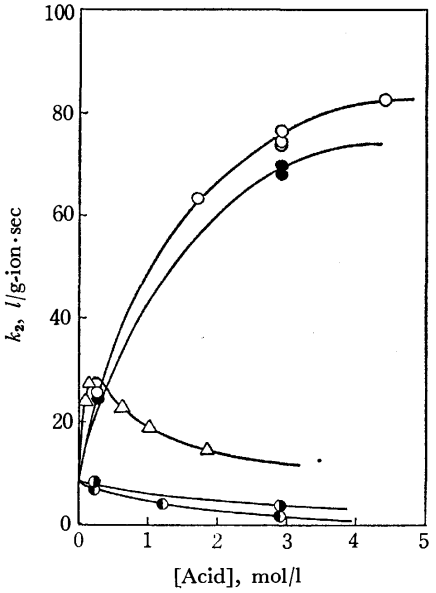

Fig. 3. The effect of anions added as proton acids on the reaction rate.
○: HCl, ●: HBr, △: H_2SO_4, ◑: HBF_4, ◐: $HClO_4$.

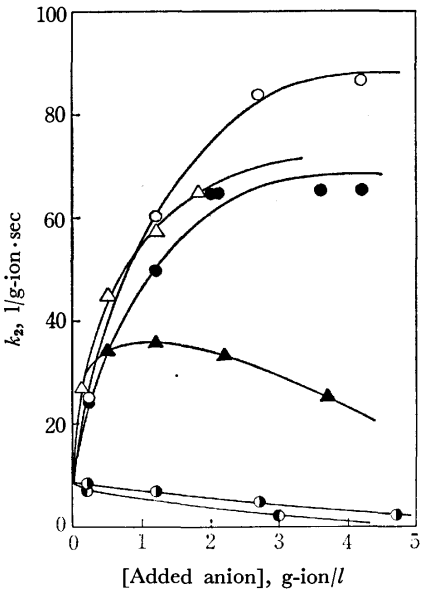

Fig. 4. The effect of anions added as sodium salts on the reaction rate.
○: Cl^-, ●: Br^-, △: SO_4^{2-}, ▲: HSO_4^-, ◑: BF_4^-, ◐: ClO_4^-.

The Analysis of Cr(III) Species. Although Cr(II) is labile to the substitution of its ligands, Cr(III) is known to be sluggish to ligand substitution.[9] Thus, the analysis of the group attached to Cr(III), which is produced as a result of Cr(II) reduction, makes it possible to deduce the nature of the activated complexes. Taking advantage of these properties, Taube and his coworkers[10] successfully demonstrated that one-electron transfer reactions from Cr(II) to several inorganic metallic complexes proceed through an activated complex in which a single anion or a molecule acts as an electron-transfer bridge. With the expectation of obtaining information on the function of the added chloride ion on the electron-transfer step, we conducted the reaction of Cr(II) with an excess of the tropylium ion in variable HCl concentrations at room

8) "Gmelins Handbuch der anorganischen Chemie," 8 Auflage, System Nr. 9, Schwefel, Teil B-2, Verlag Chemie, GmbH., Weinheim (1960), p. 737.
9) H. Taube and H. Myers, *J. Amer. Chem. Soc.*, **76**, 2103 (1954).
10) Ref. 9; H. Taube, *ibid.*, **77**, 4481 (1955).

temperature and analyzed the Cr(III) species chemically and by their visible spectra.

An excess of the tropylium ion was allowed to react with Cr(II) in 0.1 to 2.9 M aqueous HCl for 10 min (more than 100 half-lives) under nitrogen; after the subsequent extraction of the organic product, the visible spectrum of Cr(III) was taken. As is shown in Table 3 and Fig. 5, the absorption maximum of Cr(III) at longer wavelengths was found to make a bathochromic shift to 605 mμ, which corresponds to $CrCl(H_2O)_5^{2+}$,[11] with an increase in the concentration of HCl. This indicates that the Cr(III) species formed at lower HCl concentrations is a mixture of $Cr(H_2O)_6^{3+}$ (λ_{max} 575 mμ[11]) and $CrCl(H_2O)_5^{2+}$, but at higher HCl concentrations most of the Cr(III) exists as $CrCl(H_2O)_5^{2+}$. The results of the chemical analysis of the chloride ion attached to Cr(III) exhibit qualitatively the same tendency, as is shown in Table 4.

Table 3. The effect of the HCl concentration on the visible spectra of Cr(III) formed by the reaction of the tropylium ion with Cr(II)

Initial concentration			λ_{max} for Cr(III)
[HCl] N	$[C_7H_7^+]$ g-ion/l	[Cr(II)] g-ion/l	mμ
0.07	0.026	0.014	588
0.14	0.080	0.051	592
0.26	0.080	0.050	595
0.40	0.080	0.050	598
0.55	0.080	0.047	602
0.58	0.080	0.048	602
2.90	0.047	0.029	606

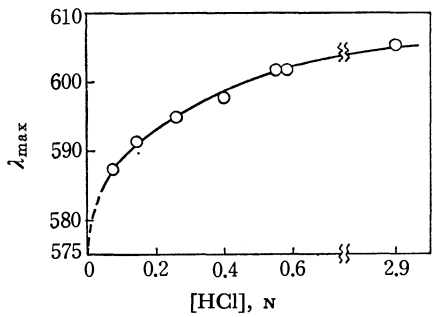

Fig. 5. The effect of HCl concentration on λ_{max} of Cr(III).

Table 4. The effect of the HCl concentration on the amount of the chloride ion bound to Cr(III)[a]

[HCl] N	Ratio of Cl bound to Cr(III) to total Cr(III)
0.072	0.47
0.110	0.51
0.139	0.53
0.175	0.59

a) [Cr(II)]: 0.014 g-ion/l, $[C_7H_7^+]$: 0.025 g-ion/l.

11) J. W. Mellor, "Comprehensive Treatise on Inorganic and Theoretical Chemistry," Vol. XI, Longmans, Green and Co., London (1954), p. 378.

Discussion

One of the simplest mechanisms for the formation of bitropyl by the reduction of the tropylium ion with Cr(II) is the radical mechanism shown below:

$$C_7H_7^+ + Cr(II) \rightarrow C_7H_7\cdot + Cr(III) \quad (2)$$

$$2C_7H_7\cdot \rightarrow (C_7H_7\text{–})_2 \quad (3)$$

At present, it still remains open whether the radical produced is entirely free or is loosely affiliated with the metal ion (Step (4)); consequently, the possibilities for the reactions through $[C_7H_7\cdots\overset{|\diagup}{\underset{\diagdown|}{Cr}}\cdots]^{2+}$, depicted in Steps (4) and (5) or in Steps (4) and (6), can not be rigorously eliminated:

$$C_7H_7\cdot + Cr(II) \rightarrow [C_7H_7\cdots\overset{|\diagup}{\underset{\diagdown|}{Cr}}\cdots]^{2+} \quad (4)$$

$$[C_7H_7\cdots\overset{|\diagup}{\underset{\diagdown|}{Cr}}\cdots]^{2+} + C_7H_7\cdot \rightarrow (C_7H_7\text{–})_2 + Cr(II) \quad (5)$$

$$[C_7H_7\cdots\overset{|\diagup}{\underset{\diagdown|}{Cr}}\cdots]^{2+} + C_7H_7^+ \rightarrow (C_7H_7\text{–})_2 + Cr(III) \quad (6)$$

Among these, however, Steps (2) and (3) seem most likely because, regardless of the acidity of the solvent, the reduction only gives the dimer, and no protonolysis product (tropilidene) which can be derived from $[C_7H_7\cdots\overset{|\diagup}{\underset{\diagdown|}{Cr}}\cdots]^{2+}$ is ever formed. Furthermore, the marked effect of the added anions on the reaction rate indicates that, in any case, the rate-determining step is Step (2), at which an anion can substantially participate.

A representative example of such an anion-affected reaction may be seen in the reduction of $[Co(NH_3)_5X]^{2+}$ with Cr^{2+}. In this case the transition state in which the anion, X, acts as an electron-transfer bridge has been proposed:[10]

$$[Co(NH_3)_5X]^{2+} + Cr^{2+} + 5H^+ \rightarrow Co^{2+} + CrX^{2+} + 5NH_4^+ \quad (7)$$

Also, in the present study, the fact that only such anions as Cl^-, Br^-, and SO_4^{2-}, which can coordinate with Cr(III), show the rate-accelerating effect would imply that these anions act as electron-transfer bridges between the tropylium ion and Cr(II). On the other hand, when the anion concentration is graphically extrapolated to zero, the rate constant still has the value of 9 (l/g.ion·sec), indicating that the electron transfer also takes place via the H_2O molecule as a bridge. Thus, in the reaction system, paths which proceed *via* an anion bridge and those which proceed *via* an H_2O bridge are both present; they give rise to $Cr(H_2O)_5X^{2+}$ and $Cr(H_2O)_6^{3+}$ respectively.

The effect of the added chloride ion on the reaction rate, however, is at most a factor of about 10 (see Fig. 4), much smaller than the factor of 10^6 found in the reaction (7) for the Cl bridging relative to the H_2O

bridging.[12] This may indicate that, although there is bridging by the chloride ion between $C_7H_7^+$ and Cr(II), it is much less effective than in the case of the reduction of $[Co(NH_3)_5X]^{2+}$, since even in the activated complex, the interaction between $C_7H_7^+$ and Cl^- is considered to be quite weak because of the complete delocalization of the positive charge in the tropylium ion.

When the reaction is conducted in the presence of HCl, the reacting species which gives rise to the chloride ion bridge is supposed to be $Cr(H_2O)_5Cl^{+}$[13] or the ion pair, $C_7H_7^+\cdots Cl^-$,[14] which is in equilibrium with $Cr(H_2O)_6^{2+}$ or with $C_7H_7^+$ respectively:

$$Cr(H_2O)_6^{2+} + Cl^- \rightleftharpoons Cr(H_2O)_5Cl^+ + H_2O \quad (8)$$

$$C_7H_7^+ + Cl^- \rightleftharpoons C_7H_7^+\cdots Cl^- \quad (9)$$

Therefore, it may be supposed that, among these species, the following reaction paths (Steps (10)—(12)) are competing with each other:

$$C_7H_7^+ + Cr(H_2O)_6^{2+} \rightarrow [C_7H_7\cdots \overset{H}{O}Cr(H_2O)_5]^{3+} \rightarrow C_7H_7\cdot + Cr(H_2O)_6^{3+} \quad (10)$$

$$C_7H_7^+\cdots Cl^- + Cr(H_2O)_6^{2+} \xrightarrow{-H_2O} [C_7H_7\cdots ClCr(H_2O)_5]^{2+}$$

$$C_7H_7^+ + CrCl(H_2O)_5^+ \rightarrow C_7H_7\cdot + CrCl(H_2O)_5^{2+} \quad (11)$$

$$C_7H_7^+\cdots Cl^- + CrCl(H_2O)_5^+ \xrightarrow{-Cl^-} [C_7H_7\cdots ClCr(H_2O)_5]^{2+} \rightarrow C_7H_7\cdot + CrCl(H_2O)_5^{2+} \quad (12a)$$

$$C_7H_7^+\cdots Cl^- + CrCl(H_2O)_5^+ \xrightarrow{-H_2O} [C_7H_7\cdots ClCrCl(H_2O)_4^+ \rightarrow C_7H_7\cdot + CrCl_2(H_2O)_4^+ \quad (12b)$$

Path (10) proceeds by means of bridging with H_2O, while Paths (11) and (12) make use of the chloride bridge. As for Path (12), it can not be determined from the analysis of Cr(III) which course, (12a) or (12b), is pertinent, since $CrCl_2(H_2O)_4^+$ is known to react readily ($k_2 \approx 10^2$ l/g.ion·sec at 2 °C[9]) with Cr^{2+} to give $CrCl(H_2O)_5^{2+}$, as is shown below:

$$CrCl_2(H_2O)_4^+ + Cr^{2+} \rightarrow CrCl(H_2O)_5^+ + CrCl(H_2O)_5^{2+} \quad (13)$$

The tendency of the rate-increasing effect of anions to approach its maximum with an increase in the anion concentration (shown in Figs. 3 and 4) can be ascribed to the shift of the equilibria (8) and (9) to the right, with the result that the reaction proceeds completely *via* the bridging with the chloride ion so that no more rate acceleration becomes observable. This is also consistent with the result, obtained from the chemical analysis, that the amount of the chloride ion attached to Cr(III) increases with an increase in the HCl concentration.

From these results, it is concluded that the one-electron reduction of the tropylium ion with Cr(II) in the aqueous acid of the appropriate concentration does not occur directly between the two reagents, but proceeds by means of the electron-transfer bridge mechanism. Therefore, it may be expected that, so long as the acid solution is used in a concentration sufficient for the bridging, the reactivity of the various stable carbonium ions in this reaction will mainly reflect the inherent electron affinity of the respective carbonium ions, and that the effect of the steric factor will be minimized. The investigation on the correlation of such a reactivity with the electron affinity of the various stable carbonium ions is now in progress and will be reported in the following paper.

Experimental[15]

Materials. Tropylium fluoroborate was prepared from tropilidene according to the method of Conrow.[16] The aqueous solutions of the chromous ion were prepared by the dissolution of chromium metal (99.99%, Nakarai Co., Ltd.) in 2.9 M respective acid solutions under nitrogen after activation in 2.9 M HCl and rinsing with distilled water. The transfer and dilution of the original chromous solution were done by the use of a hypodermic syringe; distilled water or acid solutions of appropriate concentrations had previously been deoxygenated with nitrogen. The aqueous solutions of hydrochloric, hydrobromic, sulfuric, perchloric, and fluoroboric acids, the sodium salts of the respective anions, and the sodium bisulfate were of a reagent grade and were used without further purification.

Kinetic Measurements for the Reaction of the Tropylium Ion with Cr(II). The reaction was carried out under a nitrogen atmosphere in the flow system shown in Fig. 1. Burettes and a reaction tube were covered with jackets circulated with water thermostated at 25.0±0.2 °C. The aqueous acid solutions of the tropylium ion and of the chromous ion, the concentrations of which had been determined by ultraviolet spectroscopy and by iodometry, respectively, were charged into each burette from the reservoirs and let stand for at least 10 min for temperature equilibration. The nitrogen pressure in the whole system was raised to 200 mmHg above atmospheric pressure, and then the main stopcock was opened for about 4 sec so that 20 ml each of the reagent solutions ran into a glass reaction tube 3.6 mm in inner diameter, through a mixing chamber made of T-shaped glass tube 1.0 mm in inner diameter. The reagents were allowed to react for 0.3—1.5 sec while flowing through reaction tubes of various lengths; then they flowed out into 20 ml of a magnetically-stirred "stop solution" containing 0.5 M $CuSO_4$. The operation of the main stopcock was synchronized with a buzzer switch; while the stopcock was opened the buzzer sound was recorded on a tape recorder, and from the distance of the recording tape between the starting and ending points of the buzzer sound the flowing time of the reagents was

12) J. P. Candlin, J. Halpern, and D. L. Trimm, *J. Amer. Chem. Soc.*, **86**, 1019 (1964).

13) H. L. Schlafer and H. Skoludek, *Z. Phys. Chem.* (Frankfurt am Main), **11**, 277 (1957).

14) The formation of such an ion pair can be well supposed from the observation that the charge-transfer complexes are formed between the tropylium ion and halide ions (K. M. Harmon, F. E. Cummings, D. A. Davis, and D. J. Diestler, *J. Amer. Chem. Soc.*, **84**, 120, 3349 (1962); E. M. Kosower, *J. Org. Chem.*, **29**, 956 (1964)).

15) The infrared and ultraviolet spectra were obtained on Shimadzu models IR-27 and UV-50M spectrometers respectively. The Kohlrausch bridge used for the conductometry was a Shimadzu apparatus, model BF-62.

16) K. Conrow, "Organic Syntheses," Vol. 43, p. 101 (1963).

determined. The time-distance calibration was made by the use of the standard time service of the Nippon Telegram and Telephone Corporation. Thus, when the time required for a total flow of 40 ml was determined to be 4.00 sec, for example, the reaction times were calculated to be 0.26, 0.36, 0.46, 0.60, 0.72, and 1.04 sec with reaction tubes of the length of 25.1, 35.1, 45.0, 58.8, 70.2, and 102.5 cm respectively. The reaction solution was extracted three times with 50-ml portions of *n*-hexane, washed with three 100-ml portions of 10% aqueous sodium chloride, and dried over magnesium sulfate. The solvent was evaporated under reduced pressure to give white crystals which were identified as bitropyl from the superimposability of the infrared spectrum with the spectrum of an authentic sample. The amount of the product was determined by ultraviolet spectroscopy in ethanol, using 255 mμ (ε=7080) as a characteristic band for bitropyl.[17] The rate constants were determined graphically from the ordinary second-order rate equation. The efficiency of mixing in the mixing chamber was examined by the method described by Roughton,[18] *i.e.*, the measurement of the heat of neutralization, which was evolved when equivalent aqueous solutions of HCl and NaOH were mixed together under the same conditions as in the chromous-ion reduction. It was confirmed that 100% mixing was attained within 0.02 sec after mixing.

Test for the Efficiency of the Quenching of Cr(II) with Cu(II). To 20 ml of a 2.9 M HCl solution of the tropylium ion (0.02 g.ion/l) and $CuSO_4$ (0.5 mol/l), was added 10 ml of a 2.9 M HCl solution of Cr(II) (0.04 g.ion/l) under an atmosphere of nitrogen at room temperature. After 10 min, the ultraviolet spectrum of an aliquot showed that the amount of the tropylium ion had not been affected.

The Analysis of Cr(III) Complex in Solution. By the use of an apparatus employed in the kinetic measurements, 40-ml portions each of a solution of the tropylium ion and of Cr(II) in aqueous hydrochloric acid of various concentrations were mixed and allowed to react for 10 min at room temperature under nitrogen in a Erlenmeyer flask, set under the mixing chamber. The initial concentrations of both reagents were set as is shown in Tables 3 and 4, so that the amount of the tropylium ion was a 1.5—1.8 fold excess. After the extraction of the organic product with three 60-ml portions of *n*-hexane, the aqueous layer was subjected to the measurement of its visible spectrum or to the chemical analysis of the chloride ion bound to Cr(III) as follows: the free chloride ions in the solution were first determined by conductometric titration with 0.1 M $AgNO_3$. The solution was then heated at 100 °C for 30 min and titrated again with 0.1 M $AgNO_3$. The differences in titers before and after the heating of the solution was regarded as corresponding to the amount of chloride ions bound to Cr(III).[9]

17) W. von E. Doering and L. H. Knox, *J. Amer. Chem. Soc.*, **79**, 352 (1957).

18) F. J. W. Roughton, "Technique of Organic Chemistry," Vol. 8, ed. by A. Weissberger, John Wiley & Sons, New York, N. Y. (1963), p. 711.

BULLETIN OF THE CHEMICAL SOCIETY OF JAPAN, VOL. 46, 1785—1790 (1973)

One-Electron Reduction of Carbonium Ions. IV. A Kinetic Study on the Reduction of the Substituted Tropylium Ions with Cr(II)*

Kunio Okamoto, Koichi Komatsu, Osamu Murai, Osamu Sakaguchi, and Yoshihisa Matsui**

Department of Hydrocarbon Chemistry, Faculty of Engineering, Kyoto University, Sakyo-ku, Kyoto 606

***Department of Agricultural Chemistry, Faculty of Agriculture, Shimane University, Nishikawazu-cho, Matsue 690*

(Received November 2, 1972)

The one-electron reduction of the unsubstituted, methyl-, ethyl-, isopropyl-, *t*-butyl-, triphenylmethyl-, and phenyltropylium ions with Cr(II) in a 10% HCl solution gives, quantitatively, the dimer of the corresponding substituted tropyl radical. The measurements of the reaction rate at 25 °C exhibit this order of reactivity: *t*-butyltropylium (k_2=7.98 l/g·ion·sec), isopropyltropylium (8.22), ethyltropylium (10.3), methyltropylium (11.1), tropylium (74.0), phenyltropylium (144), and triphenylmethyltropylium (567) ions. The values of log k_2 have a linear correlation with the transition energies of the charge-transfer bands observed for these carbonium ions with pyrene, and also with the polarographic half-wave potentials of the respective cations. These correlations indicate that the reactivity of the carbonium ion in the reduction with Cr(II) is determined mainly by the electron affinity inherent in the respective cations. The values of log k_2 also have a good linear correlation with the pK_{R^+} values, implying a parallelism between the electron affinity and the electrophilicity of these stable carbonium ions.

Although the one-electron reduction of carbonium ions in the gas phase has raised much theoretical interest in the ionization of organic radicals to carbonium ions, the reducibility of stable carbonium ions in solutions has received rather little attention; quantitative studies of it have been restricted to electrochemical one, such as polarography[1] and emf measurements of the cells made of equilibrated solutions of the carbonium ions and the corresponding radicals.[2] We demonstrated in previous papers[3,4] that the reducibility of the stable carbonium ion can be estimated from the reactivity

* Presented at the 22nd Symposium on Organic Reaction Mechanisms, Nagoya, October, 1971.

1) a) M. E. Vol'pin, S. I. Zhdanov, and D. N. Kursanov, *Dokl. Akad. Nauk SSSR*, **112**, 264 (1957); *Chem. Abstr.* **51**, 12057e (1957); b) P. Zuman, J. Chodkowski, H. Potesilova, and F. Santavy, *Nature*, **182**, 1535 (1958); c) M. I. James and P. H. Plesch, *Chem. Commun.*, **1967**, 508; d) R. Breslow, W. Bahary, and W. Reinmuth, *J. Amer. Chem. Soc.*, **83**, 1763 (1961).

2) E. D. Jenson and R. W. Taft, *ibid.*, **86**, 116 (1964).

3) K. Okamoto, K. Komatsu, and H. Shingu, This Bulletin, **42**, 3249 (1969).

4) K. Okamoto, K. Komatsu, S. Tsukada, and O. Murai, *ibid.*, **46**, 1780 (1973).

toward various metals and low-valent metallic ions, and that among these reductants Cr(II) is a suitable reagent for the kinetic study designed to estimate quantitatively the reducibility of stable carbonium ions in a solution.

Thus, the kinetics of the chromous-ion reduction of the substituted tropylium ions were studied with the idea that the change in the electron affinity of these ions caused by the introduction of various substituents will be reflected in the rate constants. The relative electron affinities of carbonium ions have been estimated from the transition energies of the charge-transfer bands, and also from the polarographic half-wave potentials. We will discuss the correlation of the reducibility of these carbonium ions with the relative electron affinities obtained, and also with the pK_{R^+} values measured for the respective cations, and will show the applicability of this method to the evaluation of the reducibility of stable carbonium ions of the tropylium system in a solution.

Results and Discussion

Reduction of the Substituted Tropylium Ions with Cr(II). It has been reported that the tropylium ion was readily reduced with Cr(II) to give a quantitative yield of the dimer, bitropyl.[3,5] We have ourselves examined the reduction of the substituted tropylium salts (Ia—f) with Cr(II) in 10% HCl (2.9 M);[6]

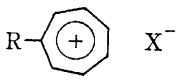

I

I a : R=CH_3, X=ClO_4 b : R=C_2H_5, X=ClO_4
c : R=i-C_3H_7, X=ClO_4 d : R=t-C_4H_9, X=ClO_4
e : R=C_6H_5, X=BF_4 f : R=$C(C_6H_5)_3$, X=BF_4

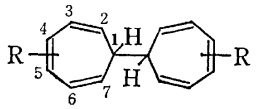

II

We ascertained that, in each case, the dimer (II) was obtained in a yield of more than 95% without the formation of any by-product. The elemental analysis of the respective reaction products gave satisfactory values for the dimers. The NMR spectra (60 MHz) of the dimers showed three groups of multiplets, centered at about τ 3.5, 3.9, and 4.8, along with a broad singlet at about 8.0, typical of a cycloheptatrienyl system, and also the signals corresponding to each substituent. The complex patterns of these multiplets and the multiplicity of the signals of the substituents suggest that the product is a mixture of isomers of x,x'-disubstituted bitropyl (II). The signals centered at τ *ca.* 3.5 ($H^{4,5}$) and at *ca.* 3.9 ($H^{3,6}$) were not fully separated; therefore, integration was made for these four protons (H^{3-6}) as one group. It was found that, although the average of from three to five integrations constantly gave the relative ratio of nearly 1 : 5 for $H^1 : H^{2-7}$, the averaged ratio for $H^{2,7} : H^{3-6}$ varied with the substituents, as is shown in Table 1. Though each integration includes the probable error of *ca.* 5%, there is still a clear tendency for the integrated value of H^{3-6} to decrease with the increase in the bulkiness of the substituent. This seems to reflect the steric hindrance exerted upon the coupling of the substituted tropyl radicals formed by one-electron transfer.[4] Each product mixture seemingly gave one or hardly separating two spots on a silica-gel thin-layer plate (*n*-hexane–benzene, 9 : 1, as the solvent), but all attempts to isolate the single isomer were unsuccessful.

Table 1. Ratio of the integrations for ring protons of x,x'-disubstituted bitropyl

Substituent	H^1	$H^{2,7}$	H^{3-6}
None	2.0	4.0	8.0
Methyl	~2[a]	2.94	7.06
Ethyl	~2[a]	3.36	6.64
Isopropyl	1.90	3.48	6.52
t-Butyl	1.80	3.76	6.24
Phenyl	1.88	4.10	5.90
Trityl	2.00	3.74	6.26

a) Not determined separately because of the substituent signals which appear at the same position.

Kinetic Measurements of the Reduction of the Substituted Tropylium Ions. In order to examine the influence of substituents on the reducibility, the rate of the chromous-ion reduction of various substituted tropylium salts (Ia—f) was measured by the use of the flow method previously described;[4] the reaction was carried out at 25 °C under a nitrogen atmosphere in 10% HCl for 0.2—1.5 sec; the conversion was determined by the ultraviolet spectroscopy of the dimers. The reaction was found to follow good second-order kinetics with respect to each substituted tropylium ion and Cr (II). The results shown in Table 2 demonstrate that, whereas the reactivity of the tropylium ion is markedly increased by the introduction of phenyl and triphenylmethyl substituents, it is suppressed by the introduction of the alkyl groups, among which the effect gradually increases in this order; methyl, ethyl, isopropyl, and *t*-butyl groups.

In a previous mechanistic study[4] it was indicated that the reduction of the tropylium ion with Cr(II) in 10% HCl proceeds through a transition state, in which the chloride ion acts as an electron-transfer bridge between the two reactants, rather than by direct interaction between them. Therefore, it was expected that the influence of the steric effect exerted by each substituent would be minimized and that the reactivity would mainly reflect the intrinsic reducibility of the

5) W. T. Bowie and M. Feldman, *J. Phys. Chem.*, **71**, 3696 (1967).

6) Throughout this work, 10% HCl was used as the standard solvent in order to ensure the enough stability of the respective tropylium ions in the aqueous solution; in the solutions with lower acidities (pH>1), slow decomposition was observed for the methyl-, ethyl-, and isopropyltropylium ions.

Table 2. Second-order rate constants for the reaction of substituted tropylium ions with Cr(II) in 10% HCl at 25 °C

Substituent	Initial concn R–$C_7H_6^+$ 10^{-2} g-ion/l	Initial concn Cr(II) 10^{-2} g-ion/l	k_2 l/g-ion·sec	k_2 average l/g-ion·sec
None	2.05	3.75	73.8	74.0
	1.80	3.05	74.1	
Methyl	1.99	4.12	11.1	11.1
	2.60	5.39	11.0	
	2.61	5.20	11.3	
Ethyl	2.48	4.87	9.90	10.3
	2.50	5.22	9.80	
	2.60	5.22	11.1	
Isopropyl	2.23	5.26	8.18	8.22
	2.46	5.31	8.26	
t-Butyl	2.07	4.83	8.16	7.98
	2.47	5.06	7.74	
	2.51	5.78	8.05	
Phenyl	0.426	0.857	140	144
	0.462	0.928	147	
Trityl	0.096	0.453	610	567
	0.099	0.288	511	
	0.103	0.312	615	
	0.113	0.226	510	
	0.114	0.253	590	

respective carbonium ions. This supposition seems to be verified by the fact that the reduction of the tropylium ion with the bulkiest substituent, the triphenylmethyl group, still proceeds most rapidly. Thus, the results of the kinetic measurements should be interpreted in terms of the difference in the intrinsic reducibility of the respective cations. From the observed results, it also appears that the inductive effect of the substituents controls the reducibility sequence (*t*-Bu<*i*-Pr<Et<Me<H<Ph<Ph_3C) and that the π-conjugative stabilization exerts very little effect in the tropylium system.

Correlation of the Reducibility with the Relative Electron Affinity of the Carbonium Ions. It seems that it would be of interest to compare the observed reducibility of each substituted tropylium ion with the electron affinity determined by the other methods. As one of such methods we made use of the measurement of the charge-transfer bands observed between carbonium ions and an aromatic hydrocarbon.[7] From the interpretation according to the donor-acceptor theory of Mulliken,[8] it can be expected that the frequency of the charge-transfer band, ν_{max}, for a series of similar stable carbonium ions with a given donor molecule would correlate with the electron affinities of these carbonium ions. Actually, Feldman and Winstein[7e] estimated the electron affinities of various organic cations, applying the principle mentioned above. In the present study, it was observed that the dissolution of each substituted tropylium salt in a 1,2-dichloroethane solution of a condensed aromatic hydrocarbon, pyrene, immediately gave a red-colored solution. It exhibits a band in the visible region which is not found in the spectrum of either component and which can be regarded as a charge-transfer band. The results are shown in Table 3, along with the values of log k_2 for the chromous-ion reduction. A plot of log k_2 against ν_{max} exhibits a linear correlation between them, as is shown in Fig. 1.

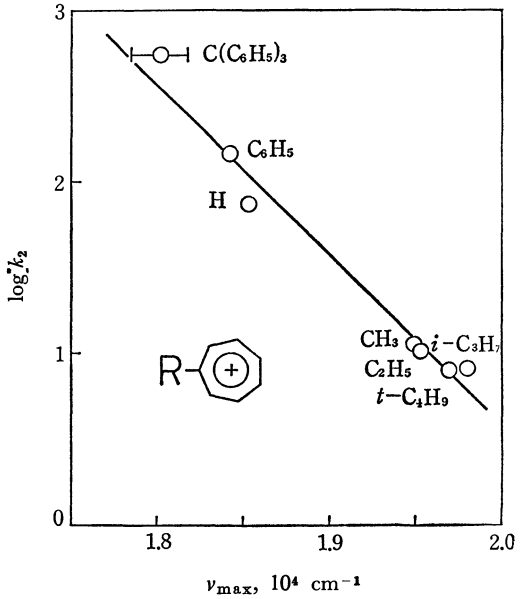

Fig. 1. The correlation of log k_2 with CT transition energies (ν_{max}).

As another measure of the electron affinity of the carbonium ions, electrochemical reduction potentials were determined by polarography with the dropping mercury electrode. The polarography of the tropylium ion was reported to include an irreversible reduction step.[1a-c] While some effects (solvation energy, *etc.*) other than electron affinity are regarded as being reflected in the half-wave potentials for such an irreversible step, for a series of similar cations the relative potentials will serve as a measure of readiness to accept an electron. The half-wave potentials measured in acetonitrile are listed in Table 3, while the correlation with log k_2 is shown in Fig. 2. The linear correlation observed in Figs. 1 and 2 clearly demonstrates that the reactivity of carbonium ions toward Cr(II) can be used satisfactorily as a measure of the electron affinity.

Correlation of the Reducibility with pK_R^+. In order to examine the correlation between the reducibility and the stability of carbonium ions, the pK_R^+ values of some representative substituted tropylium ions[9] were determined in 23% aqueous ethanol by

7) a) M. Feldman and S. Winstein, *J. Amer. Chem. Soc.*, **83**, 3338 (1961); b) M. Nepraš and R. Zahradník, *Collect. Czech. Chem. Commun.*, **29**, 1545 (1964); c) S. N. Bhat and C. N. R. Rao, *J. Chem. Phys.*, **47**, 1863 (1967); d) M. Feldman and B. G. Graves, *J. Phys. Chem.*, **70**, 955 (1966); e) M. Feldman and S. S. Winstein, *Theor. Chim. Acta*, **10**, 86 (1968); f) H. J. Dauben, Jr., and J. D. Wilson, *Chem. Commun.*, **1968**, 1629; g) T. G. Beaumont and K. M. C. Davis, *J. Chem. Soc., B*, **1968**, 1010.

8) R. S. Mulliken, *J. Chem. Phys.*, **19**, 514 (1951).

9) The pK_{R^+} values for the tropylium ions with a hydrogen atom at the α-position of the alkyl substituents could not be measured because of the decomposition of the cations in the low-acidity region; see Refs. 6 and 14.

Table 3. Results of the measurements of charge-transfer bands, polarographic half-wave potentials and pK_{R^+}'s of substituted tropylium ions

Substituent	$\log k_2$[a]	CT Band[b] λ_{max} mμ	CT Band[b] ν_{max} 10^4 cm^{-1}	$E_{1/2}$[c] V *vs.* SCE	pK_{R^+}[d]
None	1.87	540[e]	1.852	−0.126±0.002	4.3[f]
Methyl	1.05	513	1.949	−0.187±0.001	
Ethyl	1.01	512	1.953	−0.195±0.004	
Isopropyl	0.91	505	1.980	−0.235±0.002	
t-Butyl	0.90	508[g]	1.969	−0.215±0.002	5.0
Phenyl	2.16	543	1.842	−0.090±0.002	4.1
Trityl	2.75	550	1.818	−0.069±0.001	3.6
		~560	~1.786		

a) The logarithmic value of the averaged rate constant for the chromous-ion reduction of the respective tropylium ions.
b) Measured in 1,2-dichloroethane with pyrene as a donor.
c) Corrected from the values measured in acetonitrile *vs.* Ag/AgCl, whose potential was found to be −0.162 V *vs.* SCE.
d) Measured spectrophotometrically in 23% aqueous ethanol.
e) Lit., λ_{max} 535 mμ (Ref. 7d, e).
f) Lit., pK_{R^+} 4.7 (measured by potentiometric titration in water; Ref. 15).
g) Lit., λ_{max} 503 mμ (Ref. 7e).

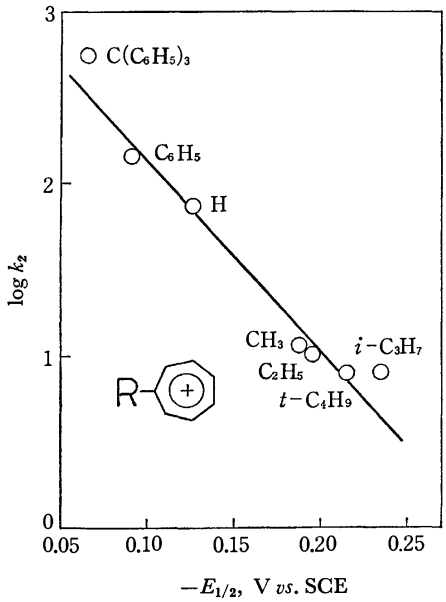

Fig. 2. The correlation of $\log k_2$ with polarographic half-wave potentials ($-E_{1/2}$).

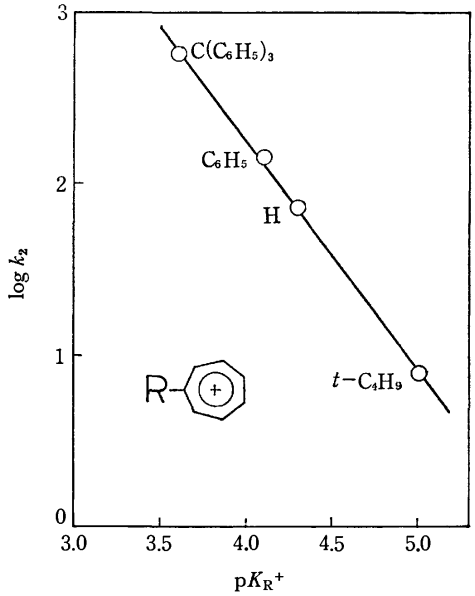

Fig. 3. The correlation of $\log k_2$ with pK_{R^+}.

the spectrophotometric method described by Breslow and Chang.[10] From the results shown in Table 3, it can be seen that, whereas the alkyl substituent increases the stability, the phenyl group rather destabilizes the cation by means of its electron-withdrawing inductive effect, as is shown by the least stability of the triphenylmethyltropylium ion. The greater contribution to the stabilization of the cation by the alkyl group than by the phenyl group has been also observed in a cyclopropenyl system.[11]

A plot of $\log k_2$ against pK_{R^+}, again, gave a good linear correlation, as is shown in Fig. 3. Since the equation for pK_{R^+} is written as Eq. (2), with the rate constants for the forward and backward reactions (k_f and k_b respectively), and since it can be assumed that the backward reaction is not greatly affected by the structural change, this correlation may be generalized to imply that the readiness of the carbonium ion to accept one electron is parallel with the reactivity of the ion toward the electron pair of the nucleophile.

$$R^+ + H_2O \underset{k_b}{\overset{k_f}{\rightleftharpoons}} ROH + H^+ \quad (1)$$

$$pK_{R^+} = \log k_b - \log k_f \quad (2)$$

Experimental[12]

Materials. All the reagents employed were of a reagent-grade quality except when otherwise noted. Aceto-

10) R. Breslow and H. W. Chang, *J. Amer. Chem. Soc.*, **83**, 2367 (1961).
11) R. Breslow, H. Hover, and H. W. Chang, *ibid.*, **84**, 3168 (1962).

12) The melting points and boiling points are uncorrected. The microanalyses were performed by the Microanalytical Center, Kyoto University, Kyoto. The infrared and ultraviolet spectra were recorded with Shimadzu spectrometers, models IR-27 and UV-50M respectively. The NMR spectra were obtained by the use of a JEOL model JNM-3H-60 spectrometer with tetramethylsilane as the internal standard. The polarograms were obtained with a Yanagimoto polarograph, model P8-DP.

nitrile and ethyl acetate were refluxed over phosphorus pentoxide and then distilled; acetonitrile, bp 81.0—81.5 °C; ethyl acetate, bp 77.0—77.4 °C.

Tropylium fluoroborate was prepared from tropilidene according to the method of Conrow.[13]

7-Methyl-, 7-ethyl-, 7-isopropyl-, and 7-*t*-butylcycloheptatrienes were obtained by the reaction of 7-ethoxycycloheptatriene with the corresponding alkyl magnesium halides, as has been reported by Nozoe and his co-workers;[14] 7-methylcycloheptatriene, bp 53 °C/63 mmHg (lit, bp 63 °C/80 mmHg[14]); 7-ethylcycloheptatriene, bp 84 °C/35 mmHg; 7-isopropylcycloheptatriene, bp 88 °C/36 mmHg (lit, bp 74 °C/33 mmHg[14]); 7-*t*-butylcycloheptatriene, 90 °C/24 mmHg (lit, bp 95—98 °C/45 mmHg.[14])

7-Phenylcycloheptatriene was prepared by the reaction of tropylium fluoroborate with phenyllithium according to the method of Doering and Knox;[15] bp 76 °C/0.4 mmHg.

7-Triphenylmethylcycloheptatriene was synthesized by reference to the thesis of Rifi.[16] In a 100-ml four-necked flask equipped with a mechanical stirrer, a thermometer, and a nitrogen inlet and outlet, there was stirred a suspension of 1.467 g (8.74 mmol) of tropylium fluoroborate in 40 ml of dry ethyl ether. To this mixture was slowly added 63 ml of a 0.14 M ethereal solution of triphenylmethylsodium (8.8 mmol), prepared from triphenylmethyl chloride and 1% sodium amalgam according to the method of Renfrow and Hauser,[17] over a 10-min period by the use of a hypodermic syringe. The dark red color of the solution of triphenylmethylsodium was instantaneously discharged when it was added to the ethereal suspension of tropylium fluoroborate. The yellowish gray mixture was stirred for a further 2 hr at 24—26 °C under nitrogen. After the addition of 100 ml of distilled water, the organic layer was separated and worked up in the usual way to give 2.928 g of a yellowish white solid, which was then chromatographed over 100 g of silica gel (Nakarai, No. II-A, 100—200 mesh). Elution with *n*-hexane–benzene (4 : 1) gave 1.263 g (3.78 mmol) of 7-triphenylmethylcycloheptatriene as white crystals; the same infrared spectrum as the authentic sample; 43.3% yield; mp 166.6—170.7 °C (dec) (lit, mps 167—170 °C (dec)[18] and 156 °C[16]).

The isomerization of 7-substituted cycloheptatrienes to the mixtures of 1-, 2-, and 3-substituted cycloheptatrienes was effected thermally by successive sigmatropic 1—5 hydrogen shifts,[19] so that the steric hindrance at the step of hydride abstraction by the triphenylmethyl cation (*vide infra*) might be diminished. 7-Methyl-, 7-ethyl-, 7-isopropyl-, 7-*t*-butyl, and 7-phenylcycloheptatrienes were sealed in Pyrex ampoules under a vacuum ($<10^{-3}$ mmHg), heated in an oil bath at 175 °C for 1.5 hr,[14] and distilled under reduced pressure; methylcycloheptatrienes, bp 65—67 °C/72 mmHg; ethylcycloheptatrienes, bp 95—98 °C/41 mmHg; isopropylcycloheptatrienes, bp 90—94 °C/35 mmHg; *t*-butylcycloheptatrienes, bp 79—80 °C/24 mmHg; phenylcycloheptatrienes, bp 77—79 °C/0.4 mmHg. 7-Triphenylmethylcycloheptatriene was dissolved in *m*-xylene and similarly sealed in a Pyrex ampoule under a vacuum. After heating at 145 °C for 5 hr, the isomer mixtures were recovered as white crystals by chromatography over silica gel (Nakarai, No. II-A, 100—200 mesh), with *n*-hexane–benzene (4 : 1) as the eluent.

Methyltropylium perchlorate (Ia) was synthesized following the method of Conrow.[20] Into a suspension of 7.00 g (0.0204 mol) of triphenylmethyl perchlorate in 40 ml of acetonitrile, we added 2.079 g (0.0195 mol) of thermally-isomerized methylcycloheptatrienes with magnetical stirring at room temperature. In 1 min, the precipitates of triphenylmethyl salt all dissolved. After 10 min, the solvent was evaporated under reduced pressure, a 50-ml portion of ethyl acetate was added, and the yellow solid mass was pulverized. Then the mixture was evaporated again, followed by the addition of another 100 ml of ether acetate and by the trituration of the solid. This time the precipitates were collected under a stream of nitrogen, washed with ten 10-ml portions of ethyl acetate, and dried in a vacuum desiccator to give 3.879 g (0.0190 mol) of crude Ia; 97.4% yield. Recrystallization from acetonitrile–ethyl ether under nitrogen gave white crystals, which rapidly decompose on exposure to air; mp 110.0—111.5 °C (lit, mp 111—112 °C[20], mp 109 °C[21]); $\lambda_{max}^{0.1\,M\,HCl}$ 287 mμ (ε, 4760) (lit, $\lambda_{max}^{conc\ H_2SO_4}$ 288 mμ (ε, 3500)[21]).

Ethyltropylium perchlorate (Ib) was obtained by the same method as white crystals with a pink tinge from the isomerized ethylcycloheptatrienes; 90.5% yield; mp 84.0—84.3 °C; $\lambda_{max}^{0.1\,M\,HCl}$ 292 mμ (ε, 4880).

Isopropyltropylium perchlorate (Ic) was similarly prepared as brownish-white crystals from the isomerized isopropylcycloheptatrienes, except that dry ethyl ether was employed instead of ethyl acetate for the washing of the product; 76.7% yield; mp 35.8—39.8 °C; $\lambda_{max}^{0.1\,M\,HCl}$ 294 mμ (ε, 5030).

t-Butyltropylium perchlorate (Id) was obtained as white crystals by the same procedure as was used in the preparation of Ia except that the reaction time was prolonged to 2 hr; 64.0% yield; mp 179.0—180.0 °C (dec); $\lambda_{max}^{0.1\,M\,HCl}$ 293 mμ (ε, 4880).

Phenyltropylium fluoroborate (Ie) was prepared as yellow crystals by the same method, except that triphenylmethyl fluoroborate was used instead of perchlorate salt; 74.9% yield; mp 151.0—152.0 °C (lit, mp 153—154 °C[22]); $\lambda_{max}^{0.1\,M\,HCl}$ 226 mμ (ε, 37700), 270.5 mμ (14800), 368 mμ (16200).

Triphenylmethyltropylium fluoroborate (If) was synthesized by an essentially similar method. In a 100-ml two necked flask equipped with a thermometer and a reflux condenser connected to soda lime tube, we charged a solution of 0.330 g (1.00 mmol) of triphenylmethyl fluoroborate in 15 ml of acetonitrile. To this solution was then added 0.336 g (1.04 mmol) of thermally-isomerized triphenylmethylcycloheptatrienes, and the whole mixture refluxed for 6.5 hr. The reaction mixture was then evaporated *in vacuo*, pulverized in 7 ml of freshly-added ethyl acetate, and evaporated again. Then an 18-ml portion of ethyl acetate was added;

13) K. Conrow, "Organic Syntheses," Vol. 43, p. 101 (1963).
14) T. Nozoe, K. Takahashi, and H. Yamamoto, This Bulletin, **42**, 3277 (1969).
15) W. von E. Doering and L. H. Knox, *J. Amer. Chem. Soc.*, **76**, 3203 (1954).
16) M. R. Rifi, Ph. D. Thesis, the University of Washington (1963), p. 105.
17) W. B. Renfrow, Jr., and C. R. Hauser, "Organic Syntheses," Coll. Vol. 2, 607 (1943).
18) K. Okamoto, K. Komatsu, T. Kinoshita, and H. Shingu, This Bulletin, **43**, 1901 (1970).
19) a) A. P. ter Borg. H. Kloosterziel, and N. van Meurs, *Rec. Trav. Chim. Pays-Bas*, **82**, 717 (1963); b) A. P. ter Borg and H. Kloosterziel, *ibid.*, **82**, 741 (1963); c) K. W. Egger, *J. Amer. Chem. Soc.*, **89**, 3688 (1967); d) T. Nozoe and K. Takahashi, This Bulletin, **38**, 665 (1965).
20) K. Conrow, *J. Amer. Chem. Soc.*, **83**, 2343 (1961).
21) H. J. Dauben, Jr., F. A. Gadecki, K. M. Harmon, and D. L. Pearson, *ibid.*, **79**, 4557 (1957).
22) J. W. Wilt and D. Piszkiewiez, *Chem. Ind.* (London), **1963**, 1761.

Table 4. Ultraviolet spectral and elementary analytical data for *x,x'*-disubstituted bitropyl

Substituent	λ_{max}^{EtOH} mμ (ε)	Formula	Elementary analysis			
			Found		Calcd	
			C%	H%	C%	H%
Methyl	254 (7400)	$C_{16}H_{18}$	91.51	8.75	91.37	8.63
Ethyl	254 (7140)	$C_{18}H_{22}$	90.81	9.53	90.69	9.31
Isopropyl	254 (7780)	$C_{20}H_{26}$	90.45	9.83	90.16	9.84
t-Butyl	251 (7810)	$C_{22}H_{30}$	89.60	10.24	89.73	10.27
Phenyl	239 (37400) [a]	$C_{26}H_{22}$	93.27	6.64	93.37	6.63
Trityl	261 (10100)	$C_{52}H_{42}$	93.37	6.35	93.65	6.35

a) With a shoulder at 275 mμ (13700).

the yellowish precipitates were then collected, washed with three 5-ml portions of ethyl ether, and dried under reduced pressure. Recrystallization of the crude product from acetonitrile–ethyl ether yielded 0.204 g (0.485 mmol) of If as white crystals with a silvery tinge; 46.6% yield; mp 243.0—243.5 °C (dec); $\lambda_{max}^{2.9\,M\,HCl}$ 226.5 mμ (ε, 46600), 260 mμ(sh) (10500), 309 mμ (5850); NMR, τ_{CH_3CN}, 0.44 (m, 6H, tropylium ring protons), 2.34 (s, 15H, phenyl protons).

Found: C, 74.25; H, 4.77%. Calcd for $C_{26}H_{21}BF_4$: C, 74.30; H, 5.04%.

The solution of chromous chloride in 10% HCl was prepared as has previously been reported.[3]

One-Electron Reduction of the Substituted Tropylium Ions with Cr(II). In a 100-ml, four-necked flask equipped with a magnetic stirring bar, a serum rubber cap, and a nitrogen inlet and outlet, there was charged a solution of 0.258 g (1.05 mmol) of Id in 40 ml of 10% HCl. To this solution was then added 5 ml of 1 M solution of chromous chloride in 10% HCl (5 mmol) by the use of a hypodermic syringe under an atmosphere of nitrogen. The reaction mixture immediately became cloudy with an organic substance dispersed in the solution. The mixture was stirred for 10 min and worked up in the usual way to give 0.157 g (0.534 mmol) of *x,x'*-di-*t*-butylbitropyl as a viscous oil; 100.1% yield; NMR, τ_{CCl_4} 3.3—4.1 (m, 6.2H, H^{3-6}), 4.7—5.1 (m, 3.8H, $H^{2,7}$), 8.2 (s, 2H, H^1), 8.8, 8.9 (two s, 18H, *t*-butyl). Reductions of Ia, b, c, e, and f were carried out in the same way. The ultraviolet spectra and the results of the elementary analyses of all the products are tabulated in Table 4.

Kinetic Measurements. The reaction rate was measured in 10% HCl at 25.0±0.2 °C by a method reported previously.[3] The products were determined by ultraviolet spectroscopy using the characteristic bands listed in Table 4.

Measurements of the Charge-Transfer Bands with Pyrene. In 5 ml of the solution of pyrene in 1,2-dichloroethane (0.2 M) was dissolved 2—4 mg of the purified sample of the substituted tropylium ion salt, so that the concentration of the cation became 2×10^{-3} g-ion/l. A red color immediately developed; the visible spectrum was then recorded to give the results shown in Table 3.

Determination of pK_{R^+}*'s.* The determination of the pK_{R^+} in 23% aqueous ethanol was carried out spectrophotometrically following the method of Breslow and Chang.[10] The ultraviolet spectrum was recorded on each cation in nine or ten solutions of buffer spaced through a pH range of about two units on each side of the pK_{R^+}. The buffer solutions were made up from various mixtures of 0.1 M citric acid and 0.2 M Na_2HPO_4 according to the procedure of Gomori.[23] The absorbancy at a wavelength characteristic of the cation, described above, was plotted against the pH to give a classical titration curve, whose mid-point was taken as the pK_{R^+}. The pH's were read on a Horiba model H pH meter calibrated with standard buffers before use.

Polarography. The polarograms were obtained on the solutions of the respective cations in acetonitrile (1.0×10^{-3} g-ion/l) containing $Et_4N^+ClO_4^-$ (0.5 M) as the supporting electrolyte at 25 °C. As the reference electrode, we used the Ag/AgCl electrode described by Popov and Geske,[24] whose potential was found to be −0.162 V *vs.* SCE.

23) G. Gomori in S. P. Colowick and N. O. Kaplan, "Methods in Enzymology," Vol. I, Academic Press, New York, N. Y. (1955), p. 138.

24) A. I. Popov and D. H. Geske, *J. Amer. Chem. Soc.*, **79**, 2074 (1957).

The Nickel-catalyzed Cyclodimerization of Butadiene. The Synthesis of 2-Methylenevinylcyclopentane and the Isomerization of 1,3,7-Octatriene

Jitsuo KIJI, Kazuyoshi YAMAMOTO, Shin-ichi MITANI, Susumu YOSHIKAWA, and Junji FURUKAWA

Department of Synthetic Chemistry, Faculty of Engineering, Kyoto University, Kyoto 606

(Received November 10, 1972)

A catalyst system of $NiX_2(R_3P)_2$–$NaBH_4$ or –R'ONa (X=halogen, R and R'=alkyl) was found to yield 2-methylenevinylcyclopentane (MVCP) and *n*-octatrienes (OT), depending on the amount of $NaBH_4$ or R'ONa, which act as a reducing agent for the nickel halide. Less than an equimolar amount of the reducing agent provides a catalyst for MVCP, whereas an excess amount provides that for *n*-octatrienes. In the latter case, the nickel halide is reduced to zero-valent nickel, which then reacts with hydrogen halide to give a catalyst for MVCP again. The catalyst (<2 : 1 ratio of reducing agent : Ni) was also effective in the isomerization of 1,3,7-octatriene to MVCP.

Some nickel catalysts have been reported to be effective catalysts for the novel cyclodimerization of butadiene to give 2-methylenevinylcyclopentane (MVCP).[1-3] Organonickels, such as arylnickel- or π-allylnickel halide, are typical catalysts which are used in the presence of a controlled amount of alcohol. The other type of the catalyst is a phosphine complex of nickel halide combined with organolithium. In both cases, the nickel compounds might be reduced by alcohols or organolithium to an active nickel species. On the other hand, sodium borohydride is an effective reducing agent for the preparation of transition-metal catalysts and is also used for the linear dimerization of butadiene by a nickel catalyst.[4,5] A mixture of cobalt halide and sodium borohydride is also effective for the dimerization of butadiene; an important intermediate has been isolated, and its structure has been studied crystallographically.[6]

It is well-known that the phosphine complex of platinum halide is also reduced to a stable platinum hydride by the action of alcoholic potassium hydroxide.[7] A similar reduction can be anticipated for nickel salts.

$$PtCl_2(Et_3P)_2 + CH_3CH_2OH + KOH \rightarrow PtHCl(Et_3P)_2 + CH_3CHO + KCl + H_2O \quad (1)$$

It has now been found that tri-*n*-butylphosphine complexes of nickel halides $NiX_2(n\text{-}Bu_3P)_2$, combined with sodium borohydride or sodium alkoxide, are also effective for the cyclodimerization of butadiene to MVCP, when the reducing agent is controlled to an equimolar amount. This paper will deal with the cyclodimerization of butadiene and the isomerization of 1,3,7-octatriene. An effort has been made to find the relationship between the two catalysts, which give linear dimers or MVCP.

Results and Discussion

When bis(tri-*n*-butylphosphine)dibromonickel and sodium borohydride or sodium alkoxide were mixed in equimolar quantities in alcohol, a yellowish-brown solution was obtained. This solution smoothly dimerized butadiene under a slightly high pressure at between 80 and 100 °C to give 2-methylenevinylcyclopentane(MVCP). In the catalyst system, the amount of sodium borohydride or sodium alkoxide plays an important role and has a strong influence on the product distribution. First, the conditions were decided under which MVCP could be formed selectively. Table 1 summarizes the effect of the amount of the reducing agent on the distribution of the dimers. In most cases, butadiene was not unchanged by the reaction. The product other than the dimers was *trans*-1,4-polybutadiene. To obtain MVCP selectively, an amount of sodium borohydride or sodium alkoxide equimolar to the nickel salt was necessary. The effect of the amount of alkoxide is shown in Fig. 1. If the nickel salt was combined with an excess (more than 1 mol) of the reducing agent, a conventional linear dimerization occurred and *n*-octatrienes were the main products.

By analogy to the reaction of platinum with alcoholic potassium hydroxide, the formation of the

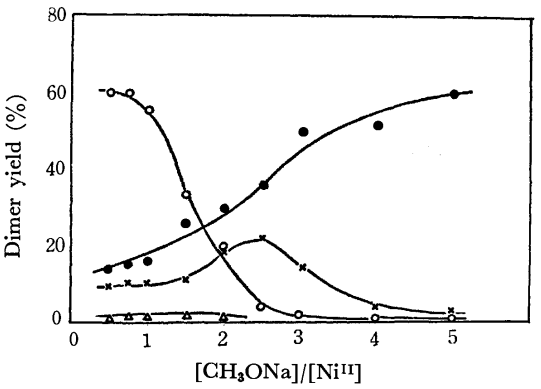

Fig. 1. Effect of [Alkoxide] on the dimerization at 80 °C for 22 hr.
(○), MVCP; (●), 2,4,6-OT; (×), 1,3,6-OT; (△), 1,3,7-OT.
Conditions: $[NiBr_2(n\text{-}Bu_3P)_2]$=0.3 mmol, [Butadiene]=25 mmol.

1) J. Kiji, K. Masui, and J. Furukawa, *Tetrahedron Lett.*, **1970**, 2561.
2) J. Kiji, K. Masui, and J. Furukawa, *Chem. Commun.*, **1970**, 1310.
3) J. Kiji, K. Masui, and J. Furukawa, This Bulletin, **44**, 1956 (1971).
4) T. Yoshida and S. Yuguchi, Presented at the 18th Annual Meeting of the Chemical Society of Japan, 1965, Osaka.
5) N. Yamazaki and T. Ohta, *J. Macromol. Sci.- Chem.*, **A3**, 1571 (1969).
6) G. Natta, V. Giannini, P. Pino, and A. Cassata, *Chim. Ind.* (Milan), **47**, 524 (1965).
7) J. Chatt and B. L. Shaw, *Chem. Ind.* (London), **1960**, 931.

TABLE 1. DIMERIZATION OF BUTADIENE[a)]

Ni Compd.	(mmol)	Reducing agent	(mmol)	Butadiene (mmol)	Solvent	Product[b)] (Yield, %) MVCP	OT	VCH	COD
$NiBr_2(n\text{-}Bu_3P)_2$	(0.3)	$NaBH_4$	(0.12)	24	Ethanol	82	—	—	—
$NiBr_2(n\text{-}Bu_3P)_2$	(1.0)	$NaBH_4$	(1.0)	24	Ethanol	80	7	—	—
$NiBr_2(n\text{-}Bu_3P)_2$	(0.3)	$NaBH_4$	(2.4)	24	Ethanol	—	12	8	1
$NiCl_2(n\text{-}Bu_3P)_2$	(0.5)	$NaBH_4$	(0.5)	12	Ethanol	30	11	—	—
$Ni(NO_3)_2(n\text{-}Bu_3P)_2$	(0.5)	$NaBH_4$	(0.5)	12	Ethanol	26	18	—	—
$Ni(SCN)_2(n\text{-}Bu_3P)_2$	(0.5)	$NaBH_4$	(0.5)	12	Ethanol	(No reaction)			
$Ni(CN)_2(n\text{-}Bu_3P)_2$	(0.5)	$NaBH_4$	(0.5)	12	Ethanol	(Polymerization)			
$NiBr_2(Et_2PhP)_2$	(0.5)	$NaBH_4$	(0.5)	12	Ethanol	71	—	—	—
$NiBr_2(Ph_3P)_2$	(0.3)	$NaBH_4$	(0.3)	25	Ethanol	27	40	—	—
$NiCl_2(Ph_3P)_2$	(0.3)	$NaBH_4$	(0.3)	25	Ethanol	33	22	—	—
$NiBr_2(n\text{-}Bu_3P)_2$	(0.3)	CH_3ONa	(0.3)	25	2-Propanol	58	28	<1	—
$NiCl_2(n\text{-}Bu_3P)_2$	(0.3)	CH_3ONa	(0.3)	25	2-Propanol	43	19	<1	—
$Ni(NO_3)_2(n\text{-}Bu_3P)_2$	(0.3)	CH_3ONa	(0.3)	25	2-Propanol	25	16	<1	—
$Ni(SCN)_2(n\text{-}Bu_3P)_2$	(0.3)	CH_3ONa	(0.3)	25	2-Propanol	—	0.3	—	—
$Ni(CN)_2(n\text{-}Bu_3P)_2$	(0.3)	CH_3ONa	(0.3)	25	2-Propanol	(No reaction)			
$NiBr_2(Ph_3P)_2$	(0.3)	CH_3ONa	(0.3)	25	2-Propanol	(No reaction)			

a) At 80 °C for 24 hr. b) MVCP, 2-methylenevinylcyclopentane; OT, mixture of isomeric *n*-octatrienes; VCH, 4-vinyl-1-cyclohexene; COD, 1,5-cyclooctadiene.

nickel hydride caused by alkoxide may be assumed (Eq. 2) when an equimolar amount of alkoxide is used. Until now only a few nickel hydrides have, however, been isolated in a stable form.

$$NiBr_2(n\text{-}Bu_3P)_2 + CH_3ONa \rightarrow [HNiBr(n\text{-}Bu_3P)_2] + NaBr + CH_2O \quad (2)$$

It has been reported that bis(tri-propylphosphine)-hydridochloronickel, $HNiCl(i\text{-}Pr_3P)_2$, is unstable and decomposes at room temperature.[9] Therefore, the hydride transiently formed according to Eq. 2 may be assumed to decompose at the reaction temperature, probably through the reductive elimination of hydrogen bromide to give an active nickel catalyst for the cyclodimerization.

$$HNiBr(n\text{-}Bu_3P)_2 \rightarrow HBr + [Ni(n\text{-}Bu_3P)_2] \quad (3)$$

Another possibility for the activation of the catalyst is that the nickel-hydrogen bond is activated by the coordination of butadiene, as in the case of the alkylnickel catalyst.[10,11] Stable $HNiCl[(C_6H_{11})_3P]_2$ has been synthesized by the reaction of $NiCl_2[(C_6H_{11})_3P]_2$ with sodium borohydride,[8] but it has no catalytic activity by itself. However, it shows a catalytic activity for the linear dimerization of butadiene in the presence of alcohol, although not for that of amine and phenol, and gives octatrienes.[12] The cyclodimerization proceeds satisfactorily in the presence of strong donor phosphines, such as tri-*n*-butylphosphine. Tricyclohexylphosphine possesses a basicity similar to that of tri-*n*-butylphosphine.[13] In the dimerization of butadiene, the bulky cyclohexyl group on phosphorus prevents the cyclodimerization to the five-membered cycle.[3] It seems reasonable to assume, on the basis of the reduction of organometals by alcohol,[14] that stable $HNiCl[(C_6H_{11})_3P]_2$ is reduced further by alcohol in the presence of butadiene, and that only after the reduction does it show the catalytic activity for the dimerization.

$$HNiCl[(C_6H_{11})_3P]_2 + C_2H_5OH \rightarrow H_2 + \{Ni[(C_6H_{11})_3P]_2\} + CH_3CHO + HCl \quad (4)$$

During this reduction or during the decomposition described above, hydrogen halide is liberated; it appears to play an important role as a cocatalyst, and

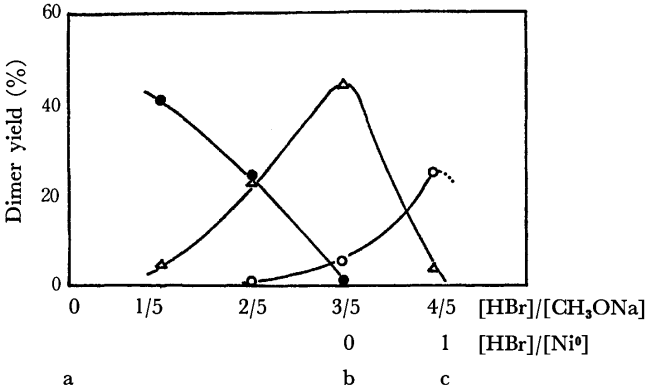

Fig. 2. Effect of [HBr] on the dimerization at 80 °C for 22 hr.
(○), MVCP; (●), 2,4,6-OT; (△), 1,3,7-OT.
Conditions: $[NiBr_2(n\text{-}Bu_3P)_2]=0.3$ mmol, $[CH_3ONa]=1.5$ mmol, [Butadiene] =20 mmol.

8) M. L. H. Green and T. Saito, *Chem. Commun.*, **1969**, 208.
9) M. L. H. Green, C. N. Street, and G. Wilkinson, *Z. Naturforsch., B*, **14**, 738 (1959).
10) A. Yamamoto, K. Morifuji, S. Ikeda, T. Saito, Y. Uchida, and A. Misono, *J. Amer. Chem. Soc.*, **87**, 4652 (1965).
11) T. Yamamoto, A. Yamamoto, and S. Ikeda, *ibid.*, **93**, 3350 (1971).
12) J. Furukawa, J. Kiji, and S. Mitani, unpublished work.
13) C. A. Tolman, *J. Amer. Chem. Soc.*, **92**, 2953 (1970).
14) D. A. White and G. W. Parshall, *Inorg. Chem.*, **9**, 2358 (1970).

the product distribution seems to vary with the concentration of hydrogen bromide. To confirm this, we examined the effect of hydrogen halide on the catalyst composed of $NiBr_2(n\text{-}Bu_3P)_2$ and an excess of sodium alkoxide. Hydrogen bromide was added incrementally to the catalyst, which gives linear dimers. The results of this study are shown graphically in Fig. 2; the reversibility of the cyclodimerization catalyst formation is there demonstrated.

The catalyst was prepared by the reaction of $NiBr_2(n\text{-}Bu_3P)_2$ with sodium methoxide (molar ratio 1 : 5) in 2-propanol. After confirming that the catalyst of this composition is effective for the linear dimerization, but not for MVCP, dry hydrogen bromide was added; the cyclodimerization catalyst was found to be thus regenerated. It is assumed that the decomposition or the reduction of the nickel hydride proceeds according to Eq. 3 or 4, and that the hydrogen bromide formed during this process in neutralized with the excess of alkoxide. It has been observed that the addition of hydrogen bromide in a 3 : 5 molar ratio of HBr: alkoxide (point (b) in Fig. 2) is still ineffective for the cyclodimerization and that *n*-octatrienes are thus formed mainly. In this region (from (a) to (b)), the isomerization of 1,3,7-octatriene to 2,4,6-octatriene decreases with an increase in the amount of hydrogen bromide, because the isomerization is catalyzed by a strong base.[15] Under these conditions, all the hydrogen bromide is neutralized by alkoxide; thus, the solution is "basic." When more hydrogen bromide (point (c)) is added, the solution reveals the catalytic activity for the cyclodimerization. At this point the molar ratio of free hydrogen bromide to nickel is assumed to be 1 : 1. Beyond this point, the further addition of hydrogen bromide produces a color change from yellow to green; this change can reasonably be attributed to the formation of the original nickel bromide, and no reaction of butadiene occurs. These observations lead to a conclusion concerning the hydrogen bromide (generally speaking, hydrogen halide) stoichiometry for the activation of the catalyst. The ratio of hydrogen bromide to zero-valent nickel must be 1 : 1 for the cyclodimerization. This reaction is demonstrated by Eq. 2. Zero-valent nickel and hydrogen bromide are formed through the transient formation of the nickel hydride, followed by rapid decomposition (Eq. (3)) or by further reduction by alcohol (Eq. (4)), when the catalyst is prepared by the equimolar reaction of $NiBr_2(n\text{-}Bu_3P)_2$ with sodium borohydride or sodium alkoxide in alcohol. The catalyst which have been reported in the previons paper[3] also satisfy these conditions. Once zero-valent nickel is formed, the formation of the bis-π-allylic intermediate (II), which is described below, is a well-known reaction.[16,17] The stabilization by forming a chelating bis-π-allylic complex seems to be a driving force for this reaction.

15) C. G. Cardenas, *J. Org. Chem.*, **35**, 264 (1970).
16) P. Heimbach, P. W. Jolly, and G. Wilke, *Advan. Organometal. Chem.*, **8**, 29 (1970).
17) B. Barnett, B. Büssemeier, P. Heimbach, P. W. Jolly, G. Krüger, I. Tkatchenko, and G. Wilke, *Tetrahedron Lett.*, **1972**, 1457.

If butadiene reacts with the nickel hydride before the reduction (Eq. (4)) or the decomposition (Eq. (3)), it forms a π-crotyl nickel.[18] This possibility can also be excluded by the observation that the position of the deuteration of the dimer (I) is at the 3-carbon atom when the dimerization is carried out in deuterium-labelling alcohol.[1]

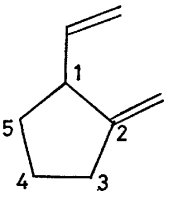

I

Therefore, in contrast to the rhodium-catalyzed dimerization of ethylene studied by Cramer,[19] where a metal hydride initiates the dimerization, nickel hydride or hydrogen bromide does not participate in the initiation reaction. Detailed information on the role of hydrogen bromide could not be obtained from the present study, but it appears that the bromide promotes the further insertion of one terminal double bond into the Ni–C bond to give the cyclic dimer before the elimination of nickel hydride.

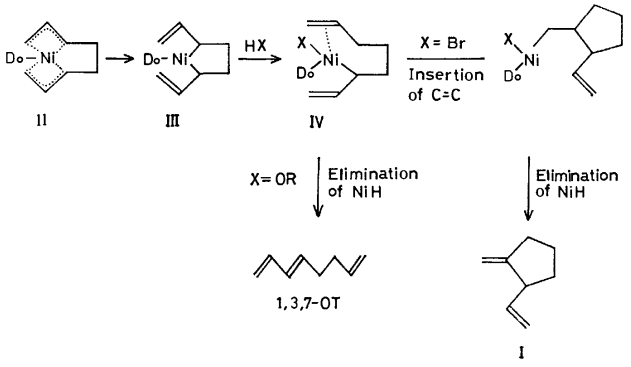

Scheme 1

Solvent. This cyclodimerization involves the migration of one hydrogen atom. It has been already proposed that alcohol participates in this reaction.[3] For this reason, in most of our studies alcohol was employed. Primary and secondary alcohols were effective for the reaction, but tertiary alcohol, benzene, tetrahydrofuran, and dimethyl sulfoxide were ineffective. In *t*-butylalcohol and dimethyl sulfoxide, *trans*-1,4-polybutadiene was the main product, while in benzene and tetrahydrofuran no appreciable reaction occurred and butadiene was recovered unchanged. In triethylsilane, no reaction of the nickel salt with sodium borohydride occurred, butadiene and triethylsilane being recovered. However, if ethanol was present in the silane, MVCP was formed in a considerable amount (≈30%). In this case, though, no product due to hydrosilation was detected.

Other Nickel Salts. The best results were obtained with tri-*n*-butylphosphine complexes of nickel

18) C. A. Tolman, *J. Amer. Chem. Soc.*, **92**, 6777 (1970).
19) R. Cramer, *ibid.*, **87**, 4717 (1965).

bromide and chloride. Since a crystalline complex could not be obtained by the reaction of nickel iodide with tri-*n*-butylphosphine, the catalytic activity of the iodide analogue has not been examined. However, it has been previously reported that (*o*-tolyl)NiI-$[(C_2H_5)_3P]_2$ is highly effective for the cyclodimerization in the presence of alcohol.[2] Therefore, hydrogen iodide has a similar effect on the reaction. The tri-*n*-butylphosphine complex of the nitrate and triphenylphosphine complexes of the bromide and the chloride gave a mixture of MVCP, *n*-octatrienes, and low-molecular-weight polybutadiene. No reaction of butadiene occurred when the isothiocyanate was used as a catalyst. The cyanate complex gave polybutadiene.

The effects of the other electron donors as auxiliary ligands have also been studied. Strong electron donors, such as tri-*n*-butylphosphine and diethylphenylphosphine, are best. The presence of an excess amount of phosphine (>2 : 1 ratio of phosphine : Ni) suppresses the formation of the dimers. The strong electron donors favor the formation of the σ-allyl complex (III), which is a transient form occurring before the alcoholysis and the cyclization. Bidentate phosphines and amines are not effective.

Isomerization of 1,3,7-*Octatriene.* 1,3,7-Octatriene may be expected to react further in the presence of the catalyst. One possibility is an isomerization through the π-allyl nickel intermediate (II), which is assumed to be formed by an intramolecular transfer of hydrogen, followed by alcoholysis. Another possibility is the direct reaction of 1,3,7-octatriene with nickel hydride to form the intermediate (IV). If this is true, it is possible to isomerize 1,3,7-octatriene to MVCP. From this point of view, the isomerization has been studied. The results are shown in Fig. 3. The nickel complex, when combined with less than 2 moles of alkoxide, isomerized 1,3,7-octatriene to MVCP. If more alkoxide was used, only the isomerization of the double bond occurred to give 2,4,6-octatriene; *e. g.*, the base-catalyzed isomerization was predominant. The other products were high-boiling oligomers.

To gain insight into the isomerization, the deuterium-labelling experiment was particularly instructive; it will, therefore, be described in some detail. Hexadeutero-1,3-butadiene and its dimer (1,3,7-OT) were used for this purpose. A solution of 0.5 mmol of $NiBr_2(n\text{-}Bu_3P)_2$, 10 mg of sodium borohydride, and 1 ml of liquified hexadeuterobutadiene were heated in 1 ml of ethanol in a sealed glass tube at 80 °C for 24 hr. The deuterated MVCP thus formed showed only one broad singlet, around 7.7 τ. Isotope (H)-labelling occurred on the 3-carbon atom. The position of the hydrogen can be explained by the assumption that the reaction proceeds through the bis-allylic nickel intermediate (II), which has been discussed previously.[1] On the other hand, 0.5 ml of perdeutero-1,3,7-octatriene was treated with 1 mmol of $NiBr_2(n\text{-}Br_3P)_2$ and sodium ethoxide in 1 ml of ethanol at 80 °C for 24 hr. The MVCP which was obtained from this isomerization showed a broad singlet around 8.2 τ. This signal is assigned to a hydrogen on the 4- or 5-carbon atom (in I). In a separate experiment we have confirmed that MVCP is stable toward the action of the catalyst under these conditions and that no appreciable exchange of hydrogen with a solvent occurs after it is formed.[20] Thus, the position of the hydrogen is quite different between these two experiments. This fact shows that the isomerization of 1,3,7-octatriene to MVCP does not proceed through the bis-π-allylic intermediate (II), which is anticipated to be formed by the nickel-catalyzed C_6—C_4 shift of hydrogen. In this case, an addition of nickel hydride occurs on the 3- and 4-carbon atoms, followed by cyclization to give the five-membered cycle, *i. e.*, nickel hydride-initiated isomerization.

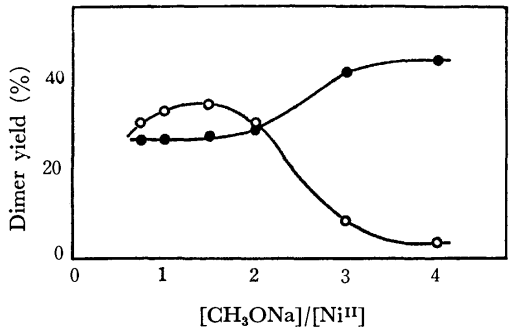

Fig. 3. Effect of [Alkoxide] on the isomerization of 1,3,7-octatriene at 80 °C for 24 hr.
(○), MVCP; (●), 2,4,6-OT.
Conditions: $[NiBr_2(n\text{-}Bu_3P)_2] = 0.3$ mmol, [1,3,7-OT] = 10 mmol.

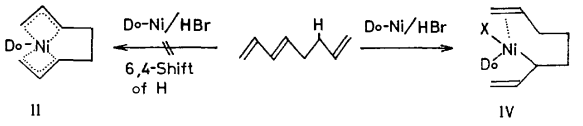

Scheme 2

This is different from the cyclodimerization of butadiene described above, which is not initiated by the addition of butadiene to the nickel hydride.

Experimental

The phosphine complexes of nickel salts were prepared by a method described earlier.[3] Commercially-available butadiene was dried over a 3A Molecular Sieve. The hexadeuterobutadiene was prepared from hexachlorobutadiene by the method of Morse.[21] The 1,3,7-octatriene was synthesized by the dimerization of butadiene with a palladium catalyst.[22] The dry hydrogen bromide was generated by adding bromine to tetralin.[23] All the solvents were purified by the conventional method and were distilled under a nitrogen atmosphere.

Gas-chromatographic analyses were carried out on a column, Silicone DC 550 on Celite, 3 m, at 100 °C. The products were identified by comparing the retention times and,

20) J. Kiji, K. Masui, K. Ueo, and J. Furukawa, presented at the 24th Annual Meeting of the Chemical Society of Japan, 1971, Osaka.
21) A. T. Morse and L. C. Leitch, *J. Org. Chem.*, **23**, 990 (1958).
22) N. Takahashi, T. Shibano, and N. Hagihara, *Tetrahedron Lett.*, **1967**, 2451.
23) A. H. Blatt, "Organic Syntheses," Coll. Vol. II, (1943), p. 338.

if necessary, the infrared and NMR spectra with those of authentic samples after separation by gas chromatography.

Cyclodimerization of Butadiene. *(i) Sodium Borohydride Method*: The nickel phosphine complex and the sodium borohydride were placed in a glass tube (20 mm in diameter). The tube was immediately fitted with a three-way stapcock. The system was placed under nitrogen by evacuating and by then filling it with nitrogen several times. When the solvent was added at room temperature, the solution turned brown or yellow, depending on the amount of sodium borohydride used. The reaction was instantaneous. The tube was cooled to −78 °C in a dry ice–acetone bath; then, liquified butadiene was added by means of a syringe through the three-way stopcock under a nitrogen atmosphere. The tube was sealed with a flame and heated. The yields of the products were determined gas chromatographically.

(ii) Alkoxide Method: To an alcoholic solution of the nickel complex in the glass tube we slowly added a 1 M solution of alkoxide by means of a syringe. At −78 °C, liquified butadiene was added, after which the tube was sealed with a flame and heated. The detailed reaction conditions and the results are given in Table 1.

Studies on Reversibility of Catalyst. The catalyst solution was prepared by the reaction of 10 ml of a 0.15 M 2-propanol solution of $NiBr_2(PBu_3)_2$ with 1.5 ml of a 5 M methanol solution of sodium methoxide. To this solution, a small amount of butadiene was then added; the mixture was allowed to stand overnight at room temperature. Five sets of experiments were made with this solution. After confirming that the only products were *n*-octatrienes and octadienyl ether, 2 ml of this solution was transferred to the glass tube under a nitrogen atmosphere. To each solution a definite amount of dry hydragen bromide was added as a 1.5 M 2-propanol solution, and then a 20-mmol portions of liquified butadiene was added at −78 °C. The tube was subsequently sealed and heated at 80 °C for 18 hr. The results are shown in Fig. 2.

Isomerization of 1,3,7-Octatriene. To the catalyst solution, 1,3,7-octatriene, instead of butadiene, was added. The mixture was then allowed to react in the sealed tube. The results are shown in Fig. 3.

BULLETIN OF THE CHEMICAL SOCIETY OF JAPAN, VOL. 46, 1795—1797 (1973)

Solvolysis of *cis*- and *trans*-4-*t*-Butylcyclohexyl Tosylates in *N*-Methylacetamide. Rates and Products Distribution

Seiki Saitô, Tatsumi Yabuki, Toshio Moriwake, and Kunio Okamoto*

Department of Synthetic Chemistry, School of Engineering, Okayama University, Tsushima, Okayama 700

**Department of Hydrocarbon Chemistry, Faculty of Engineering, Kyoto University, Sakyo-ku, Kyoto 606*

(Received November 16, 1972)

Solvolysis of *cis*- and *trans*-4-*t*-butylcyclohexyl tosylates (RX) in wet *N*-methylacetamide (H_2O content: 0.06—0.94 wt%) was carried out to give olefins (77—93%), 4- and 3-*t*-butylcyclohexyl acetates (ROAc) (6—22%), and 4- and 3-*t*-butylcyclohexanols (ROH) (2—4%). In *N*-methylacetamide with water (0.06%, wt) *trans*-4-RX gave *cis*-4-ROAc containing 18% *trans*-4-ROAc whereas *cis*-4-RX yielded *trans*-4-ROAc containing only 3% of *cis*-4-ROAc. In the course of solvolysis (75% completion) *trans*-4-RX was isomerized to *cis*-4-RX (5.9%), whereas *cis*-4-RX gave only 0.3% *trans*-4-RX. These results are characteristic of solvolysis in this amide solvent when compared with those in other hydroxylic solvents. Stereochemical results obtained from the present studies on the solvolysis in *N*-methylacetamide can not be explained by the hypothetical hydrogen-bridged carbonium ion intermediate proposed for the solvolysis of *cis*-4-RX. The nature of *N*-methylacetamide as a solvolytic solvent is discussed especially with regard to the effect of its polymeric structure on the steric course of solvolysis.

In previous studies on the solvolysis of *cis*- and *trans*-4-*t*-butylcyclohexyl tosylates (RX) in various hydroxylic solvents such as phenol, acetic acid, or 60% aqueous acetone, we demonstrated that the solvolytic *cis-trans* isomerization and 1,2-rearrangement of these tosylates, which respectively afford their geometrical isomers and their 3-derivatives (*cis*-and *trans*-3-RX), occur concurrently.[1] It was concluded that an appreciable part of the retained products is actually produced by double inversion, as is shwon in the following scheme, and the hypothesis of the hydrogen-bridged carbonium ion intermediate[2] is not necessary for an explanation of the formation of the retained products.

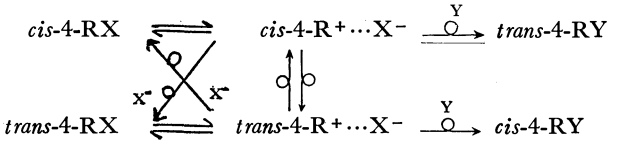

(X=OTs, Y=Nucleophile)

Scheme 1.

An investigation of these phenomena was extended to a non-hydroxylic solvent, solvolysis of this system in *N*-methylacetamide being carried out. This amide is known to possess a large dielectric constant[3] and

1) a) K. Okamoto, S. Saitô, and H. Shingu, This Bulletin, **42**, 3298 (1969); b) *ibid.*, **43**, 3008 (1970).

2) a) S. Winstein and N. J. Holness, *J. Amer. Chem. Soc.*, **77**, 5562 (1955); b) V. J. Shiner, Jr., and J. G. Jewett, *ibid.*, **87**, 1382 (1965); c) N. C. G. Campbell, D. M. Muir, R. R. Hill, J. H. Parish, R. M. Southan, and M. C. Whiting, *J. Chem. Soc., B.* **1968**, 355.

3) G. R. Leader and J. F. Gormly, *J. Amer. Chem. Soc.*, **73**, 5731 (1951); the dielectric constant of *N*-methylacetamide was determined to be 169.7 at 35 °C.

Table 1. Solvolysis products from *cis*- and *trans*-4-*t*-butylcyclohexyl tosylates at 75 °C

Solvent:	*N*-Methylacetamide[a]					PhOH–PhH[b] 1:1 by wt		AcOH[c]	
(H_2O concn., wt%)	(0.06)[d]	(0.06)[d]	(0.89)	(0.12)	(0.94)				
ROTs:	*cis*	*trans*	*cis*	*trans*	*trans*	*cis*	*trans*	*cis*	*trans*
Base:			Pyridine			Et_3N		NaOAc	
Cyclohexenes:									
Yield %	88.5	93.2	91.5	82.9	77.2	87.0	72.5	87.0	79.2
Composition %									
4-*t*-Butyl	100.0	100.0	100.0	100.0	100.0	97.4	95.3	96.6	93.0
3-*t*-Butyl	0.0	0.0	0.0	0.0	0.0	2.6	4.1	3.2	6.3
1-*t*-Butyl	0.0	0.0	0.0	0.0	0.0	0.0	0.6	0.2	0.7
Cyclohexyl Acetates or Cyclohexyl Phenyl Ethers:									
Yield %	5.7	7.0	8.4	17.1	22.4	8.7	9.4	12.8	21.9
Composition %									
trans-4-*t*-Butyl	96.1	18.0	96.1	9.2	1.2	55.0	12.9	57.0	1.8
cis-4-*t*-Butyl	3.1	77.6	1.3	88.3	97.6	20.4	69.2	5.5	89.0
trans-3-*t*-Butyl	0.8	0.0	2.6	0.0	0.0	13.7	12.8	35.2	2.3
cis-3-*t*-Butyl	0.0	4.4	0.0	2.5	1.2	10.9	5.1	2.3	6.9
Cyclohexanols or Cyclohexylphenols:									
Yield %	2.4	2.0	3.1	3.9	4.4	1.6	4.4		
Composition %									
trans-4-*t*-Butyl	96.9	28.7	97.5	12.3	2.0				
cis-4-*t*-Butyl	3.1	65.3	1.0	84.8	96.4				
trans-3-*t*-Butyl	0.0	0.0	1.5	0.0	0.0				
cis-3-*t*-Butyl	0.0	6.0	0.0	2.9	1.6				

a) ROTs concn.: 0.0922—0.0925 M; Pyridine concn.: 0.0973 M.
b) Ref. 6; ROTs concn.: 0.0913—0.0987 M; Et_3N concn.: 0.106—0.123 M.
c) Ref. 2c; data at 100 °C; NaOAc concn.: 0.05 M.
d) k_1's for *cis*- and *trans*-4-RX are 8.92×10^{-5} and 2.23×10^{-5} (sec^{-1}), respectively.

Table 2. Composition of recovered tosylates in the partial solvolysis of *cis*- and *trans*-4-*t*-butylcyclohexyl tosylates at 75 °C

ROTs	Solvent	Completion %	Composition %			
			trans-4-RX	*cis*-4-RX	*trans*-3-RX	*cis*-3-RX
cis	*N*-Methylacetamide[a]	75.0[b]	0.3	97.6	0.0	2.1
cis	PhOH–PhH (1:1 by wt)[c]	75.5	1.1	88.3	0.0	10.6
cis	AcOH[d]	74.3	2.2	82.9	0.0	14.9
trans	*N*-Methylacetamide[a]	75.0[b]	94.1	5.9	0.0	0.0
trans	PhOH–PhH (1:1 by wt)[c]	73.6	96.7	0.7	2.6	0.0

a) H_2O content: 0.05 wt%. b) Calculated from reaction time. c) Ref. 1a. d) Ref. 1b.

would be a typical solvolytic solvent. It is anticipated that the negative end of the dipole could probably solvate the carbonium ion more strongly than that of the hydroxylic solvents.

In this paper we report on the results of examination of solvolytic *cis-trans* isomerization and 1,2-rearrangement of tosylates, as well as of the rates and products studies on the solvolysis of *cis*- and *trans*-4-RX in *N*-methylacetamide. The factors determining the steric course of solvolysis are discussed in connection with the nature of the amide as a solvolytic solvent.

Results and Discussion

The solvolysis of both *cis*-4-RX and *trans*-4-RX was carried out in *N*-methylacetamide containing a small amount of water (0.06—0.94 wt%) and pyridine (equimolar amount to the tosylate). The yields and compositions were determined by means of vpc. The compositions of recovered tosylates from partially-solvolyzed reaction mixtures were determined by the method previously reported.[1b] The data are summarized in Tables 1 and 2 together with data pertinent to other solvent systems.

Both tosylates displayed good first-order behavior and the reaction proceeded at a similar rate to that of ethanolysis.[2a] This is in line with the expectation based on the Y value of *N*-methylacetamide.[4,5] As observed in S_N1 solvolysis in other solvents,[2,6] *cis*-4-RX is solvolyzed more rapidly than *trans*-4-RX in

4) a) E. Grunwald and S. Winstein, *ibid.*, **70**, 846 (1948); b) A. H. Fainberg and S. Winstein, *ibid.*, **78**, 2770 (1956).
5) K. Okamoto, M. Dohi, and S. Saitô, unpublished results; the Y value for *N*-methylacetamide has been determined to be −2.234.
6) K. Okamoto, S. Saitô, and H. Shingu, This Bulletin, **42**, 3288 (1969).

the amide by a factor of 4.0 at 75 °C (2.5—3.1 for other solvents) (Table 1). The kinetic results imply that *N*-methylacetamide is a typical solvolytic solvent.

The major product of solvolysis in the amide for both tosylates has been proved to be an olefin, exclusively 4-*t*-butylcyclohexene. This is in sharp contrast to the case of other solvent systems in which small amounts of isomeric 3- and 1-*t*-butylcyclohexenes are accompanied with 4-*t*-butylcyclohexene.

The substitution products for both tosylates are composed of a major portion of 4- and 3-*t*-butylcyclohexyl acetates (ROAc) and a minor portion of 4- and 3-*t*-butylcycohexanols (ROH). The formation of ROAc could be elucidated by a mechanism similar to the nucleophilic intervention by acetone to furnish an oxonium ion in the solvolysis of 2-octyl brosylate in 80% methanolic acetone.[7] Thus, nucleophilic attack by the amide on $R^+\cdots X^-$ would be likely to produce an oxonium ion whose subsequent reaction with water furnishes ROAc as follows.

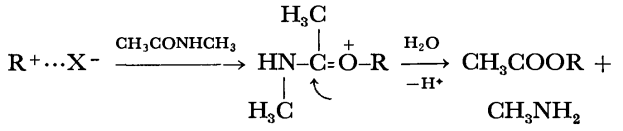

The yields of ROAc for solvolysis in the amide containing various amounts of water is a function of water concentration. This means that the second step in the above scheme is $B_{AC}2$ between the carbonyl-carbon in the pre-formed oxonium ion and water.

The composition percentage of the retained ROAc (18%) produced from the *trans*-4-RX (H_2O content: 0.06 wt%) significantly exceeds that of ROAc (3.1%) produced in the *cis*-4-RX solvolysis (H_2O content: 0.06 wt%), the formation of the rearranged ROAc being substantially less favored particularly in the case of *cis*-4-RX solvolysis. The results differ from those for the other solvent systems[2,6] (Table 1). It should be noted that the abnormal stereochemical results are incompatible with the expectation from the hypothetical hydrogen-bridged carbonium ion intermediate,[2] since such a carbonium ion should produce much of the retained or rearranged products *in the cis-4-RX solvolysis.*

The nature characteristic of this amide solvent became more evident when the composition of the recovered tosylates was examined (Table 2).

The extent of 1,2-rearrangement of the tosylate is greatly diminished, being comparable with the significant decrease in the rearranged products. Solvation of the cation by the amide in $R^+\cdots X^-$ may suppress the migration of β-hydrogen.

With regard to the superiority of *trans-cis* isomerization (5.9%) over *cis-trans* isomerization (0.3%), the following explanations are given. The amide might be operative as a nucleophile in the form of an extended polymer,[8] which would diminish the extent of attack by amide on *trans*-4-$R^+\cdots X^-$ from the back, since the approach of such a bulky nucleophile should enlarge the steric repulsion toward 1,3,5-triaxial hydrogens.[9] This would make it possible for the released tosylate anion (X^-) to compete affectively with polymerized amide to produce *cis*-4-RX from *trans*-4-RX by the S_N2-like attack on *trans*-4-$R^+\cdots X^-$ from the back (Scheme 1).

The decrease in the extent of retention for ROAc in the higher water contents, observed in the case of *trans*-4-RX solvolysis, might be explained as follows. The increase in water content lowers the degree of association of amide, increasing the extent of attack by the amide from the back on *trans*-4-$R^+\cdots X^-$, and decreasing the retained ROAc (Table 1).

The fact that the compositions of ROAc and ROH vary with the change in water content of the amide suggests the existence of an intermolecular complex between water and the amide, which competes with polymerized amide as a nucleophile to produce ROH.

Experimental

Materials. *N*-Methylacetamide was prepared according to Alelio and Ried,[10] and the water content was determined by means of Karl Fischer titration. *trans*-4-*t*-Butylcyclohexanol was prepared by the method of E. L. Eliel *et al.*,[11] other reagents being provided by the methods previously reported.[6]

Rate Measurements. Titrimetric rates were followed by placing the flask containing reaction mixture into an oil bath (75 °C±0.03) and removing 1 ml of an aliquot at various time intervals. The aliquots were transferred to a separatory funnel using 20 ml of ether and the ether solution was extracted three times with 10 ml of water. The aqueous solution was titrated with a standard aqueous sodium hydroxide using phenolphthalein as an indicator. It was not possible to obtain an experimental infinity titer, and therefore, tosylate concentrations at time t were calculated on the basis of the theoretical infinity titer. The rate constants were calculated graphically and are shown in Table 1, footnote (d).

Product Analysis and Unchanged Tosylate Analysis. The procedures were carried out as reported.[1b] except for the use of tlc for the separation of mixtures of products instead of column chromatography. The results are shown in Tables 1 and 2.

7) H. Weiner and R. A. Sneen, *J. Amer. Chem. Soc.*, **85**, 2181 (1963); **87**, 287 (1965).

8) It is considered that the much higher dielectric constant of *N*-methylacetamide is due to the formation of extended polymer by hydrogen bonding (Ref. 3).

9) The axial approach of the incoming amide should be hindered to a greater extent than the equatorial approach. For instance, S_N2 rate ratio ($k_{cis}/k_{trans}=31$ for the reaction of 4-*t*-butylcyclohexyl system with sodium thiophenoxide in 87% ethanol) is much greater than the value *ca.* 3 as expected from the ground-state energy differences alone (E. L. Eliel and R. S. Ro, *J. Amer. Chem. Soc.*, **79**, 5995 (1957)). Thus, the equatorial derivative undergoes S_N2 displacement more slowly, owing to its larger steric hindrance to the approach of the nucleophile in addition to its lower ground-state energy than the axial isomer. See also E. L. Eliel, N. L. Allinger, S. Angyal, and G. A. Morrison, "Conformational Analysis," Interscience, New York, N. Y. (1965), pp. 86—88.

10) G. F. D. Alelio and E. E. Ried, *J. Amer. Chem. Soc.*, **59**, 109 (1937).

11) E. L. Eliel, R. J. L. Martin, and D. Nasipuri, "Organic Syntheses," Vol. 47, p. 16 (1967).

Synthesis and Reactions of α-Bromoaroylacetarylamides

Ahmad S. SHAWALI,* Mohammed I. ALI, and Abdelgawad A. FAHMI
Department of Chemistry, Faculty of Science, University of Cairo, Giza, Egypt
(Received April 20, 1972)

Benzoylacetanilide and fourteen of its substituted derivatives were brominated to give α-bromobenzoylacetanilides (I). The spectral data of I indicate that they exist mainly in the keto form. Reaction of I with phenylhydrazine yielded 4-phenylazo-1,3-diaryl-2-pyrazolin-5-ones (IV). Treatment of I with thiourea and thioacetamide gave 2-amino-4-arylthiazole-5-carboxanilides (XII) and 2-methyl-4-arylthiazole-5-carboxanilides (XIII), respectively. With excess of concentrated sulfuric acid or polyphosphoric acid, α-bromobenzoylacetanilides (I) were converted into 3-bromo-4-aryl-2-quinolones (XVI). Structural assignments were based on the elemental and spectral analyses.

Aroylacetarylamides are readily available,[1] but there have been no reports on the preparation and reactions of α-bromoaroylacetarylamides (I) and their α-iodo analogs (II). Very little is known about α-chloro derivatives (III).[2] Thus, from an interest in the chemistry of aroylacetarylamides,[1,3] we have studied the preparation of two series of the α-halo derivatives (I—II) and some of their reactions.

$$RC_6H_4COCH(X)CONHC_6H_4R'$$

I, X=Br
II, X=I
III, X=Cl

a, R=R'=H	i, R=H; R'=3-NO_2
b, R=H; R'=3-CH_3	j, R=H; R'=4-NO_2
c, R=H; R'=4-CH_3	k, R=H, R'=4-$COOC_2H_5$
d, R=H; R'=4-CH_3O	l, R=Br; R'=H
e, R=H; R'=3-Cl	m, R=4-NO_2; R'=H
f, R=H; R'=4-Cl	n, R=4-CH_3O; R'=H
g, R=H; R'=3-Br	o, R=4-Cl; R'=H
h, R=H; R'=4-Br	

When benzoylacetanilide in acetic acid solution was treated with an equimolar amount of bromine in the same solvent, α-bromo derivative (Ia) was obtained in 80% yield. The other α-bromobenzoylacetanilides (Ib—o) were prepared from the corresponding benzoylacetanilides in a similar manner.

The structure assignment of I was based on elemental and spectral analyses. Thus, the NMR spectrum of Ia ($CDCl_3$) showed a multiplet absorption due to ten protons at δ 8.25—7.65 ppm and two one proton singlets at δ 4.90 (–COCHBr–) and 9.43 (–CONH–) ppm. Its IR spectrum (KBr) showed a benzoyl CO band at 1715 cm^{-1} and an anilide CO band at 1665 cm^{-1}. The high frequency position for the benzoyl carbonyl, which ordinarily falls near 1705 cm^{-1}, might be expected in view of the presence of bromine substituent on the α-carbon atom. The identity of the bromination products was also confirmed by treatment of I with acidified potassium iodide[4] to give the parent benzoylacetanilides.

It has been reported[1] that the electronic absorption pattern of benzoylacetanilides in ethanol was in each case characterised by the presence of two maxima in the 305—350 and 240—280 nm regions. These were assigned to the cinnamoyl and benzoyl chromophores of the enol and keto froms, respectively. In the UV spectra of the α-bromoanilides (Ia—o), the cinnamoyl band was absent; each exhibited only one band in the 240—270 nm region. This suggests that the α-bromobenzoylacetanilides (Ia—o), unlike their parent compounds, exist mainly in the keto form in ethanol. This might be ascribed to the instability of the enol form of I which probably results from the large steric interaction between the voluminous bromine atom and the benzene nuclei.[5]

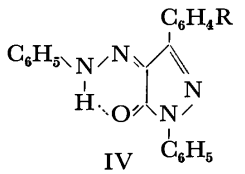

IV

a, R=H; b, R=4-Cl; c, R=4-Br; d, R=4-CH_3O

When Ia was heated with phenylhydrazine in acetic acid for 3 hr, it gave 1,3-diphenyl-4-phenylazo-2-pyrazolin-5-one (IVa). The structure of IVa was established by comparing it with an authentic sample prepared by coupling 1,3-diphenyl-2-pyrazolin-5-one with benzenediazonium chloride.[6] They were found to be identical. In order to explain this, we propose the two mechanisms represented in scheme 1 for the reaction of I with phenylhydrazine. The conversion of V into VI (or X into VIII) is similar to that for the preparation of 2-pyrazolin-5-one derivatives by the reaction of β-keto esters with phenylhydrazine.[7] This was also supported by our finding that the α-bromoanilides, If and Ij yielded IVa only when they were similarly treated with phenylhydrazine. The oxidation of the proposed hydrazine intermediates VII or IX into VIII or X, respectively, is probably effected by

* To whom all inquiries should be addressed.

1) A. S. Shawali, M. M. Naoum, and S. Ibrahim, This Bulletin, **45**, 2504 (1972).

2) A. J. Hodgkinson and B. Staskun, *J. Org. Chem.*, **34**, 1709 (1969); T. Van Es and B. Staskun, *Tetrahedron*, **25**, 5941 (1969).

3) A. S. Shawali, A. Dewidar, and M. M. Naoum, *Indian J. Chem.*, **10**, 464 (1972).

4) H. G. Garg and M. M. Bokadia, *J. Indian Chem. Soc.*, **34**, 286 (1957) and the references cited therein.

5) M. I. Kabachnik, S. T. Ioffe, E. M. Papov, and K. Vatsuro, *Tetrahedron*, **12**, 76 (1961).

6) (a) O. Dimroth and R. Schweizer, *Ber.*, **56**, 1375 (1923); (b) A. Wahl and J. Rolland, *Ann. Chim.* (Paris), **10**, 5 (1928); (c) A. Wahl and C. Silverzweig, *Bull. Soc. Chim. Fr.*, **11**, 61 (1912).

7) R. H. Wiley and P. Wiley, "Pyrazolones, Pyrazolidionones and Derivatives," Interscience Publishers, John Wiley & Sons, Inc., New York (1964).

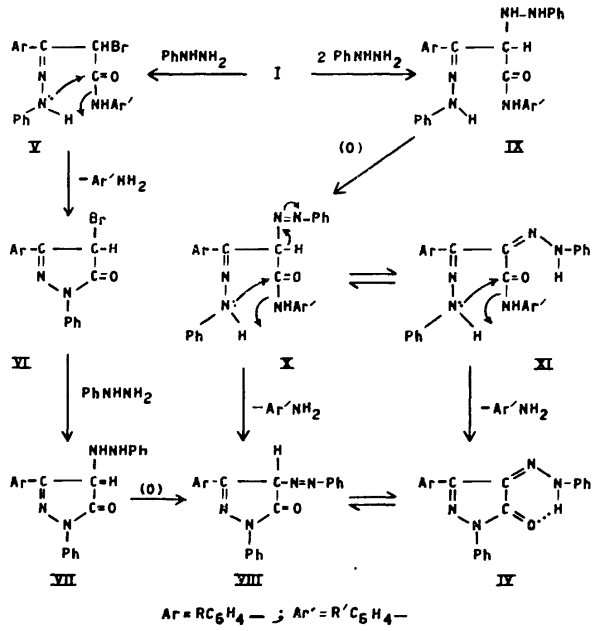

Scheme 1.

atmospheric oxygen during the course of refluxing the reaction mixture. In many cases, atmospheric oxygen suffices for such oxidation of hydrazines.[8]

Treatment of the other α-bromobenzoylacetanilides (Il, In, and Io) with phenylhydrazine in the manner described above afforded the corresponding 4-arylazo-2-pyrazolin-5-ones (IVb, IVc, and IVd), respectively. The structures of the unreported compounds in series IV were derived from their analytical and spectral data. The NMR spectrum of IVc in $CDCl_3$, as an example, exhibited a multiplet at δ 7.33 ppm due to aromatic protons and a singlet due to a highly deshielded proton at δ 13.89 ppm. The low field signal was assigned to hydrogen bonded NH group.[9] Such data indicate that the products IVa—d thus prepared exist in the assigned hydrazone structure IV. The IR spectra of IV are also compatible with this structure. Thus, each of the compounds (IVa—d) exhibited three characteristic bands at 1680 (lactam CO), 1610 (C=N), and 3280 (weak, hydrogen bonded NH) cm^{-1}.

α-Bromobenzoylacetanilides (I), when heated with thiourea, readily gave 2-amino-4-phenylthiazole-5-carboxanilides (XII). α-Bromoanilides (I) also, reacted with thioacetamide to give 2-methyl-4-phenylthiazole-5-carboxanilides (XIII). Both compounds XII and XIII have not yet been reported. Their structures were established by elemental analysis and a study of their spectral data. The UV absorption pattern of XII was in each case characterised by the presence of two maxima: one in the 320—327 (log ε 4.15$\pm$0.02) nm region and the other located between 240 and 245 nm (log ε 4.33$\pm$0.03). The 2-methyl analogs (XIII) absorb fairly intensively in the regions 306—315 (log ε 4.08$\pm$0.1) and 240—280 (log ε 4.29$\pm$0.6)

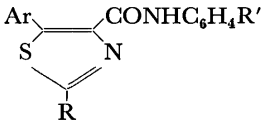

XII, R=NH_2; XIII, R=CH_3

a, Ar=C_6H_5; R′=H
b, Ar=C_6H_5; R′=3-Cl
c, Ar=C_6H_5; R′=3-NO_2
d, Ar=C_6H_5; R′=4-Br
e, Ar=4-ClC_6H_4; R′=H
f, Ar=C_6H_5; R′=4-Cl
g, Ar=4-$CH_3OC_6H_4$; R′=H

nm. All compounds (XII—XIII) showed amide-I band near 1660 cm^{-1} and an absorption band due to the C=N double bond stretching near 1620 cm^{-1} in their IR spectra. Compounds of series XII exhibited also absorption bands in the 3400—3285 cm^{-1} region due to the NH_2 stretching.

Benzoylacetanilide undergoes cyclization when heated with concentrated sulfuric acid or polyphosphoric acid (PPA) to give XIV or XV depending on the anilide to acid ratio.[10] Utilization of a higher proportion of acid in the reaction favours the formation of XIV. Cyclization of α-bromobenzoylacetanilides (Ia—o) is now being considered. With an anilide–acid (H_2SO_4 or PPA) ratio of 1: 10, the anilides I were converted into the corresponding 3-bromo-4-aryl-2-quinolones (XVI) in 60—80% yields. Attempts to cyclize α-bromoanilides If and Ij were, however, unsuccessful. This indicates that the ease of cyclization of substituted benzoylacetanilides is influenced by both the position and nature of the substituent present. In line with this finding is the observation that the nitro- and chloro-acetoacetanilides are appreciably decomposed to arylamines even with excess acid reagent.[10]

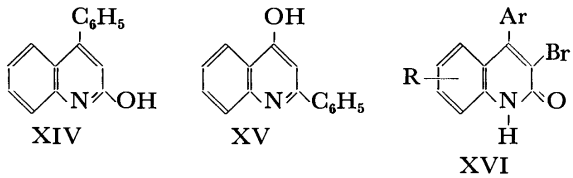

XIV XV XVI

a, R=H; Ar=C_6H_5
b, R=6-CH_3; Ar=C_6H_5
c, R=H; Ar=4-BrC_6H_4
d, R=H; Ar=4-$NO_2C_6H_4$

Staskun[10] has assigned the 2-hydroxy structure XIV for the cyclized product of benzoylacetanilide. However, the spectral data of the compounds XVIa—d prepared revealed that they have the 2-oxo form (XVI). Thus, all compounds exhibited an NH stretching bands at 3312 and 3156 cm^{-1} and a strong CO band at 1650 cm^{-1}. The products XVIa—d gave no colour with alcoholic ferric chloride. The UV absorption maxima of XVIa, as a typical example of the series, in a series of different buffer solutions were not affected by a change in pH, a fact which seems to be compatible with the proposed 2-oxo form (XVI).

Experimental

Melting points are uncorrected. IR spectra were obtained for new compounds and were recorded on a Unicam SP 200G infrared spectrophotometer (1 mg/300 mg KBr). UV

8) H. Zollinger, "Azo and Diazo Chemistry, Aliphatic and Aromatic Compounds," Intersciences Publishers, Inc., New York (1961), p. 196.

9) A. Snavely and C. H. Yoder, *J. Org. Chem.*, **33**, 513 (1968).

10) B. Staskun, *ibid.*, **29**, 1153 (1964) and the references cited therein.

spectra were determined from a Beckman DK spectrophotometer. NMR spectra were recorded on a Varian A-60 spectrometer with TMS as internal reference. Benzoylacetanilides were prepared from the appropriate arylamine and ethyl benzoylacetate.[11] Aroylacetanilides were reported by Shawali *et al.*[1]

Preparation of α-Bromoaroylacetarylamides (Ia—o). General Procedure: A solution of bromine (4.8 g, 0.03 mol) in glacial acetic acid (30 ml) was added dropwise over a period of 1 hr to the appropriate aroylacetarylamide (0.03 mol) dissolved in the same solvent (60 ml) with stirring at room temperature. After 2 hr, the mixture was poured into water and the precipitated solid was filtered. In some cases the resulting solid precipitated before dilution. The crude product was washed with water and recrystallized from dilute ethanol. The results are given in Table 1.

Table 1. α-Bromoaroylacetarylamides

Compound No	Mp, °C	Yield %	Formula	Bromine % Calcd	Bromine % Found
Ia[a]	133—134	80	$C_{15}H_{12}BrNO_2$	25.15	24.98
Ib	116—118	75	$C_{16}H_{14}BrNO_2$	24.10	24.00
Ic	141—142	77	$C_{16}H_{14}BrNO_2$	24.10	23.97
Id	144—145	70	$C_{16}H_{14}BrNO_2$	22.98	23.00
Ie	107—108	70	$C_{15}H_{11}ClBrNO_2$	22.69	22.17
If	125—126	75	$C_{15}H_{11}BrClNO_2$	22.69	22.12
Ig	129—130	75	$C_{15}H_{11}Br_2NO_2$	40.28	39.98
Ih	136—137	76	$C_{15}H_{11}Br_2NO_2$	40.28	40.00
Ii	140—142	70	$C_{15}H_{11}BrN_2O_4$	22.03	21.78
Ij	146—147	65	$C_{15}H_{11}BrN_2O_4$	22.03	21.90
Ik	130—131	60	$C_{18}H_{16}BrNO_4$	20.51	20.29
Il	181—182	70	$C_{15}H_{11}Br_2NO_2$	40.28	40.10
Im	145—147	70	$C_{15}H_{11}BrN_2O_4$	22.30	21.85
In	135—136	75	$C_{16}H_{14}BrNO_3$	22.98	23.10
Io	180—182	70	$C_{15}H_{11}BrClNO_2$	22.69	22.18

a) Calcd: C, 56.60; H, 3.77; N, 4.40%. Found: C, 56.45; H, 3.80; N, 4.38%.

Preparation of 1-Phenyl-3-aryl-4-phenylazo-2-pyrazolin-5-ones, (IVa—d). A mixture of α-bromobenzoylacetanilide (Ia) (1.6 g, 0.005 mol) and phenylhydrazine (2 ml) in acetic acid (10 ml) was refluxed for 3 hr and cooled. The precipitated product was collected and recrystallized from acetic acid. The product obtained was identified as 4-phenylazo-1,3-diphenyl-2-pyrazolin-5-one (IVa), mp 172—173 °C. Mixed mp with an authentic sample (prepared by coupling of benzenediazonium chloride with 1,3-diphenyl-2-pyrazolin-5-one as described before[6]) showed no depression. When each of the α-bromoanilides Il, In, and Io was treated with phenylhydrazine following the same procedure as for Ia, compound IVa was the only product obtained.

The other α-bromoaroylacetanilides If, Ih, and Id reacted with phenylhydrazine and yielded the following derivatives of 5-pyrazolones: IVb, mp 205 °C (55%) (lit,[6b] 203—205 °C); IVd; mp 177 °C (70%) (lit,[6c] mp 176—177 °C) and IVc, mp 201°C (65%). Found: C, 60.19; H, 3.61; Br, 18.98; N, 13.25%. Calcd for $C_{21}H_{15}BrN_4O$: C, 60.13; H, 3.57; Br, 19.09; N, 13.36%.

2-Amino-4-arylthiazole-5-carboxanilides (XII). A mixture of α-bromoaroylacetanilide (0.01 mol) and thiourea (0.8 g, 0.013 mol) in ethanol (30 ml) was refluxed for 3 hr. The reaction mixture was poured into water and made alkaline with ammonium hydroxide. The resulting solid was filtered, washed with water and finally recrystallized from ethanol. The prepared compounds and their physical constants are given in Table 2.

Table 2. 2-Substituted 4-arylthiazole-5-carboxanilides

Compound No	Mp, °C	Yield %	Formula	Sulfur % Calcd	Sulfur % Found
XIIa[a]	198—199	80	$C_{16}H_{13}N_3OS$	10.85	10.68
XIIb	193—194	85	$C_{16}H_{12}ClN_3OS$	9.72	9.38
XIIc	225—226	70	$C_{16}H_{12}N_4O_3S$	9.41	9.50
XIId	262—264	77	$C_{16}H_{12}BrN_3OS$	8.55	8.44
XIIe	243—245	80	$C_{16}H_{12}ClN_3OS$	9.72	9.54
XIIIa[b]	119—120	50	$C_{17}H_{14}N_2OS$	10.88	10.75
XIIIb	142—143	55	$C_{17}H_{13}ClN_2OS$	9.75	9.70
XIIIc	139—140	70	$C_{17}H_{13}N_3O_3S$	9.44	9.22
XIIIf	151—152	68	$C_{17}H_{13}ClN_2OS$	9.75	9.69
XIIIg	122—123	64	$C_{18}H_{16}N_2O_2S$	9.88	9.74

a) Found: C, 65.46; H, 4.24; N, 14.02%. Calcd: C, 65.07; H, 4.40; N, 14.23%.
b) Found: C, 69.13; H, 4.70; N, 9.50%. Calcd: C, 69.38; H, 4.76; N, 9.51%.

2-Methyl-4-arylthiazole-5-carboxanilides (XIII). A mixture of α-bromoaroylacetanilide (0.01 mol) and thioacetamide (0.8 g, 0.01 mol) in ethanol (30 ml) was refluxed for 3 hr and then poured into water. The resulting solid was collected, washed with water and recrystallized from ethanol. Characteristics of the compounds prepared are given in Table 2.

Table 3. 3-Bromo-4-aryl-2-quinolones

Compound No	Mp, °C	Yield %	Formula	Bromine % Calcd	Bromine % Found
XVIa[a]	228—230	65	$C_{15}H_{10}BrNO$	26.66	26.42
XVIb	288—290	85	$C_{16}H_{12}BrNO$	25.47	25.23
XVIIIc	310—312	60	$C_{15}H_9Br_2NO$	42.20	42.09
XVId	above 320	65	$C_{15}H_9BrN_2O_3$	23.18	23.00

a) Found: C, 59.89; H, 3.40; N, 4.58%. Calcd: C, 60.01; H, 3.33; N, 4.67%.

Conversion of I to 3-Bromo-2-quinolones (XVI). α-Bromoaroylacetanilide (0.005 mol) was added portionwise over a period of 20—30 min to warm concentrated sulfuric acid (10 g, *d*, 1.84, 98%) at 75—80°C, with manual stirring. Heating was continued for another 30 min at 95°C with stirring; the reaction mixture was then cooled and triturated with water. The resulting solid was collected by filtration and washed with 20 ml of aqueous sodium hydroxide (0.5M). Purification of the alkali insoluble product was effected by recrystallisation from ethanol. The mp and elemental analyses of the 3-bromo-2-quinolones prepared are given in Table 3. The same products XVIa—d were obtained when polyphosphoric acid was used in place of sulfuric acid. Anilides If and Ij could not be cyclized and were recovered unchanged when heated with concentrated sulfuric acid. When α-bromobenzoylacet-*p*-anisidide (Id) was similarly treated with the acid reagent, it gave a water solution product which could not be isolated.

11) G. H. Brown, J. F. Gueras, R. J. Gledhill, C. J. Kibler, F. C. McCrossen, S. M. Parmerter, P. W. Vittum, and A. Weissberger, *J. Amer. Chem. Soc.*, **79**, 2919 (1957).

A New Route for the Preparation of Pyrazolo[4,3-*c*]pyridines

Abdou Ahmed EL-SAYED and Masaki OHTA

Department of Chemistry, Faculty of Science, Tokyo Institute of Technology, Ookayama, Meguro-ku, Tokyo

(Received November 16, 1972)

The anhydride (II) of 4-carboxy-1,5-diphenylpyrazole-3-acetic acid (I) has been prepared. The reactions of II with primary amines resulted in the formation of the monoamides IIIa—c. 2,3-Diphenylpyrazolo[4,3-*c*]-pyridine-(5*H*,7*H*)-4,6-dione (VIIa), has been obtained by heating the ammonium salt of I in a vacuum at 220 °C. The ring closure of IIIc with acetyl chloride in benzene afforded VIIb. Compound VIIb was coupled with benzenediazonium chloride to give the 7-phenylazo derivative (XII) and also condensed with aromatic aldehydes giving 7-arylidene derivatives (XV).

We recently, prepared 4-carboxy-1,5-diphenylpyrazole-3-acetic acid (I) through the condensation of 1-benzoyl-1-phenylhydrazine with diethyl acetonedicarboxylate.[1] We wish to report on some reactions of this acid.

We have found that the acid anhydride (II) was directly obtained by dehydration of the dibasic acid (I) with acetyl chloride in anhydrous dioxane.

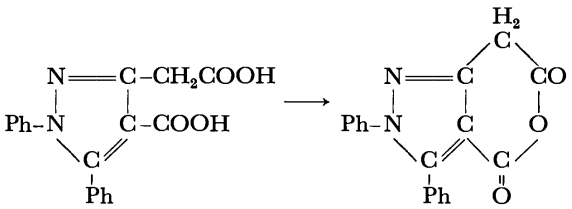

I II

The reaction of II with primary amines in anhydrous dioxane resulted in the ring opening of the anhydride at position (a) with the formation of the corresponding amides IIIa—c, rather than at position (b) to give IV.

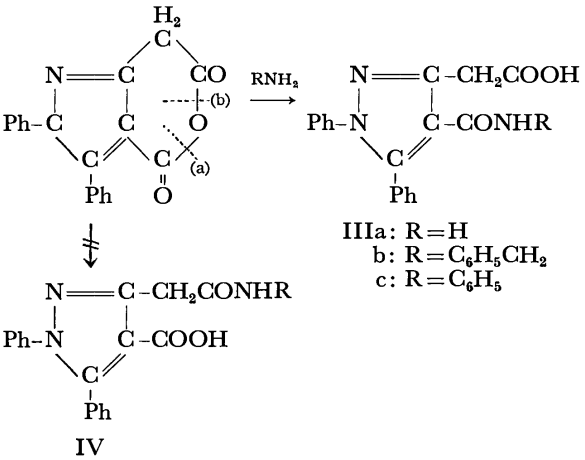

IIIa: R=H
b: R=$C_6H_5CH_2$
c: R=C_6H_5

IV

The structural elucidation of compounds III and confirmation of the ring opening of the anhydride (II) at position (a) were carrid out as follows:

Decarboxylation of the monoanilide (IIIc) at 250 °C yielded 1,5-diphenylpyrazole-4-carboxanilide (V) prepared from 4-carboxy-1,5-diphenyl-3-methylpyrazole *via* the acid chloride.[2]

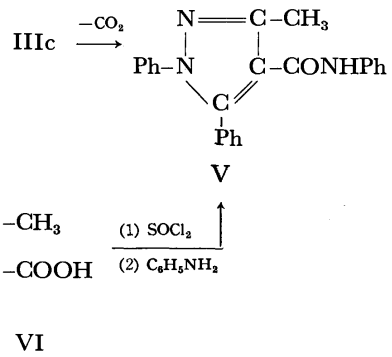

V VI

Heating of the ammonium salt of I at 220 °C in a vacuum gave 2,3-diphenylpyrazolo[4,3-*c*]pyridine-(5*H*, 7*H*)-4,6-dione (VIIa). The 5-phenyl analogue (VIIb) was obtained by the action of acetyl chloride on the monoanilide (IIIc).

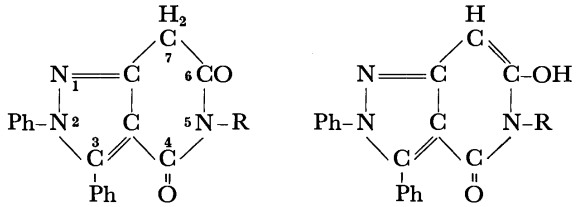

VIIa: R=H
b: R=C_6H_5

VIII

Compounds VII can also exist in the tautomeric structure VIII. However, the IR spectrum of the product shows two bands at 1720 and 1680 cm^{-1} assignable to two carbonyl groups but no absorption in the OH region. This is in favor of the keto structure VII.

A similar compound (IX) which has the same ring structure as VII was prepared by acidic hydrolysis of compound X.[3-5]

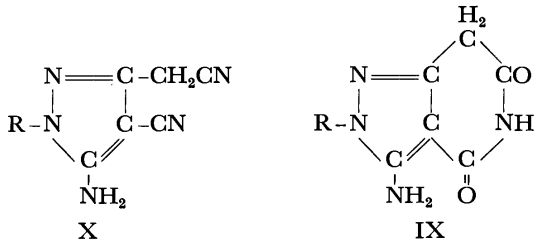

X IX

1) A. A. El-Sayed and M. Ohta, This Bulletin, **46**, 947 (1973).
2) K. V. Auwers and H. Holleman, *Ber.*, **18**, 313 (1885).
3) T. Sato, *J. Org. Chem.*, **24**, 963 (1959).
4) E. C. Taylor and K. S. Hartke, *J. Amer. Chem. Soc.*, **81**, 2452 (1959).
5) E. C. Taylor and K. S. Hartke, *ibid.*, **81**, 2456 (1959).

The reactivity of the methylene group at position 7 in pyrazolo[4,3-*c*]pyridine derivatives (VII) proved to be similar to that of the 4-methylene group in homophthalimides (XI).[6,7]

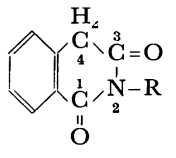

XI

Thus, compound VII was coupled with benzenediazonium chloride to give the 7-phenylazo derivative (XII) which can also be formulated as either hydrazone (XIII) or azo-enol (XIV).[8]

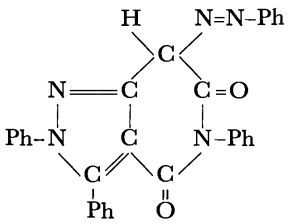

XII

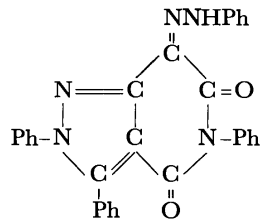

XIII

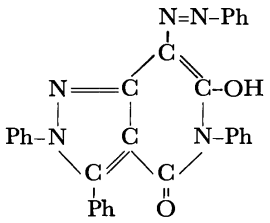

XIX

However, the IR spectrum of the product shows two absorption bands in the carbonyl region (1710, 1680 cm^{-1}), but not in either the OH or NH regions. This indicates that it exists mainly in keto-azo form XII.

Compound VIIb was also condensed with aromatic aldehyde in acetic acid to furnish the 7-arylmethylene derivatives XV in the presence of sodium acetate.

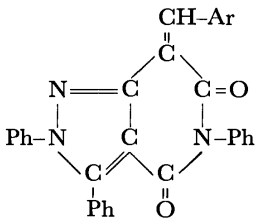

XVa: Ar = C_6H_5
b: Ar = $C_6H_4Cl(p)$

Experimental

4-Carboxy-1,5-diphenylpyrazole-3-acetic Acid Anhydride (II). To a solution of 2 g of 4-carboxy-1,5-diphenylpyrazole-3-acetic acid (I) in 50 ml of anhydrous dioxane was added 10 ml of acetyl chloride and the mixture was boiled on a water bath for 30 min. The solution was concentrated and cooled and the solid that separated (1.9 g) was crystallized from benzene to give II as colorless prismatic crystals, mp 158 °C. Found: C, 71.32; H, 3.79; N, 9.41%. Calcd for $C_{18}H_{12}O_3N_2$: C, 71.04; H, 3.98; N, 9.21%. IR: 1795, 1760 cm^{-1}.

3-Carboxymethyl-1,5-diphenylpyrazole-4-carboxamide (IIIa). Dry ammonia gas was bubbled slowly through a solution of 1.0 g of the anhydride (II) in 30 ml of anhydrous dioxane solution. The ammonium salt of the product IIIa was separated within a few minutes. Water was added after the dioxane solution has been saturated with ammonia and the clear light yellow solution was acidified with 10% hydrochloric acid solution. The resulting precipitate was filtered off to yield 0.8 g of IIIa, which was recrystallized from dilute acetic acid as colorless crystals, mp 228—230 °C. Found: C, 67.15; H, 4.50; N, 12.59%. Calcd for $C_{18}H_{15}O_3N_3$: C, 67.27; H, 4.71; N, 13.08%. IR: 3430, 3330, 1685, 1635 cm^{-1}.

3-Carboxymethyl-1,5-diphenylpyrazole-4-carboxamides (IIIb, c). A solution of II (3 g; 1 mol) in anhydrous dioxane (50 ml) was treated with appropriate amines (2.2 mol) and the mixture was refluxed for 15 min and then cooled. The reaction mixture was diluted with water (20 ml) and acidified with 10% hydrochloric acid solution. The solid that separated was collected and crystallized from the proper solvent to give IIIb, c.

3-Carboxymethyl-1,5-diphenylpyrazole-4-carboxybenzylamide (IIIb). Colorless crystals from ethanol, mp 185 °C (85%). Found: C, 72.74; H, 5.70; N, 10.10%. Calcd for $C_{25}H_{21}O_3N_3$: C, 72.98; H, 5.14; N, 10.21%. IR: 3280, 1720, 1620 cm^{-1}.

3-Carboxymethyl-1,5-diphenylpyrazole-4-carboxyanilide (IIIc). Colorless crystals from ethanol, mp 232—234 °C. Found: C, 72.22; H, 4.62; N, 10.64%. Calcd for $C_{24}H_{19}O_3N_3$: C, 72.53; H, 4.82; N, 10.57%. IR: 3400, 1698, 1665 cm^{-1}.

1,5-Diphenyl-3-methylpyrazole-4-carboxanilide (V). (Method A): Half a gram of IIIc was heated in a metal bath at 250 °C until the evolution of carbon dioxide stopped. The residue was triturated with ethanol and then crystallized from ethanol as colorless crystals, mp 178—180 °C.

(Method B): A suspension of 1.0 g of 4-carboxy-1,5-diphenyl-3-methylpyrazole (VI) in 20 ml of anhydrous benzene was treated with 3 ml of thionyl chloride and the mixture was refluxed until hydrogen chloride evolution stopped. The reaction mixture was distilled to dryness and the residue was dissolved in 50 ml of anhydrous benzene and treated with 0.7 g of aniline (2 mol). The reaction was refluxed for 2 hr, cooled and filtered to remove aniline hydrochloride. The filtrate was concentrated and cooled, and the precipitate formed was collected and recrystallized from ethanol, mp 180—181 °C. The products obtained by methods A and B were identical, as judged by mixed melting point determination and by comparison of infrared spectra. Found: C, 77.88; H, 5.38; N, 11.88%. Calcd for $C_{23}H_{19}ON_3$: C, 78.16; H, 5.42; N, 11.89%. IR: 3389, 1665 cm^{-1}.

2,3-Diphenylpyrazole[4,3-c]pyridine-(5H,7H)-4,6-dione (VIIa). Three grams of acid I was treated with 10 ml of concentrated ammonium hydroxide solution and the resulting solution was heated on a boiling water bath to dryness and then heated in a metal bath at 220 °C under reduced pressure. The residue obtained was triturated with ethanol to give a yellow solid (1.8 g) of VIIa, which was recrystallized from ethanol as yellow crystals, mp 251—252 °C. Found: C, 71.08; H, 4.40; N, 13.80%. Calcd for $C_{18}H_{13}O_2N_3$: C, 71.27; H, 4.32; N, 13.86%. IR: 3180, 3055, 1715, 1685 cm^{-1}.

2,3,5-Triphenylpyrazolo[4,3-c]pyridine-(5H,7H)-4,6-dione (VIIb). A suspension of 2 g of IIIc in 50 ml of anhydrous benzene was treated with 10 ml of acetyl chloride and the mixture was boiled on a water bath for 2 hr. The

6) A. Meyer and R. Vittenet, *Ann. Chim.*, (**10**) **17**, 272 (1932)
7) A. Meyer, *Bull. Soc. Chim. Fr.*, (**4**) **51**, 953 (1932)
8) R. C. Elderfield, "Heterocyclic Compounds," Vol. 4, John Wiley & Sons, Inc., New York, (1952), p.439.

solution obtained was concentrated to dryness and the residue was triturated with ethanol to give a pale yellow solid (1.3 g) which was crystallized from acetic acid as pale yellow crystals, mp 217—219 °C. Found: C, 75.56; H, 4.37; N, 11.22%. Calcd for $C_{24}H_{17}O_2N_3$: C, 75.97; H, 4.52; N, 11.08%. IR: 1720, 1680 cm^{-1}.

2,3,5-Triphenyl-7-phenylazopyrazolo[4,3-c]pyridine-(5H,7H)-4,6-dione (XII). A solution of 0.5 g of VIIb in 50 ml of pyridine was cooled in ice and treated with a solution of an equimolar amount of benzenediazonium chloride (prepared from 0.15 g of aniline in 2 ml of concentrated hydrochloric acid, 2 ml of water and 0.1 g of sodium nitrite), left to stand in ice for 1 hr and then diluted with water (100 ml). The product that separated was filtered off,washed thoroughly with water and crystallized from dioxane as orange voluminous crystals, mp 262—266 °C. Found: C, 74.22; H, 4.44; N, 14.27%. Calcd for $C_{30}H_{21}O_2N_5$: C, 74.52; H, 4.38; N, 14.49.% IR: 1710, 1680 cm^{-1}.

Condensation of Compound VIIb with Aromatic Aldehyde. A solution of VII (1 g) and anhydrous sodium acetate (2g) in glacial acetic acid (100 ml) was treated with an equimolar amount of appropriate aldehydes, and the mixture was refluxed for 1 hr. It was then cooled and the crystalline precipitate was filtered off. The arylidene derivatives XVa, b were yellow and gave red coloration with concentrated sulfuric acid.

7-Benzal-2,3,5-triphenylpyrazolo[4,3-c]pyridine-(5H,7H)-4,6-dione (XVa). This was recrystallized from acetic acid, mp 256—257 °C. Yield 90%. Found: C, 79.34; H, 4.46; N, 9.10%. Calcd for $C_{31}H_{21}O_2N_3$: C, 79.64; H, 4.53; N, 8.99%. IR: 1715, 1680 cm^{-1}.

7-p-Chlorobenzal-2,3,5-triphenylpyrazolo[4,3-c]pyridine-(5H,7H)-4,6-dione (XVb). This was recrystallized from acetic acid, mp 250—252 °C, yield 82%. Found: C, 73.88; H, 4.08; N, 8.29%. Calcd for $C_{31}H_{20}O_2N_3Cl$: C, 74.12; H, 3.95; N, 8.37%.

BULLETIN OF THE CHEMICAL SOCIETY OF JAPAN, VOL. 46, 1803—1806 (1973)

Spectroscopic Investigations of α-Keto Phosphorus Compounds

Takayoshi OSAKI, Junzo OTERA, and Yoshikane KAWASAKI
Department of Applied Chemistry, Osaka University, Yamadakami, Suita, Osaka 565

(Received November 18, 1972)

The NMR, IR, and UV spectra of some α-keto phosphorus compounds, $(C_2H_5)_2PCOR$, $(C_2H_5)_2P(S)COR$, and $[(C_2H_5)_2CH_3PCOR]^+I^-$ ($R=C_6H_5$ and CH_3), were measured. The carbonyl stretching frequency and the n-π^* transition show considerable red shifts, but the shifts are smaller than those of α-keto organosilicon compounds. The lowering of the carbonyl π^* level, which resulted from the interaction with a vacant d orbital of the phosphorus atom, was found to be largely responsible for the red shift of the n-π^* transition in the α-keto phosphorus compounds, particularly in $[(C_2H_5)_2CH_3PCOR]^+I^-$. The rise in the n level of the carbonyl group was found to be rather small.

Two of the characteristic properties of the α-keto derivatives of organometalloids are a large red shift of the n-π^* transition and a low carbonyl stretching frequency relative to those of the carbon analogs.[1,2] To explain these unusual red shifts of the n-π^* transition, several suggestions, especially for silicon compounds, have been put forward:

a) A large π^*-d splitting and a slight rise in the n level of the carbonyl oxygen caused by an inductive effect of the triorganosilyl group have been suggested on the basis of molecular orbital considerations.[3,4]

b) The simultaneous operation of the σ-donor and π-acceptor effects of the triorganosilyl group has been proposed.[5] Bock *et al.*[6] deduced, from a variety of experimental measurements, that the unusual red shift is due to the strong inductive rise in the n level as well as to considerable excited-state interactions, Si←π^*.

c) The inductive rise in the n level is considered to be the primary cause of the long-wavelength shift of the n-π^* transition.[7–10] Agolini *et al.*[11] have drawn the conclusion, from simple and extended Hückel molecular orbital calculations with and without d orbitals, that it is the σ-donor properties of silicon which are primarily responsible for the observed spectral shift, and that any possible p_π-d_π interactions are of minor importance.

These studies, however, were mainly made on α-keto derivatives of Group IVb organometalloids, which are very limited in organophosphorus derivatives.[12–15] In

1) A. G. Brook, *Advan. Organometal. Chem.*, **7**, 95 (1968).
2) B.G. Ramsey, "Electronic Transitions in Organometalloids," Academic Press, New York (1969), p. 95.
3) D. F. Harnish and R. West, *Inorg. Chem.*, **2**, 1082 (1963).
4) R. West, *J. Organometal. Chem.*, **3**, 314 (1965).
5) L. E. Orgel, "Volatile Silicon Compounds," *ed by* E. A. V. Ebsworth, Pergamon Press, New York (1963), p. 81.
6) H. Bock, H. Alt, and H. Seidl, *J. Amer. Chem. Soc.*, **91**, 355 (1969).
7) K. Yates and F. Agolini, *Can. J. Chem.*, **44**, 2229 (1966).
8) G. J. D. Peddle, *J. Organometal. Chem.*, **14**, 139 (1968).
9) A. G. Brook, D. G. Anderson, J. M. Duff, P. F. Jones, and D. M. MacRae, *J. Amer. Chem. Soc.*, **90**, 1076 (1968).
10) P. R. Jones and R. West, *ibid.*, **90**, 6978 (1968).
11) F. Agolini, S. Klemenko, I. G. Csizmadia, and K. Yates, *Spectrochim. Acta*, **24a**, 169 (1968).
12) K. Issleib and O. Low, *Z. Anorg. Allg. Chem.*, **346**, 241 (1966).
13) A. G. Brook, R. Kivisikk, and G. E. LeGrow, *Can. J. Chem.*, **43**, 1175 (1965).
14) R. G. Kostyanovsky, V. V. Yakshin, S. L. Zimont, and I. I. Chervin, *Izvest. Akad. Nauk SSSR, Ser. Khim.*, **1968**, 188, 190 *Chem. Abstr.*, **69**, 43987, 43988 (1968).
15) R. G. Kostyanovsky, V. V. Yakshin, and S. L. Zimont, *Tetrahedron*, **24**, 2995 (1968).

the present report, the effects of the organophosphorus group on the UV and IR spectra of the carbonyl group have been studied. For this purpose, three types of α-keto organophosphorus compounds, $(C_2H_5)_2PCOR$, $(C_2H_5)_2P(S)COR$, and $[(C_2H_5)_2CH_3PCOR]^+I^-$ (R= C_6H_5 and CH_3), have been prepared. Because the valence state of the phosphorus atom is different in these compounds, some distinguishable effects on the spectra of the carbonyl group can be expected. The internal chemical shift of the ethyl group was also measured for these compounds.

Experimental

All the experiments were performed in an oxygen-free dry nitrogen atmosphere. The solvents were purified in a stream of nitrogen prior to use.

Preparation. Benzoyldiethylphosphine (I), Benzoyldiethylmethylphosphonium Iodide (III), Acetyldiethylphosphine (IV), and Acetyldiethylmethylphosphonium Iodide (VI): These substances were synthesized by Issleib's method.[16] I, bp 102—103 °C /2.5 mmHg) (reported 98—100 °C/2 mmHg). III, mp 68—69 °C (reported 68 °C). IV, bp 58 °C/11 mmHg (reported 168 °C/760 mm and 53—54 °C/10 mmHg[14]). VI, mp121°C (reported 122 °C).

Benzoyldiethylphosphine Sulfide (II). I (2.70 g, 13.9 mmol) and trimethylstibine sulfide, $(CH_3)_3SbS$[17] (2.76 g, 13.9 mmol), were treated in dichloromethane at room temperature for 12 hr. The trimethylstibine formed was removed with a solvent *in vacuo*, and the residual liquid was extracted with *n*-hexane. After the removal of the solvent *in vacuo*, 2.63g (83%) of II were obtained as a viscous liquid, which was then gradually hydrolyzed by moisture in the air (Found: C, 58.27; H, 6.90%. Calcd for $C_{11}H_{15}OSP$: C, 58.39; H, 6.68%.). The compound could not be distilled below 100 °C under a high vacuum (1.3×10^{-3} mmHg), and it decomposed at a higher temperature. In the treatment of I with equimolar amounts of sulfur powder in tetrahydrofuran at room temperature, an exothermic reaction occurred immediately. The liquid obtained after the removal of the solvent contained II, with significant amounts of impurities.

Acetyldiethylphosphine Sulfide (V). As in the case of II, equimolar amounts of IV and trimethylstibine sulfide were treated, the liquid thus obtained was then distilled *in vacuo*, yielding 85% of V (bp 47 °C /1.1×10^{-3} mmHg); it was a faintly pale yellow liquid and was readily hydrolyzed in air (Found: C, 43.88; H, 8.05%. Calcd for $C_6H_{13}OSP$: C, 43.89; H, 7.98%.). A similar reaction took place between IV and sulfur, yielding 25% of V.

Diethylphosphine Sulfide. Soon after the mixing of diethylphosphine[18] (2.0 g, 22.2 mmol) and sulfur powder (0.64 g, 20.0 mmol) in dry ether, a vigorous reaction occurred and the sulfur powder disappeared. After the removal of the solvent, the residue was distilled *in vacuo*, yielding 1.95 g (80%) of the product (bp 57 °C/1 mmHg), which was readily hydrolyzed in air. Found: C, 39.03; H, 8.86%. Calcd for $C_4H_{11}SP$: C, 39.33; H, 9.08%. IR spectrum (neat) ν_{PH} 2297, ν_{PS} 586 cm^{-1}.

Physical Measurements. The infrared spectra in dichloromethane were measured on a Hitachi 225 grating spectrophotometer in airproof cells provided with KRS-5 windows. The electronic spectra were obtained by means of a Hitachi 124 spectrophotometer in 1 cm quartz airproof cells in cyclohexane, dichloromethane, and acetonitrile. The NMR spectra were recorded on JNM-3H-60 and JNM-PS-100 spectrometers operating at 60 and 100 MHz, respectively, at 25 °C in dichloromethane.

Analysis of the NMR Spectra. The NMR spectra of ethyl protons of I and IV were analyzed by the use of Corio's theoretical formula[19] of A_3B_2X. In other cases, the first-order analysis was performed. The reliability of the internal chemical shifts of the ethyl group was found to be ±0.02 ppm at most.

Results and Discussion

NMR Spectra. As can be seen from Table 1, the values of the internal chemical shift of the ethyl group and the indirect spin-spin coupling constants between the ethyl protons and the phosphorus nucleus increase in the following order for I—VI; tertiary phosphine<phosphine sulfide<phosphonium iodide in both benzoyl and acetyl series. The results are quite similar to those obtained for organophosphorus compounds without the keto group.[20-22] The electron-withdrawing effect on the internal chemical shift of these phosphorus compounds is considered to increase

Table 1. NMR spectral data of α-keto phosphorus compounds in dichloromethane

	Compound	H_β[a]		H_α[a]		Δ[b]	$J_{H_\alpha H_\beta}$	$PCOCH_3$		PCH_3	
		δ ppm	$^3J_{PH}$ Hz	δ ppm	$^2J_{PH}$ Hz	ppm	Hz	δ ppm	$^3J_{PH}$ Hz	δ ppm	$^2J_{PH}$ Hz
I	$(C_2H_5)_2PCOC_6H_5$	1.02	14.2	1.74	2.9	0.72	7.60				
II	$(C_2H_5)_2P(S)COC_6H_5$	1.19	19.5	2.20	11.8	1.01	7.7				
III	$[(C_2H_5)_2CH_3PCOC_6H_5]^+I^-$	1.31	20.4	3.14	12.5	1.81	7.7			2.59	13.8
IV	$(C_2H_5)_2PCOCH_3$	1.08	14.2	1.76	3.5	0.68	7.62	2.26	5.3		
V	$(C_2H_5)_2P(S)COCH_3$	1.15	19.6	1.97	11.6	0.82	7.7	2.61	4.7		
VI	$[(C_2H_5)_2CH_3PCOCH_3]^+I^-$	1.32	19.3	2.88	13.5	1.56	7.7	3.09	5.4	2.44	14.0

a) H_β and H_α are methyl and methylene protons, respectively, of the ethyl group.
b) $\Delta=\delta_{H_\alpha}-\delta_{H_\beta}$

16) K. Issleib and E. Priebe, *Chem. Ber.*, **92**, 3183 (1959).
17) M. Shindo, Y. Matsumura, and R. Okawara, *J. Organometal. Chem.*, **11**, 299 (1968); This Bulletin, **42**, 265 (1969).
18) K. Issleib and A. Tzschach, *Chem. Ber.*, **92**, 704 (1959).
19) P. L. Corio, *Chem. Rev.*, **60**, 363 (1960).
20) P. T. Narasimhan and M. T. Rogers, *J. Chem. Phys.*, **34**, 1049 (1961).
21) J. B. Hendrickson, M. L. Maddox, J. J. Sims, and H. D. Kaesz, *Tetrahedron*, **20**, 449 (1964).
22) A. G. Massey, E. W. Randall, and D. Shaw, *Spectrochim. Acta*, **21**, 263 (1965).

Table 2. Carbonyl stretching frequencies of α-keto phosphorus compounds in dichloromethane (cm^{-1})

Compound	ν_{CO}
$(CH_3)_3CCOC_6H_5$[a]	1680
$(CH_3)_3SiCOC_6H_5$[b]	1618
I	1635
II	1646
III	1663
$(CH_3)_3CCOCH_3$[c]	1718
$(CH_3)_3SiCOCH_3$[b]	1645
IV	1652
V	1687
VI	1707

a) Ref. 24.
b) Ref. 9.
c) Ref. 6.

in the above order.[23] The internal chemical shifts of I—VI are always larger than those of the corresponding phosphorus compound not containing the keto group. This is considered to be due mainly to the difference in the electron withdrawing property of the ethyl and the keto groups, although there might be some contributions of the magnetic anisotropy of the carbonyl group.

One of the most notable results is that the $^3J_{PH}$ value for the acetyl group in IV—VI is very small compared with that of the methyl protons in the ethyl group; it is almost the same for the three compounds.

IR Spectra. The carbonyl stretching frequency of I—VI is shown in Table 2, together with the carbon[6,24] and silicon[9] analogs. The low-frequency shift of the carbonyl stretching of the α-keto organosilicon compounds relative to the carbon analogs is considered to be due mainly to a small electronegativity of silicon.[1] The stretching frequency of I—VI is smaller than that of carbon analogs, but larger than that of silicon, and it increases as in the internal chemical shift in this order: I<II<III and IV<V<VI. The results are considered to be due to the increase in the electron withdrawing property of the phosphorus group. In spite of the large effective electronegativity of the phosphorus atom in III and VI relative to that of carbon as revealed from NMR spectra, the stretching frequency is a little smaller than that of the carbon analogs. These results seem to suggest that there are some p_π-d_π interactions[25] in the ground state in III and VI.

Table 3. Electronic spectra of α-keto phosphorus compounds (cm^{-1})

Compound	Solvent	A	B	C	D	E	F
		ν_{max} (ε_{max})	ν_{max} (ε_{max})	ν_{max} (ε_{max})	ν_{max} (ε_{max})	ν_{max} (ε_{max})	ν_{max} (ε_{max})
$(CH_3)_3CCOC_6H_5$[a]	*n*-C_6H_{14}	31250(103)	36500(600)	42000(8800)			50300(25400)
$(CH_3)_3SiCOC_6H_5$[a]	*n*-C_6H_{14}	23650(119)	35400(1140)	40000(11300)			50000(19450)
I	*cyc*-C_6H_{12}	26300(268)	35000sh	39100(12700)			——[d]
	CH_2Cl_2	26200(687)	——[d]	——[d]			——[d]
	CH_3CN	26600(595)	36200(3500)	41400(10500)			49500(14500)
II	*cyc*-C_6H_{12}	24600(403)	34800sh	39200(10900)		——[d]	——[d]
	CH_2Cl_2	25100(613)	——[d]	——[d]		——[d]	——[d]
	CH_3CN	25300(674)	35000sh	39200(13500)		44400(5000)	47200(11000)
III[b]	CH_2Cl_2	26400(369)		——[d]	——[d]		——[d]
	CH_3CN	27400(110)		37500(12100)	41300(16700)		48300(14700)
$(CH_3)_3CCOCH_3$[c]	*n*-C_7H_{16}	34800(23)					53800(1100)
$(CH_3)_3SiCOCH_3$[c]	*n*-C_6H_{14}	26900(126)					51200(4200)
IV	*cyc*-C_6H_{12}	30100(379)	40500(1350)				——[d]
	CH_2Cl_2	30000(608)	——[d]				——[d]
	CH_3CN	30500(517)	40800(2780)				48700(3100)
V	*cyc*-C_6H_{12}	28000(306)	37900(550)			——[d]	——[d]
	CH_2Cl_2	28400(287)	39100(442)			——[d]	——[d]
	CH_3CN	28600(329)	38900(477)			42700(6100)	48400(16000)
VI[b]	CH_2Cl_2	30700(297)			——[d]		——[d]
	CH_3CN	32000(152)			41700(14000)		48800(23700)
$(C_2H_5)_2P(S)H$	*cyc*-C_6H_{12}					45000(7900)	
	CH_3CN					47800(4100)	

a) Ref. 6.
b) The data in cyclohexane solution were not obtained because of insolubility.
c) Ref. 11.
d) Not measured.

23) If we use the relation between the internal chemical shift of the ethyl group and the electronegativity of the atom bonded to this group proposed by Narasimhan and Rogers (*J. Amer. Chem. Soc.*, **82**, 5983 (1960)), the effective electronegativities of the phosphorus and silicon atoms are found to be 2.2, 2.5, 2.8, and 1.8 for $(C_2H_5)_3P$, $(C_2H_5)_3PS$, $(C_2H_5)_4P^+$, and $(C_2H_5)_4Si$ respectively.

24) J. I. Adelfang, P. H. Hess, and N. H. Cromwell, *J. Org. Chem.*, **26**, 1402 (1961).

25) Hoffmann *et al.* have indicated that, in Extended Hückel MO calculation, the large charge separation is considerably reduced by the inclusion of the P 3d orbital in phosphonium ylide (R. Hoffmann, D. B. Boyd, and S. Z. Goldberg, *J. Amer. Chem. Soc.*, **92**, 3929 (1970)).

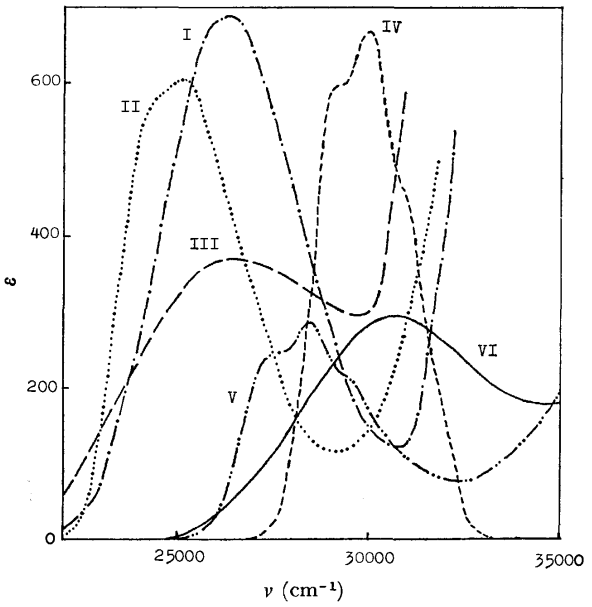

Fig. 1. The absorption bands of the n-π^* transition measured in dichloromethane.

UV Spectra. The positions and intensities of the absorption maxima of I—VI are summarized in Table 3. The values of the carbon and silicon analogs are added for the sake of comparison. Each compound exhibits several absorption bands in the 23000—50000 cm^{-1} region, these bands can be classified into six types depending on their positions and intensities. The band at the lowest frequency (A) shows a blue shift as the polarity of solvent increases, and, as is shown in Fig. 1, it has somewhat fine structure. One of the most remarkable results is that the intensity of the band is rather large as compared with that of carbon analogs. This band is presumably due to the n-π^* transition involving the carbonyl group. The band with a medium intensity or the shoulder (B) at 35000—36000 cm^{-1} in I and II is probably due to the ^1L_b band.[26] The band (B) in III may be hidden by a strong band, C. The origin of the absorption band (B) at 38000—41000 cm^{-1} in IV and V is not clear. A possible assignment of this band is a transition of the n electrons on phosphorus and sulfur to the π^* orbital of the carbonyl group. The intense band (C) at 38000—42000 cm^{-1} in I—III is probably due to the allowed ^1L_a band with an intramolecular charge-transfer character of the benzoyl group.[26] The intense band (D) at 41000—42000 cm^{-1} in III and VI was assigned tentatively to an intramolecular charge-transfer transition from the carbonyl n level to the vacant d orbitals of the phosphorus atom, because, in these compounds, the energy level of the d orbitals seems to be considerably lowered as a result of a net positive charge on the molecule. The band with medium intensity (E) at 43000—45000 cm^{-1} in II and V may be due to the P–S group, because a similar band was observed in diethylphosphine sulfide. Finally, in the highest frequency region, an intense band (F) was observed in all the compounds. The band in I—III is probably due to the intramolecular charge-transfer band with the ^1B-band character.[26] The nature of the band not containing the phenyl group IV—VI has never been definitely established. This band may be due to either the π-π^* transition or the n-σ^* transition of the carbonyl group. One notable result of this band is that, in V and VI, the intensity is very large compared with that of pinacolone or acetyltrimethylsilane.

As can be seen from Table 3, the n-π^* transition band of I—VI shows a large red shift as compared with that of the carbon analogs, but the shift is smaller than that of the silicon analogs. II and V show the largest red shift among the phosphorus compounds. The red shifts of I and III, and those of IV and VI, relative to the carbon analogs are almost the same, although the valence state of the phosphorus atom is different. As has been shown in connection with the NMR and IR spectra, the electron withdrawing property of the phosphorus group is larger than that of the silyl group. Therefore, the inductive rise in the n level of the carbonyl group may be smaller in I—VI, particularly in III and VI, than in α-keto silicon compounds. The red shift of the n-π^* transition band in III and VI may be largely responsible for the lowering of the π^* level of the carbonyl group as a result of interaction with the vacant d orbital of the phosphorus atom. In I and IV, in addition to the lowering of the carbonyl π^* level, there may be some contribution of the n level rising to the red shift. The largest red shift in II and V is also considered to be due to the large lowering of the carbonyl π^* level by the interaction with that of the P=S group. The lowering of the π^* level in the phosphorus compounds is partly supported by the following fact. In spite of the smaller red shift of the n-π^* transition in the phosphorus compounds relative to that of the silicon, the red shifts of the π-π^* transitions are larger in phosphorus compounds (see Table 3). These results seem to reveal that the d-π^* interaction occurs more easily in α-keto organophosphorus compounds than in organosilicon compounds.

We wish to express our hearty thanks to Professor Rokuro Okawara for his continuous encouragement throughout this study. We are also grateful to Drs. Masanori Wada and Yoshio Matsumura of Osaka University for their helpful discussions. The calculations needed for obtaining the NMR parameters were carried out on an NEAC-2200 at the Computation Center of Osaka University.

26) K. Kimura and S. Nagakura, *Theor. Chim. Acta* (Berl.), **3**, 164 (1965).

Reactions of Vinyloxyboranes.[1] A Convenient Method for the Preparation of β-Hydroxy Thiolesters, Esters and Ketones

Katsuhiko INOMATA, Masayoshi MURAKI, and Teruaki MUKAIYAMA

Laboratory of Organic Chemistry, Tokyo Institute of Technology, Ookayama, Meguro-ku, Tokyo 152

(Received November 27, 1972)

It was found that the reaction of thioboronites with carbonyl compounds and ketene proceeds with the initial formation of vinyloxyboranes (VII). The boranes were found to be important intermediates for the formation of β-hydroxythiolesters by the reaction with various carbonyl compounds. Vinyloxyborane derivatives can be alternatively prepared by the reactions of trialkylboranes and α-diazocarbonyl compounds. The boranes similarly reacted with carbonyl compounds to give β-hydroxyketones and β-hydroxyesters.

In a previous paper,[2] it was reported that the reaction of thioboronite with carbonyl compounds and ketene afforded β-hydroxyalkanethioates in excellent yields. This paper deals with an extention of earlier works.[2,3]

A typical reaction of thioboronite with carbonyl compounds and ketene is shown in the following. When equimolar amounts of *n*-butyl di-*n*-butylthioboronite (I) and various carbonyl compounds (IIa—g) in dry ether were treated with excess gaseous ketene at 0 °C for 2 hr followed by hydrolysis, the corresponding β-hydroxyalkanethioates (IIIa—g) were obtained in excellent yields (Scheme 1). The results are summarized in Table 1.

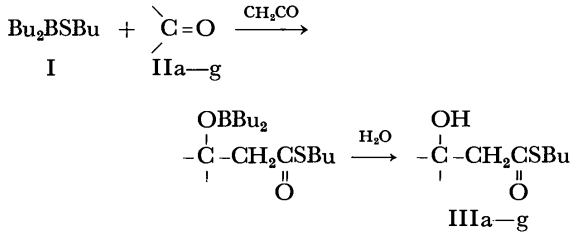

Scheme 1

In the same way, β-hydroxyalkanethioates (Va—e) were obtained by the treatment of other thioboronites (IVa—e) prepared from tri-*n*-butylborane and thiols with benzaldehyde and ketene, followed by hydrolysis, in excellent yields (Table 2). Thus, it became clear that the reaction of thioboronites with carbonyl compounds and ketene is an excellent method of preparing various β-hydroxyalkanethioates.

By utilizing this reaction, *S*-*n*-butyl ethyl β-hydroxy-β-methyl-thioglutarate (VI), the analog of β-hydroxy-β-methyl-glutaryl coenzyme A (HMG-CoA), was obtained in 81% yield from ethyl acetoacetate by the following procedure (Scheme 2).

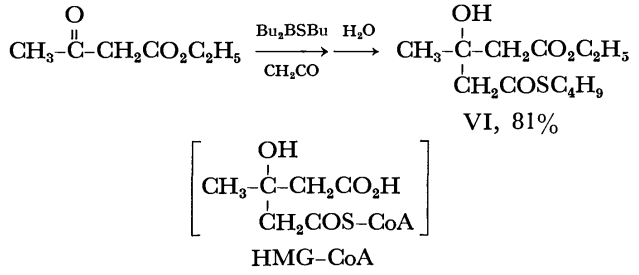

Scheme 2

TABLE 1. YIELDS AND PROPERTIES OF β-HYDROXYALKANETHIOATES[a]

IIa—g	Carbonyl compound	Product	Bp °C /mmHg	Isolated yield, %		Elemental analyses, % C	H	S
IIa	$CH_3(CH_2)_2CHO$	IIIa	97—98 /4.5	84	Found	58.51	9.92	15.87
					Calcd	58.80	9.87	15.67
IIb	C_6H_5CHO	IIIb	145—146 /4.5	90	Found	65.47	7.90	13.16
					Calcd	65.53	7.61	13.43
IIc	$C_6H_5CH=CHCHO$	IIIc	163 /0.18	90	Found	68.46	7.76	11.93
					Calcd	68.16	7.63	12.11
IId	$(CH_3)_2CO$	IIId	82—84 /3.0	98	Found	56.61	9.66	16.65
					Calcd	56.82	9.54	16.82
IIe		IIIe	112—113 /1.5	91	Found	62.59	9.69	14.12
					Calcd	62.58	9.63	13.90
IIf	$C_6H_5(C_2H_5)CO$	IIIf	139 /3.0	91	Found	67.58	8.42	12.13
					Calcd	67.64	8.33	12.01
IIg	$(C_6H_5)_2CO$	IIIg	[b]	94	Found	72.39	7.07	10.06
					Calcd	72.59	7.05	10.18

a) In ether at 0°C for 2 hr. b) Mp 75.5—76.5 °C.

1) Presented in part at the 23rd Symposium on Organic Reaction Mechanisms of the Chemical Society of Japan, Kobe, October, 1972. Preliminary communication: T. Mukaiyama, K. Inomata, and M. Muraki, *J. Amer. Chem. Soc.*, **95**, 967 (1973).

2) T. Mukaiyama and K. Inomata, This Bulletin, **44**, 3215 (1971).

3) a) T. Mukaiyama, K. Inomata, and S. Yamamoto, *Tetrahedron Lett.*, **1971**, 1097. b) T. Mukaiyama, S. Yamamoto, and K. Inomata, This Bulletin, **44**, 2807 (1971).

TABLE 2. YIELDS AND PROPERTIES OF β-HYDROXYALKANETHIOATES[a)]

$$Bu_2BSR + PhCHO \xrightarrow[ii)\ H_2O]{i)\ H_2C{=}C{=}O} PhCHCH_2CSR \quad (OH,\ O)$$

IVa—e Va—e

IVa—e	R	Product	Bp °C /mmHg (Mp °C)	Isolated yield, %		Elemental analyses, % C	H	S
IVa	$-C_6H_5$	Va	(84.5—85.5)	96	Found	69.57	5.29	12.63
					Calcd	69.74	5.46	12.41
IVb	$-CH_2C_6H_5$	Vb	182—184 /2.0	94	Found	70.93	5.66	12.06
					Calcd	70.56	5.92	11.77
IVc	$-CH_2-$(furyl)	Vc	[b)]	71	Found	64.21	5.42	12.25
					Calcd	64.09	5.38	12.23
IVd	$-C(CH_3)_3$	Vd	138—139 /2.5	93	Found	65.11	7.54	13.49
					Calcd	65.51	7.61	13.45
IVe	$-CH(CH_3)C_2H_5$	Ve	138 /2.5	97	Found	65.70	7.51	13.33
					Calcd	65.51	7.61	13.45

a) In ether at 0 °C. b) This is an oily substance and decomposed during the course of vacuum distillation.

It was postulated that the above reaction of thioboronites with carbonyl compounds and ketene proceeds with the initial formation of a coordination complex of thioboronite and a carbonyl compound, followed by a nucleophilic attack of the thiolate anion on ketene.[2] However, the present results show that this reaction proceeds through vinyloxyborane (VII), formed from thioboronite and ketene, as sketched in the following scheme.

$$H_2C{=}C{=}O + RSBR_2' \longrightarrow H_2C{=}C(SR)(OBR_2') \xrightarrow{H_2O} CH_3CSR$$

VII VIII

$$VII + \text{>C=O} \longrightarrow \left[\text{>C(H}_2\text{)–C(SR)=C(O–B(R}_2'\text{)–O)–C<}\right] \xrightarrow{H_2O} -C(OH)-CH_2CSR$$

IX

When nearly one equivalent of gaseous ketene was passed through a solution of phenyl di-*n*-butylthioboronite in carbon tetrachloride at −20——30 °C under argon, formation of VII (R=C_6H_5, R′=*n*-C_4H_9) was confirmed by the PMR spectrum of the reaction mixture which displayed two doublets for the vinyl hydrogens at δ 4.57 and 4.63 (*J*=*ca.* 1.5 Hz). On hydrolysis of this reaction mixture, phenyl thioacetate (VIII, R=C_6H_5) was isolated by preparative tlc.

It was established that the treatment of VII (R=C_6H_5, R′=*n*-C_4H_9) with acetone in ether, followed by hydrolysis, afforded phenyl β-hydroxy-isovalerothioate (IX, R=C_6H_5) in 67% yield.

Excess gaseous ketene was bubbled into a solution of equimolar amounts of thioboronites and carbonyl compounds at 0 °C in dry ether. Completion of the reaction by this procedure took a longer time as compared with the above procedure of treating vinyloxyboranes with carbonyl compounds. This might be attributed to the presence of the coordination complex of thioboronite with carbonyl compound and the necessity of ligand exchange of the carbonyl compound and ketene to proceed further.

The reactions of vinyloxyboranes prepared by other methods were studied with the expectation that these compounds would be important synthetic intermediates.

Hooz and Linke reported that the reaction of trialkylboranes and α-diazo ketones[4] or esters,[5] followed by hydrolysis, gave the corresponding α-alkyl carbonyl compounds, the intermediate being β-ketoborane.[4] Pasto and Wojtkowski[6] proposed vinyloxyborane to be an intermediate by means of NMR and UV spectra. It was found that the vinyloxyboranes (XI, Y=C_6H_5; XI′, Y=OC_2H_5), obtained from α-diazo carbonyl compounds and tri-*n*-butylborane, gave β-hydroxy ketones (XII) and β-hydroxy esters (XII′), respectively, on treatment with carbonyl compounds in THF at room temperature as follows. The results are summarized in Tables 3 and 4.

$$N_2CHCY + Bu_3B \xrightarrow{-N_2} BuCH{=}C(Y)(OBBu_2)$$

X, Y=C_6H_5; X′, Y=OC_2H_5 XI or XI′

$$XI \text{ or } XI' + \text{>C=O} \xrightarrow{H_2O} -C(Bu)-CHCY \quad (OH,\ O)$$

XII or XII′

It was found that the vinyloxyborane (XIV) prepared from tri-*n*-butylborane and ethyl α-diazohydrocinnamate (XIII)[7] reacted with benzaldehyde to give ethyl 2-*n*-butyl-2-benzyl-3-hydroxy-hydrocinnamate (XV) in 70% yield under similar conditions.

$$N_2C(CH_2C_6H_5)CO_2C_2H_5 + Bu_3B \xrightarrow{-N_2} C_6H_5CH_2(Bu)C{=}C(OC_2H_5)(OBBu_2)$$

XIII XIV

4) J. Hooz and S. Linke, *J. Amer. Chem. Soc.*, **90**, 5936 (1968).
5) J. Hooz and S. Linke, *ibid.*, **90**, 6891 (1968).
6) D. J. Pasto and P. W. Wojtkowski, *Tetrahedron Lett.*, **1970**, 215.

Table 3. Yields of β-hydroxyketones[a)]

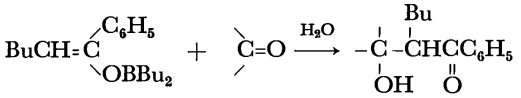

XI XIIa—d

Carbonyl compound	Time	Product	Isolated yield, %
$CH_3(CH_2)_2CHO$	10 min	XIIa	88
C_6H_5CHO	10 min	XIIb	98
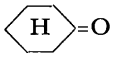	1 day	XIIc	69
$(CH_3)_2CO$	3 days	XIId	42

a) In THF at room temperature.

Table 4. Yields of β-hydroxyesters[a)]

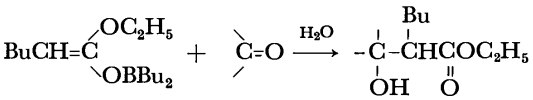

XI′ XII′a—e

Carbonyl compound	Time	Product	Isolated yield, %
$CH_3(CH_2)_2CHO$	1 day	XII′a	87
C_6H_5CHO	1 day	XII′b	81
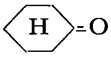	1 day	XII′c	96
$(CH_3)_2CO$	1 day	XII′d	73
$C_6H_5(C_2H_5)CO$	1 day	XII′e	68

a) In THF at room temperature.

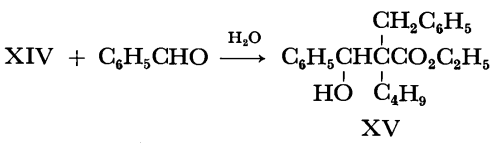

XV

Tricyclohexylborane (XVI) also reacted with ethyl diazoacetate to afford another vinyloxyborane (XVII) which further reacted with benzaldehyde to give ethyl 2-cyclohexyl-3-hydroxyhydrocinnamate (XVIII) in 87% yield.

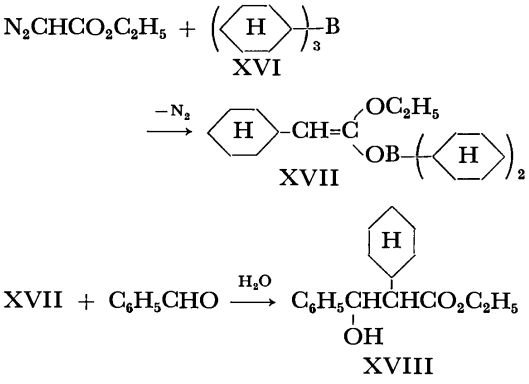

XVI XVII XVIII

It is to be noted that vinyloxyboranes, which afford the corresponding β-hydroxycarbonyl derivatives by the reaction with carbonyl compounds according to the following scheme, are useful intermediates in organic synthesis because of their high reactivity with carbonyl compounds and their availability.[6,8,9]

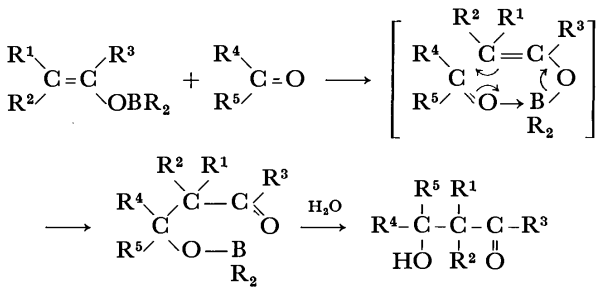

Experimental[10]

Materials. Tri-*n*-butylborane was prepared from boron trifluoride diethyl etherate and *n*-butylmagnesium bromide in dry ether under argon. Tricyclohexylborane was prepared by hydroboration of cyclohexene in THF.

s-Butyl Di-n-butylthioboronite (IVe).[11] *s*-Butylmercaptan (1.65 g, 18.3 mmol) was added to tri-*n*-butylborane (3.42 g, 18.8 mmol) in the presence of some boiling stone at room temperature under argon. The reaction mixture was then heated at 150 °C for 1 hr and distilled *in vacuo* under argon. Bp 100—103 °C/7 mmHg. 3.19 g (81.5%). PMR ($CDCl_3$) δ 0.7—1.8 (m, 26H), 3.23 (q, J=7 Hz, 1H).

Other thioboronites (IVa—e) were prepared from tri-*n*-butylborane and the corresponding mercaptans in a similar way. The results are listed in Table 5.

Table 5. Yields of thioboronites[a)]

$n\text{-}Bu_3B + RSH \longrightarrow n\text{-}Bu_2BSR$ IVa—e

Mercaptan	Conditions	Yield, %	Bp °C/mmHg
C_6H_5SH	180°, 4 hr	IVa, 80	107—108 /2
$C_6H_5CH_2SH$	160°, 3 hr	IVb, 81	157—159 /8.5
-CH_2SH	180°, 4 hr	IVc, 76	130—134 /6
$(CH_3)_3CSH$	160°, 4 hr	IVd, 81	99—102 /7
$C_2H_5(CH_3)CHSH$	150°, 1 hr	IVe, 82	100—103 /7

a) These were confirmed by PMR spectra under argon. IVa; PMR (CCl_4) δ 0.5—2.0 (m 18H), 7.14 (s 5H) IVb; ($CDCl_3$) δ 0.7—1.5 (m 18H), 3.89 (s 2H), 7.17 (s 5H). IVc; ($CDCl_3$) δ 0.7—1.4 (m 18H), 3.94 (s 2H), *ca.* 4.10 (dd, J=3 Hz, J=1 Hz, 1H), *ca.* 4.25 (dd, J=3 Hz, J=2 Hz, 1H), *ca.* 7.25 (dd, J=2 Hz, J=1 Hz, 1H). IVd; ($CDCl_3$) δ 0.7—1.8 (m 18H), 1.45 (s 9H). IVe; ($CDCl_3$) δ 0.7—1.8 (m 26H), 3.23 (sex J=6 Hz, 1H).

Reaction of n-Butyl Di-n-butylthioboronite with Benzaldehyde and Ketene. Equimolar amounts of *n*-butyl di-*n*-butylthioboronite (1.09 g, 5.1 mmol) and benzaldehyde (0.54 g, 5.1 mmol) in 15 ml dry ether were treated with ketene (prepared by thermal cracking of acetone) at 0 °C for 2 hr with stirring. After removal of the ether, the oily substance was treated with 30% H_2O_2 (4 ml) in MeOH (20 ml) at room temperature. The solution was allowed to stand overnight and water was added. The mixture was concentrated *in vacuo* to remove

7) N. Takamura, T. Mizoguchi, K. Koga, and S. Yamada, *Tetrahedron Lett.*, **1971**, 4495.

8) J. J. Tufariello, L. T. C. Lee, and P. W. Wojtkowski, *J. Amer. Chem. Soc.*, **89**, 6804 (1967).

9) R. Köster and W. Fenzl, *Angew. Chem.*, **80**, 756 (1968).

10) Melting and boiling points are uncorrected.

11) Prepared according to Mikhailov's method. B. M. Mikhailov and Yu. N. Bubrov, *Izv. Akad. Nauk SSSR., Ser. Khim.*, **1964**, 2248; *Chem. Abstr.*, **62**, 9161c (1965).

the methanol and the residue was extracted with three portions of ether. The combined ether layers were washed with 5% solution of $NaHCO_3$ and dried over anhydrous Na_2SO_4, and the solvent was evaporated to give 1.09 g (90%) of *S-n*-butyl *β*-hydroxyhydrocinnamethioate (IIIb); IR: 3440, 1670cm^{-1}. PMR ($CDCl_3$) δ 1.0—2.2 (m, 7H), 3.17 (t, J=7 Hz, 2H), *ca.* 3.20 (m, 2H), 3.74 (s, 1H), 5.42 (dd, J=8 Hz, J=6 Hz, 1H), 7.58 (s, 5H). Bp 145—146 °C/4.5 mmHg. Found: C, 65.47; H, 7.90; S, 13.16%. Calcd for $C_{13}H_{18}O_2S$: C, 65.53; H, 7.61; S, 13.43%.

Preparation of S-n-*Butyl Ethyl β-Hydroxy-β-methyl-thioglutarate (VI).* Ketene was bubbled into a solution of *n*-butyl di-*n*-butylthioboronite (973 mg, 4.55 mmol) in 15 ml dry ether at 0 °C for 15 min with stirring, and ethyl acetoacetate (545 mg, 4.19 mmol) in 10 ml dry ether was added. After bubbling ketene for 1 hr, the reaction mixture was worked up as in the preparation of IIIb to give a crude oil. The residue was separated by preparative tlc (silica gel) using methylene chloride. Elution of the main band and the evaporation under reduced pressure at *ca.* 50 °C gave 891 mg (81%) of *S-n*-butyl ethyl *β*-hydroxy-*β*-methyl-thioglutarate (VI); IR 3510, 1740, 1720 (shoulder), 1690 cm^{-1}. PMR (CCl_4) δ 0.6—1.8 (m, 13H), 2.54 (s, 2H), 2.6—3.0 (m, 2H), 2.83 (s, 2H), 3.4—3.8 (br s, 1H), 4.14 (q, J=*ca.* 7.5 Hz, 2H). Bp 119 °C/1.5 mmHg. Found: C, 54.87; H, 8.55; S, 12.48%. Calcd for $C_{12}H_{22}O_4S$: C, 54.95; H, 8.45; S, 12.20%.

Reaction of Vinyloxyborane (XI) with Benzaldehyde. To a stirred solution of diazoacetophenone (154 mg, 1.05 mmol) in 5 ml THF (dried $LiAlH_4$) was added tri-*n*-butylborane (216 mg, 1.19 mmol) at room temperature under argon. N_2 was immediately evolved. After being stirred for 45 min, the reaction mixture was treated with a solution of benzaldehyde (92 mg, 0.87 mmol) in 5 ml THF for 10 min at room temperature. The mixture was worked up as in the preparation of IIIb to give a crude oil. It was purified by preparative tlc (silica gel) using methylene chloride to give 240 mg (98%) of 2-hydroxybenzyl-1-phenylhexan-1-one (XIIb, oil); IR 3440, 1660 cm^{-1}. PMR (CCl_4) δ 0.3—2.0 (m, 9H), 3.4—3.9 (m, 2H), 4.6—4.9 (m, 1H), 6.8—7.4 (m, 8H), 7.5—8.0 (m, 2H).

The IR and PMR spectra of other *β*-hydroxyketones (XIIa—d) are consistent with the assigned structure: XIIa; IR 3430, 1660 cm^{-1}. PMR (CCl_4) δ 0.4—2.1 (m, 16H), 3.1—4.1 (m, 3H), 7.1—7.6 (m, 3H), 7.7—8.1 (m, 2H). XIIc; IR 3480, 1650 cm^{-1}. PMR (CCl_4) δ 0.3—2.4 (m, 19H), 3.19 (s, 1H), 3.50 (dd, J_A=6 Hz, J_B=8 Hz, 1H), 7.2—7.6 (m, 3H), 7.7—8.2 (m, 2H). XIId; IR 3460, 1660 cm^{-1}. PMR (CCl_4) δ 0.5—2.1 (m, 15H), 2.98 (s, 1H), 3.47 (dd, J_A=5 Hz, J_B=8 Hz, 1H), 7.1—7.6 (m, 3H), 7.7—8.1 (m, 2H).

Reaction of Vinyloxyborane (XI') with Benzaldehyde. To a solution of tri-*n*-butylborane (346 mg, 1.9 mmol) and benzaldehyde (169 mg, 1.6 mmol) in dry THF (3 ml) was added a solution of ethyl diazoacetate[12] (195 mg, 1.7 mmol, dried over P_2O_5) in THF (1 ml) at room temperature under argon with stirring. N_2 was immediately evolved and the yellow coloration characteristic of ethyl diazoacetate disappeared. The reaction mixture was allowed to stand at room temperature for 1 day. After removal of THF, the residue was treated with 30% H_2O_2 (1 ml) in MeOH (3 ml) for 2 hr and water was added. The mixture was concentrated *in vacuo* to remove most of the methanol and extracted with ether. The ether layer was washed with 5% solution of $NaHCO_3$ and saturated solution of NaCl, dried over Na_2SO_4 and the solvent was removed. The crude oil was purified by preparative tlc (silica gel, CH_2Cl_2) to give the pure oil of ethyl 2-*n*-butyl-3-hydroxyhydrocinnamate (XII'b, 320 mg, 81%); IR 3450, 1710 cm^{-1}. PMR (CCl_4) δ 0.6—1.6 (m, 9H), 1.18 (t, J=7 Hz, 3H), 2.5—2.9 (m, 1H), 3.05 (br s, 1H), 4.15 (q, J=7 Hz, 2H), 4.75 (d, J=7 Hz, 1H), 7.25 (s, 5H). Found: C, 72.02; H, 8.96%. Calcd for $C_{15}H_{22}O_3$: C, 71.97; H, 8.86%.

The IR and PMR spectra of other *β*-hydroxyesters (XII'a—d) are consistent with the assigned structure: XII'a; IR 3430, 1710 cm^{-1}. PMR (CCl_4) δ 0.7—1.6 (m, 16H), 1.25 (t, J=7 Hz, 3H), 2.25 (m, 1H), 2.68 (br s, 1H), 3.55 (m, 1H), 4.16 (q, J=7 Hz, 2H). XII'c; IR 3500, 1710 cm^{-1}. PMR (CCl_4) δ 0.65—1.9 (m, 19H), 1.25 (t, J=7 Hz, 3H), 2.30 (t, J=7 Hz, 1H), 2.79 (s, 1H), 4.15 (q, J=7 Hz, 2H). XII'd; IR 3450, 1710 cm^{-1}. PMR (CCl_4) δ 0.7—1.5 (m, 9H), 1.15 (s, 6H), 1.26 (t, J=7 Hz, 3H), 2.1—2.4 (m, 1H), 2.9 (br s, 1H), 4.14 (q, J=7 Hz, 2H). XII'e; IR 3480, 1700 cm^{-1}. PMR (CCl_4) δ 0.4—1.5 (m, 17H), 2.85 (t, J=9 Hz, 1H), 3.79 (q, J=7 Hz, 2H), 3.8 (s, 1H), 7.25 (s, 5H).

12) N. B. Searle, "Organic Syntheses," Coll. Vol. IV, p. 424 (1963).

Studies of the Synthetic Model Enzyme. The Synthesis of Cyclo(His-Glu-Cys-D-Phe-Gly)$_2$ as the Esterase Model[1]

Kiichiro NAKAJIMA and Kenji OKAWA

Department of Chemistry, Faculty of Science, Kwansei Gakuin University, Nishinomiya 662

(Received December 2, 1972)

To study the mechanism of enzyme action, cyclo(His–Glu–Cys–D–Phe–Gly)$_2$ was prepared as an esterase model from the corresponding linear decapeptide by the azide methods. The esterase-like activity of this cyclic decapeptide in reaction to *p*-nitrophenyl acetate was three times greater than that of the linear decapeptide, the curve of the catalytic coefficient *versus* the different pH is of a bell type, and the optimum pH was recorded at about 7.6. The kinetics of the hydrolysis obeyed Michaelis-Menten's typical equation.

In spite of all our knowledge of the structures of enzymes and the kinetics of enzyme-catalyzed reactions, we are still far from an adequate understanding of the mechanisms of enzyme action. To answer this problem, approaches have been made by many workers through synthetic research into model enzymes. In these cases, linear amino acid peptide[2] or polyamino acid,[3] with active sites of amino acid residues, have mostly been used as the model substances, these studies attained their first purpose to some extent.

In the present study, the authors proposed to synthesize the cyclic peptide as a model enzyme; it has a relatively low molecular weight and will have hydrolytic activity. For the above purpose, histidine, cysteine, and glutamic acid were chosen as the active-site amino acids of synthetic cyclic peptide; they are arranged along the cyclic decapeptide chain with an antiparallel structure, as is shown in Fig. 1.

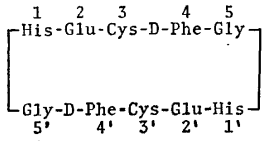

Fig. 1. Enzyme model (I)

Moreover, the cyclic decapeptide (I) could be successfully obtained by the removal of the protecting groups, followed by the cyclization of the linear decapeptide azide by using the high-dilution method. The hydrolytic activity of the synthetic model peptide has been investigated in detail by using the linear and cyclic decapeptide.

Synthesis of the Linear Decapeptide Derivative. The synthetic route of the linear decapeptide derivative (XV) is summarized in Figs. 2 and 3. Boc-dipeptide methyl ester (II) was prepared by the DCC method; then II was converted into tripeptide (IV) by the azide method. Boc-pentapeptide (X) was successively obtained from the tripeptide (V), Boc–Glu(OBzl)–OSu (VI), and Boc–His(*im*-Dnp)–OSu (IX) by the succinimide ester method. The preparation of Boc-decapeptide (XV) from X and the free pentapeptide (XII) failed, because of the difficulties of isolating the decapeptide from the reaction mixture. Also, the pure XV could be obtained by the coupling of IX and nonapeptide (XIV), which has been prepared from the Boc-tetrapeptide *p*-nitrophenyl ester (XI) and free pentapeptide (XII).

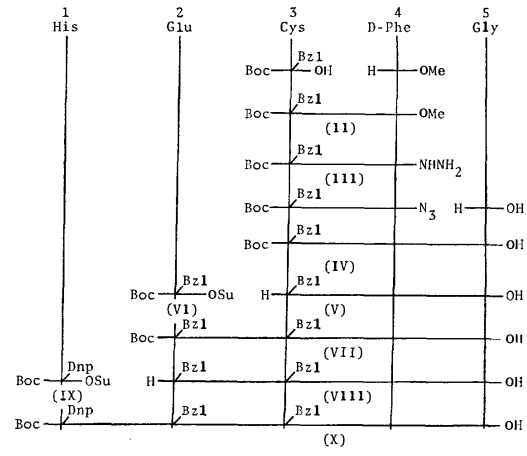

Fig. 2. Synthesis of Boc-pentapeptide (X)

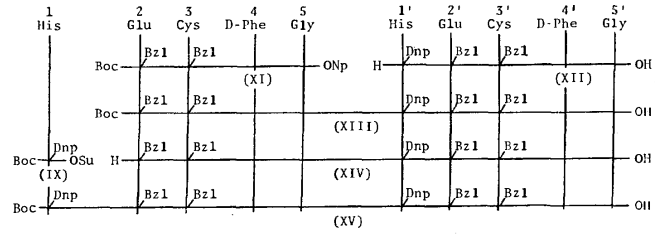

Fig. 3. Synthesis of Boc-decapeptide (XV)

The Cyclization of Linear Decapeptide Derivatives. Three different methods, using the *p*-nitrophenyl ester, *N*-hydroxysuccinimide ester, and azide, were used in the cyclization procedure (Fig. 4); the results are summarized in Table 1. The Boc-decapeptide *p*-nitrophenyl ester was obtained in a higher yield by the di-*p*-nitrophenyl sulfite method than by the DCC method, but the cyclization did not proceed satisfactorily. The Boc-decapeptide succinimide ester could be prepared in good yield by the DCC method, but

1) The abbreviations used for the amino acid residues, peptides and other abbreviations are based on the proposals by J. M. Stewart and J. D. Young, "Solid Phase Peptide Synthesis", W. H. Freeman and Co., San Francisco (1969).

2) P. Cruickshank and J. D. Sheehan, *J. Amer. Chem. Soc.*, **86**, 2070 (1964); I. Photaki, V. Bardakos, A. W. Lake, and G. Low, *J. Chem. Soc., C*, **1968**, 1860.

3) a) E. Katchalski, G. D. Fasman, E. Simons, E. R. Blout, F. R. N. Gurd, and W. L. Koltum, *Arch. Biochem. Biophys.*, **88**, 361 (1960). b) J. Noguchi and T. Saito, "Polyamino Acids, Polypeptides and Proteins", ed. by M. A. Stahmann. The Univ. Wisconsin Press, Madison (1962), p. 313.

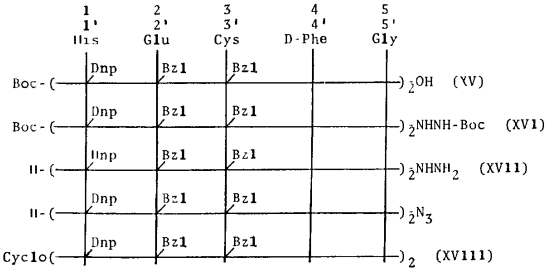

Fig. 4. Synthesis of Cyclic decapeptide (XVIII) by azide method

its active ester was not cyclized and the cyclic decapeptide derivative (XVIII) was not obtained. It was, therefore, concluded that the cyclization by the azide was the most favorable method in the present experiment, as is shown in Table 1.

TABLE 1. THE RESULTS OF THE CYCLIZATION REACTION

Method	Reaction temp. (°C)	Reaction time (hr)	Cyclo decapeptide (%)
ONp ester	60	6	52
OSu ester	rt	12	trace
Azide	0	24	87

XVIII was purified by the use of ion-exchange and gel filtration. The pure cyclic decapeptide (XVIII) was identified by thin-layer chromatography, by elemental analysis, and by molecular-weight measurements.

The Removal of the Protecting Groups from the Linear and Cyclic Decapeptide Derivatives. The benzyl ester and *s*-benzyl groups were removed from XV and XVIII by treating them with anhydrous hydrogen fluoride, and the dinitrophenyl group of the imidazole was removed by use of 2-mercaptoethanol[4] as is shown in Fig. 5.

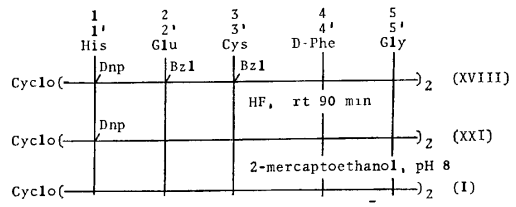

Fig. 5. Removal of the protecting groups from cyclic decapeptide (XVIII)

The free linear (XXIII) and cyclic decapeptide (I) thus obtained were purified with Sephadex G-15, and their purity was checked by means of a ninhydrin reaction, a Pauly reaction, and a nitroprusside reaction on thin-layer chromatography and paper electrophoresis. No disulfide groups were detected by the Ellman[5] and iodoacetamide methods.[6]

Hydrolytic Activity of the Synthetic Peptides, as Studied Using p-*Nitrophenyl Acetate as the Substrate.* The measurement of the catalytic action of the cyclic and linear decapeptide against *p*-nitrophenyl acetate was carried out by the method of Katchalski *et al.*;[3] the results are summarized in Table 2.

TABLE 2. HYDROLYSIS OF *p*-NITROPHENYL ACETATE IN 1/15M PHOSPHATE BUFFER, pH 7.73, CONTAINING 3.23% DIOXANE AND DMF (v/v) AT 24°C. [*p*-NITROPHENYL ACETATE]=3.23×10⁻⁵M.

Catalyst	Concn of catalyst mol l⁻¹ ×10⁴	k_1 min⁻¹ ×10³	c mol l⁻¹	k_2 l mol⁻¹ min
none		1.75		
His·HCl	5.37	2.44	5.37	1.33
Cys·HCl	5.37	20.69	5.37	32.20
I·2AcOH	3.00	13.13	6.00	19.61
XXIII·3AcOH	3.00	5.26	6.00	6.05
Chymotrypsin				10⁴

The value of the catalytic coefficient of the cyclic decapeptide was greater than those of the linear decapeptide and histidine hydrochloride, but smaller than that of cysteine hydrochloride. The results show that the active sites of the amino acid placed opposite to each in the cyclic molecule have a more effective interaction between the catalyst and the substrate than those of the linear peptide.

The initial rate of hydrolysis was determined at several concentrations of the substrate under a constant concentration of I; it was found that the reaction rate increased in parallel with the substrate concentration at a relatively lower concentration, but thereafter gradually reached the maximum rate, as is shown in Table 3.

TABLE 3. EFFECT OF CONCENTRATION ON THE RATE (V) OF *p*-NITROPHENYL ACETATE IN 1/15M PHOSPHATE BUFFER, pH 7.73, CONTAINING 3.23% DIOXANE AND DMF (v/v) AT 24°C. [DECAPEPTIDE-1]=47.6 μM

[NPA]×10⁴	V×10⁶ (M min⁻¹)
0.78	0.15
0.92	0.19
1.94	0.42
3.95	0.75
7.81	1.73
15.68	3.36
23.39	4.10

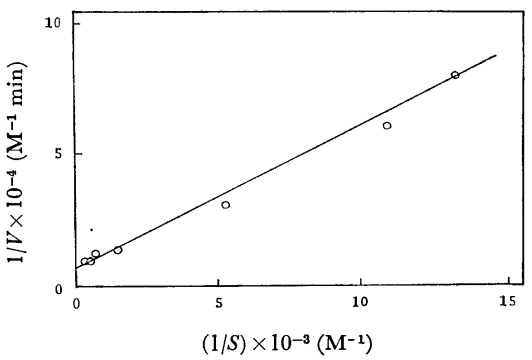

Fig. 6. Lineweaver-Burk plot for the hydrolysis of *p*-nitrophenyl acetate catalysed by Cyclic decapeptide (I) under condition indicated in Table 3

4) S. Shaltiel and M. Fridkin, *Biochemistry*, **9**, 5122 (1970).
5) G. Ellman, *Arch. Biochem. Biophys.*, **82**, 70 (1959).
6) S. Akabori, T. Kaneko, and K. Narita, "Chemistry of Proteines", Vol. 1, Kyoritsu Shuppan CO., Tokyo, (1969), p. 338.

Moreover, the Lineweaver-Burk plot of the data in Table 3 gives a straight line, as is shown in Fig. 6; the Michaelis-Menten constant, K_m, and the catalytic constant, K_{cat}, were 2.7 mM and 0.168 min^{-1} respectively. When the catalytic coefficient, K_2, was plotted against different pH values in the presence of a large excess of the substrate, the curve of K_2 was of a bell type and has an optimum pH at about 7.6, as is shown in Fig. 7.

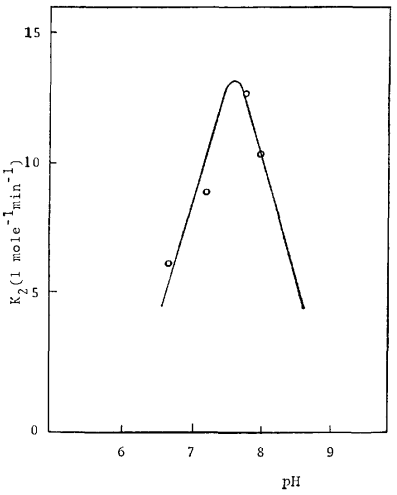

Fig. 7. PH dependance of catalytic coefficient for hydrolysis of *p*-nitrophenyl acetate by the cyclic decapeptide (I) in 1/15 M phosphate buffer containing 3.23% dioxane and DMF (v/v) at 24°C: [NPA]=1.57 mM, [Decapeptide-I]= 2.37 mM

From the above results, it may be concluded that the cyclic decapeptide behaves as an acid-base type catalyst; it seems that the reaction proceeds through a soft binding intermediate (the so-called E-S complex), as in a usual enzyme system. The kinase-like activity will be investigated by using this same cyclic decapeptide in the near future.

Experimental

All the melting points are uncorrected. The infrared spectra were measured on a Hitachi Infrared Spectrophotometer, EPI-G3. The kinetics were followed with a Hitachi Photo-Electric Spectrophotometer, EPU-2. The purity of the compound was confirmed by thin-layer chromatography on Kieselgel G.

Boc-Cys(SBzl)-D-Phe-OMe (II). Boc-Cys(SBzl)-OH[7] (from the cyclohexylamine salt; 19.8 g, 50 mmol) was treated with DCC (11.4 g, 55 mmol) and H-D-Phe-OMe (from hydrochloride; 11.9 g, 55 mmol) in methylene chloride (250 ml) at 0 °C. After the reaction mixture had been allowed to stand overnight in the refrigerator, acetic acid (2 ml) was added and the mixture was stirred for 15 min. The dicyclohexyl urea thus produced was then filtered off, and the filtrate was washed with M sodium bicarbonate, M hydrochloric acid, and water successively, dried over anhydrous sodium sulfate, and concentrated under reduced pressure. II was obtained from ethyl acetate–*n*-hexane in a 90.5% yield (21.4 g); mp 79 °C, $[\alpha]_D^{23}$ −33.3° (*c* 2.0, AcOH).

Found: C, 63.40; H, 6.90; N, 6.01; S, 6.89%. Calcd for $C_{25}H_{32}N_2O_5S$: C, 63.53; H, 6.83; N, 5.93; S, 6.78%.

Boc-Cys(SBzl)-D-Phe-NHNH$_2$ (III). 80% hydrazine hydrate (18.15 g, 300 mmol) was added to a solution of II (14.16 g, 30 mmol) in methanol (80 ml), and the solution was stirred for 30 min in an ice bath. After the reaction mixture had been kept at room temperature for one day, the addition of water to this reaction mixture gave white crystals. III was yielded; 13.9 g (98%); mp 110 °C, $[\alpha]_D^{23}$ −23.0° (*c* 2.0, AcOH).

Found: C, 60.92; H, 6.87; N, 11.59; S, 6.96%. Calcd for $C_{24}H_{32}N_4O_4S$: C, 60.99; H, 6.83; N, 11.80; S, 6.78%.

Boc-Cys(SBzl)-D-Phe-Gly-OH (IV). Into a solution of III (16.54 g, 35 mmol) in DMF (300 ml) and M hydrochloric acid (70 ml), was added, drop by drop, M sodium nitrite (35 ml, 35 mmol) under cooling at −15 °C. After stirring for 40 min, the reaction mixture was neutralized by the addition of triethylamine. A solution of glycine (7.88 g, 105 mmol), triethylamine (14.65 ml, 105 mmol), and water (35 ml) was added, drop by drop, into an azide solution at −10 °C. After the reaction mixture had then been stirred at −10 °C for 2 hr and allowed to stand overnight in a refrigerator, the mixture was acidified to pH 2 with 2 M hydrochloric acid, the precipitate appeared was collected and washed with water. The product was recrystallized from methanol-water. IV was yielded; 17.3 g (95.5%); mp 186.7—187 °C, $[\alpha]_D^{23}$ −22.0° (*c* 0.5, pyridine).

Found: C, 60.59; H, 6.55; N, 8.07; S, 6.50%. Calcd for $C_{20}H_{33}N_3O_6S$: C, 60.57; H, 6.45; N, 8.15; S, 6.22%.

H-Cys(SBzl)-D-Phe-Gly-OH·HCl (V·HCl). The dry hydrogen chloride was bubbled through a suspended solution of IV (7.73 g, 15 mmol) in ethyl acetate (90 ml) for 30 min at 0 °C; the solution was then allowed to stand in an ice bath for an additional 30 min. After the solvent had been removed under reduced pressure, anhydrous ether was added to the residual oil. The crystals (V·HCl) produced were obtained in the theoretical yield; mp 183—184 °C. $[\alpha]_D^{23}$ + 16.0° (*c* 0.5, AcOH).

Found: C, 55.82; H, 5.87; N, 9.18; S, 7.05; Cl, 7.74%. Calcd for $C_{21}H_{26}N_3O_4SCl$: C, 55.81; H, 5.80; N, 9.30; S, 7.09; Cl, 7.84%.

Boc-Glu(OBzl)-OSu (VI). Boc-Glu(OBzl)-OH[7] (from dicyclohexylamine salt, 25.94 g, 50 mmol) was treated with HOSu (6.33 g, 55 mmol) and DCC (11.4 g, 55 mmol) in methylene chloride (100 ml) at −5 °C while being stirred for 5 hr. After the reaction mixture had then been allowed to stand overnight in a refrigerator and acetic acid (1 ml) had been added, the dicyclohexyl urea thus produced was filtered off and the filtrate was washed with 0.5 M sodium bicarbonate, 0.5 M hydrochloric acid, and water successively, dried over anhydrous sodium sulfate, and concentrated under reduced pressure. The residual oil was crystallized from 2-propanol; 17.97 g (83.6%); mp 101 °C. $[\alpha]_D^{23}$ −23.4° (*c* 2.0, dioxane). ν_{max}^{KBr} 1815, 1785, 1740 cm^{-1} (ester).

Found: C, 58.35; H, 6.18; N, 6.58%. Calcd for $C_{21}H_{26}N_2O_7$: C, 58.06; H, 6.08; N, 6.48%.

Boc-Glu(OBzl)-Cys(SBzl)-D-Phe-Gly-OH (VII). The solid VI (13.1 g, 30 mmol) was added to a solution of V(from hydrochloride, 14.94 g, 33 mmol) and triethylamine (9.24 ml, 66 mmol) in 65% dioxane (100 ml) at room temperature. After stirring for 48 hr, the reaction mixture was acidified to pH 2 with M hydrochloric acid. The precipitate thus formed was extracted with ethyl acetate; the ethyl acetate solution was dried over anhydrous sodium sulfate and was concentrated under reduced pressure. The residual product was crystallized from methanol-water. VII was

7) E. Schnabel, *Ann. Chem.*, **702**, 188 (1968); E. Schnabel, H. Herzog, P. Hoffmann, E. Klauke, and I. Ugi, *ibid.*, **716**, 175 (1968).

thus yielded; 19.3 g (88%); mp 154—154.5 °C, $[\alpha]_D^{23}$ −1.83° (*c* 0.5, pyridine).

Found: C, 62.05; H, 6.28; N, 7.39; S, 4.57%. Calcd for $C_{38}H_{46}N_4O_9S$: C, 62.11; H, 6.31; N, 7.62; S, 4.36%.

*H–Glu(OBzl)–Cys(SBzl)–*D*-Phe–Gly–OH·HCl (VIII·HCl).* The dry hydrogen chloride was bubbled through a suspended solution of VII (11.01 g, 15 mmol) in dioxane (140 ml) at 0 °C for 30 min and was then allowed to stand in an ice bath for an additional 30 min. After the solvent had been removed under reduced pressure, anhydrous ether was added to the residue. White crystals were obtained in the theoretical yield; mp 178—178.5 °C. $[\alpha]_D^{23}$ +1.0° (*c* 0.5, AcOH).

Found: C, 59.25; H, 5.73; N, 8.17; S, 4.63; Cl, 5.20%. Calcd for $C_{33}H_{39}N_4O_7SCl$: C, 59.05; H, 5.86; N, 8.35; S, 4.78; Cl, 5.28%.

*Boc–His(*im*-Dnp)–OSu (IX).* Boc–His(*im*-Dnp)–OH[8] (1.58 g, 3.7 mmol) was treated with HOSu (472 mg, 4.1 mmol) and DCC (846 mg, 4.1 mmol) in dimethoxyethane (20 ml) and methylene chloride (10 ml) at 0 °C while being stirred for 10 hr. From the reaction mixture, IX was obtained by the method used in the case of VI. The product was recrystallized from ethyl acetate–ether–*n*-hexane. IX was obtained in an 83% (1.59 g) yield; mp 146—146.5 °C. $[\alpha]_D^{23}$ −3.37° (*c* 0.9, DMF). ν_{max}^{KBr} 1819, 1780, 1745 cm^{-1} (ester).

Found: C, 47.27; H, 4.25; N, 15.32%. Calcd for $C_{21}H_{22}N_6O_{10}\cdot H_2O$: C, 47.02; H, 4.51; N, 15.67%.

*Boc–His(*im*-Dnp)–Glu(OBzl)–Cys(SBzl)–*D*-Phe–Gly–OH (X).* Into a solution of VIII·HCl (6.4 g, 9 mmol) in DMF (20 ml) and water (2 ml), we stirred a solution of triethylamine (2.5 ml, 18 mmol) in DMF (5 ml) over a 20 min period at 0 °C; solid IX (7.33 g, 13.5 mmol) was then added to the above solution. After the reaction mixture had been stirred for 48 hr at room temperature, the reaction mixture was acidified to pH 2 with M hydrochloric acid, and water was added. The yellow precipitate was recrystallized from methanol–methylene chloride–ether. The yellow crystals were thus obtained in an 87.6% (8.18 g) yield; mp 153—154 °C. $[\alpha]_D^{23}$ −12.5° (*c* 0.3, DMF).

Found: C, 55.93; H, 5.18; N, 11.53; S, 3.10%. Calcd for $C_{50}H_{59}N_9O_{16}S$: C, 55.91; H, 5.54; N, 11.74; S, 2.98%.

*Boc–Glu(OBzl)–Cys(SBzl)–*D*-Phe–Gly–ONp (XI).* A solution of VII (7.35 g, 10 mmol) and *p*-nitrophenol (2.78 g, 20 mmol) in methylene chloride (10 ml) and acetonitrile (10 ml) was treated with DCC (2.27 g, 11 mmol) at 0 °C for 4 hr with stirring. After the dicyclohexyl urea thus produced had been filtered off, the reaction mixture was washed with M sodium bicarbonate, 0.1 M hydrochloric acid, and water successively, and then dried over anhydrous sodium sulfate. The solvent was evaporated under reduced pressure. The residual crystals were recrystallized from methylene chloride–ether–*n*-hexane (6.74 g, 78.7%); mp 127—128 °C, $[\alpha]_D^{24}$ −5.8° (*c* 0.3, DMF), R_f[9] 0.92 (aqueous AcOEt). ν_{max}^{KBr} 1780 cm^{-1} (ester).

Found: C, 61.53; H, 5.83; N, 7.88; S, 4.01%. Calcd for $C_{44}H_{49}N_5O_{11}S$: C, 61.74; H, 5.77; N, 8.18; S, 3.75%.

*H–His(*im*-Dnp)–Glu(OBzl)–Cys(SBzl)–*D*-Phe–Gly–OH·HCl (XII·HCl).* The dry hydrogen chloride gas was bubbled through a solution of X (1.15 g, 1.1 mmol) in ethylacetate (30 ml) containing anisole (1.5 ml) for 10 min at 0 °C; the reaction mixture was then allowed to stand at room temperature for 30 min. After the solvent had been evaporated under reduced pressure, anhydrous ether was added; the crystals thus formed were collected in the theoretical yield. The products were used immediately for the next reaction.

*Boc–Glu(OBzl)–Cys(SBzl)–*D*-Phe–Gly–His(*im*-Dnp)–Glu(OBzl)–Cys(SBzl)–*D*-Phe–Gly–OH (XIII).* The solid XI (486 mg, 0.568 mmol) was added to a solution of XII·HCl (609 mg, 0.625 mmol) and triethylamine (0.26 ml, 1.875 mmol) in DMF (5 ml). After the reaction mixture had been stirred for 3 days at room temperature, it was acidified to pH 2 by the use of M hydrochloric acid in an ice bath and the precipitate thus formed was collected by filtration. The recrystallization from DMF–water gave a pure XIII; 881 mg, (92.7% yield); mp 187 °C (decomp.), $[\alpha]_D^{32}$ −4.2° (*c* 0.4, DMF). R_f[9] 0.80 (PW), 0.80 (BAW).

Found: C, 59.58; H, 5.44; N, 10.86; S, 4.03%. Calcd for $C_{87}H_{93}N_{13}O_{21}S_2$: C, 59.59; H, 5.60; N, 10.86; S, 3.83%.

*H–Glu(OBzl)–Cys(SBzl)–*D*-Phe–Gly–His(*im*-Dnp)–Glu(OBzl)–Cys(SBzl)–*D*-Phe–Gly–OH (XIV).* The dry hydrogen chloride gas was bubbled through a solution of XIII (1 g, 0.6 mmol) in dioxane (20 ml) and methylene chloride (20 ml) containing anisole (1.5 ml) for 30 min in an ice bath. After the reaction mixture had then been allowed to stand for 1.5 hr, the solution was concentrated under reduced pressure. The addition of anhydrous ether gave yellow crystals of XIV·HCl in the theoretical yield. Free XIV was obtained by the isoelectric point precipitation method; mp 175—177 °C. $[\alpha]_D^{23}$ −21.0° (*c* 1.1, DMF).

Found: C, 58.00; H, 5.43; N, 11.68; S, 3.63%. Calcd for $C_{78}H_{89}N_{13}O_{21}S_2$: C, 58.23; H, 5.58; N, 11.32; S, 3.99%.

*Boc–(His(*im*-Dnp)–Glu(OBzl)–Cys(SBzl)–*D*-Phe–Gly)$_2$–OH (XV).* Into a solution of XIV·HCl (2.168 g, 1.347 mmol) in DMF (10 ml) and water (1 ml), we stirred triethylamine (0.376 ml, 2.7 mmol) over a 20 min period in an ice bath. Solid IX (1.4 g, 2.7 mmol) was then added to the above solution. After the reaction mixture had been stirred at room temperature for an additional 3 days, the reaction mixture was acidified to pH 2 by the addition of M hydrochloric acid and the precipitate thus fromed was collected by filtration. The recrystallization form DMF–water gave pure yellow crystals in a 90% yield (2.37 g); mp 200 °C (decomp.). $[\alpha]_D^{24}$ −10.7° (*c* 0.3, DMF). R_f[9] 0.84 (PW), 0.86 (BAW).

Found: C, 56.63; H, 4.98; N, 12.13; S, 3.53%. Calcd for $C_{95}H_{105}N_{18}O_{28}S_2$: C, 56.71; H, 5.31; N, 12.53; S, 3.19%.

*Boc–(His(*im*-Dnp)–Glu(OBzl)–Cys(SBzl)–*D*-Phe–Gly)$_2$–NH–NH–Boc (XVI).* Into a solution of XV (1.96 g, 1 mmol), Boc–NHNH$_2$ (146 mg, 1.1 mmol), HOSu (230 mg, 2 mmol) in DMF (10 ml), we stirred, drop by drop, a solution of DCC (247 mg, 1.2 mmol) in DMF (3 ml) at 0 °C; the reaction mixture was then allowed to stand for 72 hr in a refrigerator. After the addition of acetic acid (0.5 ml), the dicyclohexyl urea thus produced was filtered off and was washed with cold DMF (3 ml). The filtrate was concentrated under reduced pressure, and the residual oily product was scratched by anhydrous ether. The powder-like product was recrystallized from DMF–water in a 97% yield (2.0 g); mp 192—192.3 °C (decomp.). $[\alpha]_D^{23}$ −6.53° (*c* 0.45, DMF). R_f[9] 0.73 (aqueous AcOEt).

Found: C, 58.05; H, 5.80; N, 13.32; S, 3.37%. Calcd for $C_{100}H_{110}N_{20}O_{26}S_2$: C, 57.96; H, 5.35; N, 13.52; S, 3.09%.

*Cyclo(His(*im*-Dnp)–Glu(OBzl)–Cys(SBzl)–*D*-Phe–Gly)$_2$ (XVIII).* *a)* Via *the Azide Method*: The dry hydrogen chloride gas was bubbled through a suspended solution of XVI (1.036 g, 0.5 mmol) in anhydrous dioxane (20 ml) con-

8) F. Chillemi and R. B. Merrifield, *Biochemistry*, **8**, 4344 (1969).

9) The thin layer chromatography solvent system. aqueous AcOEt: water saturated with ethyl acetate, PW: pyridine-water (4:1 v/v), BAW: *n*-butanol–acetic acid–water (4:1:1 v/v), BAPW: *n*-butanol-acetic acid–pyridine–water (4: 1: 2: 1 v/v).

taining anisole (1 ml) for 30 min at 0 °C. After the reaction mixture had been allowed to stand for 45 min at room temperature, the solvent was removed under reduced pressure; the addition of anhydrous ether to the residual oil gave a pure yellow product of decapeptide hydrazide di-hydrochloride (XVII·2HCl) in the theoretical yield.

Found: C, 52.27; H, 5.20; N, 13.86; S, 3.39%. Calcd for $C_{90}H_{110}N_{20}O_{29}S_2Cl_2$: C, 52.19; H, 5.35; N, 13.52; S, 3.10%.

The hydrazide was used immediately in the following cyclization procedure. Into a solution of XVII·2HCl (850 mg, 0.415 mmol) in DMF (10 ml) and acetic acid (10 ml), we stirred M sodium nitrite (0.45 ml, 0.45 mmol) and M hydrochloric acid (0.415 ml, 0.415 mmol) cooling at −10—−15 °C over a 60 min period. The reaction mixture was added, drop by drop, into cold pyridine (320 ml) at 0 °C over a 5 min. After the reaction mixture was stirred for an additional 24 hr at 0 °C. After the solvent had been evaporated under reduced pressure and water had been added to the residual oil, the product was collected by filtration and was dissolved in a mixed solvent of methanol–methylene chloride–DMF–water (17: 32: 5: 6 v/v). The solution was then treated with IRC-50 (1.5×25 cm) and IR-45 (1.5×25 cm) columns. The effluent (200 ml) was concentrated under reduced pressure, and the products were purified with Sephadex LH-20 by a mixed solvent of DMF–methylene chloride (1: 1 v/v). XVIII was obtained as crystals from DMF–water in an 87.6% yield (610 mg); mp 165—166.5 °C. $[\alpha]_D^{23}$ −21.4° (*c* 0.35, DMF). R_f[9] 0.94 (PW), 0.88 (BAW).

Found: C, 55.34; H, 5.12; N, 12.46; S, 3.61%. Calcd for $C_{90}H_{90}N_{18}O_{22}S_2\cdot 6H_2O$: C, 55.49; H, 5.28; N, 12.94; S, 3.29%. Mol wt Found:[10] 1880. Calcd for $C_{90}H_{90}N_{18}O_{22}S_2$: 1840.

b) Via *the ONp Method*: Di-*p*-nitrophenyl sulfite (4 g, 12.9 mmol) was added to a solution of XV (587 mg, 0.33 mmol) in pyridine (4 ml). After the mixture had been allowed to stand for 4 days at room temperature, the solvent was evaporated under reduced pressure. The residual product (XIX) was collected by using anhydrous ether (432mg); ν_{max}^{KBr} 1775 cm^{-1} (ester). XIX was treated with formic acid (5 ml) containing anisole (1 ml) at 20 °C. After the reaction mixture had been allowed to stand for 4 hr, the solution was concentrated under reduced pressure, and the *p*-nitrophenyl ester formate was immediately dissolved in DMF (10 ml) containing a small amount of acetic acid. The DMF solution was stirred, drop by drop, into prydine (148 ml) at 60 °C over a 4 hr period; the stirring was then continued for an additional 2 hr. Cyclic decapeptide (XVIII) was obtained in a 52% yield (334 mg) by the purification procedure described in a).

c) Via *the OSu Method*: The solution of XV (1.96 g, 1 mmol) and HOSu (253 mg, 2.2 mmol) in DMF (10 ml) was treated with DCC (453 mg, 2.2 mmol) at 0 °C for 4 hr. After the dicyclohexyl urea had been filtered off, the reaction mixture was concentrated under reduced pressure and the product (XX) was collected by using anhydrous ether; ν_{max}^{KBr} 1820, 1785, and 1742 cm^{-1} (C=O and ester). The active ester was dissolved in TFA (10 ml) containing anisole (1 ml). After the mixture had been allowed to stand at 0 °C for 2 hr, the solvent was removed under reduced pressure. The addition of anhydrous ether to the residual product gave decapeptide succinimide ester trifluoroacetate. The active ester was used immediately in the following cyclization procedure. A solution of the active ester dissolved in DMF (10 ml) containing 6 drops of acetic acid was added drop by drop into anhydrous pyridine (755 ml) at room temperature over a period 12 hr with stirring. The reaction mixture was also treated by the same purification procedure as has been described in a), but XVIII was not isolated; it was only detected by thin-layer chromatography.

*Cyclo(His–Glu–Cys–*D*-Phe–Gly)$_2$·2AcOH (I·2AcOH).* *i) Removal of the Benzyl Ester and the* s*-Benzyl Group*: XVIII (1.27 g, 0.7 mmol) was treated with anhydrous HF (10 ml) containing anisole (1.5 ml) at room temperature for 90 min. After the reaction mixture had been concentrated under reduced pressure, the residual oil was dissolved in aqueous acetic acid and the residual anisole was extracted with ether from the aqueous acetic acid layer. Also, the acetic acid layer was treated with an IR-45 (1.5×30 cm, acetate form) column. The effluent (100 ml) was concentrated under reduced pressure; the addition of peroxide-free anhydrous ether to the residual oil gave a white powder (XXI).

ii) Removal of the Dinitrophenyl Group: XXI was dissolved in DMF (10 ml), and the solution was adjusted to pH 8 with 10% sodium carbonate. After 2-mercaptoethanol (60 ml)[4] had been added to the above solution, the reaction mixture was allowed to stand at room temperature for 3 hr. The reaction mixture was then neutralized by acetic acid and was concentrated under reduced pressure. The residual product was immediately treated by the use of a Sephadex G-15 (5×50 cm) column by using 50% aqueous acetic acid. When the effluent was concentrated under reduced pressure and the residue was treated with peroxide-free ether, the free cyclic decapeptide (I) was obtained in a 64.9% yield (606 mg). $[\alpha]_D^{23}$ +3.5° (*c* 0.3, DMF). The purity of I was checked by thin-layer chromatography on Kieselgel G and by paper electrophoresis. The thin-layer chromatography of I showed a single spot; R_f[9] 0.56 (BAW): Pauly reaction, nitroprusside reaction positive; ninhydrin negative. On the paper electrophoresis, I moved as a single band toward the cathode; R_{His} 0.24.[11] No disulfide bond at all was detected in I by either the Ellman[5] or iodoacetamide method.[6]

Found: C, 45.64; H, 5.94; N, 13.71; S, 4.73%. Calcd for $C_{50}H_{62}N_{14}O_{14}S_2\cdot 2AcOH\cdot 8H_2O$: C, 45.95; H, 6.14; N, 13.89; S, 4.54%.

*H–(His–Glu–Cys–*D*-Phe–Gly)$_2$–OH·3AcOH (XXIII·3AcOH).* XV (964 mg, 0.5 mmol) was treated with anhydrous HF (15 ml) containing anisole (1.5 ml) at room temperature for 1 hr. After the reaction mixture had been treated in the same way as in the case of the cyclic decapeptide (I), the debenzylated product (XXII) was obtained in a 78% yield (609 mg). XXII (151 mg, 0.1 mmol) was treated with 2-mercaptoethanol (1.56 g, 20 mmol) in DMF (5 ml) at pH 8. XXIII was purified by the same method used for the cyclic decapeptide (I). XXIII·3AcOH was thus obtained in a 44.7% yield (65 mg). $[\alpha]_D^{23}$ +1.7° (*c* 0.3, DMF). R_f[9] 0.08 (BAW). R_{His} 0.58.[11] The amount of the free thiol group was measured by the Ellman method.[5]

Found: C, 46.03; H, 5.74; N, 13.56; S, 4.70%. Calcd for $C_{50}H_{64}N_{14}O_{15}S_2\cdot 3AcOH\cdot 6H_2O$: C, 46.27; H, 6.10; N, 13.49; S, 4.43%.

Kinetic Method of Catalytic Activity. A solution of a 1/15 M phosphate buffer containing dioxane and DMF was used for all the kinetic measurements, and all the experiments were carried out at 24±1 °C. DMF was used to increase the solubility of the peptide (I or XXIII) in the buffer solution.

The linear (XXIII) and the cyclic decapeptide (I) were

10) Molecular weight was measured by a Knauer Thermoelectric Cooling Unit for cryoscopic measurements using formic acid as a solvent.

11) Solvent system: pH 1.8 (HCOOH–AcOH–MeOH–water, 1: 3: 6: 10 v/v), 1000 v/20 cm, 1 hr, Toyo Roshi No. 50.

weighed and dissolved in DMF (1 ml) and the buffer (29 ml). The buffer solution was pretreated with nitrogen gas to remove the oxygen in the solution. A solution (0.1 ml) of *p*-nitrophenyl acetate in peroxide-free dioxane was added to the peptide solution (3 ml). The reaction mixture was rapidly stirred and the liberated *p*-nitrophenol was detected by the use of a Hitachi Photo-Electric Spectrophotometer (at 400 nm[3]).

BULLETIN OF THE CHEMICAL SOCIETY OF JAPAN, VOL. 46, 1816—1819 (1973)

The Formation and Chelate-forming Properties of 2-Chloriminocyclohexanone Oxime and Its Hydrochloride

Yoshinari KOBAYASHI and Shigeru WAKAMATSU

Chemicals Research and Development Laboratories, Toray Industries, Inc., Minato-ku, Nagoya 455–91

(Received December 4, 1972)

Cyclohexane-1,2-dione dioxime (**1**) in absolute ethanol containing hydrogen chloride was subjected to an irreversible dehydration to afford 2-chloriminocyclohexanone oxime hydrochloride (**2**), which could be liberated by cautious neutralization with sodium carbonate. The novel free and salt-form compounds thus obtained reacted with metal ions, such as Cu(II), Co(II), Ni(II), and Pd(II), to afford stable complexes. The molar ratio and the consecutive stability constants of a Ni(II) complex of **2** were determined and compared with those of a complex of **1** with Ni(II). An approximate linear relationship between the logarithm of the rate constant of the *N*-chlorimination and the acidity function, H_0, was observed.

The ordinary reaction of oximes with hydrogen chloride in nonaqueous solvents affords the corresponding stable salts, which can be reversibly set free with strong bases. Cyclohexanone oxime[1a,b] and its 2-substituted derivatives,[1c,d] the substituents of which are alkyl, alkoxyl, hydroxyl, piperidinyl, morpholinyl, and so on, are typical examples. In an attempt to prepare cyclohexanedione dioxime dihydrochlorides, we have found that cyclohexane-1,2-dione dioxime (**1**) can readily be transformed into novel 2-chloriminocyclohexanone oxime hydrochloride (**2**). The conventional synthetic routes to *N*-chlorimines are the chlorination of the corresponding imines with hypochloric acid or its derivatives,[2–5] the reaction of carbonyl compounds with chloramine[6,7] and the dehydrochlorination of *N,N*-dichloro-*sec*-alkylamines by the action of strong bases.[8–10] There are few papers[11] reporting the direct conversion of hydroxyimino group into *N*-chlorimine. The present paper will report the formation of **2** from **1** by the direct displacement of one of the hydroxyl groups of the hydroxyimino groups with chloride and the chemical properties, especially, related to a ligand in chelate complexes.

Results and Discussion

Formation of 2-Chloriminocyclohexanone Oxime and Its Hydrochloride. It was found that when an absolute ethanolic solution of cyclohexane-1,2-dione dioxime (**1**) was, after the introduction of dry hydrogen chloride to saturation at temperatures between −1 and 1 °C, allowed to stand for several days at a low temperature colorless-needle-form crystalline 2-chloriminocyclohexanone oxime hydrochloride (**2**) was precipitated with the formation of its equivalent molar water.

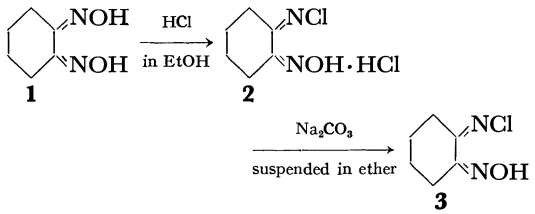

1 **2** **3**

As is shown in Fig. 1, the chloride titrations of **2** with silver nitrate indicates that the ionic chloride in **2** is equal to half of the total chlorine content. The successful liberation of **2** to 2-chloriminocyclohexanone oxime (**3**) proceeded by means of the neutralization of 2 suspended in diethyl ether with an aqueous sodium carbonate solution at temperatures between −10 and 5 °C.

1) a) H. Saito, K. Nukada, and M. Ohno, *Tetrahedron Lett.*, **1964**, 2124. b) H. Saito, *Nippon Kagaku Zasshi*, **85**, 724 (1964). c) H. Saito and K. Nukada, *J. Mol. Spectrosc.*, **18**, 1 (1965). d) H. Saito, I. Terasawa, M. Ohno, and K. Nukada, *J. Amer. Chem. Soc.*, **91**, 6696 (1969).

2) P. P. Peterson, *Amer. Chem. J.*, **46**, 325 (1911).

3) K. N. Campbell, *J. Amer. Chem. Soc.*, **59**, 2058 (1937).

4) a) H. E. Baumgarten and F. A. Bower, *ibid.*, **76**, 4561 (1954). b) H. E. Baumgarten and J. M. Petersen, *ibid.*, **82**, 459 (1960). c) H. E. Baumgarten, J. M. Petersen, and D. C. Wolf, *J. Org. Chem.*, **28**, 2369 (1963).

5) G. F. Wright, L. K. Jackson, and G. W. R. Smart, *J. Amer. Chem. Soc.*, **69**, 1539 (1947).

6) C. R. Hauser, *ibid.*, **52**, 1108 (1930).

7) B. Rudner (to W. R. Grace & Co.) U.S. 2894028 (1959).

8) S. L. Reid and D. B. Sharp, *J. Org. Chem.*, **26**, 2567 (1961).

9) G. H. Alt and W. S. Knowles, *ibid.*, **25**, 2047 (1960).

10) S. L. Reid (to Monosonto Co.) U.S. 3137728 (1964).

11) Although Hantzsch[12] had assumed the formation of *N*-chlorimines as intermediates of the Beckmann rearrangement of oximes in PCl_3, this assumption was denied by Theilacker and Mohl.[13]

12) A. Hantzsch, *Ber.*, **24**, 23 (1891).

13) W. Theilacker and H. Mohl, *Ann. Chem.*, **563**, 99 (1949).

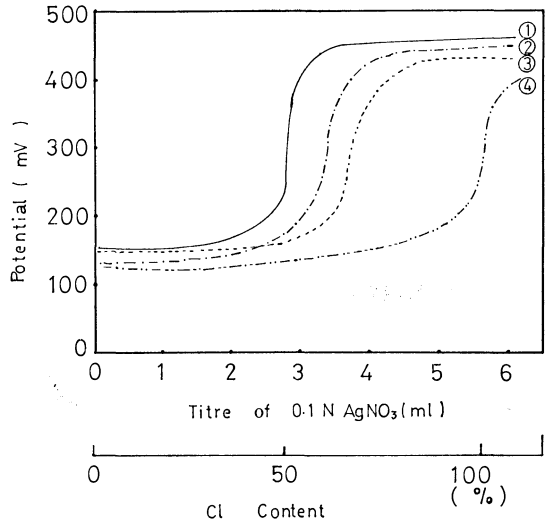

Fig. 1. $AgNO_3$ titration curves of 2-chloriminocyclohexanone oxime hydrochloride.
Condition: Sample 55.5 mg/30 ml H_2O; Temp. 25°C
1: Without buffer solution (pH 2.3); 2: Buffer solution pH 4.6; 3: Buffer solution pH 6.3—7.3; 4: Hydrolysis in alkaline solution.

The structures of **2** and **3** were supported not only by the results of the elemental analysis, the molecular-weight determinations, the titration curves and the UV and IR spectra, but also by the formation of such derivatives as cyclohexane-1,2-dione bis-(2,4-dinitrophenylhydrazone) and 1,2,3,4,6,7,8,9-octahydrophenazine: the latter was obtained by the hydrogenation of **2** in ethanol over palladium chloride. Compounds **2** and **3** also retained such chelate-forming properties as those in **1**.

Acyclic vicinal dioximes, such as dimethylglyoxime, diphenylglyoxime and di-α-furylglyoxime, normally gave the corresponding dihydrochlorides by reactions with hydrogen chloride under the same anhydrous conditions. Cyclohexane-1,3-dione dioxime monohydrochloride was immediately precipitated from an absolute ethanolic solution as soon as dry hydrogen chloride was introduced. Simple dihydrochloride, however, could not be isolated even from the solution saturated with hydrogen chloride. This result is in marked contrast with that of cyclohexane-1,4-dione dioxime, which affords the normal dihydrochloride.

From these results, we can conclude that the *N*-chlorimine formation is limited to **1**. The structure of cyclohexanone oxime hydrochloride has been reported to be one in which proton is donated to the nitrogen atom.[1] In the case of **1**, the proton transfer to the oxygen atom in one of the hydroxyimino groups is supposed to bring about a partial ionization of the hydroxyimino group as in an intermediate of the Beckmann rearrangement. The electron deficient nitrogen or nitronium thus formed may then be nucleophilically attacked by chloride to afford the *N*-chlorimine.

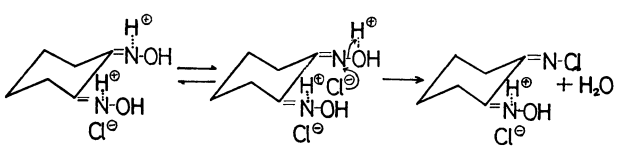

The peculiar reactivity of **1** may be ascribed to the fact that the rigid co-planarity of vicinal dioxime groups where protons donate and when counter anions, chloride anions, exist, makes the salt unstable and so likely to undergo the α-displacement described above.

Table 1. Rate constants of 2-chloriminocyclohexanone oxime hydrochloride formation from cyclohexane-1,2-dione dioxime[a] in ethanol

Temperature (°C) (±0.1)	Rate constants (hr^{-1}) × 10^{-2}		
	From the dioxime	From H_2O formed	Mean
0.0	1.72	1.48	1.60
10.0	2.88	3.22	3.05
20.0	7.66	5.27	6.45

a) The concentration of hydrogen chloride was 34.0—34.8% by weight.

Table 2. Determination of thermodynamic quantities in the formation of 2-chloriminocyclohexanone oxime hydrochloride

Solvent	E_a (kcal/mol)	(e.u.)$\Delta S^{\neq}$	Concentration of HCl (wt%)
Ethanol	11.1	−19.4	34
Dioxane	19.4	− 8.4	10
Cyclohexanone oxime dihydrochloride	7.1	−39.1	36

Kinetics. The rate of the conversion of **1** into **2** was of the first order in a non-aqueous solution at a given concentration of hydrogen chloride. Table 1 shows that the decreasing rate of **1** was approximately equal to the rate of the formation of water. The activation energy was measured in ethanol, dioxane and cyclohexanone oxime;[14] the results are shown in Table 2. These substances are all solvent-dependent, *i.e.*, smaller in more polar solvents. The rate of the *N*-chlorimination increased with an increase in the concentration of hydrogen chloride in absolute ethanol, but there was no linear relationship between them. However, when the acidity function, H_0, was measured in an absolute ethanol solution of hydrogen chloride at 10 °C, an approximate linear relationship between the logarithm of the rate constant, k, and the acidity function, H_0, was observed (Fig. 2). In discussing the probable transition state from the relationship between the rate constant and the acidity function, H_0, Hammett[15] suggested that when the conjugate acid of the reactant takes part in the rate-determining step, the $\log k = -H_0 + \text{const.}$ relation should hold. This prediction of the unit slope relationship was not realized in the authors' experiments, but there may be some significance in the approximate linear relationship between $\log k$ and H_0.

Chelate-forming Properties. The *N*-chlorimines **2** and **3** co-ordinate to various metal ions, *e.g.*, copper-

14) Cyclohexanone oxime dihydrochloride forms an oily material.[1a,1b]

15) L. P. Hammett, "Physical Organic Chemistry," McGraw-Hill Book Co., Inc., New York, N. Y. (1940), p. 273.

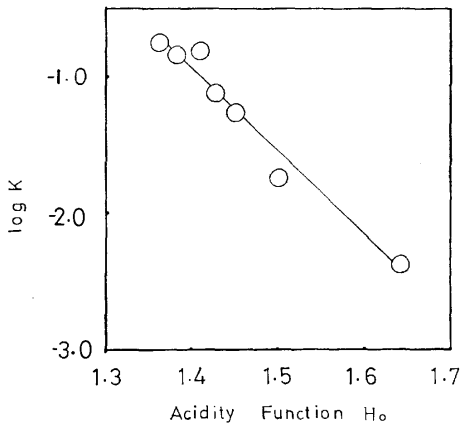

Fig. 2. The relationship between acidity H_0 and log k in 2-chloriminocyclohexanone oxime hydrochloride formation.

(II), nickel(II), cobalt(II), and palladium(II) ions, such as **1** does. However, the *N*-chlorimines are not polarographically active.

Copper(II) Complex of 2. The absorption spectra change on the change in the molar ratio of **2** to the copper(II) ion and the pH of its aqueous solution. In a neutral solution, the complex has its maximum absorption at 264 nm in the presence of an excess of copper(II) ion. However, when the molar ratio is higher than two, the complex shows its maximum at 545 nm ($\varepsilon=1.03\times10^2$). At pH values below three, the complex is not formed. A stable violet complex solution is obtained at pH value from 5 to 6. By Job's continuous variation method,[16] the molar ratio was determined to be two in the stable complex in solution.

Nickel(II) Complex of 2. The formation of the nickel(II) complex was considerably affected by the pH, and the chelate could be formed only in the alkaline range. The absorption spectrum has no maximum at pH 10, but a shoulder at 420 nm ($\varepsilon=7.10\times10^2$). In a buffer solution at pH 8.0, the molar ratio was determined to be two by Job's method. By means of Bjerrum's pH measurement method[17] and Block-McIntyre calculations[18] the consecutive stability constants were measured in 75% aqueous dioxane at 20 °C and found to be $\log k_1=7.90$ and $\log k_2=4.81$. Accordingly, appreciable amounts of the mono complex must exist in the presence of an excess of nickel(II). In contrast, vicinal dioximes give the $k_1<k_2$[19] stability constants. Especially, the nickel(II) complex of **1** has stability constants at 25 °C $\log k_1=8.52$ and $\log k_2=8.82$. Therefore, the overall stability constant ($\log k_1\cdot k_2=12.71$) of the nickel(II) complex of **2** is much smaller than that ($\log k_1\cdot k_2=17.34$) of the corresponding complex of **1**. From analogy with the metal (II)-vicinal dioxime complexes,[20] the complex was supposed to have the following structure:

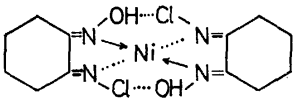

The relative instability of the nickel(II) complex of **2** and the $k_1\gg k_2$ relationship can be attributed to the weaker hydrogen bonding in the –OH···Cl bond in the complex than in the –OH···O bond in the nickel(II) complex of **1**, and to the steric effect of chlorine.

Cobalt(II) and Palladium(II) Complexes. The *N*-chlorimine **2** formed a stable complex with the cobalt(II) ion in an alkaline solution, the absorption spectrum of which had neither maximum nor shoulder. The molar ratio was also shown to be two. The palladium(II) ion readily reacted with **2** to precipitate a yellow complex.

Experimental

Apparatus. The IR spectra were measured on a Shimadzu IR spectrometer IR-27A. The electronic spectra were recorded by means of a Hitachi Spectrometer EPS-2. The pH measurements were made with a Horiba pH Meter, type M. The potentiometric titration curves were obtained by the use of a Metrohm Potentiograph E-336. The molecular weights were determined by means of a Mechrolab Vapor-pressure Osmometer.

Materials. The cyclohexanedione dioximes were prepared by the procedure described in a previous paper.[21] The copper(II), nickel(II), cobalt(II), and palladium(II) ions used were $Cu(OCOCH_3)_2\cdot H_2O$, $NiCl_2\cdot6H_2O$, $CoCl_2\cdot6H_2O$, and $PdCl_2$ respectively, all were of analytical grade purity and were used without further purification.

2-Chloriminocyclohexanone Oxime Hydrochloride (2). To a solution of **1** (90 g) in absolute ethanol (200 ml) on a brine bath at −1—1 °C, we introduced dry hydrogen chloride until the point of saturation (about 33—34% by weight). After the mixture had stood for several days in a refrigerator, colorless needle crystallines were precipitated; they were filtered off and washed with anhydrous diethyl ether. Yield, 80 g (64%). Mp 130 °C (decomp.). UV (ethanol): 224 (log $\varepsilon=4.66$), 265 nm (log $\varepsilon=4.46$). IR (KBr): 3240 (OH), 2600 (N^+–H), 1665 cm^{-1} (C=N). Found: C, 36.45; H, 4.95; O, 8.65; N, 13.69; Cl, 36.64. Calcd for $C_6H_{10}N_2OCl_2$: C, 36.57; H, 5.11; O, 8.12; N, 14.22; Cl, 36.64%. The potentiometric titration curves obtained by the use of silver nitrate are shown in Fig. 1. No such polarographic activity as that of **1**[22] was observed.

2-Chloriminocyclohexanone Oxime (3). Into a suspension of **2** (10.5 g) in diethyl ether (100 ml) on a brine bath at −5—−10 °C, was added drop an aqueous 10% sodium carbonate solution with stirring to bring the pH of the aqueous phase to about 10. After the separation of the ether phase the aqueous phase was extracted with four 25 ml portions of diethyl ether. The ether fractions were then combined and dried over anhydrous sodium sulfate. The solvent was

16) P. Job, *Ann. Chim.*, **9**, (10) 113 (1928).
17) J. Bjerrum, "Metal Ammine Formation in Aqueous Solution". P. Haase & Son. Copenhagen (1941).
18) B. P. Block and G. H. McIntyre, Jr., *J. Amer. Chem. Soc.*, **75**, 5667 (1953).
19) C. V. Banks, The Proceeding of the International Symposium, Analytical Chemistry, held at Birmingum University (U.K.). p. 131, April, 1962.
20) C. V. Banks, *Record Chem. Progr*, **25**, (2) 85 (1964).
21) Y. Kobayashi and S. Wakamatsu, *Tetrahedron*, **23**, 115 (1967).
22) a) M. Ishibashi, T. Fujinaga, and K. Kawamura, This Bulletin, **26**, 513 (1953). b) P. E. Wenger, D. Monnier, and W. Backmann-Chapuis, *Anal. Chim. Acta*, **20**, 444 (1959). c) D. Monnier and W. Haerdi, *Helv. Chim. Acta*, **41**, 2205 (1958).

distilled off, and the residue was recrystallized from water to afford colorless needles. Yield, 6.8 g (85%). Mp 115.0—116.5 °C. UV (water): 265 nm ($\log \varepsilon = 3.99$), IR (KBr); 1655 cm^{-1} (C=N). (mol. wt. by vapor-pressure osmometry in ethanol): 162 (Calcd for 160.2). Found: C, 44.55; H, 5.68; N, 17.47; O, 10.36; Cl, 22.07%. Calcd for $C_6H_9N_2OCl$: C, 44.87; H, 5.65; N, 17.44; O, 9.96; Cl, 22.08%.

Cyclohexane-1,2-dione-bis-(2,4-dinitrophenylhydrazone) from **2**. To a solution of 2,4-dinitrophenylhydrazine (2.0 g) in 95% ethanol (140 ml), conc. hydrochloric acid (100 ml) and **2** (2.0 g) were successively added. The mixture was then refluxed for 30 min with occasional stirring. After the mixture had stood overnight in a refrigerator, an orange precipitate was formed; this was filtered off and recrystallized from ethanol. Yield, 4.9 g. Mp 220—222.5 °C (decomp.); undepressed by admixture with an authentic sample derived from **1** (lit,[23] mp 220 °C). IR: superimposable with that of an authentic sample. Found: C, 45.47; H, 4.02%. Calcd for $C_{18}H_{16}O_8N_8$: C, 45.77; H, 3.42%.

1,2,3,4,6,7,8,9-Octahydrophenazine from **2**. Nine grams of **2** in absolute ethanol (220 g) were hydrogenated by palladium chloride (0.6 g as Pd) under atmospheric pressure at room temperature with constant shaking. About 2.7 l of hydrogen was absorbed. After the removal of the catalyst, the solvent was distilled off and benzene was added. The precipitated ammonium chloride was then filtered off, and the filtrate was neutralized with sodium hydroxide solution and steam-distilled. The water was removed *in vacuo*, and the residue was recrystallized from benzene or acetone to afford colorless plate crystalline: 1,2,3,4,6,7,8,9-octahydrophenazine hydrochloride hydrate (0.65 g). Mp 124—126 °C. UV (ethanol): 214 ($\log \varepsilon = 3.76$), 291 ($\log \varepsilon = 3.90$), 310 nm ($\log \varepsilon = 3.93$). IR (KBr): 2380, 1980 cm^{-1} (N^+–H), H_2O content: 8.1% (requires 7.42%), as determined by Karl Fischer's method. Found: C, 59.06; H, 7.89; N, 11.53; Cl, 14.86; O, 5.65%. Calcd for $C_{12}H_{16}N_2 \cdot HCl \cdot H_2O$: C, 59.37; H, 7.89; N, 11.54; Cl, 14.61; O, 6.59%. The base was successfully liberated by neutralization with an anionic exchanger Amberlite CG-400 (OH type), followed by steam distillation. Mp 109 °C (lit,[24] 108—109 °C). Found: C, 76.73; H, 8.44; N, 14.26%. Calcd for $C_{12}H_{16}N_2$: C, 76.55; H, 8.57; N, 14.88%.

Determination of the Rate Constants of the Dehydration Reaction of **1** *with HCl*. To a 200 ml Erlenmeyer flask with a grinding stopper containing absolute ethanol (150 ml) saturated with dry hydrogen chloride, **1** (4.5 g) was introduced with vigorous shaking. The flask was then placed in a desiccator and kept in a refrigerator at a constant temperature. The contents of both **1** and water were determined at given intervals.

Determination of **1**. About 2 g of the sample were pipetted out, accurately weighed, and then poured into water (200 ml). A 20% ammonium acetate solution was added to adjust the pH to 5.5—6.0. Then, 10 ml portion of an aqueous nickel(II) chloride solution (1 mg as Ni(II)/ml) was added, and the whole was kept standing for 3—4 hr at 40 °C. The red precipitates were filtered off with a glass-filter G4 and gravimetrically determined.

Determination of the Water Formed. About 5 g of the sample were pipetted out, poured into a mixture of absolute ethanol (10 ml) and anhydrous pyridine (5 ml), and accurately weighed. The water concentration in the solution was determined by Karl Fischer's method.

Determination of the Acidity Function, H_0. The acidity functions of the absolute ethanol–hydrogen chloride system were determined spectrophotometrically with *p*-nitroaniline at 360 nm.

23) D. D. E. Newmann and L. N. Owen, *J. Chem. Soc.*, **1952**, 4713.

24) O. Wallach, *Ann. Chem.*, **437**, 177 (1927).

BULLETIN OF THE CHEMICAL SOCIETY OF JAPAN, VOL. 46, 1819—1822 (1973)

The Structure of the Crystalline Adduct of Nitrosobenzene and 2,3-Dimethyl-1,3-butadiene

Eizo OIKAWA and Suguru TSUBAKI

Faculty of Engineering, Niigata University, Nagaoka, Niigata 940

(Received December 9, 1972)

The structure of the crystalline product obtained in up to an 18% yield in the reaction of nitrosobenzene with 2,3-dimethyl-1,3-butadiene in diethyl ether was determined to be the nitrone, II, by means of NMR, IR, and a series of reductions with lithium aluminum hydride and zinc–acetic acid, and by the ozonization of the reduction product.

Nitrosobenzene (NB) has been used as a dienophile in the Diels-Alder reaction with dienes. In the reaction with 2,3-dimethyl-1,3-butadiene (DMB) in diethyl ether, a white precipitate was obtained in a few minutes at from 0 °C to room temperature, in addition to the normal Diels-Alder adduct. This product was first reported by Arbuzov and his co-workers[1] although they did not give any structure, just the molar composition of 2NB: DMB. Hamer and Bernard[2] have carried out a very similar reaction of *p*-nitronitrosobenzene with DMB in nitromethane and obtained an orange precipitate at 0 °C in 15 min. They identified the product as 4,5-dimethyl-1,2-bis(*p*-nitrophenyl)-1,2,3,6-tetrahydropyridazine 1,2-dioxide. The present authors have now investigated the structure of the

1) Yu. A. Arbuzov, N. L. Fedyukina, V. V. Shavyrina, and R. I. Shepeleva, *Izv. Akad. Nauk SSSR, Otd. Khim. Nauk*, **1952**, 566; *Chem. Abstr.*, **47**, 4342f (1953).

2) J. Hamer and R. E. Bernard, *J. Org. Chem.*, **28**, 1405 (1963).

white product (**A**) of NB and DMB and determined it to have a nitrone structure.

Results and Discussion

The product, **A**, was obtained in a higher yield (up to 18%, based on 2 mol of NB and 1 mol of DMB) in diethyl ether and in a poor yield (5%) in benzene, but in nitromethane nothing but the normal Diels-Alder adduct was obtained. The thin-layer chromatography of **A** gave just one spot, indicating that the product was a pure material, not a mixture. The most striking characteristics of **A** were given in NMR, in which 18 protons, including 3 methyl protons, were found. This showed a clear difference in the phenyl and methyl region from the NMR of the Diels-Alder adduct of NB–DMB, 2-phenyl-4,5-dimethyl-3,6-dihydrooxazine (**B**), and from that of DMB–4,4′-dinitroazobenzene, 4,5-dimethyl-*N*,*N*-(4,4′-dinitrophenyl)-1,2,3,6-tetrahydropyridazine,[3] both of which contained 6 methyl protons. One methyl group per molecule of **A** means that one of the two initial methyl groups from DMB has reacted. This rules out a pyridazine dioxide structure. Eleven protons in the phenyl region were well observed in a $(CD_3)_2SO$ solution, as will be described in the Experimental section. The peak at δ 8.07 may be assigned to the aldo-nitrone structure, $-CH{=}N(O)Ph$.[4] These NMR analyses can give $C_{18}H_{18}N_2O_2$ as the molecular formula of the product; this formula is closer to the observed analysis that is $C_{18}H_{20}N_2O_2$ (2NB: DMB).

The nitrone structure was supported by the following experimental results. Irradiation with ultraviolet light yielded an isonitrile odor, reduced the strong peak at 1535 cm^{-1} assigned to N→O, and concurrently increased the peaks at 1665 and 1267 cm^{-1} attributed to C=O and C–N respectively. The treatment with

PCl_3 or $POCl_3$ in chloroform at room temperature overnight also reduced the peak at 1535 cm^{-1} and afforded a new peak at 1681 cm^{-1} which can be attributed to the amide group. These characteristics are generally observed in nitrone compounds.[5] One of the characteristic reactions of nitrone is the 1,3-dipolar addition to an alkene.[6] The treatment with an excess of methyl methacrylate gave colorless crystals. The NMR and elemental analyses are in good agreement with the structure of the isoxazolidine, I.

The formation of a nitrone from NB and alkene was reported long ago by Alessandri[7] in the reaction of NB with safrole and similar compounds; since then, however, very few articles have appeared.[5,8]

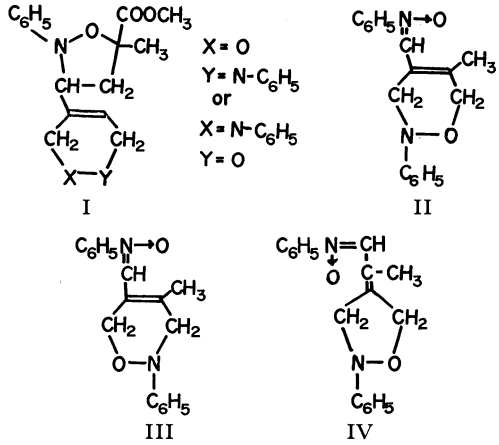

I II III IV

The possibility of the existence of a ring containing N–O from NB in **A** was indicated by the strong IR peaks at 1067 and 1082 cm^{-1}, since **B** has strong absorptions at 1047 and 1065 cm^{-1} attributable to the oxazine ring.[9] The existence of such a ring was supported by the fact that the reduction of **A** with zinc–acetic acid under conditions similar to those in the case of **B**[10] gave a solid whose IR showed no absorption at 1535 and markedly reduced absorptions at 1065 and 1082 cm^{-1}; subsequent treatment with acetic anhydride produced an acetylated solid whose IR had two carbonyl absorptions at 1735 (ester) and 1650 cm^{-1} (amide), the latter being remarkably decreased after hydrolysis with K_2CO_3 in methanol–water. The same behavior was observed in the case of **B**, and the IR absorptions of the acetylated product of **A** and **B** had nearly the same wave number and relative intensity. Furthermore, a structure which does not contain any cyclic N–O bond can not satisfy the elemental composition.

The double bond in **A** was detected with potassium permanganate and bromine.

All the foreging results obtained from the spectra, functional tests, and reduction suggest three probable structures, II, III, and IV, for **A**, but could not decide the correct structure. The final structure was determined by reduction with lithium aluminum hydride in tetrahydrofuran[8] and subsequently with zinc–acetic acid, followed by acetylation with acetic anhydride and the ozonization of the acetylated product in acetic acid. The colorless product thus obtained was identified as bis(*N*-acetylanilino)acetone, VIII. The acetoxyacetone, IX, was identified by gas chromatography.

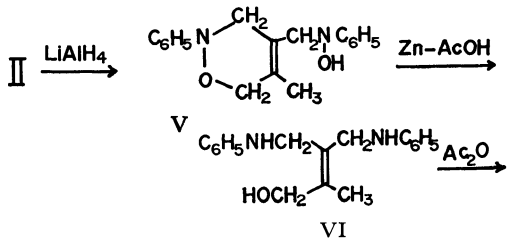

VI

3) P. Baranger, J. Levisalles, and M. Vuidart, *C.R. Acad. Sci. Paris*, **236**, 1365 (1953).

4) K. Koyano and H. Suzuki, *Tetrahedron Lett.*, **1968**, 1859; This Bulletin, **42**, 3306 (1969).

5) J. Hamer and A. Macaluso, *Chem. Rev.*, **64**, 473 (1964).

6) R. Grashey, R. Huisgen, and H. Leitermann, *Tetrahedron Lett.*, **1960**, 9; R. Huisgen, R. Grashey, H. Hauck, and H. Seidl, *Chem. Ber.*, **101**, 2043, 2548, 2559, 2568 (1968).

7) A. Angeli, L. Alessandri, and R. Pegna, *Atti Accad. Lincei*, **19**, I 650 (1910); L. Alessandri, *ibid.*, **24**, I 62 (1915); *Gazz. Chim. Ital.*, **51**, II 129 (1921).

8) R. K. Howe, *J. Org. Chem.*, **33**, 2848 (1968).

9) J. Hamer and R. E. Bernard, *Rec. Trav. Chim. Pays-Bas*, **81**, 734 (1962).

10) G. Kresze and O. Korpiun, *Tetrahedron*, **22**, 2493 (1966).

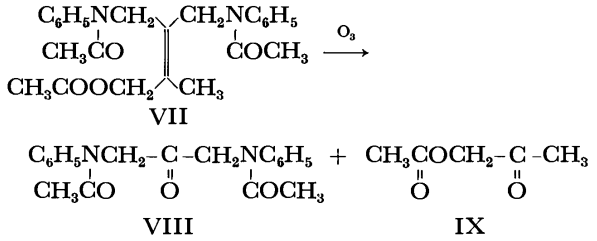

VII VIII IX

Consequently, the crystalline product, **A**, from NB and DMB was found to be the nitrone, II. This structure is also in accord with the results of catalytic hydrogenation, in which one mole of **A** consumed 6 mol of hydrogen, 3 mol for the nitrone part and the other 3 for the oxazine part.

The nitrone formation from DMB seems important because simple alkenes such as propylene, butenes, and octenes have not thus far given a nitrone.

The reaction may proceed *via* intermediate secondary hydroxylamine:[11]

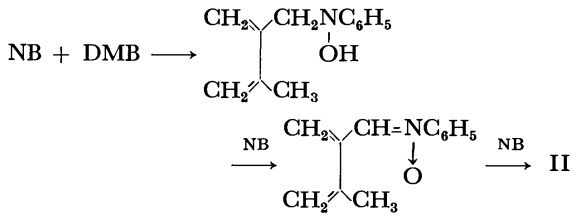

Since the first step is an "ene" reaction, the isopropenyl group may contribute to the stabilization of the transition state, facilitating the production of a nitrone in the reaction with NB:

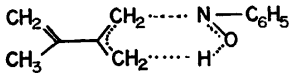

Experimental

All the melting points were corrected.

Materials. The nitrosobenzene was prepared by the reduction of nitrobenzene;[12] it was purified by sublimation before use. The 2,3-dimethyl-1,3-butadiene was prepared from acetone.[13,14] A guaranteed grade of nitromethane was purchased and was used without further purification. The other organic solvents for the reactions and for recrystallization were distilled before use. The 4,5-dimethyl *N,N*-(4,4′-dinitrophenyl)-1,2,3,6-tetrahydropyridazine was prepared by the Diels-Alder addition of 2,3-dimethyl-1,3-butadiene and 4,4′-dinitroazobenzene;[3] NMR ($(CD_3)_2SO$) δ 8.13 (d, 4, benzene ring), 7.04 (d, 4, benzene ring), 4.14 (q, J=16, 4, NCH_2), 1.67 (s, 6, CH_3).

Formation of Nitrone, II (A). A typical procedure was as follows; in a 100 ml, three-necked flask fitted with a thermometer, was placed 13.47 g (125.8 mmol) of NB and 80 ml of diethylether. After all of the nitrosobenzene had been dissolved with occasional warming, the solution was cooled to 5 °C and 9.91 g (120.5 mmol) of distilled DMB was added. The mixture was then stirred magnetically at room temperature (16 °C) for 6 hr. The white precipitate was formed within several minutes after the addition of the diene. The mixture was allowed to stand in a refrigerator overnight. The precipitate was filtered and recrystallized from ethanol or carbon tetrachloride into needles. Yield, 3.15 g (17.9% based on 2NB: DMB), mp 160.0—160.5 °C. Found: C, 73.50; H, 6.01; N, 9.29%; mol wt (cryoscopically in nitrobenzene), 294. Calcd for $C_{18}H_{20}N_2O_2$ (2NB: DMB): C, 73.00; H, 6.76; N, 9.12%; mol wt, 296; for $C_{18}H_{18}N_2O_2$: C, 73.45; H, 6.16; N, 10.87%; mol wt, 294. NMR ($CDCl_3$): δ 7.7—7.0 (m, 11), 4.75 (s, 2, OCH_2), 4.56 (s, 2, NCH_2), 1.86 (s, 3, CH_3). Phenyl region in $(CD_3)_2SO$: δ 8.07 (s, 1), 7.91—7.81 (m, 2), 7.58—7.47 (m, 3), 7.41—6.92 (m, 5).

The Diels-Alder adduct of NB–DMB, 2-phenyl-4,5-dimethyl-3,6-dihydrooxazine (**B**), was obtained from the filtrate; *i.e.*, the brown filtrate was concentrated and a small amount of ethanol was added. The solution was then cooled to about −20 °C. The white solid thus formed amounted to 9.34 g (40.9%) and was recrystallized from ethanol. Mp 37.5—38.5 °C; NMR ($CDCl_3$) δ 7.4—6.7 (m, 10, phenyl), 4.34 (s, 2, OCH_2), 3.67 (s, 2, NCH_2), 1.73 (s, 3, CH_3), 1.64 (s, 3, CH_3).

The reaction of 2 mol of NB with 1 mol of DMB and a nitrogen atmosphere did not increase the yield of **A**.

A similar treatment of 10.70 g (100 mmol) of NB and 8.10 g (98.8 mmol) of DMB in 60 ml of benzene gave 0.79 g (5.4%) of **A** and 5.84 g (31.1%) of **B**.

In nitromethane no precipitation occurred. A brown reaction mixture of 1.0 g (9.35 mmol) of NB and 0.80 g (9.73 mmol) of DMB in 40 ml of nitromethane was concentrated under reduced pressure, after which a large amount of diethyl ether was added. The solution was subsequently cooled to −10 °C, but no precipitate was formed. The evaporation of the solvent gave 0.33 g (18.7%) of **B**.

Measurements. The NMR spectra were recorded with a Japan Electron Optics Lab. Model JNM-4H-100 high-resolution spectrometer at 100 MHz at room temperature, with tetramethylsilane as the internal standard. The infrared spectra were recorded on a KRS-5 plate or by the KBr method with a Hitachi EPI-S2 double-beam spectrometer.

Thin-layer chromatography was carried out on silica gel (WAKOGEL B-5 UA) which was put on a glass plate (0.25 mm thick) and activated at 110 °C for 3 hr. A small drop of an about 1% chloroform solution of **A** was placed on the plate and developed with a mixture of chloroform–acetone (85 to 15 vol%) for 50 min. Coloring with sulfuric acid gave one spot with an R_f value of 0.59. A similar treatment with benzene–acetone (90 : 10 vol%) for 30 min gave one spot again, with an R_f value of 0.53.

Qualitative Tests of A. Irradiation by Ultraviolet Light: A small amount of **A** was placed in a quartz test tube, after which the test tube was stoppered and irradiated with a 100 W high-pressure mercury arc lamp for about half an hour. The initial white solid turned brown, and an isonitrile odor was perceived. The IR spectrum of the brown solid was recorded by the KBr pellet method.

Treatment with $POCl_3$ or PCl_3: 0.44 g of **A** was dissolved in 30 ml of chloroform, and then the mixture was ice-cooled. $POCl_3$ or PCl_3 (3 ml) was added to the cooled solution, which then turned red brown; the solution was allowed to stand overnight at room temperature. The subsequent evaporation of the solvent and an excess of the phosphorus compound gave a deep brown semisolid. It was dissolved in ethanol and cooled at −20 °C for 2 days, but no precipitate was yielded. The solution was then distilled at 60 °C under

11) G. T. Knight and M. J. R. Loadman, *J. Chem. Soc., B*, **1971**, 2107; G. T. Knight and B. Pepper, *Tetrahedron*, **27**, 6201 (1971).

12) G. H. Coleman, C. M. McCloskey, and F. A. Sturt, "Organic Syntheses" Coll. Vol. III, 668 (1955).

13) R. Adams and E. W. Adams, *ibid.*, Coll. Vol. I, 459 (1956).

14) C. F. H. Allen and A. Bell, *ibid.*, Coll. Vol. III, 312 (1955).

reduced pressure, and 0.38 g of a pale yellow liquid was obtained.

Detection of Unsaturated Group: To an acetic acid solution of **A** was added a few drops of a 0.5% potassium permanganate solution. The purple color was immediately lost. A carbon tetrachloride solution of bromine (1—2%) was added dropwise to 0.5 ml of a 1% acetic acid solution of **A**. More than two drops were needed before the color of bromine stayed.

Reaction with Methyl Methacrylate. In a 100 ml three-necked flask equipped with a condenser and a thermometer, was placed 0.50 g of **A** and an excess of methyl methacrylate (20 ml) containing a small amount of hydroquinone. The solution was then heated at 55 °C for 15 hr and at 80 °C for 2 hr. The excess methyl methacrylate was removed under reduced pressure, and the remaining pale yellow liquid was poured into petroleum ether. After a while, a white crystalline solid (I) was precipitated (0.39 g). The filtrate was concentrated, and another 0.23 g of the solid was obtained. Yield, 0.62 g (92.8%). It was recrystallized from methanol. Mp 118.0—118.5 °C. Found: C, 69.76; H, 6.29; N, 6.99%. Calcd for $C_{23}H_{26}N_2O_4$: C, 70.03; H, 6.64; N, 7.10%. NMR ($CDCl_3$): δ 7.37—6.90 (m, 10, phenyl), 4.75 (t, 1, CH), 4.39 (s, 2, OCH_2), 3.95 (s, 2, NCH_2), 3.58 (s, 3, OCH_3), 2.70 (q (two pairs), J=13, 2, CH_2(MMA)), 1.74 (s, 3, CH_3C=), 1.67 (s, 3, CH_3(MMA)).

Reductions and Acetylation. In a 100 ml Erlenmeyer flask was placed 2.14 g of lithium aluminum hydride and 60 ml of dry tetrahydrofuran; the stoppered flask was then cooled in an ice bath with magnetic stirring. To the flask was then added 3.14 g of **A** in small portions. The ice bath was removed, and the mixture was allowed to stand at room temperature for 4.5 hr with stirring. The excess of the hydride was then destroyed by adding water slowly. Diethyl ether was added to extract the product with shaking; the solution was collected by decantation. This procedure was repeated several times. The combined ether solution was dried over anhydrous sodium sulfate. The ether was removed under reduced pressure to give 2.55 g of an orange viscous liquid. About 30 ml of *n*-hexane was added to the liquid, and the mixture was heated. Because some of the liquid remained undissolved, ethanol was added with shaking until all the liquid had been dissolved. The solution was allowed to stand in a refrigerator (*ca.* 5 °C) for 2 days. The crystalline solid which formed at the bottom was removed by decantation and was found to be unreacted **A** by the measurement of the mp and IR spectra. The solution was subsequently evaporated to give 1.99 g of V.

In a 100 ml Erlenmeyer flask was placed 1.99 g of V and 25 ml of acetic acid; 6.08 g of zinc dust was then added slowly under water cooling (22 °C) and with magnetic stirring. Stirring was continued at room temperature (26 °C) for 5 hr. The mixture was then filtered, and the solid was washed with a small amount of acetic acid and then with diethyl ether. The filtrate and washings were combined, neutralized with a NaOH solution under ice cooling, and then extracted with diethyl ether. The extract was washed with water and dried over anhydrous sodium sulfate. The ether was then evaporated to give 1.42 g of VI. It was purified by distillation in a bent glass tube under highly reduced pressure. Yield, 1.28 g of a pale yellow semisolid. Found: C, 76.57; H, 7.67; N, 9.51%. Calcd for $C_{18}H_{22}N_2O$: C, 76.56; H, 7.85; N, 9.92%.

In a round-bottomed flask with a condenser was placed 1.28 g of VI, 80 ml of acetic anhydride, and about 0.2 g of anhydrous potassium acetate. The mixture was heated at 105 °C in an oil bath for 7 hr. The solution was then concentrated and neutralized with potassium carbonate. The brown crystals which came out were then dissolved in benzene. The solution was washed with water, dried over anhydrous sodium sulfate, filtered, and evaporated to dryness to give 1.76 g of crude VII. It was purified by recrystallization from *n*-hexane–diethyl ether as white crystals. Yield, 1.33 g; mp 106.0—106.5 °C. Found: C, 70.44; H, 6.61; N, 6.75%. Calcd for $C_{24}H_{28}N_2O_4$: C, 70.57; H, 6.91; N, 6.86%.

A (2.0 g) was also treated with zinc–acetic acid in a manner similar to that described above, yielding 1.1 g of a pale brown solid (softening point, 75 °C). Found: C, 77.72; H, 7.31; N, 8.51%. Calcd for $C_{18}H_{20}N_2O$: C, 77.14; H, 7.14; N, 10.00%. The subsequent acetylation of the reduction product (0.50 g) was carried out similarly, yielding 0.46 g of a brown solid (softening point, 85 °C). Found: C, 72.34; H, 6.57; N, 6.49%. Calcd for $C_{22}H_{24}N_2O_3$: C, 72.53; H, 6.59; N, 7.69%. The hydrolysis of the amide group was carried out as follows; to a methanol solution of this solid was added an aqueous potassium carbonate solution until a slight cloudiness was observed. The mixture was then heated to boil for a few minutes, and then acidified with sulfuric acid. The white precipitate thus formed was filtered and dried *in vacuo*.

Catalytic Hydrogenation. **A** was hydrogenated over a Raney Ni or Pd–$BaSO_4$ catalyst. Raney Ni was used as an isobutyl alcohol suspension after the Raney Ni alloy (Ni: Al= 1:1) had been treated with an aqueous solution of sodium hydroxide. Pd–$BaSO_4$ was prepared from palladium chloride in hydrochloric acid and a water suspension of barium sulfate from barium hydroxide and sulfuric acid. Styrene was used in a control reaction for the calibration of the results.

In a 30 ml reaction flask was placed a stirring bar and 10 ml of isobutyl alcohol containing 0.4—0.5 g of the catalyst. About 15 mg of **A** was weighed accurately in a small aluminum basket and hung on a hook in the flask. After the complete absorption of hydrogen by the catalyst and the solvent (about 3 hr), the basket was dropped and stirring was continued for from 3 to 4 hr until the manometer showed no further change. The average absorption was 6.21 mol of hydrogen per mol of **A** (294 as mol wt). When α,*N*-diphenylnitrone and **B** were treated similarly, they absorbed 3 mol of hydrogen per mol of the sample. In the former case, a primary amine was detected in the reduction mixture by a carbylamine test and a diazo test.

Ozonization. The acetylated product, VII (0.60 g), was dissolved in 4 ml of acetic acid, and an oxygen stream containing ozone was bubbled through the solution at 0 °C. The reaction was continued for 16.5 hr until the color of the solution changed from the red-brown of the initial stage to a very pale yellow. Into the solution was then added 3.0 g of zinc dust with stirring. The solution did not change the color of KI-starch paper. A gas chromatogram of the solution, recorded by using a 75 cm column of SE-30 on celite at 176 °C, had a peak at the same retention time (1.4 min) as that of the solution containing acetoxyacetone obtained by the ozonization of acetylated **B**. The acetic acid solution was filtered, and the zinc was washed with a small amount of acetic acid and then diethyl ether. The filtrate and washings were then combined and evaporated to give a white crystalline solid, VIII. It was recrystallized from ethanol. Yield, 0.23 g (48.0%); mp 137.5—138.0 °C. Found: C, 69.72; H, 6.20; N, 8.41%. Calcd for $C_{19}H_{20}N_2O_3$: C, 70.35; H, 6.21; N, 8.64%. NMR ($CDCl_3$): δ 7.36 (m, 10, phenyl), 4.49 (s, 4, NCH_2), 1.91 (s, 6, CH_3). IR: 1744 (C–C=O), 1646 (N–C=O), 1418, 1382 (δ(C–H)), 1305 (ν(N–C=)), 1596, 1496, 740, 700 cm^{-1} (benzene ring).

Synthesis and Structural Investigation of *trans*-8-Oxabicyclo[4.3.0]nonan-3-ols

Ta-Yan LEONG, Takeshi IMAGAWA, and Mituyosi KAWANISI

Department of Industrial Chemistry, Faculty of Engineering, Kyoto University, Yoshida, Sakyo-ku, Kyoto 606

(Received December 13, 1972)

Various methods of the synthesis of *trans*-8-oxabicyclo[4.3.0]nonan-3-ols were examined; the best method for *c*-3-hydroxy-*r*-1-*trans*-8-oxabicyclo[4.3.0]nonane (**2**) was found to be the LAH reduction of the epoxide of *trans*-8-oxabicyclo[4.3.0]non-3-ene (**1**), while *t*-3-hydroxy-*r*-1-*trans*-8-oxabicyclo[4.3.0]nonane (**3**) could be obtained in a high stereoselectivity by the LAH reduction of *trans*-8-oxabicyclo[4.3.0]nonan-3-one (**4**). The structures of the two isomeric alcohols were investigated by means of nuclear magnetic resonance spectroscopy using the paramagentic shift reagent. The C-1 proton of **2** is shifted to a much greater extent than that of **3**. Much as in the case of the *cis* analogues, there is almost no difference in the coordination abilities of europium ions with the alcoholic and ethereal oxygen atoms in these compounds.

We have recently reported on the synthesis and structural investigation of *cis*-8-oxabicyclo[4.3.0]nonan-3-ols.[1] In connection with the studies of the photo-induced addition of acetic acid to *trans*-8-oxabicyclo-[4.3.0]non-3-ene (**1**),[2] the hydrolysis of the adducts has been found to afford the title compounds. As an extension of this research, and also in order to compare these results with those obtained for the *cis* compounds, the synthesis of *c*-3-hydroxy-*r*-1-*trans*-8-oxabicyclo-[4.3.0]nonane (**2**) and *t*-3-hydroxy-*r*-1-*trans*-8-oxabicyclo[4.3.0]nonane (**3**)[3] has been undertaken, and the structures of the two isomeric alcohols have been investigated by means of nuclear magnetic resonance spectroscopy using the paramagnetic shift reagent.

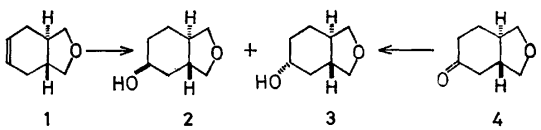

Scheme 1

Results and Discussion

As is shown in Table 1, the hydroboration of **1** with diborane gave almost an equal isomeric ratio of **2** and **3**, while hydroboration with diisopinocampheylborane did not improve the isomeric ratio. The lithium aluminum hydride (LAH) reduction of the epoxide of **1** obtained by the reaction of **1** with *m*-chloroperbenzoic acid gave **2** predominantly. The isomer **3** was obtained in a high isomeric ratio by the reduction of *trans*-8-oxabicyclo[4.3.0]nonan-3-one (**4**) with sodium in ethanol, lithium aluminum hydride, sodium borohydride, and catalytic hydrogenation over platinum oxide in acetic acid. To summarize these results, the LAH reduction of the epoxide of **1** seems to be the best method for the synthesis of the isomer **2**, while the LAH reduction of the ketone, **4**, provides the most convenient route to **3**.

A comparison of the above results with those for the *trans*-bicyclo[4.3.0]nonan-3-one[4] is included in Table 1; it can be deduced that, in this case, much as in

TABLE 1. REACTIONS OF **1** AND **4**

Starting materials	Methods of preparation		Alcohol ratio[a]	
			2(%)	**3**(%)
1	A	B_2H_6, H_2O_2	46	54
	B	DICB, H_2O_2[b]	43	57
	C	MCPBA, LAH[c]	93	7
4	D	LAH	6	94
	E	H_2, PtO_2/AcOH	20	80
	F	Na/EtOH	8	92
	G	$NaBH_4$	14	86
			β-ol	α-ol
	H	Na/EtOH	4	96
trans-Bicyclo[4.3.0]nonan-3-one	I	LAH	12	88
	J	H_2, PtO_2/AcOH	44	56

a) Percentage of ratio of alcohols **2** and **3** were determined by glc analysis.
b) DICB stands for diisopinocampheylborane.
c) MCPBA stands for *m*- chloroperbenzoic acid and LAH stands for lithium aluminum hydride.

1) K. Kimoto, T.-Y. Leong, T. Imagawa, and M. Kawanisi, *Can. J. Chem.*, **50**, 3805 (1972).
2) T.-Y. Leong, T. Imagawa, K. Kimoto, and M. Kawanisi, This Bulletin, **46**, 596 (1973).
3) To designate the relative configuration, the IUPAC 1968 Tentative Rules, Section E, have been adopted throughout this work. See *J. Org. Chem.*, **35**, 2849 (1970).
4) R. Granger, J. P. Girard, J. C. Rossi, and J. Boussinesq, *Bull. Soc. Chim. Fr.*, **1967**, 4035.

that of *cis*-8-oxabicyclo[4.3.0]nonan-3-one,[1] there seems to be no difference in the reactivities of the ketones in reductions even when one methylene group of the five-membered ring is replaced by an oxygen atom.

In order to determine the axial or equatorial nature of the protons adjacent to the hydroxyl or acetate moieties, it is helpful to observe the half-band widths of the proton NMR signal. The half-band widths of the carbinyl protons of **2** and **3** cannot be observed directly because of the overlapping with the signals of the protons α to the ethereal oxygen, even when the NMR shift reagent, Eu(DPM)$_3$, is added.[5] However, those of the respective acetates of **2** and **3** are observed to be 8 and 14 Hz[6] respectively, indicating the axial and equatorial arrangements for the acetoxy groups in the acetates of **2** and **3** respectively. Thus, the structures of **2** and **3** are unambiguously proved to have the structures shown in Figs. 1 and 2, since the fused systems have a *trans* configuration and since an inversion of the structure is impossible.

The above structures of **2** and **3** are further studied by the use of Eu(DPM)$_3$. The relationship between

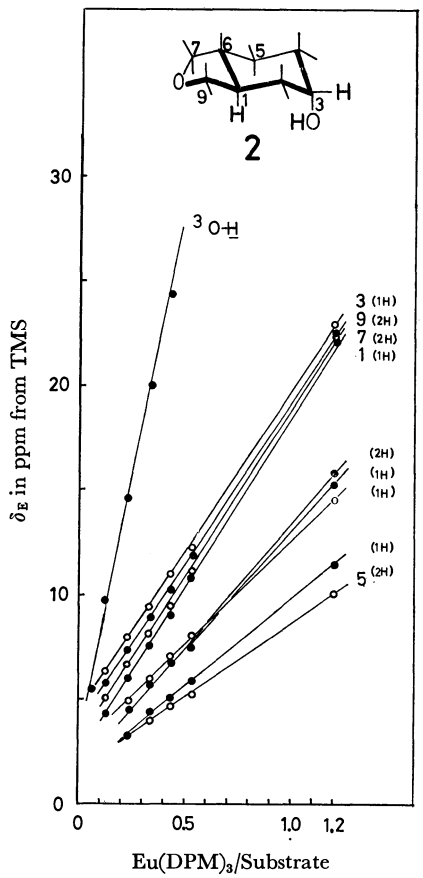

Fig. 1. Variation of chemical shift with molar ratio of Eu(DPM)$_3$/substrate for **2** in $CDCl_3$ solution.
The numerals on the lines represent protons assigned to those attached to the numbered ptorons. Numerals in parenthesis stand for the number of respective proton(s).

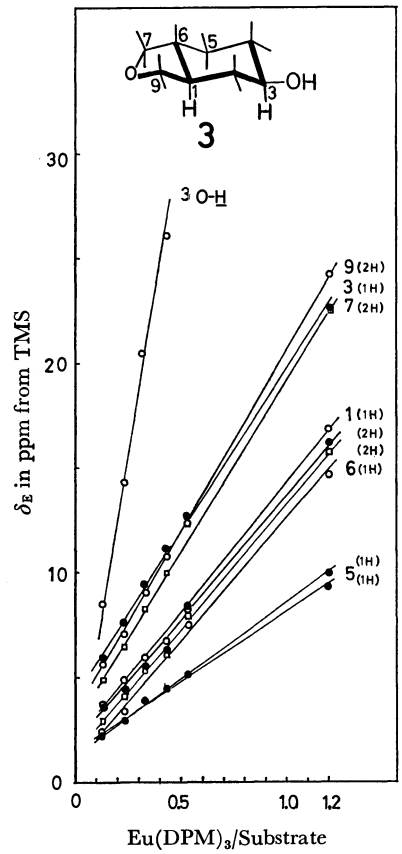

Fig. 2. Variation of chemical shift with molar ratio of Eu(DPM)$_3$/substrate for **3** in $CDCl_3$ solution.
The numerals on the lines represent protons assigned to those attached to the numbered protons. Numerals in parenthesis stand for the number of respective proton(s).

the variation in chemical shifts (δ_E) and Eu(DPM)$_3$/substrate (molar ratio) for the two isomers of **2** and **3** is shown in Figs. 1 and 2, demonstrating the linearity between δ_E and Eu(DPM)$_3$/substrate for the different protons in both isomers.

The linearities, even at the high concentration of a 1.2 molar ratio for the carbinyl protons and the four methylene protons adjacent to the oxygen atom of the five-membered rings indicate that there is no great difference in the equilibrium constants of complex formation for the alcoholic and the ethereal oxygen atoms. The same tendency has been observed in the behavior of the *cis*-8-oxabicyclo[4.3.0]nonan-3-ols toward Eu(DPM)$_3$.[1]

As is shown in Figs. 1 and 2, it is clear that the H_1 of **2** is shifted much more than that of **3**; this is the most distinct difference in the behavior of **2** and **3** upon the addition of Eu(DPM)$_3$. At the high concentration of a 1.2 molar ratio, the H_1 of **2** is unexpectedly shifted as much as H_3, H_7, and H_9, which are protons nearest to the two sites of coordination with the europium ions, whereas the H_1 of **3** is shifted to a much smaller degree. This observation supports the conformation of **2** and **3** as set forth in Figs. 1 and 2. It also implies that competitive coordination occurs at almost the same degree at the two sites in both **2** and **3**. This similar degree of competitive coordination for the two sites has been confirmed by an intermolecular

5) For pertinent references, see a) J. K. M. Sanders, S. W. Hanson, and D. H. Williams, *J. Amer. Chem. Soc.*, **94**, 5325 (1972) and b) R. von Ammon and R. D. Fischer, *Angew. Chem.*, **84**, 737 (1972) and references cited therein.

6) See Experimental Section, lit. 2.

competitive experiment on an equal molar mixture of tetrahydrofuran and cyclohexanol, as has previously been reported.[1]

Experimental

All the temperatures are uncorrected. The microanalyses were performed by Mrs. Kiyoko Fujimoto of our laboratory. The IR spectra were obtained on a Shimadzu IR-27-C spectrophotometer. The NMR spectra were taken on a JEOL C-60H spectrometer, using tetramethylsilane as the internal standard, and $CDCl_3$ as the solvent. Tris(dipivalomethanato)europium (III), $Eu(DPM)_3$, was prepared in a manner similar to that of Eisentraut;[7] it had a mp of 189.5—190 °C (lit,[8] mp 190—191 °C). The glc analyses and separations were carried out on a Shimadzu GC-4APT apparatus using a 3 m×3 mm column of Dowfax 9N9 10% on Neopak 1A, operating at 150 °C with a He flow rate of 40 cc/min. For the preparative tlc, a 1.0 mm thickness of Merck GF-254 silica gel was employed with the solvent system of diethyl ether–benzene (50: 50). The mass spectra were recorded with a Hitachi RMS-4 mass spectrometer, with an ionizing energy of 70 eV and a source temperature of 150 °C.

Starting Material. Compound **1** was prepared from dimethyl *trans*-Δ^4-tetrahydrophthalate using the method described by Eliel;[9] it had properties identical with those reported by Christol.[10]

Reactions of trans-*8-Oxabicyclo[4.3.0]none-3-ene (1).* *Hydroboration with Diborane*: Dibroane generated by adding a solution of 14 g of $BF_3 \cdot Et_2O$ in 25 ml of diglyme to 1.9 g of sodium borohydride in 50 ml of diglyme was passed over a 75 min period into a stirred solution of 5.9 g of **1** in 50 ml of THF, cooled in an ice bath. The solution was then left for 75 min at room temperature, the excess diborane was decomposed with water (15 ml), 15 ml of 3M sodium hydroxide was added, and subsequently 15 ml of 30% hydrogen peroxide was added drop by drop. The reaction mixture was then stirred for an additional hour at room temperature and extracted with dichloromethane. After the evaporation of the solvent, distillation yielded 4.1 g of a mixture of **2** and **3** (bp 120 °C/10 mmHg); the isomeric ratio of **2** to **3** was shown by glc to be 46: 54.

Hydroboration with Diisopinocampheylborane: Hydroboration with diisopinocampheylborane was carried out with 680 mg of **1** according to the method of Brown;[11] a 580 mg portion of a mixture of **2** and **3** was thus obtained, its isomeric ratio being shown by glc to be 43: 57.

Reaction of 1 with m-*Chloroperbenzoic Acid Followed by Reduction with Lithium Aluminum Hydride (LAH)*: A solution of 1.8 g of 85% *m*-chloroperbenzoic acid in 40 ml of dry chloroform was added dropwise to a stirred solution of 1 g of **1** in 10 ml of dry chloroform. The reaction mixture was stirred overnight at room temperature. The solution was then washed 2 times each with 100 ml of a 10% sodium sulfite solution, 2 times each with 100 ml of a 5% sodium bicarbonate solution, and finally with a saturated sodium chloride solution, and dried (Na_2SO_4). The chloroform was driven off at reduced pressure, and a white solid was obtained on standing. Recrystallization from petroleum ether gave the epoxide of **1** in needles; mp 53.5—54 °C, IR (KBr): 2924, 2870, 1435, 1425, 1348, 1269, 1195, 1110, 1080, 990, 885, 875, 805, 780 cm^{-1}; NMR (CCl_4): δ 4.00—3.50 (m, 2H), 3.40—2.75 (m, 4H), 2.55—1.15 (m, 6H); MS: *m/e* 140 (M^+, 23%), 110 (100), 95 (69), 82 (72), 81 (70), 79 (71%). Found: C, 68.29; H, 8.59%. Calcd for $C_8H_{12}O_2$: C, 68.54; H, 8.63%.

A solution of 640 mg of the above epoxide in 10 ml of ether was added dropwise to a stirred slurry of LAH in 10 ml of ether; the mixture was then stirred overnight at room temperature. Aqueous hydrochloric acid (10%) was added to destroy the excess hydride. Extraction (ether) and drying (Na_2SO_4), followed by evaporation, afforded 520 mg of a mixture of **2** and **3**, which was shown by glc to have an isomeric ratio of 93: 7.

Reduction of trans-*8-Oxabicyclo[4.3.0]nonan-3-one (4).* The ketone, **4**, was prepared by oxidizing the mixture of **2** and **3** obtained in the hydroboration (with diborane) of **1**. A solution of 2.84 g of a mixture of **2** and **3** in a small volume of dichloromethane was oxidized with the chromium trioxide-pyridine complex, as has been described by Ratcliffe,[12] to yield 2.2 g of **4**; bp 120—121 °C/18 mmHg, IR: 2955, 2900, 1720, 1420, 1322, 1201, 1072, 1020, 996 cm^{-1}; NMR (CCl_4): δ 4.06—3.70 (m, 2H), 3.55—3.07 (m, 2H), 2.70—1.15 (m, 8H); MS: *m/e* 140 (M^+, 100), 96 (22), 84 (41), 82 (70%). Found: C, 68.46; H, 8.88%. Calcd for $C_8H_{12}O_2$: C, 68.54; H, 8.63%.

A solution of **4** (170 mg) in 10 ml of ether was added dropwise to a stirred slurry of 60 mg of LAH in 10 ml of ether. The mixture was then stirred overnight at room temperature, dilute hydrochloric acid was added to destroy the excess hydride, and the aqueous phase was extracted with ether. After drying (Na_2SO_4), the solvent was removed; the alcohols **2** and **3** were found to have been formed in a ratio of 6: 94.

Hydrogenation of 4 over Platinum Oxide. A solution of **4** (100 mg) in 5 ml of glacial acetic acid was added to 50 mg of platinum oxide in 10 ml of glacial acetic acid, 3 drops of concentrated hydrochloric acid were added, and hydrogenation was carried out under normal atmospheric hydrogen at room temperature. A rapid uptake of hydrogen occurred, and the theoretical amount of hydrogen was absorbed in 20 min. The reaction mixture was then neutralized with aqueous sodium bicarbonate and extracted with ether. An analysis of the reaction product by glc showed that **2** and **3** were formed in a ratio of 20: 80.

Reduction of 4 with Sodium in Ethanol. A solution of 320 mg of **4** in 100 ml of absolute ethanol was placed in a flask fitted with a reflux condenser, and 1.75 g of small pieces of sodium were added to maintain reflux. After the addition of sodium had been finished, the reaction mixture was refluxed for an additional hour; it was then cooled and acidified with 10% aqueous hydrochloric acid. The ethanol was removed under diminished pressure, and the aqueous phase was extracted with ether. The ethereal solution was dried and evaporated. An analysis of the residue by glc showed that the isomers **2** and **3** were formed in a ratio of 8: 92.

Reduction of 4 with Sodium Borohydride. A solution of 170 mg of **4** in 20 ml of absolute methanol was cooled in an ice bath, and then 110 mg of sodium borohydride were slowly stirred in. After the reaction mixture had been stirred at room temperature overnight, the methanol was removed under

7) K. J. Eisentraut and R. E. Sievers, *J. Amer. Chem. Soc.*, **87**, 5254 (1965).

8) J. Selbin, N. Ahmad, and N. Bhacca, *Inorg. Chem.*, **10**, 1383 (1971).

9) E. L. Eliel and C. Pillar, *J. Amer. Chem. Soc.*, **77**, 3600 (1955).

10) H. Christol, A. Donche, and M. F. Plenar, *Bull. Soc. Chim. Fr.*, **1966**, 1315.

11) H. C. Brown, N. R. Ayyangar, and G. Zweifel, *J. Amer. Chem. Soc.*, **86**, 397 (1964).

12) R. Ratcliffe and R. Rodehorst, *J. Org. Chem.*, **35**, 4000 (1970).

diminished pressure, and ice water was added. Extraction (CH_2Cl_2) and drying (Na_2SO_4), followed by evaporation, afforded the reaction products, an analysis of which by glc showed that the isomers **2** and **3** were formed in a ratio of 14: 86.

Pure samples of **2** and **3** were secured from the reduction of epoxide of **1** and LAH reduction of **4**, respectively; by separation with preparative tlc and glc, followed by bulb-to-bulb distillation under reduced pressure, we obtained the following results, For **2**: IR (CCl_4) 3620, 3385, 2940, 2855, 1085, 1015, 995 cm^{-1}, NMR ($CDCl_3$): δ 4.40—3.80 (m, 3H), 3.60—3.18 (m, 2H), 2.40—1.30 (m, 9H), MS: *m/e* 142 (M^+, 26%), 124 (M^+-18, 30%), 69 (100%). Found: C, 67.36; H, 10.19%. Calcd for $C_8H_{14}O_2$: C, 67.57; H, 9.93%. For **3**: IR (CCl_4) 3620, 3380, 2940, 2850, 1095, 1055, 1025, 1010 cm^{-1}, NMR ($CDCl_3$): δ 4.24—3.10 (m, 5H), 2.52—0.90 (m, 9H), MS: *m/e* 142 (M^+, 11%), 124 (M^+-18, 30%), 69 (100%). Found: C, 67.30; H, 9.92%. Calcd for $C_8H_{14}O_2$: C, 67.57; H, 9.93%.

Professor Hitosi Nozaki is to be thanked for his interest in this work, and also Mr. Koichi Kimoto for his skillful technical assistance.

BULLETIN OF THE CHEMICAL SOCIETY OF JAPAN, VOL. 46, 1826—1829 (1973)

Studies of the Synthesis of Furan Compounds. XXIX.[1] Syntheses of 2-(5-Nitro-2-furyl)vinyl-1,8-naphthyridines[2]

Ichiro HIRAO, Yasuhiko KATO, Yoshimasa FUKANO, and Shinpei YANAI

Laboratory of Organic Synthesis, Department of Industrial Chemistry, Kyushu Institute of Technology, Tobata-ku, Kita-Kyushu 804

(Received December 16, 1972)

In continuing our study of the relationship between structures and antibacterial activity, 2-[2-(5-nitro-2-furyl)vinyl]-5-hydroxy- and 4-[2-(5-nitro-2-furyl)vinyl]-2,7-dihydroxy-1,8-naphthyridine and their related derivatives have been synthesized. In these compounds, 2-[2-(5-nitro-2-furyl)vinyl]-5-hydroxy- (I) and 2-[2-(5-nitro-2-furyl)vinyl]-5-hydroxy-6-ethoxycarbonyl-1,8-naphthyridine (II) showed broad spectra of antibacterial activity, and the activity of I was greater than that of II. Other compounds exhibit a strong antibacterial activity against *Diplococcus pneumoniae*, *Streptococcus hemolyticus*, and *Staphilococcus aureus*, but they show a weak activity against the other microorganisms tested.

In 1,8-naphthyridine compounds, nalidixic acid (1-ethyl-4-oxo-7-methyl-1,8-naphthyridine-3-carboxylic acid) has been known as an effective chemotherapeutic drug for Gram-negative infections. Nishigaki *et al.* reported that the derivatives of nalidixic acid and its related methyl-1,8-naphthyridines, whose methyl groups were condensed with 5-nitrofurfural, showed a broad spectrum of antibacterial activity greater than that of the parent nalidixic acid; another excellence of these compounds is that the nalidixic acid resistant-strain of *Escherichia coli* K-12 and *Shigella dysenteriae* Hanabusa are still as susceptible to these compounds as the original strains.[3,4] Several patents concerning the syntheses and the use of 2-(5-nitro-2-furyl)vinyl-1,8-naphthyridines have been granted.[5–10]

In order to compare the antibacterial activity, 2-[2-(5-nitro-2-furyl)vinyl]- and 4-[2-(5-nitro-2-furyl)-vinyl]-1,8-naphthyridine derivatives were prepared.

Results and Discussion

2-[2-(5-Nitro-2-furyl)vinyl]-5-hydroxy-1,8-naphthyridine (I) was obtained by the condensation of 2-methyl-5-hydroxy-1,8-naphthyridine[11] with 5-nitrofurfural in refluxing acetic anhydride. In a similar manner, 2-[2-(5-nitro-2-furyl)vinyl]-5-hydroxy-6-ethoxycarbonyl-1,8-naphthyridine[4] (II) was obtained from the corresponding 2-methyl-1,8-naphthyridine. I and II were converted into the corresponding 5-chloro derivatives (Ia and IIa respectively) by being heated in phosphoryl chloride. On the other hand, Ia was also obtained from 2-methyl-5-chloro-1,8-naphthyridine[11] and 5-nitrofurfural. When Ia or IIa was heated with phenol, the 5-chlorine atom was replaced by a phenoxy group to give 2-[2-(5-nitro-2-furyl)vinyl]-5-

1) Part XXVIII of this series: Y. Kato, T. Kuboyama, and I. Hirao, This Bulletin, **45**, 3165 (1972).

2) Presented at the 24th Annual Meeting of the Chemical Society of Japan, Osaka, April, 1971.

3) S. Nishigaki, F. Yoneda, K. Ogiwara, T. Naito, R. Domori, S. Kadoya, Y. Tanaka, and I. Takamura, *Chem. Pharm. Bull.*, (Tokyo), **17**, 1827 (1969); F. Yoneda, S. Nishigaki, N. Mizushima, and H. Takahashi, *J. Med. Chem.*, **14**, 638 (1971).

4) S. Nishigaki, T. Naito, Y. Oshima, R. Domori, and S. Nagasaki, Japan Pat. 69 13950; 69 13951; 69 13952, June 21, 1969.

5) S. Nishigaki, T. Naito, Y. Oshima, R. Domori, S. Nagasaki, S. Kadoya, and I. Takamura, Japan Pat. 69 13949, June 21, 1969.

6) B. Herbert, S. Kurt, D. Otto, V. Wolfgang, and S. Winfriede, S. African Pat. 69 02496, October 15, 1969.

7) T. Naito, Y. Oshima, R. Domori, S. Nagasaki, Y. Tanaka, and R. Yoshimura, Japan Pat. 70 30337, October 10, 1970.

8) R. Domori, R. Yoshimura, and T. Naito, Japan Pat. 70 39096, December 9, 1970.

9) R. Ueno and W. Kashihara, Japan Pat. 71 15632, April 27, 1971.

10) B. Herbert, G. Rudi, T. Max, V. Wolfgang, and S. Winfriede, Ger. Offen. 2030581, December 30, 1971.

11) E. V. Brown, *J. Org. Chem.*, **30**, 1607 (1965).

phenoxy-1,8-naphthyridine (Ib) and 2-[2-(5-nitro-2-furyl)vinyl]-5-phenoxy-6-ethoxycarbonyl-1,8-naphthyridine (IIb) (Scheme 1).

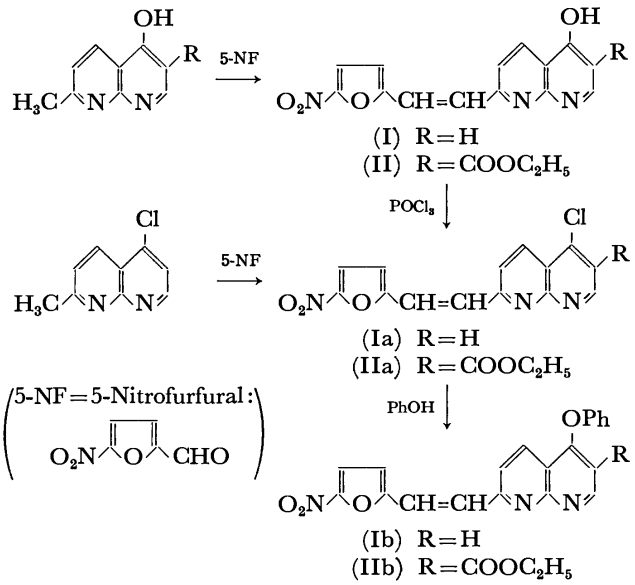

Scheme 1

It was found that the reactivity of the methyl group at the γ-position on the 1,8-naphthyridine nucleus is smaller than that at the α-position. An attempt to prepare 2-hydroxy-7-amino- (III) or 2,7-dihydroxy-4-[2-(5-nitro-2-furyl)vinyl]-1,8-naphthyridine (IV) from the corresponding 4-methyl-1,8-naphthyridines and 5-nitrofurfural was unsuccessful, although Herbert *et al.*[6] have described the preparation of the same compounds (III and IV) by this method. In our results, the raw materials were recovered as 5-nitrofurfural diacetate and 2-hydroxy-7-acetamido- or 2,7-dihydroxy-4-methyl-1,8-naphthyridine themselves in place of the desired III or IV. Another method for preparation of III and IV is the decarboxylation of 3-(5-nitro-2-furyl)-2-(2-hydroxy-7-acetamido-1,8-naphthyridin-4-yl)acrylic acid (V) and 3-(5-nitro-2-furyl)-2-(2,7-dihydroxy-1,8-naphthyridin-4-yl)acrylic acid (VI), which had themselves been prepared by the reaction of 2-hydroxy-7-amino- and 2,7-dihydroxy-1,8-naphthyridine-4-acetic acid[12] respectively with 5-nitrofurfural. While the decarboxylation of V and VI did not occur in the presence of copper bichromate in hot quinoline or in the presence of benzoyl peroxide in dimethylformamide, IV was produced as the main product in the preparation of VI. It can be assumed that IV was formed by condensation of 2,7-dihydroxy-1,8-naphthyridine-4-acetic acid with 5-nitrofurfural involved in the decarboxylation.

When IV was heated with phosphoryl chloride, the corresponding 2,7-dichloro derivative (IVa) was obtained. IVa gave 2,7-diphenoxy (IVb) and 2,7-dianilino (IVc) compounds when heated with phenol and aniline respectively.

In the IR spectra of I, II, IV, V, and VI, the C=O stretching absorption band was observed in the 1660—1650 cm^{-1} region, while it disappeared in the corresponding chloro derivatives (Ia, IIa, and IVa); this suggests that the hydroxy-naphthyridine part takes the keto structure in the solid state. The *trans*-configuration of I, Ia, b, II, IIa, b, IV, and IVa—c is supported by the presence of a C–H out-of-plane deformation vibration band in the 960—950 cm^{-1} region.

Microbiological Assays.[13] The antibacterial activities of these compounds in response to ten microorganisms were examined. The minimum amount of

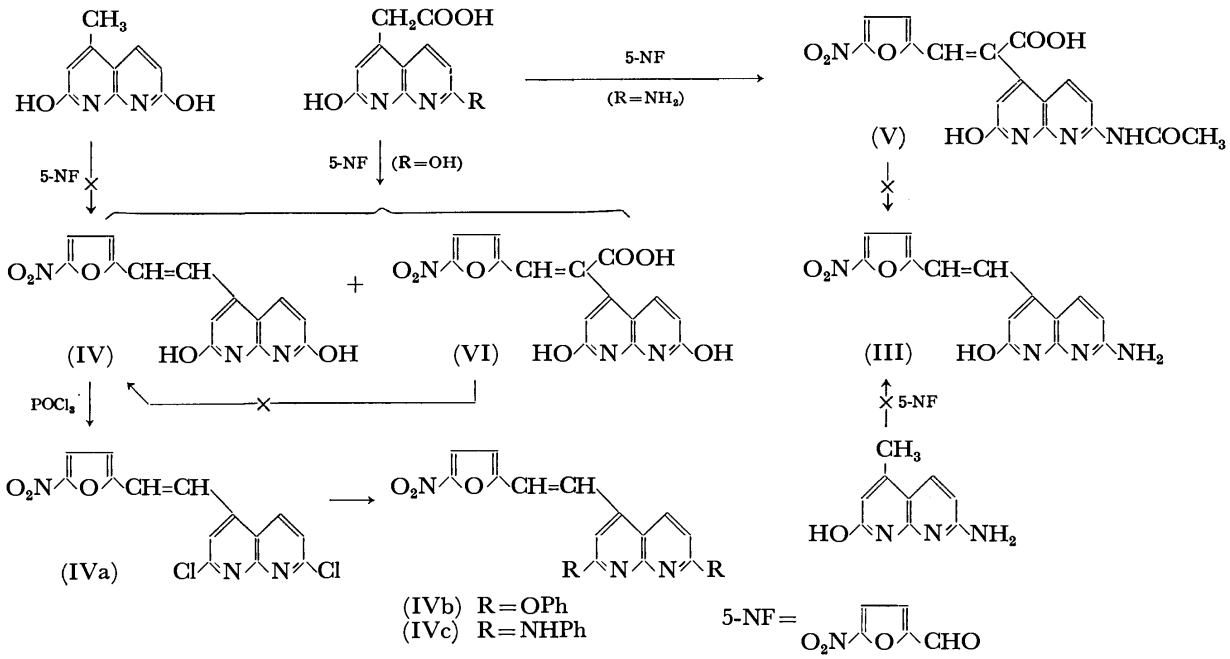

Scheme 2

12) S. Carboni, A. Da Settimo, and G. Pirisino, *Ann. Chim.* (Rome), **54**, 883 (1964).

13) The authors are indebted to Dr. R. Ueno and his staff of the Ueno Pharmaceutical Company, Ltd., for the assay.

TABLE 1. INHIBITORY ACTIVITY OF TEN COMPOUNDS ON MICROORGANISMS
Minimum inhibitory concentration, μg/ml

Compound	*Diplococcus pneumoniae* Dp-1	*Streptococcus hemolyticus* Group A 089	*Staphylococcus aureus* 209 P	*Bacillus subtilis* pcl 219	*Salmonella enteritidis* 1891	*Salmonella pullorum* Chuyu 114	*Escherichia coli* 0-55	*Klebsiella pneumoniae* ST-101	*Proteus vulgaris* HX 19	*Pseudomonus aeruginosa* 347
Type A										
I	<0.10	<0.10	0.39	—	0.39	0.78	0.39	0.39	0.39	3.13
II	0.78	0.19	0.78	—	3.13	6.25	1.56	1.56	3.13	>25
Ib	1.56	1.56	0.78	1.56	3.13	>3.13	>3.13	>3.13	1.56	>3.13
IIa	1.56	<0.19	1.56	<0.19	3.13	25	3.13	3.13	>25	>25
Type B										
IV	3.13	0.78	3.13	3.13	>25	>25	>25	>25	>25	>25
IVa	1.56	1.56	0.78	0.78	—	>25	>25	>25	1.56	>25
IVb	>25	>25	12.5	25	—	>25	>25	>25	>25	>25
IVc	1.56	—	0.78	1.56	—	>25	>25	>25	>25	>25
Type C										
V	>25	>25	>25	>25	>25	>25	>25	>25	>25	>25
VI	>12.5	0.19	>12.5	>12.5	>12.5	>12.5	>12.5	>12.5	>12.5	>12.5
Contrast[a]	12.5	0.39	1.56	1.56	0.78	1.56	1.56	3.13	6.25	25

a) 3-(5-Nitro-2-furyl)-2-(2-furyl)acrylic amide was used in the test.

each compound necessary for the complete inhibition of growth was determined by the dilution method, using the usual bouillon agar medium (pH 6.8—7.0); some of the results are shown in Table 1. The compounds employed in this test consist of three types (Table 1). I, Ib, II, and IIa are the compounds substituted by the 5-nitro-2-furylvinyl group at the 2-position on the 1,8-naphthyridine nucleus (type A), IV and IVa—c are those substituted at the 4-position (type B), and V and VI are acrylic acid derivatives (type C). The three types of compounds showed a decreasing tendency of activity in the order: type A> type B>type C.

All the compounds of type A, except for Ib, showed broad spectra of antibacterial activity; I was the most active antibacterial against all the microorganisms employed. All the compounds of type B, except IVb, showed a strong activity against *Diplococcus pneumoniae*, *Streptococcus hemolyticus*, *Staphilococcus aureus*, and *Bacillus subtilis*, but they exhibited no activity against the other microorganisms. The lack of activity in Ib and IVb may be due to the substituent (phenoxy group). The compounds of type C include almost no active antibacterial.

Experimental[14]

2-[2-(5-Nitro-2-furyl)vinyl]-5-hydroxy-1,8-naphthyridine (I). A mixture of 2-methyl-5-hydroxy-1,8-naphthyridine[11] (1.6 g, 10 mmol), 5-nitrofurfural (1.6 g, 11 mmol), and acetic anhydride (10 ml) was refluxed for 5 hr. Cooling provided 1.8 g of a crude product; when the mother filtrate was then allowed to stand for several days at room temperature, an additional 0.2 g of the product was obtained. Recrystallization from ethylene glycol monomethyl ether afforded 1.8 g (63.6%) of I as pale yellow needles; mp 316—317 °C (decomp.). IR (KBr) cm^{-1}: 1650 (ν C=O), 965 (δ C–H; *trans*).

Found: C, 59.19; H, 3.07; N, 14.60%. Calcd for $C_{14}H_9N_3O_4$: C, 59.36; H, 3.20; N, 14.83%.

2-[2-(5-Nitro-2-furyl)vinyl]-5-hydroxy-6-ethoxycarbonyl-1,8-naphthyridine (II). 2-Methyl-5-hydroxy-6-ethoxycarbonyl-1,8-naphthyridine[15] (2.6 g, 12.2 mmol) and 5-nitrofurfural (1.8 g, 12.5 mmol) were heated in acetic anhydride (10 ml) under reflux for 1.5 hr. On cooling, the precipitated product was collected and washed with ether and methanol. Crystallization from ethylene glycol monomethyl ether gave 3 g (76.5%) of II as pale yellow needles which melted, with decomposition, at 285 °C. IR (KBr) cm^{-1}: 1730 and 1710 (shoulder) (ν C=O), 960 (δ C–H; *trans*).

Found: C, 57.42; H, 3.85; N, 11.53%. Calcd for $C_{17}H_{13}N_3O_6$: C, 57.47; H, 3.69; N, 11.83%.

2-[2-(5-Nitro-2-furyl)vinyl]-5-chloro-1,8-naphthyridine (Ia). *Procedure A*: Compound I (0.4 g, 1.7 mmol) was heated in phosphoryl chloride (5 ml) for 4 hr under reflux. The reaction mixture was then poured into cold water, and the product was collected, washed with water, and then dried. Recrystallization from ethylene glycol monomethyl ether gave 0.23 g (54%) of Ia as pale yellow needles; mp 231—232 °C (decomp.). IR (KBr) cm^{-1}: 960 (δ C–H; *trans*).

Found: C, 55.76; H, 2.53; N, 13.54%. Calcd for $C_{14}H_8N_3O_3Cl$: C, 55.74; H, 2.67; N, 13.93%.

Procedure B: 2-Methyl-5-chloro-1,8-naphthyridine[11] (1 g, 5.6 mmol) and 5-nitrofurfural (0.9 g, 6.4 mmol) were heated in acetic anhydride (5 ml) under reflux for 1.5 hr. Cooling provided 1.2 g of the crude product. Work-up as above afforded 0.8 g (58.9%) of Ia; mp 231—232 °C (decomp.), undepressed on admixture with a sample prepared by *Procedure A* as has been described above for Ia.

2-[2-(5-Nitro-2-furyl)vinyl]-5-chloro-6-ethoxycarbonyl-1,8-naphthyridine (IIa). II (0.6 g, 2.12 mmol) was covered with phosphoryl chloride (*ca.* 10 ml) and refluxed for 1 hr. After cooling the reaction mixture was poured into ice water and neutralized with aqueous ammonia. The precipitated product was filtered and washed with water. Crystallization from pyridine gave 0.3 g (47.5%) of IIa as pale yellow needles

14) All the melting and decomposition points are uncorrected. The elemental analyses were carried out with a Yanagimoto CHN Corder, MT-2 type. The infrared absorption spectra (IR) were recorded with a JASCO Model IRA-2 grating infrared spectrophotometer.

15) G. R. Lappin, *J. Amer. Chem. Soc.*, **70**, 3348 (1948).

which did not melt below 300 °C. IR (KBr) cm^{-1}: 1730 (ν C=O), 960 (δ C–H; *trans*).

Found: C, 54.95; H, 3.24; N, 11.14%. Calcd for $C_{17}H_{12}N_3O_5Cl$: C, 54.63; H, 3.24; N, 11.24%.

2-[2-(5-Nitro-2-furyl)vinyl]-5-phenoxy-1,8-naphthyridine (Ib). A mixture of Ia (0.5 g, 1.7 mmol) and phenol (5 ml) was refluxed for 15—20 min. After cooling, aqueous sodium carbonate was added to the reaction mixture, and the precipitated product was filtered. Recrystallization from tetrahydrofuran afforded 0.45 g (76.5%) of Ib as a pale yellow powder which melted at 223—224 °C. IR (KBr) cm^{-1}: 950 (δ C–H; *trans*), 734 and 690 (δ C–H; mono-substituted benzene).

Found: C, 66.92; H, 3.70; N, 11.56%. Calcd for $C_{20}H_{13}N_3O_4$: C, 66.85; H, 3.65; N, 11.69%.

2-[2-(5-Nitro-2-furyl)vinyl]-5-phenoxy-6-ethoxycarbonyl-1,8-naphthyridine (IIb). The chloro compound, IIa (0.15 g, 4 mmol), was heated in 2 ml of phenol under reflux for 40 min. Aqueous sodium carbonate was then added to the reaction mixture, and the precipitates were filtered. They were subsequently crystallized from ethylene glycol monomethyl ether to afford 0.08 g (63.8%) of IIb as pale yellow granules; mp>300 °C. IR (KBr) cm^{-1}: 1730 (ν C=O), 955 (δ C–H; *trans*), 730 and 690 (δ C–H; mono-substituted benzene).

Found: C, 64.72; H, 3.98; N, 9.51%. Calcd for $C_{23}H_{16}N_3O_6$: C, 64.88; H, 3.75; N, 9.76%.

4-[2-(5-Nitro-2-furyl)vinyl]-2,7-dihydroxy-1,8-naphthyridine (IV) and 3-(5-Nitro-2-furyl)-2-(2,7-dihydroxy-1,8-naphthyridin-4-yl)acrylic Acid (VI). A mixture of potassium salt of 2,7-dihydroxy-1,8-naphthyridine-4-acetic acid[12] (4.2 g, 16.3 mmol), 5-nitrofurfural (2.6 g, 18.4 mmol), and acetic anhydride (40 ml) was heated at 66—70 °C for 4 hr. After cooling, 40 ml of glacial acetic acid was added to the reaction mixture, and then this was poured into cold water. The precipitated product was filtered and recrystallized from dimethyl sulfoxide to give 2.3 g (42%) of IV as a yellow powder; mp 317 °C (decomp.). IR (KBr) cm^{-1}: 3100—2800 (ν O–H; associated), 1663 (ν C=O), 957 (δ C–H; *trans*).

Found: C, 55.97; H, 3.24; N, 13.98%. Calcd for $C_{14}H_9N_3O_5$ (IV): C, 56.19; H, 3.03; N, 14.04%.

The mother filtrate was concentrated under reduced pressure, after which the precipitated product was collected on a filter and washed with water. Recrystallization from aqeuous acetic acid afforded 1.5 g (24%) of VI as a yellow powder; mp>320 °C. IR (KBr) cm^{-1}: 3140—2800 (ν O–H; associated), 1706 and 1658 (ν C=O).

Found: C, 52.33; H, 2.67; N, 12.45%. Calcd for $C_{15}H_9N_3O_7$ (VI): C, 52.48; H, 2.64; N, 12.24%.

4-[2-(5-Nitro-2-furyl)vinyl]-2,7-dichloro-1,8-naphthyridine (IVa). IV (1 g, 3.3 mmol) was heated in phosphoryl chloride (20 ml) under reflux for 3 hr. After cooling, the reaction mixture was poured into ice water and the precipitated product was filtered. This product was recrystallized from ethylene glycol monomethyl ether to give 0.83 g (75%) of IVa as a yellow powder which melted at 259—260 °C. IR (KBr) cm^{-1}: 957 (δ C–H; *trans*).

Found: C, 50.28; H, 2.40; N, 12.49%. Calcd for $C_{14}H_7N_3O_3Cl$: C, 50.00; H, 2.08; N, 12.50%.

4-[2-(5-Nitro-2-furyl)vinyl]-2,7-diphenoxy-1,8-naphthyridine (IVb). IVa (1 g, 3 mmol) was heated in phenol (10 ml) under reflux for 30 min. After cooling, the reaction mixture was diluted with ether, and the precipitates were collected and washed with ether. Subsequent crystallization from ethylene glycol monomethyl ether gave 0.5 g (33%) of IVb as yellow needles; mp 216—217 °C. IR (KBr) cm^{-1}: 953 (δ C–H); *trans*), 750 and 690 (δ C–H; mono-substituted benzene).

Found: C, 69.24; H, 3.64; N, 9.45%. Calcd for $C_{26}H_{17}N_3O_5$: C, 69.18; H, 3.77; N, 9.31%.

4-[2-(5-Nitro-2-furyl)vinyl]-2,7-dianilino-1,8-naphthyridine Monohydrochloride (IVc). Aniline (0.3 g, 3.2 mmol), IVa (0.5 g, 1.5 mmol), and ethylene glycol monomethyl ether (10 ml) were refluxed for 1 hr. After cooling, concentrated hydrochloric acid was added to the reaction mixture. The isolated product was then collected and washed with water. Recrystallization from aqueous methanol afforded 0.35 g (48.5%) of IVc as a crimson-colored powder; mp 147—148 °C. IR (KBr) cm^{-1}: 959 (δ C–H; *trans*), 755 and 690 (δ C–H; mono-substituted benzene).

Found: C, 64.91; H, 3.98; N, 14.04%. Calcd for $C_{26}H_{19}N_5O_3 \cdot HCl$: C, 64.26; H, 4.12; N, 14.41%.

3-(5-Nitro-2-furyl)-2-(2-hydroxy-7-acetamido-1,8-naphthyridin-4-yl)acrylic Acid (V). A mixture of potassium salt of 2-hydroxy-7-amino-1,8-naphthyridine-4-acetic acid[12] (11.7g, 45 mmol), 5-nitrofurfural (7.1 g, 50 mmol), and acetic anhydride (10 ml) was heated at 50—55 °C for 4 hr. The reaction mixture was then poured into ice water, and the separated product was filtered and washed with water. Recrystallization from glacial acetic acid gave 11.5 g (62.5%) of V as a yellow powder; mp>320 °C. IR (KBr) cm^{-1}: 3230 (ν N–H), 2925 (ν CH_3), 1707, 1693, and 1660 (ν C=O).

Found: C, 53.26; H, 3.38; N, 15.06%. Calcd for $C_{17}H_{12}N_4O_7$: C, 53.13; H, 3.13; N, 14.58%.

Studies on 3,5-pyrazolidinediones. IV. Addition of 4-Arylazo-3,5-pyrazolidinediones to Ethyl Acrylate

Mohamed Helmi ELNAGDI and Masaki OHTA

Department of Chemistry, Faculty of Science, Tokyo Institute of Technology, Ookayama, Meguro-ku, Tokyo 152

(Received December 22, 1972)

4-Arylazo-3,5-pyrazolidinediones (I) react with ethyl acrylate to yield the corresponding 1-β-ethoxycarbonylethyl derivatives (III), which were readily hydrolyzed into the acids IV. Compounds III and IV were found to react with acrylonitrile to yield the corresponding 1-substituted 2-β-cyanoethyl derivatives V and VI respectively. Whereas III and IV were recovered unchanged upon treatment with aniline or piperidine, the arylazomalonic acid dihydrazide (IX) were formed upon treatment of III or IV with hydrazine hydrate. 2-*p*-Chlorophenylazotetrahydropyrazolo[1,2-*a*]pyrazole-1,3,7-trione (XI) has been prepared by the action of phosphorus oxychloride on IVb. 3-Amino-4-phenylazo-2-pyrazolin-5-one (II) react with ethyl acrylate to yield the pyrazolo[1,5-*a*]pyrimidine derivative XII.

In a previous paper[1] it has been shown that 4-arylazo-3,5-pyrazolidinediones (I) react with acrylonitrile to yield either the 1-β-cyanoethyl or the 1,2-di(β-cyanoethyl) derivatives depending on the reaction conditions. It has also been shown that 3-amino-4-phenylazo-2-pyrazolin-5-one (II) react with the same reagent to yield a pyrazolopyrimidine derivative. As an extention of this work, it was thought worthwhile to investigate the behavior of compounds I and II toward other systems containing activated double bond. In the present paper, the behavior of I and II toward ethyl acrylate is reported.

Upon treatment of I with ethyl acrylate in molecular proportions the 1-β-ethoxycarbonylethyl derivatives (III) were formed.[2] The structure of these derivatives was established from their IR spectra and from identity with authentic specimens prepared by the action of ethanol and concentrated sulfuric acid on 4-arylazo-1-β-carboxyethyl-3,5-pyrazolidinediones (IV),[2] now obtained by the action of β-bromopropionic acid on I. Furthermore, compounds IV were formed upon treatment of III with acetic acid–hydrochloric acid mixture.

In contrast to the reported unreactivity of 4-arylazo-1-phenyl-3,5-pyrazolidinediones toward the action of acrylonitrile,[1] compounds III and IV were found to add readily to acrylonitrile to yield the 1,2-disubstituted 3,5-pyrazolidinedione derivatives, V and VI respectively. Compounds V and VI were also obtained upon treatment of III and IV with β-chloropropiononitrile respectively.

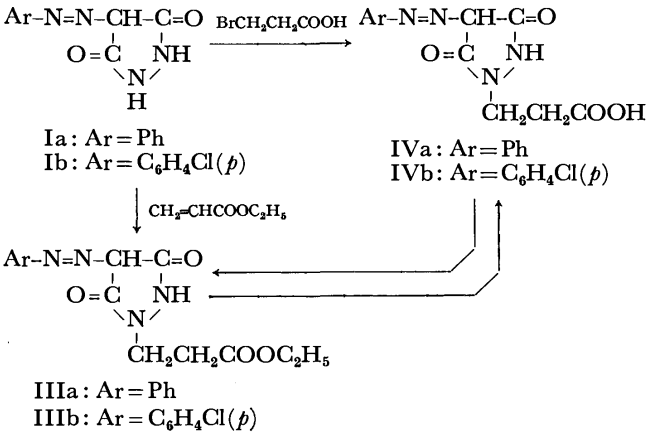

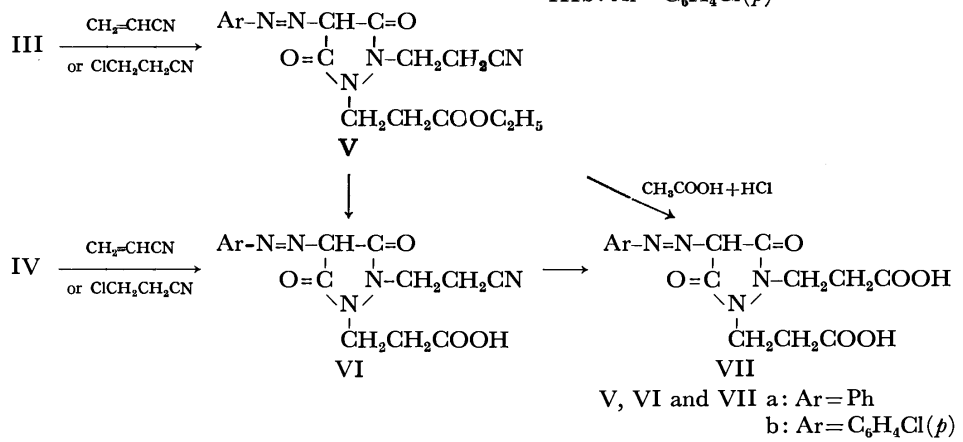

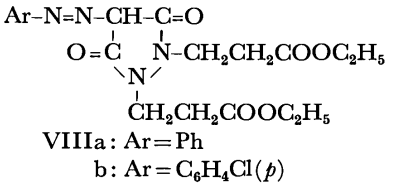

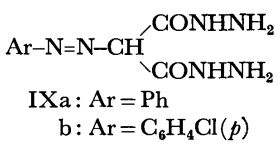

1) M. H. Elnagdi, N. A. L. Kassab, S. M. Fahmy, and F. A. El-All, *J. Prakt. Chem.*, in press.

2) For the sake of convenience, all compounds described in this paper are referred to as arylazo-3,5-pyrazolidinediones derivatives, irrespective of their actual structure.

Compounds V were readily hydrolyzed with aqueous sodium hydroxide to the corresponding VI. On the other hand, treatment of V and VI with acetic acid–hydrochloric acid mixture results in the formation of the known[1] 4-arylazo-1,2-di(β-carboxyethyl)-3,5-pyrazolidinedione derivatives (VII).

Compounds III react also with ethyl acrylate to yield the corresponding 4-arylazo-1,2-di(β-ethoxycarbonylethyl)-3,5-pyrazolidinediones (VIII). Compounds VIII are readily converted into VII by the action of acetic acid–hydrochloric acid mixture.

Whereas the compounds III and IV were recovered unchanged upon treatment with aniline or piperidine, the arylazomalonic acid dihydrazides (IX) were formed upon treatment of III with hydrazine hydrate. The stability of the pyrazolidinedione ring in III and IV toward the action of piperidine is in contrast to the reported[3,4] hetero-ring opening of 4-arylazo-1-phenyl- and 1,2-diphenyl-3,5-pyrazolidinediones by the action of the same reagent.

In a trial to effect cyclization of III into a pyrazolo-[1,2-*a*]pyrazole derivative by the action of acetic anhydride, the acetyl derivatives (X) were obtained. Although compounds III have three sites for acylation to occur,[5] compounds X were assigned the *N*-acetyl structure based on their stability toward the action of acetic acid[6] and from a study of their spectral data. The IR spectra of compound Xb, taken as an example, reveals the presence of four carbonyl sretching absorption bands at 1740, 1730, 1690, and 1675 cm^{-1}. The former two were considered to be due to the acetyl and ester carbonyl groups and the latter due to the ring carbonyl groups. Compounds X were converted readily into III on reflux with pyridine.

2-*p*-Chlorophenylazotetrahydropyrazolo[1,2-*a*]pyrazole-1,3,7-trione (XI) has now been prepared through cyclization of the acid (IVb) by the action of phosphorus oxychloride. The structure XI, presented here, finds support from analytical and spectral (IR) data. Thus, the IR spectrum was characterized by the presence of three carbonyl bands at 1770, 1710, and 1680 cm^{-1} and revealed the absence of absorption in the region of 2500—3000 cm^{-1} present in the spectrum of the starting acid (IVb).

The behavior of 3-amino-4-phenylazo-2-pyrazoline-5-one (II) toward ethyl acrylate shows that II did not add to ethyl acrylate in aqueous pyridine solution, while it react with the same reagent in the presence of catalytic amount of potassium hydroxide to yield the pyrazolo-[1,5-*a*]pyrimidine derivative (XII). This is in analogy with the recently reported behavior of 3-phenyl-5-

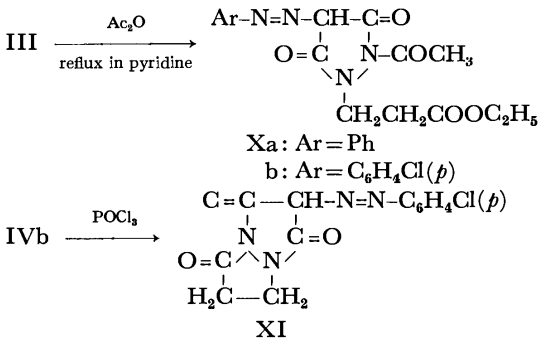

aminopyrazole toward methyl phenylpropiolate.[7] The structure proposed for compound XII finds support from analytical data, IR spectrum, and its conversion into IVa through the action of acetic acid–hydrochloric acid mixture.

The IR spectrum of compound XII does not show free hydroxyl absorption around 3600 cm^{-1} and shows a broad band (2430—2800 cm^{-1}) similar to the OH group absorption of fatty acid dimers. Similar behavior has been reported for β-keto-enols and was attributed to intramolecular conjugate chelation.[8] However, in compound XII steric considerations will prevent a direct intramolecular hydrogen bond. This may lead to the conclusion that XII, at least in solid state, exists in a highly stable dimeric structure capable of similar resonance stabilization. Similar system in which such conjugate chelation could arise from intermolecular hydrogen bond has been reported in case of 5,5-dimethyl-1,3-cyclohexanedione.[9]

In part III of this series[1] it has been shown that position 1 in compound II is the most reactive position for cyanoethylation. That this position is not involved in the reaction of II with ethyl acrylate may lead to the assumption that in case of ethyl acrylate the first step in the reaction is acylation of the amino group followed by cyclization to yield XII.

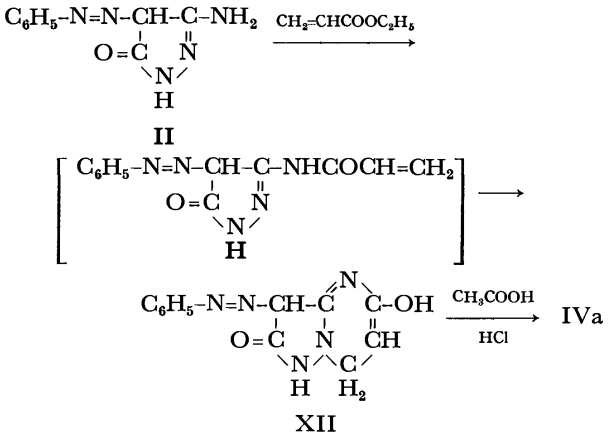

Experimental

All melting points were determined on a micro hot stage and are uncorrected. The infrared spectra were recorded

3) M. H. Elnagdi and S. M. Fahmy, *Indian J. Chem.*, **10**, 461 (1972).

4) M. H. Elnagdi, A. S. A. Shawali, and M. R. Elaukby, *ibid.*, in press.

5) *Cf.* the behavior of 3,5-pyrazolidinediones on acylation, R. H. Wiely and P. Wily, "Pyrazolones, Pyrazolidionones and Derivatives" John Wiley & Sons, New York (1964), p. 126 and 130.

6) *Cf.* the ready rearrangement of 5-acetoxy-3-phenylpyrazole into the 1-acetyl derivative by the action of acetic acid, A. Weissberger and H. D. Porter, *J. Amer. Chem. Soc.*, **65**, 1495 (1943).

7) V. Sprio and S. Plescia, *J. Heterocycl. Chem.*, **9**, 951 (1972).

8) J. L. Bellamy "The Infrared Spectra of Complex Molecules," John Wiley & Sons, Inc. New York (1958), p. 104.

9) R. S. Rasmussen, D. D. Tunnicliff, and R. R. Brattain, *J. Amer. Chem. Soc.*, **71**, 1068 (1949).

with Hitachi Grating Infrared Spectrometer Model EPI-G3. Ultraviolet spectra were measured in ethanol with Hitachi 124 Spectrophotometer.

4-Arylazo-1-β-ethoxycarbonylethyl-3,5-pyrazolidinediones (IIIa and IIIb). From I and Ethyl Acrylate: Ten mmol of I was added to a solution of ethyl acrylate (0.01 mol) in pyridine (50 ml) and water (10 ml). The reaction mixture was refluxed for 6 hr and evaporated *in vacuo* to leave a residue which was purified by recrystallization from ethanol.

IIIa. Yellow crystals, yield 80%, mp 115 °C. IR: 3150 (NH), 1725 (ester CO), 1690 and 1660 cm^{-1} (ring CO). Found: C, 55.50; H, 5.37; N, 18.69%. Calcd for $C_{14}H_{16}N_4O_4$: C, 55.25; H, 5.30; N, 18.41%.

IIIb. Orange crystals, yield 85%, mp 164 °C. IR: 3120 (NH), 1730 (ester CO), 1690 and 1660 cm^{-1} (ring CO). Found: C, 49.60; H, 4.50; N, 16.55%. Calcd for $C_{14}H_{15}N_4O_4Cl$: C, 49.63; H, 4.46; N, 16.54%.

From IV by Esterification: A suspension of IV (see below) in ethanol (30 ml) containing sulfuric acid (1.5 ml; 98%) was refluxed for 16 hr, cooled and poured into ice water. The solid product, so formed, was purified by recrystallization and identified (mp and mixed mp) as IIIa or IIIb. Yields, 60 and 67% respectively.

4-Arylazo-1-β-carboxyethyl-3,5-pyrazolidinediones (IVa and IVb). From I and β-Bromopropionic Acid: Ten mmol of I was added to a solution of β-bromopropionic acid (0.01 mol) in 100 ml of aqueous ethanol (1 : 1) containing 2.0 g of sodium carbonate and refluxed for 3 hr. Evaporation of the solvent *in vacuo* afforded a solid product which was dissolved in water (100 ml), washed with ether, and then acidified with concentrated hydrochloric acid to give crude IV.

IVa. Yellow crystals (from ethanol), yield 82%, mp 230 °C (decomp.). IR: 3000—2600 (OH), 1752 (carboxyl CO), 1690 and 1660 cm^{-1} (ring CO). Found: C, 51.94; H, 4.09; N, 19.95%. Calcd for $C_{12}H_{12}N_4O_4$: C, 52.17; H, 4.38; N, 20.28%.

IVb. Yellow needles (from acetic acid), yield 87%, mp 248 °C (decomp.). IR: 3030—2600 (OH), 1758 (CO), and 1690, 1660 cm^{-1} (CO). Found: C, 46.54; H, 3.54; N, 18.08%. Calcd for $C_{12}H_{11}N_4Cl$: C, 46.38; H, 3.56; N, 18.03%.

From III by Hydrolysis: A solution of III (2.0 g) in acetic acid (20 ml) containing concentrated hydrochloric acid (5.0 ml) was refluxed for 3 hr, allowed to cool and poured into ice-water. The solid product, so formed, was collected, crystallized and identified (mp and mixed mp) as IVa or IVb. Yields, 90 and 93% respectively.

4-Arylazo-1-β-cyanoethyl-2-β-ethoxycarbonylethyl-3,5-pyrazolidinediones (Va and Vb). From III and Acrylonitrile: Ten mmol of III was added to a solution of pyridine (50 ml) and water (10 ml) containing acrylonitrile (3 ml) and the reaction mixture was refluxed for 12 hr, left overnight at room temperature, and then evaporated *in vacuo*. The resulting oily product was triturated with petrolum ether and crystallized from ethanol.

Va. Yellow crystals, yield 75%, mp 58 °C. IR: 3154 (NH), 2230 (CN), 1730 (ester CO), 1710 and 1670 cm^{-1} (ring CO). Found: C, 57.23; H, 5.30; N, 19.26%. Calcd for $C_{17}H_{19}N_5O_4$: C, 57.13; H, 5.36; N, 19.60%.

Vb. Yield 90%, mp 100 °C. IR: 3150 (NH), 2230 (CN), 1730 (CO), 1715 and 1675 cm^{-1} (CO). Found: C, 52.03; H, 4.57; N, 17.58%. Calcd for $C_{17}H_{18}N_5O_4Cl$: C, 52.11; H, 4.63; N, 17.63%.

From III and β-Chloropropiononitrile: A mixture of III (0.01 mol), β-chloropropiononitrile (0.01 mol), sodium acetate (2.0 g) and ethanol (30 ml) was refluxed for 5 hr. The solvent was removed *in vacuo* and the remaining solid was washed with dilute hydrochloric acid and then water. The crude product was purified by recrystallization from ethanol and identified (mp and mixed mp) as Va or Vb. Yields, 70 and 72% respectively.

4-Arylazo-1-β-carboxyethyl-2-β-cyanoethyl-3,5-pyrazolidinedione (VIa and VIb). From IV and Acrylonitrile: To a solution of pyridine (50 ml) and water (10 ml) containing acrylonitrile (3 ml) 2.0 g of IV was added and refluxed for 3 hr and then evaporated *in vacuo*. The resulting crystalline mass was purified by recrystallization.

VIa. Yellow crystals (from ethanol), yield 72%, mp 195 °C. IR: 3150 (NH), 2400—2900 (OH), 2238 (CN), 1732 (carboxyl CO), 1670 and 1660 cm^{-1} (ring CO). Found: C, 54.41; H, 4.49; N, 21.14%. Calcd for $C_{15}H_{15}N_5O_4$: C, 54.71; H, 4.59; N, 21.27%.

VIb. Yellow crystals (from acetic acid), yield 75%, mp 205 °C. IR: 3125 (NH), 2400—2900 (OH), 2240 (CN), 1735 (carboxyl CO), 1660 and 1670 cm^{-1} (ring CO). Found: C, 49.16; H, 3.82; N, 19.44%. Calcd for $C_{15}H_{14}O_4N_5Cl$: C, 49.52; H, 3.87; N, 19.25%.

From V by Hydrolysis: A solution of V (2.0 g) in ethanolic aqueous sodium hydroxide (30 ml of 50% ethanol containing 1.0 g of NaOH) was refluxed for 45 min. The reaction mixture was allowed to cool and then acidified with concentrated hydrochloric acid to produce a solid product which was purified and identified as VIa or VIb.

From IV and β-Chloropropiononitrile: A mixture of IV (0.01 mol), β-chloropropiononitrile (0.01 mol), sodium carbonate (2.0 g) and ethanol (30 ml, 75%) was refluxed for 6 hr and then evaporated *in vacuo*. The remaining solid was dissolved in water and acidified with concentrated hydrochloric acid. The precipitates were purified by recrystallization and identified as V. Yields, 60 and 62% respectively.

4-Arylazo-1,2-di(β-carboxyethyl)-3,5-pyrazolidinedione (VIIa and VIIb). From V by Hydrolysis: A suspension of V (1.0 g) in acetic acid (20 ml) and hydrochloric acid (5 ml, 35%) was refluxed for 4 hr and then the solvent was removed under vacuum. The resulting crude product was treated with water, filtered and identified as VIIa or VIIb[1] after crystallization. Yields are 62 and 68% respectively.

From VI by Hydrolysis: In a similar manner as described above, hydrolysis of VI afforded VIIa or VIIb. Yields are 72 and 75% respectively.

From VIII by Hydrolysis: The procedure described above was used and the product proved to be VIIa of VIIb by mp and mixed mp.

4-Arylazo-1,2-di(β-ethoxycarbonylethyl)-3,5-pyrazolidinediones (VIIIa and VIIIb). Ten mmol of III was added to a solution of pyridine (50 ml) containing ethyl acrylate (0.02 mol) and was refluxed for 16 hr. The reaction mixture was left for two days at room temperature and then evaporated *in vacuo*. The resulting oily residue was dissolved in hot ethanol. After cooling, a small amount of unchanged material was removed by filtration. Evaporation of the filtrate afforded a crude product which was purified and identified as VIII.

VIIIa. Yellow crystals (from benzene–petroleum ether), yield 60%, mp 55 °C. Found: C, 56.69; H, 5.85; N, 13.70%. Calcd for $C_{19}H_{24}N_4O_6$: C, 56.43; H, 5.98; N, 13.86%.

VIIIb. Yellow crystals (from benzene–petroleum ether), yield 64%, mp 95 °C. IR: 1740, 1730 (ester CO), 1700 and 1680 cm^{-1} (ring CO). Found: C, 52.07; H, 5.10; N, 12.59%. Calcd for $C_{19}H_{23}N_4O_6Cl$: C, 51.99; H, 5.28; N, 12.76%.

Reaction of III or IV with Hydrazine Hydrate. Two grams of III or IV was added to a solution of ethanol (30 ml) containing hydrazine hydrate (2.0 ml) and refluxed for 3 hr. After cooling, the product was collected, recrystallized from

dioxane and proved to be arylazomalonic acid dihydrazide by mixed mp determination with an authentic sample.[3]

4-Arylazo-1-β-ethoxycarbonylethyl-2-acetyl-3,5-pyrazolidinedione (X). A mixture of III (2.0 g) and acetic anhydride (30 ml) was refluxed for 3 hr. After cooling, the reaction mixture was poured into water and stirred to decompose the excess acetic anhydride. The product, which separated out, was collected and recrystallized from ethanol.

Xa. Yellow crystals, mp 95 °C. IR: 3155 (NH), 1742 (acetyl CO), 1718 (ester CO), 1690 and 1665 cm^{-1} (ring CO). Found: C, 55.81; H, 5.26; N, 16.61%. Calcd for $C_{16}H_{18}N_4O_5$: C, 55.48; H, 5.24; N, 16.18%.

Xb. Yellow needles, mp 127 °C. IR: 3150 (NH), 1740 (acetyl CO), 1730 (ester CO), 1690 and 1675 cm^{-1} (ring CO). Found: C, 50.46; H, 4.50; N, 14.59%. Calcd for $C_{16}H_{17}N_4O_5Cl$: C, 50.46; H, 4.47; N, 14.71%.

2-p-Chlorophenylazotetrahydropyrazolo[1,2-a]pyrazole-1,3,7-trione (XI). A suspension of IVb (2.0 g) in phosphorus oxychloride (20 ml) was heated on a water bath for 3 hr. The resulting solution was then poured into ice-water and the resulting solid product was crystallized from ethanol. Yield was 50%. Yellow crystals, mp 275 °C. IR: 1770, 1710, and 1680 cm^{-1} (ring CO). Found: C, 49.09; H, 3.33; N, 18.77%. Calcd for $C_{12}H_9N_4O_3Cl$: C, 49.23; H, 3.09; N, 19.14%.

1, 2-Dihydro-5-hydroxy-3-phenylazopyrazolo[1, 5-a]pyrimidine-2-one (XII). Two grams of II was added to a solution of pyridine (50 ml) and water (10 ml) containing 1 ml of ethyl acrylate and then one drop of potassium hydroxide solution was added. The mixture was refluxed for 14 hr and then left overnight at room temperature. Removal of the solvent *in vacuo* afforded an oily residue which was dissolved in ethanol and acidified with concentrated hydrochloric acid. The crystals, which separated out, were collected and recrystallized from dimethylformamide to give 1.2 g (60%) of XII. Mp 301 °C. IR: 1690 (CO), 2430—2900 cm^{-1} (OH). Found: C, 55.62; H, 4.39; N, 27.30%. Calcd for $C_{12}H_{11}N_5O_2$: C, 56.02; H, 4.31; N, 27.23%.

Compound XII produces a red color with ferric chloride solution and is soluble in sodium carbonate solution. In the absence of potassium hydroxide, compound II was recovered unchanged after being refluxed with ethyl acrylate for 36 hr.

BULLETIN OF THE CHEMICAL SOCIETY OF JAPAN, VOL. 46, 1833—1836 (1973)

The Reaction of Dicyclopentadiene with Ethyl Diazoacetate

Tadashi SATO, Tamio MORI, and Junichi SHINODA

Department of Applied Chemistry, Waseda University, Shinjuku-ku, Tokyo 160

(Received October 5, 1972)

The reaction of *endo*-dicyclopentadiene (**1**) with ethyl diazoacetate (**3**) was carried out in the presence of several copper compounds. Two patterns of reaction were observed, depending on the type of copper compound used; the following schemes were proposed for the two reactions. I: The reaction proceeds through a coordination of the olefinic group to copper to form an olefin-copper complex, followed by an attack of the diazo compound on the complex. II: The reaction proceeds through a coordination of the diazo compound to copper to form an inversed ylide (**11**), followed by an electrophilic attack of the carbonium-ion center in **11** on the olefin to form a three-membered cyclic transition state, **12**.

It has been believed that the copper-catalyzed reactions of aliphatic diazo compounds with olefins involve copper-carbene-olefin complexes in the final stage of the reaction.[1] The scheme has been confirmed by the stereochemical relation of products with the variation in the electronic and steric factors of the ligands in the catalyst,[2] and by the introduction of chirality into the products in the reaction catalyzed by the chiral copper compounds.[3] With a view to clarifying how copper compounds participate in the transition state in these reactions, the reaction of *endo*-dicyclopentadiene with ethyl diazoacetate was carried out under several conditions.

Results

When *endo*-dicyclopentadiene (**1**) or its copper(I) chloride complex (**2**) was reacted with ethyl diazoacetate (**3**), compounds **4**—**8** were obtained in the yields shown in Table 1. Compound **9** was obtained when the reaction was carried out in the presence of triethyl phosphite (**10**). The yields were obtained by gas-chromatographic analysis, and the product identifications for new compounds were carried out as follows.

The structures of **6** and **7** were speculated to have a cyclopropane ring fused to a cyclopentane ring, judging from the IR bands characteristic of the double bond in a strained norbornene system,[4] which appeared at 1570 cm^{-1} for **6** and at 1574 cm^{-1} for **7**. The struc-

1) For a recent review, see V. Dave and E. W. Warnhoff, "Organic Reactions", Vol. 18, ed. by W. G. Dauben, John Wiley & Sons, Inc., New York, N. Y. (1970), p. 217.

2) W. R. Moser, *J. Amer. Chem. Soc.*, **91**, 1135, 1141 (1969).

3) H. Nozaki, H. Takaya, S. Moriuti, and R. Noyori, *Tetrahedron*, **24**, 3655 (1968).

4) B. W. Cook, R. Miller, and P. Todd, *J. Organometal. Chem.*, **19**, 421 (1969).

Table 1. Reaction conditions and product distributions in the reaction of **1** or **2** with **3**[a)]

Reaction	Substrate	Copper compound[b)]	Solvent[c)]	Temp(°C)	**4**	**5**	**6**	**7**	**8**	**8**/(**6**+**7**) Ratio
1	**1**	CuCl	AN	20—21	2.3	0.7	0.1	0.3	17.9	41.6
2	**2**		D	17—19	7.2	1.4	trace	trace	55.3	great
3	**1**	$CuCl_2 \cdot 2H_2O$	D–W	40—50	4.3	1.1	1.1	0.6	8.6	5.1
4	**1**	$CuSO_4$	D–W	55	1.2	1.2	0.2	0.6	6.9	8.1
5	**2**		DMSO	15—17	16.3	12.5	0.2	0.6	3.0	3.8
6	**1**	$Cu(acac)_2$[d)]	D	65	4.4	5.4	5.3	27.9	34.5	1.0
7	**1**	**2**[d)]	D	67	9.9	10.8	1.0	4.3	5.6	1.1
8[e)]	**1**	**10**·CuCl	D	40	—[f)]	2.3	2.0	5.0	7.0	1.0

a) No account was taken of the low-boiling fractions (for instance, ethyl chloroacetate).
Although the mass balance of the reaction is not satisfactory, we consider the ratio **8**/(**6**+**7**) represented in this table is still meaningful, because the ratio is independent of the reaction conditions (reaction time or length of induction period) in a respective reaction, while the actual yields of products are more or less influenced.
b) Unless otherwise stated, equimolar amount to substrate was used.
c) AN: acetonitrile; D: dioxane; D–W: dioxane–water (1:1).
d) One-tenth equivalent was used.
e) **9** (8.5%) was also obtained.
f) The peak on the gas chromatogram overlapped with that of a phosphorus-containing substance.

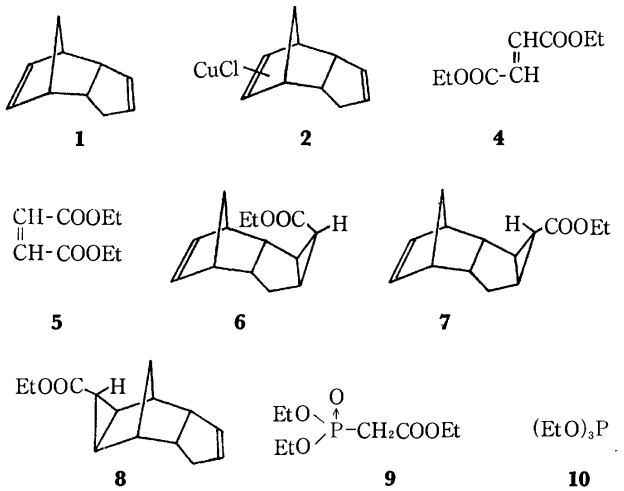

1 **2** **4** **5** **6** **7** **8** **9** **10**

Chart 1

tures were also supported by the deformation bands of C–H in a cyclopropane ring fused to a cyclopentane ring,[5)] which appeared at 999 cm^{-1} for **6** and at 1011 cm^{-1} for **7**. The *exo*-configuration of the cyclopropane ring was tentatively assigned on the basis of the steric consideration that the alternative configuration would result in an enormous nonbonded steric repulsion.[5)] Since the steric repulsion created by the ethoxycarbonyl group and the hydrogen atoms in the norbornene system would be more serious in **6** than in **7**, the structure **7** was assigned to the major product.

The structure of **8** was supported by the elemental analysis and by an IR band at 1612 cm^{-1}, characteristic of the double bond in a cyclopentene ring, and a band at 1026 cm^{-1}, the deformation band of C–H in a cyclopropane ring fused to a norbornane system.[5)] The stereochemistry of the cyclopropane ring and the ethoxycarbonyl group was assigned in a similar way.

The structure of **9** was assigned on the basis of the elemental and spectroscopic analyses. The IR spectrum showed an ester carbonyl band at 1745 cm^{-1}. The NMR spectrum showed a doublet at δ 2.73 (2H, J=20 Hz) for $-CH_2-P$, besides signals corresponding to three ethyl groups.

Discussion

Referring to the ratio of **8**/(**6**+**7**), we can classify the reactions into three groups: Class I (Reactions 1—2) with higher ratios, Class II (Reactions 3—5) with intermediate ratios, and Class III (Reactions 6—8) with lower ratios. This fact suggests that more than one mode of the participation of copper in the reaction is present. We assume that the diversity arises from the different ability of copper catalysts to coordinate to a double bond. It has been established that an olefinic ligand coordinates to a metal more readily when the metal is in a low oxidation state than when it is in a high oxidation state.[6)] The rationale behind this might be that a metal with a lower valency, because of its formal abundance of electrons, back-donates its electrons into the antibonding orbital of the ligand more efficiently than does the same metal with a higher valency, thus providing a further stabilization for the metal-olefin complex. The donation and back-donation between the metal and the olefin might result in a net excitation of electrons from bonding to antibonding orbitals in the olefin, hence stabilizing the complex, particularly when the original olefin has much I-strain.[7)] Actually, it has been established that, in the copper(I) complex of **1**, the copper atom coordinates selectively to the double bond in the strained norbornene ring, as is shown in **2**.[4)] It may be suggested that, in Reaction 1, the catalyst participates in the reaction in the state of copper(I) with a strong coordinative power. The preferential formation of **8** over **6** and **7** can be explained by assuming an initial coordination of the strained double bond to the copper(I) atom, followed

5) H. E. Simmons, E. P. Blanchard, and R. D. Smith, *J. Amer. Chem. Soc.*, **86**, 1347 (1964).

6) M. L. H. Green, "Organometallic Compounds," Vol. 2, ed. by G. E. Coates, M. L. H. Green, and K. Wade, Methuen & Co. Ltd., London, (1968), p. 19.

7) Ref. 6, p. 21.

by the attack of the diazo compound on the complex. That the reaction occurred in the near vicinity of the copper atom is evident from the fact that the complex **2** reacted with ethyl diazoacetate to form **8** predominantly (Reaction 2).

In reactions of Class III, on the other hand, both double bonds in **1** are involved in the reaction to a similar extent, thus indicating that the coordination of the metal has not played any important role in the reaction. Unlike the reactions in Class I, reactions in this class exhibit an induction period: the reactions proceeds smoothly at 40—65 °C only after the reaction has started at a higher temperature with the addition of one-third of the total amount of diazo compound. This indicates that the catalyst as such is not the actual species catalyzing the reaction. Although the exact state of this species is uncertain, we consider that copper is involved in the reaction in a state with a poor coordinative power. This consideration is consistent with the fact that the ratio (**8**/(**6**+**7**)) is quite low in Reaction 8, where the copper compound has been coordinatively saturated with the phosphorus ligand, although we observed no induction period.

Both reaction schemes (with strong and poor coordinative power of the metal) seem to occur competitively in reactions in Class II. This seems reasonable in view of the fact that copper(II) chloride is reduced partly to copper(I) chloride by ethyl diazoacetate.[8] Probably the same situation is also found with copper(II) sulfate. Furthermore, the reaction pattern of **2** (Reaction 2) was altered from Class I to Class II when the solvent was changed from dioxane to DMSO (Reaction 5). It is conceivable that a strongly coordinative solvent might partly expel copper from the complex, **2** thus providing a reaction pattern typical of reactions in Class III.

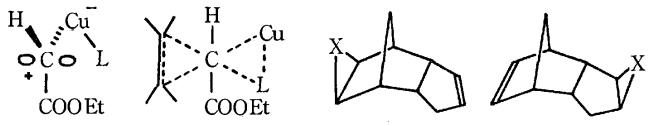

11 **12** **13** **14**

a: X=O **b**: X=CH_2

Chart 2

We feel that Moser's model,[2] which places emphasis on the coordination of copper to a double bond, is not suitable to explain the results we have presented thus far; we propose the following scheme for the reactions in Class III: the diazo compound attacks the copper compound to form an inversed ylide, **11**, and then the carbonium-ion center in **11** undergoes an electrophilic attack on the olefin to form a three-membered cyclic transition state, **12**. A three-membered cyclic transition state was proposed in view of the general belief[9] that a norbornene double bond should react in preference to a cyclopentene double bond as long as the reaction proceeds through a four-, five-, or six-membered cyclic transition state. In a separate experiment, we observed that the epoxidation of **1** with peracid, which has been confirmed to proceed through a three-membered cyclic transition state,[10] afforded **13a** and **14a** in a ratio of 1.3 (**13a**/**14a**), while epoxidation through a radical mechanism, which involves the double-bond opening,[11] afforded **13a** in preference to **14a** by a factor of 9.5.[12] Moser[2] proposed a copper-containing four-membered cyclic transition state rather than a three-membered cyclic transition state such as **12** for the present type of reaction, because no interaction causing the observed steric effects of ligands can be expected with the latter model. We are, however, of the opinion that the reaction scheme through the transition state **12** could also be susceptible to the steric effects, since the size of ligands in the copper compound **11** would sterically control the mode of approach of **11** to an olefinic group. Moreover, we consider that a transition state in which steric interaction between the reagent and the substrate are effective *to only a minor extent* is preferable in view of the following facts. The selective additions of dichlorocarbene[13] and dichloroketene[14] to the cyclopentene ring of **1** have been reported, and the unusual behavior in these cases has been interpreted in terms of the steric interaction between reagents and the hydrogen atoms in the norbornene system. Apparently, if the reaction between **1** and **3** proceeded through a transition state in which a considerable ligand effect can be expected, the formations of **6** and **7** would predominate, in contrast with the observed results. A good example favoring the present transition state, **12**, which is basically the same as that proposed for the Simmons-Smith reaction, has been provided by the observation[5] that the Simmons-Smith reaction of **1** afforded **13b** and **14b** in 12 and 11% yields respectively, as well as 63% of the diadduct.

Experimental

The IR spectra were obtained on JASCO IRS and Hitachi EPI-G3 spectrometers. The NMR spectra were measured on a JEOL MH-60 (60 MHz) spectrometer; the chemical shifts are represented in δ values relative to the internal TMS standard. The mass spectra were measured on a Hitachi RMS-4 mass spectrometer.

endo-*Dicyclopentadiene-copper(I) Chloride Complex (2).* This complex was prepared from **1**, $CuCl_2 \cdot 2H_2O$, and SO_2 in 95% ethanol by the method used for the preparation of the 1,5-cyclooctadiene-CuCl complex reported by Baird.[15] Mp 112 °C (decomp.). Lit[4]: mp 115 °C (decomp.).

Triethyl Phosphite-copper(I) Chloride Complex. This complex was prepared according to the method reported by

8) T. Saegusa, Y. Ito, T. Shimizu, and S. Kobayashi, This Bulletin, **42**, 3535 (1969).

9) R. W. Alder, R. Baker, and J. M. Brown, "Mechanism in Organic Chemistry," Wiley-Interscience, London, (1971), p. 306; J. Rocek, *J. Amer. Chem. Soc.*, **91**, 991 (1969).

10) D. Swern, "Organic Peroxides," Vol. II, ed. by D. Swern, Wiley-Interscience, New York, N. Y. (1971), p. 472.

11) S. J. Moss and H. Steiner, *J. Chem. Soc.*, **1965**, 2372.

12) T. Sato and E. Murayama, unpublished results.

13) L. Ghosez, P. Laroche, and L. Bastens, *Tetrahedron Lett.*, **1964**, 3745.

14) L. Ghosez, R. Montaigne, A. Roussel, H. Vanlierde, and P. Mollet, *Tetrahedron*, **27**, 615 (1971).

15) W. C. Baird, Jr., *J. Amer. Chem. Soc.*, **85**, 1009 (1963).

Arbusoff.[16])

Reactions of ***1*** *with* **3**. A solution of **1** (1.32 g) and copper compounds (specified amounts shown in Table 1) in 25 ml of a solvent was kept at an appropriate temperature. A solution of **3** (1.14 g) in 5 ml of the corresponding solvent was then added dropwise over a period of 2 hr. In cases where no nitrogen evolution was observed, the reaction mixture was heated to 70—80 °C after one-third of the total amount of diazo compound had been added. After the nitrogen evolution had been observed (usually in 20—90 min), the reaction mixture was cooled to the original temperature and the remainder of the diazo compound was added. The reaction mixture was poured into cold hydrochloric acid (200 ml of ice water containing 20 ml of concentrated hydrochloric acid) and shaken with ether. Ether was then removed, the residue was distilled under a vacuum, and the distillate was analyzed by gas chromatography. The six fractions, in the order of retention time, were as follows:

4 and **5**: Their retention times on gas chromatography and NMR and IR spectra were identical with those of authentic samples.

9: IR (CCl_4): 1745 (vs), 1275—1255 (b, s) and 1060—1020 cm^{-1} (b, s); NMR (CCl_4): δ 4.3—3.7 (m, 6H), 2.73 (d, J=20 Hz, 2H) and 1.4—1.1 (m, 9H).

Found: C, 43.1; H, 7.8%. Calcd for $C_8H_{17}O_5P$: C, 42.9; H, 7.6%.

6: MS: *m/e* 218 (M), 189 (M−C_2H_5), 173 (M−OC_2H_5), and 152 (base peak, M−C_5H_6); IR (CCl_4): 2940 (vs), 1730 (vs), 1570 (w), 1145 (b, vs) and 999 cm^{-1} (m).

7: MS: *m/e* 218 (M), 189 (very weak, M−C_2H_5), 173 (M−OC_2H_5), 153 (base peak, M−C_5H_5) and 152 (M–C_5H_6); IR (CCl_4): 2960 (vs), 1730 (vs), 1574 (w), 1160 (b, vs), and 1011 cm^{-1} (m); NMR (CCl_4): δ 6.15—6.0 (m, 2H), 3.95 (q, 2H), 2.9—2.6 (m), 1.7—1.0 (m), and 1.2 (t).

8: MS: *m/e* 218 (M), 189 (M−C_2H_5), 173 (M–OC_2H_5) and 152 (M–C_5H_6); IR (CCl_4): 2930 (vs), 1728 (vs), 1612 (w), 1170 (b, vs) and 1027 cm^{-1} (m); NMR (CCl_4): δ 5.8 (q, 2H), 4.2 (q, 2H), 2.7—2.2 (m), 1.7—0.9 (m), and 1.25 (t).

Found: C, 76.8; H, 8.5%. Calcd for $C_{14}H_{18}O_2$: C, 77.0; H, 8.5%.

Reactions of ***2*** *with* **3**. A solution of **2** (2.3 g) in 25 ml of a solvent was kept at an appropriate temperature. A solution of **3** (3.2 g) in 10 ml of the corresponding solvent was then added drop by drop over a period of 2 hr, after which the mixture was stirred for an additional hour. The reaction mixture was then worked-up in the way described above.

16) A. Arbusoff, *Ber.* **38**, 1171 (1905).

BULLETIN OF THE CHEMICAL SOCIETY OF JAPAN, VOL. 46, 1836—1839 (1973)

A New Synthesis of Substituted 8-Aminopurine Derivatives[1]

Fumio YONEDA, Masatsugu HIGUCHI, Takafumi MATSUMURA, and Keitaro SENGA*

Faculty of Pharmaceutical Sciences, Kumamoto University, Oe-honmachi, Kumamoto 862

**Pharmaceutical Institute, Keio University, Shinjuku-ku, Tokyo 160*

(Received November 4, 1972)

The treatment of 6-amino-5-nitrosopyrimidines with Vilsmeier-type reagents (substituted formamides and phosphorus oxychloride) afforded substituted 8-aminopurines; the treatment of 6-amino-4-hydroxy-2-methyl-5-nitrosopyrimidine gave 2-chloromethyl-8-dimethylamino-6-hydroxypurine.

Most substituted 8-aminopurine derivatives have been synthesized by the following two routes: the introduction of substituted amino groups into the preformed 8-chloro- or 8-methylmercapto-purine derivatives,[2] and the dehydrative or dethiohydrative cyclization of the 5-ureido- or 5-thioureido-6-aminopyrimidines obtained by the reaction of 5,6-diaminopyrimidines with substituted isocyanates or isothiocyanates.[3] We wish now to report a convenient new method of synthesizing substituted 8-aminopurine derivatives; the method consists of the treatment of 6-amino-5-nitrosopyrimidines with a mixture of substituted formamides and phosphorus oxychloride (Vilsmeier-type reagent).

The heating of 6-amino-1,3-dimethyl-5-nitrosouracil (**1**) with phosphorus oxychloride in dimethylformamide at 180 °C for 1 hr, the concentration of the reaction mixture by partial evaporation, and then dilution with water caused the separation of 8-dimethylaminotheophylline (**2a**) in a good yield. The structure of **2a** was established by a comparison of it with an authentic sample prepared by the treatment of 8-chlorotheophylline with dimethylformamide. This procedure is an application of the known dimethylamination of active chloro compounds using dimethylformamide.[4] Analogous reactions were observed in the condensation of **1** with methylformamide, diethylformamide, and *N*-methylformanilide in the presence of phosphorus oxychloride; in all cases, the substituted amino groups of the formamides were introduced into the 8-position of the final theophyllines. However, formamide did not react in the same way as substituted formamides to give the desired 8-aminotheophylline; rather, the formation of a small amount of 1,3-dimethylpyrimido-

1) A part of this paper has been reported in a preliminary form; see F. Yoneda, T. Matsumura, and K. Senga, *Chem. Commun.*, **1972**, 606.

2) For example, R. K. Robins, *J. Amer. Chem. Soc.*, **80**, 6671 (1958).

3) For example, A. H. Cook, and G. H. Thomas, *J. Chem. Soc.*, **1950**, 1888.

4) S. Nishigaki, K. Senga, and F. Yoneda, *Chem. Pharm. Bull.* (Tokyo), **19**, 1526 (1971).

TABLE 1. SUBSTITUTED 8-AMINOTHEOPHYLLINES

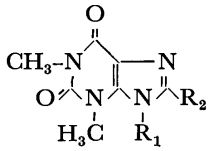

No.	R_1	R_2	Yield (%)	Recrystl. Solvent	Mp (°C)	MS (M^+)	Formula	Analyses Calcd C	Calcd H	Calcd N	Found C	Found H	Found N
2a	H	NMe_2	72	DMF	>330	223	$C_9H_{13}N_5O_2$	48.42	5.87	31.38	48.31	6.03	31.37
2b	H	NHMe	30	DMF	>330	209	$C_8H_{11}N_5O_2$	45.93	5.30	33.48	46.07	5.21	33.23
2c	H	NEt_2	43	dioxane	254	251	$C_{11}H_{17}N_5O_2$	52.57	6.82	27.87	52.30	6.79	27.65
2d	H	N(Me)Ph	40	ethanol	261	285	$C_{14}H_{15}N_5O_2$	58.93	5.30	24.55	58.84	5.38	24.44
2e	Me	NMe_2	30	methanol	295	237	$C_{10}H_{15}N_5O_2$	50.62	6.37	29.52	50.51	6.18	29.38

[4,5-*d*]pyrimidine-2,4-(1*H*,3*H*)-dione[5] was observed. The treatment of 1,3-dimethyl-6-methylamino-5-nitrosouracil (**3**) with a mixture of dimethylformamide and phosphorus oxychloride led to the formation of 8-dimethylaminoisocaffeine (**2e**). The results are summarized in Table 1.

When **1** was treated with a mixture of dimethylformamide and phosphorus oxychloride at room temperature, a dimeric product (**4**) was obtained. The latter was converted into **2a** by further heating in the same reagent or by sublimating *in vacuo*. The structure of **4** was deduced from the following evidences; the molecular ion peak at *m/e* 446 in the mass spectrum and the elemental analysis correspond to the assigned formula. The NMR spectrum (CF_3COOH) displays a pair of six-proton singlets at 3.27 and 3.74 δ corresponding to the *N*-methyl groups of uracil and a twelve-proton singlet at 3.61 δ corresponding to the dimethylamino groups. Two two-proton broad singlets, at 5.77 and 5.94 δ, were assigned to the NH and NH^+ protons respectively.

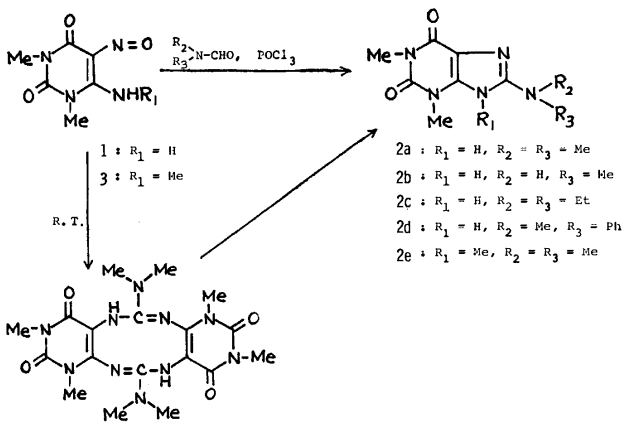

Scheme I.

The heating of 6-amino-4-hydroxy-2-methylthio-5-nitrosopyrimidine (**5**) with a mixture of dimethylformamide and phosphorus oxychloride at 130 °C for 1 hr, the subsequent concentration of the reaction mixture by partial evaporation, and the treatment of the residue with ethanol gave 8-dimethylamino-6-hydroxy-2-methylthiopurine (**6**). Similarly, 6-amino-4-hydroxy-5-nitroso-2-phenylpyrimidine (**7**) and a mixture of dimethylformamide or methylformamide and phosphorus oxychloride led to 8-dimethylamino-6-hydroxy-2-phenylpurine (**8**) or 6-hydroxy-8-methylamino-2-phenylpurine (**9**). It is interesting to note that the reaction of 6-amino-4-hydroxy-2-methyl-5-nitrosopyrimidine (**10**) with a mixture of dimethylformamide and phosphorus oxychloride under the same conditions gave 2-chloromethyl-8-dimethylamino-4-hydroxypurine (**11**) (Table 2). The nuclear magnetic resonance spectrum (CF_3COOH) of **11** shows singlets at 3.57 (NMe_2) and 4.86 δ (CH_2Cl). The mass spectrometry reveals a parent ion (*m/e* 227) and the M+2 ion, suggesting that one chlorine atom is contained in the molecule.

The new synthesis of substituted 8-aminopurines can best be explained by assuming an initial nucleophilic attack of the oxime of the imino oxime tautomeric form (**18**) of the 6-amino-5-nitrosopyrimidines on the Vilsmeier-type reagent to form the adduct (**19**). Prototropic rearrangement would then give the protonated nitrone (**20**), which is suited for intramolecular cyclization to **21**. The subsequent elimination of a dichlorophosphoric acid and deoxygenation of the purine 7-oxide (**22**) would lead to the substituted 8-aminopurine. The formation of a dimeric product (**4**) in

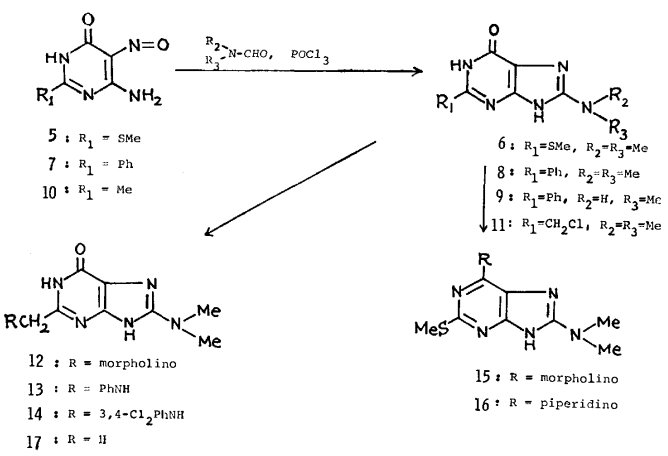

Scheme II.

5) H. Bredereck, F. Effenberger, and R. Sauter, *Chem. Ber.*, **95**, 2049 (1962).

Table 2. Substituted 8-aminopurines

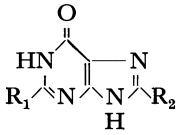

No.	R_1	R_2	Yield (%)	Recrystl. Solvent	Mp (°C)	MS (M^+)	Formula	Analyses Calcd C	Calcd H	Calcd N	Found C	Found H	Found N
6	SMe	NMe_2	75	DMF	>330	225	$C_8H_{11}N_5OS$	42.66	4.92	31.10	42.50	4.87	30.85
8	Ph	NMe_2	68	DMF	>330	255	$C_{13}H_{13}N_5O$	61.16	5.13	27.44	61.08	5.06	27.21
9	Ph	NHMe	38	DMF	>330	241	$C_{12}H_{11}N_5O$	59.74	4.60	29.03	59.85	4.52	29.24
11	CH_2Cl	NMe_2	83	AcOH	>330	227	$C_8H_{10}N_5OCl$	42.20	4.43	30.77	42.10	4.42	30.52

the reaction at a low temperature can be explained in terms of an alternative course *via* the dimerization of the initially formed nitrone (**20**), followed by the elimination of dichlorophosphoric acid and oxygen.

Compounds **6** and **11** served as starting materials for several nucleophilic reactions. For example, the displacement of the chlorine in **11** by morpholino and anilino groups yielded the respective 2-morpholinomethyl- (**12**) and 2-anilinomethyl-purine derivatives (**13** and **14**). It will be noted that the methylthio group of **6** was stable against nucleophilic substitutions. That is, in the reaction of **6** with morpholine the methylthio group survived completely and the product was 8-dimethylamino-2-methylthio-6-morpholinopurine (**15**), whose structure was established by the analytical and spectral data. Similarly, the heating of **6** with piperidine gave the corresponding 6-piperidinopurine (**16**). The reduction of **11** with triphenylphosphine in dimethylformamide gave 8-dimethylamino-6-hydroxy-2-methylpurine (**17**).

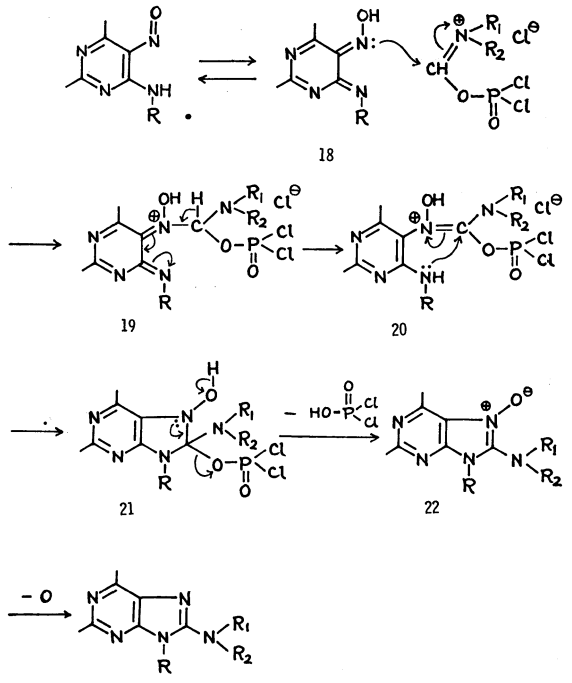

Scheme III.

Experimental

All the melting points are uncorrected. The NMR spectra were determined at 60 MHz, using tetramethylsilane as the internal standard. The chemical shifts were expressed in δ values (s: singlet, bs: broad singlet).

8-Dimethylaminopurines. General Procedure: A solution of 0.01 mol of 6-amino-5-nitrosopyrimidine and 0.015 mol of phosphorus oxychloride in 15 ml of dimethylformamide was heated at 150—180 °C for 1 hr and evaporated *in vacuo*, and water was added to the resulting residue. The solid separated was collected by filtration, washed with water, dried, and recrystallized from solvents as specified in Table 1 to give colorless needles.

8-Methylaminotheophylline (2b). A mixture of 1.84 g (0.01 mol) of 6-amino-1,3-dimethyl-5-nitrosouracil (**1**) and 2.3 g (0.015 mol) of phosphorus oxychloride in 5 ml of methylformamide was heated at 130 °C for 1 hr. The reaction mixture was diluted with methanol, and then the crystals separated were collected by filtration, washed with water, dried, and recrystallized to give colorless prisms.

8-Diethylaminotheophylline (2c). To a mixture of 0.92 g (0.005 mol) of **1** and 1 g (0.005 mol) of diethylformamide was added, 2.3 g (0.015 mol) of phosphorus oxychloride drop by drop at room temperature; the mixture was then heated at 120 °C for 30 min. After cooling, the reaction mixture was neutralized with 5% aqueous ammonia. The crystals precipitated were collected by filtration, washed with water, dried, and recrystallized to give colorless needles.

8-N-Methylanilinotheophylline (2d). To a mixture of 0.92 g (0.005 mol) of **1** and 1.35 g (0.01 mol) of *N*-methylformanilide, a 2.3 g portion (0.015 mol) of phosphorus oxychloride was added, drop by drop, at room temperature, and then the mixture was heated at 140 °C for 30 min with stirring. The reaction mixture was poured into 200 ml of ice water, and the crystals thus precipitated were collected by filtration, washed with water, dried, and recrystallized to give colorless needles.

8-Dimethylaminoisocaffeine (2e). To a mixture of 0.59 g (0.003 mol) of 1,3-dimethyl-6-methylamino-5-nitrosouracil (**3**) in 5 ml of dimethylformamide, 0.92 g (0.009 mol) of phosphorus oxychloride was added, drop by drop, at room temperature, and then the mixture was heated at 160 °C for 30 min. After the reaction mixture had been evaporated under reduced pressure, the resulting syrup was diluted with 20 ml of water, neutralized with 5% aqueous ammonia, and extracted with chloroform. The chloroform extracts were dried over anhydrous sodium sulfate, filtered, and evaporated to dryness. The residue was recrystallized from aqueous methanol to give colorless needles.

Formation of the Dimeric Product (4). Into a suspension of 1.84 g (0.01 mol) of **1** in 20 ml of dimethylformamide, 3.1 g (0.02 mol) of phosphorus oxychloride was added portionwise with stirring. The resulting clear solution was stirred at room temperature for 3 hr, during which time colorless needles were gradually separated. The crystals were collected by filtration, washed with water, dried, and recrystallized from dimethylformamide to give 1.18 g (53%) of colorless needles; mp>330 °C. MS 446 (M^+). Found: C, 48.72; H, 5.79; N, 31.09%. Calcd for $C_{18}H_{26}N_{10}O_4$: C, 48.42; H, 5.87; N, 31.38%.

Conversion of 4 into 2a. (A) A suspension of 0.8 g (0.0018 mol) of **4** and 0.77 g (0.005 mol) of phosphorus oxychloride in 10 ml of dimethylformamide was heated with stirring at 180 °C for 2 hr and then allowed to stand overnight. The crystals separated were collected by filtration and washed with ethanol to give 0.4 g (50%) of **2a**.

(B) **4** was sublimed at 260 °C under reduced pressure (10 mmHg) to yield **2a** in a good yield.

8-Dimethylamino-2-methylthio-6-morpholinopurine (15). A mixture of 0.3 g (0.0013 mol) of **6** in 10 g (0.12 mol) of morpholine was heated under gentle reflux for 1.5 hr. After the excess morpholine had been evaporated under reduced pressure, the residue was recrystallized from aqueous methanol to give 0.2 g (53%) of colorless prisms; mp>320 °C. NMR ($CDCl_3$) 2.62 (s, 3H, SMe), 3.28 (s, 6H, NMe_2), 4.01 (bs, 8H, morpholino CH_2). MS 294 (M^+). Found: C, 49.02; H, 6.15; N, 28.37%. Calcd for $C_{12}H_{18}N_6OS$: C, 48.97; H, 6.17; N, 28.56%.

8-Dimethylamino-2-methylthio-6-piperidinopurine (16). A mixture of 0.8 g (0.0036 mol) of **6** in 10 g (0.12 mol) of piperidine was treated under the same conditions to yield 1 g (95%) of colorless needles after recrystallization from aqueous methanol. MS 292 (M^+). Found: C, 53.22; H, 6.84; N, 28.49%. Calcd for $C_{13}H_{20}N_6S$: C, 53.41; H, 6.90; N, 28.75%.

2-Anilinomethyl-8-dimethylamino-6-hydroxypurine (13). A mixture of 1.5 g (0.0067 mol) of **11** and 4 g (0.043 mol) of aniline in 10 ml of dimethylformamide was heated at 130 °C for 1 hr. The reaction mixture was then evaporated under reduced pressure, and the resulting residue was recrystallized from ethanol to give 1.1 g (58%) of colorless needles; mp> 330 °C. MS 284 (M^+). Found: C, 58.97; H, 5.70; N, 29.32%. Calcd for $C_{14}H_{16}N_6O$: C, 59.14; H, 5.67; N, 29.56%.

2-(3,4-Dichloroanilino)methyl-8-dimethylamino-6-hydroxypurine (14). A mixture of 1.5 g (0.0067 mol) of 11 and 5 g (0.031 mol) of 3,4-dichloroaniline in 10 ml of dimethylformamide was heated at 160 °C for 2 hr and then treated in the manner described above to give 1.2 g (51%) of colorless needles; mp>330 °C. Found: C, 47.68; H, 4.04; N, 23.63%. Calcd for $C_{14}H_{14}H_6OCl_2$: C, 47.60; H, 3.99; N, 23.80%.

8-Dimethylamino-6-hydroxy-2-morpholinomethylpurine (12). A mixture of 0.8 g (0.0035 mol) of **11** and 10 g (0.12 mol) of morpholine was heated under reflux for 1 hr; then it was treated in the manner described for the preparation of **13** to yield 0.4 g (41%) of colorless needles (mp 260 °C) after recrystallization from methanol. MS 278 (M^+). Found: C, 51.62; H, 6.49; N, 30.31%. Calcd for $C_{12}H_{18}N_6O_2$: C, 51.78; H, 6.52; N, 30.20%.

8-Dimethylamino-6-hydroxy-2-methylpurine (17). A mixture of 0.3 g (0.0013 mol) of **11** and 0.45 g (0.0017 mol) of triphenylphosphine in 15 ml of dimethylformamide was heated under a mild reflux for 2 hr. The reaction mixture was then evaporated under reduced pressure, and the residue was diluted with 30 ml of methanol. The crystals precipitated were collected by filtration, washed with water, dried, and recrystallized from dimethylformamide to give 0.1 g (40%) of colorless prisms; mp>330 °C. MS 193 (M^+). Found: C, 50.02; H, 5.73; N, 36.03%. Calcd for $C_8H_{11}N_5O$: C, 49.73; H, 5.74; N, 36.25%.

BULLETIN OF THE CHEMICAL SOCIETY OF JAPAN, VOL. 46, 1839—1844 (1973)

The Synthesis and the Stereochemistry of 4-Chromanones and 4-Chromanols with Bulky Substituents

Kuninobu KABUTO, Yoriko KIKUCHI, Shozo YAMAGUCHI, and Naoto INOUE

Department of Chemistry, College of General Education, Tohoku University, Kawauchi, Sendai 980

(Received November 13, 1972)

The synthesis and the stereochemistry of 4-chromanones and 4-chromanols with bulky substituents have been investigated. In 3-substituted chromanones, the *t*-butyl group exists mainly in the *quasi*-axial position, while the phenyl group is still in the *quasi*-equatorial environment. The preferred conformations of the isopropyl, and of the *t*-butyl group in *cis*- and *trans*-2-substituted chromanols, are equatorial, whereas *trans*-3-*t*-butylchromanol and its benzoate exist mainly as the conformations in which the *t*-butyl group is in the axial position. The conformational preference of these compounds can reasonably be explained by considering the steric interactions ($A^{(1,3)}$ strain, *gauche*, and diaxial repulsion) of these groups. The magnitude of the $A^{(1,3)}$ strain due to the hydroxyl group was estimated to be 1.3 kcal/mol.

In a previous paper,[1] we have reported that the conformational equilibria of 3-methyl- and 3-phenylchroman-4-ols can be well interpreted on the basis of the $A^{(1,3)}$ strain together with the 1,3-diaxial repulsion.

It is still not obvious, however, how the above interaction may affect the conformational equilibrium when the bulky groups are substituted on the 2- or 3-position of 4-chromanone and 4-chromanol.

In this paper, we wish to report on the synthesis and

1) S. Yamaguchi, K. Kabuto, Y. Ninomiya, and N. Inoue, This Bulletin, **43**, 3952 (1970).

the stereochemistry of 4-chromanones and 4-chromanols with bulky groups on the heterocyclic ring.

2-*t*-Butyl-(VIII), 2-isopropylchromanone (IX) and the corresponding chromanols (IV, VI; V, VII) were synthesized according to Scheme 1. *o*-Hydroxyacetophenone was allowed to react with ethyl pivalate in the presence of sodium hydride to give the diketone, which was in turn converted to the corresponding chromone (II) with concentrated hydrochloric acid.

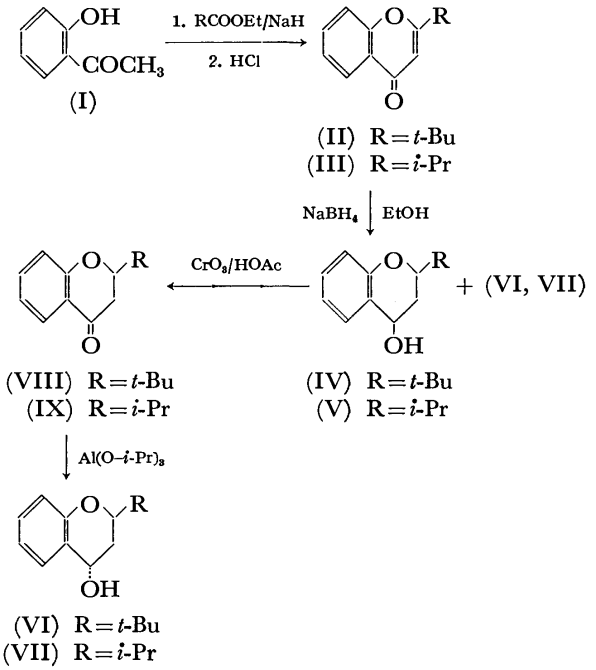

Scheme I.

When II was treated with excess sodium borohydride in boiling ethanol,[2] *cis*-2-*t*-butyl-4-chromanol (IV) was obtained as the main product. Compounds (IV) was easily oxidized by chromic acid in an acetic acid solution below 30 °C, yielding the chromanone (VIII), which subsequently afforded a mixture of *trans*- (VI, 58%) and *cis*-chromanols (IV, 22%) by Meerwein-Pondorf reduction. The NMR spectra (Table 2) of IV and VI indicate that the configurations of these compounds are *cis* and *trans* respectively. The purification of these chromanols by column or thin-layer chromatography was unsuccessful; hence, they were purified by preparative gas chromatography, using PEG 20M as the stationary phase.

The application of the synthetic route to isoflavanone[3] *via* phenoxyacetophenone cyanohydrin did not afford satisfactory results in preparing 3-*t*-butylchromanone (XIV). The chromanone (XIV) was successfully synthesized following Scheme 2, which is considered to be a suitable way for preparing chromanones with a bulky group such as the *t*-butyl group because the reaction is not so subject to steric hindrance by a bulky group.

2-*t*-Butyl-1,3-propanediol (X) was partially tosylated with tosyl chloride to give monotosylate (XI), which

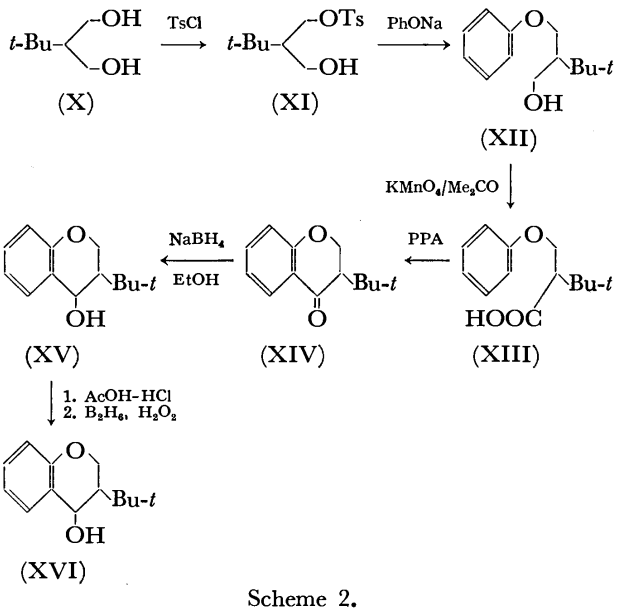

Scheme 2.

was then transformed to phenoxyalcohol (XII) with sodium phenoxide in a dimethyl sulfoxide solution. 3-*t*-Butylchromanone (XIV) was prepared by the oxidation of XII with potassium permanganate, followed by the ring closure of carboxylic acid (XIII) in PPA.

The reduction of XIV with sodium borohydride resulted almost exclusively in the formation of *cis*-3-*t*-butylchromanol (XV). Compound (XV) was easily dehydrated with boiling acetic acid–hydrochloric acid to 3-*t*-butylchromene, which was then converted to the other isomer (XVI) by hydroboration, indicating that the configurations of XV and XVI are *cis* and *trans* respectively. These results are in accordance with the findings[4] that the formation of the *cis* isomer in the hydride reduction of 3-substituted chromanones increases with an increase in the size of the substituents.

The NMR spectra of substituted 4-chromanones are summarised in Table 1.

Table 1. NMR Spectra of substituted 4-chromanones

Chromanone		Preferred conformation of alkyl group
2-*t*-Bu (VIII)	$J_{2,3}$:~13.0;[a] $\lvert J_{2,3}+J_{2,3'}\rvert=16.0$	e
2-*i*-Pr (IX)	$\lvert J_{2,3}+J_{2,3'}\rvert=16.0$	e
3-*t*-Bu (XIV)	$J_{2,3}$: 4.6, 4.2; $\lvert J_{2,3}+J_{2',3}\rvert=8.8$	a'
3-Ph	$\lvert J_{2,3}+J_{2',3}\rvert=14.0$	e'
3-Me	$J_{2,3}$: 10.8, 5.4; $\lvert J_{2,3}+J_{2',3}\rvert=16.2$[5]	e'

a) Spectrum was taken in the presence of 0.30 molar ratio of $Pr(fod)_3$ in CCl_4.

The signals of 2-H and 3-H portion of 2-*t*-butylchromanone (VIII) did not appear as the typical ABX pattern; hence the spectrum was analysed as the first-order spectrum in the presence of $Pr(fod)_3$.[5] The

2) S. Yamaguchi, S. Ito, A. Nakamura, and N. Inoue, This Bulletin, **38**, 2187 (1965).

3) N. Inoue, *Nippon Kagaku Zasshi*, **79**, 218 (1958).

4) N. Inoue, This Bulletin, **37**, 601 (1964); K. Hanaya, *ibid.*, **43**, 442 (1970).

5) Since the separation between the two strong outer lines of X part of ABX pattern is almost same to that in the absence of $Pr(fod)_3$, the geometry of chromanone ring seems not to be altered by the shift reagent.

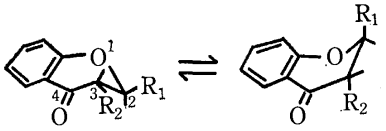

VIIIe (R_1=*t*-Bu, R_2=H) VIIIa
IXe (R_1=*i*-Pr, R_2=H) IXa
XIVe (R_1=H, R_2=*t*-Bu) XIVa

Fig. 1.

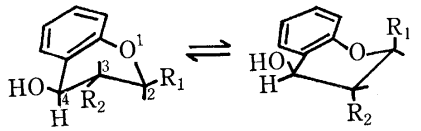

IVe (R_1=*t*-Bu, R_2=H) IVa
Ve (R_1=*i*-Pr, R_2=H) Va
XVIe (R_1=H, R_2=*t*-Bu) XVIa
XVI'e (Benzoate of XVI) XVI'a

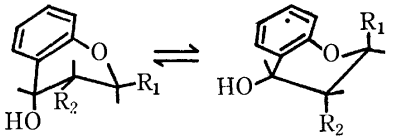

VIa (R_1=*t*-Bu, R_2=H) VIe
VIIa (R_1=*i*-Pr, R_2=H) VIIe
XVa (R_1=H, R_2=*t*-Bu) XVe

Fig. 2.

large $J_{2,3}$ value (13 Hz) and the distance between the two outside peaks of the X part of the ABX pattern[6] indicate that VIII exists exclusively in the VIIIe conformation, though there seems to be no remarkable interaction which forces VIIIa to be unfavorable.

The line separation of the X part in 2-isopropylchromanone (IX) is almost the same as that of VIII; therefore, the isopropyl group in IX also favors the equatorial orientation.

The NMR spectrum of 3-*t*-butylchromanone (XIV) was analysed as being the ABX pattern[7] ($J_{2,3}$: 4.6 and 4.2 Hz), indicating that XIV exists mainly as the XIVa conformation with the *quasi*-axial *t*-butyl group, contrary to the case of 3-methylchromanone,[8] in which the methyl group is *quasi*-equatorial.

The dihedral angle (32°) between the carbonyl group and the benzene ring, calculated from the absorbance in the ultraviolet region[9] in XIV, is almost the same as those of chromanone and 2-methylchromanone,[10] suggesting that the geometry of the chromanone ring is unchanged by the *t*-butyl group.

Although the magnitude of the 2-alkylketone effect due to the *t*-butyl group (the repulsion between the *quasi*-equatorial 3-*t*-butyl and the carbonyl group) has not yet been determined, it may be presumed to be considerably larger than that of the isopropyl group (1.7 kcal/mol).[11a] Since the 2-alkylketone effect anticipated for XIVe is considered to be considerably larger than the interaction between the *quasi*-axial *t*-butyl group and the ring oxygen in XIVa, XIVa seems more likely than XIVe.

The above considerations seem to be reasonable in the following points: (1) The interaction of an axial group with a ring oxygen is smaller than its interaction with an axial hydrogen,[12] and the repulsion between the axial *t*-butyl group and the ring oxygen in 5-*t*-butyl-2-alkyl-1,3-dioxane is estimated to be 1.4 kcal/mol,[13] which is quite small compared to the interaction with the axial hydrogen on the cyclohexane ring (4.4 kcal/mol).[13] (2) Since the interaction of an axial group with one axial hydrogen atom is reduced to one-half its normal conformational free energy,[11a,b] it may be considered that the interaction of the *quasi*-axial 3-*t*-butyl group with the ring oxygen in XIVa would be around 0.7 kcal/mol, which is considerably smaller than the 2-alkylketone effect because there is only one oxygen in the chromanone ring.

An attempt to determine the conformational equilibrium of 3-*t*-butylchromanone by studying the IR spectra using 3-d_2-chromanone and 3-*d*-3-*t*-butylchromanone was unsuccessful because of the anbiguity of the C–D stretching vibrations of these compounds.

The methylene signal in 3-phenylchromanone did not separate even in the presence of $Pr(fod)_3$. The line separation of the two strong outside peaks of the X part, however, is very close to that of 3-methylchromanone;[10] therefore, the 2-alkylketone effect in 3-phenylchromanone seems not to be sufficiently large to cause the phenyl group to occupy the axial position.

The preferred conformations of *cis*-2-isopropyl- and *cis*-2-*t*-butylchromanol are expected to be almost fixed at Ve and IVe respectively, because severe diaxial repulsion due to the bulky substituents would be considerably larger than the $A^{(1,3)}$ strain (the repulsion of *quasi*-equatorial 4-hydroxyl group with 5-H).

The magnitude of the $A^{(1,3)}$ strain for the hydroxyl group was calculated to be 1.3 kcal/mol by the procedure described in the previous paper;[1] this value was almost the same as that for the acetoxyl group.

On the other hand, *trans* isomers should be VIa and VIIa, for the sum of the diaxial repulsion (*e.g.*, 2-*t*-Bu~4-H; 2.2 kcal/mol) and the $A^{(1,3)}$ strain is much larger than the interaction due to the *quasi*-axial hydroxyl group (0.4 kcal/mol). The above considerations are supported by the NMR spectra (Table 2) of these compounds.

It is difficult to determine the preferred conformation

6) It is well known that the distance between the outermost lines of X part of ABX pattern may be used as convenient method for determining the stereochemistry: L. M. Jackman and S. Sternhell, "Application of Nuclear Magnetic Resonance Spectroscopy in Organic Chemistry," Pergamon Press, (1969), p. 133; B. J. Bolger, A. Hirwe, K. G. Marathe, E. M. Philbin, M. A. Vickers, and C. P. Lillya, *Tetrahedron*, **22**, 621 (1966).

7) H. J. Bernstein, J. A. Pople, and W. G. Schneider, *Can. J. Chem.*, **35**, 65 (1957).

8) A. R. Katritzky and B. Ternai, *J. Heterocyclic Chem.*, **5**, 745 (1968).

9) E. A. Braude and F. Sondheimer, *J. Chem. Soc.*, **1955**, 3754.

10) K. Hanaya, *Bull. Yamagata Univ., Nat. Science*, **7**, 421 (1971).

11) a) E. L. Eliel, N. L. Allinger, S. J. Angyal, and G. A. Morrison, "Conformational Analysis," Interscience Publishers, New York, N.Y. (1965), p. 114. b) *ibid.*, p. 356.

12) *ibid.*, p. 374.

13) E. L. Eliel and Sr. M. C. Knoeber, *J. Amer. Chem. Soc.*, **90**, 3444 (1968).

TABLE 2. NMR SPECTRA OF SUBSTITUTED 4-CHROMANOLS AND ITS DERIVATIVES

Chromanol	$\lvert J_{2,3}+J_{2,3'}\rvert$	$\lvert J_{3,4}+J_{3',4}\rvert$	Preferred conformation of alkyl group
cis-2-*t*-Bu (IV)	14.1	17.4	e
cis-2-*i*-Pr (V)	13.6	17.2	e
trans-2-*t*-Bu (VI)	13.8	6.0	e
trans-2-*i*-Pr (VII)	13.8	6.0	e
cis-3-*t*-Bu (XV)	$J_{3,4}$: 3.0; $\lvert J_{2,3}+J_{2',3}\rvert$=15.0		e
Benzoate of XV	$J_{3,4}$: 2.6; $\lvert J_{2,3}+J_{2',3}\rvert$=16.0		e
trans-3-*t*-Bu (XVI)	$J_{3,4}$: 4.3; $\lvert J_{2,3}+J_{2',3}\rvert$=8.6		a
Benzoate of XVI	$J_{3,4}$: 3.0; $\lvert J_{2,3}+J_{2',3}\rvert$=6.0		a

of *cis*-3-*t*-butylchromanol (XV) by the $J_{3,4}$ value (3.0 Hz) alone; however, the separations between the two strong outerlines ($\lvert J_{2,3}+J_{2',3}\rvert$) of XV and of its benzoate are 15.0 and 16.0 Hz respectively. In XV and its benzoate, the $A^{(1,3)}$ strain and the interaction of the axial *t*-butyl group with the ring oxygen would tend not to favor the XVe conformation, and the *t*-butyl group should be fixed in the equatorial environment

It is particularly interesting that the $J_{3,4}$ values in *trans*-3-*t*-butylchromanol (XVI) and its benzoate (XVI') were 4.3 and 3.0 Hz respectively, and the diaxial coupling constant expected for the XVIe conformation was not observed. Taking into account the facts that $J_{3a,4e'}$ in chromanols is as same as that of $J_{3e,4e'}$[1] and that the conformations of XV and its benzoate are homogeneous with $J_{3a,4e'}$: 3.0 and 2.6 Hz respectively, XVI and its benzoate ($J_{3,4}$: 4.3 and 3.0 Hz) can be considered to exist predominantly in the diaxial conformations (XVIa and XVI'a).

There are $A^{(1,3)}$, *gauche* (4-OR~3-*t*-Bu), and two methylhydrogen interactions due to the *t*-butyl group and C_2-methylene in XVIe and XVI'e. On the other hand, the above interactions are replaced by smaller steric interactions (4-OR~2-H, 3-*t*-Bu~ring oxygen, and one methyl-hydrogen interaction) in XVIa and XVI'a.

It is still obscure whether the chromanol ring in *trans*-3-*t*-butylchromanol has a half-chair or a half-boat conformation. If one may assume, however, that the energy difference between the half-chair and the half-boat conformation in the chroman ring is almost the same as that in the cyclohexene ring (2.7 kcal/mol),[14] the contribution of the half-boat conformation would be ruled out, because the unfavored interaction in XVIa is considered to be approximately 1.1 kcal/mol (0.4 kcal/mol: 1,3-diaxial repulsion due to 4-OH, 0.7 kcal/mol: *t*-Bu~ring oxygen).

Experimental

All the melting points are uncorrected. The NMR spectra were recorded on Varian A-60D (60 MHz) and HA-100 (100 MHz) spectrometers, using TMS as the internal standard.

2-t-Butylchromone (II). To a stirred solution of *o*-hydroxyacetophenone (I, 11 g) in ethyl pivalate (80 ml) was added, portion by portion, sodium hydride (50% in mineral oil, 15 g) at room temperature. The mixture was then stirred at 75—85 °C on a water bath for 4 hr and allowed to stand overnight at room temperature. After the excess hydride has been decomposed with a small amount of water, the reaction mixture was poured into ice water (400 ml); the separated sodium salt was then collected, decomposed with 6 M hydrochloric acid, and extracted with ether. The organic layer was washed with saturated sodium bicarbonate and water successively, and dried over sodium sulfate.

The removal of the solvent afforded pivalyl *o*-hydroxyacetophenone as a pale yellow crystals (13 g, 72%). Needles from hexane, mp 57.5—58 °C. Found: C, 70.92; H, 7.11%. Calcd for $C_{13}H_{16}O_3$: C, 70.89; H, 7.32%.

The diketone (13 g) was dissolved in concentrated hydrochloric acid (60 ml) and warmed at 40 °C for 1 hr. The solution was diluted with water (220 ml) and then extracted with ether. The organic layer was then worked up according to the usual procedure. The removal of the solvent afforded crude II, which subsequently purified by recrystallization from petroleum ether (bp 40—60 °C), mp 72—73 °C.

Found: C, 76.90; H, 6.79%. Calcd for $C_{13}H_{14}O_2$: C, 77.20; H, 6.98%. IR (KBr): 1660 cm^{-1}. NMR (CCl_4): δ 1.35 (s, 9H, *t*-Bu), 6.08 (s, 1H, C_3–H) ppm.

cis-2-t-Butyl-4-chromanol (IV). A solution of II (5 g) and sodium borohydride (5 g) in ethanol (100 ml) was refluxed for 5 hr. After the reaction mixture had then stood overnight at room temperature, the solvent was removed under reduced pressure; the residue was dissolved in 50% acetic acid (50 ml) and water (150 ml). The solution was extracted with ether, and the extract was treated as usual to give colorless crystals (4.6 g, 88%), whose vpc (20% PEG 20 M at 180 °C) showed that it was a mixture of *cis*- (94.7%) and *trans*-2-*t*-butyl-4-chromanol (5.3%). Recrystallization from pentane gave *cis*-2-*t*-butyl-4-chromanol as colorless needles; mp 58.5—60 °C.

Found: C, 75.82; H, 8.74%. Calcd for $C_{13}H_{18}O_2$: C, 75.69; H, 8.80%. IR (KBr): 3270 cm^{-1}. NMR ($CDCl_3$+D_2O): δ 1.00 (s, 9H, *t*-Bu), 3.64 (dd, 1H, C_2–H), 4.77 (dd, 1H, C_4–H) ppm.

The acetate of IV was prepared according to the usual manner with acetyl chloride and pyridine: Colorless oil. IR (neat): 1738 cm^{-1}. NMR ($CDCl_3$): δ 1.4—2.6 (m, 5H, C_3–H and –OAc), 3.76 (dd, 1H, C_2–H), 6.10 (dd, 1H, C_4–H) ppm. $\lvert J_{2,3}+J_{2,3'}\rvert$=13.6, $\lvert J_{3,4}+J_{3',4}\rvert$=16.7 Hz.

2-t-Butyl-4-chromanone (VIII). To a stirred solution of IV (3.0 g) in 80% acetic acid (20 ml) was added chromic acid (1.68 g) in the same solvent (18 ml) below 30 °C. After the stirring has been continued for an additional hour, the reaction mixture was poured into ice water (300 ml) and extracted with ether. The extract was washed according to the usual manner. The solvent was then removed to give pale yellow crystals (2.5 g, 83%); subsequent recrystallization from hexane gave colorless crystals; mp 64.5—66 °C.

Found: C, 76.59; H, 7.80%. Calcd for $C_{13}H_{16}O_2$: C,

14) C. W. Beckett, N. K. Freeman, and K. S. Pitzer, *J. Amer. Chem. Soc.*, **70**, 4227 (1948).

76.44; H, 7.90%. IR (CCl_4): 1694 cm^{-1}. NMR (CCl_4): δ 1.08 (s, 9H, *t*-Bu), 2.58 (AB part of ABX, C_3–H), 4.06 (dd, 1H, C_2–H) ppm.

trans-*2-t-Butyl-4-chromanol (VI).* A solution of VIII (2.0 g) and aluminum isopropoxide (4.0 g) in isopropyl alcohol (8.0 ml) was refluxed for 3 hr. The solution was then poured into ice water (200 ml) containing concentrated hydrochloric acid (10 ml) and extracted with ether. The ethereal layer was washed as usual. The vpc of the extract showed that it was a mixture of *trans*- (58%), *cis*-2-*t*-butyl-4-chromanol (22%), and VIII (20%). The removal of the solvent gave a pale yellow oil (1.9 g), which was then purified by preparative vpc (20% PEG 20M 3/8″ 1.2 m, at 180 °C) to yield VI. Recrystallization from pentane gave VI as colorless prisms; mp 81—82 °C.

Found: C, 75.64; H, 8.82%. Calcd for $C_{13}H_{18}O_2$: C, 75.69; H, 8.80%. IR (KBr): 3280 cm^{-1}, NMR ($CDCl_3$+D_2O): δ 1.00 (s, 9H, *t*-Bu), 3.78 (dd, 1H, C_2–H), 4.70 (t, 1H, C_4–H) ppm.

Acetate of VI: Colorless oil. IR (neat): 1736 cm^{-1}. NMR ($CDCl_3$): δ 1.5—2.1 (m, 5H, C_3–H and –OAc), 3.85 (dd, 1H, C_2–H), 6.00 (t, 1H, C_4–H) ppm. $|J_{2,3}+J_{2,3'}|=14.0$, $|J_{3,4}+J_{3',4}|=6.0$ Hz. By a procedure similar to that described above, 2-*i*-propylchromone (III, 44%), 2-*i*-propyl-4-chromanone (IX, 83%), *cis*-2-*i*-propyl-4-chromanol (V, 88%), and *trans*-2-*i*-propyl-4-chromanol (VII, 61%) were prepared.

III: Mp 42—43 °C; recrystallized from hexane. Found: C, 76.40; H, 6.39%. Calcd for $C_{12}H_{12}O_2$: C, 76.57; H, 6.43%. IR (KBr): 1660 cm^{-1}. NMR (CCl_4): δ 1.32 (Me of *i*-Pr), 6.00 (s, 1H, C_3–H) ppm.

IX: Colorless oil. Found: C, 75.79; H, 7.45%. Calcd for $C_{12}H_{14}O_2$: C, 75.76; H, 7.42%. IR (CCl_4): 1690 cm^{-1}. NMR ($CDCl_3$): δ 1.05 (Me of *i*-Pr), 2.5—2.8 (AB part of ABX, C_3–H), 4.17 (ddd, 1H, C_2–H) ppm.

V: Mp 88.5—89 °C, recrystallized from hexane. Found: C, 74.67; H, 8.27%. Calcd for $C_{12}H_{16}O_2$: C, 74.97; H, 8.39%. IR (KBr): 3250 cm^{-1}. NMR ($CDCl_3$+D_2O): δ 1.00 (Me of *i*-Pr), 3.82 (ddd, 1H, C_2–H), 4.83 (dd, 1H, C_4–H) ppm.

Acetate of V: Colorless oil. IR (neat): 1739 cm^{-1}. NMR ($CDCl_3$): δ 1.7—2.6 (m, 6H, methine of *i*-Pr, C_3–H, and –OAc), 3.90 (ddd, 1H, C_2–H), 6.07 (dd, 1H, C_4–H) ppm. $|J_{2,3}+J_{2,3'}|=13.2$, $|J_{3,4}+J_{3',4}|=16.5$ Hz.

VII: Colorless oil. Found: C, 74.70; H, 8.54%. Calcd for $C_{12}H_{16}O_2$: C, 74.97; H, 8.39%. IR (neat): 3350 cm^{-1}. NMR ($CDCl_3$+D_2O): δ 1.02 (Me of *i*-Pr), 3.91 (ddd, 1H, C_2–H), 4.67 (t, 1H, C_4–H) ppm.

Acetate of VII: Colorless oil. IR (neat): 1740 cm^{-1}. NMR ($CDCl_3$): δ 1.8—2.2 (m, 6H, methine of *i*-Pr, C_3–H, and –OAc), 3.96 (ddd, 1H, C_2–H), 5.98 (t, 1H, C_4–H) ppm. $|J_{2,3}+J_{2,3'}|=13.2$, $|J_{3,4}+J_{3',4}|=6.0$ Hz.

2-t-Butyl-1,3-propanediol Monotosylate (XI). To a stirred solution of 2-*t*-butyl-1,3-propanediol (X, 14 g) in dry pyridine (80 ml) was added, drop by drop, *p*-toluenesulfonyl chloride (20.2 g) in dry chloroform (100 ml) under ice cooling over a period of 5 hr. After the reaction mixture had then been left to stand for 2 days in a refrigerator, it was poured into ice water (500 ml) containing concentrated hydrochloric acid. The organic layer was treated in the usual way to afford a pale yellow oil (28.3 g), which was subsequently chromatographed on silica gel (400 g). Elution with benzene–ether (4: 1) afforded 2-*t*-butyl-1,3-propanediol ditosylate (8.2 g, 17.5%); mp 69.0—69.5 °C.

Found: C, 57.19; H, 6.68%. Calcd for $C_{21}H_{28}O_6S_2$: C, 57.25; H, 6.41%.

Subsequent elution gave monotosylate (XI) (16.3 g, 57.5%) as a colorless oil.

Found: C, 58.56; H, 7.93%. Calcd for $C_{14}H_{22}O_4S$: C, 58.72; H, 7.74%. IR (neat): 3450 cm^{-1}. NMR ($CDCl_3$): δ 0.90 (s, 9H, *t*-Bu) ppm.

2-t-Butyl-1,3-propanediol Monophenyl Ether (XII). To a solution of sodium ethoxide in ethanol prepared from absolute ethanol (70 ml) and sodium (1.56 g) was added phenol (6.42 g); then the solvent was removed. To the stirred suspension of sodium phenoxide in dimethyl sulfoxide (40 ml), heated at 50—60 °C, was added, drop by drop, XI (16.3 g) in dimethyl sulfoxide (30 ml) over a period of 45 min. Stirring was continued for 2 hr at 50—60 °C, and then the mixture was allowed to stand overnight at room temperature. The reaction mixture was poured into ice water (350 ml), saturated with sodium chloride, and extracted five times with ether. The combined extract was then treated as usual to give a pale yellow oil (10.6 g), which was subsequently purified by distillation, 9.7 g (83%), bp 145—147 °C/4 mmHg.

Found: C, 74.65; H, 10.05%. Calcd for $C_{13}H_{20}O_2$: C, 74.96; H, 9.68%. IR (neat): 3350 cm^{-1}. NMR ($CDCl_3$): δ 1.00 (s, 9H, *t*-Bu), 6.8—7.4 (m, 5H, aromatic-H) ppm.

p-*Nitrobenzoate of XII*: Colorless needles from ethanol–water, mp 63—63.5 °C. Found: N, 4.02%. Calcd for $C_{20}H_{23}NO_5$: N, 3.92%.

α-t-Butyl-β-phenoxypropionic Acid (XIII). To a stirred solution of XII (6.80 g) in acetone (360 ml) warmed to 30 °C was added, portion by portion, finely-powdered potassium permanganate (14 g). After the addition was complete, the stirring was continued for 24 hr. The manganese dioxide was filtered off and washed well with hot water (total volume, 300 ml). The filtrate and the washings were then combined and concentrated under reduced pressure. After 2 M sodium hydroxide (30 ml) had been added, the mixture was extracted with ether to remove the unreacted XII; the water layer was acidified with concentrated hydrochloric acid to give XIII, which was filtered, washed with water, and dried (2.67 g, 37%). Recrystallization from aqueous ethanol gave fine needles; mp 88.5—89.5 °C.

Found: C, 70.07; H, 8.12%. Calcd for $C_{13}H_{18}O_3$: C, 70.24; H, 8.16%. IR (KBr); 3300—3000 cm^{-1}. NMR ($CDCl_3$): δ 1.10 (s, 9H, *t*-Bu) ppm.

From the ether extract XII was recovered (2.85 g, 42%).

3-t-Butyl-4-chromanone (XIV). A mixture of XIII (2.85 g) and polyphosphoric acid (50 g) was kept at 90 °C for 5 hr and then poured into ice water (250 ml). Colorless crystals were collected and dissolved in ether; they were then washed with 1 M sodium hydroxide and water, and dried over sodium sulfate. The solvent was removed to give crude XIV (2.2 g, 88%) as colorless crystals, which were then distilled under reduced pressure (bath 120 °C/1 mm Hg) to yield colorless crystals; mp 37—39 °C. Recrystallization from pentane gave pure XIV; mp 41.5—42 °C.

Found: C, 76.40; H, 8.11%. Calcd for $C_{13}H_{16}O_2$: C, 76.44; H, 7.90%. IR (CCl_4): 1684 cm^{-1}. NMR ($CDCl_3$): δ 1.09 (s, 9H, *t*-Bu), 2.29 (t, 1H, C_3–H), 4.40—4.75 (AB part of ABX, C_2–H) ppm. UV (95% EtOH nm ε): 254 (8950), 324 (3360).

The alkaline extract was acidified with dilute hydrochloric acid to give unreacted XIII (145 mg, 5%).

cis-*3-t-Butyl-4-chromanol (XV).* A solution of XIV (510 mg) and sodium borohydride (70 mg) in ethanol (5 ml) was refluxed for 3 hr. The removal of the solvent afforded an oily residue, which was then dissolved in dilute acetic acid. The mixture was extracted with ether, and the organic layer was worked up according to the usual procedure to yield crude product as colorless crystals (462 mg, 90%); whose vpc indicated that it was a mixture of XV (94.4%) and

trans-3-*t*-butyl-4-chromanol (XVI, 5.6%). Recrystallization from pentane gave pure XV; mp 60.5—61.0 °C.

Found: C, 75.56; H, 8.80%. Calcd for $C_{13}H_{18}O_2$: C, 75.69; H, 8.80%. IR (KBr): 3450 cm^{-1}. NMR ($CDCl_3$+D_2O): δ 1.11 (s, 9H, *t*-Bu), 1.4—1.8 (ddd, 1H, C_3–H), 4.1—4.3 (AB part of ABX, C_2–H), 4.83 (d, 1H, C_4–H) ppm.

Benzoate of XV: Colorless crystals from pentane–benzene; mp 155 °C.

Found: C, 77.52; H, 7.15%. Calcd for $C_{20}H_{22}O_3$: C, 77.39; H, 7.14%. IR (KBr): 1710 cm^{-1}. NMR ($CDCl_3$): δ 1.06 (s, 9H, *t*-Bu), 1.8—2.2 (ddd, 1H, C_3–H), 4.4—4.6 (AB part of ABX, C_2–H), 6.50 (d, 1H, C_4–H) ppm.

trans-*3*-t-*Butyl-4-chromanol (XVI)*. A solution of XV (675 mg) in acetic acid (8 ml)-concentrated hydrochloric acid (2 ml) was kept at 120—130 °C for 20 min. The reaction mixture was then poured into ice water and extracted with ether, and the extract was washed as usual. The removal of the solvent afforded 3-*t*-butylchromene as a yellow oil (582 mg, 95%), which was then distilled under reduced pressure (bath 80—110 °C/1 mmHg). NMR ($CDCl_3$): δ 1.14 (s, 9H, *t*-Bu), 4.75 (d, 2H, C_2–H), 6.24 (bs, 1H, C_4–H) ppm.

To a stirred solution of 3-*t*-butylchromene (470 mg) and sodium borohydride (85 mg) in diglyme (3 ml) was added, drop by drop, boron trifluoride etherate (0.38 ml) in diglyme (0.4 ml) under a nitrogen atmosphere over a period of 15 min. After the reaction mixture had been stirred for 1 hr, water (1 ml) was added to decompose the excess diborane. To the above stirred solution, there were added 3 M sodium hydroxide (0.8 ml) and then, drop by drop, 30% hydrogen peroxide (0.8 ml) at 40—50 °C. After the stirring had been continued for an additional hour, the solution was poured into water and extracted with ether. The extract was treated in usual manner to give a colorless oil (450 mg, 87%) which crystallized on standing. Recrystallization from pentane afforded colorless prisms; mp 64.0—64.5 °C.

Found: C, 75.46; H, 8.88%. Calcd for $C_{13}H_{18}O_2$: C, 75.69; H, 8.80%. IR (KBr): 3260 cm^{-1}. NMR ($CDCl_3$+D_2O): δ 0.98 (s, 9H, *t*-Bu), 1.66 (q, 1H, C_3–H), 4.25 (d, 2H, C_2–H), 4.74 (d, 1H, C_4–H) ppm.

Benzoate of XVI: Colorless oil.

Found: C, 77.64; H, 7.34%. Calcd for $C_{20}H_{22}O_3$: C, 77.39; H, 7.14%. IR (neat): 1710 cm^{-1}. NMR ($CDCl_3$): δ 1.01 (s, 9H, *t*-Bu), 1.87 (q, 1H, C_3–H), 4.42 (AB part of ABX, C_2–H), 6.31 (bd, 1H, C_4–H) ppm.

BULLETIN OF THE CHEMICAL SOCIETY OF JAPAN, VOL. 46, 1844—1847 (1973)

Chemistry of α-Haloaldehydes. II.[1] Base-catalyzed Condensation of α-Haloaldehydes with Methyl Chloroacetate

Akira TAKEDA, Sadao TSUBOI, and Tōru HONGO

Department of Synthetics Chemistry, School of Engineering, Okayama University, Tsushima, Okayama 700

(Received December 15, 1972)

The Darzens-type condensation of α-haloaldehyde (**2**) with methyl chloroacetate has been studied. The reaction of aliphatic α-chloroaldehydes afforded 4-chloro-2,3-epoxyalkanoates (**4**). The reaction of 2-bromo-2-methylpropanal (**2d**) with methyl chloroacetate gave α-chloro-γ,γ-dimethyl-$\Delta^{\alpha,\beta}$-butenolide (**7**) as a major product. α-Bromo-*n*-alkanal gave a mixture of many minor products.

Two diastereomeric isomers of 4,5-dihydroxyhexanoic acid gamma lactone (**1**) have been isolated as major constituents of the aroma extracts of flour sherries.[2] In order to carry out the attempted synthesis of **1** and their derivatives we needed 4-halo-2,3-epoxys alkanoates (**4**) as starting materials. The Darzen-condensation of aldehydes and ketones may be the most convenient and common procedure for the one-step synthesis of 2,3-epoxyalkanoates, but there have been few reports on the title reaction of α-haloaldehydes (**2**).

We have been studying the reactions of α-haloaldehydes with active hydrogen compounds and reported on the Darzens-type condensation of **2** with dichloroacetate[1] giving 2,4-dichloro-2,3-epoxyalkanoates. As an extension of the previous work[1] we carried out the reaction of **2** with monochloroacetate in the presence of sodium alkoxide to prepare 4-halo-2,3-epoxyalkanoates. Ether or THF was used as solvent to prevent **2** from being transformed into α-hydroxy acetal.[3] In this paper the results of the reaction and a discussion of the reaction mechanism are given. The yields, boiling points and the analytical data are summarized in Table 1.

The cyclization of the possible intermediate (**3**) to an epoxyalkanoate may occur in such a way that the α- and γ-halogen atoms compete with each other as a leaving group to produce either 4-halo-2,3-epoxyalkanoate (**4**) (route 1) or 2-halo-3,4-epoxyalkanoate (**5**) (route 2). In the reaction of α-chloroaldehydes only 2,3-epoxyalkanoate (**4**) was obtained[4] in a 9—40% yield indicating that the oxyanion of **3** attacked more readily its α-carbon atom which was made more electron-deficient by the electron-withdrawing effect of the carboxyl group. The reaction sequence is given

1) The first paper of this series: A. Takeda, S. Tsuboi, S. Wada, and H. Kato, This Bulletin, **45**, 1217 (1972).

2) C. J. Muller, L. Maggiora, R. E. Kepner, and A. D. Webb, *J. Agr. Food Chem.*, **17**, 1373 (1969).

3) C. L. Stevens, E. Farkas, and B. Gillis, *J. Amer. Chem. Soc.*, **76**, 2695 (1954).

4) A moderate amount of resinous material was produced.

TABLE 1. PRODUCTS FROM THE REACTION OF α-HALOALDEHYDES WITH METHYL CHLOROACETATE

α-Haloaldehyde RR'C(X)-CHO				Products[a]		Yield, %	Bp, °C/mmHg (Mp)	Found, %		Calcd, %	
Code	R	R'	X	Code	Structure			C	H	C	H
2a	CH_3	H	Cl	**4a**	$CH_3CHCl\text{-}CH(O)\text{-}CHCO_2Me$	15	56—60/16	43.61	5.38	43.79	5.51
2b	CH_3	CH_3	Cl	**4b**	$(CH_3)_2CCl\text{-}CH(O)\text{-}CHCO_2Me$	40	100—103/12	46.90	6.30	47.07	6.21
2c	C_2H_5	H	Cl	**4c**	$C_2H_5CHCl\text{-}CH(O)\text{-}CHCO_2Me$	10	90—94/5	47.44	5.91	47.07	6.21
2d	CH_3	CH_3	Br	**4d**	$(CH_3)_2CBr\text{-}CH(O)\text{-}CHCO_2Me$	9	93—125/3	37.90	5.25	37.69	4.97
				and							
				7	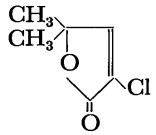	14	(94—95)	49.18	4.50	49.15	4.78
2e	C_5H_{11}	H	Cl	**4e**	$C_5H_{11}CHCl\text{-}CH(O)\text{-}CHCO_2Me$	25	130—133/5	54.13	7.87	54.42	7.77

a) All the compounds are new.

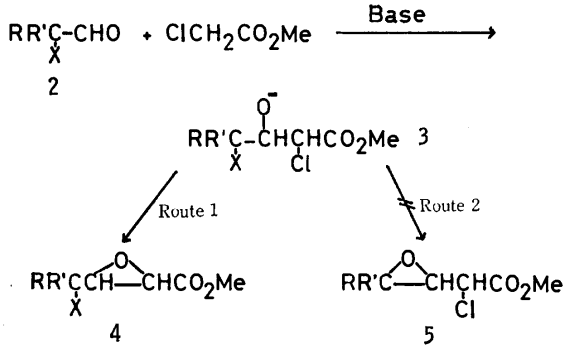

Scheme 1.

in Scheme 1. The structure of **4** was confirmed by IR spectra, NMR spectra, MS, and microanalyses. The IR bands of **4** at 1750—1755, 900—910, and 820—825 cm^{-1} [1,5a,b] are characteristic of the epoxyester. The singlets or doublets at δ 3.28—3.24 (J=0—2.3 Hz) in the NMR spectrum of **4** represent the signal from the C_2-proton. The geometry of **4** can be estimated to be *trans* from the small value of the coupling constants due to epoxy-ring protons.

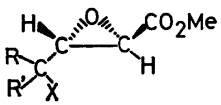

On account of a higher reactivity toward nucleophiles than their chlorine homologs α-bromoaldehydes tend to react in different ways. In contrast with α-chloroaldehydes, it is expected that in the reaction of α-bromoaldehydes the bromine atom attached to the γ-carbon of the intermediate **3** becomes a better leaving group as in the base-catalyzed condensation of α-bromoheptanal with methyl dichloroacetate.[1] As expected, the reaction of 2-bromo-2-methylpropanal (**2d**) with methyl chloroacetate gave α-chloro-γ,γ-dimethyl-$\Delta^{\alpha,\beta}$-butenolide (**7**) in a 14% yield, together with a small amount (9% yield) of methyl 4-bromo-4-methyl-2,3-epoxypentanoate (**4d**). α-Bromoheptanal (**2f**) only underwent displacement to yield α-hydroxyheptanal dimethyl acetal (**8**) and not the desired product, when methanol was used as solvent. It is not likely that acetal **8** was derived from acetal (**9**) of α-bromoaldehyde (**2f**) since α-bromoaldehyde acetal appears inactive toward nucleophiles such as sodium methoxide and sodium ethoxide as suggested by the reaction of α-bromopropanal acetal. It is reasonable to consider that the transformation of **2f** into **8** involves epoxy-ring intermediate.[3]

The $\Delta^{\alpha,\beta}$-butenolide structure of **7** is supported by IR and NMR spectra. The IR band of **7** at 1730 cm^{-1} is characteristic of the conjugated lactone carbonyl,[6] two singlets at δ 1.50 (methyl proton) and 7.35 (olefinic proton) in the NMR spectrum of **7** being indicative of butenolide structure. A possible pathway of the formation of **7** is shown in Scheme 2.

5) a) A. Takeda, S. Wada, M. Fujii, and H. Tanaka, This Bulletin, **43**, 2997 (1970); b) L. J. Bellamy, "The Infrared Spectra of Complex Molecules," 2nd Ed., Methuen & Co. Ltd., London, U. K. (1958), p. 118.

6) A. Takeda, K. Takahashi, S. Torii, and T. Moriwake, *J. Org. Chem.*, **31**, 316 (1966).

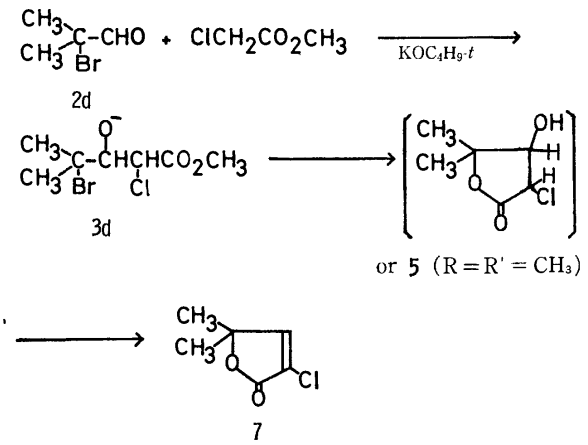

Scheme 2.

Experimental

All the boiling points and the melting points are uncorrected. α-Haloaldehydes were prepared by the method described previously.[1] The analytical determinations by glpc were performed on a Hitachi K-53 model gas chromatograph (3 mm o.d.×1 m, 10% Apiezon Grease L on Chromosorb W column); carrier gas, N_2 (0.5 kg/cm², 42 ml/min); detector, FID. The preparative glpc was performed on a Yanagimoto GCG-550T model gas chromatograph (3 mm o.d.×2.25 m, 10% Apiezon Grease L on Chromosorb W). Mass spectra were measured with a Hitachi RMS-4 model mass spectrometer and NMR spectra on a Hitachi R-24 NMR model spectrometer. Liquid samples were purified by glpc or tlc for analyses and spectral measurements.[7] The following experiments are shown as an example.

*Methyl 4-Chloro-2,3-epoxypentanoate (**4a**).* Powdered sodium methoxide (5.9 g, 0.11 mol) was added in several portions to a mixture of α-chloropropanal (9.3 g, 0.1 mol) and methyl chloroacetate (12.2 g, 0.1 mol) in dry ether (50 ml), at −30 °C.[8] After the mixture was stirred for 2 hr, it was allowed to cool to room temperature, stirring being continued for 4 hr. The reaction mixture was allowed to stand overnight and then treated with water. The ethereal layer was separated, washed several times with water and dried over $MgSO_4$. After removal of the solvent it was distilled giving 1.6 g (10%) of **4a**: bp 87—97 °C/8 mmHg; IR (cm⁻¹, liquid) 1755 (ester C=O), 900 and 825 (epoxide ring); NMR (CCl_4) δ 1.57 (d, 3H, J=6.5 Hz, $C\underline{H}_3CHCl$–), *ca.* 3.19 (q, 1H, J=1 Hz, –C<u>H</u>(O)–C<u>H</u>CO_2CH_3), 3.30 (s, 1H, –CH(O)–C<u>H</u>CO_2CH_3), 3.65 (m, 1H, >CHCl), and 3.75 (s, 3H, CO_2CH_3).

*Methyl 4-Chloro-4-methyl-2,3-epoxypentanoate (**4b**).* Powdered sodium methoxide (5.4 g, 0.1 mol) was added gradually to a solution of freshly-distilled 2-chloro-2-methylpropanal (10.6 g, 0.1 mol) and methyl chloroacetate (12.2 g, 0.1 mol) in dry ether (60 ml), at 0—3 °C. After the mixture was stirred at room temperature for 12 hr and then refluxed for 1 hr, it was treated with water. The ethereal layer was separated, washed several times with water and dried over Na_2SO_4. After removal of the solvent it was distilled to give 7.2 g (40%) of **4b**: bp 100—103 °C/12 mmHg; IR (cm⁻¹, liquid) 1750 (ester C=O), 910 and 828 (epoxide ring); NMR (CCl_4) δ 1.53 (s, 3H, >C(<u>C</u>H_3)$_2$), 1.59 (s, 3H, >C(C<u>H</u>$_3$)$_2$), 3.33 (d, 1H, J=1.7 Hz, –CH(O)–C<u>H</u>–), 3.40 (d, 1H, J=1.7 Hz, –C<u>H</u>(O)–CH–), and 3.74 (s, 3H, CO_2CH_3).

*Methyl 4-Chloro-2,3-epoxyhexanoate (**4c**).* Powdered sodium methoxide (5.4 g, 0.1 mol) was added in several portions to a mixed solution of freshly-distilled α-chloro-*n*-butanal (10.6 g, 0.1 mol) and methyl chloroacetate (10.9 g, 0.1 mol) in dry ether (30 ml) at 0—3 °C. The mixture was allowed to warm up to room temperature and then refluxed for 4 hr. The ethereal extract was worked up as usual and distilled to give 3.3 g (10% yield[9]) of the liquid, which was collected at 90—94 °C/5 mmHg. Glpc analysis showed it to consist of five components. The peaks, retention times (min), and integrated percentages[10] were: 1, 4.6, 55; 2, 6.6, 31; 3, 7.7, 5; 4, 8.3, 5; 5, 9.4, 4. Component 1 was collected by preparative glpc and identified as **4c**: IR (cm⁻¹, liquid) 1750 (ester C=O), 900 and 820 (epoxide ring); NMR (CCl_4) δ 1.10 (t, 3H, J=7.5 Hz, $C\underline{H}_3CH_2$–), 1.91 (m, 2H, $CH_3C\underline{H}_2$–), 3.19 (q, 1H, J=1 Hz, –C<u>H</u>(O)–C<u>H</u>CO_2CH_3), 3.33 (d, 1H, J=1 Hz, –CH(O)–C<u>H</u>CO_2CH_3), 3.40 (m, 1H, >CHCl), and 3.77 (s, 3H, CO_2CH_3).

Reaction of 2-Bromo-2-methylpropanal with Methyl Chloroacetate. Powdered potassium *tert*-butoxide (29.6 g, 0.26 mol) was added to a solution of freshly distilled 2-bromo-2-methylpropanal (19 g, 0.13 mol) and methyl chloroacetate (28.6 g, 0.26 mol) in dry THF (50 ml) at −5—0 °C. After addition was completed, stirring was continued for 1 hr. The reaction mixture was stirred for 5 hr at room temperature. It was allowed to stand overnight, refluxed for 1 hr and then treated with water. After the mixture was acidified with 10% HCl, the organic layer was extracted with ether, and the ethereal extract was washed several times with water and dried over Na_2SO_4. After removal of the solvent the residue was distilled to give 7 g of a liquid boiling at bp 93—125 °C/6 mmHg. The solidified material (0.9 g) was separated from the liquid, and recrystallized from *n*-hexane to give lactone **7**: mp 94—95 °C; IR (cm⁻¹, Nujol) 1730 (conjugated C=O), 1605 (conjugated C=C); NMR ($CDCl_3$) δ 1.50 (s, 6H, $(CH_3)_2C$<), and 7.35 (s, 1H, =C–H); MS (70 eV) *m/e* (relative intensity) 146 (13, M^+, 1Cl), 131 (100, M^+-CH_3), 111 (43, M^+-Cl), 103 (61), 68 (48), and 43 (73). Glpc analysis of the filtrate showed the presence of two major and six minor components. The peaks, retention times, and integrated percentages[11] were: 1, 6.0, 21%; 2, 10.6, 49%. Component 1 was collected by preparative glpc and identified as **7** by comparison of the retention times (min) and the IR spectrum with those of an authentic sample.

Component 2 was collected similarly and identified as **4d**: IR (cm⁻¹, liquid) 1750 (ester C=O), 905 and 820 (epoxide ring); NMR (CCl_4) δ 1.68 (s, 3H, $-CH_3$), 1.79 (s, 3H, $-CH_3$), 3.36 (d, 1H, J=2.3 Hz, –CH(O)–C<u>H</u>–), 3.42 (d, 1H, J=2.3 Hz, –C<u>H</u>(O)–CH–), and 3.76 (s, 3H, CO_2CH_3): MS (70 eV) *m/e* (relative intensity) 190 (1, M^+-CH_3OH), 164 (25), 162 (20), 142 (100, M^+-HBr), 135 (82), 133 (82), 104 (85), 88 (79), 54 (82), and 38 (80).

*Methyl 4-Chloro-2,3-epoxynonanoate (**4e**).* Into a solution

7) Microanalyses were carried out by Mr. Eiichiro Amano.

8) When the reaction was carried out at 0 °C, glycidate **4a** was obtained only in a poor yield, many unknown substances being obtained.

9) Estimated as compound **4c**.

10) Column temp., 150 °C.

11) Column temp., 120 °C.

of α-chloroheptanal (14.8 g, 0.1 mol) and methyl chloroacetate (12.2 g, 0.1 mol) in dry ether (60 ml), sodium methoxide (5.4 g, 0.1 mol) was added in several portions at 0—3 °C. The mixture was worked up as in the preparation of **4b** and 5.6 g (25%) of **4e** was obtained: bp 130—133 °C/5 mmHg; IR (cm^{-1}, liquid) 1755 (ester C=O), 900 and 825 (epoxide ring); NMR (CCl_4) δ 0.93 (t, 3H, $J=5$ Hz, $C\underline{H}_3(CH_2)_4$–), 1.15—2.15 (m, 8H, $CH_3(C\underline{H}_2)_4$–), 3.28 (s, 1H, –CH(O)–C<u>H</u>CO_2CH_3), 3.15—3.50 (m, 1H, –C<u>H</u>(O)–CHCO_2CH_3), 3.50 (m, 1H, >CHCl), and 3.75 (s, 3H, $CO_2C\underline{H}_3$).

*Reaction of α-Bromoheptanal (**2f**) with Methyl Chloroacetate in Methanol.* To a mixed solution of α-bromoheptanal (15.7 g, 0.081 mol) and sodium methoxide (4.4 g, 0.081 mol) in 60 ml of methanol was added 8.7 g (0.081 mol) of methyl chloroacetate with stirring, at −4 °C. Stirring was continued for 2 hr at room temperature and 0.5 hr at reflux temperature. The reaction mixture was diluted with 200 ml of water and then extracted with ether. The ethereal layer was washed several times with water, dried with $MgSO_4$ and the solvent was evaporated. The residual oil was distilled to give 10.9 g of a fraction boiling at 45—109 °C/17 mmHg. Glpc analysis of this fraction showed one major peak (58%)[12] and six minor (42% in total) peaks. The major constituent with the retention time of 8 min was collected by preparative glpc and identified as α-hydroxyheptanal dimethyl acetal (**9**) on the basis of the IR spectrum and analysis: IR (cm^{-1}, liquid) 3450 (OH), 1200, 1125, and 1070 (acetal C–O–C–O–C). Found: C, 61.06; H, 11.03%. Calcd for $C_9H_{20}O_3$: C, 61.32; H, 11.44%. Other minor products were not investigated further.

Treatment of α-bromopropanal diethyl acetal with sodium methoxide or sodium ethoxide in absolute alcohols only resulted in the recovery of starting materials.

12) Calculation based on peak area.

BULLETIN OF THE CHEMICAL SOCIETY OF JAPAN, VOL. 46, 1847—1850 (1973)

Synthesis of Alanosine

Yoshikazu Isowa, Hideaki Kurita, Muneki Ohmori, Masanari Sato, and Kaoru Mori

Sagami Chemical Research Center, Nishiohnuma, Sagamihara, Kanagawa 229

(Received January 13, 1973)

DL-2-Amino-3-(*N*-tosyl-*N*-benzyloxyamino)propionic acid (DL-V) was synthesized starting from ethyl 2,3-dibromopropionate and *N*-tosyl-*O*-benzylhydroxylamine. L-2-Benzoylamino-3-(*N*-benzoyl-*N*-hydroxyamino)propionic acid anilide (L XIV) obtained *via* the enzymatic resolution of DL-2-benzoylamino-3-benzyloxyaminopropionic acid (DL-IX) was converted by acid hydrolysis to L-2-amino-3-hydroxyaminopropionic acid (L-II). The nitrosation product of the amino-hydroxyamino acid (L-II) was identical with alanosine (L-I).

Alanosine[1,2] (L-I) is an antimicrobial agent isolated from a Streptomyces. The structure[2] of L-I was determined to be a 3-*N*-nitroso-derivative of L-2-amino-3-hydroxyamino-propionic acid (L-II), one of the α-amino-ω-hydroxyamino acid.[3-5]

A route for the synthesis of L-II starting from methyl 2-acetamino-3-chloropropionate and hydroxylamine has been reported by Lancini *et al.*[6,7] The optically active amino-hydroxyamino acid (L-II) has been obtained by the acid hydrolysis of the cinchonine salt of L-2-benzoylamino-3-(*N*-benzoyl-*N*-hydroxyamino)propionic acid (L-XI). Nitrosation of L-II with sodium nitrite in the equimolar amount of cold M hydrochloric acid gave alanosine (L-I).

In our previous paper,[8] we described the syntheses of 5-(*N*-tosyl-*N*-benzyloxy)-DL-ornithine and 5-*N*-hydroxy-L-ornithine, a higher homolog of L-II. The present paper deals with the synthesis of L-II from DL-2-amino-3-(*N*-tosyl-*N*-benzyloxy-amino)propionic acid (DL-V), which was prepared from *N*-tosyl-*O*-benzylhydroxylamine (III) and ethyl 2,3-dibromopropionate. The reaction paths were outlined in Fig. 1.

Papain-catalyzed resolution[8-11] of DL-2-acetamino-3-(*N*-tosyl-*N*-benzyloxyamino)propionic acid (DL-VI) under the same conditions (38 °C, pH 6.1, or 7.3) as in the case of 2-*N*-acetyl-5-(*N*-tosyl-*N*-benzyloxy)-DL-ornithine in the presence of aniline was unsuccessful. But optically active 2-acetamino-3-(*N*-tosyl-*N*-benzyloxyamino)propionic acid anilide (VII), $[\alpha]_D^{23}$ −113.4° (*c* 1, chloroform) was obtained at 50 °C and pH 7.3 in spite of the bulkiness of the hydroxyamino-protecting tosyl and benzyl groups at the β-position of the molecule.

On the other hand, the detosylation product of the amino acid (DL-V), DL-2-amino-3-benzyloxyamino-propionic acid (DL-VIII), which was obtained from DL-V by the action of 36% hydrogen bromide–acetic

1) Y. K. S. Murthy, J. E. Thiemann, C. Coronelli, and P. Sensi, *Nature*, **211**, 1198 (1966).
2) C. Coronelli, C. R. Pasqualucci, G. Tamoni, and G. G. Gallo, *Il Farmaco, Ed. Sci.*, **21**, 269 (1966).
3) J. B. Neilands, *Struct. Bond.*, **1**, 59 (1966).
4) G. A. Snow, *Bacteriol. Rev.*, **34**, 99 (1970).
5) H. Maehr, *Pure Appl. Chem.*, **28**, 603 (1971).
6) G. C. Lancini, A. Diena, and E. Lazzari, *Tetrahedron Lett.*, **1966**, 1769.
7) G. C. Lancini, E. Lazzari, and A. Diena, *Il Farmaco, Ed. Sci.*, **24**, 169 (1969).
8) Y. Isowa, T. Takashima, M. Ohmori, H. Kurita, M. Sato, and K. Mori, This Bulletin, **45**, 1461 (1972).
9) N. F. Albertson, *J. Amer. Chem. Soc.*, **73**, 452 (1950).
10) J. de Jersey, *Biochemistry*, **9**, 1761 (1970).
11) J. Drenth, J. N. Jansonius, R. Koekoek, and B. G. Wolthers, "Advances in Protein Chemistry," Vol. 23, Academic Press (1971), pp. 79—115.

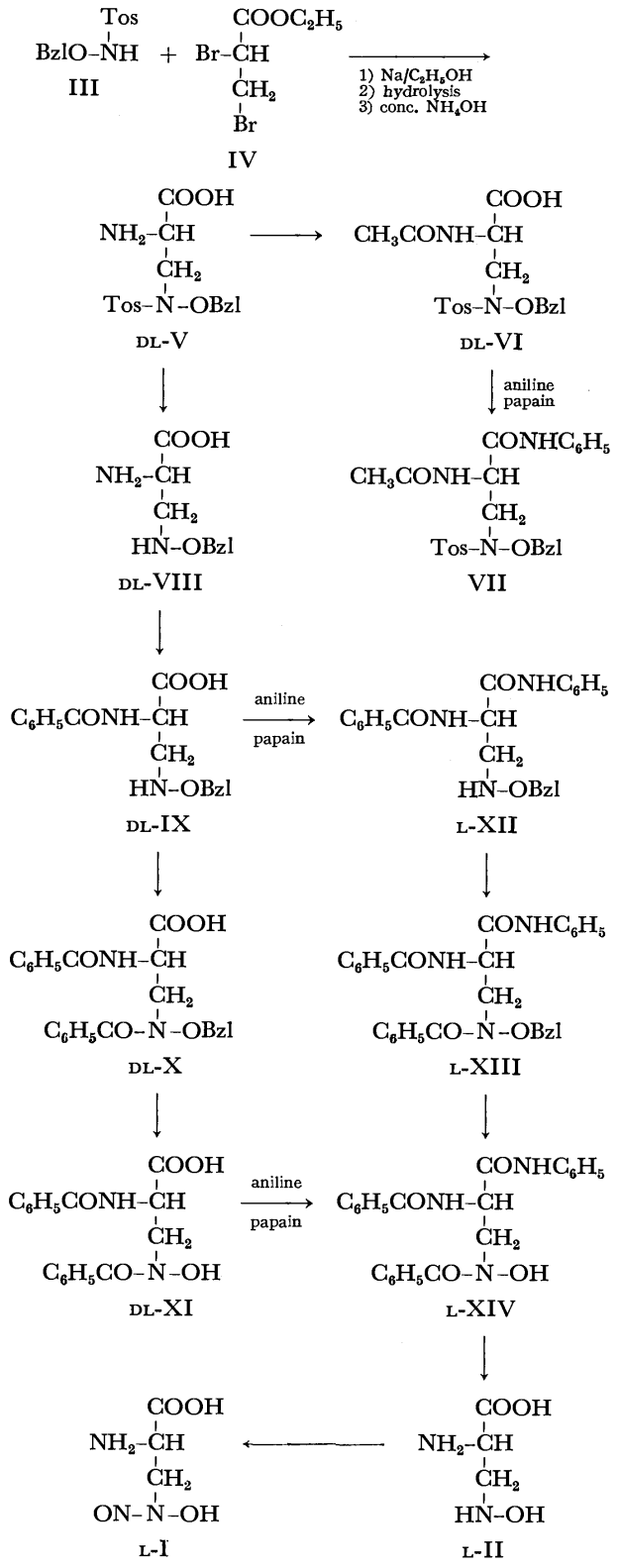

Fig. 1

acid in the presence of phenol, followed by the 2-*N*-benzoylation with *N*-benzoyloxysuccinimide, was resolved into derivatives of its optical isomers with the aid of cysteine-activated papain in the presence of aniline at 38 °C and pH 6.1; L-2-benzoylamino-3-benzyloxyaminopropionic acid anilide (L-XII), $[\alpha]_D^{26}$ −108.9° (*c* 1, chloroform) and D-2-benzoylamino-3-benzyloxyaminopropionic acid (D-IX), $[\alpha]_D^{26}$ −18.2° (*c* 1, acetic acid) were obtained.

3-*N*-Benzoylation of L-XII in pyridine with benzoyl chloride, followed by hydrogenation, yielded L-2-benzoylamino-3-(*N*-benzoyl-*N*-hydroxyamino)propionic acid anilide (L-XIV). The L-dibenzoyl derivative (L-XIV) was also obtained by resolution of DL-2-benzoylamino-3-(*N*-benzoyl-*N*-hydroxyamino)propionic acid (DL-XI), which was prepared by 3-*N*-benzoylation of monobenzoylamino acid (DL-IX) in ethyl acetate with benzoyl chloride in the presence of *N*-methylmorpholine and subsequent debenzylation.

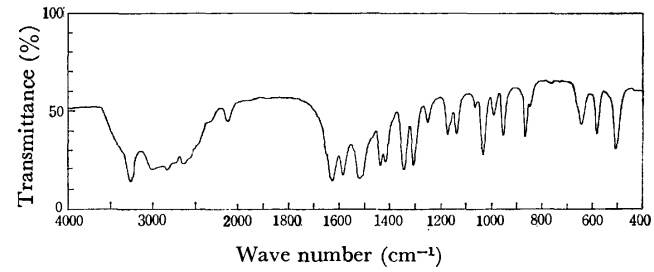

Fig. 2. L-2-Amino-3-hydroxyaminopropionic acid

Acid hydrolysis of the protected amino-hydroxyamino acid derivative (L-XIV) gave L-2-amino-3-hydroxyaminopropionic acid (L-II), which was identical, in respect of optical rotatory power, with an authentic sample obtained by another route.[6,7] The IR spectrum of L-II is shown in Fig. 2. Nitrosation of the amino-hydroxyamino acid (L-II) by the method reported by Lancini *et al.*,[7] gave L-2-amino-3-(*N*-nitroso-*N*-hydroxyamino)propionic acid, alanosine (L-I). The identity of the synthetic alanosine with natural one was confirmed by color reaction, optical rotation, and elemental analysis. The IR spectrum of L-I is shown in Fig. 3.

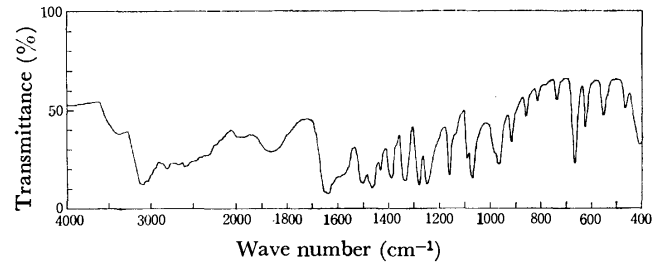

Fig. 3. L-2-Amino-3-(*N*-nitroso-*N*-hydroxyamino)propionic acid; alanosine

Experimental

Melting points were all determined with a Yanagimoto electric micromelting point apparatus, unless otherwise indicated, and are uncorrected. Optical rotations were measured with a Yanagimoto automatic polarimeter OR-50. Infrared spectra were recorded on a Hitachi EPI G-3 spectrophotometer as KBr disk. Nuclear magnetic resonance spectra were run on a Hitachi Perkin-Elmer R-20 High Resolution spectrometer, using tetramethylsilane as an internal standard. Concentration and evaporation of solutions were always carried out under reduced pressure.

DL-*2-Amino-3-(*N*-tosyl-*N*-benzyloxyamino)propionic Acid* (DL-*V*). To a solution of sodium (23 g, 1g-atom) in ethanol

(1 l) was added *N*-tosyl-*O*-benzylhydroxylamine (277 g, 1 mol). To the resultant mass, under ice-cooling and occasional shaking, ethyl 2,3-dibromopropionate (260 g, 1 mol) was added over a period of 2 hr. After stirring for 12 hr at room temperature, 5 M sodium hydroxide (210 ml) was added slowly at 0 °C and stirred for 12 hr at room temperature. Thereafter 2.5M sulfulic acid (*ca.* 210 ml) was added to the solution until pH 4 under ice-cooling and the solvent was evaporated. To the residue, ethyl acetate (1.5 l) and water (200 ml) were added, the organic layer was dried over sodium sulfate and the solvent was removed. To the viscous oily residue conc. aqueous ammonia (3 l) was added and the solution saturated with ammonia gas was stored at room temperature for 10 days. Thereafter the solution was concentrated. The crystalline deposit was collected and washed with water and methanol. Yield, 273 g (75%);mp 184—186 °C (decomp.). This crude product was used without recrystallization in the subsequent preparation. A part of the product was recrystallized from acetic acid–water to give an analytical sample, mp 187—188 °C (decomp.).

Found: C, 55.96; H, 5.23; N, 7.56%. Calcd for $C_{17}H_{20}N_2O_5S$: C, 56.03; H, 5.53; N, 7.69%.

DL-*2-Acetamino-3-(*N-*tosyl*-N-*benzyloxyamino)propionic Acid (*DL-*VI).* Crude amino acid (DL-V) (164.1 g, 0.456 mol) was mixed with glacial acetic acid (1.5 l) and acetic anhydride (60 ml) was added dropwise under stirring. After the clear solution was resulted, it was stirred for 6 hr at room temperature and then evaporated. The syrupy residue was taken up in a minimum quantity of ethyl acetate and the solution was chilled for 12 hr in a refrigerator. The resulting solid was collected by filtration. Yield, 161.0 g; mp 152—153 °C. Recrystallization from ethyl acetate gave an analytical sample, mp 156—157 °C.

Found: C, 56.11; H, 5.36; N, 6.88%. Calcd for $C_{19}H_{22}N_2O_6S$: C, 56.14; H, 5.46; N, 6.89%.

Resolution of DL-*2-Acetamino-3-(*N-*tosyl*-N-*benzyloxyamino)propionic Acid (*DL-*VI); 2-*N-*Acetamino-3-(*N-*tosyl*-N-*benzyloxyamino)propionic Acid Anilide (VII).* To the solution of the acetylamino acid (DL-VI) (20.3 g, 50 mmol) in 0.5M sodium hydroxide (300 ml) was added 0.5 M citric acid and the solution was adjusted to pH 7.3—7.35. The resultant clear solution was diluted to 500 ml and aniline (10 ml) was added together with papain (5 g) and L-cysteine hydrochloride monohydrate (5 g). The mixture was incubated at 50 °C for 48 hr. The precipitated crystals were collected, washed with 7% aqueous ammonia and water and dried. Recrystallization from *n*-propyl alcohol gave colorless crystals. Yield, 5.8 g (48.5%); mp 209—210 °C; $[\alpha]_D^{20}$ −110.2° (*c* 1, chloroform). Another recrystallization from the same solvent afforded an analytical sample, mp 211—212 °C and $[\alpha]_D^{23}$ −113.4° (*c* 1, chloroform).

Found: C, 62.05; H, 5.42; N, 8.79%. Calcd for $C_{25}H_{27}N_3O_5S$: C, 62.35; H, 5.65; N, 8.73%.

The above filtrate was adjusted to pH 1 with conc. hydrochloric acid and the deposited crystals were collected, washed with water and dried. Recrystallization from ethyl acetate gave colorless crystals, 7.45 g, mp 150—151 °C, which was identified DL-acetylamino acid (DL-VI) from the fact that this compound and the hydrolysis product, 2-amino-3-(*N*-tosyl-*N*-benzyloxyamino)propionic acid, were optically inactive and this compound gave the anilide (VII) under the above-described condition.

DL-*2-Amino-3-benzyloxyaminopropionic Acid (*DL-*VIII).* To a solution of phenol (54 g) and 36% hydrogen bromide-acetic acid (300 ml) in a glass-stoppered bottle, was added DL-V (64.5 g, 0.18 mol). After stirring for 84 hr at room temperature, the solution was evaporated to dryness at 45 °C. The residual crystals were triturated with ether and then dissolved in water (300 ml). The solution was adjusted to pH 7 with 7% aqueous ammonia under ice-cooling. After the removal of the precipitated crystals, the filtrate was concentrated to a small bulk and deposited crystals were collected. Yield, 20.55 g (54%); mp 206—210 °C (decomp.). An analytical sample was obtained by recrystallization from water, mp 210—211 °C (decomp.). IR; 3240 cm^{-1}. NMR (CF_3COOH): δ 4.46 (d, 2H), 5.12 (t, 1H), 5.53 (s, 2H), and 7.50 (s, 5H). Ninhydrin reaction was positive and triphenyltetrazolium negative.

Found: C, 57.16; H, 6.68; N, 13.54%. Calcd for $C_{10}H_{14}N_2O_3$: C, 57.13; H, 6.71; N, 13.33%.

DL-*2-Benzoylamino-3-benzyloxyaminopropionic Acid (*DL-*IX).*

a) To the suspension of DL-VIII (2.1 g, 10 mmol) in methanol (20 ml) were added 40% Triton B (4.7 ml) and *N*-benzoyloxy succinimide[12] (2.2 g, 10 mmol). After stirring for 12 hr at 50 °C, the solvent was removed and the residual oil was dissolved in water (30 ml). The water layer, after extracted with ethyl acetate, was acidified with conc. hydrochloric acid under cooling to pH 3.5. The resulting oil was scratched after standing in an ice box for 5 hr and then crystallized. Yield, 0.7 g (22.3%). Recrystallization from much water gave an analytical sample, mp 124—126 °C. NMR (CF_3COOH): 4.28 (2H), 5.32 (3H, benzylmethylene and α-methine protons), 7.49 and 7.68 (13H), and 8.16 (d, 1H, amide proton). Ninhydrin and triphenyltetrazolium test were negative.

Found: C, 65.02; H, 5.79; N, 8.93%. Calcd for $C_{17}H_{18}N_2O_4$: C, 64.95; H, 5.77; N, 8.91%.

b) The resulting oil was crystallized by adding a part of the product obtained as a) under stirring at room temperature. Yield, 64%; mp 143—147 °C. A part of the product was recrystallized from water to give an analytical sample, mp 147—149 °C. IR: 3370, 3250 cm^{-1}. NMR spectrum in trifluoroacetic acid was identical with that of the low-melting benzoylamino acid obtained as a). Ninhydrin test was negative. For the subsequent reaction this high-melting benzoylamino acid was used.

DL-*2-Benzoylamino-3-(*N-*benzoyl*-N-*benzyloxyamino)propionic Acid (*DL-*X).* To the stirred solution of DL-IX (6.28 g, 20 mmol) and *N*-methylmorpholine (2.22 g, 22 mmol) in ethyl acetate (100 ml) was added benzoyl chloride (3.08 g, 22 mmol) in ethyl acetate (20 ml) over 15 min at room temperature. The deposited crystals were collected after 12 hr and washed with ether and water. Yield, 6.84 g (81.5%); mp 175—177 °C. An analytical sample was obtained by recrystallization from ethyl acetate–ether, mp 182—183 °C.

Found: C, 68.53; H, 5.33; N, 6.79%. Calcd for $C_{24}H_{22}N_2O_5$: C, 68.89; H, 5.30; N, 6.70%.

DL-*2-Benzoylamino-3-(*N-*succinyl*-N-*benzyloxyamino)-propionic Acid.* To the stirred solution of the benzyloxyamino acid (DL-IX) (0.94 g, 3 mmol) and *N*-methylmorpholine (0.31 g, 3 mmol) in ethyl acetate (20 ml) was added succinic anhydride (0.3 g, 3 mmol). After 3 hr, water (20 ml) was added to the clear solution and the water layer was adjusted to pH 3 with 1 M hydrochloric acid. The precipitated oil was stored in an ice box for 12 hr and the resulting crystals were collected. Yield, 0.7 g (56.5%); mp 154—155 °C. Recrystallization from ethyl acetate–*n*-hexane gave an analytical sample, mp 153—154 °C. IR: 3300, 1710, 1650, 1525 cm^{-1}.

Found: C, 60.60; H, 5.24; N, 6.73%. Calcd for $C_{21}H_{22}N_2O_7$: C, 60.86; H, 5.35; N, 6.76%.

12) L. N. Nikolenko, V. N. Nezavibat'ko, and M. N. Semenova, *Zh. Obshch. Khim.*, **39**, 223 (1969).

DL-2-Benzoylamino-3-(N-benzoyl-N-hydroxyamino)propionic Acid (DL-XI). DL-X (4.18 g, 10 mmol) in methanol (130 ml) was hydrogenated in the presence of 5% palladium-charcoal (0.5 g). After 36 hr, the catalyst was removed and the filtrate was evaporated. The residual oil was dissolved in hot water and the crystalline debenzylation product was collected. Yield, 2.7 g (82.5%); mp 173—175 °C (lit,[7] mp 170 °C). Ferric chloride test was positive.

Found: C, 62.18; H, 4.90; N, 8.38%. Calcd for $C_{17}H_{16}N_2O_5$: C, 62.19; H, 4.91; N, 8.53%.

Resolution of DL-2-Benzoylamino-3-benzyloxyaminopropionic Acid (DL-IX); L-2-Benzoylamino-3-benzyloxyaminopropionic Acid Anilide (L-XII) and D-2-Benzoylamino-3-benzyloxyaminopropionic Acid(D-IX). To the suspension of DL-IX (9.42 g, 30 mmol) in 0.5 M sodium hydroxide (160 ml) was added 0.5 M citric acid and the solution was adjusted to pH 6.15. The resulting clear solution was diluted with water to 500 ml. Aniline (6 ml) was added to the solution together with papain (6 g) and L-cysteine hydrochloride monohydrate (6 g). The mixture was incubated at 38 °C. After 30 hr, the deposited L-anilide (L-XII) was collected, washed with water and recrystallized from *n*-propyl alcohol. Yield, 4.87 g (83.5%); mp 129—131 °C; $[\alpha]_D^{26}$ −108.9° (*c* 1, chloroform). IR: 3280, 1670 1630 cm^{-1}.

Found: C, 71.15; H, 6.03; N, 10.85%. Calcd for $C_{23}H_{23}N_3O_3$: C, 70.93; H, 5.95; N, 10.79%.

The above filtrate, combined with the washings was adjusted to pH 3.5 with conc. hydrochloric acid. The precipitated D-amino acid (D-IX) was collected, washed with water and recrystallized from ethyl acetate. Yield, 2.45 g (52%); mp 147—149 °C; $[\alpha]_D^{26}$ −18.2° (*c* 1, acetic acid).

Found: C, 64.89; H, 5.77; N, 8.93%. Calcd for $C_{17}H_{18}N_2O_4$: C, 64.95; H, 5.77; N, 8.91%.

L-2-Benzoylamino-3-(N-benzoyl-N-benzyloxyamino)propionic Acid Anilide (L-XIII). To the solution of the benzyloxyamino compound (L-XII) (3.89 g, 10 mmol) in pyridine (30 ml) was added benzoyl chloride (1.82 g, 13 mmol) under ice-cooling. After stirring for 12 hr at room temperature, the solvent was evaporated. The residual oil was taken up in ethyl acetate (100 ml) and washed with 1 M hydrochloric acid and water. The organic layer was dried over sodium sulfate and then evaporated. The residual crystals were recrystallized from *n*-propyl alcohol. Yield, 3.80 g (77%); mp 173—174 °C; $[\alpha]_D^{30}$ −82.6° (*c* 0.5, chloroform).

Found: C, 72.94; H, 5.45; N, 8.66%. Calcd for $C_{30}H_{27}N_3O_4$: C, 73.00; H, 5.51; N, 8.51%.

L-2-Benzoylamino-3-(N-benzoyl-N-hydroxyamino)propionic Acid Anilide (L-XIV). a) L-XIII (4.9 g, 5 mmol) in methanol (500 ml) was hydrogenated in the presence of 5% palladium-charcoal (0.5 g) at room temperature. After 72 hr, the catalyst was removed and the filtrate was evaporated. The residual crystals were recrystallized from *n*-propyl alcohol. Yield, 2.88 g (71.5%); mp 192—193 °C; $[\alpha]_D^{31}$ +55.2° (*c* 0.5, chloroform). IR: 3300, 3110, 1670, 1635 cm^{-1}. Ferric chloride test was positive.

Found: C, 68.19; H, 5.35; N, 10.72%. Calcd for $C_{23}H_{21}N_3O_4$: C, 68.47; H, 5.25; N, 10.42%.

When this reaction was performed in the presence of 10% palladium-charcoal at 40 °C, the deoxygenated product of L-XIV, L-2,3-dibenzoylaminopropionic acid anilide was obtained. Mp 257—258 °C (methanol). This compound gave a negative ferric chloride test and was sparingly soluble in chloroform, ethyl acetate, *n*-propyl alcohol and methanol.

Found: C, 70.78; H, 5.42; N, 10.60%. Calcd for $C_{23}H_{21}N_3O_3$: C, 71.30; H, 5.46; N, 10.85%.

b) To the solution of the benzoylamino acid (DL-XI) (1.64 g, 5 mmol) in 0.5 M sodium hydroxide (30 ml) was added 0.5 M citric acid and the solution was adjusted to pH 6.15. The resultant clear solution was diluted to *ca.* 60 ml and aniline (1 ml) was added together with papain (0.5 g) and L-cysteine hydrochloride monohydrate (0.5 g). The mixture was incubated at 38 °C for 30 hr. The deposited crystals were collected and washed with water and ether. Recrystallization from *n*-propyl alcohol with the aid of charcoal gave an analytical sample. Yield, 0.45 g (44.5%); mp 193—194 °C; $[\alpha]_D^{29}$ +57.6° (*c* 0.5, chloroform).

Found: C, 68.40; H, 5.30; N, 10.21%.

L-2-Amino-3-hydroxyaminopropionic Acid (L-II). The protected amino-hydroxyamino acid (L-XIV) (1.7 g, 5 mmol) was stirred with 6M hydrochloric acid (100 ml) at 90—95 °C for 8 hr. After standing at room temperature for 3 hr, the deposited crystals were removed and the filtrate, after extracted with ether, was evaporated. Water (20 ml) was added and evaporated. The residual oil was dissolved in water (5 ml) and neutralized with 7% aqueous ammonia under cooling. Ethanol was added until the solution was cloudy. The precipitated crystals were collected, after the solution was stored in an ice box for 5 hr. Yield, 260 mg (43.5%). An analytical sample was prepared by recrystallization from water–ethanol. Mp 160—161 °C (decomp.) in a sealed capillary in a liquid bath (lit,[7] mp 161—163 °C (decomp.)); $[\alpha]_D^{27}$ +12.6° (*c* 0.5, M hydrochloric acid) (lit,[7] $[\alpha]_D$ +15.7°) IR: Fig. 2 in the text. Triphenyltetrazolium and ninhydrin test were positive.

Found: C, 30.26; H, 6.63; N, 22.97%. Calcd for $C_3H_8N_2O_3$: C, 30.00; H, 6.71; N, 23.33%.

L-2-Amino-3-(N-nitroso-N-hydroxyamino)propionic Acid; Alanosine (L-I). To a stirred clear solution of the amino-hydroxyamino acid (L-II) (240 mg, 2 mmol) in M hydrochloric acid (2 ml), sodium nitrite (138 mg, 2 mmol) was slowly added at 0 °C. After 30 min, the precipitated crystals were collected and washed with ethanol and ether. Yield, 190 mg (63.7%); mp 196—198 °C (decomp.). An analytical sample was obtained by recrystallization from 1 M sodium hydroxide–acetic acid. Mp 196—197 °C (decomp.) (lit,[7] mp 190 °C (decomp.); $[\alpha]_D^{27}$ −43.2° (*c* 0.5, 0.1 M sodium hydroxide) (lit,[7] $[\alpha]_D$ −46.0°). IR: Fig. 3 in the text. Ninhydrin and ferric chloride test were positive and the characteristic reaction of the *N*-nitroso group[13] with sulphanilic acid and α-naphtylamine was also positive. Triphenyltetrazolium test was negative.

Found: C, 24.00; H, 4.95; N, 28.19%. Calcd for $C_3H_7N_3O_4$: C, 24.16; H, 4.73; N, 28.18%.

13) F. Feigl, "Spot Tests in Organic Analysis," Elsevier Pub. Co., London (1960), p. 167.

Photochemical Substitution of Ferrocene in Halogenated Hydrocarbon-Ethanol Solutions

Takeo AKIYAMA, Yoshiyuki HOSHI,* Satoshi GOTŌ,** and Akira SUGIMORI

Department of Chemistry, Faculty of Science and Technology, Sophia University, Kioi-cho 7, Chiyoda-ku, Tokyo 102

(Received January 20, 1973)

The photochemical substitution of ferrocene in several halogenated hydrocarbon–ethanol solutions was investigated. Ethoxycarbonyl, formyl, ethoxymethyl, benzyl and allyl groups were photochemically introduced into ferrocene in 25—53% yields by the UV-irradiation of ferrocene in carbon tetrachloride–, chloroform–, dichloromethane–, benzyl chloride–, and allyl bromide–ethanol solutions, respectively. The reactions proceeded effectively by the excitation of the charge transfer complexes formed between ferrocene and halogenated hydrocarbons.

Investigations have been made on the chemistry of ferrocene but only a few reports have appeared on the photochemical reactions of ferrocene. Nesmeyanov and his co-workers reported on the photochemical decomposition of several ferrocene derivatives.[1a-c]

van Riel *et al.* reported on the elimination of boric acid in the photolysis of ferroceneboronic acid in an aqueous alkaline solution.[2] Brand and Snedden observed a dissociative charge transfer absorption of ferrocene in a carbon tetrachloride solution.[3] Körner von Gustorf and his co-workers found that UV-irradiation of ferrocene in carbon tetrachloride gave ferrocenium tetrachloroferrate (III) almost quantitatively and they discussed the mechanism of its formation.[4] Spilners also reported the formation of ferrocenium tetrachloroferrate (III) in the photolysis of ferrocene in hexachlorocyclopentadiene.[5] Traverso and Scandola reported on the photochemical oxidation of ferrocene to ferrocenium ion in a carbon tetrachloride–ethanol solution, but they did not refer to the reaction product.[6] We reported the photochemical substitution of ferrocene in several organic halide–ethanol solutions.[7] The present paper deals with the photochemical introduction of ethoxycarbonyl, formyl, ethoxymethyl, benzyl, and allyl groups into ferrocene nucleus by UV-irradiation.

Experimental

Materials. Ferrocene was prepared from cyclopentadiene and iron(III) chloride by the method of Wilkinson *et al.*,[8] and was purified by column chromatography on silica gel. Mp 172—173 °C (lit,[9] 174 °C).

Carbon tetrachloride, chloroform and dichloromethane were purified by the method given in literature.[10] Benzyl chloride, benzal chloride, benzotrichloride, chlorobenzene, *n*-butyl chloride, *t*-butyl chloride, allyl chloride and allyl bromide were washed with aqueous alkaline solution and water, dried over calcium chloride and then distilled under reduced pressure just before use. Commercial *p*-nitrobenzyl chloride (Tokyo Kasei, Reagent Grade) was used without further purification.

Irradiation (General Procedure). A sample solution in a vessel equipped with gas inlet tube was irradiated internally with a high pressure mercury lamp (100 W high pressure mercury lamp, Ushio Denki, or 150 W high pressure mercury lamp, Taika Kogyo) with a quartz or a Pyrex jacket for cooling water, or a low pressure mercury lamp (120 W low pressure mercury lamp, Taika Kogyo) immersed in a sample solution. The reaction vessel was cooled externally by current water. During the course of irradiation nitrogen was bubbled through the solution. For irradiation of a comparatively small amount of solution, the sample solution in a quartz vessel was irradiated externally at the center of the spiral light source (16 W low pressure mercury lamp, Taika Kogyo) which was placed in a water bucket for cooling.

Separation of the Photoproducts (General Procedure). The irradiated solution was immediately washed with 0.1 M aqueous hydrochloric acid solution and extracted with *n*-hexane. The *n*-hexane solution was concentrated under reduced pressure below 45 °C and the residue was subjected to column chromatography on silica gel.

In the treatment of the reaction mixture from the photoreaction with less volatile chlorides such as benzyl, benzal and benzotrichloride, ether solution of anhydrous iron(III) chloride was added to the *n*-hexane solution to convert all the ferrocene and its derivatives into the corresponding ferrocenium salts. Ferrocenium salts and excess iron(III) chloride were extracted with water and then the ferrocenium salts were reconverted into ferrocene derivatives with sodium bisulfite. The reduced compounds were again extracted with *n*-hexane and dried over anhydrous sodium sulfate. After the solvent was removed, the residue was subjected to column chromatography on silica gel.

* Present Address: Fuji Photo Film Co., Ltd., Nakanuma 210, Minami-ashigara-cho, Ashigara-shi, Kanagawa.

** Present Address: Konishiroku Photo Industry Co., Ltd., Hino-shi, Sakura-cho 1, Tokyo.

1a) A. N. Nesmeyanov, V. A. Sazonova, V. I. Romanenko, N. A. Rodionova, and G. P. Zol'nikova, *Dokl. Akad. Nauk SSSR*, **155**, 1130 (1964); b) A. N. Nesmeyanov, *Pure Appl. Chem.*, **17**, 220 (1968); c) A. N. Nesmeyanov, V. A. Sazonova, V. I. Romanenko, V. N. Postov, G. P. Zol'nikova, V. A. Blonova, and R. M. Kalyanova, *Dokl. Akad. Nauk SSSR*, **173**, 589 (1967).

2) H. C. H. A. van Riel, F. C. Fischer, J. Lugtenburg, and E. Havinga, *Tetrahedron Lett.*, **1969**, 3085.

3) J. C. D. Brand and W. Snedden, *Trans. Faraday Soc.*, **53**, 894 (1957).

4) E. Körner von Gustorf, H. Köller, M.-J. Jun, and G. O. Schenck, *Chem. Eng. Tech.*, **35**, 591 (1963).

5) I. J. Spilners, *J. Organometal. Chem.*, **11**, 381 (1968).

6) O. Traverso and F. Scandola, *Inorg. Chim. Acta*, **4**, 493 (1970).

7) Y. Hoshi, T. Akiyama, and A. Sugimori, *Tetrahedron Lett.*, **1970**, 1485.

8) G. Wilkinson, F. A. Cotton, and J. M. Birmingham, *J. Inorg. Nucl. Chem.*, **2**, 95 (1956).

9) M. Rosenblum, "Chemistry of the Iron Group Metallocenes," Part I, Interscience Publishers, New York, N.Y. (1965), p. 33.

10) "Technique of Organic Chemistry," Vol. VII, ed. by A. Weissberger and E. S. Proskauer, Interscience Publishers, New York, N.Y. (1955), p. 409.

Identification of the Photoproducts. *Ethyl Ferrocenecarboxylate*: The compound was obtained in the photoreaction of ferrocene in carbon tetrachloride–ethanol solution. It was obtained as a yellow crystalline solid from the benzene fraction of column chromatography. Mp 58—61 °C. IR (KBr), 1690 cm^{-1} ($\nu_{C=O}$), 1100, 1040, 1000 cm^{-1} (mono substituted ferrocene). NMR (CCl_4), δ 4.70 (t), 2H (2,5H of the cyclopentadienyl ring of ferrocene); 4.22 (q), 2H (3,4H of the cyclopentadienyl ring of ferrocene); 4.10 (s), 5H (C_5H_5); 4.1 (q), 2H ($-CH_2-$); 1.32 (t), 3H ($-CH_3$).

Found: C, 58.0; H, 5.51%.

Formylferrocene: The compound was obtained in the photoreaction of ferrocene in chloroform–ethanol solution. Yellow orange substance was eluted with benzene on column chromatography. Mp 124—125 °C (lit,[11] 124.5 °C). IR spectrum was identical with that of the sample prepared by the method given in literature.[11]

Ethoxymethylferrocene: The compound was obtained in the photoreaction of ferrocene in dichloromethane–ethanol solution. It was eluted with *n*-hexane–benzene (9: 1) on column chromatography. Deep orange oil. Bp 112—113 °C/2 mmHg (lit,[12] 112—113.5 °C/2 mmHg). IR (direct), 2850, 1090, 920 cm^{-1} (ether), 1480, 1380 cm^{-1} ($-CH_2-$), 1100, 1020, 1000 cm^{-1} (mono substituted ferrocene). NMR (CCl_4), δ 4.11 (m), 6H ($C_5H_4-CH_2-$); 4.00 (s), 5H (C_5H_5); 3.39 (q), 2H ($-CH_2-$); 1.13 (t), 3H ($-CH_3$).

Found: C, 61.35; H, 6.39%.

1,1'-Diethoxymethylferrocene: The compound was obtained in the photoreaction of ferrocene in dichloromethane–ethanol solution. It was eluted with *n*-hexane–benzene (1: 1) after monoether had been eluted. Yellow oily substance. IR (direct), 2840, 1090, 930 cm^{-1} (ether), 1450, 1380 cm^{-1} ($-CH_2-$). The IR spectrum of this compound was nearly the same as that of monoether except for the peak at 1000 cm^{-1} which is characteristic of mono substituted ferrocene and ferrocene. NMR (CCl_4), δ 4.10 (m), 12H ($C_5H_4-CH_2-$); 3.96 (q), 4H ($-CH_2-$); 1.12 (t), 6H ($-CH_3$).

Found: C, 63.36; H, 7.14%. Calcd for $C_{16}H_{22}O_2Fe$: C, 63.59; H, 7.14%.

Benzylferrocene: The compound was obtained in the photoreaction of ferrocene in benzyl chloride–ethanol (20: 140 v/v) solution. It was obtained as a yellow orange crystalline solid (160 mg) from *n*-hexane–benzene (1: 1) fraction of column chromatography. Mp 75—76 °C (lit,[13] 74.5—76 °C). IR (KBr), 3020, 2920, 1603, 1495, 720, 699 cm^{-1} ($-CH_2-C_6H_5$), 1100, 1020, 1000 cm^{-1} (mono substituted ferrocene). NMR (CCl_4), δ 7.12 (s), 5H (C_6H_5-); 4.00 (s), 9H (C_5H_4-, C_5H_5); 3.64 (s), 2H ($-CH_2-$).

Found: C, 74.31; H, 6.39%.

Dibenzylferrocene: The compound was obtained as in the reaction described above. It was obtained as a yellow crystalline solid (50 mg) from benzene fraction of column chromatography, and was found to be a mixture of 1,2- and 1,3-dibenzylferrocene. IR (KBr), 3027, 2920, 1603, 1495, 700 cm^{-1} ($C_6H_5-CH_2-$), 1100, 1035, 1020, 1000, 940, 925, 920 cm^{-1} (homo annularly substituted ferrocene.[14]) NMR (CCl_4), δ 7.13 ($C_6H_5-CH_2-$); 7.05 ($C_6H_5-CH_2-$); 3.93 (s), (C_5H_5, C_5H_3-); 3.69 ($-CH_2-$); 3.60 ($-CH_2-$).

p-*Nitrobenzylferrocene*: The compound was obtained in the photoreaction of ferrocene with *p*-nitrobenzyl chloride in ethanol. It was obtained as a brown red substance (3.0 mg) from benzene fraction. IR (KBr), 2900, 1603, 1590, 1510, 1340, 710 cm^{-1} (p-$NO_2C_6H_4-CH_2-$), 1100, 1020, 1000 cm^{-1} (mono substituted ferrocene).

Phenylferrocene: The compound was obtained in the photoreaction of ferrocene in chlorobenzene–ethanol (10:110 v/v) solution. It was obtained as an orange crystalline solid (15 mg) from *n*-hexane–benzene (1: 1) fraction of column chromatography. IR (KBr), 3027, 1603, 1510, 690 cm^{-1} (C_6H_5-), 3080, 1100, 1020, 1000 cm^{-1} (mono substituted ferrocene). NMR (CCl_4), δ 7.20 (m), 5H (C_6H_5-); 4.50 (t), 2H (2,5H of the cyclopentadienyl ring of ferrocene); 4.16 (t), 2H (3,4H of the cyclopentadienyl ring of ferrocene); 3.90 (s), 5H (C_5H_5).

Found: C, 73.72; H, 5.20%.

Allylferrocene: The compound was obtained in the photoreaction of ferrocene in allyl bromide–ethanol (30: 250 v/v) solution. It was obtained as a dark orange liquid substance (900 mg) from *n*-hexane–benzene (2: 1) fraction of column chromatography. IR (direct), 3080, 3010, 2910, 1640, 1430, 1410 cm^{-1} (allyl group), 1100, 1020, 1000 cm^{-1} (mono substituted ferrocene). NMR (CCl_4), δ 5.70 (m), 1H ($-C\underline{H}=CH_2$); 4.90 (m), 2H ($-CH=C\underline{H}_2$); 3.96, 9H (C_5H_4-, C_5H_5); 2.98 (d), ($-CH_2-$).

Measurement. The electronic absorption spectra were measured with a Hitachi Model 124 UV–VS spectrophotometer. The NMR and IR spectra were obtained on a JEOL H-60 NMR spectrometer and a Hitachi Model 215 grating infrared spectrophotometer, respectively.

Results and Discussion

Although the UV-irradiation of ferrocene in carbon tetrachloride gave blue-gray precipitate of ferrocenium tetrachloroferrate (III) as was reported by Körner von Gustorf and his co-workers,[4] the UV-irradiation of ferrocene in a carbon tetrachloride–ethanol solution in the atmosphere of nitrogen gave ethyl ferrocenecarboxylate, a substitution product. Similar reactions were observed in the UV-irradiation of ferrocene in chloroform– and dichloromethane–ethanol solutions. Results of the reactions in these solvents are summarized in Table 1. The photoreactions can be generalized as follows.

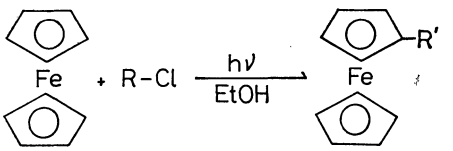

R=$-CCl_3$ R'=$-CO_2Et$
R=$-CHCl_2$ R'=$-CHO$
R=$-CH_2Cl$ R'=$-CH_2OEt$

These reactions are formally the substitution at the cyclopentadienyl ring of ferrocene by halomethyl radicals formed by the fission of R–Cl bond of halomethanes, followed by the ethanolysis of halomethyl groups. This type of reaction affords a new route for the introduction of ethoxycarbonyl, formyl and ethoxymethyl groups into ferrocene ring.

However, it was not effective for alkyl and aryl monochlorides such as *t*-butyl chloride and chlorobenzene. Of phenyl substituted chloromethanes,

11) P. J. Graham, R. V. Lindsey, G. W. Parshall, M. L. Peterson, and G. M. Whitman, *J. Amer. Chem. Soc.*, **79**, 3416 (1957).

12) A. N. Nesmeyanov, E. G. Perevalova, and Yu. A. Ustynyuk, *Dokl. Akad. Nauk SSSR*, **133**, 1105 (1960).

13) A. L. J. Beckwith and R. J. Leydon, *Tetrahedron Lett.*, **1963**, 385. M. D. Rausch, M. Vogel, and H. Rosenberg, *J. Org. Chem.*, **22**, 903 (1957).

14) Ref. (9), p. 39.

Table 1. Photochemical reactions of ferrocene in halogenated hydrocarbon–ethanol 1:1 solutions

Run	FcH[a] (g)	Solvent (ml)	Light (W)	FcH reacted (%)	Product	Yield[b] (%)
1	3.7	CCl_4–EtOH (280)	LP(16)[c] 48 hr	57	FcCOOEt	20
2	3.0	CCl_4–EtOH (140)	HP(150)[d] 8 hr	35	FcCOOEt	38
3	1.9	CCl_4–EtOH (400)	HPpy(100)[e] 7 hr	34	FcCOOEt	32
4	3.0	$CHCl_3$–EtOH (220)	LP(120) 7 hr	84	FcCHO	42
5	2.0	$CHCl_3$–EtOH (140)	HP(150) 5 hr	35	FcCHO	trace[f]
6	4.0	CH_2Cl_2–EtOH (220)	LP(120) 7 hr	72	$FcCH_2OEt$ $(C_5H_4CH_2OEt)_2Fe$[g]	43 36
7	1.0	CH_2Cl_2–EtOH (140)	HP(150) 3 hr	9	$FcCH_2OEt$ $(C_5H_4CH_2OEt)_2Fe$	53 12

a) Fc: $C_5H_5FeC_5H_4$–.
b) Yield based on unrecovered ferrocene.
c) LP: Low pressure mercury lamp.
d) HP: High pressure mercury lamp.
e) HPpy: High pressure mercury lamp with a Pyrex filter.
f) Formylferrocene is sensitive to 313 nm light.
g) 1,1′-Diethoxymethylferrocene.

Table 2. Photochemical reactions of ferrocene in halogenated hydrocarbon–ethanol solutions

Run	FcH[a] (g)	R–Cl (ml)	Light (W)	Time (hr)	FcH reacted (%)	Product	Yield[b] (%)
8	1.9	*n*-BuCl (10)	LP[c] (16)	9	—	$Fc(CH_2)_3CH_3$	trace
9	1.0	*t*-BuCl (15)	HP[d] (100)	40	7	none	
10	1.9	PhCl (10)	LP (120)	8	—	FcC_6H_5	trace
11	1.0	PhCl (10)	HPpy[e] (100)	20	35	FcC_6H_5	3.0
12	2.0	$PhCH_2Cl$ (20)	LP (16)	20	65	$FcCH_2C_6H_5$ Disubstituted	6.4 1.2
13	1.0	$PhCH_2Cl$ (20)	HPpy (100)	20	42	$FcCH_2C_6H_5$ Disubstituted	25.6 6.0
14	1.0	$PhCHCl_2$ (20)	LP (16)	45	67.5	$FcCH_2C_6H_5$	trace
15	1.0	$PhCHCl_2$ (10)	HPpy (100)	20	34	$FcCH_2C_6H_5$	trace
16	2.0	$PhCHCl_2$ (20)	HP (150)	16	45.5	$FcCH_2C_6H_5$	4.4
17	2.0	$PhCCl_3$ (20)	LP (120)	5	60.5	none	
18	2.0	$PhCCl_3$ (20)	HP (150)	16	65.0	none	
19	2.0	*p*-$NO_2C_6H_4CH_2Cl$ (3g)	LP (120)	6	6.5	*p*-$NO_2C_6H_4CH_2Fc$	1.2
20	2.0	*p*-$NO_2C_6H_4CH_2Cl$ (5g)	HP (150)	16	4.5	none	
21	2.6	$CH_2=CHCH_2Br$ (30)	LP (16)	14.5	72.5	$FcCH_2CH=CH_2$	39.1
22	2.0	$CH_2=CHCH_2Br$ (80)	HPpy (100)	20	21	$FcCH_2CH=CH_2$	45
23	1.3	$CH_2=CHCH_2Cl$ (30)	HP (150)	40	—	$FcCH_2CH=CH_2$	trace

a) Fc: $C_5H_5FeC_5H_4$–. b) Yield based on unrecovered ferrocene. c) LP: Low pressure mercury lamp. d) HP: High pressure mercury lamp. e) HPpy: High pressure mercury lamp with a Pyrex filter.

benzyl chloride gave photoproducts in considerable yields in the photoreaction with ferrocene, but benzal chloride and benzotrichloride gave only a trace of the substitution products. The results of the photoreactions of ferrocene with chlorides other than chloromethanes are listed in Table 2.

In the photoreactions of ferrocene with halides listed in Table 2, the yields of the photoproducts are lower than those shown in Table 1, except for allyl bromide.

In ferrocene–dichloromethane–ethanol system and ferrocene–benzyl chloride–ethanol system, disubstituted ferrocenes were obtained. However, the yields of the substitution products were lower in the latter system. This type of photoreaction is closely related to the formation of charge transfer complexes between ferrocene and halogenated hydrocarbons.

Brand and Snedden reported that the charge transfer absorption of ferrocene at 300—340 nm in several halogenated hydrocarbon solvents can be attributed to the electron transfer from ferrocene to the solvents.[3] The UV-spectra of ferrocene in ethanol and halogenated hydrocarbon–ethanol solutions are shown in Figs. 1 and 2. The UV-spectra of ferrocene in carbon tetrachloride, chloroform, dichloromethane, allyl bromide, ben-

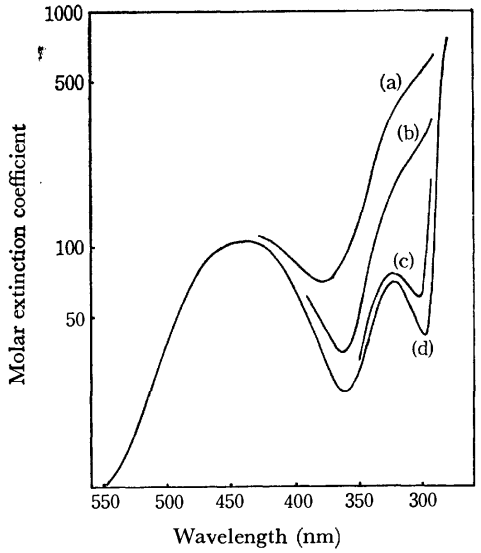

Fig. 1. UV-Spectra of ferrocene in halogenated hydrocarbon–ethanol solutions
(a) Ferrocene (5×10^{-3}mol/l) in carbon tetrachloride–ethanol (1: 1 v/v) solution.
(b) Ferrocene (5×10^{-3}mol/l) in allyl bromide–ethanol (1: 1 v/v) solution.
(c) Ferrocene (5×10^{-3}mol/l) in dichloromethane.
(d) Ferrocene (5×10^{-3}mol/l) in ethanol.
* The UV-spectra of ferrocene (5×10^{-3}mol/l) in chloroform–ethanol (1: 1 v/v) solution was nearly the same as those shown in (b). The UV-spectra of ferrocene (5×10^{-3}mol/l) in allyl chloride–ethanol (3.5×10^{-2}mol/l in ethanol) solution was nearly the same as those shown in (d).

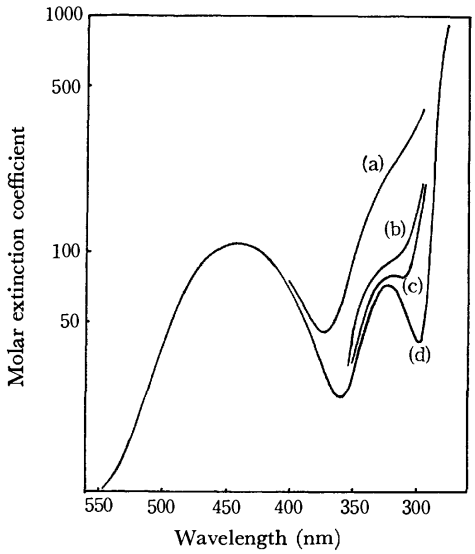

Fig. 2. UV-Spectra of ferrocene in halogenated hydrocarbon–ethanol solutions.
(a) Ferrocene (5×10^{-3}mol/l) in benzyl chloride–ethanol (7.0×10^{-1}mol/l in ethanol) solution.
(b) Ferrocene (5×10^{-3}mol/l) in benzal chloride–ethanol (5.5×10^{-1}mol/l in ethanol) solution.
(c) Ferrocene (5×10^{-3}mol/l) in benzotrichloride–ethanol (6.8×10^{-1}mol/l) solution.
(d) Ferrocene (5×10^{-3}mol/l) in ethanol.
* The UV-spectra of ferrocene (5×10^{-3}mol/l) in *n*-butyl chloride– and *t*-butyl chloride–ethanol solutions (1: 1 v/v) were nearly the same as those shown in (d). In chlorobenzene–ethanol (3.5×10^{-2}mol/l), it is similar to that in ethanol.

zyl chloride, benzal chloride, benzotrichloride and *p*-nitrobenzyl chloride showed the charge transfer absorption at 300—380 nm, but other chlorides, such as *n*-butyl chloride, *t*-butyl chloride, allyl chloride and chlorobenzene showed no charge transfer absorption.

As seen from Tables 1 and 2 and Fig. 1, the system showing charge transfer absorption afforded the photoproducts in higher yields in the irradiation with a high pressure mercury lamp (runs 1—7, Table 1, and runs 12—16, 21, 22, Table 2) than in that with a low pressure mercury lamp. Therefore, the charge transfer complex between ferrocene and halogenated hydrocarbons thus plays an important role.

In the ferrocene–chloroform–ethanol system, the low yield of the photoproducts is due to its sensitivity to 313 nm light which causes secondary decomposition.

In the ferrocene–*p*-nitrobenzyl chloride–ethanol system, the observed charge transfer absorption might be due to the interaction between ferrocene and nitro group, since the formation of ferrocenium ion was not observed and the percentage of loss of ferrocene and that of the product yield were extremely low. In the ferrocene–benzotrichloride–ethanol system, despite the high percentage of loss of ferrocene in irradiation with both high and low pressure mercury lamps, absence of the photoproduct might be due to the photo-sensitivity of benzotrichloride itself. The absorption of incident light by benzyl chloride, benzal chloride and benzotrichloride in the 300—340 nm region causes decomposition of the chlorides in irradiation with a high pressure mercury lamp. The high percentage of loss of ferrocene (runs 12—18, Table 2) might be due to the decomposition of ferrocene by the attack of chlorine atom produced by direct decomposition of the chlorides.

The Mechanism of Photo-substitution of Ferrocene in Haloalkane-Ethanol Solutions

Takeo AKIYAMA, Akira SUGIMORI, and Horst HERMANN*

Department of Chemistry, Faculty of Science and Technology, Sophia University
Kioi-cho 7, Chiyoda-ku, Tokyo 102

**Max Planck-Institut für Kohlenforschung, Abteilung Strahlenchemie, Mülheim a.d. Ruhr, Bundesrepublik Deutschland*

(Received January 20, 1973)

The mechanism of photo-substitution of ferrocene in haloalkane–ethanol solutions was investigated by the flash photolysis technique and other chemical methods mainly on the ferrocene–carbon tetrachloride–ethanol system. The photoreaction is initiated by the excitation of charge transfer state (electron transfer from ferrocene to carbon tetrachloride). In the absence of ethanol, CT-excitation leads to the decomposition of ferrocene to $FeCl_3$ with first order reaction kinetics of $k=(1.6\pm0.5)\times10^5\ s^{-1}$. The formation of $FeCl_3$ was inhibited by ethanol effectively to give ethyl ferrocenecarboxylate. Diethylamine quenched the formation of $FeCl_3$, whereas dimethyl sulfoxide, a stronger base than ethanol, is a less effective quencher than ethanol. These facts suggest that the most important role of ethanol is to ethanolyse trichloromethylferrocene, which otherwise decomposes to $FeCl_3$.

The solutions of ferrocene in haloalkanes are photochemically interesting systems. Brand and Snedden observed a CT-absorption ("dissociative charge transfer band") in ferrocene–haloalkane systems.[1] Körner von Gustorf and his co-workers reported that the irradiation of the system leads to the oxidation of ferrocene, to give $[Fe(C_5H_5)_2]^+[FeCl_4]^-$.[2]

Hoshi *et al.* and Akiyama *et al.* observed photochemical substitution of ferrocene in ferrocene–haloalkane–ethanol systems.[3] Ethyl ferrocenecarboxylate, ferrocenecarboxaldehyde and ethoxymethylferrocene (accompanied by di(ethoxymethyl)ferrocene) were isolated after the irradiation of ferrocene in carbon tetrachloride–ethanol, chloroform–ethanol and dichloromethane–ethanol solutions, respectively.

In order to elucidate the mechanism of photosubstitution and especially to clarify the role of ethanol, flash photolysis and several chemical methods were applied to ferrocene–carbon tetrachloride systems containing ethanol and other bases.

Experimental

Materials. For the flash photolysis study, commercial ferrocene (Rheinelbe Bergbau A.G.) was recrystallized twice from ethanol, mp 174—175 °C.

Spectro-grade carbon tetrachloride, acetonitrile and dimethyl sulfoxide, analytical-grade ethanol, dioxane and methanol and reagent-grade diethylamine (Merck A.G.) were used without further purification.

The materials used for other investigations by chemical methods were the same as described elsewhere.[3]

Flash Photolysis. The argon flash tube employed for photolysis discharged 50% of the total energy within 1.4 μs and 90% within 4.2 μs. The energy for a flash was about 10 J. The spectro-flash was similar except in energy. The spectral separation of the monitoring light was achieved by passing it through a Carl Zeiss double monochrometer equipped with a quartz prism. The light intensity was recorded photographically. The intensity of light was calibrated with standard filters. For kinetic measurements a monitoring flash lamp (G. 431 Vakuumtechnik, Erlangen) was used. The intensity of the transmitted light was followed with an oscillograph.

Solutions of ferrocene ($2—5\times10^{-4}$ mol/l) in ethanol or carbon tetrachloride containing various additives were flash photolyzed in a suprasil cell (50 mm in length and 7 mm in diameter). When necessary, the solution was deoxygenated by bubbling argon for 30 minutes.

Wavelength Dependence of Photoreaction. Monochromatic light of 436, 366, and 313 nm was obtained by passing the light from a high pressure 150 W mercury lamp (Ushio Denki Co.) through interference filters (Carl Zeiss monochromatic filter; M-436, M-365, and M-313). Light of 254 nm was obtained by passing the light from a low pressure mercury lamp (Ushio Denki Co.) through a filter solution containing potassium iodide and iodine.[4]

A deaerated ferrocene solution (279 mg ferrocene in 30 ml carbon tetrachloride–ethanol 1 : 1 v/v) was irradiated in a quartz vessel by monochromatic light while being stirred continuously with a magnetic stirrer. The quantities of ethyl ferrocenecarboxylate and ferrocene were determined gas chromatographically (column; SE-30 on Diasolid L of Gaschro-kogyo Co.; temperature, 176 °C) with a Perkin-Elmer gas chromatograph Model F-6.

Actinometry was performed with a potassium trioxalatoiron(III) actinometer.[5]

Results and Discussion

Excited State Responsible for Photoreaction. The absorption spectra of ferrocene in ethanol, in carbon

1) J. C. D. Brand and W. Snedden, *Trans. Faraday Soc.*, **53**, 894 (1957).

2) E. Körner von Gustorf, H. Köller, M.-J. Jun, and G. O. Schenck, *Chem. Eng. Tech.*, **35**, 591 (1963). E. Körner von Gustorf and F.-W. Grevels, *Fortschr. Chem. Forsch.*, **13**, 365 (1969).

3) Y. Hoshi, T. Akiyama, and A. Sugimori, *Tetrahedron Lett.*, **1970**, 1485., T. Akiyama, Y. Hoshi, S. Goto, and A. Sugimori, This Bulletin, **46**, 1851 (1973).

4) *Cf.* In a study by UV-spectra, Traverso and Scandola reported the formation of ferrocinium ions in a ferrocene–carbon tetrachloride–ethanol system. O. Traverso and F. Scandola, *Inorg. Chim. Acta*, **4**, 493 (1970).

4) J. G. Calvert and J. N. Pitts, "Photochemistry," John Wiley & Sons, New York, N.Y. (1966), p. 729.

5) *ibid.*, p. 783.

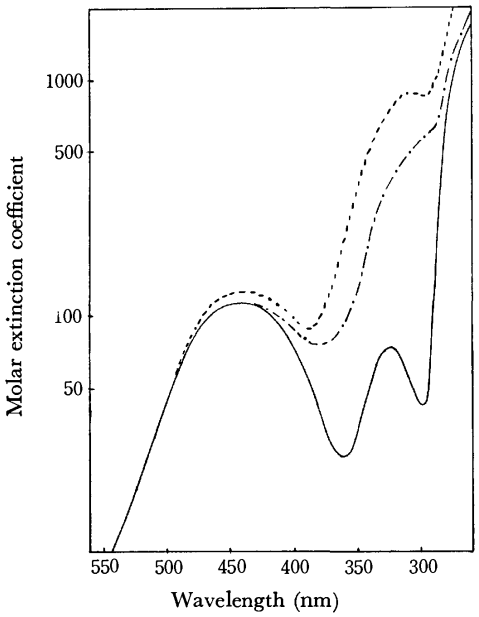

Fig. 1. UV-Spectra of ferrocene (5×10^{-3}mol/l)
—— in ethanol
- - - in carbon tetrachloride
—·— in carbon tetrachloride–Ethanol (1: 1 in volume)

tetrachloride and in carbon tetrachloride–ethanol are shown in Fig. 1.[1] Scott and Becker assigned the absorption band of ferrocene at 440 nm to d-d* transition and that at 325 nm to 3d-MO*, ring MO–MO* or symmetry forbidden π-π* transition. According to them the absorption at shorter wavelength is due to π-π* or n-π* transition.[6] The absorption at 307 nm observed in carbon tetrachloride solution is due to the charge transfer excitation.[1]

Table 1. Quantum yields in the photoreaction of ferrocene in a carbon tetrachloride–ethanol solution at various wavelengths

Wavelength (nm)	Quantum yield of ethyl ferrocenecarboxylate	Quantum yield of the decomposition of ferrocene
254	0.13	0.28
313	0.13	0.18
366	0.11	0.14
436	0.00	0.00

Wavelength dependence of the photo-substitution shown in Table 1 indicates that the excited state formed by d-d* absorption leads to no photoreaction, while the excitation of charge transfer state efficiently affords ethyl ferrocenecarboxylate. The excitation by light of a shorter wavelength brings about an increase in side reactions. Therefore, the photo-substitution arises from the electron transfer from ferrocene to carbon tetrachloride.

Reaction Succeeding CT-Excitation. It is known that the CT-excitation gives ferrocenium tetrachloroferrate (III) in the absence of ethanol.[2] However, the substitution product was obtained when ethanol is added to the above system. The problem is to clarify the role of ethanol which inhibits the decomposition of ferrocene and leads to the formation of ethyl ferrocenecarboxylate.

As reported by Brand and Snedden[1] the CT-excitation yields a radical pair.

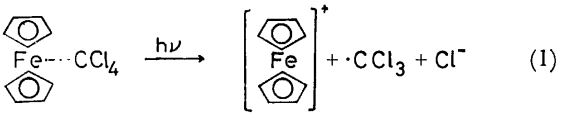

(1)

According to Beckwith and Leydon[7] ferrocenium cations are reactive toward free radicals, in contrast with ferrocene. Therefore, a reaction of the trichloromethyl radical with ferrocenium cation is plausible.

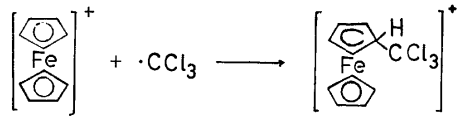

(2)

The reaction within a solvent cage would be important. The following sequence of reactions would not play an important role in this photoreaction.

(i) The formation of ferrocenium tetrachloroferrate (III), the end product in the absence of ethanol.[2]

(ii) The reaction of ferrocenium tetrachloroferrate (III) with trichloromethyl radicals.

The reasons are:

(1) The formation of ethyl ferrocenecarboxylate is linear with respect to the light absorbed (Fig. 2), excluding a two step reaction.

(2) The UV-irradiation of ferrocenium tetrachloroferrate (III) in carbon tetrachloride–ethanol solution gave no substitution product, but ferrocene, a reduction product. In this case, we obtained a comparatively large amount of hexachloroethane, the dimerization product of trichloromethyl radicals. This indicates that ferrocenium tetrachloroferrate(III) itself has a different reactivity from normal ferrocenium ions and is unreactive toward trichloromethyl radicals.

In order to complete the substitution reaction, two reaction steps are necessary, namely;

(i) proton elimination

(ii) alcoholysis of the trichloromethyl group

The results of flash photolysis are informative. Flash

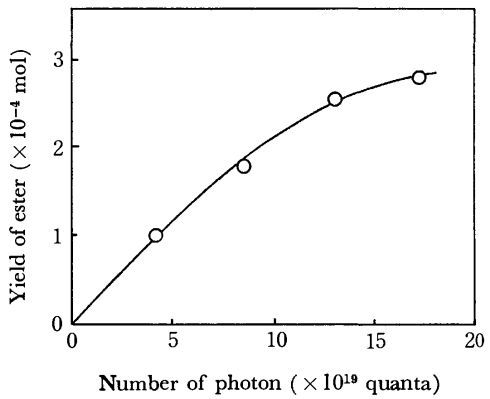

Fig. 2. The plot of the yield of ethyl ferrocenecarboxylate against quanta absorbed (at 313 nm).

6) D. R. Scott and R. S. Becker, *J. Chem. Phys.*, **35**, 516 (1961).

7) A. L. J. Beckwith and R. J. Leydon, *Tetrahedron Lett.*, **1963**, 385.

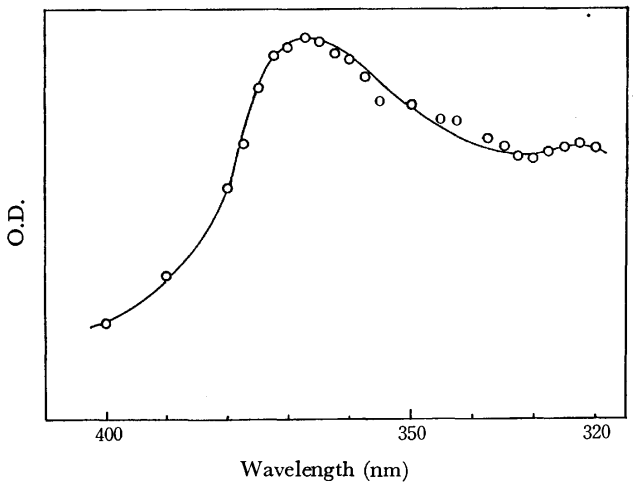

Fig. 3a. UV-Spectra of the product formed in the flash photolysis of ferrocene–CCl_4 system.

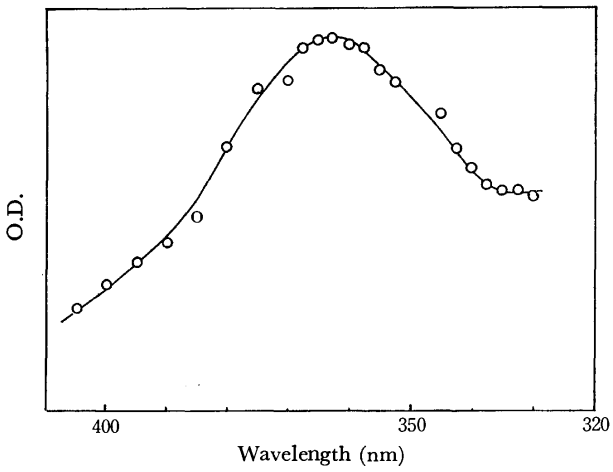

Fig. 3b. UV-Spectra of the product formed in the flash photolysis of ferrocene–CCl_4–DMSO system.

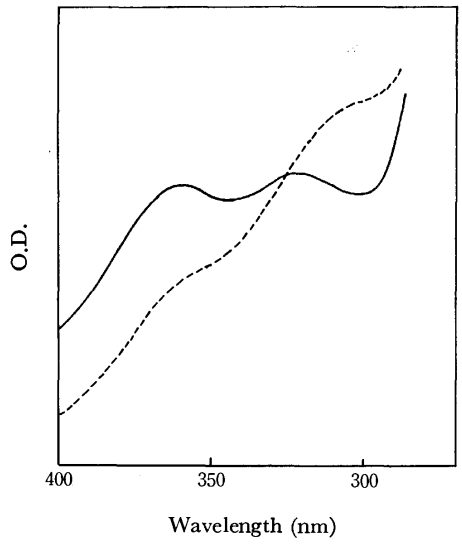

Fig. 3c. UV-Spectra of iron(III) chloride (——) and ferrocenium tetrachloroferrate (III) (- - -) in carbon tetrachloride–DMSO (DMSO 0.3 mol/l).

photolysis of ferrocene in an ethanol solution gave rise no spectral change, but that in carbon tetrachloride showed new absorption bands at 370 and 325 nm with a delay of $\sim\mu$s after the photolysis flash, though no transient absorption was observed. The absorption spectra are shown in Fig. 3a. They agree with those of iron(III) chloride (λ_{max} of the UV-spectra of iron(III) chloride are 375 and 325 nm in carbon tetrachloride solution.). The spectra of the product in carbon tetrachloride containing dimethyl sulfoxide (0.3 mol/l) also agree qualitatively with those of iron(III) chloride and not with those of ferrocenium tetrachloroferrate(III), the other possible product (Figs. 3b and 3c).

The formation of iron(III) chloride was completed in about 10 μs. An example of the intensity change of the transmitted light at 370 nm through a ferrocene solution with and without photolysis flash is shown in Fig. 4.

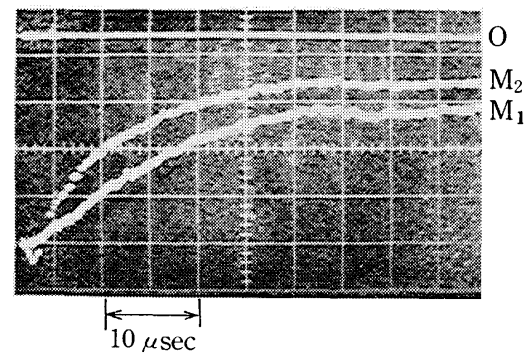

Fig. 4. The change in the intensity of the transmitted light at 370 nm.
M_1: Without photolysis flash
M_2: After photolysis flash

Kinetic analysis of the formation of iron(III) chloride is made in the following way. M_1 and M_2 are the intensities of the transmitted light without and with a photolysis flash, respectively. M_2 is smaller than M_1 due to the formation of the product. For the kinetic analysis, we should know the initial concentration of a precursor. However, the value could not be obtained in this experiment. We assume that the concentration of the precursor is equal (or proportional) to the end concentration of iron(III) chloride. Thus, we obtain the following equation for first order reaction kinetics.

$$k_1 t = \ln \frac{[FeCl_3]_\infty}{[FeCl_3]_\infty - [FeCl_3]_t}$$

where k_1 is the rate constant for a first order reaction, and $[FeCl_3]_\infty$ and $[FeCl_3]_t$ are the concentrations of iron(III) chloride after the completion of the reaction and at time t, respectively.

The expression in terms of the intensities of the transmitted light is

$$k_1 t = \ln \frac{\log (M_1/M_2)_\infty}{\log (M_1/M_2)_\infty - \log (M_1/M_2)_t}$$

In the same way, we obtain the expression for second order kinetics:

$$k_2 t = \frac{\log (M_1/M_2)_t}{\log (M_1/M_2)_\infty \{\log (M_1/M_2)_\infty - \log (M_1/M_2)_t\}}$$

Table 2. Effects of additives on the formation of $FeCl_3$ in the flash photolysis of ferrocene–CCl_4 system

Concentration of Ferrocene: 2×10^{-4} mol/l
Energy of one photolysis flash: ~10J
Cell: 50 mm in length

Additive	Concentration (mol/l)	Atmosphere	Increase in the extinction at 370 nm after the flash
—	—	Ar	0.32
Methanol	0.3	Ar	0.04
Dioxane	0.23	Ar	0.28
	1.2	Ar	0.30
Acetonitrile	1.9	Ar	0.16
—	—	Air	0.40
Ethanol	3.4	Air	0.33
Methanol	0.3	Air	0.42
Acetonitrile	1.9	Air	0.56
Dimethyl sulfoxide	4.2	Air	0.30
Dioxane	1.2	Air	0.61
Diethylamine	0.01	Air	0.10

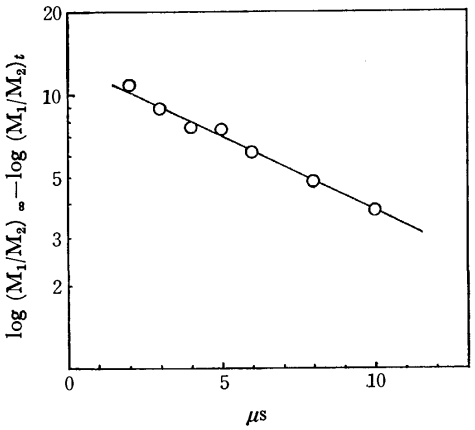

Fig. 5. First order kinetics for the formation of the product (λ_{max}=370 nm) in the flash photolysis of ferrocene–CCl_4 system.

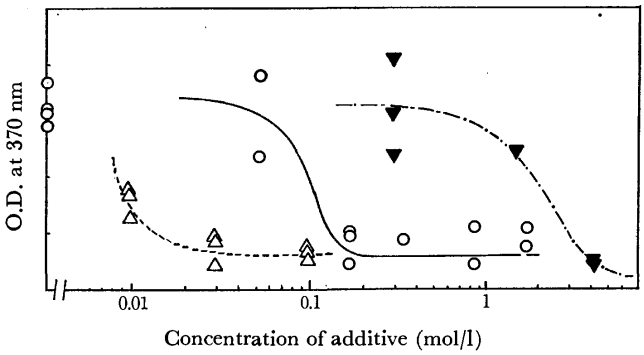

Fig. 6. Effects of additives on the formation of $FeCl_3$
△---△: Diethylamine, -○—○-: Ethanol,
▼---▼: Dimethyl sulfoxide.

The experimental data fit first order reaction kinetics as is thown in Fig. 5. The average first order rate constant is: $k_1=(1.6\pm0.5)\times10^5\ s^{-1}$.

The formation of iron(III) chloride was quenched by several additives. Figure 6 shows the quenching by ethanol, diethylamine and dimethyl sulfoxide in the function of the concentration of the additives. The quenching effect of ethanol is remarkable above 10^{-1} mol/l of ethanol concentration. Diethylamine is more effective and dimethyl sulfoxide less effective than ethanol. The quenching effect of other additives are summarized semi-quantitatively in Table 2.

If the most important role of ethanol in the photoethoxycarbonylation were to abstract the proton according to Eq. (3), the basicity of the proton acceptor would affect the quenching effect.

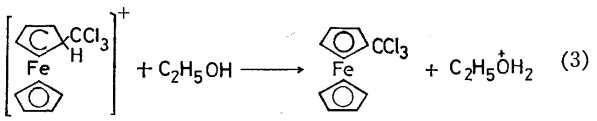

Dimethyl sulfoxide is a stronger base (pK_a of the conjugate acid of dimethyl sulfoxide is 0[8]) than alcohol (pK_a of the conjugate acid of methanol is equal to −2.[8]). The quenching effect of dimethyl sulfoxide is, however, lower by one order than ethanol and methanol. This indicates that the proton abstraction step does not determine the fate of the photoreaction.

Alcohols can solvolyze trichloromethylferrocene to give a stable product, namely, the corresponding ester of ferrocenecarboxylic acid, but dimethyl sulfoxide can not perform such a reaction. The difference in quenching effect would arise from this process.

An abnormaly high rate of solvolysis was reported for α-ferrocenylethyl chloride by Hill.[9] The solvolysis is of first order with respect to the chloride. The rate constant in ethanol (40%)–ethyl ether (60%) solution at −42.8 °C and the activation energy of the reaction are $8.9\times10^{-3}\ s^{-1}$ and 10.9 kcal/mol, respectively. Hill ascribed the high rate of solvolysis to the participation of the iron atom of ferrocene.

8) E. M. Arnett, "Progress of Physical Organic Chemistry," Vol. 1, ed. by S. G. Cohen, A. Streitwieser, and R. W. Taft, Interscience Publishers, New York, N. Y. (1963), p. 223.
9) E. A. Hill, *J. Org. Chem.*, **28**, 3586 (1963).

If the solvolysis of trichloromethylferrocene is an S_N1 type reaction, the following sequence of reactions should be considered.

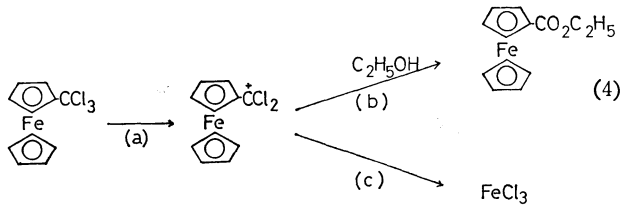

Where (a) is the rate determining process and (b) and (c) are competing processes. If this is the ca, the rate constant for process (a) should be 1.6×10^5 sec^{-1} according to our experiment. This value is large compared with that for α-ferrocenylethyl chloride (the calculated rate constant for α-ferrocenylethyl chloride at 30 °C from the data of Hill is 2.8 s^{-1}). An alternative reaction mechanism would be S_N2. We have no means of distinguishing which of these two processes actually takes place.

The presence of oxygen affects to a great extent the photochemical behavior of ferrocene, the increase in absorption at ~370 nm being greater. Alcohols hardly inhibit the increase in absorption. The shape of the spectra remained the same. This finding corresponds to the fact that the photo-substitution proceeds with no side reactions only under anaerobic conditions.

The reaction mechanism of the photo-substitution is summarized in Scheme 1.

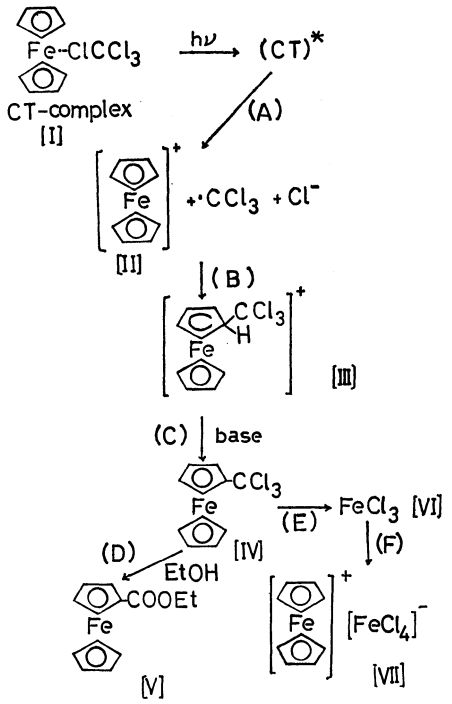

Scheme 1.

The authors wish to thank Prof. D. Schulte-Frohlinde, Dr. G. Koltzenburg and Dr. E. Körner von Gustorf of Max Planck-Institut für Kohlenforschung for their helpful discussions. They are very grateful to Frau Ch. Kuling for her assistance in experiments. A. Sugimori thanks the Alexander von Humboldt-Stiftung for a stipend.

Reaction of Alkylbenzene. IX.[1] A Study of the Reaction of Methylbenzenes under the Influence of Aluminum Chloride-Hydrogen Chloride by Means of NMR

Yoshihide Okami, Noboru Otani, Daigo Katoh, Sawako Hamanaka, and Masaya Ogawa

Department of Applied Chemistry, Faculty of Engineering, Kansai University, Senriyama, Suita, Osaka 564

(Received April 3, 1972)

The ^{1}H and ^{13}C NMR spectra of the complex layers obtained by the reaction of several methylbenzenes with aluminum chloride were measured at room temperature, and the proton exchanges were investigated. The ring ^{1}H signal shifted to a higher field as a result of fusion with the signal of the aliphatic CH_2 group of the methylbenzenonium ion, which resulted from the protonation to ring carbons. Thus, the proton exchange is considered to proceed among the ring carbons of aromatic hydrocarbon and its benzenonium ion in the complex layer intermolecularly as well as intramolecularly. This finding agrees with the results obtained from the ^{13}C NMR spectra of the complexes. The ^{13}C spectral data showed that the ease of the protonation to ring carbons depends upon the differences in the chemical shifts between the complex layer and the starting aromatic hydrocarbon, and some facts concerning the isomerization of methylbenzenes were discussed.

Investigations concerning benzenonium ions have been reported by many workers.[2-5] The presence of the benzenonium ion was supported first by measurements of vapor pressure and conductivity. The addition of the proton to an aromatic carbon atom, thus forming an "aliphatic" CH_2 group, was confirmed by observations of electronic[6] and infrared[7] spectra. More direct evidence for the structure of benzenonium ions was mainly obtained from the ^{1}H NMR spectra.

The ^{1}H NMR spectra of some methylbenzenonium ions were obtained by using $HF-BF_3$,[8,9] $HFSO_3$[10] or $HF-SbF_5$.[11] In all these experiments the spectra of benzenonium ions were measured at a low temperature in order to obtain well-resolved signals, since proton exchange occurred at higher temperatures.

Recently, Koptyug and his co-workers[12] measured the ^{13}C NMR spectrum of the mesitylenonium ion at room temperature by using aluminum chloride with hydrogen chloride and discussed how the positive charges on the ring-carbon atoms of the ion can be calculated on the basis of the relative shift differences between the mesitylenonium ion and mesitylene.

In the present work the ^{1}H and ^{13}C NMR spectra of the complex layers obtained by the reaction of several methylbenzenes with aluminum chloride were measured at room temperature in order to clarify the behavior of the methylbenzenonium ion under the influence of proton exchange.

Experimental

Preparation of the Complexes. The reaction was carried out in a long necked flask with a long side tube, as is shown in Fig. 1. About 3 g of aromatic hydrocarbon was placed in the reaction vessel (3) and about the same amount of pulverized aluminum chloride in the side tube (4). After the open end of the side tube had been sealed, the aluminum chloride was sublimed slowly under the reduced pressure of 3 mmHg by means of a ribbon heater. One-third to one-half of the aluminum chloride in the side tube was transferred into the reaction vessel, which contained the aromatic hydrocarbon which had been held at 2 °C with stirring by means of a magnetic stirrer. During the sublimation, the hydrogen chloride produced by the reaction of aluminum chloride with the moisture which existed in the system was absorbed in the aromatic hydrocarbon. Then the reaction mixture is gradually turned from a light yellow to a light vermilion as a result of the dissolving of the aluminum chloride. When the reaction mixture was left standing for a while, a colored complex of a

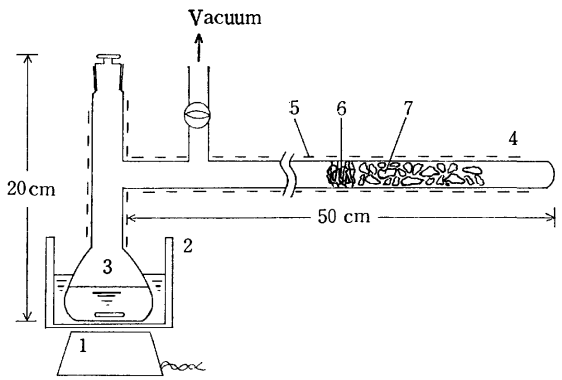

Fig. 1. Reaction flask
1. magnetic stirrer, 2. ice bath, 3. reaction vessel, 4. side tube, 5. ribbon heater, 6. glass wool, 7. $AlCl_3$.

1) Part VIII: S. Hamanaka, K. Tomimura, S. Sanada, K. Itoh, and M. Ogawa, *Kogyo Kagaku Zasshi*, **73**, 2551 (1970).
2) D. A. McCaulay and A. P. Lien, *J. Amer. Chem. Soc.*, **73**, 2013 (1951).
3) G. A. Olah and S. J. Kuhn, *Nature*, **178**, 693 (1956); *J. Amer. Chem. Soc.*, **80**, 6535 (1958).
4) W. von E. Doering, M. Saunders, H. G. Boyton, H. W. Earhart, E. F. Wadley, W. R. Edwards, and G. Laber, *Tetrahedron*, **4**, 178 (1958).
5) H. C. Brown and H. W. Pearsall, *J. Amer. Chem. Soc.*, **73**, 4681 (1951); H. C. Brown and W. J. Wallace, *ibid.*, **75**, 6268 (1953).
6) V. Gold and F. L. Tye, *J. Chem. Soc.*, **1952**, 2172.
7) H. H. Perkampus and E. Baumgarten, *Z. Elektrochem.*, 6870 (1964); *Angew. Chem.*, **76**, 965 (1964).
8) G. Dallinga, E. L. Mackor, and A. A. Verrijn Stuart, *Mol. Phys.*, **1**, 123 (1958); E. L. Mackor, A. Hofstra, and J. H. van der Waals, *Trans. Faraday Soc.*, **54**, 66 (1958).
9) C. MacLean and E. L. Mackor, *Mol. Phys.*, **4**, 241 (1961); *Discuss. Faraday Soc.*, **1962**, 165.
10) T. Birchall and R. J. Gillespie, *Can. J. Chem.*, **42**, 502 (1964).
11) G. A. Olah, *J. Amer. Chem. Soc.*, **87**, 1103 (1965).
12) V. A. Koptyug, A. I. Rezvukhin, E. T. Lippman, and T. Pehk, *Tetrahedron Lett.*, **1968**, 4009.

Table 1. The constituents of the complexes of methylbenzenes with aluminum chloride–hydrogen chloride
(Reaction temp.: 2 °C, Reaction time: 70 min)

Compound	Reaction products (wt%)	Al[a] (wt%)	Cl[a] (wt%)	Cl/Al (ratio)	ArH/Al (ratio)
Toluene	—	6.2	27.3	3.34	3.14
p-Xylene	*m*-Xylene (13.4)	6.3	28.0	3.39	2.66
m-Xylene	—	6.0	28.5	3.62	2.78
Mesitylene	—	6.4	29.7	3.53	2.24
Pseudocumene	mesitylene (1.2)	6.5	26.9	3.15	2.30
Hemimellitene	pseudocumene(3.0)	5.2	23.0	3.95	2.92

a) Al: ±0.3 wt%, Cl: ±1.0 wt%.

high viscosity was separated as a lower layer, leaving colorless hydrocarbon as the upper layer. The lower complex layer was examined by NMR and then quenched with water before submitting it to the vpc analysis for hydrocarbons.

Measurements. The ^1H NMR spectra were measured at 22.5 °C on a JEOL JNM-3H-60 spectrometer with 60 MHz, using a neat liquid. Tetramethylsilane was used as the external standard.

The ^{13}C NMR spectra were measured at 26 °C on a JEOL C-60HL spectrometer with a 15.09 MHz RF unit. The ^1H-decoupled ^{13}C spectra were obtained by means of a single scan. The chemical shifts were measured relative to CS_2.

Analyses of Hydrocarbons. The hydrocarbons in the complex layer were analyzed by means of vpc after the complex had been decomposed with water. The analyses were made at 100—130 °C by employing a vapor-phase chromatograph (Shimadzu Model GC-3AF) with a flame ionization detector and a 3 mm×3 m column packed with Benton-34 or Ucon-LB-550X; nitrogen was used as the carrier gas.

Analyses of Aluminum and Chlorine. The aluminum and chlorine in the complex layer were determined by the oxine- and the mercurimetric-titration methods,[13] respectively.

Results and Discussion

It is well known that, in the presence of hydrogen chloride, aluminum chloride dissolves in aromatic hydrocarbon by forming a benzenonium ion. In the present work, when aluminum chloride was heated, a certain amount of hydrogen chloride which was produced from the reaction of aluminum chloride with moisture evolved and was absorbed in the aromatic hydrocarbon. As more hydrogen chloride was not added in the reaction system, the amount of the complex layer seems to be proportional to that of the evolved hydrogen chloride. When both the reactants had been dehydrated extremely, aluminum chloride did not dissolve at all in aromatic hydrocarbon. Therefore, it seems that the dissolved aluminum chloride may form a certain protonic acid by reacting with hydrogen chloride or other proton donors. In each run, about a half of the aluminum chloride in the side tube dissolved in the aromatic hydrocarbon, but the excess aluminum chloride did not dissolve. Therefore, the complex layer seems to have similar constituents in each preparation under the given reaction conditions.

Analyses of Complex Layers. The constituents of the complex layers obtained by the reaction at 2 °C are shown in Table 1. Some methylbenzenes isomerized to the most stable isomer in a small amount. The ratio of Cl/Al is about 3.5. This value means that the protonic acid produced from aluminum chloride in the complex layer is not only $H^+AlCl_4^-$ but also some other acids, such as $H^+ AlCl_3OH^-$ and $H^+ Al_2Cl_7^-$.

On the other hand, the ArH/Al ratio for each complex is estimated to be between 2.24 and 3.14. This indicates that the aromatic hydrocarbon which exists in the complex layer is represented by the following equation:

$$\alpha ArH + HB + AlCl_3 \longrightarrow (\alpha - 1)ArH + ArH_2^+ \cdot AlCl_3 \cdot B^-$$

where HB is HCl or H_2O and where α is not necessarily an integer. Accordingly, the excess aromatic hydrocarbon which does not form benzenonium ions is considered to react as a solvent. The fluctuation of

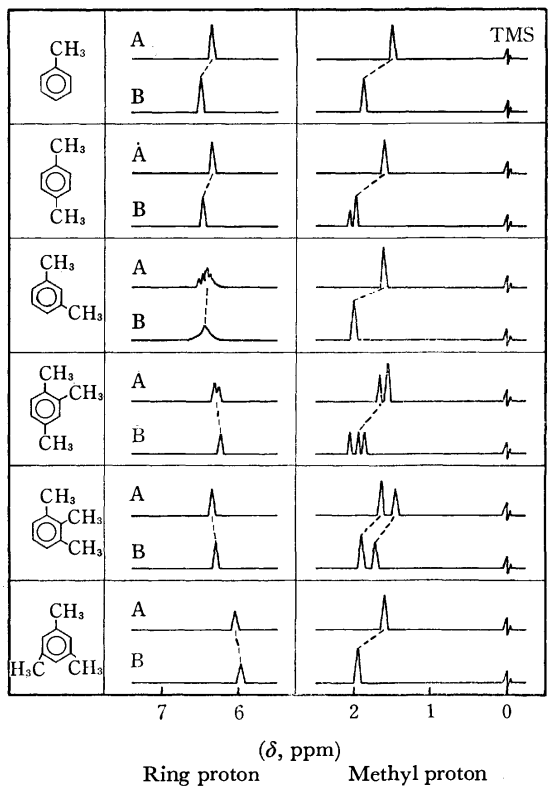

Fig. 2. The ^1H NMR spectra of the starting aromatic hydrocarbons (A) and the complexes (B).

13) Yuki Biryo Bunseki Kenkyu Kondankai, "Yuki Biryo Teiryo Bunseki," Tokyo (1969), pp. 388, 422.

Table 2. The ^1H chemical shift values of the complexes of methylbenzenes with aluminum chloride–hydrogen chloride.[a,b]

Compound	Methyl protons			Ring protons		
	Aromatic hydrocarbon (δ, ppm)	Complex (δ, ppm)	Difference ($\Delta\nu$, Hz)	Aromatic hydrocarbon (δ, ppm)	Complex (δ, ppm)	Difference ($\Delta\nu$, Hz)
Toluene	1.50	1.85	−21.0	6.35	6.50	−9.0
p-Xylene	1.60	1.96	−21.6	6.35	6.44	−5.4
		2.04[c]				
m-Xylene	1.62	1.99	−22.2	6.32	6.40	−4.8
Pseudocumene	1.65[d]	2.02	−22.2	6.31	6.26	+3.0
		1.93	−16.8			
	1.53	1.87	−19.2			
Hemimellitene	1.63	1.91	−16.8	6.36	6.31	+3.0
	1.46	1.72	−15.6			
Mesitylene	1.60	1.92	−21.0	6.06	5.96	+6.0

a) All the chemical shifts are referred to tetramethylsilane as an external standard.
b) The differences in chemical shifts between aromatic hydrocarbons and complexes are shown by Hz (positive; higher field shift, negative; lower field shift).
c) The intensity of the signal was about half of that of the signal at 1.96 ppm, and the signal could not be assigned.
d) This signal was assigned to the 1-CH_3 and 2-CH_3 groups, but it split into a doublet with an equal intensity in the complex.

the amount of such an aromatic hydrocarbon could not be interpreted.

^1H NMR Spectra. The ^1H NMR spectra of the starting aromatic hydrocarbons (A) and the complexes (B) are shown in Fig. 2. Each ^1H chemical shift (δ) of the complexes, and the difference ($\Delta\nu$) of each chemical shift between the aromatic hydrocarbon and its complex, are given in Table 2.

The proton signals of methyl groups in all of the complexes shifted about 20 Hz to a lower field. However, when cyclohexane was used as an internal reference in the complex layer, the proton signal of cyclohexane also shifted about 20 Hz to a field lower relative to the external reference. Therefore, the differences in the shifts of the methyl groups are considered to result mainly from the use of an external reference; thus, it seems that the methyl protons are not significantly affected by the formation of methylbenzenonium ions.[14]

On the other hand, the shifts of ring protons given in Table 2 are apparently up-field shifts, considering the influence of the external reference. MacLean and his co-workers,[9] who measured the NMR spectra of a mixture of aromatic hydrocarbon and its benzenonium ion in HF–BF_3, using excess HF as the solvent at various temperatures, found that signals of the ring and the methylene protons fused into a single signal at temperatures above −30 °C; this fused signal was observed between both the resolved signals.

In the present observation, the up-field shift of ring protons seems to be caused by the fusing of the signals of the ring and methylene protons.[15]

The up-field shifts of the ring protons of each complex are in the following order:

Mesitylene>Hemimellitene>Pseudocumene>*m*-Xylene>*p*-Xylene>Toluene

This order is proportional to the basicity of methylbenzenes.[2] Consequently, the proton signals of more basic benzene rings are shifted to a higher field by the fusion with the methylene signal.

The fusion of signals may result from the proton exchange. As the observed signal of the ring protons in the complex layer is a singlet, the proton exchange is considered to occur not only among the ring carbons of the same benzenonium ion intramolecularly, but also among the ring carbons of aromatic hydrocarbon and those of its benzenonium ion intermolecularly as follows:

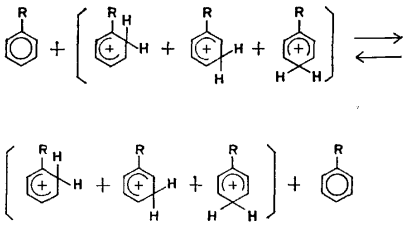

^{13}C NMR Spectra. Figure 3 shows diagrams of the ^{13}C NMR spectra of the starting aromatic hydrocarbons (A) and the complexes (B). Their chemical shift values are listed in Table 3. The assignments of the ^{13}C signals of each starting aromatic hydrocarbon were determined by reference to the literature.[16–18] The assignments of signals for the ring carbons of

14) The lowerings of the chemical shift based on the external reference are considered to be caused by some physical factors. The volume magnetic susceptibility of aluminum chloride, considered to be one of the physical factors, was determined to be $(0.70\pm0.05)\times10^{-6}$ cgs unit (measured at 100 MHz), by using hexamethyldisilane as the reference. The magnitude of the susceptibility corresponds to a lowering of the chemical shift of about 6 Hz.

15) M. Strohmeyer and C. Witte (*Ann. Chem.*, **729**, 21 (1969)) reported that aromatic hydrocarbon, which forms a stable methylbenzenonium ion in $AlCl_3$–HCl at −30 °C, must possess at least three methyl groups at the 1,3,5-positions.

16) P. C. Lauterbur, *J. Amer. Chem. Soc.*, **83**, 1838 (1961).

17) P. C. Lauterbur, *ibid.*, **83**, 1846 (1961).

18) W. R. Woolfenden and D. M. Grant, *ibid.*, **88**, 1496 (1966).

Table 3. The ^{13}C chemical shift values (ppm)[a] of pure methylbenzenes and the complexes of methylbenzenes with aluminum chloride–hydrogen chloride

Compound	Ring carbon position	Aromatic hydrocarbon observed value (w)	Calculated value[b] (s)	Difference (w−s)	Complex (x)	Difference (w−x)	Methyl carbon position	Aromatic hydrocarbon observed value (y)	Complex (z)	Difference (y−z)
Toluene	C–1	55.9[c]	55.7	0.2	46.5	9.4	1–CH_3	172.2[c]	170.3	1.9
	CH–3,5	64.3	64.3	0.0	57.8	6.5	—	—	—	—
	CH–2,6	64.9	65.0	−0.1	64.0	0.9	—	—	—	—
	CH–4	67.7	67.8	−0.1	74.2	−6.5	—	—	—	—
p-Xylene	C–1,4	58.0[c]	58.5	−0.5	57.9	0.1	1,4–CH_3	172.1[b]	171.4	0.7
	CH–2,3,5,6	64.5	64.3	0.2	63.5	−1.0	—	—	(168.0)[d]	—
m-Xylene	C–1,3	59.6[c]	55.0	4.6	45.1	14.5	1,3–CH_3	172.3[c]	169.9	2.4
	CH–5	63.2	63.6	−0.4	56.1	7.1	—	—	—	—
	CH–2	65.0	65.0	0.0	63.0	2.0	—	—	—	—
	CH–4,6	66.9	67.8	−0.9	71.9	−5.0	—	—	—	—
Mesitylene	C–1,3,5	56.4[c]	54.3	2.1	44.1	12.3	1,3,5–CH_3	172.2[c]	170.1	2.1
	CH–2,4,6	66.1	67.8	−1.7	69.8	−3.7	—	—	—	—
Pseudocumene	C–2	57.4	55.0	2.4	45.4	12.0	2–CH_3	173.5	171.5	2.0
	C–4	58.4	57.8	0.6	46.0	12.4	4–CH_3	172.1	170.4	1.7
	C–1	60.3	58.5	1.8	55.4	4.9	1–CH_3	173.8	173.3	0.5
	CH–6	62.7	63.6	−0.9	57.8	4.9	—	—	—	—
	CH–3	63.8	64.3	−0.5	64.0	−0.2	—	—	—	—
	CH–5	66.6	67.1	−0.5	77.8	−11.2	—	—	—	—
Hemimellitene	C–1,3	57.3	55.0	2.3	47.6	9.7	1,3–CH_3	172.6	171.1	1.5
	C–2	58.7	55.7	3.0	56.6	2.1	2–CH_3	177.8	177.8	0.0
	CH–4,6	65.4	66.4	−1.0	70.4	−5.0	—	—	—	—
	CH–5	67.8	67.1	0.7	60.7	−7.1	—	—	—	—

a) Referred to $^{13}CS_2$.
b) The calculated values of the chemical shifts were based on the additivity relations reported by Savitsky[19] and by Lauterbur.[17]
c) These data were assigned with Refs. 16 and 17.
d) See footnote c, Table 2.

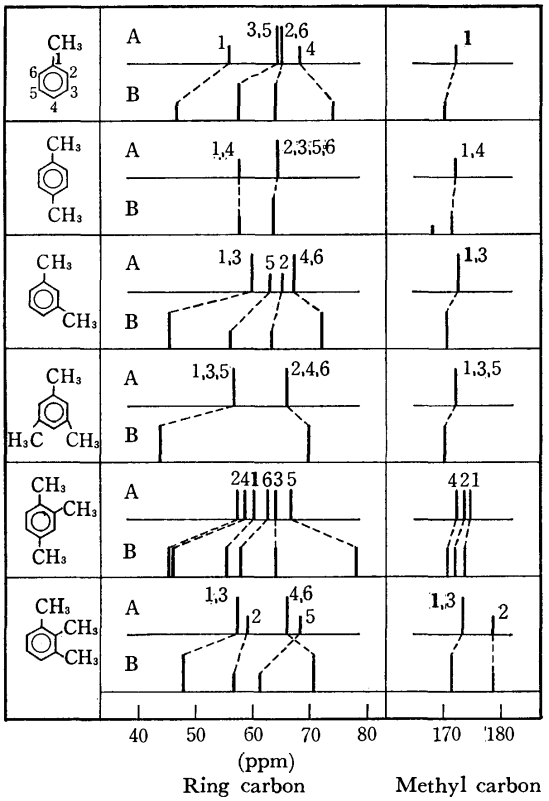

Fig. 3. The diagrams of the ^{13}C NMR spectra of the starting aromatic hydrocarbons (A) and the complexes (B).

pseudocumene and hemimellitene, the chemical shifts of which have not been reported, were performed on the basis of the peak intensities and then by using the additivity relations of chemical shifts postulated for disubstituted benzenes by Savitsky[19] and by Lauterbur.[17] The calculated values of the chemical shifts of ring carbons based on the additivity relations are also listed in Table 3. As can be seen in Table 3, the small differences between the calculated values and the observed values indicate that the above assignments of chemical shifts are acceptable.

Each ring ^{13}C signal of the complexes was also assigned by considering the peak intensities and the basicity of each ring carbon. The signals of each ring carbon were observed in the same order as those of the starting aromatic hydrocarbons, except for the signals of hemimellitene, which were ascertained by means of the peak intensities. On the other hand, the signals of the methyl groups were easily assigned by examining the peak intensities.

The mesitylenonium ion was independently prepared by introducing HCl gas into a mixture of mesitylene and two times as many moles of aluminum chloride in a stream of nitrogen. Figure 4 shows the diagrams of the ^{13}C NMR spectra of mesitylene (a), the mesitylenonium ion (b), and the complex of mesitylene (c). From the spectrum of the mesitylenonium ion (b), it

19) G. B. Savitsky, *J. Phsy. Chem.*, **67**, 2723 (1963).

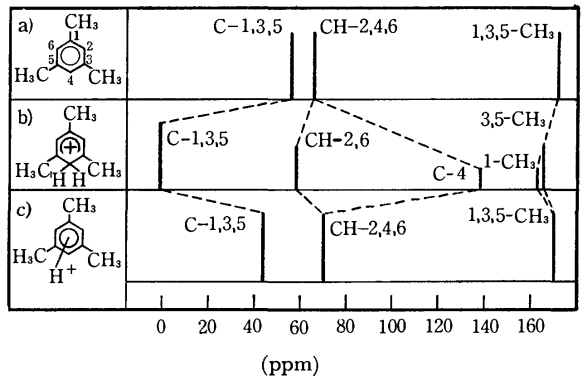

Fig. 4. The diagrams of the ^{13}C NMR spectra of mesitylene, the mesitylenonium ion and the complex of mesitylene.
a) mesitylene b) mesitylenonium ion (ArH^+_2, measured at −20 °C) c) complex (ArH: ArH_2^+)

was found that the ^{13}C signal of the methylene group resulted from the protonation to the C-4 ring carbon shifted to a higher field, similar to that of the alicyclic CH_2 group of cyclohexane (165 ppm), while the signals of the other ring carbons and of the methyl ones shifted to a lower field because of the decrease in the electron density caused by the protonation. These facts well agreed with Koptyug's findings concerning the ^{13}C NMR spectrum of the mesitylenonium ion. On the other hand, as is shown in Fig. 4 (c), the CH-2,6 and CH-4 signals of the complex were fused into a single signal, and all three signals of the complex shifted less than did the resolved signals of the mesitylenonium ion. These relations hold generally on the fused spectra of other complexes.

The following results were drawn from the data of the fused spectra in Fig. 3:

a) The protonation occurred more easily on the more basic ring carbon. Then the ring carbon signal shifted to a higher field.

b) The signals of the ring carbons with less basicity are shifted to a lower field by the decrease in electron density. Of course, such carbons also have a chance to be protonated, but the contribution of the protonation is less than that of the more basic carbon.

c) The methyl-substituted ring carbons are considered to be protonated to a small extent. Thus, their signals are shifted to a much lower field.

d) The signals of the methyl groups are shifted to a lower field, since the methyl groups are charged somewhat positively because of the decrease in the electron density through I- and H-effects.

Isomerization Mechanism. As is shown in Table 1, the complexes of some methylbenzenes, such as *p*-xylene, pseudocumene, and hemimellitene, gave small amounts of isomerized products after decomposition with water. The isomerization of methylbenzenes is known to proceed usually by means of the intramolecular 1,2-shift of methyl group;[20,21] the ease of the isomerization depends upon the ease of the protonation to the methyl-substituted carbons.

In the above three methylbenzenes, the signals of the methyl-substituted carbons showed an interesting behavior. The signals of the ring carbons, such as the C-1,4 of *p*-xylene, the C-1 of pseudocumene, and the C-2 of hemimellitene, showed small differences (w−x) compared with those of other methyl-substituted carbons. The small differences mean that such carbon atoms were protonated to a substantial extent and that then the methyl groups substituted for these atoms might have been easily rearranged to other positions. Moreover, the signals of the methyl groups attached to the above-mentioned carbons, such as the 1,4-CH_3 of *p*-xylene, the 1-CH_3 of pseudocumene, and the 2-CH_3 of hemimellitene, also shifted very slightly to a lower field compared with those of other methyl carbons. This finding indicates that the above methyl groups are charged less positively than the others and that, therefore, they may rearrange more easily.

The isomerization of hemimellitene is generally considered to proceed by means of the 1,2-shift of 1-CH_3 or 3-CH_3 groups. However, the above results suggest that hemimellitene may be isomerized by the rearrangement of the 2-CH_3 group according to the following scheme:

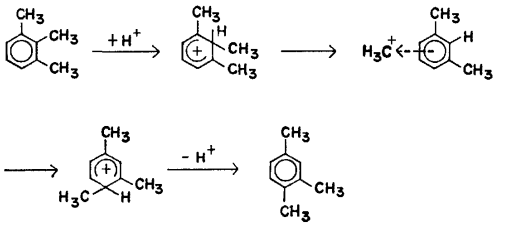

We are currently investigating this reaction further in an attempt to elucidate this mechanism.

The authors wish to thank Dr. Koichi Hatada of the University of Osaka for helpful discussions. The authors also wish to thank Mr. Hiroshi Okuda and Mr. Yoshio Terawaki of the University of Osaka for the measurements of the NMR spectra.

20) G. Baddeley, G. Holt, and D. Voss, *J. Chem. Soc.*, **1952**, 101.
21) D. M. Brouwer, *Rec. Trav. Chim. Pays-Bas*, **87**, 611 (1968).

Sterically Controlled Syntheses of Optically Active Organic Compounds. XIX. Asymmetric Syntheses of Amino Acids by the Strecker Reaction[1]

Kaoru HARADA, Tadashi OKAWARA, and Kazuo MATSUMOTO

Institute for Molecular and Cellular Evolution, and Department of Chemistry, 521 Anastasia Avenue, Coral Gables, Florida 33134, U.S.A.

(Received September 11, 1972)

The Strecker type syntheses of optically active alanine, butyrine, valine, and leucine by the use of the corresponding aldehydes, hydrogen cyanide, and optically active α-alkylbenzylamines and α-(1-naphthyl)ethylamine were carried out (reaction A). The optical purities were in the range 22—51%. The modified Strecker type syntheses of alanine from acetaldehyde cyanohydrine and optically active amines were also carried out (reaction B). The optical purities of alanine were in the range 44—48%. In reaction B, optically active phenylglycine was also used as an amino source. The optical purities of the synthesized alanine were in the range 12—17%.

Synthesis of optically active alanine by the Strecker reaction using optically active α-methylbenzylamine, acetaldehyde, and hydrogen cyanide has been reported.[2] Optically active alanine was similarly synthesized from the same amine and racemic acetaldehyde cyanohydrine.[3] In these syntheses, the isolated alanine had rather high optical purities (80—95%), but the final products were isolated from the solution by crystallization. Thus, fractionation of optical isomers of alanine would be expected to take place during the crystallization process. Recently, the addition reaction of hydrogen cyanide to the Schiff bases of several aldehydes with optically active α-methylbenzylamines was studied.[4] It was reported that the isolated amino acids were almost optically pure. Although they claimed that there was no fractionation of the synthesized optical isomers during the isolation and purification processes, it was shown that fractionation could take place in three steps.[5] The real optical purities of amino acids prepared by the addition reactions of hydrogen cyanide were found to be much lower. Similar addition reactions of benzoyl cyanide to Schiff bases composed of various aldehydes and optically active α-alkylbenzylamine were studied.[6]

In the study of syntheses of optically active amino acids by the Strecker reaction, 1) the effect of the optically active moiety, 2) the effect of the aldehyde, and 3) the optical purity of the synthesized amino acids were investigated. Two kinds of reaction were carried out. A) the Strecker reactions of aldehydes, hydrogen cyanide, and optically active amines, and B) the modified Strecker reactions of racemic aldehyde cyanohydrine with optically active amines. The optically active amines used were: *R*-(+)-α-methylbenzylamine, *S*-(−)-α-methylbenzylamine, *S*-(−)-α-ethylbenzylamine, *S*-(−)-α-(1-naphthyl)ethylamine, and *R*-(−)-phenylglycine. The aldehydes used in reaction A were: acetaldehyde, propionaldehyde, isobutyraldehyde, and isovaleraldehyde. Reaction A was carried out in absolute ethanol at room temperature, except when the reactants were mixed at −10°C. Reaction B was carried out under similar conditions, except in reactions in which (*R*)-(−)-phenylglycine was used in aqueous alkaline conditions.

Reaction (A): $RCHO + R'NH_2 + HCN \xrightarrow[H^+]{H_2O} R\text{-}\overset{*}{C}H\text{-}CN \xrightarrow[H^+]{H_2O} \xrightarrow[Pd(OH)_2/C]{H_2} R\text{-}\overset{*}{C}H\text{-}COOH$ (NHR′ / NH_2)

Reaction (B): $CH_3\text{-}CH(OH)\text{-}CN + R'NH_2 \xrightarrow[H^+]{H_2O} \xrightarrow[Pd(OH)_2/C]{H_2} R\text{-}\overset{*}{C}H\text{-}COOH$ (NH_2)

R: CH_3–, CH_3CH_2–, $(CH_3)_2CH$–, $(CH_3)_2CHCH_2$–

R′: (±)-C_6H_5-CH(CH$_3$)–, (*R*)-(+)-C_6H_5-CH(CH$_3$)–, (*S*)-(−)-C_6H_5-CH(CH$_3$)–, (*S*)-(−)-C_6H_5-CH(C_2H_5)–, (*S*)-(−)-$C_{10}H_7$-CH(CH$_3$)–, (*R*)-(−)-C_6H_5-CH(COOH)–

The resulting *N*-alkylaminonitriles synthesized in reactions A and B were hydrolyzed with 6 M hydrochloric acid. The resulting *N*-alkyl amino acids were then hydrogenolyzed with palladium hydroxide on charcoal to remove the *N*-alkyl residue. Free amino acids were isolated by the use of a Dowex 50 column. The free amino acids obtained were then converted into DNP-derivatives with 2,4-dinitrofluorobenzene, and the DNPylated amino acids were purified by means of celite column chromatography to avoid any fractionation of optical isomers. The optical purities of the resulting amino acids were measured using the DNP-amino acids.

The specific rotations, optical purities, and over-all yields of alanine, α-aminobutyric acid, valine, and leucine, by using optically active α-methylbenzylamine, α-ethylbenzylamine, and α-(1-naphthyl)ethylamine are given in Table 1. The over-all yields were in the range 19—47%. The optical purities of amino acids were in the range 22—51%. It seems that the optical purity of amino acids decreased as the size of the

1) Contribution No. 228 of the Institute for Molecular and Cellular Evolution.
2) K. Harada, *Nature*, **200**, 1201 (1963).
3) K. Harada and S. W. Fox, *Naturwissenschaften*, **51**, 106 (1964).
4) M. S. Patel and M. Worsley, *Can. J. Chem.*, **48**, 1881 (1970).
5) K. Harada and T. Okawara, *J. Org. Chem.*, **38**, 707 (1973).
6) K. Harada and T. Okawara, This Bulletin, **46**, 191 (1973).

Table 3. Synthesis of optically active alanine from acetaldehyde cyanohydrine and optically active amines under varying ratios of reactants

(*S*)-(−)-Me[a] (0.01 mol)	Racemic lacto-nitrile (0.01 mol)	Yield[b] (%)	DNP-Alanine $[\alpha]_D^{25}$ (1M NaOH) (*c*, 0.4—0.5)	Optical purity[c] (%)
3	1	29	+61.80	43
2	1	26	+48.60	34
1	1	28	+61.54	43
1	2	30	+55.0	38
1	3	31	+45.89	32
1	4	35	+37.2	26
1	5	35	+31.6	22
1	10	34	+33.7	23

(*S*)-(−)-Et[a] (0.01 mol)	Racemic lacto-nitrile (0.01 mol)	Yield[b] (%)	DNP-Alanine $[\alpha]_D^{25}$ (1M NaOH) (*c*, 0.4—0.5)	Optical purity[c] (%)
2	1	28	+63.8	44
1	1	26	+64.5	42
1	2	28	+60.2	42
1	3	29	+44.3	31
1	4	28	+41.7	29

a) (*S*)-(−)-Me, (*S*)-(−)-α-methylbenzylamine; (*S*)-(−)-Et, (*S*)-(−)-α-ethylbenzylamine.
b) The yields are calculated from the least reactant (0.01 mol).
c) Defined as $[\alpha]_D$ obsd/$[\alpha]_D$ of the compound × 100. DNP-(*S*)-(+)-alanine, $[\alpha]_D^{25}$ +143.9° (1M NaOH).

Table 4. Synthesis of optically active alanine from racemic acetaldehyde cyanohydrine using (*R*)-(−)-phenylglycine

(*R*)-(−)-Phe-Glycine (0.01 mol)	Racemic lacto-nitrile (0.01 mol)	Yield[a] (%)	DNP-(*S*)-Alanine $[\alpha]_D^{25}$ (1M NaOH) (*c*, 0.3—0.5)	Optical purity[b] (%)
4	1	77	+17.8	12
3	1	73	+23.2	16
2	1	62	+20.0	14
1	1	56	+24.1	17
1	2	67	+23.8	17
1	3	82	+21.6	15
1	4	85	+20.0	14
1	5	75	+21.9	15

a) The yields are calculated from the least reactant (0.01 mol).
b) Optical purity defined as $[\alpha]_D$ obsd/$[\alpha]_D$ of the compound × 100. DNP-(*S*)-(+)-alanine, $[\alpha]_D^{25}$ +143.9° (1M NaOH).

α-carbon of (*R*)-cyanohydrine than (*S*)-cyanohydrine because of steric factors. The (*S*)-amine reacts with (*R*)-cyanohydrine to form *N*-(*S*)-α-methylbenzyl-(*S*)-aminopropionitrile which was hydrolyzed and hydrogenolyzed to form (*S*)-alanine. However, this mechanism is not likely, because reactions carried out at a higher ratio of cyanohydrine to amine did not yield higher optical purities of alanine, but rather lower values as shown in Tables 3 and 4. On the other hand, the dissociation of cyanohydrine to aldehyde and hydrogen cyanide should be considered. The yields and optical purities of alanine prepared from reactions A and B are almost the same; therefore, these reactions might proceed by the same reaction mechanism. The addition of hydrogen cyanide to Schiff bases composed of aldehydes and amines is a possible mechanism. Such a steric course has been described[7] but the mechanism is arbitrary. In order to understand the steric course of this reaction, *syn* and *anti* structures of the Schiff base must be determined under the reaction conditions. The results shown in Tables 1 and 2 indicate that the high optical purity of isolated alanine in the earlier reports[2,3] would be due to the fractionation during the final crystallization stage.

The Strecker type reaction was also carried out by the use of racemic lactonitrile with (*R*)-(−)-phenylglycine in aqueous conditions. The resulting *N*-substituted aminonitrile was hydrolyzed and hydrogenolyzed to convert the product into optically active alanine. The yields were rather high (56—85%); however, optical purities were low (12—17%). When (*R*)-(−)-phenylglycine was used, (*S*)-alanine was produced as in the case using (*S*)-(−)-α-methylbenzylamine.[8] The results are summarized in Table 4.

Experimental

All hydrogenolyses were carried out with a Parr 3910 Shaker type hydrogenation apparatus by using palladium hydroxide on charcoal or palladium on charcoal as a catalyst. All optical activity measurements were carried out on a JASCO ORD-CD-UV 5 spectropolarimeter.

The specific rotations of optically active amines used were:
(*R*)-(+)-methylbenzylamine $[\alpha]_D^{25}$ +39.0°, benzene
(*S*)-(−)-methylbenzylamine $[\alpha]_D^{25}$ −38.5°, benzene
(*S*)-(−)-ethylbenzylamine $[\alpha]_D^{25}$ −20.0°, benzene
(*S*)-(−)-α-(1-naphthyl)ethylamine $[\alpha]_D^{25}$ −88.2°, benzene
(*R*)-(−)-phenylglycine $[\alpha]_D^{25}$ −168.0°, 5M HCl
Some of them are not completely optically pure (~95%); however, the optical purities of the resulting alanine are listed in the tables without corrections.

Syntheses of Amino Acids (Reaction A). To the solution of amine (0.012 mol) in absolute ethanol (20 ml) was added 1 ml of liqiud hydrogen cyanide (0.052 mol) at −10°C. Aldehyde (0.01 mol) was then added to the cold ethanolic solution. The sealed reaction mixture was shaken to homogenize the solution and was allowed to stand for 2 days at room temperature.

After the reaction was over, excess hydrogen cyanide and ethanol were evaporated under reduced pressure. The residue was refluxed with 20 ml of 6M hydrochloric acid for 12 hr. The hydrolyzate was extracted with ether to remove

7) In "Asymmetric Organic Reactions," by J. M. Morrison and H. S. Mosher, Prentice-Hall, Inc., Englewood Cliffs, New Jersey (1971), p. 328.

8) The steric structure of (*R*)-(−)-phenylglycine and (*S*)-(−)-α-methylbenzylamine could be expressed as shown below:

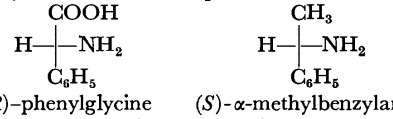

(*R*)-phenylglycine (*S*)-α-methylbenzylamine

If we regard the carboxyl and methyl groups as equivalent, the steric structures of (*R*)-(−)-phenylglycine and (*S*)-(−)-α-methylbenzylamine are the same.

Table 5. Elemental analyses of amino acids and *N*-alkyl amino acids

R: CH_3 | C_6H_5–CH–	Mp °C	Formula	Calcd (%)			Found (%)		
			C	H	N	C	H	N
N-*R*-Ala	275—276 (sublime)	$C_{11}H_{15}NO_2$	68.37	7.82	7.25	68.31	7.77	7.31
N-*R*-Buty	247—250 (sublime)	$C_{12}H_{17}NO_2$	69.54	8.27	6.96	69.61	8.23	6.88
N-*R*-Val	265—270 (sublime)	$C_{13}H_{19}NO_2$	70.56	8.65	6.33	70.18	8.85	6.34
N-*R*-Leu	256—258 (sublime)	$C_{14}H_{21}NO_2$	71.46	8.99	5.95	71.72	9.25	5.96
Ala	—	$C_3H_7NO_2$	40.44	7.92	15.72	40.20	7.86	15.49
Buty	—	$C_4H_9NO_2$	46.59	8.80	13.58	46.27	8.72	13.39
Val	—	$C_5H_{11}NO_2$	51.26	9.46	11.96	50.93	9.49	11.83
Leu	—	$C_6H_{13}NO_2$	54.94	9.99	10.68	54.91	9.87	10.64

colored material. The hydrochloric acid was evaporated to dryness under reduced pressure. The residue was dissolved in a small amount of water and was applied to a Dowex 50 column (1.9 cm×23 cm, H^+ form) and eluted with 1.5 M aqueous ammonia. The fractions containing the amino acid were combined and the solution was evaporated under reduced pressure.

When optically active amines were used, the reaction products were treated in the same way. However, the resulting *N*-alkyl amino acids were not isolated to avoid fractionation of the diastereomeric mixture. The *N*-alkyl amino acids were dissolved in a mixture of ethanol and water (*ca.* 70 ml) and were hydrogenolyzed with 0.7 g of palladium hydroxide on charcoal for 12 hr. After hydrogenolysis was over, the catalyst was removed by filtration. The solution was evaporated under reduced pressure to give free α-amino acid. A part of the α-amino acid was converted into DNP-derivatives in the usual way. The resulting DNP-α-amino acids were purified by the use of a celite column treated with pH 7 citrate-phosphate buffer[9] to measure optical purities of resulting amino acids.

When racemic α-methylbenzylamine was used, the resulting racemic *N*-α-methylbenzylamino acids were isolated by means of a Dowex 50 column. Hydrogenolysis of these compounds with palladium hydroxide on charcoal resulted in the formation of racemic amino acids. The analytical results of these amino acids are summarized in Table 5. All of these *N*-substituted amino acids are sublimable at higher temperature.

Syntheses of Alanine (Reaction B). The freshly distilled racemic acetaldehyde cyanohydrine (0.71 g, 0.01 mol) and racemic amine were mixed with 20 ml of absolute ethanol under ice cooling. The reaction mixture was then kept at room temperature for 48 hr. After the reaction was over, ethanol was evaporated under reduced pressure. After evaporation of ethanol from the reaction mixture, the residue was dissolved in 20 ml of ethyl acetate. The solution was washed twice, with 20 ml of 1% aqueous sodium hydrogen carbonate, once with 20 ml of water and was dried over anhydrous sodium sulfate. The solution was evaporated under reduced pressure and distilled. When DL-α-methylbenzylamine was used, the DL-*N*-α-methylbenzylaminonitrile was isolated. Bp. 94—97°C/1.7 mmHg, yield, 1.2 g (66%). This was converted into its hydrochloride in ether treating with gaseous hydrogen chloride. The hydrochloride was recrystallized from ethanol. Mp. 141—142°C (decomp.).

Found: C, 62.43; H, 7.27; N, 13.40%. Calcd for $C_{11}H_{15}N_2Cl$: C, 62.70; H, 7.18; N, 13.30%.

The *N*-alkyl amino nitrile was hydrolyzed with 6 M hydrochloric acid. A part of the racemic *N*-α-methylbenzylalanine was isolated by means of a Dowex 50 column and recrystallized from ethanol and water for elemental analysis. Mp 270—273°C (sublime).

Found: C, 68.02; H, 7.71; N, 7.04%. Calcd for $C_{11}H_{15}NO_2$: C, 68.37; H, 7.82; N, 7.25%.

The rest of the *N*-substituted alanine was then hydrogenolyzed by use of palladium hydroxide on charcoal and the alanine was isolated as in reaction A (Found: C, 40.47; H, 8.05; N, 15.77%).

Optically active alanine was prepared in a similar way to that described above. This was recrystallized from water and ethanol for elemental analysis (Found: C, 40.24; H, 8.00; N, 15.71%).

A part of the unfractionated alanine was converted into DNP-derivative, and was purified by the use of a celite column as in reaction A. The results are summarized in Table 2.

Synthesis of Alanine (Reaction B). Using (R)-(−)-Phenylglycine: (*R*)-(−)-Phenylglycine, 1.51 g (0.01 mol) was dissolved in 25 ml of water containing 0.01 mol of sodium hydroxide. To this solution, 0.71 g (0.01 mol) of racemic acetaldehyde cyanohydrine was added under cooling in an ice bath. The mixture was allowed to stand for 2 days at room temperature. To this, 30 ml of 6 M hydrochloric acid was added and refluxed for 6 hr. The hydrolyzate was evaporated to dryness under reduced pressure. The residue was dissolved in 50 ml of water containing 0.02 mol of sodium hydroxide. The solution was subjected to hydrogenolysis by using 2.0 g of 5% palladium on charcoal for 12 hr. After the hydrogenolysis was over, the catalyst was removed by filtration and the aqueous solution was acidified to a pH of about 2.0—1.5 and then evaporated to dryness. Synthesized alanine hydrochloride was extracted with absolute ethanol. The ethanolic solution was evaporated. The alanine hydrochloride was applied on a Dowex 50 column (H^+ form) and eluted with 1.5 M aqueous ammonia. Fractions containing alanine were combined and evaporated to obtain free alanine. A part of the alanine was DNPylated and the optical purity of alanine was measured as described earlier. The results are summarized in Table 4.

This work was supported by Grant No. NGR-10-007-052 from the National Aeronautics and Space Administration.

9) J. C. Perrone, *Nature*, **167**, 513 (1951); A. Cout, *Biochem. J.*, **58**, 70 (1954).

Sterically Controlled Syntheses of Optically Active Organic Compounds. XX. Synthesis of Optically Active Alanine from α-Bromopropionamides[1]

Tadashi OKAWARA and Kaoru HARADA

Institute for Molecular and Cellular Evolution, Department of Chemistry, University of Miami, 521 Anastasia Avenue, Coral Gables, Florida 33134, U.S.A.

(Received September 11, 1972)

The treatment of *N*-benzylchloroacetamide with sodium hydride resulted in the formation of *N,N'*-dibenzyldiketopiperazine which was converted to glycine after hydrolysis and hydrogenolysis. In a similar way, *N*-alkyl-α-bromopropionamides, in which the alkyl groups were chiral, were treated with sodium hydride and optically active alanine was obtained after hydrolysis and hydrogenolysis. When an optically active (*S*)-(−)- or (*R*)-(+)-α-methylbenzyl group was used as a chiral center, the optical activity of alanine was very low. When (*S*)-(−)-α-ethylbenzylamine was used, optically active (*S*)-alanine (optical purity 6—25%) was obtained. The use of (*S*)-(−)-α-(1-naphthyl)ethylamine resulted in the formation of (*R*)-alanine (opposite configuration, optical purity 23—27%). The overall yield of optically active alanine is in the range 11—36%.

It has been reported by Sarel and Ben-Shoshan that the α-chloropropionanilide was converted to *N*-phenyl-α-lactam by the action of sodium amide in liquid ammonia.[2] Sarel and Greenberger further reported[3] the chemical reaction of sodium hydride with α-chloro-α-phenylacetanilide (I) in dry benzene. The major product of this reaction was 1,3,4,6-tetraphenylpiperazine-2,5-dione (III), which could be converted to *N*-phenyl phenylglycine upon hydrolysis. In this reaction it was assumed that the three membered reactive intermediate (α-lactam) (II) dimerized to form a more stable six-membered ring product (III). In the inert solvent, only the dimerization reaction could take place to form the diketopiperazine derivative. Later it was reported that the postulated α-lactam and its corresponding diketopiperazine were isolated.[4] However, Sheehan and Frankenfeld[5] established that α-lactam was not found among the final products of the reaction of α-chloroanilides with sodium hydride. Baumgarten *et al.*[6] confirmed the existence of α-lactam spectroscopically. Since then, several α-lactam formations and their chemistry have been studied.[7-17]

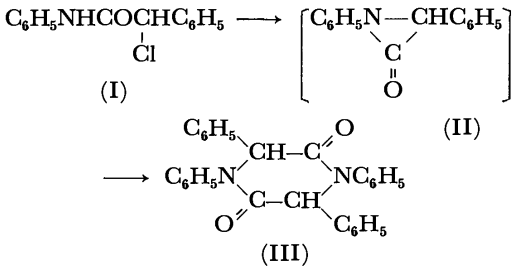

(I) (II) (III)

In this paper, the syntheses of glycine and alanine from α-haloacylamides were examined. The α-haloacylamides were prepared from several benzylic amines by acylation with α-chloroacetyl anhydride or with α-bromopropionyl bromide. The benzylic amines used were benzylamine, (±)-α-methylbenzylamine, (*R*)-(+)-α-methylbenzylamine, (*S*)-(−)-α-methylbenzylamine, (*S*)-(−)-α-ethylbenzylamine, and (*S*)-(−)-α-(1-naphthyl)-ethylamine.

In the glycine synthesis, *N*-benzyl-α-chloroacetamide (IV, X=Cl, R_1=H, R_2=H, R_3=phenyl) was treated with sodium hydride in anhydrous tetrahydrofuran at varying temperatures (0, 25, and 50°C). After evaporation of the solvent and recrystallization of the residual material, *N,N'*-dibenzylpiperazine-2,5-dione (VI) was isolated. The VI was hydrolyzed and hydrogenolyzed to form glycine (overall yield 17 to 52%).

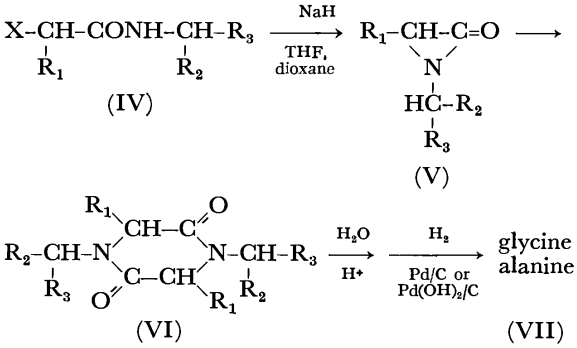

(IV) (V) (VI) (VII)

X: Cl, Br
R_1: H, Me
R_2: H, Me, Et
R_3: Phenyl, Naphthyl

1) Contribution No. 229 of the Institute for Molecular and Cellular Evolution.
2) S. Sarel and R. Ben-Shoshan, *Bull. Res. Council Israel*, **6A**, 298 (1957).
3) S. Sarel and A. Greenberger, *J. Org. Chem.*, **23**, 330 (1958).
4) S. Sarel and H. Leader, *J. Amer. Chem. Soc.*, **82**, 4752 (1960).
5) J. C. Sheehan and J. W. Frankenfeld, *ibid.*, **83**, 4792 (1961).
6) H. E. Baumgarten, R. L. Zey, and U. Krolls, *ibid.*, **83**, 4469 (1961).
7) H. E. Baumgarten, *ibid.*, **84**, 4975 (1962).
8) J. F. Fuerholzer, R. D. Clark, and R. D. Thompson, *ibid.*, **85**, 3303 (1963).
9) J. C. Sheehan and I. Lengyel, *ibid.*, **86**, 1356 (1964).
10) J. C. Sheehan and J. H. Beeson, *ibid.*, **89**, 362 (1967).
11) I. Lengyel and D. B. Uliss, *Chem. Commun.*, **1968**, 1621.
12) K. Batt, *Tetrahedron Lett.*, **1968**, 3323.
13) E. R. Talaty and A. E. Dupuy, Jr., *Chem. Commun.*, **1968**, 790.
14) J. C. Sheehan and I. Lengyel, *Angew. Chem.*, **80**, 27 (1968).
15) J. C. Sheehan and M. M. Nafissi-V, *J. Amer. Chem. Soc.*, **91**, 1176 (1969).
16) E. R. Talaty and C. M. Utermoehlen, *Chem. Commun.*, **1970**, 473.
17) M. Miyoshi, This Bulletin, **43**, 3321 (1970).

Table 1. *N*-Alkyl-α-bromopropionamide

CH_3–CH(Br)–CONHR, R[a)]	Formula	$[\alpha]_D^{25}$ (THF)	Mp, °C	Calcd % C	Calcd % H	Calcd % N	Found % C	Found % H	Found % N
(±)-Me	$C_{11}H_{14}NOBr$	—	129—130	51.58	5.51	5.47	51.59	5.64	5.58
(*R*)-(+)-Me	$C_{11}H_{14}NOBr$	+59.8	108—109	51.58	5.51	5.47	51.23	5.65	5.54
(*S*)-(−)-Me	$C_{11}H_{14}NOBr$	−59.5	108—109	51.58	5.51	5.47	51.49	5.71	5.38
(*S*)-(−)-Et	$C_{12}H_{16}NOBr$	−66.8	77—79	53.35	5.97	5.18	53.42	6.16	5.16
(*S*)-(−)-Naph	$C_{15}H_{16}NOBr$	−20.4	176—177	58.64	5.27	4.57	58.70	5.46	4.67

a) (±)-Me, (±)-α-methylbenzylamine; (*R*)-(+)-Me, (*R*)-(+)-α-methylbenzylamine; (*S*)-(−)-Me, (*S*)-(−)-α-methylbenzylamine; (*S*)-(−)-Et, (*S*)-(−)-α-ethylbenzylamine; (*S*)-(−)-Naph, (*S*)-(−)-α-(1-naphthyl)ethylamine.

Table 2. Syntheses of glycine and alanine from α-haloacylamides

	R*NHCOCH(X)R			Reaction conditions			Synthesized amino acid			
	R*[a)]	R	X	Solvent	Temp (°C)	Time (hr)	Config.	DNP-Alanine[b)] $[\alpha]_D^{25}$ (c=1.6～1.9)	Opt. purity[c)] (%)	Yield[d)] (%)
1	Benzyl	H	Cl	Anhy THF	0	12	—	—	—	17
2	Benzyl	H	Cl	Anhy THF	25	12	—	—	—	20
3	Benzyl	H	Cl	Anhy THF	50	8	—	—	—	52
4	(±)-Me	CH_3	Br	Anhy Dioxane	25	12	—	—	—	8
5	(±)-Me	CH_3	Br	Anhy Dioxane	25	36	—	—	—	38
6	(±)-Me	CH_3	Br	Anhy Dioxane	25	72	—	—	—	23
7	(*R*)-(+)-Me	CH_3	Br	Anhy THF	0	84	±	0	—	29
8	(*S*)-(−)-Me	CH_3	Br	Anhy THF	0	84	*R*	−1.9	1.3	21
9	(*S*)-(−)-Et	CH_3	Br	Anhy THF	0	84	*S*	+9.2	6.4	11
10	(*S*)-(−)-Naph	CH_3	Br	Anhy THF	0	84	*R*	−39.2	27.2	14
11	(*R*)-(+)-Me	CH_3	Br	Anhy THF	25	36	*R*	−2.4	1.7	30
12	(*R*)-(+)-Me	CH_3	Br	Anhy THF	25	72	*R*	−1.8	1.2	20
13	(*S*)-(−)-Me	CH_3	Br	Anhy THF	25	36	*S*	+2.6	1.8	20
14	(*S*)-(−)-Et	CH_3	Br	Anhy THF	25	36	*S*	+35.6	24.8	17
15	(*S*)-(−)-Naph	CH_3	Br	Anhy THF	25	12	*R*	−33.0	32.0	18
16	(*S*)-(−)-Naph	CH_3	Br	Anhy THF	25	36	*R*	−36.0	25.2	14
17	(*S*)-(−)-Naph	CH_3	Br	Anhy THF	25	72	*R*	−37.9	26.4	17
18	(*S*)-(−)-Me	CH_3	Br	Anhy THF	50	5	*S*	+3.6	2.5	27
19	(*S*)-(−)-Et	CH_3	Br	Anhy THF	50	5	*S*	+31.3	21.7	24
20	(*S*)-(−)-Naph	CH_3	Br	Anhy THF	50	5	*R*	−34.3	23.8	27

a) (±)-Me, (±)-α-methylbenzylamine; (*R*)-(+)-Me, (*R*)-(+)-α-methylbenzylamine; (*S*)-(−)-Me, (*S*)-(−)-α-methylbenzylamine; (*S*)-(−)-Et, (*S*)-(−)-α-ethylbenzylamine; (*S*)-(−)-Naph, (*S*)-(−)-α-(1-naphthyl)ethylamine.
b) Specific rotation of DNP-anlanine was measured in 1M NaOH.
c) Defined as $[\alpha]_D$ obsd/$[\alpha]_D$ of the compound ×100. DNP-(*S*)-(+)-Alanine, $[\alpha]_D^{25}$ +143.9° (1M NaOH).
d) The yields are calculated from *N*-alkyl-α-haloacidoamide by using automatic amino acid analyzer.

In a similar way, several α-bromopropionamides (IV, X=Br, R_1=CH_3, R_2=Me or Et, R_3=phenyl or naphthyl) were prepared from racemic α-bromopropionyl bromide with racemic and also optically active α-alkylbenzylamines and optically active α-(1-naphthyl)ethylamine. Table 1 shows the physical properties and elemental analyses of *N*-alkyl-α-bromopropionamides prepared. At varying temperatures, the compounds (IV) were treated with sodium hydride in dioxane as in the synthesis of glycine. After hydrolysis and hydrogenolysis of the reaction products, alanine was obtained in 11 to 36% yield. The reaction conditions, configurations, optical purities, and yields of alanine are summarized in Table 2.

As shown in Table 1, *N*-α-methylbenzyl-β-bromopropionamides were prepared using (*S*)-(−)-α-methylbenzylamine and (*R*)-(+)-α-methylbenzylamine. The melting points of these amides are identical and the magnitude of specific rotations are the same (the signs of rotation are opposite each other). However, this might not mean that the configurations of α-bromopropionyl residue of the prepared amides are racemic. It could be possible that the fractionation took place during amide formation, isolation, and purification. However, from the results shown in Table 2, the possible fractionation of the diastereomeric starting material seems not great.

The reactions were carried out at 0, 25, and 50°C. The yields of optically active alanine at these temperatures are not much different. The optical purities of alanine by the use of α-methylbenzylamine are usually low (0—2.5%) at all temperatures. The optical purity of alanine prepared using (*S*)-(−)-α-ethylbenzylamine at 0°C is rather low (6%); however, it increased considerably at higher temperatures (25% at 25°C, 22% at 50°C). The optical purities of alanine prepared

with (*S*)-(−)-α-(1-naphthyl)ethylamine are rather high at all temperatures (24—27%) and the configuration of alanine is opposite to that prepared with (*S*)-(−)-α-ethylbenzylamine.

As shown in Table 2, the yields and optical purities of the resulting optically active alanine depending on the reaction time do not show a clear relation with the reaction time. This suggests that the reactions do not follow a simple kinetic resolution type mechanism.

In this experiment, the resulting partially optically active alanine was isolated by the use of an ion exchange resin and the resulting crude alanine was converted to DNP-alanine. The partially optically active DNP-alanine was purified by the use of celite column chromatography[18] without fractionation of optical isomers.[19]

Experimental

The specific rotations of optically active amines were:
(*R*)-(+)-α-methylbenzylamine, $[\alpha]_D^{25}$ +41.5° (benzene)
(*S*)-(−)-α-methylbenzylamine, $[\alpha]_D^{25}$ −42.3° (benzene)
(*S*)-(−)-α-ethylbenzylamine, $[\alpha]_D^{25}$ −21.0° (benzene)
(*S*)-(−)-α-(1-naphthyl)ethylamine, [α]- −86.5° (benzene)

Hydrogenolysis was carried out using the Parr 3910 shaker type hydrogenation apparatus. The accuracy of reaction temperatures is about ±1°C. All optical activity measurements were carried out on the JASCO ORD-CD-UV 5 spectropolarimeter.

N-Benzylchloroacetamide (IV, X=Cl, R_1=H, R_2=H, R_3=phenyl). Benzylamine, 10.7 g (0.10 mol) and monochloroacetic anhydride, 17.1 g (0.10 mol), were dissolved in 200 ml of dry benzene and the solution was refluxed gently for 3 hr. After the reaction was over, the benzene solution was washed with 100 ml each of 1 M hydrochloric acid, 7% sodium hydrogen carbonate, and water. The benzene solution was dried with anhydrous sodium sulfate and the benzene was removed under reduced pressure. The residual material was recrystallized from 95% ethanol, yield 14.2 g (77%) mp 92—93°C.

Found: C, 58.68; H, 5.41; N, 7.30%. Calcd for $C_9H_{10}NOCl$: C, 58.86; H, 5.49; N, 7.63%.

N,N'-Dibenzylpiperazinedione (VI, R_1=H, R_2=H, R_3=phenyl). Sodium hydride (60%, 0.4 g, 0.01 mol) was suspended in 50 ml of anhydrous tetrahydrofuran (THF). To this was added slowly a solution of 1.84 g (0.01 mol) of IV in 30 ml of anhydrous THF during a period of 2 hr under cooling with ice water. After the addition was over, the solution was kept at room temperature under agitation for an additional 12 hr. After the reaction was over, precipitated sodium chloride was removed by filtration. The filtrate was divided equally into two portions. One portion was evaporated to dryness and the residue was recrystallized from ethanol, yield of VI, 0.23 g (yield 32% from IV), mp 178—180°C.

Found: C, 73.52; H, 6.21; N, 9.32%. Calcd for $C_{18}H_{18}N_2O_2$: C, 73.45; H, 6.16; N, 9.52%.

The other portion of the filtrate was evaporated to dryness under reduced pressure, and the residue was refluxed with 20 ml of 6 M HCl for 6 hr. After the hydrolysis was over, hydrochloric acid was removed under reduced pressure and the residue was applied to a Dowex 50 column (H^+ form, 19×23 cm) and *N*-benzylglycine was eluted with 1M aqueous ammonia after washing with water. The fractions containing *N*-benzylglycine were combined and evaporated. The residue was dissolved in ethanol–water mixture (1 : 1 in volume) and was hydrogenolyzed by the use of 5% palladium on charcoal. After removal of the catalyst by filtration, the filtrate was evaporated under reduced pressure. The yield of glycine was measured by automatic amino acid analyzer after appropriate dilution, yield 17.3% from I. The glycine was recrystallized from water and ethanol for elemental analysis (Found: C, 31.74; H, 6.78; N, 18.63%).

N-(+)-α-Methylbenzyl-(±)-α-bromopropionamide (IV, X=Br, R_1=Me, R_2=Me, R_3=Phenyl). The solution of (±)-α-methylbenzylamine, 12.1 g (0.1 mol), was added slowly to the solution of (±)-α-bromopropionylbromide, 10.8 g (0.05 mol), in 20 ml of benzene over a period of 1 hr under cooling with ice water. The racemic α-methylbenzylamine hydrochloride was crystallized out during the reaction. The reaction mixture was stirred for 2 hr at room temperature. The precipitated compounds were filtered and washed with benzene (60 ml) to remove amide. The benzene solution was washed with 50 ml each of 1 M hydrochloric acid, 5% sodium hydrogen carbonate, and then with water. The benzene solution was dried by anhydrous sodium sulfate. After the sodium sulfate was removed by filtration, the filtrate was evaporated to dryness under reduced pressure. The residue was recrystallized from 95% ethanol, yield 7.8 g (61%), mp 129—130°C.

Other amides were prepared in a similar way. The physical properties and elemental analyses of these α-bromopropionamides are summarized in Table 3.

(S)-Alanine (VII) from N-Alkyl-α-bromopropionamide (IV, X=Br, R_1=Me, R_2=Me, R_3=phenyl). The solution of *N*-(*S*)-(−)-α-methylbenzyl-α-bromopropionamide (IV), 1.3 g (0.005 mol), in anhydrous dioxane (20 ml) was added slowly to a suspension of sodium hydride (60%, 0.2 g, 0.005 mol) in anhydrous dioxane (20 ml) during a period of 1 hr at room temperature. After the addition was over, the reaction mixture was stirred at room temperature for another 36 hr.

Table 3. *N*-Alkyl-α-bromopropionamide

R	Mp, °C	$[\alpha]_D^{25}$ in THF	Formula	Calcd %			Found %		
				C	H	N	C	H	N
(±)-Me	129—130	—	$C_{11}H_{14}NOBr$	51.58	5.51	5.47	51.59	5.64	5.58
(*R*)-(+)-Me	108—109	+59.8	$C_{11}H_{14}NOBr$	51.58	5.51	5.47	51.23	5.65	5.54
(*S*)-(−)-Me	108—109	−59.5	$C_{11}H_{14}NOBr$	51.58	5.51	5.47	51.49	5.71	5.38
(*S*)-(−)-Et	77—79	−66.8	$C_{12}H_{16}NOBr$	53.35	5.97	5.18	53.42	6.16	5.16
(*S*)-(−)-Naph	176—177	−20.4	$C_{15}H_{16}NOBr$	58.85	5.27	4.57	58.70	5.46	4.67

(+)-Me, (+)-α-methylbenzyl;(*R*)-(+)-Me, (*R*)-(+)-α-methylbenzyl; (*S*)-(−)-Me, (*S*)-(−)-α-methylbenzyl; (*S*)-(−)-Et, (*S*)-(−)-α-ethylbenzyl; (*S*)-(−)-Naph, (*S*)-(−)-α-(1-naphthyl)ethyl.

18) J. C. Perrone, *Nature*, **167**, 513 (1951); A. Court, *Biochem. J.* **58**, 70 (1954).

19) K. Harada and K. Matsumoto, *J. Org. Chem.*, **32**, 1794 (1967); K. Harada and T. Yoshida, This Bulletin, **43**, 921 (1970).

The precipitated sodium bromide was removed by filtration. The filtrate was evaporated under reduced pressure and the residue was refluxed with 30 ml of 6 M HCl for 6 hr. The hydrolyzate was extracted with ether and the hydrochloric acid was evaporated to dryness under reduced pressure. The residue was dissolved in a small amount of water and was applied on a Dowex 50 column (H^+ form). The column was eluted with 1 M aqueous ammonia after washing the column with water. The fractions containing *N*-alkylalanine were combined and evaporated to dryness. The residual *N*-alkylalanine was dissolved in water and alcohol mixture (1: 1) and was hydrogenolyzed with 0.5 g $Pd(OH)_2/C$ for 12 hr. After the hydrogenolysis was complete, the catalyst was removed by filtration. Part of the solution was diluted in the proper way and was analyzed by an automatic amino acid analyzer to determine the yield of alanine, 19.7%. The other part of the alanine solution was evaporated to dryness and the residue was recrystallized from water and ethanol for elemental analysis of alanine (Found: C, 40.03; H, 7.84; N, 15.34%).

The other part of the alanine solution was converted to its DNP-derivative in the usual manner. The resulting DNP-alanine was purified by the use of a celite column treated with pH 7 citrate-phosphate buffer.[18] The yields, specific rotations, and optical purities of alanine preparations are summarized in Table 2.

This work was supported by Grant No. NGR-10-007-052 from the National Aeronautics and Space Administration. The authors wish to express their thanks to Dr. Kazuo Matsumoto for discussions and to Mr. Charles R. Windsor for amino acid analyses.

NOTE

BULLETIN OF THE CHEMICAL SOCIETY OF JAPAN, VOL. 46, 1873—1874 (1973)

A Theoretical Treatment of the Fragmentation Rules in the Mass Spectrometry of Organic Compounds[1]

Hiroshi ICHIKAWA and Michihiko OGATA

Hoshi College of Pharmacy, Ebara, Shinagawa-ku, Tokyo 142

(Received September 27, 1972)

The statistical theory of mass spectra[2-4] (QET) has clearly accounted for the fragmentation of saturated hydrocarbons. This approach, however, seems not to be readily adaptable to a general appreciation of the fragmentation of complex organic molecules, such as those of particular interest to organic chemists. Meanwhile, independently of the theoretical works,[5] organic chemical approaches[6] have provided some simple rules for break-down processes. These rules have been successful in predicting the major fragmentation paths of various compounds.[7] We will here propose a theoretical treatment of the fragmentation rules in terms of the QET and, at the same time, an interpretation of the relationship between the fragmentation rules and the QET.

Theory

According to the Bell[8] and Evans and Polanyi[9] (BEP) principle, the activation energy, ΔE, for a given reaction can be written in a linear form:

$$\Delta E = X + Y\Delta H, \tag{1}$$

where X and Y are constants in the same system and where ΔH is the heat of the reaction.

The QET provides several correlation formulae between the rate constant (k) and the activation energy (ΔE). Among them, for the model composed wholly of harmonic oscillators the general expression[3] in the rate constant is simply:

$$k = \nu\left(\frac{E-\Delta E}{E}\right)^{s-1}, \tag{2}$$

where E is the internal energy, ν is a constant with the dimension of cm^{-1}, and s is the effective number of degree of freedom.

If Eq. (1) holds in the mass-spectral reactions, then the ratio of the rate constants, k_1/k_2, for any two of the fragmentation paths:

$$\begin{array}{ccc} (\text{P–Q–R})^{\cdot+} & \xrightarrow[\text{Path A}]{k_1} & (\text{P–Q} + \text{R})^{\cdot+} \\ \text{Path B}\ \downarrow k_2 & & \\ (\text{P} + \text{Q–R})^{\cdot+} & & \end{array}$$

will be given by:

$$\frac{k_1}{k_2} = \left(\frac{E'-\Delta H_1}{E'-\Delta H_2}\right)^{s-1}, \tag{3}$$

where $E'=(E-X)/Y$.

Equation (3) indicates that the fracture occurs more predominantly at the position which gives the smallest ΔH; one can predict the most probable position of bond-scission by simply comparing the sum of the total energies of the fragments. That is, if the total energy of the $(\text{P–Q} + \text{R})^{\cdot+}$ state is lower than that of the $(\text{P} + \text{Q–R})^{\cdot+}$ state, the fragmentation path A will be more important.

TABLE 1. TOTAL ENERGIES OF FRAGMENTS (a.u.)

Fragment	Symmetry[a]	Radical[b]	Ion[c]
CH_3	D_{3h}	−9.1167	−8.6687
C_2H_5	C_s	−17.8337	−17.4580
$CH_3CH_2CH_2$	C_s	−26.5264	−26.1680
$CH_3(CH_2)_2CH_2$	C_s	−35.1888	−34.8077
$(CH_3)_2CH$	C_s	−26.5325	−26.2113
$(CH_3)_3C$	C_{3h}	−35.2423	−34.9561
NH_2	C_{2v}	−12.9377	−12.4110
CH_2NH_2	C_{2v}	−21.5352	−21.2964
CH_3CHNH_2	C_s	−30.2366	−30.0213
$H_2NCH_2CH_2$	C_s	−30.2471	−29.8451
$H_2N(CH_2)_2CH_2$	C_s	−38.9409	−38.5563
$CH_2CH_2CHNH_2$	C_s	−38.9268	−38.7154
$CH_2{=}CH(sp)$	C_{2v}	−16.0884	−15.7406
$CH_2{=}CHCH_2$	C_{2v}	−24.8304	−24.4726
CH_2OH	C_s	−27.5460	−27.2385
CH_3CHOH	C_s	−36.2494	−35.9788
OH	C_∞	−18.9900	−18.3504
CH_3CO	C_{3v}	−34.5607	−34.2921

a) The conformations were all set to be staggered.
b) By the open-shell CNDO/2 method.
c) By the closed-shell CNDO/2 method.

1) An MO Approach to the Interpretation of Organic Mass Spectra. II. Part I.; M. Ogata and H. Ichikawa, This Bulletin, **45**, 3231 (1972).

2) H. M. Rosenstock, M. B. Wallstein, A. L. Wahrhaftig, and H. Eyring, *Proc. Nat. Acad. Sci.*, **38**, 667 (1952).

3) H. M. Rosenstock and M. Krauss, *Adv. Mass Spectr.*, **2**, 251 (1963).

4) H. M. Rosenstock, *Adv. Mass Spectr.*, **4**, 523 (1968).

5) Among theoretical works, the quantum chemical method, based on the relationship between the scission probability and the net-charge density at the highest occupied orbital of the molecule ion, has been most successful in predicting the position of bond-scission (*e.g.*, a) J. Lennard-Jones and G. G. Hall, *Trans. Faraday Soc.*, **48**, 581 (1952); b) K. Hirota and M. Itoh, This Bulletin, **39**, 1406 (1966)). However, the inconsistence of the theory with the experimental results has also been pointed out by some authors (*e.g.*, a) N. D. Coggeshall, *J. Chem. Phys.*, **30**, 593 (1959); b) J. C. Lorquet, *Mol. Phys.*, **9**, 101 (1965)).

6) F. W. McLafferty, ed., "Mass Spectrometry of Organic Ions," Academic Press, New York, 1963, Chapter 7.

7) H. Budzikiewicz, C. Djerassi, and D. H. Willians, "Mass Spectrometry of Organic Compounds," Holden-Day, San Francisco, 1967.

8) R. P. Bell, *Proc. Roy. Soc., Ser. A*, **154**, 414 (1936).

9) M. G. Evans and M. Polanyi, *Trans. Faraday Soc.*, **32**, 1340 (1936).

Table 2. Total energies of molecule ions and produced fragments (a.u.)

Molecule ion	Total energy[a]	Fragmentation	Total energy	ΔH[b]
$CH_3CH_2NH_2$	−30.8091	1*[c] $CH_3\cdot + CH_2{=}NH_2^+$	−30.4130	0.3961
		2 $CH_3CH_2^+ + \cdot NH_2$	−30.3957	0.4134
$CH_3CH_2CH_2NH_2$	−39.4964	1 $CH_3\cdot + {}^+CH_2CH_2NH_2$	−38.9619	0.5347
		2* $CH_3CH_2\cdot + CH_2{=}NH_2^+$	−39.1301	0.3663
		3 $CH_3CH_2CH_2^+ + \cdot NH_2$	−39.1056	0.3908
$CH_3CH_2CH_2CH_2NH_2$	−48.1846	1 $CH_3\cdot + {}^+CH_2(CH_2)_2NH_2$	−47.6730	0.5116
		2 $CH_3CH_2^+ + \cdot CH_2CH_2NH_2$	−47.7051	0.4795
		3* $CH_3CH_2CH_2\cdot + CH_2{=}NH_2^+$	−47.8227	0.3619
		4 $CH_3(CH_2)_2CH_2^+ + \cdot NH_2$	−47.7454	0.4392
$CH_3CH_2CH{=}CH_2$	−33.9639	1* $CH_3\cdot + {}^+CH_2CH{=}CH_2$	−33.5893	0.3746
		2 $CH_3CH_2\cdot + {}^+CH{=}CH_2$	−33.5706	0.3933

a) Calculated by the open-shell CNDO/2 method.
b) The difference of the energies, E(radical)+E(cation)−E(molecule ion).
c) Asterisk indicates the most abundant fragmentation. See Ref. 7.

The adaptability of Eq. (3) may be responsible for the BEP principle. This principle has proved extremely valuable in a variety of chemical reactions.[10] With regard to mass-spectral reactions, some authors[11] have pointed out that the stability of the produced fragments plays an important role in the cleavage reaction. Actually, it should be pointed out that in the establishment of the fragmentation rules,[6,7] the stability of the produced fragments, based on the consideration of the ground-state chemical structure, has always been taken into account. These facts indicate that the fragmentation rules represent the approximate reactions of the electronically ground-state ion,[12] that the BEP principle mostly holds in the mass-spectral reactions, and that, therefore, the fragmentation rules suggest the path with the lower activation energy.

Results

The total energies of several cations and radicals obtained by means of the CNDO/2 method are listed in Table 1. The combination of these fragments would give a variety of fragmentation modes. Shown as examples in Table 2 are ΔH values calculated for the fragments given by the skeletal-bond cleavages of some simple amines and 1-butene, which are selected as model compounds showing the β-bond cleavage.[13] The positive charge should be put on the fragment with the lower I_p value so that the total energy of the system is made as low as possible.

The sum of the total energies of the fragments which are formed by the β-bond cleavage is generally the least, indicating that such a β-bond is most inclined to cleave. Though being qualitative, these results, of course, agree with the experimental results. We believe that the application of this method to various compounds will prove its validity and that it is possible to some extent to predict the quantitative abundance of the bond-scission for the ground-state molecule ion. Finally, though the CNDO/2 method is not well adaptable to the estimation of the total energy, as the results indicate, the method is sufficiently useful for such a qualitative problem as bond-scission.

The calculations were carried out on a HITAC 5020E computer at the Computation Center of the University of Tokyo.

10) M. J. S. Dewar, "The Molecular Orbital Theory of Organic Chemistry," McGraw-Hill, New York, 1969, Chapter 8.
11) a) H. Budzikiewicz, J. I. Brauman, and C. Djerassi, *Tetrahedron*, **21**, 1855 (1965); b) H. Budzikiewicz, C. Fenselau, and C. Djerassi, *ibid.*, **22**, 1391 (1966).
12) The main reactions of the fragmentation rules mostly give rise to metastable peaks.[7] Such reactions belong to Class I reactions, according to the classification of R. C. Dougherty (*J. Amer. Chem. Soc.*, **90**, 5780 (1968)), which occur with vibrational excitations.
13) This paper follows the definition by McLafferty.[6]

BULLETIN OF THE CHEMICAL SOCIETY OF JAPAN, VOL. 46, 1875—1876 (1973)

Phase Diagram of the Phenanthrene/Carbazole-Picric Acid System

Shigeo KOIZUMI* and Yoshio MATSUNAGA**

Department of Chemistry, Faculty of Science, Hokkaido University, Sapporo 060

(Received October 20, 1972)

By means of differential scanning calorimetry, it has been found that phenanthrene picrate exhibits an enantiotropic transition at 77 °C in addition to the one at 106 °C reported by Kofler.[1,2] The recovery of the low-temperature form is so slow that the newly-found transition cannot be observed in the second run if it is examined immediately after the first heating. Furthermore, the addition of anthracene, a major impurity in phenanthrene, has been found to slow down the recovery. As carbazole is another major impurity in phenanthrene, an examination of the phenanthrene/carbazole picrate seemed to be desirable in order to confirm the effects of impurities on the above-mentioned phase-transition.

Phenanthrene, Eastman white label, was purified according to the method reported by Feldman *et al.*,[3] and then by zone-refining. After these processes, the content of anthracene was estimated to be less than 10^{-4} mol%, because the electronic absorption maximum located at 376 nm characteristic of anthracene was no longer detectable in a cyclohexane solution. Carbazole from the Koso Chemical Co. was refluxed with acrylonitrile in toluene for ten hours to remove the anthracene, and was then recrystallized twice from benzene. Picric acid, Wako special reagent grade, was purified by recrystallization from ethanol. The picrates were crystallized from methanol containing equimolar amounts of the component compounds. Although mutual solid solubility in many pairs of molecular complexes has been examined by Rheinboldt and Senise[4] and by Lower,[5] phenanthrene/anthracene-*s*-trinitrobenzene is the only system for which a phase diagram has been described in detail. Consequently, we decided to look into the whole system rather than just the phenanthrene-rich region. Samples were prepared by melting powdered mixtures with known ratios of the parent complexes. The composition is quoted in the mole percentage of the carbazole. After storage at room temperature for a week, the melting points and transition temperatures were determined using a Rigaku Denki differential scanning calorimeter, Model 8001 SL/C, at a heating rate of 3 °C/min. X-Ray measurements on powdered samples were made at room temperature with a Toshiba recording diffractometer, Model ADG-301, using filtered copper radiation.

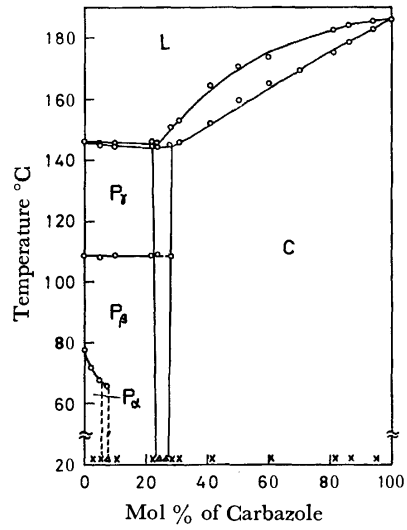

Fig. 1. The phenanthrene/carbazole-picric acid phase diagram.
○: calorimetric points, ×: single phase by X-ray diffraction, △: two phases by X-ray diffraction.

The experimental points determined by calorimetry are plotted in Fig. 1. This diagram is of the same type as that of the phenanthrene/anthracene-*s*-trinitrobenzene reported by Lower,[5] and shows the formation of two series of solid solutions, P and C, based on the two parent complex lattices, which have not previously been known. A eutectic occurs at about 24 mol% carbazole and at 145 °C. This temperature is nearly the same as the melting point of pure phenanthrene picrate. Therefore, the solidus and liquidus are almost flat and coincide with each other in the phenanthrene-rich region. The first phase-transition in the phenanthrene picrate is markedly lowered by the addition of small amounts of the carbazole picrate; *e.g.*, it becomes 66 °C at 6.86 mol%. Above this composition, the $P_\alpha \rightarrow P_\beta$ transition could not be detected by calorimetry. This result is similar to that reported for the phenanthrene/anthracene picrate.[1] Therefore, it is certain that carbazole can affect the rate of recovery as much as anthracene does. The X-ray examination revealed that the solid solution containing 5.12 mol% carbazole is single-phase, while those containing 5.91 and 6.86 mol% are mixtures of the P_α and P_β terminal solid solutions, indicating that the equilibrium condition could not be established by one week's storage. If the solid solutions containing more carbazole could be well annealed, the phase boundary between P_α and P_β would extend to about 22 mol%. On the other hand, the second phase-transition temperature is essentially independent of the composition and is detectable as

* Present address: Fuji Photo-Film Co., Minami-ashigara, Kanagawa.

** To whom inquiries may be addressed.

1) Y. Matsunaga, This Bulletin, **44**, 2868 (1971).
2) A. Kofler, *Z. Elektrochem.*, **50**, 200 (1944).
3) J. Feldman, P. Pantages, and M. Orchin, *J. Amer. Chem. Soc.*, **73**, 4341 (1951).
4) H. Rheinboldt and P. Senise, *Bols. faculdade filosofia, cienc. letras, Univ. São Paulo*, **14**, *Quimica* No. 1, 3 (1942), through *Chem. Abstr.*, **40**, 2049 (1946).
5) S. K. Lower, *Mol. Cryst. Liq. Cryst.*, **5**, 363 (1969).

far as 28 mol% carbazole. Above 26 mol%, the X-ray diffraction pattern recorded at room temperature is clearly that of the carbazole picrate, although the lattice constants increase more or less upon the addition of phenanthrene; *e.g.*, a diffraction peak located at 12.82° in the pure carbazole picrate moves to 12.30° at 30 mol% carbazole. This change corresponds to an increase of 0.30 Å in the distance of 6.91 Å in the pure carbazole picrate. The presence of a narrow miscibility gap, the width of which could be influenced by non-equilibrium effects, was confirmed by the X-ray data, as is indicated in Fig. 1.

The authors wish to express their thanks to Professor Toshio Yokokawa for letting them use the X-ray diffractometer and to Dr. Eiji Osawa for his advice concerning the purification of carbazole.

BULLETIN OF THE CHEMICAL SOCIETY OF JAPAN, VOL. 46, 1876—1878 (1973)

Infrared Spectra of CO and O_2 Adsorbed on Tungsten

G. BLYHOLOER and Masako TANAKA*

Department of Chemistry, University of Arkansas, Fayetteville, Arkansas 72701, U.S.A.

(Received January 17, 1973)

While adsorption on tungsten surfaces has received much attention[1] from workers using field emission and field ionization microscopy, LEED and flash desorption techniques there has been no successful room temperature infrared spectroscopic work reported for species chemisorbed on tungsten. Since no single technique gives a definitive view of chemisorption, it is desirable to have information from as many different techniques as possible. The main difficulty to applying the usual infrared methods[2] in surface chemistry to tungsten is its refractory nature which makes obtaining it in a highly dispersed form difficult. In the only reported[3] attempt to work with tungsten, a technique which involves evaporating a thin film of metal onto a salt plate at 170 K and then admitting the adsorbate was tried. This method produced spectra for CO on Ni, Co, Fe, and Ir but not for tungsten. If the tungsten was evaporated in 10^{-2} Torr of CO, a weak band appeared at 1970 cm^{-1} but this disappeared upon warming to room temperature. This raises the question as to whether tungsten is different from the other transition metals for which infrared spectra of adsorbed CO and other gases have been obtained.

The wide spectral range experimental technique, which has been described in detail elsewhere,[4] consists of evaporating tungsten from a filament made by twisting together 4 strands of 0.06″ diameter tungsten wire. The evaporated metal deposits in a purified hydrocarbon oil film on the salt windows of an infrared cell. Spectra are recorded before and after admission of the gas to be studied. The spectra were recorded on a Perkin-Elmer Model 457 spectrometer.

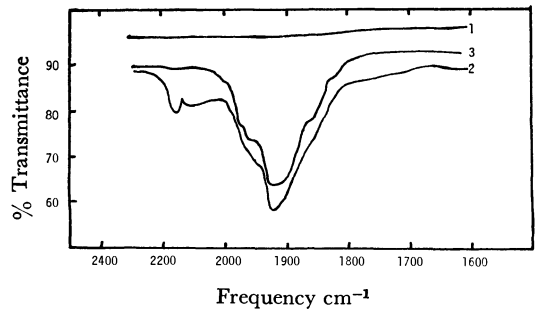

Fig. 1. Infrared spectra of CO adsorbed on tungsten. 1) background; 2) 50 Torr CO for 16 hr at room temperature; 3) evacuated at 10^{-5} Torr for 1.5 hr.

Infrared spectra of CO adsorbed on tungsten are shown in Fig. 1. After exposure to 50 Torr of CO for 16 hr at room temperature the result is curve 2, which has a band maximum at about 1920 cm^{-1} and a major shoulder at 1950 cm^{-1} as well as several lesser shoulders. The bands in the 2100—2200 cm^{-1} region are due to gas phase CO. The intensity of the band in the 1900 cm^{-1} region did not decrease appreciably after evacuation of the cell for 1.5 hr as shown in curve 3.

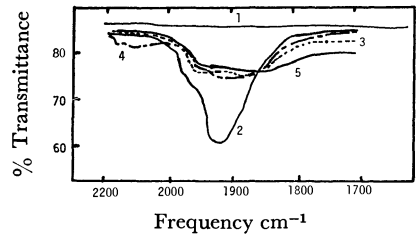

Fig. 2. Effect of heating. 1) background; 2) chemisorbed CO; 3) evacuated at 100°C for 1 hr.; 4) reexposed to 50 Torr CO for 16 hr.; 5) additional evacuation at 150 °C for 45 min.

The effect upon the spectra of mild heating is shown in Fig. 2, where curve 2 is for chemisorbed CO in an evacuated cell at room temperature. Evacuating and heating at 100 °C for 1 hr greatly decrease the band

* Present address, Department of Atomic Engineering and Nuclear Science, Hokkaido University, Sapporo 060.

1) R. R. Ford, *Advan. Catal.*, **21**, 51 (1970).

2) G. Blyholder, "Experimental Methods in Catalytic Research," Chap. 8 ed. by R.B. Anderson, Academic Press, New York, 1968.

3) F. S. Baker, A. M. Bradshaw, J. Pritchard, and K. W. Sykes, *Surface Science*, **12**, 426 (1968).

4) G. Blyholder, *J. Chem. Phys.*, **36**, 2036 (1962).

intensity in the 1920 cm^{-1} region as shown in curve 3. The permanent nature of the change caused by heating is demonstrated by exposing the cell to 50 Torr of CO for 16 hr and observing that curve 4 shows little change after this treatment. Again the bands in the 2100 cm^{-1} region are due to gas phase CO. Curve 5 shows the sample after further evacuation at 150 °C for 45 min. After noting that the background at lower wave numbers has been shifted it is evident that this last treatment has further reduced the absorption in the 1920 cm^{-1} region while that at 1970 cm^{-1} is much less decreased by the heat treatments.

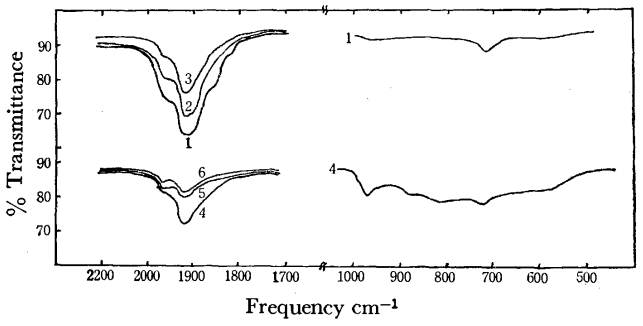

Fig. 3. O_2 addition to chemisorbed CO. 1) chemisorbed CO; 2) exposed to 30 Torr O_2 at room temperature; 3) after 6.5 hr exposure to O_2; 4) after 12 hr with 90 Torr O_2; 5) after 90 Torr O_2 at 100 °C for 30 min.; 6) evacuation at 100 °C for 5 min.

The effect of added O_2 on the chemisorbed CO is shown in Fig. 3, where curve 1 is for chemisorbed CO and the band at 720 cm^{-1} is a background oil band. After exposure to 30 Torr of O_2 at room temperature the chemisorbed CO band intensities decreased as shown in curve 2. Further exposure to O_2 for 6.5 hr gives curve 3 while 90 Torr of O_2 for 12 hr results in curve 4. By this time a broad band from 500 to 1000 cm^{-1} and a sharper band around 965 cm^{-1} have become evident. Heating the cell at 100 °C with 90 Torr of O_2 for 30 min further reduced the intensity around 1920 cm^{-1} while not changing the intensity near 1970 cm^{-1} as indicated by curve 5. Evacuation for 5 min at 100 °C resulted in curve 6.

In order to understand the bands resulting from the O_2 treatment of chemisorbed CO, a freshly evaporated tungsten surface was exposed to 115 Torr of O_2 at room temperature. The spectra obtained after 1.5 and 5 hr, shown in Fig. 4, reveal the formation of a broad absorption from 500 to 1000 cm^{-1} and a peak at 970 cm^{-1}.

In reviewing these results it is evident that tungsten

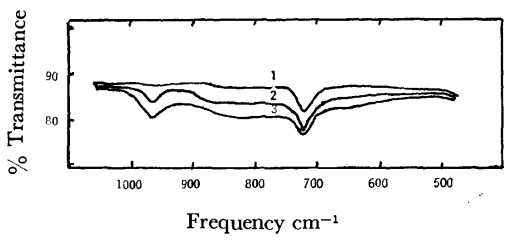

Fig. 4. O_2 adsorption on tungsten. 1) background; 2) 115 Torr O_2 at room temperature for 1.5 hr.; 3) 115 Torr O_2 at room temperature for 5 hr.

does indeed behave similarly to other transition metals with respect to the infrared spectra of chemisorbed CO. Since so much work has been done by other techniques on tungsten, it is good to have this additional evidence that tungsten is not unrepresentative of transition metals in general. The question may arise as to whether the oil matrix changes the chemical character of the metal surface. At least with respect to CO adsorption the answers seems to be no. Infrared spectra, where obtainable, for CO adsorbed on metals evaporated in high vacuum onto salt plates[3,5-7] or into an argon matrix[8,9] are like those for oil-matrix metals.[10] The spectrum obtained here by CO on tungsten is most like those for Cr, which is directly above it in the periodic table, and V which is above and one group to the left.

The decrease in infrared band intensity upon heating is more likely due to sintering than to simple thermal desorption since it occurs at 100 °C whereas the first major desorption in flash filament work occurs in the 150 to 200 °C range. That sintering can be a major cause of an infrared band intensity decrease is also shown in work with Ni in an argon matrix.[9] Noting the sintering effect and the fact that for spectra of CO on metals evaporated directly onto salt plates the intensities are always very low, it appears that most of the CO causing the large broad band centered around 1920 cm^{-1} is on surface tungsten atoms that have a low coordination number, *i.e.* that are not part of a high atom density surface plane. In view of the metal being evaporated in such a way as to inhibit sintering it is not surprising that there is large number of such sites. The band intensity around 1970 cm^{-1} suffers a less drastic decrease upon heating and oxygen treatment, suggesting that a part of this intensity is due to CO on the high atom density surface planes.

The spectral results of oxygen addition to chemisorbed CO shown in Fig. 3 indicate that the CO is displaced by the oxygen and new bands for surface species are produced in the 500 to 1000 cm^{-1} region. Subsequent adsorption of O_2 on fresh tungsten shows these bands to be entirely due to oxygen on tungsten. Thus tungsten does not behave like Ni where O_2 addition to surface CO produces a surface CO_3 species.[11]

The infrared bands produced by oxygen adsorption are quite similar to bands for tungsten oxides. Weltner and McLeod[12] report that the frequency of the terminal W=O stretch in W_2O_6 and W_3O_8 is at 989 cm^{-1} and

5) J. F. Harrod, R. W. Roberts, and E. F. Rissman, *J. Phys. Chem.*, **71**, 343 (1967).
6) A. M. Bradshaw and J. Pritchard, *Proc. Roy. Soc. Ser., A*, **316**, 169 (1970).
7) A.M. Bradshaw and O. Vierle, *Ber. Bunsenges. Phys. Chem.*, **74**, 630 (1970),
8) G. Blyholder, M. Tanaka, and J. D. Richardson, *Chem. Commun.*, **1971**, 499.
9) G. Blyholder and M. Tanaka, *J. Colloid Interfac. Sci.*, **37**, 753 (1971).
10) G. Blyholder and M. C. Allen, *J. Amer. Chem. Soc.*, **91**,3158 (1969).
11) G. Blyholder, Proc. 3rd Intern. Cong. Catalysis Amsterdam 1964, **1**, 657 (1965).
12) W. Weltner Jr., and D. McLeod, *J. Mol. Spectrosc.*, **17**, 276 (1965).

that WO_3 has a strong band at 1007 cm^{-1}. This leads to our assigning the 970 cm^{-1} band to a terminal W=O structure at the surface. The broad band in the 500—1000 cm^{-1} region is presumed due to the W–O–W structure since many W_nO_m compounds have several weak bands in this region. Thus on tungsten samples suitable for infrared studies the adsorption of O_2 is clearly dissociative. No infrared bands corresponding to O–O stretches were found. The formation of a surface structure in which an oxygen atom has a double bond to a metal atom has been found previously for V[13] and Cr[14] but not for transition metals to the right of group VIB such as Mn, Fe, Co, and Ni, which we have investigated.

Support from the National Science Foundation is acknowledged with thanks.

13) G. Blyholder and M. C. Allen, *Inorg. Chem.*, **9**, 302 (1970).
14) M. C. Allen, Ph. D. Dissertation, University of Arkansas, 1967.

BULLETIN OF THE CHEMICAL SOCIETY OF JAPAN, VOL. 46, 1878—1880 (1973)

The Synthesis of Some New Europium(II) Vanadites

Tsutomu SHIN-IKE, Ginya ADACHI,* and Jiro SHIOKAWA*

Department of Chemistry, Osaka Dental Universtiy, Makino-honmachi, Hirakata-shi, Osaka 573

(Received May 12, 1972)

This paper is concerned with the preparation of some new europium (II) double oxides by reactions between europium (II) and vanadium (III) oxides, and with the determination of their crystal structures.

Europium (III) double oxides with vanadium have been prepared previously,[1,2] but no report has appeared regarding the double oxide containing the bivalent europium ion.

We succeeded in synthesizing the double oxides containing the bivalent europium ion. The crystal structures of the double oxides were determined by an X-ray diffraction method.

Experimental

Materials. Europium sesquioxide of a 99.9% purity from the Lindsay Chemical Division, American Potash & Chemicals, vanadium trioxide of a special reagent grade, and graphite of a spectroscopic grade were all used without further purification.

The europium mono-oxide (EuO) was prepared by reducing europium sesquioxide with graphite, as has been described in the literature.[3]

Procedure. The europium mono-oxide was thoroughly mixed with vanadium trioxide by grinding in a mortar, and then pressed at 100 kg/cm^2 to a pellet. The pellet was placed in a graphite crucible and heated in an induction furnace at 1500 °C for a few minutes *in vacuo* ($\sim 10^{-4}$ mmHg).

Analyses. X-Ray diffraction patterns of the products were obtained with a Rigaku Denki Geiger-Flex D-6C diffractometer, using Ni-filtered Cu-Kα radiation at a scanning rate of 1° (2θ)/min.

The atomic ratios of europium to vanadium were determined by means of a Rigaku Denki X-ray fluorescent spectrograph unit with an NaI(Tl) scintillator, a tungsten target X-ray tube, and a lithium fluoride analyzing crystal.

Results and Discussion

The products, the color of which was black, were examined by the X-ray diffraction method. The X-ray diffraction patterns of the samples and the analyzed atomic ratios of europium to vanadium are shown in Fig. 1. The X-ray diffraction pattern, shown in Fig. 1 (a), is similar to that of Eu_2TiO_4,[4] which belongs to a tetragonal system. It seems, therefore, that the crystal structure of this compound is the same as that of Eu_2TiO_4. The arrangement of the ions in this compound may be considered to consist of alternate layers of rocksalt EuO and perovskite $EuVO_3$, as is shown in Fig. 2. Thus, by assuming that the unit cell dimensions of the product are a_0=3.856 Å and

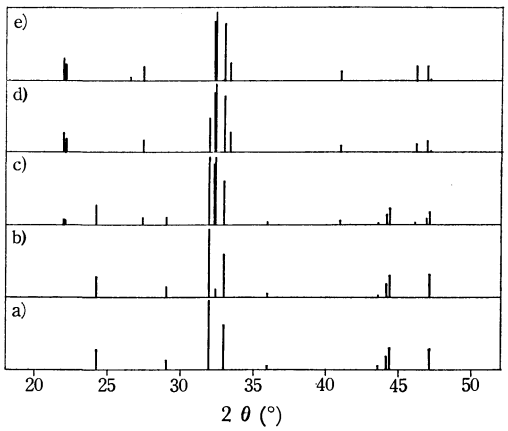

Fig. 1. X-Ray diffraction patterns
Observed Atomic Ratios of Eu: V
a) 1.0: 0.5, b) 1.0: 0.8, c) 1.0: 0.9, d) 1.0: 1.0, e) 1.0: 2.0.

* Department of Applied Chemistry, Faculty of Engineering, Osaka University, Yamadakami, Suita-shi, Osaka.

1) W. O. Milligan and L. W. Vernon, *J. Phys. Chem.*, **56**, 145 (1952).

2) A. Wold and R. Ward, *J. Amer. Chem. Soc.*, **76**, 1029 (1954).

3) M. W. Shafer, *J. Appl. Phys.*, **36**, 1145 (1965).

4) G. J. McCarthy, W. B. White, and R. Roy, *J. Inorg. Nucl. Chem.*, **31**, 329 (1969).

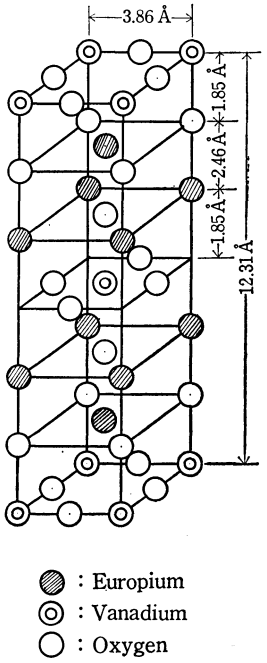

Fig. 2. The proposed structure of Eu_2VO_4

c_0=12.312 Å (in a tetragonal system), the interplanar spacing values (*d*-values) and the relative intensities were calculated. Both the calculated and the observed values are shown in Table 1.

Table 1. Powder diffraction results
(Tetragonal system; a_0=3.856Å, c_0=12.312Å)

hkl	*d*(Å) (obsd)	2θ (obsd)	*d*(Å) (calcd)	$I^{a)}$ (obsd)	$I^{a)}$ (calcd)
002	—	—	6.155	—	0.4
101	3.681	24.2	3.680	28	28
004	3.079	29.0	3.078	14	14
103	2.809	31.9	2.810	100	100
110	2.722	32.9	2.726	55	62
112	2.493	36.0	2.493	7	6
105	2.076	43.6	2.075	9	3
006	2.049	44.2	2.052	20	12
114	2.041	44.4	2.041	30	31
200	1.928	47.1	1.928	29	31
211	1.709	53.6	1.708	5	5
204	1.636	56.2	1.634	15	9
107	1.600	57.6	1.600	20	10
213	1.590	58.0	1.590	30	36
008	—	—	1.539	—	2
215	1.408	66.4	1.412	15	1
206			1.405		13

a) Relative intensities.

The density of this compound as observed by the conventional pycnometric method was 3.76 g cm^{-3}, very close to the value of 3.79 g cm^{-3} calculated using the unit cell dimensions and supposing the existence of two molecules of Eu_2VO_4 per unit cell.

When this compound was heated at 1400 °C *in vacuo* for more than 10 min, the peaks in the X-ray pattern assigned to Eu_2VO_4 gradually disappeared, while new peaks appeared. These peaks seemed to be due to another new double oxide, $Eu_3V_2O_7$, in which a

Table 2. X-Ray diffraction powder data for $Eu_3V_2O_7$
(Tetragonal system; a_0=3.94Å, c_0=19.52Å)

hkl	*d*(Å) (obsd)	2θ (obsd)	*d*(Å) (calcd)	I/I_0
101	3.86	23.1	3.86	15
103	3.37	26.5	3.37	5
006	3.25	27.4	3.25	40
110	2.78	32.2	2.78	90
105	2.77	32.3	2.77	100
112	—	—	2.68	—
008	—	—	2.44	—
114	2.42	37.2	2.42	5
107	—	—	2.28	—
116	2.11	42.8	2.11	10
200	1.97	46.1	1.97	50
0010	1.96	46.6	1.95	50
202	1.92	47.1	1.93	20
109	1.90	47.9	1.90	5
204	1.83	50.0	1.83	5

(I/I_0=relative intensities)

rocksalt-type EuO might be located at every two layers of perovskite-type $EuVO_3$. The X-ray diffraction data, given in Table 2, are indexed on a tetragonal cell with a_0=3.94 Å and c_0=19.52 Å. The reason why $Eu_3V_2O_7$ was formed may be that EuO was volatile at high temperatures, if so, the following reactions would occur:

$$2Eu_2VO_4 \longrightarrow Eu_3V_2O_7 + EuO\uparrow \quad (1)$$

The $Eu_3V_2O_7$ does not seem to be quite stable at such high temperatures, since the X-ray pattern of this compound gradually disappeared during the long period of heating. The final product was $EuVO_3$, which has the same distorted perovskite structure as the lanthanide-vanadites.[5] The $EuVO_3$ must be formed as follows:

$$Eu_3V_2O_7 \longrightarrow 2EuVO_3 + EuO\uparrow \quad (2)$$

The cell constants of $EuVO_3$ were a_0=3.88 Å, b_0=3.84 Å, c_0=3.88 Å, and β=92.50° in a monoclinic system. Both the calculated and the observed *d*-values are shown in Table 3.

Table 3. X-Ray diffraction powder data for $EuVO_3$
(Monoclinic system; a_0=3.88Å, c_0=3.88Å, b_0=3.84Å, β=92.50°)

hkl	*d*(Å) (obsd)	2θ (obsd)	*d*(Å) (calcd)	Intensities
001	3.89	22.9	3.88	m
010	3.84	23.1	3.84	w
011	2.73	32.8	2.73	s
101	2.69	33.3	2.68	m
111	2.20	41.0	2.20	w
002	1.94	46.8	1.94	w
020	1.92	47.5	1.92	w
012	1.73	53.1	1.73	w
021	1.72	53.2	1.72	m
102	1.71	53.6	1.70	w
121	1.561	59.2	1.561	m
112			1.558	
022	1.365	68.8	1.364	w

5) S. Geller, *Acta Crystallogr.*, **10**, 219 (1957).

When the Eu_2VO_4 prepared was heated in air, both $EuVO_4$ and Eu_2O_3 were formed by oxidation. This fact was confirmed by X-ray diffraction analyses. If the following reaction is supposed to occur, the weight gain should be 5.73%:

$$2Eu_2VO_4 + \frac{3}{2}O_2 \longrightarrow 2EuVO_4 + Eu_2O_3 \qquad (3)$$

The observed weight gain, on the contrary, was 7.8% Therefore, it seems that the product was a non-stoichiometric compound, like Eu_2VO_{4-x} ($0.5 \geq x \geq 0$), in which the oxygen-deficient perovskite-type $EuVO_{3-x}$ was contained, and that the reaction was as follows:

$$4EuO + V_2O_3 \longrightarrow 2Eu_2VO_{3.5} \qquad (4)$$

If excess vanadium trioxide was added, or if the reaction time was prolonged, both Eu_2VO_4 and $Eu_3V_2O_7$ were formed (see Fig. 1 (b)). If much more vanadium trioxide was used, $EuVO_{3-x}$ was formed in addition to Eu_2VO_4 and $Eu_3V_2O_7$ (see Fig. 1 (c) and (d)).

By another procedure, one in which Eu_2O_3, V_2O_3, and graphite were mixed together, in spite of using EuO and V_2O_3, and then heated in an induction furnace at 1400 °C for an hour *in vacuo*, Eu_2VO_{4-x} was also obtained.

BULLETIN OF THE CHEMICAL SOCIETY OF JAPAN, VOL. 46, 1880—1881 (1973)

Nonbridging Ligand Effects on the Reduction of Nitrilopolyaminocarboxylato-cobalt(III) Complexes by Iron(II)

Kousaburo OHASHI

Department of Chemistry, Ibaraki University, Mito 310

(Received August 19, 1972)

The effects of the nonbridging ligand on the rate of electron-transfer reactions between $Co(ox)N_4^+$-type complexes ($N_4=(NH_3)_4$, $(en)_2$, trien, $(phen)_2$, and $(dpy)_2$) and Fe^{2+} have been reported in a previous paper.[1] The results show that the variation in the rate is mainly due to the change in the enthalpy of activation. It is of interest to investigate systematically how the nonbridging ligands affect the enthalpy and entropy of activation in the Fe^{2+} reduction of the cobalt(III) complexes. The author wishes now to report on the nonbridging ligand effects on the reactivities of the nitrilotriacetato- and ethylenediamine-*N*,*N*′-diacetatocobalt(III) complexes with Fe^{2+}.

Experimental

Materials. The *cis*-α-$[Co(edda)(NH_3)_2]ClO_4$,[2,3] *cis*-α-$[Co(edda)(en)]ClO_4$,[2] $[Co(nta)(en)]$,[4,5] *trans*-(N)-K$[Co(nta),(am)]$,[6] (am=glycine, β-alanine, and γ-aminobutyric acid) were prepared by methods similar to those described in the references cited. The $Co(nta)(H_2O)(NH_2CH_2CH_3)$ solution was prepared by the dissolution of $K[Co(nta)(NH_2CH_2CH_3)(OH)]$, which has itself been prepared by modifying the method of the preparation of $[Co(nta)(en)]$[4] into a perchloric acid solution. The $Co(edda)(H_2O)_2^+$ and the $Co(nta)(H_2O)_2$ solutions were prepared by the equation of *cis*-α-Na$[Co(edda)Cl_2]$ and the dissolution of $K[Co(nta)(H_2O)(OH)]$ respectively into the perchloric acid solution.

The preparation of the iron(II) solution and the determinations of the concentrations of iron(II), the perchlorate ion, and the hydrogen ion were carried out by methods similar to those described in a previous paper.[7] Reagent-grade chemicals were used for the preparation of the reaction mixtures.

Kinetic Measurements. The reactions were followed spectrophotometrically by observing the decrease in the absorbance of the Co(III) complexes at a wavelength in the vicinity of the first absorption maximum. The determinations of the rate constants of *cis*-α-$Co(edda)(NH_3)_2^+$ and *cis*-α-$Co(edda)(en)^+$ were performed in the temperature range of 50—80 °C because of the very small solubility and reactivities of these complexes. The rate constants at 25 °C were obtained by the extrapolation of the Arrhenius plots. In the course of the reactions, the decompositions of none of the complexes were observed under the conditions adopted.

Results and Discussion

The rate constants and the activation parameters are listed in Tables 1 and 2. The reactions of *cis*-α-$Co(edda)(en)^+$ were followed under the conditions of $[H^+]=0.86$ M and $\sum[ClO_4^-]=2.45$ M; the rate constant at $\sum[ClO_4^-]=1.00$ M, $[H^+]=0.36$ M, and 25 °C should be slightly smaller than 1.65×10^{-3} $M^{-1}\cdot s^{-1}$.

The relationship between the second-order rate constant and the hydrogen ion concentration for Co(nta)(en) is shown in Fig. 1. Similar hydrogen ion effects were also observed for the *cis*-α-$Co(edda)(H_2O)_2^+$ and *cis*-α-$Co(edda)(NH_3)_2^+$. In the cases of the Fe^{2+} reduction of the positively-charged and noncharged Co(III) complexes, not such a large effect of the hydrogen ion is observed, though it has been found that the hydrogen

1) K. Ohashi, This Bulletin, **45**, 3093 (1972).
2) K. Kuroda and K. Watanabe, *ibid.*, **44**, 1034 (1971).
3) $edda^{2-}=^-O_2CCH_2NHCH_2CH_2NHCH_2CO_2^-$.
4) K. Watanabe, Presented at the 23rd Annual Meeting of the Chemical Society of Japan, Tokyo, (1970); Proceedings, p. 543.
5) $nta^{3-}=N(CH_2COO)_3^{3-}$.
6) N. Koine, N. Sakota, J. Hidaka, and Y. Shimura, This Bulletin, **42**, 1583 (1969).
7) Y. Kurimura, K. Ohashi, T. Otsuki, and K. Yamamoto, *ibid.*, **44**, 1293 (1971).

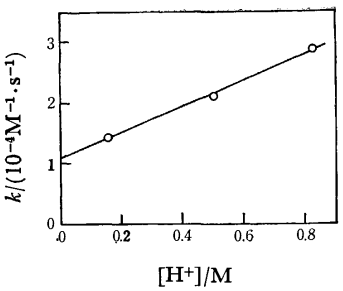

Fig. 1. The relation between the second-order rate constant k and hydrogen-ion concentration in the Fe^{2+} reduction of Co(nta)(en).
$\sum[ClO_4^-]=2.50$ M, 40.2 °C, $HClO_4$–$NaClO_4$ medium.

ion slightly accelerates the Fe^{2+} reduction rates of some negatively-charged Co(III) complexes.[8,8a] The mechanism of the hydrogen-ion dependence has not yet been made clear.

Though the electron-transfer mechanism could not be ascertained directly, it is reasonable to assume that these reactions occure *via* an inner-sphere mechanism, since the reductions of Co(HY)(H_2O), and Co(YOH)(H_2O) (Y^{4-}=the ethylenediaminetetraacetate ion and YOH^{3-}=the hydroxyethylenediaminetriacetate ion) with Fe^{2+} proceed *via* the carboxylato-bridged activated state.[8]

The experimental results presented above serve to establish how the enthalpy and entropy of the activation and reactivities change when the nonbridging ligands are varied (Table 1). The variations in the reactivities of *cis*-α-Co(edda)A_2^+ (A_2=(H_2O)$_2$, (NH_3)$_2$, and (en)), Co(nta)B_2 (B_2=(H_2O)$_2$, (H_2O)($NH_2CH_2CH_3$), and (en)), and Co(nta)(am)$^-$ (am=glycine, β-alanine, and γ-aminobutyric acid) are due primarily to the changes in the enthalpies of activation. The entropies of activation increase slightly with a decrease in the reactivities of the Co(III) complexes in the three series.

The reactivities of the Co(nta)(am)$^-$ series decrease in this order: γ-aminobutyric acid>β-alanine>glycine. In a previous paper,[9] it was mentioned that the strain on the chelate ring of the nonbridging ligand accelerates the Fe^{2+} reduction rate. The decreasing order of reactivity is consistent with that of the strain on the chelate ring of the amino acid.

It is of interst to note here that the entropies of activation of the Co(nta)(am)$^-$ and Co(nta)B_2 complexes are almost the same, though the enthalpies of the activation decrease with the reactivities of the complexes.

Table 1. The rate constants and the activation parameters for the Fe^{2+} reduction reactions of nitrilotriacetato- and ethylenediamine-*N*,*N*′-diacetato-cobalt(III) complexes

Complex ions	Rate constant $M^{-1}\cdot s^{-1}$	$\Delta H^{\ddagger}$ kcal·mol^{-1}	$\Delta S^{\ddagger}$ eu
Co(nta)(H_2O)$_2$	1.44[a]	7.1±1.0	−33.9±3.4
Co(nta)-(H_2O)($HN_2CH_2CH_3$)	9.78×10^{-3}[a]	11.6±1.5	−28.8±5.0
Co(nta)(en)	4.98×10^{-5}[a]	15.9±1.1	−24.8±3.7
Co(nta)(gly)$^-$	4.65×10^{-4}[a]	13.7±1.3	−27.9±4.5
Co(nta)(β-ala)$^-$	2.51×10^{-3}[a]	12.3±0.7	−29.0±2.5
Co(nta)-(γ-aminobut)$^-$	1.13×10^{-2}[a]	11.5±1.4	−28.7±4.7
cis-α-Co-(edda)(H_2O)$_2^+$	2.94×10^{-3}[b]	13.2±0.8	−25.8±2.7
cis-α-Co-(edda)(NH_3)$_2^+$	1.20×10^{-6}[b]	18.5±1.3	−23.5±4.4
cis-α-Co-(edda)(en)$^+$	1.65×10^{-8}[c]	24.1±0.7	−12.9±2.3

a) $\sum[ClO_4^-]=1.00$M, $[H^+]=0.10$M, 25 °C.
b) $\sum[ClO_4^-]=1.00$M, $[H^+]=0.36$M, 25 °C.
c) $\sum[ClO_4^-]=2.45$M, $[H^+]=0.84$M, 25 °C.

Table 2. The rate constants and the activation parameters for the Fe^{2+} reduction reactions of nitrilopolyaminocarboxylato-cobalt(III) complexes

Complex ions	Rate constant M^{-1} sec^{-1}	$\Delta H^{\ddagger}$ kcal·mol^{-1}	$\Delta S^{\ddagger}$ eu
Co(nta)(H_2O)$_2$	1.44[a]	7.1±1.0	−33.9±3.4
Co(edda)(H_2O)$_2^+$	2.94×10^{-3}[a]	13.2±0.8	−25.8±2.7
Co(edtaOH)(H_2O)	4.61×10^{-3}[b]	13.6±0.4	−23.5±1.4
Co(edtaH)(H_2O)	8.50×10^{-3}[b]	10.5±0.9	−33±3
Co(edta)$^-$	6.00×10^{-4}[b]	11.2±1.4	−36±5

a) This work, $\sum[ClO_4^-]=1.00$ M, $[H^+]=0.36$ M, 25 °C.
b) From Ref. 8, 25 °C, Ionic strength=1.00.

The rate constants and the activation parameters for the reductions of nitrilopolycarboxylato-Co(III) complexes by Fe^{2+} are listed in Table 2. The reactivity of the Co(nta)(H_2O)$_2$ complex is much larger than those of the other complexes. In these complexes, the efficiency of the nitrilopolycarboxylato ligand as the mediator in the electron-transfer is of almost the same degree. Therefore, the large reactivity of the Co(nta)(H_2O)$_2$ complex must be due to the smaller reorganization energy of the nonbridging ligand before electron transfer occurs. The small enthalpy of activation for the Co(nta)(H_2O)$_2$ complex supports the above-mentioned interpretation.

The author wishes to express his thanks to Professor Katsumi Yamamoto and Professor Yoshimi Kurimura for their helpful discussions, and to Mr. Takatsugu Fujita for his assistance in this work.

8) P. B. Wood and W. C. F. Higginson, *J. Chem. Soc.*, **1965**, 2116.
8a) Y. Kurimura, I. Meguro, and K. Ohashi, This Bulletin, **44**, 3367 (1971).
9) K. Ohashi, K. Yamamoto, I. Hirako, and Y. Kurimura, *ibid.*, **45**, 1712 (1972).

BULLETIN OF THE CHEMICAL SOCIETY OF JAPAN, VOL. 46, 1882—1883 (1973)

Recoil ^{82}Br Reactions with Liquid Chlorofluorocarbons

Takeshi TOMINAGA, Ren IWATA, and Yoshihiro MAKIDE*

Department of Chemistry, Faculty of Science, The University of Tokyo, Hongo, Tokyo 113

**The Institute of Physical and Chemical Research, Wako-shi, Saitama 351*

(Received November 10, 1972)

The study of recoil halogen reactions with chlorofluorocarbons appears to be interesting since one can make an intramolecular comparison of the reactivities of different types of bonds, such as C–C, C–Cl, and C–F. While recoil iodine and chlorine reactions with chlorofluoromethanes have been investigated,[1,2] the study of recoil bromine reactions with similar systems had not been reported before our preliminary work.[3] In the present article we wish to report our recent data on the recoil ^{82}Br reactions with chlorofluorocarbons, such as CF_2Cl_2, $CFCl_3$, and CF_2ClCF_2Cl.

Experimental

The samples for neutron irradiation were prepared by sealing one of the chlorofluorocarbons (CF_2Cl_2, $CFCl_3$, or CF_2ClCF_2Cl) *in vacuo* in quartz capillaries, along with varying amounts of bromine. These liquid samples were irradiated with thermal neutrons (flux: 5×10^{11} n/cm^2·s) for 5 min at room temperature in the rotary specimen rack of the TRIGA Mark II reactor at Rikkyo University. The accompanying γ dose was approximately 7×10^4 R.

The irradiated samples were analyzed after the decaying out of the shorter-lived bromine activities other than ^{82}Br. Hence, the observed radiochemical yields of recoil products were predominantly the results of the isomeric transition of ^{82m}Br.[4] The samples were directly introduced into a gas chromatograph and analyzed by means of a 5 m Silicone DC 550 column. The inorganic bromine was removed by means of a short column packed with dehydrated potassium ferrocyanide powder and placed before the main column. Procedures for the radioactivity measurement and determination of the ^{82}Br radiochemical yields of these products were the same as those in the previous work.[3]

Results and Discussion

Since radiogas chromatograms of irradiated CF_2Cl_2–Br_2 and $CFCl_3$–Br_2 systems were reported previously,[3] a typical radiogas chromatogram of ^{82}Br-labeled products from the irradiated CF_2ClCF_2Cl–Br_2 system is illustrated in Fig. 1. In the thermal conductivity measurements, only the mass peak of the parent compound could be observed (the position of the parent mass peak is indicated by an arrow in Fig. 1). The unknown radioactivity peaks were identified either by comparing their retention times with those of known

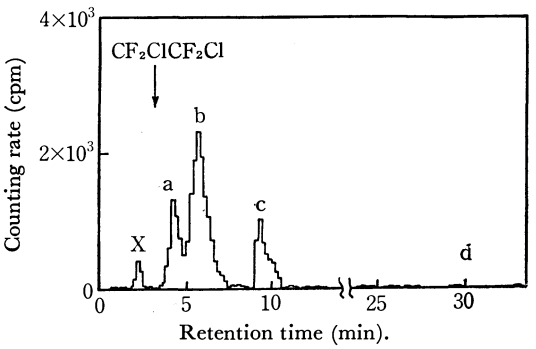

Fig. 1. Radiogas chromatogram of ^{82}Br-labeled products from the neutron-irradiated CF_2ClCF_2Cl—Br_2 system.
a: $CF_2Cl^{82}Br$; b: $CF_2ClCF_2{}^{82}Br$; c: $CF_2Br^{82}Br$; d: $CF_2ClCFCl^{82}Br$ (expected position, but not observed); X: presumably $CF_3{}^{82}Br$.

compounds added as carriers, or by applying the known correlation between the logarithm of the retention time and the composition of halogen atoms in bromochlorofluorocarbons.[5] If the carrier compounds are neither commercially available nor readily prepared by ordinary chemical syntheses, γ-irradiations up to a heavy dose of similar systems (*i.e.*, the mixtures of chlorofluorocarbons with bromine) appear to be useful

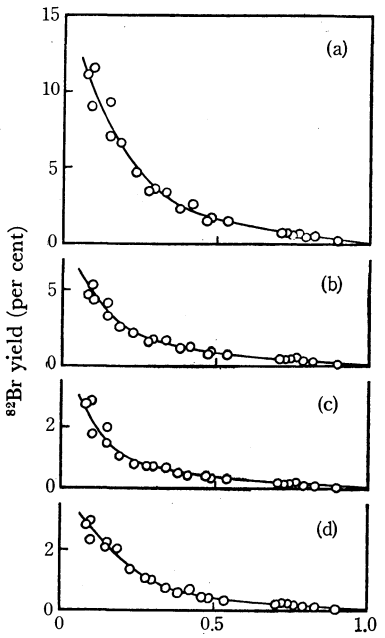

Fig. 2. Yields of major ^{82}Br-labeled products from CF_2ClCF_2Cl—Br_2 system *vs.* molar fraction of bromine.
(a) Total organic yield; (b) $CF_2ClCF_2{}^{82}Br$; (c) $CF_2Cl^{82}Br$; and (d) $CF_2Br^{82}Br$.

1) N. J. Parks and E. P. Rack, *Radiochim. Acta*, **10**, 26 (1968).
2) S. C. Lee and C. O. Hower, *J. Phys. Chem.*, **75**, 2685 (1971).
3) T. Tominaga, Y. Makide, S. Okada, Y. Kunimasa, and K. Wada, *Radioisotopes*, **20**, 541 (1971).
4) Since the reactivities of recoil ^{82}Br produced by either isomeric transition of ^{82m}Br(91%) or $^{81}Br(n,\gamma)^{82}Br$ reaction (9%) are qualitatively similar, the contribution from $^{81}Br(n,\gamma)^{82}Br$ reaction may be less than one-tenth of the overall observed results.
5) Y. Makide and N. Saito, presented at the 24th National Meeting of the Chemical Society of Japan (April 1971, Osaka).

for the preparation of the desired compounds in reasonable yields.[6] Hence, we have used mixtures of radiolysis products from the CF_2Cl_2–Br_2, $CFCl_3$–Br_2, and CF_2ClCF_2Cl–Br_2 systems preirradiated with γ-rays up to a total dose of about 10^{22} eV/g, as special samples for neutron irradiation in order only to identify the peaks of the ^{82}Br-labeled products from such systems.[7]

Figure 2 represents the radiochemical yields of the major ^{82}Br-labeled products from the CF_2ClCF_2Cl–Br_2 system as a function of the molar fraction of bromine. Very similar curves were observed for the radiochemical yields of the major ^{82}Br-labeled products from the CF_2Cl_2–Br_2 and $CFCl_3$–Br_2 systems. Bromine in these systems can scavenge carbon mixed halide radicals[6] as well as thermal ^{82}Br atoms or ions. A simple analysis of these curves, *i.e.*, an extrapolation of the almost linear portion of the curves to the yields at zero molar fraction of bromine, may reveal approximately the ^{82}Br yields from hot processes. Table 1 summarizes the ^{82}Br yields (estimated by extrapolation) of the major recoil products from the neutron-irradiated CF_2Cl_2–Br_2, $CFCl_3$–Br_2, and CF_2ClCF_2Cl–Br_2 systems. The following conclusions may be drawn from the results:

Table 1. Yields of major ^{82}Br-labeled recoil products from liquid CF_2Cl_2–Br_2, $CFCl_3$–Br_2 and CF_2ClCF_2Cl–Br_2 systems

	Product	^{82}Br yield (%)[a]
(1)	Liquid CF_2Cl_2–Br_2 system.	
	$CF_2Cl^{82}Br$	2
	$CF_2Br^{82}Br$	0.8
	$CFCl_2{}^{82}Br$	0.4
	$CFClBr^{82}Br$	0.2
(2)	Liquid $CFCl_3$–Br_2 system.	
	$CFCl_2{}^{82}Br$	6
	$CFClBr^{82}Br$	2
	$CCl_3{}^{82}Br$, $CCl_2Br^{82}Br$	not observed
(3)	Liquid CF_2ClCF_2Cl–Br_2 system.	
	$CF_2ClCF_2{}^{82}Br$	1.6
	$CF_2Cl^{82}Br$	0.6
	$CF_2Br^{82}Br$	0.7
	$CF_2ClCFCl^{82}Br$, $CFClBr^{82}Br$	not observed
	X ($CF_3{}^{82}Br$)[8]	<0.2

a) Estimated ^{82}Br yield from hot processes.

CF_2Cl_2–Br_2 System. At least four ^{82}Br-labeled species, *i.e.*, $CF_2Cl^{82}Br$, $CF_2Br^{82}Br$, $CFCl_2{}^{82}Br$, and $CFClBr^{82}Br$, were obtained from the recoil ^{82}Br reactions with CF_2Cl_2; of those the yield of $CF_2Cl^{82}Br$ (derived from ^{82}Br-for-Cl substitution) was larger than that of $CFCl_2{}^{82}Br$ (dreived from ^{82}Br-for-F substitution). Although the mechanisms for the formation of CF_2Br-^{82}Br and $CFClBr^{82}Br$ are not yet clear, it is likely that they are produced *via* radicals arising from the decomposition of the excited $CF_2Cl^{82}Br$ and $CFCl_2{}^{82}Br$ molecules.

$CFCl_3$–Br_2 System. The main ^{82}Br recoil products from the $CFCl_3$–Br_2 system were $CFCl_2{}^{82}Br$ and $CFClBr^{82}Br$, both originating from ^{82}Br-for-Cl substitution, whereas no ^{82}Br-for-F substitution product, such as $CCl_3{}^{82}Br$, was observed.

CF_2ClCF_2Cl–Br_2 System. $CF_2ClCF_2{}^{82}Br$, CF_2Cl-^{82}Br, and $CF_2Br^{82}Br$ were the major products from the CF_2ClCF_2Cl–Br_2 system,[8] indicating that ^{82}Br-for-Cl or ^{82}Br-for-CF_2Cl substituion took place predominantly. The ^{82}Br-for-F substituion product, $CF_2ClCFCl^{82}Br$, was not obtained.

In conclusion, the C–Cl and C–C bonds appear to be more reactive than the C–F bond in the recoil ^{82}Br reactions with these chlorofluorocarbons. It is worth mentioning that the C–Cl and C–C bonds are broken more readily than the C–F bond in the γ-radiolysis of these systems.[6] However, there is one point still to be clarified: whether or not such an apparent similarity between the isomeric-transition-induced ^{82}Br reactions and the γ-radiolysis reactions reflects the essential similarity of their reaction mechanisms.

Further work is in progress on the general application of the recoil technique to the selective preparation of labeled bromochlorofluorocarbons.

The present authors wish to express their thanks to Professor Nobufusa Saito, the University of Tokyo, for his encouragement and support.

6) T. Tominaga, R. Iwata, and Y. Makide, *Chem. Lett.*, **1972**, 871.

7) A variety of carbon mixed halides were produced by γ-irradiation up to a heavy dose, whereas no radiolysis products could be observed after 5 minutes' neutron irradiation in the reactor.

8) Another small unidentified peak (X) in Fig. 1 may presumably be $CF_3{}^{82}Br$, yet its origin is not fully understood.

BULLETIN OF THE CHEMICAL SOCIETY OF JAPAN, VOL. 46, 1884—1885 (1973)

Two Natural Acetylenic Aromatic Carotenoids

Toshio HAMASAKI,* Nobuhisa OKUKADO, and Masaru YAMAGUCHI

Department of Chemistry, Faculty of Science, Kyushu University, Higashi-ku, Fukuoka 812

(Received July 6, 1972)

Among seven carotenoid hydrocarbons[1] isolated from a sea-sponge "*Reniera japonica*," five major pigments, α-carotene,[1] β-carotene,[1] renieratene,[2] isorenieratene,[3] and renierapurpurin,[4] have been identified or structurally elucidated. Two other minor pigments (mp 205 and 194 °C) have remained structurally unsolved because of the paucity of materials. Recently, a considerable amount of the samples has been isolated, and, as will be shown below, enough evidence has been obtained to conclude that they have structures of acetylenic aromatic carotenoids, I (mp 205 °C) and II (mp 194 °C), respectively.

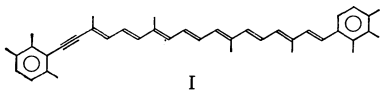

I

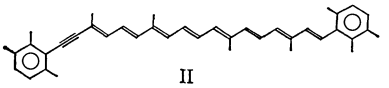

II

This is the first establishment of the natural occurrence of acetylenic aromatic carotenoids.

Experimental

Isolation of the Pigments. The extraction and isolation of the pigments were carried out according to the method described in the previous paper.[1] The pigment with a mp of 205 °C was adsorbed between renierapurpurin and renieratene in the chromatogram of the crude pigment mixture, on development on neutral alumina [Merck, deactivated by the addition of water (4%)] with a petroleum ether–benzene mixture (the benzene content being gradually increased from 30 to 75%). The pigment with a mp of 194 °C was adsorbed between renieratene and isorenieratene. Repeated chromatographic separations were necessary to obtain homogeneous zones. Several recrystallizations of the residue of each elute from a mixture of dichloromethane and petroleum ether gave a pure pigment.

Purplish red needles (referred to as the "mp 205 °C pigment"); mp 204—205 °C (uncorr.). UV max. 512, 480, 450 (benzene); 496, 465, 437 nm (*n*-hexane). IR max. (KBr disk); 3024, 2940, 2915, 2850, 1783, 1592, 1560, 1473, 1459, 1440, 1392, 1375, 1318, 1250, 1160, 1005, 960, 883, 830, 803, 776, 728 cm^{-1}.

Red needles (referred to as the "mp 194 °C pigment"); mp 194—194.5 °C (uncorr.). UV max. 500, 470, 442 (benzene); 485, 456, 431 nm (*n*-hexane). IR max. (KBr disk); 3020, 2940, 2910, 2845, 1782, 1620, 1560, 1455, 1436, 1392 1375, 1359, 1158, 997, 960, 878, 830, 805, 723 cm^{-1}.

Instruments. UV Spectra: Hitachi, Model EPS-3T. IR Spectra: Hitachi, Model 215. NMR Spectra: Hitachi, Model R-20B (60 Mc). Mass spectra: Hitachi, Model RMS-4.

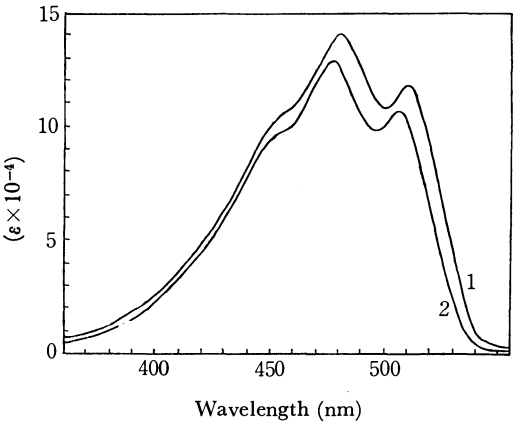

Fig. 1. Absorption spectra of the pigment, mp 205° (1) and renieratene (2) (benzene).

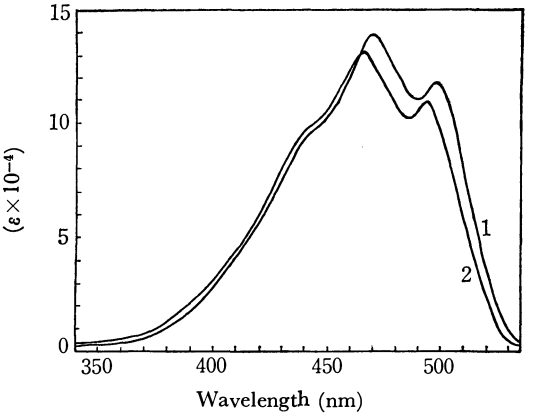

Fig. 2. Absorption spectra of the pigment, mp 194° (1) and isorenieratene (2) (benzene).

Results and Discussion

The Mp 205 °C Pigment. A brief examination of the UV, IR, NMR, and mass spectra of the pigment indicated a structurally very close relationship between the pigment and renieratene [1-(2,3,6-trimethylphenyl)-18-(2,3,4-trimethylphenyl)-3,7,12,16-tetramethyloctadecanonaene].

The mass spectrum of the pigment shows the ions [526(M), 511(M−15), 447(M−79), 434(M−92), 420 (M−106), 405(M−106−15), 393(M−133), 368(M−

* Present address: Yoshitomi Lab., Research Dept., Yoshitomi Pharmaceutical Industries, Ltd., Yoshitomi, Chikujo-gun, Fukuoka.

1) T. Tsumaki, M. Yamaguchi, and T. Tsumaki, *Nippon Kagaku Zasshi*, **75**, 297 (1954); M. Yamaguchi, This Bulletin, **30**, 111 (1957).

2) M. Yamaguchi, *ibid.*, **30**, 979 (1957); **31**, 739 (1958).

3) M. Yamaguchi, *ibid.*, **31**, 51 (1958).

4) M. Yamaguchi, *ibid.*, **33**, 1560 (1960).

158), 328(M−106−92), 301(M−133−92), 287(M−106−133), and 133(base peak)] characteristic of aromatic carotenoids.[5] The ions associated with *m/e* 133 give strong support to the presence of the trimethylphenyl group.[6] Most of the fragments are smaller by two mass units than the corresponding fragments of renieratene [528(M), 449(M−79), 436(M−92), 422(M−106), 395(M−133), 370(M−158), 330(M−106−92), 303(M−133−92), 289(M−106−133), and 133 (base peak)]. This suggests, besides other less likely structures, a possible formula where one of the double bonds of renieratene is replaced by a triple bond.

The NMR spectrum of the pigment [in $CDCl_3$, an average of 223 times: δ 2.02 (s, 6H) and 2.11 (s, 6H) ("in chain" methyl groups); 2.25 (s, 3H), 2.27 (s, 3H), and 2.34 (s, 6H) (four aromatic methyl groups); 2.45 (s, 6H) (two aromatic methyl groups); 6.10—6.90 (m, 12H) (polyene protons); 6.97 (s, 2H) (ring protons on the 2,3,6-trimethylphenyl group); double doublet centered at 6.99 (H) and 7.30 (H) (J=7.2 Hz, ring protons on the 2,3,4-trimethylphenyl group)] is quite similar to that of renieratene [in $CDCl_3$, an average of 214 times: δ 2.02 (s, 6H); 2.10 (s, 6H); 2.27—2.33 (m, 18H); 6.04—6.84 (m, 14H); 6.97 (s, 2H); 6.99 (H), and 7.29 (H) (dd, J=7.2 Hz)], indicating the presence of 2,3,6- and 2,3,4-trimethylphenyl groups.[7] It is noteworthy, however, that two (δ 2.45) out of six aromatic methyl groups are significantly deshielded when compared with those of renieratene. If the pigment is actually an acetylenic analogue of renieratene, this shift can be reasonably explained by assuming that the location of the triple bond in the polyene chain is in the moiety including the 2,3,6-trimethylphenyl group, probably neighbouring it, as is depicted in I.

The two *ortho*-standing methyl groups are considered to become more deshielded when a double bond attached to the benzene ring is replaced by a triple bond. Similar trends have been observed in alicyclic acetylenic carotenoids.[8,9] The relative abundance of the M−106 or M−92 ion (which stems from the central part of the polyene chain) in the mass spectrum also supports the conclusion.[10] This is also confirmed by the UV spectrum (Fig. 1). The small red shift of λ_{max} (3 nm in benzene) observed in going from renieratene to the pigment can be explained only by assuming that the pigment contains the triple bond in the terminal position of the central conjugated double bond system, as is observed in didehydroastaxanthin relative to astaxanthin[11] or in diatoxanthin[12] and alloxanthin[9,13] relative to zeaxanthin,[14] for example. A triple bond in other positions should give rise to a considerable hypsochromic shift.[15]

The IR spectrum also supports the (I) structure. The absence of $\nu_{C\equiv C}$ can be ascribed to the absence of polar functionality in this disubstituted acetylene. The possibility of the allenic structure, which is often encountered in natural carotenoids,[16] can be completely eliminated by a study of the IR and UV spestra.

The Mp 194 °C Pigment. The same arguments can apply to the pigment with a mp of 194 °C. The mass spectrum [526(M), 511(M−15), 447(M−79), 434(M−92), 420(M−106), 393(M−133), 301(M−133−92), 287(M−133−106), and 133(base peak)] clearly indicates that the compound can be interpreted as a dehydro derivative of isorenieratene [1,18-bis-(2,3,6-trimethylphenyl)-3,7,12,16-tetramethyloctadecanonaene; characteristic ions in the mass spectrum, 528(M, base peak), 513(M−15), 449(M−79), 436(M−92), 422(M−106), 395(M−133), 370(M−158), 330(M−106−92), 303(M−133−92), 289(M−106−133), and 133]. The NMR spectrum [in $CDCl_3$, an average of 597 times: δ 2.01 (s, 6H), 2.10 (s, 6H), 2.27—2.30 (12H), 2.44 (s, 6H), 6.05—6.90 (m, 12H), and 6.97 (s, 4H)] coincides well with that expected for the proposed formula, II, which has two 2,3,6-trimethylphenyl groups on both ends of the molecule, when compared with the spectrum of isorenieratene [in $CDCl_3$, an average of 223 times: δ 2.02 (s, 6H), 2.10 (6H), 2.31 (18H), 5.95—6.95 (m, 14H), and 6.97 (s, 4H)]. In this case again, a low-field shift by *ca.* 0.16 ppm of the signal of the *ortho*-standing methyl protons can be observed. The UV (Fig. 2) and IR spectra also prove the correctness of the (II) structure. The highest UV max. of the acetylenic analogue is again at a 3—4 nm-longer wavelength location in a benzene solution than that of isorenieratene in the same solvent.

The authors wish to thank Professor Otohiko Tsuge, Research Institute of Industrial Science, of this University, for the help he gave them in the measurements of the mass spectra.

5) Ref. 6); C. R. Enzell, G. W. Francis, and S. L. Jensen, *Acta Chem. Scand.*, **22**, 1054 (1968); H. Kjøsen, S. L. Jensen, and C. R. Enzell, *ibid.*, **25**, 85 (1971).

6) C. R. Enzell, G. W. Francis, and S. L. Jensen, *ibid.*, **23**, 727 (1969).

7) U. Schwieter, G. Englert, N. Rigassi, and W. Vetter, "Carotenoids Other than Vitamin A," Vol. 2, Butterworths, London (1969), p. 382.

8) W. Vetter, G. Englert, N. Rigassi, and U. Schwieter, "Carotenoids," ed. by O. Isler, H. Gutmann, and U. Solms, Birkhäser, Basel (1971), p. 207.

9) A. K. Mallams, E. S. Waight, B. C. L. Weedon, D. J. Chapman, F. T. Haxo, T. W. Goodwin, and D. M. Thomas, *Chem. Commun.* **1967**, 301; D. E. Loeber, S. W. Russel, T. P. Toube, B. C. L. Weedon, and J. Diment, *J. Chem. Soc., C*, **1971**, 404.

10) C. R. Enzell, "Carotenoids Other than Vitamin A," Vol. 2. Butterworths, London (1969), p. 497; Ref. 6).

11) N. A. Sørensen, S. L. Jensen, B. Børdalen, A. Haug, C. Enzell, and G. Francis, *Acta Chem. Scand.*, **22**, 344 (1968).

12) K. Aitzetmüller, W. A. Svec, J. J. Katz, and H. H. Strain, *Chem. Commun.*, **1968**, 32.

13) S. A. Campbell, A. K. Mallams, E. S. Waight, B. C. L. Weedon, M. Barbier, E. Lederer, and A. Salaque, *ibid.*, **1967**, 941.

14) P. Karrer und E. Jucker, "Carotinoide," Birkhäuser, Basel (1948), p. 182.

15) Ref. 7), p. 369.

16) O. Straub, "Carotenoids," ed. by O. Isler, H. Gutmann and U. Solms, Birkhäuser, Basel (1971), p. 771. Characteristics of IR: B. C. L. Weedon, *Chem. Brit.*, **3**, 424 (1967).

BULLETIN OF THE CHEMICAL SOCIETY OF JAPAN, VOL. 46, 1886—1887 (1973)

The Synthesis of Optically-active Valine by the Stereoselective Decarboxylation of α-(α-Methylbenzylamino)-α-isopropylmalonic Acid*

Tadao HAYAKAWA and Kazuaki SHIMIZU

Institute of High Polymer Research, Faculty of Textile Science and Technology, Shinshu University, Ueda 386

(Received July 14, 1972)

Many studies of the syntheses of optically-active α-amino acids have been reported.[1-2] Syntheses using optically-active α-methylbenzylamine as an optically-active moiety have been reported in many types of stereochemical studies.[2]

In this study, the synthesis of optically-active valine was examined by the stereoselective decarboxylation of (*S*)(−)- and (*R*)(+)-α-(α-methylbenzylamino)-α-isopropylmalonic acids.

The route of synthesis is as follows:

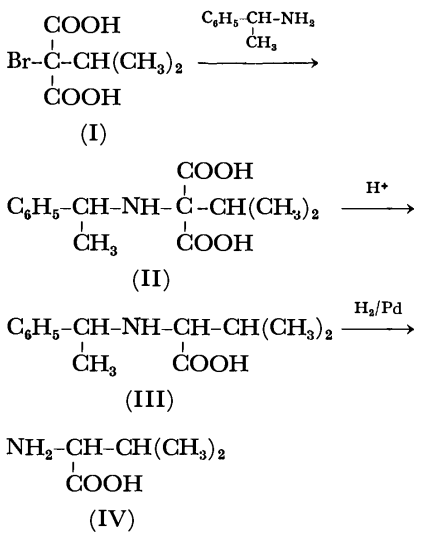

α-(α-Methylbenzylamino)-α-isopropylmalonic acid (II) was prepared by the reaction of α-brom-α-isopropylmalonic acid (I)[3] with optically-active α-methylbenzylamine. The product, II, was decarboxylated by heating it in 6 M hydrochloric acid to give *N*-(α-methylbenzyl)-valine (III). In order to check the influence of the reaction temperature on the steric effect of the decarboxylation, the reactions were carried out at various temperatures. The resulting *N*-(α-methylbenzyl)-valine was hydrogenolyzed into valine by the use of palladium hydroxide on charcoal. A part of the isolated valine (IV) was converted to DNP-valine by the use of 2,4-dinitrofluorobenzene in the usual manner.[4] The reactions of II→III→IV proceeded to give a quantitative yield. To avoid the fractionation of the partially-active valine and its methylbenzyl derivative thus synthesized, the purification of the compounds was carried out by the use of a Dowex 50×2 column (hydrogen form). The optical rotations of the valine and DNP-valine thus isolated, their optical purities, and the experimental conditions are listed in Table 1. When a decarboxylation reaction was carried out at room temperature, the higher optically-active valine (20—26%) was obtained. The optical purities of the resulting valines decreased with the rise in the reaction temperature. It is considered that, at lower reaction temperatures, the steric hindrance between the methylbenzyl group and the two carboxyl groups of the malonic acid derivative may contribute to the stereoselective decarboxylation more than at higher temperatures. The configurations of the resulting valines are also shown in Table 1. When (*S*)(−)-amine was used, (*R*)-rich valines were obtained, while (*R*)(+)-amine gave (*S*)-rich valines. In order to clarify the mechanism of this selective decarboxylation, the synthesis of another optically-active α-amino acid is now under investigation.

Experimental

α-[(S)(−)-α-Methylbenzylamino]-α-isopropylmalonic Acid (II) To a solution of 2.0 g of α-brom-α-isopropylmalonic acid (I)[3] in 7.12 ml of a 10% sodium hydroxide solution, 5.40 ml of (*S*)(−)-methylbenzylamine was added. After the mixture had been allowed to stand for 3 weeks, the unreacted amine was extracted with ether, and an aqueous layer was placed in a Dowex 50×2 column (hydrogen form). The column was washed with water. Then methylbenzylaminomalonic acid was eluted with 3 M aqueous ammonia and evaporated to dryness *in vacuo*. The residual product was dissolved in 20 ml of water, and the insoluble material was removed by filtration. After the filtrate had been acidified to congo red by the addition of dilute hydrochloric acid, the crystals thus precipitated were filtered and dried; yield, 1.0 g (38%); mp 181—183 °C (decomp.), $[\alpha]_D^{20} = -33.5°$ (*c* 1.01, 1 M NaOH).

Found: C, 63.66; H, 7.24; N, 5.31%. Calcd for $C_{14}H_{19}O_4N$: C, 63.88; H, 7.22; N, 5.28%.

α-[(*R*)(+)-α-Methylbenzylamino]-α-isopropylmalonic acid was prepared from I (2.0 g) and (*R*)(+)-methylbenzylamine

* Presented at the Annual Meeting of the Chemical Society of Japan, Hiratsuka-shi, April, 1972.

1) S. Akabori, Y. Izumi, S. Sakurai, and Y. Fujii, *Nature*, **178**, 323 (1956); K. Matsumoto and K. Harada, *J. Org. Chem.*, **31**, 1956 (1966); K. Harada, *Nature*, **212**, 1571 (1966); M. Murakami and K. Takahashi, This Bulletin, **32**, 308 (1959); R. L. Beamer, R. H. Belding, and C. S. Fickling, *J. Pharm. Sci.*, **58**, 1142, 1419 (1969); E. J. Corey, R. J. MaCaully, and H. S. Sachdev, *J. Amer. Chem. Soc.*, **92**, 2476, 2488 (1970).

2) R. G. Hiskey and R. C. Northrop, *ibid.*, **83**, 4798 (1961); J. C. Sheehan and R. E. Chandler, *ibid.*, **83**, 4795 (1961); S. Mitsui and A. Kanai, *Nippon Kagaku Zasshi*, **86**, 627 (1965); K. Harada and T. Yoshida, This Bulletin, **43**, 921 (1970); M. S. Patel and M. Worsley, *Can. J. Chem.*, **48**, 1882 (1970); J. C. Fiaud and H. B. Kagan, *Tetrahedron Lett.*, **1970**, 1813.

3) E. Koenigs and B. Mylo, *Chem. Ber.*, **41**, 4427 (1908).

4) F. Sanger, *Biochem. J.*, **39**, 507 (1945); K. R. Rao and H. A. Sober, *J. Amer. Chem. Soc.*, **76**, 1328 (1954).

Table 1. Optically-active valines prepared from (*S*) (−)- and (*R*) (+)-α-(α-methylbenzylamino)-α-isopropylmalonic acids at various temperatures

Reaction temp. (°C)	Config. of amine[a)]	Config. of isolated valine	$[\alpha]_D$ of isolated valine (5 M HCl)	Optical purity (%)[b)]	$[\alpha]_D$ of DNP-valine (1 M NaOH)	Optical purity (%)[b)]
90	*S*(−)	*R*	−1.1	3.9	−4.3	3.9
	R(+)	*S*	+1.2	4.2	+5.8	5.3
70	*S*(−)	*R*	−1.9	6.7	−9.4	8.6
	R(+)	*S*	+1.8	6.4	+7.9	7.2
60	*S*(−)	*R*	−2.2	7.8	−11.0	10.1
	R(+)	*S*	+2.8	9.9	+13.5	12.4
50	*S*(−)	*R*	−2.6	9.2	−15.1	13.8
	R(+)	*S*	+3.1	11.0	+15.6	14.3
20	*S*(−)	*R*	−5.6	19.8	−23.2	21.2
	R(+)	*S*	+6.5	23.0	+28.8	26.4

a) (*S*) (−)-α-Methylbenzylamine ($[\alpha]_D^{25}$ −41.5°, benzene); (*R*) (+)-α-Methylbenzylamine ($[\alpha]_D^{25}$ +41.0°, benzene).
b) Defined as ($[\alpha]_D$ obsd/$[\alpha]_D$ lit) × 100. *S*-Val, $[\alpha]_D^{25}$ +28.3° (5 M HCl); DNP-(*S*)-Val, $[\alpha]_D$ +109.2° (1 M NaOH). (J. P. Greenstein and M. Winitz, "Chemistry of the Amino Acids," John Wiley and Sons Inc., New York, N. Y., 1961. valine, Vol. 3 p. 2368; DNP-valine, Vol. 2 p. 1564.)

(5.40 ml) in the same way as above. Yield, 0.8 g (30%); mp 180—183 °C (decomp.), $[\alpha]_D^{20}$ = +34.0° (*c* 1.02, 1 M NaOH).

Found: C, 63.73; H, 7.18; N, 5.35%. Calcd for $C_{14}H_{19}O_4N$: C, 63.88; H, 7.22; N, 5.28%.

N-[(S)-α-Methylbenzyl]-valine (III). A solution of 0.3 g of α-[(*S*)(−)-α-methylbenzylamino]-α-isopropylmalonic acid (II) in 30 ml of 6 M hydrochloric acid was heated at room temperature (20 °C) for 24 hr, at 50 °C for 6 hr, at 60 °C for 5 hr, at 70 °C for 4 hr, and at 90 °C for 3 hr. The solution was then evaporated to dryness *in vacuo*, and the residue was dissolved in 10 ml of water. The solution was then placed in a Dowex 50×2 column (hydrogen form). The column was washed with water until the effluent became neutral. Then the methylbenzylvaline was eluted with 3 M aqueous ammonia. The effluent was evaporated to dryness *in vacuo*. The yield was nearly quantitative.

Found: C, 70.37; H, 8.63; N, 6.27%. Calcd for $C_{13}H_{19}O_2N$: C, 70.56; H, 8.65; N, 6.33%.

The *N*-[(*R*)-α-methylbenzyl]-valines were prepared by the decarboxylation of α-[(*R*)(+)-α-methylbenzylamino]-α-isopropylmalonic acids at various temperatures in the same way as above. The yields averaged 95—99%. The elemental analytical values were in good agreement with the theoretical value.

(R)(−)-Valine (IV) and DNP-(R)(−)-valine. To a solution of 0.25 g of *N*-[(*S*)-α-methylbenzyl]-valine in 30 ml of 50% ethanol containing 0.096 ml of 12 M hydrochloric acid, 0.3 g of 10% palladium hydroxide on charcoal was added; the solution was then hydrogenated at room temperature until the absorption of gas had ceased. The catalyst was removed by filtration and washed with hot water. The combined solution was evaporated to dryness *in vacuo*. After the residue had then been dissolved in 10 ml of water, the solution was placed in a Dowex 50×2 column (hydrogen form) and the valine was eluted with 3 M aqueous ammonia. The effluent was evaporated to dryness; the yields averaged 95—99%. This valine was found by paper chromatography to have the same purity as the authentic optically-active valine. The analytical sample was obtained by one recrystallization from water and ethanol.

Found: C, 51.02; H, 9.50; N, 11.84%. Calcd for $C_5H_{11}O_2N$: C, 51.26; H, 9.47; N, 11.96%.

A part of the unrecrystallized valine was converted into DNP-valine in the usual manner,[4)] and the resulting DNP-valine was purified by the use of a Celite column treated with a pH 7.0 citrate buffer.[5)] The DNP-valine was extracted with ether and crystallized.

Found: C, 46.81; H, 4.58; N, 14.71%. Calcd for $C_{11}H_{13}O_6N_3$: C, 46.64; H, 4.62; N, 14.84%.

The (*S*)(+)-valines were prepared by the hydrogenation of *N*-[(*R*)-α-methylbenzyl]-valines obtained under several conditions and were then converted to DNP-(*S*)(+)-valine by dinitrophenylation in the way described above. The optical rotations of the resulting valines and DNP-valines, and their optical purities and configulations, are shown in Table 1.

5) J. C. Perron, *Nature*, **167**, 513 (1951); A. Court, *Biochem. J.*, **58**, 70 (1954).

BULLETIN OF THE CHEMICAL SOCIETY OF JAPAN, VOL. 46, 1888—1890 (1973)

Cis- and *Trans*-Chlorination of Cyclohexene by Antimony Pentachloride and Triethyloxonium Hexachloroantimonate

Fuminori AKIYAMA, Toshio HORIE, and Minoru MATSUDA
Chemical Research Institute of Non-aqueous Solutions, Tohoku University, Sendai 980

(Received July 20, 1972)

Various methods for the preparation of *trans*-1,2-dichlorocyclohexane from cyclohexene have been reported by many investigators.[1-6] On the other hand, the formation of *cis*-1,2-dichlorocyclohexane was reported by Kawamoto and Komatsu[7] only in the case of the chlorination of cyclohexene by chlorine gas in the presence of cuprous chloride. However, the physical properties of the *cis*-1,2-dichloride reported by them are different from those reported by other investigators.[8,12] The chlorinations of cyclohexene by cupric chloride have been reported to yield *trans*-1,2-dichlorocyclohexane.[6,9] Therefore, we may suppose that the chlorination by chlorine in the presence of cuprous chloride does not give *cis*-1,2-dichloride. When we chlorinated cyclohexene by many metal halides without chlorine gas, we obtained *cis*-1,2-dichlorocyclohexane only in the case of chlorination by antimony pentachloride. While we were studying the chlorination of cyclohexene by antimony pentachloride, Uemura *et al.* reported the selective *cis*-chlorination of olefins by antimony pentachloride in carbon tetrachloride.[10] In this paper we wish to report some results on the chlorination of cyclohexene in liquid sulfur dioxide by antimony pentachloride and triethyloxonium hexachloroantimonate.

Experimental

General Procedure. The cyclohexene and antimony pentachloride were distilled into glass phials under a vacuum. The liquid sulfur dioxide was distilled into a reaction vessel in which the phials of the reactants have previously been placed. Breaking the phials, the chlorination reaction was started. After an appropriate time, an aliquot of the reaction solution was poured into a dilute alkaline aqueous solution. The products of the chlorination were analyzed by gas chromatography.

Materials. The triethyloxonium hexachloroantimonate was prepared according to the method of Meerwein *et al.*[11] Found: C, 16.26; H, 3.25%. Calcd for Et_3OSbCl_6: C, 16.46; H, 3.40%. Commercially-available metal halides and cyclohexene were purified by the usual methods. The liquid sulfur dioxide was distilled over phosphorous pentoxide.

Identification of the Chlorides. The products of the chlorination of cyclohexene were separated using 2.0 m silicone gum SE 30, 15% on a chromosorb w, column. The NMR or IR spectrum of each separated chloride coincided well with that of the respective authentic sample or that recorded in the literature.[12-14]

A. Monochlorocyclohexane

Found: C, 60.68; H, 9.25%. Calcd for $C_6H_{11}Cl$: C, 60.75; H, 9.35%.

B. *trans*-1,2-Dichlorocyclohexane——NMR: δ 3.9—4.20 (2H), 2.60—1.2 (8H); IR: 692, 738, 745 cm^{-1}.

Found: C, 47.39; H, 6.66%. Calcd for $C_6H_{10}Cl_2$: C, 47.08; H, 6.58%.

C. *cis*-1,2-Dichlorocyclohexane——NMR: δ 4.10—4.35 (2H), 1.20—2.40 (8H); IR: 696, 744 cm^{-1}.

Found: C, 47.28; H, 6.39%. Calcd for $C_6H_{10}Cl_2$: C, 47.08; H, 6.58%.

D. *trans*-1,3-Dichlorocyclohexane——NMR: δ 4.0—4.5 (2H), 1.0—2.5 (8H).

Found: C, 47.61; H, 6.60%. Calcd for $C_6H_{10}Cl_2$: C, 47.08; H, 6.58%.

Results and Discussion

We obtained only monochlorocyclohexane in the chlorination of cyclohexene by aluminum trichloride, stannic chloride, molybdenum pentachloride, and phos-

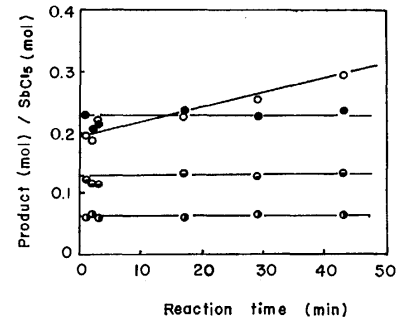

Fig. 1. The chlorination of cyclohexene by antimony pentachloride in liquid sulfur dioxide at 25°C.
$SbCl_5$ 0.14 mol/l, Cyclohexene 0.87 mol/l.
○: monochloro-, ●: *cis*-1,2-dichloro-, ◒: *trans*-1,2-dichloro-, ◑: *trans*-1,3-dichlorocyclohexane.

1) W. Markownikoff, *Ann.*, **302**, 1 (1898).
2) J. Kurokawa, *Nippon Kagaku Zasshi*, **85**, 211 (1964).
3) J. L. Cotter, L. J. Andrews, and R. M. Keefer, *J. Amer. Chem. Soc.*, **84**, 739 (1962).
4) Y. Ueno, S. Takemura, Y. Ando, and H. Terauchi, *Chem. Pharm. Bull.* (Tokyo), **13**, 1369 (1965).
5) R. E. Buckles and D. F. Knaack, *J. Org. Chem.*, **25**, 20 (1960).
6) K. Ichikawa, S. Uemura, and Y. Takagaki, *Kogyo Kagaku Zasshi*, **71**, 1657 (1968).
7) S. Komatsu and T. Kawamoto, *Nippon Kagaku Zasshi*, **52**, 685 (1931).
8) B. Carroll, D. G. Kubber, and H. A. Davis, *J. Amer. Chem. Soc.*, **73**, 5582 (1951).
9) P. P. Nicholas and R. T. Carroll, *J. Org. Chem.*, **33**, 2345 (1968).
10) S. Uemura, O. Sasaki, and M. Okano, *Chem. Commun.*, **1971**, 1064.
11) H. Meerwein, E. Battenberg, H. Gold, E. Pfiel, and C. Willfang, *J. Prakt. Chem.*, **154**, 83 (1939).
12) G. A. Russell, A. Ito, and K. Konaka, *J. Amer. Chem. Soc.*, **85**, 2988 (1963).
13) P. Klaeboe, J. J. Lothe, and K. Lunde, *Acta Chem. Scad.*, **11**, 1677 (1957).
14) H. M. van Dort and Th. J. Sekuur, *Tetrahedron Lett.*, **1963**, 1301.

Table 1. Distribution of chlorination products of cyclohexene by antimony pentachloride and triethyloxonium hexachloroantimonate

Chlorinating reagent	(mol/l)	Condition			Products mol %			
		Solvent	Temp (°C)	Cyclohexene (mol/l)	Mono-chloro-	*trans*-1,2-Dichloro-	*trans*-1,3-Dichloro-	*cis*-1,2-Dichloro-
$SbCl_5$[a]	0.14	SO_2	25	0.87	31.7	21.1	10.7	36.5
$SbCl_5$[a]	0.14	SO_2	25	2.49	29.1	20.2	14.2	36.5
$SbCl_5$[a]	0.10	SO_2	−6	0.46	26.6	22.6	12.5	38.3
$SbCl_5$[a]	0.30	*n*-hexane	25	1.86	20.8	30.7	4.0	44.5
Et_3OSbCl_6[b]	0.15	SO_2	25	0.25	82.6	5.8	2.3	9.3

a) Initial reaction products. b) Reaction products at 2040 min.

phorous pentachloride. However, in the chlorination by antimony pentachloride, we obtained four chlorination products—monochlorocyclohexane, *trans*-1,2-dichlorocyclohexane, *trans*-1,3-dichlorocyclohexane, and *cis*-1,2-dichlorocyclohexane. As the reaction of monochlorocyclohexane with antimony pentachloride did not give the dichloride under our experimental conditions, the dichlorides were considered to result from the reaction of cyclohexene with antimony pentachloride. The yields of these products in liquid sulfur dioxide at 25 °C are plotted against the reaction time in Fig. 1. The yield of monochlorocyclohexane increased with the reaction time, but the yields of the dichlorides did not change with the reaction time. In the chlorination in *n*-hexane, we observed similar time-conversion curves. The distribution of the initial reaction products is listed in Table 1. At −70 °C in liquid sulfur dioxide, the chlorination reaction was very slow. As the reaction mixture prepared and kept for several hours at −70 °C was warmed up to 25 °C, however, the yield of the chlorination increased. In this case, however, only the chlorination product was monochlorocyclohexane, as is shown in Fig. 2. These

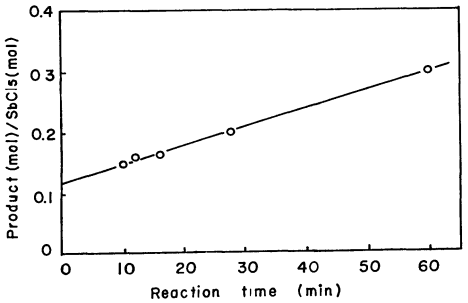

Fig. 2. The chlorination in the case that the reaction mixture was prepared at −70°C and then was warmed up to 25°C in liquid sulfur dioxide.
$SbCl_5$: 0.11 mol/l, Cyclohexene: 0.44 mol/l.
○: monochlorocyclohexane.

results may be tentatively represented by the sequence of the reactions in Scheme 1. Path (c) may resemble the Diels-Alder reaction. As Path (c) does not occur at −70 °C, all of the antimony pentachloride may be converted to an intermediate, II. The hydrochlorination of cyclohexene may be a slow reaction at −70 °C. Scarecely no change of II to I may occur with an increase in the reaction temperature from −70 to 25 °C. The II intermediate is supposed not to be able to give dichlorides. Therefore, only monochloro-

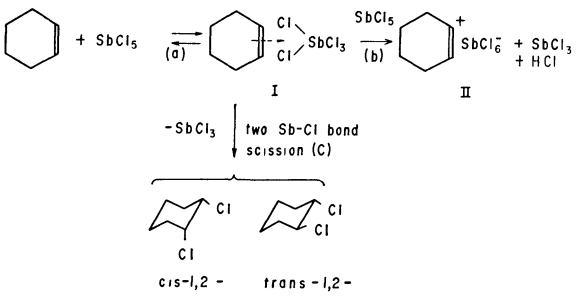

Scheme 1.

cyclohexane was obtained upon increasing the reaction temperature from −70 to 25 °C. Upon the mixing of the reagents at 25 °C, two path, (b) and (c), may occur, thus giving both mono- and dichlorides. We obtained dichlorides in the chlorination by triethyloxonium hexachloroantimonate, as is shown in Fig. 3. The product distribution at 2040 min is shown in Table 1. Since the triethyloxonium cation is more stable than the cyclohexenyl cation, a little of the free hexachloroantimonate anion can exist in the case of triethyloxonium hexachloroantimonate, but in the case of the II intermediate none can exist. The free hexachloroantimonate anion may react with cyclohexene to give

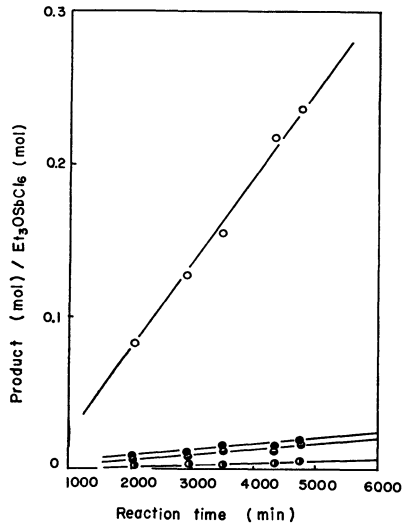

Fig. 3. The chlorination of cyclohexene by triethyloxoinum hexachloroantimonate in liquid sulfur dioxide at 25°C.
Et_3OSbCl_6 0.16 mol/l, Cyclohexene 0.25 mol/l.
○: monochloro-, ●: *cis*-1,2-dichloro-, ◒: *trans*-1,2-dichloro-, ◑: *trans*-1,3-dichlorocyclohexane.

dichlorides. However, contact-ion pairs of triethyloxonium salt or the II intermediate are considered not to give dichlorides.

The solvent effect of dichlorination is shown in Table 1. The predominance of the *cis*-chlorination is somewhat clearer in the less polar solvent, *n*-hexane, than in the more polar solvent, liquid sulfur dioxide.

At present, the mechanism of the formation of *trans*-1,3-dichlorocyclohexane is not yet clear.

BULLETIN OF THE CHEMICAL SOCIETY OF JAPAN, VOL. 46, 1890—1891 (1973)

The Synthesis of Some 2*H*-Pyrazino[2,3-*e*][1,2,4]thiadiazine 1,1-dioxides

Mitsuo HATTORI, Michiaki YONEDA, and Miki GOTO
Department of Chemistry, Gakushuin University, Toshima-ku, Tokyo 171

(Received September 29, 1972)

Some benzothiadiazine derivatives are nowadays used as potential diuretics. The object of this research is to synthesize the corresponding pyrazinothiadiazine derivatives,[1] analogues of benzothiadiazine diuretics. The ring system of pyrazinothiadiazine has not hitherto been reported. This paper deals with the synthesis of some compounds of the new heterocycles.

For the synthesis of aminopyrazine-3-sulfonamides, the conventional method applied to the synthesis of benzenesulfonamides starting from sulfonyl chloride is not adequate, as pyrazines have little tendency to react with electrophilic reagents. Aminopyrazine-3-thiols (**2**) were first converted into aminopyrazine-3-sulfonamides (**4**) *via* aminopyrazine-3-sulfenamides by a method similar to that described by Korman.[2] The sulfonamides thus obtained were condensed with ethyl orthoformate to give 2*H*-pyrazino[2,3-*e*][1,2,4]thiadiazine 1,1-dioxides (**6**).

Similarly 2*H*-quinoxalino[2,3-*e*][1,2,4]thiadiazine 1,1-dioxide (**7a**) and its 3-methyl derivative (**7b**) were synthesized from 2-aminoquinoxaline-3-thiol (**3**) as a starting material.

6,7-Dimethyl-2*H*-pyrazino[2,3-*e*][1,2,4]thiadiazine

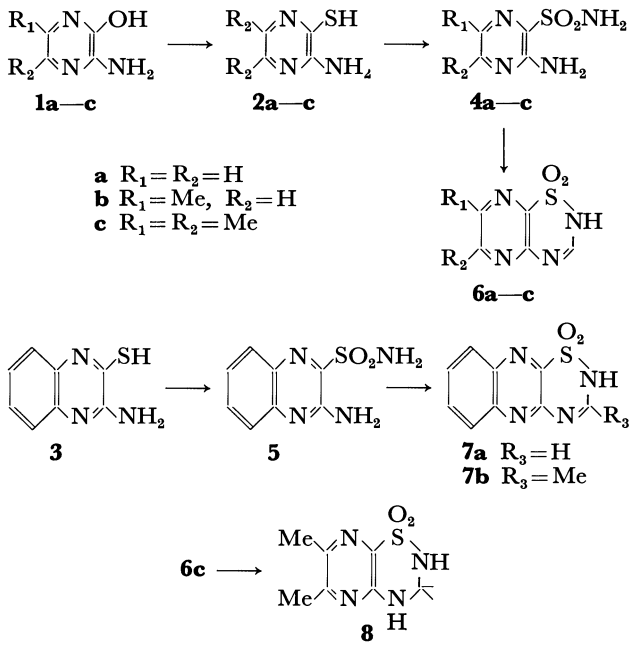

Scheme 1.

Table 1.

No	Mp °C[a]	% Yield[b]	Solv[c]	UV[d] nm (ε)		
2b	219 dec	62.3	EtOH	236 (4000)	278 (4300)	387 (6300)
2c	231 dec	61.1	EtOH	228 (4600)	275 (2800)	392 (4500)
4a	216 dec	32.8	H_2O	240 (10700)	335 (4800)	
4b	217 dec	32.1	H_2O	242 (12100)	345 (4900)	
4c	222 dec	33.1	H_2O	246 (12800)	340 (7300)	
5	224—225	42.4	H_2O	248 (23300)	301 (3200)	379 (5800)
6a	256 dec	56.6	EtOH	233 (3800)	256 (3500)	300 (6600)
6b	291 dec	52.3	EtOH	233 (4000)	267 (4600)	317 (6700)
6c	>275	59.1	EtOH	231 (4300)	276 (4100)	315 (8700)
7a	>256	60.4	DMF	246 (22700)	277 (13900)	363 (8400)
7b	>300	48.3	DMF	246 (28700)	273 (15600)	362 (9600)
8	214—215	57.7	EtOH	251 (9900)	348 (7000)	

a) All the melting points were corrected.
b) Calculated after recrystallization except for **5**.
c) Recrystallization solvent.
d) Solvent, 95% EtOH.

1) The effect of pyrazinothiadiazine 1,1-dioxides on tyrosine hydroxylase was tested preliminarily; none of them exhibited either an inhibitory or accelerating effect on the enzyme.

2) J. Korman, *J. Org. Chem.*, **23**, 1768 (1958).

Table 2. Analytical data

No	Formula	Calcd %				Found %			
		C	H	N	S	C	H	N	S
2b	$C_5H_7N_3S$	42.55	5.00	29.78	22.67	42.93	5.03	29.81	22.70
2c	$C_6H_9N_3S$	46.44	5.85	27.08	20.62	46.74	5.89	26.94	21.01
4a	$C_4H_6O_2N_4S$	27.58	3.47	32.17	18.41	27.47	3.21	32.49	18.77
4b	$C_5H_8O_2N_4S$	31.91	4.28	29.77	17.04	32.05	4.27	30.04	17.01
4c	$C_6H_{10}O_2N_4S$	35.63	4.98	27.70	15.84	35.55	4.89	27.91	15.74
5	$C_8H_8O_2N_4S$	42.85	3.59	24.99	14.30	42.68	3.36	24.88	14.52
6a	$C_5H_4O_2N_4S$	32.61	2.19	30.42	17.41	32.85	2.08	30.61	17.52
6b	$C_6H_6O_2N_4S$	36.36	3.05	28.27	16.18	36.50	2.89	28.37	16.08
6c	$C_7H_8O_2N_4S$	39.62	3.84	26.40	15.08	39.69	3.64	26.47	15.10
7a	$C_9H_6O_2N_4S$	46.15	2.58	23.92	13.69	46.33	2.42	24.20	13.81
7b	$C_{10}H_8O_2N_4S$	48.38	3.25	22.57	12.92	48.52	3.11	22.48	12.59
8	$C_7H_{10}O_2N_4S$	39.24	4.70	26.15	14.97	39.23	4.61	26.43	15.24

1,1-dioxide (**6c**) was converted into the corresponding 3,4-dihydro-compound (**8**) by reduction with sodium borohydride.

Experimental

Aminopyrazine-3-thiols (2). A mixture of aminopyrazinol[3] (**1**) (10 mmol) and phosphorus pentasulfide (1.5 g) in β-picoline (30—50 ml) was refluxed for 1.5 hr. After chilling, the solvent was evaporated *in vacuo*, and the residue was dissolved in 1 M sodium hydroxide (30—50 ml). The solution was filtered and adjusted to pH 3 with concd hydrochloric acid. After the mixture was chilled overnight, the product was collected.

Aminopyrazine-3-sulfonamides (4). Concd ammonia (15 ml) was added to aminopyrazinethiol[4] (**2**) (5 mmol) in 1.5 M sodium hydroxide (5 ml). Into the solution was then poured 10% sodium hypochlorite (3.7 ml) with stirring at 5 °C. The precipitate was collected and washed well with ice water to remove ammonia. The moist product was suspended in water (30 ml) and 5% aqueous potassium permanganate solution (15 ml) was added with vigorous stirring at room temperature. The solution was filtered, neutralized with concd hydrochloric acid and concentrated to dryness *in vacuo*. The residue was crystallized from water.

2-Aminoquinoxaline-3-sulfonamide (5). Aminoquinoxalinethiol[5] (**3**) was treated as in the synthesis of **4**. The filtered solution was concentrated to a half volume and adjusted to pH 3 with concd hydrochloric acid. After the mixture had been put to stand for 1 hr, the product was collected by filtration. The product is fairly unstable against alkaline media and boiling water. For the analysis, a small portion was recrystallized from a large amount of water (85 °C).

2H-Pyrazino[2,3-e][1,2,4]thiadiazine 1,1-Dioxides (6). A mixture of aminopyrazinesulfonamide (**4**) (5 mmol) and ethyl orthoformate (7.5 ml) was heated at 130 °C for 6 hr. After the mixture had been chilled well, the product was collected and washed with ethanol.

2H-Quinoxalino[2,3-e][1,2,4]thiadiazine 1,1-Dioxide (7a). Aminoquinoxalinesulfonamide (**5**) was treated at 110 °C for 4 hr as in the synthesis of **6**.

3-Methyl-2H-quinoxalino[2,3-e][1,2,4]thiadiazine 1,1-Dioxide (7b). A mixture of aminoquinoxalinesulfonamide (**5**) (667 mg) and ethyl orthoacetate (9 ml) was heated at 100 °C for 3 hr. After the mixture had been chilled, the product was collected and washed with ethanol.

3,4-Dihydro-6,7-dimethyl-2H-pyrazino[2,3-e][1,2,4]pyrazinothiadiazine 1,1-Dioxide (8). To sodium borohydride (47.5 mg) in water (2.25 ml) was added dimethylpyrazinothiadiazine 1,1-dioxide (**6c**) (212 mg) over a period of 30 min at room temperature. After the mixture had been put to stand for 6 hr, the product was collected.

The authors wish to express their thanks to Professors T. Nagatsu and H. Kuzuya, Aichigakuin University, for testing the enzyme.

3) F. L. Muehlmann and A. R. Day, *J. Amer. Chem. Soc.*, **78**, 242 (1956).

4) F. Chillemi and G. Palamidessi, *Farmaco. Ed. Sci.*, **18**, 566 (1963).

5) H. Saikachi and S. Tagami, *Chem. Pharm. Bull.* (Tokyo) **9**, 941 (1961).

BULLETIN OF THE CHEMICAL SOCIETY OF JAPAN, VOL. 46, 1892—1893 (1973)

Asymmetric Reactions. VIII. Stereoselectivities in Several Organometallic Reactions with *N*-Benzyl-2,3-*O*-isopropylidene-D-glyceraldimine[1]

Yoshiaki OHGO, Yaeko KONDA,[2] and Juji YOSHIMURA

Laboratory of Chemistry for Natural Products, Tokyo Institute of Technology, Meguro-ku, Tokyo 152

(Received October 17, 1972)

The present authors have previously reported differences in stereoselectivity between phenyllithium and phenylmagnesium bromide reactions with α-aminonitriles bearing 1,3-dioxolane rings at α-positions,[3] 2,3-*O*-isopropylidene-D-glyceraldimines,[3,4] or 2,3-*O*-isopropylidene-D-glyceraldehyde,[5] *i.e.*, phenyllithium reactions gave *threo* products and Grignard reactions *erythro* products predominantly. The stereoselectivity of the phenyllithium reactions is consistent with Cram's rigid model,[6] but that of the Grignard reaction cannot be explained by this model. The anomalous stereoselectivity has been explained[3-5] in terms of the coordination ability of magnesium to C_3-oxygen, together with C_1-oxygen or C_1-nitrogen, and C_2-oxygen (Fig. 1). Support for this assumption was obtained[1] from the fact that no stereoselectivity difference was observed between the tworeactions with substrates having no C_3-oxygen.

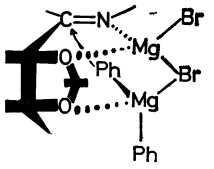

Fig. 1.

It is of interest to investigate other organometallic reactions in connection with the stereoselectivity which might result from the coordination ability of the attacking species. This paper will report on the stereoselectivity exhibited by organometallic compounds of Be, Ca, and Zn.

The phenylcalcium iodide was prepared in ether according to Gilman's method.[7] The other organometallic reagents were prepared by the addition of the corresponding metal halides into an ether solution of phenyllithium.[7]

N-Benzyl-D-glyceraldimine was treated with 2—3 molar equivalents of the reagents in ether. The reaction mixture was then decomposed with ice water, and the addition products obtained from ether layer were hydrolyzed to give a diastereomeric mixture of 1-benzylamino-1-deoxy-1-*C*-phenyl-*threo*- and -*erythro*-D-glyceritols. The product was confirmed by thin-layer chromatography. The analytical results agreed. In the case of the reaction with phenylcalcium iodide, there appeared in the thin-layer chromatography two spots other than the desired products. Therefore, the sample was purified by preparative thin-layer chromatography. The purified sample gave a single spot and agreeing analytical results.

The diastereomeric ratio was calculated from the optical rotation of the product by reference to that of each sample of the *threo* and *erythro* isomers. The results are shown in Table 1.

Table 1. Diastereomer ratios produced by the reaction with organometallic reagents

Run	Reagent (moles to substrate)	$[\alpha]_D$	Products *threo* (%)	Products *erythro* (%)
1	PhCaI (3)	−31.5	67	33
2	Ph_2Be+$BeCl_2$ (3) (0.6)	+15	35	65
3	Ph_2Zn (2)	+17	34	66
4	Ph_2Zn+$ZnCl_2$ (1.5) (1.5)	+34	23	77

As is shown in Table 1, the reactions with organometallics of Be and Zn showed a stereoselectivity similar to that of the organomagnesium reaction (giving the *erythro* product predominantly). It is worthy of mention that, in contrast to these reactions, the organocalcium reaction gives *threo* product predominantly, despite the fact that calcium belongs to the alkaline earth group (like Be and Mg) in the periodic table. Investigations[7] of the relative reactivities of organoalkaline and -alkaline earth metal compounds suggested that organocalcium has a rather ionic character, which could explain the stereoselectivity of the organocalcium reaction. At this stage, however, no clear explanation can be given.

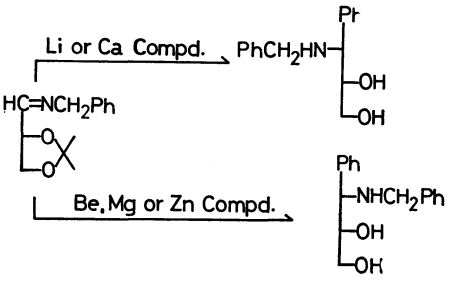

Scheme 1.

1) Asymmetric Reactions. VII. J. Yoshimura, Y. Ohgo, K. Ajisaka, and Y. Konda, This Bulletin, **45**, 916 (1972).

2) Present address: School of Pharmacy, Kitazato University, Minato-ku, Tokyo.

3) J. Yoshimura, Y. Ohgo, and T. Sato, *J. Amer. Chem. Soc.*, **86**, 3858 (1964).

4) Y. Ohgo, J. Yoshimura, and T. Sato, This Bulletin, **42**, 728 (1969).

5) Y. Ohgo, J. Yoshimura, M. Kono, and T. Sato, *ibid.*, **42**, 2957 (1969).

6) D. J. Cram and K. R. Kopecky, *J. Amer. Chem. Soc.*, **81**, 2737 (1959).

7) H. Gilman and J. C. Bailie, *J. Org. Chem.*, **2**, 84 (1937).

Experimental

Reaction of N-*Benzyl-2,3-*O-*isopropylidene-*D-*glyceraldimine with Phenylcalcium Iodide.* An ethereal solution of *N*-benzyl-2,3-*O*-isopropylidene-D-glyceraldimine (10 g) was added with stirring at 0—5 °C into an ethereal solution of phenylcalcium iodide prepared from calcium (5.5 g) and phenyliodide (28 g). The reaction mixture was refluxed with stirring for 10 hr and then decomposed with ice water. The products were extracted with ether. The ether layer was concentrated *in vacuo* to a syrup. The syrup was hydrolyzed with 6 M hydrochloric acid (30 ml) at 100 °C for 2 hr, thereafter the hydrolysate was decolorized with activated carbon and then extracted four times with 50 ml portions of ethyl acetate after the adjustment of the pH to about 10 with a sodium hydroxide solution. The combined ethyl acetate solution was washed with water, dried over anhydrous sodium sulfate, and concentrated under reduced pressure to give crude products which showed two spots on a tlc besides those of the desired products. The crude products were purified by preparative thin-layer chromatography. The purified sample gave a single spot on a tlc (R_f, 0.45; solvent, acetone–benzene (3:5)). Found: C, 74.83; H, 7.20; N, 5.93%. Calcd for $C_{16}H_{19}O_2N$: C, 74.68; H, 7.44; N, 5.44%. The specific rotation of the sample was also measured; the result is shown in Table 1.

Reaction of N-*Benzyl-2,3-*O-*isopropylidene-*D-*glyceraldimine with Organoberyllium and Organozinc Compounds.* Organoberyllium and organozinc compounds were prepared from anhydrous beryllium chloride or zinc chloride, and phenyllithium according to the Gilman method.[7] For example, beryllium chloride (9 g) was added, portion by portion,into a stirred solution of phenyllithium prepared from lithium (2.7 g) and phenylbromide (20.1 ml). The mixture was refluxed for 30 min after the addition has been completed. To the resulting solution was added an ethereal solution of *N*-benzyl-2,3-*O*-isopropylidene-D-glyceraldimine with cooling and stirring; subsequently, the same procedure as was used in the phenylcalcium iodide reaction gave a diastereomeric mixture. Each sample gave a single spot on a tlc (R_f, 0.45; solvent, acetone–benzene (3:5)). The diastereomeric ratios produced by each reaction were calculated from the optical rotation of the sample and pure D-*threo* and D-*erythro* isomers. The analytical results agreed. Found: [C, 74.64; H, 7.20; N, 5.73% (Run 2)], [C, 74.21; H, 7.64; N, 5.97% (Run 3)], [C, 74.57; H, 7.56; N, 6.24% (Run 4)]. Calcd for $C_{16}H_{19}O_2N$: C, 74.68; H, 7.44; N, 5.44%.

BULLETIN OF THE CHEMICAL SOCIETY OF JAPAN, VOL. 46, 1893—1895 (1973)

The Synthesis of a Sweet Peptide, α-L-Aspartyl-L-phenylalanine Methyl Ester, without the Use of Protecting Groups

Yasuo ARIYOSHI, Tetsuo YAMATANI, Noboru UCHIYAMA, Yohko ADACHI, and Naotake SATO

Central Research Laboratories, Ajinomoto Co., Inc., Suzuki-cho, Kawasaki-ku, Kawasaki 210

(Received November 6, 1972)

The large-scale preparation of α-aspartyl peptides which are entirely free from the corresponding β-isomers is not easily accomplished. In a previous paper the present authors reported a convenient one-step preparation of the hydrochloride and hydrobromide of L-aspartic anhydride, which might be useful intermediates for preparing aspartyl peptides.[1] It then appeared of interest to prepare α-L-aspartyl-L-phenylalanine methyl ester (α-APM), which has a sweet taste,[2] by the direct condensation of L-aspartic anhydride hydrochloride with methyl L-phenylalaninate. Although Kovacs *et al.* described the condensation of L-aspartic anhydride hydrobromide with ethyl glycinate to give a mixture of α- and β-aspartyl glycine ethyl esters,[3] its practical use for peptide synthesis has not yet been reported in the literature.

Simply by mixing L-aspartic anhydride hydrochloride and methyl L-phenylalaninate in an organic solvent, we can obtain a mixture of α- and β-APM in a fairly good yield. This coupling reaction, however, is always accompanied with side-reactions, such as the self-condensation of L-aspartic anhydride and the further condensation between the unchanged anhydride and the resulting dipeptide ester, since the amino group of the aspartyl residue is unprotected. In order to overcome these disadvantages and, in particular, to increase the formation of the α-isomer, the reaction conditions, such as the temperature, the solvent effects, and the molar ratios of the two reactants, were investigated. It was found that the reaction could be effected by adding such weak acids as acetic acid, by employing an excess of methyl L-phenylalaninate, and by conducting it at a low temperature. This method would appear to have considerable promise for conveniently preparing α-APM on a large scale, but it is necessary to separate the α-APM from the reaction mixture.

In the course of investigations of this peptide, we had occasion to attempt to hydrolyze the methyl ester group of α-APM in dilute hydrochloric acid. Contrary to expectations, α-APM hydrochloride (α-APM·HCl) readily crystallized out when α-APM was dissolved in dilute hydrochloric acid. This finding is interesting, since most peptides usually increase their

1) Y. Ariyoshi, T. Yamatani, N. Uchiyama, and N. Sato, This Bulletin, **45**, 2208 (1972).

2) R. H. Mazur, J. M. Schlatter, and A. H. Goldkamp, *J. Amer. Chem. Soc.*, **91**, 2684 (1969).

3) J. Kovacs, H. N. Kovacs, and R. Ballina, *ibid.*, **85**, 1839 (1963).

solubilities in such an acidic solution; *e.g.*, some closely related compounds, such as α-L-aspartyl-D-phenylalanine methyl ester hydrochloride and α-L-aspartyl-L-phenylalanine ethyl ester hydrochloride, are too soluble to be isolated. α-APM was also sparingly soluble in aqueous hydrobromic acid, while β-APM was almost freely soluble in both dilute hydrochloric and hydrobromic acids.

This characteristic was used successfully in the separation of α- and β-APM. After the separation, the recovery of the α-APM from the salt, and that of the β-APM from the mother liquor, could be accomplished easily and in an excellent yield by conventional neutralization. The ester group and the peptide bond were stable enough for the separation procedure.

The treatment of L-aspartic anhydride hydrochloride with 4 molecular equivalents of methyl L-phenylalaninate in the presence of acetic acid in ethylene dichloride at −20 °C gave a mixture of α- and β-APM, from which α-APM was isolated in a 37% yield (from the anhydride) by separation through its hydrochloride, followed by the neutralization of the salt with sodium carbonate and subsequent column chromatography.

On the other hand, when the reaction was conducted in acetone in the absence of acids, β-APM was formed predominantly and was isolated in a 36% yield.

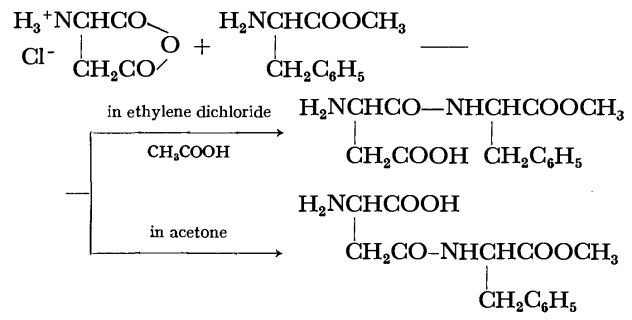

Experimental

All the melting points are uncorrected. The peptides used here were left over from a previous investigation.[4] The optical rotations were measured by means of a visual polarimeter. The determination of the α- and β-APM by paper electrophoresis was carried out according to the method described in a previous paper.[5]

α-L-Aspartyl-L-phenylalanine Methyl Ester Hydrochloride Dihydrate (α-APM·HCl). α-APM (5.0 g) was dissolved in 1 M hydrochloric acid (50 ml) with slight warming, and then the solution was kept in a refrigerator overnight. The crystals thus formed were collected by filtration; yield, 5.2 g (86%); mp 127—128 °C (decomp., partly melted at 103 °C); $[\alpha]_D^{25}$ +1.3° (*c* 2, water). Lit,[6] mp 105—110 °C. Found: C, 45.86; H, 6.18; N, 7.55; Cl, 9.73%. Calcd for $C_{14}H_{18}O_5N_2 \cdot HCl \cdot 2H_2O$: C, 45.84; H, 6.32; N, 7.64; Cl, 9.67%.

α-L-Aspartyl-L-phenylalanine Methyl Ester Hydrobromide Dihydrate (α-APM·HBr). This salt was obtained from a solution of α-APM (5.0 g) in 1M hydrobromic acid (100 ml) by the procedure used in the preparation of α-APM·HCl; yield, 4.3 g (63%); mp 155 °C (decomp.); $[\alpha]_D^{2.5}$ +1.0° (*c* 2, water). Found: C, 41.13; H, 5.76; N, 6.85; Br, 19.39%. Calcd for $C_{14}H_{18}O_5N_2 \cdot HBr \cdot 2H_2O$: C, 40.89; H, 5.64; N, 6.81; Br, 19.43%.

Separation of α- and β-APM. α-APM (10 g) and β-APM (10 g) were dissolved in 1 M hydrochloric acid (100 ml) with slight warming. The solution was then kept in a refrigerator overnight. The crystals thus formed were collected by filtration; yield, 9.4 g (78%). The IR spectrum (Nujol) of the crystals was identical with that of the authentic α-APM·HCl. The crystals (9.3 g) were dissolved in water (90 ml), and the solution was adjusted to pH 4.8 with a 5% aqueous sodium bicarbonate solution while being stirred at 50 °C. The solution was then kept in a refrigerator overnight. The crystals thus formed were collected by filtration and washed with a small amount of chilled water; yield, 6.7 g (67%). The crystals were found by paper electrophoresis to be free from the β-isomer. For elemental analysis, the crystals were recrystallized from water; mp 235—236 °C (decomp.); $[\alpha]_D^{25}$ +32.0° (*c* 1, acetic acid). Lit,[2] mp 95 °C and 245—247 °C. Lit,[7] mp 246—247 °C. Lit,[4] mp 235—236 °C; $[\alpha]_D$ +32° (*c* 1, acetic acid). Found: C, 55.52; H, 6.13; N,9.32%. Calcd for $C_{14}H_{18}O_5N_2 \cdot 1/2H_2O$: C, 55.44; H, 6.31; N, 9.24%.

The filtrate from the α-APM·HCl was adjusted to pH 4.8 with a 5% aqueous sodium bicarbonate solution while being stirred at 50 °C; then the solution was treated in the manner described above to give 5.3 g (53%) of β-APM as needles. These needles were found by paper electrophoresis to be free from the α-isomer; mp 198—199 °C; $[\alpha]_D^{23}$ +40.5° (*c* 1, acetic acid). Lit,[2] mp 196—197 °C. Lit,[4] mp 198—199 °C; $[\alpha]_D$ +40.5° (*c* 1, acetic acid). Found: C, 55.29; H, 6.36; N, 9.27%. Calcd for $C_{14}H_{18}O_5N_2 \cdot 1/2H_2O$: C, 55.44; H, 6.31; N, 9.24%.

Synthesis of α-APM. A solution of methyl L-phenylalaninate hydrochloride (90 g) in water (450 ml) was neutralized with sodium carbonate (24 g), and the resulting free ester was extracted with two 350-ml portions of ethylene dichloride. To the organic solution there were then added acetic acid (9 g) and methanol (8 ml). Into this solution, L-aspartic anhydride hydrochloride (15.2 g)[1] was stirred at −20 °C. After stirring for 30 min at this temperature, hot water (350 ml, 70—80 °C) and an aqueous solution (300 ml) of sodium carbonate (5.7 g) were added successively to the reaction mixture. After the removal of the excess of methyl L-phenylalaninate by two extractions with 150-ml portions of ethylene dichloride, the aqueous layer was adjusted to pH 4.8 with dilute hydrochloric acid. The solution was found by paper electrophoresis to contain 18.2 g (60%) of α-APM and 6.1 g (20%) of β-APM. The solution was concentrated *in vacuo* to about 100 ml, and 36% hydrochloric acid (30 ml) was added to the concentrate. The solution was kept in a refrigerator overnight. The crystals (α-APM·HCl, 21.3 g, 58%) thus formed were collected by filtration and dissolved in water (200 ml). The solution was adjusted to pH 4.8 with a 5% aqueous sodium carbonate solution while being stirred at 50 °C, and then kept in a refrigerator overnight. The crystals thus formed were collected by filtration; yield, 13.0 g (43%). The crystals were dissolved in water (500 ml) and passed through a column (1×20 cm) of Dowex 1×4 (acetate form) maintained at 45 °C, and then the column was washed with water (20 ml). The eluate and washings were concentrated *in vacuo* to give α-APM, which was recrystallized from water; yield, 11.2 g (37%); mp 235—236 °C (decomp.); $[\alpha]_D^{22}$ +32.0° (*c* 1, acetic acid).

4) Y. Ariyoshi and N. Sato, This Bulletin, **45**, 2015 (1972).
5) Y. Ariyoshi and N. Sato, *ibid.*, **45**, 942 (1972).
6) P. M. Hardy, G. W. Kenner, R. C. Sheppard, and J. S. Morley, Brit. 1042484 (1966).
7) J. M. Davey, A. H. Laird, and J. S. Morley, *J. Chem. Soc., C*, **1966**, 555.

Found: C, 55.30; H, 6.19; N, 9.36%.

Synthesis of β-APM. To a stirred solution of methyl L-phenylalaninate (72 g) in acetone (750 ml), there was added L-aspartic anhydride hydrochloride (30.3 g) at −30 °C. After having been stirred for 1 hr at this temperature, the reaction mixture was allowed to attain room temperature and then concentrated *in vacuo*. The residue was dissolved in water (750 ml) containing sodium bicarbonate (20 g). The aqueous solution was extracted with two 500-ml portions of ethylene dichloride to remove the excess methyl L-phenylalaninate. The aqueous layer was adjusted to pH 4.8 with dilute hydrochloric acid and then concentrated to about 400 ml *in vacuo*. After storage in a refrigerator overnight, the crystals thus formed were collected by filtration; yield, 27.0 g (45%). Recrystallization from water gave 23.5 g (36%) of β-APM as needles, which were confirmed by paper electrophoresis to be free from the α-isomer; mp 198—199 °C; $[\alpha]_D^{28}$ +40.5° (*c* 1, acetic acid). Found: C, 55.79; H, 6.07; N, 9.39%.

BULLETIN OF THE CHEMICAL SOCIETY OF JAPAN, VOL. 46, 1895—1896 (1973)

The Inhibitory Effect of Several Olefins on the Formation of the Zinc-carbenoid Reagent from Diethylzinc and Chloroiodomethane

Sotaro MIYANO and Harukichi HASHIMOTO

Department of Applied Chemistry, Faculty of Engineering, Tohoku University, Aramaki, Sendai 980

(Received November 16, 1972)

In a previous paper[1] we reported that styrene greatly inhibits the formation of the zinc-carbenoid reagent from diethylzinc and diiodomethane or chloroiodomethane. In this respect, it appeared of interest to examine the effects of several olefins on the zinc-carbenoid reaction of cyclohexene with diethylzinc and chloroiodomethane (Table 1). Norcarane was obtained

TABLE 1. EFFECT OF THE ADDITION OF AN OLEFIN ON THE ZINC-CARBENOID REACTION[a)]

Added olefin	Norcarane yield[b)], (%)	Reacted CH_2ClI (mmol)
None	67	9.8
2-Heptene	65	9.7
1-Heptene	64	10
Isoprene	45	8.3
trans-Stilbene	34	5.8
1,4-Diphenyl-1,3-butadiene	25	4.7
Styrene	22	4.6
α-Methylstyrene	16	3.1
1,1-Diphenylethylene	12	2.3
1-Phenyl-1,3-butadiene	8	1.8

a) Reaction conditions: diethylzinc; 10 mmol, chloroiodomethane; 15 mmol, cyclohexene; 10 mmol, added olefin; 5 mol % based on cyclohexene, 35°C, 5 hr, under a nitrogen atmosphere.
b) Based on cyclohexene.

in a good yield when diethylzinc was allowed to react with a mixture of cyclohexene and chloroiodomethane under a nitrogen atmosphere. On the other hand, in the presence of 5 mol % of 1-phenyl-1,3-budadiene only 18% of the initial chloroiodomethane was consumed within 5 hr. When dry air was introduced into the reaction mixture, chloroiodomethane completely reacted within 0.5 hr, giving norcarane in the yield of 98%.[2] This shows that 1-phenyl-1,3-butadiene retards the step of the formation of the zinc-carbenoid reagent from diethylzinc and chloroiodomethane. The order of the inhibiting effect of an added olefin on the zinc-carbenoid reaction seems to be in accordance with that of the reactivity of the olefin toward radicals. These results are consistent with the proposed radical-chain mechanism for the formation of the zinc-carbenoid reagent (Eqs. (1)—(3));[1] that is, the more reactive the olefin is toward radicals, the more the olefin seems to trap the ethyl or chloromethyl radiacl, and stop the chain:

$$EtZnR \xrightarrow{\text{initiator}} Et\cdot \quad (1)$$

$$Et\cdot + CH_2ClI \longrightarrow EtI + \cdot CH_2Cl \quad (2)$$

$$\cdot CH_2Cl + EtZnR \longrightarrow ClCH_2ZnR + Et\cdot \quad (3)$$

(R = Cl or Et)

The reason why isoprene was not so effective as was expected from its reactivity toward the methyl radical[3] or from the Q-value is not yet obvious, but the absence of a conjugating phenyl group and/or its volatility (bp 34 °C, while the reaction temperature was 35 °C) may be partly responsible.

Experimental

Materials. The 1-phenyl-1,3-butadiene[4] (bp 81.5 °C/9 mmHg), 1,4-diphenyl-1,3-butadiene[5] (mp 152—152.5 °C), and 1,1-diphenylethylene[6] (bp 111—113 °C/2 mmHg) were

1) S. Miyano and H. Hashimoto, This Bulletin, **46**, 892 (1973).

2) For the accelerating effect of oxygen on the zinc-carbenoid reaction, see Ref. 1).

3) a) F. Leavitt, M. Levy, M. Szwarc, and V. Stanett, *J. Amer. Chem. Soc.*, **77**, 5493 (1955). b) A. Rajkenbach and M. Szwarc, *Proc. Roy. Soc. Ser., A*, **251**, 394 (1959).

4) H. Hashimoto, M. Hida, and S. Miyano, *J. Organometal. Chem.*, **10**, 518 (1967).

5) B. B. Corson, "Organic Syntheses," Coll. Vol. II (1948), p. 229.

6) C. F. Allen and S. Converse, "Organic Syntheses," Coll. Vol. I (1956), p. 226.

prepared by conventional methods. The other materials were purified by methods which have been reported before.[1]

Reaction Procedure. The following procedure is representative. The reaction was carried out in a 100 ml, round-bottomed flask equipped with a magnetic stirrer, a reflux condenser, a pressure-equilibrating dropping funnel topped with a gas inlet cock, thermometer, and inlet carrying a rubber septum cap. The flask was flushed with nitrogen. In the flask was placed 30 ml of benzene containing 15.4 mmol of chloroiodomethane, 10.2 mmol of cyclohexene, and 0.865 g of ethylbenzene. To the solution we then added 67.2 mg 1-phenyl-1,3-butadiene (5.2 mmol). The temperature of the solution was kept at 35 °C, and 1 ml of diethylzinc (10 mmol) was injected into the solution with a hypodermic syringe through the septum cap. The reaction was then carried out under a nitrogen atmosphere for 5 hr at 35 °C. At the end of the reaction period, a sample (*ca.* 1 ml) was withdrawn through the septum cap with a hypodermic syringe and quenched with 3 ml of a dilute hydrogen chloride solution which had been saturated with nitrogen. After three extractions of the aqueous layer with benzene, the combined organic phase was analysed by glc. The amounts of the products were estimated from the peak areas, using ethylbenzene as the internal standard. Dry air was passed into the space above the remaining reaction mixture at a rate of 10 ml/min for 0.5 hr, after which the reaction products were analysed similarly.

BULLETIN OF THE CHEMICAL SOCIETY OF JAPAN, VOL. 46, 1896—1897 (1973)

Organic Synthesis by Means of Noble Metal Compounds. L.[1] Palladium Catalyzed Reactions of Enamines with Butadiene and Allyl Acetate

Jiro TSUJI

Basic Research Laboratories, Toray Industries, Inc., Kamakura 248

(Received February 16, 1973)

Recently extensive studies have been carried out on the palladium catalyzed dimerization reactions of butadiene, which can be classified into two types.[3] The first one is the dimerization reaction, especially with incorporation of a nucleophile such as water, alcohols, carboxylic acids, ammonia, amines, and some active methylene compounds to give 1-substituted 2,7-octadienes. Another one is the cocyclization reaction with a dipolar double bond such as aldehydes and isocyanates to give six-membered heterocyclic compounds.

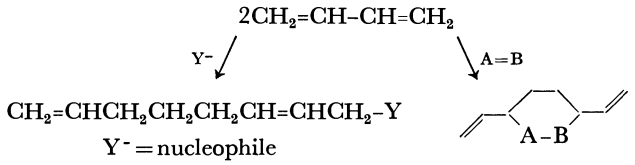

We have investigated a reaction of enamine with butadiene in the presence of a palladium catalyst based on the following considerations. Enamines are considered to be a strong nucleophile and their nucleophilic reactions are well known.[4] In addition, enamines have dipolar double bond, which takes part in cyclization reactions to form six- or four-membered rings. Thus with these dual reactivities of butadiene and enamines in mind, we have carried out the reaction of enamine with butadiene in the presence of a palladium catalyst in order to determine which type of the reaction, namely nucleophilic attack or cocyclization of enamine, takes place. Concerning the interaction of enamine with a palladium complex, we have shown before that enamines are allylated with π-allylpalladium chloride.[5]

Pyrrolidine enamine of cyclohexanone was allowed to react with butadiene by using palladium acetate combined with triphenylphosphine as the catalyst. The reaction observed was not the cocyclization, but the introduction of 2,7-octadienyl moiety at the α position of cyclohexanone took place. In addition, 2,6-disubstituted cyclohexanone was obtained as a minor product. Pyrrolidine enamine of cyclopentanone behaved similarly giving 2-(2,7-octadienyl)cyclopentanone as a main product, accompanied by 2,5-di(2,7-octadienyl)-cyclopentanone.

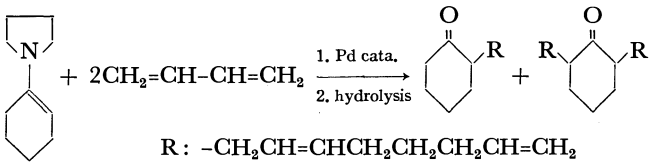

The reaction undoubtedly proceeds through nucleophilic attack of the enamine on an intermediate π-allylic palladium complex formed from butadiene and the palladium compound. Formation of the intermediate π-allylic complex was proposed by Hagihara and his co-workers for dimerization of butadiene in the presence of nucleophiles.[6] Allyl acetate is known to form the most simple π-allylpalladium complex,

1) Part XLIX. T. Susuki and J. Tsuji, This Bulletin, **46**, 655 (1973).

2) The content of this paper was presented with other reactions at the 23rd Intern. Congr. Pure Appl. Chem., July 1971, Boston, *Pure Appl. Chem. Suppl.*, **2**, 107 (1972).

3) For references: J. Tsuji, *Accounts Chem. Res.*, **6**, 8 (1973).

4) A. G. Cook, "Enamines", Marcel Dekker, Inc., New York, N. Y. (1969).

5) J. Tsuji, H. Takahashi, and M. Morikawa, *Tetrahedron Lett.*, 1965, 4387.

6) S. Takahashi, H. Yamazaki, and N. Hagihara, This Bulletin, **41**, 254 (1968).

which is expected to react with enamines in the presence of the palladium catalyst. Thus we carried out the reaction of allyl acetate with the enamine of cyclohexanone, and 2-allylcyclohexanone was obtained as expected.[7]

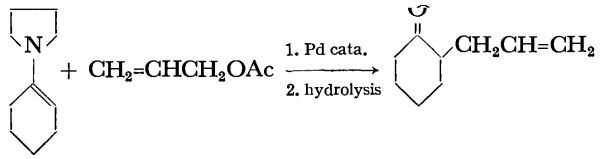

Experimental

Reaction of the Cyclohexanone Enamine. A solution of 1-pyrrolidinocyclohexene (15 g), palladium acetate (100 mg), triphenylphosphine (200 mg) in acetonitrile (40 ml) was placed in an autoclave, and butadiene (12 g) was introduced. The autoclave was shaken for 3 hr at 80 °C. Two layers were formed, which were subjected to hydrolysis with hydrochloric acid at 50 °C for 30 min. Dichloromethane (100 ml) was added and the solution was washed with water. After being dried, the solvent was evaporated. The residue was distilled to give 2-(2,7-octadienyl)cyclohexanone (13.5 g) and 2,6-di(2,7-octadienyl)cyclohexanone (6.8 g), which were identified by the following data.

2-(2,7-Octadienyl)cyclohexanone. Bp 130—135 °C/3 mmHg, IR (neat); 993, 911 ($CH=CH_2$), 968 cm^{-1} (*trans* olefin). The NMR spectrum (CCl_4) showed complex olefin bands at τ 3.5—4.8 (=CH–) and τ 4.8—5.4 ($=CH_2$), which were identical with the olefin bands of the NMR spectrum of the known methyl 2,7-octadienyl ether.[8]

Found: C, 81.66; H, 10.73%; mol wt (mass spectrum), 206. Calcd for $C_{14}H_{22}O$: C, 81.50; H, 10.75%; mol wt, 206.32.

2,4-Dinitrophenylhydrazone, mp 93—94 °C. Found: C, 62.54; H, 6.81; N, 14.51%. Calcd for $C_{20}H_{26}O_4N_4$: C, 62.16; H, 6.78; N, 14.50%.

2,6-Di(2,7-octadienyl)cyclohexanone. Bp 170—175 °C/1 mmHg, showed the similar NMR olefinic bands as those of the above-shown monoderivative. Found: mol wt, 314. Calcd for $C_{22}H_{34}O$: 314.49. Hydrogenation over platinum oxide absorbed 4 mol of hydrogen to give 2,6-dioctylcyclohexanone, bp 160—165 °C/0.5 mmHg, mp 37—38 °C (from methanol–ether).

Found: C, 82.16; H, 12.84%; mol wt, 322. Calcd for $C_{22}H_{42}O$: C, 81.91; H, 13.13%; mol wt. 322.56.

Reaction of Cyclopentanone Enamine. A mixture of the enamine (10 g), butadiene (9 g), dimethylformamide (30 ml), palladium acetate (100 mg), and triphenylphosphine (200 mg) was allowed to react at 85 °C for 5 hr. After the usual work-up, 2-(2,7-octadienyl)cyclopentanone (8.2 g) and 2,5-di(2,7-octadienyl)cyclopentanone (4.2 g) were obtained.

2-(2,7-Octadienyl)cyclopentanone. Bp 100—105 °C/3 mmHg. The NMR spectrum showed the similar olefinic pattern as that of the corresponding cyclohexanone derivative.

Found: C, 81.36; H, 10.60%; mol wt. 192. Calcd for $C_{13}H_{20}O$: C, 81.20; H, 10.48%; mol wt. 192.29.

2,5-Di(2,7-octadienyl)cyclopentanone. Bp 155—165 °C/2 mmHg.

Found: C, 83.76; H, 10.68%; mol wt. 300. Calcd for $C_{21}H_{32}O$: C, 83.94; H, 10.73%; mol wt. 300.47.

Hydrogenation gave 2,5-dioctylcyclopentanone, mp 45—47 °C.

Found: C, 81.86; H, 12.90%; mol wt. 308. Calcd for $C_{21}H_{40}O$: C, 81.75; H, 13.07%; mol wt. 308.53.

Reaction of Allyl Acetate and Cyclohexanone Enamine. A mixture of 1-pyrrolidinocyclohexene (18 g), allyl acetate (15 g), acetonitrile (30 ml), palladium acetate (100 mg), and triphenylphosphine (200 mg) was stirred at 80 °C for 5 hr. Then 10 ml of concd hydrochloric acid and 10 ml of water were added and the mixture was stirred for 30 min. After the usual work-up, distillation gave 2-allylcyclohexanone (7.2 g, 70—73 °C/3 mmHg) and 2,6-diallylcyclohexanone (3 g, 85—95 °C/3 mmHg). They were identified with authentic samples prepared by the known method[9] by NMR and IR spectra and mixed mp determination of 2,4-dinitrophenylhydrazones (148—150 and 113—115 °C).

7) The same reaction was reported recently by; H. Onoue, I. Moritani, and S. Murahashi, *Tetrahedron Lett.*, **1973**, 121.

8) S. Takahashi, T. Shibano, and N. Hagihara, This Bulletin, **41**, 454 (1968).

9) G. Opitz, H. Mildenberger, and H. Suhr, *Ann.*, **649**, 47 (1961).

BULLETIN OF THE CHEMICAL SOCIETY OF JAPAN, VOL. 46, 1898—1899 (1973)

The Preparation of *N*-(Alkylthio)- and *N*-(Arylthio)succinimides[1]

Yasuo ABE, Takeshige NAKABAYASHI, and Jitsuo TSURUGI
Radiation Center of Osaka Prefecture, Shinke-cho, Sakai 593

(Received December 19, 1972)

N-(Organothio)succinimides have been known as useful starting materials for syntheses of various organic sulfur compounds and have previously been synthesized by the reactions of: (1) organic sulfides with *N*-bromosuccinimide (NBS),[2] (2) organic disulfides with NBS,[3] and with NBS in the presence of benzoyl peroxide[4] or pyridine,[5] and organic disulfides and trisulfides with *N*-chlorosuccinimide (NCS) in the presence of pyridine,[6] (3) sulfenyl halides with potassium succinimide[5] and with succinimide in the presence of triethylamine,[7] and (4) lead bisthiolates with NBS or NCS.[8] It has been reported that mercaptans react with NBS or NCS to give disulfides,[5] sulfenyl bromides, or chlorides.[9] In a benzene solution, thiophenol was reacted with NCS to give phenylsulfenyl chloride and succinimide at room temperature.[9]

However, we have found that an exactly equimolar mixture of mercaptans and NCS, after the addition of triethylamine, gives *N*-(organothio)succinimides. Aryl, aralkyl and alkyl mercaptans can give the corresponding *N*-(organothio)succinimides in good yields. The identification was performed by studying the IR spectra and by elemental analyses. Table 1 gives the various types of thiosuccinimides prepared by this method, together with the yields, melting points, and IR data.

The reaction of disulfide and trisulfide with NCS in the presence of pyridine as a catalyst was proposed by Hayashi to proceed by a radical mechanism which involved the cleavage of NCS to a succinimido radical and a chloro radical in the first step.[6] The present reaction between mercaptan and NCS would then seem to proceed through the initial formation of sulfenyl chloride by the electrophilic chlorination of mercaptan.[8] It follows that the sulfenyl chloride and succinimide produced simultaneously would be dehydrochlorinated by the addition of triethylamine, much as in the reaction of sulfenyl chloride and succinimide:[7]

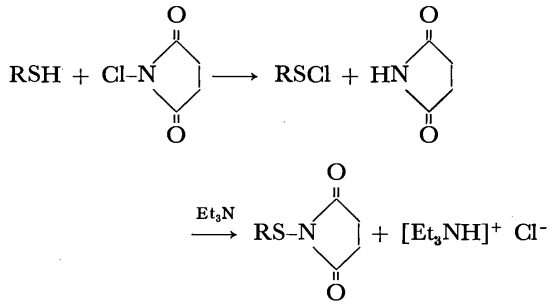

TABLE 1. THE YIELDS, MP, AND IR SPECTRA OF THE PREPARED *N*-(ALKYLTHIO)- AND *N*-(ARYLTHIO)SUCCINIMIDES[a]

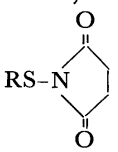

R	Yield (%)	Mp (°C)	(lit mp) (°C)	IR (C=O)[b] (cm^{-1})
Phenyl	78.2	117—117.5	(118—119)[5]	1740
o-Tolyl	71.2	88—88.5	(85.5—86)[2]	1730
m-Tolyl	86.4	108—109	(100—102)[7]	1725
p-Tolyl	75.6	114.5—115	(113.5)[2]	1725
p-Chlorophenyl	79.3	146—147	(142.5—143.5)[2]	1730
Benzyl	66.4	164—165	(165—166)[3]	1725
Benzhydryl	64.7	155—156		1725
Ethyl	34.2	48—49		1725
Isopropyl	68.6	48.5—49.5		1725
t-Butyl	79.6	156.5—157.5		1725
Cyclohexyl	74.5	106.5—107	(99)[7]	1725

a) Satisfactory elemental analyses were obtained for all compounds. Analytical data for the new compounds are shown in Experimental section.
b) All IR spectra were measured in KBr pellets.

1) Chemistry of *N*-(Organothio)imides. III. For part II, see Y. Abe and J. Tsurugi, *Chemistry Lett.*, **1972**, 811.
2) W. Groebel, *Chem. Ber.*, **92**, 2887 (1959).
3) K. H. Büchel and A. Conte, *ibid.*, **100**, 1248 (1967).
4) W. Groebel, *ibid.*, **93**, 284 (1960).
5) H. Miyoshi and R. Oda, *Kogyo Kagaku Zasshi*, **59**, 224 (1956).
6) M. Furukawa, Y. Fujino, Y. Kojima, M. Ono, and S. Hayashi, *Chem. Pharm. Bull.* (Tokyo), **20**, 2024 (1972).
7) M. Behforouz and J. E. Kerwood, *J. Org. Chem.*, **34**, 51 (1969).
8) B. C. Pant and J. G. Noltes, *Inorg. Nucl. Chem. Lett.*, **7**, 63 (1971).
9) H. Emde, Ger, 804572 (1951); *Chem. Abstr.*, **46**, 529 (1952).

The red or orange coloration in the mixture solution of mercaptan, NCS, and benzene may be attributed to the formation of sulfenyl chloride. After the addition of triethylamine to this solution, the color of the reaction mixture fades. This indicates the consumption of sulfenyl chloride.

The use of an excess of mercaptan must be avoided. Otherwise, the product will be obtained in a lower yield than that shown in Table 1, because the *N*-(organothio)succinimide produced will react with the excess mercaptan to produce disulfide.[10,11]

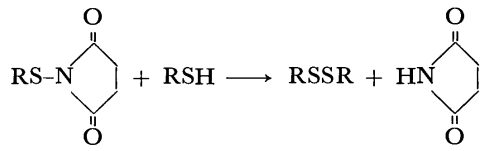

Therefore, the purity of NCS must be determined by iodometrical titration and a calculated equimolar amount of NCS must be used. For example, in the case of the preparation of *N*-(phenylthio)succinimide, the yield increased from 55.1 to 78.2% as the NCS became more pure. The yield is still not quantitative, however. This may be because a part of the mercaptan is oxidized to disulfide by the reaction with NCS in spite of the major route to sulfenyl chloride. In fact disulfides were detected as by-products in all runs.

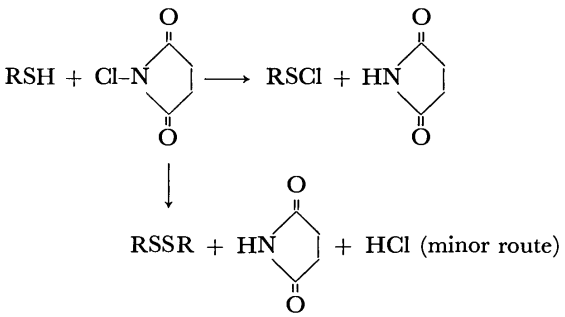

This method for the preparation of *N*-(organothio)-succinimide is superior to the method using chlorine gas[7] because the amount of NCS required as a chlorinating agent can be exactly and conveniently weighed, and it needs only one reaction vessel, even though the method involves two steps.

Experimental

All the melting points are uncorrected. The IR spectra were recorded with a JASCO IR-S spectrometer. The mercaptans were used without further purification. The purity of the NCS was determined by iodometrical titration before use.

General Procedure for the Preparation of N-*(Alkylthio)- and* N-*(Arylthio)succinimides.* A solution of mercaptan (20 mmol) in benzene (20 ml) at room temperature (*ca.* 20 °C) was added, all at once, to a suspension of NCS (20 mmol) in benzene (110 ml). After being stirred for 5 min, the mixture turned red or orange and the temperature rose to 30—35 °C. After the temperature had been depressed to 25 °C, a solution of triethylamine (21 mmol) in benzene (20 ml) was added, drop by drop, over a period of 5 min at 20—30 °C with cooling. The reaction mixture faded; it was then allowed to stand for 30 min, was washed thoroughly with water, and was then dried over anhydrous sodium sulfate. After the removal of the solvent, it was recrystallized from ethanol.

N-*(Benzhydrylthio)succinimide.* Found: C, 68.22; H, 5.02; N, 4.43; S, 10.52%. Calcd for $C_{17}H_{15}NO_2S$: C, 68.66; H, 5.08; N, 4.71; S, 10.78%.

N-*(Ethylthio)succinimide.* Found: C, 45.33; H, 5.74; N, 8.75; S, 20.04%. Calcd for $C_6H_9NO_2S$: C, 45.27; H, 5.70; N, 8.80; S, 20.14%.

N-*(Isopropylthio)succinimide.* Found: C, 48.36; H, 6.48; N, 8.11; S, 18.72%. Calcd for $C_7H_{11}NO_2S$: C, 48.53; H, 6.40; N, 8.09; S, 18.51%.

N-*(t-Butylthio)succinimide.* Found: C, 51.39; H, 7.04; N, 7.45; S, 17.14%. Calcd for $C_8H_{13}NO_2S$: C, 51.31; H, 7.00; N, 7.48; S, 17.12%.

The authors are grateful to Dr. Tsugio Fukumoto for his kind advice, to Mr. Toyokazu Horii for the supply of benzhydryl mercaptan, and to Mr. Ryuichi Akaki for his elemental analyses.

10) K. S. Boustany and A. B. Sullivyan, *Tetrahedron Lett.*, **1970**, 3547.

11) D. N. Harpp, D. K. Ash, T. G. Back, J. G. Greason, B. A. Orwig, W. H. VanHorn, and J. P. Snyder, *ibid.*, **1970**, 3551.

BULLETIN OF THE CHEMICAL SOCIETY OF JAPAN, VOL. 46, 1900 (1973)

Dielectric Relaxation in α,ω-Dichloroalkanes in Benzene Solution

Suresh CHANDRA* and R. A. YADAV
Physics Department, University of Gorakhpur, Gorakhpur, India
(Received June 16, 1972)

We have recently reported the asymmetric dielectric behaviour for α,ω-dichloroalkanes in pure liquid.[1] In order to confirm the behaviour, dielectric studies have been made in dilute solutions since the result would give an idea of the molecular structure in quasi-isolated state. Dielectric constants and loss of five α,ω-dichloroalkanes (1,2-dichloroethane; 1,4-dichlorobutane; 1,6-dichlorohexane; 1,8-dichlorooctane; and 1,10-dichlorodecane) have been measured at frequencies 450 KHz, 1.8 GHz, 4.0 GHz, and 23.7 GHz in dilute benzene solution at 35°C. The experimental arrangement and procedure are the same as described earlier.[2,3] An asymmetric distribution of relaxation time has been obtained for all cases giving skewed arcs when the dielectric loss slope is plotted against the dielectric constant slope (Fig. 1).

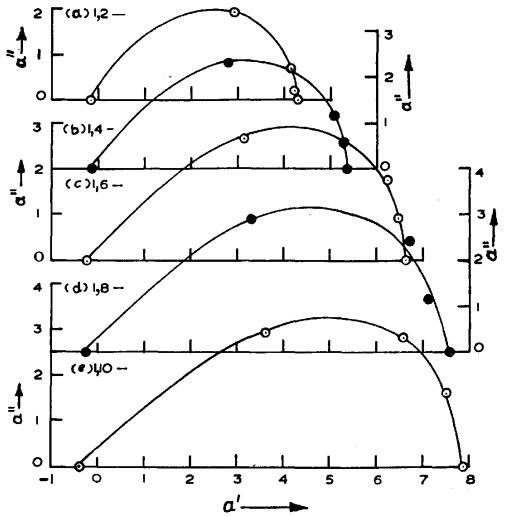

Fig. 1. Complex plot between a'' and a' for some α,ω-Dichloroalkanes in benzene solution.

The results have been analysed in terms of the Davidson-Cole plot.[4] They indicate the presence of some cooperative phenomenon in case of associated liquids[7,8] with a few exceptions.[1,5,6] Skewed arc behaviour in α,ω-dichloroalkanes can be understood in terms of intramolecular cooperative relaxation mechanism, *viz*; the intramolecular group rotations are such that the rotating electric moments interact sufficiently with one another and the reorientation of one segment triggers many other reorientations. Thus this intramolecular cooperative phenomenon has similar effect to that of intermolecular cooperative phenomena known to give skewed arc dielectric behaviour.

TABLE 1. DIELECTRIC RELAXATION PARAMETERS OF α,ω-DICHLOROALKANES IN BENZENE SOLUTION AT 35°C ASSUMING A DAVIDSON-COLE TYPE DISTRIBUTION

Parameters	1,2-DCE	1,4-DCB	1,6-DCH	1,8-DCO	1,10-DED
$\tau_{cs} \times 10^{12}$ (s)	7.3	11.6	16.5	23.6	31.6
β_{sol}	0.67	0.64	0.61	0.59	0.57

The characteristic relaxation time (τ_{cs}) and asymmetric distribution parameter (β_{sol}) in solution are presented in Table 1. We see that the value of τ_{cs} increases with increasing chain-length. The value of β_{sol} increases with decreasing chain-length suggesting more rigid structure with decreasing chain-length.

The authors are thankful to Prof. D. Sharma for his interest in the work.

* Present address: Physics Department, Ravishankar University, Raipur, M. P. India.

1) S. Chandra and R. A. Yadav, *J. Chim. Phys.*, **69**, 1018 (1972).
2) S. Chandra and D. Nath, *J. Chem. Phys.*, **51**, 5299 (1969).
3) S. Chandra and J. Prakash, *ibid.*, **54**, 5366 (1971).
4) D. W. Davidson and R. H. Cole, *ibid*, **19**, 148 (1951).
5) S. Chandra and J. Prakash, *J. Phys. Chem.*, **75**, 2616 (1971).
6) F. I. Mopsik and R. H. Cole, *J. Chem. Phys.*, **44**, 1015 (1966).
7) D. J. Denney and R. H. Cole, *ibid.*, **19**, 1484 (1951).
8) N. Koizumi and T. Hanai, *ibid.*, **60**, 1496 (1956).

BULLETIN OF THE CHEMICAL SOCIETY OF JAPAN, VOL. 46, 1901—1902 (1973)

Sterically Controlled Syntheses of Optically Active Organic Compounds. XXI. The Temperature Dependence of Hydrogenolytic Asymmetric Transamination between Optically Active Phenylglycine and α-Keto Acids*

Kaoru HARADA, Tameo IWASAKI, and Tadashi OKAWARA

Institute for Molecular and Cellular Evolution, Department of Chemistry, University of Miami, 521 Anastasia Avenue, Coral Gables, Florida 33134, U.S.A.

(Received September 25, 1972)

Generally, temperature is one of the most important factors in determining the molecular conformation in asymmetric syntheses. Several studies of the effect of temperature on asymmetric syntheses have been recorded in the literature.[1-7]

A temperature dependent asymmetric synthesis by hydrogenolytic asymmetric transamination between ethyl pyruvate and optically active benzylic amines was reported from this laboratory.[8,9] It was found that the difference of entropy of activation ($\Delta\Delta S^{\neq}$) for the diastereomeric transition states was the important factor in the asymmetric synthesis. These facts agreed with the previously proposed explanation (chelation hypothesis) for the steric course of the sterically controlled reaction.[10-12]

In the previous study from this laboratory, the hydrogenolytic asymmetric transamination between α-keto acids and optically active α-phenylglycine in aqueous alkaline solution was examined.[13,14] The possible steric course of this asymmetric synthesis was discussed.[14] The chelated intermediate formed between the substrate and the catalyst would not be expected to be as important in this reaction as in similar asymmetric reactions using organic solvents[10-12] because of the high dielectric constant of the solvent used.

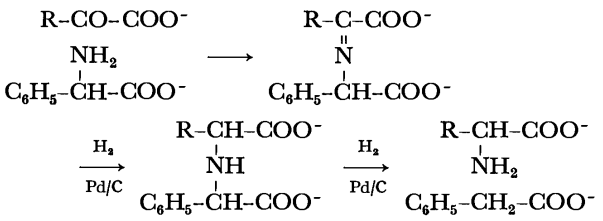

This investigation examines the temperature dependence of the hydrogenolytic asymmetric transamination between (*R*)-α-phenylglycine and (A) pyruvic acid or (B) α-ketoglutaric acid. The reaction temperatures used ranged from 0 to 70°C. The hydrogenation reactions were carried out at 1 atmosphere of hydrogen using palladium on charcoal (5%) in an aqueous solution that contained an equimolar amount of sodium hydroxide to the carboxyl groups in the substrate. The reaction procedures are similar to those described in an earlier paper.[13,14] The results are summarized in Table 1. When (*R*)-phenylglycine was used, (*R*)-alanine and (*R*)-glutamic acid were synthesized. The optical purities ranged from 31 to 57% for alanine and from 4 to 46% for glutamic acid. At 0°C, the optical purities of amino acids were the highest and the optical purities decreased as the reaction temperature was increased.

Formation of optically active amino acids in the asymmetric synthesis is due to the difference between the rates of formation of the two diastereomers from the starting material (substrate*). The rates of formation of the diastereomeric activated complexes are determined by the difference of the free energies of activation ($\Delta G^{\neq}$) for two diastereomeric transition states. According to the transition state theory, the rate of formation of an activated complex [(*R*)-substrate* complex]$^{\neq}$ in the transition state is expressed as follows:[2,15-18]

$$k_R = \kappa_R \frac{kt}{h} e^{-\Delta G_R^{\neq}/RT}$$

If we assume that the transmission coefficient κ_R is equal to κ_S, the *R*-product*/*S*-product* is expressed as shown below:

$$R\text{-product}^*/S\text{-product}^* = \frac{R}{S} = \frac{k_R}{k_S} = \exp\frac{\Delta S_R^{\neq} - \Delta S_S^{\neq}}{R} \exp\frac{-(\Delta H_R^{\neq} - \Delta H_S^{\neq})}{RT}$$

$$= \exp\frac{\Delta\Delta S_{R\text{-}S}^{\neq}}{R} \exp\frac{-\Delta\Delta H_{R\text{-}S}^{\neq}}{RT}$$

$$\log\frac{R}{S} = \log\frac{k_R}{k_S} = \frac{\Delta\Delta S_{R\text{-}S}^{\neq}}{2.3R} - \frac{\Delta\Delta H_{R\text{-}S}^{\neq}}{2.3RT}$$

* Contribution No. 231 of the Institute for Molecular and Cellular Evolution, University of Miami. Part XX, Tadashi Okawara and Kaoru Harada, This Bulletin, **46**, 1869 (1973).

1) H. Pracejus, *Ann.*, **634**, 9, 23 (1960).
2) H. Pracejus and A. Tille, *Chem. Ber.*, **96**, 854 (1963).
3) H. Pracejus and H. Mae je, *J. Prakt. Chem.*, **24**, 195 (1964).
4) H. Pracejus, *Tetrahedron Lett.*, **1966**, 3809.
5) S. Win er and H. Pracejus, *Chem. Ber.*, **99**, 151 (1966).
6) U. Folli, D. Iarossi, F. Montanari, and G. Torre, *J. Chem. Soc., C*, **1968**, 1317.
7) C. A. Brown, *J. Amer. Chem. Soc.*, **91**, 5901 (1969).
8) K. Harada and T. Yoshida, *Chem. Commun.*, **1970**, 1071.
9) K. Harada and T. Yoshida, *J. Org. Chem.*, **37**, 4366 (1973).
10) K. Harada and K. Matsumoto, *ibid.*, **32**, 1794 (1967).
11) K. Harada and K. Matsumoto, *ibid.*, **33**, 4466 (1968).
12) K. Harada and T. Yoshida, This Bulletin, **43**, 921 (1970).
13) K. Harada, *Nature*, 212, 1571 (1966).
14) K. Harada, *J. Org. Chem.*, **32**, 1790 (1967).
15) S. Glasston, K. J. Laidler, and H. Eyring, "The Theory of Rate Process," McGraw-Hill Book Co., Inc., New York (1941).
16) C. A. Eckert, *Ind. Eng. Chem.*, **59**, No. 9, 20 (1967).
17) E. I. Klabunovskii and E. S. Levitina, *Russ. Chem. Rev.*, **39**, 1035 (1970).
18) The $\Delta G^{\neq}$ of the equation includes external factors such as solvents and catalysts, which cause to change the free energy of activation of the reactions, *Cf.* Chapters 4 and 8 of literature 15.

TABLE 1. ASYMMETRIC SYNTHESIS OF AMINO ACIDS AT VARYING TEMPERATURES

Reaction		Reaction temp. (°C)	Phegly config.	Synthesized amino acid		DNP-Amino acid	
				Config. of amino acid	Yield[a] (%)	$[\alpha]_D^{25}$[b]	Optical purity[c] (%)
A	Ala	10	*R*	*R*	—[d]	−82.0	57
		20	*R*	*R*	33	−74.5	52
		30	*R*	*R*	29	−66.0	46
		40	*R*	*R*	26	−59.8	42
		50	*R*	*R*	46	−56.2	39
		60	*R*	*R*	44	−44.8	31
		70	*R*	*R*	40	−50.8	35
B	Glu	10	*R*	*R*	30	+37.4	46
		20	*R*	*R*	24	+31.0	38
		30	*R*	*R*	29	+21.8	27
		40	*R*	*R*	27	+16.6	20
		50	*R*	*R*	36	+10.8	13
		60	*R*	*R*	34	+ 9.8	12
		70	*R*	*R*	35	+ 3.2	4

a) Yields were calculated from phenylglycine.
b) Specific rotation of DNP-alanine was measured in 1M NaOH. Specific rotation of DNP-glutamic acid was measured in glacial acetic acid.
c) Optical purity was defined as $[\alpha]_D$ obsed/$[\alpha]_D$ of the compound ×100; DNP-(*R*)-(−)-alanine, $[\alpha]_D^{25}$ −143.9° (1M NaOH), DNP-(*R*)-(+)-glutamic acid, $[\alpha]_D^{25}$ +80.8° (AcOH).
d) A part of the sample was lost.

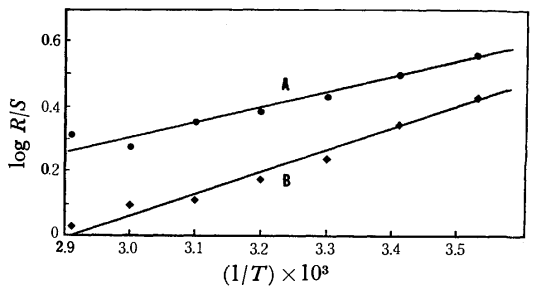

Fig. 1. Temperature dependence of hydrogenolytic asymmetric transamination. Reaction A, alanine: Reaction B, glutamic acid.

Figure 1 shows the plot of log R/S against $1/T$ from the results obtained in the asymmetric transamination reactions. In both reactions A and B, the plots are almost linear in the range from 10 to 70°C. From this plot, $\Delta\Delta H^{\ddagger}_{R-S}$ and $\Delta\Delta S^{\ddagger}_{R-S}$ of reactions A and B were calculated.

reaction A $\Delta\Delta H^{\ddagger}_{R-S} = -5.0$ kcal mol^{-1}

$\Delta\Delta S^{\ddagger}_{R-S} = -11.8$ cal mol^{-1} deg^{-1}

reaction B $\Delta\Delta H^{\ddagger}_{R-S} = -7.5$ kcal mol^{-1}

$\Delta\Delta S^{\ddagger}_{R-S} = -22.0$ cal mol^{-1} deg^{-1}

These results indicate that the free energy of activation ($\Delta G^{\ddagger}$) is independent of the reaction temperature and that the asymmetric hydrogenation reaction proceeds by a single mechanism in this temperature range.

Experimental

All the asymmetric transamination reactions were carried out as described in reference 14, except for the reaction temperature and the apparatus. Hydrogenation and hydrogenolysis were carried out in a three neck flask (100 ml) at one atmosphere with magnetic stirring at varying temperatures. The accuracy of the reaction temperature is about ±1°C. (*R*)-Phenylglycine (1.5 g, 0.001 mol, $[\alpha]_D^{25}$ −168.0°, *c* 1.11, 5M HCl) and 0.01 mol of α-keto acids were dissolved in 20 ml (30 ml in the case of α-ketoglutaric acid) fo aqueous sodium hydroxide (1M). Palladium on charcoal (5%, 2.5 g) was added to the solution and hydrogenation and hydrogenolysis were carried out. The hydrogenation and hydrogenolysis reactions proceeded at different rates depending on the temperature used. At 70°C, 20 min was sufficient to complete the reaction; however, at 10°C, more than 100 hr was necessary. After hydrogenolysis, the resulting amino acids were isolated by the use of a Dowex 50 column. A part of the amino acid was converted to DNP-amino acid by the use of 2,4-dinitrofluorobenzene. The resulting amino acids were purified by the use of Celite column chromatography in the usual manner[19] without fractionation of optical isomers. The DNP-amino acids were used for measurement of optical purity of amino acid. The dinitrophenylation was especially necessary in these asymmetric syntheses because the resulting crude amino acids contained impurities which had amphoteric properties. Therefore, the yield of alanine and glutamic acid was determined by the use of an automatic amino acid analyzer after appropriate dilution. The elution pattern of alanine in the amino acid analyzer showed 4—7 peaks other than alanine. However, the elution pattern of glutamic acid showed a single peak.

This work was supported by Grant No. NGR-10-007-052 from the National Aeronautics and Space Administration. The authors wish to express their thanks to Mr. Charles R. Windsor for amino acid analyses.

19) J. C. Perrone, *Nature*, **167**, 513 (1951); A. Court, *Biochem. J.*, **58**, 70 (1954).

Ionic Photodissociation of Electron Donor-Acceptor Complexes

Motoo SHIMADA, Hiroshi MASUHARA, and Noboru MATAGA

Department of Chemistry, Faculty of Engineering Science, Osaka University, Toyonaka, Osaka 560

(Received June 12, 1972)

Ionic photodissociation of electron donor-acceptor (EDA) complexes of *s*-tetracyanobenzene (TCNB) and pyromellitic dianhydride (PMDA) with 2-methyltetrahydrofuran (MTHF) has been investigated by means of nsec flash photolysis and transient photocurrent measurements. The solvent-shared ion-pair of TCNB anion and MTHF cation is formed from the excited charge-transfer (CT) singlet state of a TCNB–MTHF complex, dissociating into solvated ions. TCNB complexes with aromatic hydrocarbons dissociate directly into ions from the lowest excited CT singlet state. Dissociation of PMDA complexes occurs in the CT triplet state in nonpolar solvents and mainly in the excited CT singlet state in polar solvents. The relative rate constant of radiationless process, which competes with ionic dissociation in the excited singlet state, can be deduced from the effect of solvent on ionic photodissociation. It has been confirmed for the first time that the ionic dissociation of a TCNB–benzene–1,2-dichloroethane (DCE) system occurs in the excited Franck-Condon (FC) state. It is pointed out that the latter dissociation mechanism is not inconsistent with all the results obtained for TCNB and PMDA complexes under various conditions.

Ionic photodissociation is one of the most important processes of EDA complexes. At the present stage of our investigation on the electronic structures and dynamic behaviors of EDA complexes in the excited state, the results on weak EDA complexes may be summarized as follows. TCNB complexes with methyl-substituted benzenes as well as some other aromatic donors such as naphthalene in polar solvents dissociate into ions in the excited singlet state, while in nonpolar solvents, ionic dissociation does not occur but only the CT fluorescence is observed.[1,2] It has become clear that a TCNB–α-methylstyrene complex in amylalcohol at low temperature dissociates in the CT triplet state.[3] Dissociation of PMDA complexes with mesitylene and hexamethylbenzene (HMB) occurs also in the CT triplet state.[4] The dissociative state of tetracyanoethylene (TCNE) complexes with tetrahydrofuran (THF), dimethylsulfoxide, *N*,*N*-dimethylformamide and acetone donors was concluded to be CT triplet state by means of ESR experiments.[5,6] A flash photolysis study on a TCNE–THF complex gave the same conclusion.[7] The present work deals with the complex formation and ionic dissociation of TNCB–MTHF and PMDA–MTHF complexes. The dissociation mechanism of TCNB complexes will be discussed in detail on the basis of present and previous results.

Experimental

Experimental methods are the same as reported previously.[2] Acetonitrile and butyronitrile were refluxed over phosphorus pentoxide and distilled from anhydrous calcium carbonate. MTHF was refluxed over metallic sodium for a few hours, distilled and stocked in a vacuum. Spectrograde DCE, 1,4-dioxane, THF, ethanol (Nakarai Chemicals) and benzene (Merck) were used without further purification. TCNB, PMDA and naphthalene were the same samples as used before.[2] All the solutions were degassed by the usual freeze-pump-thaw method.

Results

Absorption and Luminescence Spectra of MTHF Complexes. The absorption spectra of TCNB–MTHF–DCE and PMDA–MTHF–DCE systems are given in Figs. 1 and 2, respectively. As the concentration of the donor increases, the intensity of the absorption band of the acceptor decreases, the swelling and tail appearing at 280 and 330 nm, respectively. The isosbestic points can be recognized in both systems. A spectrum, obtained by normalizing spectra (a) and (c) at the 320 nm peak and subtracting the former from the latter, has broad bands with peaks at 280 and 323 nm. Both bands satisfy approximately the relation between the absorption maxima of TCNB complexes and the ioniza-

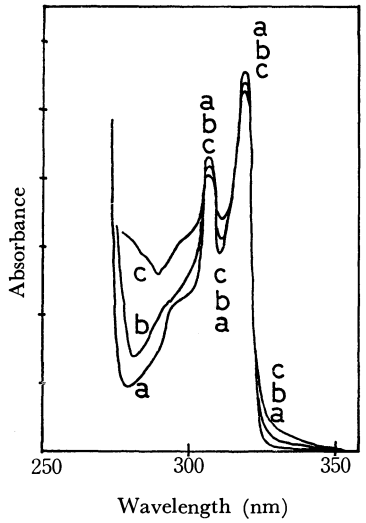

Fig. 1. The absorption spectra of TCNB–MTHF–DCE system; the concentration of TCNB is 2.12×10^{-4} M. Concentrations of MTHF; (a) 0 M, (b) 2 M, (c) 7.9 M.

1) H. Masuhara, M. Shimada, and N. Mataga, This Bulletin, **43**, 3316 (1970).
2) H. Masuhara, M. Shimada, N. Tsujino, and N. Mataga, *ibid.*, **44**, 3310 (1971).
3) M. Irie, S. Tomimoto, and K. Hayashi, *J. Phys. Chem.*, **76**, 1419 (1972).
4) R. Potashnik, C. R. Goldschmidt, and M. Ottolenghi, *ibid.*, **73**, 3170 (1969).
5) D. F. Ilten and M. Calvin, *J. Chem. Phys.*, **42**, 3760 (1965).
6) F. E. Stewart, M. Eisner, and W. R. Carper, *ibid.*, **44**, 2866 (1966).
7) Y. Achiha, S. Katsumata, and K. Kimura, *Chem. Phys. Lett.*, **13**, 213 (1972); This Bulletin, **45**, 1272 (1972).

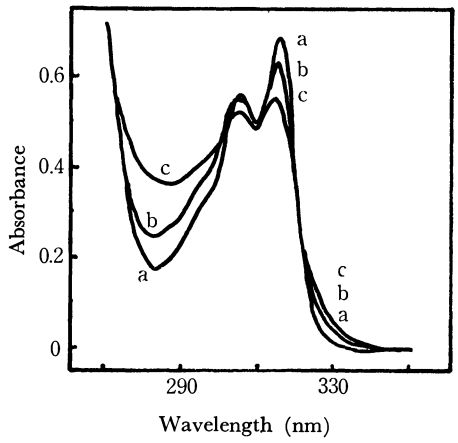

Fig. 2. The absorption spectra of a PMDA–MTHF–DCE system; the concentration of PMDA is 2.61×10^{-4} M. Concentrations of MTHF; (a) 0 M, (b) 2 M, (c) 7.9 M.

tion potential of the donor,[8] although the precise value of the ionization potential of MTHF is not known. Hence, they may be assigned to CT transitions of MTHF complexes with TCNB and PMDA. Absorption spectra were measured with a high concentration of the acceptor, and the molar extinction coefficient of the CT band as well as the equilibrium constant of the complex formation were evaluated. Since the original band of the acceptor has a small absorption intensity in the wavelength region examined, the following equation was used.

$$\varepsilon^* - \varepsilon_A = (\varepsilon - \varepsilon_A)/(1 + 1/Kc_D)$$
$$\varepsilon^* = D/c_A l$$

where D is the absorbance at the wavelength examined and l is the optical path length of the cell in cm. ε_A and ε represent molar extinction coefficients of the acceptor and the EDA complex at that wavelength, respectively. c_A and c_D are the concentrations of the donor and the acceptor, respectively. K is the equilibrium constant. The results for the TCNB–MTHF–DCE system are shown in Fig. 3, where the measure-

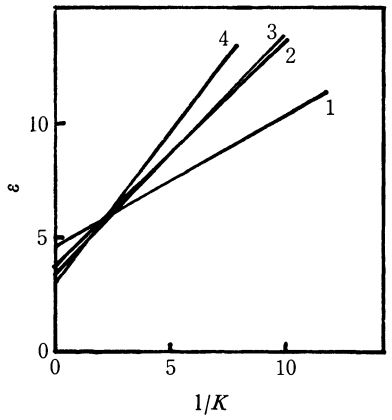

Fig. 3. The relation between ε and $1/K$ of a TCNB–MTHF–DCE system; the concentration of TCNB is 1.06×10^{-2} M. Concentrations of MTHF; (1) 3.36 M, (2) 1.38 M, (3) 0.99 M, (4) 0.49 M.

8) N. Mataga and Y. Murata, *J. Amer. Chem. Soc.*, **91**, 3144 (1969).

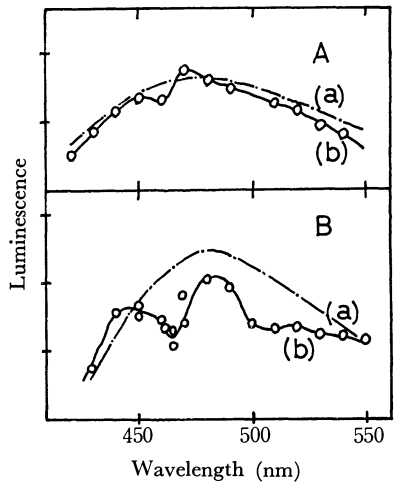

Fig. 4. Fluorescence spectra of a TCNB–MTHF complex at room temperature (A), and at 77 K (B): (a) —— by spectrophotofluorometer, (b) —○—○— by laser excitation.

ments were made at 350 nm. The complex formation of MTHF, a weak electron-donor reagent, with TCNB and PMDA is thus confirmed. K was obtained as 0.45 and ε was calculated to be 6 at 350 nm. The extinction coefficients of CT bands at 323 and 280 nm were 700 and 1100, respectively.

Fluorescence spectra of the TCNB–MTHF complex observed at room temperature and at 77 K by exciting the CT absorption band are shown in Fig. 4. The fluorescence lifetime at room temperature is *ca.* 5 ns at all the wavelengths in the fluorescence band, while at 77 K the lifetime depends on the fluorescence wavelength. It increases from *ca.* 20 to 40 ns as the wavelength increases. A re-absorption of the CT fluorescence by the excited complex or by photoproduced transients was observed in the case of laser excitation. A phosphorescence spectrum of the TCNB–MTHF complex has a peak at about 500 nm with a lifetime 28.4 ms. Flourescence of the PMDA–MTHF complex has a peak at 390 nm with a very short lifetime (a few ns). No re-absorption effect by laser excitation was observed.

Ionic Dissociation of MTHF Complexes. The transient absorption spectrum obtained by exciting the TCNB–MTHF complex at 347 nm is shown in Fig. 5. Since the absorption spectrum on the wave-

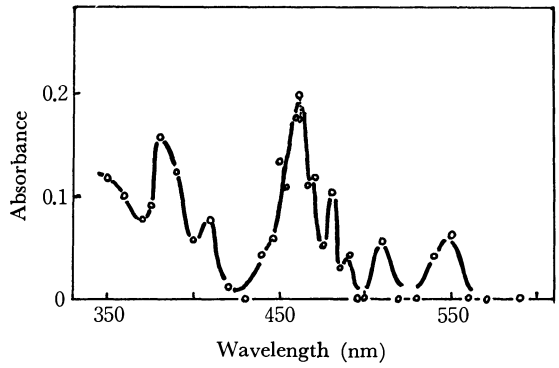

Fig. 5. The transient absorption spectra observed immediately after excitation of a TCNB–MTHF complex; the concentration of TCNB is 0.1 M.

length region smaller than 500 nm is similar to that of TCNB anion, it is confirmed that the excitation of the complex leads to ionic dissociation. On the other hand, the bands in the wavelength region greater than 500 nm, which cannot be observed by the ordinary stationary measurements, may be due to the excited state of a photoproduct, since the absorbances of these bands increase by the irradiation of CT band with a steady Xe-lamp. The kinetic relation between the transmittance at 462 nm and the transient photocurrent is given in Fig. 6. The transimittance is almost constant in the course of several μs after excitation, while the peak photocurrent is attained during *ca.* 2 μs. The current decays slowly ($\tau_{1/2}\sim 10$ μs). The difference between transmittance and photocurrent may be ascribed to a transient, which gives no current but shows an absorption spectrum similar to that of TCNB anion. The transient is deemed to be an ion-pair of TCNB anion and MTHF cation, which is produced rapidly by laser excitation, dissociating gradually into ions. The results in the case of the aerated system are the same as those in the degassed case.

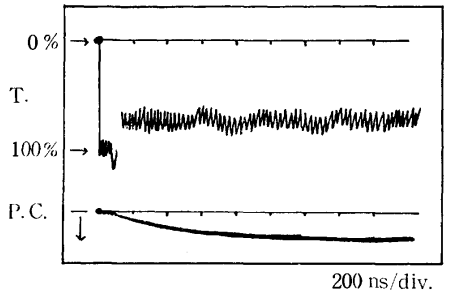

Fig. 6. The kinetic relation between the transient photocurrent and the transmittance of a TCNB anion at 462 nm, induced by exciting TCNB–MTHF complex.

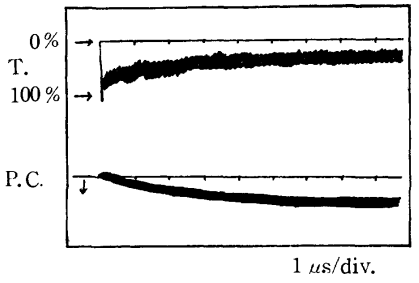

Fig. 7. The kinetic relation between the transient photocurrent and the transmittance of a PMDA anion at 660 nm, induced by exciting a PMDA–MTHF complex.

The dissociation process was also examined in an ethanol solution, where the volume ratio of MTHF to ethanol was 1:1. The transient absorption was similar to that of a TCNB anion. The transmittance was constant with respect to time, while most of the photocurrent was induced rapidly, the delayed ($\sim$100 ns) photocurrent being also detected.

Assuming that an extinction coefficient of the ion-pair is equal to that of the dissociated ions, the quantum yields of dissociation as well as ion-pair formation for the systems of TCNB–MTHF and TCNB–MTHF–ethanol were estimated according to the same method as reported previously.[2] Values for the quantum yield were 0.03 and 0.089, respectively.

Since all the measurements were carried out under a high concentration of TCNB, effect of the direct excitation of the tail of the original TCNB band should be examined. A small and rapidly rising photocurrent was induced in the TCNB–DCE system, which may be due to ionization of TCNB itself. A slowly rising curve of laser-induced photocurrent similar to that of the TCNB–MTHF system was observed by exciting the TCNB–MTHF–DCE system, where the concentration of TCNB was equal to that of the TCNB–DCE system. Thus, it might be concluded that the present results are due to the ionic dissociation of the TCNB–MTHF complex.

We have confirmed that a PMDA anion is produced by exciting a PMDA–MTHF complex with a 347 nm laser pulse at room temperature. Oscillograms showing the transmittance at the wavelength of the PMDA anion absorption (660 nm) as well as a laser-induced photocurrent are given in Fig. 7. The peak photocurrent was measured at *ca.* 8 μs after excitation. It decayed slowly ($\tau_{1/2}\sim 300$ μs). The rise curve of the photocurrent is in good agreement with that of absorption band of a PMDA anion. At 77 K the measurement of transient absorption spectra is impossible because of a laser-induced cracking of an MTHF rigid solution. No appropriate condition could be found in which the rise of a PMDA anion can be related to the decay of the phosphorescence. In the aerated system the peak photocurrent was measured at *ca.* 2.5 μs after excitation, its value being *ca.* one fifth of that in the degassed system.

The effect of solvents on the dissociation of a PMDA–MTHF complex was examined by photocurrent measurement. A schematic representation of oscillograms is given in Fig. 8. In a DCE solution, the peak photocurrent was reached slowly, while in polar solvents such as acetonitrile and butyronitrile rapid as well as slow productions of ions were observed. The rise of a laser-induced photocurrent is in good agreement with

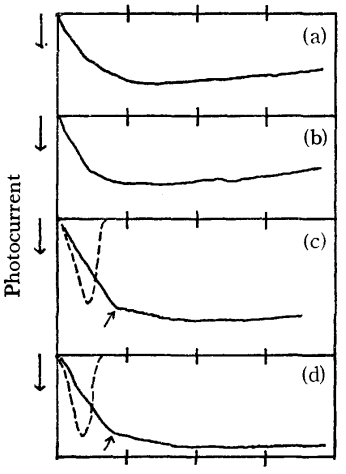

Fig. 8. The rise and decay curves of photocurrent induced by exciting a PMDA–MTHF complex. Solvents; (a) Without other solvent, (b) DCE, (c) butyronitrile, (d) acetonitrile. Horizontal scale; (a), (b) 5 μsec per division, (c), (d) 50 nsec per division. ------Observed exciting pulse.

that of transmittance of a PMDA anion in the case of a PMDA–MTHF–acetonitrile system. The photocurrent of a PMDA–acetonitrile system was also confirmed under the same concentration of PMDA as that of a PMDA–MTHF–acetonitrile system. Only rapid rise of the photocurrent was observed, which is *ca.* one fifth of that of a PMDA–MTHF–acetonitrile system. Hence, the present result is concluded to be due to the dissociation of a PMDA–MTHF complex.

We also made an investigation on TCNB–1,4-dioxane, PMDA–1,4-dioxane and PMDA–THF complexes in DCE solutions. The peak photocurrents were observed at several μs after excitation, the delayed formation of ions being confirmed. The effect of excitation light intensity on the production of ions was examined by transient photocurrent measurement. Since the decay of a photocurrent is slower than the rise, the peak photocurrent is approximately proportional to the concentration of dissociated ions. The linear relations obtained between the excitation light intensity and the peak photocurrent show that the ionic dissociation of the present complexes in several solvents is a one-photon process.

Ionic Dissociation of TCNB and PMDA Complexes with Benzene and Naphthalene Donors. TCNB complexes with benzene and naphthalene donors and a PMDA–benzene complex were investigated in several solvents. The transient photocurrent measurements show that these complexes dissociate into ions immediately after excitation. The PMDA–benzene complex was examined in DCE and acetonitrile, where the volume ratio of benzene donor *vs.* solvent was fixed to 1:2. The results obtained on the TCNB–naphthalene complex are listed in Table 1, where the values of dielectric

TABLE 1. IONIC DISSOCIATION OF TCNB–NAPHTHALENE COMPLEX IN ITS LOWEST EXCITED SINGLET STATE

Solvent	ε[a)]	φ_{ion}[b)]
Ethylether	4.34	0.0019
DCE	10.36	0.095
Butyronitrile	20.3	0.24
Acetonitrile	27.5	0.57
Standard[c)]	25.8[d)]	1.00

a) Dielectric constant of solvent.
b) Relative quantum yields of ionic dissociation determined by measurement of photocurrent.
c) The TCNB–toluene–acetonitrile system.[2)]
d) Calculated dielectric constant.[2)]

constant and viscosity coefficient are corrected by the method described previously. Although the measurement of the photocurrent has been reported,[2)] we examined the TCNB–benzene–DCE system in more detail, with a 1:2 volume ratio of benzene to DCE. The rise and decay curves obtained for the fluorescence and photocurrent are shown in Figs. 9A and B. The observed fluorescence lifetime is about 20 ns. The simulated curves, considering a duration of an exciting pulse, are given in Fig. 9C, where (a), (b), and (c) represent the observed exciting pulse and the rise curves of radical ions from the fluorescent state ($\tau\sim$20 ns) and excited FC states, respectively. The present observation of photocurrent agrees with (c). From an

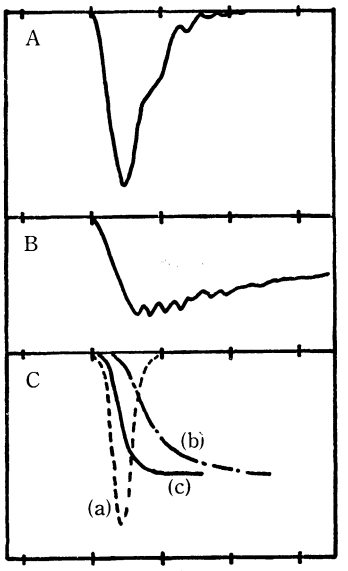

Fig. 9. TCNB–benzene–DCE system.
A. The rise and decay of fluorescence.
B. The rise and decay of laser-induced photocurrent.
C. The simulated rise and decay curves of photocurrent;
(a) Observed exciting pulse, $p(t')$,
(b) $\int_0^t p(t')\,(1-\exp\text{-}(-(t'-t)/\tau))\,dt'$, $\tau\sim$20 ns,
(c) $\int_0^t p(t')dt'$.

examination of the effect of excitation light intensity upon photocurrent, it has been confirmed that this ionic dissociation is a one-photon process. The photocurrent of TCNB in DCE was confirmed to be much smaller than that of the present system.

Discussion

The Electronic Structure of a TCNB–MTHF Complex in the Ground and Excited States. It has been shown that the 1st and the 2nd CT absorption bands of TCNB–mesitylene and TCNB–HMB complexes are due to transitions from the highest occupied molecular orbital (MO) of the donor to the lowest and the 2nd lowest vacant MO's of the acceptor, respectively.[9)] In the case of benzene and toluene donors the 2nd CT band was not observable since there are absorption bands of the donor in this wavelength region. In the case of the TCNB–MTHF complex, two CT bands were observed since there is no absorption band of the donor. The energy gap between the 1st and the 2nd new bands was estimated to be 0.56 eV, from the observed frequencies of the two bands. The value differs somewhat from the gap between the lowest and the 2nd lowest MO's of TCNB (0.68 eV). The difference may be related to the relative locations of the CT and the original bands of TCNB. In the case of mesitylene and HMB donors, two CT's are observed in the wavelength region longer than the original TCNB band, which results in the small configuration interaction (CI) between the CT and the locally excited (LE) configurations. On the other hand, the CT bands of

9) S. Iwata, J. Tanaka, and S. Nagakura, *J. Amer. Chem. Soc.*, **88**, 894 (1966).

the present complex were observed in the same wavelength region as that of the original bands of the acceptor. Hence, it is expected that the extent of CI between the CT and the LE configurations is rather large. Thus, the energy gap between the two bands of the TCNB–MTHF complex is not connected directly with the gap between two MO energies.

According to Iwata *et al.*,[9] the CT degree in the excited singlet FC state of TCNB complexes increases as the ionization potensial of the donor decreases. The ionization potential of MTHF is not known but may be larger than that of benzene (9.24 eV), since the ionization potensial of THF is 9.49 eV. The large interaction between the CT and the LE configurations is expected in the TCNB–MTHF complex. The LE character in the excited FC state may be rather high.

Fluorescence spectra of a TCNB–MTHF complex at room temperature show a large Stokes shift of about 10200 cm^{-1}. This can be explained by the same consideration as that on TCNB complexes with other donors. The large Stokes shift of TCNB–methylsubstituted benzene complexes was concluded to be due to differences in energy and geometrical structure between the excited FC and the fluorescent state. This conclusion was deduced from fluorescence studies as well as from direct observations of excited singlet-singlet absorption spectra.[8,10–12] Since the LE character of the excited FC state of the TCNB–MTHF complex seems to be high and the value of Stokes shift is quite large, it is considered by analogy to the case of the TCNB–methylsubstituted benzene complexes that the CT character of the fluorescent state is rather high. The fluorescence spectrum of a TCNB–MTHF complex by laser excitation are re-absorbed by some transients photoproduced from the excited FC state. Absorption spectra of the transient estimated from the re-absorption are similar to those of TCNB anion. Due to the short fluorescence lifetime it was difficult to analyze fluorescence decay curves at several wavelengths, though this is necessary for assigning the transient to the fluorescent state of the complex.[13] Nevertheless, similarity of the spectra of the fluorescent state to those of a TCNB anion is consistent with the large value of the Stokes shift and with the above argument concerning the high CT character of the fluorescent state. Hence, the changes in energy as well as electronic structure of the TCNB–MTHF complex occur in the course of the process from the excited FC to the relaxed fluorescent states, just as in the case of TCNB–methylsubstituted benzene complexes.

The Stokes shift of the present complex at 77 K is almost the same as that at room temperature, differing from the case of TCNB complexes with methylsubstituted benzenes.[8,10] Dependence of fluorescence lifetime on the observed wavelength was not observed in the case of the latter TCNB complexes at 77 K. The fact that the lifetime increases with the fluorescence wavelength may be ascribed to the relaxation process including surrounding molecules from the excited FC state to the equilibrium state. This particular behavior might be due to the fact that the electron donating orbital is the lone pair orbital of oxygen atom and the structural change involving environments is possible even at 77 K.

Ionic Dissociation of TCNB Complexes. Dissociation mechanism of TCNB complexes should be discussed in detail in consideration of the results of previous[2] and present works. All these complexes with cyclic ethers, methylsubstituted benzenes and naphthalene have a quite polar structure in the fluorescent state and form ion-pair or dissociate into ions rapidly in various solvents. In the case of cyclic ether donors, ions are produced rather slowly through the ion-pair state from the excited CT singlet state in nonpolar and slightly polar solvents. In moderately and strongly polar solvents the new process of direct dissociation, not through the ion-pair, is observed in addition to the above delayed process. Stabilization of ion-pair state may be partially due to the Coulomb attraction force between the cation and the anion. Since the positive charge is localized on an oxygen atom, this attractive force may be rather large. In the case of TCNB complexes with methylsubstituted benzenes, dissociation occurs spontaneously in the lowest excited CT singlet state in various solvents and the ion-pair is not observed. We have pointed out that the ionic dissociation yield increases with the increase of ionization potential of the donor.[2] However, the dissociation yield of a TCNB–naphthalene complex in acetonitrile is larger than that of a TCNB complex with mesitylene, although the ionization potential of naphthalene is lower than that of mesitylene. This may be ascribed to the difference of the Coulomb attractive force between the donor cation and the acceptor anion, if one assumes that the larger Coulomb attraction leads to the stronger nondissociative quenching of the excited state. The Coulomb force between a TCNB anion and a naphthalene cation seems to be rather small, since the positive charge in naphthlene is more delocalized than that in methylsubstituted benzene as well as in cyclic ether. From this consideration and the solvent effect on ionic dissociation of some TCNB complexes, it is concluded that the ionic dissociation of TCNB complexes depends upon the solvation energy on the one hand and upon the Coulomb force between ions on the other.

In the above discussion, the difference of solvation energies of different donor cations was not considered explicitly. The particular behavior of TCNB–cyclic ether complexes may be attributed partly to the property of the donor solvent itself, since cyclic ether is a well-known solvent which stabilizes ion-pair rather than dissociated ions. For example, Briegleb and Lind showed the ion-pair formation in the case of THF–nitrosubstituted benzenes by analyzing an ESR hyperfine pattern.[14] The ion-pair formation was reported

10) T. Kobayashi, K. Yoshihara, and S. Nagakura, This Bulletin, **44**, 2603 (1971).
11) H. Masuhara and N. Mataga, *Chem. Phys. Lett.*, **6**, 608 (1970).
12) H. Masuhara and N. Mataga, *Z. Phys. Chem. N. F.*, **80**, 113 (1972).
13) H. Masuhara and N. Mataga, This Bulletin, **45**, 43 (1972).
14) G. Briegleb and G. Lind, *Z. Naturforsch.*, **23a**, 1747, 1752 (1968).

also by Pilette and Weiss by analysing the decay of a PMDA anion,[15] produced by exciting the CT bands of PMDA complexes. They interpreted the results in terms of the equilibrium between ion-pair and dissociated ions as well as of the degradation of ion-pairs. In the case of TCNB–methylsubstituted benzene complexes, it is not certain whether the ion-pair was produced or not. Direct observation of the rapid formation of ion-pair was achieved for the first time for a TCNB–MTHF complex.

It should be noted that the ion-pair is a solvent-shared one. From the study on the electronic structure of the EDA complexes we have made it clear that the fluorescent state of these complexes is a contact ion-pair.[11,12] The excited equilibrium state of a TCNB–MTHF complex also seems to be quite polar. The lifetime of this fluorescent ion-pair is *ca.* 5 ns while that of the other ion-pair deduced from the absorption as well as the photocurrent measurement is a few μs. Since the difference of lifetime is very large, the difference between both ion-pairs cannot be ascribed to the difference of relative orientation of the donor cation and the acceptor anion. The long-lived ion-pair observed in μs time region is concluded to be a solvent-shared ion-pair.

Ionic Dissociation of PMDA Complexes. From the delayed formation of a PMDA anion and the oxgen effect on the dissociation, it is concluded that the PMDA–MTHF complex dissociates in the CT triplet state. Ions were produced not through the ion-pair state with rather long life, which differs from that of a TCNB–MTHF complex. This different behavior can be interpreted as follows. In the case of a PMDA–MTHF complex the rate constant of ion-pair formation might be small and in the same order as the dissociation of an ion-pair. Thus, the concentration of the latter is low and not detectable. In polar solvents, however, rapid production of a PMDA anion was observed in addition to the slow formation process. Due to the strong solvation of the donor cation and the acceptor anion by polar solvents, ionic dissociation may compete with intra-complex processes including intersystem crossing in the excited state. This suggests also a delicate balance between intra-complex interaction and solvation.

In the case of benzene and its derivative donors, dissociation has been confirmed to occur in the lowest CT triplet state. Potashnik *et al.* reported the dissociation from the CT triplet states of PMDA–mesitylene and PMDA–HMB complexes.[4] Recently, this dissociation from the triplet state has been demonstrated also by energy transfer experiments in some solvents.[7] In the present work, we observed the rapid dissociation of a PMDA–benzene complex in DCE as well as in acetonitrile. The rapid dissociation of a PMDA–mesitylene complex in acetonitrile was confirmed previously.[2] In the case of the latter system Achiba *et al.*,[7] have pointed out no participation of the CT triplet state to ionic dissociation. All these results on the PMDA complexes show a delicate effect of environments on the dissociation

15) Y. P. Pilette and K. Weiss, *J. Phys. Chem.*, **75**, 3805 (1971).

The relative rate constant of radiationless processes such as direct degradation as well as intersystem crossing, which compete with ionic dissociation in the excited singlet state, can be deduced from the effect of a solvent on ionic photodissociation. Assuming the same rate constants of photodissociation of TCNB and PMDA complexes, the intersystem crossing process of PMDA complexes may be faster than those of TCNB complexes. The process of PMDA–MTHF is faster than that of PMDA–methylsubstituted benzenes.

Ionic Dissociation from the Excited FC State. Although the dissociative states of EDA complexes have been classified as CT singlet or CT triplet state, the following experimental results seem to suggest the possibility of ionic dissociation in the excited FC state. (1) The electronic structure and geometrical configuration of the fluorescent state differ considerably from those of excited FC state in the case of TCNB complexes. The fluorescent state is therefore produced in nonpolar solvent through relaxation from the excited FC state.[12] In polar solvents, ionic dissociation was observed instead of fluorescence. (2) The intersystem crossing process of TCNB complexes is very rapid and direct formation of the phosphorescent state from the FC state was observed by means of ns flash photolysis studies on the rigid solution of TCNB–toluene complex in the mixture of 2- and 1-propanols.[16] In liquid mixture, ionic dissociation was observed, but not the formation of phosphorescent state. These results suggest that ionic dissociation and intersystem crossing compete with each other in the excited FC state. (3) The solvent effect on the fluorescence quantum yield and lifetime of a TCNB–benzene complex was examined and direct radiationless process was proved to occur from the excited FC state as well as in the course of the relaxation from the excited FC to the relaxed fluorescent states.[2] (4) Energy levels of several states of a TCNB–MTHF complex are given in Fig. 10. The energy levels of a solvent-shared ion-pair as well as dissociated ions are cited from results by Taniguchi *et al.*[17] It should be noted that there is a large gap between the fluorescent and solvent-shared ion-pair states. The ion-pair may be formed from the excited FC state.

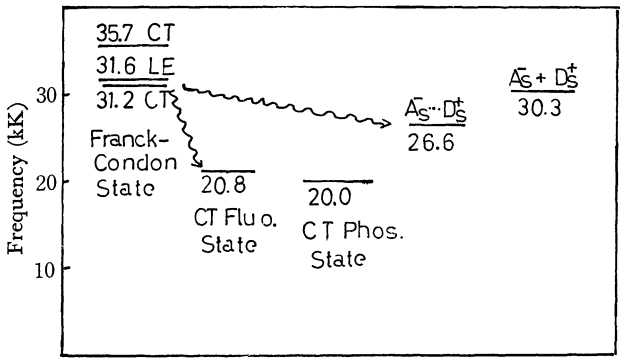

Fig. 10. Energy diagram of a TCNB–MTHF system.

16) H. Masuhara, N. Tsujino, and N. Mataga, *Chem. Phys. Lett.*, **12**, 481 (1972).

17) Y. Taniguchi, Y. Nishina, and N. Mataga, This Bulletin, **45**, 764 (1972).

We have directly confirmed that ions are produced immediately after exciting the CT band of a TCNB–benzene complex in DCE, not through the fluorescent state. It is concluded that the ionic dissociation of the present complex occurs in the excited FC state. This is the first direct observation of rapid dissociation of EDA complexes which are stable in the ground state. In more polar solvents the fluorescence lifetime of this complex is too short to be analysed, while no photocurrent is observed in less polar solvents.[18] Investigations on other systems are difficult because of short fluorescence lifetime. Hence, a TCNB–benzene–DCE system is the only example at the present stage of investigations. All the results obtained for TCNB and PMDA complexes under various conditions are not inconsistent with the present mechanism of dissociation in the excited FC state.

18) We used a 50Ω resistor for obtaining ns time resolution.

BULLETIN OF THE CHEMICAL SOCIETY OF JAPAN, VOL. 46, 1909—1913 (1973)

Reaction of Mo^{5+} Formed on Supported Molybdena Catalysts with Oxygen or Water

Masamichi AKIMOTO and Etsuro ECHIGOYA

Department of Chemical Engineering, Tokyo Institute of Technology, Ookayama, Meguro-ku, Tokyo 152

(Received August 4, 1972)

Reactivity of Mo^{5+} formed on supported molybdena catalysts with oxygen or water was investigated by means of ESR spectroscopy. Mo^{5+} formed on the alumina carrier could not be oxidized with gaseous oxygen even at 450 °C and was poisoned by water at 200 °C losing its ESR signal. The Mo^{5+} formed on the titania carrier disappeared by reaction with either oxygen or water. The mechanism for the reactions was investigated and the different reactivities of Mo^{5+} with oxygen as regards carrier effect on the structure were discussed.

The surface area of a catalyst determined by the BET method has long been used as a measure of catalytic activity. However, in the case of supported catalysts, the surface area also contains that of carrier and does not give the actual surface area of the active site. The need to determine this area increases particularly in the case where catalysts of the same or similar compositions show different activity and selectivity. Various methods have been presented to determine the number of active sites. As an example, adsorption of hydrogen or carbon monoxide was used to estimate the active surface area of platinum supported on alumina. Carbon monoxide was also utilized in the analysis of real surface area of supported nickel catalyst. For the case of supported metal oxide catalysts, the actual surface area of chromic oxide[1] supported on either alumina, silica or silica-alumina and of bismuth molybdate[2] on silica was estimated by reducing these catalysts with hydrogen followed by the determination of the amount of oxygen required for reoxidation.

We observed Mo^{5+} which cannot be oxidized even at 450 °C, denoted as Mo^{5+} (A), in molybdena catalysts supported on alumina and magnesia.[3] Mo^{5+} formed on silica and zinc oxide carrier, denoted as Mo^{5+} (B), was easily oxidized and showed good selectivity for maleic anhydride in the vapor phase oxidation of butadiene. Both Mo^{5+} (A) and Mo^{5+} (B) appeared in titania supported molybdena catalyst. In order to investigate the mechanism for carbon dioxide and maleic anhydride formation during the course of oxidation of butadiene, a method is desirable for estimating the amount of Mo^{5+} on the surface of supported molybdena catalysts. Thus, the reaction of Mo^{5+} formed in supported molybdena catalysts with oxygen or water was investigated by means of ESR, their structure being discussed with respect to different reactivities.

Amounts of Mo^{5+} (A) and Mo^{5+} (B) formed in MoO_3–TiO_2 catalyst and their distribution on the surface and in bulk were also determined.

Experimental

The reactivity of Mo^{5+} formed in a supported molybdena catalyst was investigated by means of ESR with a glass instrument consisting of a 5 mm o.d. quartz tube, 150 mm long with a glass cock. The amount of catalyst was 0.100 g. Evacuation was carried out with a conventional apparatus consisting of an oil diffusion pump. Heating was carried out by means of a cylindrical thermal air bath. Oxygen was introduced into the reaction vessel from a reservoir connected with the evacuation apparatus and water as saturated vapor at room temperature. First, the catalyst was evacuated for 30 min at 10^{-4}—10^{-5} mmHg and the Mo^{5+} was determined at room temperature by means of ESR using Mn^{2+} as an internal standard. Oxygen or water was then introduced into the vessel at room temperature and the vessel was heated to start the reaction. After the elapse of a certain time, the reaction mixture was cooled to room temperature and evacuated for 30 min. The amount of decreased Mo^{5+} was also determined by ESR at room temperature. The effect of temperature on the amount of

1) H. Charcossett, A. Revillon, and A. Guyot, *J. Catal.*, **8**, 334 (1967).

2) E. H. Lee, *ibid.*, **12**, 314 (1968).

3) M. Akimoto and E. Echigoya, *Chem. Lett.*, **1972**, 305.

adsorbed oxygen species was also measured by a similar method to that described above. However, in this case the catalyst (50 mg) was evacuated at 540 °C for 1 hr, and oxygen was introduced at a pressure of 5 mmHg at about −100 °C. A temperature-programmed cavity was used for ESR studies at −100—+250 °C. For temperatures above 250 °C, the vessel was heated at various temperatures for a fixed time followed by the determination of the amount of adsorbed oxygen species at room temperature. The catalysts were prepared by wet mixing of alumina sol or titania gel with an aqueous solution of ammonium paramolybdate.[3]

The surface area of the catalysts was determined by the BET method using nitrogen adsorbate. The structure of these catalysts was investigated by X-ray diffraction using nickel-filtered Cu$K\alpha$ radiation. It was found that molybdena can dissolve in anatase titania to the extent of 25—30 mol% and MoO_3–Al_2O_3 catalyst is amorphous within a 66.7 mol% molybdena content.

Results and Discussion

Reaction of Mo^{5+} with Oxygen or Water. Figure 1 shows the effect of reaction temperature and time on the amount of Mo^{5+} decreased as a result of the reaction. Mo^{5+} was formed by the evacuation of MoO_3–TiO_2 (1 : 3) catalyst at 365 °C for 30 min and then reacted. The same result was previously obtained for oxygen pressures of 20 and 200 mmHg. Therefore, gaseous oxygen of 20 mmHg was used in all experiments. We see that water does not react with Mo^{5+} at 100 °C but easily does so at 200 °C. Mo^{5+} is oxidized rapidly with oxygen at 200 °C in contrast with the case at 100 °C.

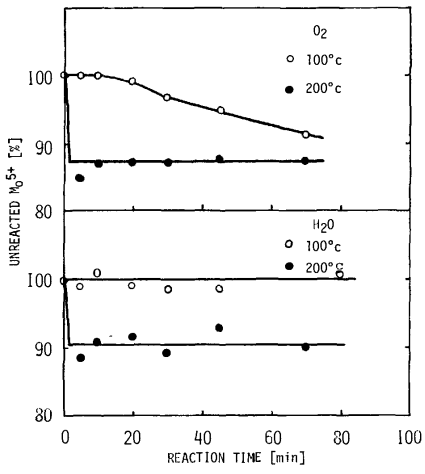

Fig. 1. Reaction of Mo^{5+} with oxygen or water. Effect of reaction time.
catalyst: MoO_3–TiO_2 (MoO_3 25.0 mol%)

The effect of reaction temperature is shown in Fig. 2. Decrease in the amount of Mo^{5+} was observed on reaction with water above 200 °C but not below 175 °C. However, the amount above 250 °C was found to exceed the initial amount presumably due to the formation of new Mo^{5+} in the bulk with a loss of lattice oxygen above 250 °C.

Based on the oxidation temperature, the reaction step can be broadly divided into (a) 57—150 °C, (b) 150—300 °C, and (c) 300—450 °C, attributable to the different reactivities of Mo^{5+} formed on the surface and in the bulk. At 57—150 °C, Mo^{5+} (B) on the surface seems to be oxidized slowly in contrast with the oxidation at 150—300 °C. However, when the temperature exceeds 300 °C, oxygen is assumed to penetrate into the bulk and oxidize Mo^{5+} (B) formed in the lattice. It is notable that the amount of Mo^{5+} decreased on reaction with water at 200—250 °C is approximately equal to that with oxygen. This suggests that water also reacts with surface Mo^{5+} (B) at 200—250 °C. Stable Mo^{5+} was observed in the catalyst not oxidized even at 450 °C. This is in accordance with Mo^{5+} (A) in MoO_3–Al_2O_3 catalyst.

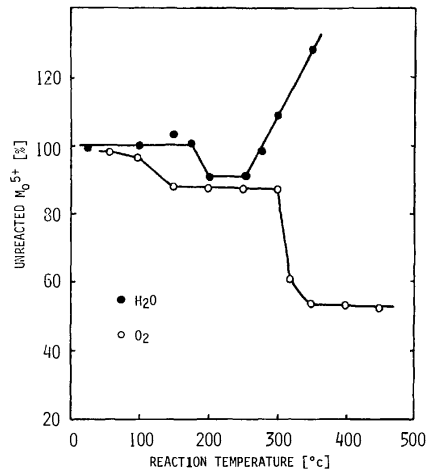

Fig. 2. Reaction of Mo^{5+} with oxygen or water. Effect of reaction temperature.
catalyst: MoO_3–TiO_2 (MoO_3 25.0 mol%)
reaction time: 30 min

The effect of evacuation temperature on the formation of Mo^{5+} in MoO_3–TiO_2 (1 : 3) catalyst is shown in Fig. 3. The catalyst was evacuated for 30 min at 10^{-4}—10^{-5} mmHg and Mo^{5+} was oxidized at 350 °C. The Mo^{5+} disappearing on oxidation is accordingly Mo^{5+} (B) and the rest is Mo^{5+} (A). Mo^{5+} (B) is possibly formed at the sites where lattice oxygen is lost by evacuation. The amount of Mo^{5+} (A) was found to be independent of evacuation temperature, thus suggesting that Mo^{5+} (A) is formed during the preparation of the catalyst. It is possible that water penetrates into the bulk and dissociates to form a bond M–OH (M: Mo^{6+} or Ti^{4+}) during the preparation and that these hydroxyl groups are dehydrated to give water with formation of a bond $-Ti^{4+}$–O–Mo– on heating in water-free atmosphere at higher temperatures. This molybdenum ion is expected to be Mo^{5+} (A). This gives an evidence for the amount of Mo^{5+} (A) exceeding the total amount formed on evacuation below 200 °C.

Figure 3 also shows that the total amount of Mo^{5+} formed on evacuation at 200 °C is nearly equal to that of Mo^{5+} (A), formation of Mo^{5+} (B) being negligible, thus suggesting that dehydration occurs above 200 °C in accordance with the formation of Mo^{5+} (B). From these results, it can be concluded that the Mo^{5+} disappearing on reaction with oxygen or water at 200—250 °C is surface Mo^{5+}.

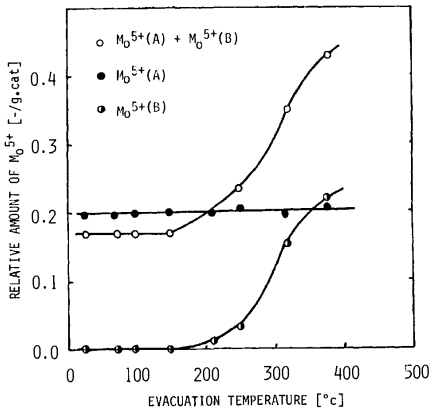

Fig. 3. Correlation between the amount of Mo^{5+} formed and evacuation temperature.
catalyst: MoO_3–TiO_2 (MoO_3 25.0 mol %)
evacuation time: 30 min
oxidation: 350 °C, 30 min, O_2 20 mmHg

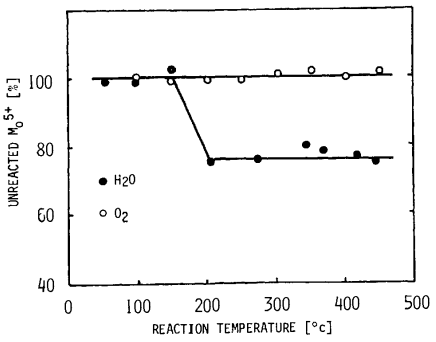

Fig. 4. Reaction of Mo^{5+} with oxygen or water.
catalyst: MoO_3–Al_2O_3 (MoO_3 18.2 mol %)
reaction time: 30 min

Figure 4 shows the result of reaction of oxygen or water with Mo^{5+} formed in MoO_3–Al_2O_3 (2: 9) catalyst, in which the intensity of ESR signal attributable to Mo^{5+} (A) does not decrease on reaction with oxygen even at 450 °C but does so with water above 200 °C. The reactivity of Mo^{5+} (A) with water was thus found to be similar to that of Mo^{5+} (B) on MoO_3–TiO_2 catalyst. The Mo^{5+} (A) disappearing on reaction with water is surface Mo^{5+} (A) since hydroxyl groups are dehydrated easily at higher temperatures and water cannot penetrate into the bulk.

Structure of Mo^{5+}. The amount of Mo^{5+} formed on MoO_3–TiO_2 catalyst was measured by the above method (Table 1). It is of interest to note that the amount of surface Mo^{5+} determined by means of oxidation is approximately equal to that obtained by reaction with water. Decrease in the amount of Mo^{5+} was not observed on reaction with water at 200 °C when Mo^{5+} was previously oxidized at 225 °C. These results suggest that most of Mo^{5+} on the surface is Mo^{5+} (B). The amount of Mo^{5+} (A) increases with a rise in molybdena content to reach a maximum amount at MoO_3 30 mol%, *i.e.*, at a maximum solubility of molybdena in anatase titania, which provides an evidence for the conclusion that most of Mo^{5+} (A) is present in the bulk as predicted by the mechanism for its formation.

Table 1. Distribution of the amount of Mo^{5+} in MoO_3–TiO_2 catalyst

MoO_3 content (mol %)	Surface area (m^2/g)	Surface amount of Mo^{5+} (%) by H_2O	Surface amount of Mo^{5+} (%) by O_2	Total Mo^{5+} [a]	Mo^{5+} (A) [b]
0.0	60	—	—	0.000	0.000
5.0	85	33.3	44.4	0.122	0.050
10.0	126	28.7	37.1	0.247	0.105
13.0	129	25.5	33.6	0.274	0.148
18.0	119	22.0	20.0	0.473	0.190
25.0	63	19.2	18.5	0.576	0.260
30.0	37	18.7	14.0	0.598	0.317
40.0	23	14.4	16.4	0.419	0.264
50.0	23	20.1	14.8	0.436	0.215

a) Evacuated at 365 °C for 30 min.
b) Oxidized with oxygen at 350 °C for 30 min.

Asmolov and Krylov[4,5] investigated the structure of molybdena supported on magnesia or alumina by means of ESR and optical diffuse reflactance spectroscopy, and revealed that Mo^{6+} and Mo^{5+} on the surface are present in octahedric or tetrahedric and square-pyramid coordination, respectively. Mo^{4+} and Mo^{3+} were also found to occupy the lattice points in these carriers in octahedric coordination. It is possible that Mo^{5+} (A) in the bulk has a similar structure to that of Mo^{4+} and Mo^{3+}. Thus, the structure of surface or bulk Mo^{5+} is assumed to be that shown in (1). The structure of Mo^{5+} (B) in the bulk seems to be similar to that of Mo^{5+} (A) in the bulk, but at least one of the oxygen surrounding molybdenum ions is lost with formation of anion vacancy and M is not always metal ion of carrier. In the case of surface Mo^{5+}, M is expected to be metal ion of carrier (Mo^{5+} (A)) or molybdenum ion and metal ion of carrier (Mo^{5+} (B)). Thus, most of Mo^{5+} (A) in the bulk is presumably formed by dispersion and dissolution of molybdena into these carriers followed by the occupation of molybdenum ion at the lattice points of Al^{3+} or Ti^{4+}. Excess electrons appear around the molybdenum ion and are trapped by Mo^{6+} rather than by Al^{3+} or Ti^{4+} forming Mo^{5+} (A). This mechanism is similar to that of acid and base formation in aluminosilicate.[6] Mo^{5+} (A) in the bulk does not seem to be oxidized even at higher temperatures, which agrees with our result. On the contrary, Mo^{5+} (B) is presumably formed with a loss of lattice oxygen at the sites where molybdena is not so dispersed as in the case of Mo^{5+} (A) formation in MoO_3–TiO_2 catalyst. Decrease in the amount of Mo^{5+} on MoO_3–Al_2O_3 and MoO_3–TiO_2 catalyst was observed on reaction with water in contrast with the oxidation. This suggests that the reactions of water with Mo^{5+} (A) and Mo^{5+} (B) follow the same mechanism.

4) G. N. Asmolov and O. V. Krylov., *Kinet. Katal.*, **11**, 1028 (1970).
5) G. N. Asmolov and O. V. Krylov, *Izv. Akad. Nauk SSSR, Ser. Khim.*, No. 10, 2414 (1970).
6) C. L. Thomas, *Ind. Eng. Chem.*, **41**, 2564 (1949); R. C. Hansfold, "Advances in Catalysis," Vol. 3, Academic Press Inc., New York (1952), pp. 1, 7; M. Mcd. Baker, and G. I. Jenkins, *ibid.*, Vol. 7, (1955), p. 39.

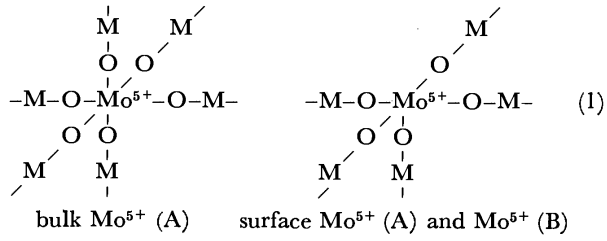

bulk Mo^{5+} (A) surface Mo^{5+} (A) and Mo^{5+} (B)

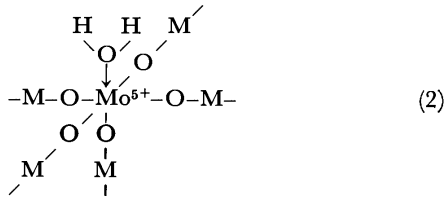

(2)

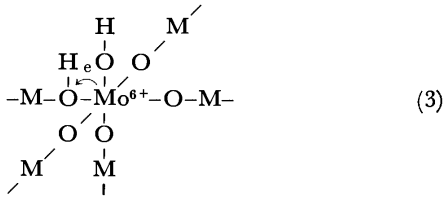

(3)

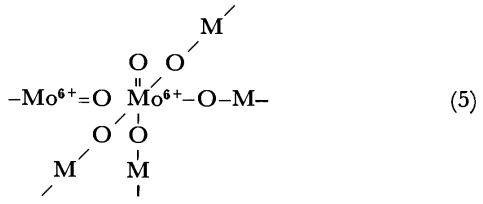

(5)

Mechanism for the Reaction of Mo^{5+} with Water.

Basolo and Pearson[7] showed that $(MoO)^{3+}$ is a hard Lewis acid which interacts more easily with a hard Lewis base than with a soft one. Based on this conception, Mo^{5+} formed on MoO_3–TiO_2 (1 : 3) catalyst by evacuation at 365 °C was reacted with either pyperidine, *n*-butylamine or tetrahydrothiophene as hard Lewis bases or toluene or benzene as soft Lewis bases at 200—250 °C. Pyridine was also used as a hard and soft Lewis base. However, decrease in the signal intensity was not observed in these reactions, thus suggesting that Mo^{5+} does not shift to Mo^{4+} even by the formation of a coordination bond between acidic Mo^{5+} and these Lewis bases. Accordingly, disappearance of the ESR signal on reaction with water can not be attributed to the formation of a complex (2) but to some other mechanism.

It is very possible that coordinated water in (2) dissociates above 200 °C to make a σ-bond with molybdenum ion as shown in (3). In proportion to the evacuation temperature, the amount of Mo^{5+} (A) formed in MoO_3–Al_2O_3 catalyst was found to increase with a decrease in the intensity of a broad absorption band due to OH stretching (3000—3600 cm^{-1}). IR measurement also revealed the presence of molecular water on MoO_3–Al_2O_3 catalyst on admission of water. These results provide a powerful evidence for the mechanism (3). Hence, it is concluded that Mo^{5+} shifts to Mo^{6+} with disappearance of its ESR signal by formation of the σ-bond with OH and extraction of electron by a neighboring oxygen. This mechanism is similar to that of Brønsted acid formation from Lewis acidic site in the presence of water at higher temperatures.[8]

Mechanism for the Reaction of Mo^{5+} with Oxygen.

It is interesting to note that Mo^{5+} on MoO_3–TiO_2 is oxidized with oxygen in contrast with Mo^{5+} on MoO_3–Al_2O_3 catalyst. For the purpose of clarifying this carrier effect, the mechanism for oxidation was studied by observation of adsorbed oxygen species with ESR.

Many papers[9] have appeared on the ESR spectra of oxygen species adsorbed on metal oxides. Shvets and Kazansky[10] investigated the spectra of oxygen species adsorbed on reduced molybdena and identified the triplet signal with $g=2.018$, 2.010, and 2.004 with O_2^-. Ishii and Matsu-ura[11] also studied the spectra on molybdena and ascribed the triplet signal with $g=2.04$, 2.01, and 2.00 to O_2^- and a sharp singlet signal with $g=2.00$ to O^-.

In our experiments, no ESR signal of adsorbed oxygen species appeared on alumina and silica even at −100 °C, but the signal was observed on supported molybdena catalysts. At room temperature, a triplet signal with $g=2.019$, 2.009, and 2.003 was observed on MoO_3–TiO_2 (1 : 99) catalyst on admission of oxygen. At 60—100 °C, the signal intensity at $g=2.019$, and 2.009 decreased and at the same time the signal with $g=2.002$ became sharp and increased. When N_2O was adsorbed on the MoO_3–TiO_2 catalyst at 100 °C, a sharp singlet signal with $g=2.002$ was obtained. Thus, the triplet signal with $g=2.019$, 2.009, and 2.003 can be ascribed to O_2^-, and a sharp singlet signal with $g=2.002$ to O^-. This signal of O^- is similar to that of Setaka and Kwan[9] and of Ishii and Matsu-

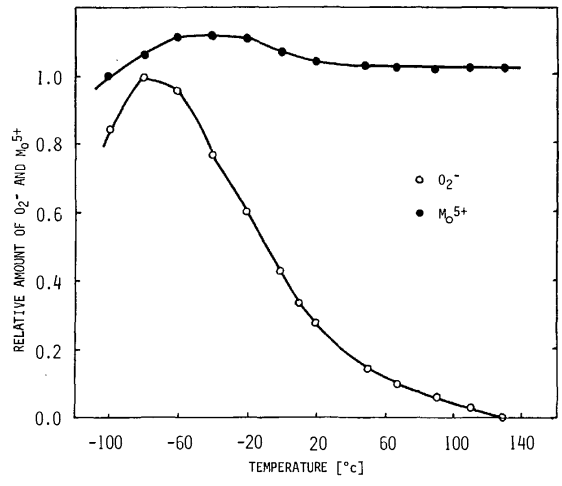

Fig. 5. Effect of temperature on the amount of O_2^- and Mo^{5+} ion.
catalyst: MoO_3–Al_2O_3 (MoO_3 18.2 mol %)

7) F. Basolo and R.G. Pearson, "Mechanism of Inorganic Reactions. A Study of Metal Complexes in Solution," John Wiley & Sons, Inc., New York (1967), p. 25.

8) M. W. Tamele, *Discuss. Faraday Soc.*, **8**, 270 (1950).

9) T. Kwan and Y. Fujita, *Shokubai*, **5**, 206 (1963); R. J. Kokes, *J. Phys. Chem.*, **66**, 99 (1962); K. M. Sancier and T. Freund, *J. Catal.*, **5**, 293 (1965); M. Setaka and T. Kwan, This Bulletin, **38**, 1414 (1965).

10) V. A. Shvets and V. B. Kazansky, *J. Catal.*, **25**, 123 (1972).

11) Y. Ishii and I. Matsu-ura, *Nippon Kagaku Zasshi*, **89**, 553 (1968).

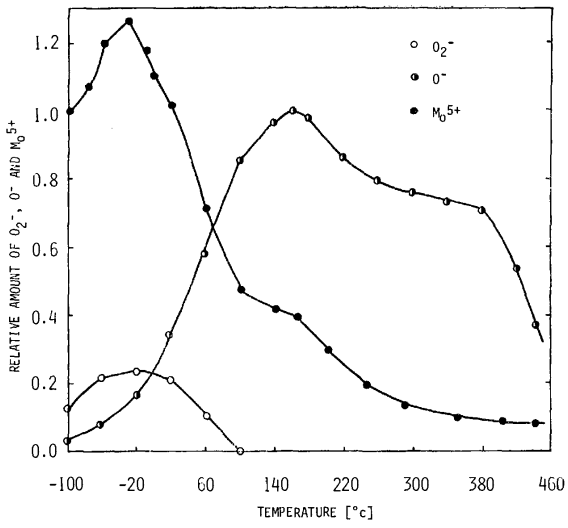

Fig. 6. Effect of temperature on the amount of O_2^-, O^-, and Mo^{5+} ion.
catalyst: MoO_3–TiO_2 (MoO_3 1.0 mol%)

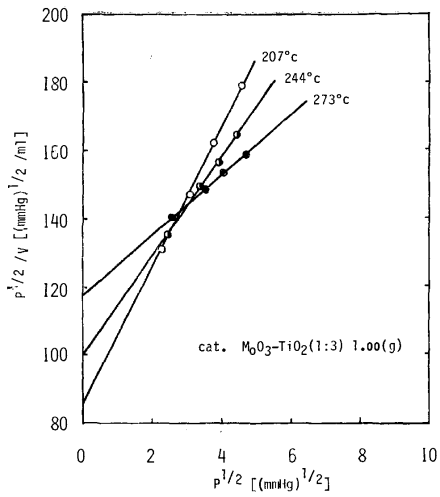

Fig. 7. Langmuir plot of oxygen adsorption on MoO_3–TiO_2 catalyst.
catalyst: pre-evacuated at 540 °C for 1 hr
P: oxygen pressure (mmHg)
V: volume of adsorbed oxygen (NTP ml)

ura[11] but does not agree with the results of Shvets and Kazansky.[10] In the case of anatase titania, there appeared only one adsorbed oxygen species O_2^- which showed the maximum amount at 50 °C and disappeared at 230 °C. On the contrary, the MoO_3–TiO_2 catalyst showed the maximum amount of O_2^- at −20 °C and the ion disappeared at 100 °C with formation of a great amount of O^- which showed a maximum at 150 °C, thus suggesting that these oxygen species are not formed on titanium ions but on molybdenum ions.

The effect of temperature on the amount of adsorbed oxygen species formed on MoO_3–Al_2O_3 (2: 9) and MoO_3–TiO_2 (1: 99) catalyst is shown in Figs. 5 and 6, the amount of Mo^{5+} modified with temperature also being shown. Only O_2^- was observed on the MoO_3–Al_2O_3 catalyst, the ion disappearing at 130 °C without any decrease in the amount of Mo^{5+} (Fig. 5). In the case of the MoO_3–TiO_2 catalyst, the amount of Mo^{5+} and O_2^- decreased at higher temperatures with formation of O^-. Thus, the following reaction can be assumed to proceed on the catalyst surface at higher temperatures.

$$O_2(g) \xrightarrow{e} O_2^- \xrightarrow{e} 2O^- \xrightarrow{2e} 2O^{2-} \qquad (4)$$

O^{2-} combines with molybdenum ion to form Mo^{6+}.

Adsorption of oxygen on Mo^{5+} (B) at higher temperatures follows a dissociative mechanism of Langmuir type (Fig. 7), which supports the above reaction mechanism. In contrast with Mo^{5+} (B), this reaction does not seem to proceed on Mo^{5+} (A) formed on MoO_3–Al_2O_3 catalyst, to which the inactivity of Mo^{5+} (A) for oxygen is attributable.

As shown in Figs. 5 and 6, increase in the amount of Mo^{5+} was observed at −100—+20 °C, which is presumably due to formation of Mo^{4+} on these catalysts on evacuation at 540 °C and of Mo^{5+} and O_2^- on admission of oxygen.

These different reactivities of Mo^{5+} with oxygen are presumably attributed to the different dispersions of molybdena in the carriers, *i.e.*, molybdena seems to be finely dispersed in alumina and magnesia with formation of the molybdates in contrast with anatase titania and silica. Accordingly, it is possible that the bond Mo–O–Al^{3+} in MoO_3–Al_2O_3 is strong and difficult to be cut off in contrast with Mo–O–Mo in MoO_3–TiO_2 catalyst. Hence, Mo^{5+} (B) on the latter catalyst is expected to be oxidized with oxygen through cutting off the weak Mo–O–Mo bond followed by formation of the double bond as shown in (5). By IR analysis, the double bond type lattice oxygen was proved to be reduced easily with hydrogen and recovered by reoxidation,[12] which supports the above mechanism for the oxidation of surface Mo^{5+} (B). The formation of this double bond is presumably impossible in the case of alumina and magnesia carriers.

In conclusion, the nature of the Mo^{5+} formed when molybdena is supported on a carrier is remarkably affected by the property of the carrier through its dispersion and formation of the chemical bond. Mo^{5+} (A) on the surface has extra ability in making a single bond, while Mo^{5+} (B) on the surface can make, in addition, a double bond.

12) M. Akimoto and E. Echigoya, to be published.

Equilibrium Composition of 1-Butanol-Water-Alkali Hydroxide System and Distribution of the Base

Norio YUI, Yoichi KUROKAWA, and Isozi SAKURABA

Department of Applied Science, Faculty of Engineering, Tohoku University, Aoba, Aramaki, Sendai 980

(Received September 6, 1972)

Equilibrium compositions of 1-butanol–water–MOH systems were studied at 25 °C, where MOH represents LiOH, NaOH, and KOH. Water and 1-butanol were determined by means of gas chromatography and the bases by titration. Apparent distribution ratio K_{obs} (molality of MOH in the aqueous phase/molality of MOH in the 1-butanol phase) was dependent on the concentration of base. A considerable amount of water was transferred from 1-butanol to the aqueous phase giving rise to an increase of base concentration. This suggests that the variation of K_{obs} depends principally on the variation of solvent composition. K_{obs} was expressed semi-empirically, considering the activity coefficients calculated by Miller's equation and also the change in the standard free energy resulting from the variation in solvent composition. Decrease of 1-butanol in the aqueous phase with the base concentration obeyed the salting-out equation. The calculated salting-out coefficients were: LiOH 0.176, NaOH 0.192, and KOH 0.184. These values are correlated to Gurney's unitary entropy. The results were compared with those previously obtained for alkali halides.

Solvent extraction of inorganic species was reviewed by Marcus,[1] a good summary being given by Marcus and Kartes.[2] There are a few theoretical treatments on extraction including a thermodynamical treatment by Dyrssen *et al.*[3] and Friedman and Haugen,[4] and a regular solution treatment by Skytte-Jensen.[5]

The authors investigated the change of solvent composition with salt concentration for the distribution of alkali halides between the 1-butanol and aqueous phases at atmospheric pressure and room temperature.[6–10] The relation between solvent composition and distribution ratio or salting-out coefficient was described. It was found that the changes in distribution ratio accompanied by the change of solvent composition could be classified into two groups; one showing a decrease of distribution ratio with an increase of salt concentration and the other an increase of distribution ratio. The greater the change of distribution ratio, the greater the change of solvent composition. Namely, the water transfer from 1-butanol to the aqueous phase increased with an increase of salt concentration. As to 1-butanol, the increase of it in the 1-butanol phase and the decrease in the aqueous phase were observed.

A semi-empirical treatment of distribution was made by using Miller's equation for the activity coefficient and also by assuming that the standard free energy depends linearly on the mole fraction of water in the 1-butanol phase.[9] It was found that the decrease of 1-butanol in the aqueous phase is represented by the salting-out equation, the decrease being correlated to Gurney's unitary partial molar entropy.[10] This study was undertaken to examine the applicability of the above treatment to the 1-butanol–water–alkali hydroxide systems.

Experimental

Reagents. Lithium Hydroxide, Sodium Hydroxide, Potassium Hydroxide, and 1-Butanol: Chemicals of reagent grade were used without purification. Conductivity water was prepared by passing distilled water through a mixed bed of ion exchange resins. The specific conductance was less than 2×10^{-7} ohm^{-1} cm^{-1}.

Procedure. 100 ml of aqueous and 1-butanol solutions of known composition were shaken mechanically in a thermostat for one hour at 25±0.1 °C and then let to stand in the thermostat for one hour. Distribution equilibrium was reached within 15 min. A portion of each solution was taken for analysis.

Analysis. The method has been described.[7] Solvents were analyzed by gas chromatography, and alkali hydroxide by titration with standard hydrochloric acid using phenolphthalein. A mean of three determinations was taken. The solvent was separated from the base by vacuum distillation for avoiding attachment of the base to gas chromatography detector. *t*-Butanol was added to the sample, separated into two phases on removal of base in order to bring about a single phase. Analysis was then carried out. For molality and wt % calculation, density of the solution was determined with a pycnometer (10 ml).

Various stationary liquids for analyzing a water–alcohol mixture have been reported.[11] We found that cetyl alcohol containing a small amount of triethanol amine gave a satisfactory result. The packing column had a support with 60—80 mesh cellite containing stationary liquid (20 wt%). The column was 100 cm long and made of a ϕ 6 mm stainless steel tube bent into a U shape. This was installed in a HITACHI KGL-2A type gas chromatography apparatus equipped with a thermal conductivity detector. Conditions of operation were: Column temperature 95 °C, carrier gas

1) Y. Marcus, *Chem. Rev.*, **62**, 139 (1963).
2) Y. Marcus and A. S. Kertes, "Ion Exchange and Solvent Extraction of Metal Complexes," Wiley-Interscience (1969), p. 575.
3) D. Dyrssen, J. O. Liljenzin, and J. Rydberg, "Solvent Extraction Chemistry," North-Holland Publishing Company (1967), p. 195.
4) H. L. Friedman and G. R. Haugen, *J. Amer. Chem. Soc.*, **76**, 2060 (1954); H. L. Friedman, *J. Phys. Chem.*, **59**, 161 (1955); H. L. Friedman and G. R. Haugen, *ibid.*, **67**, 1757 (1963).
5) Ref. 2, p. 517.
6) N. Yui, Y. Kurokawa, Y. Takamura, and M. Maeda, *Nippon Kagaku Zasshi*, **87**, 1138, 1143 (1966).
7) N. Yui, Y. Kurokawa, and Y. Otomo, *ibid.*, **88**, 273 (1967).
8) N. Yui, Y. Kurokawa, M. Sono, and T. Hiramoto, *ibid.*, **89**, 483 (1968).
9) N. Yui and Y. Kurokawa, *ibid.*, **89**, 487 (1968).
10) N. Yui and Y. Kurokawa, *ibid.*, **88**, 276 (1967).
11) S. Musha and T. Nishimura, *Bunseki Kagaku*, **14**, 803 (1965); W. T. Casazza and R. J. Stelenkamp, *J. Gas Chromatog.*, **3**, (8), 253 (1965).

(He) flow rate 50 ml/min, bridge current 180 mA and output signal 16 mV. A peak ratio was adopted for the analysis, since a linear relation holds between the peak ratio of solvent and its weight ratio, when the peak of 1-butanol is kept constant. A different method was used for the analysis of the aqueous phase to avoid tailing of the water peak. Weighed toluene and sodium chloride as salting-out agent were added to a weighed sample with shaking, causing the separation into two layers. The toluene phase containing the salted-out 1-butanol was analyzed by gas chromatography. Water was determined by subtracting the amounts of solute and 1-butanol from the total amount.

Results and Discussion

Mutual solubilities of the 1-butanol–water system in the absence of alkali hydroxide are given in Table 1.

Table 1. Mutual solubilities of 1-butanol and water at 25 °C

	Aqueous phase	1-Butanol phase
Water	92.69 (98.12)	20.36 (51.24)
1-Butanol	7.31 (1.88)	79.64 (48.76)

wt% (mol %)

Our result is consistent with those of Butler *et al.*,[12] and Hill and Malisoff.[13] The equilibrium composition of the system in the presence of alkali hydroxide is given in Tables 2—4, where m denotes molality, suffixes a and b indicate the aqueous and 1-butanol phases, respectively. The apparent distribution ratio K_{obs} is defined by m_a/m_b. Its determination is restricted to the system in the liquid-liquid distribution region. No determination was carried out in the vicinity of saturated solution and in higher concentration of lithium hydroxide for the sake of precision (particularly aqueous phase). We see that as the base concentration increases, in the 1-butanol phase the amount of water decreases and that of 1-butanol increases, and in the aqueous phase 1-butanol decreases. The behavior of each base shows the same trend as in the case of alkali halides.[6-8]

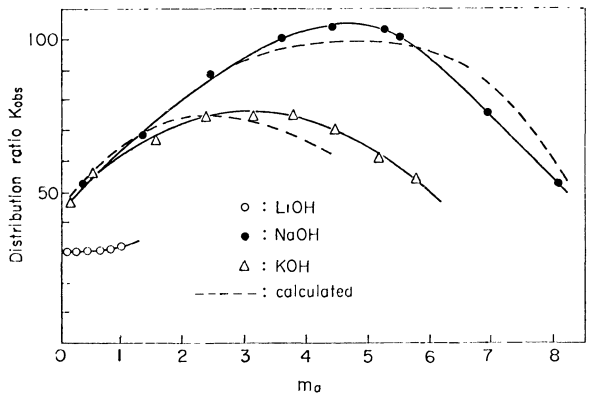

Fig. 1. Distribution ratio of base *vs.* molality in the aqueous phase at 25 °C.

The plots of K_{obs} against m_a are shown in Fig. 1. The distribution ratio of lithium hydroxide is almost constant at 31—33. At a higher concentration the same behavior as in sodium hydroxide and potassium hydroxide is expected. The ratios for sodium hydroxide and potassium hydroxide reach maximum at around 5 m_a and 3 m_a respectively, and then decrease. With the increase of base concentration the base tends to go into the 1-butanol phase. At a low concentration, the base might undergo primary solvation with water molecules even in the 1-butanol phase and secondary solvation with 1-butanol or more water molecules through primary solvation shell. The hydrated base may form bonds with an appreciable portion of 1-butanol molecules and the butanol phase loses its availability for extracting more base. Thus K_{obs} increases with the increase of base concentration. However, at a higher concentration any change in solvation and increase of ionic association might occur. The base might undergo primary solvation with both water and 1-butanol molecules, and is extracted to a greater extent into the 1-butanol phase, making K_{obs} decrease. The m_a at the maximum of K_{obs} is not identical with m_a at the minimum of activity coefficient in the aqueous phase.[14] A ternary diagram for the 1-butanol–water–sodium hydroxide system is given in Fig. 2. **A** indicates two liquid phases and one solid one, **B** one liquid and one solid phase in the aqueous region, **C** and **D** homogeneous phases. Oblique lines are the tie lines and the region is the range of separation of two liquids. An exact comparison of the results with the iso-butanol–water–sodium hydroxide system by Fritzche can no tbe made, but they seem to show a similar trend.[15]

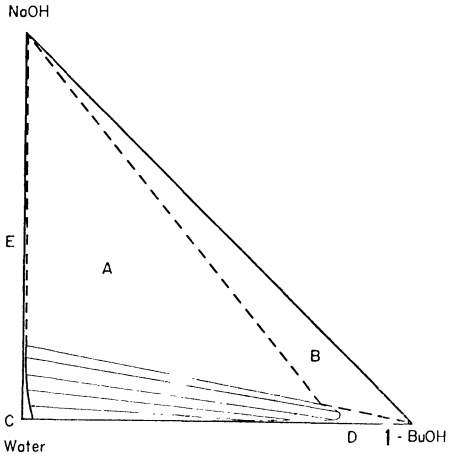

Fig. 2. Ternary diagram for 1-butanol–water–NaOH system at 25 °C, mol %.

The amounts of transfer of 1-butanol and water were determined. 50 mol of 1-butanol and 100 mol of water were taken. Alkali hydroxide was added to the latter and the resulting change of distribution of solvents between the two phases was determined. The result

12) J. A. V. Butler, D. W. Thomson, and W. H. Maclennan, *J. Chem. Soc.*, **1933**, 674.

13) A. E. Hill and W. M. Malisoff, *J. Amer. Chem. Soc.*, **48**, 918 (1926).

14) H. S. Harned and B. B. Owen, "The Physical Chemistry of Electrolytic Solution," Reinhold Publishing Co. (1964), pp. 498, 161.

15) R. H. Fritzche and D. L. Stockton, *Ind. Eng. Chem.*, **38**, 737 (1946); H. Stephen and T. Stephen, "Solubilities of Inorganic and Organic Compounds Vol. 2," Pergamon Press (1964), pp. 85, 86.

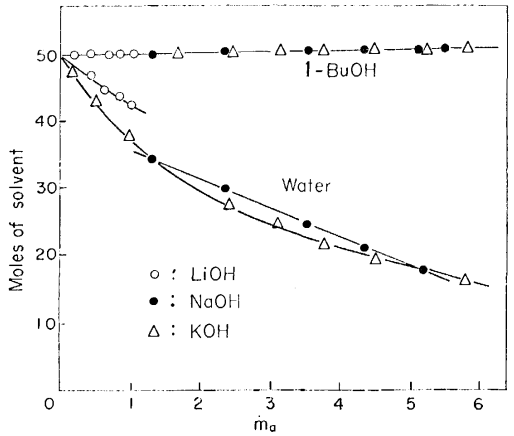

Fig. 3. The change of solvent with base concentration for the butanol phase.

of calculation is shown in Fig. 3. The number of moles of 1-butanol in the 1-butanol phase 49 is almost constant, but transfer of a greater amount of water took place from 1-butanol to the aqueous phase. The decrease of 1-butanol in the aqueous phase appears to be due to the salting-out effect but can not be attributed apparently to the salting-out effect.

Distribution Ratio. Alkali halides can be classified into two groups according to their distribution ratio between 1-butanol and water phases: (a) chlorides, fluorides and bromides which show a significant variation of ratio with the salt concentration, and (b) iodides which show no variation.[9] A semi-empirical treatment was made by assuming that the standard free energy of salt changes linearly with the mole fraction of water in the 1-butanol phase and Miller's equation is applicable to the calculation of activity coefficient. A reasonable agreement was obtained between calculated and observed values. Assuming the equilibrium in which electrolyte is completely dissociated in 1-butanol phase and also in the aqueous phase, we obtain

$$M_b^+ + OH_b^- \overset{K}{=} M_a^+ + OH_a^- \qquad (1)$$

where the subscripts a and b refer to the aqueous and 1-butanol phases, respectively. Thus, the equilibrium constant K is obtained as

$$K = \frac{a_a^+ \cdot a_a^-}{a_b^+ \cdot a_b^-} = \frac{(\gamma_\pm)_a^2}{(\gamma_\pm)_b^2} K_{obs}^2 \qquad (2)$$

where a: activity, γ: mean activity coefficient. It follows that

$$K_{obs} = \frac{(\gamma_\pm)_b}{(\gamma_\pm)_a} \exp\left\{\frac{(\mu_\pm^0)_a - (\mu_\pm^0)_b}{2RT}\right\} \qquad (3)$$

where $\mu_\pm^\circ$: the standard free energy term in chemical potential. Thermodynamic relations have been derived for the distribution of salts between the two phases, assuming that the salts in the organic phase are completely associated. However, this is not always valid in the phase with higher dielectric constant or high water content. Hesford and Mckay reported that perchloric acid is largely ionized when extracted into TBP alone.[16] Conductivity measurements on the 1-butanol phase containing alkali halides indicate that the salts are appreciably dissociated.[17] Friedman and Haugen showed that alkali perchlorates are strong electrolytes in the nitromethane phase.[18]

The standard free energies of transfer of various alkali halides from 1-butanol to aqueous phase were calculated, by assuming Eq. (1) and by applying the modified Born's equation proposed by Stokes.[19] The distribution ratio is independent of the concentration of the salts only in the case of complete immiscibility of phases and non-existence of any interaction between the salts and solvents. Dependency of K_{obs} on concentration might result from variation of activity coefficients and that of solvent composition with salt concentration. Solvent composition changes considerably with the addition of alkali hydroxide (Tables 2—4). Identification of the butanol phase containing a large amount of salt with one containing no salt is no longer valid. We assume that the standard free energy term in chemical potential of salt changes linearly with the mole fraction of water in the 1-butanol phase. Thus

$$\{(\mu_\pm^0)_a - (\mu_\pm^0)_b\}/2RT = -A_1 N_b + A_2 \qquad (4)$$

where N_b: mole fraction of water in the 1-butanol phase, A_1, A_2: adjustable parameters empirically determined. The variation of solvent composition in the aqueous phase which was considerably less than that

Table 2. LiOH–water–1-butanol

1-Butanol phase				Aqueous phase				K_{obs}
LiOH	m_b	Water	1-BuOH	LiOH	m_a	Water	1-BuOH	(m_a/m_b)
0.02	(0.0037)	50.61	49.37	0.23	(0.122)	98.08	1.69	32.9
0.03	(0.0062)	49.99	49.98	0.36	(0.193)	98.02	1.62	31.2
0.06	(0.0130)	48.49	51.44	0.76	(0.407)	97.75	1.49	31.3
0.09	(0.0196)	47.07	52.84	1.15	(0.619)	97.45	1.40	31.6
0.12	(0.0256)	46.78	53.10	1.54	(0.838)	97.23	1.23	32.7
0.15	(0.0306)	45.94	53.91	1.88	(1.03)	97.00	1.12	33.6

Equilibrium composition (mol %) at 25°C, m in parenthesis is molality

16) E. Hesford and H. A. C. Mckay, *J. Inorg. Nucl. Chem.*, **13**, 156 (1960).

17) M. Nakayama, Y. Kurokawa, and N. Yui, This Bulletin, **46**, 1027 (1973); Y. Kurokawa and N. Yui, *Technology Reports Tohoku Univ.*, **37**, 153 (1972).

18) H. L. Friedman and G. R. Haugen, *J. Amer. Chem. Soc.*, **76**, 2060 (1954).

19) Y. Kurokawa and N. Yui, *Nippon Kagaku Zasshi*, **87**, 1135 (1966).

Table 3. NaOH–water–1-butanol

1-Butanol phase				Aqueous phase				K_{obs}
NaOH	m_b	Water	1-BuOH	NaOH	m_a	Water	1-BuOH	(m_a/m_b)
0.03	(0.0052)	45.22	54.75	0.52	(0.276)	97.78	1.70	52.7
0.09	(0.0184)	40.78	59.13	2.27	(1.25)	96.80	0.93	68.1
0.13	(0.0258)	37.30	62.57	4.08	(2.32)	95.39	0.54	89.9
0.19	(0.0341)	32.82	66.99	5.94	(3.47)	93.74	0.32	102
0.23	(0.0403)	29.09	70.68	7.19	(4.27)	92.56	0.25	106
0.32	(0.0521)	24.37	75.32	8.88	(5.38)	90.94	0.17	103
0.54	(0.0854)	19.89	79.58	10.95	(6.80)	88.93	0.13	79.6
0.89	(0.1410)	18.43	80.68	12.66	(8.02)	87.23	0.11	56.9
2.11	(0.3480)	18.71	79.18	14.86	(9.65)	85.03	0.11	28.3
4.42	(0.7556)	22.09	73.50	16.68	(11.87)	83.22	0.10	14.7

Table 4. KOH–water–1-butanol

1-Butanol phase				Aqueous phase				K_{obs}
KOH	m_b	Water	1-BuOH	KOH	m_a	Water	1-BuOH	(m_a/m_b)
0.01	(0.0029)	48.95	51.03	0.27	(0.142)	98.10	1.63	49.0
0.04	(0.0082)	46.23	53.73	0.86	(0.464)	97.77	1.36	56.6
0.08	(0.0153)	42.80	57.12	1.68	(0.918)	97.27	1.05	60.0
0.12	(0.0238)	46.11	59.77	2.87	(1.59)	96.35	0.78	67.0
0.18	(0.0327)	35.32	64.51	4.20	(2.39)	95.22	0.58	73.1
0.23	(0.0412)	32.81	66.96	5.30	(3.06)	94.26	0.44	74.3
0.29	(0.0502)	29.28	70.43	6.35	(3.73)	93.32	0.33	74.2
0.37	(0.0637)	27.80	71.83	7.46	(4.44)	92.27	0.27	69.7
0.48	(0.0820)	26.24	73.27	8.48	(5.08)	91.13	0.39	61.9
0.63	(0.105)	24.15	75.21	9.45	(5.75)	90.33	0.22	54.6

in the 1-butanol was neglected. Dielectric constants of the 1-butanol phase change a great deal with the presence of water. These values for the calculation of the theoretical slope were estimated from those for pure water and 1-butanol assuming that the dielectric constant of the 1-butanol–water mixture is given by a linear function of the weight fraction analogous with the behavior of ethanol–water mixture.

Of the theories on the activity coefficient of salt, those of Robinson-Stokes[20] and Miller[21] are useful. Miller's theory has no solvent activity term, and is convenient for computation. He derived an equation for the molality activity coefficient in terms of the hydration number n and ion size a. We assumed that the ions solvate water molecules selectively, both in the 1-butanol and aqueous phases. Thus, for calculation of γ in the two phases, the hydration number and ion size parameters given by Miller[21] were used. Water molecules are much smaller in size than 1-butanol molecules in the solution. More water than 1-butanol dipoles can pack around a cation to form its primary solvation shell.[22] Thus, the energy of the primary solvation by water is greater than that of 1-butanol. This means that the cation carries its primary water shell with it, and then in the 1-butanol phase undergoes further solvation of the hydrated species by 1-butanol. The following semi-empirical equations were obtained for K_{obs} as

$$\text{NaOH: } K_{obs} = (\gamma_\pm)_b/(\gamma_\pm)_a \exp(-6.60N_b + 7.30) \quad (5)$$

$$\text{KOH: } K_{obs} = (\gamma_\pm)_b/(\gamma_\pm)_a \exp(-9.34N_b + 8.45) \quad (6)$$

The values obtained by means of these equations are given in Fig. 1. The agreement between the calculated and observed values is reasonable. Parameters A_1 and A_2 were determined to fit K_{obs} by combining Eqs. (3) and (4). Theoretically, A_1 should be equivalent to A_2. However, it is not as is evident from the calculation for alkali halides.[9] The errors resulting from the calculation of activity coefficient and the inadequacy of assumption at high concentration are included in A_1 and A_2. This treatment might not be always applicable to other extraction systems. But it is thought to be advisable to investigate the treatment of the two liquid phase system accompaning a great change of solvent composition.

Salting-out Coefficient. The decrease of 1-butanol in the aqueous phase by the addition of salt follows the Setchenow equation[23,24]

$$\log f = \log S^0/S = kc \quad (7)^{25}$$

where f is the activity coefficient of non-electrolyte, S^0 and S are the solubility of non-electrolyte in pure water (mol/l) and in salt solution (mol/l), respectively, k is the salting-out coefficient and c is the concentration

20) R. H. Stokes and R. A. Robinson, *J. Amer. Chem. Soc.*, **70**, 1870 (1948).
21) D. G. Miller, *J. Phys. Chem.*, **60**, 1296 (1956).
22) R. M. Diamond, *ibid.*, **63**, 659 (1959).
23) Ref. 14, p. 531.
24) F. A. Long and W. F. McDevit, *Chem. Rev.*, **51**, 119 (1952).
25) It is assumed that the activity coefficient of 1-butanol in a saturated aqueous solution is unity.

of salt in mol/l. In general, the salting-out effect is influenced by the kind of non-electrolyte, but not by concentration and temperature. The values of k determined by means of Eq. (7) are as follows: LiOH 0.176, NaOH 0.184, KOH 0.192. The data of alkali halides and alkali hydroxides are well represented by Eq. (7), and this linear relation holds up to the salt concentration of one mole. On comparing the coefficients of alkali hydroxides with those of alkali halides, we see that the values are larger found for the latter. The values of k decrease in the order LiOH<NaOH<KOH, similar to that for alkali halides.[10] The above order is virtually the same for other non-electrolytes. In the case of alkali metal cations, the order of salting-out is generally Cs<Rb≃Li<K<Na and for the anion I<Br<Cl<F.[24] The small or highly charged ions which are strongly hydrated show a greater salt effect. There are, however, exceptions such as lithium and hydrogen ions. It is well-known that the tendency for complex ion formation between cation and non-electrolyte is greater for lithium ion.[26]

The relation of k to Gurney's unitary entropy will be discussed. The standard free energy change per mole for transfer of 1-butanol from a solution in pure water to one in which electrolyte is added is given by multiplying Eq. (7) by RT.[27] Combining the latter and the thermodynamic relation we have [10,27]

$$2.3kc = \Delta H/RT - \Delta S/R \qquad (8)$$

where ΔH, temperature slope, is small and almost of the same order as for the alkali hydroxides and alkali halides studied, ΔS being dominant. Gurney succeeded in correlating many properties of electrolytes using the partial entropy of salts. He showed that entropy of salts in water contained a constant or a cratic term depending not on the species of particles but only on the number of particles that have been mixed.[28]

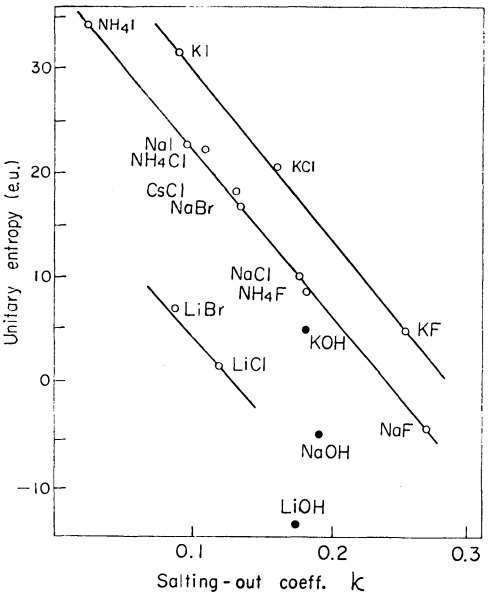

Fig. 4. Unitary entropies *vs.* salting-out coefficients at 25 °C

Subtracting the cratic term 8 e.u. from the observed partial molal entropy, he obtained the values as a unitary term which should be characteristic of ion. Higgins correlated salting-out coefficient with unitary entropy, assuming that all the cations beyond lithium behaved as if they were protons.[5] However, his assumption appears to be oversimplified. Without using it we compared unitary entropies for salts against the corresponding salting-out coefficients and consequently obtained three linear relationships, Li, K, and an other ion group.[10] It is interesting to see to what extent our approach could be applied to the problem of alkali hydroxides. Considerable deviation from lineality were seen for hydroxides as shown in Fig. 4. This might be due to specific interaction between hydroxides and 1-butanol, and to significant difference between temperature effects on salting-out coefficients of alkali halides and alkali hydroxides. The situation may be more complicated than this classification implies.

26) E. E. Schrier and E. B. Schrier, *J. Phys. Chem.*, **71**, 1851 (1967).
27) C. E. Higgins, W. H. Boldwin, and B. A. Soldna, *ibid.*, **63**, 113, 118 (1959).
28) R. W. Gurney, "Ionic Processes in Solution," McGraw-Hill Book Co., Inc. (1953), pp. 89, 97.

An Interstitial-Electron Model for the Structure of Metals and Alloys. III. Interpretation and Correlation of Properties of Group I—V Metals

Oliver JOHNSON*

Research Institute for Catalysis, Hokkaido University, Sapporo 060

(Received August 9, 1971)

The interstitial-electron model for metals supplements the concepts of band theory to give a detailed interpretation of the properties of metals. The instantaneous picture of vacant and electron-occupied interstices given by the model clarifies the complex gradations in electrical conductivity which are not explained by an electron per unit volume term. The consideration of polarization of the itinerant electron cloud by ion cores with high positive fields and of interpenetration of the more deformable ion cores by itinerant electrons is another new feature of the model. The interstitial-electron model leads to the expectation of parallel gradations for electronic heat capacity and magnetic susceptibility and an inverse relation of both of these properties with electrical conductivity. The presence of ($\bar{e}_2$) in the metal structure is associated with a positive Hall Coefficient for a metal, and a new correlation between positive Hall Coefficient and superconductivity for a metal is pointed out.

The interstitial-electron model for metals postulates an interstitial localization of electron density in close-packed metal structures.[1] The different interstice distances, the degree to which an $\bar{e}$ in an interstice is screened by ion cores, and requirement of alternating electron spin in adjoining interstices leads to variations in occupation of octahedral and tetrahedral interstices in metals. It was shown[2] that electron occupancy of interstices could be specified quite closely for metals of Group I—V. The definition of an electron in an interstice as an itinerant electron moving predominantly in a binding region provides a rigorous basis for handling interactions of $\bar{e}$ and ion cores on an electrostatic basis.[1]

The difference in the present interpretation with those of the band theory of metals is illustrated by the lack of a "density of states" term in the present paper. This arises because band theory uses energy and momentum coordinates while the interstitial model uses space coordinates. Band theory has given quantitative accounting of many properties of lower valent metal and much work is currently published on more complex metals.[3]

Electrical Conductivity of Metals

The four major factors which determine electrical conductivity of metals are (1) the number of electrons moving under the influence of the electric field, (2) the velocity of these electrons, (3) the scattering of electrons by metal ion cores due to their displacement during lattice vibrations, and (4) the degree of interpenetration of the ion cores by itinerant electrons. From the interstitial-electron model it is obvious that the number of electrons which can move under the influence of the electric field is directly proportional to the number of vacant interstices in the metal structure. The velocity of electrons will depend on electron energy, and the maximum electron velocities are for electrons at the Fermi Surface. The relative velocities of electrons in two metals can be compared from estimates of Fermi energies.[4] Electrons moving with maximum velocity will dominate the conduction process. The spin requirements of the lattice must be obeyed in relation to both factors (1) and (2). The greater the amplitude of lattice vibration, the greater the scattering of itinerant electrons by ion cores, and thus lowering of electrical conductivity. Lattice displacements are known experimentally.[5] Interpenetration of ion cores will reduce conductivity and, as discussed in part II, is expected to be largest for ion cores containing d-electrons (non-rare gas shells).

Conductivity Trends in Metals. The new concept in the interstitial-electron model is the presence of vacant interstices, and it is of interest to demonstrate the role of vacant interstices in the conductivity process. Electrical conductivity will be discussed in this paper in terms of molar conductivity (specific conductivity × atomic volume).

The molar conductivity for alkali metals increases from Li to K and then declines to Rb and Cs. See Fig. 1. The interstitial-electronic structures are the

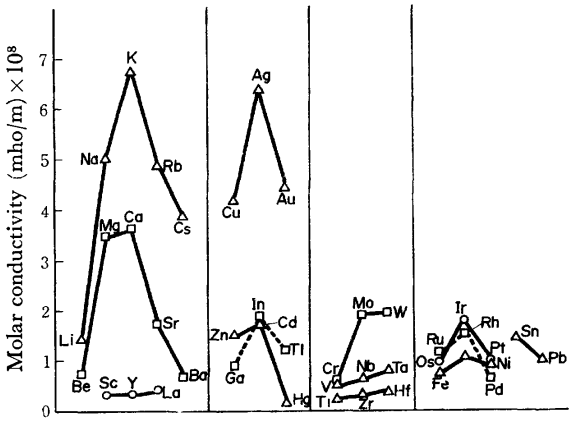

Fig. 1. Variations in molar conductivity for groups of metals.

* Present address: Institute of Physics, University of Uppsala, Uppsala, Sweden.

1) O. Johnson, Part I of Series, This Bulletin, **45**, 1599 (1972).

2) O. Johnson, Part II, of Series *ibid.*, **45**, 1607 (1972).

3) W. M. Lomer, *Prog. Materials Sci.*, **14**, 99 (1969).

4) R. A. Smith, "Wave Mechanics of Crystalline Solids," Chapman and Hall, Ltd., London (1969).

5) G. V. Samsonov, "Handbook of Physicochemical Properties of the Elements," Plenum, New York (1968).

same for all the alkali metals, and the number of vacant interstices is the same. Electron velocities are expected to increase monotonically from Li to Cs, with the decrease in positive field of the ion core with increase in size. The amplitude of lattice vibrations also increases monotonically from Li to Cs, but this is expected to lead to the opposite effect, a decrease in conductivity. The combination of these two opposing factors leads to the maximum at K (See Fig. 1) with decreasing conductivity for Rb and Cs due to larger effect of lattice vibrations. These same two factors account for the maximum at Ca in the series Be to Ba (See Fig. 1). For the latter series changes in crystal structure modify the trends of Mg to Ca as shown in Fig. 1. The maximum for Ag in the series Cu, Ag, Au cannot have the same explanation since the lattice displacements are very nearly the same for Ag and Au. There is an unusually high positive field in case of Au,[6] leading to lower electron velocity and lower conductivity. These are all manifestations of greater interpenetration of the Au^{25+} ($4f^{14}$, $5d^{10}$) ion core by itinerant electrons.

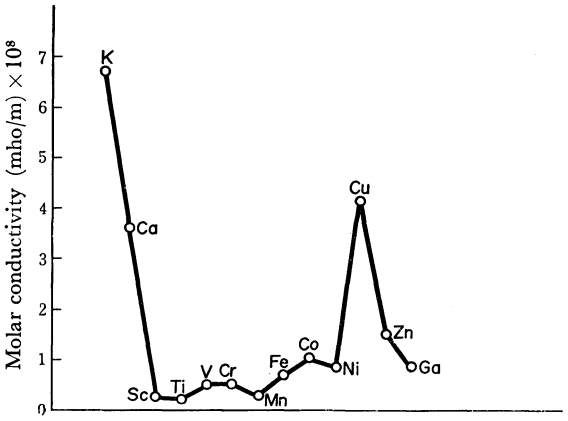

Fig. 2. Gradations in molar conductivity for metals.

It is of interest to note the relatively few metals with high molar conductance in Figs. 1 and 2. Those with values above 3.5 are Na, K, Rb, Cs, Cu, Ag, Au, Mg, Ca, and Al. All of the other metals including many not shown in Figs. 1 and 2 have molar conductivities below 2. Since there is a large variation in both E_f and amplitude of lattice vibration in both groups, the preponderance of metals with high conductivity which have large number of vacancies is a strong support for emphasis of this property of metals.

The sharp decrease in the order K, Ca, Sc, in Fig. 2 has not been explained previously. It will be noted that conductivities remain low for the series of 1st row transition metals until Cu is reached. For the series K, Ca, Sc the lattice displacements decrease so this factor should lead to increased conductivity. There is an increase in positive field, and this factor could cause a small decrease in conductivity (perhaps 2-fold). However, the 20-fold drop in conductivity is unexpected and must be connected with the decline in number of vacant interstices. There are 5 vacant interstices per metal ion core in K, 4 in Ca and only 1 in Sc (See Part 1). The series Cu, Zn, Ga represents a similar series, but the non-close packed structure of Ga may have influence here.

The gradations in conductivity Na>Cu and Mg>Zn show the effect of d-shell ion cores in lowering electron velocities due to the interpenetration of the d-shell by itinerant electrons.[2] The similar conductivities of Mg and Al are in sharp contrast to the sharp decline from Ca to Sc. In the above example there is a change from HCP to CCP for Mg to Al and from CCP to HCP for Ca to Sc. Due to pairing in the Al structure (See Part 1) there are a larger than normal number of vacant interstices. The especially low conductivities of Sc, Y, and La can all be traced to the distortion of the HCP lattice for these metals which reduces the number of tetrahedral interstices from 2 to 1 (bipyramical interstice) and thus reduces the total number of interstice vacancies. Vacancies listed above are based on 6 $\bar{e}$ (or 3 $\bar{e}_2$) in the normal 2 tet and 1 oct interstice per ion cores. A 1-electron vacancy and a 2-electron vacancy could be distinguished.

The interstitial-electron model also leads to the expectation of a dependence of conductivity on lattice structure. It is especially clear from the geometry that the pathways for itinerant electrons are more direct in HCP than CCP for non-distorted lattices (See Part I and II). This can explain the low position of Ca (CCP) in Fig. 1 as compared to Mg (HCP). A greater conductivity would be expected in normal HCP metals parallel to the c-axis than perpendicular to the axis. This is as observed for HCP magnesium.

Comparison of Interpretations of Conductivity. Band theory has accounted for the major effects observed experimentally for electrical conductivity, and it is generally assumed that it gives a quantitative interpretation. This is the case for Na and K metals, but with Li, Rb, and Cs there are 2—4 fold differences between calculated electrical conductivity and observed values, similar discrepancies for noble metals and poor results for higher valent metals.[7] From the interpretations of the interstitial-electron model it would appear that two factors have not been taken into account in the band theory treatment of conductivity. One is the concept of vacant interstices (on an instantaneous picture) although a term for $\bar{e}$ per unit volume partially takes care of this. The second factor is the polarization of the itinerant electron cloud by ion cores of strong positive field and interpenetration of deformable ion cores by itinerant electrons. The latter factor explains the very low conductivities for Li and Be and the trends for the noble metals.

The marked advantage of the Interstitial-Electron Model over previous attempts to account for gradations in electrical conductivity is demonstrated in Table 1. The first comparison is Bardeen's[7] Band Theory calculation where only Na and K show calculated values within 20% of the experimental conductivity. The second comparison is that of Ziman's[8] reduced re-

6) O. Johnson, *J. Chem. Educ.*, **47**, 43, (1970).

7) W. Bardeen, *J. Appl. Phys.*, **11**, 88 (1940).

8) J. M. Ziman, "Electrons and Phonons," Oxford, Clarendon Press (1968).

TABLE 1. COMPARISON OF THREE APPROACHES TO EXPLANATION OF GRADATIONS IN ELECTRICAL CONDUCTIVITY

	Band theory calculations (Bardeen[7])						
	Li	Na	K	Rb	Cu	Ag	Au
Obsd	11.8	23.4	16.4	8.6	64	66	49
Calcd	28	23	20	5.3	174	143	142

Ziman[8] $\left(\text{Reduced Resistivity} = \frac{4e^2M\alpha\theta^2}{n^2h^3n^{-1/2}Q_D T}\rho(T)\right)$

Li	1.63	Be	3.76	Al	1.98	Zn	3.94
Na	1.04	Mg	2.36	Ca	3.12	Cd	4.42
K	2.08	Ca	2.30	In	4.26	Hg	7.76
Rb	2.62	Sr	11.3	Tl	5.76		
Theory	1		1.6		2		1.6

Interstitial-Electron model[a]

	Conductivity	$(\text{Vac})^2$	$\frac{\text{Cond.}}{(\text{Vac})^2}$		Conductivity	$(\text{Vac})^2$	$\frac{\text{Cond.}}{(\text{Vac})^2}$
K	6.75	25	0.27	Cu	4.17	25	0.16
Ca	3.6	16	0.23	Zn	1.50	16	0.09
Sc	0.28	1	0.28	Mg	3.5	16	0.22
Be	0.75	4	0.19	Li	1.39	25	0.06
Mg	3.5	16	0.22	Be	0.75	4	0.19
Ca	3.6	16	0.23				
Al	3.82	9	0.42	Na	5.06	25	0.20
Sc	0.18	1	0.28	Mg	3.5	16	0.22

a) (Vac)=Vacant interstices

sistivity values where Na and Al give the only close correlation with the theoretical values. A correlation of electrical conductivity and *square* of number of vacancies is given for the interstitial-electron model. The reason for using $(\text{vac})^2$ involves the direct dependence of conductivity on vacancies *via* number of electrons moving and an indirect dependence since the velocity of electrons is also directly dependent on the number of vacancies. In the table the deviations of the ratios of $\text{cond}/(\text{vac})^2$ from the mean value of about 0.23 are all within 20% except for Li, Zn, and Al. This is a rather remarkable correlation when it is considered that a single parameter is used and that effects of lattice vibrations have not been directly included. The latter become important *e.g.* in extending the comparisons to Rb, Cs.

Thermal Conductivity of Metals

The same factors responsible for the gradations in electrical conductivity influence thermal conductivity: (1) the number of electrons moving as a result of the temperature gradient is directly proportional to the number of vacant interstices, (2) the velocity of electrons which move depend on the Fermi Energy, and those at the Fermi Level dominate the thermal conduction, (3) lattice vibration and (4) ion core interpenetration reduces thermal conductivity. In addition there is an influence of temperature since the number of electrons involved in heat conduction is a function of kT.

Electronic Heat Capacity of Metals

The interstitial-electron model accounts for the abnormally low value of the electronic heat capacity of metals in the same way as does band theory. While the movement of electrons which accounted for electrical conductivity did not depend on an excitation of electrons, the heat absorption by electrons does depend on excitation of electrons to a higher energy level. The electronic heat capacity, γ, depends also on the number of electrons at the Fermi Level which can be excited (absorb heat). Since kT is very small (0.02 eV at room temperature) relatively few electrons will be excited, and the expected electronic heat capacity will be a small fraction of 3/2 k. Because kT is small, the number of electrons at E_f is expected to be the decisive factor in determining electronic heat capacities of metals. From the interstitial model the number of electrons is directly proportional to the occupied interstices (and inversely proportional to the number of vacancies). This leads to the expectation of an inverse relation between electrical conductivity and electronic heat capacity since the conductivity is directly proportional to the number of vacancies. The influence of energy of excitation will be expected to show up in series of metals with the same number of vacancies (*e.g.* alkali metals).

The interstitial-electron model accounts for the major trends in γ for the metals as follows: (1) The small increase in γ in the order Na–Cs, metals which all have the same number of $\bar{e}$ at E_f is due to a decrease in the energy of excitation of $\bar{e}$. This is expected for the larger ion cores and indicated by band widths, but the larger value of Li than Na is due to an unexpectedly weak field of Li^+. This comes about by polarization of the $\bar{e}$ cloud and has been commented on in part II. (2) There is a monotonic increase from Be to Sr followed by a drop in γ at Ba. The first increase parallels the increase observed for the alkalis. The low value for Ba is associated with the change to BCC structure with a greater energy for excitation of $\bar{e}$ as compared to HCP. (3) The noble metals have γ values about 4 times smaller than the corresponding alkali metals and there also is lower electronic heat capacity for Zn, Cd, and Hg than the alkaline earths. This also is due to the larger excitation energy resulting from the 18-shell ion cores of the noble metals and Zn, Cd, and Hg. (4) In group 3 metals there is a large increase in γ from Al to Sc, Y, and La. In this case the distorted HCP lattice of the latter three metals leads to high occupancy of the fewer interstices. The larger number of $\bar{e}$ at E_f leads to the higher γ values. (5) The relatively high values of γ for group IV and group V metals also reflects the high occupancy of interstices in these metals. It is believed that across a row in the periodic table the increase Ca to Sc and Zr to V represents the normal trend of increased interstice occupancy, and the very high values for Sc, Y, and La are abnormal and due to restricted number of interstices in the distorted HCP lattice. (6) In general γ increases from M^+ to M^{2+} to M^{3+}, *etc.*, in proportion to the occupancy of interstices even though excitation energy increases in that order. The close proximity of tet interstices in HCP leads to the expectation of higher electronic heat capacity for HCP than BCC or FCC at least for high

occupancy of interstices. This is the observation for Ti and Zr.[9] The γ values for BCC Fe and Mn are higher than for FCC structures.

The discussion of electronic heat capacity has considered the number of $\bar{e}$ at E_f (occupied interstices) as well as the difference in energy of electron energy levels. These are usually considered as "density of states" in band theory. The density of states which is defined as the number of electron energy levels per ev is a theoretically derived concept and not an experimental number. There does appear to be a direct relation of the intensity of X-ray spectra to density of states.

Magnetic Susceptibility of Metals

The reason for weak paramagnetism in many metals is that only the $\bar{e}$ near E_f can have the spins reversed by the applied magnetic field. The gradations in paramagnetic susceptibility as for γ will depend primarily on the number of $\bar{e}$ at E_f but also on the energy required to reallign the electron spin. Thus, magnetic susceptibility should parallel the gradations in γ with the additional effect that electron pairs among the itinerant electrons can reduce the paramagnetism of the metal. Figure 3 shows the expected parallel behavior of γ and χ.

The diamagnetism of Be is an example of a divergence of magnetic properties from the observed gradation of γ. The diamagnetism of Be is undoubtedly the result of greater electron pairing of $\bar{e}$ in the distorted HCP structure ($c/a=1.567$) of Be (See Part II). There is a minimum in magnetic susceptibility at Na for the alkali metals which reflects the abnormally high value for Li. This is due to polarization of the itinerant electron cloud by the high field of Li^+. It can be looked on as the result of an increase in electron density around the Li^+ core. The trends in magnetic susceptibility for the heavier metals are difficult to interpret because of the large correction for the diamagnetism of the ion core. The χ values in Fig. 3 are not corrected for core diamagnetism.

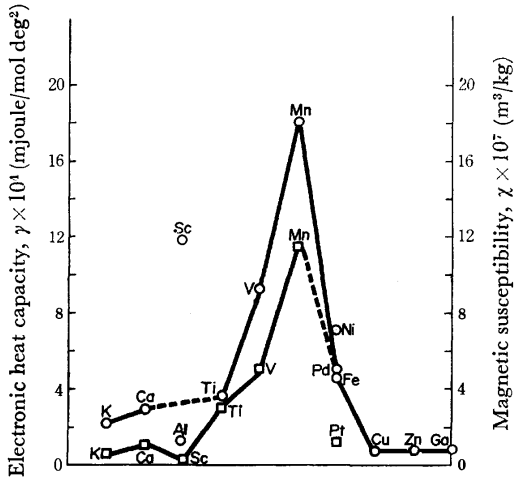

Fig. 3. Electronic heat capacity and magnetic susceptibility of metals.
(○: Electronic heat capacity, □: Magnetic susceptibility)

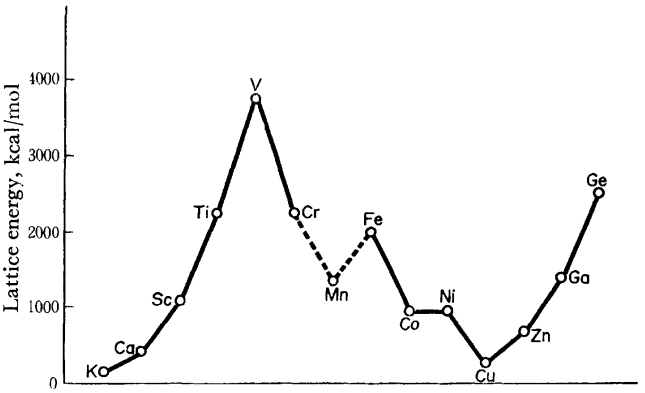

Fig. 4. Variation in lattice energy with group in periodic table.

Hall Coefficients of Metals

When a magnetic field is applied to a metal through which an electric current is passing, there is a drift of electrons in the direction of the magnetic field. The derived Hall Coefficients of metals have been taken as a measure of whether there are + or − carriers of electric current.

The alkali metals, noble metals, Mg, Ca, Al, and several other metals have −Hall Coefficients, while Be, Zn, Cd, V, Cr, Mn, Fe, and a number of other metals have +Hall Coefficients.[9] The explanation has been given tha tthe metals with +Hall Coefficient have positive hole conduction. The interstitial-electron model gives the following different interpretation. It is noticeable that the metals with +Hall Coefficients are those which contain electron pairs in their structure. It is proposed that in the conduction process an $\bar{e}$ dissociates from an $(\bar{e})_2$ and moves to an adjacent interstice. Then an $\bar{e}$ from a neighboring $(\bar{e})_2$ takes the place of the first $\bar{e}$. This process can continue and the resulting chain is equivalent to the movement of an $\bar{e}$ in the direction opposite to the movement of the first $\bar{e}$. This parallels the hole conduction explanation, but there are additional consequences of $(\bar{e})_2$ in metal lattices which are completely different from those of "holes" and which have been discussed in connection with other metal properties.

It is of great interest that with very few exceptions the metals with +Hall Coefficients are superconducting metals. The exceptions, *i.e.* superconductors which have −Hall Coefficients are La, Ga, In, Sn, all of which have unusual or distorted lattices. Th and Ti, also exceptions, have very low Hall Coefficients. This correlation between superconductivity and +Hall Coefficient has not been pointed out previously, and the role of $(\bar{e})_2$ in the superconducting state will be discussed in detail in Part VI of this series of papers.

Physical Properties of Metals

Only some general comments will be made relating to the very extensive area of physical and metallurgical properties of metals. The greater the degree of localiza-

9) R. J. Weiss, "Solid State Physics for Metallurgists," Pergamon, Oxford (1963).

tion of $\bar{e}$ density in a metal structure, the more brittle and hard the metal or alloy. This shows up in some of the metal alloys with large number of $(\bar{e})_2$ postulated for their structures and will be discussed in Part V for intermetallic phases. The localization of $\bar{e}$ density can also come *via* electron preference for occupancy of one type of interstice, or by asymmetry in $\bar{e}$ density in an interstice. The greater ductility of CCP metals as compared to HCP or BCC is probably connected to with the greater symmetry of $\bar{e}$ distribution in CCP.

BULLETIN OF THE CHEMICAL SOCIETY OF JAPAN, VOL. 46, 1923—1928 (1973)

An Interstitial-Electron Model for the Structure of Metals and Alloys. IV. Magnetic Properties of Metals and Electronic Structures of Group VI—VIII Metals

Oliver JOHNSON*

Research Institute for Catalysis, Hokkaido University, Sapporo 060

(Received August 9, 1971)

The interstitial-electron model leads to localization of d-electrons on the metal ion cores starting with group 6 metals which would have all the tetrahedral and octahedral interstices occupied by itinerant electrons. In the model the itinerant electrons play the role of ligands and determine the degeneracy of the d-orbitals localized on the ion core. There are mutual accomodations as far as location of itinerant electrons in specific interstices and d-electrons in preferred orbitals. Consideration of metal properties, especially Hall Coefficients, leads to reasonable values for both localized and itinerant magnetic moments. The relatively large spatial extension of 3d-orbitals at low intermetallic distances accounts for the magnetic moments in Cr, Mn, Fe, Co, and Ni. A striking consequence of the application of the interstitial-electron model to Fe is that it reproduces in detail the regions of positive and negative magnetization (including the interlocking rings on edges and faces) observed in neutron diffraction studies by Shull and Mook.

This paper will treat the magnetic properties of metals and show how the interstitial-electron model[1] accounts for the very complex magnetic behavior of metals like Cr and Mn, the ferromagnetism of Fe, Co, and Ni and the lack of a magnetic moment for metals of 2nd and 3rd transition series.

The first paper in the series indicated that the model would require localization of d-electrons on the metal ion core at M^{6+} since 6 itinerant electrons would completely fill the 2 tetrahedral and 1 octahedral interstice with electron pairs. The problem then for the metals starting with chromium (Cr^{6+} ion core) is to decide how many d-electrons are localized. Since it is desirable to predict magnetic moments, the starting point will be to examine the metal properties to see if the number of itinerant electrons can be specified as they were in Group I—V metals. Properties such as electrical conductivity, electronic heat capacity and Hall Coefficient are indicative of number and kind of itinerant electrons.

Itinerant Electrons and d-Electrons in Metals

Just as for non-transition metals there will be a structure determined preference for electron occupancy of octahedral or tetrahedral interstice, but extension of d-orbitals into each type of interstice can influence the distribution of itinerant electrons. A localization of itinerant electron density in binding regions (interstices) has been described in detail.[1] The alternate "instantaneous" description of electrons in interstices is the unique new feature of the interstitial-electron model. These electrons or $(\bar{e})_2$ can be treated as ligands in determining the degeneracy of the localized d-orbitals on the metal ion cores. This differs from the use of ligand field theory in metals by both Trost[2] (orbital constructions) and Goodenough.[3] It is believed that the objection made by Brooks to the use of ligand field theory in metals does not hold for this model, since his objections were directed toward the use of d-orbitals on other ion cores as ligand fields. Elliot[4] also discusses crystal fields in metal and suggests methods for their use.

Thus, ligand field theory can give the value of the magnetic moment on the ion core once the electronic structure with number of itinerant electrons and localized d-electrons and orientation of d-orbitals with respect to lattice axes is decided. In cases where there is unequal distribution of itinerant electrons among octahedral ($\uparrow$) and tetrahedral interstices ($\downarrow$), there can be a magnetic moment of itinerant electrons. The combination and interaction of these two kinds of moments can lead to ferromagnetism, antiferromagnetism and itinerant ferromagnetism.

* Present address: Institute of Physics, University of Uppsala, Uppsala, Sweden.

1) O. Johnson, This Bulletin, **45**, 1599, 1607 (1972).

2) W. R. Trost, *Can. J. Chem.*, **37**, 460 (1959).

3) J. B. Goodenough, "Magnetism and the Chemical Bond," J. Wiley and Sons, N. Y, (1963).

4) R. J. Elliot, *Comments Solid State Phys.*, **1**, 85 (1968).

The nature of interaction between itinerant electrons and d-electrons has not been specified. The simple picture of ion cores and itinerant electrons in binding regions (See Part I) no longer holds for metals with localized d-electrons. It is assumed that the extension of 3d-orbitals at least is such that itinerant electrons in the interstice involved would have an electron spin *opposite* to that of the d-electron. This also assumes that the two electron energies are about equal which is a reasonable assumption and consistent with the band theory of metals. This description of the interaction of $\bar{e}$ and d-electrons is essentially the "indirect exchange" used by Zener[5] but with antiparallel spin allignment as proposed by Vonsovsky and Vlasov[6] and Mott and Stevens.[7]

Trost[2] has argued for a strong interaction of adjacent 3d-orbitals on adjoining metal ion cores. He points out that the ratio of size of the $(n-1)$ shell to the n shell has the smallest value for the first transition period. The two factors involved are the decreasing separation of ns, np, and $(n-1)$ d atomic orbital energy and the increasing relative size of the $(n-1)$ d-orbitals as n increases. This implies that the $(n-1)$ d-orbitals become more important for binding and explains the increase in mp, bp, in transition metals as n increases (it decreases for non-transition metals). This effect of size and separation of d-orbitals reaches its maximum around Mn, Fe, and Co. It is believed that Trost's analysis is an even stronger argument for interaction of 3d electrons with itinerant electrons than his proposed interactions of 3d-3d on adjacent ion cores. In the present paper it is assumed that there are potential interactions between itinerant $\bar{e}$ and d-electrons of all 3 transition series, but that the very low intermetallic distances for the 1st transition series is crucial for determining magnetic properties.

In a metal lattice the ion cores can have an orientation such that its d-orbital axes are identical to the crystal axes or they may be at an appropriate angle, *e.g.* 45°. This orientation will be determined by the magnitude of repulsive interactions between itinerant electrons and d-electrons as compared to interactions between d-electrons on two adjacent ion cores. It is assumed that the onset of magnetic properties corresponds to the condition where the d-electron interactions determine the orientation, and empirically this occurs for metals with interatomic distances of 2.6 Å or less. This can now be compared directly to the treatment of magnetic properties by Goodenough.[3] Goodenough assumes a critical separation of $R_c = 2.9 \pm 0.1$ Å, below which there is localization of d-electrons on ion cores and above which the d-electrons are considered itinerant. The treatment by the interstitial-electron model proposed the localization of d-electrons to occur after M^{5+} and at M^{6+} (the intermetallic distances here are close to R_c above). The additional criterion is that at $R \leq 2.6$ Å, the $M^{n+}(d) - M^{n+}(d)$ interactions become more important than the $M^{n+}(d)$–$\bar{e}$ interactions in determining the orientation of the axes of the d-orbitals on the ion core.

The above principles will now be used in formulating interstitial-electron structures, and thus magnetic properties, for metals of Groups VI—VIII.

Interstitial-Electron Structures for Group VI Metals

Chromium metal has many unusual properties such as a very high positive Hall Coefficient, low electronic heat capacity (γ) for a transition metal, high work function, low electric conductivity and small amplitude of lattice displacement. It is also likely that the Cr structure differs from that of Mo and W since it exhibits a complex antiferromagnetism and the latter two are paramagnetic. To assign a valence to Cr, and thus an ion core charge and the number of localized d-electrons, it is pertinent to note that Cr has the BCC structure as does V^{5+} and Ti^{4+} (at high temperatures). The relatively low value of γ, comparable to that of Ti, suggests an ion core charge of 4. The very high positive Hall Coefficient (+36) suggests at least 4 as the number of itinerant electrons to account for a large number of ($\bar{e}_2$) (or filled interstices) in the structure. Tentatively, the structure will be taken as:

$$\left| \begin{matrix} Cr^{6+}(d^2),\ 4\bar{e} \\ \text{tet rings} \end{matrix} \right|_{BCC}$$

It is inherent in the BCC crystal structure that the corner and body center ion cores are not equivalent. However, for an equal distribution of itinerant electron in the face tetrahedral and edge tetrahedral rings (See Part I) there is the same degeneracy of d-orbitals on both corner and body center ion cores. The degeneracy given below is based on $\bar{e}$ in tet rings as ligands with equal $\bar{e}$ density on all faces and d-orbital axes 45° to crystal axes:

$\overline{xz}$ $\overline{yz}$ (directed to Cr)

$\overline{xy}$ $\overline{z^2}$ (directed to edges)

$\overline{x^2-y^2}$ (directed to face center)

Corner or Body Center $Cr^{6+}(d^2)$

This degeneracy is based on usual crystal field theory considerations. The 45° orientation is chosen since it conforms to the observed magnetic properties and has no occupied d-orbitals directed to Cr.

The degeneracy of d levels is such that the d^2 configuration of the Cr ion core leads to pairing of these localized d-electrons, and spatially they extend from corner ion cores (atoms) diagonally along horizontal faces and from body center ion cores perpendicular to the vertical face centers. The proposed structure for chromium has the following instantaneous distribution (See Part I[1]) of itinerant electrons in tetrahedral rings: 3 $\bar{e}$ in each tet ring on 4 faces of the Cr unit cell (xz, yz planes) and 2 $\bar{e}$ in each tet ring on two faces (xy plane). This is a total of 16 $\bar{e}$ on faces, 8 $\bar{e}$ per unit cell or 4 per Cr ion core. The e in tet rings on the 2 horizontal faces will be paired and the remain-

5) C. Zener, *Phys. Rev.*, **81**, 440 (1951); *Rev. Mod. Phys.*, **25**, 191 (1953).

6) S. V. Vonsovski and K. B. Vlasov, *Zh. Eksp. Teor. Fiz.*, **25**, 327 (1953).

7) N. F. Mott and K. W. H. Stevens, *Phil. Mag.*, **2**, 1364 (1957).

ing 6 ē do not have any spin allignment except that adjacent ē in tet rings will have opposite spins. Thus, there can be 1 ē on each of 4 faces with undetermined spin, and this can lead to 0,1 or 2 ē with the same spin per unit cell or 0, 1/2 or 1 unpaired spin per Cr. This lies within the observed magnetic moment for Cr of 0.54 μ_B per Cr.

The model proposes that any itinerant moment is to be distributed among the 4 vertical faces of the unit cell. The theoretical prediction of an helical spin state as the ground state for magnetic systems,[8] and consideration of linear spin density waves for Cr makes it reasonable that the undetermined spin above leads to an itinerant moment on Cr of approximately 0.5 μ_B per Cr.

Neutron diffraction studies show that below 312K Chromium exhibits a complex antiferromagnetic behavior. There are not the usual two sublattices associated with antiferromagnetism but a sinusoidal modulation of moment over at least 21 unit cells *i.e.* the total moment varies with position. The model gives a physical picture of this complex behavior in terms of electrons with free spins in each of the 4 vertical faces of the Cr unit cell. It is understandable that this could easily revert to a paramagnetic state as temperature is increased and as is observed above 312K.

The smaller Hall Coefficient and greater electrical conductivity suggest fewer itinerant electrons for *Mo and W* than for Cr. This leads to the proposal of a d^4 localization of d electrons on Mo and W. A different localization is expected as well on the basis of the non-magnetic properties of Mo and W. The proposed itinerant-electron structure for Mo and W is:

$$\left| \begin{matrix} M^{6+}(d^4),\ 2\bar{e} \\ \text{tet rings} \end{matrix} \right|_{BCC}$$

The intermetallic distance for Mo and W (1.39 and 0.41 Å) places it in the group of metals where the interaction of localized d-electrons is expected to be larger than between ē and localized d-orbitals on adjacent ion cores. A 45° orientation of the axes of d-orbitals in respect to the crystal axis gives the minimum ē-d interaction, and the degeneracy of d levels is as follows:

$\underline{z^2}$ $\underline{xy}$ (to edge tet ring)

$\underline{x^2-y^2}$ (to face tet ring)

$\underline{\uparrow\downarrow xy}$ $\underline{\uparrow\downarrow yz}$ (directed to M^{n+})

This degeneracy leads to complete pairing of d-electrons for d^4 and accounts for the normal metallic paramagnetism of metallic Mo and W. The degeneracy is based on distribution of itinerant electrons as 1 ē per tet ring on each of 2 horizontal faces (xy plane) and 1 ē per tet ring on each of 4 edges (z^2 and xy of d-orbital axes). In such an arrangement electron spins can be random as in the cases of Ba metal (also BCC). Each ē has 4 interstitial locations and different spins in adjoining interstices. This contrasts with the greater restriction of ē spin in Cr. No itinerant moment (or SDW) have been observed in neutron diffraction studies of Mo or W.

Interstitial-Electronic Structures for Group VII Metals

α-Manganese, the form of manganese metal stable from ordinary temperature to 710°C, has more than one type of Mn ion core in the structure. β-Manganese is paramagnetic and stable from 710—1079°C. It has 20 atoms per unit cell of which 8 are of higher valence (smaller size) than the remaining 12. A structure similar to those proposed for β-phases which have the same structure[9] is the following:

$$\left| 8Mn^{7+}(d^4),\ 12Mn^{7+}(d^6),\ 36\bar{e} \right|_{\beta\text{-Mn}}$$

This gives a number of itinerant electrons per unit cell which is close to the *e/a* ratio of 3/2 observed in β-phases. The structure has interstices which are not homogeneous in terms of ion cores around an interstitial electron. This is discussed in detail in Part V,[9] and in the case of Mn it leads to localization of ē in the structure as electron pairs and is associated with the hardness and brittleness of β-Mn.

γ-Manganese, stable in the temperature range 1079—1143°C, has a face-centered tetragonal structure when stabilized at room temperature and is CCP in its normal state. The room temperature modification has been observed to be antiferromagnetic[7] with a magnetic moment of 2.4 μ_B. The only data available to help establish the ion core charge is the relatively low atomic volume of 12.7 Å^3. This is reasonable for a divalent ion core, $Mn^{7+}(d^5)$, also indicated by magnetic properties. In the antiferromagnetic face-centered tetragonal structure, Mn has 8 neighbors at 2.58 Å and 4 neighbors at 2.67 Å. It is proposed that in a distorted structure like this, the Mn ion cores in the top and bottom faces (short distances) have a 45° orientation of d-orbital axes which minimizes Mn–Mn interactions, and the face center Mn on vertical faces (larger distance) have a 90° orientation of d-orbital axes with respect to the tetragonal cell. This leads to the following degeneracy for $|Mn^{7+}(d^5),\ 2\bar{e}|$ FCTetr.

$\overline{z^2-y^2}$ (Mn–Mn face)

$\underset{xz}{\uparrow}$ $\underline{yz}$ (tet)

$\underline{\uparrow\downarrow}$ xy (oct)

$\underline{\uparrow\downarrow}$ z^2 (oct, large d)

Mn ion cores on top and bottom face

$\overline{xy}$ (Mn–Mn, short d.)

$\overline{x^2-y^2}$ (oct)

$\underline{\downarrow}$ z^2 (oct, large d.)

$\underline{\uparrow\downarrow}$ xz $\underline{\uparrow\downarrow}$ yz (Mn–Mn, large d.)

Mn ion cores on Vert. Face Centers

8) A. W. Overhauser and A. Arrott, *Phys. Rev. Lett.*, **4**, 226 (1960).

9) O. Johnson, This Bulletin, **46**, 1929 (1973).

This degeneracy leads to one unpaired ē localized on the Mn ion cores of the top and bottom faces of a tetragonal unit cell and one unpaired ē on the Mn ion cores on centers of vertical faces. The former are directed into tet interstices and the latter into oct interstices so they will have opposite spins, and the total moment difference corresponds to 2 μ_B. In addition there is the chance of considerable imbalance in the itinerant electron spins since there is much more ē density from d-electrons directed into oct interstices. A distribution, *e.g.* of 1/2 ē in oct and 1 1/2 ē in tet would lead to an itinerant moment of 1 ↑/unit cell or 0.25 ↑ per Mn ion core.

Tc and Re both form HCP lattices with *c/a* values close to normal. Little data is available on Tc, but Re has a high Hall Coefficient and moderate electronic heat capacity; both metals have low conductivity. The structure proposed below with 3 itinerant electrons is reasonable for these properties:

$$\left|M^{7+}(d^4),\ 3\bar{e}\right|_{HCP}$$

The degeneracy of d levels, discussed in detail for Co, leads to pairing of localized d-electrons and thus normal paramagnetism for these metals.

Interstitial-Electron Structures for Fe, Ru, and Os

The Hall Coefficient for metallic iron is positive but not as high as that of Cr. It also has a high electronic heat capacity for a group 8 metal. These properties suggest an electronic structure with at least 4 itinerant electrons as follows:

$$\left|Fe^{8+}(d^4),\ 4\bar{e}\right|_{BCC}$$

A d^2 structure as proposed by Lomer and Marshall[10] is not compatible with the interstitial electron model since it would have 6 itinerant electrons, postulated not to give metallic properties.

In deriving the degeneracy of d-orbitals it is assumed that the 4 ē are distributed evenly among the tet rings on faces and edges of the BCC unit cell. An orientation of d-orbital axes of the Fe ion cores at 45° to the crystal axes leads both to the expected localized moment on the Fe ion cores and to the location of the magnetic lobes according to neutron diffraction studies.[11] The following degeneracy holds for both body-center and corner ion cores:

$\overline{xz}$ $\overline{yz}$	(directed to Fe)
$\uparrow$ $\uparrow$	
$\overline{z^2}$ $\overline{xy}$	(along edges or to face centers)
$\uparrow\downarrow$	
$\overline{x^2-y^2}$	(directed diagonally to tet rings)

The above electronic structure and degeneracy of d levels leads to d^2-orbitals along horizontal faces and directed to vertical edges from the body-centered ion cores. Unpaired d-electrons extend along all edges and from the body center Fe ion core to centers of all faces. The 4 itinerant electrons (or 8 ē per unit cell) on an instantaneous picture can be pictured as occupying 4 face tet with 3 ē each and the remaining 2 face tet per unit cell with 2 ē each. Thus, the small negative magnetization (0.2 μ_B) is associated with the interlocking tet rings. It is striking that the model proposed here reproduces in detail the spatial arrangement of localized moments on Fe ion cores as well as the itinerant moment found by Shull and Mook,[11] in neutron diffraction studies of Fe.

The difference in magnetic properties of Fe and Cr requires comment. The lack of a localized moment in Cr is accounted for on the basis of its d^2 configuration. The two metals in BCC have the same number of itinerant electrons according to the proposed structures. The unpaired d-electrons in Fe must greatly restrict the location of itinerant electrons in tet ring interstices. This restriction of ē in Fe is in keeping with the normal value of magnetic entropy ($k \ln 3$) observed for Fe and the very low magnetic entropy in the case of Cr.[11]

Os and Ru have HCP structures with *c/a* values of 1.57 and 1.59 and are expected to have 1 oct interstice and 1 Bipyramidal interstice per M^{n+}. This accounts for the very high Hall Coefficient of Ru if it has a d^4 structure (like Fe). The lower Hall Coefficient and electronic heat capacity suggest the following d^6 structure for Os:

$$\left|Os^{8+}(d^6),\ \bar{e}_{oct},\ \bar{e}_{BP}\right|_{HCP}$$

The degeneracy in HCP (see discussion, Part II[1]) leads to complete pairing of electrons for both Ru and Os, and the structure accounts for the normal paramagnetism of these metals.

Interstitial-Electron Structures for Co, Rh, and Ir

The Hall Coefficient is strongly negative for cobalt metal, an indication of lower electron occupancy of interstices and much less liklihood for presence of electron pairs in interstices. The electrical conductivity is higher than for iron, an indication of lower interstice occupancy than iron or of less interference in the conduction process by d-electrons.

These properties suggest a low ion core charge for Co relative to Fe, and the stability of Co^{2+} makes it a reasonable choice. The ion core structure below has the high d localizations as has been used by Lomer and Marshall[10] and others and applies to paramagnetic Co.

$$\left|Co^{9+}(d^7),\ 2\bar{e}\right|_{HCP}$$

The axes of the d-orbitals are placed so the z-axis corresponds to the c-axis of the hexagonal cobalt structure, the x-axis is placed along a line connecting 2 cobalt ion cores and the y-axis then passes 1/2 way between two other cobalt ion cores. This gives rise

10) W. M. Lomer and W. Marshall, *Phil. Mag.*, **3**, 185 (1958).
11) G. G. Shull and H. A. Mook, *Phys. Rev. Lett.*, **16**, 14 (1966); *Phys. Rev.*, **136**, A195 (1964); *ibid.*, **148**, 495 (1966).

to the following degeneracy for ferromagnetic Co:

$\overline{x^2-y^2}$ (to M^+)

$\underline{\uparrow(\downarrow)_{0.2}}_{yz}$ $\underline{\uparrow}_{z^2}$ (M^+, oct) (tet)

$\underline{\uparrow\downarrow}_{xz}$ $\underline{\uparrow\downarrow}_{xy}$ (no $\bar{e}$ or ion cores)

The above degeneracy of d levels for $Co^{9+}(d^7)$ leads to unpaired d-electrons extending into tet interstices and 0.8 unpaired d-electrons extending near oct and another ion core. It is not likely that other orientations of the d-axes would lead to more favorable d-electron distribution as far as ion core interactions are concerned.

The spin requirements of oct interstices[1] in HCP leads to only 0.4↑ occupancy since an unpaired d-electron from the Co ion core directed to oct requires an opposite itinerant electron spin. This gives the following interstitial-electron structure for cobalt metal:

$$\left| Co^{9+}(d^{6.2}),\ \bar{e}_{0.4}(\bar{e}_2)_{0.6oct},\ \bar{e}_{1.2tet} \right| HCP$$

This placement of additional $\bar{e}$ in tet is also in keeping with the preference for tet occupancy in HCP lattices below 2 $\bar{e}$ and accounts for a negative moment on $\bar{e}$.

The proposed structure has a magnetic moment corresponding to 1.8↑ on each Co ion core with spins alligned *via* tet electrons. The oct $\bar{e}$ (0.4 $\bar{e}$) have all one spin and the $\bar{e}$ in tet interstices can have a range of unpaired spins. Depending on whether these spins cancel or add, there could be no itinerant moment in Co or a maximum of 0.4↑. The observed moment of 1.7 μ_B lies within the range allowed by the above structure. The model would not give structures which would have more than 2 unpaired electrons localized on Co.

Rhodium and Iridium have a small positive Hall Coefficient so higher occupancy of interstices by electrons is indicated. The normal valence of 3 is thus indicated for the CCP structures of Rh and Ir.

$$\left| Rh^{9+}(d^6),\ \bar{e}_{oct},\ \bar{e}_{tet},\ (\bar{e}_2)_{1/2tet} \right| CCP$$

The distribution of electrons in interstices is that normally required in the CCP lattice to give balanced spins and preference for tet occupancy. The degeneracy for the d-electrons in this structure and the comparable Ir structure is:

$\underline{z^2}$ $\underline{x^2-y^2}$ (directed to edges)

$\underline{\uparrow\downarrow}_{xy}$ $\underline{\uparrow\downarrow}_{xz}$ $\underline{\uparrow\downarrow}_{yz}$ (directed to M^{n+})

The degeneracy given above is for placement of axes of d-orbitals coincident with crystal axes. This leads to non-magnetic properties for Rh and Ir.

Interstitial-Electron Structures for Ni, Pd, and Pt

Mook[11] has shown by neutron diffraction for Ni a ferromagnetic moment of 0.71 μ_B (0.656, 3d and 0.055, orbital) is localized around the ion core with a negative magnetization of 0.105 μ_B. It has also been maintained that the moment is itinerant[12,13] for Ni. In the following a structure is proposed which attempts to resolve these conflicting interpretations.

As with cobalt metal, the negative Hall Coefficient, relatively low electronic heat capacity and moderate electrical conductivity make it reasonable that Nickel has a Ni^{2+} ion core. The following ion core structure is proposed:

$$\left| Ni^{10+}(d^8),\ 2\bar{e} \right| CCP$$

To determine the d level degeneracy, the d-orbital axis is placed at 45° to the crystal axis since this gives the minimum extension of d-orbitals toward other Ni ion cores (R=2.5 Å). The degeneracy is as follows:

$\overline{x^2-y^2}$ (toward Ni)

$\underline{\uparrow\downarrow}_{xz}$ $\underline{\uparrow(\downarrow)_{0.3}}_{yz}$ (toward tet)

$\underline{\uparrow\downarrow}_{xy}$ $\underline{\uparrow\downarrow}_{z^2}$ (toward oct)

The degeneracy has occupied d-orbitals extending into both oct and tet interstices. The resultant repulsive interaction between d^2 electrons and itinerant electrons could lead to a shift of $\bar{e}$ from tet to oct (greater distance from ion core) or to a transfer of some d-electrons to tet interstices as itinerant electrons. The former requires $\bar{e}$ pairing so the latter is considered more likely. Assuming a transfer of 0.7 $\bar{e}$ from a localized d-orbital to tet interstice, the following structure results:

$$\left| Ni^{10+}(d^{7.3}),\ \bar{e}_{oct},\ (\bar{e}_2)_{0.3}\bar{e}_{1.1tet} \right| CCP \quad \text{(Ferromagnetic Ni)}$$

This electronic structure accounts for the observed moment around the Ni ion core observed by Mook and also its itinerant character. The equilibrium state can be looked on as having an occupied d-orbital extending into a tet interstitial region with a d-electron of one spin near the ion core and a d-electron of the opposite spin (and now indistinguishable from an itinerant electron) near the centre of a tet interstice. On an instantaneous basis there will be 30% regions of $Ni^{10+}(d^8)$, 1 $\bar{e}_{tet}$ (no magnetic moment) and 70% regions of $Ni^{10+}(d^7)$, 2 $\bar{e}$ (with 1 unpaired electron). Above 700° where Ni shows paramagnetism a small additional shift of electrons can give the following structure with no coupling of spins:

$$\left| Ni^{10+}(d^7),\ \bar{e}_{oct},\ \bar{e}_{tet},\ (\bar{e}_2)_{1/2tet} \right| CCP \quad \text{(Paramagnetic Ni)}$$

A similar equilibrium between d^2 electrons localized on Co ($d^{4.2}$) and tet itinerant electrons can explain the total localized moment and form factor for Co.

Palladium and Platinum have higher electronic heat capacities and lower electrical conductivities than expected for these group 8 metals. This suggests more itinerant electrons than ferromagnetic Ni. An ion core structure with M^{3+} can account for the above properties and the paramagnetism of these metals.

$$\left| M^{10+}(d^7),\ \bar{e}_{oct},\ \bar{e}_{tet},\ (\bar{e}_2)_{1/2tet} \right| CCP$$

12) A. Arrott, "Magnetism," Vol. 2B, Ed. by G.T. Rado and H. Suhl, Acad. Press, New York (1966), Chap. 4.

13) C. Herring, "Magnetism," Vol. 4, Ed. by G. T. Rado, H. Suhl, Acad. Press, New York (1966).

This structure is the same as that proposed for paramagnetic Ni. This proposed structure has the same degeneracy as shown for Rh and Ir and leads to d^2 electrons directed toward other M^{n+} and an unpaired electron directed toward 1/2 of the oct interstices. No coupling of spins is expected.

Discussion

The interstitial-electron model has been used to formulate structures for the magnetic and non-magnetic metals of groups VI—VIII. Ion core charges were established by comparison of properties of these metals (Hall Coefficient, electronic heat capacity and electrical conductivity) with metals of known ion core charge. The view is taken that when d-orbitals of the ion core extend into interstices, electrons occupying these two positions will have anti-parallel spins. The placing of the axes of the d-orbitals of the ion cores is based on empirical choice of an intermetallic distance of 2.6 Å above which interactions between d-electrons on adjacent ion cores becomes less important than interactions between these d-electrons and itinerant electrons in metal interstices. The itinerant electrons are treated as ligands to establish the d level degeneracy for d-electrons localized on the ion cores. The more complex splitting of d-levels than the usual e_g-t_{3g} splitting provides a new basis for discussing magnetic form factor.

The model leads to a magnetic structure of iron which has 2 unpaired electrons localized on the ion core, and a small additional moment associated with itinerant electrons. The magnetic entropy value and the spherical form factor found in neutron diffraction studies support this structure. The model proposes a magnetic moment originating on the itinerant electrons for nickel. This is supported by the observation that for Ni and Co metals, orbital magnetic moments are completely quenched (g value approx 2) and by the anisotropic form factor observed in neutron diffraction. For cobalt the model leads to 1.8 unpaired electron localized on the ion core and an additional moment on itinerant electrons. There have been unsuccessful attempts to locate itinerant electron spin density waves in Ni and Co. The experiments appear to have been scans in the 1, 1, 1 direction. The model indicates, *e.g.*, for Ni that unpaired electrons would be in tet interstices which are not centered on the 1, 1, 1 plane. The interpretation of the antiferromagnetism of Chromium offers a useful physical picture of the unusual itinerant magnetism (spin density waves). The model suggests that the antiferromagnetism of γ-Manganese is like that of an oxide system with itinerant electrons providing the antiferromagnetic allignment of spins.

The scheme of localization of electrons in interstices has provided a basis for explaining the complex magnetic properties of group VI—VIII metals. The electron distributions formulated for metals in this paper have been the result of mutual accomodations of localized d-electrons and itinerant electrons as is inherent in ligand field theory. This resultant more uniform electron density is an important property of the transition metals, and it is anticipated that it will give valuable insight into metal properties.

An Interstitial-Electron Model for the Structure of Metals and Alloys. V. Metal Alloys and Intermetallic Compounds

Oliver JOHNSON*

Research Institute for Catalysis, Hokkaido University, Sapporo 060

(Received September 17, 1971)

On the basis of the interstitial-electron model for metals the essential feature of the metallic state is the relatively free movement of electrons, ($\bar{e}$), between interstices in a close-packed array of metal ions (positive cores). For a solid solution of one metal in another in which the metal ions have nearly the same size and core charge, the interstitial-electron structures which incorporate spatial and spin correlation of electrons are the same as for metals. Metallic properties can also result when the ratios of two less similar metals in an alloy are such as to give interstices with a constant ratio of the two metals surrounding them. Occupancy of such "homogeneous interstices" is the basis for intermetallic compounds and accounts for the Hume-Rothery rules. Intermetallic compounds such as γ phases (*e.g.* Cu_5Zn_8) are unique in that $\bar{e}$ and electron pairs must be assigned to two or more types of interstices which have different ratios of the two metal ions around them. This localization of $\bar{e}$ density explains the very poor conductivity, the hardness, the brittleness and the large diamagnetic susceptibility of γ phases. The structural framework of the interstitial-electron description accounts for the large composition range of the interstitial phases and can naturally include effects of ion core size and charge. Interpenetration of d^{10} ion cores by itinerant electrons which gives a balancing of the positive fields of the 2 ion cores accounts for the preponderance of d^{10} metals among intermetallic phases.

Of the metals, only Manganese has ions of two different core charges (and sizes), and Mn has unusual properties for a metal. However, with metal alloys there are always two or more ions of different size or core charge to be accomodated into the metallic structure. Where there are not large differences in effective positive fields of the metal ions making up the alloy the disruption of the periodic field will not be great enough to lead to large changes in properties. This situation holds for a great many alloys of similar metals. When the differences in positive field are very large, metallic salts or alloy salts[1] are formed. Some examples are Li_3B, Mg_3Sb_2, and Mg_2Sn. They have a metallic appearance but have unusually high melting points, are brittle and are very poor conductors of electricity. The alloy salt CsAu has been given[1] the structure Cs^+Au^-.

Between these two extremes of alloys, the solid solutions of one metal in another and the metallic salts, there are a large number of intermediate alloys which are called secondary alloys or intermetallic compounds. They are clearly metal-like but may deviate from metals in some property *e.g.* the intermetallic compound may be less ductile, it may be harder or brittle, or it may be a poor conductor.

There are a large number of different types of intermetallic compounds. The best known of these are the ones classified by Hume-Rothery[2] on the basis of the number of electrons per atom in the compound (or intermetallic phase). This ratio is 3/2 for β phases, 21/13 for γ phases and 7/4 for ε phases. All three types of intermetallic compounds form over rather wide composition ranges so the ratios are only approximate. In addition it has to be assumed that group VIII metals contributed no electrons in order to fit them into the ratio pattern.

Recent reviews[3–5] show the highly complex behavior and interrelations of α, β, γ, μ, and ε phases including both size effects and electronic effects.

The relations between the electronic structures of intermetallic compounds and that of metals, as well as the inter-relation between the various phases still remains obscure. Since the intermetallic compounds all form close-packed or nearly close-packed structures, it is anticipated that the interstitial-electron model[6] of metal structure can be applied to understanding the binding in intermetallic compounds as well as in metals. The term electron in an interstice refers to electron density considered to be localized in the interstitial binding region of the close-packed metal structure.[6]

Interstices in Intermetallic Compounds

It is proposed that a stable metallic structure can result for intermetallic compounds if the ratio of the two metal ions around an interstice is the same throughout the structure. This homogeneity of interstices can lead to the same free movement of electrons through the intermetallic structure as is observed for the metals themselves. The observed deviations from stoichiometry are understandable since a given structure can accomodate some deviation from homogeneity of interstices just as is the case for the solid solutions.

With this postulated basis for the formation of intermetallic compounds the structures for the various types of intermetallic phases can be considered and formulated using the Interstitial Electron Model.

---

* Present address: University of Physics, University of Uppsala, Uppsala, Sweden.

1) R. G. Nyholm, Proc. Tihany Symposium on Coordination Chemistry, Tihany, Hungary, 1965.

2) W. Hume-Rothery, *J. Inst. Metals*, **35**, 295 (1926).

3) M. V. Nevitt, "Electronic Structure and Alloy Chemistry of Transition Elements," ed. by P. A. Beck, Intersciences, New York (1963).

4) T. B. Massalski and H. W. King, *Prog. Materials Sci.*, **10**, 5 (1961).

5) J. M. Sivertson and M. E. Nicholson, *ibid.*, **9**, 305 (1961).

6) O. Johnson, This Bulletin, **45**, 1599, 1607 (1972).

β Phases

A typical example of a β phase occurs with a 50–50 Cu–Zn alloy which is known as β-brass. Other examples are Cu_3Ga, AlFe, and Cu_5Sn. They have Body-Centered Cubic (BCC) structures and ordinarily form a random structure of the two metals (β-form); tempering converts them to an ordered structure known as a "superlattice" (β′-form). For CuZn each ion forms its own simple cubic lattice. For Cu_3Al a double unit must be taken, and no superlattice has been observed for Cu_5Sn.

In formulating an electronic structure for the BCC β-phases based on the interstitial-electron model, the first question is which interstices are most likely to be occupied. Unsymmetrical oct interstices are chosen as most likely to be occupied by electrons in an unsymmetrical structure with two different metal ion cores. The relatively poor conductivity compared to pure metals and the low ductility of β-phases also makes it unlikely that tet rings of interstices are occupied by $\bar{e}$.

For CuZn (β-brass) the ion cores Cu^+ and Zn^{2+} give up 3 itinerant electrons to the BCC lattice of the intermetallic compound. The two unsymmetrical oct interstices can be designated as (Cu_2Zn_4) and (Cu_4Zn_2). A preference for electron occupancy of (Cu_2Zn_4) interstices is expected because of the stronger positive field exerted by Zn^{2+} as compared to Cu^+. There are 2 such interstices per unit cell of CuZn, and there can be occupancy of all 3 by $\bar{e}$. The geometry of interstices is discussed in detail in Part I.[6]

In such an arrangement of electrons, the $\bar{e}$ are separated widely enough to have random spins (see Part I).[6] Thus, the proposed low occupancy by $\bar{e}$ would give low paramagnetic susceptibility for the itinerant electrons and is in keeping with the diamagnetism of the β-phases. As far as the structure as a whole is concerned there is a network of adjoining homogeneous interstices, in this case the (Cu_2Zn_4), through which electrons can move as in other metallic structures.

The model characterizes β-phases as having occupancy of one of the two types of oct interstices which gives an electron/atom ratio of 3/2. The 3 interstices of one type can accomodate as few as 1 $\bar{e}$ or with electron pairing as many as 6 electrons per unit cell. This would give e/a ratios of 1/2 to 3 with the major number expected at 3/2 which is occupancy by $\bar{e}$ of one type of the oct interstices in BCC and presumably the occupancy with optimum binding energy for a metal. The 3/2 ratio is found for CuZn, Cu_3Al, Cu_5Zn, PdCu and related compounds. It is 5/2 for AlCo, FeAl, NiAl, NiGa, and NiIn and 6/2 for TiFe, VFe, and AlNd.

Some β-phases are ferromagnetic and offer an additional test for the model. There are also intermetallic compounds containing Fe, Co, or Ni which are not ferromagnetic. The compound NiAl is one such example. According to the interstitial-electron model the electronic structure for NiAl would be $|Al^{3+}, Ni^{10+}(d^8), 5e_{oct}|_{BCC}$. If the Ni ion cores occupy body center positions, electron occupancy will be of the (Ni_2Al_4) interstices on faces of the unit cell. The d-orbital axis of the $Ni^{10+}(d^8)$ core will be at 45° to the lattice axis because this directs d-orbitals toward Al^{3+} and not to itinerant electrons. The degeneracy of d-orbitals will be:

$\overline{xy}$ (to $\bar{e}_2$ on faces)

$\overline{z^2}$ (to $\bar{e}$ on faces)

$\underline{\uparrow\downarrow}$ $\overline{x^2-y^2}$ (to edges)

$\underline{\uparrow\downarrow}$ $\overline{xz}$ $\underline{\uparrow\downarrow}$ $\overline{yz}$ (toward Al)

This leads to complete pairing of d-electrons so no magnetic moment is expected on the Ni ion core. Electron occupancy of the (Ni_2Al_4) interstices by $5\bar{e}$ requires $2(\bar{e})_2$ and $\bar{e}$ per unit cell. This high ratio of $\bar{e}_2/\bar{e}$ is in keeping with the +Hall Coefficient observed for NiAl. For FeAl the structure $|Fe^{8+}(d^6), Al^{3+}, \bar{e}, 2(\bar{e}_2)_{oct}|_{BCC}$ is proposed and leads to all paired d-electrons for Fe iron cores as corner atoms in the unit cell and $\bar{e}$ and $(\bar{e})_2$ on faces. This is in agreement with the observed paramagnetism of FeAl. The magnetic properties of the compound CoAl have not been reported. The structure expected from the interstitial-electron model is $|Co^{9+}(d^7), Al^{3+}, \bar{e}, 2(\bar{e}_2)_{oct}|_{BCC}$, and the same degeneracy of d-orbitals to the NiAl and FeAl leads to 1 unpaired electron in an orbital toward a face. This alligns with an itinerant electron so this alloy is expected to be ferromagnetic. A $Co^{9+}(d^6)$ ion core would lead to no magnetic moment on cobalt. The background for this method of interpreting magnetic properties is given in Part IV.[7]

Magnetic properties are known for the series TiFe, VFe, and CrFe. Both TiFe and VFe form ordered β-phases. TiFe is not ferromagnetic while VFe has a saturation moment of 0.80 μ_B localized on Fe. Cr does not form a β-phase but is related and will be considered as having similar oct interstices; it has a saturation magnetization of 1.8 μ_B per iron atom. The interstitial-electron structure proposed for TiFe has a high d-localization which is necessary to limit the number of itinerant electrons to 6 which appeared to be the maximum observed for β-phases.

$$\left|Ti^{4+}, Fe^{8+}(d^6), 3(\bar{e}_2)_{oct}\right|_{BCC}$$

When Fe ion cores are at body-centered positions the electron pairs are expected to be on face oct interstices (Ti_4Fe_2). The degeneracy expected is

$\overline{z^2}$ $\overline{xy}$ (to $2\bar{e}$ on faces)

$\underline{\uparrow\downarrow}$ $\overline{x^2-y^2}$ (to $\bar{e}$ on edge)

$\underline{\uparrow\downarrow}$ $\overline{xz}$ $\underline{\uparrow\downarrow}$ $\overline{yz}$ (to Ti).

There is no magnetic moment associated with this structure, in agreement with experimental data.

For VFe there must be still greater localization of d-electrons to keep within the maximum of 6 itinerant electrons. Thus an ion core $Fe^{8+}(d^7)$ is proposed for VFe.

7) O. Johnson, This Bulletin, **46**, 1923 (1973).

$$\left|V^{5+},\ Fe^{8+}(d^7),\ 3(\bar{e}_2)_{oct}\right|_{BCC}$$

This degeneracy of d-orbitals is the same as for TiFe, and with 7 d-electrons there will be one unpaired electron on the iron core. This is close to the observed magnetic moment for VFe. The increase in lattice contraction[3] from VFe to TiFe is probably due to the removal of some screening of the Fe ion core in going from 7 to 6 d-electrons (core charge from Fe^+ to Fe^{2+}).

The following structure is proposed for FeCr assuming it has the same occupancy of interstices as the β-phases:

$$\left|Fe^{8+}(d^6),\ Cr^{6+}(d^4),\ (\bar{e}_2),\ 2\bar{e}\right|_{oct}$$

Using the model, the unsymmetrical distribution of $\bar{e}$ and $(\bar{e})_2$ leads to 2 unpaired electrons on Fe and paired electrons on Cr. The data of Shull and Wilkenson[8] show a moment of 2 μ_B on Fe and no moment on Cr for the 50% alloy of Cr and Fe. The proposed structure for FeCr has fewer itinerant electrons (lower total ion core charges) than TiFe or VFe and weaker binding is expected. This agrees with the absence of lattice contraction[3] in FeCr.

There is a preponderence of intermetallic phases containing metal ion cores with d-electrons (*e.g.* Cu, Ag, Zn, Cd, *etc.*). This has been discussed by Nevitt[3] for β-phases. He suggests a special affinity for β-phase formation by the combination Group IV (*e.g.* Ti) and the Fe group and by Sc and the Cu, Zn group. There are two differences in the ion cores which contain d-electrons which may be responsible for stability of intermetallic phases with d-shell metals. One is the presence of d-electrons which can add to the binding strength. These d-electrons will be directed spatially in regions not occupied by interstitial electrons. The other difference is that d-shells are more easily deformed by positive fields of other ion cores and are more penetrable by itinerant electrons. This makes it possible for them to adapt to structures with another metal ion core and give greater homogeneity of interstices.

β-Manganese Phases

The β-Manganese type of compound has the same electron/atom concentration as the β-phases just discussed and will be included here for comparison. The crystal structure of β-Mn phases is a complex cubic type (tetragonal) with 20 atoms per unit cell. There are relatively few intermetallic compounds of this type which are also referred to as μ-phases.[4] These phases do not form superlattices. The interstitial-electron structures are given in Table 1.

Examination of the β-Mn structure indicates that interstices are approximately as in a face-centered cubic lattice, *i.e.* an oct edge interstice surrounded by 4 face and 2 corner ion cores and a central oct interstice surrounded by 6 face-centered ion cores. This is the basis for the interstices given in Table 1 and occupancy of a preferred 3/4 of the oct interstices (and the equivalent number of tet interstices) is the key to the 3/2 electron to atom ratio.

The interstitial-electron structure for Cu_5Si has three types of interstices. The stoichiometry requires that there is a 2/1 ratio of Cu/Si as corner atoms in the CCP scheme applied to interstices. In this case it is assumed that occupancy of 2 types of oct interstices is preferred to $\bar{e}$ pairing in tet. This provides an explanation for the difference in composition[4] for Cu_5Si as compared to Ag_3Al and $CoZn_3$.

It appears that $CoZn_3$ fits into the series by having additional $\bar{e}$ in tet interstices when the homogeneous oct interstices are occupied. The interstitial-electron structure proposed for $CoZn_3$ is

$$\left|Co^{9+}(d^7),\ 3Zn^{2+},\ 3\bar{e}_{oct},\ 3\bar{e},\ \bar{e}_{2tet}\right|\ \beta\text{-Mn}$$

The degeneracy of d-orbitals for a corner cobalt ion core is as follows (where d-orbital axes are in coincidence with lattice axes):

$$\underset{z^2}{\uparrow} \qquad \underset{x^2-y^2}{\overline{}} \qquad \text{(to edges, } \bar{e} \text{ in oct)}$$

$$\underset{xy}{\uparrow\downarrow} \qquad \underset{xz}{\uparrow\downarrow} \qquad \underset{yz}{\uparrow\downarrow} \qquad \text{(to Zn)}$$

This gives a magnetic moment on Co of 1 unpaired $\bar{e}$ which is directed to oct $\bar{e}$. This makes the additional $\bar{e}$ in tet interstices a reasonable structure for balancing $\bar{e}$ distribution. The $CoZn_3$ (β-Mn phase) has been observed to be ferromagnetic by Koster and Schmidt.[9] The structure for $CoZn_3$ is a further demonstration of the limited nature of the electron concentration/atom approach which requires Group VIII metals to be zero valent to fit the ratios.

The structure for β-Mn was given in Part IV[7] as $|8Mn^{3+}, 12Mn^{+}, 36e|\beta$-Mn. This fits the present scheme with 15 $\bar{e}$ in oct interstices, 15 $\bar{e}$ and 3 $\bar{e}_2$ in tet interstices. This fits the paramagnetism observed (assume the d^4 and d^6 ion cores have d-electrons paired), and the

Table 1. Interstitial-electron structures for β-manganses phases[a]

Intermetallic compound	Composition range electrons/atom	Oct interstices	Tet interstices	Electron/atom ratio
Ag_3Al,[b] $(Ag_3^+Al^{3+})$	~1.4	$3(Ag_4Al_2)$, $1(Ag_2)$ $3\bar{e}\uparrow$	$8(Ag_3Al)$ $3\bar{e}\downarrow$	3/2
$2Cu_5Si$, $2(Cu_5^+Si^{4+})$	~1.5	$6(Cu_4Si_2)$, $3(Cu_5Si)$, $3(Cu_6)$ $6\bar{e}\uparrow$ $3\bar{e}\uparrow$	$16(Cu_3Si)$, $8(Cu_4)$ $9\bar{e}\downarrow$	3/2
$CoZn_3$, $(Co^{2+}Zn^{2+})$	~1.4	$3(Co_2Zn_4)$, $1(Zn_6)$ $3\bar{e}\uparrow$	$8(CoZn_3)$ $3\bar{e}\downarrow$, $\bar{e}_2$	2

a) See text concerning interstices occupied. b) Also Au_3Al.

8) C.G. Shull and M.K. Wilkenson, *Phys. Rev.*, **97**, 304 (1955).

9) W. Koster and H. Schmidt, *Z. Metallk.*, **46**, 468 (1955).

localization of e_2 in tet accounts for the brittleness and hardness.

ε-Phases

The ε-phase for brass occurs at approximately 75 atomic % zinc, and the structure is written $CuZn_3$. ε-Phases have hexagonal close packing (HCP) with less than the normal ratio for c/a, and the metal ion cores are randomly arranged in HCP ε-phases. The lattice distortion of HCP gives the structure 4 oct and 4 bipyramidal interstices[6] per 4 ion cores ($CuZn_3$). For bipyr interstices to be completely occupied there must be only 1/2 occupancy of oct interstices because of the specific electron spin restrictions of the distorted HCP (see Part I).[6] The other restrictions on interstice occupancy, *e.g.* for $CuZn_3$, are (1) there is preferential occupancy of $CuZn_5$ oct interstices over $CuZn_4$ oct due to the difference in fields of the ion cores. (2) There is preferential occupancy of $CuZn_4$ bipyr over Cu_2Zn_3 bipyr which are in ratio of 3 $CuZn_4$ to 1 Cu_2Zn_3. In placing itinerant electrons in the interstices the maximum of 3 $\bar{e}$ are placed in $CuZn_4$ bipyr and the remaining 4 as $\bar{e}$ and $\bar{e}_2$ in $CuZn_5$ oct and $\bar{e}$ in $CuZn_4$. Thus, the electronic structure for $CuZn_3$, a typical example of the β-phase is:

$$\left|Cu^{+},\ 3Zn^{2+},\ \bar{e}_2,\ 2\bar{e}_{oct},\ 3\bar{e}_{bipyr}\right|_{HCP}$$

The unique requirements of the distorted HCP lattice explains the 7/4 e/a ratio of Hume-Rothery for most of the ε-phases, and the greater electron density in oct interstices is as expected for distortion of the HCP lattice in the non-axial direction (see Part II).[6] See Table 2.

Table 2. Interstitial-electron structures for ε-phases

Intermetallic compound	Electron/atom conc. range	Fractional occupancy of interstices		Electron/atom ratio
		bipyr.	Oct	
$CuZn_3$[a]	1.78—1.85	3/4	$1/2\bar{e}$, $1/4\bar{e}_2$	7/4
Cu_3Sn[b]	1.75	3/4	$1/2\bar{e}$, $1/4\bar{e}_2$	7/4
Ag_5Al_3[c]	1.54—1.86	3/4	$1/2\bar{e}$, $1/4\bar{e}_2$	7/4
$FeZn_7$	—	$5/8(\bar{e}_2)$	$3/4\bar{e}$	8/4
Sb_3Cu_{13}[d]	—	3/4	$1/2\bar{e}$, $1/4\bar{e}_2$	7/4

a) Also $CuBe_3$, $CuCd_3$, $AgZn_3$, $AgCd_3$, $AuZn_3$, $AuCd_3$.
b) Also Cu_3Ge, Ag_3Sn, Au_3Sn, Cu_3Si.
c) Also Au_5Al_3.
d) Also Sb_3Ag_{10}.

The interstitial-electron structure proposed for FeZn is (where bp=bipyramidal interstice)

$$\left|Fe^{8+}(d^6),\ 7Zn^{2+},\ 6\bar{e}_{oct},\ (5\bar{e}_2)_{bp}\right|_{HCP}$$

This stoichiometry $FeZn_7$ gives a ratio of $5(FeZn_4)$ and $3(Zn_5)$ bp interstices and a ratio of $6(FeZn_5)$ and $2(Zn_6)$ oct interstices. To place 16 $\bar{e}$ in conformity with lattice restrictions requires 5 $\bar{e}_2$ in B.P. and 6 $\bar{e}$ in oct. The degeneracy of d-orbitals on Fe in $FeZn_7$ is expected to be the same as for Ru metal in HCP (see Part IV),[7] and the six d-electrons are all paired. The Ag_5Al_3 ε-phase has a still different pattern of interstices, and Massalski[4] has not included it with the ideal ε-phases. A possible electron structure is

$$\left|5Ag^{+},\ 3Al^{3+},\ 2(\bar{e}_2),\ 4\bar{e}_{oct},\ 6\bar{e}_{bipyr}\right|_{HCP}$$

Here the bp interstices are in a ratio of $7Ag_3Al_2$ to one Ag_4Al and the oct interstice $6Ag_4Al_2$ to $1Ag_3Al_3$. A greater range of composition is expected since one more $\bar{e}$ can be accommodated in bp interstices. The Cu_3Sn phase fits the scheme for the other ε-phases if Cu is taken to have the stronger field in influencing preference within the bipyr interstices. This may be the case since the work function for Cu (4.4) is greater than that of Sn (4.2 eV).

None of the pairs of occupied interstices in ε-phases can be considered to be homogeneous, and there is relatively large localization of $\bar{e}$ in certain interstices proposed in the above structure so the movement of electrons from the occupied to vacant interstices will be more difficult than in pure metals. This restriction of electrons is reflected in the greater hardness and brittleness and relatively low electrical conductivity of ε-phases as compared to β-phases.

γ-Phases

As seen in Table 3 the compositions of γ-phases are rather complicated. These intermetallic compounds are exceptionally hard and brittle, and they have low electrical conductivity. They show a pronounced maximum in diamagnetic susceptibility over the small increases shown *e.g.* for brass by the β and ε phases.

A neutron diffraction study[10] has confirmed the structure of Cu_5Cd_8 and Cu_9Al_4, and the authors discussed the arrangement of ions in terms of inner and outer tetrahedral and octahedral positions in agreement with recent X-ray data[11] indicating a close-packed structure. The symmetry of Cu_9Al_4 is slightly different than that of the two other intermetallic phases. The γ-phase structure can also be discussed in terms of the small BCC units, and as in β-phases it is assumed that $\bar{e}$ will occupy the unsymmetrical octahedral interstices of these individual BCC unit cells. This can be done in a straight-forward manner even for these complex lattices if the true unit cell of 52 ions is broken up into individual AB unit cells with corner and body center ions assigned so as to give the correct over all composition.

For Cu_5Zn_8 (unit cell is $Cu_{20}Zn_{32}$) the structure can be divided into the following groups of BCC unit cells:

$$\left|8(Cu_7Zn_1,\ Zn_8),\ 1(Cu_5Zn_3,\ Zn_8),\ 1/2(Cu_2Zn_2,\ Zn_4)\right|$$

where for each group the first two atoms listed are the corner atoms and the last one the body center atoms. All of the face oct and edge oct interstices in these units can be listed and when grouped together they are:

face oct; $\underline{18(Cu_2Zn_4)}$, $24(Cu_4Zn_2)$ and $36(Cu_3Zn_3)$ total=78
edge oct; $\underline{42(Cu_2Zn_4)}$ and $36(CuZn_5)$ total=78

10) O. Heidenstam, A. Johansson, and S. Westman, *Acta Chem. Scand.*, **22**, 653 (1968).
11) W. B. Pearson, J. K. Brandon, R. K. McMillan, and R. Brizzard, *Acta Crystallogr.*, **A28**, 596 (1972).

Table 3. Electronic structure of γ-phases[e]

Compound	Unit cell groups	Face oct	Edge oct	Interstice occupancy[f]	
Cu_5Zn_8[a]	$8(Cu_7Zn_1, Zn_8)$	$\underline{18Cu_2Zn_4}$	$\underline{42Cu_2Zn_4}$	$18\bar{e}\uparrow$	$18\bar{e}\downarrow$
$(Cu_{20}Zn_{32})$	$1(Cu_5Zn_3, Zn_8)$	$24Cu_4Zn_2$	$36CuZn_5$		$24(\bar{e})_2$
	$1/4(Cu_4Zn_4, Zn_8)$	$36Cu_3Zn_3$			
Cu_9Al_4[b]	$3(Cu_3Al_5, Cu_8)$	$\underline{42Cu_4Al_2}$	$\underline{18Cu_4Al_2}$	$18\bar{e}\uparrow$	$18\bar{e}\downarrow$
$(Cu_{36}Al_{16})$	$1/4(Cu_4Al_4, Cu_8)$	$36Cu_3Al_3$	$60Cu_5Al$	$24(\bar{e})_2$	
$Li_{10}Pb_5$	$2(Li_5Pb_3, Li_8)$	$\underline{42Li_4Pb_2}$	$\underline{18Li_5Pb_2}$	$18\uparrow$	$18\downarrow$
$(Li_{40}Pb_{12})$	$1(Li_5Pb_3, Li_8)$	$24Li_5Pb$	$42Li_5Pb$	$24(\bar{e})_2$	$(4\bar{e}?)$
	$1/4(Li_4Pb_4, Li_8)$	$12Li_3Pb_3$	$18Li_6$		
$Cu_{31}Sn_8$[c]	$4(Cu_5Sn_3, Cu_8)$	$63Cu_4Sn_2$	$\underline{24Cu_4Sn_2}$	$24\uparrow$	$24\downarrow$
$(Cu_{62}Sn_{16})$	$3/8(Cu_4Sn_4, Cu_8)$	$48Cu_5Sn_1$	$42Cu_5Sn$	$39\bar{e}_2$	
	$1/2(Cu_3Sn_5, Cu_8)$	$6Cu_3Sn_3$	$3Cu_4$		
$Li_{10}Ag_3$	Assume 1/3 occupancy of oct interstices			$26\uparrow$	$26\downarrow$
$(Li_{40}Ag_{12})$					
Fe_5Zn_{21}[d]	$1(Zn_6Fe_2, Zn_8)$	$84Fe_2Zn_4$	$\underline{120FeZn_5}$		$48\bar{e}_2$
$(Fe_{20}Zn_{84})$	$4(Zn_5Fe_3, Zn_8)$	$\underline{72FeZn_5}$	$36Zn_6$	$72\bar{e}\uparrow$	$72\bar{e}\downarrow$
	$1\ 1/2(Zn_4Fe_4, Zn_8)$				

a) Also Cu_5Cd_8, Ag_5Zn_8, Ag_5Cd_8, Au_5Zn_8, Au_5Cd_8, and Au_5Hg_8.
b) Also Cu_9Ga_4, Cu_9In_4, and Ag_9Al_4.
c) Also $Ag_{31}Sn_8$ and $Na_{31}Pb_8$ (unit of $Cu_{62}Sn_{16}$ has 117 unit cells, 128 $\bar{e}$)
d) Also Ni_5Zn_{21}, Rh_5Zn_{21}, Pd_5Zn_{21}, Pt_5Zn_{21}, and Ni_5Cd_{21}. (Ternary systems are $Cu_7Zn_4Al_2$, Cu_6Zn_6Al, and $Cu_2Al_3Zn_2$.)
e) Underlined interstices assumed to be occupied by electrons.
f) Most frequent e/a ratio is 21/13. The exceptions are $Li_{10}Ag_{13}$ (13/13), $Li_{10}Pb_3$ (22/13) and Fe_5Zn_{21} (26/13).

The criteria for deciding electron occupancy will be (1) the greatest homogeneity of interstices, (2) the maximum field of ions and (3) the balancing of electron spins. These preferred interstices are underlined above and in Table 3. The following distribution of electrons places the maximum number of $\bar{e}$ in these two interstices with the additional interstices occupied by electron pairs (there is complete occupancy of the preferred interstices):

$\underline{18Cu_2Zn_4}$ (face oct), $18\bar{e}$ $\underline{42Cu_2Zn_4}$ (edge oct), $18\bar{e}$, $24(\bar{e})_2$

This assignment of the 84 $\bar{e}$ of $Cu_{20}^{+}Zn_{32}^{2+}$ gives a structural explanation of the 84/52 or 21/13 Hume-Rothery ratio for γ-phases. The localization of $\bar{e}$ in certain interstices and presence of a large number of electron pairs is in keeping with the extreme hardness and brittleness and the low electrical conductivity of γ-phases as well as their high diamagnetic susceptibility (reduction in paramagnetic susceptibility). (An alternate placement of $\bar{e}$ as 24 $\bar{e}$ in Cu_4Zn_2, 18 $\bar{e}$ in Cu_2Zn_4 face oct and 42 $\bar{e}$ in Cu_2Zn_4 edge oct is also a possibility but would not account for the unusual properties.)

Table 3 lists some other γ-phases and lists the interstices in the same way as illustrated above for Cu_5Zn_8. The interstice pattern accounts for the electron/atom ratio is all of the cases except $Li_{10}Ag_3$. Here it is considered that this compound is an exception due to the weak forces of the two metal ion cores. It has an electron to atom ratio of 13/13. A 1/3 occupancy of edge and face oct can explain the electron/atom ratio. It would appear that the similarity to other γ-phases is coincidental for $Li_{10}Ag_3$.

The structure for $Li_{10}Pb_3$ suggests similarity to other γ-phases, but the Hume-Rothery e/a ratio is 22/13. The structure given in Table 4 requires placement of 4 additional electrons (out of 88). It may be that the stoichiometry $Li_{10}Pb_3$ is not exact, or it may be that the large difference in ion cores leads to occupancy of more than one type of interstice.

The compound Fe_5Zn_{21} is also included in the same interstice scheme as the majority of γ-phases with an ion core of $Fe^{8+}(d^4)$. This leads to no unpaired electrons on the iron since the degeneracy of d-orbitals is the same as for β-phases. As given in Table 3 the preferred interstices for Fe_5Zn_{21}, are 8 $\bar{e}$ (out of 248) short of being completely occupied. This can reflect the extension of $\bar{e}$ in d-orbitals into interstices and a small stoichiometry change would be indicated. Another possibility is that interstices surrounded only by Zn are preferred by itinerant electrons because of absence of d-electrons directed into these interstices.

The small Hall Coefficient[4] for γ-phases can be explained by the presence of both $\bar{e}_2$ and vacancies in the structure. In cases like this electric current can be carried both by dissociation of $\bar{e}_2$ and by $\bar{e}$ movement through interstices. The strong interstice preference in γ-phases with resultant presence of many $(\bar{e})_2$ leads to a polarity in the structure; regions of vacant interstices have a net positive charge and regions with $(e)_2$ a net negative charge.

Laves Phases

A special group of intermetallic compounds which is composed of metal ions of different sizes and which have more exact compositions than the intermetallic phases considered above are the Laves phases. These compounds are all close-packed structures and include both binary (AB_2) and ternary (A, BC) compounds. As an example of structure, $MgCu_2$ has cubic close packing, and the two metal ions form two interpenetrating lattices; Mg^{2+} is surrounded by 12 Cu^{+} and Cu^{+} by 6 Mg^{2+}. A few Laves phases are listed in Table 4 with proposed interstitial electron structure.

TABLE 4. INTERSTITIAL-ELECTRON STRUCTURES FOR LAVES PHASES

	Compound (AB_2)	Occupancy of interstices[b]		
		Tetrahedral		Octahedral
		($4AB_3$)	($2A_2B_2$)	$3(A_2B_4)$
Type 1 (CCP)	$MgCu_2$	—	$2\bar{e}\uparrow$	$2\bar{e}\downarrow$
	$AgBe_2$	$2\ 1/2\bar{e}\uparrow$	—	$2\ 1/2\bar{e}\downarrow$
	$NaAu_2$	—	$1\ 1/2\bar{e}\uparrow$	$1\ 1/2\bar{e}\downarrow$
	Mg(NiZn)	$3\bar{e}\uparrow$	—	$3\bar{e}\downarrow$
	KBi_2	$\uparrow 3\bar{e}, 1/2\bar{e}_2$	—	$3\bar{e}\downarrow$
	ZrW_2	$\uparrow 3\bar{e}$	—	$3\bar{e}\downarrow$
	$ZrZn_2$[a]	$\uparrow 3\bar{e}$, $(\bar{e})_2$ or $(\bar{e})$?		$3\bar{e}\downarrow$
Type 2 (HCP)	$MgZn_2$	$3\bar{e}\uparrow$	—	$3\bar{e}\downarrow$
	$CaMg_2$	$3\bar{e}\uparrow$	—	$3\bar{e}\downarrow$
	Ca(AgAl)	$3\bar{e}\uparrow$	—	$3\bar{e}\downarrow$
	$TiFe_2$	$\uparrow 3\bar{e}, \bar{e}_2$	—	$3\bar{e}\downarrow$
Type 3	$MgNi_2$	$3\bar{e}\uparrow$	—	$3\bar{e}\downarrow$
	Mg(CuAl)	$3\bar{e}\uparrow$	—	$3\bar{e}\downarrow$
	$TiCo_2$	$\uparrow 3\bar{e}, \bar{e}_2$	—	$3\bar{e}\downarrow$
	$ScFe_2$	$\uparrow 3\bar{e}, 1/2\bar{e}_2$	—	$3\bar{e}\downarrow$
	$ThMg_2$	$\uparrow 3\bar{e}, \bar{e}_2$	—	$3\bar{e}\downarrow$
	$NbZn_2$	$\uparrow 3\bar{e}, 1/2\bar{e}_2$	—	$3\bar{e}\downarrow$

a) Ferromagnetic Laves Phase (S. J. Pickart, H. A. Alperin, G. Shirane, and R. Nathans, *Phys. Rev. Lett.*, **12**, 444 (1964)).
b) Fractions used for a single unit cell.

Close-packed structures of the type AB_2 have octahedral interstices (A_2B_4 neighbors) which are all identical, but the tetrahedral interstices are of two types (AB_3 and A_2B_2 neighbors). It appears most likely that the electrons will occupy octahedral interstices and those tetrahedral interstices with highest + fields. When ion core A has the highest+field, the tet interstice A_2B_2 is occupied; when ion core B has the highest+ field, interstice AB_3 is occupied. This is done for the compounds in Table 4. These compounds cover a wide range of electron/atom ratios (given by Nevitt[3]). The compounds which have more electrons than the number which fill the preferred octahedral and tetrahedral interstices with single $\bar{e}$ are those with ions having unfilled d-shells. This is a classification pointed out by Raynor,[12] and these compounds also show considerable lattice contraction upon formation. The proposed structures for these latter compounds have $\bar{e}_2$ in tet interstices.

The Laves phase KBi_2 represents an exceptional compound. It has a melting point of 553°C, and there is a very large lattice contraction upon formation of KBi_2. Since Bi metal does not have a close-packed structure and may have electron pairs within the layer of bismuth ions[6] there may be a greater change in pattern of $\bar{e}$ in interstices of KBi_2 than in formation of other Laves phases. The structure as given in Table 4 assumes an ion core of Bi^{3+} for Bismuth and does have $\bar{e}_2$ in the tet interstice.

When a transition metal with localized d-electrons is present there is interaction between the ($\bar{e}$) of the interstices and the localized d-electrons. This could explain the non-existence of $TiNi_2$ whereas $TiFe_2$ and $TiCo_2$ both form. This probably comes about because the degeneracy of d-orbitals in the HCP lattice (see Part IV) directs d-electrons toward tet interstices for Fe(d^6) and Co(d^6) but to both oct and tet for Ni(d^8).

The interstitial-model indicates that the key to the $\bar{e}$ distribution in Laves phases is the change in occupancy of A_2B_2 tet interstices as there is a change from B to A as the ion core with highest+field. Lattice contractions appear to be associated with $(\bar{e})_2$ in the structure. It is of interest that the Laves phase $ZrZn_2$ exhibits itinerant ferromagnetism. As indicated in Table 4 this could come about if an unpaired $\bar{e}$ went into the A_2B_2 tet interstice instead of $\bar{e}_2$ in AB_3. Pairing of $\bar{e}$ is observed for Laves phases with d-electrons localized on ion cores and for KBi_2, $ThMg_2$, and $NbZn_2$ and may not occur in the case of $ZrZn_2$.

Miscellaneous Alloy Phases

The Na–Pb System is of interest because there are maxima in the phase diagram, but $Na_{31}Pb_8$ (a γ-phase) appears to be the only definite intermetallic compound. The special stability for certain compositions can be accounted for on the basis of the interstitial-electron model in the following way. The Na–Pb system forms a CCP lattice ($AuCu_3$ structure) with Na in corner positions and with a small portion of the Pb face center ions replaced by Na. The ideal phase $NaPb_3$ would have 13 $\bar{e}$ to be distributed among 4 oct and 8 tet interstices and is not observed. The phase maximum at Na_2Pb_5 represents replacement of 1Pb out of 18 (5.5%) by Na. Such a structure of 7 ion cores would have 7 oct and 14 tet interstices (11 of which are homogeneous with oct). Occupancy of oct by $7\bar{e}(\uparrow)$ and tet by $7\bar{e}(\downarrow)$ and $4(\bar{e})_2$ gives complete occupancy of preferred interstices. Greater % of Na leads to insufficient $\bar{e}$ to occupy all preferred interstices for an $AuCu_3$ structure. It appears that there is a stability for Na_2Pb_5 based on interstice occupancy which is similar to other intermetallic phases, but the small fraction of (or random nature of) face-centered Pb replaced by Na is insufficient to lead to a definite compound.

Discussion

The Interstitial-Electron Model gives reasonable structures for the wide variety of alloy phases and accounts for the existence and stability of intermetallic phases in the following way. A combination of 2 or more metal ion cores can achieve stability and metallic properties when a given structure provides an appropriate number of homogeneous interstices for the number of itinerant electrons available. A given structure will have an optimum number of interstices and variations in this optimum are expected with variations in core charge and ion core size. In this way the model incorporates the Hume-Rothery *e/a* ratio as a special case, and makes it possible to include discussion of the effect of d-electrons, of lattice contraction and changes in many properties in the framework of a comprehensive model for metals and alloys.

12) G. V. Raynor, "Physical Chemistry of Metallic Solutions and Intermetallic Compounds, Symposium," Vol. 1, Chemical Publishing Co., New York (1960).

The focussing on electrons in interstices gives insight into the variation in properties of an intermetallic compound in cases where electron concentration or radius-ratio failed to account for changes in properties. An example given by Nowotny *et al.*[13] is $LaNi_2$, a Laves phase which shows a strong lattice contraction. Nowotny suggests the polarity of La^+Ni^- but points out that Pauling assumed the opposite polarity on the basis of his interatomic distance relationships. The polarity arising in the Interstitial-Electron Model requires neither of these extremes. As pointed out for γ-phases for structures with strong preference for $\bar{e}$ occupancy of certain interstices, there will be interstitial regions with net + charge and others of net − charge. Lattice contractions to compensate for this lead to more uniform charge distribution.

13) H. Nowotny, F. Holub, and A. Wittmann, *ibid.*, Vol. 1.

BULLETIN OF THE CHEMICAL SOCIETY OF JAPAN, VOL. 46, 1935—1940 (1973)

An Interstitial-Electron Model for the Structure of Metals and Alloys. VI. Interpretation of Superconductivity

Oliver JOHNSON*

Research Institute for Catalysis, Hokkaido University, Sapporo 060

(Received September 17, 1971)

A physical interpretation of the superconducting state based on the interstitial-electron model for metals is given within the framework of the BCS theory. The following conditions for itinerant electrons ($\bar{e}$) and metal ion cores (M^{n+}) are postulated as necessary for superconductivity: (1) There must be a matching of $\bar{e}$ energies (velocity) and binding strength of M^{n+} so $\bar{e}$ initiation of a lattice vibration is possible. (2) Movement of $\bar{e}$ and M^{n+} must be synchronized so there is enhancement of $\bar{e}$-phonon coupling. (3) There must be $\bar{e}$ of one spin available to enter such $\bar{e}$-phonon "chains". The model leads to $\bar{e}$ of opposite spin in phonon chains 500—5000 Å apart. It gives physical interpretations of the thermodynamic properties of superconductors and clearly shows that type of lattice influences superconductivity. It shows the basis for the new correlation observed between superconductivity and a positive Hall Coefficient. Since the model can incorporate the presence of anions as well as $\bar{e}$, it provides a related explanation for superconductivity in non-metals.

The phenomenon of superconductivity has been known since 1911[1] and major efforts have been expended to discover superconducting materials with the highest possible T_c. The range of T_c for materials now known is from a fraction of a degree K to the region of 20K. The major advances have been achieved by Matthias and coworkers[2] whose experiments were based on very careful considerations of the periodic relationships involved. There are several different types of superconductors, and the BCS theory[3] does not explain all of them.[4] It was therefore of great interest to see what additional information and insight the interstitial-electron model[5] might offer for the understanding of superconductivity. It was anticipated that the spatial location of electrons as well as the inherently chemical approach would supplement the correlations of Matthias.[2,4]

Theoretical discussions on superconductivity have emphasized that it is a quantum phenomenon not to be understood on a classical basis. The interpretation presented in this paper is largely in classical terms, but the interstitial-electron model does incorporate all of the essential elements of quantum chemistry and indicates how a microscopic quantum state arises. This is possible because the model introduces spin correlation of electrons in its fundamental postulate of localization of $\bar{e}$ density in interstitial positions (or binding regions).[5] If this approximation of $\bar{e}$ density is reasonably accurate it should lead to the same interpretations of metal properties as the approximations of band theory using wave mechanical calculations involving overlap and exchange terms for atomic wave functions. The viewpoint in this paper follows from the ideas of Föhlich,[6] London[7] Pippard,[8] and Matthias[4] and it contains the essential energy gap[9] of the BCS theory.[3]

Description of the Superconducting State

The basis idea of an electron-phonon interaction,[6] which was incorporated into the BCS theory,[3] will be

* Present address: Institute of Physics, Uppsala University, Uppsala, Sweden.

1) H. K. Onnes, *Leiden. Commun*, **1201**, 1226 (1911).

2) B. T. Matthias, T. H. Geballe, and V. B. Compton, *Rev. Mod. Phys.*, **35**, 1 (1963).

3) J. Bardeen, L. N. Cooper, and J. R. Schrieffer, *Phys. Rev.*, **108**, 1175 (1957).

4) B. T. Matthias, "Superconductivity," Vol. I, ed. by P. R. Wallace, Gordon and Breach, Sc. Pub., New York (1969).

5) O. Johnson, This Bulletin, **45**, 1599, 1607 (1972); *ibid.*, **46**, 1923 (1973).

6) H. Fröhlich, Reports on Prog. in Physics, XXIV, 1 (1961).

7) F. London, "Superfluids," Vol. I, Wiley, New York (1950).

8) A. B. Pippard, *Prov. Roy. Soc. Ser. A*, **216**, 547 (1953).

9) R. A. Smith, "Wave Mechanics of Crystalline Solids," Chapman and Hall, Ltd., London (1969).

used in the physical picture for superconductivity according to the Interstitial-Electron Model. The treatment of metal properties in Parts I—V of this series of papers emphasized an instantaneous picture of a small degree of localization of electron density as "electrons-in-interstices". The Hellmann-Feynman Theorem was used to justify the electrostatic treatment of the quantum-mechanical electron distribution, and the interstitial electrons were pictured as moving between octahedral (oct) and tetrahedral (tet) binding regions separated by a triangle of 3 M^{n+} (positive ion cores). To treat the phenomenon of superconductivity the dynamic movement of electrons and ion cores must be included. In the normal metal, dynamic movement of $\bar{e}$ throughout the lattice is seen as part of a continuous reestablishment of equilibrium as $\bar{e}$ move to new positions in response to lattice vibrations. All of the properties of $\bar{e}$, including interstice preference and spin correlation are postulated to persist in the dynamic picture.

The concept of an electron initiating a lattice vibration[3,6] is used in qualitative discussions of superconductivity, but the details have not been explored beyond the postulate that upon movement of 2 M^{n+} closer together a second electron will be attracted to this region. At the critical temperature for superconductivity (T_c) the conditions must be such that electron motion can influence lattice vibrations. The Interstitial-Electron Model requires that the following conditions be fulfilled for superconductivity:

(1) There must be a matching of energy of electrons (velocity) and binding strength of M^{n+} for initiation of lattice vibrations. Taking a fixed electron velocity at T_c, when the amplitude of lattice vibrations is larger than optimum (low binding strength of M^{n+}) the lattice will not be significantly modified by motions of $\bar{e}$ in the vicinity of M^{n+}; when the amplitude is smaller than optimum (high binding strength), lattice vibrations cannot be initiated.

(2) The movement of $\bar{e}$ and M^{n+} must be synchronized so an $\bar{e}$ passes between $2M^{n+}$ at the precise time to give enhancement of lattice vibration. This condition includes the requirement of availability of a sufficient number of $\bar{e}$ at such critical positions and thus has a geometric component. This condition also implies that electrons not involved in the superconduction process do not scatter the phonons. This condition is in keeping with the treatment of superconductivity as a many body problem.[6]

(3) There must be a sufficient number of electrons of 1 spin in the above positions to sustain an electron-phonon chain. The detailed way in which these conditions lead to superconductivity can best be described by the interpretation of the persistent current and diamagnetism of the superconducting state.

The existence of the *persistent current* is the most spectacular consequence of the postulated electron-phonon coupling. The situation before application of an electric field is that there is relatively small amplitude of lattice vibration and random movement of $\bar{e}$. When electrons are set into motion by the electric field they will move from oct to tet between 2 (or 3) ion cores. Under conditions favorable for superconductivity the $\bar{e}$ will attract the ion cores toward each other and initiate or enhance a lattice vibration at that point. The initial moving electron, now moving faster than thermal velocity, continues on its path while a second electron is attracted to the region where the ion cores have moved even closer together. Thus, there is a phonon induced by the electron movement, and it has been proposed above that each phonon involves electrons of one spin type. This follows from the association of electron spin with an interstice type in the interstitial-electron model.[5] Thus, the second electron moving into the interstice vacated by the first moving electron must have the same spin. The same is true of subsequent electrons which are attracted. Along with the phonon, then, there is a group of $\bar{e}$ of the same spin moving through the lattice, and this has been termed an $\bar{e}$-phonon chain.

When the lattice vibration induced by the first moving electron is at minimum displacement (1/2 way through the vibration cycle), it will begin to move closer to metal ion cores in the adjoining layer in the lattice and thus attract an electron there, this time an electron of the opposite spin since it involves an adjoining interstice separated by an ion core. A new phonon chain is induced by the movement of electrons of spin opposite to the initial phonon chain and follows it by 1/2 of a vibration cycle, and a second group of $\bar{e}$ of opposite spin move in the same direction as the first group. If the vibration frequency induced is 10^{13} sec^{-1}, and the velocity of the electrons 10^8 cm/sec, the spacing of the two groups of $\bar{e}$ will be about 500 Å. For electrons of 10^9 cm/sec, the distance between these groups of $\bar{e}$ of opposite spin would be 5000 Å. These electron groups of opposite spins, in a sense bound together by induced phonons, are the counterpart to "Cooper Pairs" in the interstitial-electron model. It is easily seen that in a lattice like those of metals there is mutual reinforcement of all the phonons and consequently a persistent current in the superconducting state. It is also obvious that a metal surface as well as interstice vacancies or impurities will modify this effect, and this will be discussed in the next section. The range of distances of Cooper Pairs would represent a minimum since the lattice vibration in the adjoining layer may not always initiate a phonon.

Since lattice vibrations are a sensitive function of temperature it is reasonable that at a sufficiently low temperature (T_c for superconductivity), the optimum conditions for initiation of a phonon by an $\bar{e}$ would be reached. At T_c it becomes energetically more favorable for $\bar{e}$ of one spin to move in groups through the lattice as parts of a phonon chain than for $\bar{e}$ to move *via* the normal means of consecutive occupancy of vacant lattice interstices (energy gap). Since the new path has zero resistance there is a sharp drop in resistance over a small temperature interval as the electron transport shifts more and more to the new pathway.

The postulated $\bar{e}$-phonon chains with alternating spins associated with the moving itinerant electrons in a superconductor means that the superconducting metal

will exhibit *perfect diamagnetism* (Meissner Effect[10]). The interstitial-electron model gives a picture of the superconducting metal as a giant diamagnetic molecule which is a macroscopic manifestation[11] of the quantization of electrons (Pauli Principle). The diamagnetism of a superconductor is probable its most important property.

Properties of the Superconducting State

The model leads to a unique interpretation of the influence of crystal lattice on superconductivity and also to a new correlation with positive Hall Coefficient. These will be presented in detail, and then some major properties of the superconducting state will be briefly listed and commented on.

It has been observed that with few exceptions *superconducting metals have positive Hall Coefficients*. This appears to be an important correlation which has not been reported previously (See Paper III in Series). The interstitial-electron model for metals has interpreted a positive Hall Coefficient as indicative of electron pairs in the interstices of the metal in question. The presence of electron pairs goes along with high occupancy of interstices, large field of the metal ion core and fewer spin restrictions to the arrangement of electrons, all properties which favor the transition to a superconducting state. A small Hall Coefficient indicates nearly equal numbers of $\bar{e}$ and $\bar{e}_2$ in the interstices of the metal lattice, and metals with small Hall Coefficients are also expected to be potential superconductors. Another possibility is that the remaining $\bar{e}$ in the structure are more restricted (less phonon scattering) by the surrounding $(e)_2$ than in metals without these electron pairs. The $(e)_2$ also provide a source of $\bar{e}$ for the phonon interaction. Somewhat the same restriction may obtain in superconducting compounds such as NbN or MoC. The C^{4-} and N^{3-} anions in the structure restrict the movement of $\bar{e}$ which are present in the metallic structure and at the same time provide a source of additional $\bar{e}$ to propagate the phonon (*via* dissociation of electrons from the relatively unstable anion). The absence of a Hall Effect in the superconducting state provides confirmation of the proposed mechanism of superconductivity. A movement of chains of electrons of alternating spin with $\bar{e}_2$ as a major source of these electrons would not be affected by a magnetic field.

The type of crystal lattice is also expected to influence

Properties of Superconductor (S) Compared to Normal Metal (M)	Comments
1) There is an energy gap of approximately $3.5\,kT_c$ between S and M.	The $\bar{e}$-phonon chains give a pathway of lower potential energy; $\bar{e}$ kinetic energy may be higher.[12]
2) S has lower thermal conductivity than M.	Lattice vibrations are enhanced in S; this scatters $\bar{e}$ and there is lower dissipation of thermal energy.
3) At T_c, the electronic heat capacity (ν) increases for S.	In S, electrons require greater energy for excitation and more electrons are available. (See Text, Sect IV)
4) Penetration Depth for S is observed to be approximately 500 Å.	The 10—30% greater amplitude of lattice vibrations at the surface can disrupt phonon chains; proposed reinforcement at 1/2 of a vibration will be out of phase, effect is expected to extend at least 500 Å below the surface.
5) Coherence length (ε) of Pippard[8] (or correlation distance of BCS Theory) has been calculated[13] from the relation, $\varepsilon = 0.18\hbar V_f/kT_c$ to be (in Å) 830 for Pb, 2300 for Sn, 3800 for Nb, 7600 for Cd and 16000 for Al.	This is the spatial definition of the superconducting electron and is proposed to be in the range 500—5000 Å by the model. Gradation appears consistent with frequency of vibration expected for different M^{n+}.
6) For non-transition metals $T_c \propto m^{-1/2}$. For transition metals, no mass dependence or small dependence.	This isotope effect was the first demonstration of a relation between lattice vibration (frequency $\propto m^{-1/2}$) and S. Model suggests interaction of $\bar{e}$ and localized d-electrons in transition metals may provide a source of $\bar{e}$ of 1 spin and thus a modified mechanism of S.
7) Ferromagnetic or anti-ferromagnetic materials are not S.	The allignment of $\bar{e}$ with spin of d-electrons localized on ion cores interferes with $\bar{e}$-phonon chains.
8) S can be quenched by passing a critical transport current (Silsbee effect).	The greater number of moving $\bar{e}$ can disrupt $\bar{e}$-phonon chains.

10) W. Meissner and R. Ochenfeld, *Naturwissenschaften*, **21**, 787 (1933).
11) J. E. Mercereau, "Superconductivity", Vol. I, ed. by R. D. Parks, Marcel Dekker, Inc., New York (1966), Chap. 8, p. 174.
12) R. J. Weiss, "Solid State Physics for Metallurgists," Pergammon, Oxford (1963).
13) Ref. 11, Chap. 3, Vol. I by R. Meservey and B. B. Schwartz.

the possibility of superconductivity both by its determining influence on phonon paths but also by its indirect affect on localization of electrons in interstices. The cubic close-packed lattice (CCP) is expected to offer favorable pathways for $\bar{e}$ of one spin through the lattice because it has the largest number of interconnected oct and tet interstices. Of the various hexagonal close-packed lattices (HCP), the La structure (ABACAB arrangement of layers) is more favorable than normal HCP or HCP with c/a greater than 1.632. The HCP structure with c/a less than 1.632 is less favorable because with bipyramidal interstices occupied by $\bar{e}$ the oct interstices can be only 1/2 occupied with $\bar{e}$. This restriction is removed, however, when $\bar{e}_2$ occupy these interstices. The details of the symmetry of interstices was given in paper I.[5] In the BCC structure the $\bar{e}$ are well dispersed in interlocking tet rings and would be favorable for superconductivity only for high occupancy of interstices. Tendency for superconductivity is expected to decrease in the order CCP>HCP-(La)>HCP($c/a \geq 1.632$)>HCP($c/a < 1.632$)>BCC.

TABLE 1. SUPERCONDUCTING TRANSITION TEMPERATURE AND LATTICE TYPE

CCP	HCP (La)	HCP ($c/a>1.632$)		HCP ($c/a<1.632$)	BCC	
La 6.3	La 4.9	Ti 0.4	Zn 0.9	Be 8.0	V	5.0
Al 1.2		Zr 0.6	Cd 0.5	(as thin film	Nb	9.1
Ir 0.14		Hf 0.2		only)	Ta	4.5
Pb 7.2		Tc 9.3	Tl 2.4		Mo	0.9
Th 1.4		Re 1.7			W	0.9
		Ru 0.5				
		Os 0.65				

Several examples with values for T_c (in K) are tabulated below. In general these expectations agree with the observations of Matthias[2,4] as far as frequency of superconductors of various lattice types. Superconductors with high T_c values do occur for all types of metal lattices. It is the frequency of occurrence of superconductivity in many alloy systems and compounds which is the criterion for the gradations with lattice type. Matthias[4] mentions that the β-tungsten structure is particularly favorable and that it has strings of transition metal ions which do not intersect. This observation is in keeping with the postulation of phonon chains as one of the requirements of superconductivity.

Correlation of Physical Properties with T_c

The three interrelated conditions postulated for superconductivity in a metal can be best related to the transition temperature (T_c) through well-known metal properties. The onset of superconductivity must represent a very delicate balance of electron energies since the lowering of energy in the superconducting state is very small.

Electron velocity can be estimated from band width (X-ray spectra), but the data is sometimes controversial. *Lattice energy* will also reflect electron velocity, and Fig. 1 shows that there is a rough correlation of T_c and lattice energy. Lattice energy should be a good correlating parameter since it is a measure of $\bar{e}$-lattice interaction. The deviations in Fig. 1 may indicate some optimum favorable lattice energy.

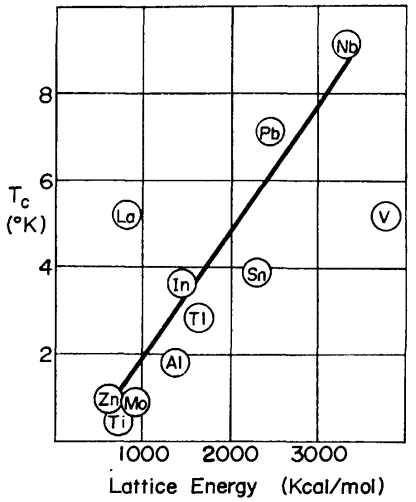

Fig. 1. Dependence of T_c on lattice energy of metal.

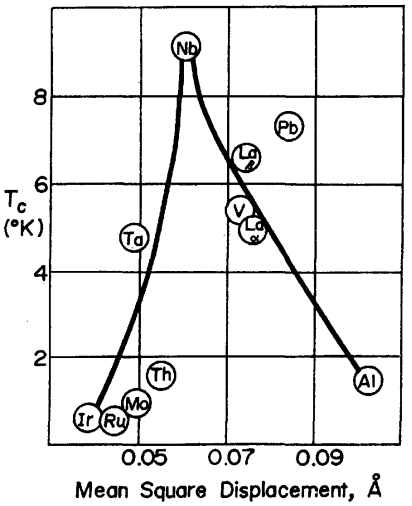

Fig. 2. Dependence of T_c on lattice displacement in thermal vibration.

Lattice displacement is directly related to ion core repulsion, and there is expected an increase in T_c as lattice displacement decreases followed by a decrease in T_c for ion core repulsions beyond the optimum for superconductivity. The data in Fig. 2 can be interpreted as showing such an optimum. The optimum may well be different for ion cores with completed d-shells. The relations in Fig. 2 show that T_c is inversely proportional to lattice displacement above values of 0.06 and directly proportional to $\sqrt{\bar{u}_0^2}$ for values below 0.06. The optimum may be 0.08 for d^{10} metals. In connection with the suggested optimum in Hall Coefficient it should be mentioned that although $\bar{e}_2$ are proposed to exist in the lattices of all superconducting metals, these $\bar{e}_2$ are not the "Cooper pairs" referred to above. The unusual gradation of T_c for group V metals (Nb>V≥Ta), not previously explained, appears to be due to an optimum lattice

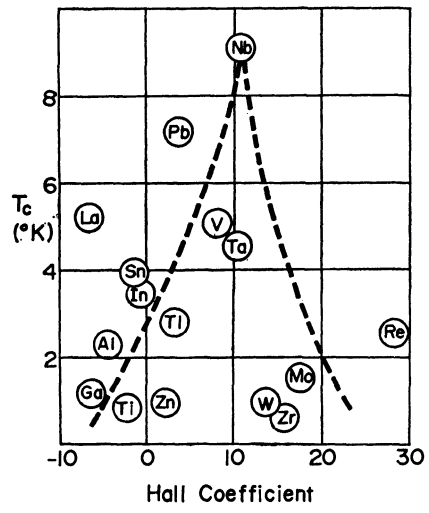

Fig. 3. Suggested dependence of T_c on Hall coefficient.

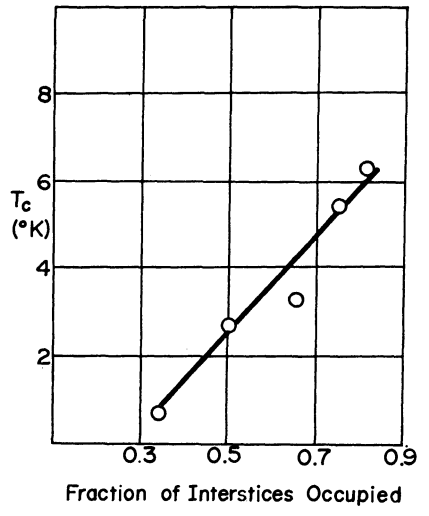

Fig. 4. Dependence of T_c on occupancy of metal interstices (average values)

displacement for Nb, less than optimum for Ta and more than optimum for V. The high T_c observed for La (as seen in Figs. 1 and 3) is due to the high favorability for superconductivity of the La-type packing in the lattice according to the interstitial-electron model.

The correlation with electron occupancy is shown in Fig. 4 and is based on values of electron occupancy of interstices given in Part II.[5] This appears to be a good correlation as expected. The largest deviations from the average line in Fig. 3 are for metals where other factors have a strong effect, *e.g.* for Pb (T_c= 7.2) and Ti, Zr, and Hf (0.2—0.6K) with 2/3 occupancy of interstices and for La (T_c=6.3) and Ir (0.14) both with 1/2 occupancy of interstices. The correlation with *Hall Coefficient* is shown in Fig. 3, where a maximum is suggested. This is a rough correlation and is given for illustration purposes. The interstitial-electron model clarifies the partial relation between *electronic heat capacity* (γ) and T_c. Qualitatively T_c and γ correlate[14] for M^{4+} to M^{6+} metals. There are opposite trends for M^{3+} (Sc, Y, and La) and for M^{7+}-M^{10+} ion cores. The lack of correlation for M^{3+} results from special $\bar{e}$ distribution due to lattice distortion in these metals (see Part II).[5] In groups 7 and 8 the localized d-electrons influence γ and no correlation with T_c is expected. These conclusions are related to the findings of Ishikawa and Totts[15] that a superconducting electron-phonon interaction parameter has a different behavior for d^{10} metals and transition metals. These authors use a correlation of T_c with a parameter combining γ and θ_D (Debye temperature).

The correlations given above offer a means of relating metal properties to the onset of superconductivity. It may be possible as well to relate these factors to superconductivity in non-metal materials. Factors which are more specific are the effects of type of lattice (sect. III) and effect of d-electrons localized on the ion core. Partially filled d-shells may lead to an interference with superconductivity due to asymmetry of ion core fields. For the ion cores with completed d-shells (Zn, Cd, Ga, In, Tl, Sn, Pb) the high positive field which results from the poor screening by d-electrons increases the chances of superconductivity. The greater $\bar{e}$ penetrability of the d^{10} ion cores also increases the chances of e-phonon interaction. Matthias[4] has pointed out the greater ease of preparing this group of superconductors.

Discussion

The interstitial-electron model for metals gives a detailed interpretation of the superconducting state as based on phonons induced by $\bar{e}$, very much as the general suggestions made by Fohlich[6] and Bardeen.[17] It also gives a qualitative physical interpretation of the energy gap which is the essential element of the BCS Theory. The model makes it possible to relate metal properties such as lattice energy, electron velocity, lattice displacement, type of metal lattice, and electron occupancy of interstices to the critical temperature(T_c) for superconductivity. These correlations can be the basis for further explorations for superconducting metals.

On the basis of the model all metals are not expected to become superconductors even at the lowest temperatures attainable. It is believed that the alkali metals and Cu, Ag, and Au have too many vacant interstices to allow superconductivity. In addition, certain intermetallic compounds with strong localization of $\bar{e}$ and $\bar{e}_2$ (inhomogeneous interstices, see Part IV) are not expected to allow superconductivity. The model does suggest that compounds with unstable anions (dissociable electrons) such as O^{2-}, S^{2-}, Se^{2-}, Te^{2-}, N^{3-}, P^{3-}, and C^{4-} are all possible superconductors when in metal-like compounds. (High pressure CS is superconducting.)

The present model gives a different interpretation from that of Matthias[18] for the gradations of T_c across

14) Ref. 11, Chap. 13, Vol. II by G. Gladstone, M. A. Jensen, and J. R. Schrieffer.

15) M. Ishikawa and L.E. Totts, *Solid State Commun.*, **9**, 799 (1971).
16) B. W. Roberts, "Progress in Cryogenics," Vol. IV, ed. by K. Mendelsohn, Academic Press (1964).,
17) J. Bardeen, *Rev. Mod. Phys.*, **23**, 261 (1951).
18) B. T. Matthias, "Progress in Low Temperature Physics," Vol. II, Interscience, New York (1955).

the rows in the periodic table. The maximum at Group V and VII and for Group IVB are considered to be the result of optima in lattice displacements and only indirectly a function of place in the periodic table. For example, the decreases from Nb to Mo followed by an increase to T_c are taken as due to changes in lattice displacement which reflect the different localization of d-electrons on the ion cores for Mo and T_c whereas Nb has no localized d-electrons. As mentioned earlier the maximum in T_c for Nb (and Pb) at a lattice displacement of approximately 0.06 Å (0.08 for Pb) represents the point at which strong ion core repulsion leads to low amplitude of lattice vibration but is not sufficiently strong to prevent initiation of phonons by $\bar{e}$. In the d^{10} group the inherently stronger forces lead to a larger optimum displacement and also lead to distorted structures and non-metallic properties beyond Group IV.

There are many superconductors not discussed in this paper. A detailed analysis of data on superconducting alloys would be needed to determine the effect of more than one ion core on superconductivity. It is anticipated for alloys with transition metals that the way the model allows ligand field theory to be used would be helpful in interpreting the effect of localized d-electrons in alloys on superconductivity.

The author wishes to thank the Japan Society for the Promotion of Science for the invitation to Hokkaido University as a Visiting Scientist (1971—1972) and to express appreciation to Professor Toya and the Staff of the Research Institute for Catalysis for valuable suggestions during Seminar discussions of this series of papers. The assistance of Miss M. Azuma, Miss T. Kawai, and Miss A. Hiratsuka in preparation of this series of manuscripts is much appreciated.

BULLETIN OF THE CHEMICAL SOCIETY OF JAPAN, VOL. 46, 1940—1945 (1973)

Dipole Correlation Functions of Non-interacting Symmetric Vib-rotors

Teruyo YAMASHITA* and Hiroshi SHIMIZU**

Faculty of Pharmaceutical Sciences, Kyushu University, Katakasu, Fukuoka 812

(Received September 13, 1972)

Dipolar correlation functions of non-interacting symmetric top molecules were obtained by quantum mechanical calculation. The effect of the rotation-vibration interaction on the correlation function is discussed, taking the constant ζ of the Coriolis coupling and the asymmetry I_x/I_z as parameters. It is shown that the decay of the correlation function for perpendicular vibrations very much depends on the sign and the magnitude of ζ. Some relationships between the shape of the correlation function and the value of the parameters are given.

Detailed information on the reorientational motion of molecules in the liquid state is obtained by infrared spectroscopy; the dipolar correlation function $\Xi(t)$ is given[1,2] from infrared spectrum $I(\omega)$ according to the Fourier transform

$$\Xi(t) = \int_{-\infty}^{+\infty} I(\omega) \exp(i\omega t) d\omega.$$

A number of studies[1-13] have shown that molecular reorientation of small molecules is not of rotational diffusion as described by Debye[14] but to some extent of free rotation. Contribution from this deviates the form of correlation function $\Xi(t)$ from exponential decay curves. Qualitatively, the function $\Xi(t)$ is represented by that of free rotors followed by an exponential curve.[2,5] The molecular motion can be treated more quantitatively, considering the effect of free rotation rigorously.[3,14-19] The form and the relaxation time of $\Xi(t)$ for non-interacting molecules give useful information for the study of observed functions. Thus, $\Xi(t)$ has been calculated for free diatomic,[1,2] spherical[5,20] and symmetric top[21] molecules.

* Present Address: Daiichi College of Pharmaceutical Sciences, Tamagawa-cho, Takamiya, Fukuoka, 815.

** Present Address: Faculty of Sciences, Kyushu University, Hakozaki, Fukuoka, 812.

1) R. G. Gordon, *J. Chem. Phys.*, **43**, 1307 (1965).
2) H. Shimizu, *ibid.*, **43**, 2453 (1965).
3) R. G. Gordon, *ibid.*, **44**, 1830 (1966).
4) J. T. Shimozawa and M. K. Wilson, *Spectrochem. Acta.*, **22**, 1609 (1966).
5) H. Shimizu, This Bulletin, **39**, 2385 (1966).
6) C. E. Favelukes, A. A. Clifford, and B. Crawford, Jr., *J. Phys. Chem.*, **72**, 962 (1968).
7) R. L. Armstrong, S. M. Blumenfeld, and C. G. Gray, *Can. J. Phys.*, **46**, 1331 (1968).
8) T. Fujiyama and B. L. Crawford, Jr., *J. Phys. Chem.*, **73**, 4040 (1969).
9) A. Cabana, R. Bardoux, and A. Chamberland, *Can. J. Chem.*, **47**, 2915 (1969).
10) W. G. Rothschild, *J. Chem. Phys.*, **51**, 5187 (1969).
11) W. G. Rothschild, *ibid.*, **53**, 990 (1970).
12) W. G. Rothschild, *ibid.*, **53**, 3265 (1970).
13) W. G. Rothschild, *ibid.*, **55**, 1402 (1971).
14) M. Fixman and K. Rider, *ibid.*, **51**, 2425 (1969).
15) R. E. D. McClung, *ibid.*, **51**, 3842 (1969).
16) B. J. Berne, T. P. Boon, and S. A. Rice, *ibid.*, **45**, 1086 (1966).
17) G. D. Harp and B. J. Berne, *Phys. Rev.*, **2**, 975 (1970).
18) D. Kivelson, M. G. Kivelson, and I. Oppenheim, *J. Chem. Phys.*, **52**, 1810 (1970).
19) K. Kometani and H. Shimizu, *J. Phys. Soc. Jap.*, **30**, 1036 (1971).
20) W. A. Steele, *J. Chem. Phys.*, **38**, 2411 (1963).
21) W. A. Steele, *Phys. Rev.*, **184**, 172 (1969).

The most important merit of the IR method may be that detailed and quantitative information is obtained on the anisotropy in molecular reorientation as predicted by theories.[1,2] Shimozawa and Wilson[4] first reported the observation of the anisotropic rotation in liquids by the IR method by using *trans*-dichloroethylene. The reorientational motion of acetone in various polar and non-polar solution was recently studied by Koga *et al.*[22] They found that the anisotropy was influenced by the density and polarizability of the solvent.

Observation of the anisotropy is difficult, however, because observed functions often differ much from theoretical ones.[14,22] The most significant contribution to the difference seems to result from the Coriolis' coupling as pointed out by Rothschild.[23] In the present paper we will show how the function $\Xi(t)$ of free symmetric top molecules is influenced by the Coriolis' coupling, taking the coupling constant ζ and the ratio of the moments of inertia, I_x/I_z, as parameters.

Methods of Calculation

In order to take into account the Coriolis' coupling at full length, we may write the Hamiltonian of a vib-rotor[24] as

$$H = H_v + H_r + H', \tag{1}$$

where

$$H_v = (1/2)\sum_i p_i^2 + V_0 + (1/2)l_z^2/I_z, \tag{2}$$

$$H_r = (1/2)(J_x^2/I_x + J_y^2/I_y + J_z^2/I_z) \tag{3}$$

and

$$H' = -J_z l_z/I_z. \tag{4}$$

x, y, and z in (2)—(4) refer to the principal inertial axes of molecule with components of the moment of inertia I_x, I_y, and I_z, respectively; J_x, J_y, and J_z are the components of the total angular momentum $\boldsymbol{J}$ onto the same axes; l_z is the z component of the vibrational angular momentum $\boldsymbol{l}$; p_i is the momentum conjugate to the i-th normal coordinate; and V_0 is the intra-molecular potential. We neglect anharmonicity in vibrations as well as vibration-rotation interactions higher than the first order one H'. We are interested only in the relative frequency of component lines to the center of vibration-rotation bands and not in absolute value. The anharmonicity can therefore be neglected, since it contributes mainly to shifting the whole band spectrum with band center. Vibration-rotation interactions of higher order shift energy levels of vibrationally excited states in the wave number of the order of the rotational constant B ($=\hbar/4\pi cI_x$, where c is the light velocity). The energy change in wave number is of the order of 10^{-2} cm^{-1} for an ordinary molecule. Displacements of the component line of the order of 10^{-2} cm^{-1} can be safely neglected, since neighboring lines are generally separated from each other about the wave number of the order of 1 cm^{-1}.

The eigenfunctions and eigenvalues for the Hamiltonian H may be rewritten in terms of conventional notation corresponding to (1) as follows.

$$H|v, l, k, M) = \hbar\omega(v, l, J, k)|v, l, k, M) \tag{5}$$

with

$$\omega(v, l, J, k) = \omega_v(v, l) + \omega_r(J, k) + \omega'(k, l) \tag{6}$$

$$\omega_v(v, l) = \begin{cases} (v+1/2)\omega_v \\ \qquad \text{for non-degenerate vibrations} & \text{(7a)} \\ (v+1)\omega_v + \hbar\zeta^2 l^2/2I_z \\ \qquad \text{for degenerate vibrations} & \text{(7b)} \end{cases}$$

$$\omega_r(J, k) = \hbar J(J+1)/2I_x + \hbar k^2/[2(1/I_z - 1/I_x)]$$
$$\omega'(k, l) = \hbar\zeta kl/I_z, \tag{8}$$

where $l=\pm 1$ is the quantum number for l_z, *viz.*, the projection of vibrational angular momentum $\boldsymbol{l}$ onto the molecular axis. The Coriolis' coupling appears only when vibrational states are degenerated. Such degenerate vibrations have an induced dipole moment in the x-y plane perpendicular to the molecular axis. In the following treatment the set of quantum numbers v, l, J, k, and M may be concisely represented in a symbolic way by a single letter n. In other words, all the possible quantum states are properly numbered from $n=1$ to infinity. The Schrödinger equation (4) is briefly rewritten as

$$H|n) = \hbar\omega_n|n) \tag{9}$$

with

$$|n) = |n_v)|n_r) \equiv |v, l)|J, k, M).$$

The dipole correlation function $\Xi(t)$, a normalized and dimensionless quantity, may be defined by

$$\Xi(t) = N\langle\mu_z(0), \mu_z(t)\rangle, \tag{10}$$

where μ_z refers to the projection of the induced moment μ onto the space fixed Z-axis which is taken arbitrarily in a plane perpendicular to the direction of propagation of the IR light; $\langle A, B\rangle$ represents the canonical average between variables A and B; and $N=\langle\mu_z(0), \mu_z(0)\rangle^{-1}$ is the normalization constant which makes $\Xi(0)=1$. When molecules are free from intermolecular interactions, energy H is a constant of motion. The correlation function is then conveniently expressed in terms of eigenfunctions $|n)$ and eigenvalues ω_n as follows.[25]

$$\Xi(t) = N\sum_{n,n'}(\beta\hbar\omega_{nn'})^{-1}\exp(-\beta\hbar\omega_n)\{\exp(\beta\hbar\omega_{nn'})-1\} \times \exp(i\omega_{nn'}t)(n|\mu_z|n')(n'|\mu_z|n), \tag{11}$$

where

$$\omega_{nn'} \equiv \omega_n - \omega_{n'}$$

and $\beta\equiv 1/kT$ with Boltzmann constant k and absolute temperature T. The angular frequency $\omega_{nn'}$ may be given by

$$\omega_{nn'} = \omega_{nn'}^c + \omega_{nn'}^* \tag{12}$$

where $\omega^c(n; n')\equiv\omega_{nn'}^c$, the angular frequency of the center of fundamental band $\{n\to n'\}$, is independent of the sets of rotational quantum numbers n_r and n_r' in the present approximation; namely,

22) K. Koga, Y. Kanazawa, and H. Shimizu, *J. Molec. Spectrosc.* (in press).
23) W. G. Rothschild, *J. Chem. Phys.*, **57**, 991 (1972).
24) H. H. Nielsen, *Phys. Rev.*, **60**, 794 (1941).
25) R. Kubo and K. Tomita, *J. Phys. Soc. Jap.*, **9**, 45 (1954).

$$\omega^c(n, n') = \omega^c(n_v; n_{v'}) \tag{13}$$

with $v=0$ and $v'=1$. By utilizing (12) the correlation function (11) may be rewritten as

$$\Xi(t) = \Xi^*(t) \exp [i\omega^c(n_v; n_{v'})t]$$

with

$$\Xi^*(t) = N'\sum_{n,n'}(\beta\hbar\omega_{nn'})^{-1} \exp(-\beta\hbar\omega_{n_r}) [\exp(\beta\hbar\omega_{nn'})-1] \times \exp(i\omega^*_{nn'}t)(n|\mu_z|n')(n'|\mu_z|n), \tag{14}$$

where N' is the normalization factor of $\Xi^*(t)$. The Fourier transform of $\Xi^*(t)$ gives the "normalized" and dimensionless rotation-vibration spectrum $S^*(\omega)$ relative to the band center ω^c. The inverse Fourier transformation of $S^*(\omega)$ results in $\Xi^*(t)$. In classical limit $\beta\hbar\omega_{nn'} \ll 1$, (14) is reduced to

$$\Xi^*_{cl}(t) = N'\sum_{n,n'} \exp(-\beta\hbar\omega_{n_r}) \times \exp(i\omega^*_{nn'}t)(n|\mu_z|n')(n'|\mu_z|n). \tag{15}$$

Further calculation of $\Xi(t)$ is possible when μ_z in the matrix elements of (11) is given in terms of variables defined in molecular-fixed coordinate systems. Wigner's rotation matrix $A_{mm'}{}^{(1)}(\Omega)$ can be most conveniently used for this purpose:[26]

$$\mu_z = \sum_{m=-1}^{1} A^{(1)}_{m0}(\Omega)\mu_m \tag{16}$$

with

$$\begin{pmatrix}\mu_{+1}\\ \mu_0\\ \mu_{-1}\end{pmatrix} = \begin{pmatrix}-1/\sqrt{2}\,(\mu_x+i\mu_y)\\ \mu_z\\ 1/\sqrt{2}\,(\mu_x-i\mu_y)\end{pmatrix} \tag{17}$$

and Ω refers to Eulerian angles between the space-fixed and molecule-fixed coordinate systems. We obtain

$$(n'|\mu_z|n) = \sum_{m=-1}^{1}(n_r'|A^{(1)}_{m0}(\Omega)|n_r)(n_v'|\mu_m|n_v), \tag{18}$$

where $(n_{v'}|\mu_m|n_v)$ have non-vanishing values only when $v'=v\pm1$ and $l'=l+m$.

We obtain the function $\Xi(t)$ corresponding to fundamental bands from (11) by confining ourselves to states $|n)$ with $v=0$ and $l=0$, or such states where $|n_v)=|n_0)$. Hence, non-vanishing elements appear when $v'=1$ and $l'=m$. Since the induced moment μ_m is given in terms of the normal coordinate Q_i by

$$\mu_m \simeq Q_i(\partial\mu_m/\partial Q_i)e, \tag{19}$$

nonvanishing elements become

$$(1, 0|\mu_0|0, 0) = [\hbar/2\omega_v]^{1/2}(\partial\mu_0/\partial Q_i)_e$$
$$(1, \pm1|\mu_{\pm1}|0, 0) = \mp[\hbar/\omega_v]^{1/2}(\partial\mu_{\pm1}/\partial Q_i)_e. \tag{20}$$

Matrix elements $(n_r'|A_{m0}{}^{(1)}|n_r)$ may be conveniently given in terms of Clebsch-Gordan coefficients[15] as

$$(J', K', M'|A^{(1)}_{m0}|J, K, M) = [J+1]^{1/2}C(J, 1, J'; K, m), \tag{21}$$

which have non-vanishing values only when

$$\Delta J \equiv J' - J = 0, \pm1 \tag{22}$$

and

$$\Delta K \equiv K' - K = m.$$

26) M. E. Rose, "Elementary Theory of Angular Momentum," John Wiley & Sons, Inc., N. Y. (1957), p. 52.

Results and Discussion

Parallel Bands. The excited states in the present case have no vibrational angular momentum, *i.e.* $l'=0$. Thus (18) is transformed into

$$(n'|\mu_z|n) = (n_r'|A^{(1)}_{00}(\Omega)|n_r)(n_v'|\mu_0|n_v) \tag{23a}$$
$$= (J', K, M'|A^{(1)}_{00}(\Omega)|J, K, M)(1, 0|\mu_0|0, 0)$$
$$= C(J, 1, J'; K, 0)[\hbar(J+1)/2\omega_v]^{1/2}(\partial\mu_0/\partial Q_i)_e \tag{23b}$$

by utilizing (20), (21) and (22). The quantity C in (23b) is non-vanishing only when $J'=J-1$, J, and $J+1$:

$$C(J, 1, J-1; K, 0) = [J^2-K^2]^{1/2}/[J(2J+1)]^{1/2}$$
$$C(J, 1, J; K, 0) = K/[J(J+1)]^{1/2}$$
$$C(J, 1, J+1; K, 0) = [(J+1)^2-K^2]^{1/2}/[(J+1)(2J+1)]^{1/2}. \tag{24}$$

We have

$$\omega^*_{nn'} = \begin{cases}-2BJ & \text{for } J' = J-1\\ 0 & J' = J\\ +2BJ & J' = J+1.\end{cases} \tag{25}$$

The reduced correlation function $\Xi^*(t)$ is easily obtained from (7), (14), (23b), (24), and (25).

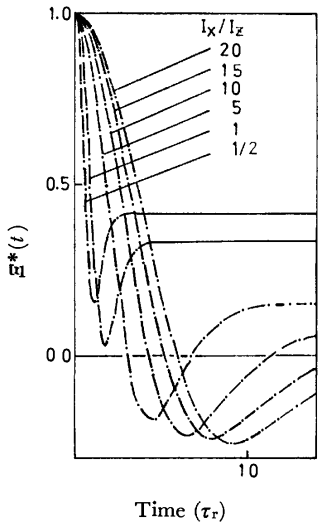

Fig. 1. Time correlation functions $\Xi^*(t)$ for parallel band obtained at $T=300$ K and $\omega_{nn'}{}^c=2{,}000\ \mathrm{cm}^{-1}$ in units of $\tau_r \equiv (I_z/kT)^{1/2}$, the mean period of rotation.

The functions $\Xi^*(t)$ at 300 K and $\omega_{nn'}{}^c=2000\ \mathrm{cm}^{-1}$ are shown in Fig. 1, taking the ratio I_x/I_z as a parameter. The value of I_z is assumed to be 5×10^{-40} g·cm^2, which is nearly the same with the moment of inertia of CH_3X. The calculated functions are clearly of non-exponential form with non-vanishing limiting value $\Xi^*(\infty)$, which results from the Q branch of spectrum. The limiting value $\Xi^*(\infty)$ is directly related to the relative intensity the Q branch. The proof is very simple. The spectrum $S^*(\omega^*)$ may be composed of the sum of the P and R branches, $S_1{}^*(\omega^*)$, and the Q branch, $S_2{}^*(0)\delta(\omega^*)$. The Fourier transform of $S^*(\omega^*)$ gives

$$\Xi^*(t) = \int_{-\infty}^{\infty} S_1{}^*(\omega^*)e^{i\omega^*t}d\omega^* + S_2{}^*(0)\int_{-\infty}^{\infty}\delta(\omega^*)e^{i\omega^*t}d\omega^*,$$

where the first term in the RHS vanishes when $t\to\infty$. Hence, $\Xi^*(\infty)=S_2^*(\omega_{nn'^c})$.

It is noted that the magnitude of the transition moment $(n|\mu_z|n')$ is independent of the moment of inertia of molecule as indicated by (23) and (24). This means that the relative intensity S_2^* of the Q branch is varied only by the statistical factor, the Boltzmann distribution factor $\exp(-\hbar\omega_n/kT)$, which is a function of the ratio of ω_n and temperature T. The eigenvalues (6)—(8) lead to the result that an increase in the moment of inertia I_x decreases the magnitude of ω_n/T and, hence, the relative intensity S_2^*. A similar effect is expected by increasing temperature T instead of I_x. On the other hand, there is the relation $\Xi^*(\infty)=S_2^*$ as shown above. Therefore, $\Xi^*(\infty)$ is a decreasing function of I_x as well as T.

It was shown by one of us (H.S.)[5] that the non-dissipative relaxation of the dipolar correlation $\Xi^*(t)$ is characterized by two dynamical factors, the mean period τ_f of rotation and the relaxation time τ_p of the phase coherence among dipole moments which are in phase at initial time $t=0$. The rate of the initial decay of the correlation function $\Xi^*(t)$ for non-interacting molecules is inversely proportional to τ_f, or estimated qualitatively by $<|\hbar/\omega_{nn'}^*|>$, where $<\ >$ refers to the ensemble average. In other words, the rate of the initial decay of the function $\Xi^*(t)$ is proportional to $<|\omega_{nn'}^*|>$ in a qualitative sense. The results (25) leads to $<|\omega_{nn'}^*|>\propto B\propto 1/I_x$, indicating that the smaller the moment of inertia I_x for a fixed value of I_z, the larger the rate of initial decay. The tendency is demonstrated in Fig. 1. The relaxation of the phase coherence gives rise to the disappearance of the oscillatory behavior of the correlation function and makes the function approach zero. The depth of the minimum Ξ_m^* of the correlation function is, therefore, an increasing function of τ_p, or the relaxation time of the phase coherence and is inversely proportional to $<|\Delta\omega_{nn'}^*|>\equiv<|\omega_{nn'}^*-<\omega_{nn'}^*>|>$. The rates of reorientation of molecular frame, (25), indicate that $<|\Delta\omega_{nn'}^*|>$ is further proportional to B or $1/I_x$. Thus, the larger the ratio I_x/I_z in Fig. 1 the deeper the minimum of the correlation function. The time t_m where the correlation function takes the minimum value Ξ_m^* is linearly proportional to $[I_z/I_x]^{1/2}$ as shown in Fig. 2. t_m is given in Fig. 3 as a function of $[I_z/I_x]^{1/2}$, indicating that it is proportional to $[I_z/I_x]^{1/2}$. In other words, t_m multiplied by Ξ_m^* is constant.

In classical limit, $\beta\hbar\omega_{nn'}\ll 1$, no vibrational effect

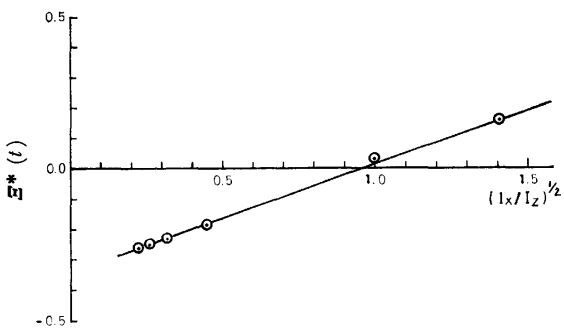

Fig. 2. The minimum values of Fig. 1 as a function of $(I_z/I_x)^{1/2}$.

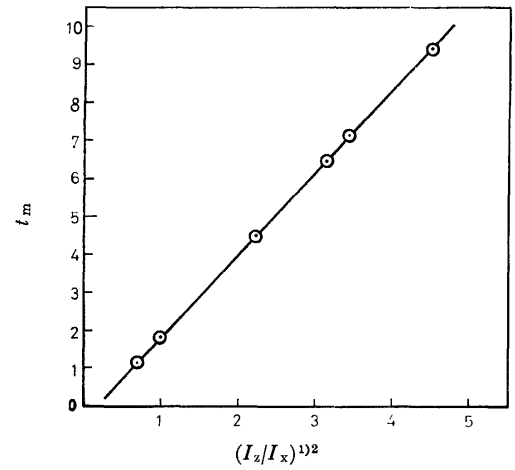

Fig. 3. The position of the minimum of $\Xi^*(t)$ in units of $t_m=t(I_z/kT)^{1/2}$ as a function of $(I_x/I_z)^{1/2}$.

exists in the correlation function $\Xi^*(t)$, because matrix elements $(n'|\mu_z|n)$ in (15) can be replaced by $(n_r'|A_{00}^{(1)}|n_r)$ and, the vibrational contributions, $(n_v'|\mu_0|n_v)$, can be included in the normalization factor N'. Hence, the correlation function in classical limit $\Xi_{cl}^*(t)$ represents the dipole correlation of rotor but not of vib-rotor. On the other hand, $\Xi^*(t)$ describes that of free vib-rotor.

Perpendicular Bands. In the present case where $l'\geq 1$, vibrations interact with molecular rotation through the Coriolis' coupling and vibration and rotation are often influenced substantially. From (20), (21) and (22), (18) becomes

$$(n'|\mu_x|n)=(n_r'|A_{\pm 10}^{(1)}(\Omega)|n_r)(n_v'|\mu_{\pm 1}|n_v) \tag{26a}$$

$$=(J',K',M|A_{\pm 10}^{(1)}(\Omega)|J,K,M)(1,\pm 1|\mu_{\pm 1}|0,0)$$

$$=C(J,1,J';K,\pm 1)[\hbar(2J+1)/\omega_v]^{1/2}(\partial\mu_{\pm 1}/\partial Q)_e. \tag{26b}$$

The coefficients C in (26b) have non-vanishing values only when $J'=J-1$, J, and $J+1$ and $K'=K-1$, and $K+1$:

$$\begin{aligned}&C(J,1,J-1;K,\pm 1)\\&\quad=[(J\mp K+1)(J\mp K)]^{1/2}/[2J(2J+1)]^{1/2}\\&C(J,1,J;K,\mp 1)\\&\quad=-[(J\mp K+1)(J\pm K)]^{1/2}/[2J(J+1)]^{1/2}\\&C(J,1,J+1;K,\pm 1)\\&\quad=[(J\pm K+1)(J\pm K)]^{1/2}/[2(J+1)(2J+1)]^{1/2}.\end{aligned} \tag{27}$$

We have[27]

$$\omega_{nn'}=\omega_v-B+\zeta(\zeta-2)A\pm 2K[(1-\zeta)A-B]\mp 2BJ, \tag{28a}$$

where the upper sign refers to $J'=J+1$, $K'=K-1$ and $l'=l-1$, and the lower one to $J'=J-1$, $K'=K+1$ and $l'=l+1$, and $A=\hbar/4\pi cI_z$. Similarly, we have

$$\omega_{nn'}=\omega_v-B+\zeta(\zeta-2)A\pm 2K[(1-\zeta)A-B], \tag{28b}$$

where the upper sign refers to $J'=J$, $K'=K+1$ and $l'=l+1$, and the lower $J'=J$, $K'=K-1$ and $l'=l-1$. For $J'=J+1$, $K'=K+1$ and $l'=l+1$ and for $J'=$

27) H. H. Nielsen, "Handbuch der Physik," Band 37-1, Atom 3-Molekül 1, Springer-Verlag Berlin, Göttingen, Heidelberg (1959), p. 254.

$J-1$, $K'=K-1$ and $l'=l-1$ we write

$$\omega_{nn'} = \omega_v - B + \zeta(\zeta-2)A \pm 2K[(1-\zeta)A-B] \pm 2BJ. \quad (28c)$$

From (7), (14), (26b), (27), (28a), (28b), and (28c), the reduced correlation function $\Xi^*(t)$ is easily calculated. In Figs. 4—9 are shown the dipole correlation functions at $T=300$ K and $\omega_{nn'^c}=2000$ cm^{-1}, regarding the Coriolis' coupling constant ζ as a parameter. When $\zeta \neq 0$, correlation function is affected not only by rotational state but also by interactions of the vibration and the rotation. Generally, the correlation function of degenerate vibrations obtained from infrared spectrum significantly differs from the dipole correlation functions of rotors as shown in Figs. 4—9.

Symmetric top molecules are classified into two groups, the oblate symmetric top (in the case of $I_z>I_x$)

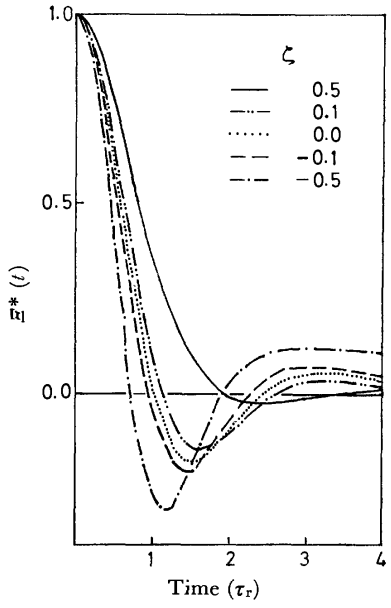

Fig. 4. Time correlation fuctions $\Xi^*(t)$ for perpendicular band at $I_x/I_z=1/2$, $T=300$ K and $\omega_{nn'^c}=2,000$ cm^{-1} in units of $(I_z/kT)^{1/2}$.

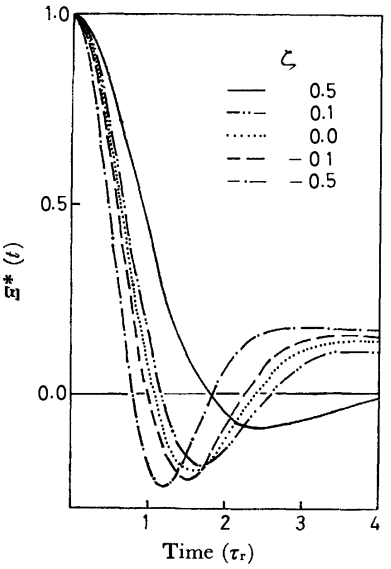

Fig. 5. Time correlation fuctions $\Xi^*(t)$ for perpendicular band at $I_x/I_z=3/4$, $T=300$ K and $\omega_{nn'^c}=2,000$ cm^{-1}.

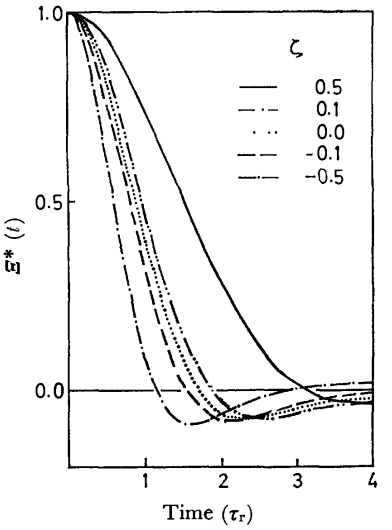

Fig. 6. Time correlation functions $\Xi^*(t)$ for perpendicular band at $I_x/I_z=5$, $T=300$ K and $\omega_{xx'^c}=2,000$ cm^{-1}.

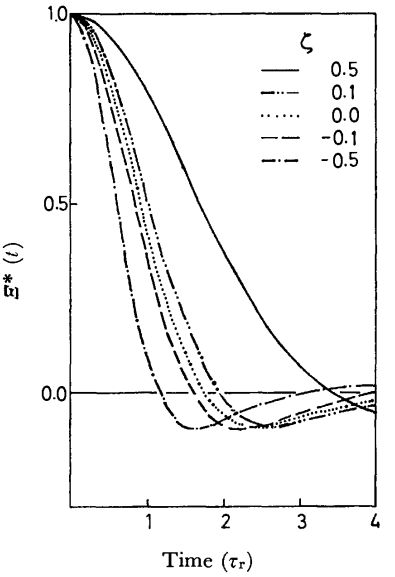

Fig. 7. Time correlation functions $\Xi^*(t)$ for perpendicular band at $I_x/I_z=10$, $T=300$ K and $\omega_{nn'^c}=2,000$ cm^{-1}.

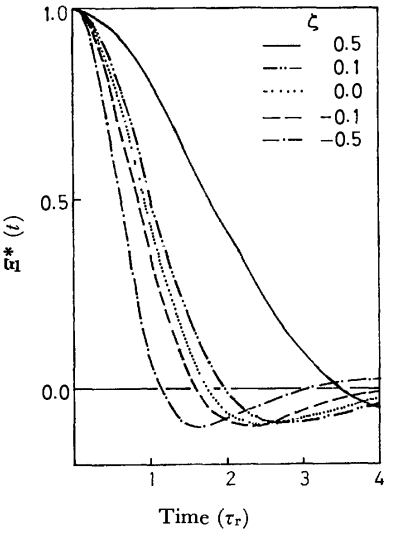

Fig. 8. Time corrlation functions $\Xi^*(t)$ for perpendicular band at $I_x/I_z=15$, $T=300$ K and $\omega_{nn'^c}=2,000$ cm^{-1}.

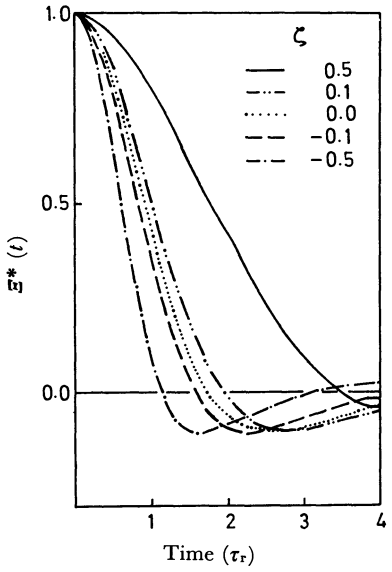

Fig. 9. Time correlation functions $\Xi^*(t)$ for perpendicular band at $I_x/I_z=20$, $T=300$ K and $\omega_{nn'^c}=2{,}000$ cm^{-1}.

and prolate symmetric top ($I_z<I_x$), the functions $\Xi^*(t)$ for the oblate and prolate molecules being shown in Figs. 4—5 and in Figs. 6—9, respectively. The dependence of the correlation function on I_x/I_z is more pronounced in oblate molecules than in prolate ones.

We will discuss the form of the correlation function more in detail by considering the two dynamical factors as in the case of parallel bands. In the present case the orientation of the dipole moment is changed by molecular vibrations with non-vanishing angular momentum as well as by molecular rotations. When $\zeta<0$ vibration and rotation change the orientation of the dipole moment in the same direction whereas in opposite directions for $\zeta>0$. Therefore, the rate of the initial decay of the function $\Xi^*(t)$ is evidently larger when $\zeta<0$ than when $\zeta>0$. Relations (28) demonstrate that $\omega_{nn'}^*\equiv\omega_{nn'}-\omega_v$ decreases as Ξ is increased for constant A and B from -1 to $+1$. This means that $<|\omega_{nn'}^*|>$ or the rate of the initial decay is also a decreasing function of ζ when the values of I_x and I_z are fixed. On the other hand, when I_x changes with constant I_z and ζ, the variable part of $\omega_{nn'}^*$ is $\mp 2(J+K)B$. This indicates that $<|\omega_{nn'}^*|>$ or the rate of the initial decay of the correlation function decreases as B is decreased, *i.e.*, as I_x/I_z is increased. Equations (28) show that the ζ-dependence of the rate of the initial decay becomes sharper as the ratio $I_x/I_z=A/B$ is increased.

In contrast to the case of parallel bands, the larger the rate of the initial decay of the function $\Xi^*(t)$ the deeper the minimum Ξ_m^* as seen in Figs. 4—9. The tendency may be explained as follows in terms of the relaxation of the phase coherence among dipole moments.

The rate of the change of the orientation of induced moments depends not only on the rotational quantum number J but also on the quantum number K of component of angular momentum along molecular axis. To estimate the effect caused by the K-dependence of molecular reorientation on τ_p, it will be convenient to utilize the relation $\tau_p\simeq\hbar/<\Delta\omega^*>$, where $<\Delta\omega^*>$ is the width of band spectrum in angular frequency units. Equations (28) together with (27) give an inhomogenous distribution of component lines and the spectrum is made from a subband structure. The wings of the whole spectrum are mainly contributed from P and Q branches of sub-bands, respectively, and give rapidly relaxing components in the phase correlation, since separations from the band center are large. The relaxation time τ_p is, therefore, contributed most effectively by Q branches which gather rather closely in the central part of the spectrum and gives a slowly relaxing component. In other words, the width of the spectrum is contributed most effectively from the Q branches as far as the phase relaxation is concerned. Hence, we have in a rough measure

$$\tau_p\simeq\hbar/\langle|\Delta\omega_{nn'}^*(Q)|\rangle, \tag{29}$$

where $\Delta\omega_{nn'}^*(Q)$ is the position of the Q branches relative to the center of the spectrum, namely,

$$\Delta\omega_{nn'}^*(Q)=2AK[(1-\zeta)-I_z/I_x], \tag{30}$$

from (28) for a fixed value of I_z.

When the ratio I_x/I_z is increased from zero, we obtain a decrease in the value of $<|\Delta\omega_{nn'}^*(Q)|>$ and its minimum value, *i.e.* the maximum value of τ_p, at

$$I_x/I_z=1/(1-\zeta). \tag{31}$$

Further increase of I_x/I_z leads to an increase of $<|\Delta\omega_{nn'}^*(Q)|>$ or a decrease of τ_p. Equation (30) indicates that the main contribution to τ_p results from the term $1-\zeta$, provided that

$$I_x/I_z\gg 1/(1-\zeta). \tag{32}$$

Equation (31) leads to the result that the larger the Coriolis' coupling constant ζ the larger the ratio I_x/I_z which gives the maximum τ_p. Comparison of the correlation functions for $=-0.5$ and $=0.5$ in Figs. 4—9 support the above discussion.

One of the authors, T. Yamashita, wishes to express her sincere thanks to Dr. K. Nishiyama and Mr. K. Kometani, Faculty of Science, Kyushu University, for discussions. She is also grateful to Prof. Y. Ueda and Dr. Y. Kanazawa, Faculty of Pharmaceutical Sciences, Kyushu University, and Prof. H. Yano, Daiichi College of Pharmaceutical Sciences, for their continuous encouragement.

On the Interaction of Sodium Alkyl Sulfate with Alkylpyridinium Chloride and with Alkyltrimethylammonium Bromide in a Solution

Masaru MITSUISHI and Mieko HASHIZUME

Faculty of Textile Science and Technology, Shinshu University, Ueda, Nagano 386

(Received September 21, 1972)

The interaction between sodium alkyl sulfate and alkylpyridinium chloride or alkyltrimethylammonium bromide has been studied quantitatively by means of the conductometric method. The equilibrium constants of the reactions between them have been found to increase with an increase in the length of the alkyl chain. When the sum of the carbon atoms in an alkyl sulfate and of those of an alkylpyridinium chloride or of alkyltrimethylammonium bromide is less than twenty, no reaction has been found to take place. When it is larger than twenty-six, precipitates of the complex have been found. The interaction has been found to depend greatly on the length of the alkyl chain. The interaction decreases the heat content and increases the entropy.

The interaction between the oppositely-charged organic ions in aqueous solution have been examined by means of UV-spectroscopic,[1-5] NMR-spectroscopic,[6] conductometric,[7] and polarographic procedures.[8] The experimental evidence suggests that the hydrophobic groups in the organic ions play an important role in the ion-pair formation between oppositely-charged organic ions. However, very few quantitative investigations of the ion-pair formation between oppositely-charged organic ions, and of the factors involved in the determination of the interactions between them, have been carried out. Therefore, it seems valuable to make a quantitative examination of the role of the hydrophobic groups in the ion-pair formation between oppositely-charged organic ions by means of conductometric measurements of the solution.

Experimental

Materials. The alkyltrimethylammonium bromides (ATB) and alkylpyridinium chlorides (APC) used were as follows: hexyltrimethylammonium bromide (C_6TB), octyltrimethylammonium bromide (C_8TB), decyltrimethylammonium bromide ($C_{10}TB$), dodecyltrimethylammonium bromide ($C_{12}TB$), tetradecyltrimethylammonium bromide ($C_{14}TB$), hexadecyltrimethylammonium bromide ($C_{16}TB$), dodecylpyridinium chloride ($C_{12}PC$), and hexadecylpyridinium chloride ($C_{16}PC$).

The ATB was obtained by boiling a mixture of trimethylamine and the corresponding alkyl bromide in ethanol, by removing the ethanol, and by then recrystallizing it from acetone and/or benzene.

The APC was obtained by recrystallizing commercial agents from acetone and benzene.

The sodium alkyl sulfates (SAS) used were as follows: sodium amyl sulfate (SC_5S), octyl sulfate (SC_8S), sodium decyl sulfate ($SC_{10}S$), sodium dodecyl sulfate ($SC_{12}S$), sodium tetradecyl sulfate ($SC_{14}S$), sodium hexadecyl sulfate ($SC_{16}S$), and sodium octadecyl sulfate ($SC_{18}S$). They were prepared by adding an excess of sulfuric acid to a solution of the corresponding alkyl alcohol, by neutralizing alkyl sulfate with sodium hydroxide, and by then recrystallizing the sodium alkyl sulfate from ethanol.

Conductance Measurements of a Solution. A solution of alkyl sulfate and one of alkylpyridinium chloride or alkyltrimethylammonium bromide were mixed in varied proportions; the conductance measurements on the mixtures were made with a Yokogawa-Hewlett Packard Universal Bridge BV-Z-13B at 15, 25, 35 and 45 ± 0.01 °C. A simple dilution cell with a cell constant of 0.0514 at 25 °C was used.

Results and Discussion

The interaction of SAS with APC or ATB may be represented by Eq. (1), since all the examinations of the reactions between them have been carried out on a solution below the CMC of each electrolyte;

$$C^+ + nA^- \rightleftarrows CA_n \qquad (1)$$

Here, C^+ is an organic cations, like the alkylpyridinium ion (AP^+) or the alkyltrimethylammonium ion (AT^+), and A^- is an organic anion, like the alkyl sulfate ion (AS^-). The counter ion of AP^+ or AT^+, like Cl^- or Br^-, and the counter ion of AS^-, like Na^+, are assumed not to take part in the reaction at all, because the concentrations of the electrolytes are very low and the electrolytes are supposed to dissociate completely. In order to determine the n in Eq. (1) by the conductometric continuous-variation method,[9] a solution of C and one of A with the same molar concentration are mixed in various proportions and the conductances of the mixtures are measured.

Figure 1 shows the results obtained by the conductometric continuous-variation method for the interaction of $C_{16}TB$ with SC_8S. The mixture is made by the addition of x_1 liter ($x_1 \leqq 1$) of SC_8S of 1.0×10^{-4} mol/l to x_2 liter ($x_2=1-x_1$) of $C_{16}TB$ of 1.0×10^{-4} mol/l, the conductance measurement is carried out, and then specific conductance of the mixture is plotted against the composition. The straight lines, AB and CD, indicate the specific conductances of the SC_8S and $C_{16}TB$ solution respectively. When no reaction between SC_8S and $C_{16}TB$ takes place, the specific conductance of the mixture must be on the straight line BD. Since the

1) M. Koizumi and N. Mataga, *Nippon Kagaku Zasshi*, **75**, 273 (1954).
2) T. Kondo, *ibid.*, **76**, 50 (1955).
3) M. C. Corrin and W. D. Harkins, *J. Amer. Chem. Soc.*, **69**, 683 (1947).
4) R. Haque and W. U. Malik, *ibid.*, **67**, 2082 (1963).
5) W. U. Malik and S. P. Verma, *J. Phys. Chem.*, **70**, 26 (1966).
6) R. P. Taylor and I. D. Kunz, *J. Amer. Chem. Soc.*, **92**, 4813 (1970).
7) K. Yamaki, *Kogyo Kagaku Zasshi*, **65**, 1854 (1962).
8) S. Hayano, K. Kageyama, and T. Suzuki, *ibid.*, **68**, 126 (1965).
9) P. Job, *Ann. Chim.*, [10] **9**, 113 (1928).

Table 1. Equilibrium constants of the interactions between sodium alkyl sulfates and alkylpyridinium chlorides

Alkyl-pyridinium chlorides	Sodium alkyl sulfates	Temperature (°C) 15	25	35	45
$C_{12}PC$	$SC_{10}S$	1.19×10^5	9.06×10^4	7.22×10^4	
	$SC_{12}S$		1.11×10^6	8.11×10^5	6.28×10^5
$C_{16}PC$	SC_8S	1.43×10^6	1.07×10^6	7.22×10^5	

specific conductance is found to be the smallest in the equimolar mixture, the n in Eq. (1) is 1, *i.e.*, an equimolecular complex with no charge is formed in the mixture.

Figure 2 shows the specific conductance *vs.* composition plot of a mixture of SC_5S and $C_{12}PC$ at 25 °C. The specific conductance of the mixture is equal to the sum of the specific conductances of SC_5S and $C_{12}PC$ with the corresponding concentrations. The results

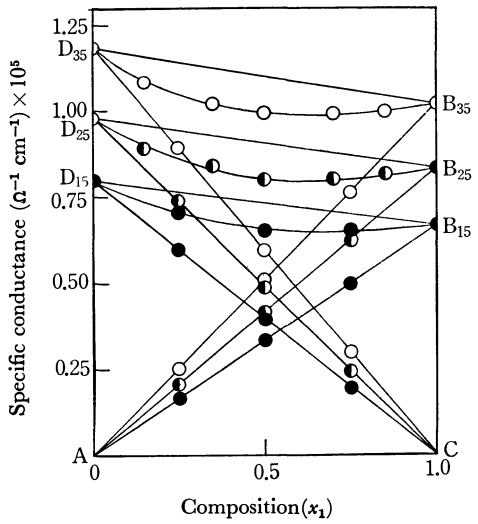

Fig. 1. The specific conductances of the mixture of x_1 liters of sodium octyl sulfate of 1.0×10^{-4} mol/l and $(1-x_1)$ liters of hexadecyltrimethylammonium bromide of 1.0×10^{-4} mol/l at 15 (●), 25 (◐), and 35 °C (○).

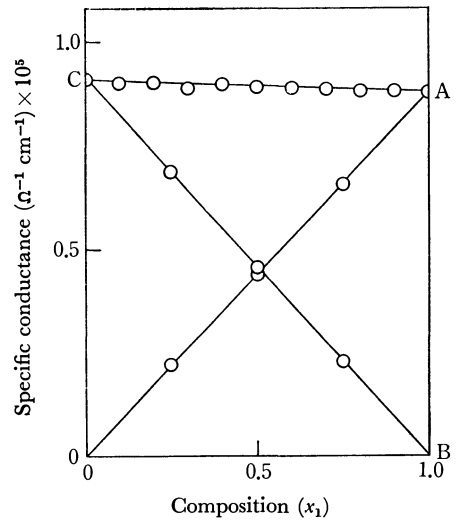

Fig. 2. The specific conductances of the mixture of x_1 liters of sodium amyl sulfate of 1.0×10^{-4} mol/l and $(1-x_1)$ liters of dodecylpyridinium chloride of 1.0×10^{-4} mol/l at 25 °C.

indicate that no reaction between SC_5S and $C_{12}PC$ takes place in the mixture.

The specific conductance *vs.* composition plots for the mixtures of the other substances, SAS and APC or ATB, are to be similar to either Figs. 1 or 2.

When the reaction between SAS and APC or ATB takes place, only the equimolecular complex is formed in the solution. The equilibrium constant, K, of Eq. (1) is given by Eq. (2);

$$K = \frac{X_{CA}}{X_{C^+}X_{A^-}} \tag{2}$$

Here, the X denotes the mole fraction of each component.

When the reaction takes place in a mixture of x_1 liter of C of c mol and x_2 liter of A of c mol, the specific conductance, κ, of the mixture is given by Eq. (3);

$$\kappa = (cx_1-z)\frac{\alpha}{10^3} + (cx_2-z)\frac{\beta}{10^3} + \frac{z(\gamma_-+\delta_+)}{10^3} \tag{3}$$

Here, z is the concentration of the product, CA, in the reaction. The α and β symbols are the equivalent conductances of the C electrolyte and the A electrolyte respectively. The γ_- and δ_+ symbols are the equivalent ionic conductance of the counter ion of C^+ and that of A^- respectively.

The concentration of the product, z, is obtained by means of Eq. (4);

$$z = \frac{c(x_1\alpha+x_2\beta)-10^3\kappa}{(\alpha+\beta)-(\gamma_-+\delta_+)} \tag{4}$$

The equilibrium constants shown in Tables 1 and 2 were calculated from Eqs. (4) and (2). It may be seen that the equibrium constants increase with the number of carbon atoms in the alkyl chain.

Table 2. Equilibrium constants of the interactions between sodium alkyl sulfates and alkyltrimethyl ammonium bromides

Alkyl-trimethyl-ammonium-bromides	Sodium alkyl sulfates	Temperature (°C) 15	25	35
CT_6B	$SC_{16}S$	2.66×10^5	2.08×10^5	1.62×10^5
	$SC_{18}S$	1.58×10^6	9.83×10^5	6.89×10^5
CT_8B	$SC_{14}S$	5.43×10^5	4.23×10^5	3.36×10^5
	$SC_{16}S$	2.04×10^6	1.53×10^6	1.12×10^6
$CT_{10}B$	$SC_{12}S$	9.67×10^4	7.28×10^4	5.34×10^4
	$SC_{14}S$	1.01×10^6	8.28×10^5	6.78×10^5
$CT_{12}B$	$SC_{10}S$	7.44×10^4	5.78×10^4	4.42×10^4
	$SC_{12}S$	1.03×10^6	9.28×10^5	8.06×10^5
$CT_{14}B$	SC_8S	6.17×10^4	4.76×10^4	3.71×10^4
	$SC_{10}S$	1.47×10^6	1.17×10^6	8.72×10^5
$CT_{16}B$	SC_8S	1.17×10^6	8.89×10^5	6.72×10^5

Table 3. Thermodynamic parameters of the interactions between sodium alkyl sulfates and alkylpyridinium bromides at 25 °C

Alkyl-pyridinium chlorides	Sodium alkyl sulfates	K_{298}	$-\Delta H°$ (kcal/mol)	$-\Delta G°$ (kcal/mol)	$\Delta S°$ (cal/K mol)
$C_{12}PC$	$SC_{10}S$	9.06×10^4	2.4	6.8	15
	$SC_{12}S$	1.11×10^6	5.0	8.2	11
$C_{16}PC$	SC^3S	1.07×10^6	5.5	8.2	9

Let N_1 and N_2 be the carbon atoms of the alkyl groups of SAS and APC or ATB respectively. When the sum of the carbon atoms of N_1 and N_2 is less than twenty, as in the mixture of SC_5S and $C_{12}PC$, no reaction takes place between SAS and ATB in the solution. When the sum is twenty-two, the equilibrium constant is smaller than 6×10^5, whereas it is larger than 6×10^5 when the sum reaches twenty-four. At a value for the sum of more than twenty-six, the reaction is found to be heterogeneous, for precipitates appear.

It is obvious from Tables 1 and 2 that the interaction of SAS with APC or ATB is highly dependent on the length of the alkyl group, though the behavior of the hydrophobic group in the complex is not clear.

The enthalpy changes, $\Delta H°$, in the reaction of SAS with APC or ATB were obtained from the slopes of the straight lines of the $\log K$ *vs.* $1/T$ plot over the whole temperature range; they are shown in Tables 3 and 4. The $\Delta H°$ values, which are always negative, are comparable with those of the interactions between the acid dye (C. I. Acid Blue 120) and some nonionic surface-active agents,[10] and with those of the interactions between the oppositely-charged organic ions, such as ionic dyes and ionic surface-active agents.[7]

Table 4. Thermodynamic parameters of the interactions between sodium alkyl sulfates and alkyltrimethylammonium bromides at 25 °C

Alkyl-trimethyl ammonium chlorides	Sodium alkyl sulfates	K_{298}	$-\Delta H°$ (kcal/mol)	$-\Delta G°$ (kcal/mol)	$\Delta S°$ (cal/K mol)
C_6TB	$SC_{16}S$	2.08×10^5	4.4	7.3	10
	$SC_{18}S$	9.83×10^5	7.3	8.2	3
C_8TB	$SC_{14}S$	4.23×10^5	4.3	7.7	12
	$SC_{16}S$	1.53×10^6	5.3	8.4	10
$C_{10}TB$	$SC_{12}S$	7.18×10^4	5.2	6.6	5
	$SC_{14}S$	8.28×10^5	3.5	8.1	15
$C_{12}TB$	$SC_{10}S$	5.78×10^4	4.6	6.5	6
	$SC_{12}S$	9.28×10^5	2.2	8.1	20
$C_{14}TB$	SC_8S	4.76×10^4	4.5	6.4	6
	$SC_{10}S$	1.17×10^6	4.6	8.3	12
$C_{16}TB$	SC_8S	8.89×10^5	4.9	8.1	11

The $\Delta S°$'s of the interaction between SAS and APC or ATB are found to be positive, as are shown in Tables 3 and 4. It can be presumed that the iceberg structure of water around the hydrophobic groups in the organic ions weakens when alkyl chains in both the ions are held together.

10) Y. Nemoto and T. Imai, *Kogyo Kagaku Zasshi*, **62**, 1286 (1954).

BULLETIN OF THE CHEMICAL SOCIETY OF JAPAN, VOL. 46, 1948—1953 (1973)

The Photoconductivity of Poly(*N*-vinylcarbazole). I. The Photoconductivity in a Surface-type Cell*

Kenichi OKAMOTO,** Shigekazu KUSABAYASHI,** and Hiroshi MIKAWA

Department of Applied Chemistry, Faculty of Engineering, Osaka University, Yamadakami, Suita, Osaka 565

(Received June 19, 1972)

The photoconductivity of poly-*N*-vinylcarbazole in a surface-type cell was measured both in a high vacuum and in the air. Fresh films showed a large photocurrent in the lower π-π^* absorption region and a small photocurrent in the visible region. The threshold of the photocurrent was found at about 600 mμ. By heat treatment or by pre-irradiation with UV-light or γ-ray, the photocurrent increased throughout the spectral region and its threshold shifted to a longer wavelength. Both the dark current and the photocurrent in the visible and the near IR regions must be due to the thermal or optical reexcitation of the trapped carriers. The activation energies of the dark current (0.4—1.3 eV) and the photocurrent (0.06—1.0 eV) differ according to the temperature range, the light wavelength, and the film history (whether fresh film or one of various pre-treated films). The activation energies are needed for carrier migration and can be explained by the "trapping conduction mechanism".

Recently many vinyl polymers with large pendant π-electron systems have been synthesized in expectation of their having good photoconductive properties. These polymer materials will be useful for electrophotography. The polymers synthesized and examined for photoconductivity measurements are poly-*N*-vinylcarba-

* The experimental results in this paper were presented at the 22th Symposium of the Society of Electrophotography of Japan, Kyoto, November, 1968.

** Present address: Department of Chemical Engineering, Faculty of Engineering, Yamaguchi University, Ube, Yamaguchi 755.

zole (PVCz),[1-9] polyvinylanthracene,[10,11] polyvinylpyrene,[12] polypyrenylmethylvinylether,[13] polyvinylacridine,[14] and polyacenaphthylene.[15] PVCz is one of the most photoconductive polymers, and it is now being used as a material for electrophotography.

In the present series of papers on the electrical properties of PVCz, the authors have examined the photoconductivity of PVCz purified as far as possible, especially under a high vacuum, for the purpose of clarifying the origin of the photoconductivity of PVCz. These studies can be expected to give us some guiding principles for preparing new photoconductive polymers with high sensitivity.

This paper will deal with the photoconductivity of fresh films in a surface-type cell. The effect of air, heating, or pre-irradiation with UV light or γ-rays will also be investigated.

Experimental

Materials. *N*-Vinylcarbazole was recrystallized three times from methanol and three times from *n*-hexane; it was then polymerized by heating it together with azobisisobutyronitril in benzene at 70 °C for 2 hr. The polymer was purified three times by reprecipitation from benzene–methanol. The molecular weight was determined to be 110000 by means of a membrane osmometer.

Measurements. The following four kinds of films were used.

a) Fresh film. A 0.2 ml portion of a 5 wt% benzene solution of the polymer was placed on a quartz plate (20×25 mm^2), and the solvent was evaporated slowly in the dark under a nitrogen atmosphere. The thickness of the film was determined to be about 15 μ by studying the UV absorption. The film showed an absorption edge at 357 mμ.

b) Film irradiated with UV light. A fresh film was irradiated with UV light in the air for 15 hr, 50 cm distant from a 500 W xenon lamp without a condenser lens.

c) Film irradiated with γ-rays. A fresh film was irradiated with γ-rays (^{60}Co) in the air for 1—50 hr (dose amount; 5×10^4—2×10^6 R).

d) Hot-pressed film. The powder of the polymer was compressed to a disk under a pressure of 80 kg/cm^2 and then hot-pressed at 220—240 °C in the air to a transparent film. There was no difference in either the IR spectrum or the UV spectrum among these four kinds of films. The γ-irradiated film showed a broad ESR signal ($g=2.0$) which was very stable and which did not disappear even after the film has been heated at 100 °C for 2 hr in a high vacuum.

In order to prepare a surface-type cell, Au or Ag comb-type electrodes (50 mm in length and 0.18 mm in electrode distance) were evaporated on the film, and then lead wires were placed in these electrodes by means of silver paste. A high-vacuum evaporation apparatus was prepared to obtain a clean vacuum of the order of 10^{-8} mmHg, according to the method reported by Maruyama *et al.*[16] This enabled us to measure photo- and dark-currents larger than 5×10^{-16} A in a high vacuum at 10—200 °C. The DC conductivity was measured by means of a vibrating-reed electrometer (Takeda Riken TR 84M). A stabilized 500 W xenon lamp was used as the light source; it was monochromatized by means of a prism monochromator. The light intensity was measured by means of a thermopile (Kipp and Zonen CA 1) or an actinometer by the use of potassium ferric oxalate. The intensity was changed by the use of neutral filters. The following data were taken using cells left for more than a few hours in the dark with an applied DC voltage.

Results

Shape of the Photoresponse Curve. In the pattern of photoresponse, the time required to reach the steady-state was between a second and a few minutes for the fresh films in a high vacuum. For the samples exposed in the air and also for the pre-treated ones, the response time was a little longer than that of the fresh film.

The decay curve of the photocurrent after the light had been turned off did not obey either the first- or second-order decay, and it showed a long tail, especially in the case of pre-treated films.

Voltage-dependence. The dark current of the fresh film left in the dark for a long time was too small to be observed at room temperature in a high vacuum. Its surface specific resistivity (ρ_{20}) was larger than $10^{19}\Omega$. On the other hand, the dark current of the pre-treated film was large enough to be measured (for instance, $\rho_{20}=1\times10^{18}\Omega$ for a UV-light-irradiated film in a high vacuum) and obeyed Ohm's law.

The photocurrents of both films obeyed also Ohm's law regardless of the wavelength of the illuminating light and the ambient gas.

Light-intensity Dependence. Figure 1 shows the light-intensity dependence of the photocurrent. The α value in the equation $i_{ph}\propto L^{\alpha}$, where L is the light intensity, was 1.0 in a high vacuum and 0.6—0.8 in the air for the fresh film. On the other hand, for the pre-treated films the α values were 0.6—0.9 both in a high vacuum and in the air. The lowering of the α value may be due to the introduction of some shallow trap levels by air or by pre-treatment, as has been reported in the case of polyethylene film by Yahagi *et al.*[17]

1) K. Okamoto, Y. Hasegawa, S. Kusabayashi, and H. Mikawa, This Bulletin, **41**, 2563 (1968).
2) Y. Hayashi, M. Kuroda, T. Imura, and A. Inami, *Kobunshi Kagaku*, **21**, 557 (1964).
3) M. Lardon, E. L. Doller, and J. W. Weigl, *Mol. Crystals*, **2**, 241 (1967).
4) P. J. Regensburger, *Photochem. Photobiol.*, **8**, 429 (1968).
5) A. Szymanski and M. M. Labes, *J. Chem. Phys.*, **50**, 3568 (1969).
6) D. M. Pai, *ibid.*, **52**, 2285 (1970).
7) A. I. Lakatos and J. Mort, *Phys. Rev. Lett.*, **21**, 1444 (1968).
8) H. Bauser and W. Klöpffer, *Chem. Phys. Lett.*, **7**, 137 (1970).
9) R. C. Hughes, *ibid.*, **8**, 403 (1971).
10) H. Inoue, K. Noda, S. Takiuchi, and E. Imoto, *Kogyo Kagaku Zasshi*, **65**, 146 (1962).
11) K. Morimoto, E. Ishida, and A. Inami, *J. Poly. Sci. A-1*, **5**, 1699 (1967).
12) K. Tanikawa, T. Ishizuka, K. Suzuki, S. Kusabayashi, and H. Mikawa, This Bulletin, **41**, 2719 (1968).
13) S. Yoshimoto, K. Okamoto, H. Hirata, S. Kusabayashi, and H. Mikawa, This Bulletin, **46**, 358 (1973).
14) S. Moriwaki, K. Okamoto, S. Kusabayashi, and H. Mikawa, to be published in this Bulletin.
15) K. Morimoto, Y. Murakami, and M. Ikeda, *National Technical Reports*, (Kadoma), **15**, 125 (1969) (in Japanese).
16) Y. Maruyama and H. Inokuchi, This Bulletin, **39**, 1418 (1966).
17) K. Yahagi and K. Shinohara, *J. Appl. Phys.*, **37**, 310 (1966).

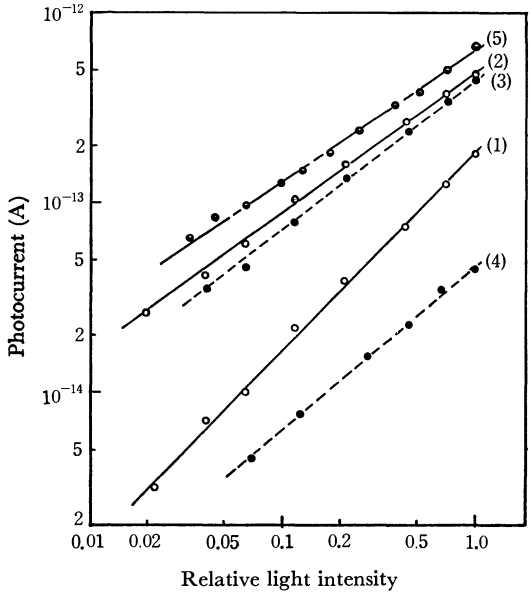

Fig. 1. Light intensity dependence of the photocurrent in a PVCz surface-type cell.
360 mμ (or 500 mμ) light at 24 °C under 3000 V/cm.
(1) a fresh film in high vacuum, (2) a fresh film in the air, (3) a film irradiated with γ-ray in high vacuum, (4) a film irradiated with γ-ray in high vacuum (500 mμ illumination), and (5) hot-pressed film in the air.

Spectral Response. Figures 2 and 3 show the spectral responses of the photocurrent for various films, the current being normalized for the relative light

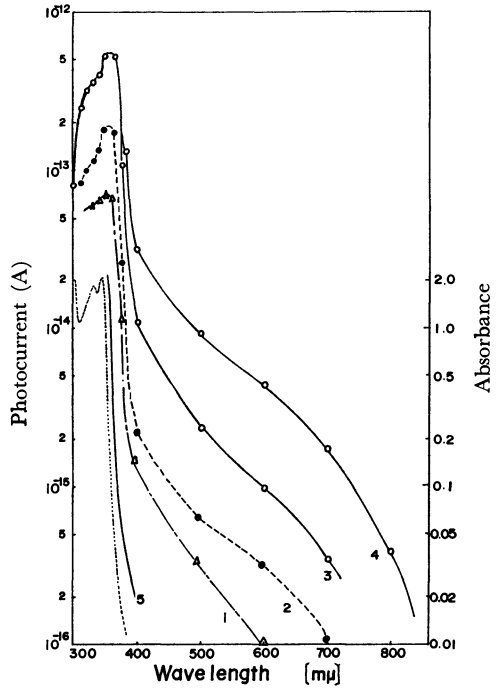

Fig. 2. Spectral dependence of the photocurrent of the fresh film in a surface-type cell for the light of 2×10^{13} photons/cm^2 s under 3000 V/cm at 23 °C.
(1) first run in high vacuum, (2) after heat treatment at 120 °C for 10 hr in high vacuum, (3) first run in the air, (4) after standing for a long time in the air, (5) absorption spectrum of the film 15 μ thick (The absorption spectrum of a film 3 μ thick is also given by a dotted line order to show the π–π^* absorption band).

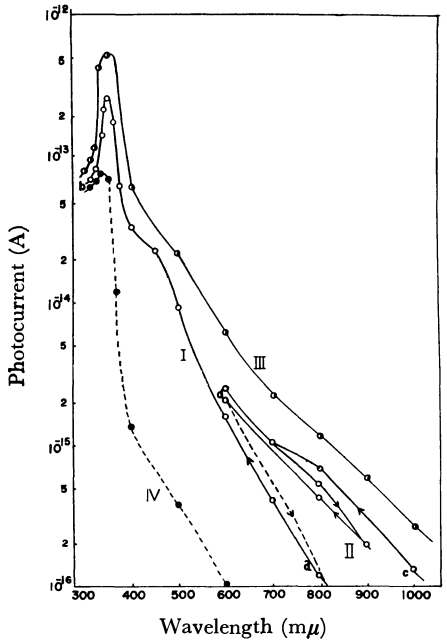

Fig. 3. Spectral dependence of the photocurrent in surface-type cells of the pre-treated films for the light of 2×10^{13} photons/cm^2 s. Effect of the repeated illumination of near-IR light was investigated. 3000 V/cm in high vacuum at 20 °C.
(I) The photocurrent of a UV-light irradiated film was measured from the wavelength (a) to (b). (II) Immediately after (b), the photocurrent was measured in the near-IR region from (c) to (d). This shows that the repeated illumination with near-IR light lowers the photocurrent progressively to the curve (I). (III) a film irradiated with γ-ray (2×10^6R). (IV) Fresh film, for comparison.

intensity according to the results shown in Fig. 1.

Fresh films have the photocurrent peak at 350—360 mμ and the threshold at 600 mμ. The wavelength for the minimum detectable photocurrent, 10^{-16} A, was taken as a threshold. After the film had been heated for a long time in a high vacuum (120 °C, 10 hr) or illuminated many times with UV light in a high vacuum, the photocurrent became larger in the UV as well as in the visible region and the threshold shifted to a longer wavelength region. The introduction of air had the same effect. As is shown by Curve (4) in Fig. 2, the photocurrent became larger in the air and the threshold shifted to 900 mμ. This effect of air was reversible so long as the cell was not exposed to UV illumination for a long time in the air.

In the case of the pre-treated films, the photocurrent was larger than that of the fresh film in all the wavelength regions, especially in the visible and near-IR regions, and showed the threshold at 1000 mμ even in a high vacuum, as is shown in Fig. 3. This large photocurrent in the visible and near-IR regions became still larger with pre-illumination by UV light and gradually became smaller with repeated illuminations by visible or near-IR light, as is shown in Fig. 3. Films with large photocurrents in the visible and near-IR regions showed quite large dark currents compared with that of the fresh film. Thus, there was a resemblance in the effect of the pre-treatments on the photocurrent in the visible or near-IR regions and on the dark

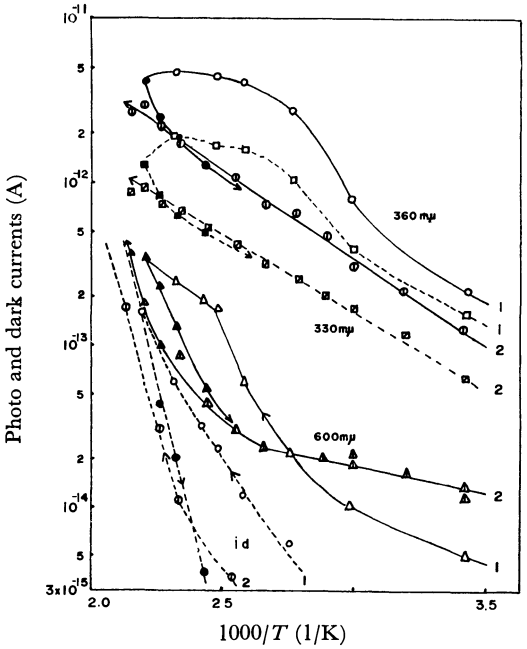

Fig. 4. Temperature dependence of the dark and photo current in a PVCz surface-type cell.
A fresh film under 3000 V/cm in high vacuum. 1 and 2; first and second heating runs, respectively.

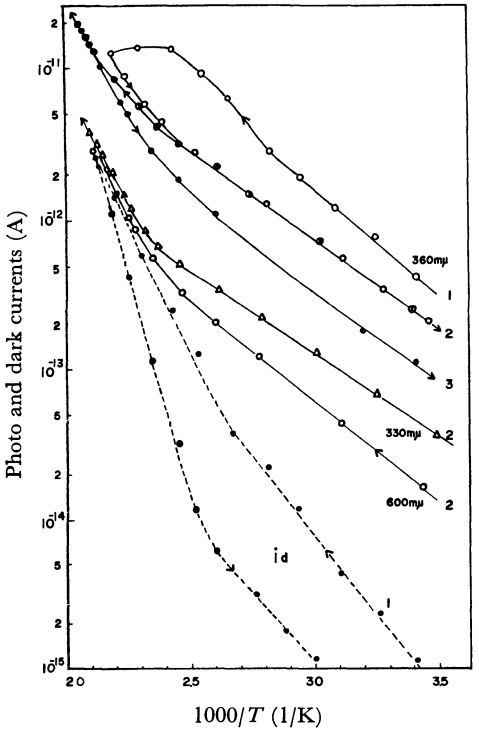

Fig. 5. Temperature dependence of the dark and photo currents in a PVCz surface-type cell.
A film irradiated with γ-ray (1×10^6R) under 3000 V/cm in high vacuum. 1, 2, and 3; first, second and third heating runs, respectively.

current.

Temperature-dependence and Activation Energies. Figures 4 and 5 show the temperature dependence of the photo and dark currents for the fresh film as well as for the pre-treated films. In these figures, the photocurrent in the first heating run increases steeply at first, reaches the saturation point, and finally even decreases in some cases. This initial increases must be due to some unknown heat effect, while the subsequent saturation or decrease (at higher temperatures, above 120 °C) must be due to the desorption of oxygen. It has been reported that, in molecular crystals, the complete elimination of the adsorbed oxygen molecules was possible only by sublimation in a high vacuum.[16] The temperature dependence of dark and photo currents observed after two or three heating cycles was inferred to be free from the above-mentioned heat effect and oxygen desorption effect. The values of activation energies (ΔE_d and ΔE_{ph}) shown in Table 1 were thus obtained.

Discussion

Effects of Air, Hot-press, and Irradiation with UV light or γ-Rays. It is well known that the ambient gas exerts significant effects on the electrical conduction

Table 1. Activation energies for dark and photo conductivities (ΔE_d and ΔE_{ph}) in a PVCz surface-type cell[a]

Sample	ΔE (eV)					
	ΔE_d		ΔE_{ph} (Visible light illumination)		ΔE_{ph} (UV light illumination)	
	low	high	low	high	low	high
Fresh film[c]	(b)	1.0—1.3 (120—200 °C)	0.06—0.20 (20—120 °C)	0.7—1.0 (~200 °C)	0.16—0.22 (20—120 °C)	0.16—0.22 (~200 °C)
Fresh film[d]	0.7—0.8 (50—120 °C)	—	0.3—0.6 (20—120 °C)	—	0.5—0.6 (20—120 °C)	—
Film irradiated with UV light[c]	0.47 (50—100 °C)	0.80 (80—200 °C)	0.20 (20—100 °C)	0.70 (~200 °C)	0.23 (20—130 °C)	0.68 (~200 °C)
Film irradiated with γ-rays[c]	0.4—0.5 (40—110 °C)	0.8—1.0 (~200 °C)	0.24 (20—130 °C)	0.40 (~200 °C)	0.23 (20—140 °C)	0.40 (~200 °C)

a) Activation energy (ΔE) is represented by the equation $i \propto \exp(-\Delta E/kT)$.
b) Only on the first heating, a fresh film showed a small dark current similar to the thermally stimulated current at this low temperature range. Thereafter, the current was too small to be measured.
c) In high vacuum under 3000 V/cm.
d) In air under 3000 V/cm.

in a surface-type cell.[18] The following effects of air on the electrical conduction were observed in a PVCz film: (a) an increase in the dark current with a lowering of ΔE_d; (b) an increase in the photocurrent in all the wavelength regions and a red shift of the threshold of the photocurrent; (c) a lowering of the α value of the light-intensity dependence of the photocurrent; (d) an increase in ΔE_{ph}, and (e) an increase in the rise time of the photocurrent and a long tail in the decay curve of the photocurrent.

The oxygen molecule acts as an electron acceptor because of its large electron affinity, and the resulting O_2^- molecule may act as a hole-trapping center.[19] These effects of air may be explained by supposing that, in the air, impurity levels acting as shallow hole-trapping centers are introduced into a PVCz film by oxygen molecules.

Such pre-treatments in the air as hot-press and irradiation by UV light or γ-rays had effects on the photocurrent similar to the effects of air. Any electron-accepting or hole-trapping levels may be introduced by these pre-treatments.

Origin of Both the Dark Current and the Photocurrent in the Visible and Near-IR Regions. The resemblance in the effects of the pre-treatments on the photocurrent in the visible and near-IR regions and on the dark current suggest that, in both cases, the carriers are generated from the same origins, which are increased by air, hot-press, or irradiation with UV light or γ-rays. In every film the value of ΔE_d was less than 1.3 eV. As this value is much smaller than the estimated band gap energy (~4.4 eV[20]), the intrinsic carrier generation must be ruled out. Other possible carrier generation process in the dark are (1) carrier injection from the electrode and (2) the ionization of acceptors or donors, which can release carriers by means of the thermal process.

The possibility of the carrier injection from the electrode can be ruled out on the basis of the following findings: (a) the dark current did not obey the Schottky equation, but Ohm's law[21]; (b) the electrode materials (Au, Ag, Cu, and Al) had no effect on the dark and photo currents,[21] and (c) the magnitude of the dark and photo currents was strongly influenced by UV pre-illumination or by repeated near-IR illuminations.

In a PVCz surface-type cell the dark current and the photocurrent may, therefore, be mainly due to the thermal or optical reexcitation of trapped carriers. In the pre-treated films, trapped carriers will increase with an increase in the number of trap centers introduced by the pre-treatments, thus resulting in an enhanced dark current and photocurrent in the visible and near-IR regions.

Activation Energy for Dark and Photo Conductions. As is evident from Table 1, the values of ΔE_d and ΔE_{ph} change considerably both with the temperature and with the wavelength of illuminated light. Except in the case of ΔE_{ph} for UV illumination in a fresh film, in every film the values of ΔE_d and ΔE_{ph} in the high temperature range are considerably larger than the values in low temperature range; the former values are also large as compared with those in the case of such aromatic hydrocarbons as anthracene. A similar phenomenon has been reported for polyethylene[23] and for the polymers prepared by glow-discharged polymerization.[24] In polyethylene Tanaka *et al.* have explained this phenomenon in terms of a "trapping conduction mechanism".[23] As has been mentioned above, both the dark current and the photocurrent in the visible and near-IR regions are due to the reexcitation of trapped carriers. The process of the reexcitation by light must not need a large activation energy. The large values of ΔE_{ph} in the high temperature range, therefore, suggest that these activation energies are needed mainly for carrier migration. A trapping conduction mechanism similar to the case of polyethylene is applicable to the photo- and dark-conductions in a PVCz surface-type cell as follows.

The exact profile of trap distribution is not yet available. However, if one considers a "hypothetical trap" which is defined as a discrete level corresponding to a special distribution of trapped carriers under conditions leading to a measured ΔE_d or ΔE_{ph}, then one can draw an energy diagram such as is shown in Fig. 6. In this diagram, a deep trap (E_{t4}) is also shown, though it has not been dicussed in this paper.

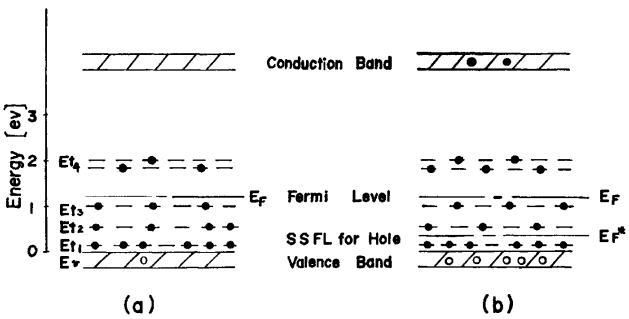

Fig. 6. Energy level model for a PVCz fresh film in high vacuum. As concerns the levels (E_{t1}~E_{t4}), see text.
(a) in the dark in low temperature range. (b) under UV or visible illumination in low temperature range.

Supposing that the Fermi level (E_F) exists between E_{t2} and E_{t3} or a little higher than E_{t3} below 120 °C, as the reexcitation of holes from the energy states much higher than E_F (E_{t3} or E_{t4} in the present case) is negligible, the energy states a little lower than E_F (E_{t2} or E_{t3} in the present case) will play an important role in

18) F. Gutmann and L. E. Lyons, "Organic Semiconductors," John Wiley & Sons, Inc., New York, (1967), p. 197.

19) H. Kokado and W. G. Schneider, *J. Chem. Phys.*, **40**, 2937 (1964). A. Bree and R. A. Kydd, *ibid.*, **40**, 1775 (1964).

20) W. Klöpffer, *Z. Naturforsch.*, **24a**, 1923 (1969).

21) As will be reported in the succeeding paper of this series,[22] sandwichtype cells were examined over a wide range of field strengths up to 330000 V/cm with several kinds of electrode materials. The information thereby obtained also suggests the impossibility of electrode injection.

22) K. Okamoto, S. Kusabayashi, and H. Mikawa, This Bulletin, **46**, 1953 (1973).

23) T. Tanaka and T. Inuishi, *Jap. J. Appl. Phys.*, **6**, 1371 (1967).

24) T. Hirai and O. Nakada, *Reports on Progress in Polymer Physics in Japan*, **VIII**, 333 (1965). A. Bradley, *Trans. Faraday Soc.*, **61**, 773 (1965).

trapping hole carriers. The ΔE_d value in this temperature range, which could not be measured in the present study, may thus be estimated to be E_{t2} or E_{t3}, that is, 0.7—1.0 eV or 1.0—1.3 eV. With UV illumination, some holes and electrons are created by the extrinsic mechanism[25] and the distribution of holes in the dark (Fig. 6(a)) changes, thus resulting in Fig. 6(b). The increasing concentration of holes in the valence band leads to a lowering of the Fermi level to the steady-state Fermi level for hole (E_F*), and the trap level below E_F* acts as a shallow trap and the level above E_F* as a deep trap.[26] Now, supposing that E_F* exists between E_{t1} and E_{t2}, the trap levels associated with E_{t2} must be filled with holes and the levels associated with E_{t1} must act as effective trapping centers for migrating holes. Therefore, the ΔE_{ph} value under UV illumination is 0.1—0.2 eV ($=E_{t1}$) in the low-temperature range.

In the case of visible illumination in the low-temperature range, the photocurrent is much larger than the dark current. Therefore, the steady-state Fermi level must be lowered so far as below E_{t2} according to the increase in the current under visible illumination. The trap levels associated with E_{t1} act as effective trapping centers for migrating holes, and the ΔE_{ph} value under visible illumination is 0.1—0.2 eV in the low-temperature range. Above 120 °C the Fermi level probably rises to much above E_{t3}. In the dark the trap levels associated with E_{t3} act as effective trapping centers and the ΔE_t value is 1.0—1.3 eV.

Under UV illumination the steady-state Fermi level is probably lowered so far as below E_{t2} according to the number of holes created, in the same manner as in the case of the low-temperature range, and the ΔE_{ph} value is 0.1—0.2 eV even at high temperatures. In the case of visible or near-IR illumination, the photocurrent is not so large as the dark current in the high-temperature range and the steady-state Fermi level for hole is lowered to near E_{t3} or E_{t2} at most. The ΔE_{ph} value in this case becomes 0.7—1.0 or 1.0—1.3 eV.

A similar explanation is possible for the conductions in the pre-treated films.

25) K. Okamoto, S. Kusabayashi, and H. Mikawa, This Bulletin, in press.

26) A. Rose, *RCA Rev.*, **1951**, 362, *Phys. Rev.*, **97**, 322 (1955).

BULLETIN OF THE CHEMICAL SOCIETY OF JAPAN, VOL. 46, 1953—1959 (1973)

The Photoconductivity of Poly(*N*-vinylcarbazole). II. Dark Conductivity in a Sandwich-type Cell

Kenichi OKAMOTO,* Shigekazu KUSABAYASHI,* and Hiroshi MIKAWA

Department of Applied Chemistry, Faculty of Engineering, Osaka University, Yamadakami, Suita, Osaka 565

(Received January 17, 1972)

The dark conductivity in a sandwich-type cell of PVCz films was investigated in a high vacuum, taking the temperature, the applied voltage, and the film thickness as parameters. In low fields, the conductivity was proportional to the applied voltage. In high fields, however, it was proportional to the fourth power of the applied voltage. This nonohmic dark conductivity in high fields may be attributed to the Pool-Frenkel effect. A model of the energy-level diagram is presented which can explain the dark conductivity in both low and high fields.

In the previous paper the authors have reported the photo and dark conductivities in a surface-type cell of poly-*N*-vinylcarbazole (PVCz) films.[1] Although PVCz has a large π-electron system as a pendant group, its dark conductivity is too small to be measured at moderate temperatures in a high vacuum. In the present paper, the dark conductivity was investigated in a sandwich-type cell. Interesting behavior was observed in the high-field conductivity, as will be mentioned below.

Experimental

PVCz was prepared as has been described in the previous paper.[1] A certain amount of a 5 wt% benzene solution of the polymer was poured onto a nesa-coated quartz plate, and the solvent was evaporated slowly in the dark. Films 8, 15, and 24 μ thick were thus prepared, to which three lead wires were attached by using silver paste, as is shown in Fig. 1 (a). The film with lead wires was set in the apparatus

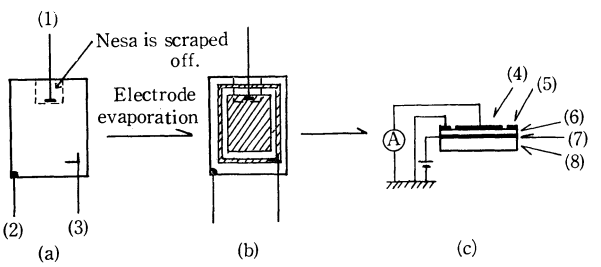

Fig. 1. Sandwich-type cell.
(1) metal electrode lead wire, (2) nesa-electrode lead wire, (3) guard ring lead wire, (4) evaporated metal electrode, (5) evaporated guard ring electrode, (6) PVCz film, (7) nesa-electrode coated on quartz plate, (8) quartz plate (20×25×1 mm).

* Present address: Department of Chemical Engineering, Faculty of Engineering, Yamaguchi University, Ube, Yamaguchi 755.

1) K. Okamoto, S. Kusabayashi, and H. Mikawa, This Bulletin, **46**, 1948 (1973).

for the electrical measurement described in the previous paper and was kept in a high vacuum (10^{-7} mmHg) for several hours. Semitransparent main and guard electrodes were evaporated on the film to prepare the sandwich-type cell, as is shown in Fig. 1 (b, c). Several kinds of metals, such as Au, Ag, Cu, and Al, were used as the electrode material. The sandwich-type cell thus prepared was subjected to the electrical conductivity measurements after it had stood for a day in the dark in a high vacuum, without exposure to air after the evaporation of the metal electrodes. The measurements were carried out by means of a vibrating-reed electrometer (Takeda Riken TR 84M) in a high vacuum (10^{-7} mmHg).

Results

Time-dependence of the Dark Current. The dark current slowly decreased with the time after applying the voltage, as is shown in Fig. 2. The dark current requires from several hours to a day to reach a steady-state value. After the voltage was taken off, a fairly large back current was observed in the short circuit.

In low fields the dark current showed the time-dependence given by Eq. (1), where n was 0.4—0.7, and reached the steady-state value in scores of minutes or in a few hours at room temperature, as is shown in Fig. 3.

$$i_d \propto t^{-n} \qquad (1)$$

In high fields the dark current obeyed Eq. (1) for only a short period after the voltage was applied and the current continued to decrease slowly with the time even after ten hours. It reached the steady-state value after more than 20 hr at room temperature.

Voltage-dependence of the Dark Current. The voltage-dependence of the forward dark current (abbreviated as "dark current") is shown in Fig. 4(a), taking the time after the application of voltage as a parameter, and in Fig. 4(b), taking the temperature and the polarity of the electrode as parameters. The voltage-dependence of the dark current showed a dramatic change at a certain voltage (transition voltage, V_t); that is, the dark current was proportional to the applied voltage below the transition voltage and to the fourth power of the applied voltage above that. This voltage-dependence

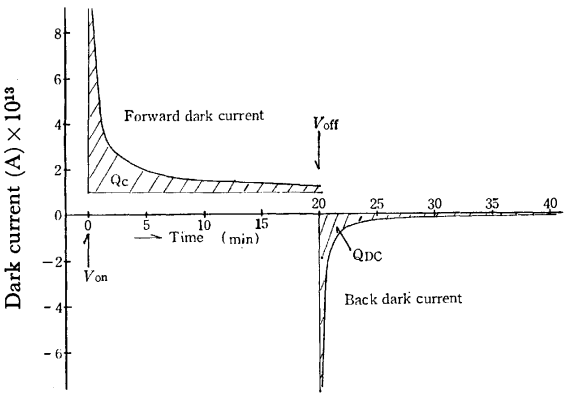

Fig. 2. Dark current-time response curves in the sandwich-type cell.
Au-PVCz-Nesa sandwich-type cell, Film thickness; 15 μ, applied voltage; 20 V (nesa-electrode biased positively), 20 °C.

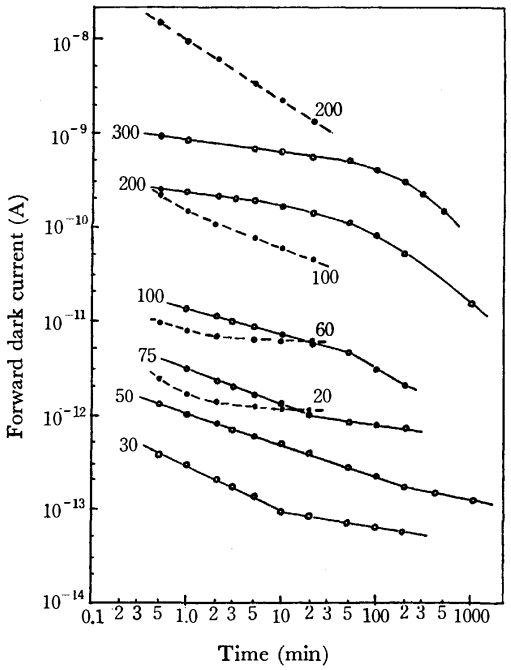

Fig. 3. Time dependence of the dark current in the Au-PVCz-Nesa sandwich-type cell.
The numerical values show the applied voltage when the nesa-electrode was biased positively. Solid lines; at 20 °C, dotted lines; at 106 °C. Film thickness; 15 μ.

was observed for the dark current (charging absorption current) within several minutes after the application of the voltage as well as for the steady-state dark current. The transition voltage changed with the temperature, the polarity of the electrode, and the thickness of the film. In the asymmetric Au–PVCz–Nesa sandwich-type cell of the film 15 μ thick, the transition voltage was about 35 V at room temperature or 60 V at 106 °C when the nesa-electrode was biased positively, while the transition voltage was about 90 V when the nesa-electrode was biased negatively at 20 °C. On the other hand, it was 60—80 V at 20 °C in the symmetric Au–PVCz–Au sandwich-type cell. Sandwich-type cells with other electrode materials (Ag, Cu, and Al) acted the same.

At a constant applied voltage, the dark current was inversely proportional to the thickness of the film below the transition voltage and apparently so to the fourth power of the thickness above the transition voltage, as is shown in Fig. 5(a). The transition voltage was proportional to the thickness of the film, as is shown in Fig. 5(b).

Temperature-dependence of the Dark Current. Figure 6(a) shows the temperature-dependence of the ohmic dark current below the transition voltage. Though the measurement was carried out after the cell had stood with an applied voltage of 7000 V/cm for a day in the dark, on the first heating the dark current behaved in a manner similar to that of the thermally stimulated current. After the subsequent cooling and heating cycles, the dark current showed a reproducible temperature-dependence. The activation energy[2] was

2) The activation energy (ΔE) is represented by the equation: $i_d \propto \exp(-\Delta E/kT)$.

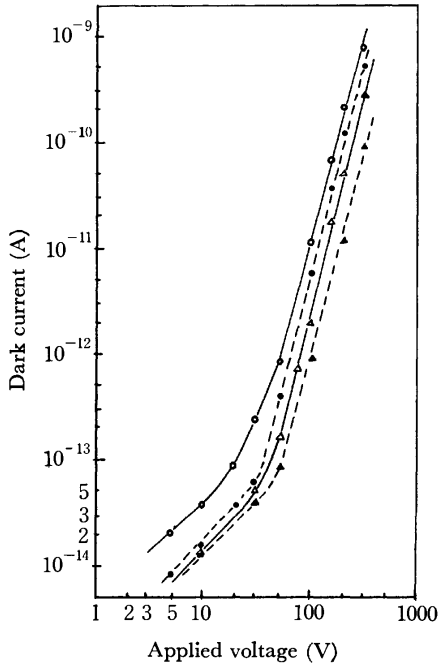

Fig. 4(a). Voltage dependence of the dark current in the sandwich-type cell.
Au-PVCz-Nesa sandwich-type cell, film thickness 15 μ. The nesa-electrode was biased positively at 20 °C. Dark current was measured the following minutes after application of the voltage; —○— 2 min., ---●--- 20 min., —△— 180 min., and ---▲--- 1000 min.

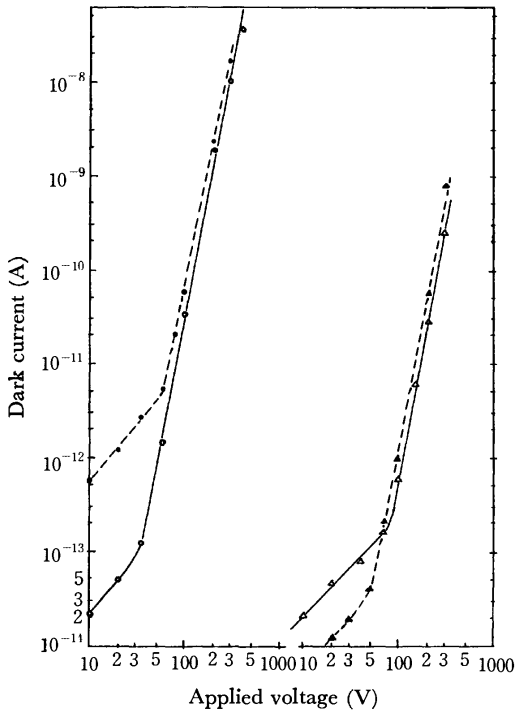

Fig. 4(b). Voltage dependence of the dark current in the sandwich-type cell. Dark current was measured 10 minutes after applying voltage.
Au-PVCz-Nesa sandwich-type cell (film thickness 15 μ); —○— at 20 °C, nesa-electrode biased positively, ---●--- at 106 °C, nesa-electrode biased positively, —△— at 20 °C, nesa-electrode biased negatively. Au-PVCz-Au sandwich-type cell (film thickness 15 μ); ---▲--- at 20 °C.

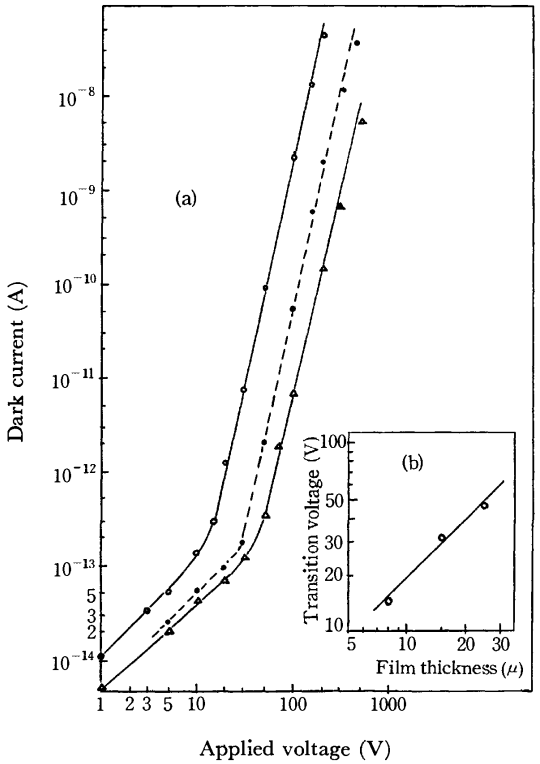

Fig. 5. Effect of the film thickness on the dark conductivity in the sandwich-type cell.
Dark current was measured in Au-PVCz-Nesa sandwich-type cell (film thickness 15 μ) 15 minutes after applying voltage at 27 °C.
(a) Dark current *vs.* applied voltage.
—○— 8 μ thick, ---●--- 15 μ thick, —△— 24 μ thick.
(b) Transition voltage *vs.* film thickness.

1.1—1.3 eV, which was identical with that measured in the surface cell in the high-temperature range (100—200 °C) in a high vacuum. After the thermodynamic equilibrium had been built up, the dark conductivity was very small; the specific conductivity was only $1\times10^{-18}\ \Omega^{-1}\,cm^{-1}$ at 90 °C.

Figure 6(b) shows the temperature-dependence of the nonohmic dark current above the transition voltage. In the applied field (200000 V/cm), the activation energy of this dark current was 0.6—0.8 eV, which was considerably smaller than that of the ohmic dark current.

Discharging Absorption Current. When the applied voltage was taken off, the back dark current was observed in the short circuit. This back dark current is referred to the discharging absorption current. For many cells this current followed Eq. (1), as is shown in Fig. 7(a), and the n value was 1.0—1.4 regardless of the field strength. The discharging absorption current, was proportional to the pre-applied voltage in any voltage region, as is shown in Fig. 7(b). It should be noted that the discharging absorption current showed a linear dependence on the pre-applied voltage even in the high-voltage region, where the dark current showed the nonohmic dependence.

The temperature-dependence of the discharging absorption current was small in comparison with that of the dark current; that is, the discharging absorption

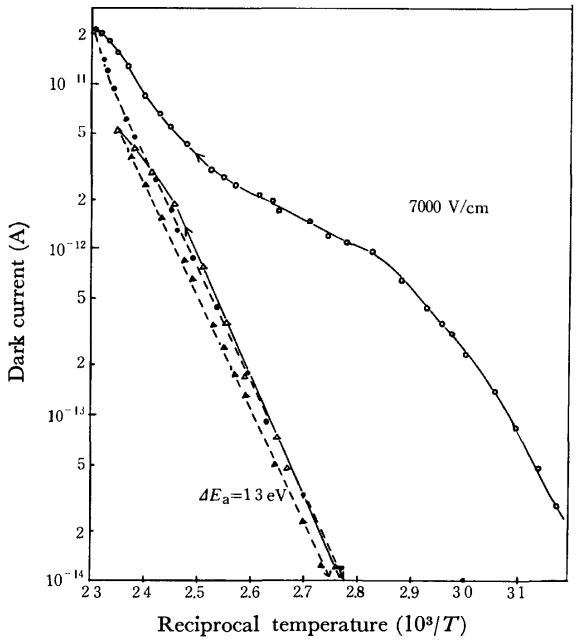

Fig. 6(a). Temperature dependence of the ohmic dark current at low field in the PVCz sandwich-type cell.

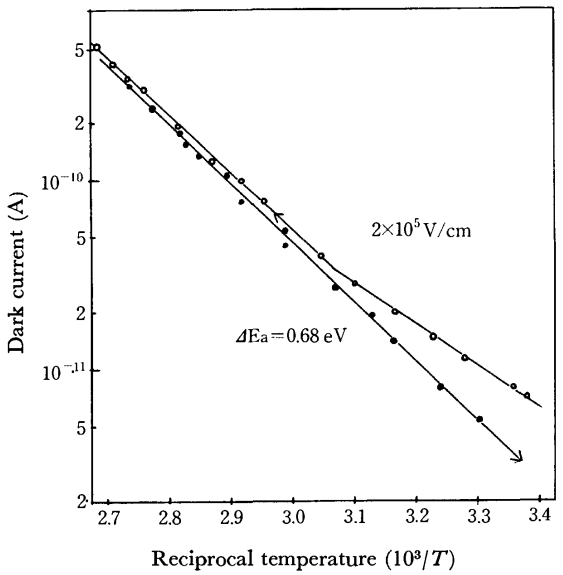

Fig. 6(b). Temperature dependence of the nonohmic dark current at high field in the PVCz sandwich-type cell.

current was approximately doubled in magnitude with a rise in the temperature from 20 to 100 °C.

The amount of the electric charge carried by the charging absorption current, which is indicated by the symbol Q_C in Fig. 2, did not depend on the structure of the electrodes, but that carried by the discharging absorption current (Q_{DC} in Fig. 2) was affected by the structure of the electrodes. In the asymmetric Au–PVCz–Nesa sandwich-type cell, the Q_{DC} value was about three times that in the symmetric Au–PVCz–Au sandwich-type cell. Furthermore, the Q_{DC} value was much smaller than the Q_C value; that is, the Q_{DC}/Q_C ratio was 1 : 2 in the asymmetric sandwich-type cell and 1 : 6 in the symmetric one in the ohmic voltage region.

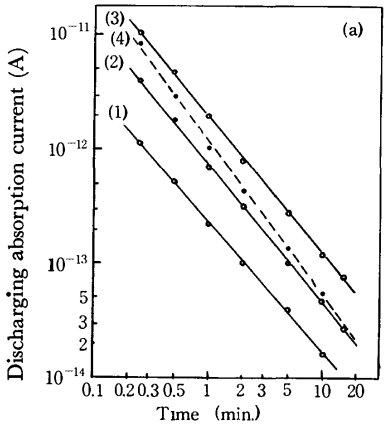

Fig. 7(a). Time dependence of the discharging absorption current in the Au-PVCz-Nesa sandwich-type cell. $i_{DC}= i_0 t^{-n}$, $n=1.1-1.4$.
Film thickness; 15 μ, nesa-electrode biased positively.
(1) 35 V, 20 °C, (2) 100 V, 20 °C, (3) 300 V, 20 °C, (4) 100 V, 106 °C.

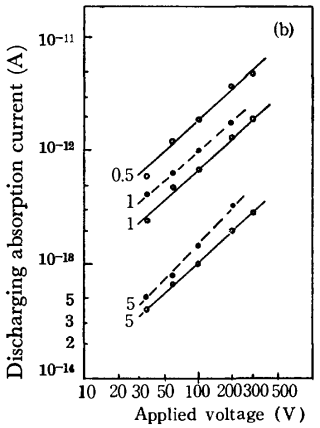

Fig. 7(b). Voltage dependence of the discharging absorption current in the Au-PVCz-Nesa sandwich-type cell.
Film thickness; 15 μ. The numerical values show the time (min.) after closing the external circuit. Solid lines are measured at 20 °C and dotted lines at 106 °C.

Discussion

Absorption Current. It is well known that, for many insulating polymers, both charging and discharging absorption currents obey Eq. (1), where the n value is equal to 0.7—1.1.[3-5] In the case of the polymers such as polymethylmethacrylate, the two absorption currents equal one another in magnitude (superposition principle) and are attributable to the slow orientation of the permanent electric dipoles or ionic charges by the applied voltage.[3] On the other hand, for the polymers such as polyethylene the superposition principle fails to hold and the Q_C value is usually several times larger than the Q_{DC}. Another mechanism besides the orientation of the permanent electric dipoles (for example, the accumulation or dissipation of space charge) must, therefore, be used

3) R. J. Munick, *J. Appl. Phys.*, **27**, 1114 (1956).
4) S. Ieda and G. Sawa, *J. Inst. Elect. Eng. Jap.*, **89**, 812 (1969).
5) G. Lengyel, *J. Appl. Phys.*, **37**, 807 (1966).

for both absorption currents of these polymers.[3,6]

In the case of PVCz, the discharging absorption current had an n value, 1.1—1.4, similar to those of polyethylene and others, but the charging absorption current showed a very small n value, 0.1—0.7, especially in the high-voltage region. The Q_C value was two or six times larger than the Q_{DC} value, and the superposition principle failed to hold. Both absorption currents in a PVCz sandwich-type cell, therefore, should not be attributed to the orientation of the permanent dipoles by the applied voltage, but to another mechanism in the same manner as in the case of polyethylene. The accumulation of space charges could be the reason for the charging absorption current in the low-voltage ohmic region, but not for that in the high-voltage nonohmic region, because the back electromotive force which would be caused by that is too large compared with the applied voltage.

Lindmayer has applied Eq. (2) to the discharging absorption current in the Au–SiO_2–Si system; he attributed this relation to the asymmetric field caused by the space charges trapped inhomogeneously in the bulk by the trap levels distributed energetically:[7]

$$I_{ext}(=i_{DAC}) = f \cdot g \cdot C \cdot V_a/t \qquad (2)$$

where I_{ext}, is the discharging absorption current; C, the capacity of the sandwich-type cell; f, the charge in the insulator divided by $C \cdot V_a$; V_a, the applied voltage; g, the charge appearing in the discharging current (Q_{DC}) divided by $C \cdot V_a$ and t, the time after the electrodes were short-circuited. Now, Eq. (2) was used for the PVCz sandwich-type cell the following $f \cdot g$ values were obtained; $f \cdot g = 0.8—1.0 \times 10^{-3}$ (20 °C) or $1.2—1.6 \times 10^{-3}$ (106 °C). These values are in agreement with the requirement that $f \cdot g < 0.06$.[7]

The Q_{DC} value in the asymmetric Au–PVCz–Nesa sandwich-type cell was larger than that in the symmetric Au–PVCz–Au one. The asymmetric structure of the electrodes, therefore, seems to contribute to the formation of the asymmetric field to a fairly large extent.

Ohmic Dark Current under a Low Field Strength. The ohmic dark current under a low field strength in a sandwich-type cell showed a behavior similar to that in a surface-type cell described in the previous paper.[1] The dark current increased upon UV-light pre-illumination and decreased upon repeated IR-light illumination. The activation energy of the ohmic dark current was quite small, while the dark current was fairly large, because of the effect of the previous history. After the thermodynamic equilibrium was achieved, it was, however, the same value, 1.0—1.3 eV, as that observed in a surface-type cell in a high vacuum in the high-temperature range.[1] These facts suggest that the ohmic dark current in a sandwich-type cell may be due to the thermal reexcitation of the trapped carriers, just as in the case of a surface-type cell.

On the other hand, the considerable effect of air on the dark conductivity observed in a surface-type cell was not observed for a sandwich-type cell; that is, there were no significant differences in the magnitude of the dark current and the dark activation energy between that in the air and in a high vacuum. This suggests that the trap level which gave an activation energy of 0.7—1.0 eV in a surface-type cell (trap level E_{t2} shown in Fig. 6 in the previous paper[1]) is negligibly small in a sandwich-type cell. This trap level was introduced by air or the irradiation of UV-light or γ-ray, and may, therefore, be attributed to some surface impurity. In a sandwich-type cell, the layer containing both some surface impurity and adsorbed oxygen molecules will be covered by the evaporated electrode layer.

Nonohmic Dark Current under a High Field Strength. The nonohmic dark current under a high field strength was different from the ohmic dark current under a low field strength in the following three characteristics; (1) $i_d \propto V^4$, (2) a small activation energy, and (3) the dark current decreased very slowly with time. The dark current with a superlinear dependence on the applied voltage has often been attributed to the space-charge limited current (SCLC), the Schottky conductivity, or the Poole-Frenkel conductivity.[8]

When there are trap levels with an energetic distribution such as an exponential one, the SCLC is proportional to the n-th power ($n>1$) of the applied voltage and the transition voltage from the ohmic current to the SCLC is proportional to the second power of the film thickness.[9,10] This kind of SCLC has been reported for anthracene,[10] stilbene,[11] and polyethyleneterephthalate.[12] In a sandwich-type cell of PVCz film, the nonohmic dark current was proportional to the fourth power of the applied voltage and inversely proportional to the same power of the film thickness. The nonohmic dark current, therefore, showed the same value for films with different thicknesses under the same field strength; that is, there was no effect of the film thickness. Furthermore, the transition voltage was

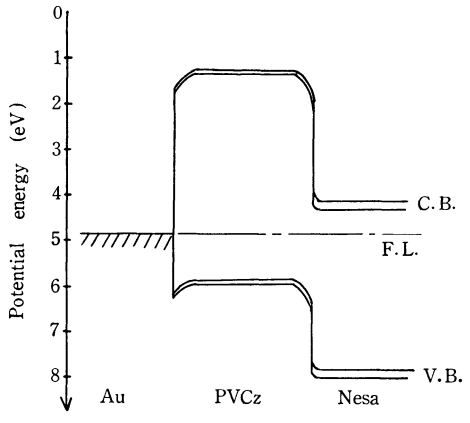

Fig. 8. Energy level diagram of the Au-PVCz-Nesa system.

6) R. H. Partridge, *Polym. Lett.*, **5**, 205 (1967).
7) J. Lindmayer, *J. Appl. Phys.*, **36**, 196 (1965).
8) D. R. Lamb, "Electrical Conduction Mechanisms in Thin Insulating Films," Methuen and Co., Ltd., London, p. 3 (1967).
9) A. Rose, *Phys. Rev.*, **97**, 1538 (1955).
10) P. Mark and W. Herfrich, *J. Appl. Phys.*, **33**, 205 (1962).
11) N. I. Gritsenko and M. V. Kurik, *Phys. State. Sol.* (a), **3**, K57 (1970).
12) G. Caserta, B. Rispoli, and A. Serra, *Phys. Stat. Sol.*, **35**, 237 (1969).

proportional to the film thickness. The carrier injection from the electrodes is difficult, as will be discussed below. The nonohmic dark current can not, therefore, be explained by the SCLC for these three reasons.

Figure 8 shows the energy diagram for the Au–PVCz–Nesa sandwich-type cell. The work function of gold is 4.83 eV.[13] The ionization potential and the electron affinity of nesa coating are 7.2 and 3.6 eV respectively.[14] The ionization potential of PVCz has been reported to be 6.1 eV from the measurement of the photoinjected hole current from the gold electrode,[15] and its electron affinity has been estimated to be only the polarization energy, the estimated value being 1.5 eV.[16] From Fig. 8 the hole injection from a gold electrode to PVCz is most conceivable, and the electron injection from a gold or nesa electrode to PVCz is not conceivable. As the nesa coating is a *n*-type semiconductor, the possibility of a hole injection from a nesa electrode to PVCz can be neglected. When a nesa-electrode was biased positively, the transition voltage was usually smaller and the nonohmic dark current was usually larger, as is shown in Fig. 4(b). For the nonohmic dark current to be attributed to the Schottky emission, an electron injection from a gold electrode to PVCz must be supposed. This injection, however, is difficult, as has been discussed above. The other electrode materials (Ag, Al, and Cu) which have a lower work function than that of Au, did not affect either the magnitude of the dark current or the transition voltage. From these facts, it can be said that the nonohmic dark current can not be explained by the Schottky emission from the electrode.

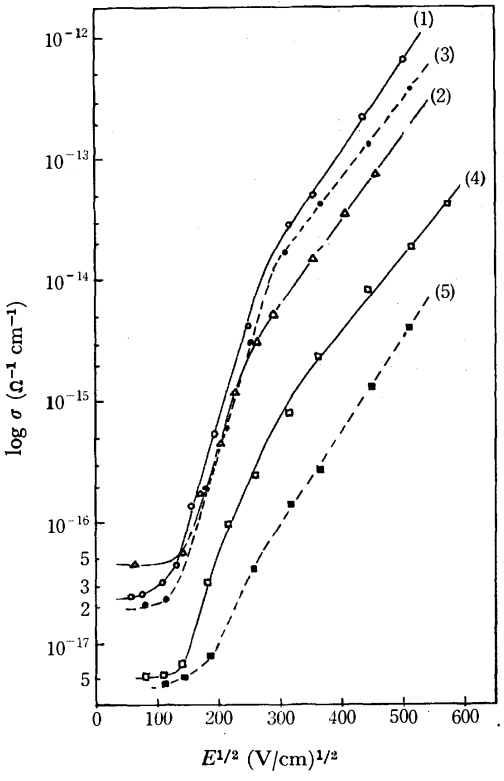

Fig. 9. Poole-Frenkel plot of dark conductivity *vs.* applied field for the PVCz sandwich-type cell.
(1) 8μ thick, 27 °C, 15 min. after application of voltage.
(2) 15 μ thick, 27 °C, 15 min. after application of voltage.
(3) 24 μ thick, 27 °C, 15 min. after application of voltage.
(4) 15 μ thick, 20 °C, 20 min. after application of voltage.
(5) 15 μ thick, 20 °C, steady state value.

Now the application of the Poole-Frenkel effect was attempted in the case of the nonohmic dark current. This effect is not concerned with the electrode limited conductivity, but with the bulk conductivity. The Poole-Frenkel effect gives the conductivity a field dependence of this form:[17]

$$\sigma_{PF} = \sigma_0 \exp(\beta_{PF} E^{1/2}/kT) \quad (3)$$

$$\beta_{PF} = (q^3/\pi K \varepsilon_0)^{1/2} \quad (4)$$

where σ_0 is the low-field conductivity of the system, q is the unit of electric charge, ε_0 is the permitivity of free space, K is the high-frequency dielectric constant of the film, and E is the electric field strength in the film. When the voltage-dependence of the dark current given in Figs. 4 and 5 is replotted, with log σ as ordinate and $E^{1/2}$ as abscissa, a straight line is obtained in the high field strength region, as is shown in Fig. 9. The Poole-Frenkel constant, β_{FP}, was obtained from the slope of the straight line in Fig. 9; it is shown in Table 1. On the other hand, this constant is calculated to be 4.1×10^{-5} eV m$^{1/2}$ V$^{-1/2}$ from Eq. (4) by assuming K as 3.0.[18] As is shown in Table 1, the agreement between the calculated and the experimentally found values of the β_{PF} constant are very good. The nonohmic dark current under the high-field strength in the sandwich-type cell of the PVCz film thus satisfies well Eqs. (3) and (4) and may, therefore, be attributed to the Poole-Frenkel conductivity. A similar behavior has been reported for the high-field conductivity of the polymers, such as polyethylene[19] and polyacrylonitrile,[20] and has been attributed to the Poole-Frenkel effect.

In order to exhibit the Poole-Frenkel conductivity under a high-field strength, a trap is required to be

TABLE 1. THE β_{PF} VALUES OBSERVED FOR THE PVCz FILMS

Film thickness	β_{PF} Observed[a]	β_{PF} Calculated
8μ	4.3×10^{-5} eV (m/V)$^{1/2}$	
15	4.4×10^{-5} [b]	4.1×10^{-5} eV (m/V)$^{1/2}$
24	4.0×10^{-5}	

a) Measured for the dark current in 15 minutes after application of voltage at 27 °C.
b) The same value was obtained for the steady-state dark current at 20 °C.

13) P. A. Anderson, *Phys. Rev.*, **115**, 553 (1959).
14) M. Nagasawa, *Oyo Buturi*, **39**, 465 (1970); H, Hurukawa, T. Takeuchi, A. Ebina, and T. Takahashi, The report for the JSPS 125th Committee. (Conversion between Light and Electricity).
15) A. I. Lakatos and J. Mort, *Phys. Rev. Lett.*, **21**, 1444 (1968).
16) J. H. Sharp, *J. Phys. Chem.*, **71**, 2587 (1967); W. Klöppfer, *Z. Naturforsch.*, **24a**, 1923 (1969).
17) J. G. Simmons, *Phys. Rev.*, **155**, 657 (1967).
18) R. C. Hughes, *Chem. Phys. Lett.*, **8**, 403 (1971).
19) T. Tanaka, Thesis, Osaka University (1969); S. Kato, G. Sawa, and S. Ieda, The anual meeting of the Institute of Electrical Engineering of Japan, No. 242 (1971).
20) O. Nakata and T. Hirai, *Rep. Progr. Poly. Phys. Jap.*, **8**, 339 (1965).

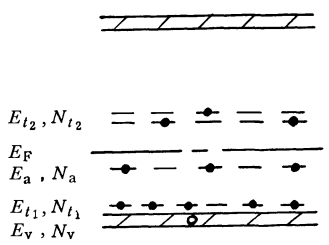

Fig. 10. Energy level diagram explaining the dark conductivity in PVCz sandwich-type cell.
The symbols E_v (=0), E_{t_1} (=0.1—0.3 eV), E_{t_2} (=2 eV), E_a (=1.0—1.3 eV) and E_F express the potential energy of each level measured above the valence band edge. The values in parentheses were obtained from the activation energy for the dark current. The symbols N_v, N_{t_1}, N_{t_2}, and N_a express the density of each level.

positively (or negatively) charged; that is, it must be charged when empty and uncharged when filled (donor or aceeptor), and these traps must be the main source of the dark conductivity under a low-field strength. A model must, therefore, be presented which can explain both the low-field and high-field conductivities. The energy level, 0.7—1.0 eV, above the valence band was negligibly small in the sandwich-type cell, as has been mentioned above, and so it has been excluded from Fig. 10. An acceptor level was considered as the trap level causing the Poole-Frenkel effect, because holes are the majority carriers in PVCz.

We located the position of the Fermi level by equating e number of holes missing from the acceptor centers with the number of the deep traps occupied by holes, the number of holes in the valence band being negligibly small. The thermodynamic Fermi level, E_F, as measured above from the valence band edge, is therefore, given by Eq. (5).

$$E_F = E_a - kT\log\{(N_a - N_{t2})/N_a\} \quad (5)$$

At a zero (or low) field, the number of free holes, p, is given by:

$$P = \{N_v(N_a - N_{t2})/N_a\}\exp(-E_a/kT) \quad (6)$$

The low-field conductivity σ_0 is, therefore, given by:

$$\sigma_0 = Pq\mu_h = \{q\mu N_v(N_a - N_{t2})/N_a\}\exp(-E_a/kT) \quad (7)$$

where μ_h is the hole carrier mobility. In the high field, the acceptor barrier is lowered by the Poole-Frankel effect, so that the number of free holes in the valence band increases to:

$$P = \{N_v(N_a - N_{t2})/N_a\}\exp\{-(E_a - \beta_{PF}E^{1/2})/kT\} \quad (8)$$

and the dark conductivity is given by Eq. (3). The magnitude of the lowering of the activation energy for the dark conductivity was 0.3—0.5 eV at the field strength of 2×10^5 V/cm, which is in approximate agreement with the calculated value, 0.2 eV. Thus, the energy-level model given in Fig. 10 can give a reasonable explanation of the dark conductivity in the sandwich-type cell of the PVCz film in both low- and high-fields.

The authors wish to thank the Fuji Photo Film Co. for its finacial support of this work.

BULLETIN OF THE CHEMICAL SOCIETY OF JAPAN, VOL. 46, 1959—1963 (1973)

Lone Pair Ionization Potentials of Carboxylic Acids Determined by He(I) Photoelectron Spectroscopy

Iwao WATANABE, Yu YOKOYAMA, and Shigero IKEDA

Department of Chemistry, Faculty of Science, Osaka University, Toyonaka, Osaka 560

(Received October 2, 1972)

Photoelectron spectra of some simple carboxylic acids and halogen substituted acetic acids were observed. Each spectrum contains a band which is associated with the ionization from an oxygen lone pair (n_O) orbital of carboxyl group. The band associated with the n_O orbital is clearly separated from other bands, and its shape and width are quite similar among the various carboxylic acids. In the spectra of halogen substituted acetic acids, n_O band appears around the region of the lone pair bands of halogen atoms. The ionization potentials for oxygen lone pair orbital of carboxylic acids are measured and compared with the results of some semi-empirical SCF MO calculations. The agreements are quite satisfactory when ionization potentials are obtained from the difference of total energies of neutral molecule and its corresponding cation calculated using CNDO/2 or INDO method. MINDO/2 method also gives excellent values when Koopmans' theorem is applied.

When a certain functional group of a molecule is expected to play a special role in a chemical reaction, it is desired to know the intrinsic properties of the group. There are many physicochemical techniques being used for that purpose, *e.g.* IR, Raman, UV, NMR, *etc.* If a functional group has electron orbitals which are considered to be essentially localized on the group, the orbital energies should be a measure of the intrinsic properties of the group, too. The orbital energies have usually been determined experimentally as ionization potentials of molecules from vacuum ultraviolet absorption spectrum, electron impact, or

photoionization method. Photoelectron spectroscopy, developed by Turner *et al.*,[1] has recently been recognized to have great potentialities as a tool which measures ionization potentials of various free molecules. It enables us to observe all orbitals of molecules which have less binding energy than the energy of irradiating light, frequently helium resonance line 584 Å (21.22 eV). The shape and/or structure of each band in the high resolution photoelectron spectrum are useful for the assignment of the bands.

Carboxyl group is known to have an oxygen lone pair (n_o) orbital and π orbitals. Theoretical calculations predict that the n_o orbital is composed mainly (50—80 per cent) of carbonyl oxygen atomic orbitals in various carboxylic acids.

It was our interest to study the extent of disappearance of the feature of these particular bands in the photoelectron spectra and the orbital energy variation as carboxylic acid molecule becomes larger. This paper deals with the results of some simple mono carboxylic acids and halogen substituted acetic acids. They are compared with the results of semi-empirical molecular orbital calculations such as CNDO/2,[2] INDO,[2] and MINDO/2[3] method to know how well these calculations can predict the ionization potentials of various carboxylic acids.

Experimental

The details of the photoelectron spectrometer used have already been reported.[4] The exciting light was He(I) resonance line which was produced by DC discharge through a glass capillary with a hollow cathode. The electron energy analyser was of an electrostatic type with parallel plates coated with benzene soot. With this spectrometer the peak width of Xe $^2P_{3/2}$ was 27.5 meV. Although the most of the sample gases were measured at this resolution, we had to decrease the resolution to about 50 meV for measuring monoiodo acetic acid, since its vapor pressure was small.

All samples were of G.R. grade and used without any further purification. Variations of appearance potentials of photoelectron peaks for carboxylic acids during measurements were so large that preliminary mixing of reference gas, xenon, into the sample gas was essentially needed to measure the ionization potentials accurately. Usually the spectra were measured after more than 30 min running of sample gas, since shift of the kinetic energy of photoelectron to lower energy side with the elapse of time was always noticed.

Results and Discussion

In Fig. 1, the photoelectron spectrum of formic acid is shown. At least five bands are distinguishable and three of them have clear vibrational structures. The spectrum appears quite similar to the spectrum

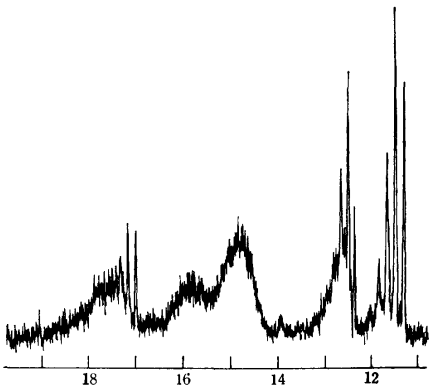

Fig. 1. Photoelectron spectrum of formic acid.

reported by Turner and co-workers.[1,5] However the structures of the second band are somewhat different from their results. Measurements for DCOOD, DCOOH, and HCOOD have also been performed and their vibrational structures have been studied. The details of the results will be reported elsewhere.[6]

In Figs. 2—5, the spectra of a series of aliphatic carboxylic acids are shown. The larger the alkyl group, the less clear the vibrational structures, and the closer the bands overlap. However it is observed that the first band is always separated from the second, that its shape and width are much the same, and that there always appears a band at a potential of 16—18 eV.

The spectra of trifluoro-, monochloro-, monobromo-,

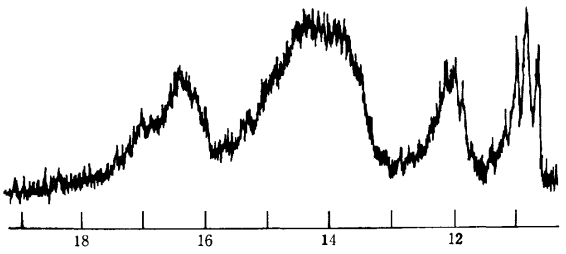

Fig. 2. Photoelectron spectrum of acetic acid.

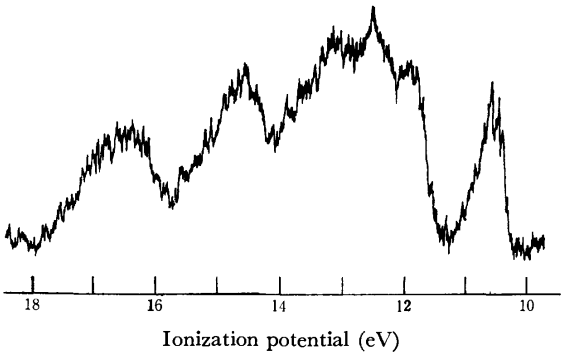

Fig. 3. Photoelectron spectrum of propionic acid.

1) D. W. Turner, C. Baker, A. D. Baker, and C. R. Brundle, "Molecular Photoelectron Spectroscopy," Wiley-Interscience, New York (1970).

2) J. A. Pople and D. L. Beveridge, "Approximate Molecular Orbital Theory," McGraw-Hill, New York (1970).

3) N. Boder, M. J. S. Dewar, A. Harget, and E. Haselbach, *J. Amer. Chem. Soc.*, **92**, 3854 (1970).

4) Y. Yokoyama, I. Watanabe, and S. Ikeda, *Bunseki Kagaku*, **20**, 1502 (1971).

5) C. R. Brundle, D. W. Turner, M. B. Robin, and H. Basch, *Chem. Phys. Lett.*, **3**, 292 (1969).

6) I. Watanabe, Y. Yokoyama, and S. Ikeda, *ibid.*, **19**, 406 (1973).

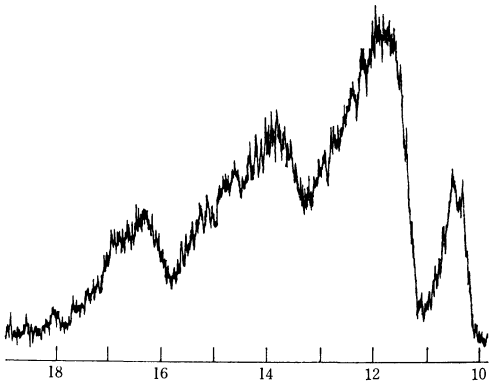

Fig. 4. Photoelectron spectrum of *n*-butyric acid.

and monoiodo-acetic acids are shown in Figs. 6, 7, 8, and 9, respectively. Although the intensity of the peaks of trifluoroacetic acid is relatively weak and the spectrum has a lot of noise, six bands are clearly separated. In this spectrum no vibrational structure is distinguishable. The first and the second bands are a little broader than those of acetic acid and, however, the band shapes and the separation of these bands are almost identical. The molecular orbital calculations indicate these bands are associated with the ionizations from n_0 and antisymmetric π (π_2) orbital of carboxyl group.

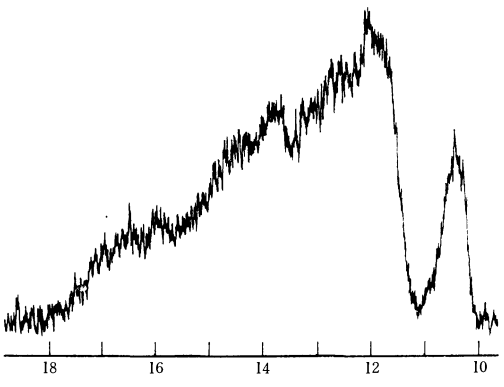

Fig. 5. Photoelectron spectrum of *iso*-butyric acid.

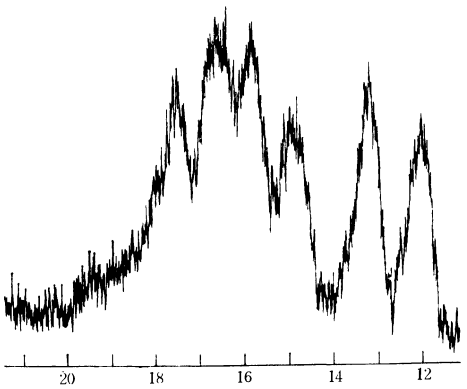

Fig. 6. Photoelectron spectrum of trifluoroacetic acid.

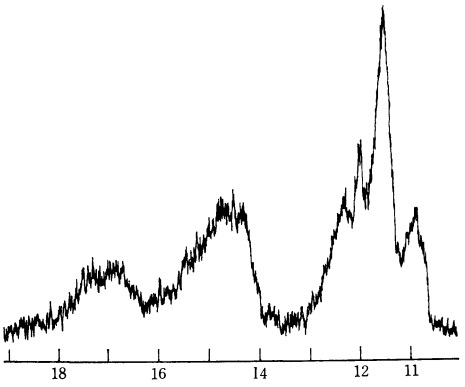

Fig. 7. Photoelectron spectrum of monochloroacetic acid.

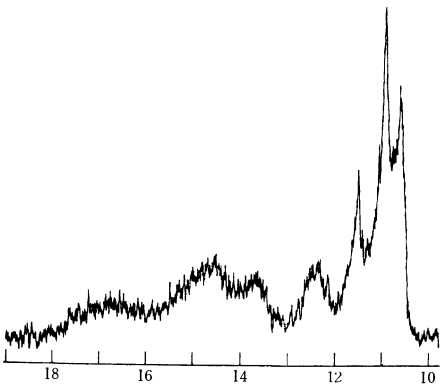

Fig. 8. Photoelectron spectrum of monobromoacetic acid.

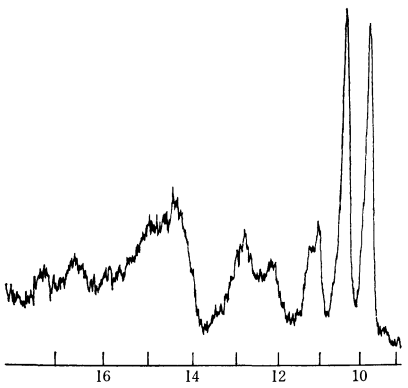

Fig. 9. Photoelectron spectrum of monoiodoacetic acid.

The spectra of the other three halogen substituted acetic acids are more complex, since around the bands from the orbitals localized mainly on the carboxyl group appear halogen lone pair bands which split into two components by the effect of the spin-orbit interaction. The spin-orbit splittings for many molecules containing halogen atoms have been reported to be about 80 meV for chlorine, 0.3 eV for bromine, and 0.6 eV for iodine.[1,7] With the aid of these values the

7) a) A. B. Cornford, D. C. Frost, C. A. McDowell, J. L. Ragle, and I. A. Stenhouse, *J. Chem. Phys.*, **54**, 2651 (1971); *b*) J. L. Ragle, I. A. Stenhouse, D. C. Frost, and C. A. McDowell, *ibid.*, **53**, 178 (1970).

TABLE 1. IONIZATION POTENTIALS FOR OXYGEN LONE PAIR ORBITALS (eV)

	CNDO/2		INDO		MINDO/2	P. I.	Present work	
	a)	b)	a)	b)	a)	c)	Vertical	Adiabatic
HCOOH	14.69	12.11	13.70	11.38	11.44	11.05	11.52	11.33
CH_3COOH	13.87	11.22	12.96	10.61	10.95	10.37	10.84	10.65
C_2H_5COOH	13.46	11.01	12.65	10.42	10.65	10.24	10.72	10.54
$CH_3(CH_2)_2COOH$	13.33	10.89	12.51	10.31	10.46	10.16	10.64	10.46
$(CH_3)_2CHCOOH$	13.28	10.87	12.55	10.32	10.57	10.02	10.50	10.33
$CH_3(CH_2)_3COOH$	13.21	10.84	12.42	10.26	10.29		10.5 (3)	
$(CH_3)_2CHCH_2COOH$	13.18	10.74	12.43	10.20	10.45		10.5 (1)	
CF_3COOH	14.56	12.82	13.87	12.26			12.00	
$ClCH_2COOH$	13.75	11.55					10.99	
$BrCH_2COOH$							11.0	
ICH_2COOH							11.03	

a) Obtained by the use of Koopmans' theorem.
b) The difference between the total energies of molecule and its corresponding cation.
c) The results of photoionization method. Ref. 8.
Ionization potentials of carboxylic acids determined by others are, formic (adia. 11.33,[d] 11.35,[e] vert. 11.51,[d] 11.52[e]), acetic (adia. 10.70,[d] 10.69,[e] vert. 10.87,[d] 10.86,[e]), propionic (adia. 10.44,[e] vert. 10.70[e]), isobutyric (adia. 10.33,[e] vert. 10.50[e]), trifluoroacetic (vert. 12.0[e]).
d) Ref. 13.
e) Ref. 14.

spectra are interpreted.

The first band in the spectrum of monochloro acetic acid is originated from n_O orbital of carboxyl oxygen and the next sharp peak from chlorine lone pair orbital. The spin-orbit splitting for chlorine atom is not observed because of the broadness of the peak. The order of halogen lone pair orbital and n_O orbital of carboxyl group is reversed in the case of monoiodoacetic acid. In the spectrum of monobromoacetic acid, the first two bands are originated from bromine lone pair orbital and the n_O band is considered to coincide with the second peak of the bromine lone pair bands.

Comparison of the Results Obtained by Photoelectron Spectroscopy and Photoionization Method. In Table 1, ionization potentials for various mono carboxylic acids determined by the photoelectron spectroscopy and photoionization method[8] are listed. The photoionization method always gives smaller adiabatic ionization potentials by 0.28—0.31 eV than the photoelectron spectroscopy does. The differences are quite the same. The first band of all of these molecules originates from oxygen lone pair orbital and photoelectron spectra show that the bands so much resemble each other in both shape and band width, and that the first band is clearly separated from the second. Since the photoionization method is particularly sensitive to the structure around the onset potential for the highest occupied orbital, these special conditions should be the main reason for the differences of the ionization potentials obtained by the photoionization method from our results to be constant.

Ionization Potentials Predicted from MO Calculations. In many cases, ionization potentials have been estimated by applying Koopmans' theorem to the results of molecular orbital energy calculation. When semi-empirical SCF MO calculations, such as CNDO or INDO, are performed, it is well known that each eigen value after multiplication by about 0.8[9] or subtraction of about 4 eV[10] approximately agrees with ionization potential experimentally measured. It is also known that the correlation between the eigen values calculated by MINDO/2 method and ionization potentials is quite satisfactory.[3]

We have performed CNDO/2, INDO, and MINDO/2 calculations. Ionization potentials have been estimated by the use of Koopmans' theorem. In addition, ionization potentials have been obtained from the difference between the total energy of the neutral molecule, E^0, and that of the corresponding cation radical in the same geometry, E^+, calculated by the unrestricted CNDO/2 and INDO method. The values obtained are listed in Table 1 and should be compared with the vertical ionization potentials observed.

The orbital energies by CNDO/2 and INDO method are steadily larger than the observed ionization potentials, and the agreement of the differences, E^+-E^0, with the observed ionization potentials is excellent. On the occasion of application of Koopmans' theorem to calculation by CNDO/2 and INDO methods, the discrepancy of energy in calculated and observed values is derived from errors due to arbitrariness of parameters used in calculation by CNDO/2 and INDO methods as well as both neglect of reorganization energy and assumption of constancy of relativistic and correlation energies.[11] On the other hand, the errors could successfully be cancelled in the difference, E^+-E^0.

Ionization potentials taken as the difference, E^+-E^0,

8) K. Watanabe, T. Nakayama, and J. Mottl, *J. Quant. Spectrosc. Radiat. Transfer*, **2**, 369 (1962).

9) J. W. Rabalais, *J. Chem. Phys.*, **57**, 960 (1972).

10) a) D. W. Davies, *Chem. Phys. Lett.*, **2**, 173 (1968); b) D. C. Frost, F. G. Herring, C. A. McDowell, M. R. Mustafa, and J. S. Sandhu, *ibid.*, **2**, 663 (1968); c) G. R. Branton, D. C. Frost, F. G. Herring, C. A. McDowell, and I. A. Stenhouse, *ibid.*, **3**, 581 (1969).

11) W. G. Richards, *Int. J. Mass Spectr. Ion Phys.*, **2**, 419 (1969).

using CNDO/2 method are larger than the observed ones. The same procedure using INDO method gives smaller values. MINDO/2 method is superior in predicting ionization potentials to the above methods from the view point of simplicity of calculation. Our computer program for INDO method was available only for trifluoroacetic acid and CNDO/2 program for trifluoro- and monochloroacetic acid among the halogenated acids. The difference method using INDO predicts excellent value for trifluoroacetic acid.

All calculations we have performed predicted that the level of n_O orbital is higher than that of π_2 orbital in all carboxylic acids, and that the n_O orbital is the highest occupied orbital in the aliphatic carboxylic acids.

Difference of n_O-π_2 Levels. In RCOX where X is OH, OR′, or NR′$_2$, it has been reported that the separation between n_O and π_2 orbital varies with R and X groups and that the π_2 orbital is particularly sensitive to changes in the X group and the n_O orbital is sensitive to changes in the R group, since the π_2 orbital has a large population on the X group and the n_O orbital has a greater population on the carbonyl carbon than the π_2 does.[12]

In the present work, as the alkyl group of the carboxylic acid becomes larger, the separation between the first and the second band increases. The gap between the first and the second band in the *iso*-tutyric acid is wider by 0.2 eV than that in the *n*-butyric acid. The electron releasing effect of the alkyl group and the atomic orbital population analysis seem to explain these results. However, such an explanation is not always applicable, since the substitution of all hydrogen atoms in the methyl group in acetic acid with fluorine atoms which have a strong electron withdrawing effect considerably shifts the n_O and π_2 bands to greater energy side but the gap in trifluoroacetic acid is almost the same as in acetic acid.

The molecular orbital calculations have been carried out on a NEAC 2200/N700 computer at Osaka University Computer Center.

Notes Added in Proof

After the completion of this paper came to hand two very important papers dealing with the photoelectron spectra of carboxylic acids.[13,14] Ionization potentials reported in these papers are added in a margin of Table 1. The spectra of dimers and complexes of carboxylic acids have been reported by Thomas.[14] From his calculated dimer-monomer ratios and spectra of dimers, we believe that contribution of dimers in the present work is negligible.

From our expanded spectrum of n_O band of acetic acid, from which we have determined the ionization potentials, it appears that the band has at least three vibrational components and is more complex than the one reported by Sweigart and Turner.[13] This might cause the ionization potentials of acetic acid in the present work to be a little smaller than the values reported by them.

It was recognized that the spectrum of the second band (π_2) of formic acid reported by Turner and co-workers[1] may contain a peak (12.61 eV) from impurity water.[15]

12) J. Daintith, R. Dinsdale, J. P. Maier, D. A. Sweigart, and D. W. Turner, "Molecular Spectroscopy 1971, Proc. of the 5th Conf. on Molecular Spectroscopy, Brighton, 1971," Institute of Petroleum, (1972), p. 16.

13) D. A. Sweigart and D. W. Turner, *J. Amer. Chem. Soc.*, **94**, 5592 (1972).

14) R. K. Thomas, *Proc. Roy. Soc. Ser. A*, **331**, 249 (1972).

15) D. W. Turner, Private communication.

Effect of Additives on Thermal Decomposition of Basic Magnesium Carbonate[1]

Kayoko AMITA and Genzo HASHIZUME

Industrial Research Institute of Hyogo Pref., Yukihira-cho, Suma-ku, Kobe 654

(Received January 31, 1972)

The effect of eleven halides on the thermal decomposition of basic magnesium carbonate ($4MgCO_3 \cdot Mg(OH)_2 \cdot 4H_2O$) has been studied by means of thermogravimetry (TG), differential thermal analysis (DTA) and gas chromatography. The size of crystallite of magnesium oxide prepared by heating the carbonate containing halide was determined by X-ray diffractometry, the oxides being studied by transmission electron microscopy. The thermal decomposition of basic magnesium carbonate was influenced by the addition of beryllium chloride tetrahydrate, magnesium chloride hexahydrate, calcium chloride hexahydrate and magnesium bromide hexahydrate. The DTA curve was changed with the amount of additive, *i.e.*, three endothermic peaks (at about 300, 430, and 530 °C) and an exothermic peak (at 490 °C) turned to only two endo-thermic peaks in the case where the molar ratio of an additive to the carbonate exceeded 0.005, the peak at higher temperature becoming sharp with shift toward lower temperature. The results of TG of basic magnesium carbonate corresponded to those of DTA. Gas chromatographic data showed that the composition of evolved gas varied with temperature. The activation energies of decarbonation and dehydration were obtained by gas chromatography by use of Freeman-Carroll's technique. Increase in the amount of additive caused a decrease in the activation energy of decarbonation, but not in that of dehydration except for magnesium bromide hexahydrate. The size of crystallite of magnesium oxide prepared by calcination at 600 °C for 2 hr, increased with the increase in the amount of additive.

The effect of impurities or additives on the thermal properties of compounds and the characteristics of materials produced by thermal decomposition have been extensively investigated.[2-4]

Basic magnesium carbonate shows the DTA curve as seen in Fig. 1c, which is similar to that given by Mackenzie.[5] We also reported that the DTA curve was influenced by the addition of magnesium chloride hexahydrate and environmental atmosphere.[6] Sawa reported that the addition of lithium fluoride also affected the shape of the curve.[7]

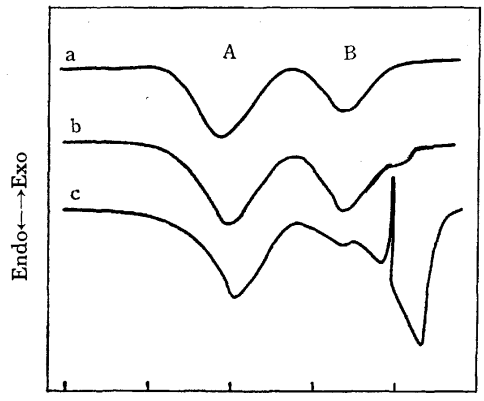

Fig. 1. DTA curves of basic magnesium carbonate Heating rate of a, b, and c was 1, 3, and 20 °C/min respectively. Sample weight was about 18 mg.

In this paper, the effect of halides (mainly chlorides) which affect the decomposition of magnesium hydroxide prepared from sea salt,[8] on the decomposition of basic magnesium carbonate was investigated by the measurement of DTA and TG curves, the calculation of apparent activation energy (referred to hereafter as "activation energy") of decarbonation and dehydration, and the determination of the size of crystallite of magnesium oxide prepared from basic magnesium carbonate.

Experimental

Materials. Basic magnesium carbonate (Earth Seiyaku Co., Ltd.) and additives of reagent grade were used. X-Ray diffractometry showed the structure of basic magnesium carbonate to be $4MgCO_3 \cdot Mg(OH)_2 \cdot 4H_2O$ although the composition is known to be either $5MgO \cdot 4CO_2 \cdot 5H_2O$ or $4MgO \cdot 3CO_2 \cdot 5H_2O$ according to the mode of preparation.

The following additives were used. Alkali metal chlorides (lithium chloride, sodium chloride, potassium chloride, and rubidium chloride) alkaline earth metal chlorides (beryllium chloride tetrahydrate, magensium chloride hexahydrate, strontium chloride hexahydrate, and barium chloride dihydrate), and magnesium halides (magnesium fluoride, magnesium bromide hexahydrate, and magnesium iodide).

Procedure. A given volume of methanolic solution of additive or a given weight of solid additive was mixed with a given weight of basic magnesium carbonate in an automatic mortar for a short time.

Simultaneous DTA–TG was performed with a Rigaku Denki Thermoflex 8002. DTA–TG runs were made at a

1) Studies on Technical Analytical Methods by Differential Scanning Calorimetry, Differential Thermal Analysis and Thermogravimetry, IV. Part III of this series: G. Hashizume and K. Amita, *Bunseki Kagaku*, **20**, 340 (1971).

2) G. V. S. Rao, M. Natarajan, and C. N. R. Rao, *J. Amer. Ceram. Soc.*, **51**, 179 (1968).

3) J. M. Schempf, F. E. Freeberg, and F. M. Angeloni, *Anal. Chem.*, **37**, 1704 (1965).

4) G. Hashizume, Y. Arai, M. Ishino, and S. Takashima, *Reports of Industrial Research Institute, Hyogo Pref.*, 5 (1966); I. F. Guilliatt and N. H. Brett, *Trans. Brit. Ceram. Soc.*, **69**, 1 (1970).

5) Ed. by R. C. Mckenzie, "Differential Thermal Analysis," Vol. 1, Academic Press (1970), p. 315.

6) G. Hashizume and K. Amita, *Bunseki Kiki*, **8**, 388 (1970).

7) H. Sawa and M. Oya, The 24th Annual Meeting of Chemical Society of Japan, Preprints page 970 (Apr. 1971).

8) Unpublished.

heating rate of 3 °C/min under dry nitrogen flow of 100 ml/min, except for that of 20 °C/min in the measurement of a sample containing 1 mol% of an additive. The weight of sample was about 18 mg.

Gas evolved during the course of decomposition was measured with a gas chromatograph (Hitachi Ltd., Model 063) connected with DTA–TG apparatus equipped with an automatic gas sampler. A katharometer was used as a detector. The glass column was packed with Porapak-Q 80/100 (Water Associate Inc.). The column temperature was 110 °C. The time interval to collect a gas sample was 15 s.

The size of crystallite was determined by a Rigaku Denki Geigerflex X-ray diffractometer. Ni-filtered CuKα-radiation was used. The size of magnesium oxide samples was calculated from half width of diffraction peak by Sherrer's equation, taking that of magnesium oxide prepared by the combustion of magnesium metal as a standard.

Particle forms were observed with a transmission electron microscope (Japan Electron Optics Laboratory Co., Ltd., model JEM-T6S). A specimen was prepared by placing a sample on a collodion membrane, and carrying out vacuum-evaporation with carbon to prevent sintering of the sample by an electron beam. Samples used for X-ray diffractometry and transmission electron microscopy were prepared by calcination at 600 °C for 2 hr.

Results and Discussion

Effect of Additives on DTA Curve. The DTA curve of basic magnesium carbonate changes with environmental atmosphere[9] and heating rate. Four transitions were observed on the DTA curve at a heating rate of 20 °C/min (Fig. 1c): Endothermic peak (1) at about 300 °C due to dehydration, (2) at about 430 °C due to partial decarbonation, (3) at about 520 °C due to decarbonation, and an exothermic peak at 490 °C attributable either to crystallization of amorphous magnesium oxide or recombination of magnesium oxide with carbon dioxide evolved. When the heating rate decreased, the DTA curve showed two endothermic peaks (Fig. 1a).

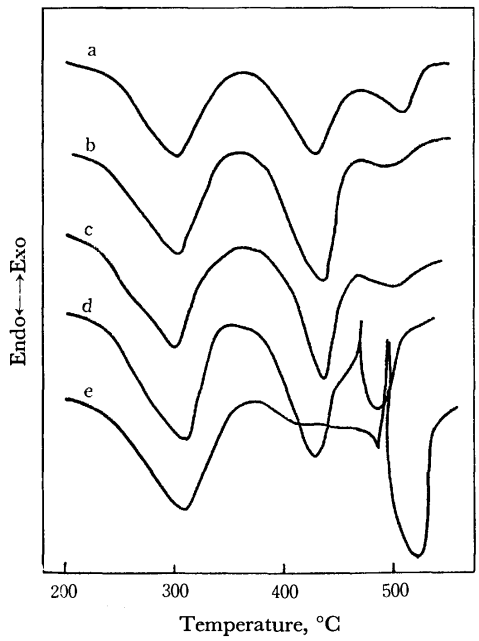

Fig. 2. Comparison of DTA curves of basic magnesium carbonate with those of additives.
a: $BeCl_2 \cdot 4H_2O$, b: $MgCl_2 \cdot 6H_2O$, c: $CaCl_2 \cdot 6H_2O$,
d: $SrCl_2 \cdot 6H_2O$, e: $BaCl_2 \cdot 2H_2O$.

The DTA curves of the sample containing 1 mol% of alkali earth metal chlorides are given in Fig. 2. Decomposition was greatly influenced by the addition of beryllium chloride tetrahydrate, magnesium chloride hexahydrate, calcium chloride hexahydrate and magnesium bromide hexahydrate, but the effect of strontium chloride hexahydrate was small and no effects were observed by other additives.

We see that all the additives with considerable effect contain four or six molecules of water of crystallization which would cause the hydrolytic cleavage of hydrogen chloride from the halides at relatively low temperature, as suggested from the following reaction scheme.[10]

$$MgCl_2 \cdot 6H_2O \longrightarrow MgCl_2 \cdot 4H_2O + 2H_2O \quad 95—115°C$$
$$MgCl_2 \cdot 4H_2O \longrightarrow MgCl_2 \cdot 2H_2O + 2H_2O \quad 135—180°C$$
$$MgCl_2 \cdot 4H_2O \longrightarrow MgOHCl + HCl + 3H_2O$$
$$MgCl_2 \cdot 2H_2O \longrightarrow MgCl_2 \cdot H_2O + H_2O \quad 185—230°C$$
$$MgCl_2 \cdot 2H_2O \longrightarrow MgOHCl + HCl + H_2O$$
$$MgCl_2 \cdot H_2O \longrightarrow MgCl_2 \cdot H_2O \quad \text{over above } 230°C$$
$$MgCl_2 \cdot H_2O \longrightarrow MgOHCl + HCl$$
$$MgOHCl \longrightarrow MgO + HCl$$

Evolution of hydrogen chloride or hydrogen bromide was also detected from three other additives by gas chromatography. The temperature of liberation of hydrogen chloride was the same as or very close to that of decarbonation and dehydration of basic magnesium carbonate.

Effect of the Amount of Additive on DTA Curve. Concentrations of four additives greatly influenced DTA curves. The DTA curves for various concentrations of magnesium chloride hexahydrate are shown in Fig. 3. The other three additives also show similar tendency. With increase in the amount of additive endothermic peak A at a lower temperature shifted somewhat to a higher temperature and peak B at a higher temperature shifted considerably to a lower temperature. The change in the maximum temperature of peak B is illustrated in Fig. 4. Of the four additives, magnesium bromide showed the largest temperature shift (80°) to lower side.

Effect of Additive on the TG Curve. In Fig. 5 are shown the TG curves of the sample containing magnesium chloride hexahydrate in the region 300—500 °C, where decarbonation, partial dehydration from basic magnesium carbonate and decomposition of additive are known to occur. The other three additives also show a similar tendency. It is thus evident that the TG curve is also influenced by additive. It appears that the rate of decomposition increases with the increase in the amount of additive.

9) H. Hashimoto, T. Tomizawa, and M. Mitomo, *Kogyo Kagaku Zasshi*, **71**, 480 (1968); R. M. Dell and S. W. Weller, *Trans. Faraday Soc.*, **55**, 2203 (1959).

10) "Jikken Kagaku Koza," ed. by Chemical Society of Japan, Vol. 9, Maruzen, Tokyo (1970), p. 143.

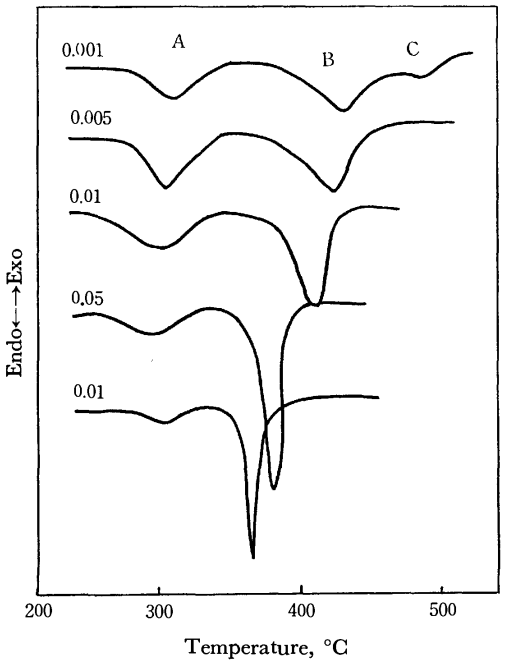

Fig. 3. DTA curves of $4MgCO_3 \cdot Mg(OH)_2 \cdot 4H_2O$-$MgCl_2 \cdot 6H_2O$.
0.001—0.1: $[MgCl_2 \cdot 6H_2O]/[4MgCO_3 \cdot Mg(OH)_2 \cdot 4H_2O]$

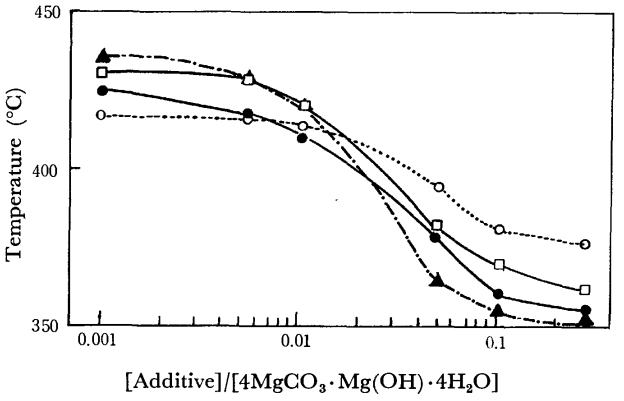

Fig. 4. Variation of the peak maximum temperature of decarbonation
○—○ $BeCl_2 \cdot 4H_2O$ ●—● $MgCl_2 \cdot 6H_2O$
□—□ $CaCl_2 \cdot 6H_2O$ ▲—▲ $MgBr_2 \cdot 6H_2O$

Effect of Additive on the Activation Energy. To evaluate the activation energy from the TG curve, we employed Freeman-Carroll's technique[11] and Coat's technique.[12] An abnormally high activation energy was obtained for decomposition of the sample containing additive at about 450 °C, although the decomposition occurred more abruptly and at a lower temperature than that for an additive-free sample. Reason why the above high value was obtained was considered as follows: Weight loss obtained by TG might be attributed to the decomposition of basic magnesium carbonate and additive. Not only the rate of decomposition but also the composition of the evolved gas varied with the amount of additive (Fig. 6).

11) E. S. Freeman and B. Carroll, *J. Phys. Chem.*, **62**, 394 (1958).
12) A. W. Cats and J. P. Redfern, *Nature*, **201**, 68 (1964).

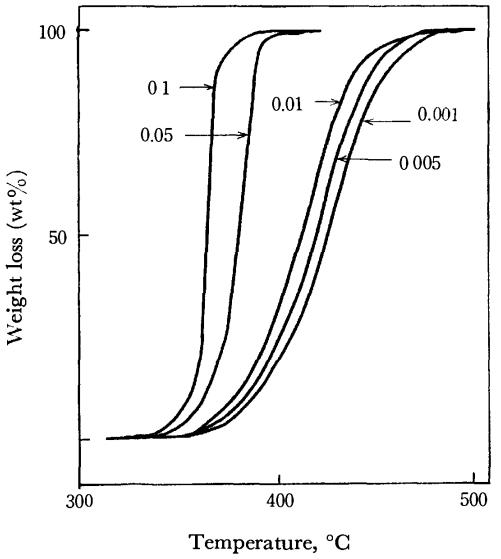

Fig. 5. Effect of magnesium chloride hexahydrate on TG curve of basic magnesium carbonate in the region of 300 to 500 °C.
0.001—0.1: $[MgCl_2 \cdot 6H_2O]/[4MgCO_3 \cdot Mg(OH)_2 \cdot 4H_2O]$

We employed gas chromatography for the evaluation of activation energy using the Freeman-Carroll equation:

$$\frac{-E}{2.3R}\frac{\Delta\frac{1}{T}}{\Delta \log Wr} = -x + \frac{\Delta \log \frac{dw}{dt}}{\Delta \log Wr}$$

where E, T, R, and x represent the activation energy, the absolute temperature at which gas is collected, the gas constant and the order of reaction with respect to the component, respectively, dw/dt being the rate of

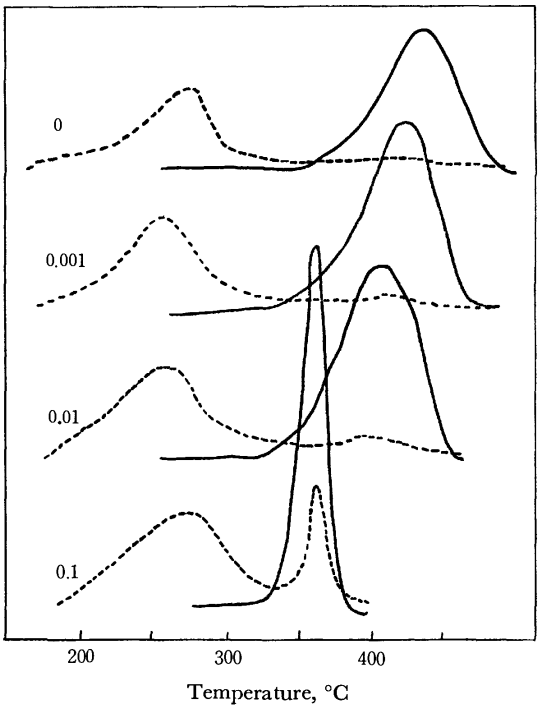

Fig. 6. Rate of dehydration and decarbonation
0—0.1: $[MgCl_2 \cdot 6H_2O]/[4MgCO_3 \cdot Mg(OH)_2 \cdot 4H_2O]$
——: CO_2, ------: H_2O

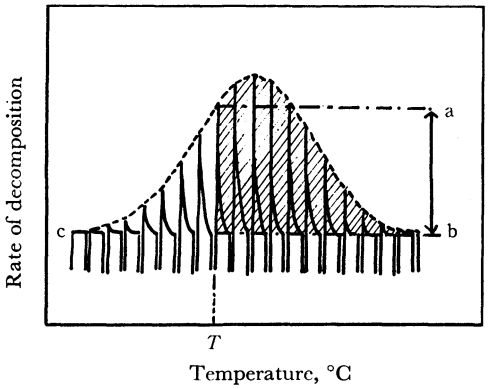

Fig. 7. Gas chromatogram obtained by thermal decomposition.

decomposition at T K, and Wr the difference between the weight loss at completion of reaction and total weight loss up to T K. Gas chromatograms obtained are shown in Fig. 7. The differential curve given by a dotted line (namly dw/dt *vs.* t) corresponds to the rate of decomposition. The length from (a) to (b) is the rate of decomposition reaction (dw/dt) at T K. The areas bound by a dotted line and basement (b—c) represent the total amount of water or carbon dioxide. Wr corresponds to the shaded part. Thus dw/dt and Wr can be determined directly from the curve (dotted line), and the activation energy could be readily calculated by plotting $(\Delta\log dw/dt)/\Delta\log Wr$ against $(T^{-1})/\Delta\log Wr$.

Validity of this gas chromatographic method is clear from the following evidences. Although basic magnesium carbonate evolved water vapor only in a very small amount in the range 350—500 °C, this does not seem to affect the evaluation of activation energy. Thus the values of $\Delta\log dw/dt$ and $\Delta\log Wr$ determined by gas chromatography for the additive-free sample seems to be the same as those by TG. The activation energies calculated from gas chromatogram agreed with the one from the TG curve, *viz.*, 47.7 and 47 kcal/mol.

The activation energies of decarbonation obtained by gas chromatography are shown in Fig. 8. The rate of decomposition was too large for the evaluation of activation energy for the sample containing an additive in a molar ratio greater than 0.05.

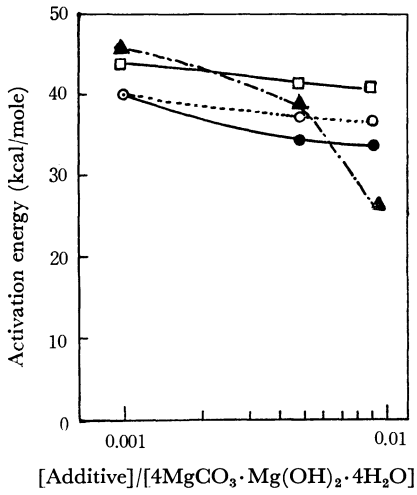

Fig. 8. Variation of the activation energy of basic magnesium carbonate with additives
○---○ $BeCl_2\cdot4H_2O$ ●—● $MgCl_2\cdot6H_2O$
□—□ $CaCl_2\cdot6H_2O$ ▲-·-▲ $MgBr_2\cdot6H_2O$

Although the effect of additive on dehydration at about 200 °C of basic magnesium carbonate is not clear since dehydration of the additive took place in a similar temperature range, the influence on the activation energy of dehydration would be neglected due to a very low concentration of additive. The activation energies of dehydration of the sample containing beryllium chloride tetrahydrate, magnesium chloride hexahydrate, calcium chloride hexahydrate, and additive-free were 13, 15, 23, and 25 kcal/mol, respectively. They were not affected by the amount of additive. On the other hand, the values for the sample containing magnesium bromide hexahydrate in the molar ratio range 0.001—0.01 varied from 25 to 15 kcal/mol.

The amount of magnesium bromide hexahydrate affects the activation energies of both decarbonation and dehydration remarkably. The effect might be mainly ascribed to hydrogen bromide generated in addition to the difference in the mode of decomposition of additive.

Effect of Additive on the Size of Crystallite of Magnesium Oxide. Sizes of the crystallite of magnesium oxide are shown in Fig. 9.

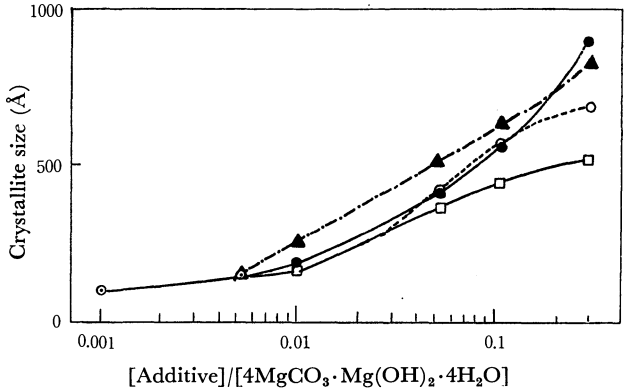

Fig. 9. Variation of the crystallite size of MgO with concentration of additives
○---○ $BeCl_2\cdot4H_2O$ ●—● $MgCl_2\cdot6H_2O$
□—□ $CaCl_2\cdot6H_2O$ ▲-·-▲ $MgCl_2\cdot6H_2O$

Transmission electron micrographs of basic magnesium carbonate and magnesium oxides are shown in Fig. 10. Magnesium oxide exists as an aggregate of small particles of the oxide. The shape of the aggregate is similar to that of basic magnesium carbonate, the particle size of magnesium oxide increasing with the increase of the amount of additive. The results obtained the micrographs (Fig. 10) are in line with those obtained with X-ray diffractometry. Since it is known that sintered magnesia of large size is prepared by heating magnesium oxide under a flow of hydrogen chloride,[13] it seems that the growth of crystal of magnesium oxide is influenced by hydrogen halide evolved

13) T. Titani, "Muki Kagaku," Sangyo Tosho, Tokyo, (1959).

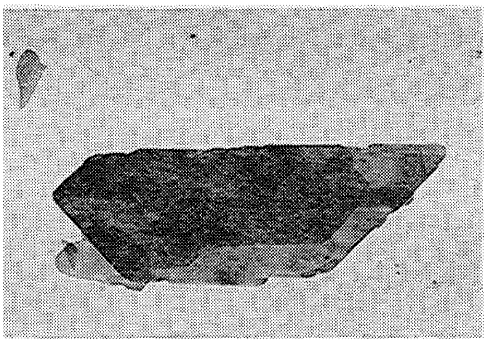

Basic magnesium carbonate

0

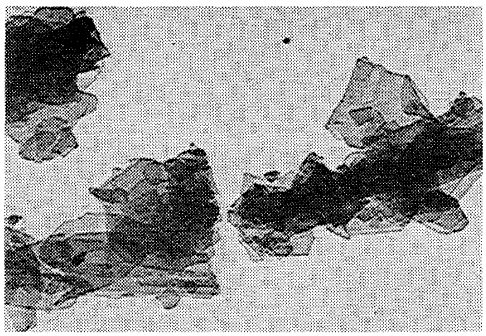

0.001

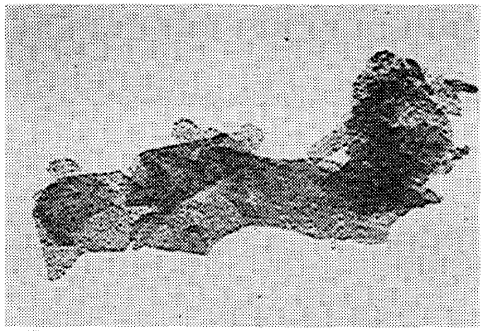

0.01

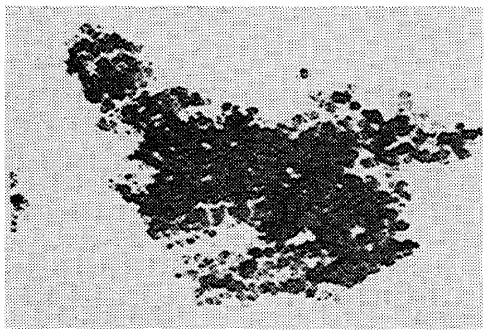

0.1

Fig. 10. Electron micrographs of basic magnesium carbonate and magnesium oxide.
0—0.1: $[MgCl_2 \cdot 6H_2O]/[4MgCO_3 \cdot Mg(OH)_2 \cdot 4H_2O]$

by the decomposition of an additive.

It should be noted that thermal decomposition of basic magnesium carbonate and the size of the crystallite of magnesium oxide prepared from basic magnesium carbonate are influenced by hydrogen halide evolved from an additive.

Spectroscopic and Coordination Behavior of α-Cyanothioacetamide

Arabinda RAY and D. N. SATHYANARAYANA

Department of Inorganic and Physical Chemistry, Indian Institute of Science, Bangalore-12, India

(Received June 14, 1972)

α-Cyanothioacetamide (CTAM) complexes of cuprous chloride CuCl–2CTAM and cuprous bromide CuBr–2CTAM have been prepared. The infrared spectra of CTAM and its complexes, and the laser Raman spectrum of CTAM have been recorded. Assignment of the frequencies of the ligand has been made on the basis of a normal coordinate analysis using the Urey-Bradley force field. The copper (I) complexes are inferred to have thiocarbonyl sulfur and amide nitrogen bonded CTAM as evidenced from infrared and electronic spectra.

α-Cyanothioacetamide is a potentially tridentate ligand. The coordination complexes of its oxygen anologue α-cyanoacetamide have been studied recently.[1,2] The results of detailed spectroscopic investigations of thioacetamide[3] and malononitrile[4] are also available. In this connection, we considered it interesting to study in detail the spectroscopic and coordination behavior of α-cyanothioacetamide (CTAM). The location of thiocarbonyl stretching frequency was also of considerable interest. We report here the infrared and laser Raman spectra of CTAM and the assignment of its vibrational frequencies with the aid of a normal coordinate treatment. The complexes of CTAM with cuprous chloride and cuprous bromide are also included. The assignment of the vibrational frequencies and the frequency shifts in metal complexes are discussed.

Experimental

Materials. α-Cyanoacetamide was prepared by reacting ethylcyanoacetate (Boehringer Ingelheim reagent) with liquor ammonia.[5] CTAM was synthesised from α-cyanoacetamide by being refluxed with phosphorus pentasulfide (Fluka) in ethylacetate[6] (BDH reagent). The product was recrystallized from A.R. benzene. The salts $CuCl_2 \cdot 2H_2O$ and $CuBr_2$ were of A.R. grade. Ethanol (99%) was used for the preparation.

Preparations. *CuCl–2CTAM*: An ethanol solution of the ligand was mixed with cupric chloride dihydrate in ethanol when cupric chloride was reduced and a yellow precipitate of the cuprous chloride complex was obtained. It was filtered off, washed with ethanol and dried in a vacuum. Found: Cu, 20.73; S, 20.99%. Calcd for CuCl–2CTAM: Cu, 21.26; S, 21.4%.

CuBr–2CTAM: The above procedure was followed for the preparation of CuBr–2CTAM. The resulting yellow precipitate was filtered, washed with ethanol and dried in a vacuum. Found: Cu, 18.70; S, 18.33%. Calcd for CuBr–2CTAM: Cu, 18.48; S, 18.63%.

Analysis. Copper in the complexes was estimated by the thiosulfate method and sulfur as barium sulfate.

Infrared Spectra. The infrared spectra of CTAM and its complexes were taken in Nujol mull and KBr pellets on a Carl-Zeiss UR 10 spectrophotometer in the range 4000—400 cm^{-1}, and on a Perkin-Elmer 521 grating spectrophotometer in the range 400—250 cm^{-1}.

Raman Spectra. The Raman spectrum of the powdered sample of CTAM sealed in a thin capillary tube was taken on a Cary 81 Raman spectrophotometer equipped with an argon ion laser.[7]

Electronic Spectra. The electronic spectrum of CTAM in acetonitrile was taken on a Unicam SP 700A recording spectrophotometer. The electronic spectra of the complexes were recorded in Nujol mull.

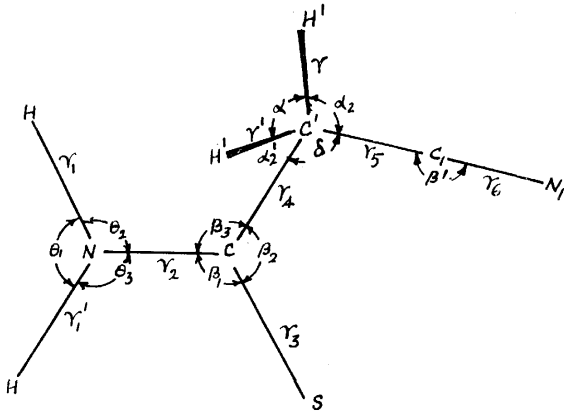

Fig. 1. Internal coordinates.

Normal Coordinate Analysis. The molecule CTAM belongs to the point group C_s and its 24 fundamental vibrations are distributed as 16 A′ and 8 A″ types. Calculations have been carried out for the A′ vibrations only since the frequencies of interest in the present study belong to this species. The internal coordinates are defined in Fig. 1 and the internal symmetry coordinates are given in Table 1. The molecular parameters of CTAM based on the available structural data for formamide,[8] α-cyanoacetamide,[9] and thioacetamide[10] are given in Table 2. The secular equation of Wilson's GF matrix was solved using Miyazawa's method[11] on a IBM 360/44 computer.

Force Field. Because of its effectiveness for thio-

1) S. C. Jain and R. Rivest, *Can. J. Chem.*, **45**, 139 (1967).
2) R. C. Paul and S. L. Chadha, *Aust. J. Chem.*, **22**, 1381 (1969).
3) I. Suzuki, This Bulletin, **35**, 1449 (1962).
4) T. Fujiyama and T. Shimanouchi, *Spectrochim. Acta*, **20**, 829 (1964).
5) B. B. Corson, R. W. Scott, and C. E. Vose, "Inorganic Synthesis," Vol. 1, 179 (1947).
6) V. Grinsteins and L. Serina, *Latvijas PSR Zinatnu Akad. Vestis, Kim. Ser.*, **4**, 469 (1968); *Chem. Abstr.*, **60**, 5391 h.
7) The spectrum was kindly recorded for us by Dr. James R. Scherer, the U.S. Department of Agriculture, Albany, California.
8) C. C. Costain and J. M. Dowling, *J. Chem. Phys.*, **32**, 158 (1960).
9) P. C. Chieh and J. Trotter, *J. Chem. Soc., A*, **1970**, 184.
10) M. R. Truter, *J. Chem. Soc.*, **1960**, 997.
11) T. Miyazawa, *J. Chem. Phys.*, **29**, 246 (1958).

Table 1. Internal symmetry coordinates

Symmetry coordinate	Mode	
$S_1 = (\Delta r + \Delta r')/\sqrt{2}$	CH stretching	ν_sCH
$S_2 = (\Delta r_1 + \Delta r_1')/\sqrt{2}$	NH sym stretching	ν_sNH
$S_3 = (\Delta r_1 - \Delta r_1')/\sqrt{2}$	NH asym stretching	ν_aNH
$S_4 = \Delta r_6$	C≡N stretching	νC≡N
$S_5 = (\Delta r_4 + \Delta r_5)/\sqrt{2}$	CC sym stretching	ν_sCC
$S_6 = (\Delta r_4 - \Delta r_5)/\sqrt{2}$	CC asym stretching	ν_aCC
$S_7 = \Delta r_2$	CN stretching	νCN
$S_8 = \Delta r_3$	CS stretching	νCS
$S_9 = (2\Delta\theta_1 - \Delta\theta_2 - \Delta\theta_3)/\sqrt{6}$	NH_2 bending	δNH_2
$S_{10} = (\Delta\theta_2 - \Delta\theta_3)/\sqrt{2}$	NH_2 rocking	ρNH_2
$S_{11} = (2\Delta\beta_1 - \Delta\beta_2 - \Delta\beta_3)/\sqrt{6}$	NCS bending	δNCS
$S_{12} = (\Delta\beta_2 - \Delta\beta_3)/\sqrt{2}$	CCS bending	δCCS
$S_{13} = \Delta\beta'$	CC≡N bending	δCC≡N
$S_{14} = (5\delta - \Delta\alpha - \Delta\alpha_1 - \Delta\alpha_1' - \Delta\alpha_2 - \Delta\alpha_2')/\sqrt{30}$	CCC bending	δCCC
$S_{15} = (4\alpha - \Delta\alpha_1 - \Delta\alpha_1' - \Delta\alpha_2 - \Delta\alpha_2')/\sqrt{20}$	CH_2 bending	δCH_2
$S_{16} = (\Delta\alpha_1 + \Delta\alpha_2' - \Delta\alpha_2 - \Delta\alpha_1')/\sqrt{2}$	CH_2 wagging	ωCH_2

Table 2. Molecular parameters

Bond length		Bond angle		
N–H	1.002 Å	HNH	120°	
C–H	1.093 Å	HNC	120°	
C–N	1.324 Å	NCS	120°	
C–S	1.713 Å	SCC′	120°	
C–C′	1.540 Å	C′C_1N	180°	
C′–C_1	1.458 Å	Angles around		109°28′
C≡N	1.162 Å	C′ carbon		

Table 3. Urey-Bradley force constants (md/Å)

Stretching		Bending		Repulsion	
K_{CH}	4.14	H_{HNH}	0.41	F_{HNH}	0.04
K_{NH}	5.85	H_{HNC}	0.32	F_{HCH}	0.05
K_{CN}	6.45	H_{HCH}	0.39	F_{HNC}	0.44
K_{CS}	3.81	$H_{HC'C}$	0.29	$F_{HC'C}$	0.50
$K_{CC'}$	2.45	$H_{HC'C_1}$	0.31	$F_{HC'C_1}$	0.55
$K_{C'C_1}$	2.90	H_{NCS}	0.22	$F_{NCC'}$	0.70
$K_{C\equiv N}$	18.20	$H_{C'CS}$	0.10	F_{NCS}	1.20
k (intramolecular tension) = −0.05 (md/Å)		$H_{C'CN}$	0.10	$F_{SCC'}$	0.44
		$H_{CC'C_1}$	0.62	$F_{CC'C_1}$	0.42
		$H_{C'C_1N_1}$	0.40	$F_{C'CN_1}$	0.50

amides,[3,12-14] the Urey-Bradley force field (UBFF) was chosen for the calculations. The initial set of force constants were taken from thioacetamide (TAM)[3] and malononitrile (MNL, set I).[4] From the results of calculation, the force constants were modified by an iterative procedure so as to get the best fit between the calculated and the observed frequencies. Table 3 shows the final force constants thus obtained. A comparison of the force constants of CTAM with those of TAM and MNL indicates that only three bending force constants differ considerably while all other force constants are nearly the same as those in either TAM or MNL. Thus the transferability of these force constants is good.

12) I. Suzuki, This Bulletin, **35**, 1286, 1456 (1962).
13) G. Durga Prasad, D. N. Sathyanarayana, and C. C. Patel, *ibid.*, **44**, 316 (1971).
14) C. N. R. Rao and G. C. Chaturvedi, *Spectrochim. Acta*, **27A**, 520 (1971).

Table 4. Observed and calculated vibrational frequencies and their assignments

Frequencies, cm^{-1} Obsd	Calcd	Δ[a]	Assignments (PED, %)[b]
3375	3375	0	ν_a(NH)(100)
3295	3289	0.18	ν_s(NH)(99)
2895	2898	0.10	ν_s(CH)(99)
2268	2268	0	ν(C≡N)(91)
1630	1627	0.18	$\delta(NH_2)(77)+\nu$(CN)(21)
1460	1450	0.69	ν(CN)(41)+$\omega(CH_2)$(27)+ $\delta(NH_2)$(10)
1415	1419	0.28	$\delta(CH_2)$(88)
1385	1386	0.07	$\omega(CH_2)(59)+\nu$(CN)(24)
1260	1262	0.16	$\rho(NH_2)(30)+\nu$(CS)(17)+ ν_a(CC)(16)+ν_s(CC)(16)+ δ(NCS)(11)
1001	1001	0	$\rho(NH_2)(49)+\nu_s$(CC)(20)+ δ(CCC)(14)
955	955	0	ν_a(CC)(63)+ν_s(CC)(13)
760	764	0.53	ν(CS)(63)+δ(CC≡N)(14)
630	629	0.16	ν_s(CC)(35)+δ(CC≡N)(25)+ δ(NCS)(13)
421	421	0	δ(NCS)(77)+δ(CC≡N)(10)
335	333	0.60	δ(CCS)(49)+δ(CC≡N)(27)+ δ(CCC)(10)
105[c]	102	2.94	δ(CCS)(39)+δ(CCC)(36)+ δ(CC≡N)(20)

a) Percentage deviation.
b) Contribution less than 10 per cent is not included.
c) Taken from Raman data.

The calculated frequencies are compared with the observed ones in Table 4, in which the assignments of the bands based upon the calculated potential energy distribution (PED) are also given.

Results and Discussion

The assignments are compared with those of the closely related TAM and MNL molecules.

3400—2000 cm^{-1} Region. The bands at 3375 and 3295 cm^{-1} in CTAM are due to N–H asymmetric and symmetric stretching vibrations. The CH symmetric and antisymmetric (A″) modes are located at 2895 and 2930 cm^{-1}, respectively. The C≡N stretching occurs at 2268 cm^{-1}.

1650—1000 cm^{-1} Region. The 1630 cm^{-1} band is due to NH_2 bending. The C–N stretching mode is coupled and is distributed in the frequencies at 1630, 1460, and 1385 cm^{-1}, its contribution being maximum (41 per cent) in the 1460 cm^{-1} band. In TAM, NH_2 bending and C–N stretching modes occur, respectively, at *ca.* 1630 and 1400 cm^{-1}. The bands at 1415 and 1385 cm^{-1} due to CH_2 bending and CH_2 wagging, respectively, are compatible with those in MNL[4] and other related molecules.[15]

In the 1300—1250 cm^{-1} region, there are two intense absorptions at 1260 and 1295 cm^{-1}. The 1260 cm^{-1}

15) H. A. Szymanski, "Theory and Practice of IR Spectroscopy," Plenum Press, New York (1961), pp. 225, 302.

Table 5. Observed infrared frequencies[a] (in cm^{-1}) of CTAM and its complexes

CTAM	CuCl·2CTAM	CuBr·2CTAM
3375 s	3280 mb	3290 m
3295 s	3180 mb	3180 m
3170 sb	—	—
2930 m	2935 m	2935 w
2895 m	2855 vw	2880 w
	2275 vw	2270 vw
2268 m	2190 sb	2200 sb
1740 vw	1750 w	1745 w
1685 shw	1690 w	1695 w
1630 vsb	1632 vs	1618 vs
1460 vsb	1470 vs	1475 vsb
1415 m	—	—
1385 m	1385 s	1385 vs
1295 s	1300 sb	1325 sb
1260 sb	1201 mb	1205 mb
	1090 w	1100 mw
1001 s	1040 mw	1030 m
	1010 mw	
955 s	960 vw	965 vw
905 mw	920 m	925 m
	890 vw	885 sh
855 vw	825 shw	850 wsh
	785 msh	780 sh
760 s	700 s	710 s
715 msh	695 s	700 m
696 vs (695 s)		
630 vsb		
495 mw	525 w	525 w
	480 m	470 vw
421 mw (422 m)	440 w	430 vw
390 w		
380 w	378 vw	380 vw
365 mw	364 w	360 vw
335 s (331 m)	328 vw	328 vw
(145 mw)		
(105 s)		
(92 s)		
(72 m)		

a) Values in parantheses are Raman frequencies. Because of poor signal/noise ratio in the Raman spectrum, only the prominent bands are given.

band has been included in A′ vibrations in preference to the 1295 cm^{-1} one. The 1260 cm^{-1} band has a complicated mode of coupling with a slightly higher contribution from NH_2 rocking (Table 4). The 1295 cm^{-1} band has been assigned to CH_2 twisting (A″) in accordance with the CH_2 twisting mode at 1225 cm^{-1} in MNL.[4] The 1295 cm^{-1} band is not much affected on complex formation with metals while that at 1260 cm^{-1} shows a large red shift (Table 5). The infrared spectra of the deuterated ligand and the reaction product with HCl gas also showed that the 1295 cm^{-1} band is not affected while the 1260 cm^{-1} band showed a large variation. These findings might support the assignments.

The bands at 1001 and 1260 cm^{-1} have, respectively, 50 and 30 per cent NH_2 rocking mode. Comparable frequencies in TAM appear at 1310, 1030, and 965 cm^{-1} having, respectively, 50, 20, and 16 per cent contribution from NH_2 rocking vibration.[3]

950—700 cm^{-1} Region. The asymmetric C–C stretching mode in CTAM is observed at 955 cm^{-1} while the symmetric mode is distributed amongst 1001, 955, and 630 cm^{-1} bands. The asymmetric mode is comparable with the 985 cm^{-1} band in MNL.[4] The symmetric C–C stretching in MNL occurs as a pure band around 890 cm^{-1}. The symmetric C–C vibration in CTAM is comparable with the C–C stretching mode in TAM, where it is distributed in the bands in the 1400—700 cm^{-1} region.[3]

The band at 760 cm^{-1} is of considerable interest and is due, mainly, to C=S stretching in agreement with an earlier empirical assignment.[16] The C=S stretching occurs at 720 cm^{-1} in TAM.[3] Occurrence of C=S stretching at a higher frequency in CTAM could be attributed to the electron withdrawing effects of the CN group. This band shifts to lower frequency in metal complexes (where sulfur is presumed to be the donor) which may be taken as a support to the above assignment.

650—100 cm^{-1} Region. The CCC bending mode is observed at 580 cm^{-1} in MNL, while in the present case, it is highly coupled and appears in the bands at 1001, 335, and 105 cm^{-1}, the contribution being the largest (36 per cent) in the 105 cm^{-1} band.

The assignment of bands at 421 and 335 cm^{-1} to predominantly NCS and CCS bending modes needs some comment. The corresponding bands in TAM have been observed at 470 and 390 cm^{-1}. One would be inclined therefore to assign empirically the 495 and 421 cm^{-1} in CTAM to NCS and CCS bending vibrations, respectively. The frequencies obtained from the initial trial set were very close to 420 and 330 cm^{-1}. To raise these bands to 495 and 420 cm^{-1}, it was necessary to employ unusually large bending force constants. When this was done, the assignments obtained for some of the higher frequencies were of "unacceptable" nature. Hence, the present assignments for 421 and 335 cm^{-1} were preferred. The lowering of NCS and CCS bending frequencies in CTAM may be attributed to its coupling with CC≡N bending. The CC≡N "in-plane" bending modes in MNL[4] occur at 365 and 165 cm^{-1}.

Out-of-plane Vibrations. Mention should be made of the A″ vibrations although no calculations have been carried out to assign the frequencies to these modes. There are 8 A″ vibrations. The CH_2 antisymmetric stretching occurs at 2930 cm^{-1}. A band at 1295 cm^{-1} is assigned to CH_2 twisting. The CH_2 rocking mode is assigned at 905 cm^{-1} in comparison with that at 936 cm^{-1} in MNL.[4] A strong band at 695 (715) cm^{-1} is assigned to NH_2 wagging in agreement with that in TAM[3] and acetamide,[17] while a very weak band at 855 cm^{-1} is assigned to NH_2 torsional vibration in comparison with that around 800 cm^{-1} in acetamide.

Of the remaining four modes, the band at 495 cm^{-1}

16) K. A. Jensen and P. H. Nielsen, *Acta. Chem. Scand.*, **20**, 597 (1966).

17) T. Uno, K. Machida, and Y. Saito, *Spectrochim. Acta*, **27A**, 833 (1971).

may be due to C–C out-of-plane bending and is compatible with that at 530 cm^{-1} in TAM.[3] An out-of-plane C–C≡N bending mode is assigned to 365 cm^{-1} in comparison with the one at 371 cm^{-1} in MNL.[4] The C=S out-of-plane bending is tentatively placed at 380, 390 cm^{-1}. The bands below 150 cm^{-1} in Raman spectrum (excepting 105 cm^{-1}) may be due to lattice modes.

Metal Complexes. Except for the copper(I) complexes, the initial efforts to prepare complexes of other metals were unsuccessful. The cuprous complexes are insoluble in most solvents, thus restricting the studies. The site of coordination of CTAM in the complexes were inferred from the infrared data based on the assignments for the ligand bands discussed above. The changes in the infrared frequencies of CTAM on coordination to copper(I) can be seen in Table 5.

A strong band at 760 cm^{-1} due mainly to C=S stretching is lowered by 50 to 60 cm^{-1} in the complexes. This large red shift clearly indicates the coordination of CTAM through sulfur.

The NH_2 stretching modes are found to shift to lower frequencies by about 100 cm^{-1} in the complexes. No perceptible variation is observed in the NH_2 bending frequency. The NH_2 rocking frequencies at 1260 and 1001 cm^{-1} are affected differently. The 1260 cm^{-1} band which has considerable C=S stretching decreases to ~1200 cm^{-1} while the 1001 cm^{-1} shows two or three bands at higher frequencies at 1030—1100 cm^{-1}. Similar variations in the $-NH_2$ group frequencies have been noted in the case of (glycine[18]), urea[19] and thiourea[20] complexes of metals when coordination is said to have taken place through nitrogen. This indicates that in CTAM the bonding to copper(I) through amide nitrogen is likely.

The decrease in C≡N stretching frequency at 2268 cm^{-1} to ~2200 cm^{-1} in metal complexes is puzzling. Normally, coordination through the nitrogen of the cyanide group should increase the C≡N frequency, as has been observed in almost all the cases, including α-cyanoacetamide.[1,21] A decrease in C≡N stretching frequency has been found in cases where the coordination to the metal is through the π-bonding of the CN group.[21] Such a possibility is not thought of seriously in this case, although it cannot be completely ruled out. The intense broad band at 630 cm^{-1} in CTAM disappears in the complexes or appears as a weak band at 525 cm^{-1}. If the latter is the case, the unusually large shift is rather difficult to explain, if CN group is not coordinated.

The complexes of α-cyanothioacetamide are likely to be polymeric and may have complicated stereochemistry.

Electronic Spectra. The electronic spectrum of CTAM in acetonitrile shows bands at 270 mμ (ε 10000) and at 358 mμ (ε 200). These are due to $\pi \rightarrow \pi^*$ and $n \rightarrow \pi^*$ transitions of the C=S chromophore. The electronic spectra of the complexes in solid state give a well-defined peak ~225 mμ. This band may correspond to the π—π^* transition at 270 mμ of the ligand. This blue shift may be attributed to the coordination of the thiocarbonyl sulfur to the metal.

The authors thank Prof. C. C. Patel for helpful discussions, and Prof. A. R. Vasudeva Murthy for his keen interest and encouragement.

18) R. A. Condrate and K. Nakamoto, *J. Chem. Phys.*, **42**, 2590 (1965).

19) R. B. Penland, S. Mizushima, C. Curran, and J. V. Quagliano *J. Amer. Chem. Soc.*, **73**, 1575 (1957).

20) R. Rivest, *Can. J. Chem.*, **40**, 2234 (1962).

21) J. Grundes and P. Klaboe, "The Chemistry of the Cyano group," ed. by Z. Rappoport, Interscience (1970), Chap. 3.

A Study of Solute-Solvent Interaction in Solvents of Medium Dielectric Constant from the Apparent Molal Volume Data. I

Ram GOPAL,* D. K. AGARWAL, and Rajendra KUMAR
Department of Chemistry, Lucknow University, Lucknow, India
(Received July 28, 1972)

A study of the apparent molal volume (ϕ_v) of some common salts and the tetraalkylammonium iodides in DMSO has been reported in this communication. All the salts studied here, including those containing the larger R_4N^+ ions, have a positive slope in the ϕ_v *vs.* $\sqrt{C}$ curves, indicating a strong ionic interaction, apparently due to the medium dielectric constant of the solvent. This dielectric constant also promotes ion-association at higher concentrations and thus mutual penetration of the R_4N^+ ions is prevented. As a result, no negative slope in the ϕ_v *vs.* $\sqrt{C}$ curves of the larger R_4N-iodides is observed in this solvent. The effect of temperature on the limiting apparent molal volume, $\phi°$, reveals that the ion-solvent interaction is comparatively stronger in the non-hydrogen bonded solvents like DMSO and DMF than that in strongly hydrogen-bonded solvents like NMA and NMP. Addition of a CH_2-group to each of the four R-chains of the R_4N^+ ion increases its volume by about 70 ml per mole in DMSO, DMF, and NMA.

Dependence of the apparent molal volume, ϕ_v, on concentration and temperature has been employed as a tool to study ion-ion and ion-solvent interactions in some non-aqueous solvents of high dielectric constant during the last few years.[1-8] The usual idea that the salts, containing the small common ions have only a positive slope in the linear ϕ_v *vs.* $\sqrt{C}$ curves, is not universally true and the slope for some of these salts in the solvents of very high dielectric constant, like *N*-methylacetamide (NMA, $\varepsilon_{25°}=171.7$) and *N*-methylpropionamide (NMP, $\varepsilon_{30°}=164.3$) is negative.[5-8] It was suggested that in such cases, perhaps, the small ions are accommodated inside the voids left in the packing of the large solvent molecules. Because of the weak ion-ion interaction, due to the very high dielectric constant of the solvents, such systems would behave, more or less, like a mixture of two molecular species widely different in size. This fact and some electrostatic ion-solvent interaction somehow combine to give a negative slope even for the salts containing small and compact ions. It was believed that the extension of studies on apparent molal volumes in solvents of medium dielectric constant[9] should prove useful and may give a better insight into ion-ion and ion-solvent interaction in general. Hence dimethylsulphoxide ($\varepsilon_{25°}=46.6$) has been chosen as the solvent for the present study in which the apparent molal volumes of some salts containing small common ions and of some tetraalkylammonium iodides have been determined and examined.[10]

Experimental

Dimethylsulphoxide (Fluka, purum) was refluxed for several hours on freshly ignited quicklime and then distilled under reduced pressure, the middle fraction being retained; this was again distilled under reduced pressure and the middle fraction was collected. This process was continued until the electrical conductance of the sample was reduced to 10^{-7} mho or less. The purified sample was stored in dark colored

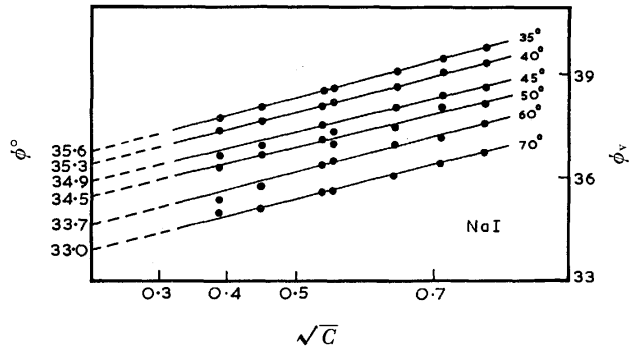

Fig. 1a. ϕ_v *vs.* $\sqrt{C}$ curves of NaI in DMSO at different temperatures.

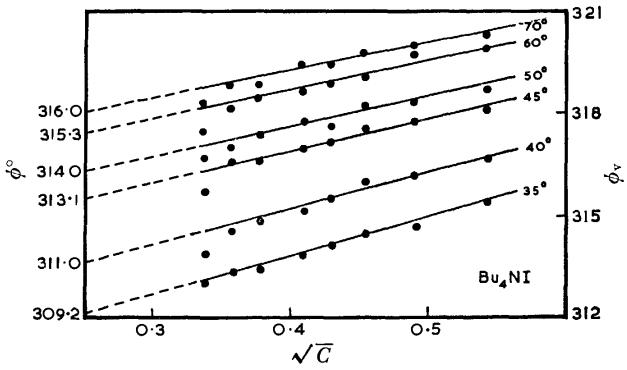

Fig. 1b. ϕ_v *vs.* $\sqrt{C}$ curves of Bu_4NI in DMSO at different temperatures.

* To whom the correspondence should be addressed.

1) Ram Gopal and R. K. Srivastava, *J. Phys. Chem.*, **66**, 207 (1962).
2) Ram Gopal and R. K. Srivastava, *J. Indian Chem. Soc.*, **40**, 99 (1963).
3) Ram Gopal and M. A. Siddiqi, *J. Phys. Chem.*, **72**, 1814 (1968).
4) Ram Gopal and M. A. Siddiqi, *ibid.*, **73**, 3390 (1969).
5) Ram Goppal and M. A. Siddiqi, *Z. Phys. Chem. N. F.*, **67**, 122 (1969).
6) F. J. Millero, *J. Phys. Chem.*, **72**, 3209 (1968).
7) Ram Gopal, M. A. Siddiqi, and K. Singh, *J. Indian Chem. Soc.*, **47**, 504 (1970).
8) Ram Gopal, M.A. Siddiqi, and K. Singh, *Z. Phys. Chem., N. F.*, **75**, 7 (1971).
9) K. Singh, Ph. D. Thesis, 1971, Lucknow University.
10) D. D. Macdonald and J. B. Hyne, *Can. J. Chem.*, **48**, 2416 (1970). Some ϕ_v-studies in DMSO–water mixtures have been reported in this paper.

bottles and kept in a dry box until used. The tetraalkylammonium iodides and the common salts, used in the present study, were purified in the usual manner, dried and kept in a vacuum desiccator. The rest of the experimental procedure for determining the density of the solutions and calculating the apparent molal volume therefrom, was the same as detailed in some earlier communications.[3,4]

From the ϕ_v-data, thus obtained, ϕ_v *vs.* $\sqrt{C}$ curves were drawn and are given in Fig. 1a for NaI and in Fig. 1b for Bu_4NI. The ϕ_v *vs.* $\sqrt{C}$ curves for other salts are very much similar to those given in Figs. 1a and 1b and hence have been omitted.

From these figures it is clear that the ϕ_v *vs.* $\sqrt{C}$ curves are almost linear with a positive slope[11] for all the salts studied here. Obviously, the Masson's empirical relation, namely,

$$\phi_v = \phi^\circ + S_v\sqrt{C}$$

is satisfied within the concentration range studied here. The limiting apparent molal volumes, ϕ°, obtained from extrapolation of the ϕ_v *vs.* $\sqrt{C}$ curves to infinite dilution, for various salts at different temperatures, are given in Tables 1 and 2. The ϕ°-values of some salts in DMF are also included in these Tables for the sake of comparison (quoted from Ref. 9).

Table 1. Limiting apparent molal volumes of some common salts in DMSO and DMF (ml/mol)

Salt	ϕ° in ml per mole at					
	35 °C	40 °C	45 °C	50 °C	60 °C	70 °C
	In DMSO					
KBr	24.65	25.40	26.25	25.90	25.00	23.24
KNO_3	33.70	33.85	—	33.32	32.46	30.72
NaBr	19.14	18.82	18.55	18.20	17.22	16.54
NaI	35.65	35.42	34.92	34.40	33.72	33.15
$NaNO_3$	27.94	—	27.70	27.30	25.76	23.85
CsI	46.92	47.75	48.05	47.92	47.25	45.94
	In DMF					
$NaNO_3$	24.10	23.82	23.35	22.94	22.90	22.32
NaI	21.25	20.74	—	20.40	20.12	19.75
NH_4NO_3	41.25	40.72	—	40.12	39.45	38.90
NH_4Br	32.22	32.00	—	31.72	31.45	31.10
NH_4I	38.10	37.80	—	37.50	37.22	36.92

Table 2. Limiting apparent molal volumes of some R_4N-iodides in DMSO and DMF (ml/mol)

Salt	ϕ° in ml per mole at					
	35 °C	40 °C	45 °C	50 °C	60 °C	70 °C
	In DMSO					
Et_4NI	172.7	173.3	173.9	174.7	175.1	174.4
Pr_4NI	*242.2*	*243.6*	*245.6*	*246.1*	*247.2*	*248.1*
Bu_4NI	309.2	311.0	313.1	314.1	315.3	316.0
Pen_4NI	378.5	383.3	386.0	387.6	390.2	391.0
Hep_4NI	519.4	521.3	523.7	525.8	528.0	531.1
	In DMF					
Et_4NI	166.1	167.0	—	168.6	170.1	171.9
Pr_4NI	238.8	240.0	—	241.6	243.5	245.0
Bu_4NI	307.6	308.9	—	311.0	313.6	315.6
Pen_4NI	377.9	379.0	—	381.6	384.4	387.0
Hex_4NI	449.1	450.7	—	453.0	455.6	457.9
Hep_4NI	515.1	516.6	—	520.1	523.9	527.5

Note: Due to limited range of concentrations that could be studied in many cases on account of low solubility and also because of our inability to handle dilute solutions (<0.1 m) for want of proper equipment, values of ϕ° given in Tables 1 and 2 should be considered only approximate.

Discussion

Variation of the Apparent Molal Volume with Concentration. As has been pointed out earlier, both the common salts and the R_4N iodides, have a positive slope in the ϕ_v *vs.* $\sqrt{C}$ curves in DMSO and DMF[11] both of which have a medium dielectric constant. It may also be recalled that the slope for some R_4N bromides (R= CH_3 to C_4H_9) and common salts is positive in methanol.[12,13] The positive slope, even for the larger R_4N-salts in these solvents is rather surprising since the interionic penetration[14] which is expected to occur when the large R_4N^+ ions are involved, should also be present in DMSO and DMF. These solvents, of course differ from solvents like water, formamide, NMA and NMP (in which negative S_v values have been reported) in having a much lower dielectric constant and negligible hydrogen bonding.

A comparison of the results obtained in DMSO and DMF on the one hand and in water, formamide, NMA and NMP on the other, suggests a possible explanation for the absence of the negative S_v values (*i.e.* the negative slope) for the R_4N-salts, in the former set of solvents. Although at infinite dilution, R_4N- and common salts are completely dissociated in all these solvents, the situation in the two types would be different at the higher concentrations. While in the solvents of high dielectric constant like water, the salts would remain completely ionized, even at fairly high concentrations, so that appreciable interionic penetration may occur and this may give rise to a negative slope in the ϕ_v *vs.* $\sqrt{C}$ curves in salts containing the larger R_4N^+ ions, the situation would be somewhat different in solvents of medium dielectric constant in which the ionic association would be quite appreciable at the higher concentrations and this would result in weakening of the ion-solvent interaction. So the ion-solvent interaction, which would be maximum at infinite dilution and would cause maximum electrostriction and contraction of the solvent, would be significantly lowered at higher concentrations. This would result in net positive volume changes per mole of the added solute since now electrostriction is less as compared to that at the lower concentrations, even if some interionic penetration, involving the large uncommitted R_4N^+ ions, occurs. As far as the common ions of small radii and compact nature are concerned,

11) It may be mentioned that similar results, *i.e.* a positive slope in the ϕ_v *vs.* $\sqrt{C}$ curves of some common as well as tetraalkylammonium salts have been obtained in dimethylformamide (DMF); see Ref. 9.

12) J. Padova and L. Abrahamer, *J. Phys. Chem.*, **71**, 2112 (1967).

13) J. B. Stark and E. C. Gilbert, *J. Amer. Chem. Soc.*, **59**, 1818 (1937); W. C. Vosburgh, L. C. Connell, and J. A. V. Butler, *J. Chem. Soc., A*, **1933**, 933.

14) This concept has been used to explain the negative slope in the ϕ_v *vs.* $\sqrt{C}$ curves and other properties of the larger R_4N-salts in different solvents.

the question of interionic penetration does not arise; at the higher concentrations, strong electrostatic ion-ion interaction would cause ionic association and weaken the ion-solvent interaction and this would result in positive S_v values.

Variation of Limiting Apparent Molal Volume, ϕ°, with Temperature. The effect of temperature on ϕ° of the salts in DMSO is shown in Figs. 2a and 2b. Similar results have been obtained in DMF also. It may be noted that as far as the salts containing the small common ions are concerned, ϕ° *vs.* t curves pass through a maximum around 35—45°C, after which ϕ° steadily decreases with the rise in temperatures. The nature of the curves clearly suggests strong ion-solvent dipole interaction so that some of the solvent molecules remain firmly associated with the solute ions even at higher temperatures and hence are not available for expansion so that the solution expands less rapidly than the pure solvent. This behavior is somewhat similar to that in water, formamide *etc.* except that the maximum in the ϕ° *vs.* t curves occurs at lower temperatures in DMSO and DMF.

Turning now to the R_4N-iodides, it may be noted that the ϕ° *vs.* t curve for Et_4NI salt almost passes through a maximum around 60°; however, for the larger R_4N iodides, although ϕ° increases with the rise in temperature throughout the temperature range

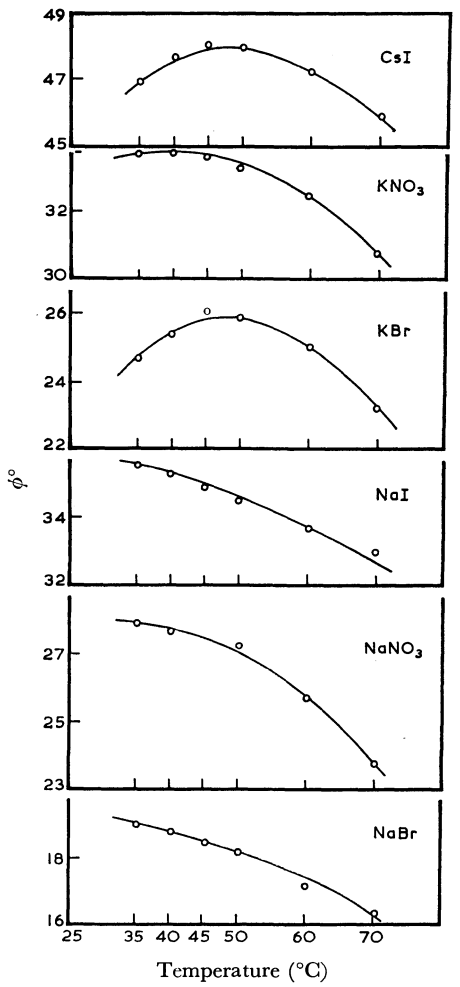

Fig. 2a. ϕ° *vs.* t curves of some common salts in DMSO.

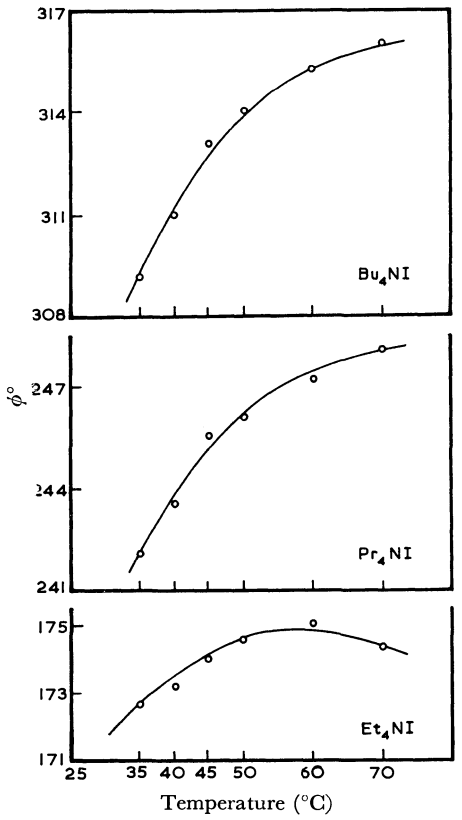

Fig. 2b. ϕ° *vs.* t curves of Et_4NI, Pr_4NI, and Bu_4NI in DMSO.

studied here, $d\phi^\circ/dt$ appears to decrease significantly, indicating the occurrence of a maximum at somewhat higher temperatures.[15] Thus the nature of the ϕ° *vs.* t curves appears to show that ion-solvent interaction is quite appreciable for the R_4N^+ ions in DMSO, the extent of interaction decreasing with increase in the radius of the R_4N^+ ion. It may be recalled that for the larger R_4N iodides, $d\phi^\circ/dt$ is almost a constant in protic solvents like formamide, NMA and NMP (not water in which ϕ° increases almost exponentially with temperature[3]), perhaps, due to release of the solvent molecules loosely bound to the R_4N^+ ions and of the solvent molecules which may be accomodated inside the larger R_4N^+ ions as well as due to uncoiling of the long coiled-up R-chains at higher temperatures. The same should be true in DMSO and DMF as well and the observed appreciable decrease in the $d\phi^\circ/dt$ values for the R_4N iodides in these solvents at higher temperatures indicates electrostatic interaction. Some other factors also appear to play an important role in controlling the general variation of ϕ° with temperature in different solvents.

A close look into the two types of the solvents appears to suggest a solution to this riddle. While DMSO and DMF are, more or less, non-hydrogen bonded-solvents, formamide, NMA and NMP, are strongly hydrogen bonded. The ion-solvent dipole interaction energy in DMF and DMSO, in the absence of any appreciable hydrogen-bond breaking energy, would be appreciable and the attachment of the solvent molecules even to

15) The ϕ° *vs.* t curves for Pen_4NI and Hep_4NI are almost similar to those for Bu_4NI although slightly steeper.

the R_4N^+ ions may not be loose; at the same time, no structure formation would occur in the solvents around the ions.[16] On the other hand, in formamide, NMA and NMP, a similar ion-solvent dipole interaction will lead to the breaking of the strong intermolecular hydrogen bonds and loosening up of the solvent structure around the ions so that the attachment of the solvent molecules to the R_4N^+ ions should be weaker, on account of the competing intermolecular hydrogen-bondre formation energy. The net result will be a weaker solvation[17] and loosening of the hydrogen bonded structure of the solvent[15,16] around the ions. Now in DMF and DMSO, some solvent molecules would be associated with the R_4N^+ ions while outside the ion-sphere, the solvent structure would be almost the same as in the pure solvent; so the expansion of the solution on heating would be comparatively less than that of the pure solvent and $d\phi^\circ/dt$ would decrease with the rise in temperature. In formamide, NMA and NMP, due to net structure breaking of the solvent[16,18] in presence of the R_4N^+ ions and their comparatively weaker solvation, solution may expand more rapidly than the pure solvent and $d\phi^\circ/dt$ may remain almost a constant (if the R_4N^+ is not too small like Me_4N^+ and Et_4N^+ ions). Thus it appears that the variation of ϕ° with temperature in different solvents can be satisfactorily explained on the concept of the ion-solvent interaction alone without invoking the idea of the release of the solvent molecules locked inside the large R_4N^+ ions or of the uncoiling of the coiled up large R-chains[4,5] of the R_4N^+ ions at the higher temperatures.

Some Remarks on the Values of ϕ° of R_4N Iodides in Various Solvents. An interesting fact to which the attention may now be drawn is that the difference $(\phi^\circ_{(RR_{n+1})_4NI} - \phi^\circ_{(R_n)_4NI})$ in formamide,[5] NMA[4,8] DMF[9] and DMSO is around 70 and is almost independent of temperature. Further, this difference *i.e.* 70 ml, very nearly corresponds to the difference in the intrinsic volumes, obtained from the relation $4\pi r^4N/3$ (r being the radius of the ions in question) of the R_4N^+ ions, using the radius as given by Robinson and Stokes.[19] This observation suggests that the electrostriction in presence of the R_4N^+ ions is very little in these solvents and also that the addition of one CH_2-group to the R-chains of the R_4N^+ ions, increases the volume of the ion by about 70 ml per mole. Since our ϕ° data have been obtained by extrapolation of the ϕ_v *vs.* $\sqrt{C}$ curves from higher concentrations and in many cases, density could be measured only within a very narrow range of concentrations due to solubility restrictions, it would be safer not to make any quantative deductions. However, since the results indicate that R_4N^+-solvent interaction is very slight, one wonders whether the variation of ϕ° with temperature, in the case of the larger R_4N iodides, is only governed by I^--solvent interaction alone. It is hoped that studies on apparent molal volumes in dilute solutions would throw more light on the behavior of the R_4N^+ ions.

Financial assistance given by the CSIR, India and the Society of the Sigma Xi of USA, is gratefully acknowledged. One of us (R.K.) is thankful to the CSIR, India, for the grant of a Junior Research Fellowship.

16) Ram Gopal and P.P. Rastogi, *Z. Phys. Chem., N. F.*, **69**, 1 (1970).

17) Situation would be different with the small common ions with high surface charge density which would produce a much stronger ion-solvent interaction than the hydrogen bond energy. This would usually lead to strong primary and secondary solvation depending upon the radius of the ion concerned.

18) R. D. Singh, P. P. Rastogi, and Ram Gopal, *Can. J. Chem.*, **46**, 3524 (1968).

19) R. A. Robinson and R. H. Stokes, "Electrolytes Solutions," Butterworths Publishing Co., London (1959), p. 124.

The Bromination of *p*-Nitrophenol in Acetic Acid

N. SRIDHAR, J. RAJARAM, and J. C. KURIACOSE
Department of Chemistry, Indian Institute of Technology, Madras, India
(Received April 1, 1972)

Bromination of aromatic substrates like *p*-bromophenol, anisole, *etc.* by molecular bromine in acetic acid follows the rate expression, Rate=k[ArH][Br_2]+k'[ArH][Br_2]^2. For the bromination of *p*-nitrophenol in acetic acid, variable orders in bromine and *p*-nitrophenol have been observed on varying the concentrations of reactants. A rate expression of the type, Rate=k[ArH][Br_2]+k'[ArH][Br_2]^2+k''[ArH]^2[Br_2] has been proposed. The observations conform to a general mechanism for bromination provided a bromine molecule, a substrate molecule or solvent molecules can be the electrophile in the rate determining step, depending upon the conditions employed for the reaction.

Bromination of aromatic compounds by molecular bromine in acetic acid medium usually exhibits complex kinetics, the overall orders being dependent on the relative concentration of substrate and bromine.[1,2] The rate is usually expressed in the form

$$\text{Rate} = k[\text{ArH}][Br_2] + k'[\text{ArH}][Br_2]^2.$$

The accepted mechanism for the third order process involves the electrophilic attack of the complex formed between the substrate and bromine by a molecule of bromine in the rate-determining step.[3] In the second order process, it has been suggested that the complex undergoes electrophilic attack by the solvent molecules.[2] That certain substrates can also act as electrophiles has been shown in the bromination of *p*-bromophenol in CCl_4.[4] In acetic acid however, it has not been possible to establish conditions where *p*-bromophenol acts as an electrophile. A more powerful electron-withdrawing group like $-NO_2$ in the *para* position of phenol might make it function as an electrophile capable of competing with both Br_2 and CH_3COOH, leading to a second order in substrate and first order in Br_2. The bromination of *p*-nitrophenol (ArH) in acetic acid has been taken up to investigate this possibility.

Experimental

Glacial acetic acid (GR, SM) was purified according to Orton's procedure,[5] potassium permanganate being used instead of chromic acid. Bromine (AR, BDH) was used without further purification. *p*-Nitrophenol was recrystallized from two percent hydrochloric acid. The kinetics of the bromination of *p*-nitrophenol was followed by determining the concentration of bromine iodometrically as a function of time. The reactions were carried out by the batch method.[6] The orders have been determined by the isolation method using the initial rates. This procedure eliminates the influence of the products formed in the reaction. The slopes at various concentrations were taken from the concentration-time curve by the mirror method.[7] For each experiment a plot of log rate *vs.* log concentration was made from which the initial rate was obtained for the corresponding initial concentration. The initial rate was also evaluated by the method of least-squares. The values obtained for initial rates by both methods were within 5% deviation. With the use of these initial rates, orders were obtained by plotting the logarithms of initial rates against the corresponding initial concentrations. The orders and rate constants were again evaluated by the least-squares analysis of the data. The deviations in rate constants in most cases were within 10%.

Results and Discussion

The interaction of *p*-nitrophenol with bromine in acetic acid follows 1:1 stoichiometry. At higher concentrations of reactants (0.29—0.14M) under equimolar conditions, the overall order is three and at lower concentrations of reactants (0.099—0.018M) it is less than three (Fig. 1). It is apparent that the reaction is complicated by the occurence of variable orders. The individual ordres are given in Table 1.

The variation in order in ArH from 0.80 to 1.58 is more than to be expected from experimental error.

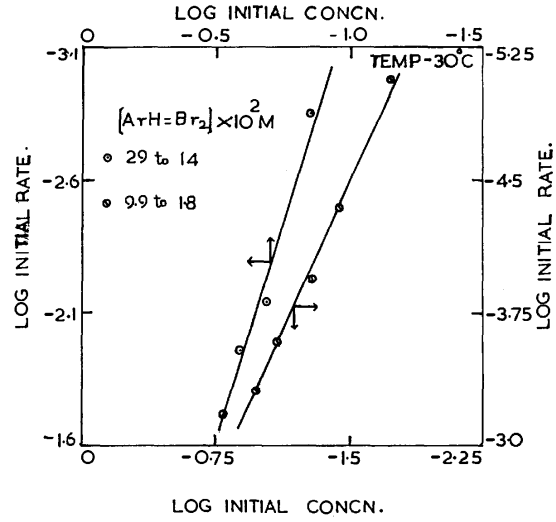

Fig. 1. Logarithmic plots of initial rates *vs.* initial concentrations for the determination of overall order.

1) N. S. Gnanapragasam and L. M. Yeddanapalli, *J. Indian Chem. Soc.*, **36**, 745 (1959).
2) J. Rajaram and J. C. Kuriacose, *Aust. J. Chem.*, **21**, 3069 (1968).
3) R.O.C. Norman and R. Taylor, "Electrophilic Substitution in Benzenoid Compounds," Elsevier, Amsterdam (1965), p. 128.
4) J. Rajaram and J. C. Kuriacose, *Indian J. Chem.*, **8**, 1145 (1970).
5) K. J. P. Orton and A. E. Bradfield, *J. Chem. Soc.*, **1927**, 823.
6) L. M. Yeddanapalli and N. S. Gnanapragasam, *ibid.*, **1956**, 4934.
7) W. H. Pearlson and J. H. Simons, *J. Amer. Chem. Soc.*, **67**, 354 (1945).

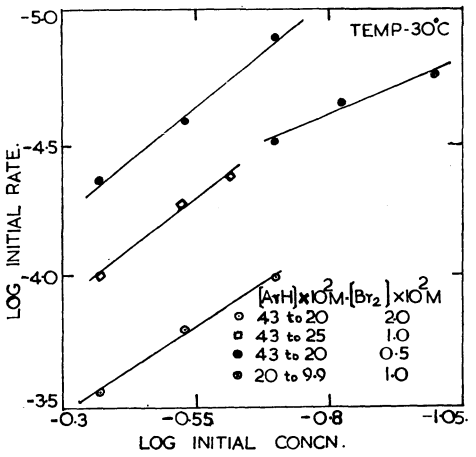

Fig. 2. Logarithmic plots of initial rates *vs.* initial concentrations for the determination of order in *p*-nitrophenol.

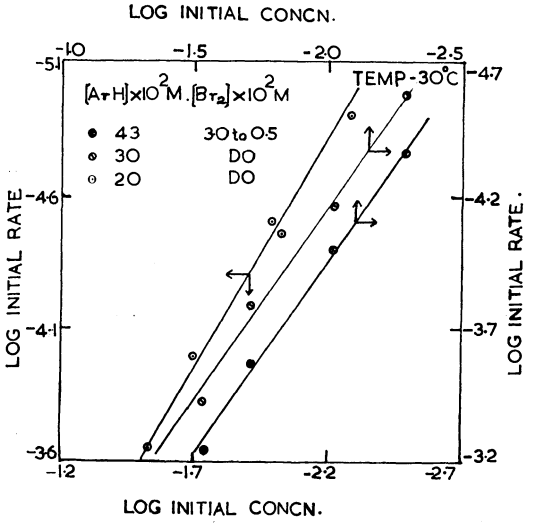

Fig. 3. Logarithmic plots of initial rates *vs.* initial concentrations for the determination of the order in bromine.

TABLE 1. INDIVIDUAL ORDERS AT DIFFERENT CONCENTRATION RANGES

Order in *p*-nitrophenol (Fig. 2)			Order in bromine (Fig. 3)		
Concentrations (mol/l)		order	Concentrations (mol/l)		order
ArH	Br_2		ArH	Br_2	
0.43—0.20	0.020	1.40	0.43	0.03—0.005	1.56
0.43—0.25	0.010	1.58	0.30	0.03—0.005	1.50
0.43—0.20	0.005	1.40	0.20	0.03—0.005	1.64
0.20—0.10	0.010	0.80			

The fractional orders observed in ArH and bromine at different concentrations of reactants suggest the possibility of either substrate molecules or bromine molecules or solvent molecules playing a vital role in the rate-determining step of the general mechanism:

$$ArH + Br_2 \rightleftharpoons ArHBr_2$$

$$ArHBr_2 + E \xrightarrow{slow} ArHBr^+ + EBr^-$$

$$ArHBr^+ \xrightarrow{fast} ArBr + H^+$$

$$H^+ + EBr^- \xrightarrow{fast} HBr + E$$

E can be ArH, bromine or solvent. When the bromine concentration is comparatively high, the electrophile will be bromine itself. As the concentration of ArH is increased, the substrate, being in excess, may satisfy the role of electrophile. This is possible in the case of *p*-nitrophenol, due to the highly electron-withdrawing nature of the nitro group which will make the molecule more electrophilic towards the removal of Br^- from the $ArHBr_2$ complex. Hence the fractional orders in reactants observed in the bromination of *p*-nitrophenol suggest a rate expression of the type

$$\text{Rate} = k[ArH][Br_2] + k'[ArH][Br_2]^2 + k''[ArH]^2[Br_2]$$

This equation can be rearranged as

$$\frac{\text{Rate}}{[ArH][Br_2]} = k + k'[Br_2] + k''[ArH]$$

At constant concentrations of bromine, the values on the left hand side of this equation can be plotted against [ArH]. The value of k'' can be obtained from the slope (Fig. 4). Different values of intercepts will be

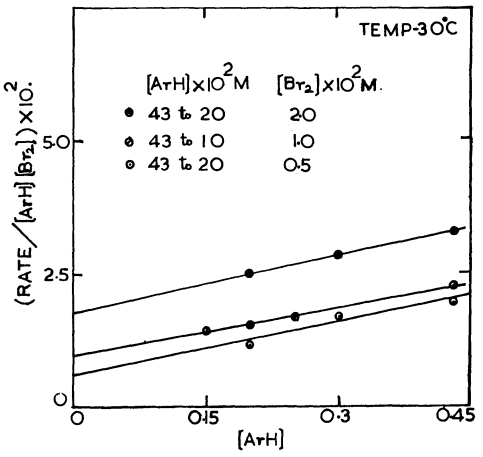

Fig. 4. Composite order plots.

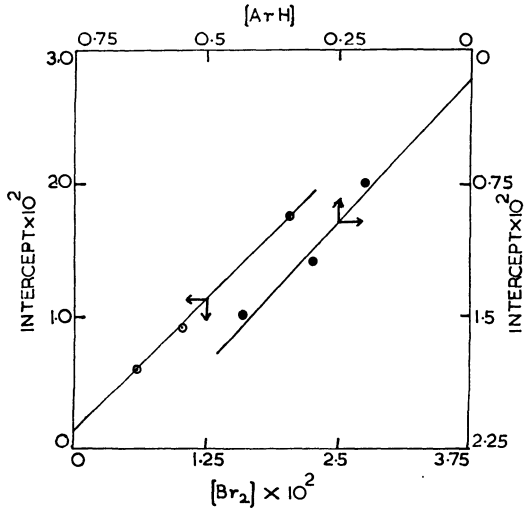

Fig. 5. ⊙ Intercept *vs.* [bromine] for different constant concentrations of bromine. ● Intercept *vs.* [*p*-nitrophenol] for different constant concentrations of *p*-nitrophenol.

Table 2. Rate constants

Data from Figs. 4 and 5			Data from Figs. 5 and 6			Data from Fig. 6
k ($l\ mol^{-1}\ min^{-1}$)	k' ($l^2\ mol^{-2}\ min^{-1}$)	k''	k ($l\ mol^{-1}\ min^{-1}$)	k' ($l^2\ mol^{-2}\ min^{-1}$)	k''	$(k'+k'')$ ($l^2\ mol^{-2}\ min^{-1}$)
		0.02991		1.088		
0.00102	0.884	0.03296	0.0011	1.066	0.03055	0.7299
		0.03254		0.996		

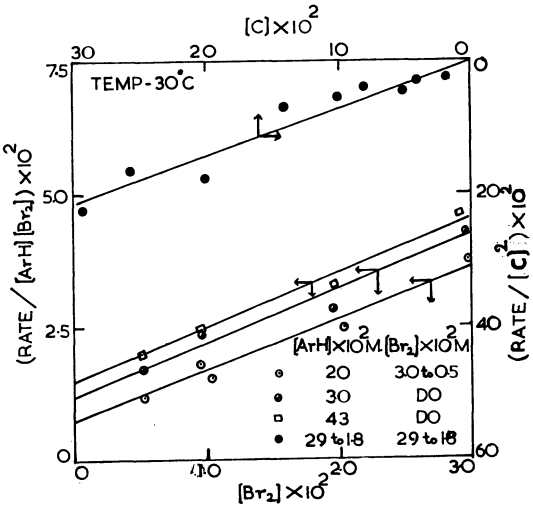

Fig. 6. Composite order plots.

obtained for different constant concentrations of bromine. A plot of the values of the intercepts obtained against the corresponding $[Br_2]$ should give a straight line with a slope k' and an intercept k (Fig. 5). Similar analysis of the data can be made for experiments where the concentration of ArH is kept constant and that of bromine is varied. The linear relationship is actually verified (Fig. 6) and another set of values of k, k', and k'' are obtained (Table 2). There is satisfactory agreement between these two sets of values. For the experiments carried out to determine the overall order, since equimolar concentrations are used, the rate expression can be written as

$$\text{Rate} = k[C]^2 + (k'+k'')[C]^3$$

where $[C]=[ArH]=[Br_2]$. The plot of Rate/$[C]^2$ *versus* [C] should be a straight line. This is verified as can be seen in Fig. 6. The intercept in agreement with value of k already determined is almost zero. The value of $(k'+k'')$ obtained is presented along with the rate constants obtained from the other analysis, in Table 2. The overall second order process may not be significant under these conditions.

The values of the rate constants indicate that the process in which bromine acts as the electrophile is much faster than the one in which ArH acts as the electrophile, which in turn is faster than the one in which the solvent molecules take an active part. The appearance of higher orders in substrate indicates that structural features induce a molecule to play an active role in the rate-determining step. In the case of *p*-nitrophenol, this may be due to the inductive effect of the nitro group which makes the substrate more electrophilic for the removal of Br^- from the $ArHBr_2$ complex than *p*-bromophenol.

Since ArH is in excess of bromine, even if there is a significant complex formation between the reactants, the total concentration of ArH and the free concentration of ArH are not different. But the total bromine concentration and the free bromine concentration will be different. Hence

$$\text{Rate} = \frac{k_1[ArH][Br_2]_T}{1+K[ArH]} + \frac{k_1'[ArH][Br_2]_T^2}{(1+K[ArH])^2} + \frac{k_1''[ArH]^2[Br_2]_T}{1+K[ArH]}$$

where K is the equilibrium constant for the complex formation. On transformation this expression can be written as

$$\frac{\text{Rate}}{[ArH][Br_2]_T} = \frac{k_1}{1+K[ArH]} + \frac{k_1'[Br_2]_T}{(1+K[ArH])^2} + \frac{k_1''[ArH]}{1+K[ArH]}$$

At constant concentration of ArH, the left hand side of the above expression can be plotted against $[Br_2]_T$ to give a straight line. The experimental results plotted in this manner yields a straight line with an intercept equal to $(k_1+k_1''[ArH])/(1+K[ArH])$. From the different values of the intercepts for different concentrations of ArH, the values of K, k_1, and k_1'' can be calculated. The value of K thus obtained is about 23. Eventhough the value of k_1'' obtained is positive, the value of k_1 is negative which is absurd. A similar plot made for the results obtained for varying concentrations of ArH but constant concentration of bromine is also a straight line. This should not be so if there is significant complex formation. Spectroscopic studies also suggest that the concentration of the complex is very small. It is therefore justified to consider that actually K is very small and the free bromine concentration can be taken to be equal to the total bromine concentration.

One of the authors (NS) is grateful to the CSIR, New Delhi for a research fellowship.

Neutral Salt Effect on the Interaction of Poly-α,L-glutamic Acid with Acridine Orange

Yukio SATO, Masahiro HATANO, and Michio YONEYAMA*

The Chemical Research Institute of Non-Aqueous Solutions, Tohoku University, Katahira, Sendai 980

(Received October 7, 1972)

The effect of potassium chloride on the absorption and optical rotatory properties of the poly-α,L-glutamic acid-acridine orange system in an aqueous solution was studied under various conditions. The stability of the helical conformation of poly-α,L-glutamic acid in this system was examined at different potassium chloride concentrations by estimating the helix fraction of the polymer. At pH 4.5, where poly-α,L-glutamic acid exists in the helix, it was found that the added potassium chloride raised the stability of the helical conformation of the polymer in this system. In this case, it was assumed that the added potassium chloride lowers the disturbance of helix formation by the bound acridine orange cation. However, when the solution's pH was raised, the added potassium chloride lowered the extent of the helix fraction in this system. These phenomena were discussed on the basis of several experimental findings on the circular dichroism of the systems. Furthermore, from the change in the intensities of the circular dichroism with the variation in the potassium chloride concentration, it was presumed that the positive circular dichroism band at about 520 nm was due to the binding of dimeric acridine orange molecules to the polymer.

Many investigators[1-3] have studied the interaction of biopolymers, such as polynucleotides,[4,5] or polypeptides,[6,7] with dyes. It is well known that an extrinsic optical activity is induced in the region corresponding to the absorption bands of acridine orange (AO) only when the dye combines with the helical form of poly-α,L-glutamic acid (PLGA) in an acidic solution. Furthermore, in the course of studies of the interaction of PLGA with AO under conditions of various pH or R/D (the ratio of glutamyl residues to dye molecules) ratios,[8,9] we found that, in the case of a R/D of around unity, the induced Cotton effects can also be observed even when the AO molecules are bound to PLGA in the neutral and alkaline pH region.[8] In this case, it was confirmed that the PLGA–AO complex had a helical conformation. Thus, extrinsic optical activity can be expected in the aqueous solution system of PLGA–AO, in which PLGA forms a helix.[10] Ballard *et al.*[2] assigned the induced circular dichroism (CD) bands of the PLGA–AO complex in an aqueous solution by measuring the CD spectrum of the complex under streaming conditions. Yamaoka and Resnik[11] discussed the optical activity in this system at very large R/D values. They proposed that the induced Cotton effects could arise from monomeric dye bound near the asymmetric environment of the α-carbon atom of the peptide residue.

In this paper, we will discuss the effect of potassium chloride on the interaction of PLGA with AO. The origin of the CD band at 520 nm will also be considered on the basis of the effect of potassium chloride at small R/D values, and will be compared with the dimer formation of AO.

Experimental

Materials. The sodium poly-α,L-glutamate used here was supplied by the Ajinomoto Co., Inc. The degree of polymerization of the polymer was 650. The AO was purified according to the method described in previous paper.[9]

Procedure. The mixtures were prepared by adding an aqueous AO solution to an aqueous PLGA solution with a pH of 4.5 in the presence or absence of potassium chloride, and then the pH of the mixed solutions was brought to the desired value by the addition of 1/10N NaOH. The R/D value was varied from 1 to 10, but the final concentration of AO was fixed at 2×10^{-5} M. The spectra of all the mixed solutions were measured within a few hours after their preparation. The CD and absorption spectra were measured by means of a JASCO Model ORD/UV-5 dichrograph with a CD attachment and by means of a Hitachi Model EPS-3T spectrometer respectively, both times at room temperature. The pH values of the solutions were measured by means of a Toa Denpa Kogyo Model HM-8 pH meter under a streaming of nitrogen gas. All the data presented below are reduced to the molar basis of the total dye concentration or the glutamyl residue concentration, and are expressed by the molar extinction coefficient, ε, and the molar ellipticity, $[\theta]$. As for the dependence of the concentration on the ellipticities, we refer to each figure.

Results and Discussion

Effect on Absorption Spectra. AO molecules aggregate in an aqueous solution. Thus, in the concentration range from 10^{-3} to 10^{-6} M of AO, as the concentration increases, the intensity of the monomer band at 492 nm (α-band) gradually decreases and the dimer band at about 470 nm (β-band) appears.[12]

* Present address: Department of Highpolymer Science, Hokkaido University, Sapporo.

1) D. F. Bradley and M. K. Wolf, *Proc. Natl. Acad. Sci.*, **45**, 944 (1959).
2) R. E. Ballard, A. J. McCaffery, and S. F. Mason, *Biopolymers*, **4**, 97 (1966).
3) E. J. Eyring, H. Kraus, and J. T. Yang, *ibid.*, **6**, 703 (1968).
4) B. J. Gardner and S. F. Mason, *ibid.*, **5**, 79 (1967).
5) M. Zama and S. Ichimura, *ibid.*, **9**, 53 (1970).
6) B. C. Myhr and J. G. Foss, *ibid.*, **10**, 425 (1971).
7) S. Ikeda and T. Imae, *ibid.*, **10**, 1743 (1971).
8) Y. Sato, M. Yoneyama, and M. Hatano, This Bulletin, **45**, 1941 (1972).
9) M. Hatano, M. Yoneyama, and Y. Sato, *Biopolymers*, **12**, 895 (1973).
10) L. Stryer and E. R. Blout, *J. Amer. Chem. Soc.*, **83**, 1411 (1961).
11) K. Yamaoka and R.A. Resnik, *J. Phys. Chem.*, **70**, 4051 (1966).
12) V. Zanker, *Z. Phys. Chem.*, **199**, 225 (1952).

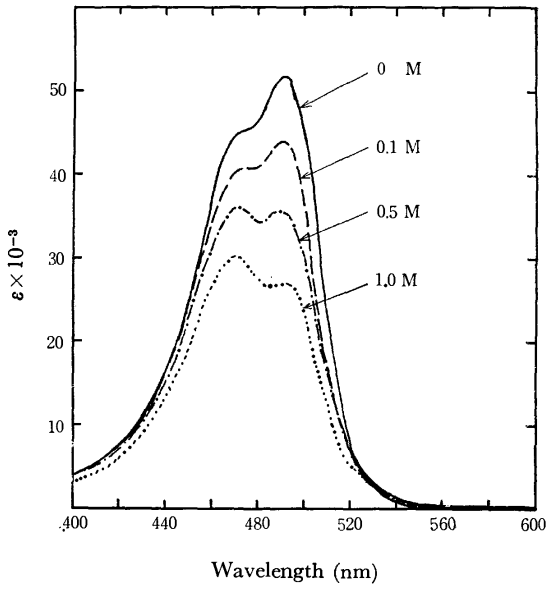

Fig. 1. Absorption spectra of AO at various KCl concentrations (pH=4.5, [AO]=2×10^{-5}M).

With a further increase in the concentration of AO, the β-band shifts toward a shorter wavelength (γ-band, about 450 nm); this corresponds to the formation of higher aggregates.

Figure 1 shows the change in the absorption spectrum of AO with a variation in the potassium chloride concentration. As the concentration of potassium chloride increases, the intensity of the monomer band becomes weak, while the dimer band increases in intensity. There is an isosbestic point at about 520 nm, indicating that only two molecular species, the AO monomer and the dimer, are present in the system. The AO dimer is probably held by dispersion force and/or hydrophobic interaction between the π-electron system, which overcomes the electrostatic repulsion force between the two AO cations. From Fig. 1, it is obvious that potassium chloride promotes the dimerization of AO. This may be due to the fact that the binding of the chloride anions to the AO cation reduces the electrostatic repulsion force between the cations of AO. The coulombic repulsion between the AO cations is minimized when the charged amino groups on both sides lie along opposite edges of the sandwich,[13] and the anions are attached laterally to the dye cation without affecting the internal coupling of AO. Therefore, it is reasonable that Fig. 1 shows the extent of the dimerization of the AO cations.

If the association is enhanced through an increase in the concentration of Cl^-, the following two equilibria can be considered for the association step of the AO cations in the presence of the anion:[14]

$$2D^+ + A^- \rightleftarrows (D_2A)^+ \quad (1)$$

$$2D^+ + 2A^- \rightleftarrows (D_2A_2) \quad (2)$$

where D^+ and A^- denote the dye cation and the anion respectively.

13) K. Bergmann and C. T. O'Konski, *J. Phys. Chem.*, **67**, 2169 (1963).

14) G. R. Haugen and E. R. Hardwick, *ibid.*, **67**, 725 (1963).

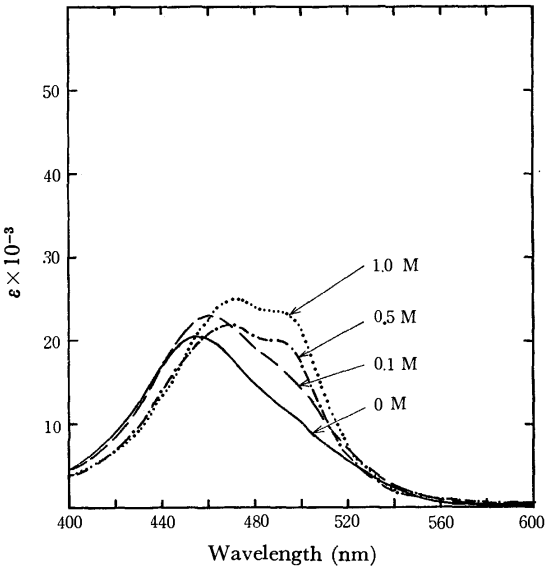

Fig. 2. Absorption spectra of PLGA–AO system at various KCl concentrations (R/D=10, pH=4.5, [AO]=2×10^{-5}M).

Figure 2 shows the change in the absorption spectrum of AO in an aqueous solution with various potassium chloride concentrations at pH=4.5 and R/D=10. The intensity of the γ-band is stronger than those of the α-band and the β-band; however, with an increase in the potassium chloride concentration the intensity of the β-band becomes rather strong. This spectral profile is scarcely influenced by the variation in R/D values. From these results, it can be concluded that the addition of potassium chloride to the AO system promotes the dimerization of the AO cation, even in the presence of PLGA.

Effect on the Helix-coil Transition of PLGA. Figure 3 shows the helix-coil transition of PLGA at various potassium chloride concentrations. The helix-coil transition of PLGA occurs in the pH range from 5.6 to 6.8. However, the transition range of pH was gradually lowered with an increase in the potassium chloride con-

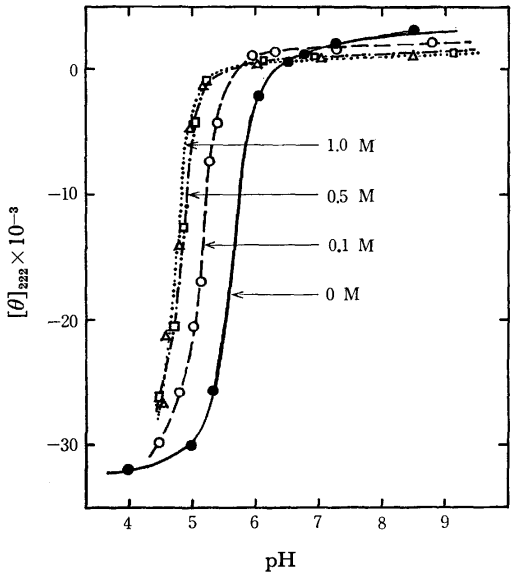

Fig. 3. Helix-coil transition of PLGA at various KCl concentrations.

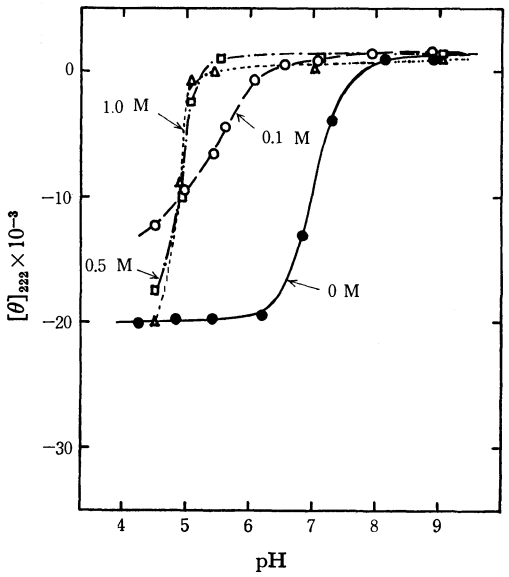

Fig. 4. Helix-coil transition of PLGA in PLGA–AO system at various KCl concentrations (R/D=6, [AO]=2×10^{-5}M).

centration. This indicated that the apparent pK_a value of PLGA was lowered by the electrostatic interaction between the carboxylate anions of side chains and the potassium cations.[15]

Figure 4 shows the effect of the addition of potassium chloride on the helix-coil transition of PLGA in the PLGA–AO system. At lower concentrations of potassium chloride, the transition range of pH remained unchanged, as dose the range in the case of the PLGA solution. When the R/D values are small, *e.g.*, smaller than about 10, the AO cations come to bind to the carboxylate anions of PLGA with an increase in the pH value in the absence of potassium chloride and stabilize the helical structure of PLGA.[9]

On the contrary, the results in Fig. 4 show that, at higher concentrations of potassium chloride, the stabilization of the helical structure of PLGA by AO molecules is lowered. In this case, this phenomenon may be elucidated by the fact that the neutral AO dimer is formed according to Eq. (2), thus reducing the binding of AO cations to PLGA.

At various concentrations of potassium chloride in the PLGA–AO system, the helix fraction (f_H) of PLGA was estimated in order to examine the influence of potassium chloride on the helix stability of PLGA (Fig. 5). It was found that f_H values tended to increase with a decrease in the R/D values when potassium chloride was added to the PLGA–AO system. This implies that the decrease in f_H value results from reducing the ionic coupling of the AO cation with the carboxylate anion. Therefore, the interaction of PLGA with AO is lowered and the stability of helical structure increases with a decrease in the R/D value and with an increase in the concentration of potassium chloride.

Relation between Dimer Formation and CD. The magnitude of CD is also dependent on the potassium chloride concentration, as may be seen in Fig. 6. While the magnitude of the positive CD band at about 435 nm and that of the negative CD band at about 465 nm decrease with an increase in the potassium chloride concentration, the magnitude of the positive CD band at about 520 nm increases with an increase in the concentration of potassium chloride. This spectral change is elucidated by the fact that, at higher concentrations of potassium chloride, the dyes aggregated in a helical fashion along the peptide chain decrease. The extent of the increase in the ellipticity of the CD band at 520 nm is larger when the potassium chloride concentration is lower. Since Eq. (1) is applicable in the case of lower concentrations of potassium chloride, where the cationic AO dimer is easily formed, AO dimer can be bound to the ionized carboxyl groups of PLGA. At higher concentrations, however, Eq. (2) seems to be more reasonable; if it holds, the binding of the AO dimer would be reduced. The change in the ellipticity of the CD band at 520 nm can be explained as follows. From the correlation between the positions of the absorption bands of the AO dimer, it can be demonstrated that the CD band at 520 nm is

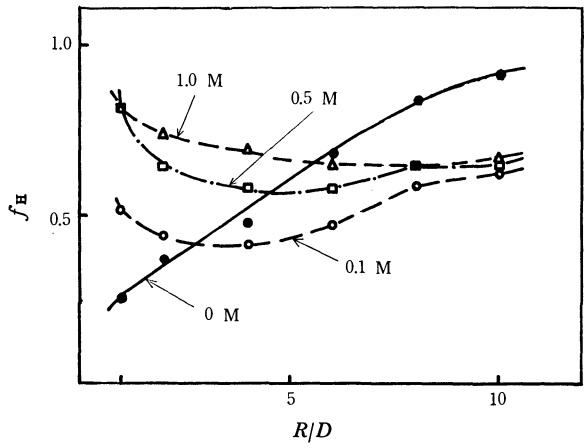

Fig. 5. R/D dependence of helix fraction (f_H) of PLGA in PLGA–AO system at various KCl concentrations (pH=4.5, [AO]=2×10^{-5}M).

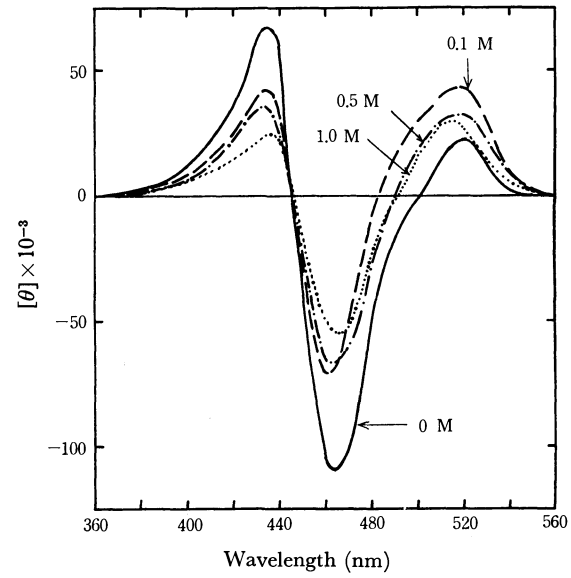

Fig. 6. CD spectra of PLGA–AO system at various KCl concentrations (R/D=10, pH=4.5, [AO]=2×10^{-5}M).

15) E. Iizuka and J. T. Yang, *Biochemistry*, **4**, 1249 (1965).

due to the binding of the dimeric AO molecule to the isolated site in an asymmetric environment of PLGA. Thus, the positive CD band at 520 nm can be ascribed to the Cotton effect originating from the AO dimer bound to PLGA. This assumption is consistent with the information obtained from the electronic spectrum of the AO dimer.[12,16,17]

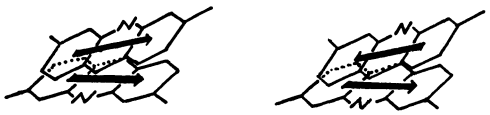

(a) (b)

Fig. 7. AO dimer on PLGA–AO complex. The arrows are direction-pair of the monomer transition dipoles.

The dimer spectrum of the AO molecule has two peaks, a strong one at about 465 nm and a weak one at about 510 nm, which can be explained in terms of the simple exciton theory.[18] The stronger band at the shorter wavelength can be assigned to an allowed transition, and the weaker band at the longer wavelength, to a forbidden transition. When AO molecules in the dimer state are oriented at small angles to each other in binding to PLGA, an optical activity is induced and the CD band arising from the dimer on PLGA may split into two components, having signs opposite to each other.

In the staggered conformation for the dimeric AO, we can consider two modes for the direction-pair of the monomer transition dipoles: (a) the directions of the monomer transition dipoles are the same, and (b) the directions of the monomer transition dipoles are opposite to one another. In the case of (a), a negative CD band arises at a shorter wavelength, whereas a positive CD band arises at a longer wavelength in the case of (b). The weak negative dichroism, concealed under the larger negative CD band, can be expected at a shorter wavelength, besides a positive dichroism at 520 nm.

Yamaoka and Resnik[11] proposed that the induced Cotton effects could arise from the dye monomers bound near the asymmetric carbon atoms in polypeptide in the case of very large R/D values. Under these conditions, the Cotton effects may be induced mainly by an interaction between dyes in the monomeric state on PLGA, since the aggregation of dye on the polymer is not plausible. On the other hand, in the case of smaller R/D values the Cotton effects may be induced mainly by an exciton interaction between dye dimers bound to PLGA.

16) R. E. Ballard and C. H. Park, *Spectrochim. Acta*, **26** (A), 399 (1970); *Idem*, *J. Chem. Soc., A*, **1970**, 1340.

17) M. E. Lamm and D. M. Neville, Jr., *J. Phys. Chem.*, **69**, 3872 (1965).

18) M. Kasha, M. A. El-Bayyoumi, and W. Rhodes, *J. Chim. Phys.*, **58**, 916 (1961).

BULLETIN OF THE CHEMICAL SOCIETY OF JAPAN, VOL. 46, 1983—1987 (1973)

The Structure and Reactivity of Nickel Hydroxide

Masao SAKASHITA and Norio SATO

Electrochemistry Labolatory, Faculty of Engineering, Hokkaido University, Sapporo 060

(Received October 4, 1972)

This paper examines the correlation between the structure and the reactivity of nickel hydroxide, using X-ray diffraction, DTA, IR spectroscopy, and gravimetry during dehydration. The degree of crystallization of β-nickel hydroxide depends on the preparation conditions of the hydroxide. Highly-crystallized β-nickel hydroxide has "free" hydroxyl groups, as is to be expected from its brucite structure. Poorly-crystallized β-hydroxide, however, has "hydrogen-bonded" hydroxyl groups, this finding is in disagreement with a previous result that "hydrogen-bonded" hydroxyl groups were found to exist only in α-form nickel hydroxide. The dehydration of the hydroxide is shown to take place in first-order kinetics with an activation energy which increases as the crystallization extends.

Nickel hydroxide and nickel oxide are produced during the corrosion of nickel and constitute surface-oxide film.[1] Nickel hydroxide is also used as an active material for the positive electrode of a nickel-cadmium battery. Many attempts have been made to determine the structure of nickel hydroxide,[2-6] and it has been proposed that nickel hydroxide exists in the α-form and the β-form. The α-nickel hydroxide contains crystallized water with "hydrogen-bonded" hydroxyl groups, while the β-form hydroxide contains no excess water and has "free" hydroxyl groups with no hydrogen-bond. McEwen,[7] however, found, by using electron microscopy and diffraction, that the α-form nickel hydroxide proposed by Bode can not exist. In

1) N. Sato, K. Kudo, and M. Miki, *Kinzoku Gakkaishi*, **35**, 1007 (1971).

2) W. Feitknecht, H. R. Christen, and H. Studer, *Z. Anorg. Allgem. Chem.*, **283**, 88 (1956).

3) H. Bode, K. Dehmelt, and J. Witte, *Chem-Ingr-Techn.*, **36**, 671 (1964); *Electrochim. Acta*, **11**, 1079 (1966).

4) F. P. Kober, *J. Electrochem. Soc.*, **112**, 1064 (1965); *ibid.*, **114**, 215 (1967).

5) M. A. Aia, *ibid.*, **114**, 418 (1967).

6) W. Dennsted and W. Loser, *Electrochim. Acta*, **16**, 429 (1971).

7) R. S. McEwen, *J. Phys. Chem.*, **75**, 1782 (1971).

spite of the many results reported, the structures and the reactivities have not been established exactly.

This paper will examine the correlation between the structures of nickel hydroxide prepared under several conditions and the dehydration kinetics by using the X-ray diffraction, DTA, IR, and gravimetry.

Experimental

Materials. Four types of nickel hydroxide powders were prepared from nickel nitrate and ammonia water under the conditions described below.

Sample *a* was a fresh hydroxide prepared by mixing 0.2 M $Ni(NO_3)_2$ with 0.2 M NH_3H_2O at room temperature; it was washed by water immediately after precipitation, Sample *b* was prepared under the same conditions except for the solution being 1.0 M NH_3H_2O and the temperature of preparation being 60~70 °C. Samples *c* and *d* were prepared by aging Sample *b* at 30 °C for 24 hr (Sample *c*) and 35 days (Sample *d*).

All of the precipitated nickel hydroxides were dried in a vacuum of 10^{-2} mmHg at 110 °C for 4 hr after having been dried in a desiccator over silica gel in 20 mmHg for 2 days. The sample was ground (200 to 300 mesh) and calcinated in a vacuum at 110 °C before measurements.

The specific surface area of each sample was determined by the BET method using N_2 gas adsorption; the values are listed in the first column of Table 1.

Table 1. Characteristics of nickel hydroxide samples

Sample	Specific surface area m^2/g	Mean particle diameter Å	Total weight loss % (w/w)	E_a [a] kcal/mol
a	59	150	20.2	20
b	45	420	19.5	30
c	31	650	19.0	33
d	30	700	19.2	49

a) Activation energy in dehydration reaction.

X-Ray Diffraction. The samples were examined by the powder method with Cu*Kα* radiation. As the diffractometer a Geigerflex 2030/P apparatus (Rigaku Denki Co., Ltd.) was used. The mean particle diameter was calculated approximately by the line-broadening method, referring to highly pure silicon as the standard.

Differential Thermal Analysis (DTA). The DTA of nickel hydroxide which had been preheated in 10^{-3} mmHg at 110 °C was carried out in air, using Al_2O_3 as the standard. A thermoflex 8001 apparatus (Rigaku Denki Co., Ltd.) was used, and the rate of heating was 10 °C/min.

IR Spectroscopy. Disks transparent to infrared radiation were prepared by pressing nickel hydroxide to about 10 ton/cm^2. Their thicknesses were between 0.03 and 0.05 mm. The disks were then placed in an IR cell with sodium chloride windows and could be connected with a conventional high-vacuum system. The spectra were taken at room temperature after treatment at the desired temperatures using a Hitachi grating spectrometer, IR-G2.

Dehydration of Nickel Hydroxide. The weight loss during the dehydration of the hydroxide, which had been dried in a vacuum at 110 °C for 1 hr, was measured gravimetrically by using a quartz spring balance placed in a quartz tube and a cathetometer (0.01 mm=0.0392 mg) under isothermal and isobaric conditions, with air provided, in 40 mmHg. The weight loss measured was then corrected by taking the buoyancy effect into account; its magnitude was separately measured with anhydrous nickel oxide. In order to reduce the pressure change caused by the water vapour produced during the dehydration, silica gel was placed in a drying tube connected to the spring balance system. The temperature was measured outside a quartz tube placed in a furnace and was controlled within an accuracy of ±1 °C. The total weight loss in the dehydration was checked in a vacuum at 400 °C.

Results and Discussion

Structure of Nickel Hydroxide. It has been reported in the literature[5,8] that the α-form nickel hydroxide can be prepared by precipitation in a mixture of nickel nitrate and diluted ammonia water at temperatures lower than 25 °C and that the β-form can be formed by mixing nickel nitrate with concentrated ammonia water at temperatures above 60 °C.

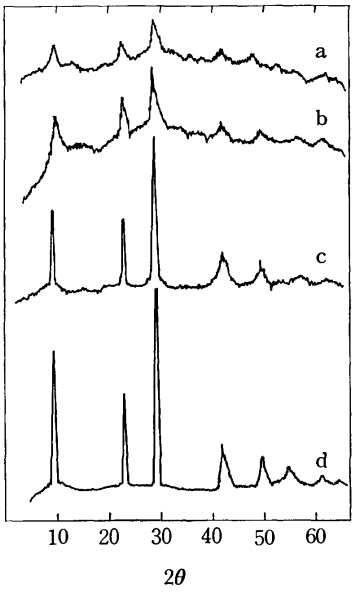

Fig. 1. X-Ray diffraction patterns of nickel hydroxide (sample *a* to *d*)

Since the α-form hydroxide proposed by Bode[3] is markedly different from the β-form, it is possible how to identify the crystal form. The conditions under which Sample *a* was prepared seem to coincide with the conditions of preparing the α-form given by the literature.[5,8] All the nickel hydroxide prepared in this work, however, shows the pattern of the β-form in the X-ray diffraction, as is shown in Fig. 1. It may also be seen in Fig. 1 that, as the crystallization extends, the X-ray diffraction pattern becomes sharp for the β-form from Samples *a* to *d*. The crystallization of nickel hydroxide is seen to increase as the concentration of ammonia in the solution for precipitation increases, as the temperature of precipitation rises, and as the aging of the hydroxide extends. The mean particle diameters of the four samples are listed in the second column of Table 1.

8) H. Bode, K. Dehmelt, and J. Witte, *Z. Anorg. Allg. Chem.*, **366**, 1 (1969).

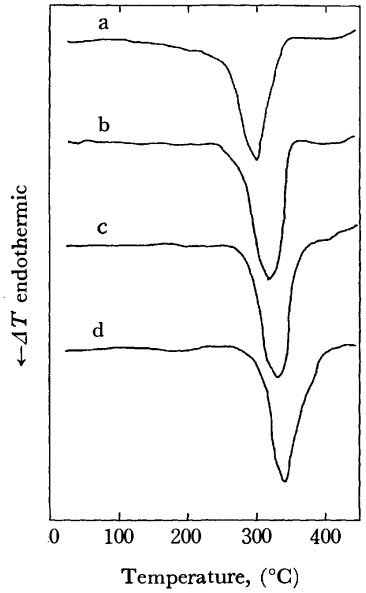

Fig. 2. DTA of nickel hydroxide dried in 10^{-2}mmHg at 110 °C for 4 hr.

The DTA curves of four samples are shown in Fig. 2. For all samples, one endothermic peak due to the dehydration is observed between 200 and 400 °C. This indicates that the nickel hydroxide, in which physically-adsorbed water is dehydrated in a vacuum at 110 °C, contains only one kind of water species to be dehydrated. The rate of the dehydration of highly-crystallized nickel hydroxide is expected to be small, because the temperature of the peak is shifted to a higher temperature in the order from Samples *a* to *d*, that is, in the order of crystallization.

The dehydration phenomenon shown in the DTA curves in Fig. 2 is coincident with the weight loss of Samples *a* and *c* during the nonisothermal dehydration shown in Fig. 3, in which the weight loss was measured as the temperature rose at the rate of 5 °C/min in air at 40 mmHg. In Fig. 3, α represents the dehydration ratio referred to the total weight loss. Since the total weight loss in reference to the initial weight shown in the third column of Table 1 is 19~20% (w/w) and is nearly equal to 1 mol% of water for all samples, it seems that the excess water or bound water previously

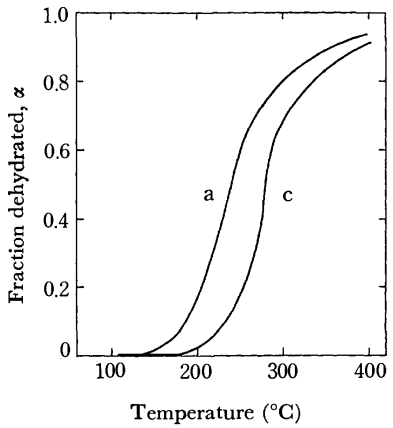

Fig. 3. Weight loss with dehydration of nickel hydroxide (sample a and c)

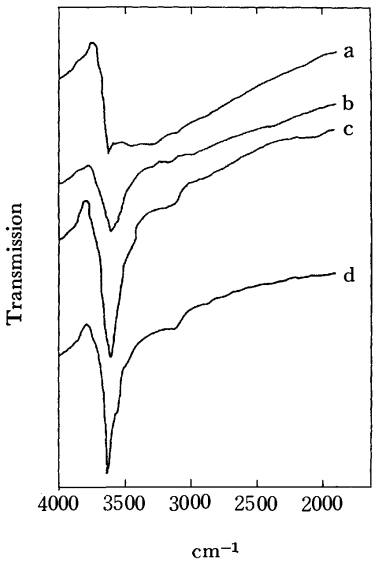

Fig. 4. IR spectra of nickel hydroxide dried in 10^{-5}mmHg at 25 °C.

observed in ferric oxide[9] is not present in nickel hydroxide.

The IR spectra of four samples in the range between 4000 and 2000 cm^{-1} are shown in Fig. 4. The bands due to the antisymmetric stretching of the hydroxyl group broaden in the order from Samples *d* to *a*. This indicates that Sample *a* has a hydroxyl group "hydrogen-bonded," while Sample d has a nearly "free" hydroxyl group at 3620 cm^{-1}. Samples *b* and *c* have an intermediate hydroxyl group between Samples *a* and *d*.

The variations in the IR spectra of Samples *a* and *d* with the temperature of the heat treatment above 100 °C in 10^{-5} mmHg for 1 hr are shown in Figs. 5 and 6. It may be seen in Fig. 5 that the hydroxyl

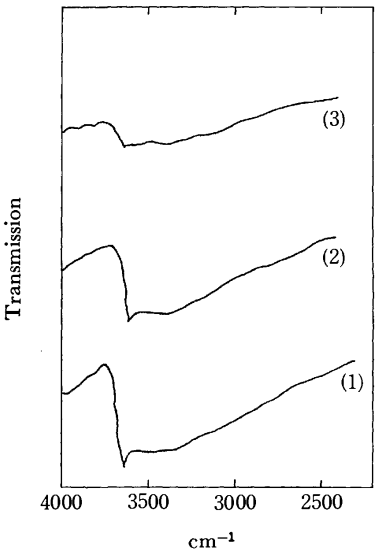

Fig. 5. Variations of IR spectrum of nickel hydroxide (sample a) with calcination in 10^{-5}mm Hg for 1 hr; (1) 110 °C, (2) 150 °C, (3) 200 °C.

9) R. Furuichi, N. Sato, and G. Okamoto, *Chimia*, **23**, 455 (1969).

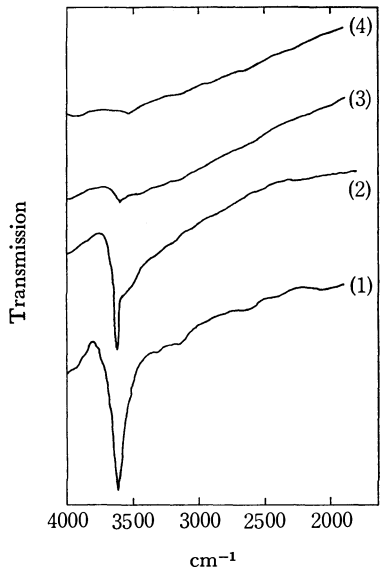

Fig. 6. Variations of IR spectrum of nickel hydroxide (sample d) with calcination in 10^{-5}mmHg for 1 hr; (1) 110 °C, (2) 200 °C, (3) 250 °C, (4) 300 °C.

group in Sample *a* is hydrogen-bonded not only in the initial state, but also in partially-dehydrated states. As Fig. 6 shows, Sample *d* has the "free" hydroxyl group in the partially-dehydrated states as well as in the initial state. As has already been discussed, the samples of nickel hydroxide used in this work were all of the β-form, as is indicated by the X-ray diffraction and by the fact that no excess water was present. In the brucite structure of β-form, it is structually impossible to form a hydrogen bond between hydroxyl groups. The hydrogen bond present in Sample *a* may, therefore, be attributed to the formation of a hydrogen bond between hydroxyl groups on the surface of crystallite.

At any rate, it is a fact that the hydrogen-bonded hydroxyl group exists in poorly-crystallized β-form nickel hydroxide; hence, a hydrogen bond is not always the characteristic of the α-form. It should also be noted that the bonding state of the hydroxyl group in each sample does not change during the dehydration, as is shown in Figs. 5 and 6.

Dehydration Kinetics. The overall dehydration reaction that was measured by the weight loss may be written by:

$$Ni(OH)_{2(solid)} \longrightarrow NiO_{(solid)} + H_2O_{(gas)} \quad (1)$$

and the normalized rate equation, by:

$$F(\alpha) = F(\alpha=0.5)t/t_{0.5}, \quad (2)$$

where α is the fraction of water dehydrated in time t and where $t_{0.5}$ is the time required for 50% dehydration. $F(\alpha)$ can be theoretically derived by assuming the reaction mechanism proposed by many workers for several solid-state reactions.[10-12]

As is shown in Fig. 7, all the dehydration data for the four types of nickel hydroxide conformed to the

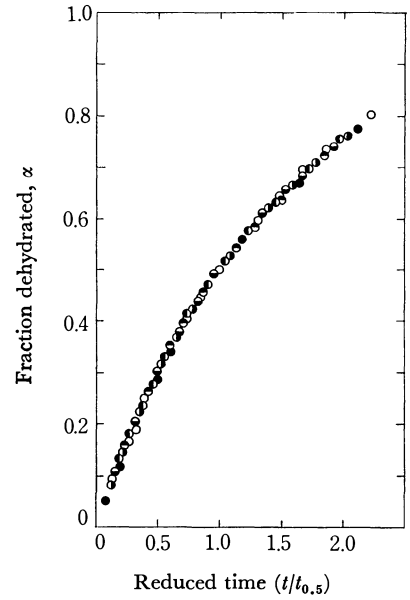

Fig. 7. Fraction dehydrated, α, *versus* reaction time, $t/t_{0.5}$, in reference to the time for 50% dehydration of nickel hydroxide in 40 mmHg air at 225 °C (●) for a sample a, at 242 °C (○) for sample b, at 245 °C (◐) and 268 °C (◑) for sample c, at 243 °C (◒) and 250 °C (◓) for sample d.

same curve of α *vs.* $t/t_{0.5}$. This indicates that the same reaction mechanism operates in all the samples examined.

If the reaction is controlled by a diffusion in the solid, one obtain this equation: $D_1(\alpha)=\alpha^2=0.25\times t/t_{0.5}$, for one-dimensional diffusion and this equation: $D_3(\alpha)=[1-(1-\alpha)^{1/3}]^2=0.0426\times t/t_{0.5}$, for three-dimensional diffusion. In the case of phase-boundary controlled reactions, one has this equation: $R_2(\alpha)=1-(1-\alpha)^{1/2}=0.293\times t/t_{0.5}$, for a two-dimensional reaction and this equation: $R_3(\alpha)=1-(1-\alpha)^{1/3}=0.206\times t/t_{0.5}$, for a three-dimensional reaction. If the dehydration process occurring in the particle is the limiting step, the de-

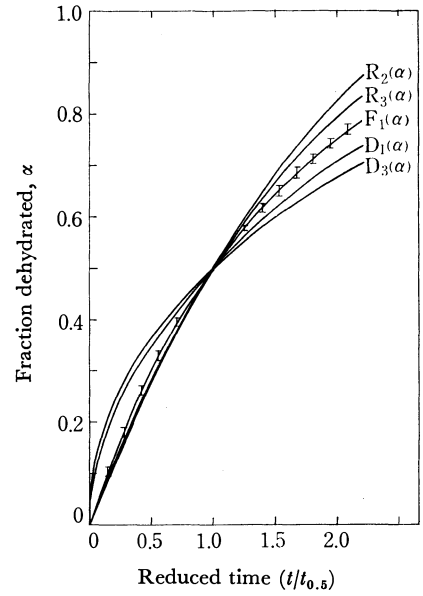

Fig. 8. Comparison of observed values, indicated by vertical line segment, with calculated α versus $t/t_{0.5}$ relation for various dehydration mechanisms.

10) R. E. Carter, *J. Chem. Phys.*, **34**, 2010 (1961).
11) E. A. Giess, *J. Amer. Ceram. Soc.*, **46**, 374 (1963).
12) J. H. Sharp, G. W. Brindley, and B. N. N. Achar, *ibid.*, **49**, 379 (1966).

hydration is of the first-order kinetics represented by this equation: $F_1(\alpha)=\ln(1-\alpha)=-0.693\times t/t_{0.5}$. The α and $t/t_{0.5}$ for each mechanism calculated are compared with the experimental results in Figs. 7 and 8. All the experimental data are seen to be in good agreement with $F_1(\alpha)$. Accordingly, the first-order reaction mechanism is operative.

Another mechanism has been proposed by Hazell *et al.*,[13] who examined the thermal decomposition of iron(II), cobalt(II), and nickel(II) hydroxides and assumed a phase-boundary reaction mechanism in the range of α less than 0.6. The first-order kinetics, however, is valid not only in the $\alpha<0.6$ range, but also in the $\alpha>0.6$ range.

The first-order kinetics assuming that the dehydration extends in the bulk of crystals is also supported by the electronmicrographical finding[14] which shows the hexagonal crystal form of the original nickel hydroxide to remain in the partially-dehydrated state. If the diffusion mechanism operated, there would be some diffusing water or hydrated hydroxyl groups in the bulk of the crystals and, hence, the IR spectrum would show a broadening peak in the partially-dehydrated state. Since the IR spectrum of Sample *d* shown in Fig. 6, however, has a sharp peak of the "free" hydroxyl groups in the partially-dehydrated state, it seems that the diffusion is unlikely to limit the reaction rate.

The Arrhenius activation energies for the four types of nickel hydroxide are listed in the fourth column in Table 1.

The table indicates that the activation energy also increases with the degree of crystallization. All the activation energies are seen to be larger than the heat of dehydration of nickel hydroxide, $\Delta H^\circ=12.4$ kcal/mol, a finding which is in agreement with the usual conception.

Conclusion

Nickel hydroxide samples prepared from nickel nitrate and ammonia water in the range of concentration from 0.2 to 1.0 M at temperatures between 20 and 60 °C are all β-form, in disagreement with the work of Bode. The more extended crystallization results from the more concentrated ammonia solution, the higher temperature of precipitation, and the more extended time of the aging of the precipitates.

The β-nickel hydroxide contains, in addition to the physically-adsorbed water, only one kind of water which exists in the form of hydroxyl groups corresponding to an endothermic peak in DTA between 200 and 400 °C. The endothermic peak shifts to higher temperatures as the degree of the crystallization rises.

The hydroxyl group of β-nickel hydroxide is "free" in the highly-crystallized particle, but "hydrogen-bonded" in the poorly-crystallized particle.

The dehydration reaction of nickel hydroxide is represented by a first-order reaction mechanism, with an activation energy which increases with the extent of crystallization.

13) I. F. Hazell and R. J. Irving, *J. Chem. Soc. A*, **669** (1966).
14) F. P. Larkins, P. J. Fensham, and J. V. Sanders, *Trans. Faraday Soc.*, **66**, 1748 (1970).

BULLETIN OF THE CHEMICAL SOCIETY OF JAPAN, VOL. 46, 1987—1990 (1973)

Crystal Structure of the Potassium Salt of Chloranil

Michiko KONNO, Hayao KOBAYASHI, Fumiyuki MARUMO, and Yoshihiko SAITO
The Institute for Solid State Physics, The University of Tokyo, Roppongi 7, Minatoku, Tokyo 106
(Received October 23, 1972)

The crystal structures of K^+(chloranil)$^-$ have been studied by X-ray diffraction. Several polymorphs were recognized, two of which (α- and β-forms) grew into comparatively good crystals. The α-form is orthorhombic, space group $P2_12_12_1$ with unit cell dimensions: $a=13.49$, $b=17.02$, $c=4.03$ Å. The β-form is orthorhombic, space group $P22_12$ with unit cell dimensions: $a=14.13$, $b=17.35$, $c=3.71$ Å. The structure of the α-form was deduced from the Patterson synthesis and refined by the block-diagonal least-squares method. The final R value was 0.13 for 146 observed reflections. Chloranil anions are stacked with equal intervals in the crystal, forming columns parallel to the c axis, the interplanar spacing being 3.47 Å. The electrostatic energy calculated by Evjen's method was about -148 kcal/mol, indicating that the structure is essentially ionic.

The magnetic, optical and electronic properties of chloranil anion radical (CA^-) salts of alkali metals[1-5] have been extensively studied in an effort to obtain information on the electronic structures of these radical salts. It is of interest that the absorption spectra of Li^+CA^- and Na^+CA^- greatly differ from those of K^+CA^- and Rb^+CA^-. The two former salts show a strong intermolecular charge-transfer band in the near infrared region and a blue shifted band originating from the monomer band in the visible region, whereas the latter salts show a weak charge-transfer band in the

1) J. J. André, J. Clémentz, R. Jesser, and G. Weill, *C. R. Acad. Sci., Paris, Ser. B*, **266**, 1057 (1968).
2) J. J. André and G. Weill, *ibid.*, **269**, 499 (1969).
3) J. J. André and G. Weill, *Mol. Phys.*, **15**, 97 (1968).
4) Y. Iida, This Bulletin, **43**, 2772 (1970).
5) N. Sakai, I. Shirotani, and S. Minomura, *ibid.*, **44**, 675 (1971).

near infrared region and a band quite similar to the anion radical monomer band. This seems to indicate stronger charge-transfer interaction between the anion radicals in lithium and sodium salts than in potassium and rubidium salts. A knowledge of the crystal structure is highly desirable for understanding the difference between the electronic structures of these radical salts. The crystal of K^+CA^- has been subjected to X-ray crystal analysis as a part of our systematic studies on the radical salts.

Experimental

Dark green crystals of K^+CA^- were grown from an acetone solution by the diffusion method according to Torrey and Hunter.[6] The shape of the crystals depends on the conditions of growing. Sometimes they are needle-like and sometimes platy. Several polymorphs were recognized from X-ray diffraction patterns, two of which (referred to as α- and β-forms) were orthorhombic and had comparatively good crystallinity. The structure of the α-form was determined in the present study. The cell dimensions and possible space groups were obtained from oscillation and Weissenberg photographs. Since the c axis is very short in both modifications, it is impossible to decide whether the systematic absences observed for $00l$ reflections were due to the space group symmetries of crystals or merely due to an accidental extinction. Important crystallographic data are given in Table 1. A crystal with the dimensions $0.04\times0.38\times0.15$ mm^3 was used for the intensity measurements of the α-form. Equi-inclination Weissenberg photographs were taken around the b axis (0th to 7th layer) and around the c axis (0th and 1st layer), utilizing the multiple film technique with Cu$K\alpha$ radiation. The intensities were estimated visually with a calibrated intensity scale. Accuracy of the measurements was bad, the diffraction spots being markedly diffuse owing to poor crystallinity of the specimen. In total, intensities of only 146 independent reflections could be collected. The usual Lorentz, polarization and spot shape corrections were applied, but no corrections were made for absorption.

TABLE 1. CRYSTALLOGRAPHIC DATA OF α- AND β-MODIFICATION OF K^+CA^- CRYSTALS

Chemical formula Crystal system	α $KC_6O_2Cl_4$ Orthorhombic	β $KC_6O_2Cl_4$ Orthorhombic
a	13.49±0.02 Å	14.13 Å
b	17.02±0.01	17.35
c	4.03±0.01	3.71
Space group	$P2_12_12_1$	$P22_12$
Z	4	4
D_c	2.04 g·cm^{-3}	2.08 g·cm^{-3}

Structure Determination of the α-Form

Three-dimensional Patterson maps were synthesized. The space groups $P2_12_12_1$ and $P2_12_12$ can be distinguished by examining the peak distribution in the Patterson maps. The space group $P2_12_12_1$ was found to be the true space group of this crystal. The positions of chlorine atoms were derived from the Patterson maps with the aid of the known molecular structure of chloranil.[7] All the remaining atoms were located from successive Fourier and difference Fourier syntheses. The structure was refined by a block-diagonal least-squares program HBLS-IV due to Dr. Ashida, assigning anisotropic temperature factors to Cl and K atoms and isotropic temperature factors to all the remaining atoms. The weighting scheme used was $w=1.0$ for $F_0\geq20.0$ and $w=0.5$ otherwise. The atomic scattering factors were taken from the International Tables for X-Ray Crystallography.[8] The final R-value was 0.13 for 146 observed reflections. The final atomic parameters are given in Table 2 with their standard deviations. The observed and calculated structure factors are compared in Table 3.

Description of Structure and Discussion

The structure viewed along the b and c axes is presented in Figs. 1(a) and (b), respectively. Chloranil anions are planar and stacked with equal intervals,

TABLE 2. FINAL POSITIONAL PARAMETERS AND THERMAL PARAMETERS FOR α-FORM WITH THEIR e.s.d.'s IN PARENTHESES

The temperature factor expression used was $\exp[-(h^2B_{11}+k^2B_{22}+l^2B_{33}+2hkB_{12}+2hlB_{13}+2klB_{23})]$

	x	y	z	B_{11}	B_{22}	B_{33}	B_{12}	B_{13}	B_{23}
K	0.405(3)	0.364(2)	0.732(9)	0.034(5)	0.003(1)	0.139(35)	0.001(3)	0.001(14)	−0.013(9)
Cl(1)	0.694(3)	0.070(2)	−0.089(10)	0.017(4)	0.003(1)	0.093(32)	−0.001(2)	−0.008(12)	0.007(9)
Cl(2)	0.616(3)	0.248(2)	−0.087(12)	0.018(4)	0.002(1)	0.168(46)	−0.001(2)	−0.012(16)	0.014(10)
Cl(3)	0.294(3)	0.148(2)	0.565(12)	0.019(4)	0.007(2)	0.219(55)	0.000(3)	−0.007(16)	−0.004(16)
Cl(4)	0.382(3)	−0.024(2)	0.593(13)	0.025(5)	0.004(2)	0.148(46)	−0.002(3)	−0.020(16)	0.013(10)
O(1)	0.567(6)	−0.041(5)	0.258(27)	11(3)					
O(2)	0.420(6)	0.259(5)	0.237(25)	11(3)					
C(1)	0.588(9)	0.093(7)	0.099(41)	10(4)					
C(2)	0.550(8)	0.167(8)	0.094(38)	10(4)					
C(3)	0.458(9)	0.190(7)	0.239(39)	10(5)					
C(4)	0.403(8)	0.126(7)	0.396(36)	10(4)					
C(5)	0.442(9)	0.053(7)	0.399(41)	10(4)					
C(6)	0.536(9)	0.032(7)	0.252(41)	10(5)					

isotropic thermal parameters (in Å^2)

6) H. A. Torrey and W. H. Hunter, *J. Amer. Chem. Soc.*, **34**, 702 (1912).

7) Shirley. S. C. Chu, G. A. Jeffrey, and T. Sakurai, *Acta Crystallogr.*, **15**, 661 (1962).

8) International Tables for X-Ray Crystallography, Vol. III p. 202, (1962), Kynoch Press, Birmingham.

TABLE 3. OBSERVED AND CALCULATED STRUCTURE FACTORS FOR α-FORM

h	k	F_o	F_c	h	k	F_o	F_c	h	k	F_o	F_c	h	k	F_o	F_c	h	k	F_o	F_c	h	k	F_o	F_c
l=0				6	3	20	29	1	9	17	11	9	1	16	5	4	5	27	32	5	1	20	14
2	0	54	56	7	3	22	25	2	9	18	10	0	2	50	52	0	6	36	41	1	2	29	31
4	0	91	86	0	4	8	4	6	9	32	34	1	2	75	74	1	6	24	21	3	2	17	21
6	0	54	55	2	4	44	45	0	10	95	91	2	2	64	65	2	6	16	28	4	2	42	34
8	0	21	22	4	4	44	43	1	10	58	51	4	2	24	30	4	6	23	22	6	2	22	15
10	0	21	12	8	4	19	17	3	10	19	28	5	2	15	15	1	8	44	41	7	2	24	11
1	1	10	13	1	5	59	54	3	11	30	26	6	2	21	19	2	8	29	27	4	3	35	25
2	1	15	18	2	5	144	136	3	12	31	32	9	2	14	12	2	9	25	27	5	3	30	22
3	1	11	16	4	5	52	50	2	13	47	53	1	3	32	39	4	9	37	33	3	4	33	32
4	1	17	22	5	5	13	14	2	14	19	22	2	3	64	67	1	10	34	37	4	4	30	26
5	1	27	26	6	5	14	12	l=1				3	3	42	49	2	10	30	29	0	5	40	31
6	1	27	32	8	5	18	19	2	0	149	158	4	3	48	44	1	12	35	31	1	5	44	34
7	1	17	20	0	6	24	16	3	0	94	94	5	3	36	34	l=2				3	5	34	31
8	1	10	9	3	6	20	20	4	0	16	12	6	3	16	22	1	0	40	58	1	6	34	30
9	1	11	9	1	7	66	66	5	0	10	7	7	3	21	16	2	0	33	36	l=3			
0	2	13	26	3	7	50	46	8	0	18	20	0	4	16	24	3	0	14	7	3	0	15	17
1	2	40	35	5	7	19	16	9	0	19	16	1	4	32	31	4	0	11	1	5	0	12	9
3	2	35	35	0	8	58	58	0	1	35	38	2	4	17	16	5	0	22	20	0	2	21	16
5	2	60	69	1	8	31	35	1	1	22	25	6	4	30	33	6	0	16	9	1	4	33	23
7	2	25	27	2	8	18	21	2	1	20	25	7	4	22	24	11	0	14	66	5	4	27	19
2	3	21	25	3	8	23	22	3	1	20	19	0	5	113	113	1	1	22	18				
3	3	98	87	4	8	61	57	4	1	31	35	1	5	83	89	2	1	38	39				
4	3	32	36	5	8	35	35	5	1	19	24	2	5	50	55	3	1	30	33				
5	3	19	23	6	8	25	23	8	1	13	7	3	5	52	56	4	1	20	14				

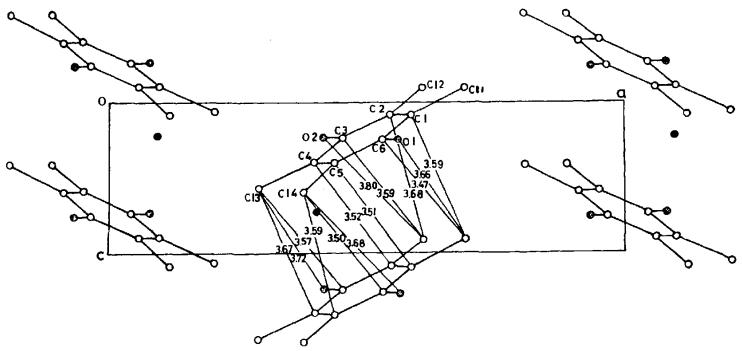

Fig. 1(a). Projection of the structure of α-form along the b axis.

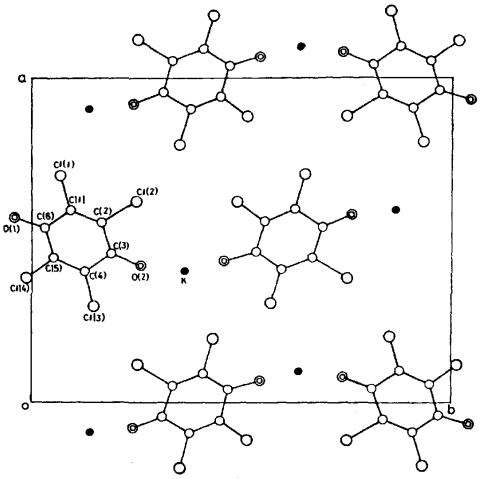

Fig. 1(b). Projection of the structure of α-form along the c axis.

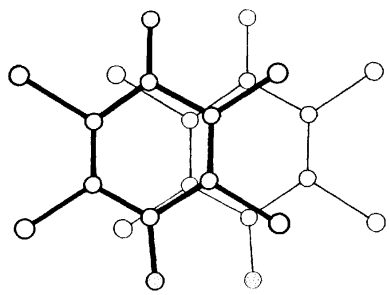

Fig. 2. Nearest-neighbor packing within the column of CA^- anions. Direction of view is perpendicular to the molecular plane.

forming columns parallel to the c axis. These columns are held together through K^+ ions. Since chloranil anions are inclined at an angle of 30° with respect to (001), an anion does not fall exactly upon the adjacent one in the same column when the structure is viewed perpendicularly to the molecular plane (Fig. 2). The least-squares plane through the atoms of anion is

$$0.468x + 0.190y + 0.863z = 4.35$$

where x, y, and z are coordinates in Å units referred to the crystal axes a, b, and c, respectively. The interplanar spacing is 3.47 Å. Intermolecular atomic distances are given in Fig. 1(a). Bond distances and angles within an anion are shown in Fig. 3. Since the number of observable reflections is small, the

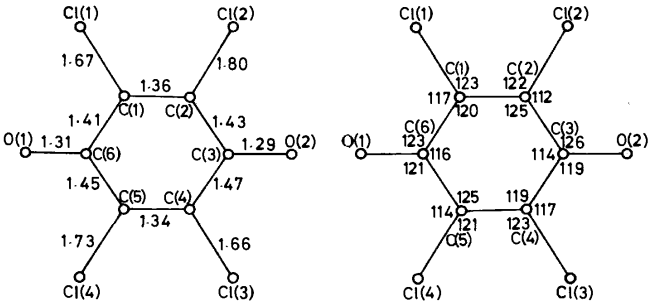

Fig. 3. Bond lengths(Å) and bond angles(degrees) within CA^- anion.

estimated standard deviations are extremely large: 0.22 Å for C–C, 0.19 Å for C–O, 0.16 Å for C–Cl. Thus it may not be practicable to discuss the interatomic distances and bond angles in detail. The average distances of chemically equivalent bonds are 1.35 Å for C=C, 1.44 Å for C–C, and 1.30 Å for C–O. Bond distances of C=C, C–C, and C–O in a chloranil anion were deduced by Iida[9] from infrared absorption spectra to be 1.37, 1.45, and 1.31 Å, respectively. The observed values of C=C, C–C, and C–O are in good accordance with these values. The K^+ ion lies at the center of a rectangle formed by two O(1) and two O(2) atoms related by c translation, respectively. The K–O distances are in the range 2.58—2.68 Å (Fig. 1(b)).

The structure does not contain dimeric CA^- anions, and the overlap between two adjacent CA^- anions in the column is rather small as shown in Fig. 2. This is in line with the spectroscopic study of this anion radical salt in crystals.

Electrostatic interactions seem to play the most important role in this anion radical salt. For the sake of confirmation, the electrostatic energy was calculated by Evjen's procedure.[10] The structure was divided into electrically neutral shells in the form of a rhombus as indicated in Fig. 4, which shows the structure of the α-form viewed along the a axis. Centers of CA^- anions drawn with solid lines are at the same level as K^+ ions with solid circles, while those drawn with broken lines are shifted by $a/2$ with respect to those drawn with solid lines. The charge of CA^- anion was assumed to be located equally at the two oxygen atoms. This assumption was supported by the theoretical calculation by Giacometti.[11] The electrostatic energy of K^+ ions and anions in each shell was calculated in the usual way. The summation of the energy converged quickly, giving a value of −148 kcal/mol. This amounts to 3/4 of the electrostatic energy of NaCl crystal and is much greater than the contributions of the van der Waals energy, charge-transfer energy, *etc.* The arrangement of K and O atoms appears to be determined mainly by electrostatic energy. When positions of two O atoms in a CA^- anion are fixed in the structure, freedom of rotation remains around the line joining the two O atoms for the anion molecule. The optimum orientation of the anion molecule was estimated for the α-form by adopting the following form for the potential energy V due to the van der Waals and repulsive forces.

$$V = \sum_i \sum_j \left(\frac{a_{ij} \exp(-b_{ij} r_{ij})}{r_{ij}^{d_{ij}}} - \frac{c_{ij}}{r_{ij}^6} \right)$$

where r_{ij} is the distance between the i-th atom in a CA^- molecule and the j-th atom in the neighboring molecules, and a_{ij}, b_{ij}, c_{ij}, and d_{ij} are the constants depending on atomic species, the values tabulated by De Santis *et al.*[12] being given. The summation for i is taken over all atoms in the CA^- molecule under consideration and that for j is taken over atoms in all the 16 neighboring molecules. During the calculation, the shape of the molecule and the symmetry of the crystal were conserved. The structure was calculated to be most stable when the molecular plane makes an angle of 34° with the (001) plane as illustrated in Fig. 5. This is in good agreement with the experimental value of 30°.

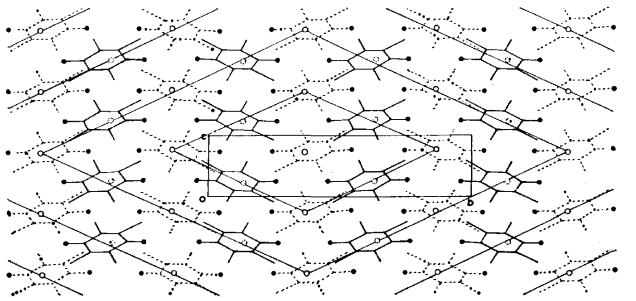

Fig. 4. Projection of the structure of α-form along the a axis, showing scheme for dividing the electrically neutral shells. Oxgen atoms are indicated by black circles.

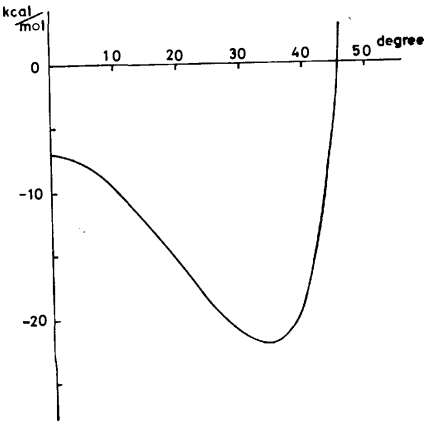

Fig. 5. Variation of non-bonded interaction energy with the change in rotation of the CA^- anion.

9) Y. Iida, This Bulletin, **43**, 345 (1970).
10) H. M. Evjen, *Phys. Rev.*, **39**, 675 (1932).
11) G. Giacometti, P. L. Nordio, and G. Rigatti, *Nuovo Cimento*, **23**, 433 (1962).
12) P. De Santis, E. Giglio, A. M. Liquori, and A. Ripamonti, *J. Polym. Sci., Part A-1*, 1383 (1963).

ESR Studies of Stable Free Radical Pairs in the Diamagnetic Matrix Crystal

Osamu TAKIZAWA, Jun YAMAUCHI,* Hiroaki OHYA-NISHIGUCHI, and Yasuo DEGUCHI**

Department of Chemistry, Faculty of Science, Kyoto University, Kyoto 606
**The Institute for Chemical Research, Kyoto University, Uji 611*
***College of Liberal Arts and Science, Kyoto University, Kyoto 606*

(Received October 24, 1972)

The radical pair system of a stable free radical, di-*p*-anisyl-nitric-oxide (DANO), has been observed in the magnetically-diluted crystal of 4,4-dimethoxy-benzophenone. The existence of the radical pair has been ascertained by the characteristic ESR absorptions, which give rise to the zero-field splitting and half-field resonance, of the powdered sample as well as by a comparison of the magnitude of the hyperfine coupling constant of the isolated radical with that of the pair system. The precise ESR measurements were performed using a single crystal containing 7.5% DANO radicals oriented well in the diamagnetic matrix. The fine structure parameters, $|D|$ and $|E|$, have been determined to be 186 Gauss and 2 Gauss respectively, from which the distance between the two radical molecules in the pair system is estimated to be 5.4 Å. In order to deduce the structures of the radical pair, the *g*-value and the hyperfine coupling constant of the isolated radical have also been determined.

Paramagnetic entities diluted in the crystals have been fruitfully investigated by electron spin resonance (ESR) techniques in order to gather information on the structures and magnetic properties of solids. Many of these works are concerned with the color center or with the radiation damage in diamagnetic matrix crystals, and some authors have studied the stable radicals in the matrix.[1–3] One of the present authors (Y.D.) has reported on the ESR measurement of the organic stable radical, diphenyl-nitric-oxide (DPNO), in a diamagnetic matrix crystal of benzophenone.[1] Analyzing the dependence of the line shape on the radical concentration, he elucidated the property of an exchange interaction between neighboring radicals and discussed the effects of exchange narrowing in the concentrated radical solid. He has also found that, in the very diluted radical crystal, the exchange interaction is so weak that the ESR line-width broadening is attributable dominantly to the dipolar interaction between two radicals. Griffith *et al.* established experimentally an exact and approximate method for determining the $\tilde{g}$- and hyperfine-tensors of the nitroxide free radical, di-*tert*-butyl-nitric-oxide.[2]

On the other hand, the triplet states of radical pairs in the irradiated organic crystals and polymers have been found by many authors.[4,5] By determining the $\tilde{g}$-tensors and the fine and hyperfine splitting tensors of the radical pair in the X-ray-irradiated single crystal of dimethyl-glyoxime at the temperature of liq. N_2, Kurita has elucidated the position of the radiation damage in the molecule and clarified the tructures of the radical pairs formed between the two neighboring molecules.[4]

The ESR of the triplet state has been utilized for the analysis of the magnetic properties of solids after the work of Bleany and Bowers.[6] One such study has been of the triplet state in the crystal of anion radical salt of 7,7,8,8-tetra-cyanoquinodimethane (TCNQ) reported by Chesnut *et al.*, who have observed the mobile triplet exciton.[7] From the analysis of the temperature dependence of the signal intensity, they have also determined the magnitude of a singlet-triplet energy separation, which is in fairly good agreement with the results of some other magnetic measurements.

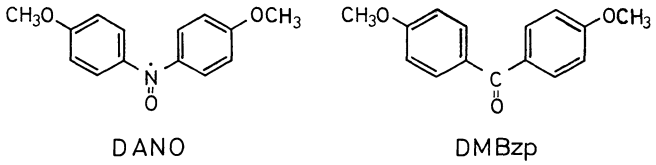

Fig. 1. Molecular structures of the radical and diamagnetic matrix.

In the present work we observed the "radical pair" of a stable free radical DANO diluted in a diamagnetic matrix crystal in order to discuss the structures and properties of DANO radical pairs. The diamagnetic matrix carefully chosen was 4,4-dimethoxy-benzophenone (DMBzp), in which the radical molecules are considered to be uniformly oriented. From the angular dependence of the ESR spectra of the radical pairs and the isolated radicals, the magnitude of the dipolar interaction is estimated and the structure of the radical pair in the diamagnetic matrix is clarified. We will discuss only the sample with a 7.5% radical concentration, the concentration dependence of the ESR spectrum will also be discussed in the last part of this paper.

Experimental

The DANO radical was synthesized by the method of Meyer *et al.*[8] After the recrystallization from ether, the

1) Y. Deguchi, This Bulletin, **34**, 910 (1961).
2) O. H. Griffith, D. W. Cornell, and H. M. McConnel, *J. Chem. Phys.*, **43**, 2909 (1965); L. J. Libertini, and O. H. Griffith, *ibid.*, **53**, 1359 (1970).
3) R. W. Holmberg, R. Livingston, and W. T. Smith, Jr., *ibid.*, **33**, 541 (1960).
4) Y. Kurita, *ibid.*, **41**, 3926 (1964); Y. Kurita, *Nippon Kagaku Zasshi*, **85**, 833 (1964).
5) M. Iwasaki and T. Ichikawa, *J. Chem. Phys.*, **46**, 2851 (1967).
6) B. Bleany and K. D. Bowers, *Proc. Roy. Soc., Ser A*, **214**, 451 (1952).
7) D. B. Chesnut and P. Arthur, Jr., *J. Chem. Phys.*, **36**, 2969 (1962); D. B. Chesnut and W. D. Phillips, *ibid.*, **35**, 1002 (1961); D. B. Chesnut, *ibid.*, **41**, 472 (1964); J. C. Bailey and D. B. Chesnut, *ibid.*, **51**, 5118 (1969).
8) K. H. Meyer and G. Brilloth, *Ber.*, **52**, 148 (1919); K. H. Meyer and W. Reppe, *ibid.*, **54**, 330 (1921).

radical and DMBzp were dissolved together in an acetone–ethanol mixed solvent. The sample crystals were obtained by recrystallization from a slow evaporation of the solvent. The radical concentration was determined by a precise ultimate analysis of the amount of nitrogen in the sample. The appearance of the mixed crystal was greatly dependent on the radical concentration. In the concentrated region, the single crystal could not be grown well; it formed only a thin, plate-like feather.[9] In the low-concentration region (especially less than 10% concentration) well crystallized samples like needles or oblique prisms were obtained. The simplicity of the ESR spectra obtained from these crystals indicate that the radical molecules are almost uniformly mixed with the matrix molecules.

The DMBzp single crystal containing 7.5% DANO radicals was grown in the form of a mono- or triclinic prism. As the crystallographic study has not yet been done, a rectangular coordinate system, a, b, and c, was defined for convenience from its shape. The c axis was selected parallel to the long edge, and the a axis, normal to the well-developed face. One of the single crystals is shown in Fig. 2, with a, b, and c axis.

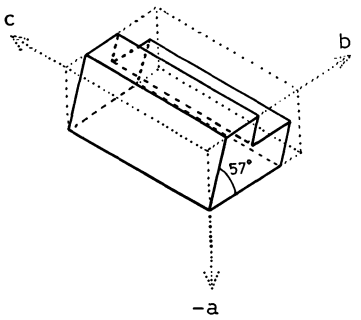

Fig. 2. A sketch of a single crystal of DMBzp containing 7.5% DANO radical. a, b, and c indicate a rectangular coordinate system adopted in the present paper.

The ESR measurements were carried out using a X-band spectrometer ME3X of JEOLCO at room temperature. The angular dependence of the ESR spectra was obtained by rotating the crystal around the a, b, or c axis, which is set perpendicular to the magnetic-field direction. The magnetic field was calibrated by the hyperfine splittings of Mn^{2+} doped in MgO and of the peroxylamine-disulfonate ion,[10] as well as by the signal of DPPH (g=2.0036).

Results

ESR Spectrum of Powdered Sample. The ESR spectrum in the g=2 region (near 3300 Gauss) is shown in Fig. 3a). In addition to a sharp absorption due to isolated radicals in the matrix, there exist a pair of broad peaks separated by about 185 Gauss and some other feeble and broad absorptions in both the higher and lower external fields. The side peaks are regarded as the triplet absorptions due to radical pairs, and so the zero-field splitting parameters, $|D|$ and $|E|$, are evaluated as 185 and 0 Gauss respectively by the method of Wasserman *et al.*[11]

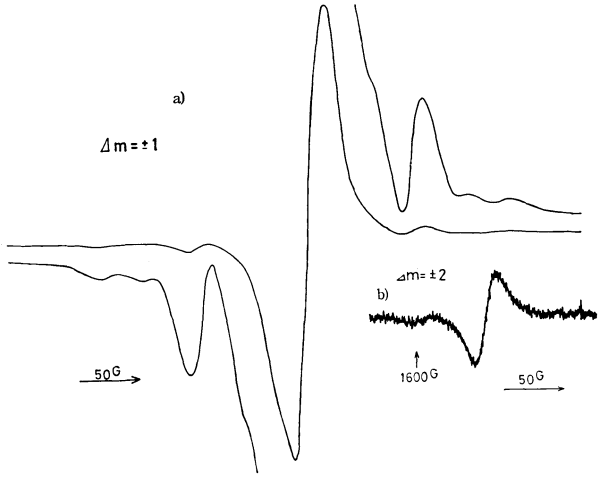

Fig. 3. a) ESR spectrum of the powdered sample of diluted DANO radical, b) $\Delta m_s = \pm 2$ transition spectrum of powdered sample.

The absorption near g=4 (1650 Gauss) shown in Fig. 3b) is the characteristic triplet absorption due to the $\Delta m_s = \pm 2$ transition. This forbidden transition was observed under the conditions of about a 100-times higher ESR spectrometer gain than that for the allowed triplet absorption, $\Delta m_s = \pm 1$ in Fig. 3a).

ESR Spectra from Single Crystal. Some of the typical ESR spectra of the single crystal are shown in Fig. 4. In (a) a pair of absorptions can be seen, one on each side of the central peak. Some other pairs of absorptions which are hidden in (a) appear in (b). When the hyperfine (hf) splitting of the central peak becomes large in some field directions, the absorptions at both sides split further into several peaks, as

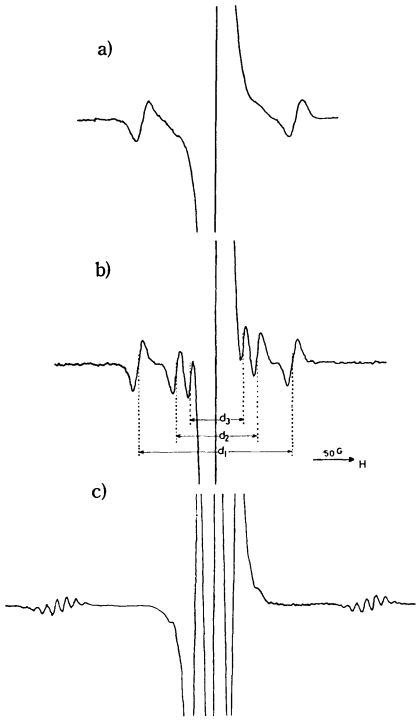

Fig. 4. Some of the ESR spectra of a single crystal of diluted DANO radical. The spectra are explained in the text. a) a//***H***, b) b//***H***, c) c//***H***.

9) A. W. Hanson, *Acta. Crystallogr.*, **6**, 32 (1953).
10) G. E. Pake, J. Townsent, and S. I. Weissman, *Phys. Rev*, **85**, 682 (1952).
11) E. Wasserman, L. C. Snyder, and W. A. Yager, *J. Chem. Phys.*, **41**, 1763 (1964).

is sohwn in (c). These can be attributed to the hf structure of two nitrogen nuclei in triplet-state radical pairs. This explanation is also supported by the fact that the splitting width of the side peaks is about half as wide as that of the central peak. The observed splittings due to the zero-field interaction are denoted by d_1, d_2, and d_3 in Fig. 4b).

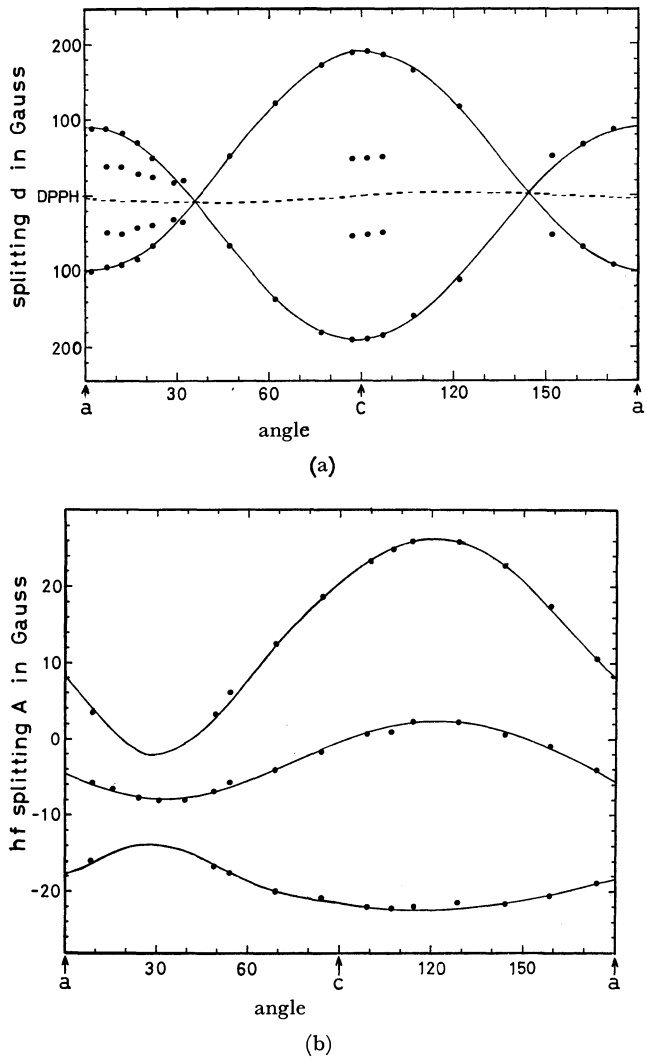

Fig. 5. Angular variation of the spectral line position in the ca plane. The position are measured from the absorption of DPPH.
a) Doublet splittings due to radical pair.
b) Nitrogen hf splittings of isolated radical.

The angular dependences of d_1 and d_2, as measured with the external magnetic field, H, in the ac plane, are shown in Fig. 5a). The nitrogen hf splitting and the g-value (denoted as g_{isol}) of the isolated radicals in the matrix, measured on the same plane, are also shown in Fig. 5b). The well-separated structures of the central peak and the simple angular variation in the hf structure parameter and g_{isol} indicate that the $\tilde{\boldsymbol{g}}$- or $\tilde{\boldsymbol{A}}_N$-tensor has the same principal axes and principal values for all radicals in the matrix.

The d_1 of the triplet-state absorption as well as the g_{isol} and hf parameters of the isolated radicals are also discussed.

Discussion

Two-spin System. In order to analyze the zero-field splittings observed, we can introduce the spin Hamiltonian of the triplet state of the radical pair, assuming that the principal axes of the $\tilde{\boldsymbol{g}}$-tensors of the two radicals are common;

$$\boldsymbol{H} = \beta \boldsymbol{H}\cdot\tilde{\boldsymbol{g}}\cdot\boldsymbol{S} + \boldsymbol{S}\cdot\tilde{\boldsymbol{D}}\cdot\boldsymbol{S} \quad (1)$$

where $\boldsymbol{S}=\boldsymbol{S}^{1}+\boldsymbol{S}^{11}$ and where the subscripts 1 and 11 indicate the radicals which form the radical-pair system. The energy levels and the separation, d, of the dipole-dipole doublet splitting at an arbitrary crystal orientation relative to the magnetic field are analyzed by Kurita[4] in the case of the axially-symmetric $\tilde{\boldsymbol{D}}$-tensor; this method is well suited for triplet species of the radical pair in the irradiated single crystal. For the nonaxial $\tilde{\boldsymbol{D}}$-tensor, if the principal axis can be set parallel or perpendicular to the external field, $\boldsymbol{H}$, the method of analysis without approximation has been reported by many authors.[12,13] In this paper the approximate method using the perturbation theory given by Itoh[14] will be used, for it needs no supposition about its crystal structure and principal-axis direction. In this method, the following assumptions are made: 1) the g-anisotropy is small, and 2) $g\beta\boldsymbol{H} \gg |D|, |E|$. Both of these assumptions are considered to be valid in the present case of the organic radical.

The method may be summarized as follows: the second term of Eq. (1) is treated as a perturbing Hamiltonian, and then the $\tilde{\boldsymbol{D}}$-tensor is represented as D_{ij} (i, j=a, b, c) on the basis of the rectangular coordinate axes, a, b, and c, which are fixed in the crystal. When the crystal is rotated around the c axis and when the external field, $\boldsymbol{H}$, makes an angle, θ, with the a axis, the resonance-field separation of the two absroptions is given, after second-order perturbation calculations, by:

$$d = 3(g_e/g_{zz})(D_{aa}\cos^2\theta + 2D_{ab}\sin\theta\cdot\cos\theta + D_{bb}\sin^2\theta) \quad (2)$$

where g_e is the g-factor of the free electron, g_{zz} is the zz-component of the $\tilde{\boldsymbol{g}}$-tensor, and z refers to the external-field direction. The tensor components with respect to the experimental coordinate system were determined by the least-squares method. Then, the $\tilde{\boldsymbol{D}}$-tensor was diagonalized to obtain the principal values.

We will not discuss the hfs of the radical-pair system in detail, but when $\boldsymbol{A}^{1}=\boldsymbol{A}^{11}$ the hfs Hamiltonian can be expressed[4] as:

$$\boldsymbol{H}_{hfs} = (1/2)\boldsymbol{I}\cdot\tilde{\boldsymbol{A}}\cdot\boldsymbol{S} \quad (3)$$

This equation suggests that a hf coupling of the pair system will be observed with a half of that of the isolated radicals, as may be seen in Fig. 4c).

One-spin System. An organic radical oriented in

12) R. W. Brandon, G. L. Closs, and C. A. Hutchison, *ibid.*, **37**, 1878 (1962); C. A. Hutchison and B. W. Mangum, *J. Chem. Phys.*, **29**, 952 (1958), **34**, 908 (1961).
13) J. R. Morton, *Chem. Rev.*, **64**, 453 (1964).
14) K. Itoh, "Jikken Kagaku Koza," ed. by the Chemical Society of Japan, Maruzen, Tokyo (1967), Vol. 13, p. 153.

the diamagnetic crystal can be described by the following Hamiltonian:

$$\boldsymbol{H} = \beta \boldsymbol{S}\cdot\tilde{\boldsymbol{g}}\cdot\boldsymbol{H} + \boldsymbol{I}\cdot\tilde{\boldsymbol{A}}\cdot\boldsymbol{S} \quad (4)$$

The results of the calculation when $I=1$, and especially in nitroxide radicals, have been reported by Griffith *et al.*[2] In the present paper, as the crystal structure is not known, the method described in the textbook of Carrington and McLachlan[15] is used. The principal values of $\tilde{\boldsymbol{g}}$- and hf-tensors and their directions can be obtained by the next equations:

$$(g_{obs})^2 = g_{aa}^2\cos^2\theta + 2g_{ab}^2\sin\theta\cdot\cos\theta + g_{bb}^2\sin^2\theta \quad (5a)$$

$$(A_{obs})^2 = A_{aa}^2\cos^2\theta + 2A_{ab}^2\sin\theta\cdot\cos\theta + A_{bb}^2\sin^2\theta \quad (5b)$$

where θ and the a, b, and c indices are defined as in the discussion of the two-spin system and where g^2_{ij} and A^2_{ij} are defined as the ij components of the $\boldsymbol{g}^2=({}^t\tilde{\boldsymbol{g}}\cdot\tilde{\boldsymbol{g}})$ and $\boldsymbol{A}^2=({}^t\tilde{\boldsymbol{A}}\cdot\tilde{\boldsymbol{A}})$ tensors respectively. The treatment of Eq. (5) is the same as that of Eq. (2).

Table 1. Experimental parameters for DANO radical in DMBzp

	Principal value	Angle with a	b	c	Parameters
	Radical pair				
D_x	± 63.7 ±0.5	0	90	90	$\|D\|=186\pm1$ G
D_y	± 59.7 ±0.5	90	0	90	$\|E\|=2\pm1$ G
D_z	∓124.4 ±1.0	90	90	0	$r=5.4\pm0.11$ Å
	Isolated radical				
g_1	2.0089±0.0002	31	92	59	
g_2	2.0059±0.0002	86	4	90	
g_3	2.0022±0.0002	121	89	31	
A_1	9.4±0.1	33	97	58	
A_2	4.4±0.1	84	7	87	
A_3	24.6±0.2	122	90	32	

Structure of the Two-spin System in the Matrix. The $\tilde{\boldsymbol{D}}$-tensor is analyzed for the side peak, d_1, which is clearly observed in all the external-field directions. The principal values and principal axes of the $\tilde{\boldsymbol{D}}$-, $\tilde{\boldsymbol{g}}$-, and hf-tensors are shown in Table 1. The D value is consistent with the data estimated from the powdered sample in Fig. 3a). By applying the measured D and E values to the equation of the resonance field of the $\Delta m_s=\pm2$ transition, $g\beta H_{dq}=\sqrt{(1/4)(h\nu)-(1/3)(D^2+3E^2)}$, one can obtain $H_{dq}=1620$ Gauss, which also agrees well with our measurement of the powdered sample (Fig. 3b).

The radical pairs in the organic crystal produced by irradiation have been reported to be $E=0$ or $E/D\neq0$: this is considered to be due to the localization of the unpaired electron in the molecule.[16] This holds also in the present case for the DANO stable radical pair. Comparing with a transition-metal complex or a TCNQ salt, in which the E/D value is not small (~0.1), the unpaired electron of the DANO radical, which has a spin density of more than 70% on the N=O bond, may be considered as a point dipole. By applying the equation: $|D|=3g^2\beta^2/2r^3$, where r is the distance between the two radicals, one can obtain $r=5.4$ Å. From the principal axes of $\tilde{\boldsymbol{D}}$, one can also determine the direction of the radical-pair axis to be parallel to the c axis.

Since one-site spectra are obtained for the isolated radical in any crystalline orientation, all the DANO radicals are considered to be oriented with the N=O bond aligned along the unique direction in the matrix even if there is more than one site in a unit cell. Consequently, one can assume that the $\tilde{\boldsymbol{g}}$-tensor orientation of radicals forming a radical pair is the same as that of the isolated radicals.

Kikuchi has calculated the g-values of several nitric-oxide radicals using the CNDO/2 molecular orbital calculation method.[17] The calculated principal g-values in the case of H_2NO and a conjugated radical, diphenyl-nitric-oxide (DPNO), are cited in Table 2, along with the principal axes from his paper. The principal values are in fairly good agreement with those of our results shown in Table 1.

Table 2. Calculated g-values for some nitric-oxide radicals[17]

	$H_2N\dot{O}$	DPNO	Axis
g_x	2.0062	2.0046	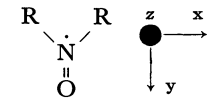
g_y	2.0091	2.0086	
g_z	2.0023	2.0023	
g_{av}	2.0059	2.0051	

Assuming the same principal axis system, one can estimate the orientation of the paired DANO molecules in the matrix crystal. Figure 6 shows a model of the two-spin system obtained from the relative orientation of the $\tilde{\boldsymbol{D}}$- and $\tilde{\boldsymbol{g}}$-tensors. Although the crystal structure of the matrix crystal is not known, the distance of the two radical molecules, r, and their alignment in the matrix determined experimentally may be compared with the crystal structure of DANO[9] cited in Fig. 7. The crystal structure of the DANO radical in Fig. 7 is orthorhombic, with four sites per unit cell; all the N=O bonds of molecules, however,

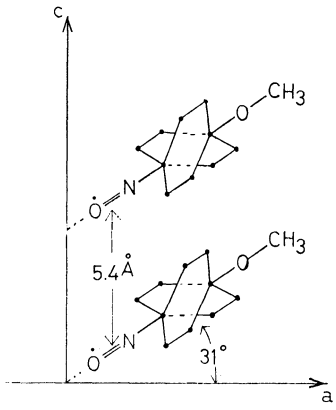

Fig. 6. A model of two spin system in a diamagnetic matrix crystal.

15) A. Carrington and A. D. McLachlan, "Introduction to Magnetic Resonance," Harper and Row, New York (1967).

16) H. Ohigashi and Y. Kurita, This Bulletin, **40**, 704 (1967).

17) O. Kikuchi, *ibid.*, **42**, 47, 1187, 1472 (1969).

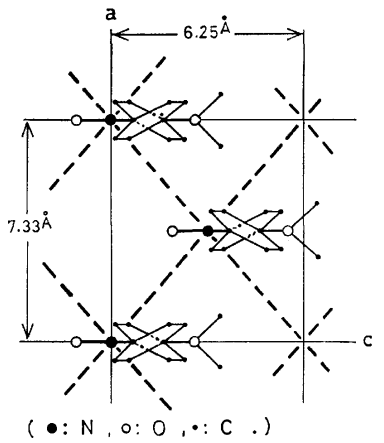

Fig. 7. Crystal structure of DANO reported by Hanson,[9] as viewed on a (010) projection
------: the nearest neighbor direction (4.81 Å)

are aligned along the c axis direction of the crystal. The distance of the nearest neighbor molecule of DANO is 4.81 Å, which is of the same order of experimental value, 5.4 Å, for DANO in DMBzp. Unlike the DANO crystal with the two distinct directions of the nearest-neighbor molecules, there is only one nearest-neighbor direction in DMBzp. This may mean a lower symmetry of the DMBzp crystal than that of the DANO crystal.

Our model for the radical pairs diluted in DMBzp is appropriate considering the alignment and the packing structure of the molecules in the matrix crystal.

Effect of the Radical Concentration. The radical concentration has great effects on both the line shape and the triplet absorption intensity. In the crystal with more than 30% DANO, the triplet absorption was not clearly observed because of the exchange narrowing effect. In a very diluted system, on the other hand, it was observed with a very weak intensity. For the 7.5% sample, the main subject of the present paper, the integrated absorption intensity ratio of the side peaks to the main peak was estimated to be 1900/11000~0.17. Assuming a one-dimensional lattice containing the radical molecule with the fractional concentration, c, the probabilities of making the radical pair and the isolated radical are approximately $2c^2$ and $c-2c^2$ respectively in the small c region. By this simple model with $c=0.075$, one can enumerate the ratio, $2c^2/(c-2c^2)$, as 0.18, which is consistent with the experimental intensity ratio.

The other peaks in Fig. 4b), whose intensities are nearly equal to each other, are considered to be due to the next-nearest neighbor molecules in the matrix. The other weak absorptions in Fig. 3a) suggest the possibility of another radical pair or a three-spin system. No more detailed discussions of these ESR absorptions can be done at present because the crystal structure of a matrix crystal is not known.

Conclusion

The existence of the stable radical triplet state is confirmed from: (1) the ESR line shape of the powdered sample; (2) the D and E values of the triplet state obtained from measurements of powdered and single-crystal samples, (3) a comparison of the hf coupling in the pair system with that in the isolated radical; (4) the forbidden transition of $\Delta m_s=\pm 2$, and (5) the ESR intensity compared with the estimation of the chance of making the two-spin system in the small radical-concentration region. The magnetic properties of this triplet radical pair and isolated radicals have been discussed. The structure of the radical pair in the diamagnetic matrix has been proposed on the basis of an analysis of the ESR spectra.

The authors are much obliged to Professor Hideo Takaki for his continuous encouragement throughout this work, and also to Dr. Mamoru Mekata and other members of his laboratory for their helpful discussions.

The Chlorination of Benzene with a Sodium Chloride-Ferric Chloride Melt

Yasukatsu TAMAI and Yasuo OHTSUKA

Chemical Research Institute of Non-Aqueous Solutions, Tohoku University, Katahira, Sendai 980

(Received October 24, 1972)

The chlorination of C_6H_6 with a NaCl–$FeCl_3$ (52: 48 in mol) melt was studied in a batch reactor at 250 °C and at a constant pressure. The main chlorinated products were monochlorobenzene (MCB) and dichlorobenzene (DCB). The isomers in DCB were *ortho* and *para*, and did not include the *meta* form. The rate of chlorination was nearly proportional to the benzene pressure in the range from 0.5 to 2.0 atm. When O_2 was introduced into the reaction system, both the rate of chlorination and the selectivity of MCB increased with the increase in the partial pressure of O_2. These facts suggest that chlorination proceeds by the electrophilic substitution on the melt surface. It was indicated by an X-ray diffraction examination of the powder of the salts used, which lost the activity for chlorination after a prolonged experiment in the presence of O_2, that the source of Cl was $FeCl_3$ and not NaCl in this reaction.

Molten salts have relatively high thermal conductivities and heat capacities. These thermal characteristics are favorable to reaction-temperature control when the salts are used as chemical-reaction media, especially in highly exothermic reactions. Furthermore, the higher mobility of ions in fused salts seems to give an interesting difference from solid salts where the ion plays an important role as a component of the expected reaction. In view of these facts, studies have recently been done on the use of molten salts as organic reaction media, mainly as catalysts.[1] Only a few studies have, however, been made on the use of molten salts as reagents;[2] especially, little work has been reported on the reaction of aromatic hydrocarbons with molten chlorides. Therefore, we studied the chlorination of C_6H_6 with a NaCl–$FeCl_3$ melt, and examined the effect of O_2 on it; this effect is of interest in connection with oxychlorination.

Experimental

Scope of Experiment. The choice of the NaCl–$FeCl_3$ melt as a chlorinating agent was based on the following considerations. The chlorination of C_6H_6 with molten chlorides took place when their metallic cations, of a polyvalent type, were used in the form of a higher valence state.[3] NaCl–$FeCl_3$ (52: 48 in mol) melt has a low melting point (*ca.* 160 °C), and the vapor pressure is very small below 500 °C.[4] C_6H_6 was selected because the product distribution, especially the isomer distribution of DCB, suggests whether the reaction mechanism is radical or ionic. The benzene pressure was varied to see where the chlorination occurred—that is, in the gas phase, at the interface, or in the bulk molten phase. To examine the effect of O_2 on the chlorination, chlorination was done at various partial pressures of O_2—that is, at different ratios of O_2 to C_6H_6. Many runs were made repeatedly with the same melt charge. The purpose is to investigate the influence of the aging of the melt on the chlorination. The contact time was varied to see whether chlorination proceeded successively or simultaneously by examining the subsequent change in the ratio of MCB to DCB.

Materials. The anhydrous $FeCl_3$ was 98.5% pure, and the NaCl and C_6H_6 were guaranteed reagents from Wako Pure Chemicals Industries, Ltd. The oxygen was 99.8% pure and was obtained from the Miyagi Sanso Co. These materials were used without further purification.

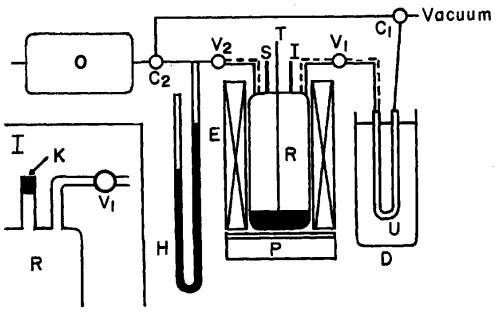

Fig. 1. Apparatus.
C: glass cock, D: dry-ice methanol trap, E: electric furnace, H: Hg-manometer, I: injection mouth of benzene, K: silicone rubber, O: oxygen reservoir, P: plate heater, R: reactor, S: charging mouth of salts, T: thermocouple, U: U-tube, V: teflon needle valve, – – –: electrically tracing.

Apparatus. The apparatus is illustrated in Fig. 1. The reactor (R) consisted of a Pyrex vessel 60 mm in diameter and 130 mm long. It was equipped with two open stems: one (S) was to charge salts, and the other (I), to introduce C_6H_6. As is shown in the detailed figure, at the top of (I) a plug of silicone rubber (K) was attached, through which C_6H_6 was injected. (R) was heated by a surrounding electric furnace (E) and by a plate heater (P) at the bottom. The reaction temperature was measured with a chromel-alumel thermocouple (T) located in a well embedded in the melt, and was controlled within ±5 °C. (R) was connected to the oxygen reservoir (O) and a U-tube (U) in a dry-ice methanol trap (D; *ca.* −75 °C) through two separate Pyrex tubings. Each tubing had a Teflon needle valve (V), by which the influence of grease contamination was avoided, to close or open the line. The Pyrex lines were electrically heated to prevent chlorination products from condensing.

1) a) W. Sundermeyer, *Angew. Chem.*, **77**, 241 (1965), (Review). b) R. T. Struck, W. E. Clark, P. J. Dudt, W. A. Rosenhoover, C. W. Zielke, and E. Gorin, *Ind. Eng. Chem. Process Res. Develop.*, **8**, 546 (1969). c) S. Kikkawa, T. Hayashi, T. Tani, and H. Osima, *Kogyo Kagaku Zasshi*, **73**, 964 (1970). d) C. N. Kenney and R. Takahashi, *J. Catal.*, **22**, 16 (1971).

2) a) R. B. Temple, C. Fay, and J. Williamson, *Chem. Commun.*, **1967**, 966. b) T. Kunugi, H. Tominaga, A. Sawanobori, and M. Nushi, *Kogyo Kagaku Zasshi*, **72**, 2385 (1969).

3) Y. Ohtsuka, K. Saegusa, and Y. Tamai, Preprint, the 26th Annual Meeting of the Chemical Society of Japan, Tokyo, 1972.

4) C. M. Cook, Jr., and W. E. Dunn, Jr., *J. Phys. Chem.*, **65**, 1505 (1961).

Procedure. The salts were ground separately and mixed together by weight (15.2 g of NaCl and 38.9 g of $FeCl_3$) in a dry box of flowing nitrogen. The mixed salts were charged quickly through (S) into (R) in laboratory air. After charging, (S) was sealed off. Then, the salts were heated to melt and then further continuously up to the reaction temperature under a vacuum produced by a rotary pump. After 30–60 mins' preheating under a vacuum, (V_1) and (V_2) were closed, and a given amount of C_6H_6 was injected through (I) into (R) with a syringe. In the following discussion, this time of injection was taken as the time of initiation of the reaction.

In this reactor, the gas volume above the melt was 250 cm^3, and the contact area was 23.7 cm^2.

After a definite contact time, (V_1) was opened to introduce the products into (U), which was then evacuated with special care so as to condense the products perfectly. To make sure that all the contents of (R) were taken out, (V_2) was opened to measure the residual pressure by means of a Hg-manometer (H). When the condensation was finished, (V_1) was closed and (U), containing the condensed materials, was removed into a Dewar vessel for storage.

The next run was usually conducted immediately after the foregoing run without changing the melt used. The procedure was repeated in the exactly same way and the melt was under a vacuum all the time between the runs.

To study the effect of O_2, the following procedures were employed. At first, the melt was preheated under a vacuum in the way described above, and then (V_1) was closed and the three-way cock (C_2) was opened to let the oxygen gas in (O) flow into the reactor until the scheduled pressure was reached (this pressure could be read with (H)). After this introduction of O_2, (V_2) was closed and a calculated amount of C_6H_6 was injected so that the total pressure could reach the atmospheric level.

Conditions of Chlorination. *General Conditions*: Unless otherwise stated, the chlorination was studied under the following conditions; amount of salts, 15.2 g of NaCl and 38.9 g of $FeCl_3$; reaction temperature, 250 °C; contact time, 50 min; total pressure, 1.0 atm. The melt was newly-prepared prior to every run in all the examinations, except when the effect of the aging of the melt was studied. The variables were as follows.

Partial Pressure of O_2: 0–0.33 atm at a constant total pressure of 1.0 atm.

Benzene Pressure: 0.5–2.0 atm in the absence of O_2.

Number of Runs: 6–9 runs with the same melt charge at constant partial pressures of O_2, 0–0.33 atm.

Contact Time: 20–120 min at a constant partial pressure of O_2, 0.33 atm.

Analytical Method. *Benzene Derivatives*: The liquid products, collected in a dry-ice methanol trap, were analyzed by the gas-chromatography method with 5% Bentone 34 and 5% DIDP on 60–80 mesh Celite 545 as the partitioning agent.[5]

Cl_2 and HCl: The Cl_2 evolved from the melt in the absence of C_6H_6 was detected by iodometry. The HCl formed by chlorination was identified by the use of an aqueous solution of ammonia.

Salts Used: To analyze the salts used, the following special experiment was conducted. That is, the chlorination of C_6H_6 in the presence of O_2 was run as follows; many runs were made with an unchanged melt charge of a rather small amount, that is, 3.0 g of NaCl and 7.8 g of $FeCl_3$ (52: 48 in mol), using the same procedure as has been described before, until the melt did not react with C_6H_6. At that time the reaction conditions were slightly modified; temperatures, 250–450 °C; contact time, 50 min; partial pressure of O_2, 0.33 atm; total pressure, 1.0 atm. Then, the melt was solidified in the vessel under a vacuum and taken out to be ground. The ground powder was analyzed by means of a standard X-ray diffraction unit, cobalt $K\alpha$ radiation being used.

5) S. Abe, A. Hongo, and E. Shirakawa, *Bunseki Kagaku*, **16**, 399 (1967).

Results and Discussion

The main chlorinated products were monochlorobenzene (MCB) and dichlorobenzene (DCB). A small amount of trichlorobenzene (TCB) was also formed. HCl was evolved as a by-product. The isomers in DCB were *ortho* and *para*, and did not include the *meta* form. Most of the TCB was the 1,2,4-isomer. These results were common findings throughout the experiments whether O_2 existed in the reaction system or not. In addition, the chlorination of MCB under the same conditions as in this work gave the same isomer distributions of DCB and TCB as do the present results on C_6H_6.[6]

It has been reported that, in the gas-phase chlorination of C_6H_6 with Cl_2 in the absence of the catalyst above 400 °C, the orientation is reversed and the products containing *m*-DCB and 1,3,5-TCB are obtained.[7] With the chlorination of MCB at 275 to 500 °C, all three DCBs are formed, with the *meta*-isomer predominating.[8] These gas-phase chlorinations in the absence of the catalyst proceed by the radical substitution, the initiation of which is the formation of a Cl radical by the thermal activation.

The present isomer distributions of DCB and TCB differ markedly from these, suggesting that the chlorination of C_6H_6 with the NaCl–$FeCl_3$ melt proceeds by the electrophilic substitution.

The chlorination of C_6H_6 in the presence of O_2 gave the same isomer distributions of DCB and TCB as in the absence of O_2. The formation of phenol as an oxidation product was expected, but not found. Carbon, CO, CO_2, and H_2O, all of which may be formed by the combustion of C_6H_6, were not identified. A very small amount of a liquid material was obtained; it was immiscible with C_6H_6 and chlorinated benzenes and was soluble in acetone and H_2O. This material may be H_2O. Furthermore, a carbon-like material was observed on the reactor wall. This material was insoluble in hot water and hydrochloric acid. These materials may be combustion products. Their amounts, however, are negligible, because, according to the observed mass balance, the charged benzene is almost completely converted to chlorinated benzenes. The formation of a compound like H_2O may also suggest the chlorination of C_6H_6 by the HCl formed and O_2 introduced, that is, oxychlorination. To elucidate its process, a quantitative analysis of HCl and H_2O should be made.

6) Y. Tamai and Y. Ohtsuka, unpublished.

7) J. P. Wibaut, L. M. F. van der Lande, and G. W. A. Wallagh, U.S. 2123857 (1938).

8) J. W. Engelsma, E. C. Kooyman, and J. R. van der Bij, *Rec. Trav. Chim.*, **76**, 325 (1957).

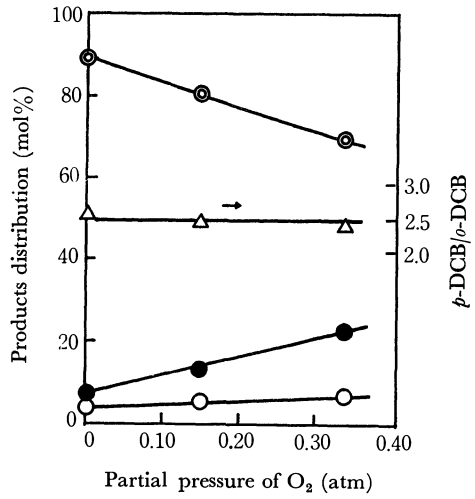

Fig. 2. Effect of partial pressure of O_2 on products distribution.
◎ unreacted C_6H_6, △: *p*/*o*, ●: MCB, ○: DCB.

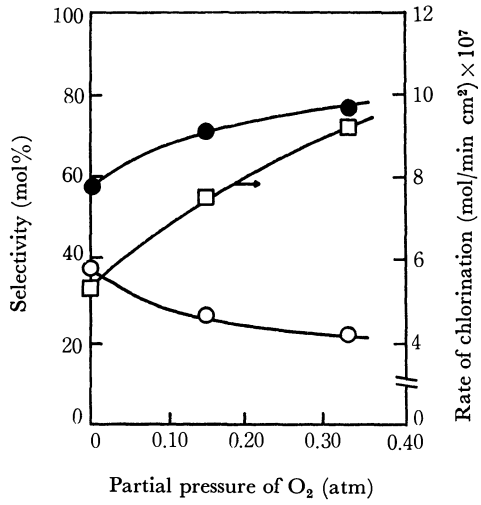

Fig. 3. Dependence of rate of chlorination and selectivity of MCB and DCB on partial pressure of O_2.
●: MCB, ○: DCB, □: rate of chlorination.

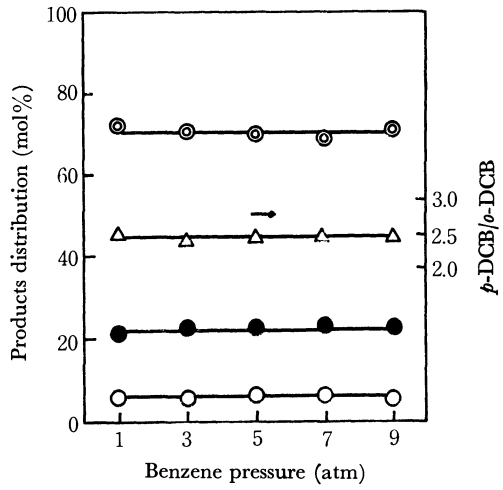

Fig. 4. Influence of benzene pressure on products distribution.
◎: unreacted C_6H_6, △: *p*/*o*, ●: MCB, ○: DCB.

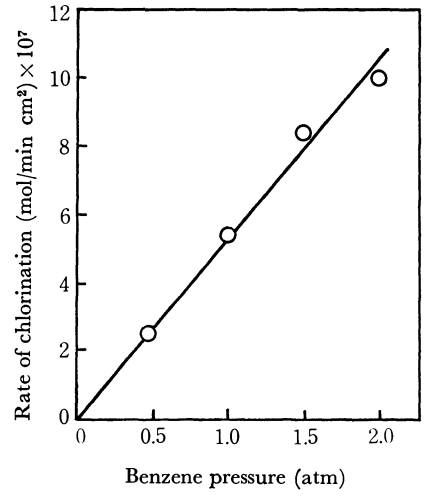

Fig. 5. Dependence of rate of chlorination on benzene pressure.

The effect of the O_2 introduced into the reaction system on the chlorination is shown in Figs. 2 and 3. Figure 2 shows that the conversion of C_6H_6 increases with the increase in the partial pressure of O_2, that is, the decrease in the partial pressure of C_6H_6. It is shown in Fig. 3 that the O_2 introduced raises both the rate of chlorination, which is expressed as moles of chlorinated benzenes formed per unit of contact time per unit of contact area, and the selectivity of MCB. In other words, O_2 promotes the chlorination and favors the formation of MCB.

The fact that the O_2 introduced raises the rate of chlorination seems to support the above suggestion of the electrophilic substitution, for, the O_2 molecule generally behaves as an inhibitor in the radical reaction because of its easy bonding to a radical. Therefore, if the radical mechanism were predominant in this chlorination, the effect of O_2 described above would not be observed.

The influence of the benzene pressure on the chlorination is shown in Figs. 4 and 5. Figure 4 shows that the products distribution is independent of the benzene pressure. The rate of chlorination is nearly proportional to the benzene pressure in the range from 0.5 to 2.0 atm, as is shown in Fig. 5. A very small amount of free Cl_2 was evolved from the melt in the absence of C_6H_6. The pressure of Cl_2 on the NaCl–$FeCl_3$ (54: 46 in mol) melt at 250 °C was estimated to be about 10^{-5} mmHg. This estimation was made by using the pressure of the $FeCl_3$ vapor, which existed almost entirely in the form of Fe_2Cl_6 at 250 °C, about 10^{-4} mmHg,[4] and the equilibrium constant between Cl_2 and Fe_2Cl_6.[9] The gas-phase chlorination by free Cl_2, however, is not considerable, because it proceeds by the radical mechanism, which gives isomer distributions of DCB and TCB different from the present results.

It is considered that the chlorination in the bulk of the melt is not appreciable because of the poor solubility of organic compounds in molten salts.[1a] By the way, the solubility of Cl_2 in molten chlorides, which is larger than those of other inorganic gases, is 3.65×10^{-7}

9) L. E. Wilson and N. W. Gregory, *J. Phys. Chem.*, **62**, 433 (1958).

mol per cm^3 of the NaCl–KCl (50: 50 in mol) melt at 750 °C.[10]

These discussions suggest that the chlorination of C_6H_6 with the NaCl–$FeCl_3$ melt takes place mainly on the melt surface. Accordingly, the rate of chlorination may be represented as the product of the rate constant, the concentration of the adsorbed benzene on the melt surface, and that of the active species. Therefore, the fact that the rate of chlorination is nearly proportional to the benzene pressure suggests that the adsorption of C_6H_6 is of a Henry-type in the pressure range from 0.5 to 2.0 atm.

The effect of the aging of the melt on the chlorination is shown in Figs. 6 and 7. The decrease in reactivity is not observed within the conducted runs whether O_2 exists in the reaction system or not, as is shown in these figures. These results may throw some doubt on the above suggestion that chlorination occurs mainly on the melt surface, for, as the numbers of runs increase, that is, as the reaction time gets longer, the composition of the melt surface should change because of the consumption of Cl. Therefore, the reactivity should decrease if the surface reaction is predominant. However, the fact that the reactivity does not decrease does not necessarily conflict with the surface-composition change resulting from the consumption of Cl. The color of the surface layer of the solidified salts used turned dark-green after many runs in the absence of O_2 and red-brown in the presence of O_2. Such changes suggest the formation of $FeCl_2$ and Fe_2O_3 respectively; Fe_2O_3 was identified by X-ray diffraction, as will be shown later. However, in the working state, the $FeCl_2$ and Fe_2O_3 formed do not stay on the melt surface as a solid, but dissolve or are suspended in the bulk of the melt. In other words, the active species of chlorination easily diffuses from the bulk to the interface. To elucidate further the suggestion that chlorination takes place predominantly on the melt surface, the effect of changes in the contact area on the chlorination, the determination of the surface tension of the melt during chlorination, and so on should be studied in the future.

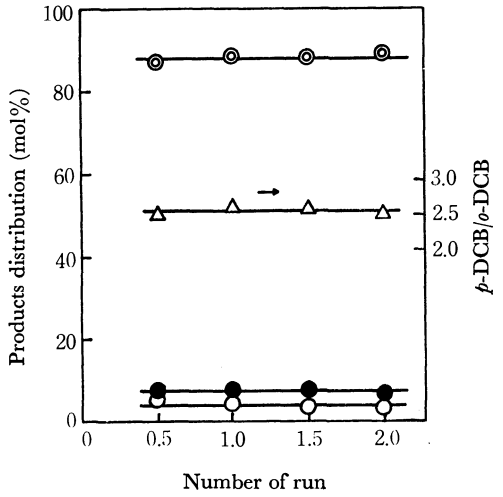

Fig. 6. Products distribution as a function of number of run in the absence of O_2.
◎: unreacted C_6H_6, △: *p*/*o*, ●: MCB, ○: DCB.

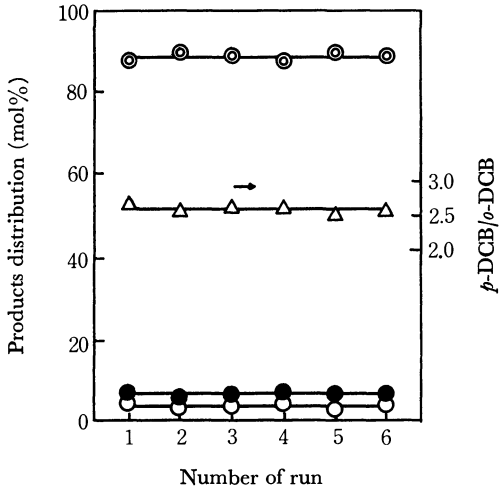

Fig. 7. Products distribution as a function of number of run in the presence of O_2.
◎: unreacted C_6H_6, △: *p*/*o*, ●: MCB, ○: DCB.

10) N. R. Thompson and B. Tittle, "Halogen Chemistry," Vol. 2, ed. by V. Gutmann, Academic Press, New York (1967), p. 387.

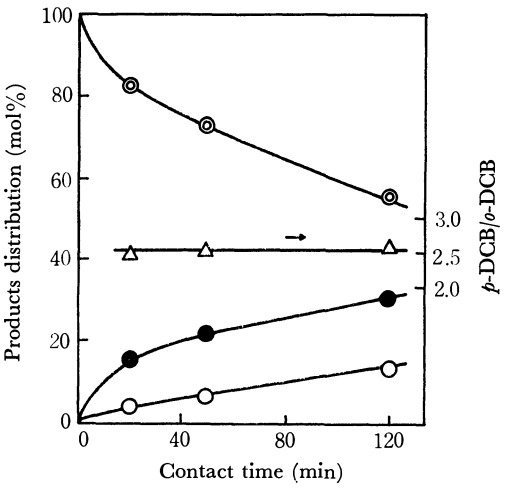

Fig. 8. Dependence of products distribution on contact time.
◎: unreacted C_6H_6, △: *p*/*o*, ●: MCB, ○: DCB.

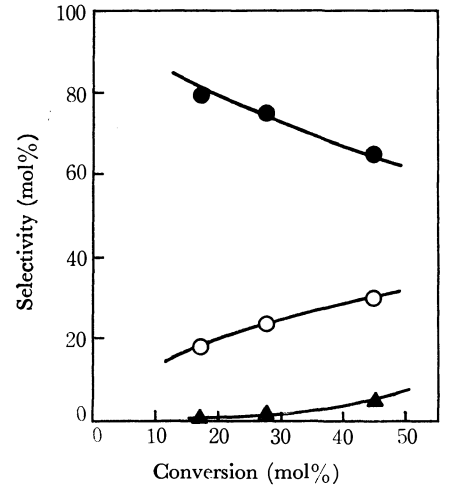

Fig. 9. Selectivity of chlorinated benzenes as a function of conversion of benzene.
●: MCB ○: DCB ▲: TCB

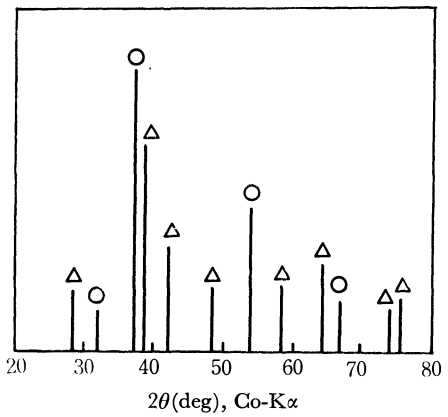

Fig. 10. X-ray diffraction pattern of used salts.
○: NaCl △: α-Fe_2O_3

The dependence of the chlorination on the contact time is shown in Figs. 8 and 9. It is shown in Fig. 9 that the selectivities of poly-substituted DCB and TCB get higher as the conversion of C_6H_6 higher. This tendency was observed whether O_2 existed in the reaction system or not. It suggests the possibility that chlorination proceeds consecutively; to confirm this mechanism, runs at shorter or longer contact times should be examined.

Figure 10 shows the X-ray diffraction pattern of the salts used, which became inactive to chlorination in the presence of O_2. The observed peaks were assigned to NaCl and α-Fe_2O_3. These results indicate that the source of Cl was $FeCl_3$ and not NaCl in this reaction. This indication gives the impression that only $FeCl_3$ participated in the chlorination. The following result, however, suggests that NaCl also participates in the chlorination. That is, when KCl was used in place of NaCl and when the chlorination of C_6H_6 with the KCl–$FeCl_3$ (52: 48 in mol; mp *ca.* 230 °C) was conducted under the same conditions as in this work, the reactivity decreased.[6] Cook *et al.* showed the existence of $NaFeCl_4$ by examinations of the vapor pressure above the NaCl–$FeCl_3$ melts and by the X-ray diffraction of their powder,[4] and Gruen *et al.* indicated the existence of $FeCl_4^-$ by studying the absorption spectra of $FeCl_3$ in a LiCl–KCl eutectic.[11] These reports also suggest that NaCl participates in this reaction.

11) G. Harrington and B. R. Sundheim, *Ann. N. Y. Acad. Sci.*, **79**, 950 (1960).

BULLETIN OF THE CHEMICAL SOCIETY OF JAPAN, VOL. 46, 2000—2003 (1973)

Water Content on Metal Oxides. I. Water Content on Silica Gel, Magnesium Oxide, Zinc Oxide, and Titanium Dioxide

Tetsuo MORIMOTO and Hiromitu NAONO*

Department of Chemistry, Faculty of Science, Okayama University, Tsushima, Okayama 700

(Received October 30, 1972)

The surface water content has been determined on silica gel, magnesium oxide, zinc oxide, and titanium dioxide by means of active hydrogen analysis and by the successive-ignition-loss method. Except for magnesium oxide pretreated at 100 °C, it has been found that the water contents obtained from the two methods on every oxide tested are in good agreement with each other. The successive-ignition-loss method gives an extraordinarily high value of water content on magnesium oxide pretreated at 100 °C, probably because of the retention of inner hydroxyl groups. The present results indicate that the two methods are equally reliable for the quantitative determination of the water content on metal oxides. Moreover, the simultaneous application of both methods make it possible to estimate each amount of surface hydroxyl groups and physisorbed water molecules.

The surface hydroxyl groups on metal oxide play an important role in the adsorption of molecules. Several methods have thus far been examined in estimating the surface hydroxyl groups.[1-13] Morimoto *et al.* have studied the metal oxide surface by measuring the water content by means of the successive-ignition-loss method.[14-16] On the other hand, Fripiat *et al.* adopted Zerewitinoff's method to determine active

* Present address: Department of Chemistry, Faculty of Science, Kwansei Gakuin University, Uegahara, Nishinomiya, Hyogo.

1) I. Shapiro and H. G. Weiss, *J. Phys. Chem.*, **57**, 219 (1953).
2) G. J. Young, *J. Colloid Sci.*, **13**, 67 (1958).
3) H. Duel, J. Wartmann, K. Hutsehneker, U. Schobinger, and C. Grüdel, *Helv. Chim. Acta*, **42**, 1160 (1959).
4) H. P. Boehm and M. Schneider, *Z. Anorg. Allg. Chem.*, **301**, 326 (1959).
5) W. Noll, K. Damm, and R. Fauss, *Kolloid-Z.*, **169**, 18 (1960).
6) M. Folman, *Trans. Faraday Soc.*, **57**, 2000 (1961).
7) J. J. Fripiat and J. Uytterhoeven, *J. Phys. Chem.*, **66**, 800 (1962).
8) J. Uytterhoeven and H. Naveau, *Bull. Soc. Chim. Fr.*, **1962**, 27.
9) V. Ya Davydov, A. V. Kiselev, and L. T. Zhuravlev, *Trans. Faraday Soc.*, **60**, 2254 (1964).
10) G. Wirzing, *Naturwissenschaften*, **51**, 211 (1964).
11) J. Uytterhoeven, M. Sleen, and J. J. Fripiat, *Bull. Soc. Chim. Fr.*, **1965**, 1800.
12) H. P. Boehm, *Angew. Chem. Int. Ed. Ergl.*, **5**, 533 (1966).
13) R. Flaig-Baumann, H. D. Neuwinger, and H. P. Boehm, *Fortsch. Kolloid Polym.*, **55**, 7 (1971).
14) T. Morimoto, K. Shiomi, and H. Tanaka, This Bulletin, **37**, 392 (1964).
15) T. Morimoto, M. Nagao, and F. Tokuda, *ibid.*, **41**, 1533 (1968).
16) T. Morimoto, M. Nagao, and J. Imai, *ibid.*, **44**, 1288 (1971).

hydrogen in the analysis of the water content on silica gel.[7]

In order to obtain reliable data on the water content, it is desirable to compare the water content as determined by different methods and to investigate the characteristic features of each method. The water content on silica gel has been examined by various methods,[12] but for the other metal oxides few works have been reported and different methods have not been compared. In connection with this problem, the active hydrogen analysis and the successive-ignition-loss method have been used for measuring the water content on several metal oxides pretreated at different temperatures. This paper will report the finding that both methods give, except in special cases, consistent data on the water content of silica gel, magnesium oxide, zinc oxide, and titanium dioxide.

Experimental

Materials. The metal oxides used in this work were silica gel, magnesium oxide, zinc oxide, and titanium dioxied. The silica gel was prepared by the hydrolysis of ethyl orthosilicate, which had been purified by redistillation.[17] Zinc oxide furnished by the Sakai Chemical Co. was the sample which was prepared by burning zinc metal in air. Titanium dioxide furnished by the Teikoku Kako Co. was prepared by the hydrolysis of titanium sulfate; it was purified further by washing it with dilute ammonia water, nitric acid, and then thoroughly with distilled water. The magnesium oxide was synthesized *via* methylate. Twenty grams of magnesium metal (99.9% purity) were allowed to react with 300 g of purified methyl alcohol at 50—60 °C for 4 hr. The methyl alcohol solution of magnesium methylate thus obtained was kept at *ca.* 5 °C for one night. The crystals of magnesium methylate thus deposited were then further recrystallized from methyl alcohol. The magnesium hydroxide was made by hydrolyzing 30 g of magnesium methylate in 1000 g of distilled water at 60 °C for 7 hr. The excess water and methyl alcohol evolved by the hydrolysis were evaporated out. The magnesium oxide was obtained by calcining magnesium hydroxide at 800 °C for 3 hr in the atmosphere.

The methyl magnesium iodide used for active hydrogen analysis was synthesized by reacting 50 g of methyl iodide with 9 g of magnesium metal in 150 g of dried *n*-butyl ether at 60—70 °C for 4 hr. After the sedimentation of the excess magnesium metal, the supernatant solution was used for active hydrogen analysis.

Specific Surface Areas of the Oxides. The nitrogen adsorption isotherms were measured on the powdered samples at the temperature of liquid nitrogen. Assuming that the nitrogen molecular area was 16.2 Å^2, the surface areas of the powder were calculated by using the BET equation. The specific surface areas of silica gel, magnesium oxide, zinc oxide, and titanium dioxide pretreated *in vacuo* for 4 hr are given in Table 1.

Table 1. Specific surface area of metal oxides

Pretreatment temperature (°C)	Metal oxides (m^2/g)			
	SiO_2	MgO	ZnO	TiO_2
100	423	67	6.4	9.7
200			5.5	
300	422	71	5.6	9.9
500	431	65	4.4	9.3
800	396	77		
1000	333			

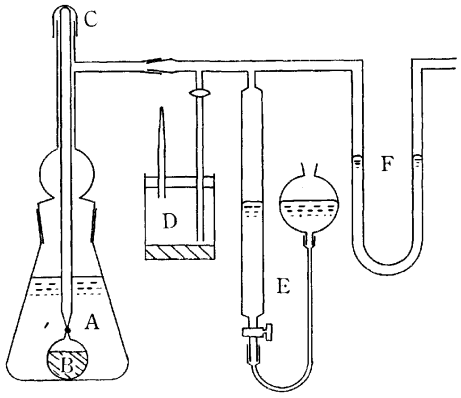

Fig. 1. Apparatus for active hydrogen on metal oxide.
A, methyl magnesium iodide solution; B, oxide powder; C, rubber cup; D, dry box (P_2O_5); E, gas burette; F, balance manometer.

Water-content Measurement by Means of Active Hydrogen Analysis. The measuring apparatus for active hydrogen on metal oxide is shown in Fig. 1; it was constructed by modifying the apparatus used for the determination of the active hydrogen of organic compounds by Krynitsky *et al.*[18] The oxide powder used at one time was 0.3—2.0 g; it was pretreated *in vacuo* for 4 hr in a thin-walled glass bulb. The degree of vacuum attained in the pretreatment was 10^{-5} Torr at 100, 200, and 300 °C, and 10^{-3} Torr at 500, 800, and 1000 °C. After the pretreatment had finished, the neck of the bulb was sealed off and connected to a glass rod by fusion. The bulb was then transferred into reaction vessel containing 80 ml of a methylmagnesium iodide solution, and then it was broken in the solution by pushing in a glass rod. Since the reaction between methylmagnesium iodide and active hydrogen on metal oxide generates methane gas, the gas volume was measured by means of a gas burette at appropriate intervals. Prior to the measurements, the apparatus was calibrated by using pure benzoic acid; the volume of methane evolved from the reaction of benzoic acid with methyl magnesium iodide was confirmed to coincide with the calculated value.

Water-content Measurement by Means of the Successive-Ignition-Loss Method. The water content in metal oxides was determined by a procedure described previously.[14] By this method, water molecules can be removed from the surface through the condensation dehydration of surface hydroxyl groups; moreover, the physisorbed water, if present, can be desorbed.

Results and Discussion

Methane gas is evolved by the reaction of methylmagnesium iodide with the surface hydroxyl groups or with the physisorbed water molecules:[7]

$$CH_3MgI + HO\text{-(oxide surface)} \longrightarrow CH_4 + MgIO\text{-(oxide surface)}$$

$$CH_3MgI + H_2O \longrightarrow CH_4 + MgI(OH)$$

17) T. Morimoto and H. Naono, This Bulletin., **45**, 700 (1972).

18) J. A. Krynitsky, J. E. Johnson, and H. W. Carhart, *J. Amer. Chem. Soc.*, **70**, 486 (1948).

The volume of methane gas, V(ml(STP)/g oxide), is given by this equation:

$$V = \left\{V_1 - \left(V_2 - \frac{W}{\rho}\right)\right\} \cdot \frac{1}{W} \cdot \frac{273}{273+t}$$

where V_1 is the volume as measured by means of a gas burette, V_2 is the volume of a glass bulb, W and ρ are the weight and density of the oxide powder, and t is the measuring temperature (23—27 °C). In Figs. 2 and 3, V is plotted against the reaction time at various pretreatment temperatures for silica gel, magnesium oxide, zinc oxide, and titanium dioxide. It can be seen from these figures that the evolution of methane gas ceases within 30—50 min.

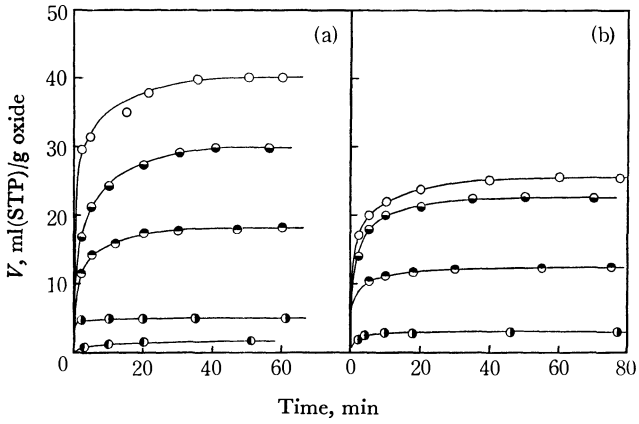

Fig. 2. Reaction of methylmagnesium iodide with active hydrogen on silica gel (a) and magnesium oxide (b). Pretreatment temperatures, ○: 100 °C, ◒: 300 °C, ◓: 500 °C, ◑: 800 °C, ◐: 1000 °C.

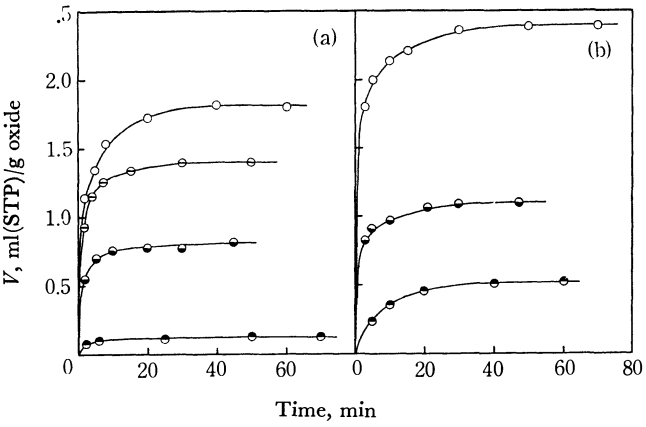

Fig. 3. Reaction of methylmagnesium iodide with active hydrogen on zinc oxide (a) and titanium dioxide (b). Pretreatment temperatures, ○: 100 °C, ⊖: 200 °C. ◒: 300 °C, ◓: 500 °C.

In all the cases of oxides, the volume of the methane gas decreases with an increase in the pretreatment temperature; that is, the active hydrogen is removed from the oxide surface by pretreating oxides at elevated temperatures *in vacuo*. On the basis of the reaction of methylmagnesium iodide with the solid surface, we can calculate the water content on metal oxides from the amount of methane gas evolved. Taking into account the specific surface areas listed in Table 1, the water content can be expressed in the number of

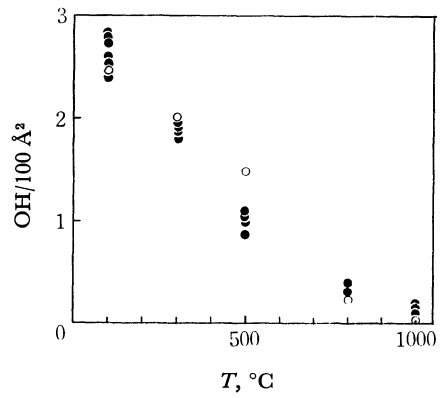

Fig. 4. Water content on silica gel measured by the active hydrogen analysis (●) and the successive-ignition-loss method (○).

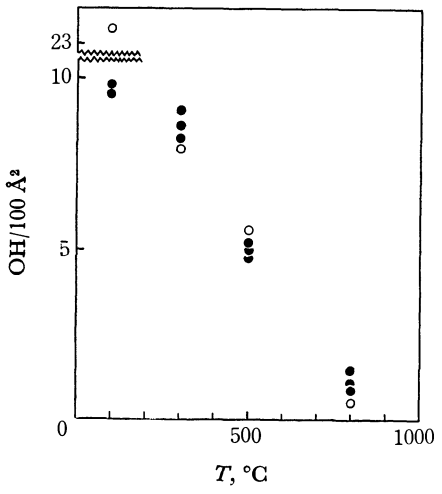

Fig. 5. Water content on magnesium oxide measured by the active hydrogen analysis (●) and the successive-ignition-loss method (○).

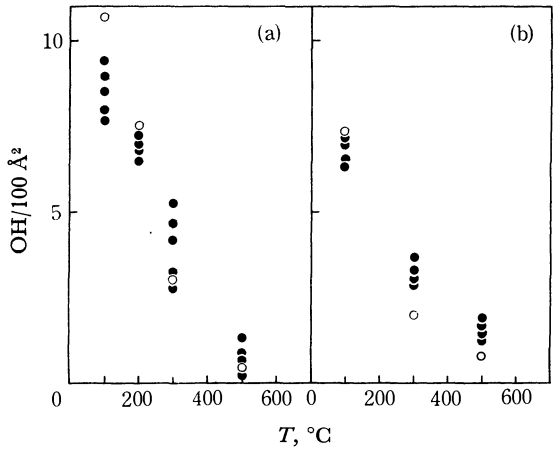

Fig. 6. Water content on zinc oxide (a) and titanium dioxide (b) measured by the active hydrogen analysis (●) and the successive-ignition-loss method (○).

hydroxyl groups on an area of 100 Å², as is shown in Figs. 4—6. In these figures, the values of the water content, as determined by the active hydrogen analysis, are illustrated, together with those obtained by the successive-ignition-loss method.

Silica Gel. As can be seen from Figs. 2 and 3, the evolution of methane gas from silica gel occurs as rapidly as that from the other oxides, though the specific surface area of silica gel is much larger than those of the others. Furthermore, as may be seen from Fig. 4, the water contents on silica gel, as determined by the two methods, are in good agreement with each other. Therefore, it may be considered from these results that methylmagnesium iodide molecules react readily with all the active hydrogen atoms on silica gel.

Generally, on metal oxides pretreated at lower temperatures the surface may possibly retain physisorbed water molecules, together with chemisorbed water as surface hydroxyl groups, though only the latter exist on surfaces pretreated at higher temperatures. Here, it will be very interesting to analyze the water content into the surface hydroxyl groups and the physisorbed water. As has been stated above, one water molecule can be estimated to contain one hydroxyl group by the methylmagnesium iodide method, and two hydroxyl groups by the successive-ignition-loss method. Accordingly, when an appreciable amount of the physisorbed water exists on the metal surface, the water content obtained by the latter method should be larger than that obtained by the former one, as will be reported with regard to the water content on alumina pretreated at 100 °C *in vacuo*.[19] Since the water contents obtained on silica gel by the two methods accord well with each other, it may be concluded that only the surface hydroxyl groups exist on silica gel pretreated above 100 °C *in vacuo*.

Magnesium Oxide. Figure 5 shows that the water contents obtained on magnesium oxide by the active hydrogen analysis agrees fairly well those obtained by the successive-ignition-loss method, except for the sample pretreated at 100 °C. On 100 °C-treated sample, however, the two methods give very different values as to the water content; it is found to be 9.6 OH/100 Å^2 by the former, and 23.4 OH/100 Å^2 by the latter method. As has been described above, if physisorbed water exists on magnesium oxide, the latter method will give a larger value for the water content. Now, assuming that the difference between the values of the water content obtained by the two methods is due to the presence of the physisorbed water, we can calculate each of the surface hydroxyl groups and the physisorbed water. The calculation results in a negative value (−4.2 OH/100 Å^2) as the density of the surface hydroxyl groups. Thus, the large difference between the data obtained by the two methods cannot be explained only by the existence of physisorbed water.

With the successive-ignition-loss method it is possible to detect the hydroxyl groups in the inner layer of the solid besides those on the surface, because the oxide powder is ignited at elevated temperatures. On the contrary, in the active hydrogen analysis, only the surface hydroxyl groups can be determined, because methylmagnesium iodide molecules can react only the surface of the solid. The extraordinarily high value obtained by the successive-ignition-loss method stated above makes it possible to infer that the hydroxyl groups exist not only on the surface, but also in the inner layer of magnesium oxide crystals.

Assuming that a hydroxyl group is formed on a surface magnesium atom, the surface hydroxyl groups on the (100) face of magnesium oxide can be calculated crystallographically to be 11.3 OH/100 Å^2. The calculated water content approximates the value obtained by the active hydrogen analysis, being about twice as large as the value obtained by the successive-ignition-loss method. Thus, the water content obtained by the successive-ignition-loss method on the 100 °C-treated magnesium oxide corresponds to the two-layer coverage of hydroxyl groups. It is known that magnesium oxide is gradually changed into magnesium hydroxide by the reaction with water. Therefore, the value of 23.4 OH/100 Å^2 obtained on 100 °C-treated magnesium oxide may reasonably be said to originate from the chemisorption of water vapor from the atmosphere during preservation. On the samples treated above 300 °C, the two methods give similar results for the water content below the monolayer coverage, which shows that only the surface hydroxyl groups exist on magnesium oxide.

So far, methylmagnesium iodide has been mainly used for the determination of the hydroxyl groups on silica, which is known as a weakly acidic surface. On the contrary, magnesium oxide is well known as a basic solid; its basicity was intestigated by Tanabe and Yamaguchi by using bromo-thymol-blue as an indicator.[20] It is very interesting to note that the hydroxyl groups on such a basic solid as magnesium oxide react quantitatively with methylmagnesium iodide. In conclusion, all the hydroxyl groups on the acidic and basic surfaces can be measured quantitatively by means of the present active hydrogen analysis.

Zinc Oxide and Titanium Dioxide. The water content on zinc oxide and titanium dioxide is shown in Fig. 6 as a function of the pretreatment temperature. As can be seen from Fig. 6, the data obtained by different methods are, as a whole, in agreement with each other and the water content decreases remarkably with the increase in the pretreatment temperature. In these cases, an appreciable fluctuation of the data is observed in the active hydrogen analysis, probably because of the small quantities of methane gas evolved. A trend can be seen that the successive-ignition-loss method gives a slightly higher value in the water content on the 100 °C-treated zinc oxide than does the other method; this greater value may be attributed to the existence of the physisorbed water.

The above results lead to the conclusion that the surface hydroxyl groups can reasonably be measured quantitatively by both active hydrogen analysis and the successive-ignition-loss method. Furthermore, it is possible to estimate the values of both physisorbed water and surface hydroxyl groups by the simultaneous application of the two methods.

The authors wish to express their thanks to Miss Toshie Takeshita for her experimental assistance.

19) T. Morimoto and H. Naono, To be published.

20) K. Tanabe and T. Takeshita, "San Enki Shokubai (Acid-Base Catalysis)," Sangyo Tosho, Tokyo (1966).

Energy Transfer in the Radiolysis of Neopentane-Alkane Mixture in the Solid Phase at 77 K

Masaki KATO, Yoshiyuki SAITAKE, Tetsuo MIYAZAKI,* and Zen-ichiro KURI

Department of Synthetic Chemistry, Faculty of Engineering, Nagoya University, Chikusa-ku, Nagoya 464

(Received November 2, 1972)

When neopentane containing a small amount of cyclohexane is γ-irradiated at 77 K, the cyclohexyl radical is mainly formed by the energy transfer from neopentane to cyclohexane. The addition of CCl_4, which is an electron scavenger and an excitation acceptor, to the mixture suppresses the formation of the cyclohexyl radical. This fact indicates that the energy transfer is not due to an ion-molecule reaction. When CO_2, which can capture an electron in the neopentane matrix to form CO_2^-, is added to the neopentane–cyclohexane mixture, scarcely any CO_2^- is formed by the irradiation. When ethyl chloride or nitrous oxide is added to the neopentane–cyclohexane mixture, the formation of the cyclohexyl radical is not suppressed, although these additives capture electrons effectively in the solid neopentane. The addition of tetramethylethylene (TME) to the neopentane–cyclohexane–carbon dioxide mixture does not affect the formation of the cyclohexyl radical, although an appreciable amount of TME^+ is formed. These results show that the energy transfer is not due to the ionic process, but to a non-ionic process. The energy transfer is explained by two possible mechanisms, a selective abstraction reaction by the hydrogen atom and an excitation transfer *via* a highly-excited state.

We have previously studied the radiolysis in the solid state in order to elucidate the primary process of radiolysis in the solid state and in order to obtain information about reaction kinetics in the solid state. The quite peculiar phenomena[1-6] we then found could not be explained by applying the mechanism of the radiolysis in the gas and liquid phases to the solid phase.

Therefore, we have indicated that two important problems must be solved in order to elucidate the cause of the peculiar phenomena in the radiolysis of solid hydrocarbons. One problem is the energy transfer in the primary process; the other is how the state of the solid matrix, such as its phase or defects, affects the reaction in the solid phase.

When neopentane containing a small amount of another alkane is γ-irradiated in the solid phase at 77 K, the solute radical is mainly formed by the energy transfer from the γ-irradiated neopentane to the solute.[6] Even if the ionization potential and the energy of the first singlet excited state of the solute are higher than those of neopentane, the solute radical is effectively formed. It was suggested, from the point of view of energetics, that the energy transfer may occur *via* a non-ionic process.[6]

We have here obtained clearer results demonstrating the mechanism of the non-ionic energy transfer in the radiolysis of neopentane containing cyclohexane in the solid phase.

Experimental

The neopentane and cyclopentane supplied by the Tokyo Kagaku Seiki Co. were more than 99.9% pure. Spectrograde cyclohexane and toluene were passed through a 1 m column packed with silica gel and then distilled on a vacuum line before use. The tetramethylethylene supplied by the Tokyo Kagaku Seiki Co. was more than 99.0% pure. The ethane and carbon dioxide supplied by the Takachiho-Shoji Co. were of a high purity and were used without further purification. The carbon tetrachloride was used after distillation on a vacuum line.

Samples were irradiated with γ-rays from a ^{60}Co source at 77 K and at a dose rate of 7.8×10^5 rad/hr. The total dose was 2.0×10^5 rad. The ESR spectra of irradiated samples were measured at 77 K on a JES-3BX ESR spectrometer.

Results and Discussion

Radiolysis of Neopentane Containing Cyclohexane in the Solid Phase at 77 K. When neopentane containing a small amount of cyclohexane is γ-irradiated at 77 K, the cyclohexyl radical is mainly formed, while the formation of the solvent radical is suppressed. The ESR spectra of the irradiated samples were shown in a previous paper.[6] The yields of the cyclohexyl radical are shown in Fig. 1 as a function of the concentration of cyclohexane. Cyclohexane at a concentration of over 0.2% accepts energy efficiently from the irradiated neopentane. When neopentane containing other alkanes, such as ethane, propane, and cyclopentane, is γ-irradiated at 77 K, the energy transfer from neopentane to the solute also occurs efficiently.[6] Since the ionization potential and the first excited state of these alkanes are higher than those of neopentane, a charge transfer from the neopentane cation in a ground state and/or an excitation transfer from neopentane in the first excited state to the solute are impossible. Therefore, we will discuss here whether the energy

* To whom correspondence should be addressed.

1) a) T. Wakayama, T. Kimura, T. Miyazaki, K. Fueki, and Z. Kuri, This Bulletin, **43**, 1017 (1970). b) T. Miyazaki, T. Yamada, T. Wakayama, K. Fueki, and Z. Kuri, *ibid.*, **44**, 934 (1971).

2) T. Wakayama, T. Miyazaki, K. Fueki, and Z. Kuri, *J. Phys. Chem.*, **74**, 3584 (1970).

3) T. Miyazaki, Y. Fujitani, T. Wakayama, K. Fueki, and Z. Kuri, This Bulletin, **44**, 984 (1971).

4) T. Wakayama, T. Miyazaki, K. Fueki, and Z. Kuri, *ibid.*, **44**, 2619 (1971).

5) M. Fukaya, T. Wakayama, T. Miyazaki, Y. Saitake, and Z. Kuri, 14th Japanese Conference on Radiation Chemistry, Sept. 1971, Sapporo, Japan; This Bulletin, **46**, 1036 (1973).

6) T. Miyazaki, T. Wakayama, M. Fukaya, Y. Saitake, and Z. Kuri, 14th Japanese Conference on Radiation Chemistry, Sept. 1971, Sapporo, Japan; This Bulletin, **46**, 1030 (1973).

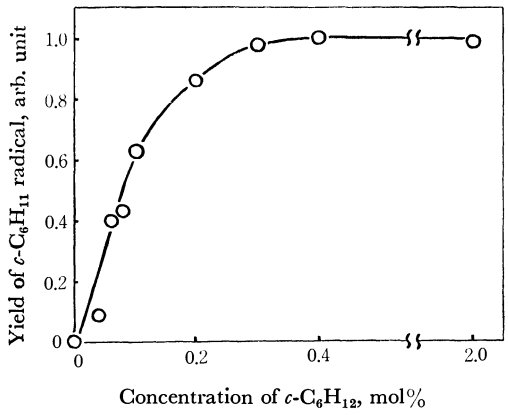

Fig. 1. Formation of cyclohexyl radical as a function of the concentration of cyclohexane in the radiolysis of solid neopentane at 77 K.

transfer is due to an ionic process, such as an ion-molecule reaction and a positive charge transfer *via* an excited ion, or to a non-ionic process.

Ion-Molecule Reaction. Willard *et al.* proposed that the solvent radical may be formed by the ion-molecule reaction in the radiolysis of 3-methylpentane in the solid phase.[7] According to this mechanism, the formation of the solute radical in the radiolysis of neopentane containing alkane may be represented as follows:

$$\text{neo-}C_5H_{12} \rightsquigarrow C_5H_{12}^+ + e^- \quad (1)$$

$$C_5H_{12}^+ + \text{neo-}C_5H_{12} \longrightarrow C_5H_{13}^+ + C_5H_{11}\cdot \quad (2)$$

$$C_5H_{12}^+ + RH \longrightarrow C_5H_{13}^+ + R\cdot \quad (3)$$

$$C_5H_{13}^+ + e^- \longrightarrow C_5H_{12} + H \quad (4)$$

$$H + H \longrightarrow H_2 \quad (5)$$

where RH represents some alkane as a solute. In the previous paper,[6] it was suggested that, for the following reasons, these reactions seem unlikely.

First, when neopentane containing cyclopentane is γ-irradiated at 77 K, the cyclopentyl radical is mainly formed. If the formation of the cyclopentyl radical is due to Reaction (3), neither the amounts of the $C_5H_{13}^+$ ion nor the yields of hydrogen (Reactions (4) and (5)) change upon the addition of cyclopentane. The experimental results, however, show that the yields of hydrogen increase sharply upon the addition of cyclopentane.

Second, the ion-molecule reaction between a neopentane parent ion and an ethane molecule (Reaction (3)) is expected to be endothermic.

Third, though the proton-transfer reaction of polar molecules has been found by means of the mass spectrometer, the reaction cannot be detected in any alkane systems except for methane and ethane. The reaction seems to become more difficult as the molecular weight of alkane increases.[8] It has been reported, from a study of the high-pressure mass spectrometry of propane, that the protonated alkane ion was not detected at all, but only a clustered parent ion.[9]

In the present study we have obtained clear results which support the previous suggestion. Carbon tetrachloride, which is an electron scavenger and an excitation acceptor,[1,10] was added to the neopentane-cyclohexane mixture. If Reactions (1)—(3) occur in the solid phase, CCl_4 will capture the electron (Reaction (6)) and prolong the lifetime of the cation:

$$e^- + CCl_4 \longrightarrow Cl^- + CCl_3\cdot \quad (6)$$

Therefore, the ion-molecule reaction (3) should be promoted by the addition of CCl_4, as has been observed in the radiolysis of liquid neopentane.[11] The effect of CCl_4 on the formation of the cyclohexyl radical is shown in Fig. 2. The formation of the cyclohexyl radical, however, is suppressed by the addition of CCl_4. The formation of solute radicals in the radiolysis of neopentane containing ethane or cyclopentane is also suppressed by the addition of CCl_4. Since carbon tetrachloride does not react with the neopentane cation in the liquid phase,[12,13] it may be a source of difficulty that carbon tetrachloride disturbs the ion-molecule reaction (3). Therefore, Reactions (1)—(3) are not responsible for the formation of solute radicals in the radiolysis of neopentane containing alkane.

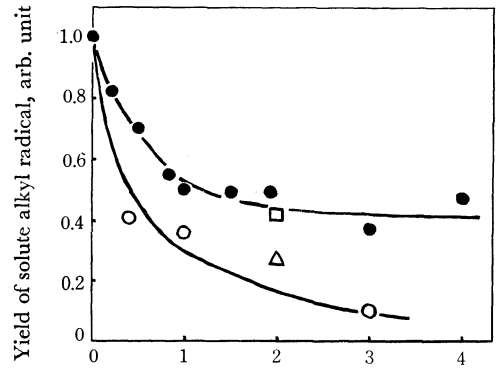

Fig. 2. Effect of CCl_4 on the formation of solute alkyl radical in the radiolysis of neopentane containing alkane at 77 K.
●—●: cyclo-C_6H_{11} in the radiolysis of neo-C_5H_{12}—cyclo-C_6H_{12} (2%).
○—○: cyclo-C_6H_{11} in the radiolysis of neo-C_5H_{12}—cyclo-C_6H_{12} (0.4%).
△: C_2H_5 in the radiolysis of neo-C_5H_{12}—C_2H_6(2%).
□: cyclo-C_5H_9 in the radiolysis of neo-C_5H_{12}—cyclo-C_5H_{10} (2%).

Positive Charge Transfer. Hamill *et al.* proposed that a charge transfer in the irradiated 3-methylpentane glass may occur *via* the excited state of the solvent cation.[14] According to this mechanism, the formation

7) a) M. Shirom and J. E. Willard, *J. Phys. Chem.*, **72**, 1702 (1968). b) D. Timm and J. E. Willard, *ibid.*, **73**, 2403 (1969).
8) F. P. Abramson and J. H. Futrell, *ibid.*, **71**, 3791 (1967).
9) L. W. Sieck, S. Searles, and P. Ausloos, *J. Chem. Phys.*, **54**, 91 (1971).
10) P. K. Ludwig and C. D. Amata, *J. Phys. Chem.*, **72**, 3725 (1968).
11) A. A. Scala, S. G. Lias, and P. J. Ausloos, *J. Amer. Chem. Soc.*, **89**, 3677 (1967).
12) J. A. Stone and G. Matsushita, *Can. J. Chem.*, **49**, 3287 (1971).
13) G. J. Collin and P. Ausloos, *J. Amer. Chem. Soc.*, **93**, 1336 (1971).
14) W. H. Hamill, "Ionic Process in Irradiated Organic Solids," a chapter in "Radical Ions," E. T. Kaiser and L. Kevan, Eds., John Wiley and Sons, New York, N. Y., 1968.

of the solute radical in the radiolysis of neopentane containing cyclohexane may be represented as follows:

$$\text{neo-}C_5H_{12} \rightsquigarrow C_5H_{12}^{+*} + e^- \quad (7)$$

$$C_5H_{12}^{+*} + \text{cyclo-}C_6H_{12} \longrightarrow C_5H_{12} + C_6H_{12}^{+} \quad (8)$$

$$C_6H_{12}^{+} + e^- \longrightarrow C_6H_{11}\cdot + H \quad (9)$$

where $C_5H_{12}^{+*}$ represents an excited cation. Though the information on the excited ion is very scanty at present, we will point out some drawbacks to this mechanism.

First, carbon dioxide captures an electron in the solid phase to form CO_2^- (Reaction (10)), and its formation can be easily detected by ESR spectroscopy:

$$e^- + CO_2 \longrightarrow CO_2^- \quad (10)$$

If Reaction (7) occurred in the radiolysis of neopentane, CO_2^- should be formed upon the addition of CO_2. Since cyclohexane traps the mobile excited cation in Reaction (8), it is expected that the electron may be more easily captured by CO_2 in the presence of cyclohexane, as has been discussed in connection with the radiolysis of 3-methylpentane.[14,15] The yields of CO_2^- in the radiolysis of neopentane–cyclohexane–CO_2 (2%) mixture are shown in Fig. 3. The yields of CO_2^- are quite small, contrary to the expectation based on Reactions (7), (8), (9), and (10). The G-values of CO_2^- are only 0.04—0.01, although the yields of the cyclohexyl radical amount to 2 G-units in the radiolysis of the neopentane–cyclohexane(3%)–CO_2(2%) mixture and cyclohexane captures a large amount of active species. There is a possibility that CO_2 is not dissolved into the neopentane matrix and that it cannot capture an electron in this matrix. This possibility is, however, obviated by the following experimental results. When tetramethylethylene is added to the neopentane–CO_2 (2%) mixture, an appreciable amount of CO_2^- is formed (Fig. 3).

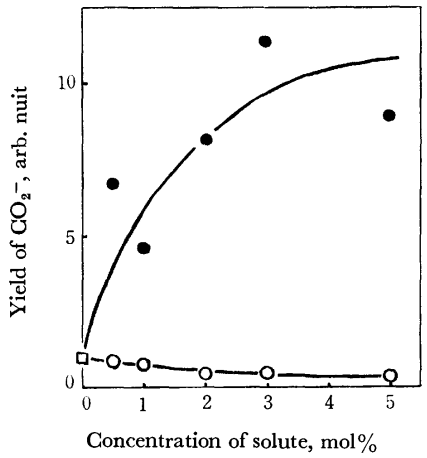

Fig. 3. Effect of solute on the formation of CO_2^- in the radiolysis of neopentane containing CO_2 (2%) at 77 K.
●—●: Yields of CO_2^- in the presence of tetramethylethylene.
○—○: Yields of CO_2^- in the presence of cyclohexane.
□: Yields of CO_2^- in the absence of the solute.

15) M. Shirom, R. F. C. Claridge, and J. E. Willard, *J. Chem. Phys.*, **47**, 286 (1967).

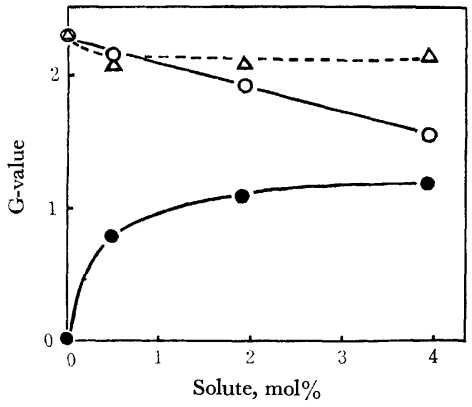

Fig. 4. Effect of C_2H_5Cl and N_2O on the formation of cyclohexyl radical in the radiolysis of neopentane–cyclohexane (2%) mixture at 77 K.
○—○: cyclohexyl radical upon the addition of C_2H_5Cl.
●—●: ethyl radical upon the addition of C_2H_5Cl.
△—△: cyclohexyl radical upon the addition of N_2O.

Second, since the efficiency of electron capture by carbon dioxide is relatively small, we have used more efficient electron scavengers, such as ethyl chloride and nitrous oxide. Figure 4 shows the effects of ethyl chloride and nitrous oxide on the formation of the cyclohexyl radical in the radiolysis of the neopentane–cyclohexane (2%) mixture at 77 K. When ethyl chloride captures an electron, it produces the ethyl radical by dissociative electron attachment. The yields of the ethyl radical, which represent the amounts of electrons captured by ethyl chloride, are also shown in the figure. The yields of the cyclohexyl radical decrease gradually upon the addition of ethyl chloride, while the yields of the ethyl radical increase sharply upon the addition of a small amount of ethyl chloride. The decreases in the yields of the cyclohexyl radical are much smaller than the yields of the ethyl radical at the concentrations of 0.5 and 2% ethyl chloride. It has been reported that nitrous oxide can efficiently capture an electron in the radiolysis of solid neopentane at 77 K.[16] According to the product analysis, the $G(N_2)$ in the radiolysis of neopentane containing nitrous oxide (4%) at 77 K was about 0.5, suggesting that nitrous oxide captures an electron in the solid neopentane at 77 K. The yields of the cyclohexyl radical do not decrease at all upon the addition of nitrous oxide. Therefore, the neutralization reaction does not participate in the formation of the cyclohexyl radical in the radiolysis of neopentane containing cyclohexane at 77 K.

Third, Fig. 5 shows the effect of tetramethylethylene (TME) on the formation of the cyclohexyl radical in the radiolysis of the neopentane–cyclohexane(1%)–CO_2 (2%) mixture at 77 K. Though an appreciable amount of TME^+ is formed upon the addition of TME, and though $G(TME^+)$ amounts approximately to 1—1.5 at 2% of TME, the yields of cyclohexyl radical do not decrease at all. Therefore, the charge transfer reaction does not participate in the formation of cyclohexyl radical.

16) J. Lin and F. Williams, *J. Phys. Chem.*, **72**, 3707 (1968).

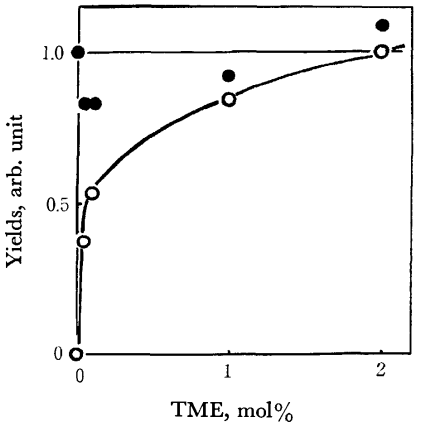

Fig. 5. Effect of TME on the formation of cyclohexyl radical in the radiolysis of neopentane-cyclohexane (1%)-CO_2(2%) mixture at 77 K.
●: yield of cyclohexyl radical.
○: yields of TME^+.

Fourth, since the neopentane parent ion is quite unstable and decomposes in the period of one vibration in the gas[17] and liquid phases,[13,18,19] the excited ion may decompose before charge transfer.

From the present discussions, it seems to be difficult to explain the energy transfer in the radiolysis of solid neopentane by the ionic processes. In the present poor state of knowledge of the radiolysis in the solid phase, we cannot decide the true mechanism of the energy transfer. We will try, however, to explain the energy transfer by two possible non-ionic processes as a basis for further study.

Selective Abstraction Reaction by the Hydrogen Atom. The formation of the solute radical in the radiolysis of neopentane may be explained by the selective abstraction reactions:

$$\text{neo-}C_5H_{12} \rightsquigarrow C_5H_{12}^* \quad (11)$$

$$C_5H_{12}^* \longrightarrow C_5H_{11}\cdot + H \quad (12)$$

$$H + H \text{ or } R\cdot \longrightarrow H_2 \text{ or } RH \quad (13)$$

$$H + C_5H_{12} \longrightarrow C_5H_{11}\cdot + H_2 \quad (14)$$

$$H + C_2H_6 \longrightarrow C_2H_5\cdot + H_2 \quad (15)$$

where $C_5H_{12}^*$ and R· represent an excited neopentane molecule and some radical respectively. If the H atom in these reactions is a hot hydrogen atom, the rate constant of Reaction (14) is a little larger than that of Reaction (15) in the gas phase.[20] Therefore, it cannot be expected that the ethyl radical is formed selectively in the radiolysis of neopentane containing a small amount of ethane. If the H atom is a thermal hydrogen atom, Reaction (15) cannot occur at 77 K because of its high activation energy. Therefore, we must assume that the reaction of the hydrogen atom in the crystalline neopentane is quite different from that in the gas and liquid phases, and that the H-atom reacts selectively with ethane with a low activation energy at 77 K.

It has been reported recently that H-atom abstraction reaction by a thermal methyl radical occurs with low activation energy in the solid phase.[21] Recently we have found that the hot hydrogen atom produced by the photolysis of hydrogen iodide reacts selectively with solute alkane in the neopentane matrix at 77 K.[22] The result, which cannot be explained by this mechanism, is that the yields of solvent radicals in the radiolysis of neopentane or isobutane decrease below 50% of the initial yields upon the addition of an additive.

Excitation Transfer via a Highly-excited State. According to the mechanism of the excitation transfer, the reaction scheme may be represented as follows:

$$\text{neo-}C_5H_{12} \rightsquigarrow C_5H_{12}^* \quad (11)$$

$$C_5H_{12}^* \longrightarrow C_5H_{11}\cdot + H \quad (12)$$

$$\searrow\ C_4H_9\cdot + CH_3\cdot \quad (16)$$

$$C_5H_{12}^* + RH \longrightarrow C_5H_{12} + RH^* \quad (17)$$

$$RH^* \longrightarrow R\cdot + H \quad (18)$$

Reaction (17) is the excitation transfer to other alkane. Since an appreciable quantity of solute radicals is formed by the addition of ethane, propane, and cyclopentane, whose first excited states are higher than that of neopentane, the excitation transfer may occur *via* the highly-excited state.

The excitation transfer has also been proposed in the radiolysis of isobutane[1] and polyethylene[23] in the solid phase. From the calculation, it was suggested that the excitation transfer is possible in the alkane.[24]

The authors wish to express their appreciation to Professor John E. Willard of the University of Wisconsin for his kind discussion.

17) H. D. Beckey, *Z. Naturforsch.*, **A16**, 505 (1961).
18) K. Tanno, T. Miyazaki, K. Shinsaka, and S. Shida, *J. Phys. Chem.*, **71**, 4290 (1967).
19) J. A. Ward and W. H. Hamill, *J. Amer. Chem. Soc.*, **89**, 5116 (1967).
20) R. J. Carter, W. H. Hamill, and R. R. Williams, *ibid.*, **77**, 6457 (1955).
21) a) E. D. Sprague and F. Williams, *ibid.*, **93**, 787 (1971). b) A. Campion and F. Williams, *ibid.*, **94**, 7633 (1972).
22) T. Wakayama, T. Miyazaki, K. Fueki, and Z. Kuri, to be published.
23) R. H. Partridge, *J. Chem. Phys.*, **52**, 2491 (1970).
24) T. Miyazaki, This Bulletin, **46**, 329 (1973).
The equation (1) in the paper is misprinted and should be corrected as $u = -3f(ea_0)^2 \cdot R/\Delta E \cdot \Omega/r^3$.

Radioactive Iodine Exchange and the Dushman Reaction

Ryusaburo FURUICHI* and Herman A. LIEBHAFSKY

Department of Chemistry, Texas A & M University, College Station, Texas 77843, U.S.A.

(Received November 7, 1972)

Critical studies were made on the Dushman reaction, $6H^+ + 5I^- + IO_3^- = 3I_2 + 3H_2O$. Rate measurements of radioactive iodine exchange away from chemical equilibrium gave results which made the rate law for the Dushman reaction doubtful. Measurements of $d(H^+)/dt$ confirmed the rate law. The contrary interpretation resulted because existing chemical information was not considered. This situation holds in many radioactive iodine exchange experiments done on the Dushman reaction.

The reaction between iodate and iodide ions in acid solution was first studied systematically by Dushman.[1] Its rate law in simplified form was found to be[2,3]

$$-\frac{[IO_3^-]}{dt} = [IO_3^-][H^+]^2\{2.4\times10^4[I^-] + 7.6\times10^{10}[I^-]^2 + 5.5\times10^{10}[I^-][I_3^-]\} \quad \text{at } 25°C \qquad (1)^4$$

The $[I^-]$ and $[I^-]^2$ terms contribute equally to the rate when $[I^-]$ is near 10^{-7}. The $[I_3^-]$ term is negligible when $[I^-]$ greatly exceeds $[I_3^-]$, which is the case when IO_3^- and I^- are the only iodine species initially mixed.

Measurements of the rate of radioactive iodine isotope exchange have placed Eq. (1) in doubt. Measurements at chemical equilibrium[5-7] led to different formulations of the $[I^-]$ term. Measurements away from equilibrium in nearly neutral solution by Myers and Kennedy[6] showed no exchange under conditions where it was expected that the rate of exchange *via* the $[I^-]^2$ term could easily be measured.

A survey of literature on the relevant exchange measurements away from chemical equilibrium[6,8-15] shows a marked discrepancy (Table 1).

The Dushman reaction participates in the oscillatory decomposition[16] of H_2O_2. In particular, $[I^-]$ during the $[I^-]$ pulses changes about 10-fold at concentrations where the $[I^-]^2$ term of Eq. (1) contributes significantly to the rate, indicating that the contribution changes by almost 100-fold during a single pulse (see Ref. 16, Fig. 1). Such fluctuations could trigger oscillations. There is no hope of understanding the oscillatory

TABLE 1. RADIOACTIVE EXCHANGE OF IODINE SPECIES WITH IODATE ION

No	Ref.	Species	Acidity	T(°C)	Time	Exchange reported
1	8	I_2	1M	Room (?)	Not given	No
2	8	I_2	20M	"Hot"	Not given	Yes
3	9	I^-	Neutral[a]	100	3 hr	No
4	10	I_2	Neutral[a]	Not given	Not given	No
5	10	I^-	Alkaline	Not given	Not given	No
6	6	I^-	Neutral[a]	50	1600 hr	No
7	11, 12	I_2	Acid	b)	b)	Yes
8[c]	13	I_2, I^-	pH=5.1	Room (?)	24 hr	Yes
9[c]	13	I_2, I^-	pH=1	Room (?)	24 hr	No
10	13	I^-	Ammoniac	Room	12 hr	Trace
11	14	I^-	Neutral[a]	200—300	——	Slow
12	15	I^-	Neutral[a]	240	up to 24 hr	Yes[d]

a) Not strictly defined.
b) Equivalent quantities of I^- and IO_3^- in 0.5 M HNO_3 were boiled for 35 min after standing for 40 hr at room temperature.
c) 0.2 mCi ^{131}I added as iodide.
d) Induction period observed.

* Present address: Department of Applied Chemistry, Faculty of Engineering, Hokkaido University, Sapporo, 060.

1) S. Dushman, *J. Phys. Chem.*, **8**, 453 (1904).
2) E. Abel and K. Hilferding, *Z. Phys. Chem.*, **136**, 186 (1928).
3) E. Abel and F. Stadler, *ibid.*, **122**, 49 (1926).
4) Concentrations in mol/l actually existing, or calculated to exist, are denoted by ( ). Terms for mol/l added to make the reaction mixture are denoted by [ ]. Time in min.
5) R. E. Connick and Z. Z. Hugus, Jr., Brookhaven Conf. Report BNL-C-8, *Chem. Conf.*, No. 2, 164 (1948).
6) O. F. Myers and J. F. Kennedy, *J. Amer. Chem. Soc.*, **72**, 897 (1950).
7) R. Furuichi, I. Matsuzaki, R. Simic, and H. A. Liebhafsky, *Inorg. Chem.*, **11**, 952 (1972).
8) D. E. Hill, C. H. Shiflett, and S. C. Lind, *J. Amer. Chem. Soc.*, **58**, 535 (1936).
9) A. Polessitsky, *Compt. Rend. (Doklady) USSR*, **24**, 540 (1939).
10) R. Daudel, P. Daudel, and M. Martin, *C. R. Acad. Sci. Paris, Ser. C*, **219**, 129 (1944).
11) M. Cottin, M. Haissinsky, and D. Pechanski, *J. Chim. Phys.*, **48**, 500 (1951).
12) M. Cottin and M. Haissinsky, *C. R. Acad. Sci. Paris, Ser. C*, **224**, 1636 (1947).
13) H. Hellauer and H. Spitz, *Biochem. Z.*, **325**, 40 (1953).
14) Yu. Ya. Fialkov, *Izvest. Vysshik Ucheb. Zavedenniy, Khim. i Khim. Tekhnol.*, **4**, 314 (1961); *Chem. Abstr.*, 13206e (1962).
15) H. Arnikar and R. Tipathi, *J. Chromatogr.*, **7**, 362 (1962).
16) I. Matsuzaki, J. H. Woodson, and H. A. Liebhafsky, This Bulletin, **43**, 3317 (1970).

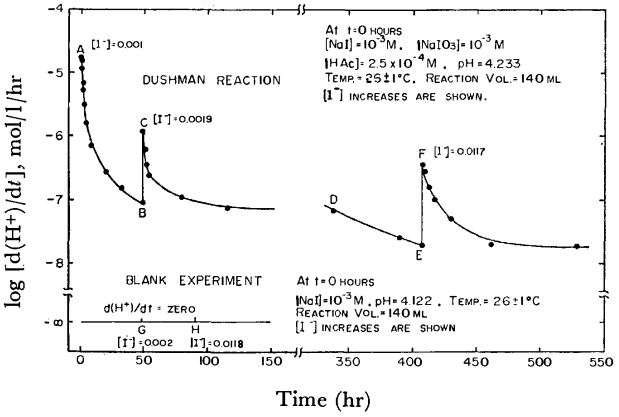

Fig. 1. Decrease of $d(H^+)/dt$ with time in the reaction mixtures of the figure.
Note the breaks in the coordinate axes.

decomposition so long as the present confusion about the Dushman reaction continues.

Experimental

Abel and Stadler[3] carried out their work on the $[I^-]^2$ term in acid solution. Myers and Kennedy[6] used a reaction mixture which they considered nearly neutral. The difference in $[H^+]$ seemed to be responsible for any conflict between the two investigations.

The Dushman reaction may be written as

$$6H^+ + 5I^- + IO_3^- = 3I_2 + 3H_2O \qquad (2)$$

Hydrogen ion is rapidly consumed as the reaction proceeds. If the $[H^+]^2$ term in Eq. (1) is correct, the rate of reaction will decrease rapidly as $[H^+]$ decreases. Working near $(H^+)=10^{-7}$ will be difficult because formation of even a small amount of I_2 (or I_3^-) will cause large relative change in (H^+) and thus in the rate. Hence it is desirable to follow the rate by measuring $d(H^+)/dt$.

Preliminary experiments with $HClO_4$ confirmed the above. Good measurements of $d(H^+)/dt$ could not be made because the rate decreased too rapidly. Measurements in buffered solutions were also difficult. Consequently, acetic acid (HAc) was chosen as a medium between strong acid and buffered solution as regards $d(H^+)/dt$. It can give rates in reaction mixtures with $[I^-]$ and $[IO_3^-]$ large enough to be considered constant during the experiment.

The reaction mixtures were prepared by mixing NaI, $NaIO_3$, and HAc (J. T. Baker Chemical Co.) solutions. The initial composition is given in Fig. 1. The reaction mixture was contained in a stoppered flask kept in the dark at room temperature except during the pH measurements, which were carried out with a glass electrode (Orion Type 801 Digital Ionalyser). The solution became yellowish as the reaction proceeded. Values of $d(H^+)/dt$ for the logarithmic ordinate of Fig. 1 were obtained by graphical differentiation of the curves of pH against time. Addition of NaI is indicated by points B and E.

A blank experiment was carried out because the oxygen from air can sometimes oxidize I^- to form I_2 and I_3^- with the consumption of H^+. The result was satisfactory.

Discussion of the Results of New Rate Measurements

Figure 1 is qualitatively in accord with Eq. (1): the decreases in rate beyond points A, C, and F point to an $(H^+)^2$ term in the rate law. The perpendicular increases along BC and EF seem in accord with an $(I^-)^2$ term. For a quantitative comparison, one must remember that the progress of reaction is measured by $d\sum(H^+)/dt$, and that

$$\sum(H^+) = (H^+) + (HAc) \qquad (3)$$

$$[HAc] = (HAc) + (Ac^-) = 2.5\times10^{-4}\ \text{mol/l} \qquad (4)$$

and

$$\frac{(H^+)(Ac^-)}{(HAc)} = 1.8\times10^{-5} \quad \text{at } 25°C \qquad (5)$$

from which it follows that

$$\frac{d\sum(H^+)}{dt} = \frac{d(H^+)}{dt} + \frac{d(HAc)}{dt} = \frac{d(H^+)}{dt}\left[1+\frac{4.5\times10^{-9}}{\{(H^+)+1.8\times10^{-5}\}^2}\right] \qquad (7)$$

The $d\sum(H^+)/dt$ calculated by means of Eq. (7) from the measured $d(H^+)/dt$ and (H^+) should be equal to the rate calculated from the rate equation found by Abel and Stadler[3] for HAc solutions.

Agreement is satisfactory (Table 2) considering the difficulties and the fact that Abel and Stadler measured the rate in a different way (iodimetric determination of $-d(IO_3^-)/dt$). We thus conclude that Table 1 contains no evidence that the Dushman reaction does not proceed as expected. It seems clear that all chemical information available should be considered in designing and interpreting radioisotope exchange experiments on this reaction and others.

General Discussion of the Dushman Reaction

Chemical Information. The following three equilibria should be considered.

$$6H^+ + 5I^- + IO_3^- \rightleftharpoons 3I_2 + 3H_2O$$
$$K_8 = 1.6\times10^{47} \quad \text{at } 25°C[6,17] \qquad (8)$$

$$I_2 + H_2O \rightleftharpoons H^+ + HIO + I^-$$
$$K_9 = 5.4\times10^{-13} \quad \text{at } 25°C[18] \qquad (9)$$

$$I_3^- \rightleftharpoons I_2 + I^-$$
$$K_{10} = 1.4\times10^{-3} \quad \text{at } 25°C[19] \qquad (10)$$

In (8), the forward rate is fast in acid solution as Eq. (1) indicates, the reverse rate being slow. For (9) and (10), forward and reverse rates are fast.[20] I_2 does not react directly with IO_3^-.

Isotope exchange between I_2 and IO_3^- cannot occur directly. Exchange between I^- and IO_3^- is possible *via* the Dushman reaction. Equilibria (9) and (10) make an accompanying indirect exchange between I_2 and IO_3^- possible.

Radioactive Iodine Exchange at Chemical Equilibrium. There is no confusion of experimental results for radioactive iodine exchange between I_2 and IO_3^- at chemical

17) W. O. Lundberg, C. S. Vestling, and J. E. Ahlberg, *J. Amer. Chem. Soc.*, **59**, 264 (1937).
18) T. L. Allen and R. M. Keefer, *ibid.*, **77**, 2957 (1955).
19) A. D. Awtrey and R. E. Connick, *ibid.*, **73**, 1842 (1951).
20) M. Eigen and K. Kustin, *ibid.*, **84**, 1355 (1962).

TABLE 2. QUANTITATIVE EVALUATION OF FIG. 1

	$t=0$	$t=10$	$t=B$	$t=C$	$t=D$	$t=E$	$t=F$
$(H^+)\times 10^5$ (mol/l)	5.85	3.11	2.25	2.20	0.706	0.628	0.600
$(Ac^-)\times 10^5$ (mol/l)	5.85	9.11	11.0	11.2	17.9	18.4	18.7
$(HAc)\times 10^4$ (mol/l)	1.90	1.57	1.38	1.37	0.70	0.64	0.62
$d(H^+)/dt$ (mol/l/min)[a]	1.9×10^{-5}	6.0×10^{-7}	9.0×10^{-8}	1.2×10^{-6}	8.0×10^{-8}	2.0×10^{-8}	3.8×10^{-7}
$d\sum(H^+)/dt$ (mol/l/min)[b]	3.4×10^{-5}	1.7×10^{-6}	3.4×10^{-7}	4.6×10^{-7}	5.4×10^{-7}	1.4×10^{-7}	2.7×10^{-6}
Calculated rate (mol/l/min)[3]	7.0×10^{-5}	1.7×10^{-5}	8.4×10^{-6}	3.3×10^{-6}	3.1×10^{-6}	2.4×10^{-6}	5.7×10^{-5}

a) Measured $d(H^+)/dt$ from Fig. 1.
b) To be compared with calculated rate.

equilibrium.[5-7] The rate of exchange is[6,21]

$$R=\frac{2\{I_2\}\{IO_3^-\}}{2\{I_2\}+\{IO_3^-\}}\times\frac{\ln 2}{T_{1/2}} \qquad (11)$$

where $T_{1/2}$ is the half time for the exchange and R the constant rate, since the system is in chemical equilibrium. For Eq. (11) to be valid, either of the two iodine species added should be initially inactive, and exchange should proceed along a single path which in this case is that of the Dushman reaction. The braces in the equation enclose gram-formula weight of the iodine species.

The measured rates of radioisotope exchange agree fairly well with rates calculated from Eq. (1) for the equilibrium concentrations.[7] Only the $[I^-]$ term is significant in this calculation.

Radioactive Iodine Exchange Away from Chemical Equilibrium. The rate of exchange is determined by Eq. (1), in which the $[I^-]^2$ term has been confirmed. Only the most important case will be discussed.

When radioactive I^- is mixed with excess nonradioactive IO_3^- in acid solution at concentrations such that no solid I_2 is formed, the Dushman reaction will proceed at a rate given by Eq. (1). I_2 and I_3^-, both radioactive, will be produced. As the reaction proceeds, (H^+), (IO_3^-), and (I^-) will decrease, as will the rate of reaction (Fig. 1). As (I^-) decreases, the order of reaction with respect to $[I^-]$ will change as Eq. (1) requires. (I_3^-) will decrease along with (I^-) in conformity with Equilibrium (10). Radioactive IO_3^- will begin to form when steps in the reverse Dushman reaction begin to proceed at an appreciable rate. In equilibrium, forward and reverse rates will be equal, and Eq. (11) will hold.

Experiment 127 of Myers and Kennedy. Myers and Kennedy[6] reported that in an extention of their equilibrium exchange measurements to higher iodide concentrations, Experiment 127 was performed with $[NaI]=5\times10^{-3}$ and $[NaIO_3]=0.1$ in nearly neutral solution at 50 °C. No measurable exchange was found in any of the five samples of solution taken over a period of 1600 hr. They concluded that $T_{1/2}$ in Eq. (11) exceeded 5×10^5 hr at 50 °C.

By use of Eq. (11), they calculated the expected $T_{1/2}$ of 2.8×10^4 hr at 25 °C for the experiment. The calculation is not acceptable because their system was not in equilibrium. They used a value of R calculated from the $[I^-]^2$ term of Eq. (1) with $(H^+)=10^{-7}$. As (H^+) is drastically reduced during the approach to chemical equilibrium, the rate at equilibrium should be far less than their value of R to obtain $T_{1/2}=2.8\times10^4$ hr.

It is possible to calculate the expected equilibrium rate for Experiment 127. Here H_2O plays somewhat the same role as HAc in Fig. 1, and OH^- is analogous to Ac^-. Here the Dushman reaction is

$$3H_2O + 5I^- + IO_3^- = 3I_2 + 6OH^- \qquad (12)$$

Further, Equilibrium (10) requires that 3.6 mol of I_3^- form at 25 °C for each mole of I_2, which means that 2×4.6 mol OH^- will be formed for each mole of I_2 produced in Reaction (12). Thus

$$(OH^-)_{eq} = 10^{-7} + 9.2\times(I_2)_{eq} \qquad (13)$$

for an initially neutral reaction mixture that has gone to equilibrium. Obviously,

$$(H^+)_{eq}=\frac{10^{-14}}{10^{-7}+9.2\times(I_2)_{eq}} \quad \text{at 25°C} \qquad (14)$$

For known $[I^-]$ and $[IO_3^-]$, Equilibrium (8) gives the relation of $(H^+)_{eq}$ to $(I_2)_{eq}$ because

$$K_8=\frac{(I_2)^3}{(H^+)^6(I^-)^5(IO_3^-)}=1.6\times10^{47} \quad \text{at 25°C} \qquad (15)$$

The last two equations give the rounded values $(I_2)_{eq}=7.6\times10^{-7}$ and $(H^+)_{eq}=1.4\times10^{-9}$ for Experiment 127. The expected value of $T_{1/2}$ is

$$T_{1/2}=2.8\times10^4\left\{\frac{10^{-7}}{1.4\times10^{-9}}\right\}^2=1.4\times10^8 \text{ hr} \quad \text{at 25°C} \qquad (16)$$

The expected half time $T_{1/2}$ at 50 °C will be lower, perhaps 10-fold lower, than the value in Eq. (16). This lower half time still exceeds 5×10^5 hr. Therefore, our calculated value is in accord with the results of Experiment 127.

There is thus no conflict between the results of Experiment 127 and the $[I^-]^2$ term in Eq. (1). Considerations about mechanism[6,22] that assumed such a conflict are invalid. To verify the $[I^-]^2$ term by measuring the rate of isotope exchange, one ought to make the measurements on reaction mixtures at chemical equilibrium.

In order to clarify the discrepancies in Table 1, each conclusion therein should be examined as in Experiment 127, and all available chemical information be given due consideration.

We thank Professor Emile Schweikert for helpful discussions and the Robert A. Welch Foundation for support of the work.

21) O. E. Myers and R. J. Prestwood, in "Radioactivity Applied to Chemistry," Editors, A. C. Wahl and M. Bonner, John Wiley & Sons, New York (1951), pp. 7, 8, 32, 33.

22) K. J. Morgan, M. Peard, and C. F. Cullis, *J. Chem. Soc.*, **1951**, 1865.

The Crystal Structure of Orotic Acid Monohydrate (Vitamin B_{13})

Fusao TAKUSAGAWA and Akira SHIMADA

Department of Chemistry, Faculty of Science, Osaka City University, Sugimoto-cho, Sumiyoshi-ku, Osaka 558

(Received November 17, 1972)

The crystal structure of orotic acid monohydrate (Vitamin B_{13}) has been determined by the method of X-ray diffraction. The crystals are triclinic with the space group of $P\bar{1}$ and with cell dimensions of $a=9.561$, $b=7.261$, $c=5.895$ Å, $\alpha=117.6°$, $\beta=107.6°$, and $\gamma=90.4°$. The structure was determined by an inspection of the sharpened Patterson map. The final R value was 5.75% for 1345 observed reflections. The uracil group of orotic acid resembles uracil itself in its molecular dimensions. The molecules are arranged in layers closely parallel to the $(\bar{2}\ 1\ 1)$ plane. The orotic acid molecules are linked through two kinds of N–H···O hydrogen bonds in zig-zag chains extending in the [1 1 1] direction. Each chain is joined, by three kinds of O–H···O hydrogen bonds through the medium of a water molecule, with two neighboring chains, and each forms a sheet parallel to the $(\bar{2}\ 1\ 1)$ plane. The hydrogen bond of the water molecule as an acceptor is of the F type, in which the bisector of lone pairs in the oxygen atom is directed toward a donor group.

This work is a part of a series of X-ray studies of aromatic carboxylic acids. The series has already covered pyromellitic acid dihydrate,[1] trimellitic acid,[2] hemimellitic acid dihydrate,[3] dipicolinic acid monohydrate,[4] dinicotinic acid,[4] quinolinic acid,[4] and cinchomeronic acid.[4] These investigations have given several interesting results, and it is of interest to elucidate the molecular structure of the carboxylic acid based on the pyrimidine ring and the mode of hydrogen-bond formation. Moreover, the orotic acid is vitamin B_{13} and is a biologically-important substance, as are uracil, thymine, and other compounds with a uracil group. In view of the fact that the crystal structures of many uracil derivatives have been determined by the X-ray method, it is also of interest to compare uracil itself with its derivatives in molecular dimensions and in the hydrogen-bond system of the uracil group.

Experimental

A sample of orotic acid was supplied by the Sigma Chemical Co.; crystallization from water yielded crystals of a suitable size. The unit cell dimensions were measured from zero-layer Weissenberg photographs, which were calibrated with superimposed Al powder lines. The crystal data are given in Table 1. Using a spherically-shaped crystal with an average diameter of 0.3 mm, the intensity data were collected for the 0—6 layers around the c axis and the 0—2 layers around the b axis by the use of the multiple-film equi-inclination integrating Weissenberg technique, with Cu$K\alpha$ radiation. The intensities were estimated visually by comparison with a calibration-intensity standard. Of the 1562 possible reflections within the Cu$K\alpha$ sphere, 1488 independent reflections were measured; 143 were too weak to be observed. No absorption correction was applied. The space group $P\bar{1}$ was assigned on the basis of the statistical average for normalized structure factors.

Table 1. Crystal data for orotic acid monohydrate

Molecular formula	$C_5H_4N_2O_4 \cdot H_2O$
Molecular weight	174.06
Crystal system	Triclinic
Space group	$P\bar{1}$
Cell dimensions;	
a	9.561±0.006Å
b	7.261±0.006
c	5.895±0.006
α	117.6±0.09°
β	107.6±0.08
γ	90.4±0.09
V	340.7±0.4Å^3
Z	2
Density (calculated)	1.697 g/cm^3
Density (by flotation)	1.68
Linear absorption coefficient for Cu$K\alpha$	15.4 cm^{-1}
The atom numbering	

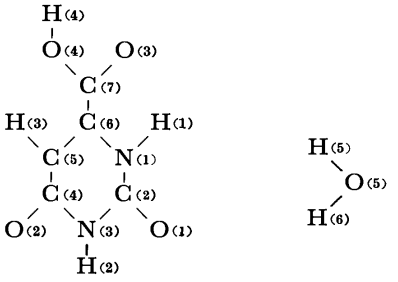

Structure Determination and Refinement

The crystal structure was determined by the inspection of a sharpened Patterson map, which was resolved sufficiently enough to give the orientation and location of the orotic acid molecule in the unit cell. The first postulated structure gave an R value of 63%, which decreased to 35% in three cycles of least-squares refinement with individual isotropic thermal parameters. A difference Fourier map clearly showed the position of water oxygen atom. Since the $\bar{2}\ 1\ 1$ reflection seemed to have a strong extinction effect, it was removed from the later refinements.

Anisotropic thermal parameters were introduced, and

1) F. Takusagawa, K. Hirotsu, and A. Shimada, This Bulletin, **44**, 1274 (1971).

2) F. Takusagawa, K. Hirotsu, and A. Shimada, to be published.

3) F. Takusagawa, K. Hirotsu, and A. Shimada, to be published.

4) F. Takussgawa, K. Hirotsu, and A. Shimada, *Acta Crystallogr.*, **A28**, S15 (1972).

TABLE. 2. THE OBSERVED AND CALCULATED STRUCTURE FACTORS. F_O, F_C, and DF have been multiplied by 10. The unobserved reflections are indicated by an asterisk. The reflections with $|F_O-F_C|/|F_O|$ larger than 0.3 are indicated by a plus sign.

H	FO	FC	DF	H	FO	FC	DF	H	FO	FC	DF	H	FO	FC	DF	H	FO	FC	DF	H	FO	FC	DF	H	FO	FC	DF
K=L= 0	0		7	79	80	0	7	14	13	0	-5	220	223	-2	3	83	-79	-4	2	18	19	0	-3	408	-391	-16
2	292	-305	13	8	11	-13	1	8*	0	0	0	-4	170	-171	0	4	21	21	0	3*	0	0	0	-2	270	-281	11
3	252	248	4	9*	0	-5	5	9+	3	-1	-1	-3	80	80	0	5	70	-77	7	4	87	-95	8	-1	179	157	21
4	114	-119	4	K=L=	5	0		K=L=	-5	1		-2	190	-193	2	6	33	-30	-3	5	38	-36	-1	0	135	-142	7
5	76	-68	-7	-10*	0	-4	4	-9	6	5	0	-1	118	-117	-1	7	37	41	-3	6	20	21	0	1	157	150	6
6	43	-40	-3	-9*	0	-4	4	-8	18	18	0	0+	25	-33	8	8	24	-24	0	7	9	-10	0	2	35	30	5
7	33	-29	-3	-8	7	-9	1	-7	42	-39	-2	1	66	-64	-2	9+	6	-12	5	8+	5	-7	2	3	176	-161	-15
8	83	-82	-1	-7	51	48	2	-6	55	52	2	2	171	-183	12	K=L=	4	1		K=L=	-6	2		4	49	57	-8
9	11	-11	0	-6	40	38	1	-5	35	-35	0	3	247	-237	-9	-11*	0	-1	1	-8	21	19	1	5	97	95	2
10+	13	8	5	-5	15	-16	0	-4	282	-272	-10	4	80	87	-6	-10	21	-19	-1	-7	27	-27	0	6	130	-128	-1
11	35	-31	-4	-4	31	-31	0	-3	20	21	0	5	14	-14	0	-9*	0	-2	2	-6	34	34	0	7	10	-12	1
K=L=	1	0		-3	97	-89	-7	-2	69	70	-1	6	28	31	-2	-8	9	-7	-1	-5	29	29	0	8	103	95	7
-11*	0	-2	2	-2	67	63	4	-1	72	-68	-3	7	121	113	7	-7	21	-22	0	-4	26	-26	0	9*	0	-1	1
-10	45	-45	0	-1	42	41	1	0	36	38	-1	8	12	12	0	-6	37	-36	-1	-3	25	-28	3	10	7	5	1
-9+	18	12	6	0	68	-63	-4	1	94	87	7	9	13	-15	1	-5*	0	2	-2	-2	50	48	2	K=L=	-1	2	
-8	15	-14	-1	1	27	27	0	2*	0	0	0	10	36	35	0	-4	65	-60	-5	-1*	0	3	-3	-12	9	9	0
-7+	5	-8	2	2	37	34	2	3	30	30	0	11*	0	-5	5	-3	50	-49	0	0	32	-32	0	-11	28	28	0
-6	7	-9	1	3	13	13	0	4	47	49	-2	K=L=	0	1		-2	51	51	0	1	27	29	-2	-10	18	20	-2
-5	177	-173	-3	4	18	-16	-2	5	7	-7	0	-12*	0	3	-3	-1+	13	-5	-7	2	26	-27	1	-9	14	-13	0
-4	74	78	-4	5	5	6	0	6	24	26	-1	-11	67	-60	-6	0*	0	-3	3	3	28	-28	0	-8	56	57	-1
-3	125	126	0	6	8	-7	0	7	20	21	-1	-10	45	-41	-4	1	64	59	4	4	17	19	-1	-7	60	62	-1
-2	326	338	-11	7	19	16	2	8	9	10	-1	-9	19	17	1	2	65	60	4	5	16	16	0	-6	23	-28	5
-1	179	173	6	K=L=	6	0		9	11	-11	0	-8	12	11	0	3	29	-27	-2	6	34	-33	0	-5	26	-26	0
0	169	-167	-1	-9	7	8	0	10	12	-12	0	-7	67	62	4	4	14	15	0	7	17	18	0	-4	95	103	-7
1	93	93	0	-8	8	9	0	K=L=	-4	1		-6	93	-85	-8	5	38	41	-3	8	39	37	2	-3	155	-162	6
2	96	97	0	-7*	0	1	-1	-10+	7	12	-5	-5	85	-79	-5	6	11	14	-2	9+	17	-23	6	-2	241	-252	11
3	104	-105	1	-6	11	11	0	-9	21	22	0	-4	88	81	7	7*	0	6	-6	K=L=	-5	2		0	222	-232	10
4	133	-139	5	-5+	5	2	3	-8	11	-11	0	-3	60	63	-3	K=L=	5	1		-9	23	20	2	1	43	-43	0
5	89	89	0	-4*	0	3	-3	-7*	0	1	-1	-2	155	-149	-5	-10+	3	5	-2	-8	12	-13	1	2	52	-53	1
6+	7	4	3	-3	48	50	-1	-6	19	-23	4	-1	135	132	2	-9	24	-23	0	-7	47	-49	2	3	95	-96	0
7	21	26	-5	-2	19	15	3	-5	12	14	-2	0	316	331	-14	-8*	0	-6	6	-6	46	50	-3	4	54	-54	0
8	65	-67	2	-1	36	-32	-4	-4	25	25	0	1	135	134	1	-7	13	14	0	-5	80	-84	4	5	23	-27	3
9	109	-106	-2	0	53	50	2	-3	45	47	-1	2	102	101	1	-6*	0	-4	4	-4	144	-143	-1	6	258	244	14
10	14	11	3	1	10	9	0	-2	117	-117	0	3	271	-254	-16	-5	9	10	0	-3	45	-48	3	7	69	70	-1
11+	3	-4	1	2	166	-160	-6	-1	50	46	3	4	5	-4	0	-4	41	-42	0	-2	36	-40	3	8	22	-23	1
K=L=	2	0		3	28	-24	-3	0	152	148	3	5+	8	-1	-7	-3	73	-68	-4	-1	115	119	-3	9	45	44	0
-11	11	-11	0	4	39	36	2	1	206	-199	-7	6	29	-27	-2	-2	22	21	0	0*	0	2	-2	10*	0	-4	4
-10*	0	1	-1	5	32	-31	-1	2	57	-54	-3	7	32	35	-2	-1	21	21	0	1	86	85	0	K=L=	0	2	
-9	61	62	0	6	13	12	1	3	46	-49	3	8	80	-75	-4	0	31	29	2	2	48	50	-2	-12+	5	-3	-1
-8	25	25	0	K=L=	7	0		4	100	98	1	9*	0	-2	2	1*	0	-6	6	3	39	-41	2	-11	31	-27	-3
-7*	0	-3	3	-7*	0	-1	1	5	131	127	4	10*	0	3	-3	2	22	20	1	4	87	91	-4	-10+	7	-2	-5
-6	38	40	-2	-6	8	9	0	6	25	-25	0	K=L=	1	1		3	55	49	5	5	26	27	0	-9	25	-24	0
-5	110	-115	4	-5	18	19	-1	7	7	5	1	-11	4	-5	1	4	21	22	0	6	10	-11	0	-8	99	94	5
-4	92	-98	6	-4	8	7	1	8	14	-14	0	-10	39	-36	-2	5	53	52	1	7	8	-8	0	-7	113	101	12
-3	30	-25	-5	-3	12	11	1	9	15	-14	-1	-9	13	-12	0	6	7	-7	0	8	23	-24	1	-6	80	-79	0
-2+	18	-9	-9	-2*	0	-4	4	10*	0	-2	2	-8	18	-17	-1	K=L=	6	1		9	12	-14	2	-5	21	25	-3
-1	94	-100	6	-1	14	-12	-1	K=L=	-3	1		-7	57	-50	-6	-9+	9	14	-5	K=L=	-4	2		-4	98	-96	-2
0	170	-173	3	0	68	-62	-6	-10	10	-11	0	-6	54	-55	0	-8	13	12	0	-10	13	15	-1	-3	52	-58	5
1	87	83	3	1	54	-47	-7	-9	72	72	0	-5	120	125	-4	-7	4	-3	-1	-9	39	-35	-4	-2	24	-20	-4
2	183	-186	3	2	25	24	1	-8	30	22	8	-4	167	-170	3	-6	14	-14	0	-8	50	51	-1	-1	70	-63	-6
3	253	261	-8	3	21	-19	-2	-7	73	72	1	-3	8	9	0	-5	34	-32	-1	-7	36	-37	0	0	171	-154	-16
4	257	254	2	4	12	-12	0	-6	37	41	-4	-1	38	37	0	-4	21	21	0	-6	313	-302	-11	1	239	-217	-21
5	108	-110	1	K=L=	8	0		-5	11	-11	0	0	246	-251	5	-3	31	26	4	-5	18	22	-4	2	83	84	-1
6	30	29	0	-4	5	-4	0	-4	99	96	3	1	222	227	-4	-2	26	-23	-2	-4	71	77	-6	3	17	-18	0
7	73	-77	4	-3	6	-6	0	-3	17	18	0	2	117	-120	2	-1	9	10	-1	-3	93	-94	0	4	32	37	-3
8	31	-27	-3	-2*	0	-1	1	-2	119	118	1	3	68	-65	-2	0	35	30	4	-2	59	60	-1	5	139	141	-2
9	37	41	-4	-1	14	-13	-1	-1	397	-407	9	4	52	-54	1	1	9	7	1	-1	128	126	1	6	22	21	1
10	21	-21	0	0	8	-8	0	0	267	-256	-10	5	38	-37	0	2	12	-10	-1	0*	0	0	0	7	14	-13	0
K=L=	3	0		K=L=	-8	1		1	128	129	0	6	116	-114	-1	3	5	5	0	1	77	74	2	8	52	47	4
-11	30	30	0	-3	10	10	0	2	103	-107	4	7	16	-17	1	4	3	-3	0	2	117	124	-7	9+	5	-3	-1
-10	93	88	4	-2	35	32	3	3	95	93	1	8	21	17	4	K=L=	7	1		3	27	-29	2	K=L=	1	2	
-9*	0	-6	6	-1	8	8	0	4	11	12	-1	9	49	-44	-5	-7*	0	-3	3	4	55	56	-1	-12	18	-18	0
-8	36	-36	0	0	17	17	0	5	118	-112	-6	10+	11	-4	-6	-6*	0	3	-3	5	41	43	-2	-11	7	7	0
-7	20	-24	3	1*	0	2	-2	6	34	36	-1	K=L=	2	1		-5	25	23	1	6	15	16	-1	-10	11	9	1
-6	20	-23	2	2	4	4	0	7	49	48	0	-11*	0	-1	1	-4	3	4	0	7	18	-20	2	-9	30	30	0
-5	30	-28	-2	3*	0	0	0	8	89	-86	-3	-10*	0	-3	3	-3	11	-11	0	8	29	-30	1	-8	37	-36	0
-4	116	-116	0	4	13	11	1	9*	0	-3	3	-9	5	-6	1	-2	32	28	4	9	5	5	0	-7	45	-48	2
-3	30	32	-1	5*	0	-1	1	10	60	59	1	-8*	0	-6	6	-1*	0	3	-3	10	11	-13	1	-6	43	42	1
-2	178	-174	-4	6	45	-43	-2	11*	0	3	-3	-7	55	-56	1	0	67	-70	3	K=L=	-3	2		-5	15	17	-2
-1	139	-135	-4	K=L=	-7	1		K=L=	-2	1		-6	29	30	-1	1	13	-13	0	-11	13	14	-1	-4	84	-79	-5
0	129	130	-1	-6	14	15	0	-11+	10	6	4	-5	58	60	-2	2	14	17	-3	-10	10	-10	0	-3	49	52	-2
1+	11	-16	5	-5	21	-18	-2	-10	12	13	0	-4	179	168	10	K=L=	-9	2		-9+	7	-4	-2	-2	151	143	8
2	16	-19	2	-4	25	24	1	-9	38	42	-4	-3	109	107	1	-1*	0	5	-5	-8	29	-27	-2	-1	62	63	0
3	92	96	-4	-3	25	24	1	-8	29	31	-1	-2	94	-89	-4	0	13	-14	0	-7+	7	1	5	0	57	54	2
4	110	114	-3	-2	20	-17	-2	-7	22	-25	3	-1	53	58	-5	1	19	-18	0	-6	20	24	-4	1	173	-167	-6
5	30	-32	2	-1	21	-21	0	-6	110	112	-1	0	72	71	0	2	3	3	0	-5	44	46	-2	2*	0	1	-1
6	26	29	-2	0	15	14	0	-5	98	99	0	1	87	-87	0	3*	0	2	-2	-4	120	-123	3	3+	15	9	5
7	43	48	-4	1	7	-6	0	-4	27	-35	7	2	115	-120	5	K=L=	-8	2		-3	52	48	3	4	20	-19	0
8	12	14	-2	2	15	-14	0	-3	29	-31	1	3	79	74	4	-5	52	47	5	-2	221	203	17	5	33	38	-5
9	7	9	-1	3	7	8	0	-2	163	176	-13	4*	0	-4	4	-4	12	11	1	-1	261	-272	11	6	87	-82	-4
10	24	25	-1	4	16	-16	0	-1	223	-218	-4	5	17	22	-4	-3+	3	6	-2	0	74	-65	-8	7*	0	0	0
K=L=	4	0		5	14	-12	-1	0	297	-314	16	6	66	-71	4	-2	18	17	1	1	82	-84	2	8*	0	5	-5
-11*	0	0	0	6	14	14	0	1	98	104	-5	7	127	-125	-2	-1	4	-3	0	2	181	177	4	9	4	5	-1
-10	48	-44	-4	7	9	8	1	2	242	-243	1	8	19	17	1	0	6	6	0	3	255	234	20	K=L=	2	2	
-9	16	13	2	8	12	-12	0	3	36	-36	0	9	7	-9	1	1	32	30	1	4	52	-54	1	-12	9	-11	2
-8	15	16	0	K=L=	-6	1		4	41	-45	3	K=L=	3	1		2	11	-10	0	5	29	34	-5	-11*	0	-2	2
-7	58	-57	-1	-7	22	21	1	5	73	-71	-2	-11	26	26	0	3	19	-19	0	6	31	-35	4	-10+	4	-6	2
-6*	0	-3	3	-6	13	-14	1	6	53	-50	-2	-10	19	18	0	4	52	46	6	7	19	-21	2	-9	31	-29	-1
-5	39	37	2	-5	40	-40	0	7	14	-15	1	-9*	0	1	-1	5	10	-11	0	8	8	8	0	-8	12	-14	2
-4	35	-35	0	-4	42	41	1	8	178	173	4	-8	12	11	1	6	50	-47	-3	9	33	-33	0	-7	39	43	-3
-3	45	49	-4	-3	78	-74	-4	9	54	53	0	-7	24	-25	1	K=L=	-7	2		10	24	-22	-1	-6	64	-70	6
-2	122	-122	0	-2	105	-110	4	10	18	-17	0	-6	25	-26	0	-7	12	11	0	K=L=	-2	2		-5	10	9	0
-1	208	-207	0	-1	29	-31	1	11	26	26	0	-5	6	-5	-1	-6	34	-30	-3	-11	38	39	-1	-4	418	398	20
0	65	65	0	0	20	-20	0	K=L=	-1	1		-4*	0	-2	2	-5	20	21	-1	-10	14	15	-1	-3	30	31	-1
1	23	24	0	1	53	51	2	-11	30	31	0	-3	50	-49	0	-4	52	51	0	-9	44	46	-1	-2	113	-111	-1
2	70	69	1	2	9	10	0	-10	17	-15	-2	-2	82	-75	-6	-3	7	8	-1	-8	30	32	-1	-1	106	102	4
3	9	-10	0	3	49	45	3	-9	48	-52	4	-1	31	30	0	-2	43	45	-1	-7*	0	-3	3	0	50	-53	2
4	35	35	0	4	22	23	0	-8	18	13	4	0	105	-97	-7	-1	9	-7	-1	-6	70	71	0	1	49	-43	-6
5	74	73	0	5	12	-11	-1	-7	71	-73	2	1	145	153	-8	0	16	17	0	-5	13	16	-3	2	38	-36	-1
6	19	24	-5	6	36	34	2	-6	207	202	5	2	163	170	-7	1	16	16	0	-4	96	100	-3	3	29	-30	0

TABLE 2. Continued.

H	FO	FC	DF	H	FO	FC	DF	H	FO	FC	DF	H	FO	FC	DF	H	FO	FC	DF	H	FO	FC	DF	H	FO	FC	DF
4	87	-95	8	3	20	-18	-1	-2	48	-44	-3	-8	26	-28	1	-6	53	56	-2	-6	60	-57	-3	5*	12	16	-3
5	14	-17	3	4	103	-95	-7	-1	73	-68	-5	-7	5	5	0	-5	16	-15	0	-5	23	21	2	K,L=	-6	5	
6	16	18	-2	5*	0	-4	4	0	190	169	20	-6	128	124	4	-4	28	33	-4	-4	17	-17	0	-9	47	46	0
7	42	-42	0	6	12	-12	0	1	266	247	19	-5	18	20	-2	-3	47	45	1	-3	59	56	3	-8	24	22	1
8*	0	-1	1	7	6	-7	0	2	66	-63	-3	-4	38	-41	3	-2	24	23	1	-2	17	15	2	-7	8	10	-1
K,L=	3	2		K,L=	-6	3		3	44	49	-5	-3	34	35	-1	-1*	9	4	5	-1	82	-76	-6	-6	33	-34	0
-11*	0	-3	3	-9	16	12	4	4	45	-49	4	-2	7	-8	1	0	223	-206	-17	0	30	31	-1	-5	45	-48	2
-10*	0	-2	2	-8	30	-30	0	5	23	-24	0	-1	24	-25	0	1	79	-81	2	1	61	53	7	-4*	0	4	-4
-9	8	-8	0	-7	25	26	-1	6	18	19	-1	0	14	-14	0	2	25	27	-1	2	97	-93	-3	-3	13	-10	-2
-8	9	7	1	-6	62	58	3	7	50	-50	0	1	16	-15	0	3	27	-28	1	3	18	-19	0	-2	23	22	0
-7	17	21	-3	-5*	0	5	-5	8	36	-35	0	2	49	-51	1	4	11	-14	2	4	83	78	5	-1	7	6	1
-6	68	74	-5	-4	68	68	0	9	10	-9	0	3	9	-12	2	5	20	24	-3	5	12	-11	-1	0*	0	-1	1
-5	55	51	3	-3	21	-20	-1	K,L=	-1	3		4	9	11	-2	6	16	19	-2	6*	0	2	-2	1	26	27	0
-4	41	-44	3	-2	30	32	-2	-12	8	7	0	5	23	-27	3	7	15	15	0	K,L=	1	4		2	25	24	0
-3*	10	14	-3	-1	47	41	6	-11	17	20	-2	K,L=	4	3		K,L=	-4	4		-11	10	10	0	3	11	-13	1
-2	36	36	0	0	22	23	0	-10	17	19	-1	-10*	0	1	-1	-11	9	-11	2	-10	3	-2	0	4	4	4	0
-1	52	-54	2	1*	0	1	-1	-9*	5	3	2	-9	5	6	0	-10	16	18	-2	-9*	0	-6	6	5	14	15	0
0	66	-62	-4	2	168	-167	-1	-8	30	31	0	-8	26	30	-4	-9	23	23	0	-8*	0	4	-4	K,L=	-5	5	
1	34	36	-2	3	66	-64	-1	-7	14	16	-1	-7	23	22	0	-8	12	-14	1	-7	19	-21	1	-10	14	14	0
2*	0	-6	6	4	26	28	-1	-6	40	43	-2	-6	21	-20	0	-7	11	-11	0	-6	26	-27	0	-9	3	4	0
3	9	9	0	5	19	-20	1	-5	179	-187	8	-5*	0	0	0	-6	48	50	-1	-5*	12	16	-4	-8	15	13	2
4	50	-47	-3	6	11	-12	0	-4	151	-154	3	-4	16	14	1	-5	12	14	-1	-4	25	-23	-2	-7	11	-13	1
5	100	-95	-5	7	19	22	-2	-3	78	84	-6	-3	28	-27	0	-4	35	-37	1	-3	29	-30	0	-6*	0	2	-2
6	12	12	0	8	10	12	-2	-2	73	-77	4	-2	28	-26	-1	-3	45	44	1	-2	19	-20	1	-5	37	40	-2
7*	0	-5	5	K,L=	-5	3		-1	125	115	10	-1	11	13	-1	-2	45	-46	1	-1	14	-14	0	-4	17	-18	0
K,L=	4	2		-10	19	16	2	0	95	31	4	0*	0	-3	3	-1	61	-61	0	0	38	-35	-3	-3	68	-64	-3
-10*	0	2	-2	-9	23	-23	0	1	154	-136	-17	1*	0	1	-1	0*	17	11	6	1	23	-22	0	-2	112	115	-3
-9*	0	0	0	-8	31	31	0	2	49	54	-5	2	18	-20	2	1	25	24	1	2	144	133	10	-1	17	-15	-1
-8*	0	-1	1	-7	31	29	1	3	101	97	4	3	41	-48	6	2	78	-82	4	3	49	49	0	0	150	-143	-6
-7*	0	0	0	-6	23	-24	1	4	131	-131	0	4*	0	3	-3	3	17	22	-4	4	17	-19	2	1	7	9	-2
-6	5	-5	0	-5	22	-23	1	5	17	-21	4	K,L=	5	3		4	104	99	4	5	30	37	-6	2	28	-27	0
-5	22	-24	1	-4	72	68	3	6	114	106	7	-7*	0	-10	10	5	78	-75	-3	6*	0	-2	2	3	3	-5	1
-4	23	-24	1	-3	14	16	-2	7	9	-9	0	-6	10	-7	-2	6	22	-23	1	K,L=	2	4		4	22	23	0
-3*	0	0	0	-2	48	-47	-1	8*	7	5	2	-5*	7	-3	-3	7	8	9	-1	-10	7	-8	0	5*	0	4	-4
-2	35	-34	0	-1	55	52	2	K,L=	0	3		-4*	4	-11	7	K,L=	-3	4		-8	8	-6	-1	6	2	-2	0
-1	58	53	5	0	37	-41	3	-12	11	10	1	-3	10	12	-1	-11	10	-11	1	-7	8	-7	-1	K,L=	-4	5	
0	73	69	3	1	50	-49	-1	-11	7	-6	-1	-2*	12	21	-9	-10	27	26	0	-6*	4	-7	3	-10	23	23	0
1	27	-27	0	2	15	16	-1	-10	20	18	2	-1	2	-3	0	-9	38	-37	-1	-5	18	-17	0	-9*	0	3	-3
2*	0	3	-3	3	23	23	0	-9	31	28	3	0*	0	-2	2	-8	74	-76	1	-4	23	-22	-1	-8	26	25	1
3	54	-53	0	4	63	-66	2	-8	13	-12	-1	1	26	-27	1	-7	23	-28	4	-3	23	-22	-1	-7*	0	0	0
4	20	-20	0	5	22	22	0	-7	14	-14	0	K,L=	-9	4		-6	17	-19	1	-2	7	7	0	-6	21	20	0
5	26	31	-4	6	73	72	0	-6	28	30	-1	-3	6	7	-1	-5	73	76	-3	-1	4	-3	0	-5	24	23	1
6	16	-17	0	7	56	-51	-4	-5	68	-66	-1	-2	31	-26	-4	-4	6	-6	0	0	31	30	1	-4	24	21	2
K,L=	5	2		8	17	-19	2	-4	102	-100	-2	-1	18	-17	-1	-3	64	63	1	1	70	67	2	-3	6	6	0
-9	11	-11	0	9*	0	3	-3	-3	45	44	0	0	3	3	0	-2	55	53	2	2	10	9	0	-2	177	-168	-8
-8	8	-10	2	K,L=	-4	3		-2	102	-97	-4	1	11	10	1	-1	62	-59	-2	3	5	-6	0	-1	75	-73	-2
-7*	0	-1	1	-11	16	16	0	-1	44	-37	-7	2	10	9	0	0	151	138	12	4	24	26	-1	0	19	22	-3
-6	18	-17	0	-10	12	-12	0	0	42	-38	-4	3+	9	13	-4	1	35	33	1	K,L=	3	4		1	26	-28	2
-5	14	-14	0	-9	32	-32	0	1	57	-57	0	K,L=	-8	4		2	28	-29	0	-9*	0	-1	1	2	12	-13	1
-4	13	13	0	-8	44	42	2	2	50	-46	-3	-6	3	3	0	3	25	-25	0	-8	17	-19	1	3	19	22	-3
-3*	0	-2	2	-7	66	-66	0	3	29	-30	0	-5	6	-7	0	4	51	-51	0	-7+	3	5	-1	4	18	21	-2
-2*	0	0	0	-6	120	-125	4	4	243	223	20	-4	7	-7	0	5	28	-27	0	-6	22	21	0	5	19	19	0
-1	29	27	1	-5	42	-46	3	5	72	68	3	-3	14	13	1	6	8	-6	-1	-5	5	6	0	6	17	16	1
0	16	18	-2	-4	38	-39	1	6	26	-24	-1	-2	41	-42	0	8*	6	8	-2	-4*	0	3	-3	K,L=	-3	5	
1	20	-18	-1	-3	133	137	-4	7	58	50	7	-1*	0	-4	4	K,L=	-2	4		-3*	0	-5	5	-11	13	13	0
2*	0	2	-2	-2*	0	-7	7	8*	3	-6	2	0	12	-12	0	-11	13	-15	1	-2	7	6	0	-10	4	-4	0
3	24	27	-3	-1	100	101	0	K,L=	1	3		1	6	-6	0	-10	110	-105	-5	-1	11	10	0	-9	3	-2	0
4	10	11	-1	0	65	71	-6	-12	4	-5	0	2	33	35	-1	-9	6	-6	0	0	6	7	0	-8	21	21	0
K,L=	6	2		1	67	-74	6	-11*	0	-3	3	3	9	10	-1	-8	42	42	0	1*	0	0	0	-7*	0	3	-3
-7*	0	1	-1	2	150	151	0	-10	30	32	-1	4	7	8	0	-7	34	-35	1	2	24	-27	3	-6	17	-16	-1
-6	12	-12	0	3	36	37	-1	-9	31	30	1	5+	4	6	-2	-6	20	18	1	3*	0	0	0	-5	18	18	0
-5	19	-18	0	4	27	-27	0	-8	26	-26	0	K,L=	-7	4		-5	68	67	1	K,L=	4	4		-4	39	-37	-2
-4	5	6	0	5	19	-20	1	-7*	0	-1	1	-8	25	-25	0	-4	18	16	1	-8+	27	36	-8	-3	46	-51	5
-3	11	12	0	6	39	-42	3	-6	30	-29	0	-7	67	65	1	-3	54	52	2	-7	8	9	-1	-2	7	8	-1
-2	8	8	0	7	24	-25	0	-5	20	-21	1	-6	29	27	1	-2	84	100	-15	-6	11	-13	2	-1	19	18	1
-1*	0	-3	3	8*	0	-1	1	-4	11	-10	0	-5*	10	14	-4	-1	21	-20	0	-5	11	11	0	0	60	-61	1
0	8	9	-1	9	18	17	1	-3	37	-36	0	-4	38	-38	0	0	50	50	0	-4*	0	2	-2	1	16	19	-3
1	23	24	0	K,L=	-3	3		-2	67	-68	0	-3	51	-52	1	1	45	46	0	-3	10	-11	1	2	85	88	-2
2	13	14	-1	-11	23	-21	-2	-1	97	-93	-4	-2*	0	5	-5	2	11	8	3	-2*	0	-4	4	3	70	-67	-3
K,L=	-9	3		-10	32	33	0	0	34	36	-2	-1	11	-9	-2	3	27	-30	3	-1	7	-6	0	4	18	-19	0
-2*	4	-1	-2	-9	27	-28	0	1	8	-8	0	0	20	19	0	4	57	-54	-2	0	20	-21	1	5	9	11	-2
-1	6	5	1	-8	219	-213	-6	2	37	39	-2	1	8	9	0	5	13	12	1	1*	0	-5	5	6	4	-4	0
0	24	-24	0	-7*	0	5	-5	3	117	116	0	2+	4	1	3	6	24	-23	0	K,L=	-9	5		K,L=	-2	5	
1	3	-3	0	-6	61	66	-4	4	19	18	1	3	17	18	0	7	7	-6	0	-2	15	18	-3	-11	17	-16	-1
2	7	-8	0	-5	70	-73	2	5	7	-9	1	4	14	14	0	K,L=	-1	4		-1	19	-19	0	-10	38	-35	-2
3*	0	-2	2	-4	46	48	-2	6	40	42	-2	5	10	-12	1	-11	9	-8	-1	0	27	-31	3	-9	10	-12	1
K,L=	-8	3		-3	119	114	5	7*	0	-2	2	6*	0	1	-1	-10	25	22	3	K,L=	-8	5		-8	4	-5	1
-5	61	62	-1	-2+	8	11	-2	K,L=	2	3		K,L=	-6	4		-9	11	12	0	-6	10	-9	0	-7	22	20	1
-4	28	24	4	-1	88	87	1	-11	11	11	0	-9	58	54	3	-8	29	-28	0	-5	7	8	-1	-6*	0	-3	3
-3	14	11	2	0	167	160	6	-10	13	-14	0	-8	18	17	0	-7	38	35	2	-4	34	-35	0	-5	24	22	2
-2	29	-28	-1	1	42	-40	-1	-9	22	-24	1	-7+	5	7	-1	-6	65	61	3	-3	22	-20	-2	-4	24	22	1
-1	36	-38	2	2	73	74	0	-8	17	16	1	-6	24	24	0	-5	78	-74	-4	-2	6	6	0	-3	21	-19	-2
0	4	4	0	3	60	59	1	-7*	0	0	0	-5+	10	-14	3	-4	24	-22	-2	-1	17	16	0	-1	24	21	2
1*	0	-1	1	4	14	15	-1	-6	39	-42	3	-4*	0	6	-6	-3	27	-27	0	0	14	14	0	0	14	-14	0
2	11	9	1	5	26	-29	2	-5	15	18	-2	-3	43	50	-7	-2	84	87	-2	1	23	23	0	1	18	-16	-1
3	11	11	0	6	50	-51	0	-4	53	54	0	-2	20	-20	0	-1	131	143	-11	2*	0	-1	1	2	41	-40	0
4*	0	5	-5	7	10	9	0	-3	18	20	-2	-1	74	-76	2	0	42	-37	-5	3	6	-6	0	3	24	-22	-1
5	7	7	0	8	21	-22	0	-2	14	16	-1	0	132	125	6	1	26	26	0	K,L=	-7	5		4	5	-6	1
6	4	3	0	9	8	-7	-1	-1	49	-50	1	1	23	-21	-1	2	36	-36	0	-7	8	-8	0	5	24	24	0
K,L=	-7	3		K,L=	-2	3		0	5	5	0	2	148	-142	-5	3	16	-18	1	-6	9	-8	0	K,L=	-1	5	
-7	61	62	-1	-12	5	-5	0	1	14	13	0	3*	0	4	-4	4	14	15	0	-5	14	13	0	-11	5	-6	1
-6	17	16	1	-11	7	-6	0	2*	0	0	0	4	24	-24	0	5	52	-49	-2	-4	44	-46	1	-10	20	21	0
-5+	6	9	-2	-10	20	-24	4	3	16	16	0	5	5	-6	1	6	35	-36	1	-3*	0	-4	4	-9	13	-12	0
-4	29	25	4	-9	9	-7	-1	4	56	-56	0	6	16	18	-1	7	14	-14	0	-2	11	-12	0	-8*	5	2	3
-3	9	-9	0	-8	28	28	0	5*	0	0	0	7+	12	5	7	K,L=	0	4		-1	6	-8	1	-7	31	33	-1
-2	9	8	1	-7	24	27	-2	6*	0	2	-2	K,L=	-5	4		-11	5	4	1	0	47	47	0	-6	14	13	0
-1	42	46	-3	-6	69	-73	4	K,L=	3	3		-10	17	-18	0	-10	12	10	1	1	11	12	0	-5	20	18	2
0	18	-17	-1	-5	49	46	2	-11+	10	-13	3	-9	17	19	-1	-9	12	11	0	2	12	13	0	-4	43	37	5
1	50	-50	0	-4	143	139	3	-10*	0	-2	2	-8	47	45	2	-8	15	14	1	3+	3	5	-1	-3*	4	0	-3
2	99	90	9	-3	177	-186	9	-9	12	13	-1	-7*	0	4	-4	-7	62	-59	-2	4	20	21	0	-2	23	20	3

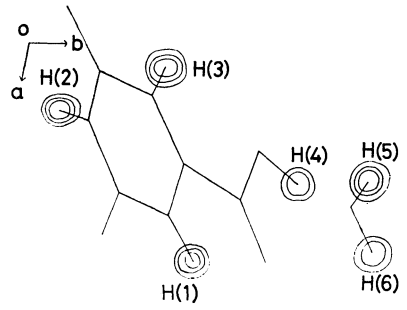

Fig. 1. A composite drawing of the electron density associated with the hydrogen atoms. The contours are at intervals of 0.2 e Å^{-3}, beginning with the 0.2 e Å^{-3} contour.

the block-diagonal least-squares refinement was continued, reducing the R value to 8.1%. At this stage, a difference Fourier map was computed, from which the positions of six hydrogen atoms were then found (Fig. 1). There was no unexplainable peak on this map except those due to hydrogen atoms. With anisotropic thermal parameters for non-hydrogen atoms and isotropic thermal parameters for hydrogen atoms, the final R value was found to be 5.75%, excluding unobserved reflections. The $\sum w(F_o-F_c)^2$ function was minimized, where;

$$w = 0.5 \text{ for } |F_o| \leqq 0.5,$$
$$w = 1.0 \text{ for } 0.5 < |F_o| < 5.0 \text{ and}$$
$$w = 5.0/|F_o| \text{ for } 5.0 \leqq |F_o|.$$

The atomic scattering factors used were those listed in the International Table for X-ray Crystallography for C, N, and O atoms and the spherical scattering factors proposed by Stewart, Davidson, and Simpson[5] for the H atom. The observed and calculated structure factors are listed in Table 2, while the fractional coordinates and thermal parameters are listed in Table 3.

Results and Discussion

Molecular Structure of Orotic Acid. The bond lengths and angles are listed, along their estimated standard deviations, in Table 4 and are shown in Fig.

TABLE 3. THE FINAL PARAMETERS AND THEIR ESTIMATED STANDARD DEVIATIONS (IN PARENTHESES)
The coordinates of the non-hydrogen atoms have been multiplied by 10^4; those of the hydrogen atoms, by 10^3. The anisotropic thermal parameters of non-hydrogen atoms are of the form $\exp[-(B_{11}h^2+B_{22}k^2+B_{33}l^2+B_{12}hk+B_{13}hl+B_{23}kl)]$, and have been multiplied by 10^5. For the hydrogen atoms the values listed are isotropic thermal parameters B(Å^2).

Atom	x	y	z	B (Å^2)
N (1)	3299(2)	4692(3)	1900(4)	—
C (2)	2931(2)	3262(3)	2603(4)	—
N (3)	1531(2)	2073(3)	1065(4)	—
C (4)	547(2)	2116(3)	−1141(4)	—
C (5)	1028(2)	3630(3)	−1787(4)	—
C (6)	2373(2)	4868(3)	−237(4)	—
C (7)	2984(2)	6557(3)	−638(4)	—
O (1)	3750(2)	3045(3)	4484(4)	—
O (2)	−671(2)	917(3)	−2384(3)	—
O (3)	4204(2)	7570(3)	792(4)	—
O (4)	2079(2)	6773(3)	−2625(4)	—
O (5)	3148(2)	9579(3)	−3310(4)	—
H (1)	424(3)	557(4)	297(6)	4.4(0.5)
H (2)	123(3)	116(4)	151(6)	3.2(0.6)
H (3)	28(3)	376(4)	−336(6)	4.1(0.6)
H (4)	267(3)	788(4)	−274(6)	6.4(0.8)
H (5)	250(3)	962(4)	−464(6)	7.4(0.9)
H (6)	400(3)	1021(4)	−267(6)	9.6(1.1)

Atom	B_{11}	B_{22}	B_{33}	B_{12}	B_{13}	B_{23}
N (1)	892(19)	2273(43)	4086(74)	−444(45)	129(60)	3100(96)
C (2)	870(21)	2264(48)	3939(82)	−208(51)	265(66)	2950(106)
N (3)	852(19)	2305(42)	4213(76)	−426(44)	194(60)	3426(96)
C (4)	860(21)	2114(46)	3934(82)	−253(49)	357(66)	2664(103)
C (5)	916(21)	2280(48)	4093(85)	−78(51)	456(68)	3286(108)
C (6)	927(21)	2079(45)	3968(82)	155(50)	952(68)	2844(103)
C (7)	1067(24)	2191(49)	4224(89)	−77(54)	877(74)	2974(111)
O (1)	1022(18)	3151(47)	5151(76)	−611(46)	−452(59)	5033(103)
O (2)	931(17)	2899(44)	5033(76)	−1030(43)	−429(57)	4536(98)
O (3)	1326(23)	3602(56)	6438(98)	−1703(58)	−559(75)	5983(127)
O (4)	1134(19)	2934(45)	5619(80)	−357(46)	541(62)	5096(104)
O (5)	1244(22)	3636(55)	6317(94)	−747(54)	−48(72)	6550(127)

5) R. F. Stewart, E. R. Davidson, and W. T. Simpson, *J. Chem. Phys.*, **42**, 3175 (1965).

TABLE 4. BOND LENGTHS AND BOND ANGLES

Bond	Length(Å)	e.s.d.(Å)	Bond	Angle(°)	e.s.d.(°)
N(1)–C(2)	1.363	0.003	C(2)–N(1)–C(6)	122.7	0.2
C(2)–N(3)	1.373	0.003	N(1)–C(2)–N(3)	114.7	0.2
N(3)–C(4)	1.369	0.003	C(2)–N(3)–C(4)	126.4	0.2
C(4)–C(5)	1.433	0.004	N(3)–C(4)–C(5)	115.5	0.2
C(5)–C(6)	1.346	0.004	C(4)–C(5)–C(6)	119.0	0.2
C(6)–N(1)	1.365	0.003	C(5)–C(6)–N(1)	121.7	0.2
C(2)–O(1)	1.227	0.003	N(1)–C(2)–O(1)	124.1	0.2
C(4)–O(2)	1.237	0.003	N(3)–C(2)–O(1)	121.2	0.2
C(6)–C(7)	1.498	0.004	N(3)–C(4)–O(2)	119.5	0.2
C(7)–O(3)	1.197	0.004	C(5)–C(4)–O(2)	125.0	0.2
C(7)–O(4)	1.306	0.003	C(5)–C(6)–C(7)	124.3	0.2
N(1)–H(1)	0.94	0.04	N(1)–C(6)–C(7)	114.1	0.2
N(3)–H(2)	0.89	0.04	C(6)–C(7)–O(3)	120.5	0.2
C(5)–H(3)	1.03	0.03	C(6)–C(7)–O(4)	114.1	0.2
O(4)–H(4)	1.02	0.04	O(3)–C(7)–O(4)	125.4	0.2
O(5)–H(5)	0.85	0.03	C(2)–N(1)–H(1)	117	2
O(5)–H(6)	0.82	0.03	C(6)–N(1)–H(1)	121	2
			C(2)–N(3)–H(2)	117	2
			C(4)–N(3)–H(2)	116	2
			C(4)–C(5)–H(3)	117	2
			C(6)–C(5)–H(3)	124	2
			C(7)–O(4)–H(4)	105	2
			H(5)–O(5)–H(6)	121	3

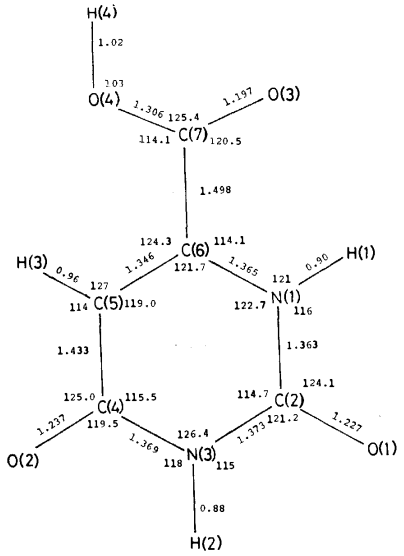

Fig. 2. Dimensions of the orotic acid molecule.

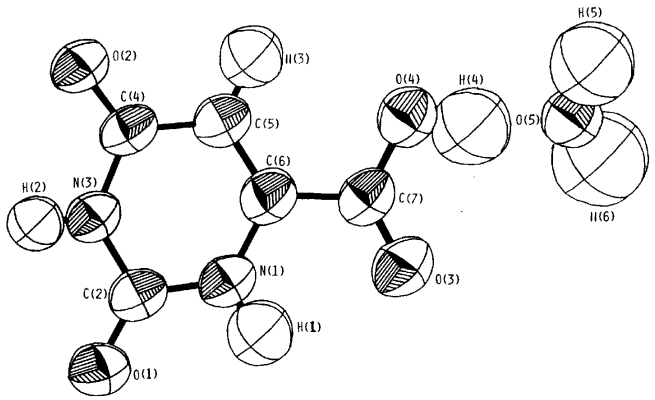

Fig. 3. The anisotropic thermal ellipsoids of non-hydrogen atoms and the isotropic thermal ellipsoids of hydrogen atoms. Ellipsoids are scaled to include the 74% probability.

2. Figure 3 shows the anisotropic thermal ellipsoids of non-hydrogen atoms and the isotropic thermal ellipsoids of hydrogen atoms. Ellipsoids are scaled to include the 74% probability.

The orotic acid molecule may be a mixture of tautomers, such as;

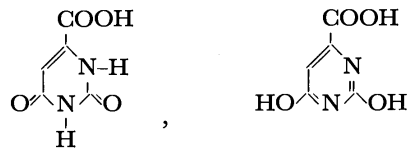

However, according to the present study, the molecule clearly takes the keto form in the crystal. This is quite evident from the assignment of hydrogen atoms in the difference Fourier map. It is also confirmed by the C(2)–O(1) and C(4)–O(2) bond lengths, 1.227(3) and 1.237(3) Å, and the C(2)–N(3)–C(4) and C(2)–N(1)–C(6) bond angles, 122.7(2)° and 126.4(2)° respectively

TABLE 5. THE DISTANCES FROM THE LEAST-SQUARES PLANE DEFINED BY THE SIX NON-HYDROGEN ATOMS OF PYRIMIDINE RING

Atom	Deviation (Å)	Atom	Deviation (Å)
N(1)	0.005	O(3)	0.039
C(2)	−0.018	O(4)	0.100
N(3)	0.019	O(5)	0.134
C(4)	−0.005	H(1)	0.04
C(5)	−0.009	H(2)	0.02
C(6)	0.009	H(3)	0.04
C(7)	0.053	H(4)	0.05
O(1)	−0.043	H(5)	0.16
O(2)	0.002	H(6)	−0.01

TABLE 6. THE COMPARISONS BETWEEN THE CORRESPONDING BOND LENGTHS AND BOND ANGLES OF OROTIC ACID AND URACIL, THYMINE, METHYLTHYMINE, THYMIDINE, METHYLURIDINE, AND DEOXYURIDINE

Bond length	(a)	(b)	(c)	(d)	(e)	(f)	(g)	(g')
N(1)–C(2)	1.363	1.371	1.355	1.379	1.385	1.377	1.39	1.43
C(2)–N(3)	1.373	1.376	1.361	1.379	1.381	1.376	1.36	1.36
N(3)–C(4)	1.369	1.371	1.391	1.375	1.378	1.384	1.37	1.37
C(4)–C(5)	1.433	1.430	1.447	1.432	1.453	1.437	1.44	1.36
C(5)–C(6)	1.349	1.340	1.349	1.346	1.343	1.345	1.31	1.36
C(6)–N(1)	1.365	1.358	1.382	1.383	1.374	1.361	1.37	1.34
C(2)–O(1)	1.227	1.215	1.234	1.214	1.206	1.196	1.23	1.23
C(4)–O(2)	1.237	1.245	1.231	1.237	1.230	1.223	1.20	1.19
Bond angle								
C(2)–N(1)–C(6)	122.7	122.7	122.8	120.6	121.8	121.6	121.8	118.2
N(1)–C(2)–N(3)	114.7	114.0	115.2	115.4	113.7	114.1	112.4	115.1
C(2)–N(3)–C(4)	126.4	126.7	126.3	126.3	127.5	127.2	128.5	126.8
N(3)–C(4)–C(5)	115.5	115.5	115.6	116.1	115.8	115.4	114.4	114.7
C(4)–C(5)–C(6)	119.0	118.9	118.2	118.3	117.2	117.6	121.2	121.9
C(5)–C(6)–N(1)	121.7	122.3	121.8	123.3	124.1	124.2	121.6	123.0
N(1)–C(2)–O(1)	124.1	123.7	122.7	123.3	124.3	123.0	126.7	124.1
N(3)–C(2)–O(1)	121.2	122.3	122.1	121.3	122.0	122.9	120.9	120.5
N(3)–C(4)–O(2)	119.5	119.2	118.3	120.0	119.7	119.2	123.8	121.5
C(5)–C(4)–O(2)	125.0	125.3	126.1	123.9	124.5	125.4	121.8	123.8

(a) Orotic acid (This Paper). (b) Uracil.[6] (c) Thymine.[7] (d) 1-Methylthymine.[8] (e) Thymidine.[9] (f) 5-Methyluridine.[10] (g) and (g') Deoxyuridine.[11]

TABLE 7. HYDROGEN BOND DISTANCES (Å) AND ANGLES (degree)

X—H·····O	Symmetry	X···O	e.s.d.	X–H	e.s.d.	H···O	e.s.d.	Angle	e.s.d.
N(1)–H(1)···O(1)	(1, 1, 5)	2.874	0.003	0.94	0.04	1.95	0.04	167	3
N(3)–H(2)···O(2)	(1, 1, 2)	2.816	0.003	0.89	0.04	1.92	0.04	177	3
O(4)–H(4)···O(5)	(1, 1, 1)	2.520	0.003	1.02	0.04	1.52	0.03	165	3
O(5)–H(5)···O(2)	(1, 1, 3)	2.772	0.003	0.85	0.03	1.95	0.03	162	3
O(5)–H(6)···O(3)	(1, 1, 4)	2.777	0.003	0.82	0.03	1.98	0.03	164	3
X—O·····H	Symmetry	Angle	e.s.d.						
C(2)–O(1)···H(1)	(1, 1, 5)	132	1	Symmetry codes		1=(x, y, z)			
C(4)–O(2)···H(2)	(1, 1, 2)	123	1			2=(−x, −y, −z)			
C(4)–O(2)···H(5)	(1, 1, 3)	131	1			3=(−x, 1−y, −1−z)			
C(7)–O(3)···H(6)	(1, 1, 4)	163	1			4=(1−x, 2−y, −z)			
H(5)–O(5)···H(4)	(1, 1, 1)	113	2			5=(1−x, 1−y, 1−z)			
H(6)–O(5)···H(4)	(1, 1, 1)	124	3						
H(2)···O(2)···H(5)	(2, 1, 3)	105	1						

TABLE 8. π-BOND ORDERS AND NET CHARGES CALCULATED BY CNDO METHOD

Bond	Bond order	Calcd[a] (Å)	Obsd (Å)	Calcd−Obsd (Å)	Atom	Net charge
N(1)–C(2)	0.389	1.366	1.363	0.003	N(1)	−0.252
C(2)–N(3)	0.394	1.365	1.373	−0.008	C(2)	+0.522
N(3)–C(4)	0.376	1.368	1.369	−0.001	N(3)	−0.326
C(4)–C(5)	0.346	1.450	1.433	0.017	C(4)	+0.437
C(5)–C(6)	0.848	1.359	1.346	0.013	C(5)	−0.212
C(6)–N(1)	0.369	1.370	1.365	0.005	C(6)	+0.163
C(2)–O(1)	0.793	1.227	1.227	0.000	C(7)	+0.409
C(4)–O(2)	0.821	1.222	1.237	−0.015	O(1)	−0.406
C(6)–C(7)	0.243	1.468	1.498	−0.030	O(2)	−0.375
C(7)–O(3)	0.875	1.212	1.197	0.015	O(3)	−0.315
C(7)–O(4)	0.361	1.305	1.306	−0.001	O(4)	−0.267
					H(1)	+0.173
					H(2)	+0.181
					H(3)	+0.082
					H(4)	+0.186

a) The bond lengths are calculated by the following equations,
$D_{C-C}=1.512-0.180P$
$D_{C-N}=1.436-0.180P$
$D_{C-O}=1.370-0.180P$
K. Nishimoto and L. S. Forster, *Theor. Chim. Acta* (Berl.), **4**,155 (1966).

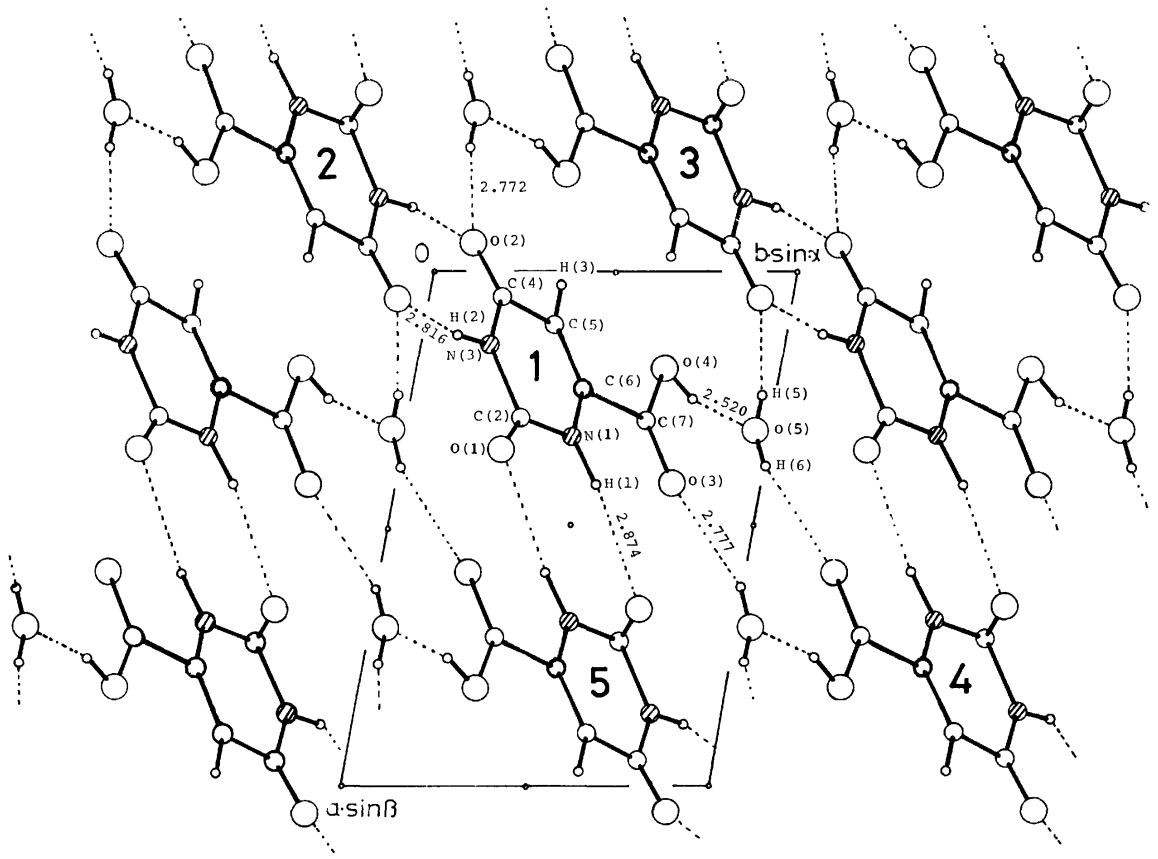

Fig. 4. A view of the crystal structure down the *c* axis. The hydrogen bonds are shown by broken lines.

(the values in parentheses denote the e.s.d.'s in the last digits, here and throughout this paper).

The pyrimidine ring is planar. The equation of the least-squares plane through six atoms of the pyrimidine ring is:

$$-0.6557X + 0.4402Y + 0.6134Z = 0.0078$$

where X, Y, and Z are coordinates in Å referred to an orthogonal set of axes, where X and Z are parallel to the a and c^* axes, and where Y lies in the ab plane; this coordinate system is used throughout this paper. The maximum deviation of a ring atom from this plane is 0.019 Å. The displacements of all the atoms from the plane are listed in Table 5.

The comparisons between the corresponding bond lengths and bond angles of orotic acid, and uracil,[6] thymine,[7] methylthymine,[8] thymidine,[9] methylthymidine,[10] and deoxyuridine[11] are given in Table 6. Those of uracil are in good agreement with those found in orotic acid, except for the C(2)–O(1) bond length and the N(3)–C(2)–O(1) bond angle. This means that the substitution of the carboxyl group does not appreciably change the bond lengths and angles of the uracil group. The C(2)–N(3)–C(4) bond angle is 3.7(2)° larger than the C(2)–N(1)–C(6) bond angle. Many other compounds which have the uracil group show a similar tendency. The net charges on each atom have been calculated by the CNDO method;[12] they are listed, along the π-bond orders, in Table 8. The C(2) atom has the most positive charge (0.522), and the C(4) atom has the second (0.437) in the uracil group. Therefore, the C(2)–N(3)–C(4) bond angle might be larger than the C(2)–N(1)–C(6) bond angle, since the repulsion between the C(2) and C(4) atoms is clearly stronger than that between the C(2) and C(6) atoms. There is a significant difference between the two bond angles, N(1)–C(6)–C(7) (114.1(2)°) and C(5)–C(6)–C(7) (124.3(2)°). A similar difference between the two angles is also observed in uracil. There is a difference of 0.010(3) Å between the C(2)–O(1) and C(4)–O(2) bond lengths. Although this difference

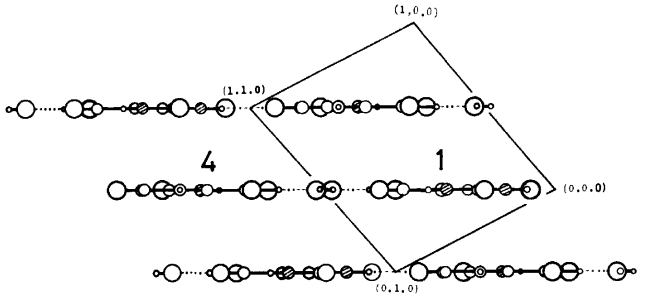

Fig. 5. A view of the crystal structure parallel to the ($\bar{2}$ 1 1) plane. The hydrogen bonds are shown by broken lines.

6) R. F. Stewart, *ibid.*, **23**, 1102 (1967).
7) R. Gerdil, *ibid.*, **14**, 333 (1961).
8) K. Hoogsteen, *ibid.*, **16**, 28 (1963).
9) D. W. Young, P. Tollin, and H. R. Wilson, *ibid.*, **B25**, 1423 (1971).
10) J. Hunt and E. Subramanian, *ibid.*, **B25**, 2144 (1969).
11) A. Rahman and H. R. Wilson, *ibid.*, **B28**, 2260 (1972).
12) J. A. Pople and D. L. Beverige, "Approximate Molecular orbital Theory," McGraw-Hill Book Co., New York (1970).

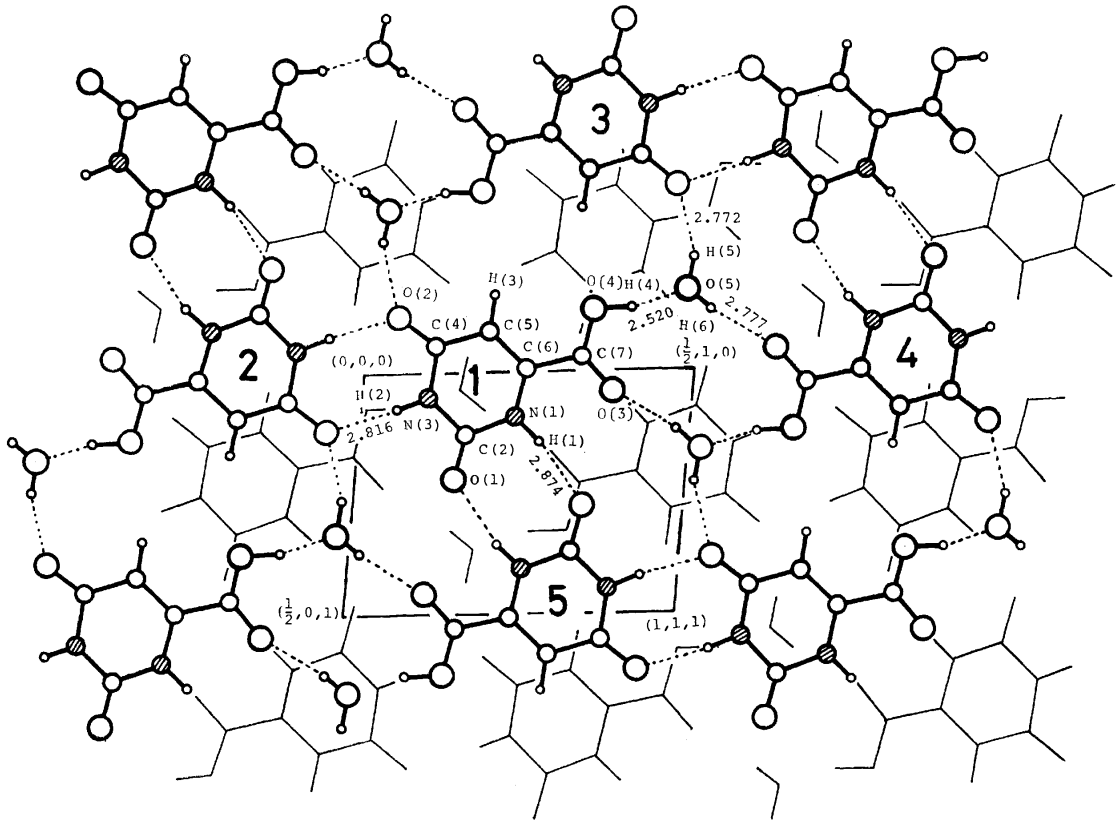

Fig. 6. A view of the crystal structure perpendicular to the ($\bar{2}$ 1 1) plane, showing the relative orientation of the molecules in two adjacent layers parallel to the ($\bar{2}$ 1 1) plane.

may be on the borderline of experimental error, similar differences between the two C=O bond lengths are also observed in thymidine,[9] methyluridine,[10] deoxyuridine,[11] methylthymine,[8] and uracil.[6] The π-bond orders of the C(2)–O(1) and C(4)–O(2) bonds are 0.793 and 0.821 respectively. These values are contrary to the observed lengths, as is shown in Table 8. The difference between the N(3)–C(2)–O(1) and N(3)–C(4)–O(2) bond angles is 1.7(2)°. Similar differences are also observed in uracil, thymine, methylthymine, thymidine, and methyluridine. In a carboxyl group, the C(7)–O(3) bond length is 0.109(3) Å shorter than the C(7)–O(4) bond length. Hence, the carboxyl group clearly consists of carbonyl and hydroxyl groups. The carboxyl group is twisted by 2.2° out of the plane of the pyrimidine ring.

Molecular Arrangement and Hydrogen-bond System.

The crystal structure is shown in Figs. 4, 5, and 6, while the distances and angles of hydrogen bonds are listed in Table 7. The molecules are arranged in layers closely parallel to the ($\bar{2}$ 1 1) plane. This plane has a spacing of 3.102 Å. The best plane, calculated by a least-squares analysis, through the carbon, nitrogen and oxygen atoms of two molecules, 1 and 2, is:

$$-0.6514X + 0.4183Y + 0.6289Z = 0.0000 \quad \text{(i)}$$

The best planes through the molecules, 1 and 3, and the molecules, 1 and 4, are found by the same procedure to be:

$$-0.6573X + 0.4183Y + 0.6289Z = -0.0630 \quad \text{(ii)}$$

$$-0.6580X + 0.4216Y + 0.6239Z = -0.0558 \quad \text{(iii)}$$

respectively. The dihedral angles which these best planes make with the ($\bar{2}$ 1 1) plane are 0.4° (i), 0.6° (ii), and 0.7° (iii). Figures 5 and 6 show the views parallel and perpendicular to the ($\bar{2}$ 1 1) plane respectively, illustrating the relative orientation of the molecules in two neighboring layers. The upper layer in Fig. 6, containing the molecules drawn with heavy lines, passes through the point of origin (0, 0, 0). In Figs. 4, 5, and 6, the same numerals designate the same molecules. The symmetry codes corresponding to these numbers are shown in Table 7.

In crystals of uracil and thymine, one of the oxygen atoms is hydrogen-bonded to the nitrogen atoms, N(1) and N(3), of two different molecules, while the other is not hydrogen-bonded to any nitrogen atom. However, in the case of the orotic acid monohydrate, each oxygen atom of the uracil group is hydrogen-bonded to one nitrogen atom of each of two different molecules. In uracil and thymine, the distances of the two N–H···O hydrogen bonds are equal within the limits of experimental error. There is, however, a significant difference between the two N–H···O hydrogen bond distances, 2.874(3) and 2.816(3) Å, in this crystal. The O(2) atom participates in two kinds of hydrogen bonds (O···H–N; 2.816(3) Å, O···H–O; 2.772(3) Å), while the O(1) atom participates in only one hydrogen bond (O···H–N; 2.874(3) Å).

Each molecule is joined, through two kinds of N–H···O hydrogen bonds around the center of symmetry, with two neighboring molecules and forms a zig-zag chain along the [1 1 1] direction. Each chain

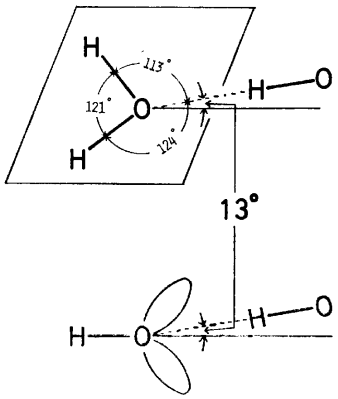

Fig. 7. Diagrammatic view of the water molecule in orotic acid. The value 13° indicates the angle between the O···H vector and the plane of the water molecule.

is joined, by three kinds of O–H···O hydrogen bonds through the medium of the water molecule, with two neighboring chains and forms a sheet parallel to the ($\bar{2}$ 1 1) plane. These three hydrogen-bond distances are 2.772(3) and 2.777(3) Å for O···HOH, which are equal within the limits of experimental error, and 2.520(3) Å for H_2O···HO, which seems to be a nearly symmetrical hydrogen bond.

Each water molecule is hydrogen-bonded to three oxygen atoms. The coordination of a water molecule is approximately trigonal planar. The hydrogen-bonding angles are H(4)–O(5)–H(5)=113(2)°, H(4)–O(5)–H(6)=124(3)°, and H(5)–O(5)–H(6)=121(3)°. The angle which the O(5)···H(4) vector of the hydrogen bond makes with the plane of the water molecule is 13° (Fig. 7). Therefore, the water molecule in this crystal is of the F type, according to the classification of Chidambaram, Sequeira, and Sikka;[13] that is, the bisector of lone pairs of the water oxygen atom is directed toward a hydrogen-bond donor group. In the hydrogen bond O(5)–H(6)···O(3), the C(7)–O(3)···H(6) hydrogen-bonding angle is 163(1)°. This value also indicates that the bisector of lone pairs in the carbonyl oxygen atom O(3) is directed toward a hydrogen-bond donor group.

Computer Programs. All the calculations were performed on a FACOM 270-30 computer at the Computer Center of Osaka City University, using these modified programs: RSLC-3 (cell constant),[14] RSSFR-3 (Fourier synthesis),[15] HBLS-IV (block-diagonal least-squares refinement),[16] DAPH (bond length, bond angle, least-squares plane),[17] SCALE (film factor, Lp, and layer scaling),[18] TE-I (thermal ellipsoid),[19] and CNINDO (CNDO and INDO calculations).[12]

The authors wish to express their thanks to Dr. K. Nishimoto of this faculty for his useful advice on the CNDO calculations.

13) R. Chidambaram, A. Sequeira, and S. K. Sikka, *J. Chem. Phys.*, **41**, 3616 (1964).
14) T. Sakurai, "The Universal Crystallographic Computing System (I)," ed. by T. Sakurai, Japanese Crystallographic Association, 1967 p. 18.
15) T. Sakurai, Ref. 14, p. 45.
16) T. Ashida, Ref. 14, p. 65.
17) T. Ashida, Ref. 14, p. 76.
18) H. Yoshioka, K. Hirotsu, and F. Takusagawa, unpublished work.
19) F. Takusagawa, unpublished work.

The Crystal Structure of Dipicolinic Acid Monohydrate

Fusao TAKUSAGAWA, Ken HIROTSU, and Akira SHIMADA

Department of Chemistry, Faculty of Science, Osaka City University, Sugimoto-cho, Sumiyoshi-ku, Osaka 558

(Received December 4, 1972)

The crystal structure of the dipicolinic acid monohydrate has been determined by the method of X-ray diffraction. The crystal is orthorhombic, with a space group of $P2_12_12_1$ and with cell dimensions of $a=12.233$, $b=9.399$, and $c=6.817$ Å. The crystal structure was solved by an inspection of the Patterson map. The final R value was 5.67% for 964 observed reflections. The pyridine ring has the C_{2v} symmetry within the limits of experimental error. The protonation does not occur on the nitrogen atom of the pyridine ring, and two carboxyl groups consist of carbonyl and hydroxyl groups. There is a simple relation between the C–O bond length and the C–C–O bond angle. The molecules are arranged in layers closely parallel to the (0 0 1) plane. Each molecule on the same plane is hydrogen-bonded to form an endless chain along the b axis. These two chains on the planes at $z=1/8$ and 3/8 are linked together by the O–H···N hydrogen bond between the water and pyridine ring to form a double chain along the b axis. In this case, the angle between the N···H(7) vector of the hydrogen bond and the plane of the pyridine ring is 28°. This situation can be explained by the fact that two adjacent and bulky carboxyl groups wrap up the nitrogen atom as an acceptor of the hydrogen bond. The double chains are packed only by the van der Waals forces. The thermal diffuse scattering observed on Weissenberg photographs can be explained by this hydrogen-bond system.

This work is a part of series of X-ray diffraction studies on the O–H···N hydrogen bonding system in pyridine-dicarboxylic acids, which also cover dinicotinic acid,[1] quinolinic acid,[1] and cinchomeronic acid.[1] In connection with this work, the crystal structures of nicotinic acid[2] and benzoic acid[3] have also been established; they all have similar frameworks and isoelectronic structures. However, these two structures were found to be quite different from each other in the way of hydrogen-bond formation. The most remarkable feature is that the hydroxyl group in nicotinic acid is hydrogen-bonded not to the oxygen atom but to the nitrogen atom, although the hydrogen bond is plausible between two carboxyl groups, as in benzoic acid. This was explained by Wright and King[2] on the basis of the packing mode of the moelcules, which does not permit the O–H···O hydrogen bond in this case. Hence, it is of interest to elucidate the effect of the nitrogen atom in the pyridine ring on the hydrogen-bond formation in solids. The crystal structures of calcium dipicolinate trihydrate,[4] strontium dipicolinate tetrahydrate,[5] and some coordination compounds[6-8] containing dipicolinate were also determined by the X-ray method. It is also of interest to compare the molecular dimensions of dipicolinic acid itself with those of its salts and coordination compounds.

Experimental

The crystals were obtained in the form of colorless prisms by recrystallization from an aqueous solution. Weissenberg photographs showed the crystals to be orthorhombic, with the space group of $P2_12_12_1$. The unit cell dimensions were measured from zero-layer Weissenberg photographs taken with Cu$K\alpha$ radiation ($\lambda=1.5418$ Å); these photographs were calibrated with the superimposed Al powder lines ($a=4.0494$ Å). They are given, along other crystal data, in Table 1. There are four molecules in the unit cell, corresponding to the density of 1.56 g/cm³ observed by the flotation method. One crystal was in the shape of a sphere with the average diameter of 0.4 mm. The intensity data were collected for the 0—10 layers around the a axis and the 0—6 layers around the c axis by the use of the multiple-film equi-inclination integrating Weissenberg technique, with Cu$K\alpha$ radiation. The intensities of the diffraction spots

TABLE 1. CRYSTAL DATA FOR DIPICOLINIC ACID MONOHYDRATE

Molecular formula	$C_7H_5NO_4\cdot H_2O$
Molecular weight	185.14
Crystal size	$\sim 0.4\times 0.4\times 0.4$ mm
Crystal system	Orthorhombic
Space group	$P2_12_12_1$
Cell dimensions;	
a	12.233 ± 0.003 Å
b	9.399 ± 0.001
c	6.817 ± 0.006
V	783.8 ± 0.8 Å³
Z	4
Density (calculated)	1.569 g/cm³
Density (observed)	1.56
Radiation	Cu$K\alpha$ ($\lambda=1.5418$ Å)
Linear absorption coefficient	13.54 cm^{-1}
Number of independent reflections	1026
The atom numbering	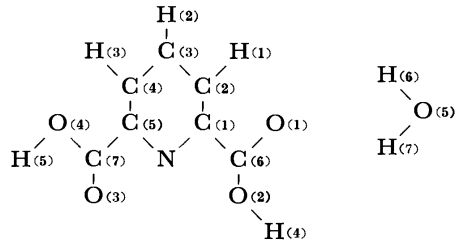

1) F. Takusagawa, K. Hirotsu, and A. Shimada, *Acta Crystallogr.*, **A28**, S15 (1972).
2) W. B. Wright and G. S. D. King, *ibid.*, **6**, 305 (1953).
3) G. A. Sim, J. M. Robertson, and T. H. Goodin, *ibid.*, **8**, 157 (1955).
4) G. Strahs and R. E. Dickerson, *ibid.*, **B24**, 571 (1968).
5) K. J. Palmer, R. Y. Wong, and J. C. Lewis, *ibid.*, **B28**, 233 (1972).
6) R. E. Drew and F. W. B. Einstein, *ibid.*, **A28**, S86 (1972).
7) P. P. Quaglieri, H. L. G. Thomas, *ibid.*, **B28**, 2583 (1972).
8) D. Schwarzenbach, *Inorg. Chem.*, **9**, 2391 (1970).

Table 2. THE OBSERVED AND CALCULATED STRUCTURE FACTORS.

F_o, F_c and DF have been multiplied by 10. The unobserved reflections are indicated by an asterisk. The reflections, for which the $|F_o-F_c|/|F_o|$ is larger than 0.3, are indicated by a plus sign.

H	FO	FC	DF	H	FO	FC	DF	H	FO	FC	DF	H	FO	FC	DF	H	FO	FC	DF	H	FO	FC	DF	H	FO	FC	DF
K,L=	0	0		11*	0	4	-4	6	100	99	1	K,L=	9	1		1	73	72	0	2	54	48	6	8	19	19	0
2	750	779	-29	12*	0	4	-4	7	89	94	-4	0	121	111	10	2	345	346	0	3+	35	23	11	9	27	30	-2
4	429	443	-14	13	36	34	1	8	45	43	1	1	49	42	7	3	204	191	13	4	95	95	0	10	50	53	-3
6	401	407	-5	K,L=	7	0		9	46	48	-1	2	68	69	-1	4	241	229	11	5	110	108	2	11	17	19	-2
8	210	198	12	1	94	84	10	10+	17	8	8	3	55	55	0	5	132	134	-2	6	22	22	0	12	11	13	-2
10	175	179	-4	2	157	161	-4	11*	0	13	-13	4	55	51	3	6	56	54	1	7+	12	7	4	K,L=	7	3	
12	103	99	3	3	42	41	1	12	40	40	0	5	45	41	3	7	56	54	2	8	53	49	3	0	42	44	-1
14	76	60	16	4*	0	0	0	13	40	40	0	6	29	30	-1	8	192	198	-5	9	30	32	-2	1	30	33	-2
K,L=	1	0		5	63	64	0	14	19	18	0	7	48	49	-1	9	82	81	0	10*	0	8	-8	2	64	66	-2
1	59	62	-2	6	104	111	-6	15	20	14	5	8	35	28	6	10	108	106	2	11	44	44	0	3	61	65	-3
2	319	327	-8	7	25	31	-5	K,L=	3	1		9	38	36	1	11	15	14	0	12	18	18	0	4	39	40	-1
3	176	187	-10	8	49	56	-7	0	21	24	-2	10	38	36	1	12	35	34	0	13	16	18	-2	5	62	66	-4
4	215	209	6	9	88	88	0	1	218	222	-4	K,L=	10	1		13	36	39	-3	14	9	10	-1	6	27	27	0
5	213	209	4	10+	11	7	3	2	266	267	0	0	83	74	9	14	11	11	0	K,L=	1	3		7	16	15	0
6	102	98	4	11	45	42	2	3	259	260	0	1	56	50	6	K,L=	5	2		0	115	110	5	8	26	29	-2
7	81	75	5	12	45	40	5	4	239	239	0	2	31	28	3	0	14	14	0	1	141	123	18	9+	11	5	6
8	96	86	9	K,L=	8	0		5	124	126	-1	3	47	44	2	1	82	82	0	2	161	146	15	10	12	10	2
9	66	52	14	0	37	34	3	6	61	60	0	4	43	43	0	2	55	51	3	3	99	82	17	11+	11	18	-6
10	20	18	1	1	47	47	0	7	136	141	-5	5	77	71	6	3	174	171	3	4	90	88	1	K,L=	8	3	
11	83	85	-1	2	82	84	-2	8	189	201	-12	6	46	41	5	4	73	74	0	5	122	106	15	0	163	160	2
12	53	48	5	3	19	21	-1	9	179	176	3	7	23	23	0	5	52	51	0	6	155	148	7	1	294	287	7
13	71	70	0	4	15	15	0	10	191	181	9	8	15	16	0	6	34	32	2	7	154	150	3	2	119	125	-6
14	19	21	-2	5	31	32	0	11	112	106	6	K,L=	11	1		7	172	174	-2	8	49	53	-3	3	114	116	-2
15	27	21	5	6	22	22	0	12	63	58	4	0	37	34	3	8	195	209	-13	9	22	23	0	4	24	27	-3
K,L=	2	0		7	29	29	0	13+	18	11	6	1	42	39	2	9	75	71	4	10	48	49	-1	5	82	93	-10
0	234	261	-27	8	84	81	2	14	22	15	6	2	35	30	4	10	41	40	1	11	92	93	-1	6	43	46	-3
1	229	235	-6	9	26	26	0	15	36	31	4	3	82	79	3	11	87	92	-4	12	62	67	-5	7	64	68	-4
2	410	402	8	10*	0	0	0	K,L=	4	1		4	75	72	3	12	15	12	3	13+	14	19	-4	8	51	51	0
3	218	230	-11	11	15	12	2	0	100	97	2	5	37	30	6	13	19	18	0	14	13	16	-2	9	32	31	1
4	593	588	4	K,L=	9	0		1	448	449	0	6+	17	11	5	K,L=	6	2		K,L=	2	3		10	34	36	-1
5	141	143	-1	1	29	26	2	2	397	388	8	K,L=	12	1		0	24	23	1	0+	11	4	7	K,L=	9	3	
6	135	133	1	2*	0	9	-9	3	231	233	-2	0	75	64	11	1	127	129	-1	1	82	77	4	0	84	81	2
7	129	144	-14	3	14	14	0	4	122	111	11	K,L=	0	2		2	115	114	0	2	243	230	13	1	49	50	-1
8	12	9	3	4	75	78	-2	5	116	106	10	0	461	478	-16	3	130	128	2	3	71	72	-1	2	37	39	-1
9+	28	19	8	5	71	74	-2	6	52	59	-6	1	657	1678	-21	4	43	41	2	4	128	115	12	3	42	45	-2
10	24	19	4	6	44	49	-5	7	118	120	-2	2	243	250	-6	5	62	62	0	5	120	115	4	4	24	23	0
11	65	61	4	7	14	12	2	8	189	186	3	3	192	181	11	6	19	19	0	6	44	42	1	5	32	31	0
12	39	33	5	8	37	37	0	9	190	193	-3	4	124	117	6	7	64	64	0	7	95	96	0	6	22	23	0
13*	0	1	-1	9	69	57	11	10	49	46	3	5	328	302	26	8	27	28	-1	8+	13	7	5	7	22	27	-4
14	25	20	5	10	75	65	9	11	44	38	6	6	67	60	7	9	11	13	-1	9	29	29	0	8	22	24	-2
15+	20	13	7	K,L=	10	0		12	25	23	1	7	327	315	11	10	26	27	0	10	27	30	-2	K,L=	10	3	
K,L=	3	0		0	18	19	0	13	31	27	3	8	41	39	1	11	11	12	-1	11*	0	6	-6	0	27	28	-1
1	181	189	-7	1	25	24	0	14	22	18	4	9	82	85	-3	12	10	13	-2	12	22	24	-2	1	43	42	0
2	178	182	-4	2	12	10	2	K,L=	5	1		10	28	23	5	13	15	16	-1	13	21	25	-4	2	15	19	-3
3	314	326	-11	3	15	11	3	0	100	104	-3	11	86	83	2	K,L=	7	2		14*	0	5	-5	3	25	25	0
4	49	43	6	4	86	87	0	1	59	54	4	12	25	20	4	0	87	92	-4	K,L=	3	3		4	27	28	0
5	108	115	-6	5	81	77	4	2	167	172	-4	13	87	94	-7	1	42	40	2	0	33	33	0	5	29	29	0
6*	0	8	-8	6	56	49	6	3	131	126	5	14	17	18	-1	2	50	51	0	1	20	22	-1	6	34	37	-3
7*	0	14	-14	7+	14	9	5	4	19	21	-2	15	8	6	1	3	120	122	-1	2	187	164	23	K,L=	11	3	
8	22	23	0	8	15	16	0	5	109	105	3	K,L=	1	2		4	53	56	-3	3	188	180	8	0	32	37	-5
9	189	193	-3	K,L=	11	0		6	80	81	0	0	184	187	-2	5	27	29	-1	4	85	85	0	1+	7	4	3
10	82	82	0	1	110	97	13	7	88	92	-4	1	538	561	-22	6	18	16	1	5	69	73	-4	2	28	30	-2
11	70	58	12	2	22	17	5	8	126	128	0	2	87	89	-2	7	106	122	-16	6	31	38	-6	3	38	42	-4
12*	0	14	-14	3	54	47	6	9	158	160	-1	3	214	212	2	8	50	56	-5	7	77	79	-2	K,L=	0	4	
13	82	76	6	4	63	54	8	10	89	87	1	4	27	24	2	9	19	17	1	8	157	149	8	1	299	284	15
14	44	43	0	5+	33	22	11	11	41	34	6	5	34	32	2	10	28	29	0	9	141	136	4	2	153	171	-17
15	23	19	4	6	20	18	1	12	29	29	0	6	155	157	-1	11	12	14	-1	10	84	81	2	3	141	140	1
K,L=	4	0		K,L=	12	0		13	14	15	0	7	41	44	-2	12	73	72	0	11	83	95	-12	4	139	122	17
0	374	392	-17	0	145	132	12	14	52	48	4	8	43	42	1	K,L=	8	2		12	34	36	-1	5	78	77	1
1	302	306	-4	1	66	51	15	K,L=	6	1		9	76	71	5	0	18	17	1	13	15	18	-2	6	150	141	8
2	335	333	1	K,L=	0	1		0	19	23	-3	10	13	14	0	1	31	29	2	14	11	10	0	7	48	50	-2
3	425	455	-29	1	238	220	17	1	50	53	-3	11	14	15	-1	2	33	36	-2	K,L=	4	3		8	68	67	0
4	142	136	6	2	24	20	3	2	144	155	-11	12	64	68	-3	3+	14	9	4	0+	18	10	8	9+	10	3	6
5	146	150	-3	3	45	42	3	3	215	222	-6	13	25	26	-1	4	28	29	-1	1	189	177	12	10	76	76	0
6	129	120	9	4	150	148	2	4	103	94	9	14	27	31	-4	5	23	25	-2	2	270	261	9	11	32	30	1
7	134	137	-3	5	136	121	14	5	58	57	0	15	15	10	4	6	25	29	-4	3	84	85	-1	12	40	42	-1
8	35	40	-4	6	49	44	5	6	20	21	0	K,L=	2	2		7	53	50	2	4	127	122	5	13+	15	21	-6
9	232	251	-19	7	97	91	6	7	61	61	0	0	59	55	3	8	37	40	-2	5	25	23	2	14+	15	23	-7
10	84	85	-1	8	69	71	-2	8	22	24	-2	1	324	314	10	9	11	10	1	6	44	43	0	K,L=	1	4	
11*	0	1	-1	9	100	93	6	9	47	51	-4	2	204	199	4	10	12	11	0	7	82	84	-2	0	40	42	-1
12*	0	2	-2	10	23	26	-2	10	72	71	0	3	236	224	12	11	30	30	0	8	172	172	0	1	84	84	0
13	25	18	7	11	32	36	-3	11	54	48	5	4	113	110	2	K,L=	9	2		9	78	78	0	2	120	109	10
14	47	40	7	12	21	18	2	12+	25	14	10	5	121	121	0	0	27	26	0	10	59	64	-5	3	60	57	2
K,L=	5	0		13	58	52	5	K,L=	7	1		6	110	110	0	1	23	25	-1	11	18	22	-3	4	62	53	9
1	17	19	-1	14	16	13	2	0	55	58	-2	7	59	54	4	2	25	25	0	12	22	28	-6	5	48	48	0
2	104	104	0	15+	13	8	5	1	50	49	1	8	44	40	3	3	12	14	-2	13	14	14	0	6	27	26	0
3+	26	16	9	K,L=	1	1		2	77	81	-3	9	19	17	1	4	27	29	-1	K,L=	5	3		7	24	29	-4
4	120	116	4	0	190	193	-2	3	70	71	0	10	26	26	0	5	79	85	-6	0	50	52	-2	8	46	49	-3
5	158	140	17	1	276	270	5	4	124	127	-3	11	55	60	-4	6	62	64	-1	1+	13	5	8	9	19	23	-3
6	197	200	-3	2	144	147	-3	5	68	71	-2	12	37	36	1	7	11	9	1	2	140	140	0	10*	0	0	0
7	160	176	-16	3	198	193	4	6	56	55	1	13	34	35	-1	8	33	32	1	3	63	56	6	11	25	25	0
8	116	110	5	4	203	193	10	7	18	17	0	14	18	17	0	9	13	13	0	4	35	30	5	12	22	29	-6
9	169	176	-7	5	162	159	2	8	28	28	0	K,L=	3	2		K,L=	10	2		5	25	28	-3	13+	16	22	-5
10	132	134	-2	6	276	306	-29	9+	13	3	9	0	74	68	5	0*	0	2	-2	6	83	83	0	K,L=	2	4	
11*	0	9	-9	7	206	199	7	10	25	25	0	1	120	121	0	1	17	20	-2	7	68	73	-4	0	54	52	1
12	46	37	8	8	158	147	11	11	13	10	3	2	198	195	2	2	35	34	0	8	82	85	-3	1	78	69	8
13	24	17	6	9+	46	22	24	12	22	16	6	3	262	252	10	3	66	69	-3	9	85	87	-1	2	109	100	1
14	49	37	11	10	106	104	1	K,L=	8	1		4	202	185	16	4	36	38	-1	10	83	86	-2	3	63	55	8
K,L=	6	0		11	116	112	4	0	380	416	-35	5	131	133	-2	5	23	18	4	11+	14	20	-6	4	175	163	12
0	136	148	-12	12	98	93	4	1	315	330	-14	6	13	13	0	6	25	23	2	12+	13	18	-4	5	33	32	0
1	116	117	-1	13	31	26	5	2	264	260	4	7	87	92	-5	7	9	10	0	13	15	13	2	6	56	57	0
2	62	60	1	14	16	12	4	3	99	101	-1	8	71	68	3	K,L=	11	2		K,L=	6	3		7	32	32	0
3	69	68	1	15	19	17	1	4	112	113	-1	9	44	45	-1	0	70	64	6	0	13	12	1	8*	0	9	-9
4	181	179	2	K,L=	2	1		5	76	84	-7	10	139	144	-4	1	37	36	0	1	32	29	2	9+	10	5	5
5	63	66	-2	0	15	17	-2	6	102	109	-6	11	49	46	2	2	74	73	1	2	117	119	-2	10*	0	7	-7
6	190	197	-7	1	167	165	1	7	66	69	-3	12	43	44	0	3	23	22	0	3	79	81	-2	11	22	26	-3
7	24	20	4	2	343	345	-2	8	61	68	-7	13+	11	6	4	4+	10	7	3	4	40	40	0	12*	0	4	-4
8	13	11	1	3	237	238	0	9	73	70	2	14	20	23	-3	5	37	38	-1	5	43	48	-5	13*	0	1	-1
9	47	46	0	4	206	205	1	10	61	57	3	K,L=	4	2		K,L=	0	3		6	16	19	-2	K,L=	3	4	
10	31	31	0	5	325	331	-5	11	50	44	5	0	54	46	9	1	21	27	-5	7	25	29	-3	0	47	39	7

TABLE 2. Continued.

H	FO	FC	DF	H	FO	FC	DF	H	FO	FC	DF	H	FO	FC	DF	H	FO	FC	DF	H	FO	FC	DF	H	FO	FC	DF
1	15	14	0	5	12	10	1	K=L=	2	5		5	24	26	0	11	7	5	1	0	46	43	3	2	38	39	0
2	100	103	-2	6	39	39	0	0	18	17	1	6	9	8	1	K=L=	2	6		1	33	31	2	3*	0	5	-5
3	96	98	-2	7	25	24	1	1	38	33	5	7	14	12	1	0	14	12	2	2	30	31	-1	4	28	30	-2
4	39	38	0	8	20	21	-1	2	43	40	3	8+	3	3	4	1	32	34	-1	3	32	33	0	5	8	7	1
5	51	48	2	9	29	32	-3	3	60	61	0	9	12	13	-1	2	22	23	-1	4	11	10	0	6	23	24	-1
6	25	25	0	10	9	7	1	4	33	32	1	10	15	19	-3	3	16	15	0	5	11	11	0	7+	10	26	-16
7	24	28	-4	K=L=	8	4		5	64	62	2	K=L=	7	5		4	15	19	-3	6	13	10	3	K=L=	5	7	
8	45	45	0	0+	12	2	9	6	30	30	0	0+	9	4	5	5	12	11	1	7	20	23	-2	0	14	13	0
9	63	69	-5	1	15	18	-3	7	44	40	4	1	29	28	1	6	10	7	2	K=L=	8	6		1	15	13	1
10	52	57	-4	2	33	33	0	8*	0	9	-9	2	25	26	0	7	11	8	2	0	10	8	1	2	14	15	-1
11	26	32	-5	3	18	18	0	9	20	22	-2	3	14	12	2	8	3	2	0	1	15	15	0	3	23	24	-1
12*	0	8	-8	4	22	23	0	10	22	20	1	4	39	39	0	9*	0	3	-3	2	8	6	2	4*	0	3	-3
13+	26	34	-8	5	30	32	-1	11	9	10	-1	5	9	8	0	10*	0	5	-5	3	9	11	-1	5	9	9	0
K=L=	4	4		6	14	14	0	12	9	9	0	6	21	21	0	11	9	8	0	4	11	13	-2	6	15	16	0
0	132	124	8	7	22	26	-3	K=L=	3	5		7	10	10	0	K=L=	3	6		5*	0	9	-9	7	23	21	1
1	108	103	5	8	22	25	-2	0	34	27	6	8	6	5	1	0	27	25	2	K=L=	0	7		K=L=	6	7	
2	109	105	3	9	11	13	-1	1	34	33	0	9	8	9	0	1	17	14	2	1+	19	11	8	0*	0	1	-1
3	162	155	6	K=L=	9	4		2	33	35	-1	K=L=	8	5		2	13	14	-1	2*	0	2	-2	1	14	12	2
4	64	60	4	0+	13	18	-5	3	20	21	0	0	178	172	5	3	64	62	1	3+	12	7	4	2	10	10	0
5	48	51	-2	1	26	28	-1	4	70	69	1	1	60	66	-6	4	35	35	0	4	23	24	-1	3	9	9	0
6	66	71	-5	2	14	18	-3	5	12	13	-1	2	106	107	-1	5	13	11	1	5	12	13	-1	4*	0	2	-2
7	52	53	-1	3	12	11	0	6	16	15	0	3	10	12	-2	6	21	19	2	6	23	16	6	K=L=	7	7	
8	49	50	-1	4	29	32	-3	7	55	55	0	4	60	60	0	7	29	28	1	7+	6	1	4	0*	0	0	0
9	105	117	-12	5	35	39	-3	8	70	65	4	5	10	10	0	8	19	17	2	8+	12	8	3	1	8	10	-2
10	50	54	-4	6+	11	17	-6	9	50	48	2	6	44	50	-5	9	27	26	0	9	7	7	0	K=L=	0	8	
11	11	10	0	7+	12	15	-3	10	71	71	0	7	11	11	0	10	27	30	-3	K=L=	1	7		0	89	73	16
12*	0	8	-8	K=L=	10	4		11	19	23	-3	K=L=	9	5		K=L=	4	6		0	58	50	8	1	63	58	5
K=L=	5	4		0	6	6	0	12	22	26	-4	0	48	50	-1	0	29	25	4	1*	0	8	-8	2	17	18	0
0	13	14	0	1	11	12	-1	K=L=	4	5		1	24	26	-1	1	24	23	1	2	41	43	-1	3	35	37	-1
1	27	31	-4	2	9	8	0	0	15	13	2	2	15	16	0	2	60	60	0	3	19	19	0	4	10	9	1
2	16	14	1	3	12	16	-3	1	107	105	1	3+	8	11	-3	3	38	37	1	4*	0	9	-9	5	21	24	-2
3	46	48	-1	4+	20	27	-6	2	44	47	-3	4	18	21	-2	4	41	42	-1	5	9	8	1	6	13	15	-2
4	31	27	4	5	18	20	-2	3	70	68	1	5	11	12	0	5	35	39	-3	6	36	33	3	K=L=	1	8	
5	39	42	-2	K=L=	0	5		4*	0	7	-7	K=L=	10	5		6*	14	8	5	7+	23	13	9	0*	0	2	-2
6	74	75	-1	1	50	48	1	5	54	59	-5	0*	0	19	-19	7	39	37	1	8+	8	3	5	1	20	20	0
7	83	90	-6	2	35	28	6	6	32	31	1	K=L=	0	6		8	45	47	-2	9	11	9	2	2	14	15	0
8	51	52	-1	3*	0	4	-4	7	68	63	4	0	161	157	4	9	33	40	-6	K=L=	2	7		3*	0	2	-2
9	70	73	-2	4	34	34	0	8	52	54	-2	1	181	185	-4	10	25	30	-5	0	12	8	3	4*	0	3	-3
10	58	61	-3	5	68	68	0	9	88	87	0	2	96	100	-4	K=L=	5	6		1*	0	7	-7	5*	0	2	-2
11	24	29	-4	6	14	14	0	10	10	8	1	3	16	14	2	0	17	17	0	2	22	25	-3	6*	0	0	0
12	16	20	-3	7*	0	1	-1	11	15	18	-2	4	66	64	2	1	21	21	0	3*	0	0	0	K=L=	2	8	
K=L=	6	4		8	15	14	0	K=L=	5	5		5	48	49	0	2	25	27	-1	4*	0	4	-4	0*	0	7	-7
0	54	52	1	9	29	26	3	0	35	37	-2	6	36	35	1	3	14	15	-1	5+	9	5	4	1*	0	7	-7
1	51	53	-1	10	35	30	5	1	17	15	1	7	53	52	1	4	17	17	0	6	12	9	2	2	12	12	0
2	25	28	-2	11	17	21	-4	2	44	40	4	8	17	18	-1	5	9	8	1	7	14	14	0	3*	0	4	-4
3	27	28	-1	12	8	7	0	3	47	47	0	9	22	21	0	6	20	22	-2	8	10	8	2	4	10	8	1
4	51	56	-5	K=L=	1	5		4	26	24	2	10	21	19	2	7	35	35	0	9	13	14	-1	5*	0	1	-1
5	21	20	0	0	44	43	1	5	31	32	-1	11	18	18	0	8	44	51	-6	K=L=	3	7		K=L=	3	8	
6	78	74	3	1	109	103	5	6	19	14	5	K=L=	1	6		9	16	19	-3	0+	12	8	4	0*	0	1	-1
7	25	25	0	2	29	26	2	7	30	24	5	0	71	65	5	K=L=	6	6		1*	0	9	-9	1	11	10	0
8	23	24	-1	3+	18	12	5	8	54	59	-4	1	71	70	1	0	18	15	2	2*	0	8	-8	2	15	16	0
9	27	29	-1	4	36	27	8	9	55	57	-1	2	12	9	3	1	15	16	0	3	22	23	-1	3	10	12	-1
10	7	6	1	5	53	51	2	10	19	20	0	3	13	11	1	2	25	24	0	4	10	9	1	4	9	11	-2
11*	0	3	-3	6	59	60	-1	11	9	11	-2	4	12	10	1	3	20	19	1	5	13	15	-2	5*	0	11	-11
K=L=	7	4		7	32	29	3	K=L=	6	5		5*	0	4	-4	4	9	9	0	6	16	13	2	K=L=	4	8	
0	26	27	-1	8	24	29	-5	0	22	19	2	6	16	18	-2	5	17	14	2	7+	11	19	-8	0*	10	5	5
1	72	72	0	9	9	7	2	1	12	12	0	7*	0	3	-3	6	12	9	3	8	28	32	-3	1	15	14	0
2	75	77	-2	10	48	44	4	2	22	24	-1	8+	7	5	2	7+	9	4	4	K=L=	4	7		2	13	17	-3
3	22	25	-2	11	33	35	-1	3	46	47	0	9	23	21	2	8	7	6	0	0+	10	6	4	3+	15	20	-5
4*	0	5	-5	12	30	36	-5	4	15	16	0	10*	0	0	0	K=L=	7	6		1*	0	11	-11				

were estimated visually by comparison with an intensity standard. Of the 1071 possible reflections within the Cu$K\alpha$ sphere, 1026 independent reflections were measured; 62 were too weak to be observed. No absorption correction was applied. The appreciable thermal diffuse scattering along the a^* and c^* axes was observed on Weissenberg photographs.

Structure Determination and Refinement

At first, the crystal structure determination was attempted by the symbolic addition method. However, the statistical average for normalized structure factors showed an abnormal distribution as if this crystal had a centro-symmetric structure. Therefore, the phase refinement by the use of the tangent formula did not lead to the determination of the crystal structure. An effort was then made to solve the structure by the Patterson method. The sharpened Patterson map was resolved sufficiently to give the orientation and location of the molecule in the unit cell. The first postulated structure gave an R value of 52%, which decreased to 31% in three cycles of least-squares refinement with individual isotropic thermal factors. A difference Fourier map which was calculated by the use of these parameters clearly showed the position of the water oxygen atom. Since the 0 0 4 reflection seemed to have a strong extinction effect, this reflection was removed from the later refinements.

The coordinates and anisotropic thermal factors were refined in a block-diagonal least-squares procedure, minimizing the function $\sum w(F_o-F_c)^2$, where:

$$w = 0.5 \text{ for } |F_o| \leqq 0.5,$$
$$w = 1.0 \text{ for } 0.5 < |F_o| < 7.0 \text{ and}$$
$$w = 7.0/|F_o| \text{ for } 7.0 \leqq |F_o|.$$

The atomic scattering factors used were those listed in the International Table for X-ray Crystallography for C, N, and O atoms, and the spherical scattering factors proposed by Stewart, Davidson, and Simpson[9] for the H atom. At the stage of $R=7.9\%$, a difference Fourier map was computed, from which the positions of the seven hydrogen atoms were found (Fig. 1). With anisotropic thermal parameters for non-hydrogen atoms and isotropic thermal parameters for hydrogen atoms, the final R value was 5.67%, excluding unobserved reflections. The observed and calculated structure factors are listed in Table 2. The fractional coordinates and thermal parameters are listed in Table 3.

9) R. F. Stewart, E. R. Davidson, and W. T. Simpson, *J. Chem. Phys.*, **42**, 3175 (1965).

TABLE 3. THE FINAL PARAMETERS AND THEIR ESTIMATED STANDARD DEVIATIONS (IN PARENTHESES)

The coordinates of the non-hydrogen atoms have been multiplied by 10^4; those of the hydrogen atoms, by 10^3. The anisotropic thermal parameters of non-hydrogen atoms are of the form $\exp[-(B_{11}h^2+B_{22}k^2+B_{33}l^2+B_{12}hk+B_{13}hl+B_{23}kl)]$, and have been multiplied by 10^5. For the hydrogen atoms, the values listed are isotropic thermal parameters B(Å^2).

Atom	x	y	z	B(Å^2)	B_{11}	B_{22}	B_{33}	B_{12}	B_{13}	B_{23}
N	2166 (2)	2793 (3)	1491 (5)	—	523 (19)	569 (26)	2419 (76)	−64 (38)	256 (80)	−174 (98)
C (1)	2651 (3)	4067 (3)	1396 (7)	—	645 (25)	691 (33)	2188 (88)	−219 (51)	200 (98)	−76 (119)
C (2)	3783 (3)	4246 (4)	1256 (7)	—	662 (27)	811 (38)	2950 (111)	−414 (55)	86 (111)	52 (144)
C (3)	4440 (3)	3066 (4)	1234 (8)	—	485 (24)	1303 (53)	3645 (133)	−389 (59)	110 (117)	−33 (182)
C (4)	3950 (3)	1745 (4)	1312 (8)	—	594 (25)	847 (39)	3472 (124)	230 (55)	22 (118)	−29 (155)
C (5)	2820 (3)	1655 (3)	1443 (7)	—	575 (23)	689 (33)	2369 (91)	−47 (49)	130 (96)	58 (123)
C (6)	1940 (3)	5376 (3)	1388 (7)	—	723 (27)	671 (35)	2509 (96)	−146 (54)	214 (105)	−22 (127)
C (7)	2243 (3)	233 (3)	1496 (7)	—	622 (25)	605 (34)	2802 (104)	105 (49)	197 (105)	43 (129)
O (1)	2367 (2)	6544 (3)	1464 (7)	—	901 (24)	554 (25)	5309 (127)	−338 (44)	681 (116)	−203 (130)
O (2)	900 (2)	5163 (2)	1330 (6)	—	648 (18)	601 (24)	3800 (88)	94 (37)	303 (84)	−205 (103)
O (3)	1285 (2)	81 (3)	1484 (7)	—	602 (18)	605 (26)	5778 (127)	−180 (37)	518 (102)	177 (127)
O (4)	2953 (2)	−816 (3)	1538 (8)	—	695 (21)	530 (25)	6869 (156)	167 (39)	−105 (120)	15 (136)
O (5)	−102 (2)	7556 (3)	1321 (5)	—	569 (18)	729 (26)	3994 (90)	155 (38)	359 (87)	−150 (113)
H (1)	401 (3)	528 (5)	119 (7)	4.9 (0.9)						
H (2)	516 (3)	318 (5)	107 (7)	5.3 (1.0)						
H (3)	434 (3)	100 (4)	126 (7)	4.7 (0.9)						
H (4)	64 (3)	603 (4)	147 (7)	4.1 (0.8)						
H (5)	267 (3)	−153 (5)	151 (7)	6.2 (1.1)						
H (6)	13 (3)	822 (4)	144 (6)	4.6 (0.9)						
H (7)	−65 (5)	744 (7)	190 (9)	9.7 (1.6)						

TABLE 4. INTRAMOLECULAR BOND LENGTHS AND BOND ANGLES

Bond	Length(Å)	e.s.d.(Å)	Bond	Angle(°)	e.s.d.(°)
N −C (1)	1.338	0.005	C (1)−N −C (5)	116.8	0.4
C (1)−C (2)	1.399	0.006	N −C (1)−C (2)	123.4	0.4
C (2)−C (3)	1.372	0.007	N −C (1)−C (6)	118.4	0.4
C (3)−C (4)	1.378	0.007	C (2)−C (1)−C (6)	118.2	0.4
C (4)−C (5)	1.388	0.006	C (1)−C (2)−C (3)	118.9	0.5
C (5)−N	1.336	0.005	C (2)−C (3)−C (4)	118.2	0.5
C (1)−C (6)	1.507	0.006	C (3)−C (4)−C (5)	119.4	0.5
C (5)−C (7)	1.511	0.006	C (4)−C (5)−N	123.3	0.4
C (6)−O (1)	1.217	0.006	C (4)−C (5)−C (7)	121.4	0.4
C (6)−O (2)	1.280	0.005	N −C (5)−C (7)	115.3	0.4
C (7)−O (3)	1.181	0.006	C (1)−C (6)−O (1)	119.2	0.4
C (7)−O (4)	1.315	0.006	C (1)−C (6)−O (2)	116.3	0.4
C (2)−H (1)	1.02	0.05	O (1)−C (6)−O (2)	124.4	0.5
C (3)−H (2)	0.89	0.05	C (5)−C (7)−O (3)	124.8	0.5
C (4)−H (3)	0.85	0.05	C (5)−C (7)−O (4)	110.8	0.4
O (2)−H (4)	0.88	0.05	O (3)−C (7)−O (4)	124.4	0.5
O (4)−H (5)	0.76	0.05	C (1)−C (2)−H (1)	113	3
O (5)−H (6)	0.69	0.04	C (3)−C (2)−H (1)	128	3
O (5)−H (7)	0.79	0.06	C (2)−C (3)−H (2)	119	3
			C (4)−C (3)−H (2)	123	3
			C (3)−C (4)−H (3)	119	3
			C (5)−C (4)−H (3)	121	3
			C (6)−O (2)−H (4)	102	3
			C (7)−O (4)−H (5)	111	4
			H (6)−O (5 (−H (7)	115	5

Results and Discussion

Molecular Structure. The bond lengths and bond angles are listed, along their estimated standard deviations, in Table 4 and are shown in Fig. 2. Figure 1 shows a difference Fourier map along the c axis. There are three peaks around the water oxygen atom. Two of them correspond to the hydrogen atoms of the water molecule, while one may be a ghost peak or a peak due to disordered hydrogen atoms. There is no other

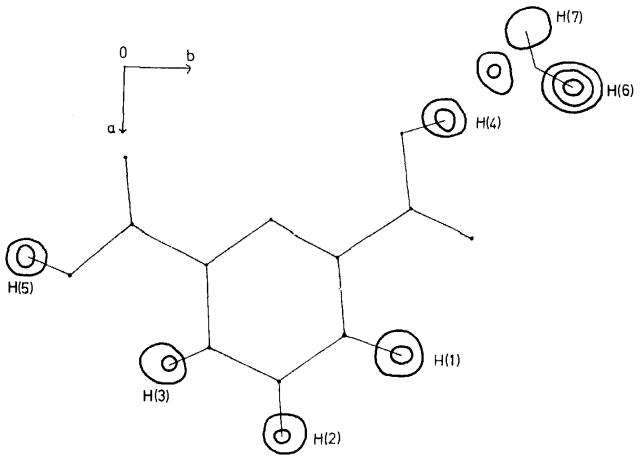

Fig. 1. A composite drawing of the electron density associated with the hydrogen atoms. The contours are at intervals of 0.1 e Å^{-3}, beginning with the 0.3 e Å^{-3} contour.

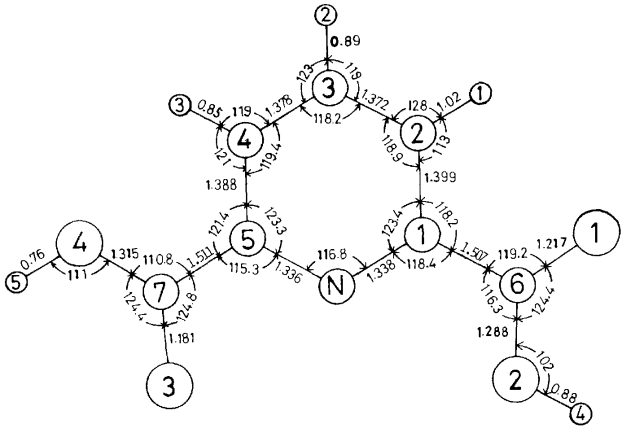

Fig. 2. Dimensions of the dipicolinic acid molecule.

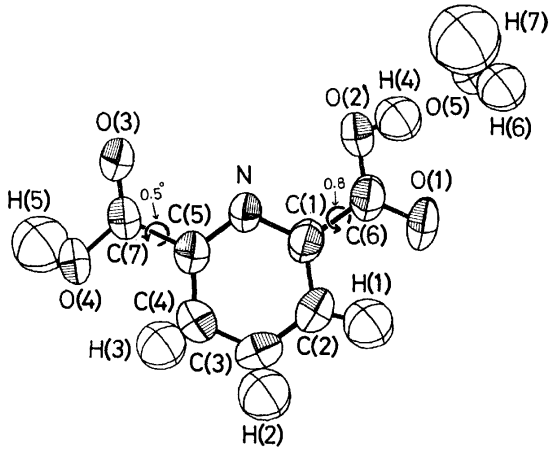

Fig. 3. The anisotropic thermal ellipsoids of non-hydrogen atoms and the isotropic thermal ellipsoids of hydrogen atoms. Ellipsoids are scaled to include 74% probability.

unexplainable peak in this difference Fourier map. Figure 3 shows the anisotropic thermal ellipsoids of non-hydrogen atoms and the isotropic thermal ellipsoids of hydrogen atoms. Ellipsoids are scaled to include 74% probability.

The pyridine ring is planar, and the maximum deviation of a ring atom from the least-squares plane is 0.007 Å. The equation of the least-squares plane through the six non-hydrogen atoms of the pyridine ring is;

$$0.0622X + 0.0208Y + 0.9979Z = 1.2303$$

where X, Y, and Z are coordinates in Å referred to an orthogonal set of axes and parallel to the a, b, and c axes. The displacements of all the atoms from the plane are listed in Table 5.

Table 5. The distances from the least-squares plane defined by the six non-hydrogen atoms of pyridine ring

Atom	Deviation (Å)	Atom	Deviation (Å)
N	−0.004	O (3)	0.121
C (1)	0.000	O (4)	0.025
C (2)	0.005	O (5)	0.192
C (3)	−0.007	H (1)	0.01
C (4)	0.003	H (2)	0.05
C (5)	0.002	H (3)	0.02
C (6)	0.034	H (4)	0.06
C (7)	0.038	H (5)	0.03
O (1)	−0.073	H (6)	0.08
O (2)	0.156	H (7)	−0.16

The comparisons between the corresponding bond lengths and bond angles of dipicolinic acid and calcium dipicolinate,[4] strontium dipicolinate[5] and pyridine[10] are given in Table 6. The pyridine ring has the C_{2v} symmetry within the limits of experimental error. The dimensions of the pyridine ring are in good agreement with those of pyridine itself, except for the C(2)–C(3) and C(3)–C(4) bond lengths. The net charges and π-bond orders calculated by the "complete neglect of the differential overlap (CNDO)" method[11] are shown in Fig. 4. The bond orders of the C(2)–C(3), C(3)–C(4), C(1)–C(2), and C(4)–C(5) bonds are 0.674, 0.659, 0.637, and 0.651 respectively. The first two bond orders are larger than the two others. These are in good correlation with the bond lengths obtained experimentally. The pyridine ring of dipicolinic acid

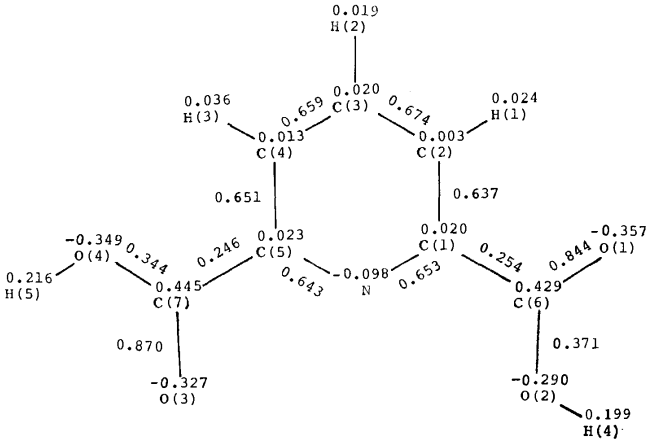

Fig. 4. The net charges and π-bond orders calculated by the CNDO method.

10) B. Bak, L. H. Nygaard, and J. R. Andersen, *J. Mol. Spectrosc.*, **2**, 361 (1958).

11) J. A. Pople and D. L. Beveridge, "Approximate Molecular Orbital Theory," McGraw-Hill Book Co., New York (1970).

Table 6. The comparisons between the corresponding bond lengths and angles of dipicolinic acid and calcium dipicolinate, strontium dipicolinate and pyridine

Bond length	(a)	(b)	(c)	(d)
N –C (1)	1.338 Å	1.339 Å	1.335 Å	1.340 Å
C (1)–C (2)	1.399	1.395	1.381	1.390
C (2)–C (3)	1.372	1.395	1.385	1.400
C (3)–C (4)	1.378	1.374	1.385	1.400
C (4)–C (5)	1.388	1.379	1.381	1.390
C (5)–N	1.336	1.326	1.335	1.340
C (1)–C (6)	1.507	1.500	1.525	
C (5)–C (7)	1.511	1.508	1.525	
C (6)–O (1)	1.217	1.240	1.245	
C (6)–O (2)	1.288	1.256	1.258	
C (7)–O (3)	1.181	1.245	1.258	
C (7)–O (4)	1.315	1.254	1.245	
Bond angle				
C (5)–N –C (1)	116.8°	119.6°	118.8°	116.7°
N –C (1)–C (2)	123.4	122.4	122.4	124.0
C (1)–C (2)–C (3)	118.9	116.9	118.7	118.6
C (2)–C (3)–C (4)	118.2	120.1	118.9	118.1
C (3)–C (4)–C (5)	119.4	119.0	118.7	118.6
C (4)–C (5)–N	123.3	121.6	122.4	124.0
N –C (1)–C (6)	118.2	114.9	115.4	
C (2)–C (1)–C (6)	118.4	122.7	112.4	
N –C (5)–C (7)	115.3	114.8	115.4	
C (4)–C (5)–C (7)	121.4	123.3	122.4	
O (1)–C (6)–C (1)	119.2	117.6	117.4	
O (2)–C (6)–C (1)	116.3	116.9	117.2	
O (1)–C (6)–O (2)	124.4	125.4	125.5	
O (3)–C (7)–C (5)	124.4	116.4	117.2	
O (4)–C (7)–C (5)	110.4	118.1	117.4	
O (3)–C (7)–O (4)	124.4	125.5	125.3	

(a) Dipicolinic acid (This study).
(b) Calcium dipicolinate (G. Strahs and R. E. Dickerson, *Acta. Crystallogr.*, **B24**, 571 (1968)).
(c) Strontium dipicolinate (K.J. Palmer, R.Y. Wong, and J. C. Lewis, *ibid.*, **B28**, 233 (1972)).
(d) Pyridine (B. Bak, L. H. Nygaard, and J. R. Andersen, *J. Mol. Spectrosc.*, **2**, 361 (1958)).

also agrees considerably well in dimensions with those of the salts of calcium and strontium.

The C(1)–N–C(5) bond angel is 116.8°; this means that the protonation did not occur on the nitrogen atom of the pyridine ring. The lengths of two C–C bonds joining the ring to the carboxyl groups are equal within the limits of experimental error; the average value is 1.509 Å, which is quite normal. The two C–O bond lengths in each carboxyl group are clearly different from each other. The bonds between the carbon and carbonyl oxygen atoms, C(6)–O(1) and C(7)–O(3), are shorter than those between the carbon and hydroxyl oxygen atoms, C(6)–O(2) and C(7)–O(4), by an average value of 0.108 Å. This finding also supports the fact that the hydrogen atoms of dipicolinic acid are definitely associated with the hydroxyl oxygen atoms. In both carboxyl groups, the C–C–O angles associated with the shorter C–O bonds are larger than those associated with longer C–O bonds, as is usually observed in carboxylic acids. There is a very simple relation between the C–O bond length and the C–C–O bond angle. This relation is $1/d=e\cdot\sin\theta+f$, where d is the C–O bond length, where θ is the C–C–O bond angle shown as follows;

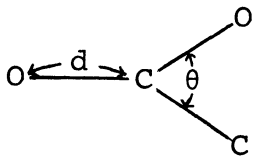

and where e and f are constants. This relation is shown in Fig. 5. In spite of the simplicity of this equation, there is a good correlation between the experimental values.

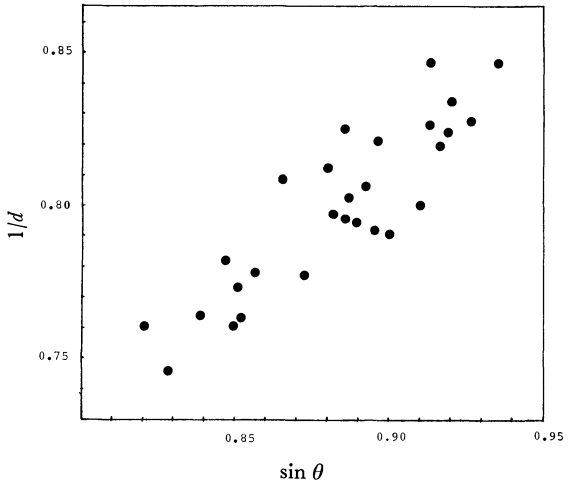

Fig. 5. The relation between the C–O bond lengths and C–C–O bond angles in carboxyl groups. The plotted compounds are dipicolinic acid, dinicotinic acid, quinolinic acid, cinchomeronic acid, calcium dipicolinate, strontium dipicolinate and oxalic acid.

The differences between the N–C(1)–C(6) and N–C(5)–C(7) bond angles, and between the C(2)–C(1)–C(6) and C(4)–C(5)–C(7) bond angles, are 3.1° and −3.2° respectively. These differences are significant, judging from their estimated standard deviations, and were not observed in calcium dipicolinate[4] and strontium dipicolinate.[5] This means that such differences depend on the orientation of the carboxyl groups and on the formation of hydrogen bonds. One carboxyl group (C(6)O(1)O(2)H(4)) is twisted by 0.8° out of the plane of the pyridine ring, while the other (C(7)O(3)O(4)H(5)) is twisted by 0.5° in the directions shown in Fig. 3.

Molecular Arrangement and Hydrogen-bond System. The crystal structure is shown in Figs. 6, 7, and 8. The distances and angles of hydrogen bonds are listed in Table 7. The dipicolinic acid and water molecules are arranged in layers closely parallel to the (0 0 1) plane, except the one hydrogen atom of the water molecule, and lie on the planes at $z=1/8$, 3/8, 5/8, and 7/8. These planes have a spacing of 1.704 Å. The best plane through the non-hydrogen atoms of a dipicolinic acid and a water molecule is calculated by the least-squares analysis to be:

$$0.0343X + 0.0171Y + 0.9993Z = 1.1129.$$

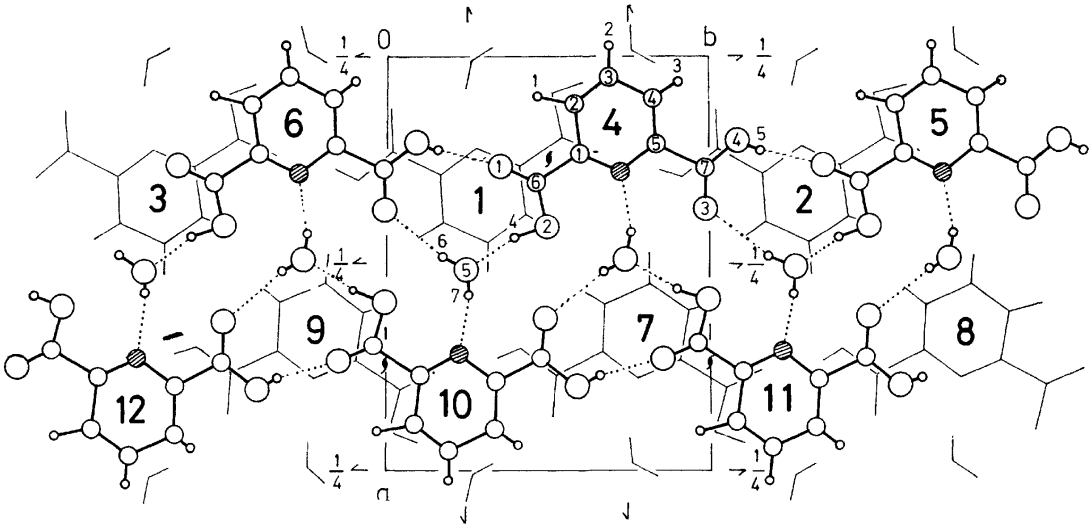

Fig. 6. A view of the crystal structure along the *c* axis, showing the relative orientation of the molecules in two adjacent layers parallel to the (0 0 1) plane. The hydrogen bonds are shown by broken lines.

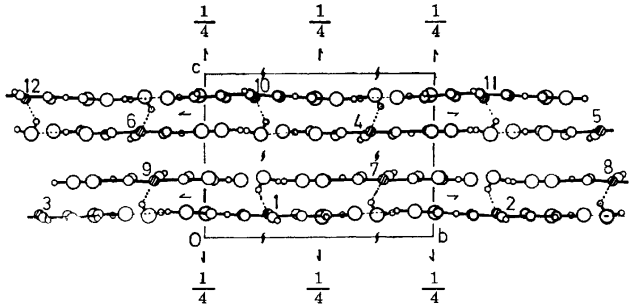

Fig. 7. A view of the crystal structure down the *a* axis. The hydrogen bonds are shown by broken lines.

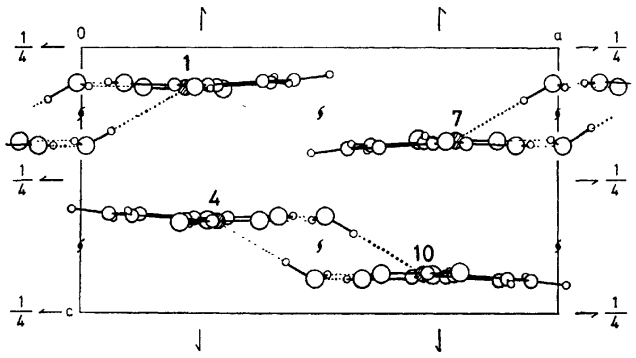

Fig. 8. A view of the crystal structure down the *b* axis. The hydrogen bonds are shown by broken lines.

The dihedral angle which it makes with the (0 0 1) plane is 2.1°. Figures 7 and 8 show the view parallel to the (0 0 1) plane, while Fig. 6 shows a view normal to the (0 0 1) plane, which illustrates the relative orientations of the molecules in two neighboring layers. The upper layer of the molecules drawn with heavy lines in this figure involves the molecules on the planes at $z=5/8$ and 7/8. In Figs. 6, 7, and 8, the same numerals designate the same molecules. The symmetry codes involving molecules which have these numbers are shown in Table 6.

Each molecule on the same plane is joined, through three hydrogen bonds, O(4)–H(5)···O(1), O(2)–H(4)···O(5), and O(5)–H(6)···O(3), with two neighboring molecules, and each forms an infinite chain along the *b* axis. In the O(4)–H(5)···O(1) hydrogen bond,

Table 7. Hydrogen bond distances (Å) and angles (degree)

O——H·····X	Symmetry	O···X	e.s.d.	O–H	e.s.d.	H···X	e.s.d.	Angle	e.s.d.
O (2)–H (4)···O (5)	(4, 4, 4)	2.561	0.005	0.88	0.05	1.70	0.05	165	5
O (4)–H (5)···O (1)	(4, 4, 5)	2.584	0.007	0.75	0.05	1.85	0.05	164	5
O (5)–H (6)···O (3)	(4, 4, 6)	2.920	0.006	0.69	0.04	2.25	0.04	164	5
O (5)–H (7)···N	(4, 4, 10)	2.941	0.005	0.79	0.06	2.17	0.06	163	6

X——O·····H	Symmetry	Angle	e.s.d.	X——Y·····O	Symmetry	Angle	e.s.d.
C (1)–N ···H (7)	(4, 4, 11)	123	2	C (1)–N ···O (5)	(4, 4, 11)	118.2	0.3
C (5)–N ···H (7)	(4, 4, 11)	114	2	C (5)–N ···O (5)	(4, 4, 11)	117.8	0.3
C (6)–O (1)···H (5)	(4, 4, 6)	166	2	C (6)–O (1)···O (4)	(4, 4, 6)	170.6	0.4
C (7)–O (3)···H (6)	(4, 4, 5)	136	1	C (7)–O (3)···O (5)	(4, 4, 5)	132.5	0.4
H (6)–O (5)···H (4)	(4, 4, 4)	122	4	N·····O (5)···O (2)	(10, 4, 4)	118.4	0.2
H (7)–O (5)···H (4)	(4, 4, 4)	108	4	O (3)···O (5)···O (2)	(6, 4, 4)	115.8	0.2

Symmetry
1=(*x*, *y*, *z*)
2=(*x*, 1+*y*, *z*)
3=(*x*, −1+*y*, *z*)
4=(1/2−*x*, 1−*y*, 1/2+*z*)
5=(1/2−*x*, 2−*y*, 1/2+*z*)
6=(1/2−*x*, −*y*, 1/2+*z*)
7=(1−*x*, 1/2+*y*, 1/2−*z*)
8=(1−*x*, 3/2+*y*, 1/2−*z*)
9=(1−*x*, −1/2+*y*, 1/2−*z*)
10=(1/2+*x*, 1/2−*y*, 1−*z*)
11=(1/2+*x*, 3/2−*y*, 1−*z*)
12=(1/2+*x*, −1/2−*y*, 1−*z*)

the C(6)–O(1)···H(5) and C(6)–O(1)···O(4) hydrogen bonding angles are 166° and 170.6° respectively. These values indicate that the bisector of the lone pairs in the carbonyl oxygen atom O(1) is directed toward a hydrogen-bond donor group. On the other hand, the C(7)–O(3)···H(6) and C(7)–O(3)···O(5) hydrogen bonding angles are 136° and 132.5° in the O(5)–H(6)···O(3) hydrogen bond. In this case, one of the lone pairs in the carbonyl oxygen atom O(3) is directed toward a hydrogen-bond donor group, as is usually observed in hydrogen bonds.

These two chains on the planes at $z=1/8$ and 3/8 are linked together by the O–H···N hydrogen bond between the water and the pyridine ring, and form a double chain along the b axis. The angle between the N···H(7) vector of the hydrogen bond and the plane of the pyridine ring is 28°, and the distances between N and H(7) and between N and O(5) are 2.07 and 2.941 Å respectively. Since the two carboxyl groups in α-positions prevent the formation of the O–H···N hydrogen bond which is parallel to the pyridine plane, the donor group of the hydrogen bond may deviate from the pyridine plane. In spite of such a steric hindrance and the presence of some other acceptors of the hydrogen bond, the O–H···N hydrogen bond is formed in this crystal. This suggests that the O–H···N hydrogen bond is more energetically favored than the O–H···O hydrogen bond in solids. The hydrogen-bonding system is also the same in the two chains on planes at $z=5/8$ and 7/8. These double chains are not joined by the hydrogen bond, but only by the van der Waals forces. Thus, the hydrogen-bond system in dipicolinic acid monohydrate plays an important role in connecting the molecules along the b axis.

The relation between the thermal diffuse scattering and the crystal structure can be explained on the basis of this hydrogen-bond system. There is an anisotropy of the bonding forces joining the molecules in the crystal. The molecules are linked by a strong hydrogen bond along the double chains (along the b axis in the crystal), but only the weak van der Waals forces act between chains (that is, perpendicular to the b axis). The nature of the bonding forces suggests that the vibrations are almost out-of-phase among different chains (almost an independent motion of one chain with respect to the others), but there should be a strong interaction in the motion of the molecules along the same chain. Therefore, the continuous thermal diffuse scattering appears along the directions of the a^* and c^* axes. Similar patterns were also observed in the crystals with molecules joined in the chain by hydrogen bonds.[12]

It will be of interest to compare the crystal structure of the present compound with that of isophthalic acid,[13] since they have similar frameworks and isoelectronic structures. The crystals of isophthalic acid which were recrystallized from the aqueous solution are not hydrates, and the molecules of isophthalic acid are linked together by hydrogen bonds between carboxyl groups. The reason for this difference between the crystal structures of these two compounds is the presence of a nitrogen atom in dipicolinic acid and the O–H···N hydrogen-bond formation with the aid of a water molecule.

Computer Programs. All the calculations were performed on a FACOM 270-30 computer at the Computer Center of Osaka City University using the following programs: RSLC-3 (cell constant),[14] RSSFR-3 (Fourier synthesis),[15] HBLS-IV (block-diagonal least-squares refinement),[16] DAPH (bond length, bond angle, and least-squares plane,[17] SCALE (film factor, Lp, and layer scaling),[18] TE-I (thermal ellipsoid),[19] PHASE-I, II, III (symbolic addition),[20] and CNINDO (CNDO and INDO calculations).[11]

The authors wish to express their thanks to Dr. K. Nishimoto of this faculty for his useful advice on the CNDO calculations.

12) J. L. Amóros and M. Amóros, "Molecular Structures," John Wiley and Sons., New York (1968), pp. 250—265.
13) R. Alcala and S. M. Carrera, *Acta Crystallogr.*, **B28**, 1671 (1972).
14) T. Sakurai, "The Universal Crystallographic Computing System (I)," ed. by T. Sakurai, Japanese Crystallographic Association (1967), p. 18.
15) T. Sakurai, *ibid.*, p. 45.
16) T. Ashida, *ibid.*, p. 65.
17) T. Ashida, *ibid.*, p. 76.
18) H. Yoshioka, K. Hirotsu, and F. Takusagawa, unpublished work.
19) F. Takusagawa, unpublished work.
20) K. Nakatsu and K. Hirotsu, unpublished work.

Deuteron and Niobium-93 Magnetic Resonance Studies of the Nb-D System. Comments on the Effects of Interstitial Impurities

Keikichi NAKAMURA

National Resarch Institute for Metals, 2-3-12, Nakameguro, Meguro-ku, Tokyo 153

(Received November 22, 1972)

The deuteron and niobium magnetic resonance in the Nb–D system have been measured over a wide range of deuterium concentrations. It has been found that the order-disorder ($\beta \rightarrow \alpha$) phase transition temperature depends on the small amount of interstitial impurities as well as on the concentration of the deuterium. From the concentration dependency of deuterium (Nb) in the α phase, one can determine the amount of deuterium (Nb) in the β phase coexisting with that in the α phase. On the basis of this finding, a tentative Nb–D phase diagram has been proposed. It has been confirmed that the interstitial impurities decrease the deuterium concentration of the β phase which is in equilibrium with the α phase. The niobium signal intensity has been found to be greatly reduced by the interstitial oxygen and other impurities, while the line width is not affected. For the interpretation of these findings, a simple model has been proposed in which only the interstitial atoms, which are present within the spherical sphere of a critical radius, r_c, from a niobium atom, eliminate the niobium resonance by means of the second-order quadrupole interaction.

Numerous studies have been made of the Va metal–Hydrogen system.[1] In these systems, the number of interstitial sites is greater than that of the interstitial hydrogen atoms, and a ninteresting phenomenon related to the order-disorder phase transition[2] has been reported. By the method of neutron diffraction, Somenkov *et al.*[3] have determined the atomic arrangement in niobium deuteride with a composition close to the equiatomic ratio (0.88~0.95 D/Nb) and have found that, at room temperature, the arrangement of deuterium atoms is ordered, filling four tetrahedral sites of the face-centered orthorhombic cell of niobium metal. As the temperature increases, the arrangement of deuteriums becomes disordered. They proposed two possible structures for the high-temperature form (α form). One of the structures, however, seems to be unlikely from the NMR point of view, as will be discussed below.

In the previous paper (hereafter denoted as I),[4] the present author has shown that the deuteron quadrupole splitting spectrum in the ordered β Ta_2D can be accounted for if deuteriums occupy tetrahedral sites with the largest principal component of the electric-field gradient (EFG) parallel to the c axis. In I, it has also been shown that the sharp single resonance line observed for the disordered α Ta is an indicative of the random distribution of deuterium in the tetrahedral interstices of the body-centered cubic metal.

The Nb–D system, like the Ta–D system, shows a spectrum of quadrupole splitting in its ordered state.[5,6] This is consistent with the existence of superlattice diffractions[3] in the same system. In spite of the resemblance of the Nb–D and Ta–D systems in their quadrupole splitting spectra and the superlattice diffraction patterns, there are considerable differences between the two systems. For instance, the deuteride phase (β phase) of the Ta–D system, which is in equilibrium with the metallic phase (α phase), has the composition of Ta_2D, while that for the Nb–D system has a composition close to Nb_4D_3.[7,8] The Ta–D phase diagram, as determined by X-ray measurement,[9] is consistent with the proton[10] and deuteron magnetic resonance[4] results. However, the Nb–H phase diagram, as determined by means of the proton and niobium magnetic resonance[11] is different from the phase diagram as determined by X-rays and by thermal analysis.[8] It is one of the purposes of this paper to reexamine the phase diagram of the Nb–D system.

Together with the tendency to deuteride formation, Va metals have a strong affinity to oxygen. Commercially-available niobium metal powder usually contains about 0.3~0.4 wt% oxygen. In this paper, we will show that discrepancies in the composition of the ordered phase, the phase-transition temperatures, and the solubility of hydrogen in the metallic phase are due to differences in the contents of oxygen and other interstitial impurities.

Experimental

Two types of niobium specimens with different oxygen contents were used for the preparation of deuterides. One specimen was a powdered niobium obtained from Herman Stark; it contained about 3900 ppm oxygen, 560 ppm nitrogen, and 200 ppm carbon (hereafter denoted as the S–II series). This powdered niobium metal was purified by using a electron-beam melting furnance. The purification was carried out

1) For reviews, see G. G. Libowitz, *J. Nucl. Mater.*, **2**, 1 (1960). H. Asano and M. Hirabayashi, *Buturi*, **26**, 273 (1971).

2) W. G. Saba, W. E. Wallace, H. Sandmo, and R. S. Craig, *J. Chem. Phys.*, **35**, 2148 (1961).

3) V. A. Somenkov, A. V. Gurskaya, M. G. Zemlyanov, M. E. Cost, N. A. Chernoplekov, and A. A. Chertkov, *Soviet Physics-Solid State*, **10**, 1076 (1968); **10**, 2123 (1969).

4) K. Nakamura, This Bulletin, **45**, 3356 (1972).

5) B. Pedersen and D. D. Slotfeld-Ellingsen, *J. Less-Common Metals*, **23**, 223 (1971).

6) H. Lütgemeir, H. G. Bohn, and R. R. Arons, *J. Magn. Resonance*, **8**, 80 (1972).

7) G. Brauer and R. Hermann, *Z. Anorg. Chem.*, **274**, 11 (1953).

8) R. J. Walter and W. T. Chandler, *Trans. AIME*, **223**, 762 (1965).

9) T. R. Wait, W. E. Wallace, and R. S. Draig, *J. Chem. Phys.*, **24**, 634 (1956).

10) B. Pedersen, T. Krogdahl, and O. Stokkeland, *ibid.*, **42**, 72 (1965).

11) D. Zamir and R. M. Cott, *Phys. Rev.*, **134**, A666 (1964).

four times. The purified ingot was rolled to make a foil 0.05 mm thick. The final oxygen content, as determined by the inert gas fusion method, was 12 ± 2 ppm. The other interstitial impurities were 30 ppm carbon and 17 ppm nitrogen. This foil was used to prepare deuterides of the S–I series. The deuteration was carried out as follows. The niobium specimen was placed in a quartz tube and subjected to thermal treatment in a vacuum of 1.2×10^{-5} mmHg at about 800 °C. Then, a known amount of deuterium gas as purified by means of Hydrogen Purifier[12] (Pd membrane method), was introduced, after which the sample was cooled to 150 °C and kept about two hours. The deuteride foil was then crushed to powder. In this deuteration process, the oxygen content increased from 12 ppm to 70~80 ppm for the S–I series, and from 3900 ppm to 4100~4500 ppm for the S–II series. The accuracy in the composition determination was within $\pm0.4\%$. The D/Nb atomic ratios of the deuterides examined were as follows:

S–I series: 0.236, 0.347, 0.480, 0.532, 0.587, 0.612, 0.699, 0.715, 0.738, 0.746, 0.796, 0.804, 0.822, 0.855, 0.899, 0.945.

S–II series: 0.232, 0.340, 0.426, 0.562, 0.646, 0.727, 0.807, 0.837, 0.874, 0.890.

The deuteron and niobium-93 resonance measurements were made by using a Varian VF-16 wide-line NMR spectrometer, operating mainly at 6.53 MHz for the deuteron and at 10.47 MHz for the niobium resonance. In some cases, other frequencies were employed to see the effect of the magnetic-field strength. The temperatures of the samples were controlled with a Varian variable-temperature accessory.

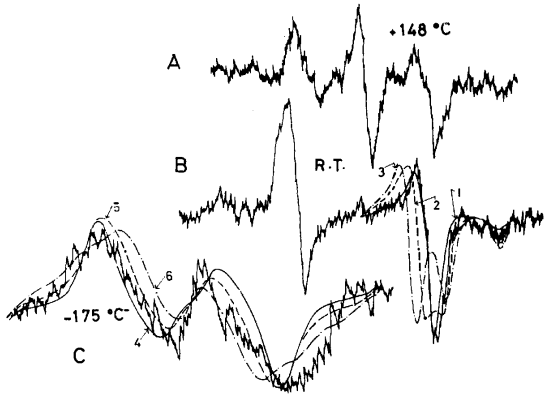

Fig. 1. Observed deuteron resonance spectra of $NbD_{0.855}$ (S-I series). Smoothed curves (1—6) are drawn with $e^2qQ/h=32.8$ KHz and with various values of asymmetry parameters, η, and individual line width, σ.

	$\sigma/(3e^2qQ/4h)$	α
1	0.05	0.03
2	0.05	0.15
3	0.05	0.25
4	0.15	0.13
5	0.15	0.23
6	0.15	0.40

Results

Deuteron Resonance at Room Temperature. The room-temperature deuteron resonance spectra of the Nb–D system resemble those of the Ta–D system.[4] In the case of a D/Nb atomic ratio of less than ≈0.65, the powder pattern consists of two parts; one is a sharp, single line located at the center of the spectrum, and the other is a pair of lines which are characteristic of a nuclei with $I=1$ in the presence of an approximately axially-symmetrical EFG. However, for the samples with D/Nb atomic ratios larger than ≈0.65, the central line becomes unobservable. According to the Nb–H phase diagram (Fig. 2), the central line can be attributed to the deuterium of the α phase and the satellites to the β-phase deuterium.

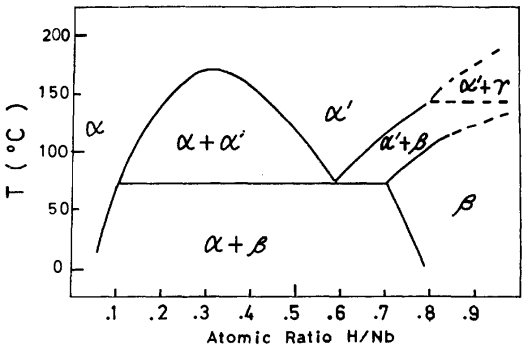

Fig. 2. The phase diagram of Nb–H system[8]

Table 1. Room temperature's deuteron quadrupole coupling constants, e^2qQ/h, and asymmetry parameters for the Nb–D system (S–I and S-II series)

	D/Nb	e^2qQ/h (KHz)[a]	η[b]
S-I	0.945	31.8	0.07
	0.822	32.8	0.04
	0.796	33.2	0.04
	0.738	33.4	0.03
	0.612	33.2	0.03
S-II	0.890	31.2	0.05
	0.874	31.6	0.04
	0.837	31.6	0.04
	0.727	32.2	0.03

a) The mean errors in the e^2qQ/h are less than 0.3 KHz
b) The mean errors in the η are less than 0.02.

A detailed analysis of the powder pattern for the nuclei with $I=1$ in the presence of an asymmetric-field gradient has been shown in the Appendix of I. The quadrupole coupling constants and the asymmetry parameters obtained by using the analytical method of I are shown in Table 1. The observed quadrupole coupling constants and the asymmetry parameters in the same series are almost concentration-independent up to ≈0.822 D/Nb (S-I). However, slight decreases in the quadrupole coupling constants are observed in the highest deuterium-concentration range for both series. The quadrupole coupling constants of the Nb–D system (S-II) containing oxygen are smaller by about 0.6~1.0 KHz than those of the oxygen-free Nb–D system (S-I).

Deuteron Resonance and Phase Transition above Room Temperature. As the temperature of the sample increased from room temperature, the apparent signal intensity of the central line began to increase and that of the satellite line began to decrease, indicating that the $\beta\rightarrow\alpha$ phase transition occurred. Since the line-

12) Japan Pure Hydrogen Co., Ltd.

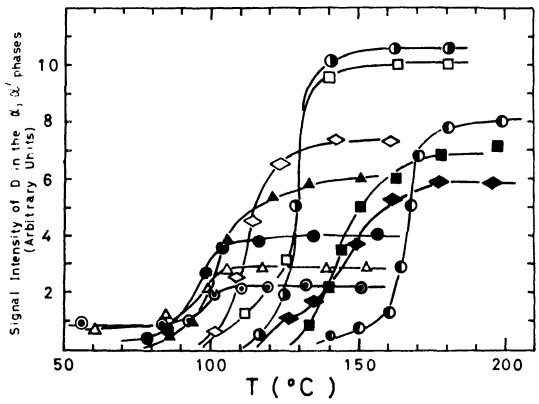

Fig. 3. Temperature dependence of the deuteron central line intensity of the S–I series.

D/Nb	D/Nb	D/Nb
◎ 0.236	▲ 0.587	◆ 0.855
△ 0.347	◇ 0.699	■ 0.899
● 0.480	□ 0.738	◐ 0.945
	◑ 0.804	

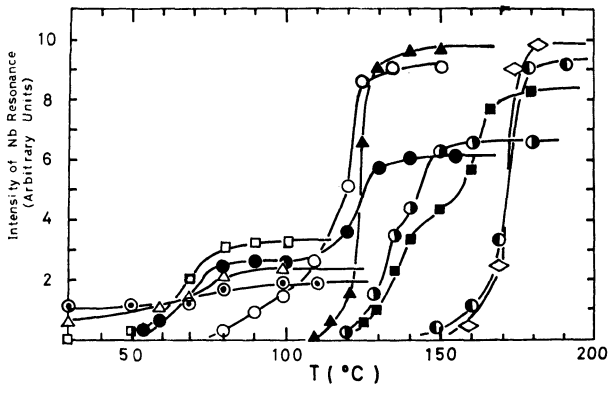

Fig. 4. Temperature dependence of the deuteron central line intensity of the S–II series.

D/Nb	D/Nb
⊙ 0.232	▲ 0.727
△ 0.340	◑ 0.807
□ 0.426	■ 0.837
● 0.562	◐ 0.874
○ 0.646	◇ 0.890

width of the central line above room temperature is mainly determined by the bulk magnetization of the deuterides,[11] and since the line-width is constant above room temperature ($\Delta H_{msl} \approx 0.5$ G at 10 KG.), the signal intensity (apparent peak to peak intensity $\times 1/T$) of the central line is taken as proportional to the concentration of the deuterium atoms in the α phase. In Figs. 3 and 4, the signal intensities of the central lines are shown as a function of the temperature. These figures suggest that the phase-transition temperatures of the S-I series are higher than those of the S-II series by about 25 to 10 °C. The following have been noted for the two series.

S-I series: As may be seen in Fig. 3, a sharp phase transition occurs at three different temperatures, about 95, 130, and 170 °C, although some gentle phase-transition curves can be seen at the intermediate temperatures for the samples with intermediate compositions, which will be discussed below. For $NbD_{0.587}$, which is in the $\beta+\alpha$ region at room temperature, the $\beta+\alpha \rightarrow \alpha$ phase transition is initiated at about 90 °C and is finished at a temperature close to the $\beta \rightarrow \alpha$ phase-transition temperature of $NbD_{0.738\sim0.804}$ ($\approx$130 °C). The existence of such a broad two-phase region may be related to the presence of two types of α forms, α and α'. The solubility of deuterium in the α' form is greater than that in the α form. The fact that two types of α forms exist is consistent with the findings in the Nb–H phase diagram.[8]

As has been mentioned above, gentle phase-transition curves are observed with the samples of $NbD_{0.855}$ and $NbD_{0.945}$ in the intermediate region between curves of $NbD_{0.855}$ and $NbD_{0.945}$. This indicates that there is a relatively broad $\beta+\alpha'$ region in the temperature range from 130 to 170 °C. Thus, it may be concluded that, in this two-phase region, the β phase, which is in equilibrium with the α' phase, must have a composition larger than 0.899 D/Nb. For $NbD_{0.899}$, the $\beta \rightarrow \beta+\alpha'$ phase-transition begins at a temperature close to the $\beta \rightarrow \alpha'$ phase-transition temperatures of $NbD_{0.738\sim0.804}$. The $\beta+\alpha' \rightarrow \alpha'$ phase transition for the same sample is finished at a temperature close to the $\beta \rightarrow \alpha'$ phase transition temperature of $NbD_{0.945}$. These facts may be well interpreted by assuming that the β phase consists of two types of β forms. This deuteron magnetic resonance behavior shows a good agreement with the niobium resonance, which will be discussed later.

S–II series: The phase-transition behavior of the S–II series is approximately analogous to that of the S–I series. However, the following points of disagreement are observed. a) The $\beta+\alpha \rightarrow \alpha+\alpha'$ phase-transition temperatures from $NbD_{0.232}$ to $NbD_{0.426}$ are lower by about 20 to 25 °C than those of the corresponding deuterides of the S–I series. The $\beta \rightarrow \alpha'$ phase-transition temperature of $NbD_{0.727}$ is lower by about 10 °C than that of the corresponding deuteride of the S–I series. b) The compositions where the sharp $\beta \rightarrow \alpha'$ ($\approx$130 and $\approx$170 °C) phase transitions occur are lower by about 0.06 D/Nb than those of the S-I series.

Deuteron Resonance below Room Temperature. As the temperature of the sample decreased, the signal intensity of the α form decreased, until finally it vanished in the temperature range from −10 to −70 °C. The quadrupole coupling constants and the asymmetry parameters measured at −50 °C show no significant change as compared with those at room temperature. As the temperature decreased from −70 °C, the satellite lines became broad; this broadening ended at about −120 °C. This is consistent with the temperature dependence of the proton line width in the Nb–H system.[13] In Fig. 1-(C), three calculated line shapes with different asymmetry parameters are shown. The value of the line-width, σ, is taken from the D–Nb dipole-dipole interaction.

Niobium Magnetic Resonance. At room temperature, the observed niobium magnetic resonance intensity is roughly proportional to the concentration of the cubic α phase, which coexists with the unobservable orthorhombic β phase. This is consistent with the findings

13) B. Stalinski and O. J. Zogal, *Bull. Acad. Poln. Sci. Ser. Chem.*, **13**, 397 (1965).

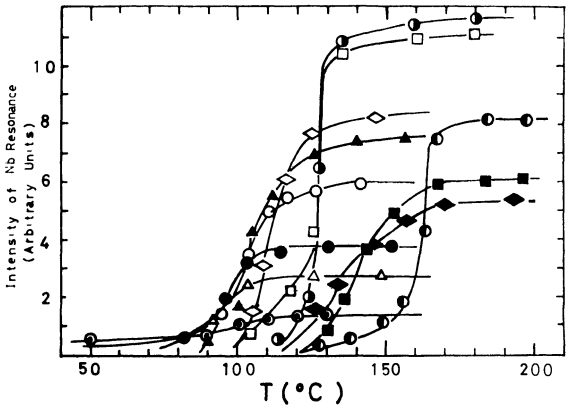

Fig. 5. Temperature dependence of the niobium-signal intensity of the S–I series. The assignments of the marks in the figure are the same as those of Fig. 3.

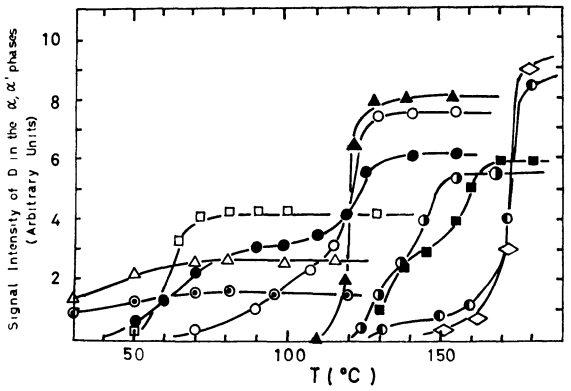

Fig. 6. Temperature dependence of the niobium-signal intensity for the S–II series. The assignments of the marks in the figure are the same as those of Fig. 4.

on the niobium magnetic resonance in the Nb–H system.[11] Since the variation in the line-width of the α Nb with the temperature is very small as compared with the variation in the apparent signal intensity, the signal intensity may be useful for the investigation of the phase-transition behavior of the Nb–D system. The temperature dependences of niobium-signal intensities shown in Figs. 5 and 6 agree well with the temperature dependence of the deuteron-signal intensities.

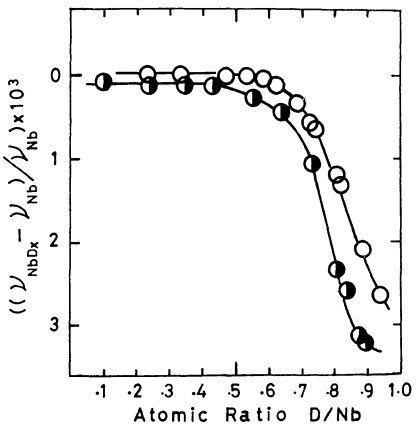

Fig. 7. Concentration dependence of the niobium resonance shift in the NbD_x relative to that in the pure Nb metal.
○: S–I series ◑: S–II series

The concentration dependence of the niobium Knight shift change measured at +180 °C is shown in Fig. 7. The variation in the niobium Knight shift up to 0.7 D/Nb agrees well with the previous results.[11] However, in this case, sharp decreases in the Knight shift are observed in the concentration range from 0.7 D/Nb to the highest concentration studied for both series.

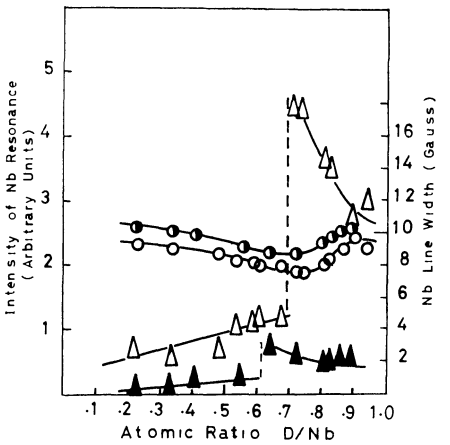

Fig. 8. Concentration dependence of niobium-signal intensity (△ S–I series, ▲ S–II series) and niobium line-width (○ S–I series, ◑S–II series).

The concentration dependence of the niobium-signal intensity shown in Fig. 8 is not so simple as has been indicated in one previous paper.[11] The niobium resonance intensity of Nb metal is affected strongly not only by its heat treatment, but also by the small amount of interstitial impurities. In the Nb–D system, the niobium resonance intensity decrease due to the interstitial impurities is observed for the S–II series, while the line-width increase is unexpectedly small.

A deuterium concentration dependence of the niobium-signal intensity is also observed in this study. A sharp, discontinuous increase in the niobium-signal intensity is observed at about 0.73 D/Nb for the S–I series. However, the line-width change at this concentration is small and gradual. At this temperature, niobium deuteride is in the cubic phase for all the deuterium concentrations. Thus, these sharp and discontinuous intensity changes can not be interpreted in terms of the present phase diagram.

Discussion

Probable Deuterium Arrangement in the β Form. As has previously been shown, the deuteron quadrupole splitting spectra at low temperatures, where the dipolar width of an individual line is assumed to be equal to the rigid lattice one, are essentially the same as that at room temperature. This fact shows that the deuteron quadrupole coupling constant is independent of the translational motion of deuteriums; that is, all the positions occupied by deuterium atoms must be equivalent. For the face-centered orthorhombic cell (a= 4.83, b=4.89, and c=3.44 Å),[7] of the β form, only the following 8 positions are equivalent: 1/4 1/4 1/4, 1/4 1/4 3/4, 1/4 3/4 1/4, 1/4 3/4 3/4, 3/4 1/4 1/4, 3/4

1/4 3/4, 3/4 3/4 1/4, and 3/4 3/4 3/4. This consideration confirms the finding of an recent neutron diffraction study[3] that the deuteriums are in the 2a (1/4 1/4 1/4, 3/4 3/4 3/4) and 2b (3/4 1/4 1/4, 1/4 3/4 3/4) positions of the face-centered orthorhombic cell (space group, Pnnn).

It is of particular interest to see the concentration dependency of the quadrupole coupling constant and the asymmetry parameter of the β form. An X-ray diffraction study[14] of the niobium hydride phase has shown that both the distortion from cubic symmetry and the increase in the lattice parameters occur as the concentration of hydrogen increases from $\approx$0.7 H/Nb. The former effect may increase the asymmetry of the EFG, while the latter decreases the principal component of the EFG. On the other hand, although the electrostatic potential from the positively-charged interstitial deuterium atoms is fairly screened,[16] the increase in the deuterium concentration may increase the quadrupole coupling constant. From a simple electrostatic calculation,[4] this effect can also be seen to increase the asymmetry of the EFG. The experimental results shown in Table 1 exhibit a significant increase in the asymmetry parameters of the S–I series. However, no significant change in the asymmetry parameters is observed for the S–II series. Thus, from the significant change in the quadrupole coupling constants, it may be concluded that the electrostatic potential from the interstitial deuteriums is almost screened and that the effect of lattice expansion is dominant in this case.

Deuteron Resonance Line Shape and Deuterium Arrangement in the Low-temperature Region. Somenkov *et al.*[15] have shown that the partially-ordered deuteride which was found in the solid solution of 3 atomic percent deuterium becomes ordered at -100 °C. The composition of the ordered phase was found to be Nb_4D_3. The crystal has a cell which is double in all directions with respect to the ordered $NbD_{1.0}$ cell. The structure is shown in Fig. 9. An examination of the figure will show that the unit cell consists of four $NbD_{1.0}$-type ordered cells and four Ta_2D-type ordered cells. Since the EFG at the deuterium atom in the Ta_2D-type ordered cell is characterized by a relatively large asymmetry parameter ($\simeq$0.24),[4] the EFG of the ordered Nb_4D_3 is considered to have an asymmetry parameter larger than that for the room-temperature form.

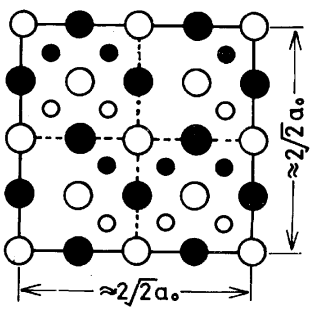

Fig. 9. Projection onto (001) plane of ordered Nb_4D_3 structure.[15] Nb's are at z=0, 1/2 (large open circles) and at z=1/4, 3/4 (large full circles). D's are at z=1/8, 5/8 (small open circles) and at z=3/8, 7/8 (small full circles).

In Fig. 1-(C), the calculated line shapes for three values of asymmetry parameters are shown. Because of the poor signal-to-noise ratio of the observed spectrum, it is difficult to decide which one of the calculated line shapes fits the observed one. Another difficulty in the decision may lie in the approximate-line-shape calculation, for we have disregarded the increase in the EFG due to lattice contraction and the angle dependency of the individual line-width.

Nb–D Phase Diagram as Determined by Deuteron and Niobium Magnetic Resonance. The Nb–H phase diagram proposed by Walter and Chandler[8] is shown in Fig. 2. Apart from the difference in the phase-transition temperature, the essential features of this phase diagram may be used in discussing the Nb–D system. The following features are in accord with our results:

1) At room temperature, the α phase is between 0 and $\simeq$0.1 H/Nb, while $\alpha+\beta$ is between $\simeq$0.1 and $\simeq$0.75 H/Nb.

2) In the concentration range of less than 0.5 H/Nb, the $\alpha+\beta\rightarrow\alpha+\alpha'$ phase transition occurs at about 60 °C, lower by about 20$\sim$30 °C than that for the Nb–D system.

3) In the concentration range between 0.75 and 0.85 H/Nb, the phase transition proceeds according to $\beta\rightarrow\beta+\alpha'\rightarrow\alpha'$.

However, the following aspects of the phase transition behavior can not be interpreted in terms of the Nb–H phase diagram:

4) $\alpha+\beta\rightarrow\alpha'+\beta\rightarrow\alpha'$ two-step phase transition for $NbD_{0.532\sim0.699}$.

5) $\beta\rightarrow\alpha'$ sharp phase transition for $NbD_{0.738\sim0.804}$.

6) $\beta\rightarrow\alpha'$ one-step phase transition for $NbD_{0.945}$.

7) Between 0.7 and 0.8 H/Nb, the Nb–H phase diagram shows that the phase transition proceeds according to $\beta+\alpha\rightarrow\beta\rightarrow\beta+\alpha'\rightarrow\alpha'$. However, if we take into consideration the neutron diffraction[3,15] and the heat capacity findings[9] that the β phase is in an ordered state and that the α phase is in a disordered state, the $\beta+\alpha\rightarrow\beta$ phase transition may be thought to be a disorder-order phase transition. Therefore, the $\alpha+\beta/\beta$ boundary line must be perpendicular to the X axis (composition axis) or, at least, must be a rising gradient.

As has been described previously, the existence of two sharp phase transitions, 5) and 6), can be accounted for if the β phase consists of two types of β forms with similar structures. However, this assumption contradicts the X-ray diffraction finding[14] that the change in the lattice parameters in the β-phase region (0.7 to 0.9 H/Nb) is continuous. A tentative Nb–D phase diagram which is consistent with both our NMR and the X-ray

14) C. Wainright, A. J. Cook, and B. E. Hopkins, *J. Less-Common Metals*, **6**, 362 (1964).

15) V. A. Somenkov, V. F. Petrunin, S. Sh. Shil'shtein, and A. A. Chertkov, *Soviet Physics-Crystallography*, **14**, 522 (1970).

16) N. F. Mott and G. H. Johnes "Theory of the Properties of the Metals and Alloys," Oxford Univ. Press, New York (1936), p. 86.

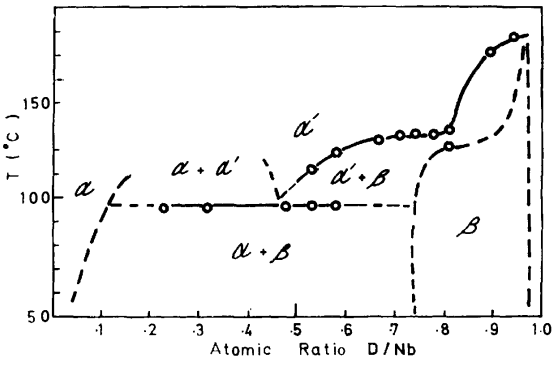

Fig. 10. Proposed phase diagram for Nb–D system.

diffraction results[14] is shown in Fig. 10. This diagram is quite different from any phase diagrams for a binary system ever published. In this phase diagram, the change in the $\alpha'+\beta/\beta$ boundary against the deuterium concentration occurs in one step, as if there are two types of β phases. However, this one-step change in the $\alpha'+\beta/\beta$ boundary may be explained by the schematic free energy-composition diagram shown in Fig. 11.

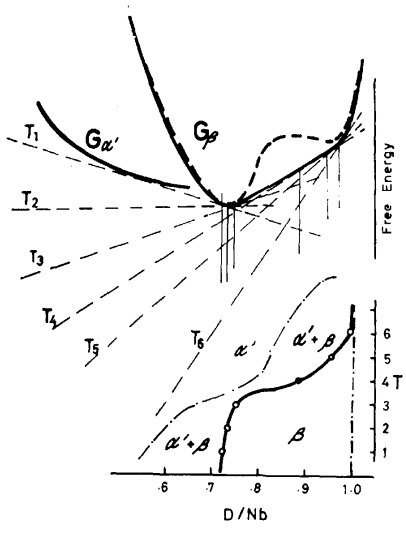

Fig. 11. Common tangents to the schematic free energy-composition curves for the β and α' phases at temperatures from T_1 to T_6 (upper). Only $G_{\alpha'}$ for T_1 is shown. Dotted line shows the free energy curve for the case where two β phase coexists. $\beta+\alpha'/\alpha'$ bundary derived from the upper diagram is shown below.

In Fig. 11, the $\alpha'+\beta/\beta$ boundary may be determined by a common tangent with the free energy-composition curves for the β and α' phases ($G_{\alpha'}$ and G_{β}). For the sake of simplicity, the shape for $G_{\beta'}$ is assumed to be temperature-independent. Since the β phase is an ordered one, while the α phase is a disordered one, the change in the gradient of the common tangent with the increase in the temperature from T_1 to T_6 must be positive. If the G_{β} curve is almost linear between $\simeq$0.7 to $\simeq$1.0 D/Nb, a sharp change in the $\alpha'+\beta/\beta$ boundary may be observed from T_3 to T_5. The resultant phase diagram closely resembles that in which two β phases of different compositions coexist.

Effect of Interstitial Impurities on Niobium Resonance Intensities.[17] In the course of this investigation, we have found large differences between the properties of niobium deuterides prepared from electron beam-melted niobium metal (S–I series) and those prepared from commercially-available powdered niobium metal (S–II series). The major interstitial impurity in the S–II series is oxygen. One of the most outstanding phenomena is the niobium signal intensity reduction in the S–II series. As is shown in Fig. 8, the addition of about 2.3 atomic percent (0.4 wt%) of oxygen reduces the intensity to about 10~40% of that of oxygen-free deuterides. If the dissolved oxygen is used to form a NbO-type oxide, the reduction of the intensity will be of an order of only a few percent. Since the observed reduction is far larger than 2.3%, then, most of the dissolved oxygen atoms must be randomly distributed over the interstices of the metal. This is possible in view of the relatively large solubility of oxygen in the metallic niobium.[18]

In Fig. 8, the maximum resonance intensity is observed for $NbD_{0.738}$ of the S–I series. The intensities of the $NbD_{0.236\sim0.587}$ of the same series are about 13~17% of its maximum intensity. If the satellite lines are eliminated by the first-order quadrupole interaction, and if the observed resonance is due to the $1/2\leftrightarrow-1/2$ transition only, the theoretical intensity should be 15.1% of its maximum intensity. Thus, the intensity loss of the S–I series seems to be due to the first-order quadrupole interaction.

The mechanism of the intensity loss due to the addition of interstitial impurities is somewhat different from that of the S–I series. For samples with D/Nb ratios lower than $\approx$0.5, where the observed resonance is due to the $1/2\leftrightarrow-1/2$ transition only, the reduction of intensity due to the addition of interstitial impurities must be caused by the second-order quadrupole interaction. A comparision of the resonance intensities of the S–I and S–II series shows that the intensity loss of the S–II series is about 87—83%. However, the line-width increase of the same series is less than 10% and the change in the line shape is small. This is contrary to what might be expected from a consideration of the second-order line broadening of the central line.[17]

To account for the above contradiction, we will present a simple model for the intensity loss due to the interstitial oxygen. This model is similar to that proposed by Bloembergen and Rowland[19] for the Cu–Zn substitutional alloy. Since the major impurity is oxygen, it is not unreasonable to confine the discussion to a case where interstitial oxygen is dominant. Consider that there are two niobium atoms and N interstitial sites accessible for oxygen in a unit cell. If the atomic concentration of oxygen is C, the probability

17) As for static quadrupole broadening in metals, refer to M. H. Cohen and F. Reif, "Solid State Physics Vol. 5", Academic Press, New York (1957), pp. 365—420.

18) A. Taylor and N. J. Doyle, *J. Less-Common Metals*, **13**, 313 (1967).

19) N. Bloembergen and J. J. Rowland, *Acta Met.*, **1**, 731 (1953).

that an interstitial site is occupied by an oxygen atom is $C/(N/2)$. We assume that oxygen atoms within a sphere of a critical radius, r_c, from a given niobium atom casuse a field gradient sufficiently large to make the niobium resonance unobservable. The number of interstitial sites, n_c, within a radius of r_c is $(4\pi/3)\cdot(r_c/a_o)^3\cdot N$. Therefore, $(1-C/(N/2))n_c$ is the fraction of niobium atoms whose resonance is observable.

To calculate n_c, we must take into consideration the intensity loss due to the small line broadening. The fraction of niobium resonance observable has been calculated to be about $0.21\sim0.28$. The number of interstitial sites in a unit cell is 12 for tetrahedral occupation and 6 for octahedral occupation. With an atomic fraction of oxygen of 0.024, and with a fraction of niobium observable of 0.24, n_c and r_c/a_o have been calculated; these values are listed in Table 2. It should be noted that there are small amounts of other interstitial and substitutional impurites, and that the calculated r_c values are the upper limits.

TABLE 2.

	N	n_C	r_C/a_O
Tetra	12	328	1.87
Oct	6	168	1.88

The author expresses his deep gratitude to Professor Shizuo Fujiwara, Drs. Ichiro Morimoto, Ryoji Watanabe and Yasuo Sasaki for their helpful advice and encouragement. Thanks are also given to Dr. Tokuzo Tsujimoto for his helpful advice on phase diagram and to Dr. Nobuhiko Iwao for his assistance in the sample preparation.

BULLETIN OF THE CHEMICAL SOCIETY OF JAPAN, VOL. 46, 2034—2039 (1973)

Geometrical Structures of Excited States of Conjugated Molecules. II. The Calculated Vibronic Intensity Distributions in the Absorption Spectra of Naphthalene

Yuichi FUJIMURA, Masamune ONDA, and Takeshi NAKAJIMA

Department of Chemistry, Tohoku University, Sendai 980

(Received November 27, 1972)

The normal coordinates and the vibrational frequencies in the first excited singlet ($^1B_{2u}$), the second excited singlet ($^1B_{1u}$), and the first excited triplet ($^3B_{1u}$) states of naphthalene, whose geometries were calculated by a semi-empirical method, are evaluated by assuming a simplified valence force field. The relation between the normal coordinates of two different electronic states is expressed on the basis of the Franck-Condon principle. The mixing among the excited-state normal coordinates, expressed in terms of the ground-state normal coordinates, is neglected in the present treatment. By using the simple relation between the normal coordinates of two different electronic states, the vibronic intensity distributions in the absorption spectra ($^1B_{2u}\leftarrow{}^1A_g$, ^1L_b, $^1B_{1u}\leftarrow{}^1A_g$, ^1L_a, and $^3B_{1u}\leftarrow{}^1A_g$, ^3L_a) have been calculated. The vibronic intensity distribution of the $^1B_{2u}\leftarrow{}^1A_g$ transition has been calculated, taking into consideration the intensity of the interpenetrating sets of the vibronic band groups on the basis of the Herzberg-Teller perturbation theory.

In the previous paper,[1] we proposed a computational method for determining the molecular symmetries and C–C bond distances in the electronically-excited states of conjugated molecules on the basis of the semiempirical SCF LCAO MO theory, and examined the geometrical structures of the lower excited states of benzene, naphthalene, azulene, and heptalene.

Many phenomena in the excited states of molecules, such as photochemical reactions or intramolecular nonradiative transitions, depend primarily on the geometrical structures of the excited states which are expressed by the multidimensional potential energy surfaces. For example, the large geometrical changes brought about by electronic excitation may lead to predissociation in small molecules,[2] or to photoisomerization[3–9] or to electrocyclic reactions,[10,11] in large

1) Y. Fujimura, H. Yamaguchi, and T. Nakajima, This Bulletin, **45**, 384 (1972).

2) G. Herzberg, "Molecular Spectra and Molecular Structure, Vol. III. Electronic Spectra and Electronic Structure of Polyatomic Molecules," D. Van Nostrand Company Inc., Princeton, New Jersey (1966), p. 429.

3) G. N. Lewis, T. T. Magel, and D. Lipkin, *J. Amer. Chem. Soc.*, **62**, 2973 (1940).

4) D. Schulte-Frohlinde, H. Blume, and H. Güsten, *J. Phys. Chem.*, **66**, 2486 (1962).

5) G. S. Hammond, J. Saltiel, A. A. Lamola, N. J. Turro, J. S. Bradshow, D. O. Cowan, R. C. Counsell, V. Vogt, and C. Dalton, *J. Amer. Chem. Soc.*, **86**, 3197 (1964).

6) W. M. Gelbart and S. A. Rice, *J. Chem. Phys.*, **50**, 4775 (1969).

7) E. E. van Tamlen and S. P. Pappas, *J. Amer. Chem. Soc.*, **85**, 3297 (1963).

8) A. W. Burgsthlen and P. L. Chien, *ibid.*, **86**, 2940 (1964).

9) D. Bryce-Smith and H. C. Longuet-Higgins, *Chem. Commun.*, **1966**, 593.

10) R. B. Woodword and R. Hoffmann, *J. Amer. Chem. Soc.*, **87**, 395 (1965).

11) R. Hoffmann and R. B. Woodword, *ibid.*, **87**, 2046, 4388 (1965).

aromatic molecules, all of which may be interpreted by the strong coupling scheme. On the other hand, small geometrical changes in large aromatic molecules lead to nonradiative transitions, such as internal conversions or intersystem crossings, which may be interpreted by the weak coupling scheme.[12-18]

Another interesting manifestation of the geometrical changes on excitation is the appearance of the vibronic intensity distribution in the electronic absorption and emission spectra. As is well known from the Franck-Condon principle, the vibronic intensity distribution depends on the relative displacements of the potential energy surfaces of the two electronic states in the equilibrium positions. The geometrical structures of the excited state of interest can be estimated from the vibronic intensity measurement, provided the ground-state geometrical structure has been established. By analyzing the vibronic intensity distribution in the 2600 Å transition of benzene, Craig[19] has suggested that all the C–C bonds in the $^1B_{2u}$ state are longer by 0.037 Å than those in the ground state. Coon *et al.*[20] have also determined the excited-state molecular geometries of SO_2 and ClO_2 by using the same procedure. Similarly, Anno and Sadô[21] have applied the Franck-Condon principle to the analysis of the 4500 Å absorption system of *p*-benzoquinone. Hunt *et al.*[22] have given a conventional method for calculating the vibronic intensity distribution in aromatic hydrocarbons. Their calculation is based on the assumption that only one vibrational mode or set of degenerate modes contributes to the vibrational progressions. Miller and Murrell[23] have calculated the vibronic intensity distribution in the L_a bands of polyacenes, and have attempted to explain why a vibrational progression of about 1400 cm^{-1} appears in these bands. They have performed the normal coordinate analysis on the assumption that all the rings of polyacenes are hexagonal in the ground state and that the frequencies and the normal modes in the ground and the excited states are identical. Diner and Malrieu[24] have tried to reproduce the vibrational structures in the first UV band of linear polyenes, using the method proposed by Hunt *et al.*[22]

It is our purpose in this paper to examine theoretically the vibronic intensity distribution in the absorption spectrum ($^1B_{2u}\leftarrow{}^1A_g$, ^1L_b) of naphthalene, which is complicated by the occurrence of false origins, and the vibronic intensity distributions in the absorption spectra of the next singlet transition ($^1B_{1u}\leftarrow{}^1A_g$, ^1L_a) and of the lowest triplet transition ($^3B_{1u}\leftarrow{}^1A_g$, ^3L_a).

The following section will describe the relation between the normal coordinates of two different electronic states. In Section 3, a conventional method for determining molecular force fields will be described by using a simplified valence-force-field. The Badger relation[25] is used to obtain the C–C stretching force constant from the corresponding bond distance. The results of the normal coordinate analysis of the ground and excited states are also given in this section. In Section 4, the vibronic intensity distributions in the various absorption spectra of naphthalene are evaluated.

The Relation between the Normal Coordinates of Two Different Electronic States

Let us describe a method for the transformation of the normal coordinates of an electronic state, subjected to interaction with an electromagnetic field, into those of the resultant electronic state. First, let us consider a system in the absorption process. The progression-forming modes of large aromatic molecules are generally totally symmetric in so far as vibronic couplings such as the Jahn-Teller coupling or the pseudo-Jahn-Teller coupling may be neglected. It is recognized that molecular geometries in the lower electronic states of naphthalene belong to the D_{2h} symmetry. In the present calculations, the totally symmetric modes will be restricted to the C–C skeletal stretching modes. These modes are thought to have the strongest effects on the vibronic intensity distribution. Naphthalene has four skeletal stretching normal modes belonging to the A_g irreducible representation of the D_{2h} point group.

The internal symmetry coordinates for the totally-symmetric skeletal stretching modes of naphthalene in the ground state may be specified as follows:

$$S_1 = \frac{1}{2}\sum_{j=1}^{4}\Delta r_j, \qquad S_2 = \frac{1}{2}\sum_{j=5}^{8}\Delta r_j,$$
$$S_3 = \frac{1}{\sqrt{2}}\sum_{j=9}^{10}\Delta r_j, \text{ and } S_4 = \Delta r_{11} \tag{1}$$

where $\Delta r_j = r_j - r_j^0$, and where r_j^0 and r_j are the C–C bond distance at the vibrational equilibrium point and the corresponding instantaneous bond distance respectively. For the excited states also, the same relationships as above hold. (For the r_j^0 values, see Table 1.) By equating the instantaneous bond distances of the ground and excited electronic states, we obtain:

$$S' = S + D, \tag{2}$$

where the primed quantity refers to the excited states. The i-th component of the column matrix, D, is expressed in the form of $a_i\sum_j(r_j^0 - r_j^{0\prime})$, where a_i is a normalization constant for the i-th internal symmetry coordinate. The internal symmetry coordinates are

12) R. Willams and G. J. Goldsmith, *J. Chem. Phys.*, **39**, 2008 (1963).
13) G. B. Kistiakowsky and C. S. Parmenter, *ibid.*, **42**, 2942 (1965).
14) R. J. Watts and S. J. Strickler, *ibid.*, **44**, 2423 (1966).
15) E. M. Anderson and G. B. Kistiakowsky, *ibid.*, **48**, 4787 (1968).
16) J. Jortner and R. S. Berry, *ibid.*, **48**, 2757 (1968).
17) M. Bixon and J. Jortner, *ibid.*, **50**, 3284 (1969).
18) R. Englman and J. Jortner, *Mol. Phys.*, **18**, 145 (1970).
19) D. P. Craig, *J. Chem. Soc.*, **1950**, 2146.
20) J. B. Coon, R. E. DeWames, and C. M. Loyd, *J. Mol. Spectry.*, **8**, 285 (1962).
21) T. Anno and A. Sadô, *J. Chem. Phys.*, **32**, 1611 (1960).
22) G. R. Hunt, E. F. McCoy, and I. G. Ross, *Australian J. Chem.*, **18**, 591 (1962).
23) K. Miller and J. N. Murrell, *Theoret. Chim. Acta* (Berl.), **3**, 231 (1965).
24) S. Diner and J. P. Malrieu, *ibid.*, **7**, 15 (1967).
25) R. M. Badger, *J. Chem. Phys.*, **2**, 128 (1934).

TABLE 1. C–C BOND DISTANCES (IN Å) IN NAPHTHALENE

Bonds	Electronic states			
	^1A_g [a]	$^1B_{2u}$ [b]	$^1B_{1u}$ [b]	$^3B_{1u}$ [c]
r_1^0	1.364	1.399	1.427	1.422
r_5^0	1.421	1.421	1.417	1.424
r_9^0	1.415	1.430	1.382	1.393
r_{11}^0	1.418	1.457	1.427	1.419

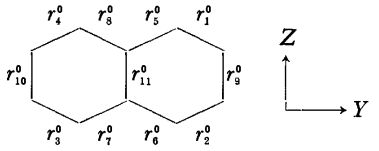

a) D. W. J. Cruickahank, and R. A. Sparks, *Proc. Roy. Soc., Ser. A*, **258**, 270 (1960).
b) Data taken from Ref. 1.
c) M. Onda, Thesis, Univ. of Tohoku, Sendai (1971).

connected with the normal coordinates, Q, by the transformation matrix, L_s:

$$S = L_s Q \tag{3}$$

and

$$S' = L_s' Q'. \tag{3'}$$

From Eqs. (2), (3), and (3'), the normal coordinates of the excited states are expressed in terms of those of the ground state in the form of:

$$Q' = C_a Q + \Delta Q, \tag{4}$$

$$C_a = (L_s')^{-1} L_s, \tag{5}$$

and

$$\Delta Q = (L_s')^{-1} D, \tag{6}$$

where the subscript, a, refers to the ground state. For the emission process, the following formula can be obtained:

$$Q = C_e Q' - \Delta Q', \tag{7}$$

with:

$$C_e = (L_s)^{-1} L_s', \tag{8}$$

and:

$$\Delta Q' = (L_s)^{-1} D, \tag{9}$$

where the subscript, e, refers to the emitting state.

We have thus obtained the formulas indicating the relation between the normal coordinates of two different electronic states. The off-diagonal matrix elements of the C_a and C_e matrices are related to the magnitudes of the mixing among the normal coordinates of the two relevant electronic states (the Duschinsky effect).[26] In the following section, we will show that the diagonal parts of the C_a matrix in Eq. (4) make the dominant contribution to the transformation of the normal coordinates of the electronic states, and that the Duschinsky effect can be neglected for the totally symmetric skeletal stretching modes in naphthalene. Consequently, Eq. (4) may be safely expressed as follows:

$$Q' = Q + \Delta Q. \tag{10}$$

Determination of the Molecular Force Fields

The molecular force field assumed is of a valence-force type consisting of the C–C stretching force constants, all the interaction constants being neglected. In order to obtain the C–C stretching force constants, k, the following relation is used:

$$k = A(r^0 - B)^{-3} \tag{11}$$

where k is given in millidynes per Å, A and B are the constants to be determined so as to reproduce the observed frequencies. The above relation between the equilibrium bond distances and the corresponding force constants has been proposed by Badger.[25] The relation is applicable not only for the force fields in the ground state, but also for those in excited states, with the proper choice of constants.

TABLE 2. CALCULATED FREQUENCIES AND THE TRANSFORMATION MATRIX IN THE GROUND STATE OF NAPHTHALENE

	Q_1	Q_2	Q_3	Q_4
Calcd (cm^{-1})	784	1032	1400	1545
Obsd[a]	762	1025	1380	1579
S_1	0.09333	0.16182	−0.21210	0.29459
S_2	0.18579	−0.08149	−0.19265	−0.29731
S_3	0.06778	0.25882	0.24496	−0.18730
S_4	0.14779	−0.13561	0.27487	0.22557

a) D. E. Freeman and I. G. Ross, *Spectrochim. Acta*, **16**, 1393 (1960).

The best values of A and B obtained by the variational procedure for the molecular force fields in the ground state of naphthalene are 2.4 millidyne Å^2 and 0.64 Å respectively. The results of the normal coordinate analysis for the ground-state naphthalene obtained by using Eq. (11) are given in Table 2. The fairly good agreement between the calculated and the observed frequencies supports the validity of the molecular force fields determined by the above procedure.

TABLE 3. CALCULATED FREQUENCIES AND THE TRANSFORMATION MATRIX IN THE $^1B_{2u}$ STATE OF NAPHTHALENE

	Q_1	Q_2	Q_3	Q_4
Calcd (cm^{-1})	757	993	1342	1495
Obsd[a]	702	987	1390	1435
S_1	0.09417	0.17379	−0.20016	0.29586
S_2	0.16647	−0.05821	−0.20789	−0.30389
S_3	0.06433	0.24507	0.25863	−0.18863
S_4	0.17148	−0.15571	0.26017	0.21290

a) Ref. 27.

TABLE 4. CALCULATED FREQUENCIES AND TRANSFORMATION MATRIX IN THE $^1B_{1u}$ STATE OF NAPHTHALENE

	Q_1	Q_2	Q_3	Q_4
Calcd (cm^{-1})	770	1024	1401	1513
Obsd[a]	710	995	1390	1520
S_1	0.11901	0.22766	−0.18282	0.25933
S_2	0.17044	−0.07946	−0.19191	−0.30737
S_3	0.05489	0.18317	0.29812	−0.20305
S_4	0.15177	−0.16472	0.23914	0.24354

a) Ref. 35.

26) F. Duschinsky, *Acta Physiochim. U. R. S. S.*, **7**, 551 (1937).

Table 5. Calculated frequencies and the matrix elements of the L_s matrix in the $^3B_{1u}$ state of naphthalene

	Q_1	Q_2	Q_3	Q_4
Calcd (cm^{-1})	766	1020	1394	1510
Obsd[a)]	712	1024	1343	1562
S_1	0.11267	0.21829	−0.21333	0.24661
S_2	0.17651	−0.08444	−0.16541	−0.31784
S_3	0.05628	0.19928	0.30275	−0.17924
S_4	0.14650	−0.15098	0.22883	0.26466

a) Ref. 38.

In order to obtain the molecular force fields in the excited states, Eq. (11) with the constants, A and B, determined for the ground-state molecular force fields will be used. The results of the normal coordinate analysis for the $^1B_{2u}$, $^1B_{1u}$, and $^3B_{1u}$ excited states are shown in Tables 3, 4, and 5 respectively.

The Vibronic Intensity Distributions in Electronic Spectra

According to the Franck-Condon principle, the vibronic intensity distribution accompanied by a pure electronic transition is obtained by evaluating the square of the overlap integral between the vibrational wave functions for the relevant electronic states. If the geometrical changes on excitation are relatively small, and if the magnitudes of the off-diagonal matrix elements in the C_a or C_e matrix may be neglected, the vibrational wave function for each electronic state can be expressed in terms of the product of the harmonic-oscillator wave functions. The vibronic intensity distribution of the r-th mode relative to the 0—0 intensity in the electronic spectra is given as follows:

$$I_{I-J}(Q_r) = \frac{S^2_{I-J}(Q_r)}{S^2_{0-0}(Q_r)} \tag{12}$$

where $S_{I-J}(Q_r)$ is the overlap integral between the I and J quantum harmonic oscillators belonging to the normal coordinate, Q_r. The total vibronic intensity distribution relative to the 0—0 intensity is given by the product of the relative vibronic intensity distributions over the possible normal modes.

Because of the small energy separation between the lowest ($^1B_{2u}$) and the second ($^1B_{1u}$) singly-excited states of naphthalene, these two electronic states are strongly subjected to vibronic perturbation from each other, and the shifts of the point of origin, which correspond to the frequencies of b_{3g} vibrations (438 and 911 cm^{-1}), are observed in the absorption spectrum ($^1B_{2u}\leftarrow{}^1A_g$).[27] (see Fig. 1) The vibronic intensity in the absorption spectrum, where the vibronic bands are subjected to vibronic perturbation by a nontotally symmetric mode, Q_p, can be expressed by using the Herzberg-Teller perturbation theory.[28] The perturbed vibronic intensity distribution of the totally symmetric mode, Q_r, relative to the 0—0 vibronic transition of the pure electronic transition is approximately given as follows:

$$I_{I-J}(Q_r) = C(Q_p)\frac{S^2_{I-J}(Q_r)}{S^2_{0-0}(Q_r)} \tag{13}$$

where $C(Q_p)$ is the square of the ratio of the transition moment induced by a unit displacement along the p-th nontotally symmetric normal coordinate to the zeroth-order transition moment. Equation (13) has been derived on the assumption that the two excited states are subjected to vibronic perturbation by the inducing mode, Q_p, the frequency of which is the same in both ground and excited states, and on the assumption that the electronic wavefunction corresponding to the lowest excited state is expanded about the nuclear configuration in the ground state at the vibrational equilibrium to the first order of Q_p in the perturbation theory. $C(Q_p)$ will be evaluated empirically in the present calculation. The analysis of the vibronic intensity distribution in the spectra ($^1B_{2u}\leftarrow{}^1A_g$) of naphthalene vapor shows that the vibronic-band intensity of the false origin at 0+438 cm^{-1} (vs)[29] is five or ten times stronger than that of the 0—0 group (m),[29] and that the intensity of the false origin at 0+911 cm^{-1} (ms)[29] is somewhat stronger than that of the 0—0 group.[28] From the above experimental facts, for the 438 and 911 cm^{-1} inducing modes of b_{3g} the values of $C(Q_p)$ were taken to be 6.0 and 2.0 respectively.

The overlap integrals, $S_{I-J}(Q_r)$, were evaluated by using the formula derived in the previous paper.[30]

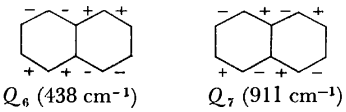

Fig. 1. b_{3g} modes inducing the vibronic perturbation between the $^1B_{2u}$ and $^1B_{1u}$ states. Quantities in parentheses indicate frequencies in the $^1B_{2u}$ state.

Discussion

The mixing among the excited-state normal coordinates expressed in terms of the ground-state ones was neglected in the calculation. This is sufficiently supported by the small off-diagonal matrix elements in the transformation matrixes C_a, *e.g.* for $^1B_{2u}\leftarrow{}^1A_g$ (see Table 6). Consequently, the Duschinsky effect can not be expected for the a_g skeletal stretching modes of naphthalene. On the other hand, for the nontotally

Table 6. The C_a matrix elements for the absorption spectrum ($^1B_{2u}\rightarrow{}^1A_g$) of naphthalene

	Q_1	Q_2	Q_3	Q_4
Q'_1	0.99684	−0.01834	0.03975	0.04397
Q'_2	0.02392	0.99659	−0.07259	−0.01761
Q'_3	−0.03969	0.07338	0.99700	0.01009
Q'_4	−0.04273	0.01701	−0.01240	0.99890

27) D. P. Craig, J. M. Hollas, M. F. Redies, and S. C. Wait, Jr., *Phil. Trans. Roy. Soc.*, **A253**, 543 (1961).

28) G. Herzberg and E. Teller, *Z. Physik. Chem.* (Leipzig), **B21**, 410 (1933).

29) The symbols in parentheses denote the qualitative measure of the band intensity in the absorption spectra observed by Craig *et al.*[27] The measures are as follows: vs–very strong, ms–medium strong, and m–medium.

30) N. Shimakura, Y. Fujimura, and T. Nakajima, This Bulletin, **45**, 695 (1972).

symmetric modes, which induce the vibronic coupling between the first and the second singlet electronic states, the Duschinsky effect must be operative.[31] The neglect of the mixing among the excited-state normal coordinates will be valid in the calculation of the vibronic intensity distribution of the large aromatic molecules, such as polyacenes, with small relative displacements in the points of origin of the normal coordinates. However, in calculating the vibronic intensity distribution of azulene, which retains the C_{2v} molecular symmetry in the first singlet excited state,[1,32] we cannot neglect the mixing among the normal coordinates in the a_g vibrational modes, because there are substantial geometrical changes, especially a shortening of the central bond in the first singlet excited state compared with that in the ground state. In fact, from the analysis of the 7000 Å absorption spectra of azulene vapor, Hunt and Ross[32] concluded that the upper-state vibrational frequencies are difficult to correlate with those of the ground state. The Duschinsky effect for the totally symmetric modes will also have to be explicitly taken into account in calculating the vibronic intensity in the absorption spectra ($S_1 \leftarrow S_0$) of heptalene, which is observed to suffer drastic changes in molecular symmetry on excitation; heptalene has C_{2h} and D_{2h} symmetries in the ground and the first excited states respectively.[1,33,34] The effect of the mixing among normal coordinates will be reflected in the appearance of the combination bands in the vibronic spectra.

The calculated vibronic intensity distributions in the absorption spectra will now be compared with the observed ones.

The analysis of the absorption spectrum ($^1B_{2u} \leftarrow {}^1A_g$)

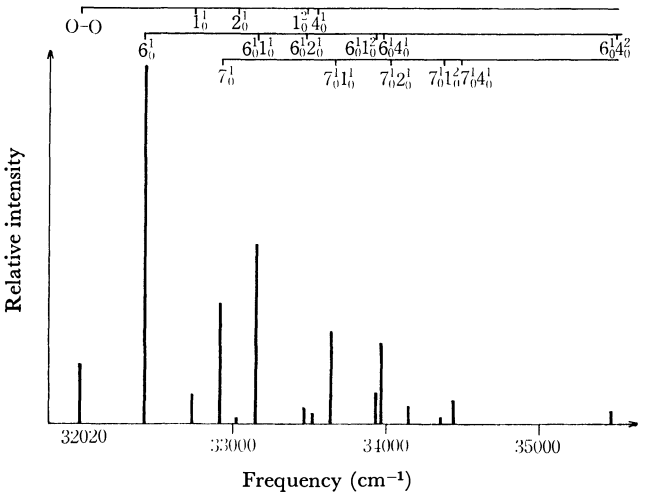

Fig. 2. Calculated vibronic intensity distribution in the absorption spectrum ($^1B_{2u} \leftarrow {}^1A_g$) of naphthalene. The numbers give the normal modes which are involved in the transition. Superscripts and subscripts give the number of vibrational quanta excited in the upper and lower states, respectively.

of naphthalene vapor indicates that the vibrational structures consist of three main interpenetrating sets of band groups which originate at the pure electronic origin and at false origins, 0+438 cm^{-1} and 0+911 cm^{-1}; it indicates further that the progression-forming modes are those with frequencies of 702, 987, and 1435 cm^{-1} with two quantum intervals, while for the 987 and 1435 cm^{-1} modes the one-quantum addition gives a band weaker than the fundamental.[27] On the other hand, for the 702 cm^{-1} mode, the one-quantum addition gives a band much weaker than the fundamental. The vibronic intensity distribution calculated for the absorption spectrum, $^1B_{2u} \leftarrow {}^1A_g$ is shown in Fig. 2. The progression-forming modes calculated are mainly those with frequencies of 757, 993, and 1495 cm^{-1}. For these modes, progressions with two-quantum intervals, in addition to the fundamentals, are thought to appear with significant intensities. It can be recognized that the vibronic intensity distribution calculated is in fairly good agreement with the observed one. However, a slight discrepancy remains between them: for the mode belonging to the lowest vibrational frequency in the calculation, the over-tone band intensity is somewhat stronger than the observed one. This indicates that the relative displacement along its mode on excitation has been slightly overestimated in calculating the geometrical structures in the $^1B_{2u}$ state.

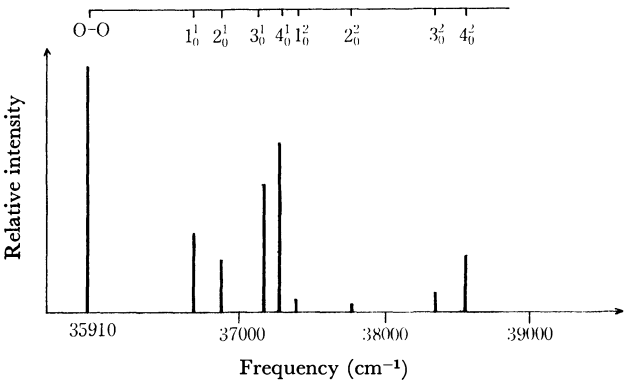

Fig. 3. Calculated vibronic intensity distribution in the absorption spectrum ($^1B_{1u} \leftarrow {}^1A_g$) of naphthalene.

The calculated vibronic intensity distribution in the absorption spectrum of the second singlet transition ($^1B_{1u} \leftarrow {}^1A_g$, ^1L_a) is shown in Fig. 3. The vibronic bands originating from the Herzberg-Teller vibronic coupling are neglected. The vapor absorption spectrum of naphthalene at 2900~2500 Å indicates that the 0—0 band is located at 35910 cm^{-1} and that the strong bands can be explained as resulting from two vibrations, with the 1390 and 485 cm^{-1} bands assigned to the totally symmetric skeletal stretching and bending vibrations respectively.[35] Miller and Murrell[23] have calculated the normal coordinate displacements between the second singlet, $^1B_{1u}$, and the ground states of naphthalene. There is a considerable difference in the vibronic intensity distribution of the absorption spectrum ($^1B_{1u} \leftarrow {}^1A_g$) between their results and ours. Their results indicate that the displacements with higher

31) G. J. Small, *J. Chem. Phys.*, **54**, 3300 (1971).
32) G. R. Hunt and I. G. Ross, *J. Mol. Spectry.*, **9**, 50 (1962).
33) H. J. Dauben, Jr. and D. J. Bertelli, *J. Amer. Chem. Soc.*, **83**, 4659 (1961).
34) T. Nakajima and A. Toyota, *Chem. Phys. Lett.*, **3**, 272 (1969).
35) H. Sponer and C. D. Cooper, *J. Chem. Phys.*, **23**, 646 (1955).

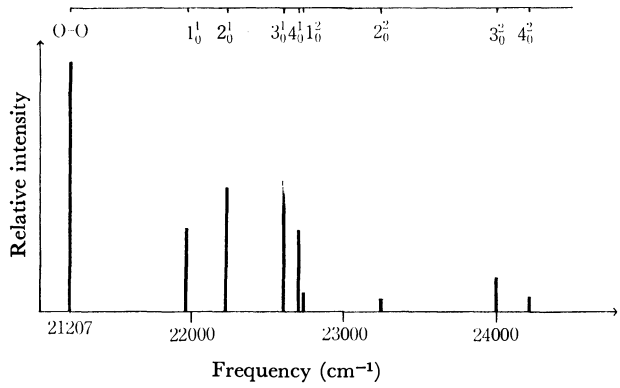

Fig. 4. Calculated vibronic intensity distribution in the absorption spectrum ($^3B_{1u}\leftarrow{}^1A_g$) of naphthalene.

frequencies are larger, and that the main intense bands of the spectrum correspond to the frequencies around 1500 and 1400 cm^{-1}. In our treatment, the changes of the C–C skelton on excitation are nearly equally distributed into the totally symmetric normal coordinates considered. These differences can be in part ascribed to the choice of the geometrical structures of the ground state of naphthalene.

Experimental studies of the $^3B_{1u}\leftarrow{}^1A_g$ absorption spectrum on naphthalene have been reported by many authors.[36–38] Castro and Robinson[38] have obtained the high-resolution $^3B_{1u}\leftarrow{}^1A_g$ absorption spectrum of crystalline naphthalene at 4.2 K. The absorption spectrum reported by them consists of the strong a_g modes (498 and 1343 cm^{-1}) primarily polarized normal to the molecular plane and, further, weak antisymmetric fundamentals that behave as false origins for the strong progression-forming modes. The most intense of the antisymmetric modes exhibits an intensity 15 times weaker than the 0—0 band. On the basis of the above experimental evidence, the vibronic spectrum of the lowest triplet transition is calculated, neglecting the bands originating from the false origins (Fig. 4). The calculated largest displacement of the C–C stretching normal coordinates between the lowest triplet and the ground states is that with the frequency of 1393 cm^{-1}. The band of the 1393 cm^{-1} mode with three-quantum intervals appears with a significant intensity. This is in agreement with the observed result. On the other hand, the other normal coordinate diplacements calculated indicate a more uniform distribution in the a_g normal coordinates of the C–C stretching modes than in the observed ones.

The lack of agreement between the calculated and observed $^3B_{1u}\leftarrow{}^1A_g$ spectra mainly originates from the neglect of the contribution of the in-plane C–C–C deformation on excitation.

One of the present authors (Y. F.) wishes especially to thank Professor A. Sadô for his useful discussions of normal coordinate analysis. This research was supported in part by a grant from the Takeda Science Foundation.

36) G. Porter and F. J. Write, *Trans. Faraday Soc.*, **51**, 1025 (1955).
37) A. P. Marchetti and D. R. Kearns, *J. Amer. Chem. Soc.*, **89**, 768 (1967).
38) G. Castro and G. W. Robinson, *J. Chem. Phys.*, **50**, 1159 (1969).

BULLETIN OF THE CHEMICAL SOCIETY OF JAPAN, VOL. 46, 2039—2044 (1973)

The X-Ray Emission Spectra of the Compounds of Third-period Elements. VI.* The Relationship between the $K\alpha$ and $K\beta$ Spectra

Yoshihito TAKAHASHI

Government Industrial Development Laboratory, Hokkaido, 41-2 Higashi-Tsukisamu, Toyohira, Sapporo 061-01

(Received December 4, 1972)

Data on the $K\beta$ spectra for several compounds of silicon, aluminum, and sulfur are shown. The intensity of the $K\beta'$ line is affected not by the kinds of thrid-period atoms, but by their charges and by the kinds of ligand atoms. The degree of the contribution of each bonding group to the relative intensity of the $K\beta'$ line and to the chemical shift of the $K\alpha_{1,2}$ lines are shown; they have additivity in the molecule. Therefore, the chemical shift of the $K\alpha_{1,2}$ lines can be estimated from the molecular structural formula; the charge of the atom can also be estimated.

Concerning some compounds of sulfur,[3] chlorine,[4] and phosphorus,[5] the fine structures of the $K\beta$ spectra have been investigated with relation to the chemical bonds. On these oxygen-included compounds, a satellite line, $K\beta'$ line, is observed in the spectrum; the relative intensity of the satellite line is related to the energy shift of the $K\alpha_{1,2}$ lines. In addition, it has been

* Our papers first named "An X-Ray Emission Spectroscopic Investigation of the Chemical Bond of Sulfur I~III"[1-3] have been renamed Parts III~V of this series.

1) T. Sato, Y. Takahashi, and K. Yabe, This Bulletin, **40**, 298 (1967).

2) Y. Takahashi, K. Yabe, and T. Sato, *ibid.*, **42**, 2707 (1969).

3) Y. Takahashi and K. Yabe, *ibid.*, **42**, 3064 (1969).

4) Y. Takahashi, *ibid.*, **44**, 587 (1971).

5) Y. Takahashi, *ibid.*, **45**, 4 (1972).

reported that the $K\beta'$ line is also observed in the spectra of compounds of third-period elements in which electronegative elements other than oxygen, such as fluorine, chlorine, and nitrogen, are included as ligands.[6-8] In order to check the character of the $K\beta'$ line and other satellite lines in detail, in this paper the characteristics of the K spectra of several compounds of silicon and aluminum, and also these of a few fluoro-compounds of sulfur and phosphorus, will be discussed.

Many reports have been published on the spectra of the compounds of silicon and aluminum;[6,7,9-11] these reliable reports shall be referred to in this paper as much as necessary. However, in order to compare the band-width and the chemical shift of the line, some easily measurable data were measured anew, consistently with some of the new data, such as those on tetraethylorthosilicate, silicon tetrachloride, aluminium propoxide, sulfur tetrafluoride, by means of our own apparatus.

Experimental

The details of the measurement apparatus and the conditions were presented in previous papers.[1,3] Analyzing crystals were used: EDDT (020) for the measurements of the Si and Al K spectra, germanium (111) for the P K spectra, and sodium chloride (200) for the S K spectra. In the measurements of gaseous samples, the samples were made to flow through a cell at a steady pressure. The gas-sample cell is a stainless-steel vessel with Mylar film window 25 mm × 30 mm, and 25 mm in depth.

The separation of the $K\beta$ spectrum into component peaks was done in a manner similar to that described in previous paper,[3-5] adopting the P $K\beta_1$ line of anhydrous sodium phosphate[5] as the standard shape of the component peak. Previously, we adopted the S $K\beta_1$ line of anhydrous sodium sulfide as the standard shape in peak separation for the S $K\beta$ spectra.[3] However, concerning the peak separation for two sulfur fluoro-compounds, we could find little difference between the results of the two methods.

Results and Discussion

Silicon Compounds. The Si $K\beta$ spectra of the compounds which were measured are shown in Fig. 1. The characteristic values on the $K\alpha_{1,2}$ and the $K\beta$ lines for each compound are listed in Table 1. The chemical shifts of the $K\alpha_{1,2}$ lines were determined with silicon metal as the standard material.

The energy differences between the $K\beta_1$ line (C peak) and the $K\beta'$ line (A peak) are about 14 eV for oxy-compounds, 19 eV for sodium hexafluorosilicate, and 8.6 eV for silicon tetrachloride.

The Si $K\beta$ spectrum of silicon dioxide consists of two main peaks; the $K\beta_1$ (C) and the $K\beta'$ (A). The

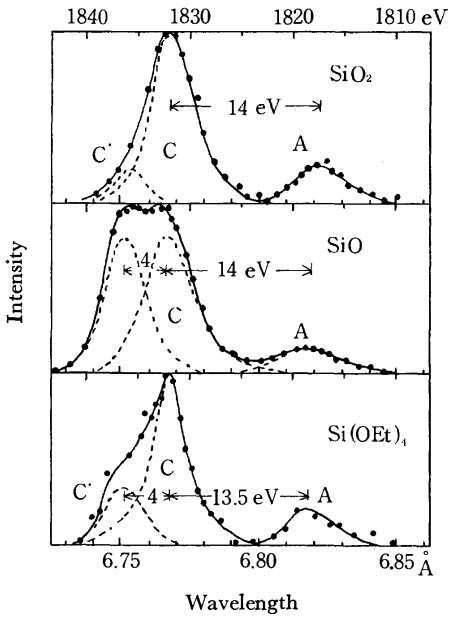

Fig. 1a. Silicon $K\beta$ spectra of some silicon compounds
A: $K\beta'$ line, C: $K\beta_1$ line.

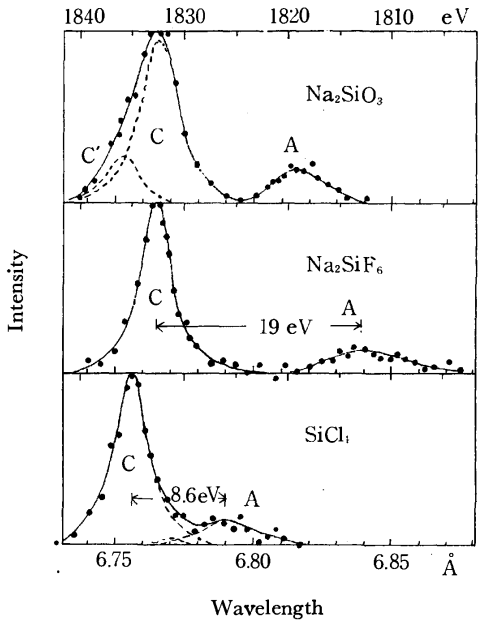

Fig. 1b. Silicon $K\beta$ spectra of some silicon compounds
A: $K\beta'$ line, C: $K\beta_1$ line.

$K\beta_1$ line is about 1.4 times wider than those of the spectra of sodium hexafluorosilicate and silicon tetrachloride. It seems that the spectrum contains a satellite line which is like the C' peak in the P $K\beta$ spectra of molecular phosphorus compounds.[5]

The C peak in the spectrum of silicon monoxide[13] seems to consist of two component peaks. White said that the component peak on the short-wavelength side was the $K\beta_1$ line, which was attributable to the zero valent silicon atom, and that the other was the $K\beta_1$ line of the plus-4 valent silicon atom.[14]

6) K. Ohno, *Bunseki Kagaku*, **20**, 308 (1971).
7) D. F. Lawrence and D. S. Urch, *Specrtochim. Acta*, **25B**, 305 (1970).
8) W. L. Baun and D. W. Fischer, *ibid.*, **21**, 1471 (1965).
9) C. G. Dodd and G. L. Glen, *J. Appl. Phys.*, **39**, 5377 (1968).
10) E. W. White and G. V. Gibbs, *Amer. Mineralogist*, **52**, 985 (1967).
11) S. Maruno and S. Fujii, *Jap. J. Appl. Phys.*, **9**, 1428 (1970).
12) Landolt-Börnstein, "Zahlenwerte und Funktionen," 6 Aufl. I/4 (1952), S. 859.

Table 1. Chemical shift of the $K\alpha_{1,2}$ lines and characteristic values of the $K\beta$ spectrum of silicon compounds

Compound	$K\alpha_{1,2}$ Chemical shift (eV)	$K\beta$ Peak position (eV)			$K\beta$ Relative intensity	
		A	C	C′	A	C′
SiO_2	0.72	1818.4	1832.4	1835.6	0.18	0.11
SiO	0.40	18.1	31.8	36.2	0.12	0.40
$Si(OEt)_4$	0.68	17.9	31.8	35.6	0.16	0.19
Na_2SiO_3	0.66	18.4	32.6	35.6	0.16	0.16
$Al_2(SiO_3)_3$	0.75	18.4	23.1	35.4	0.18	0.17
Na_2SiF_6	1.05	13.6	32.6		0.19	
$SiCl_4$	0.66	26.8	35.4		0.18	
σ	0.06	0.3	0.3		0.02	0.03
SiC	0.22[a]				0.19[b]	

a) Ref. 12.
b) The value was estimated from the spectrum of Ref. 15.

Tetraethylorthosilicate ($Si(OEt)_4$) and sodium metasilicate (Na_2SiO_3) are molecules which have tetrahedral structures,[15] and their silicon atoms do not have any lone pairs. Consequently, it is inferred that, in these spectra, the satellite peak which is so-called D peak does not appear.[17] In their spectra, the energy difference between the shorter-wavelength peak and the $K\beta_1$ line (C) is about 4 eV. This value is close to the energy difference between the $K\beta_1$ line (C) and the C′ peak in the P $K\beta$ spectrum of phosphorus pentoxide, 5 eV. On the other hand, the difference between the $K\beta_1$ line and the D peak is about 7 eV in the spectra of sulfite, chlorite, and sulfur tetrafluoride. Hence, the shortest-wavelength peak may be the C′ peak.

Table 2. Chemical shift of the $K\alpha_{1,2}$ lines and cha racteristic values of the $K\beta$ spectrum of aluminum compounds

Compound	$K\alpha_{1,2}$ Chemical shift (eV)	$K\beta$ Peak position (eV)		$K\beta$ Relative intensity
		A	C	A
Al_2O_3	0.41	1536	1553	0.11
$Al(OPr)_3$	0.37	1537	1553	0.14
AlF_3	0.64	1530	1550	0.12
AlF_3 (dry)	0.57	1532	1551	0.11
σ	0.07	0.5	0.5	0.03
Na_3AlF_6	0.52[a]	1531[b]	1552[b]	0.12[c]
AlN	0.29[a]			0.09[d]
Al_4C_3	0.13[a]			0.16[d]

a) Ref. 12.
b) Ref. 7.
c) The value was estimated from the spectrum of Ref. 7.
d) The value was estimated from the spectrum of Ref. 6.

13) 99.9%; it was produced by Nakarai Chemicals, Ltd.
14) E. W. White, *Solid State Commun.*, **2**, 151 (1964).
15) The structure of $Si(OEt)_4$ was determined by analogy with that of $Si(OMe)_4$.[16]
16) R. Kiriyama and H. Kiriyama, "Kozo-Mukikagaku, II," (1966), p. 213.
17) The D peak appears in the $K\beta$ spectrum of a compound in which the central atom has a lone pair, such as sulfite, sulfur tetrafluoride, and phosphorus trichloride.[5]

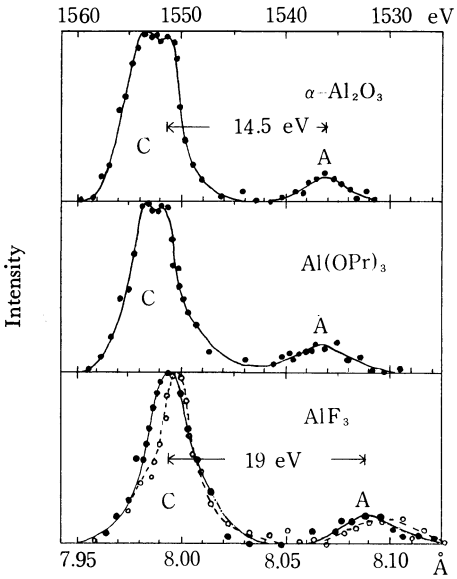

Fig. 2. Aluminum $K\beta$ spectra of some aluminum compounds
A: $K\beta'$ line, C: $K\beta_1$ line.

Aluminum Compounds. The measured Al $K\beta$ spectra are shown in Fig. 2. The data on the $K\alpha_{1,2}$ lines and the $K\beta$ lines of each compound are listed in Table 2. The standard material for the $K\alpha_{1,2}$-line shifts is aluminium metal.

In the spectra of aluminum oxide and aluminum propoxide, the top of the $K\beta_1$ line splits into two peaks, so one may guess that the C′ peak exists in the spectrum. Concerning the spectrum of aluminum oxide, a theory has been advanced attributing the shorter-wavelength peak to the transition of the π-electron, and the longer one, to the σ-electron.[9] The differences between these peaks and the $K\beta'$ line (A) are 16 and 14.5 eV respectively.

The Al $K\beta$ spectrum of aluminum fluoride, the specimen of which was not dried enough (however, it was confirmed to be anhydride by X-ray diffraction), is different from that of the dried specimen and from that which was measured in the vacuum. In the former spectrum, a puff which seems to be the C′ peak is observed, but it is absent in the latter.

Sulfur and Phosphorus Compounds. The measured S $K\beta$ spectra of sulfur hexafluoride, sulfur tetrafluoride, and sulfur dioxide in a gaseous state are shown in Fig. 3. The energy differences between the $K\beta_1$ (C) and the $K\beta'$ (A) lines are 18.5, 17.8, and 15.5 eV for SF_6, SF_4, and SO_2 respectively. The D peak is observed in the spectra of SF_4 and SO_2. The characteristic values of the $K\alpha_{1,2}$ and the $K\beta$ lines for these sulfur compounds and potassium hexafluorophosphate (KPF_6), are listed in Table 3. As the standard materials for the line shift, rhombic sulfur and red phosphorus were chosen.

The $K\beta'$ Line in All the Measured Spectra. The values of the energy difference between the $K\beta_1$ and the $K\beta'$ lines in the oxy-compound are spread from

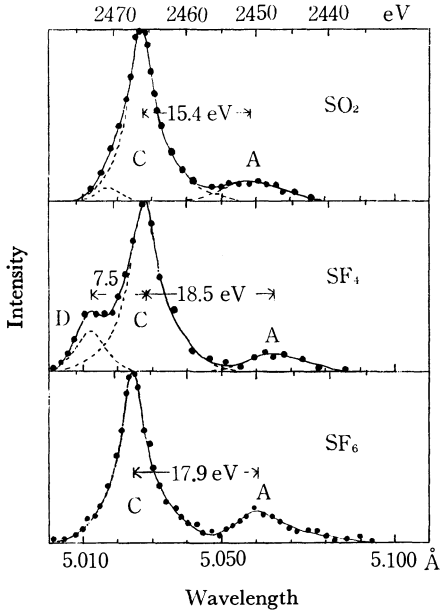

Fig. 3. Sulfur $K\beta$ spectra of some sulfur compounds
A: $K\beta'$ line, C: $K\beta_1$ line.

TABLE 3. CHEMICAL SHIFT OF THE $K\alpha_{1,2}$ LINES AND CHARACTERISTIC VALUES OF THE $K\beta$ SPECTRUM OF SOME SULFUR AND PHOSPHORUS COMPOUNDS

Compound	$K\alpha_{1,2}$ Chemical shift (eV)	$K\beta$ Peak position (eV) A	C	D	$K\beta$ Relative intensity A	C	D
SF_6	1.59	2449.2	2467.1		0.25	0.75	
SF_4	0.94	2447.3	2465.8	2473.6	0.15	0.72	0.13
SO_2	0.65	2451.1	2466.5	2470.7	0.16	0.79	0.05
KPF_6	0.87	2120[a]	2138[a]		0.2_0[b]	0.8_0[b]	
σ	0.04	0.5	0.4	1.0	0.02	0.02	0.03

a) Ref. 7.
b) The value was estimated from the spectrum of Ref. 7.

13.6 to 15.6 eV. Particularly, those of oxy-anions, such as ClO_4^-, ClO_3^-, SO_4^{2-}, and PO_4^{3-}, are less than 14 eV, while in many cases of molecular compounds, such as sulfone, sulfoxide, and SO_2, they are more than 14 eV.[3-5] On the other hand, in the cases of fluoro-compounds and chlorine-compounds (which have chlorine atoms as ligands), the values are 17.9~21 eV[7] and about 8.5 eV[5] respectively. According to Ohno's report,[6] in which several Al $K\beta$ spectra are given, the values are estimated to be about 12 eV for nitride and 8 eV for carbite. In the Si $K\beta$ spectrum, the value of carbite is 9 eV[18] (Table 4). Consequently, the energy difference between the $K\beta_1$ and the $K\beta'$ lines actually differs according to the kind of ligand atom.

The relationship between the relative intensity of the $K\beta'$ line (the ratio of the integral intensity of the A peak to that of the total of the $K\beta$ lines) and the chemical shift of the $K\alpha_{1,2}$ lines for each compound is shown in Fig. 4. In this figure, our results and those of some other researchers are collected. Two points are clear; the measured points make a linear relation for each ligand element, and these linear relations are almost independent of the kind of central atom in the molecule. It has become clearer, therefore, than in the results presented in a previous paper[4] that the intensity of the $K\beta'$ line is affected not by the kinds of central atoms, but by their charges, and by the kinds of ligand atoms. This deduction as to the effects of ligand elements is consistent with Nefedow's theory,[19] in which

18) G. Wiech, "Soft X-Ray Band Spectra," ed. by D. J. Fabian, Academic Press, London and New York (1968), p. 59.

TABLE 4. ENERGY DIFFERENCE BETWEEN $K\beta_1$ AND $K\beta'$ LINES

Compound	$\Delta E_{K\beta_1-K\beta'}$	Compound	$\Delta E_{K\beta_1-K\beta'}$
$NaClO_4$	13.6 eV	SF_6	17.9 eV
$NaClO_3$	13.6	SF_4	18.5
$NaClO_2$	14.3	KPF_6	18[a]
Na_2SO_4	14.0	Na_2SiF_6	19.0
$PhSO_3H$	14.2	AlF_3	19
$(EtO)_2SO_2$	14.4	Na_3AlF_6	21[a]
$(CH_3)_2SO_2$	14.2		
Na_2SO_3	14.2	PCl_5	8.5
$(CH_3)_2SO$	15.6	PCl_3	8.5
SO_2	15.4	$SiCl_4$	8.6
Na_3PO_4	13.9		
Na_2HPO_3	13.9	AlN	12[b]
NaH_2PO_2	14.2		
SiO_2	14.0	SiC	9[c]
Na_2SiO_3	14.2	Al_4C_3	8[d]

a) Ref. 7.
b) The value was estimated from the spectrum of Ref. 6.
c) The value was estimated from the spectrum of Ref. 15.

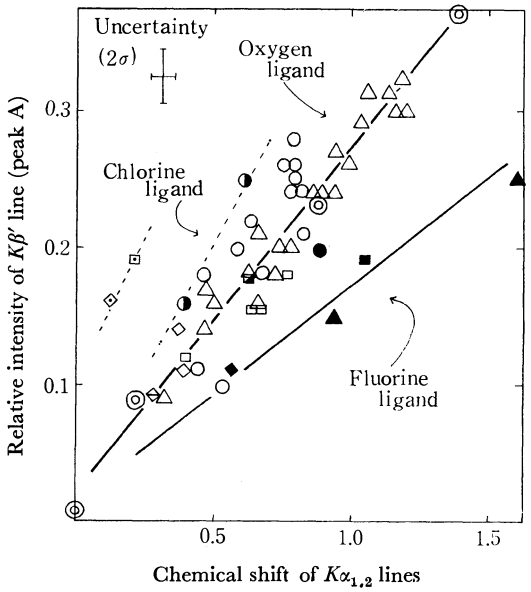

Fig. 4. Relationship between the relative intensity of $K\beta'$ line and the chemical shift of $K\alpha_{1,2}$ lines
◎: Chlorine compound, △, :▲ Sulfur compound, ○, ●, ◑: Phosphorus compound, □, ■, ◪: Silicon compound, ◇, ◆: Aluminum compound.
white point: Oxygen ligand compound, black point: Fluorine ligand compound, half-black point: Chlorine ligand compound.
⊡: SiC, ◈: Al_4C_3, ⟐: AlN.

19) W. I. Nefedow, *Zh. Strukt. Khim.*, **8**, 686, 1037 (1967).

Table 5. Contribution of an atom bonded with a sulfur atom to the relative intensity of S $K\beta'$ line and the chemical shift of S $K\alpha_{1,2}$ lines

=O	0.10 (0.38 eV)	-C	~0.00 (0.00 eV)
-O	0.05 (0.19)	-Cl	0.03 (0.12)
=N	0.07 (0.26)	-F	0.04 (0.26)
-N	0.04 (0.16)	lone pair	−0.02 (−0.08)

( ): value for the contribution to the chemical shift of $K\alpha_{1,2}$ lines

he proposes that, in MO_4-type oxy-anions of third-period elements, the $K\beta'$ line is substantially due to the electronic transition from the O_{2s} state to the M_{1s} state.

Table 6. Contribution of an atom bonded with a chlorine atom to the relative intensity of Cl $K\beta'$ line and the chemical shift of Cl $K\alpha_{1,2}$ lines

=O	0.12	(0.46 eV)
-O	~0.00	(0.00)
lone pair	−0.02	(−0.08)

( ): value for the contribution to the chemical shift of Cl $K\alpha_{1,2}$ lines

Table 7. Contribution of an atom bonded with a phosphorus atom to the relative intensity of P $K\beta'$ line and the chemical shift of P $K\alpha_{1,2}$ lines

=O	0.14 (0.40 eV)	-Cl	0.05 (0.12 eV)
-O	0.04 (0.13)	-H	~0.00 (0.00)

( ): value for the contribution to the chemical shift of $K\alpha_{1,2}$ lines

Table 8. Comparison of the estimated value with the observed value on the relative intensity of S $K\beta'$ line

Compound	Rel. int. of $K\beta'$	
	Estd	Obsd[a]
Na_2SO_4	0.30	0.30
$(EtO)_2SO_2$	0.30	0.30
H_2NSO_3H	0.29	0.29
$PhSO_3H$	0.25	0.26
$(CH_3)_2SO_2$	0.20	0.20
SF_6	0.24	0.25
Cl_2SO_2	0.26	0.27
p-$EtPhSO_2Cl$	0.23	0.24
$PhSO_2NH_2$	0.24	0.24
$PhSO_2NHBu$	0.24	0.24
p-$EtPhSO_2NEt_2$	0.24	0.21
Na_2SO_3	0.18	0.20
$(EtO)_2SO$	0.18	0.18
$HOCH_2SO_2Na$	0.13[b]	0.16
$PhSO_2Na$	0.20[c]	0.18
$(CH_3)_2SO$	0.08	0.09
SF_4	0.14	0.15
Cl_2SO	0.14	0.15
SO_2	0.18	0.16
PhNSO	0.15	0.17

a) from Ref. 3.
b) The value was estimated as a thionyl compound.
c) The value was estimated as a sulfonyl compound.

Table 9. Comparison of the estimated value with the observed value on the chemical shift of $K\alpha_{1,2}$ lines

Compound	Chemical shift (eV)	
	Estd	Obsd
Na_2SO_4	1.14	1.15[a]
$(EtO)_2SO_2$	1.14	1.16[a]
H_2NSO_3H	1.11	1.04[a]
$PhSO_3H$	0.95	0.96[a]
$PhSO_2NH_2$	0.92	0.93[a]
$PhSO_2NHBu$	0.92	0.95[a]
p-Et-$PhSO_2NEt_2$	0.92	0.95[a]
Cl_2SO_2	1.00	0.99[a]
p-Et-$PhSO_2Cl$	0.88	0.85[a]
$(CH_3)_2SO_2$	0.76	0.75[a]
SF_6	1.56	1.59[a]
Na_2SO_3	0.68	0.74[a]
$NaHSO_3$	0.68	0.65[a]
$(EtO)_2SO$	0.68	0.61[a]
Cl_2SO	0.54	0.65[a]
$(CH_3)_2SO$	0.30	0.33[a]
PhNSO	0.56	0.46[a]
SO_2	0.68	0.65[a]
SF_4	0.96	0.94[a]
$HOCH_2SO_2Na$	0.49[c]	0.49[a]
$PhSO_2Na$	0.76[d]	0.70[a]
Na_3PO_4	0.79	0.79[b]
Na_2HPO_4	0.79	0.76[b]
NaH_2PO_4	0.79	0.80[b]
H_3PO_4	0.79	0.79[b]
$(P_2O_5)_2$	0.79	0.82[b]
$(PhO)_3PO$	0.79	0.70[b]
PCl_5	0.60	0.59[b]
$POCl_3$	0.76	0.58[b]
Na_2HPO_3	0.66	0.66[b]
H_3PO_3	0.66	0.59[b]
$(PhO)_3P$	0.39	0.54[b]
PCl_3	0.36	0.41[b]
NaH_2PO_2	0.53	0.48[b]
H_3PO_2	0.53	0.45[b]
$NaClO_4$	1.38	1.38[b]
$NaClO_3$	0.84	0.87[b]
$NaClO_2$	0.30	0.22[b]

a) from Ref. 2.
b) from Ref. 4 or 5.
c) The value was estimated as a thionyl compound.
d) The value was estimated as a sulfonyl compound.

The degree of the contribution of each bonding group which is linked to the sulfur atom to the relative intensity of the S $K\beta'$ line is shown in Table 5. The effects of these groups have additivity in each molecule. For example, in diethyl sulfate ($(EtO)_2SO_2$), the sulfur atom is linked by two double-bonded oxygen atoms and two single-bonded oxygen atoms, so the relative intensity of the $K\beta'$ line is estimated to be 0.30 ($2\times 0.10+2\times 0.05$); in benzenesulfonamide ($PhSO_2NH_2$), the sulfur atom is linked by two double-bonded oxygen atoms, one nitrogen atom (amino group), and one carbon atom (phenyl group), so the value is estimated to be 0.24 ($2\times 0.10+0.04+0.00$), and in sulfur dioxide, the sulfur atom has two double-bonds and one lone

BULLETIN OF THE CHEMICAL SOCIETY OF JAPAN, VOL. 46, 2044—2052 (1973)

Vibrational Assignments of Ethylmethylsilane

Michiro HAYASHI, Keiichi OHNO, and Hiromu MURATA
Department of Chemistry, Faculty of Science, Hiroshima University, Hiroshima 730

(Received December 12, 1972)

The infrared spectra of ethylmethylsilane, $CH_3CH_2SiH_2CH_3$, its deuterated species, $CH_3CH_2SiD_2CH_3$, and a mixture of $CH_3CH_2SiHDCH_3$, $CH_3CH_2SiH_2CH_3$, and $CH_3CH_2SiD_2CH_3$ have been measured in the gaseous, liquid, and crystalline states. The Raman spectrum of ethylmethylsilane has also been measured in the liquid state. Vibrational assignments have been made in relation to the rotational isomerism, on the basis of a modified Urey-Bradley force field, in which the force constants have been transferred from those for dimethylsilane and ethylsilane. The conclusion regarding the molecular forms of the rotational isomers, which has been obtained from the experimental evidence of the SiHD deformation vibrations for an asymmetrically-deuterated species, $CH_3CH_2SiHDCH_3$, can be considered to be also supported by the present results of the normal vibration calculations.

In previous notes, we have reported the existence of the rotational isomers in ethylmethylsilane[1] and have determined the molecular forms of the isomers from the SiHD deformation vibrations for the asymmetrically-deuterated species, $CH_3CH_2SiHDCH_3$, experimentally.[2] In the present paper, we will deal with the molecular forms of the isomers and with the vibrational assignments based on the normal vibration calculation using a modified Urey-Bradley force field.

Experimental

The samples of ethylmethylsilane and its deuterated species were prepared by the method of making CH_3CH_2MgBr react with CH_3SiCl_3 in ethylether and by reducing the resultant $CH_3CH_2SiCl_2CH_3$ with $LiAlH_4$, $LiAlD_4$, or an equimolar

1) M. Hayashi, K. Ohno, and H. Murata, This Bulletin, **45**, 298 (1972).
2) M. Hayashi, K. Ohno, and H. Murata, *ibid.*, **46**, 684 (1973).

mixture of $LiAlH_4$ and $LiAlD_4$ in *n*-butylether.[3] The purities of the samples of $CH_3CH_2SiH_2CH_3$ and $CH_3CH_2SiD_2CH_3$ were found to be better than 95% by a study of the infrared spectra and the gas chromatograph. Though the sample prepared using the mixture of $LiAlH_4$ and $LiAlD_4$ was a mixture of $CH_3CH_2SiHDCH_3$, $CH_3CH_2SiH_2CH_3$, and $CH_3CH_2SiD_2CH_3$, it was used in the measurements without further attempts at isolation.

The infrared spectra in the region from 200 to 4000 cm^{-1} were recorded on a Perkin-Elmer instrument (model 621) using conventional techniques.[1,2] The Raman spectrum in the liquid state was measured with a JEOL Raman spectrometer.

Rotational Isomerism

The observed infrared and Raman spectra of ethylmethylsilane, $CH_3CH_2SiH_2CH_3$, are given in Table 1. The infrared spectra of its deuterated species, $CH_3CH_2SiD_2CH_3$, and the mixture of $CH_3CH_2SiHDCH_3$, $CH_3CH_2SiH_2CH_3$, and $CH_3CH_2SiD_2CH_3$ are also given in Tables 2 and 3. As has been reported in the previous notes,[1,2] from a comparison of the spectra in the gaseous and liquid states with those in the crystalline state in the region from 300 to 950 cm^{-1}, definite evidence of the rotational isomers is obtained, as is shown in Fig. 1; that is, some of the bands existing in both the gaseous and liquid states disappear in the crystalline state. On the other hand, the existence of the isomers cannot be concluded from the spectra in the region from 950 to 1500 cm^{-1} alone, since the infrared spectra in the liquid and crystalline states are not so much different.

Normal Vibration Calculation

A normal vibration calculation based on a modified Urey-Bradley force field was carried out, with the force constants being transferred from those for dimethylsilane and ethylsilane,[4] except the force constant of

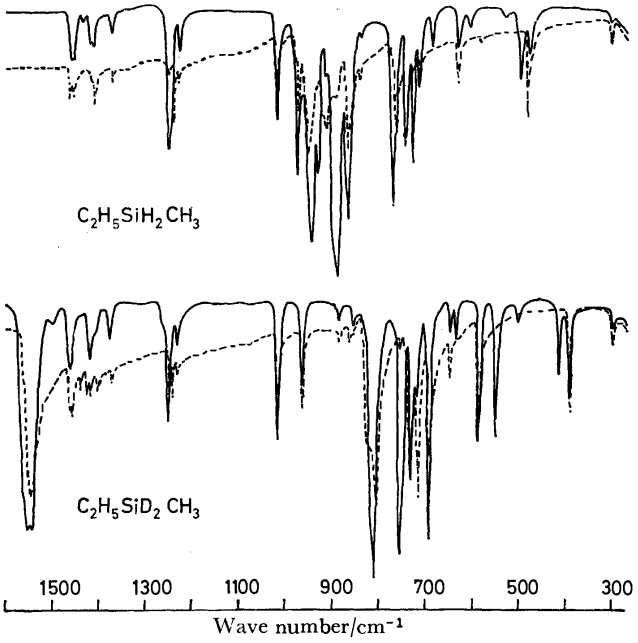

Fig. 1. The infrared spectra of ethylmethylsilane and its deuterated species, ——: in the liquid state (19 °C), ------: in the crystalline state.

Table 1. Infrared and Raman spectra of $CH_3CH_2SiH_2CH_3$[a] (cm^{-1})

Infrared						Raman		Assignment
Gas	Int.	Liquid	Int.	Crystal	Int.	Liquid	Int.	
2972	s							
2966	s			2962	m	2961	m	
2962	sh s	2950	s	2950	s			
						2939	m	
2926	b s	2928	w	2928	w	2930	sh m	
		2913	w	2914	m	2911	s	C–H str. T,G
2896								
2890	m	2891	w	2895	m	2899	s	
2882		2870	m	2870	w	2880	s	
		2800	vw	2800	vw			
2150	vs							
2146	vs							SiH_2 str. T,G
2139	vs	2126	vs	2126	vs	2137	vs	
1463	w	1462	sh m	1463	m	1463	s	CCH_3 asym. def.
1455	w	1455	sh m	1455	m			(A′,A″) T,G
1444	w							
		1437	vw			1437	sh m	
1431	sh							
1420	w	1422	sh m	1418	vw	1423	m	CH_2 sci., $SiCH_3$ asym. def. (A′, A″) T,G
1414		1413	sh m	1410	m			
1385	w	1377	w	1373	w			CCH_3 sym. def. T,G
1351	b vw							
						1298	w	

3) F. S. Kipping, *Proc. Chem. Soc.*, **20**, 15 (1904); W. Dilthey, *Ber.*, **37**, 319 (1904); A. E. Finholt, A. C. Bond, Jr., and H. I. Schlesinger, *J. Amer. Chem. Soc.*, **69**, 1199 (1947).

4) K. Ohno, M. Hayashi, and H. Murata, *J. Sci. Hiroshima Univ., Ser A*, **36**, 121 (1972).

Infrared						Raman		Assignment
Gas	Int.	Liquid	Int.	Crystal	Int.	Liquid	Int.	
1266								
1261	m	1251	s	1250	w	1254	m	$SiCH_3$ sym. def. T,G
1255								
				1244	m			
1227	w	1230	m	1230	w	1228	m	CH_2 wag., CH_2 twist. T,G
						1122	vw	
1031								
1023	m	1021	s	1021	m	1022	m	C–C str. T,G
1016								
983				981	sh vw			
977	s	977	s	975	m	971	m	CCH_3 rock. (A′,A″) T,G
969								
958								
952	vs	946	vs	952	s	953	m	SiH_2 sci. T
945								
		933	s	—				SiH_2 sci. G
		914	vw	915	b m			
908								
900	vs	890	vs	—				SiH_2 wag. G
892								
873	m	868	s	869	s			SiH_2 wag. T
		840	vw	841	vw	842	w	$SiCH_3$ rock. (A″) T,G
772	m	770	s	765	s	772	vw	CH_2 rock. T
740								
730	m	743	s	746	s	741	w	$SiCH_3$ rock. (A′) T
723		730	s	—				$SiCH_3$ rock. (A′) G, CH_2 rock. G
715	m	715	m	719	m	714	m	C–Si str. T
690	w	687	m	—		686	m	C–Si str. G
639	sh w	630	m	630	m	628	vs	C–Si str. T
619	w							
		606	w	—				C–Si str. G
		577	vw	580	w	590	m	SiH_2 twist. T
		530	w	—				
492	w	498	m			500	vw	SiH_2 rock. G
482	sh w	480	m	480	m			SiH_2 rock. T
						331	vw	
294	sh w	301	vw	301	w	298	m	C–C–Si bend. T
280	w							
215	? vvw					216	? vw	CCH_3 torsion T,G
						200	? vw	
170	? vvw					167	w	C–Si–C bend. T
87	? w							CH_2–SiH_2 torsion T,G

a) Int.=intensity; s, m, w=strong, medium, weak; v=very; b=broad; sh=shoulder; T=*trans* isomer; and G=*gauche* isomer.

TABLE 2. INFRARED SPECTRA OF $CH_3CH_2SiD_2CH_3$[a] (cm^{-1})

Infrared						Assignment
Gas	Int.	Liquid	Int.	Crystal	Int.	
2972	s					
2966	s			2964	w	
		2951	vs	2951	m	
2927	b m	2932	m	2932	w	C–H str. T,G
		2916	m	2916	w	
2905	m					
2898		2893	m	2896	w	
2889	m	2874	s	2871	w	
2882						
		2828	vvw	2825	vw	

Infrared						Assignment
Gas	Int.	Liquid	Int.	Crystal	Int.	
1561	vs	1561 sh	s	1562 sh	m	Si–D str. T,G
1556 b	vs	1552	vs	1549	vs	
		1542	vs			
		1499	vw	1504 sh	w	
1473	w					
1466	w	1463	m	1463	m	CCH_3 asym. def. (A′, A″) T,G
1458 b	w	1458 sh	m	1458	m	
		1437	vw	1440	w	
1427	w			1427	w	CH_2 sci., $SiCH_3$ asym. def. (A′, A″) T,G
1417	w	1419	m	1418	w	
1410 sh	w	1408	w	1403	w	
				1386	vw	
		1378	m	1373	w	CCH_3 sym. def. T,G
1263	m	1263	w			$SiCH_3$ sym. def. T,G
1261	m	1251	s	1250	m	
1256	m					
				1243	m	
		1232	m	1230	w	CH_2 wag., CH_2 twist. T,G
1026	m	1015	s	1014	s	C–C str. T,G
1018	m					
1010	m					
966	m	963	s	960	s	CCH_3 rock. (A′, A″) T,G
		893	vw	896	vw	
		883	w	885	w	
867	vw			863	w	
		852	w	857	w	
820 b	s			822 sh	s	$SiCH_3$ rock. (A′, A″) T,G
812	s	810	vs	814 sh	s	
				805	vs	
762 b	s	753	vs	—		CH_2 rock. G
755 b	s					
749 b	s	730	vs	732	vs	CH_2 rock. T
743	s					
741	s					
723	s	719	s	716	vs	C–Si str. T,G
719	s					
701	m	691	vs	691	vs	SiD_2 sci. T,G
695	m					
688	m					
653	w	644	w	646	m	C–Si str. T
643	w					
		633	w	—		C–Si str. G
592	m	584	s	587	s	SiD_2 wag. T
585	m					
578	m					
554	m	548	s	—		SiD_2 wag. G
547	m					
541	m					
498	w	501	w	—		SiD_2 twist. G
422 sh	m	414	s	—		SiD_2 rock. G
412	m					
402 sh	m					
393	m	390	s	390	s	SiD_2 rock. T
380 sh	m					
		294	m	294	m	C–C–Si bend. T

a) See a) of Table 1.

Table 3. Infrared spectra of the mixture of $CH_3CH_2SiHDCH_3$, $CH_3CH_2SiH_2CH_3$ ($-d_0$), and $CH_3CH_2SiD_2CH_3$ ($-d_2$)[a] (cm^{-1})

Infrared[b] Liquid	Int.	Crystal	Int.	Assignment
893	sh s			
890	sh s	888	sh s	$-d_0$
879	s	876	s	$-d_0$
862	sh vs	866	s	$-d_0$
856	sh vs	852	b vs	SiHD sci. T, G
849	vs			$SiCH_3$ rock. T,G
808	vs	809	vs	$-d_2$
796	s	798	s	$SiCH_3$ rock. T,G
766	vs	765	s	CH_2 rock. T, $-d_0$
748	vs	748	vs	CH_2 rock. G, $-d_2$
740	sh s	740	s	CH_2 rock. G, $-d_0$
726	s	726	s	C–Si str. T, G, $-d_2$
716	s	714	s	C–Si str. G, $-d_0$, $-d_2$
687	s	689	s	$-d_0$, $-d_2$
677	m	678	s	SiH def. T, G
640	w	640	w	C–Si str. T
624	m	625	m	$-d_0$
666	w	—		C–Si str. G
578	m	578	m	$-d_2$
543	m	—		$-d_2$
519	w	—		SiD def. G
508	sh w	—		SiD def. G
495	m	486	m	SiD def. T, $-d_0$
477	w	477	m	$-d_0$
443	m	—		SiHD rock. G
434	m	—		SiHD rock. G
		422	m	SiHD rock. T
413	m	—		$-d_2$
390	w	391	w	$-d_2$
293	vw	294	vw	C–C–Si bend.

a) The vibrational assignments are only described for $CH_3CH_2SiHDCH_3$. See also a) of Table 1.
b) The spectra were not measured in the region from 900 to 4000 cm^{-1}.

F(C·C·Si), which was adjusted in order to reproduce the observed C–C–Si bending vibration.

The Urey-Bradley force field was modified as follows: 1) the internal rotation force constants for CH_3–C, CH_2–Si, and Si–CH_3 groups were assumed to be the calculated values from the barrier heights of 3.49, 1.24, and 1.24 kcal/mol respectively; 2) the *trans* and *gauche* coupling constants between the CH_3 and SiH_2 groups, between the CH_2 and SiH_2 groups, and between the Si–C–H bendings and the C–Si–C bending were added, and these values were transferred from dimethylsilane and ethylsilane, and 3) the C–H bond interaction constant was added in order to reproduce the observed C–H stretching frequencies.

The bond lengths used in the calculation were the values transferred from those for methylsilane and ethylsilane.[5] All of the valency angles were assumed to be tetrahedral.

The force constants and the observed and calculated frequencies of ethylmethylsilane are given in Tables 4—7. Since the adjustment was made only for F(C·C·Si), while the other transferred force constants were fixed at the original values, relatively larger differences were found between the observed and calculated frequencies of some of the hydrogen deformation modes. However, the results of the calculation were considered still to be valid for the assignments of the observed spectra.

From the calculated potential energy distributions, considerably larger mixings of the modes were found in the following pairs of modes: 1) the CH_2 scissoring and CCH_3 symmetric deformation, 2) the SiH_2 wagging and $SiCH_3$ rocking, 3) the CH_2 rocking and SiH_2 twisting for $CH_3CH_2SiH_2CH_3$, 4) the CH_2 scissoring and CCH_3 symmetric deformation, and 5) the C–Si stretching and SiD_2 scissoring for $CH_3CH_2SiD_2CH_3$. The localization of the CH_2 rocking mode for the

Table 4. Force constants for ethylmethylsilane[a]

K(C–H), CCH_3	4.297	κ (CCH_3)	0.029
K(C–H), CH_2	4.297	κ (CH_2)	−0.040
K(C–H), $SiCH_3$	4.403	κ (SiH_2)	0.104
K(Si–H)	2.462	κ ($SiCH_3$)	0.014
K(C–C)	2.400	Y(C–C)	0.109
K(Si–C)	1.991	Y(C–Si)	0.039
H(C–C–H), CCH_3	0.164	F(C · C · H), CCH_3	0.470
H(H–C–H), CCH_3	0.370	F(H · C · H), CCH_3	0.200
H(C–C–Si)	0.087	F(C · C · Si)	0.540[b]
H(Si–C–H), CH_2	0.123	F(Si · C · H), CH_2	0.271
H(C–C–H), CH_2	0.278	F(C · C · H), CH_2	0.540
H(H–C–H), CH_2	0.331	F(H · C · H), CH_2	0.200
H(C–Si–C)	0.133	F(C · Si · C)	0.040
H(C–Si–H)	0.092	F(C · Si · H)	0.149
H(H–Si–H)	0.180	F(H · Si · H)	0.041
H(Si–C–H), $SiCH_3$	0.102	F(Si · C · H), $SiCH_3$	0.271
H(H–C–H), $SiCH_3$	0.349	F(H · C · H), $SiCH_3$	0.200
t(CH_2, SiH_2)[c]	0.072	t(SiH_2 $SiCH_3$)[c]	0.057
t(Si–C–H, C–Si–C)[c]	0.030	p(C–H)	−0.084

a) The units of the force constants are in mdyn/Å for stretching, K; bending, H; repulsion, F; and bond interaction, p; and in mdyn·Å for intramolecular tension, κ; internal rotation, Y; and *trans* coupling, t. Force constants were transferred from dimethylsilane and ethylsilane.
b) The value was adjusted in order to reproduce the observed C–C–Si bending frequency.
c) *Gauche* coupling constants were assumed to be $g=-0.5t$.

5) M. Hayashi and C. Matsumura, This Bulletin, **45**,732 (1972).

Table 5. Observed and calculated frequencies for $CH_3CH_2SiH_2CH_3$ (cm^{-1})

	No.	*Trans* form		*Gauche* form		P.E.D.[a]
		Obsd	Calcd	Obsd	Calcd	
A'	ν_1	2950	2965	*A* 2950	2965	CCH_3 asym. str.
	ν_2	2950	2964	2950	1964	$SiCH_3$ asym. str.
	ν_3	2928	2933	2928	2933	CH_2 sym. str.
	ν_4	2913	2901	2913	2901	$SiCH_3$ sym. str.
	ν_5	2870	2900	2870	2900	CCH_3 sym. str.
	ν_6	2126	2148	2126	2148	SiH_2 sym. str.
	ν_7	1462	1461	1462	1461	CCH_3 asym. def.
	ν_8	1422	1429	1422	1429	CH_2 sci.
	ν_9	1413	1413	1413	1413	$SiCH_3$ asym. def.
	ν_{10}	1377	1377	1377	1377	CCH_3 sym. def.
	ν_{11}	1251	1254	1251	1254	$SiCH_3$ sym. def.
	ν_{12}	1230	1189	1230	1188	CH_2 wag.
	ν_{13}	1021	1021	1021	1022	C–C str.
	ν_{14}	977	965	977	965	CCH_3 rock.
	ν_{15}	946	948	933	945	SiH_2 sci.
	ν_{16}	868	865	890	865	SiH_2 wag.
	ν_{17}	743	760	730	745	$SiCH_3$ rock.
	ν_{18}	715	714	687	711	C–Si str.
	ν_{19}	630	656	606	644	C–Si str.
	ν_{20}	301	301	—	317	C–C–Si bend.
	ν_{21}	167	186	—	187	C–Si–C bend.
A''	ν_{22}	2950	2975	*A* 2950	2975	CH_2 antisym. str.
	ν_{23}	2950	2964	2950	2964	CCH_3 asym. str.
	ν_{24}	2950	2959	2950	2959	$SiCH_3$ asym. str.
	ν_{25}	2126	2148	2126	2148	SiH_2 antisym. str.
	ν_{26}	1455	1458	1455	1458	CCH_3 asym. def.
	ν_{27}	1413	1413	1413	1413	$SiCH_3$ asym. def.
	ν_{28}	1230	1244	1230	1248	CH_2 twist.
	ν_{29}	977	975	977	968	CCH_3 rock.
	ν_{30}	840	840	840	840	$SiCH_3$ rock.
	ν_{31}	770	790	730	758	CH_2 rock.
	ν_{32}	577	594	—	622	SiH_2 twist.
	ν_{33}	480	487	498	498	SiH_2 rock.
	ν_{34}	215	243	—	250	C–CH_3 torsion
	ν_{35}	—	147	—	144	Si–CH_3 torsion
	ν_{36}	87	65	—	67	CH_2–SiH_2 torsion

a) Only the predominant symmetry coordinates are shown.

Table 6. Observed and calculated frequencies for $CH_3CH_2SiD_2CH_3$ (cm^{-1})

	No.	*Trans* form		*Gauche* form		P.E.D.[a]
		Obsd	Calcd	Obsd	Calcd	
A'	ν_1	2951	2965	*A* 2951	2965	CCH_3 asym. str.
	ν_2	2951	2964	2951	2964	$SiCH_3$ asym. str.
	ν_3	2932	2933	2932	2933	CH_2 sym. str.
	ν_4	2916	2901	2916	2901	$SiCH_3$ sym. str.
	ν_5	2874	2900	2874	2900	CCH_3 sym. str.
	ν_6	1542	1537	1542	1537	SiD_2 sym. str.
	ν_7	1463	1461	1463	1461	CCH_3 asym. def.
	ν_8	1419	1428	1419	1429	CH_2 sci.
	ν_9	1408	1413	1408	1413	$SiCH_3$ asym. def.
	ν_{10}	1378	1377	1378	1377	CCH_3 sym. def.
	ν_{11}	1251	1254	1251	1254	$SiCH_3$ sym. def.
	ν_{12}	1232	1189	1232	1188	CH_2 wag.
	ν_{13}	1015	1020	1015	1020	C–C str.
	ν_{14}	963	964	963	964	CCH_3 rock.
	ν_{15}	810	819	810	818	$SiCH_3$ rock.
	ν_{16}	719	731	719	721	C–Si str.
	ν_{17}	691	698	691	688	SiD_2 sci.
	ν_{18}	644	638	633	629	C–Si_2 str.
	ν_{19}	584	579	548	572	SiD_2 wag.
	ν_{20}	294	297	—	305	C–C–Si bend.
	ν_{21}	—	184	—	186	C–Si–C bend.
A''	ν_{22}	2951	2975	*A* 2951	2975	CH_2 antisym. str.
	ν_{23}	2951	2964	2951	2964	CCH_3 asym. str.
	ν_{24}	2951	2959	2951	2959	$SiCH_3$ asym. str.
	ν_{25}	1552	1552	1552	1552	SiD_2 antisym. str.
	ν_{26}	1458	1458	1458	1458	CCH_3 asym. def.
	ν_{27}	1408	1413	1408	1413	$SiCH_3$ asym. def.
	ν_{28}	1232	1243	1232	1247	CH_2 twist.
	ν_{29}	963	971	963	963	CCH_3 rock.
	ν_{30}	810	816	810	816	$SiCH_3$ rock.
	ν_{31}	730	761	753	750	CH_2 rock.
	ν_{32}	—	451	501	464	SiD_2 twist.
	ν_{33}	390	392	414	406	SiD_2 rock.
	ν_{34}	—	239	—	246	C–CH_3 torsion
	ν_{35}	—	146	—	144	Si–CH_3 torsion
	ν_{36}	—	64	—	65	CH_2–SiD_2 torsion

a) See a) of Table 5.

gauche form was worse than that for the *trans* form.

For the SiHD deformation modes of $SiHDCl_2$ and $(CH_3)_2SiHD$, it was found that the SiHD wagging and twisting modes should be more properly called the SiH and SiD deformation modes respectively, while the SiHD scissoring and rocking modes keep their original modes.[4] In $CH_3CH_2SiHDCH_3$, the situation was nearly the same as in $SiHDCl_2$ and $(CH_3)_2SiHD$ for the SiHD rocking and SiD deformation modes, while the SiHD scissoring and SiH deformation modes were different and were considerably mixed with the C–Si stretching, CH_2 rocking, and $SiCH_3$ rocking modes.

Molecular Forms and Vibrational Assignments

The infrared spectra of ethylmethylsilane in the region from 1000 to 1500 cm^{-1} are not much different in the liquid and crystalline states; also, they are close to the superposition of the spectra of ethylsilane and methylsilane. The results of the calculations indicate that, as the coupling between the ethyl and methyl groups seems to be negligible, the calculated frequencies for the *trans* and *gauche* forms are essentially identical with each other. Therefore, the assignments of the observed spectra in this region can easily be obtained from the reported assignments for ethylsilane and methylsilane, without regard to the rotational isomerism.

On the other hand, it can be expected from the calculation that spectra sensitive to the molecular forms of the isomers exist in the region from 650 to 1000 cm^{-1}. Actually, in this region, ten infrared bands are observed in the liquid state for $CH_3CH_2SiH_2CH_3$, while four of them disappear in the crystalline state. For $CH_3CH_2SiD_2CH_3$, six infrared bands are observed in the liquid state; one of them disappears in the

Table 7. Observed and calculated frequencies for $CH_3CH_2SiHDCH_3$[a] (cm^{-1})

	No.	*Trans* form		*Gauche* form (G)[b]		*Gauche* form (G')[c]		P.E.D.[d]
		Obsd	Calcd	Obsd	Calcd	Obsd	Calcd	
A	ν_{21}	—	974	—	965	—	965	CCH_3 rock.
	ν_{22}	—	965	—	964	—	964	CCH_3 rock.
	ν_{23}	856	857	856	858	856	857	SiHD sci.
	ν_{24}	849	843	849	844	849	838	$SiCH_3$ rock.
	ν_{25}	796	810	796	811	796	810	$SiCH_3$ rock.
	ν_{26}	766	776	740	739	748	754	CH_2 rock.
	ν_{27}	726	732	726	736	716	721	C–Si str.
	ν_{28}	677	689	677	682	677	699	SiH def.
	ν_{29}	640	654	616	642	616	642	C–Si str.
	ν_{30}	486	489	519	503	508	496	SiD def.
	ν_{31}	422	422	443	438	434	430	SiHD rock.
	ν_{32}	293	299	—	307	—	315	C–C–Si bend.
	ν_{33}	—	241	—	248	—	248	C–CH_3 torsion
	ν_{34}	—	185	—	187	—	186	C–Si–C bend.
	ν_{35}	—	146	—	144	—	144	Si–CH_3 torsion
	ν_{36}	—	65	—	66	—	66	CH_2–SiHD torsion

a) The calculated frequencies for the other vibrations are omitted in the Table.
b) The CCH_3 group occupies the *trans* position to the deuterium of the SiHD group.
c) The CCH_3 group occupies the *trans* position to the hydrogen of the SiHD group.
d) Only the predominant symmetry coordinates are shown.

crystalline state.

For $CH_3CH_2SiH_2CH_3$, the strong infrared band at 977 cm^{-1} and the pairs of strong bands around 940 and around 879 cm^{-1} are easily assigned to the CCH_3 rocking, SiH_2 scissoring, and SiH_2 wagging modes respectively, since the band at 940 cm^{-1} and the pair of bands around 879 cm^{-1} are not observed for CH_3-$CH_2SiD_2CH_3$, and since the CCH_3 rocking modes are observed at 979 cm^{-1} for ethylsilane, and the SiH_2 scissoring and wagging modes are observed at 959 and 919 cm^{-1} for dimethylsilane.

There are a weak infrared band at 840 cm^{-1}, a strong band at 770 cm^{-1}, and two pairs of strong bands around 736 cm^{-1} and around 700 cm^{-1}, which correspond to the weak Raman bands at 842, 772, and 741 cm^{-1} and two medium bands around 700 cm^{-1} respectively, while the lower-frequency infrared bands of the two pairs disappear in the crystalline state.

On the basis of a comparison of the spectra with those for methylsilane, ethylsilane, and dimethylsilane, they can be assigned to the CH_2 rocking, $SiCH_3$ rocking of the A' and A'' species, and asymmetric C–Si stretching modes. That is, since the averaged frequency of the observed $SiCH_3$ rocking modes of the A_1 and B_1 species for dimethylsilane is about 780 cm^{-1}, either the band at 770 cm^{-1} or the pair of the bands around 736 cm^{-1} may be the $SiCH_3$ rocking modes of the A' species for both the *trans* and *gauche* isomers, while the weak band at 840 cm^{-1} can be assigned to the $SiCH_3$ rocking modes of the A'' species for both isomers, since the averaged frequency of the $SiCH_3$ rocking modes of the A_2 and B_2 species for dimethylsilane is about 840 cm^{-1}. On the other hand, since the CH_2 rocking mode is found at 764 cm^{-1} for ethylsilane, the CH_2 rocking mode can also be expected in this region for the $SiCH_3$ rocking mode.

As the calculated frequencies of the CH_2 rocking mode are 790 cm^{-1} for the *trans* form and 758 cm^{-1} for the *gauche* form, while those of the $SiCH_3$ rocking mode are 760 and 745 cm^{-1}, the band at 770 cm^{-1} can be assigned to the CH_2 rocking mode for the *trans* isomer, the higher frequency band (743 cm^{-1}) of the pair can be assigned to the $SiCH_3$ rocking mode for the *trans* isomer, and the lower-frequency band (730 cm^{-1}) of the pair can be regarded as the overlapping band of the $SiCH_3$ rocking and CH_2 rocking modes for the *gauche* isomer.

The pair around 700 cm^{-1} can be easily assigned to the asymmetric C–Si stretching mode for the *trans* and *gauche* isomers, since the mode is to be expected in the range of 695—805 cm^{-1}, as has already been pointed out by Janz and Mikawa,[6] and since the corresponding mode can be found at 728 cm^{-1} for dimethylsilane.

For $CH_3CH_2SiD_2CH_3$, three independent infrared bands at 810, 719, and 691 cm^{-1} and a pair of strong bands around 742 cm^{-1} are observed in the liquid state, while the higher-frequency band of the pair disappears in the crystalline state.

Since the $SiCH_3$ rocking modes are found around 800 cm^{-1} for the analogous deuterated molecules such as dimethylsilane, the band at 810 cm^{-1}, which shows a complicated pattern in the crystalline state, may be assigned to the overlapping band of the $SiCH_3$ rocking modes of the A' and A'' species.

Although the above assignments seem questionable at first glance from the fact that the corresponding modes of the A' and A'' species for $CH_3CH_2SiH_2CH_3$ are greatly separated from each other, it may be understood that the $SiCH_3$ rocking modes of the A' species at 743 and 730 cm^{-1} for $CH_3CH_2SiH_2CH_3$ are pushed down by the SiH_2 wagging modes at 868 and 890 cm^{-1}, since the calculation shows that the larger mode mixing

6) G. J. Janz and Y. Mikawa, This Bulletin, **34**, 1495 (1961).

is found between these modes, while the $SiCH_3$ rocking modes of the A'' species at 840 cm^{-1} stay at the original frequency. On the other hand, for $CH_3CH_2SiD_2CH_3$, both of the two $SiCH_3$ rocking modes, belonging to the A' and A'' species, exist in the 800—830 cm^{-1} region, outside the influence of the SiD_2 hydrogen deformation modes which exist in the far lower frequency region, as the calculations indicate.

From the results of the calculations and the comparison of the spectra for $CH_3CH_2SiD_2CH_3$ with those for $CH_3CH_2SiH_2CH_3$, the pair of the bands around 742 cm^{-1} and the two bands at 719 and 691 cm^{-1} can be assigned to the CH_2 rocking, C–Si asymmetric stretching, and SiD_2 scissoring modes respectively.

It is noticeable that the CH_2 rocking mode for the *trans* isomer has a higher frequency than that for the *gauche* isomer for $CH_3CH_2SiH_2CH_3$, while they are the reverse in frequency for $CH_3CH_2SiD_2CH_3$. This is understandable for the following reasons, obtained by an examination of the calculated potential energy distributions.

First of all, for the *trans* form, from the symmetry the coupling is possible between the modes belonging to the same species. Therefore, the CH_2 rocking mode for the *trans* form is pushed up by the SiH_2 twisting mode for $CH_3CH_2SiH_2CH_3$, while the corresponding mode stays at the unaffected frequency for $CH_3CH_2SiD_2CH_3$ since the SiD_2 twisting mode goes to a far lower frequency.

However, for the *gauche* form, as the molecular symmetry is lowered, coupling is possible between all of the modes. For $CH_3CH_2SiH_2CH_3$, the CH_2 rocking mode, which is influenced by the SiH_2 twisting mode, is also affected by the $SiCH_3$ rocking mode corresponding to that of the A' species for the *trans* form, which may be at a slightly higher frequency than the unaffected frequency for the CH_2 rocking mode. Therefore, as the pushing-up effect of the SiH_2 twisting mode may be cancelled by the pushing-down effect of the $SiCH_3$ rocking mode, the CH_2 rocking mode can be found around the unaffected frequency. For $CH_3CH_2SiD_2CH_3$, though the $SiCH_3$ rocking mode in question exists at a higher frequency with a diminishing influence on the CH_2 rocking mode, the SiD_2 scissoring and C–Si stretching modes corresponding to those of the A' species for the *trans* form appear anew at the lower frequencies and push the CH_2 rocking mode up to a higher frequency.

Therefore, the CH_2 rocking mode for the *gauche* form is found at a lower frequency than that for the *trans* form for $CH_3CH_2SiH_2CH_3$, while it is found at a higher frequency than that for the *trans* form for $CH_3CH_2SiD_2CH_3$.

In the region from 350 to 650 cm^{-1}, two pairs of the bands for $CH_3CH_2SiH_2CH_3$ and three pairs of the bands for $CH_3CH_2SiD_2CH_3$ are observed in the liquid state. Since the symmetric C–Si stretching mode is found at 659 cm^{-1} for dimethylsilane, the pairs around 620 and 638 cm^{-1} can be assigned to the symmetric C–Si stretching modes for $CH_3CH_2SiH_2CH_3$ and $CH_3CH_2SiD_2CH_3$ respectively, while the lower-frequency bands in each pair vanish in the crystalline state and belong to the *gauche* isomers.[7]

The SiH_2 and SiD_2 twisting modes can be expected to be very weak bands, since the corresponding band is infrared-inactive because of the symmetry for dimethylsilane. Therefore, another pair of bands, that around 490 cm^{-1} for $CH_3CH_2SiH_2CH_3$ can easily be assigned to the SiH_2 rocking mode; this pair corresponds to the pair around 402 cm^{-1} for $CH_3CH_2SiD_2CH_3$.

The pair around 566 cm^{-1} for $CH_3CH_2SiD_2CH_3$ can be assigned to the SiD_2 wagging mode. As for the SiH_2 and SiD_2 twisting modes, there are no distinct pairs of bands except for the very weak bands in the region expected from the calculations.

For $CH_3CH_2SiH_2CH_3$, a weak band at 577 cm^{-1}, which is found in both the liquid and crystalline states and which corresponds to a medium Raman band at 590 cm^{-1}, may be assigned to the SiH_2 twisting mode for the *trans* isomer, while the mode for the *gauche* isomer cannot be found in the expected region around 620 cm^{-1} where the bands assigned to the C–Si stretching mode are also present.

For $CH_3CH_2SiD_2CH_3$, the weak band at 501 cm^{-1}, existing only in the liquid state, may be assigned to the SiD_2 twisting mode for the *gauche* isomer, while the mode for the *trans* isomer cannot be found in the expected region (around 450 cm^{-1}).

In the region below 350 cm^{-1}, two skeletal bending and three torsional modes are expected. The Raman bands at 298 and 167 cm^{-1} in the liquid state, and the infrared bands at 301 cm^{-1} in the crystalline state and at about 170 cm^{-1} in the gaseous state, are observed for $CH_3CH_2SiH_2CH_3$. These bands may be assigned to the C–C–Si and C–Si–C bending modes for the *trans* isomer.

In Table 3, the observed and calculated frequencies fot the mixture of $CH_3CH_2SiHDCH_3$, $CH_3CH_2SiH_2CH_3$, and $CH_3CH_2SiD_2CH_3$ are shown as a basis for finding the vibrational assignments for $CH_3CH_2SiHDCH_3$, especially in the range from 250 to 900 cm^{-1}, where the bands sensitive to the molecular forms of

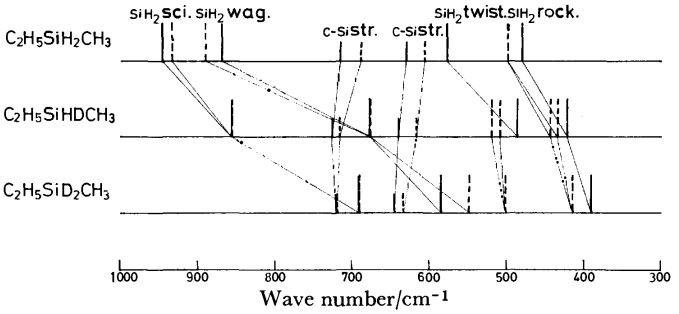

Fig. 2. Observed frequencies for the SiH_2, SiD_2, SiHD deformation modes and the C–Si stretching mode. ——: the spectra which persist in the crystalline state. ·····: the spectra which disappear in the crystalline state.

7) In the previous note (Ref. 1), the pair around 620 cm^{-1} for $CH_3CH_2SiH_2CH_3$ has been erroneously assigned to the SiH_2 wagging mode from the reported assignments for dimethylsilane given by Ball *et al.* (D. F. Ball, P. L. Goggin, D. C. McKean, and L. A. Woodward, *Spectrochim. Acta*, **16**, 1358 (1960).) However, the normal vibration calculation indicates the present assignment is correct for both dimethylsilane and ethylmethylsilane.

the isomers can be expected to exist. A comparison of the spectra of the mixture with the other species easily leads to the vibrational assignments for CH_3CH_2-$SiHDCH_3$ in this region. The correlation of the spectra for the three isotopic species is found to be excellent, as is shown in Fig. 2, where only the SiH_2 hydrogen deformation and C–Si stretching modes are shown. The results of the normal vibration calculations also prove the correctness of the present assignments, as is shown in Table 7.

So far, the vibrational assignments have been made without any impropriety on the assumption of the co-existence of the *trans* and *gauche* isomers in the gaseous and liquid states. In general, the calculated frequencies can be considered to reproduce the observed frequencies well, though most of the force constants are transferred from those for other, similar molecules without any adjustments. Therefore, the co-existence and the molecular forms of the isomers can be regarded as also proved by the present normal vibration calculations.

The authors wish to express their thanks to Professor Tatsuo Miyazawa of Osaka University and to the staff of his research group for allowing us to use their instruments and for their technical assistance.

BULLETIN OF THE CHEMICAL SOCIETY OF JAPAN, VOL. 46, 2052—2056 (1973)

Ionic Equilibria in Mixed Solvents. VIII. Solvent Effects on the Dissociation of Diprotic Acids in Aqueous Methanol Mixtures

Hitoshi OHTAKI and Masunobu MAEDA

Department of Electrochemistry, Tokyo Institute of Technology, O-okayama, Meguro-ku, Tokyo 152

(Received December 11, 1972)

Dissociation constants of protonated 1,6-hexanediamine, 1,8-octanediamine, 1,10-decanediamine, 1,11-undecanediamine, and 1,12-dodecanediamine in aqueous mixtures of 0 to 90% (w/w) methanol were determined potentiometrically at 25 °C, 0.1 M sodium chloride being used as an ionic medium. Values of pK_2-pK_1 of diamines were practically independent of the solvent composition in contrast to those of dicarboxylic acids, which increase monotonously with methanol concentration. Variations of pK_1, pK_2, and pK_2-pK_1 of diamines with solvent composition were discussed in comparison with those of dicarboxylic acids.

It is known that the acid dissociation constant of a monoprotic acid of neutral type (*e.g.* acetic acid or phenol) decreases with an increase in the concentration of an organic solvent in aqueous organic mixtures.[1-11] The solvent effect on dissociation constants of dicarboxylic acids[9,11-18] is similar to that of monocarboxylic acids. This can be explained qualitatively in terms of the electrostatic interaction between a leaving proton on an acid group and the conjugate base radical. On the other hand, the dissociation of a charged acid such as ammonium ion as well as other protonated mono- and diamines is enhanced by the addition of an organic solvent into aqueous solution, decreasing steeply after passing through a maximum.[1,5,9,10,14,19-21]

Kotaka and others[22] studied the association of ammonia in aqueous propanol solution by conductometry and confirmed that the association constant of the reaction

$$NH_4^+ + OH^- = NH_3 + H_2O$$

increases monotonously with solvent composition, and the variation of the dissociation constant of ammonium ion in mixed solvents described in terms of the reaction

$$NH_4^+ + H_2O = NH_3 + H_3O^+; \quad K = \frac{[NH_3][H^+]}{[NH_4^+]}$$

is essentially attributed to the variation of the autoprotolysis constant of the solvent with solvent composition.

1) L. Michaelis and M. Mizutani, *Z. Phys. Chem.*, **116**, 135 (1925).
2) E. Grunwald and B. J. Berkowitz, *J. Amer. Chem. Soc.*, **73**, 4939 (1951).
3) H. S. Dunsmore and J. C. Speakman, *Trans. Faraday Soc.*, **50**, 236 (1954).
4) T. Shedlovsky and R. L. Kay, *J. Phys. Chem.*, **60**, 151 (1956).
5) R. G. Bates, "Determination of pH," John Wiley and Sons, Inc., New York, p. 195 (1964).
6) R. Gaborioud and G. Champetier, *C. R. Acad. Sci. Paris.*, **263**. 911 (1966).
7) G. Douhéret, *Bull. Soc. Chim. Fr.*, **1967**, 1412.
8) J. O. Frohlinger, R. G. Gartska, H. W. Irwin, and O. W. Stewart, *Anal. Chem.*, **40**, 1408 (1968).
9) R. Gaborioud, R. Schaal, and O. Fillaux, *J. Chim. Phys.*, **66**, 730 (1969).
10) H. Ohtaki, This Bulletin, **42**, 1573 (1969).
11) S. K. Pal and S. C. Lahiri, *Z. Phys. Chem.* (Leipzig), **246**, 81 (1971).
12) M. Mizutani, *Z. Phys. Chem.*, **118**, 318 (1925).
13) G. Schwarzenbach, *Helv. Chim. Acta*, **16**, 522 (1933).
14) J. C. Speakman, *J. Chem. Soc.*, **1943**, 270.
15) M.-L. Dondon, *J. Chim. Phys.*, **54**, 290 ,304 (1957).
16) M. Yasuda, This Bulletin, **32**, 429 (1959).
17) G. Bonhomme and M.-L. Dondon, *C. R. Acad. Sci. Paris*, **263**, 1097 (1966).
18) G. Bonhomme, *Bull. Soc. Chim., Fr.* **1968**, 60.
19) M. Paabo, R. G. Bates, and R. A. Robinson, *J. Phys. Chem.*, **70**, 247 (1966).
20) J. Leliévre and R. Gaborioud, *C. R. Acad. Sci. Paris*, **266**, 1725 (1968).
21) H. Ohtaki and N. Tanaka, *J. Phys. Chem.*, **75**, 90 (1971).
22) M. Kotaka, E. Kubota, Y. Mori, and M. Yokoi, *Nippon Kagaku Zasshi*, **92**, 18 (1971).

In a previous paper[10] we showed that the variation of dissociation constant of a monoprotic acid with solvent composition in aqueous alcoholic solutions, regardless of neutral or charged type, could be explained in terms of free energy changes of transfer of species from water to a mixed solvent taking into account the equilibrium between hydronium and alkoxonium ions:

$$H_3O^+ + ROH = H_2O + ROH_2^+ \quad (1)$$

For protonated diamines we found that dissociation constants vary in the same manner as those of monoamines.[21] A remarkable difference was observed between variations of pK_2-pK_1 for diamine and carboxylic acid. For the latter not only pK_1 and pK_2 but also pK_2-pK_1 increase with solvent composition, as predicted from electrostatic theories.[23-26] On the other hand, values of pK_2-pK_1 for diamines remain practically constant, or in some cases decrease with an increase of the methanol content.

We have attempted to clarify these phenomena of dissociation reactions of diprotic acids in mixed solvents.

Experimental

A. Reagents. Dihydrochlorides of 1,6-hexanediamine, 1,8-octanediamine, 1,10-decanediamine, 1,11-undecanediamine, and 1,12-dodecanediamine (Aldrich Chemical Co., Inc., Milwaukee, Wis., U.S.A.) were prepared by the method described previously.[21] Recrystallization of the salts was repeated three times from water. When a salt was colored, the colored substance was removed with active charcoal before recrystallization. The salts thus prepared were dried *in vacuo* at room temperature and kept in the dark.

Sodium Chloride (ultra pure) from E. Merck Co. was dried at 500 °C.

Sodium Hydroxide was prepared by the method described previously[21] and was stored in a polyethylene bottle under nitrogen. Transfer of the sodium hydroxide solution from the bottle to a buret was carried out under an atmosphere of nitrogen gas.

Methanol. Reagent grade methanol was distilled and stored in a glass bottle.

B. Apparatus. Beckman glass electrodes (No. 40495 and 39301) were used. No difference was observed between two types of electrodes in pH measurements. A silver-silver chloride electrode was prepared according to Brown[27] and was set in the "Wilhelm" type of a reference half-cell.[28] A Radiometer PHM-4d pH-meter (Copenhagen) was used.

Dissociation constants of the diprotonated diamines were determined in aqueous mixtures of 0—90% (w/w) methanol. Experimental conditions were the same as those mentioned previously.[21] The pH values never exceeded 10.4 in the course of measurements in all systems.

Hydrogen ion concentrations in solution at equilibrium were determined from emf measurements by application of the Nernst equation

$$E = E_0 + 59.15 \log [H^+]_s + 59.15 \log f_H + E_j \quad (2)$$

23) M. Born, *Z. Phys.*, **1**, 45 (1920).
24) N. Bjerrum, *Z. Phys. Chem.*, **106**, 219 (1923).
25) J. G. Kirkwood and F. H. Westheimer, *J. Chem. Phys.*, **6**, 506 (1938).
26) F. H. Westheimer and J. G. Kirkwood, *ibid.*, **6**, 513 (1938).
27) A. S. Brown, *J. Amer. Chem. Soc.*, **56**, 646 (1934).
28) W. Forsling, S. Hietanen, and L. G. Sillén, *Acta Chem. Scand.*, **6**, 901 (1952).

Table 1. Dissociation constants of 1,6-hexanediamine, 1,8-octanediamine, 1,10-decanediamine, 1,11-undecanediamine, and 1,12-dodecanediamine in various water–methanol mixtures containing 0.1M NaCl

Concn of methanol %(w/w)	pK_1	pK_2	pK_2-pK_1
1,6-Hexanediamine			
0	10.08	10.79	0.71
10	9.98	10.67	0.69
20	9.87	10.55	0.68
30	9.72	10.40	0.68
40	9.56	10.21	0.65
50	9.49	10.12	0.64
60	9.29	9.93	0.64
70	9.18	9.95	0.77
80	9.16	9.94	0.78
90	9.43	10.13	0.70
1,8-Octanediamine			
0	10.16	10.76	0.60
10	10.11	10.71	0.60
20	10.01	10.54	0.53
30	9.82	10.48	0.66
40	9.67	10.26	0.59
50	9.51	10.13	0.62
60	9.39	9.99	0.60
70	9.31	9.94	0.63
80	9.35	9.97	0.62
90	9.46	10.09	0.63
1,10-Decanediamine			
0	10.36	10.93	0.57
10	10.19	10.75	0.56
20	10.04	10.62	0.58
30	9.88	10.44	0.56
40	9.70	10.28	0.58
50	9.54	10.12	0.57
60	9.40	10.01	0.61
70	9.28	9.93	0.65
80	9.29	9.94	0.65
90	9.56	10.16	0.60
1,11-Undecanediamine			
0	10.37	10.95	0.58
10	10.22	10.77	0.55
20	10.08	10.64	0.55
30	9.89	10.42	0.53
40	9.69	10.34	0.65
50	9.55	10.10	0.55
60	9.43	9.97	0.54
70	9.36	9.98	0.62
80	9.37	10.03	0.66
90	9.60	10.18	0.58
1,12-Dodecanediamine			
0	10.34	10.92	0.58
10	10.24	10.81	0.57
20	10.10	10.66	0.56
30	9.90	10.52	0.62
40	9.82	10.44	0.62
50	9.57	10.17	0.60
60	9.44	10.05	0.61
70	9.35	9.94	0.59
80	9.37	9.90	0.53
90	9.61	10.16	0.56

and the liquid junction potential E_j in 90% methanol–water mixture was corrected with the relation $E_j = -450 \pm 50$ mV/M·$[H^+]_s$, where $[H^+]_s$ denotes the concentration of hydrogen ion at equilibrium. In other solutions the liquid junction potential was corrected by the use of E_j values reported previously.[21]

Results and Discussion

Dissociation constants for each diamine were determined from the formation function $\bar{n} = ([H^+]K_2^{-1} + 2[H^+]^2K_1^{-1}K_2^{-1})/(1 + [H^+]K_2^{-1} + [H^+]^2K_1^{-1}K_2^{-1})$ by means of a generalized least-squares method with the aid of an electronic computer FACOM 230-60 in order to make the error square sum ($U = \sum(\bar{n} - \bar{n}_{calcd})^2$) minimum for the set of dissociation constants K_1 and K_2. The results are summarized in Table 1.

In order to assess the solvent effects on the dissociation of diprotic acids, the variation of the dissociation constants of dicarboxylic acids with the methanol concentration is discussed first, the values of pK_1 and pK_2 of the dicarboxylic acids being quoted from literature. Variations of pK_1 and pK_2 of diamines with solvent composition are treated next.

(1) Variation of $pK_2 - pK_1$ for Dicarboxylic Acids with the Solvent Composition. In 1937 Kirkwood and Westheimer[25,26] proposed the following equation for the $pK_2 - pK_1$ value of a diprotic acid in aqueous solution.

$$pK_2 - pK_1 = \frac{Ne^2}{a\varepsilon_e RT \ln 10} + \log \sigma \qquad (3)$$

If we assume that the equation is applicable to a diprotic acid not only in aqueous solution but also in a mixed solvent and that Kirkwood-Westheimer's spherical model can be used, we can calculate from the data of $pK_2 - pK_1$ the radius of the sphere b, the distance between a charge and the center of the sphere r, the angle between lines from the center to the charges θ and the distance between charges a of the model. The values of $pK_2 - pK_1$ found in literature are satisfactorily reproduced with the parameters best chosen by means of the least-squares method over the whole range of methanol concentration (Fig. 1). Parameters thus obtained are given in Table 2. The value of θ decreases as the methylene chain becomes longer. The value of $2r = l$ for an acid is very close to l_{max}. These results lead to a conclusion that a dicarboxylic acid is bent in a nearly V- or U-shape in solution and the bending may be enhanced with chain length. The fact that *p*-phthalic acid has a larger value of θ than that of *o*-phthalic acid supports the model we used. Values of a obtained from $pK_2 - pK_1$ values in aqueous solu-

Table 2. Parameters of various dicarboxylic acids

	a (Å)	θ (°)	$l = 2r$ (Å)	l_{max} (Å)
$HOOCCH_2COOH$	2.81	100	3.67	
$HOOCCH(CH_3)COOH$	2.58	100	3.37	
$HOOCC(CH_3)(C_2H_5)COOH$	2.12	100	2.77	
$HOOCC(C_2H_5)_2COOH$	1.84	100	2.40	
$HOOC(CH_2)_4COOH$	5.53	70	8.38	9.02[a], 6.65[b]
$HOOC(CH_2)_5COOH$	5.78	70	10.07	9.91[a], 7.40[b]
$HOOC(CH_2)_8COOH$	5.60	70	9.76	11.46[b]
$HOOC(CH_2)_{10}COOH$	7.10	70.2	12.37	13.93[b]
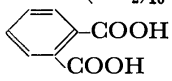	2.72	100	3.55	
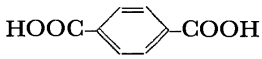	3.03	145	3.18	

a) Ref. 29.
b) Ref. 31.

Table 3. Values of a of dicarboxylic acids estimated by various authors

	Tanford[30] (Westheimer Shookhoff)[29]	Peek and Hill[33]	Ninomiya and Tōei[32]	Present work
$HOOCCH_2COOH$	4.10			2.81
$HOOCCH(CH_3)COOH$	4.05			2.58
$HOOCC(C_2H_5)_2COOH$	3.75			1.84
$HOOCC(CH_3)(C_2H_5)COOH$	4.10			2.12
$HOOC(CH_2)_4COOH$	7.75	5.99	5.72	5.53
$HOOC(CH_2)_5COOH$	8.30	6.57	6.79	5.78
$HOOC(CH_2)_6COOH$	9.30	7.59	7.64	
$HOOC(CH_2)_7COOH$	9.85	8.22	7.86	
$HOOC(CH_2)_8COOH$	9.60	9.17	8.21	5.60
$HOOC(CH_2)_{10}COOH$	11.20	10.37	8.81	7.10

29) F. H. Westheimer and M. W. Shookhoff, *J. Amer. Chem. Soc.*, **61**, 555 (1939).
30) C. Tanford, *ibid.*, **79**, 5348 (1957).
31) H. M. Peek and T. L. Hill, *ibid.*, **73**, 5304 (1951).
32) A. Ninomiya and K. Tōei, *Nippon Kagaku Zasshi*, **90**, 655 (1969).

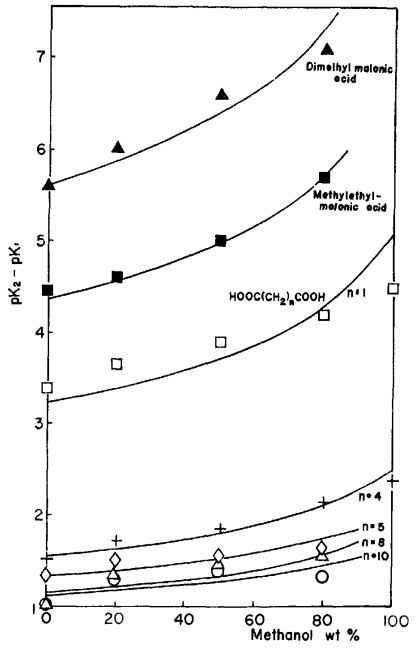

Fig. 1. pK_2—pK_1 of some dicarboxylic acids in water–methanol mixtures. Solid lines show calculated values of pK_2—pK_1 of the acids with parameters listed in Table 2.

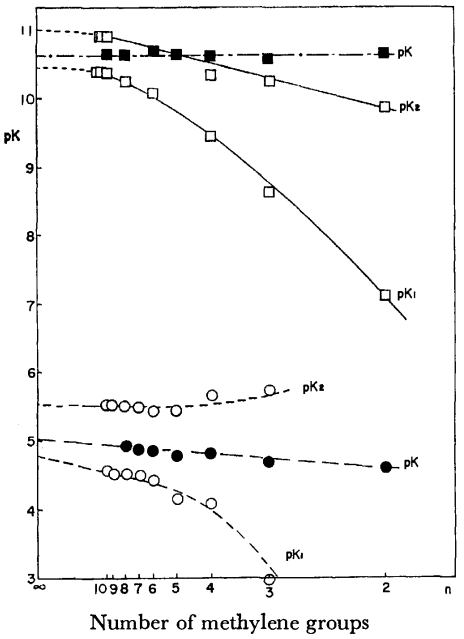

Fig. 2. Variations of pK_1 and pK_2 of dicarboxylic acids[32] and diamines in aqueous solutions with the number of methylene groups in the molecule: ○ dicarboxylic acids, ● monocarboxylic acid, □ diamines, ■ monoamines.

tions are summarized in Table 3. The values calculated by the present method are slightly smaller than others but seem reasonable.

(2) Variation of pK_2-pK_1 for Diamines with Solvent Composition. The value of pK_2-pK_1 varied with solvent composition in a different manner from that of dicarboxylic acids; the pK_2-pK_1 value was practically independent of methanol concentrations. As ε_e in Eq. (3) is expected to decrease with the increase of the methanol concentration, a should increase in order to keep the pK_2-pK_1 value in solution constant independent of solvent compositions. Increase of a caused by the addition of methanol into aqueous solution may be qualitatively interpreted in terms of the following effects: (1) Electrostatic repulsion between charged sites increases with the decrease of the effective dielectric constant. (2) It is known that hydrophobic groups in molecules tend to gather in hydrophilic solvent. However, the addition of methanol makes the solvent less hydrophilic so that hydrophobic coagulation of methylene groups may be reduced and the molecule turns out to be stretched. (3) The hydrogen bond between amino groups through water molecules may partly be broken by the addition of methanol, although no definite evidence for the hydrogen bond formation between amino groups in a molecule has been found.

(3) Variation of pK_1 and pK_2 for Diamines with Chain Length and with Solvent Composition. In aqueous solution both pK_1 and pK_2 of a diamine are smaller than the pK of the corresponding monoamine when the chain is short, pK_2 increasing with chain length in such a way to cross pK's of monoamines (Fig. 2). At a given solvent composition variations of pK_1 and pK_2 are similar to those of pK's of monoamines. Since the interaction between charges, that is pK_2-pK_1, in a diamine molecule can be assumed to be practically constant, we can assume that free energy changes caused by the interaction between charges is independent of solvent composition and therefore, variations of pK_1 and pK_2 can be treated separately as if there were two independent acids, each having dissociation constants of pK_1 and pK_2. Therefore, equations proposed to monoamines can be used also for diamines. For an acid of BH^+ type, $\Delta pK=pK(s)-pK(w)$ is written as follows:

$$\Delta pK = [(\mu^\circ_{BH}(w)-\mu^\circ_{BH}(s))+(\mu^\circ_{H_2O}(w)-(1-x)\mu^\circ_{H_2O}(s) - x\mu^\circ_{ROH}(s))+(\mu^\circ_{B}(s)-\mu^\circ_{B}(w))+((1-x)\mu^\circ_{H_2O}(s) + x\mu^\circ_{ROH_2}(s)-\mu^\circ_{H_2O}(w))]/RT\ln 10 \quad (4)$$

where $\mu^\circ(w)$ and $\mu^\circ(s)$ stand for standard chemical potentials of a relevant species in water and an aqueous methanol solution, respectively, x a fraction of meth-

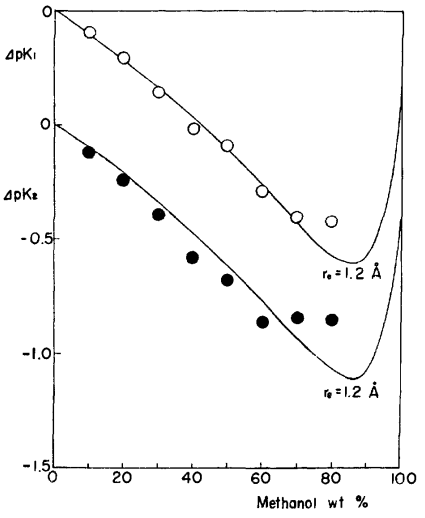

Fig. 3. Variations of ΔpK_1 and ΔpK_2 of 1,6-hexanediamine with the solvent composition.

oxonium ion formed from one mole of proton and is given by the equation

$$x = \frac{\kappa y}{1-y+\kappa y} \quad (5)$$

where y represents the mole fraction of methanol in the solvent. κ is the equilibrium constant of reaction (1).

By application of models proposed by one of the authors (H. O.),[10] we can calculate free energy changes of transfer of species from aqueous solution to a mixed solvent and thus ΔpK, assuming an effective size of a functional group r_e in a diamine molecule. Typical results for ΔpK_1 and ΔpK_2 are shown in Fig. 3 for 1,6-hexanediamine. The effective sizes of each amino group in the diamine were evaluated to be $r_e=1.2$ Å. The value 1.2—1.3 Å of r_e was found for other diamines regardless of the chain length. For ammonium and diethylethanol ammonium ions, the effective sizes of the functional groups were estimated to be 1.4—1.5 Å. The slightly smaller values of r_e for diamines than those for ammonium and diethylethanol ammonium ions may be due to the interaction between charged groups in diamine molecules, the solvent effect on which is neglected in calculation of ΔpK of diamines. The different interactions between an ammonium ion or a tertiary amino group in diethylethanol ammonium ion and a primary amino group of a diamine with solvent molecules might give rise to different values of r_e.

BULLETIN OF THE CHEMICAL SOCIETY OF JAPAN, VOL. 46, 2056—2060 (1973)

The Triplet Excitons in the Anion Radical Salts of $[(C_6H_5)_3PCH_3]_{1-x}^+$ $[(C_6H_5)_3AsCH_3]_x^+$ $(TCNQ)_2^+$, $(0 \leq x \leq 1)$

Yukio Suzuki and Yôichi Iida

Department of Chemistry, Faculty of Science, Hokkaido University, Sapporo 060

(Received December 16, 1972)

The electron spin resonance (ESR) absorption and its variation with the temperature were measured with single crystals of the anion radical salts containing the mixed cations, $[(C_6H_5)_3PCH_3]_{1-x}^+$ $[(C_6H_5)_3AsCH_3]_x^+$ $(TCNQ)_2^-$, $(0 \leq x \leq 1)$. The paramagnetic excited state of these salts is triplet in character, as was shown from the anisotropic zero-field splitting at low temperatures. The triplet state is not localized, but, rather, corresponds to the triplet exciton state. The exciton exchange frequency and its temperature dependence were determined by analyzing the line shapes of the ESR spectra. The exciton motion in the mixed crystal system was investigated in order to establish the character of the triplet excitons in ion radical salts.

Much attention has been paid to the solid anion radical salts of 7,7,8,8-tetracyanoquinodimethane (TCNQ) because of their prominent electronic properties.[1-24] In particular, the anion radical salts of $[(C_6H_5)_3PCH_3]^+$ $(TCNQ)_2^-$ and $[(C_6H_5)_3AsCH_3]^+$ $(TCNQ)_2^-$ have been found to possess non-singlet, excited crystal states lying very close to a singlet ground state.[6] These excited states are triplet in character, as has been demonstrated by electron spin resonance (ESR) studies of the anisotropic zero-field splitting.[1] The excited states of such a system are thought not to be localized, but, rather, to correspond to the exciton states; that is, the excitation may propagate as a quasi-particle (*i.e.*, a triplet exciton).[4]

On the other hand, one can prepare anion radical salts containing the mixed cations represented by $[(C_6H_5)_3PCH_3]_{1-x}^+$ $[(C_6H_5)_3AsCH_3]_x^+$ $(TCNQ)_2^-$, $(0 \leq x \leq 1)$.[2] In the present paper, we found that these mixed crystals also show the ESR spectra charac-

1) D. B. Chesnut and W. D. Phillips, *J. Chem. Phys.*, **35**, 1002 (1961).
2) L. R. Melby, R. J. Harder, W. R. Hertler, W. Mahler, R. E. Benson, and W. E. Mochel, *J. Amer. Chem. Soc.*, **84**, 3374 (1962).
3) D. B. Chesnut and P. Arthur, Jr., *J. Chem. Phys.*, **36**, 2969 (1962).
4) M. T. Jones and D. B. Chesnut, *ibid.*, **38**, 1311 (1963).
5) W. J. Siemons, P. E. Bierstedt, and R. G. Kepler, *ibid.*, **39**, 3523 (1963).
6) R. G. Kepler, *ibid.*, **39**, 3528 (1963).
7) D. B. Chesnut and A. Suna, *ibid.*, **39**, 146 (1963); H. M. McConnell and C. G. Montgomery, *ibid.*, **39**, 252 (1963).
8) D. B. Chesnut, *ibid.*, **41**, 472 (1964).
9) D. B. Chesnut, *ibid.*, **40**, 405 (1964).
10) Y. Iida, M. Kinoshita, M. Sano, and H. Akamatu, This Bulletin, **37**, 428 (1964).
11) Y. Iida, M. Kinoshita, A. Kawamori, and K. Suzuki, *ibid.*, **37**, 764 (1964).
12) H. M. McConnell and Z. G. Soos, *J. Chem. Phys.*, **42**, 586 (1964).
13) A. W. Merkl, R. C. Hughes, L. J. Berliner, and H. M. McConnell, *ibid.*, **43**, 953 (1965).
14) Z. G. Soos and H. M. McConnell, *ibid.*, **43**, 3780 (1965).
15) Y. Marechal and H. M. McConnell, *ibid.*, **43**, 4126 (1965).
16) P. Nordio, Z. G. Soos, and H. M. McConnell, *Ann. Rev. Phys. Chem.*, **17**, 237 (1966).
17) Z. G. Soos and R. C. Hughes, *J. Chem. Phys.*, **46**, 253 (1967).
18) J. C. Bailey and D. B. Chesnut, *ibid.*, **51**, 5118 (1969).
19) Y. Iida, This Bulletin, **42**, 71, 637 (1969).
20) Y. Iida, *ibid.*, **43**, 578, 3685 (1970).
21) A. Kosaki, Y. Iida, M. Sorai, H. Suga, and S. Seki, *ibid.*, **43**, 2280 (1970).
22) Y. Iida, *J. Phys. Soc. Jap.*, **30**, 583 (1971); Y. Iida, *J. Chem. Phys.*, in press.
23) Y. Iida, *Bussei*, **12**, 198 (1971).
24) Y. Iida, This Bulletin, **44**, 3344 (1971).

teristic of the triplet excitons. At various temperatures, the exchange frequencies due to triplet exciton motion were evaluated by analyzing the line shapes of the observed ESR spectra. In these mixed crystals, if the mixed cations are randomly arranged, the crystal lattice will no longer be periodic. At this time, the triplet exciton exchange and the exciton motion will be much affected in the field of the irregular crystal lattice. In this respect, it is interesting to compare the results of our study with those of the regular crystal lattice for $[(C_6H_5)_3PCH_3]^+$ $(TCNQ)_2^-$ or $[(C_6H_5)_3AsCH_3]^+$ $(TCNQ)_2^-$.[4]

Experimental

Materials. The preparation of TCNQ has been described by Acker and Hertler.[25] It was purified by recrystallization from acetonitrile. The anion radical salts containing the mixed cations, $[(C_6H_5)_3PCH_3]_{1-x}^+$ $[(C_6H_5)_3AsCH_3]_x^+$ $(TCNQ)_2^-$, $(0\leq x\leq 1)$, were synthesized according to the method of Melby *et al.*[2] Six salts with the compositions of $x=0.00$, 0.20, 0.40, 0.60, 0.80, and 1.00 were prepared. They were taken from the same batches as those previously used for the differential scanning calorimeter (DSC) measurements and the electrical conductivity measurements.[20,22,23]

Measurements. The ESR spectra of the single crystals (5 mm×5 mm×1 mm) in the temperature range from 112 K to 333 K were measured by means of a JES-ME X-band spectrometer. The steady magnetic field was modulated at 100 KHz, with a modulation amplitude of 0.32 gauss. The temperature of the specimen was controlled to within ±1 K by means of the temperature equipment.

Results

The ESR spectra of the triplet excitons in the anion radical salts of $[(C_6H_5)_3PCH_3]^+$ $(TCNQ)_2^-$, $(x=0.00)$, and $[(C_6H_5)_3AsCH_3]^+$ $(TCNQ)_2^-$, $(x=1.00)$, have been described by Jones and Chesnut.[4] Therefore, let us examine the mixed crystals below. As an example, the salt of $[(C_6H_5)_3PCH_3]_{0.20}^+$ $[(C_6H_5)_3AsCH_3]_{0.80}^+$ $(TCNQ)_2^-$, $(x=0.80)$, will be investigated in detail.

The ESR absorption of a single crystal of $[(C_6H_5)_3PCH_3]_{0.20}^+$ $[(C_6H_5)_3AsCH_3]_{0.80}^+$ $(TCNQ)_2^-$ and its variation with the temperature were measured for three arbitrary orientations. Figure 1 shows the experimental results for one of the orientations. Striking temperature effects were found in the ESR spectra. At low temperatures (approximately at 112 K), doublet components of the triplet-state fine structure and a central paramagnetic impurity signal[26] were observed. The doublet components are sharp (about 0.7_0 gauss in width) and well-resolved. These doublet components, the separation of which is quite anisotropic, arise from the zero-field splitting of the triplet state in the absence of the triplet exciton exchange.[1] As the temperature is raised, the doublet components broaden and move together, eventually collapsing into a single line which becomes progressively sharper, approaching

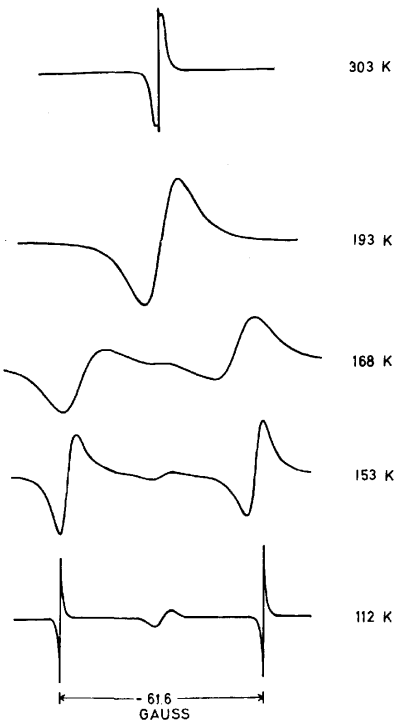

Fig. 1. The temperature dependence of the ESR absorption of a single crystal of the $[(C_6H_5)_3PCH_3]_{0.20}^+$ $[(C_6H_5)_3AsCH_3]_{0.80}^+$ $(TCNQ)_2^-$ salt for the $d_0=61.6$ gauss orientation. The spectra were obtained with different spectrometer gain settings at the different temperatures.

a limit of about 1.9_0 gauss in width at room temperature;[27] these changes were found to be thermally reversible. This spectroscopic behavior is characteristic of an exchange interaction, a process which first removes the fine structure (exchange broadening) and then sharpens up the single remaining resonance line (exchange narrowing).

Figure 2 demonstrates the temperature dependence of the ESR spectra of the same salt for another orientation, where the separation of the fine-structure splitting at low temperature is narrower than that in Fig. 1. In this case, the temperature at which the doublet components collapse into a single line was found to be lower than that in Fig. 1. However, the line-widths of the absorptions at the low and high temperature limits were practically the same as those in Fig. 1.

Discussion

There have been various treatments of exchange-narrowing phenomena in magnetic resonance spectra.[28,29] Jones and Chesnut have applied Bloch equa-

25) D. S. Acker and W. R. Hertler, *J. Amer. Chem. Soc.*, **84**, 3370 (1962).

26) The ESR absorption intensity of the central absorption decreased, as the temperature was raised, according to the Curie law.

27) It was noticed that, in addition to the exchange-narrowed absorption, a sharp spike of absorption appeared in the room-temperature ESR spectra. However, no such sharp spike was observed when another smaller crystal was taken as a specimen. The extra absorption may arise from some skin effect, since this material is known to show high electrical conduction.

28) H. S. Gutowsky and A. Saika, *J. Chem. Phys.*, **21**, 1688 (1953); H. S. Gutowsky and C. H. Holm, *ibid.*, **25**, 1228 (1956); H. M. McConnell, *ibid.*, **28**, 430 (1958); L. H. Piette and W. A. Anderson, *ibid.*, **30**, 899 (1959).

29) P. W. Anderson, *J. Phys. Soc. Jap.*, **9**, 316 (1954); D. Kivelson, *J. Chem. Phys.*, **27**, 1087 (1957).

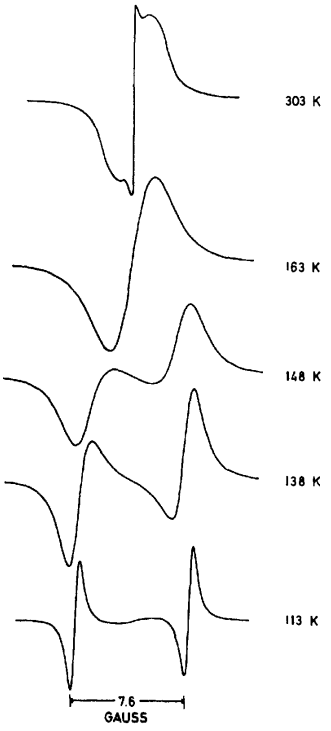

Fig. 2. The temperature dependence of the ESR absorption of a single crystal of the $[(C_6H_5)_3PCH_3]_{0.20}^+$ $[(C_6H_5)_3AsCH_3]_{0.80}^+$ $(TCNQ)_2^-$ salt for the $d_0=7.6$ gauss orientation.

tions modified to include the effect of exchange to the systems of $[(C_6H_5)_3PCH_3]^+$ $(TCNQ)_2^-$, $(x=0.00)$, and $[(C_6H_5)_3AsCH_3]^+$ $(TCNQ)_2^-$, $(x=1.00)$,[4] which show two-line spectra arising from the zero-field splitting of $S=1$ species. In the following discussion, we shall also examine the exchange effects of the triplet state in the mixed crystals by applying this method to $[(C_6H_5)_3PCH_3]_{0.20}^+$ $[(C_6H_5)_3AsCH_3]_{0.80}^+$ $(TCNQ)_2^-$, $(x=0.80)$, and will compare them with those for the regular crystal lattices for $[(C_6H_5)_3PCH_3]^+$ $(TCNQ)_2^-$ and $[(C_6H_5)_3AsCH_3]^+$ $(TCNQ)_2^-$.

For the ESR absorption of the simple two-line case, we can express the line separation, d, and the line width, ΔH, in terms of the exchange frequency, ν. For the slow exchange region $(d_0 \gg \sqrt{2}\nu/\gamma)$:

$$\gamma^2(d_0^2-d^2) = 2\nu^2, \tag{1}$$

$$\gamma(\Delta H-\Delta H_0) = \nu/\sqrt{3}, \tag{2}$$

while for the fast exchange region $(d_0 \ll \sqrt{2}\nu/\gamma)$:

$$2\sqrt{3}(\Delta H-\Delta H_0) = \gamma d_0^2/\nu, \tag{3}$$

$$d = 0, \tag{4}$$

where ΔH and ΔH_0 are the linewidths in gauss measured from the points of maximum slope of the first derivative of the absorption in the presence and in the absence of exchange respectively. d and d_0 are the separation of the two lines in gauss with and without exchange respectively, and γ is the gyromagnetic ratio of the electron. These equations demonstrate that, when the exchange frequency is increased, each of the two spectral lines broadens and shifts towards the center of the spectrum, and then the two lines collapse into a single broad line, which becomes progressively sharper. The limiting line width in both extremes is given by ΔH_0.

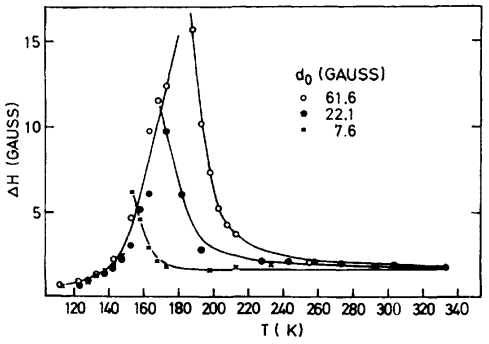

Fig. 3. Plots of line width of the ESR absorption *versus* temperature in K for various orientations of a single crystal of the $[(C_6H_5)_3PCH_3]_{0.20}^+$ $[(C_6H_5)_3AsCH_3]_{0.80}^+$ $(TCNQ)_2^-$ salt.

These theoretical features agree well with those of our experimental results in Fig. 3, which shows the line-width measurements of the ESR absorptions of $[(C_6H_5)_3PCH_3]_{0.20}^+$ $[(C_6H_5)_3AsCH_3]_{0.80}^+$ $(TCNQ)_2^-$, $(x=0.80)$, as functions of the temperature (and, thus, of the exchange frequency) for several crystal orientations (different values of d_0). The various curves in Fig. 3 intersect at the point where $\nu=\gamma d_0$. In the left region of this point (in the lower temperature region), we observed a two-line spectrum for slow exchange, but in the right region (in the higher temperature region), we observed a single-line spectrum for fast exchange. The application of the above simple two-line analysis to our experimental results is supported by the fact that the intersection at $\nu=\gamma d_0$ takes place at lower temperatures as d_0 is decreased and that, in the slow-exchange region, ΔH is found to depend only on the temperature.

For $[(C_6H_5)_3PCH_3]_{0.20}^+$ $[(C_6H_5)_3AsCH_3]_{0.80}^+$ $(TCNQ)_2^-$, $(x=0.80)$, the values of the exchange frequencies, ν, were determined from the observed ESR spectra as a function of the temperature. For three crystal orientations, the calculations were made by the use of the approximations expressed by Eqs. (1), (2), and (3) respectively. The values of d_0 were taken as the limiting values of d at low temperatures. ΔH_0 was taken in a similar way, using the high- or low-temperature limits. For the three d_0 orientations, the estimated values of ν *versus* the temperature are illustrated in Figs. (4)—(6), in which the signs of $\nu(1)$, $\nu(2)$, and $\nu(3)$ indicate the values estimated by using Eqs. (1), (2), and (3) respectively.

In general, it was found that a good linear relation was obtained when the logarithm of the exchange frequency was plotted against the reciprocal of the absolute temperature. Therefore, the exchange frequency, ν, was described by:

$$\nu = \nu_0 \exp(-\Delta E/kT), \tag{5}$$

where ΔE is the activation energy for exchange. The parameters of ν_0 and ΔE were determined from the slow-exchange line collapse of Eq. (1), the slow-exchange line broadening of Eq. (2), and the fast-exchange line narrowing of Eq. (3). They are denoted as $\nu_0(i)$ and $\Delta E(i)$ $(i=1, 2, \text{and } 3)$ respectively. The estimated values are collected in Table 1, together with those for

Table 1. Exchange parameters of $\nu_0(i)$ and $\Delta E(i)$, ($i=1$, 2, and 3), for the anion radical salts of $[(C_6H_5)_3PCH_3]_{1-x}^+$ $[(C_6H_5)_3AsCH_3]_x^+$ $(TCNQ)_2^-$, ($0 \leq x \leq 1$)[a]

Composition parameter, x	d_0 (gauss)	$\nu_0(1)$ (Hz)	$\Delta E(1)$ (eV)	$\nu_0(2)$ (Hz)	$\Delta E(2)$ (eV)	$\nu_0(3)$ (Hz)	$\Delta E(3)$ (eV)	Reference
0.80	7.6	5.6×10^{10} (±2.0)	0.11 (±0.01)	1.6×10^{13} (±0.9)	0.20 (±0.01)	—	—	This work
	22.1	5.4×10^{11} (±2.3)	0.14 (±0.01)	2.9×10^{13} (±1.1)	0.22 (±0.02)	1.5×10^{13} (±3.9)	0.19 (±0.02)	This work
	61.6	4.0×10^{9} (±1.4)	0.048 (±0.003)	9.2×10^{11} (±2.1)	0.15 (±0.01)	1.4×10^{13} (±3.6)	0.17 (±0.02)	This work
0.00	—	1.4×10^{10} (±0.2)	0.042 (±0.001)	1.6×10^{12} (±0.9)	0.13 (±0.01)	5.4×10^{14} (±4.6)	0.19 (±0.01)	4
1.00	—	2.8×10^{10} (±1.2)	0.050 (±0.007)	3.5×10^{12} (±4.8)	0.11 (±0.02)	3.3×10^{13} (±2.5)	0.16 (±0.01)	4

a) The values of $\nu_0(i)$ and $\Delta E(i)$, ($i=1$, 2, and 3), were derived from Eqs. (1), (2), and (3), respectively.

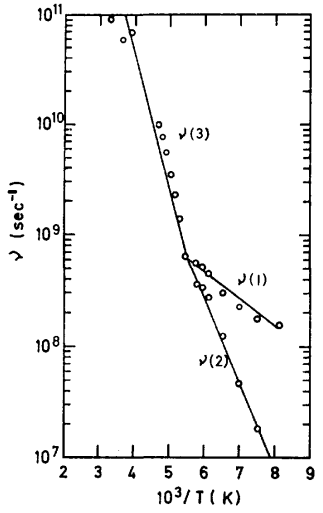

Fig. 4. Semilog plot of ν *versus* $1/T$ K for the $d_0=61.6$ gauss orientation of a single crystal of the $[(C_6H_5)_3PCH_3]_{0.20}^+$ $[(C_6H_5)_3AsCH_3]_{0.80}^+$ $(TCNQ)_2^-$ salt. $\nu(1)$, $\nu(2)$, and $\nu(3)$ indicate the values derived from Eqs. (1), (2), and (3), respectively.

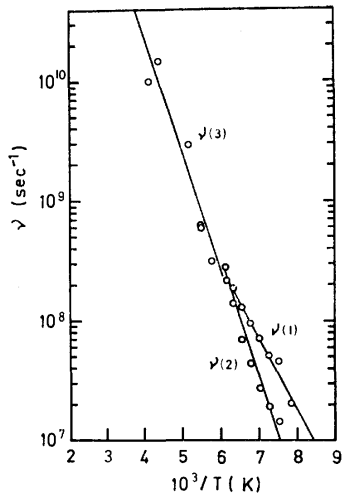

Fig. 5. Semilog plot of ν *versus* $1/T$ K for the $d_0=22.1$ gauss orientation of a single crystal of the $[(C_6H_5)_3PCH_3]_{0.20}^+$ $[(C_6H_5)_3AsCH_3]_{0.80}^+$ $(TCNQ)_2^-$ salt.

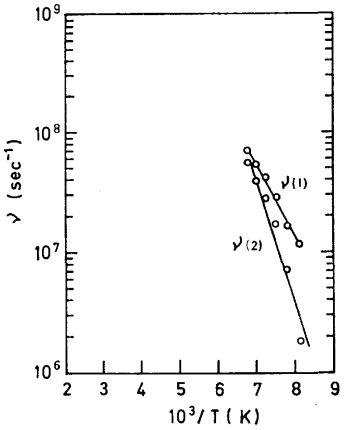

Fig. 6. Semilog plot of ν *versus* $1/T$ K for the $d_0=7.6$ gauss orientation of a single crystal of the $[(C_6H_5)_3PCH_3]_{0.20}^+$ $[(C_6H_5)_3AsCH_3]_{0.80}^+$ $(TCNQ)_2^-$ salt.

the salts of $[(C_6H_5)_3PCH_3]^+$ $(TCNQ)_2^-$, ($x=0.00$), and $[(C_6H_5)_3AsCH_3]^+$ $(TCNQ)_2^-$, ($x=1.00$).[4] These parameters were obtained by the method of least-squares. For the $d_0=7.6$ gauss orientation, however, we could scarcely determine the $\nu_0(3)$ and $\Delta E(3)$ values, since the estimation of $\nu(3)$ *versus* the temperature could not be made over the wide temperature range.

For $[(C_6H_5)_3PCH_3]_{0.20}^+$ $[(C_6H_5)_3AsCH_3]_{0.80}^+$ $(TCNQ)_2^-$, ($x=0.80$), the data given in Table 1 show that $\Delta E(3) \geqslant \Delta E(2) > \Delta E(1)$ and $\nu_0(3) \geq \nu_0(2) > \nu_0(1)$. As has been pointed out by Jones and Chesnut,[4] for the exchange effect of the triplet exciton system, the simple two-site exchange model may yield different ν_0 and ΔE values, depending on whether one uses Eqs. (1), (2), or (3). This is also shown by the experimental results we give in Table 1. Rigorously speaking, according to the calculations by Lynden-Bell,[30] the simple two-site model is not always applicable to the triplet-exciton system. However, for purposes of comparison with those for $[(C_6H_5)_3PCH_3]^+$ $(TCNQ)_2^-$ and $[(C_6H_5)_3AsCH_3]^+$ $(TCNQ)_2^-$, the simple two-site analysis was applied to the present case. Except for the small d_0 crystal orientation, the values of $\nu_0(i)$ and $\Delta E(i)$ ($i=1$, 2, and 3) in $[(C_6H_5)_3PCH_3]_{0.20}^+$ $[(C_6H_5)_3AsCH_3]_{0.80}^+$ $(TCNQ)_2^-$ were found to coincide well

30) R. M. Lynden-Bell, *Mol. Phys.*, **8**, 71 (1964).

with those for the regular crystal lattice in $[(C_6H_5)_3PCH_3]^+$ $(TCNQ)_2^-$ or $[(C_6H_5)_3AsCH_3]^+$ $(TCNQ)_2^-$ respectively, within the limits of experimental error.[4] The apparent values of $\Delta E(i)$ ($i=1$, 2, and 3) were found to be somewhat anisotropic; larger values of $\Delta E(i)$ were obtained for the smaller d_0 crystal orientation. As d_0 approaches zero, however, the straight application of Eqs. (1)—(3) may cause apparent ΔE anisotropy, since one can hardly measure the linewidth accurately because of the overlap of the two lines.

The exchange effect of the triplet state can be understood in terms of the movement of pseudo-particles with spin 1 (*i.e.*, triplet excitons). The ESR spectra of the triplet excitons do not show any hyperfine structure, even at low temperatures, since their mobility causes its motional narrowing. At higher temperature, as the concentration of the excitons is increased, the mutual collisions of the triplet excitons lead to an exchange-narrowing effect of the triplet-state fine structure. Thus, we can relate the exchange frequency, ν, to the collision frequency of the triplet excitons:

$$\nu \propto n\sigma v, \tag{6}$$

where n is the concentration of triplet excitons; v, an average propagation velocity, and σ, an effective cross-section for triplet-exciton collisions. For our system below room temperature, we can approximately take:

$$n \propto [\exp(J/kT)+3]^{-1} \approx \exp(-J/kT), \tag{7}$$

where J is the energy difference between the singlet ground state and the triplet excited state. According to Kepler's susceptibility measurements,[6] $J=0.065$ eV below room temperature for the salts of $[(C_6H_5)_3PCH_3]_{1-x}^+$ $[(C_6H_5)_3AsCH_3]_x^+$ $(TCNQ)_2^-$, $(0\leq x\leq 1)$. Judging from our experimental expression of $\nu=\nu_0 \exp(-\Delta E/kT)$ for the salt with $x=0.80$, the $\Delta E\approx J$ equality should exist if we assume that σ and v are not strongly temperature-dependent. However, our experimental results given in Table 1 show this correlation not to be generally correct. In general, $\Delta E(1)$, $\Delta E(2)$, $\Delta E(3)>J$, except $\Delta E(1)<J$ for the $d_0=61.6$ gauss crystal orientation. Jones and Chesnut have considered that ΔE might exceed J if the propagation of the triplet exciton could involve an activated process (*i.e.*, a diffusional propagation) with an activation energy of $\Delta E_v=\Delta E-J$, that is:[4]

$$v \propto \exp(-\Delta E_v/kT). \tag{8}$$

In this case, the foregoing anisotropy of the ΔE values, if it exists, seems to be attributable to that of the ΔE_v values.

According to the X-ray diffraction studies by McPhail *et al.*,[31] the crystal structures of both $[(C_6H_5)_3PCH_3]^+$ $(TCNQ)_2^-$ and $[(C_6H_5)_3AsCH_3]^+$ $(TCNQ)_2^-$ are triclinic and isomorphous.[32] The planar TCNQ molecules are stacked face-to-face to form a column along the b-axis. Four TCNQ molecules form a repeating unit in the column. The ion radius of the arsonium cation is somewhat longer than that of the phosphonium cation. It is almost certain that the crystal structures of the salts containing the mixed cations are identical with that of the phosphonium or arsonium salt. This kind of molecular stacking should then lead to anisotropic ΔE_v values if the triplet exciton can be described by the diffusional process. At present, a question remains in which crystal direction the activation energy, ΔE_v, has its maximum and minimum values.

Up to now, extensive investigations have been made to distinguish whether or not the triplet excitons in ion radical salts can be characterized by "localized excitons" or "free excitons."[7,8,13–16] The localized exciton carries a distortion with it as it goes through the crystal lattice. The exciton motion is, then, represented by a hopping from one cell to the next through a random walk (*i.e.*, diffusional process). On the other hand, the free exciton goes through the crystal lattice, carries with it essentially no crystal distortion, and has a long mean free path. The free exciton is, then, expressed by extended wave packets distributed over the whole lattice. In the salts containing mixed cations, if the mixed cations are randomly arranged, the crystal lattices will no longer be periodic. In this case, the free excitons are strongly scattered by the irregular crystal lattices, while the localized excitons are not. The present ESR experimental results support the model of localized triplet excitons, since the observed ν_0 and ΔE values for $[(C_6H_5)_3PCH_3]_{0.20}^+$ $[(C_6H_5)_3AsCH_3]_{0.80}^+$ $(TCNQ)_2^-$ coincide well with those in the regular crystal lattices for $[(C_6H_5)_3PCH_3]^+$ $(TCNQ)_2^-$ and $[(C_6H_5)_3AsCH_3]^+$ $(TCNQ)_2^-$ respectively.[4] Soos and McConnell have found that the activation energy for diffusion, ΔE_v, is essentially $\Delta/2$ where Δ is the "self-trapping energy" of the triplet exciton due to exciton-phonon interaction.[14] These results suggest that, at least in the anion radical salts of $[(C_6H_5)_3PCH_3]_{1-x}^+$ $[(C_6H_5)_3AsCH_3]_x^+$ $(TCNQ)_2^-$, $(0\leq x\leq 1)$, the best picture of the triplet-exciton motion is one in which a localized exciton rapidly hops from one site to the next. The motion is, then, "random walk" or diffusional.

31) A. T. McPhail, G. M. Semeniuk, and D. B. Chesnut, *J. Chem. Soc., A*, **1971**, 2174.

32) The electronic state and the crystal properties of the phosphonium salt are very similar to those of the arsonium salt, except for the occurrence of the phase transition of the phosphonium salt at 315.7 K. See Refs. 1,2,4–6,9–11,16,19–24.

The Simultaneous Detection of Gas Phase Atoms and Free Radicals Produced in a Microwave Discharge by ESR Spin Trapping Methods

Edward G. JANZEN,* Toshio KASAI, and Keiji KUWATA

Department of Chemistry, Faculty of Science, Osaka University, Toyonaka, Osaka 560

* *Department of Chemistry, The University of Georgia, Athens, Georgia, 30601 U.S.A.*

(Received December 16, 1972)

The simultaneous detection of gas phase atoms and free radicals produced in a 2450 MHz discharge is demonstrated by use of a previously described technique called spin trapping. The atoms or radicals are allowed to react with phenyl *N*-*t*-butyl nitrone to give relatively stable nitroxide radicals. The ESR spectra of these nitroxides provide the analytical data for identification of the atoms or radicals trapped.

In previous communications we have described a technique for the detection and identification of gas phase free radicals which depends on the rapid radical addition to phenyl *t*-butyl nitrone (PBN) to produce relatively stable nitroxyl radicals:[1,2]

$$R\cdot + C_6H_5CH{=}N(O)C(CH_3)_3 \longrightarrow C_6H_5CH(R)\overset{+}{N}(\overset{-}{O})\cdot C(CH_3)_3$$

The ESR spectra of the nitroxyl radicals recorded at room temperature in liquid solutions (*e.g.* in benzene) provide ideally an unique set of parameters for each radical (R·) trapped. We have called this technique spin trapping and the nitroxyl radicals produced spin adducts.[3,4]

The previously reported gas phase work demonstrated the feasibility of detecting radicals at atmospheric pressures in a carrier gas (N_2) *e.g.* methyl, ethyl, and perfluoroethyl,[1] or at total pressures as low as 0.1 Torr in the presence of the radical precursor *e.g.* methyl from acetone or azomethane, ethyl from 3-pentanone, tetraethyllead or diethylmercury.[2] We now wish to report that hydrogen atoms can be detected simultaneously with radicals in the gas phase by spin trapping methods.

Experimental

A well established source of hydrogen atoms is the microwave discharge of hydrogen molecules. By placing powdered PBN in a 8 mm glass tube about 10—20 cm downstream from the microwave discharge of hydrogen in an apparatus similar to the one shown in Fig. 1, Ref. 2, benzyl *t*-butyl nitroxide, the hydrogen atom adduct of PBN is readily detected in a benzene solution of either the powdered PBN itself or the material collected in the liquid nitrogen trap downstream;

$$H_2 \longrightarrow H\cdot \xrightarrow{PBN} C_6H_5CH_2N(O\cdot)C(CH_3)_3$$

Results and Discussion

Deuterium molecules (D_2) gave the deuterium atom spin adduct in addition to some hydrogen atom addition product (see Table 1 for splitting constants). In some experiments with H_2 or D_2 an additional triplet of doublets was also observed which is tentatively assigned to the hydroxy radical spin adduct presumably produced from the discharge of water vapor inadvertently present in the system. Assignment of this structure is based on the results obtained from water vapor discharge which itself produces a strong hydrogen atom adduct signal and the same triplet of doublets. A previous spectral assignment to this spin adduct does not appear to be correct.[1] Ammonia discharge has only given the hydrogen atom adduct (and the hydroxy radical adduct in some cases). No amino radicals have been detected to date but this result is not considered final.

Fig. 1. ESR spectrum of hydrogen atom and methyl radical addition products of phenyl *N*-*t*-butyl nitrone (benzyl and α-methyl *t*-butyl nitroxides) in benzene at room temperature isolated from microwave discharge of methane (see Table 1); top: experimental result; bottom: computer simulated sum of the two spectra.

The nature of the products of microwave discharge of organic compounds has been the subject of some interest in the past.[5-7] Hydrogen, acetylene, and

* On leave from the Department of Chemistry, The University of Georgia, Athens, Georgia, U.S.A., January–June, 1972.

1) E. G. Janzen and J. L. Gerlock, *Nature*, **222**, 867 (1969).

2) E. G. Janzen and I. G. Lopp, *J. Phys. Chem.*, **76**, 2056 (1972).

3) E. G. Janzen and B. J. Blackburn, *J. Amer. Chem. Soc.*, **91**, 4481 (1969).

4) For reviews of this technique, see E. G. Janzen, *Accounts Chem. Res.*, **4**, 31 (1971); C. Lagercrantz, *J. Phys. Chem.*, **75**, 3466 (1971); M. J. Perkins, *Chem. Soc. Spec. Publ.*, No. 24, 97 (1970).

5) R. L. McCarthy, *J. Chem. Phys.*, **22**, 1360 (1954).

6) A. Streitwieser, *J. Amer. Chem. Soc.*, **84**, 1065 (1962); A. Streitwieser and H. R. Ward, *ibid.*, **85**, 539 (1963).

7) "Chemical Reactions in Electric Discharges," Advances in Chemistry Series, No. 80, American Chemical Society, Washington, D. C., 1969; see for example: J. P. Wightman and N. J. Johnston, p. 322; D. D. Neiswender, p. 338.

TABLE 1. HYPERFINE SPLITTING PARAMETERS OF NITROXYLS PRODUCED IN THE REACTION OF ATOMS AND RADICALS WITH PHENYL *N*-*t*-BUTYL NITRONE
$C_6H_5CH(R)N(O\cdot)C_4H_9$

R	Source	A_N	A_β^H	A_β^D	Reference
H·	$H_2 \rightsquigarrow H\cdot$ (2.5 Torr, 1 hr)	14.84	7.42		This work
H·	$(n\text{-Bu})_3SnH + PBN + h\nu$	14.88[a)]	7.44[a)]		3
D·	$D_2 \rightsquigarrow D\cdot$ (1 Torr, 2.5 hr)	15.10	7.67	1.15	This work
D·	$(n\text{-Bu})_3SnD + PBN + h\nu$	14.64	7.45	1.15	8
H·	$H_2O \rightsquigarrow H\cdot + HO\cdot$	14.98	7.50		This work
HO·	(0.55 Torr, 2 hr)	14.63	2.88		This work
D·	$D_2O \rightsquigarrow D\cdot + DO\cdot$	14.94	7.66	1.14	This work
DO·	(0.6 Torr, 1 hr)	14.70	2.61		This work
H·	$CH_4 \rightsquigarrow H\cdot + CH_3\cdot$	15.06	7.54		This work
CH_3·	(0.8 Torr, 1.3 hr)	14.94	3.30		This work
CH_3·	$CH_3COCH_3 + h\nu$	14.82	3.47		2

a) Corrected values; see reference 3, p. 4483.

polymers are obtained from methane discharge but experimental evidence of methyl radical detection has not been reported. In our experiments hydrogen atoms and methyl radicals are readily detected (see Fig. 1) in the microwave discharge of methane. The ratio of these products varies from one experiment to another but the determining factors have not been ascertained.

From these preliminary experiments it can be seen that gas phase spin trapping techniques appear to be potentially useful in studies where simultaneous detection of atoms and radicals is desired. Further application of this technique are in progress.

The microwave discharge was operated at 2450 MHz by a 200 watt power supply. Either a rectangular or a cylindrical (Broida) type cavity was used.

Partial support by the Environmental Protection Agency Air Pollution Control Office, Public Health Service, Grant APD 1096 is gratefully acknowledged.

Grateful acknowledgement is hereby made to the U.S.-Japan Cooperative Science Program of the National Science Foundation for support in this endeavor.

8) Unpublished results of Mr. Dale Nutter, Department of Chemistry, The University of Georgia, Athens, Georgia.

BULLETIN OF THE CHEMICAL SOCIETY OF JAPAN, VOL. 46, 2062—2065 (1973)

Determination of the Molecular Arrangement in Liquid Crystals. A New Method of Determining the Molecular Arrangement in Liquid Crystals by the Use of the Polarization of the Fluorescence

Sakumitsu SAKAGAMI, Akira TAKASE, Minoru NAKAMIZO, and Hitoo KAKIYAMA

National Industrial Research Institute, Kyushu, Tosu, Saga 841

(Received December 19, 1972)

The molecular order in the liquid crystal states of *p*-*n*-octyloxybenzoic acid (OOBA) has been measured by means of a new method utilizing the polarization of the fluorescence. The polarized components of the fluorescence observed for the isotropic liquid state are independent of the rotation angle; this indicates that no molecular order exists in the liquid state. The polarized components of the fluorescence observed for the nematic state show that the molecular order of the aligned nematic state can be represented by a partially uniaxial orientation. The results observed for the nematic phase are also quantitatively discussed by the use of the uniaxial prolate ellipsoidal orientation pattern. On the other hand, the smectic state of OOBA is not affected by the surface action, and the observed patterns of the polarization of the fluorescence have very little angular dependence, in contrast with those for the nematic state. Furthermore, the molecular orientation for the crystal state of OOBA is briefly described.

It is well established that liquid crystals have properties similar to liquid in mobility, yet are crystal in structure, and that they can be classified into three basic types, *i.e.*, smectic, nematic, and cholesteric. These liquid crystal states are all characterized by a more or less complete orientation of the molecules with their long molecular axes parallel. In particular, the parallel orientation of the nematic state can usually be described by the degree of order: $S=(1/2)\cdot\langle 3\cos^2\theta-1\rangle_{av}$, where θ is the angle between a molecular axis and the preferred axis, which gives the average deviation of orientation of the molecular axes. Saupe and

Maier have shown that this degree of order can be determined by various experimental method[1-5] the principal refractive indices, the principal diamagnetic susceptibilities, the UV or IR dichroism, and the magnetic resonance.

In this paper, we wish to report a new method of determining the molecular order in the liquid crystalline states on the basis of the polarization of the fluorescence from molecules dispersed in liquid crystals. This method has the advantage that it is, in principle, possible to measure not only the extent of orientation, but also the type of orientation, because it utilizes the two-fold optical anisotropy of fluorescent molecules.

Theoretical

The theoretical background of this method has been given by Nishijima *et al.*[6-9] in their studies of molecular orientation in polymer solids; it consists of the application of a simple oscillator model of classical electrodynamics to the polarization phenomena of fluorescence on the assumption that the absorbing and emitting oscillators are linear oscillators whose directions coincide with a single molecular axis. The theory gives the intensities of the parallel and perpendicular components of the polarized fluorescence emitted from a system with a certain degree of optical anisotoropy, $I_{//}$ and $I_{\perp}$, whose electric vectors are, respectively, parallel and perpendicular to the direction of the electric vector of the linearly-polarized exciting light.

$$I_{//} = \frac{K}{2\pi}\int_0^{2\pi}\int_0^{\pi/2} N(\omega, \varphi)M_x^2M_x^2 \sin\omega d\omega d\varphi, \quad (1)$$

$$I_{\perp} = \frac{K}{2\pi}\int_0^{2\pi}\int_0^{\pi/2} N(\omega, \varphi)M_x^2M_z^2 \sin\omega d\omega d\varphi, \quad (2)$$

where K is the proportionality constant, where $N(\omega,\varphi)$ is an angular distribution function in the orientation coordinate system (a, b, c) fixed to the specimen, as is shown in Fig. 1, and where M_x and M_z are the components of the linear axis, **M**, of the fluorescent molecule in the directions of the X and Z axes in the optical coordinate system. The components in the optical coordinate system, M_x, M_y, and M_z, can easily be obtained from its components, M_a, M_b, and M_c, in the orientation coordinate system using a transformation matrix (T):

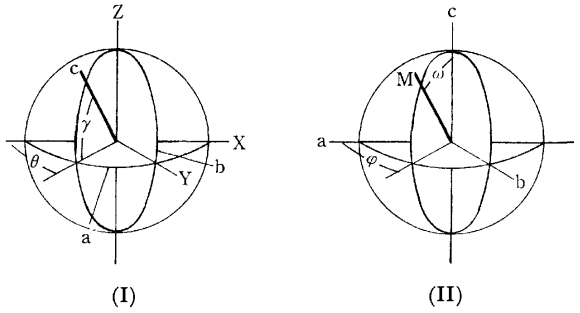

Fig. 1. Coordinate systems. (I): optical coordinate system, (II): orientation coordinate system.

$$\begin{pmatrix} M_x \\ M_y \\ M_z \end{pmatrix} = (T)\begin{pmatrix} M_a \\ M_b \\ M_c \end{pmatrix} \quad (3)$$

$$(T) = \begin{pmatrix} \cos\theta\sin\gamma & -\sin\theta & \cos\theta\cos\gamma \\ \sin\theta\sin\gamma & \cos\theta & \sin\theta\cos\gamma \\ -\cos\gamma & 0 & \sin\gamma \end{pmatrix} \quad (4)$$

The extent as well as the type of molecular orientation in the system can be obtained from measurements of the angular dependency of $I_{//}$ and $I_{\perp}$, and of the degree of polarization of fluorescence, P, which is defined by Eq. (5):

$$P = \frac{I_{//}-I_{\perp}}{I_{//}+I_{\perp}} \quad (5)$$

Experimental

Apparatus. The optical system used in this study is schematically illustrated in Fig. 2. The light of the 365 nm wavelength was separated from a mercury lamp using a monochromator, M, and was used as an exciting light; it illuminated fluorescent molecules dispersed in liquid crystals after passing through a polarizer, P. The wavelength of the exciting light coincides with that of the maximum of the principal absorption peak, which itself corresponds to the electronic transition between the ground and lowest excited states of the fluorescent molecules. The polarized components of the fluorescence intensity are measured by a photomultiplier, PM, through an analyzer, A, and a cut-off filter, CF, and are then recorded as the sample is being rotated through 360° on the rotating stage. The analyzer can also be rotated so that the direction of the electric vector of the fluorescent light lies either parallel ($I_{//}$) or perpendicular ($I_{\perp}$) to that of the exciting light. An ordinary polarizing microscope was modified as the optical system passed from the polarizer to the analyzer. The observed sample area is around 100 μm in diameter.

Materials. The liquid crystal compound used in this study is *p-n*-octyloxybenzoic acid (OOBA), which was purchased from the Tokyo Kasei Co.; it was recrystallized several

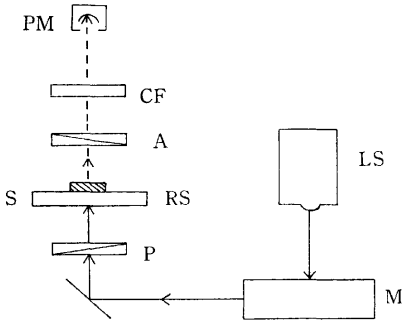

Fig. 2. Schematic diagram of the apparatus. LS: light source, M: monochromator, P: polarizer, RS: rotating stage, S: sample, A: analyzer, CF: cut-off filter, PM: photomultiplier.

1) A. Saupe and W. Maier, *Z. Naturforsch.*, **16a**, 816 (1961).
2) W. Maier and K. Markau, *Z. Phys. Chem., N.F.* **28**, 190 (1961).
3) W. Maier and A. Saupe, *Z. Naturforsch.*, **13a**, 564 (1958).
4) W. Maier and G. Englert, *Z. Elektrochem.*, **64**, 689 (1960).
5) V. D. Neff, L. W. Gulrich, and G. H. Brown, *Mol. Cryst.*, **1**, 225 (1966).
6) Y. Nishijima, Y. Onogi, and T. Asai, *J. Polym. Sci. Part C*, **15**, 237 (1966).
7) Y. Nishijima, *ibid.*, **31**, 353 (1970).
8) Y. Nishijima and T. Asai, *Repts. Progr. Polym. Phys. Jap.*, **11**, 419 (1968).
9) Y. Nishijima, Y. Onogi, and T. Asai, *ibid.*, **10**, 461 (1967).

times from ethanol and benzene to insure a higher degree of purity. The phase transition of OOBA are:[10-12]

$$C_2 \overset{68^\circ C}{\longleftrightarrow} C_1 \overset{102^\circ C}{\longleftrightarrow} S_m(C) \overset{108^\circ C}{\longleftrightarrow} N \overset{145^\circ C}{\longleftrightarrow} I$$

1,6-Diphenyl-1,3,5-hexatriene was used as the fluorescent compound.[13] This fluorescent molecule can be considered to be an approximately perfect linear oscillator, because the measurement of the degree of the polarization of the fluorescence in various solvents with a wide range of viscosities has given the value of 0.5 at the extrapolation of $T/\eta=0$ theoretically anticipated by the perfect anisotropic molecule.

A mixture of the liquid crystal compound and fluorescent substances of about 10^{-3} wt% was dissolved in chloroform in order to obtain a uniformly-dispersed system, and then the solvent was removed by evaporation at room temperature under reduced pressure. The liquid crystal state was attained by heating this mixture to the isotropic state of the liquid crystal between a glass slide and a cover slip on a microscopic stage with a heating block, and by then slowly cooling it to the mesomorphic state. The sample thickness was approximately 5 μm. The aligned nematic state was obtained by the well-known method of rubbing the glass surface.[14-19]

Results and Discussion

The polarized components of the fluorescence intensity, $I_{//}$ and $I_{\perp}$, observed at each state are shown in Figs. 3 and 4 as a function of the angle of rotation, γ.

As is apparent from Fig. 3, in the isotropic state both $I_{//}$ and $I_{\perp}$ are independent of the angle, γ. This can easily be understood by considering that a molecular ordering in the liquid state is at random because of the

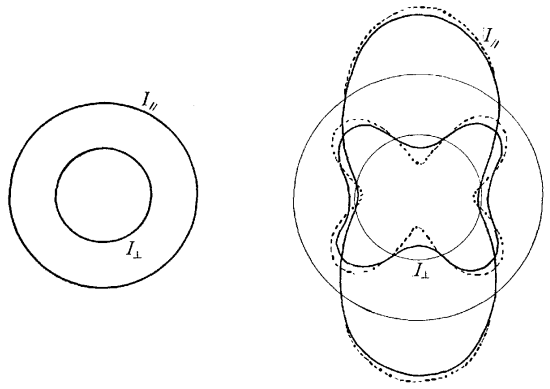

Fig. 3. Angular distributions of the polarized components of fluorescence observed in the aligned nematic state (N) and the isotropic liquid state (I). The dotted lines indicate the calculated intensities of the polarized components of fluorescence corresponding to $\alpha=5$ and $\theta=60°$.

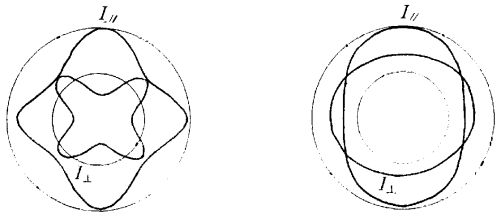

Fig. 4. Angular distributions of the polarized components of fluorescence observed in the smectic C state (S_mC) and the crystalline state (C_1).

vigorous thermal motion of the molecules. In the case of a completely random distribution, the intensity of the polarized component of fluorescence can be expressed by:

$$I_{//} = \frac{3}{15}K\Phi, \tag{6}$$

$$I_{\perp} = \frac{1}{15}K\Phi, \tag{7}$$

where K and Φ are independent of the angle of rotation and are correlated to the maximum probability of excitation and the quantum yield of the fluorescence respectively.[6,9] These equations indicate that the polarized components of the fluorescence for the completely random system are independent of the angle, γ, and that the intensity ratio of the fluorescence, $I_{//}/I_{\perp}$, is equal to 3. The observed polarized components of the fluorescence coincide entirely with those expected from the above equations so far as the angular dependence is concerned. However, the observed intensity ratio of the polarized components of the fluorescence is somewhat smaller than the ratio, $I_{//}/I_{\perp}=3$, theoretically expected from the above equations. This discrepancy is mainly attributable to the facts that the viscosity of the isotropic liquid state is low and that the molecules are very mobile in the liquid state.

At the phase transition from the liquid to the nematic, both $I_{//}$ and $I_{\perp}$ drastically change, as is illustrated in Fig. 3. Although the angular distribution of $I_{//}$ and $I_{\perp}$, in this nematic state, varied little with the measured place of the liquid crystal compound, the substantial features of angular dependence were the same as those shown in Fig. 3. In addition, no significant change in either $I_{//}$ or $I_{\perp}$ with the variation in the temperature was observed throughout the nematic state, except that the fluorescence intensity decreased slightly as the temperature decreased. As is shown in Fig. 3, $I_{//}$ has a maximum intensity at a definite angle of γ, whereas $I_{\perp}$ exhibits a fluorescence pattern with a four-leaf shape. It is evident from the angular dependence of $I_{//}$ and $I_{\perp}$ that the nematic state has a partially uniaxial molecular orientation.

The distribution function, $N(\omega,\varphi)$, is indispensable to explaining quantitatively the observed angular dependence of both $I_{//}$ and $I_{\perp}$. Taking account of the partially parallel molecular orientation in the nematic state, we assume that the molecular orientation for the nematic state can be expressed by the uniaxial prolate ellipsoidal pattern, as is illustrated in Fig. 5. Fur-

10) G. W. Gray and B. Jones, *J. Chem. Soc.*, **1953**, 4179.
11) A. J. Herbert, *Trans. Faraday Soc.*, **63**, 555 (1967).
12) D. Demus and H. Sackmann, *Z. Phys. Chem.*, **222**, 127 (1963).
13) K. W. Hausser, R. Kuhn, and E. Kuhn, *Z. Phys. Chem.*, **29**, 417 (1935).
14) A. Saupe, *Mol. Cryst. Liquid Cryst.*, **16**, 87 (1972).
15) G. P. Ceasar, R. A. Levenson, and H. B. Gray, *J. Amer. Chem. Soc.*, **91**, 772 (1969).
16) R. Williams, *J. Chem. Phys.*, **56**, 147 (1972).
17) W. Helfrich, *ibid.*, **51**, 2755 (1969).
18) P. A. Penz, *Phys. Rev. Lett.*, **24**, 1405 (1970).
19) M. Schadt and W. Helfrich, *Appl. Phys. Lett.*, **18**, 127 (1971).

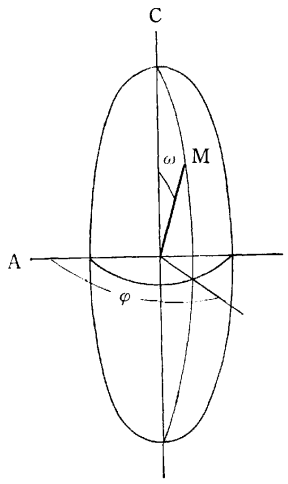

Fig. 5. Schematic representation of the distribution function $N(\omega, \varphi)$.

thermore, it seems quite reasonable to assume that the distribution function, $N(\omega,\varphi)$, is proportional to the cube of the distance from the center of the prolate ellipsoidal of rotation. $N(\omega,\varphi)$ is, then, given by:

$$N(\omega, \varphi) \propto \frac{1}{(\alpha^2 \sin^2 \omega + \cos^2 \omega)^{3/2}}, \quad (8)$$

where α is the axial ratio, C/A. The angular distribution of $I_{//}$ and $I_{\perp}$ can be straightforwardly computed by substituting this distribution function for $N(\omega,\varphi)$ in Eqs. (1) and (2). The final equations representing $I_{//}$ and $I_{\perp}$ include both γ and θ as parameters. The results of the calculations at $\alpha=5$ and $\theta=60°$ are shown by the dotted line in Fig. 3; these results agree well with the observed angular distributions of $I_{//}$ and $I_{\perp}$, aside from a very small difference in the intensity of $I_{\perp}$. This good accordance distinctly indicates that the molecular orientation in the nematic state lies essentially parallel and can be expressed by the uniaxial prolate ellipsoidal pattern, as has been discussed above. The fact that α is equal to 5 indicates that the molecules in the nematic state can be regarded as adopting an almost perfect parallel alignment over regions larger than the molecular dimensions. It is known that the molecular order of the nematic state is not seriously disturbed by the presence of a solute, but is clearly dependent on the molecular shape and size of a solute,[20] although it has thus far been assumed that the molecular order of the fluorescent molecules used as a probe is completely consistent with that of the nematic phase. Therefore, further detailed arguments concerning the molecular order in the nematic state are impossible.

The $I_{//}$ and $I_{\perp}$ observed for the smectic C state of OOBA are strikingly different from those for the nematic state, as is shown in Fig. 4. Both $I_{//}$ and $I_{\perp}$ are very little dependent upon the angle of rotation, γ, in contrast to those of the nematic state, with their sharp angular dependence. Furthermore, microscopic observations also indicate that this smectic C state exhibits the smectic schlieren texture[21,22] characteristic of the smectic C state, while the nematic state gives the pattern of the so-called aligned layers[14] due to the surface action. This suggests that the smectic C liquid crystal, unlike the nematic liquid crystal, is not easily aligned by rubbing glass surfaces.

It is well known that the smectic C state has such a layer structure that the long molecular axis is tilted to a layer and has optically biaxial properties.[23–27] Recently, the present authors have proposed, on the basis of optical observations,[28] twisted smectic layers for the molecular arrangements of the smectic C state. In these twisted smectic layers, the molecules are arranged in layers and have their long molecular axes successively twisted with respect to the normal layer. If this is the case, the observed $I_{//}$ and $I_{\perp}$, which are substantially independent of the rotation angle, are reasonable, since the molecular order in the twisted smectic layers is likely to be essentially distributed at random over the whole region where the polarization measurement of the fluorescence from the system is made.

The polarized fluorescence intensity decreases at the phase transition from the smectic to the crystalline state. The $I_{//}$ and $I_{\perp}$ for the crystalline state (C_1) are also significantly different from those observed for the nematic and smectic states, discussed above, in the angular dependence as well as in the intensity, as is shown in Fig. 4. The angular dependence of $I_{//}$ and $I_{\perp}$ suggests that the crystal state (C_1) of OOBA attained on cooling the smectic state has an approximately perfect biaxial molecular orientation, although a birefringence effect in the crystalline state must be considered for an accurate determination of the molecular orientation.[29]

The authors wish to thank Professor Yasunori Nishijima of Kyoto University for his valuable suggestions.

20) S. H. Glarum and J. H. Marshall, *J. Chem. Phys.*, **46**, 55 (1967).
21) H. Sackmann and D. Demus, *Mol. Cryst.*, **2**, 81 (1966).
22) E. F. Carr, *Mol. Cryst. Liquid Cryst.*, **13**, 27 (1971).
23) G. R. Luckhurst and F. Sundholm, *Mol. Phys.*, **21**, 349 (1971).
24) S. Diele, P. Brand, and H. Sackmann, *Mol. Cryst. Liquid Cryst.*, **16**, 105 (1972).
25) J. G. Chistyakov and W. M. Chaikowsky, *ibid.*, **7**, 269 (1969).
26) T. R. Taylor, J. L. Fergason, and S. L. Arora, *Phys. Rev. Lett.*, **24**, 359 (1970).
27) T. R. Taylor, S. L. Arora, and J. L. Fergason, *ibid.*, **25**, 722 (1970).
28) S. Sakagami, A. Takase, M. Nakamizo, and H. Kakiyama, *Mol. Cryst. Liquid Cryst.*, **19**, 303 (1973).
29) Y. Onogi and Y. Nishijima, *Repts. Progr. Polym. Phys. Jap.*, **14**, 533 (1971).

The *G*-values of Nitrogen Obtained from the Gas-phase γ-Radiolysis of Nitrous Oxide–Hydrocarbon Systems

Kiyoshi Okazaki, Rei Yugeta, and Shin Sato

Department of Applied Physics, Tokyo Institute of Technology, Ookayama, Meguro-ku, Tokyo 152

(Received January 5, 1973)

The gas-phase γ-radiolysis of a N_2O–1-butene system has been reinvestigated. The other hydrocarbons used for the substrate are ethylene, propylene, 1,3-butadiene, cyclopropane, propane, and *n*-butane. The *G*-value of nitrogen from any system increased with an increase in the pressure of N_2O and was saturated at about 4 mol% of N_2O. The saturated value, $G(N_2)_{max}$, was much larger than the *G*-value of electrons estimated from the *W*-value of the hydrocarbon used and was rather strongly dependent upon the irradiation temperature, the dose rate, and the total dose. Some of the results were not consistent with those reported by the previous investigators. The reason for this discrepancy, and also the possible reaction mechanism to explain the large $G(N_2)_{max}$, have been discussed.

Nitrous oxide has been used as an electron scavenger in the gas- and liquid-phase radiolyses of hydrocarbons.[1-3] If the yield of nitrogen is consistent with the amount of scavenged electrons, we can study many features of the radiolysis. Generally, however, the *G*-value of nitrogen from the gas-phase radiolysis of a hydrocarbon in the presence of nitrous oxide is higher than that to be expected from the *W*-value of the hydrocarbon. This excess nitrogen yield has usually been explained in terms of the reactions between nitrous oxide and negative species produced in the electron-scavenging reaction of nitrous oxide.

According to the paper of Warman,[4] there are two groups of alkenes. One consists of isobutene and propylene, which give $G(N_2)_{max}=G_e$. Here, $G(N_2)_{max}$ is the maximum *G*-value of nitrogen which results from the electron scavenging of nitrous oxide and G_e is the *G*-value of electrons, as estimated from the *W*-value of the hydrocarbon. The other group consists of 1-butene and *cis*- and *trans*-2-butene, which give $G(N_2)_{max}=2\,G_e$. On the other hand, in the gas-phase radiolysis of alkanes (C_2, C_3, and C_4), $G(N_2)_{max}=1.55\,G_e$ has been reported. The data so far introduced were obtained at room temperature.

Holtslander and Freeman[5] reported that, in the γ-radiolysis of methylcyclohexane at 110 °C, the *G*-value of nitrogen attains as high as $5\,G_e$; they attributed this high yield to the ionic chain reaction between the oxygen atom ion and the hydrocarbon. In the case of the benzene-nitrous oxide system at room temperature, the $G(N_2)_{max}$ is reported to be $8.2\,G_e$, and the $G(C_6H_5OH)$, to be $6.4\,G_e$.[6] The authors explained this result in terms of the chain reaction including $C_6H_6O^-$ as the chain carrier.

The present authors hoped to find a more systematic explanation of these rather conflicting data, and so reinvestigated the gas-phase γ-radiolysis of 1-butene in the presence of nitrous oxide. For comparison, several experiments were performed with ethylene, propylene, 1,3-butadiene, cyclopropane, propane, and *n*-butane.

Experimental

The nitrous oxide (Showa Denko Co.), ethylene, propylene 1-butene, propane, *n*-butane, cyclopropane, 1,3-butadiene (Takachiho Chemical Co.), and sulfur hexafluoride (Matheson Co.) were used after several bulb-to-bulb distillations. The volume of the irradiation cell was 50 ml. Before preparing the irradiation sample, the cell was heated with a torch under a vacuum. The pressure of the hydrocarbon was around 600 Torr in all the experiments. The irradiation temperatures were 0 °C, room temperature, and 100 ± 1 °C.

For the measurement of the dose rate, use was made of the Fricke dosimeter. In order to check the difference between the gas-phase radiolysis and the liquid one, the radiolysis of ethylene was carried out. The obtained *G*-value of hydrogen from ethylene was 1.30 ± 0.02, which is in agreement with the literature value, 1.31.[7]

The amount of the non-condensable products at 77 K (N_2, H_2, and CH_4) was measured with a Toepler pump equipped with a gas buret. This non-condensable gas was passed through a furnace of cuprous oxide at 300 °C in order to combust the hydrogen into water, which was then trapped at 77 K. After the measurement of the amount, the remaining gas was analyzed by mass spectrometry.

Results

Figure 1 shows the *G*-values of nitrogen as a function of the mol% of nitrous oxide. The hydrocarbons used are propylene, ethylene, 1,3-butadiene, and cyclopropane. The pressure is 600 Torr, and the irradiation temperature is room temperature. The dose rate used here is 2×10^{-13} eV ml^{-1} sec^{-1}. As may be seen in Fig. 1, the $G(N_2)_{max}$'s are 6.5 for propylene, 9.2 for ethylene and 1,3-butadiene, and 10.3 for cyclopropane. The data obtained with 1-butene is not shown because of considerable scattering, although the $G(N_2)_{max}$ was found in the range from 12 to 13. It may be worthwhile to mention here that the $G(N_2)_{max}$ values for propylene and for 1-butene are 1.5 times larger than those reported by Warman.[4]

Since we found considerable scattering data in the

1) G. Scholes and M. Simic, *Nature*, **202**, 895 (1964).
2) S. Sato, R. Yugeta, K. Shinsaka, and T. Terao, This Bulletin, **39**, 156 (1966).
3) G. R. A. Johnson and J. M. Warman, *Nature*, **203**, 73 (1964).
4) J. M. Warman, *J. Phys. Chem.*, **71**, 4066 (1967).
5) W. J. Holtslander and G. R. Freeman, *Can. J. Chem.*, **45**, 1661 (1967); *J. Phys. Chem.*, **71**, 2562 (1967).
6) S. J. Rzad and J. M. Warman, *ibid.*, **72**, 3013 (1968).
7) G. G. Meisels, *J. Chem. Phys.*, **41**, 51 (1964).

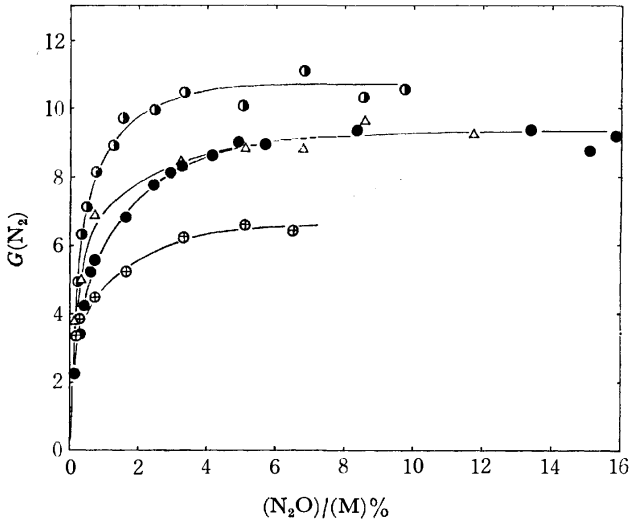

Fig. 1. G-values of nitrogen from N_2O–hydrocarbon systems as a function of the $[N_2O]/[M]$ ratio. △: ethylene, ⊕: propylene, ●: 1,3-butadiene, ◑: cyclopropane.

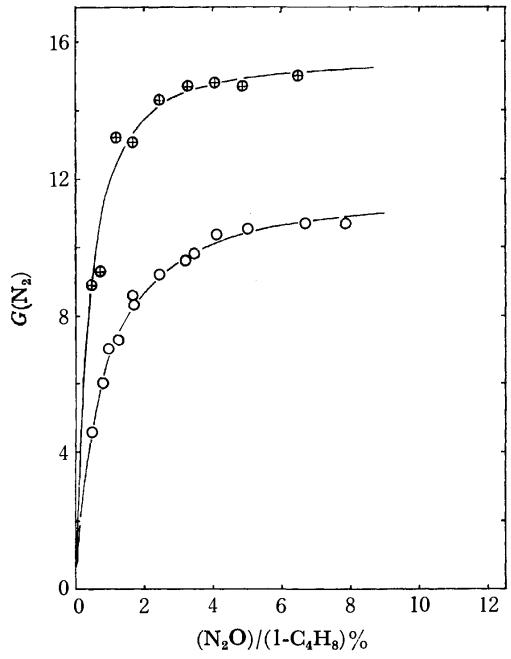

Fig. 2. G-values of nitrogen from a N_2O–1-butene system as a function of the $[N_2O]/[1\text{-butene}]$ ratio.
○: 0 °C, ⊕: 100 °C.

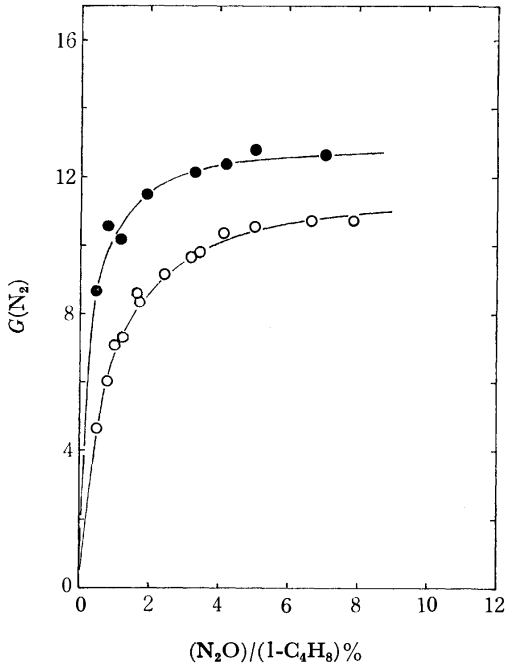

Fig. 3. The effect of dose rate on the G-value of nitrogen from a N_2O–1-butene system. ○: 1.9×10^{13} eV ml^{-1}s ec^{-1}, ●: 3.6×10^{12} eV ml^{-1} sec^{-1}.

Table 1. $G(N_2)_{max}$ from N_2O–hydrocarbon systems and the effect of the addition of SF_6

Substrate (600 Torr)	$G(N_2)_{max}$ Room temperature This work	Literature values	0 °C This work	$G(N_2)$ in the presence of 0.03 mol % SF_6 at 0 °C
Propane	—	7.5,[3] 6.5,[4] 8.7[20]	8.2	0.2
n-Butane	—	6.5[4]	8.8	0.3
Ethylene	8.7	—	8.0	0.2
Propylene	6.3	4.2[4]	5.0	0.3
1-Butene	14.8[a]	8.4[4]	10.4	0.3
Cyclopropane	10.4	—	7.3	0.2
1,3-Buradiene	8.6	—	6.2	0.1

a) Obtained at 100 °C.
b) $G(N_2)$ from a 4.1 mol% N_2O–hydrocarbon system.

case of 1-butene, we controlled the irradiation temperatures at 0 and 100 °C. Figure 2 shows the results. From this figure, we can understand that the G-value of nitrogen is rather strongly temperature-dependent.

The dose rate-dependence of $G(N_2)$ from the N_2O–1-butene system has also been investigated. The results are shown in Fig. 3. The dose rates are 1.9×10^{13} and 3.6×10^{12} eV ml^{-1} sec^{-1}. The irradiation temperature is 0 °C, and the total dose is 1.9×10^{17} eV ml^{-1}. The $G(N_2)_{max}$ values are 10.7 for the higher dose rate and 12.7 for the lower. When the total dose was changed from 1.9×10^{17} to 9.6×10^{17} eV ml^{-1}, the $G(N_2)_{max}$ decreased from 10.3 to 8.4. With doses lower than 1.9×10^{17} eV ml^{-1}, the $G(N_2)_{max}$ did not change from 10.3.

Table 1 summarizes the $G(N_2)$'s from seven hydrocarbons containing 4.1 mol% nitrous oxide at 0 °C, along with the values at room temperature and the $G(N_2)$'s in the presence of 0.03 mol% SF_6. The dose rate and the total dose used here are 1.9×10^{13} eV ml^{-1} sec^{-1} and 1.9×10^{17} eV ml^{-1}.

Since the dosimetry by the decomposition of nitrous oxide plays an important role in the explanation of the present results, we measured the $G(N_2)$ from pure nitrous oxide at three different temperatures. The results are summarized in Table 2, together with the

Table 2. $G(N_2)$ from pure N_2O

$G(N_2)$	Source	Temperature	Reference
12.0	^{60}Co γ	room	Johnson
10.9	4 MeV X	room	Hearne
11.25	T β	room	
10.0	^{210}Po α	25 °C	Sears
7.6	^{222}Rn α	25 °C	
9.9	^{60}Co γ	10 °C	
10.0	1 MeV e$^-$	24 °C	Jones
12.4		70 °C	
14.1		100 °C	
17.9		150 °C	
21.1		200 °C	
10.1	^{60}Co γ	room	Takao
10.9	^{60}Co γ	room	This work
9.3		0 °C	
12.5		100 °C	

data of previous workers.[8-12] The obtained temperature dependence was very similar to that reported by Jones and Sworski,[11] who used 1 MeV electrons from a Van de Graaff apparatus as the irradiation source. Our data were independent of the dose rate used in the range from 2.8×10^{12} to 1.5×10^{13} eV ml^{-1} sec^{-1}.

Discussion

Accumulating evidence[13-19] seems to establish that a third-body reaction is necessary for thermalized electrons to attach to nitrous oxide. According to Warman and Fessenden,[18] the rate constant of this third-body reaction at 300 K is $5.6\pm0.2\times10^{-33}$ ml^2 molecules^{-2} sec^{-1}, while Johnson and Redpath[13] estimated it to be 2×10^{-31} ml^2 molecules^{-2} sec^{-1}. On the other hand, Holtslander and Freeman[5] estimated the lifetime of the decomposition of N_2O^- into N_2 and O^- in the atmosphere of methylcyclohexane at 110 °C to be in the range from 10^{-4} to 10^{-3} sec.

As is shown in Table 1, the presence of a very small amount of SF_6, a well-known electron scavenger, suppressed the formation of nitrogen from the γ-radiolyses of seven hydrocarbons containing 4.1 mol% N_2O. The precursor of nitrogen, therefore, must be thermalized electrons. A pressure of 600 Torr of hydrocarbons is probably high enough to thermalize electrons before the occurrence of the dissociative electron-capture process of N_2O.

The reactions of electrons in the present system, therefore, may be expressed as follows:

$$e^- + N_2O \xrightarrow{+M} N_2O^- \quad (1)$$

$$e^- + M^+ \longrightarrow \text{products} \quad (2)$$

Here, M and M^+ stand for a hydrocarbon molecule and its positive ion. The G-values of electrons estimated from the W-values of hydrocarbons are to be around 4; accurate values are known for propane (4.27), n-butane (4.37), ethylene (3.86), propylene (4.03), and 1-butene (4.10).[7] Therefore, all of the $G(N_2)_{max}$ values obtained in the present experiment are larger than the G_e's. The excess nitrogen yield ranges from 0.25 G_e for propylene at 0 °C to 2.5 G_e for 1-butene at 100 °C.

As Table 1 shows, there are rather serious discrepancies between the $G(N_2)_{max}$ reported by Warman and his co-workers[3,4,20] and ours. Therefore, we carefully compared their experimental conditions with ours—the dose rate, the total dose, the pressure of the sample, the irradiation temperature, and so on, but we could not find the reason for this discrepancy. The ethylene dosimetry has also been checked; they used $G(H_2)=1.31$, which is in good agreement with our result, $G(H_2)=1.30\pm0.02$. Since most of their experiments were carried out with a cell of about 150 ml, while ours was 50 ml, we also used the same-size cell as theirs; however, the data we thus obtained were the same as those observed with the 50 ml cell. The question of the discrepancy in the $G(N_2)_{max}$ value, therefore, is still open.

In the studies of the γ-radiolysis of propane containing N_2O, Warman reported $G(N_2)_{max}=7.5$,[3] 6.5,[4] and 8.7.[20] The difference between 6.5 and 7.5 is probably due to the dose-rate dependence, although they did not mention it. The large value of 8.7 probably resulted from the nitrous oxide dosimetry; Warman used $G(N_2)=12.0$, but the most reliable G-value at present is 10.0 at room temperature.[11] According to the present measurements, the $G(N_2)$ from the 4.1 mol% N_2O–propane system at 0 °C is 8.2, larger than that reported by Warman. Recently, Johnson and Redpath.[13] reported $G(N_2)=7.5$ from the 2 mol% N_2O–propane system. This result is in accord with ours.

In order to explain the excess nitrogen yield observed in the present experiment, we propose the following reaction scheme:

$$N_2O^- + M \longrightarrow \begin{cases} N_2 + X^- & a \\ N_2 + P^- & 1-a \end{cases} \quad (3)$$

$$X^- + N_2O \longrightarrow N_2O^- + \text{residue} \quad (4)$$

$$N_2O^- + M^+ \longrightarrow N_2 + \text{residue} \quad (5)$$

$$P^- + M^+ \longrightarrow \text{products} \quad (6)$$

Here, a is the branching ratio of the reactions of N_2O^- with a hydrocarbon. X^- and P^- are unspecified ions, which we will discuss below. The essential difference between the X^- and P^- ions in the above scheme is that X^- can react readily with N_2O to produce its ion, while P^- cannot. In this scheme, we have excluded

8) G. R. A. Johnson, *J. Inorg. Nucl. Chem.*, **24**, 461 (1962).
9) J. A. Hearne and R. W. Hummel, *Rad. Res.*, **15**, 254 (1961).
10) J. T. Sears, *J. Phys. Chem.*, **73**, 1143 (1969).
11) F. T. Jones and T. J. Sworski, *ibid.*, **70**, 1546 (1966).
12) S. Takao, S. Shida, Y. Hatano, and H. Yamazaki, This Bulletin, **41**, 2221 (1968).
13) G. R. A. Johnson and J. L. Redpath, *Trans. Faraday Soc.*, **66**, 861 (1970).
14) J. F. Paulson, *Adv. Chem. Series*, **58**, 28 (1966).
15) J. L. Moruzzi and J. T. Dakin, *J. Chem. Phys.*, **49**, 5000 (1968).
16) J. Schaefer and J. M. S. Henis, *ibid.*, **49**, 5377 (1968).
17) J. F. Paulson, *ibid.*, **52**, 959 (1970).
18) J. M. Warman and R. W. Fessenden, *ibid.*, **49**, 4719 (1968).
19) A. V. Phelps and R. E. Voshall, *ibid.*, **49**, 3246 (1968).
20) G. R. A. Johnson and J. M. Warman, *Trans. Faraday Soc.*, **61**, 1709 (1965).

the neutralization reaction between X^- and M^+ ions. As is shown in Table 1, 0.03 mol% SF_6 was effective enough to suppress the formation of nitrogen. This suggests that the following charge-transfer reaction:

$$N_2O^- + SF_6 \longrightarrow N_2O + SF_6^-$$

takes place very readily and that, in the presence of 0.03 mol% SF_6, this reaction occurs much faster than the neutralization reaction, Reaction (5). If X^- ions are very reactive to N_2O, the neutralization reaction between X^- and M^+ ions may be ignored in the presence of a certain amount of N_2O.

Recently, Bohme and his co-workers[21,22] observed the reactions between O^- ions and several hydrocarbons by using the afterglow method and reported that their specific rates are of the order of 10^{-9} ml molecules^{-1} sec^{-1}:

$$O^- + RH \longrightarrow R^- + OH \quad a'$$
$$\searrow \quad OH^- + R \quad 1-a'$$

They also showed that the branching ratio of these two reactions is strongly dependent on the kind of hydrocarbon. Reaction (3) in the above reaction scheme is analogous with this reaction.

The steady-state treatment based on Reactions (1)~(6) gives the following relationship:

$$\frac{1}{G(N_2)} = \frac{1}{G(N_2)_\infty}\left(1+\frac{k_2}{\sqrt{k_a k_1}}\sqrt{\frac{D}{W}}\frac{1}{[N_2O]}\right) \qquad (I)$$

Here,

$$k_a = \frac{k_2[e^-]+k_6[P^-]}{[e^-]+[P^-]}$$

and D stands for the dose rate, and W, for the W-value of the hydrocarbon used. $G(N_2)_\infty$ is the G-value of nitrogen when all of the ejected electrons are scavenged by N_2O. By using the pulse radiolysis technique, Lias *et al.*[23] measured the rates of the neutralization of the t-butyl ion by an electron and by the SF_6^- ion, and reported $k(t\text{-}C_4D_9^+ + e^-) = 1.92 \times 10^{-6}$ ml molecules^{-1} sec^{-1} and $k(t\text{-}C_4D_9^+ + SF_6^-) = 4.0 \times 10^{-7}$ ml molecules^{-1} sec^{-1}. If we take these values for our k_2 and k_6 respectively, the k_a value may be said to be in between those two values.

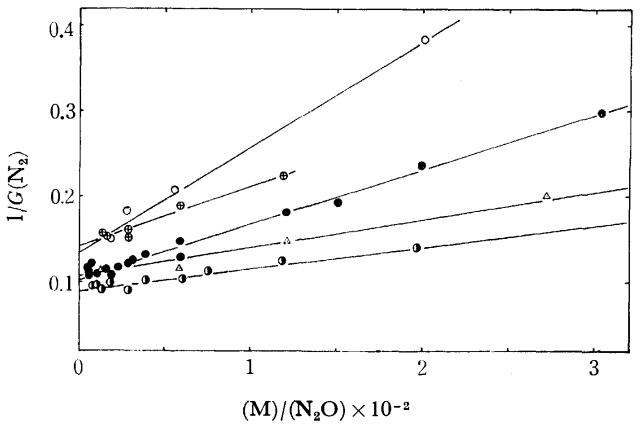

Fig. 4. Plots for Eq. (I). ○: 1,3-butadiene at 0 °C, ●: 1,3-butadiene at r. t., △: ethylene, ⊕: propylene, ◑: cyclopropane.

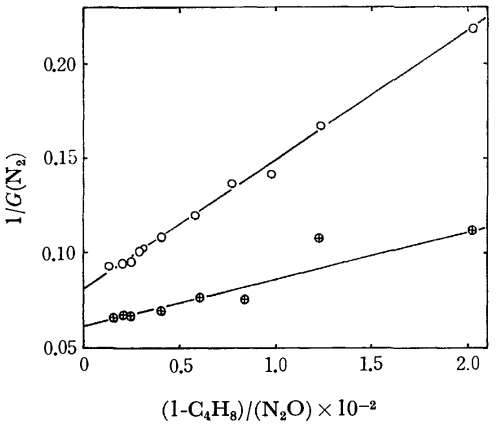

Fig. 5. Plots for Eq. (I) on 1-butene. ○: 0 °C, ⊕: 100 °C.

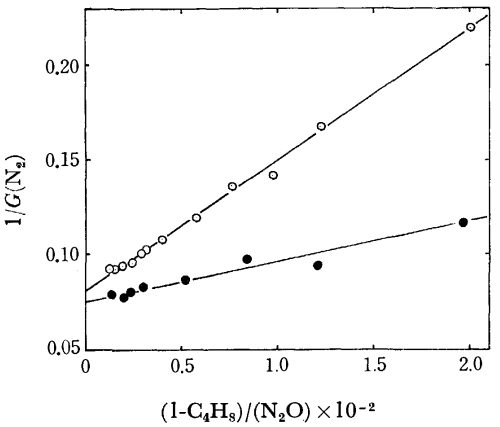

Fig. 6. Plots for Eq. (I), on 1-butene.
○: 1.9×10^{13} eV ml^{-1} sec^{-1}, ●: 3.6×10^{-12} eV ml^{-1} sec^{-1}.

Table 3. Calculated values of $G(N_2)_\infty$ and a

Substrate	Dose rate eV ml^{-1} sec^{-1}	$G(N_2)_\infty$	$k/(\sqrt{k_a k_1})$ (molec·ml^{-1} sec)$^{1/2}$	a	
1-Butene	1.9×10^{13}	12.1	1.7×10^{11}	0.71	0 °C
	3.6×10^{12}	13.2	1.4×10^{11}		
	1.8×10^{13}	16.0	8.3×10^{10}	0.78	100 °C
1,3-Butadiene	1.8×10^{13}	7.9	2.2×10^{11}	0.51	0 °C
	2.1×10^{13}	9.9	1.3×10^{11}	0.62	room temp.
Ethylene	1.1×10^{13}	9.2	1.1×10^{11}	0.60	
Propylene	1.6×10^{13}	7.2	1.3×10^{11}	0.46	
Cyclopropane	2.0×10^{13}	11.1	7.2×10^{10}	0.67	

Figure 4 shows the plots of $1/G(N_2)$ against the $[M]/[N_2O]$ ratio, where M's are ethylene, propylene, 1,3-butadiene, and cyclopropane. Figures 5 and 6 show the results obtained with 1-butene. From these linear relationships, we can calculate $G(N_2)_\infty$ and $k_2/(\sqrt{k_a k_1})$, which are summarized in Table 3. All of the $k_2/(\sqrt{k_a k_1})$ values are of the order of 10^{11} (molecules ml^{-1} sec)$^{1/2}$. From this value, the third-body reaction rate of Reaction (1) can be estimated to be 10^{-33} ml^2 molecules^{-2} sec^{-1} by assuming $k_a = 10^{-6}$ ml mole-

21) D. K. Bohme and L. B. Young, *J. Amer. Chem. Soc.*, **92**, 3301 (1970).
22) D. K. Bohme and F. C. Fehsenfeld, *Can. J. Chem.*, **47**, 2717 (1969).
23) S. G. Lias, R. E. Rebbert, and P. Ausloos, *J. Chem. Phys.*, **57**, 2080 (1972).

cules^{-1} sec^{-1} and by taking into account the fact that the pressure of hydrocarbons used in the present experiment is 600 Torr. The estimated value, 10^{-33}, may be compared with that of 5.6×10^{-33} reported by Warman and Fessenden.[18]

From the reaction scheme proposed above, this relationship:

$$\frac{G_e}{G(N_2)_\infty} = 1 - a\left(1+\frac{k_5}{\sqrt{k_a k_3}}\sqrt{\frac{D}{W}}\frac{1}{[M]}\right)^{-1} \quad \text{(II)}$$

can also be derived. In the case of 1-butene at 0 °C, we have a pair of data on the $G(N_2)_\infty$ for two different dose rates. The substitution of these data into Eq. (II) gives:

$$a = 0.71$$

and: $$\frac{k_5}{\sqrt{k_a k_3}} = 1.1\times10^{12} \text{ (molecules ml}^{-1}\text{ sec)}^{1/2}.$$

If we can assume the value of 1.1×10^{12} even for other hydrocarbons and for different temperatures, we can calculate the a values for other hydrocarbons. These values are also listed in Table 3. The accuracy of these numbers is open to further investigation, but we believe that these values can become an index for estimating the $G(N_2)_\infty$.

Speculations for X^- and P^- Ions. When olefins are used as the substrate, Reactions (3) and (4) may be written as follows, by analogy with the O^- reactions:[21]

$$\begin{aligned} N_2O^- + RH &\longrightarrow N_2 + R^- + OH \quad a \\ &\searrow N_2 + R + OH^- \quad 1-a \end{aligned} \quad (3')$$

$$R^- + N_2O \longrightarrow N_2O^- + R \quad (4')$$

As has been shown above, the branching ratio, a, obtained with 1-butene at 0 °C was 0.71, which is not inconsistent with the a' value, 0.6 ± 0.1, reported by Bohme *et al.* However, in the case of propylene, the a value was 0.46, while the a' value was reported to be 0.05 ± 0.05. A more serious difference was observed in the case of ethylene. According to Bohme *et al.*, the reaction between O^- ions and ethylene gives ethylene oxide and electrons. We checked the presence of ethylene oxide in the products of the γ-radiolysis of C_2H_4 containing N_2O, but we could not observe it by gas chromatography. The only product we could observe, except nitrogen, was water, although we did not measure it quantitatively.

In the case of paraffins, the a' values have been reported to be zero.[22] If the a values are also zero, the $G(N_2)_{max}$ cannot be more than the G_e's. The experimental results obviously contradict this. One possible explanation for this contradiction, and also for the discrepancy between the a and a' values for propylene and ethylene, is that the reaction between N_2O^- ions and RH produces the excited OH^{-*} ions, which can then react with other RH's to produce R^- ions.

In order to establish the reaction mechanism of the formation of nitrogen, it is necessary to continue further investigations, probably using a different approach.

BULLETIN OF THE CHEMICAL SOCIETY OF JAPAN, VOL. 46, 2070—2074 (1973)

Crystal Structure of μ-Peroxo-bis[nitrobis(ethylenediamine)-cobalt(III)] Dinitrate Tetrahydrate[1)]

Takashi SHIBAHARA, Shigetaka KODA,* and Masayasu MORI

Faculty of Science, Osaka City University, Sugimoto-cho, Sumiyoshi-ku, Osaka 558

(Received January 5, 1973)

The crystal and molecular structure of μ-peroxo-bis[nitrobis(ethylenediamine)cobalt(III)] dinitrate tetrahydrate, $[NO_2(en)_2CoO_2Co(en)_2NO_2](NO_3)_2 \cdot 4H_2O$ has been determined using visual intensity data of three dimensional Weissenberg photographs taken with Ni-$K\alpha$ radiation. The brown-black salt is monoclinic with space group $P2_1/n$ and cell dimensions $a=10.755\pm0.011$, $b=12.941\pm0.008$, $c=9.709\pm0.006$ Å, and $\beta=100.4\pm0.1°$. The least-squares refinement with anisotropic temperature factors gave an R index of 0.106. The coordinating ligands form nearly regular octahedra about the cobalt atoms, with Co–N(en), Co–N(NO_2), and Co–O distances of about 1.95, 1.94, and 1.89 Å, respectively. Both NO_2^-'s are *trans* to the O–O bridge, and the geometry of Co–O–O–Co is *trans* planar with O–O distance of 1.53 Å and Co–O–O angle of 110°. The two Co–$(en)_2$ moieties have $\delta\delta$ and $\lambda\lambda$ conformations.

It is well-known that a cobalt-ammonia solution takes up molecular oxygen in aqueous solution to give a brown diamagnetic decaammine μ-peroxo dicobalt complex, which can be oxidized further by Cl_2, $KMnO_4$, *etc.* to yield a green paramagnetic decaammine μ-superoxo dicobalt complex. Several instances of X-ray analyses of decaammine μ-O_2 (both peroxo and superoxo) dicobalt complexes $[(NH_3)_5CoO_2Co(NH_3)_5]^{n+}$

* Present address: Research Laboratories, Fujisawa Pharmaceutical Co. Ltd., Higashiyodogawa-ku, Osaka, Japan.

1) Presented at the 22nd Conference on Coordination Chemistry of the Chemical Society of Japan, Osaka, November (1972), Proceedings, p. 1.

(n=4, 5) have been reported.[2-5] The O–O distances were reported to be 1.31—1.32 Å for superoxo complexes; the O–O distance in KO_2 is 1.28 Å. For peroxo complexes, Schaefer reported 1.47 Å,[5] although Vannerberg had given a considerably longer O–O distance (1.65 Å).[4] Recently we found that $[NH_3(en)_2CoO_2Co(en)_2NH_3]^{4+}$ reacts with NO_2^- in a neutral solution to give $[NO_2(en)_2CoO_2Co(en)_2NO_2]^{2+}$ without causing any cleavage of the O_2-bridge.[6] The present report deals with the crystal and molecular structure of this new complex. This seems to be the first example of an O_2-single-bridged dicobalt complex with coordinated nitro groups as studied by X-ray analysis.

Studies have been carried out on the *cis-trans* problem of a mononuclear complex, but very little is known about *cis-trans* configuration in binuclear complexes, partly because most of the binuclear dicobalt complexes so far determined by X-ray analyses were of the unsubstituted ammine type. It seemed worthwhile to investigate the geometrical isomerism of binuclear complexes.

Experimental

Crystals of μ-peroxo-bis[nitrobis(ethylenediamine)cobalt(III)] dinitrate tetrahydrate recrystallized from an aqueous solution are monoclinic brown-black prisms. The compound is stable against air oxidation. Cell dimensions were obtained from zero-level Weissenberg films, taken about the a and b axes, on which the diffraction pattern of silicon powder (a= 5.43066 Å) was superimposed for calibration. The space group $P2_1/n$ was indicated on Weissenberg photographs by a systematic absence of reflections $h0l$ with $h+l$ odd and $0k0$ with k odd. The density of the compound was determined by flotation in a chloroform–bromoform mixture. The crystal data are listed in Table 1. The intensities were measured visually on integrated multi-film equiinclination Weissenberg photographs taken with Ni-$K\alpha$ radiation, for layers from $0kl$ through $7kl$ and from $h0l$ through $h8l$. The intensities were corrected for Lorentz, polarization and absorption factors. In all, 2331 independent (1994 non-zero) reflections were obtained.

Table 1. Crystal data

$[NO_2(en)_2CoO_2Co(en)_2NO_2](NO_3)_2 \cdot 4H_2O$
Monoclinic
$a=10.755\pm0.011$, $b=12.941\pm0.008$, $c=9.709\pm0.006$ Å
$\beta=100.4\pm0.1°$
$D_m=1.70$ g cm^{-3} $D_c=1.70$ g cm^{-3}
$Z=2$, space group $P2_1/n$
Linear absorption coefficient for Ni-$K\alpha$ radiation,
$\mu=28.39$ cm^{-1}

Structure Determination

Approximate coordinates of the cobalt atom were found from three-dimensional Patterson synthesis. The center of the μ-peroxo group lies on the crystallographic center of symmetry. A three dimensional electron density map was then calculated on the basis of cobalt contribution. R index ($\Sigma||F_o|-|F_c||/\Sigma|F_o|$) was 0.435. Several cycles of Fourier and differential Fourier syntheses revealed all the non-hydrogen atoms. The atomic parameters and individual isotropic temperature factors were refined by three cycles of the block diagonal least-squares method. At this stage the R index was 0.154. Three more cycles of refinement were carried out on introduction of anisotropic temperature factors. The following weighting scheme was employed:

$$w = 0.15, \text{ if } F_o \leqq F_{min} (=4.04);$$

Table 2. Atomic parameters and their estimated standard deviatons[a] ($\times 10^4$)
Temperature factors are of the form: $\exp[-(B_{11}h^2+B_{22}k^2+B_{33}l^2+B_{12}hk+B_{13}hl+B_{23}kl)]$

Atom	x/a	y/b	z/c	B_{11}	B_{22}	B_{33}	B_{12}	B_{13}	B_{23}
Co	1139(1)	1348(1)	1046(1)	57(1)	37(1)	66(1)	−9(2)	−6(2)	−5(2)
O(1)	171(5)	505(4)	−330(5)	39(5)	17(3)	30(6)	−31(6)	−10(8)	15(7)
O(2)	2198(10)	2101(9)	3667(8)	183(13)	132(10)	62(9)	−198(19)	−44(18)	−16(15)
O(3)	2718(9)	2989(7)	2073(9)	167(12)	62(6)	129(12)	−154(15)	55(19)	−72(14)
O(4)	1074(8)	1352(8)	−3268(8)	116(10)	167(9)	72(9)	67(16)	7(15)	16(15)
O(5)	639(11)	2978(11)	−3277(18)	146(14)	143(13)	472(35)	51(22)	−99(37)	−419(37)
O(6)	−300(7)	2011(7)	−4904(8)	81(8)	86(7)	68(8)	45(12)	−33(13)	−33(12)
O(7)	1700(8)	−129(7)	4864(8)	110(9)	62(6)	110(10)	15(12)	65(16)	28(12)
O(8)	861(14)	4412(14)	−780(23)	200(18)	203(19)	616(50)	−252(30)	−310(51)	506(52)
N(1)	2314(7)	1582(5)	−231(8)	51(7)	21(4)	65(8)	−9(9)	2(12)	8(9)
N(2)	2150(6)	164(6)	1740(7)	32(6)	32(5)	47(7)	3(9)	−2(11)	14(9)
N(3)	−77(6)	1074(6)	2272(7)	38(6)	31(5)	47(7)	−6(9)	3(11)	−8(9)
N(4)	45(7)	2511(5)	328(7)	49(6)	25(4)	62(8)	6(9)	−17(12)	−9(10)
N(5)	2133(7)	2241(6)	2430(8)	57(7)	42(5)	53(8)	−2(10)	−12(13)	10(11)
N(6)	486(8)	2133(8)	−3816(10)	49(7)	85(8)	103(11)	35(13)	26(15)	−68(16)
C(1)	3109(9)	617(8)	−267(11)	56(9)	47(7)	109(13)	10(13)	62(18)	20(15)
C(2)	3392(9)	186(9)	1237(12)	42(8)	55(8)	131(15)	17(13)	29(18)	60(17)
C(3)	−1220(9)	1751(8)	1841(10)	46(8)	47(6)	75(11)	1(12)	21(15)	−26(14)
C(4)	−738(9)	2782(8)	1360(10)	61(9)	39(6)	78(11)	19(12)	4(16)	−27(13)

a) Standard deviations of least significant figures are given in parentheses.

2) W. P. Schaefer and R. E. Marsh, *Acta Crystallogr.*, **21**, 735 (1966).
3) R. E. Marsh and W. P. Schaefer, *ibid.*, **B24**, 246 (1968).
4) N. G. Vannerberg, *ibid.*, **18**, 449 (1965).
5) W. P. Schaefer, *Inorg. Chem.*, **7**, 725 (1968).
6) T. Shibahara and M. Mori, This Bulletin, **45**, 1433 (1972).
7) International Tables for X-ray Crystallography, Vol. III, Kynoch Press, Birmingham (1962), p. 202.

TABLE 3. CALCULATED HYDROGEN ATOM POSITIONS[a] ($\times 10^4$)

Atom		x/a	y/b	z/c
N(1)	H(1)	2818	2122	66
	H(2)	1883	1719	−1095
N(2)	H(3)	1730	−418	1433
	H(4)	2292	168	2682
N(3)	H(5)	279	1210	3166
	H(6)	−309	405	2204
N(4)	H(7)	−452	2332	−485
	H(8)	520	3058	178
C(1)	H(9)	3910	790	−595
	H(10)	2630	95	−917
C(2)	H(11)	3755	−526	1243
	H(12)	4007	642	185
C(3)	H(13)	−1662	1864	2650
	H(14)	−1821	1422	1058
C(4)	H(15)	−1462	3229	927
	H(16)	−227	3158	2169

a) All hydrogen atoms were assigned isotropic temperature factors, B=3.5 Å^2.

$w = 1.0$, if $F_{min} < F_o < F_{max}$ (=30.7);

$w = F_{max}/F_o$, if $F_o > F_{max}$

The atomic scattering factors were taken from the International Tables for X-ray Crystallography.[7] The R index was 0.113 for all the observed reflections. The positions of fourteen hydrogen atoms attached to ethylenediamine molecules were apparent from difference maps, but residual two hydrogen-atom positions were obscure. Although least-squares refinement including hydrogens gave R of 0.103, it indicated some unreasonable short C–H and N–H distances. Thus, neither their coordinates nor their temperature factors were refined. Instead, the hydrogen-atom positions were calculated assuming a tetrahedral configuration about the carbon and nitrogen atoms in ethylenediamine molecules, and C–H and N–H distances of 1.00 and 0.90 Å.[5,8] Inclusion of these assumed hydrogen positions gave R index of 0.106.

The final atomic coordinates and anisotropic temperature factors of the form: $\exp(-(B_{11}h^2+B_{22}k^2+B_{33}l^2+B_{12}hk+B_{13}hl+B_{23}kl))$ together with their estimated standard deviations are given in Table 2, and the calculated hydrogen-atom parameters in Table 3. A complete list of the observed and calculated structure factors is preserved by the Chemical Society of Japan.[9]

Description and Discussion of Structure

A perspective drawing of the complex cation is given in Fig. 1, and the atomic arrangement in the crystal in projection along the b axis in Fig. 2. Interatomic distances and bond angles within the ions are listed, along with their estimated standard deviations, in Tables 4 and 5. Each cobalt atom is surrounded octahedrally by four nitrogen atoms of ethylenediamine molecules, a nitrogen atom of the nitro group, and an oxygen atom of the bridging group. As the center of the μ-peroxo group lies on the crystallographic center of symmetry, the geometry of Co–O–O–Co is *trans* coplanar. The torsion angle (180°) about the O–O bond is thus much larger than 146° found for the decaammine μ-peroxo dicobalt (4+) cation reported by Schaefer.[5] This is probably due to the greater steric hindrance between coordinated ethylenediamine groups across the bridge than that between coordinated ammine groups. The short distances across the bridge are those of C(1)···C(3′) and C(3)···C(1′), and are both 3.83 Å, *i.e.* less than twice the van der Waals radius (2.0 Å) of C–H. The nitro ligand has *trans* configuration to the μ-peroxo bridge. The O–O distance in the bridge is 1.53 Å, somewhat longer than that found in H_2O_2 (1.47—1.49 Å)[10,11] and BaO_2

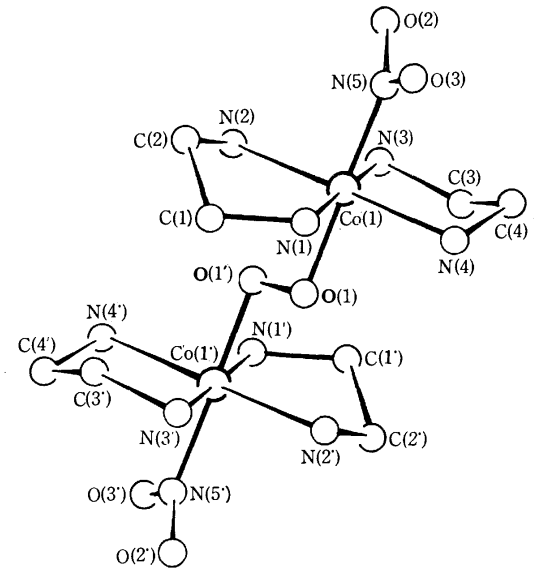

Fig. 1. Perspective drawing of $[NO_2(en)_2CoO_2Co(en)_2NO_2]^{2+}$ cation.

TABLE 4. INTERATOMIC DISTANCES WITHIN THE IONS

Distance	Value, Å	Distance	Value, Å
Co(1)–O(1)	1.887(6)	N(5)–N(1)	2.761(11)
–N(1)	1.947(8)	–N(2)	2.772(11)
–N(2)	1.927(7)	–N(3)	2.796(11)
–N(3)	1.953(7)	–N(4)	2.770(11)
–N(4)	1.960(7)	O(1)–N(1)	2.681(9)
–N(5)	1.940(8)	–N(2)	2.687(9)
N(5)–O(2)	1.204(14)	–N(3)	2.691(9)
–O(3)	1.238(13)	–N(4)	2.684(9)
O(1)–O(1′)	1.529(9)	O(1′)–N(1)	3.907(9)
N(1)–C(1)	1.515(13)	–N(2)	2.756(9)
N(2)–C(2)	1.503(14)	–N(3)	2.769(9)
N(3)–C(3)	1.507(13)	–N(4)	3.910(9)
N(4)–C(4)	1.462(12)	N(6)–O(4)	1.258(15)
C(1)–C(2)	1.542(16)	–O(5)	1.211(21)
C(3)–C(4)	1.534(14)	–O(6)	1.238(14)

8) D. J. Hodgson, P. K. Hale, and W. E. Hatfield, *Inorg, Chem.*, **10**, 1061 (1971).

9) The complete data of the F_o—F_c table are kept as Document No. 7312 at the office of the Bulletin of the Chemical Society of Japan.

10) P. A. Giguere and V. Schoemaker, *J. Amer. Chem. Soc.*, **65**, 2025 (1943).

11) S. C. Abrahams, R. L. Collin, and W. N. Lipscomb, *Acta Crystallogr.*, **4**, 15 (1951).

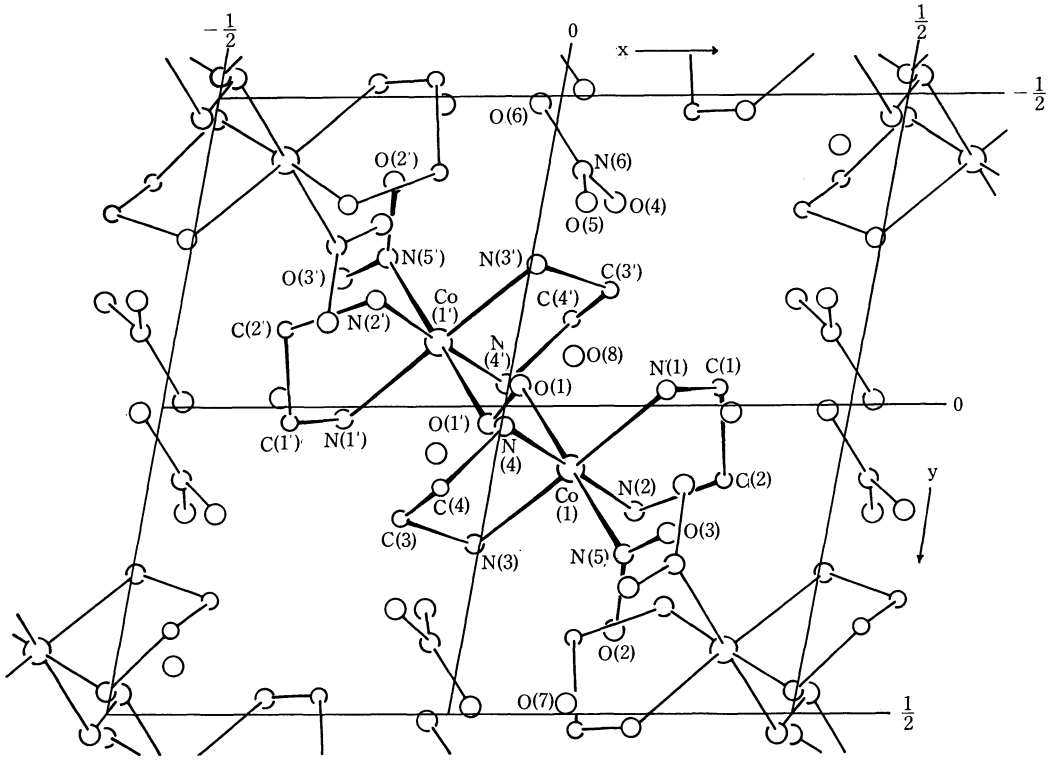

Fig. 2. The atomic arrangement in projection along the b axis.

Table 5. Bond angles

Angle	Deg.	Angle	Deg.
Co(1)–O(1)–O(1')	110.0(6)	Co(1)–N(1)–C(1)	108.6(6)
O(1)–Co(1)–N(1)	88.7(3)	Co(1)–N(2)–C(2)	110.4(6)
O(1)–Co(1)–N(2)	89.5(3)	Co(1)–N(3)–C(3)	109.1(6)
O(1)–Co(1)–N(3)	89.0(3)	Co(1)–N(4)–C(4)	108.9(6)
O(1)–Co(1)–N(4)	88.5(3)	N(1)–C(1)–C(2)	107.1(8)
N(1)–Co(1)–N(2)	87.5(3)	N(2)–C(2)–C(1)	106.1(9)
N(3)–Co(1)–N(4)	86.1(3)	N(3)–C(3)–C(4)	106.7(8)
N(1)–Co(1)–N(4)	94.1(3)	N(4)–C(4)–C(3)	105.5(8)
N(2)–Co(1)–N(3)	92.3(3)	O(1)–Co(1)–N(5)	178.7(3)
Co(1)–N(5)–O(2)	121.8(8)	N(1)–Co(1)–N(3)	177.6(3)
Co(1)–N(5)–O(3)	121.1(7)	N(2)–Co(1)–N(4)	177.4(3)
O(2)–N(5)–O(3)	117.1(10)	O(4)–N(6)–O(5)	121.6(13)
N(5)–Co(1)–N(1)	90.5(3)	O(5)–N(6)–O(6)	120.2(13)
N(5)–Co(1)–N(2)	91.5(3)	O(6)–N(6)–O(4)	118.1(10)
N(5)–Co(1)–N(3)	91.8(3)		
N(5)–Co(1)–N(4)	90.5(3)		

(1.49 Å).[12] The Co–O distance is 1.89 Å about the same as that found in the μ-O_2 decaammine (both superoxo and peroxo) complexes. The Co–N(NO_2) distance is 1.940(8) Å, essentially the same as the value 1.92(2) Å in $[CoNO_2(NH_3)_5]Br_2$.[13] Thus, there appeares no significant structural *trans* effect of the O_2 and NO_2 groups. This is in agreement with the fact that $[NO_2(en)_2CoO_2Co(en)_2NO_2]^{2+}$ is stable in an aqueous solution. The Co–O–O angle is 110°, somewhat smaller than that reported for the μ-O_2 compound. An average of 1.947(8) Å was obtained for the four Co–N(en) distances, comparable with Co(III)–N(sp^3) distances given in literature such as $[(NH_3)_5CoO_2Co(NH_3)_5](SO_4)_2 \cdot 4H_2O$, 1.962(9) Å; *trans* $[CoCl(NO)(en)_2]ClO_4$,[14] 1.964(5) Å; and $[Co(NH_3)_6]I_3$,[15] 1.936 (15) Å.

The Co–$(en)_2$ moieties have unusual $\delta\delta$ and $\lambda\lambda$ con-

Table 6. Puckering of the ethylenediamine rings

Plane defined by atoms	Atom	Deviation from plane, Å
Co(1), N(1), N(2)	C(1)	−0.36
	C(2)	0.32
Co(1), N(3), N(4)	C(3)	−0.26
	C(4)	0.49

12) S. C. Abrahams and H. A. Levy, *J. Chem. Phys.*, **7**, 838 (1954).
13) F. A. Cotton and W. T. Edwards, *Acta Crystallogr.*, **B24**, 474 (1968).
14) D. A. Snyder and D. L. Weaver, *Inorg. Chem.*, **9**, 2760 (1970).
15) N. E. Kime and J. A. Ibers, *Acta Crystallogr.*, **B25**, 168 (1969).

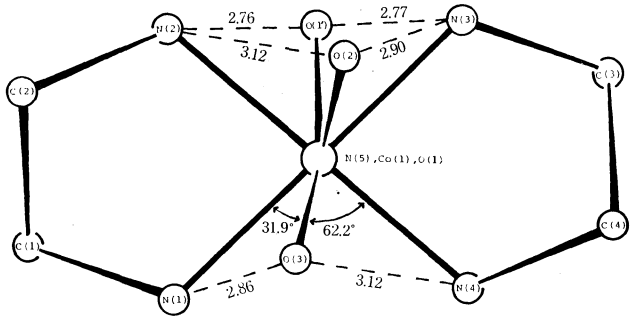

Fig. 3. The view of half of the cation along the N(5), Co(1), O(1) bonds.

figurations. The out-of-plane distances in relation to the puckering of the ethylenediamine rings are listed in Table 6. All *trans* bis(ethylenediamine) complexes so far determined by X-ray analyses have $\delta\lambda$ conformation[16,17] except for $[CoCl(NO)(en)_2]ClO_4$. As is shown in Fig. 3, the NO_2 plane does not bisect the N(1)–Co(1)–N(4) angle, in contrast to $[CoNO_2(NH_3)_5]Br_2$, and O(3)–N(1) and O(2)–N(3) have rather short distances 2.86 and 2.90 Å, respectively, implying hydrogen bonding. Existence of hydrogen bonding can also be inferred between O(1′) and N(2) (2.76 Å) as well as between O(1′) and N(3) (2.77 Å). The two sp^3-type unshared electron orbitals of bridging oxygen O(1′) should point toward the vicinity of hydrogen atoms attached to N(2) and N(3) atoms. These may be partly respondible to the $\delta\delta$ and $\lambda\lambda$ configurations of the complex ion. The possible hydrogen bondings

16) C. J. Hawkins, "Absolute Configuration of Metal Complexes," ed. by F. A. Cotton and G. Willkinson, Wiley-Interscience, New York, N. Y. (1971), p. 128.

17) A. Nakahara, Y. Saito, and H. Kuroya, This Bulletin, **25**, 331 (1952).

TABLE 7. POSSIBLE HYDROGEN BONDINGS[a)]

From	To	Distance, Å
N(1)	O(3), a	2.86
	O(4), a	3.02
	O(6), d	3.12
N(2)	O(1′), a	2.76
	O(7), a	3.18
N(3)	O(1′), a	2.77
	O(2), a	2.89
	O(6), a	3.05
N(4)	O(8), a	2.89
O(4)	O(7), a	2.80
O(6)	O(7), b	2.87
O(7)	O(8), c	2.68

a) The translations are as follows:
(a) x, y, z; (b) $-x, -y, -z$;
(c) $-x, +y, -z$; (d) $+x, -y, +z$.

with N–H···O distances less than 3.3 Å and O–H···O distances less than 3.0 Å are listed in Table 7. It is interesting that both the first example of $\delta\delta$ and $\lambda\lambda$ configuration ($[CoCl(NO)(en)_2]^+$) and the present one ($[NO_2(en)_2CoO_2Co(en)_2NO_2]^{2+}$) have rather abnormal ligands such as –NO or –O–O– considered to give some specific π-bonding character. The nitro group is planar within experimental error, with N–O distances of 1.21—1.26 Å and O–N–O angles of 118.1—121.6°. The short distances between N(4)–O(8), O(8)–O(7), O(7)–O(4), and O(7)–O(6) appear to be due to intermolecular hydrogen bonds. Cations and anions alternately form layers parallel to the plane ($\bar{1}01$).

The authors wish to express their thanks to Dr. S. Ooi for his kind suggestions. They are also indebted to Mr. K. Hirotsu, for adaptation of the HBLS-4 and RSSFR-3 computer programs to the FACOM 270-30 computer at Osaka City University.

Photovoltaic Effect of Aromatic Diamine in Solution

Takeshi IMURA, Seishi TAKAGI, and Kazuo KAWABE

Electrophysics Laboratory, Department of Electrical Engineering, Faculty of Engineering, Osaka University, Suita, Osaka 565

(Received January 12, 1973)

Photovoltaic behaviors are described of *N,N,N',N'*-tetramethyl-*p*-phenylenediamine dissolved in various polar solvents. Positive photovoltage is observed on the illuminated electrode in highly polar solvents such as methanol and acetonitrile, and none in moderately polar ones such as ethanol and acetone. The influence of a few electrode metals on photovoltage has been examined. The electromotive force increases with the work function of metals from tantalum to platinum. Conditions for the appearance of photovoltage are discussed and the photo-ionization process of the aromatic diamine is considered.

Photovoltaic effects are sometimes observed when an electrode immersed in some organic solution is irradiated with light. This phenomenon has been utilized by a few researchers for studying photochemical or photobiological reactions where ionic species play an important role. Methanol solutions of chlorophyll containing benzoquinone were shown to produce photovoltages which depend upon the pH of the solutions.[1,2] Photovoltage measurements were also carried out in tetracyanoethylene dissolved in tetrahydrofuran by exciting the charge-transfer band.[3] The first problem was to identify the active species inducing electromotive force, identification being carried out by means of ESR, flash photolysis and other spectroscopic techniques. The active species are generally the anions or cations which are generated in solutions by photo-ionization, and held on the electrode by adsorption.

The present work deals with the photovoltaic behaviors of *N,N,N',N'*-tetramethyl-*p*-phenylenediamine (TMPD) in polar solvents. This system seems to be the best for general and exhaustive investigation of photoelectric phenomena in organic fluid solutions, since a number of detailed studies have clarified the primary products and processes which take place on the photo-ionization of TMPD.[4-14]

When TMPD is photo-ionized in solution, a fairly large photocurrent is observed,[4,8,10-13] suggesting the generation of voltaic effect. Although the photovoltaic effect is a phenomenon taking place on the interface between liquid solvent and solid metal, detailed information is scarce as regards the properties and reactions of the active species which produces photo-emf on the interface. It was thought desirable to carry out experiments from the viewpoint of surface phenomenon. In this paper discussions are given on the influence of electrode metals and solvents upon the photovoltaic effect of TMPD solutions.

Experimental

Materials. TMPD was obtained as described.[4] Ethanol for spectroscopy (Nakarai Chemicals), spectrosol-grade acetone and methanol (Dotite), and luminasol-grade dimethylformamide (Dotite) were used without purification for the preparation of solutions. Acetonitrile was refluxed, fractionally distilled twice over phosphorus pentoxide, and finally distilled over potassium carbonate.

Apparatus and procedure. The cell for photovoltaic measurement is shown in Fig. 1. It is made from a quartz tube, the top of the cell being a ground joint fitted to the upper cover, from which 5 mm × 50 mm electrodes are suspended with two tungsten rods.

The electrode metals were cleaned as follows. Platinum and tantalum were washed successively with a solution of a surfactant (R.B.S. 25, Chemical-Products R. Borghgraef), deionized water and distilled methanol, and were then dried. Copper was treated with dilute hydrochloric acid, washed with deionized water and distilled methanol, and then dried.

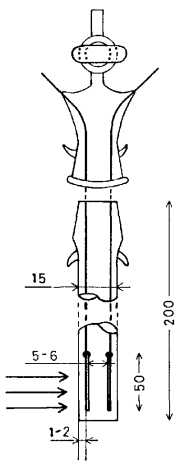

Fig. 1. Cell for the measurement of photo-emf.

1) E. Fujimori, and M. Tavla, *Photochem. Photobiol.*, **8**, 31 (1968).
2) W. H. Simpson, R. A. Freeman, and P. J. Reucroft, *ibid.*, **11**, 319 (1970).
3) P. J. Reucroft, P. L. Kronick, and E. E. Hillman, *J. Electrochem. Soc.*, **114**, 1054 (1967).
4) T. Imura, N. Yamamoto, and H. Tsubomura, This Bulletin, **43**, 1670 (1970).
5) Y. Nakato, M. Ozaki, A. Egawa, and H. Tsubomura, *Chem. Phys. Letters*, **9**, 615 (1971).
6) Y. Nakato, N. Yamamoto, and H. Tsubomura, This Bulletin, **40**, 2480 (1967).
7) J. T. Richards and J. K. Thomas, *Trans. Faraday Soc.*, **66**, 621 (1970).
8) T. Imura, N. Yamamoto, H. Tsubomura, and K. Kawabe, This Bulletin, **44**, 3185 (1971).
9) A. Singh, H. D. Gesser, and A. R. Scott, *Chem. Phys. Letters*, **2**, 271 (1968).
10) H. S. Pilloff and A. C. Albrecht, *J. Chem. Phys.*, **49**, 4891 (1968).
11) N. Houser and R. C. Jarnagin, *ibid.*, **52**, 1069 (1970).
12) M. Tamir and M. Ottolenghi, *Chem. Phys. Lett.*, **6**, 369 (1970).
13) S. S. Takeda, N. E. Hauser, and R. C. Jarnagin, *J. Chem. Phys.*, **54**, 3195 (1971).
14) R. Potashnik, M. Ottolenghi, and R. Bensasson, *J. Phys. Chem.*, **73**, 1912 (1969).

Table 1. Effect of polarity and viscosity of solvent[15] on the photo-emf of TMPD solution (5×10^{-3} M)

	Dielectric constant (25 °C)	Dipole moment (D)	Viscosity (cp, 25 °C)	Photo-emf (mV)	$TMPD^+$ spectrum	Appearance[4] of phto-current
Acetone	20.7	2.90	0.304	—	—	···
Ethanol	24.3	1.69	1.078	—	+	—
Methanol	32.6	1.69	0.545	10.2(±15%)	+	···
Dimethylformamide	36.7	3.86	0.802	8.6(±10%)	+	+
Acetonitrile	37.5	3.92	0.325 (30 °C)	40.5(±15%)	+	+

The sample solution was introduced into the cell, the electrodes inserted, and high-purity nitrogen (more than 99.999%) was bubbled into the solution for a few minutes through a fine Teflon tube to remove dissolved oxygen. The tube was then pulled out, the upper ground stopper being closed before each experiment.

Only the front electrode was illuminated by light from a high-pressure mercury lamp (250 W, Ushio) with quartz lenses and a glass filter (UV-D1C, Toshiba) which passes only light having energy 3.1—4.1 eV. The distance between the lamp and the cell was fixed at about 400 mm. The lower part of the front electrode was illuminated over a 20 mm× 2—3 mm area.

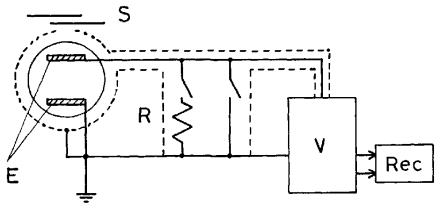

Fig. 2. Schematic diagram of measureing circuit.
S: Shutter, E: Electrodes, R: 100 kΩ resistor, V: Vibrating-reed electrometer, Rec: Recorder.

The apparatus for measurement of photovoltage is shown in Fig. 2. The entire cell was put in a brass pipe to be protected from electrical noise. A vibrating-reed electrometer (TR-84 M Takeda Riken) was used to read photo-induced voltage. Photovoltage was recorded with values across a shunt resistor of 100 kΩ. This helped improve the reproducibility of measurement and produce the stable value of voltage, though the magnitude of the observed voltage became smaller. The resistance of the sample solutions were in the range 4×10^5—5×10^6 Ω, differing with solvent. The lower limit of the detection of photovoltage was down to 0.05 mV.

Results

The photovoltage responses are shown in Table 1 for 5×10^{-3} M solutions of TMPD in various polar solvents. Positive photovoltages were observed on the illuminated electrode in methanol, dimethylformamide, and acetonitrile. Experiments in dimethylformamide were repeated several times for each sample, the deviation from the mean value being within ±10%. In the other solvents the error, partly due to the optical system, was estimated to be within ±15%.

No photo-emf was detected in moderately polar solvents, acetone or ethanol. The positive sign in the column of $TMPD^+$ spectrum in Table 1 indicates that the sample solution turns bluish after the irradiation for measurement of the photo-voltage, *viz.*, $TMPD^+$ is photo-generated and exists either in the form of the free or paired ion in the solution. Appearance of the photocurrent indicates the existence of photo-generated free ions, not paired, in the solution.[4]

The effect of electrode metal on the photovoltage response is shown in Table 2 for 5×10^{-4} M solutions of TMPD in dimethylformamide. The electromotive force shows a tendency to increase with the work function of the metal.

Table 2. Effect of work functions of electrode metals on the photo-emf of TMPD solutions (5×10 M) in dimethylformamide

	Work function[16] (eV)	Photo-emf (mV) (±15%)
Pt	5.4	10.2
Cu	4.5	4.7
Ta	4.1	0.5

The maximum quantity of the photo-emf was obtained over the concentration range 10^{-3}—10^{-4} M. The phtovoltage decreased remarkably when the solution was diluted to 10^{-5} M or less. In concentrated solution ($\geqq10^{-2}$ M) photovoltage response became small due to the diminution in intensity of the exciting light on the surface of the electrode caused by the inner filter effect in the front portion of the sample solution. The molar extinction coefficient was determined to be $(2.6\pm0.1)\times10^3$ M^{-1} cm^{-1} for the first absorption maximum of TMPD at 3.8 eV in dimethylformamide.

No photovoltage (more than 0.05 mV) was generated by irradiating the system containing no TMPD and composed of only solvent and electrodes.

Discussion

Cationic and anionic species should be photo-generated in equal concentration. However, the photovoltage appeared positively on the illuminated electrode. The concentration gradient of charged species in the vicinity of the electrode can be induced from the difference in the diffusion velocity between $TMPD^+$ and anionic species. The latter might have a larger

15) J. A. Riddick and W. B. Bunger, "Techniques of Chemistry," ed. A. Weissberger, Vol. 2, "Organic Solvent," third ed., John Wiley & Sons, Inc., N. Y. (1970).

16) A. J. Dekker, "Solid State Physics," Asian ed., Maruzen Co., Ltd., Tokyo (1960), p. 223.

diffusion velocity since the electron is to react easily with the solvent molecules and to be transferred successively. On the contrary, stable $TMPD^+$ has ordinary diffusion velocity of the solvated ion. It is well-known that either cation or anion is adsorbed preferentially from electrolyte solution onto the metal surface. $TMPD^+$ might be adsorbed preferably onto the surface of the illuminated electrode.

No response of photo-emf was detected in acetone (Table 1). Ultraviolet excitation of TMPD in acetone produced no absorption of $TMPD^+$. Thus the cation, active species, does not seem to be generated in the solution. In ethanol the photo-generation of $TMPD^+$ surely occurs (Table 1), but neither photocurrent nor photovoltage was detected. This implies that $TMPD^+$ observed spectroscopically in ethanol is to be present in the form of ion-pair which gives rise to absorption but cannot contribute to photoelectric effect. The particular situation in ethanolic solution was discussed in other papers.[4,7] The polarization energy seems to be somewhat short in acetone or ethanol for the photo-generation of ion-pair or dissociation into free ions.

Methanol, dimethylformamide, and acetonitrile, in which the photoelectric effects could be observed are highly polar. The fall in the ionization level by polarization energy or the ease for photo-ionization should be in the order of polarity of the solvents. The magnitude of the photovoltage, however, was not in the order of polarity, and seems to depend on the viscosity of solvents as well (Table 1). Actually, the photo-emf was hardly observed in *N*-methylpropionamide which has a high dielectric constant ($\varepsilon = 172$[14] at 25 °C) and high viscosity (5.2 cp[14] at 25 °C) due to the hydrogen-bonded aggregation. A lower viscosity may accelerate the formation of the concentration gradient of the active ionic species. Higher viscosity of dimethylformamide in spite of its large polarity, would prevent the generation of a larger photo-emf than in methanol. Photoelectric responses were especially large in acetonitrile. A possible explanation might be that the anionic species in acetonitrile is very mobile and diffuses away rapidly.

The cation present in the adjacent neighborhood of the electrode was supposed to be the active species to produce electromotive force. The cation will pull out the electron from electrode metal if the metal had a small work function, and will be changed to neutral TMPD which cannot produce electromotive force. The electron-transfer process between $TMPD^+$ and metal or the oxidation-reduction reaction on the metal surface can take place more easily as the work function of the metal decreases. Thus the photovoltage obtained gets smaller, as the work function of electrode metal becomes smaller (Table 2). If the work function is smaller than the energy of the state of $TMPD^+$, no photovoltage response would be detectable, because of the instant reduction of cation to neutral molecule.

It is concluded that photo-generation of dissociated $TMPD^+$ is necessary for the appearance of photovoltage in the solution. The magnitude of photo-emf seems to be determined by the quantity of $TMPD^+$ in the vicinity of the electrode.

The Emission Spectra of Hexamminechromium(III) Hexacyanocobaltate(III), $[Cr(NH_3)_6][Co(CN)_6]$

Hiroshi KATAOKA

Department of Chemistry, Faculty of Science, Rikkyo University, Nishi-ikebukuro, Toshima-ku, Tokyo 171

(Received August 15, 1972)

Spin-forbidden absorption bands of $K_3[Co(CN)_6]$ were reexamined employing conventional transmission spectroscopy, diffuse reflectance spectroscopy, and microspectrophotometry. A small but very distinct shoulder ($\varepsilon \approx 0.3$—0.4) obtained at a low temperature at 26000 cm^{-1} was assigned to the $^3T_{1g} \leftarrow {}^1A_{1g}$ transition. Another very small band ($\varepsilon \approx 0.001$) at 16300 cm^{-1} was probably due to an impurity. The emission spectra of $K_3[Co(CN)_6]$ powder in the temperature range from room temperature to that of liquid hydrogen were observed by means of a modified Hitachi 203 fluorescence spectrophotometer. The broad emission band at room temperature showed some vibrational structures at low temperatures. The emission spectra of powders of $[Cr(NH_3)_6](NO_3)_3$ and $[Cr(NH_3)_6][Co(CN)_6]$ were also measured. The following results were obtained: i) Similar emission spectra, which seemed to originate from $[Cr(NH_3)_6]^{3+}$, were observed with both complexes $[Cr(NH_3)_6](NO_3)_3$ and $[Cr(NH_3)_6][Co(CN)_6]$ using mercury lines at 313, 365, and 435 nm for excitation. ii) With 254 nm excitation, such emission spectra as i) were not observed with $[Cr(NH_3)_6](NO_3)_3$, but the same emission spectra as in i) were observed with $[Cr(NH_3)_6][Co(CN)_6]$. iii) The ratio of the emission intensities at 15000 cm^{-1} with 435 and 313 nm excitations was 1 : 0.25—0.30 for $[Cr(NH_3)_6](NO_3)_3$, but it was 1 : 1.5—1.7 for $[Cr(NH_3)_6][Co(CN)_6]$. From these results, it was presumed that, in $[Cr(NH_3)_6][Co(CN)_6]$, there occurred an energy transfer from the complex anion to the complex cation. Furthermore, emission spectra were observed with $[Cr(NH_3)_6](ClO_4)_3$ and the equimolar mixture of complex salts $[Cr(NH_3)_6](ClO_4)_3$–$K_3[Co(CN)_6]$ and $[Cr(NH_3)_6](NO_3)_3$–$K_3[Co(CN)_6]$ for the purpose of confirming the energy transfer in $[Cr(NH_3)_6][Co(CN)_6]$. The temperature dependence of the emission intensity was also discussed.

Recently it has been found by many authors that chromium(III) complexes show emission spectra,[1] and several papers have been published presenting evidence for energy transfer in chromium complexes in solutions[2] and in solids.[3,4]

On the other hand, although there have been extensive studies of the absorption spectra of cobalt(III) complexes, there have been few papers on their emission spectra. Those reported up to this time are $Na_5[Co(SO_3)_2(CN)_4]$,[5] $Ag_3[Co(CN)_6]$,[6], and $K_3[Co(CN)_6]$.[7-10] Several papers on energy transfer with cobalt(III) complexes in solutions have also been presented,[11-13] but there have been few papers on that in solids. One of the reasons why the relationship between the absorption and the emission spectrum has not been discussed fully in those reports seem to have been the difficulty of observing the very weak spin-forbidden absorption band. Some authors have observed the spin-forbidden band of $K_3[Co(CN)_6]$,[7,10,14] but differing results have been reported.

In the present work, $K_3[Co(CN)_6]$ was studied in order to establish the relationship between the emission band and the spin-forbidden absorption band. Furthermore, the double complex salt $[Cr(NH_3)_6][Co(CN)_6]$ was studied to get information on the emission spectrum and energy transfer. The reasons why the double complex salt $[Cr(NH_3)_6][Co(CN)_6]$ was selected were as follows: i) The relation between the emission spectrum and the spin-forbidden band of $[Cr(NH_3)_6]^{3+}$ has been elucidated by extensive studies.[15] ii) The absorption spectra of the double complex salt nearly form a superposition of the spectra of the complex cation $[Cr(NH_3)_6]^{3+}$ and the complex anion $[Co(CN)_6]^{3-}$. Therefore, the selective excitation of the complex anion or cation is possible if a suitable wavelength is selected for the excitation. Furtheremore, $[Cr(NH_3)_6](NO_3)_3$, $[Cr(NH_3)_6](ClO_4)_3$, and an equimolar mixture of the complex salts $[Cr(NH_3)_6](ClO_4)_3$–$K_3[Co(CN)_6]$ and

1) For example a) E. Koglin and W. Krasser, *Ber. Bunsenges. Phys. Chem.*, **76**, 401 (1972). b) H. L. Schläfer, M. Martin, H. Gausmann, and H. H. Schmidtke, *Z. Phys. Chem. (N.F.)*, **76**, 61 (1971). c) S. L. Barker, *Chem. Commun.*, **1971**, 363. d) N.A.P. Kane-Maguire and C. H. Langford, *ibid.*, **1971**, 895. e) G. Gliemann and H. Yersin, *Ber. Bunsenges. Phys. Chem.*, **75**, 1257 (1971). f) F. D. Camassei and L.S. Forster, *J. Chem. Phys.*, **50**, 2603 (1969). g) J. C. Hemple and F. A. Matsen, *ibid.*, **73**, 2502 (1969). h) P. Cancellieri, E, Cervone, C. Furlani, and G. Sartori, *Z. Phys. Chem. (N.F.)*, **62**, 35 (1968).

2) a) I. Fujita and H. Kobayashi, *Ber. Bunsenges. Phys. Chem.*, **76**, 115 (1972). b) V. Balzani, R. Ballardini, M. T. Gandolfi and L. Moggi, *J. Amer. Chem. Soc.*, **93**, 339 (1971). c) A. Vogler and A. W. Adamson, *J. Phys. Chem.*, **74**, 67 (1970). d) T. Ohno and S. Kato, This Bulletin, **42**, 3385 (1969). e) M. R. Edelson and R. A. Plane, *J. Phys. Chem.*, **63**, 327 (1959).

3) H. Gausmann and H. L. Schläfer, *J. Chem. Phys.*, **48**, 4056 (1968).

4) H. L. Schläfer, H. Gausmann, and C. H. Möbius, *Inorg. Chem.*, **8**, 1137 (1969).

5) F. Zuloaga and M. Kasha, *Photochem. Photobiol.*, **7**, 549 (1968).

6) A. D. Kirk, H. L. Schläfer, and A. Ludi, *Can. J. Chem.*, **48**, 1065 (1970).

7) G.B. Porter and M. Mingardi, *J. Chem. Phys.*, **44**, 4354 (1966).

8) G. A. Crosby, *J. Chem. Phys.*, **64**, 160 (1967).

9) A. D. Kirk, A. Ludi, and H. L. Schläfer, *Ber. Bunsenges. Phys. Chem.*, **73**, 669 (1969).

10) H. Kataoka, Y. Yamamoto, M. Nakahara, and Y. Kondo, *Nippon Kagaku Zasshi*, **92**, 274 (1971).

11) G. B. Porter, *J. Amer. Chem. Soc.*, **91**, 3980 (1969).

12) L. Moggi, F. Bolletta, F. Balzani, and F. Scandola, *J. Inorg. Nucl. Chem.*, **28**, 2589 (1966).

13) A. W. Adamson, *Coord. Chem. Rev.*, **3**, 169 (1968).

14) S. Kida, J. Fujita, K. Nakamoto, and R. Tsuchida, This Bulletin, **31**, 79 (1958).

15) For example a) H. H. Eysel, *Z. Phys. Chem. (N.F.)*, **72**, 82 (1970). b) A. W. Adamson and T. M. Dunn, *J. Mol. Spectrosc.*, **18**, 83 (1965). c) G. B. Porter and H. L. Schläfer, *Z. Phys. Chem. (N.F.)*, **40**, 280 (1964). d) H. L. Schläfer, *J. Phys. Chem.*, **69**, 2201 (1965).

$[Cr(NH_3)_6](NO_3)_3$–$K_3[Co(CN)_6]$ were studied for the purpose of confirming the energy transfer.

Recently, energy transfer in the double complex salt composed of $[Ru(bipy)_3]^{2+}$ and $[Cr(ox)_3]^{3-}$ (bipy: bipyridine, ox: oxalate ion) was studied by Fujita and Kobayashi.[16] Their observations provided interesting evidence for an electronic excitation energy transfer between complexes with different central metals.

Experimental

Preparation of Materials. $K_3[Co(CN)_6]$, $[Cr(NH_3)_6](ClO_4)_3$, and $[Cr(NH_3)_6](NO_3)_3$ were prepared according to the published methods.[17,18] These compounds were recrystallized three times from an aqueous solution.

The double complex salt $[Cr(NH_3)_6][Co(CN)_6]$ was prepared by adding an aqueous solution of $K_3[Co(CN)_6]$ (0.02 mol/l, 500 ml), with rigorous stirring, drop by drop into an aqueous solution of $[Cr(NH_3)_6](NO_3)_3$ (0.02 mol/l, 500 ml).[19] The fine precipitate thus obtained was filtered using a 4G-glass filter, washed with a large amount of water, and dried in a vacuum desiccator.

An equimolar mixture of the complexes was obtained by grinding powder of $[Cr(NH_3)_6](NO_3)_3$ and $K_3[Co(CN)_6]$ or $[Cr(NH_3)_6](ClO_4)_3$ and $K_3[Co(CN)_6]$ in an equimolar ratio.

The Growing of a Single Crystal of $K_3[Co(CN)_6]$. Because of the small molar extinction coefficient of the spin-forbidden bands of $K_3[Co(CN)_6]$,[7,14] a large single crystal was necessary for measuring its absorption spectrum. This single crystal was grown using equipment similar to that of Galsbøl.[20] The solution was prepared by dissolving about 150 g of $K_3[Co(CN)_6]$ in 300 ml of water containing a small amount of KCN at 50—55 °C. The vessel was then covered with a wrap sheet and placed in a thermostated bath at 50 °C. After one day, the solution was decanted into a 300 ml beaker, and then again placed in the thermostated bath as quickly as possible. A small seed[21] (*ca.* $1.5\times1\times1$ mm or larger) was put on the bottom of the beaker, and the surface was covered with a small amount of liquid paraffine in order to avoid evaporation. The solution at 50 °C was slowly cooled to room temperature at a velocity of 2.50 ± 0.01 °C/day. The temperature controller was a Jumo (Western Germany) model MS.D.B.P.8.66. After 10—15 days, a large single crystal weighing 23 g (approximately $25\times30\times20$ mm) was obtained.[22] It was greenish yellow and had some fine cracks, only a small portion being available for measuring the spectra.

Measurements of Absorption and Diffuse Reflectance Spectra. The absorption spectra of aqueous solutions were measured with a Hitachi EPS-3T recording spectrophotometer. The inside of the monochromator was filled with nitrogen gas during the measurement in the 190—220 nm region. The visible and ultraviolet spectra of a single crystal (thickness: 1.5 mm) of $K_3[Co(CN)_6]$ were measured with this spectrophotometer using a microspectrophotometric attachment constructed in this laboratory at room temperature (*ca.* 295 K) and at the temperature of liquid nitrogen (77 K).

The visible and near-infrared spectra of a large single crystal (*ca.* $25\times30\times20$ mm) were also measured by the conventional method at room temperature using a Cary-14 recording spectrophotometer.

The diffuse reflectance spectra were measured with a Hitachi EPS-3T spectrophotometer, using a reflectance accessory at room temperature.

The infrared spectra in the 700—4000 cm^{-1} region and in the 200—700 cm^{-1} region were obtained with, respectively a JASCO DS-301 infrared spectrophotometer and a JASCO Model IR-F far-infrared spectrophotometer, using the Nujol-mull method.

Measurement of Emission Spectra. For the present purpose, a Hitachi 203 fluorescence spectrophotometer (with two grating monochromators for the excitation and the detection) was modified as follows: i) the sample chamber of the Hitachi 203 spectrophotometer was modified to accommodate a cryostat-type AC-2 apparatus made by Air Products and Chemicals;[23,24] ii) the usual Hamamatsu R-212 (maximum sensitive wavelength 340 nm) photomultiplier was replaced with two photomultipliers, a Hamamatsu R-406 (S-1 characteristic, maximum sensitive wavelength 800 nm) and an R-136 (maximum sensitive wavelength 430 nm), for the purpose of detecting weak emission spectra in the near-infrared and red regions; iii) in most cases, the sample was excited with a mercury lamp (120 W, Ushio, UM-102) but in a few cases it was excited with a xenon lamp (150 W, Ushio, UXI-151D), and iv) in order to record the emission spectra automatically a Hitachi wavelength driving apparatus and a Hitachi QPD-53 recorder were used.

The emission spectra were passed through a yellow cut-off filter in order to remove the exciting light, and were detected at the right angle to the exciting light. Furthermore, the correction for the small amount of stray light from the exciting light source was made by means of powdered magnesium oxide, as has been described by Kirk and his co-workers.[9] The sample temperature was measured using a calibrated chromel-constantan thermocouple and a reference junction. The entrance and exit slit widths were 0.8 mm in all the measurements. The emission spectra thus obtained were not corrected for the spectrophotometer, incident light intensity, detector, and particle size. The measurement region was 500—780 nm, while the temperatures ranged from room temperature to the temperature of liquid hydrogen (20 K). The measurement error of the temperature was $\pm0.5\%$ near 250 K, $\pm1.0\%$ near 150 K, and $\pm5\%$ near 50 K. The errors of the emission intensity measurement were $\pm5\%$.

Wavelength calibrations of the Hitachi EPS-3T spectrophotometer and Hitachi 203 fluorescence spectrophotometer were made by the use of mercury lines.

Results and Discussion

Diffuse Reflectance Spectra. Figure, 1 shows the diffuse reflectance spectra of the complex salts $[Cr(NH_3)_6](NO_3)_3$, $[Cr(NH_3)_6](ClO_4)_3$, $K_3[Co(CN)_6]$, and the double complex salt $[Cr(NH_3)_6][Co(CN)_6]$. The diffuse reflectance spectra of an equimolar mixture of complex salts $[Cr(NH_3)_6](NO_3)_3$–$K_3[Co(CN)_6]$ and $[Cr(NH_3)_6](ClO_4)_3$–$K_3[Co(CN)_6]$ are shown in Fig. 2.

16) a) I. Fujita, and H. Kobayashi *J. Chem. Phys*,. **52**, 4904 (1970). b) I. Fujita and H. Kobayashi, private communication.

17) "Inorganic Synthesis," Vol. II, ed. by W. C. Fernelius, (1946), p. 225.

18) M. Mori, *Nippon Kagaku Zasshi*, **74**, 253 (1953).

19) S. M. Jørgensen, *J. Prakt. Chem.*, **30**, 31 (1884).

20) F. Galsbøl, *Rev. Sci. Instrum.*, **36**, 1367 (1965).

21) Small seeds were obtained easily by the evaporation of the concentrated $K_3[Co(CN)_6]$ solution.

22) It was easy to obtain crystals which were thick enough to observe the very weak band, but usually they had many fine cracks and could not be used for the spectral measurement. Thick and transparent crystals could be obtained only very rarely.

23) D. White and K. E. Mann, *Rev. Sci. Instrum.*, **34**, 1370 (1963).

24) T. Ueno and K. Yoshiwara, *Teion Kogaku*, **4**, 106 (1969).

TABLE 1. SPECTRAL DATA OF $K_3[Co(CN)_6]$

	LF-I[d] Band			LF-II[d] Band			CT[e] Band		
	Maxima (cm^{-1})	log ε	$f \times 10^{-3}$	Maxima (cm^{-1})	log ε	$f \times 10^{-3}$	Maxima (cm^{-1})	log ε	$f \times 10^{-1}$
This work	32090	2.28	4.27	38800	2.12	3.30	49800	4.39	6.62
G. B. Porter *et al.*[a]	32100	2.26	—	38600	2.20	—	50000	4.20	—
M. Mingardi *et al.*[b]	32050	—	3.0	38460	—	2.8	48500	—	3.2
S. Kida *et al.*[c]	32500	2.29	—	39000	2.09	—	—	—	—

a) Ref. 7.
b) Ref. 25a).
c) Ref. 14.
d) Spin-allowed ligand field bands.
e) Charge transfer bands.

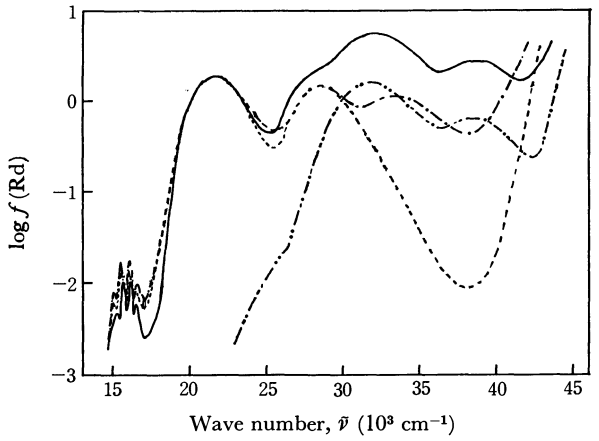

Fig. 1. Diffuse reflectance spectra of $[Cr(NH_3)_6](NO_3)_3$, $[Cr(NH_3)_6](ClO_4)_3$, $K_3[Co(CN)_6]$ and $[Cr(NH_3)_6][Co(CN)_6]$.
-·-·- $[Cr(NH_3)_6](NO_3)_3$ ····· $[Cr(NH_3)_6](ClO_4)_3$
-··-·· $K_3[Co(CN)_6]$ ——— $[Cr(NH_3)_6][Co(CN)_6]$

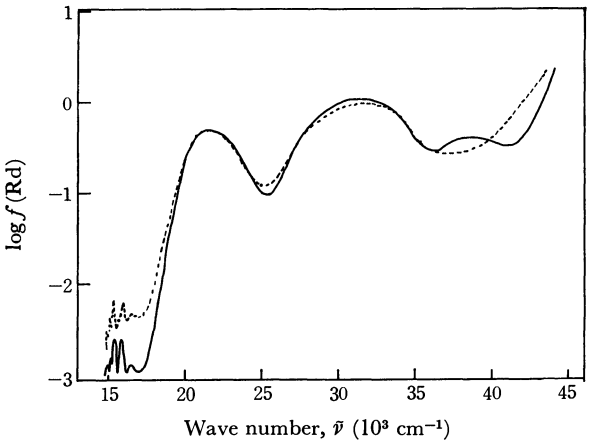

Fig. 2. Diffuse reflectance spectra of equimolar mixture of complex salts.
------$[Cr(NH_3)_6](ClO_4)_3$–$K_3[Co(CN)_6]$
———$[Cr(NH_3)_6](NO_3)_3$–$K_3[Co(CN)_6]$

From these figures it is evident that the spectrum of the double complex salt compares well with the spectra of equimolar mixtures, which are considered to be the sum spectra of the individual spectra of the component complexes.

The Absorption Spectrum of $K_3[Co(CN)_6]$. Spin-allowed ligand-field bands and the charge-transfer band of $K_3[Co(CN)_6]$ were measured in an aqueous solution. The position (cm^{-1}) and the logarithms of the molar extinction coefficients of the bands are shown in Table 1, together with other workers' data. The oscillator strength, f, was calculated by the use of:

$$f = 4.32 \times 10^{-9} \int \varepsilon d\bar{\nu} = 5.6 \times 10^{-9} \varepsilon_{max} \Delta\bar{\nu} \quad (1)$$

where ε is the molar extinction coefficient; $\bar{\nu}$, the wave number, and $\Delta\bar{\nu}$, the half-band width.[25a] There is a rather good agreement between the present data and those of others.

Spin-forbidden bands for a number of cobalt(III) complexes have been reported by many workers.[26] Those of $K_3[Co(CN)_6]$ were also reported by Kida *et al.*[14] and Porter *et al.*[7] The former found a shoulder at 24000 cm^{-1} and suggested that it represented a spin-forbidden band. The latter workers obtained a weak band ($\varepsilon \approx 0.01$) at 18500 cm^{-1} and assigned it to the $^3T_{1g} \leftarrow {}^1A_{1g}$ transition. The Tanabe-Sugano diagram[27] suggests that two spin-forbidden bands ($^3T_{1g}$, $^3T_{2g} \leftarrow {}^1A_{1g}$) exist in the near-ultraviolet and visible regions. It is thus necessary to elucidate whether the weak bands obtained by the above authors originate from similar transitions or from different transitions. In this paper, the spin-forbidden absorption bands of $K_3[Co(CN)_6]$ were reexamined employing conventional transmission spectroscopy, diffuse reflectance spectroscopy, and microspectrophotometry.

With the conventional transmission method, using various concentrations, it was impossible to obtain an absorption spectrum that showed a clear shoulder at 24000 cm^{-1}. Thus, the weak band might have been covered by the tail of the first spin-allowed band. A curve analysis of the first spin-allowed band was made using the equation presented by Shimura and Tsuchida.[28] Their equation is a modification of Kuhn

25) a) M. Mingardi and G. B. Porter, *Spectrosc. Lett.*, **1**, 293 (1968). b) M. K. DeArmond and J. E. Hillis, *J. Chem. Phys.*, **54**, 2247 (1971).
26) a) J. Fujita and Y. Shimura, This Bulletin, **36**, 1281 (1963). b) M. Linhard and M. Weigel, *Z. Phys. Chem. (N.F.)*, **11**, 308 (1957). c) C. K. Jørgensen, *Advan. Chem. Phys.*, **5**, 33 (1963). d) D. A. Johnson and A. G. Sharpe, *J. Chem. Soc., A*, **1966**, 798.
27) Y. Tanabe and S. Sugano, *J. Phys. Soc. Jap.*, **9**, 753, 766 (1954).
28) Y. Shimura and R. Tsuchida, This Bulletin, **28**, 572 (1955).

and Braun's[29] containing as a correction term δ, the inclination parameter.

On account of the superposition of the first and second spin-allowed ligand field bands of $K_3[Co(CN)_6]$, the true half-width of the first band was expected to be smaller than that obtained from the experimental curve. Thus, curve analyses were done in which the parameters, l (half-width of the band) and δ, were changed in the regions of 3300—5000 cm^{-1} and 0—300 cm^{-1} respectively. The best agreement between the experimental curve and the calculated one in the region 28000—35000 cm^{-1} was found when l and δ were 4900 and 170 cm^{-1} respectively. These two curves are shown in Fig. 3. However, much larger inconsistencies than those found in most cobalt(III) complexes were found in the wave number region below 28000 cm^{-1}. This must have been due to the presence of a small band ($\log \varepsilon \approx 0.4$) at about 27000 cm^{-1}.

An indistinct shoulder appeared at about 25000 cm^{-1} in the diffuse reflectance spectrum of $K_3[Co(CN)_6]$ (Fig. 1). The absorption spectra obtained by microspectrophotometry are shown in Fig. 4. Although no maximum or shoulder in the region in question was found at room temperature, a small but very distinct shoulder was obtained at 26000 cm^{-1} at the temperature of liquid nitrogen. The subtraction of the tail of the first spin-allowed band from this spectrum gave a small band whose maximum was at about 26000 cm^{-1}, its molar extinction coefficient was about 0.3—0.4. This small band may be the spin-forbidden band of $K_3[Co(CN)_6]$.[30]

Furthermore, a very weak band ($\varepsilon \approx 0.001$) was observed at 16300 cm^{-1} using a 10 cm cell and a concentrated solution (1.24 mol/l). This band was also observed at about the same position using a single crystal (thickness, 20 mm). The half-width of this band was about 1000 cm^{-1}.

The single crystal showed two very strong bands, at 4246 and 4279 cm^{-1}, and some other bands at 4155, 4160, 4290, 6333, and 6341 cm^{-1} in the near-infrared region. The two strong bands at 4246 and 4279 cm^{-1} were assigned by Jones to the combination bands for $(\nu_3+\nu_6)$ and $(\nu_1+\nu_6)$.[34] The two very weak bands in the 6000 cm^{-1} region may be due to the combination band for 2 (ν_1, ν_3, or ν_6)+(ν_1, ν_3, or ν_6). The next combination band, related to ν_1, ν_3, and ν_6, could be expected to appear in about the 8500 cm^{-1} region; however, no band was observed until the weak and broad band at 16300 cm^{-1} was reached. Therefore, this band might also be due to the spin-forbidden band of K_3-$[Co(CN)_6]$ (Fig. 5).

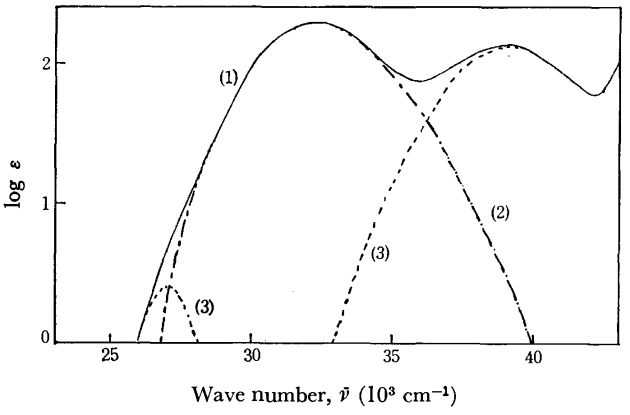

Fig. 3. Curve analysis of $[Co(CN)_6]^{3-}$.
(1): Experimental curve
(2): From Shimura and Tsuchida's equation, where l= 4900 cm^{-1} and δ=170 cm^{-1}
(3): (1)—(2).

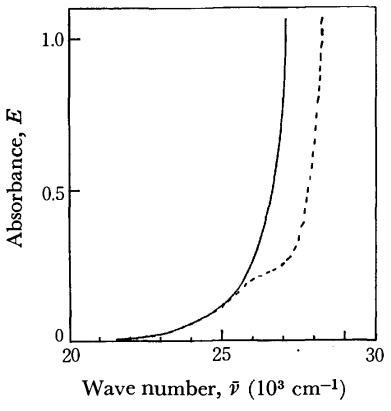

Fig. 4. Absorption spectra of a $K_3[Co(CN)_6]$ crystal by microspectrophotometry.
———: Room temperature
– – –: Liquid nitrogen temperature

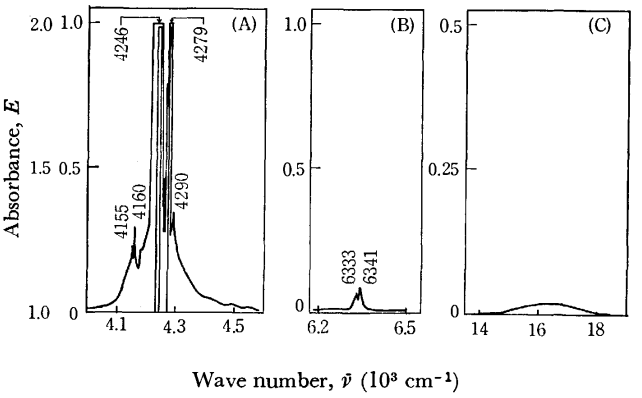

Fig. 5. Absorption spectrum of $K_3[Co(CN)_6]$ in the red and near-infrared regions.
(A), (B) Absorbance scale is left side
(C) Absorbance scale is right side

29) W. Kuhn and E. Braun, *Z. Phys. Chem.*, **B8**, 281 (1930).

30) If a small amount of $K_2[Co(CN)_5H_2O]$ exists in a $K_3[Co(CN)_6]$ crystal, a shoulder might appear at about 26000 cm^{-1}, because $K_2[Co(CN)_5H_2O]$ has the first spin-allowed band at 26300 cm^{-1} ($\varepsilon \approx 260$).[31] It is well-known in the preparation of $K_3[Co(CN)_6]$ that the uptake of the sixth cyanide by $[Co(CN)_5H_2O]^{2-}$ is a slow process at room temperature,[32] but very rapid at 95°C.[33] Thus, the reaction solution was boiled long enough to avoid contamination with $[Co(CN)_5H_2O]^{2-}$. Recrystallization was repeated several times. It is, therefore, more reasonable to attribute the small shoulder at 26000 cm^{-1} to the spin-forbidden band of $K_3[Co(CN)_6]$.

31) A. Haim and W. K. Wilmarth, *J. Amer. Chem. Soc.*, **83**, 509 (1961).

32) N. K. King and M. E. Winfield, *ibid.*, **83**, 3366 (1961).

33) L. C. Smith, J. Kleinberg, and E. Griswold, *ibid.*, **75**, 449 (1953).

34) L. H. Jones, *J. Chem. Phys.*, **36**, 1209 (1962).

However, it is more probable that this band is due to an impurity[35] contained in $K_3[Co(CN)_6]$. This is for the following reasons. i) There is a linear relation, as found by Fujita and Shimura, between the positions of the first spin-forbidden band and the first spin-allowed band of cobalt(III) complexes.[26a] The position of the band in question shifted very much from that expected from this relationship. The band found at 26000 cm^{-1}, however, is in agreement with the relationship, thus, it should be assigned to the $^3T_{1g}\leftarrow{}^1A_{1g}$ transition. The $^3T_{2g}\leftarrow{}^1A_{1g}$ band will exist at higher wave numbers, thus being covered completely by the first spin-allowed band. ii) Based on a theoretical calculation, Alexander and Gray concluded that the spin-forbidden $^3T_{1g}\leftarrow{}^1A_{1g}$ band will appear at about 27000 cm^{-1}.[36] iii) The intensity of this band ($\varepsilon\approx 0.001$) is abnormally small compared with those of the spin-forbidden bands of other cobalt(III) complexes ($\varepsilon=0.1$—1). iv) The separation between the positions of this band and the phosphorescence band seems to be too small if it is assumed that this band is due to the $^3T_{1g}\leftarrow{}^1A_{1g}$ transition.[37] v) The position (16300 cm^{-1}) and the intensity ($\varepsilon\approx 0.001$) of the band found in this work differ very much from the position (18500 cm^{-1}) and the intensity ($\varepsilon\approx 0.01$) reported by Porter *et al.*

Energy Level Diagram. The evergy level diagram based on the results of the conventional transmission and diffuse reflectance measurements on $[Cr(NH_3)_6](ClO_4)_3$, $K_3[Co(CN)_6]$ and $[Cr(NH_3)_6][Co(CN)_6]$ is shown in Fig. 6. The positions of the maxima of the absorption bands are shown by solid lines and dashed lines, and the half-widths of the bands, by hatched areas. The solid lines and dashed lines represent the electronic states possessing the same multiplicity and different multiplicities with respect to that of each ground state respectively. The electronic configurations of each level are given in parentheses. The wavelengths of the light used for excitation are also shown by the arrows on the left of the diagram.

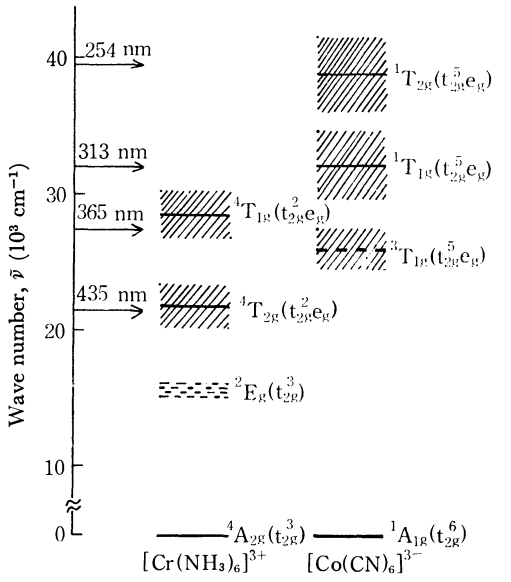

Fig. 6. Energy level diagram of $[Cr(NH_3)_6]^{3+}$ and $[Co(CN)_6]^{3-}$

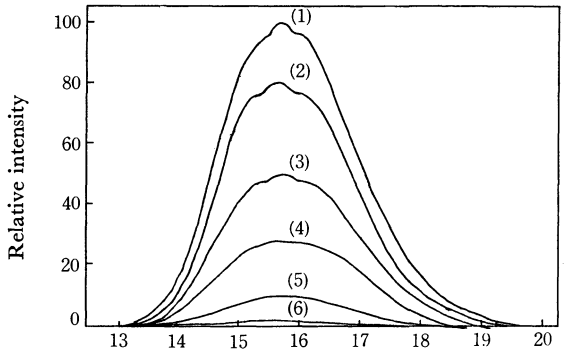

Fig. 7. Emission spectra of $K_3[Co(CN)_6]$ excited with 313 nm light.
Temperature (K): (1): 20, (2) : 100, (3): 151, (4): 190, (5): 235, (6): 295.

Emission Spectrum of $K_3[Co(CN)_6]$. The emission spectra at various temperatures excited with 313 nm light, which has almost the same energy as that of the maximum of the first spin-allowed band, are shown in Fig. 7.[38] It was found that the extremely weak and broad structureless emission band at room temperature gradually increased in intensity with a decrease in the temperature and that it showed some vibrational structures below *ca.* 150 K. Excitations with 365 nm light, and with 254 nm light, which has almost the same energy as that of the maximum of the second spin-allowed band, gave the same spectral pattern as that obtained by excitation with 313 nm light. The temperature dependence of the emission spectra excited with 313 and 254 nm light showed practically the same behavior.

The emission band of $K_3[Co(CN)_6]$ had been observed previously by Porter and Mingardi[7,25a] with a crystal at 4.2 and 77 K at 14000 cm^{-1} and assigned to the $^3T_{1g}\rightarrow{}^1A_{1g}$ phosphorescence of $[Co(CN)_6]^{3-}$, mainly on the basis of the mirror-image relationship between the emission band and the absorption band (18500 cm^{-1}), and on the basis of the lifetime measurement of the emission band (6.8×10^{-4} sec). A broad structureless band with a maximum at 14000 cm^{-1} was also obtained by Kirk *et al.*[9] The discrepancy in the

35) One possible impurity may be a binuclear cyanoaquo Co(II)-Co(III) complex with, in the low wave number visible region, a spin-allowed band, a charge transfer band, or an interaction absorption band. According to the conditions of synthesis, the complex with a band at 16300 or 18500 cm^{-1} will be produced.

36) J. J. Alexander and H. B. Gray, *Coord. Chem. Rev.*, **2**, 29 (1967).

37) Since the maximum of the absorption band lies at 16300 cm^{-1}, and since the half-width of the band is about 1000 cm^{-1}, the 0-0 position of the band must lie at about 15300 cm^{-1}, which limits the position of the phosphorescence band to wave numbers smaller than this. If a phosphorescence band larger than 15300 cm^{-1} is found, it should be an anti-Stokes band and thus should show a decrease of intensity with a decrease in the temperature. This was not the case in our experiment, as may be seen in Fig. 7.

38) The maximum of the phosphorescence band of $K_3[Co(CN)_6]$ shifted to a low wave number of about 1000 cm^{-1} when an R-406 tube was used instead of an R-136 tube. However, only the results obtained by the latter tube are shown throughout this work because the sensitivity of the former tube is much lower than that of the latter.

phosphorescence band position between this work (14700 cm^{-1} using an R-406 tube) and other authors' works may be due to the use of different experimental setups.

As has been stated above, the weak absorption band at 26000 cm^{-1} was assigned to the $^3T_{1g} \leftarrow {}^1A_{1g}$ transition. Thus, the emission band at 14700 cm^{-1} should be assigned to the $^3T_{1g} \rightarrow {}^1A_{1g}$ transition. The position of the emission band might seem to be too far apart from the position of the absorption band, the difference being about 10000 cm^{-1}. However, a similar large difference has been observed by Mingardi *et al.*[25a] in a d^6 cyano-complex, $K_4[Ru(CN)_6]$. They found the corresponding absorption and emission bands at 31000 and 22650 cm^{-1} respectively. The large Stokes shifts 11600 and 17200 cm^{-1} in other d^6 complexes have also been found by DeArmond *et al.* in $[Rh(en)_3]Cl_3$ and $[Ir(en)_3]Cl_3$ (en=ethylenediamine) respectively.[25b]

Schläfer *et al.* observed the phosphorescence of $K_3[Cr(CN)_6]$ in a glycerol/H_2O (1 : 1) rigid solution and in a fine crystal state at −190 °C and assigned the interval (*ca.* 350 cm^{-1}) between the vibrational structures of the phosphorescence band to the Cr–C stretching vibration.[39] The mean interval, 400 cm^{-1}, in the phosphorescence spectrum of $K_3[Co(CN)_6]$ in this work may be due to the Co–C stretching or Co–CN bending vibration.

Emission Spectra of $[Cr(NH_3)_6](NO_3)_3$ *and* $[Cr(NH_3)_6](ClO_4)_3$. The emission spectra of $[Cr(NH_3)_6](NO_3)_3$ and $[Cr(NH_3)_6](ClO_4)_3$ are shown in Figs. 8 and 9. The following results were obtained:

i) The emission spectra excited with 313, 365, and 435 nm light showed the same pattern in both complexes.[40,41] On the other hand, with 254 nm light it was very difficult to distinguish between the emission spectrum and the noise signal at any temperature used in this work.

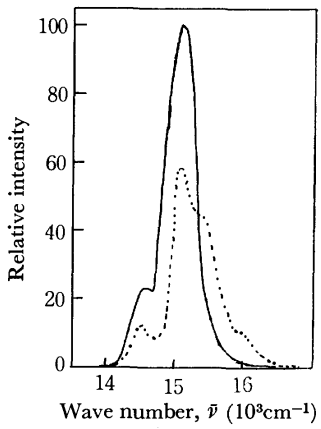

Fig. 8. Emission spectra of $[Cr(NH_3)_6](NO_3)_3$ excited with 313 nm light.
——: 20 K --------: 295 K

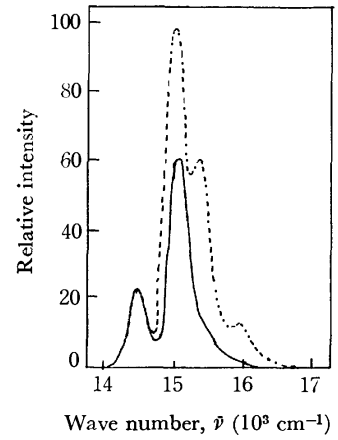

Fig. 9. Emission spectra of $[Cr(NH_3)_6](ClO_4)_3$ excited with 435 nm light.
——: 20 K -----: 295 K

ii) In $[Cr(NH_3)_6](NO_3)_3$, the two emission bands at 15390 and 15970 cm^{-1} decreased in intensity with a decrease in the temperature and almost disappeared at 20 K. However, the other two bands at 14470 and 15040 cm^{-1}, increased in intensity with a decrease in the temperature.

iii) In $[Cr(NH_3)_6](ClO_4)_3$, the emission band at 14550 cm^{-1} did not change in intensity with a decrease in the temperature. The other three bands, at 15020, 15390, and 15900 cm^{-1}, decreased in intensities with a decrease in the temperature.

As may be seen from the results shown in ii), the two bands at 15390 and 15970 cm^{-1} can be assigned to the transitions from the higher vibrational levels of the ^2E_g state to the ground state. The band at 15390 cm^{-1} may correspond to the 15120 cm^{-1} band reported by Porter *et al.*,[15c] which was assigned to the 0–0 band. However, it is more reasonable to assign the band at 15040 cm^{-1} to the 0–0 band, judging from the findings on the temperature dependence of the emission spectra (see Fig. 8).

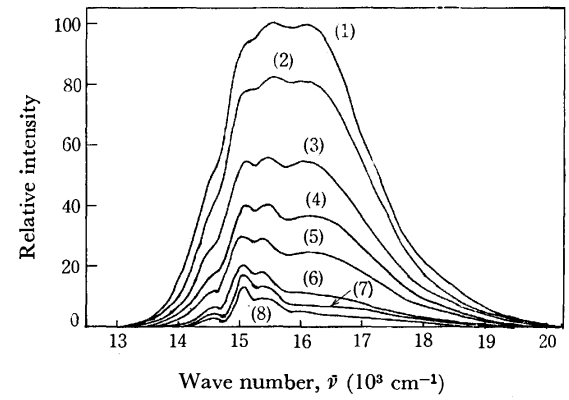

Fig. 10. Emission spectra of equimolar mixture of complex salts $[Cr(NH_3)_6](ClO_4)_3$–$K_3[Co(CN)_6]$ excited with 313 nm light.
Temperature (K)
(1): 20, (2): 57, (3): 115, (4): 150, (5): 170, (6): 222, (7): 235, (8): 295.

39) H. L. Schläfer, H. Gausman, H. F. Wasgestian, and H. U. Zander, *Z. Phys. Chem.*, (*N.F.*) **51**, 274 (1966).

40) The position of the maxima of the phosphorescence band of $[Cr(NH_3)_6]^{3+}$ shifted to a low wave number of about 200 cm^{-1} when an R-406 tube was used instead of an R-136 tube.

41) The emission spectra excited with 435 nm light are shown in $[Cr(NH_3)_6](ClO_4)_3$. This is because the emission intensity was very weak with 313 nm light, which has the same energy as that of the valley between the second spin-allowed band and the charge-transfer band (see Fig. 1).

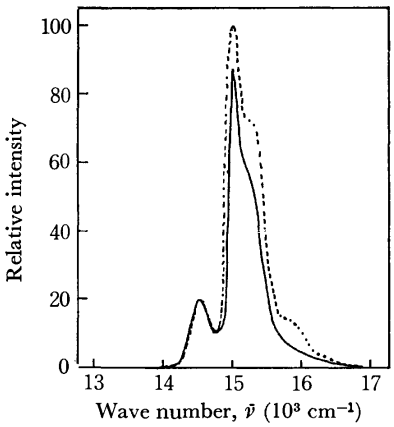

Fig. 11. Emission spectra of equimolar mixture of complex salts $[Cr(NH_3)_6](ClO_4)_3$–$K_3[Co(CN)_6]$ excited with 435 nm light. ——: 20K ------: 295 K

Emission Spectra of Equimolar Mixtures of Complex Salts $[Cr(NH_3)_6](NO_3)_3$–$K_3[Co(CN)_6]$ *and* $[Cr(NH_3)_6](ClO_4)_3$–$K_3[Co(CN)_6]$. The emission spectra for these two equimolar mixtures of complex salts were observed. All the results obtained could be explained by considering the superposition of the spectra of the component complexes. Some of the results are shown in Figs. 10 and 11. Figure 10 gives the emission spectra of an equimolar mixture of $[Cr(NH_3)_6](ClO_4)_3$–$K_3[Co(CN)_6]$ excited with 313 nm light at various temperatures. It is evident from the figure that the spectra consist of the emission bands of $[Cr(NH_3)_6]^{3+}$ and $[Co(CN)_6]^{3-}$. Figure 11 shows the emission spectra of an equimolar mixture of $[Cr(NH_3)_6](ClO_4)_3$–$K_3[Co(CN)_6]$ at 20 and 295 K excited with 435 nm light. As may be seen from Fig. 1, $[Co(CN)_6]^{3-}$ absorbs little in this region; thus, only the emission spectrum due to $[Cr(NH_3)_6]^{3+}$ is observed.

Emission Spectra of $[Cr(NH_3)_6][Co(CN)_6]$. The emission spectra of the double complex salt $[Cr(NH_3)_6][Co(CN)_6]$ are shown in Fig. 12.[42] The following results were obtained:

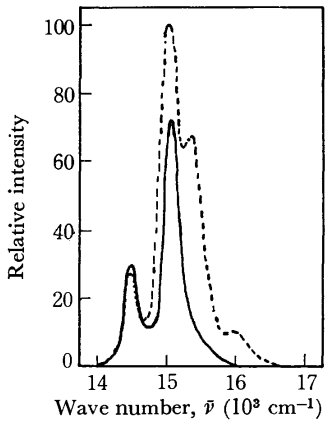

Fig. 12. Emission spectra of $[Cr(NH_3)_6][Co(CN)_6]$ excited with 313 nm light. ——: 20 K ------: 295 K

i) The emission spectra excited with 254, 313, 365, and 435 nm light were different from the emission spectra of the equimolar mixtures of the complex salts excited with 313 nm light, but had nearly the same pattern and position as those of the emission spectra of $[Cr(NH_3)_6](NO_3)_3$ or $[Cr(NH_3)_6](ClO_4)_3$. The only difference was that the two emission bands in the higher wave number region observed as shoulders in $[Cr(NH_3)_6](NO_3)_3$ and $[Cr(NH_3)_6](ClO_4)_3$ showed distinct maxima in this double complex salt. The emission intensity of $[Cr(NH_3)_6]^{3+}$ in the double complex was several times stronger than that of $[Cr(NH_3)_6]^{3+}$ in equimolar mixtures.

ii) The ratio of the emission intensities at 15000 cm^{-1} excited with 435 and 313 nm light was 1 : 1.5—1.7 at room temperature, and the ratio hardly changed at 20 K. The ratio was 1 : 0.25—0.30 in the case of $[Cr(NH_3)_6](NO_3)_3$.[43]

iii) The two bands at 15400 and 15970 cm^{-1} decreased in their intensities with a decrease in the temperature and almost disappeared at 20 K; the intensity of the emission band at 15000 cm^{-1} also decreased with a decrease in the temperature. However, no temperature dependence of the intensity was observed with the emission band at 14470 cm^{-1}.

Energy Transfer. The fact that the emission spectra of the double complex salt had nearly the same pattern as that of $[Cr(NH_3)_6](NO_3)_3$ or $[Cr(NH_3)_6](ClO_4)_3$ and did not resemble that of $K_3[Co(CN)_6]$, even if 254 nm light, which was mostly absorbed by the complex anion, was used, strongly suggests that some energy transfer occurs from the complex anion to the complex cation in the double complex salt. This becomes clearer when we compare the phosphorescence band of the double complex salt (Fig. 12) with that of the equimolar mixture of the complexes (Figs. 10 and 11) in which the energy transfer cannot be considered and in which the spectrum thus consists of those of the component complexes. Additional evidence is given by the ratio of the intensities of the emission bands at 15000 cm^{-1} excited with 435 and 313 nm light. If the two ratios mentioned above are compared, it is more reasonable to consider that the increase in the ratio from 1 : 0.25—0.30 in $[Cr(NH_3)_6](NO_3)_3$ to 1 : 1.5—1.7 in $[Cr(NH_3)_6][Co(CN)_6]$ corresponds to the increase in the absorption due to [Co-

42) The intensity of the emission band excited with 254 nm light was weak because of the low intensity of the light source in this region. However, it was confirmed that the pattern and position of this band were similar to those of the emission band excited with 313 nm light. Thus, the emission spectrum excited with 254 nm light was not shown; that excited with 313 nm light was shown instead.

43) The intensities of the 313 and 435 nm emission lines of the Ushio UM-102 mercury lamp were almost the same (private communication from Ushio, Incorporated). The sensitivities of the photomultiplier R-136 at 313 and 435 nm were 1 : 2 (Hamamatsu Corporation Information Bulletin, **1972**, 8). When powdered magnesium oxide was irradiated with these mercury light, the Hitachi 203 fluorescence spectrophotometer out-put indicated the 1 : 2 ratio at these wavelengths. Therefore, the transmittance of the fluorescence spectrophotometer was considered to be nearly the same at these wavelengths. From these results, it was concluded that the ratios of the emission band at 15000 cm^{-1} excited with 313 and 435 nm were not much different from the true value if we neglect the problems concerning the samples, that is, the inner-filter effect, the particle size effect, etc. A more detailed experiment concerning the quantitative aspects of this work using ferrioxalate solutions in a chemical actinometer is now under way in this laboratory.

$(CN)_6]^{3-}$.[44]

As possible energy transfer paths, the following two are suggested. They satisfy the spin conservation rule in consideration of the energy level diagram shown in Fig. 6:

$$^1T_{2g} \dashrightarrow {}^1T_{1g} \begin{cases} \nearrow {}^4T_{1g} \dashrightarrow {}^4T_{2g} \rightsquigarrow {}^2E_g \\ \searrow {}^4T_{2g} \rightsquigarrow {}^2E_g \end{cases}$$

where→means energy transfer; ⇢, internal conversion, and ⇝, intersystem crossing. However, if the formation of the molecular orbitals between the complex cation and the complex anion are considered, the following two paths are also possible, as in the case of $[Ru(bipy)_3]_3[Cr(ox)_3]_2$ (bipy: 2,2'-bipyridyl, ox: oxalate ion) studied by Fujita and Kobayashi:[16]

$$^1T_{2g} \dashrightarrow {}^1T_{1g} \rightsquigarrow {}^3T_{1g} \begin{cases} \nearrow {}^4T_{2g} \rightsquigarrow {}^2E_g \\ \searrow {}^2E_g \end{cases}$$

It is interesting to note that the latter paths are prohibited if importance is attached to the simple consideration of the spin conservation rule, although they are usually considered to be more favorable from the point of view of the longer lifetime of $^3T_{1g}$.

Temperature Dependence of the Emission Intensity. The temperature dependence of the emission intensity of $K_3[Co(CN)_6]$, $[Cr(NH_3)_6](NO_3)_3$, $[Cr(NH_3)_6](ClO_4)_3$, and $[Cr(NH_3)_6][Co(CN)_6]$ is shown in Figs. 13—16.

These data may be classified into two groups according to whether the emission intensity increases or decrease with a decrease in the temperature. The emission intensity in $K_3[Co(CN)_6]$ and $[Cr(NH_3)_6](NO_3)_3$ increases with a decrease in the temperature. These phenomena can be explained in terms of the usual emission process competing with the nonradiative relaxation process.

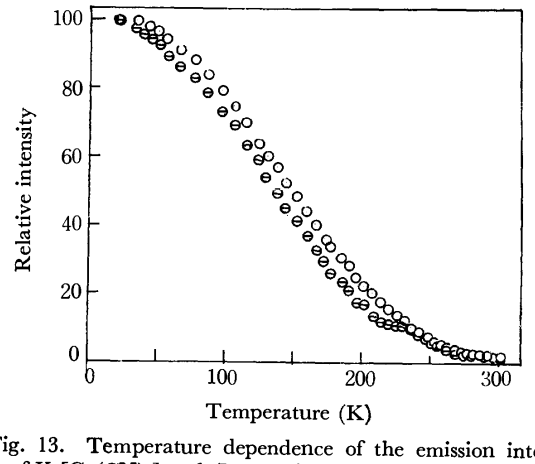

Fig. 13. Temperature dependence of the emission intensity of $K_3[Co(CN)_6]$ at 15700 cm^{-1}.
○: excited with 313 nm light
⊖: excited with 254 nm light
Relative intensity of the emission spectra was obtained by normalizing its value at 20 K to 100.

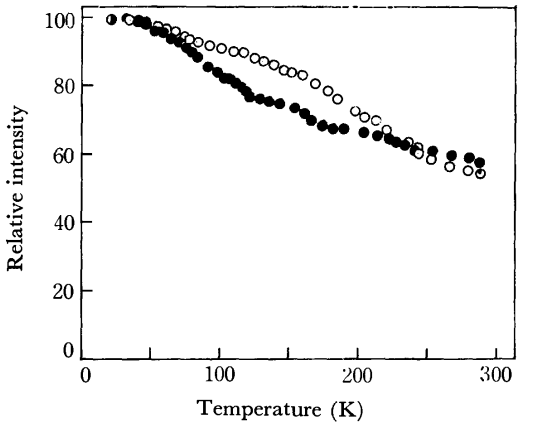

Fig. 14. Temperature dependence of the emission intensity of $[Cr(NH_3)_6](NO_3)_3$ at 15040 cm^{-1}.
●: excited with 435 nm light
○: excited with 313 nm light
Relative intensity of the emission spectra was obtained by normalizing its value at 20 K to 100.

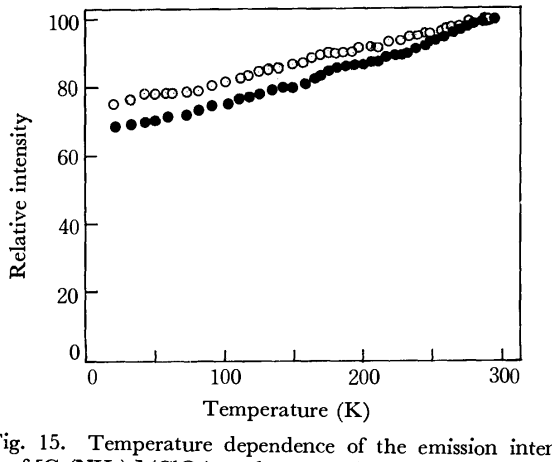

Fig. 15. Temperature dependence of the emission intensity of $[Cr(NH_3)_6](ClO_4)_3$ at 15000 cm^{-1}.
●: excited with 435 nm light
○: excited with 313 nm light
Relative intensity of the emission spectra was obtained by normalizing its value at room temperature to 100.

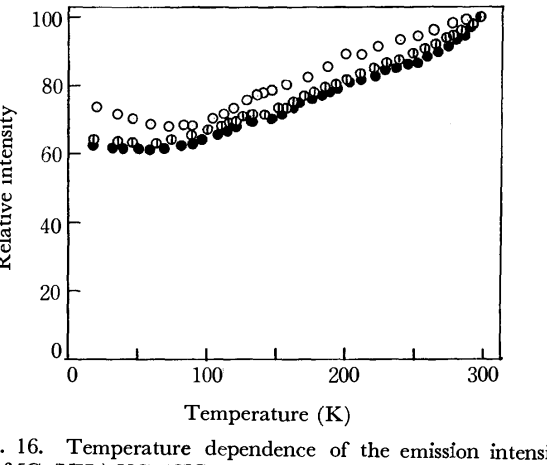

Fig. 16. Temperature dependence of the emission intensity of $[Cr(NH_3)_6][Co(CN)_6]$ at 15000 cm^{-1}
●: excited with 435 nm light
◐: excited with 365 nm light
○: excited with 313 nm light
Relative intensity of the emission spectra was obtained by normalizing its value at room temperature to 100.

44) Kirk and Schläfer proposed a crystal perturbation theory against an energy transfer in order to explain an abnormal emission spectrum of $[Cr(atp)_6][Cr(CN)_6]$ (atp: antipyrin). Their case must be the result of a special ligand which prohibits the energy transfer, as they pointed out.[45]

45) A.D. Kirk and H.L. Schläfer, *Z. Phys. Chem.*, **52**, 2411 (1970).

However, the temperature dependence of the emission intensity of $[Cr(NH_3)_6](ClO_4)_3$ and $[Cr(NH_3)_6][Co(CN)_6]$ is anomalous; that is, the intensity decreases with a decrease in the temperature except in the cases of the bands at 14550 and 14470 cm^{-1} respectively. The explanation of this anomalous temperature effect is very difficult. Flint studied the emission spectra of crystalline $2[Cr(en)_3]Cl_3 \cdot KCl \cdot 6H_2O$ and $[Cr(en)_3]Cl_3 \cdot 3H_2O$ (en=ethylenediamine) at temperatures down to 5 K.[46] He found that the emission band at 14880 cm^{-1} (N-band) having vibronic structure to lower energy due to $^2E \rightarrow {}^4A_2$ was quenched at temperatures below 200 K, and that a new broader emission band appeared at *ca.* 14500 cm^{-1} (B-band) and increased in intensity with a decrease in the temperature. He explained this new emission band as being due to a transition within a new Cr(III) center associated with lattice defects. Probably a similar explanation would hold for $[Cr(NH_3)_6](ClO_4)_3$ and $[Cr(NH_3)_6][Co(CN)_6]$. That is, if we assume that, in our case, the bands 15020 and 15000 cm^{-1} correspond to the N-bands, the anomalous decrease in the intensity with the decrease in the temperature can be explained. Therefore, the bands at 14550 and 14470 cm^{-1} should be assigned to the B-bands. The fact that the B-bands in our case do not show any increase in intensity with a decrease in the temperature may be explained by the overlap of the decreasing lower-energy part of the N-band.

The temperature dependence of the emission intensity of equimolar mixtures of complex salts, $K_3[Co(CN)_6]$-$[Cr(NH_3)_6](ClO_4)_3$, are shown in Fig. 17. In these cases, the temperature dependence can be explained by a superposition of those of the component complexes.

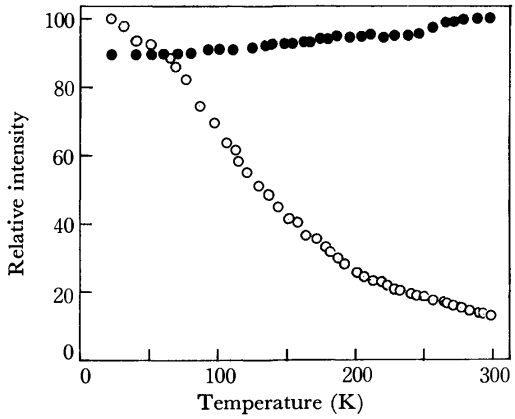

Fig. 17. Temperature dependence of the emission intensity of equimolar mixture of complex salts $[Cr(NH_3)_6](ClO_4)_3$-$K_3[Co(CN)_6]$ at 15040 cm^{-1}
●: excited with 435 nm light
○: excited with 313 nm light
Relative intensity of the emission spectra excited with 435 nm light was obtained by mornalizing its value at room temperature to 100, and relative intensity of the emission spectra excited with 313 nm light was obtained by normalizing its value at 20 K to 100.

The author wishes to express his gratitude to Professor Y. Kondo and Professor M. Nakahara for their stimulating suggestions and discussion during this work. He is also indebted to Dr. A. Kuboyama (The Government Chemical Industrial Research Institute) for the use of a Cary-14 spectrophotometer, and to Mr. A. Urushiyama for his help with the microscopic measurements. Special thanks are also due to Professor H. Kobayashi and Dr. I. Fujita (Tokyo Institute of Technology) for pre-prints of their reports. He also wishes to thank Professor Gene S. Lehman for his kindness in reading the original manuscript.

46) C. D. Flint, *J. Chem. Phys.*, **52**, 168 (1970).

Phase Equilibria in the V_2O_3-VO_2 System at High Temperatures

Hozumi ENDO, Masataka WAKIHARA, Masao TANIGUCHI, and Takashi KATSURA*

Department of Synthetic Chemistry, Tokyo Institute of Technology, Ookayama, Meguro-ku, Tokyo 152
**Department of Chemistry, Faculty of Science, Tokyo Institute of Technology, Ookayama, Meguro-ku, Tokyo 152*

(Received August 19, 1972)

The phase equilibria in the V_2O_3–VO_2 system were established at 1307 K by varying the oxygen partial pressures from 10^{-4} to 10^{-12} atm. Eight phases, V_2O_3, V_3O_5, V_4O_7, V_5O_9, V_6O_{11}, V_7O_{13}, V_8O_{15}, and VO_2, were observed under these experimental conditions. Vanadium sesquioxide has an extensive range of solid solutions at 1307 K. Also, the phase diagram and isobaric lines of oxygen partial pressure in the V_2O_3 phase were determined from 1307 to 1700 K on the basis of our present and previous studies. Quenching and thermogravimetric methods were applied under a controlled oxygen atmosphere. The oxygen partial pressures were determined by means of a solid electrolyte cell composed of $(ZrO_2)_{0.85}(CaO)_{0.15}$. The standard free energies of the oxidation of V_2O_3 to V_3O_5, of V_3O_5 to V_4O_7, of V_4O_7 to V_5O_9, of V_5O_9 to V_6O_{11}, of V_6O_{11} to V_7O_{13}, of V_7O_{13} to V_8O_{15}, and of V_8O_{15} to VO_2 were determined on the basis of the equilibrium oxygen partial pressure at 1307 K. The enthalpy and entropy data of the oxidations of V_2O_3 to V_3O_5 and of V_3O_5 to V_4O_7 were evaluated from the oxygen partial pressures on the basis of the present results and previous data.

Among early studies,[1-5] Andersson[4,5] investigated a series of compounds formulated by V_nO_{2n-1} (n: integer) at temperatures from 800 to 900 °C, and distinguished such compounds as varied in n value from 2 to 8. Kosuge *et al.*[6] found V_nO_{2n-1} phases in which the n value varied from 2 to 7 at 800 °C. Later, Okinaka *et al.*[7] presented a general-phase diagram of the V_2O_3–VO_2 system up to 1600 K based on their previous data.

In spite of a number of studies of the V_2O_3–VO_2 system at lower temperatures, only a few works have been reported about the thermochemical properties of the V_2O_3–VO_2 system at higher temperatures except for the V_2O_3 and VO_2 phases. Katsura and Hasegawa[8] reconfirmed the phase equilibria studied by Andersson,[4,5] and presented the standard free energies of the compounds which exist in the V_2O_3–VO_2 system at 1600 K. Wakihara and Katsura[9] reported thermodynamic data on the V_2O_3, V_3O_5, and V_4O_7 phases from 1400 to 1700 K. Recently, Anderson and Khan[10] and Okinaka *et al.*[7] studied the V_2O_3–VO_2 system up to 1423 K, and from 600 to 1200 °C, respectively, and reported some thermodynamic data of this system.

The present objectives are: (1) to obtain a detailed phase equilibria of the V_2O_3–VO_2 system at 1307 K in order to establish the phase diagrams at higher temperatures on the basis of both the present and previous studies,[8,9] and also to compare our results with the estimated phase diagrams proposed by several previous investigators; (2) to obtain linear free-energy equations at higher temperatures by determining three thermodynamic functions $\Delta G°$, $\Delta H°$, and $\Delta S°$, and (3) to ascertain the phase transition of V_6O_{11}, which had a different structure at 1600 K from that obtained by Andersson at around 1000 °C.

Experimental

The quenching and thermogravimetric methods were adopted in the present study. Since the details of the procedure have been previously described by Katsura and Muan[11] and by Katsura and Hasegawa,[8] only a brief description of the general procedure will be given here.

In the thermogravimetric method, a pre-reduced vanadium oxide sample was heated at 1307 K in an atmosphere of a CO_2 and H_2 mixture (ratio of 1: 1). The pellet thus obtained was suspended in a furnace by means of a Pt-40%Rh wire connected to a quick-weighing balance. The oxide had a chemical formula of $VO_{1.500}$ as this oxygen partial pressure and temperature. It was also found that the substantially stoichiometric V_2O_3 phase was stable at lower oxygen partial pressures than 10^{-12} atm. Thus, the weight of $VO_{1.500}$ prepared at an oxygen partial pressure of 10^{-12} atm was chosen as the reference weight standard.

In the quenching method, an oxide sample was heated at 1307 K and at a particular oxygen pressure until an equilibrium was attained between the gas and condensed phases. The sample was then quenched rapidly to the temperature of ice by burning away the thin platium wire with an electric current and by allowing the sample to drop into an ice-cooled tube. The sample thus obtained was used for identifying the phases present by means of the powder X-ray diffraction method and for determining the compositions by means of gravimetric analysis.

The atmospheres of the desired oxygen partial pressures were obtained by using mixtures of CO_2 and H_2. In the present study, the ratios of CO_2/H_2 were changed from 1.0 to 4000, and the flow rate in the furnace was set at 0.8 cm/sec. The actual partial pressures of oxygen in the gas mixture were stably and accurately measured by inserting a solid electrolyte cell, $(ZrO_2)_{0.85}$ $(CaO)_{0.15}$, into the furnace tube before a sample was suspended in it. The error of $\log P_{O_2}$ was estimated to be within ± 0.01. The details of the procedure have been described in the authors' previous papers.[8,9]

1) E. Hoschek and W. Klemm, *Z. Anorg. Allg. Chem.*, **242**, 63 (1939).
2) W. Klemm and L. Grimm, *ibid.*, **250**, 42 (1942).
3) F. Aebi, *Helv. Chim. Acta*, **31**, 8 (1948).
4) G. Andersson, *Acta Chem. Scand.*, **8**, 1599 (1954).
5) G. Andersson, *ibid.*, **10**, 623 (1956).
6) K. Kosuge, T. Takada, and S. Kachi, *Nippon Kagaku Zasshi*, **83**, 1243 (1962).
7) H. Okinaka, K. Kosuge, and S. Kachi, *Trans. JIM*, **12**, 44 (1971).
8) T. Katsura and M. Hasegawa, This Bulletin, **40**, 561 (1967).
9) M. Wakihara and T. Katsura, *Met. Trans.*, **1**, 363 (1970).
10) J. S. Anderson and A. S. Khan, *J. Less-Common Metals*, **22**, 209 (1970).
11) T. Katsura and A. Muan, *Trans. A. I. M. E.*, **230**, 77 (1964).

Results and Discussion

Phase Equilibria. The data obtained at 1307 K are summarized in Table 1 and are graphically illustrated in Fig. 1.

TABLE 1. EQUILIBRIA OF THE V_nO_{2n-1} PHASES AT 1307K

$-\log P_{O_2}$	CO_2/H_2	Value of x in VO_x	Phase
11.99 (±0.02)	10.0	1.500 (±0.001)	V_2O_3
10.50	40.6	1.503	V_2O_3
10.45	42.9	1.505	V_2O_3
10.38	45.4	1.506	V_2O_3
10.33	47.5	1.506	V_2O_3
10.32	48.3	1.509	V_2O_3
10.24	51.9	1.507	V_2O_3
10.18	54.9	1.510	V_2O_3
10.13	56.4	1.512	V_2O_3
10.04	61.8	1.512	V_2O_3
9.90	68.9	1.520	V_2O_3
9.85 (±0.02)	72	1.667 (±0.008)	V_3O_5
9.73	79	1.667	V_3O_5
8.00	430	1.667	V_3O_5
7.96	450	1.674	V_3O_5
7.93 (±0.02)	470	1.753 (±0.008)	V_4O_7
7.80	540	1.748	V_4O_7
7.42	870	1.747	V_4O_7
7.40	880	1.750	V_4O_7
7.39	910	1.757	V_4O_7
7.31	960	1.756	V_4O_7
7.19	1070	1.760	V_4O_7
7.11 (±0.02)	1130	1.798 (±0.008)	V_5O_9
7.00	1200	1.808	V_5O_9
6.66	1460	1.803	V_5O_9
6.55	1550	1.803	V_5O_9
6.49 (±0.05)	1610	1.830 (±0.008)	V_6O_{11}
6.26	1830	1.830	V_6O_{11}
5.91	2230	1.836	V_6O_{11}
5.80 (±0.06)	2370	1.859 (±0.008)	V_7O_{13}
5.63	2590	1.861	V_7O_{13}
5.57 (±0.06)	2680	1.918 (±0.008)	$V_8O_{15}+VO_2$
5.50	2770	1.901	$V_8O_{15}+VO_2$
5.32 (±0.06)	3100	1.997 (±0.008)	VO_2
4.86	4000	1.997	VO_2

The following eight phases were found to be stable under the present experimental conditions: V_2O_3, with a corundum-type structure and various V/O ratios; V_3O_5, with a monoclinic structure showing no significant variation in the V/O ratio; V_4O_7, V_5O_9, V_6O_{11}, V_7O_{13}, and V_8O_{15}, showing no significant variations in the V/O ratio, and VO_2, with a monoclinic rutil-type structure.

According to the previous paper,[8] the V_6O_{11} phase had a wide range of composition, from $VO_{1.833}$ to $VO_{1.905}$, and $VO_{1.905}$ was in equilibrium with the stoichimoetric VO_2. In addition, it is significant that the structural powder X-ray patterns of $VO_{1.834}$, $VO_{1.853}$, and $VO_{1.898}$ obtained at 1600 K, all of which compositions belong to the V_6O_{11} phase, were identical with each other, but definitely different from that of

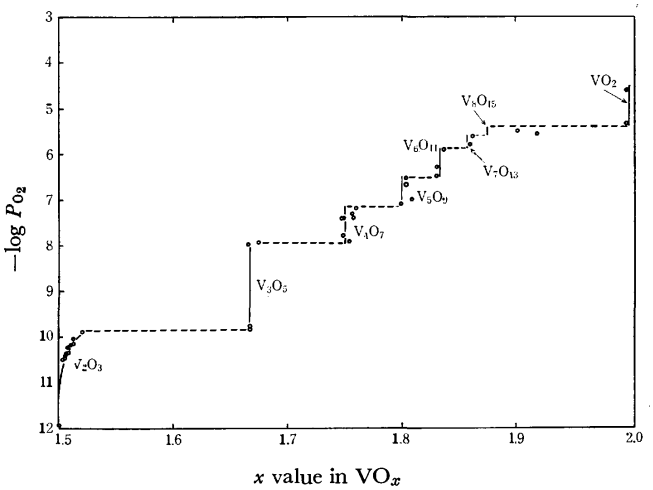

Fig. 1. Relationship between composition of oxide and oxygen partial pressure represented by logarithmic scale on the V_nO_{2n-1} phases at 1307 K.

the V_6O_{11} phase obtained by Andersson[4] at around 1000 °C. Under the present experimental conditions, the stoichiometric V_6O_{11} phase was in equilibrium with the stoichiometric V_7O_{13} phase at the oxygen partial pressure of $10^{-5.91}$ atm. Also, the structural powder X-ray pattern of the present V_6O_{11} phase was identical with that obtained by Andersson.[4] This leads to the conclusion that the transition point must be located at a temperature between 1307 and 1600 K.

The compositions of $VO_{1.901}$ and $VO_{1.918}$ in Table 1 correspond to a mixture of the V_8O_{15} and VO_2 phases. The single phase of V_8O_{15} could not be obtained under the present conditions, because the stable range of oxygen partial pressure to the V_8O_{15} phase was too narrow for us to obtain an equilibrated single phase of V_8O_{15} at the present temperature; therefore, no exact composition range of the V_8O_{15} phase was determined.

As is shown in Fig. 2, the homogeneous region and

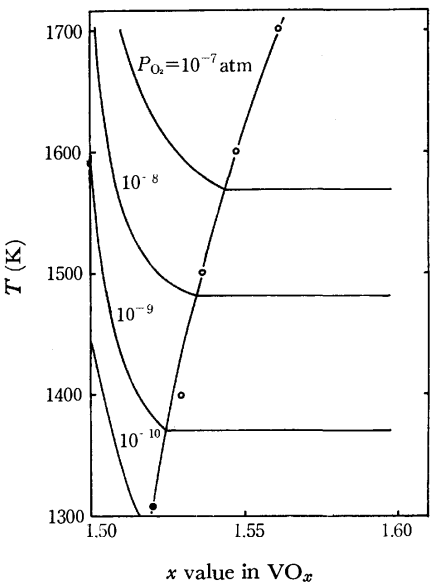

Fig. 2. Isobaric lines of oxygen partial pressure and the homogeneous range in the V_2O_3 solid solution at temperatures from 1300 to 1700 K.

the isobaric lines of the oxygen pressure relating to the change in composition and temperature in the V_2O_3 phase were determined from 1300 to 1700 K on the basis of the present study and previous results.[8,9] The compositions of the V_2O_3 phase were determined by applying the thermogravimetric method, while the compositions from V_3O_5 to VO_2 phase were obtained using the quenching method, because of the appreciable amounts of sublimation in these samples.

Andersson[4] pointed out a narrow homogeneity range in the V_3O_5 phase at 900 °C. On the other hand, Kosuge *et al.*[6,7] suggested a fairly wide range of variations in the V/O ratio in the phases of V_3O_5, V_4O_7, and V_6O_{11}, as well as that in the phase of V_2O_3 over a wide range of temperature. However, a wide homogeneous range was seen only in the phase of V_2O_3 at 1307 K. The results in the present study may be reliable because the samples were quenched in an equilibrium state. Also, in a preliminary experiment, no change in the composition was found in any phase between before and after quenching. By way of summarizing both the present and previous results,[8,9] the phase diagram of the V_2O_3–VO_2 system at higher temperatures is briefly given in Fig. 3; this diagram is somewhat different from that of Okinaka *et al.*[7]

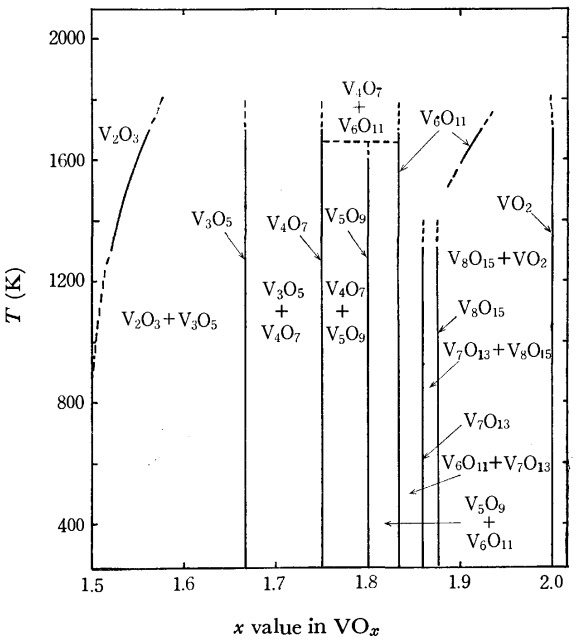

Fig. 3. Phase diagram of the V_2O_3–VO_2 system based on the present and previous data.[8,9]

Thermodynamic Properties of Oxidation. Since the oxygen partial pressure at which two oxide phases coexist had been determined, the standard free energy of the oxidation of each oxide could readily be estimated by means of the van't Hoff equation except for Reaction (1), as is shown in Table 2. It may be necessary for Reaction (1) to use a correction term because of the existence of homogeneity in the V_2O_3 phase. The method of calculating the standard free energy of the formation of a solid solution has been derived from the expansion of the Gibbs-Duhem equation described in previous papers.[8,9] In the present study, the correction term for the standard free energy was estimated to be about 21 cal. Since the establishment of a discrete oxygen partial pressure for the V_8O_{15} phase was impossible, the proper oxygen partial pressure for the stoichiometric V_8O_{15} phase was estimated (Table 2) on the basis of the powder X-ray pattern. The standard free energies of the oxidation of Reactions (1) to (7) are summarized in Table 2.

Table 2. Oxidation reactions and corresponding free energies at 1307K

Reaction	$-\log P_{O_2}$	Free energy $\Delta G°$ (cal)
$VO_{3/2}+1/12\ O_2=VO_{5/3}$(1)	9.88±0.05	−4955± 50
$VO_{5/3}+1/24\ O_2=VO_{7/4}$(2)	7.95±0.05	−1981± 30
$VO_{7/4}+1/40\ O_2=VO_{9/5}$(3)	7.15±0.07	−1069± 10
$VO_{9/5}+1/60\ O_2=VO_{11/6}$(4)	6.52±0.05	− 650± 5
$VO_{11/6}+1/84\ O_2=VO_{13/7}$(5)	5.86±0.12	− 417± 10
$VO_{13/7}+1/112\ O_2=VO_{15/8}$(6)	5.60±0.09	− 299± 5
$VO_{15/8}+1/16\ O_2=VO_2$(7)	5.41±0.17	−2022± 60
$VO_{3/2}+1/4\ O_2=VO_2$(8)		−11393± 170
[Mah *et al.*[12]]		−12604± 200]
[Coughlin[13]]		−10879±1000]
[Okinaka *et al.*[7]]		−11922± 100]

The summation of these reactions gives Reaction (8) and the corresponding free energy, shown in Table 2. The value thus obtained is compared with those obtained by Mah *et al.*,[12] by Coughlin[13] and by Okinaka *et al.*[7] in the same table.

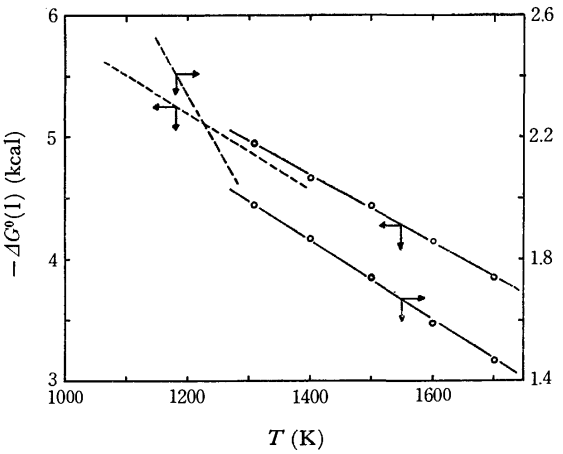

Fig. 4. Free energy change *vs.* temperature of reactions (1) and (2). Solid lines indicate our data, while dashed lines are derived from the data of Okinaka *et al.*[7]

The values of $\Delta G°(1)$ and $\Delta G°(2)$ are plotted against the temperatures from 1307 to 1700 K in Fig. 4, on the basis of the present and our previous data,[9] together with the relationships of Okinaka *et al.*[7] It may be expected from Fig. 4 that the linear free-energy equations for Reaction (1) are in pretty good agreement with each other, but for Reaction (2) there is a slight difference in slope. The standard entropy changes in Reactions (1) and (2) were evaluated from the slope

12) A. D. Mah and K. K. Kelley, *U. S. Bur. Mines Rept. Invest.*, (1961), p. 5858.
13) J. P. Coughlin, *U. S. Bur. Mines, Bulletin*, **542**, (1954).

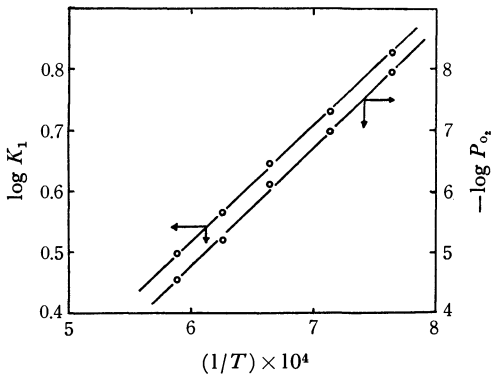

Fig. 5. log K_1 corresponding to Eq. (1) and equilibrium oxygen partial pressure in Eq. (2) *vs.* reciprocal absolute temperature, $1/T$.

in Fig. 4. The least-squares method was used to estimate the standard entropy changes of the two reactions. Also, the entropy changes of Reactions (1) and (2) were evaluated by means of the van't Hoff equation. The logarithmical equilibrium constant of Reaction (1) was calculated from the following equation:

$$\log K_1 = \log \frac{P_{O_2}(1)}{a_{V_2O_3}} = -\frac{\Delta G^\circ(1)}{RT}$$

The relationship between $\log K_1$ and $1/T$ was substantially linear, as is illustrated in Fig. 5. Hence, the following equation may be deduced from the above equation:

$$\frac{\mathrm{d}\log K_1}{\mathrm{d}(1/T)} = -\frac{\Delta H^\circ(1)}{2.303R}$$

where $\Delta H^\circ(1)$ and R are the heat of Reaction (1) and the gas constant respectively. The heat of Reaction (2), $\Delta H^\circ(2)$, may be estimated from this reaction:

$$\frac{\mathrm{d}(-\log P_{O_2}(2))}{\mathrm{d}(1/T)} = -\frac{\Delta H^\circ(2)}{2.303R}$$

The equilibrium constant of Reaction (2), K_2, is equal to the equilibrium oxygen partial pressure ($P_{O_2}(2)$).

TABLE 3. ESTIMATED RESPECTIVE THERMODYNAMIC FUNCTIONS AT TEMPERATURES FROM 1300 TO 1700 K

$\Delta H^\circ(1) = -8310$	(± 230)	(cal)
$\Delta H^\circ(2) = -3716$	(± 250)	(cal)
$\Delta S^\circ(1) = -2.73$	(± 0.30)	(e.u.)
$\Delta S^\circ(2) = -1.32$	(± 0.13)	(e.u.)
$\Delta G^\circ(1) = -8310+2.73T$	(± 630)	(cal)
$\Delta G^\circ(2) = -3716+1.32T$	(± 430)	(cal)

The respective entropy and enthalpy data are shown in Table 3. The linear equations of the standard free energies of Reactions (1) and (2) were estimated by using the entropy and enthalpy data obtained above over the temperature range from 1307 to 1700 K. The equations are also listed in the last two lines of Table 3.

BULLETIN OF THE CHEMICAL SOCIETY OF JAPAN, VOL. 46, 2090—2092 (1973)

Analysis of Metals by Solid-Liquid Separation. Spectrophotometric Determination of Cadmium by Extraction of Cadmium Salt of Oxine with Melted Naphthalene

Taitiro FUJINAGA,* Masatada SATAKE, and Tatsuo YONEKUBO

*Faculty of Science, Kyoto University, Sakyo-ku, Kyoto 606
Faculty of Engineering, Fukui Universtiy, Fukui 910

(Received September 22, 1972)

A method is described for the spectrophotometric determination of a minute quantity of cadmium. A cadmium complex stable at 90 °C is easily extracted with melted naphthalene. The resulting mixture of cadmium complex and naphthalene is dissolved in dimethylformamide and absorbance of the solution is measured at 400 nm. Effects of pH, amounts of oxine, naphthalene and diverse salts are given.

Oxine (8-hydroxyquinoline) reacts with various metal ions to form stable complexes which have been widely used for spectrophotometric determination of metal ions by extraction from aqueous solution into organic solvents such as chloroform or benzene. However, this method cannot be applied to metals such as zinc, magnesium and cadmium, since their salts of oxine are insoluble in organic solvents; zinc and magnesium salts extracted are not very soluble, those of cadmium and beryllium are hardly soluble.

We found that most metal salts of oxine in aqueous solution can be easily extracted with melted organic compounds such as naphthalene and diphenyl as in the case of liquid-liquid extraction. The method was named "analysis by solid-liquid separation", and applied to the spectrophotometric determination of copper,[1] zinc,[2] and magnesium.[3] It is particularly convenient for the determination of metals whose salts of oxine are strongly hydrated. The method is also applicable to the determination of nickel[4] and palla-

1) T. Fujinaga, T. Kuwamoto, T. Yonekubo, and M. Satake, *Bunseki Kagaku*, **18**, 1113 (1969).

2) T. Fujinaga, M. Satake, and T. Yonekubo, *ibid.*, **19**, 216 (1970).

3) M. Satake, *Memoirs of the Faculty of Engineering, Fukui University*, **18**, 225 (1970).

4) T. Fujinaga, M. Satake, and T. Yonekubo, *Bunseki Kagaku*, **20**, 1255 (1971).

dium[5] using dimethylglyoxime as the chelating reagent.

Cadmium was chosen in the present work, and its salt of oxine was extracted completely with melted naphthalene from aqueous solution at pH above 5.5. The solidified naphthalene crystals containing the metal salt of oxine were separated and dissolved in dimethylformamide, the absorbance of the solution being measured at 400 nm against the reagent blank. Effects of diverse ions were studied. The method seems to be promising since the extract with naphthalene has adequate solubility, colour intensity and stability in dimethylformamide. Cadmium salt of oxine is insoluble in organic solvents except dimethylformamide.

Experimental

Reagents. Reagents of analytical grade were used without purification. Water used was redistilled after deionization.

Standard cadmium solution, 1.997×10^{-3} g per ml: Prepared by dissolving 0.99855 g of cadmium metal (purity 99.999%) in 3 ml of concentrated nitric acid, diluted to 500 ml with water. More dilute cadmium solution (19.97 μg per ml) was prepared as required.

Oxine solution, 1%: Prepared by dissolving 1.0 g of oxine in glacial acetic acid (2 ml) on a water bath, diluted to 100 ml with water.

Alkali metal salt solutions, 10 mg of the corresponding salt per ml: Prepared by dissolving 1.000 g of the salt in water, diluted to 100 ml.

Other metal salt solutions, 1 mg of the individual salt per ml: Prepared by dissolving 0.100 g of each salt in water. In some cases, a small amount of acid was added to prevent hydrolysis.

Apparatus. A Hitachi Model 124 spectrophotometer was employed for the absorbance measurements with matched 10 mm glass cells. A Toa-Denpa HM-6A pH meter equipped with combined glass and calomel electrodes was used for all pH measurements.

Procedure. Pipet a sample solution containing 10—160 μg of cadmium into an 80 ml tightly stoppered Erlenmeyer flask, and dilute with water to *ca.* 30 ml. Add 1.5 ml of 1% oxine and adjust the pH of the solution to 6—10 with 0.5—1.0 N ammonia. Heat the flask on a water bath to precipitate cadmium salt of oxine completely. Add 2.0 g of naphthalene and warm the flask at 90 °C until naphthalene melts completely. Remove the flask from the bath and shake vigorously. Naphthalene will be solidified forming fine crystals suspended in the solution. Warm the flask again and melt slowly the fine crystals. Cool the mixture to room temperature. Larger crystalline deposits will grow up in the solution. Filter the mixture and wash the solidified deposits on the filter paper with water. Remove the water from the filter paper with a separate piece of paper. Spread the yellow deposits on a dry filter paper for air-drying. Transfer them to a volumetric flask and add dimethylformamide so that the final volume becomes 10 ml. Shake well and measure the absorbance of the solution in a 10 mm cell against the reagent blank. The amount of cadmium can be determined using a calibration curve.

Results and Discussion

Absorption Spectra. Cadmium in the test solution containing 99.86 μg of cadmium was extracted with melted naphthalene as complex salt of oxine at pH *ca.* 7.5. The mixture of cadmium-oxine complex and naphthalene was dissolved in dimethylformamide, and the absorbance of the solution was measured at various wavelengths between 360 and 470 nm. The result is shown in Fig. 1. Curves 1 and 2 show the absorption spectra of the reagent blank and the complex, respectively. Curve 3 shows the absorption spectra of the complex against the reagent blank. The curve has a maximum at 400 nm, beyond which the absorbance decreases gradually and becomes insignificant beyond 470 nm. Wavelength 400 nm was chosen for the measurement.

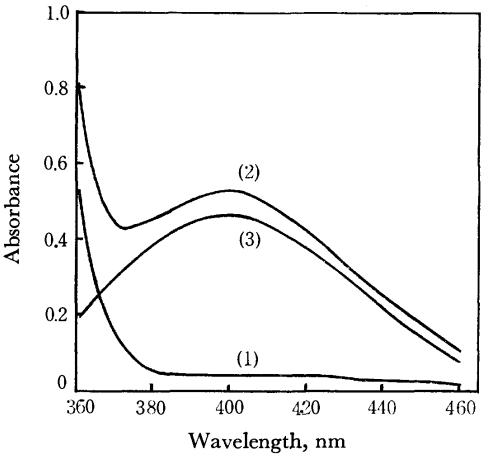

Fig. 1. Absorption spectra of oxine and cadmium oxinate in naphthalene-dimethylformamide.
Cadmium: 99.86 μg, 1% oxine: 1.5 ml, pH: 7.5, naphthalene: 2.0 g, (1) Reagent blank *vs.* water, (2) Cadmium oxinate *vs.* water, (3) Cadmium oxinate *vs.* reagent blank.

Effect of pH. The pH of a solution containing 99.86 μg of cadmium and 1.5 ml of 1% oxine solution was carefully controlled to 4—10 with dilute ammonia. The solution was heated on a water bath till the precipitate of complex salt between cadmium and oxine appeared, and the complex salt was extracted with melted naphthalene. The absorbance of the mixture of the salt and naphthalene in dimethylformamide was

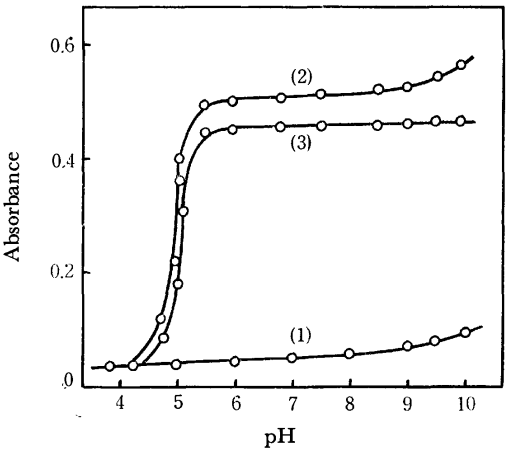

Fig. 2. Effect of pH on absorbance.
Cadmium: 99.86 μg, 1% oxine: 1.5 ml, naphthalene: 2.0 g, wavelength: 400 nm, (1) Reagent blank *vs.* water, (2) Cadmium oxinate *vs.* water, (3) Cadmium oxinate *vs.* reagent blank.

5) T. Fujinaga, M. Satake, and T. Yonekubo, *Talanta*, **19**, 689 (1972).

measured. Curves 1 and 2 show respectively the effect of pH on the absorbance of the reagent blank and on that of the salt in the solution against water. Curve 3 shows the difference in the absorbances between the reagent blank and the salt at each pH value. We see that extraction starts from pH 4.0, increases sharply with increasing pH and reaches the maximum, then becomes constant beyond pH 6.0. Thus the pH range 6—10 is suitable.

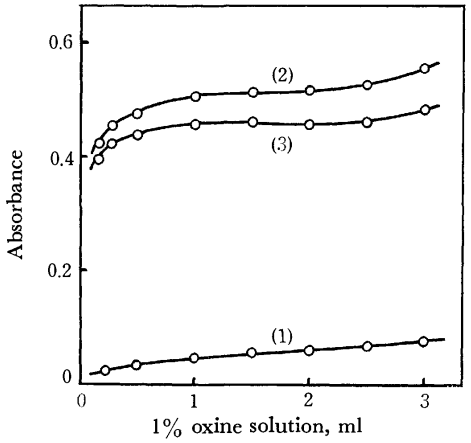

Fig. 3. Effect of oxine concentration on absorbance
Cadmium: 99.86 μg, pH: 7.5, naphthalene: 2.0 g, wavelength: 400 nm, (1) Reagent blank *vs.* water, (2) Cadmium oxinate *vs.* water, (3) Cadmium oxinate *vs.* reagent blank.

Effect of Oxine Concentration and Amount of Naphthalene. Various amounts of oxine were added to the solution containing 99.86 μg of cadmium at pH about 7.5, and the effect of variation in the oxine concentration on the absorbance of the complex salt has been studied. The absorbance increased with increasing amounts of oxine up to 1 ml of 1% oxine solution, whereas addition of 1—2 ml of it gave difinite absorbance, and the absorbance increased again when more than 2 ml was added. Thus, 1.5 ml of oxine solution was found to be the proper amount. On the other hand, addition of 0.5—3.0 g of naphthalene gave almost no difference.

Effect of Shaking Time and Stability. A mixture containing 99.86 μg of cadmium and 1.5 ml of 1% oxine solution was heated till larger particles of the precipitate of the complex salt were formed. Extraction of the salt was then carried out with melted naphthalene by vigorous shaking, and the absorbance of the extract in the dimethylformamide solution was measured. It was observed that the speed of extraction was very rapid and the salt was easily extracted from aqueous solution merely by contact with melted naphthalene. For the sake of good reproducibility, the precipitate of the salt should be digested sufficiently before extraction with naphthalene. The extracted salt was very stable in naphthalene-dimethylformamide solution as well as in naphthalene, and the absorbance remained unchanged for a long time.

Calibration Curve, Sensitivity and Reproducibility. A linear relationship was obtained between the concentration of cadmium and the absrobance in the range of 10—160 μg of cadmium per 10 ml of dimethylformamide. The molar absorptivity of the extracted complex salt was found to be 5.45×10^4 l·mol^{-1}·mm^{-1} at 400 nm and the sensitivity for the absorbance of 0.001 was 0.00263 μg cadmium per cm^2.

An average of ten determinations on 99.86 μg of cadmium gave a mean absorbance of 0.484 with a standard deviation of 0.0041 (relative standard deviation, 0.85%).

Table 1. Effect of diverse salts

Salts	Added (mg)	Absorbance
—	—	0.484
NaF	50	0.488
	100	0.547
KH_2PO_4	50	0.479
	100	0.484
$Na_2HPO_4\cdot12H_2O$	50	0.477
	100	0.484
NaCl	50	0.471
	100	0.475
NH_4Cl	50	0.415
	100	0.332
$CH_3COONa\cdot3H_2O$	50	0.543
	100	0.623
CH_3COONH_4	50	0.485
	100	0.487
	325	0.489
$CuSO_4\cdot5H_2O$	0.25	0.931
$Co(NO_3)_2\cdot6H_2O$	0.25	1.009
$MnCl_2\cdot4H_2O$	0.25	1.323
$ZnCl_2$	0.25	0.869
$Ni(NO_3)_2\cdot6H_2O$	0.25	0.989
Mohr's salt	0.25	0.713
Potassium alum	0.26	0.715
Iron alum	0.10	1.159

Effect of Diverse Ions. Solutions containing 99.86 μg of cadmium were prepared with varying amounts of salt and the determination of cadmium was performed. Some results are given in Table 1. One hundred milligrams of the following salts gave no interference: NaCl, KCl, Na_2SO_4, KH_2PO_4, $Na_2HPO_4\cdot12H_2O$, CH_3COONH_4, $Na_2C_2O_4$, sodium tartrate and sodium citrate. Fifty milligrams of sodium fluoride gave no interference, but 100 mg of it did. Sodium acetate and ammonium chloride gave considerable interference, while even a small amount of EDTA gave serious interference. Many metal ions reacting with oxine to form complex salt at pH 4—10 interfered with the determination. Of the metal salts tested, the following gave interference: $CuSO_4\cdot5H_2O$, $Co(NO_3)_2\cdot6H_2O$, $MnCl_2\cdot4H_2O$, $ZnCl_2$, $Ni(NO_3)_2\cdot6H_2O$, Mohr's salt, potassium alum, iron alum. Magnesium and calcium gave no interference when pH was adjusted to *ca.* 6.5 with ammonium acetate and dilute ammonia or with phosphate buffer. Copper and iron can be removed by oxine-chloroform extraction at pH 3.5—4.0. The interference should be completely suppressed before extraction by some methods such as ion-exchange separation,[6] addition of masking reagent or pH adjustment.[7]

6) T. Yamabe, "Muki Bunri Kagaku," Gihodo, Tokyo (1971), p. 91.

7) Nippon Bunseki Kagaku Kai, "Bunri Bunseki Ho (the last volume)" Kyoritsu, Tokyo (1963), p. 25.

Reductions of Cobalt(III) Complexes by Iron(II) Chelates. I. The Kinetics and Mechanisms of the Reductions of Acidopentaamminecobalt(III) Complex Ions by Iron(II) Chelates of Nitrilopolycarboxylic Acids

Yoshimi KURIMURA

Chemical Laboratory, College of General Education, Ibaraki University, Mito 310

(Received October 24, 1972)

Kinetic studies have been made of the reactions of $FeEDTA^{2-}$ with complex ions of the $Co(NH_3)_5X^{2+}$ ($X=F^-$, Cl^-, Br^-, I^-, NO_3^-, NCS^-, and N_3^-) type. The pattern of reactivity suggests that $FeEDTA^{2-}$ reacts with $Co(NH_3)_5X^{2+}$ mainly through an innersphere mechanism. The variation in the rate of the reactions of $Fe^{II}Z_m^-$ ($Z=$EDTA, CyDTA, EDTA-OH, and DTPA), in which the Z ligand is varied, with $Co(NH_3)_5Cl^{2+}$ can be explained in terms of the steric effect, the charge effect, and the stabilization effect.

The ferrous-ion reductions of cobalt(III) complexes of several types have been investigated. However, rate studies of only a relatively small number of redox reactions between iron(II)–nitrilopolycarboxylate complex ions and metal complex ions have been reported. The reactions of $FeEDTA^{2-}$–$MnCyDTA^-$,[1,2] $FeEDTA^{2-}$–$FeCyDTA^-$,[1] and $CrEDTA^{2-}$–$FeEDTA^-$ [3] are known to be rapid reactions, and the reductions of Co(III)-chelate by Fe(II)-chelates such as $FePDTA^{2-}$–$CoEDTA^-$ [3] and $FePDTA^{2-}$–$CoCyDTA^-$,[3] to be relatively slow reaction. All of the above reactions seem to proceed *via* the outer-sphere activated states.[1,3] On the other hand, the inner-sphere nature of the reactions was suggested in the $FePDTA^{2-}$ reductions of RX^{2+} ($R=Co(NH_3)_5$, $X=Cl^-$, Br^-, N_3^-, and NCS^-).[3]

The pattern of reactivity for the reduction of RX^{2+} by several reducing agents has been studied: the dependence of the rate for the reductions of RX^{2+} by a given reductant would give information about whether the mechanism of the electron-transfer reaction is of outer- or inner-sphere type, though it is a less direct manner.

This article will describe our investigations of the kinetics of the $Fe^{II}EDTA$ reductions of RX^{2+} and the $Fe^{II}Z$ ($Z=$EDTA, CyDTA, EDTA-OH, and DTPA) reductions of RCl^{2+}. The observed rate data will be explained in terms of the effects of the charge, the steric hindrance of $Fe^{II}Z$, and the free energy change from the ferrous to the ferric chelate.

Experimental

Materials. The cobalt(III) complexes of the perchlorate form, $[RF](ClO_4)_2$,[5] $[RCl](ClO_4)_2$,[6] $[RBr](ClO_4)_2$,[7] $[RI](ClO_4)_2$,[8] $[RNO_3](ClO_4)_2$,[6] $[RNCS](ClO_4)_2$,[9] and $[RN_3](ClO_4)_2$[10] were prepared according to the published procedures. The identity and purity of the cobalt(III) products were confirmed analytically and spectrophotometrically. The wavelengths and molar absorption coefficients of the first absorption maximum of the cobalt(III) complexes prepared are summarized in Table 1.

Table 1. Spectral data ($R=Co(NH_3)_5$)

Complex	λ_{max}[a,b] nm	ε_{max}[b]
$[RF](ClO_4)_2$	509 (510)	44 (44)
$[RCl](ClO_4)_2$	531 (533)	49 (49)
$[RBr](ClO_4)_2$	549 (550)	55 (53)
$[RI](ClO_4)_2$	582 (580)	82 (80)
$[RNO_3](ClO_4)_2$	501 (500)	58 (57)
$[RNCS](ClO_4)_2$	496 (497)	191 (192)
$[RN_3](ClO_4)_2$	518 (520)	260 (265)

a) Wavelength for first absorption maximum.
b) Values in parentheses are from the literature.[4]

The preparation of the ferrous perchlorate solution and the determinations of the concentrations of hydrogen and perchlorate ions in the solution were carried out by methods similar to those described previously.[11] The disodium salts of the ethylenediaminetetraacetic acid, cyclohexanediaminetetraacetic acid, hydroxyethylethylenediaminetriacetic acid, and diethylenetriaminepentaacetic acid used were Dotite reagents and were used without further purification. The ferrous chelate solutions were prepared by mixing a deaerated solution of ferrous perchlorate and a slight excess of a deaerated solution of a chelating agent which had been prepared by neutralizing a solution of the chelating agent with a dilute sodium hydroxide solution. The solutions of the cobalt(III) complexes were prepared by dissolving weighed amounts of a cobalt(III) complex into an acetate buffered solution. The ionic strength of the reaction mixture was maintained at 0.50 by the addition of sodium perchlorate. All the reactant solutions were prepared under a nitrogen atmosphere. For all the reactions except for $RNCS^{2+}$ it was necessary to use a stopped-flow technique. The spectrophotometers used

1) R. G. Wilkins and R. E. Yelin, *Inorg. Chem.*, **7**, 2667 (1968).
2) The abreviation for the chelating agents used here are: EDTA, ethylenediaminetetraacetic acid; CyDTA; cyclohexanediaminetetraacetic acid; PDTA; propylenediaminetetraacetic acid; EDTA-OH; hydroxyethylethylenediaminetriacetic acid; DTPA, diethylenetriaminepentaacetic acid.
3) B. Grossman and R. G. Wilkins, *J. Amer. Chem. Soc.*, **89**, 4230 (1967).
4) J. P. Candlin, J. Halpern, and D. L. Trimm, *ibid.*, **86**, 1019 (1964).
5) F. Basolo and R. K. Murmann, "Inorganic Syntheses," Vol. 4, P. 171 (1953).
6) W. A. Hynes, L. K. Yanowski, and M. Shuller, *J. Amer. Chem. Soc.*, **60**, 3053 (1938).
7) H. Diehl, H. Clark, and H.H. Willards, "Inorganic Syntheses," Vol. 1, P. 186 (1939).
8) A. Haim and H. Taube, *J. Amer. Chem. Soc.*, **85**, 495 (1963).
9) A. Werner and H. Muller, *Z. Anorg. Chem.*, **22**, 102 (1900).
10) M. Linhard and H. Flygare, *Z. Anorg. Allgem. Chem.*, **262**, 328 (1950).
11) Y. Kurimura, K. Ohashi, T. Ohtsuki, and K. Yamamoto, This Bulletin, **44**, 1293 (1971).

were a Yanagimoto Model SPS-1 stopped-flow apparatus and a Hitachi Model 124 recording spectrophotometer. The reactions were followed under pseudo-first-order conditions in which the concentration of the ferrous chelate was at least 10 times greater than that of the Co(III) complex. The reactions were monitored by following the variation in the absorbance of the reaction mixture in the vicinity of the first absorption maximum of the Co(III) complex. The pH value of the solution was measured by means of a Hitachi-Horiba F-5 type pH meter. The hydrogen-ion concentration of the reaction mixture was calculated using the relationship: $-\log[H^+]=pH-0.10$. In this calculation, the activity coefficient of the hydrogen ions was estimated to 0.8 at $\mu=0.5$ from the data obtained by Kielland ($f_{H^+}=0.83$ at $\mu=0.2$).[12]

Results

The observed rate constant, k_{obsd}, defined by:

$$-d[Co(III)]/dt = k_{obsd}[Co(III)][Fe(II)] \quad (1)$$

was obtained from the slope of log (A_t-A_∞) *vs.* the time plot (A_t is the absorbance at time t, and A_∞, that at the time the reaction was completed). The plots were linear for at least for 2 half-lives in all cases The initial reactant concentrations were generally varied over at least a two-fold range, and a first-order dependence on the reactants was confirmed for the Co(III) and Fe(II).

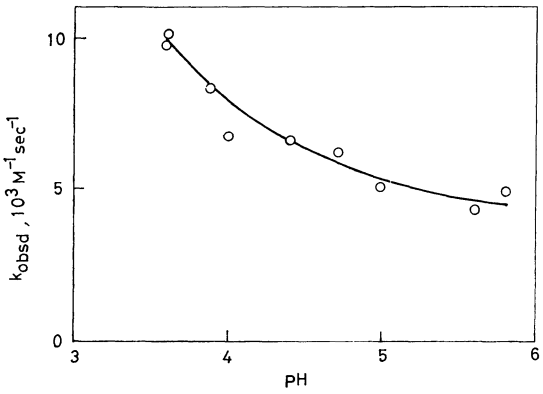

Fig. 1. Rate profile for the reduction of $Co(NH_3)_5Cl^{2+}$ by $Fe^{II}EDTA$.
$[Co(NH_3)_5Cl^{2+}]=8-10\times10^{-4}$M, $[Fe^{II}EDTA]=1.0\times10^{-2}$M, $\mu=0.50$, 25 °C.

Reduction of $Co(NH_3)_5Cl^{2+}$ by $Fe^{II}EDTA$. The values of k_{obsd} for the $Fe^{II}EDTA$ reduction of RCl^{2+} depend on the hydrogen-ion concentration. The rate profile for the reaction is shown in Fig. 1. The variation in the k_{obsd} with the pH indicates the following competition reactions:

$$Co(NH_3)_5Cl^{2+} + FeEDTA^{2-} \xrightarrow{k_n} Co(II) + Fe(III) \quad (2)$$

$$Co(NH_3)_5Cl^{2+} + FeHEDTA^{-} \xrightarrow{k_p} Co(II) + Fe(III) \quad (3)$$

The $FeHEDTA^-$ is the protonated species of Fe^{II}-EDTA, and k_n and k_p are the rate constants for the (2) and (3) reactions respectively. The amounts of free ferrous ion can be neglected under the present experimental conditions. The concentration of Fe(II) can be expressed by:

$$[Fe(II)] = [FeEDTA^{2-}] + [FeHEDTA^{-}] \quad (4)$$

The rate equation derived from Eqs. (2) and (3) is:

$$\text{Rate} = \frac{k_n+k_pK_{FeHY}[H^+]}{1+K_{FeHY}[H^+]}[Co(III)][Fe(II)] \quad (5)$$

where K_{FeHY} is the formation constant for the protonated ferrous chelate. From a comparison of Eqs. (1) and (5), we obtain:

$$k_{obsd}(1+K_{FeHY}[H^+]) = k_n + k_pK_{FeHY}[H^+] \quad (6)$$

The plots of $k_{obsd}(1+K_{FeHY}[H^+])$ *vs.* $[H^+]$ form straight lines, and the slope and intercept of the line give the values of k_p and k_n respectively if the redox reaction can be expressed by the (2) and (3) reactions. The relationship between $k_{obsd}(1+K_{FeHY}[H^+])$ *vs.* $[H^+]$ for the $Fe^{II}EDTA$ reduction is shown in Fig. 2. The value of K_{FeHY} used was $10^{2.8}$ [13]; this value was obtained under conditions of $\mu=0.1$ and 25 °C, and was used without any correction. The values of k_n and k_p, as calculated from the intercept and slopes of the straight line in Fig. 2, are 4.7×10^3 $M^{-1}sec^{-1}$ and 3.5×10^4 $M^{-1}sec^{-1}$ respectively at 25 °C and $\mu=0.50$.

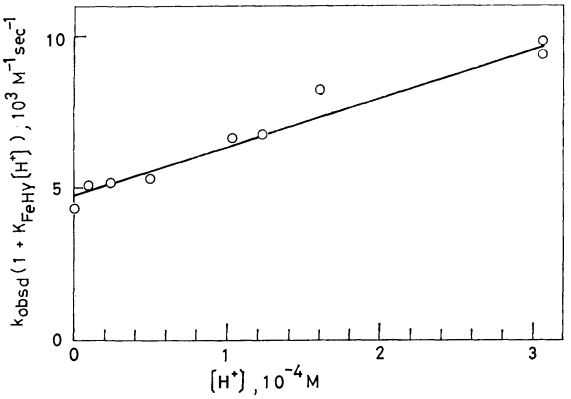

Fig. 2. Plots of $k_{obsd}(1+K_{Fe^{II}HY}[H^+])$ *vs.* $[H^+]$ for the reduction of $Co(NH_3)_5Cl^{2+}$ by $Fe^{II}EDTA$.

Reductions of RX^{2+} ($X=F^-$, Cl^-, Br^-, I^-, NO_3^-, NCS^-, and N_3^-) by $FeEDTA^{2-}$. The rate constants for the $FeEDTA^{2-}$ reduction of RX^{2+} were obtained in the higher pH region (pH=4—5). In this pH region, the protonated species of the ferrous chelate is less important; the only species to be considered is the $FeEDTA^{2-}$. The second-order rate constants obtained are shown in Table 2.

TABLE 2. RATE CONSTANTS FOR THE $FeEDTA^{2-}$ REDUCTION OF PENTAAMMINECOBALT(III) COMPLEXES AT 25 °C AND $\mu=0.50$

Complex ($R=Co(NH_3)_5$)	k, $M^{-1}sec^{-1}$
RF^{2+}	6.0×10^3
RCl^{2+}	4.7×10^3 (3.5×10^4)[a]
RBr^{2+}	3.8×10^3
RI^{2+}	3.4×10^3
RNO^{3+}	~50
$RNCS^{2+}$	0.13
RN_3^{2+}	7.3×10^3

a) Rate constant for the $FeHEDTA^-$ reduction.

12) J. Kielland, *J. Amer. Chem. Soc.*, **59**, 1675 (1937).

13) A. Ringbom, "Complexation in Analytical Chemistry," John Wiley and Sons, New York, 1963.

Reduction of $Co(NH_3)_5Cl^{2+}$ by $Fe^{II}Z^{m-}$ (Z=CyDTA, EDTA-OH, and DTPA). In the Fe^{II}CyDTA–RCl^{2+} and Fe^{II}EDTA-OH–RCl^{2+} reactions, the only predominant species of the ferrous chelate are the normal ones, $FeCyDTA^{2-}$ and $FeEDTA\text{-}OH^{-}$ respectively, under the experimental conditions employed. Therefore the second-order rate constants for these two reactions can simply be obtained from the rates evaluated in the pH region between 4 and 5. The rate constants thus obtained are shown in Table 3.

Table 3. Rate constants for the $FeCyDTA^{2-}$ and $FeEDTAOH^{-}$ reductions of $Co(NH_3)_5Cl^{2+}$ at 25 °C and μ=0.50

Reductant	pH	k, $10^3 M^{-1} sec^{-1}$	Average value ($M^{-1} sec^{-1}$)
$FeCyDTA^{2-}$	4.0	2.6	
	4.4	2.9	
	5.0	2.9	2.9×10^3
$FeEDTAOH^{-}$	4.0	4.4	
	4.5	4.5	
	5.0	4.4	4.4×10^3

The rate constants for the $FeHDTPA^{2-}$–RCl^{2+} and $FeDTPA^{2-}$–RCl^{2+} reactions were obtained in the manner employed in the case of the Fe^{II}EDTA–RCl^{2+} reaction. The value of $K_{Fe^{II}HL}$ used for the calculation was $10^{5.4}$ (μ=0.1 and 25 °C).[13] The second-order rate constants were 4.8×10^3 $M^{-1} sec^{-1}$ for $FeHDTPA^{2-}$ and $\sim10^2$ $M^{-1} sec^{-1}$ for $FeDTPA^{3-}$. The rate constant for the $FeDTPA^{3-}$ may be less accurate, since the intercept of the straight line of the $k_{obsd}(1+K_{MHL}[H^+])$ *vs.* $[H^+]$ plot is relatively small.

Discussion

The relative rates for the reductions of Co(III)-pentaammine complexes by several reductants are shown in Table 4. It may be possible to assume that the reductions of RX^{2+} by Cr^{2+} [18] and, perhaps, by Fe^{2+} proceed *via* the inner-sphere mechanism, and those by $Cr(bipy)_3^{2+}$ [4] and $Ru(NH_3)_6^{2+}$,[19] *via* the outer-sphere mechanism. If we accept the suggestion that Cr^{2+} reacts by means of a bridging mechanism,[19] is possible to suggest that the ligand, X, acts as the bridge in the Fe^{II}EDTA reductions of RX^{2+}. Furthermore, the large value of $k_{N_3^-}/k_{NCS^-}$ ($=5.5\times10^5$), which can often be used to distinguish between an inner-sphere and an outer-sphere mechanism,[20] also indicates the inner-sphere nature of the reactions in the present system. Since the $Fe^{II}Z^{m-}$ complex ion is labile for the ligand exchange, one of the coordinated positions of the chelate could easily be open, so a bridged intermediate of the $[R\cdot X\cdot FeZ]^{(n-m)+}$ form might be formed prior to electron-transfer.

In the cases of $X=F^-$, Cl^-, Br^-, and I^-, the variation in the rate constants for FeY^{2-} ($Y=EDTA^{4-}$) shows the same tendency as Fe^{2+}; that is, the reactivity of the FeY^{2-} toward the RX^{2+} shows an "inverted order" of bridging efficiency:[18] $RF^{2+}>RCl^{2+}>RBr^{2+}>RI^{2+}$.

The relative rates for the reduction of RCl^{2+} by several ferrous chelate species are presented in Table 5. The results show that the decreasing order of the reactivities of the ferrous chelates is: $FeHEDTA^{-}>FeHDTPA^{2-}=FeEDTA^{2-}>FeEDTA\text{-}OH^{-}>FeCyDTA^{2-}>FeDTPA^{3-}$. This order shows that the rate does not depend so much on the charge of the chelate. The decreasing order of the values of "relative stabiliza-

Table 4. Relative rates[a] for the reductions of acidopentaammminecobalt (III) complexes at 25 °C and μ=1.0 (R=$Co(NH_3)_5$)

Complex	Reductant: $FeEDTA^{2-}$[b]	$FePDTA^{2-}$[c]	Fe^{2+}	Cr^{2+}	$Ru(NH_3)_6^{2+}$	$Cr(bipy)_3^{2+}$[j]
RF^{2+}	1.3	—	4.8[d]	0.4[g]	—	2×10^{-3}
RCl^{2+}	1.0	1.0	1.0[d]	1.0[g]	1.0[h]	1
RBr^{2+}	0.81	0.82	0.58[d]	2.3[g]	6.2[h]	6
RI^{2+}	0.72	—	—	5.0[g]	26[h]	—
RNO_3^{2+}	~0.01	—	—	6.4×10^{-4}[h]	—	—
$RNCS^{2+}$	2.7×10^{-5}	1.2×10^{-4}	1.8×10^{-3}[e]	1.4×10^{-5}[h]	—	1.3×10^{-2}
RN_3^{2+}	1.6	3.2	5.4[f]	0.5[h]	4.6×10^{-3}[i]	5×10^{-2}

a) Ratio of rate constant of RX^{2+} to that of RCl^{2+},
b) This work (μ=0.50),
c) From ref. 3,
d) From ref. 14 (μ=1.7),
e) From ref. 15,
f) From ref. 16,
g) From ref. 17,
h) From ref. 4,
i) From ref. 17 (μ=0.22),
j) From ref. 4 (μ=0.18).

14) H. Diebler and H. Taube, *Inorg. Chem.*, **4**, 1029 (1965).
15) J. H. Espenson, *ibid.*, **4**, 121 (1965).
16) A. Haim, *J. Amer. Chem. Soc.*, **86**, 2352 (1964).
17) J. P. Candlin and J. Halpern, *Inorg. Chem.*, **4**, 766 (1966).
18) H. Taube, *Advan. Inorg. Chem. Radiochem.*, **1**, 1 (1959).
19) J. F. Endicott and H. Taube, *J. Amer. Chem. Soc.*, **86**, 1686 (1964).
20) F. Basolo and R. G. Pearson "Mechanism of Inorganic Reaction," 2nd Ed., John Wiley and Sons, New York (1958), p. 482.

TABLE 5. COMPARISON OF REACTIVITY FOR FeZ^{m-} REDUCTIONS OF $Co(NH_3)_5Cl^{2+}$ AT 25 °C AND $\mu=0.50$

Complex	Relative rate
$FeEDTA^{2-}$	1.0
$FeCyDTA^{2-}$	0.62
FeEDTA-OH$^-$	0.94
$FeDTPA^{3-}$	0.02
FeHEDTA$^-$	6.0
$FeHDTPA^{2-}$	1.0

TABLE 6. VALUES OF log $K_{Fe^{III}Z}/K_{Fe^{II}Z}$ OF Fe(III)–Fe(II) REDOX COUPLES

Redox couple	log $K_{Fe^{III}Z}/K_{Fe^{II}Z}$ (R_s)[a]
$FeEDTA^-/FeEDTA^{2-}$	0.25
FeEDTA-OH/FeEDTA-OH$^-$	0.21
$FeCyDTA^-/FeCyDTA^{2-}$	0.21
$FeDTPA^{2-}/FeDTPA^{3-}$	0.24
$FeEDT^-/FeHEDTA^-$ [b]	0.95
$FeDTPA^{2-}/FeHDTPA^{2-}$ [b]	0.71

a) The values are calculated using formation constants estimated at 25 °C and $\mu=0.1$.[13]

tion," which is expressed by R_s, in Table 6 is: $FeHEDTA^- > FeHDTPA^{2-} > FeEDTA^{2-}$ $FeDTPA^{3-} > FeEDTA\text{-}OH^- = FeCyDTA^{2-}$. For the $FeHEDTA^-$ and $FeHDTPA^{2-}$ reductions, the predominant species of the oxidized forms which are formed in the solutions are normal ferric chelates, $Fe^{III}EDTA^-$, and $Fe^{III}DTPA^{2-}$ respectively under the experimental conditions employed. Therefore, the values of R_s for $FeHEDTA^-$ and $FeHDTPA^{2-}$ are evaluated on the basis of the change from a protonated ferrous chealte to a normal ferric chelate. The decreasing order of reactivity agrees with that of R_s except for $FeDTPA^{3-}$. Such a correspondence between the order of reactivity and that of R_s suggests that one of the most important factors controlling the rates of the ferrous chelate reductions of RX^{2+} is the effect of the relative stabilization (stabilization effect). This indicates that there is some correlation between ΔF and ΔF^* for the reaction. The smaller reactivity for $FeDTPA^{3-}$ may be due to the steric hindrance of the bulky ligand.

The author wishes to express his thanks to Mr. Kosaburo Ohashi, Miss Ikuko Sekine, and Miss Chiyoko Endo for their help in part of the measurements and in the syntheses of the complexes.

BULLETIN OF THE CHEMICAL SOCIETY OF JAPAN, VOL. 46, 2096—2101 (1973)

Some β-Diketone Chelate Complexes with Uranium(IV), Thorium(IV), and Cerium(IV). Preparation and IR Spectra

Tetsuhiko YOSHIMURA,* Chie MIYAKE, and Shosuke IMOTO

Department of Nuclear Engineering, Faculty of Engineering, Osaka University, Suita, Osaka 565

(Received August 9, 1972)

The tetrakis β-diketonates of U(IV), Th(IV), and Ce(IV) with acetylacetone, trifluoroacetylacetone, hexafluoroacetylacetone, benzoylacetone, dibenzoylmethane, benzoyltrifluoroacetone, and thenoyltrifluoroacetone have been prepared and their infrared spectra measured in the range 4000—200 cm^{-1}. In every chelate, a strong, broad and metal sensitive band related to the M–O stretching mode was found in the 200—250 cm^{-1} region.

Many β-diketones coordinate to various metal ions as a bidentate ligand, generally forming stable chelates. Acetylacetone and thenoyltrifluoroacetone are well-known as extraction reagent for various metal ions and as metal indicator in chelatometry. The β-diketonato chelates of actinoid and lanthanoid elements are of particular interest, since they are used as solvent extraction reagent for the actinoid elements in the reprocessing of spent fuel and the separation of actinoid elements from fission products.[1] The possibility of their use as nuclear fuel with organic moderator has been suggested. Most β-diketonato chelates are so volatile that they are often purified by means of sublimation, and the volatility of the β-diketonates of uranium has been investigated from the view point of isotope separation.[2]

The measurements of the infrared spectra for tetrakis β-diketonates of uranium(IV), thorium(IV), and cerium(IV) have been carried out for acetylacetonates and thenoyltrifluoroacetonates.[3,4] Fay and Pinnavaia[3] measured the IR and Raman spectra of $M(acac)_4$ (M=Zr(IV), Hf(IV), Ce(IV), and Th(IV)) and assigned the IR absorption bands in the 1600—500 cm^{-1} region according to the assignments for the

* Present address: The Environmental Science Institute of Hyogo Prefecture, Hyogo-ku, Kobe.

1) J. J. Katz and G. T. Seaborg, "The Chemistry of the Actinide Elements," Methuen and Co., London (1957).

2) a) H. I. Schlesinger, H. C. Brown, J. J. Katz, S. Archer, and R. A. Lad, *J. Amer. Chem. Soc.*, **75**, 2446 (1953). b) H. Gilman, R. G. Jones, E. Bindschardler, D. Blume, G. Karmas, G. A. Martin, Jr., J. F. Nobis, J. R. Thirtle, H. L. Yale, and F. A. Yoeman, *ibid.*, **78**, 2790 (1956). c) H. A. Swain, Jr. and D. G. Karraker, *Inorg. Chem.*, **9**, 1766 (1970).

3) R. C. Fay and T. J. Pinnavaia, *ibid.*, **7**, 508 (1968).

4) Y. Baskin and N. S. K. Prasad, *J. Inorg. Nucl. Chem.*, **25**, 1001 (1963).

β-diketonato chelates with transition metal ions reported by Behnke and Nakamoto.[5] They also assigned some metal sensitive bands in the 500—70 cm^{-1} region to the M–O band. The IR study for the effect of replacement of the methyl groups of the acetylacetonates in the β-diketonato chelates with Cu(II) and Ni(II) has been made by Nakamoto *et al.*[6]

This paper deals with the preparation of several tetrakis-β-diketonates of U(IV), Th(IV), and Ce(IV) with acetylacetone, trifluoroacetylacetone, hexafluoroacetylacetone, benzoylacetone, dibenzoylmethane, benzoyltrifluoroacetone and thenoyltrifluoroacetone and their IR spectra in the range 4000—200 cm^{-1} together with the substituent effects on the M–O bond.

Experimental

Preparation. Hydrochloric acid (6N) solution of U(IV) (supplied by Power Reactor and Nuclear Fuel Corporation, Tokai works) was used for preparation of uranium(IV) chelates. The solution contained 302.8 g U(IV) per liter. Thorium tetrachloride hydrate and cerium(IV) ammonium sulfate tetrahydrate, both of GR grade, were used for the preparation of thorium(IV) and cerium(IV) chelates, respectively. All the ligands and other reagents were of GR grade and used without further purification. As the U(IV) ion in solution is particularly sensitive towards oxidation, the syntheses and purification of U(IV) chelates were carried out in a dry box filled with argon or nitrogen gas. The seven β-diketonato ligands used are denoted by: acetylacetonato, acac; trifluoroacetylacetonato, tfac; hexafluoroacetylacetonato, hfac; benzoylacetonato, bzac; dibenzoylmethanato, dbm; benzoyltrifluoroacetonato, bfac; thenoyltrifluoroacetonato, TTA. The chelates of uranium(IV), thorium(IV) and cerium(IV) were prepared as follows.

(1) $U(acac)_4$, $Th(acac)_4$, and $Ce(acac)_4$. Acetylacetone was added to a dilute U(IV) hydrochloric acid solution, aqueous thorium tetrachloride solution and the aqueous cerium(IV) ammonium sulfate solution each with the metal ion to acetylacetone ratio 1:4. These solutions were then gradually neutralized with concd. aqueous ammonia. The precipitates were filtered off, washed with water and dried *in vacuo*. The products were recrystallized twice from benzene-petroleum ether or toluene–petroleum ether and dried *in vacuo*. Found: C, 37.81; H, 4.40; U, 37.60%. Calcd. for $U(acac)_4$ (slightly greenish brown): C, 37.86; H, 4.45; U, 37.52%. Found: C, 38.08; H, 4.58; Th, 36.2%. Calcd for $Th(acac)_4$ (white): C, 38.22; H, 4.49; Th, 36.92%. Found: C, 44.51; H, 5.14; Ce, 25.82%. Calcd for $Ce(acac)_4$ (brown): C, 44.77; H, 5.26; Ce, 26.11%.

(2) $U(hfac)_4$, $Th(hfac)_4$, and $Ce(hfac)_4$. The U(IV) ion, Th(IV) ion and Ce(IV) ion were extracted from dilute U(IV) hydrochloric acid solution, aqueous Th(IV) solution and aqueous Ce(IV) solution respectively with a hexafluoroacetylacetone benzene solution. The products crystallized from these benzene solutions were recrystallized twice from benzene and dried *in vacuo*. Found: C, 23.77; H, 0.88%. Calcd for $U(hfac)_4$ (brown): C, 22.53; H, 0.38%. Found: C, 21.13; H, 0.52%. Calcd for $Th(hfac)_4$ (white): C, 22.66; H, 0.38%. Found: C, 23.12; H, 0.63%. Calcd for $Ce(hfac)_4$ (brown): C, 24.81; H, 0.42%.

(3) $U(tfac)_4$, $Th(tfac)_4$, $U(bfac)_4$, $Th(bfac)_4$, $U(bzac)_4$, $Th(bzac)_4$, $U(bdm)_4$, $Th(dbm)_4$, and $U(TTA)_4$. The ethanol solution of ligand was added to aqueous Th(IV) solution or U(IV) hydrochloric acid solution diluted with water or ethanol (metal ion: ligand≒1:4). The precipitates thus obtained were filtered, washed with water, dried *in vacuo* and purified as in the case of acetylacetonates. Found: C, 28.17; H, 2.10%. Calcd for $U(tfac)_4$ (yellowish brown): C, 28.25; H, 1.90%. Found: C, 28.62; H, 2.18%. Calcd for $Th(tfac)_4$ (white): C, 28.45; H, 1.91%. Found: C, C, 44.24; H, 1.98%. Calcd for $Th(bfac)_4$ (pale orange): C, 43.97; H, 2.21%. Found: C, 43.66; H, 2.13%. Calcd for $U(bfac)_4$ (reddish brown): C, 43.73; H, 2.20%. Found: C, 54.58; H, 4.39; U, 27.15%. Calcd for $U(bzac)_4$ (reddish brown): C, 54.42; H, 4.11; U, 26.97%. Found: C, 55.02; H, 4.42; Th, 26.88%. Calcd for $Th(bzac)_4$ (white): C, 54.79; H, 4.14; Th, 26.47%. Found: C, 63.89; H, 3.88; U, 21.17%. Calcd for $U(dbm)_4$ (reddish brown): C, 63.71; H, 3.92; U, 21.05%. Found: C, 63.84; H, 3.85; Th, 20.6%. Calcd for $Th(dbm)_4$ (yellow): C, 64.05; H, 3.94; Th, 20.63%. Found: C, 34.34; H, 1.74%. Calcd for $U(TTA)_4$ (reddish brown): C, 34.23; H, 1.44%. Found: C, 34.79; H, 1.50%. Calcd for $Th(TTA)_4$ (pale yellow) :C, 34.42; H, 1.44%.

(4) $Ce(tfac)_4$, $Ce(bfac)_4$, $Ce(bzac)_4$, $Ce(dbm)_4$, and $Ce(TTA)_4$. The ethanol solution of ligand was added to aqueous Ce(IV) solution. The chelates thus formed were extracted from the crude precipitates with benzene or toluene. The products crystallized from these benzene or toluene solutions were purified as in the case of hexafluoroacetylacetonates. Found: C, 31.99; H, 2.40%. Calcd for $Ce(tfac)_4$ (buff brown): C, 31.92; H, 2.15%. Found: C, 47.51; H, 2.35%. Calcd for $Ce(bfac)_4$ (brownish purple): C, 48.01; H, 2.42%. Found: C, 60.48; H, 4.63; Ce, 18.3%. Calcd for $Ce(bzac)_4$ (brown): C, 61.21; H, 4.62; Ce, 17.86%. Found: C, 69.53; H, 4.49; Ce, 13.54%. Calcd for $Ce(dbm)_4$ (reddish brown): C, 69.75; H, 4.30; Ce, 13.56%. Found: C, 37.58; H, 1.51%. Calcd for $Ce(TTA)_4$ (reddish brown): C, 37.50; H, 1.57%.

Measurements. IR absorption spectra were recorded on Hitachi-Perkin-Elmer 225 (4000—250 cm^{-1}) and Hitachi EPI-L (700—200 cm^{-1}) IR grating spectrophotometers, using the technique of Nujol mull and HCB mull supported between caesium iodide plates.

Results and Discussion

The yield of U(IV) β-diketonates was quantitative by the present method. However, yields of Th(IV)- and Ce(IV)-β-diketonates were not quantitative because of the fact that Th(IV)- and Ce(IV)-ion are easily hydrolyzed and their hydrolyzed products are less soluble in water. Generally, the yields of metal chelates with acetylacetone, trifluoroacetylacetone and hexafluoroacetylacetone were lower than those with the other four ligands, benzoylacetone, dibenzoylmethane, benzoyltrifluoroacetone and thenoyltrifluoroacetone. The U(IV) β-diketonates were gradually oxidized and discolored in air at room temperature, except for the chelates with the ligand containing phenyl and thienyl groups which were relatively stable in air. It was found from the absorption spectra in visible region that $U(acac)_4$, $U(tfac)_4$, and $U(hfac)_4$ were not stable even in organic solution. All the U(IV) β-diketonates were kept in a vacuum container, and all operations involved in preparations and measurements were carried out as rapidly as possible.

Tetrakis-bidentate chelate, to which all tetrakis β-

5) G. T. Behnke and K. Nakamoto, *Inorg. Chem.*, **6**, 433 (1967).
6) K. Nakamoto, Y. Morimoto, and A. E. Martell, *J. Phys. Chem.*, **66**, 346 (1962).

diketonato chelates belong, has the coordination number of eight around the central metal ion. The configuration of tetrakis β-diketonato chelates has been determined for two chelates $M(acac)_4$ (M=Zr, Ce, Th, and U)[7] and $M(dbm)_4$ (M=Ce, Th, and U)[8] to be square antiprism with D_2 symmetry and dodecahedron with D_{2d} symmetry, respectively. It seems that the tetrakis β-diketonato chelates with the other kind of ligand dealt with are also isomorphous for Ce(IV), Th(IV), and U(IV).

IR Spectra. In Fig. 1 are shown the IR spectra in the 1800—600 cm^{-1} region of $U(acac)_4$, $U(tfac)_4$, $U(hfac)_4$, $U(bzac)_4$, $U(dbm)_4$, $U(bfac)_4$, and $U(TTA)_4$ chelates. Above 1800 cm^{-1}, no absorption band is found except the C–H stretching bands (not given in the figure) of the methyl group, the γC–H bond, the phenyl group and the thienyl group near 3000 cm^{-1}.

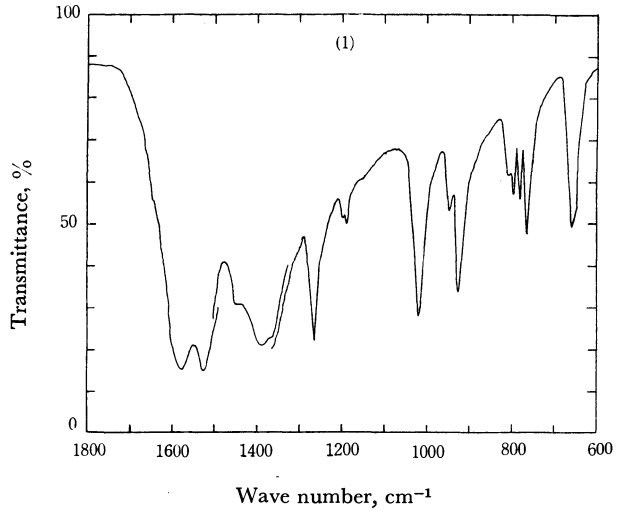

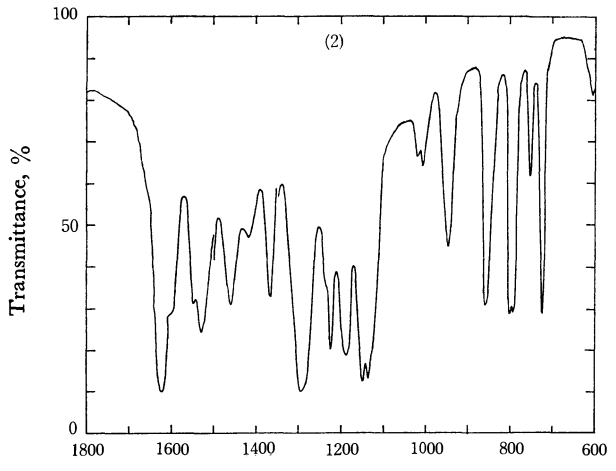

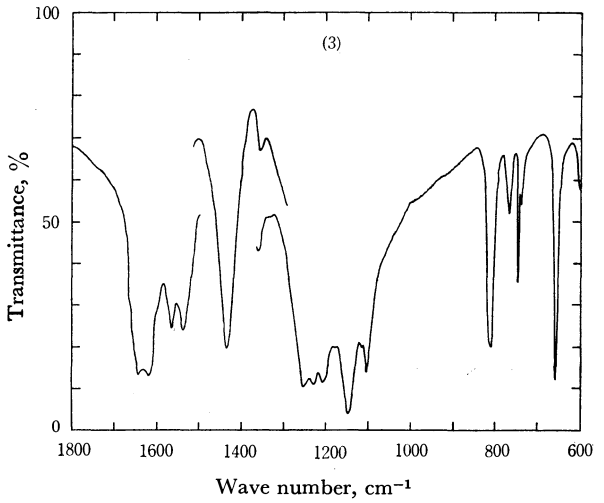

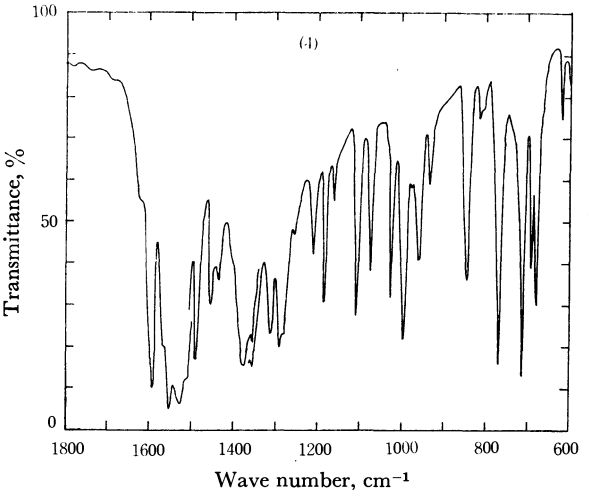

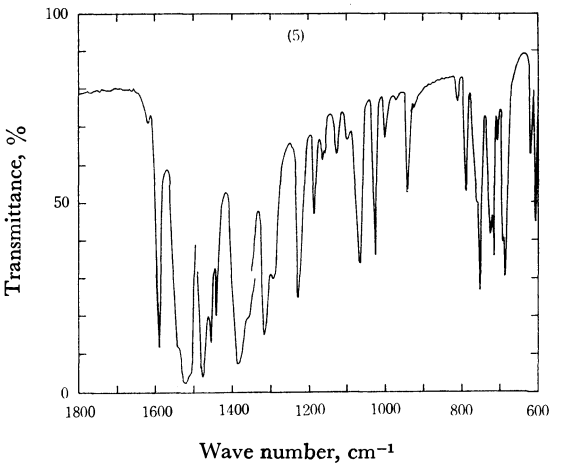

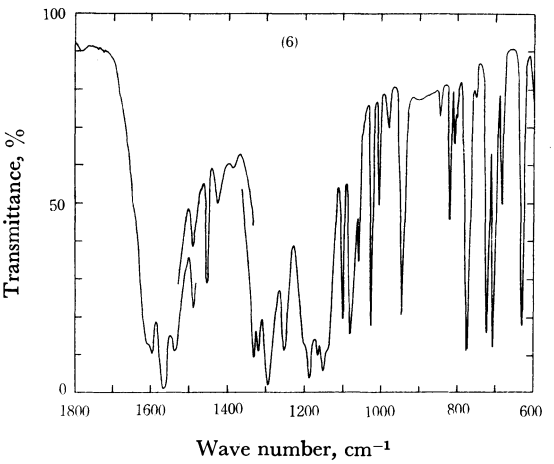

7) J. L. Hoard and J. V. Silverton, *Inorg. Chem.*, **2**, 235 (1963).
8) V. L. Wolf and H. Barnighausen, *Acta Crystallogr.*, **13**, 778 (1960).

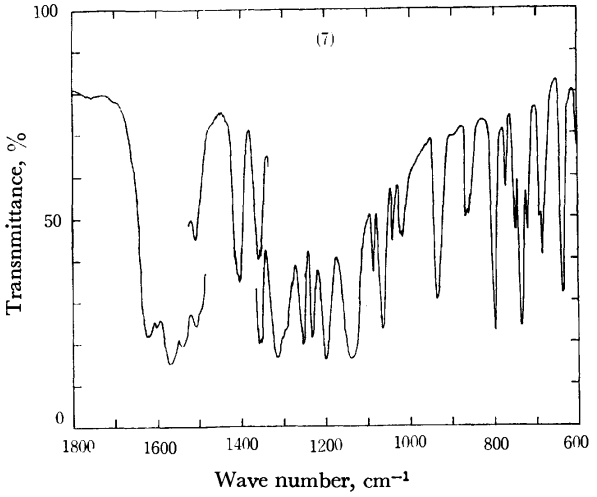

Fig. 1. Infrared spectra of the tetrakis β-diketonates of U(IV). (1) $U(acac)_4$, (2) $U(tfac)_4$, (3) $U(hfac)_4$, (4) $U(bzac)_4$, (5) $U(dbm)_4$, (6) $U(bfac)_4$, (7) $U(TTA)_4$. 200—1350, 1500—2700 cm^{-1}: Nujol mull. 1350—1500, 2700—4000 cm^{-1}: HCB mull.

The IR spectra of acetylacetonates of uranium reported by Lecomte[9] do not show the valence state of uranium. The present result differs from that given by Lecomte, but is in line with $Th(acac)_4$ given by Fay and Pinnavaia.[3] The spectra of $M(acac)_4$ (M= U(IV), Th(IV), and Ce(IV)) in the 1600—500 cm^{-1} region are very similar to each other and to those of $Pt(acac)_2$ and $Cu(acac)_2$.[5,10] They are independent of both mass and coordination number of the central metal ion. The absorption bands of each chelate in the 1700—500 cm^{-1} region can be assigned on the basis of β-diketonato chelates with bivalent- or trivalent-transition metal ion reported by Nakamoto *et al.*,[5,6] Mikami *et al.*,[10] and also based on the result reported by Fay and Pinnavaia.[3] The infrared frequencies and tentative assignments for $U(acac)_4$ are given in Table 1.

In the spectra of tetrakis β-diketonates other than tetrakis acetylacetonates, intense bands are found in the region 1500—1700 cm^{-1}, corresponding to the C=O+C=C stretching bands in the spectra of $M(acac)_4$. Other bands are possibly a combination band of bands appearing in the 700—800 cm^{-1} region such as CH

Table 2. Frequencies of the intense bands in the 1500—1700 cm^{-1} (cm^{-1})

Metal	Ligand						
	acac	tfac	hfac	bzac	dbm	bfac	TTA
U(IV)	1577	1620	1643	1590	1590	1605	1618
		1600	1619	1562		1595	1600
	1525	1545	1568	1552	1542	1564	1570
		1530	1538	1525	1522	1535	1540
Th(IV)	1580	1620	1645	1589	1591	1605	1622
		1590	1620	1560		1595	1604
	1523	1545	1570	1551	1542	1565	1573
		1530	1543	1524	1520	1536	1544
Ce(IV)	1575	1618	1643	1587	1589	1606	1617
		1595	1620	1560		1595	1598
	1518	1545	1564	1545	1540	1564	1570
		1525	1535	1520	1520	1535	1542

Table 1. Infrared frequencies for $M(acac)_4$ chelates

$U(acac)_4$	$Th(acac)_4$	$Ce(acac)_4$	Predominant mode[a]
1577 vs[b]	1580 vs	1575 vs	ν(C=O)+ν(C=C)
1525 vs	1523 vs	1518 vs	ν(C=C)+ν(C=O)
1448 m	1448 m	1440 sh	δd(CH_3)
1390 vs	1390 vs	1386 vs	δ(C–H)+ν(C=O)
1365 sh	1365 sh	1365 sh	δs(CH_3)
1267 s	1267 s	1267 s	ν(C–CH_3)+ν(C=C)
	1199 vw	1198 vw	
1189 w	1192 w	1190 w	δ(CH)+ν(C–CH_3)
1019 s	1020 s	1020 s	ρr(CH_3)
944 w	943 w	945 w	ν(C–CH_3)
924 s	924 s	924 s	ν(C=C)+ν(C=O)
803 w	803 vw	803 vw	π(CH)
794 w	794 w	793 w	
779 w	780 w	779 w	
764 m	765 m	764 m	
656 s	657 s	658 m	δ(C–CH_3)+ring
647 sh	650 sh	650 sh	π(CH_3CCO)
562 vw	561 vw	560 vw	ring
524 s	524 s	525 m	
	404 sh		
399 s	397 s	400 s	δ(C–CH_3)+ν(M–O)
221 s	225 m	250 m	ν(M–O)

a) ν, stretching; δ, in-plane deformation; π, out-of-plane deformation; ρ r, rocking; s, symmetric; d, degenerated; ring, ring deformation; R. substituent.
b) v, very; s, strong; m, medium; w, weak; sh, shoulder.

9) J. Lecomte, *Discuss. Farad. Soc.*, **9**, 225 (1950).

10) M. Mikami, I. Nakagawa, and T. Shimanouchi, *Spectrochim. Acta*, **23A**, 1037 (1967).

out-of-plane deformation bands[10] and/or the split C···O+C=C stretching absorption bands as a result of the lowered symmetry induced by the asymmetrical

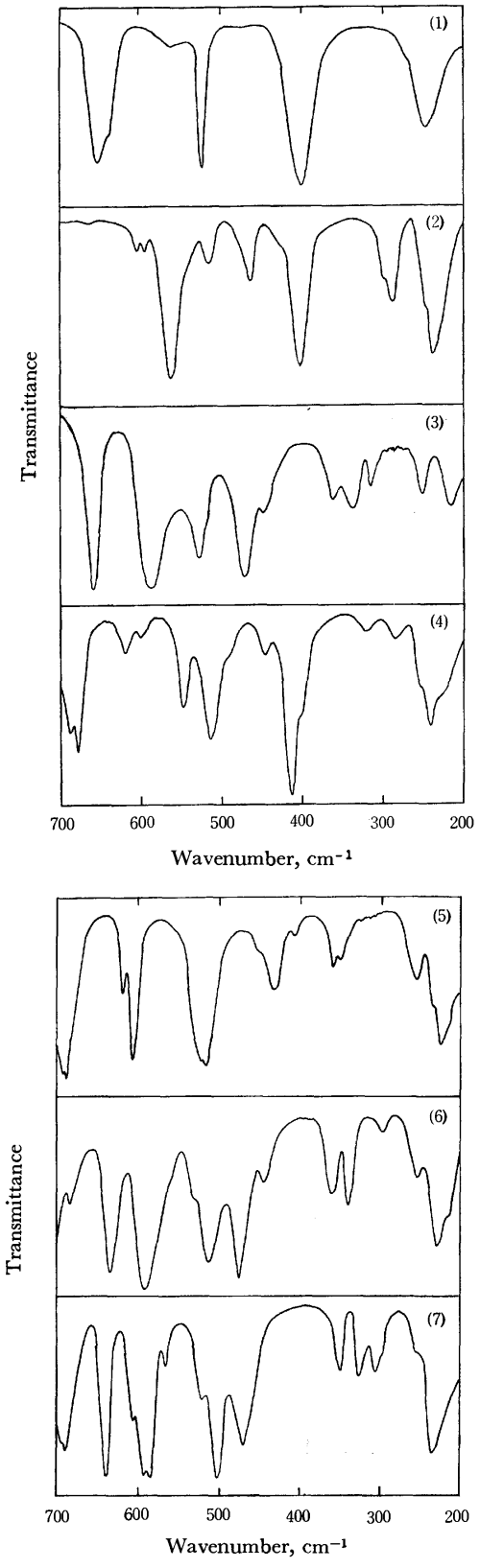

Fig. 2. Low-frequency infrared spectra of the tetrakis β-diketonates of Ce(IV).
(1) $Ce(acac)_4$, (2) $Ce(tfac)_4$, (3) $Ce(hfac)_4$, (4) $Ce(bzac)_4$, (5) $Ce(dbm)_4$, (6) $Ce(bfac)_4$, (7) $Ce(TTA)_4$.

ligands such as tfac, bzac, bfac, and TTA in the chelate. The frequencies of the intense bands in the 1500—1700 cm^{-1} are summarized in Table 2.

In Fig. 2 are shown the IR spectra of the seven β-diketonates of Ce(IV) in the region 200—700 cm^{-1}. Vibrational bands contributed by appreciable amounts of M–O stretching mode are expected in the 500—200 cm^{-1} region. The spectra of $M(acac)_4$ show a strong band in the 220—250 cm^{-1} region and one in the 397—400 cm^{-1} region. The former band is relatively broad and metal sensitive, having a tendency to shift towards lower frequency side with an increase in the mass of the central metal, and can be assigned to the nearly pure M–O stretching mode, after the assignments for $M(acac)_4$ (M=Zr(IV), Hf(IV), Ce(IV), and Th(IV)) reported by Fay and Pinnavaia. The latter was assigned to a predominant M–O stretching mode.[3]

In tetrakis β-diketonates other than $M(acac)_4$, a strong, broad and metal sensitive band is found in the region 200—240 cm^{-1}. This band is also considered to be the nearly pure M–O stretching band corresponding to the 220—250 cm^{-1} band of $M(acac)_4$. The frequencies of the M–O stretching band in the lower frequency side are given in Table 3. They decrease for each metal ion in the order: $M(acac)_4 > M(bzac)_4 > M(tfac)_4 > M(TTA)_4 > M(dbm)_4 > M(hfac)_4$. In $U(hfac)_4$ and $Th(hfac)_4$ no such band was observed since it shifts out of the frequency region due to the mass effect of central metal ion.

Table 3. Frequencies of M–O stretching band (cm^{-1})

Metal	Ligand						
	acac	bzac	tfac	TTA	bfac	dbm	hfac
U(IV)	221	213	219	215	210	207	—
Th(IV)	225	215	212	212	210	210	—
Ce(IV)	250	242	240	233	230	225	218

In the β-diketonates containing the trifluoromethyl group, the M–O stretching band is found in the lower frequency side than that for $M(acac)_4$. This shows that the M–O bond is weakened because electron density on the carbonyl oxygens decreases by the strong electron-withdrawing property of the trifluoromethyl group. In the $M(bzac)_4$ and $M(dbm)_4$ which contain the phenyl group, the M–O stretching band is also found in the lower frequency side than that of $M(acac)_4$, showing that the M–O bond is weakened by the substitution of phenyl group for methyl group. This is in contradiction to the result reported by Nakamoto *et al.* in the study of the bis β-diketonates with Cu(II) and Ni(II), that the M–O bond is strengthened as a result of the mesomeric interactions of the phenyl group with the chelate ring.[6] The mesomeric interactions of the phenyl group with the chelate ring are assumed to occur only when the phenyl group is coplanar with the chelate ring. It has been suggested, however, by X-ray structure analysis for $M(dbm)_4$ (M=U(IV), Th(IV), and Ce(IV)) that the phenyl group is not coplanar with the chelate ring because of a steric hindrance.[8] The phenyl group seems hardly to release the electron by the mesomeric effect, but like

the trifluoromethyl group, to act as an electron-withdrawing group by its inductive effect. Thus, in the β-diketonates with the phenyl group and probably with the 2-thienyl group, the M–O bond is weakened and the frequencies of the M–O stretching band are lowered as in the case of the trifluoromethyl group.

As the strength of the M–O bond changes with substituent, so is that of the C=O and C=C bonds expected to change. In fact, the C=O+C=C stretching bands move to the higher frequency side as the M–O stretching band moves to the lower. Thus, as the M–O bond weakens, the C=O and the C=C bonds are generally strengthened and their bands move to the higher frequency side. These tendencies are particularly remarkable in the β-diketonates with the trifluoromethyl group.

BULLETIN OF THE CHEMICAL SOCIETY OF JAPAN, VOL. 46, 2101—2105 (1973)

Electron-transfer Kinetics of Transition-metal Complexes in Lower Oxidation States. Part I. Electron Spin Resonance Measurements of the Electron-exchange Rate between $Cr(bipy)_3^{1+}$ and $Cr(bipy)_3$

Tetsuo SAJI and Shigeru AOYAGUI

Faculty of Engineering, Tokyo Institute of Technology, Ohokayama, Meguro-ku, Tokyo 152

(Received November 2, 1972)

The rate of the electron-exchange reaction between $Cr(bipy)_3^{1+}$ and $Cr(bipy)_3$ was measured in *N*,*N*-dimethylformamide by the ESR method, with the line-broadening procedure. The width of the partly-overlapped hyperfine lines was determined by comparing the observed spectrum with the computer-simulated one. The observed second-order rate constant was $(1.5\pm0.4)\times10^9\ M^{-1}\ sec^{-1}$ at 25 °C. When corrected for diffusion, this yielded the activation-controlled rate constant of $2.0\times10^9\ M^{-1}\ sec^{-1}$. It was pointed out that the rate constant obtained here was the largest of all those ever reported for the electron-exchange reactions in which the transition-metal complexes participated. The observed rate constant was in good agreement with the one calculated non-empirically according to the theory of R. A. Marcus. Although the value for the molecular radius must be chosen somewhat arbitrarily in applying this theory, the "good" radius was a reasonable one in view of the molecular geometry and dimensions of the reactants. The rate constant of the Heisenberg spin-exchange process was also determined to be $1.8\times10^9\ M^{-1}\ sec^{-1}$ at 25 °C in the same solvent.

From the mechanistic point of view, the electron-transfer reactions of transition-metal complexes may be divided into two groups: one is the group of reactions proceeding *via* an outer-sphere activated complex, and the other, an inner-sphere activated complex.[1,2] In the reactions of the former group, the inner coordination shells of the reactant complex ions are left intact in the transition state; in the latter, two reactants share the ligands of their first coordination spheres in the transition state. In general, it may be difficult to show which mechanism is realized in an electron-transfer reaction. However, it is known that reactions of some kind proceed with the outer-sphere mechanism: they are the fast electron-transfer reactions between substitution-inert complexes. Particularly, the electron-exchange rate constant is very large for a pair of complexes differing by one in the number of electrons in the lower t_{2g} orbitals, which are not used in ligand bondings.[1] For example, the electron-exchange reaction between $Fe(phen)_3^{3+}(t_{2g}^5)$ and $Fe(phen)_3^{2+}(t_{2g}^6)$ is too fast to be measured by the NMR method; the largest second-order rate constant observable by this method is of the order of $10^7\ M^{-1}\ sec^{-1}$. The lower limit of the rate constant of this reaction has been reported by Larsen and Wahl to be $3\times10^7\ M^{-1}\ sec^{-1}$ at 25 °C in aqueous solutions.[3]

Among the methods for measuring the rates of isotopic exchange-reactions, the ESR method is probably the only one which is applicable to such fast reactions as were mentioned above. This method has been applied extensively to electron-transfer reactions between aromatic hydrocarbons and their anion radicals. On the other hand, there has been only one report on the application of this procedure to the transition-metal complexes.[4] This may be because of the following difficulties: most of the ESR spectra of these complexes thus far reported are very broad at ordinary temperatures, and they scarcely ever exhibit a hyperfine structure. Moreover, the rate constants measurable by this method must be larger than $10^6\ M^{-1}\ sec^{-1}$.

The present investigation deals with the ESR measurement of the rate of electron-exchange between

1) F. Basolo and R. G. Pearson, "Mechanisms of Inorganic Reactions," 2nd ed., John Wiley & Sons Inc., New York, N.Y. (1967), Chap. 6.

2) W. L. Reynolds and R. W. Lamry, "Mechanisms of Electron Transfer," The Ronald Press Co., New York, N. Y. (1966).

3) D. W. Larsen and A. C. Wahl, *J. Chem. Phys.*, **43**, 3765 (1965).

4) R. A. Stewart, L. W. Reeves and S. Fujiwara,, This Bulletin, **41**, 2832 (1968).

$Cr(bipy)_3^{1+}$ and $Cr(bipy)_3$ in *N,N*-dimethylformamide (DMF). The latter complex is diamagnetic,[5] while the former complex yields the ESR spectra with the most resolved nitrogen hyperfine splittings of all the tris-bipyridyl complexes of transition metals ever reported.[6,7] Furthermore, the electronic configurations of $Cr(bipy)_3^{1+}$ and $Cr(bipy)_3$ are t_{2g}^5 and t_{2g}^6 respectively, as in $Fe(phen)_3^{3+}$ and $Fe(phen)_3^{2+}$; it may thus be expected that the reaction rate for this pair of complexes is sufficiently fast for it to be measured by the ESR method. The determination of the hyperfine linewidth is made by comparing the observed ESR spectrum with the computer-simulated one. The observed rate constants are discussed in comparison with those predicted by the theory of R. A. Marcus on the electron-transfer reactions with the adiabatic outer-sphere mechanism.[8]

The present discussion is based on the following premises: (1) both complexes, $Cr(bipy)_3^{1+}$ and $Cr(bipy)_3$, are substitution-inert, and (2) the electron-transfer reaction between them proceeds *via* an outer-sphere activated complex. Experimental evidence for the validity of the former premise will be described elsewhere. In regard to the latter one, there is no data which assures us of its validity. However, it may reasonably be considered that this reaction has a fair chance of being an outer-sphere reaction because of its very large rate constant, which will be seen in the later part of this article.

Experimental

Reagents. All the reagents and solvents were commercially obtained. The 2,2′-bipyridine was supplied by the Tokyo Chemical Industry Co., Ltd. The DMF used as the solvent was refluxed over calcium hydride, distilled *in vacuo*, and then stored in an evacuated ampoule already containing solid $Cr(bipy)_3(ClO_4)_2$ and magnesium powder in order to remove the trace of oxygen.

Complexes. Tris(2,2′-bipyridyl)chromium(1+) perchlorate[9] and tris(2,2′-bipyridyl)chromium(0)[10] were prepared in a nitrogen atmosphere or in a vacuum, according to the procedures described in the literature cited. They were identified by means of their electronic spectra[11] and by elemental analyses.

Found: C, 57.8; H, 3.79; N, 13.9. Calcd for $Cr(bipy)_3ClO_4$: C, 58.1; H, 3.90; N, 13.6.

Found: C, 67.0; H, 4.60; N, 16.0. Calcd for $Cr(bipy)_3$: C, 69.2; H, 4.65; N, 16.2.

Solutions. Solutions of $Cr(bipy)_3ClO_4$ with various concentrations were required in order for us to evaluate the contribution to the linewidth of the $Cr(bipy)_3^{1+}$ spectrum from the Heisenberg spin-exchange process. They were prepared separately in the ESR sample tubes by diluting each aliquot from the stock solution of $Cr(bipy)_3ClO_4$ to a desired concentration with the solvent distilled from the stock solution *in vacuo*. Their concentrations were determined ESR-spectroscopically.

The sample solutions used in the measurement of the electron-exchange rates contained both $Cr(bipy)_3ClO_4$ and $Cr(bipy)_3$; they were prepared by dissolving a known amount of solid $Cr(bipy)_3$ into a $Cr(bipy)_3ClO_4$ solution of a known concentration in such an ampoule as is shown in Fig. 1.

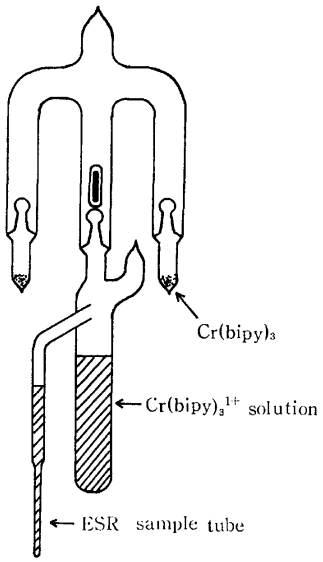

Fig. 1. Apparatus for preparation of ESR sample solutions.

In handling the sample solutions, all the operations were performed on a vacuum line by the use of glassware fitted with a breakable seal.

ESR Measurements. The ESR spectra of $Cr(bipy)_3^{1+}$ were measured in solutions with and without $Cr(bipy)_3$ added under experimental conditions otherwise identical. A JEOL-3SB spectrometer was operated at a frequency near 9.7 kMHz, with a 100 kHz field modulation and with a modulation amplitude of 0.5 gauss. The measurements were carried out at room temperature maintained at 25±1 °C. Calculations of the linewidth were performed on a FACOM 270-20/30 computer using a FORTRAN program.

Results and Discussion

Let the rate of the electron-transfer reaction between a diamagnetic and a paramagnetic molecule be described by the following equation:

$$\text{rate} = k[P][D] = [P]/\tau_p$$

where k is the second-order rate constant and τ_p, the mean life of the paramagnetic species; [D] and [P] are the concentrations of $Cr(bipy)_3$ and $Cr(bipy)_3^{1+}$ respectively, in this case. The hyperfine linewidth as a function of τ_p can be linearlized with regard to τ_p and $1/\tau_p$ respectively, under the following fast-limit and slow-limit conditions:[12]

$$\text{fast-limit: } |\omega_i-\omega_j|\tau_p \ll 1 \quad \text{for all i's}$$

$$\text{slow-limit: } |\omega_i-\omega_j|\tau_p \gg 1 \quad \text{for all i's}$$

5) S. Herzog and K. Renner, *Chem. Ber.*, **92**, 872 (1959).
6) B. Elschner and S. Herzog, *Arch. Sci.* (Geneva), **11**, 160 (1958).
7) E. König, *Z. Naturforsch., A*, **19**, 1139 (1964).
8) R. A. Marcus, *J. Chem. Phys.*, **24**, 966, 979 (1956).
9) V. F. Hein and S. Herzog, *Z. Anorg. Allgem. Chem.*, **267**, 337 (1952).
10) S. Herzog, K. Renner, and W. Schön, *Z. Naturforsch., B*, **12**, 809 (1957).
11) E. König and S. Herzog, *J. Inorg. Nucl. Chem.*, **32**, 585 (1970).
12) J. A. Pople, W. G. Schneider, and H. J. Bernstein, "High-resolution Nuclear Magnetic Resonance," McGraw-Hill, New York, N. Y. (1959), Chap. 10.

where ω's are the resonance frequencies of the designated hyperfine lines. As will be seen below, it is necessary that [D] be larger than 1 M to fulfill the fast-limit condition. This is not possible in the present investigation, however, because of the poor solubility of the D species; thus, in the present experiment the rate constant is determined by the line-broadening procedure, with the slow-limit approximation. The rate constant is, then, given by Eq. (1), when the broadened hyperfine lines are assumed to maintain the Lorentzian lineshape:[13]

$$k = (1.5\times10^7)\Delta(\Delta H_{pp})/[D] \quad (1)$$

where $\Delta(\Delta H_{pp})$ is the increase in the peak-to-peak linewidth of the first derivative spectra caused by electron exchange.

Although evidence has been reported for the disproportionation of $Cr(bipy)_3^{1+}$ ions,[14] their absorption spectrum obtained in DMF exhibited no sign of absorption due to either $Cr(bipy)_3^{2+}$ or $Cr(bipy)_3$; it was identical with the spectrum reported by König and Herzog in methanol.[11] Hence, the disproportionation was not taken into consideration.

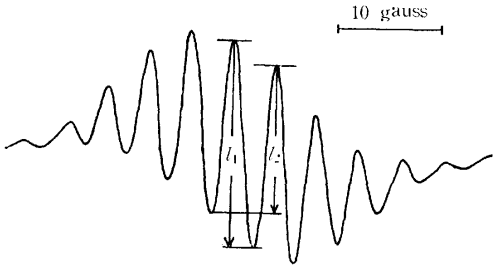

Fig. 2. ESR spectrum of 0.7 mM $Cr(bipy)_3^{1+}$ in DMF.

The ESR spectrum of $Cr(bipy)_3^{1+}$, shown in Fig. 2, exhibits eleven poorly-resolved lines with a spacing of about 3.05 gauss. They may be attributed to the hyperfine interaction due to six equivalent nitrogen nuclei of three bipyridyls. Such an interaction would give rise to thirteen lines. Because of the broadening in linewidth and poor signal-to-noise ratio, not all the thirteen lines were observed. The following procedure was used in order to determine the hyperfine linewidth of such a poorly-resolved spectrum as this. A linewidth parameter is defined here as l_2/l_1, where l_1 and l_2 are taken in the way shown in Fig. 2. The parameter was calculated for each given width of the hypothetical unoverlapping hyperfine lines and is shown plotted *vs.* the latter quantity in Fig. 3. From the observed values for the linewidth parameter, the true or unoverlapped hyperfine linewidths are obtained by the use of this figure.

Figure 4 illustrates a plot of the linewidth *vs.* the concentration of $Cr(bipy)_3ClO_4$. The experimental points lie on a straight line; this may serve to support this procedure for the linewidth determination. From the slope of this line, the second-order rate constant

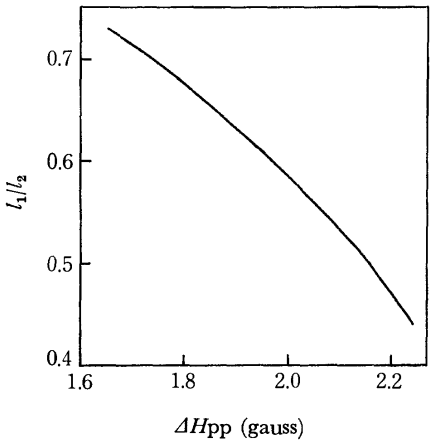

Fig. 3. Linewidth parameter *vs.* unoverlapped hyperfine linewidth.

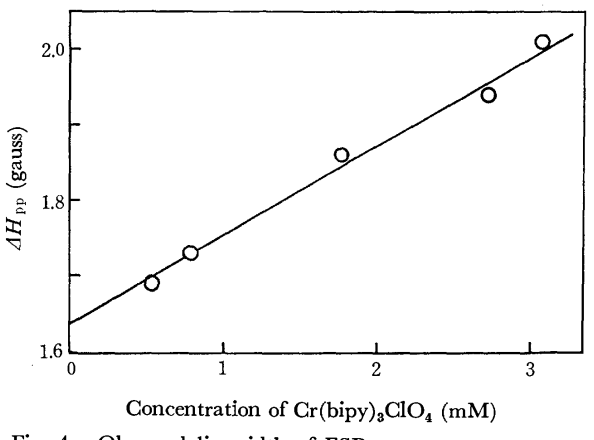

Fig. 4. Observed linewidth of ESR spectrum *vs.* concentration of $Cr(bipy)_3ClO_4$.

of the Heisenberg spin-exchange process[15] was estimated to be $1.8\times10^9\ M^{-1}\,sec^{-1}$. An inevitable increase in the concentration of $Cr(bipy)_3ClO_4$ is caused by the addition of $Cr(bipy)_3$;[16] this can be corrected by a procedure described elsewhere.[17] The increase, however, was less than 0.02 mM; its effect on the linewidth is negligible.

Figure 5 shows with circles the observed increase in the linewidth plotted *vs.* the concentration of added $Cr(bipy)_3$. The second-order rate constant of the electron-exchange reaction was determined from the slope of the straight line drawn through the point of origin and the circles as $k_{obs}=(1.5\pm0.4)\times10^9\ M^{-1}\,sec^{-1}$. No such a large rate constant exceeding $10^9\ M^{-1}\,sec^{-1}$ has, to our knowledge, ever been reported for the electron-exchange reactions of transition-metal complexes. The observed rate constant must be corrected for diffusion because of its large value, approaching the value for the diffusion-controlled rate constant. The correction was performed using the following relation:

13) R. L. Ward and S. I. Weissman, *J. Amer. Chem. Soc.*, **79**, 2086 (1957).

14) U. P. Geiger and E. Class, *Experientia*, **17**, 444 (1961).

15) M. P. Eastman, R. G. Kooser, M. R. Das, and J. H. Freed, *J. Chem. Phys.*, **51**, 2690 (1969). M. P. Eastman, G. V. Bruno J. H. Freed, *ibid.*, **52**, 2511 (1970).

16) When a known amount of $Cr(bipy)_3$ is added to the solution of $Cr(bipy)_3^{1+}$, a part of $Cr(bipy)_3$ may inevitably be oxidized by oxygen to yield $Cr(bipy)_3^{1+}$.

17) S. Suga and S. Aoyagui, This Bulletin, **45**, 1375 (1972).

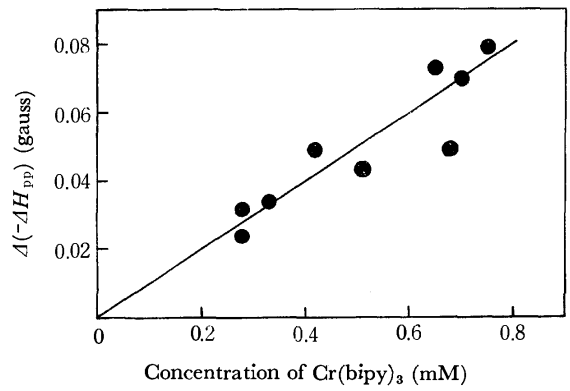

Fig. 5. Increase in linewidth of ESR spectrum *vs.* concentration of added Cr(bipy)$_3$.

$$k_{act}^{-1} = k_{obs}^{-1} - k_{dif}^{-1}$$

where k_{act} is the corrected or activation-controlled rate constant, and k_{obs} and k_{dif} are the observed and the diffusion-controlled rate constant respectively. The last one was estimated in the following way. When one of the reactants is neutral and when, accordingly, the electrostatic interaction between the reactants is negligibly small or zero, the diffusion-controlled second-order rate constant in $M^{-1}\,sec^{-1}$ may be given by:[18]

$$k_{dif} = 4\pi\sigma DN/1000 \qquad (2)$$

where σ is the collision diameter; D, the sum of the diffusion coefficients of the two reactants, and N, Avogadro's number. The value for σ was assumed to be equal to the sum of the molecular radii of the reactants; the latter quantities were estimated from the molecular geometry of Cr(bipy)$_3$, drawn in Fig. 6 on the basis of the X-ray diffraction data[19] as well as the van der Waals radius of the hydrogen atom (1.2 Å). It may reasonably be assumed that a common value can be attributed to the radii of Cr(bipy)$_3^{1+}$ and Cr(bipy)$_3$. In the subsequent calculations, this common molecular radius is designated by a and taken in the two ways shown in Fig. 6: 7.1 and 6.1 Å. The diffusion coefficients of Cr(bipy)$_3$ and Cr(bipy)$_3^{1+}$ are both 3.2×10^{-6} cm^2 sec^{-1} at 25 °C in DMF.[20] The diffusion-controlled rate constants calculated from Eq. (2) with the a values of 7.1 and 6.1 Å were 7×10^9 and 6×10^9 $M^{-1}\,sec^{-1}$ respectively. Both k_{dif} values, however, actually yielded the same k_{act} value, 2.0×10^9 $M^{-1}\,sec^{-1}$. The limiting condition for slow-exchange

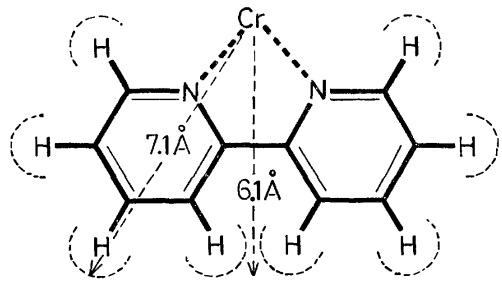

Fig. 6. Molecular geometry of Cr(bipy)$_3$.

18) M. V. Smoluchowski, *Z. Phys. Chem.*, **92**, 129 (1917).
19) G. Albrecht, *Z. Chem.*, **3**, 182 (1963).
20) T. Saji and S. Aoyagui, to be published.

is obviously fulfilled with the observed k value of 1.5×10^9 $M^{-1}\,sec^{-1}$ and the minimum value for $|\omega_i-\omega_j|$, 3.05 gauss, as well as the maximum value for $[D]$, 0.7 mM. On the other hand, the limiting condition for fast-exchange requires that $[D]$ be significantly larger than 0.4 M when the maximum value for $|\omega_i-\omega_j|$, *ca.* 30 gauss, is applied.

According to the theory of Marcus,[8] the rate constant of the electron-exchange reaction between a neutral and a charged species is, the inner-sphere reorganization being neglected:

$$k_{act} = Z\exp(-\Delta G^*/RT)$$
$$= Z\exp[-(e^2/8a)(1/D_{op}-1/D_s)] \qquad (3)$$

where Z, the collision number between two uncharged species in solution, is assumed to be 10^{11} $M^{-1}\,sec^{-1}$; ΔG^* is the reorganization free energy of solvent molecules in forming the activated complex; e is the electronic charge, and D_{op} and D_s are the optical and the static dielectric constants respectively. The activation-controlled rate constant was calculated from Eq. (3) for each radius mentioned above. They are listed in

Table 1. Comparison of the corrected observed rate constant with the calculated one in the electron exchange reaction between Cr(bipy)$_3^{+1}$ and Cr(bipy)$_3$

k_{act} (M^{-1} sec^{-1})	Radius (Å)	k_{calc} (M^{-1} sec^{-1})	ΔG^* (kcal/mol)
	6.1	3.7×10^8	3.3
	7.1	1.2×10^9	2.6
2.0×10^9	8.2	2.0×10^9	2.2

Table 1, together with the corrected observed rate constant. The agreement between k_{act} and k_{calc} was satisfactory. In order for k_{calc} to be in exact agreement with k_{act}, a should be taken as 8.2 Å, a reasonable value in view of the molecular dimensions of Cr(bipy)$_3$. This suggests that the inner-sphere reorganization energy contributes to the activation free energy to only a small extent in this reaction. However, the value of k_{calc} is quite sensitive to that of a, and unfortunately a is not a sufficiently definite quantity for the Marcus theory to be applied to the existing molecules. Thus, the theory must be tested experimentally with regard to a variety of aspects of its theoretical expression for the rate constant before we can consider that the theory is successful in the nonemiprical prediction of the electron-exchange rate constant. Such an extensive examination of this theory has recently been attempted for the electron-transfer reactions between aromatic hydrocarbons and their anion radicals.[21] The theoretical calculation of the rate constant can be done more reasonably for the reactions participated by the octahedral complex ions than for those participated by the planar aromatic hydrocarbons, because of the premise of a spherical molecular shape in this theory. However, there may be more difficulties in finding a suitable reactant among the former complexes than among the latter.

21) K. Suga and S. Aoyagui, This Bulletin, **46**, 755, 808 (1973).

One of the most outstanding features of the Marcus theory is that it can treat the homogeneous and the electrochemical electron-transfer reactions in a unified way.[22] An attempt to test this theory in the electrochemical electron-transfer reaction of the $Cr(bipy)_3^{1+}$/$Cr(bipy)_3$ redox couple, the corresponding homogeneous reaction having been revealed to be the fastest of all the electron-transfer reactions participated by the transition-metal complexes, is now in progress in our laboratory. It will be reported in the near future.[20]

22) R. A. Marcus, *J. Chem. Phys.*, **43**, 679 (1965).

BULLETIN OF THE CHEMICAL SOCIETY OF JAPAN, VOL. 46, 2105—2107 (1973)

Studies on Mass Spectrometry of Metal Chelates. I. Mass Spectrometry of Oxine Metal Chelates[1]

Yoshinori KIDANI, Shinobu NAGA, and Hisashi KOIKE

Faculty of Pharmaceutical Sciences, Nagoya City University, Tanabe-dori, Mizuho-ku, Nagoya 467

(Received November 8, 1972)

With a view to applying mass spectrometry to the studies of metal chelates, we investigated the mass spectrometry of divalent metal oxinates (Mn, Co, Ni, Cu, Zn, Pb, and Pd). The molecular ion I, whose peaks correspond to the metal chelates in a 2: 1 ratio, were observed in every spectrum. A loss of 144 mass units from I, corresponding to one molecule of coordinated oxine, occurred to afford the fragment ions II of metal chelates in a 1: 1 ratio. The peaks of the fragment ions III which lost 28 mass units (CO) from II were observed for Mn, Co, Ni, Cu, and Pd chelates. In order to study the stability of metal chelates against electron impact, special attention was paid to the peaks of I and II, which are supposed to be affected strongly by the *d*-electron number, electronegativity, ionization potential, and the ionic radius of central metal atoms. The intensity ratios of peaks I to II were obtained in the order Zn>Ni>Pd≈Co>Mn>Cu>Pb. It has been shown that the intensity ratios are related to the charge-radius ratio (e/r) of central metal atoms and the stability constants ($\log k_2$) of oxine metal chelates.

Studies have been carried out on metal chelates of acetylacetone and its derivatives by mass spectrometry.[2] With respect to the metal chelates of 8-quinolinol (oxine) and its derivatives, Jenkins *et al.* reported on the determination of metal purity in the order of 10^{-12} g as a form of oxine metal chelate by mass spectrometry.[3] Charalambous *et al.* recently reported on the fragmentation of oxine chelates with trivalent metals.[4] Budzikiewicz *et al.* found that fragmentation of the side chain in 2-*n*-butyloxine chelates was affected by their central metal atoms.[5] Although studies on mass spectrometry have been carried out to confirm the molecular weight of the metal complexes isolated,[6] no investigation has been made from the viewpoint of coordination chemistry. We have thus investigated mass spectrometry of oxine metal chelates in order to examine the stability of metal chelates against electron impact.

Results and Discussion

Mass spectra of divalent metal oxinates are shown in Fig. 1.

The fragmentation sequences are summarized in Chart 1. A peak of the molecular ion (M^+, I) appeared in the highest portion of the mass number of each metal chelate, attributable to the chelates in a 2: 1 ratio. A loss of 144 mass units was observed in each spectrum in common. This may be explained by the loss of one molecule of the coordinated oxine from I, affording fragment ion II of a 1: 1 complex. The peaks of III produced by the loss of 28 mass units from II are observed for Mn, Co, Ni, Cu, and Pd chelates. This can be explained by the loss of CO since the metastable ion peaks are observed distinctly in these spectra (ex. $Ni(oxine)_2$; *m/e* 202→174, calcd 149.8812, found 150.0). However, the peak of fragment ion III has not been detected for both Zn and Pb chelates. A plausible explanation for the lack of ion III in the mass spectra of both Zn and Pb chelates is that ion IV is directly produced from ion II, ion III being skipped, but the reason why the fragmentation schemes of these two chelate compounds are different from other chelates has not yet been clarified.

No peak at *m/e* 144 due to the oxinate ion was observed in almost all the chelates, that at *m/e* 145 (oxine ion) being found instead. (A similar phenomenon was

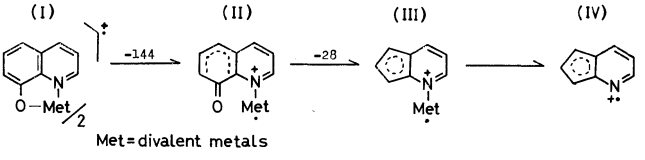

Chart 1. Fragmentation sequences of divalent metal oxinates.

1) Y. Kidani, S. Naga, and H. Koike, *Chem. Lett.*, **1972**, 507.
2) C. G. MacDonald and J. S. Shannon, *Aust. J. Chem.*, **19**, 1545 (1966); S. Sasaki, Y. Itagaki, T. Kurokawa, and K. Nakanishi, This Bulletin, **40**, 76 (1967).
3) A. E. Jenkins, J. R. Majer, and M. J. A. Reade, *Talanta*, **14**, 1213 (1967).
4) J. Charalambous, M. J. Frazer, R. K. Lee, A. H. Qureshi, and F. B. Taylor, *Org. Mass Spectrom.*, **5**, 1169 (1971).
5) H. Budzikiewicz and E. Plöger, *ibid.*, **3**, 709 (1970).
6) P. R. Scherer and Q. Fernando, *Anal. Chem.*, **40**, 1938 (1968).

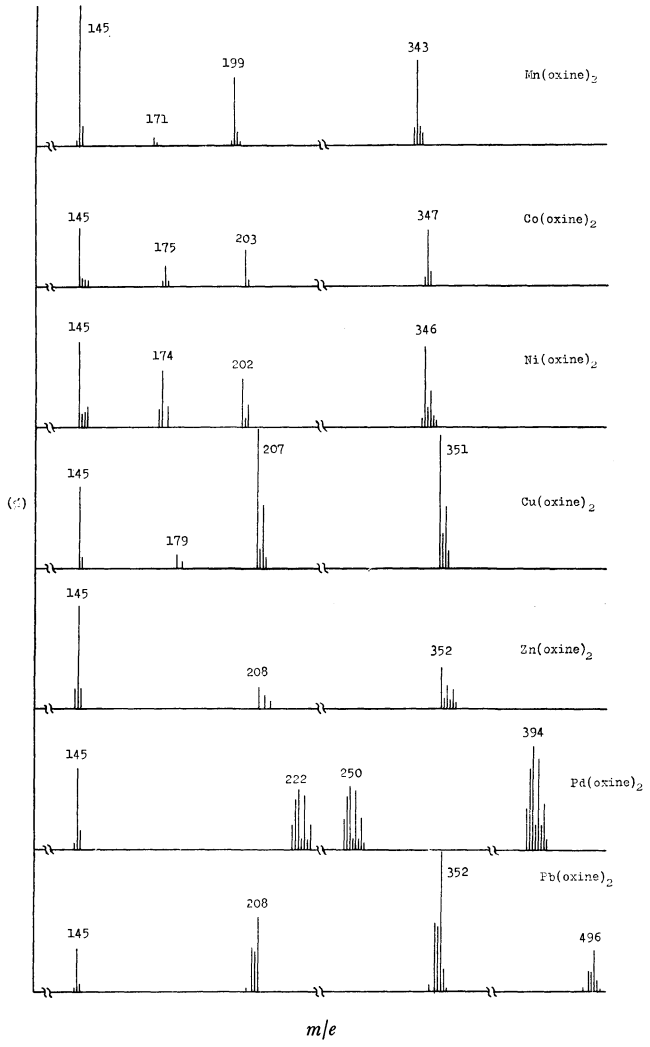

Fig. 1. Mass spectra of divalent metal oxinates
(*m/e* values are given for the ions containing ^{58}Ni, ^{63}Cu, ^{64}Zn, ^{106}Pd, and ^{208}Pb).

also observed in the mass spectra of acetylacetone metal chelates; no peak at *m/e* 99, acetylacetonate ion, but one at *m/e* 100, acetylacetone ion, being found.[2] This can be explained as follows: (a) the peak at *m/e* 144 is afforded by the production of the oxinate ion, but it is very unstable and does not reach the ion collector in the mass spectrometer, (b) the peak at *m/e* 145 can be attributed to the oxine, whose oxinate ion produced from I may pick up one hydrogen atom affording the peak at *m/e* 145. However, in this experiment, the sample was introduced by a direct inlet system, being the little possibility for a hydrogen atom to be picked up in the mass spectrometer. The peak at *m/e* 145 is regarded to arise from the oxine molecule produced by thermal decomposition prior to the vaporization of sample. Charles studied the differential thermal analyses of oxine metal chelates and reported that the heat stability at melting point was in the order Cu>Pb>Zn>Ni>Co>Mn>Mg.[7] The intensity ratio of the peak at *m/e* 145 to I were therefore obtained, since the peak of I was supposed to be unaffected by thermal decomposition. The order of the ratios is Mg>Zn>Mn>Co>Ni>Pb>Cu, coinciding well with the heat instability order by Charles, since the peak at *m/e* 145 was considered to be due to the oxine molecule produced by thermal decomposition.

In order to compare the stability of metal chelates against electron impact, special attention was paid to the relationship between ions I and II, both of which might be affected strongly by the *d*-electron number, electronegativity, ionization potential and ionic radius of central metal atoms. In order to find the stability of ion I of the chelates with various metals, the intensity ratios of the peaks were substituted into formula I/(I+II), the stability of the molecular ions against electron impact being found to be in the order Zn> Ni>Pd≈Co>Mn>Cu>Pb (Table 1).

Table 1. Intensity ratios of the molecular ion, I, to the fragment ion, II

	Zn	Ni	Pd	Co	Mn	Cu	Pb
I/(I+II)%	67	63	61	61	55	48	22

By plotting the values of the intensity ratio against the charge-radius ratio (*e/r*),[8] a linear relationship was obtained (Fig. 2). It was found that the greater the charge-radius ratio of metal atoms, the higher the stability of ion I.

The correlation between the stability constants of oxine metal chelates in solution[9] and the stabilities to electron impact is given in Fig. 3. The process which produced ion II from I may be understood in relation

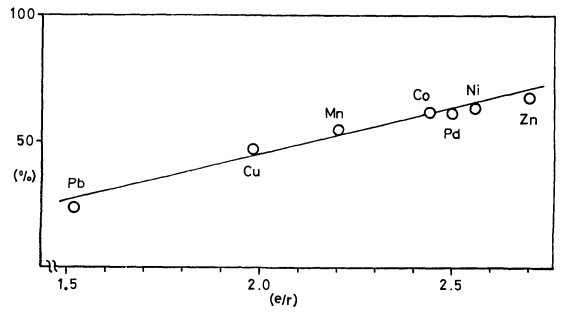

Fig. 2. Correlation between the stability upon electron impact and the charge-radius ratio.

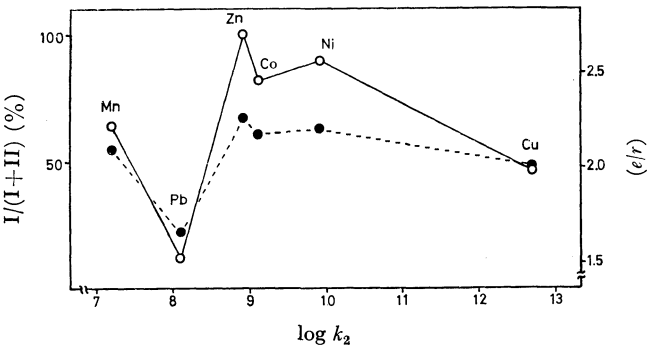

Fig. 3. Plots of intensity ratio and charge-radius ratio against stability constant log k_2.
---●--- Intensity ratio, —○— Charge-radius ratio.

7) R. G. Charles, *Anal. Chim. Acta*, **27**, 474 (1962).

8) Pauling's value was taken for ionic radii.

9) Stability constants were taken from: W. D. Johnston and H. Freiser, *J. Amer. Chem. Soc.*, **74**, 5239 (1952).

to the step of the second stability constant ($\log k_2$). From the plot intensity ratio *vs.* $\log k_2$, (broken line) we see that there is a correlation between the stability constant and the charge-radius ratio, showing a linear relationship for the stability of ion I, against electron impact. A similar, plot e/r *vs.* $\log k_2$ (solid line) is given. The plots are similar in form, indicating that intensity ratio is correlated to stability constant.

In conclusion, the binding ratios of the ligands to metals can be easily determined by measurements of the mass spectra of metal chelates with a trace amount of the sample. Helpful information can be obtained for the stability of metal chelates against electron impact.

Experimental

Mass spectra were measured by a Hitachi RMU-7 mass spectrometer according to a direct inlet system under the following conditions: ionizing voltage 70 eV, ion accelerating voltage 1800 V, total emission current 80 μA, ion source temperature 250 °C. Metal oxinates were prepared by the usual method,[10] their purity being confirmed by elemental analyses.

The authors' thanks are due to Professor Akira Tatematsu, Faculty of Pharmacy, Meijo University, for the use of apparatus, and to Professor Hisao Nakata, Department of Chemistry, Aichi Kyoiku University, for valuable discussions.

10) H. Goto, *Nippon Kagaku Zasshi*, **54**, 725 (1933).

BULLETIN OF THE CHEMICAL SOCIETY OF JAPAN, VOL. 46, 2107—2111 (1973)

Polarographic Study of Monosaccharides in Unbuffered Solution and Its Application to the Determination of the Mutarotation Rate Constants

Tokuji IKEDA and Mitsugi SENDA

Department of Agricultural Chemistry, Faculty of Agriculture, Kyoto University, Sakyo-ku, Kyoto 606

(Received November 8, 1972)

The polarographic behavior of monosaccharides in unbuffered neutral solution was investigated. The limiting current was ascertained to be an autocatalytic current which could be caused by the production of hydroxyl ion at the electrode surface. Equations for the characteristic limiting current and for the shape of current-potential curve were derived by use of the reaction layer concept. Experimental results for D-glucose, D-galactose, and D-xylose were fairly well expressed by these equations. The wave can also be applied to the determination of the mutarotation rate constants of monosaccharides, the values obtained (D-glucose: 0.53×10^{-3} s^{-1}, D-galactose: 0.54×10^{-3} s^{-1}, and D-xylose: 1.31×10^{-3} s^{-1}) being in fairly good agreement with those obtained by the polarimetric method (D-glucose: 0.4×10^{-3} s^{-1}, D-galactose: 0.5×10^{-3} s^{-1}, and D-xylose: 1.3×10^{-3} s^{-1}).

The polarographic behavior of monosaccharides in buffered solutions has been investigated by a number of workers.[1-4] The limiting current of the wave in buffered solutions has a kinetic character; it depends on the pH as well as the concentration of buffer salts. The mutarotation rate constants of monosaccharides have been determined by detailed analysis of the polarographic limiting currents.[5]

Little attention has been paid to their polarographic behavior in unbuffered solutions. We have observed that in unbuffered solutions the polarographic wave of monosaccharide gives a limiting current, which seems to be an autocatalytic current. The present investigation was undertaken to elucidate the characteristic behavior of the polarographic wave of monosaccharide in unbuffered media. Application of the wave to the determination of the mutarotation rate constants of monosaccharide has also been studied.

Experimental

Materials. Commercial D-glucose, D-galactose and D-xylose of reagent grade were used. Pure α-D-glucose: $[\alpha]_D^{25}=+112$ (*c* 4 in water), mp 146 °C, was supplied by Tokai Togyo Co., Ltd. Pure α-D-galactose[6] and α-D-xylose[7] were prepared by recrystallization from ethanol and water, respectively; α-D-galactose: $[\alpha]_D^{25}=+150$ (*c* 4 in water), mp 167 °C, α-D-xylose: $[\alpha]_D^{25}=+94$ (*c* 1 in water), mp 145 °C. Commercial potassium chloride and tetraethyl ammonium iodide (TEAI) of reagent grade were used as supporting electrolytes. The latter was used after recrystallization from methanol.

1) K. Wiesner, *Collect. Czech. Chem. Commun.*, **12**, 64 (1947).
2) P. Delahay and J. E. Strasner, *J. Amer. Chem. Soc.*, **74**, 893 (1952).
3) W. G. Overend, A. R. Peacocke, and J. B. Smith, *J. Chem. Soc.*, **1961**, 3487.
4) B. Capon, A. A. Levy, and W. G. Overend, *Carbohyd. Res.*, **5**, 93 (1967).
5) J. M. Los, L. B. Simpson, and K. Wiesner, *J. Amer. Chem. Soc.*, **78**, 1564 (1957).
6) M. L. Wolfrom and A. Tompson, "Method in Carbohydrate Chemistry," Vol. 1, ed. by R. L. Whistler and M. L. Wolfrom, Academic Press, New York and London (1962), p. 120.
7) K. Anno and N. Seno, "Jikken Kagaku Koza," Vol. 23, ed. by S. Akabori and S. Funahashi, (in Japanese) Maruzen, Tokyo (1957), p. 336.

Apparatus. Polarograms were recorded with a Yanagimoto PE 21-TB2S polarograph connected to a Yokogawa 3077 X-Y recorder. Polarimetry was carried out with a Yanagimoto polarimeter OR-20.

Measurements were carried out with an H-type cell. A saturated calomel electrode (SCE) was used as reference electrode. In order to minimize accumulation of hydroxyl ions in the close neighbourhood of the electrode, which could be caused by unsufficient stirring of the neighbouring solutions after the detachment of the individual mercury drops, a pencil-sharpened capillary (tip outside-diameter 1 mm) was used. The capillary characteristics of the dropping mercury electrode measured in 0.1 M potassium chloride (open circuit) at a mercury reservoir height of 52.5 cm were $m=1.306$ mg s^{-1} and $t=5.65$ s. All experiments were carried out at 25± 0.05 °C. The procedure for measuring the polarographic current has been described previously.[8]

Theory

Limiting Current. According to Los, Simpson and Wiesner,[5] the strictly rate-controlled limiting current $\bar{i}_l$ of reaction scheme (1)

$$\alpha\text{-pyranose} \underset{k_{-1}}{\overset{k_1}{\rightleftharpoons}} \gamma(\text{reducible form}) \underset{k_2}{\overset{k_{-2}}{\rightleftharpoons}} \beta\text{-pyranose} \quad (1)$$

is given by

$$\bar{i}_l = nF\bar{q}\bar{\mu}(k_1C_\alpha + k_2C_\beta) \quad (2)$$

$$\bar{\mu} = (D_s/(k_{-1}+k_{-2}))^{1/2}, \quad (3)$$

where n denotes the number of electrons consumed in the electrolysis per one molecule of monosaccharide, F Faraday constant, $\bar{q}$ the mean electrode surface area, D_s the diffusion coefficient of monosaccharide, C_α and C_β the bulk concentration of α- and β-pyranose, respectively, and $\bar{\mu}$ the mean thickness of the reaction layer. Equation (2) was later derived by one of us (M.S.)[9] and Paldus and Koutecký[10] on the basis of a rigorous mathematical procedure.

The rate constants k_i (i=1, 2, −1, and −2) of Eq. (1) depend on the concentrations (activities) of acid and base catalysts. In unbuffered aqueous solutions, they are generally given by[11,12]

$$k_i = k_{i,w} + k_{i,H}(H^+) + k_{i,OH}(OH^-), \quad (4)$$

where $k_{i,w}$ represents the catalytic constant of water, $k_{i,H}$ and $k_{i,OH}$ the catalytic coefficients of the catalysts indicated by subscripts, and the symbols in brackets the concentrations (activities) of the catalysts, H^+ and OH^- being hydrogen ion and hydroxyl ion, respectively.

In the reaction layer the solution is basic because of the production of hydroxyl ions by the electro-reduction of monosaccharide at the electrode surface. For example, a rough estimation (see below) shows pH is 9.8 at the electrode when 0.006 M D-xylose solution is reduced at d.m.e. in unbuffered solution. The catalytic effect of hydrogen ion can be neglected in such a basic solution. The first term on the right hand side of Eq. (4), $k_{i,w}$, can also be neglected in comparison with the third term. Accordingly, the rate constants k_i ($i=1$, 2, −1, and −2), in the reaction layer are eventually expressed, in the first approximation, by

$$k_i = k_{i,OH}(OH^-)^\circ, \quad (5)$$

where $(OH^-)^\circ$ represents the mean concentration of hydroxyl ions at the electrode surface, which may be assumed to be approximately constant throughout the reaction layer due to the thinness of the layer.

Since hydroxyl ions diffuse into the solution and the concentration of hydroxyl ion is practically zero in the bulk solution, the limiting current of monosaccharide is related to the concentration of hydroxyl ions at the electrode surface, with the aid of the Ilković equation[13]

$$\bar{i}_l = \bar{\kappa}_{OH}(OH^-)^\circ, \quad (6)$$

where $\bar{\kappa}_{OH}$ denotes the Ilković constant for hydroxyl ion.

Substitution of Eqs. (5) and (6) into Eq. (2) gives

$$\bar{i}_l = 1.322\bar{\kappa}_s(D_s/D_{OH})^{1/2}\tau(k_{-1,OH}+k_{-2,OH})^{-1} \times (k_{1,OH}C_\alpha + k_{2,OH}C_\beta)^2, \quad (7)$$

where $\bar{\kappa}_s$ denotes Ilković constant for the hypothetical diffusion current for monosaccharide with $n=2(\bar{\kappa}_s = 2(D_s/D_{OH})^{1/2}\bar{\kappa}_{OH})$, D_{OH} the diffusion coefficient of hydroxyl ion and τ the drop time. For the solution of equilibrated mixture of monosaccharide, Eq. (7) is reduced to

$$\bar{i}_l = 1.322\bar{\kappa}_s(D_s/D_{OH})^{1/2}\tau(k_{1,OH}+k_{2,OH}K)^2(C_{\alpha,eq}+C_{\beta,eq})^2 \times (k_{-1,OH}+k_{-2,OH})^{-1}(1+K)^{-2} \quad (7')$$

where $C_{\alpha,eq}$ and $C_{\beta,eq}$ represent the equilibrated concentrations of α- and β-pyranose, respectively, and K the equilibrium constant defined by $K=C_{\beta,eq}/C_{\alpha,eq}$. The sum $C_{\alpha,eq}+C_{\beta,eq}$ is equal to the total concentration of monosaccharide because the concentration of the intermediate γ-form is negligibly small.

Electrode reaction of the same mechanism as that described above was proposed for the electro-reduction of formaldehyde in unbuffered solution by Brdička[13] and a mathematically rigorous solution of the process was given by Koutecký.[14] The result requires that the numerical coefficient of Eq. (7'), 1.322, should be replaced by 0.966. The value was adopted in the following.

Current Potential Curve. Since the electroactive intermediate γ-form is formed from α- and β-pyranose, the current at a point of the kinetic wave of monosaccharide can be given by

$$\bar{i} = nF\bar{q}\bar{\mu}(k_1C_\alpha^\circ + k_2C_\beta^\circ - (k_{-1}+k_{-2})C_\gamma^\circ), \quad (8)$$

where C_α°, C_β°, and C_γ° represent the mean concentration of α-, β-, and γ-form, respectively, in the reaction layer. Provided that the limiting current has a strictly kinetic character as given by Eq. (2), there is no significant depletion of α- and β-pyranose in the reaction layer. Thus substitution of Eq. (2) in Eq. (8) gives

8) T. Ikeda and M. Senda, This Bulletin, **46**, 1650 (1973).
9) M. Senda, *Rev. Polarogr.* (Kyoto), **6**, 95 (1958).
10) J. Paldus and J. Koutecký, *Collect. Czech. Chem. Commun.*, **23**, 376 (1958).
11) H. S. Isbell and W. Pigman, "Advances in Carbohydrate Chemistry and Biochemistry," Vol. 24, ed. by M. L. Wolfrom and R. S. Tipson, Academic Press. London (1969), p. 13.
12) B. Capon, *Chem. Rev.*, **69**, 407 (1969).
13) a) R. Brdička, *Collect. Czech. Chem. Commun.*, **20**, 387 (1955). b) R. Brdička, *Z. Electrochem.*, **59**, 787 (1955).
14) J. Koutecký, *Collect. Czech. Chem. Commun.*, **21**, 652 (1956).

$$\bar{i} = \bar{i}_l - nF\bar{q}\bar{\mu}(k_{-1}+k_{-2})C_\gamma^\circ \quad (8')$$

Based on the theory of slow discharge, the current intensity can be given by

$$\bar{i} = nF\bar{q}k_{el}\exp\left((-\alpha_a n_a F/RT)(E-E_0)\right)C_\gamma^\circ, \quad (9)$$

where k_{el} represents the standard rate constant at the standard potential E_0, $\alpha_a n_a$ the product of the transfer coefficient and the number of electrons in discharge process, R the gas constant and T the absolute temperature. Other symbols were defined above.

In unbuffered solutions the current intensity can also be related to the concentration of hydroxyl ion at the electrode surface by

$$\bar{i} = \bar{k}_{OH}(OH^-)^\circ \quad (6')$$

Substituting the appropriate values from Eqs. (5), (6'), and (9) into Eq. (8'), we obtain after rearrangement

$$E = E_0 + \frac{RT}{\alpha_a n_a F}\ln\left[\frac{k_{el}(\bar{k}_{OH})^{1/2}}{(D_s(k_{-1,OH}+k_{-2,OH}))^{1/2}}\right] + \frac{RT}{\alpha_a n_a F}\ln\left[\frac{\bar{i}_l-\bar{i}}{\bar{i}^{3/2}}\right], \quad (10)$$

here it is assumed that Eq. (5) holds.

Results and Discussion

Experiments were carried out for several monosaccharides (D-glucose, D-galactose, and D-xylose) in unbuffered solutions of 0.1 M potassium chloride.

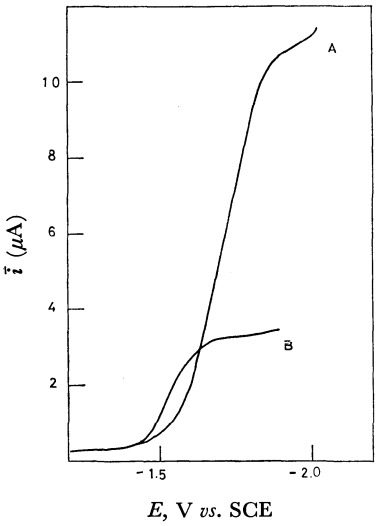

Fig. 1. Polarogram of 0.06M D-xylose in 0.1M potassium chloride A, 0.2M ammonia buffer pH 8.59 B.

Curve A in Fig. 1 shows an example of the polarographic wave of D-xylose in unbuffered neutral solution. The wave is very large in comparison with that of D-xylose of the same concentration (curve B in Fig. 1) in buffered solution of 0.2 M ammonia at pH 8.59. Similar large waves were observed for all other monosaccharides studied. The value of $\bar{i}_l/\bar{i}_d$ is shown in Table 1, $\bar{i}_d$ being the hypothetical diffusion current of monosaccharide. The limiting current $\bar{i}_l$ is still small enough to be considered as strictly kinetic-controlled in the concentration ranges studied. Thus the use of Eq. (2) in deriving the theoretical equations is justified.

Table 1. Dependence of the limiting current $\bar{i}_l$ on the height of mercury reservoir h
(Current sens 0.2 μA/cm Temp. 25 °C)

	D-Xyl.(10mM)[a]		D-Glu.(60mM)[b]		D-Gal.(14mM)[c]	
h (cm)	$\bar{i}_l$ (cm)	$\bar{i}_l(h^{1/2})$	$\bar{i}_l$ (cm)	$\bar{i}_l(h^{1/2})$	$\bar{i}_l$ (cm)	$\bar{i}_l(h^{1/2})$
42.5	5.16	34	4.26	28	4.51	29
52.5	4.80	35	4.16	30	4.25	31
62.5	4.45	35	3.87	31	4.10	32

at h=52.5 cm a) $\bar{i}_l/\bar{i}_d=2.1\times10^{-2}$ b) $\bar{i}_l/\bar{i}_d=3.0\times10^{-3}$ c) $\bar{i}_l/\bar{i}_d=1.3\times10^{-2}$

It is expected from Eq. (7') that $\bar{i}_l$ is approximately proportional to $m^{2/3}\tau^{7/6}$. Since m is proportional to the height of mercury reservoir h, and τ is inversely proportional to h, $\bar{i}_l$ is eventually proportional to $h^{-1/2}$. Experimental results (Table 1) show that $\bar{i}_l$ decreases with increasing height of mercury reservoir and is approximately proportional to $h^{-1/2}$.

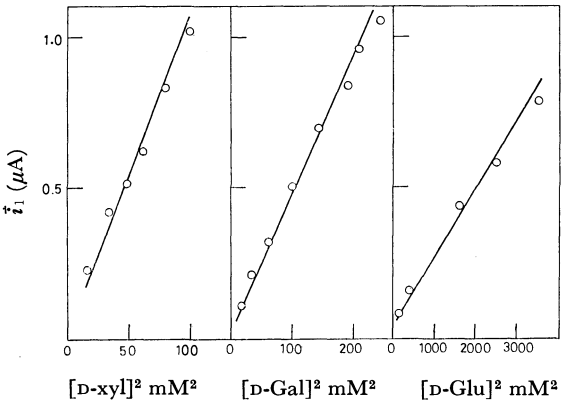

Fig. 2. Relationship between the limiting current $\bar{i}_l$ and the square of the concentration of monosaccharides.

Figure 2 shows the plot of $\bar{i}_l$ against the square of the monosaccharide concentration $(C_\alpha+C_\beta)^2$. In accordance with theoretical consideration, all the data in Fig. 2 are distributed along a straight line, deviating downward from the line at higher concentrations of monosaccharides. A similar deviation from linearity was also observed for the limiting current of formaldehyde in unbuffered solutions by Brdička,[13] who attributed the deviation to the streaming of the solution in the neighbourhood of the electrode.

The concentration of hydroxyl ions in the reaction layer $(OH^-)^\circ$ can be calculated with the aid of the Ilković equation (6). Even at the lowest concentration studied (0.04 M D-xylose) $\bar{i}_l$ reached 0.23 μA. Thus $(OH^-)^\circ$ may be estimated as 3.6×10^{-5} M or more, where $D_{OH}=5.23\times10^{-5}$ cm² s^{-1} was used.[15] In view of the numerical values of the rate constants,[8] *i.e.* $k_{1,w}=2.4\times10^{-3}$ s^{-1} and $k_{1,OH}=1.2\times10^3$, the catalytic effect of water may be considered to be of secondary significance under the present experimental conditions. Thus the use of Eq. (5) in place of Eq. (4) is justified.

The mean thickness of the reaction layer $\bar{\mu}$, which

15) J. Heyrovský and J. Kůta, "Principle of Polarography," Academic Press, New York and London (1966), p. 105.

is now given by $\bar{\mu}=(D_{xy}/(k_{-1,OH}(OH^-)^o+k_{-2,OH}(OH^-)^o))^{1/2}$, is calculated to be 9.3×10^{-4} cm when $(OH^-)^o=3.6\times10^{-5}$ M, D_{xy}[16] $=6.7\times10^{-6}$ cm^2 s^{-1}, $k_{-1,OH}=8.4\times10^4$ s^{-1} l mol^{-1}, and $k_{-2,OH}=11.5\times10^4$ s^{-1} l mol^{-1}. The numerical value of the rate constants used were obtained in the present study (Table 3). The magnitude of $\bar{\mu}$ is less than one twentieth of the thickness of the mean diffusion layer for hydroxyl ion, ($\delta\simeq2.3\times10^{-2}$ cm). This is acceptable.

Similar arguments can also be applied to D-glucose and D-galactose.

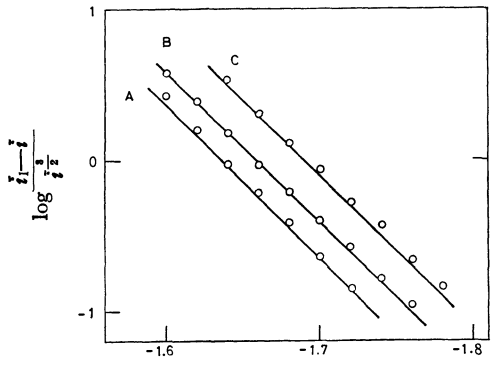

E, V *vs.* SCE

Fig. 3. Log$((\bar{i}_l-\bar{i})/\bar{i}^{3/2})$ *vs.* E plot for the polarographic current of D-xylose(8 mM) A, D-glucose(40 mM) B, D-galactose (12 mM) C, in 0.1M potassium chloride. Reciplocal slope of the solid lines: 100 mV.

Figure 3 shows the plot of $\log[(_{l}\bar{i}-\bar{i})/\bar{i}^{3/2}]$ against E. The experimental points lie on a straight line, as expected from Eq. (10) with a reciprocal slope 2.303 $RT/\alpha_a n_a F\sim100$ mV per log unit.

The general solution of the current-potential curve of the kinetic wave in buffered solutions has been given by Koutecký.[17] Rewriting his result for the current-potential curve of monosaccharide in buffered solutions, we obtain

$$E=E_0+\frac{RT}{\alpha_a n_a F}\ln[k_{el}(D_s(k_{-1}+k_{-2}))^{-1/2}]+\frac{RT}{\alpha_a n_a F}\ln\left[\frac{\bar{i}_l-\bar{i}}{\bar{i}}\right] \quad (11)$$

Figure 4 shows the plot of $\log[(\bar{i}_l-\bar{i})/\bar{i}]$ *vs.* E for the polarographic current of monosaccharides in buffered solution of pH 8.56. As expected from Eq. (11), a straight line was obtained. The value of the slope 2.303 $RT/\alpha_a n_a F$ was again *ca.* 100 mV; this is reasonable provided that the discharge process of monosaccharides is identical both in buffered and in unbuffered solutions.

From Eq. (10) we obtain

$$E_{1/2}=E_0+\frac{RT}{\alpha_a n_a F}\ln\left[\frac{k_{el}(\bar{k}_{OH})^{1/2}}{(D_s(k_{-1,OH}+k_{-2,OH}))^{1/2}}\right]-\frac{RT}{\alpha_a n_a F}\ln\left[\frac{\bar{i}_l}{2}\right]^{1/2} \quad (12)$$

for the half-wave potential of the polaragraphic wave in unbuffered solutions. Figure 5 shows the plot of

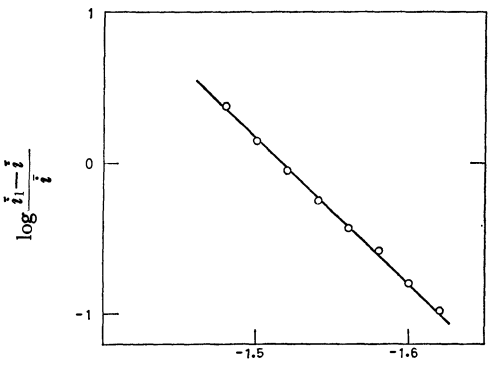

E, V *vs.* SCE

Fig. 4. Log$((\bar{i}_l-\bar{i})/\bar{i})$ *vs.* E plot for the polarographic current of D-xylose (0.06 M) in ammonia buffer pH 8.56. Reciprocal slope of the solid line: 100 mV.

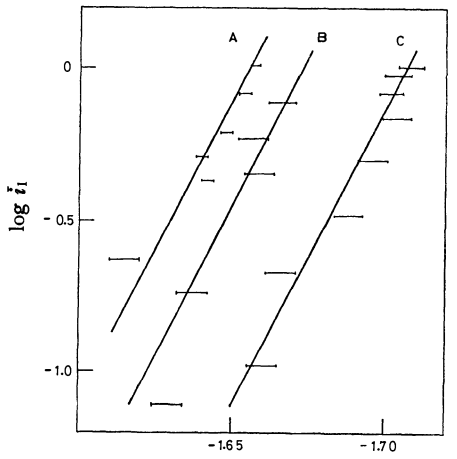

$E_{1/2}$ V *vs.* SCE

Fig. 5. Log$(\bar{i}_l)$ *vs.* $E_{1/2}$ plot for the polarographic current of D-xylose A, D-glucose B, and D-galactose C, in 0.1M potassium chloride. Reciprocal slope of the solid lines: −50 mV.

log $\bar{i}_l$ against $E_{1/2}$. As expected from Eq. (12), the data are distributed along a straight line with a reciprocal slope $RT/2\alpha_a n_a F\sim-50$ mV. The fact that the values of $\alpha_a n_a$ are nearly identical for all monosaccharides investigated (Figs. 3 and 4) suggests the similarity of the discharge process for these monosaccharides.

In conclusion, the current-potential relationship of the monosaccharide is fairly well reproduced by Eq. (10). It is to be noted that in deriving Eq. (10), k_{el} is assumed to be independent of the concentrations of acid and/or base at the electrode surface. However, there is a reason to believe that the discharge process should depend on acid and/or base.

When TEAI was used as a supporting electrolyte, the half-wave potential of the monosaccharide appeared in more negative potential than in KCl solution. The reciprocal slope of the plot of $\log[(\bar{i}_l-\bar{i})/\bar{i}^{3/2}]$ against E became 200 mV or even greater. A similar effect was observed[3,4] when tetramethylammonium phosphate was used as the supporting electrolyte. This effect may be attributed to the adsorption of the quarternary

16) L. Friedman and P. G. Carpenter, *J. Amer. Chem. Soc.*, **61**, 1745 (1939).

17) J. Koutecký, *Collect. Czech. Chem. Commun.*, **20**, 116 (1955).

ammonium cation on the electrode surface,[18] which results in the retardation of the electro-reduction of monosaccharide.

Determination of the Mutarotation Rate Constant

When a weighed amount of a monosaccharide in pure α-pyranose form was dissolved in 0.1 M potassium chloride, the limiting current decreased with time and reached a constant value corresponding to the value for the equilibrated mixture of the monosaccharide. This behavior is very much similar to that in buffered solutions and the mutarotation rate constants may be obtained by analyzing the limiting current with the aid of Eq. (7) as a function of time.

When we start from α-pyranose, the change of concentrations of α- and β-pyranose with time is given as follows,[5]

$$C_\alpha = C_{\alpha,eq}(1+Ke^{-k_{o,w}t})$$
$$C_\beta = C_{\beta,eq}(1-e^{-k_{o,w}t}), \quad (13)$$

where $k_{o,w}$ is the overall mutarotation constant of water and is defined by four individual rate constants as follows.

$$k_{o,w} = (k_{1,w}k_{-2,w}+k_{-1,w}k_{2,w})/(k_{-1,w}+k_{-2,w}) \quad (14)$$

Substitution of Eq. (13) into Eq. (7) gives

$$\bar{i}_1(t)^{1/2} = (0.966\bar{\kappa}_s(D_s/D_{OH})^{1/2}\tau)^{1/2}(k_{-1,OH}+k_{-2,OH})^{-1/2} \times (1+K)^{-1}(C_{\alpha,eq}+C_{\beta,eq})((k_{1,OH}+Kk_{2,OH}) +K(k_{1,OH}-k_{2,OH})e^{-k_{o,w}t}) \quad (15)$$

Subtraction of the expression corresponding with Eq. (15) at time $t+\Delta t$ and taking logarithms leads to the result

$$\ln[\bar{i}_1(t)^{1/2}-\bar{i}_1(t+\Delta t)^{1/2}] = \ln[(0.966\bar{\kappa}_s(D_s/D_{OH})^{1/2}\tau)^{1/2} \times (k_{-1,OH}+k_{-2,OH})^{-1/2}(1+K)^{-1}K(k_{1,OH}-k_{2,OH}) \times (C_{\alpha,eq}+C_{\beta,eq})(1-e^{-k_{o,w}\Delta t})] - k_{o,w}t \quad (16)$$

Plotting $\log[\bar{i}_1(t)^{1/2}-\bar{i}_1(t+\Delta t)^{1/2}]$ with constant Δt *vs.* t, according to the method of Guggenheim,[19] should give a straight line with slope $-k_{o,w}$, and

$$\text{intercept} = \ln[(0.966\bar{\kappa}_s(D_s/D_{OH})^{1/2}\tau)^{1/2} \times (k_{-1,OH}+k_{-2,OH})^{-1/2}(1+K)^{-1}K(k_{1,OH}-k_{2,OH}) \times (C_{\alpha,eq}+C_{\beta,eq})(1-e^{-k_{o,w}\Delta t})] \quad (17)$$

At $t\to\infty$, Eq. (15) is reduced to

$$\bar{i}_1(t\to\infty)^{1/2} = (0.966\bar{\kappa}_s(D_s/D_{OH})^{1/2}\tau)^{1/2} \times (k_{-1,OH}+k_{-2,OH})^{-1/2}(1+K)^{-1}(C_{\alpha,eq}+C_{\beta,eq}) \times (k_{1,OH}+Kk_{2,OH}) \quad (18)$$

Namely, the overall catalytic rate constant $k_{o,w}$ is determined from the slope of the Guggenheim plot. Furthermore, if the overall catalytic rate coefficient of hydroxyl ion $k_{o,OH}$ and the equilibrium constant K are known, Eqs. (17) and (18) in combination with the following two equations

$$k_{o,OH} = (k_{1,OH}k_{-2,OH}+k_{-1,OH}k_{2,OH})/(k_{-1,OH}+k_{-2,OH}) \quad (19)$$
$$K = C_{\beta,eq}/C_{\alpha,eq} = k_{1,OH}k_{-2,OH}/k_{-1,OH}k_{2,OH} \quad (20)$$

can be solved with respect to four individual rate coefficients $k_{1,OH}$, $k_{2,OH}$, $k_{-1,OH}$, and $k_{-2,OH}$.

18) Ref. 15), p. 301.
19) E. A. Guggenheim, *Phil. Mag.*, **2**, 538 (1926).

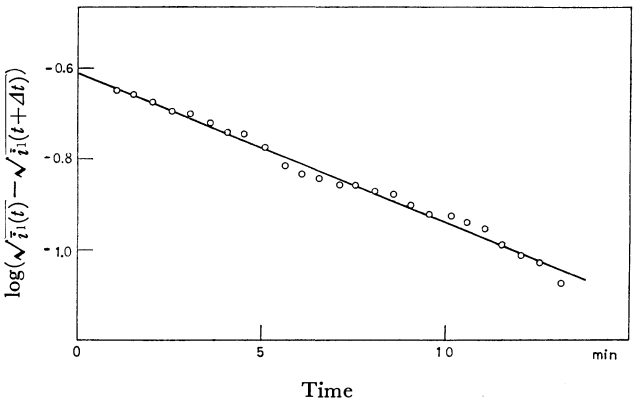

Fig. 6. Analysis of $\bar{i}_1$ *vs.* time curve of (α—β) D-xylose in 0.1M potassium chloride solution. Δt=15 min.

An example of the Guggenheim plot according to Eq. (16) is shown in Fig. 6. The values of $k_{o,w}$ determined by the present method and by the polarimetric method are given in Table 2. The results are in good accordance with each other.

Table 2. The overall mutarotation rate constant $k_{o,w}$ in 0.1M KCl solution (Temp. 25 °C)

	$k_{o,w}$ (s^{-1})	
	Polarography	Polarimetry
D-Xylose	1.31×10^{-3}	1.3×10^{-3}
D-Glucose	0.53×10^{-3}	0.4×10^{-3}
D-Galactose	0.54×10^{-3}	0.5×10^{-3}

Table 3. The forward and backward rate coefficients $k_{i,OH}$ (i=1,2, −1, and −2) (Temp. 25 °C)

	$k_{1,OH}$	$k_{2,OH}$	$k_{-1,OH}$	$k_{-2,OH}$
	($l\ mol^{-1}\ s^{-1}$)			
D-Xylose	8.2×10^2	6.0×10^2	8.4×10^4	11.5×10^4
D-Glucose	11.6×10	6.5×10	9.1×10^4	8.9×10^4

Table 3 shows the individual rate coefficients of hydroxyl ion for D-xylose and D-glucose, $k_{o,OH}$= $8\times10^2\ s^{-1}\ l\ mol^{-1}$ (D-xylose),[8] $9\times10\ s^{-1}\ l\ mol^{-1}$ (D-glucose),[11] D_{xy}[16]$=6.71\times10^{-6}\ cm^2\ s^{-1}$, D_{glu}[16]$=6.65\times10^{-6}\ cm^2\ s^{-1}$, K_{xy}[20]$=1.87$ and K_{glu}[20]$=1.74$ being used. The forward rate coefficients $k_{1,OH}$ and $k_{2,OH}$ for D-xylose are in fair agreement with those obtained from the analysis of the polarographic currents in buffered media.[8] The ratio of the concentration of the intermediate γ-form $C_{\gamma,eq}$ to that of α- and β-pyranose form, $C_{\alpha,eq}+C_{\beta,eq}$, was 3×10^{-1}% for D-xylose and 4×10^{-2}% for D-glucose. The results are also in the same order as those obtained from the experiments in buffered media.[8]

The authors thank Tokai Togyo Co., Ltd. for supplying α-D-glucose.

20) W. Pigman and H. S. Isbell, "Advances in Carbohydrate Chemistry," Vol. 23, ed. by M. L. Wolfrom and R. S. Tipson, Academic Press, New York and London (1968), p. 11.

Thermal and Spectrophotometric Studies of 8-Mercaptoquinoline-5-sulfonic Acid and Its Sodium Salt

Eiichi SEKIDO, Junichi TANAKA, and Yoshitaka MASUDA

Department of Chemistry, Faculty of Science, Kobe University, Nada-ku, Kobe 657

(Received November 9, 1972)

Thermal and spectrophotometric studies of 8-mercaptoquinoline-5-sulfonic acid and its sodium salt synthesized by an improved method are reported. In order to determine the best formula for the weighing of organic reagent, the thermal stabilities of 8-mercaptoquinoline-5-sulfonic acid and its sodium salt and the amount of water of crystallization were examined with a thermal balance. It was found that the disodium dihydrate was of the best form. The ultraviolet and visible absorption spectra in aqueous-ethanol solution were measured, the tautomeric constant K_t between neutral and zwitterion forms being estimated and acid dissociation constants obtained spectrophotometrically. The absorption spectra and the equilibrium constants of the reagents were compared with those of 8-mercaptoquinoline, 8-hydroxyquinoline and 8-hydroxyquinoline-5-sulfonic acid.

Analytical application of 8-mercaptoquinoline, a typical organic reagent containing nitrogen and sulfur ligand atoms, has recently been studied by many analytical chemists. Stoichiometric studies of 8-mercaptoquinoline have been reported by a few investigators,[1-3] but they are not as extensive and systematic as those of 8-hydroxyquinoline and its metal chelates. This may be attributed to the difficulty of finding a favorable organic solvent capable of dissolution of many kinds of metal 8-mercaptoquinoline chelates.

Introduction of a sulfonic acid group at 5-position of the quinoline nucleus makes its metal chelates soluble in water. Thus it is possible to study stoichiometrically the various metal 8-mercaptoquinoline-5-sulfonic acid chelates as water soluble metal 8-mercaptoquinoline chelates.

The present paper deals with the thermal and spectrophotometric studies of 8-mercaptoquinoline-5-sulfonic acid and its sodium salt synthesized by an improved method. Their thermal stabilities, air oxidation, acid dissociation constants and ultraviolet and visible absorption spectra are compared with those of 8-mercaptoquinoline, 8-hydroxyquinoline, and 8-hydroxyquinoline-5-sulfonic acid.

Experimental

Materials. 8-Mercaptoquinoline-5-sulfonic acid and its derivatives have been synthesized by Vogt and Hein[4] and Bankovskis *et al.*[5] In order to raise the yield of the reagents, an improved synthesis from 8-hydroxyquinoline was attempted.

8-Hydroxyquinoline-5-sulfonic Acid: The methods by Coll and Coll[6] and Matsumura[7] were adopted for the synthesis from 8-hydroxyquinoline. Yield: 90%.

8-Aminoquinoline-5-sulfonic Acid: The synthesis of 8-aminoquinoline from 8-hydroxyquinoline by Vorozhtzov and Kogan[8] was utilized. 8-Hydroxyquinoline-5-sulfonic acid (45 g, 0.20 mol), ammonium sulfite (70 g, 0.52 mol), 28% ammonia (50 ml, 0.36 mol) and 100 ml of water are charged in an autoclave and heated at 150—160 °C, for 6—7 hr. under 10—15 atm. The gray green precipitate formed was dissolved with water, insoluble residues being filtered off. When the filtrate was concentrated to 300 ml followed by addition of 36% hydrochloric acid (50 ml, 0.58 mol), yellow to orange precipitate was formed. This was filtered and washed with water. One litre of water was added to the crude 8-aminoquinoline-5-sulfonic acid (10 g). A small amount of active carbon was added to the solution and heated for 30 min. After filtration, the filtrate was concentrated to 500 ml. On cooling, pure 8-aminoquinoline-5-sulfonic acid (*ca.* 6 g) was obtained.

Found: C, 44.55; H, 3.99; N, 11.32%. Calcd for $C_9H_{10}N_2O_4$: C, 44.62; H, 4.16; N, 11.56%. 8-Aminoquinoline-5-sulfonic acid was obtained by recrystallization from water as a mixture of yellow needle crystal and orange cube crystal. Both exist as monohydrate at room temperature, their anhydride being obtained by drying at 100—110 °C. Decomposition temperature is 220 °C.

8-Mercaptoquinoline-5-sulfonic Acid Disodium Salt Trihydrate: The synthesis of 8-mercaptoquinoline from 8-aminoquinoline by Kealey and Freiser[9] was utilized. 8-Aminoquinoline-5-sulfonic acid monohydrate (4.84 g, 0.02 mol) once at least recrystallized, was added to 150 ml of 24% hydrobromic acid solution (0.65 mol) and heated for dissolution. After complete dissolution, the solution was rapidly cooled in an ice-bath to deposit the fine crystal. To the resulting suspension, was added 10% sodium nitrous acid solution dropwise in an ice-bath until potassium iodide-starch paper turned blue. Excess sodium nitrous acid was decomposed by addition of 2 M sulfamic acid solution. The diazotized solution was gradually added to a solution of thiourea (1.7 g, 0.022 mol) dissolved in 50 ml of water at 30—40 °C, the solution then being heated at 90 °C for a short time. The reacting solution changed to red and a white precipitate was formed. To the resulting solution containing the precipitate was added hypophosphorous acid (2—5 equivalent amounts of 8-aminoquinoline-5-sulfonic acid) and heated to dissolve the precipitate. After the solution was filtered, the filtrate was cooled in an ice-bath and 100 g of solid sodium hydroxide

1) A. Corsini, Q. Fernando, and H. Freiser, *Anal. Chem.*, **35**, 1424 (1963).
2) Yu. A. Bankovskii, L. M. Chera, and A. F. Ievin'sh, *Zh. Analit. Khim.*, **18**, 668 (1963).
3) P. D. Anderson and D. M. Hercules, *Anal. Chem.*, **38**, 1703 (1966).
4) K. H. Vogt and Fr. Hein, *J. Prakt. Chem.*, **31**, 240 (1966).
5) J. Bankovskis, M. Cirule, J. Asaks, A. Ievins, and V. Vanags, *Latv. PSR Zinat. Akad. Vestis Kim. Ser.*, **1967**, 441.
6) A.-L. Coll and G. P. Coll, *Afinidad*, **28**, 163 (1951).
7) K. Matsumura, *J. Amer. Chem. Soc.*, **49**, 810 (1927).
8) N. N. Vorozhtzov and I. M. Kogan, *Ber.*, **65**, 142 (1932).
9) D. Kealey and H. Freiser, *Talanta*, **13**, 1381 (1966).

was gradually added with sufficient stirring under nitrogen gas. 8-Mercaptoquinoline-5-sulfonic acid disodium salt trihydrate formed as a yellow precipitate. After being filtered, the precipitate was washed twice with 90% ethanol. It was then dried for 1—2 hr under reduced pressure by means of a water-jet pump.

Yield: 80—90%. The crude product of 5—6 g was throughly dissolved in 50 ml of water and then 150 ml of ethanol was added. A yellow cube crystal was formed. After filtration, the precipitate was washed twice with 10 ml of ethanol and dried for 1—2 hr under reduced pressure by means of water-jet pump and then kept in a desiccator with silica gel under nitrogen.

Yield: 60—65%. Yellow cube crystals.

Found: C, 31.68; H, 3.19; N, 3.97%. Calcd for $C_9H_5NO_3S_2Na_2$: C, 31.86; H, 3.27; N, 4.13%.

8-Mercaptoquinoline-5-sulfonic Acid: To 8-mercaptoquinoline-5-sulfonic acid disodium salt trihydrate (3.3 g, 0.01 mol) dissolved in 45 ml of water was added 2.5 ml of 35% hydrochloric acid solution and 2.5 ml of 50% hypophosphorous acid, and the resulting red solution was heated for 1—2 hr on a water-bath and allowed to stand overnight. Faint yellow to faint brown silk thread-like 8-mercaptoquinoline-5-sulfonic acid was formed from the deep red solution. After the precipitate was filtered, it was washed twice with 3—4 ml ethanol and dried for 1—2 hr under reduced pressure, and kept in a desiccator with silica gel under nitrogen. The crude product was recrystallized from water containing hypophosphorous acid.

Yield: 63%.

8,8'-Diquinolyldisulfide-5,5'-disulfonic Acid Trihydrate: To 8-mercaptoquinoline-5-sulfonic acid disodium salt trihydrate (3.43 g, 0.01 mol) dissolved in 50 ml of water was added 2 ml of 35% hydrochloric acid and then 3% hydrogen peroxide solution until the red color disappeared completely. The resulting solution was allowed to stand overnight. Faint yellow cube crystal was formed.

Yield: 70%.

Found: C, 40.15; H, 3.42; N, 5.49%. Calcd for $C_{18}H_{18}N_2O_9S_4$: C, 40.44; H, 3.39; N, 5.24%.

Apparatus. Ultraviolet and visible absorption spectra were measured with a Hitachi 124 type spectrophotometer with 1 cm quartz cells. A Horiba Model P pH meter with glass and calomel electrodes was standardized against aqueous buffer (pH 4.01 and 6.86). Thermogravimetric curves were obtained with a Cho Thermobalance apparatus.

Thermogravimetric Measurement. About 100 mg of sample powder was weighed out into a holder for thermobalance and the temperature was elevated at a rate of 5 °C/min. The weight and temperature were read at regular time intervals.

Spectrophotometric Measurement. All the solutions were deaerated by bubbling with nitrogen. The absorption spectra were measured at 20±1 °C under nitrogen atmosphere. The solutions were buffered with perchloric acid, sodium hydroxide, acetic acid and disodium hydrogen phosphate and were adjusted with sodium perchlorate to maintain the ionic strength at 0.1 except for the solution with pH below 1.0.

Determination of Acid Dissociation Constants. All the acid dissociation constants for 8-mercaptoquinoline-5-sulfonic acid were determined spectrophotometrically. The macroscopic acid dissociation constants K_a at the ionic strength 0.1 and at 20±1 °C were determined by the equation

$$pK_{a_i} = \log (d_b - d)/(d - d_a) + pH \quad (1)$$

where d is the absorbance at 454 or 278 nm at the particular pH, d_b the absorbance in 1.00×10^{-3} M perchloric acid and d_a the absorbance in 5 M perchloric acid. The values of pK_{a_1} obtained for each pH were averaged. pK_{a_2} was determined in a similar way. pK_a' was estimated roughly by a graphical method. The values of the microscopic acid dissociation constants K_{a_A}, K_{a_B}, K_{a_C}, and K_{a_D} were obtained by the following equation and the values of K_{a_1}, K_{a_2} and the tautomeric constant K_t.

$$K_t = [\text{zwitterion}]/[\text{neutral}] = K_{a_D}/K_{a_C} \quad (2)$$

$$K_{a_1} = K_{a_A} + K_{a_B} \quad (3)$$

$$1/K_{a_2} = 1/K_{a_C} + 1/K_{a_D} \quad (4)$$

Determination of Tautomeric Constant. The tautomeric constant K_t was roughly estimated by two methods. 1) On the assumption that both extinction coefficients for 8-methylmercaptoquinoline-5-sulfonic acid and the neutral form of 8-mercaptoquinoline-5-sulfonic acid are the same at a corresponding wavelength, the ratio of the extinction coefficient at 339 nm of 8-methylmercaptoquinoline-5-sulfonic acid to the apparent extinction coefficient of 8-mercaptoquinoline-5-sulfonic acid in aqueous solution at 322 nm gives the fraction of the neutral form of 8-mercaptoquinoline. 7980 was taken[4] as the molar extinction coefficient at 339 nm for 8-methylmercaptoquinoline-5-sulfonic acid. 2) It is possible to estimate the expected absorbance at 322 nm for 100% neutral form of 8-mercaptoquinoline-5-sulfonic acid by using the data that the ratios of the increment of the absorbance at 322 nm to the decrement of the absorbance of the absorption maxima around 450 nm in various v/v% ethanol solution are approximately 1.6. The ratio of the absorbance in aqueous solution at 322 nm to the expected absorbance as 100% neutral form at the same wavelength gives the fraction of the neutral form of 8-mercaptoquinoline-5-sulfonic acid.

Results and Discussion

Thermal Stability. In order to find the best formula for gravimetry of the reagent, the thermal stability of 8-mercaptoquinoline-5-sulfonic acid and its sodium salt and the amount of water of crystallization were examined with a thermal balance. The thermogravimetric curves are given in Fig. 1 and the results in Table 1. We see that 8-mercapto and 8-hydroxyquinoline-5-sulfonic acids are less stable than the corresponding sodium salts and that 8-mercaptoquinoline-

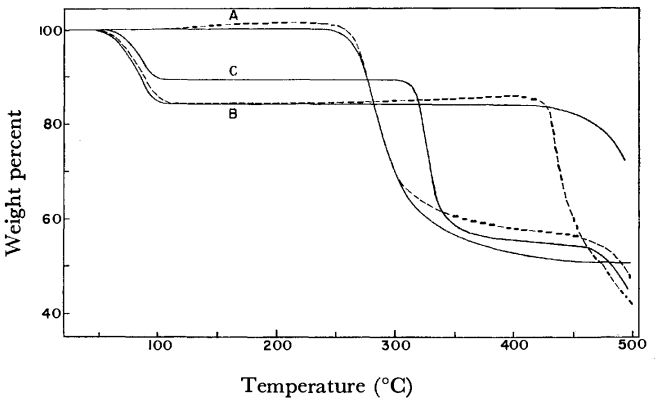

Fig. 1. Thermogravimetric curves of 8-mercaptoquinoline-5-sulfonic acid and its disodium salt.
A: 8-mercaptoquinoline-5-sulfonic acid
B: 8-mercaptoquinoline-5-sulfonic acid disodium salt trihydrate
C: 8,8'-Diquinolyldisulfide-5,5'-disulfonic acid trihydrate
——: in nitrogen gas, ------: in air.

Table 1. Thermogravimetric results for 8-mercapto and 8-hydroxyquinoline -5-sulfonic acid and their derivatives

Reagent	Dehydration		Decomposition begins at
	Temperature	Weight loss%	
8-Mercaptoquinoline-5-sulfonic acid disodium salt trihydrate	50—105°C	Found: 15.90% Calcd for $C_9H_5NO_3S_2Na_2 \cdot 3H_2O$: $3H_2O$, 15.93%	415°C
8-Mercaptoquinoline-5-sulfonic acid			240°C
8,8′-Diquinolyldisulfide-5,5′-disulfonic acid trihydrate	60— 95°C	Found: 10.10% Calcd for $C_{18}H_{12}N_2O_6S_4 \cdot 3H_2O$: $3H_2O$, 10.11%	300°C
8-Hydroxyquinoline-5-sulfonic acid disodium salt 3.5 hydrate	40— 78°C	Found: 14.00% Calcd for $C_9H_5NO_4SNa_2 \cdot 5H_2O$: $2.5H_2O$ 14.42%	355°C
	78—110°C	Found: 6.04% Calcd for $C_9H_5NO_4SNa_2 \cdot 3.5H_2O$: H_2O, 5.77%	
8-Hydroxyquinoline-5-sulfonic acid dihydrate	70—105°C	Found: 7.23% Calcd for $C_9H_7NO_4S \cdot 2H_2O$: H_2O, 6.90%	270°C
	105—147°C	Found: 6.42% Calcd for $C_9H_7NO_4S \cdot 2H_2O$: H_2O, 6.90%	

5-sulfonic acid and its sodium salt are more stable than the corresponding 8-hydroxy compounds. 8-Mercaptoquinoline-5-sulfonic acid sodium salt anhydride is so hygroscopic that it rapidly increases about 11.8% in wt. when exposed to air for 1 hr. It may be concluded that the form of 8-mercaptoquinoline-5-sulfonic acid disodium dihydrate is the best for weighing. In the thermogravimetric curves in air for 8-mercaptoquinoline-5-sulfonic acid and its disodium salt (dashed lines of curves A and B, respectively), the former increases in weight by 1.0—1.2% in the temperature range 120—240 °C, the latter by 1.8—2.1% in the range 240—408 °C. A similar phenomenon was found with the sodium salts of 8-mercaptoquinoline[10] and 8-selenoquinoline.[11] It is assumed that the sodium salt of 8-mercaptoquinoline-5-sulfonic acid is oxidized by air.

Ultraviolet and Visible Absorption Spectra of the Reagent. Ultraviolet and visible spectra of 8-mercaptoquinoline-5-sulfonic acid were measured in order to know the stability of the reagent in aqueous solution against oxidation, species existing in various pH, acid dissociation constant, and tautomeric constant.

Oxidation in Aqueous Solution: When 8-mercaptoquinoline-5-sulfonic acid in aqueous solution is allowed

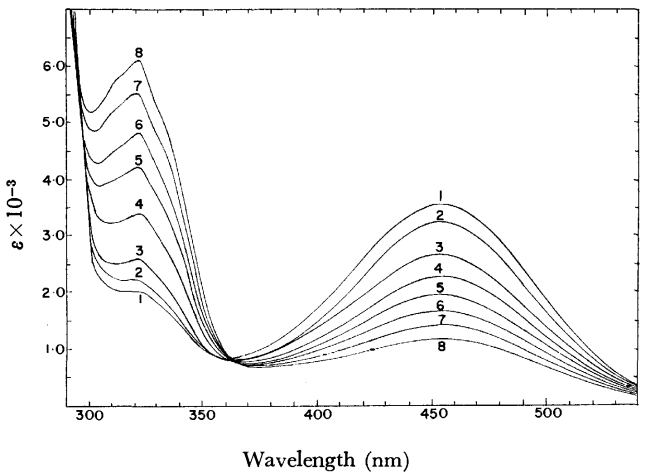

Fig. 2. Time dependence of the spectra of 1.00×10^{-4}M 8-mercaptoquinoline-5-sulfonic acid solution in 1.00×10^{-3}M perchloric acid at 35 °C.
Standing time: 1: 0 hr., 2: 1 hr, 3: 5 hr, 4: 10 hr, 5: 15 hr, 6: 20 hr, 7: 25 hr, 8: 30 hr.

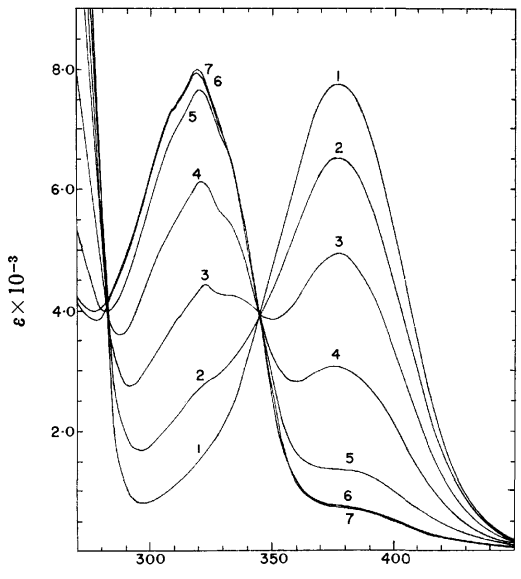

Fig. 3. Time dependence of the spectra of 1.00×10^{-4}M 8-mercaptoquinoline-5-sulfonic acid solution at pH 10.02 and at 35 °C.
Standing time: 1: 0 hr, 2: 2 hr, 3: 4 hr, 4: 6 hr, 5: 8 hr, 6: 10 hr, 7: 12 hr.

10) Y. Mido and E. Sekido, This Bulletin, **44**, 2127 (1971).

11) E. Sekido and I. Fujiwara, *Talanta*, **19**, 647 (1972).

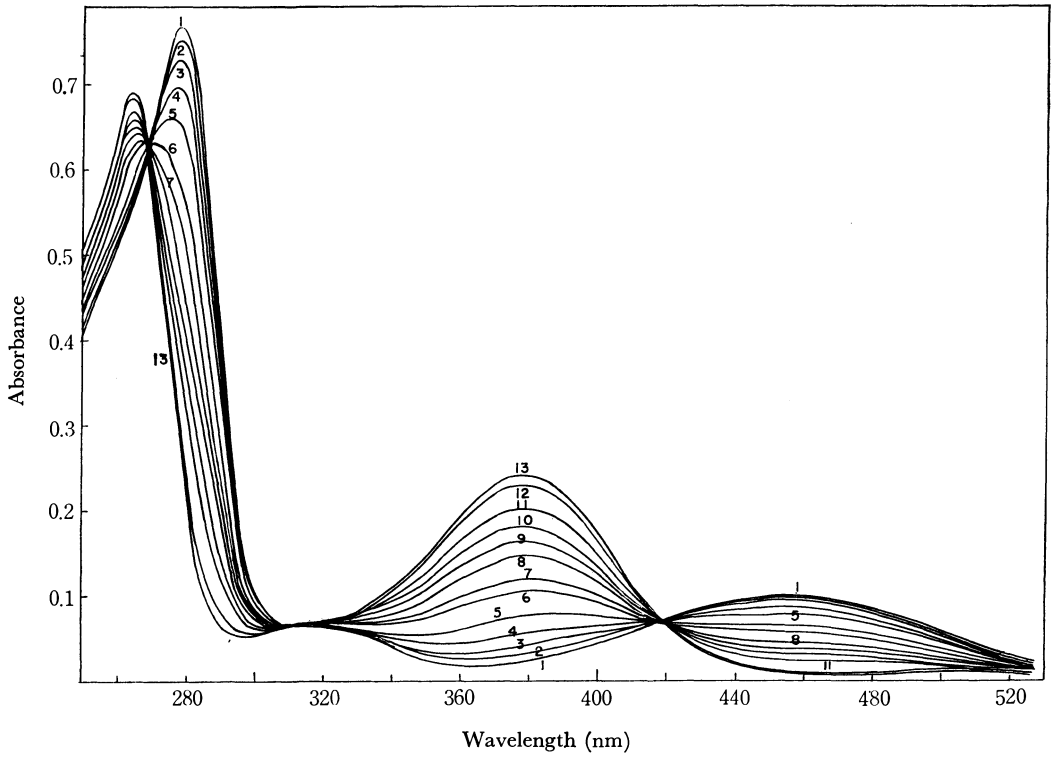

Fig. 4. Absorption spectra of 8-mercaptoquinoline-5-sulfonic acid at various acid concentration of perchloric acid and at $\mu=1.00$.
Concentration of the reagent: 3.00×10^{-5}M. Concentration of perchloric acid: 1: 1.00×10^{-3}M, 2: 1.00×10^{-2}M, 3: 2.00×10^{-2}M, 4: 3.00×10^{-2}M, 5: 5.00×10^{-2}M, 6: 8.00×10^{-2}M, 7: 1.00×10^{-1}M, 8: 2.00×10^{-1}M, 9: 3.00×10^{-1}M, 10: 5.00×10^{-1}M, 11: 1.00M.

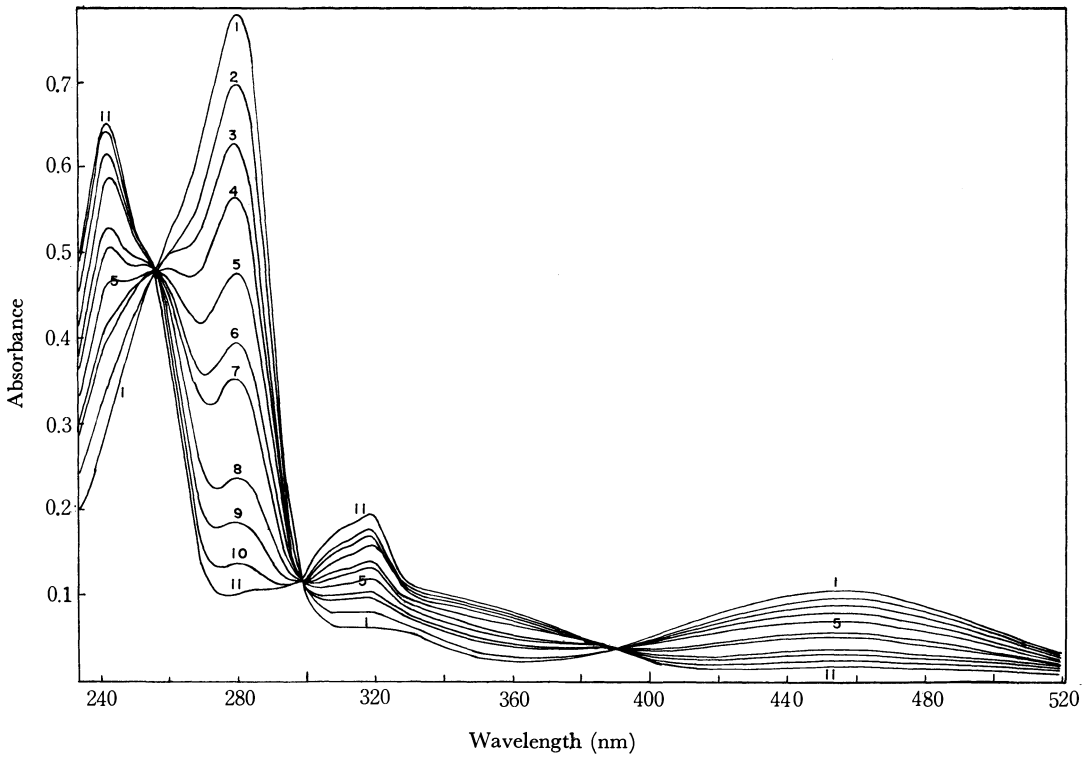

Fig. 5. Absorption spectra of 8-mercaptoquinoline-5-sulfonic acid in various pH solution at $\mu=0.10$.
Concentration of the reagent: 3.00×10^{-5}M. pH: 1: 2.73, 2: 4.82, 3: 6.18, 4: 6.75, 5: 7.10, 6: 7.26, 7: 7.46, 8: 7.56, 9: 7.74, 10: 8.02, 11: 8.42, 12: 9.00, 13: 11.03.

to stand in air, it is gradually oxidized giving rise to the formation of 8,8′-diquinolyldisulfide-5,5′-disulfonic acid. Changes in the ultraviolet and visible absorption spectra by air oxidation at pH 3.0 and 10.0 were examined at 35 °C at which temperature oxidation is more accelerated than that at room temperature. The results are shown in Figs. 2 and 3, respectively. The intensities of the absorption maxima at 454 and 279 nm for pH 3.0 and at 378 nm for pH 10.0 decrease with time, while those at 322 and 243 nm for pH 3.0 and at 378 nm for pH 10.0 increase with time. The time required to oxidize half the amount of reagent at 35 °C is about 12 hr for pH 3.0 and about 5 hr for pH 10. The reagent is more rapidly oxidized with increase in pH. It is assumed that electron donation, or the oxidation of the $-S^-$ group of the anion (IV) existing in a high pH solution, accelerated to a greater extent than in the other species (I), (II), (III_a), and (III_b) of the reagent.

Ultraviolet and Visible Absorption Spectra of 8-Mercaptoquinoline-5-sulfonic Acid in Aqueous Solution: The ultraviolet and visible absorption spectra of 1.00×10^{-4} M 8-mercaptoquinoline-5-sulfonic acid at various concentrations of perchloric acid from 1.00×10^{-3} to 10.0 M and those in the pH range 3.0—12.0 are shown in Figs. 4 and 5, respectively. The relationship between the absorption maxima of 8-mercaptoquinoline-5-sulfonic acid and pH is shown in Fig. 6. The intensities of absorption at 454 and 279 nm decrease with the concentration of perchloric acid and disappear above 3.0 M. The absorption maximum at 322 nm in the solution of pH 3.0 shifts slightly toward 318 nm with acid concentration. The intensity increases and a weak absorption appears around 360 nm as a shoulder of the absorption at 318 nm. The weak absorption of 311 nm hardly recognized as an absorption at pH 3.0 appears as a shoulder of the absorption of 318 nm. The isosbestic points appear at 389 and 298 nm in the pH range 5.0—0, but the absorption bands in perchloric acid with concentration above 3 M deviate from these points. The absorption bands at 454 and 279 nm which exhibit the constant maximum absorbance in the pH range 3.0—5.0 decrease with alkaline concentration. Those at 378 and 265 nm increase. Isosbestic points exist at 419, 323, and 270 nm. (Fig. 5).

The ultraviolet and visible absorption spectra for 8-mercaptoquinoline-5-sulfonic acid in various pH solutions are similar to those for 8-mercaptoquinoline[2,3] except for the change in absorption at 318 nm below pH 0. Thus the changes in absorption spectra correspond to those of the structures I↔II↔III↔IV as follows:

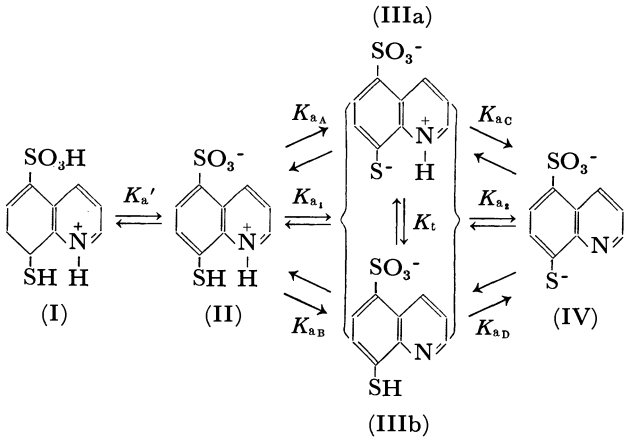

From the changes of absorbance at 454 nm in the acidic and alkaline sides we obtained the values $pK_{a_1}=0.90\pm0.03$ and $pK_{a_2}=7.50\pm0.04$, respectively. Similarly from the changes of absorbance at 278 nm, $pK_{a_1}=0.90\pm0.01$ and $pK_{a_2}=7.48\pm0.09$ were obtained in good accordance with above.

The following results are found for the absorption band at 318 nm. 1) The absorption curves of the reagent in perchloric acid with concentration above 1.00 M deviate from the isosbestic points at 389 and 298 nm. 2) The plot of the absorbance *vs.* pH at

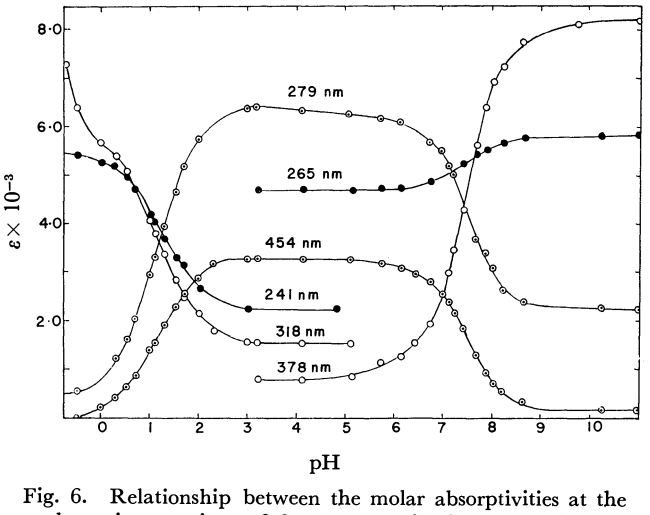

Fig. 6. Relationship between the molar absorptivities at the absorption maxima of 8-mercaptoquinoline-5-sulfonic acid and pH.

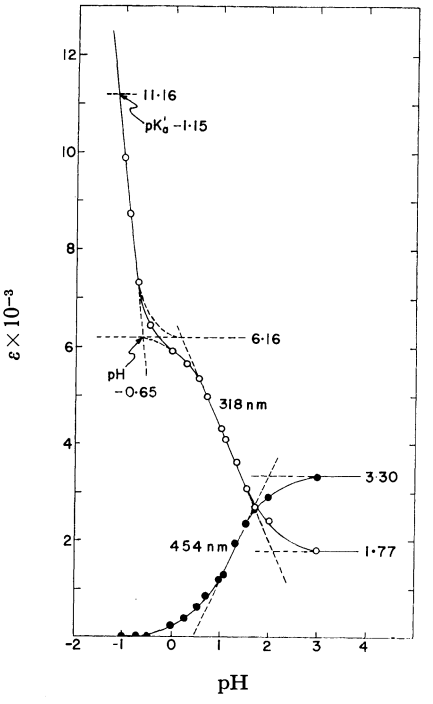

Fig. 7. Graphical determination of p*Ka*′.

Table 2. Relationship between absorbance of 8-mercaptoquinoline-5-sulfonic acid and concentration of perchloric acid

Concentration of perchloric acid (M)	Absorbance at 454 nm	Absorbance at 318 nm	$\frac{A_{318}-0.177}{0.330-A_{454}}$
1.00×10^{-3}	0.330	0.177	
1.00×10^{-2}	0.292	0.237	
2.00×10^{-2}	0.261	0.267	
3.00×10^{-2}	0.232	0.305	
5.00×10^{-2}	0.195	0.359	1.35
8.00×10^{-2}	0.155	0.403	1.29
1.00×10^{-1}	0.140	0.429	1.33
2.00×10^{-1}	0.087	0.495	1.31
3.00×10^{-1}	0.065	0.532	1.34
5.00×10^{-1}	0.041	0.562	1.33
1.00	0.023	0.590	1.35
		Mean	1.33 ± 0.04
3.00	0.002	0.640	1.41
5.00	0	0.731	1.61
8.00	0	0.870	2.10
10.00	0	0.987	2.45

318 nm has a point of inflexion around pH 0 (Fig. 7). 3) The ratio of the increase in absorbance at 318 nm to its decrease at 454 nm becomes greater in perchloric acid with concentration above 1 M (Table 2). These results are obtained also in the case of hydrochloric acid. This indicates that species (I) may be formed in a strong acid solution. The value of pK_a' for the equilibrium $I \rightleftarrows II + H^+$ is estimated as follows. The absorbances at 454 and 318 nm of the 1.0×10^{-4} M reagent in various concentrations of perchloric acid solution in the range 1.00×10^{-3}—10.0 M were measured. The ionic strength at 1.0 was maintained in the range 1.00×10^{-3}—1 M perchloric acid. The results are given in Table 2, and the plots of absorbances at 454 and 318 nm *vs.* pH in Fig. 7. $pK_{a_1}=1.14\pm0.02$ ($\mu=1.0$) was obtained from the values of absorbance at 454 nm and Eq. (1). If species (I) is not formed in a strong acid solution, the upper limit of the absorbance at 318 nm will be estimated as $d_a=0.330\times1.33\pm0.177=0.616$. Using $d_a=0.616$ and $d_b=0.177$, $pK_{a_1}=1.13\pm0.02$ ($\mu=1.0$) could be obtained. This is in good accordance with 1.14 ± 0.02 mentioned above. The plot of the absorbance at 318 nm *vs.* pH below -0.5 is found to be linear with a slope -1 (Fig. 7). Thus the value of pK_a' was roughly estimated to be -1 (dotted line, Fig. 7).

Ultraviolet and Visible Absorption Spectra of 8-Mercaptoquinoline-5-sulfonic Acid in Ethanol-Water Media: The absorption spectra of 8-mercaptoquinoline-5-sulfonic acid in aqueous-ethanol mixtures containing 1.00×10^{-3} M of perchloric acid are sohwn in Fig. 8. The wavelength of the absorption maxima and the molar extinction coefficients of the species in several kind of aqueous-ethanol mixtures are given in Table 3. The

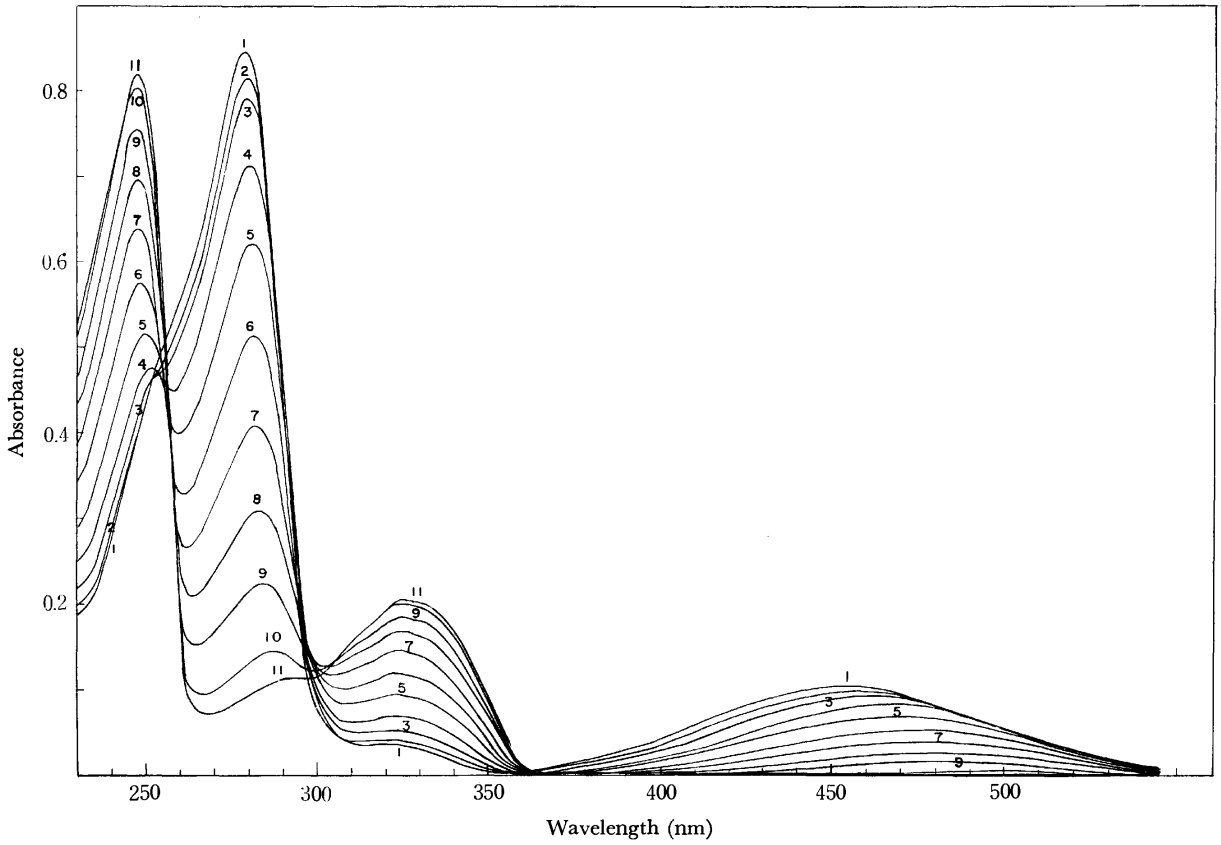

Fig. 8. Absorption spectra of 8-mercaptoquinoline-5-sulfonic acid in aqueous ethanol containing 1.00×10^{-3}M of perchloric acid at $\mu=0.005$.
Concentration of the reagent: 3.33×10^{-3}M. Concentration of ethanol (v/v%): 1: 0%, 2: 10%, 3: 20%, 4: 30%, 5: 40%, 6: 50%, 7: 60%, 8: 70%, 9: 80%, 10: 90%, 11: 95%.

Table 3. Effect of the concentration of ethanol on absorption maxima (nm) and molra absorptivity ($l \cdot mol^{-1} \cdot cm^{-1}$) of 8-mercaptoquinoline-5-sulfonic acid

Concn of ethanol % (v/v)	Cation (II) in 1.02 M $HClO_4$							
	λ[a]	ε	λ	ε	λ	ε	λ[a]	ε
0	241	2.13×10^4	(311)	4.67×10^3	318	5.45×10^3	(340)	3.00×10^3
30	241	2.20×10^4	(310)	4.77×10^3	318	5.28×10^3	(340)	3.00×10^3
60	242	2.23×10^4	(310)	5.00×10^3	319	5.20×10^3	(340(	3.12×10^3
80	241	2.21×10^4	(310)	5.17×10^3	319	5.20×10^3	(340)	3.24×10^3
90								

Zwitterion (IIIa) in 1.00×10^{-3} M $HClO_4$				Neutral (IIIb) in 1.00×10^{-3} M $HClO_4$				Anion (IV) in 1.09×10^{-2} M NaOH			
λ	ε	λ	ε	λ[a]	ε	λ	ε	λ	ε	λ	ε
279	2.53×10^4	454	3.26×10^3	(255)	1.50×10^4	322	1.42×10^3	265	2.32×10^4	378	8.47×10^3
281	2.14×10^4	466	2.64×10^3	252	1.43×10^4	324	2.48×10^3	266	2.41×10^4	382	8.47×10^3
282	1.23×10^4	478	1.34×10^3	247	1.92×10^4	324	4.91×10^3	267	2.48×10^4	387	8.47×10^3
285	6.67×10^3	488	6.3×10^2	247	2.25×10^4	324	6.14×10^3	268	2.53×10^4	389	8.47×10^3
288	4.32×10^3	494	2.0×10^2	247	2.41×10^4	325	6.58×10^3	268	2.53×10^4	391	8.47×10^3

a) Figures in parentheses indicates shoulder.

Table 4. Equilibrium constants of 8-mercaptoquinoline-5-sulfonic acid and 8-mercaptoquinoline in aqueous solution

Compunds	pK_a'	pK_{a_1}	pK_{a_2}	K_t	pK_{a_A}	pK_{a_B}	pK_{a_C}	pK_{a_D}
8-MQ-5-SO_3H[a]	−1.15	0.91±0.03	7.50±0.04	5.6[c]	0.98	1.73	7.43	6.68
				3.9[d]	1.01	1.59	7.40	6.81
8-MQ[b]		2.0 ±0.1[e]	8.36±0.1[f]	3.8[g]	2.10	2.68	8.26	7.68

a) 8-MQ-5-SO_3H: 8-Mercaptoquinoline-5-sulfonic acid.
b) 8-MQ: 8-Mercaptoquinoline.
c) by method 1.
d) by method 2.
e) Ref. 12.
f) Ref. 13.
g) Ref. 2.

absorption maximum in aqueous solution shifts to longer wavelength with the increase of ethanol content, its intensity decreasing significantly. Thus in 95% ethanol solution the absorption maximum shifts from 454 nm in aqueous solution to 498 nm in 95% ethanol and the apparent extinction coefficient decreases from 3.26×10^3 to 1.8×10^2. On the other hand, the absorption maximum at 322 nm in aqueous solution shifts slightly to longer wavelength 325 nm in 95% ethanol, but the apparent extinction coefficient increases from 1.42×10^3 to 6.58×10^3. In the range 300—200 nm, the absorption maximum at 279 nm decreases with the increase of ethanol content and that at 255 nm increases. It is assumed that zwitterion form IIIa is transferred into neutral form IIIb with the increase of ethanol content which causes the lowering of the dielectric constant of the solution. The absorption bands having peaks at 454 and 279 nm correspond to the zwitterion form and those at 323 and 255 nm to the neutral form. The absorption maxima of both the cation and the neutarl having –SH group are slightly shifted, but those at the longer wavelengths of both the zwitterion and anion having $-S^-$ group are significantly shifted to longer wavelength with the increase of the ethanol content (Table 3). This is remarkable for the zwitterion. Increase of the water content may stabilize the ground state to a greater extent for zwitterion (IIIa) or anion (IV) and the absorption maximum will shift to the blue side. Thus these absorption bands might be assigned to the charge transfer absorption in which $-S^-$ group takes part.

Equilibrium Constants of 8-Mercaptoquinoline-5-sulfonic Acid in Aqueous Solution. The tautomeric constant K_t=[zwitterion]/[neutral] was calculated to be 5.6 by method (1), and 3.9 by method (2). It was found that 80—85% of the reagent exists as the zwitterion and 20—15% as the neutral form in aqueous solution. Table 4 shows the equilibrium constants of 8-mercaptoquinoline-5-sulfonic acid and 8-mercaptoquinoline. The values of pK_{a_1} and pK_{a_2} for 8-mercaptoquinoline-5-sulfonic acid are lower than the corresponding ones for 8-mercaptoquinoline. This can be attributed to the electron with drawing power of the sulfonic acid group substituted at 5-position of the quinoline nucleus. The difference for pK_{a_1} (1.09) is larger than that for pK_{a_2} (0.86). The somewhat larger decrease of pK_{a_1} seems to be due to the fact that the value of K_t 3.9—5.6 for 8-mercaptoquinoline-5-sulfonic acid is somewhat larger than that for 8-mercaptoquinoline, 3.8.

12) E. Sekido, Q. Fernando, and H. Freiser, *Anal. Chem.*, **36**, 1768 (1964).
13) N. Nakamura and E. Sekido, *Talanta*, **17**, 515 (1970).

Stability of Fused Rings in Metal Chelates. X. Structures and Stability Constants of the Copper(II) Complexes of Tripeptides Composed of Glycine and/or β-Alanine

Osamu YAMAUCHI, Yasuo NAKAO, and Akitsugu NAKAHARA

Institute of Chemistry, College of General Education, Osaka University, Toyonaka, Osaka 560

(Received November 15, 1972)

On the basis of comparative studies of the equilibria involving copper(II) and triglycine (G·G·G), glycylglycyl-β-alanine (G·G·β-A), glycyl-β-alanylglycine (G·β-A·G), or β-alanylglycylglycine (β-A·G·G), the structures of the complexes formed at various pH values and the structure-stability relationship between the fused-ring chelates have been discussed in reference to the equilibrium constants determined by potentiometric titration at 25° (μ=0.1 (KNO_3)) and the properties of the copper(II) chelates isolated. For each tripeptide, the stability constant K_1 for the 1 : 1 complex and the constants for the deprotonation reactions K_{c_1} and K_{c_2} were calculated by the method of non-linear least-squares. For G·G·G, G·G·β-A, and G·β-A·G, the equilibrium indicating the formation of a protonated complex was detected at pH 3.5—4.5. The relatively small difference in the log K_1 values (5.25—5.60) and the $-\log K_{c_1}$ values (5.23—5.36) and the larger difference in the $-\log K_{c_2}$ values (5.54—6.73) have been interpreted in terms of the steric requirements around copper(II) in the fused-ring chelates. Relative stabilities of the fused-ring systems in the deprotonated chelates have been inferred from the $K_1K_{c_1}K_{c_2}$ values to be in the order 5-6-5(G·β-A·G–Cu(II))≃6-5-5(β-A·G·G–Cu(II))>5-5-6(G·G·β-A–Cu(II))>5-5-5(G·G·G–Cu(II)).[1]

In view of the importance of the metal-protein interactions in biological systems, attention has been paid to various fundamental aspects of the protein-metal bonding, such as the bonding modes and the extents or strengths of the interactions in simplified systems. The complex formation between peptides and metal ions has been extensively investigated.

However, there still exist some ambiguities about the nature of the metal–peptide binding in aqueous solution, which is a prerequisite for understanding the interactions in the biological fluid. In this connection we have extended our studies on the copper(II) complexes of the dipeptides[2] and the amino acid amides[3] to the tripeptides composed of glycine and β-alanine, in order to reveal their behavior toward copper(II) ion.

Valuable findings characterizing the triglycine-copper(II) complexes in solution have accumulated by detailed potentiometric,[4-8] thermodynamic,[9,10] kinetic,[11,12] and spectral studies.[6,7,13] The coordination sites in the complexes in aqueous solution have been inferred from these findings and the results of X-ray crystal structure analyses[14,15] to be the amino nitrogen and the peptide oxygen in the acid region (structure **1**), and the amino nitrogen, the peptide nitrogens and the carboxyl oxygen in the neutral and alkaline regions (structure **2**). Probably because of the steric requirements around copper(II), the triglycine complex isolated from the alkaline solution has a dimeric structure,[15] where the carboxyl group coordinates to the copper(II) above (or below) the plane of the chelate ring considered and one of the peptide nitrogens axially interacts with that copper(II).

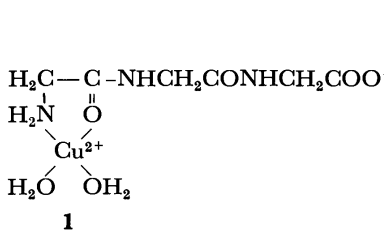

1

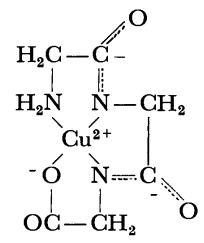

2

We considered it to be of basic importance to investigate how and to what extent the steric requirements in the consecutive chelate rings affect the stability in solution of the copper(II)–tripeptide complexes and, if possible, to infer the bonding modes in the fused-ring chelates. Since replacement of a glycyl group of triglycine with a β-alanyl group is expected to introduce a six-membered ring which would affect the stability of the fused-ring system, we have investigated the solution equilibria of the copper(II) complexes of several tripeptides containing glycine and/or β-alanine, and attempted to elucidate the structure-stability relationship between them.

1) Such notations are used throughout the text to express arrangement and size of the individual rings involved in the fused-ring system.

2) O. Yamauchi, Y. Hirano, Y. Nakao, and A. Nakahara, *Can. J. Chem.*, **47**, 3441 (1969).

3) O. Yamauchi, H. Miyata, and A. Nakahara, This Bulletin, **44**, 2716 (1971).

4) H. Dobbie and W. O. Kermack, *Biochem. J.*, **59**, 257 (1955).

5) C. B. Murphy and A. E. Martell, *J. Biol. Chem.*, **226**, 37 (1957).

6) W. L. Koltun, R. H. Roth, and F. R. N. Gurd, *ibid.*, **238**, 124 (1963).

7) M. K. Kim and A. E. Martell, *J. Amer. Chem. Soc.*, **88**, 914 (1966).

8) R. Österberg and B. Sjöberg, *J. Biol. Chem.*, **243**, 3038 (1968).

9) A. P. Brunetti, M. C. Lim, and G. H. Nancollas, *J. Amer. Chem. Soc.*, **90**, 5120 (1968).

10) G. H. Nancollas, *Coord. Chem. Rev.*, **5**, 407 (1970).

11) G. K. Pagenkopf and D. W. Margerum, *J. Amer. Chem. Soc.*, **90**, 6963 (1968).

12) H. Hauer, E. J. Billo, and D. W. Margerum, *ibid.*, **93**, 4173 (1971).

13) M. K. Kim and A. E. Martell, *ibid.*, **91**, 872 (1969).

14) H. C. Freeman, G. Robinson, and J. C. Schoone, *Acta Crystallogr.*, **17**, 719 (1964).

15) H. C. Freeman, J. C. Schoone, and J. G. Sime, *ibid.*, **18**, 381 (1965).

TABLE 1. ELEMENTAL ANALYSIS AND SOME PROPERTIES OF TRIPEPTIDE-COPPER(II) CHELATES

Complex	Elemental analysis C(%) Calcd	C(%) Found	H(%) Calcd	H(%) Found	N(%) Calcd	N(%) Found	Absorp. max. Dec. temp.[b] (°C)	Absorp. max. ($\times 10^3$ cm^{-1}) (log ε)	pH[c]
Na[Cu–G·G·G]·2H$_2$O[a]	23.34	23.24	3.93	3.63	13.61	13.57	250—263	17.9 (2.16)	9.0
Na[Cu–G·G·β-A]·4H$_2$O	23.43	23.75	5.07	4.90	11.71	11.31	235—245	18.0 (2.02)	8.6
K[Cu–G·β-A·G]·2H$_2$O	24.80	25.08	4.17	4.52	12.40	12.29	240—253	18.4 (1.77)	7.5
Na[Cu–β-A·G·G]·5H$_2$O	22.31	22.37	5.36	4.96	11.15	11.18	255—260	17.8 (1.92)	8.8

a) The corresponding chelate used by Freeman *et al*[15] for X-ray study was a monohydrate.
b) Determined on a micro melting point apparatus.
c) Values of 5.0×10^{-3}M aqueous solutions of the chelates.

For the present purpose, we chose triglycine (G·G·G), glycylglycyl-β-alanine (G·G·β-A), glycyl-β-alanylglycine (G·β-A·G), and β-alanylglycylglycine (β-A·G·G) as typical ligands, and carried out potentiometric titration and preparation of the copper(II) chelates. Determination of the equilibrium constants and the discussion of the structures and relative stabilities of the complexes in solution constitute the main subjects.

Experimental

Ligands. *G·G·G*: This was purchased from Nakarai Chemicals Co., Ltd. and checked by elemental analysis and amino acid analysis with a Yanagimoto amino acid analyzer LC-5.

G·G·β-A: To a cooled and stirred solution of glycyl-β-alanine[16] (7.8 g) in 4 M sodium hydroxide (13.4 ml) was added, alternately, chloroacetyl chloride (9.1 g) and 4 M sodium hydroxide (20.4 ml) at such a rate that the reaction mixture could be maintained alkaline at a temperature below 5 °C. After addition was over, stirring was continued for 10 min, and the pH of the solution was adjusted to *ca.* 2 with concd. hydrochloric acid. The colorless precipitate formed was collected by filtration and recrystallized from acetone to give chloroacetylglycyl-β-alanine, mp 158—159 °C (uncor.). Found: C, 37.75; H, 4.83; N, 12.20%. Calcd for $C_7H_{11}N_2O_4Cl$: C, 37.76; H, 4.99; N, 12.58%.

Chloroacetylglycyl-β-alanine was treated with aqueous ammonia as for chloroacetyl-β-alanine,[16] and the product was recrystallized from water–ethanol to give G·G·β-A, which was checked by melting point[16] and elemental analysis.

G·β-A·G: This was prepared by catalytic reduction[16] of carbobenzoxyglycyl-β-alanylglycine prepared from β-alanylglycine[17] and carbobenzoxyglycyl chloride,[18] and checked by melting point and elemental analysis.

β-A·G·G: This was prepared and checked analogously.[16]

(1) Copper(II) Chelates: All the chelates were prepared by the method described for sodium glycylglycylglycinatocuprate(II) monohydrate[15] and dried over silica gel. The analytical data and the spectral properties of the four chelates isolated are summarized in Table 1.

(2) Measurements of Spectra: Visible spectra were measured for 5.0×10^{-3} M aqueous solutions with a Shimadzu QR-50 spectrophotometer.

(3) pH Titrations: *(a) Reagents*: 0.1 M Potassium hydroxide, 0.1 M nitric acid, and 0.01 M copper(II) nitrate were prepared in the same manner as described.[3] All the reagents used were of analytical grade, distilled and deionized water being used.

(b) Apparatus: A Radiometer PHM 4d pH meter equipped with a G202B glass electrode and a K401 calomel electrode was used after standardization with a Horiba and a Radiometer standard buffer solution (pH 4.01 and 6.48 at 25 °C).

(c) Procedure: The procedure was essentially the same as that reported.[3] An aqueous solution containing nitric acid and equimolar amounts of a ligand and copper(II) nitrate (*ca.* 0.004 M) was titrated with 0.1 M potassium hydroxide, the pH being measured at 25±0.05 °C under a nitrogen atmosphere. The ionic strength was adjusted to 0.1 with potassium nitrate. The ligands were titrated in the absence of copper(II) nitrate under the same conditions. Conversion of pH to $-\log[H^+]$ and determination of the apparent ion product of water were made as reported.

Results

Titration Curves and Equilibria. The titration curves obtained for the tripeptides in the absence and the presence of copper(II) are given in Figs. 1 and 2, respectively. All the peptides give similar titration curves with four protons dissociating from the protonated peptide molecule in the presence of copper(II). The same reaction sequence can thus be reasonably assumed for all the systems. The G·G·G–Cu(II) system has been expressed by the following equilibria in acid and neutral solutions corresponding to *a* values (moles of KOH added per mole of ligand) of 1—4:[4-8]

$$Cu^{2+} + H_2L^- \overset{K_1}{\rightleftharpoons} Cu(H_2L)^+ \quad (1)$$

$$Cu(H_2L)^+ \overset{K_{c_1}}{\rightleftharpoons} Cu(HL) + H^+ \quad (2)$$

$$Cu(HL) \overset{K_{c_2}}{\rightleftharpoons} CuL^- + H^+ \quad (3)$$

where Cu^{2+} and H_2L^- refer to free copper(II) ion and free ligand, respectively, and equilibria (2) and (3) express the dissociation of protons from the peptide groups in the complex. The equilibrium constants are

16) H. T. Hanson and E. L. Smith, *J. Biol. Chem.*, **175**, 833 (1948).
17) Y. Nakao, H. Ishibashi, and A. Nakahara, This Bulletin, **43**, 3457 (1970).
18) M. Bergmann and L. Zervas, *Ber.*, **65**, 1192 (1932).

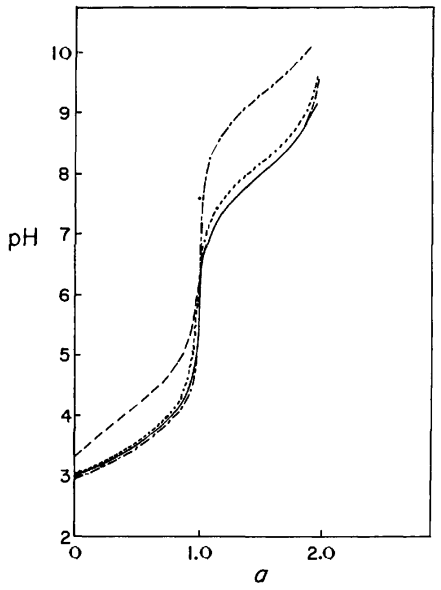

Fig. 1. Titration curves for the tripeptides.
———: G·G·G, – – – –: G·G–β-A, ------: G·β-A·G, — – —: β-A·G·G.
a: moles of KOH added per mole of ligand.

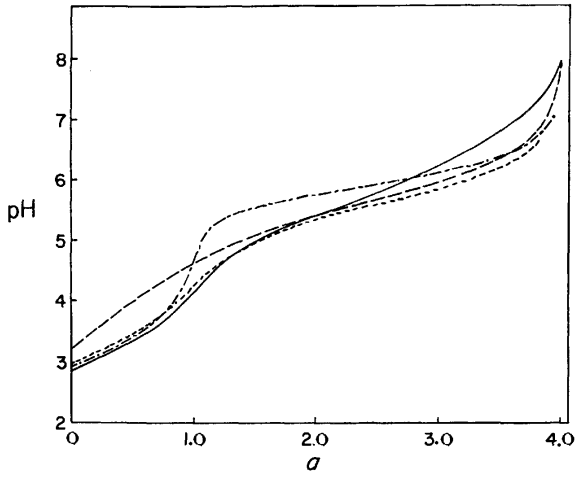

Fig. 2. Titration curves for the 1:1 tripeptide–copper(II) systems.
———: G·G·G–Gu(II), – – – –: G·G·β-A–Cu(II), --------: G·β-A·G–Cu(II), —·—·—: β-A·G·G–Cu(II).

defined by the following equations.

$$K_1 = \frac{[Cu(H_2L)^+]}{[Cu^{2+}][H_2L^-]} \quad (4)$$

$$K_{c_1} = \frac{[H^+][Cu(HL)]}{[Cu(H_2L)^+]} \quad (5)$$

$$K_{c_2} = \frac{[H^+][CuL^-]}{[Cu(HL)]} \quad (6)$$

In the pH range 3.5—4.5, pH depressions due to complex formation with copper(II) are small but not negligible for the G·G·G–, G·G·β-A–, and G·β-A·G–Cu(II) systems, whereas hardly any depression is observed for the β-A·G·G–Cu(II) system. In order to achieve better fit to the titration curves in this region, it was found necessary to add the following equilibria when the tripeptides have glycine residue as the NH_2-terminus:

$$Cu^{2+} + H_3L \overset{K^H}{\rightleftharpoons} Cu(H_3L)^{2+} \quad (7)$$

$$Cu(H_3L)^{2+} \overset{K_a^H}{\rightleftharpoons} Cu(H_2L)^+ + H^+ \quad (8)$$

where H_3L is the zwitterionic species of the tripeptides and $Cu(H_3L)^{2+}$ the protonated complex. The equilibria involving such a protonated complex have been reported for G·G·G at $\mu=3.0$ ($NaClO_4$) by Österberg and Sjöberg,[8] and they seem to exist also in the other tripeptide–Cu(II) systems in 0.1 M KNO_3.

Method of Calculation. On the basis of equations for the mole balance for total ligand and total metal ion concentrations C_L and C_M and for the electroneutrality of solution, the equilibrium constants K^H, K_1, K_{c_1}, and K_{c_2} were calculated by the method of non-linear least-squares with the aid of a NEAC 2200/500 computer. Constant K_a^H for the equilibrium (8) was calculated by

$$K_a^H = \frac{K_{a_2}K_1}{K^H} \quad (9)$$

where K_{a_2} refers to the acid dissociation constant of the amino group.

Details of the computer calculations are the same as those reported previously.[3] The Newton-Raphson iterations for calculating the free ligand and free metal ion concentrations at each data point were continued until satisfactory convergence had been attained. When the residuals $|C_L(\text{observed}) - C_L(\text{calcd})|$ and $|C_M(\text{observed}) - C_M(\text{calcd})|$ failed to converge to within $10^{-5}\times C_L(\text{observed})$ and $10^{-5}\times C_M(\text{observed})$, respectively, after 150 iterations, the calculation was abandoned, and the computer proceeded to the next data point. When the total number of such non-convergent data points amounted up to 10, the initial constants were replaced by another set of estimates. Least-squares refinements were complete after 5—10 cycles when the initial estimates were nearly satisfactory, but 30 or more cycles were necessary when they were poor. Usually, 70—100 data were subjected to the least-squares treatment, which afforded the constants that could satisfactorily reproduce the titration curves. The difference between the observed and calculated titers of 0.1 M potassium hydroxide was less than 0.03 ml for all the data points with the titers ranging from 2.0 to 6.5 ml. The acid dissociation constants for each ligand were calculated from 40—50 data points.

Equilibrium Constants. Table 2 shows the equilibrium constants for the tripeptides and the two dipeptides included for comparison. The excellent fit of the theoretical titration curves to the observed ones over all the data points used substantiates the equilibria considered and the relevant constants in the 1:1 tripeptide–Cu(II) systems. When the theoretical curves were described by the three constants K_1, K_{c_1}, and K_{c_2} calculated from the data corresponding to $a=1$—4, serious deviations (*ca.* 8% when expressed in the titer) from the experimental curves were observed at $a<1$ for G·G·G–, G·G·β-A–, and G·β-A·G–Cu(II) systems. In the case of the β-A·G·G–Cu(II) system, calculation of the reliable values of K^H was not successful probably because of the very low stability of

Table 2. Equilibrium constants (25 ± 0.05 °C; $\mu=0.1$ (KNO_3))[a]

Ligand	pK_{a_1}	pK_{a_2}	log K^H	$pK_a^{Hb)}$	log K_1	pK_{c_1}	pK_{c_2}	log $K_1K_{c_1}K_{c_2}$
G·G·G	3.26±0.002	7.93±0.009	1.7[c]	4.4	5.25±0.003	5.23±0.003	6.73±0.002	−6.71
G·G·β-A	4.08±0.005	7.93±0.005	1.9	4.6	5.25±0.004	5.27±0.006	6.08±0.002	−6.10
G·β-A·G	3.34±0.005	8.09±0.002	1.8	4.2	5.60±0.003	5.36±0.004	5.74±0.003	−5.50
β-A·G·G	3.23±0.003	9.29±0.007	<1		5.28±0.018	5.32±0.027	5.54±0.011	−5.58
G·G[d]	3.14±0.006	8.09±0.006	negligible		5.50±0.001	4.10±0.001	[e]	
β-A·G[d]	3.22±0.009	9.45±0.009	negligible		5.45±0.001	4.09±0.001	[e]	

a) Variances are expressed in standard deviations estimated from the elements of the inverted matrix and the assumed error (0.01 ml) for the titers of 0.1 M potassium hydroxide. b) Calculated by eq. (9). c) The value reported by Österberg and Sjöberg[8] is 1.58 at 25° (μ=3.0($NaClO_4$)). d) Previously reported.[3] e) Not measured.

the protonated complex. Log K^H and hence the pK_a^H ($=-\log K_a^H$) values may not be sufficiently accurate, and we may safely use two significant figures for each. Some characteristic features of chelate stability can be seen from Table 2. The log K_1 values for G·G·G, G·G·β-A, and β-A·G·G are nearly the same, the value for G·β-A·G being slightly higher. A somewhat different trend is observed for the log K^H values which indicate the importance of the size of the NH_2-terminal chelate ring and the pK_a of the amino group. It is also evident from the values for G·G·G and G·G·β-A that the nature of the COOH-terminus has practically no influence on the stability constants.

Replacement of a glycine residue of G·G·G with a β-alanine residue does not seem to affect the log K_1 and pK_{c_1} ($=-\log K_{c_1}$) values greatly, but the steric effects associated with it are most clearly reflected in the pK_{c_2} ($=-\log K_{c_2}$) values, which vary from 5.54 of β-A·G·G to 6.73 of G·G·G.

The relative abundances of the species present at various pH in the tripeptide–copper(II) systems were calculated from the equilibrium constants and plotted against pH (Figs. 3(a)—(d)).

Discussion

The sequence and mode of coordination to copper(II) of the amino, peptide, and carboxyl groups of peptides have been discussed by many investigators. As regards the structures of the protonated copper(II) complexes $Cu(H_3L)^{2+}$ in acid solution, the log K^H values suggest the structure like **3** where the amino group in the coordination sphere of copper(II) is

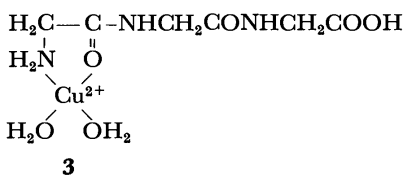

3

assumed with the carboxyl group left un-ionized. Such a structure seems to explain the higher stability of the protonated G·G·G–, G·G·β-A–, and G·β-A·G–Cu(II) complexes, which have a stable five-membered ring as compared with the less stable six-membered ring in the β-A·G·G–Cu(II) complex. The structure is not inconsistent with the crystal structure for $Cu(H_2L)^+$ [14] formed upon dissociation of a proton from $Cu(H_3L)^{2+}$ and is also in line with the NMR studies by Li *et al.*[19] and Kim and Martell[13] on the pH-dependent disappearance of the signals of the three CH_2-groups in the G·G·G–Cu(II) complex. On the other hand, no appreciable formation of the protonated complexes was detected for glycylglycine(G·G) and β-alanylglycine(β-A·G). Their titration curves could be reproduced without serious deviations by K_1 and K_{c_1} over the range covering $a=0$—3. Since the pK_a values of G·G do not differ much from those of G·G·G, the lack of the intermediate step similar to reaction 7 in the G·G–Cu(II) system suggests that the complex formation therein must be achieved, even before dissociation of the peptide proton, by the coordination of the amino, peptide, and carboxyl groups (structures **4a** and **4b**). This mode of coordination may be due to the quite favorable locations of these groups in the ligand molecule for constructing a fused-ring chelate. The reason for the behavior of β-A·G may in part be the same as that for β-A·G·G.

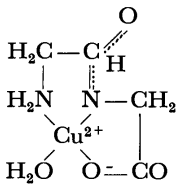

4a

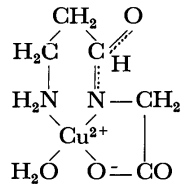

4b

We have disclosed by X-ray crystal structure analysis[20] that chloroglycylglycinatocopper(II) monohydrate, which corresponds to the tripeptide complexes of the type $Cu(H_2L)^+$, has a dimeric structure very similar to that of the G·G·G–Cu(II) complex. Although the crystal structure generally gives evidence to the structures in solution, it seems unlikely that the carboxyl groups maintain the dimeric structure even in dilute aqueous solution.[2,3] In this connection, Bair and Larsen[21] inferred from spectral studies on the isolated chelates that the binding sites in the G·G–Cu(II) chelate of the type $Cu(HL)^+$ (HL^- refers to the free G·G ion) were the amino and peptide nitrogens, although contribution of the carboxyl group remained

19) N. C. Li, R. L. Scruggs, and E. D. Becker, *J. Amer. Chem. Soc.*, **84**, 4650 (1962).

20) M. Shiro, Y. Nakao, O. Yamauchi, and A. Nakahara, *Chem. Lett.*, **1972**, 123.

21) M. L. Bair and E. M. Larsen, *J. Amer. Chem. Soc.*, **93**, 1140 (1971).

unknown.

The complexes of the type Cu(HL), where one of the peptide hydrogens is removed, have been expressed by a fused-ring structure like **5** which is also consistent with our finding about the pK_{c_1} values. We see from Table 2 that the pK_{c_1} values for the four tripeptides are very close to each other. If we assume the coordination by the tripeptides to be bidentate, we should expect a

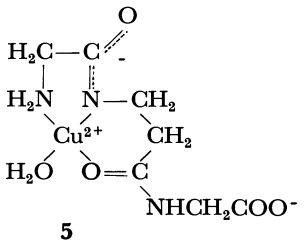

5

higher pK_{c_1} value for β-A·G·G from the usual rule for the steric effects of the ring size on stability, because pK_{c_1} can be taken as a measure of the steric accessibility of the peptide group to copper(II). The degrees of formation of Cu(HL) can be compared at a constant pH by the $K_1K_{c_1}$ values according to the following equation[2]

$$\frac{[Cu(HL)]}{[Cu^{2+}][H_2L^-]} = \frac{K_1K_{c_1}}{[H^+]} \qquad (10)$$

The small difference between the ligands (less than 0.28 log unit) is similar to that in the results obtained for the dipeptide–copper(II) systems and may be considered as indicative of approximately equal stability of 5-5-membered systems (G·G·G– and G·G·β-A–Cu(II)) and 6-5-(or 5-6-)membered systems (β-A·G·G– and G·β-A·G–Cu(II)).

In contrast to the log K_1 and pK_{c_1} values, a striking difference is observed between the pK_{c_2} values. The value for G·G·G is the highest, which may reasonably be interpreted as resulting from the steric strain due to the fused 5-5-5-membered ring (structure **2**), where the accumulated ring strains can not be relieved by a six-membered ring existing in the complexes of the other three β-alanine-containing tripeptides, whose pK_{c_2} values are more than 0.6 log unit lower.

The relative stability of the complexes of the type CuL^- at a constant pH inferred from the $K_1K_{c_1}K_{c_2}$ values in the following equation clearly indicates the effects of the overall steric requirements around copper(II) on the stability of the chelates:

$$\frac{[CuL^-]}{[Cu^{2+}][H_2L^-]} = \frac{K_1K_{c_1}K_{c_2}}{[H^+]^2} \qquad (11)$$

We see that the values decrease in the order G·β-A·G≈ β-A·G·G>G·G·β-A>G·G·G (Scheme 1), being the manifestation of accumulation of, or release from, the strains in the rigid fused-ring systems composed of three individual rings. The low stability of the probably monomeric G·G·G–Cu(II) formed in neutral and alkaline solutions might give rise to the formation of a dimer with a less hindered structure in the crystalline state.[15] Hence, it may be expected that the

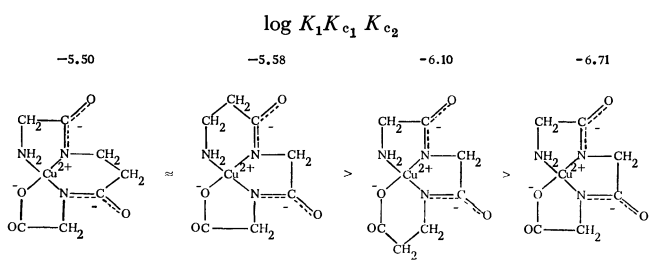

Scheme 1. Relative stabilities of the tripeptide–Cu(II) chelates of the type CuL^-

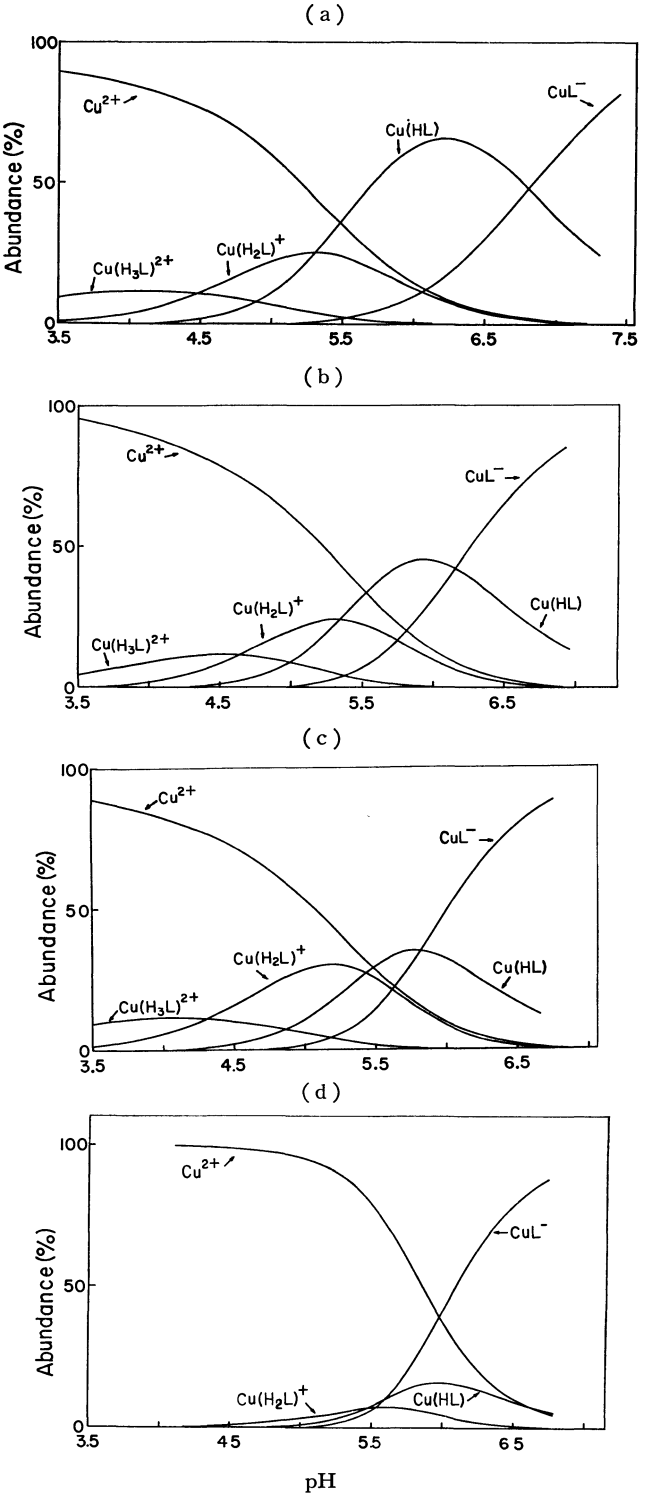

Fig. 3. Calculated abundances of the coordinated species in the 1:1 tripeptide–copper(II) systems.
(a): G·G·G–Cu(II) system, (b): G·G·β-A–Cu(II) system, (c): G·β-A·G–Cu(II) system, (d): β-A·G·G–Cu(II) system.

chelates are monomeric also in the crystalline state when the steric strains are cancelled by a β-alanine residue. It is of particular interest to note in this connection that the recent studies[22] on temperature dependence of magnetic susceptibilities of the chelates isolated as crystals indicated no copper(II)-copper(II) interactions. This supports the view that in the crystalline state the chelates of the β-alanine-containing tripeptides may have monomeric structures. On the other hand, the dimeric G·G·G–Cu(II) chelate exhibits such interactions owing to the short distance (3.077 Å)[15] between the copper(II) ions constituting the dimeric structure.

Figures 3(a)—(d) show the pH dependence of the relative amounts of the species present in the 1:1 tripeptide–copper(II) systems. In acid solution, the protonated complexes are present over considerably wide pH ranges. The four coordinated species $Cu(H_3L)^{2+}$, $Cu(H_2L)^{+}$, Cu(HL), and CuL^{-} are present at pH 5—6 in the systems of the tripeptides with glycine at the NH_2-terminus. In the G·G·G–Cu(II) system, there is a distinct peak for Cu(HL) at pH 6.2 ascribable as being due to the difficulty of deprotonation from the peptide group nearest the carboxyl terminus. Thus, formation of the species CuL^{-} in this system occurs at higher pH values as compared with other systems. However, the predominant species at pH above 7 is CuL^{-} in all the systems investigated, which may be taken as evidence for the bonding modes in the biological fluid.

The authors wish to thank members of the Osaka University Computation Center for computations. The investigation was supported in part by a grant from the Japanese Ministry of Education.

22) W. Mori, Y. Nakao, O. Yamauchi, M. Kishita, and A. Nakahara; Proceedings of the 21st Annual Symposium of Coordination Chemistry, Nagoya, p. 285 (1971).

BULLETIN OF THE CHEMICAL SOCIETY OF JAPAN, VOL. 46, 2124—2128 (1973)

The Metal Ammine Cyanide Aromatics Clathrates. XVI. Wide-Line NMR Studies of the Three-Spin Systems of Ligand Ammonia in Paramagnetic Hofmann-type Clathrates

Taku NAKANO*

Department of Chemistry, Faculty of Science, The University of Tokyo, Hongo, Tokyo 113

(Received November 7, 1972)

Wide-line NMR studies of ammonia molecules in Hofmann-type clathrates with the general formula jo $M(NH_3)_2M'(CN)_4 \cdot 2C_6D_6$ are reported. In the Hofmann-type clathrates, two ammonia molecules coordinate to the paramagnetic metal ions in *trans* positions and have only a slight interaction with each other. In powder samples, the proton NMR spectra of ammonia give fine structures with three components, which are caused by dipolar interaction between protons of the rotating triangular three-spin system. The signals shift to the higher-field side under the influence of the paramagnetic moments of the metal ions. The temperature dependence of the shifts and line shapes, where M is iron(II), cobalt(II), nickel(II), and copper(II), will be reported on. No rigid ammonia was found, even at the temperature of liquid nitrogen.

Previously, in this laboratory, the Hofmann-type clathrates with general formula of $M(NH_3)_2M'(CN)_4 \cdot 2G$ have been prepared.[1-4] Their structure, determined on the basis of the single-crystal X-ray diffraction data, are illustrated in Fig. 1.[5-8] The clathrates consist of an inorganic host lattice formed infinite net planes, $[M(NH_3)_2M'(CN)_4]_\infty$, and aromatic guest molecules, G, such as benzene or aniline, trapped

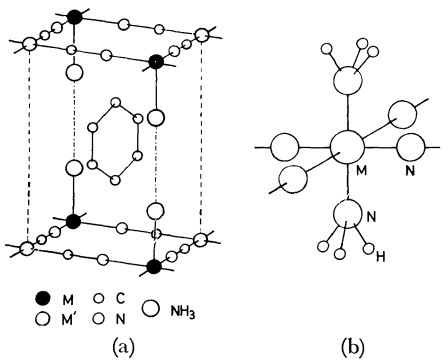

Fig. 1. Structure of Hofmann-type clathrates, $M(NH_3)_2M'(CN)_4 \cdot 2C_6H_6$.
(a) A cavity for one benzene molecule.
(b) Coordination of ammonia molecule to a divalent metal ion.

* Present address: Faculty of Pharmaceutical Sciences, University of Toyama, Gofuku, Toyama 930.

1) T. Iwamoto, T. Miyoshi, T. Miyamoto, Y. Sasaki, and S. Fujiwara, This Bulletin, **40**, 1174 (1967).
2) T. Nakano, T. Miyoshi, T. Iwamoto, and Y. Sasaki, *ibid.*, **40**, 1297 (1967).
3) M. Morita, T. Miyoshi, T. Iwamoto, T. Miyamoto, and Y. Sasaki, *ibid.*, **40**, 1556 (1967).
4) T. Iwamoto, T. Nakano, M. Morita, T. Miyoshi, T. Miyamoto, and Y. Sasaki, *Inorg. Chim. Acta*, **2**, 313 (1968).
5) J. H. Rayner and H. M. Powell, *J. Chem. Soc.*, 319 (1952).
6) Y. Sasaki, This Bulletin. **42**, 2412 (1969).
7) T. Miyoshi, *Inorg. Chim. Acta*, in press.
8) K. Kuroda, Master Thesis, The University of Tokyo, 1971.

in the lattice. Here, M means the divalent transition metal ions, Mn, Fe, Co, Ni, Cu, Zn, and Cd, which occupy the octahedral site, $M(NH_3)_2(NC)_4$, and M′ is divalent Ni, Pd, or Pt, in the square-palnar site, $M'(CN)_4$. To the metal ion, M, four bridging cyanide ions coordinate with nitrogen atoms in the square-planar configuration and two ammonia molecules in *trans* positions (Fig. 1b).

As has been reported in previous papers, the clathrates whose octahedral sites are occupied by Zn or Cd are diamagnetic, and those containing paramagnetic divalent transition metals are high-spin complexes. The temperature dependence of the paramagnetic susceptibility obeys Curie's law throughout the range from 76 to 300 K.[4]

Beside the structure determination, wide-line NMR studies were undertaken, and the motion of the guest molecules was successfully studied.[9] Two ammonia ligands attached to an octahedral metal ion appear to be magnetically well shielded from each other, and the NMR signals split into fine structures which could not be observed in other, ordinary metal ammine complexes.[10]

A diamagnetic clathrate, $Cd(NH_3)_2Ni(CN)_4\cdot 2C_6D_6$, has already been studied by Miyamoto.[11] He used single crystals containing deuterated benzene and analyzed the ammonia spectra by the use of the three-spin-system model of Andrew and Bersohn;[12] he thus obtained the proton-proton distance from the line splitting in the fine structures, and also from the second-moment data. No rigid ammonia was found at the temperature of liquid nitrogen.

In paramagnetic substances, a wide-line NMR is influenced by electron spins and so is the source of much information about structures. The subjects of the present report are paramagnetic Hofmann-type clathrates containing divalent transition metals, Mn, Fe, Co, Ni, and Cu, in the high-spin state.

Apart from their interest in the connection with the phenomena of clathration, these compounds were used to study the general problem of the magnetic behavior of ammonia molecules coordinated to paramagnetic cations. The situations are favorable; the NMR spectra show fine structures, the metals take a series of electron configurations from d^5 to d^9, and moreover, all the complexes are isostructural.

The only data previously available were those of Umemoto and Danyluk[13] for $Ni(NH_3)_2Ni(CN)_4\cdot 2C_6H_6$ and $2C_6D_6$; our interpretations are different from theirs.

Experimental

Materials. The clathrates investigated were prepared by the methods described in the previous papers.[2,4] When M was Mn, Fe, or Co, the preparations and measurements were carried out in a nitrogen atmosphere to protect the metal ions from oxidation. The powder samples of about one gram for each species were sealed in a glass tube 10 mm in diameter, avoiding the oxidation of the sample and the escape of benzene from the clathrates.

Apparatus. The NMR spectra were recorded with a JEOL-JNM-W30 spectrometer (30 MHz) of the Anderson-bridge type. The spectra of the clathrates were recorded as derivative curves at temperatures from 100 to 296 K, the measurements being made with a copper-constantan thermocouple. The samples were cooled with a cold nitrogen stream from a liquid nitrogen bottle. To ascertain the values of the shifts of the signals from the Larmor frequency, isopentane (mp 113 K) in a capillary on the wall of the sample tube was used as the reference compound.

Results and Discussion

The Wide-line NMR Spectra of $M(NH_3)_2Ni(CN)_4\cdot 2C_6H_6$. The superimposed spectra of the protons of benzene and ammonia molecules in Hofmann-type clathrates at room temperature are shown in Fig. 2.

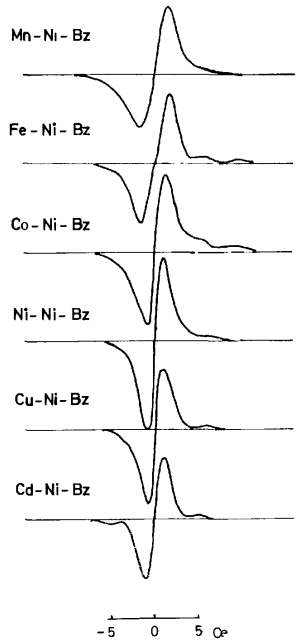

Fig. 2. Wide-line NMR spectra of ammonia protons and benzene protons in Hofmann-type clathrates, $M(NH_3)_2Ni(CN)_4\cdot 2C_6H_6$ at 296 K.

The signal of diamagnetic clathrate is symmetric with respect to the Larmor frequency, whereas the signals of the paramagnetic ones are asymmetric; the degree of asymmetry grows with the paramagnetic moments of the compounds. Apparently, the asymmetry is mainly due to the large shift of the ammonia protons. The signals of benzene protons do not vary for different clathrates at room temperature.

The Spectra of $M(NH_3)_2Ni(CN)_4\cdot 2C_6D_6$. As is shown in Fig. 3, ammonia in the Hofmann-type clathrates which contain deuterated benzene gives NMR spectra at 296 K with fine structures, typical of a trianglar three-spin system, except in the case of the manganese compound.

In Figs. 4—7, the signals of ammonia in four complexes in the derivative form at various temperatures are

9) T. Miyamoto, T. Iwamoto, and Y. Sasaki, *J. Mol. Spectrosc.*, **35**, 244 (1970).
10) P. H. Kim, *J. Phys. Soc. Jap.*, **15**, 445 (1960).
11) T. Miyamoto, *Inorg. Chim. Acta*, **3**, 511 (1969).
12) E. R. Andrew and R. Bersohn, *J. Chem. Phys.*, **18**, 159 (1950).
13) K. Umemoto and S. S. Danyluk, *J. Phys. Chem.*, **71**, 450 (1967).

shown. All the spectra show a higher-field shift at lower temperatures, though they have delicate variations in shape. If they are compared as integral forms, the distances between the three peaks are constant. The shift increases to the higher-field side, and the tails of the signals are more elongated to the lower-field side, so that the accurate computation of the second moments was not possible, in practice. As will be shown later, the long tailing in the spectra demonstrates that the shift depends upon the angle of the *c*-axis of the crystallines in the magnetic field.

Analyses of Ammonia Spectra. The above features of the spectra were explained theoretically and provide knowledge of the molecular structure.

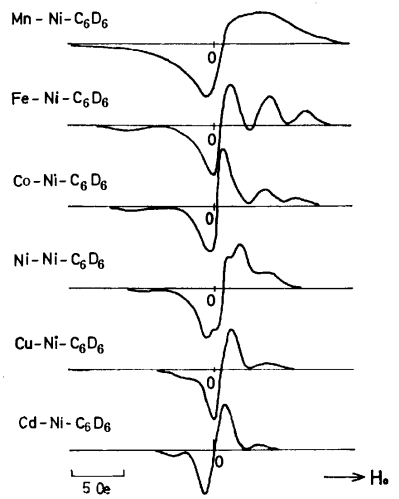

Fig. 3. Wide-line NMR spectra of ammonia protons in Hofmann-type clathrates, $M(NH_3)_2Ni(CN)_4\cdot 2C_6D_6$ at 296 K.

In order to consider the system,[10,11] we take the effective spin Hamiltonian of the system as:

$$H_{\text{eff}} = H^\circ + H_1' + H_2' + H_3'$$

$$H^\circ = -\sum_{j=1}^{3}\gamma_N\hbar I_{zj}H_0$$

$$H_1' = \sum_{i>j}\frac{\gamma_N^2\hbar^2(3\cos^2\theta_{ij}-1)}{2r_{ij}}(\mathbf{I}_i\cdot\mathbf{I}_j - 3I_{zj}I_{zi})$$

$$H_2' = -\sum_{j=1}^{3}\frac{\gamma_N\hbar(3\cos^2\theta_j-1)}{r_j^3}(\gamma_e\hbar\langle S_z\rangle)I_{zj}$$

$$H_3' = \sum_{j=1}^{3}a_j\langle S_z\rangle I_{zj}$$

$$a_j = \frac{8\pi}{3}\gamma_N\gamma_e\hbar^2\delta_j$$

$$\delta_j \equiv \langle\Psi_1|\sum_k\delta(r_{kj})S_{kz}|\Psi_1\rangle/S_z \qquad (1)$$

where the four terms, H°, H_1', H_2', and H_3', are the Zeeman term, the dipolar interaction between three protons, the dipolar interaction between paramagnetic moment and protons, and the Fermi-type contact interaction respectively. In Eq. (1), r_{ij} is the distance between the i and j nuclei, r_j is the distance between the metal ion and the j nucleus, θ_j is the angle between the applied field, $\boldsymbol{H}_0$, and $\boldsymbol{r}_j$, a_j is the coefficient of the contact interaction, Ψ_1 is a wave function of the electrons, and $\boldsymbol{r}_{kj}$ is the vector between the electron and j nucleus. The other symbols have their usual meanings.

In the present compounds, the paramagnetism obeys Curie's law, so we assumed the time-average value of the z component of the electron spin, $\langle S_z\rangle$, to be:

$$\langle S_z\rangle = \frac{\gamma_N\hbar S(S+1)}{3kT}\boldsymbol{H}_0 \qquad (2)$$

When the applied magnetic field is large enough, *i.e.*, $H^\circ \gg H'$, H' is treated as a first-order perturbation.

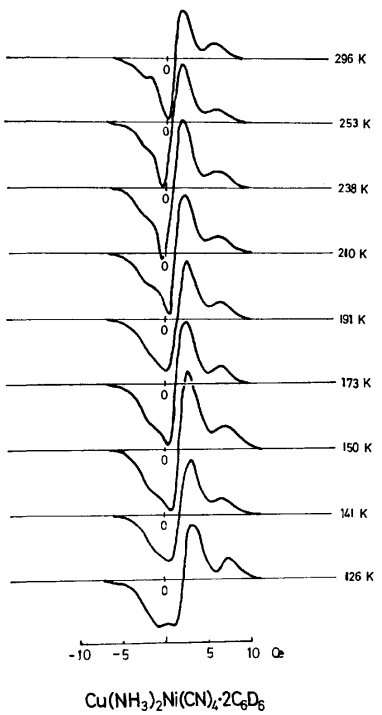

Fig. 4. Wide-line NMR spectra of ammonia of $Cu(NH_3)_2Ni(CN)_4\cdot 2C_6D_6$ at various temperatures,

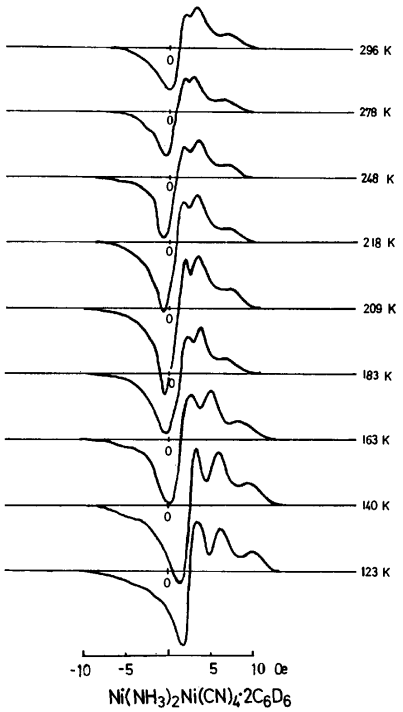

Fig. 5. Wide-line NMR spectra of ammonia of $Ni(NH_3)_2Ni(CN)_4\cdot 2C_6D_6$ at various temperatures.

Taking the spin eigenfunctions of the three-spin system ($\mathbf{I}_i=1/2$), and assuming that the ammonia molecules rotate about the three-fold axes, parallel to the c-axis of the crystals, we may obtain the diagonal matrix and then the energy diagram for this system shown in Fig. 9. The possible transitions are shown in Fig. 9; the selection rules are $\Delta M_I=\pm 1$, $\Delta\mathbf{J}=0$, and $\Delta\mathbf{I}=0$, where $\mathbf{J}=\mathbf{I}_1+\mathbf{I}_2$ and $\mathbf{I}=\mathbf{J}+\mathbf{I}_3$.

Since $\gamma_N\hbar\boldsymbol{H}^*=h\nu$, the absorptions occur at:

$$\begin{aligned}
&\mathbf{1} \quad \boldsymbol{H}_0=\boldsymbol{H}^*+\frac{1}{\gamma_N\hbar}(\mathrm{B}+4\mathrm{X}) \quad |-\tfrac{1}{2}\rangle\rightarrow|-\tfrac{3}{2}\rangle\\
&\mathbf{2,3} \quad \boldsymbol{H}_0=\boldsymbol{H}^*+\frac{1}{\gamma_N\hbar}\mathrm{B} \quad |\tfrac{1}{2}\rangle\rightarrow|-\tfrac{1}{2}\rangle\\
&\mathbf{4} \quad \boldsymbol{H}_0=\boldsymbol{H}^*+\frac{1}{\gamma_N\hbar}(\mathrm{B}-4\mathrm{X}) \quad |\tfrac{3}{2}\rangle\rightarrow|\tfrac{1}{2}\rangle \qquad (3)
\end{aligned}$$

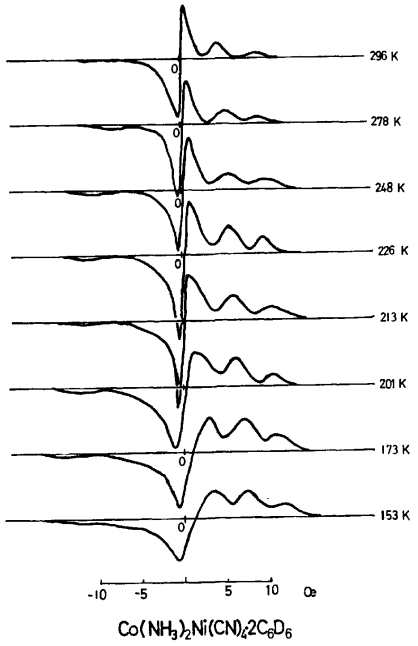

Fig. 6. Wide-line NMR spectra of ammonia of $Co(NH_3)_2$-$Ni(CN)_4\cdot 2C_6D_6$ at various temperatures.

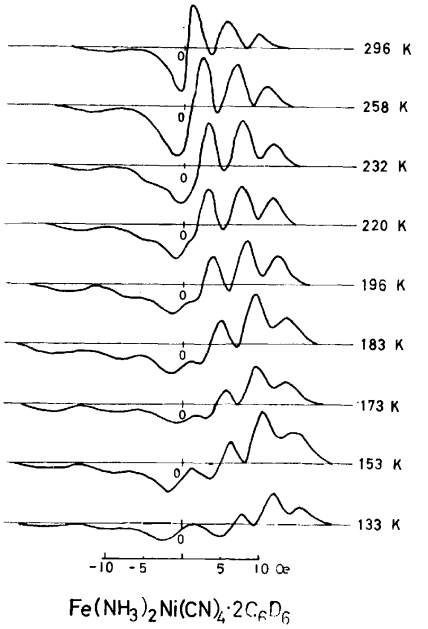

Fig. 7. Wide-line NMR spectra of ammonia of $Fe(NH_3)_2$-$Ni(CN)_4\cdot 2C_6D_6$ at various temperatures.

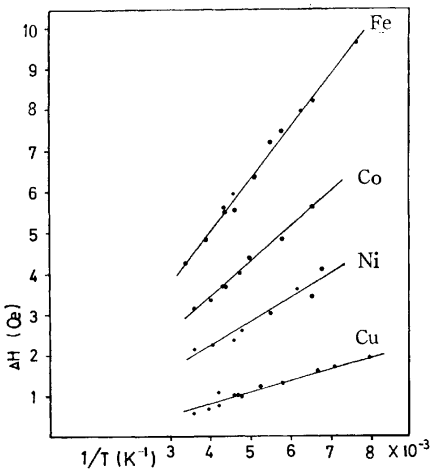

Fig. 8. Temperature dependency of paramagnetic shifts of Hofmann-type clathrates.

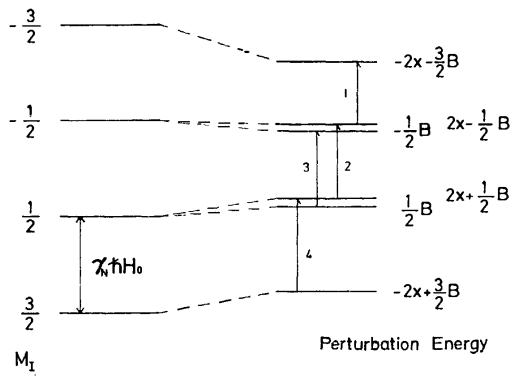

Fig. 9. Energy diagram for the three-spin system perturbed by a paramagnetic moment.

where

$$\mathrm{X}=\frac{3}{16}\gamma_N^2\hbar^2(1-3\cos^2\theta)r_{p\text{-}p}^{-3}$$

$$\mathrm{B}=\frac{1}{2}\gamma_N\hbar(3\cos^2\gamma-1)(1-3\cos^2\theta)r_{p\text{-}p}^{-3}$$

$$\times\ \gamma_e\hbar\langle S_z\rangle+a\langle S_z\rangle$$

and where θ and γ are angles between c-axis and the applied magnetic field and between c-axis and the vector $\boldsymbol{r}_j$ respectively.

The probabilities of the transitions are 1/4, 1/2, and 1/4 respectively. The theoretical spectra are illustrated in Fig. 10. In terms of the dipole-dipole interactions among protons, the signal consists of three components and the distance is $4X/\gamma_N\hbar$, while the paramagnetic shift, $B/\gamma_N\hbar$, equally contributes to each component and depends upon the reciprocal absolute temperature.

In powder samples, fine crystallites are distributed over the angle, θ, on which the positions of the signals for the segments depend. The theoretical line shape for polycrystalline samples is obtained in calculating $g(h)=P\cdot d(\cos\theta)/dh$, where P is a transition probability and where $h=\boldsymbol{H}_0-(\boldsymbol{H}^*+C)$; it is shown in Fig. 10; $g(h)=(-h/\alpha_i+1)^{-1/2}$; α_i and C are given in the caption of Fig. 10.

The Shift Caused by the Paramagnetic Moment. The observed spectra can be satisfactorily explained by

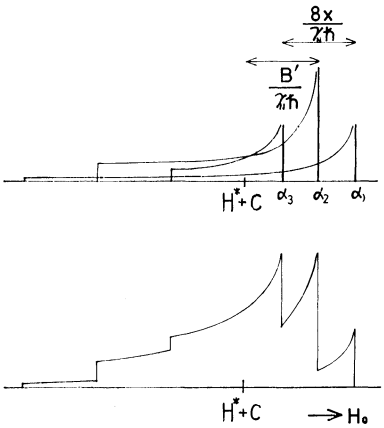

Fig. 10. Paramagnetic shifts and theoretical line shapes for components, where
$\alpha_1=1/2\,\gamma_e\hbar\langle S_z\rangle(3\cos^2\gamma-1)r_{p\text{-}e}^{-3}+3/4\,\gamma_N\hbar r_{p\text{-}p}^{-3}$
$\alpha_2=1/2\,\gamma_e\hbar\langle S_z\rangle(3\cos^2\gamma-1)r_{p\text{-}e}^{-3}$
$\alpha_3=1/2\,\gamma_e\hbar\langle S_z\rangle(3\cos^2\gamma-1)r_{p\text{-}e}^{-3}-3/4\,\gamma_N\hbar r_{p\text{-}p}^{-3}$
$C=a/\gamma_N\hbar\langle S_z\rangle$, $B'=B-a\langle S_z\rangle$
$r_{p\text{-}p}$ is the distance between adjacent protons, $r_{p\text{-}e}$ is the distance between metal ion and protons, and γ is the angle between $r_{p\text{-}e}$ and c-axis.

the above theoretical treatment of the shifts and line shapes. Both the isotropic and anisotropic paramagnetic interactions cause the signals to shift to the higher-field side; this makes the signal very asymmetric.

As the central peak in the three components does not always have the highest intensity in the powder samples shown in Fig. 10, we should read the value of the paramagnetic shift not at the highest peak, as has been done,[13] but at the central peak, *i.e.*, the second one from the higher-field side.

When the fine structure does not appear, as in the case of the previously-reported metal ammine complexes, the value of the shift cannot be read with certainty.

The linearity of the paramagnetic shift expressed by Eq. (2) is seemingly well demonstrated in Fig. 8. The paramagnetic shift thus measured contains the dipolar and the contact interaction, both of them proportional to $1/T$. The former is angular-dependent, but the latter is not. By the use of single-crystal samples, these two kinds of shifts could be measured separately.

The sole data[14] of the contact shift for metal ammine complexes have been obtained by the use of liquid ammonia solutions, in which the angular-dependent shift vanishes because of the thermal motion. The reported values for the hexammine complex ions, $[Mn(NH_3)_6]^{2+}$, $[Co(NH_3)_6]^{2+}$, $[Ni(NH_3)_6]^{2+}$, and $[Cu(NH_3)_6]^{2+}$, at 311 K are −0.68, 0.17, 0.50, and 0.34 Oe (recalculated for 30 MHz) respectively. In the present systems, the contact shifts may be of the same order and may be rather small compared to the total shift values.

The fine structure of the spectra indicates that the ammonia molecule in the compounds does not interact with the neighboring one at the *trans* position and the other nuclei; then, width become narrower than that of other ammine complexes. Furthermore, the fact that the values of the paramagnetic moments scarcely affect the dipolar broadening of the components, except for manganese clathrate, means that the electron spins on the metal ions next to the one to which ammonia coordinates do not interact with protons.

Structure and Motion of Ammonia. Using the above model, it is possible to obtain the proton-proton distance if the value of the line splitting X, in Eq. (3), is known with enough accuracy.

The spectra were transformed into the integral form and then analyzed to obtain the proton-proton distances by means of Eq. (3). The values of $r_{p\text{-}p}=1.7_0-1.7_9$ Å were obtained for all the clathrates, though the accuracy is not very high. The assumption of rigid ammonia would also explain the fine structure with three peaks, but numerical calculations lead to an abnormally long proton-proton distance.

The constancy of the X value on the change in the temperature suggests that ammonia molecules are not rigid even at the temperature of liquid nitrogen, and that the proton-proton interaction is not decoupled by the paramagnetism of the metal cation to which the ammonia molecules are coordinated.

The values of the shifts and the shape of the spectra of the ammonia protons were thus explained by the model of the triangular rotating three-spin system perturbed by the paramagnetism of the transition metal cation to which the ammonia ligands are coordinated.

Although the lattice is composed of infinite net planes with bridges of cyanide ions, the d-electrons of the metal ion appear to be around the divalent cations and are not delocalized.

The manganese clathrate is different from the other compounds; independent study of it necessary.

The author wishes to thank Professor Yukiyoshi Sasaki for encouraging him throughout this work.

14) B. B. Wayland and W. L. Rice, *Inorg. Chem.*, **6**, 2270 (1967).

Cathodic Waves of *o*-Hydroxyphenylmercury Chloride in Aqueous Nitric Acid Medium. Inhibition by Reaction Product and Reduction of Precipitate

Teisuke MURAYAMA and Motonobu MORIOKA

Department of Industrial Chemistry, Faculty of Engineering, Shizuoka University, Johoku, Hamamatsu 432

(Received December 1, 1972)

Polarographic behavior of *o*-hydroxyphenylmercury chloride was examined in aqueous nitric acid medium. An abnormal first wave and a peculiar angular-shaped second wave were observed. Equations of the current-potential curves of the first and second waves are derived on the following assumptions: the first wave is inhibited by a reduction product adsorbed on the surface of the dropping mercury electrode as solid particles, the adsorbed precipitate being reduced at the second wave. The equations agree well with the observed results.

In a previous paper, inhibition of an electrode process by a reduction product of another electroactive species was discussed in relation to its current-time behavior.[1] This paper reports inhibition of an electrode process by its own reduction product.

Polarographic behavior of *o*-hydroxyphenylmercury chloride (*o*-HPMC) in 80% ethanol solution was studied by Sato.[2] He observed double one-electron waves of normal shape. This compound is soluble in water. We examined its polarographic behavior in aqueous solutions and observed an abnormal first wave and a peculiar angular-shaped second wave in aqueous nitric acid medium. It was revealed that the first wave is inhibited by a reduction product which is adsorbed on the surface of the dropping mercury electrode (DME) as solid particles, and that the adsorbed precipitate is reduced at the second wave.

Experimental

o-HPMC was prepared according to the method of Whitmore and Middleton,[3] and recrystallized from water several times: mp 152 °C (lit.[4] 152.5 °C). A stock solution was made by dissolving a weighed amount.

The nitric acid medium, used as a supporting electrolyte solution, was a mixture of 0.05 M nitric acid and 0.45 M sodium nitrate. Acetate buffer solutions, whose ionic strength was controlled to 0.50 with sodium nitrate, were also used as supporting electrolyte solution. All the supporting electrolyte solutions contained also 0.005% gelatin.

All solutions were prepared with redistilled water. Test solutions were degassed with nitrogen and thermostated at 25.0±0.1 °C.

The capillary constant ($m^{2/3}t^{1/6}$) of a DME was 1.810 $mg^{2/3}\,sec^{-1/2}$ at zero applied potential *vs.* SCE and at mercury pressure of 1000 mm. The cell and salt bridge are described elsewhere.[5] A manual instrument was used for the measurement of polarograms. Polarograms were corrected for the internal resistance (*iR* drop) across the cell and the residual current.

Results and Discussion

Figure 1 shows typical polarograms of *o*-HPMC in aqueous solutions. Polarograms in acetate buffer solutions have a normal shape and their diffusion currents increase linearly with increasing concentration of *o*-HPMC. The polarogram in the nitric acid medium, however, has a peculiar angular-shaped second wave. The first wave shifts to negative potentials with increasing concentration of *o*-HPMC in spite of its irreversibility. In the following discussion is confined to the behavior in the nitric acid medium.

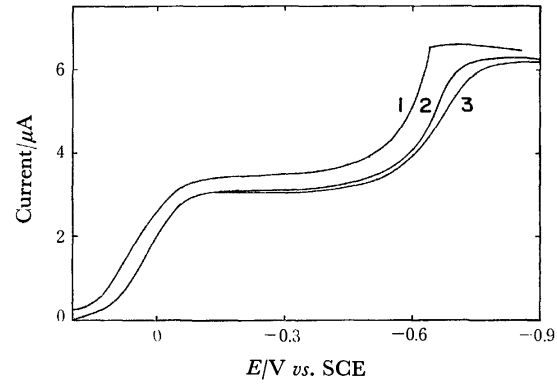

Fig. 1. Polarograms of *o*-HPMC.
Concentration of *o*-HPMC, 1.000 mM. Supporting electrolyte solution: 1, nitric acid medium; 2, acetate buffer (pH 4.38); 3, acetate buffer (pH 5.21).

The first wave in the nitric acid medium is preceded by a small wave, which does not exist in polarograms in acetate buffer solutions (Fig. 1). The height of this small wave increases slowly with degassing time. Dimroth decomposed *o*-HPMC by boiling with hydrochloric acid, and obtained phenol and mercuric chloride.[6] Thus it seems that the small wave is due to mercuric ions produced by the protolysis of *o*-HPMC. The current measured at 0.20 V *vs.* SCE was identified as diffusion current of mercuric ions produced by the protolysis reaction, and subtracted from the current due to *o*-HPMC. The current corrected in this way is denoted by i^{I}.

Logarithmic plots of the first wave are given in Fig. 2, where i_d^{I} is the diffusion current of the first wave.

1) T. Murayama and A. Takayanagi, This Bulletin, **45**, 2233 (1972).

2) H. Sato, *Eisei Shikenjo Hokoku*, **75**, 50 (1957).

3) F. C. Whitmore and E. B. Middleton, *J. Amer. Chem. Soc.*, **43**, 619 (1921).

4) L. G. Makarova and A. N. Nesmeyanov, "Methods of Elemento-Organic Chemistry," Vol. 4, North-Holland Publishing Co., Amsterdam (1967), p. 83.

5) T. Murayama, T. Sawaki, and S. Sakuraba, This Bulletin, **43**, 2820 (1970).

6) O. Dimroth, *Ber.*, **31**, 2154 (1898).

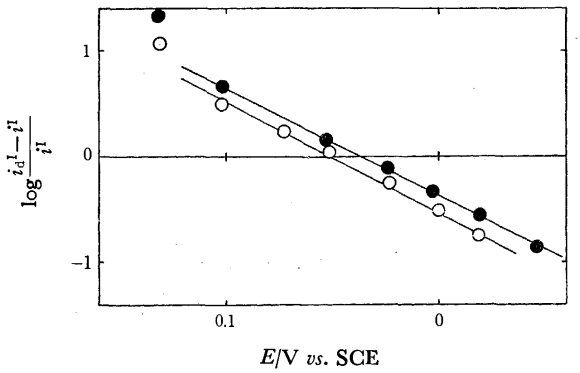

Fig. 2. Relation of log $(i_d^I-i^I)/i^I$ *vs.* E.
Mercury pressure, 1000 mm. Concentration of *o*-HPMC: ○, 0.400 mM; ●, 1.000 mM.

The slope of these plots indicates that the electrode process is totally irreversible. Thus the half-wave potential of the wave is expected to be constant and independent of the concentration of the electroactive species.[7] However, the half-wave potential shifts actually to negative with increasing concentration of *o*-HPMC. The first wave is abnormal in this respect.

The result of measurement of the electrocapillary curve indicates that a considerable adsorption takes place on the surface of DME in the range of potentials between the first and second waves (Fig. 3). This suggests that a reduction product of the first wave is adsorbed on the electrode surface and reduced further to non-adsorbable species at the potential of the second wave.

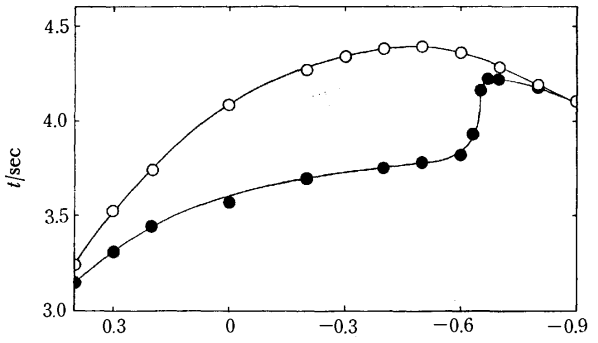

Fig. 3. Effect of *o*-HPMC on the electrocapillary curve.
○, nitric acid medium; ●, nitric acid medium + 1.000 mM *o*-HPMC.

If this is the case, the electrode reaction at the second wave may be written as

$$A + e \xrightarrow{k_2} B \qquad (1)$$

where A is the reduction product of the first wave and adsorbable on the surface of DME, B the reduction product of the second wave and non-adsorbable, and k_2 the rate constant of the electrode process. The rate constant k_2 varies with the electrode potential E according to the equation

$$k_2 = k_2^\circ \exp\left[-\frac{\alpha_2 F}{RT}(E-E_2^\circ)\right] \qquad (2)$$

where E_2° is the standard potential of reaction (1), k_2° the rate constant at E_2°, α_2 the transfer coefficient, F the Faraday constant, R the gas constant, and T the absolute temperature. The current of the second wave is given by

$$i^{II} = Fqk_2C_A^* \qquad (3)$$

where i^{II} is $i^I-i_d^I$, q the mean surface area of DME, and C_A^* the concentration of A at the electrode surface.

In order to account for the peculiar shape of the second wave we assume that A is a precipitate with very low solubility. Thus C_A^* is given by

$$C_A^* = S_A \qquad (4)$$

where S_A is the solubility of A. Introduction of Eqs. (2) and (4) into Eq. (3) results

$$i^{II} = FqS_Ak_2^\circ \exp\left[-\frac{\alpha_2 F}{RT}(E-E_2^\circ)\right]$$

This equation can be written in the form

$$E = E_2^\circ + \frac{2.303RT}{\alpha_2 F}\log FqS_Ak_2^\circ - \frac{2.303RT}{\alpha_2 F}\log i^{II} \qquad (5)$$

It is evident from Eq. (5) that a plot of log i^{II} *vs.* E should produce a straight line with a reciprocal slope equal to $2.303\,RT/(\alpha_2 F)$. The plot constructed from observed polarograms is shown in Fig. 4. The reciprocal slope of the straight line is 0.167 V, consistent with the total irreversibility of reaction (1).

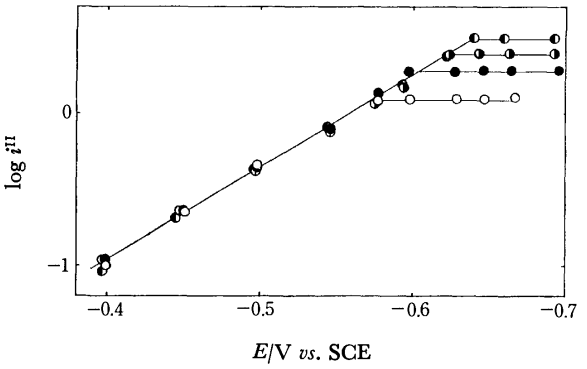

Fig. 4. Relation of log i^{II} *vs.* E.
Concentration of *o*-HPMC: ○, 0.400 mM; ●, 0.600 mM; ◑, 0.800 mM; ◐, 1.000 mM.

If A is a precipitate and is adsorbed on the electrode surface, it is expected that A inhibits the electrode process of the first wave. In the absence of inhibition the electrode reaction of the first wave may be written as

$$Z + e \xrightarrow{k_1} A \qquad (6)$$

where Z is *o*-HPMC, and k_1 is the rate constant of the electrode reaction in the absence of inhibition. The rate constant k_1 varies with E as given by

$$k_1 = k_1^\circ \exp\left[-\frac{\alpha_1 F}{RT}(E-E_1^\circ)\right] \qquad (7)$$

where E_1° is the standard potential of reaction (6), k_1° the rate constant at E_1°, and α_1 the transfer coefficient. If k_1 varies according to Eq. (7), the electrode potential

7) J. Heyrovský and J. Kůta, "Principles of Polarography," Academic Press, New York, N. Y. (1966), p. 213.

is given by

$$E = E_1^\circ + \frac{RT}{\alpha_1 F} \ln 0.886 k_1^\circ D_Z^{-1/2} t^{1/2} + \frac{RT}{\alpha_1 F} \ln \frac{i_d^I - i^I}{i^I} \quad (8)$$

where t is the drop time of DME, and D_Z the diffusion coefficient of Z.[7]

In the presence of inhibition the electrode reaction at the surface covered with A proceeds with the rate constant k_{1c}, differing from that at free surface. As a first approximation, the effective rate constant k_{ef} can be written as

$$k_{ef} = k_1(1-\Theta) + k_{1c}\Theta \quad (9)$$

where Θ is the mean surface fraction of the electrode covered with A.[8] The rate constant k_{1c} is given by

$$k_{1c} = k_{1c}^\circ \exp\left[-\frac{\alpha_{1c} F}{RT}(E - E_1^\circ)\right] \quad (10)$$

where k_{1c}° is the rate constant at E_1°, and α_{1c} the transfer coefficient at the covered surface. Substituting k_{ef} for k_1 in the derivation of Eq. (8) one obtains

$$E = E_1^\circ + \frac{RT}{\alpha_1 F} \ln 0.886 k_1^\circ D_Z^{-1/2} t^{1/2} + \frac{RT}{\alpha_1 F} \ln\left[1 - \left(1 - \frac{k_{1c}}{k_1}\right)\Theta\right] + \frac{RT}{\alpha_1 F} \ln \frac{i_d^I - i^I}{i^I} \quad (11)$$

The half-wave potential is given by

$$E_{1/2} = E_1^\circ + \frac{RT}{\alpha_1 F} \ln 0.886 k_1^\circ D_Z^{-1/2} t^{1/2} + \frac{RT}{\alpha_1 F} \ln\left[1 - \left(1 - \frac{k_{1c}}{k_1}\right)\Theta\right]_{1/2} \quad (12)$$

where the subscript 1/2 indicates the value at the half-wave potential. The first and second terms in the right-hand side are independent of the concentration of *o*-HPMC, whereas the third term becomes zero by decreasing the concentration to zero.

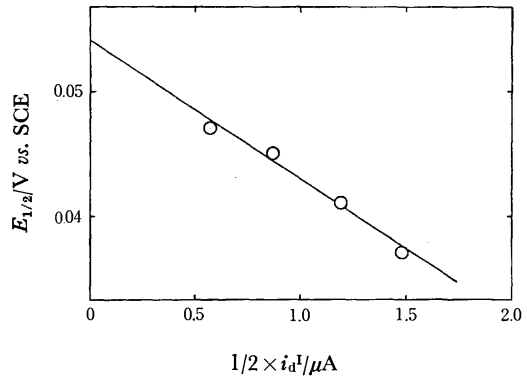

Fig. 5. Relation of $E_{1/2}$ *vs.* $i_d^I/2$.
Mercury pressure, 1000 mm.

The observed $E_{1/2}$ shifts linearly to negative by increasing the current at $E_{1/2}$, *i.e.* $i_d^I/2$, as shown in Fig. 5. One may write as

$$E_{1/2} = a + b(i_d^I/2) \quad (13)$$

where a and b are constants. Comparison of Eqs. (12) and (13) results

$$b\left(\frac{i_d^I}{2}\right) = \frac{RT}{\alpha_1 F} \ln\left[1 - \left(1 - \frac{k_{1c}}{k_1}\right)\Theta\right]_{1/2} \quad (14)$$

The fraction of covered surface increases proportionately with the amount of A on the surface of DME, which is proportional to $i^I t$. Hence Θ is given by

$$\Theta = \frac{si^I t}{q} \quad (15)$$

where s is a proportionality constant.

By introducing Eq. (15) into Eq. (14), expanding the logarithm, and retaining only the first term, one get

$$b\left(\frac{i_d^I}{2}\right) = -\frac{RTst}{\alpha_1 Fq}\left[1 - \left(\frac{k_{1c}}{k_1}\right)_{1/2}\right]\frac{i_d^I}{2} \quad (16)$$

where

$$\left(\frac{k_{1c}}{k_1}\right)_{1/2} = \frac{k_{1c}^\circ}{k_1^\circ} \exp\left[\frac{(\alpha_1 - \alpha_{1c})F}{RT}(E_{1/2} - E_1^\circ)\right] \quad (17)$$

Division of Eq. (16) by $i_d^I/2$ results

$$b = -\frac{RTst}{\alpha_1 Fq}\left[1 - \left(\frac{k_{1c}}{k_1}\right)_{1/2}\right] \quad (18)$$

Since the half-wave potential of a totally irreversible wave is more negative than the standard potential of the reaction, $E_{1/2} - E_1^\circ$ is not equal to zero. Hence the right-hand side of Eq. (18) does not generally remain constant. To keep this remaining constant one must conclude that

$$\alpha_1 - \alpha_{1c} = 0 \quad (19)$$

By expansion of the logarithm and introduction of Eqs. (15) and (19), the third term in the right-hand side of Eq. (11) can be approximately written as

$$\frac{RT}{\alpha_1 F} \ln\left[1 - \left(1 - \frac{k_{1c}}{k_1}\right)\Theta\right] = -\frac{RTst}{\alpha_1 Fq}\left(1 - \frac{k_{1c}^\circ}{k_1^\circ}\right) i^I \quad (20)$$

Combination of this with Eq. (11) yields

$$E = E_1^\circ + \frac{2.303RT}{\alpha_1 F} \log 0.886 k_1^\circ D_Z^{-1/2} t^{1/2} - \frac{RTst}{\alpha_1 Fq}\left(1 - \frac{k_{1c}^\circ}{k_1^\circ}\right) i^I + \frac{2.303RT}{\alpha_1 F} \log \frac{i_d^I - i^I}{i^I} \quad (21)$$

The half-wave potential is now given by

$$E_{1/2} = E_1^\circ + \frac{2.303RT}{\alpha_1 F} \log 0.886 k_1^\circ D_Z^{-1/2} t^{1/2} - \frac{RTst}{\alpha_1 Fq}\left(1 - \frac{k_{1c}^\circ}{k_1^\circ}\right)\frac{i_d^I}{2} \quad (22)$$

Rearranging Eq. (21) one has

$$E + \frac{RTst}{\alpha_1 Fq}\left(1 - \frac{k_{1c}^\circ}{k_1^\circ}\right) i^I = E_1^\circ + \frac{2.303RT}{\alpha_1 F} \log 0.886 k_1^\circ D_Z^{-1/2} t^{1/2} + \frac{2.303RT}{\alpha_1 F} \log \frac{i_d^I - i^I}{i^I} \quad (23)$$

It is evident from Eq. (23) that a plot of $\log (i_d^I - i^I)/i^I$ *vs.* $E + RTst(1 - k_{1c}^\circ/k_1^\circ) i^I/(\alpha_1 Fq)$ should produce a straight line as far as q and t are kept constant. This is in agreement with results shown in Fig. 6, where a value of 0.011_1 V μA^{-1}, calculated from the slope of the straight line in Fig. 5, is used for $RTst(1 - k_{1c}^\circ/k_1^\circ)/(\alpha_1 Fq)$. A value of 0.081 V is obtained for the reciprocal slope of the plot, which is given as $2.303RT/(\alpha_1 F)$ in Eq. (23). This is in accord with the assumption of total irreversibility of reaction (6).

8) J. Heyrovský and J. Kůta, "Principles of Polarography," Academic Press, New York, N. Y. (1966), p. 307.

TABLE 1. COMPARISON OF OBSERVED AND CALCULATED VALUES OF THE HALF-WAVE POTENTIAL OF *o*-HPMC[a)]

Mercury pressure mm	Drop time ratio[b)]	$i_d^I/2$ μA	$\Delta E_{1/2}$[c)] V	$E_{1/2}$ *vs.* SCE, V Calcd	Obsd
1000	1	1.49	0	(0.036)	0.036
700	1.423	1.24	0.003	0.039	0.038
500	2.000	1.07	0.005	0.041	0.039

a) Concentration of *o*-HPMC, 1.000 mM.
b) The ratio of drop time to the one at mercury pressure of 1000 mm, calculated from the ratio of mercury pressure.
c) The difference between $E_{1/2}$ and the one at mercury pressure of 1000 mm, calculated according to Eq. (22).

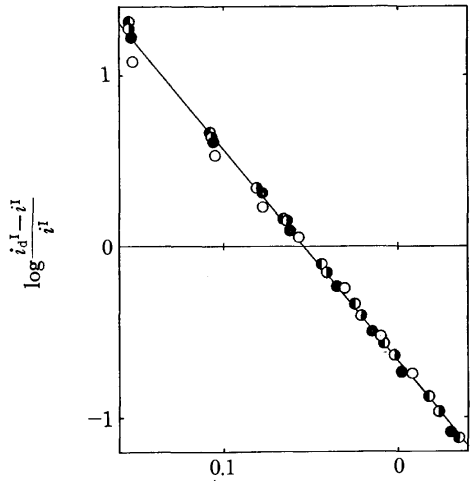

Fig. 6. Relation of log $(i_d^I-i^I)/i^I$ *vs.* $E+0.011_1\, i^I$.
Mercury pressure, 1000 mm. Concentrations are same as in Fig. 4.

The half-wave potential shifts to positive when t increases. As shown in Table 1, the observed results are in good agreement with theoretical prediction given by Eq. (22).

The results support the assumptions that the first wave is inhibited by a reduction product adsorbed on the surface of DME as solid particles, and that the adsorbed precipitate is reduced at the second wave. Benesch and Benesch reported that an organomercury free radical RHg· is formed by one-electron reduction of organomercury compound RHgX.[9] At present we are not certain whether $HOC_6H_4Hg\cdot$ corresponds to the sparingly soluble precipitate A or its dimer $(HOC_6H_4Hg)_2$ does. Because of its irreducibility $(HOC_6H_4)_2Hg$ should be excluded from possible reaction intermediates. However, a slow chemical reaction will produce $(HOC_6H_4)_2Hg$ from $HOC_6H_4Hg\cdot$ or $(HOC_6H_4Hg)_2$ as a final product at the first wave. These considerations lead to the following mechanism:

First wave

$$HOC_6H_4HgCl + e \longrightarrow HOC_6H_4Hg\cdot\text{(or 1/2 mol of its dimer)} + Cl^-$$

$$2HOC_6H_4Hg\cdot\text{(or 1 mol of its dimer)} \longrightarrow (HOC_6H_4)_2Hg + Hg$$

Second wave

$$HOC_6H_4HgCl + e \longrightarrow HOC_6H_4Hg\cdot\text{(or 1/2 mol of its dimer)} + Cl^-$$

$$HOC_6H_4Hg\cdot\text{(or 1/2 mol of its dimer)} + H^+ + e \longrightarrow C_6H_5OH + Hg$$

9) R. Benesch and R. E. Benesch, *J. Amer. Chem. Soc.*, **73**, 3391 (1951).

Studies of Ruthenium Complexes. IV. The Solvent Effect on the Isotopic Ligand-exchange Reaction of the *cis*-Dibromotetraammineruthenium(III) Complex

Akira OHYOSHI, Tetsuo SHINOHARA, Yoshihiro HOSOYAMADA, Takato YAMADA, and Yutaka HIROSHIMA

Department of Industrial Chemistry, Faculty of Engineering, Kumamoto University, Kumamoto-shi, Kumamoto 860

(Received December 4, 1972)

The isotopic ligand-exchange reactions of *cis*-dibromotetraammineruthenium(III) were studied in aqueous and methanol–water solutions in order to distinguish them from those in the case of the monobromocomplex and in order to ascertain the role of the water molecule with respect to the reaction mechanism. In an aqueous solution, the reaction proceeds through the rate-determining aquation step with the S_N2 mechanism: $Ru(NH_3)_4Br_2^+ + H_2O \rightarrow Ru(NH_3)_4(H_2O)Br^{2+} + Br^-$, $Ru(NH_3)_4(H_2O)Br^{2+} + {}^*Br^- \rightarrow Ru(NH_3)_4Br{}^*Br^+ + H_2O$. This result is similar to that for the monobromocomplex. In the methanol solution ($H_2O \sim 1.5\%$), the exchange reaction proceeds through the S_N1 mechanism: $Ru(NH_3)_4Br_2^+ \rightarrow Ru(NH_3)_4Br^{2+} + Br^-$, $Ru(NH_3)_4Br^{2+} + {}^*Br^- \rightarrow Ru(NH_3)_4Br{}^*Br^+$. When the concentration of water becomes very low, the number of solvated water molecules decreases; therefore, the coordinated bromide ion may easily be liberated. When the concentration of water is higher than 10%, the rate constant increases with the increase in the water concentration. Since the electronic spectra did not change during the exchange reaction, it would seem that the water molecule attacks a *cis*-position as a nucleophile. These results can be interpreted by postulating a hydrogen-bond between the proton of the water molecule and the coordinated bromide ion.

In our previous work,[1] it was found that the rate-determining step in the isotopic ligand-exchange reaction of halogenopentaammineruthenium(III) is the aquation process, which proceeds through the S_N2 mechanism, however, the role of the water molecule in connection with this reaction was not yet clear. For this purpose, it was necessary to use a considerably soluble complex in a mixed solution of methanol and water, because the monohalogenopentaamminecomplexes are less soluble in this solution. Thus, the *cis*-dibromotetraammine complex was chosen as a basis for a study of the ligand-exchange reaction.

In the present paper, the comparison of the reaction rate in the cases of mono- and dibromocomplexes in aqueous solutions, and the reaction mechanisms for the latter complex in a methanol–water solution, will be discussed in connection with those in the aqueous solution.

Experimental

Reagents. All the chemicals used were of a reagent grade. The radio-isotope, $^{82}Br(NH_4Br)$, was obtained from the Japan Radioisotope Association, Tokyo, and was used as a radioactive tracer. Doubly-distilled water was used in all the kinetic runs. The ionic strength and the acidity of the reaction mixture were adjusted with *p*-toluenesulfonic acid and its sodium salt. The sodium salt was prepared by the neutralization of the acid with sodium hydroxide.

Preparation of Complexes and Kinetic Measurements. Chloropentaammineruthenium(III) was dissolved in an ammonia solution, and then transformed into a hydroxo-complex. Oxalic acid was subsequently added to make the solution acidic. This solution was heated for about ten minutes, after it has then been cooled, sodium dithionate was added and the solution was left alone. The yellow precipitates thus obtained consisted of *cis*-$[Ru(NH_3)_4C_2O_4]_2S_2O_6$, and the molar extinction coefficient was $4.87 \times 10^3\ M^{-1}\ cm^{-1}$ (at 283 mμ).

Concentrated hydrobromic acid was added to this oxalato-complex, and the solution was heated for a few minutes. When the electronic spectrum showed *cis*-$Ru(NH_3)_4Br_2^+$, ethanol was added to isolate *cis*-$[Ru(NH_3)_4Br_2]Br$ as a precipitate. The final product was obtained by three recrystallizations from distilled water. The molar extinction coefficient of this compound was $1.67 \times 10^3\ M^{-1}\ cm^{-1}$ (at 442 mμ) and $1.22 \times 10^3\ M^{-1}\ cm^{-1}$ (at 370 mμ).

Found: H, 2.91; N, 13.82%. Calcd for $[Ru(NH_3)_4Br_2]Br$: H, 2.94; N, 13.70%.

The procedures of kinetic measurement and the apparatus and technique for radiometry used in this work were similar to those already described.[1] A reaction vessel with a refluxing apparatus was used to avoid the loss of any volatile material. A Hitachi Model 124 spectrophotometer was used to determine the absorption spectra of the complexes.

Results and Discussion

Estimation of the Exchange Rate, R, and the Rate Constant, k_{ex}. The reactions have been carried out for a period of 8—10 times half-time, and the exchange rates were calculated by means of McKay's equations.[2]

$$\ln(1 - X/X_\infty) = -[(a+b)/ab]Rt \quad (1)$$

$$R = 0.693ab/[(a+b)\cdot T_{1/2}] \quad (2)$$

where R is exchange rate; t, time; a and b, the initial concentrations of the complex and the halide ion, and X and X_∞, the radioactivity of the *cis*-dibromotetraammine complex at time t and at an infinite time. From the plots in Fig. 1, the half-time of the exchange reaction was determined.

From the measurements of the reaction rates varying

1) T. Shinohara T. Yamada N. Takebayashi, S. Hiraki, and A. Ohyoshi, This Bulletin, **45**, 3081 (1972).

2) H. A. C. McKay, *J. Amer. Chem. Soc.*, **65**, 702 (1943).

Table 1. Rate constants (at 70 °C) and activation parameters for ligand-exchange reactions

Complex ion	k_{ex}(sec^{-1})	E_a(kcal/mol)	ΔS(e.u.)
$Ru(NH_3)_5Br^{2+}$	1.5×10^{-4} a)	23.2±0.9	−9±2
cis-$Ru(NH_3)_4Br_2^+$ in aqueous solution	4.8×10^{-4}	23 ±3	−7±8
in 98.5% Metanol solution	4.2×10^{-4} b)	24.8±0.6	−0.1±0.1

a) This value was obtained by extrapolating the value obtained at 80 °C.
b) This value was obtained by extrapolating the value obtained at 55 °C.

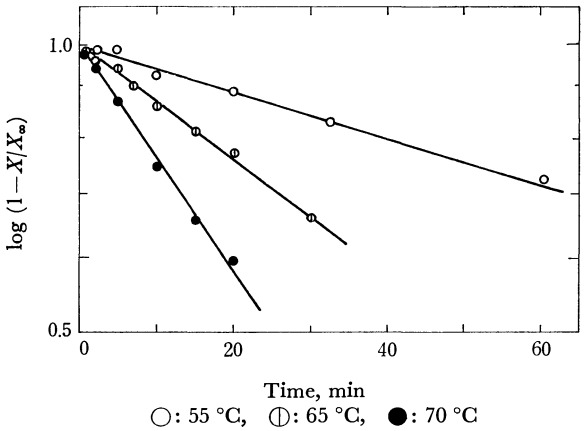

Fig. 1. Plots of $\log(1-X/X_\infty)$ *vs.* reaction time.

with the concentration of the complex in aqueous and methanolic solutions, it is found that both the exchange reactions are first-order with respect to the concentration of the complex. No influence of the concentrations of the bromide ion and the hydrogen ion on the reaction rate has been observed, and no practical salt effect on the rate is found in either solution. Thus, the reaction rate, R, and the rate constant, k_{ex}, can be expressed by the following equations, just as in the case of the monobromopentaammine complex.[1]

$$R = k_{ex}[\text{complex}] \quad (3)$$

$$k_{ex} = 0.693b/[(a+b)\cdot T_{1/2}] \quad (4)$$

The values of the rate constants of the exchange reactions are listed, along with that of the reference reaction, in Table 1.

Ligand-exchange Reaction of the cis-*Dibromotetraammine Complex in an Aqueous Solution.* To ascertain the dependence of the rate on the ionic strength, experiments were carried out while varying the ionic strength of the aqueous solution from 4.0 to 5.0 using sodium *p*-toluenesulfonate. From the plot of k_{ex} *vs.* ionic strength (Fig. 2), it was found that the rate constant decreases slightly with the increase in the ionic strength. By succesive measurements of the absorption spectrum of the reaction solution, it was confirmed that the exchange reaction was accompanied by aquation as a side reaction. The extent of this decomposition was about 9% when 8 times the half-time had elapsed at the ionic strength of 5.0.

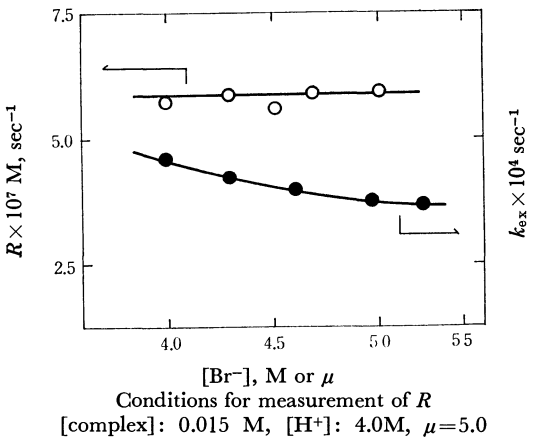

Fig. 2. Effects of bromide-ion concentration and ionic strength on the exchange rate in aqueous solution at 70 °C.

It is plausible that the exchange rate is essentially independent of the ionic strength; therefore, the charged species is not involved in the rate-determining step. Thus, it may be concluded that the exchange reaction proceeds through the aquation process (5) and that the anation reaction (6) follows:

$$cis\text{-}Ru(NH_3)_4Br_2^+ + H_2O \longrightarrow cis\text{-}Ru(NH_3)_4BrOH_2^{2+} + Br^- \quad (5)$$

$$cis\text{-}Ru(NH_3)_4BrOH_2^{2+} + {}^*Br^- \longrightarrow cis\text{-}Ru(NH_3)_4Br{}^*Br^+ + H_2O \quad (6)$$

The former step is presumably the rate-determining one. These reaction schemes are similar to those of the monobromocomplex.[1]

The rate constant of the dibromocomplex is nearly three times greater than that of the monobromocomplex (Table 1). The difference between these rate constants may be statistically understood, as will be described below.

In the aquation reaction of halogenoamminecobalt(III), the rate constant for the *cis*-dichlorotetraammine complex is 100 times that for monochloropentaammine.[3] On the basis of this evidence, it was concluded that the aquation reaction proceeded by means of the S_N1 mechanism.

In the present study, such a discrepancy between the two rate constants is seen to be small in comparison with that in the above case. It would seem that the dissociative mechanism could not be involved in the rate-determining step expressed by Eq. (5). From the measurements of the absorption spectra in the present study, it was found that the steric configuration of the *cis*-dibromocomplex was retained during the exchange reaction. This fact suggests that the water molecule enters from the front side of coordinated bromide ions. The process of Eq. (5) involves an intermediate which is formed by hydrogen bondings between coordinated bromide-ions and the protons of the water molecule, that is, the S_N2 Front-side mech-

3) R. G. Pearson, C. R. Boston, and F. Basolo, *J. Phys. Chem.*, **59**, 304 (1955).

anism. This mechanism has also been reported in the acid-hydrolysis reaction of *cis*-dihalogenodiethylendiammineruthenium(III) by Broomhead and Maguire.[4]

The fact that the exchange rate for the dibromocomplex is three times as fast as that for the monobromocomplex can be interpreted by indicating that the probability of the hydrogen-bond formation in the former case is twice as much as that in the latter case.

Exchange Reaction in Water-Methanol Mixed Solutions. In the aqueous solution, the ligand exchange reaction was found to proceed through the S_N2, F.S. mechanism. To ascertain the role of water molecule for the reaction mechanism, therefore, experiments were carried out varying the water concentration with a methanol solvent. The plot of the observed rate constant *vs.* the water content (mol %) in a methanol solution is shown in Fig. 3. In the region where the concentration of

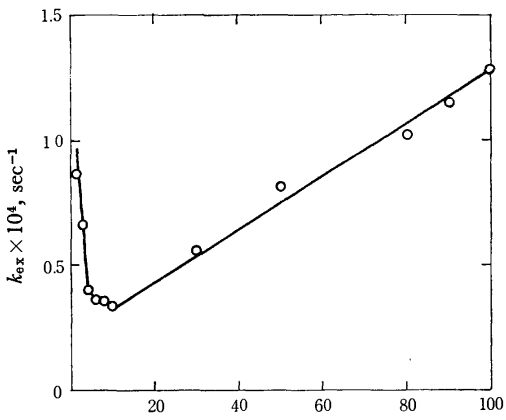

Fig. 3. Effect of water concentration on the exchange rate constant.

water is lower than 10%, the sign of the slope is negative, while it is positive in the concentration region higher than 10%. It appears that the water molecule behaves as a nucleophile in the rate-determining process (5). This action of the water molecule gives an evidence for the S_N2, F.S. mechanism discussed in a previous paragraph. When the water concentration is less than 10%, the exchange reaction mechanism may be different from the above one; that is, the following mechanisms may be presumed: (1) the S_N1 dissociative mechanism, (2) a S_N2 mechanism involving the bromide-ion as a nucleophile, or (3) a mechanism which involves methoxide ion or methanol molecule in the intermediate. The last mechanism is the most improbable, because it is difficult for the methoxide to exist in a hydrogen-ion solution of 0.05 M and a methanol molecule has even less coordination ability. To distinguish the S_N1 mechanism (1) from the S_N2 mechanism (2), both the concentration of the bromide ion and the ionic strength were varied. As is shown in Fig. 4, on neither the bromideion concentration nor the ionic strength depends the exchange rate constant; that is, both the bromide ion and charged species are not involved in the rate-

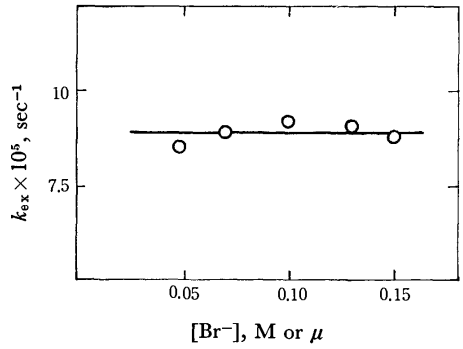

Fig. 4. Effects of bromide-ion concentration and relative ionic strength on the rate constant in 98.5% methanol solutions at 55 °C.

determining step, and the S_N2 mechanism may be concluded to be impossible. Moreover, when the S_N2 mechanism proceeds, the bromide-ion should attack the bromide ligands from the opposite side because a front-side attack is difficult because of the electrostatic repulsion between the nucleophile-bromide and the ligand-bromide ions. This is schematically expressed by Eq. (7):

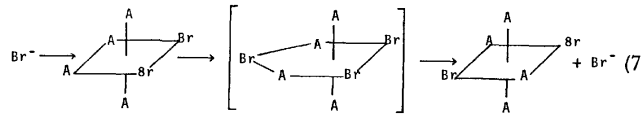

For this reason, the reaction product should be a *trans*-isomer. Since there is no change in the absorption spectrum during the exchange reaction, no isomerization of the *cis*-dibromocomplex occurs; therefore, the S_N2 mechanism (2) is also improbable. As for the remaining mechanism, that is, the dissociative

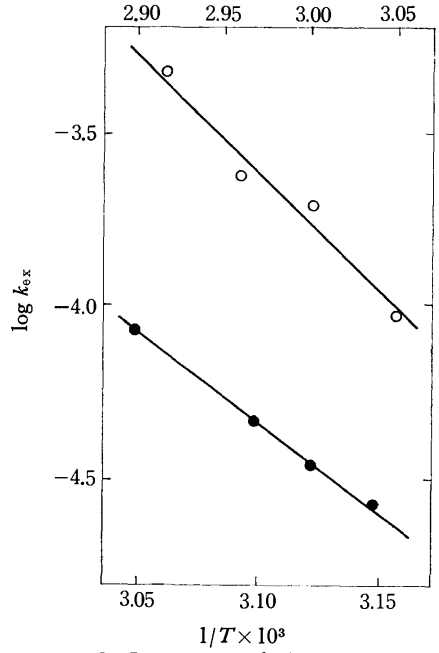

Fig. 5. Arrhenius plots for isotopic ligand-exchange reactions.

4) J. A. Broomhead and L. Kane-Maguire, *Inorg. Chem.*, **7**, 2519 (1968).

S_N1 mechanism may be considered acceptable on the basis of the following explanation. The rate constant increases with the decrease in the water concentration in the region less than 10% (Fig. 3). When the water concentration is comparatively high, the solvated water molecule in the second coordination sphere can be repressed until the bromide ion dissociates. When the water concentration is extremely low, the decrease in the solvated molecule facilitates the dissociation of the bromide ion. Thus, it may be concluded that the exchange reaction proceeds through two reaction processes, (8) and (9), and that the former using the S_N1 mechanism is the rate-determining step.

$$cis\text{-}Ru(NH_3)_4Br_2^+ \longrightarrow Ru(NH_3)_4Br^{2+} + Br^- \quad (8)$$

$$Ru(NH_3)_4Br^{2+} + {}^*Br^- \longrightarrow cis\text{-}Ru(NH_3)_4Br{}^*Br^+ \quad (9)$$

Figure 5 shows the Arrhenius plots, while the activation parameters are listed, along with those of the reference reactions, in Table 1. The values of the activation energies are nearly the same for all the reactions, though the value of the activation entropy for the reaction in the 98.5% methanol solution is extremely small. The degree of entropy change in the transition state of the S_N1 mechanism was estimated to be $-2 \sim -20$ e.u. for the aquations of carboxylatopentaammineruthenium(III) in aqueous solutions.[5] The small value of entropy change for the same mechanism in the methanolic solution may be ascribed to the poor solvation ability of the methanol molecule compared with that of the water molecule.

5) A. Ohyoshi, A. Jyo, and N. Shin, This Bulletin, **45**, 2121 (1972).

BULLETIN OF THE CHEMICAL SOCIETY OF JAPAN, VOL. 46, 2136—2139 (1973)

The Synthesis of Some *N,N*-Dialkylselenocarbamate Complexes of Tin(IV), and Their Infrared and PMR Spectra

Koji TANAKA, Shigeo ARAKI, and Toshio TANAKA

Department of Applied Chemistry, Faculty of Engineering, Osaka University, Yamada-kami, Suita, Osaka 565

(Received December 21, 1972)

Several *N,N*-dialkylselenocarbamate complexes of tin(IV), $(CH_3)_2Sn[OSeCNR_2]_2$ (**1**), $(CH_3)_2ClSn[OSeCNR_2]$ (**2**) ($R=CH_3$ and C_2H_5) and $(CH_3)_3Sn[OSeCN(CH_3)_2]$ (**3**), have been prepared, and their infrared and proton magnetic resonance spectra have been examined. The results indicate that in **1** and **2** the selenocarbamate ligands are coordinated to the tin atom in a bidentate manner, although the coordination of the oxygen atom is weak. On the other hand, **3** has a tetra-coordinate tin with a free carbonyl bond. The configurations of these complexes are discussed and compared with those of the corresponding thio-, dithio-, diseleno-, and thioselenocarbamate complexes of tin(IV).

In previous papers, one of the present authors has demonstrated that dimethyltin(IV) bis(*N,N*-dimethyldithio-[1] and -diselenocarbamates,[2] $(CH_3)_2Sn[Y_2CN(CH_3)_2]_2$ (Y=S and Se), have a distorted octahedral *trans*-configuration (I), and that dimethylchlorotin(IV) *N,N*-dimethyldithio-[1] and -diselenocarbamates,[2] $(CH_3)_2ClSn[Y_2CN(CH_3)_2]$, form a trigonal bipyramid, with the (Sn–)CH_3 groups being located in equatorial positions (II); we reached these conclusions on the basis of the infrared and proton magnetic resonance spectra.

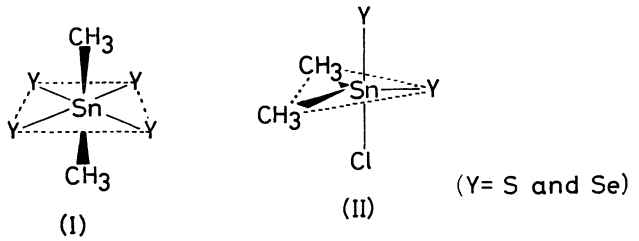

These structures have been confirmed by the X-ray crystallographic analysis of $(CH_3)_2Sn[S_2CN(CH_3)_2]_2$[3] and $(CH_3)_2ClSn[S_2CN(CH_3)_2]$.[4] Similar configurations have been suggested for the *N,N*-dimethylthioselenocarbamate complexes of tin(IV), $(CH_3)_2Sn[SSeCN(CH_3)_2]_2$ and $(CH_3)_2ClSn[SSeCN(CH_3)_2]$, in which the Sn–Se bond is more ionic than the Sn–S bond, judging from the benzene-induced solvent shifts of the N–CH_3 proton signals in the PMR spectra.[5]

It seems to be of interest at this stage to prepare other types of tin(IV)-carbamates, such as thio- and selenocarbamates, and to compare their spectroscopic properties with those of the complexes described above. Concerning the thiocarbamates, only the trimethyltin(IV) derivative has been reported on thus far,[6,7]

1) M. Honda, M. Komura, Y. Kawasaki, T. Tanaka, and R. Okawara, *J. Inorg. Nucl. Chem.*, **30**, 3231 (1968).

2) T. Kamitani, H. Yamamoto, and T. Tanaka, *ibid.*, **32**, 2621 (1970).

3) T. Kimura, N. Yasuoka, and N. Kasai, This Bulletin, **45**, 1649 (1972).

4) K. Furue, T. Kimura, N. Yasuoka, N. Kasai, and M. Kakudo, *ibid.*, **43**, 1661 (1970).

5) T. Kamitani and T. Tanaka, *Inorg. Nucl. Chem. Lett.*, **6**, 91 (1970).

6) R. F. Dalton and K. Jones, *J. Chem. Soc.*, **A**, **1970**, 590.

7) C. H. Yoder, A. Komiyama, J. E. Kochanowski, and F. H. Saydam, *J. Amer. Chem. Soc.*, **93**, 6515 (1971).

although a few transition metal complexes have been characterized.[8]

The present paper was undertaken to prepare some *N,N*-dialkylselenocarbamate complexes of tin(IV), $(CH_3)_2Sn[OSeCNR_2]_2$, $(CH_3)_2ClSn[OSeCNR_2]$ (R= CH_3 and C_2H_5), and $(CH_3)_3Sn[OSeCN(CH_3)_2]$, which are the first metal-selenocarbamates, and to elucidate their configurations and the bonding between the ligand anions and the tin(IV) on the basis of the infrared and PMR spectra.

Experimental

Dimethylammonium N,N-*Dimethylselenocarbamate, $[(CH_3)_2NH_2](dmsc)$ (dmsc: $OSeCN(CH_3)_2$), and Diethylammonium* N,N-*Diethylselenocarbamate, $[(C_2H_5)_2NH_2](desc)$ (desc: $OSeCN(C_2H_5)_2$).* These starting substances were synthesized by the reaction of dimethyl- or diethylamine, selenium powder, and carbon monoxide in tetrahydrofuran according to a procedure described elsewhere.[9]

*Dimethyltin Bis(*N,N-*dimethylselenocarbamate), $(CH_3)_2Sn(dmsc)_2$.* A solution of $(CH_3)_2SnCl_2$ (2.54 g, 11.5 mmol) in dry benzene (25 ml) was stirred, drop by drop, into a solution of $[(CH_3)_2NH_2]$(dmsc) (4.53 g, 23.0 mmol) in tetrahydrofuran (25 ml) at room temperature; the mixture was then stirred further for 2 hr. Then the precipitate which appeared, $(CH_3)_2NH_2Cl$, was filtered off, and the filtrate was evaporated under reduced pressure. The resulting product was recrystallized from carbon tetrachloride to give pale yellow crystals (4.93 g, 10.9 mmol); mp 166 °C.

Found: C, 21.06; H, 3.96; N, 6.07%; mol wt, 458. Calcd for $C_8H_{18}N_2O_2Se_2Sn$: C, 21.31; H, 4.02; N, 6.21%; mol wt, 458.

*Dimethyltin Bis(*N,N-*diethylselenocarbamate), $(CH_3)_2Sn(desc)_2$.* This compound was similarly prepared by the reaction of $(CH_3)_2SnCl_2$ (1.87 g, 8.50 mmol) with $[(C_2H_5)_2NH_2]$(desc) (4.31 g, 17.0 mmol) in benzene. Recrystallization from petroleum ether gave yellow crystals (4.08 g, 8.05 mmol); mp 81—83 °C.

Found: C, 28.62; H, 5.47; N, 5.31%; mol wt, 528. Calcd for $C_{12}H_{26}N_2O_2Se_2Sn$: C, 28.43; H, 5.17; N, 5.53%; mol wt, 507.

Dimethylchlorotin N,N-*Dimethylselenocarbamate, $(CH_3)_2ClSn(dmsc)$.* A mixture of $(CH_3)_2Sn(dmsc)_2$ (4.73 g, 10.5 mmol) and $(CH_3)_2SnCl_2$ (2.32 g, 10.5 mmol) in dry benzene was stirred for 2 hr at room temperature. Then the solution was evaporated under reduced pressure, and the resulting product was recrystallized from carbon tetrachloride to give pale yellow crystals (6.34 g, 18.9 mmol); mp 75 °C.

Found: C, 17.96; H, 3.86; N, 4.06%; mol wt, 352. Calcd for $C_5H_{12}NClOSeSn$: C, 17.91; H, 3.61; N, 4.18%; mol wt, 355.

Dimethylchlorotin N,N-*Diethylselenocarbamate, $(CH_3)_2ClSn(desc)$.* A mixture of $(CH_3)_2Sn(desc)_2$ (3.25 g, 6.41 mmol) and $(CH_3)_2SnCl_2$ (1.41 g, 6.41 mmol) in carbon tetrachloride was treated as in the case of $(CH_3)_2ClSn$(dmsc). The resulting oily product was dissolved in an ether–petroleum ether mixture, and then the solution was cooled to −78 °C to give pale yellow crystals (4.07 g, 11.2 mmol); mp 31 °C.

Found: C, 22.85; H, 4.74; N, 3.99%; mol wt, 373. Calcd for $C_7H_{16}NClOSeSn$: C, 23.12; H, 4.44; N, 3.86%; mol wt, 363.

Trimethyltin N,N-*Dimethylselenocarbamate, $(CH_3)_3Sn(dmsc)$.* A solution of $(CH_3)_3SnCl$ (1.34 g, 6.72 mmol) in benzene was added to a solution of $[(CH_3)_2NH_2]$(dmsc) (1.32 g, 6.72 mmol) in tetrahydrofuran, after which the mixture was stirred for 3 hr at room temperature. After the precipitate of $(CH_3)_2NH_2Cl$ had been filtered off, the filtrate was evaporated under reduced pressure; the resulting product was recrystallized from tetrahydrofuran to give brownish yellow crystals (1.27 g, 4.03 mmol); mp 32 °C.

Found: C, 22.76; H, 5.05; N, 4.54%; mol wt, 325. Calcd for $C_6H_{15}NOSeSn$: C, 22.89; H, 4.80; N, 4.45%; mol wt, 325.

Physical Measurements. The molecular-weight determinations were carried out by the use of Mechrolab vapor pressure osmometer in the 0.018—0.034 M range in chloroform. The infrared spectra were recorded in Nujol and in hexachlorobutadiene mulls on a Hitachi-Perkin 225 Spectrophotometer, while the proton magnetic resonance spectra were measured at 100 MHz on a Japan Electron Optics PS-100 Spectrometer, equipped with a variable-temperature probe and controller. The chemical shifts were measured against tetramethylsilane as the internal standard.

Results and Discussion

Properties. All the complexes are soluble in common organic solvents, except for $(CH_3)_2Sn(dmsc)_2$ and $(CH_3)_2ClSn$(dmsc), which are less soluble in petroleum ether. They are stable to air and moisture, in contrast with the very hygroscopic property of $[(CH_3)_2NH_2]$(dmsc) and $[(C_2H_5)_2NH_2]$(desc), but somewhat sensitive to the light in the solid state and in solution. The molecular-weight determination indicates that the selenocarbamate complexes are all monomeric in chloroform.

Configurations. The relevant infrared frequencies of the present complexes are listed in Table 1. All the complexes exhibit an intense band about 1600 cm^{-1};

Table 1. Relevant infrared frequencies (cm^{-1} in Nujol) of selenocarbamate-tin(IV) complexes[a]

Compound	ν(C=O)	ν_{as}(Sn–C)	ν_s(Sn–C)	ν(Sn–Se)	ν(Sn–Cl)
$(CH_3)_2Sn(dmsc)_2$	1592 s	557 s	519 s	337 m	
$(CH_3)_2Sn(desc)_2$	1586 s	552 s	517 s	322 m	
$(CH_3)_2ClSn(dmsc)$	1590 s	563 s	524 s	343 m	290 s
$(CH_3)_2ClSn(desc)$	1587 s	558 s	524 s	325 m	288 s
$(CH_3)_3Sn(dmsc)$	1620 s	534 s	511 s	328 m	

a) The abbreviations used in this table are as follows: s, strong; m, medium.

8) B. J. McCormick and B. P. Stormer, *Inorg. Chem.*, **11**, 729 (1972), and the references cited therein.

9) N. Sonoda, T. Yasuhara, K. Kondo, T. Ikeda, and S. Tsutsumi, *J. Amer. Chem. Soc.*, **93**, 6344 (1971); K. Kondo, N. Sonoda, Y. Yoshida, M. Koishi, and S. Tsutsumi, *Chem. Lett.*, **1972**, 401.

Table 2. PMR spectra of selenocarbamate-tin (IV) complexes

Compound		τ ppm, in CCl_4	τ ppm, in C_6H_6	Δ[a] ppm	$J(^{119}Sn-CH_3)$[b] Hz
$(CH_3)_2Sn(dmsc)_2$	N-CH_3	6.89	7.54	+0.65	
		7.06	7.60	+0.54	
	Sn-CH_3	8.90	8.48	−0.42	76
$(CH_3)_2Sn(desc)_2$	N-CH_2	6.59	6.98	+0.39	
		6.70	7.00	+0.30	
	C-CH_3	8.77	9.14	+0.37	
		8.87	9.16	+0.29	
	Sn-CH_3	8.91	8.47	−0.44	77
$(CH_3)_2ClSn(dmsc)$	N-CH_3	6.91	7.85	+0.94	
		7.08	7.88	+0.80	
	Sn-CH_3	8.92	8.95	+0.03	73
$(CH_3)_2ClSn(desc)$	N-CH_2	6.64	7.23	+0.59	
		6.75	7.29	+0.54	
	C-CH_3	8.70	9.31	+0.61	
		8.77	9.35	+0.58	
	Sn-CH_3	8.90	8.94	+0.04	73
$(CH_3)_3Sn(dmsc)$	N-CH_3	6.72	7.41	+0.69	
		6.91	7.52	+0.61	
	Sn-CH_3	9.28	9.42	+0.14	55

a) $\Delta=\tau(C_6H_6)-\tau(CCl_4)$.
b) The values in CCl_4.

this band can tentatively be assigned to the ν(C=O).[11] In the $(CH_3)_3Sn(dmsc)$ complex, the ν(C=O) frequency is in agreement with those of the desc anion (1620 cm^{-1})[12] and of $(CH_3)_3Sn[OSCN(CH_3)_2]$ (1621 cm^{-1}), the latter of which has a tetracoordinate tin with the tin-sulfur bond.[6] It may, therefore, be assumed that in $(CH_3)_3Sn(dmsc)$ only the selenium atom, not the oxygen, attaches to the tin. The similar tetra-coordinate tin was also reported on in recent X-ray structure determinations for the two modifications (orthorhombic and monoclinic) of trimethyltin *N,N*-dimethyldithiocarbamate, $(CH_3)_3Sn[S_2CN(CH_3)_2]$.[13]

On the other hand, the dimethyltin(IV) complexes exhibit the ν(C=O) band at a frequency lower by about 30 cm^{-1} than $(CH_3)_3Sn(dmsc)$. In addition, all the complexes, including $(CH_3)_3Sn(dmsc)$, commonly show an medium intense band due to the ν(Sn-Se) in the 322—343 cm^{-1} range. There seems to be no band ascribable to the ν(Sn-O) vibration down to 200 cm^{-1}. In view of these results, the selenocarbamate anions can be said to act as bidentate ligands in the dimethyltin(IV) complexes, but the coordination of the oxygen to the tin atom is weak.

The weak coordination of the oxygen atom brings about a stereochemical characteristic of the selenocarbamate complexes of tin(IV), which may be examined by comparing the intensities of the ν_{asym}(Sn-C) and ν_{sym}(Sn-C) bands in the infrared spectra. The intensity ratio of $I\nu_{sym}$(Sn-C)/$I\nu_{asym}$(Sn-C) (abbreviated as I_s/I_a) of $(CH_3)_2Sn(dmsc)_2$ (0.61) is appreciably larger than those of the corresponding dithio-,[1] diseleno-,[2] and thioselenocarbamate[5] complexes (0.21, 0.23, and 0.19 respectively). In the PMR spectra of both $(CH_3)_2Sn(dmsc)_2$ and $(CH_3)_2Sn(desc)_2$, the $J(^{119}Sn-CH_3)$ values (Table 2) are considerably smaller than those (83—84 Hz) of the analogous dithio-,[1] diseleno-,[2] and thioselenocarbamates.[5] These infrared and PMR results may be interpreted as much more a distortion of the $(CH_3)_2Sn$ moiety in $(CH_3)_2Sn(dmsc)_2$ and $(CH_3)_2Sn(desc)_2$ from the *trans*-octahedron(I) configuration, which may result in a configuration like a *cis*-one, although a detailed structure has to await the X-ray structure determination.

The I_s/I_a value of $(CH_3)_2ClSn(dmsc)$ (0.95) is close to those of the corresponding dithio-,[1] diseleno-,[2] and thioselenocarbamates[5] (0.97, 0.93, and 0.91 respectively). Furthermore, the $J(^{119}Sn-CH_3)$ values are virtually invariant (73—75 Hz; Table 2 and Refs. 1, 2, and 5) among all of these complexes, including $(CH_3)_2ClSn(desc)$. Thus, the present dimethylchlorotin(IV) complexes may be concluded to have the configuration shown by II.

Description of the PMR Spectra. The dmsc complexes in solution exhibit a doublet for the N-CH_3 proton signals at room temperature (Table 2), as expected from the restricted rotation around the carbamate C=N bond. The down-field signal is smaller in height and broader than the up-field one both in carbon tetrachloride and in benzene. These appearances are quite similar to the case of $(CH_3)_2ClSn[SSeCN(CH_3)_2]$ in carbon tetrachloride;[5] therefore, the former signal may be assigned to the $CH_3^{(A)}$ protons *trans* to the selenium atom with respect to the

11) The dithio-,[1] diseleno-,[2] and thioselenocarbamate[5] complexes of tin(IV) exhibit an intense band due to ν(C=N) in the 1490—1550 cm^{-1} range. It may, therefore, be more reasonable to identify the band at about 1600 cm^{-1} as the ν(N=C=O). However, the ν(C=N) dose not very largely contribute to this frequency, since the partial double-bond character is not large, as will be described below.

12) The wave number of $[(C_2H_5)_2NH_2]$ (desc); the spectrum of $[(CH_3)_2NH_2]$ (dmsc) has not been recorded because of its extremely hygroscopic property.

13) G. M. Sheldrick and W. S. Sheldrick, *J. Chem. Soc.*, **A**, **1970**, 490.

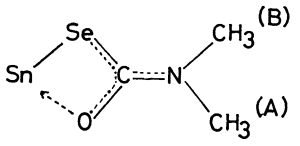

C=N bond in the planar selenocarbamate. The desc complexes in benzene[14] show doublets of a quartet and of a triplet for the N–CH_2 and C–CH_3 proton signals respectively at room temperature. By the analogy with the dmsc complexes, the down-field signals of each pair may be ascribed to the N–CH_2 or C–CH_3 protons *trans* to the selenium atom with respect to the C=N bond.

The N–CH_3 proton chemical shifts of $(CH_3)_2Sn(dmsc)_2$ in varying volume ratios of carbon tetrachloride to benzene are depicted in Fig. 1, which indicates that the solvent effect in benzene is a little larger with the $CH_3^{(A)}$ than with the $CH_3^{(B)}$. This is also the case with the remaining dmsc and desc complexes (Table 2). It may further be noticed in Table 2 that the *N*-alkyl protons of $(CH_3)_2ClSn(dmsc)$ and $(CH_3)_2ClSn(desc)$ undergo profound benzene shifts compared with those of $(CH_3)_2Sn(dmsc)_2$ and $(CH_3)_2Sn(desc)_2$ respectively. This may be responsible for decreasing the electron density of the nitrogen atom of the former complexes relative to the latter; this idea is supported by the fact that the coalescence temperatures of the N–CH_3 proton signals of $(CH_3)_2ClSn(dmsc)$ are a little higher than those of $(CH_3)_2Sn(dmsc)_2$, 55 and 50 °C in nitrobenzene respectively. These temperatures are considerably lower than that of $(CH_3)_2ClSn[SSeCN(CH_3)_2]$ (110 °C in 1,1,2,2-tetrachloroethane),[15] indicating, although only qualitatively, that the C=N double bond character of the selenocarbamate complexes of tin(IV) is not very large. This conclusion is in accordance with the weak coordination of the carbonyl oxygen of the selenocarbamates to the tin atom.

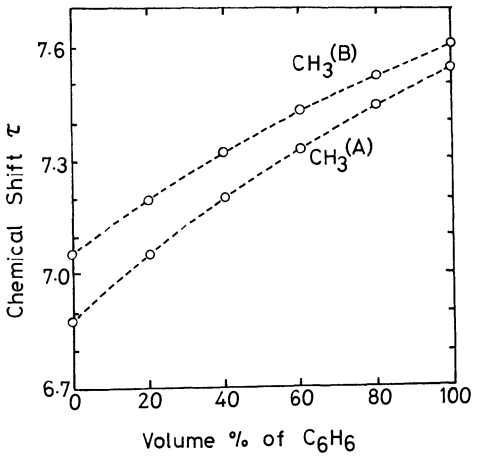

Fig. 1. Chemical shifts of the N–CH_3 protons of $(CH_3)_2Sn(dmsc)_2$ in CCl_4–C_6H_6 mixtures.

The authors wish to express their hearty thanks to Professor Noboru Sonoda and Mr. Kiyoshi Kondo of this University for giving them guidance in preparing the starting materials, $[(CH_3)_2NH_2](dmsc)$ and $[(C_2H_5)_2NH_2](desc)$; they are also grateful to the Shinko Chemical Co., Ltd., Osaka, for supplying the elemental selenium.

14) In carbon tetrachloride, the N–CH_2 proton signals occur as a quintet (1:4:6:4:1), a superposition of two quartets.

15) T. Tanaka and T. Kamitani, unpublished work.

Adducts of Neodymium(III) and Lanthanum(III) Acetylacetonate with some Bidentate Organic Bases[1]

Isao YOSHIDA, Hiroshi KOBAYASHI, and Keihei UENO

Department of Organic Synthesis, Faculty of Engineering, Kyushu University, Fukuoka 812

(Received January 16, 1973)

Several bidentate uncharged organic base adducts of neodymium(III) and lanthanum(III) acetylacetonate were prepared by the reaction of the free bases with tris(acetylacetonato)neodymium(III) monohydrate and tris-(acetylacetonato)lanthanum(III) dihydrate in ethyl acetate, respectively. Elemental analyses, molecular weight determinations, NMR, IR, and visible absorption spectra indicate that the adducts are of the general formula $Ln(AA)_3(BB)$, where AA, BB, and Ln denote acetylacetonate ion, bidentate uncharged base and lanthanide ion, respectively. Thermal stability of the base adducts as well as the hydrates was studied by differential thermal analysis (DTA) and thermogravimetric analysis (TGA). Coordination of the additional ligand having reactive hydrogen atoms resulted in poor thermal stability of the addition complexes. This might be explained by assuming that the coordinated acetylacetonate ion reacts readily with the reactive hydrogen atom of the neighboring ligand to liberate acetylacetone molecule, though the nature of the resulting pyrolyzed products is unknown.

It is well-known that the reaction of a lanthanide ion with acetylacetone in an aqueous solution affords always hydrated chelates[2,3] of hepta-[4,5] or octa-coordinate[6,7] structure. Dehydration from the hydrated chelates gave no anhydrous lanthanide acetylacetonate but a polymerized hydroxo chelate by liberating an acetylacetone molecule.[3,8] Przystal and his co-workers[9] obtained anhydrous chelates by the reaction of lanthanide hydrides with acetylacetone. However, the anhydrous chelates hydrolyzed easily to the hydroxo complex accompanied by weight loss when they were exposed to the moist air.

With the hope of obtaining thermally stable lanthanide complexes,[10] bidentate organic base adducts of tris(acetylacetonato)neodymium(III) and -lanthanum-(III) were prepared.

The organic bases used were ethylenediamine(en), 1,2-propanediamine(pn), 2,2′-dipyridyl(2-dipy), 4,4′-dipyridyl(4-dipy), 1,10-phenanthroline(phen), and isopropanolamine(ipa). These uncharged bidentate bases are expected to occupy the coordination sites of hydrated water to afford the mixed ligand uncharged complexes of the general formula of $Ln(AA)_3(BB)$, where AA, BB and Ln denote acetylacetonate ion, bidentate base and lanthanide ion, respectively. The structures and thermal properties of these addition complexes were studied.

Experimental

Materials. Lanthanide nitrates, organic bases and acetylacetone were of reagent grade and used without further purification. Chloroform and pyridine used for spectral measurements were dried and distilled according to standard procedures.

Preparation of Addition Complexes. Neodymium and lanthanum acetylacetonate of unknown degree of hydration, prepared by a slight modification of the standard procedure,[2] were recrystallized from ethyl acetate and the products were dried at room temperature to obtain $Nd(AA)_3 \cdot H_2O$ and $La(AA)_3 \cdot 2H_2O$[11] respectively, their compositions being confirmed by elemental analyses.

The base adduct was prepared by dissolving 0.8 g of a hydrated complex in 25 ml of warm (60—70 °C) ethyl acetate containing an appropriate amount of an organic base. The insoluble residue was filtered off after about ten minutes and the filtrate was cooled to about 0 °C. The neodymium-(III) and lanthanum(III) adducts precipitated as red-purple and white crystalline products, respectively. They were collected by filtration, and dried at room temperature under reduced pressure. Yield: 40—80%. Results of elemental analyses are shown in Table 1.

Diaquo complex, $Nd(AA)_3 \cdot 2H_2O$[11] was also prepared by recrystallizing 0.8 g of monohydrate from about 25 ml of ethyl acetate–water–acetone mixture (90: 5: 5 in volume). Similarly mono pyridine adduct of the formula $Ln(AA)_3(Py)-(H_2O)_2$ was obtained by recrystallizing 0.8 g of the corresponding dihydrate from 20 ml of warm pyridine–cyclohexane mixture (95: 5). Compositions of these complexes were confirmed by elemental analyses.

Measurements. IR measurements were carried out with a JASCO-DS-403G spectrophotometer. A Hitachi-124 spectrophotometer was used to observe visible absorption spectra. DTA was measured with Rigaku Denki-thermoflex-8001 in nitrogen atmosphere using α-alumina as a reference. TGA was measured with a Shimadzu-thermobalance TB-10B in a nitrogen stream. The thermal analyses were carried out mostly at a heating rate of 10 °C min^{-1}. NMR spectra were obtained by use of a Varian A-60 NMR spectrometer in deuterated chloroform using TMS as an internal reference. Molecular weight was determined with a Mechrolab 301A vapor pressure osmometer.

1) Contribution No. 308 from the Department of Organic Synthesis, Faculty of Engineering, Kyushu University.

2) J. G. Stites, C. N. McCarthy, and L. L. Quill, *J. Amer. Chem. Soc.*, **70**, 3142 (1948).

3) G. W. Pope, J. F. Steinbach, and W. F. Wagner, *J. Inorg. Nucl. Chem.*, **20**, 304 (1961).

4) J. A. Cunningham, D. E. Sands, W. F. Wagner, and M. F. Richardson, *Inorg. Chem.*, **8**, 22 (1969).

5) E. D. Watkins, II, J. A. Cunningham, T. Phillips, II, D. E. Sands, and W. F. Wagner, *ibid.*, **8**, 29 (1969).

6) T. Phillips, II, D. E. Sands, and W. F. Wagner, *ibid.*, **7**, 2295 (1968).

7) J. A. Cunningham, D. E. Sands, and W. F. Wagner, *ibid.*, **6**, 500 (1967).

8) T. Moeller, D. F. Martin, L. C. Thompson, R. Ferrus, G. R. Feistel, and W. J. Randall, *Chem. Rev.*, **65**, 1 (1965).

9) J. K. Przystal, W. G. Bos, and I. B. Liss, *J. Inorg. Nucl. Chem.*, **33**, 679 (1971).

10) I. Yoshida, Y. Oono, H. Kobayashi, and K. Ueno, This Bulletin, **45**, 174 (1972).

11) M. F. Richardson, W. F. Wagner, and D. E. Sands, *Inorg. Chem.*, **7**, 2495 (1968).

Table 1. Analytical results

Compound	Molecular formula	Elemental analysis					
		C%		H%		N%	
		Found	Calcd	Found	Calcd	Found	Calcd
$Nd(AA)_3(en)$	$C_{17}H_{29}N_2O_6Nd$	40.68	40.72	5.51	5.78	5.78	5.59
$Nd(AA)_3(pn)$	$C_{18}H_{31}N_2O_6Nd$	41.71	41.94	6.07	6.01	5.40	5.49
$Nd(AA)_3(2\text{-dipy})$	$C_{25}H_{29}N_2O_6Nd$	50.00	50.25	5.05	4.85	4.66	4.69
$Nd(AA)_3(4\text{-dipy})$	$C_{25}H_{29}N_2O_6Nd$	49.45	50.25	5.10	4.85	4.57	4.69
$Nd(AA)_3(phen)$	$C_{27}H_{29}N_2O_6Nd$	52.27	52.17	5.07	4.67	4.27	4.51
$Nd(AA)_3(ipa)$	$C_{18}H_{30}NO_7Nd$	41.17	41.86	5.91	5.81	3.02	2.71
$La(AA)_3(en)$	$C_{17}H_{29}N_2O_6La$	41.26	41.16	5.80	5.85	4.27	4.51
$La(AA)_3(pn)$	$C_{18}H_{31}N_2O_6La$	41.93	42.38	5.91	6.08	5.43	5.49
$La(AA)_3(ipa)$	$C_{18}H_{30}NO_7La$	41.38	42.30	5.89	5.87	2.90	2.74
$La(AA)_3(phen)$[a]	$C_{27}H_{29}N_2O_6La$	52.47	52.62	4.74	4.71	4.53	4.55

a) The product as isolated from an ethyl acetate solution contained one mole of ethyl acetate as a lattice solvent. Found: C, 52.42; H, 4.86; N, 4.16%. Calcd for $La(AA)_3(phen)$ (ethylacetate): C, 52.94; H,5.12; N, 3.98%. IR(Nujol): $\nu_{C=O}$= 1732 cm^{-1}. NMR in $CDCl_3$ (TMS reference): 1.27$_t$ ($-CH_2\underline{CH_3}$); 2.05$_s$ ($\underline{CH_3}CO$); 4.16 ppm$_q$ ($-\underline{CH_2}CH_3$). Ethylacetate can be removed by drying at about 80°C under reduced pressure to give a complex having the formula shown in the table.

Results and Discussion

Structures of Complexes. The structures of the addition complexes were elucidated by IR, visible and NMR spectral data.

Elemental Analysis and Molecular Weight. Results of elemental analyses (Table 1), indicate the formation of a 1: 1 addition complex with each bidentate base, suggesting that the bidentate base occupies the coordination sites of hydrated water through ligand exchange reaction.

Table 2. Molecular weights(37 °C)

Compound	Molecular weight		Solvent
	Found	Calcd	
$Nd(AA)_3(pn)$	532	515.44	Pyridine
$La(AA)_3(pn)$	548	510.11	Pyridine
$Nd(AA)_3(phen)$	564	621.53	Pyridine
$La(AA)_3(phen)$	601	616.20	Chloroform
$Nd(AA)_3(2\text{-dipy})$	620	597.51	Pyridine
	810		Chloroform
$Nd(AA)_3(4\text{-dipy})$		597.51	
	327		Pyridine

Molecular weights of the bidentate base adducts were measured with a vapor pressure osmometer. Results are summarized in Table 2 together with solvents used. Observed values agreed fairly well with those calculated from the formula of mononuclear 1: 1 adducts, except for the 4,4′-dipyridyl adduct. Thus, the addition complexes, with exception of the 4,4′-dipyridyl adduct, can be considered to be of octa-coordinated mononuclear structure.

As regards the 4,4′-dipyridyl adduct, both terminal nitrogen atoms can not coordinate to the central metal ion simultaneously, and the resulting adduct may be of polymeric form bridged by 4,4′-dipyridyl. The 4,4′-dipyridyl adduct in chloroform showed a molecular weight slightly larger than that corresponding to the monomeric structure, suggesting that the depolymerization occurred upon dissolution of the polymeric complex in chloroform. On the other hand, the molecular weight of the adduct in pyridine was half the value of monomeric form, showing the complete dissociation of 4,4′-dipyridyl from the addition complex by coordination of pyridine molecule.

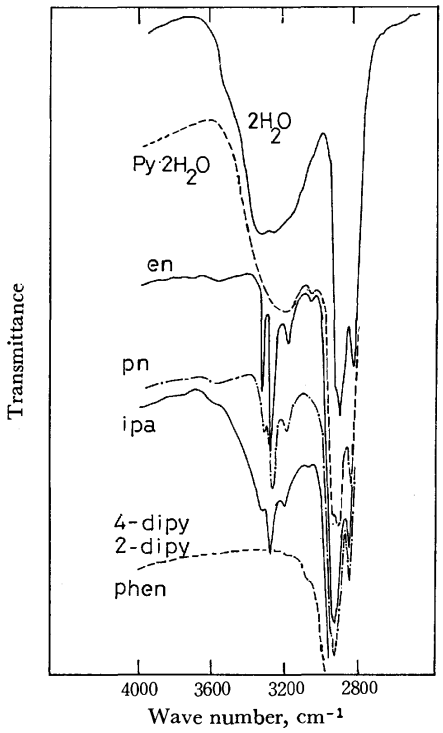

Fig. 1. IR spectra of $Ln(AA)_3(BB)$ in which BB represents the respective base (or bases) indicated in the figure.

Infrared Spectra. IR spectra of the base adducts as well as the hydrated complexes are given in Fig. 1 in the region 2800—4000 cm^{-1}. The dihydrate and the pyridine adducts show a relatively intense and broad absorption at about 3200—3300 cm^{-1} region due to ν_{OH}, and at about 1670—1690 cm^{-1} region due to δ_{OH} of water.[11]

Table 3. Absorption bands (500—600 nm) of neodymium complexes

Compound	Solvent	Absorption peak(nm) / Molar absorptivity									
$Nd(AA)_3(en)$	$CHCl_3$	513	525	528	572	575_{sh}	581	584_{sh}	587	598	
		2.9	5.2	5.2	19.0	12.5	22.8	19.6	17.1	4.5	
	Py	513		527	571	575_{sh}	581				
		2.8		5.8	22.6	14.6	28.7				
$Nd(AA)_3(pn)$	$CHCl_3$	513	525	528	572	575_{sh}	581	584_{sh}	587	598_{sh}	
		2.3	4.4	4.6	19.6	11.8	22.6	18.9	16.6	4.3	
	Py	512		527	571	575_{sh}	581				
		2.4		5.7	24.0	14.7	28.5				
$Nd(AA)_3(ipa)$	$CHCl_3$	513		527	571	575_{sh}	581	584	587	598_{sh}	
		2.4		5.1	17.7	13.8	22.6	21.1	18.2	4.9	
	Py	512		527	571	575_{sh}	581	583			
		2.7		6.4	23.0	15.1	28.4	27.4			
$Nd(AA)_3(2\text{-dipy})$	$CHCl_3$	513		526	571	575_{sh}	582	584	588	591	598_{sh}
		2.1		4.5	17.4	12.7	20.6	17.8	15.0	12.0	4.9
	Py	512		527	571	575_{sh}	581	583			
		2.1		7.0	23.1	16.4	31.4	32.5			
$Nd(AA)_3(phen)$	$CHCl_3$	514		527	572	576	582	585	588	593	600_{sh}
		2.2		5.1	21.2	13.8	22.2	17.7	15.6	11.4	4.2
$Nd(AA)_3(4\text{-dipy})$	$CHCl_3$	513		526	571	575_{sh}	582	584	589	591	598_{sh}
		2.4		4.9	15.5	12.8	20.8	19.0	15.7	12 3	3.0
	Py	512		527	571	575	581	583			
		3.1		7.4	23.1	16.7	31.8	33.1			

On the other hand, 2,2′-dipyridyl, 4,4′-dipyridyl and 1,10-phenanthroline adduct show no absorption band due to water molecule. Ethylenediamine and 1,2-propanediamine adducts show sharp triplet absorptions in the 3300 cm^{-1} region due to ν_{NH}. Isopropanolamine adducts show a rather complicated spectra in the 3300 cm^{-1} region due to the superimposition of ν_{NH} and ν_{OH}.

IR absorptions of the β-diketone moiety of these addition complexes appear at 1590—1600 and 1510—1520 cm^{-1} for $\nu_{C=O}$ and $\nu_{C=C}$, respectively.[11,12]

Visible Absorption Spectra of Neodymium Complexes. Visible absorption spectra of the 2,2′-dipyridyl adducts are shown in Fig. 2 and the numerical data for a series of neodymium complexes in Table 3 in the range 500—600 nm. The spectral characteristics of the base adducts are very similar to each other regardless of the kind of base. The absorption intensity was found to be higher in pyridine than in chloroform. A similar increase in absorption intensity was observed when excess bidentate base was added to the chloroform solution of the corresponding addition complex.

Although the shape of absorption band of the base adduct in chloroform is similar to that for neodymium β-diketonates[13] believed to be heptacoordinate, the present addition complexes are definitely octacoordinate even in chloroform solution as evidenced by NMR spectra. Thus, the diagnosis on the coordination structure of lanthanide chelates from the hypersensitive absorption bands may be useful only within a limited

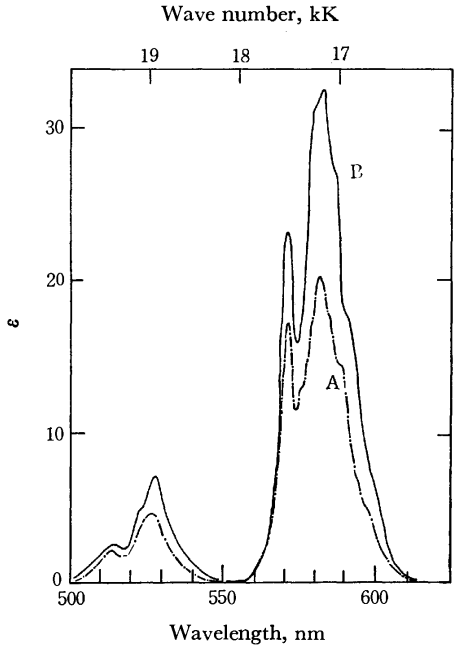

Fig. 2. Visible absorption spectra of $Nd(AA)_3$ (2-dipy) in chloroform(A) and pyridine(B).

combination of ligands.[13,14]

NMR Spectra of Lanthanum Complexes. NMR spectral data for several addition complexes of lanthanum(III) are summarized in Table 4. NMR signals of acetylacetone moiety of the complexes appear at 1.73—1.87 ppm for methyl protons and at 5.19—5.30 ppm for methine proton as a relatively broad singlet

12) S. Pinchas, B. L. Silver, and I. Laulicht, *J. Chem. Phys.*, **46**, 1506 (1967).

13) D. G. Karraker, *Inorg. Chem.*, **6**, 1863 (1967).

14) D. G. Karraker, *ibid.*, **7**, 473 (1968).

Table 4. Proton NMR absorption peaks of lanthanum complexes in deuteriochloroform(TMS reference)

Compound	Chemical shift (ppm)		
$La(AA)_3(en)$	$1.85_s(CH_3)$	$1.98_s(NH_2)^u$	$2.76_s(CH_2)^u$
	$5.30_s(CH)$		
en	$1.27_s(NH_2)^u$	$2.72_s(CH_2)^u$	
$La(AA)_3(pn)$[e]	$1.08_d(CH_3)^u$	$1.87_s(CH_3)$	$2.14_s(NH_2)^u$
	$5.22_s(CH)$		
$CH_3{}^dCH^c(NH_2)CH^bH^aNH_2$	$1.03_d(CH^d{}_3)^u$	$1.48_s(NH_2)^u$	$2.38_q(CH^a)^u$
	$2.68_q(CH^b)^u$	$2.76_{hd}(CH^c)^u$	
$La(AA)_3(phen)$	$1.73_s(CH_3)$	$5.19_s(CH)$	$7.63_q(H^b)^u$
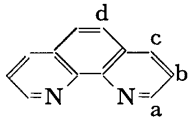	$7.78_s(H^d)^u$	$8.30_q(H^c)^u$	$9.41_q(H^a)^u$
	$7.56_q(H^b)^u$	$7.71_s(H^d)^u$	$8.19_q(H^c)^u$
	$9.14_q(H^a)^u$		

s) Singlet peak. d) Doublet peak. q) Quartet peak. hd) Sixteen multiplet peak. u) proton signals of the uncharged base. e) A part of proton signals could be assigned as shown in table, multiplet peaks of others appearing at 2.3—2.9 ppm region.

Superscripts, a, b, c, ·····, denote the signals from the corresponding protons indicated on the structural formula.

peak. Other signals can be assigned to those of the base coordinated to the complexes.

Amine protons of the free ethylenediamine and 1,2-propanediamine are known to give a singlet peak, while those of the coordinated ligands were found to shift remarkably to the lower field (0.71 ppm for ethylenediamine and 0.66 ppm for propanediamine). This deshielding effect of the amine protons obviously suggests the coordination of amino groups to the lanthanide ion.

Deshielding shifts of proton signals due to ethylene- or propylene moiety of the corresponding coordinated diamines were apparent but very slight. A remarkable change in the adduct formation arose on the spin-spin coupling constants, presumably due to fixation of the most favorable conformation for chelation of the metal ion. The coupling constants of the ring protons on a rigid 1,10-phenanthroline nucleus in $La(AA)_3(phen)$ remained equal to those in the free base, although the signals appeared at 0.27—0.07 ppm field lower than those of the free base.

Base adducts of paramagnetic neodymium chelate showed very broad proton signals, giving no high resolution signals due to base. This suggests that the coordinated base did not dissociate from the neodymium(III) adduct in deuteriochloroform.

The structure of base adducts of the general formula $Ln(AA)_3(BB)$ is very likely to be of a mononuclear octa-coordination, in which each of three acetylacetonate ion and an uncharged bidentate base occupy *cis*-coordination sites.[15] In the case of 4,4'-dipyridyl adducts, the structure is still octa-coordinate but may be polymeric. The coordination site of the base is not certain.

Thus it is interesting to note that most unidentate uncharged bases gave no bis-adduct with acetylacetonate chelate under similar conditions. For example, pyridine afforded a mono pyridine adduct of the general formula $Ln(AA)_3(Py)(H_2O)_2$ when the hydrated chelate was recrystallized from pyridine. The only known example for bis-base adduct is of dipivaloylmethane chelates such as $Eu(DPM)_3(Py)_2$[16] and $Ho(DPM)_3(4\text{-pic})_2$,[17] where DPM and 4-pic denote dipivaloylmethanate ion and 4-picoline, respectively.

The relative lower preference of forming bis-adduct with unidentate base in comparison with bidentate base can be understood to be due to the chelate effect of the latter. The formation of bis base adduct of dipivaloylmethane chelates can then be ascribed to the increased hydrophobic interaction between the hydrocarbon moieties of the diketone ligand and water molecules.

Thermal Properties. Thermal properties of the addition complexes were examined by DTA and TGA methods. Those of the hydrate complexes were also studied for comparison. Numerical data are summarized in Table 5.

$Nd(AA)_3(H_2O)_2$ released one mole of water at 68 °C giving a monohydrate, which subsequently liberated one-half mole of acetylacetone at 110—116 °C. Residual polymeric complex[3,9] decomposed at about 200 °C. DTA curve also showed three endotherms at temperatures corresponding to the above reactions. $La(AA)_3(H_2O)_2$ also showed similar DTA and TGA curves.

Pyridine adducts $Ln(AA)_3(Py)(H_2O)_2$ showed three DTA endotherms. One mole each of water and pyridine was released at about 80 °C forming monohydrates, then at about 120 °C one-half mole of acetylacetone was liberated from the monohydrates. Liberated water, pyridine and acetylacetone upon pyrolysis were identified by gas-chromatographic analysis.

$Ln(AA)_3(en)$ and $Ln(AA)_3(pn)$ showed irreversible pyrolytic DTA endotherms and subsequent exotherms in the range 130—160 °C. $Ln(AA)_3(ipa)$ also decomposed at 123—124 °C, accompanied by weight loss corresponding to the elimination of isopropanolamine.

15) W. H. Watson, R. J. Williams, and N. R. Stemple, *J. Inorg. Nucl. Chem.*, **34**, 501 (1972).

16) C. C. Hinckley, *J. Amer. Chem. Soc.*, **91**, 5160 (1969).

17) W. D. Horrocks, Jr., J. P. Sipe, III, and J. R. Luber, *ibid.*, **93**, 5258 (1971).

Table 5. DTA and TGA data of base adducts

Compound	Peak temp. (°C) on DTA curve		
	Weight loss (%) on TGA curve at corresponding peak temp.[a]		
$Nd(AA)_3(H_2O)_2$	68	110	207
	4.0 (3.8)[d]	15.0 (14.3)[e]	22
$La(AA)_3(H_2O)_2$	100	116_{sh}	184
	10	14.5 (14.4)[e]	16
$Nd(AA)_3(Py)(H_2O)_2$	81	118	208
	18.0 (17.4)[f]	28.0 (26.4)[g]	33
$La(AA)_3(Py)(H_2O)_2$	80	116	186
	19.0 (17.7)[f]	29.0 (26.8)[g]	30
$Nd(AA)_3$(ipa)	70	124	
	0	14 (14.5)[j]	
$La(AA)_3$(ipa)	75	123	203
	0	15 (14.7)[j]	33 (34.3)[k]
$Nd(AA)_3$(en)		160	162.5[c]
		17.0 [p]	17.5[p]
$La(AA)_3$(en)		128	134[c]
		6.0 [p]	7.5[p]
$Nd(AA)_3$(pn)		161	166[c]
		15 (14.4)[h]	35 (33.8)[i]
$La(AA)_3$(pn)		159	162[c]
		21 (13.4)[h]	33 (31.0)[l]
$Nd(AA)_3$(2-dipy)		188	209
		25.0 (27.0)[l]	38.5 (43.8)[m]
$Nd(AA)_3$(4-dipy)		209	218
		32 [p]	41 (43.8)[n]
$Nd(AA)_3$(phen)		229	246
		29.0 (29.2)[o]	34.0[p]
$La(AA)_3$(phen)		209	224
		14.0 [p]	30.0 (29.5)[o]

a) Temperatures with superscript c) indicate exothermic peaks, those without endothermic peaks.
b) Numbers in parentheses indicate the calculated values of weight loss accompanied by the elimination of components shown by the following superscripts. d) H_2O, e) H_2O+0.5 acetylacetone, f) H_2O+pyridine, g) H_2O+pyridine+0.5 acetylacetone, h) propanediamine, i) propanediamine+acetylacetone, j) isopropanolamine, k) isopropanolamine+acetylacetone, l) dipyridyl, m) 2,2′-dipyridyl+acetylacetone, n) 4,4′-dipyridyl+acetylacetone, o) phenanthroline, p) values are only approximate due to the close succession of DTA peaks.

On the other hand, $Ln(AA)_3$(phen), $Nd(AA)_3$(2-dipy) and $Nd(AA)_3$(4-dipy) showed pyrolysis in the range 190—200 °C.

Thermal stability increased in the following order, hydrate and unidentate base adducts<bidentate primary amine and isopropanolamine adducts<bidentate heterocyclic nitrogen base adducts.

Ease with which acetylacetone evolves from the hydrates, could be ascribed to the structure of complexes in which acetylacetone moieties were so arranged that they react readily with hydrogen atom in a coordinated water, forming hydrogen bonding between the carbonyl oxygen and the water hydrogen atoms.[11,18] Such a hydrogen bonding should also exist in the primary amine adducts. The relatively high thermal stability of the addition complexes with the bases such as dipyridyl or 1,10-phenanthroline may be thus understood to be due to the absence of reactive hydrogen atoms.

18) T. S. Davis and J. P. Fackler, *Inorg. Chem.*, **5**, 242 (1966).

Hexaammine, Tris(ethylenediamine), Glycinato, and L-Alaninato Complexes of a Triperiodatotetracobaltate(III) Condensed Anion

Tomoharu AMA,* Jinsai HIDAKA, and Yoichi SHIMURA

**Faculty of Literature and Science, Kochi University, Asakura, Kochi 780*

Department of Chemistry, Faculty of Science, Osaka University, Toyonaka, Osaka 560

(Received January 29, 1973)

Malaprade's triperiodatotetracobaltate(III) heteropoly condensed acid, $H_3[Co_4I_3O_{18}(OH_2)_6]\cdot nH_2O$, was characterized by examination of its coordination derivatives with ammonia, ethylenediamine, glycinato, or L-alaninato ligands. It was concluded that the ion of parent acid and its derivatives, $[Co_4I_3O_{18}X_6]^{n-}$ ($X_6=(OH_2)_6$, $(NH_3)_6$, en_3, $(OH_2)_4$(gly), or $(OH_2)_4$(L-ala)), commonly have a hexol-like arrangement of four cobalt(III) octahedra so that the whole skeletons are based on the Anderson structure. The hexol-like configuration is chiral, this being demonstrated by the separation of two diastereomers of $[Co_4I_3O_{18}(OH_2)_4(L\text{-ala})]^{4-}$ ion.

A dark green heteropoly condensed acid $H_3[Co_4I_3O_{24}H_{12}]\cdot nH_2O$ was first separated by Malaprade.[1] Nyman and Plane[2] proposed two possible structures, one being based on the so-called Anderson structure.[3] The Anderson structure consists of seven octahedra condensed by edge sharing into a flat aggregate of trigonal symmetry and includes some important examples such as $[TeMo_6O_{24}]^{6-}$,[4] and $[CrMo_6O_{18}(OH)_6]^{3-}$.[5] If this is the case for $H_3[Co_4I_3O_{24}H_{12}]$, the arrangement of four cobalt(III) octahedra in the green acid have a chiral configuration same as that in a hexol-cobalt(III) ion $[Co\{(\mu\text{-}OH)_2Co(NH_3)_4\}_3]^{6+}$, and accordingly the green acid should be optically resolved into enantiomers. Our attempts at optical resolution of this acid were unsuccessful but we obtained several coordination derivatives of the acid, and finally two diastereomers of $[Co_4I_3O_{18}(OH_2)_4(L\text{-ala})]^{4-}$ ion, which proves the chiral configuration of the skeleton of the starting acid. Details of preparation and electronic absorption and circular dichroism (CD) spectral studies are presented. These compounds may be new examples of a hybrid between ordinary metal complex and heteropoly condensed compound. So far only a few examples of this compound have been reported, such as $Na_5[CoNb_6O_{19}(OH_2)(en)]\cdot 17H_2O$[6] and $K_5[SiCoW_{11}O_{39}(NH_3)]\cdot 14H_2O$.[7]

Experimental

Preparation. *1)* $H_3[Co_4I_3O_{24}H_{12}]\cdot nH_2O$: This was prepared by the method described in literature.[8] Previous authors reported $n=3$[8] or $n=6$,[2,9] but the following elemental analysis showed our samples to be an octahydrate with $n=8$. Found: H, 2.62; I, 32.56%. Calcd for $H_3[Co_4I_3O_{24}H_{12}]\cdot 8H_2O$: H, 2.69; I, 32.83%.

Sodium salt of this acid was also prepared. Found: H, 2.81; I, 29.28%. Calcd for $Na_3[Co_4I_3O_{24}H_{12}]\cdot 12H_2O$: H, 2.80; I, 29.33%.

2) $H_3[Co_4I_3O_{18}(en)_3]\cdot 5H_2O$: The starting acid $H_3[Co_4I_3O_{24}H_{12}]\cdot 8H_2O$ was reacted with 98% ethylenediamine at 55 °C for 3 hr. The reaction mixture was filtered and the resulting solid was washed with methanol. The crude product was dissolved in a minimum amount of water and the insoluble material was filtered off. To the filtrate was gradually added 15% perchloric acid and the complex deposited was purified by adding 15% perchloric acid to an alkaline solution (pH=about 12) of the complex. The reddish brown precipitate was filtered and washed with water, methanol and finally with acetone. Found: N, 7.20; C, 6.14; H, 3.18; I, 32.28%. Calcd for $H_3[Co_4I_3O_{18}(en)_3]\cdot 5H_2O$: N, 7.14; C, 6.12; H, 3.17; I, 32.32%.

3) $H_3[Co_4I_3O_{18}(NH_3)_6]\cdot 9.5H_2O$: This was derived from $H_3[Co_4I_3O_{24}H_{12}]\cdot 8H_2O$. Five grams of the starting acid was dried *in vacuo* overnight and was added in an excess of liquid ammonia at room temperature. The suspension was allowed to stand for 30 hr to complete the reaction. The solid phase gradually turned brown from green. Both the green starting compound and the reddish brown reaction product were sparingly soluble in liquid ammonia. The resulting solid was filtered and washed with a large amount of methanol. The crude product was dissolved in a minimum amount of water and the insoluble material was filtered off. An appropriate amount of methanol was added to the filtrate, a reddish brown precipitate being formed. This was recrystallized from a minimum amount of water by addition of methanol. When an aqueous solution of the complex was acidified, it precipitated immediately. Found: N, 7.10; H, 3.40%. Calcd for $H_3[Co_4I_3O_{18}(NH_3)_6]\cdot 9.5H_2O$: N, 7.12; H, 3.41%.

4) $(NH_4)_7H[Co_4I_3O_{18}(OH_2)_4(gly)]_2\cdot 14H_2O$: Two and a half grams of glycine was dissolved in a solution containing 5 g of $H_3[Co_4I_3O_{24}H_{12}]\cdot 8H_2O$ in 1.5 l of water. This solution was kept at 65 °C for 10 hr, during which the pH of the solution was about 2.8. After the solution had been cooled to room temperature and filtered, the filtrate was poured into a column (length *ca.* 0.5 m, diameter 3 cm) containing an anion exchanger, QAE-Sephadex A-25 chloride form. The dark green layer adsorbed at the top of the column was eluted with a solution of NaCl (5 g in 1 l of 1M acetic acid). It was confirmed from measurements of absorption spectra that the first eluted green band is the original aquo complex (sodium salt). The second eluted dark green species was adsorbed again on a column of QAE-Sephadex and eluted with NH_4Cl (100 g in 1 l of 1M acetic acid). When an appropriate amount of methanol was added to the eluate,

1) L. Malaprade, *Bull. Soc. Chim. Fr.*, **6**, 223 (1939).
2) C. J. Nyman and R. A. Plane, *J. Amer. Chem. Soc.*, **83**, 2617 (1967).
3) J. C. Anderson, *Nature*, **140**, 850 (1937).
4) H. T. Evans, Jr., *J. Amer. Chem. Soc.*, **90**, 3275 (1968); **70**, 1291 (1948).
5) A. Perloff, *Inorg. Chem.*, **9**, 2228 (1970).
6) C. M. Flynn, Jr., and G. D. Stucky, *ibid.*, **8**, 178 (1969).
7) L. C. W. Baker and J. S. Figgis, *J. Amer. Chem. Soc.*, **92**, 3794 (1970).
8) J. M. Williams and C. J. Nyman, "Inorganic Syntheses," **9**, 142 (1967).
9) Y. Yoshino, T. Takeuchi, and H. Kinoshita, *Nippon Kagaku Zasshi*, **86**, 978 (1965).

the dark green complex was precipitated. This was recrystallized from a minimum amount of water by addition of NH_4Br and methanol. Found: N, 5.03; C, 1.92; H, 3.28; I, 30.07%. Calcd for $(NH_4)_7H[Co_4I_3O_{18}(OH_2)_4(gly)]_2 \cdot 14H_2O$: N, 5.08; C, 1.94; H, 3.29; I, 30.69%.

5) $(NH_4)_2H_2[Co_4I_3O_{18}(OH_2)_4$(L-ala)$]\cdot 9H_2O$: This was obtained by the same procedure as for 4), using 2.5 g of L-alanine instead of glycine. The L-alaninato complex was recrystallized from water by addition of methanol. The ammonium salt of the complex was less soluble than that of the glycinato complex. Found: N, 3.30; C, 2.65; H, 3.33; I, 29.79%. Calcd for $(NH_4)_2H_2[Co_4I_3O_{18}(OH_2)_4$ (L-ala)$]\cdot 9H_2O$: N, 3.32; C, 2.85; H, 3.35; I, 30.10%.

6) $(+)_{589}$-$Na_4[Co_4I_3O_{18}(OH_2)_4$(L-ala)$]\cdot 8H_2O$ *and* $(-)_{589}$-$Na_4[Co_4I_3O_{18}(OH_2)_4$(L-ala)$]\cdot 9H_2O$: For the separation of isomers of L-alaninato complex, the reaction mixture prepared in 5) was chromatographed by use of an eluent containing 3 g of NaCl in 1 l of 1M acetic acid and a column of 1.5 m length and 3 cm diameter. The first eluted band was the starting aquo complex (sodium salt) as in the case of the glycinato complex, and the second eluted band was broader than that of the glycinato complex. In this band, the species eluted faster showed a positive rotation at 589 nm and that eluted more slowly a negative one. These were sorbed separately on QAE-Sephadex columns, each adsorbed band being eluted again with a solution of NaCl (100 g in 1 l of 1M acetic acid). The sodium salts of L-alaninato isomers were obtained by adding methanol to each purified eluate and recrystallized from water by addition of methanol. Found: N, 0.79; C, 2.50; H, 2.36; I, 29.76%. Calcd for $(+)_{589}$-$Na_4[Co_4I_3O_{18}(OH_2)_4$(L-ala)$]\cdot 8H_2O$: N, 1.08; C, 2.77; H, 2.32; I, 29.27%. Found: N, 0.92; C, 2.78; H, 2.48; I, 28.84%. Calcd for $(-)_{589}$-$Na_4[Co_4I_3O_{18}(OH_2)_4$(L-ala)$]\cdot 9H_2O$: N, 1.06; C, 2.73; H, 2.45; I, 28.87%.

Measurements. The electronic absorption spectra were measured with Shimadzu QR-50 and Hitachi EPS-3T recording spectrophotometers. The CD spectra were recorded with a Roussel-Jouan dichrographe. All the measurements except for $[Co_4I_3O_{18}(en)_3]^{3-}$ were made in aqueous solutions at room temperature. The spectra of $[Co_4I_3O_{18}(en)_3]^{3-}$ were measured in 1/10M NaOH aqueous solution.

Results and Discussion

Nyman and Plane[2] proposed two possible structures for the dark green triperiodatotetracobaltate(III) heteropoly acid $H_3[Co_4I_3O_{30}H_{24}]\cdot nH_2O$ (Fig. 1), one chain and the other hexol-like, which have a notable difference in the number of water molecules coordinating to the cobalt(III) ions; *viz.*, 12 for the former and 6 for the latter. $[Co_4I_3O_{18}(NH_3)_6]^{3-}$ and $[Co_4I_3O_{18}(en)_3]^{3-}$ were derived from the reactions of the dark green acid with liquid ammonia and 98% ethylenediamine, respectively. This supports the view that the original dark green acid has structure (a) in Fig. 1. The formation of ethylenediamine complex indicates out that every two of the six water molecules take a *cis* position to each other. The dark green acid and its derivatives are thus assigned to have a hexol-like structure. One monoglycinato and two mono(L-alaninato) complexes resulted from the reactions of the dark green starting acid and glycine or L-alanine. The two L-alaninato isomers separated by column chromatographic method are assigned to a pair of diastereomers (Fig. 2) from their CD behaviors.

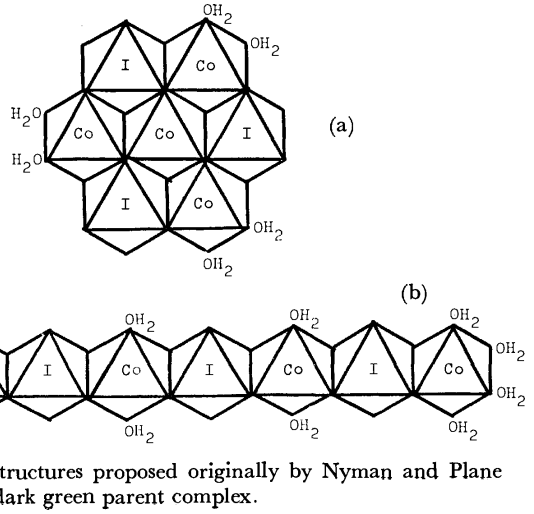

Fig. 1. Structures proposed originally by Nyman and Plane for the dark green parent complex.

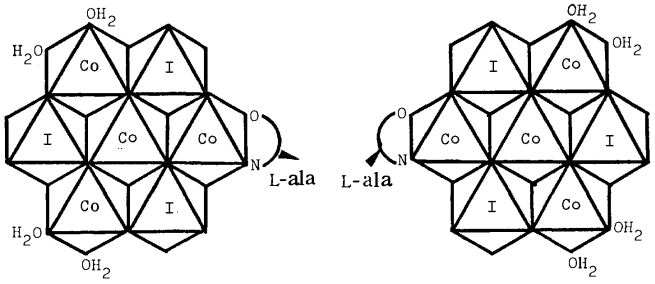

Fig. 2. Two diastereomers of the L-alaninato complex.

The absorption curves of the complexes are on the whole similar to each other (Figs. 3 and 4). Each complex shows three absorption bands in the region from visible to near-ultraviolet. Of these bands a shoulder at about $25—30\times10^3$ cm^{-1} is assigned to the "poly-nuclear band"[10-12] due to a charge-transfer transition in the group $Co\langle_O^O\rangle Co$, from a comparison of the spectra of present complexes to those of $[(ox)_2Co(\mu\text{-}OH)_2Co(ox)_2]^{4-}$,[13] and $[Co_2Mo_{10}O_{34}(OH)_4]^{6-}$,[12,14]. This assignment is emphasized by the fact that the mono-nuclear complexes $[CoMo_6O_{24}H_6]^{3-}$,[12] and $[CoW_6O_{22}]^{5-}$,[15] did not have this kind of absorption band.

The first absorption band for the dark green parent complex $[Co_4I_3O_{18}(OH_2)_6]^{3-}$ appears at 16.8×10^3 cm^{-1} which agrees well with the behavior of several $[Co(O)_6]$ type complexes[12,16] (Table 1). The first bands of the

10) Y. Inamura and Y. Kondo, *ibid.*, **74**, 627 (1953).
11) Y. Sasaki, J. Fujita, and K. Saito, This Bulletin, **42**, 146 (1969).
12) Y. Shimura, H. Ito, and R. Tsuchida, *Nippon Kagaku Zasshi*, **75**, 560 (1954).
13) Diffuse reflectance spectrum of $K_4[Co_2(OH)_2(ox)_4]\cdot 3H_2O$, measured by N. Matsuoka (Department of Chemistry, Faculty of Science, Osaka University), showed three absorption bands at 16.6, 24.1 and 30.6×10^3 cm^{-1}, the last one being the poly-nuclear band.
14) T. Ama, J. Hidaka, and Y. Shimura, This Bulletin, **43**, 2654 (1970).
15) M. Shibata, *Nippon Kagaku Zasshi*, **87**, 771 (1966).
16) N. Matsuoka, J. Hidaka, and Y. Shimura, This Bulletin, **40**, 1868 (1967).

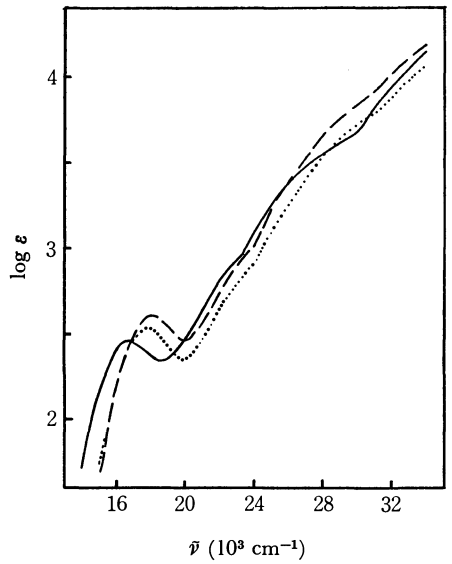

Fig. 3. Absorption curves of $[Co_4I_3O_{18}(OH_2)_6]^{3-}$ (———), $[Co_4I_3O_{18}(NH_3)_6]^{3-}$ (····) and $[Co_4I_3O_{18}(en)_3]^{3-}$ (– – – –).

ammine and ethylenediamine complexes shift to somewhat higher energy, *i.e.*, 17.7 and 18.0×10^3 cm^{-1}, respectively (Fig. 3). These positions may be reasonable, since the hexol-like complexes containing six ammonia or three ethylenediamine ligands have one $[Co(O)_6]$ and three *cis*-$[Co(O)_4(N)_2]$ type chromophores. A similar consideration is applicable to the first absorption bands of glycinato and L-alaninato complexes, which are contributed from three $[Co(O)_6]$ and one $[Co(O)_5(N)]$ type chromophores (Fig. 4 and Table 1). The second absorption bands appear at about $20—25\times10^3$ cm^{-1} as a vague shoulder on the strong poly-nuclear band in all of the present complexes.

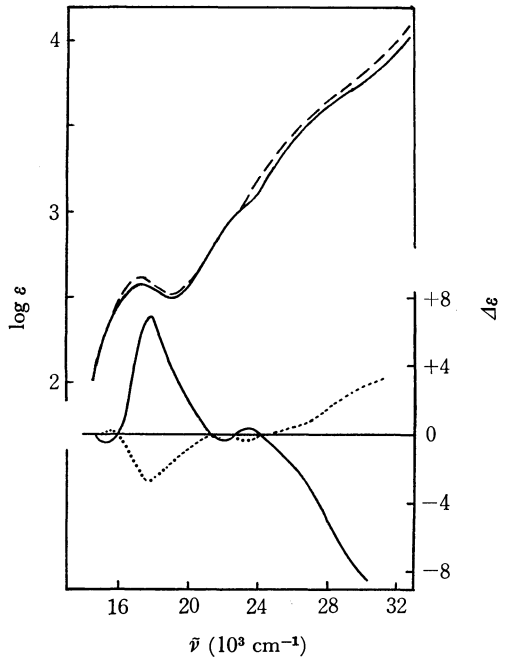

Fig. 4. Absorption and CD curves of $(+)_{589}$-$[Co_4I_3O_{18}(OH_2)_4$(L-ala)$]^{4-}$ (——), absorption curve of $[Co_4I_3O_{18}(OH_2)_4$(gly)$]^{4-}$ (– – –) and CD curve of $(-)_{589}$-$[Co_4I_3O_{18}(OH_2)_4$(L-ala)$]^{4-}$ (····).

The CD curves of the two L-alaninato complexes are shown in Fig. 4. Roughly speaking two CD curves are antipodal to each other, indicating that the two complexes are a diastereomeric pair, *Δ*L and *Λ*L. Two CD bands with opposite signs to each other appear in the first absorption band region ($14—21\times10^3$ cm^{-1}); that at lower energy is weak and the other at higher energy comparatively intense and broad. Broadening

Table 1. Absorption maximum data for the first absorption band

Complex	$\tilde{\nu}_{max}$, 10^3 cm^{-1}	log ε_{max}	log ε(Co)[a]
$[Co_4I_3O_{18}(OH_2)_6]^{3-}$	16.8	2.47	1.87
$[Co_4I_3O_{18}(NH_3)_6]^{3-}$	17.7	2.54	1.94
$[Co_4I_3O_{18}(en)_3]^{3-}$ in 1/10 M NaOH	18.0	2.60	2.00
$[Co_4I_3O_{18}(OH_2)_4(gly)]^{4-}$	17.2	2.62	2.02
$(+)_{589}$-$[Co_4I_3O_{18}(OH_2)_4$(L-ala)$]^{4-}$	17.2	2.57	1.97
$(-)_{589}$-$[Co_4I_3O_{18}(OH_2)_4$(L-ala)$]^{4-}$	17.2	2.57	1.97
$[CoMo_6O_{18}(OH)_6]^{3-}$,[12]	16.5	1.29	1.29
$(+)_{589}$-$[Co_2Mo_{10}O_{34}(OH)_4]^{6-}$,[14]	16.5	1.96	1.66
$[CoNb_6O_{19}(OH_2)(en)]^{5-}$,[6]	16.7	1.81	1.81

a) intensity calculated per one cobalt(III) ion.

Table 2. CD in the $[Co(O)_6]$ chromophore band region

Complex	$\tilde{\nu}_{ext}$, 10^3 cm^{-1} ($\Delta\varepsilon$)	$\tilde{\nu}_{ext}$, 10^3 cm^{-1} ($\Delta\varepsilon$)	Ref.
$(+)_{589}$-$[Co_4I_3O_{18}(OH_2)_4$(L-ala)$]^{4-}$	15.3 (−0.5)	17.8[a] (+6.9)	
$(-)_{589}$-$[Co_4I_3O_{18}(OH_2)_4$(L-ala)$]^{4-}$	15.5 (+0.2)	17.6[a] (−2.7)	
$(-)_{589}$-$[Co_4(OH)_6(NH_3)_{12}]^{6+}$	14.7 (*ca.* −4)[b]	16.5 (*ca.* +15)[b]	17)
$(-)_{589}$-$[Co_4(OH)_6(en)_6]^{6+}$ (L_I-isomer)	14.6 (−5.0)	16.5 (+16.0)	18)
$(-)_{589}$-$[Co_4(OH)_6$(L-pn)$_6]^{6+}$	14.3 (−1.1)	16.2 (+10.8)	19)
$(+)_{589}$-$[Co_4(OH)_6$(L-pn)$_6]^{6+}$	14.5 (+1.3)	16.3 (−13.3)	19)
$(+)_{589}$-$[Co_2Mo_{10}O_{34}(OH)_4]^{6-}$	15.6 (−2.20)	17.1 (+1.35)	14)

a) Overlapped with the bands due to $[Co(O)_4$(L-ala)$]$ chromophore.
b) Estimated from figure.

in the latter suggests a contiguity of two CD bands of the same sign. The CD bands in the second absorption band region ($21—25\times10^3$ cm^{-1}) are weak as compared with those in the first band region. The CD in the poly-nuclear band region is considerably strong.

As seen in Table 2, the CD behavior in the region of d-d absorption band due to the $[Co(O)_6]$ chromophore ($14—18\times10^3$ cm^{-1}) is quite similar to that observed for some hexol-cobalt(III) ions with ammonia,[17] ethylenediamine,[17,18] and L-propylenediamine[19] in the corresponding region. Thus, it is concluded that the complexes have the hexol-like Anderson structure. For the absolute configurations of hexol-cobalt(III) ions with ammonia, ethylenediamine or L-propylenediamine, Mason *et al.*[17] and Douglas *et al.*[19] gave reversed assignments, but Wentworth *et al.*[18] none. Since the one X-ray study of this type of compound is confined to the racemic ammine hexol,[20] we have not attempted to assign the absolute configurations of the L-alaninato diastereomers. Nevertheless, it is evident from Table 2 that the $(+)_{589}$-L-alaninato diastereomer has the same configuration as the $(-)_{589}$-isomers of the ammine-, ethylenediamine-, and L-propylenediamine-hexols.

17) S. F. Mason and J. W. Wood, *Chem. Commun.*, **1967**, 209.
18) R. D. Kern and R. A. D. Wentworth, *Inorg. Chem.*, **6**, 1018 (1967).
19) I. Masuda and B. E. Douglas, *J. Coord. Chem.*, **1**, 189 (1971).
20) U. Thewalt, *Chem. Ber.*, **104**, 2657 (1971).

BULLETIN OF THE CHEMICAL SOCIETY OF JAPAN, VOL. 46, 2148—2151 (1973)

Polarographic Reductions of Some Alkali and Alkaline Earth Metal Ions in Dimethylacetamide. Effect of Cation of the Supporting Electrolyte

Kosuke IZUTSU,* Sachiko SAKURA, and Taitiro FUJINAGA

Department of Chemistry, Faculty of Science, Kyoto University, Sakyo-ku, Kyoto 606

(Received February 19, 1973)

Polarographic reductions of lithium, barium, strontium, and calcium ions in dimethylacetamide (DMA) have been examined in the supporting electrolytes of various kinds of tetraalkylammonium perchlorates. As having been observed in hexamethylphosphoramide, the reductions of these metal ions in DMA are influenced significantly by the cation of the supporting electrolyte. When the cation of the supporting electrolyte is small in size and easily adsorbed onto the negatively charged electrode surface, as in the case in Et_4NClO_4, the reductions of these metal ions are difficult and they either do not occur at all until the reduction of the supporting electrolyte itself or, if they occur, the limiting currents are small and controlled by some preceding processes. With the increase of the cationic size of the supporting electrolyte, the reductions become much easier. Thus, in Bu_4NClO_4 and in Hex_4NClO_4, these metal ions are reduced almost reversibly. The effect of cation of the supporting electrolyte on the reduction of lithium ion has also been examined briefly in dimethylsulfoxide, dimethylformamide and propylenecarbonate.

In our recent papers,[1-3] we reported that the polarographic reductions of alkali and alkaline earth metal ions in hexamethylphosphoramide (HMPA) are strongly influenced by the cation of the supporting electrolyte. As an example, the behavior of sodium ion in various kinds of perchlorate solutions is shown in Fig. 1: In 0.05 M Et_4NClO_4, sodium ion is not reduced until the reduction of the supporting electrolyte. In 0.05 M Pr_4NClO_4 or in Bu_4NClO_4, however, a small sodium wave is observed and its limiting current is controlled kinetically. In 0.05 M Hex_4NClO_4, the sodium wave becomes much higher, but still partly controlled by the kinetic process. If 0.05 M $LiClO_4$ is used instead of tetraalkylammonium salts, the reduction of sodium ion becomes reversible and diffusion controlled. We showed that these effects are mainly due to the pheno-

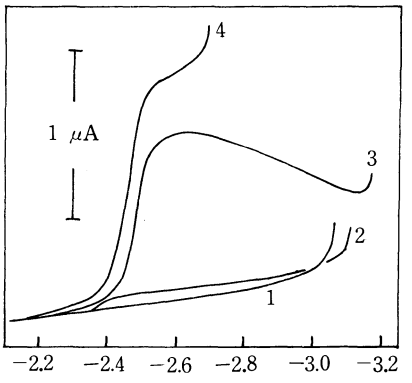

Fig. 1. Polarograms of 1 mM $NaClO_4$ in HMPA. Supporting electrolyte: curve 1, Et_4NClO_4; 2, Bu_4NClO_4; 3, Hex_4NClO_4; and 4, $LiClO_4$. Each in 0.05 M.

* Present Address: Department of Chemistry, Faculty of Science, Shinshu University, Matsumoto 390.

1) K. Izutsu, S. Sakura, and T. Fujinaga, This Bulletin, **45**, 445 (1972).

2) K. Izutsu, S. Sakura, K. Kuroki, and T. Fujinaga, *J. Electroanal, Chem.*, **32**, A pp. 11—44 (1971).

3) K. Izutsu, S. Sakura, and T. Fujinaga, This Bulletin, **46**, 493 (1973).

mena occurring near the electrode double layer. At extremely negative potentials, smaller cations are preferentially attracted onto the electrode surface. Thus, Et_4N^+ ion, which is smallest of the cations used in Fig. 1, is most easily adsorbed and inhibits the reduction of heavily solvated sodium ion completely. The inhibition seems to be due mainly to electrostatic effect but steric effect may also be involved. In Pr_4NClO_4 or in Bu_4NClO_4, Bu_4N^+, or Pr_4N^+ ion is still adsorbed rather easily and the reduction of sodium ion must be preceded by a process, which may be considered to be either a (partial) desolvation of the sodium ion or its penetration through the layer of the adsorbed tetraalkylammonium ion, and the rate of the preceding process controls the limiting current of the sodium wave. In $LiClO_4$, on the contrary, sodium ion is more easily attracted onto the electrode surface than lithium ion and its reduction is not inhibited at all.

Polarographic reductions of alkali and alkaline earth metal ions in dimethylacetamide (DMA) have already been studied by Gutmann *et al.*[4,5] and by Broadhead and Elving,[6] but they used only tetraethylammonium salt as the supporting electrolyte. In the present paper, the reductions of these metal ions in DMA and in several other dipolar aprotic solvents have been examined by using various kinds of tetraalkylammonium perchlorates as the supporting electrolytes.

Apparatus and Reagents

Most of the apparatus are the same as those used in the previous reports.[1,3] Except the measurement of Fig. 8, the dropping mercury electrode had the following characteristics in 0.05 M Et_4NClO_4–DMA and at $h=62$ cm; $m=1.88$ mg/sec with the circuit open and $t=1.31$ sec at -3.1 V *vs.* Ag/0.1 M $AgClO_4$ (DMA) reference electrode. The DME for Fig. 8 had $m=1.62$ mg/sec at $h=62$ cm and with the circuit open.

DMA was distilled following the method of Gutmann *et al.*[4] All perchlorates used in this experiment are the same as those in the previous reports[1,3] and were dried before use. Measurements were carried out at 25 ± 0.1 °C.

Results and Discussion

Alkali Metal Ions in DMA: Gutmann *et al.*[4] have shown that lithium ion is irreducible in truly anhydrous DMA by using 0.1 M Et_4NClO_4 as the supporting electrolyte.

Figure 2 shows the effect of the cation of the supporting electrolyte on the lithium wave. In accordance with the Gutmann's results, lithium ion is irreducible in 0.1 and 0.05 M Et_4NClO_4 untill the reduction of the supporting electrolyte, though a very small wave becomes to be observed in 0.02 M Et_4NClO_4. In 0.05 M Bu_4NClO_4 and Hex_4NClO_4, the lithium wave is AC polarographically reversible and the DC limiting current is diffusion controlled, though a big polarographic

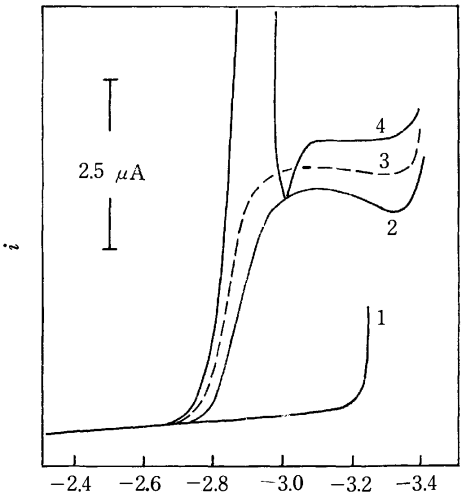

Fig. 2. Polarograms of 1.9 mM Li^+ in DMA.
Supporting electrolyte: curve 1, Et_4NClO_4; 2, Pr_4NClO_4; 3, Bu_4NClO_4; and 4, Hex_4NClO_4. Each in 0.05 M.

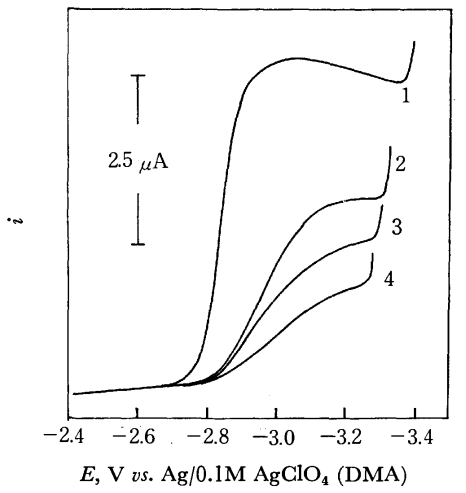

Fig. 3. Effect of Et_4NClO_4 on the reduction wave of 2.1 mM Li^+ in 0.05 M Bu_4NClO_4–DMA.
Concn. of Et_4NClO_4: curve 1, 0 mM; 2, 2 mM; 3, 4 mM; and 4, 10 mM.

maximum of the first kind appears. In 0.05 M Pr_4NClO_4, the limiting current is still somewhat smaller than that expected for diffusion controlled process. In 0.05 M Bu_4NClO_4–DMA, $E_{1/2}$ is -2.8_5 V.

Figure 3 shows how the addition of Et_4NClO_4 affects the lithium wave in 0.05 M Bu_4NClO_4. The addition of as small as 2 mM Et_4N^+ ion decreases the limiting current to about a half of its original value.

Though the reduction wave of lithium ion in DMA is influenced by the cation of the supporting electrolyte, the reversible reduction wave of cesium, rubidium, potassium, and sodium ion is not influenced. For an example, the wave of cesium ion has $E_{1/2}$, -2.4_6 V in all the supporting electrolytes used.

Alkaline Earth Metal Ions in DMA:

Polarograms of barium, strontium and calcium ions are shown in Figs. 4, 5, and 6, respectively.

In 0.05 M Pr_4NClO_4 and Bu_4NClO_4, diffusion con-

4) V. Gutmann, M. Michlymayr, and G. Peychal-Heiling, *Anal. Chem.*, **40**, 619 (1968).

5) V. Gutmann, M. Michlmayr, and G. Peychal-Heiling, *J. Electroanal. Chem.*, **17**, 153 (1968).

6) J. Broadhead and P.J. Elving, *J. Electrochem. Soc.*, **118**, 63 (1971).

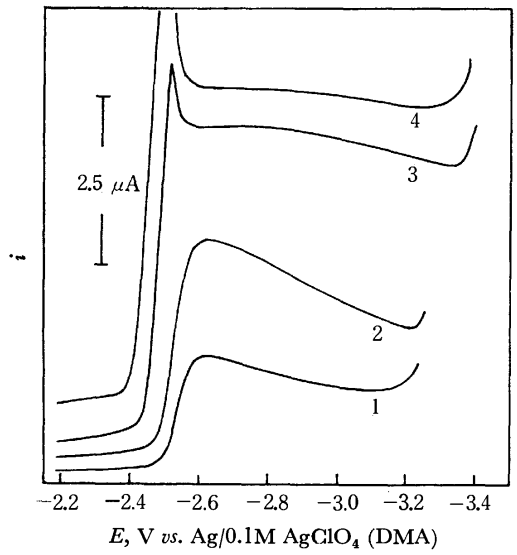

Fig. 4. Polarograms of 1.0 mM Ba^{2+} in DMA.
Supporting electrolyte: curve 1, 0.1 M Et_4NClO_4; 2, 0.05 M Et_4NClO_4; 3, 0.05 M Pr_4NClO_4; and 4, 0.05 M Bu_4NClO_4.

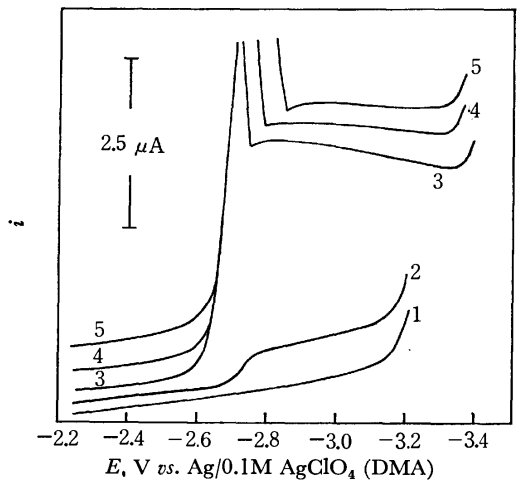

Fig. 5. Polarograms of 0.8 mM Sr^{2+} in DMA.
Supporting electrolyte: curve 1, 0.1 M Et_4NClO_4; 2, 0.05 M Et_4NClO_4; 3, 0.05 M Pr_4NClO_4; 4, 0.05 M Bu_4NClO_4; and 5, 0.05 M Hex_4NClO_4.

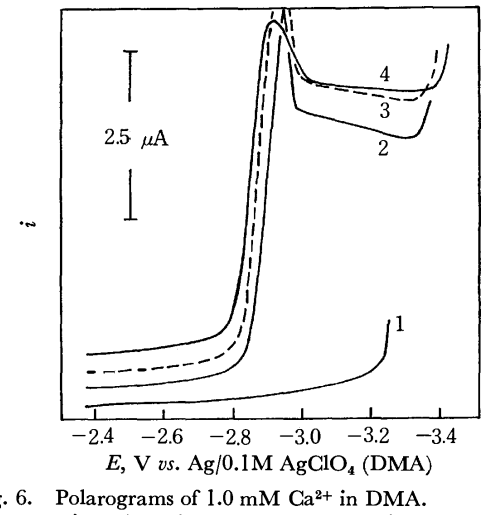

Fig. 6. Polarograms of 1.0 mM Ca^{2+} in DMA.
Supporting electrolyte: curve 1, Et_4NClO_4; 2, Pr_4NClO_4; 3, Bu_4NClO_4; and 4, Hex_4NClO_4. Each in 0.05 M.

trolled barium wave with $E_{1/2}$ of *ca.* -2.4_5 V is observed. AC polarographic measurement shows that the wave is reversible. The barium wave in 0.1 M and 0.05 M Et_4NClO_4, on the other hand, is partly controlled kinetically (Fig. 7) and its limiting current is smaller than that expected for the diffusion process.

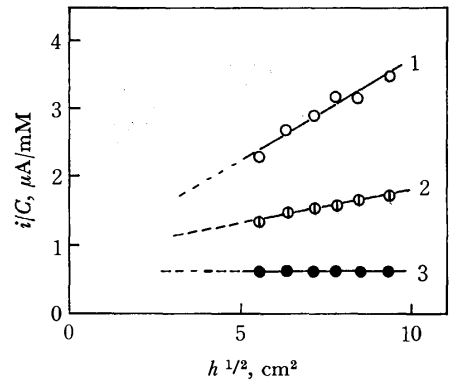

Fig. 7. Change of the limiting currents with the height of the mercury column.
Curve 1, 1.0 mM Ba^{2+} in 0.05 M Et_4NClO_4–DMA; 2, 1.0 mM Ba^{2+} in 0.1 M Et_4NClO_4–DMA; and 3, 0.9 mM Sr^{2+} in 0.05 M Et_4NClO_4–DMA.

Strontium ion is irreducible in 0.1 M Et_4NClO_4 but gives a small, kinetically controlled wave in 0.05 M Et_4NClO_4 (Fig. 7). In 0.05 M Pr_4NClO_4, Bu_4NClO_4, and Hex_4NClO_4, strontium wave is diffusion controlled with $E_{1/2}$ of *ca.* -2.6_8 V.

Calcium ion is irreducible in 0.05 M Et_4NClO_4, but in other supporting electrolytes, the wave is reversible and diffusion controlled with $E_{1/2}$ of *ca.* -2.8_5 V.

These effects of cation of the supporting electrolyte can be explained almost in the same way as in the case in HMPA. Figure 8 shows the drop-time potential curves. The drop-time at extremely negative potentials differs considerably by the cation of the supporting

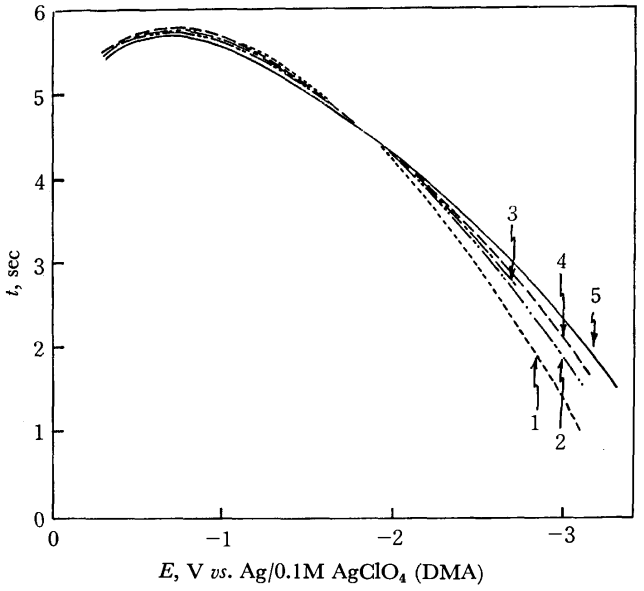

Fig. 8. Drop time—potential curves in 0.05 M perchlorates in DMA.
Curve 1, Et_4NClO_4; 2, Pr_4NClO_4; 3, $LiClO_4$; 4, Bu_4NClO_4; and 5, Hex_4NClO_4.

electrolyte. For tetraalkylammonium ions, it increases in the order $Et_4N^+ < Pr_4N^+ < Bu_4N^+ < Hex_4N^+$ and the drop time in 0.05 M $LiClO_4$ is approximately the same as that in 0.05 M Bu_4NClO_4. From these results, it is apparent that Et_4N^+ ion is preferentially adsorbed onto the electrode surface in the presence of other cations. Thus, for the metal ions to be reduced in Et_4NClO_4 solutions, they must approach to the electrode surface through the layer of adsorbed Et_4N^+ ions. If metal ions are lightly solvated and with moderate sizes, this process will be relatively easy. But, for heavily solvated, bulky metal ions, the process must be difficult, from both electrostatical and sterical points of view. The reduction either does not occur at all or, even if it occurs, it may take place at the rate controlled by the preceding process of the approach of solvated forms or somewhat desolvated forms of metal ions to the electrode surface.

Lithium Ions in DMF, DMSO, and PC: The reductions of lithium ion in Et_4NClO_4–DMSO and Et_4NClO_4–DMF have been reported to be irreversible.[6] Figure 9 shows the effect of supporting electrolytes on the lithium wave in DMF. In 0.05 M Me_4NClO_4 and Et_4NClO_4, lithium wave is irreversible as having been reported in literatures. But in solutions with larger tetraalkylammonium ions, the reduction of lithium ion becomes much more reversible. Similar increase of reversibility of lithium wave by the increase of the size of the cation of the supporting electrolyte is observed also in DMSO.

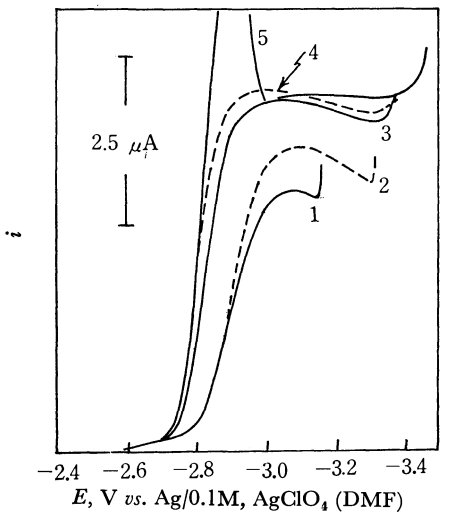

Fig. 9. Polarograms of 2.0 mM Li^+ in DMF.
Supporting electrolyte: curve 1, Me_4NClO_4; 2, Et_4NClO_4; 3, Pr_4NClO_4; 4, Bu_4NClO_4; and 5, Hex_4NClO_4. Each in 0.05 M.

In propylenecarbonate, in which the solvation of lithium ion is considered to be moderate, the lithium wave keeps almost reversible in all the tetraalkylammonium perchlorates solutions used.

BULLETIN OF THE CHEMICAL SOCIETY OF JAPAN, VOL. 46, 2151—2155 (1973)

Polarography of Ammonium 1-Pyrrolidinecarbodithioate and Ammonium 2-Carboxy-1-pyrrolidinecarbodithioate at the Dropping Mercury Electrode

Toyokichi KITAGAWA and Koji TAKU

Department of Chemistry, Faculty of Science, Osaka City University, Sugimoto-cho, Sumiyoshi-ku, Osaka 558

(Received February 22, 1973)

Direct current and alternating current polarographic behaviors of ammonium 1-pyrrolidinecarbodithioate (APCD) and ammonium 2-carboxy-1-pyrrolidinecarbodithioate (ACPCD) were investigated at the dropping mercury electrode. APCD showed an adsorption pre-wave (−0.70 V *vs.* SCE) and one-electron oxidation wave (−0.42 V). ACPCD showed only an adsorption wave (−0.65 V). These results were also confirmed by the investigation of the electrocapillary curves and the current-time curves. The surface excess of APCD or ACPCD on the surface of mercury drop electrode at the potential which the adsorption process was observed were 5.76×10^{-10} mol/cm^2 and 2.62×10^{-10} mol/cm^2, respectively.

APCD forms insoluble complexes with various metal ions and these complexes are much more stable than 1,1-diethylcarbodithioate complexes for heat and acidity. This reagent has been used for colorimetric determinations[1] and atomic absorption spectrophotometric determinations[2] since it was found that these precipitates were extracted with organic solvents.[3] On the other hand, ACPCD forms soluble complexes with various metal ions in aqueous solution.

This paper concerns the polarographic behaviors of APCD and ACPCD at the dropping mercury electrode. The mechanism of electrode reactions and the number of moles adsorbed per unit area of the electrode surface of these substances are also discussed.

Experimental

APCD was prepared according to Mallisa and Schöff-

1) R. W. Looyenga and D. F. Boltz, *Talanta*, **19**, 82 (1972).
2) R. R. Brooks, B. J. Presley, and I. R. Kaplan, *ibid.*, **14**, 809 (1967).
3) W. Doll und H. Specker, *Z. Anal. Chem.*, **161**, 354 (1958).

mann.[4]

ACPCD was prepared by the following procedure. Dissolve 0.1 mol of 2-carboxypyrrolidine(L-proline) in the minimum amount of methanol and add 6 ml of carbon disulfide. Saturate the solution with ammonia gas at 0 °C. Filter off the product and recrystallize twice by dissolving in methanol and precipitating with ethyl ether. Found: C, 32.05; H, 6.80; N, 18.37%. Calcd for $C_6H_{15}O_2N_3S_2$: C, 31.98; H, 6.71; N, 18.65%. All other reagents were A.R. grade.

Polarographic curves were recorded using Yanagimoto P-8 type Polarograph in conjunction with a H-type cell with a saturated calomel electrode and a spiral platinum wire as an auxiliary electrode. The dropping mercury electrode used had the following characteristics; mercury flow rate $m=1.32$ mg/s, drop time $t=5.57$ s at open circuit and at a height of mercury reservoir 65 cm in 0.1 M sodium hydroxide. The current-time curves were recorded using National Oscilloscope VP-546A in conjunction with the polarograph.

A freshly prepared sample solution which contained 0.1 M sodium hydroxide as a supporting electrolyte, was taken into the H-type cell. The dissolved oxygen was removed by bubbling with highly purified nitrogen and then the polarogram was recorded. Experiments were carried out in alkaline solution at 25.0±0.1 °C in order to prevent the decomposition of the sample.[5,6]

Results

Ammonium 1-Pyrrolidinecarbodithioate (APCD).

Direct Current (DC) Polarography: Figure 1 shows the DC and AC polarograms of 5×10^{-4} M APCD in 0.1 M sodium hydroxide solution. Only one DC wave A is observed at −0.70 V in APCD solution less than 1.5×10^{-4} M. When the concentration of APCD exceeds 1.5×10^{-4} M, however, another DC wave B appears at −0.42 V. The limiting current of wave A does not change with increasing concentration of APCD above 1.5×10^{-4} M. The limiting current of total wave (A+B), however, increases linearly with the concentration of APCD less than 2×10^{-3} M as shown in Fig. 2. The effect of the height of the mercury reservoir is shown in Table 1. The height of wave A is approximately proportional to $h_{corr.}$ linearly, while the total wave height is approximately proportional to $h_{corr.}^{1/2}$ The temperature coefficient of the limiting current of the total wave is +1.3% per degree in the temperature range of 5 to 40 °C (Fig. 3). These results show that

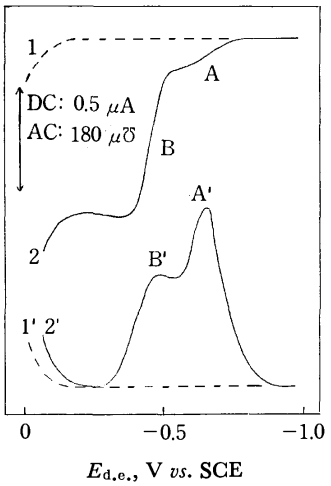

Fig. 1. Polarograms of APCD in 0.1 M NaOH at 25 °C. 1, 1′: 0 M APCD, 2, 2′: 5×10^{-4}M APCD, 1,2: DC polarograms, 1′, 2′: AC polarograms.

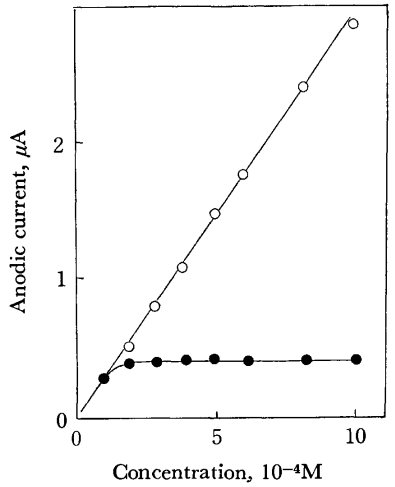

Fig. 2. Calibration curves of DC waves of APCD in 0.1 M NaOH at 25 °C.
(●—●): pre-wave A, (○—○): total wave (A+B)

TABLE 1. THE EFFECT OF THE HEIGHT OF THE MERCURY RESERVOIR ON THE PRE-WAVE A AND THE TOTAL WAVE (A+B) OF 5×10^{-4}M APCD IN 0.1M NaOH AT 25 °C

h, cm	$\bar{i}_A$, nA	$\bar{i}_{A+B}$, nA	$\bar{i}_A/h_{corr.}$	$\bar{i}_{A+B}/\sqrt{h_{corr.}}$
45.0	220	1450	5.0	210
55.0	280	1580	5.2	210
65.0	320	1770	5.0	220
75.0	380	1920	5.1	220
85.0	420	2060	5.0	230
95.0	480	2200	5.1	230

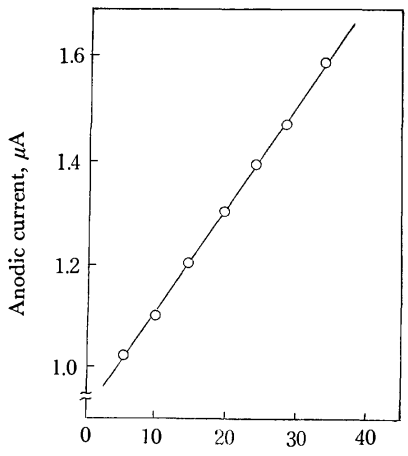

Fig. 3. The effect of temperature on the height of DC total wave of 5×10^{-4}M APCD in 0.1M NaOH.

4) H. Malissa und E. Schöffmann, *Mikrochim. Acta*, **1**, 187 (1955).

5) S. J. Joris, K. I. Aspila, and C. L. Chakrabarti, *J. Phys. Chem.*, **74**, 860 (1970).

6) S. J. Joris, K. I. Aspila, and C. L. Chakrabarti, *Anal. Chem.*, **43**, 1529 (1971).

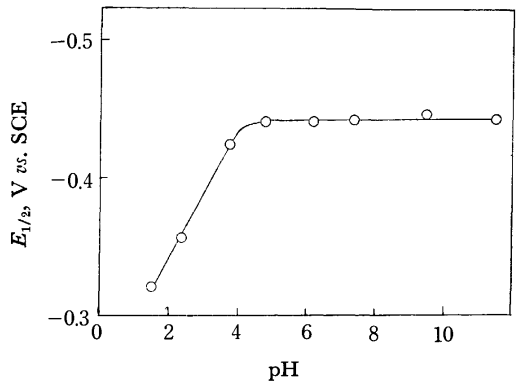

Fig. 4. The effect of pH on the half-wave potential of the wave B of APCD (Britton-Robinson buffers).

wave A is an adsorption wave and that the total anodic wave of APCD is diffusion controlled. The effect of pH on the half-wave potential was also studied. The results are shown in Fig. 4. The half-wave potential of wave B shifts to more negative potential with increasing pH in the pH range less than 4.2 and at higher pH value the half-wave potential of wave B is almost pH independent. This result shows that hydrogen ion participates in the anodic oxidation process of APCD in the pH range less than 4.2.

Alternating Current (AC) Polarography. Two AC waves are observed (Fig. 1, curve 2', A' and B'). AC peak A' is observed in the potential region in which DC wave A is observed, and AC peak B' in the region of DC wave B. The peak height of A' is considerable high in comparison with the corresponding small DC wave A.

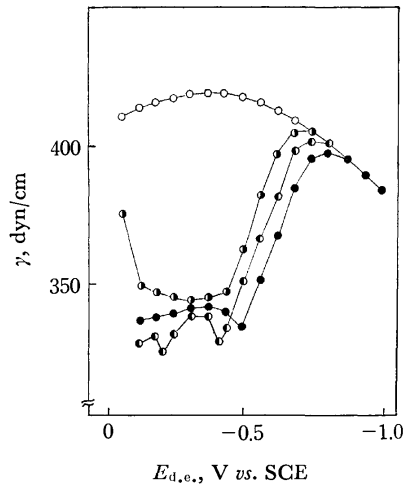

Fig. 5. Electrocapillary curves of APCD in 0.1M NaOH at 25 °C.
(○—○): 0 M, (◑—◑): 10^{-4}M, (◐—◐): 2×10^{-4}M, (●—●): 10^{-3}M.

Electrocapillary Curves. The electrocapillary curves of APCD are shown in Fig. 5. In the presence of APCD, marked decrease of the surface tension of mercury is observed in the potential range between 0 and −0.7 V. At more negative potential than −0.7 V, the surface tension of mercury in the presence of APCD is almost equal to that in its absence. This indicates that APCD adsorbs on the mercury surface strongly in the potential region between 0 and −0.7 V.

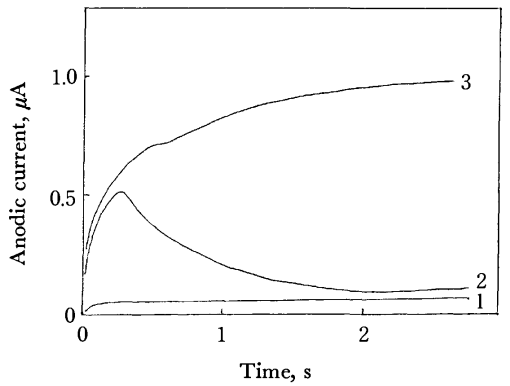

Fig. 6. The effect of the potential on *i-t* curves of 3×10^{-4}M APCD in 0.1M NaOH at 25 °C.
1: −0.80 V, 2: −0.47 V, 3: −0.20 V.

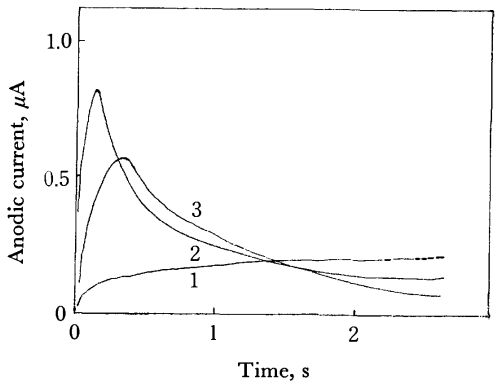

Fig. 7. The effect of the concentration on *i-t* curves of APCD at −0.47 V.
1: 10^{-4}M, 2: 3×10^{-4}M, 3: 5×10^{-4}M.

Current-Time Curves. A series of the current-time (*i-t*) curves of APCD during single mercury drop life was measured. The results are shown in Figs. 6 and 7. At the potential more positive than −0.4 V, the *i-t* curves of 5×10^{-4} M APCD show the diffusion current, which are approximately proportional to $t^{1/6}$. At the potential −0.47 V, however, the *i-t* curves are deformed anomalously. The current increases rapidly for a short time, and then decreases slowly. The time t_m, at which the *i-t* curves reaches maximum, decreases with increasing concentration of APCD, and the height of the maximum current i_m increases with increasing concentration of APCD. These facts are discussed later. This shape of *i-t* curve is the same as that for 1,1-diethylcarbodithioate.[7]

From DC and AC polarograms, electrocapillary curves and *i-t* curves, it seems to be considered that the wave A is adsorption controlled and the total wave is diffusion controlled.

According to Ilkovič equation, the diffusion current constant I of APCD can be calculated; $I=1.77$ μA·mg$^{-2/3}$·s$^{1/2}$·mM^{-1}. This value indicates that the number of electron in the oxidation process of APCD is one and the diffusion coefficient of APCD is 8.52×10^{-6} cm^2·s^{-1}.

7) Unpublished data.

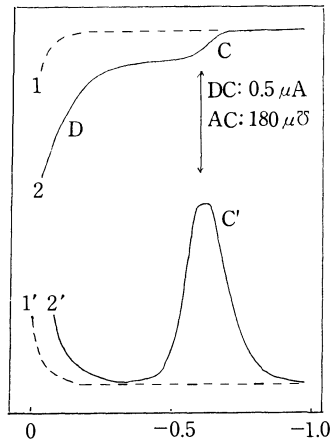

Fig. 8. Polarograms of ACPCD in 0.1M NaOH at 25 °C.
1, 1′: 0 M ACPCD, 2, 2′: 5×10^{-4}M ACPCD, 1, 2: DC porlarograms, 1′, 2′: AC polarograms.

Ammonium 2-Carboxy-1-pyrrolidinecarbodithioate (ACPCD). DC and AC Polarography: Figure 8 shows the DC and AC polarograms of 5×10^{-4} M ACPCD in 0.1 M sodium hydroxide. ACPCD shows DC wave C at −0.65 V, and the limiting current becomes constant above 10^{-4} M. Another DC wave D which appears at more positive potential is overlapped with the anodic dissolution of mercury and can not be analyzed. An AC peak C′ is observed at the potential corresponding to the DC wave. The height of the AC peak is considerably high in comparison with the corresponding DC wave.

From these results, it is found that the DC wave C of ACPCD corresponds to the DC wave A of APCD and that the wave C is also adsorption controlled. The fact that the DC wave D of ACPCD shifts to more positive potential than the DC wave B of APCD may be attributed to the difference of the formation constant of their mercuric complexes, that is, mercury(II) PCD complex is more stable than mercury(II) CPCD complex.

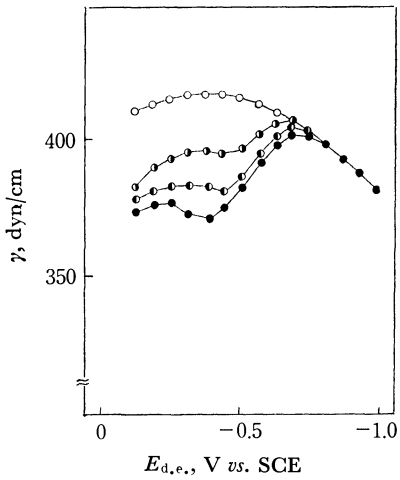

Fig. 9. Electrocapillary curves of ACPCD in 0.1 M NaOH at 25 °C.
(○—○): 0 M, (◑—◑): 10^{-4}M, (◐—◐): 5×10^{-4}M, (●—●): 10^{-3}M.

Electrocapillary Curves. The electrocapillary curves of ACPCD are shown in Fig. 9. ACPCD also causes a decrease of the surface tension of mercury in the potential range between 0 and −0.65 V. However, the degree of decrease of the surface tension is not so remarkable as that of APCD.

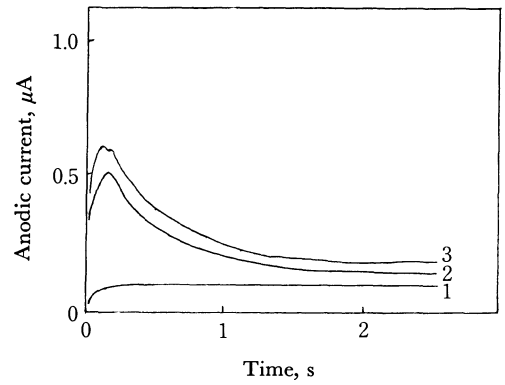

Fig. 10. The effect of the potential on *i-t* curves of 4×10^{-4}M ACPCD in 0.1 M NaOH at 25 °C.
1: −0.75 V, 2: −0.49 V, 3: −0.38 V.

Current-Time Curves. The results of the *i-t* curves of ACPCD are shown in Fig. 10. The *i-t* curves of ACPCD are similar to those of APCD, and it is found that ACPCD also adsorbs on the surface of mercury electrode in the potential range below −0.5 V.

Discussion

The Electrode Reaction Mechanism. The following electrode reactions are considered at the potential which the adsorption process occurs

$$Hg \overset{\text{reversible}}{\rightleftharpoons} Hg^{2+} + 2e^- \quad (1)$$

$$Hg^{2+} + 2L \rightleftharpoons HgL_2 \quad (2)$$

where L stands for a ligand (*e.g.*, PCD^- or $CPCD^{2-}$). It is assumed that Hg^{2+} and HgL_2 are absent in the bulk of the solution and that the mass transfer of L and HgL_2 is controlled by diffusion.

The current is expressed in a following equation.[8]

$$i = i_d/(1+\xi\theta) \quad (3)$$

$$i_d = 7.08\times10^4 nm^{2/3}t^{1/6}D^{1/2}C \quad (4)$$

$$\xi = \exp\frac{nF}{RT}(E^0 - E_{1/2}) \quad (5)$$

$$\theta = \exp\frac{nF}{RT}(E - E^0) \quad (6)$$

The net current until the surface of the mercury electrode is completely covered with HgL_2 is;

$$i = \int_0^{t_m} i\,dt = nF\Gamma_m A \quad (7)$$

$$A = 0.85m^{2/3}t^{2/3} \quad (8)$$

where Γ_m is a surface excess of L and A is a surface area of electrode.

From Eqs. (3)—(8), the time t_m till which the current reaches maximum is;

8) E. Laviron and C. Dogrand, *Bull. Soc. Chim. Fr.*, **1964**, 864.

$$t_m = 1.82\Gamma_m^2(1+\xi\theta)^2/C^2D \quad (9)$$

and at $t=t_m$, the maximum current i_m is;

$$i_m = 7.08\times10^4 nm^{2/3}D^{1/3}\Gamma_m^{1/3}C^{2/3}/(1+\xi\theta)^{2/3} \quad (10)$$

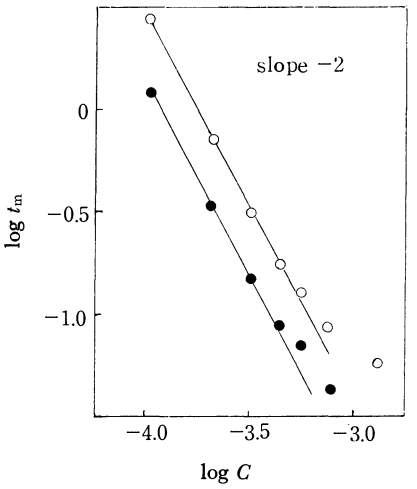

Fig. 11. The effect of concentration on the time till which the current reaches maximum.
(○—○): APCD, (●—●): ACPCD.

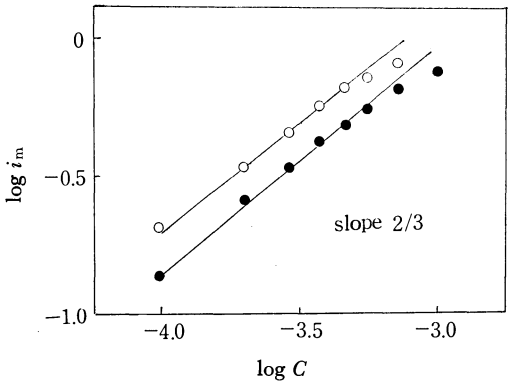

Fig. 12. The effect of concentration on the maximum currents.
(○—○): APCD, (●—●): ACPCD.

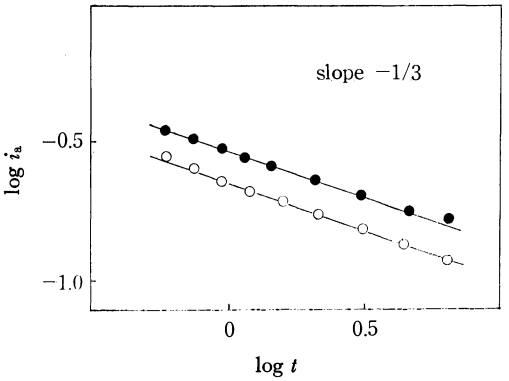

Fig. 13. Log plots of i-t curves of 10^{-3}M of APCD (○—○) and ACPCD (●—●) in 0.1M NaOH at 25 °C.

and in case of $t>t_m$, the adsorption controlled current i_a is;

$$i_a = 5.47\times10^4 nm^{2/3}\Gamma_m/t^{1/3} \quad (11)$$

then the values of

$$\partial \log t_m/\partial \log C = -2,$$

$$\partial \log i_m/\partial \log C = 2/3,$$

and

$$\partial \log i_a/\partial \log t = -1/3$$

can be obtained. In Figs. 11—13, the log plots of these experimental values are shown and the results are in accordance with the theoretical values.

Surface Excess. The values of surface excess of APCD and ACPCD can be calculated from the following three methods.

The first method is based upon a mean adsorption current of DC polarogram using the following equation.[9]

$$\Gamma_s = i_a\tau^{1/3}/8.17\times10^4 nm^{2/3} \quad (12)$$

where τ is a drop time.

The second method is a calculation from the surface tensions at the constant potential E using the following equation.[10]

$$\Gamma_i = -(1/RT)(\partial\gamma/\partial \ln C)_E \quad (13)$$

where γ is the surface tension.

Third method is a calculation from the maximum currents of the i-t curves using Eq. (9).

Table 2. Surface excess of carbodithioates

Substance	Γ, 10^{-10} mol/cm^2
APCD	6.9[a]
	5.8[b]
	3.7[c]
ACPCD	4.8[a]
	2.6[b]
	2.5[c]

a) Calculated from adsorption wave (i_a).
b) Calculated from surface tention (γ).
c) Calculated from current-time curve (t_m).

The results are shown in Table 2. The second method seems to be the most accurate experimentally. In all cases, the values of the surface excess of APCD are larger than that of ACPCD. This will be due to the steric hindrance of mercuric CPCD complex owing to the presence of carboxy group at 2 position.

The authors thank the Ministry of Education for financial support.

9) K. Hasebe and T. Kambara, *Rev. Polarog.* (Kyoto), **15**, 37 (1968).
10) B. B. Damaskin, O. A. Petrii, and V. V. Batrakov, "Adsorption of Organic Compounds on Electrodes," Plenum Press, New York-London, (1971), p. 22.

Reactions of *N*-Sulfinylamines with Carbodiimides[1a]

Toru MINAMI, Michihiko FUKUDA, Masahiro ABE, and Toshio AGAWA
Department of Petroleum Chemistry, Faculty of Engineering, Osaka University, Yamadakami, Suita, Osaka 565

(Received August 29, 1972)

N-Sulfinylsulfonamides **1a, b** reacted with carbodiimides **2** to give the 1,2-cycloadducts, 3-imino-1,2,4-thiadiazetidin-1-oxides **3**, which were readily thermolyzed to sulfonylcarbodiimides **4** and *N*-sulfinylamines **5**. The alkaline or acidic hydrolysis of the cycloadducts **3a, b, d** in ethanol gave the corresponding 1,3-disubstituted-2-*p*-toluenesulfonylguanidines **6a, b, d** in good yields. Reduction of **3a** by the Raney Ni produced similarly **6a** in 87% yield. Reactions of *N*-sulfinylacylamides **1c, d** with **2** led to the formation of an oily mixture of the 1,2-cycloadducts, 3-imino-4-acyl-1,2,4-thiadiazetidin-1-oxides **7** and the 1,4-cycloadducts, 5-imino-1,2,4,6-thiaoxadiazines **8**. Thermal decomposition of the mixture gave **5**, isocyanates **9**, nitriles **10**, and amides **13** as major products.

We reported on the exchange reactions[1b,2a] between *N*-sulfinylamine and heterocumulenes such as isocyanate and isothiocyanate *via* the intermediate 1,2-cycloadducts, which are not isolated.

$$R\text{-}N{=}S{=}O + R'\text{-}N{=}C{=}O \rightleftarrows \begin{bmatrix} R\text{-}N\text{—}S{=}O \\ | \quad | \\ O{=}C\text{—}N\text{-}R' \end{bmatrix} \rightleftarrows R'\text{-}N{=}S{=}O + R\text{-}N{=}C{=}O$$

$$R\text{-}N{=}S{=}O + R'\text{-}N{=}C{=}S \rightleftarrows \begin{bmatrix} R\text{-}N\text{—}S{=}O \\ | \quad | \\ S{=}C\text{—}N\text{-}R' \end{bmatrix} \rightleftarrows R'\text{-}N{=}S{=}O + R\text{-}N{=}C{=}S$$

However use of carbodiimide instead of the above heterocumulenes gave rise to the formation of unstable 1:1-cycloadducts.[2b] This paper deals with the structures of the unstable cycloadducts and their reactivities.

Results and Discussion

N-Sulfinylsulfonamide. The reaction of *N*-sulfinyl-*p*-toluenesulfonamide (**1a**) with dicyclohexylcarbodiimide (**2a**) in ether afforded immediately a 1:1-cycloadduct **3a**, which was precipitated on standing, in 95% yield. The infrared spectrum (Nujol) of the adduct **3a** showed the characteristic absorption bands for the C=N group and the S=O group at 1635 and 1145 and 1100 cm^{-1}, respectively. The mass spectrum exhibited the molecular ion at *m/e* 423 and the fragment ions at 278 and 145 due to $(Ts\text{–}NCN\text{–}C_6H_{11})^+$ and $(C_6H_{11}\text{–}NSO)^+$. Thus, the structure of **3a** was assigned as 2-cyclohexyl-3-cyclohexylimino-4-*p*-toluenesulfonyl-1,2,4-thiadiazetidin-1-oxide. The structure was confirmed by chemical degradation as follows. The cycloadduct **3a** readily decomposed into *p*-toluenesulfonylcyclohexylcarbodiimide (**4a**) and *N*-sulfinylcyclohexylamine (**5a**) under refluxing benzene. Both basic and acidic hydrolysis of **3a** in ethanol gave 1,3-dicyclohexyl-2-*p*-toluenesulfonylguanidine (**6a**) in good yield. Reduction of **3a** by the Raney Ni afforded **6a** in 87% yield.

The reactions of **1a** with other carbodiimides **2b—d** also gave the 1,2-cycloadducts **3b—d**.

In the reaction between *N*-sulfinylmethanesulfon-

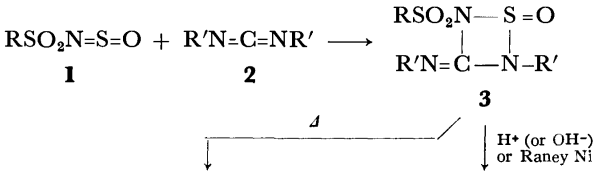

1a, R=*p*-$CH_3C_6H_4$
1b, R=CH_3
2a, **5a**, R'=C_6H_{11}
2b, **5b**, R'=*n*-C_4H_9
2c, **5c**, R'=C_6H_5
2d, **5d**, R'=$(CH_3)_2CH$

3a, **4a**, **6a**, R=*p*-$CH_3C_6H_4$, R'=C_6H_{11}
3b, **4b**, **6b**, R=*p*-$CH_3C_6H_4$, R'=*n*-C_4H_9
3c, **4c**, R=*p*-$CH_3C_6H_4$, R'=C_6H_5
3d, **4d**, **6d**, R=*p*-$CH_3C_6H_4$, R'=$(CH_3)_2CH$
3e, **4e**, R=CH_3, R'=C_6H_{11}
4f, R=CH_3, R'=*n*-C_4H_9
4g, R=CH_3, R'=C_6H_5

Scheme 1.

TABLE 1. CYCLOADDUCTS **3** FROM *N*-SULFINYLSULFONAMIDE AND CARBODIIMIDE

3 (Substituents, R, R')	mp, °C	yield, %	Formula	Calcd %			Found %		
				C	H	N	C	H	N
3a ($CH_3C_6H_4$, C_6H_{11})	149	95	$C_{20}H_{29}N_3O_3S_2$	56.72	6.90	9.90	56.76	6.75	9.82
3b ($CH_3C_6H_4$, *n*-C_4H_9)	58	45	$C_{16}H_{25}N_3O_3S_2$	51.74	6.79	11.32	51.61	6.85	11.30
3c ($CH_3C_6H_4$, C_6H_5)	125	85	$C_{20}H_{17}N_3O_3S_2$	58.39	4.17	10.22	58.35	4.13	9.98
3d ($CH_3C_6H_4$, *iso*-C_3H_7)	90	77	$C_{14}H_{21}N_3O_3S_2$	48.97	6.17	12.24	48.97	6.28	12.49
3e (CH_3, C_6H_5)	119	45	$C_{14}H_{25}N_3O_3S_2$	48.76	7.39	12.25	48.41	7.25	12.25

1a) Presented in part at the 23 rd Annual Meeting of the Chemical Sosiety of Japan, Tokyo, April 1970, Abstracts Vol. 3, p. 1591.

1b) T. Minami, H. Miki, and T. Agawa, *Kogyo Kagaku Zasshi*, **70**, 1831 (1967).

2a) T. Minami and T. Agawa, *Tetrahedron Lett.*, **1968**, 2651.

2b) Note added in proof. These results in part now appear in: H. Ulrich, B. Tucker and A. A. R. Sayigh, *J. Amer. Chem. Soc.*, **94**, 3484 (1972).

amide (**1b**) and **2a**, the 1,2-cycloadduct **3e** was obtained. However, the expected adducts **3f—g** from **2b—c** and **1b** could not be isolated in pure form since they are unstable and readily thermolyzed to generate the corresponding methanesulfonylcarbodiimides **4f—g** and *N*-sulfinylamines **5b—c**. The physical and analytical data and yields of the cycloadducts obtained above are shown in Table 1.

N-*Sulfinylacylamide.* *N*-Sulfinylbenzamide (**1c**) reacted easily with **2a** to afford an oily product which could not be crystallized even after prolonged standing at −20 °C, and which exhibited carbonyl and C=N absorption bands at 1655 and 1620 cm^{-1}, respectively, in the IR spectrum. For confirmation of structure, the product was pyrolyzed at 110 °C under reduced pressure to give a volatile liquid consisting of *N*-sulfinylcyclohexylamine (**5a**, 42%), cyclohexylisocyanate (**9a**, 17%) and benzonitrile (**10c**, 6%) and the residual solid, which was chromatographed on alumina to afford 1,3-dicyclohexyl-2-benzoylguanidine (**11a**, 14%), 2,4-diphenyl-6-cyclohexylamino-*s*-triazine (**12a**, 6%), and *N*-cyclohexylbenzamide (**13a**, 6%). The product seems to be a mixture of the 1,2-cycloadduct, 2-cyclohexyl-3-cyclohexylimino-4-benzoyl-1,2,4-thiadiazetidin-1-oxide (**7a**) and the 1,4-cycloadduct, 5,6-dihydro-3-phenyl-5-cyclohexylimino-6-cyclohexyl-1,2,4,6-thiaoxadiazine (**8a**), since the guanidine derivative **11a** would be formed *via* hydrolysis of the 1,2-cycloadduct **7a** containing the carbonyl absorption band in the IR spectrum and cyclohexylisocyanate (**9a**) and benzonitrile (**10c**) *via* thermolysis of the 1,4-cycloadduct **8a**. The difference in yield between **5a** and **9a** suggests that **5a** would arise from the thermal decomposition of both cycloadducts **7a** and **8a**, since an equimolar amount of **5a** and **9a** from **8a** should be obtained. However, the benzoylcyclohexylcarbodiimide moiety, which would be formed by elimination of **5a** from **7a**, could not be isolated because of instability. The triazine derivative **12a** might be yielded from **10c** and **11a** in the presence of sulfur dioxide, which would be generated by thermolysis of **1c** or hydrolysis of **7a** in the reaction system, as known in the synthesis of 2,4-diaryl-6-amino-*s*-triazine[3] from arylnitrile, sulfur trioxide and guanidine. Accordingly, the formation of **13a** is explicable by the elimination of cyclohexylcyanamide moiety, which would be used for the formation of **12a** from **11a**.

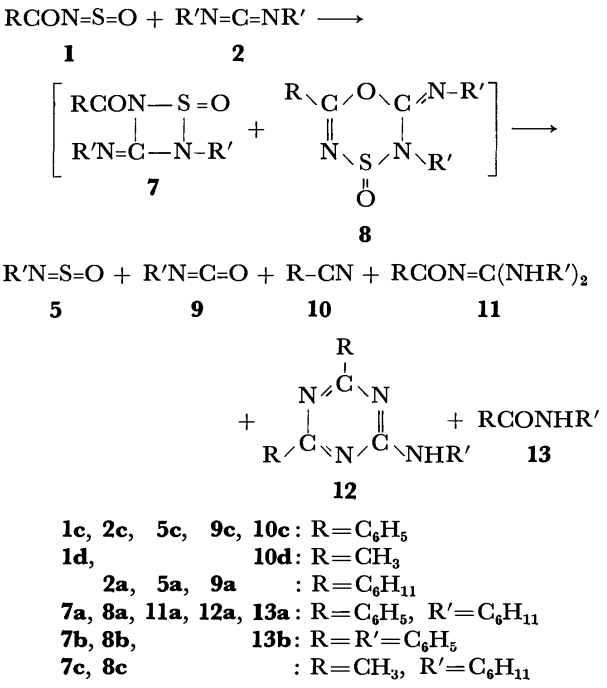

1c, 2c, 5c, 9c, 10c: R=C_6H_5
1d, 10d: R=CH_3
2a, 5a, 9a: R=C_6H_{11}
7a, 8a, 11a, 12a, 13a: R=C_6H_5, R'=C_6H_{11}
7b, 8b, 13b: R=R'=C_6H_5
7c, 8c: R=CH_3, R'=C_6H_{11}

Scheme 2.

In thermal decomposition of the reaction product between **1c** and diphenylcarbodiimide (**2c**), *N*-sulfinylaniline (**5c**), phenylisocyanate (**9c**), **10c**, and benzanilide (**13b**) were obtained in 47, 19, 10, and 12% yields, respectively, but no guanidine **11b** and triazine **12b** corresponding to **11a** and **12a**.

Thermolysis of the reaction product between *N*-sulfinylacetamide (**1d**) and **2a** gave a similar result (Table 3).

In contrast to reactive *N*-sulfinylamine attached to the polar group such as the sulfonyl and carbonyl groups, *N*-sulfinylarylamine and *N*-sulfinylalkylamine gave no cycloadduct in the reaction with carbodiimide.

Table 2. The exchange reaction between *N*-sulfinylsulfonamide **1** and carbodiimide **2**

Starting material (Substituent)		Product (yield %)	
1	**2**	**4**	**5**
1a ($CH_3C_6H_4$),	**2a** (C_6H_{11})	**4a** (76),	**5a** (75)
1a ($CH_3C_6H_4$),	**2b** (*n*-C_4H_9)	**4b** (74),	**5b** (57)
1a ($CH_3C_6H_4$),	**2c** (C_6H_5)	**4c** (70),	**5c** (48)
1a ($CH_3C_6H_4$),	**2d** (*iso*-C_3H_7)	**4d** (42),	**5d** (48)
1b (CH_3),	**2a** (C_6H_{11})	**4e** (78),	**5a** (68)
1b (CH_3),	**2b** (*n*-C_4H_9)	**4f** (52),	**5b** (47)
1b (CH_3),	**2c** (C_6H_5)	**4g** (72),	**5c** (62)

Experimental

All melting points were determined with a YANAGIMOTO micro melting apparatus and uncorrected. The NMR spectra were taken with a JOELLMM 3H-60 spectrometer with tetra-

Table 3. Thermolysis of the reaction products from *N*-sulfinylacylamide and carbodiimide

Starting material (Substituent)		Product (Yield[a] %)			
1	**2**	**5**	**9**	**10**	**13**
1c (R=C_6H_5)	**2a** (R=C_6H_{11})	**5a** (42)	**9a** (17)	**10c** (6)	**13a** (6)
1c (R=C_6H_5)	**2c** (R=C_6H_5)	**5c** (47)	**9c** (19)	**10c** (10)	**13b** (12)
1d (R=CH_3)	**2a** (R=C_6H_{11})	**5a** (15)	**9a** (7)	**10d** (22)	—

a) Based on carbodiimide

3) F. C. Schaefer, "The Chemistry of the Cyano Group," ed. by Z. Rappoport, Interscience Publishers, New York, N. Y. (1970). p. 246.

methylsilane as an internal standard. The IR spectra were recorded with a JASCO IR-E spectrometer. The mass spectra were taken with a HITACHI RMU-6E spectrometer.

Materials. *N*-Sulfinyl-*p*-toluenesulfonamide,[4] *N*-sulfinylmethanesulfonamide,[4] *N*-sulfinylbenzamide,[5,6] *N*-sulfinylacetamide,[5] di-*n*-butylcarbodiimide,[7] and diphenylcarbodiimide[8] were prepared according to the established procedures. Commercial dicyclohexylcarbodiimide and diisopropylcarbodiimide were purified by distillation before use.

*2-Cyclohexyl-3-cyclohexylimino-4-*p*-toluenesulfonyl-1,2,4-thiadiazetidin-1-oxide (3a).* Dicyclohexylcarbodiimide (**2a**, 5.15 g, 25 mmol) in 20 ml of dry ether was added dropwise to a stirred solution of 5.43 g (25 mmol) of *N*-sulfinyl-*p*-toluenesulfonamide (**1a**) in 40 ml of dry ether. After being stirred at ambient temperature for 1 hr, the solution was allowed to stand overnight to give 10.2 g (95%) of a white solid **3a**. Recrystallization from hexane–benzene afforded the analytical sample, mp 149—149.5 °C; IR (Nujol) ν 1635 (C=N), 1290 (SO_2), 1185 (SO_2), 1145 (SO), and 1100 cm^{-1} (SO); NMR ($CDCl_3$) δ 1.05—2.25 (m, 20H, cyclohexyl protons), 2.43 (s, 3H, $-CH_3$), 7.28 (d, J=8 Hz, 2H, phenyl protons), and 7.84 (d, J=8 Hz, 2H, phenyl protons); mass spectrum (70 eV) *m/e* 423 (M^+), 278 $(TsNCNC_6H_{11})^+$, 206 $(C_6H_{11}NCNC_6H_{11})^+$, and 145 $(C_6H_{11}NSO)^+$.

*2-n-Butyl-3-n-butylimino-4-*p*-toluenesulfonyl-1,2,4-thiadiazetidin-1-oxide (3b).* This was prepared in the same way as for **3a**, from the reaction of di-*n*-butylcarbodiimide (**2b**, 3.85 g, 25 mmol) with **1a** (5.43 g, 25 mmol). After removal of solvent *in vacuo*, the resulting residue was recrystallized from petroleum ether–ether to give 4.16 g (45%) of pure **3b**, mp 58.5—59 °C as a white crystal; IR (Nujol) ν 1635 (C=N), 1290 (SO_2), 1150 (SO), and 1095 cm^{-1} (SO); NMR ($CDCl_3$) δ 0.96 (t, J=5 Hz, 6H, methyl protons), 1.13—1.95 (m, 8H, methylene protons), 2.40 (s, 3H, $\underline{H}_3CAr$), 3.60 (t, J=6 Hz, 4H, N–$C\underline{H}_2$–), 7.16 (d, J=8 Hz, 2H, phenyl protons), and 7.70 (d, J=8 Hz, 2H, phenyl protons); mass spectrum (70 eV) *m/e* 371 (M^+), 252 (TsNCN-*n*-Bu)$^+$, and 119 (*n*-BuNSO)$^+$.

*2-Phenyl-3-phenylimino-4-*p*-toluenesulfonyl-1,2,4-thiadiazetidin-1-oxide (3c).* This was prepared in the same way as for **3a** from the reaction of diphenylcarbodiimide (**2c**, 4.70 g, 25 mmol) with **1a** (5.43 g, 25 mmol) at ether refluxing temperature for 2 hr. The crude product was recrystallized from acetone to give 8.50 g (85%) of pure **3c**, mp 125—126 °C; IR (Nujol) ν 1650 (C=N), 1320 (SO_2), 1200 (SO_2), 1160 (SO), and 1095 cm^{-1} (SO); NMR ($CDCl_3$) δ 2.35 (s, 3H, $-CH_3$) and 7.00—7.90 (m, 14H, phenyl protons); mass spectrum (70 eV) *m/e* 272 $(TsNCNPh)^+$, 194 $(PhNCNPh)^+$, and 139 $(PhNSO)^+$.

*2-Isopropyl-3-isopropylimino-4-*p*-toluenesulfonyl-1,2,4-thiadiazetidin-1-oxide (3d).* This was prepared in the same way as for **3a**, from the reaction of **1a** (4.10 g, 20 mmol) with diisopropylcarbodiimide (**2d**, 2.52 g, 20 mmol). The crude product was recrystallized from ether–petroleum ether to give 5.10 g (77%) of pure **3d**, mp 90 °C as a white granular crystal; IR (Nujol) ν 1625 (C=N), 1280 (SO_2), 1180 (SO_2), 1150 (SO), and 1090 cm^{-1} (SO); NMR ($CDCl_3$) δ 1.37 (d, J=7 Hz, 12H, methyl protons), 2.37 (s, 3H, $\underline{H}_3CAr$), 4.35 (qq, J=7 Hz, 2H, methine protons), 7.25 (d, J=9 Hz, 2H, phenyl protons), and 7.80 (d, J=9 Hz, 2H, phenyl protons); mass spectrum (70 eV) *m/e* 343 (M^+), 238 (TsNCN-*iso*-Pro)$^+$ and 105 (*iso*-Pro–NSO)$^+$.

2-Cyclohexyl-3-cyclohexylimino-4-methanesulfonyl-1,2,4-thiadiazetidin-1-oxide (3e). This was prepared in the same way as for **3a** except that the reaction temperature was kept below 10 °C. The crude product was recrystallized from hexane–benzene to give pure **3e** (45%), mp 119—119.5 °C; IR (Nujol) ν 1620 (C=N), 1290 (SO_2), 1185 (SO_2), and 1135 cm^{-1} (SO); mass spectrum (70 eV) *m/e* 374 (M^+), 202 $(CH_3SO_2NCNC_6H_{11})^+$, and 147 $(C_6H_{11}NSO)^+$.

Thermolysis of 3a. The compound (4.23 g, 0.01 mol) was pyrolyzed at 180 °C under reduced pressure (15 mmHg) for 1 hr. The distillate (1.11 g, 75%) was identified as *N*-sulfinylcyclohexylamine (**5a**) by comparison of its IR spectrum and glpc behavior with those of an authentic sample.[9,10] Vacuum distillation of the residue gave 1.57 g (76%) of *p*-toluenesulfonylcyclohexylcarbodiimide (**4a**), bp 165 °C/0.05 mmHg (lit,[11] bp 203—206 °C/0.3 mmHg).

Thermolysis of 3d. The compound (3.40 g, 10 mmol) was thermolyzed at 80—100 °C under reduced pressure (10 mmHg) for 1 hr. The yellow liquid **5d** (0.50 g, 48%) identified as *N*-sulfinylisopropylamine by comparison of its IR spectrum with that of an authentic sample, bp 95—100 °C prepared from isopropylamine and thionyl chloride according to the established procedure[12] was trapped in an ice cooled flask. Vacuum distillation of the residue afforded 1.0 g (42%) of *p*-toluenesulfonylisopropylcarbodiimide (**4d**), bp 90—100 °C/0.01 mmHg (lit,[11] 168 °C/0.1 mmHg); IR (neat) ν 2180 (SO_2N=C=N), 1340 (SO_2), and 1160 cm^{-1} (SO_2).

Found: C, 55.25; H, 5.90; N, 11.26%. Calcd for $C_{11}H_{14}N_2O_2S$: C, 55.45; H, 5.92; N, 11.76%.

Exchange Reaction between 1a and 2b. To 5.43 g (25 mmol) of **1a** in 20 ml of benzene was added dropwise 3.85 g (25 mmol) of **2b** in 10 ml of benzene. The mixture was stirred for 2 hr at ambient temperature. After evaporation of solvent under reduced pressure, vacuum distillation of the residue yielded 1.04 g (57%) of *N*-sulfinyl-*n*-butylamine (**5b**), bp 30 °C/20 mmHg (lit,[9] bp 30 °C/20 mmHg) and 4.66 g (74%) of *p*-toluenesulfonyl-*n*-butylcarbodiimide (**4b**), bp 150—155 °C/0.1 mmHg (lit,[11] bp 155—158 °C/0.2 mmHg); IR (neat) ν 2180 (SO_2N=C=N).

Exchange Reaction between 1a and 2c. In a similar way, the reaction of **1a** (5.43 g, 25 mmol) with **2c** (4.85 g, 25 mmol) was carried out. Vacuum distillation of the reaction mixture yielded 1.67 g (48%) of *N*-sulfinylaniline (**5c**), bp 80 °C/12 mmHg (lit,[9] bp 84 °C/12 mmHg) and 7.50 g of the sticky residue whose IR spectrum displayed a characteristic band of the SO_2N=C=N group at 2180 cm^{-1}. Upon addition of the residue to wet acetone, *N-p*-toluenesulfonyl-*N'*-phenylurea (5.10 g, 70%), mp 171 °C (lit,[13] mp 169—170 °C) was obtained.

Exchange Reaction between 1b and 2a. In a similar way, the reaction of **1b** (2.82 g, 0.02 mol) with **2a** (4.10 g, 0.02 mol) was carried out, vacuum distillation of the reaction mixture yielding 1.95 g (68%) of **5a** and 3.14 g (78%) of methanesulfonylcyclohexylcarbodiimide (**4e**), bp 165 °C/0.1 mmHg; IR (neat) ν 2180 cm^{-1} (SO_2N=C=N).

4) G. Kresze and W. Wucherpfennig, *Angew. Chem.*, **79**, 109 (1967).
5) O. J. Scherer and R. Schmitt, *Chem. Ber.*, **101**, 3302 (1968).
6) O. Tsuge and S. Mataka, This Bulletin, **44**, 2836 (1971).
7) E. Schmidt, F. Hitzler, and E. Lahde, *Ber.*, **71**, 1933 (1938).
8) Y. Ohshiro, Y. Mori, T. Minami, and T. Agawa, *J. Org. Chem.*, **35**, 2076 (1970).
9) D. Klamann, C. Sass, and M. Zelenka, *Chem. Ber.*, **92**, 1910 (1959).
10) T. Minami, H. Miki, and T. Agawa, *Kogyo Kagaku Zasshi*, **70**, 1829 (1967).
11) H. Ulrich, B. Tucker, F. A. Stuber, and A. A. R. Sayigh, *J. Org. Chem.*, **34**, 2250 (1969).
12) A. Michaelis, and O. Storbeck, *Ann.*, **274**, 187 (1893).
13) C. King, *J. Org. Chem.*, **25**, 352 (1960).

*Exchange Reaction between **1b** and **2b**.* In a similar way, the reaction of **1b** (2.82 g, 0.02 mol) with **2b** (3.80 g, 0.02 mol) was carried out, vacuum distillation yielding 1.12 g (47%) of **5b** and 2.0 g (52%) of methanesulfonyl-*n*-butylcarbodiimide (**4f**), bp 100 °C/0.2 mmHg (lit,[14] bp 103—105 °C/0.3 mmHg); IR (neat) ν 2180 cm^{-1} ($SO_2N{=}C{=}N$).

*Exchange Reaction between **1b** and **2c**.* In a similar way, the reaction of **1b** (2.82 g, 0.02 mol) with **2c** (3.88 g, 0.02 mol) was carried out, vacuum distillation yielding 1.72 g (62%) of **5c** and 2.86 g (72%) of methanesulfonylphenylcarbodiimide (**4g**), bp 145 °C/0.1 mmHg; IR (neat) ν 2180 cm^{-1} ($SO_2N{=}C{=}N$).

*Base Catalyzed Hydrolysis of **3a**.* A solution of **3a** (0.85 g, 2 mmol) in 95% ethanol (15 ml) containing sodium hydroxide (0.08 g, 2 mmol) was refluxed for 8 hr. After removal of the solvent, the residue was washed with water, followed by drying. The white solid obtained was recrystallized from benzene–hexane to give pure 1,3-dicyclohexyl-2-*p*-toluenesulfonylguanidine (**6a**, 0.69 g, 91%), mp 158 °C (lit,[15] mp 161 °C).

*Acid Catalyzed Hydrolysis of **3a**.* A solution of **3a** (0.85 g, 2 mmol) in 95% ethanol (15 ml) containing 48% aqueous HBr (2 ml) was refluxed for 5 hr. After removal of the solvent, the residue was recrystallized from benzene–hexane to afford 0.70 g (93%) of **6a**.

*Base Catalyzed Hydrolysis of **3b**.* A solution of **3b** (1.48 g, 4 mmol) in ethanol was treated under the same condition as for **3a**. After a similar work-up, the white solid obtained was recrystallized from ether–petroleum ether to give pure 1,3-dibutyl-2-*p*-toluenesulfonylguanidine (**6b**, 1.24 g, 95%), mp 82 °C; IR (Nujol) ν 3350 (NH) and 1580 cm^{-1} (C=N).

Found: C, 58.86; H, 8.37; N, 12.91%. Calcd for $C_{16}H_{27}N_3O_2S$: C, 59.05; H, 8.36; N, 12.91%.

*Base Catalyzed Hydrolysis of **3d**.* The reaction was carried out as described above using **3d** (2.60 g, 7.6 mmol). After removal of the solvent, the residue was recrystallized from hexane–benzene to give pure1,3-diisopropyl-2-*p*-toluenesulfonylguanidine (**6d**, 1.85 g, 82%), mp 120 °C; IR (Nujol) ν 3350 (NH) and 1590 cm^{-1} (C=N).

Found: C, 56.77; H, 7.91; N, 13.91%. Calcd for $C_{14}H_{23}N_3O_2S$: C, 56.55; H, 7.80; N, 14.13%.

*Reduction of **3a**.* A solution containing **3a** (0.85 g, 2 mmol) and the Raney Ni (1 g) in 30 ml of ethanol was refluxed for 5 hr. The organic layer was separated and concentrated under reduced pressure. The residue was recrystallized from benzene–hexane to give pure **6a** (0.65 g, 86%).

*Reaction between **1c** and **2a**.* The reaction between **1c** (2.70 g, 16 mmol) and **2a** (3.33 g, 16 mmol) was carried out in a similar way to that described for the exchange reaction between **1a** and **2a**. After removal of the solvent under reduced pressure, the oily residue was dissolved in ether–petroleum ether and allowed to stand at −20 °C for a week, but no crystallization took place. Vacuum distillation of the oily product yielded 1.40 g of a mixture, bp 53—56 °C/7—8 mmHg, of **5a** (0.95 g, 42%), cyclohexylisocyanate (**9a**, 0.35 g, 17%) and benzonitrile (**10c**, 0.10 g, 6%), whose ratio was determined by gas chromatography by use of a 1 m Silicon Gum column at 176 °C. The residue was chromatographed on alumina using hexane, hexane–benzene and benzene as eluent to give 0.30 g (6%) of 2,4-diphenyl-6-cyclohexylamino-*s*-triazine (**12a**), 0.76 g (14%) of 1,3-dicyclohexyl-2-benzoylguanidine (**11a**) and 0.20 g (6%) of *N*-cyclohexylbenzamide (**13a**). The structure of **12a** was confirmed by comparison of mp and IR with those of an authentic sample prepared from 2,4-diphenyl-6-chloro-*s*-triazine[16] and cyclohexylamine. The analytical and physical data of the products are as follows.

12a: mp 148 °C; IR (Nujol) ν 3330 (NH), 1590, 1560, and 1530 cm^{-1} (C=N and N–H); mass spectrum (70 eV) *m/e* 330 (M^+) and 248 ($M^+-C_6H_{10}$).

Found: C, 76.27; H, 6.67; N, 16.86%. Calcd for $C_{21}H_{22}N_4$: C, 76.33; H, 6.71; N, 16.96%.

11a: mp 158 °C; IR (Nujol) ν 3310 (N–H), 1605 (C=O), 1590 and 1570 cm^{-1} (C=N); mass spectrum (70 eV) *m/e* 327 (M^+) and 245 ($M^+-C_6H_{10}$).

Found: C, 73.55; H, 9.02; N, 12.91%. Calcd for $C_{20}H_{29}N_3O$: C, 73.35; H, 8.93; N, 12.83%.

13a: mp 151 °C (lit,[17] mp 153 °C); IR (Nujol) ν 3320 (NH), 1625 (C=O), and 1530 cm^{-1} (NH).

*Reaction between **1c** and **2c**.* In a similar way, the reaction of **1c** (2.40 g, 14.4 mmol) with **2c** (2.79 g, 14.4 mmol) was carried out, vacuum distillation of the oily product yielding 1.42 g of a mixture, bp 70—73 °C/9 mmHg, of **5c** (0.95 g, 47%), phenylisocyanate (**9c**, 0.32 g, 19%) and **10c** (0.15 g, 10%), whose ratio was determined as described above. The residue was chromatographed on alumina to give 0.34 g (12%) of benzanilide (**13b**) and a small amount of *N*-phenyl-*N'*-benzoylurea, which were identified by comparison of their IR spectrum and mp with those of authentic samples.[18,19]

*Reaction between **1d** and **2a**.* In a similar way, the reaction of **1d** (2.0 g, 19 mmol) with **2a** (3.68 g, 18 mmol) was carried out, distillation of the oily product yielding 0.20 g (22%) of acetonitrile (**10d**), bp 68—73 °C/760 mmHg (lit, 77 °C/760 mmHg), and a mixture, bp 55—57 °C/5—6 mmHg, of **5a** (0.40 g, 15%) and **9a** (0.15 g, 7%), whose ratio was determined as described above. No identification of the residue was attempted.

14) H. Ulrich and A. A. R. Sayigh, *Angew. Chem.*, **76**, 781 (1964).
15) W. V. Farrar, *J. Chem. Soc.*, **1965**, 856.
16) J. Ephraim, *Chem. Ber.*, **26**, 2226 (1893).
17) W. Scharwin, *Chem. Ber.*, **30**, 2863 (1897).
18) C. N. Webb, "Organic Syntheses," Coll. Vol. I, p. 82 (1956).
19) E. Beckmann and A. Köster, *Ann.*, **274**, 28 (1893).

Ferricyanide Oxidation of 4-Arylazo-2,6-di-*t*-butylphenols

Eiichiro MANDA

National Chemical Laboratory for Industry, Honmachi, Shibuya-ku, Tokyo 151

(Received June 10, 1972)

Alkaline ferricyanide oxidation of 4-arylazo-2,6-di-*t*-butylphenols (I) gave molecular nitrogen, diphenyl derivatives (VI), 2,6-di-*t*-butyl-*p*-benzoquinone-*N*-(3′,5′-di-*t*-butyl-4′-hydroxyphenyl)arylhydrazone (V) and red tarry compounds. Picryl derivative of phenol (I) gave 2,6-di-*t*-butyl-*p*-benzoquinone-picrylanil (X) instead of hydrazone (V). The reaction path was studied on the basis of isolated compounds.

4-Arylazo-2,6-di-*t*-butylphenols (I) have been found to give some mixtures of stable free radicals by alkaline ferricyanide oxidation.[1] The oxidation products of phenols (I: Ar=*p*-nitrophenyl, *p*-chlorophenyl, phenyl, *p*-methoxyphenyl, and picryl) and the reaction path were studied, and the results are reported in this paper. A few papers have appeared on the oxidation of hydroxyazo dyes as studied by the synthesis of azoxy compounds, photochemical or oxidative color fading,[2,3] and the effect of chemical structure on reactivity.[4–7] Azoxy compounds, phthalic acid and some phenolic compounds were obtained by hydrogen peroxide oxidation,[2] and quinone derivatives and other compounds were obtained by oxidation with ceric sulphate,[3] lead peroxide,[4] ferric chloride,[5] sodium hypochlorite,[7] and molecular oxygen.[6] These oxidation reactions were carried out under acidic conditions and little is known about the reaction path.

Results and Discussion

Benzene solution of phenols (I: Ar=*p*-nitrophenyl, *p*-chlorophenyl, phenyl, *p*-methoxyphenyl, and picryl), prepared from 2,6-di-*t*-butyl-*p*-benzoquinone and aryl hydrazine hydrochlorides, were oxidized with an aqueous solution of potassium ferricyanide and potassium hydroxide accompanied by vigorous evolution of molecular nitrogen. The reaction was stopped in a few minutes at the end of vigorous gas evolution, though slight gas evolution was observed to continue for a few hours. Picryl derivative of phenol (I: Ar=picryl), which has strong electron-attracting groups and exists completely as a hydrazone tautomer,[8] showed quite slow gas evolution and required a longer period of oxidation than the other four phenols (I). After the organic layer of the reaction mixture was left standing until stable free radicals in it had almost faded away, tarry residual compounds were obtained by distilling off the solvent. Appropriate purification of the residual compounds gave 2,6-di-*t*-butyl-*p*-benzoquinone-*N*-(3′,5′-di-*t*-butyl-4′-hydroxyphenyl)arylhydrazones (V: Ar=*p*-nitrophenyl, *p*-chlorophenyl, phenyl, and *p*-methoxyphenyl), diphenyl derivatives (VI: Ar=*p*-nitrophenyl, *p*-chlorophenyl, phenyl, *p*-methoxyphenyl, and picryl), 2,6-di-*t*-butyl-*p*-benzoquinone (VIII), 3,3′,5,5′-tetra-*t*-butyldiphenoquinone (IX), 2,6-di-*t*-butyl-*p*-benzoquinonepicrylanil (X) and a large amount of red brown tarry compounds. The chemical structures of these oxidation products were determined by means of their melting points, elemental analyses, infrared spectra, and mass spectra. The presence of ν_{OH} band at 3630 cm^{-1}, the value of the molecular ion peak (M^+) and elemental analyses offered two isomeric forms (V) and (V′) for hydrazones (V). However, (V′) was excluded since the peak of a fragment ion 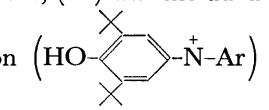 was observed in the mass spectra, but the characteristic strong absorption bands (1670 and 1630 cm^{-1}) of 4-substituted-2,5-cyclohexadienone[9,10] were not observed in the infrared spectra.

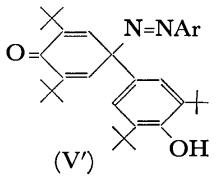

(V′)

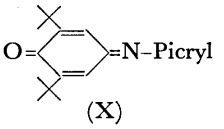

(X)

One of the oxidation products of picryl derivative of phenol (I: Ar=picryl) was found to be an anil derivative (X) from its mass spectrum (M^+), infrared spectrum (absence of ν_{OH} band) and elemental analysis. Diphenyl derivatives (VI) were isolated from the oxidation products of each phenol (I). A very small amount of 3,3′,5,5′-tetra-*t*-butyldiphenoquinone (IX) was isolated from the oxidation products of nitro derivative of phenol (I: Ar=*p*-nitrophenyl), and a trace amount of 2,6-di-*t*-butyl-*p*-benzoquinone (VIII) was detected in the oxidation products of unsubstituted derivative of phenol (I: Ar=phenyl). Their melting points were the same as those in literature and their infrared spectra were consistent with the structures. The rest of the oxidation products were tarry materials which could not be crystallized, and were found to be of phenolic character from the infrared spectra. The yields of oxidation products are given in Table 1. The yields of hydrazones (V) and diphenyl derivatives (VI) are not high. Substituent effect on the yield seems apparent. This might be caused by the difficulty of isolating these compounds. High yields of diphenyl derivative (VI) and molecular nitrogen, and low yields of hydrazone (V) were ob-

1) E. Manda, This Bulletin, **41**, 1743 (1968).
2) D. Haller and G. Ziersch, *Melliand textilber.*, **10**, 951 (1923).
3) A. N. Desai and C. H. Giles, *J. Soc. Dyers. Colourists.*, **65**, 639 (1949).
4) R. Willstäter and M. Benz, *Ber.*, **39**, 3482 (1906).
5) O. N. Witt and J. Dedichen, *ibid.*, **30**, 2655 (1897).
6) T. Zincke and P. Wiegand, *Ann.*, **286**, 85 (1895).
7) A. Seyewetz and E. Chaix, *Bull. Soc. Chim. Fr.*, **41**, 332 (1927).
8) E. Manda, This Bulletin, **44**, 1620 (1971).
9) E. Müller and K. Ley, *Chem. Ber.*, **87**, 922 (1954).
10) N. P. Neureiter, *J. Org. Chem.*, **28**, 3486 (1963).

Table 1. Oxidation products of phenols (I)

Ar of (I)	Oxidizing agent (mole ratio)	Reaction time (min)	Yields of oxidation products (%) (V)	(VI)	Other compound	N_2
p-Nitrophenyl	1.1	7	27.2	15.0	trace of IX	40.8
	5.0	30	18.0	33.0	trace of IX	59.2
	7.5	420	—	24.2	—	75.0
p-Chlorophenyl	1.1	5	20.0	5.3	—	38.2
	5.0	30	6.0	19.0	—	65.0
Phenyl	1.1	4	12.1	2.2	trace of VIII	39.2
	5.0	30	—	40.0	—	53.3
p-Methoxyphenyl	1.1	5	14.7	10.9	—	44.6
	5.0	30	2.0	14.3	—	46.7
Picryl	5.0	120	—	11.9	21.1% of X	48.1

tained when large amounts of oxidizing agent were used for long period of oxidation. When nitro derivative of phenol (I: Ar=*p*-nitrophenyl) was treated with 7.5 mol of oxidizing agent, the resulting products were 4-nitrodiphenyl, molecular nitrogen and a red tarry compound. Disappearance of hydrazone (V) is due to its oxidative degradation since it has also an oxidizable phenol group. Thus, the oxidation of hydrazone (V) was carried out at 10 °C with an excess aqueous alkaline solution of potassium ferricyanide. The reaction proceeded slowly and evolution of nitrogen gas continued for several hours. The ESR spectra (Fig. 1) indicate that more than two species of stable free

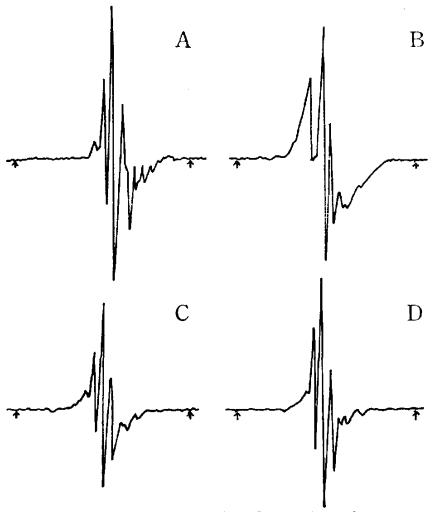

Fig. 1. ESR spectra observed in the oxidation of hydrazones (V).
A) V; Ar=*p*-nitrophenyl, B) V; Ar=*p*-chlorophenyl, C) V; Ar=phenyl, D) V; Ar=*p*-methoxyphenyl.
↑: ESR signals of Fremy's salt as a marker (The center line is not shown).

radicals exist in the organic layer of the reaction mixture of hydrazone (V), and the location of the peaks in the ESR spectrum of each derivative of hydrazone (V) is the same as that observed in the oxidation of the corresponding derivative of phenol (I) (Fig. 2). Thus, it is very likely that the stable radicals observed in the oxidation of phenol (I) are not radical (II) but other radicals originating from hydrazone (V). One might be radical (VII), and the others might be some radicals possibly formed during the process of degradation of

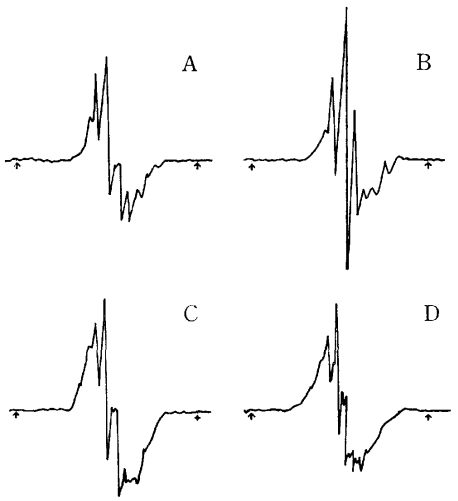

Fig. 2. ESR spectra observed in the oxidation of phenols (I)
A) I; Ar=*p*-nitrophenyl, B) I; Ar=*p*-chlorophenyl, C) I; Ar=phenyl, D) I; Ar=*p*-methoxyphenyl.
↑: ESR signals of Fremy's salt as a marker (The center line is not shown.)

radical (VII). Diphenyl derivatives (VI), 2,6-di-*t*-butyl-*p*-benzoquinone (VIII), 3,3′,5,5′-tetra-*t*-butyldiphenoquinone (IX) and red tarry compound were obtained from the organic layer which had been kept standing for about four weeks to allow stable radicals to disappear (Table 2). The result shows that some

Table 2. Oxidation products of hydrazones (V)

Ar of (V)	Reaction time (hr)	Yields of oxidation products (%) (VI)	(VIII)	(IX)	N_2
p-Nitrophenyl	6.5	40.2	34.1	1.2	54.0
p-Chlorophenyl	5	21.1	20.5	1.7	71.0
Phenyl	4	16.2	25.0	0.7	65.0
p-Methoxyphenyl	3	16.3	22.7	0.5	60.0

parts of diphenyl derivative (VI) and 3,3′,5,5′-tetra-*t*-butyldiphenoquinone (IX) in the oxidation products of phenol (I) originated from hydrazone (V). The path of oxidation presumed from the isolated compounds is given in Fig. 3. Oxidizing agent will generate free radical (II) by the abstraction of a hydrogen atom from phenol (I). Radical (II) might disappear thorugh a few routes. One possible reaction is homolytic sub-

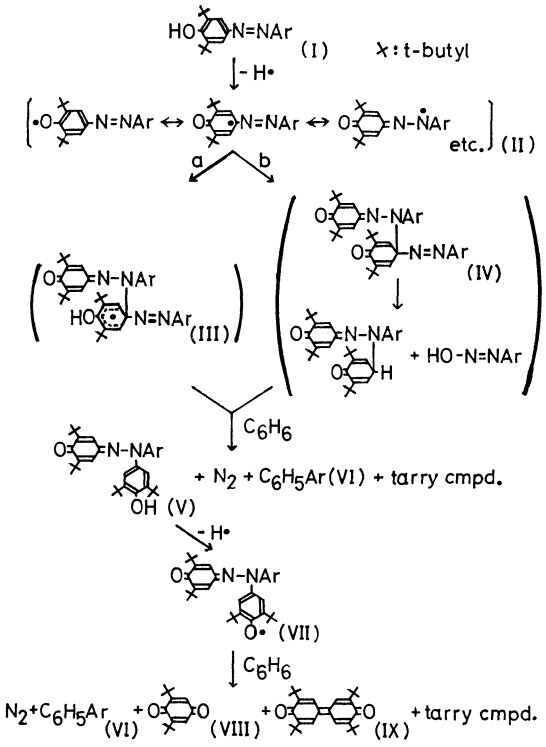

Fig. 3. Presumed reaction path.

stitution (route a). Radical (II) attacks phenol (I), and hydrazone (V) is formed from the intermediate (III) through elimination of arylazo radical, which gives out molecular nitrogen and diphenyl derivative (VI) through the reaction with benzene used as solvent. Another possible reaction is the recombination of radical (II) (route b). The self-coupling of radical (II) at carbon and nitrogen atom forms a dimer (IV), which is hydrolyzed to aryldiazonium hydroxide and hydrazone (V) *via* its dienone form. Aryldiazonium hydroxide undergoes decomposition to yield molecular nitrogen and diphenyl derivative (VI).[11] As for recombination reaction of radical (II), modes of coupling other than oxygen-oxygen coupling[12] and polymerization are possible since the maximum yield of molecular nitrogen based on the used phenol (I) is 75% and a large amount of tarry materials which may consist of the compounds through such a reaction path are obtained. Oxidizing agent will give a phenoxy radical (VII) by abstraction of a hydrogen atom from hydrazone (V), and radical (VII) will decompose to yield the final oxidation products (Table 2).

Picryl derivative of phenol (I; Ar=picryl) gave picrylbenzene (VI: Ar=picryl) and an anil derivative (X) instead of hydrazone (V). The strong electron-attracting power of picryl group might weaken and cleave the nitrogen-nitrogen bonding (=N–N<) of the dimer (IV), and an anil derivative might be formed as a result of the elimination of quinone-imino nucleus and picrylazo group.

11) W. E. Bachmann and R. A. Hoffman, "Organic Reactions," John Wiley and Sons, Inc., New York, N. Y. (1940), Vol. 2, p. 224.
12) T. Matsuura and A. Nishinaga, "Yuri-ki no Kagaku," ed. by H. Sakurai and K. Tokumaru, Nanko-do, Tokyo (1967), p. 176.

Experimental

4-Arylazo-2,6-di-t-butylphenols (I). Phenols (I) were prepared by the same method as reported previously.[1]

Oxidation of 4-Arylazo-2,6-di-t-butylphenols (I). An aqueous solution (0.2 mol/l) of potassium ferricyanide and potassium hydroxide was placed in a Schlenk tube equipped with a gas buret. A solution of phenol (I) in benzene was placed in another Schlenk tube. Both solutions were degassed three times by freezing with dry ice–acetone, then argon gas was led into both Schlenk tubes. While the temperature of each solution was kept at 10 °C, a benzene solution of phenol (I) was carefully added to the aqueous solution of the oxidizing agents. The mixture was then stirred for several minutes (Table 1), and the volume of evolved gas was determined with the gas buret in the course of stirring. The reaction was stopped by pouring the reaction mixture to degassed water in a separatory funnel of Schlenk type. The organic layer was washed with degassed water and dried over anhydrous sodium sulphate under the atmosphere of argon until the ESR spectrum showed almost complete absence of radical species in the organic layer. A tarry residual compound was obtained after distilling off benzene from the organic layer and the oxidation products of each phenol (I) were separated from the residual tarry compound according to the following.

Oxidation Products of 4-p-Nitrophenylazo-2,6-di-t-butylphenol (I: Ar=p-nitrophenyl) (1.75 g, 5.0 mmol) in benzene (200 ml): Yellow brown powder was obtained by washing the tarry compounds with cyclohexane, and yellow brown needles of nitro derivative of hydrazone (V: Ar=*p*-nitrophenyl) (0.76 g, 27.2%) were recrystallized from methanol solution of this powder. Mp 197.0—199.0 °C *m/e* 559.344 (M^+). Found: C, 72.22; H, 8.18; N, 7.51%. Calcd for $C_{34}H_{45}O_4N_3$: C, 72.96; H, 8.10; N, 7.32%. IR (KBr) cm^{-1}: 3630 (ν_{OH}), 3030, 2950 (ν_{CH}), 1640 ($\nu_{C=N}$), 1625 ($\nu_{C=O}$), 1610 ($\nu_{C=C}$), 1510, 1355 (ν_{NO_2}), 1260 (*t*-butyl), 845, 820 (δ_{CH}). 4-Nitrodiphenyl (VI: Ar=*p*-nitrophenyl) (0.15 g, 15.0%) was isolated from the filtrate. Mp 113.0—114.0 °C. (lit,[13] 114 °C). All the resulting filtrate and washing were collected and the solvent was completely distilled. Chromatographic separation of *n*-hexane solution of residual compound on a column of silica gel yielded some phenolic red brown tarry compound, a small amount of hydrazone, 4-nitrodiphenyl and 3,3′,5,5′-tetra-*t*-butyldiphenoquinone (IX) (1 mg) mp 247.0—248.0 °C (lit,[14] 247.0 °C) *m/e* 408.311 (M^+).

Oxidation Products of 4-p-Chlorophenylazo-2,6-di-t-butylphenol (I: Ar=p-chlorophenyl) (3.44 g, 10.0 mmol) in Benzene (50 ml): Yellow powder was obtained by washing the red brown tarry compound with *n*-hexane. By recrystallization of the powder from *n*-hexane solution, yellow needles of chloro derivative of hydrazone (V: Ar=*p*-chlorophenyl) (1.1 g, 20.0%) were obtained. Mp 203.0—205.0 °C. *m/e* 548.319 (M^+). Found: C, 74.05; H, 8.28; N, 5.15; Cl, 6.37%. Calcd for $C_{34}H_{45}O_2N_2Cl$: C, 74.36; H, 8.26; N, 5.10; Cl, 6.46%. IR (KBr) cm^{-1}: 3630 (ν_{OH}), 3030, 2950 (ν_{CH}), 1625 ($\nu_{C=N}$), 1615 ($\nu_{C=O}$), 1605 ($\nu_{C=C}$), 1260 (*t*-butyl), 880, 820 (δ_{CH}). Chromatographic separation of the washing on a column of alumina gave pale yellow plates of 4-chlorodiphenyl (VI: Ar=*p*-chlorophenyl) (0.1 g, 5.3%), mp 74.5—76.0 °C (lit,[13] 77.5 °C), a small amount of hydrazone and a red tarry compound.

Oxidation Products of 4-Phenylazo-2,6-di-t-butylphenol (I: Ar=phenyl) (3.10 g, 10.0 mmol) in Benzene (60 ml): Chromato-

13) "Handbook of Chemistry," ed. by N. A. Lange, McGraw-Hill Book Company, Inc., New York, N. Y. (1961), p. 382
14) H. Hart and F. Cassis, *J. Amer. Chem. Soc.*, **73**, 3179 (1951).

graphic separation of *n*-hexane solution of the red tarry compound gave colorless plates of diphenyl (VI: Ar=phenyl) (0.03 g, 2.2%), mp 69.0—69.5 °C (lit,[13] 70.5 °C), a red brown tarry compound and yellow brown plates of unsubstituted derivative of hydrazone (V: Ar=phenyl) (0.5 g, 12.1%), mp 151.0—153.0 °C. Found: C, 78.45; H, 8.86; N, 5.29%. Calcd for $C_{34}H_{46}O_2N_2$: C, 79.33; H, 9.01; N, 5.44%. IR (KBr) cm^{-1}: 3630 (ν_{OH}), 3030, 2950 (ν_{CH}), 1640 ($\nu_{C=N}$), 1620 ($\nu_{C=O}$), 1605 ($\nu_{C=C}$), 1255 (*t*-butyl), 880, 750 (δ_{CH}). A very small amount of 2,6-di-*t*-butyl-*p*-benzoquinone (VIII) was detected inside the flask containing the red brown tarry compound after it had been left standing for a long time. Mp 65.5—67.0 °C (lit,[15] 68.0 °C).

Oxidation Products of 4-p-Methoxyphenylazo-2,6-di-t-butylphenol (I: Ar=p-methoxyphenyl) (3.41 g, 10.0 mmol) in Benzene (50 ml): Yellow powder was obtained by washing the red brown tarry compound with *n*-hexane. By recrystallization of this powder from methanol solution, yellow plates of hydrazone (V: Ar=*p*-methoxyphenyl) (0.73 g, 14.7%) were obtained. Mp 181.0—182.0 °C, *m/e* 544.355 (M^+). Found: C, 76.65; H, 8.86; N, 4.89%. Calcd for $C_{35}H_{48}N_2O_3$: C, 77.16; H, 8.88; N, 5.14%. IR (KBr) cm^{-1}: 3630 (ν_{OH}), 3030, 2950 (ν_{CH}), 1625 ($\nu_{C=N}$), 1615 ($\nu_{C=O}$), 1610 ($\nu_{C=C}$), 1245 (*t*-butyl), 1020 (ν_{OMe}) 880, 825 (δ_{CH}). Chromatographic separation of the washing on a column of alumina gave yellow plates of 4-methoxydiphenyl (VI: Ar=*p*-methoxyphenyl) (0.2 g, 10.9 %), mp 87.0—88.0 °C (lit,[13] 90 °C), and a red brown tarry compound.

Oxidation Products of 4-Picrylazo-2,6-di-t-butylphenol (I: Ar=picryl) (0.41 g, 0.9 mmol) in Benzene (35 ml): Yellow brown powder was obtained by washing the red brown tarry compound with cyclohexane. Chromatographic separation of benzene solution of this powder on a column of silica gel gave a yellow compound, pale yellow plates of picrylbenzene (0.03 g, 11.9%) mp 130.0—131.5 °C (lit,[16] 130.0 °C), a small amount of starting material and a dark red tarry compound. Yellow plates of anil (X) (0.08 g, 19.1%) were recrystallized from methanol solution of the yellow compound. Mp 176.0—177.0 °C, *m/e* 430.152 (M^+). Found: C, 56.03; H, 4.91; N, 12.97%. Calcd for $C_{20}H_{22}O_7N_4$: C, 55.81; H, 5.15; N, 13.02%. IR (KBr) cm^{-1}: 3030, 2950 (ν_{CH}), 1660 ($\nu_{C=N}$), 1640 ($\nu_{C=O}$), 1620 ($\nu_{C=C}$), 1540, 1345 (ν_{NO_2}), 1250 (*t*-butyl), 880, 820 (δ_{CH}).

Oxidation of Hydrazone (V). A solution of hydrazone (V) (1.0 mmol) in benzene (60 ml) was oxidized with an aqueous alkaline solution of potassium ferricyanide (5.0 ml) at 10 °C until cessation of nitrogen gas evolution, and the reaction mixture was treated in the same way as in the oxidation of phenols (I). The solvent was distilled off after the stable radicals in the organic layer had disappeared, and isolation of oxidation products from the residual compounds was carried out as described below.

Oxidation Products of Nitro Derivative of Hydrazone (V: Ar=p-nitrophenyl): The yellow brown residual compound was dissolved in *n*-hexane and a small amount of insoluble material remained. The starting material (9 mg, 1.6%) was obtained by recrystallization of this insoluble material from methanol solution. The *n*-hexane solution was passed through a column of alumina, and 3,3′,5,5′-tetra-*t*-butyldiphenoquinone (X) (5 mg, 1.2%), 2,6-di-*t*-butyl-*p*-benzoquinone (VIII) (75 mg, 34.1%), 4-nitrodiphenyl (VI: Ar=*p*-nitrophenyl) (80 mg, 40.2%) and a red brown tarry compound were obtained.

Oxidation Products of Chloro Derivative of Hydrazone (V: Ar=p-chlorophenyl): The red brown residual compound was dissolved in *n*-hexane and passed through a column of alumina. 4-Chlorodiphenyl (VI: Ar=*p*-chlorophenyl) 40 mg, 21.1%), 3,3′,5,5′-tetra-*t*-butyldiphenoquinone (IX) (7 mg, 1.7%), 2,6-di-*t*-butyl-*p*-benzoquinone (VIII) 45 mg, 20.5%) and a red brown tarry compound were obtained.

Oxidation Products of Unsubstituted Derivative of Hydrazone (V: Ar=phenyl): The red brown residual compound was dissolved in *n*-hexane and passed through a column of alumina. Diphenyl (VI: Ar=phenyl) (25 mg, 16.2%), 3,3′,5,5′-tetra-*t*-butyldiphenoquinone (VIII) (3 mg, 0.7%), 2,6-di-*t*-butyl-*p*-benzoquinone (VIII) (55 mg, 25.0%) and a red brown tarry compound were obtained.

Oxidation Products of Methoxy Derivative of Hydrazone (V: Ar=p-methoxyphenyl): Red brown residual compound was dissolved in *n*-hexane and passed through a column of alumina. 3,3′,5,5′-Tetra-*t*-butyldiphenoquinone (IX) (2 mg, 0.5%) was obtained from the first yellow band. The eluent from the second yellow brown band was passed through a column of silica gel, and 4-methoxydiphenyl (VI: Ar=*p*-methoxydiphenyl) (30 mg, 16.3%), 2,6-di-*t*-butyl-*p*-benzoquinone (VIII) (50 mg, 22.7%) and a red brown tarry compound were obtained.

All the melting points were uncorrected. The infrared spectra were taken with a Shimadzu IR-27G grating spectrophotometer. The ESR spectra for the benzene-diluted organic layer of the reaction mixture, which had been dried over anhydrous sodium sulphate for a few minutes directly following cessation of oxidation, were taken with a Hitachi 771 electron spin resonance spectrometer.

The author is indebted to Mr. Wasada for the mass spectra.

15) M. S. Kharash and B. S. Joshi, *J. Org. Chem.*, **27**, 651 (1962).
16) H. C. Gull and E. E. Turner, *J. Chem. Soc.*, **1929**, 498.

Selective Formations of Several Carboxylic Acids by Carbonylation in the $SbCl_5$–Liquid Sulfur Dioxide System*

Masakatsu YOSHIMURA, Masatomo NOJIMA, and Niichiro TOKURA

Department of Applied Chemistry, Faculty of Engineering, Osaka University, Suita, Osaka 565

(Received September 4, 1972)

The carbonylations of *cis*- and *trans*-4-*t*-butyl-1-methylcyclohexanols, *exo*- and *endo*-2-methyl-2-norbornanols and *exo*- and *endo*-2-norbornanols were carried out in $SbCl_5$–liq.SO_2 at −70°. From both the *cis*- and *trans*-4-*t*-butyl-1-methyl-cyclohexanols, *cis*-4-*t*-butyl-1-methylcyclohexanecarboxylic acid was formed exclusively in an excellent yield (over 90%). Both *exo*- and *endo*-2-methyl-2-norbornanols gave only *endo*-2-methyl-*exo*-2-norbornylcarboxylic acid in a high yield. The reason for the stereoselectivity of the reactions was discussed.

A convenient carbonylation of alkyl halides with carbon monoxide at −70 °C in the $SbCl_5$–SO_2 system to give carboxylic acids or esters in good yields and with a high selectivity has been reported in a preceding paper.[1] In the present paper we wish to describe the results of the carbonylation of alicyclic alcohols, whose stereochemistries had previously been confirmed, in order to investigate the steric course of the carbonylation in this system along with the mechanism of the reaction. The reactions of *cis*- and *trans*-4-*t*-butyl-1-methylcyclohexanols, *exo*- and *endo*-2-methyl-2-norbornanols and *exo*- and *endo*-2-norbornanols have been carried out. The results thus obtained are gathered in Table 1.

From both *cis*- and *trans*-4-*t*-butyl-1-methylcyclohexanols (I and II), *cis*-4-*t*-butyl-1-methylcyclohexanecarboxylic acid (III) was obtained exclusively in a yield of over 90%. *exo*- and *endo*-2-Methyl-2-norbornanols (IV and V) also gave 2-*endo*-methyl-2-*exo*-norbornanecarboxylic acid (VI) exclusively in a high yield. Furthermore, *exo*- and *endo*-2-norbornanols (VII and VIII) were carbonylated to give only *exo*-norbornane-2-carboxylic acid (IX). The yield of IX from VII is very good (92%), but that of IX from VIII is low (16%). These results seem to be important from the preparative point of view, and also to be suggestive of the reaction mechanism. Whereas the carbonylation reaction of the mixture of I and II with formic acid and sulfuric acid (Koch's method) has been reported to give III (*cis*-carboxylic acid) in a 35% yield along with six other isomeric carboxylic acids,[2] III was obtained stereospecifically in the present reaction.

The stereochemistry of the reactions of a number of nucleophiles with 4-*t*-butyl-1-methylcyclohexanol in the presence of acetic acid and sulfuric acid has previously been studied. According to Beeby and Sternhell, the stereoselectivity of the reaction was found to depend upon the size of the attacking nucleophile.[2] The stereochemistry of the product is determined by the stability of the oxocarbonium ion (B) and not by the attacking facility of carbon monoxide on the carbonium ion (A), although the attack of carbon monoxide seems to be possible from the equatorial direction because of the lack of 1,3-diaxial interaction. Carbon monoxide, whose steric bulkiness is comparable to that of acetylene,[3] is much smaller than the methyl group. The formation of III in the $SbCl_5$–SO_2 system with a high selectivity and a high yield seems to be due to the irreversible formation of 1:1 donor acceptor complex (C) between acyl halide and $SbCl_5$ from B, which is predominantly formed under those reaction conditions. The reaction course is depicted in Chart 1.

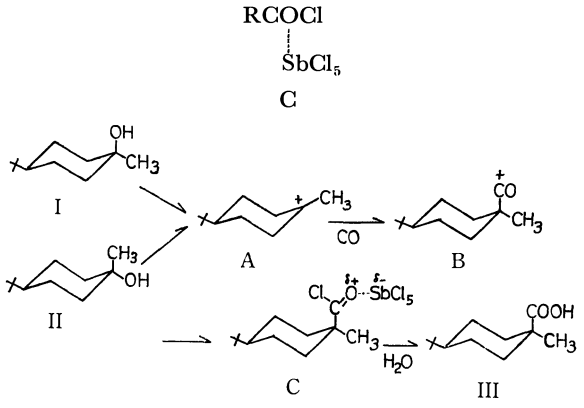

Chart 1.

In the Koch reaction, the formation of olefin is frequently encountered, this gives other side products

Table 1. Carbonylation of alicyclic alcohols in $SbCl_5$–liq. SO_2 at −70 °C

Alcohol	Product (yield %)
cis-4-*t*-Butyl-1-methylcyclohexanol (I)	*cis*-4-*t*-Butyl-1-methylcyclohexanecarboxylic acid (III), (94)
trans-4-*t*-Butyl-1-methylcyclohexanol (II)	III, (90)
exo-2-Methyl-2-norbornanol (IV)	2-*endo*-Methyl-2-*exo*-norbornanecarboxylic acid (VI), (96)
endo-2-Methyl-2-norbornanol (V)	VI, (85)
exo-2-Norbornanol (VII)	*exo*-Norbornane-2-carboxylic acid, (IX), (92)
endo-2-Norbornanol (VIII)	IX, (16)

* Carbonylation in Liq. SO_2, part II: Preceding Paper, Ref. 1.

1) M. Nojima, K. Tatsumi, and N. Tokura, This Bulletin, **44**, 2001 (1971).

2) P. J. Beeby and S. Sternhell, *Aust. J. Chem.*, **24**, 809 (1971).

3) J. A. Hirsch in "Topics in Stereochemistry," ed. by N. L. Allinger and E. L. Eliel, Interscience Pablishers, New York, Vol. **1**. (1967), p. 199.

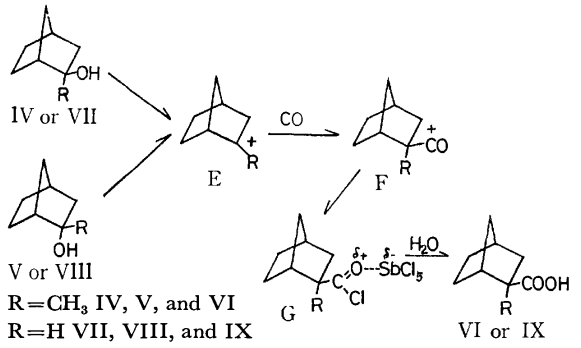

Chart 2.

in the reaction.[4] In the present reaction, the formation of olefin, polymerization, and oxidation were depressed for the reason described before.

The selective formations of *endo*-2-methyl-*exo*-2-norbornanecarboxylic acid from *exo*- and *endo*-2-methyl-2-norbornanols and *exo*-2-norbornanecarboxylic acid from *exo*- and *endo*-2-norbornanols are interesting. It was clarified by Hogeveen and Roobeek[5] that the formation of F in Koch's reaction is kinetically controlled, while, under thermodynamically-controlled conditions, both *exo*- and *endo*-norbornyl oxocarbonium ions were formed to the same extent, the ratio of the *exo*- and *endo*-norbornanecarboxylic acids produced being 51 to 49.

These results suggest that, in our reaction, the same carbonium ion was formed from epimers and was subsequently carbonylated by the stereospecifical *exo* attack of CO on an oxocarbonium ion, followed by the formation of a 1:1 donor-acceptor complex[6] of acyl halide and $SbCl_5$.

The *exo* attack of the nucleophilic reagent on norbornyl and 2-methylnorbornyl cations in kinetically-controlled reactions, has been well confirmed.[7] The present results seem to be consistent with these facts and with the formation of the norbornyl cation and the 2-methylnorbornyl cation, followed by the attack of carbon monoxide from the *exo* direction.

In the carbonylation of *endo*-2-norbornanol (VIII), the conversion to the product, IX, was very low, the starting norbornanol was almost all recovered, and no olefinic or polymeric material was found in the reaction mixture. These results suggest that the formation of the carbonium ion is the rate-determining step in this reaction and that the attack of carbon monoxide on this carbonium ion is a very fast step, as has already been indicated by Hogeveen.[5]

The authors wish to express their deep gratitude to the Seitetsu Kagaku K.K. for its donation of liquid sulfur dioxide. They are also grateful for the grant from the Ministry of Education, Japan, which supported this project.

Experimental

Materials. *cis*-4-*t*-Butyl-1-methylcyclohexanol (I) was obtained by the oxymercuration of 4-*t*-butyl-1-methylcyclohexene.[8] *trans*-4-*t*-Butyl-1-methylcyclohexanol (II) was prepared by the method of Corey.[9] *exo*-2-Methyl-2-norbornanol (IV) was obtained by the oxymercuration and reduction of 2-methylnorbornene-2.[10] *endo*-2-Methyl-2-norbornanol (V) was obtained by the reaction of 2-norbornanone with methylmagnesium iodide.[11] By the hydrolysis of *exo*-2-norbornyl formate, *exo*-2-norbornanol (VII) was obtained.[10] *endo*-2-Norbornanol (VIII) was prepared by the reduction of 2-norbornanone with lithium aluminum hydride.[12]

General Procedure of Carbonylation. Into a mixture of 20 g (0.07 mol) of $SbCl_5$ and 50 ml of liq. SO_2, an alcohol in 20 ml of dichloromethane was dropped at −70 °C over a thirty-minute period while a current of carbon monoxide gas was being bubbled into the flask at a velocity of 70 ml per minute, after which the reaction was continued for an additional thirty minutes. Then the reaction mixture was poured into ice-cold aqueous sodium hydroxide, and the neutral products were extracted by ether. Then the acidic products were extracted with ether after the water layer had been acidified with aqueous hydrogen chloride. After the evaporation of the ether, the product was characterized by NMR, infrared, and mass spectroscopies.

The Reaction of I and II. *cis*-4-*t*-Butyl-1-methylcyclohexanol, (I) (1.70 g, 0.01 mol), was allowed to react with carbon monoxide following the general procedure. After the evaporation of the ether, 1.86 g of a solid (III) was obtained. III was identified as 4-*t*-butyl-1-methylcyclohexanecarboxylic acid by comparing it with the physical data of an authentic sample;[2] mp 132—133 °C (lit,[2] 132—133 °C). The crude product was reduced by lithium aluminum hydride and was analyzed by glc; the glc showed the formation of only *cis*-4-*t*-butyl-1-methylcyclohexylcarbinol.[2]

By the reaction of II (1.70 g, 0.01 mol), III was obtained in a 90% yield.

The Reaction of IV and V. From *exo*-2-methyl-2-norbornanol (IV) (1.26 g, 0.01 mol), 1.48 g (96% yield) of 2-*endo*-methyl-2-*exo*-norbornanecarboxylic acid were obtained; mp 50—51 °C (lit,[13] 50—52 °C). The physical data were identical with those of an authentic sample.[13]

The selective formation of VI was clarified by the glc analysis of the reduction products with lithium aluminum hydride. From V, VI was obtained exclusively in an 85% yield.

The Reaction of VII and VIII. By the reaction of VII (1.12 g, 0.01 mol) under these reaction conditions, 1.29 g (92% yield) of 2-*exo*-norbornanecarboxylic acid (IX) was obtained; mp 52—53 °C (lit,[14] 52—53 °C).

In the reaction of *endo*-2-norbornanol (VIII), IX was obtained as the acidic product in a 16% yield, and from the neutral part 80% of the starting material, VIII, was recovered.

4) H. Hogeveen and C. F. Roobeek, *Rec. Trav. Chim.*, **89**, 1121 (1970).
5) H. Hogeveen and C. F. Roobeek, *Tetrahedron Lett.*, **1969**, 4941.
6) M. Nojima, F. Shiba, M. Yoshimura, and N. Tokura, *Chem. Lett.*, **1972**, 1133. The formation of a free oxocarbonium ion as the stable intermediate was not detected by NMR spectroscopy. A tight acyl halide-$SbCl_5$ complex has been proposed.
7) H. C. Brown and K. Ti Lngiu, *J. Amer. Chem., Soc.* **89**, 3900 (1967).
8) D. J. Pasto and J. A. Gontarz, *J. Amer. Chem. Soc.*, **92**, 7480 (1970).
9) E. J. Corey and M. Chaykovsky, *ibid.*, **87**, 1353 (1965).
10) J. H. Markgrof and P. Tong Leung, *J. Chem. Educ.*, **47**, 707 (1970).
11) S. Beckmann and R. Mezger, *Chem. Ber.*, **90**, 1564 (1957).
12) J. P. Schaefer and D. S. Weinberg, *J. Org. Chem.*, **30**, 2635 (1964).
13) J. A. Berson, J. S. Walia, A. Remanic, P. Reynolds-Warnhoff, and D. Willner, *J. Amer. Chem. Soc.*, **83**, 3186 (1961).
14) R. Reubke, *Chem. Ber.*, **91**, 1516 (1958).

The Mass Spectra of 3-Aryl-5-chloromethyl-1,2,3-oxathiazolidine-2-oxides

Tomihiro NISHIYAMA and Fukiko YAMADA

Department of Applied Chemistry, Faculty of Engineering, Kansai University, Senriyama, Suita, Osaka 564

(Received September 19, 1972)

The mass spectra of 3-phenyl- (I), 3-tolyl- (II), 3-chlorophenyl- (III), and 3-trichlorophenyl- (IV), -5-chloromethyl-1,2,3-oxathiazolidine-2-oxides have been obtained. The major path in the electron impact-induced cleavage of all the compounds involves the loss of SO_2 and Cl from each molecular ion (M). The $M-SO_2-Cl$ ions show the loss of $CH{=}CH_2$, followed by the loss of the hydrogen radical and HCN. On the other hand, in compounds II, III, and IV, the $M-SO_2-Cl$ ions show the loss of the ring-substituted methyl or chloro radical. The above fragmentation pathways associated with metastable transitions or the chlorine isotopic clusters for each ion of III or IV have been outlined and discussed for each group of compounds.

Recently, we have reported the mass spectra of 3-aryl-1,2,3-oxathiazolidine-2-oxides[1] and 3-aryl-5-methyl-1,2,3-oxathiazolidine-2-oxides.[2] This time we wish to report the mass spectral data of new compounds of oxathiazolidines as an extension of our previous work. That is, the 3-aryl-5-chloromethyl-1,2,3-oxathiazolidine-2-oxides have been easily prepared by a previously-reported method,[3] and the mass spectra of the following eight compounds have been determined.

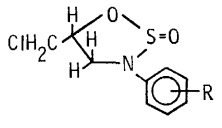

I, R=H (*cis*)
IIa, R=*o*-CH_3 (*cis*)
IIb, R=*m*-CH_3 (*trans*)
IIc, R=*p*-CH_3 (*cis*)
IIIa, R=*o*-Cl (*cis*)
IIIb, R=m-Cl (*trans*)
IIIc, R=*p*-Cl (*cis*)
IV, R=2,4,6-Cl (*trans*)

The present work is concerned with the fragmentation schemes of the above oxathiazolidines.

Experimental

Materials. All the eight oxathiazolidines examined were prepared by the reported method, and the general structures of these compounds were confirmed by means of the NMR spectral data.[3]

Compound IV: mp 77.5—78.7 °C (uncorrected), elemental analysis, Found: C, 32.31; H, 2.10; N, 4.25; S, 9.51; Cl, 42.10%. Calcd for $C_9H_7NSO_2Cl_4$: C, 32.24; H, 2.09; N, 4.18; S, 9.55; Cl, 42.38%.

Measurement. The high-resolution mass spectra were obtained by means of a Japan Electron Optics Co. Ltd., JMS-O1SG Mattauch-Herzog double-focusing mass spectrometer, at an ionizing voltage of 75 eV, an emission current of 200 μA, an accelerating voltage of 6.4 kV, and a vapor pressure of 1.0×10^{-6} mmHg. The ion-source temperature varied between 100 and 150 °C. The accurate masses and elemental compositions were determined by a previously-reported method.[1]

Results and Discussion

The mass spectral data of compounds I, II, and III, are summarized in Table 1, while their fragmentation pathways are shown in Scheme 1. It has previously been established that the oxathiazolidines exist in the *cis* and *trans* configurations between the S=O group and the chloromethyl group in the 5-position.[3] On the other hand, we have found that the fragmentation patterns of the oxathiazolidines are the same in the *cis* and *trans* configurations.[2] Thus, the fragmentation pattern for each compound will be discussed on the basis of the data obtained in the case of either the *cis* or *trans* isomer.

The molecular ions of these compounds are of low abundance. The base peaks of compounds I, IIb and c, and IIIc appeared at the mass numbers of 132, 146, and 166 respectively, corresponding to that of the

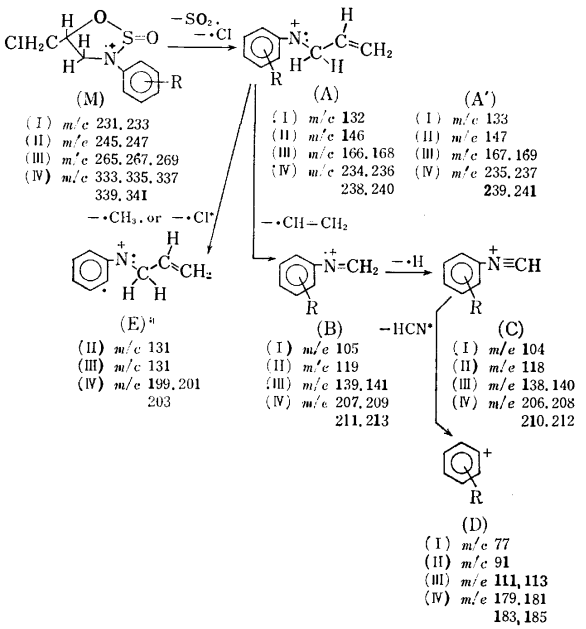

* Asterisks denote the processes for which metastable transitions were observed.

a) The radical on the benzene ring exists at *ortho*, *meta*, and *para* position in the corresponding compounds, II and III.

Scheme 1. The major fragmentation pathways of oxathiazolidines, I, II, III, and IV.

1) F. Yamada, T. Nishiyama, Y. Fujimoto, and M. Kinugasa, This Bulletin, **44**, 1152 (1971).
2) T. Nishiyama and F. Yamada *ibid.*, **45**, 928 (1972).
3) T. Nishiyama and F. Yamada *ibid.*, **44**, 3073 (1971).

Table 1. Mass spectral data of compounds I, II, and III (75 eV)

m/e	Compound I	
	Ion composition[a]	Rel. Int. (%)
233	$C_9H_{10}NSO_2Cl$	10
231	$C_9H_{10}NSO_2Cl$	27
133	$C_9H_{11}N$	11
132	$C_9H_{10}N$	100
105	C_7H_7N	30
104	C_7H_6N	91
77	C_6H_5	70

m/e	Compound II			
	Ion composition	Rel. Int. (%)		
		IIa	IIb	IIc
247	$C_{10}H_{12}NSO_2Cl$	9	14	13
245	$C_{10}H_{12}NSO_2Cl$	25	36	35
147	$C_{10}H_{13}N$	8	13	12
146	$C_{10}H_{12}N$	64	100	100
131	C_9H_9N	7	9	9
130	C_9H_8N	6	7	8
119	C_8H_9N	18	28	32
118	C_8H_8N	100	70	82
91	C_7H_7	45	68	71

m/e	Compound III			
	Ion composition	Rel. Int. (%)		
		IIIa	IIIb	IIIc
269	$C_9H_9NSO_2Cl_2$	4	2	5
267	$C_9H_9NSO_2Cl_2$	18	12	26
265	$C_9H_9NSO_2Cl_2$	28	18	37
168	C_9H_9NCl	31	29	32
167	$C_9H_{10}NCl$	11	11	12
166	C_9H_9NCl	81	92	100
141	C_7H_6NCl	8	12	10
140	C_7H_5NCl	33	37	31
139	C_7H_6NCl	27	38	30
138	C_7H_5NCl	100	100	78
131	C_9H_9N	9	13	13
130	C_9H_8N	25	18	15
113	C_6H_4Cl	17	25	14
111	C_6H_4Cl	40	74	46

a) The high-resolution mass spectra of these compounds gave the correct composition of all the ions mentioned in the table within an error of ±5millimass units.

$R-C_6H_4NC_3H_5$ ion (A). In the case of compounds IIa, IIIa, and IIIb, the $R-C_6H_4NCH$ cation (C) was the base peak. The ion A was formed from the molecular ion by the loss of the SO_2 group and a chloro radical. In the fragment ion A, the isotope peaks (A') appeared.

Our reports which have appeared in recent years have indicated that in the electron impact-induced cleavage of the 3-aryl-1,2,3-oxathiazolidine-2-oxides[1] and the 3-aryl-5-methyl-1,2,3-oxathiazolidine-2-oxides[2] the major path involves the loss of sulfur dioxide from the molecular ions. In view of these findings, it was interesting to find that the mass spectra of the 3-aryl-5-chloromethyl-1,2,3-oxathiazolidine-2-oxides showed no such $(M-SO_2)^{+\cdot}$ peak at all. Each showed peaks representing the loss of SO_2 and Cl. In none of these spectra were Cl-, SO_2-, or SO_2–Cl-positive ions present. The probable mechanism is indicated by the following diagram.

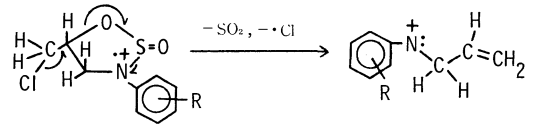

This decomposition implied that the loss of SO_2 and Cl is either concerted or so nearly so that no substantial amount of the $(M-SO_2)^{+\cdot}$ ion or $(M-Cl)^{+\cdot}$ ion is formed.

The ion B is formed from the ion A by the loss of the $CH=CH_2$ radical, and the resulting ion loses a hydrogen radical to give the ion C. In compound I, the peak at mass 77 due to the hydrocarbon ion (D), $C_6H_5^+$, is about 70% of the base peak intensity and was produced by the loss of the HCN group from the ion C. Similar methyl- or chloro-substituted hydrocarbon ions, $R-C_6H_4^+$, can also be observed in the spectra of compounds II, III, and IV and are abundant. This fragmentation pathway, (C)→(D), is verified by the metastable peaks at *m/e* 57.0, 70.2, and 89.3 respectively. On the other hand, no metastable peak was observed in Compound IV. Moreover, there have been many reports concerning the fragmentation pathway of $R-C_6H_4N^+\equiv CH \longrightarrow R-C_6H_4^+ + HCN$.[1,2,4,5]

In the spectra of II, the ion at *m/e* 131, which is of a 7% abundance for the *ortho* isomer, 9% for the *meta*, and 9% for the *para*, is present. This ion, corresponding to the C_9H_9N cation (E), is formed from the ion A. On the other hand, in the oxathiazolidines having the ring-substituted chloro atom, such as IIIa, IIIb, and IIIc, the ion at *m/e* 131, which is of a 9% abundance for the *ortho*, 13% for the *meta*, and 13% for the *para* isomer, is observed. In this case, the metastable peaks at *m/e* 103.3 are also observed. In the case of IV, the $C_9H_7NCl_2$ ion (*m/e* 199, 201, and

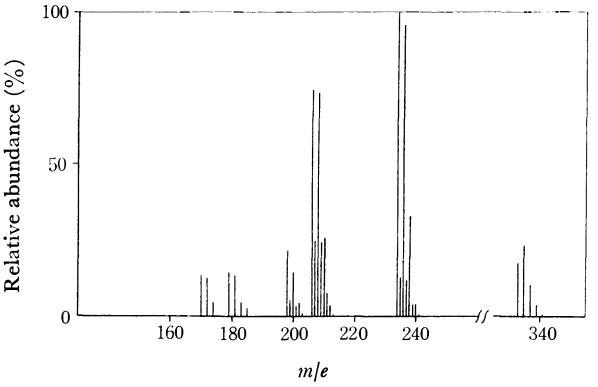

Fig. 1. Relative abundance of the fragment ions of the compound IV (75 eV).
The peaks below *m/e* 160 are omitted here.

4) F. Yamada, Y. Fujimoto, and T. Nishiyama, *ibid.*, **45**, 280 (1972).
5) D. J. Elias and R. G. Gillis, *Aust. J. Chem.*, **19**, 251 (1966).

203), with two ring-substituted chloro atoms, is present (E in Scheme 1). The above results suggest that these ions are produced by the loss of the methyl- or chloro-radical from the ion A.

It is interesting to compare these spectra with the spectra of the other oxathiazolidines reported by Deyrup and Moyer.[6,7] They reported that the mass spectrum of 2-oxo-3-*t*-butyl-4-chloromethyl-1,2,3-oxathiazolidines showed the $M-CH_3$ and $M-CH_3-SO_2$ peaks. The molecular ion is obviously of low abundance, and there are intense peaks at *m/e* 162 and *m/e* 106 as a result of the loss of the chloromethyl radical, followed by the loss of the isobutylene.

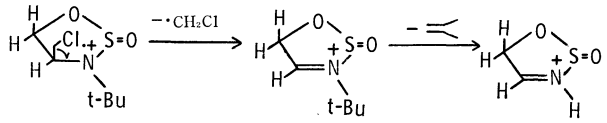

m/e 162 *m/e* 106 (Base peak)

On the contrary, in the cases of compounds I, II, III, and IV, the $M-CH_2Cl$ peaks are extremely small (4—5% of the base peak). These differences can be explained by the substituted groups on the oxathiazolidine ring. The fragmentations are influenced by the presence of the *N*-substituted aromatic nucleus and the position of the chloromethyl group (4- or 5-position).

The present fragmentation pathways are further illustrated by those of the 2,4,6-trichlorophenyl-5-chloromethyl-1,2,3-oxathiazolidine-2-oxide (IV). The mass-spectral data of IV are shown in Fig. 1, and the major fragmentation pathways are shown in Scheme 1.

6) J. A. Deyrup and C. L. Moyer, *J. Org. Chem.*, **34**, 175 (1969).

7) C. L. Moyer, 2-Oxo-1,2,3-oxathiazolidines, Dissertations, II, Harvard University (1968), (Avail. Univ. Microfilms, Ann, Arbor, Mich., Order No. 68–16878), p. 134; *Chem. Abstr.*, **70**, 77677d (1969).

BULLETIN OF THE CHEMICAL SOCIETY OF JAPAN, VOL. 46, 2168—2174 (1973)

Synthesis and Biological Activity of Peptides Related to Eledoisin. III.[1] *C*-Terminal Hexapeptide Amides Modified in Methionine and Isoleucine Residues[2,3]

Hiroshi SUGANO

Department of Synthetic Chemistry, Research Laboratory of Applied Biochemistry, Tanabe Seiyaku Co., Ltd., Kashima-cho, Higashiyodogawa-ku, Osaka 532

(Received September 16, 1972)

New analogs of hexapeptide related to eledoisin containing *N*-methylmethionine and α-hydroxy-γ-methylthiobutyric acid in place of the methionine, and α-hydroxyisovaleric acid in place of the isoleucine, were synthesized in order to obtain some information about the role of the amide bond in the peptide backbone. The former two were practically inactive in the rabbit pressure assay. These results indicated that the amide bond between the leucine and the methionine residues was important for the depressor activity of eledoisin. The last one showed very little activity. The results supported the suggestion made previously that the amide bond between the phenylalanine and the isoleucine residues is important in eliciting the biological response. The role of the amide bonds in the peptide backbone of eledoisin was also discussed.

Eledoisin, Pyroglu–Pro–Ser–Lys–Asp–Ala–Phe–Ile–Gly–Leu–Met–NH_2, is a potent, naturally occurring depressor substance. A number of data have accumulated on the relation between the structure of eledoisin and the biological activity. The *C*-terminal pentapeptide sequence, H–Phe–Ile–Gly–Leu–Met–NH_2, is of particular importance for the depressor activity.[4] The low depressor activity (1%) of this sequence is enhanced to almost full hormonal activity by introducing lysine to the *N*-terminus.[5] It has also been reported that the amino acid residues, phenylalanine, isoleucine, leucine, and methionine are the essential elements for the depressor activity.[4] The hydrophobic side chains in these residues may play a role in interaction with the biological receptor site.

However, there is practically no knowledge as to the part played by the amide bond which is a structural element of the polypeptide chain of eledoisin.

1) Part II of this series; H. Sugano, K. Higaki, and M. Miyoshi, This Bulletin, **46**, 231 (1973)

2) Presented in part at the 9th Symposium on Peptide Chemistry, Shizuoka, November, 1971.

3) The abbreviations recommended by the IUPAC-IUB commission on Biological Nomenclature (*J. Biol. Chem.*, **241**, 2491 (1966); **242**, 555 (1967) have been used throughout. In addition: Glyc=glycolic acid, HyMeV=α-hydroxy-β-methylvaleric acid, Phlac=β-phenyllactic acid, HyIc=α-hydroxyisocaproic acid, HyIv=α-hydroxyisovaleric acid, and HyMtb=α-hydroxy-γ-methylthiobutyric acid residues. Amino acid, α-hydroxy acid, and *N*-methylamino acid symbols except Gly, Glyc, and Sar denote the L-configuration.

4) E. Schröder and K. Lübke, "The Peptides," Academic Press, New York and London (1966), p. 127.

5) L. Bernardi, G. Bosisio, F. Chillemi, G. De Caro, R. De Castiglione, V. Erspamer A. Glaesser, and O. Goffredo, *Experientia*, **20**, 306 (1964).

In previous papers,[1,6] the present author chose the [Lys^6]-eledoisin-(6-11)-hexapeptide (I) as a model compound of eledoisin and described the synthesis and the biological activity of several analogs. In these peptides, some amide bonds in I were replaced by ester bonds or *N*-methylamide bonds by the replacement of the parent amino acids with α-hydroxy acids or *N*-methylamino acids. These studies gave us some information about the relationship between the structure of the peptide backbone of eledoisin and the activity. It was found that, in the case of the substitution of the amide group in the peptide I by an ester group or an *N*-methylamide group without any change in the amino acid side chain, the potency of the activity was dependent upon the position substituted. The replacement of the amide bond between the phenylalanine and the isoleucine residues by an ester bond or an *N*-methylamide bond led to a much less active compound. These facts suggest that the amide bond between the phenylalanine and the isoleucine residues is essential for the activity.

In order to provide further information concerning the role of the amide bond in the peptide backbone, the author will report, in the present paper, on the synthesis of [Lys^6, MeMet^{11}]-eledoisin-(6-11)-hexapeptide (XIV) and [Lys^6, HyMtb^{11}]-eledoisin-(6-11)-hexapeptide (VIII) and on their depressor activities. In these peptides the amide bond between the leucine and the methionine residues was replaced by an *N*-methylamide bond or an ester bond. In addition, to confirm the necessity of the amide bond between the phenylalanine and the isoleucine residues for the activity, [Lys^6, HyIv^8]-eledoisin-(6-11)-hexapeptide (IV) was synthesized and its activity was estimated.

A synthetic route to the [Lys^6, MeMet^{11}]-analog (XIV) is shown in Scheme 1.

Boc-Leu-OH + H-MeMet-OEt (**1**)
↓ DCC
Boc-Leu-MeMet-OEt (**2**)
↓ NH_3 in MeOH
Boc-Leu-MeMet-NH_2 (**3**)
↓ i) HCl in dioxane ii) Boc-Gly-ONp
Boc-Gly-Leu-MeMet-NH_2 (**4**)
↓ i) HCl in dioxane ii) Aoc-Phe-Ile-N_2H_3 HNO_2
Aoc-Phe-Ile-Gly-Leu-MeMet-NH_2 (**5**)
↓ i) HCl in dioxane ii) di-Boc-Lys-ONp
di-Boc-Lys-Phe-Ile-Gly-Leu-MeMet-NH_2 (**6**)
↓ HCl in AcOH
H-Lys-Phe-Ile-Gly-Leu-MeMet-NH_2·2HCl (XIV)

Scheme 1.

Optically active *N*-methylmethionine was prepared by the method reported by Izumiya *et al.*[7] Boc-leucine was condensed with *N*-methylmethionine ethyl ester with dicyclohexylcarbodiimide (DCC) to yield the Boc-dipeptide ester, **2**, which was then converted to the amide, **3**. After the removal of the protecting group, the resulting dipeptide amide was coupled with Boc-glycine *p*-nitrophenyl ester to form the Boc-tripeptide amide, **4**. The condensation of the azide derived from *t*-amyloxycarbonylphenylalanylisoleucine hydrazide, Aoc-Phe-Ile-N_2H_3, with the tripeptide amide gave an acylpentapeptide amide, **5**. The di-Boc-hexapeptide amide, **6**, was obtained *via* the *p*-nitrophenyl ester method. Since all attempts to crystallize the intermediates **2**—**6** were unsuccessful, the products were purified by column chromatography on silica gel after each coupling step.

The [Lys^6, HyMtb^{11}]-analog (VIII) was synthesized by the method shown in Scheme 2.

H-HyMtb-OH (**7**) ⟶ H-HyMtb-OMe (**8**)
⟶ H-HyMtb-NH_2 (**9**)
Boc-Leu-OH + **9**
↓ CDI
Boc-Leu-HyMtb-NH_2 (**10**)
↓ i) HCl in dioxane ii) Boc-Ile-Gly-ONp
Boc-Ile-Gly-Leu-HyMtb-NH_2 (**11**)
↓ i) HCl in dioxane ii) Boc-Phe-ONp
Boc-Phe-Ile-Gly-Leu-HyMtb-NH_2 (**12**)
↓ i) HCl in dioxane ii) di-Boc-Lys-ONp
di-Boc-Lys-Phe-Ile-Gly-Leu-HyMtb-NH_2 (**13**)
↓ HCl in AcOH
H-Lys-Phe-Ile-Gly-Leu-HyMtb-NH_2·2HCl (VIII)

Scheme 2.

L-α-Hydroxy-γ-methylthiobutyric acid (**7**) was prepared from L-methionine by the procedure of Winitz *et al.*[8] The α-hydroxy acid, **7**, was converted to the methyl ester, **8**; subsequent amidation yielded the corresponding amide, **9**. Boc-leucine was coupled with the free hydroxyl by the use of *N*,*N*′-carbonyldiimidazole (CDI)[9] to yield the Boc-didepsipeptide amide, **10**, in a good yield. After the removal of the Boc-group of **10**, the resulting didepsiptide amide was condensed with Boc-isoleucylglycine *p*-nitrophenyl ester to yield the Boc-tetradepsipeptide amide, **11**. The di-Boc-hexapeptide amide, **13**, was prepared by two successive stepwise elongations *via* the *p*-nitrophenyl ester method.

In the synthesis of [Lys^6, HyIv^8]-analog (IV), benzenesulfonyl chloride and pyridine were used for the formation of the depsipeptide bond, as had been reported previously for the synthesis of [Lys^6, HyMeV^8]-analog (III)[6] (Scheme 3).

The peptides, XIV, VIII, and IV, were obtained by the removal of the Boc group of the di-Boc-hexapeptide amides with hydrogen chloride in acetic acid.

6) H. Sugano, K. Higaki, and M. Miyoshi, This Bulletin, **46**, 226 (1973).
7) N. Izumiya, A. Nagamatsu, and S. Ota, *Kyushu Mem. Med. Sci.*, **4**, 1 (1953).
8) M. Winitz, L. Bloch-Frankenthal, N. Izumiya, S. M. Birnbaum, C. G. Baker, and J. P. Greenstein, *J. Amer. Chem. Soc.*, **78**, 2423 (1956).
9) H. A. Staab, *Angew. Chem.*, **71**, 194 (1959).

Boc-Phe-OH + H-HyIv-OBzl
↓ $C_6H_5SO_2Cl$/pyridine
Boc-Phe-HyIv-OBzl
↓ H_2/Pd
Boc-Phe-HyIv-OH (**14**) + H-Gly-Leu-Met-NH_2
↓ EtOCOCl/Et_3N
Boc-Phe-HyIv-Gly-Leu-Met-NH_2 (**15**)
↓ i) HCl in dioxane
↓ ii) di-Boc-Lys-ONp
di-Boc-Lys-Phe-HyIv-Gly-Leu-Met-NH_2 (**16**)
↓ HCl in AcOH
H-Lys-Phe-HyIv-Gly-Leu-Met-NH_2·2HCl (IV)

Scheme 3.

They were found to be homogeneous by the criteria of paper chromatography, paper electrophoresis, and elementary analysis. The presence of the depsipeptide bond was confirmed by IR, which showed an ester carbonyl band near 1750 cm^{-1}.

TABLE 1. PHARMACOLOGICAL RESULTS ON THE BLOOD PRESSURE IN RABBITS

Peptide		Relative[a] potency
H-Lys-Phe-Ile-Gly-Leu-Met-NH_2	(I)	100
H-Lys-Phlac-Ile-Gly-Leu-Met-NH_2	(II)	90[b]
H-Lys-Phe-HyMeV-Gly-Leu-Met-NH_2	(III)	10[b]
H-Lys-Phe-HyIv-Gly-Leu-Met-NH_2	(IV)	6
H-Lys-Phe-Ile-Glyc-Leu-Met-NH_2	(V)	30[b]
H-Lys-Phe-Ile-Gly-HyIc-Met-NH_2	(VI)	120[b]
H-Lys-Phlac-Ile-Gly-HyIc-Met-NH_2	(VII)	30[b]
H-Lys-Phe-Ile-Gly-Leu-HyMtb-NH_2	(VIII)	0.1
H-Lys-MePhe-Ile-Gly-Leu-Met-NH_2	(IX)	10[b]
H-Lys-Phe-MeIle-Gly-Leu-Met-NH_2	(X)	0.1[b]
H-Lys-Phe-Ile-Sar-Leu-Met-NH_2	(XI)	200[b]
H-Lys-Phe-Ile-Gly-MeLeu-Met-NH_2	(XII)	120[b]
H-Lys-MePhe-Ile-Gly-MeLeu-Met-NH_2	(XIII)	10[b]
H-Lys-Phe-Ile-Gly-Leu-MeMet-NH_2	(XIV)	0.1

a) The activity of the reference standard (I) is taken as 100. The potency of the other peptides is compared on a weight basis which causes fall of 20 mmHg of the blood pressure and expressed in per cent.
b) Taken from the previous papers.[1,6]

Results and Discussion

Table 1 shows the biological activities of the analogs synthesized here, together with those reported previously. In the rabbit blood pressure assay, the peptides VIII and XIV possessed 0.1% and the peptide IV possessed 6% of the depressor activity of the reference standard (I). The inactivity of the former two analogs strongly suggests the necessity of the amide bond between the leucine and the methionine residues for the biological activity. Although IV still had an appreciable activity, its potency was more decreased than those of II, V, VI, and VII, in which the phenylalanine, the glycine, or the leucine was replaced by the α-hydroxy acid. This low activity may be due not to the change in the side chain, but to the change in the backbone, because α-hydroxyisovaleric acid has a β-branched side chain like isoleucine, and because a [Val[8]]-eledoisin-(6-11)-hexapeptide, in which the isoleucine is replaced by valine, retains the same activity as the parent *C*-terminal hexapeptide of eledoisin.[10] These results support the suggestion made previously that the amide bond between the phenylalanine and the isoleucine residues is probably important for the depressor activity.[6]

Summarizing the results obtained in this series of studies, both the amide bond between the phenylalanine and the isoleucine residues and that between the leucine and the methionine residues are indispensable in manifesting the depressor activity of eledoisin. The analogs which are lacking in either of the essential amide bonds show much less activity.

Apart from minor differences in geometry, such as the steric effect of the *N*-methyl group, the amide bond differs fundamentally from the ester bond or the *N*-methylamide bond in its ability of hydrogen-bond formation. This loss of activity may indicate that the hydrogen bonding is required to maintain a favorable conformation of the peptide for the activity or to bind the molecule with the biological receptor site.

To gain some insight into conformational changes in solution following chemical alteration, circular dichroism (CD) spectroscopy was applied. Figures 1 and 2 show representative CD spectra in water between 250 and 210 nm. The biologically active hexapeptide analog of eledoisin (I) shows a trough at 233 nm ($[\theta]=-2800$). The CD curves of the biologically active analogs, such as [Lys[6], Phlac[7]]-analog (II), [Lys[6], Glyc[9]]-analog (V), [Lys[6], HyIc[10]]-analog (VI),

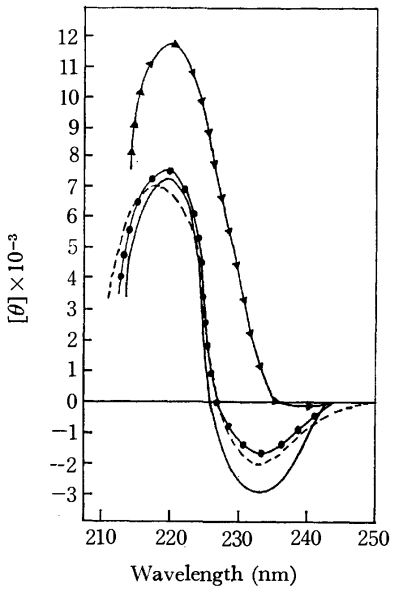

Fig. 1. Circular dichroism of depsipeptide analogs in the region 210—250 nm in water; concentration 1 mg/ml.
———: [Lys[6]]-eledoisin-(6-11)-hexapeptide (I)
– – – –: [Lys[6], Phlac[7]]-analog (II)
▶—▶: [Lys[6], HyMeV[8]]-analog (III)
●—●: [Lys[6], HyMtb[11]]-analog (VIII)

10) K. Lübke, E. Schröder. R. Hempel, and R. Schmiechen, Japan, 26004 (1967).

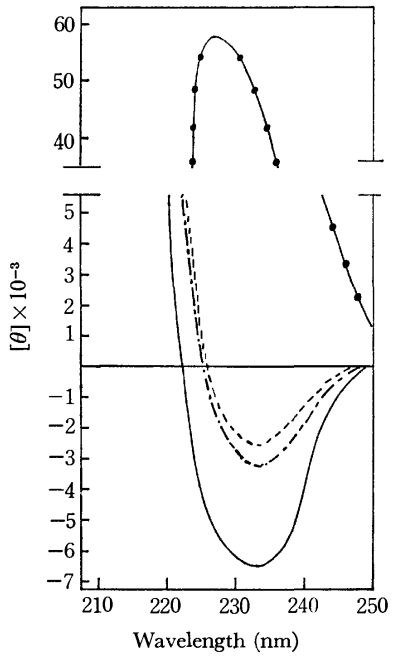

Fig. 2. Circular dichroism of *N*-methylpeptide analogs in the region 210—250 nm in water; concentration 1 mg/ml.
———: [Lys^6, MePhe^7]-analog (IX)
●—●: [Lys^6, MeIle^8]-analog (X)
— — —: [Lys^6, Sar^9]-analog (XI)
------: [Lys^6, MeMet^{11}]-analog (XIV)

[Lys^6, Phlac^7, HyIc^{10}]-analog (VII), [Lys^6, Sar^9]-analog (XI), and [Lys^6, MeLeu^{10}]-analog (XII), are very similar to that of the standard peptide (I). On the other hand, in the spectra of the less active peptides, such as [Lys^6, HyMeV^8]-analog (III) and [Lys^6, HyIv^8]-analog (IV), the positions of the troughs are shifted to longer wavelengths and the troughs are shallower. In the inactive compound, [Lys^6, MeIle^8]-analog (X), an anomalous spectrum is observed. However, [Lys^6, MeMet^{11}]-analog (XIV) and [Lys^6, HyMtb^{11}]-analog (VIII), which are devoid of biological activity, give spectra like that of I. These findings suggest that all the active peptides have very similar molecular conformations, and that the less active ones, such as III, IV, and X, are different from the active ones in backbone conformation. Furthermore, in the spectra of the less active compounds, such as [Lys^6, MePhe^7]-analog (IX) and [Lys^6, MePhe^7, MeLeu^{10}]-analog (XIII), the shapes and the positions of the troughs are almost identical with that of I, but the depths of the troughs are much enhanced ($[\theta]=-6500$ and -5900 respectively). Although the origin of the Cotton effect at about 233 nm is considered to be the n-π^* peptide transition, the contribution from the absorption of the aromatic group cannot be disregarded. From this point of view, the author assumes that these two peptides (IX and XIII) are different from I in the aromatic side chain conformation due to the steric effect of the *N*-methyl group in the *N*-methylphenylalanine residue.

Judging from these observations, the amide bond between the phenylalanine and the isoleucine residues probably restricts the favorable conformation of eledoisin. Such a conformation would facilitate an orientation of the side chains of the phenylalanine, the isoleucine, the leucine, and the methionine to a position in space in which a productive interaction with the biological receptor could occur. When *N*-methylisoleucine was introduced in place of the isoleucine, the conformation would be destroyed because of the lack of hydrogen bonding and also because of the steric effect of the *N*-methyl group. This is a factor which accounts for the much lower activity of the peptide, X, and for the anomalous spectrum. The exchange of the amide bond between the phenylalanine and the isoleucine residues by the ester bond appears to change the conformation to a considerable degree, but it does not completely destroy the molecular shape in spite of the lack of hydrogen bonding. In addition, the replacement of the amide bond between the lysine and the phenylalanine residues by the *N*-methylamide bond would cause a change in the orientation of the aromatic side chain and thereby affect the interaction with the receptor site.

From the fact that the peptides, VIII and XIV, were inactive even though they had favorable conformations, one can also guess that the amide bond between the leucine and the methionine residues plays an important role in exhibiting the biological activity. The possibility of binding *via* hydrogen bonding between the amide bond and the receptor site may be considered.

Experimental

The melting points are uncorrected. All the intermediates containing *N*-methylmethionine were purified by column chromatography on silica gel (Merck, 70-325 mesh). Each fraction was checked by thin-layer chromatography (tlc) on silica gel G(Merck); the products were determined by NMR in $CDCl_3$, which showed *N*-methyl protons (2.8—3.1 ppm) and *S*-methyl protons (2.0—2.1 ppm). The CD spectra were recorded on a JASCO Model ORD/UV-5 spectrophotometer. The amino acid analysis was performed as had been described previously.[1]

Pharmacological Assay. White male rabbits (2—3 kg) were anesthetized subcutaneously with 1.2 g/kg of urethane. Anesthesia was maintained with additional doses as needed. Arterial blood pressure was measured from a canulated carotid artery and recorded on a Kymograph by mercury manometer. All the peptides were dissolved in physiological saline and were injected into the femoral vein. Each dose was tested on five animals and was always checked against the reference standard material, I. The activity of the peptides was compared on a weight basis. The data were obtained with five animals per group.

H-MeMet-OEt·HCl (1). Thionyl chloride (22 g, 180 mmol) was added to absolute ethanol (200 ml) at 0—2 °C. To this solution, *N*-methylmethionine[7] (9.8 g, 60 mmol) was added, after which the solution was stirred at room temperature for 5 hr. After the removal of the solvent, this procedure was repeated two times. The oily residue thus obtained was dissolved in water, and the solution was filtered with activated charcoal and made alkaline by the addition of sodium bicarbonate. The oil thus separated was extracted repeatedly with ether, and the extracts were washed with saturated sodium chloride solution and dried over magnesium sulfate. To the filtered solution, dry hydrogen chloride was introduced, and the precipitated white crystals were collected

and recrystallized from ethanol–ether; yield, 6.7 g (29%); mp 95—97 °C; $[\alpha]_D^{25}$ +35.7° (*c* 1, EtOH). Found: C, 42.40; H, 7.78; N, 5.80; S, 13.98; Cl, 15.78%. Calcd for $C_8H_{18}NO_2SCl$: C, 42.19; H, 7.91; N, 6.15; S, 14.06; Cl, 15.60%.

Boc–Leu–MeMet–OEt (2). To a solution of Boc–Leu–OH·H_2O (8.3 g, 33 mmol) in chloroform (100 ml), DCC (7.2 g, 35 mmol) was added with stirring at −5—0 °C. After 1 hr, there was added a solution of **1** (6.7 g, 30 mmol) and triethylamine (4.2 ml, 30 mmol) in chloroform (50 ml). After the mixture had been stirred overnight at room temperature, the dicyclohexylurea was filtered off. The filtrate was washed successively with 4% sodium bicarbonate, 1 M hydrochloric acid, and water, and dried over magnesium sulfate. The filtrate was evaporated *in vacuo* to yield an oil (11 g), which was then chromatographed on silica gel, with elution by a mixture of benzene and ethyl acetate (9: 1). In this solvent system, the by-products (R_f 0.8 and 0.9) were eluted. The desired product (R_f 0.4) was then removed by a mixture of ethyl acetate and methanol (8: 2). The fractions containing the product, as detected by tlc, were combined and evaporated *in vacuo* to yield a colorless oil; yield, 6.5 g (51%); $[\alpha]_D^{25}$ −64.8° (*c* 2.6, MeOH). NMR δ ($CDCl_3$): 3.03 (s, 3H, $-NCH_3$), 2.08 (s, 3H, $-SCH_3$), 1.43 (s, 9H, $-C(CH_3)_3$), 4.16 (q, 2H, $-OCH_2-$), 0.95 (dd, 6H, $-CH(CH_3)_2$).

Boc–Leu–MeMet–NH_2 (3). A solution of compound **2** (6.5 g) in methanol (100 ml) was saturated with dry ammonia gas at 0 °C, and the solution was allowed to stand for 40 hr at room temperature. The reaction mixture was then concentrated to dryness under reduced pressure, and the residual oil (6 g) was chromatographed on silica gel, with elution by a mixture of benzene and ethyl acetate (6: 4). After removal of the unreacted ester **2** (R_f 0.9), the product was eluted by a mixture of benzene and ethyl acetate (4: 6). The fractions containing the product (R_f 0.7, benzene–AcOEt (3: 7)) were pooled and evaporated, yield of oil, 5.45 g (86%); $[\alpha]_D^{25}$ −26.4° (*c* 0.7, MeOH). NMR δ ($CDCl_3$): 3.08 (s, 3H, $-NCH_3$), 2.10 (s, 3H, $-SCH_3$), 1.43 (s, 9H, $-C(CH_3)_3$), 6.45 (s, 2H, $-NH_2$).

Boc–Gly–Leu–MeMet–NH_2 (4). Compound **3** (5.6 g, 15 mmol) was dissolved in 3M hydrogen chloride in dioxane (450 ml), and the solution was allowed to stand at room temperature for 30 min. The solvent was distilled off *in vacuo*, and the residue was triturated with ether. The H–Leu–MeMet–NH_2·HCl thus obtained was dissolved in chloroform (30 ml), neutralized with triethylamine (2.1 ml), and then subjected to a reaction with Boc–Gly–ONp[11] (6 g, 20 mmol). After standing overnight at room temperature, the solution was diluted with ethyl acetate (350 ml), washed successively with 1 M hydrochloric acid, 4% sodium bicarbonate, and water, and dried over magnesium sulfate. The solvent was distilled off *in vacuo*, and the remaining oil was chromatographed on silica gel, with elution by a mixture of benzene and ethyl acetate (9: 1). In this solvent system, the unreacted Boc–Gly–ONp (R_f 0.8) was eluted, while the product was not eluted ($R_f < 0.1$). The product was removed from the column by a mixture of ethyl acetate and benzene (9: 1). The fractions containing the product, as determined by tlc (R_f 0.35, $CHCl_3$–MeOH–AcOH (95: 5: 3)) was pooled and evaporated *in vacuo*; yield of oil, 4.3 g (66%); $[\alpha]_D^{25}$ −25.0° (*c* 1, MeOH). Found: C, 52.41; H, 8.27; N, 12.00; S, 7.01%. Calcd for $C_{19}H_{36}N_4O_5S$: C, 52.77; H, 8.33; N, 12.96; S, 7.40%.

Aoc–Phe–Ile–Gly–Leu–MeMet–NH_2 (5). Compound **4** (2.2 g, 5 mmol) was treated with 2M hydrogen chloride in dioxane (30 ml) for 30 min at room temperature. After evaporation, the residue was triturated with ether; the remaining oil, corresponding to H–Gly–Leu–MeMet–NH_2·HCl, was used without further purification. To a solution of Aoc–Phe–Ile–$NHNH_2$[6] (2 g, 5 mmol) in a mixture of 2 M hydrochloric acid (10 ml) and dimethylformamide (100 ml), was added with stirring a chilled solution of sodium nitrite (350 mg, 5 mmol) in water (1 ml) over a period of 15 min at −15—−13 °C. After 20 min, a solution of previously prepared tripeptide amide hydrochloride, dissolved in dimethylformamide (20 ml), was added to the reaction mixture, and then the pH was adjusted to 7 with triethylamine. Stirring was continued for 3 hr at 0 °C and the mixture was then poured into cold water (500 ml). The oil thus separated was extracted with ethyl acetate, and the extract was washed successively with 0.5M sulfuric acid, 4% sodium bicarbonate, and water, and dried over magnesium sulfate. The dried solution was concentrated to an oil, which was subsequently chromatographed with elution by a mixture of ethyl acetate and methanol (95: 5). After the undesired products had been eluted (R_f 0.9, 0.8, and 0.6, AcOEt), the desired product (R_f 0.1, AcOEt; 0.35, $CHCl_3$–MeOH–AcOH (95: 5: 3)) was eluted with methanol; yield of oil, 700 mg (20%); $[\alpha]_D^{25}$ −24.8° (*c* 1, MeOH). Found: C, 58.34; H, 8.41; N, 11.29; S, 4.28%. Calcd for $C_{35}H_{58}N_6O_7S \cdot H_2O$: C, 58.01; H, 8.28; N, 11.60; S, 4.42%.

Di-Boc–Lys–Phe–Ile–Gly–Leu–MeMet–NH_2 (6). Compound **5** (700 mg, 1 mmol) was treated with 3M hydrogen chloride in dioxane (7 ml) for 40 min at room temperature. After evaporation, the residue was dissolved in dimethylformamide (5 ml), neutralized with triethylamine (0.13 ml), and subjected to a reaction with di-Boc–Lys–ONp[12] (700 mg) for 24 hr at room temperature. Ethyl acetate (100 ml) was then added to the reaction mixture, and the solution was washed with 1% hydrochloric acid, 4% sodium bicarbonate, and water, and dried over magnesium sulfate. The solution was concentrated to dryness, and remaining oil was purified by silica gel column chromatography, by elution with a mixture of ethyl acetate and methanol (9: 1). After the unreacted di-Boc–Lys–ONp ($R_f \fallingdotseq 1.0$, AcOEt–MeOH (9: 1)) had been eluted, the product ($R_f < 0.1$, AcOEt–MeOH (9: 1); 0.3, $CHCl_3$–MeOH–AcOH (95: 5: 3)) was eluted with methanol; yield of oil, 660 mg (70%); $[\alpha]_D^{25}$ −34.0° (*c* 1, MeOH). Found: C, 57.39; H, 8.28; N, 11.20; S, 3.14%. Calcd for $C_{45}H_{76}N_8O_{10}S \cdot H_2O$: C, 57.50; H, 8.30; N, 11.92; S, 3.40%.

H–Lys–Phe–Ile–Gly–Leu–MeMet–NH_2·2HCl (XIV). Compound **6** (200 mg) was dissolved in 2M hydrogen chloride in acetic acid (5 ml), and the solution was allowed to react at room temperature for 20 min. The product was precipitated by adding ice-cold dry ether (20 ml), and the precipitate was collected by filtration, washed well with ether, and dried over sodium hydroxide *in vacuo*. The product was dissolved in 60% methanol (4 ml), and an insoluble material was filtered off. The filtrate was concentrated to dryness over phosphorus pentoxide *in vacuo* to afford the final product; yield, 170 mg; mp 80—120 °C; $[\alpha]_D^{25}$ −34.0° (*c* 0.5, H_2O); R_f, 0.74;[13] amino acid ratios in the acid hydrolysate: Lys, 1.14; Phe, 1.03; Ile, 1.02; Gly, 0.95; Leu, 1.00; MeMet, 1.09. Found: C, 51.26; H, 7.88; N, 12.92; S, 3.68%. Calcd for $C_{35}H_{60}N_8O_6S \cdot 2HCl \cdot 2H_2O$: C, 50.66; H, 7.96; N, 13.51; S, 3.86%.

11) E. Bayer, G. Jung, and H. Hagenmaier, *Tetrahedron*, **24**, 4853 (1968).

12) E. Sandrin and R. A. Boissonnas, *Helv. Chim. Acta*, **46**, 1637 (1963).

13) Paper chromatography was carried out on Toyo Roshi No. 50 with *n*-butanol–acetic acid–water (4: 1: 1).

H–HyMtb–OH (7). This was prepared by the nitrous acid deamination of L-methionine (150 g) by the procedure reported by Winitz *et al.* for L-α-hydroxy-β-methylvaleric acid;[8] yield of oil, 27 g (16.7%). A sample for analysis was dissolved in ether; the subsequent addition of dicyclohexylamine to the solution gave crystalline dicyclohexylammonium salt, which was then recrystallized from ethyl acetate–petroleum ether; mp 130—131 °C; $[\alpha]_D^{25}$ −20.3° (*c* 1, EtOH). Found: C, 61.49; H, 10.15; N, 4.28; S, 9.92%. Calcd for $C_5H_{10}O_3S \cdot C_{12}H_{23}N$: C, 61.63; H, 9.96; N, 4.22; S, 9.66%.

H–HyMtb–OMe (8). Thionyl chloride (28 g, 230 mmol) was added with stirring to methanol (150 ml) at −2—2 °C. To the solution, compound **7** (33 g, 220 mmol) was added and the mixture was stirred for 1 hr at 0 °C and 3 hr at room temperature. After the solution had then been concentrated *in vacuo*, the remaining oil was distilled to give the ester (**8**); yield, 22 g (62%); bp 91—93 °C/3 mmHg; $[\alpha]_D^{25}$ −16.4° (*c* 1, MeOH). IR cm^{-1} (liq. film): 3450 (OH), 1740 (C=O). NMR δ ($CDCl_3$): 4.30—4.50 (dd, 1H, –CH–), 3.82 (s, 3H, $-OCH_3$), 3.15 (s, 1H, –OH), 2.54—2.82 (m, 2H, $-CH_2S$–), 2.15 (s, 3H, $-SCH_3$), 1.82—2.20 (m, 2H, $-CH_2$–).

H–HyMtb–NH₂ (9). A solution of compound **8** (18 g, 110 mmol) in methanol (300 ml) was saturated with dry ammonia gas at 0 °C. After standing for 48 hr at room temperature, the solution was concentrated to dryness; yield of oil, 16 g (100%); $[\alpha]_D^{25}$ −55.0° (*c* 0.65, H_2O). NMR δ ($CDCl_3$): 6.88 (d, 2H, $-NH_2$), 5.34 (s, 1H, –OH), 4.13—4.34 (dd, 1H, –CH–), 2.45—2.75 (m, 2H, $-CH_2S$–), 2.10 (s, 3H, $-SCH_3$), 1.60—2.18 (m, 2H, $-CH_2$–).

Boc–Leu–HyMtb–NH₂ (10). To a solution of carbonyldiimidazole[9] (13 g, 80 mmol) in tetrahydrofuran (80 ml) was added a solution of Boc–Leu–OH·H_2O (20 g, 80 mmol) in tetrahydrofuran (50 ml) at 0 °C over a period of 30 min. Then there was added a solution of compound **9** (11.5 g, 80 mmol) in tetrahydrofuran (20 ml); the reaction mixture was stirred at 0 °C for 1 hr and then at room temperature for 2 days. Water (20 ml) was added to the solution, and the solvent was removed under reduced pressure. The residue was dissolved in ethyl acetate, and the ethyl acetate solution was washed with 1% hydrochloric acid, 4% sodium bicarbonate, and water, and dried over magnesium sulfate. The evaporation of the solvent gave white crystals, which were then recrystallized from ethyl acetate–petroleum ether; yield, 20 g (69%); mp 97—99 °C; $[\alpha]_D^{25}$ −56.5° (*c* 1, EtOH). Found: C, 52.98; H, 8.32; N, 7.61; S, 8.77%. Calcd for $C_{16}H_{30}N_2O_5S$: C, 53.02; H, 8.34; N, 7.73; S, 8.82%.

Boc–Ile–Gly–Leu–HyMtb–NH₂ (11). Compound **10** (4 g, 11 mmol) was treated with 3M hydrogen chloride in dioxane for 30 min. After evaporation, the residue, corresponding to didepsipeptide amide hydrochloride, was dissolved in dimethylformamide (50 ml), neutralized with triethylamine (1.5 ml), and subjected to a reaction with Boc–Ile–Gly–ONp[14] (3.6 g, 9 mmol) for 24 hr at room temperature. Ethyl acetate (500 ml) was then added to the reaction mixture, and the solution was washed thoroughly with 1M ammonia, 1% hydrochloric acid, and water, and dried over magnesium sulfate. On removal of the solvent a crystalline residue was obtained; this was recrystallized from ethyl acetate–petroleum ether; yield, 2.8 g (60%); mp 114—115 °C; $[\alpha]_D^{25}$ −39.1° (*c* 1, MeOH). Found: C, 54.47; H, 8.41; N, 10.43; S, 5.88%. Calcd for $C_{24}H_{44}N_4O_2S$: C, 54.12; H, 8.33; N, 10.52; S, 6.00%.

Boc–Phe–Ile–Gly–Leu–HyMtb–NH₂ (12). Compound **11** (2.7 g, 5 mmol) was treated with 3M hydrogen chloride in dioxane for 40 min. The solvent was evaporated under reduced pressure, and the residue was dissolved in dimethylformamide (25 ml), neutralized with triethylamine, and subjected to a reaction with Boc–Phe–ONp[11] (2 g, 5 mmol) for 24 hr at room temperature. Ethyl acetate (200 ml) was then added to the reaction mixture, and the solution was treated as described for the preparation of **11**. The crude product was recrystallized from ethyl acetate–methanol–petroleum ether; yield, 3.1 g (92%); mp 179—183 °C; $[\alpha]_D^{25}$ −35.5° (*c* 1, MeOH). Found: C, 58.81; H, 7.84; N, 10.13; S, 4.50%. Calcd for $C_{33}H_{53}N_5O_8S$: C, 58.32; H, 7.80; N, 10.30; S, 4.71%.

Di-Boc–Lys–Phe–Ile–Gly–Leu–HyMtb–NH₂ (13). Compound **12** (700 mg, 1 mmol) was treated with 3M hydrogen chloride in dioxane for 30 min. After evaporation, the residue was dissolved in dimethylformamide (5 ml), neutralized with triethylamine, and subjected to a reaction with di-Boc–Lys–ONp (450 mg, 0.97 mmol) for 48 hr. Ethyl acetate (100 ml) was then added to the reaction mixture, and the solution was treated as described for the preparation of **11**. The crude product was recrystallized from ethyl acetate–methanol–petroleum ether; yield, 700 mg (75%); mp 172—175 °C; $[\alpha]_D^{25}$ −47.4° (*c* 1, MeOH). Found: C, 58.30; H, 8.21; N, 10.69; S, 3.23%. Calcd for $C_{44}H_{93}N_7O_{11}S$: C, 58.19; H, 8.10; N, 10.79; S, 3.53%.

H–Lys–Phe–Ile–Gly–Leu–HyMtb–NH₂·2HCl (VIII). This was obtained from compound **13** (200 mg) as described for the preparation of XIV; yield, 165 mg; mp 225—227 °C; $[\alpha]_D^{25}$ −36.6° (*c* 0.21, H_2O); R_f, 0.76;[13] amino acid ratios in the acid hydrolysate: Lys, 1.01; Phe, 0.98; Ile, 1.10; Gly, 0.95; Leu, 1.00. Found: C, 50.81; H, 7.48; N, 12.08; S, 3.80%. Calcd for $C_{34}H_{57}N_7O_7S \cdot 2HCl \cdot 2H_2O$: C, 51.12; H, 7.64; N, 12.28; S, 4.01%.

Boc–Phe–HyIv–OH (14). To a solution of Boc–Phe–OH (15 g, 57 mmol) in a mixture of pyridine (100 ml) and tetrahydrofuran (100 ml), was added with stirring benzenesulfonyl chloride (8.8 g, 50 mmol) at −10 °C over a period of 10 min. After 10 min, a solution of benzyl L-α-hydroxyisovalerate[15] (10 g, 48 mmol) in pyridine (30 ml) was added to the solution. The mixture was then allowed to stand at 0 °C for 1 hr and at room temperature for 8 hr, and subsequently poured into water (1000 ml). The oil thus separated was extracted with ether. The extract was washed repeatedly with 2% hydrochloric acid, 4% sodium bicarbonate, and water, and dried over magnesium sulfate. The solvent was distilled off *in vacuo* to leave an oil (19.6 g); this oil was then dissolved in methanol (100 ml) and hydrogenated in the presence of 10% palladium on charcoal. The filtrate from the catalyst was evaporated to dryness, and the crude acid was dissolved in 4% sodium bicarbonate, washed with ether, and acidified with 1% hydrochloric acid. The oil thus separated was extracted with ether. The ethereal solution was washed with water and dried over magnesium sulfate. The ether was removed under reduced pressure; yield of oil, 15 g (88%). IR cm^{-1} (liq. film): 1740, 1720, 1705 (C=O).

Boc–Phe–HyIv–Gly–Leu–Met–NH₂ (15). To a solution of **14** (7.3 g, 20 mmol) and triethylamine (2.8 ml) in chloroform (200 ml), was added ethyl chloroformate (2.2 g, 20 mmol) at −15—−10 °C. After 15 min, there was added a solution of H–Gly–Leu–Met–NH_2·HCl[16] (7.3 g, 20 mmol)

14) H. Niedrich, *Chem. Ber.*, **100**, 3273 (1967).

15) G. Losse and G. Bachmann, *ibid.*, **97**, 2671 (1964). P. Quitt, R. O. Studer, and K. Volger, *Helv. Chim. Acta*, **47**, 166 (1964).

16) E. Schröder, R. Schmiechen, and H. Gibian, *Ann. Chem.*, **679**, 195 (1964).

and triethylamine (2.8 ml) in dimethylformamide (50 ml) at −15—−10 °C, and this mixture was allowed to stand at room temperature overnight. The mixture was poured into cold water (1000 ml), and the resulting solid material was extracted with chloroform. The extract was washed successively with 2% hydrochloric acid, 4% sodium bicarbonate, and water. The solvent was then evaporated *in vacuo*, and the crude product thus obtained was recrystallized from ethyl acetate–methanol–petroleum ether; yield, 9.4 g (71%); mp 160—164 °C; $[\alpha]_D^{25}$ −43.3° (*c* 1, MeOH). Found: C, 57.32; H, 7.80; N, 10.26; S, 4.75%. Calcd for $C_{32}H_{51}N_5O_8S$: C, 57.73; H, 7.72; N, 10.52; S, 4.80%.

*Di-Boc–Lys–Phe–HyIv–Gly–Leu–Met–NH$_2$ (**16**).* Compound **15** (5.32 g, 8 mmol) was dissolved in 3M hydrogen chloride in dioxane (70 ml) at room temperature. After 20 min, the solution was evaporated to dryness *in vacuo*. The pentadepsipeptide amide hydrochloride thus obtained was dissolved in dimethylformamide (40 ml) and then neutralized with triethylamine (1.2 ml). Di-Boc–Lys–ONp (4.2 g, 9 mmol) was added to the solution, and the mixture was allowed to stand at room temperature for 20 hr. Water was added to the reaction mixture to precipitate the product, which was then collected by filtration, washed well with 2% hydrochloric acid, 1M ammonia, and water, and dried. Recrystallization from ethyl acetate–petroleum ether gave 4.2 g (58%) of a product; mp 198—201 °C; $[\alpha]_D^{25}$ −40.2° (*c* 1, MeOH). Found: C, 57.53; H, 8.08; N, 11.05; S, 3.85%. Calcd for $C_{43}H_{71}N_7O_{11}S$: C, 57.76; H, 8.00; N, 10.96; S, 3.58%.

H–Lys–Phe–HyIv–Gly–Leu–Met–NH$_2$·2HCl (IV). This was obtained from **16** (200 mg) as described for the preparation of XIV; yield, 180 mg; mp 95—100 °C; $[\alpha]_D^{25}$ −42.2° (*c* 0.265, H_2O); R_f, 0.68;[13] amino acid ratios in the acid hydrolysate: Lys, 0.96; Phe, 0.95; Gly, 0.98; Leu, 1.00; Met, 0.81. Found: C, 50.25; H, 7.66; N, 12.21; S, 4.11; Cl, 8.69%. Calcd for $C_{33}H_{55}N_7O_7S\cdot H_2O$: C, 50.51; H, 7.52; N, 12.50; S, 4.08; Cl, 9.05%.

The author wishes to express his thanks to Professor N. Izumiya of Kyushu University and Director Dr. I. Chibata of this laboratory for their encouragement in the course of this study. Thanks are also due to Associate Professor Y. Mukohata of Osaka University for his helpful discussions and to Dr. K. Higaki for his biological assay.

BULLETIN OF THE CHEMICAL SOCIETY OF JAPAN, VOL. 46, 2174—2176 (1973)

The Synthesis of γ-3,4,5,6-Tetrachlorocyclohexene (γ-BTC) by Means of a Diels-Alder Reaction

Kiichi SHINODA

Nishiki Research Laboratory of Kureha Chemical Industry Co., Ltd., Nishiki-machi, Iwaki-shi, Fukushima 974

(Received October 2, 1972)

γ-3,4,5,6-Tetrachlorocyclohexene (γ-BTC) was synthesized in a yield of 14—30% by a Diels-Alder reaction between *trans,trans*-1,4-dichloro-1,3-butadiene and *trans*-dichloroethylene. The *s-cis* requirement and stereochemical relationships consistent with Alder's rule are shown. Antioxidants are effective in this reaction.

Orloff *et al.*[1,2] isolated 3,4,5,6-tetrachlorocyclohexene (benzene tetrachloride, BTC) isomers and clarified their conformations and their relationships with 1,2,3,4,5,6-hexachlorocyclohexane (BHC) isomers. By Orloff's method, however, the yield of γ-BTC is very low and the isolation procedure is very laborious. Kurihara *et al.*[3] obtained γ-BTC from α-BTC, which is the main product in Orloff's method, through several routes.

In this report, the synthesis of γ-BTC by a Diels-Alder reaction between 1,4-dichloro-1,3-butadiene (I) and 1,2-dichloroethylene (II) will be described.

Results and Discussion

Each isomer of 1,4-dichloro-1,3-butadiene, which had been prepared[4-6] by the dechlorination of 1,3,4,4-tetrachlorobutene, was reacted in a small bomb with *trans*-dichloroethylene (IIa), under the conditions below: temperature, 150 °C; time, 30 hr; molar ratio, I/IIa= 1/20.

The results are shown in Table 1. γ-BTC was obtained in the reactions of *trans,trans*-I (Ia), *trans,cis*-I (Ib) and an isomer mixture of I with IIa. None of the BTC could be obtained by the reaction of *cis,cis*-I (Ic) with IIa. γ-BTC was identified by IR, its mp (87—88 °C, Orloff *et al.*,[2] mp 88.2—88.8 °C), and by photochlorination to BHC. As has already been clarified by Orloff *et al.*,[2] γ-BTC formed α, γ, and δ-BHC upon photochlorination.

Stereochemical Relationships. It has been illustrated in many cases that, in Diels-Alder reactions, dienes

1) G. Calingeart, M. E. Griffing, E. R. Kerr, A. J. Kolka, and H. D. Orloff, *J. Amer. Chem. Soc.*, **73**, 5224 (1951).
2) H. D. Orloff, A. J. Kolka, G. Calingaert, M. E. Griffing, and E. R. Kerr, *ibid.*, **75**, 4243 (1953).
3) N. Kurihara, Y. Sanemitsu, T. Kimura, M. Kobayashi, and M. Nakajima, *Agr. Biol. Chem. Jap.*, **34**, 784 (1970).
4) R. Criegee, W. Hörauf, and W. D. Schellenberg, *Chem. Ber.*, **86**, 126 (1953).
5) H. G. Viehe and E. Franchimont, *ibid.*, **97**, 602 (1964).
6) P. D. Batlett and G. E. H. Wallbillich, *J. Amer. Chem. Soc.*, **91**, 409 (1969).

must take the cisoid conformation.[7] It is probable that, in our case, only Ia can exist in the *s-cis* conformation and react with IIa. In the case of Ib, it is clear that Ib is isomerized to Ia, and then enters into the reaction, because the recovered I was a mixture of I isomers.

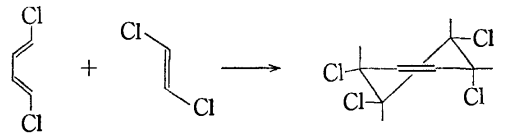

Ia IIa γ-BTC

According to Alder's rule,[7,8] the chlorine atoms at the 4,5-position of BTC produced from Ia and IIa must be *trans* (aa or ee) to each other, while those of 3,6 must be *cis* (ae). Therefore, the BTC have to be γ ($\overline{\text{HH}}$ aeee⇄$\overline{\text{HH}}$ eaaa). Our results shown in Table 1 are consistent with Alder's rule.

Table 1. Diels-Alder reaction of 1,4-dichloro-1,3-butadiene isomers (I) with *trans*-dichloroethylene (IIa)
Temp. 150 °C, 30 hr, Molar ratio I/IIa=1/20

I isomer	Product	Yield %	Recovered I %	Ia	Ib	Ic
trans, trans(Ia)[a]	γ-BTC	14.3	36.3	24.9	48.8	26.3
trans,cis (Ib)[a]	γ-BTC	0.03	41.6	4.9	90.0	5.1
cis,cis (Ic)[a]	no BTC	0			4.2	95.8
Isomer mixture[b] Ia:Ib:Ic= 18.1:46.4:25.5	γ-BTC	16.8[c]	58.5	13.3	48.2	38.3

a) The amounts used were Ia 1.12 g, Ib 1.23 g, and Ic 1.23 g, respectively.
b) The amount used was 4.1 g. Molar ratio I/IIa was 1/5.
c) The yield is based on Ia charged initially.

Effects of Antioxidants and Temperature. The reaction mixture, after the excess II and the unreacted I had been removed, was generally reddish-brown in color. This colored material seemed to be the decomposition product of I. In order to suppress the decomposition of I, the effect of the antioxidants was examined. The results are shown in Table 2. The effect of the antioxidants was obvious; the effective ones were *p*-phenylenediamine and *p*-aminophenol.

Table 2. Diels-Alder reaction of *trans,trans*-1,4-dichloro-1,3-butadiene (Ia) with *trans*-dichloroethylene (IIa). Effect of antioxidants and temperature
Molar ratio Ia/IIa=1/20

Antioxidants[a]	Atmosphere	Temp. (°C)	Time (hr)	γ-BTC Yield (%)
Hydroquinone	air	150	30	19.3
1,3,5-Trinitrobenzene	air	150	30	19.1
p-Phenylenediamine	air	150	30	31.1
None	N_2	150	30	18.3
p-Aminophenol	N_2	150	30	30.9
None	N_2	200	14	3.2
p-Phenylenediamine	N_2	200	14	Trace
Lauryl disulfide	N_2	200	14	15.7

a) The amounts used were 1.0 mol % *vs.* Ia.

Effect of Friedel-Crafts Catalysts. There have been reports[9,10] that, in some cases, Friedel-Crafts-type metal halides function as catalysts in Diels-Alder reactions. We tried several metal halides—anhydrous $AlCl_3$, $FeCl_3$, $TiCl_4$, and $SnCl_4$, but no BTC was obtained because of the decomposition-promoting property of metal halides.

Experimental

All the melting points are uncorrected. The IR spectra were recorded with a Nihonbunko DS-301 or a Shimadzu IR-27 spectrophotometer.

1,3,4,4-Tetrachlorobutene (IV).[11,12] *cis*-Dichloroethylene (IIb) (700 g) was refluxed for 80 hr, with 1.0 g of benzoyl peroxide being added every 5 hr. The reaction mixture was then subjected to distillation at reduced pressure, and a fraction boiling at 79—85 °C/15 mmHg was collected. The yield was 28.9%, based on the IIb used.

Similarly, IV was prepared from IIa. The yield was 5.3%. The IV obtained consisted of 39% *trans*- and 61% *cis*-isomer.

Dechlorination of IV. Criegee's procedure[4] was followed, and a fraction boiling at 50—55 °C/50 mmHg was collected. The yield was 60—80%. The isomer ratio (Ia: Ib: Ic) was measured by glc (Shimadzu polyethylene glycol 6000). In general, the Ia: Ib: Ic ratio was 15: 50: 35.

Separation of 1,4-Dichloro-1,3-butadiene Isomers (Ia, Ib, and Ic). The separation of isomers was carried out by preparative glc; apparatus, Shimadzu GC-10A, using polyethylene glycol.

Ia, purified by sublimation at reduced pressure, has a mp of 36—37 °C (37—38 °C,[4] 38—39.6 °C[6]). Ib is a liquid (bp 53.0—55.0 °C/50 mmHg). Ic is also a liquid (bp 48.0—48.5 °C/50 mmHg). From 54.9 g of a mixture of I, pure Ia (1.5 g (after sublimation)), Ib (10.9 g), and Ic (8.4 g (after distillation)) were obtained.

In order to obtain only pure Ia from the isomer mixture, the mixture was cooled with dry ice–methanol, partially frozen, and then filtered under cooling with dry ice. The solid collected was purified by sublimation under reduced pressure. This Ia was pure enough for the reaction.

Diels-Alder Reaction between I and IIa. Usually IIa (19.4 g, 0.20 mol) was weighed in a 50 ml autoclave, and then the I isomer (1.23 g, 0.01 mol) was added, the solution was mixed well, and the autoclave was sealed. Then, the autoclave was placed in an oil bath kept at 150 or 200 °C. After the reaction, the excess IIa and unreacted I were removed by distillation under reduced pressure, first at about 100 mmHg and then 15 mmHg. The residue, usually a reddish brown solid with a little oily matter, was subjected to column chromatography. The column chromatography was carried out as follows: absorbent, activated alumina (Kanto Chemical, for chromatography); solvent, methanol or *n*-hexane; column dia., 15 mm; height of alumina layer, 50 mm. About 100 ml of the elute had been taken up, the solvent was removed under reduced pressure. The white solid thus obtained, a little yellowish in color, was found by

7) J. G. Martin and R. K. Hill, *Chem. Rev.*, **61**, 537 (1961).
8) J. Sauer, *Angew. Chem. Int. Ed.*, **6**, 16 (1967).
9) P. Yates and P. Eaton, *J. Amer. Chem. Soc.*, **82**, 4436 (1960).
10) G. I. Fray and R. Robinson, *ibid.*, **83**, 249 (1961).
11) C. E. Frank and A. U. Blackham, *ibid.*, **72**, 3283 (1950).
12) K. E. Weale, *J. Chem. Soc.*, **1952**, 2223.

IR to be almost pure γ-BTC. The yields were calculated on the basis of the weights at this stage. After recrystallization from ethanol, mp was 87—88 °C.

Photochlorination of γ-BTC to BHC. Pure γ-BTC (0.44 g, 0.002 mol), chlorine (0.17 g, 0.0024 mol), and 10 ml of dry distilled carbon tetrachloride were charged in an ampoule (1.2×15 cm). The air in the ampoule and the carbon tetrachloride were then replaced by dry nitrogen. The ampoule was immersed in a methanol–dry ice bath kept at -10 ± 2 °C, and a 10 W blue fluorescent lamp (Mazda) was placed at a distance of 14 cm as the light source. The photochlorination was over within one hour.

After the reaction, the reaction mixture was subjected to steam distillation and a white solid (0.515 g, 88.9% as BHC) was obtained.

By IR the reaction product was found to consist of γ, α, and δ-BHC. The amount of each BHC isomer was determined by IR according to Milone.[13] The key bands for the isomers were α, 15.93; γ, 20.70; and δ, 17.65 μ. By our experiment, at -10 °C in carbon tetrachloride the produced BHC contained α, 37.6; γ, 56.0; and δ, 6.4%.

The author wishes to thank Mr. Shigeto Ohtsuka and Dr. Hiromichi Watanabe for their encouragement, and Mr. Tadashi Uzuki and Mr. Eiji Yokoyama for their experimental help.

13) M. Milone and E. Borello, *Gazz. Chim. Ital.*, **83**, 255 (1953); *Chem. Abstr.*, **47**, 12133 (1953).

BULLETIN OF THE CHEMICAL SOCIETY OF JAPAN, VOL. 46, 2176—2180 (1973)

The Formation of Tin-Nitrogen Bonds. V. The Selective 1-Substitution Reaction of Tetrazoles by the Reaction of 5-Substituted 2-(Tri-*n*-butylstannyl)tetrazoles with Methyl Iodide, Methyl *p*-Toluenesulfonate, Dimethyl Sulfate, and Ethyl Bromoacetate

Tyûzô Isida, Tetsuo Akiyama, Kiyoshi Nabika, Keiiti Sisido, and Sinpei Kozima*

Department of Industrial Chemistry, Faculty of Engineering, Kyôto University, Sakyô-ku, Kyôto 606

**Department of Chemistry, College of Liberal Arts and Sciences, Kyôto University, Sakyô-ku, Kyôto 606*

(Received October 11, 1972)

The selective 1-substitution reaction of tetrazole was developed by the treatment of 5-substituted 2-(tri-*n*-butylstannyl)tetrazoles with methyl iodide, methyl *p*-toluenesulfonate, dimethyl sulfate, or ethyl bromoacetate at room temperature. This selectivity was introduced by blocking the 2-nitrogen with the tri-*n*-butyltin group against the 2-substitution. In the case of 5-substituted 2-(trimethylstannyl)tetrazoles, a low selectivity was observed. The possible reaction pathways have been discussed.

In continuation of our research into the preparation and reaction of tetrazoles and their derivatives,[1] this paper will describe a highly selective 1-methylation method of tetrazoles.

The *N*-alkylation of 5-substituted tetrazoles has, until now, always been carried out by the reaction of tetrazole with either alkyl halide[2-10] or dialkyl sulfate[4,7,11,12] in the presence of a base, and also with diazomethane.[12-14] These reactions, in general, have provided the 2-alkyl isomers in a greater proportion than the 1-alkyl isomers.

It has now been found that the treatment of 5-substituted 2-(tri-*n*-butylstannyl)tetrazoles (I) with methyl iodide at room temperature for several hours afforded the 1-methyl isomer with a high selectivity (1-methyl-: 2-methyl isomer=90: 10). For the preparation of 5-substituted 1-methyltetrazole (III), this method is facile and comparable to the steady route of Harville, Herbst, Schreiner, and Roberts,[15] who prepared 1,5-disubstituted tetrazole from *N*-monosubstituted amide. Since the 2-(tri-*n*-butylstannyl)tetrazoles (I) can be prepared very easily by mixing free tetrazoles with bis(tri-*n*-butyltin) oxide,[1a] the 1-methylation can be carried out

1) a) K. Sisido, K. Nabika, T. Isida, and S. Kozima, *J. Organometal. Chem.*, **33**, 337 (1971). b) T. Isida, S. Kozima, K. Nabika, and K. Sisido, *J. Org. Chem.*, **36**, 3807 (1971). c) T. Isida, S. Kozima, S. Fujimori, and K. Sisido, This Bulletin, **45**, 246 (1972). d) T. Isida, S. Fujimori, K. Nabika, K. Sisido, and S. Kozima, *ibid.*, **45**, 1471 (1972).

2) J. S. Mihina and R. M. Herbst, *J. Org. Chem.*, **15**, 1082 (1950).

3) R. A. Henry, *J. Amer. Chem. Soc.*, **73**, 4470 (1951).

4) R. A. Henry and W. G. Finnegan, *ibid.*, **76**, 923 (1954).

5) W. G. Finnegan and R. A. Henry, *J. Org. Chem.*, **24**, 1565 (1959).

6) W. P. Norris, *ibid.*, **27**, 3248 (1962).

7) R. N. Butler and F. L. Scott. *ibid.*, **31**, 3182 (1966).

8) R. Raap and J. Howard, *Can. J. Chem.*, **47**, 813 (1969).

9) F. Einberg, *J. Org. Chem.*, **35**, 3978 (1970).

10) L. Huff and R. A. Henry, *J. Med. Chem.*, **13**, 777 (1970).

11) R. Huisgen, J. Sauer, and M. Seidel, *Chem. Ber.*, **94**, 2503 (1961).

12) K. Hattori, E. Lieber, and J. P. Horwitz, *J. Amer. Chem. Soc.*, **78**, 411 (1956).

13) O. Gryszkiewicz-Trochimowski, *C. R. Acad. Sci., Paris.*, **246**, 2627 (1958).

14) J. H. Margraf, W. T. Bachmann, and D. P. Hollis, *J. Org, Chem.*, **30**, 3472 (1965).

15) E. K. Harville, R. M. Herbst, F. C. Schreiner, and C. W. Roberts., *ibid.*, **15**, 662 (1950).

by the simple procedure of dissolving a mixture of tetrazole and bis(tri-*n*-butyltin) oxide in methyl iodide. Additionally, the tri-*n*-butyltin iodide formed by the methylation process can be easily removed from the reaction mixture by extraction with light petroleum ether.

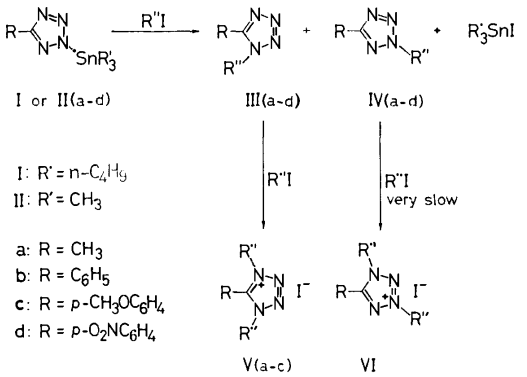

When 2-(tri-*n*-butylstannyl)-5-methyltetrazole (Ia) was dissolved in excess methyl iodide at room temperature and the solution was kept standing overnight, the *N*-methylation was completed. The ratio of 1,5-dimethyltetrazole (IIIa) and 2,5-dimethyltetrazole (IVa) was found to be 92: 8 by NMR analysis. Since 2,5-dimethyltetrazole (IVa) is much more volatile[1a,14] and far less reactive toward methyl iodide[1a] than IIIa, the evaporation of IVa and the surplus methyl iodide from the reaction products gave a mixture of IIIa and tri-*n*-butyltin iodide. Tri-*n*-butyltin iodide was also removed by simple extraction with light petroleum ether. Analytically pure 1,5-dimethyltetrazole (IIIa) was isolated in a good yield. 1,5-Dimethyltetrazole (IIIa) reacted gradually with excess methyl iodide at room temperature to give crystalline 1,4,5-trimethyltetrazolium iodide (Va), which began to precipitate after about 30 hr. When the reaction of Ia with excess methyl iodide was carried out at a higher temperature, a greater part of the IIIa was converted into the thermally stable tetrazolium iodide (Va).[1d]

A similar selective 1-methylation was also observed in the reactions of 5-phenyl and 5-(*p*-methoxyphenyl) analogues (Ib and Ic) with methyl iodide (Table 1). In the reaction of Ib with methyl iodide, the reaction temperature should be maintained at room temperature for the preparation of the 1-methyl isomer (IIIb), because on heating IIIb is easily converted into the 2-methyl isomer (IVb) in the presence of methyl iodide.[1b]

A less selective and much slower *N*-methylation was found in the reaction of 2-(tri-*n*-butylstannyl)-5-(*p*-nitrophenyl)tetrazole (Id) (Table 1). There occurred no further methylation of IIId to form the 1,4-dimethyltetrazolium salt (Vd). These results can be interpreted in terms of the electron-withdrawing character of the *p*-nitrophenyl group, which preferentially decreased the electron density of the 1- and 4-nitrogen atoms of the tetrazole ring, analogously to the reaction of potassium or sodium 5-substituted tetrazolate with methyl iodide.[4,6-8]

When the reaction of Ia—d with methyl iodide was carried out in the presence of methanol,[16] little change was found either in the isomer ratios of the products or in the reaction rate in comparison with the case of a reaction without methanol. This shows that the associative polymeric structure[1b] can not be involved in the selective 1-substitution reaction pathway.

Table 1. Distribution of III and IV formed by the reaction of I with methyl iodide

Compound	5-Substituent	Distribution (%) III	IV
Ia	CH_3	92	8
Ib	C_6H_5	90	10
Ic	p-$CH_3OC_6H_4$	91	9
Id	p-$O_2NC_6H_4$	68	32

It might be reasonable to consider that both the electron densities and steric requirements of the nitrogen atoms of tetrazole ring govern the site of the *N*-substitution. Since 2-substituted (or 2,5-disubstituted) tetrazoles react with methyl iodide[1b] or methyl *p*-toluenesulfonate[19] to yield exclusively 1,3-disubstituted (or 1,3,5-trisubstituted) tetrazolium salts, the 4-nitrogen of the 2-substituted tetrazole must be the most favorable site among the nitrogens to be attacked.[20] Analogously, it is probable that the *N*-methylation of 2-(trialkylstannyl)-5-substituted tetrazole (I or II) occurs preferentially on the 4-nitrogen.

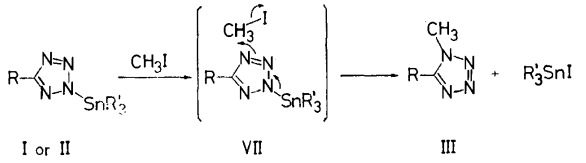

The minor product, the 2-methyl isomer (IV), could be formed by the methylation of the 2- or 3-nitrogen of I (or II). Since the formation of 2,3,5-trisubstituted tetrazolium salt from 2,5-disubstituted tetrazole has never been observed by spectroscopic investigations,[1d] the *N*-methylation of the 3-nitrogen of I (or II) might

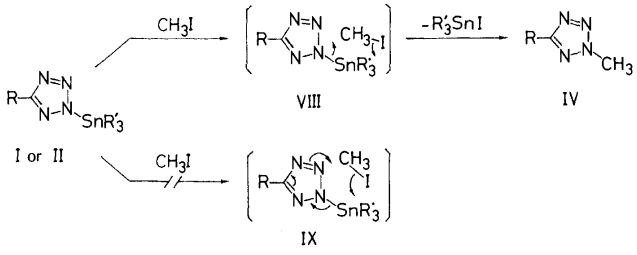

16) Addition of ligands such as alcohol to the toluene solution of tri-*n*-butylstannylimidazole has been reported to lower the viscosity, and hence the associative polymeric structure was fractured by the ligand to be the monomeric one.[17] Analogous fact has also been observed in the case of Ia—d.[18]

17) M. J. Janssen, J. G. A. Luijten, and G. J. M. van der Kerk, *J. Organometal. Chem.*, **1**, 286 (1963).

18) T. Isida, S. Kozima, and K. Sisido, unpublished results.

19) W. P. Norris and R. A. Henry, *Tetrahedron Lett.*, **1965**, 1213.

20) Formation of the 1,2,5-trisubstituted tetrazolium salts has never been reported and hence the 1-substitution of 2-substituted tetrazole can be excluded since the 1-nitrogen is sterically much more hindered than the 4-nitrogen.

be much less probable; a possible process can be the direct methylation of the 2-nitrogen bonded to the tin atom *via* VIII.

In this selective methylation, consequently, the tri-*n*-butyltin group blocked the 2-nitrogen against the 2-methylation and led the methyl group into the 4-nitrogen. A comparable protection of the 1-nitrogen of 4-substituted imidazole by the benzoyl group has been reported for the specific preparation of 5-substituted 1-methylimidazole.[21,22]

Table 2. Distribution of III and IV formed by the reaction of II with methyl iodide

Compound	5-Substituent	Distribution (%)	
		III	IV
IIa	CH_3	40	60
IIb	C_6H_5	38	62
IIc	p-$CH_3OC_6H_4$	49	51
IId	p-$O_2NC_6H_4$	21	79

In the reaction of 5-substituted 2-(trimethylstannyl)-tetrazoles (II) with methyl iodide in methanol, the 2-methyl isomers (IV) have been produced in greater yields than the 1-methyl isomers (III) (Table 2). In the case of 2-(trimethylstannyl)-5-(*p*-nitrophenyl)tetrazole (IId), the distribution ratio of the 1-methyl *vs.* 2-methyl isomer was smaller than those in the case of the other homologs (IIa, IIb, and IIc). The electron-withdrawing *p*-nitrophenyl group apparently decreased the ratio of the 1-methylation, much as in the case of 2-(tri-*n*-butylstannyl) derivatives of tetrazoles with methyl iodide. In the presence of the electron-donating *p*-methoxyphenyl group in the 5-position, the 1-methyl isomer was obtained in a greater proportion than the cases of the phenyl and *p*-nitrophenyl groups. This is an additional case of how the electronic effect of the 5-substituent greatly influences the ratio of the 1-methylation *vs.* 2-methylation. The low selectivity in the *N*-methylation of 5-substituted 2-(trimethylstannyl)-tetrazoles (II) (Table 2), compared with the case of the 2-(tri-*n*-butylstannyl) analogues (I) (Table 1), is apparently correlated to the higher polarity of the tin-nitrogen bond in II. Because IIa is insoluble in non-polar solvents and is undistillable, while Ia is soluble and distillable,[1a] the trimethyltin-nitrogen bond in II is considered to be more polar than the tri-*n*-butyltin-nitrogen bond in I. As the polarity of the tin-nitrogen bond in II increases, the direct methylation of the 2-nitrogen atom *via* VIII could possibly increase. This trend has been supported by the predominant 2-methylation in the case of lithium salt of tetrazole (X), in which the lithium-nitrogen bond has a strongly ionic character (Table 3).

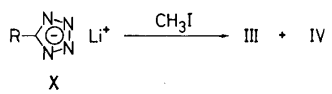

X

Table 3. Distribution of III and IV formed by the reaction of X with methyl iodide

Compound	5-Substituent	Distribution (%)	
		III	IV
Xb	C_6H_5	21	79
Xc	p-$CH_3OC_6H_4$	29	71
Xd	p-$O_2NC_6H_4$	19	81

Highly selective 1-methylation was also found in the reaction of 5-substituted 2-(tri-*n*-butylstannyl)tetrazole (I) with methyl *p*-toluenesulfonate or dimethyl sulfate (Table 4). In contrast to the easy removal of surplus methyl iodide from the products by evaporation, the use of these methyl esters as a methylating reagent is not preferred for the synthesis of III, since it is troublesome to remove the residual reagents and tri-*n*-butyltin salts from the product (III) by simple evaporation or extraction.

Table 4. Distribution of III and IV formed by the reaction of I with methyl *p*-toluenesulfonate, dimethyl sulfate, and ethyl bromoacetate

Compound	5-Substituent	Reagent	Distribution (%)	
			III	IV
Ia	CH_3	CH_3OTs[a]	79	21
Ib	C_6H_5	CH_3OTs	92	8
Ib	C_6H_5	$(CH_3O)_2SO_2$	93	7
Ia	CH_3	$BrCH_2CO_2C_2H_5$	90	10
Ib	C_6H_5	$BrCH_2CO_2C_2H_5$	91	9
Ie	$C_6H_5CH_2$	$BrCH_2CO_2C_2H_5$	94	6
Ib	C_6H_5	$ClCH_2CO_2C_2H_5$	No reaction	

a) Methyl *p*-toluenesulfonate.

A similar specific 1-substitution of tetrazole has also been achieved in the reaction of I with ethyl bromoacetate (Table 4). The synthesis of 5-substituted tetrazolylacetic acids and esters has been investigated for pharmaceutical purposes.[8,9,23,24] This method will provide a convenient route for the preparation of 5-substituted 1-tetrazolylacetic or -propionic acids and their esters.

Experimental

5-Substituted 2-(tri-*n*-butylstannyl)- and 2-(trimethylstannyl)tetrazoles (Ia—e and IIa—d) were prepared as has previously been described.[1a] The distribution of the 1-methyl and 2-methyl isomers was determined by studying the NMR spectrum, which was taken on a JEOL C-60HL spectrometer. All the melting points are uncorrected.

*Reaction of 2-(Tri-*n*-butylstannyl)-5-methyltetrazole (Ia) with Methyl Iodide.* A solution of 0.200 g of Ia in 0.25 ml of methyl iodide and 0.25 ml of $CDCl_3$ was kept in an NMR tube at room temperature for one day. The NMR spectrum of the reaction mixture was then measured. The distribution of the IIIa and IVa was determined to be 92:8 by

21) R. A. Olofson and R. V. Kendall, *J. Org. Chem.*, **35**, 2246 (1970).
22) H. C. Beyerman, L. Meat, and A. Vauzor, *Rec. Trav. Chim. Pays-Bas*, **91**, 245 (1972).
23) R. T. Buckler, S. Hayao, O. J. Lorenzetti, L. F. Sancilio, H. E. Hartzler, and W. G. Strycker, *J. Med. Chem.*, **13**, 725 (1970),
24) A. K. Sorensen and N. A. Klitgaard, *Acta Chem. Scand.*, **26**. 541 (1972).

means of the integral ratio of the peak areas at δ 4.14 and 4.34 ppm respectively.[1c,d,14]

A mixture of 3.362 g (9.00 mmol) of Ia and 7 ml of methyl iodide was kept at room temperature for two days. The subsequent evaporation of the surplus methyl iodide and IVa from the reaction mixture gave a pasty liquid containing colorless crystals. To the residue was added 50 ml of light petroleum ether (bp 40—48 °C); fine crystals were then separated by filtration and rinsed twice with petroleum ether. The crystals were identified as IIIa; mp 70—71 °C (lit,[14] mp 71.8—72.6 °C), 0.515 g (58%).

*Reaction of 2-(Tri-*n*-butylstannyl)-5-phenyltetrazole (Ib) with Methyl Iodide.* A solution of Ib (4.009 g, 9.22 mmol) in 5.0 ml of methyl iodide was kept at room temperature for 3 days. The subsequent evaporation of the residual methyl iodide *in vacuo* gave 5.230 g of a liquid containing crystals. To the residue was then added three 20 ml portions of light petroleum ether to extract tri-*n*-butyltin iodide. The petroleum ether was then evaporated off to give 3.723 g (97%) of tri-*n*-butyltin iodide. The crystals (1.491 g), insoluble in petroleum ether, consisted of IIIb and IVb in a ratio of 90:10. The NMR peaks at δ 4.15 and 4.35 ppm were assigned to the *N*-methyl protons of IIIb and IVb respectively.[25] The recrystallization of the crystals from *n*-hexane gave 1.252 g (78%) of pure IIIb;[1b,15] mp 103—104 °C (lit,[15] mp 101—102 °C).

*Reaction of 2-(Tri-*n*-butylstannyl)-5-(*p*-methoxyphenyl)tetrazole (Ic) with Methyl Iodide.* A solution of 1.447 g (3.12 mmol) of Ic in 3 ml of methyl iodide was kept at room temperature for two days. The subsequent evaporation of the surplus methyl iodide gave 1.871 g of a liquid containing crystals. The proportional ratio of IIIc and IVc in the reaction mixture was determined to be 91:9; the peaks at δ 4.11 and 4.34 ppm were assigned to IIIc and IVc respectively. The reaction mixture was treated with two 20 ml portions of petroleum ether to remove the tri-*n*-butyltin iodide. The resulting crystals, 0.492 g (84.7%), were recrystallized from a mixture of diisopropyl ether and tetrahydrofuran (4:1) to give 1-methyl-5-(*p*-methoxyphenyl)tetrazole (IIIc); mp 121—122 °C.[26] NMR ($CDCl_3$): δ 3.84 (s, 3H, methoxy protons), 4.11 (s, 3H, 1-methyl protons), 7.24 (d, 2H, *meta*-protons with respect to the tetrazole ring, $J_{o,m}$ 8.7 Hz), 7.67 ppm (d, 2H, *ortho*-protons).

*Reaction of 2-(Tri-*n*-butylstannyl)-5-(*p*-nitrophenyl)tetrazole (Id) with Methyl Iodide.* A solution of 0.460 g (0.955 mmol) of Id in 5 ml of methyl iodide was kept at room temperature for 40 days. The subsequent evaporation of the surplus methyl iodide gave 0.587 g of solids. The NMR spectrum of the solids had two peaks, at δ 4.25 and 4.42 ppm, assignable to the *N*-methyl protons of IIId and IVd respectively.[25] The integral ratio of the two peaks showed the distribution of IIId and IVd to be 68:32. The reaction mixture was subsequently treated with 100 ml of diethyl ether to extract the tri-*n*-butyltin iodide, IVd, and the recovered Id. The resultant crystals, insoluble in ether, were treated with hot diisopropyl ether to isolate 0.107 g (55%) of IIId; mp 122—123 °C (lit,[25] mp 121—123 °C). The ether solution was then concentrated and treated with hot diisopropyl ether. From the insoluble part 0.048 g (25%) of IVd was isolated by column chromatography (Silica Gel, benzene–tetrahydrofuran 10:2); mp 173—174 °C (lit,[25] mp 171—172 °C).

Reaction of 2-(Trimethylstannyl)-5-methyltetrazole (IIa) with Methyl Iodide. A solution of 0.062 g (0.23 mmol) of IIa in 0.25 ml of methyl iodide and 0.1 ml of methanol was kept in an NMR tube at room temperature for 4 days. Long needles of Va were found in the reaction mixture. In the NMR spectrum of the mixture there were not the peaks at δ 4.14 and 0.74 ppm characteristic of IIIa and the starting ingredient, IIa respectively, but there were peaks at δ 4.34 and 0.87 ppm assignable to the 2-methyl protons of IVa and the methyl protons of trimethyltin iodide respectively. Methanol, IVa, and surplus methyl iodide were evaporated off from the reaction mixture *in vacuo* to leave crystalline Va and trimethyltin iodide. The iodide was then removed by extraction with ether. The resultant crystals were identified as Va, 0.0242 g (40%); mp 266 °C (dec).[1d] The distribution of IIIa and IVa was determined to be 40:60 on the basis of the following facts: the starting IIa was completely converted into IIIa and IVa, and the resultant IIIa reacted with methyl iodide quantitatively to give Va, while little reaction occurred between IVa and methyl iodide.[1d]

Reaction of 2-(Trimethylstannyl)-5-phenyltetrazole (IIb) with Methyl Iodide. A solution of 0.378 g (1.22 mmol) of IIb in 2 ml of methyl iodide and 5 ml of methanol was kept at room temperature for two days. Evaporation of methanol and surplus methyl iodide *in vacuo* gave 0.383 g of crystals, which were then treated with benzene to separate the insoluble IIb, which was recovered unchanged; 0.158 g (42%). From the benzene extract the trimethyltin iodide was removed by extraction with water. The resultant benzene solution was concentrated to give a mixture of IIIb and IVb; 0.085 g (44%); IIIb:IVb=38:62.

Reaction of 2-(Trimethylstannyl)-5-(p-methoxyphenyl)tetrazole (IIc) with Methyl Iodide. A solution of IIc (0.351 g) in 1 ml of methyl iodide and 2 ml of methanol was kept at room temperature for 5 days. Methanol and surplus methyl iodide were then evaporated off *in vacuo* to give 0.362 g of crystals, whose components were determined by NMR analysis to be IIc (49%) and IVc (51%).

Reaction of 2-(Trimethylstannyl)-5-(p-nitrophenyl)tetrazole (IId) with Methyl Iodide. A solution of 0.088 g (0.25 mmol) of IId in 0.25 ml of methyl iodide and 0.25 ml of methanol was kept at room temperature for 5 days. The subsequent evaporation of methanol and surplus methyl iodide gave yellowish crystals (0.076 g) which were then treated with chloroform to extract *N*-methyl isomers and leave the recovered IId (0.012 g, 14%). The chloroform solution was evaporated off to give 0.057 g of the yellowish crystals. The ratio of IIId and IVd in the crystals was determined by NMR analysis to be 21:79.

Reaction of Lithium 5-Phenyltetrazolate (Xb) with Methyl Iodide. The monohydrate of Xb (0.1062 g, 0.625 mmol), prepared from an equimolar mixture of lithium hydride and 5-phenyltetrazole, was dissolved in 1.0 ml of methyl iodide and 2.0 ml of methanol. The solution was kept at room temperature for 3 days. The subsequent evaporation of methyl iodide and methanol gave 0.226 g of a pasty liquid, which was then extracted with dry ether. The ether solution was evaporated off to give 0.106 g of a liquid. The distribution of IIIb and IVb was determined by NMR analysis to be 21:79.

Reaction of Lithium 5-(p-Methoxyphenyl)tetrazolate (Xc) with Methyl Iodide. A solution of 0.094 g (0.47 mmol) of Xc in 0.25 ml of methanol and 0.25 ml of methyl iodide was kept at room temperature for two days. The subsequent evaporation of methanol and methyl iodide *in vacuo* gave 0.216 g of brownish crystals which were dissolved in chloroform. The chloroform solution was evaporated off to give 0.081 g (91%) of crystals. The ratio of IIIc and IVc in the crystals was determined by NMR analysis to be 21:79. The separation of IVc from IIIc was carried out by column

25) R. R. Fraser and K. E. Haque, *Can. J. Chem.*, **46**, 2855 (1968).

26) Although the melting point was different from the reported one (mp 93—94 °C),[15] not only the elemental analysis but also the NMR and mass spectra were consistent with the structure of IIIc.

chromatography (silica gel, benzene–chloroform 2:1) to isolate 0.055 g of IVc; mp 86.5—87.5 °C, NMR: δ 3.86 (s, 3H, methoxy protons), 4.37 (s, 3H, 2-methyl protons), 7.02 (d, 2H, *meta*-protons with respect to the tetrazole ring, $J_{o,m}$ 9.0 Hz), 8.12 ppm (d, 2H, *ortho*-protons).

Found: C, 57.17; H, 5.19; N, 30.05%. Calcd for $C_9H_{10}N_4O$: C, 56.83; H, 5.30; N, 29.46%.

From the later fraction 0.015 g of IIIc was collected.

Reaction of Lithium 5-(p-Nitrophenyl)tetrazolate (Xd) with Methyl Iodide. A solution of 0.076 g (0.35 mmol) of the monohydrate of Xd in 0.25 ml of methanol and 0.25 ml of methyl iodide was kept at room temperature for two days. The subsequent evaporation of the methanol and surplus methyl iodide gave 0.176 g of brownish crystals, which were then dissolved in chloroform. The solution was treated with water to remove the lithium iodide and Xd. From the chloroform layer was obtained 0.060 g (83%) of brownish-yellow crystals in which IIId and IVd were present in a ratio of 19:81.

Reaction of Ia with Methyl p-Toluenesulfonate. An equimolar solution of Ia and methyl *p*-toluenesulfonate in $CDCl_3$ was kept in an NMR tube at room temperature. After 21 days, the conversion of Ia into IIIa and IVa reached 42%. The distribution of IIIa and IVa was 79:21.

Reaction of Ib with Methyl p-Toluenesulfonate. A solution of 0.870 g (2 mmol) of Ib and 0.372 g (2 mmol) of methyl *p*-toluenesulfonate in 5 ml of ether was kept at room temperature for one day. The subsequent purification of the reaction mixture by column chromatography (silica gel, benzene: ether=1:1) yielded 0.280 g (89%) of crystals, which contained IIIb and IVb (92:8).

Reaction of Ib with Dimethyl Sulfate. A solution of 0.383 g of Ib and 0.200 g of dimethyl sulfate in 10 ml of ether was kept at room temperature for 8 days. After the evaporation of the ether, the reaction mixture was extracted with petroleum ether. The remaining crystals (0.087 g) were pure IIIb. From the extract, 0.015 g of a mixture of IIIb and IVb (1:1) was obtained by column chromatography. Consequently, the ratio of IIIb and IVb was found to be 93:7.

Reaction of Ib with Ethyl Bromoacetate. A solution of 0.671 g (1.5 mmol) of Ib and 0.259 g (1.5 mmol) of ethyl bromoacetate in 10 ml of benzene was refluxed for 10 days. The subsequent separation of the products by column chromatography (silica gel, benzene: ether=1:1) gave 0.327 g (91%) of crystalline ethyl 5-phenyl-1-tetrazolylacetate[8] and 0.033 g (9%) of ethyl 5-phenyl-2-tetrazolylacetate.[8] These esters were converted into the corresponding acids by alkali hydrolysis. 5-Phenyl-1-tetrazolylacetic acid, mp 169—170 °C (*n*-hexane) (lit,[8] mp 148—150 °C). Although the melting point is different from the reported one, the NMR and elemental analyses are consistent with the structure. NMR ($CDCl_3$: CF_3COOH=1:2): δ 7.70 (s, 5H, phenyl protons), 5.37 ppm (s, 2H, methylene protons). 5-Phenyl-2-tetrazolylacetic acid, mp 183—184 °C (*n*-hexane), (lit,[8] mp 182—184 °C). NMR ($CDCl_3$: CF_3COOH=1:2): δ 8.0 (m, 2H, *ortho*-protons), 7.55 (m, 3H, *meta*- and *para*-protons), 5.64 ppm (s, 2H, methylene protons).

Reaction of Ia with Ethyl Bromoacetate. An analogous treatment of Ia with ethyl bromoacetate for four days gave a mixture of the 1- and 2-substituted isomers. The NMR spectrum of the mixture showed that the ratio of the 1- and 2-substituted isomers was 90:10. The peaks at δ 5.23 and 5.40 ppm were assigned to the methylene protons of the 1- and 2-substituents respectively.[8] 5-Methyl-1-tetrazolylacetic acid was isolated by the hydrolysis of the ester; mp 183—184 °C (dec) (*n*-hexane and ethyl acetate) (lit,[8] mp 184—186 °C (dec)).

Reaction of 2-(Tri-n-butylstannyl)-5-benzyltetrazole (Ie) with Ethyl Bromoacetate. An analogous treatment of Ie with ethyl bromoacetate gave a mixture of the 1- and 2-substituted isomers in a ratio of 94:6. 5-Benzyl-1-tetrazolylacetic acid was isolated by the hydrolysis of the ester; mp 181—182°C (ethanol). NMR ($CDCl_3$: CF_3COOH=1:2): δ 7.6—7.0 (m, 5H, phenyl), 5.10 (s, 2H, $C\underline{H}_2COOH$), 4.43 ppm (broad s, 2H, $C_6H_5C\underline{H}_2$–).

Found: C, 54.95; H, 4.63; N, 25.43%. Calcd for $C_{10}H_{10}N_4O_2$: C, 55.04; H, 4.62; N, 25.68%.

A Study on the Photochemistry of α,β-Unsaturated γ-Lactones. II. Photoisomerization of 3-Ethylidene-4,5-dihydro-2(3*H*)-furanone[1]

Kazuya Ohga and Taku Matsuo

Department of Organic Synthesis, Faculty of Engineering, Kyushu University, Hakozaki, Fukuoka 812

(Received December 8, 1972)

On irradiation of *cis*-3-ethylidene-4,5-dihydro-2(3*H*)-furanone with 2537 Å light, both the *cis-trans* isomerization of the exocyclic double bond and transformation into the β,γ-unsaturated isomer, 3-vinyl-4,5-dihydro-2(3*H*)-furanone, were observed. By the use of sensitizers such as acetone, acetophenone, *p*-methoxyacetophenone and benzophenone, it was possible to induce *cis-trans* isomerization exclusively. On the basis of the solvent effect and the wavelength dependence of the reactions, transformation into the β,γ-unsaturated isomer and *cis-trans* isomerization were suggested to proceed *via* $T_2(n,\pi^*)$ and $T_1(\pi,\pi^*)$ states, respectively.

In contrast to the case of α,β-unsaturated ketones, information on the excited states of α,β-unsaturated esters and their analogues is scarce on account of the fact that systematic studies have not been made on the photochemistry of the latter.[2] The n,π* absorption bands of esters and their analogues are extremely blue-shifted from those of the corresponding α,β-unsaturated ketones as a result of conjugation between the carbonyl group and the adjacent hetero atom.[3] Hence, one may expect the photochemical behaviors ascribable to the n,π* excited state to differ considerably. We reported on the photodimerization of 2(5*H*)-furanone where no significant difference in stereo-selectivity and solvent effects on the yield were observed as compared with those of 2-cyclopentenone.[4] On irradiation of 2(5*H*)-furanone in 2-propanol, we obtained the same type of compound as in the case of the photoaddition of 2-cyclopentenone to 2-propanol;[5] the yield of the adduct in the former system, however, was very large in contrast to that of the latter system.[6] In order to investigate the photochemical behaviors of α,β-unsaturated lactones, we synthesized 3-ethylidene-4,5-dihydro-2(3*H*)-furanone, which is a new α,β-unsaturated lactone having a carbon-carbon double bond exocyclic to the lactone ring. The photochemical reactions of this compound are dealt with in this paper.

Results and Discussion

Synthesis and Identification of Starting Materials and Reaction Products. In order to synthesize the starting material, *trans*-3-ethylidene-4,5-dihydro-2(3*H*)-furanone (I), some modifications were made in the method by Zimmer and Rothe who mainly prepared 3-benzylidene derivatives of 4,5-dihydro-2(3*H*)-furanone.[7] The product contained at least two impurities which could not be removed by either repeated distillation or preparative vapor phase chromatography (vpc). The benzene solution was then irradiated in the presence of acetone as a sensitizer to yield *cis*-3-ethylidene-4,5-dihydro-2(3*H*)-furanone (II), which was readily isolated by preparative vpc. By the use of either acetone or benzophenone as a sensitizer, II was further photoisomerized back to I. Isolation of I from a small amount of the by-product III was achieved by the use of preparative vpc. The IR and NMR spectroscopic data of I and II given in Table 1 are in line with those of the isomeric 3-ethylidene-4,5-dihydro-2(3*H*)-furanones. The mass spectra and results of elementary analyses are in agreement with the assigned structure. A large difference in the chemical shift of methyl and methine protons on the exocyclic double bond can be seen in the NMR spectra. In the case of five- or six-membered ketones or lactones with structures analogous to compounds I and II, the methine proton signals for the *trans*-isomer are observed at lower field than those for *cis*-isomer, while a reverse tendency is observed for methyl proton signals.[8] Hence, compounds I and II were assigned to *trans*- and *cis*-3-ethylidene-4,5-dihydro-

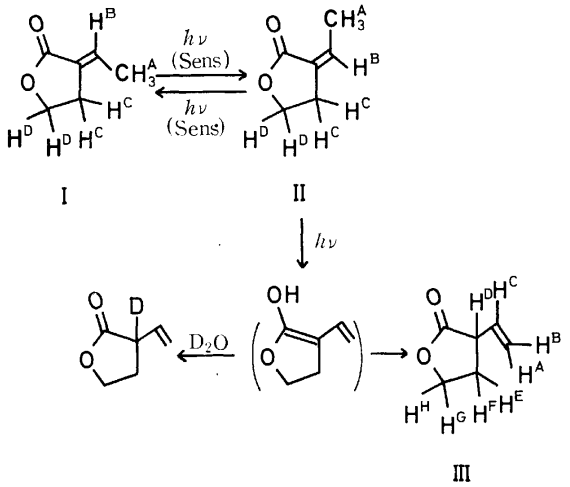

1) Contribution No. 303 from the Department of Organic Synthesis, Faculty of Engineering, Kyushu University.

2) N. J. Turro, "Technique of Organic Chemistry," Vol. XIV, ed. by P. A. Leermakers and A. Weissberger, Interscience Publishers, New York, N.Y. (1969), pp. 202 and 225.

3) W. D. Closson, S. F. Bradry, and P. J. Orenski, *J. Org. Chem.*, **30**, 4026 (1965).

4) K. Ohga and T. Matsuo, This Bulletin, **43**, 3505 (1970).

5) P. de Mayo, J.-P. Pete, and M. Tchir, *Can. J. Chem.*, **46**, 2535 (1968).

6) K. Ohga and T. Matsuo, unpublished results. Presented at the Discussion Meeting on the Photochemistry (Osaka, November, 1972).

7) H. Zimmer and J. Rothe, *J. Org. Chem.*, **24**, 28 (1959).

8) a) L. M. Jackmann and S. Sternhell, "Application of Nuclear Magnetic Resonance Spectroscopy in Organic Chemistry, 2nd ed,". Pergamon Press, New York, N.Y. (1969), p. 222. b) J. E. Dubois and M. Dubois, *C. R. Acaid. Sci., Paris*, **256**, 915 (1963). c) N. Baumann, M. Sung and E. F. Ullmann, *J. Amer, Chem. Soc.*, **90**, 4157 (1968). d) A. Hassner and T. C. Mead, *Tetrahedron*, **20**, 2201 (1964).

TABLE 1. NMR[a] AND IR[b] SPECTRA OF THE THREE ISOMERS (I, II, AND III)

Compound	Chemical shifts (δ, ppm)		Coupling constants (Hz)			Characteristic IR absorptions (cm^{-1})	
I	H^A 1.87		J_{AB} 7.1			$\nu_{C=O}$	1753
	H^B 6.81		J_{AC} 2.0			ν_{C-O-C}	1215
	H^C 2.85		J_{BC} 3.0			$\nu_{C=C}$	1681
	H^D 4.38		J_{CD} 7.3			ν_{CH}	3015
II	H^A 2.17		J_{AB} 7.2			$\nu_{C=O}$	1752
	H^B 6.36		J_{AC} 2.4			ν_{C-O-C}	1211
	H^B 2.92		J_{AC} 2.3			$\nu_{C=C}$	1673
	H^D 4.33		J_{CD} 7.4			ν_{CH}	3015
III	H^A 5.28[c]	H^E 2.20	J_{AB} 1.5[c]	J_{CD} 5.9	J_{EH} 8.1	$\nu_{C=O}$	1771
	H^B 5.30[c]	H^F 2.48	J_{BC}10.5[c]	J_{DE}10.0	J_{FG} 6.4	ν_{C-O-C}	1218
	H^C 5.92[c]	H^G 4.27	J_{AC}17.5[c]	J_{DF} 8.5	J_{FH} 4.5	$\nu_{C=C}$	1646
	H^D 3.27	H^H 4.38	J_{AD} 1.5	J_{EF}13.0	J_{GH} 9.0	ν_{CH}	3080
			J_{BD} 1.6	J_{EG} 8.6		δ_{CH}	1005, 927

a) Obtained in $CDCl_3$ with TMS as an internal standard.
b) Liquid sample.
c) Obtained by the simulation of the vinyl proton signals (ABC type) of III, deuterated at the α-position.

2(3*H*)-furanones, respectively. In the following experiments, the *cis*-isomer II (prepared as described above) was used as the starting material for photochemical investigations.

In addition to the *trans*-isomer I, another compound III was also produced when the acetonitrile solutions of isomer II in a sealed quartz tube was irradiated with a high-pressure mercury lamp. Compound III was isolated by preparative vpc, and the mass spectra as well as the result of elementary analysis indicate that III is another isomer. The spectral data are also summarized in Table 1. The wave number of the carbonyl absorption band (1771 cm^{-1}) indicates that the structure of γ-lactone is still retained in III but the carbonyl group is not conjugated with the carbon-carbon double bond. The IR spectra suggest the presence of a terminal vinyl group (δ_{CH}, 1005, 927 cm^{-1}). This was confirmed by the observation of ABC-type proton signals ascribable to the vinyl group in the NMR spectra of the sample, which was deuterated at the α-position with respect to the carbonyl group. Compound III was thus assigned to β,γ-unsaturated 3-vinyl-4,5-dihydro-2(3*H*)-furanone(β,γ-isomer).

Direct Irradiation of cis-*Isomer II.* Acetonitrile solutions of II were irradiated with a low-pressure mercury lamp in nitrogen atmosphere. The variation of each component with time was monitored by the use of vpc (Fig. 1). A very small amount of an unidentified compound (X) is produced together with the main products (I and III). The NMR spectra of the irradiated solution also indicates that isomers I and III are absolutely predominant reaction products and that the formation of X is negligible compared with those of I and III. The absorption maximum in the UV spectra shifted to shorter wavelength and the absorbance decreased with time. These changes can be accounted for by the formation of β,γ-unsaturated isomer III. Thus we see that the direct excitation of II induces both *cis-trans* isomerization between I and II and transformation from II to III.

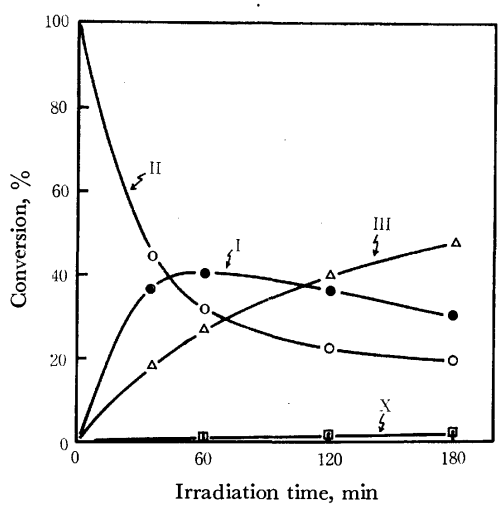

Fig. 1. Variation in the population of each component during the direct irradiation of II in acetonitrile (3×10^{-3}M).

When irradiation was carried out in D_2O–acetonitrile mixed solvent (4: 1), the methine group α to the carbonyl group of III was deuterated up to 89% as determined by NMR spectra. The formation of III is considered to proceed through an enol intermediate produced by the intramolecular hydrogen abstraction in analogy with the isomerization of α,β-unsaturated esters[9] or 5-methyl-3-hexen-2-one.[10]

Photosensitized cis-trans *Isomerization.* In Fig. 2 is shown the variation of isomer ratio with irradiation time, when either the *cis*- or *trans*-isomer was irradiated with a high-pressure mercury lamp in the presence of

9) a) M. J. Jorgenson and L. Gundel, *Tetrahedron Lett.*, **1968**, 4991. b) J. A. Barltrop and J. Wills, *ibid.*, **1968**, 4987. c) M. J. Jorgenson, *J. Amer. Chem. Soc.*, **91**, 198 (1969). d) M. Itoh, M. Tokuda, K. Seguchi, K. Taniguchi, and A. Suzuki, *Kogyo Kagaku Zasshi*, **72**, 219 (1969). e) P. J. Kropp and H. J. Krauss, *J. Org. Chem.*, **32**, 3222 (1967).
10) N. C. Yang and M. J. Jorgenson, *Tetrahedron Lett.*, **1964**, 1203.

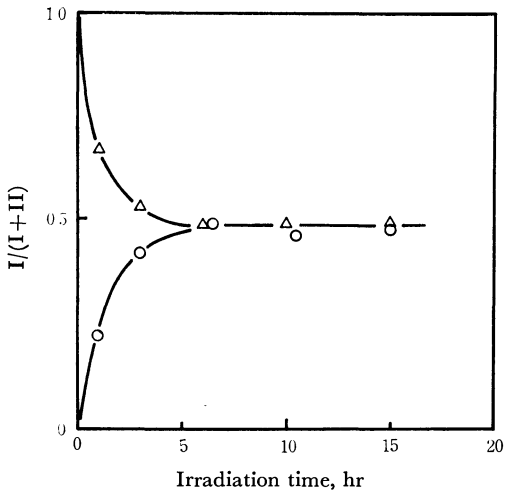

Fig. 2. Variation of the isomer ratio along the elapsed time in the acetophenone photosensitized isomerization of I and II.

Table 2. The isomer ratio at the photostationary state in the photosensitized isomerization between I and II[a)]

Sensitizer	[Sensitizer] M	E_T of the sensitizer kcal/mol	Isomer ratio[b)] I/II
Acetone	0.11	80	1.0
Acetophenone	0.01	74	0.96
p-Methoxy-acetophenone	0.01	72	1.0
Benzophenone	0.01	69	1.7

a) The concentrations of both I and II were 2.0×10^{-2}M. The reactions were carried out in an ordinary glass sample tube except for the case of acetone sensitization where a Pyrex tube was utilized.
b) Average values for the two reactions started from the pure sample of either of the two isomers. The errors are within 5%.

acetophenone as a sensitizer. The isomer ratio was determined by vpc analysis, assuming that both isomers can be detected with equal sensitivity. The isomer ratios at the photostationary states in the presence of a series of sensitizers were investigated in a similar way and the results are summarized in Table 2. The relationship between the triplet energy of the sensitizer and the isomer ratio at the photostationary state indicates that the triplet energy of the *cis*-isomer is lower than that of the *trans*-isomer estimated to be approximately 70 kcal/mol.

On direct excitation of the *cis*-isomer with 2537 Å light, the β,γ-isomer was obtained in 45% yield of the *trans*-isomer. In the case of the photosensitized reaction, the formation of the β,γ-isomer was completely suppressed. Thus, the excited precursor of the β,γ-isomer seems to differ from that of the *trans*-isomer. Since it is clear that *cis-trans* isomerization proceeds *via* the lowest triplet state (T_1) in the photosensitized reaction, the excited precursor leading to the β,γ-isomer seems to be either an excited singlet state (S_1) or the second-lowest triplet state (T_2) located above the triplet energy of acetone.

Solvent Effects of the Relative Yields of the β,γ-Isomer on the Direct Excitation of the cis-Isomer. When the

Table 3. Solvent effects on the relative quantum yields of the *trans*-isomer and the β,γ-isomer in the direct excitation of the *cis*-isomer

Solvent	[II] $\times 10^2$ M	Product yield (%) I	Product yield (%) III	Φ_I in solv.[a)] / Φ_I in C_6H_{12}	Φ_{III}[b)] / Φ_I
C_6H_{12}	2.07	6.4	1.1	1.0	0.18
CH_3CN	2.08	5.6	2.6	1.0	0.45
CH_3OH	2.04	5.5	2.3	1.0	0.41

a) The relative quantum yield for the formation of I in the given solvent with respect to that in cyclohexane.
b) The relative quantum yield for the formation of III with respect to that of I.

cis-isomer in various solvents was irradiated with 2537 Å light, the relative quantum yield of the β,γ-isomer varied considerably with solvent polarity (Table 3), while that of the *trans*-isomer was unaffected by the change of solvent. The quantum yield of the β,γ-isomer in cyclohexane is reduced to a value less than 50% of that in either methanol or acetonitrile (Table 3).

A similar solvent effect has been reported also on the photoisomerization of α,β-unsaturated esters: conversion of ethyl *trans*-crotonate into the β,γ-unsaturated isomer proceeds much more easily in ethanol than in *n*-hexane.[9d)] This is explained by the effect of crossing between the π,π* triplet and the n,π* triplet levels on the change of solvents. The n,π* triplet seems to be the reactive species responsible for the formation of the β,γ-isomer.

It is quite likely that the solvent dependence of the quantum yield can also be explained by assuming the crossing of two closely separated energy levels with different reactivities. The plausibility of this speculation was further examined by studying the electronic absorption spectra. The UV-spectra of the *cis*-isomer II are shown in Fig. 3. The strong absorption band at the shorter wavelength is assigned to π,π* absorption in analogy with the case of α,β-unsaturated esters.[3)] We see that a week absorption band is superimposed on the tail of the π,π* absorption band in the cyclo-

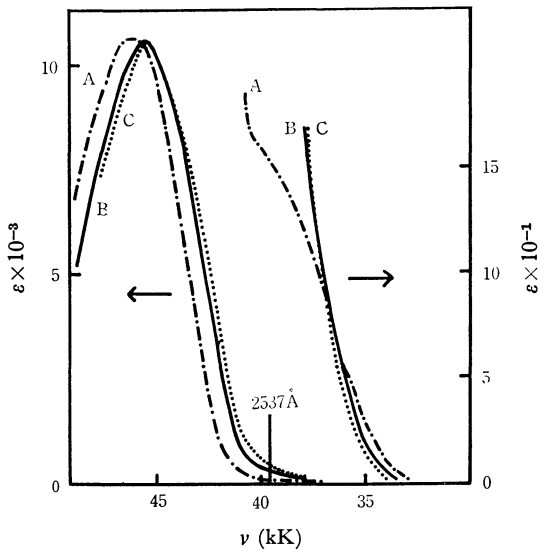

Fig. 3. UV absorption spectra of the *cis*-isomer II. A, in cyclohexane,; B in acetonitrile; C, in methanol.

hexane solution. On closer examination it can be seen to be associated with a series of broad vibrational structures frequently observed with n,π^* absorptions. The weak absorption band observed in cyclohexane is concealed under the red-shifted π,π^* absorption in acetonitrile and methanol. Hence, the weak absorption band is suggested to be either unaffected or slightly blue-shifted in polar solvents. We thus assigned the weak absorption band to the n,π^* transition of the *cis*-isomer II. As far as the singlet states of the *cis*-isomer II are concerned, the energy level of the lowest n,π^* excited state is concluded to be very close to that of the lowest π,π^* excited state in both acetonitrile and methanol. The 2537 Å exciting light is situated in the middle of the region where the n,π^* transition is superposed on the tail of the π,π^* transition (Fig. 3). Hence, the ratio in population between the n,π^* singlet and the π,π^* singlet species obtained in the excitation should vary with solvent. This might be why the relative yield of the β,γ-isomer considerably varies with the solvent while that of the *trans*-isomer remains the same (Table 3).

It should be noted, however, that the solvent effect on the yield of Norrish type II photolysis of valerophenone has been explained as being due to stabilization of the hydroxyl biradical intermediate which is capable of making a hydrogen bonding with the polar solvent molecules.[11] An *enol* type intermediate is suggested to be involved in the isomerization from II to III. The solvent effect on the secondary processes after the photoexcitation might be partly responsible for the variation in the relative yield of the β,γ-isomer with the change of solvent.

Dependence of the Relative Quantum Yields on the Wavelength of the Exciting Light. If the solvent effect on the relative yield of the β,γ-isomer is due to the change in population ratio between the n,π^* singlet and the π,π^* singlet just after excitation, the yield should show an appreciable variation with the wavelength of the exciting light, when examined in the absorption edge of the sample in a given solvent. The experiment was carried out under two different irradiation conditions: (a) with 2537 Å light from a low-pressure mercury lamp and (b) with a xenon short arc lamp filtered through carbon tetrachloride layer of 15 mm thickness, the incident lights being limited to be those with wavelength longer than 260 mμ. The results are summarized in Table 4. In cyclohexane, the ratio of the relative yield of the β,γ-isomer to that of the *trans*-isomer under conditions (b) is reduced to 35% of that under conditions (a). The isomer ratio (β,γ-isomer/*trans*-isomer) in acetonitrile under the same conditions varies only by 20%. The n,π^* absorption band of the *cis*-isomer in cyclohexane appears as a clear shoulder superimposed on the tail of the π,π^* absorption band (Fig. 3). Hence the longer the wavelength of the excitation light, the larger the population ratio between the $S_1(n,\pi^*)$ and $S_2(\pi,\pi^*)$. Thus, the rapid decrease in the isomer ratio in cyclohexane is nicely correlated to the increase in the relative population of the first n,π^* singlet state. Analogously, the small wavelength dependence of the isomer ratio in the acetonitrile solution is suggested to correspond to the fact that the n,π^* absorption band is located in almost the same wavelength region where the π,π^* absorption is observed. It is thus difficult to enhance selectively the relative population of the n,π^* excited species only by selection of the wavelength of exciting light.

Table 4. Dependence of the ratio of the relative quantum yields (III/I) on the wavelength of the exciting light (λ)[a]

Solvent	$\lambda>260$ mμ[b]	$\lambda=254$ mμ
C_6H_{12}	0.059	0.17
CH_3CN	0.33	0.41

a) The relative yield was estimated from the vpc chart by assuming that the molar sensitivities of the two isomers are the same.
b) Obtained by the use of Xe lamp in combination with CCl_4.

Proposal of a Reaction Scheme. As regards solvent effects and wavelength effects on the relative quantum yields of the β,γ- and the *trans*-isomer, we might suggest that the former mainly comes from the π,π^* singlet state and the latter from the n,π^* singlet state. The relative heights of the n,π^* and π,π^* singlet energy levels can be determined from the UV absorption spectra of the *cis*-isomer (Fig. 3). We have no data for the location of the triplet energy levels. However, the following theoretical consideration can be given.

On spectroscopic evidences, Marsh *et al.* have shown that the energy of n,π^* triplet state of steroidal enones is very close to that of the π,π^* triplet state.[12] This may be also true for other α,β-unsaturated ketones in general. In the case of esters and lactones, the conjugation between the carbonyl group and the adjacent oxygen atom raises the n,π^* state considerably and leaves the π,π^* state almost unchanged in comparison with those of the corresponding ketones or aldehydes.[13] The lowest n,π^* triplet state of an ester or a lactone is thus expected to be located much above the lowest π,π^* triplet state so that the change of solvents can not reverse the relative heights of these energy levels. A schematic energy-level diagram for the relevant states of the *cis*-isomer is shown in Fig. 4.

Intramolecular hydrogen abstraction is generally considered to take place at the n,π^* excited state. In the present experiment, however, $S_1(n,\pi^*)$ species is considered to hardly contribute to the hydrogen abstraction reaction since the relative yield of the β,γ-isomer decreases on irradiation of the *cis*-isomer in cyclohexane with the longer wavelength light which predominantly induces n,π^* transition. Formation of the β,γ-isomer should be correlated to the population of $S_2(\pi,\pi^*)$ species, since the relative quantum yield on the irradiation with 2537 Å light decreases in cyclohexane, where an appreciable blue shift of the π,π^* absorption band

11) P. J. Wagner, *J. Amer. Chem. Soc.*, **89**, 5898 (1967).

12) G. Marsh, D. R. Kearns, and K. Schaffner, *ibid.*, **93**, 3129 (1971).

13) a) H. H. Jaffe and M. Orchin, "Theory and Application of Ultraviolet Spectroscopy," John Wiley & Sons, Inc., New York, N.Y. (1962), p. 179. b) R. Simonaitio and J. N. Pitts, Jr., *J. Amer. Chem. Soc.*, **90**, 1389 (1968).

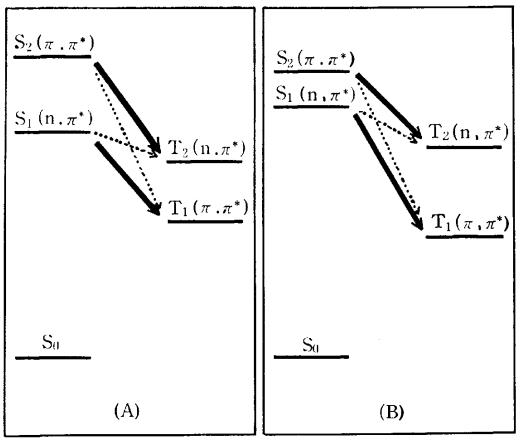

Fig. 4. Schematic energy level diagram for the relevant states of the *cis*-isomer: A (in cyclohexane) and B (in acetonitrile). The solid and dotted arrows represent the intersystem crossing manifolds with the higher- and the lower-efficiency, respectively.

is observed. The quantum yield of the *cis-trans* isomerization, in turn, should be related to the population of $S_1(n,\pi^*)$ species. However, it is rather unusual that the *cis-trans* isomerization takes place directly at the $S_1(n,\pi^*)$ state, since this type of reaction is known to proceed *via* π,π^* state. Taking into account the fact that *cis-trans* isomerization is sensitized by the triplet sensitizers, and that the lowest triplet state is estimated to be a π,π^* state, it is more likely that *cis-trans* isomerization takes place at $T_1(\pi,\pi^*)$ state which mainly comes from $S_1(n,\pi^*)$ state even in direct excitation. The results on the formation of the β,γ-isomer, are well accounted for if we consider that the hydrogen abstraction reaction takes place at $T_2(n,\pi^*)$ state which mainly comes from $S_2(\pi,\pi^*)$ state. This is in accordance with the general principle on the reactive species in the photochemical hydrogen abstraction reactions.

On the basis of theoretical arguments and experimental observations on the radiation yields of ketones, El-Sayed proposed a selection rule for the intersystem crossing at the excited states: the intersystem crossing between the levels of different nature [$S(n,\pi^*)\rightarrow T(\pi,\pi^*)$ and $S(\pi,\pi^*)\rightarrow T(n,\pi^*)$] should be faster than those between the levels of the same nature [$S(\pi,\pi^*)\rightarrow T(\pi,\pi^*)$ and $S(n,\pi^*)\rightarrow T(n,\pi^*)$] by a factor of 10^3.[14] If this selection rule holds also in the case of the photoexcited states of II, the routes for photoisomerization can be reasonably accounted for as shown in Fig. 4, where the intersystem crossing with higher efficiency is denoted by a broad solid arrow, and that with lower efficiency by a dotted arrow.

In order to confirm the reaction scheme, we made several attempts to quench the excited states in the photoisomerization of II on direct excitation. However, no positive results were obtained. This is understandable from the fact that the lifetimes of the concerned states are expected to be extremely short in the present case. We can not completely disregard the contribution of singlet species to isomerization on direct excitation at this stage. The present model might be adopted as reasonable means for explaining the characteristics of the photoisomerization of α,β-unsaturated γ-lactones.

14) a) M. A. El-Sayed, *Accounts Chem. Res.*, **1**, 8 (1968). b) S. K. Lower and M. A. El-Sayed, *Chem. Rev.*, **66**, 199 (1966).

Experimental

Instrumental Analysis. The NMR spectra were measured with a Varian Model A-60 analytical spectrometer. The IR, UV, and mass spectra were recorded on a JASCO Model DS-301 IR spectrometer, a Shimadzu Model UV-200 spectrophotometer, and JEOL Model JMS-01SG mass spectrometer, respectively. Vapor phase gas-chromatography for qualitative analysis was carried out by the use of a Shimadzu Model GC-2C chromatograph equipped with a thermal conductivity detector. Analysis was carried out by the use of a column (2.25 m × 3 mm) with packings made by coating polyphenyl ether 5-rings (10%) on Chamelite CS (DMCS-treated Celite 545) support. The column temperature was kept to 175 °C. The preparative vpc was also carried out under the same conditions. The quantitative analyses were carried out at either 120 or 130 °C by the use of a Shimadzu Model GC-3BF gas chromatograph equipped with a flame ionization detector.

Preparation of trans-*3-Ethylidene-4,5-dihydro-2(3H)-furanone (I).* Preparation of I was carried out by a modification of the method reported by Zimmer and Rothe.[7] Acetaldehyde (18 g) and γ-butyrolactone (70 g) in benzene (500 ml) were maintained at 5 °C in the presence of powdered sodium ethoxide for 1.5 hr, and the reaction was completed by heating the solution up to 45 °C for 15 min. Dilute sulfuric acid (10%, 360 ml) was added to the solution, and the organic layer was separated from the aqueous phase. The aqueous phase was extracted with 350 ml of benzene, and the extract was combined with the previously separated organic layer. The benzene solution was successively washed with water, aqueous sodium hydroxide and finally with water. Benzene was removed by distillation and the succeeding distillate was collected (up to 114 °C/6 mmHg). The same procedure was repeated and crude products were combined (21.7 g), which yielded 6.2 g of the final product (72.5—76.0 °C/5 mmHg) after fractional distillation. In addition to the main product I, several other byproducts were involved in the collected distillate. Preparative vpc was then applied to obtain I, which was still accompanied by small amounts of two other impurities difficult to separate. An attempt was also made to prepare I according to Pinder's method[15] for the preparation of the benzylidene analogue of I, but the yield was too small for the method to be adopted.

Preparation of cis-*3-Ethylidene-4,5-dihydro-2(3H)-furanone (II).* The *trans*-isomer I (1.8 g), together with small amounts of accompanying impurities were dissolved in 100 ml of benzene. Acetone (10 g) was added as a sensitizer, and the solution was internally irradiated with a high-pressure mercury lamp (Riko-Sha UVL-700P) equipped with a pyrex water-jacket in nitrogen atmosphere for 21 hr. According to the vpc analysis, the *cis*-isomer II was the sole product. The *cis*-isomer was isolated by fractional distillation followed by preparative vpc. Yield, 325 mg; m/e=112 (M^+). Found: C, 64.18; H, 7.28%. Calcd for $C_6H_8O_2$: C, 64.27; H, 7.19%.

Photosensitized Reaction of cis-*3-Ethylidenedihydro-2(3H)-furanone (II).* *(A) Preparation of the Authentic Sample of* trans-*Isomer (I):* The *cis*-isomer II (179 mg) and benzophenone (5 mg) were dissolved in 1 ml of benzene. The

15) A. R. Pinder, *J. Chem. Soc.*, **1952**, 2236.

solution was placed in a pyrex tube which was sealed after evacuation under nitrogen atmosphere. The sample was externally irradiated with a high-pressure mercury lamp (Toshiba H-400P) for 22 hr at room temperature. The NMR and vpc of the irradiated sample indicated that the *trans*-isomer I was formed together with a small amount of III. Preparative vpc was applied to isolate I. Yield, 39 mg; $m/e=112$ (M^+); Found: C, 64.05; H, 7.37%. Calcd for $C_6H_8O_2$: C, 64.27; H, 7.19%.

(B) Determination of the Isomer Ratio between I and II at the Photostationary State: Acetone was purified by treating with potassium permanganate followed by fractional distillation. Acetophenone (reagent grade) was also purified by fractional distillation under reduced pressure just before use. *p*-Methoxyacetophenone was recrystallized from *n*-hexane–benzene mixed solvent (mp 39.1—40.1 °C). Benzophenone was recrystallized from methanol (mp 51.2—51.5 °C). Each sample tube was sealed after flushing with nitrogen and irradiated with a high-pressure mercury lamp (Riko-Sha UVL-700P) equipped with a pyrex glass filter. The reaction was carried out at 20.2 °C, and the products were analyzed by vpc at 130 °C.

Direct Irradiation of cis-*Ethylidene-4,5-dihydro-2(3H)-furanone II.* *(A) Preparation of β,γ-Unsaturated 3-Vinyl-4,5-dihydro-2(3H)-furanone III*: The *cis*-isomer II (73 mg) was dissolved in 0.5 ml of acetonitrile, and the solution was irradiated in a quartz tube under exactly the same conditions, as for the preparation of I, except for the absence of the sensitizer. The main products were isomers I and III, the latter being isolated by distillation under reduced pressure followed by vpc in a preparative scale. Yield, 20 mg; $m/e=112$ (M^+); Found: C, 63.89; H, 7.28%. Calcd for $C_6H_8O_2$: C, 64.27; H, 7.19%.

(B) Variation of UV Spectra during Irradiation: Acetonitrile solution of II (3×10^{-3}M, 150 ml) was internally irradiated with a low-pressure mercury lamp (Riko-Sha UVL-303Q) under nitrogen atmosphere at room temperature. Four ml of the sample was periodically extracted from the irradiated solution, and a quarter of the sample was used for measurement of the UV spectra after being diluted with acetonitrile to one hundredth of the initial concentration. The remaining 3 ml of the sample was concentrated to approximately one twentieth in volume, and was analyzed by vpc. After irradiation for 3 hr most of the acetonitrile was removed by distillation under reduced pressure and the residue was analyzed by NMR spectroscopy. No absorption was observed due to the compound other than the three isomers.

(C) Irradiation in D_2O-Acetonitrile System: Approximately 60 mg of the *cis*-isomer was dissolved in a mixed solvent consisting of D_2O (0.8 ml) and acetonitrile (0.2 ml). A quartz tube containing the solution was sealed under reduced pressure, after the remaining oxygen had been replaced with purified nitrogen. The sample was externally irradiated for 12 hr with a high-pressure mercury lamp. After irradiation was completed, the products were extracted into benzene (20 ml), and successively distilled under reduced pressure. The NMR spectra in deuterochloroform indicated the isomers I, II, and III to be 24, 9, and 67%, respectively.

Solvent Effect on the Quantum Yield of the Isomers on the Irradiation of II with 2537 Å Light. The *cis*-isomer was purified by vpc on a preparative scale and successive distillation under reduced pressure (2 mmHg) so that it gave a single peak in the vpc. The purified *cis*-isomer was dissolved in solvents of spectrograde purity. Eight ml of each solution was pippetted into a quartz tube (15 mm inner diameter), fused to a pyrex tubing of the same diameter with a graded seal. The air inside the sample tube was purged by a stream of purified nitrogen, and the tube was sealed under reduced pressure (2 mmHg) after it was cooled by being dipped into dry ice–methanol mixture. In the case of the acetonitrile and methanol solutions, the samples were also prepared by the use of a vacuum line (less than 10^{-4} mmHg) for degassing. Good agreement was observed with the pair of samples prepared by the above two methods. Each sample tube was set in a cylindrical glass holder, mounted on a turn table with a radius of 12 cm. A square window (10×30 mm) on the wall of the holder allowed more than 99% of the incident 2537 Å light to be absorbed in the sample at the concentration of the experiment. At the center of the turn table was placed a low-pressure mercury lamp (Riko-Sha UVL-303Q), surrounded by a layer of aqueous 2,7-dimethyl-3,6-diazocyclohepta-1,6-diene perchlorate filter solution (175 mg/l)[16] of approximately 2 cm thickness. Under such conditions, the sample absorbs only 2537 Å light from the low-pressure mercury lamp since no absorption band is observed for the *cis*-isomer at the wavelength longer than 300 mμ. The characteristic of each sample tube was calibrated in advance by monitoring the change in the potassium ferrioxalate actinometer solution in each tube when it was irradiated by the light filtered through an aqueous solution containing $NiSO_4\cdot xH_2O$ (450 g), $CoSO_4\cdot 6H_2O$ (150 g), and 2,7-dimethyl-3,6-diazocyclohepta-1,6-diene perchlorate (175 mg).[17] The relative quantum yield of each isomer was determined after irradiation of the sample for 1,5 hr. The reaction was carried out at 20.0 °C by immersing the whole irradiation unit in a thermostat bath. The content of the sample tube was concentrated, under nitrogen stream, down to approximately one tenth of the initial volume and the residue was analyzed by vpc in the presence of β-methylnaphthalene as an internal standard. On irradiation of the cyclohexane solution, small amounts of a by-product other than the three isomers were also detected. No further attempt was made to identify the by-product since the yield was extremely small.

Determination of the Relative Quantum Yield on Irradiation of Light with Wavelength longer than 260 mμ. Either acetonitrile solution (2.2×10^{-2}M) or cyclohexane solution (2.18×10^{-2}M) was placed in a cylindrical cell, ($25\phi\times10$ mm) which was sealed under reduced pressure (2 mmHg) after being flushed with nitrogen. The light beam from a xenon lamp (Ushio UXL-500D) was filtered through a layer of carbon tetrachloride (15 mm), and was irradiated on the optically flat surface of the cylindrical cell. Irradiation was continued for 4.5 hr at a constant temperature (19—20 °C), and the product was analyzed by vpc.

16) G. Schwarzenbach and K. Lutz, *Helv. Chim. Acta*, **23**, 1139 (1952).

17) B. M. Monroe and S. A. Weiner, *J. Amer. Chem. Soc.*, **91**, 450 (1969).

Syntheses of Organic Phosphates. III. Syntheses and Properties of 2-Amino-3-pyridylmethyl and 2-Chloro-3-pyridylmethyl Phosphates[1]

Yukito MURAKAMI, Junzo SUNAMOTO, Seiichiro KINUWAKI, and Haruomi HONDA

Department of Organic Synthesis, Faculty of Engineering, Kyushu University, Hakozaki, Higashi-ku, Fukuoka 812

(Received December 25, 1972)

Two substituted pyridylmethyl phosphates, 2-amino-3-pyridylmethyl (I) and 2-chloro-3-pyridylmethyl phosphates (II), were prepared and their properties were discussed. Acid dissociation constants and NMR data suggested that the neutral species of I exists in the zwitterion form consisting of the protonated amino group and the monoanionic phosphate moiety, while that of II in the dihydrogen phosphate form analogous to the simple alkyl phosphates. In addition, physical properties of 2-amino-3-pyridylmethanol and 2-chloro-3-pyridylmethanol, which are respectively precursors of phosphates I and II, as well as 1,2-dihydro-2-oxo-3-hydroxymethylpyridine, were examined by IR and NMR measurements.

In a series of our studies on the chemistry of organic phosphates, some phosphates, which carry a heteroaromatic moiety, have been prepared.[2-5] Their hydrolytic behaviors have been investigated with particular attention to the intramolecular catalysis brought about by the proximity participation of a functional group.[4-7] In order to search for further evidence of the proximity catalysis in hydrolysis, two phosphates, 2-amino-3-pyridylmethyl (I) and 2-chloro-3-pyridylmethyl phosphates (II), were synthesized in this work.

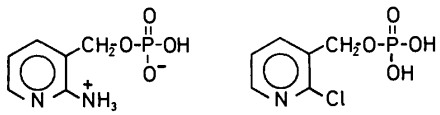

I II

2-Chloro-3-pyridylmethanol (XI) which is the precursor of II was also found to be a new material. On the other hand, Cislak has already prepared 2-amino-3-pyridylmethanol (VII), the precursor of I, by a method different from the present one.[8] Their physical properties were examined in this work.

Pyridylmethanols. Both pyridylmethanols, VII and XI, were prepared from the same starting material, 2-aminonicotinic acid (III),[9] according to the processes shown in Scheme 1. The synthesis of 1,2-dihydro-2-oxo-3-hydroxymethylpyridine (IX) was also carried out.

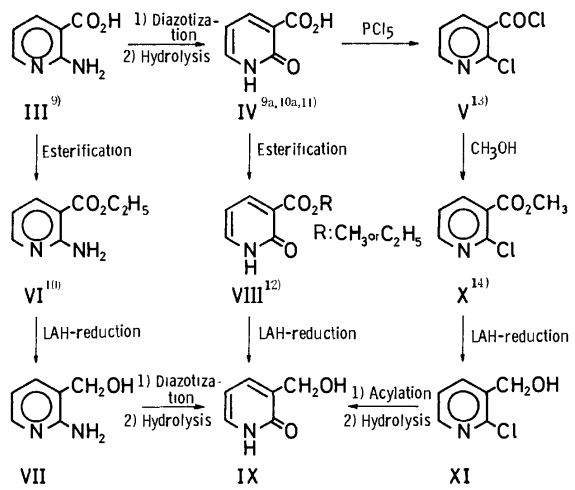

Scheme 1.

The following tautomerism would be considered for 2-aminopyridines.[15] In the case of 2-amino-3-pyridylmethanol, however, we confirmed the absence of such a tautomerism on the basis that the correlation between the symmetric and asymmetric N–H stretching vibrational modes for this alcohol is in good agreement with the Bellamy-Williams relationship for the aromatic primary amines.[16] The alcoholic hydroxyl proton only

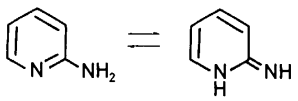

1) Contribution No. 301 from this Department.
2) Y. Murakami, M. Takagi, and H. Nishi, This Bulletin, **39**, 1197 (1966).
3) Y. Murakami, J. Sunamoto, H. Sadamori, H. Kondo, and M. Takagi, *ibid.*, **43**, 2518 (1970).
4) Y. Murakami, J. Sunamoto, and H. Ishizu, *ibid.*, **45**, 590 (1972).
5) Y. Murakami, J. Sunamoto, and N. Kanamoto, *ibid.*, **46**, 871 (1973).
6) Y. Murakami and M. Takagi, *J. Amer. Chem. Soc.*, **91**, 5130 (1969).
7) Y. Murakami and J. Sunamoto, This Bulletin, **44**, 1939 (1971).
8) F. E. Cislak, U. S. 2807619 (Sept., 1957).
9) a) F. G. Mann and J. A. Reid, *J. Chem. Soc.*, **1952**, 2057; b) A. Phillips, *Ber.*, **27**, 839 (1894).
10) a) A. Dornow and P. Karlson, *Ber.*, **73**, 542 (1940); b) H. H. Fox, *J. Org. Chem.*, **17**, 547 (1952).
11) a) F. G. Mann and J. H. Jurnbull, *J. Chem. Soc.*, **1951**, 761; b) S. Carboni, *Gazz. Chim. Ital.*, **83**, 637 (1953); *Chem. Abstr.*, **49**, 1039 (1955).
12) For the methyl ester, A. Kirpal, *Monatsh. Chem.*, **27**, 371 (1906); for the ethyl ester, A. Dornow, *Ber.*, **73**, 153 (1940).
13) Mp 40—41 °C. This compound was converted by hydrolysis to 2-chloronicotinic acid; mp 192—193 °C. The acid has been prepared by Seide; O. Seide, *Ber.*, **57**, 1802 (1924).
14) S. Sugasawa and Y. Ban, *J. Pharm. Soc. Jap.*, **72**, 1336 (1952).
15) A. Albert, R. Goldacre, and J. Phillips, *J. Chem. Soc.*, **1948**, 2240; the ionic strength is not certain.
16) L. J. Bellamy and R. L. Williams, *Spectrochim. Acta*, **9**, 341 (1957).

Table 1. NMR data of 2-substituted 3-pyridylmethanols[a)]

Substituted 3-pyridyl-methanol	Solvent	Chemical shift, ppm					Coupling constant, Hz			
		CH_2	H-4	H-5	H-6	Others	$J_{4,5}$	$J_{4,6}$	$J_{5,6}$	J_{CH_2-OH}
2-Chloro-	Acetone[b)]	4.70, s	8.00, q	7.40, q	8.30, q	–OH; 4.67, br.s	4.5	2.0	7.5	—
	DMSO[c)]	4.57, d	7.95	7.43	8.19	–OH; 5.49, t	4.5	2.0	7.5	5.5
2-Amino-	Acetone[d)]	4.58, s	7.40, sx	6.55, q	7.90, q	$-NH_2$ / $-OH$); 4.99, br.s	5.0	2.0	7.5	—
	DMSO[c)]	4.34	8.18	6.50	7.81	($-NH_2$; 3.91, br.s / $-OH$; 5.04, br.s	5.0	2.0	7.0	—
1,2-Dihydro-2-oxo-	DMSO[c)]	4.28, s	7.22, m	6.17 t	7.38 m	–OH; 4.91, br.s	6.5	1.5	6.5	—

a) All the spectra were referred to TMS as an internal reference at ordinary temperature. Multiplicity: s=singlet, br. s=broad singlet, d=doublet, t=triplet, q=quartet, sx=sextet, m=multiplet.
b) 12 wt% in acetone.
c) 2.8 mol% in dimethyl sulfoxide.
d) 10 wt% in acetone.

gave a broad singlet NMR signal even in dimethyl sulfoxide. Apparently, the hydrogen bonding of the hydroxyl proton with the solvent must be disturbed by a strong intramolecular hydrogen bonding involving both hydroxyl and amino groups. This interaction may give rise to a slow hydrogen exchange, causing NMR line-broadening. The result is consistent with configuration XII. The appropriate data for NMR chemical shifts are summarized in Table 1.

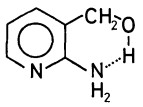

XII

Albert *et al.* reported the pK_a-value of the protonated 2-aminopyridine as 6.86 at 20 °C.[15] The pK_a value of the protonated 2-amino-3-pyridylmethanol was determined in this work to be 6.35 at 25 °C (μ= 0.10 with potassium chloride). Although the hydroxymethyl group is an electron-withdrawing substituent ($\sigma^*=+0.555$),[17] the decrease in pK_a upon substitution with the group ($\Delta pK_a=0.51$) seems to be too large to be attributed wholly to its electronic nature: pK_a, 9.94 for phenol, 9.92 for 2-hydroxymethylphenol, 9.83 for 3-hydroxymethylphenol, and 9.82 for 4-hydroxymethylphenol at 25 °C;[18] 3.99 for benzoic acid and 3.84 for 2-hydroxymethylbenzoic acid at 20 °C.[19] Consequently, the intramolecular hydrogen bonding, XII, may take place and result in the enhanced dissociation of proton from the protonated 2-amino group.

For 2-chloro-3-pyridylmethanol, the NMR hydroxyl proton resonance in dimethyl sulfoxide was well resolved into a triplet through coupling with the α-methylene. The strong hydrogen bonding of the hydroxyl group with dimethyl sulfoxide seems to be responsible for the inhibition of the hydroxyl proton exchange. As a result, pyridylmethanol does not involve an intramolecular hydrogen bonding strong enough to reject the interaction with dimethyl sulfoxide.

1,2-Dihydro-2-oxo-3-hydroxymethylpyridine (IX) showed a broad hydroxyl proton resonance signal in its NMR spectrum, indicating the existence of an intramolecular hydrogen bonding (XIII).

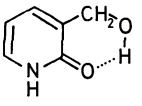

XIII

Pyridylmethyl Phosphates. Both phosphates, I and II, were prepared from the corresponding pyridylmethanols according to the established procedures.[2-5]

For simple alkyl phosphate monoesters, three species have to be considered, in general, where $pK_{H_2A}=1$—2 and $pK_{HA}=5$—7. Meanwhile, an additional ionic species must be considered for pyridylalkyl phosphates as shown typically for 3-pyridylmethyl phosphate in Scheme 2.[2] The second acid dissociation constant

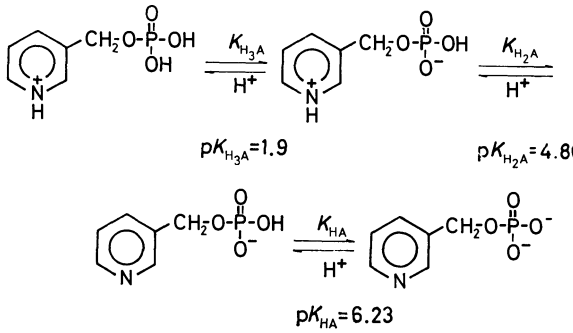

Scheme 2.

found for 2-chloro-3-pyridylmethyl phosphate (pK_{H_2A}= 2, Table 2) is considerably smaller than those for the other pyridylalkyl phosphates ($pK_{H_2A}=4$—5).[2-5] Brown and McDaniel obtained the pK_a value of 0.72 for 2-chloropyridine in an aqueous media at 25 °C.[20] The phosphorylated hydroxymethyl group acts as an electron-withdrawing group to some extent.[2] Consequently, the pK_a-value for dissociation of a pyridinium proton in 2-chloro-3-pyridylmethyl phosphate should

17) R. W. Taft, Jr., "Steric Effects in Organic Chemistry," ed. by M. S. Newman, John Wiley & Sons, Inc., New York, N.Y. (1956), Chapt. 13.
18) G. R. Sprengling and C. W. Lewis, *J. Amer. Chem. Soc.*, **71**, 2624 (1949).
19) M. M. Delépine and M. J. Tironflet, *C. R. Acad. Sci. Paris*, **236**, 1426 (1953).
20) H. C. Brown and D. H. McDaniel, *J. Amer. Chem. Soc.*, **77**, 3753 (1955).

Table 2. Acid dissociation constants for the phosphates at μ=0.10 (KCl or KNO_3)

Phosphate	pK_{H_2A}		pK_{HA}	
	25 °C	80 °C	25 °C	80 °C
2-Chloro-3-pyridylmethyl	2.17	1.8[a]	5.97	6.3[a]
2-Amino-3-pyridylmethyl	5.42	5.11[b]	7.03	7.40[b]
3-Pyridylmethyl	4.86[c]	4.43[d]	6.23[c]	6.48[d]

a) Quoted from Ref. 21.
b) At 70.0 °C.
c) Quoted from Ref. 2.
d) Quoted from Ref. 6.

be less than that for 2-chloropyridine. If the pK_{H_2A} refers to the dissociation of the first phosphate proton, a little larger value (2.2), relative to that of 3-pyridylmethyl phosphate (1.9), can be attributed to trapping of the phosphate proton by the chlorine atom through an intramolecular hydrogen bonding.[21] Therefore, the plausible acid dissociation processes for the phosphate are reasonably presented in Scheme 3. The neutral species of 2-chloro-3-pyridylmethyl phosphate does not exist in the zwitterion form but in the dihydrogen phosphate. This characteristic structural feature was closely reflected on its hydrolytic behavior.[21]

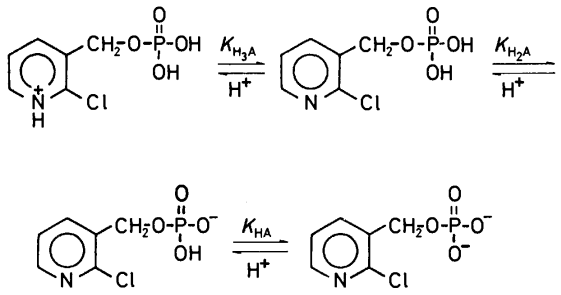

Scheme 3.

Since 2-amino-3-pyridylmethyl phosphate is tetrabasic, the acid dissociation processes become somewhat complex. The pK_a value of the protonated 2-amino group can be reduced by the phosphorylated 3-hydroxymethyl group playing as an electron-withdrawing substituent, while the acid dissociation of the last-dissociating proton on the phosphate moiety is somewhat depressed by the substitution of an electron-donating 2-amino group. The most plausible acid dissociation processes for the phosphate are reasonably given in Scheme 4.

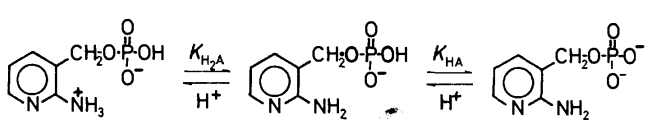

Scheme 4.

For both phosphates of the present study, the dissociation of the pyridinium proton seems to be much enhanced by the presence of an electron-withdrawing group, protonated amino group or chlorine, and the reliable pK_a value for such dissociation was not evaluated under present experimental conditions.

21) Y. Murakami, J. Sunamoto, and N. Kanamoto, This Bulletin, **46**, 1730 (1973).

Experimental

2-Amino-3-pyridylmethanol (VII). A mixture of 16.3 g of lithium aluminum hydride (LAH) and 1 l of dry ether was stirred for 20 min at room temperature. The reaction flask was assembled with a Soxhlet extraction apparatus equipped with an extraction thimble in which 30.0 g of ethyl 2-aminonicotinate was placed. With care for vigorous reaction, the ether–LAH mixture was gently refluxed. After most of the ester was dissolved in ether, an additional 29.3 g sample of the ester was placed in the thimble. Upon refluxing for about 60 hr, the reaction mixture was cooled down to room temperature. After decomposing the excess hydride with water, the ether layer was separated and concentrated to crystallize the crude alcohol (22.9 g). From the residue containing metal hydroxide, 10.5 g of the alcohol was recovered. Both crops of the crude alcohol were combined and recrystallized from ether: colorless leaflet, mp 70 °C. Found: C, 58.11; H, 6.44; N, 22.54%. Calcd for $C_6H_8N_2O$: C, 58.04; H, 6.50; N, 22.57%. UV (methanol): 235.5 (log ε 3.97) and 295.5 nm (log ε 3.66). IR (KBr disk): ν_{NH}, 3410, 3335; δ_{NH}, 1650; ν_{ring}, 1605, 1575; ν_{C-O}, 1036, 1006; δ_{CH}, 791 and 756 cm^{-1}. NMR data are given in Table 1.

2-Chloro-3-pyridylmethanol (XI). A 27.1 g sample of methyl 2-chloronicotinate was treated with LAH in an established manner; yield 11 g (48%), bp 105—112 °C/0.20 mmHg. After being left overnight at room temperature, the distillate was solidified and recrystallized from chloroform: white needles, mp 63—64 °C. Found: C, 50.46; H, 4.24; N, 9.86%. Calcd for C_6H_6NOCl: C, 50.20; H, 4.21; N, 9.76%. UV (methanol): 265.5 nm (log ε 3.62). IR (KBr disk): ν_{OH}, 3280; ν_{ring}, 1588, 1571; ν_{C-O}, 1054, 1044; δ_{CH}, 817, 796, 734, and 718 cm^{-1}. NMR data are given in Table 1.

1,2-Dihydro-2-oxo-3-hydroxymethylpyridine (IX). (i) By the LAH reduction of ethyl 1,2-dihydro-2-oxonicotinate (1.0 g) according to the general procedure, the corresponding alcohol was obtained in poor yield (63 mg); mp 134 °C.

(ii) A solution containing 28.4 g of 2-amino-3-pyridylmethanol in 253 ml of 10% sulfuric acid was poured onto 950 ml of water warmed at 60—70 °C. At the same temperature, 230 ml aqueous solution of sodium nitrite (22.15 g) was added dropwise in 1 hr. After addition of aqueous nitrite was completed, the mixture was continuously stirred at the same temperature for additional 1 hr. The acidic solution was neutralized with anhydrous sodium carbonate and concentrated to 200 ml, to which double volume of ethyl acetate was added. The precipitated inorganic salt was removed. This procedure was repeated until inorganic salt was not detected any longer. Needle-like crystals were recovered from the cooled ethyl acetate solution, and recrystallized from ethanol: yield 19.9 g (70%), mp 137.5—138.4 °C. Found: C, 57.63; H, 5.78; N, 11.11%. Calcd for $C_6H_7O_2N$: C, 57.59; H, 5.64; N, 11.19%. UV (methanol): 230 (log ε 3.79) and 299 nm (log ε 3.77). IR (KBr disk): ν_{NH}, 3400; $\nu_{C=O}$, 1647; ν_{ring}, 1620, 1567; ν_{C-O}, 1040; δ_{CH}, 765 cm^{-1}. NMR data are listed in Table 1.

(iii) The pyridone IX was also obtained through acylation of the alcohol XI, followed by hydrolysis with diluted hydrochloric acid in the presence of sodium acetate; very poor yield.

2-Amino-3-pyridylmethyl Phosphate (I) 2-Amino-3-pyridylmethanol (VII) (1.0 g) was mixed with pyrophosphoric

acid, which was freshly prepared by brief heating of 85% orthophosphoric acid (6.5 g) and phosphorus pentoxide (5.0 g), at 50 °C under protection from moisture. The reaction mixture was heated at 70—80 °C for 20 hr, diluted with 20 ml of water, and heated again in order to hydrolyze any coexisting polyphosphate. The resulting hydrolyzate was poured onto 250 ml of acetone and allowed to stand overnight in a refrigerator. White precipitates were separated and washed sufficiently with acetone; yield 1.18 g. Further recrystallization from water gave white crystals; neutralization equivalence, 102.62 (calcd. 102.06). Found: C, 34.92; H, 4.84; N, 13.42%. Calcd for $C_6H_9O_4N_2P$: C, 35.31; H, 4.44; N, 13.72%. IR (KBr disk): $\nu^{+}_{NH_3}$, 3300, 3130, 2600, 2400, 2020, 1980; $\delta^{+}_{NH_3}$, 1685, 1646; $\nu_{P=O}$, 1247, 1150, 1130; $\nu_{P-O-C(alk)}$, 1020 and 946 cm^{-1}. UV (10^{-4}M, water): 232.5 (ε 8080) and 303.0 nm (ε 6840).

2-Chloro-3-pyridylmethyl Phosphate (II). A 1.44 g sample of 2-chloro-3-pyridylmethanol (XI) was phosphorylated with 12.7 g of pyrophosphoric acid at 80—100 °C for 4 hr according to the method similar to that used for 2-amino-3-pyridylmethanol. The resulting mixture was neutralized with concentrated aqueous ammonia and evaporated to dryness. The residue was extracted twice with a 100 ml portion of hot ethanol. The extracts were evaporated to 10 ml and white crystals (the diammonium salt) were recovered; yield 440 mg. Found: P, 12.1%. Calcd for $C_6H_{13}O_4N_3PCl$: P, 12.02%. The ammonium salt of the phosphate was converted to the free acid form with the use of cation exchange resin, Dowex-50W×8; neutralization equivalence, 108.90 (calcd. 111.77). Found: C, 32.22; H, 3.31; N, 6.12%. Calcd for $C_6H_7NO_4PCl$: C, 32.24; H, 3.16; N, 6.27%. UV (10^{-4}M, water): 266 (ε 3140) and 272 nm (ε 2840). IR (KBr disk): ν_{OH}, ~3400; $\nu_{P=O}$, 1287, 1230—1195 (broad), 1110; $\nu_{P-O-C(alk)}$, 1054 and 1010—970 cm^{-1} (broad). NMR (0.71M, dimethyl sulfoxide-d_6, TMS as an internal reference): δ 5.03 (2H, d, $J_{CH_2-^{31}P}$=8.0 Hz, $-C\underline{H}_2-$), 6.61 (2H, s, $-O\underline{H}$), 7.54 (1H, q, J_{4-5}=7.5 Hz and J_{5-6}=5.0 Hz, H-5), 8.02 (1H, q, J_{4-6}=2.0 Hz, H-4), and 8.46 (1H, q, H-6).

Acid Dissociation Constants. Acid dissociation constants of the pyridylmethyl phosphates and the pyridylmethanols were measured by potentiometric titrations of the corresponding aqueous solutions (2.0×10^{-3}M) with standard base or acid at an ionic strength of 0.10 (KCl or KNO_3). All the measurements were checked by duplicate runs. The procedures for measurements were essentially the same as those adopted in the previous studies.[2-5] A set of electrodes used for pH measurements were glass electrode TOA HG-6005 and reference electrode TOA HC-605, which were connected to the TOA HM-9A expandomatic pH meter. The evaluated acid dissociation constants are listed in Table 2 along with the previous data for comparison.

Thanks are due to Miss Chieko Gondo for her assistance in part of the potentiometric measurements.

BULLETIN OF THE CHEMICAL SOCIETY OF JAPAN, VOL. 46, 2190—2193 (1973)

Chemical Studies on the Mistletoe. II.[1] The Structure of Viscumamide, a New Cyclic Peptide Isolated from *Viscum album* Linn. *var. coloratum* Ohwi

Yasuaki OKUMURA and Atsushi SAKURAI

Chemical Institute, Faculty of Science, Shizuoka University, Ohya, Shizuoka 420

(Received December 25, 1972)

A new cyclic peptide, viscumamide ($C_{30}H_{55}N_5O_5$) was isolated from *Viscum album* Linn. *var. coloratum* Ohwi, and the structure Ia ($\overline{\text{→L-Leu→L-Ileu→L-Leu→L-Ileu→L-Leu—}}$) was assigned to this substance from gas-chromatographic studies on the products of partial hydrolysis.

During our studies on the constituents of a mistletoe, *Viscum album* Linn. *var. coloratum* Ohwi, we isolated a new cyclic peptide and named it viscumamide.

The mistletoe which occurred on a hackberry (*Celtis sinensis* Pers. *var. japonica* Nakai) was collected and extracted with methanol in the usual way. The extract was fractionated into the neutral, basic, and acidic fractions. The neutral fraction was chromatographed on a column of activated alumina and gave a crystalline substance of mp 349.5—351 °C. This substance, viscumamide is optically active, $[\alpha]_D^{25}$ −49.1°. Elemental analyses and the mass spectrum (Fig. 1) show that viscumamide has a composition of $C_{30}H_{55}N_5O_5$ and a molecular weight of 565.8. The infrared spectrum of this substance (Fig. 2) shows absorption bands at

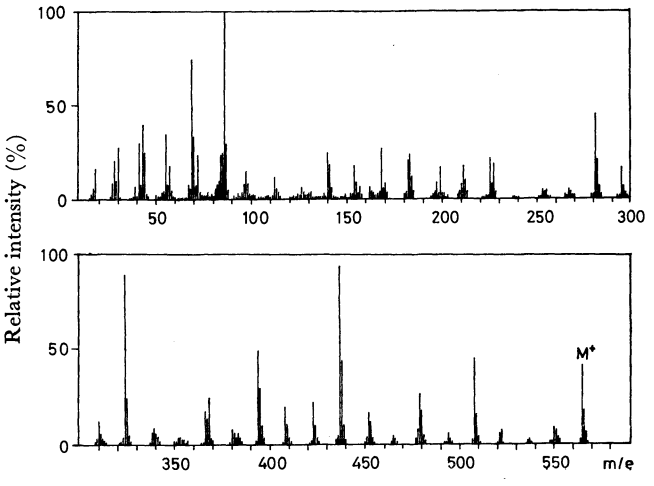

Fig. 1. Mass spectrum of viscumamide.

1) Part I: A. Sakurai and Y. Okumura, Reports of Faculty of Science, Shizuoka University, **6**, 63 (1971).

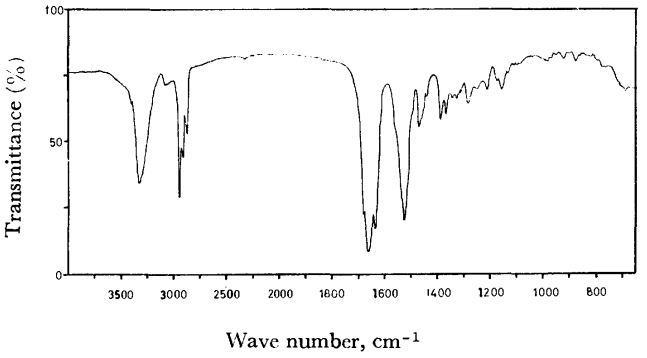

Fig. 2. Infrared spectrum of viscumamide.

3315, 3050, 1658, and 1530 cm^{-1} ascribed to secondary amide groups, and shows no absorption band indicative of the existence of a free amino group or a carboxyl group. The potentiometric titration of viscumamide in a dilute hydrochloric acid solution with potassium hydroxide shows that the substance has no dissociating group. And this substance shows a negative reaction with ninhydrin and is sparingly soluble in numerous solvents. These results suggest a cyclic structure linked by five peptide bonds for viscumamide.

Hydrolysis of viscumamide with 6M hydrochloric acid according to the method described by Harfenist[2] gave a mixture of leucine (60.6%) and isoleucine (39.4%). Gas-chromatographic analysis of the hydrolysate after esterification and treatment with trifluoroacetic anhydride[3] also showed to be a mixture of leucine and isoleucine, and showed the absence of alloisoleucine.

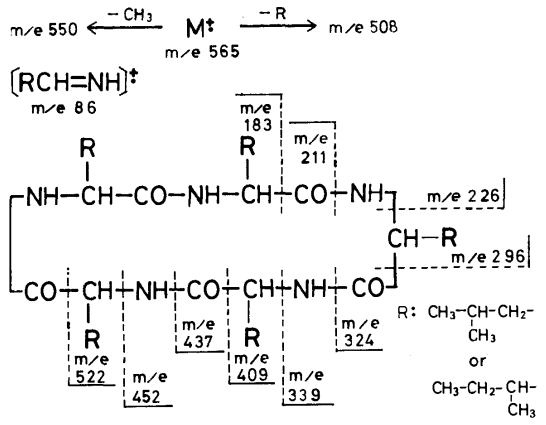

Scheme.

The mass spectrum of the homocyclic hexapeptide[4] has been investigated and shows that its fragmentation obeys the simple rules established with cyclodipeptides[5] as follows: the lower mass range is governed by the amine fragments ($RCH{=}\overset{+}{N}H_2$), while in the higher mass range expulsion of HNCO followed by several alternating losses of RCH=NH and carbon monoxide can be discerned. The mass spectrum of viscumamide shows fragmentations according to the fragmentation rules of these cyclopeptides. A primary process in the fragmentation of viscumamide is the loss of a HNCO fragment from $M^{\ddagger}$ (*m/e* 565) which gives a fragment ion peak at *m/e* 522. Then, the successive eliminations of RCH=NH (R=*i*-butyl or *s*-butyl) followed by loss of carbon monoxide occur, and intensive fragment ion peaks are formed at *m/e* 437, 409, 324, 296, 211, and 183, respectively. The amine fragments ($RCH{=}\overset{+}{N}H_2$) in the lower mass range appear at the same mass number, *m/e* 86, as the base peak. These results lead to a fragmentation sequence and a possible partial structure for viscumamide, which is shown in the scheme.

Table. Specific optical rotation of amino acids

Amino acid		$[\alpha]_D^{27}$	*c* in 20% HCl
Amino acids isolated from the hydrolysate of viscumamide	Leucine	+12.1°	0.40
	Isoleucine	+34.8°	0.39
Amino acids treated under the same conditions as the hydrolysis of viscuammide	L-Leucine	+13.2°	0.40
	L-Isoleucine	+33.8°	0.41

Specific optical rotation of leucine and isoleucine, which were isolated from the hydrolysate of viscumamide by chromatography on a column of Dowex 50×4, are summarized in the table and are in good agreement with the data of L-leucine and L-isoleucine, respectively, which were treated under the same conditions as the hydrolysis of viscumamide. These results indicate that this substance is constructed of three molecules of L-leucine and two molecules of L-isoleucine. And this leads to two possible structures, Ia and Ib for viscumamide.

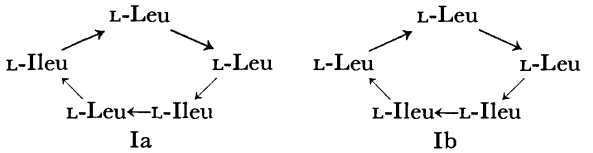

Partial hydrolysis of viscumamide with alcoholic hydrochloric acid gave a mixture of five substances, which were analyzed by gas-chromatography after esterification and treatment with trifluoroacetic anhydride. The gas-chromatogram of this mixture showed five peaks.

The substances of the first and the second peaks in order of the retention time in the gas-chromatogram were identified as *n*-butyl *N*-trifluoroacetylisoleucinate and *n*-butyl *N*-trifluoroacetylleucinate, respectively. After being fractionated by gas-chromatography, the substances of the third, the fourth and the fifth peaks were hydrolyzed respectively with 6M hydrochloric acid. And each hydrolysate was analyzed by gas-chromatography in the form of *N*-trifluoroacetylated *n*-butyl ester. The gas-chromatograms of the hydrolysates showed that upon hydrolysis, both the substances of the third and the fourth peaks gave isoleucine and leucine in equal amounts, and that the substance of the fifth peak gave only leucine. By comparison with

2) E. J. Harfenist, *J. Amer. Chem. Soc.*, **75**, 5528 (1953).
3) G. W. Gehrke and W. M. Lamkin, *Chem. Eng. News*, **42**, 62 (1964).
4) K. Heyns and H.F. Grützmacher, *Ann. Chem.*, **669**, 189 (1963).
5) H. J. Svec and G. A. Junk, *J. Amer. Chem. Soc.*, **86**, 2278 (1964).

synthetic samples of dipeptide, the substances of the third, the fourth and the fifth peaks were identified as *n*-butyl *N*-trifluoroacetylisoleucylleucinate, *n*-butyl *N*-trifluoroacetylleucylisoleucinate and *n*-butyl *N*-trifluoroacetylleucylleucinate, respectively.

Thus, partial hydrolysis of viscumamide gave leucine, isoleucine, isoleucylleucine (II), leucylisoleucine (III), and leucylleucine (IV). The absence of isoleucylisoleucine (V) in the partial hydrolysate eliminates the validity of the structure Ib for viscumamide, and all experimental results described above support the structure of Ia for viscumamide.

Experimental

All melting points are uncorrected. Infrared spectrum was measured in KBr disk with a model EPI-G3 Hitachi spectrophotometer and gas-chromatogram was measured with a model K-53 Hitachi gas-chromatograph.

Extraction and Isolation of Viscumamide. The mistletoe (10 kg)[6] was extracted with methanol in the usual way, and the extract was concentrated under reduced pressure. The concentrate was dissolved in ethyl acetate and fractionated into the basic, acidic, and neutral fractions by shaking with dilute hydrochloric acid and then with sodium carbonate solution. The neutral fraction was concentrated to a syrup *in vacuo*. This syrup was digested with boiling *n*-hexane and the insoluble residue was collected by filtration. The faintly brown residue (18.2 g) was dissolved in hot methanol (100 ml), and activated alumina (50 g) was added to this solution and stirred. The suspension was evaporated to dryness *in vacuo*. The alumina which adsorbed the residue was placed on the top of a column of activated alumina (450 g), and the column was eluted with solvents. Elution with a mixture of ethyl acetate and ethanol and recrystallization from ethanol gave colorless needles, mp 349.5—351 °C (158 mg, 0.0158% from wet plant). $[\alpha]_D^{25}$ −49.1° (*c* 0.199, ethanol).

Found: C, 63.52; H, 10.07; N, 12.55%. Calcd for $C_{30}H_{55}N_5O_5$: C, 63.68; H, 9.80; N, 12.38%.

Potentiometric Titration of Viscumamide. Viscumamide (5.6 mg) in 0.01*M* hydrochloric acid (20 ml) was titrated with 0.1M sodium hydroxide using a Hiranuma Rat-1(P) autotitrator. The titration curve was identical with that of blank titration. This results showed that the substance has no dissociating group.

Hydrolysis of Viscumamide. Viscumamide (1.51 mg) in 6M hydrochloric acid (2 ml) was heated in a sealed tube at 110 °C for 120 hr according to the method described by Harfenist.[2] The reaction mixture was evaporated to dryness *in vacuo* and was dissolved in water. This solution was analyzed with a model KLA-3B Hitachi amino acid analyzer and showed to be a mixture of 0.91 mg of leucine (60.6%) and 0.59 mg of isoleucine (39.4%) at the recovery rate of 86.3%.

Separation of Leucine and Isoleucine from the Hydrolysate of Viscumamide. Viscumamide (100 mg) in 6M hydrochloric acid (20 ml) was hydrolyzed in the same manner as described above. The reaction mixture evaporated to dryness *in vacuo*, was dissolved in water (5 ml) and was submitted to chromatography on a column of Dowex 50 X 4 (150×2 cm, H^+ form, 200—400 mesh; developer: hydrochloric acid, pH value being changed continuously from 1M hydrochloric acid (1 l) to 12M hydrochloric acid (1 l). The fractions containing a mixture of leucine and isoleucine were evaporated to dryness *in vacuo*, and the residue of the mixture was chromatographed again in the same manner. The respective fractions containing pure leucine and isoleucine were evaporated to dryness *in vacuo*, and dissolved in ethanol (2 ml) and treated with ethyl acetate. The solutions were allowed to stand at 0 °C. Leucine hydrochloride (15 mg) and isoleucine hydrochloride (13 mg) were obtained as colorless powder.

Specific rotations of these amino acid hydrochlorides were measured in 20% hydrochloric acid, and the data were summarized in the table.

Preparation of Amino Acids for the Measurement of Specific Rotation. L-Leucine and L-isoleucine were respectively treated with 6M hydrochloric acid in the same manner as described above. The solutions were evaporated to dryness *in vacuo*. The residue was dissolved in ethanol and treated with ethyl acetate. The specific rotations of the resulted L-leucine hydrochloride and L-isoleucine hydrochloride were measured and the data were summarized in the table.

Preparation of L-Isoleucyl-L-Leucine (II). To a solution containing carbobenzoxy-L-isoleucine[7] (1.6 g) in dry chloroform (20 ml), dry triethylamine (0.6 g) was added at 0 °C and ethyl chloroformate (0.65 g) was added to this solution. After 30 min methyl L-leucinate dissolved in chloroform (10 ml) was added in about 20% excess of the calculated amount. The solution was allowed to stand at room temperature for 1 hr and then washed successively with 1M hydrochloric acid, sodium bicarbonate, and water. The solution was dried over sodium sulfate and evaporated to dryness *in vacuo*. The residue was dissolved in ether (10 ml) and treated with petroleum ether (15 ml, bp 50—80 °C). After being chilled, methyl carbobenzoxy-L-isoleucyl-L-leucinate (1.9 g) was obtained as colorless needles; 83% of the theoretical yield and mp 121.5—122 °C.

The above-described ester (1.5 g) in acetone (15 ml) was saponified by treating with 1M sodium hydroxide (4.2 ml) at room temperature for 45 min. The solution was acidified until acid to Congo red with concentrated hydrochloric acid and was concentrated *in vacuo*. Then the product was extracted with ethyl acetate and the extract was dried over sodium sulfate. By adding petroleum ether, carbobenzoxy-L-isoleucyl-L-leucine (1.2 g) was obtained as colorless crystals; 85% of the theoretical yield and mp 130—131 °C (lit,[8] mp 130—131 °C).

The carbobenzoxydipeptide (500 mg) was hydrogenated in methanol (6 ml) containing water (0.30 ml) and glacial acetic acid (0.30 ml) in the presence of palladium black. The catalyst was removed by filtration and the filtrate was concentrated *in vacuo* with repeated additional methanol. Ether was added to complete the crystallization. After recrystallization from methanol–water, L-isoleucyl-L-leucine (243 mg)was obtained as colorless needles; 71% of the theoretical yield and $[\alpha]_D^{18}$ −11° (*c* 1, 1M sodium hydroxide).

Found: C, 58.71; H, 10.02; N, 11.36%. Calcd for $C_{12}H_{24}N_2O_3$: C, 58.99; H, 9.90; N, 11.47%.

Preparation of L-Leucyl-L-isoleucine (III). L-Leucyl-L-isoleucine was prepared in 58% yield in the same manner as described above *via* methyl carbobenzoxy-L-leucyl-L-isoleucinate, colorless needles, mp 64.5—65.5 °C (lit,[9] mp 64—65 °C) and carbobenzoxyl-L-leucyl-L-isoleucine, colorless crystals, mp 99—101 °C (lit,[10] mp 101—101.5 °C) from carbo-

6) The mistletoe was collected at Futamata of Tenryu City in the winter of 1969.

7) H. E. Carter, R. L. Frank, and H. W. Johnston, "Organic Synthesis," Coll. Vol., 3, p. 167 (1955).

8) D. Theodoropoulos and L. C. Craig, *J. Org. Chem.*, **20**, 1169 (1955).

9) K. Isono and R. W. Curtis, *Phytochemistry*, **3**, 276 (1964).

10) E. Smith, D. H. Spackman, and W. J. Polglase, *J. Biol. Chem.*, **199**, 803 (1952).

benzoxy-L-leucine[6] (1.6 g) and methyl L-isoleucinate (1.0 g); colorless needles, $[\alpha]_D^{20}$ +19° (*c* 1, water) (lit,[10] $[\alpha]_D^{23}$ +20.9° (*c* 1, water)).

Found: C, 54.49; H, 9.78; N, 10.48%. Calcd for $C_{12}H_{24}N_2O_3 \cdot H_2O$: C, 54.94; H, 9.99; N, 10.68%.

Preparation of L-*Leucyl*-L-*leucine (IV).* L-Leucyl-L-leucine was prepared in 65% yield in the same manner as described above *via* methyl carbobenzoxy-L-leucyl-L-leucinate, colorless needles, mp 98.5—99 °C (lit,[10] mp 97.5—98.5 °C) and carbobenzoxy-L-leucyl-L-leucine, colorless crystals, mp 98.5—100 °C (lit,[10] mp 98—101 °C) from carbobenzoxy-L-leucine[7] (1.6 g) and methyl L-leucinate (1.0 g); colroless needles, $[\alpha]_D^{20}$ −13.6° (*c* 5, 1M sodium hydroxide)).

Found: C, 55.11; H, 9.49; N, 10.69%. Calcd for $C_{12}H_{24}N_2O_3 \cdot H_2O$: C, 54.94; H, 9.99; N, 10.68%.

Preparation of L-*Isoleucyl*-L-*isoleucine (V).* L-Isoleucyl-L-isoleucine was prepared in 63% yield in the same manner as described above *via* methyl carbobenzoxy-L-isoleucyl-L-isoleucinate, colorless needles, mp 132—132.5 °C and carbobenzoxy-L-isoleucyl-L-isoleucine, colorless crystals, mp 120.5—122°C from carbobenzoxy-L-isoleucine[7] (1.6 g) and methyl L-isoleucinate (1.0 g); colorless needles, $[\alpha]_D^{20}$ +7° (*c* 0.1, water).

Found: C, 55.05; H, 9.79; N, 10.79%. Calcd for $C_{12}H_{24}N_2O_3 \cdot H_2O$: C, 54.94; H, 9.99; N, 10.68%.

Preparation of N-*Trifluoroacetylated Amino Acid* n-*Butyl Esters and* N-*Trifluoroacetylated Dipeptide* n-*Butyl Esters.* These substances were prepared by a modification of the procedure described by Gehrke and Lamkin.[3] One mg of amino acid or dipeptide was treated with methanol (1 ml) saturated with hydrogen chloride at room temperature for 4 hr. The reaction mixture was evaporated to dryness *in vacuo*, and the residue was dissolved in *n*-butanol (1 ml) saturated with hydrogen chloride. And then the mixture was heated in a sealed tube at 120 °C for 2 hr. After the solvent was removed *in vacuo*, the resulted *n*-butyl ester was treated with trifluoroacetic anhydride (1 ml) in dichloromethane (1 ml) at room temperature for 15 min. After the solvent was removed *in vacuo*, the residue was dissolved in dichloromethane and was submitted to gas-chromatography.

Gas-Chromatogram of the Hydrolysate of Viscumamide. The hydrolysate of viscumamide was esterified and was treated with trifluoroacetic anhydride in the same manner as described above. The resulted *N*-trifluoroacetylated amino acid *n*-butyl esters showed the identity with authentic *n*-butyl *N*-trifluoroacetylleucinate and *n*-butyl *N*-trifluoroacetylisoleucinate, but not with authentic *n*-butyl *N*-trifluoroacetylalloisoleucinate in gas-chromatography (column: 3 mm×4 m stainless steel column, stationary phase; 20% diethylene glycol adipate on Celite 545, column bath temperature; 175 °C, carrier gas; He, 20 ml/min). The retention times of *n*-butyl *N*-trifluoroacetylleucinate, *n*-butyl *N*-trifluoroacetylisoleucinate and *n*-butyl *N*-trifluoroacetyl-alloisoleucinate were 31.6, 25.6, and 24.2 min, respectively.

Partial Hydrolysis of Viscumamide. Viscumamide (10 mg) in a mixture of 6M hydrochloric acid (10 ml) and ethanol (10 ml) was refluxed for 4 hr. After being evaporated to dryness *in vacuo*, the hydrolysate was esterified and treated with trifluoroacetic anhydride in the same manner as described above. The resulted *N*-trifluoroacetylated amino acid *n*-butyl esters and *N*-trifluoroacetylated dipeptide *n*-butyl esters were submitted to gas-chromatography (column; 3 mm×2 m stainless steel column, stationary phase; 20% diethylene glycol adipate on Celite 545, column bath temperature; 200 °C, carrier gas; He, 40 ml/min) and fractionated. The chromatogram of this mixture showed five peaks and the retention times of these peaks were 1.0, 1.2, 20.4, 22.1, 23.5 min. The fractions of the first and the second peaks in order of the retention time showed the identity with authentic *n*-butyl *N*-trifluoroacetylisoleucinate and *n*-butyl *N*-trifluoroacetylleucinate, respectively. The fraction of the third peak was hydrolyzed with 6M hydrochloric acid, and then was esterified and treated with trifluoroacetic anhydride in the same manner as described above. The reaction mixture showed the identity with a mixture (1 : 0.99) of authentic *n*-butyl *N*-trifluoroacetylisoleucinate and *n*-butyl *N*-trifluoroacetylleucinate in gas-chromatography. The fraction of the fourth peak was treated in the same manner as the fraction of the third peak and showed the identity with a mixture (0.96: 1) of authentic *n*-butyl *N*-trifluoroacetylisoleucinate and *n*-butyl *N*-trifluoroacetylleucinate. The fraction of the fifth peak was treated in the same manner and showed the identity with only authentic *n*-butyl *N*-trifluoroacetylleucinate. And the fractions of the third, the fourth and the fifth peaks showed to be *n*-butyl *N*-trifluoroacetylisoleucylleucinate, *n*-butyl *N*-trifluoroacetylleucylisoleucinate and *n*-butyl *N*-trifluoroacetylleucylleucinate, respectively, by gas-chromatographic comparison with the synthetic samples.

The authors wish to express their thanks to Professor Yoshimasa Hirata of Nagoya University for the measurement of mass spectrum, Dr. Takayuki Naito of Bristol-Banyu Research Institute for microanalyses and Mr. Koichi Mochizuki of Japan Spectroscopy Co. Ltd. for the measurement of specific rotation.

Crystal and Molecular Structure of ω-Amino Acids, ω-Aminosulfonic Acids and Their Derivatives. III. The Crystal and Molecular Structure of γ-Guanidino-β-hydroxypropane Sulfonic Acid

Yang Bae KIM, Akio WAKAHARA, Takaji FUJIWARA, and Ken-ichi TOMITA
Faculty of Pharmaceutical Sciences, Osaka University, Toneyama, Toyonaka, Osaka 560
(Received December 28, 1972)

γ-Guanidino-β-hydroxypropane sulfonic acid $C_4H_{11}O_4N_3S$ crystallizes in the monoclinic space group $P2_1/c$, with four formula units in a unit cell of dimensions, $a=7.44$, $b=9.89$, $c=11.11$ Å and $\beta=97.75°$. The crystal structure was determined by the heavy atom method and refined by block-diagonal least-squares to an R-value of 0.12 using intensity data collected photographically. The molecule takes the zwitterionic form, $(NH_2)_2{}^+CNHCH_2CH(OH)CH_2SO_3{}^-$. The skeletal conformation of the molecule is planar *trans* zigzag. The molecules are held together in the crystal by a three-dimensional network of NH···O and OH···O hydrogen bonds.

γ-Guanidino-β-hydroxypropane sulfonic acid (GGBOPSA) is one of the derivatives of chemical transmitter in the central nervous system[1-3] such as γ-aminobutyric acid (GABA), γ-amino-β-hydroxybutyric acid (GABOB), homotaurine and taurine. This work is a part of a series of structural studies on the derivatives of the above compounds. Details of action mechanisms are not clear. However, it was reported that guanidino derivatives of ω-aminosulfonic acid such as GGBOPSA and γ-guanidinopropane sulfonic acid (GGPSA) act as a depressant for the lowering of blood pressure, whereas homotaurine and γ-amino-β-hydroxypropane sulfonic acid (GABOPSA) show an excitatory action for it.[4] It would be of great interest to elucidate the correlation between structural specificities and biological implications of these compounds.

Some structural features of GGBOPSA and its related compounds have been reported.[5] This paper deals with the precise structure analysis of GGBOPSA and comparison of the molecular structure with that of the related compounds.

Experimental

A racemic sample of GGBOPSA (supplied by Prof. S. Tsunoo, Medical School of Showa University) was recrystallized from water at room temperature as colorless, transparent prisms elongated along the a-axis. The space group and cell constants were determined from Weissenberg and precession photographs. The crystal data are presented in Table 1. Intensity data of 1452 independent reflections around a and b-axes were collected from equi-inclination Weissenberg photographs by the multiple film method with Cu$K\alpha$ radiation and estimated by visual comparison with a calibrated scale. Lorentz, polarization and spot-shape corrections were applied, but no absorption correction was made. The approximate scale factor and over-all temperature factor were calculated by Wilson's method.

TABLE 1. CRYSTAL DATA OF GGBOPSA

Molecular Formula: $C_4H_{11}O_4N_3S$	M.W.=197.21
Colorless transparent prism, Monoclinic system	
$a=7.44\pm0.02$ Å	$b=9.89\pm0.02$ Å
$c=11.11\pm0.03$ Å	$\beta=97.75\pm0.5°$
Volume of the unit cell, 810.02 Å^3	
Density (by flotation) 1.621 g cm^{-3}	
Density(calculated) 1.617 g cm^{-3}	
$Z=4$	$F(000)=416$
Absent spectra: $h0l$ when $l=2n+1$	
$0k0$ when $k=2n+1$	
Space group, $P2_1/c$	

Structure Determination and Refinement

The structure was solved by the usual heavy-atom procedure. By interpretation of high peaks on sharpened Patterson function, the coordinates of sulfur atom were easily determined. From the Fourier synthesis with only the heavy atom phase, all the non-hydrogen atoms could be found. R-index, $R=\sum||F_o|-|F_c||/\sum|F_o|$, was reduced from 0.32 to 0.18 by block-diagonal least-squares refinement with isotropic temperature factors, the unit weight being applied for the non-zero reflections. Refinement was continued with anisotropic temperature factors and R-index was reduced to 0.14. The used anisotropic temperature factors are of the form: $\exp\{-(B_{11}h^2+B_{22}k^2+B_{33}l^2+B_{12}hk+B_{13}hl+B_{23}kl)\}$.

A difference Fourier synthesis calculated in this stage revealed all the hydrogen atoms which were included in the further refinement. The final R-value was 0.12. The used atomic scattering factors were taken from *International Tables for X-ray Crystallography*.[6]

All the computations were carried out on NEAC 2200-500 and 2200-700 machines at this University and on FACOM 230-60 at the University of Kyoto, using the programs of UNICS system.

Results and Discussion

The final positional and thermal parameters are listed in Tables 2-a and b, together with their estimated

1) K. Tomita, *Tetrahedron Lett.*, **1971**, 2587.
2) A. N. Davison and L. K. Kaczmarek, *Nature*, **234**, 107 (1971).
3) T. Hayashi and K. Nagai, Proc. 20th Int. Physiol. Cong., (1956), Brussels, Belgium, p. 410.
4) S. Tsunoo, K. Horisaka, H. Tanaka, T. Chida, S. Nakajima, and Z. Fukai, *J. Showa Med. Assoc.*, **30**, 521(1970).
5) Y. B. Kim, A. Wakahara, T. Fujiwara, and K. Tomita, *Chem. Lett.*, **1972**, 891.
6) "International Tables for X-ray Crystallography," Vol. 3, Kynoch Press, England (1962).

Table 2-a. Final positional and thermal parameters with their estimated standard deviations in parentheses ($\times 10^4$)

The anisotropic temperature factors are expressed in the form of

$$\exp\{-(B_{11}h^2+B_{22}k^2+B_{33}l^2+B_{12}hk+B_{13}hl+B_{23}kl)\}$$

Atom	x/a	y/b	z/c	B_{11}	B_{22}	B_{33}	B_{12}	B_{13}	B_{23}
S	12216(3)	950(2)	3718(2)	62(4)	18(2)	37(2)	−1(5)	44(4)	−25(3)
O(1)	12240(10)	−269(7)	2972(7)	111(14)	59(7)	82(7)	34(17)	41(16)	−111(12)
O(2)	13224(10)	2062(7)	3271(7)	86(13)	66(7)	84(7)	−38(17)	138(16)	13(12)
O(3)	12792(10)	671(7)	4996(6)	125(14)	42(6)	34(5)	20(15)	−30(13)	−1(9)
O(4)	10181(9)	3873(6)	3945(6)	86(13)	29(6)	64(6)	−30(14)	47(14)	−21(10)
C(1)	9914(12)	1461(9)	3591(8)	70(17)	30(7)	45(8)	30(19)	31(18)	−23(12)
C(2)	9597(12)	2679(8)	4408(8)	52(16)	25(7)	46(7)	−2(18)	23(17)	5(12)
C(3)	7640(13)	2772(9)	4561(9)	76(18)	28(8)	52(8)	−9(19)	60(19)	−4(12)
C(4)	6069(12)	3934(9)	6090(8)	73(17)	42(8)	28(6)	−9(20)	15(16)	−27(12)
N(1)	7362(10)	3888(7)	5370(7)	65(14)	27(6)	41(6)	−1(16)	30(14)	−13(10)
N(2)	6060(10)	5015(7)	6836(7)	67(14)	35(7)	48(6)	−11(16)	91(16)	−11(11)
N(3)	4869(11)	2987(8)	6121(7)	101(16)	40(7)	51(7)	−62(18)	71(17)	−22(12)

Table 2-b. Fractional coordinates of hydrogen atoms ($\times 10^4$)

Atom	Bound to	x	y	z	
H(1)	O(4)	9371	4211	3279	
H(2)	C(1)	8986	556	3887	
H(3)	C(1)	9596	1635	2605	
H(4)	C(2)	10178	2399	5368	
H(5)	C(3)	7328	1700	5079	Over-all isotropic
H(6)	C(3)	6938	2960	3645	temperature factor
H(7)	N(1)	8501	4679	5425	is 1.156Å²
H(8)	N(2)	5157	5227	7297	
H(9)	N(2)	6953	5635	6917	
H(10)	N(3)	4084	2982	6855	
H(11)	N(3)	4764	2383	5455	

standard deviations. The observed and calculated structure factors are listed in Table 3. Figure 1 shows bond distances and angles with the numbering of atoms. The bond lengths and angles are compared in Table 4 with those of other compounds such as L-arginine dihydrate,[7] taurine,[8,9] homotaurine,[10] GABA,[11] GABOB,[12] and γ-guanidinobutyric acid hydrochloride (GGBA·HCl).[13] Similarly, in the cases of taurine and homotaurine, the guanidyl group is protonated by one hydrogen atom of the sulfonate group, the three S–O bonds of the resultant $-SO_3^-$ group being equivalent in the state of resonance. The average O–S–O and C–S–O angles in the sulfonate group are 112.1 and 106.7°, respectively. Deviations from the tetrahedral angles are probably due to the repulsion between the adjacent oxygen atoms which lie at the short contact distances of 2.42 Å as discussed in taurine by Sutherland and Young.[8]

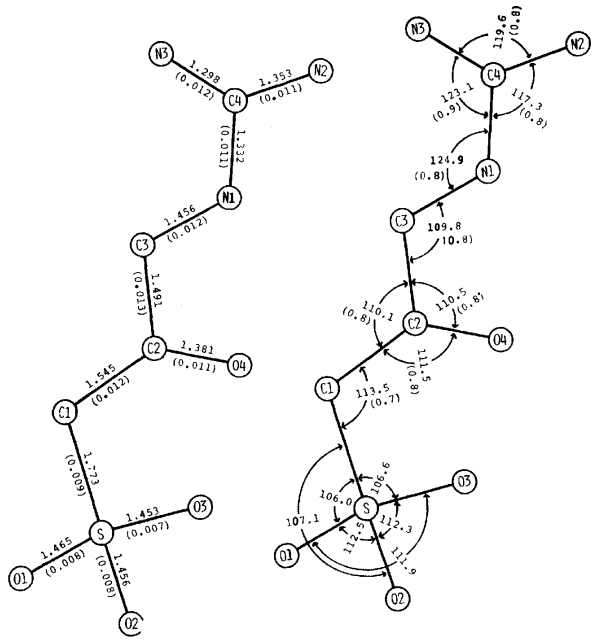

Fig. 1. Bond lengths (Å) and angles (°) of GGBOPSA. Estimated standard deviations are listed in the parentheses and those of angles around sulfur atom are 0.5°.

The guanidyl group is planar and the equation of the least-squares plane through the four atoms, N(1), C(4), N(2), and N(3), is

$$-0.51539X + 0.47909Y - 0.71053Z = -4.76419.$$

Deviations of the individual atoms from this plane are N(1): −0.0027, C(4): 0.0081, N(2): −0.0026 and N(3): −0.0028 Å. The dihedral angle between this plane and that passing through C(1)–C(2)–C(3) is 27.4°. In L-arginine dihydrate,[7] the deviations of the individual atoms from the least-squares plane of guanidyl group are N(1): −0.0005, C(4): 0.0015, N(2): −0.0005, and N(3): −0.0005 Å. Thus, the planarity of the guanidyl group in GGBOPSA is in good agreement with that of L-arginine dihydrate. All the C–N bond distances of the guanidyl group are halfway between the value of single bond (1.47 Å) and that of double bond (1.24 Å) proposed by Shomaker and

7) I. L. Karle and J. Karle, *Acta Crystallogr.*, **17**, 835 (1964).
8) H. H. Sutherland and D. W. Young, *ibid.*, **16**, 897 (1963).
9) Y. Okaya, *ibid.*, **21**, 726 (1966).
10) S. Ueoka, T. Fujiwara, and K. Tomita, This Bulletin, **45**, 3634 (1972).
11) K. Tomita, T. Fujiwara, and H. Higashi, *Jap. J. Brain Physiol.*, **111**, 111 (1971).
12) M. Harada, H. Higashi, T. Fujiwara, and K. Tomita, unpublished result.
13) T. Maeda, T. Fujiwara, and K. Tomita, This Bulletin, **45**, 3628 (1972).

TABLE 3. OBSERVED AND CALCULATED STRUCTURE FACTORS

K	Fo	Fc	K	Fo	Fc	K	Fo	Fc	K	Fo	Fc	K	Fo	Fc	K	Fo	Fc	K	Fo	Fc	K	Fo	Fc	K	Fo	Fc	K	Fo	Fc
H,L=	0	0	5	42	-39	2	169	-174	H,L=	2	4	8	38	-36	H,L=	3	12	H,L=	4	2	3	55	40	1	80	-82	5	91	82
2	83	68	6	109	-88	3	31	-35	0	144	-129	9	49	33	0	95	84	0	79	59	5	133	127	2	239	-246	6	59	-47
4	104	-90	7	81	67	4	167	149	1	131	114	10	27	-25	3	27	-19	1	134	147	6	97	-77	3	148	-151	H.L=	6	-5
6	199	-216	8	96	75	5	19	19	2	68	43	H,L=	2	-8	H,L=	3	-1	2	126	-146	8	86	72	4	123	117	1	78	-72
8	110	84	9	148	174	6	92	80	3	156	153	1	77	-65	1	194	-219	3	116	108	H,L=	4	-8	5	32	22	2	118	-117
10	183	201	10	83	-66	7	93	-70	4	48	32	2	98	-104	2	252	-273	4	53	37	0	136	128	6	59	42	3	61	46
H,L=	0	1	11	33	32	8	174	184	7	140	-164	3	59	-37	3	52	-37	7	146	-144	1	55	43	7	44	28	5	90	100
1	52	-34	H,L=	1	1	9	52	47	9	54	-47	4	97	85	4	173	-169	H,L=	4	3	2	89	75	8	43	-29	7	47	59
2	269	-302	1	238	-257	11	59	48	10	78	86	6	131	148	5	129	-116	1	193	185	3	126	108	9	68	58	H.L=	6	-6
3	141	-137	2	466	520	12	87	-86	11	27	35	7	26	26	6	98	86	2	41	40	4	119	-98	10	38	-56	0	126	147
4	120	105	3	94	78	H,L=	1	-4	H,L=	2	5	10	46	-51	8	174	197	3	55	-45	6	35	-28	H,L=	5	-3	2	103	-96
5	113	105	4	115	94	0	178	187	1	51	33	H.L=	2	-9	10	50	34	4	97	81	7	56	-56	1	75	70	4	106	-103
6	74	58	5	43	-43	1	28	3	2	49	-44	1	124	139	11	29	-27	5	121	-112	9	60	-66	2	108	96	6	130	-130
7	72	55	6	39	32	2	112	-122	3	179	193	2	108	-90	H,L=	3	-2	6	102	-89	H,L=	4	-9	3	76	-69	H,L=	6	-7
8	161	142	7	90	81	3	131	114	4	66	-62	3	83	-81	0	190	224	7	48	28	1	126	-117	4	37	26	2	124	115
9	137	131	8	236	-267	4	327	345	5	89	64	4	134	-141	1	245	-272	8	76	-57	2	77	61	5	88	-76	4	72	70
10	66	56	9	50	-30	5	87	-66	6	70	-56	5	130	-132	2	99	101	9	103	109	3	50	40	6	34	31	7	40	-45
11	64	-67	10	37	28	6	96	78	7	83	64	6	74	51	3	177	177	H,L=	4	4	4	65	54	7	121	-146	H,L=	6	-8
12	37	-45	11	74	-81	7	95	-87	8	102	102	7	85	-78	4	128	-119	0	57	-46	5	113	109	10	32	20	1	96	-94
H,L=	0	2	12	54	55	8	56	-45	9	88	-90	8	60	57	5	117	114	1	26	-16	6	56	-44	H,L=	5	-4	6	46	59
0	173	175	H,L=	1	2	9	68	-63	10	45	48	9	50	51	6	182	-179	2	108	118	7	82	73	0	150	-171	7	41	44
1	292	330	0	567	614	10	34	39	11	23	-21	H.L=	2	-10	9	53	-33	3	119	-113	8	34	28	2	140	-134	H,L=	6	-9
2	176	-171	1	468	523	11	48	40	H.L=	2	6	0	59	-51	10	50	37	4	84	66	H,L=	4	-10	3	123	122	1	154	153
3	162	155	2	168	185	H,L=	1	-5	0	232	-257	1	53	35	11	59	-56	6	73	59	0	35	29	4	287	279	3	51	-53
4	143	-134	3	37	-17	1	173	-167	1	140	131	2	53	-53	H,L=	3	-3	9	65	67	1	96	-82	5	67	-58	H,L=	6	-10
6	221	-207	4	66	-50	2	89	-68	3	157	165	3	67	62	1	139	-184	10	29	-40	2	42	31	6	114	99	0	72	-81
7	178	-177	5	136	-139	4	82	-85	5	92	72	4	93	-76	2	150	-135	H,L=	4	5	3	130	-145	7	109	-102	3	45	45
9	80	-66	6	113	-115	5	168	177	6	99	102	5	71	55	3	98	-70	1	84	-74	4	34	-30	8	50	-35	H,L=	6	-11
H,L=	0	3	7	197	-197	6	93	73	7	73	-61	8	37	34	4	77	-60	2	162	176	6	42	-35	9	45	-44	2	104	-117
1	94	74	8	89	75	9	83	-68	9	94	-89	H,L=	2	-11	5	254	289	3	54	-44	7	85	84	10	72	-80	H,L=	7	0
2	224	-224	9	45	-22	10	42	-19	10	57	-59	1	60	51	6	106	-88	4	88	74	8	46	-68	H.L=	5	-5	0	88	-76
3	186	-183	10	138	159	11	63	-68	H,L=	2	7	2	99	-95	7	141	73	5	34	-33	H,L=	4	-11	2	102	-104	1	63	-55
4	155	-149	11	77	87	H,L=	1	-6	1	73	70	4	81	-81	9	74	-57	8	97	-90	1	33	-37	3	31	-24	H.L=	7	1
5	74	-51	12	45	51	0	25	-13	2	33	-30	6	74	66	10	59	-40	H,L=	4	6	2	81	80	4	79	-69	1	62	46
6	76	39	H,L=	1	3	1	35	12	3	76	-70	H,L=	2	-12	11	84	-99	0	77	63	5	62	62	5	156	180	2	29	-28
7	60	-47	1	167	178	2	104	-81	4	77	-72	0	86	108	H,L=	3	-4	1	102	-97	6	33	28	6	72	52	5	72	-146
8	46	35	2	125	135	3	87	90	5	141	-168	1	54	48	1	103	-75	2	59	42	H,L=	4	-12	7	76	-77	7	19	8
9	97	80	3	73	60	4	167	-158	7	119	-137	2	71	69	2	49	36	3	161	-170	0	162	-150	8	64	61	H.L=	7	2
10	58	46	4	45	53	5	99	-89	8	36	19	4	50	-52	3	130	-135	4	126	-138	2	41	33	9	31	6	3	100	-93
12	97	-92	5	101	86	6	149	-157	9	31	30	6	36	-44	4	39	14	6	104	-104	3	51	-67	H.L=	5	-6	H,L=	7	3
H,L=	0	4	6	86	81	8	45	-43	H,L=	2	8	H,L=	3	0	6	82	-58	7	71	63	4	35	37	0	62	53	1	85	-76
0	295	-315	7	121	117	10	44	56	0	77	-75	0	212	208	7	173	189	9	34	31	H,L=	4	-13	1	125	116	2	95	69
1	75	-57	8	43	31	11	34	34	1	77	-66	1	71	61	8	52	-37	H,L=	4	7	1	44	64	3	105	100	4	54	58
2	90	71	10	83	82	H,L=	1	-7	2	58	-53	2	86	-72	9	58	47	1	111	-111	2	38	-39	8	47	26	H,L=	7	4
3	53	-57	11	31	-40	1	112	-94	5	61	-40	3	173	179	10	64	63	2	59	-38	H,L=	5	0	9	55	-58	0	81	68
4	224	240	12	34	-49	2	206	220	6	89	92	4	79	-58	11	45	-55	3	73	72	0	180	190	H,L=	5	-7	2	91	79
5	94	106	H,L=	1	4	3	47	33	7	63	57	5	67	54	H,L=	3	-5	4	50	-36	1	44	40	1	89	-82	4	50	-28
6	109	94	0	246	-257	4	155	139	H,L=	2	9	7	125	-115	1	82	84	5	94	79	2	111	132	3	108	104	H,L=	7	5
8	46	-41	1	271	287	5	124	130	1	118	129	8	74	57	2	77	57	6	101	106	3	137	-154	4	51	37	1	54	-59
9	82	62	2	81	-83	6	56	-45	2	37	48	9	130	-110	3	38	33	7	63	55	4	102	-95	5	109	114	5	125	124
10	132	-140	3	32	37	7	37	-30	4	71	72	10	43	-42	4	116	120	9	30	-39	5	32	20	7	34	26	H.L=	7	6
11	37	-24	4	82	-64	8	88	-80	8	39	-54	11	51	-43	6	60	-47	H,L=	4	8	6	68	-42	8	49	36	3	102	99
H,L=	0	5	5	28	29	9	54	-50	H,L=	2	10	12	46	-20	7	40	44	0	107	110	7	56	39	9	56	-56	H,L=	7	7
1	88	-95	7	149	-150	H,L=	1	-8	0	66	57	H,L=	3	1	8	81	-61	1	35	24	8	105	115	H,L=	5	-8	2	75	-85
2	172	173	8	62	-40	1	53	-49	1	76	-59	1	309	350	9	36	38	2	61	50	9	92	77	0	101	85	H,L=	7	-1
3	75	78	9	68	-66	2	84	78	5	49	-36	2	199	-198	10	32	-27	4	49	-32	10	62	64	1	117	-125	1	63	64
4	90	-71	11	87	100	3	145	-157	7	54	66	3	104	95	11	36	32	7	27	28	H,L=	5	1	3	106	-104	2	144	-149
5	93	-66	H,L=	1	5	5	87	-81	8	18	39	4	47	-28	H,L=	3	-6	H,L=	4	9	1	46	-65	4	89	-93	4	84	-74
6	68	44	1	107	109	6	64	52	H,L=	2	11	5	184	-178	0	46	45	2	117	-126	5	66	48	5	56	-44	H,L=	7	-2
7	63	51	3	186	-167	7	67	56	4	33	26	6	30	-20	1	51	37	4	54	-44	6	92	94	6	85	-72	0	139	127
8	120	-123	4	82	-69	9	38	29	5	42	57	8	37	25	2	49	-38	6	58	64	8	73	-60	7	85	77	2	124	111
11	67	68	5	149	-150	H,L=	1	-9	6	50	-57	9	158	164	4	92	76	7	28	25	9	33	-24	8	26	19	3	59	43
H,L=	0	6	7	127	-122	1	57	46	H,L=	2	12	11	87	102	5	93	-69	H,L=	4	10	10	46	48	H.L=	5	-9	H,L=	7	-3
0	144	134	8	52	28	2	126	122	0	38	26	H,L=	3	2	6	128	108	0	65	-61	H,L=	5	2	2	100	97	1	99	-101
1	66	-51	11	75	81	3	50	28	3	64	78	0	114	-118	7	52	28	3	30	22	0	44	-28	4	77	77	2	71	-63
2	105	81	H,L=	1	6	4	120	119	H,L=	2	-1	1	130	138	9	34	10	4	47	55	1	121	132	5	109	-110	H,L=	7	-4
3	295	-325	0	140	-134	5	99	-97	1	439	467	2	69	56	10	58	-58	6	17	32	2	28	12	H,L=	5	-10	0	124	122
4	55	33	1	188	-189	6	67	-56	2	216	-200	3	64	-55	H,L=	3	-7	H,L=	4	11	3	60	49	0	105	-103	4	82	-78
5	38	32	2	58	44	8	31	-34	3	162	155	4	64	48	1	34	42	1	26	27	4	108	-112	1	146	-149	6	161	-152
6	37	14	3	141	-135	9	37	33	4	119	-122	5	70	64	3	81	-67	2	25	34	5	47	-36	3	49	-43	H,L=	7	-5
7	109	100	4	74	58	H,L=	1	-10	5	157	-137	6	66	54	4	144	-126	3	27	-33	6	86	-82	4	42	40	1	61	-39
8	55	-40	6	151	167	0	141	-159	6	131	124	7	135	128	5	268	-264	4	22	29	7	126	-144	6	55	59	2	161	157
9	36	25	7	56	38	1	79	-77	7	105	-86	8	59	43	6	52	29	H,L=	4	12	10	48	45	7	57	75	4	56	42
11	41	-36	9	69	55	2	43	-33	8	149	149	9	59	54	7	60	-47	0	24	-39	H,L=	5	3	H,L=	5	-11	7	36	48
H,L=	0	7	10	75	-81	3	37	-23	9	103	87	10	64	-61	9	73	65	H,L=	4	-1	1	70	61	1	146	147	H.L=	7	-7
1	148	-156	11	49	-47	4	97	93	11	125	120	H,L=	3	3	H,L=	3	-8	1	152	-183	4	105	-98	2	56	-54	1	80	80
2	77	58	H,L=	1	7	6	82	87	12	56	-62	1	82	-73	0	33	-37	2	40	21	5	76	-72	4	29	30	2	90	68
3	106	85	1	46	51	8	33	-27	H,L=	2	-2	2	111	107	1	100	90	3	114	-109	6	96	88	5	50	-45	5	47	-66
4	64	45	2	107	92	H,L=	1	-11	0	82	70	3	182	-189	2	44	46	4	80	-59	8	34	22	H,L=	5	-12	H,L=	7	-8
5	128	123	3	98	95	1	51	46	1	88	90	4	48	-38	3	193	210	5	184	199	9	53	-44	0	104	-99	0	74	-63
6	83	64	4	133	130	2	105	-116	2	88	-80	6	34	-28	4	173	-149	6	76	51	10	49	68	3	42	54	1	53	58
7	76	76	5	94	-92	4	49	-23	3	59	-64	7	74	-51	5	64	42	9	60	45	H,L=	5	4	H,L=	6	0	H,L=	7	-9
8	72	-60	8	57	-46	5	54	-55	4	193	200	8	110	-126	7	91	-93	10	43	-36	0	156	-186	0	65	-65	2	103	-101
9	54	-44	10	38	-34	6	61	63	5	126	108	H,L=	3	4	8	49	37	11	74	-94	1	107	124	2	143	-120	4	36	-52
H,L=	0	8	H,L=	1	8	H,L=	1	-12	6	111	100	0	49	40	9	69	-60	H,L=	4	-2	2	72	-65	3	122	-125	H,L=	7	-10
0	141	126	0	44	31	0	54	-59	7	79	-68	1	118	-118	10	24	-46	0	248	266	3	57	44	5	65	61	0	55	54
1	91	69	1	132	-124	H,L=	1	-13	8	74	59	3	130	-114	H,L=	3	-9	1	81	-81	4	81	88	6	86	67	3	65	63
2	86	66	2	72	49	2	78	-83	9	156	-178	6	95	-88	1	35	36	2	83	82	5	44	23	7	72	94	H,L=	8	0
3	69	-53	3	163	-177	H,L=	2	0	H,L=	2	-3	7	101	83	2	74	-61	3	213	-251	6	117	121	H,L=	6	1	0	97	96
4	197	-218	4	119	-99	0	280	-279	1	195	-211	8	92	-90	3	37	35	4	47	-37	7	81	-67	2	72	52	1	79	82
6	125	-128	5	80	-81	1	93	91	2	172	-187	9	62	49	4	111	-99	5	55	43	8	47	-35	4	77	68	H,L=	8	1
7	40	28	7	86	85	2	256	-267	3	22	-21	10	31	37	7	63	60	6	149	-137	9	39	-36	6	85	-71	1	140	134
8	45	-33	9	71	83	3	161	-181	4	296	-300	11	46	-59	8	73	78	7	178	178	H,L=	5	5	H,L=	6	2	2	61	-49
9	23	-2	10	35	39	4	42	32	5	45	-46	H,L=	3	5	H,L=	3	-10	8	61	48	1	89	86	0	117	93	H.L=	8	3
10	61	76	H,L=	1	9	5	93	95	6	169	165	1	184	-197	0	111	109	9	69	46	2	107	94	1	63	42	1	69	63
H,L=	0	9	1	56	-48	6	165	178	8	100	94	3	96	78	1	59	55	10	53	58	5	79	-73	2	136	134	2	76	50
1	88	-84	3	62	52	7	119	122	9	121	-124	4	66	-49	2	132	127	H,L=	4	-3	6	71	-72	4	63	-62	H,L=	8	4
2	153	-149	4	109	112	8	64	56	10	44	28	5	227	235	3	66	50	1	109	96	7	35	-39	H,L=	6	3	1	62	-61
3	84	-78	7	81	82	10	101	-98	11	66	-64	6	24	19	4	101	-90	2	143	142	8	44	-30	5	77	80	H,L=	8	5
4	98	-88	8	37	-38	11	33	-23	12	87	-85	7	79	60	5	51	43	3	81	63	H,L=	5	6	7	66	81	1	46	-49
5	34	29	9	52	-71	12	40	-46	H,L=	2	-4	8	58	50	6	75	-67	4	146	158	0	82	-80	H,L=	6	4	H,L=	8	6
6	79	75	H,L=	1	10	H,L=	2	1	0	264	-273	9	92	-98	7	60	-58	5	28	26	1	54	-53	0	109	-103	2	26	31
7	38	37	0	37	28	1	107	100	3	128	121	H,L=	3	6	8	23	41	6	110	-102	2	44	29	3	146	151	H,L=	8	-1
8	48	37	2	83	75	2	51	43	4	83	-73	0	90	83	H,L=	3	-11	7	94	69	3	76	-71	4	60	-67	1	80	-98
H,L=	0	10	3	58	42	3	130	-142	5	76	67	3	91	78	1	82	-85	8	70	-66	5	36	-30	7	80	-95	H,L=	8	-2
0	49	38	4	108	-112	4	78	71	6	162	-163	5	64	60	2	36	33	9	72	68	6	110	121	H,L=	6	5	0	80	94
2	102	92	5	50	-40	5	37	-29	10	35	32	7	37	-28	4	49	46	10	66	-65	8	26	13	2	100	-78	H,L=	8	-3
3	106	111	6	76	-88	6	105	-92	H,L=	2	-5	8	76	-72	5	66	61	H,L=	4	-4	H,L=	5	7	4	81	-91	1	69	-70
5	23	7	H,L=	1	11	7	166	170	1	75	-80	9	55	-42	6	58	-50	0	91	-97	2	89	96	5	80	-69	2	124	130
7	61	-54	3	55	-56	8	167	-169	2	18	12	10	47	50	7	62	77	1	93	-81	3	44	27	H,L=	6	6	H,L=	8	-4
8	41	-44	H,L=	1	12	10	37	-29	3	117	101	H,L=	3	7	H,L=	3	-12	2	110	-95	4	98	106	0	119	-137	0	87	-88
H,L=	0	11	3	62	64	11	51	33	4	82	62	1	83	-85	3	69	-66	3	81	-72	8	36	-51	3	55	61	1	78	-90
1	69	57	H,L=	1	13	12	48	55	5	203	216	2	166	-192	H,L=	3	-13	4	153	148	H,L=	5	8	4	53	68	4	81	87
2	64	-59	1	87	82	H,L=	2	2	6	76	-56	3	85	64	2	46	45	5	115	-119	1	71	-62	6	86	107	H,L=	8	-5
4	32	-26	H,L=	1	-1	0	165	-191	8	103	-89	4	90	-85	H,L=	4	0	8	34	-35	4	136	-134	H,L=	6	8	1	75	81
5	62	-62	1	110	120	1	125	-137	9	112	-110	5	101	95	0	412	446	9	46	40	5	44	-49	1	59	-32	2	83	58
6	27	11	2	299	335	2	43	-28	11	89	-112	8	92	104	1	23	9	10	69	-69	6	51	-56	H,L=	6	-1	4	77	93
7	50	56	3	69	-50	3	35	38	H,L=	2	-6	H,L=	3	8	2	47	-27	H,L=	4	-5	7	27	25	1	87	63	H,L=	8	-6
H,L=	0	12	4	176	188	4	34	24	0	138	-125	0	79	-75	3	38	32	1	34	-31	H,L=	5	9	3	61	44	0	79	-87
0	101	-110	5	42	-31	5	57	-46	1	45	-30	1	59	60	4	118	-128	2	93	79	2	46	-49	4	109	-95	3	73	50
1	56	-60	6	87	-62	6	30	13	3	128	-119	3	120	128	5	39	-31	3	93	-78	H,L=	5	10	5	93	-108	4	57	66
4	50	56	7	152	-146	7	48	36	4	55	34	4	66	56	6	162	-153	4	111	101	0	29	43	6	106	81	H,L=	8	-7
6	47	60	0	112	-129	9	146	171	5	52	-49	5	37	36	7	111	-88	5	224	-225	2	38	36	7	73	-82	2	86	-85
H.L=	0	13	9	71	65	11	67	-58	6	82	59	6	73	67	9	48	-35	6	48	-24	3	35	39	H,L=	6	-2	H,L=	8	-8
1	38	-39	H,L=	1	-2	H,L=	2	3	7	83	76	9	34	-42	10	53	53	7	75	-54	H,L=	5	-1	0	178	-205	0	69	72
2	49	52	0	423	-422	1	176	-208	8	54	32	H,L=	3	9	H,L=	4	1	9	32	24	1	81	77	2	64	-61	2	59	-57
3	34	27	1	188	-187	2	153	172	9	81	62	1	37	31	1	26	-15	H,L=	4	-6	2	118	123	4	126	132	3	98	100
4	29	43	2	231	-258	3	126	122	11	38	-48	2	38	-27	2	87	-74	0	97	-82	3	91	83	5	80	82	H,L=	9	-1
H,L=	0	14	3	251	-283	4	98	91	H,L=	2	-7	3	59	-54	3	98	-87	3	259	309	4	122	127	6	106	96	1	61	-76
0	24	-23	4	266	254	5	113	109	1	103	89	5	80	-93	4	51	-38	4	63	40	6	108	-100	H,L=	6	-3	H,L=	9	-2
1	23	-34	5	35	-24	6	73	-63	2	69	56	7	41	-29	5	28	-23	5	118	-103	7	26	-25	2	169	-161	1	62	-85
H,L=	1	0	6	139	122	7	102	102	3	51	41	H,L=	3	10	6	150	136	6	64	44	8	114	-127	4	186	-176	H,L=	9	-3
1	67	-64	10	131	-134	8	83	-64	4	133	148	0	63	-66	8	79	74	7	135	-151	9	42	34	6	121	132	1	100	91
2	53	-29	12	35	-41	9	193	-185	5	93	-75	H,L=	3	11	9	63	55	10	83	-98	10	34	-33	H,L=	6	-4			
3	174	-173	H.L=	1	-3	10	50	49	6	79	-60	1	48	30	10	52	49	H,L=	4	-7	H,L=	5	-2	1	109	108			
4	174	-176	1	175	174	11	79	-87	7	77	-59	2	70	82	11	30	-30	2	76	-58	0	104	-111	2	93	93			

Table 4. Comparison of bond lengths (Å) and angles (°) with related compounds

Length	GGBOPSA	Homo-taurine	Taurine	L-Arginine	GGBA·HCl	GABA	GABOB
C(1)–C(2)	1.545	1.526	1.520	1.540	1.557	1.519	1.525
C(2)–C(3)	1.491	1.508	—	1.517	1.528	1.502	1.516
C(3)–N(1)	1.456	1.486	1.484	1.471	1.477	1.469	1.477
C(4)–N(1)	1.332	—	—	1.351	1.317	—	—
C(4)–N(2)	1.353	—	—	1.340	1.338	—	—
C(4)–N(3)	1.298	—	—	1.322	1.318	—	—
S–O(1)	1.465	1.445	1.461	—	—	—	—
S–O(2)	1.456	1.469	1.448	—	—	—	—
S–O(3)	1.453	1.469	1.465	—	—	—	—
S–C(1)	1.773	1.761	1.780	—	—	—	—
C(2)–O(4)	1.381	—	—	—	—	—	1.425
Angle							
O(1)–S–O(2)	112.5	112.5	113.7	—	—	—	—
O(1)–S–O(3)	111.9	112.5	110.9	—	—	—	—
O(2)–S–O(3)	112.3	110.7	113.0	—	—	—	—
C(1)–S–O(1)	106.0	107.3	105.8	—	—	—	—
C(1)–S–O(2)	107.1	106.7	106.9	—	—	—	—
C(1)–S–O(3)	106.6	106.7	105.8	—	—	—	—
S–C(1)–C(2)	113.5	112.0	112.9	—	—	—	—
C(1)–C(2)–C(3)	110.1	110.7	—	110.1	107.1	113.0	110.8
C(2)–C(3)–N(1)	109.5	109.8	112.6	111.1	107.8	111.8	109.5
C(3)–N(1)–C(4)	124.9	—	—	123.2	123.7	—	—
N(1)–C(4)–N(2)	117.3	—	—	121.0	120.9	—	—
N(1)–C(4)–N(3)	123.1	—	—	118.9	120.3	—	—
N(2)–C(4)–N(3)	119.6	—	—	120.2	118.7	—	—
C(1)–C(2)–O(4)	111.5	—	—	—	—	—	111.1
C(3)–C(2)–O(4)	110.5	—	—	—	—	—	107.0

Stevensen,[14] the average being 1.328 Å. We see from Table 4 that C–N distances of the guanidyl group differ (greater than 2σ) from those of GGBA·HCl. This difference is probably due to the difference of molecular environments, *i.e.*, GGBOPSA molecule is in free state while GGBA molecule is in hydrochloride salt state. Three C–N bonds of GGBOPSA have somewhat double bond character and calculation by Pauling's method[15] indicates that the double bond characters of C(4)–N(1), C(4)–N(2), and C(4)–N(3) bonds are 32, 25, and 43%, respectively, whereas the corresponding values for GGBA·HCl are 35, 29, and 36%.[13]

It is of interest to note that C(2)–O(4) distance of the hydroxyl group is 1.381 Å, significantly shorter than that of found in GABOB (1.425 Å) which is normal C–O single bond. Other bond distances and angles in the molecule are quite normal.

The skeletal conformation of GGBOPSA molecule (Fig. 2) is of *trans* zigzag form as found in GGBA·HCl, GABA·HCl, GABOB, and homotaurine. The torsion angles around C(1)–C(2) and C(2)–C(3), which are in the skeletal conformation of the molecules, are both almost 180° in homotaurine, GABA·HCl, and GGBA·HCl. On the other hand, the corresponding values of GGBOPSA are 161.9 and 177.8°, and those of GABOB, 173.7 and 168.8°, respectively. The effect of β-hydroxyl group in the molecule might be one of the factors influencing the restricted conformation and

Table 5. Hydrogen bond lengths (Å) and angles (°) of GGBOPSA

Bond length (Å)		Bond angle (°)	
O(4)–H(1)—O(1) (I)	2.732	C(2)–O(4)–O(1) (I)	110.4
N(1)–H(7)—O(4) (II)	2.907	C(3)–N(1)–O(4) (II)	127.0
N(2)–H(8)—O(2) (II)	2.944	C(4)–N(2)–O(2) (II)	137.0
N(2)–H(8)—O(4) (II)	3.231	C(4)–N(2)–O(4) (II)	91.7
N(2)–H(9)—O(1) (III)	3.271	C(4)–N(2)–O(1) (III)	111.9
N(3)–H(10)—O(2) (III)	2.827	C(4)–N(3)–O(2) (III)	114.4
N(3)–H(11)—O(3) (IV)	2.945	C(4)–N(3)–O(3) (IV)	150.9
(I) (2.0−x, 0.5+y, 0.5−z)		(II) (2.0−x, 1.0−y, 1.0−z)	
(III) (−1.0+x, 0.5−y, 0.5+z)		(IV) (−1.0+x, y, z)	

14) V. Shomaker and D. P. Stevensen, *J. Amer. Chem. Soc.*, **63**, 37 (1941).

15) L. Pauling, "The Nature of the Chemical Bond," 3rd. ed., Cornell University Press, Ithaca (1960), p. 232.

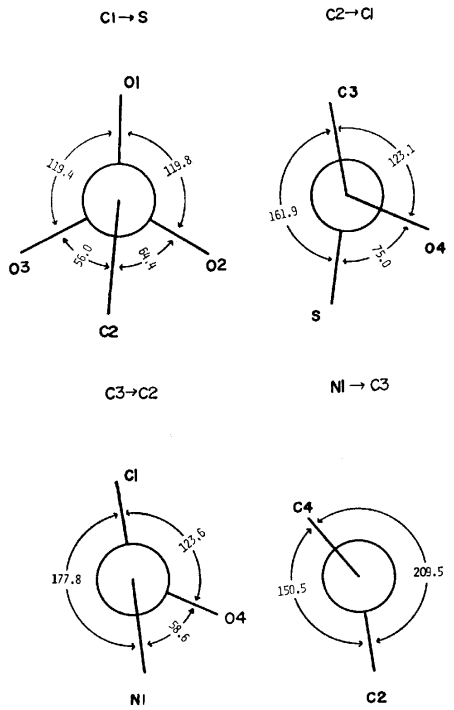

Fig. 2. Newman projection of atoms around four bonds. The arrow indicates the bond direction viewing down from front to back of paper.

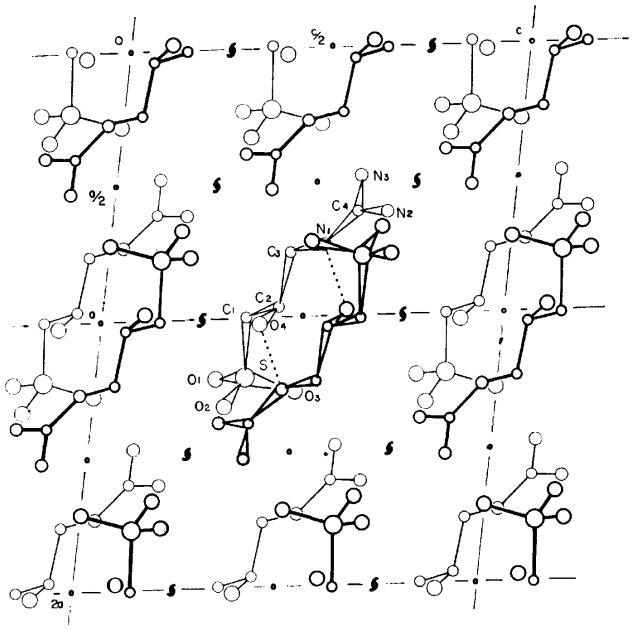

Fig. 3. The crystal structure projected along *b*-axis.

also the physiological action. Torsion angles of sulfonate group have similar values to those of homotaurine. The torsion angle around C(3)–N(1) is 150.5°, which is similar to 162.0° of L-arginine dihydrate[7] calculated.

Similarly in the case of L-arginine dihydrate, GGBOPSA molecule occurs in zwitterionic form, $(NH_2)_2^+$-$CNHCH_2CH(OH)CH_2SO_3^-$.

Distances and angles of hydrogen bonds are listed in Table 5. As shown in Fig. 3, *d*- and *l*-forms of GGBOPSA molecules were dimerized through the N(1)–H···O(4) hydrogen bonds (2.907 Å) related by a center of symmetry. This cyclic *d*–*l*, dimerization can be also seen in GABOB,[12] which were dimerized through OH···O hydrogen bond between β-OH group and oxygen atom of carboxyl group related by a center of symmetry. In these cases, however, the oxygen atom, O(4), of β-hydroxyl group of GGBOPSA molecule takes part in the intermolecular hydrogen bond system as an acceptor, while β-OH of GABOB is used to form intra- and intermolecular bifurcated hydrogen

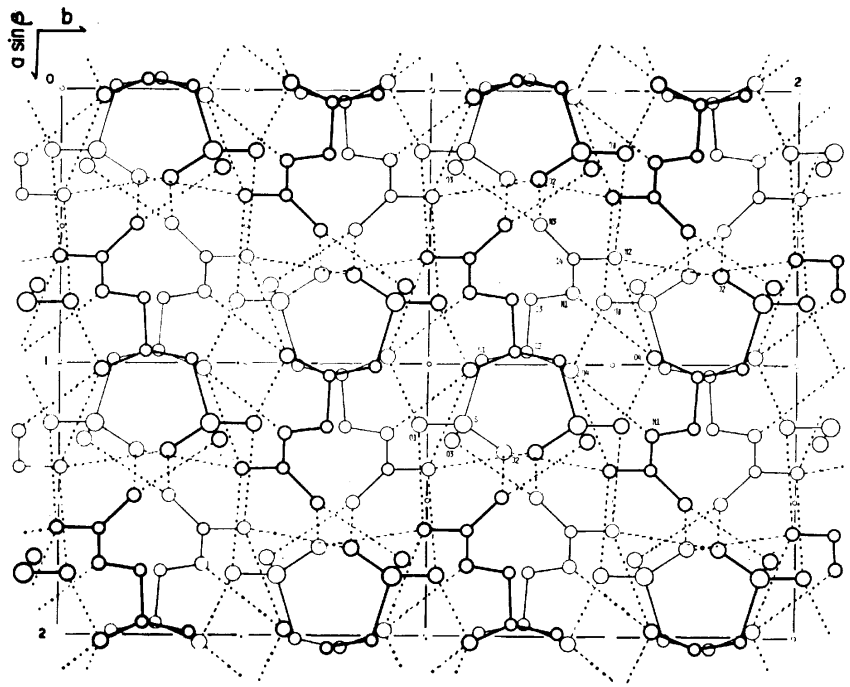

Fig. 4. The crystal structure projected along *c*-axis. The broken lines indicate the hydrogen bonds.

bond as a donor.

The crystal structure projected downward to *c*-axis is shown in Fig. 4. Among the hydrogen atoms in the molecule, all the feasible ones are utilized to form hydrogen bonds and the molecules are held together by three-dimensional network of NH···O and OH···O hydrogen bonds. The guanidyl group is connected with three neighboring molecules by six hydrogen bonds, the sulfonate group acting as an acceptor of five hydrogen bonds, and oxygen atom of hydroxyl group as both acceptor and donor. The distances of N(2) to O(2) and to O(4) by a translational operation (2.0-*x*, 1.0-*y*, 1.0-*z*) are 2.994 and 3.231 Å, respectively, H(8) atom being located on a line bisecting these two directions. Thus, the H(8) atom seems to contribute to form a bifurcated hydrogen bond. On the other hand, homotaurine molecules are jointed with each other with three NH···O hydrogen bonds to form a three-dimensional network, while in taurine, there are three NH···O intermolecular hydrogen bonds and one intramolecular hydrogen bonding. The intermolecular contacts between adjacent molecules are kept by normal van der Waals distances.

This work was partly supported by a research grant from the Ministry of Education.

BULLETIN OF THE CHEMICAL SOCIETY OF JAPAN, VOL. 46, 2199—2204 (1973)

Crystal and Molecular Structure of ω-Amino Acids, ω-Amino Sulfonic Acids and Their Derivatives. IV. The Crystal and Molecular Structure of γ-Aminobutyric Acid (GABA), a Nervous Inhibitory Transmitter

Ken-ichi TOMITA, Hideko HIGASHI, and Takaji FUJIWARA

Faculty of Pharmaceutical Sciences, Osaka University, Toneyama, Toyonaka, Osaka 560

(Received December 28, 1972)

The structure of γ-aminobutyric acid (GABA), $C_4H_9NO_2$, was determined by single-crystal X-ray diffraction analysis using the data collected on a four-circle diffractometer. The compound was crystallized from an aqueous ethanol solution as needles of the monoclinic space group $P2_1/c$ with four molecules in the following unit cell; $a=7.193$, $b=10.120$, $c=8.260$ Å and $\beta=111.05°$. The structure was solved directly by a symbolic addition method and refined by a least-squares procedure. The final R is 9.3%. The molecular geometry is not a planar *trans*-zigzag configuration as found in γ-guanidinobutyric acid hydrochloride or homotaurine, but a *gauche* configuration with respect to $C_\alpha-C_\beta$ bond. The expected zwitterionic structure is evident from the locations of the hydrogen atoms in a difference Fourier map, each molecule being connected with three N–H···O hydrogen bonds to form a three-dimensional network.

Unusual amino acids, in particular ω-amino acids, are of interest with respect to their characteristic biological actions. γ-Aminobutyric acid (GABA) occurs especially in the mammalian brain[1] where it is enzymatically produced.[2] By virtue of its potent synaptic effect and other extensive evidence, GABA may play the physiological role of "inhibitory transmitter" in the mammalian central nervous system.[3-7]

It seems important to determine the molecular structure of such biologically active compounds and to compare it with that of other related derivatives in order to elucidate the close relation between molecular conformation and its specific physiological action.

The crystal data and some structural features of GABA and its derivatives were reported briefly.[8] As a part of this project, the details of structure analysis of homotaurine and γ-guanidinobutyric acid hydrochloride and hydrobromide were recently given.[9-10] This paper deals with precise analyses of crystal and molecular structure of γ-aminobutyric acid.

Experimental

Commercial γ-aminobutyric acid (GABA) was used, colorless needle-like crystals elongated along *a* axis being obtained by slow evaporation of an aqueous ethanol solution. They were somewhat hygroscopic and were used for X-ray investigation on being sealed in a quartz capillary together with a few piece of ssilica gel. Oscillation and Weissenberg photographs showed the crystals to be monoclinic. Systematic extinctions, $0k0$ absent with k odd and $h0l$ absent with l odd, indicated the space group to be $P2_1/c$. Unit-cell dimensions, $a=7.193(4)$, $b=10.120(5)$, $c=8.260(5)$ Å and $\beta=$

1) J. Awapara, A. J. Landua, R. Fuerst, and B. Seale, *J. Biol. Chem.*, **187**, 35 (1950).
2) E. Roberts and S. Frankel, *ibid.*, **187**, 55 (1950).
3) D. P. Purpura, M. Girado, and H. Grundfest., *Science*, **125**, 1200 (1957).
4) D. R. Curtis and J. C. Watkins, *Pharmac. Rev.*, **17**, 347 (1965).
5) J. F. Mitchell and V. Srinivasan, *Nature*, **224**, 663 (1969).
6) D. R. Curtis, A. W. Duggan, D. Felix, and G. A. R. Johnston, *ibid.*, **226**, 1222 (1970).
7) K. Krnjević, *ibid.*, **228**, 119 (1970).
8) K. Tomita, *Tetrahedron Lett.*, **1971**, 2587.
9) S. Ueoka, T. Fujiwara, and K. Tomita, This Bulletin, **45**, 3634 (1972).
10) T. Maeda, T. Fujiwara, and K. Tomita, *ibid.*, **45**, 3628 (1972).

111.05(7)° were determined on a diffractometer. The calculated density corresponding to four molecules in the unit cell is 1.226 g·cm^{-3} and in good agreement with the observed density of 1.225 g·cm^{-3}, determined by flotation in a mixture of benzene and carbon tetrachloride. Using a cuboid crystal with an edge of 0.3 mm, all the intensities of 1243 independent reflections within $2\theta<55°$ were measured on a Rigaku-Denki computer-controlled four-circle diffractometer with Zr-filtered MoK_α radiation. The ω-2θ scanning was employed at a rate of 2° per min, and backgrounds were measured for 10 sec at each start and end point of the scan interval. Lorentz and polarization corrections were applied, but neither extinction nor absorption corrections were considered. The observed structure factors were adjusted to their absolute values by Wilson's method and then normalized structure factors $|E|$ were obtained.

Structure Determination and Refinement

The crystal structure of GABA was determined by direct phase determination using the symbolic addition procedure.[11] From a $\sum_2$ list for 169 reflections with $|E|\geqq1.5$ and with probability greater than 97%, the signs of three reflections were chosen for specifying the origin and four symbols for initiating the sign determinations (Table 1). The signs were determined as follows by many different combinations in $\sum_2$ interactions; A=B=C=− and D=+. An E map calculated with the signs of 161 reflections revealed the locations of all atoms except hydrogen atoms in the unit cell. Refinement of the structure was carried out using a block-diagonal least-squares program (BLLS) with unit weight for non-zero reflections. Atomic scattering factors were taken from "International Tables for X-ray Crystallography" (1962). Application of isotropic temperature factor to non-hydrogen atoms decreased the R index ($R=\sum||F_o|-|F_c||/\sum|F_o|$) to 0.21 after five cycles. The following five cycles of anisotropic refinement lowered R to 0.13. A difference Fourier synthesis at this stage was calculated and all hydrogen atoms were shown in this map. The final cycles of refinement including the hydrogen atoms with isotropic temperature factors reduced the R index to 0.093 (0.127 including $|F_o|=0$). The final positional and thermal parameters are given in Table 2, and the observed and calculated structure factors in Table 3.

All the numerical computations were carried out on NEAC 2200-500, NEAC 2200-700 computers in the computing center of this University, and FACOM 230-60 in the data processing center of Kyoto University, using the programs written by Dr. Tamaichi Ashida and by the authors.

Table 1. Starting set for the symbolic addition procedure

h	k	l	sign	|E|
2	2	−7	+	3.593
4	3	3	+	3.475
3	1	5	−	2.671
0	2	1	A	3.745
1	1	8	B	3.072
6	1	−4	C	2.934
8	3	−7	D	3.963

Results and Discussion

The bond lengths and angles of GABA are shown in Figs. 1(a) and 1(b), respectively. The C4–N bond length of 1.469 Å is very close to the sum of each covalent bond radius for the carbon and nitrogen atom (1.47 Å), being a little less than the average value of 1.487 Å found in α-amino acids.[12] The

Table 2. Final positional and thermal parameters

All values × 10^4 for O, N, and C atoms; for H, position parameters × 10^3. E.s.d.'s in parentheses are in units of least significant digit. Isotropic B's for H atoms in Å^2; for other atoms, the expression is: $\exp[-(B_{11}h^2+B_{22}k^2+B_{33}l^2+B_{12}hk+B_{13}hl+B_{23}kl)]$.

Atom	x	y	z	B_{11} or B	B_{22}	B_{33}	B_{12}	B_{13}	B_{23}
O1	−196(4)	1513(3)	1757(3)	180(6)	170(4)	179(5)	79(9)	154(9)	82(8)
O2	2268(4)	500(4)	3730(4)	251(8)	217(6)	243(7)	70(11)	185(12)	244(11)
N	8163(4)	1591(3)	4316(4)	176(7)	112(4)	136(5)	−27(8)	123(10)	1(7)
C1	1544(5)	1052(4)	2320(5)	148(7)	102(4)	139(6)	1(9)	72(11)	31(9)
C2	2790(5)	1211(4)	1185(5)	149(8)	150(6)	139(7)	−8(11)	97(11)	−8(10)
C3	4989(5)	907(4)	2091(5)	166(8)	107(5)	168(7)	6(10)	134(12)	−39(9)
C4	6082(5)	1962(4)	3353(5)	164(8)	105(4)	156(7)	−2(9)	131(12)	−33(9)
H1	238(7)	230(5)	85(6)	4.4(12)					
H2	219(6)	71(5)	3(6)	4.0(12)					
H3	557(6)	81(4)	127(5)	3.1(10)					
H4	498(6)	7(4)	254(6)	3.0(10)					
H5	558(6)	210(4)	412(5)	3.5(11)					
H6	607(5)	280(4)	273(5)	2.0(8)					
H7	835(6)	70(5)	520(6)	4.2(12)					
H8	874(6)	245(4)	516(6)	3.4(10)					
H9	905(6)	170(4)	347(6)	4.0(11)					

11) H. Hauptman and J. Karle, "Solution of the Phase Problem," A. C. A. Monograph No. 3. Polycrystal Book Service, Pittsburgh (1953), Chapter I.

12) R. E. Marsh and J. Donohue, *Advan Protein Chem.*, **22**, 235 (1967).

TABLE 3. OBSERVED AND CALCULATED STRUCTURE FACTORS (×10)

Reflections with asterisk were omitted from the least-squares refinement.

H FO FC	H FO FC	H FO FC	H FO FC	H FO FC	H FO FC	H FO FC	H FO FC
K,L= 6 -1	1 89-101	7 52 53	9* 0 -11	8 61 50	7 9 16	6 17 -19	6* 0 -9
1* 0 -8	2 49 76	8* 0 -3	K,L= 2 -4	9 21 20	8 16 15	7 21 24	7* 0 16
2* 0 6	3 115 114	9* 0 3	1 48 -53	K,L= 2 -5	9 23 12	8 73 -65	8 5 -6
3 74 -74	4 66 63	K,L= 4 -3	2* 0 14	1 10 20	K,L= 1 -6	K,L= 2 -7	K,L= 3 -8
4 33 -34	5 9 -11	1 44 -62	3 37 41	2 69 -61	1 36 40	1 53 53	1 36 -36
5 53 51	6 91 92	2 45 47	4 26 -44	3 207-214	2 34 41	2 191 189	2 28 -30
6 72 -67	7 18 23	3 116 124	5 14 -18	4 2 -12	3 39 47	3 44 45	3 83 83
7 28 -29	8* 0 17	4 97 96	6 45 44	5 7 18	4 60 59	4 52 -57	4* 0 -8
8* 0 3	K,L= 5 -2	5* 0 1	7 28 -35	6 65 67	5 25 21	5 27 20	5 30 29
K,L= 7 -1	1 131-124	6 100 -95	8* 0 8	7 22 19	6 39 48	6 54 46	6 28 -23
1 12 -12	2 28 -21	7 57 61	9 35 -25	8* 0 -3	7 42 -46	7 30 29	7* 0 -3
2 53 -50	3 79 -75	8 17 15	K,L= 3 -4	9 21 -14	8 81 71	8 12 11	K,L= 4 -8
3 71 73	4 60 -55	K,L= 5 -3	1 110 110	K,L= 3 -5	9 37 33	K,L= 3 -7	1 31 27
4 16 18	5 24 23	1 122-119	2 129-145	1 104-112	K,L= 2 -6	1 5 19	2 54 45
5 9 -10	6 31 24	2 66 73	3 59 -55	2 45 -44	1 49 51	2 50 58	3* 0 1
6 44 -37	7 20 -25	3 22 27	4* 0 1	3 37 -44	2 39 -47	3 52 62	4 21 21
7 3 -16	8 25 -20	4 22 -30	5 68 69	4 45 -46	3 63 -70	4 27 -30	5 17 15
K,L= 8 -1	K,L= 6 -2	5 50 -55	6 30 -30	5 80 -78	4* 0 16	5 12 -14	6 28 24
1 59 63	1 25 19	6 13 -11	7 24 -24	6 113-113	5 12 13	6* 0 4	7* 0 -11
2 34 -40	2 12 -13	7 7 7	8 45 -38	7 32 27	6 3 15	7 15 12	K,L= 5 -8
3 71 66	3 140-140	8 33 32	9 20 17	8* 0 -7	7 30 -25	8 77 66	1 1 9
4 50 45	4 79 -72	K,L= 6 -3	K,L= 4 -4	K,L= 4 -5	8 35 -33	K,L= 4 -7	2* 0 5
5 61 58	5 47 -46	1 41 -36	1) 0 -23	1 108-110	K,L= 3 -6	1* 0 -4	3 7 12
6 14 -14	6 70 64	2 41 -33	2* 0 -16	2 29 37	1* 0 2	2 3 -17	4 19 -21
7 3 -7	7 21 -23	3 43 55	3 77 72	3 109 110	2 64 70	3* 0 3	5 21 -18
K,L= 9 -1	8* 0 -11	4 5 -6	4 39 40	4* 0 -4	3 109-103	4* 0 -1	6 30 -18
1 43 42	K,L= 7 -2	5* 0 9	5 33 -34	5 17 -20	4 36 36	5 50 -45	7 40 34
2* 0 -14	1 19 21	6 54 51	6 63 -69	6 13 -13	5 11 7	6* 0 5	K,L= 6 -8
3 28 -28	2 46 53	7* 0 -10	7* 0 -5	7* 0 -7	6 18 21	7 39 -38	1 33 -31
4* 0 -1	3 6 7	8 31 22	8 32 -28	8 37 38	7 17 -19	8 14 -11	2* 0 12
5 15 -14	4* 0 -4	K,L= 7 -3	K,L= 5 -4	K,L= 5 -5	8 48 38	K,L= 5 -7	3 24 28
6 3 -5	5* 0 19	1 86 -81	1 169 176	1 25 22	K,L= 4 -6	1 32 25	4* 0 -5
K,L= 10 -1	6 16 20	2 53 -44	2 67 58	2 123-129	1* 0 8	2 58 58	5 62 -54
1 20 18	7* 0 10	3 40 -36	3* 0 -5	3 91 94	2 139-142	3 114-108	6 29 -25
2 8 -12	K,L= 8 -2	4 32 30	4 12 -9	4 34 38	3 119-120	4* 0 10	K,L= 7 -8
3 24 15	1* 0 -3	5 44 -40	5 86 87	5 26 23	4* 0 2	5 20 -20	1* 0 0
4 20 -20	2 40 36	6 13 -12	6 97 89	6 19 -18	5 54 59	6 23 22	2 8 0
5 13 -11	3 41 -39	7 29 -25	7 18 16	7 13 -9	6* 0 -8	7* 0 2	3 26 -23
K,L= 11 -1	4 4 10	K,L= 8 -3	8 27 -21	8 16 -17	7 17 -18	K,L= 6 -7	4 21 23
1* 0 -5	5 13 13	1 32 -42	K,L= 6 -4	K,L= 6 -5	8* 0 -3	1 7 -12	5 32 -26
2 21 20	6 37 -40	2 25 -30	1 74 74	1 33 -35	K,L= 5 -6	2 33 -31	K,L= 1 -9
3 15 -8	7* 0 -5	3 88 -84	2 49 49	2 55 61	1 3 3	3 33 -36	1* 0 13
4 4 3	K,L= 9 -2	4 4 5	3* 0 12	3 79 77	2 53 -56	4 20 -22	2* 0 2
K,L= 12 -1	1* 0 13	5 11 2	4* 0 -19	4 40 40	3 73 -74	5 20 27	3 49 -53
1 24 -14	2* 0 -4	6 23 21	5 1 -8	5 75 -74	4* 0 -7	6 21 -20	4 26 -25
2 2 8	3 56 51	7 14 -14	6* 0 -12	6* 0 -8	5 25 -32	7 15 12	5 24 -17
3 25 -19	4 24 -21	K,L= 9 -3	7 36 39	7 14 18	6 12 -8	K,L= 7 -7	6 24 21
K,L= 13 -1	5 22 13	1 23 21	8* 0 -1	8 22 -19	7 9 -9	1 9 5	7 18 14
1 15 -13	6 14 -12	2* 0 7	K,L= 7 -4	K,L= 7 -5	8 25 -18	2* 0 -12	K,L= 2 -9
K,L= 0 -2	K,L= 10 -2	3 12 4	1 46 -40	1* 0 -3	K,L= 6 -6	3 30 -25	1 3 -4
1 378 306	1 37 33	4* 0 -3	2 83 77	2 42 36	1* 0 5	4 20 -13	2 36 -36
2 552-535	2 8 -13	5 30 31	3 26 -29	3 36 31	2* 0 25	5* 0 0	3 8 15
3 16 37	3 65 60	6* 0 10	4 44 -45	4* 0 0	3 33 22	6 38 32	4 64 -58
4 109-104	4 22 21	K,L= 10 -3	5 39 -42	5 64 63	4 9 10	K,L= 8 -7	5 20 -23
5 108-104	5* 0 8	1 8 -11	6 10 -1	6 10 4	5 8 7	1 52 50	6* 0 4
6 146-133	6* 0 -10	2 22 17	7 9 2	7 25 20	6 9 -5	2* 0 2	7* 0 4
7 38 -38	K,L= 11 -2	3 3 2	K,L= 8 -4	K,L= 8 -5	7 26 20	3* 0 -17	K,L= 3 -9
8* 0 -11	1* 0 7	4 15 19	1 17 16	1 17 10	K,L= 7 -6	4* 0 -5	1* 0 5
9* 0 -4	2 18 -14	5 24 -20	2 30 -31	2* 0 8	1 22 -25	5 18 15	2 20 19
K,L= 1 -2	3 22 -21	6 14 -10	3 11 -9	3* 0 11	2 81 -76	6 37 32	3 26 22
1 287 253	4 12 13	K,L= 11 -3	4 24 -29	4 42 -42	3 87 84	K,L= 9 -7	4 30 32
2 394 397	5 5 -12	1* 0 -8	5 48 39	5* 0 -1	4 40 43	1 10 -10	5* 0 0
3 36 101	K,L= 1 -3	2* 0 -5	6* 0 11	6 1 4	5 27 22	2 4 2	6 7 7
4 75 73	1 22 -33	3 31 27	7 12 -17	7* 0 7	6 26 -26	3 23 23	7 30 -22
5 182-181	2 335-336	4 4 -7	K,L= 9 -4	K,L= 9 -5	7 4 -8	4* 0 9	K,L= 4 -9
6* 0 5	3 169-169	5 16 13	1* 0 8	1 8 15	K,L= 8 -6	K,L= 0 -8	1* 0 2
7 85 84	4 26 24	K,L= 12 -3	2 8 -16	2 64 53	1 3 -11	1 34 -43	2 12 -12
8 21 16	5 177 173	1* 0 7	3* 0 -32	3 17 -21	2* 0 7	2 131-133	3 25 -21
9* 0 -2	6 90 -88	2* 0 3	4* 0 18	4 51 -50	3 29 26	3 5 21	4 30 30
K,L= 2 -2	7 84 -85	3 41 30	5 2 -39	5 46 -40	4 36 28	4* 0 6	5 55 52
1 309-281	8 23 -25	K,L= 0 -4	6* 0 6	6 20 17	5 27 -29	5 54 -54	6* 0 -1
2 38 62	9 25 25	1 73 61	K,L= 10 -4	K,L= 10 -5	6* 0 9	6 23 -38	K,L= 5 -9
3 227 227	K,L= 2 -3	2 337 342	1 9 -16	1 11 9	K,L= 9 -6	7 25 -21	1* 0 -7
4 66 87	1 11 25	3 272-260	2* 0 -12	2* 0 2	1 15 -12	8 6 -9	2 3 -1
5 22 25	2 420-424	4 118-130	3 3 -41	3 6 -3	2* 0 1	K,L= 1 -8	3 10 16
6 75 -93	3 45 56	5 23 -16	4* 0 29	4 11 -12	3 12 15	1 27 -31	4 8 -20
7 40 47	4 57 56	6 154 155	5* 0 9	5 14 12	4 17 14	2 24 -24	5 52 50
8 14 14	5* 0 -1	7 86 82	K,L= 11 -4	K,L= 11 -5	5 28 26	3 33 27	6 6 -12
9 17 17	6 141-137	8* 0 1	1* 0 -2	1* 0 5	K,L= 10 -6	4 52 47	K,L= 0-10
K,L= 3 -2	7 55 -57	9 9 -7	2* 0 -12	2* 0 5	1 34 -28	5 10 9	1* 0 -13
1 17 -10	8 15 -20	K,L= 1 -4	3* 0 -9	3 15 -14	2* 0 -3	6 10 -12	2 7 20
2 228 229	9* 0 -9	1 149-153	K,L= 1 -5	4 6 0	3 2 11	7 23 -16	3* 0 2
3 94 108	K,L= 3 -3	2 106-105	1 22 -28	K,L= 0 -6	4 12 -8	8 52 -51	4 71 73
4 79 -83	1 349 350	3 51 -53	2 40 43	1 70 65	K,L= 1 -7	K,L= 2 -8	5 19 -22
5 119-121	2 120 125	4 78 -86	3 35 37	2 214 211	1 46 -44	1 8 -4	6 29 -28
6 11 13	3 14 16	5 5 16	4 109 105	3 149 149	2 37 -38	2* 0 -7	
7 37 37	4 45 50	6 159-155	5 8 -2	4 100 -91	3 67 63	3 20 -19	
8 40 37	5 20 -23	7 19 -23	6 57 61	5 24 18	4 9 -17	4 16 24	
K,L= 4 -2	6 100 100	8 10 -6	7 27 -26	6 19 7	5* 0 -4	5 47 46	

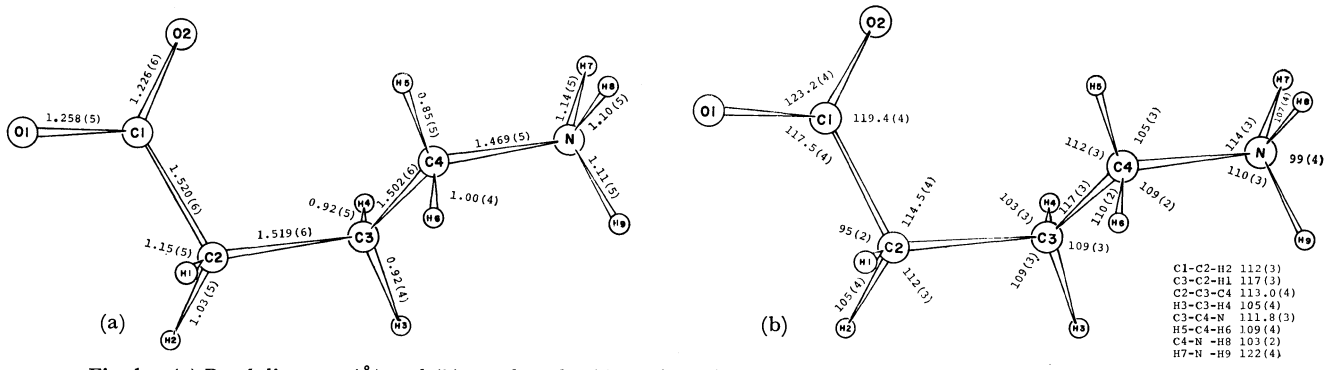

Fig. 1. (a) Bond distances (Å) and (b) Bond angles (°). The estimated standard deviations are shown in parentheses.

(Table 3. continued)

H FO FC	H FO FC	H FO FC	H FO FC	H FO FC	H FO FC	H FO FC	H FO FC
K,L= 0 0	3 24 -17	4 24 18	K,L= 8 2	2 6 2	K,L= 9 4	1 17 18	0 13 -11
1 114 94	4 25 -23	5 24 20	0 13 -12	3 60 61	0 4 6	2 70 -70	K,L= 0 8
2 130-124	5 12 -18	K,L= 10 1	1 55 -51	4 14 17	1 35 34	3 51 46	0* 0 -9
3 192-214	K,L= 11 0	0* 0 6	2* 0 3	5 2 -7	2 12 -2	4 10 8	1 9 14
4 192 196	1 24 -27	1 18 -12	3 80 74	K,L= 9 3	3 24 24	5* 0 0	2 4 -7
5 125 135	2 46 -39	2 24 33	4* 0 -7	0 17 -13	4 30 -23	K,L= 2 6	3* 0 -11
6 77 79	3 8 16	3* 0 2	5 10 -13	1 13 13	K,L= 10 4	0 15 -24	K,L= 1 8
7 28 23	4 5 9	4 10 -6	6 9 13	2 29 29	0 24 24	1 13 -12	0 24 25
8 41 40	K,L= 12 0	5* 0 -3	K,L= 9 2	3 23 25	1 50 43	2 35 -41	1 88 -81
K,L= 1 0	0* 0 8	K,L= 11 1	0 21 -21	4 5 -7	2* 0 1	3 6 -14	2 5 -12
1 52 50	1* 0 3	0* 0 -2	1 3 12	K,L= 10 3	3* 0 -11	4 11 16	3* 0 0
2 42 -50	2* 0 12	1* 0 2	2 20 -20	0 11 1	K,L= 11 4	5 6 -11	K,L= 2 8
3 262 264	3 27 -20	2 19 -16	3 50 -44	1 18 16	0 36 -30	K,L= 3 6	0 35 46
4 73 -61	K,L= 1 1	3 14 -16	4* 0 -3	2 11 -13	1 8 -8	0 65 -61	1 13 24
5 15 -13	0 112 -88	4* 0 1	5 21 -14	3 23 -21	2* 0 -2	1 30 31	2 22 -18
6 96 103	1 355-321	K,L= 12 1	K,L= 10 2	4* 0 -11	K,L= 12 4	2 20 14	3* 0 4
7 30 20	2 83 79	0 23 -21	0 48 -51	K,L= 11 3	0 10 14	3 46 44	K,L= 3 8
8 10 8	3 249 283	1 15 9	1* 0 -3	0* 0 -3	K,L= 1 5	4* 0 -4	0 8 18
K,L= 2 0	4 80 80	2* 0 8	2 12 23	1 18 19	0 134 135	5* 0 -5	1 49 -46
0* 0 -30	5 57 -60	3 6 9	3 25 28	2* 0 5	1 77 79	K,L= 4 6	2* 0 -15
1 45 -49	6 41 50	K,L= 13 1	4 10 10	3 17 16	2 27 31	0 35 45	K,L= 4 8
2 173-144	7 50 41	0* 0 -3	K,L= 11 2	K,L= 12 3	3 125-123	1 17 -19	0 5 2
3 160-162	8 5 7	K,L= 0 2	0* 0 -7	0 25 21	4 12 18	2 30 -31	1* 0 -4
4 116 115	K,L= 2 1	0 395-370	1 12 -8	1 27 18	5 30 34	3 26 -25	2 13 11
5 65 -74	0 971-991	1 131-107	2 40 36	K,L= 0 4	6 32 31	4 49 -44	K,L= 5 8
6* 0 0	1 334-336	2 159-161	3 21 15	0 172-172	K,L= 2 5	K,L= 5 6	0 11 14
7 33 -27	2 84 -81	3 45 -49	K,L= 12 2	1 60 -55	0 34 33	0 63 -59	1 26 24
8* 0 4	3 105 98	4 5 4	0* 0 1	2* 0 20	1 7 2	1 20 15	2 19 19
K,L= 3 0	4 48 -53	5 79 72	1 8 6	3 42 -44	2 36 32	2 57 56	K,L= 6 8
1 436-401	5* 0 7	6 7 -10	2 29 -30	4 62 -66	3 93 88	3* 0 12	0 38 -39
2* 0 -2	6 43 -46	7 10 0	K,L= 1 3	5 55 -51	4 69 66	4 43 -35	1 24 -24
3 86 90	7 34 -30	K,L= 1 2	0 103-124	6 34 33	5 23 23	K,L= 6 6	K,L= 7 8
4 68 65	8 57 -51	0 5 14	1 45 -67	K,L= 1 4	K,L= 3 5	0 26 37	0* 0 -5
5 6 6	K,L= 3 1	1 60 -44	2 53 -54	0 172 180	0 57 -54	1 17 13	K,L= 1 9
6* 0 20	0* 0 7	2 37 37	3 61 60	1 150 150	1 52 -52	2 18 16	0 31 36
7 41 32	1 201-191	3 161-152	4 96 -98	2 21 18	2 67 -67	3 26 23	1 40 -38
8 19 -24	2 22 -41	4 183-183	5 43 -34	3 127-120	3 60 50	4* 0 4	K,L= 2 9
K,L= 4 0	3 166-163	5 9 14	6 47 -42	4 94 96	4* 0 -7	K,L= 7 6	0 6 7
0 409-413	4 67 -67	6 46 -46	7 7 5	5 50 50	5 18 -16	0* 0 -3	1* 0 -5
1 160-161	5 6 9	7 6 -9	K,L= 2 3	6 36 35	K,L= 4 5	1 36 -38	K,L= 3 9
2 1 -25	6 58 -62	K,L= 2 2	0 109-113	K,L= 2 4	0 16 -14	2 16 -18	0 33 -32
3 45 35	7 25 -22	0 69 -67	1* 0 4	0 5 -4	1 40 -31	3 16 -16	1 30 24
4 72 -80	8 29 -19	1 258 277	2 101 98	1 33 -29	2 109-113	K,L= 8 6	K,L= 4 9
5* 0 14	K,L= 4 1	2* 0 15	3* 0 -20	2 122 128	3 1 -5	0* 0 -13	0 17 -20
6 77 -78	0 14 -13	3 78 79	4 42 -39	3 22 -24	4 40 40	1 33 31	1 34 -33
7 43 -42	1 276 279	4 91 -92	5 64 -55	4 29 -32	5* 0 -4	2* 0 0	K,L= 5 9
8* 0 -7	2 93 95	5 43 40	6* 0 7	5* 0 -5	K,L= 5 5	3 24 -18	0 4 -5
K,L= 5 0	3 112 113	6* 0 13	7 32 -25	6* 0 8	0 41 -51	K,L= 9 6	K,L= 1 -1
1 154-164	4 130-129	7 3 -7	K,L= 3 3	K,L= 3 4	1 41 48	0 35 25	1 249 252
2 121-117	5 78 78	K,L= 3 2	0 206 211	0 169 168	2 40 44	1 32 -30	2 333 325
3 30 35	6 17 21	0 135-143	1 54 58	1 37 34	3 37 31	2 13 9	3 37 -48
4 63 60	7 18 14	1 186 185	2 89 -96	2 18 -12	4 13 -12	K,L= 1 7	4 10 -20
5 23 -26	K,L= 5 1	2 96 -87	3 2 14	3 110-103	5* 0 -12	0 29 -34	5 93 -95
6 79 -75	0 149-160	3 24 -15	4 183 184	4 24 26	K,L= 6 5	1 83 78	6 25 -32
7 29 -30	1 184 197	4 50 -45	5 49 49	5 51 45	0 39 52	2* 0 -5	7 8 21
8* 0 4	2* 0 10	5 17 -14	6 12 7	6 31 24	1 58 -53	3* 0 16	8 7 15
K,L= 6 0	3 34 36	6 23 -23	7 2 -6	K,L= 4 4	2 6 -13	4 1 -1	K,L= 2 1
0* 0 21	4 37 -34	7 17 -16	K,L= 4 3	0* 0 9	3 20 -22	K,L= 2 7	1 194-172
1 112 118	5 31 -39	K,L= 4 2	0 68 78	1 22 19	4 42 -37	0* 0 8	2 38 39
2* 0 17	6 14 -11	0 103 101	1 99-102	2* 0 0	5* 0 6	1 22 23	3 29 -44
3 82 87	7* 0 -12	1 186 207	2 93 82	3 85 88	K,L= 7 5	2 18 -16	4 166 203
4 13 -12	K,L= 6 1	2 123 131	3 79 -88	4 46 42	0 14 -11	3 26 -27	5 104 108
5 94 94	0 61 49	3 108-115	4* 0 -3	5 5 -6	1 59 56	4 31 -29	6 90 105
6* 0 0	1 146 144	4 12 -17	5 15 -10	6* 0 -4	2 16 11	K,L= 3 7	7 17 24
7 17 10	2 57 53	5 34 -29	6 27 19	K,L= 5 4	3 18 17	0 38 -39	8 6 13
K,L= 7 0	3 91 -88	6* 0 9	K,L= 5 3	0 107-117	4 43 -35	1 62 -63	K,L= 3 -1
1 98 99	4* 0 15	7* 0 10	0 176 172	1 36 -40	K,L= 8 5	2 41 40	1 82 68
2 13 15	5 28 -27	K,L= 5 2	1 54 -49	2 29 28	0* 0 17	3* 0 8	2 11 -24
3 24 20	6 19 21	0 117 115	2 33 -37	3 11 -4	1 47 41	4 14 -18	3 58 -65
4 31 -28	7 33 28	1* 0 18	3 62 -59	4 41 -40	2 29 25	K,L= 4 7	4 163-167
5 35 -36	K,L= 7 1	2 29 -28	4 16 15	5 35 -39	3 11 4	0 69 73	5 66 84
6 10 -9	0 35 29	3 108 106	5 39 32	6* 0 -1	4* 0 -1	1 19 18	6 105 110
7 12 6	1 19 12	4 134 124	6 5 3	K,L= 6 4	K,L= 9 5	2 19 -14	7* 0 -14
K,L= 8 0	2 67 69	5 29 30	K,L= 6 3	0 51 -56	0 28 -26	3 12 17	8 18 -19
0* 0 -15	3 50 47	6 17 -16	0 33 -31	1 70 -67	1 42 -39	K,L= 5 7	K,L= 4 -1
1 48 44	4 23 19	7* 0 9	1 46 -46	2 79 -80	2* 0 -7	0* 0 6	1 74 101
2* 0 -9	5 9 10	K,L= 6 2	2 34 -39	3 46 46	3* 0 -12	1 32 -28	2 82 -81
3* 0 2	6 11 -9	0 48 45	3 109 110	4 36 38	K,L= 10 5	2 12 -14	3 204-212
4 17 11	7 34 30	1 101-106	4 21 19	5* 0 0	0 13 13	3 9 -15	4 27 -27
5 37 -36	K,L= 8 1	2* 0 -20	5 19 -19	K,L= 7 4	1 4 9	K,L= 6 7	5 80 -90
6 19 14	0 14 17	3 85 -92	6 17 12	0 25 -23	2 1 -9	0 20 -22	6 51 54
K,L= 9 0	1 81 -83	4 31 27	K,L= 7 3	1 56 57	K,L= 11 5	1* 0 16	7 39 -35
1 15 -10	2* 0 -10	5* 0 -12	0 69 -74	2 25 33	0 7 13	2 11 13	8* 0 0
2 64 55	3 39 -41	6 21 18	1* 0 1	3 14 16	K,L= 0 6	3 25 -21	K,L= 5 -1
3* 0 -4	4* 0 0	K,L= 7 2	2 31 28	4 5 -13	0 9 6	K,L= 7 7	1 81 -98
4* 0 3	5 19 -23	0 150 149	3 68 -60	5 9 -1	1 48 -44	0 47 43	2* 0 11
5* 0 -3	6 5 7	1 58 -46	4 35 -30	K,L= 8 4	2 31 27	1* 0 -10	3 13 -13
6 2 -2	K,L= 9 1	2 64 -70	5 40 -37	0 15 17	3 91 84	2* 0 8	4 49 40
K,L= 10 0	0 59 54	3 64 -67	6 21 20	1 19 -17	4 64 62	K,L= 8 7	5 36 37
0 20 20	1 35 -31	4 15 15	K,L= 8 3	2* 0 10	5 39 38	0 18 -17	6 14 13
1 59 -55	2 72 -71	5 27 28	0 71 -69	3 29 -30	K,L= 1 6	1* 0 -6	7 13 9
2* 0 19	3 30 -29	6* 0 4	1 48 -49	4 26 -24	0 23 -21	K,L= 9 7	8 36 -39

GABA molecule has the zwitterionic structure as well as γ-amino-β-hydroxybutyric acid[13] or α-amino acids so far investigated. The molecular projections of GABA around the C2–C3 (C_α–C_β) and C1–C2 bonds are shown in Fig. 2. Three hydrogen atoms attached to the amino nitrogen atom are shown clearly in the difference Fourier map. This indicates that the rotation around the N–C4 bond is so restricted as having the most stable *trans* configuration (Fig. 2). The GABA molecule has no planar zigzag configuration but a somewhat twisted structure, *i.e.*, the C3–C4 bond has the *gauche* configuration to the C1–C2 bond with respect to the C2–C3 bond, the torsion angle around the C2–C3 bond being 73.6°. On the other hand, the carboxyl C1–O1 and C1–O2 bonds have nearly the *trans* and *cis* configuration to the C2–C3 bond with respect to the C1–C2 bond, and the torsion angles are 167.3 and 11.9°, respectively. It is of particular interest that the twisted molecular structure of GABA in the present work and the extended *trans*-zigzag one

13) K. Tomita, T. Fujiwara, H. Higashi, and M. Harada, presented at the Anual Meeting of Pharmaceutical Society of Japan (1971). Full detail will be published in the near future in this Bulletin.

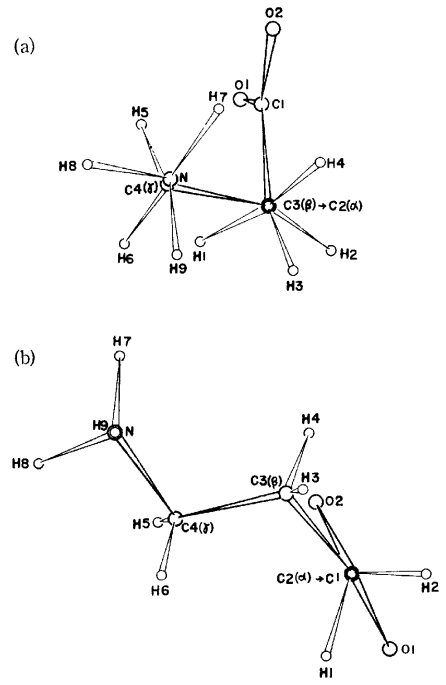

Fig. 2. Projections of the molecule. (a) around the C3–C2 (C_β–C_α) bond, (b) around the C2–Cl bond.

in GABA hydrochloride[14] are also found in bis(γ-aminobutyrato)copper(II)[15] and its dihydrate,[15] respectively. Three atoms, Cl, O1, and O2, of the carboxyl group and the C2 atom are exactly in one plane (mean deviation from the least-squares plane is 0.001 Å), another plane being formed by the C2, C3, C4, and N atoms with the mean deviation of 0.03 Å. The dihedral angle between these two planes is 79.1°, which coincides well with 68.4° in bis(γ-aminobutyrato)-copper(II). Similar dihedral angles between the plane of carboxyl group and that containing C_α, C_β, and N atoms have been observed in β-alanine (83.8°),[16] bis-β-alaninatocopper(II) hexahydrate (about 70°)[17] and bis(β-amino-*n*-butyrato)copper(II) dihydrate (about 67°).[18]

The GABA molecule is thought to be like a chemical condenser which is composed of the amino terminal with a positive charge, the carboxyl end with a negative charge and three non-conductive methylene linkages connecting both ends. It is also of interest to assume that the GABA molecule is a biological on-off switch which works with the change of surrounding environments such as pH, the concentration of Na^+ and Cl^- ions and so on. GABA is well-known as a chemical transmitter in the central nervous system. Which of the two observed configurations around the C2–C3 bond is the active form is not yet certain but correlation between configuration and charge of the GABA molecule, such as monovalent cationic, monovalent anionic and zwitterionic, is probably substantial for the interaction to its receptor. The intramolecular distances between the nitrogen and oxygen atoms are listed in Table 4 together with those of the related compounds.

The crystal structure of GABA is shown in projection along the crystallographic *b* and *c* axes in Figs. 3 and 4, respectively. Distances and angles about the hydrogen

Table 4. Intramolecular distances in GABA and related compounds

From atom	To atom	Distance (in Å)	Compound
O1	N	5.612 (0.006)[a]	GABA (this work)
O2	N	4.238 (0.007)	
O1	N	6.052 (0.007)	γ-Amino-β-hydroxybutyric acid[13]
O2	N	5.027 (0.007)	
O1	N	6.11 (0.02)	GABA·HCl[14]
O2	N	5.15 (0.02)	

a) Estimated standard deviations are in parentheses.

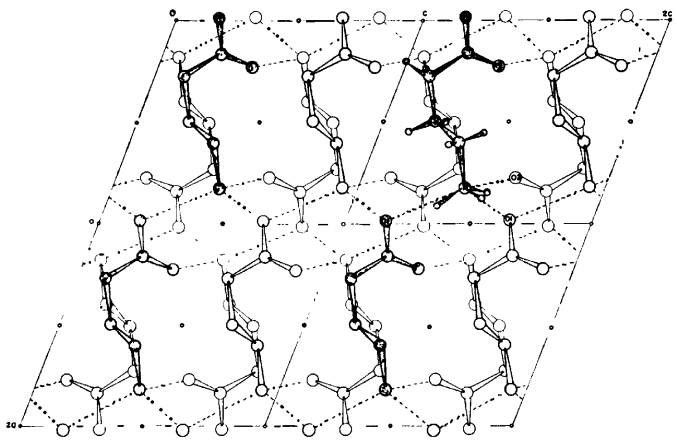

Fig. 3. The crystal structure projected along *b* axis. The broken lines indicate the hydrogen bonds.

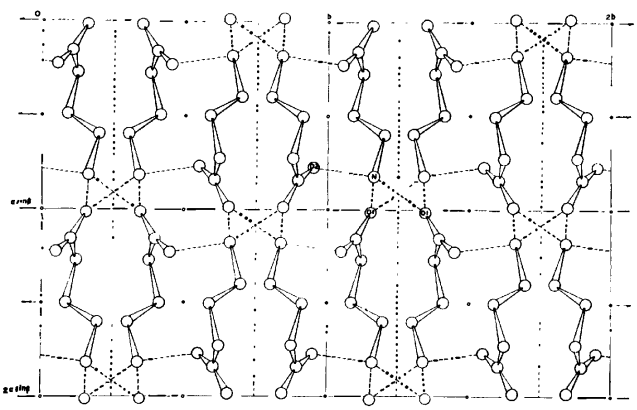

Fig. 4. The crystal structure projected along *c* axis. The broken lines indicate the hydrogen bonds.

14) K. Tomita, *Jap. J. Brain Physiol.*, **61**, 1 (1965).
15) A. Takenaka, E. Oshima, S. Yamada, and T. Watanabé, *Acta Crystallogr.*, **B29**, 503 (1973).
16) J. Jose and L. M. Pant, *ibid.*, **18**, 806 (1965).
17) K. Tomita, This Bulletin, **34**, 397 (1961).
18) B. R. Bryan, R. J. Poljak, and K. Tomita, *Acta Crystallogr.*, **14**, 1125 (1961).

Table 5. Hydrogen bond distances and angles in GABA

Distance (in Å)				Angle (in degrees)	
donor (original) acceptor					
N···O1 (I)	2.768 (0.006)[a]			C4–N···O1 (I)	103.0 (0.3)[a]
N···O1 (II)	2.726 (0.006)			C4–N···O1 (II)	107.9 (0.3)
N···O2 (III)	2.746 (0.007)			C4–N···O2 (III)	101.9 (0.3)
original		x	y	z	
(I)		$1+x$	y	z	
(II)		$1+x$	$1/2-y$	$1/2+z$	
(III)		$1-x$	$-y$	$1-z$	

a) Estimated standard deviations are in parentheses.

Table 6. Intermolecular distances less than 4.0 Å in GABA

From (original)	To	Distance (in Å)
N	O2 (I)[a]	3.346 (0.007)[b]
N	C1 (I)	3.436 (0.007)
C3	O1 (I)	3.624 (0.007)
C4	O1 (I)	3.413 (0.007)
N	C1 (II)	3.664 (0.007)
N	C2 (II)	3.836 (0.007)
C4	O1 (II)	3.471 (0.007)
N	Cl (III)	3.807 (0.007)
C4	O2 (III)	3.372 (0.007)
O2	C3 (III)	3.598 (0.007)
O2	O2 (III)	3.867 (0.010)

a) See symmetry codes in Table 5.
b) Estimated standard deviations are in parentheses.

bonds are listed in Table 5 and intermolecular distances less than 4.0 Å in Table 6. GABA molecules in the crystal are connected by three-dimensional networks of NH···O hydrogen bonds. Each hydrogen bond has nearly equal distance, three C4–N···O angles being also almost tetrahedral. The O2 atom is the acceptor of two hydrogen bonds whereas the O1 atom accepts only one hydrogen bonding. There are no unusual short contacts in this crystal, the shortest one of 3.346 Å being found between the N and O2 atoms.

The authors wish to thank the late Professor Masaji Tomita, Kobe Women's College of Pharmacy, for his valuable advice and continuous encouragement during the course of this work. The investigation was partly supported by a research grant from Ministry of Education.

BULLETIN OF THE CHEMICAL SOCIETY OF JAPAN, VOL. 46, 2204—2207 (1973)

The Electrochemical Fluorination of Benzenes and Pyridines[1)]

Yoshio INOUE,* Shunji NAGASE, Kazuo KODAIRA, Hajime BABA, and Takashi ABE
Government Industrial Research Institute, Nagoya, Kita-ku, Nagoya 462

(Received January 25, 1973)

The electrochemical fluorination of several aromatic compounds (benzene, fluorobenzene, chlorobenzene, *m*-dichlorobenzene, anisole, *o*-chloroanisole, thiophenol, *p*-chlorothiophenol, *m*-thiocresol, 2-chloropyridine, and 3-chloropyridine) has been carried out. Perfluorocyclohexane was the principal product from benzene and fluorobenzene. In addition, chloro-derivatives of perfluorocyclohexane were produced from chlorobenzenes. Anisoles gave fully-saturated perfluoroethers, together with cleaved products. Extensive cleavage was observed in the fluorination of thiophenols and chloropyridines, and fluorocarbons and sulfur hexafluoride or nitrogen trifluoride were characteristic products. New compounds were also formed, trifluoromethyl 2-chlorodecafluorocyclohexyl ether from *o*-chloroanisole, and 3-chlorodecafluoropiperidine and 2-chloroundecafluoropentane from 3-chloropyridine.

Although a number of papers dealing with the fluorination of aromatic compounds with elemental fluorine[2)] and with higher valency metallic fluoride[3)] have appeared, works on the electrochemical fluorination of these compounds are rare. A patent[4)] mentioned the electrochemical fluorination of several aromatic compounds, but no details were given. Shepard

* Present address: Nippon Oil Seal Industry Co., Ltd., Fujisawa, Kanagawa.

1) Presented in part at the Autumn Meeting of the Chemical Society of Japan, Nagoya, October, 1971.

2) a) L. A. Bigelow, "Fluorine Chemistry," Vol. 1, ed. by J. H. Simons, Academic Press, New York, N. Y., (1950), p. 380. b) J. M. Tedder, "Advances in Fluorine Chemistry," Vol. II, ed. by M. Stacey, J. C. Tatlow, and A. G. Sharpe, Butterworths Scientific Publications, London (1961), p. 129.

3) a) M. Stacey and J. C. Tatlow, "Advances in Fluorine Chemistry," Vol. I, ed. by M. Stacey, J. C. Tatlow, and A. G. Sharpe, Butterworths Scientific Publications, London (1960), p. 166. b) W. A. Sheppard and C. M. Sharts, "Fluorine Organic Chemistry," W. A. Benjamin, New York, N. Y., (1969), p. 72.

4) J. H. Simons, U. S. 2519983 (1950).

and Dannels,[5] and Kokhanov and Per'kova[6] have discussed a fluorine-containing polymer formed by the electrochemical fluorination of benzene. The difficulty of the fluorination of benzene itself by the electrochemical process has been described.[7] Soviet chemists have reported on the electrochemical fluorination of fluorinated anisole[8] and *N*,*N*-dimethylaniline,[9] but they have also described their failure in the fluorination of unfluorinated anisole.[8]

The present paper will deal with the electrochemical fluorination of benzene and its derivatives in order to clarify their behavior in the fluorination. For the sake of comparison with the fluorination of chlorobenzenes, the fluorination of chloropyridines was also included in the present work. Pyridine has often been subjected to electrochemical fluorination,[10] but no works on chlorinated pyridines have been reported.

The reaction conditions for the electrochemical fluorination of benzene and its derivatives, and pyridines, and the results obtained, are shown in Tables 1 and 2 respectively. Benzene was only slightly soluble in anhydrous hydrogen fluoride,[11] and the resulting solution did not have enough electric conductivity; therefore, its electrochemical fluorination required the use of a conductivity additive, sodium fluoride.

From benzene, perfluorocyclohexane, which consitituted a high percentage of the product composition, and perfluoro(methylcyclopentane) were produced, together with fragmented products. A considerable amount of tarry material in the cell and on the electrodes was also found. No simple fluorinated aromatic compound could be isolated. The formation of perfluorocyclohexane and perfluoro(methylcyclopentane) has also been reported in the electrochemical fluorination of 1,1-difluorocyclohexane.[7]

The mechanism for the fluorination of benzene to form perfluorocyclohexane may be of the free-radical type. The initial attack of the fluorine radical is presumably by direct addition to benzene nucleus to form the fluorocyclohexadienyl radical. This combines with the fluorine radical; the resulting intermediate is fluorinated further to yield hexafluorocyclohexane or a similar compound. The replacement of the hydrogens of the cyclohexane by fluorines follows to produce perfluorocyclohexane. The cleavage of the carbon-carbon bond probably occurs in this replacement stage by the energy which is liberated from the formation of the hydrogen-fluorine and carbon-fluorine bonds. Perfluoro(methylcyclopentane) may be yielded by the rearrangement of the carbon skeleton of partially-fluorinated cyclohexanes. The ease of the isomerization of the cyclohexane ring to methylcyclopentane has been established.[12]

No partially fluorinated products except trifluoromethane were obtained. Even if such compounds were formed, their amounts would be small and they would be dissolved in anhydrous hydrogen fluoride. The tarry material would be formed by radical mech-

Table 1. Conditions for fluorination

Run No.	Sample[a]	Voltage (V)	Electricity[b,c] passed (A. hr)	Procedure[d,e]
1	Benzene	5.2—9.0	64 (65)	A
2	Fluorobenzene	4.0—7.4	87	A
3	Chlorobenzene	4.8—6.1	94	A
4	*m*-Dichlorobenzene	4.9—5.8	106	A
5	Anisole	5.4—9.0	86 (74)	A
6	*o*-Chloroanisole	6.0—9.0	97 (85)	A
7	Thiophenol	5.0—6.3	131	B
8	*p*-Chlorothiophenol	6.2—6.8	131	B
9	*m*-Thiocresol	5.0—5.5	164	B
10	2-Chloropyridine	5.0—5.2	87	B
11	3-Chloropyridine	5.3—6.0	87	B

a) The amount of the starting material used was 0.20 mol except *o*-chloroanisole, 0.175 mol.
b) The amount of electricity supplied was 1.1 times of the theoretical one that was, as indicated below, assumed to be required to form perfluorocyclohexane from benzene and its derivatives, and undecafluoropiperidine from pyridines, respectively. For example,
$C_6ClH_5 + 18\,F \longrightarrow c\text{-}C_6F_{12} + 5\,HF + ClF$
$ClC_5H_4N + 16\,F \longrightarrow C_5F_{11}N + 4\,HF + ClF$
c) The anodic current density was adjusted as 1.2—1.5 A/dm^2; however, in runs 1, 5, and 6, the current block occurred. The numerical values in the parentheses shows the percentage of electricity used to the theoretical amount.
d) Cell temperature was kept at 5—8 °C.
e) A: sodium fluoride (10 g) was used; B: Carried out without using the additive.

5) A. F. Shepard and B. F. Dannels, *J. Polym. Sci.*, A-1, **4**, 511 (1966); U. S. 3386899 (1968).
6) G. N. Kokhanov and S. A. Per'kova, *Electrokhimiya*, **3**, 977 (1967).
7) M. Sander and W. Blöchl, *Chem. Ingr. Tech.*, **37**, 7 (1965).
8) N. A. Ryabinin, I. P. Kolenko, L. N. Pushkina, V. F. Kollegov, and B. N. Lundin, *Zh. Obshch. Khim.*, **39**, 2716 (1969).
9) V. S. Plashkin, L. N. Pushkina, S. L. Mertsalov, V. F. Kollegov, and S. V. Sokolov, *Zh. Org. Khim.*, **6**, 1006 (1970).
10) See, for example, S. Nagase, "Fluorine Chemistry Reviews," Vol. 1, ed. by P. Tarrant, Marcel Dekker, New York, N. Y., (1967), p. 93.
11) Ref. 2-a), p. 239.
12) A. L. Glasebrook and W. G. Lovell, *J. Amer. Chem. Soc.*, **61**, 1717 (1939).

TABLE 2. RESULTS WITH THE FLUORINATION OF BENZENES AND PYRIDINES

Run No.	Product obtained (g)	Total[a] yield (%)	Product composition[b] (%)							
			Common product							Others
			CF_4	CHF_3	C_2F_6	C_3F_8	n-C_4F_{10}	n-C_5F_{12}	cyclo-C_6F_{12}	
1	7.1	15.4	11.1	18.0	1.6	1.0	1.3	+	54.2	n-C_6F_{14}(+), CF_3-cyclo-C_5F_9 (12.7)
2	17.7	29.2	5.3	0.7	0.3	0.9	+	+	74.1	n-C_6F_{14}(0.2), CF_3-cyclo-C_5F_9 (18.5)
3	15.6	27.4	3.4	2.0	0.5	0.2	0.2	1.8	40.6	n-C_6F_{14} (0.4), $CClF_3$ (5.6), CF_3-cyclo-C_5F_9 (3.5), cyclo-C_6ClF_{11} (41.8)
4	8.1	17.1	21.3	4.9	0.9	1.7	2.0	4.1	19.8	n-C_6F_{14} (2.1), $CClF_3$ (9.9), cyclo-C_6ClF_{11} (23.6), cyclo-$C_6Cl_2F_{10}$ (9.6)
5	9.1	15.1	30.1	0.2	+	+	+	0.3	0.8	n-C_6F_{14}(+), CF_3O-n-C_6F_{13} (7.9), CF_3O-cyclo-C_6F_{11} (60.4)
6	9.8	25.0	16.5	6.0	1.9	8.1	+	6.1	4.9	n-C_6F_{14} (1.7), $CClF_3$ (21.3), CF_3O-n-C_6F_{13} (6.2), CF_3O-cyclo-C_6F_{11} (12.4), cyclo-C_6ClF_{11} (5.6), CF_3O-cyclo-C_6ClF_{10} (9.3)
7	25.6	64.3	9.1	+	5.3	+	+	0.6	23.5	n-C_6F_{14} (+), CF_3-cyclo-C_5F_9 (2.3), SF_6 (59.2)
8	18.1	39.6	10.7					2.5	34.0	n-C_6F_{14} (+), CF_3-cyclo-C_5F_9 (1.5), cyclo-C_6ClF_{11} (13.1), $CClF_3$ (3.2), SF_6 (35.0)
9	34.4	94.6	30.3	+	+	+	+	+	2.0	CF_3-cyclo-C_6F_{11} (23.8), SF_6 (43.8)
10	16.6	52.7	3.0	+	+	+	1.5	26.6		$C_5F_{11}N$ (3.3), C_5ClF_{11} (7.7), $CClF_3$ (+), NF_3 (57.9)
11	16.0	49.0	6.2	9.3	+	+	1.4	15.8		$C_5F_{11}N$ (2.0), C_5ClF_{11} (19.8), $C_5ClF_{10}N$(+), NF_3 (45.4)

a) In the calculation, the total number of mole of the products including fragmented ones was divided by the mole of starting material fed.
b) Expressed in mole percent.

anism: the addition of the fluorine radical to the benzene nucleus occurs, and the fluorohexadienyl radical thus formed would attack benzene to produce another radical; this process could be repeated and would ultimately result in the formation of a highly polymerized material.

Halobenzenes and anisoles also produced considerable amounts of a resinous material. These aromatic compounds, similar to benzene, seemed to have only a limited solubility in anhydrous hydrogen fluoride. Their fluorinations were carried out by the use of the conductivity additive. Fluorobenzene was converted into perfluorocyclohexane in a better yield than benzene was. Chlorobenzene gave chloroundecafluorocyclohexane,[13] in addition to perfluorocyclohexane, together with cleaved products. 1,3-Dichlorodecafluorocyclohexane[13] was produced from *m*-dichlorobenzene in a small yield. The fluorination of *m*-dichlorobenzene was carried out with some difficulty. Explosions often occurred in the reaction system. Among the compounds subjected to the present fluorination, *m*-dichlorobenzene appeared to have the least solubility in anhydrous hydrogen fluoride. The generation of free fluorine was presumably the cause of the explosion.

The ether linkage was relatively stable in the electrochemical fluorination, and anisole and *o*-chloroanisole gave fully-fluorinated derivatives which retained the original ether linkage. *o*-Chloroanisole yielded a new compound, trifluoromethyl 2-chlorodecafluorocyclohexyl ether, but the yield was low. From these results, it may be stated that the chlorine in the aromatic nucleus is retained in the electrochemical fluorination, and chlorinated polyfluorocyclohexyl derivatives are given.

In contrast to the behavior of the compounds described above, thiophenol, *p*-chlorothiophenol, *m*-thiocresol, 2-chloropyridine, and 3-chloropyridine gave an electro-conducting solution as would be expected by their basic character. Therefore, their fluorinations were accomplished without using the conductivity additive. These thiophenols and pyridines afforded the perfluorinated products and did not yield any tarry material.

However, extensive cleavage occurred at the site of the hetero-atoms, such as nitrogen or sulfur, resulting in the formation of nitrogen trifluoride or sulfur hexafluoride, along with fluorocarbons. These phenomena may be caused mainly by the weakness of the carbon-nitrogen and carbon-sulfur bonds, whose single-bond energies are 69.7 and 62.0 kcal/mol respectively (carbon-carbon bond energy, 83.1 kcal/mol).[14] As has been shown in connection with the electrochemical fluorination of amines,[15] the adsorption of the hetero-compounds at the active sites on the nickel anode may give the conditions for the preferential attack of fluorine on the hetero-atoms.

As the principal products, thiophenol and *m*-thiocresol afforded perfluorocyclohexane and perfluoro(methyl-

13) a) J. C. Tatlow and R. E. Worthington, *J. Chem. Soc.*, **1952**, 1251. b) P. L. Coe, B. T. Croll, and C. R. Patrick, *Tetrahedron*, **20**, 2097 (1964).

14) L. Pauling, "The Nature of the Chemical Bond," 3rd Ed., Cornell University Press, N. Y. (1960), p. 85.

15) B. Chang, H. Yanase, K. Nakanishi, and N. Watanabe, *Electrochim. Acta*, **16**, 1179 (1971).

cyclohexane) respectively, in reasonable yields while *p*-chlorothiophenol yielded perfluorocyclohexane and chloroundecafluorocyclohexane. The formation of the perfluorocyclohexyl-[16] or chloropolyfluorocyclohexyl-derivative of sulfur hexafluoride could not be confirmed under the reaction conditions used. Chloropyridines yielded nitrogen trifluoride, perfluoropentane, and 1-chloro- or 2-chloroundecafluoropentane as the main products. 3-Chloropyridine gave a small amount of a new compound, 3-chlorodecafluoropiperidine.

Experimental

Materials and Apparatus. The starting materials subjected to the fluorination were all of a reagent grade. Their purities were confirmed by gas chromatography. Anhydrous hydrogen fluoride was more than 99.5% pure. The electrolytic cell used was the same as that described in a previous paper.[17] The product identifications and analyses were performed by means of gas chromatography (Shimadzu GC-2C model chromatograph) and IR spectroscopy (Hitachi EPI-S2 spectrometer), as before.[18] Mass spectrometry-(Hitachi RMU-7 spectrometer) was frequently used.

Procedure A (for a poor electro-conducting solution). As a typical example, the procedure for the fluorination of chlorobenzene (Run 3) will be described. In electrically-purified anhydrous hydrogen fluoride (1.28 l) in the cell, sodium fluoride (10 g) was dissolved. Then, while the current was being passed through the hydrogen fluoride solution, chlorobenzene (22.5 g, 0.20 mol) was charged in over a period of 2.5 hr by the use of a mechanical micro-pump.

The reflux condenser of the cell was kept at −15 °C. Helium (200 ml/min) was introduced through the bubbler placed at the bottom of the cell in order to agitate the solution and also to carry away the fluorinated products from the cell. In the begining of the electrolysis, the cell voltage was 4.8 V, with an anodic current density of 1.2 A/dm² (effective surface areas of the anodes and cathodes, 20 dm²), and the cell temperature was 6—8 °C; however, the voltage rose gradually until it reached 6.1 V at the end of the operation. The total amount of electricity supplied over the 4-hr period was 94 A·hr. The passing of the cold brine through the reflux condenser was stopped for the last 30 min of the electrolysis. The blowing of helium was continued for 2 hr after the electrolysis was over.

The fluorinated products evolving from the cell were passed through the sodium fluoride tubes[17] (for the removal of the hydrogen fluoride) and gas-washing bottles (for the removal of a small amount of oxygen difluoride); these bottles were filled with an aqueous solution of sodium sulfite containing a small amount of potassium iodide. The products were further guided to a series of cold traps kept in ice and in liquid nitrogen.

The products thus obtained were separated into a lower-boiling (0.7 g) and a higher-boiling (14.9 g) fraction in the usual manner. The former was analyzed by gas chromatography, using a silica gel column at 80 and 120 °C, with helium as the carrier gas. It consisted of carbon tetrafluoride, trifluoromethane, chlorotrifluoromethane, perfluoroethane, perfluoropropane, and traces of other compounds. These and the compounds described below were identified by a comparison of their IR spectra (and of their mass spectra if necessary) with those of authentic specimens.

The higher-boiling portion was analyzed with a column packed with 30% of Daifl oil #50 (Daikin Industries Co.) on Chromosorb P-AW, 60—80 mesh (Johns-Manville Co.), at room temperature. It consisted of perfluorobutane, perfluoropentane, perfluoro(methylcyclopentane), perfluorohexane, perfluorocyclohexane, chloroundecafluorocyclohexane, and small amounts of unidentified compounds. The product distribution (mol%) and total yield are shown in Table 2, Run 3.

Most of the hydrogen fluoride used was distilled off from the cell, and the residual solution, containing much tarry material, was extracted with 1,1,2-trichloro-1,2,2-trifluoroethane and with ethyl ether; however, from the extract no pure individual compound was isolated.

By means of Procedure A, trifluoromethyl 2-chlorodecafluorocyclohexyl ether was obtained from *o*-chloroanisole (Run 6), although in a low yield (2.3%), together with cleaved products. The ether was a colorless liquid with a bp of 104 °C, n_D^{20} 1.3052. Found: Cl, 9.4; F, 64.0%; mol wt (mass), 382. Calcd for $C_7ClF_{13}O$: Cl, 9.3; F, 64.6%; mol wt, 382.5. The mass spectrum had peaks at 382 [M], 347 [M−Cl], 313 [M−CF_3], 247 [C_5F_9O], and 247 [C_5F_8Cl].

Procedure B (for an electro-conducting solution). As a representative example, the procedure for the fluorination of 3-chloropyridine (Run 11) will be described below. Several minor points were different from Procedure A. 3-Chloropyridine (22.7 g, 0.20 mol) was fed into the cell by the use of the micro-pump. The electrolysis was carried out with the anodic current density of 1.3 A/dm², the cell voltage of 5.3—6.0 V, and the cell temperature of 6 °C. Helium (200 ml/min) was blown into the cell.

The gases evolving from the cell were led to the sodium fluoride tubes, to gas-washing bottles filled with an aqueous solution of potassium hydroxide, to traps (Trap A) immersed in ice and in CO_2–acetone, to gas-washing bottles filled with an aqueous solution of sodium sulfite containing potassium iodide, and finally to traps (Trap B) immersed in ice and in liquid nitrogen. These were connected in a series. A total of 87 A·hr was consumed over a 3.5-hr period. Passing the cold brine through the reflux condenser was stopped for the last 30 min of the electrolysis, and the blowing of helium was continued for 1.5 hr after the electrolysis was over.

The product (11.0 g) obtained in Trap A was analyzed by means of a column packed with 30% of Daifl oil #50 on Chromosorb P-AW and one packed with 30% of dinonyl phthalate on Chromosorb P-AW at room temperature. It contained perfluoropentane, undecafluoropiperidine, and 2-chloroundecafluoropentane, together with small amounts of unidentified compounds. 3-Chlorodecafluoropiperidine was also detected, but its amount was very small and it was identified only by mass specrtometry. 2-Chloroundecafluoropentane, obtained in a 9.7% yield, was a colorless liquid with a bp of 61 °C, $n_D^{20}<1.28$. Found: Cl, 11.6; F, 68.1%; mol wt (mass), 304. Calcd for C_5ClF_{11}: Cl, 11.6; F, 68.6%; mol wt, 304.5. The mass spectrum had peaks at 304 [M], 285 [M−F], 269 [M−Cl], and 235 [M−CF_3].

The mass spectrum of 3-chlorodecafluoropiperidine had peaks at 299 [M], 280 [M−F], 264 [M−Cl], 261 [M−F_2], 245 [M−ClF], 183 [M−C_2F_3Cl], and 116 [C_2F_3Cl].

The product (5.0 g) in Trap B was analyzed by means of a silica gel column at 0 and 80 °C; it was found to consist of carbon tetrafluoride, trifluoromethane, perfluorobutane, and nitrogen trifluoride. The over-all results are shown in Table 2, Run 11.

16) R. D. Dresdner, T. M. Reed, III, T. E. Taylor, and J. A. Young, *J. Org. Chem.*, **25**, 1464 (1960).

17) S. Nagase, H. Baba, K. Tanaka, and T. Abe, *Kogyo Kagaku Zasshi*, **67**, 2062 (1964).

18) For example, S. Nagase, T. Abe, H. Baba, and K. Kodaira, This Bulletin, **43**, 2980 (1970).

Autoxidation of Trimethyl Phosphite Initiated by One-Electron Transfer from Phosphite to Quinones*

Yoshiro OGATA and Mitsuji YAMASHITA

Department of Applied Chemistry, Faculty of Engineering, Nagoya University, Chikusa-ku, Nagoya 464

(Received January 29, 1973)

The reaction of trimethyl phosphite (I) with acenaphthenequinone (II) under air affords quantitatively trimethyl phosphate (III) and 1:2 adduct (IV), which was converted into δ-lactone (V) and III by addition of water, while only IV was obtained quantitatively under N_2 atmosphere. ESR and UV spectra, decolorization of 1,1-diphenyl-2-picrylhydrazyl (DPPH), and initiation of styrene polymerization suggest the transient formation of radical ions VI and VII. The rate law for the autoxidation of I is expressed as: $v=k[I][II]^{0.7-1.0}$. The reaction in chloroform proceeds faster than that in dioxane. The reaction of I with chloranil is much slower, and no reaction occurs with phenanthrenequinone and anthraquinone which have low reduction potentials. A mechanism which involves one-electron transfer from phosphite to acenaphthenequinone followed by autoxidation was proposed for the reaction under air.

The reaction of trimethyl phosphite with acenaphthenequinone was reported to give a 1:2 adduct under nitrogen atmosphere.[1] Trimethyl phosphite is stable toward molecular oxygen in the absence of a radical source or light.[2] The peculiar behavior in the reaction of phosphite with acenaphthenequinone, *i.e.*, the rapid red-shift of color of the reaction mixture followed by a slow blue-shift,[3] prompted us to study the reaction in detail.

Some reactions of trivalent phosphorus compounds with carbonyl compounds are of radical character, but little evidence is available.[4] The present paper is a summary of our study on the products and mechanism of the autoxidation of trimethyl phosphite initiated by one-electron transfer reaction from phosphite to acenaphthenequinone.

Results and Discussion

The reaction of trimethyl phosphite (I) with acenaphthenequinone (II) proceeds exothermally at room temperature. The color of II fades rapidly,[3] producing trimethyl phosphate (III) in the air as the only liquid product together with a white solid. The former was confirmed by glc, tlc, IR and NMR spectra, and latter was identified by means of NMR to be an adduct of I to II in a molar ratio of 1:2. The adduct after treatment with water and recrystallization gave 8-[hydroxy(2-oxo-acenaphthenylidene)methyl]-1-naphthoic acid δ-lactone (V) [see Experimental].

The reaction of acenaphthenequinone with a large excess of trimethyl phosphite under oxygen atmosphere gives an excess equivalent of trimethyl phosphate, while under nitrogen atmosphere the yield is lower, most of trimethyl phosphite being recovered as shown in Table 1. This shows that the autoxidation of I occurs under O_2 atmosphere. The 1:2 adduct (IV) does not initiate the autoxidation. An increase of ratio of trimethyl phosphite to acenaphthenequinone under O_2 atmosphere results in a higher yield of phosphate (based on the used quinone), indicating a long length of radical chain (Table 2).

Stoichiometry. Stoichiometry of the autoxidation of trimethyl phosphite in the presence of acenaphthenequinone was determined in dioxane at 25.0 °C by use of an apparatus for kinetic study.[3] The reaction produced a quantitative amount of trimethyl phosphite with consumption of a half equivalent of molecular oxygen (Table 3). As reported by Ramirez and Ramanathan,[1] acenaphthenequinone is converted into a 1:2 adduct (IV) with trimethyl phosphite [(1a), (1b)]. We found that the adduct gives δ-lactone (V) and trimethyl phosphate (III) by treatment with water. Both reaction (1a) and (1b) take place in the air, but only (1b) under N_2.

Detection of Radicals. When trimethyl phosphite was added to a dioxane solution of acenaphthenequinone, the yellow color of the solution deepened (red-shift) and then faded away gradually. Immeasurably fast change of color was observed in chloroform. ESR spectra in dioxane showed a broad signal.[5] On addition of DPPH to the reaction mixture, the color

Table 1. Effect of oxygen on the yield of trimethyl phosphate at room temperature[a]

Acenaphthenequinone (mmol)	Trimethyl phosphite (mmol)	Atmosphere	Yield of trimethyl phosphate[b] [mmol (%)]
0.53	25	Air	5.6 (1100)
0.62	11	N_2	0.75 (120)

a) Neat.
b) Based on acenaphthenequinone.

* Contribution No. 191.

1) F. Ramirez and N. Ramanathan, *J. Org. Chem.*, **26**, 3041 (1961).
2) Y. Ogata and M. Yamashita, *J. Chem. Soc. Perkin II*, **1972**,493.
3) Y. Ogata and M. Yamashita, *ibid.*, **1972**, 730.
4) R. F. Hudson, "Structure and Mechanism in Organo-Phosphorus Chemistry," Academic Press, London (1965), Chapter 9.
5) Y. Ogata and M. Yamashita, *J. Org. Chem.*, in press.

Table 2. Effect of molar ratio of trimethyl phosphite (I) *vs.* acenaphthenequinone (II) on the yield of trimethyl phosphate in $CHCl_3$ at room temperaturee for 10 hr

Concentration		Ratio of	Yield of trimethyl phosphate[a]
[I], (10^{-1}M)	[II], (10^{-2}M)	I to II	(%)
29	8.1	28	590
15	8.1	14	380
7.3	8.1	6.9	230
29	4.1	56	830
29	2.0	100	1400

a) Based on II.

Table 3. The stoichiometry of autoxidation of trimethyl phosphite in dioxane at 25 °C[a]

$P(OMe)_3$ (10^{-4} mol)	Consumed oxygen (10^{-4} mol)	$2\ O_2/P(OMe)_3$[b]
2.58	1.19	0.92
6.49	3.08	0.95
11.4	9.90	0.89

a) Acenaphthenequinone used was 9.0×10^{-6} – 3.4×10^{-5} mol.
b) Molar ratio of oxygen to trimethyl phosphite.

$$P(OMe)_3 + \frac{1}{2}O_2 \xrightarrow{\text{acenaphthenequinone (II)}} P(O)(OMe)_3 \quad (1a)$$

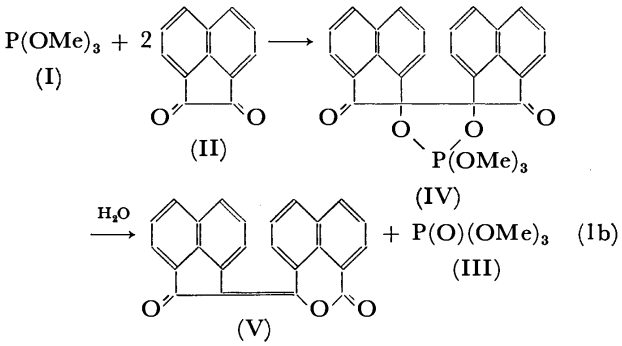

(1b)

of DPPH vanished rapidly, but it did not vanish by the action of IV, I, or II. The decolorization rate of DPPH was much faster in chloroform than in dioxane. A similar decolorization was observed for the reaction with chloranil (though slow in the initial period), but not with phenanthrenequinone.[3] These facts suggest that the reaction of trimethyl phosphite with acenaphthenequinone produces radical species by one-electron transfer as in the case of chloranil and that the autoxidation is initiated by these radicals. The formation of a charge-transfer complex of I with II is less probable, since no autoxidation of I would occur in the stage of charge-transfer complex.

Triphenylphosphonium radical cation ($Ph_3P^{\cdot+}$) may be an intermediate in the reaction of triphenylphosphine with some quinones.[6] The ESR spectra of some semiquinone radicals are well-known,[7] while those of phosphoranyl radicals[8] and phosphoranylperoxy radicals,[9] prepared by the photolysis of di-*t*-butyl peroxide in the presence of trivalent phosphorus compounds, have been reported recently. The observed broad signal may be either an anion radical of ketyl or a cation radical of phosphorus, or both.

Kinetics. The kinetics of the autoxidation was studied by the manometric method.[3] As shown in

Table 4. Rate constants for the autoxidation of trimethyl phosphite (I) with acenaphthenequinone (II) in dioxane at total pressure of 760 mmHg

Concentration		Partial pressure of O_2 (mmHg)	Temp. (°C)	Rate and rate constant	
$[I]_0$ (10^{-1} M)	$[II]_0$ (10^{-3} M)			$10^5\ v$[a] (M sec^{-1})	$10^2\ k_2$[b] (M^{-1} sec^{-1})
1.90	4.27	159	25.0	2.54	1.57
3.25	9.20	760	25.0	8.33	1.39
3.25	9.20	159	25.0	8.11	1.36
4.86	4.60	159	25.0	6.96	1.64
2.03	6.00	159	25.0	4.32	1.78
0.508	6.00	159	25.0	1.08	1.78
2.11	8.50	159	35.0	3.06	1.71
1.99	8.45	159	45.0	3.51	2.09
1.99	8.45	159	60.0	4.08	2.43

a) $v=-d[O_2]/dt$.
b) $v=k_2[I][II]$.

6) a) F. Ramirez and S. Dershowitz, *J. Amer. Chem. Soc.*, **76**, 5614 (1956). b) F. Ramirez and S. Dershowitz, *J. Org. Chem.*, **22**, 856 (1957).

7) a) M. Adams, M. S. Blois, Jr., and R. H. Sands, *J. Chem. Phys.*, **28**, 774 (1958). b) E. Warhust and A. M. Wilds, *Trans. Faraday Soc.*, **65**, 1413 (1969). c) A. G. Evans, J. E. Evans, and E. H. Godden, *J. Chem. Soc., B*, **1969**, 546. d) G. A. Russell, "Radical Ions," ed. by K. T. Kaiser and L. Kevan, Interscience Publishers, New York (1968), Chapter 3.

8) a) J. K. Kochi and P. J. Krusic, *J. Amer. Chem. Soc.*, **91**, 3944 (1969). b) A. G. Davies, D. Griller, and B. P. Roberts, *J. Chem. Soc. Perkin II*, **1972**, 993. c) P. J. Krusic, W. Mahler, and J. K. Kochi, *J. Amer. Chem. Soc.*, **94**, 6033 (1972).

9) G. B. Watts and K. U. Ingold, *ibid.*, **94**, 2528 (1972).

Table 4, the rate is independent of partial pressure of oxygen as expressed by

$$v = k[\mathrm{I}][\mathrm{II}]^{0.7\text{-}1.0} \quad (2)$$

It is also shown that the temperature effect is small, which reflects a small activation energy for the initiation. Chloranil initiates the autoxidation very slowly,[10] while rapid autoxidation is observed with AIBN (Table 5).

TABLE 5. SECOND-ORDER RATE CONSTANTS FOR AUTOXIDATION OF TRIMETHYL PHOSPHITE IN DIOXANE AT 60.0 °C

$[(MeO)_3P]_0$ (10^{-1} M)	Added compound (concentration) (10^{-3} M)	k_2 [a] ($M^{-1}sec^{-1}$)
1.99	Acenaphthenequinone (8.45)	2.43×10^{-2}
1.99	AIBN (9.40)	4.84×10^{-2}
1.99	Chloranil (7.95)	1.61×10^{-7}

a) $v=k_2[(MeO)_3P][\text{Added compound}]$.

Mechanism. The above fact suggest that the one-electron transfer occurs at the initiation step, and the radicals formed initiate the autoxidation of trimethyl phosphite. Thus a probable initiation reaction is expressed as follows.

Initiation:

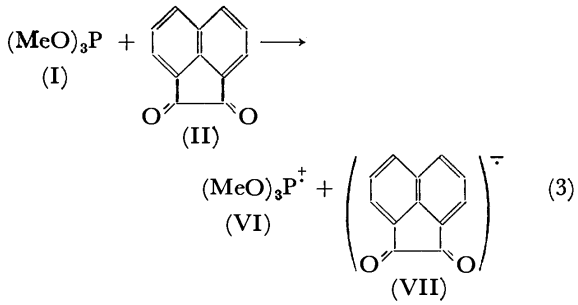

(I) (II) (VI) (VII) (3)

Radicals VI and/or VII, represented by R·, may initiate the autoxidation.

The propagation reaction can be expressed by the mechanism involving alkyl, alkoxy, and alkylperoxy radicals as chain carriers,[3] *e.g.*,

$$(MeO)_3P + RO_2\cdot \longrightarrow (MeO)_3PO + RO\cdot$$

$$\text{or } (MeO)_3P + RO\cdot \longrightarrow (MeO)_3PO + R\cdot.$$

The termination reaction can be expressed as follows.

$$2RO_2\cdot \longrightarrow RO_4R \text{ or other inactive products} \quad (4)$$

$$RO_2\cdot \longrightarrow \text{inactive products} \quad (5)$$

$$RO_2\cdot + R'\cdot \longrightarrow \text{inactive products} \quad (6)$$

where R'· represents radicals other than $RO_2\cdot$.

If step (4) is favorable for termination, the order with respect to II in the rate law should be 0.5, while if steps (5) and/or (6) occur, the order should be 1,[3] on applying the steady state approximation to this mechanism. Actually, the order in II Eq. (2) is 0.7—1.0. This might be explained by assuming the occurrence of bimolecular termination [step (4)] along with unimolecular termination [steps (5) and (6)]. The radical chain may need small energy of activation, thus the temperature dependence of the autoxidation rate is small (E_a=5.9 kcal/mol and ΔS^*=−54 e.u. at 25.0 °C).

Formation of trimethyl phosphate is due to the autoxidation of I but not to the hydrolysis of phosphorus intermediate reported in the reaction of phosphite with chloranil.[11] One-electron transfer occurred in the reaction of trimethyl phosphite with acenaphthenequinone or chloranil, but none in that with phenanthrenequinone or anthraquinone. The different behaviors in these quinones can be attributed to the difference of reduction potentials of quinones,[12] *i.e.*, reduction potentials of quinones: chloranil (0.712 V),[12b] phenanthrenequinone (0.458 V),[12c] anthraquinone (0.157 V),[12d] and acenaphthenequinone (0.78 V). The last has not been reported.

Polymerization. Copolymerization of added styrene-divinylbenzene was initiated during the reaction of trimethyl phosphite with acenaphthenequinone at 60 °C under O_2 or N_2, while formed IV did not initiate the polymerization. This indicates the presence of a free radical in the reaction mixture of trimethyl phosphite with acenaphthenequinone and the fact that the radical has a life long enough to initiate polymerization.

Experimental

Apparatus. The NMR spectra were measured with a JNM-C60-HL model of Japan Electron Optics Laboratory Co., Ltd; IR spectra with a Perkin-Elmer 337 grating infrared spectrophotometer; ESR spectra with a JES-ME1X model of Japan Electron Optics Laboratory Co., Ltd; UV spectra with a Hitachi 124 spectrophotometer; and mass spectra with a Hitachi RMS-4 model. A Yanagimoto GCG 550F gas chromatograph was used for glc analysis, and a Yanagimoto P8-DPR polarograph for the measurement of reduction potentials.

Materials. Trimethyl phosphite (bp 58 °C/116 mmHg; lit,[13] bp 111—112 °C), acenaphthenequinone (mp 261 °C; lit,[14] mp 259—260 °C), chloranil (mp 299 °C; lit,[15] mp 291—293 °C), styrene (bp 49—50 °C/25 mmHg; lit,[16] bp 54 °C/30 mmHg), phenanthrenequinone (mp 210 °C; lit,[17] mp 208.5—210 °C), and solvents were purified before use.

Reaction of Trimethyl Phosphite (I) with Acenaphthenequinone (II). The reaction of I with II was carried out at room temperature in neat or in a dioxane or chloroform solution. The tlc analysis (silica gel/acetone) of the reaction mixture gave two spots, one (R_f=0.59) being detected by $CoCl_2$, and the other (R_f=0.80) by I_2. After separation of formed precipitate by filtration (reaction in neat), the solid

10) F. Ramirez and S. Dershowitz, *J. Amer. Chem. Soc.*, **81**, 587 (1959).

11) F. Ramirez, E. H. Chen, and S. Dershowitz, *ibid.*, **81**, 4338 (1959).

12) a) F. J. Lopez and W. A. Waters, *J. Chem. Soc.*, 4666 (1952). b) K. Wallenfels and W. Möhle, *Ber.*, **76**, 924 (1943). c) L. F. Fieser, *J. Amer. Chem. Soc.*, **51**, 3101 (1929). d) J. B. Conant and L. F. Fieser, *ibid.*, **46**, 1855 (1924).

13) Wm. W. Marshall, U. S. Patent, 2,848,474 (1958); *Chem. Abstr.*, **53**, 1144c (1959).

14) C. F. H. Allen and J. A. VanAllan, "Organic Syntheses," Coll. Vol. III, 1 (1955).

15) S. S. C. Chu, G. A. Jeffrey, and T. Sakurai, *Acta Crystallogr.*, **15** 661 (1962).

16) H. B. Dykstra, *J. Amer. Chem. Soc.*, **56**, 625 (1934).

17) R. Wendland and J. LaLoude, "Organic Syntheses," Coll. Vol. IV, 757 (1963).

product was washed with water, then extracted by $CHCl_3$. The extract gave a solid which was identified to be 8-[hydroxy (2-oxo-1-acenaphthenylidene)methyl]-1-naphthoic acid δ-lactone (V) mp 274 °C.

Found: C, 82.1; H, 3.52%. Calcd for $C_{24}H_{12}O_3$: C, 82.8; H, 3.47%.

The NMR spectra gave only aromatic protons (in $CDCl_3$). The mass spectra are shown in Table 6. The UV spectra in CH_3CN are as follows: λ_{max} 249 nm (log ε 4.92), 285 nm (4.64), 301 nm (4.61), 316 nm (4.60), and 342 nm (4.53). The crude yield of V was quantitative. The filtrate gave only one peak in glc (Apiezon Grease L 3% on Celite 545), whose structure was confirmed to be trimethyl phosphate (III) by NMR (6.26 τ, doublet, J_{PH}=11 Hz) and IR (P=O; 1267 cm^{-1}, P–O–C; 1035 cm^{-1}). The reaction in dioxane or in $CHCl_3$ gave the same results as described above. The structure of 1:2 adduct (IV) was determined by NMR spectra without purification (1.5—2.5 τ, multiplet, 12H; 6.28 τ doublet, J_{PH}=10.6 Hz, 9H).

Kinetics. A dioxane solution of trimethyl phosphite (2 ml) and a doixane solution of acenaphthenequinone (2 ml) was mixed under 159 mmHg partial pressure of oxygen. The autoxidation rate was measured manometrically.[3] The stoichiometry was determined by the consumed amount of oxygen after being kept standing for a long time.

ESR Spectra. A dioxane solution of acenaphthenequinone was introduced into an ESR tube and frozen out at liquid nitrogen temperature under N_2 flow. A dioxane solution of trimethyl phosphite was then introduced into the tube and also frozen out. Two separate layers were gradually mixed by raising the temperature. The observed broad ESR signal having center at 3150 G soon reached a maximum intensity and then gradually vanished.

Table 6. Mass spectra of δ-lactone (V)

m/e	Relative intensity
126	100
154	85
182	38
320	12
348 (M^+)	30 (100) [a]
349 (M^++1)	(25)
350 (M^++2)	(3.7)

a) Numerals in parenthesis denote relative intensity based on M^+. The calculated intensity of M^++1 and M^++2 is 26.1 and 1.3, respectively ($C_{24}H_{12}O_3$) [J. H. Beynon, "Mass Spectrometry and its Application to Organic Chemistry," Elsevier, Amsterdam (1960), p. 305)].

Polymerization of Styrene. Acenaphthenequinone (0.007 g) was dissolved in a mixture of 4 ml styrene and 0.1 ml divinylbenzene. Bubbling nitrogen gas, 1 ml trimethyl phosphite was added to the mixture at 60 °C and then the tube was sealed. The homo and popcorn polymerization was almost complete after two days, but no such polymerization was observed without trimethyl phosphite and acenaphthenequinone.

Reduction Potential. The reduction potential of quinones was measured in 50% aqueous ethanol containing 0.1M HCl as a saturated solution of substrate at 20 °C by means of a Yanagimoto P8-DPR polarograph potentiostated with a calomel electrode.

BULLETIN OF THE CHEMICAL SOCIETY OF JAPAN, VOL. 46, 2211—2215 (1973)

The Oxidative Coupling of Alkyl Aryl Ketones by Iron(III) Chloride

Hiroo INOUE, Mitsuya SAKATA, and Eiji IMOTO

Department of Applied Chemistry, College of Engineering, University of Osaka Prefecture, Sakai-shi Osaka 591

(Received February 3, 1973)

The oxidative carbon-carbon coupling of two enolizable ketones, propiophenone and butyrophenone, with iron(III) chloride is investigated. The ketones are converted to γ-diketones (II) and 2,5-diphenylfurans (III) in high yields, while iron(III) chloride is reduced to iron(II) chloride. III is produced by the dehydration of II with iron(III) chloride and/or hydrogen chloride. During the reaction, iron(III) chloride is regenerated partially by the oxidation of iron(II) chloride with oxygen in the presence of hydrogen chloride. However, oxygen enhances the formation of III and the polymeric material. The addition of pyridine, calcium oxide, or zinc oxide to the iron(III) chloride-ketone system brings about the selective formation of α-chloroketones. A combination of iron(III) chloride with copper(II) chloride or oxide is effective for the oxidative coupling. Under irradiation, the reactions result both in oxidative coupling and in chlorination at the α-position of the carbonyl group, accompanied by chlorination at the β-position.

The oxidative coupling with phenols of compounds containing the -CH=C(OH)- group has been well known.[1] As the oxidizing agents, $K_3Fe(CN)_6$,[1] $VOCl_3$,[2] VCl_4,[2] Mn(acetylacetonate)$_3$,[3] [Fe(dimethylformamide)$_3$Cl$_2$][FeCl$_4$],[4] and the Cu-amine-O_2 system[1] have been investigated. In recent years considerable attention has been given to the mechanistic aspects of the coupling of phenoxy radicals.[5-7] We

1) W. I. Taylor and A. R. Battersby, "Oxidative Coupling of Phenols," Marcel Dekker, New York, N. Y. (1967).
2) W. L. Carrick, G. L. Karapinka, and G. T. Kwiatkowski, *J. Org. Chem.*, **34**, 2388 (1969); M. A. Schwartz, R. A. Holton, and S. W. Scott, *J. Amer. Chem. Soc.*, **91**, 2800 (1969).
3) M. J. S. Dewar and T. Nakaya, *ibid.*, **90**, 7134 (1968).
4) S. Tobinaga and E. Kotani, *ibid.*, **94**, 309 (1972).
5) W. A. Waters, *J. Chem. Soc., B*, **1971**, 2026.
6) M. Chauhan, F. M. Dean, K. Hindley, and M. Robinson, *Chem. Commun.*, **1971**, 1141.
7) L. R. Mahoney and S. A. Weiner, *J. Amer. Chem. Soc.*, **94**, 1412 (1972).

have now examined the oxidative carbon-carbon coupling of enolizable ketones with iron(III) chloride. The carbon-carbon coupling of the compounds containing the activated CH, CH_2, or CH_3 groups has been investigated with a large variety of oxidants.[8] However, no method for the direct coupling of the α-carbon of simple ketones has been reported. We will describe herein a new reaction in which propiophenone (Ia) or butyrophenone (Ib) successfully undergoes carbon-carbon coupling by iron(III) chloride to give the γ-diketones (II) and 2,5-diphenylfurans (III). Furthermore, we will report on the influence of additives, such as pyridine, water, copper(II) chloride, metal oxides, and metal, upon the reactions. Some of the results of this investigation have been reported in a previous communication.[9]

$$\underset{\text{I}}{C_6H_5COCH_2R} \xrightarrow{FeCl_3} \underset{\text{II}}{C_6H_5COCHCHCOC_6H_5}$$

a: R=CH_3
b: R=CH_3CH_2

$$+ \underset{\text{III}}{\text{(2,5-diphenylfuran)}} + \underset{\text{IV}}{C_6H_5COCHR}$$

Results and Discussion

Oxidative Coupling. When a solution of anhydrous iron(III) chloride in I was heated without a solvent at 70 °C under an atmosphere of air, γ-diketones (II) were obtained, together with 2,5-diphenylfurans (III) and α-chloroketones (IV). Iron(III) chloride was reduced to iron(II) chloride, which was precipitated as white crystals. The formation curve of the products against the reaction time is shown in Fig. 1. In a separate experiment, it was observed that II was converted to III with the aid of hydrogen chloride and iron(III) chloride. Therefore, III would be produced consecutively by the dehydration of II with hydrogen chloride and/or iron(III) chloride. II was produced parallel with IV without an induction period. In order to investigate whether or not II is produced from IV, a solution of IV in I in the presence of iron(II) or iron(III) chloride was heated at 70 °C. IV was recovered unchanged. This means that II is not produced either by the reductive coupling of IV by iron(II) chloride or by the reaction of IV and the enol of I with iron(III) chloride.

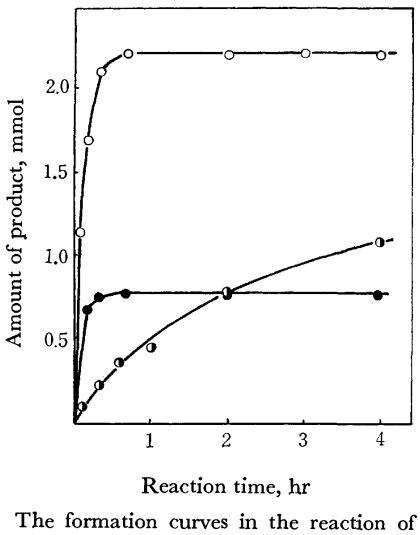

Fig. 1. The formation curves in the reaction of Ia (15 ml) with iron (III) chloride (4.5 mmol) at 70°C.
○: IIa, ◑: IIIa, ●: IVa.

The formation of II and IV together with iron(II) chloride indicates that the initial step involves the oxidation of the ketone by iron(III) chloride, thus leading to the α-keto radical (V). Such a process has also been found in the oxidation of ketones by either manganic or ceric ions.[10-12] The α-keto radicals couple with each other to form II, or are oxidized by the iron(III) chloride to give α-chloroketone (IV).[13]

$$\underset{\text{I}}{} \xrightarrow{FeCl_3} \underset{\text{V}}{[C_6H_5\dot{C}OCHR]} \begin{cases} \xrightarrow{\text{V}} \underset{\text{II}}{} \xrightarrow{FeCl_3\text{-}HCl} \underset{\text{III}}{} \\ \xrightarrow[FeCl_3]{} \underset{\text{IV}}{} \end{cases}$$

When the yields of II, III, and IV were calculated by this equation: 200×(the number of moles of the products/the number of moles of iron(III) chloride), the sum of the yields was higher than 100%, as Table 1 shows.

Effect of Oxygen. The oxidation of iron(II) salts by oxygen in an aqueous or nonaqueous solvent has already been studied.[14-16] We carried out the reaction of Ia with iron(III) chloride under an oxygen atmosphere. As Table 1 shows, the reaction resulted in a decreased yield of IIa and an increased yield of IIIa. In addition, a polymeric material, the IR spectrum of which exhibited bands at 3050, 2900, 1700, 1600, 1495, 1440, 1370, 1000, 750, and 695 cm^{-1}, was isolated. Furthermore, we carried out the experiment of heating a dispersed solution of iron(II) chloride in Ia at 70 °C under a slow flow of oxygen and hydrogen chloride for 30 min. In this case, IIa was obtained in a 54% yield, based on the iron(II) chloride. In the absence of hydrogen chloride and oxygen, IIa and IIIa were not obtained at all. Thus, the presence of oxygen

8) H. A. P. De Jongh, C. R. H. I. De Jonge, and W. J. Mijs, *J. Org. Chem.*, **36**, 3160 (1971). Many examples are described in this literature.

9) H. Inoue, M. Sakata, and E. Imoto, This Bulletin, **44**, 3490 (1971).

10) E. I. Heiba and R. M. Dessau, *J. Amer. Chem. Soc.*, **93**, 524 (1971).

11) R. VanHelden and E. C. Kooyman, *Rec. Trav. Chim. Pays-Bas*, **80**, 57 (1961); H. J. den Hertog, Jr. and E. C. Kooyman, *J. Catal.*, **6**, 357 (1966).

12) G. A. Russell and J. Lokensgard, *J. Amer. Chem. Soc.*, **89**, 5059 (1967).

13) J. K. Kochi and D. M. Mog, *ibid.*, **87**, 552 (1965); J. K. Kochi, *Rec. Chem. Progr.*, **27**, 207 (1966).

14) V. V. Ermilov, Yu .P. Romanteev, and Yu. A. Shchurovskii, *Tr. Inst. Met. Obogashch., Akad. Nauk Kaz. SSR*, **30**, 55 (1969); *Chem. Abstr.*, **71**, 95410 m (1969).

15) A. N. Dokuchaeva, L. Liepina, and B. P. Macejevskis, *Latv. PSR Zinat. Akad. Vestis, Kim. Ser.*, **2**, 167 (1969); *Chem. Abstr.*, **71**, 74568 d (1969).

16) G. S. Hammond and Chin-Hua S. Wu, *Advan. Chem. Ser.*, **77**, 186 (1968).

Table 1. The thermal reaction of Ia or Ib with iron(III) chloride[a)]

Ketone	$FeCl_3$, mmol	Atmosphere	Reaction time, hr	Products, mmol × 10			
				γ-Diketone	Furan	α-Chloro-ketone	$FeCl_2$
Ia	1.5	Air	24	7.2	4.7	1.9	10.2
Ia	0.3[b)]	Air	24	1.8	1.1	1.3	—
Ia	1.5	O_2	5	3.6	5.1	3.0	—
Ia	1.5	O_2	24	3.5	6.5	2.3	9.6
Ia	1.5	N_2-flowed[c)]	2	7.7	0.0	2.8	—
Ia	1.5	N_2-flowed[c)]	24	19.8	3.5	2.4	8.3
Ib	1.4	Air	48	3.4	—	3.8	9.4
Ib	1.4	N_2	48	4.6	—	3.2	—

a) Experiments were carried out without solvent at 70—75°C, using 5 ml of I.
b) The reaction was carried out in 3 ml of Ia.
c) Nitrogen gas was flowed at 30 ml/min.

and hydrogen chloride brought about the regeneration of iron(III) chloride from iron(II) chloride, but the yield of II decreased due to the consecutive formation of III and the polymeric material. The rate of the formation of the products was not accelerated by oxygen.

In order to remove the excess of oxygen and hydrogen chloride, the reaction was carried out with a slow flow of gaseous nitrogen. As Table 1 shows, II was obtained in a high yield, along with III and IV in low yields. The fact that the yield of II was over 100% indicates that oxygen present in the reaction system contributes to the regeneration of iron(III) chloride. Thus, for preventing the consecutive reaction of II it was effective to remove the excess of oxygen and hydrogen chloride.

Effect of Concentration of Iron(III) Chloride. The amounts of II and III produced after a certain reaction time increased with an increase in the concentration of iron(III) chloride up to nearly the saturation point of iron(III) chloride. When iron(III) chloride came to be dispersed in I, however, the amount of IV increased, while the amounts of II and III decreased.

Effects of Solvents. The use of such solvents as benzene and diglyme was not preferred for the oxidative coupling reaction: the reaction of Ia with iron(III) chloride in diglyme gave mainly IVa in an 80% yield (concentration of iron(III) chloride and Ia, 0.33 mol/l; reaction time, 48 hr; reaction temperature, 70—80 °C).

Effects of Additives. Pyridine or Water: When pyridine was added to a solution of iron(III) chloride in I, an iron(III) chloride–pyridine complex was precipitated. The complex was dispersed in I and was then heated at 70—75 °C for 24 or 48 hr. As Table 2 shows, the yield of IV increased with an increase of the pyridine/iron(III) chloride ratio up to the molar ratio of 1—2: 1, accompanied by a decrease in the yields of II and III. At the molar ratio of 5: 1, however, no product was obtained. These facts indicate that II, III, and IV are produced through the coordination of I to iron(III) chloride and that the addition of pyridine to the iron(III) chloride–I system alters the reaction pathway to the course of the formation of IV:

$$\mathrm{I} \xrightarrow{FeCl_3\text{–}C_5H_5N} \mathrm{IV}$$

The reaction pathway was also influenced by the addition of water instead of pyridine. The increase in the water/iron(III) chloride molar ratio brought about a decrease in the yields of II and III, along with a slight increase in that of IV.

Table 2. Effects of pyridine and water on the thermal reaction of I with iron(III) chloride[a)]

Ketone	Additive	Molar ratio Additive /$FeCl_3$	Yields of products, %[b)]		
			γ-Diketone	Furan	α-Chloro-ketone
Ia	C_5H_5N	0	96	63	25
Ia	C_5H_5N	0.5	5	0	69
Ia	C_5H_5N	0.9	0	0	65
Ia	C_5H_5N	2.0	0	0	43
Ia	C_5H_5N	5.0	0	0	0
Ia	H_2O	2.0	42	40	36
Ia	H_2O	6.0	27	23	52
Ib	C_5H_5N	0.5	23	—	18
Ib	C_5H_5N	1.0	0	0	63

a) The starting amount of iron(III) chloride was 1.5 mmol in 5 ml of I. The reactions were carried out under atmosphere at 70—75 °C for 24 hr (Ia) and 48 hr (Ib).
b) The yield was calculated by 200× (the number of moles of the products that of iron(III) chloride).

Copper(II) Chloride, Metal Oxide, and Metal. The reaction of Ia with iron(III) chloride in the presence of copper(II) chloride was carried out under conditions similar to those in the absence of copper(II) chloride. Since copper(II) chloride was insoluble in Ia, it was dispersed under stirring in a solution of iron(III) chloride in Ia. As is shown in Table 3, the maximum yield of IIa, along with low yields of IIIa and IVa, was observed in the iron(III) chloride/copper(II) chloride plus iron(III) chloride ratio of 0.2: 1. The yield, being over 100%, was higher than in the absence of copper(II) chloride. The amount of IIIa produced increased with an increase in the ratio. On the other hand, the reaction of Ia with copper(II) chloride gave only IVa. The amount of IVa produced decreased with the addition of iron(III) chloride to the copper(II) chloride–I system. Thus, the binary iron(III) chloride–copper(II) chloride system was effective for the oxidative coupling reaction, although the mechanism of the action of the binary metal salts is not as yet clear.

Table 3. Effects of copper(II) chloride on the thermal reaction of Ia with iron(III) chloride[a]

$FeCl_3/(FeCl_3+CuCl_2)$[b] ratio	Products, mmol × 10		
	γ-Diketone	Furan	α-Chloroketone
0	0	0	4.0
0.1	1.4	0	1.8
0.2	7.8	1.8	1.5
0.3	7.0	4.2	1.5
0.5	6.1	4.2	1.5
1.0	4.3	3.0	1.1

a) Experiments were carried out under air atmosphere at 70—75 °C for 24 hr, using 3 ml of Ia.
b) The starting amount of iron(III) chloride plus copper(II) chloride was 0.9 mmol.

The presence of CaO and ZnO in the iron(III) chloride–Ia system resulted in the selective formation of IVa in a high yield, although Ia did not react with CaO and ZnO, as is shown in Table 4. In the cases of TiO_2, Fe_2O_3, and Cr_2O_3, IIa, IIIa, and IVa were obtained. The $FeCl_3$–CuO system gave IIa in a high yield, plus IIIa and IVa in low yields. These results also support the idea of the effectiveness of the Fe(III)–Cu(II) combination system for the oxidative coupling reaction. The reaction of Ia with iron(III) chloride in the presence of Fe^0 or Cu^0 resulted in the formation of IVa without IIa and IIIa, as Table 4 shows.

As has been described above, the effects of the concentrations, the additives, and the solvents on the reaction pathway suggest that the course of either coupling or chlorination is governed by the state of an aggregate of iron(III) chloride in the solution—for example, a dimer form of iron(III) chloride, although the details are uncertain. Furthermore, it is interesting to note that a combination of iron(III) chloride and an oxidizing agent is effective for the coupling reaction.

Table 4. Effects of metal oxide and metal on the thermal reaction of Ia with iron(III) chloride[a]

Additive	Product, mmol × 10		
	γ-Diketone	Furan	α-Chloroketone
CaO	0.4	0	8.4
ZnO	0.4	0	7.0
Cr_2O_3	10.9	6.5	2.4
TiO_2	4.9	4.2	2.5
Fe_2O_3	4.8	5.0	5.2
CuO	11.6	0.7	2.2
Fe	0	0	4.6
Cu	0.6	0	4.4

a) The amount of iron(III) chloride used was 1.5 mmol in 5 ml of Ia. The metal oxide or metal /iron(III) chloride molar ratio was 1. The reactions were carried out under air atmosphere at 70—75 °C for 24 hr.

Under Irradiation. A solution of iron(III) chloride in I, which had been placed in a quartz tube, was irradiated with a 100 W high-pressure mercury lamp at a distance of 4 cm under an atmosphere of air at room temperature for 24 hr. During the reaction, white crystals of iron(II) chloride were precipitated. As is shown in Table 5, Ia was converted to IIa, IIIa, and IVa in lower yields than in the case of the thermal reaction. In the case of Ib, however, 3-chlorobutyrophenone (VI), acetophenone, and ethylene were obtained in addition to IIb and IVb. Acetophenone and ethylene were produced after the complete conversion of the iron(III) chloride to iron(II) chloride. The reaction probably proceeded by means of a Norrish Type II process.[17] When pyridine was added to the reaction system in the pyridine/iron(III) chloride molar ratio of 1:1, the reaction resulted in chlorination at the α- and/or β-position of the carbonyl group. In the case of Ib, however, crotophenone (VII) was produced by the dehydrochlorination of VI.

$$\mathrm{Ib} \xrightarrow{h\nu} \mathrm{C_6H_5COCH_3} + \mathrm{CH_2{=}CH_2}$$

$$\mathrm{Ib} \xrightarrow[\mathrm{FeCl_3\text{–}C_5H_5N}]{h\nu} \mathrm{IVb} + \underset{\mathrm{VI}}{\mathrm{C_6H_5COCH_2\overset{Cl}{\overset{|}{C}}HCH_3}} + \underset{\mathrm{VII}}{\mathrm{C_6H_5COCH{=}\overset{}{\overset{|}{C}}HCH_3}}$$

Other Ketones. The reactions of acetophenone and aliphatic ketones, such as acetone, 2-heptanone, and cyclohexanone, with anhydrous iron(III) chloride at 70 °C resulted in aldol condensation, giving the corresponding α,β-unsaturated ketones. That is, the oxidative coupling by iron(III) chloride was specific for the α-methylene group of alkyl aryl ketones.

$$\mathrm{C_6H_5COCH_3} \xrightarrow{\mathrm{FeCl_3}} \mathrm{C_6H_5COCH{=}\overset{CH_3}{\overset{|}{C}}\text{–}C_6H_5}$$

Table 5. The photo-reactions of I with iron(III) chloride

Ketone	Molar ratio[a] $C_5H_5N/FeCl_3$	Yields of products, %[b]				
		γ-Diketone	Furan	α-Chloroketone	β-Chloroketone	$FeCl_2$
Ia	0	40	29	25	—	94
Ia	1	0	0	20	—	—
Ib	0	26	—	26	14	83
Ib[c]	1	0	0	48	14	—

a) The amount of iron(III) chloride used was 1.5 mmol in 5 ml of I. The reactions were carried out under air atmosphere at room temperature for 24 hr.
b) The yield was calculated by 200 × (the number of moles of the products/that of iron(III) chloride).
c) Crotophenone was obtained in 6% yield.

17) J. G. Calvert and J. N. Pitts, Jr., "Photochemistry," John Wiley & Sons, Inc., New York, N. Y. (1967), p. 382.

Experimental

Materials. The aliphatic ketones, acetophenone, metal salts, metal oxides, and metal were purchased from commercial sources. The aliphatic ketones and acetophenone were distilled twice before use. The propiophenone and butyrophenone were prepared by the methods described in the literature.[18] The anhydrous iron(III) chloride was prepared by the sublimation of the commercial iron(III) chloride under the reduced pressure of 1 mmHg at 300 °C. The purity of the iron(III) chloride used was 99—99.8%; it was measured from the content percentage of Fe(III) and chloride ions. Furthermore, the UV absorption spectrum of the iron(III) chloride in dry dioxane coincided with that described in the literature.[19]

Reactions. Similar procedures were used for all the reactions. A solution of 1.3—1.5 mmol of iron(III) chloride in 5 ml of ketones was heated at 70—75 °C or was irradiated with a 100 W high pressure mercury lamp at room temperature for the desired time. II, III, and IV were isolated by gas chromatography after a work-up. The isolation of II and III was carried out by the following method. After a reaction period, dry ether was added to the reaction mixture, the resulting solution was filtered off, and the filtrate was washed repeatedly with water and dried over calcium chloride. After the ether and then the starting ketone and IV had been removed, the residue was distilled under the reduced pressure of 3×10^{-3} mmHg at 100—110 °C. The high-boiling components containing II and III were submitted to chromatography on silica gel (elution with dry carbon tetrachloride), and then to gas chromatography, thus leading to the isolation of II and III.

The NMR spectrum (CCl_4) of IIa showed signals of δ 1.35 and 1.50 (d, 6H, CH_3), 4.25 and 5.60 (q, 2H, CH), and 7.1—8.0 (m, 10H, aromatic protons). The IR spectrum of IIa exhibited strong bands at 1680 cm^{-1} (CO). Mass *m/e*; 266 (parent peak).

Found: C, 81.33; H, 6.80%. Calcd for $C_{18}H_{18}O_2$: C, 81.20; H, 6.76%.

IIb exhibited NMR (CCl_4) signals at δ 0.7—1.3 (m, 6H, CH_3), 1.6—2.1 (m, 4H, CH_2), 4.05 and 5.55 (q and t, 2H, CH), and 6.9—8.0 (m, 10H, aromatic protons), and an IR (liquid film) peak at 1680 cm^{-1} (CO). Mass *m/e*; 294 (parent peak).

Found: C, 81.56; H, 7.55%. Calcd for $C_{20}H_{22}O_2$: C, 81.60; H, 7.53%.

IIIa, mp 52—54 °C, exhibited NMR (CCl_4) signals at δ 2.16 and 2.33 (s, 6H, CH_3), and 7.2—7.8 (m, 10H, aromatic protons). Mass *m/e*; 248 (parent peak).

Found: C, 86.92; H, 6.50%. Calcd for $C_{18}H_{16}O$: C, 87.09; H, 6.45%.

The other products were identified by a comparison of their IR and NMR spectra, the results of elementary analyses of their 2,4-dinitrophenylhydrazones, their retention times in gas chromatography, and their molecular weights with those of authentic specimens.

Analyses. After a reaction period, the iron(II) chloride produced was filtered off, washed by *n*-hexane, dried over calcium chloride, and then weighed. The determination of the iron(III) chloride and iron(II) chloride was carried out by the methods described in the literature.[20] The amounts of the products were determined by means of gas chromatography using a 3 mm×2 m column of 30% high-vacuum Silicone grease on Celite 545 (80—100 mesh).

18) W. T. Read, *J. Amer. Chem. Soc.*, **44**, 1746 (1922); W. A. Riddell and C. R. Noller, *ibid.*, **54**, 290 (1932).

19) P. A. McCusker and S. M. S. Kennard, *ibid.*, **81**, 2976 (1959).

20) H. Inoue, N. Komakine, and E. Imoto, This Bulletin, **41**, 2726 (1968).

BULLETIN OF THE CHEMICAL SOCIETY OF JAPAN, VOL. 46, 2215—2218 (1973)

Reactions of Phenylhydrazinium Thiocyanate with Ketones and Aldehydes

Isamu ARAI

Department of Chemistry, College of Science, Rikkyo (St. Paul's) University, Nishi-Ikebukuro, Toshima-ku, Tokyo 171

(Received February 5, 1973)

Reactions of phenylhydrazinium thiocyanate with various ketones and aldehydes gave 1-phenyl-3-alkyl-5-mercapto-Δ^4-1,2,4-triazoline compounds in 80—90% yield by the cycloaddition of thiocyanic acid to the phenylhydrazones intermediately formed from phenylhydrazine and the ketones or aldehydes. Their structure were determined by elemental analyses, spectral data (IR, NMR, and MS) and chemical reactions. Many 2-phenylthiosemicarbazone and 1-phenyl-1,2,4-triazole derivatives were synthesized in good yields.

We have reported that hydrazinium thiocyanate (I') reacts with aldehydes and ketones to give 1,2,4-triazolidine (II') and triazolo-triazole (III') compounds.[1)]

We considered that the 1,2,4-triazolidine compounds (II') were produced by the cycloaddition of thiocyanic acid to the hydrazones intermediately formed from ketones or aldehydes with hydrazine. Attempts to isolate these intermediate hydrazones from the reaction mixture failed because the hydrazones were not stable and readily changed to the corresponding azines.[2)]

In this paper we deal with the formation of 1,2,4-

1) I. Arai, S. Abe, and A. Hagitani, This Bulletin, **46**, 677 (1973).

2) H. H. Szmant and C. Mc Ginnis, *J. Amer. Chem. Soc.*, **72**, 2890 (1950).

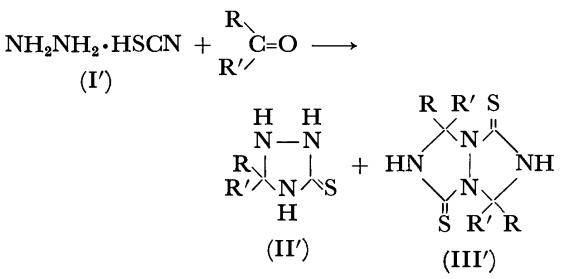

triazolidine compounds and their derivatives, using phenylhydrazine as the starting material instead of hydrazine. New useful methods are given for the preparation of 2-phenylthiosemicarbazone and 1-phenyl-1,2,4-triazole derivatives.

Results and Discussion

When a ketone or aldehyde was added to an aqueous solution of phenylhydrazinium thiocyanate (I) and the mixture was allowed to stand at room temperature, 1-phenyl-3-alkyl-5-mercapto-Δ^4-1,2,4-triazoline (II) was obtained in an 80—90% yield. Elemental analyses (Table 1) and mass spectral data of (II) gave a reasonable molecular formula. The IR spectra of (II) showed absorption bands at 3135—3136 (NH) and 1590—1595 (C=N) cm^{-1}, and the NMR spectral data of (II) also gave a reasonable structure (see Experimental). From these data and the results of chemical reactions (hydrolysis, thermolysis, oxidation, and desulfurization) of (II), the structure was assigned to be 1-phenyl-3-alkyl-5-mercapto-Δ^4-1,2,4-triazoline.

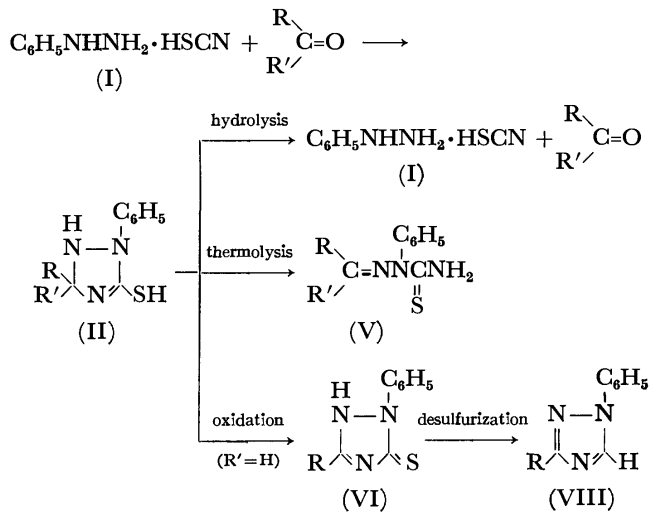

This was also supported by the mass spectral data of (II); *i.e.*, peaks of $C_6H_5NCS^+$ and $C_6H_5NH^+$ at *m/e* 135 and 92 respectively. Fragmentations resulting from the loss of R, R′ or HSCN from the molecular ion were also observed.

The yields of the products are given in Table 2 and those of (IIa) *versus* reaction time in Fig. 1.

From the above results and those of previous work,[1] the following path is proposed for the formation of (II). First the ketone or aldehyde reacts with phenylhydrazine in the presence of an acid catalyst to produce phenylhydrazone (IV). The intermediate then reacts with thiocyanic acid to form (II). Formation of this

Table 1. 1-Phenyl-3-alkyl-5-mercapto-Δ^4-1,2,4-triazoline (II)

II	R	R′	Mp (decomp) (°C)	Formula	Analysis (%) Found (Calcd)			
					C	H	N	S
IIa	CH_3	CH_3	134.0	$C_{10}H_{13}N_3S$	57.85 (57.96)	6.71 (6.32)	20.25 (20.28)	15.19 (15.44)
IIb	C_2H_5	CH_3	113.5	$C_{11}H_{15}N_3S$	59.92 (59.71)	6.85 (6.83)	19.38 (18.99)	14.43 (14.46)
IIc	*n*-C_3H_7	CH_3	112.0	$C_{12}H_{17}N_3S$	61.18 (61.24)	7.94 (7.28)	17.80 (17.85)	
IId	*iso*-C_3H_7	CH_3	130.5	$C_{12}H_{17}N_3S$	61.13 (61.24)	6.70 (7.28)	18.26 (17.85)	
IIe	*t*-C_4H_9	CH_3	167.0	$C_{13}H_{19}N_3S$	61.99 (62.62)	7.95 (7.68)	16.81 (16.85)	
IIf	*iso*-C_4H_9	CH_3	136.5	$C_{13}H_{19}N_3S$	62.69 (62.62)	7.30 (7.68)	16.58 (16.85)	
IIg	C_2H_5	C_2H_5	119.0	$C_{12}H_{17}N_3S$	61.22 (61.24)	7.40 (7.28)	17.64 (17.85)	13.35 (13.16)
IIh			148.8	$C_{13}H_{17}N_3S$	62.91 (63.12)	6.70 (6.93)	16.99 (16.99)	
IIi	CH_3	H	96.5	$C_9H_{11}N_3S$	55.71 (55.93)	6.15 (5.74)	21.35 (21.74)	
IIj	C_2H_5	H	125.0	$C_{10}H_{13}N_3S$	58.31 (57.96)	6.30 (6.32)	20.06 (20.28)	
IIk	*n*-C_3H_7	H	125.5	$C_{11}H_{15}N_3S$	59.51 (59.71)	7.21 (6.83)	18.76 (18.99)	
IIl	*iso*-C_3H_7	H	130.0	$C_{11}H_{15}N_3S$	59.98 (59.71)	7.11 (6.83)	18.79 (18.99)	

Table 2. Reactions of phenylhydrazinium thiocyanate (I) with ketones and aldehydes

Ketone	Yield (%) of (II)	Aldehyde	Yield (%) of (II)
CH_3COCH_3	78.7	CH_3CHO	78.3
$C_2H_5COCH_3$	83.5	C_2H_5CHO	84.6
n-$C_3H_7COCH_3$	77.4	*n*-C_3H_7CHO	87.6
iso-$C_3H_7COCH_3$	80.7	*iso*-C_3H_7CHO	92.6
t-$C_4H_9COCH_3$	70.3		
iso-$C_4H_9COCH_3$	53.6		
$C_2H_5COC_2H_5$	90.2		
	93.4		

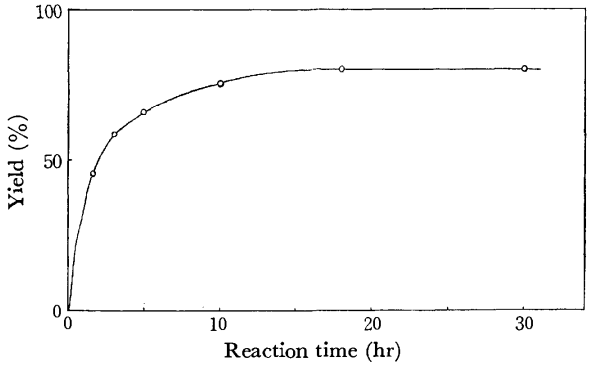

Fig. 1. Yield of (IIa) *versus* reaction time, $C_6H_5NHNH_2 \cdot HSCN$ (0.05 mol), acetone (0.05 mol), and water (200 ml)

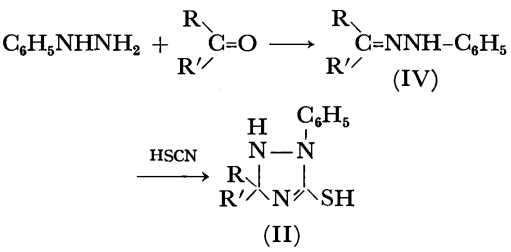

intermediate (IV) was detected by tlc[3] and confirmed by isolating it from the reaction mixture.

Reactions (IV)+HSCN→(II) were carried out to confirm the above path. (II) was obtained in higher yields (Table 3) than in the original reactions ((I)+$\begin{matrix}R'\\R\end{matrix}$>C=O→(II)). The results reveal that the reactions

Table 3. Reactions of phenylhydrazones(IV) with thiocyanic acid

IV	$\begin{matrix}R\\R'\end{matrix}$>C=NNH-$C_6H_5$ (IV)		Yield (%) of (II)
	R	R′	
IVa	CH_3	CH_3	91.2
IVb	C_2H_5	CH_3	93.7
IVc	*n*-C_3H_7	CH_3	92.8
IVd	*iso*-C_3H_7	CH_3	89.9
IVe	*t*-C_4H_9	CH_3	94.6
IVf	*iso*-C_4H_9	CH_3	81.2
IVg	C_2H_5	C_2H_5	91.1
IVh			92.7
IVi	CH_3	H	80.0
IVj	C_2H_5	H	88.9
IVk	*n*-C_3H_7	H	95.0
IVl	*iso*-C_3H_7	H	90.2

of (I) with ketones or aldehydes pass through phenylhydrazone (IV) as an intermediate, and those of (I′) also pass through hydrazone.

Thermolysis of (II) gave 2-phenyl-thiosemicarbazone (V) almost quantitatively. This is a convenient method for synthesizing thiosemicarbazone derivatives since to synthesize them by the conventional method requires several steps.[4]

Oxidation of (IIi—l) gave 1-phenyl-3-alkyl-Δ^3-1,2,4-triazoline-5-thione (VI). This is also a new method to synthesize Δ^3-1,2,4-triazoline-5-thione derivatives and demonstrates the interesting fact that the hydrogen atom attached to a ring carbon of an saturated heterocyclic compound is easily released under mild conditions. Table 4 shows the yields and elemental analyses of (VI).

(VI) was readily methylated with dimethyl sulfate or methyl iodide to give 1-phenyl-3-alkyl-5-methylthio-1,2,4-triazole (VII). (VII) was further desulfurizated with Raney nickel to give 1-phenyl-3-alkyl-1,2,4-triazole (VIII). (VIII) was also prepared by desulfurization of (VI) with Raney nickel. (VIII) was identified by comparison (mp and UV) with an authentic sample.[5] The reactions indicated the presence of a 1,2,4-triazoline skeleton in (II). They also represent a new

Table 4. 1-Phenyl-3-alkyl-Δ^3-1,2,4-triazoline-5-thione (VI)

VI	R	Mp (°C)	Yield (%)	Formula	Analysis (%) Found (Clacd)		
					C	H	N
VIi	CH_3	177.0—178.0	58.62	$C_9H_9N_3S$	56.47 (56.52)	4.73 (4.74)	21.96 (21.97)
VIj	CH_3	147.0—147.5	57.56	$C_{10}H_{11}N_3S$	58.49 (58.51)	5.40 (5.40)	20.47 (20.47)
VIk	*n*-C_3H_5	135.5—136.5	62.57	$C_{11}H_{13}N_3S$	60.19 (60.25)	5.99 (5.97)	19.25 (19.16)
VIl	*iso*-C_3H_7	161.5—162.2	79.08	$C_{11}H_{13}N_3S$	60.29 (60.25)	5.98 (5.97)	19.17 (19.16)

3) On silica gel with methanol–chloroform (1: 100 v/v).
4) "Beilsteins Handbuch der Organischen Chemie," Vol. 15, 281.
5) M. R. Atkinson, E. A. Parkes, and J. B. Polya, *J. Chem. Soc.*, **1954**, 4256.

useful method for th preparation of 1,2,4-triazole derivatives.

Experimental

All melting and boiling points are uncorrected. The IR spectra were recorded from KBr pellets, using a 215 Hitachi grating infrared spectrophotometer. The NMR spectra were measured in a solution of deuteriochloroform with a JNM C-60HL spectrometer using tetramethylsilane as an internal standard. The mass spectra were obtained on a CEC 21-110B spectrometer at 70 eV.

Reaction of Phenylhydrazinium Thiocyanate (I) with Ketone and Aldehyde. Ketone or aldehyde (0.05 mol) was added dropwise to a solution of phenylhydrazine hydrochloride (7.23 g, 0.05 mol) and sodium thiocyanate (4.05 g, 0.05 mol) in 0.25 M hydrochloric acid (200 ml) with stirring. The solution was stirred at room temperature for 18 hr under shield from light. A white precipitate formed which was filtered and washed with water several times. It was recrystallized with 1,2-dichloroethane to give 1-phenyl-3-alkyl-5-mercapto-Δ^4-1,2,4-triazoline (II).

(IIa): IR; 3150, 2970, 1595, 1490, 1380, 1170, 745 cm^{-1}. NMR; δ 1.50 (s, $-CH_3$), 4.80 (s, –SH), 7.18—8.20 ($-C_6H_5$ and –NH–). Mass spectra; *m/e* 207 ($C_{10}H_{13}N_3S^+$), 192 ($C_9H_{10}N_3S^+$), 148 ($C_9H_{12}N_2^+$), 135 ($C_6H_5NCS^+$), 92 ($C_6H_5NH^+$).

(IIi): IR; 3150, 2960, 1590, 1475, 1400, 1239, 760 cm^{-1}. NMR; δ 1.45 (d, J=6.0 Hz, $-CH_3$), 4.75 (broad s, –SH) 4.92 (q, J=6.0 Hz, =CH–), 7.00—8.20 ($-C_6H_5$ and –NH–). Mass spectra; *m/e* 193 ($C_9H_{11}N_3S^+$), 191 ($C_9H_9N_3S^+$), 178 ($C_8H_8N_3S^+$), 135 ($C_6H_5NCS^+$), 134 ($C_8H_{10}N_2^+$), 92 ($C_6H_5NH^+$).

Phenylhydrazone (IV). To a cooled solution of 0.1 mol of phenylhydrazine in ether (100 ml) were added 0.1 mol of ketone or aldehyde and a few drops of acetic acid and the solution was heated for several minutes. Sodium hydroxide was added to the solution, and it was allowed to stand at room temperature overnight. The ethereal solution was separated from the sodium hydroxide by decantation and then evaporated. The residue was distilled under reduced pressure to give ketone or aldehyde phenylhydrazone (IV).

(IVa); bp 127.0 °C/9.5 mmHg, (IVb); bp 136.5—137.5 °C/7.5 mmHg, (IVc); bp 158.0—160.0 °C/18.5 mmHg, (IVd); bp 156.0—157.0 °C/21.0 mmHg, (IVe); bp 111.8—113.8 °C/1.5 mmHg, (IVf); bp 127.0—128.7 °C/3.0 mmHg, (IVg); bp 157.0—158.0 °C/20.0 mmHg, (IVh); mp 73.0—75.0 °C, (IVi); bp 110.0—111.0 °C/3.5 mmHg, (IVj); bp 126.0—128.5 °C/7.0 mmHg, (IVk); bp 110.0—111.5 °C/2.0 mmHg, (IVl); bp 142.5—144.0 °C/16.0 mmHg.

Reaction of Phenylhydrazone(IV) with Thiocyanic Acid. Sodium thiocyanate (8.10 g, 0.05 mol) was added in one portion to a solution of 0.05 mol of (IV) in acetic acid (40 ml) with stirring. The solution was stirred at room temperature for 18 hr with a light shield. A white precipitate formed which was filtered and washed with water. It was recrystallized with dichloroethane to give 1-phenyl-3-alkyl-5-mercapto-Δ^4-1,2,4-triazoline (II).

Hydrolysis of 1-Phenyl-3,3-dimethyl-5-mercapto-Δ^4-1,2,4-triazoline (IIa). A mixture of 1.0 g of (IIa) in water (30 ml) was refluxed for a few minutes, and distilled at atmospheric pressure until 5 ml of a solution was collected. The distillate was poured into a solution of 2,4-dinitrophenylhydrazine in 6 M hydrochloric acid. A yellow precipitate formed which was filtered and recrystallized from ethanol to give acetone 2,4-dinitrophenylhydrazone, mp 125 °C. The liquor remaining on distillation was evaporated under reduced pressure, and chloroform was added to the residue. An insoluble material (0.40 g) was recrystallized with methanol–ether to give phenylhydrazinium thiocyanate (I), mp 108 °C (decomp). The products were identified by comparison (IR spectra and mp) with an authentic sample.

Thermolysis of 1-Phenyl-3,3-dimethyl-5-mercapto-Δ^4-1,2,4-triazoline (IIa). A solution of 1.0 g of (IIa) in 2-butanol (50 ml) was refluxed for 1.5 hr, and then evaporated under reduced pressure. The residue (1.0 g) was recrystallized from 75 vol% ethanol to give acetone 2-phenylthiosemicarbazone (Va), mp 133.0—134.0 °C (lit,[4] mp 135.0 °C).

Found: C, 57.94; H, 6.32; N, 20.27%. Calcd for $C_{10}H_{13}N_3S$: C, 58.18; H, 6.41; N, 20.23%.

Oxidation of 1-Phenyl-3-alkyl-5-mercapto-Δ^4-1,2,4-triazoline (IIi—l). Oxygen was passed into a mixture of 1.0 g of (IIi—l) in 1 M sodium hydroxide (100 ml) with stirring until (IIi—l) was dissolved. The solution was then acidified with 1 M hydrochloric acid. A white precipitate formed which was filtered and recrystallized from 50 vol% ethanol to give 1-phenyl-3-alkyl-Δ^3-1,2,4-triazoline-5-thione (VI).

IR of (VIi): 3000, 2890, 2700, 1610, 1490, 1225, 1010, 755, 687 cm^{-1}. NMR of (VIi): δ 2.36 (s, $-CH_3$), 7.30—8.25 ($-C_6H_5$ and –NH–).

Methylation of 1-Phenyl-3-methyl-Δ^3-1,2,4-triazoline-5-thione (VIi). 1) With methyl iodide. A solution of 2.0 g of (VIi) and methyl iodide (1.48 g) in ethanol (50 ml) was refluxed for 3.5 hr, and then evaporated under reduced pressure. Fifty milliliters of 1 M sodium hydroxide was added to the residue, and the mixture was extracted with chloroform. The extract was evaporated. The residue (2.07 g) gave 1-phenyl-3-methyl-5-methylthio-1,2,4-triazole (VIIi). (VIIi) was an oil and formed a hydrochloride, mp 141 °C decomp. (from tetrahydrofuran).

Found: C, 49.60; H, 4.87; N, 17.73%. Calcd for $C_{10}H_{12}N_3SCl$: C, 49.69; H, 5.01; N, 17.38%. IR: 2990, 2600, 2470, 1595, 1585, 1505, 1480, 1245, 1025, 770, 690 cm^{-1}. NMR: δ 2.78 (s, $-CH_3$), 3.20 (s, $-SCH_3$), 7.68 (s, $-C_6H_5$).

2) With dimethyl sulfate. To a cooled solution of 0.5 g of (VIi) in 1 M sodium hydroxide (20 ml) was added dropwise dimethyl sulfate (0.33 g). The mixture was then stirred at room temperature for 24 hr and extracted with chloroform. The extract was evaporated and the residue (0.34 g) gave (VIIi).

1-Phenyl-3-methyl-1,2,4-triazole (VIIIi). 1) A mixture of 0.5 g of 1-phenyl-3-methyl-Δ^3-1,2,4-triazoline-5-thione (VIi) and *ca.* 5 g of Raney nickel (W-2) in ethanol (25 ml) was refluxed for 24 hr. The solution of ethanol was then separated from Raney nickel by filtration and evaporated. The residue (0.34 g) was recrystallized with *n*-hexane to give (VIIIi), mp 89.5 °C (lit,[5] mp 89.0 °C).

Found: C, 68.10; H, 6.00; N, 26.27%. Calcd for $C_9H_9N_3$: C, 67.91; H, 5.70; N, 26.40%. IR: 3100, 1600, 1530, 1500, 1310, 765, 695 cm^{-1}. UV λ_{max}^{EtOH} 244 nm (lit,[5] 244 nm). NMR: δ 2.53 (s, $-CH_3$), 7.35—7.90 ($-C_6H_5$), 8.59 (s, =CH–).

2) A mixture of 1.0 g of 1-phenyl-3-methyl-5-methylthio-1,2,4-triazole (VIIi) and *ca.* 10 g of Raney nickel (W-2) was refluxed for 24 hr. It was worked up as in the previous experiment to give (VIIIi), 0.70 g.

The author wishes to thank Professor A. Hagitani, Professor I. Muramatu, and assistant Professor Y. Satoh for many helpful discussions and suggestions during this work, and he also indebted to Mr. S. Kodaka and Mr. T. Shimada for their assistance in the experiments.

Peptides. IV. Racemization Suppression by the Use of Ethyl 2-Hydroximino-2-cyanoacetate and Its Amide

Masumi ITOH

Research Laboratories, Fujisawa Pharmaceutical Co., Ltd. Kashima-cho, Higashiyodogawa-ku, Osaka 532

(Received February 6, 1973)

Racemization suppression by the addition of ethyl 2-hydroximino-2-cyanoacetate (IIIa) or 2-hydroximino-2-cyanoacetamide (IIIb), during coupling stages in peptide synthesis, was studied. The effectiveness of IIIa was compared with these of known additives by the help of Bodanszky's test, which is a simple and accurate method for racemization detection.

There are so many literatures reported about racemization suppression during coupling stages in peptide synthesis.[1,2] These have recommended the use of restricted amount of base,[3] the use of weaker bases which have sufficient basicity to proceed the reaction,[4-6] or the addition of some acidic and nucleophilic compounds for racemization suppression.[7-11] A combination of dicyclohexylcarbodiimide (DCC) with *N*-hydroxysuccinimide (I) practically seems to be an attractive coupling reagent, but it has also known that I is not so stable and that the combination of DCC with I occasionally leads to some side reactions.[12,13] Later 1-hydroxybenzotriazole (II) and its derivatives have been proposed as superior additives than I.[10] In the DCC method using additives, Anderson has concluded that a major factor for racemization suppression was not neutralization of basicity of DCC by an additive, but its nucleophilic reactivity.[14] Some oximes reported as alcoholic components of active esters[15-18] seem to be good nucleophiles, but the reactivity of these esters is somewhat lower than those of other types of active esters. It was expected, therefore, that strongly acidic and nucleophilic oximes, which possess electron-withdrawing groups in the molecule, might be suitable as additives. The author intended to search for more promising additives and alcoholic components of active esters, and now wishes to report the use of strongly acidic oximes, ethyl 2-hydroximino-2-cyanoacetate (IIIa) and 2-hydroximino-2-cyanoacetamide (IIIb), as suitable additives for the same purpose.

Results

The pK_a values of several oximes prepared were compared (Table 1), and acidic oximes, IIIa and IIIb, were chosen as possible additives among them. At the same time several acylamino acid oxime esters shown in Table 2 were prepared and examined their reactivities with ethyl glycinate by the help of thin layer chromatography. It was also shown that those esters with IIIa and IIIb were more reactive than others tested. Both of IIIa and IIIb are stable, acidic compounds and are used in organic syntheses.

TABLE 1. APPARENT pK_a VALUES OF OXIMES, $HON{=}C\langle^{R_1}_{R_2}$

R_1	R_2	pK_a
CN	COOEt	4.6
CN	$CONH_2$	5.2
$COCH_3$	COOEt	7.0
COOEt	COOEt	7.1
$COCH_3$	$COCH_3$	7.4
H	$COCH_3$	8.4
H	CH_3	>11

Racemization with these additives were examined first by Anderson's test.[19] The coupling reaction of *N*-benzyloxycarbonylglycyl-L-phenylalanine with ethyl glycinate gave no racemate by the use of DCC with IIIa or IIIb in tetrahydrofuran at room temperature, while the control experiment, without additive, gave 8% of racemate. The effectiveness of IIIa was further examined by Young's test.[20] The crude coupling product, ethyl *N*-benzoylleucylglycinate, showed 93.6% optical purity calculated from the optical rotation, which was raised to 97% by recrystallization. This method is not satisfactory for the detection of small

1) E. Schröder and K. Lübke, "The Peptides," Vol. I, Academic Press Inc., New York, N.Y. (1966), p. 325.
2) M. Bodanszky and M. A. Ondetti, "Peptide Synthesis," Interscience Publishers, New York, N.Y. (1966), p. 137.
3) G. W. Anderson, F. M. Callahan, and J. E. Zimmerman, *Acta Chim. Acad. Sci. Hung.*, **44**, 51 (1965).
4) G. W. Anderson, J. E. Zimmerman, and F. M. Callahan, *J. Amer. Chem. Soc.*, **88**, 1338 (1966); *ibid.*, **89**, 5012 (1967).
5) S. Sakakibara and M. Itoh, This Bulletin, **40**, 656 (1967).
6) M. Bodanszky and A. Bodanszky, *Chem. Commun.*, **1967**, 591.
7) J. Kovacs, L. Kisfaludy, and M. Q. Ceprini, *J. Amer. Chem. Soc.*, **89**, 183 (1967).
8) F. Weygand, D. Hoffmann, and E. Wünsch, *Z. Naturforsch., B*, **21**, 426 (1966).
9) E. Wünsch and F. Dress, *Chem. Ber.*, **99**, 110 (1966).
10) W. König and R. Geiger, *ibid.*, **103**, 788, 2024, 2034 (1970).
11) G. C. Windridge and E. C. Jorgensen, *J. Amer. Chem. Soc.*, **93**, 6318 (1971).
12) H. Gross and L. Bilk, *Tetrahedron*, **24**, 6935 (1968).
13) F. Weygand, W. Steglich, and N. Chytil, *Z. Naturforsch., B*, **23**, 1391 (1968).
14) G. W. Anderson, "Peptides, Chemistry and Biochemistry," ed. by B. Weinstein and S. Lande, Marcel Dekker, Inc., New York, N.Y. (1970), p. 255.
15) S. Bittner, Y. Knobler, and M. Frankel, *Tetrahedron Lett.*, **1965**, 95.
16) G. Losse, K. H. Hoffmann, and G. Hetzer, *Ann. Chem.*, **684**, 236 (1965).
17) M. Fujino and O. Nishimura, *Chem. Pharm. Bull.* (Tokyo), **17**, 1937 (1969).
18) B. O. Handford, J. H. Jones, G. T. Young, and T. F. N. Johnson, *J. Chem. Soc.*, **1965**, 6814.
19) G. W. Anderson and F. M. Callahan, *J. Amer. Chem. Soc.*, **80**, 2902 (1958).
20) M. W. Williams and G. T. Young, *J. Chem. Soc.*, **1963**, 881.

Table 2. Some esters of acylamino acids with oximes

Esters[a]	Yield (%)	Mp °C	Analysis (Calcd) C %	H %	N %
Cbz–Gly–ON=CHCOCH$_3$	83	60.5— 62[b]	56.34	5.16	10.31
			(56.11	5.07	10.07)
Cbz–Gly–ON=C$\langle^{COCH_3}_{COCH_3}$	76	83 — 85[c]	56.43	5.22	8.56
			(56.24	5.03	8.75)
Cbz–Gly–ON=C$\langle^{CN}_{COOEt}$	72	119 —121[c]	53.86	4.32	12.54
			(54.05	4.54	12.61)
Cbz–Gly–ON=C$\langle^{CN}_{CONH_2}$	60	141 —143[d]	51.52	3.86	18.33
			(51.31	3.98	18.42)

a) Cbz–Gly=*N*-Benzyloxycarbonylglycyl residue.
b) Recrystallized from ether–petroleum ether.
c) Recrystallized from ethyl acetate–petroleum ether.
d) Recrystallized from 2-propanol–petroleum ether.

Table 3. Comparison of effectiveness of the additives

Acetyl-L-isoleucine	Ethyl glycinate hydrochloride	Triethylamine	Additive	Extent of racemization (%)[a]
1.0 mmol	1.0 mmol	1.0 mmol	none	35
1.0	1.0	1.0	I 1.2 mmol	2.7
1.0	1.0	1.0	II 1.2	8.8
1.0	1.0	1.0	IIIa 1.2	1.8

a) Racemization during hydrolysis was not subtracted.

quantity of racemate, because it does not give accurate percentage of racemization if the protected dipeptide is contaminated with unconcerned impurities. Therefore, Bodanszky's test[21] was chosen as a more simple and sensitive procedure for racemization detection. For a comparison of additives, I, II, and IIIa, coupling of *N*-acetyl-L-isoleucine and ethyl gylcinate with DCC was carried out in dimethylformamide (DMF), in which significant racemization occurs. The crude product, ethyl *N*-acetylisoleucylglycinate, was hydrolyzed by 6M hydrochloric acid at 110 °C and the hydrolyzate was subjected to amino acid analysis to detect D-alloisoleucine. About 0.7% of racemization occured during hydrolysis of *N*-acetyl-L-isoleucine itself under the same condition. The results obtained are summarized in Table 3, which shows that all of additives examined suppress racemization potently. Unexpectedly, II is less effective than I. Although this is incompatible with previously reported results by König and Geiger,[10] it is difficult to discuss because the racemate detection systems are completely different.

Apart from such a problem the combination of DCC with IIIa seems to be a promising approach in coupling reactions.

Experimental

Capillary melting points were observed on a Hoover "Uni-Melt" apparatus and are uncorrected.

Measurement of pK_a *Values of Several Oximes in Aqueous Solution.* A solution of small amount of sample (2—7 mg) in 0.02 M potassium hydroxide (6.0 ml) was titrated by the use of an automatic titrator, Metrohm E 336. The pK_a values measured are listed in Table 1. Oximes were prepared according to the literatures: ethyl 2-hydroximino-2-cyanoacetate (IIIa),[22] 2-hydroximino-2-cyanoacetamide (IIIb),[22] ethyl 2-hydroximino-2-acetoacetate,[23] diethyl 2-hydroximinomalonate,[24] 3-hydroximinopentan-2,4-dione,[25] and 3-hydroximinopropan-2-one.[26]

Preparation of Esters of Acylamino Acids with Oximes. A typical example is as follows: DCC (1.05 g) was added to a solution of *N*-benzyloxycarbonyl-L-proline (1.25 g) and IIIb (0.56 g) in dioxane (10 ml) at 0 °C. The mixture was allowed to react for 2 hr at the same temperature and to stand for 16 hr at room temperature. After filtration the filtrate was evaporated to dryness. The product was filtered with small amount of 2-propanol and petroleum ether, and was recrystallized from same solvent system; yield 1.5 g (85%); mp 136—138 °C.

Found: C, 55.74; H, 4.71; N, 15.76%. Calcd for $C_{16}H_{18}O_4N_4$: C, 55.81; H, 4.68; N, 16.27%.

The other esters prepared are listed in Table 2.

Investigation of the Effectiveness of IIIa and IIIb for Racemization Suppression. a) Anderson's Test:[19] *N*-Benzyloxycarbonylglycyl-L-phenylalanine (1.78 g, 5 mmol), ethyl glycinate (0.52 g, 5 mmol) and IIIb (0.68 g, 6 mmol) were dissolved in dry tetrahydrofuran (25 ml). DCC (1.20 g, 5.8 mmol) was added to the solution at room temperature and the mixture was stirred for 4 hr. After the addition of acetic acid (0.05 ml), the mixture was filtered. The filtrate was evaporated completely, and the residue was taken up in ethyl acetate, washed with 1 M sodium bicarbonate solution, water, 1 M hydrochloric acid and water, and dried over mag-

21) M. Bodanszky and L. E. Conklin, *Chem. Commun.*, **1967**, 773.
22) M. Conrad and A. Schulze, *Ber.*, **42**, 735 (1909).
23) M. Z. Jovitchitch, *ibid.*, **35**, 151 (1902).
24) V. Cerchez, *Bull. Soc. Chim. Fr.*, **47**, 1279 (1930).
25) L. Wolff, *Ann. Chem.*, **325**, 139 (1902).
26) P. Fréon, *Ann. Chim.* (Rome), **11**, 453 (1939); *Chem. Abstr.*, **33**, 7733 (1939).

nesium sulfate. After evaporation of the solvent crude ethyl *N*-benzyloxycarbonylglycyl-L-phenylalanylglycinate was obtained. Fractional recrystallization from ethanol gave no racemate; yield of pure L isomer, 2.03 g (92%); mp 116—118 °C.

The use of IIIa (0.71 g) in place of IIIb gave similar result. In control experiment, without additive, 8% of racemate, ethyl *N*-benzyloxycarbonylglycyl-DL-phenylalanylglycinate (mp 130—132 °C), was obtained from crude protected tripeptide by fractional recrystallization.

b) Young's Test:[20] DCC (0.52 g, 2.52 mmol) was added to a solution of *N*-benzoyl-L-leucine (0.60 g, 2.55 mmol), free ethyl glycinate (0.30 g, 2.91 mmol) and IIIa (0.35 g, 2.46 mmol) in ethyl acetate (5 ml) at 0 °C. The mixture was stirred for 3 hr at the same temperature, and was filtered. The filtrate was diluted with ethyl acetate, washed with 1 M sodium bicarbonate solution, water, 1 M hydrochloric acid and water, and dried over magnesium sulfate. After evaporation of the solvent the residue was filtered with ether–petroleum ether mixture; yield, 0.73 g; mp 145—152 °C; $[\alpha]_D^{25}$ −30.9° (*c* 3, EtOH). Recrystallization from ethyl acetate–petroleum ether gave 0.61 g of product; mp 151—153 °C; $[\alpha]_D^{25}$ −33.0° (*c* 3, EtOH).

c) Bodanszky's Test:[21] A typical example is as follows: Ethyl glycinate hydrochloride (140 mg, 1.0 mmol) was dissolved in dry DMF (3.0 ml) and neutralized with triethylamine (0.14 ml, 1.0 mmol) under ice-cooling. Then IIIa (170 mg, 1.2 mmol) and *N*-acetyl-L-isoleucine[27] (173 mg, 1.0 mmol) were dissolved in the above solution. A solution of DCC (206 mg, 1.0 mmol) in dry DMF (2.0 ml) was added into the solution, and the mixture was allowed to react for 3 hr at +5 °C. After standing overnight DMF was evaporated completely under nitrogen gas, and the residue was extracted with ethyl acetate. The filtered extract was washed with water, 1 M sodium bicarbonate solution (4 times), water, 1 M hydrochloric acid and water, and dried over magnesium sulfate. After evaporation of the solvent the residue was filtered with small amount of ether–petroleum ether mixture; yield of crude ethyl *N*-acetylisoleucylglycinate, 178 mg (69%). A small amount of the sample was hydrolyzed by 6 M hydrochloric acid at 110 °C in a sealed tube for 16 hr. The hydrolyzate was subjected to an amino acid analyzer, and 1.8% of racemization was detected. The extent of racemization was calculated according to the following formula:

$$\text{Racemization (\%)} = \frac{\text{alloisoleucine} \times 100}{\text{alloisoleucine} + \text{isoleucine}}$$

During hydrolysis of *N*-acetyl-L-isoleucine under the same condition, very small amount of alloisoleucine (0.7%) was formed and detected by following amino acid analysis.

The results obtained are summarized in Table 3.

The author wishes to express his deep gratitude to Professor Miklos Bodanszky of Case Western Reserve University, Cleveland, U.S.A., for his kind advice and encouragement.

27) J. P. Greenstein, L. Levintov, C. G. Baker, and J. White, *J. Biol. Chem.*, **188**, 647 (1951).

BULLETIN OF THE CHEMICAL SOCIETY OF JAPAN, VOL. 46, 2221—2225 (1973)

Studies of Enamines. III.[1] The Reaction of 4-(1-Piperidyl)- and 4-(1-Pyrrolidinyl)-3-penten-2-ones with Aryl Isothiocyanates

Otohiko TSUGE[2] and Akitaka INABA

Research Institute of Industrial Science, Kyushu University, Hakozaki, Higashi-ku, Fukuoka 812

(Received February 7, 1973)

The reaction of enamino ketones, derived from acetylacetone and piperidine or pyrrolidine, with aryl isothiocyanates has been investigated. In contrast with phenyl isocyanates, phenyl isothiocyanates react with the enamino ketones to yield the corresponding 3-phenylthiocarbamoyl derivatives (1 : 1 adducts). The reaction with 1-naphthyl isothiocyanate forms 3-naphthylthiocarbamoyl and/or 2-thiopyridone derivatives, depending on the reaction conditions.

We have reported that 4-(1-piperidyl)- (Ia) and 4-(1-pyrrolidinyl)-3-penten-2-one (Ib) react with phenyl isocyanates to give 3,5-diphenylcarbamoyl (**A**), 2-pyridone (**B**) and/or its 3-phenylcarbamoyl derivatives (**C**), depending on the reaction conditions.[1] The reaction with 1-naphthyl isocyanate afforded the 1 : 1 adduct (**D**).

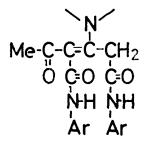

A

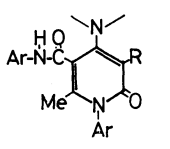

B (R=H)
C (R=CONHAr)

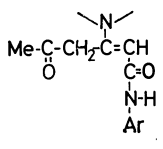

D

The only example involving the reaction of enamino ketones with isothiocyanates was reported by Goerdeler and Keuser;[3] cyclic enamino ketones derived from cyclohexane-1,3-dione and its 5,5-dimethyl derivative reacted with aryl isothiocyanates to yield the corresponding 2-thiocarbamoyl compounds.

For comparison with the reactions of enamino ketones I with isocyanates, and those of cyclic enamino ketones with isothiocyanates, it seemed to be of interest to investigate the reaction of I with isothiocyanates.

1) Part II of this series: O. Tsuge and A. Inaba, This Bulletin, **46**, 286 (1973).
2) To whom inquiries should be directed.
3) J. Goerdeler and U. Keuser, *Chem. Ber.*, **97**, 2209 (1964).

Results and Discussion

When a solution of equimolar amounts of enamino ketone Ia and phenyl isothiocyanate (IIa) in benzene was refluxed for 5 hr, a 1 : 1 adduct IIIa was obtained in a good yield. Enamino ketone Ia reacted with phenyl isocyanate to give 1 : 2 adduct **A** and its derivatives **B** and **C**.[1] However, the 1 : 1 adduct IIIa was also formed even when excess IIa was employed.

Similarly, the reaction of Ia with *p*-chlorophenyl isothiocyanate (IIb), and that of enamino ketone Ib with IIa afforded the corresponding 1 : 1 adducts IIIb and IIIc, respectively.

The IR spectra of all III exhibited no well-defined bands ascribable to ν_{NH} absorptions, but their structures were assigned to those of the corresponding 3-arylthiocarbamoyl-4-amino-3-penten-2-ones on the basis of their NMR spectral data and chemical conversion. The NMR spectra in deuteriochloroform ($CDCl_3$) displayed signals at δ about 14 (1H, broad, N**H**), and 2.8, 1.8 ppm (each 3H, s, C**H**$_3$), besides methylene and aromatic protons. These observations indicate that III exists as the chelating form[4] as shown in Scheme 1.

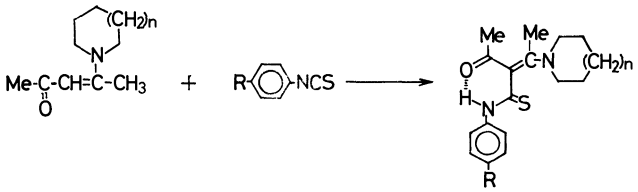

I a: n=1 b: n=0 — II a: R=H b: R=Cl — III a: n=1, R=H b: n=1, R=Cl c: n=0, R=H

Scheme 1

Hydrolysis of both IIIa and IIIc with 18% hydrochloric acid at room temperature for 6 hr, followed by neutralization with aqueous sodium hydroxide, afforded the same product, phenylthiocarbamoylacetone (IV).[5] When the hydrolyzed product of IIIa under same conditions was treated with ammonium hydroxide, 1-phenylthiocarbamoyl-2-aminopropene (V) was obtained; V was transformed into IV on further acidic hydrolysis.

Hydrolysis of III is assumed to proceed *via* the initial formation of 1-phenylthiocarbamoyl-2-(1-piperidyl or 1-pyrrolidinyl)propene (VI) as shown in Scheme 2. 1-Phenylthiocarbamoyl-2-(1-pyrrolidinyl)propene (VIa) was isolated by the hydrolysis of IIIc under mild conditions.

The structures of IV, V, and VIa were confirmed on the basis of their spectral data and microanalyses. The NMR spectrum of IV indicates that IV exists as a 5 : 3 mixture of hydrogen-bonded froms IV-1 and IV-2 in $CDCl_3$; signals appear at δ 1.98 (9/8H, s, C**H**$_3$ in IV-2), 2.34 (15/8H, s, C**H**$_3$ in IV-1), 4.13 (5/4H, s, C**H**$_2$), 5.56 (3/4H, s, =C**H**), 7.20—7.9 (5H, m, aromatic protons), 10.6—10.9 (3/8H, broad, N**H** and O**H** in IV-2), and 14.45 ppm (5/8H, broad singlet, N**H** in IV-1) in the spectrum.

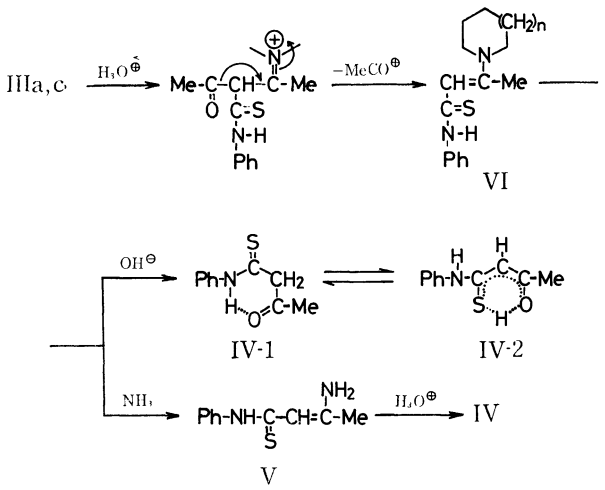

VI — IV-1 — IV-2 — V — IV

Scheme 2.

Treatment of IIIc with hydrazine hydrate afforded 3(5)-methyl-4-acetyl-5(3)-anilinopyrazole (VII), 3,5-dimethyl-4-phenylthiocarbamoylpyrazole (VIII), and hydrazone (IX) of VII. Similarly, IIIa reacted with hydrazine hydrate to give VII, VIII, and IX. The structures of VII and IX were confirmed by their spectral data and microanalyses. The reaction of VII with hydrazine hydrate gave hydrazone IX, which was easily hydrolyzed to VII. Purification of VIII was difficult owing to contamination with sulfur, the NMR spectrum of crude VIII exhibited a signal ascribable to two methyls at δ 2.38 ppm. Acetylation of VIII with acetic anhydride afforded 1-acetyl-3,5-dimethyl-4-phenylthiocarbamoylpyrazole (X) in a good yield. On the other hand, IIIc reacted with phenylhydrazine to form 1-phenyl-3-methyl-5-anilinopyrazole (XI), whose structure was deduced from its spectral data and the mode of its formation (Scheme 3).

The reaction of IIIc with *p*-chlorophenyl isocyanate afforded bis(*p*-chlorophenylcarbamoyl) derivative XIII, instead of the expected product XII.

3-(1-Naphthylthiocarbamoyl) compound XVa, a product of the same type as III, was obtained, when enamino ketone Ia was treated with 1-naphthyl isothiocyanate (XIV) in refluxing benzene. The structure of XVa was confirmed by its spectral data as well as by its microanalysis. In the same reaction under reflux in xylene two products XVa and XVIa were formed in low yields. Under reflux in both benzene and xylene, however, enamino ketone Ib gave XVIb but not 1 : 1 adduct XVb corresponding to XVa.

The molecular formulas of XVIa and XVIb corresponded to those of the compounds derived from 1 : 1 adducts with loss of water. The IR spectra of both XVI exhibited bands assignable to $\nu_{C=C}$, but no absorption bands of ν_{NH}. Both NMR spectra displayed two olefinic protons besides methyl, methylene and aromatic protons. Thus, XVI were concluded to be the corresponding 1-(1-naphthyl)-4-amino-6-methylpyrid-2-thiones, whose structures correspond to those derived

4) Goerdeler and Keuser[3] reported that 1-amino-2-arylthiocarbamoylcyclohexen-3-ones exist as double chelating forms.

5) Similarly, hydrolysis of bis(phenylcarbamoyl) derivative **A** afforded 1,3-bis(phenylcarbamoyl)acetone with loss of acetyl group.[1]

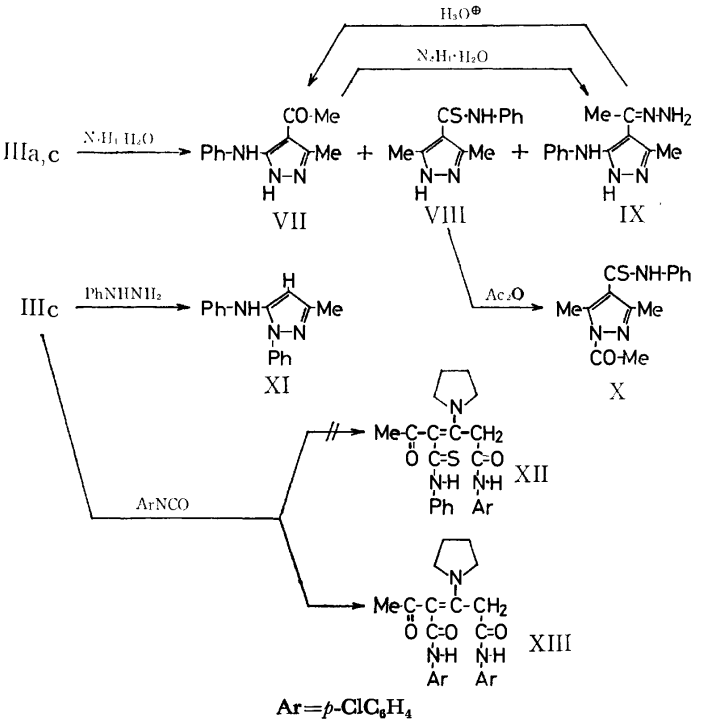

Scheme 3.

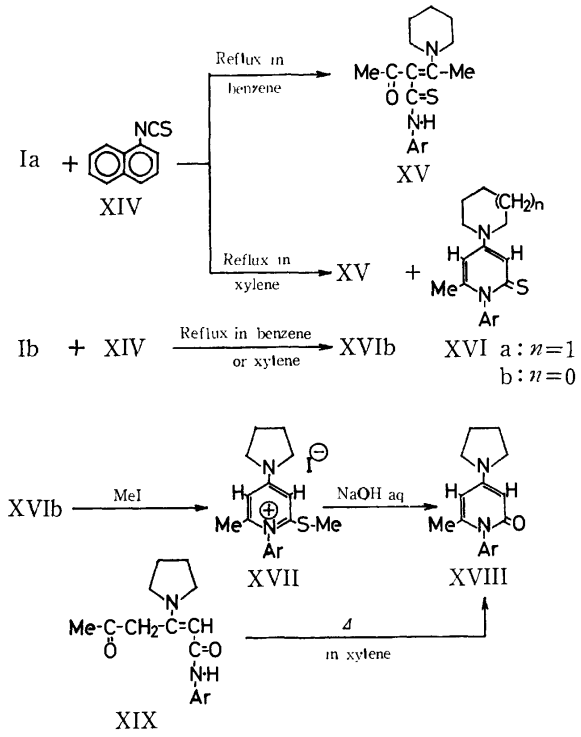

Scheme 4.

from isomers of XV, 4-amino-5-(1-naphthylthiocarbamoyl)-4-penten-2-ones, with dehydration.

Compounds XVIa and XVIb remained unchanged on both acidic and alkaline hydrolysis under various conditions. The reaction of XVIb with methyl iodide afforded S-methyl pyridinium iodide XVII, which was treated with ethanolic sodium hydroxide to give 1-(1-naphthyl)-4-(1-pyrrolidinyl)-6-methylpyrid-2-one (XVIII). The structure of XVIII was confirmed by its spectral data as well as by identification with an authentic sample prepared from 4-(1-pyrrolidinyl)-5-(1-naphthylcarbamoyl)-4-penten-2-one (XIX).[1] This supports the proposed structure for XVI.

Experimental

All melting points are uncorrected. The IR spectra were measured as KBr pellets by a Nippon Bunko IR-S spectrophotometer, and the NMR spectra were determined at 60 MHz on a Hitachi R-20 NMR spectrometer with TMS as an internal reference. The mass spectra were obtained on a Hitachi RMS-4 mass spectrometer with a direct inlet and an ionization energy of 70 eV. Microanalyses were carried out by Miss M. Akita with a Yanagimoto C.H.N. Corder MT-1.

Materials. 4-(1-Piperidyl)- (Ia) and 4-(1-pyrrolidinyl)-3-penten-2-one (Ib) were prepared from acetylacetone and the corresponding amines.[1] Commercial phenyl (IIa), *p*-chlorophenyl (IIb), and 1-naphthyl isothiocyanate (XIV) were used.

Reaction of 4-(1-Piperidyl)-3-penten-2-one (Ia) with Phenyl Isothiocyanate (IIa). 1.67 g (0.01 mol) of Ia and 1.35 g (0.01 mol) of IIa were dissolved in 50 ml of benzene and the solution was refluxed for 5 hr, and concentrated *in vacuo* to give crystals which, on recrystallization from ethanol, afforded 2.53 g (84%) of 3-phenylthiocarbamoyl-4-(1-piperidyl)-3-penten-2-one (IIIa), mp 135—136 °C (decomp.), as yellow prisms.

Found: C, 67.30; H, 7.60; N, 9.33%. Calcd for $C_{17}H_{22}N_2OS$: C, 67.52; H, 7.33; N, 9.27%.

NMR (in $CDCl_3$) δ ppm: 1.78 (3H, s, CH_3), 1.85 (6H, m, CH_2), 2.80 (3H, s, CH_3), 3.93 (4H, m, CH_2), 7.0—7.95 (5H, m, aromatic protons), 13.98 (1H, broad, NH).

Similarly, the reaction of 4-(1-pyrrolidinyl)-3-penten-2-one (Ib) with IIa gave 3-phenylthiocarbamoyl-4-(1-pyrrolidinyl)-3-penten-2-one (IIIc), mp 131—132 °C (decomp.), as yellow

prisms (from ethanol). Yield, 83%.

Found: C, 66.65; H, 7.03; N, 9.71%. Calcd for $C_{16}H_{20}N_2OS$: C, 66.64; H, 6.99; N, 9.72%.

NMR (in $CDCl_3$) δ ppm: 1.80 (3H, s, CH_3), 2.11 (4H, m, CH_2), 2.73 (3H, s, CH_3), 3.88 (4H, m, CH_2), 7.0—8.0 (5H, m, aromatic protons), 13.89 (1H, broad, NH).

A similar reaction of Ia with *p*-chlorophenyl isothiocyanate (IIb) at room temperature for 10 hr afforded 3-*p*-chlorophenylthiocarbamoyl-4-(1-piperidyl)-3-penten-2-one (IIIb), mp 141—142 °C (decomp.), as yellow prisms (from ethanol). Yield, 44%.

Found: C, 60.85; H, 6.32; N, 8.27%. Calcd for $C_{17}H_{21}N_2OSCl$: C, 60.62; H, 6.24; N, 8.59%.

NMR (in $CDCl_3$) δ ppm: 1.80 (3H, s, CH_3), 1.88 (6H, m, CH_2), 2.81 (3H, s, CH_3), 3.96 (4H, m, CH_2), 7.1—7.9 (4H, m, aromatic protons), 14.04 (1H, broad, NH). Mass spectrum *m/e*: 336, 338 (M^+, rel. intensity 3: 1).

Hydrolysis of 1: 1 Adduct III. *i)* A solution of 1.0 g of IIIa in 10 ml of 18% hydrochloric acid was stirred at room temperature for 6 hr, and neutralized (*a*) with aqueous sodium hydroxide or (*b*) with ammonium hydroxide as follows. (a) The solution was neutralized with aqueous sodium hydroxide and then extracted with diethyl ether. The ether extract was concentrated to give crystals which on recrystallization from ethanol–petroleum ether mixture afforded 0.38 g (60%) of phenylthiocarbamoylacetone (IV), mp 61—62.5 °C (decomp.), as yellow prisms.

Found: C, 62.09; H, 5.75; N, 7.30%. Calcd for $C_{10}H_{11}NOS$: C, 62.16; H, 5.74; N, 7.25%.

IR cm^{-1}: 3290, 3220 (NH or OH), 1630 (C=O or C=C). Mass spectrum *m/e*: 193 (M^+).

(b) The solution was treated with 20% ammonium hydroxide and the resulting precipitate was filtered. Recrystallization from ethanol–petroleum ether mixture afforded 0.25 g (40%) of 1-phenylthiocarbamoyl-2-aminopropene (V), mp 155—157 °C (decomp.), as pale yellow needles.

Found: C, 62.28; H, 6.35; N, 14.50%. Calcd for $C_{10}H_{12}N_2S$: C, 62.48; H, 6.29; N, 14.58%.

IR cm^{-1}: 3300 (NH), 1672 (C=C). NMR (in $CDCl_3$) δ ppm: 1.93 (3H, s, CH_3), 5.32 (1H, s, =CH), 7.0—7.5 (7H, m, aromatic protons (5H) and NH (2H)), 8.0 (1H, broad, NH). Mass spectrum *m/e*: 192 (M^+).

The hydrolysis of V with 18% hydrochloric acid gave IV quantitatively.

ii) A solution of 1.0 g of IIIc in 10 ml of 18% hydrochloric acid was stirred at room temperature for 2 hr, and neutralized with aqueous sodium hydroxide. The resulting precipitate was filtered. Recrystallization from ethanol afforded 0.37 g (43%) of 1-phenylthiocarbamoyl-2-(1-pyrrolidinyl)propene (VIa), mp 156—157 °C, as yellow plates.

Found: C, 68.08; H, 7.42; N, 11.34%. Calcd for $C_{14}H_{18}N_2S$: C, 68.27; H, 7.37; N, 11.37%.

IR cm^{-1}: 3290 (NH), 1580 (C=C).

A trace of IV was obtained from the filtrate by a treatment similar to i)-(a).

Reaction of 1: 1 Adduct IIIc with Hydrazine Hydrate. A solution of 2.35 g of IIIc and 1 ml of hydrazine hydrate in 10 ml of ethanol was stirred at room temperature for 2 hr and then poured into 30 ml of water. The resulting precipitate was collected by filtration. Recrystallization from ethanol–petroleum ether mixture afforded 0.5 g (28.5%) of 3(5)-methyl-4-acetyl-5(3)-anilinopyrazole (VII), mp 236—237 °C (decomp.), as colorless prisms.

Found: C, 66.90; H, 6.14; N, 19.29%. Calcd for $C_{12}H_{13}N_3O$: C, 66.95; H, 6.09; N, 19.52%.

IR cm^{-1}: 3320, 3220 (NH), 1600 (C=O). NMR (in $CDCl_3$) δ ppm: 2.42, 2.53 (each 3H, s, CH_3), 6.85—7.8 (6H, m, aromatic protons (5H) and NH), 9.36 (1H, broad, NH). Mass spectrum *m/e*: 215 (M^+), 200 (M^+—Me), 172 (M^+—COMe), 124 (M^+—PhNH), 104, 77.

The filtrate was concentrated *in vacuo* to leave a residue which was triturated with benzene to give 50 mg of 3,5-dimethyl-4-phenylthiocarbamoylpyrazole (VIII) contaminated with sulfur. Its purification was very difficult.

Crude VIII; mp 148—149 °C (decomp.), yellow prisms. IR cm^{-1}: 3220, 3120—2800 (NH). NMR (in $CDCl_3$) δ ppm: 2.38 (6H, broad singlet, CH_3), 7.0—8.0 (6H, m, aromatic protons (5H) and NH), 9.1 (1H, broad, NH). Mass spectrum *m/e*: 231 (M^+), 198 (M^+—SH), 139 (M^+—PhNH, base peak), 122 (139^+—NH_3), 93, 77.

The benzene solution which was removed VIII was concentrated *in vacuo* to give crystals, which on recrystallization from ethanol–petroleum ether afforded 0.32 g (17%) of hydrazone IX, mp 175—177 °C (decomp.), as colorless prisms.

Found: C, 63.20; H, 6.85; N, 30.36%. Calcd for $C_{12}H_{15}N_5$: C, 62.86; H, 6.60; N, 30.55%.

IR cm^{-1}: 3280, 3150, 3040—2800 (NH), 1640 (C=N). NMR (in $CDCl_3$) δ ppm: 2.1 (6H, broad singlet, CH_3), 4.8—6.0 (3H, broad, NH), 6.5—7.5 (6H, m, aromatic protons (5H) and NH). Mass spectrum *m/e*: 229 (M^+), 198 (M^+—N_2H_3), 137 (M^+—PhNH), 120 (137^+—NH_3), 93, 77.

Similarly, the reaction of IIIa with hydrazine hydrate afforded three pyrazoles VII, VIII, and IX in similar yields to those in the case of IIIc.

1-Acetyl-3,5-dimethyl-4-phenylthiocarbamoylpyrazole (X). A solution of crude VIII (20 mg) in 10 ml of acetic anhydride was stirred at room temperature for 5 hr and then poured into water. The resulting precipitate was filtered. Recrystallization from ethanol–petroleum ether mixture afforded 20 mg of X, mp 163—164 °C (decomp.), as yellow needles.

Found: C, 61.48; H, 5.65; N, 15.17%. Calcd for $C_{14}H_{15}N_3OS$: C, 61.53; H, 5.53; N, 15.38%.

IR cm^{-1}: 3310 (NH), 1730 (C=O). Mass spectrum *m/e*: 273 (M^+), 240 (M^+—SH), 230 (M^+—COMe), 198 (230^+—S), 181 (M^+—PhNH), 139 (181^+—CH_2CO, base peak).

Reaction of 1: 1 Adduct IIIc with Phenylhydrazine. A solution of 1.15 g of IIIc and 0.5 g of phenylhydrazine in 30 ml of ethanol was stirred at room temperature for 7 hr and then concentrated *in vacuo* to leave a solid, which was chromatographed on alumina using benzene as an eluent to give 1-phenyl-3-methyl-5-anilinopyrazole (XI), mp 119—120 °C (decomp.) (lit,[6] mp 120 °C), as red prisms. Yield, 0.3 g (34.7%).

Found: 77.32; H, 6.12; N, 16.70%. Calcd for $C_{16}H_{15}N_3$: C, 77.08; H, 6.06; N, 16.86%.

IR cm^{-1}: 3200 (NH). NMR (in $CDCl_3$) δ ppm: 2.28 (3H, s, CH_3), 5.67 (1H, broad, NH), 5.98 (1H, s, =CH), 6.7—7.6 (10H, m, aromatic protons).

Reaction of 1: 1 Adduct IIIc with p*-Chlorophenyl Isocyanate.* A solution of 1.5 g of IIIc and 1.53 g of *p*-chlorophenyl isocyanate in 30 ml of benzene was refluxed for 5 hr. After cooling, filtration gave crystals, which on recrystallization from benzene afforded 2.0 g (85%) of bis(*p*-chlorophenylcarbamoyl)-4-(1-pyrrolidinyl)-3-penten-2-one (XIII), mp 162—163 °C (lit,[1] mp 162—163 °C), as colorless needles.

Reaction of Enamino Ketone I with 1-Naphthyl Isothiocyanate (XIV). *i)* A solution of 1.67 g (0.01 mol) of Ia and 1.85 g (0.01 mol) of XIV in 30 ml of benzene was refluxed for 5 hr. It was concentrated *in vacuo* to give crystals, which on recrystallization from ethanol afforded 1.58 g (45%) of 3-(1-naphthylthiocarbamoyl)-4-(1-piperidyl)-3-penten-2-one

6) A. Michaelis and E. Grunkel, *Ber.*, **34**, 723 (1901).

(XVa), mp 123—124 °C (decomp.), as yellow needles.

Found: C, 71.73; H, 6.96; N, 7.66%. Calcd for $C_{21}H_{24}N_2OS$: C, 71.57; H, 6.86; N, 7.95%.

NMR (in $CDCl_3$) δ ppm: 1.77 (6H, m, CH_2), 1.82, 2.77 (each 3H, s, CH_3), 3.83 (4H, m, CH_2), 7.2—8.6 (7H, m, aromatic protons), 14.40 (1H, broad, NH).

ii) After a solution of 1.67 g of Ia and 1.85 g of XIV in 20 ml of xylene had been refluxed for 1 hr, it was concentrated *in vacuo* to leave a residue. The residue was chromatographed on alumina using chloroform as an eluent to give 0.26 g (7.8%) of 1-(1-naphthyl)-4-(1-piperidyl)-6-methylpyrid-2-thione (XVIa) and 0.46 g (13%) of XVa.

Compound XVIa; mp 215—217 °C (decomp.), pale orange prisms.

Found: C, 75.62; H, 6.68; N, 8.62%. Calcd for $C_{21}H_{22}N_2S$: C, 75.42; H, 6.63; N, 8.38%.

IR cm^{-1}: 1622 (C=C). NMR (in $CDCl_3$) δ ppm: 1.70 (6H, m, CH_2), 1.87 (3H, s, CH_3), 3.47 (4H, m, CH_2), 6.31, 7.21 (each 1H, d, =CH, J=3 Hz), 7.3—8.1 (7H, m, aromatic protons). Mass spectrum *m/e*: 334 (M^+), 302 (M^+-S).

Similarly, Ib reacted with XIV in refluxing benzene to afford a 17.2% yield of 1-(1-naphthyl)-4-(1-pyrrolidinyl)-6-methylpyrid-2-thione (XVIb), mp 298—300 °C (decomp.), as pale orange prisms.

Found: C, 75.18; H, 6.33; N, 8.55%. Calcd for $C_{20}H_{20}N_2S$: C, 74.99; H, 6.29; N, 8.74%.

IR cm^{-1}: 1620 (C=C). NMR (in $CDCl_3$) δ ppm: 1.88 (3H, s, CH_3), 2.05, 3.45 (each 4H, m, CH_2), 6.14, 7.00 (each 1H, d, =CH, J=3 Hz), 7.4—8.1 (7H, m, aromatic protons). Mass spectrum *m/e*: 320 (M^+), 288 (M^+-S).

1-(1-Naphthyl)-4-(1-pyrrolidinyl)-6-methylpyrid-2-one (XVIII). *i)* A solution of 1.0 g of pyrid-2-thione XVIb in 10 ml of methyl iodide was stirred at room temperature for 2 hr, during which time crystals were precipitated. The crystals were collected by filtration and washed with petroleum ether to give 1.4 g (97%) of *S*-methyl pyridinium iodide XVII, mp 200—202 °C (decomp.), as colorless crystals.

NMR (in $CDCl_3$) δ ppm: 2.12, 2.56 (each 3H, s, CH_3), 2.18, 3.82 (each 4H, m, CH_2), 6.48, 6.99 (each 1H, d, =CH, J=3 Hz), 7.2—8.2 (7H, m, aromatic protons).

XVII was hydrolyzed without further purification. A solution of 1.0 g of XVII in 10 ml of ethanol was stirred with 10 ml of 5 M aqueous sodium hydroxide at room temperature for 5 hr, and then was poured into water to precipitate crystals, which on recrystallization from ethanol afforded 0.48 g (73%) of XVIII, mp 233—234 °C, as colorless prisms.

Found: C, 79.25; H, 6.65; N, 9.22%. Calcd for $C_{20}H_{20}N_2O$: C, 78.92; H, 6.62; N, 9.20%.

IR cm^{-1}: 1655 (C=O). NMR (in $CDCl_3$) δ ppm: 1.78 (3H, s, CH_3), 2.01, 3.37 (each 4H, m, CH_2), 5.53, 5.81 (each 1H, d, =CH, J=3 Hz), 7.3—8.1 (7H, m, aromatic protons). Mass spectrum *m/e*: 304 (M^+).

ii) A solution of 100 mg of 4-(1-pyrrolidinyl)-5-(1-naphthylcarbamoyl)-4-penten-2-one (XIX)[1] in 10 ml of xylene was refluxed for 5 hr, and then concentrated *in vacuo*. The residue was then extracted with petroleum ether. The solvent was removed from the extract to leave crystals. Recrystallization from ethanol gave 25 mg (26%) of colorless prisms, which were identical with XVIII.

NOTES

BULLETIN OF THE CHEMICAL SOCIETY OF JAPAN, VOL. 46, 2226—2227 (1973)

The Viscosity *B*-Coefficients of the Anionic Species of Benzoic Acid and Its Monosubstituted Derivatives

Motoo YASUDA and Kiyoshi MIZUTANI
Department of General Education, Nagoya University, Chikusa-ku, Nagoya 464

(Received March 14, 1972)

The viscosities of aqueous electrolyte solutions have been measured for a large number of electrolytes. According to Jones and Dole,[1] who first measured accurately the viscosity of the aqueous electrolyte solutions up to the range of extremely high dilution, the specific viscosity, η_{sp}, of aqueous solutions of strong electrolytes is related to the solute molarity, c, by the equation:

$$\eta_{sp} = \frac{\eta}{\eta_0} - 1 = A\sqrt{c} + Bc$$

where η and η_0 are the viscosities of the solution and of water respectively. A is a coefficient depending on the ion-ion interaction between the solute ions; it can be calculated theoretically. B is a coefficient depending on the size of the ions and on the interaction between the ions and the surrounding solvent; it is usually called the Jones-Dole's viscosity B-coefficient.

In the course of measurements of the B-coefficients of isomers of metal complexes, we felt that a thorough study of the viscosity of the benzoate anion and its derivatives might supply useful information concerning the contribution of substituents to the viscosity. A study was, therefore, made of the viscosities of the benzoic acid and its derivatives.

Experimental

Measurements. The viscosities were measured with a Cannon-Fenske capillary viscometer with an efflux time of *ca.* 300 seconds for distilled water. The viscosities and densities of the solutions were measured in a water bath maintained at 25±0.01 °C. The efflux times, measured with a stopwatch to 0.1 sec, were easily reproducible to 0.2 sec.

Materials. Samples of benzoic acid and its derivatives of a guaranteed reagent grade were used. From stock solutions, prepared from benzoic acids and potassium hydroxide, solutions containing 0.04—0.15 mol/l potassium benzoate were made by dilution and were then used for the viscosity and density measurements. In each case, the pH value of the solution was controlled so as to be about 2 or 3 pH units higher than the pK value of the parant acid.

Calculations. The B-coefficient was evaluated by plotting $\eta_{sp}/\sqrt{c}$ *vs.* $\sqrt{c}$ (Fig. 1). A straight line was obtained in each case at concentrations below 0.15 mol/l. The intersection of the resulting straight line on the ordinate gives the value of the A-coefficient. In each case, the A-coefficient was found to be zero within the limits of experimental error. The slope of the resulting straight line gives the value of the B-coefficient. As has been discussed by Gurney,[2] the B-coefficient is composed additively of contributions from each of the solute species present in the solution. Moreover, the B-value of the benzoate anion can be obtained by subtracting a correction for the other solute species present in the solution.

Results and Discussion

As the pH value of the solution was at least 2 pH units higher than the pK value of the parent benzoic acid, the contribution of the un-ionized benzoic acid to the viscosity of the solution may be practically neglected. The concentrations of the hydrogen and hydroxide ions are very low compared with that of the benzoate anion in the pH range (5—10) studied here. Moreover, their B-coefficients are themselves quite small compared with that of the benzoate anion,[2] and so their contribution to the viscosity of the solution may also be practically neglected. On the other hand, the concentration of the potassium ion is comparable to that of the benzoate anion. Hence, a correction, a relatively small one, for the potassium ion is necessary, although its B-value is actually the lowest of those of the chemical species under consideration.[2] The B-coefficients studied here are listed in Table 1.

Table 1. Viscosity B-coefficients of benzoate derivatives

Substituent	*o*-	*m*-	*p*-
H		(0.41)	
OH	0.31	0.41	0.45
CH_3	0.49	0.49	~0.49
Cl	0.49	0.47	0.47
NO_2	0.44	0.41	0.41
OCH_3	0.50	—	0.46
COO^-	0.61	0.61	0.61

As has been reported by Charles,[3] the values of η_{sp}/c for the copper chelate with an enforced planar *cis*-configuration about the metal were higher than those found for the corresponding alkyl-substituted chelates with planar *trans*-configurations, evidently the result of the permanent dipole moment associated with the *cis*-configuration. However, as may be seen from Table 1, no essential difference between the B-coefficients of *o*-, *m*-, and *p*-isomers is found, even for COO^--derivatives, with the exception of the OH-derivatives. In the latter case, the B-value of the *o*-hydroxybenzoate, *i.e.*, the salicylate anion, is appreciably lower than that

1) G. Jones and M. Dole, *J. Amer. Chem. Soc.*, **51**, 2950 (1929).
2) R. W. Gurney, "Ionic Processes in Solution," McGraw-Hill Book Company, New York (1953).
3) R. G. Charles, *J. Amer. Chem. Soc.*, **81**, 1793 (1959).

of its isomers. This may by due mainly to the formation of an intramolecular hydrogen bond, as has been discussed by Davies and Malpass[4] in connection with the difference in *B*-values between maleic acid and its isomer, fumaric acid.

For *o*-phthalic acid, the viscosity measurements were carried out over the 4.4—11.8 pH range. The slope of the straight lines obtained by plotting $\eta_{sp}/\sqrt{c}$ *vs.* $\sqrt{c}$ depend on the pH values lower than about 6. However, for the pH values higher than about 6.7, where phthalic acid, H_2A, is present virtually as the A^{2-} anion the satisfactory agreement of all the points with a single straight line indicates that the *B*-value of the phthalate anion, A^{2-}, is independent of the pH value, as has been expected.

Figure 1 shows two straight lines at the pH values of 4.6 and 7.2. The *B*-coefficient of hydrogenphthalate, HA^-, was tentatively calculated as 0.42 using the data for the lower pH range, where the A^{2-} and HA^- species are present predominantly, together with the *B*-value of A^{2-} and the acid dissociation constants of phthalic acid.

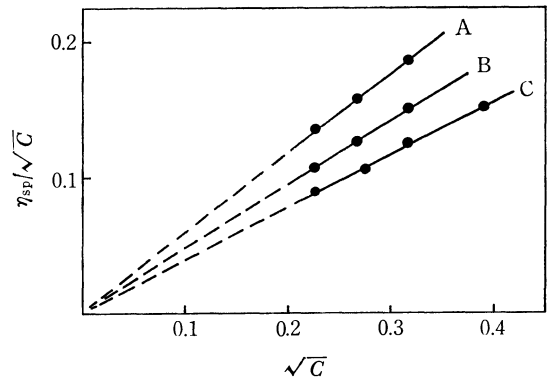

Fig. 1. $\eta_{sp}/\sqrt{C}$ for aqueous potassium benzoate and potassium *o*-phthalate solutions at 25 °C as a function of $\sqrt{C}$
A: potassium *o*-phthalate, pH=7.2, B: potassium *o*-phthalate, pH=4.6, C: potassium benzoate, pH=10.0.

4) C. W. Davies and V. E. Malpass, *Trans. Faraday Soc.*, **60**, 2075 (1964).

BULLETIN OF THE CHEMICAL SOCIETY OF JAPAN, VOL. 46, 2227—2229 (1973)

The CNDO-type Molecular Orbital Calculations of MnO_4^-, CrO_4^{2-}, PdX_4^{2-}, and PdX_6^{2-}

Shigeyoshi SAKAKI and Hiroshi KATO*

Department of Hydrocarbon Chemistry, Faculty of Engineering, Kyoto University, Sakyo-ku, Kyoto 606

**Department of General Education, Nagoya University, Chikusa-ku, Nagoya 464*

(Received August 3, 1972)

Since the molecular orbital (MO) calculations of MnO_4^- and CrO_4^{2-} were presented by Wolfsberg and Hermholz,[1] various MO methods have been used in the MO calculations of transition-metal complexes; the Extended Hückel,[2] SCCC,[3] CNDO-type,[4] INDO-type,[5] *ab-initio*,[6] and the others[7] methods. However, none of these methods was perfectly satisfactory, because an effective method for some compounds can not always give reasonable results in other cases. In order to re-examine the usefulness of the CNDO-type MO calculation of transition-metal complexes except for the estimation of the intra-atomic triplet transition, we calculated the electronic structures of MnO_4^-, CrO_4^{2-}, PdX_4^{2-}, and PdX_6^{2-} (X=halogen), for the CNDO-type approximation avoids the difficulties of the rotation invariance and of the estimation of the one-center exchange integral. The calculated results of the electronic population, the strength of the Pd–X bonds, and the electronic spectra of these complexes will be presented in this paper.

Method

We start from Roothaan's familiar closed-shell SCF equation[8] and separate the Hartree-Fock matrix element, F_{rs}, into the one-electron part, H_{rs}, and the two-electron part;

$$\begin{aligned} &|F_{rs}-\varepsilon S_{rs}| = 0 \\ &F_{rs} = H_{rs} + \sum_{t,u}^{occ} P_{tu}[(rs|tu)-0.5(rt|su)] \end{aligned} \quad (1)$$

where r, s, t, and u denote the atomic orbitals and whose P_{tu} is the t, u density matrix element. Then, the following approximations are introduced into Eq. (1): (I) The zero-differential overlap approximation[9] is introduced:

1) M. Wolfsberg and L. Hermholz, *J. Chem. Phys.*, **20**, 837 (1952).
2) C. J. Ballhausen and H. B. Gray, *Inorg. Chem.*, **1**, 111 (1962).
3) R. F. Fenske and C. C. Sweeney, *ibid.*, **3**, 1105 (1964).
4) a) R. D. Brown, B. H. James, M. F. O'Dwyer, and K. R. Roby, *Chem. Phys. Lett.*, **1**, 459 (1967). b) R. D. Brown, B. H. James, and M. F. O'Dwyer, *Theor. Chim. Acta*, **17**, 262, 279 (1970).
5) a) L. Oleari, G. De Michelis, and L. De Sipio, *Mol. Phys.*, **10**, 111 (1966). b) W. Th. A. M. Van Der Lugt, *Chem. Phys. Lett.*, **10**, 117 (1971).
6) I. H. Hillier and V. R. Saunders, *Proc. Roy. Soc. Ser A*, **320**, 161 (1970).
7) H. Katô, This Bulletin, **45**, 1281 (1972).
8) C. C. J. Roothaan, *Rev. Mod. Phys.*, **23**, 69 (1951).
9) J. A. Pople, D. P. Santry, and G. A. Segal, *J. Chem. Phys.*, **43**, s 129 (1965).

$$S_{rs} = \delta_{rs} \quad (2)$$

$$(rs|tu) = \delta_{rs}\delta_{tu}(rr|tt) \quad (3)$$

(II) The diagonal element, H_{rr}, of the one-electron part can be written as follows:[10]

$$H_{rr} = U_{rr} + \sum_{B \neq A} (B|rr) \quad (4)$$

$$U_{rr} = -I_r - (N_r - 1)(rr|rr) - \sum_{s \neq r}^{A} N_s(rr|ss) \quad (5)$$

$$(B|rr) = -\sum_{s}^{B} N_s(rr|ss) \quad (6)$$

where N_r and I_r represent the number of electrons on the atomic orbital (AO), r, in the neutral atom, A, and the ionization potential of AO r respectively. $\sum^A$ indicates the summation on the A atom.

(III) The off-diagonal element, H_{rs} ($r \neq s$), is approximated according to Wolfsberg and Hermholz:[1]

$$H_{rs} = -0.5kS_{rs}(I_r + I_s) \quad (7)$$

where k is a parameter equal to 1.1.

(IV) The one-center Coulomb repulsion integral (rr|rr) and the two-center Coulomb repulsion integral (rr|ss) are estimated by Pariser's approximation[11] and Ohno's approximation[12] respectively.

In order to calculate S_{rs}, Clementi's AO[13] and Burns' AO[14] were used for ligands and metals respectively. The same orbital exponents were used for s- and p-orbitals. The values obtained by Hinze and Jaffé.[15] were used for the I_r and (rr|rr) values of ligands. The values used for the metals are listed in Table 1.

Table 1. The ionization potential (I_r) and one-center Coulomb repulsion integral (J_{rr})

		I_r(eV)	J_{rr}[18](eV)
Cr	3d	−20.28[16]	14.03
	4s	−14.73	6.80
	4p	−10.31	5.80
Mn	3d	−21.64[16]	14.70
	4s	−15.35	7.09
	4p	−10.62	5.95
Pd	4d	− 8.54[17]	13.87
	5s	− 7.60	7.46
	5p	− 3.84	6.22

Results and Discussion

MnO_4^- and CrO_4^{2-}. For the purpose of comparing our results with previous ones,[4-6] we calculated the MO's of MnO_4^- and CrO_4^{2-}. The net charge on the Mn atom in MnO_4^- was found to be 1.28 from the metal K–X ray spectra.[4b] However, in our results, negative net charge on the Mn atom was obtained. This may be due to the too large electron population of the 4s and 4p orbitals of the Mn atom compared with the results of Oleari *et al.*[5a] and Hillier and Saunders[6] (MnO_4^-; 4s, 0.81 and 4P, 0.78: CrO_4^{2-}; 4s, 0.81 and 4p, 0.78 in our results).

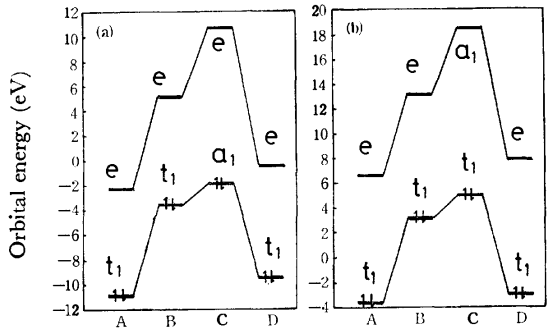

Fig. 1. HOMO and LUMO of MnO_4^- (a) and CrO_4^{2-}(b) by various Methods.
⇅ : HOMO, —; LUMO
A: Oleari *et al.*[5b] by INDO, B: Brown *et al.*[4a] by VE-SCF-CNDO. C: Hillier *et al.*[6] by *ab-initio*, D: ours by CNDO.

The highset occupied (HO) MO and the lowest unoccupied (LU) MO are considered to be represented by t_1[4,5] and e[19] respectively. Our results with respect to HOMO and LUMO are compared with previous ones in Fig. 1. The results of Oleari *et al.*[5a] seem to be quite reasonable. However, the calculation by Brown *et al.*[4b] gave a positive orbital energy for the HOMO of CrO_4^{2-}. Also, in the case of Hillier's calculation,[6] the representations of HOMO and LUMO are not t^1 and e respectively, and the HOMO of CrO_4^{2-} has a positive orbital energy. In contrast to these results, our result are reasonable regarding the orbital energy and the orbital symmetry.

The calculated transition energies are given in Table 2. Our results agree fairly with the experimental results.

PdX_4^{2-} and PdX_6^{2-}. We then calculated the MO's of PdX_4^{2-} and PdX_6^{2-} in order to examine the validity of our method for different types of complexes. The net charge of Pd decreases with a decrease in the electronegativity of halogens, as is shown in Table 3. This tendency agrees with the results obtained by means of photoelectron spectroscopy.[21] However, we obtained a negative net charge on the Pd atom due to the large electron population of 5s- and 5p-orbitals. As is shown in Table 3, the absolute value of the two atomic part of the total energy, $|E_{Pd-Cl}|$,[9] is larger than $|E_{Pd-Br}|$ in PdX_4^{2-} and PdX_6^{2-}, and $|E_{Pd-X}|$ in

10) T. Yonezawa, K. Yamaguchi, and H. Kato, This Bulletin, **40**, 536 (1967); H. Kato, H. Konishi, H. Yamabe, and T. Yonezawa, *ibid.*, **40**, 2761 (1961).
11) R. Pariser, *J. Chem. Phys.*, **21**, 568 (1953).
12) K. Ohno, *Theor. Chim. Acta*, **2**, 219 (1964).
13) E. Clementi and D. L. Raimondi, *J. Chem. Phys.*, **38**, 2686 (1963).
14) G. Burns, *ibid.*, **41**, 1521 (1964).
15) J. Hinze and H. H. Jaffé, *J. Amer. Chem. Soc.*, **84**, 540 (1961); *J. Phys. Chem.*, **67**, 1504 (1963).
16) C. J. Ballhausen and H. B. Gray, "Molecular Orbital Theory," W. A. Benjamin, Inc., New York (1965), p. 120.
The electron configuration of neutral Mn atom is d^5s^2. However, we can not obtain the I_r for d^5s^2 except with I_{4s}, because of the lack of the observed atomic spectra. Therefore we investigated the effect of I_r and choose the suitable values. We show this value in Table 1.
17) I. H. Hillier and R. M. Canadine, *Discuss. Faraday Soc.*, **47**, 27 (1969).
18) L. De Sipio, E. Tondello, G. De Michelis, and L. Oleari, *Chem. Phys. Lett.*, **11**, 287 (1971).
19) A. Carrington, D. J. E. Ingram, K. A. K. Lott, D. S. Schonland, and M. C. R. Symons, *Proc. Roy. Soc., Ser. A*, **254**, 101 (1960).

TABLE 2. TRANSITION ENERGIES OF MnO_4^-, CrO_4^{2-}, AND $PdCl_6^{2-}$

	Experimental (eV)		Calculated (eV)	
MnO_4^- [20b]	1.79	$^3T_1$ or $^1T_1$ [20a]	1.44	$^1T_1$
	2.38	$^1T_2$	2.45	$^1T_2+^1E$
			3.65	$^1T_2$
	3.44	$^1T_1$	4.27	$^1T_1$
	4.13	$^1T_2$	4.47	$^1T_2$
CrO_4^{2-} [20c]	3.00	$^1T_1$	3.36	$^1T_1$
			3.78	$^1T_1$
	3.56	$^1T_2$	5.15	$^1T_2$
	4.65	$^1T_2$	6.47	$^1T_2$
	6.20		6.70	$^1T_1$
$PdCl_6^{2-}$ [24]	2.27		3.98	T_{1g}
	3.64		4.13	T_{2g}
			5.94	T_{1u}
	5.17		6.45	T_{2u}

PdX_6^{2-} is larger than $|E_{Pd-X}|$ in PdX_4^{2-}. These results agree with the experimental results.[22]

Though the order of bond strength agrees with the experimental results, we failed to obtain reasonable transition energies for PdX_4^{2-}. The calculated first transition energies seem too small for $PdCl_4^{2-}$ (0.019 eV) and $PdBr_4^{2-}$ (0.028 eV). Furthermore, neither is the d-d transition which is to be expected as the first transition.[23] For $PdCl_6^{2-}$, the calculation gives almost reasonable results, as is shown in Table 2.

As has been described above, by treatment with the same approximation as was used in MnO_4^- and CrO_4^{2-} we can obtain reasonable trends of electron population and bond strength for Pd-halogen complexes, but not successful results for any transition energies except PdX_6^{2-}. Attempts to improve this approximation are under way, for example the inclusion of one-center exchange integrals and further refinements in the parametrization of H_{rs} will be described in the near future.

TABLE 3. ELECTRON POPULATION AND E_{Pd-X} OF PdX_4^{2-} AND PdX_6^{2-}

	Electron Population			Net Charge on Pd			Obsd[22]	
	Pd		X	Calcd	Expt.[21]	E_{Pd-X} [c]	f_{Pd-X} [a]	ν_{Pd-X} [b]
	d	sp						
$PdCl_4^{2-}$	8.075	2.259	7.417	−0.333	0.42	-15.882_{ev}	1.355	310
$PdBr_4^{2-}$	8.049	2.343	7.402	−0.392	0.23	−14.688		187
PdF_6^{2-}	7.137	2.219	7.441	0.644		−19.124		
$PdCl_6^{2-}$	7.177	3.043	7.297	−0.220	0.72	−16.300	1.90	317
$PdBr_6^{2-}$	7.157	3.203	7.273	−0.360		−14.920	1.58	198

a) The force constant of Pd-X stretching vibration. (mdyn/Å)

b) The symmetric stretching frequency of Pd-X. (cm^{-1})

c) $E_{A-B}=2\sum_r^A\sum_s^B P_{rs}H_{rs}-\frac{1}{2}\sum_r^A\sum_s^B P_{rs}^2(rr/ss)+\sum_r^A\sum_s^B(P_{rr}-N_r)(P_{ss}-N_s)(rr/ss)$

20) a) P. Day, L. De Sipio, and L. Oleari, *Chem. Phys. Lett.*, **5**, 533 (1970); b) L. W. Johnson and S. P. McGlynn, *J. Chem. Phys.*, **55**, 2985 (1971); c) L. W. Johnson and S. P. McGlynn, *Chem. Phys. Lett.*, **7**, 618 (1970).

21) G. Kumer, J. R. Blackburn, R. G. Albridge, W. E. Moddeman, and M. M. Jones, *Inorg. Chem.*, **11**, 296 (1972).

22) P. J. Hendra and P. J. D. Park, *Spectrochim. Acta*, **23A**, 1635 (1967).

23) A. J. MacCaffery, P. N. Schatz, and P. J. Stephens, *J. Amer. Chem. Soc.*, **90**, 5730 (1968).

24) C. K. Jorgensen, *Adv. Chem. Phys.*, **5**, 119 (1963); *Mol. Phys.*, **2**, 309 (1959).

BULLETIN OF THE CHEMICAL SOCIETY OF JAPAN, VOL. 46, 2230—2231 (1973)

Catalytic Codimerization of Styrene with Lower Olefins by Rhodium and Ruthenium Catalysts

Hiroshi UMEZAKI, Yuzo FUJIWARA, Kenichi SAWARA, and Shiichiro TERANISHI
Faculty of Engineering Science, Osaka University, Toyonaka, Osaka 560

(Received July 7, 1972)

We have investigated the codimerization reaction of styrene with lower olefins such as ethylene, propylene or 1-butene in the presence of rhodium(III) or ruthenium(III) compounds as a catalyst.

Results and Discussion

The results are summarized in Tables 1 and 2. We see that the reaction of styrene with ethylene gives 3-phenyl-1-butene (**1**), 2-phenyl-2-butene (**2**) and 2-phenyl-1-butene (**3**) in high yields.[1)]

In order to determine the initial product of codimerization, the relative yields of three phenylbutenes **1**, **2** and **3** were examined as a function of the length of the reaction time. It was possible to monitor the yields as shown in Fig. 1. The rate of formation of **1** is initially high. That of **2** becomes greater after about 3 hr, indicating that the initially formed product from the reaction of styrene and ethylene by rhodium (III) chloride is **1** which is then isomerized to its isomers **2** and **3**.[2)]

We see from Tables 1 and 2 that the codimerization reaction of styrene with lower olefins has the following characteristics: (1) Rhodium(III) and ruthenium(III) catalysts give *internally* phenyl-substituted codimers while palladium(II) catalyst gives *terminally* phenyl-substituted products.[3)] (2) Although accurate comparison is not practical owing to the lack

Table 1. Codimerization of styrene with ethylene

Catalyst	Solvent	Codimer yield, %[a)]		
		1	**2**	**3**
$RhCl_3 \cdot 3H_2O$	Methanol	932	584	84
$RhCl_3 \cdot 3H_2O$	None	482	47	trace
$RhCl_3 \cdot 3H_2O$	Acetic acid	37	121	trace
$RhCl_3 \cdot 3H_2O$	Furfural	37	—	—
$RhCl_3 \cdot 3H_2O$	Benzene+phenol (1 : 1)	21	—	—
$[Rh(C_2H_4)_2Cl]_2$	Methanol	—	21	48
$[Rh(C_2H_4)_2Cl]_2$	None	—	trace	—
$RhCl(PPh_3)_3$	Benzene	—	—	—
$RuCl_3 \cdot H_2O$	Methanol	3	3	1
$RuCl_3 \cdot H_2O$[b)]	Acetic acid	14	36	14
$RuCl_3 \cdot H_2O$	Acetonitrile	trace	trace	trace
$[PdCl_2 \cdot \text{styrene}]_2$[c)]	None	*trans*-1-phenyl-1-butene,		1278
		cis-1-phenyl-1-butene,		57
		trans-1-phenyl-2-butene,		170

a) Yields are based on the catalyst used. b) α-phenylethyl acetate was also formed in 293% yield. c) Reference. 3.

Table 2. Codimerization of styrene with propylene and 1-butene

Olefin (5 atm)	Catalyst (1.9 mmol)	Solvent (30 ml)	Product and yield, %[a)]
Propylene[b)]	$RhCl_3 \cdot 3H_2O$	Methanol	CH_3–PhCH–CH=CH–CH_3, 20
Propylene	$RuCl_3 \cdot H_2O$	Methanol	—
Propylene	$[PdCl_2 \cdot \text{styrene}]_2$[c)]	None	Ph–CH=CH–C_3H_7, 72
1-Butene	$RhCl_3 \cdot 3H_2O$	Methanol	—
1-Butene	$RuCl_3 \cdot H_2O$	Methanol	—
1-Butene	$[PdCl_2 \cdot \text{styrene}]_2$	None	Ph–CH=CH–C_4H_9, trace

a) Reactions were performed at 50°C for 6 hr and yields are based on the catalyst used. b) Acetophenone was also formed in 33% yield. c) Styrene dimers were also obtained in 56% yield.

1) Lindsey *et al.*[2)] reported that the rhodium(III) chloride catalyzed codimerization reaction of ethylene with styrene under high pressure (1000 atm) gives only **2** in 40% conversion. The three isomers **1**, **2** and **3** we obtained presumably result from the difference in reaction pressure.

2) T. Alderson, E. L. Jenner, and R. V. Lindsey, *J. Amer. Chem. Soc.*, **87**, 5638 (1965).

3) K. Kawamoto, T. Imanaka, and S. Teranishi, This Bulletin, **43**, 2512 (1970) and the literature therein.

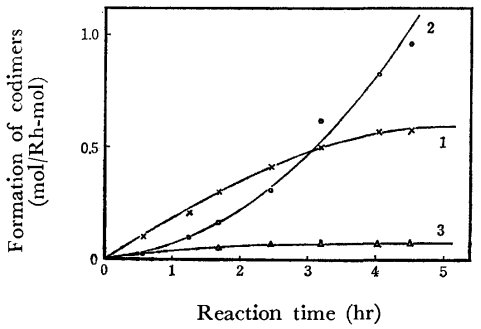

Fig. 1. Formation of 3-Phenyl-1-butene(×), 2-pheny-2-butene (○) and 2-phenyl-1-butene (△) during the reaction of styrene and ethylene with $RhCl_3$-MeOH.

of a solvent which dissolves all of these catalysts, the catalytic activity appears to decrease in the order Pd(II)>Rh(III)>Ru(III) (3) The reactivity of the gaseous olefins decreases in the order ethylene>propylene>1-butene. (4) **1** is the initial codimerization product in the case of the reaction of styrene with ethylene by rhodium(III) chloride.

In the rhodium(III) chloride catalyzed dimerization of olefins, the reaction proceeds through a rhodium hydride from a protonic solvent.[4] Thus, the present codimerization by rhodium(III) chloride seems to proceed also *via* a rhodium hydride as shown in Fig. 2. For the sake of clarity, the case with styrene, ethylene and methanol-d_1 is shown.

A rhodium hydride complex (**4**) would be formed

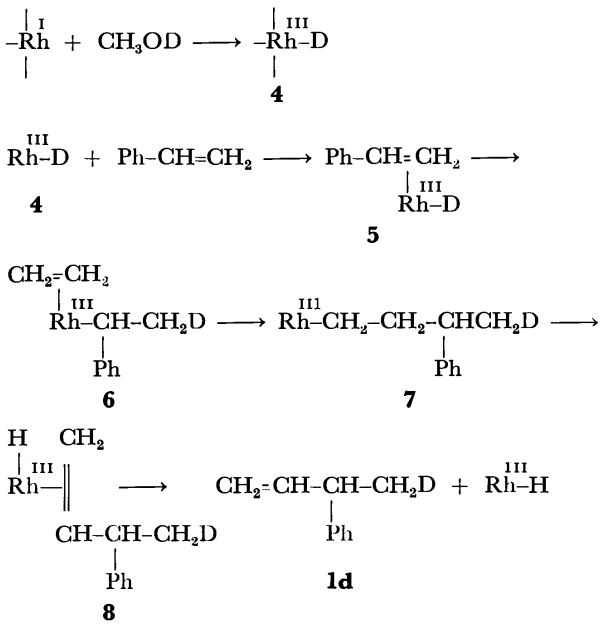

Fig. 2. Mechanism of Codimerization by Rhodium Compound.

4) R. Cramer, *ibid.*, **87**, 4717 (1965).

5) Since the rhodium-ethylene complex has low catalytic activity (Table 1), styrene could be considered to coordinate first with rhodium.

first and then styrene coordinates with **4** giving a styrene-rhodium hydride π complex (**5**).[5] Complex **5** is transformed into a σ, π complex (**6**) through the addition of Rh-D to styrene, followed by the coordination of ethylene. In this insertion step, there are two modes of addition giving **A** or **B**, the former being favoured because of an electronic effect shown below in **C**.

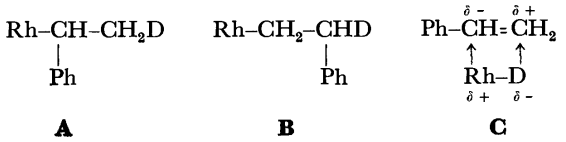

Complex **6** undergoes rearrangement to a butylrhodium compound (**7**). Finally the elimination of β hydrogen gives **1d** and Rh–H *via* a complex **8**. The reformed rhodium hydride would serve as an active catalyst for codimerization.

Experimental*1

Di-μ-chlorotetrakis(ethylene)dirhodium(I) was prepared according to the method of Cramer.[6]

General Procedure for the Codimerization of Styrene with Lower Olefins by Rhodium Chloride. A glass autoclave was charged with rhodium(III) chloride (1.9 mmol), styrene (27 g, 0.26 mol) and the solvent (30 ml). The autoclave was flushed with ethylene and the pressure was elevated to 5 atm., the mixture being stirred at 50°C for 6 hr. The resulting mixture was distilled under reduced pressure to remove styrene, and then diluted with petroleum ether. The mixture was filtered to remove rhodium(III) chloride, and the filtrate was evaporated. The residue was analyzed and purified by glpc. The products were identified by IR and NMR. 3-phenyl-1-butene (**1**): IR (direct): 990, 910 (-HC=CH_2), 755 and 695 cm^{-1} (-Ph). NMR (CCl_4): 8.66 (d, 3H), 6.58 (m, 1H), 5.04 (m, 2H), 3.77—4.32 (m, 1H) and 2.87 τ (m, 5H). 2-Phenyl-2-butene (**2**): IR (direct): 935 (C=CH–), 752 and 697 cm^{-1} (-Ph). NMR (CCl_4): 8.24 (d, 3H), 8.02 (s, 3H), 4.29 (q, 1H) and 2.02 τ (s, 5H). 2-Phenyl-1-butene (**3**): IR (direct): 893 (CH_2=C<), 780 and 700 cm^{-1} (-Ph). NMR (CCl_4): 8.95 (t, 3H), 7.53 (q, 2H), 5.04 (d, 1H), 4.83 (d, 1H) and 2.76 τ (m, 5H).

Codimerization reactions of styrene with propylene and 1-butene were similarly carried out with use of the same autoclave and reaction conditions as above. *trans*-4-Phenyl-2-pentene; IR (direct): 966 (*trans* HC=CH), 762 and 700 cm^{-1} (-Ph). NMR (CCl_4): 8.72 (d, 3H), 8.36 (d, 3H), 6.68 (m, 1H), 4.55 (m, 2H) and 2.92 τ (m, 5H). *trans*-1-Phenyl-1-pentene: IR (direct): 960 (*trans* HC=CH), 740 and 695 cm^{-1} (-Ph). NMR (CCl_4): 9.03 (t, 3H), 8.51 (m, 2H), 7.82 (q, 2H), 3.78 (m, 2H) and 2.83 τ (m, 5H).

This work was supported by the TAKEDA Science Foundation.

*1 IR spectra were taken on a JASCO Model IR-E spectrometer. NMR spectra were obtained using JNM-4H-100 or JNM-C60HL spectrometers. Rhodium(III) and ruthenium(III) chlorides were of commercial grade.

6) R. Cramer, *J. Inorg. Chem.*, **1**, 722 (1962).

BULLETIN OF THE CHEMICAL SOCIETY OF JAPAN, VOL. 46, 2232 (1973)

Polarography of Europium(III)-DL-Tryptophan Complex

Sudarshan LAL

The Thomas Hunt Morgan Institute of Genetics, Inc., 628 N. Broadway, Lexington, KY 40508, U.S.A.

(Received April 1, 1972)

Polarographic studies of europium(III) at the dropping mercury electrode (d.m.e.) in various electrolytes and organic chelating agents have been reported in literature. Holleck[1] claimed that no complexation occurs between Eu(III) and amino acids. However, a recent polarographic study[2] on Eu(III)-L-Proline system indicated definite complexation. In this note, polarographic results on the interaction of Eu(III)-DL-Tryptophan are described.

Experimental

Reagent grade chemicals were used. Solution of europium was prepared by dissolving a weighed amount of Eu_2O_3 (Moly Corp., Colorado) in minimum amount of perchloric acid and diluting with distilled water. M/100 solution of DL-tryptophan (Nutritional Biochem. Corp.) was prepared in double distilled water. The ionic strength was kept constant (μ=0.1) by adding requisite quantity of $NaClO_4$.

PAR Electrochemistry system 170 was used in conjunction with a droptimer for the record of current-voltage curves. The capillary had the characteristics $m^{2/3}t^{1/6}=1.46$ $mg^{2/3}$ $sec^{-1/2}$ in 0.1M $NaClO_4$ in the open circuit. Three electrode circuitry was used with a mercury pool as the counter electrode and voltages measured *vs.* S.C.E. Triple distilled (Bethlehem Instrument) mercury was used for the d.m.e. The temperature of the cell was maintained at 25±0.1C. Linde's prepurified nitrogen was used for deaeration.

Results and Discussion

Solutions containing 0.5 mM Eu(III) with different concentrations of tryptophan (pH=2.4) were polarographed. In each case, a well-defined reduction wave was obtained and $E_{1/2}$ shifted more negatively with increasing concentration of tryptophan. Plots of i_d against h_{eff} were linear depicting it to be a diffusion-controlled process. The plots of log $(i_d-i)/i$ *vs.*$E_{\text{d.e.}}$ were linear but slopes were higher than 59 mV which implied an irreversible process. Although the reduction, in the present case, is diffusion controlled yet is not reversible. $E^r_{1/2}$ (reversible halfwave potential) and kinetic parameters were determined by Gellings[3] method.

The tryptophanate anion [Tr$^-$] concentration at pH=2.4 was calculated with the knowledge of pK value=2.38 of tryptophan. The plot of $E^r_{1/2}$ against $-\log C_x$ is a straight line. Lingane's method[4] for the complex formation studies was applied with the equation:

$$\Delta E_{1/2} = (E^r_{1/2s}) - (E^r_{1/2})_c = \frac{0.0591}{n}\log p + p\frac{0.0591}{n}\log C_x \quad \text{at } 25°C$$

The slope of the plot $(E^r_{1/2})_c$ *vs.* $-\log C_x$ is given by the relation

$$\frac{\Delta E^r_{1/2}}{\Delta \log C_x} = -\frac{0.0591p}{n}$$

and the coordination number, p, is determined. The intercept on the potential axis corresponding to C_x= 1M, gives the instability constant of the complex. In the present case for n=1; p=1 and the intercept= −1.03 V is obtained. The instability constant of the complex $[Eu(Tr)]^{2+}$ is 1.63×10^{-7}.

TABLE 1. $E^r_{1/2}$ AND KINETIC PARAMETERS OF Eu(III)-DL-TRYPTOPHAN SYSTEM

Concn ×10³M Tryptophan	Tr ×10⁻³M	$-E^r_{1/2}$V *vs.* SCE	α	$k_s\times10^3$ cm/sec
0.00	0.000	0.654	0.88	6.25
0.005	0.002	0.668		
0.01	0.004	0.685		
0.02	0.008	0.705		
0.05	0.021	0.736		
0.10	0.041	0.747	0.89	5.75
0.20	0.082	0.762		
0.30	0.123	0.780		
0.40	0.164	0.788		
0.80	0.328	0.804	0.88	5.10
1.00	0.411	0.812		
2.00	0.822	0.831		
3.00	1.233	0.842	0.89	4.86
6.00	2.466	0.862	0.88	4.17
8.00	3.288	0.866	0.87	3.34

The rate constants and transfer coefficients of the process have been evaluated and summarized in Table 1. The apparent rate constants tend to decrease with increasing tryptophan concentration and the reduction appears to be quasireversible.[5]

The author expresses his profound thanks to the Chemistry Department, University of Kentucky and Dr. H. H. Bauer for providing necessary facilities.

1) L. Holleck, *Z. Naturforsch.*, **2b**, 81 (1947); *Chem. Abstr.*, **42**, 4084 (1948).
2) S. Lal, *Aust. J. Chem.*, **25**, 1571 (1972).
3) P. J. Gellings, *Z. Electrochem., Ber. Bunsenges. Phys. Chem.*, **66**, 477, 481, 799 (1962); **67**, 167 (1963).
4) J. J. Lingane, *Chem. Rev.*, **29**, 1 (1941).
5) L. Meites, "Polarographic Techniques," Interscience, New York (1965), p. 236.

BULLETIN OF THE CHEMICAL SOCIETY OF JAPAN, VOL. 46, 2233—2234 (1973)

The Absolute Configurations and Optical Rotations of (−)-4-Hydroxy-2-pentanone and (−)-2,4-Pentanediol

Tadashi TANABE*

Division of Organic Chemistry, Institute for Protein Research, Osaka University, Suita, Osaka 565

(Received September 28, 1972)

In order to calculate the asymmetric yield and the contents of the stereoisomers of the products obtained by the asymmetric hydrogenation of acetylacetone using Raney nickel catalysts modified with L$_s$-glutamic acid and D$_s$-tartaric acid, the absolute configurations and the optical rotations of (−)-4-hydroxy-2-pentanone and (−)-2,4-pentanediol were studied in the present work.

As the direct resolutions of the optical isomers of 2,4-pentanediol were not successful because of difficulty in separating the *racemic* and *meso* compounds, the optical rotation was decided by the following method.

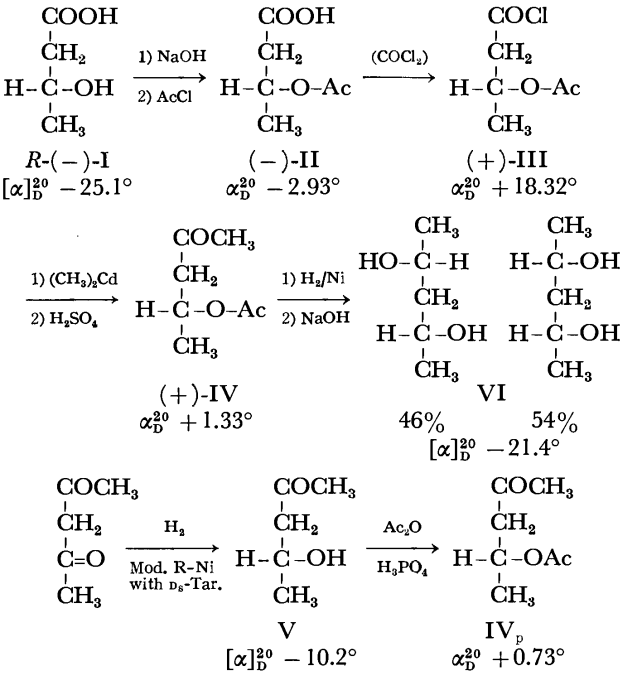

Scheme 1.

Sodium salt of *R*-(D$_s$)-3-hydroxybutyric acid ((−)-I)[1] ([α]$_D^{20}$ −25.1° (*c* 10, water)) was converted into (−)-3-acetoxybutyric acid ((−)-II), which was then treated with oxalyl chloride to yield (+)-3-acetoxybutyryl chloride ((+)-III). By the action of dimethylcadmium, (+)-4-acetoxy-2-pentanone ((+)-IV) was prepared from (+)-III. As IV was a comparatively labile compound under both acidic and alkaline conditions, direct hydrolysis with a base or acid was difficult. (+)-IV was reduced with a Raney nickel catalyst, and the product was hydrolyzed with an aqueous sodium hydroxide solution to yield a mixture of (−)- and *meso*-2,4-pentanediol ((−)- and *meso*-VI). On the other hand, the partially optically-active 4-hydroxy-2-pentanone (V) ([α]$_D^{20}$ −10.2°) obtained by the asymmetric hydrogenation of acetylacetone using a Raney nickel catalyst modified with D$_s$-tartaric acid was acetylated with acetic anhydride in the presence of phosphoric acid to give a partially optically-active IV (IV$_p$) ([α]$_D^{20}$ +0.73°), as is shown in Scheme 1. As (+)-IV and IV$_p$ had the same sign of optical rotation, the absolute configuration of (−)-4-hydroxy-2-pentanone was identified as *R*. From the ratio of the optical rotations of (+)-IV and IV$_p$, and from the optical rotation of V, the optical rotation of *R*-(−)-4-hydroxy-2-pentanone was calculated to be −18°.

The contents of *R*-(−)- and *meso*-VI were determined to be 46 and 54% respectively by means of the glc and NMR spectroscopy of 2,4-*O*-benzylidene-2,4-pentanediol, which had been derived from *R*-(+)-IV. From the contents of *R*-(−)-VI and the optical rotation of the mixture of *R*-(−)- and *meso*-VI, the optical rotation of *R*-(−)-2,4-pentanediol was calculated to be −47°.

Experimental

Determination of the Ratio of racemic *and* meso *2,4-Pentanediols (VI).* *Preparation of* meso-*VI*: A mixture of *racemic* and *meso*-VI was prepared by the hydrogenation of acetylacetone with a Raney nickel catalyst modified with DL-malic acid at pH 5.0, 0 °C.[2] The hydrogenation product was distilled under reduced pressure. Thirty-five grams of the boric ester of VI was prepared from 20 g of VI, 20 g of boric acid, and 4 ml of water according to the method of Nagai *et al.*[3] Twenty grams of the boric ester was recrystallized three times from chloroform; mp 76 °C (lit.,[3] mp 85 °C). Found: C, 45.36; H, 8.61%. Calcd for $C_5H_{11}O_3B$: C, 46.55; H, 8.53%.

Six and a half grams of the boric ester was refluxed with 100 ml of methanol for six hours, and then the methanol and methyl borate were removed under reduced pressure. The residual diol was distilled *in vacuo*. Bp 104 °C/15 mmHg; yield, 3.5 g. Found: C, 56.04; H, 11.90%. Calcd for $C_5H_{12}O_2$: C, 57.66; H, 11.61%. The IR spectrum corresponded with that of *meso*-VI reported in the literature,[3] and the product was used as the standard compound of *meso*-VI.

Preparation of 2,4-O-Benzylidene-2,4-pentanediol (VII): A mixture of 1.2 g of *meso*-VI (or a mixture of *racemic* and *meso*-VI) and 5 ml of benzaldehyde was stirred with 0.5 g of anhydrous zinc chloride[4] for 12 hr at room temperature. The reaction mixture was then distilled two times under reduced pressure, and a fraction with a bp of 130—132 °C/

* Present address: Faculty of Medicine, Kyoto University, Sakyo-ku, Kyoto, 606.

1) P. A. Levene and H. L. Haller, *J. Biol. Chem.*, **65**, 49 (1925).

2) T. Tanabe, This Bulletin, **46**, 1482 (1973).

3) E. Nagai, S. Kuribayashi, M. Shiraki, and M. Ukita, *J. Polym. Sci.*, **35**, 295 (1959).

4) L. Zervas, *Ber.*, **64**, 2293 (1931).

16 mmHg was collected.[5] Found: C, 74.25; H, 8.09%. Calcd for $C_{12}H_{16}O_2$: C, 74.97; H, 8.39%.

Determination of the Contents of meso *and* racemic *VII by Gas Chromatography*: The gas chromatography of VII was carried out under the following conditions: column, 1.5% PEG 20 M on Chromosorb W, 3 m; temp., 140 °C. The retention times of VII from *meso* and *racemic* VI were 5.3 and 7.1 min respectively. The ratio of the areas of *meso* and *racemic* VII in the gas chromatograph was in good agreement with the ratio of the intensities of the signals from the proton of the methine group $\left(\begin{matrix}C_6H_5\\H\end{matrix}\!\!>\!C\!<\!\!\begin{matrix}O-\\O-\end{matrix}\right)$ in the NMR spectra. This fact shows that the contents of the *meso* and *racemic* VI can be determined by glc like those of VII.

Preparation of the Sample of VII for Gas-chromatographic Analysis. Twenty to thirty milligrams of VI was dissolved in a solution of 0.4 ml of absolute benzene and 0.2 ml of freshly-distilled benzaldehyde, and then 25 mg of anhydrous zinc chloride and 50 mg of anhydrous potassium carbonate were added to the solution. The mixture was shaken for 1 hr and then allowed to stand for 24 hr at 30 °C. Under these conditions, the conversion of VI to VII was found to be quantitative by gas chromatography.

Determination of the Absolute Configurations and Specific Rotations of (−)-4-Hydroxy-2-pentanone ((−)-V) and (−)-VI. Preparation of (−)-3-Acetoxybutyric Acid ((−)-II): Fifty grams of sodium salt of *R*-(D_s)-(−)-3-hydroxybutyric acid ((−)-I) ($[\alpha]_D^{20}$ −25.1° (*c* 10, water)), prepared by the method of Levene *et al.*, and 16 g of anhydrous sodium acetate were dissolved in 100 ml of glacial acetic acid. Forty-two milliliters of acetyl chloride was then stirred into the mixture at 10 °C, after which the stirring was kept up for another hour at room temperature. One hundred and fifty milliliters of ether was then added, and the inorganic salts were removed by filtration. A fraction with a bp of 98—99 °C/1.5 mmHg was collected. 39.3 g $[\alpha]_D^{20}$ −2.93° (without dilution). Found: C, 48.67; H, 6.92%. Calcd for $C_6H_{10}O_4$: C, 49.31; H, 6.90%.

Preparation of (+)-3-Acetoxybutyryl Chloride ((+)-III): Fifteen milliliters of oxalyl chloride[6] was added to 20 g of (−)-II in 10 ml of absolute benzene,[7] and the resulting solution was allowed to stand for 12 hr at room temperature. The benzene was removed under reduced pressure, and the residual liquid was distilled. Bp 79—81 °C/12 mmHg; yield, 21.3 g; $[\alpha]_D^{20}$ +18.32° (neat) IR: 1730, 1800 cm^{-1} (C=O).

Preparation of (+)-4-Acetoxy-2-pentanone ((+)-IV): Nineteen grams of (+)-III in 50 ml of benzene was added at 0 °C, over a period of twenty seconds, to a benzene solution of dimethylcadmium prepared from 6.2 g of magnesium, 20.8 g of methyl iodide, and 26 g of anhydrous cadmium chloride.[8] The reaction mixture was then kept for 15 min at room temperature, carefully decomposed with 80 g of ice water, and acidified with 1.5 M sulfuric acid. The organic layer was separated, washed with water and then with saturated sodium hydrogencarbonate solution, and dried over anhydrous sodium sulfate. After the removal of the benzene, the residue was distilled *in vacuo*. A fraction with a bp of 80—90 °C/14 mmHg was redistilled. Bp 85—90 °C/14 mmHg; yield, 6.3 g.

(+)-IV was obtained by further purification using silica gel column chromatography. (Column: Kiesel Gel, 0.05—0.2 mesh, 1.6×75 cm. Eluent solvent: benzene.) Bp 92 °C/20 mmHg; yield, 2.3 g, $[\alpha]_D^{20}$ +1.33° (neat). Found: C, 56.43; H, 8.33%. Calcd for $C_7H_{12}O_3$: C, 58.31; H, 8.39%.

Preparation of IV from Partially Optically-active 4-Hydroxy-2-pentanone (V) and Calculation of the Specific Rotation of Optically-pure V: Five milliliters of partially optically-active V ($[\alpha]_D^{20}$ −10.2° (d^{20} 0.986), neat), prepared by the asymmetric hydrogenation of acetylacetone using a modified Raney nickel catalyst with D_s-tartaric acid at pH 5.0, 100 °C,[2] was acetylated with 6 ml of acetic anhydride and a catalytic amount of phosphoric acid.[9] After the removal of the acetic acid under reduced pressure, partially optically-active IV (IV_p) was obtained by distillation *in vacuo*. Bp 43 °C/2 mmHg; yield, 4 g, $[\alpha]_D^{20}$ +0.73° (neat).

The specific rotation of (−)-4-Hydroxy-2-pentanone was calculated by the following procedure; $[\alpha]_D^{20}$ of V×($[\alpha]_D^{20}$ of (+)-IV/$[\alpha]_D^{20}$ of IV_p)=−10.2°×(1.33/0.73)=−18°.

Preparation of a Mixture of (−)- and meso*-VI and the Specific Rotation of (−)-VI*: Two grams of (+)-IV ($[\alpha]_D^{20}$ +1.33°) in 5 ml of methanol was reduced using 0.6 g of a Raney nickel catalyst in an autoclave at 70 °C under an initial pressure of 90 kg/cm^2.[10] The product was hydrolyzed with 0.6 g of sodium hydroxide in 0.6 ml of water and 3 ml of methanol. The resulting solution was neutralized with 3 M hydrochloric acid and concentrated *in vacuo*, and then the VI was extracted with acetone. After the acetone had been removed, the residue was distilled. Bp 107—108 °C/17 mmHg; yield, 0.6 g, $[\alpha]_D^{20}$ −21.4° (*c* 10.5, ethanol). Found: C, 56.27; H, 11.57%. Calcd for $C_5H_{12}O_2$: C, 57.66; H, 11.61%. The content of (−)-VI was 46%. The specific rotation of optically-pure (−)-2,4-pentanediol was calculated by means of the following equation: −21.4°×(100/46)=−47° (*c* 10.5, ethanol).

The author wishes to express his thanks to Professor Yoshiharu Izumi for his continuous guidance and encouragement. He also wishes to thank Miss Kiku Koike and Mrs. Nobuko Okuhara for the elemental analyses.

5) As, under these conditions, the conversion of VI to VII was not perfect, and as the distillation process changed the diastereomeric component ratio of VII, the method is inadequate for the preparation of samples for diastereomeric analysis by glc.

6) H. Staudinger, *Ber.*, **41**, 3563 (1908).

7) R. Adams and L. H. Ulich, *J. Amer. Chem. Soc.*, **70**, 2427 (1948).

8) J. Cason and F. S. Prout, *J. Amer. Chem. Soc.*, **66**, 46 (1944).

9) V. Isaguljaz and F. Amoljaninova, *Riechstoff-ind. u. Kosm.*, **8**, 194 (1933).

10) Y. Izumi, M. Imaida, H. Fukawa, and S. Akabori, This Bulletin, **36**, 24 (1963).

BULLETIN OF THE CHEMICAL SOCIETY OF JAPAN, VOL. 46, 2235—2236 (1973)

Electronic Properties of the Tautomers of Hydroxy-substituted Purines and Pyrimidines

Mamoru KAMIYA

Shizuoka College of Pharmacy, Oshika, Shizuoka-shi 420

(Received September 30, 1972)

The purines and pyrimidines bearing potential amino- or hydroxyl-groups have been the subjects of a number of spectroscopic studies, since they present several interesting problems concerning tautomerism in solution. One of the most useful methods for approaching this problem has been a comparison of the UV spectrum of a given compound with those of the reference compounds, such as the *N*-methyl derivatives. In recent years, the SCF-MO calculation has also been used in the inspection of the correlation between the electronic spectrum and the tautomeric structure of biological purines and pyrimidines.[1-4] These works led to the finding that the P-P-P method, when properly modified, can afford to support fairly well the observations of the predominant tautomers on the basis of the π-electronic transitions and energies. In this work, a more general consideration of the keto-enol tautomerism of purines and pyrimidines was made using the P-P-P method coupled with the variable-β procedure.[5]

The calculations were performed including all singly excited configurations. The variable-β procedure was adopted in order to take account of the remarkable π-bond localization at the keto-tautomers. The parametrizations adopted are analogous to that used previously.[6] The observed transition energies of pyrimidine can be explained well by the present calculation, provided that the second weak band is reduced to $n\rightarrow\pi^*$ in accord with the assignment by Clark and Tinoco.[7] It has been indicated that the 2-, 4-, and 2,4-hydroxypyrimidines take keto-forms in an aqueous solution.[8-10] In this respect, the present calculation of the electronic spectrum shows that the predominant forms of the 2- and 4-isomers are certainly keto-forms, but that of the dihydroxypyrimidine is not necessarily restricted to the diketo-form. In view of the π-electronic energy, the predominance of the diketo-form is supported.

The calculations of purines were performed on the basis of the N(9)H form of purine, since the majority of biological purines exist essentially as derivatives of this form; the calculated data of the electronic spectrum of this form are in good accord with the observed data. The UV spectra of monohydroxypurines in an aqueous solution suggested that the 2- and 8-isomers exist largely in a keto-form type of –CO–NH–, but the 6-isomer is likely to take the enol-form which might contain an intramolecular hydrogen-bond.[11] The above suggestions for the 2- and 8-isomers are well

Table 1. Experimental UV data of purines and pyrimidines

	ΔE[a] ($\varepsilon_{max}\times 10^{-3}$)
Pyrimidine derivatives	
None[f]	5.12 (2.0), 5.90 (1.0), 6.53 (6.0)
2-Hydroxy[c]	4.14 (4.6), 5.77 (10.0)
4-Hydroxy[d]	4.77 (3.7), 5.59 (7.4)
2,6-Dihydroxy[b]	4.77 (9.0)
Purine derivatives	
None[f]	4.68 (6.9), 5.17 (3.0), 6.20 (18.1), 6.59 (21.1)
2-Hydroxy[e]	3.94 (4.9), 5.21 (2.9),
6-Hydroxy[e]	4.98 (10.5)
8-Hydroxy[e]	4.47 (11.2), 5.28 (3.2)
2,6-Dihydroxy[e]	4.64 (7.9)
2,8-Dihydroxy[e]	4.00 (5.0), 5.39 (7.9)
6,8-Dihydroxy[e]	4.43 (5.7), 4.82 (12.0)

a) ΔE is transition energy in eV obtained from spectra in neutral solution.
b) L. F. Cavalieri *et al.*, *J. Amer. Chem. Soc.*, **72**, 2587 (1950).
c) M. P. V. Boarland *et al.*, *J. Chem. Soc.*, **1952**, 3716.
d) D. J. Brown *et al.* *J. Chem. Soc.*, **1953**, 331.
e) S. F. Mason, *J. Chem. Soc.*, **1954**, 2071.
f) L. B. Clark *et al.*, *J. Amer. Chem. Soc.*, **87**, 11 (1965).

1) C. Giessner-Prette and A. Pullman, *Theore. Chim. Acta*, **9**, 279 (1968).
2) B. Pullman, "Quantum Aspects of Chemical and Biochemical Heterocycles," *Proc. Int. Symp.*, 2nd, 292 (1969).
3) A. Julg and P. Carles, *Theore. Chim. Acta*, **17**, 301 (1970).
4) B. Pullman and H. Berthod, *Tetrahedron*, **26**, 1483 (1970).
5) K. Nishimoto and L. S. Forster, *Theore. Chim. Acta*, **4**, 155 (1966).
6) M. Kamiya and Y. Akahori, *Nippon Kagaku Zasshi*, **92**, 118 (1971).
7) L. B. Clark and I. Tinoco, Jr., *J. Amer. Chem. Soc.*, **87**, 11 (1965).
8) M. P. V. Boarland and J. F. W. McOmie, *J. Chem. Soc.*, **1952**, 3716.
9) D. J. Brown and L. N. Short, *ibid.*, **1953**, 331.
10) J. R. Marshall and J. Walker, *ibid.*, **1951**, 1004.
11) S. F. Mason, *ibid.*, **1954**, 2071.

TABLE 2. THEORETICAL DATA OF THE UV SPECTRUM AND π-ELECTRONIC ENERGY

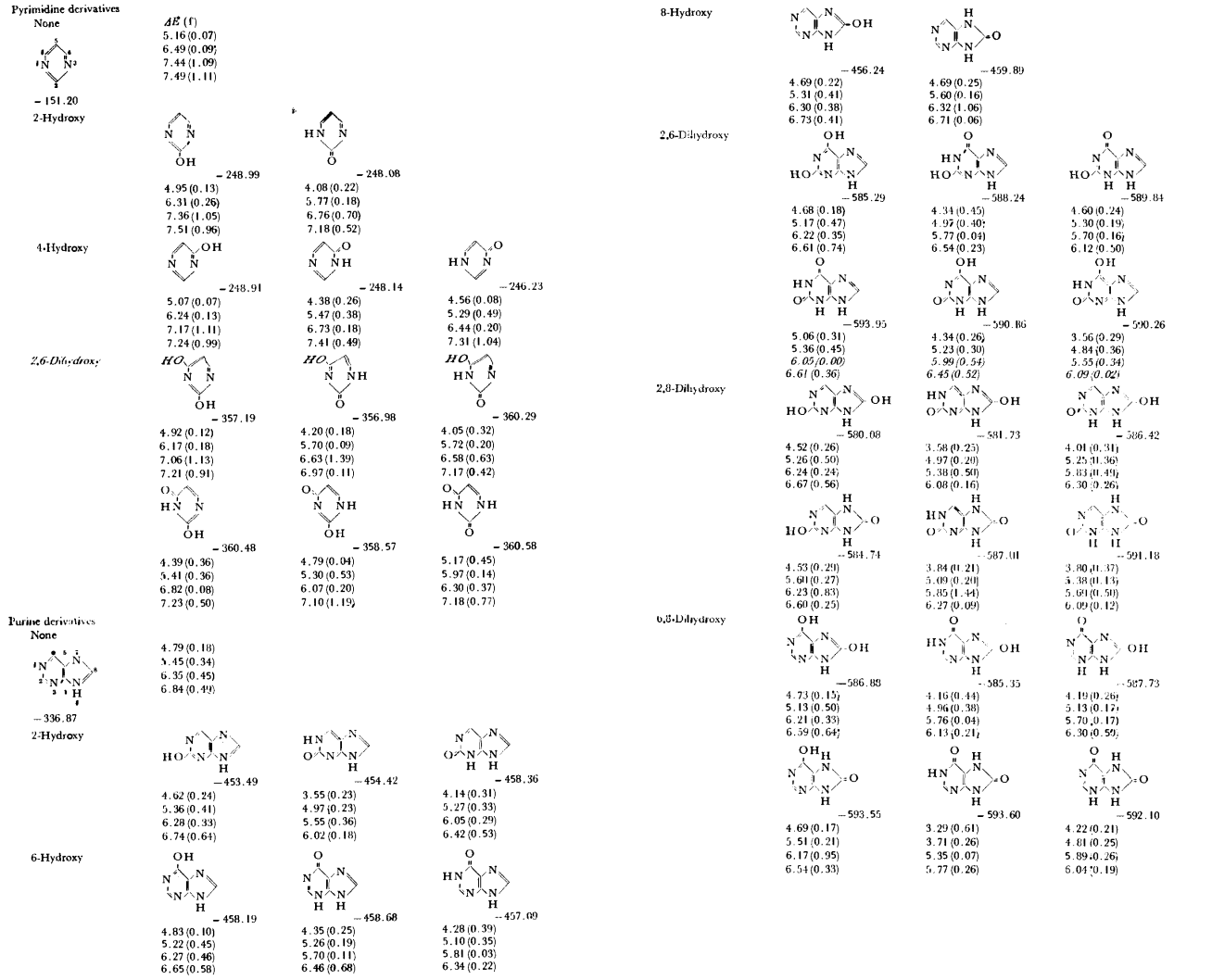

a) ΔE is singlet-singlet transition energy in eV.

b) f is oscillator strength.

c) The valence-state ionization potential and electron affinity are taken as follows:

	=C-	=N-	-N-	=O	-O-
Ionization potential (eV)	11.16	14.12	28.72	17.28	34.75
Electron affinity (eV)	0.03	1.78	11.96	2.01	13.57

The two-center Coulomb integral is evaluated with the Nishimoto-Mataga formula. Parametrization for the evaluation of the core-resonance integral by the variable-β method is as follows:

$\beta_{C-C} = -0.51\, P_{C-C} - 2.04$,

$\beta_{C-N} = -0.53\, P_{C-N} - 2.24$,

$\beta_{C-O} = -0.56\, P_{C-O} - 2.44$.

d) Numerals under the structural formula are π-electronic energies in eV.

supported by the present calculations of the electronic transitions and energies. In the case of the 6-isomer, the predominance of the keto-form –CO–NH–, can not be confirmed by the calculated results. As regards the dihydroxypurines, the calculated data of the electronic spectra of diketo-forms satisfy the relative sequence of the observed first-transition energies. Moreover, the π-electronic energies support the predominance of diketo-forms.

In conclusion, the variable β–P-P-P calculation of the π-electronic transitions and energies was found to be rather useful for the prediction of the predominant tautomers of the compounds in the title.

The calculations were performed on a HITAC 5020-E computer at the University of Tokyo. The author wishes to thank Professor Yukio Akahori for his useful suggestions.

BULLETIN OF THE CHEMICAL SOCIETY OF JAPAN, VOL. 46, 2237—2238 (1973)

X-Ray Photoelectron Spectra of Copper-Tetracyanoquinodimethane Complexes

Isao IKEMOTO, John M. THOMAS, and Haruo KURODA*

Edward Davies Chemical Laboratories, The University College of Wales, Aberystwyth, U.K.
**Department of Chemistry, Faculty of Science, The University of Tokyo, Hongo, Tokyo 113*

(Received March 14, 1973)

Copper forms[1] two types of complexes with tetracyano-*p*-quinodimethane (TCNQ). Metathesis of cupric sulphate and Li(TCNQ), and related reactions, yield a solid corresponding to the formula $Cu(TCNQ)_2$, whereas the product formed when the parent TCNQ reacts either with metallic copper or certain cuprous salts, has a composition Cu(TCNQ). From their mode of production it seems reasonable to suppose that these complexes contain cupric and cuprous ions, respectively; the formula have been written as $Cu^{2+}(TCNQ^-)_2$(A) and $Cu^+(TCNQ^-)$ (B). Whilst formulation B is consonant with the observed properties of the complex, there are difficulties associated with A. First, no Cu^{2+} signal is detectable in the ESR spectrum of the $Cu(TCNQ)_2$, and, second, static magnetic susceptibility measurements reveal that the so-called cupric compound is apparently diamagnetic.[2] In addition, the IR absorption spectrum of this compound clearly indicates the presence of TCNQ as well as $TCNQ^-$.[2] Hence feasible alternative representations for A are $Cu^+(TCNQ^-)(TCNQ)$ or $(Cu^+)_2(TCNQ^-)_2(TCNQ)_2$, and it has been suggested[1] that the following equilibria might be set up in the solid state:

$$2Cu^{2+}(TCNQ^-)_2 \rightleftharpoons (Cu^+)_2(TCNQ^-)_2(TCNQ)_2$$
$$\rightleftharpoons (Cu^+)_2(TCNQ^{2-})(TCNQ)_3$$

The X-ray induced photoelectron spectra (ESCA) of the two compounds (hitherto represented as A and B above) have been recorded (on an AEI ES100) under conditions which have been fully descibed[3] for other complexes. The materials were synthesized according to the procedures given in Ref. 1 and the binding energies (Table 1) have been accurately determined using the gold-decoration technique,[4] the subsidiary standard being 84.0 eV for the binding energy of the Au $4f_{7/2}$ level.[5]

TABLE 1. BINDING ENERGIES (eV)

Compounds	Cu $2p_{1/2}$	Cu $2p_{3/2}$	Cu 3s	Cu 3p	Cu 3d	N1s
Cu(TCNQ)	951.0	931.2	121.8	74.8	2.2	398.1
$Cu(TCNQ)_2$	950.4	930.4	121.5	74.5	2.1	(398.3)[a]

a) The peak is broad, and the value is approximate. (Precision throughout is ±0.3 eV).

It is to be expected from other works[6] that a chemical shift of about 1.5 eV occurs between copper in +2 and +1 formal oxidation states, yet the metal core level binding energies for the two complexes are almost coincident. Significantly the shapes and half-widths of the Cu 2p and the Cu 3s peaks (Fig. 1) are indistinguishable for the two compounds, and in each case there are no satellites[7] on the higher-binding energy side of the Cu 2p peaks, nor any signs of spin-spin splitting of the Cu 3s levels that is expected for a $3d^9$ configuration. These facts prove that the copper ion has, in both cases, the $3d^{10}$ configuration.

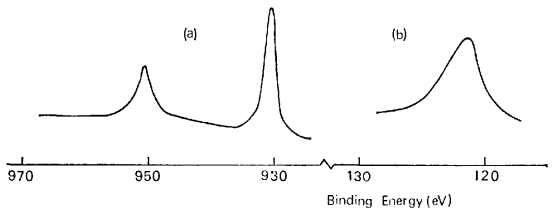

Fig. 1. Copper peaks of $Cu(TCNQ)_2$ (a) Cu 2p (b) Cu 3s.

N1s peaks for the two compounds are, however, revealingly different (Fig. 2). They both exhibit the higher-binding energy satellites, which we have shown elsewhere[3] to be a general feature of TCNQ complexes and which we now know to arise from an intramolecular shake-up (two-electron) mechanism. But of greater significance is the differences in widths of the main peaks. The breadth of the N1s peak in $Cu(TCNQ)_2$ signifies, as does the IR spectra,[2] the presence of two types of nitrogen, namely those due to ($TCNQ^-$) and (TCNQ). Using the N1s peaks observed on TCNQ crystal and K(TCNQ), we synthesized the N1s peak which is expected for the system containing equivalent

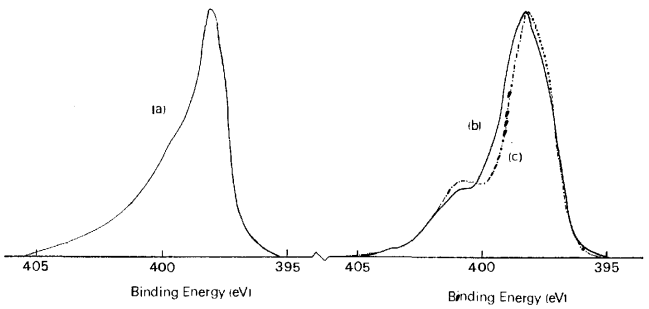

Fig. 2. N1s peaks (a) Cu(TCNQ), (b) $Cu(TCNQ)_2$, (c) Synthesized N1s peak for $Cu(TCNQ)_2$.

1) L. R. Melby, R. J. Harder, W. R. Hertler, W. Hahler, R. E. Benson, and W. E. Mochel, *J. Amer. Chem. Soc.*, **84**, 3374 (1962).
2) M. Sano, T. Ohta, and H. Akamatu, This Bulletin, **41**, 2204 (1968).
3) I. Ikemoto, J. M. Thomas, and H. Kuroda, *Discuss. Faraday Soc.*, (1972), in press.
4) J. M. Thomas, E. L. Evans, M. Barber, and P. Swift, *Trans. Faraday Soc.*, **67**, 1875 (1971).
5) C. S. Fadley, Ph. D. Thesis (Univ. of California), (1970).
6) T. Novakov, *Phys. Rev.*, **B3**, 2693 (1971).
7) Just as for cuprous compounds free of adsorbed impurities.[8]
8) T. Novakov and R. Prins, *Solid. State Commun*, **9**, 1975 (1971).
9) The observed diamagnetism of this complex seems to be brought from the interaction between ($TCNQ^-$) anion radicals.

amounts of (TCNQ) and ($TCNQ^-$). As shown in Fig. 2, the observed N1s peak of $Cu(TCNQ)_2$ well agrees with the synthesized one. Thus, a possible formulation in place of A is $Cu^+(TCNQ^-)(TCNQ)$ or $(Cu^+)_2(TCNQ^-)_2(TCNQ)_2$.[9]

$Cs_2(TCNQ)_3$ as well as $(Ph_3PMe)(TCNQ)_2$ is also known to be a 'mixed' complex, frequently formulated as $(Cs^+)_2(TCNQ^-)_2(TCNQ)$ and $(Ph_3PMe)(TCNQ^-)$-(TCNQ), but its N1s peak shape is distinctly different from that shown here for the mixed cuprous complex. For these two complexes it is not possible to reproduce the N1s peak by a simple superposition of the N1s peaks of TCNQ and K(TCNQ). If there is a significant electron delocalization between ($TCNQ^-$) and (TCNQ), we should naturally expect a disagreement between synthesized and actual spectra. Thus, the good agreement between the observed and synthesized N1s peaks in the case of $Cu(TCNQ)_2$ seems to indicate small electron delocalization between ($TCNQ^-$) and (TCNQ).

Thanks are due to the S.R.C. for financial support.

BULLETIN OF THE CHEMICAL SOCIETY OF JAPAN, VOL. 46, 2238—2240 (1973)

A Potentiometric Study on Complex Formation of Oxovanadium(IV) with Malonic Acid

Satoshi Ito,* Hiroshi Tomiyasu,** and Hitoshi Ohtaki***

Department of Electrochemistry, Tokyo Institute of Technology, O-okayama, Meguro, Tokyo 152

***Department of Chemistry, Faculty of Science, Shinshu University, Asahi-machi, Matsumoto 390*

(Received February 1, 1973)

In the previous work we found a protonated oxovanadium(IV)-glycine complex MHGly (where M and Gly denote VO^{2+} and glycinate ions, respectively) along with the MGly and $M(Gly)_2$ complexes (charges are omitted for simplicity) by spectrophotometric measurements.[1] In the present study we employed potentiometric titrations for studying reactions between oxovanadium(IV) ion and malonic acid as another topic of the complex formation of multidentate ligands with metal ions.

Experimental

Reagents. Oxovanadium(IV) perchlorate solution was prepared by the method described in the preceding papers.[1,2] Sodium perchlorate and sodium hydroxide solutions were prepared and purified by the usual methods. Reagent grade malonic acid (Wako Pure Chemicals, Co. Ltd.) was recrystallized twice from distilled water and dried under a reduced pressure in a desiccator over silica gel.

Apparatus. A six-neck titration vessel was used, which was set with a glass electrode and the "Wilhelm" type reference electrode,[3] burets and glass tubes for nitrogen gas inlet and outlet. Nitrogen gas free from carbon dioxide was preequilibrated with 3 M $NaClO_4$ aqueous solution. Glass electrodes of Beckman No. 40498 were used in combination with a Radiometer PHM-4d pH meter (Copenhagen).

Emf measurements were carried out at 25.00 ± 0.01 °C in a paraffin oil thermostat in a room thermostated at 25 ± 1 °C. 3 M sodium perchlorate was used as an ionic medium.

Method of Measurements. Potentiometric titrations were carried out in 3 M $NaClO_4$ aqueous solution at a constant total metal concentration during the course of the titrations. The hydrogen ion concentration at equilibrium [H] was determined by means of emf measurements by the use of the Nernst equation;

$$E = E^\circ + 59.15 \log [H] + E_j \qquad (1)$$

under an assumption of a constant activity coefficient of hydrogen ion. The liquid junction potential E_j was calculated from the relation $E_j = -16.5[H]$ mV/M.[4] Since malonic acid dissociates to some extent even in an acid solution (pH ~2), E° was determined by means of a Gran plot[5] at each titration in a constant ionic solution which contained oxovanadium(IV) perchlorate but no malonic acid in the pH range where oxovanadium(IV) ions did not appreciably hydrolyze. After the determination of E° a suitable amount of malonic acid solution was added to prepare a test solution, the mole ratio of V(IV): malonic acid being controlled to be 1: 10. The concentration of V(IV) covered the range of 0.0007562 to 0.007499 M.

Results and Discussion

Dissociation constants of malonic acid were determined as $pK_1=2.82\pm0.01$ and $pK_2=5.78\pm0.01$ in 3 M $NaClO_4$ at 25 °C. Hydrolysis of oxovanadium(IV) ion in 3 M $NaClO_4$ has been studied by Rossotti and Rossotti[6] who reported values $\log \beta_{11}=-6.0\pm0.1$ and $\log \beta_{22}=-6.88\pm0.04$. In the present work we used these values in preliminary calculations of stability constants of oxovanadium(IV) malonate complexes, although we will briefly discuss whether the values of β_{11} and β_{22} are reasonalbe or not at the final stage of refinement of the results by computer calculations.

Titration curves of mixtures of oxovanadium(IV) perchlorate and malonic acid are shown in Fig. 1.

* Present address: Department of Chemistry, Faculty of Science, Hiroshima University, Higashisenda-machi, Hiroshima 730.

*** To whom correspondence should be addressed.

1) H. Tomiyasu and G. Gordon, *J. Coord. Chem.*, in press.

2) H. Tomiyasu, K. Dreyer, and G. Gordon, *Inorg. Chem.*, **11**, 2409 (1972).

3) W. Forsling, S. Hietanen, and L. G. Sillén, *Acta Chem. Scand.*, **6**, 901 (1952).

4) G. Biedermann and L. G. Sillén, *Ark. Kemi.*, **5**, 425 (1953).

5) G. Gran, *Analyst* (London), **77**, 661 (1952).

6) F. J. C. Rossotti and H. S. Rossotti, *Acta Chem. Scand.*, **9**, 117 (1955).

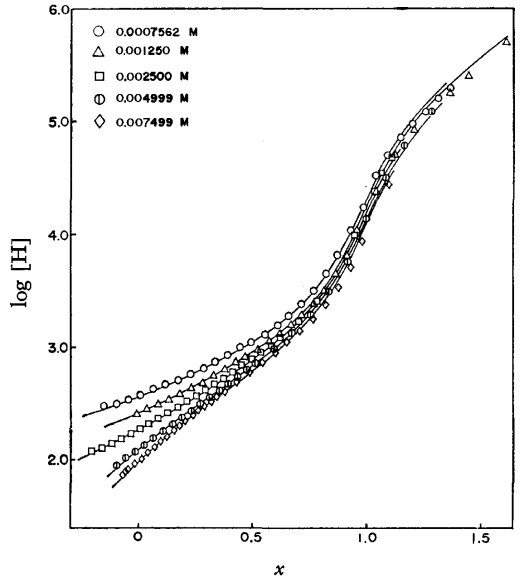

Fig. 1. Titration curves of mixtures of oxovanadium(IV) perchlorate and malonic acid in 3M $NaClO_4$. Curves are plotted against the degree of neutralization of malonic acid, x, at various total oxovanadium(IV) concentrations. Solid lines are calculated titration curves with $pK_1=2.82$, $pK_2=5.78$, $\log \beta_{11}=-6.0$, $\log \beta_{22}=-6.88$, and $\log \beta_{111}=7.41$.

Data obtained in an acid region where no hydrolysis of oxovanadium(IV) ion is expected were used for the first approach of stability constants. Since the concentration of malonate ion A^{2-} could be neglected in the pH range less than 3, the complex formation of oxovanadium(IV) ion with malonic acid may, in general, be described by the following equation:

$$pVO^{2+} + rHA^- + (q-r)H^+ = (VO)_pH_qA_r^{(2p+q-2r)+} \quad (2)$$

The equilibrium constant of the reaction (2) is defined as

$$\kappa_{pqr} = \frac{[M_pH_qA_r]}{[M]^p[HA]^r[H]^{q-r}} \quad (3)$$

The total concentrations of malonic acid (C_A) and proton to be dissociated (C_H) are given as follows:

$$C_A = [H_2A] + [HA] + \sum_r r[M_pH_qA_r] \quad (4)$$

$$C_H = C_A + H = [H] + [H_2A] + \sum_{q-r}(q-r)[M_pH_qA_r] \quad (5)$$

where H represents the analytical excess of hydrogen ion in a test solution. Since C_A is about ten times larger than the total metal C_M in any solution, it is reasonably assumed that the term $\sum_r r[M_pH_qA_r]$ is much smaller than the sum of C_A and H so that [HA] can be obtained, without introduction of any serious error, as follows:

$$[HA] = \frac{(C_A+H-[H])K_1}{[H]} \quad (6)$$

The average number of HA combined with V(IV) in solution $\bar{n}_{M(HA)}$ is given as

$$\bar{n}_{M(HA)} = \frac{C_A-[H_2A]-[HA]}{C_M} = \frac{\sum_r r[M_pH_qA_r]}{C_M} = \frac{\sum_r r\kappa_{pqr}[M]^{p-1}[HA]^r[H]^{q-r}}{1+\sum_p p\kappa_{pqr}[M]^{p-1}[HA]^r[H]^{q-r}} \quad (7)$$

Almost all points of $\bar{n}_{M(HA)}$ plotted against log [HA] fell on a single curve which was drawn by a normalized function $y=x/(1+x)=f(\log x)$ and no systematic scattering of data was observed with varying C_M and [H]. This result showed that Eq. (7) was not a function of [M] and [H] and thus, $p-1=0$ and $q-r=0$. Therefore, we concluded that the complex formed in this pH range was MHA. The equilibrium constant κ_{111} was determined as $10^{1.65}$ by means of curve fitting, or $\beta_{111}=[MHA]/[M][H][A]=10^{7.43}$.

In the range of pH larger than 3, hydrolysis of oxovanadium(IV) must be taken into account in evaluation of stability constants of complexes. If the formula of a complex present in solution is generally described as $M_pH_qA_r$, the mole balances lead to following relations:

$$C_H = 2C_A + H = [H] + [H][A]K_2^{-1} + 2[H]^2[A]K_1^{-1}K_2^{-1} - \beta_{11}[M][H]^{-1} - 2\beta_{22}[M]^2[H]^{-2} + \sum_q q\beta_{pqr}[M]^p[H]^q[A]^r \quad (8)$$

$$C_M = [M] + \beta_{11}[M][H]^{-1} + 2\beta_{22}[M]^2[H]^{-2} + \sum_p p\beta_{pqr}[M]^p[H]^q[A]^r \quad (9)$$

$$C_A = [A] + [H][A]K_2^{-1} + [H]^2[A]K_1^{-1}K_2^{-1} + \sum_r r\beta_{pqr}[M]^p[H]^q[A]^r \quad (10)$$

Since we found the MHA complex in the acid solution, we examined if we could explain whole data by assuming the formation of only the complex. Under the present assumption the following relations could readily be derived from Eqs. (9) and (10):

$$[A] = \frac{C_A}{1+[H]K_2^{-1}+[H]^2K_1^{-1}K_2^{-1}+\beta_{111}[M][H]} \quad (11)$$

$$[M] = [\{(1+\beta_{11}[H]^{-1}+\beta_{111}[H][A])^2 + 8C_M\beta_{22}[H]^{-2}\}^{1/2} - (1+\beta_{11}[H]^{-1}+\beta_{111}[H][A])]/4\beta_{22}[H]^{-2} \quad (12)$$

Successive approximations were repeated until [A] and [M] converged to certain values with which Eqs. (11) and (12) were satisfied simultaneously, β_{111} being known. The average number of malonate ion per oxovanadium(IV) ion $\bar{n}$ is calculated by the following equation after the correction of hydrolysis of oxovanadium(IV) ions;

$$\bar{n} = \frac{C_A-([A]+[H][A]K_2^{-1}+[H]^2[A]K_1^{-1}K_2^{-1})}{C_M-\beta_{11}[M][H]^{-1}-2\beta_{22}[M]^2[H]^{-2}} \quad (13)$$

and was plotted against log [H]+log [A] as seen in Fig. 2. All points fitted very well a normalized curve drawn by the function $y=x/(1+x)=f(\log x)$. This shows that experimental results are satisfactorily explained in terms of the formation of the MHA complex and no other ones, besides the hydrolyzed species MOH and $M_2(OH)_2$, over the whole range of pH and the metal concentration studied.

The stability constants of complexes in solution were refined by means of a non-linear least squares method with the help of an electronic computer. If we set constant K_1, K_2, β_{11}, and β_{22} and variable β_{111}, the value of $\beta_{111}=10^{7.41}$ was obtained as the best one to interprete experimental data. When we set K_1 and K_2 as constants and β_{11}, β_{22}, and β_{111} as variable parameters, a slightly better agreement between calculated

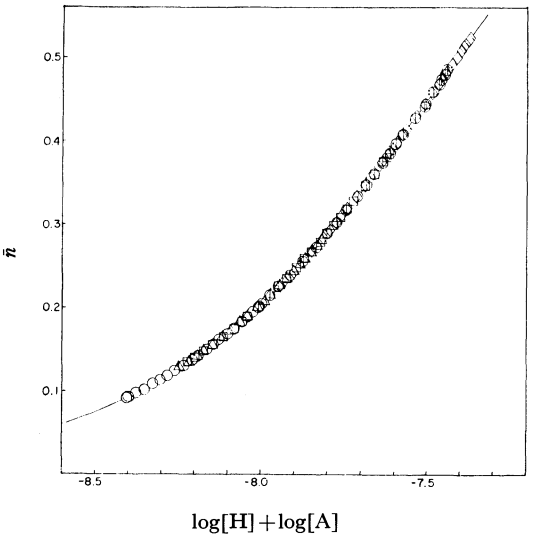

Fig. 2. Relationship between $\bar{n}$ and log [H] + log [A]. A solid line is a curve drawn by a normalized function, $y=x/(1+x)=f(\log x)$ at the position of best fit. Symbols are the same as those used in Fig. 1.

and experimental titration curves was obtained with values of $\beta_{11}=10^{-5.0}$, $\beta_{22}=10^{-6.71}$, and $\beta_{111}=10^{7.50}$. However, the value $10^{-5.0}$ is far beyond the uncertainty of β_{11} estimated by Rossotti and Rossotti,[6] although diversed values of the stability constant of the $VOOH^+$ complex appear in literature.[7] Therefore, we finally adopted the value $\beta_{111}=10^{7.41\pm0.02}$, which is in good agreement with the value obtained in the acid region, instead of $10^{7.50}$. The results were not improved by the assumption of formation of two complexes HMA and MA together with MOH and $M_2(OH)_2$. Thus we concluded that only the MHA complex is formed in solutions we examined. Other complexes such as MA and MA_2 may be formed in more basic solution containing malonic acid of much higher concentration.

The complex MHA is so stable that the complex does not release a proton even at pH$\simeq$6. This fact shows that the dissociation constant of MHA to MA and H must be less than 10^{-6}, which is smaller than K_2. In many protonated complexes of highly charged metal ions, the dissociation of a proton in a complex is usually more enhanced than that of the corresponding free acid by electrostatic repulsion between a leaving proton and the central metal ion. However, the dissociation of a proton in the protonated oxovanadium(IV) malonate complex is not the case. This phenomenon may be interpreted in terms of formation of an intramolecular hydrogen bond between the oxygen atom in VO^{2+} ion and a proton in a malonic acid molecule coordinated as a monodentate ligand to the central metal ion.

7) L. G. Sillén and A. E. Martell, "Stability Constants," The Chemical Society, London (1964); 2nd ed. (1971).

BULLETIN OF THE CHEMICAL SOCIETY OF JAPAN, VOL. 46, 2240—2242 (1973)

A Common Feature in the 2+2 Cycloadditions of Benzyne and $^1\Delta_g$ Molecular Oxygen to Ethylene Derivatives

Satoshi INAGAKI and Kenichi FUKUI

Department of Hydrocarbon Chemistry, Faculty of Engineering, Kyoto University, Kyoto 606

(Received October 2, 1972)

The abnormal behavior of $^1\Delta_g$ molecular oxygen in the cycloaddition reaction previously stimulated our interest in a well-established, close connection between orbital interaction and stereoselection,[1] since the singlet oxygen gives 2+2 and 4+2 cycloadducts, both retaining the configuration of the substrate olefins.[2] A consideration of the orbital interaction scheme[1] was previously found to suggest that the singlet oxygen may approach ethylene, as is represented by Model I.[3] This sort of reaction path for 2+2 cycloaddition was novel and is clearly different from the symmetry-allowed 2_s+2_a process generally proposed for concerted cycloaddition by Woodward and Hoffmann.[4] The preference for this nuclear configuration has been attributed to the fact that the interaction between the highest occupied (HO) molecular orbital (MO) of ethylene as an electron-donor and the lowest unoccupied (LU) MO of the oxygen molecule as an electron-acceptor is most favored in this nuclear configuration. The prediction of the addition mechanism

1) The essence of this concept may be briefly said as follows; a majority of chemical reactions should take place at the position and in the direction where the particular interaction between the frontier orbitals is most favored.

For further particulars on the HOMO-LUMO interaction scheme, see the following articles; K. Fukui, *Accounts Chem. Res.*, **4**, 57 (1971); K. Fukui and H. Fujimoto, "Mechanisms of Molecular Migrations," Vol. 2, ed. by B. S. Thyagarajan, Interscience, New York, N. Y. (1969), p. 118; K. Fukui, "Theory of Orientation and Stereoselection," Springer-Verlag, Heidelberg, (1970).

2) For stereospecific *cis*-[2+2] cycloaddition, P. D. Bartlett and A. P. Schaap, *J. Amer. Chem. Soc.*, **92**, 3223 (1970) and for 4+2 cycloaddition with the stereochemical integrity of retention, see the following review; D. R. Kearns, *Chem. Rev.*, **71**, 395 (1971).

3) S. Inagaki, S. Yamabe, H. Fujimoto, and K. Fukui, This Bulletin, **45**, 3510 (1972).

4) R. B. Woodward and R. Hoffmann, "The Conservation of Orbital Symmetry," Verlag Chemie, Academic Press, N. Y. (1970).

tempts us to seek the most favorable path of the reaction between olefinic C=C double bonds and benzyne, which exhibits a similar behavior toward unsaturated hydrocarbons.[5] Here, this problem will also be probed by means of the HOMO–LUMO interaction scheme.[1]

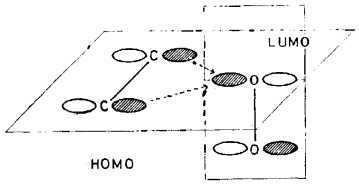

I

The electronic state of benzyne has been presented in several papers,[6] and it has been shown that the HOMO (II) and the LUMO (III) have the same symmetry property as normal mono-olefins.[6a] Accordingly, it can readily be found that the simple symmetry arguments of the Woodward-Hoffmann method[3] predict that suprafacial-suprafacial[3] cycloaddition is symmetry-forbidden and that the other mode of suprafacial-antarafacial process is not probable for the following reasons. No antarafacial mode on benzyne is conceivable since the particular MO's of benzyne extend their lobes exclusively outward from the benzene nucleus[6a] (see II and III). On the other hand, the antarafacial interaction is possible on the side of ethylene, but this $2\pi_s+2\pi_a$ process ends in the inversion of the ethylene derivative configuration, which is inconsistent with the experimental observations.[5] It follows that the simple application of the Woodward-Hoffmann dichotomy of symmetry-allowed 2_s+2_a and symmetry-forbidden 2_s+2_s processes cannot produce fruitful information on the reaction between benzyne and ethylene.

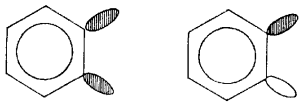

II III

Here, the electronic structure of benzyne, particularly the LUMO with an abnormally low energy or with a negative eigenvalue (the result of *ab initio* calculation),[6b] should be noted; this suggests the strong electrophilicity of benzyne.[7] This characteristic is markedly different from normal olefins, but is similar to the $^1\Delta_g$ oxygen molecule.[4] It may, therefore, be considered that benzyne may also provide the LUMO for the critical orbital interaction with ethylene.

The above discussion allows us to predict the most favorable reaction path, using the degree of interaction between the HOMO of ethylene and the LUMO of benzyne as the primary measure. We will examine the same sorts of models (IV, V, and VI) as with the singlet oxygen. Here, the IV candidate corresponds to that which was predicted to be the most feasible with $^1\Delta_g$ oxygen,[4] in which the benzyne structure lies in the bisecting plane of the ethylenic C–C bond with one of its particular carbon atoms in the vertical plane of ethylene. The V illustration represents some models with C_2 symmetry, including a symmetry-forbidden $2\pi_s+2\pi_s$ process, where the molecular plane of benzyne intersects the plane containing the ethylene π-orbital at the angles of 0°, 30°, and 90°. The last model, VI, is intended for a step-by-step reaction, whether ionic or radical-like. The parallel relation between the C=C bond of ethylene and the C≡C bond of benzyne is broken a little (5°) in the coplane. The overlap integrals between the HOMO of ethylene and the LUMO of benzyne are calculated for each model in order to estimate the degree of orbital interaction between them.[8] The results show that the overlap integral for the IV model is the largest (0.026) among those of the models examined (*cf.* 0.000 for V's and 0.003 for VI).[9] On comparing these values, we see that the IV model is the most appropriate. The prediction made here on the basis of the HOMO–LUMO interaction is consistent with that drawn from the total energy by extended Hückel calculations (−701.501 eV for IV and higher than −701.440 eV for V's and VI).[9]

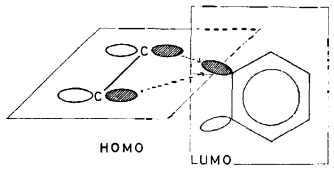

IV

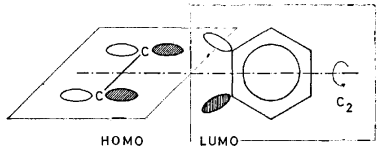

V

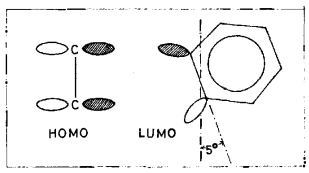

VI

The nuclear configuration IV is also shown to have good grounds for the most probable structure of the transition state or the intermediate structure in the 2+2 cycloaddition between benzyne and ethylene. Here it is

5) For example, see the review, I. Tabushi and H. Yamada, *Yuki Gosei Kyokai Shi*, **28**, 667 (1970).

6) a) R. Hoffmann, A. Imamura, and W. J. Hehre, *J. Amer. Chem. Soc.*, **90**, 1499 (1968), T. Yonezawa, H. Konishi, and H. Kato, This Bulletin, **42**, 933 (1969); b) D. L. Wilhite and J. L. Whitten, *J. Amer. Chem. Soc.*, **93**, 2858 (1971).

7) In fact, benzyne readily reacts with a variety of nucleophiles such as anion (alkoxide, metal amide and carbanion), sulfides, phosphorus compounds, amines, ethers, and so on; see the Ref. 5.

8) K. Fukui and H. Fujimoto, This Bulletin, **41**, 1989 (1968).

9) These values are obtained by the calculation on each model where the distance between the relevant C=C bond of benzyne and that of ethylene is 3 Å apart from each other. For more detailed calculation, D. M. Hayes and R. Hoffmann, *J. Phys. Chem.*, **76**, 656 (1972).

noteworthy that good electron-acceptors, *e.g.*, ketenes[10] and tetracyanoethylene,[11] also afford 2+2 cycloadducts with a retention of the configuration. Whether or not these cycloadditions are intrinisically identical with those of $^1\Delta_g$ molecular oxygen and benzyne is a question requiring further study,[12] but it can be expected that this mechanism is pervasive throughout 2+2 cycloadditions between electron-donating and electron-accepting multiple bonds.

10) See the article cited in the Ref. 4.

11) See; P. D. Bartlett, *Quart. Rev. Chem. Soc.*, **24**, 473 (1970).

12) Subsequent to the submission to this manuscribt, a detailed calculation on the ketene [2+2] addition has appeared and has drawn entirely the same conclusion as is proposed here [R. Sustmann, A. Ansmann, and F. Vahrenholt, *J. Amer. Chem. Soc.*, **94**, 8099 (1972)].

BULLETIN OF THE CHEMICAL SOCIETY OF JAPAN, VOL. 46, 2242—2244 (1973)

The Vibrational Spectra of the Zn-Acrylonitrile Complex

Tomoichi KAMO, Sumio NAGAI, and Masao KIMURA*

Department of Chemistry, Faculty of Science, Hokkaido University, Sapporo 060

(Received December 6, 1972)

In a previous paper,[1] the present authors reported on the infrared spectra of zinc-halide complexes with acetonitrile; these complexes form σ-bonds between the Zn atom and the N atoms of the nitrile groups. In the present study the infrared spectrum of the zinc chloride-acrylonitrile complex has been investigated; it was also expected to be a σ-complex.

Experimental

The sample of $[ZnCl_2 \cdot CH_2CHCN]_n$ was prepared from $ZnCl_2$ and acrylonitrile by the method described in the previous paper.[1]

The infrared spectra, ranging from 4000 to 96 cm^{-1}, were measured by the mull method on a JASCO IR-G infrared spectrophotometer in the near-infrared region, and on a Hitachi FIS-21 infrared spectrophotometer in the far-infrared region.

Assignment and Normal Coordinate Analysis

A complete assignment for the in-plane vibrational modes of acrylonitrile has been made by Halverson *et al.*[2] and has been supported by Fritz and Schrauzer[3] and also by Devlin *et al.*[4] In the present study, the assignment of bands for the ligand was made by correlation with the spectra for the free acrylonitrile, while that for the skeleton about the Zn atom was made by referring to the spectra of analogous complexes.[1,5]

In order to see the strength of the coordination bond, normal coordinate analyses were carried out in two steps using the simple Urey-Bradley force fields. In the first step (Calculation 1), only the intra-ligand vibrations for the $CH_2 \cdot CH \cdot CN \cdot Zn$ system were treated by assuming them to be separable from the skeletal vibrations about the central Zn atom. The molecular geometry of gaseous acrylonitrile[6] was assumed to be maintained in the complexed ligand. All the force constants associated with the ligand vibrations except for the C≡N stretching, $\nu_{C\equiv N}$, were transferred from those which had been determined by the present authors by applying the overlay technique[4,7] to the observed frequencies for both acrylonitrile and fumaronitrile in the free states. In the second step (Calculation 2), the complex was assumed to be a Cl-bridged dimer of C_{2h} symmetry, in which the two-fold axis was the line connecting the two bridging chlorine atoms and in which the two linear R–C≡N–Zn (R: H_2C=CH) frames are located at *trans* positions on the horizontal plane. The bond distances and angles about the Zn atoms were assumed to be as follows: Zn–Cl=2.30 Å, Zn–N=2.00 Å, and all the valence angles were 109.5°. The force constants, K_{R-C}, $K_{C\equiv N}$, K_{Zn-N}, and $H_{Cl^bZnCl^b}$, were then determined so as to reproduce the observed frequencies by transferring the other force constants from those obtained for the acetonitrile complexes.[1] The observed and calculated frequencies and their assignments are shown in Table 1, while the force constants are shown in Table 2.

Results and Discussion

For comparison, the observed frequencies for the free ligand are reproduced in Table 1. Tables 1 and 2 indicate that the coordination has an appreciable effect only on the $\nu_{C\equiv N}$, and that the slight increase in the $K_{C\equiv N}$ value satisfactorily explains the observed frequencies for the acrylonitrile moiety. Such an effect of coordination has also been observed in the Zn-aceto-

* To whom correspondence should be addressed.

1) T. Kamo and M. Kimura This Bulletin, **45**, 3309 (1972).

2) F. Halverson, R. F. Stamm, and J. J. Whalen. *J. Chem. Phys.*, **16**, 808 (1948).

3) H. P. Fritz and G. N. Schrauzer, *Chem. Ber.*, **94**, 650 (1961).

4) D. Devlin, J. Overend, and B. Crawford, Jr., *Spectrochim. Acta*, **20**, 23 (1964).

5) See, e.g., G. E. Coats and D. Ridley, *J. Chem. Soc.*, **1964**, 166.

6) a) C. C. Costain and B. P. Stoicheff, *J. Chem. Phys.*, **30**, 777 (1959); b) I. Fukuyama and K. Kuchitsu, *J. Mol. Struct.*, **5**, 131 (1970).

7) J. H. Schachtschneider and R. G. Snyder, *Spectrochim. Acta*, **19**, 117 (1963).

TABLE 1. THE OBSERVED AND CALCULATED FREQUENCIES AND THEIR ASSIGNMENTS FOR ACRYLONITRILE AND THE $ZnCl_2$–ACRYLONITRILE COMPLEX (in cm^{-1})

Acrylonitrile		$ZnCl_2$–Acrylonitrile			Assignment[d]
Obsd[a]	Calcd	Obsd	Calcd 1.[b]	Calcd 2.[c]	
3120	3120	3125	3118		$a\nu_{CH_2}$
3070	3065	3083	3067		ν_{CH}
3030	3031	3048	3031		$s\nu_{CH_2}$
2239	2237	2283	2282	2282	$\nu_{C\equiv N}$
1609	1603	1610	1605		$\nu_{C=C}$
1414	1419	1416	1428		δ_{CH_2}
1292	1277	1284	1281		ρ_{CH}
1098	1101	1095	1110		ρ_{CH_2}
875	881	895	894	890	ν_{C-C}
575	596	581	602		$\delta_{C=CC}$
236	247	348	274	310	$\delta_{C-CN}+\nu_{Zn-Cl^t}$
				305	$\nu_{Zn-Cl^t}+\delta_{C-C\equiv N}$
		328		339	ν_{Zn-Cl^b}
		280		263	$\nu_{Zn\cdot Cl^b}$
		153	151	155	ν_{Zn-N}
		110		97	ρ_{Zn-Cl^t}
				92	ν_{Zn-Cl^t}
				88	ρ_{Zn-L}
				76	γ_{Zn-Cl^t}
				29	$\delta_{Zn-NC}{}^{i.p.}$
				16	$\delta_{Zn-NC}{}^{o.p.}$

a) Frequencies observed by the present authors; see also Ref. 2.
b) Calculated for the ligand; see text.
c) Calculated for the normal modes of A_u and B_u species of the skeleton; see text.
d) Cl^t, terminal Cl; Cl^b, bridging Cl; i.p., in plane; o.p., out of plane.

TABLE 2. UREY-BRADLEY FORCE CONSTANTS FOR THE $ZnCl_2$–ACRYLONITRILE COMPLEX (in mdyn/Å)[a]

Ligand (Calc. 1)					
$K_{C=C}$	(7.02)	$H_{C=CH_2}$	(0.22)	$F_{C=CH_2}$	(0.60)
$K_{C\equiv N}$[b]	17.58	$H_{C=CH}$	(0.15)	$F_{C=CH}$	(0.77)
K_{C-C}	(4.99)	H_{H-CH}	(0.31)	F_{H-CH}	(0.041)
K_{CH_2}	(4.78)	H_{C-CH}	(0.14)	F_{C-CH}	(0.37)
K_{CH}	(4.46)	$H_{C=CC}$	(0.31)	$F_{C=CC}$	(0.91)
K_{ZnN}	0.40	H_{C-CN}	(0.17)	F_{C-CN}	(0.0)
		H_{C-NZn}	(0.025)	F_{C-NZn}	(0.0)
Skeleton (Calc. 2)					
$K_{C\equiv N}$	17.32	H_{NZnCl^t}	(0.013)	F_{N,Cl^t}	(0.016)
K_{R-C}	6.84[c]	$H_{Cl^bZnCl^b}$	0.035	$F_{Cl^bCl^b}$	(0.075)
K_{Zn-N}	0.40	$H_{Cl^bZnCl^t}$	(0.075)	$F_{Cl^bCl^t}$	(0.075)
K_{Zn-Cl}	(1.10)	H_{ZnClZn}	((0.025))	$F_{Zn,Zn}$	((0.025))
		H_{CNZn}	(0.025)	$F_{C,Zn}$	(0.0)
		H_{RCN}	(0.12)	$F_{R,N}$	(0.0)

a) Values in parentheses were transferred; see text. Values in double parentheses were assumed.
b) The $K_{C\equiv N}$ for the free ligand, 16.70 mdyn/Å.
c) An effective value obtained by treating the olefinic group as a single mass point.

nitrile complexes; it may be considered to be characteristic of σ-coordination. In Calculation 2, the olefinic group was treated as a single mass point. This treatment produces only an insignificant change in the $K_{C\equiv N}$ value and no change in the K_{Zn-N} value, as compared with the results of Calculation 1. The K_{Zn-N} value was thus determined to be 0.40 mdyn/Å in both calculations, 1 and 2. This value is of the same order of magnitude as that in the Zn-acetonitrile complex, 0.65 mdyn/Å. This suggests that the Zn atom coordinates to the N atom of the nitrile group with a similar bond strength to that of the coordination bonds in the Zn-acetonitrile complexes.[1]

As the geometry of the present complex has not yet been known, we assumed a bridged structure so as to account for the results of the chemical analysis. Then, the three bands observed at 348, 328, and 280 cm^{-1} were assigned to the three Zn–Cl stretching vibrations; the highest frequency band at 348 cm^{-1} may be due to the Zn-terminal Cl stretching, ν_{Zn-Cl^t}, while the

broad band observed at 328 cm^{-1} is probably composed of two bands, one of which originates from the ν_{Zn-Cl^t} and the CCN deformation. Since a Zn atom forms usually a tetrahedral coordination, and since the observed spectra could be interpreted on the basis of a Cl-bridged structure, the assumed structure for this complex seems most probable. In the present normal coordinate calculation, no particular attention was paid to the Zn–Cl stretching vibrations, all the Zn–Cl bonds being assumed to have the same force constant. If different Zn–Cl force constants are used for the terminal- and bridging-Cl atoms, the agreement between the observed and calculated frequencies will be improved. However, no further refinement was made.

BULLETIN OF THE CHEMICAL SOCIETY OF JAPAN, VOL. 46, 2244—2246 (1973)

Interaction between Lone Pair Electrons on the Nitrogen Atoms in 1,5-Diazabicyclo[3.2.1]octane

Yoshiaki HAMADA, Akiko Y. HIRAKAWA, Masamichi TSUBOI, and Hitoshi OGATA*

Faculty of Pharmaceutical Sciences, The University of Tokyo, Hongo, Bunkyo-ku, Tokyo 113

**Department of Industrial Chemistry, Faculty of Engineering, The University of Tokyo, Hongo, Bunkyo-ku, Tokyo 113*

(Received January 24, 1973)

In the course of our studies on the electronic spectra of amines,[1-3] we have been interested in the intramolecular interaction between the nitrogen lone pairs. Hoffmann *et al.*[4] made a theoretical study on the interaction of two orbitals (n_1 and n_2) separated by a number of intervening σ bonds. They showed that the interaction should be dependent only on the orientation of the σ bonds between the orbital lobes in question and the orientation of the lobes themselves, but not on the specific molecule. By extended Hückel calculations, they predicted, for example, that in arrangement (a) of Fig. 1, the antisymmetric (n_1-n_2) level should be

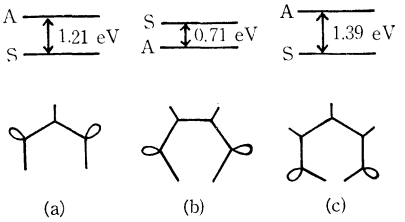

Fig. 1. Interaction patterns in some model arrangements of orbital lobes (n_1 and n_2) and intervening σ bonds, as given by Hoffmann *et al.*[4] The amount of splitting of the S (symmetric, n_1+n_2) and A (antisymmetric, n_1-n_2) levels is given in eV for each model arrangement.

higher by 1.21 eV than the symmetric (n_1+n_2) level, while in arrangement (b) the symmetric level should be higher by 0.71 eV than the antisymmetric level. Therefore, for 1,4-diazabicyclo[2.2.2]octane (I), a splitting of some 2.1 eV ($\fallingdotseq 0.71\times 3$) is expected between the two levels of the lone pair electrons. This was

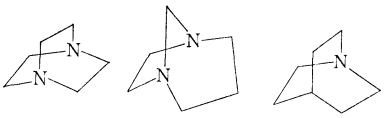

shown to be the case by Bischof *et al.*[5] They found in the photoelectron spectrum of I two bands at 7.5 and 9.5 eV which are assignable to the ionizations of electrons from two orbitals strongly localized on the nitrogen lone pairs. The assignment was also supported by Dewar and Wasson[6] by the use of a semiempirical SCF MO procedure (MINDO/2).

We now report here the result of our similar examination on 1,5-diazabicyclo[3.2.1]octane (II), in which two nitrogen atoms are connected by three σ-bond-bridges corresponding to arrangements (a), (b), and (c) in Fig. 1 (instead of three type-(b) bridges in I). On the basis of the study of Hoffmann and his collaborators,[4] the amount of splitting should be somewhat smaller in II than in I, and the ordering of the symmetric and antisymmetric levels should be reversed. In Fig. 2, are given the photoelectron spectra of I and II observed in their gaseous states. To help the assignments of the observed peaks, we have made a semiempirical SCF MO (MINDO/2) calculation for quinuclidine (III), as well as for I and II. In the calculation for III, the orbital energy of an MO in which the nitrogen lone pair has the greatest contribution came out to be −8.64 eV, and this is in agreement with the position of the observed peak (8.02 eV) in the photoelectron spectrum of III assignable to the lone pair orbital (highest occupied MO).[5] For I and II, the calculated energy values of the MO's in which the main contributions come from the nitrogen lone

1) M. Tsuboi, A. Y. Hirakawa, and H. Kawashima, *J. Mol. Spectrosc.*, **29**, 216 (1969).

2) A. Y. Hirakawa, H. Miyazaki, and M. Tsuboi, This Bulletin, **45**, 757 (1972).

3) Y. Hamada, A. Y. Hirakawa, and M. Tsuboi, *J. Mol. Spectrosc.*, in press.

4) R. Hoffmann, A. Imamura, and W. J. Hehre, *J. Amer. Chem. Soc.*, **90**, 1499 (1968).

5) P. Bischof, J. A. Hashmall, E. Heilbronner, and V. Hornung, *Tetrahedron Lett.*, **1969**, 4025.

6) M. J. S. Dewar and J. S. Wasson, *J. Amer. Chem. Soc.*, **92**, 3506 (1970).

Table 1. Energy levels (eV) of I and II

Orbital	Molecule I Obsd	Molecule I MINDO/2	Molecule II Obsd	Molecule II MINDO/2
A vacant MO	(−2.77)[a]	—	(−2.64)[a]	—
Highest occupied MO	−7.70	− 8.27(S)	−8.24	−8.83(A)
Other lone pair combination	−9.71	−10.17(A)	−8.95	−9.10(S)
(A–S Splitting)	(2.01)	(−1.90)	(0.71)	(+0.27)

a) Obtained by adding the transition energy of the observed absorption band to the orbital energy of the highest occupied MO.

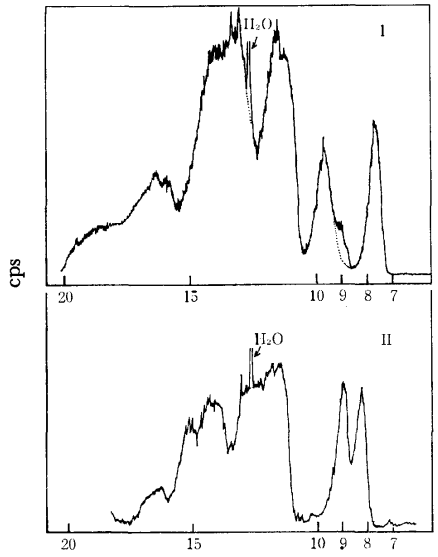

Fig. 2. Photoelectron spectra of I and II. Ordinate is the count rate in arbitrary units. The photoelectron spectrum of I was observed also by Bischof *et al.*,[5] and their result is in a good agreement with ours, shown here. A small peak at 9 eV in the spectrum of I is considered to be caused by an impurity.

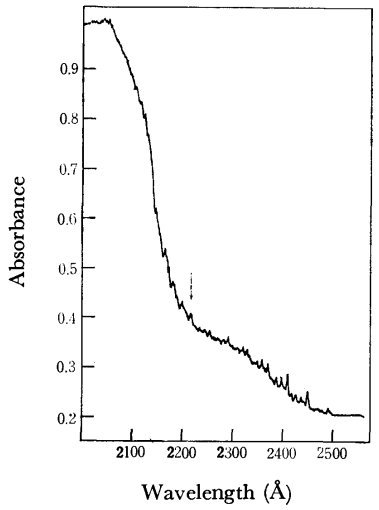

Fig. 3. Ultraviolet absorption spectrum of II in its gaseous state. The arrow indicates a band assigned to 0-0 transition.

pairs are given in Table 1. As may be seen in this table, the calculated values for I are in good agreement with the observed values. In view of such an agreement (both for III and I), we may expect an equally good prediction for our MINDO/2 calculation of the orbital energy in II. Hence, the assignments can be made on the observed peaks in the photoelectron spectrum of II as shown in Table 1. In other words, we may conclude that, assuming the validity of Koopmans' theorem, the two highest occupied MO's of II at −8.24 and −8.95 eV are attributed mostly to the nitrogen lone pairs, the higher one ($E_A = -8.24$ eV) to the antisymmetric MO ($n_1 - n_2$) and the lower one ($E_S = -8.95$ eV) to the symmetric MO($n_1 + n_2$). The amount of splitting ($E_A - E_S$) due to the lone pair interaction is +0.71 eV. This is somewhat smaller than a simple estimate from the study of "basic coupling units" of Hoffmann *et al.*,[4] but slightly greater than the value estimated by our MINDO/2 procedure.

We like to mention here the result of our ultraviolet absorption measurement of II in its vapor phase. This is shown in Fig. 3. The apparent 0—0 transition of the strong absorption band is found at 2216 Å. By adding this transition energy to the orbital energy of the highest occupied MO (−8.24 eV), the approximate orbital energy of the vacant MO now in question is given as −2.64 eV. By a similar procedure, the corresponding orbital energy is found to be −2.77 eV in I and −2.6 eV in III. It is interesting that this vacant MO is located at almost equal height for all of these molecules (I, II, and III).

Experimental

The sample of 1,5-diazabicyclo[3.2.1]octane (II) was prepared from homopiperazine and formaldehyde by the method of Poppelsdorf.[7] Solvent used was toluene, and the product was purified by a recrystallization and sublimation procedure.

The photoelectron spectra were recorded on a Jasco PE-1 High-resolution Photoelectron Spectrometer. Excitation was made by photons from the 584 Å He resonance line. For calibration of the ionization potential (IP), H_2O (IP, 12.61_6 eV), O_2 (12.07_0), and N_2 (15.57_9) were used as internal standards.

The ultraviolet absorption spectrum was observed by the use of a Hitachi EPS-3T spectrometer with a quartz prism. The calibration was made by the absorption lines of the γ system of nitric oxide in the region from 1955 to 2270 Å.

MINDO/2 Calculation

For I and III, a set of the molecular parameters given by Yokozeki and Kuchitsu[8] (N–C, 1.472 Å;

7) F. Poppelsdorf, U.S. 3120336 (Cl. 260—239).
8) A. Yokozeki and K. Kuchitsu, This Bulletin, **44**, 72 (1971).

C–C, 1.562 Å; C–H, 1.110 Å; ∠NCC, 110.2°; ∠CNC, 108.7°; ∠HCH, 111.5°; angle of twisting ϕ defined by Yokozeki and Kuchitsu, 10°) has been used. For II, the following parameters were used: N–C, 1.472 Å; C–C, 1.562 Å; C–H, 1.110 Å; ∠NCN, 109.7°; ∠CNC, 108.7°; ∠NCC, 110.2°; ∠CCC, 109.7°; ∠HCH, 111.5°, dihedral angle HCCH, 0°. The calculation was made by the use of HITAC 5020E. The SCF procedure was repeated until the change in total electronic energy becomes smaller than 0.0005 eV.

The sequence which follows is analogous to that proposed by Kolthoff *et al.*[1]

$$CO_2^- + O_2 \rightleftharpoons O_2CO_2^- \quad (3)$$

$$O_2CO_2^- + Mn^{II}Ox + 2H^+ \longrightarrow H_2O_2 + Mn^{III}Ox + CO_2 \quad (4)$$

$$Mn^{III}Ox \longrightarrow Mn^{II}Ox + CO_2 + CO_2^- \quad (5)$$

The sequence of Reactions (3), (4), and (5) constitutes a chain reaction. The terminating reaction probably occurs *via* Eq. (6):

$$Mn^{III}Ox + CO_2^- \longrightarrow Mn^{II}Ox + CO_2 \quad (6)$$

where $Mn^{II}Ox$ and $Mn^{III}Ox$ indicate the various forms of oxalato-manganese(II) and (III) respectively. The assumption of steady-state concentrations of CO_2^-, $O_2CO_2^-$, and $Mn^{III}Ox$ leads to Eq. (7):

$$[H_2O_2]_{formed} = \sqrt{\frac{kk_4k_5K[O_2][Mn^{II}Ox][Co(C_2O_4)_3^{3-}]}{2k_6}}[H^+]\tau \quad (7)$$

where $k=k_1+k_2[H^+]$, where k_n indicates the rate constant of the reaction (n), where K is the equilibrium constant of Reaction (3), and where τ means the time of standing of the reaction mixtures. It may be presumed that the concentrations, $[O_2]$, $[H^+]$, and $[Mn^{II}Ox]$ are constant under the conditions of Tables 1 and 2. Under these circumstances Eq. (7) predicts a linear relation in the plot of $[H_2O_2]_{formed}/[Co(C_2O_4)_3^{3-}]^{1/2}$ *vs.* τ. This is verified experimentally in Fig. 1. The above reaction mechanisms are properly

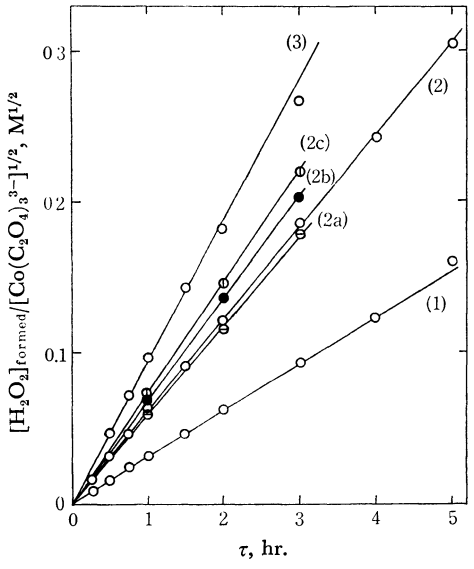

Fig. 1. Plot of $[H_2O_2]_{formed}/[Co(C_2O_4)_3^{3-}]^{1/2}$ *vs.* τ.
Conditions as in Table 1. Concentrations of manganese(II) sulfate are 0.001M (1), 0.01M (2), and 0.1M (3). (2a), (2b), and (2c) are as in (2) except 0.005M, 0.05M, and 0.1M in oxalic acid respectively, instead of 0.01M oxalic acid.

borne out by the fitness of the kinetic treatment. Since the concentration of oxalate does not appear in Eq. (7), the amount of hydrogen peroxide formed must be essentially independent of the concentration of the uncomplexed oxalate ion. However, the following facts should be noted. Manganese(III) as well as manganese(II) forms various complexes with oxalate, and the redox decomposition of Mn(III)Ox occurs at different rates (k_5);[4,5] In acidic solutions under conditions such as are shown in Tables 1 and 2, mono- and di-oxalato complexes of manganese(III) would be presumably predominant species, and the oxalato complexes of manganese(II) may be highly dissociated. The equilibria should be shifted by any change in the concentrations of oxalate and manganese(II) sulfate. Accordingly, the formation of hydrogen peroxide would be dependent on the oxalate concentration. As may be seen in Table 2, a small dependence of

Table 2. Effect of the oxalic acid concentration on the formation of hydrogen peroxide[a]

$[H_2C_2O_4]_{added}$, M[b]	$[H_2O_2]_{formend} \times 10^3$, M Time of standing, hr			
	0.5	1	2	3
0	1.3	2.5	4.4	6.1
0.005	1.7	3.2	5.4	7.3
0.01	1.8	3.4	5.7	7.7
0.05	1.8	3.8	7.2	9.6
0.1	1.8	4.2	7.6	10.4
0.1 M HCOOH instead of $H_2C_2O_4$	1.1	2.2	3.9	5.2

a) Conditions as in Table 1 except for the varied concentrations of oxalic acid and the 0.01 M value of manganese(II) sulfate.
b) The concentrations of oxalic acid listed here indicate those in the initial solutions.

the oxalate concentration was observed. However, the amount of hydrogen peroxide formed at 0.5 hr was practically independent of the concentration of oxalic acid. Finally, formic acid was compared with oxalic acid in respect of the hydrogen peroxide formation. As can be seen in Table 2, the amount of hydrogen peroxide formed does not increase when formic acid is added instead of oxalic acid; rather, it decreases slightly. It appears that the following reactions, (4′) and (5′) hardly occur under these conditions:

$$O_2CO_2^- + Mn^{II} + 2H^+ \longrightarrow H_2O_2 + Mn^{III}(formate) + CO_2 \quad (4')$$

$$Mn^{III}(formate) \longrightarrow Mn^{II} + CO_2^- + H^+ \quad (5')$$

4) a) H. Taube, *J. Amer. Chem. Soc.*, **69**, 4118 (1947); b) H. Taube, *ibid.*, **70**, 1216 (1948).
5) S. J. Adler and R. M. Noyes, *ibid.*, **71**, 2036 (1955).

BULLETIN OF THE CHEMICAL SOCIETY OF JAPAN, VOL. 46, 2248—2249 (1973)

A Facile, Stereospecific Preparation of Olefins from Pinacols

Tamejiro HIYAMA and Hitosi NOZAKI

Department of Industrial Chemistry, Kyoto University Yoshida, Kyoto 606

(Received November 30, 1972)

Considerable attention has been drawn to stereospecific or stereoselective olefin syntheses.[1] Among them, the deoxygenation of pinacols constitutes a convenient route to olefins, especially symmetric ones.[2] The desulfurization of thioncarbonates of pinacols with phosphite[3] is well known, but the method requires not-easily-available thiocarbonyldiimidazole as well as a high reaction temperature. The reaction of benzaldehyde acetal of pinacols with *n*-butyllithium[4] proceeds at a low temperature and has been successfully applied to the preparation of *trans*-cyclooctene, but the attempt to prepare stilbene from dihydrobenzoin has been reported to be unfruitful. In contrast, a third method, discovered by Eastwood *et al.*[5], has proven to be quite useful in the preparation of alkylsubstituted stilbenes and cyclic olefins. The present note will describe the experimental details of these new applications.

A mixture of the pinacol **1b**, for example, an excess of ethyl orthoformate, and a catalytic amount of benzoic acid was heated at 100 °C for 2 hr and subsequently at 170—190 °C for 2 hr to afford, stereospecifically, the **2b** olefin in a good yield. The results are summarized in Table 1, which shows that the sequence provides a beneficial route to stilbestrol.[6] Since the pure *threo* diols, **1d** and **1f**, were unaccessible, a mixture of diastereomers was subjected to the reaction in the case of **1d**. The yields of the *trans*-olefins, **2d** and **2f**, were improved by the isomerization of the corresponding *cis*-olefins (**2c** and **2e**).

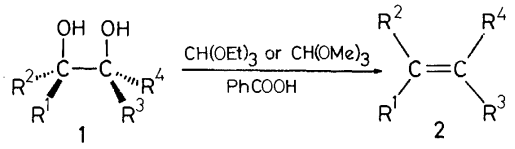

TABLE 1. YIELDS OF OLEFINS FROM PINACOLS

	Pinacol	Olefin	Y(%)
a: $R^1=R^3=$Ph, $R^2=R_4=$Me	**1a**	**2a**	100
b: $R^1=R^4=$Ph, $R^2=R^3=$Me	**1b**	**2b**	83
c: $R^1=R^3=p$-$MeOC_6H_4$, $R^2=R^4=$Et	**1c**	**2c**	86
d: $R^1=R^4=p$-$MeOC_6H_4$, $R^2=R^3=$Et	**1d** (+**1c**)[a]	**2d**	37[b]
e: $R^1=R^3=p$-$MeOC_6H_4$, $R^2=R^4=$H	**1e**	**2e**	c)
f: $R^1=R^4=p$-$MeOC_6H_4$, $R^2=R^3=$H	**1e**	**2f**	36
g: R^1, $R^4=-(CH_2)_6-$, $R^2=R^3=$H	**1f**	**2g**	53
h: R^1, $R^3=-(CH_2)_8-$, $R^2=R^4=$H	**1h**	**2h**	67

a) A mixture of stereoisomers obtained by pinacolic reduction.
b) The yield based on *p*-methoxypropiophenone.
c) Not isolated. See experimental.

Experimental

Preparation of trans-*2,3-Diphenyl-2-butene (2b).* A mixture of *dl*-2,3-diphenylbutane-2,3-diol (**1b**, 642 mg, 2.65 mmol), ethyl orthoformate (600 mg, 5.6 mmol), and benzoic acid (20 mg, 0.16 mmol) was stirred at 100 °C for 2 hr. The subsequent evaporation of the produced ethanol and the excess orthoformate *in vacuo* gave the crude 1,3-dioxolane (IR 1120—1050 cm^{-1}). Benzoic acid (300 mg) was then added, and the mixture was heated at 170—190 °C for 2 hr, during which time the evolution of carbon dioxide and the refluxing of ethanol were observed. After cooling, dichloromethane (20 ml) was added, and the solution was washed with saturated sodium bicarbonate (four 5 ml portions) and dried with anhydrous potassium carbonate. Concentration gave crystalline **2b** (593 mg). Recrystallization from methanol afforded an analytically-pure sample (460 mg); mp 103—104 °C (lit,[9] 106 °C). NMR (δ, CCl_4): 1.85 (s, 6H) and 7.15 (s, 10H). Mass spectrum: *m/e* 208 (M^+, 100%).

cis-*2,3-Diphenyl-2-butene (2a)* (402 mg) was obtained from **1a** (484 mg). NMR (δ, CCl_4): 2.10 (s, 6H) and 6.85 (s, 10H).

cis-*3,4-Di*-p-*methoxyphenyl-3-hexene (2c).* The heating of **1c** (660 mg, 2 mmol), ethyl orthoformate (300 mg), and benzoic acid (50 mg) at 170 °C for 1 hr and a subsequent work-up gave **2c** (510 mg); bp 190 °C (bath temperature)/4 mmHg. NMR (δ, CCl_4): 0.90 (t, 6H), 2.44 (q, 4H), 3.52 (s, 6H), 6.40 (d, J=8.4 Hz, 4H), and 6.68 (d, J=8.4 Hz, 4H). Mass spectrum: *m/e* 296 (M^+, 100%).

trans-*3,4-Di*-p-*methoxyphenyl-3-hexene (2d).* An isomer mixture of the **1c** and **1d** pinacols obtained by the redcution[6] of *p*-methoxypropiophenone (2.80 g, 17 mmol) was heated at

1) D. J. Faulkner, *Synthesis*, 175 (1971); J Reucroft and P. E. Sammes, *Quart. Rev.* (London), **25**, 135 (1971).

2) Sharpless and Flood have reported recently direct deoxygenation of vicinal diols using tungsten (IV): I. B. Sharpless and T. C. Flood, *Chem. Commun.*, **1972**, 370. The reaction proceeds with poor stereospecificity.

3) E. J. Corey, F. A. Carey, and R. A. E. Winter, *J. Amer. Chem Soc.*, **87**, 934 (1965); E. J. Corey and J. I. Shulman, *Tetrahedron Lett.*, **1968**, 3655.

4) J. N. Hines, M. J. Peagram, G. H. Whitham, and M. Wright, *Chem. Commun.*, **1968**, 1593.

5) J. S. Josan and F. W. Eastwood, *Aust. J. Chem.*, **21**, 2013 (1968); G. Crank and F. W. Eastwood, *ibid.*, **17**, 1392 (1964). See also, F. W. Eastwood, K. J. Harrington, J. S. Josan, and J. L. Pura, *Tetrahedron Lett.*, **1970**, 5223.

6) K. Sisido and H. Nozaki, *J. Amer. Chem. Soc.*, **70**, 776 (1948).

7) The glycol **1h** (mp 130—131 °C) was obtained by sodium borohydride reduction of sebacoin. Cf. ref 11).

8) All temperatures are uncorrected. Infrared spectra were taken on a Shimadzu IR-27G, NMR spectra on a JEOL C-60H, mass spectra on a Hitachi RMU-6L. Benzoic acid used was recrystallized from benzene. Commercial orthoformates were distilled before use.

9) J. K. Cline, E. Campaingne, and J. W. Spies, *J. Amer. Chem. Soc.*, **66**, 1136 (1944).

170—180 °C for 2 hr with ethyl orthoformate (4 ml) and benzoic acid (0.5 g). The addition of *n*-hexane precipitated unchanged **1c** (230 mg). The concentration of the filtrate and the recrystallization of the residue (1.8 g) gave **2d** (640 mg); mp 118—120 °C (lit,[6] 124 °C). The mother liquor was concentrated (*ca.* 1.0 g), and dissolved in chloroform (10 ml) and iodine (0.5 g). The solution was then heated under reflux for 3.5 hr, washed thoroughly with aqueous sodium bisulfite and then with water and dried (sodium sulfate). The subsequent concentration of the solution, followed by the recrystallization of the residue, gave additional **2d** (420 mg). A total of 1.06 g of **2d** was obtained. NMR (δ, CCl_4): 0.75 (t, 6H), 2.09 (q, 4H), 3.74 (s, 6H), 6.72 (d, J=8.4 Hz, 4H), and 6.98 (d, J=8.4 Hz, 4H). Mass spectrum: *m/e* 296 (M^+, 100%).

trans-p,p'-*Dimethoxystilbene (**2f**)*. The heating of hydroanisoin (**1e**) (822 mg, 3 mmol) with ethyl orthoformate (900 mg) for 1 hr at 170—180 °C, followed by the evaporation of the excess orthoformate and ethanol *in vacuo*, gave an oil (**2e**) (1.2 g). This oil was heated with iodine (0.50 g) in chloroform (10 ml) under reflux for 3 hr. Work-up and recrystallization (*n*-hexane–acetone) afforded colorless needles (260 mg); mp 216—218 °C (lit,[10] 214—215 °C).

trans-*Cyclooctene (**2g**)*. *trans*-Cyclooctane-1,2-diol (**1g**) (385 mg, 2.7 mmol), methyl orthoformate (0.5 ml), and benzoic acid (20 mg) were heated at 90—100 °C for 2 hr. The methanol and excess orthoformate were then evaporated under reduced pressure. Benzoic acid (50 mg) was added, and the mixture was heated at 160—170 °C. The olefin thus produced was distilled as were carbon dioxide and methanol. The distillate was placed in dichloromethane, washed with aqueous sodium bicarbonate, and dried (sodium sulfate). Concentration gave crude **2g** quantitatively. Distillation at 90—100 °C (bath temperature)/95 mmHg gave **2g** (155 mg). IR (neat): 3020, 1650, and 982 cm^{-1}. Gas-chromatographic analysis (High Vacuum Silicone Grease, 10%, on Celite 545, 2 m, 60 °C) showed a single peak.

cis-*Cyclodecene (**2h**)*. *cis*-Cyclodecane-1,2-diol (**1h**) (860 mg, 5 mmol), methyl orthoformate (1.0 ml), and benzoic acid (50 mg) were heated at 90—100 °C for 2 hr. After concentration *in vacuo*, benzoic acid (100 mg) was added and the mixture was heated at 160—170 °C for 1 hr. Work-up gave **2h** (465 mg); bp 120—130 °C (bath temperature)/106 mmHg. IR (neat)[11]: 706 cm^{-1}.

Financial support from the Ministry of Education, Japanese Government is acknowledged with pleasure.

10) P. Hoerings and K. P. Gralert, *Ber.*, **42**, 1204 (1909).

11) A. T. Blomquist, R. E. Burge, Jr., and A. C. Sucsy, *J. Amer. Chem. Soc.*, **74**, 3636 (1952).

BULLETIN OF THE CHEMICAL SOCIETY OF JAPAN, VOL. 46, 2249—2251 (1973)

The Catalytic Decomposition of 9-Diazofluorene by Metal Carboxylates

Tamio SHIRAFUJI, Katuzi KITATANI, and Hitosi NOZAKI

Department of Industrial Chemistry, Kyoto University, Yoshida, Sakyo-ku, Kyoto 606

(Received December 14, 1972)

We have found that Cu(II) carboxylates in aq DMF catalyze the decomposition of 9-diazofluorene (I), thus affording fluorenone pinacol diesters (II) in addition to bifluorenylidene (III). The reaction is, therefore, analogous to that of diphenyldiazomethane recorded previously.[1] Though fluorenone pinacol diacetate may alternatively be obtained by treating fluorenone (IV) with zinc and acetyl chloride,[2] the present reaction does furnish a practical, simple method for preparing this class of esters, II.

$$(RCO_2)_2Cu(II) + Ar_2CN_2 \longrightarrow$$
$$\underset{I}{}$$
$$\underset{RCOO\ \ OCOR}{\overset{Ar_2C-CAr_2}{|\quad\ |}} + Ar_2C{=}CAr_2 + Ar_2C{=}O + Ar_2C{=}N\rangle_2$$
$$\underset{II}{}\qquad\qquad\underset{III}{}\qquad\underset{IV}{}\qquad\underset{V}{}$$

Ar_2=2,2′-biphenylene

Table 1 summarizes the reactions of I with Cu(II) carboxylates in aq. DMF to give II, III, and IV. Diacetate IIa was identified by means of the spectral and analytical data, and by the thermal decomposition,[3] which afforded IV and fluorenyl acetate (VI) at 170°C. In contrast to Cu(II) carboxylates such as acetate, propionate, and *n*-butyrate, the Cu(II) isobutyrate afforded IId in an inferior yield, whereas the Cu(II) tartrate gave no pinacol diester, II, but mainly III, along with fluorenone azine (V). Such a difference between Cu(II) carboxylates and the chelate salt may be attributed to the mobility of ligands around the central Cu(II) ion toward the newly-attached fluorenylidene moiety. Chelate ligands are tightly bound to the central metal ion and should be less accessible than simple carboxylate anions.

TABLE 1. REACTIONS OF I WITH Cu(II) CARBOXYLATES IN aq DMF

Cu(II) cabroxylate	Reaction		Products (yield in %)[a]			
	temp (°C)	time (hr)	II	III	IV	V
a Acetate	40	18	55	24	15	—
b Propionate	40	19	47	17	18	—
c *n*-Butyrate	40	20	51	16	23	—
d Isobutyrate	40	17	36	36	19	—
e Tartrate	40	6	—	85	—	12

a) Recovery was not considered in calculation of yields.

1) T. Shirafuji, Y. Yamamoto, and H. Nozaki, *Tetrahedron*, **27**, 5353 (1971).
2) C. Gräbe and H. Stindt, *Ann. Chem.*, **291**, 1 (1896).
3) For a similar decomposition of benzopinacol diesters, see Ref. 4.
4) T. Shirafuji, Y. Yamamoto, and H. Nozaki, This Bulletin, **45**, 2574 (1972).

$$\text{Metal acetate} + \underset{\text{I}}{Ar_2CN_2} \longrightarrow \underset{\text{VI}}{Ar_2CHOAc} + \underset{\text{IIa}}{\begin{matrix} Ar_2C-CAr_2 \\ | \quad | \\ AcO \quad OAc \end{matrix}} + \underset{\text{VII}}{Ar_2C(OAc)_2}$$

Ar_2=2,2′-biphenylene

Table 2. Oxidation of I with various metal acetates

Metal acetate	Reduction potential in water (eV)[a]	Reaction		Solvent	Products (Yield in %)[b]			
		°C	hr		VI	IIa	VII	IV
$Cr(III)(OAc)_3$	−0.41	60	23	aq DMF	9	—	—	55
$Cu(II)(OAc)_2$	+0.15	40	18	aq DMF	—	55	—	15[c]
$Tl(III)(OAc)_3$	+1.21	25	19	CH_2Cl_2	—	—	42	56
$Pb(IV)(OAc)_4$	+1.69	25	25	CH_2Cl_2	—	—	61	30

a) These data were taken from N. A. Lange, "Handbook of Chemistry" 10th ed. McGraw-Hill (1961), p. 1212.
b) Recovery was not considered in calculation of yields. c) A 24% yield of III was obtained.

Being interested in oxidation reactions brought about by metal ions,[5] we then investigated the decomposition of I by means of various other metal acetates, as is shown in Table 2. The Cr(III) acetate catalyzed the decomposition of I to afford VI in a low yield, while the Tl(III) or Pb(IV) acetate gave fluorenone diacetate (VII) as the major product.[6] This behavior is parallel to that of diphenyldiazomethane with the metal acetates.[1]

Experimental

All the melting points are uncorrected. The NMR spectra were obtained on a 60 MHz instrument (JEOL C-60-H spectrometer) in $CDCl_3$ unless otherwise stated. The chemical shifts are given in ppm from the TMS internal standard, and the abbreviations of s, d, t, q, and m are used with their common meanings.

The mass spectra were obtained on a Hitachi RMU 6L spectrometer. The microanalyses were performed by Mrs. K. Fujimoto.

General Procedure of the Catalytic Decomposition of 9-Diazofluorene (I) with Metal Salts. Under N_2, metal salts were dissolved in aq DMF (1:1) or methylene chloride so as to give a *ca.* 0.3 M solution; this solution was then kept at an appropriate reaction temperature (25—60 °C) with stirring. To this we then added, drop by drop, a solution (*ca.* 0.5 M) of I in the same solvent. The molar ratio of diazo compound/metal salt was taken to be 1:1 unless otherwise stated. Heating and stirring were continued until the evolution of N_2 had ceased. The mixture was then worked up as usual. The crude products were separated by glc, recrystallization, or column chromatography, and then identified. The following descriptions will be concerned with cases which are not covered sufficiently by Tables 1 and 2.

Preparation of Fluorenone Pinacol Diesters (II). The diazo compound I was treated with solutions of Cu(II) carboxylates in aq DMF. The chromatography of the reaction mixture on a short silica gel column (benzene elution) gave bifluorenylidene,[7] II, and fluorenone. The spectral

Table 3. Physical properties of II

Compd II R	Mp °C [a]	IR (cm^{-1}) [b]	NMR (δ ppm)
Me[c]	252 (decomp)	1742, 1363, 1291, 1225, 1197, 1073, 1023, 976, 950	7.70—6.67(m, 16H, aromatic), 2.13 (s, 6H, –OAc)
Et[d]	244 (decomp)	1735, 1267, 1210, 1191, 1060, 1008, 990, 931	7.51—6.55 (m, 16H, aromatic),2.45 (q, 4H, $-C\underline{H}_2Me$), 1.10 (t, 6H, $-C\underline{H}_3$)
n-Pr[e]	169 (decomp)	1740, 1248, 1202, 1157, 1070, 1010, 970, 940	7.50—6.65 (m, 16H, aromatic), 2.43 (t, 4H, $-C\underline{H}_2Et$), 1.17 (m, 4H, $-C\underline{H}_2Me$), 0.95 (t, 6H,$-C\underline{H}_3$)
iso-Pr[f]	210—211 (decomp)	1743, 1254, 1210, 1186, 1142, 1109, 1050, 963	7.45—6.65 (m, 16H, aromatic), 2.78 (m, 2H, methines), 1.21 (d, 12H, methyls)

a) Recrystallized from benzene–ethanol (1:1).
b) KBr disk unless otherwise stated.
c) Found: C, 80.6;H, 4.9%. Calcd for $C_{30}H_{22}O_4$: C, 80.7; H, 5.0%. Mass *m/e* (relative abundance): 344 (70), 328 (40), 180 (100).
d) Found: C, 81.1; H, 5.6%. Calcd for $C_{32}H_{26}O_4$: C, 81.0; H, 5.5%. Mass *m/e* (relative abundance): 344 (7), 328 (4), 180 (4), 29 (100).
e) Found: C, 81.4; H, 5.9%. Calcd for $C_{34}H_{30}O_4$: C, 81.3; H, 6.0%. Mass *m/e* (relative abundance): 344 (60), 328 (30), 180 (21), 43 (100).
f) Found: C, 81.2; H, 5.8%. Calcd for $C_{34}H_{30}O_4$: C, 81.3; H, 6.0%. Mass *m/e* (relative abundance): 344 (26), 328 (26), 180 (21), 43 (100).

5) a) T. Shirafuji, Y. Yamamoto, and H. Nozaki, *Tetrahedron Lett.*, **1971**, 4713; b) C. L. Jenkins and J. K. Kochi, *J. Amer. Chem. Soc.*, **94**, 843, 856 (1972).

6) A. Stojiljković, N. Orbović, S. Sredojević, and M. Lj. Mihailović, *Tetrahedron.* **26**, 1101 (1970).

7) R. J. S. Jennings and A. Fowler-Williams, *J. Appl. Chem.* (London), **3**, 426 (1953).

and analytical data of II are shown in Table 3.

Reaction of I with Tl(III) Acetate. I (370 mg, 1.94 mmol) was treated with Tl(III) acetate (1530 mg, 4.0 mmol) in methylene chloride (20 ml) at room temperature for 19 hr. After filtration, the reaction mixture was concentrated *in vacuo*. The products were recrystallized from carbon tetrachloride to give fluorenone diacetate (230 mg, 42%); mp 138—140 °C. IR (Nujol): 1740, 1200, 999 cm^{-1}. NMR (CCl_4, 10%): δ 7.80—7.20 (m, 8H, aromatic) and 2.20 (s, 6H, –OAc). Mass spectrum (relative abundance): *m/e* 180 (100), 152 (36), 105 (15), 76 (20), 43 (84).

Found: C, 72.1; H, 5.0%. Calcd for $C_{17}H_{14}O_4$: C, 72.3; H, 5.0%.

The subsequent concentration of the filtrate gave fluorenone (200 mg, 56%).

Financial support from the Ministry of Education, Japanese Government, and from Toray Science Foundation is acknowledged with pleasure.

BULLETIN OF THE CHEMICAL SOCIETY OF JAPAN, VOL. 46, 2251—2252 (1973)

The Carbonylation of Furan and Thiophene Mercuric Compounds with Palladium Salt

Taeko IZUMI, Toshio IINO, and Akira KASAHARA

Department of Applied Chemistry, Faculty of Engineering, Yamagata University, Yonezawa, Yamagata 992

(Received January 12, 1973)

Heck[1] has reported that diarylketones were formed in moderate yields from arylmercuric salts and carbon monoxide with a transition-metal-salt catalyst. Furthermore, we have ourselves described the carbonylation of 1,1′-bis(chloromercuri)-ferrocene in the presence of a palladium salt.[2] In this report, we wish to report on the carbonylation reactions of chloromercuri-derivatives of furan and thiophene in methanol with a palladium salt.

The carbonylation of 2-chloromercurifuran (I–1) was carried out at 100 °C under a carbon monoxide pressure of 50 atm in the presence of lithium chloropalladite in methanol; the main products were 2,2′-difurylketone (II–1) and methyl furoate (III–1), plus a small amount of 2,2′-bifuryl (IV–1). The carbonylations of 5-methoxycarbonyl-2-chloromercurifuran (I–2) and 2-chloromercurithiophene (I–3) were performed under the same conditions. The mechanism of the formation of II–1 from I–1, as has been pointed out by Heck,[1] probably involves the reaction of an acylpalladium compound with a furylpalladium compound or I–1. III–1 and IV–1 are probably formed by side reactions.

$$ArHgCl + Li_2PdCl_4 \longrightarrow (ArPdCl) + HgCl_2 + 2LiCl$$

$$(ArPdCl) + CO \longrightarrow (ArCOPdCl)$$

$$(ArCOPdCl) + (ArPdCl) \longrightarrow ArCOAr + PdCl_2 + Pd$$

or

$$(ArCOPdCl) + ArHgCl \longrightarrow ArCOAr + HgCl_2 + Pd$$

$$2(ArPdCl) \longrightarrow Ar\text{-}Ar + PdCl_2 + Pd$$

or

$$(ArPdCl) + ArHgCl \longrightarrow Ar\text{-}Ar + HgCl_2 + Pd$$

$$(ArCOPdCl) \longrightarrow ArCOCl + Pd$$

$$ArCOCl + CH_3OH \longrightarrow ArCOOCH_3 + HCl$$

[Ar = furyl]

On the other hand, the carbonylation of 2,5-dichloromercurifuran (V–1) under the same conditions gave a mixture of 5,5′-dimethoxycarbonyl-2,2′-difurylketone (II–2), 2,5-dimethoxycarbonylfuran (III–2), and the keto-ester polymer (VIII). The structure of VIII was identified by means of the measurement of the molecular weight and by means of the spectral data. In the IR spectrum, very intensive absorption bands at 1735 cm^{-1} due to ester streching, at 1630 cm^{-1} due to carbonyl streching, and at 880 cm^{-1} due to the furan ring were observed. However, the carbonylation of 2,5-dichloromercurithiophene (V–2) yielded a mixture of 5,5′-dimethoxycarbonyl-2,2′-dithienylketone (VI) and 2,5-dimethoxycarbonylthiophene (VII).

Experimental

All the melting and boiling points are uncorrected. The IR spectra were recorded on a Hitachi 215 spectrometer, while the NMR spectra were obtained in $CDCl_3$ at 90 MHz with a Hitachi R-22 NMR spectrometer, using TMS as the internal standard.

Materials. The 2-chloromercurifuran (I-1) and 2,5-dichloromercurifuran (V-1) were synthesized by the method of Gilman *et al.*[3] The 2-chloromercurithiophene (I-3) and 2,5-dichloromercurithiophene (V-2) were prepared by the method of Cherbuliez and Giggey.[4]

The 5-methoxycarbonyl-2-chloromercurifuran (I-2) was synthesized from methyl furoate, mercuric chloride, and sodium acetate by a modification of the method of Gilman and Wright[3] Mp 243—245 °C. Yield, 60%. Found: C, 19.69; H, 1.15%. Calcd for $C_6H_5O_3HgCl$: C, 19.95; H, 1.36%.

General Procedure for The Carbonylation of Chloromercuric Compounds. A lithium chloropalladite solution was prepared by stirring 0.84 g (20 mmol) of lithium chloride with 1.77g

1) R. F. Heck, *J. Amer. Chem. Soc.*, **90**, 5546 (1968).
2) A. Kasahara, T. Izumi, and S. Ohnishi, This Bulletin, **45**, 951 (1972).
3) H. Gilman and G. F. Wright, *J. Amer. Chem. Soc.*, **55**, 3302 (1933).
4) E. Cherbuliez and C. Giggey, *Helv. Chim. Acta*, **35**, 160 (1952).

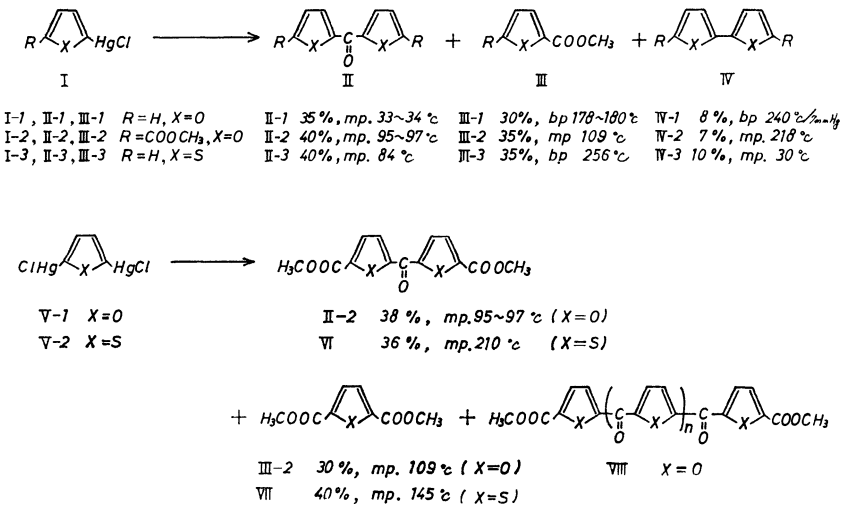

Fig. 1.

(10 mmol) of anhydrous palladium chloride overnight at room temperature in 100 ml of methanol. Into this solution, chloromercuric compound in an equivalent amount was then carbonylated at 100 °C under a carbon monoxide pressure (50 atm) for 6 hr with shaking. The reaction mixture was filtered to remove precipitated palladium, and the solvent was distilled under reduced pressure. The residue was dissolved in benzene and then purified by column chromatography on neutral alumina, or separated by preparative gas chromatography (Hitachi K-53 gas chromatograph, SE-30 column). The structures of the products were confirmed by an observation of the IR and NMR spectra and by comparing the retention time with those of authentic samples. The following results were obtained.

a) The carbonylation of I-1 afforded 2,2′-difurylketone (II-1) (35%, mp 33—34 °C (lit,[5] 33—34 °C)), methyl furoate (III-1) (30%, bp 178—180 °C (lit,[6] 181 °C)), and 2,2′-bifuryl (IV-1) (8%, bp 240 °C/7 mmHg (lit,[7] 240—245 °C/7 mmHg)).

b) The carbonylation of I-2 afforded 5,5′-dimethoxycarbonyl-2,2′-difurylketone (II-2) (40%, mp 95—97 °C, IR 1735, 1640, 880 cm^{-1}, NMR δ 3.88 (s, 6, $-COOCH_3$), 7.15 (d, 2, H on C_3 and $C_{3'}$), 7.34 (d, 2, H on C_4 and $C_{4'}$). Found: C, 56.05; H, 3.53%. Calcd for $C_{13}H_{10}O_7$: C, 56.12; H, 3.62%). 2,5-Dimethoxycarbonylfuran (III-2) (35%, mp 109 °C (lit,[8] 111—112 °C)), and 5,5′-dimethoxycarbonyl-2,2′-bifuryl (IV-2) (7%, mp 218 °C, IR 1728, 878 cm^{-1}, NMR δ 3.89 (s, 6, $-COOCH_3$), 6.87 (d, 2, H on C_3 and $C_{3'}$), 7.22 (d, 2, H on C_4 and $C_{4'}$). Found: C, 57.51; H, 3.96%. Calcd for $C_{12}H_{10}O_6$: C, 57.60; H, 4.03%).

c) The carbonylation of I-3 afforded 2,2′-dithienylketone (II-3) (40%, mp 84 °C (lit,[9] 87—88 °C)), 2-methoxycarbonylthiophene (III-3) (35%, bp 256 °C (lit,[10] 117 °C/30 mmHg)), and 2,2′-bithienyl (IV-3) (10%, mp 30 °C(lit,[11] 33 °C)).

d) The carbonylation of V-1 afforded II-2 (38%), III-2 (30%), and the ketoester polymer (VIII) 7%, IR 1735 (C=O, ester), 1630 (C=O, ketone), 880 (furan ring), mol wt 1212 (in benzene)).

e) The carbonylation of V-2 afforded 5,5′-dimethoxycarbonyl-2,2′-dithienylketone (VI) (36%, mp 210 °C, IR 1710, 1610, 700 cm^{-1}, NMR δ 3.91 (s, 6, $-COOCH_3$), 7.23 (d, 2, H on C_3 and $C_{3'}$), 7.44 (d, 2, H on C_4 and $C_{4'}$), Found: C, 50.25; H, 3.07%; Calcd for $C_{13}H_{10}O_5S_2$: C, 50.33; H, 3.25%), and 2,5-dimethoxycarbonylthiophene (VII), (40%, mp 145 °C (lit,[12] 148—149 °C)).

5) T. Reichstein, *Helv. Chim. Acta*, **13**, 356 (1930).
6) C. C. Price, E. C. Chapin, A. Goldman, E. Krebs, and H. M. Shafer, *J. Amer. Chem. Soc.*, **63**, 1857 (1941).
7) T. Reichstein, A Grussner, and H. Zschokke, *Helv. Chim. Acta*, **15**, 1066 (1932).
8) E. Votocek and S. Malachta, *Coll. Czechoslov. Chem. Commun.* **6**, 241 (1934).
9) V. Thomas and V. Couderc, *Bull. Soc. Chim. Fr.*, [4] **23**, 280 (1918).
10) O. Twilli and M. Gandino, *Ann. Chim.* (Rome), **53**, 1687 (1963).
11) A. Tohl, *Ber.*, **27**, 665 (1894).
12) J. M. Griffing and L. F. Salislury *J. Amer. Chem. Soc.*, **70**, 3416 (1948).

BULLETIN OF THE CHEMICAL SOCIETY OF JAPAN, VOL. 46, 2253—2254 (1973)

Photochemical Reactions of Some Thiocarbonyl Trimers

Takehiko NISHIO, Michikazu YOSHIOKA, Hiromu AOYAMA, and Noboru SUGIYAMA

Department of Chemistry, Tokyo Kyoiku University, Otsuka, Tokyo 112

(Received May 24, 1972)

Although the photochemical reactions of diaryl thiocarbonyls have been extensively studied,[1] those of dialkyl or alkyl-aryl thiocarbonyls have not yet been given attention. Generally, monomeric dialkyl or alkyl-aryl thiocarbonyls are unstable and readily trimerize at room temperature. Previously, we reported the photochemical formation of a monomeric thiocarbonyl from the corresponding trimer.[2] In this paper we want to report that the irradiation of some thiocarbonyl trimers give a thiophene, a dithietane, and/or a disulfide.

When the thioacetophenone trimer (**1**) in cyclohexane was irradiated, the solutlon turned blue (λ_{max} 575 nm),[3] showing the formation of thioacetophenone (**7**). After irradiation for 2 hr, the product was treated with cyclopentadiene to give an 1:1-adduct (**8**) of **7** and cyclopentadiene. The NMR spectrum of **8** showed two singlets, at τ 8.49 and 8.39 and in a ratio of 1.9:1.1, assignable to methyl protons at C-3. The product, **8**, was therefore considered to be a mixture of *endo*- and *exo*-isomers. The prolonged irradiation (24 hr) of **1** gave 2,4-diphenylthiophene (**9**) (15%), 9,10-dimethylphenanthrene (**10**) (8%), and an unidentified product (**11**) (3.75%), which was then converted into **9** by distillation (175—178 °C/2 mmHg). The structure of **9** was established on the basis of the results of elemental analysis and the spectral data by comparison with an authentic sample.[4] The formation of **10** seems to proceed through the cyclization of dimethylstilbene,[5] which is photochemically derived from **7**, whlie thiobenzophenone gives tetraphenylethylene on irradiation.[1a]

The irradiation of the thiobenzaldehyde trimer (**2**) in dioxane gave *cis*-stilbene (**12**), *trans*-stilbene (**13**) (combined yield, 3.5%), and phenanthrene (**14**) (3.5%). Compounds **12** and **13** may be derived from a thiobenzaldehyde monomer like **1** and are presumed to be precursors of **14**.[5]

The irradiation of the cyclohexanethione trimer (**3**) in cyclohexane yielded 7,14-dithiadispiro[5.1.5.1]-tetradecane (**15**) (20%) and dicyclohexyl disulfide (**16**)

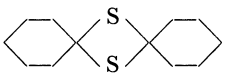

(**15**)

(10%). The formation of **15** is presumed to proceed through the dimerization of cyclohexanethione, formed from **3** by light, because on irradiation the solution of **3** immediately turns pink (λ_{max} 504 nm),[6] showing the formation of cyclohexanethione. On the other hand, Compound **16** probably arises from **15**, since Berchtold *et al.*[7] reported that the photolysis of 1,4-dithiaspiro[4.5]decane afforded **15** and was followed by the formation of **16**.

The irradiation of the thioacetone trimer (**4**) in cyclohexane yielded 2,2,4,4-tetramethyl-1,3-dithietane (**17**) (35%) and diisopropyl disulfide (**18**) (21%). These photoproducts undoubtedly arise from the thioacetone monomer, which may be formed by an initial C–S bond cleavage of **4**.

The irradiation of other thiocarbonyl trimers (**5**) and (**6**) gave the corresponding disulfides, (**19**) (15%) and (**20**) (20%) respectively. The disulfide **20** was confirmed by unequivocal synthesis from benzylacetone.

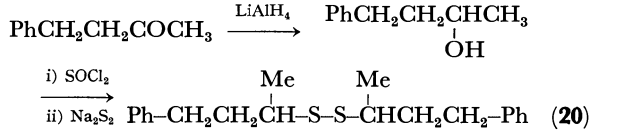

(**20**)

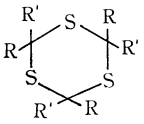

1 R=Ph R′=Me **4** R=R′=Me
2 R=Ph R′=H **5** R=PhCH$_2$ R′=H
3 R=R′=–(CH$_2$)$_5$– **6** R=PhCH$_2$CH$_2$ R′=Me

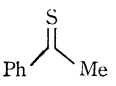

7

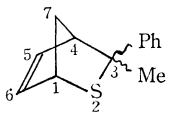

8

Experimental

Materials. The thiocarbonyl trimers, **1**, **2**, **4**, and **5**, were prepared according to previouly-proposed procedures.[8-11] **3** was synthesized by modifying the method of Baumann;[8] mp 99—100 °C (lit,[12] 102 °C).

2,4,6-Triphenethyl-2,4,6-trimethyl-1,3,5-trithiane (6). Dry HCl was bubbled through a solution of 25 g of benzylacetone in 250 ml of ethanol with stirring below 0 °C for

1) a) Y. Omote, M. Yoshioka, K. Yamada, and N. Sugiyama, *J. Org. Chem.*, **32**, 3676 (1967). b) K. Yamada, M. Yoshioka, and N. Sugiyama, *ibid.*, **33**, 1240 (1968). c) G. Oster, L. Citarel, and M. Goodman, *J. Amer. Chem. Soc.*, **84**, 703 (1962). d) A. Ohno, Y. Ohnishi, and G. Tsuchihashi, *ibid.*, **91**, 5083 (1969). e) G. Tsuchihashi, M. Yamauchi, and M. Fukuyama, *Tetrahedron*, **23**, 1971 (1967). f) A. Schonberg, and A. Mustafa, *J. Chem. Soc.*, **1943**, 275.

2) N. Sugiyama, M. Yoshioka, H. Aoyama, and T. Nishio, *Chem. Comm.*, **1971**, 1603.

3) R. Mayer, J. Morgenstein, and J. Fabian, *Angew. Chem.*, **76**, 157 (1964).

4) T. K. Hauson, and L. M. Kinnard, *Brit.* 696439 (1953).

5) N. J. Turro, "Molecular Photochemistry," W. A. Benjamin, Inc., New York, (1967), p. 233.

6) M. J. Jansen, *Rec. Trav. Chim. Pay-Bas.*, **79**, 464 (1960).

7) J. D. Willet, J. R. Grandwell, and G. A. Berchtold, *J. Org. Chem.*, **33**, 2297 (1968).

8) E. Baumann and E. Fromm, *Ber.*, **28**, 895 (1895).

9) E. Baumann and E. Fromm, *ibid.*, **24**, 1436 (1891).

10) I. B. Douglass and W. R. Hydro, *J. Amer. Chem. Soc.*, **73**, 3507 (1951).

11) H. Bohne, H. Pfeifer, and E. Schneider, *Ber.*, **75**, 900 (1942).

12) J. Jentzsch, J. Fabian, and R. Mayer, *Chem. Ber.*, **95**, 1764 (1962).

30 min. Then H_2S was passed through until precipitation formation came to the end. The precipitates were collected by filtration and were recrystallized from acetone to give 10 g of **6**; mp 130—131 °C. IR: ν_{max}^{KBr} cm^{-1}, 3020, 1600, 1490, 1365, 753, 730, 700. NMR: (τ in $CDCl_3$) 8.17 (s, 9H, 3×Me), 7.86—6.92 (A_2B_2 m, 12H, 6×CH_2), 3.10—2.63 (m, 15H, 3×Ph). Found: C, 73.25; H, 7.51%. Calcd for $C_{30}H_{36}S_3$: C, 73.14; H, 7.37%.

Irradiation of **1**. (a) When a solution of 1 g of **1** in 150 ml of cyclohexane was irradiated with a low-pressure mercury lamp in a quartz tube under nitrogen, the blue color of **7** gradually appeared with time. After irradiation for 2 hr, 1 g of cyclopentadiene was added to the reaction mixture and it was stirred until the blue color disappeared at room temperature. After the removal of the solvent, the residue was chromatographed on a silica-gel column. Elution with *n*-hexane–benzene(9: 1) gave 100 mg of 3-phenyl-3-methyl-2-thianorbornene (**8**); IR: ν_{max}^{film} cm^{-1}, 3050, 1598, 1575, 1490, 765, 748, 702. NMR: (τ in $CDCl_3$) 8.49 (s, 1.9H, *endo*-Me) and 8.39 (s, 1.1H, *exo*-Me), 8.11 (m, 2H, CH_2), 6.63 and 6.03 (m, 2H, 2×CH), 3.90 and 3.68 (m, 2H, vinyl), 3.05—2.2 (m, 5H, Ph). Found: C, 77.24; H, 6.60%. Calcd for $C_{13}H_{14}S$: C, 77.20; H, 6.98%.

(b) A solution of 1 g of **1** in 150 ml of cyclohexane was irradiated for 24 hr. After the removal of the solvent, the residue was chromatographed on a silica gel column with *n*-hexane–benzene (19: 1) to give 150 mg of **9**, 80 mg of **10**, and 37.5 mg of **11**.

(i) 2,4-Diphenylthiophene (**9**); mp 118.5—120.5 °C (lit,[13] 121.0—121.5 °C). UV: $\lambda_{max}^{cyclohexane}$ nm (ε), 223.5 (sh. 19900), 256 (54200), 301 (sh. 11400).

(ii) 9,10-Dimethylphenanthrene (**10**); mp 138—139 °C (lit,[14] 139 °C). NMR: (τ in $CDCl_3$) 8.30 (s, 6H, 2×Me), 2.58—2.30 (m, 4H, aromatic), 2.06—1.78 (m, 2H, aromatic), 1.48—1.20 (m, 2H, aromatic).

Irradiation of **2**. A solution of 1 g of **2** in 150 ml of dioxane was irradiated for 15 hr. After the removal of the solvent, the residue was chromatographed on a silica gel column with *n*-hexane–benzene (9: 1) to give 15 mg of **12**, 20 mg of **13**, and 35 mg of **14**. Each product was identified with the corresponding authentic sample by comparing the spectral data.

Irradiation of **3**. A solution of 1 g of **3** in 150 ml of cyclohexane was irradiated for 15 hr. After the removal of the solvent, the residue was chromatographed on a silica gel column with *n*-hexane–benzene (9: 1) to give 200 mg of **15**, 100 mg of **16**, and 150 mg of unchanged **3**.

(i) 7,14-Dithiadispiro[5.1.5.1]tetradecane (**15**); Recrystallizations from *n*-hexane afforded prisms; mp 131—132 °C (lit,[15] 132—133 °C). NMR: (τ in $CDCl_3$) 9.0—8.18 (m, 12H, 6×CH_2), 8.18—7.62 (m, 8H, 4×CH_2). Mass spectrum: *m/e*, 228 (M^+), 114 ($M-C_6H_{10}S$) and 81.

(ii) Dicyclohexyl disulfide (**16**); bp 125—128 °C/4—5 mmHg (lit,[7,17] 98 °C/2 mmHg, 100 °C/0.01 mmHg). NMR: (τ in $CDCl_3$) 9.40—7.40 (m, 20H, 10×CH_2), 7.30 (br s, 2H, 2×CH). Mass spectrum: *m/e*, 230 (M^+), 148 ($M-C_6H_{10}$), 115 ($M-C_6H_{11}S$) and 83.

Irradiation of **4**. A solution of 1 g of **4** in 150 ml of cyclohexane was irradiated for 20 hr. After the removal of the solvent, the residue was chromatographed on a silica gel column with *n*-hexane–benzene (9: 1) to give 350 mg of **17** and 210 mg of **18**.

(i) 2,2,4,4-Tetramethyl-1,3-dithietane (**17**). Recrystallization from *n*-hexane afforded needles; mp 77—78 °C (lit,[16] 77—77.5 °C). UV: $\lambda_{max}^{cyclohexane}$ nm (ε), 233.5 (180), 303.5 (20). Mass spectrum: *m/e*, 148 (M^+), 74 ($M-C_3H_6S$) and 59.

(ii) Diisopropyl disulfide (**18**); bp 72—75 °C/20 mmHg (lit,[17] 70 °C/20 mmHg). IR: ν_{max}^{film} cm^{-1}, 1380, 1368. NMR: (τ in $CDCl_3$) 8.70 (d, 12H, 4×Me), 7.01 (sep, 2H, 2×CH). Mass spectrum: *m/e*, 150 (M^+), 107 ($M-C_3H_7$), 75 ($M-C_3H_7S$) and 59.

Irradiation of **5**. A solution of 1 g of **5** in 150 ml of tetrahydrofuran was irradiated for 20 hr. After the removal of the solvent, the residual oil was chromatographed on a silica gel column with *n*-hexane–benzene (4: 1) to give 150 mg of diphenethyl disulfide (**19**); bp 159—161 °C/4—5 mmHg (lit,[18] 150—155 °C/1 mmHg. NMR: (τ in $CDCl_3$) 7.05 (s, 8H, 4×CH_2), 2.77 (s, 10H, 2×Ph). Mass spectrum: *m/e*, 274 (M^+), 169 ($M-C_6H_5CH_2CH_2$), 137 ($M-C_6H_5CH_2CH_2S$), 105 ($M-C_6H_5CH_2CH_2SS$) and 91.

Irradiation of **6**. A solution of 1 g of **6** in 150 ml of cyclohexane was irradiated for 15 hr. After the removal of the solvent, the residual oil was chromatographed on a silica gel column with *n*-hexane–benzene (4: 1) to give 200 mg of (1,1′-dimethyl-3,3′-diphenyl)dipropyl disulfide (**20**); bp 185—187 °C/4—5 mmHg. IR: ν_{max}^{film} cm^{-1}, 3030, 2924, 2855, 1605, 1490, 1370, 750, 700. NMR: (τ in $CDCl_3$) 8.67 (d, 6H, 2×Me), 8.42—7.75 (m, 4H, 2×CH_2), 7.27 (t, 4H, 2×CH_2), 7.20 (m, 2H, 2×CH), 2.77 (s, 10H, 2×Ph). Mass spectrum: *m/e*, 330 (M^+), 197 ($M-C_6H_5CH_2CH_2C(Me)H$), 166 ($M-C_6H_5CH_2CH_2C(=S)Me$), 165 ($M-C_6H_5CH_2CH_2CH(Me)S$), 132 ($M-C_6H_5CH_2CH_2CH(Me)SSH$). Found: C, 72.08; H, 7.99%. Calcd for $C_{20}H_{26}S_2$: C, 72.67; H, 7.90%.

Synthesis of **20** *from Benzylacetone*. To a solution of 1 g of $LiAlH_4$ in 30 ml of ether, a solution of 5 g of benzylacetone in 30 ml of ether was added. The solution was refluxed for 20 hr, poured into ice water, and then extracted with ether. The extract was dried over anhydrous Na_2SO_4 and evaporated to leave 4-phenylbutan-2-ol (5 g). The crude alcohol (5 g) was dissolved in 30 ml of DMF, and then thionyl chloride (5 g) was stirred in drop by drop. The whole was stirred for 12 hr, poured into ice water, and extracted with ether. The extract was washed with water, dried (Na_2SO_4), and evaporated. The solution of the crude product (5 g) in 10 ml of alcohol was stirred into a solution of Na_2S_2 (from Na_2S–$9H_2O$ (5 g), S (0.6 g), and H_2O (5 ml)). The whole was then heated to 60 °C, stirred at that temperature for 7 hr, and extracted with *n*-hexane. The extract was then dried and evaporated. When the residual oil was chromatographed on a silica gel column with *n*-hexane–benzene (4: 1), it gave an oil which was subsequently distilled (bp 185—187 °C/4—5 mmHg) and found to be identical with the photoproduct (IR and NMR spectra and tlc) (2.5 g).

13) H. Wynberg, H. van Driel, R. M. Kellogg, and J. Buter, *J. Amer. Chem. Soc.*, **89**, 3487 (1967).

14) S. I. Heibron, "Dictionary of Organic Compounds," Eyre and Spottiswoode, London, Vol. I, (1953), p. 330.

15) A. R. Katritzky, R. Mayer, J. Morgenstein, and M. J. Sewell, *J. Chem. Soc.*, **1965**, 5953.

16) R. E. Kohrman and G. A. Berchtold, *J. Org. Chem.*, **36**, 3971 (1971).

17) K. J. Rosengren, *Acta Chem. Scand.*, **16**, 1401 (1962).

18) *Chem. Abstr.*, **52**, 4544a (1958).

BULLETIN OF THE CHEMICAL SOCIETY OF JAPAN, VOL. 46, 2255—2256 (1973)

Oxosulfonium Salts. II. Nitration of Dimethylphenyloxosulfonium Salt

Kenji KAMIYAMA, Hiroshi MINATO, and Michio KOBAYASHI

Department of Chemistry, Faculty of Science, Tokyo Metropolitan University, Fukazawa, Setagaya, Tokyo 158

(Received February 24, 1973)

The effects of the positively charged substituents of arenes on the rates and isomer distributions in electrophilic aromatic substitution have been studied by various investigators. In connection with the question whether or not the $p\pi$—$d\pi$ resonance exists between aromatic rings of aryl onium salts and the positively charged hetero atoms, electrophilic aromatic substitution of anilinium salts[2] and onium salts of some hetero atoms involving d-orbitals (P, Se, As, and S)[3] have recently been reported. In the substitution reaction of the aryl onium salts of selenium and sulfur the ortho and para substituted products were found in considerable yields, and the existence of $p\pi$—$d\pi$ resonance was proposed in these cases.[4-6]

Oxosulfonio groups, $-\overset{\oplus}{\underset{\underset{O}{\|}}{S}}R_2$, are expected to be more strongly electron-withdrawing than sulfonio groups, $-\overset{\oplus}{S}R_2$. Studies on aromatic substitution of $Ar\overset{\oplus}{\underset{\underset{O}{\|}}{S}}R$ would yield useful information on the presence or absence of resonance between the aromatic ring and the tetrahedral sulfur atom of an oxosulfonio group. Although alkyloxosulfonium salts are fairly reactive with nucleophilic agents and act as methylating agents of thiolate or hydroxide ions, they are very stable toward oxidizing agents and electrophiles. Therefore, it is possible to investigate the electrophilic substitution on oxosulfonio-arenes. However, the electrophilic substitution of aryl oxosulfonium salts has not been reported in the literature, because the preparation of aryl oxosulfonium salts is rather difficult.

In order to determine the electronic effect of oxosulfonio groups on electrophilic aromatic substitution, the nitration of dimethylphenyloxosulfonium salt has been investigated.

Results and Discussion

Product Study. Dimethylphenyloxosulfonium perchlorate (I) remained unchanged when it was heated in concd nitric acid at 70 °C. When a solution of I in a mixture of concd sulfuric acid and fuming nitric acid (*d*, 1.52) (*v*/*v* 2/1) was heated at 80 °C for 3 hr, dimethylnitrophenyloxosulfonium perchlorate (II) was obtained in 80—87% yield. When II was refluxed in a solution of sodium iodide in acetone and the sulfoxide (III) obtained was oxidized to the corresponding sulfone, only the *m*-nitro isomer was found. No *ortho* and *para* isomer were detected with a flame-ionization gas chromatography.

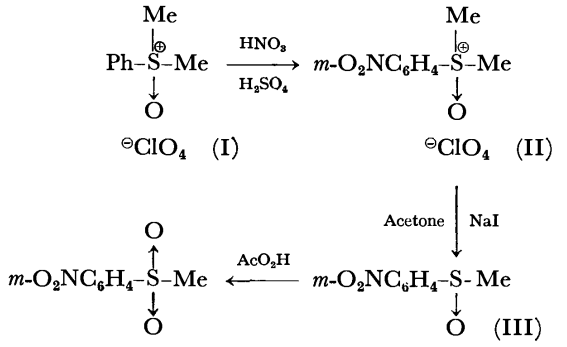

TABLE 1. ISOMER DISTRIBUTION IN THE NITRATION OF SOME AROMATICS POSSESSING POSITIVE POLES

Aromatics	Nitro-aromatics			Reference
	ortho%	*meta*%	*para*%	
$Ph\overset{\oplus}{N}Me_3$	0	89	11	7)
$Ph\overset{\oplus}{P}Me_3$	0	97	3	7)
$Ph\overset{\oplus}{As}Me_3$	0	96	4	7)
$Ph\overset{\oplus}{Se}Me_2$	2.6	91.3	6.1	4)
$Ph\overset{\oplus}{S}Me_2$	3.6	90.4	6.0	4)
	2.18	93.87	3.95	6)
$PhMe_2\overset{\oplus}{S}=O$	0	100	0	This work

The results are shown in Table 1 together with the data on nitration of other onium salts. The nitration of dimethylphenylsulfonium ion gave the *o*- and *p*-nitro derivatives in 5—10% yields, whereas that of dimethylphenyloxosulfonium ion gave no *o*- and *p*- derivatives.

The stretching frequencies of S–O of *p*-substituted phenyldimethyloxosulfonium ions were found to be proportional to the Hammett σ^+ values;[8] this finding suggests a 2p—3p resonance between the benzene ring and the S=O bond.

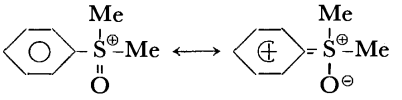

The fact that only *m*-nitro product was formed in nitration of I is ascribable to the inductive effect of the dimethyloxosulfonio group but also the resonance des-

1) Organic Sulfur Compounds. Part XXXVIII.

2) M. Brickman, J. M. P. Utley, and J. H. Ridd, *J. Chem. Soc.*, **1965**, 6851.

3) J. W. Baker and W. G. Moffitt, *ibid.*, **1930**, 1722.

4) H. M. Gilaw and G. L. Walker, *J. Org. Chem.*, **32**, 2580 (1967).

5) H. M. Gilaw, M. De Shazo, and W. C. Van Cleave, *ibid.*, **36**, 1745 (1971).

6) N. C. Marziano, E. Maccarone, and R. C. Passerini, *Tetrahedron Lett.*, **1972**, 17.

7) J. H. Ridd and J. H. Utley, *Proc. Chem. Soc.*, **1964**, 24.

8) K. Kobayashi, K. Kamiyama, H. Minato, Y. Oishi, Y. Takada, and Y. Hattori, This Bulletin, **45**, 3703 (1972).

cribed above. In order to ascertain this, the kinetics of nitration was also investigated.

Kinetic Study. Nitration of I in a mixture of 98% H_2SO_4 and fuming HNO_3 (*d*, 1.52) (*v/v*, 2/1; $[HNO_3]=8.23$ M) was followed by the increase of the UV absorption at 250 nm ascribable to II. (λ_{max} of II, 250 nm, $\varepsilon_{II}=7.063$; ε_I at 250 nm is 328). The reaction was first order in I, and good linear relationship was observed. The rate constants obtained are shown in Table 2.

Table 2. The rate constants of nitration of I in concd H_2SO_4

Temperature (°C)	$10^5 \times k$ (M^{-1} sec^{-1})
40.0	0.917±0.04
50.0	2.11 ±0.06
60.0	4.30 ±0.06

Table 3 compares the rate parameters of nitration of I and dimethylphenylsulfonium ion in concentrated sulfuric acid. The rate of nitration of I is very much smaller than that of the sulfonium ion (by a factor of 500), and this smaller rate is ascribable to the greater activation energy. These data show that the benzene ring of I is considerably deactivated because of the 2p—3p resonance between the ring and the $-\overset{\oplus}{S}(=O)Me_2$.

Very small rates of nitration of I suggest that the σ-value of an oxosulfonio group is very large. When the σ_m-value of $-\overset{\oplus}{S}(=O)Me_2$ was calculated from the rates of nitration at *meta* and *para* positions of $PhN\overset{\oplus}{M}e_3$, $Ph\overset{\oplus}{S}Me_2$, and $PhMe_2\overset{\oplus}{S}=O$, 1.38±0.04 was obtained. This σ-value is the greatest among the σ values known except the values for diazonium ion $-\overset{\oplus}{N}_2$ (σ_m 1.76; σ_p 1.91),[9] and much greater than σ_m of $-\overset{\oplus}{N}Me_3$ (1.01) and $-\overset{\oplus}{S}Me_2$ (1.00). The diazonium group is unstable and reactive whereas the oxosulfonio group is stable and much less reactive. Therefore, the oxosulfonio groups are expected to be very useful for the studies on the effects of substituents on various organic reactions or the properties of various organic compounds.

Experimental

Preparation of Dimethylphenyloxosulfonium Perchlorate (I). After a mixture of mercury(II) iodide (20 g, 44 mmol) and methyl iodide (30 ml) was deaerated in a 100 ml flask by bubbling nitrogen, it was stirred with a magnetic stirrer for 30 min under nitrogen. Then methyl phenyl sulfoxide (20 g, 142 mmol) was added, and the mixture was refluxed for 65 hr. When the excess methyl iodide was removed by distillation and the unchanged sulfoxide was removed by extraction with ether, reddish brown residue was obtained, which crystallized when extraction with ether was repeated few more times. Recrystallization from methanol gave light yellow leaflets of dimethylphenyloxosulfonium mercuritriiodide; yield, 14.0 g; mp 138—139 °C (decomp.); IR, 1230, 750 cm^{-1}; NMR (acetone-d_6), δ, 4.43 (s, 6H), 8.27 (m, 5H).

The mercuritriiodide salt (22.2 g) was dissolved in acetone (200 ml), and an acetone solution of silver perchlorate was added until no more precipitates (AgI, HgI_2) were formed. After the precipitates were filtered off, the acetone was removed under reduced pressure. When the residue was recrystallized from methanol several times, I was obtained as white needles; yield, 5.5 g (73%); mp 158—159 °C; IR, 1230 (ν_{S-O}), 1100, 750 cm^{-1}. Found: C, 37.67; H, 4.31%. Calcd for $C_8H_{11}O_5SCl$: C, 37.71; H, 4.35%.

Table 3. Activation parameters for nitration of sulfonium and oxosulfonium salts in concd H_2SO_4

	E_a (kcal/mol)	ΔS (e.u.)	$10^5 k_{25°C}$ ($M^{-1}sec^{-1}$)	$10^6 k_{0.5°C}$ ($M^{-1}sec^{-1}$)
$Ph-\overset{\oplus}{S}Me_2$	12.9	−28.0	133[a]	150[b]
$Ph-\overset{\oplus}{S}Me_2$ (=O)	16.0	−32.4	0.245	0.218[c]

a) Ref. 6.
b) Determined in the mixed acid used for nitration of $PhMe_2\overset{\oplus}{S}=O$
c) Calculated by use of E_a.

Measurements of the Rates of Nitration of I. A mixture of 98% sulfuric acid and fuming nitric acid (*d*, 1.52) (v/v= 2/1) was used. The concentration of HNO_3 was 8.23 M. A solution of I (about 1 mmol) in the mixed acid (10 ml) was placed in a constant temperature bath, and the samples withdrawn after suitable intervals were diluted with water (1000 times by volume), and the UV absorptions were determined against the reference (the mixed acid diluted by the same factor).

Identification of the Product of Nitration of I. After a mixture of I (318.4 mg), 98% sulfuric acid (2 ml) and fuming nitric acid (1 ml) was heated at 80.0 °C for 3 hr, it was diluted with ice water (20 ml), and the crystals formed were filtered. When the filtrate was made weakly alkaline and an aqueous $NaBPh_4$ solution was added, $O_2NC_6H_4\overset{\oplus}{S}(=O)Me_2$ $Ph_4\overset{\ominus}{B}$ precipitated. The total amount of II isolated (the crystals plus the tetraphenylborate salt obtained from the filtrate) amounted to 87%. Dimethylnitrophenyloxosulfonium perchlorate. Found: C, 32.13; H, 3.40; N, 4.85%. Calcd for $C_8H_{10}O_7ClNS$: C, 32.03; H, 3.36; N, 4.68%.

After the nitrated salt was refluxed in an acetone solution (40 ml) of sodium iodide (0.435 g) for 2 hr, the acetone was removed under reduced pressure, and the residue obtained was heated with 30% hydrogen peroxide (2.0 g) and acetic acid (5 ml) at 70—90 °C for 2 hr. Then the solution was diluted with water, and extracted with dichloromethane. The extracts combined were concentrated, and the residue was subjected to gas-chromatographic analysis (a Hitachi K-51 Gas Chromatograph; column, Silicone XF 1105 on Chromosorb W, 2 m).

Determination of Rates of Nitration of Dimethylphenylsulfonium Perchlorate. In 10.0 ml of the mixed acid used for the nitration of I, about 1 mmol of dimethylphenylsulfonium perchlorate was dissolved, and the mixture was let to react in a constant temperature bath. After suitable intervals, samples were withdrawn and diluted with water (1000 times by volume). The rate constant was calculated from the increase of the UV absorptions at 256 nm (ε of dimethylphenylsulfonium salt is 555, whereas that of the nitrated salt is 7256).[5]

9) E. S. Lewis and M. D. Johnson, *J. Amer. Chem. Soc.*, **81**, 2070 (1959).

BULLETIN OF THE CHEMICAL SOCIETY OF JAPAN, VOL. 46, 2257—2258 (1973)

$N^2 \rightarrow N^1$ Migration of *s*-Triazinyl Group in the Reaction of N^1-Acetyl-N^2-(*s*-triazinyl)alkylenediamines

Seiichi UNO, Kenji NAKAMURA, Yukio INOUE, Shizen SEKIGUCHI, and Kohji MATSUI

Department of Synthetic Chemistry, Gunma University, Tenjincho, Kiryu, Gunma

(Received August 2, 1972)

A report was given by West and Stewart[1] on the anionic migration of an aryl group in arylhydrazines. We studied the $N^1 \rightarrow N^2$ rearrangement of an s-triazinyl group in N^1,N^1-bis(*s*-triazinyl)-*o*-phenylenediamines.[2] The reactions of N^1-acetyl-N^2-(4,6-dichloro-*s*-triazin-2-yl)alkylenediamines with cyanuric chloride (CC) were carried out in order to obtain information on the migration of an s-triazinyl group in N^2,N^2-bis(*s*-triazinyl)alkylenediamines.

Reaction of N^1-*Acetyl*-N^2-*(4,6-dichloro*-s-*triazin-2-yl)-ethylenediamine with Cyanuric Chloride.* Two moles of cyanuric chloride at −20 °C under alkaline conditions to give N^1-acetyl-N^2-(4,6-dichloro-*s*-triazin-2-yl) ethylenediamine (II). One mole of I was subjected to reaction with two moles of cyanuric chloride at 0—5 °C under alkaline conditions to give N^1-acetyl-N^1,N^2-bis(4,6-dichloro-*s*-triazin-2-yl)ethylenediamine (III). Two singlets appeared at δ 7.91 and 9.00, assignable to N^1-H and N^2-H, respectively, in the NMR spectrum of II, and a singlet at δ 9.00 (assignable to N^2-H in that of III, their structures being shown to be as follows.

$$CH_3CON^1HCH_2CH_2N^2H_2\ (I) \xrightarrow{CC} CH_3CON^1HCH_2CH_2N^2H\text{–}X\ (II) \xrightarrow{CC} CH_3CON^1CHCH_2N^2H\text{–}X\ (III)$$

(X = Cl)

X, A=Cl
Y, A=$N(CH_3)_2$
Z, A=OCH_3

For the sake of confirmation, II and III were treated with excess dimethylamine to give N^1-acetyl-N^2-[4,6-bis(dimethylamino)-*s*-triazin-2-yl]- (IV) and N^1-acetyl-N^1,N^2-bis[4,6-bis(dimethylamino)-*s*-striazin-2-yl] ethylenediamines (V), since II and III are slightly unstable. In the NMR spectrum of IV the two singlets at δ 7.83 and 6.53 are assignable to N^1–H and N^2–H, respectively, and in that of V the singlet at δ 6.53 to N^2–H.

$$II \xrightarrow{NH(CH_3)_2} CH_2CON^1HCH_2CH_2N^2H\text{–}Y\ (IV)$$

$$III \xrightarrow{NH(CH_3)_2} CH_3CON^1CH_2CH_2N^2H\text{–}Y\ (V)$$

(Y)

II and III were treated with excess sodium methoxide to give N^1-acetyl-N^2-(4,6-dimethoxy-*s*-triazin-2-yl)-ethylenediamine (VI) and N^1,N^2-bis(4,6-dimethoxy-*s*-triazin-2-yl)ethylenediamine (VII) under cleavage of an acety lgroup. In the NMR spectrum of VI two singlets appeared at δ 7.83 and 7.92, assignable to N^1–H and N^2–H, respectively, and in that of VII a singlet at δ 7.88 only, assignable to N^1–H (or N^2–H).

$$II \xrightarrow{NaOCH_3} CH_3CON^1HCH_2CH_2N^2H\text{–}Z\ (VI)$$

$$III \xrightarrow{NaOCH_3} Z\text{–}N^1HCH_2CH_2N^2H\text{–}Z\ (VII)$$

The following reactions were carried out to clarify whether cyanuric chloride reacts directly with the N^1–H group to produce III, or with the N^2-H group to produce III *via* the transition state or the intermediate (VIII). It is not clear whether VIII is the transition state or the intermediate. Neither *N*-methyl acetamide nor N^1,N^2-diacetylethylenediamine (XIX) reacted with cyanuric chloride under alkaline conditions, but ethylamine did so under the same conditions to give *N*-(4,6-dichloro-*s*-triazin-2-yl)(IX)[3] and *N,N*-bis(4,6-dichloro-*s*-triazin-2-yl)-ethylamines (X).[4] These results confirm the $N^2 \rightarrow N^1$ migration of a dichlorotriazinyl group.

VIII

$$CH_3CONHCH_3 \xrightarrow{CC} \text{no reaction}$$

$$C_2H_5NH_2 \xrightarrow{CC} CH_3NH\text{–}X\ (IX) \xrightarrow{CC} CH_3N(X)_2\ (X)$$

Cyanuric chloride did not react with *N*-(4,6-dimethoxy-*s*-triazin-2-yl)ethylamine[5] or VI under alkaline conditions. This indicates that cyanuric chloride does not react directly with the N^1-H group and supports the view that the $N^2 \rightarrow N^1$ migration of a dichlorotriazinyl group occurs in the reaction of II with cyanuric chloride.

$$C_2H_5NH\text{–}Z \xrightarrow{CC} \text{no reaction}$$

$$CH_3CON^1HCH_2CH_2N^2H\text{–}Z\ (VI) \xrightarrow{CC} \text{no reaction}$$

The NMR measurement on the reaction of II with triethylamine was carried out in order to determine with which nitrogen atom cyanuric chloride reacts at first. When triethylamine (0.00020 mol) was added to II (0.00010 mol) in DMSO-d_6–$CDCl_3$ (1 : 3 vol) at 0 °C, the peak (N^2-H) at δ 9.16 immediately decreased, but the peak (N^1–H) at δ 8.33 did not change. The area ratio of the peaks at δ 8.33 and 9.16 was

1) R. West and H. F. Stewart, *J. Amer. Chem. Soc.*, **92**, 853 (1970).

2) K. Nakamura, N. Nohara, and K. Matsui, This Bulletin, **45**, 3140 (1972).

3) O. Diels, *Ber.*, **32**, 691 (1899).

4) N. Nohara, S. Sekiguchi, and K. Matsui, *J. Heterocyclic Chem.*, **7**, 519 (1970).

5) K. Stammbach, H. Kilchler, K. Freiedrich, M. Larser, and G. Szekely, *Weed. Red.*, **4(1)**, 64 (1964).

about 2. The ratio remained constant for 25 min after addition of triethylamine, the peak area at δ 8.33 being unchanged. This supports the veiw that cyanuric chloride reacts at first with N^2 atom under alkaline conditions.

Reaction of N^1-*Acetyl*-N^2-*(4,6-dichloro-s-triazin-2-yl)-tri- (XI) or -hexamethylenediamine (XII) with Cyanuric Chloride.* Under alkaline conditions cyanuric chloride reacted with XI and XII to give N^1-acetyl-N^2,N^2-bis(4,6-dichloro-*s*-triazin-2-yl)tri- (XIII) and -hexamethylenediamines (XIV),[6] respectively. A singlet appeared at δ 7.75 only, assignable to N^1–H, in both NMR spectra of the dimethylamino derivatives of XIII and XIV. This indicates that two dichlorotriazinyl groups are attached to N^2 atom in XIII and XIV, no rearrangement of an *s*-triazinyl group taking place. It is therefore concluded that the number of methylene groups in alkylenediamines plays an important role in the $N^2 \rightarrow N^1$ migration of an *s*-triazinyl group in the title reaction.

$$CH_3CON^1H(CH_2)_nN^2H\text{–}X \xrightarrow{CC} CH_3CON^1H(CH_2)_nN^2(X)X$$

XI ($n=3$) XII ($n=6$) XIII ($n=3$) XIV ($n=6$)

$$\xrightarrow{NH(CH_3)_2} CH_3CON^1H(CH_2)_nN^2(Y)Y$$

XV ($n=3$) XVI ($n=6$)

Experimental

N^1-*Acetylethylenediamine (I),* N^1-*Acetyltri- (XVII), and -hexamethylenediamines (XVIII), and* N^1,N^2-*Diacetylethylenediamine (XIX).* Compounds I and XIX were prepared by the method of Hill and Aspinall.[7] Compounds XVII and XVIII were prepared in the same manner as for I. Yield for I 56%; bp 143°C/10 mmHg (lit,[7] bp 128°C/3 mmHg). Yield for XVII 65%; bp 140°C/6 mmHg (lit,[10] bp 146—8°C/15 mmHg). Yield for XVIII 52%; bp 165°C/3 mmHg, d_{25}^{25} 0.9738 $n_D^{22.5}$ 1.4778. Found: C, 61.01; H, 11.69%. Calcd for $C_8H_{18}N_2O$: C, 60.72; H, 11.46%. Compound XIX was obtained as a by-product in the preparation of I, yield *ca.* 10%, mp 174—5°C (lit,[7] 172°C).

Table 1. *s*-Ariazine derivatives of *N*-acetyl-alkylneediamines

Compound No.	Yield (%)	Mp (°C)	Recryst. Solv.
II	44	134—134.5	Benzene
III	40	153—154	Benzene-Ligroin
IV	85	116—117	Ligroin
V	92	197—197.5	Ligroin
VI	67	142—142.5	Acetone
XI	64	179—179.5	Dioxane-Ligroin
XII	57	111—111.5	Benzene-Ligroin
XV[b]	33	142—142.5	Ligroin
XVI	57	145—145.5	Ligroin

a) These values agreed with the calculated ones within the usual limit of variation of elemental analysis.
b) Mass spectrometry, *m/e* 446 (medium, attributable to the parent peak; Hitachi RMS-4 mass spectrometre).

N^1-*Acetyl*-N^2-*(4,6-dichloro-s-triazin-2-yl)ethylenediamine (II).* A solution of 6.7 g (0.036 mol) of cyanuric chloride in 70 ml of acetone was added dropwise at −20°C to a stirred solution of 7.5 g (0.073 mol) of I in 100 ml of acetone. After stirring for 2.5 hr, the mixture was poured into 200 ml of ice–water. The precipitate was filtered and dried.

N^1-*Acetyl*-N^1,N^2-*bis(4,6-dichloro-s-triazin-2-yl)ethylenediamine (III).* A solution of 15 g (0.015 mol) of I in 30 ml of acetone was added dropwise at 0—5°C to a stirred solution of 5.4 g (0.029 mol) of cyanuric chloride and then 7.8 ml of a 20% sodium carbonate solution dropwise. After being stirred for 2 hr, the mixture was processed according to the procedure for II.

N^1-*Acetyl*-N^2-*[4,6-bis(dimethylamino)-s-triazin-2-yl]-(IV) and* N^1-*Acetyl*-N^1,N^2-*bis[4,6-bis(dimethylamino)-s-triazin-2-yl]-ethylenediamine (V).* These compounds were prepared from 1.0 g (0.0040 mol) of II and 2.4 g (0.0060 mol) of III, respectively, by the method described previously.[8]

N^1-*Acetyl*-N^2-*(4,6-dimethoxy-s-triazin-2-yl)ethylenediamine (VI).* To a stirred solution of 3.5 g (0.02 mol) of 4,6-dimethoxy-2-chloro-*s*-triazine (CDMT)[9] in 50 ml of acetone was added dropwise at 0—5 °C a solution of 2.1 g (0.020 mol) of I in 20 ml of acetone and then 5.3 ml of a 20% sodium carbonate solution dropwise. After being stirred for 6.5 hr at the same temperature, the mixture was stirred at *ca.* 20°C for 6 hr. The mixture was then concentrated under reduced pressure and cooled. The precipitate was filtered and dried.

N^1,N^2-*Bis(4,6-dimethoxy-s-triazin-2-yl)ethylenediamine (VII).* A solution of 3 g (0.050 mol) of ethylenediamine in 30 ml of acetone was added dropwise at *ca.* 20°C to a stirred solution of 17.6 g (0.10 mol) of CDMT in 100 ml of acetone. After being stirred for 30 min, 26.5 ml of a 20% sodium carbonate solution was added dropwise to the mixture. After being stirred for 4 hr at 30°C, the mixture was poured into 300 ml of ice–water, filtered and dried. Recrystallization from dioxane yielded 17.0 g (quantitative), mp 237.0—237.5°C. Found: C, 42.64; H, 5.64; N, 32.93%. Calcd for $C_{12}H_{18}N_8O_4$: C, 42.60; H, 5.36; N, 33.11%.

N^1-*Acetyl*-N^2-*(4,6-dichloro-s-triazin-2-yl)tri- (XI) and -hexamethylenediamines (XII).* These compounds were prepared from 2.3 g (0.020 mol) of XVII and 4.7 g (0.030 mol) of XVIII in the same manner as for III.

N^1-*Acetyl*-N^2,N^2-*bis[4,6-bis(dimethylamino)-s-triazin-2-yl]-tri- (XV) and -hexamethylenediamines (XVI).* A solution of 4.5 g (0.017 mol) of XI in 80 ml of acetone was added dropwise at 0°C to a stirred solution of 4.8 g (0.026 mol) of cyanuric chloride in 120 ml of dioxane–acetone (1 : 1 vol). After 1.46 g (0.026 mol) of potassium hydroxide in 4 ml of water had been added in small portions, the mixture was stirred for 5 hr at 0—5 °C. The mixture was processed according to the procedure described previously.[8]

Yields and melting points are summarized in Table 1. The results in elemental analysis are within the experimental error. NMR spectral data are in DMSO-d_6

6) Since XIII and XIV were too unstable to be isolated, they were prompty transformed into dimethylamino derivatives.
7) A. J. Hill and S. R. Aspinall, *J. Amer. Chem. Soc.*, **61**, 822 (1939).
8) Y. Fukushima, N. Nohara, Y. Hashida, S. Sekiguchi, and K. Matsui, This Bulletin, **44**, 794 (1971).
9) J. R. Dudley, J. T. Thurston, F. C. Schaefer, D. H. Hansen, C. J. Hull, and P. Adams, *J. Amer. Chem. Soc.*, **73**, 2986 (1961).
10) H. Mkolajewska and A. Kotelko, *Acta Polon. Pharm.*, **22 (3)**, 219 (1965).

BULLETIN OF THE CHEMICAL SOCIETY OF JAPAN, VOL. 46, 2259—2260 (1973)

Effect of Crown Ether in the Reduction of Ketones with Sodium Borohydride in Aromatic Solvent

Tsutomu MATSUDA and Kenichi KOIDA

Department of Organic Synthesis, Faculty of Engineering, Kyushu University, Hakozaki, Higashi-ku, Fukuoka 812

(Received November 28, 1972)

Cyclic polyethers, firstly synthesized by Pedersen[1a] and known as crown ethers, have been attracted much attention because of their unusual capability to form stable complexes with a variety of metallic or non-metallic cations.[1] Asides of their utility in physico-chemical phenomena[1b] they are also interesting in the application of the function to organic synthesis. Pedersen[1a] reported a successful saponification of the sterically hindered esters of 2,4,6-trimethylbenzoic acid with potassium hydroxide in aromatic hydrocarbon in the presence of dicyclohexyl-18-crown-6. Subsequent papers[2] have revealed dominating feature of the cyclic polyethers in enhancement of anion reactivity by com-

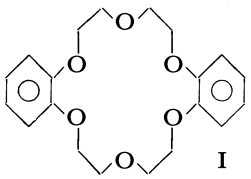

I

plex formation with a counter cation in low dielectric solvents. In this paper, we report an effectiveness of dibenzo-18-crown-6 (I) in sodium borohydride reduction of some ketones in aromatic hydrocarbon.

Results and Discussion

Effect of the Addition of Various Ethers. A ketone (0.12 mol) was allowed to react with sodium borohydride (0.03 mol) in 100 ml toluene for 5 hr under reflux in the presence of three ethereal additives (0.03 mol). The results for four ketones were illustrated in Table 1. Table 2 shows the influence of relative amount of I to sodium borohydride in the reduction of cyclohexanone. The presence of 5 mol% of I to the reducing agent was found to be almost as effective as equimolar combination of I. Because of the low solubility of sodium borohydride under the conditions, the ratio of I to sodium borohydride above 5 mol% does not have a practical importance. Use of potassium borohydride required a prolonged reaction period. Sullivan and Hinckley[3] reported that in the reduction of acetophenone tricaprylmethylammonium borohydride afforded a 20% yield of the corresponding alcohol at 25 °C (4 hr) and a 8% at 65 °C (2 hr) in benzene solvent. Present reduction which was carried out at higher temperature and with longer reaction time gave much improved yields, but was inevitably accompanied by the formation of by-product. The by-product in the reduction of cyclohexanone was found to be mostly consisted of 2-(cyclohexen-1-yl)-cyclohexanol (III, a mixture of *cis* and *trans* isomers) and the corresponding ketone (II). Table 3 suggests the occurrence of base-catalyzed condensation of the ketone. 3,3,5-Trimethyl-

Table 1. Effect of ethereal additives on the reduction of ketones[a]

Ketone		Product,[b] %		
		I	Diglyme	Dimethoxy-ethane
Acetophenone	Alcohol	49	42	23
	Ketone	0	38	40
	Residue	28	12	13
Cyclohexanone	Alcohol	50	28	19
	Ketone	0	32	56
	Residue	37	17	8
Methyl *n*-amyl ketone	Alcohol	41	27	14
	Ketone	3	9	34
	Residue	29	22	18
Methyl *iso*-propyl ketone	Alcohol	23	11	0
	Ketone	63	74	78
	Residue	10	6	5

a) Solvent; toluene, reflux for 5 hr.
b) The values show weight percent to the amount of ketone utilized.

Table 2. Influence of relative amount of I to $NaBH_4$ in the reduction of cyclohexanone

Product[a] %	Ratio of I to $NaBH_4$							
	1	0.5	0.25	0.125	0.05	0.02	0.01	0
Alcohol	50	43	40	47	42	13	0	0
Ketone	0	0	0	1	2	45	84	85
Residue	37	48	42	48	43	25	3	trace

a) See footnote in Table 1.

Table 3. Time dependence in the reduction of cyclohexanone[a]

Time, min	Product,[b] %			
	Ketone	Alcohol	III	II
10	97	3	0	0
20	47	33	30	0
40	7	58	27	8
60	0	56	16	28
90	0	57	6	37

a) Equimolar amount of $NaBH_4$ was used.
b) The values show relative peak areas of gas chromatogram for undistilled raw products.

1) a) C. J. Pedersen, *J. Amer. Chem. Soc.*, **89**, 7017 (1967). b) C. J. Pedersen, *ibid.*, **92**, 391 (1970); C. J. Pedersen and H. F. Frensdorff, *Angew. Chem.*, **84**, 16 (1972).

2) J. N. Roitman and D. J. Cram, *J. Amer. Chem. Soc.*, **93**, 2231 (1971); L. M. Thomassen, T. Ellingsen and J. Ugelstad, *Acta Chem. Scand.*, **25**, 3024 (1971); J. Zavada, M. Svoboda, and M. Pankova, *Tetrahedron Lett.*, **1972**, 711; D. J. Sam and H. E. Simmons, *J. Amer. Chem. Soc.*, **94**, 4024 (1972).

3) E. A. Sullivan and A. A. Hinckley, *J. Org. Chem.*, **27**, 3731 (1962).

Table 4. Stereochemical outcome in the reduction of cyclic ketones

Ketone	Conditions			Products,[a] %			
				Ketone	Alcohol		
	$\frac{I}{NaBH_4}$	Time, hr	Solvent[b]		*cis*(*exo*)[c]	*trans*(*endo*)[c]	$\frac{cis}{trans}\left(\frac{exo}{endo}\right)$[c]
4-Methylcyclohexanone	1	5	T	0	26	74	26
4-*t*-Butylcyclohexanone	1	5	T	3	22	75	23
	0.5			0	21	79	21
3,3,5-Trimethylcyclohexanone	1[d]	5	T	77	10	13	44
	1			31	52	17	75
	1			15	68	17	80
	0.1			25	62	13	83
	0.05			27	56	16	78
2-Norbornanone	1	5	T	84	5	11	31
	1	9	T	78	6	16	29
	1	3.5	X	41	20	39	34
	1	5	X	4	31	65	32

a) Weight percent for distillate. b) T=toluene, X=*o*-xylene. c) For 2-norbornanone.
d) The reaction was carried out at 100 °C, and the others were under reflux.

cyclohexanone was more resistant to the reduction than less hind ered substituted cyclohexanones; 4-methyl- and 4-*t*-butylcyclohexanone (Table 4). The reduction of 2-norbornanone required a higher reaction temperature to achieve a good conversion and camphor did not react to a measureable extent.

Effect of I on the Stereochemical Course. It is known that the stereochemical course of sodium borohydride reduction is subjected to various factors, such as steric[4] or polar effect[5] in substituted ketones, as well as the nature of solvent.[6] The isomer distributions of the product alcohols obtained in the reduction of substituted cyclohexanones and 2-norbornanone were tabulated in Table 4. Reduction of 4-methyl- and 4-*t*-butylcyclohexanone yielded alcohols in 74 and 77% abundance of *trans* isomer, respectively, which are in good accordance with the reported *trans* contents of 76 and 78% for the reductions in 2-propanol.[5]

In the borohydride reduction of 3,3,5-trimethylcyclohexanone the *cis* alcohol was always an unfavorable isomer in the product and its abundance varies from 27 to 45% depending on the solvent utilized.[6] On the other hand, the *cis* isomer was found to become the predominant product in the present reduction. The present results can be explained in terms of a smaller effective size of reducing agent in nonpolar solvent; toluene. The increased yield (29—34%) of *exo* alcohol from 2-norbornanone as compared to the result in 2-propanol (14%)[4b] can again be accommodated with the idea.

The observed order of facility of reduction in toluene, cyclohexanone $\approx$ 4-substituted cyclohexanones $>$ 3,3,5-trimethylcyclohexanone ($\approx$methyl isopropyl ketone) $>$ 2-norbornanone $\gg$ camphor, also suggests that an unsolvated borohydride anion in toluene still suffers the similar kind of steric hindrance as observed in conventional solvent,[4b] possibly because of close proximity of sodium ion complexed with the cyclic polyether to borohydride anion.

Experimental

Materials. Dibenzo-18-crown-6-(2,3,11,12-dibenzo-1,4,7,10,13,16-hexaoxacyclooctadeca-2,11-diene) was prepared by the procedure described by Pedersen,[1a] mp 163.2—164.5 °C (lit,[1a] 164 °C). 2-Norbornanone[7] and methylisopropyl ketone[8] were obtained by the standard methods. Other liquid ketones used were commercial products and distilled prior to use. Sodium borohydride and camphor were used without purification.

Procedures. A typical procedure is as follows. A mixture of I (10.8 g, 0.03 mol), finely pulverized sodium borohydride (1.13 g, 0.03 mol) and dry toluene (100 ml) was refluxed for 0.5 hr under stirring. Cyclohexanone (11.8 g, 0.12 mol) in toluene (20 ml) was added in a period of 10 min and the mixture was refluxed for 5 hr under stirring. The reaction mixture was cooled and hydrolyzed by addition of dil. hydrochloric acid and let stand at 0 °C. Crystalline I precipitated was removed by filtration and the water layer was extracted three times with ether. The combined organic layer was neutralized, dried and concentrated. Distillation of the concentrate yielded cyclohexanol (6.7 g, 50% bp 89—92 °C/80 mmHg) and a residue (4.4 g). A distillate from the residue (3.9 g, bp 80—100 °C/2 mmHg) was found to be composed mainly of *cis*- and *trans*-2-(cyclohexen-1-yl)-cyclohexanol and small amounts of the corresponding ketone and an unidentified compound by gas chromatography (compared with authentic specimen[9]). Extent of the reduction and isomer ratios of the products were determined by gas chromatography on Ucon Oil HB5100 10%-Celite column or 1,2,3-tris(2-cyanoethoxy)propane 10%-Shimalite column (for isomers of 4-methyl- and 4-*t*-butylcyclohexanol).

4) a) W. G. Dauben, G. J. Fonken, and D. S. Noyce, *J. Amer. Chem. Soc.*, **78**, 2579 (1956). b) H. C. Brown and J. Muzzio, *ibid.*, **88**, 2811 (1966).
5) H. Kwart and T. Takeshita, *ibid.*, **84**, 2834 (1962).
6) H. Haubenstock and E. L. Eliel, *ibid.*, **84**, 2363 (1962).
7) D. C. Kleinfelter and P. V. R. Schleyer, "Organic Syntheses," Vol. **42**, p. 79 (1962).
8) M. S. Newman and A. S. Smith, *J. Org. Chem.*, **13**, 592 (1948).
9) J. Plesek, *Chem. Listy*, **50**, 246 (1956); *Chem. Abstr.*, **50**, 7732b (1956).

BULLETIN OF THE CHEMICAL SOCIETY OF JAPAN, VOL. 46, 2261—2262 (1973)

Synthetic Studies of Carbohydrate Derivatives with Photochemical Reaction. VIII.[1] Photochemical Desulfurization of Some Sugar Diethyl Dithioacetal Acetates into the Corresponding 1-*S*-Ethyl-1-thioalditol Acetates

Kazuo MATSUURA, Younosuke ARAKI, and Yoshiharu ISHIDO

Department of Chemistry, Faculty of Science, Tokyo Institute of Technology, Ookayama, Meguro-ku, Tokyo 152

(Received February 13, 1973)

In the series of this investigation, a facile photochemical addition of thiols to enoses has briefly been reported from our laboratory.[1,2] As a part of this investigation, the present authors wish to report successively a photochemical desulfurization of some sugar diethyl dithioacetal acetates into the corresponding 1-*S*-ethyl-1-thioalditol acetates since such a conversion has been known solely with respect to D-galactose diethyl dithioacetal which affords 1-*S*-ethyl-1-thiogalactitol.[3] The photochemical desulfurization of diethyl dithioacetal acetates of D-arabinose, D-ribose, D-xylose, and D-glucose are described herewith.

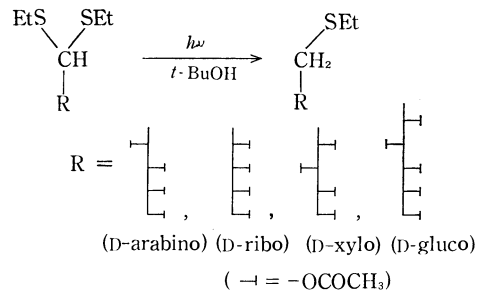

The corresponding 1-*S*-ethyl-1-thioalditol acetates were easily obtained in excellent yields by a chromatography on a column of silica gel (eluting solvent: 1%-acetone–benzene) of each sirup resultant from the concentration of the solution which was obtained by a previous irradiation of a *t*-butyl alcohol solution of the sugar diethyl dithioacetal acetates with a low pressure mercury lamp at room temperature under nitrogen atmosphere for 20 hr; the yields of 1-*S*-ethyl-1-thio-D-arabinitol, -D-ribitol, -D-xylitol, and -D-glucitol acetates were 79.3%, 85.3%, 86.9%, and 84.1%, respectively. The NMR data showed good agreement with their expected structures. According to the result of Horton and Jewell,[3] incidentally, 1-*S*-ethyl-1-thio-D-galactitol was obtained in a 55% yield by irradiation of methanolic solution of D-galactose diethyl dithioacetal with a low pressure mercury lamp (450 W) for 36 hr. The results described here were thus considerably superior to this result with respect to the yields of the photochemical reaction. The superiority may depend on the use of mercaptal acetates and *t*-butyl alcohol as the reaction solvent in place of methanol.

t-Butyl alcohol may probably facilitate the reaction in comparison with the reaction in methanol; 1-deoxy-D-galactitol (L-fucitol) is already produced in the latter case as a result of concomitant process of further elimination of the ethylthiyl radical, and, in addition, the diethyl dithioacetal is yet remained in the reaction mixture.[3]

Two procedures have generally been known for the preparation of 1-*S*-alkyl-1-thioalditols; 1) Partial reduction of sugar mercaptals by the use of an aged Raney nickel as the catalyst.[4] 2) Reduction of 1-halogeno-1-alkylthioalditol derivatives, which was obtained from sugar mercaptals by halogenation, with lithium aluminum hydride.[5] The yield of the product in problem were, however, not so good in these procedures. Consequently, the procedure described in this article can be concluded to be practically feasible for the general synthetic method of 1-*S*-alkyl-1-thioalditols.

Experimental

Melting points are uncorrected. The irradiations were carried out by the use of a low pressure mercury lamp (6 W) of Ushio Electric Co. Inc. at room temperature under nitrogen atmosphere. NMR spectra were taken with a JEOL JNM-H-100 at 100 MHz in deuterochloroform by the use of tetramethylsilane as the internal standard. The acetates of diethyl dithioacetals of D-arabinose, D-ribose, D-xylose, and D-glucose were prepared according to the usual method.[6]

2,3,4,5-Tetra-O-acetyl-1-S-ethyl-1-thio-D-arabinitol: A solution of 2,3,4,5-tetra-*O*-acetyl-D-arabinose diethyl dithioacetal (1.00 g) in *t*-butyl alcohol (170 ml) was irradiated with the UV lamp under nitrogen atmosphere at room temperature for 20 hr. Resultant solution was evaporated *in vacuo* to afford brown sirup, which was subsequently chromatographed on a silica gel column (3×20 cm) by eluting with benzene containing 1% volume of acetone. The starting material (4 mg, 0.4%) was eluted out as the first portion, and 2,3,4,5-tetra-*O*-acetyl-1-*S*-ethyl-1-thio-D-arabinitol was as the second portion. The eluate was concentrated *in vacuo* to a sirup which was soon crystallized on standing at room temperature and is already pure enough for the elemental analysis. Yield

1) Part VII: Y. Araki, K. Matsuura, Y. Ishido, and K. Kushida, *Chem. Lett.*, **1973**, 383.

2) K. Matsuura, S. Maeda, Y. Araki, and Y. Ishido, *Tetrahedron Lett.*, **1970**, 2869.

3) D. Horton and J. S. Jewell, *J. Org. Chem.*, **31**, 509 (1966).

4) J. K. N. Jones and D. L. Mitchell, *Can. J. Chem.*, **36**, 206 (1958).

5) H. Zinner, R. Kleeschätzky, and P. Neels, *Chem. Ber.*, **98**, 1492 (1965).

6) a) S. M. Olin, "Methods in Carbohydrate Chemistry," Vol. 1, ed. by R. L. Whistler and M. L. Wolfrom, Academc Press, New York and London (1962), p. 148. b) M. L. Wolfrom and A. Thompson, *ibid.*, Vol. 2, (1963), p. 427. c) J. Stanĕk, M. Černý, J. Kocourek, and J. Pacák, "The Monosaccharides," Academic Press, New York and London, and Publishing House of the Czechoslovak Academy of Science, Prague (1963), p. 589.

0.681 g (79.3%), mp 56—58 °C, $[\alpha]_D^{22}$ +43.3° (*c* 1.0, Me_2CO) {lit,[7] mp 58 °C, $[\alpha]_D$ 38±4° (*c* 1.3, $CHCl_3$)}. NMR: δ 1.25 (3H, t, $J_{CH_3-CH_2}$=7.0 Hz, C–C$\underline{H}_3$), 2.56 (2H, q, –C$\underline{H}_2$–Me), 2.58 (1H, q, $J_{1,1'}$=13.5 Hz, $J_{1,2}$=7.0 Hz, H-1), 2.60 (1H, q, $J_{1',2}$=6.0 Hz, H-1'), 5.23 (1H, oct, $J_{2,3}$=2.5 Hz, H-2), 5.45 (1H, q, $J_{3,4}$=8.5 Hz, H-3), 5.15 (1H, oct, $J_{4,5}$=5.0 Hz, $J_{4,5'}$=3.5 Hz, H-4), 4.15 (1H, q, $J_{5,5'}$=12.5 Hz, H-5), 4.23 (1H, q, H-5'), 2.05, 2.06, 2.08, and 2.14 (4×–OCOC$\underline{H}_3$).

The other mercaptal acetates (1.00 g) were respectively treated in the same way as had been described in the above experiment, and the results thus obtained were summarized as below.

2,3,4,5-Tetra-O-*acetyl-1*-S-*ethyl-1-thio*-D-*ribitol*: Yield 0.733 g (85.3%), mp 59—61 °C, $[\alpha]_D^{22}$−4.7° (*c* 1.0, Me_2CO). Found: C, 49.69; H, 6.85; S, 8.59%. Calcd for $C_{15}H_{24}O_8S$: C, 49.45; H, 6.64; S, 8.78%. NMR: δ 1.23 (3H, $J_{CH_3-CH_2}$=7.5 Hz, CH_2–C$\underline{H}_3$), 2.55 (2H, q, –S–C$\underline{H}_2$–Me), 2.70 (1H, $J_{1,1'}$=13.5 Hz, $J_{1,2}$=8.0 Hz, H-1), 2.82 (1H, q, $J_{1',2}$=5.0 Hz, H-1'), 5.05—5.45 (3H, m, H-2, H-3, and H-4), 4.16 (1H, q, $J_{4,5}$=6.0 Hz, $J_{5,5'}$=12.0 Hz, H-5), 4.37 (1H, q, $J_{4,5'}$=3.0 Hz, H-5'), 2.05, 2.09, and 2.10 (3H, 6H, and 3H, –OCOC$\underline{H}_3$). The starting material was recovered in a 2.5% yield (25 mg) in this case.

2,3,4,5-Tetra-O-*acetyl-1*-S-*ethyl-1-thio*-D-*xylitol*: Yield 0.747 g (86.9%), sirup, $[\alpha]_D^{22}$ −21.7° (*c* 1.1, Me_2CO). Found: C, 49.31; H, 6.49; S, 9.08%. Calcd for $C_{15}H_{24}O_8S$: C, 49.45; H, 6.64; S, 8.78%. NMR: δ 1.24 (3H, t, $J_{CH_3-CH_2}$=7.5 Hz, –CH_2–C$\underline{H}_3$), 2.57 (2H, q, –S–C$\underline{H}_2$–Me), 2.66 (1H, q, $J_{1,1'}$=13.5 Hz, $J_{1,2}$=6.5 Hz, H-1), 2.68 (1H, q, $J_{1',2}$=6.0 Hz, H-1'), 5.17 (1H, oct, $J_{2,3}$=4.5 Hz, H-2), 5.49 (1H, q, $J_{3,4}$=6.0 Hz, H-3), 5.27 (1H, sex, $J_{4,5}$=6.0 Hz, $J_{4,5'}$=3.5 Hz, H-4), 4.02 (1H, q, $J_{5,5'}$=12.5 Hz, H-5), 4.33 (1H, q, H-5'), 2.05, 2.08, and 2.11 (3H, 3H, and 6H, –OCOC$\underline{H}_3$).

2,3,4,5,6-Penta-O-*acetyl*-*1*-S-*ethyl*-*1*-*thio*-D-*glucitol*: Yield 0.739 g (84.1%), mp 84—86 °C, $[\alpha]_D^{22}$ +1.3° (*c* 1.0, Me_2CO) {lit,[4] mp 82 °C, $[\alpha]_D^{26}$ 5±1° (*c* 1.1, $CHCl_3$)}. NMR: δ 1.24 (3H, t, $J_{CH_3-CH_2}$=7.5 Hz, –CH_2–C$\underline{H}_3$), 2.57 (2H, q, –S–C$\underline{H}_2$–Me), 2.66 (1H, q, $J_{1,1'}$=14.0 Hz, $J_{1,2}$=6.5 Hz, H-1), 2.74 (1H, q, $J_{1',2}$=5.5 Hz, H-1'), 4.95—5.2 (2H, m, H-2 and H-5), 5.51 (1H, q, $J_{2,3}$=5.0 Hz, $J_{3,4}$=4.0 Hz, H-3), 5.43 (1H, q, $J_{4,5}$=10.5 Hz, H-4), 4.14 (1H, q, $J_{5,6}$=5.5 Hz, $J_{6,6'}$=12.5 Hz, H-6), 4.25 (1H, q, $J_{5,6'}$=3.5 Hz, H-6'), 2.04, 2.06, 2.09, and 2.12 (3H, 6H, 3H, and 3H, –OCOC$\underline{H}_3$). The starting material was recovered in a 1.3% yield (13 mg) in this case.

7) L. Hough, J. K. N. Jones, and D. L. Mitchell, *Can. J. Chem.*, **37**, 725 (1959).

BULLETIN OF THE CHEMICAL SOCIETY OF JAPAN, VOL. 46, 2262—2264 (1973)

Three-Membered Ring-formation Reactions. V. The Cyclopropane Derivative Obtained from the α-Halogenoacrylic Ester by Means of Zinc Alkyl-Active Methylene Chelate Compounds

Yusuke KAWAKAMI and Teiji TSURUTA

Department of Synthetic Chemistry, Faculty of Engineering, The University of Tokyo, Hongo, Bunkyo-ku, Tokyo 113

(Received September 16, 1972)

It was previously reported that two molecules of methyl α-chloroacrylate undergo a ring-formation reaction with ethylzinc chloride to produce dimethyl 1-chloro-2-propyl-*cis*-1,2-cyclopropanedicarboxylate (I).[1-3] The reaction was considered to proceed according to a step-by-step mechanism:

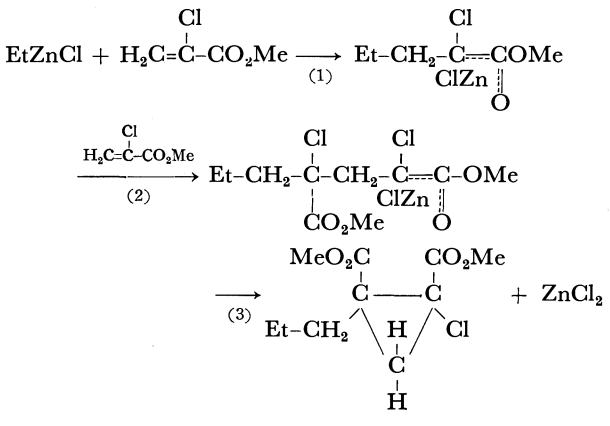

(I)

Diethylzinc, instead of ethylzinc chloride, was also effective in the ring-formation reaction.[4] It was further confirmed that the zinc alkyl–active methylene chelate compound[5] behaved in a different fashion from ethylzinc chloride or diethylzinc,[3] as is exemplified by Reaction (4):

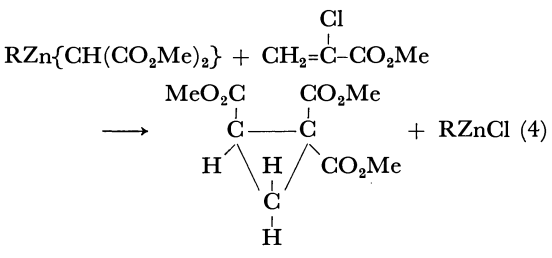

(II)

Only one molecule of methyl α-chloroacrylate participates in Reaction (4). Since it was considered that the second active hydrogen atom in the intermediate (A1) may play an essential role as is shown below (Reaction (5)) in the ring-formation reaction (4), we

1) Y. Kawakami and T. Tsuruta, *Tetrahedron Lett.*, **1971**, 1173.
2) Y. Kawakami and T. Tsuruta, *ibid.*, **1971**, 1959.
3) T. Tsuruta and Y. Kawakami, *Tetrahedron*, in press.
4) T. Tsuruta Y. Kawakami, and R. Tsushima, *Makromol. Chem.*, **149**, 135 (1971).
5) Y. Kawakami and T. Tsuruta, This Bulletin, **44**, 247 (1971).

Table 1. Reaction of methyl α-halogenoacrylate with metal alkyl–active methylene chelate compounds[a)]

Acrylate[b)]	Chelate compound	Product yield (%)				
		II	III	IV	V	VI
MCA	*n*-BuZn{$CH(CO_2Me)_2$}	60.0	—	—	—	—
MBA	*n*-BuZn{$CH(CO_2Me)_2$}	75.2	—	—	—	—
MCA	EtClAl{$CH(CO_2Me)_2$}	13.0	—	—	—	—
MCA	*n*-BuZn{$C(CH_3)(CO_2Me)_2$}	—	—	22.6	21.5	—
MCA	*n*-BuZn{$C(Br)(CO_2Me)_2$}	—	—	—	—	15.0
MA	*n*-BuZn{$C(Br)(CO_2Me)_2$}	22.2	—	—	—	—
MCA	*n*-BuZn{$CH_3COCHCO_2Me$}	—	16.0[c)]	—	—	—

a) Reaction for 2 hr in benzene at 70 °C.
b) MCA, MBA, and MA are methyl α-chloroacrylate, methyl α-bromoacrylate, and methyl acrylate, respectively.
c) The yield was calculated based on 1/2 [MCA].

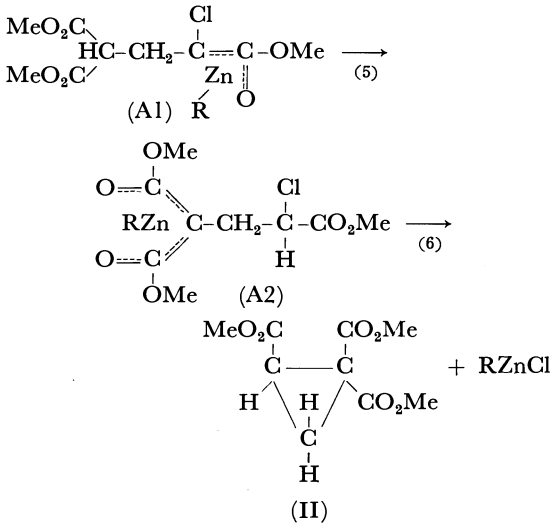

have undertaken a study of the reactions of methyl α-chloroacrylate with metal alkyl–active methylene chelate compounds, which have substituents on the α-carbon of the active methylene component.

Experimental

The NMR spectra were recorded at 100 MHz in benzene, TMS being used as the internal standard.

The metal alkyl-active methylene chelate compounds were prepared by a method reported before.[5)] Methyl α-chloroacrylate and methyl α-bromoacrylate were prepared according to the literature.[6)]

To a benzene solution of methyl α-chloroacrylate, equimoles of metal alkyl–active methylene chelate compounds were added at 70 °C. After a given time interval, the reaction was stopped by pouring the reaction system into water containing a small amount of hydrochloric acid. The organic layer was then separated and distilled. The results obtained are shown in Table 1.

The structures of the products in Table 1 were established to be as follows:

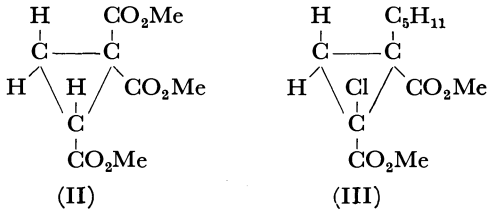

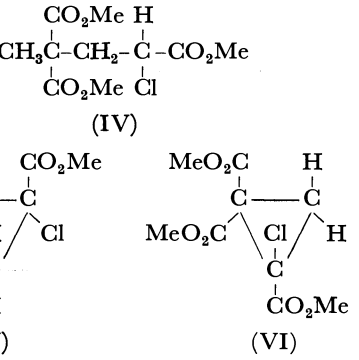

Compounds II (n_D^{20} 1.4518, d_4^{20} 1.17, bp 108 °C/1 mmHg) and III (n_D^{20} 1.4618, d_4^{20} 1.08, bp 90 °C/2 mmHg) were identified by comparing their NMR spectra with those reported previously.[1,4)] Compounds IV and V were obtained in 22.5 and 21.5% yields respectively from *n*-butyl(dimethylmethylmalonato)zinc and methyl α-chloroacrylate. Moreover, Compound VI was obtained in a 15% yield from *n*-butyl(dimethyl bromomalonato)zinc and methyl α-chloroacrylate.

IV: n_D^{20} 1.4577, d_4^{20} 1.22, bp 115.5 °C/1 mmHg; NMR: δ 4.50 (1H, t, >CH), δ 3.38, 3.37, 3.32 (9H, s, $-CO_2CH_3$), δ 2.76, 2.47 (2H, q, $-CH_2-$), δ 1.29 (3H, s, CH_3-).

Found: C, 45.36; H, 5.97; Cl, 13.14%. Calcd for $C_{10}H_{15}ClO_6$: C, 45.02; H, 5.67; Cl, 13.30%.

V: n_D^{20} 1.4838, d_4^{20} 1.26, bp 165 °C/1 mmHg.

Found: C, 48.25; H, 5.76; Cl, 9.74%. Calcd for $C_{14}H_{19}ClO_8$: C, 47.92; H, 5.46; Cl, 10.11%.

VI: n_D^{20} 1.4638, bp 116 °C/1 mmHg; NMR: δ 3.28, 3.20 (9H, s, $-CO_2CH_3$), δ 2.09 (2H, q, $>CH_2$).

Found: C, 43.22; H, 4.77; Cl, 14.03%. Calcd for $C_9H_{11}ClO_6$: C, 43.11; H, 4.43; Cl, 14.15%.

Results and Discussion

When dimethyl methylmalonate was used as an active methylene component in the reaction with methyl α-chloroacrylate, the first-step addition product, IV, of dimethyl methylmalonate to methyl α-chloroacrylate was isolated from the reaction mixture along with V. Thus, a close similarity in the mode of formation can be seen between I and V. The results can be reasonably explained in terms of the lack of the exchange reaction (5), because no active hydrogen

6) C. S. Marvel, J. Dec, H. G. Cooke, and J. C. Cowan, *J. Amer. Chem. Soc.*, **62**, 3495 (1940).

atom exists in the intermediate formed by the addition reaction of *n*-butyl(dimethyl methylmalonato)zinc to the acrylate.

When dimethyl α-bromomalonate was used as the active methylene component, an elimination reaction of bromine atom predominate to form VI, because the bromine atom is a good leaving group. In conformity with this, dimethyl α-bromomalonate could undergo a ring-formation reaction, even with methyl acrylate (Table 1, No. 6). In the reaction of *n*-butyl(methyl acetoacetato)zinc with methyl α-chloroacrylate, methyl acetoacetate component did not act as an addendum, but *n*-butyl group underwent the addition reaction, giving dimethyl 1-chloro-2-amyl-*cis*-1,2-cyclopropanedicarboxylate.[4] These results may be ascribed to the chelate ring of methyl acetoacetate being much more stable than that of dimethyl malonate.

Some results on the asymmetric synthesis by zinc alkylactive methylene chelate compounds in the presence of Et_2Zn-*l*-menthol are shown in Table 2.

The rather small value of the optical rotation in II should be ascribed to an exchange reaction (for example, Reaction (5)) between RZn and H groups, which may also be a cause of the racemization around the chiral center in II.

From the results presented above, it seems reasonable to conclude that the mode of the ring-formation reaction of α-halogenoacrylate with alkylzinc–active methylene chelate compounds is strongly influenced by the nature of substituents at the α-carbon atom of an active methylene component, and also by the stability of the chelating systems.

Table 2. Asymmetric synthesis by zinc alkyl–active methylene chelate compounds in the presence of Et_2Zn–*l*-menthol (1.0:1.2) system[a]

$[\alpha]_D^{20}$ in benzene	Chelate	Product
−6.6°	*n*-BuZn{$CH(CO_2Me)_2$}	II
−8.0°	*n*-BuZn{$CH_3COCHCO_2Me$}	III

a) One to one mole ratio of the chelate compound to Et_2Zn was used.
Et_2Zn–*l*-menthol system was prepared as reported.[2,7]

7) a) J. M. Bruce and D. W. Farren, *Polymer*, **6**, 509 (1965). b) M. Ishimori, T. Tomoshige, and T. Tsuruta, *Makromol. Chem.*, **120**, 161 (1968).

BULLETIN OF THE CHEMICAL SOCIETY OF JAPAN, VOL. 46, 2265—2266 (1973)

The Light Resistance of the Complex Salts of Flavones and Flavonols

Makoto KANETA and Noboru SUGIYAMA*

Fukushima Technical College, Iwaki-shi, Fukushima 970

**Department of Chemistry, Tokyo Kyoiku University, Otsuka, Tokyo 112*

(Received November 22, 1972)

In a previous paper,[1] we showed that flavones, in contrast to flavonols (3-hydroxyflavones), show a high degree of resistance to light, and made clear that dyes from the plants *Arthraxon hispidus*,[2] *Reseda luteola*, and *Miscanthus tinctorius*[3] are superior to dyes from other grasses in their resistance to light because they contain flavones, such as arthraxin, luteolin, and tricin.

Since silk threads normally soaked in a mordant of lye made from leaves and stems of trees, such as *Eurya ochacea* and *Camellia japonica*, after being dyed with dyes from the above-mentioned plants, we examined the light resistance of the complex salts of flavones and flavonols by following the time change in the UV spectra of the following complexes substances: quercetin (**1**), morin (**2**), arthraxin (**3**), luteolin (**4**), and tricin (**5**).

Because of the similarity in the molecular structures of these substances, their molecular extinction coefficients will be considered to be approximately equal.

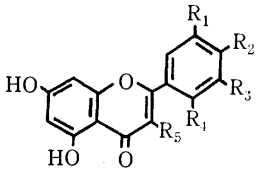

1 R_1, R_2, R_5=OH R_3,R_4=H
2 R_2,R_4,R_5=OH R_1,R_3=H
4 R_1,R_2=OH R_3,R_4,R_5=H
5 R_2=OH R_1,R_3=OMe R_4,R_5=H

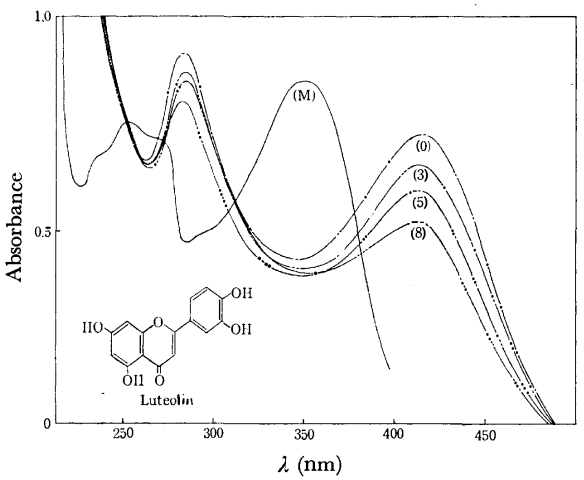

Fig. 1. Time change during irradiation of the spectrum of luteolin complex formed with *Camellia* lye.
(M): Methanol solution of luteolin, (0): 0 hr irradiation, (3): 3 hr irradiation, (5): 5 hr irradiation, (8): 8 hr irradiation.

We can, therefore, measure the light resistance of the substances by means of the decrease in the ratio of the absorption intensity.

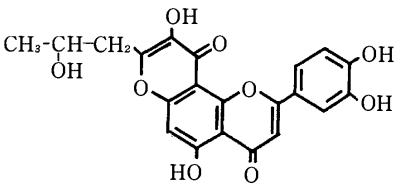

3

TABLE 1. DECREASE RATIO OF INTENSITY OF BAND I AFTER FIVE-HOUR IRRADIATION

	Flavonol		Flavone		
	Quercetin (371)[a]	Morin (370)	Arthraxin (340)	Luteolin (350)	Tricin (350)
Lye of plant *Camellia*[5]	53% (438)	57 (403)	30 (403)	19 (415)	24 (375)
Lye of plant *Eurya*	51 (443)	54 (395)	12 (408)	15 (412)	20 (377)
Na_2CO_3	100 (385)	75 (395)	24 (401)	20 (395)	37 (418)
$AlCl_3$	92 (456)	38 (420)	31 (408)	22 (425)	17 (392)
Al_2O_3	100 (380)	75 (392)	16 (353)	3 (360)	24 (367)
CuO(NaOHaq)	100 (425)	100 (455)	15.3 (415)	25 (405)	15 (425)

$$\text{Decrease ratio} = \frac{\text{Intensity at 0 hr} - \text{Intensity at 5 hr}}{\text{Intensity at 0 hr}} \times 100\%$$

a) λ max of band I of the samples and their complexes are shown in the respective parentheses.

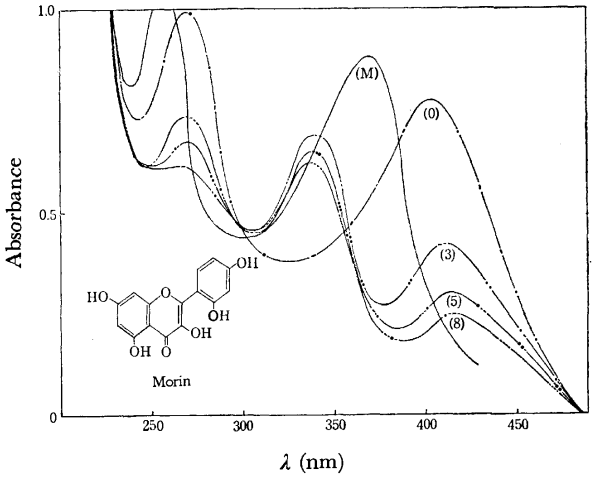

Fig. 2. Time change during irradiation of the spectrum of morin complex formed with *Camellia* lye.
(M): Methanol solution of morin, (0) 0 hr irradiation, (3): 3 hr irradiation, (5): 5 hr irradiation, (8): 8 hr irradiation.

1) M. Kaneta and N. Sugiyama, This Bulletin, **44**, 3211 (1971).
2) M. Kaneta and N. Sugiyama, *ibid.*, **42**, 2084 (1969).
M. Kaneta and N. Sugiyama, *J. Chem. Soc., C*, **1971**, 1892
3) M. Kaneta and N. Sugiyama, This Bulletin, **45**, 528 (1972).

Fifty ml portions of methanol solutions of the samples were prepared so as to show approximately equal absorption intensities of Band I, with Band I defined as the peak absorption band in the 350—450 nm region. To each solution, we then added a few drops of a saturated solution of salts (Na_2CO_3, $AlCl_3$) or lye of leaves and stems of *Eurya ochacea*, and *Canellia japonica* in order to make a complex.[4] The methanolic solutions of the complexes were irradiated under the same conditions with an immersion-type Taika HLV-A 200-W high-pressure mercury lamp through a quartz glass tube under bubbling air. The UV spectrum of an aliquot was then recorded at intervals of 1, 2, 3, 5, 8, 12, and 24 hr.

The results tabulated in Table 1 indicate that the complex salts of flavones, in contrast with flavonol-salt complexes, show a high power of resistance to the light when air is bubbled into the methanol solution. This result also agrees with the observations reported in a previous paper,[1] so it becomes clear that flavones are more stable than flavonols (3-hydroxyflavone) to irradiation both in the free state and in the complex-salt state.

4) For information about the "complexes" of flavones and flavonols, the reader is referred to T. J. Mabry, K. R. Markham and M. B. Thomas, "The Systematic Identification of Flavonoids," Springer-Verlag, New York (1970), p. 51.

5) The main metals contained in these plants were found to be Na, K, Ca, Mn, Al, Fe, and Cu by Mr. Ryokichi Negishi, Kanagawa Prefectural Industrial Experiment Station.

Application of the RRKM Theory to Energized Ethylene Formed in the Vacuum-ultraviolet Photolysis of *n*-Paraffins

Hajime Akimoto, Kinichi Obi, and Ikuzo Tanaka

Department of Chemistry, Tokyo Institute of Technology, Ohokayama, Meguro-ku, Tokyo 152

(Received October 5, 1972)

The Rice-Ramsperger-Kassel-Marcus treatment has been applied to the energized ethylene produced in the vacuum-ultraviolet photolysis of C_2H_6, C_2D_6, C_3H_8, C_3D_8, n-C_4H_{10} and n-C_4D_{10}. The energy spread in the energized ethylene has been evaluated assuming modified statistical distribution of liberated energy among fragment species. The calculated nonequilibrium unimolecular decomposition rate constant for the process $C_2H_4(C_2D_4)\rightarrow C_2H_2(C_2D_2)+H_2(D_2)$ could satisfactorily reproduce the experimental pressure dependence of ethylene to acetylene ratio. Non-statistical kinetic energy E_k seems to appear for the primary decomposition of the n-paraffins. Its value ranges from zero for the elimination of methane and ethane from propane and n-butane, respectively, at 147.0 nm to about 25 kcal mol^{-1} for the elimination of hydrogen from ethane at 123.6 nm.

In the vacuum-ultraviolet photolysis of n-paraffin hydrocarbons in the gas phase, ethylene and acetylene are always among the major products.[1-11] From the analysis of products the following reaction schemes have been proposed[9,12] for the production of ethylene and acetylene in the photolysis of ethane, propane and n-butane.

$$C_2H_6 + h\nu \xrightarrow{\phi_{1a}} H_2 + C_2H_4^{**} \xrightarrow{k_d} C_2H_2 + H_2 \quad (1)$$

$$\xrightarrow{k_s[M]} \xrightarrow{\phi_{1b}} H_2 + C_2H_4^{*} \longrightarrow C_2H_4 \quad (2)$$

$$\xrightarrow{\phi_2} H + C_2H_4 + H \quad (3)$$

$$C_3H_8 + h\nu \xrightarrow{\phi_{1a}} CH_4 + C_2H_4^{**} \xrightarrow{k_d} C_2H_2 + H_2 \quad (4)$$

$$\xrightarrow{k_s[M]} \xrightarrow{\phi_{1b}} CH_4 + C_2H_4^{*} \longrightarrow C_2H_4 \quad (5)$$

$$\xrightarrow{\phi_2} H + C_2H_4 + CH_3 \quad (6)$$

$$n\text{-}C_4H_{10} + h\nu \xrightarrow{\phi_{1a}} C_2H_6 + C_2H_4^{**} \xrightarrow{k_d} C_2H_2 + H_2 \quad (7)$$

$$\xrightarrow{k_s[M]} \xrightarrow{\phi_{1b}} C_2H_6 + C_2H_4^{*} \longrightarrow C_2H_4 \quad (8)$$

$$\xrightarrow{\phi_2} \begin{cases} H + C_2H_4 + C_2H_5 & (9) \\ CH_3 + C_2H_4 + CH_3 & (10) \end{cases}$$

Experimental studies[5,12] revealed that two kinds of ethylene should be obtained through the molecular detachment processes; one which undergoes unimolecular decomposition into acetylene and hydrogen competing with collisional stabilization to ethylene and the other which does not decompose even at very low pressure. These two kinds of ethylene are designated as $C_2H_4^{**}$ and $C_2H_4^{*}$, respectively, their relative yields being referred to as ϕ_{1a} and ϕ_{1b}, respectively. The assumption that the ethylene produced in Eqs. (3), (6), (9) and (10) does not decompose is easily justified in terms of the large endothermicity of the reactions.

With respect to energized ethylene the following points should be clarified: (1) How the unimolecular decomposition rate k_d can be correlated to the internal energy retained in the energized ethylene $C_2H_4^{**}$. How the internal energy can be correlated to the maximum energy available in the processes. (2) The nature of $C_2H_4^{*}$. (3) Whether ethylene is originally produced in the form of ethylidene CH_3CH which then isomerizes to C_2H_4, or it is originally formed as C_2H_4.

By means of the classical Kassel formula,[13] Hampson and McNesby[5] first attempted to correlate the experimentally determined unimolecular decomposition rate to the internal energy of ethylene produced in the photolysis of n-paraffin hydrocarbons, diazoethane and methylketene. Assuming *a priori* that 80% of the maximum energy available in the process would be retained in ethylene, they succeeded in showing reasonably good correlation in a semi-quantitative manner. Their results suggest that energized ethylene $C_2H_4^{**}$ is vibrationally excited ethylene in its ground electronic state. They also suggested that $C_2H_4^{*}$ is a long-lived triplet ethylene.

Kirk and Tschuikow-Roux[14] applied the Rice-Ramsperger-Kassel-Marcus (RRKM) treatment to the decomposition of ethylene produced in the photolysis of 3-methyldiazirine assuming that ethylene is produced in the photolysis with a wide spread of internal energy, whose distribution was selected arbitrarily to fit the experimental data. According to this model ethylene produced in the photolysis has a continuous distribution of internal energy from zero to maximum value allowed in the process, and both $C_2H_4^{**}$ and $C_2H_4^{*}$

1) J. R. McNesby and H. Okabe, *Advan. Photochem.*, **3**, 157 (1964).
2) R. F. Hampson, Jr., J. R. McNesby, H. Akimoto, and I. Tanaka, *J. Chem. Phys.*, **40**, 1099 (1964).
3) H. Akimoto, K. Obi, and I. Tanaka, *ibid.*, **42**, 3864 (1965).
4) R. F. Hampson, Jr. and J. R. McNesby, *ibid.*, **42**, 2200 (1965).
5) R. F. Hampson, Jr. and J. R. McNesby, *ibid.*, **43**, 3592 (1965).
6) S. G. Lias, G. J. Collin, R. E. Robbert, and P. Ausloos, *ibid.*, **52**, 1841 (1970).
7) P. Ausloos and S. G. Lias, *ibid.*, **44**, 521 (1966).
8) P. Ausloos and S. G. Lias, *Ber. Bunsenges. Physik. Chem.*, **72**, 187 (1968).
9) H. Akimoto and I. Tanaka, *ibid.*, **72**, 135 (1968).
10) D. W. L. Griffiths and R. A. Back, *J. Chem. Phys.*. **46**, 3913 (1967).
11) K. Obi, H. Akimoto, Y. Ogata, and I. Tanaka, *ibid.*, **55**, 3822 (1971).
12) H. Akimoto and I. Tanaka, *J. Phys. Chem.*, **71**, 4135 (1967).
13) L. S. Kassel, *ibid.*, **32**, 225 (1928).
14) A. W. Kirk and E. Tschuikow-Roux, *J. Chem. Phys.*, **51**, 2247 (1969).

can be in the ground electronic state with different amounts of internal energy. Energized ethylene C_2H_4** can then be interpreted as ethylene whose internal energy is greater than a certain critical value necessary to decomposition, and C_2H_4* as that which retains less energy than the critical value.

This model was further developed[15] for ethylene formed in the photolysis of alkanes at 147.0 nm. In order to predict the distribution of internal energy of ethylene more systematically, a statistical model proposed by Campbell and Schlag[16] was employed. Although the RRKM calculation could predict the nonequilibrium unimolecular decomposition rate in fair agreement with experimental data, we had to introduce a correction parameter (A in Eq. (22) of the paper[15]) whose value was hard to reconcile with the statistical model of energy distribution.

This paper presents a modified version of our previous treatment. In the new model a restriction to the statistical calculation for the initial distribution of internal energy of ethylene has been introduced. In order to test the validity of the new model, comparison with experimental data for the photolysis of ethane, propane, and *n*-butane at different excitation wavelengths and also for the photolysis of fully deuterated compounds was made. The new model was found to give good agreement with all sets of data tested and could predict the wavelength effect and isotope effect quantitatively.

Method

Calculation of k_E. Suppose that ethylene with internal energy E is produced through a molecular elimination process in a vacuum-ultraviolet photolysis of *n*-paraffin. A specific rate constant k_E of the decomposition of energized ethylene into acetylene and hydrogen can be given by the RRKM theory[17,18] as follows.

$$k_E = \frac{1}{h}\frac{\sigma}{\sigma^+}\frac{\sum P(E-E_0)}{N(E)} \tag{11}$$

where σ and σ^+ are the symmetry numbers of the active molecule and the activated complex, respectively. $N(E)$ is the energy level density for the active molecule at energy E, $\sum P(E-E_0)$ the energy-level sum for the activated complex and E_0 the critical energy required for the decomposition of energized ethylene into acetylene and hydrogen. A contribution from the change in moment of inertia between the active molecule and activated complex has been neglected since it is known[15] to be small in the case of a hydrogen elimination process.

In the absence of an internal free rotation as is the case here, $N(E)$ and $\sum P(E-E_0)$ can be approximated by

$$N(E) = \frac{(E+aE_z)^{s-1}}{\Gamma(s)\Pi h\nu_i} \tag{12}$$

$$\sum P(E-E_0) = \frac{(E-E+a^\dagger E^\dagger_z)^{s\dagger}}{\Gamma(s^\dagger+1)\Pi h\nu_i^\dagger} \tag{13}$$

as proposed by Whitten and Rabinovitch.[19] In Eqs. (12) and (13) s and $s^\dagger$ are the numbers of vibrational degrees of freedom, E_z and E_z^+ are the zero point energy, and ν_i and $\nu_i^\dagger$ are vibrational frequencies of active molecule and activated complex, respectively. Energy dependence of parameters a and $a^\dagger$ are calculated using analytical expressions given by Whitten and Rabinovitch[19]

An activated complex having a four-membered ring structure has been considered.[15] The activated complex is assumed to be rigid and the frequencies are taken to be equal to those of ground state ethylene except for one CH stretching mode (B_{2u}) which is taken as a reaction coordinate. All the frequencies used are given in the Appendix. Since the pyrolysis of ethylene proceeds through radical chain mechanism rather than molecular elimination of hydrogen,[20,21] no direct experimental data is available for the value of E_0. Benson and Haugen[22] estimated the activation energy of the reverse reaction, $H_2+C_2H_2\rightarrow C_2H_4$, to be 40 kcal mol^{-1}. From this value and the heat of reaction of the process 41.7 kcal mol^{-1}, *ca.* 80 kcal mol^{-1} is obtained for the activation energy of decomposition as a first approximation. The E_0 value of 78 kcal mol^{-1} for C_2H_4 is chosen since it was found to give the most consistent results. Taking into account the difference in zero point energy between the active molecule and the activated complex, 1 kcal mol^{-1} should be raised, giving 79 kcal mol^{-1} for the decomposition of C_2D_4.

Calculation of $f(E)$. It is expected that ethylene molecules produced in the photolyses of *n*-paraffins will have certain energy spread rather than monoenergetic energy. However, at present there exists no *a priori* method to determine the energy distribution of the products of the reactions. In the photolysis of ethane, propane and *n*-butane, molecular elimination of hydrogen, methane and ethane would respectively give rise to energized ethylene. In such a system the maximum energy E_t available for the energized ethylene can be given by

$$E_t = E_p - \Delta H \tag{14}$$

where E_p is the energy of photon used in the photolysis of parent *n*-paraffin and ΔH the heat of reaction of each molecular elimination process. The values of ΔH we used are 32.7, 19.4 and 22.5 kcal mol^{-1} for the photolysis of ethane, propane and *n*-butane, respectively. Energy E_t may either be distributed among each degree of freedom of product fragments more or less statistically or appear as non-statistical kinetic energy of fragments.

During the course of molecular elimination the following type of transition state is expected:

15) Y. Ogata, K. Obi, H. Akimoto, and I. Tanaka, This Bulletin. **44**, 2671 (1971).
16) R. J. Campbell and E. W. Schlag, *J. Amer. Chem. Soc.*, **89**, 5103 (1967).
17) G. M. Wieder and R. A. Marcus, *J. Chem. Phys.*, **37**, 1835 (1962).
18) B. S. Rabinovitch and D. W. Setser, *Advan. Photochem.*, **3**, 1 (1964).
19) G. Z. Whitten and B. S. Rabinovitch, *J. Chem. Phys.*, **38**, 2466 (1963).
20) I. D. Gay, R. D. Kern, G. B. Kistiakowsky, and H. Niki, *ibid.*, **45**, 2371 (1966).
21) S. W. Benson and G. R. Haugen, *J. Phys. Chem.*, **71**, 1735 (1967).
22) S. W. Benson and G. R. Haugen, *ibid.*, **70**, 3337 (1966).

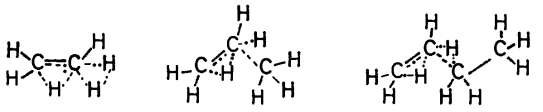

C_2H_6 C_3H_8 n-C_4H_{10}

It is postulated that one of the hydrogen atoms of the methyl group in the "ethylene" part of parent molecule would start to transfer to the adjacent atom while the molecular elimination of H_2, CH_4, and C_2H_6 starts to occur. We assume that the statistical part of the liberated energy would be distributed among "active" vibrational modes which can be defined as vibrational modes whose associated normal coordinates undergo drastic changes during passage through the transition state. The drastic changes mean those of bond length and bond angle for newly formed bond and those of bond angles accompanying a change of hybridization from sp^3 to sp^2. The following vibrational modes should be taken as inactive; three CH stretching modes of "ethylene" part of all n-paraffins; three CH stretching and three CH_3 deformation modes of "methane" part of propane; and five CH stretching, one CC stretching, three CH_3 deformation, one CH_2 scissors, two CH_3 rocking, one CH_2 wagging, one CH_2 twisting and one CH_3 tortional modes of "ethane" part of n-butane. Using a statistical model proposed by Campbell and Schlag,[16] a fraction of the energized ethylene which retains a vibrational energy E out of the total available energy, E_t, can be written as

$$f(E) = \frac{N_{C_2H_4}(E)N_R(E_t-E-E_k)}{\sum N_{C_2H_4}(E_l)N_R(E_t-E_l-E_k)} \quad (15)$$

where E_k is non-statistical kinetic energy, $N_{C_2H_4}(E)$ the energy-level density of the "active" ethylene part of the n-paraffin and $N_R(E_t-E-E_k)$ that of the "active" remaining part of the n-paraffin. The energy-level densities were calculated by means of Eq. (12). All vibrational frequencies used are given in the Appendix.

Comparison with Experiments. Now that the energy distribution of energized ethylene $f(E)$ and the specific rate constant k_E have been calculated, the apparent rate constant k_d can be given[18] by

$$k_d = \frac{\int \frac{k_E}{k_E+\omega} f(E)dE}{\int \frac{1}{k_E+\omega} f(E)dE} \quad (16)$$

where ω is the rate of deactivation of energized ethylene. Throughout this work a strong collision model is assumed, *viz.*, ω is assumed to be equal to the kinetic collision frequency independent of the energy of ethylene. Kinetic treatment[9] of the reaction schemes in Eqs. (1)—(10) gives the relation

$$\frac{\phi(\text{Ethylene})}{\phi(\text{Acetylene})} = \frac{\phi_2+\phi_{1b}}{\phi_{1a}} + \frac{k_s}{k_d}\left(1+\frac{\phi_2+\phi_{1b}}{\phi_{1a}}\right)P \quad (17)$$

which allows us to compare the experimentally determined quantity ϕ(Ethylene)/ϕ(Acetylene) with the calculable quantity of the right hand side of the scheme. In Eq. (17), P is the pressure of n-paraffin, k_s the simple collisional rate constant given by gas kinetics in accordance with the strong collision model ($\omega=k_sP$). The values of k_s we used are 1.43×10^7, 1.58×10^7 and 1.72×10^7 $Torr^{-1}\,s^{-1}$ for ethane, propane and n-butane, respectively. The ϕ_{1a}, ϕ_{1b} and ϕ_2 are defined in schemes (1)—(10). The values of ϕ_2 were determined[2,3,9,11] experimentally. The values we used are given in Table 1 together with the calculated quantities. The values of ϕ_{1a} and ϕ_{1b} are calculated using the energy distribution function $f(E)$, *i.e.* under the restriction of $\phi_{1a}+\phi_{1b}+\phi_2=1$; ϕ_{1a} is put to be equal to the fraction of energized ethylene with energy greater than E_0 and ϕ_{1b} put to be equal to that of energized ethylene with energy less than E_0.

Under the restrictions of all selected values of parameters, only the value of E_k has been left as an adjustable parameter. Selection of the E_k value to give the best fit of calculated curve to the experimental points has been made for each case.

Results and Discussion

The validity of model has been tested by comparing the calculation with the experimental data of the photo-

Table 1. Values of excess energy E_t, relative yields ϕ_{1a}, ϕ_{1b} and ϕ_2, average energy of ethylene $\overline{E}$ and average energy of decomposing ethylene $\overline{E_d}$ associated with non-statistical energy parameter E_k

Parent n-Paraffin	Wavelength nm	E_t kcal mol^{-1}	ϕ_{1a}	ϕ_{1b}	ϕ_2[a]	$\overline{E}$ kcal mol^{-1}	$\overline{E_d}$ kcal mol^{-1}	E_k kcal mol^{-1}
C_2H_6	157.7	149	0.60	0.35	0.05	84	97	13
	147.0	162	0.59	0.26	0.15	88	99	20
	123.6	199	0.50	0.07	0.43	107	113	25
C_2D_6	147.0	162	0.62	0.23	0.15	93	103	10
	123.6	199	0.52	0.05	0.43	115	120	10
C_3H_8	147.0	175	0.26	0.14	0.60	87	101	0
	123.6	212	0.33	0.09	0.58	101	110	10
C_3D_8	147.0	175	0.24	0.14	0.62	87	101	0
	123.6	212	0.39	0.10	0.52	103	112	5
n-C_4H_{10}	147.0	172	0.23	0.14	0.63	85	99	0
	123.6	209	0.24	0.06	0.70	101	110	5
n-C_4D_{10}	147.0	172	0.22	0.15	0.63	85	100	0
	123.6	209	0.28	0.07	0.65	104	113	0

a) Experimentally determined. See Ref. 9, 15, 23.

lysis of C_2H_6,[11,12] C_2D_6,[23] C_3H_8,[11] C_3D_8,[23] n-C_4H_{10}[11] and n-C_4H_{10}[23] at two exciting wavelengths, 147.0 and 123.6 nm. The data for the photolysis of C_2H_6 at 157.7 nm are also available[9] for comparison. The results are presented in Figs. 1—4. The best fit curves were obtained by varying the value of E_K after selecting all other parameters. It should be noted that except E_K the best fit curves for all data were obtained with a common activated complex model, a systematic way of calculation for $f(E)$, and common values of E_0.

Taking into account the fact that the calculated results are very sensitive to selected parameters, and the range of selection of each parameter is not so wide as regards its physical meaning, successful reproduction of experimental data should not be taken as only fortuitous. Calculated values of relative yields ϕ_{1a} and ϕ_{1b}, average internal energy of ethylene $\overline{E}$ and average energy of decomposing ethylene $\overline{E_d}$ are given in Table I, together with the selected values of E_k. An important feature of the model is the successful reproduction of the curvature of the plots[9] of ϕ(Ethylene)/ϕ(Acetylene) *vs.* P in the photolysis of C_2H_6 at 157.7 nm.

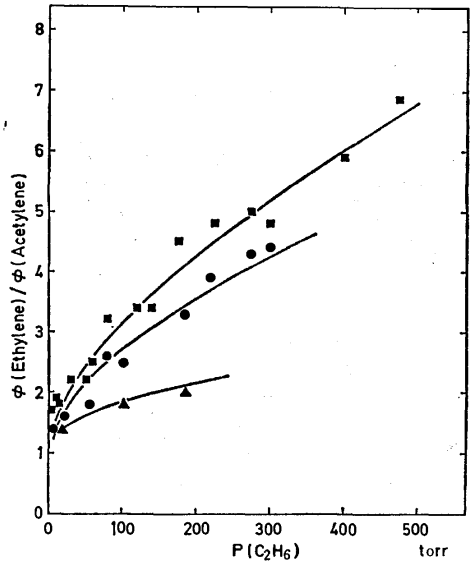

Fig. 1. Calculated ratio of ethylene to acetylene in the photolysis of C_2H_6 (solid lines), compared to experimental results at 157.7 (■), 147.0 (●) and 123.6 nm (▲).

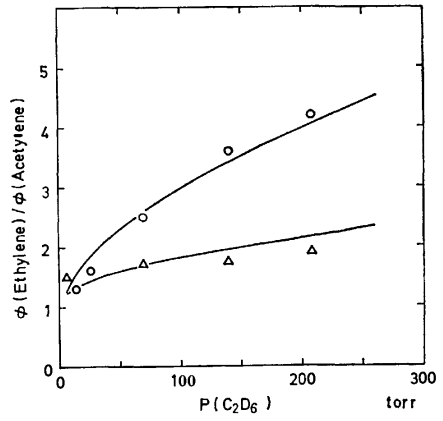

Fig. 2. Calculated ratio of ethylene to acetylene in the photolysis of C_2D_6 (solid lines), compared to experimental results at 147.0 (○) and 123.6 nm (△).

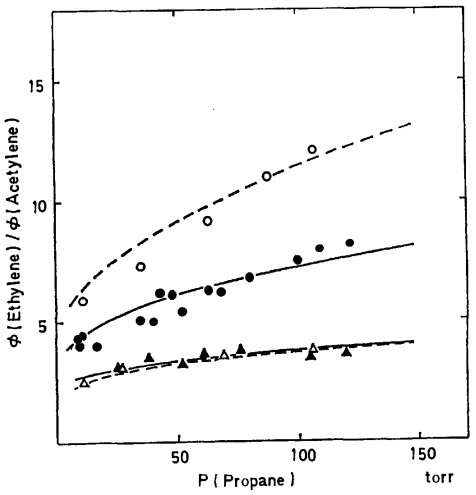

Fig. 3. Calculated ratio of ethylene to acetylene in the photolysis of C_3H_8 (solid lines) and C_3D_8 (dashed lines), compared to experimental results for C_3H_8 at 147.0 (●) and 123.6 nm (▲), and C_3D_8 at 147.0 (○) and 123.6 nm (△).

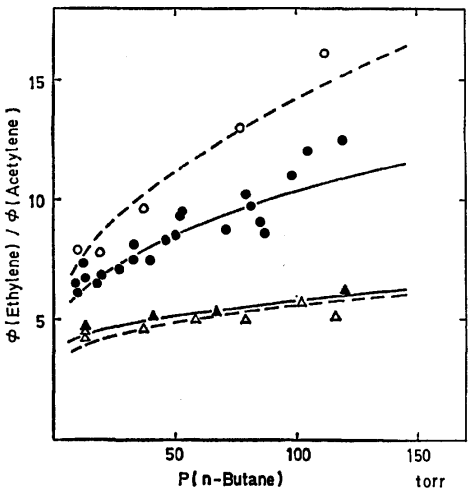

Fig. 4. Calculated ratio of ethyiene to acetylene in the photolysis of n-C_4H_{10} (solid lines) and n-C_4D_{10} (dashed lines), compared to experimental results for n-C_4H_{10} at 147.0 (●) and 123.6 nm (▲) and n-C_4D_{10} at 147.0 (○) and 123.6 nm (△).

According to the present model the curvature results from a very wide spread of internal energy of the energized ethylene formed in the photolysis. Although in all other cases the scatter of experimental points does not allow us to make a clear preference, the non-linear correlation seems to fit the experimental results better than the linear one. The values of ϕ_{1a} and ϕ_{1b} given in Table 1 differ somewhat from those obtained from linear correlation of ϕ(Ethylene)/ϕ(Acetylene) *vs.* pressure plots.[9,12,15] We believe that the linear correlation is true only in appearance and that the k_s/k_d and ϕ_{1a}/ϕ_{1b} values thus obtained are no more than those in a zero approximation. The latter situation has been pointed out by Campbell

23) H. Akimoto and I. Tanaka, unpublished data.

et al.[24] who stated linear plots may not be a sufficient guarantee against a simple two step mechanism.

Production of vibrationally excited polyatomic species in photodissociative processes has been reported in several species. These include the photolysis of cyclobutanone,[16,25] cyclopentanone,[25] methylketene,[26] tetrahydrofuran,[27] 2,3-diazabicyclo[2,2,1]hept-2-ene,[28] *t*-pentyl nitrite,[29] 1-pyrazoline,[30] diazoethane,[31] and 3-methyl diazirine.[32] Generally the excess photon energy has been found to be distributed over the products so that the species formed have a spread of energy. For the case of energized cyclopropane formation, the statistical model which assumes the microscopic equilibration of liberated energy among all degrees of freedom of products, was found[16,30] to be inappropriate to predict the energy partitioning for cyclopropane. Thus the assigned energy for cyclopropane was an underestimate in the case of cyclobutanone and an overestimate in the case of 1-pyrazoline. For the energized ethylene formation in the photolysis of *n*-paraffins,[15] such simple statistical model also failed to predict the energy partition particularly in the case of *n*-butane, where a large negative correction factor was required to reproduce the experimental data. In this work the modified statistical model which introduced an "active" model of energy partitioning was found to be satisfactory at least for the reproduction of experimental data. Although clear justification cannot be made without more information on the potential surface of photodissociation, the assumption we employed is consistent with the general view[29] that a change in an equilibrium bond distance or bond angle during the course of dissociation may lead to preferential excitation of vibrational modes involving the affected bond.

As shown in Table 1 the average energy of decomposing ethylene $\overline{E}_d$ ranges from 97 to 120 kcal mol^{-1}, which is roughly 20—40 kcal mol^{-1} higher than the critical energy E_0. Thus, if an energy quanta transferred by a single collision between *n*-paraffin is as much as 40 kcal mol^{-1}, the strong collision model we used can be justified. Data on an amount of energy transferred by a single collision for deactivation of highly vibrationally excited species are still scarce. Setser *et al.*[33] have shown that ethylene and cyclopropane remove energy from vibrationally excited cyclopropane and methylcyclopropane, respectively, in average steps of at least about 30 kcal mol^{-1} at room temperature. Taking into account the similarity of molecular complexity and the average energy of around 110 kcal mol^{-1} contained in energized cyclopropane and methylcyclopropane in their system, our present system may be analogous to theirs. Thus their conclusion would be applicable to our case and the strong collision assumption may be justified. On the other hand, the photolysis of paraffins in the presence of nitrogen indicates[15] that the collision efficiency of ethane against energized ethylene would be smaller than unity. If this is the case, the best fit of the data is obtained at higher values of E_k, and those given in Table 1 should be taken as a lower limit.

An activated complex model which has the same frequencies as in the ground state molecule except for the reaction coordinate is of course a conventional one. But the selection of the "rigid" model is in accord with the results of quasi-equilibrium theory of ion fragmentation where molecular elimination of hydrogen from a hydrocarbon parent ion is assumed to proceed through a "rigid" activated complex.[34] An activated complex with lower frequencies naturally yields a higher decomposition rate and could not reproduce the experimental data even if other parameters were adjusted.

As shown in Table 1, 13, 20 and 25 kcal mol^{-1} are assigned as suitable values of the non-statistical energy E_k in the photolysis of ethane at 157.7, 147.0 and 123.6 nm respectively. While it is indicated to be close to zero at 147.0 nm in the photolysis of propane and *n*-butane, E_k appears to increase with excitation energy in the case of C_2H_6, and E_k for C_2D_6 appears to be smaller than that for C_2H_6. In the photolysis at 123.6 nm an appreciable amount of E_k may be implied for the elimination of methane from propane and less amount for the elimination of ethane from *n*-butane. Although the assignment of specific values of E_k is difficult for these cases due to the insensitivity of the calculated results to the value of E_k, the trend may be noted that the E_k is smaller for the deuterated compound. Since the reduction of the value of E_0 can be compensated to some extent by the increase of the value of E_k to reproduce experimental data, the value of E_k can not be defined unambiguously. Nevertheless the set of values of E_k would be correct at least relatively (Table 1) since a common value of E_0 was used throughout the calculation.

Non-statistical kinetic energy has been observed in some ion fragmentation processes.[34] Taubert[35] determined experimentally translational energies of some fragment ions after the ionization of paraffins by electron impact. His data suggested that in the elimination of neutral methane from $C_3H_8^+$, the excess energy remains mostly as internal energy of the fragments while in the elimination of a hydrogen molecule from $C_3H_8^+$ and $C_2H_6^+$, part of the excess energy appears as non-statistical kinetic energy to the amount *ca.* 13 and

24) R. J. Campbell, E. W. Schlag, and B. W. Ristow, *J. Amer. Chem. Soc.*, **89**, 5098 (1967).
25) R. F. Klemm, D. N. Morrison, P. Gilderson, and A. T. Blades, *Can. J. Chem.*, **43**, 1934 (1965).
26) D. P. Chong and G. B. Kistiakowsky, *J. Phys. Chem.*, **68**, 1793 (1964).
27) B. C. Roquitte, *ibid.*, **70**, 1334 (1966).
28) D. Durant and G. R. McMillan, *ibid.*, **70**, 2709 (1966).
29) T. F. Thomas, C. I. Sutin, and C. Steel, *J. Amer. Chem. Soc.*, **89**, 5107 (1967).
30) P. Cadman, H. M. Meunier, and A. F. Trotman-Dickenson, *ibid.*, **91**, 7640 (1969).
31) C. L. Kibby and G. B. Kistiakowsky, *J. Phys. Chem.*, **70**, 126 (1966).
32) H. M. Frey and I. D. R. Stevens, *J. Chem. Soc.*, **1965**, 1700.
33) D. W. Setser, B. S. Rabinovitch, and J. W. Simons, *J. Chem. Phys.*, **40**, 1751 (1964).
34) M. L. Vestal, "Ionic Fragmentation Processes," Fundamental Processes in Radiation Chemistry, P. Ausloos ed., Interscience Publishers, New York, N. Y. (1968), p. 59.
35) R. Taubert, *Z. Naturforsch.*, **199**, 911 (1964).

8 kcal mol^{-1}, respectively.[34] Our results agree with this observation, and the parameter E_k would be justified as non-statistical kinetic energy.

Following the present scheme, C_2H_4* has been interpreted to be an electronic ground state ethylene which contains less vibrational energy than a critical value necessary for decomposition. Since experimental data have been reproduced successfully according to this scheme, it seems unnecessary to invoke another long-lived electronic state of ethylene unless direct evidence indicates the presence of such species.

Energized ethylene formed in Eqs. (1), (2), (4), (5),(7) and (8) has been sometimes quoted[12] as "ethylidene". However, so far there is no experimental evidence that ethylidene is produced in a primary process in the photolysis of *n*-paraffins. We could exclude primary processes such as

$$C_2H_6 + h\nu \longrightarrow H_2 + CH_3CH: \quad (18)$$

$$CH_3CH: \longrightarrow C_2H_4** \quad (19)$$

According to an extended Hückel MO calculation,[36] ground state ethylidene CH_3CH: lies 81 kcal mol^{-1} above the ground state of ethylene. Thus ethylene produced through the isomerization of ethylidene should have at least 81 kcal mol^{-1} of internal energy even if ethylidene formed in Eq. (18) is in the lowest vibrational state. Since E_0 is about 80 kcal mol^{-1}, all of the ethylene thus formed should be able to decompose at low enough pressure and should be interpreted as C_2H_4**. Thus there should be another process which forms exclusively ethylene whose internal energy is lower than 80 kcal mol^{-1}, which would hardly be accepted. Formation of ethylidene in the primary step of the photolysis of *n*-paraffin seems improbable.

36) O. P. Strausz, R. J. Norstrom, D. Salahub, R. K. Gosavi, H. E. Gunning, and I. G. Csizmadia, *J. Amer. Chem. Soc.*, **92**, 6395 (1970).

Appendix

The vibrational frequencies of C_2H_4 (C_2D_4) are taken[37] to be 3000(2250), 1600(1500), 1350(1000), 1000(800), 3100-(2300), 1250(900), 950(700), 950(800), 3100(2350), 800-(600), 3000(2200), 1450(1100) cm^{-1} for ν_1 to ν_{12} in order. Exactly the same frequencies were used in activated complex, except for ν_9 which was taken as reaction coordinate.

For normal mode frequencies[37] of *n*-paraffin the average values were assigned to the same type of mode. They are given below, where numbers in parentheses are the number of modes, the two successive numbers being the frequencies in cm^{-1} for hydrogenated and deuterated compounds, respectively. For C_2H_6 and C_2D_6: CH strecthing (6), 3000, 2200; CC stretching (1), 1000, 850; CH_3 deformation (6), 1450, 1100; CH_3 rocking (4), 1000, 800; and CH_3 torsion (1), 300, 200. Three CH stretching modes which correlate to ethylene part were taken as inactive for the calculation of $f(E)$. For C_3H_8 and C_3D_8: CH stretching (8), 3000, 2200; CC stretching (2), 1000, 950; CH_3 deformation and CH_2 scissors (7), 1450, 1100; CH_3 rocking (4), 1100, 800; CH_2 rocking (1), 700, 550; CH_2 twisting and wagging (2), 1300, 950; CCC bending (1), 400; 300; and CH_3 torsion (2), 200, 150. Three CH stretching modes which correlate to ethylene part, and three CH stretching and three CH_3 deformation modes which correlate to methane part were taken as inactive for the calculation of $f(E)$. For *n*-C_4H_{10} and *n*-C_4D_{10}: CH stretching (10), 3000, 2200; CC stretching (3), 1000, 950; CH_3 deformation and CH_2 scissors (8), 1450, 1100; CH_3 rocking (4), 1100, 800; CH_2 rocking (2), 700, 550; CH_2 twisting and wagging (4), 1300, 950; CCC bending (2), 400, 300; CH_3 torsion (2) 200, 150; and CH_2CH_2 torsion (1), 100, 90. Three CH stretching modes which correlate to ethylene part and five CH stretching, one CC stretching, four CH_3 deformation and CH_2 scissors, two CH_3 rocking, two CH_2 twisting and wagging and one CH_3 torsion modes which correlate to ethane part were taken as inactive for the calculation of $f(E)$.

37) T. Shimanouchi, "Table of Molecular Vibrational Frequencies," Part 1, U. S. Department of Commerce, National Bureau of Standards (1967).

Measurement of Negative Ions Formed by Electron Impact. IX. Negative Ion Mass Spectra and Ionization Efficiency Curves of Negative Ions of *m/e* 25, 26, 27, 38, 39, 40 and 50 from Acrylonitrile

Satoru TSUDA, Akira YOKOHATA, and Toshikatsu UMABA

Department of Chemistry, Faculty of Engineering, University of Hiroshima, Senda-machi, Hiroshima 730

(Received November 4, 1972)

Negative ion mass spectra of acrylonitrile were measured for the electron energies of 80, 40 and 9.5 eV. Emphasis was laid on the abundance of the negative ions relative to the positive ions measured for the energies of 80, 40 and 15 eV, respectively. The ionization efficiency (IE) curves were also determined up to 25 eV for the ions of *m/e* 25(C_2H^-), 26(CN^-), 27(HCN^-), 38(C_2N^-), 39($CHCN^-$), 40(CH_2CN^-) and 50(C_3N^-). The electron impact of 80 eV and 40 eV gave almost the same distribution of *m/e* for negative ion mass spectra. Besides the most intense peak of CN^- ions, relatively strong peaks of C_3N^-, C_2H^-, C_2^- and C_2N^- ions were observed. In 9.5 eV, CN^- ions predominated over other ions. Yields of the ions showed a good linearity against the pressure in the range used for usual chemical analysis, irrespective of electron energy. Comparison of the yield of CN^- ions with that of $C_2H_3CN^+$ gave the values 1.2×10^4 and 1.9×10^4 for $C_2H_3CN^+/CN^-$ at 80 eV and 40 eV, respectively, and 47.6 at 9.5 eV (15 eV for the positive ions). The plausible reaction schemes expected to occur at each onset observed in the IE curves were also sought thermochemically by using ΔH_f values of the reactant and products. A value $\gtrsim 2$ eV was obtained for the electron affinity of C_2H.

Studies have been reported on the measurement of negative ion mass spectra by the electron impact method.[1–5] However, they were restricted to a limited number of compounds. Data of ionization efficiency (IE) curves of negative ions are also very limited.[6–10]

IE curves were given for NO_2^-, O^-, $CH_2NO_2^-$, CN^- and CNO^- ions from nitroalkanes,[11] O^- and OH^- ions from *n*-propyl and isopropyl alcohols,[12] O^-, C_2H^- and C_2HO^- ions from tetrahydrofuran,[13] Cl^- ions from alkyl chlorides,[13] CN^-, HCN^-, C_2N^- and $CHCN^-$ ions from methyl and ethyl cyanides.[15] Investigation was extended to acrylonitrile. In this paper we report on negative ion mass spectra for 80eV, 40eV and 9.5 eV, with emphasis on relative abundances to the positive ions for 80 eV, 40 eV and 15 eV, and the IE curves of *m/e* 25(C_2H^-), 26(CN^-), 27(HCN^-), 38(C_2N^-), 39 ($CHCN^-$), 40(CH_2CN^-) and 50(C_3N^-) ions.[16]

Experimental

Experiments were performed on a Hitachi RMU-6D mass spectrometer equipped with a T-2M ion source having a rhenium filament. The ion detector consisted of a ten-stage electron multiplier and a Faraday collector. Experimental conditions: total emission current=20 μA, ion accelerating voltage=3.6 kV, electron multiplier voltage=2.8 kV, sourve pressure $\simeq 10^{-6}$ mmHg. The ionizing current varied from 10.5 μA above 10 eV to 6.4 μA at ~3 eV.[14] The energy scale was calibrated in every measurement by the vanishing current method in comparison with the ionization potential of argon (for positive ions) and the appearance potential of *m/e* 16(O^-) from carbon monoxide, carbon dioxide and oxygen (for negative ions).[11,14] The repeller voltage was adjusted to the best condition to collect positive and negative ions. The sample used was of reagent grade.

Results and Discussion

Negative Ion Mass Spectra. The relative abundances of negative ions for 80 eV, 40 eV and 9.5 eV electron energies are shown in Table 1. Since the data were taken at a pressure of $\sim 10^{-6}$ mmHg in the source, the possibility of ions being induced by ion-molecule reactions may be ruled out. The electron impact of 80 eV and 40 eV gave almost the same distribution of *m/e* for negative ion mass spectra.

The spectra obtained are as follows.

m/e 12(C^-), *m/e* 13(CH^-), *m/e* 14(CH_2^-), *m/e* 24(C_2^-), *m/e* 25(C_2H^-), *m/e* 26(CN^-), *m/e* 27(HCN^-), *m/e* 36(C_3^-), *m/e* 37(C_3H^-), *m/e* 38(C_2N^-), *m/e* 39($CHCN^-$), *m/e* 40(CH_2CN^-), *m/e* 50(C_3N^-), *m/e* 51(HC_3N^-), *m/e* 52($H_2C_3N^-$)

The parent ion (*m/e* 53, $H_3C_3N^-$) was not detected.

1) C. E. Melton, "Mass Spectrometry of Organic Ions," ed by F. W. McLafferty, Academic Press, New York, N. Y. (1963), p. 163.
2) E. W. McDaniel, "Collision Phenomena on Ionized Gases," John Wiley & Sons Inc., New York (1964), p. 368.
3) F. Fiquat-Fayard, *Actions Chim. Biol. Radiations.*, **8**, 31 (1965).
4) R. T. Aplin, H. Budzikieweiz, and C. Djerassi, *J. Amer. Chem. Soc.*, **87**, 3180 (1965).
5) D. F. Munro, J. E. Ahnell, and W. S. Koski, *J. Phys. Chem.*, **72**, 2682 (1968).
6) L. G. Christophorou, R. N. Compton, G. S. Hurst, and P. W. Rienhardt, *J. Chem. Phys.*, **45**, 536 (1966).
7) L. G. Christophorou and R. N. Compton, *Health Physics.*, **13**, 1277 (1967).
8) R. N. Compton and L. G. Christophorou, *Phys. Rev.*, **154**, 110 (1967).
9) T. Sugiura, T. Seguchi, and K. Arakawa, This Bulletin, **40**, 2992 (1967).
10) R. N. Compton, J. A. Stockdale, and P. W. Reinhardt, *Phys. Rev.*, **180**, 111 (1969).
11) S. Tsuda, A. Yokohata, and M. Kawai, This Bulletin, **42**, 614, 1515 (1969).
12) S. Tsuda, A. Yokohata, and M. Kawai, *ibid.*, **42**, 2514 (1969).
13) S. Tsuda, A. Yokohata, and M. Kawai, *ibid.*, **42**, 3115 (1969).
14) S. Tsuda, A. Yokohata, and M. Kawai, *ibid.*, **43**, 1649 (1970).
15) S. Tsuda, A. Yokohata, and T. Umaba, *ibid.*, **44**, 1486 (1971).
16) Recently, the measurement of IE curves of a few ion species was reported. However, no discussion is given on the plausible reaction schemes expected to appear at each onset value (T. Sugiura, Discussion Meeting of the Research Reactor Institute of Kyoto University, January 14, (1968)).

Table 1. Relative abundances of negative ions (normalized to $[CN^-]=100$)

m/e	Probable negative ion	Relative abundances		
		80 eV	40 eV	9.5 eV
12	C	1.46	0.76	
13	CH	0.39	0.85	0.07
14	CH_2	0.06	0.05	0.04
24	C_2	11.20	7.26	0.10
25	C_2H	34.20	36.80	0.91
26	CN	100.00	100.00	100.00
27	HCN	1.47	1.26	1.32
36	C_3	2.39	1.76	
37	C_3H	0.58	0.78	
38	C_2N	2.90	3.55	0.46
39	CHCN	0.89	0.81	2.31
40	CH_2CN	0.04	0.04	0.26
50	C_3N	50.80	61.70	4.45
51	C_2HCN	1.86	2.88	0.78
52	C_2H_2CN	0.47	0.76	0.02

Relatively strong peaks were observed at *m/e* 50(C_3N^-), *m/e* 25(C_2H^-) and *m/e* 24(C_2^-) ions for 80 eV and 40 eV, besides the most intense peak at *m/e* 26(CN^-). The situation is quite similar to that for ethyl cyanide. This shows that C_3N^-, C_2H^- and C_2^- ions are stable, while electron affinities of C_3N and C_2 between them are known to be $EA(C_3N)=2.4$ eV[17] and $EA(C_2)=3.1$ eV.[18] However, the values of $EA(C_2H)$ and $EA(C_2N)$ are not known. The change of relative abundances with electron energies (80→40 eV) was relatively great for C^-, CH^-, C_2^-, C_3^-, C_3HN^- and $C_3H_2N^-$ ions.

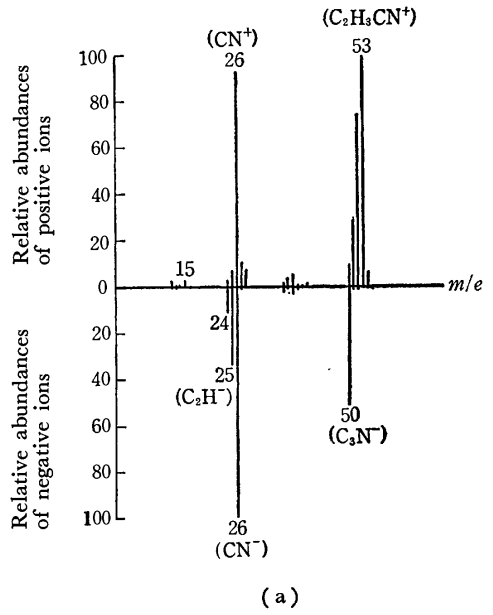

(a)

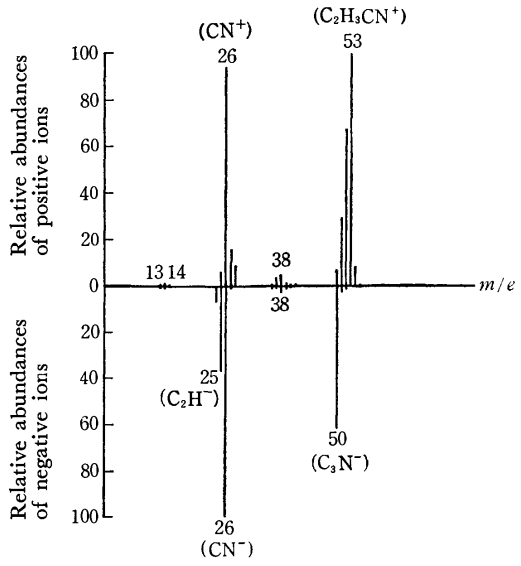

(b)

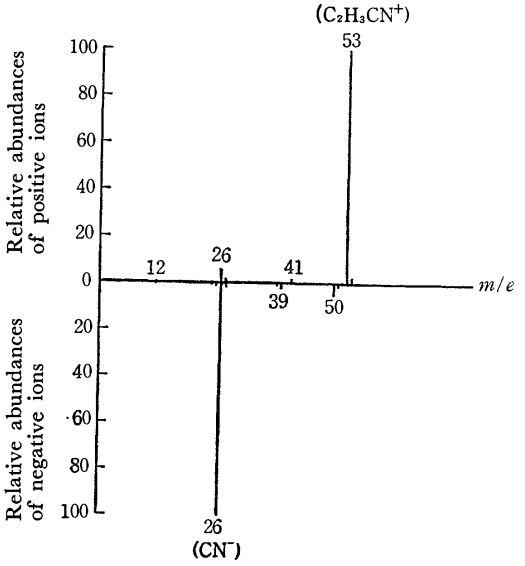

(c)

Fig. 1. Positive and negative ion mass spectra of acrylonitrile (Pressure in the source, $\sim 10^{-6}$ mmHg).
(a): 80 eV, $C_2H_3CN^+/CN^- \simeq 1.2\times 10^4$
(b): 40 eV, $C_2H_3CN^+/CN^- \simeq 1.9\times 10^4$
(c): 15 eV for positive ions, 9.5 eV for negative ions, $C_2H_3CN^+/CN^- \simeq 47.6$

In 9.5 eV electron energy, *m/e* 26(CN^-) ions predominated over other negative ions. Since the dissociative electron capture process governs the reaction in a lower energy region, the yield should depend on the cross section of each process. The IE curves of CN^-, C_3N^-, C_2H^-, C_2N^-, HCN^-, $CHCN^-$ and CH_2CN^- ions are given.

Figure 1 shows the negative ion mass spectra for 80 eV, 40 eV and 9.5 eV electron energies in relation to the positive ion mass spectra at 80 eV, 40 eV and 15 eV.[19] Comparison of the yield of CN^- ions with

17) V. H. Dibeler, R. M. Reese, and J. L. Franklin, *J. Amer. Chem. Soc.*, **83**, 1813 (1961).

18) C. I. Vedeneyev, L. V. Gurvich, V. N. Kandrat'yev, V. A. Medvedev, and Ye. L. Frankevich, "Bond Energies, Ionization Potentials and Electron Affinities," Bulter Tranner Ltd., London (1966) p. 194.

19) Since the formation of positive fragment ions cannot be expected from the impact of 9.5 eV electrons, the data for 15 eV electrons were used for comparison for the sake of convenience.

that of $C_2H_3CN^+$ ions (the most intense peak among the positive ions) gave $C_2H_3CN^+/CN^- \simeq 1.2\times10^4$ and 1.9×10^4 at 80 eV and 40 eV electron energies, respectively. The ratio of the yield of CN^- ions at 9.5 eV to that of $C_2H_3CN^+$ ions at 15 eV gave the value $C_2H_3CN^+/CN^- \simeq 47.6$.

Effect of Pressure. Figure 2 shows the plot of the yield of *m/e* 26(CN^-), 50(C_3N^-), 38(C_2N^-) and 39($CHCN^-$) ions against pressure, where the electron energy used was 80 eV. All the results showed a good linearity, which are consistent with the findings for *m/e* 1(H^-) ion from hydrogen,[20] *m/e* 39(CH_3CC^-) ion from methylacetylene,[21] *m/e* 46(NO_2^-), 16(O^-), 26(CN^-) and 42(CNO^-) ions from nitroalkanes,[11] *m/e* 26(CN^-), 27(HCN^-), 38(C_2N^-), 39($CHCN^-$) and 40(CH_2CN^-) ions from methyl- and ethylcyanides.[22] The linear correlations against pressure were independent of electron energy. The pressure dependency may become complicated at higher pressures because of the occurrence of ion-molecule reactions.

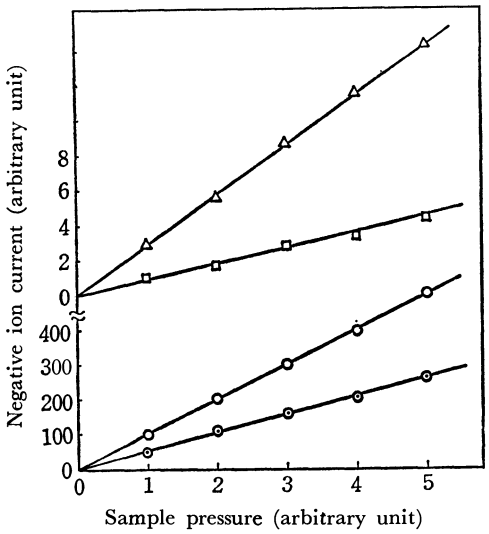

Fig. 2. Plot of negative ion current against pressure. (electron energy, 80 eV)
○ CN^- ⊙ C_3N^- △ C_2N^- □ $CHCN^-$

IE Curves; CN^- ions. Figure 3(a) shows the IE curve of *m/e* 26(CN^-) ions. At least three processes appear to take place. The first process appears at lower energies than 2 eV, the second process at ~3.0 eV[23] and the third process at ~5.8 eV. The shape of the IE curve suggests a dissociative electron capture process except for the part in a higher energy region.

The appearance potential (*AP*) of reaction (1) can be expressed by Eq. (2), if the kinetic energies of the fragment are ignored and the ions formed are in the ground state.

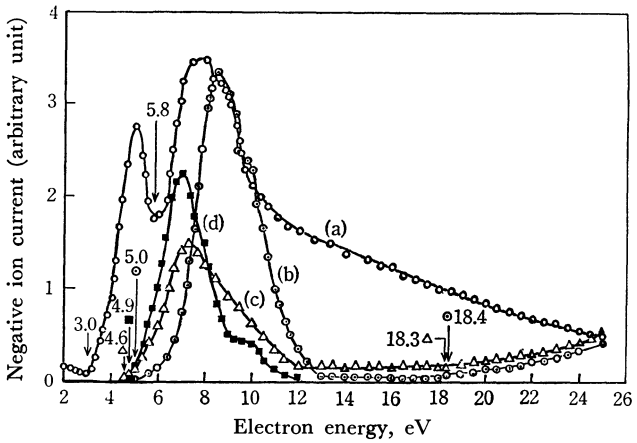

Fig. 3. Ionization efficiency curves of *m/e* 26(CN^-), *m/e* 25(C_2H^-) and *m/e* 38(C_2N^-) ions.
○ CN^- ⊙ C_3N^- △ C_2H^- ■ C_2N^-

$$XYZ + e^- \longrightarrow X^- + YZ \quad (1)$$

$$AP_{calcd} = \Delta H = \Delta H_f(X^-) + \Delta H_f(YZ) - \Delta H_f(XYZ) \quad (2)^{24}$$

In the case of ion pair formation ($XYZ \rightarrow X^-YZ^+$), the following equation holds.

$$AP_{calcd} = \Delta H = \Delta H_f(X^-) + \Delta H_f(YZ^+) - \Delta H_f(XYZ) \quad (3)$$

From Eqs. (2) and (3), schemes of the reactions expected to occur at each onset value (AP_{obsd}) were sought thermochemically.

For the first process, we have

$$C_2H_3CN + e^- \longrightarrow CN^- + C_2H_3 (AP_{calcd} = 1.3\ eV) \quad (4)$$

In the estimation of AP_{calcd}, the values of $\Delta H_f(C_2H_3CN) = 2$ eV,[25] and $\Delta H_f(CN^-) = 0.47$ eV and $\Delta H_f(C_2H_3) = 2.83$ eV[26] were used. The first process appearing at <2 eV would probably correspond to reaction (4). Combining $\Delta H_f(C_2H_3CN) = 2$ eV with $\Delta H_f(CH_2) = 2.5$ eV[26] and $\Delta H_f(CHCN) = 4.2$ eV,[15] we obtain $D(CH_2{=}CHCN) = 4.7$ eV. This is reasonable as compared with $D(CH_2{=}CH_2) = 5.2$ eV.[18] The CN radical is expected to weaken the C=C bond. A previous value $\Delta H_f(CHCN) = 4.2$ eV[15] might also be mentioned.

For the second process, we have

$$C_2H_3CN + e^- \longrightarrow CN^- + C_2H_2 + H \quad (AP_{calcd} = 3.08\ eV) \quad (5)$$

$$\longrightarrow CN^- + C_2H + H_2 \quad (AP_{calcd} = 3.47\ eV) \quad (6)$$

Estimation of each AP_{calcd} value was made with the use[26] of $\Delta H_f(C_2H_2) = 2.35$ eV, $\Delta H_f(H) = 2.26$ eV and $\Delta H_f(C_2H) = 5.0$ eV. A good consistency of $AP_{calcd} = 3.08$ eV with $AP_{obsd} \simeq 3.0$ eV suggests the possibility of the occurrence of reaction (5) rather than (6).

For the third process, we have

20) G. J. Schulz, *Phys. Rev.*, **113**, 816 (1959).
21) T. Sugiura, T. Seguchi, and K. Arakawa, This Bulletin, **40**, 2992 (1967).
22) S. Tsuda, A. Yokohata, and T. Umaba, *ibid.*, **43**, 3383 (1970).
23) Exact determination of appearance potential of the 2nd and 3rd processes is difficult, since the tailing due to the 1st and 2nd processes and their appearance might overlap. In this work, the minimum values in the IE curves have been discussed as by Schulz (G. J. Schulz, *Phys. Rev.*, **113**, 816 (1959)).
24) ΔH (X): heat of formation of X.
25) From $\Delta H_f(C_3H_3N^+) = 12.8$ eV and $IP(C_2H_3CN) = 10.75$ eV, $\Delta H_f(C_2H_3CN) \simeq 2$ eV can be estimated (J. D. Morrison and A. J. C. Nicholson, *J. Chem. Phys.*, **20**, 1021 (1952)).
26) R. R. Bernecker and F. A. Long, *J. Phys. Chem.*, **65**, 1565 (1961).

$$C_2H_3CN + e^- \longrightarrow CN^- + CH_2 + CH \quad (AP_{calcd} = 7.13\ eV)^{27)} \quad (7)$$

$$\longrightarrow CN^- + C_2H + 2H \quad (AP_{calcd} = 7.99\ eV) \quad (8)$$

$$\longrightarrow CN^- + C_2 + H + H_2 \quad (AP_{calcd} = 9.25\ eV)^{28)} \quad (9)$$

However, each AP_{calcd} value does not fit $AP_{obsd} \simeq 5.8$ eV. Reaction (10) might be possible. The value of C_2H_2* can be estimated to be $\sim$2.7 eV.

$$C_2H_3CN + e^- \longrightarrow CN^- + C_2H_2^* + H \quad (10)$$

C_3N^- Ions. Figure 3(b) shows the IE curve of *m/e* 50(C_3N^-) ions with relatively strong peaks. Its shape suggests a dissociative electron capture process and an ion pair formation process. The former appears at $\sim$5 eV and the latter at $\sim$18.4 eV.

On the basis[17] of $\Delta H_f(C_3N) = 131$ kcal/mol and $EA(C_3N) = 55$ kcal/mol,[29] AP_{calcd} values of reactions (11) and (12) can be estimated as follows.

$$C_2H_3CN + e^- \longrightarrow C_3N^- + H_2 + H \quad (AP_{calcd} = 3.57\ eV) \quad (11)$$

$$\longrightarrow C_3N^- + H_2 + H^+ \quad (AP_{calcd} = 17.16\ eV) \quad (12)$$

The difference between AP_{obsd} and AP_{calcd}, $\sim$1.43 eV or $\sim$1.23 eV would be ascribed to an excess energy of C_3N^- ion.

C_2H^- Ions. Figure 3(c) shows the *IE* curve of *m/e* 25(C_2H^-) ions, where the first process appears at $\sim$4.6 eV and the second process at $\sim$18.3 eV. The values of $\Delta H_f(C_2H) \simeq 5$ eV, $\Delta H_f(HCN) = 1.3$ eV and $\Delta H_f(CN) = 3.87$ eV result in $AP_{calcd} = 6.56$ eV for reaction (13) and $AP_{calcd} = 6.87$ eV for reaction (14).

$$C_2H_3CN \longrightarrow C_2H + H + HCN \quad (AP_{calcd} = 6.56\ eV) \quad (13)$$

$$\longrightarrow C_2H + H_2 + CN \quad (AP_{calcd} = 6.87\ eV) \quad (14)$$

If an electron affinity of C_2H is assumed to be 1.96 eV, we have the following schemes.

$$C_2H_3CN + e^- \longrightarrow C_2H^- + H + HCN \quad (AP_{calcd} = 4.6\ eV) \quad (15)$$

$$\longrightarrow C_2H^- + H_2 + CN \quad (AP_{calcd} = 4.91\ eV) \quad (16)$$

$$\longrightarrow C_2H^- + H^+ + HCN + e^- \quad (AP_{calcd} = 18.19\ eV)^{30)} \quad (17)$$

$$\longrightarrow C_2H^- + H + HCN^+ + e^- \quad (AP_{calcd} = 18.46\ eV)^{31)} \quad (18)$$

$$\longrightarrow C_2H^- + H_2 + CN^+ + e^- \quad (AP_{calcd} = 20.04\ eV)^{32)} \quad (19)$$

If we assume $EA(C_2H) = 2.27$ eV we get the following results.

$$C_2H_3CN + e^- \longrightarrow C_2H^- + H + HCN \quad (AP_{calcd} = 4.29\ eV) \quad (20)$$

$$\longrightarrow C_2H^- + H_2 + CN \quad (AP_{calcd} = 4.6\ eV) \quad (21)$$

$$\longrightarrow C_2H^- + H^+ + HCN + e^- \quad (AP_{calcd} = 17.88\ eV) \quad (22)$$

$$\longrightarrow C_2H^- + H + HCN^+ + e^- \quad (AP_{calcd} = 18.15\ eV) \quad (23)$$

$$\longrightarrow C_2H^- + H_2 + CN^+ + e^- \quad (AP_{calcd} = 19.73\ eV) \quad (24)$$

Reaction (19) or (24) might be excluded. This suggests the possibility of reaction (15) rather than reaction (16). Introduction of $EA(C_2H) = 1.96$ eV appears to make the assignment of reactions (15) and (17) or (18) possible. To assume $EA(C_2H) = 2.27$ eV requires 0.31 eV and 0.42 eV or 0.15 eV for an excess energy of C_2H^- ion under the assignment of reactions (20) and (22) or (23). Although the possibility of excess energy of the fragment makes the situation complicated, it should be noted that the value of the electron affinity of C_2H is relatively large and the value of $EA(C_2H) \gtrsim 2$ eV is reasonable.

C_2N^- Ions. As shown in Fig. 3(d), the shape of the IE curve is a little complicated in the range 9—11 eV. We got $AP_{obsd} \simeq 4.9$ eV. The values of $\Delta H_f(C_2N) = 5.3$ eV and $\Delta H_f(CH_3) = 1.39$ eV give a value of 4.69 eV for AP_{calcd} of reaction (25), $AP_{calcd} = 8.06$ eV also for reaction (26).

$$C_2H_3CN \longrightarrow C_2N + CH_3 \quad (AP_{calcd} = 4.69\ eV) \quad (25)$$

$$\longrightarrow C_2N + CH_2 + H \quad (AP_{calcd} = 8.06\ eV) \quad (26)$$

Combining AP_{calcd} (=8.06 eV) with AP_{obsd} ($\simeq$4.9 eV), we have $EA(C_2N) \simeq 3.16$ eV. Judging from $EA(CN) = 3.4$ eV, $EA(C_3N) = 2.4$ eV and $EA(C_5N) = 2.3$ eV, the value of $EA(C_2N) \simeq 3.16$ eV is reasonable, in other words, the following reaction would be assigned.

$$C_2H_3CN + e^- \longrightarrow C_2N^- + CH_2 + H \quad (27)$$

The following ion-pair process was difficult to detect.

$$C_2H_3CN + e^- \longrightarrow C_2N^- + H^+ + CH_2 + e^- \quad (AP_{calcd} \simeq 18.5\ eV) \quad (28)$$

HCN^-. Three processes were observed (Fig. 4(a)). The values of AP_{obsd} were $\ll$2 eV, 3.0 eV and 5.6 eV. Although the possibility of $C_2H_3^-$ ions for *m/e* 27 ions might be considered, combining of AP_{calcd} (=4.7 eV) of reaction (29) with AP_{obsd} lower than 2 eV leads to $EA(C_2H_3)$ larger than 2.7 eV. This seems to be too large to be acceptable. Thus, it can be excluded:

$$C_2H_3CN \longrightarrow C_2H_3 + CN \quad (AP_{calcd} = 4.7\ eV) \quad (29)$$

Using $EA(HCN) \gtrsim 1$ eV[15] and $(C_2H_2)^* = 2.7$ eV (introduced temporarily) the following reactions might be assigned.

$$C_2H_3CN + e^- \longrightarrow HCN^- + C_2H_2 \quad (AP_{calcd} \lesssim 0.65\ eV) \quad (30)$$

$$\longrightarrow HCN^- + C_2H_2^* \quad (AP_{calcd} \lesssim 3.35\ eV) \quad (31)$$

27) $\Delta H_f(CH) = 6.16$ eV (refer to 26).
28) $\Delta H_f(C_2) = 8.52$ eV (refer to 18).
29) $EA(X)$: electron affinity of X.
30) $IP(H) = 13.59$ eV (refer to 26). $IP(X)$: ionization potential of X.
31) $IP(HCN) = 13.86$ eV (refer to 18).
32) $IP(CN) = 15.13$ eV (refer to 18).

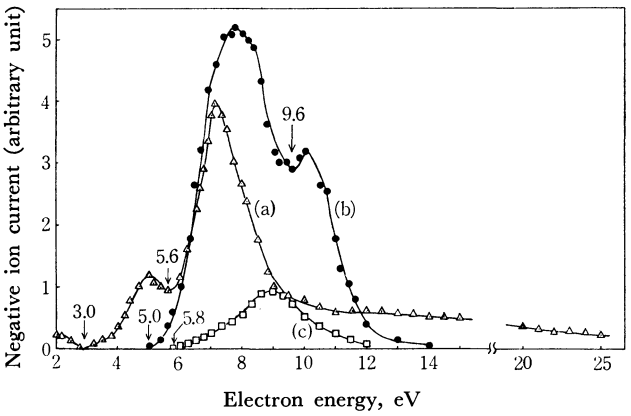

Fig. 4. Ionization efficiency curves of *m/e* 27(HCN^-), *m/e* 39($CHCN^-$) and *m/e* 40(CH_2CN^-) ions.
△ HCN^- ● $CHCN^-$ □ CH_2CN^-

$$\longrightarrow HCN^- + C_2H + H \quad (AP_{calcd} \leq 5.56\ eV) \qquad (32)$$

$CHCN^-$ Ions. Figure 4(b) shows $AP_{obsd}=5.0$ eV and 9.6 eV. By using $\Delta H_f(CHCN)=4.2$ eV[15] we have

$$C_2H_3CN \longrightarrow CHCN + CH_2 \quad (AP_{calcd} = 4.7\ eV) \qquad (33)$$

Moreover, $EA(CHCN) \geqq 1.1$ eV[15] leads to the following result.

$$C_2H_3CN + e^- \longrightarrow CHCN^- + CH_2 \quad (AP_{calcd} \leq 3.6\ eV) \qquad (34)$$

Thus, combining of AP_{calcd} with AP_{obsd} (=5.0 eV) requires a value of $\geqq 1.4$ eV as an excess energy of the fragment.

Next, let us consider the possibility of $C_3H_3^-$ ions.

$$C_2H_3CN \longrightarrow C_3H_3 + N \quad (AP_{calcd} = 5.9\ eV)^{33} \qquad (35)$$

Introduction of $EA(C_3H_3)=0.9$ eV appears to make possible the interpretation of $AP_{obsd}=5$ eV. Since no $C_3H_3^-$ ion from hydrocarbons has been obtained, they may be excluded.

For $AP_{obsd}=9.6$ eV, the following reaction would be assigned.

$$C_2H_3CN + e^- \longrightarrow CHCN^- + CH + H \quad (AP_{calcd} \leq 9.52\ eV) \qquad (36)$$

CH_2CN^- Ions. These ions show only one process having the appearance potential at ~5.8 eV (Fig. 4(c)). $\Delta H_f(CH_2CN)=1.96$ eV,[15] $EA(CH_2CN) \geqq 1.64$ eV[15] and $\Delta H_f(CH)=6.16$ eV give a value of $\leqq 4.48$ eV for AP_{calcd} of the following reaction.

$$C_2H_3CN + e^- \longrightarrow CH_2CN^- + CH \quad (AP_{calcd} \leq 4.48\ eV) \qquad (37)$$

The reaction might also be accompanied with an excess energy of fragments; $\geqq 1.32$ eV.

33) $\Delta H_f(C_3H_3)=3.0$ eV (refer to 26). $\Delta H_f(N)=4.9$ eV (refer to 18).

BULLETIN OF THE CHEMICAL SOCIETY OF JAPAN, VOL. 46, 2277—2279 (1973)

Improvement of Zone Melting Apparatus. I. Zone Melting Apparatus with a Device to Prevent Breakage of a Sample Tube

Nobuko I. WAKAYAMA, Yasuko NAKANO, and Yo-ichiro MASHIKO
National Chemical Laboratory for Industry, Honmachi, Shibuya-ku, Tokyo 151

(Received November 14, 1972)

A glass sample tube is widely used in zone melting of organic substances since it is transparent, inert to most substances and easily prepared in the laboratory. The glass tube, however, is frequently broken owing to the volume increase of the sample. A new device was worked out to prevent breakage of the sample tube, to purify the sample efficiently and to make replacement of the atmosphere inside the sample tube possible. The apparatus requires much less space than for one ever reported and consists of a sample tube with a set of stainless steel spring and Teflon plug and a new mechanism for carrying it. It was successfully used for biphenyl and *p*-dichlorobenzene.

Zone melting with a sample container is sometimes useful in preparing very pure materials which have high vapor pressure and low surface tension. A glass tube is usually used as a sample container because of its transparency, inertness to most substances and applicability up to 500 °C. However, it undergoes frequent breakage due to volume increase of the sample during zone melting. This paper deals with a new zone melting apparatus which prevents breakage and operates safely and reliably.

The following two methods have been reported to prevent breakage of the sample tube. (a) A glass plug is inserted into the open end of a Teflon sample tube, or a Teflon stick is used as a plug of a glass sample tube for absorbing the volume change of the sample.[1,2] (b) A spring and a tapered glass are put at the bottom of the sample tube for the same purpose.[3]

In order to obtain ultra-pure organic compounds by the zone melting method, gases which react with molten organic compounds and produce some impurities must be removed. Thus for the preparation of the ultra-pure sample for phosphorescence and fluorescence

1) M. J. Joncich and D. R. Bailey, *Anal. Chem.*, **32**, 1578 (1960).
2) N. J. G. Bollen, M. J. van Essen, and W. M. Smit, *Anal. Chim. Acta*, **38**, 279 (1967).
3) F. Ordway, *Anal. Chem.*, **37**, 1178 (1965).

measurement, the atmosphere of the sample tube should be kept under vacuum or replaced by an inert gas. When compounds such as alkali halides, which decompose at melting in the air are to be purified, the atmosphere should be replaced by gases such as halogens.

Thus attention should be focused on replacement of atmosphere as well as protection from breakage of the sample tube. Method (a) is insufficient for replacing atmosphere because of lack in air-tightness.

In our method we used a sealed glass sample tube containing a Teflon plug and a stainless steel spring as a buffer for volume change of sample as shown in Fig. 1 (a), (b). A Teflon plug is more easily made than a glass bar. It is inert to organic compounds and has low thermal conductivity, but is not suitable for use at temperature above 250 °C. When this sample tube is used, each molten zone should be formed first at a point adjacent to the Teflon plug with the heater H 1 in order that the volume increase caused by melting is absorbed by the spring.

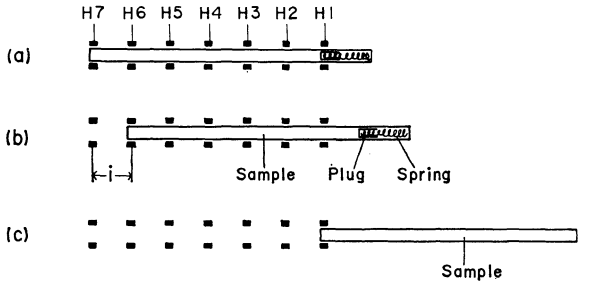

Fig. 1. Reciprocal motion in zone melting. In our mechanism a sample tube reciprocates the distance i between the position (a) and (b). With Sloans' mechanism, at first a sample tube starts from the position (c).

Sloan and McGowan[4] reported a method preventing breakage of the sample tube without the use of a spring and a plug. All the heaters are kept on during the operation in their case. At first a sample tube is located out of the row of the heaters as shown in Fig. 1(c). It slowly moves through the row of the heaters till the left end of the sample tube comes across the left end heater. Then the sample tube reciprocates the distance between the two neighbouring heaters.

We have devised a new mechanism of carriage which requires half the space used by Sloan and McGowan for movement of the sample tube. It operates automatically from beginning to end. First the tube is located at position (a) in Fig. 1. While the heater H 1 is on, it travels one interval i slowly to position (b). The volume increase of molten zone pushes the plug in order to be absorbed by the spring. The tube then returns to the initial position (a) in a few seconds. The zone molten by H 1 is now located at the position H 2. At this moment the heater H 2 is switched on and the sample tube moves from position (a) to (b) again slowly. The heater H 1 makes a new molten zone again. The volume increase of a newly molten zone is also absorbed by the spring. Thus at each return the heaters are switched on one by one, H 1, H 2, H 3, ····· starting from the bottom of the sample tube. After all the heaters are switched on, they are maintained until the end of the zone melting operation.

Even if any buffer is placed at one end of the sample tube, it cannot absorb the volume increase in the middle of the tube when all the heaters are switched on at once. Thus when many heaters are used to improve the efficiency of zone melting, mere insertion of a plug and a spring is unsatisfactory for preventing breakage perfectly. Our new mechanism of carrying the sample tube and switching on the heaters makes the spring absorb every volume increase of a molten zone, thus preventing breakge of the sample tube perfectly, purifying the sample efficiently and requiring much less space than that previously reported. In addition the replacement of atmosphere is accomplished.

Description of Apparatus

A diagram of the sample tube is given in Fig. 1 (a), (b). Tubes with 10 or 25 mm in outer diameter and 1200 mm in length were used. The apparatus is shown in Fig. 2. The sample tube driven by a motor M 1 travels horizontally one interval i (50 mm) for 2/3, 1, 2 or 4 hours and returns rapidly by another motor M 2 through the row of sixteen heaters H and seventeen coolers C. The rate of the tube is changeable by the combination of the gears G 1,2. Water flows through the coolers. The heaters are made of nichrome wire. Switching on the heaters and movement of the tube are controlled by a microswitch Ms. The tube supported by a roller R rotates by a motor M 3 (44 r.p.m.) to make the concentration of liquid zone uniform.

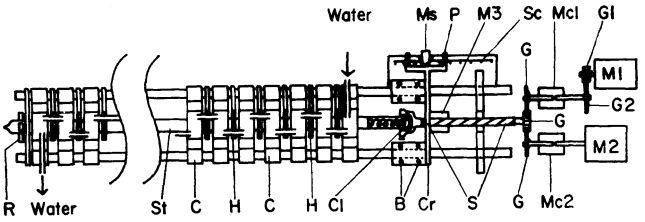

Fig. 2. The figure of zone meting apparatus.
B: Ball-bearing, C: Cooler, Cl: Clamp to connect St and M3, Cr: Carriage of M3, Cl and P, G, Gl, 2: Gear, H: Heater, Ml, 2: Synchronous motor to move Cr, M3: Motor to rotate St, Mc: Magnetic clutch, Ms: Microswitch, P: Piece to push microswitch Ms, R: Roller to support St, S: Male and female screw, Sc: Scale, St: Sample tube.

Results and Discussion

Most organic compounds expand when they melt. The apparatus was tested with biphenyl (volume change 12%, mp 71 °C) and *p*-dichlorobenzene (22%, 53 °C) in nitrogen atmosphere. In the case of biphenyl the sample near the plug was colorless and transparent crystals with cracks. Far from the plug yellowish crystals rich in impurities were observed. When biphenyl was zone refined using a 25 mm O. D. sample tube, the movement of the plug was observed. The result was as follows: The number of zone passes 3- the distance of the movement 7 mm, 8—18 mm,

4) G. J. Sloan and N. H. McGowan, *Rev. Sci. Instr.*, **34**, 60 (1963).

13—26 mm, 24—41 mm, 27—50 mm. A similar result was obtained for *p*-dichlorobenzene. The apparatus will be useful for other organic compounds which expand on melting.

The authors are indebted to Mr. K. Tsuji of the Institute for Solid State Physics, the University of Tokyo, for his valuable advice and technical help in the construction of the apparatus.

BULLETIN OF THE CHEMICAL SOCIETY OF JAPAN, VOL. 46, 2279—2284 (1973)

ESR Studies on Radical Anions of Calicene Derivatives

Shiro KONISHI, Shigeya NIIZUMA, Hiroshi KOKUBUN, and Masao KOIZUMI
Department of Chemistry, Faculty of Science, Tohoku University, Aoba, Aramaki, Sendai 980

(Received December 18, 1972)

Two calicene derivatives, 1,2,3,4-tetrachloro-5,6-diphenylcalicene and 1,2,3,4-tetrachloro-5,6-di-*n*-propylcalicene, were reduced with an alkali metal in degassed tetrahydrofuran and the ESR spectra of the resluting mono-anion radicals were investigated. It was found that in both anion radicals the unpaired spin does not exist on the five-membered ring, and is localized only on the other part. In the latter anion radical, the five-membered and three-membered rings were found to be twisted toward each other at about 45°, a line width alternation caused by hindered internal rotation of two adjacent *n*-propyl groups being observed. The potential barrier for the hindered rotation was determined to be about 1.5 kcal/mol.

Cycloheptatrienecyclopentadiene, commonly called calicene, has a very unique structure consisting of unsaturated five-membered and three-membered rings bonded to each other. Its derivatives were first synthesized by Kende and Izzo,[1,2] Jones and Pyron[3] and also by Prinzbach and Fischer.[4] Since then, many derivatives have been synthesized, their physical and chemical properties being studied extensively. However, no ESR studies on their ion radicals have yet been reported.

Using two species of calicene derivatives, 1,2,3,4-tetrachloro-5,6-diphenylcalicene [PhC] and 1,2,3,4-tetrachloro-di-*n*-propylcalicene [PrC], we succeeded in preparing their anion radicals. This paper reports the details of ESR studies on these anion radicals which were briefly reported previously.[5]

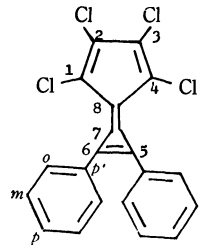

[PhC]

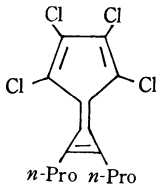

[PrC]

Experimental

Materials. Two calicene derivatives PhC and PrC were prepared by Ueno *et al.* and Kitahara *et al.*[6,7] Tetrahydrofuran [THF] (Wako Junyaku Co.) was distilled after being refluxed over sodium wire for several hours, dehydrated with sodium-potassium alloy and degassed by freeze-thaw cycles. Sodium (Wako Junyaku Co.) and potassium (Kanto Kagaku Co.) metals were used.

Procedures. Anion radicals were prepared by bringing degassed THF solutions of calicenes into contact below −30 °C with a sodium or a potassium mirror deposited by vacuum evaporation.

In the case of PhC, the solution turned bluish green when it was warmed slowly up to room temperature. The anion radical thus obtained was very stable at room temperature giving a well resolved ESR spectrum. However, it turned reddish brown and lost the ESR signal when kept in contact with the mirror for a long time.

In the case of PrC, the ESR signals observed at low temperatures disappeared rapidly when warmed to room temperature. We therefore introduced the degassed solution previously cooled in a dry ice-methanol bath into a glass capillary also degassed, with an alkali metal mirror deposited on the wall, and immediately inserted the capillary into a low temperature apparatus attached to an ESR cavity. In this way the light yellow solution gave a stable ESR signal below −30 °C where the temperature dependence was reversible. With a gradual rise of temperature above −30 °C, the pattern of the signal changed irreversibly and finally disappeared at room temperature.

A JEOL P-10 type ESR spectrometer (X band, 100 kHz modulation) was used. A NEAC 2200 MODEL 500 Electronic Computer in the Calculation Center of Tohoku University was used for the simulation of ESR spectra and the calculation of spin densities.

Results and Discussion

Hyperfine Structure. Figure 1 shows the observed and simulated ESR spectra of PhC anion radical obtained with the use of sodium and potassium. Only

1) A. S. Kende and P. T. Izzo, *J. Amer. Chem. Soc.*, **87**, 1609 (1965).
2) *idem*, *ibid.*, **87**, 4142 (1965).
3) W. M. Jones and R. S. Pyron, *ibid.*, **87**, 1608 (1965).
4) H. Prinzbach and U. Fischer, *Angew. Chem.*, **77**, 258 (1965).
5) S. Niizuma, S. Konishi, H. Kokubun, and M. Koizumi, *Chem. Lett.*, **1972**, 643.
6) M. Ueno, I. Murata, and Y. Kitahara, *Tetrahedron Lett.*, **1965**, 2967.
7) Y. Kitahara, I. Murata, M. Ueno, K. Sato, and H. Watanabe, *Chem. Commun.*, **1966**, 180.

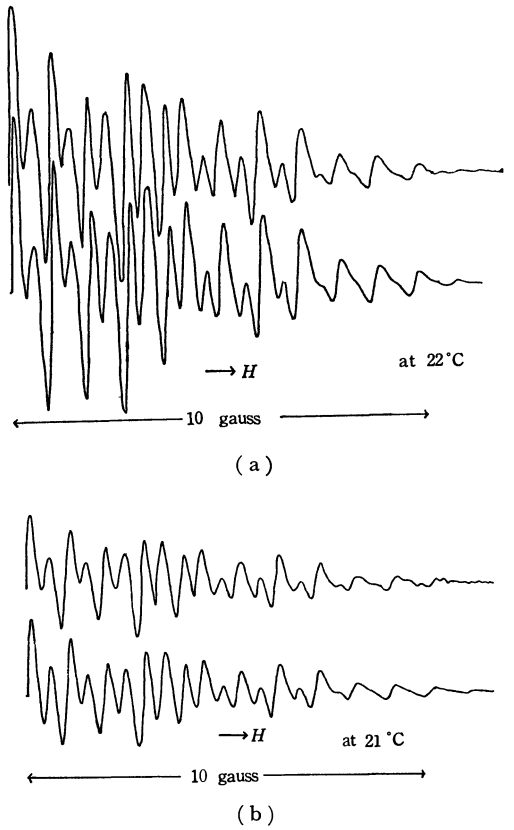

Fig. 1. ESR spectra of PhC anion radical.
(a) K reduction upper; observed lower; simulated
(b) Na reduction upper; observed lower; simulated

the right halves of ESR spectra are illustrated because of their symmetry with respect to the central lines. The simulated spectra agree satisfactorily with the observed ones. Simulations were performed by assigning a set of different hfs constants to two sets of four protons and one set of two protons. These protons naturally belong to two equivalent phenyl groups. The total separation of the hyperfine structure due to the protons of the two phenyl groups is about 22 Gauss. This implies that the unpaired spin mainly exists on the two phenyl groups.

Spin Density Calculation of PhC Anion Radical. The unpaired spin densities of PhC anion radical were calculated by the simple Hückel and McLachlan methods to interpret the observed hfs constants, assuming all rings are coplanar. It has been reported that for the calculation of electronic states of PhC neutral molecule, consideration of bond length alternation[8] is desirable; accordingly a similar treatment was also taken into account in the present calculation.

The results are shown in Table 1. It is evident that the unpaired spin does not exist (simple Hückel) or scarcely exists (McLachlan) on the five-membered ring and also on the 7-carbon atom. This conclusion is quite independent of bond length alternation.

According to results from the simple Hückel method,

8) T. Nakajima, S. Kohda, A. Tajiri, and S. Karasawa, *Tetrahedron*, **23**, 2189 (1967).

Table 1. Observed hfs constants and calculated spin densities

Position	Observed hfs const.		●	○	◉	△
1			0	−0.005	0	−0.001
1-Cl			0	−0.001	0	−0.000
2			0	−0.004	0	−0.004
2-Cl			0	−0.001	0	−0.001
7			0	−0.032	0	−0.005
8			0	−0.003	0	−0·011
6			0.192	0.265	0.156	0.217
p'	K	Na	0.047	0.015	0.085	0.068
o	2.80	2.90	0.075	0.094	0.062	0.072
m	0.95	1.00	0.006	0.027	0.014	0.022
p	3.20	3.35	0.098	0.115	0.109	0.128

Parameters used
$\alpha_{Cl}=\alpha_C+1.8\beta$, $\beta_{Cl}=0.8\beta$, $\alpha_{C'}=\alpha_C+0.18\beta$
McLachlan's parameter $\lambda=1.0$
in the case of bond length alternation
$\beta_{single}=0.59\beta_{double}$
$\beta_{phenyl}=0.80\beta_{double}$

●: Hückel
○: McLachlan
◉: Hückel with bond length alternation
△: McLachlan with bond length alternation

the orbital occupied by the unpaired spin belongs to a_2, corresponding to the lowest vacant orbital of *cis*-stilbene. Thus the PhC anion radical is almost the same as the *cis*-stilbene anion radical. The ESR of the latter, however, has not yet been reported, the transform being much more stable.

The localization of the unpaired spin on two phenyl groups and on C_5 and C_6 agrees very well with the expectation based on the analysis of ESR spectra. Spin densities evaluated by the four methods are plotted against hfs constants in Fig. 2. A fairly good straight line passing through the origin can be drawn for the values obtained by McLachlan method without bond length alternation. From its slope,

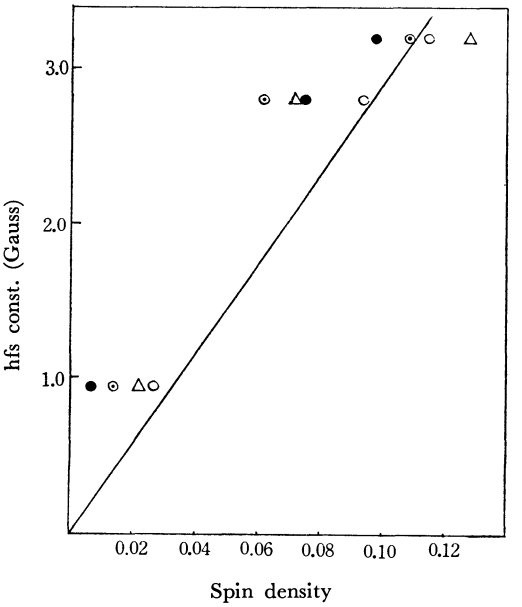

Fig. 2. A plot of hfs constants *vs.* spin densities.

the ordinary McConell's Q-value of 29 Gauss is obtained. Consideration of bond length alternation does not give any improvement. A similar result was reported by Ikegami *et al.* for the case of the tropone anion radical.[9]

The observed and the simulated ESR spectra of PrC anion radical at −51 °C are shown in Fig. 3.

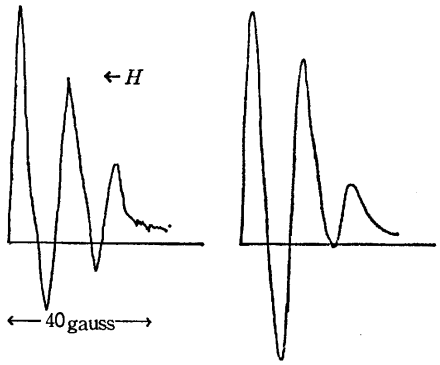

Fig. 3. ESR spectra of PrC anion radical at −51 °C.
left side; observed
right side; simulated

Under over modulation, the spectrum consists of five lines with the approximate intensity ratio 1 : 4 : 6 : 4 : 1. Thus the simulation was carried out by considering four equivalent protons. A hfs constant was found to be 14 Gauss. These must be β-protons of two n-propyl groups.

Generally, a hfs constant of β-protons of an alkyl group a_β^H is given by the following equation.[10]

$$a_\beta^H = B\langle\cos^2\theta\rangle\rho_C$$

where ρ_C is the spin density of carbon atom to which the alkyl group attaches, B is a constant in the range 40∼56 Gauss and θ is the angle between the axis of ring carbon $2p_z$ orbital and the carbon-hydrogen bond both projected on the plane perpendicular to $C_\alpha-C_\beta$ axis. If free rotation of the alkyl group is is allowed, $\langle\cos^2\theta\rangle$ is equal to 1/2. Then from the above equation ρ_C becomes equal to or greater than 1/2 in the present case. Thus we can say that the spin is localized only on C_5 and C_6.

Spin Density Calculation of PrC. In calculating the unpaired spin densities of PrC, we must consider whether the three-membered and five-membered rings are coplanar or not. A molecular model for PrC demonstrates that chlorine atom bonded to C_1 or C_4 and δ-hydrogen atom of n-propyl groups collide with each other if free rotation is assumed for the latter group. To allow this free rotation without collision with chlorine atoms, the three-membered and five-membered rings should be twisted at an angle greater than 45°. In view of the fact that free rotation around the C_7—C_8 bond has been reported for 1-formyl-5,6-di-n-propylcalicene[11] at temperatures higher than room temperature on the basis of NMR data, the above geometry for PrC in our case seems to be quite reasonable although the radical is ionic and the temperature is below room temperature.

Thus, it was assumed that the five-membered and three-membered rings are not in general coplanar. In calculating the spin densities of PrC, a parameter $\cos^2\alpha$ (α is an angle between two rings) was introduced for the resonance integral between C_7 and C_8 and the calculation was made for various α-values. In the case of PhC anion radical, the unpaired spin densities were found to be independent of α, but there is no steric hindrance according to the model constructed, so that all the rings are considered to be coplanar in the PhC anion radical.

The effect of hyperconjugation was taken into account since it is generally believed that the hfs constant of an alkyl group is mainly due to this. In the actual calculation we regarded a n-propyl group as —C≡H_2R and used the following parameters.[12,13]

$$C_{5\,(\text{or }6)} \overset{1.0\beta}{\text{——}} \underset{\alpha-0.1\beta}{C_\beta} \overset{2.5\beta}{\text{═══}} \underset{\alpha-0.5\beta}{H_2R}$$

We considered that the above procedure is sufficient as a first approximation and made no use of other more refined methods.[14,15] Only the result by Hückel method is shown in Fig. 4, because McLachlan method gives an essentially similar result. When α is greater than 40°, the spin densities on C_5, C_6 and on H_2R are respectively 0.42 and 0.076 (Fig. 4). The latter leads to a splitting constant of a methylene proton $508\times0.076\times1/3=12.9$ Gauss which agrees fairly well with the observed value.

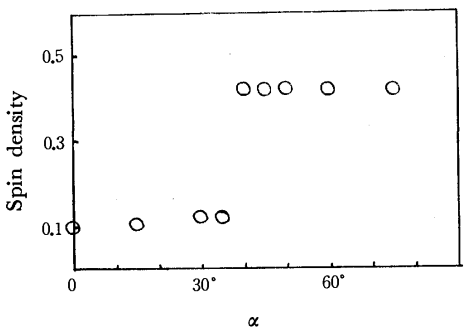

Fig. 4. A plot of spin density on position 5 or 6 *vs.* twisting angle α.

Reason for a Sudden Spin Density Change at around 40°. An unusual dependence of spin density on α appears, increasing only very little from $\alpha=0$ to $\alpha<40°$, but suddenly jumping at 40° and then remaining constant. The reason for this is as follows.

The PrC anion radical is a 21 π-electron system including hyperconjugation of two n-propyl so that the unpaired electron occupies the 11th orbital. According to results obtained by the simple Hückel

9) Y. Ikegami, H. Watanabe, and S. Seto, This Bulletin, **45**, 1976 (1972).
10) C. Heller and H. M. McConnell, *J. Chem. Phys.*, **32**, 1535 (1960).
11) A. S. Kende, P. T. Izzo, and U. Fulmor, *Tetrahedron Lett.*, **1966**, 3697.
12) C. A. Coulson and V. A. Crawford, *J. Chem. Soc.*, **1953**, 2052.
13) R. Bersohn, *J. Chem. Phys.*, **24**, 1066 (1956).
14) J. P. Colpa and E. deBoer, *Mol. Phys.*, **7**, 333 (1963).
15) D. H. Levy, *ibid.*, **10**, 233 (1966).

calculation the energy for two types of orbitals either depends or does not depend on angle α. These orbitals belong to b_1 and a_2 respectively, assuming PrC molecule has C_{2v} symmetry. The 11th orbital occupied by the unpaired electron at $\alpha=0$ belongs to the former and the 12th orbital to the latter. The energy of the 11th orbital increases with the increase in α, moving above the 12th level for $\alpha>40°$. Inversion occurs at 40° between 11th and 12th levels. Thus when α exceeds 40°, the unpaired electron occupies the 12th orbital (when $\alpha=0$) whose energy is independent of α. The angle α at which the inversion occurs depends slightly on the parameters of hyperconjugation. The increase of the total electronic energy due to twisting is about 0.42 β/mol which is equal to 6.9 kcal/mol at $\alpha=45°$ if resonance integral β is assumed to be 16.5 kcal/mol.[8]

Observation of Line Width Alternation. In the ESR spectrum of PrC anion radical (Fig. 3), the second line from the right is broader than the others. We examined the temperature dependence of ESR spectra, the results for potassium and sodium reduction being given in Figs. 5 and 6. Line width changes remarkably only in the second line. The temperature dependence is almost completely reversible, and is considered to be due to the line width alternation.

Hindered Rotation as a Cause of Line Width Alternation. The line width alternation might be attributed to the hindered rotation of two *n*-propyl groups. The molecular model constructed shows that the free rotation

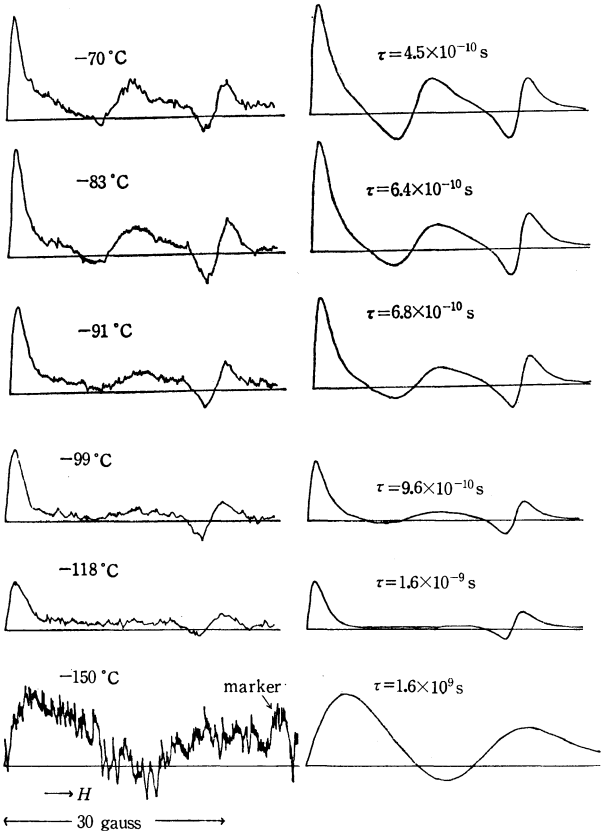

Fig. 5. ESR spectra of PrC anion radical at different temperatures (K reduction).
left side; observed
right side; simulated

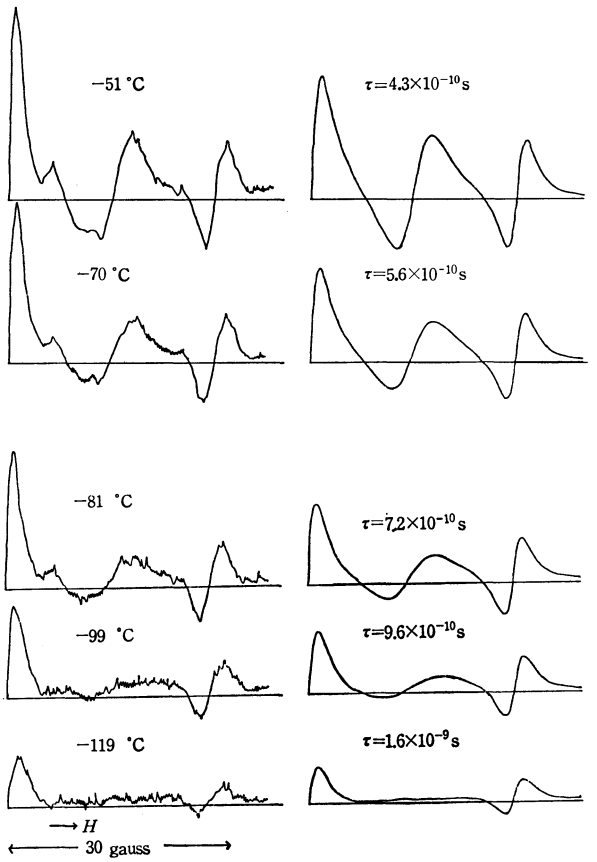

Fig. 6. ESR spectra of PrC anion radical at different temperatures (Na reduction).
left side; observed
right side; simulated

of each *n*-propyl group around C_α–C_β, $C_{\alpha'}$–$C_{\beta'}$ axis is not allowed because of mutual steric hindrance of the two groups. It is expected that certain stable conformations exist and the transformation from one to another occurs with characteristic frequencies determined by the potential barriers between them. In the frozen state at −150 °C, PrC anion radical gives a spectrum with the intensity ratio 1 : 2 : 1, suggesting that the spectrum arises mainly from only two equivalent protons and that the other protons have fairly small hfs constants. This implies that the C_β—H or $C_{\beta'}$—H bond belonging to the former group has a small angle to the axis of $2p_z$ orbital of C_5 or C_6 and the one belonging to the latter a large angle.

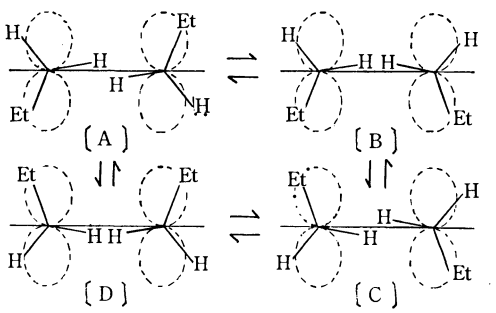

Fig. 7. Equilibrium four conformations.

The four conformations shown in Fig. 7 are most plausible as stable ones. All other conformations conceivable can be eliminated because of a strong steric hindrance between two R-groups.

Simulation Analysis of Line Width. In order to analyze the present result we made use of a theory developed and applied successfully to a similar system to ours.[16,17] According to the theory, the average magnetization to the four conformations (Fig. 7) is expressed as follows.

$$\langle\overline{G}\rangle = -i\omega_1 M_0 \times \left\{ \frac{(2+3\eta\tau)(2+2\eta\tau)+\tau^2(1+\eta\tau)(\eta_C\eta_D+\eta_A\eta_B)}{2\eta+3\eta^2\tau+\tau(1+2\eta\tau)(\eta_C\eta_D+\eta_A\eta_B)+\tau^3\eta_A\eta_B\eta_C\eta_D} \right\}$$

where $\omega_1 M_0$ is a constant intensity factor, subscripts A, B, C, D refer to the four conformations and τ[18] is the lifetime of each conformation. The η's are defined by the following expression.

$$\eta_A = 1/T_2 - i(\omega_0 - \omega + \omega_A)$$
$$2\eta = \eta_A + \eta_B = \eta_C + \eta_D$$

where $1/T_2$ is the line width in the absence of conformation change, ω_0 the Larmor precession frequency of the electron in the absence of hyperfine interaction and ω_A the shift in resonance frequency due to interactions with protons in conformation A. The imaginary part of $\langle\overline{G}\rangle$ gives an absorption spectrum. In the present case ω_A's were determined for each state of sixteen nuclear spin states and $1/T_2$ was equated to the observed line width of the end line. For simulation the absorption line was converted into the first differential by numerical differentiation for comparison with the observed spectra. Calculations were made by use of an electronic computer.

In the case of potassium reduction (Fig. 5), a constant quantity of absorption, about 1/20 of the total, should be added to the central line in order to get a good agreement with the experiment. This may be due to an impurity or a certain radical produced by some side reaction. Simulation spectra agree very well with the observed ones. Simulation was similarly made for sodium reduction (Fig. 6). For the end line and its adjacent line the agreement between observed and simulated ones is good. However, the simulated spectra differ from the observed ones in the central region where the latter is more intensive and has a small shoulder. The disagreement may be due to the same reason as in the case of potassium reduction. This is supported by the fact that strength of the central line increases and the shoulder becomes remarkable with the rise in temperature, and that this is not reversible. The best values for the hfs constants of protons are 24 and 4 Gauss for both potassium and sodium reduction and are quite consistent with the conformation in Fig. 7.

Potential Barrier Height of Hindered Rotation. The potential barrier height of the hindered rotation of *n*-propyl groups can be determined from the temperature dependence of lifetime τ or the first-order rate constant k $(=1/\tau)$. A plot of $\log_{10}(1/\tau)$ against $1/T$ is given in Fig. 8. The linearity is satisfactory. Activation energies E_A and frequency factors k_0 are determined from the slopes and the intercepts of two lines, the values being 1.6_5 kcal/mol, 1.3×10^{11} s^{-1} for potassium reduction and 1.4_1 kcal/mol, 6.2×10^{10} s^{-1} for sodium reduction. The difference in values for the two cases may be due to the difference in the perturbation by cations.

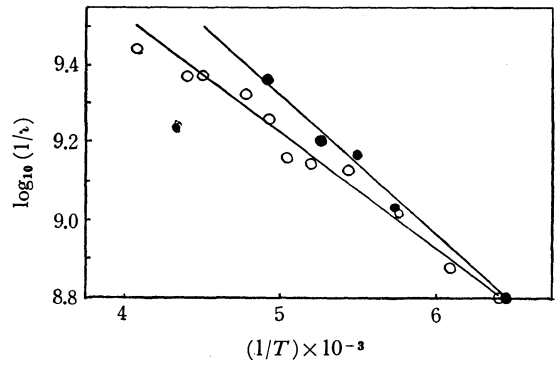

Fig. 8. A plot of $\log_{10}(1/\tau)$ *vs.* $1/T$.
○: Na reduction, ●: K reduction

Stone and Maki[19] discussed the internal rotation of an alkyl group of nitroalkane anion radical in solution from a quantum mechanical viewpoint. According to them the height of the potential barrier for internal rotation is 1.4 kcal/mol, and the spin density on nitrogen atom to which an alkyl group links is 0.7±0.1. Ishizu *et al.* also reported a similar equilibrium conformation for 2,2′-dialkylbiphenyl.[20]

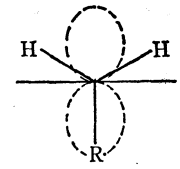

Fig. 9. Possible equilibrium conformation for RCH_2-Ar.

The conformation is given in Fig. 9. The hindered rotation of the present system is similar to that of this compound. Miyagawa and Itoh[21] obtained 3.6±0.2 kcal/mol and $(10\pm4)\times10^{12}$ s^{-1} as the value of E_A and k_0 respectively for rotation of a methyl group in $CH_3\dot{C}HCOOH$ radical produced in a single crystal of L-alanine by γ-ray irradiation. Iwaizumi and Isobe[22] have reported on the inversion of two benzene ring planes in 4,5,9,10-tetrahydropyrene anion radical (non-planer molecule) $2.0—9.0\times10^{-6}$ s (−90 °C)

16) A. Carrington, *Mol. Phys.*, **5**, 425 (1962).
17) J. R. Bolton, A. Carrington, and P. F. Todd, *Mol. Phys.*, **6**, 169 (1963).
18) We defined τ as the reciprocal of the angular frequency of the transformation.
19) E. W. Stone and A. H. Maki, *J. Chem. Phys.*, **37**, 1326 (1962).
20) K. Ishizu, K. Mukai, H. Hasegawa, K. Kubo, H. Nishiguchi, and Y. Deguchi, This Bulletin, **42**, 2808 (1969).
21) I. Miyagawa and K. Itoh, *J. Chem. Phys.*, **36**, 2157 (1962).
22) M. Iwaizumi and T. Isobe, This Bulletin, **38**, 1547 (1965): Abstract of Symposium on ESR, in Kanazawa, October, p. 1 (1972).

and gave 4~5 kcal/mol as the values of the lifetime of individual configuration and the energy barrier. The values we have obtained are reasonable as compared with the above.

The authors wish to thank Professor Y. Kitahara for the supply of valuable samples. H.K. and S.N. are indebted to the Ito Science Foundation for financial support.

BULLETIN OF THE CHEMICAL SOCIETY OF JAPAN, VOL. 46, 2284—2287 (1973)

Bond Distortions and Related Phenomena in *Peri*-Condensed Tetracyclic Nonbenzenoid Aromatic Hydrocarbons

Azumao TOYOTA and Takeshi NAKAJIMA

Department of Chemistry, Faculty of Science, Tohoku University, Sendai 980

(Received December 25, 1972)

On the basis of the second-order Jahn-Teller effect and SCF MO method, we have examined the geometrical structures with respect to bond length and the ground-state multiplicity and stability of *peri*-condensed tetracyclic nonbenzenoid aromatic hydrocarbons. It was found that of the molecules examined, dibenzo[cd, gh]pentalene (III) and its seven-membered analogue (IV) should have a triplet ground-state, exhibiting no appreciable double-bond fixation in the peripheral carbon skeleton. The other molecules were predicted to suffer the first-order or second-order bond distortions, showing a more or less marked double-bond fixation. The electronic spectra were calculated using the bond distances obtained on the basis of SCF MO method.

In a previous paper[1] we developed a symmetry rule for predicting the stable molecular shapes with respect to C–C bond length in the ground and electronically-excited states of conjugated molecules. The symmetry rule[2–7] is based on the second-order Jahn-Teller effect, occurring when a certain bond distortion mixes two electronic states which are nearly degenerate in the symmetrical nuclear arrangement. On the basis of this theory, we examined the bond-length distributions and stabilities of a large number of non-alternant hydrocarbons.

In this paper we examine the bond distortions and related phenomena in *peri*-condensed tetracyclic nonbenzenoid aromatic hydrocarbons containing a pentalene or a heptalene nucleus (Fig. 1). Of these systems, the dianion of dibenzo[cd, gh]pentalene(III) has recently been synthesized by Trost and Kinson.[8]

There are two equilibrium nuclear arrangements in the ground state for pentalene, the closest derivative of which, 1-methylpentalene, has recently been synthesized by Bloch *et al.*[9] and for heptalene, which has already been synthesized by Dauben and Bertelli.[10] One belongs to molecular symmetry group D_{2h} which exhibits only a slight degree of double-bond fixation in the peripheral carbon skeleton, and the other to molecular symmetry group C_{2h} exhibiting a marked double-bond fixation.[1,11–15] It was revealed that the latter is energetically more stable than the former. These predictions are in good agreement with experimental results.[9,10] This aroused our interest in an examination of the stable nuclear arrangements and molecular symmetries of condensed hydrocarbons containing a pentalene or a heptalene nucleus.

One interesting prediction of molecular orbital theory is the possibility that certain symmetrical molecules may have a triplet ground state. For example, in the case of 1.2-5.6-dibenzopentalene, the triplet state is predicted to be more stable than the closed-shell singlet state in the symmetrical C_{2v} conformation (Fig. 2). However, in this molecule the closed-shell singlet interacts strongly with the first excited singlet state through the b_2 nuclear displacement because of the small energy gap between them.[1] As a result, the ground state turns out to be a singlet with C_s conformation.

Breslow *et al.*[16] observed a thermally accessible triplet state of pentaphenylpentadienyl cation in equilibrium with a singlet state, and also the stable triplet ground state of pentachlorocyclopentadienyl cation. Van Willigen *et al.*[17] observed the triplet ground states of triphenylbenzene dianion, triphenylene dianion *etc.*, and suggested that in triphenylene dianion the trigonal symmetry is lost. The origin of the molecular sym-

1) T. Nakajima, A. Toyota, and S. Fujii, This Bulletin, **45**, 1022 (1972).
2) R. F. Bader, *Mol. Phys.*, **3**, 137 (1960).
3) R. F. Bader, *Can. J. Chem.*, **40**, 1164 (1962).
4) R. G. Pearson, *J. Amer. Chem. Soc.*, **91**, 4947 (1969).
5) R. G. Pearson, *ibid.*, **91**, 1252 (1969).
6) R. G. Pearson, *J. Chem. Phys.*, **52**, 2167 (1970).
7) L. Salem, *Chem. Phys. Lett.*, **3**, 99 (1969).
8) B. M. Trost and P. L. Kinson, *J. Amer. Chem. Soc.*, **92**, 2591 (1970).
9) R. Bloch, R. A. Marty, and P. de Mayo, *ibid.*, **93**, 3071 (1971).
10) H. J. Dauben and D. J. Bertelli, *ibid.*, **83**, 4659 (1961).
11) P. C. den Boer-Veenendaal, J. A. Vliegenthart, and D. H. W. den Boer, *Tetrahedron*, **18**, 1325 (1962).
12) T. Nakajima and S. Katagiri, *Mol. Phys.*, **7**, 149 (1963).
13) T. Nakajima, Y. Yaguchi, R. Kaeriyama, and Y. Nemoto, This Bulletin, **37**, 272 (1964).
14) P. François and A. Julg, *Theoret. Chim. Acta*, **11**, 128 (1968).
15) A. Tajiri, N. Ohmichi and T. Nakajima, This Bulletin, **44**, 2347 (1971).
16) R. Breslow, H. W. Chang, R. Hill, and E. Wasserman, *J. Amer. Chem. Soc.*, **89**, 1112 (1967).
17) H. van Willigen, J. A. M. van Broekhoven, and E. de Boer, *Mol. Phys.*, **12**, 533 (1967).

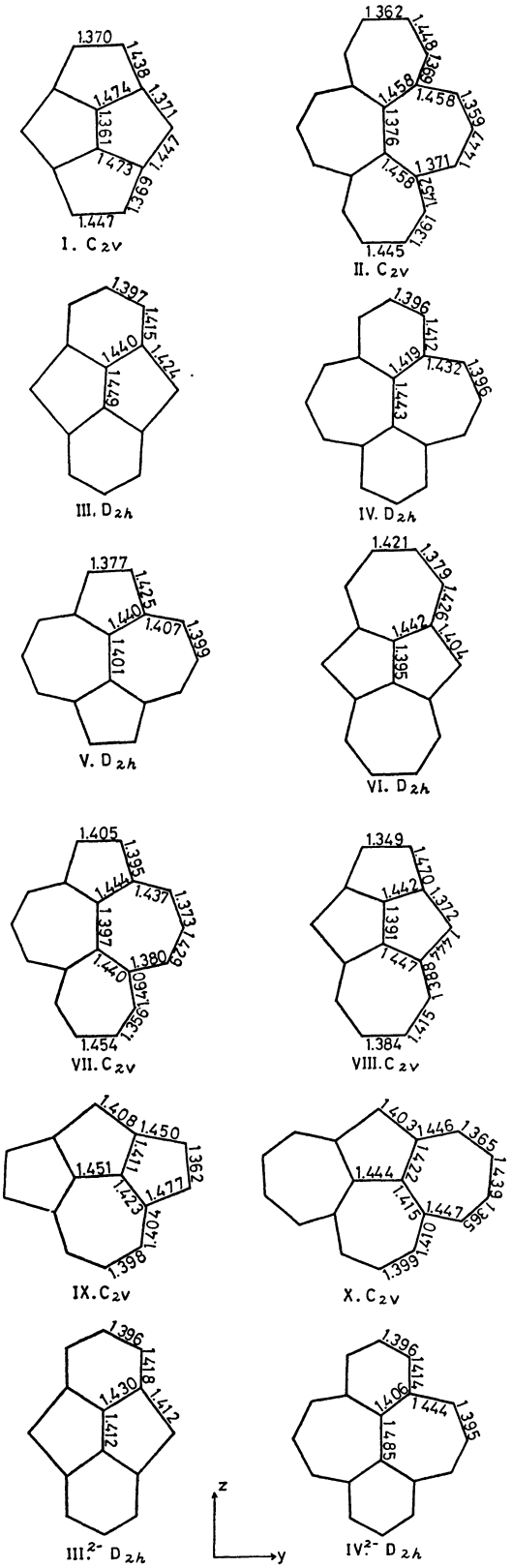

Fig. 1. Molecular symmetry groups, bond lengths (in Å), and choice of axes.

metry reduction has been ascribed to the perturbing effect of alkali counterions, since in this molecule the energy gap between the lowest triplet ground and the first excited triplet states is relatively large, and

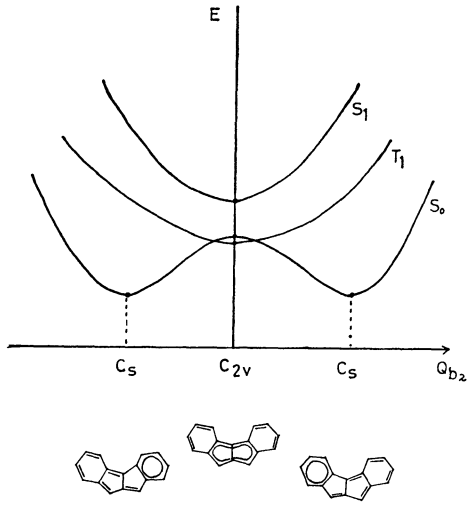

Fig. 2. The potential energy curves for the lowest singlet (S_0), the first singlet excited (S_1) and the lowest triplet states (T_1) of 1.2-5.6-dibenzopentalene.

there is no possibility for the second-order Jahn-Teller distortion to occur.[18,19]

The purpose of this paper is to predict the ground-state multiplicities, energetically most favorable symmetry groups and the equilibrium bond length of the *peri*-condensed nonalternant hydrocarbons, using the symmetry rule which is based on the second-order perturbation theory and the variable bond length SCF MO method.[20] The ground-state π-electronic properties and the electronic spectra were also examined.

Theoretical

We start by assuming a particular symmetrical nuclear configuration for a molecule. This will place the molecule in a certain fully-symmetrical point group. We treat the nuclear displacements as perturbations and use the second-order perturbation theory. On the basis of the same approximation as used previously, we find that the force constant for the ith normal nuclear-displacement in the ground state may be written as

$$f_0{}^i = k - 2\sum_n{}' \frac{\left|\langle\psi_n\left|\frac{\partial H_\pi}{\partial Q_i}\right|\psi_0\rangle\right|^2}{(E_n - E_0)}$$

where k and H_π are the force constant for an sp^2 hybridized C–C σ-bond and the Hamiltonian for π-electrons, respectively. ψ_0 and ψ_n represent the ground and the nth excited wavefunctions with respective energies E_0 and E_n.

The symmetry rules for predicting the stable molecular shapes in the ground state are as follows: the symmetry of the normal nuclear displacement with

18) J. A. M. van Broekhoven, H. van Willigen, and E. de Boer, *Mol. Phys.*, **15**, 101 (1968).
19) J. L. Sommerdijk and E. de Boer, *J. Chem. Phys.*, **50**, 4771 (1969).
20) H. Yamaguchi, T. Nakajima, and T. L. Kunii, *Theoret. Chim. Acta*, **12**, 349 (1968).

the smallest force constant is identical with that of the lowest excited state, ψ_1. If the energy gap ($E_1 - E_0$) is smaller than the critical value, about 1.2 eV, the molecule would be distorted into a less symmetrical nuclear configuration. The most favorable type of bond distortion is predicted by examining the distribution of the transition densities ρ_{01} over the molecular skeleton.

The symmetry rule gives only the type of most favorable bond distortion since it is based on the second-order perturbation theory. In order to obtain information on the actual magnitudes of distortions or the equilibrium bond lengths at which the nuclei of the real molecule will settle, we use the variable bond-length SCF MO method.[20]

Results and Discussion

Ground-State Molecular Symmetries and Multiplicities. The symmetries and energies (measured from the lowest singlet state) of the first excited singlet states for the fully-symmetrical nuclear arrangements of the *peri*-condensed hydrocarbons and some of their dianions are given in Table 1, and the two-center components of the transition densities for some selected molecules in Fig. 3.

Table 1. Symmetries and energies of first excited singlet states of *peri*-condensed nonalternant hydrocarbons

Molecule (Point group)	First excited state	
	$E_1 - E_0$ (eV)	Symmetry
I (D_{2h})	0.91	B_{2u}
II (D_{2h})	0.39	B_{2u}
III (D_{2h})	1.13	B_{3g}
III^{2-} (D_{2h})	3.28	B_{3g}
IV (D_{2h})	1.09	B_{3g}
IV^{2-} (D_{2h})	1.10	B_{2u}
V (D_{2h})	1.81	B_{3g}
VI (D_{2h})	1.86	B_{3g}
VII (C_{2v})	1.45	B_2
VIII (C_{2v})	1.34	B_2
IX (C_{2v})	1.34	B_2
X (C_{2v})	1.19	B_2

Molecule II was predicted to have a triplet ground state in the fully-symmetrical D_{2h} conformation. However, in molecules I and II, the energy gap between the lowest singlet and first excited singlet states $E_1 - E_0$ is small, as compared with the critical value 1.2 eV for the molecular symmetry reduction in the ground state. Thus, these molecules might undergo the second-order bond distortions making their ground-state molecular symmetry groups reduced to C_{2v} from D_{2h} by the interaction of the lowest state with the first excited state through the b_{2u} normal displacement.

We may predict that molecules V, VI, VII and VIII undergo no second-order Jahn-Teller distortion, since the energy gap is relatively large as compared with the critical value.

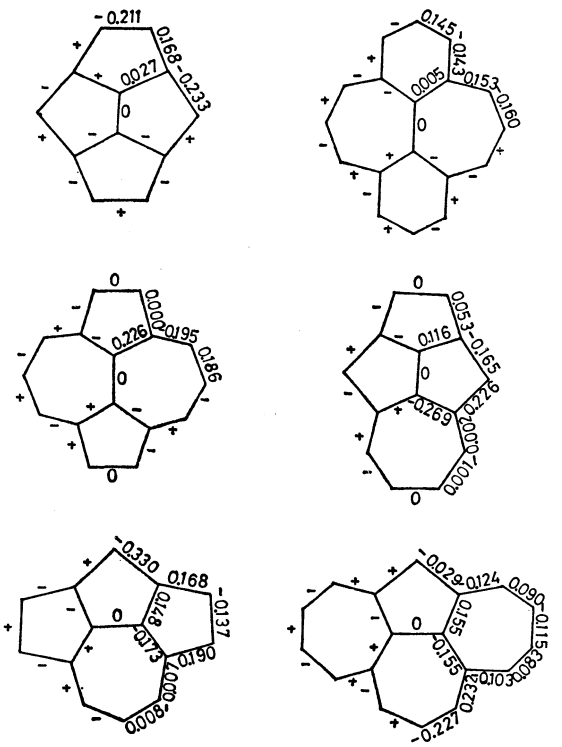

Fig. 3. Two-center components of transition densites (ρ_{01}).

The energy gap in III and IV is comparable with the critical value, and in the symmetrical D_{2h} conformation the ground state is not singlet but triplet.

The energy gap in molecules IX and X is also comparable with the critical value, but the ground state is singlet in the symmetrical C_{2v} conformation.

In order to investigate the ground-state molecular-symmetry groups, geometries and multiplicities, we have performed the SCF calculation, taking into account a distorted structure as the starting geometry.[21] The form of the displacement vector has been estimated from the distributions of two-center components of transition density ρ_{01} (Fig. 3).

SCF MO calculations revealed that molecules I and II undergo the second-order bond distortion, as predicted from the symmetry rule, their ground-state molecular symmetry groups being lowered from D_{2h} to C_{2v}. The prediction is in good agreement with the theoretical investigation of Binsch.[22] The stabilization energies which favor the lower-symmetry nuclear arrangements are estimated to be 3.1 and 17.5 kcal mol^{-1}, respectively. It is of interest to note that the second-order effect in molecules containing the seven-membered rings is greater than that in its five-membered analogues, as in the case of heptalene and pentalene.[23]

On the other hand, it turns out that III and IV undergo no second-order bond distortions. Thus, we may conclude that both their stable ground states are triplet states ($^3B_{1u}$), which are energetically more stable than the singlet states by 3.9 and 8.5 kcal, respectively.

21) T. Nakajima and A. Toyota, *Chem. Phys. Lett.*, **3**, 272 (1969).
22) G. Binsch, "Aromaticity, Pseudoaromaticity and Antiaromaticity." The 3rd Jerusalem Symposium, The Israel Academy of Sciences and Humanities, Jerusalem (1971), p. 25.
23) T. Nakajima, A. Toyota and H. Yamaguchi, *ibid.*, p. 227.

V, VI, VII, VIII, IX, and X were predicted not to undergo second-order bond distortions and all the ground-state molecular symmetries to belong to the fully-symmetrical group.

Dianions of III and IV undergo no second-order bond distortions, both their ground-state multiplicities being singlet.

Ground-State π-Electronic Properties. The calculated equilibrium bond length at the energetically favorable geometrical structures of the molecules examined are shown in Fig. 1. Since all the stable conformations of I, II, VII, VIII, IX and X belong to the molecular symmetry group C_{2v}, they have dipole moments in the ground state. The dipole moments calculated using the theoretical charge densities are 1.16, 1.23, 2.30, 2.70, 2.05, and 1.12 D, respectively

Concerning the distribution of bond length, it is of interest to note that in molecules I and II there is a marked double-bond fixation in the periphery and vinyl segment located at the center of molecule, but no appreciable one in III and IV. The bond lengths of the two benzene rings are very much smoothed out as those of the free benzene molecule.

In V and VI, the C–C skeleton is composed of two distinguishable parts: one in which bond lengths are highly equalized (in a pentalene or a heptalene core), and the other in which there is a marked double-bond fixation (in the remainder of the periphery).

In VII and VIII, a strong first-order double-bond fixation exists in the peripheral C–C skeleton, the bond length of vinyl segment located at the center of molecule being 1.4 Å.

In IX and X, there is a moderate first-order double-bond fixation in the peripheral C–C skeleton.

In dianions of III and IV, the bond lengths of a pentalene or a heptalene core are almost same as those of the free pentalene or heptalene dianion in which bond lengths are nearly equal throughout the whole molecular skeleton.

Electronic Spectra. In calculating electronic spectra, configuration mixing of the singly excited states is partially included: the number of configuration interactions considered is 28 for each molecule. The lower singlet transition energies and intensities calculated using the geometrical structures corresponding to the energetically most stable nuclear configuration are summarized in Table 2. The transition symmetries are also included. Unfortunately, there are at present no experimental spectral data available for a direct comparison of theory and experiment.

Table 2. Transition energies and intensities

Molecule (Point group)	Transition symmetry	ΔE (eV)	f (c. g. s.)	Molecule (Point group)	Transition symmetry	ΔE (eV)	f (c. g. s.)
I (C_{2v})	$^1A_1$	1.20	0.008	V (D_{2h})	$^1B_{3g}$	1.81	Forb.
	$^1B_2$	1.68	0.005		$^1B_{2u}$	2.62	0.163
	$^1A_1$	3.05	0.030		^1A_g	3.19	Forb.
	$^1B_2$	3.90	0.482		$^1B_{1u}$	3.46	0.015
	$^1B_2$	4.60	0.101		$^1B_{2u}$	4.19	0.051
II (C_{2v})	$^1B_2$	1.38	0.004	VI (D_{2h})	$^1B_{3g}$	1.86	Forb.
	$^1A_1$	1.41	0.000_1		$^1B_{2u}$	2.68	0.254
	$^1A_1$	2.79	0.004		^1A_g	3.21	Forb.
	$^1B_2$	2.90	0.274		$^1B_{1u}$	3.47	0.058
	$^1B_2$	3.46	0.164		$^1B_{2u}$	3.93	0.007
III (D_{2h})	$^3B_{3g}$	1.21	0.005	VII (C_{2v})	$^1B_2$	1.45	0.017
	$^3B_{2u}$	1.78	Forb.		$^1B_2$	2.24	0.006
	$^3B_{1u}$	2.96	Forb.		$^1A_1$	2.90	0.001
	^3A_g	3.17	0.628		$^1A_1$	3.22	0.000_1
	$^3B_{3g}$	3.53	0.635		$^1B_2$	4.55	0.019
III^{2-} (D_{2h})	$^1B_{3g}$	3.28	Forb.	VIII (C_{2v})	$^1B_2$	1.34	0.024
	$^1B_{2u}$	3.44	0.577		$^1B_2$	2.14	0.028
	$^1B_{1u}$	3.67	0.218		$^1A_1$	2.89	0.069
	$^1B_{3g}$	4.30	Forb.		$^1A_1$	3.45	0.033
	^1A_g	4.51	Forb.		$^1B_2$	3.74	0.046
IV (D_{2h})	$^3B_{3g}$	1.38	0.004	IX (C_{2v})	$^1B_2$	1.34	0.003
	$^3B_{2u}$	1.79	Forb.		$^1A_1$	2.16	0.000_3
	$^3B_{3g}$	2.89	0.501		$^1B_2$	3.40	0.012
	^3A_g	3.09	0.547		$^1A_1$	3.77	0.004
	$^3B_{1u}$	3.31	Forb.		$^1A_1$	4.12	0.029
VI^{2-} (D_{2h})	$^1B_{2u}$	1.10	0.004	X (C_{2v})	$^1B_2$	1.19	0.017
	$^1B_{3g}$	1.14	Forb.		$^1A_1$	2.29	0.005
	$^1B_{3g}$	2.08	Forb.		$^1B_2$	3.18	0.191
	$^1B_{2u}$	3.06	0.828		$^1A_1$	3.36	0.117
	^1A_g	3.26	Forb.		$^1A_1$	3.54	0.208

Time-Resolved Fluorescence Studies on the Dual Fluorescence Process of *p*-(Dimethylamino)benzonitrile

Nobuaki NAKASHIMA, Hidetoshi INOUE, Noboru MATAGA,* and Chiyoe YAMANAKA**

Department of Chemistry, Faculty of Engineering Science, Osaka University, Toyonaka, Osaka 560

***Department of Electrical Engineering, Faculty of Engineering, Osaka University, Suita, Osaka 565*

(Received December 28, 1972)

Time-resolved fluorescence spectra and the fluorescence rise and decay curves have been measured for *p*-(*N*,*N*-dimethylamino)-benzonitrile. The results demonstrate the relaxation process to be due to the interaction between the solvent and the ^1L_a state of the solute, leading to dual fluorescence.

In some molecules such as *p*-(dimethylamine)benzonitrile (DMABN)[1] and indole[2] the lowest excited singlet state is a slightly polar state of the ^1L_b type, and the highly polar ^1L_a state is not far from it. In such a case, there is a possibility that the solvent effect causes the inversion of two different energy states since the solvent effect on these two excited states seems to differ considerably. In relation to such a solvent effect, the fluorescence of DMABN has been studied in detail.[1]

In a nonpolar solvent such as cyclohexane, DMABN shows only one fluorescence band due to the transition from the ^1L_b state. However, in a polar solvent, fluorescence spectra have two peaks, since the ^1L_a state can be strongly stabilized in the excited equilibrium state because of the large dipole-dipole interaction and turn out to be the lowest excited state. Actually, from the solvent shift of the fluorescence, the dipole moment of the ^1L_a state, $\vec{\mu}(^1L_a)$,has been evaluated to be 23 D.[1]

So far no direct confirmation of the above relaxation process has been made. We have undertaken to observe the process by means of ns time-resolved fluorescence spectroscopy.

Experimental

The fluorescence rise and decay curves as well as time-resolved fluorescence spectra were obtained by exciting the solution with a 337 nm light pulse of nitrogen gas laser. Details of the apparatus were described elsewhere.[3] For the measurement of ordinary luminescence spectra, calibrated Aminco-Bowman and Hitachi MPF-2A spectrophotofluorometers were used. The absorption spectra were measured with Cary 15 and Shimadzu MPS-50L spectrometers. The temperature of a solution was controlled by a constant flow of cold nitrogen gas in a metal Dewar with quartz windows.

DMABN was recrystallized several times from cyclohexane. 2-Methyltetrahydrofuran (MTHF) was refluxed over metallic sodium wire, fractionally distilled and finally distilled under vacuum in the presence of lithium aluminum hydride. Spectrograde benzonitrile and cyclohexane were used without further purification.

Results and Discussion

DMABN shows ^1L_b fluorescence (F_b) at 365 nm and ^1L_a fluorescence (F_a) at 425 nm in MTHF solution at room temperature. The fluorescence quantum spectra at several temperatures are given in Fig. 1.

When the temperature of the solution is lowered from room temperature to −110 °C, F_a shows a remarkable red shift while F_b shows no shift at all. The former can be ascribed to the very polar structure of the ^1L_a state and increase of solvent polarity by temperature lowering, and the latter to the nonpolar nature of the ^1L_b state.[1]

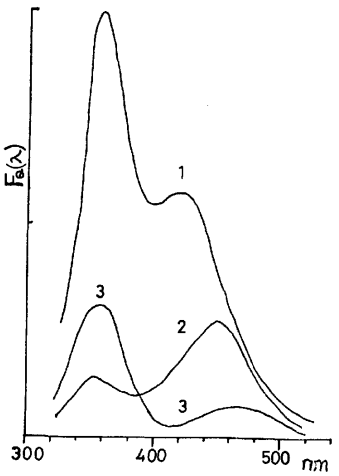

Fig. 1. Fluorescence quantum spectra of DMABN in MTHF at various temperatures.
1: room temperature (~20 °C), 2: −50 °C, 3: −110 °C

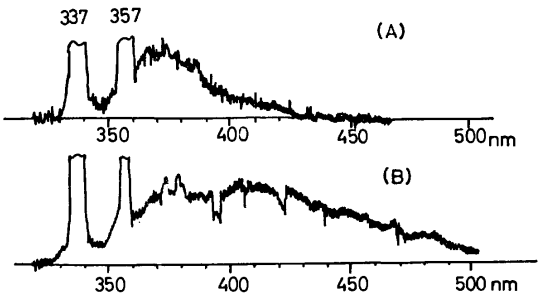

Fig. 2. Time-resolved fluorescence spectra of DMABN in MTHF at −115 °C.
(A) T_d=2.0 ns, (B) T_d=7.0 ns.
The spectra are not corrected, and the correction will shift the F_a band to the longer wavelength side. The lines at 337 and 357 nm are due to the scattered exciting pulse.

** To whom correspondence should be addressed.

1) E. Lippert, W. Lüder, and H. Boos, "Advances in Molecular Spectroscopy," Pergamon Press, (1962), p. 443.

2) N. Mataga, Y. Torihashi, and K. Ezumi, *Theoret. Chim. Acta* (Berl.) **2**, 158 (1964).

3) N. Nakashima, N. Mataga, F. Usio, and C. Yamanaka, *Z. Phys. Chem. N. F.*, **79**, 150 (1972).

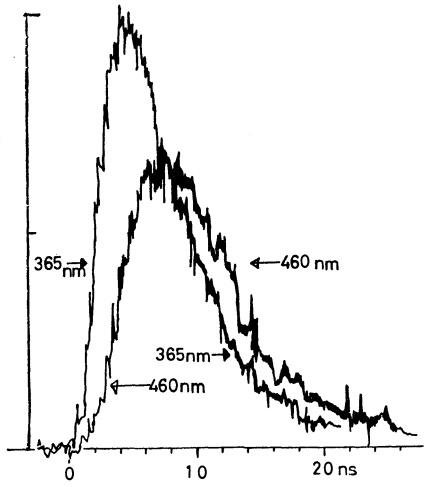

Fig. 3. Rise and decay curves of F_b and F_a bands.
(It has been confirmed that the intensity of the scattered exciting pulse can be neglected at 365 nm.)

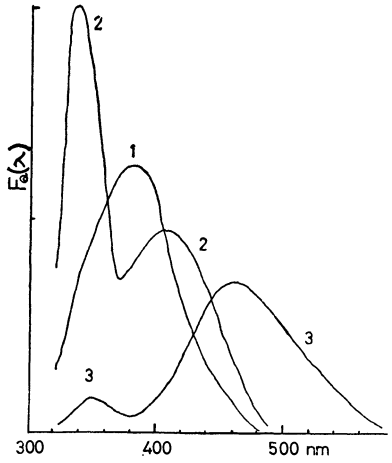

Fig. 4. Fluorescence quantum spectra of DMABN-benzonitrile system in cyclohexane at various temperatures.
[DMABN] = 5.0×10^{-4} M, [Benzonitrile] = 5.0×10^{-3} M.
1: room temperature (~20°C) 2: 0°C, 3: −10°C.

In order to observe directly the solvent relaxation process leading to dual fluorescence, we have made the time-resolved fluorescence measurements as shown in Figs. 2 and 3. It can be seen that at the delay time (T_d) of 2 ns from the exciting pulse the F_b band is predominant and the intensity of the F_a band is very weak (Fig. 2). At $T_d=7$ ns, the intensity of the F_a band becomes comparable with that of the F_b band. The relaxation process can be demonstrated also by measuring the fluorescence rise and decay curves of the F_b and F_a bands. We see that the fluorescence rise time of the F_a band measured at 460 nm is longer than that of the F_b band, in agreement with the results in Fig. 2. The decay times of both bands are approximately the same, which seems to indicate the equilibrium or reaction between the two states, ^1L_b and ^1L_a. The results prove unambiguously the solvation process of the ^1L_a state which causes the dual fluorescence. The results given in Figs. 2 and 3 were obtained at −115 °C, but we have made measurements on the same system also at room temperature where the relaxation process is much faster than that at −115 °C. Thus even at small delay times, the intensity of the F_a band is fairly strong. Nevertheless, we observed that the intensity ratio $I(F_b)/I(F_a)$ at a small T_d value is larger than that at a large one.

In relation to the very polar nature of the ^1L_a state of DMABN, we have examined the possibility that the ^1L_a DMABN forms the complex with benzonitrile by electrostatic dipolar interaction. Such a possibility has already been examined by Chandross and Thomas[4] in the case of DMABN-propionitrile system in methylcyclohexane. They observed three fluorescence maxima upon successive additions of propionitrile to a methylcyclohexane solution. We studied the effect of temperature upon the fluorescence of the DMABN-benzonitrile system in cyclohexane, the results of which are shown in Fig. 4.

4) E. A. Chandross and H. T. Thomas, *Chem. Phys. Lett.*, **9**, 397 (1971).

At 70 °C, we observed only one fluorescence band which may be ascribed to a free DMABN molecule. The spectra at room temperature seem to be a superposition of the band due to the free DMABN and that of the complex. At 0 °C as well as at −10 °C, we can clearly recognize two bands, the shorter being ascribable to the free DMABN and the longer to the complex. The fluorescence band due to the complex shows a remarkable red shift by temperature lowering. Presumably, the spectra of the complex at lower temperatures are not due to the 1 : 1 dipolar complex but can be attributed to a 1 : n complex or a 1 : 1 complex strongly solvated by benzonitrile.

We also examined temperature effect on the cyclohexane solution of DMABN itself. At low temperatures, this system shows a long wavelength fluorescence band with peaks at 390 and 460 nm together with the ^1L_b band of the free DMABN. Since the positions of the long wavelength fluorescence peaks and the ratio of their intensities do not change with temperature lowering or with the increase of DMABN concentration, the long wavelength band might be ascribed to the 1 : 1 dipolar complex (self-complex) of DMABN.

The fluorescence decay time at 390 and 460 nm was about 9 ns, while that measured at F_b band was shorter than 5 ns. A slightly longer lifetime of the long wavelength fluorescence may be explained based on the above dimer model. We assume the sandwich dimer configuration where the dimethylamino group comes over the cyano group, and take the excition type wavefunction $\Psi_\pm=(\Psi_1^a\Psi_2^o\pm\Psi_1^o\Psi_2^a)/\sqrt{2}$, assuming the perturbation Hamiltonian of the dipole-dipole interaction, where Ψ^a represents the ^1L_a state. Thus, the energies of these states may be written as $E_+=E_a-\{(|\vec{\mu}_e|\cdot|\vec{\mu}_g|+\mu_t^2)/R^3\}$, $E_-=E_a-\{(|\vec{\mu}_e|\cdot|\vec{\mu}_g|-\mu_t^2)/R^3\}$, where E_a is the energy of the ^1L_a state, $\vec{\mu}_e$ and $\vec{\mu}_g$ the dipole moments of the ^1L_a state and the ground state, respectively, and $\vec{\mu}_t$ the transition moment. Thus, $E_+<E_-$ and the transition between the ground state

$\Psi_1^\circ \cdot \Psi_2^\circ$ and Ψ_+ is forbidden. Presumably, this sort of exciton type interaction in addition to the permanent dipole-dipole interaction is responsible for making the lifetime of the long wavelength band a little longer.

In view of the above results of complex formation, short range dipolar interactions might be important even in the case of the interaction between ^1L_a DMABN and MTHF.

BULLETIN OF THE CHEMICAL SOCIETY OF JAPAN, VOL. 46, 2290—2292 (1973)

Mass Spectrometric Study of the Primary Processes in Photochemical Reactions I. Photodecomposition of 1,1′-Azopropane

Shigeru YAMASHITA and Teruo HAYAKAWA

Department of Chemistry, Faculty of Liberal Arts and Sciences, University of Osaka Prefecture, Mozu-Umemachi, Sakai, Osaka 591

(Received January 11, 1973)

Primary processes of the photolysis of 1,1′-azopropane were studied using a high intensity light beam and a collision-free photochemical reactor incorporated in the ion-source of a mass spectrometer. The photofragments produced by the following three one-bond fission primary processes were found.

$$CH_3CH_2CH_2N_2CH_2CH_2CH_3 + h\nu \longrightarrow CH_3CH_2CH_2N_2CH_2 + CH_2CH_3 \quad (1)$$

$$CH_3CH_2CH_2N_2CH_2CH_2CH_3 + h\nu \longrightarrow CH_3CH_2CH_2N_2 + CH_2CH_2CH_3 \quad (2)$$

$$CH_3CH_2CH_2N_2CH_2CH_2CH_3 + h\nu \longrightarrow 2\,CH_3CH_2CH_2N \quad (3)$$

The lifetime of these photofragments seems to be longer than 50 μs considering the experimental conditions.

Several mass spectroscopic instruments have been reported for the study of primary processes of photochemical reactions. The essential part of these instruments is the photolysis reactor connected with the ion source of the mass spectrometer for prompt detection of photofragments produced in the primary processes.[1-4] Information has been obtained for many reaction systems.

However, in these mass spectroscopic intruments, collision of the photofragments with each other and with the reactor wall is inevitable. Most reaction products detected were molecular species and a few free radicals in certain cases.[5-7]

One of us reported on the photolysis of mercaptans and alkyl sulfides with a mass spectrometer connected with a fast-flow reactor.[8,9] We were interested in the use of molecular flow of reactant in the photolysis reactor involved in the ion source of the mass spectrometer. A mass spectrometric investigation of the primary processes in the photolysis of 1,3-butadiene with a pulsed flash-lamp and the molecular beam of the reactant vapor was reported by Bergmann and Demtröder.[10]

We attempted the use of steady illumination with a high-intensity light beam and the molecular flow type gas-lead of a Pyrex glass tube in the ion source of a mass spectrometer for studying primary processes of photochemical reactions.

From an interest in re-examination of the primary processes of 1,1′-azopropane, we carried out the photolysis of azopropane using the above instrument. The present paper describes the results.

The primary process was found to be[11]

$$CH_3CH_2CH_2N{=}NCH_2CH_2CH_3 + h\nu \longrightarrow 2\,CH_3CH_2CH_2 + N_2 \quad (a)$$

indicating simultaneous two-bond-splitting. Gowenlock *et al.* pointed out the possibility of the single bond-splitting process in their electron impact study of azo-*n*-alkanes,[12] suggesting that the products ($2\,CH_3CH_2CH_2 + N_2$) in process (a) might be derived from a preceding state ($CH_3CH_2CH_2N_2 + CH_3CH_2CH_2$).

We expected to find photofragments such as $CH_3CH_2CH_2N_2$ produced by single bond-rupture with a collision-free reactor incorporated in the ion source of the mass spectrometer. Collisions during the time between the photon impact and the detection of the photofragments could be neglected provided that the experimental conditions for the molecular flow of the reactant were satisfied by use of proper arrangement of gas-leak orifice and reservoir pressure.

1) F. P. Lossing, D. G. H. Marsden, and J. B. Farmer, *Can. Chem.*, **34**, 701 (1956).
2) G. B. Kistiakowsky and P. H. Kydd, *J. Amer. Chem. Soc.*, **79**, 4825 (1957).
3) H. Okabe, H. D. Beckey, and W. Groth, *Z. Naturforsch.*, **21a**, 135 (1966).
4) R. T. Meyer, *J. Sci. Instr.*, **44**, 422 (1967).
5) F. P. Lossing, *Can. J. Chem.*, **35**, 305 (1957).
6) J. B. Farmer, F. P. Lossing, D. G. H. Marsden, and E.W.R. J. Steacie, *J. Chem. Phys.*, **23**, 1169 (1955).
7) R. F. Pottie, A. G. Harrison, and F. P. Lossing, *Can. J. Chem.*, **39**, 102 (1961).
8) A. Jones, S. Yamashita and F. P. Lossing, *ibid.*, **46**, 833 (1968).
9) S. Yamashita and F. P. Lossing, *ibid.*, **46**, 2925 (1968).
10) K. Bergmann and W. Demtröder, *J. Chem. Phys.*, **48**, 18 (1968).
11) J. A. Kerr and J. G. Calvert, *J. Amer. Chem. Soc.*, **83**, 3391 (1961).
12) B. G. Gowenlock, J. R. Majer, and D. R. Snelling, *Trans. Faraday Soc.*, **58**, 670 (1962).

Experimental

Figure 1 shows a schematic diagram of the photolysis reactor and ion source. The mass spectrometer was a modified Hitachi RMU-5 type instrument, the ion current being detected by a ten-stage secondary electron multiplier.

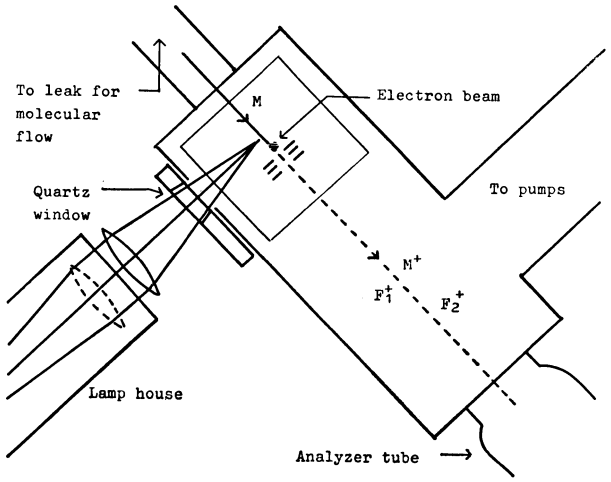

Fig. 1. Illustration of the reactor in the ion source. M means the reactant azopropane, M^+ denotes the ion from unreacted azopropane and F_1^+, F_2^+ show the ions from the photofragments.

Molecular flow of the reactant azopropane was supplied from a 5-l gas reservoir kept in the dark into the ion source through an orifice and a Pyrex glass gas-lead. The pressure in the reactor was about 10^{-5} Torr.

The light source for the photolysis was a USH-500D 500W high-pressure mercury lamp (Ushio Electric Co.). The light output was collimated in a housing fitted with a condensing lens system and a spherical mirror to obtain maximum intensity. The total light flux was estimated by ferrioxalate actinometer to be about 3×10^{18} quanta/s. The light flux from the lamp house was focused on the molecular flow of the reactant in the Pyrex gas-lead tube through a quartz window fixed on a side hole of the ion source block. In order to cut off wavelengths shorter than 300 nm, a Toshiba UV-29 filter was installed before the quartz window. Most of the incident light-quanta into the reactor were of 365 nm with small contribution from that of 334 nm. No light-exit window[10] was installed in this work, but the effect of scattered light was considered insignificant because of the fact that several metal pieces of the ionization chamber effectively shield the scattered light.

The mass spectrum obtained for each run was a superposition of the cracking patterns of the photofragments and that of unreacted azopropane. The mass spectrum of the photofragment mixture was obtained after subtracting the contribution from unreacted azopropane.

For detecting the signal of the photofragments, sufficient concentration of the photofragments relative to that of unreacted azopropane was necessary. This could be achieved by using a highly intense light beam focused on the molecular flow of the reactant and by using a reactant with a very high molecular extinction coefficient in the wavelength range of the light source. Since azopropane has absorption in near ultraviolet (Fig. 2), the high-intensity mercury lamp was proved to be effective for detecting the photofragments from azopropane.

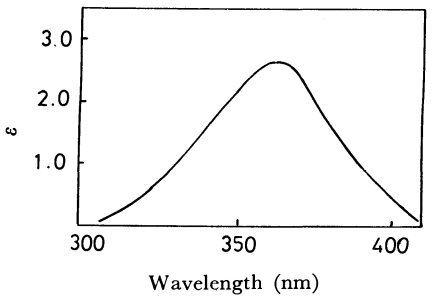

Fig. 2. Absorption spectrum of 1,1'-azopropane CH_3CH_2-$CH_2NNCH_2CH_2CH_3$ (gas phase).

Results and Discussion

The procedure to obtain the mass spectrum of the photofragment mixture from the recorded mass spectrum is given in Table 1. By subtracting the contribution from unreacted azopropane (third column) from the recorded peak height (second column), we obtain the residue Δ, the sum of the mass spectrum of the photofragments. Only the residues of significant magnitude are shown. Subtraction was done by normalizing at the mass number 114, the parent peak of azopropane.

Table 1. Mass spectrum of the photolyte flow of 1,1'-azopropane
(in arbitrary units)

m/e	Peak height	Azopropane contribution	Δ	Assignment
27	7.5	6.4	1.1	
28	75.0	75.0	—	
29	46.5	37.2	9.3	C_2H_5
30	14.0	13.0	1.0	
39	26.3	27.2	—	
41	99.0	97.4	1.6	
42	27.1	25.2	1.9	
43	239.5	231.0	8.5	C_3H_7
56	3.8	3.0	0.8	
57	5.6	3.1	2.5	C_3H_7N
71	7.9	6.9	1.0	$C_3H_7N_2$
85	2.1	1.6	0.5	$C_3H_7N_2CH_2$
114	20.0	20.0	—	Azopropane

The residue at *m/e* 28 was found to be negligible, indicating that N_2 was not a primary product. Some process preceding (a) might be expected.

The residues at *m/e* 85, 71 and 57 (Table 1) could be assgined as the ion peaks of $CH_3CH_2CH_2N_2CH_2$, $CH_3CH_2CH_2N_2$ and $CH_3CH_2CH_2N$, respectively. Presumably these photofragment radicals were produced in the following primary processes:

$$CH_3CH_2CH_2N_2CH_2CH_2CH_3 + h\nu \rightarrow CH_3CH_2CH_2N_2CH_2 + CH_2CH_3 \quad (1)$$

$$CH_3CH_2CH_2N_2CH_2CH_2CH_3 + h\nu \rightarrow CH_3CH_2CH_2N_2 + CH_2CH_2CH_3 \quad (2)$$

$$CH_3CH_2CH_2N_2CH_2CH_2CH_3 + h\nu \rightarrow 2\,CH_3CH_2CH_2N \quad (3)$$

TABLE 2. MASS SPECTRA OF THE PHOTOFRAGMENT MIXTURES

m/e	27	28	29	30	39	41	42	43	56	57	71[a)]	85
Run 1	0.6	—	7.0	2.5	1.3	—	3.6	4.8	0.5	0.4	1.0	0.1
Run 2	0.6	—	8.0	0.6	—	—	3.0	—	0.4	1.0	1.0	0.8
Run 3	0.3	—	4.5	2.0	2.5	0.7	1.2	2.0	0.2	0.7	1.0	0.2
Run 4	—	—	2.1	1.9	2.6	0.1	2.6	2.4	0.3	0.9	1.0	0.1
Run 5	0.5	—	5.8	1.9	—	1.5	1.1	12.5	0.6	1.4	1.0	0.1
Run 6	1.1	—	9.3	1.0	—	1.6	1.9	8.5	0.8	2.4	1.0	0.5
Run 7	1.5	—	12.8	3.8	3.2	2.3	6.0	4.4	0.9	0.6	1.0	0.3

a) Peak heights are normalized to unity at *m/e* 71.

The ion peak at m/e 43 was due to the unreacted azopropane whose concentration is several tens of times higher than the sum of the concentration of photofragments. Thus fluctuation of the peak height of *m/e* 43 affected its Δ-value of photofragments to such an extent to make it unreliable.

The residues at lower mass numbers were taken for mass spectral fragment ion peaks of the primary photofragments induced by electron impact. There was contribution from the ions of the photofragments $CH_3CH_2CH_2$ and CH_3CH_2 at *m/e* 43 and 29.

The results are summarized in Table 2, where the peak heights are normalized to unity at *m/e* 71. Assuming the same sensitivity for the three of photofragments of the mass numbers 85, 71 and 57, the probability of the occurrence of the primary processes (1), (2) and (3) seems to be approximately comparable with each other.

From the geometry of the instrument and the experimental conditions, the lifetime of these photofragments seems to be longer than 50 μs.

BULLETIN OF THE CHEMICAL SOCIETY OF JAPAN, VOL. 46, 2292—2299 (1973)

The Crystal Structure of Dinicotinic Acid

Fusao TAKUSAGAWA, Ken HIROTSU and Akira SHIMADA

Department of Chemistry, Faculty of Science, Osaka City University, Sugimoto-cho, Sumiyoshi-ku, Osaka 558

(Received January 13, 1973)

The crystal structure of dinicotinic acid has been determined by X-ray diffraction method. Two kinds of twinning crystals were obtained by changing the pH of the aqueous solution by recrystallization. The crystals are monoclinic with the space group of $P2_1/c$ and with cell dimensions of $a=9.702$, $b=11.153$, $c=6.587$ Å, and $\beta=107.8°$. The crystal structure was solved by an inspection of the sharpened Patterson map. The final R value is 5.93% for 1181 observed reflections. The dinicotinic acid molecule takes an intermediate structure between the neutral molecule and the zwitter ion with an approximate C_{2v} symmetry. The bond lengths and angles related by the C_{2v} symmetry are equal within the limits of experimental error for those of the two carboxyl groups. The C(2)–N(1)–C(6) bond angle is 119.8°, which lies between those of protonated and unprotonated species of the pyridine ring. The molecules lie approximately on planes parallel to the (001) plane at $z=1/4$ and 3/4. Each molecules on the same plane is joined through two kinds of hydrogen bonds (O–H···O; 2.594 Å, O···H···N; 2.515 Å), related by two-fold screw axes, with four neighboring molecules. In the O···H···N hydrogen bond, the hydrogen bonding distance and angle are 2.515 Å and 174° and the O–H and N–H distances are 1.23 and 1.29 Å, which are equal within the limits of experimental error. Therefore, it may be considered as an example of the single minimum hydrogen bond of the O–H···N hydrogen-bond type. The existence of two kinds of twins may be interpreted on the basis of the layer structure.

This work is a part of a series of studies on the O–H···N hydrogen bonding by the X-ray crystal structure analyses of several carboxylic acids with a pyridine ring. In their crystal structures studied hitherto, the O–H···N or $^+$N–H···O hydrogen bonds are found to play an important role without exception. Thus, this type of hydrogen bond is formed in nicotinic acid,[1] although the formation of the O–H···O hydrogen bond might also be plausible between carboxyl groups, as has been found in isoelectronic benzoic acid.[2] The same situation has also been revealed in dipicolinic acid,[3] which has a framework similar to that of isophthalic acid.[4] This dipicolinic acid has two bulky carboxyl groups in both α-positions so as to shield the nitrogen atom in a pyridine ring from the hydrogen-bond donor group, but it forms a hydrogen bond between nitrogen and oxygen atoms with the aid of a water molecule. The dinicotinic acid in the present

1) W. B. Wright and G. S. D. King, *Acta Crystallogr.*, **6**, 305 (1953).

2) G. A. Sim, J. M. Robertson, and T. H. Goodin, *ibid.*, **8**, 157 (1955).

3) F. Takusagawa, K. Hirotsu, and A. Shimada, This Bulletin **46**, 2020 (1973).

4) R. Alcala and S. M. Carrera. *Acta Crystallogr.*, **B28**, 1971 (1972).

study is also isoelectronic with isophthalic acid, and it will be of interest to elucidate the effect of the nitrogen atom in a pyridine ring on the hydrogen-bond formation in solids. Furthermore, the melting point of this compound is the highest of the six pyridine-dicarboxylic acids. Therefore, a rather strong hydrogen bond might be expected to exist in this crystal.

Experimental

Two kinds of crystals were obtained by changing the pH of the aqueous solutions by recrystallization, one in the form of colorless pillars from an aqueous solution and the other in the form of colorless prisms from an aqueous solution containing a few drops of HCl. Weissenberg photographs showed that the crystals recrystallized from an aqueous solution had the a^*b^* twinning plane, and that the other crystals recrystallized from an aqueous acidic solution has the b^*c^* twinning plane. The intensity ratio of the two individuals in the former twin is about 1.0 to 1.0, while that in the latter is 1.0 to 0.15.

The crystals were monoclinic with the space group of $P2_1/c$. The cell dimensions were measured from zero-layer Weissenberg photographs, which were calibrated with superimposed Al powder lines. They are given, along with other crystal data, in Table 1. One of the crystals which had the b^*c^* twinning plane was shaped to a sphere with the average diameter of 0.4 mm. The intensity data were collected for the 0—9 layers around the b axis and the 0—2 layers around the c axis by the use of the multiple-film equi-inclination-integrating Weissenberg technique, using Cu$K\alpha$ radiation. The intensities of the diffraction spots were estimated visually by comparison with an intensity standard. The intensities of the overlapped spots were estimated from $I \times 0.87$, where I is the intensity of the overlapped spot and where 0.87 is $1.0/(1.0+0.15)$. Of the possible 1555 reflections within the Cu$K\alpha$ sphere, 1289 independent reflections were measured; 108 were too weak to be observed. No absorption correction was applied.

Table 1. Crystal data for dinicotinic acid

Molecular formula	$C_7H_5NO_4$
Molecular weight	167.12
Crystal size	$\sim 0.4\times0.4\times0.4$ mm
Crystal system	Monoclinic
Space group	$P2_1/c$
Cell dimensions;	
a	9.702 ± 0.004 Å
b	11.153 ± 0.007
c	6.587 ± 0.004
β	$107.80\pm0.05°$
V	$678.5\ \pm0.7$ Å^3
Z	4
Density (calculated)	1.636 g/cm^3
Density (observed)	1.63
Radiation	Cu$K\alpha$ ($\lambda=1.5418$ Å)
Linear absorption coefficient	13.65 cm^{-1}
Number of independent reflections	1289
Atom numbering	

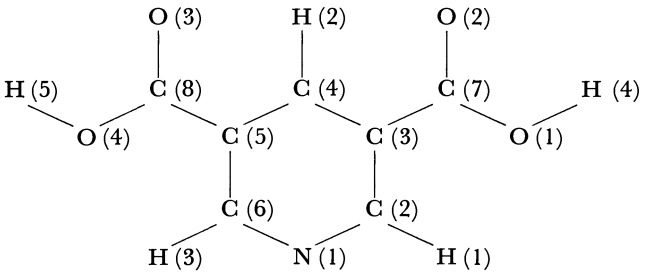

Structure Determination and Refinement

The crystal structure was solved by an inspection of the sharpened Patterson map, which was resolved sufficiently enough to give the orientation and the location of molecules in the unit cell. The first postulated structure gave an R value of 42%, which decreased to 13% in three cycles of least-squares refinement with individual isotropic thermal factors. Since the 0 0 2 reflection was seemingly influenced by the strong extinction effect, this reflection was removed from the later refinements.

The coordinates and anisotropic thermal parameters were refined by the block-diagonal least-squares procedure, minimizing the function $\Sigma w(F_o-F_c)^2$, where:

$w=0.5$ for $|F_o|\leqq 0.5$,

$w=1.0$ for $0.5<|F_o|<6.0$ and

$w=6.0/|F_o|$ for $6.0\leqq|F_o|$.

The atomic scattering factors used were those listed in the International Table for X-ray Crystallography for C, N and O atoms and the spherical scattering factors proposed by Stewart, Davidson, and Simpson[5] for the H atom. At the stage of $R=7.9\%$, a difference Fourier map was computed, from which five hydrogen atoms were located (Fig. 1). With anisotropic thermal parameters for non-hydrogen atoms and isotropic thermal parameters for hydrogen atoms, the final R value was 5.93%, excluding unobserved reflections. The observed and calculated structure factors are listed in

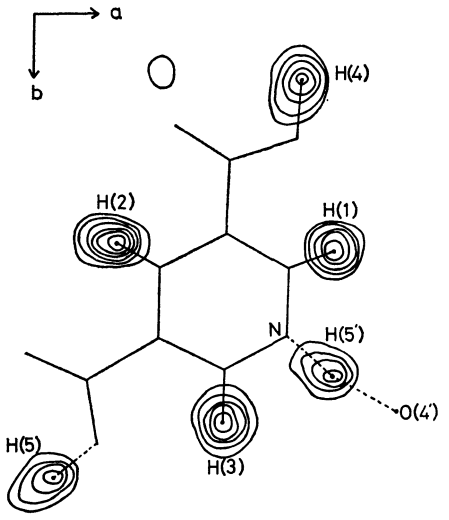

Fig. 1. A composite drawing of the electron density associated with the hydrogen atoms. The contours at intervals of 0.1 e·Å^{-3}, beginning with 0.2 e·Å^{-3} contour.

5) R. F. Stewart, E. R. Davidson, and W. T. Simpson, *J. Chem. Phys.*, **42**, 3175 (1965).

Table 2. The observed and calculated structure factors

F_o, F_c and DF have been multiplied by 10. The unobserved reflection is indicated by an asterisk. The reflection, for which the $|F_o-F_c|/|F_o|$ is larger than 0.3, is indicated by a plus sign.

H	FO	FC	DF	H	FO	FC	DF	H	FO	FC	DF	H	FO	FC	DF	H	FO	FC	DF	H	FO	FC	DF
K=L= 0 0				-5	378	-346	-32	2*	0	-6	6	4	46	54	-7	1	56	-56	0	-2	68	65	2	K=L= 4 2			
1	41	-41	0	-4	193	194	-1	3	48	50	-1	5	44	-48	4	2*	0	11	-11	-1	17	18	0	-11+	11	-15	4
2	90	103	-13	-3	236	-229	-6	4	20	-23	2	6	7	9	-1	3+	10	0	9	0	61	-63	2	-10	21	25	-4
3	70	-68	-1	-2	528	500	28	5	67	65	1	7+	6	9	-2	K=L=	2	8		1	65	-64	0	-9	18	20	-1
4	665	-653	-11	-1	447	448	-1	6	11	-12	1	8	53	-53	0	-6*	0	-1	1	2*	0	-2	2	-8	105	-112	7
5	234	232	22	0	23	25	-2	7+	8	-5	-2	9	11	8	2	-5	31	30	1	3	89	-86	-2	-7	23	27	-4
6	109	100	9	1	533	-528	-4	K=L=	1	6		10	45	-40	-5	-4	19	-21	2	4	27	26	0	-6	15	14	0
7	112	111	1	2	316	-314	-1	-10	4	4	0	K=L=	2	3		-3	27	28	0	5	40	40	0	-5+	13	7	6
8	100	-110	10	3	260	273	-13	-9	10	-9	-1	-12+	31	15	15	-2	5	6	-1	6	36	-35	0	-4	209	206	3
9	78	-74	-4	4	123	-131	8	-8	21	-24	2	-11	16	-15	-1	-1	24	-25	0	7	75	72	3	-3	88	97	-8
10	71	68	3	5	309	294	14	-7	11	-10	-1	-10+	7	12	-5	K=L=	3	0		8	35	-33	-2	-2	75	76	-1
11	17	-18	1	6	46	49	-3	-6*	0	-1	1	-9	46	-47	0	1	206	-211	4	K=L=	3	5		-1	115	122	-7
K=L=	0	2		7	27	-29	2	-5	25	-25	0	-8	49	-46	-3	2	167	-180	12	-11	4	3	0	0*	0	-9	9
-12+	13	-8	-4	8	49	56	-7	-4	41	-44	3	-7	123	126	-2	3	316	-289	-26	-10	59	59	0	1	33	37	-4
-11+	4	11	-6	9	86	91	-5	-3	43	45	-1	-6	79	-80	0	4	49	46	2	-9*	0	-1	1	2	16	16	0
-10	82	-91	8	10+	9	-12	3	-2	25	27	-1	-5+	35	-21	-14	5	129	149	-19	-8	44	41	3	3	83	89	-6
-9	87	92	-5	11	14	-15	0	-1	64	62	1	-4	162	-174	11	6	69	-73	3	-7*	0	-3	3	4	117	128	-10
-8	47	61	-13	K=L=	1	2		0	46	48	-2	-3	146	-143	-3	7	172	186	-13	-6	93	95	-1	5	23	-27	3
-7	161	-182	21	-12+	13	-19	5	1*	0	4	-4	-2	56	-56	0	8	121	-123	1	-5*	0	7	-7	6+	9	-14	5
-6	130	-137	6	-11	76	-78	1	2	47	-47	0	-1	101	-103	1	9	35	-35	0	-4	37	-37	0	7	51	-56	4
-5	246	-245	-1	-10+	32	-11	-20	3*	0	-3	3	0	121	118	3	10+	9	-5	-3	-3	8	-10	2	8	82	-79	-3
-4	725	679	45	-9	45	-47	2	4*	0	4	-4	1	330	-322	-8	11	26	-23	-2	-2	68	-63	-4	9	24	25	0
-3	83	-87	4	-8	20	-23	3	5*	0	-5	5	2	17	-19	1	K=L=	3	1		-1	52	-52	0	K=L=	4	3	
-2	119	-109	-9	-7	121	-125	3	K=L=	1	7		3	81	-82	1	-11	13	-10	-2	0	15	15	0	-11	86	78	7
-1	160	-171	11	-6	150	-158	7	-9	51	50	0	4*	0	6	-6	-10	108	113	-4	1	44	-46	1	-10+	9	-4	-5
0	1312	122	-8	-5	65	-69	4	-8+	4	1	3	5	69	60	9	-9	53	56	-3	2	73	-60	-12	-9	148	136	11
1	242	241	1	-4	279	-278	0	-7*	0	-2	2	6	45	39	5	-8	158	162	-3	3*	0	6	-6	-8	146	140	6
2	21	-17	-3	-3	227	220	7	-6	5	7	-1	7	31	28	2	-7	21	20	0	4	15	11	3	-7	70	-71	1
3	122	144	-22	-2	45	46	-1	-5	22	29	-6	8	19	20	0	-6	77	85	-8	5	17	17	0	-6	195	-196	1
4	298	333	-35	-1	245	232	12	-4	33	-34	0	9	31	27	3	-5	147	152	-4	6	14	13	0	-5	116	-110	-5
5	90	-99	8	0	154	156	-2	-3	14	-13	0	K=L=	2	4		-4	4	-4	0	K=L=	3	6		-4	184	185	-1
6	37	-44	6	1	42	40	2	-2	33	-36	2	-12	41	-53	12	-3	178	168	9	-10	22	19	2	-3	18	17	0
7	23	-22	0	2	74	-83	8	-1*	0	-5	5	-11	61	58	2	-2+	18	-25	6	-9	20	-19	-1	-2	397	377	20
8	86	85	0	3	70	-78	7	0	9	-10	0	-10	37	38	0	-1	80	-91	11	-8	55	-50	-4	-1	76	81	-5
9	34	36	-1	4	154	166	-11	1	60	60	0	-9	13	17	-3	0	14	-14	0	-7	117	108	8	0	118	-120	1
10	42	-43	0	5	25	28	-2	2	7	-7	0	-8	11	7	3	1	13	-13	0	-6	26	-27	0	1	150	156	-5
K=L=	0	4		6	145	151	-5	3	11	-13	1	-7	140	-142	1	2	139	-145	6	-5	25	28	-2	2	203	190	12
-12*	0	17	-17	7	25	28	-2	K=L=	1	8		-6	50	-54	3	3	183	-175	-8	-4	33	-37	3	3	17	-17	0
-11*	0	11	-11	8*	0	1	-1	-7*	0	-7	7	-5	56	59	-2	4	15	-17	1	-3	38	-37	0	4+	8	-14	5
-10	78	86	-8	9*	0	9	-9	-6*	0	0	0	-4	68	-64	-3	5	88	-101	12	-2	20	-19	-1	5	105	-106	1
-9	64	-67	2	10*	0	15	-15	-5	14	14	0	-3	127	126	0	6	10	-11	1	-1	12	13	0	6	93	-93	0
-8+	6	-1	-4	K=L=	1	3		-4	13	16	-3	-2	32	31	0	7	23	-29	6	0	28	28	0	7	42	-39	-2
-7	135	140	-5	-12	19	-21	2	-3	12	-15	3	-1	193	-196	3	8	125	-128	3	1	13	15	-2	8	95	90	5
-6	82	90	-8	-11	5	7	-1	-2	10	-10	0	0	107	101	6	9	49	-50	1	2	15	-16	0	9+	8	4	3
-5	101	110	-8	-10	6	7	-1	-1	19	-22	3	1	130	-128	-2	10	62	-62	0	3	37	37	0	K=L=	4	4	
-4	434	-393	-40	-9	116	136	-20	K=L=	2	0		2+	19	2	16	K=L=	3	2		4	11	-11	0	-11+	10	16	-5
-3	82	92	-10	-8	68	71	-2	0	152	164	-12	3+	7	10	-2	-11	42	-34	-7	5	13	-15	1	-10	26	-28	2
-2	38	35	2	-7	40	-41	0	1	513	-535	22	4	22	-22	0	-10+	9	6	3	K=L=	3	7		-9	13	-13	0
-1	97	110	-12	-6	111	109	1	2	35	44	-8	5	32	30	1	-9	42	-42	0	-9	9	12	-2	-8	56	58	-2
1	168	-177	8	-5	231	205	25	3	179	177	1	6+	7	10	-3	-8	125	-139	13	-8+	8	-5	-2	-7	54	-60	6
2	16	-16	0	-4	143	-155	12	4	88	-92	3	7	17	14	3	-7	213	211	1	-7	8	-6	-2	-6	12	-11	-1
3	83	-85	2	-3	57	67	-9	5	49	53	-3	8	25	21	4	-6	61	-67	5	-6	58	-54	-4	-5	10	10	0
4	122	-121	-1	-2	330	-329	-20	6	47	-53	6	K=L=	2	5		-5	140	152	-11	-5	10	10	0	-4	95	-110	15
5	18	22	-4	-1	129	-133	4	7	70	-84	14	-11	22	21	0	-4+	11	-2	-9	-4	18	18	0	-3	23	-29	6
6	17	21	-4	0	34	-40	6	8	74	77	-3	-10*	0	1	-1	-3	242	-244	1	-3	5	6	-1	-2	32	-36	4
7*	0	-8	8	1	288	283	5	9+	18	6	11	-9	57	55	1	-2	162	-155	-7	-2	23	26	-3	-1	64	-64	0
8	39	-38	0	2	78	84	-5	10	65	63	1	-8	25	23	2	-1	122	-112	-9	-1	21	21	0	0+	22	33	-11
K=L=	0	6		3	148	-146	-1	11	24	28	-4	-7	89	-80	-8	0	78	87	-4	0	15	-19	0	1*	0	0	0
-10	42	-51	9	4	62	61	1	K=L=	2	1		-6	79	73	5	1	174	165	8	1	26	27	-1	2*	0	1	-1
-9	33	32	1	5	161	-156	-5	-12	18	-16	-1	-5	26	28	-1	2	67	76	-9	2	21	16	4	3	42	-44	2
-8	9	-10	0	6*	0	1	-1	-11+	5	0	-5	-4	55	58	-2	3	189	183	6	K=L=	3	8		4	44	-48	4
-7	59	-61	1	7	17	14	2	-10	19	-23	4	-3	21	21	0	4	45	-49	3	-5*	0	-3	3	5	23	23	0
-6	27	-29	1	8	15	-16	1	-9*	0	-1	1	-2	10	-10	0	5	72	-89	16	-4	20	20	0	6	9	10	0
-5	16	-21	4	9	47	-47	0	-8	48	37	10	-1*	0	1	-1	6	53	57	-3	-3	8	7	0	7	40	38	1
-4	172	170	1	K=L=	1	4		-7	136	-140	3	0	29	-23	0	7	130	-128	-2	-2*	0	3	-3	8	31	31	0
-3	39	-46	7	-12+	13	17	-4	-6	27	28	-1	1	146	138	7	8	71	72	-1	K=L=	4	0		K=L=	4	5	
-2*	0	-5	5	-11	58	59	-1	-5	46	-42	-3	2	13	-11	-2	9	24	23	1	0	21	-25	3	-11	78	-71	-6
-1	37	-36	0	-10+	6	2	3	-4	212	207	4	3	13	13	0	10	12	10	1	1	112	-114	1	-10	15	-13	-1
0	236	-228	-8	-9	31	31	0	-3	311	297	13	4+	14	-10	-4	K=L=	3	3		2	57	-65	7	-9	115	-110	-5
1	84	83	0	-8	21	27	-5	-2	156	149	6	5	27	-27	0	-11+	8	-3	-4	3	136	-132	-4	-8	71	-69	-2
2	10	11	-1	-7	66	66	0	-1	416	423	-7	6	22	-20	-2	-10	113	-112	-1	4	219	-220	1	-7	33	32	1
3	30	32	-1	-6	40	44	-3	0	290	-303	12	7*	0	0	0	-9	25	-29	4	5*	0	5	-5	-6	157	146	10
4	29	34	-5	-5	42	44	-1	1	512	568	-55	K=L=	2	6		-8	124	-116	-7	6*	0	3	-3	-5+	21	29	-8
5*	0	-4	4	-4	124	124	0	2	100	109	-8	-10	13	-14	0	-7*	0	1	-1	7	31	34	-2	-4	76	-76	0
K=L=	0	8		-3	120	-118	-2	3	225	239	-13	-9*	0	-8	8	-6	129	-122	-7	8	123	123	0	-3*	0	5	-5
-6*	0	1	-1	-2	43	-45	2	4	72	76	-3	-8	15	15	0	-5	73	-78	4	9	24	-25	1	-2	174	-163	-11
-5*	0	3	-3	-1	151	-151	0	5	86	-85	-1	-7	86	79	6	-4	42	41	0	10+	8	-13	5	-1	8	8	0
-4	53	-62	8	0	114	-107	-6	6	29	-33	3	-6	17	17	0	-3	39	-39	0	11+	5	9	-3	0	32	31	0
-3+	13	18	-5	1	33	-29	-3	7	90	-89	0	-5	52	-50	-2	-2	111	106	5	K=L=	4	1		1	35	-38	3
-2*	0	0	0	2	77	77	0	8*	0	1	-1	-4	36	39	-2	-1	100	97	2	-10+	19	25	-6	2	76	-75	0
K=L=	1	0		3	20	20	0	9	33	-34	0	-3	63	-64	1	0	8	5	2	-9	102	-97	-4	3	20	22	-1
1	97	98	0	4	39	-45	5	10	12	-14	2	-2	19	-16	-3	1	54	57	-3	-8	175	-178	3	4	19	21	-1
2	54	57	-3	5*	0	0	0	11*	0	-4	4	-1	78	73	4	2	145	136	8	-7	100	100	0	5	36	40	-3
3	218	196	21	6	69	-66	-3	K=L=	2	2		0	70	-63	-7	3	64	57	6	-6	201	208	-7	6	39	37	1
4	344	-317	-26	7*	0	4	-4	-12	69	61	7	1	50	50	0	4*	0	0	0	-5	196	202	-6	K=L=	4	6	
5	60	-65	5	8*	0	1	-1	-11	55	-53	-1	2*	0	6	-6	5	12	12	0	-4	217	-204	-12	-10	19	19	0
6	230	-222	-7	K=L=	1	5		-10	65	-62	-3	3	13	10	3	6	18	-19	0	-3	56	-48	-8	-9	7	8	0
7	93	-97	3	-11	10	-8	-2	-9	26	-18	-7	4+	8	5	2	7+	9	18	-8	-2	623	-586	-37	-8	15	-18	2
8	13	-12	0	-10	5	-5	0	-8	57	-54	-2	5	17	-14	-3	8	74	72	1	-1	299	-288	-10	-7	42	45	-3
9	28	-31	3	-9	90	-96	6	-7	156	157	0	K=L=	2	7		9	29	26	3	0	276	243	33	-6*	0	0	0
10	20	-15	-5	-8	23	-25	1	-6	75	80	-4	-9	37	-32	-4	K=L=	3	4		1	331	-330	0	-5	18	-21	2
11	62	-61	0	-7	18	19	-1	-5	57	-55	-2	-8*	0	-5	5	-11	45	39	6	2	439	-443	3	-4	39	43	-3
K=L=	1	1		-6	46	-49	2	-4	99	93	5	-7	43	41	1	-10	18	-17	-1	3	26	-22	-3	-3*	0	-2	2
-12	26	27	-1	-5	76	-78	2	-3	195	-196	0	-6	52	-47	-5	-9	37	34	2	4	69	-74	5	-2	8	9	0
-11*	0	6	-6	-4	76	82	-5	-2	48	-53	4	-5	9	-11	1	-8	99	100	-1	5	183	190	-7	-1	25	25	0
-10*	0	0	0	-3	6	7	-1	-1	415	432	-17	-4*	0	-2	2	-7	174	-175	1	6	157	163	-5	0	19	-23	4
-9	122	-134	11	-2	129	126	3	0	144	-132	-11	-3	10	9	0	-6	43	45	-2	7	84	82	2	1*	0	-2	2
-8	81	-90	9	-1	24	29	-4	1	290	315	-25	-2	18	18	0	-5	81	-87	5	8	149	-146	-3	2*	0	0	0
-7	43	44	-1	0	20	21	0	2	17	-18	1	-1	6	5	0	-4	29	37	-7	9	39	-37	-1	3	17	19	-1
-6	110	-115	4	1	136	-136	0	3	71	-82	10	0*	0	-2	2	-3	118	115	3	10	26	27	-1	4	10	13	-2

TABLE 2. Continued

H	FO	FC	DF	H	FO	FC	DF	H	FO	FC	DF	H	FO	FC	DF	H	FO	FC	DF	H	FO	FC	DF	H	FO	FC	DF
5+	2	-11	9	K=L=	5	4		9	12	-12	0	-7	12	12	0	5	49	45	4	-4+	6	-9	2	3	79	78	1
K=L=	4	7		-11	93	89	10	10	61	54	7	-6	51	-50	0	6	40	-44	4	-3	39	-38	-1	4	12	-14	1
-8	19	22	-2	-10	27	-26	-1	K=L=	6	2		-5	14	15	0	K=L=	7	5		-2	33	-36	3	5	12	11	0
-7	8	-9	1	-9	56	-53	-3	-11	36	38	-1	-4	11	11	0	-9	23	23	0	-1	36	-35	0	6	34	30	4
-6	87	-84	-2	-8	70	-66	-3	-10	81	-74	-6	-3*	0	-4	4	-8	13	14	0	0	33	-36	2	7*	0	0	0
-5*	0	1	-1	-7	373	-385	11	-9	17	18	-1	-2	35	37	-2	-7	34	38	-3	1	119	-115	-4	K=L=	9	3	
-4	16	14	1	-6	147	152	-4	-8	18	18	0	-1*	0	-4	4	-6	145	-131	-13	2	44	-46	1	-9	73	-61	-11
-3*	0	-3	3	-5	45	48	-3	-7	33	-33	0	0*	0	0	0	-5	19	21	-2	3*	0	0	0	-8	16	-15	0
-2	55	58	-2	-4	60	68	-6	-6	73	70	2	K=L=	7	0		-4	25	-26	0	4	29	31	-2	-7	16	16	0
-1	16	-16	0	-3	150	158	-7	-5	80	-80	0	1	99	-105	5	-3+	6	3	2	5+	9	16	-7	-6	56	-61	4
0+	4	-2	-2	-2	123	-121	-2	-4	20	20	0	2	46	-46	0	-2	82	74	7	6	21	21	0	-5	178	-201	22
1*	0	1	-1	-1	26	-25	-1	-3	197	-210	12	3	35	-35	0	-1*	0	0	0	7*	0	0	0	-4	57	61	-3
2	26	30	-3	0	45	47	-2	-2	82	-81	-1	4	28	-31	3	0	25	-26	1	K=L=	8	4		-3+	8	14	-5
K=L=	4	6		1	105	103	2	-1	94	-102	7	5	100	108	-8	1	43	43	0	-9	38	-39	1	-2	174	177	-3
-5	12	14	-1	2	58	59	0	0	201	-204	2	6	119	-118	-1	2*	0	4	-4	-8	38	36	1	-1	174	172	2
-4+	11	-15	3	3	131	-129	-2	1	29	35	-5	7	25	24	1	3	18	20	-2	-7*	0	1	-1	0	9	10	0
-3	6	6	0	4	29	26	2	2	97	-97	0	8	92	-88	-4	4*	0	3	-3	-6	40	35	4	1	186	-198	12
-2*	0	-1	1	5+	9	3	9	3	109	-116	7	9	67	-68	1	5	8	-11	2	-5	14	-17	3	2	33	-39	5
K=L=	5	0		6+	7	0	-6	4	15	16	-1	10	8	10	-1	K=L=	7	6		-4	71	75	-3	3	35	38	-2
1	211	228	-17	7	148	138	9	5	21	-20	-1	K=L=	7	1		-8	40	-37	-3	-3+	13	-21	7	4+	9	-6	-3
2	356	353	2	K=L=	5	5		6	97	94	2	-10	44	-38	-5	-7	26	29	-2	-2	18	-17	-1	5	154	137	16
3	392	-378	-14	-10	9	7	1	7	41	41	0	-9*	9	12	-3	-6	20	-21	0	-1	44	45	0	6+	3	-8	4
4+	18	27	-9	-9	18	-19	1	8	47	49	-1	-8	49	-42	-6	-5+	10	14	-3	0	189	-173	-15	K=L=	9	4	
5	28	-32	3	-8	64	-65	1	9	13	-13	0	-7	87	88	-1	-4	16	-15	0	1	41	39	1	-9	8	-7	-1
6	34	-32	-1	-7+	17	12	5	K=L=	6	3		-6	182	-182	0	-3*	0	2	-2	2	12	-11	0	-8	21	19	1
7	520	511	8	-6	63	-65	1	-11*	0	0	0	-5	53	-57	3	-2	13	13	0	3	26	30	-3	-7	10	-11	1
8	20	21	-1	-5	66	69	-2	-10	37	-39	2	-4	116	-121	4	-1	18	20	-2	4	21	21	0	-6	16	14	1
9+	18	24	-5	-4	33	34	-1	-9	33	36	-2	-3	102	-97	-5	0	39	41	-2	5	21	22	0	-5	23	-19	-3
10	9	-10	0	-3+	14	-9	-5	-8	57	61	-3	-2	176	167	9	1	21	22	-1	6+	6	-8	2	-4	15	16	0
11	55	-57	1	-2	42	49	-7	-7	51	56	-4	-1	14	16	-2	2	28	-27	0	K=L=	8	5		-3	59	63	-4
K=L=	5	1		-1	32	-33	1	-6	95	-98	2	0	7	-9	2	K=L=	7	7		-9	12	15	-2	-2	11	-14	2
-11	15	11	3	0	15	19	-4	-5+	17	-7	-9	1+	21	14	6	-6	63	68	-5	-8	45	47	-2	-1	73	67	5
-10*	0	-5	5	1	28	30	-1	-4	24	27	-3	2	86	-87	0	-5	26	-27	0	-7	21	-22	0	0	59	-56	-2
-9	15	-17	2	2	6	-8	1	-3	59	-67	8	3	125	120	4	-4+	4	5	-1	-6	52	52	0	1	55	-52	-2
-8	133	-144	10	3*	0	5	-5	-2	172	163	9	4	87	98	-10	-3*	0	-3	3	-5	39	38	0	2	16	13	3
-7+	26	5	20	4	29	-33	3	-1	36	39	-2	5	37	42	-4	-2	28	-26	-2	-4	6	-6	0	3	37	-36	0
-6	96	-96	0	5	9	-9	0	0	19	19	0	6	100	108	-7	-1*	0	4	-4	-3	7	7	0	4	9	9	0
-5	72	82	-10	6+	5	7	-2	1	32	35	-2	7	67	-68	1	K=L=	8	0		-2+	15	-3	-12	5+	5	-8	2
-4	145	152	-6	K=L=	5	6		2	89	83	6	8	55	57	-1	0	372	-362	-10	-1+	16	-6	-10	K=L=	9	5	
-3	126	-129	-3	-9	27	27	0	3	94	-91	-2	9+	8	-12	3	1	83	96	-12	0+	11	19	-8	-8*	0	-1	1
-2	144	135	8	-8	41	40	0	4	27	-27	0	K=L=	7	2		2	71	-67	-3	1	52	59	-6	-7	11	-9	-2
-1	185	-186	1	-7	201	186	15	5	29	-29	0	-10	23	23	0	3*	0	3	-3	3	14	-10	-3	-6	33	31	1
0	24	29	-4	-6	108	-106	-2	6	10	-8	-2	-9	85	-82	-2	4+	55	73	-17	4	14	-14	0	-5	117	104	13
1	173	175	-1	-5	21	-22	1	7	25	26	0	-8	91	-89	-1	5	22	20	1	K=L=	8	6		-4	57	-50	-6
2	83	-82	0	-4	45	-46	0	8	60	59	1	-7	18	17	0	6	41	36	4	-7	8	-6	-2	-3	33	-31	-2
3	104	107	-2	-3	51	-56	5	K=L=	6	4		-6	90	-92	2	7	11	-12	1	-6	15	-16	0	-2	106	-90	-15
4	123	-133	9	-2	32	33	0	-10	79	75	3	-5	93	97	-3	8	41	40	0	-5+	12	16	-3	-1	85	-81	-4
5	35	-41	6	-1	10	13	-2	-9	18	-21	2	-4	28	-36	8	9	37	-39	1	-4	47	-49	1	0*	0	-1	1
6	57	58	-1	0	23	-22	0	-8	29	29	0	-3*	14	-10	-4	K=L=	8	1		-3	10	9	0	1	112	110	2
7+	8	5	9	1	28	-29	1	-7	44	46	-2	-2	34	-30	-4	-10	62	-59	-3	-2*	0	5	-5	2*	0	0	0
8	92	104	-11	2	10	-11	0	-6	36	-29	-7	-1+	14	-18	4	-9	42	-43	1	-1	23	-22	0	3	10	-10	0
9+	4	7	-3	3	50	53	-3	-5	16	16	0	0	62	67	-4	-8	69	66	3	0	82	84	-1	K=L=	9	6	
10+	10	2	8	4	10	-11	0	-4	16	-16	0	1	137	126	10	-7	23	-23	0	1	15	-16	1	-6*	0	-1	1
K=L=	5	2		K=L=	5	7		-3	111	112	0	2	7	6	1	-6	38	37	0	2*	0	-1	1	-5	15	11	4
-11	85	-79	-6	-8	20	22	-2	-2	13	11	1	3	40	43	-2	-5	34	32	1	K=L=	9	0		-4	15	-13	-1
-10+	12	8	4	-7*	0	-2	2	-1	88	84	4	4+	14	-2	-12	-4*	0	1	-1	1	148	-155	6	-3	26	-27	0
-9	53	57	-3	-6	26	32	-6	0	45	50	-5	5	82	-81	0	-3	59	61	-1	2	22	22	0	-2+	3	6	-3
-8	66	66	0	-5	29	-32	3	1	36	-38	1	6	82	88	-5	-2	81	87	-6	3	97	-116	18	-1	29	-26	-3
-7	561	555	6	-4+	5	-7	2	2	44	45	-1	7	34	-34	0	-1	127	122	4	4+	4	8	-4	0	36	31	4
-6	120	-118	-2	-3*	0	-3	3	3	51	52	-1	8	61	59	2	0	53	56	-3	5	5	-4	-1	1	12	15	-2
-5	50	-57	7	-2+	11	-17	5	4	13	-14	0	K=L=	7	3		1	162	160	1	6	36	-41	4	K=L=	10	0	
-4	45	-41	-3	-1	7	7	0	5+	7	-4	-2	-10	34	33	0	2	85	86	0	7*	0	-3	3	0	460	-433	-27
-3	331	-318	-13	0+	3	-4	1	6	63	-55	-8	-9	17	-19	1	3	30	35	-4	8+	8	-11	2	1*	0	1	-1
-2	328	289	38	1	9	-10	0	7	33	-32	-1	-8+	5	8	-2	4	24	-28	4	9	27	23	4	2+	7	9	-2
-1	91	98	-6	K=L=	6	0		K=L=	6	5		-7	71	-73	2	5+	18	-3	-15	K=L=	9	1		3	7	-5	-1
0	47	-59	12	0	315	321	-6	-10	13	13	0	-6	191	189	1	6*	0	-5	5	-9	90	68	21	4+	63	84	-21
1	203	-215	12	1	34	41	-6	-9	20	-24	4	-5	19	17	1	7	11	-13	1	-8	24	23	0	5	32	-36	4
2	203	-202	-1	2	134	134	0	-8	24	-27	3	-4	76	75	0	8	33	32	0	-7	12	-10	-1	6	60	-67	6
3	253	256	-2	3	203	209	-5	-7	28	-30	1	-3	24	27	-2	9	67	-55	-12	-6	53	59	-6	7	13	-16	3
4	42	-47	4	4	20	-16	-3	-6	85	81	4	-2	163	-146	-16	K=L=	8	2		-5	240	277	-36	8	70	60	10
5+	16	6	9	5	72	74	-2	-5	16	-13	-3	-1	14	-14	0	-10	73	66	7	-4	36	-43	7	1+	7	-12	4
6*	0	-3	3	6	111	-108	-3	-4	24	-23	-1	0	19	23	-4	-9	46	50	-3	-3	41	39	2	2	78	77	1
7	311	-307	-3	7	16	-14	-2	-3	21	25	-3	1	39	-42	3	-8	47	-43	-3	-2	215	-208	-7	3	57	-60	2
8+	15	20	-4	8	55	-58	2	-2	91	-87	-3	2	11	14	-2	-7	10	9	0	-1	272	-259	-13	4	90	87	3
9	10	7	2	9*	0	-2	2	-1+	8	-5	-3	3	74	-70	-3	-6	54	-49	-5	0	10	-8	-2	5*	0	-5	5
K=L=	5	3		10	52	47	4	0*	0	-3	3	4	35	-38	3	-5*	0	6	-6	1	247	269	-22	6	39	42	-3
-11+	11	-7	-4	K=L=	6	1		1*	0	1	-1	5*	0	-3	3	-4	75	-86	11	2	125	132	-6	7	56	51	5
-10*	0	0	0	-10	60	59	1	2	28	-31	3	6	38	-41	2	-3	23	23	0	3	59	-65	5	0	40	40	0
-9	20	23	-3	-9	28	-30	2	3	45	44	0	7	35	36	0	-2	47	47	0	4	15	17	-2	1	36	39	-2
-8	124	124	0	-8	90	-86	-3	4	17	17	0	8	45	-46	0	-1	75	-77	2	5	247	-240	-7	2	22	27	-4
-7+	26	-17	-9	-7	62	-68	5	5	10	8	2	K=L=	7	4		0	284	293	-8	6	23	-22	-1	3	25	18	6
-6	92	97	-5	-6	66	78	-11	K=L=	6	6		-10	34	-31	-3	1	79	-74	-5	7*	0	3	-3	4	42	41	0
-5	95	-98	3	-5	37	41	-4	-9	13	13	0	-9	60	57	3	2	47	45	2	8	11	-11	0	5*	0	8	-8
-4	96	-94	-1	-4*	0	-6	6	-8	38	-39	0	-8	70	64	5	3	28	-31	3	K=L=	9	2		6*	0	-9	9
-3	57	59	-1	-3	116	119	-3	-7	24	-28	4	-7	27	-26	0	4	42	-46	3	-9	23	18	5	1	28	-31	2
-2	100	-106	5	-2	249	-224	-24	-6	18	13	5	-6	45	45	0	5	33	-32	-1	-8	23	-23	0	2	13	14	-1
-1	101	101	0	-1	87	-85	-2	-5	24	26	-1	-5	47	-52	5	6+	11	-8	-3	-7+	4	2	2	3	73	68	4
0	36	-43	6	0	53	-49	-4	-4*	0	4	-4	-4	21	23	-2	7	5	5	0	-6	32	-33	1	4*	0	3	-3
1	86	-86	0	1	81	-83	1	-3	35	-34	0	-3+	12	-1	-11	8	29	-26	-3	-5	16	13	3	5	17	18	0
2	25	27	-1	2	196	-176	-19	-2	10	9	1	-2	6	-4	-1	K=L=	8	3		-4*	0	-7	7	0	4	-5	0
3	40	-41	1	3	126	131	-5	-1	47	-47	0	-1	20	-21	1	-10	55	54	1	-3	92	-108	15	1	16	19	-2
4	72	75	-2	4	22	22	0	0*	0	5	-5	0	69	-69	0	-9+	5	7	-1	-2	23	21	1	2	42	-39	-2
5	16	19	-2	5	47	50	-2	1	15	16	0	1	75	-71	-4	-8	73	-73	0	-1	142	-128	-14				
6	21	-23	1	6	31	37	-6	2	18	-21	2	2	28	28	0	-7	26	25	1	0	58	55	2				
7*	0	-4	4	7	50	-51	1	3	20	-24	3	3	27	-28	1	-6	65	-63	-2	1	124	115	8				
8	50	-53	2	8	86	-84	-2	K=L=	6	7		4	19	23	-4	-5	48	-52	3	2	21	-18	-3				

Table 2. The fractional coordinates and thermal parameters are listed in Table 3.

Results and Discussion

Molecular Structure. The bond lengths and angles are shown with their estimated standard deviations in Fig. 2. Figure 1 shows the difference Fourier map along the *c* axis, in which there is no high peak except for those due to the hydrogen atoms. Figure 3 shows the anisotropic thermal ellipsoids of non-hydrogen atoms and the isotropic thermal ellipsoids of hydrogen atoms.

The dinicotinic acid molecule in the crystal was found by this study to have a structure intermediate between the neutral molecule and the zwitter ion, as

TABLE 3. THE FINAL PARAMETERS AND THEIR ESTIMATED STANDARD DEVIATIONS (IN PARENTHESES)

The coordinates of non-hydrogen atoms have been multiplied by 10^4; those of the hydrogen atoms by 10^3. The anisotropic thermal parameters of non-hydrogen atoms are of the form $\exp[-(B_{11}h^2+B_{22}k^2+B_{33}l^2+B_{12}hk+B_{13}hl+B_{23}kl)]$ and have been multiplied by 10^4. For the hydrogen atoms the values listed are isotropic thermal parameters B (Å^2).

Atom	x	y	z	B (Å^2)	Atom	x	y	z	B (Å^2)
N (1)	8186 (2)	6534 (2)	2128 (3)	—	O (2)	3892 (2)	4711 (2)	2650 (3)	—
C (2)	6835 (2)	6576 (2)	2266 (4)	—	O (3)	8457 (2)	2272 (2)	2453 (3)	—
C (3)	6120 (2)	5539 (2)	2516 (3)	—	O (4)	10381 (2)	3419 (2)	2819 (4)	—
C (4)	6808 (2)	4453 (2)	2625 (4)	—	H (1)	638 (3)	732 (2)	214 (4)	3.5 (0.6)
C (5)	8204 (2)	4406 (2)	2476 (4)	—	H (2)	630 (3)	367 (2)	284 (4)	3.0 (0.5)
C (6)	8856 (2)	5475 (2)	2235 (4)	—	H (3)	985 (3)	551 (2)	213 (4)	3.9 (0.6)
C (7)	4609 (2)	5591 (2)	2641 (4)	—	H (4)	303 (4)	676 (3)	263 (5)	6.0 (0.8)
C (8)	9039 (2)	3260 (2)	2588 (4)	—	H (5)	1110 (3)	252 (3)	275 (5)	5.6 (0.8)
O (1)	4167 (2)	6697 (2)	2717 (4)	—					

Atom	B_{11}	B_{22}	B_{33}	B_{12}	B_{13}	B_{23}	Atom	B_{11}	B_{22}	B_{33}	B_{12}	B_{13}	B_{23}
N (1)	81 (2)	39 (2)	33 (6)	−6 (3)	132 (6)	18 (5)	C (7)	74 (2)	45 (2)	25 (6)	9 (3)	110 (6)	8 (5)
C (2)	85 (2)	39 (2)	30 (7)	1 (3)	128 (7)	1 (6)	C (8)	86 (3)	43 (2)	29 (7)	−6 (3)	117 (7)	−13 (6)
C (3)	77 (2)	40 (2)	23 (6)	1 (3)	103 (6)	3 (5)	O (1)	96 (2)	44 (2)	52 (8)	24 (3)	245 (7)	18 (5)
C (4)	83 (2)	40 (2)	26 (6)	−3 (3)	110 (6)	1 (5)	O (2)	91) 2)	53 (2)	34 (6)	−16 (3)	159 (5)	2 (5)
C (5)	76 (2)	39 (2)	26 (6)	7 (3)	101 (6)	−3 (5)	O (3)	90 (2)	40 (2)	44 (7)	−7 (3)	193 (6)	−9 (5)
C (6)	72 (2)	50 (2)	30 (7)	0 (3)	125 (6)	−3 (6)	O (4)	73 (2)	46 (2)	53 (8)	7 (3)	169 (6)	−39 (5)

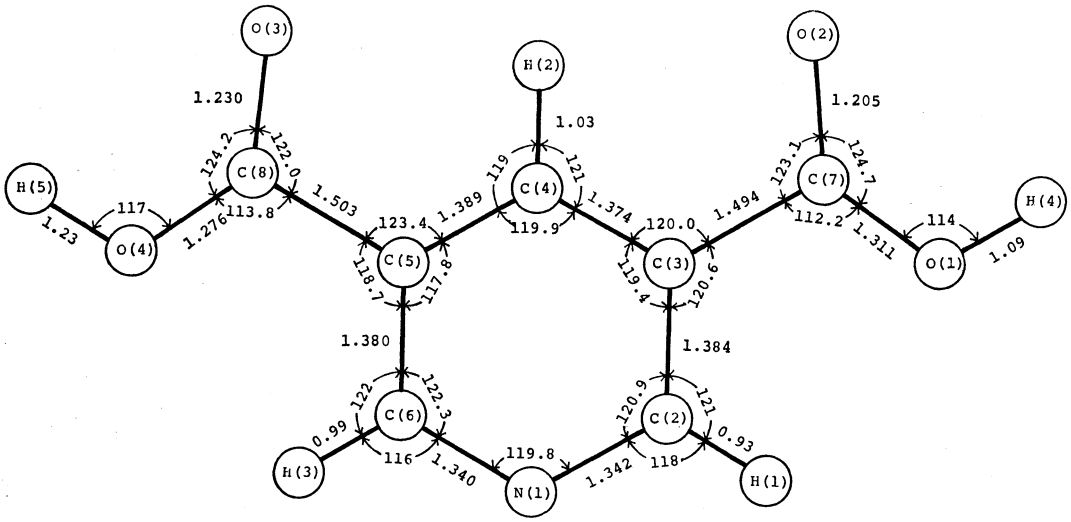

Fig. 2. Dimensions of dinicotinic acid molecule.
The estimated standard deviations are as follows:
X-X=0.003−0.004 Å X-H=0.03−0.04 Å
X-X-X=0.2−0.3° X-X-H=2°
where X and H are non-hydrogen atom and hydrogen atom, respectively.

is shown below;

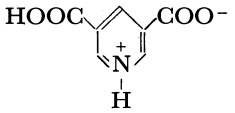

The existence of the molecule in this form is evident from the position of the hydrogen atom in the difference Fourier map. It is also confirmed by the C(2)–N(1)–C(6) bond angle of 119.8 (2)° and the O(4)–H(5) and H(5)–N(1) bond lengths, which are 1.23(4) and 1.29 (4) Å, respectively (the values in parentheses denote the e.s.d.'s in the last digits).

A dinicotinic acid molecule is approximately planar, with the maximum deviation of 0.229 Å, and its pyridine ring is essentially planar and the maximum deviation of a ring atom from the least-squares plane is 0.002 Å. The equations of the two planes through twelve non-hydrogen atoms of a molecule and six non-hydrogen atoms of the pyridine ring are:

$$0.0523X+0.0736Y+0.9951Z=2.3097 \quad \text{and}$$

$$0.0677X+0.0906Y+0.9936Z=2.4951,$$

respectively, where X, Y and Z are coordinates in Å referred to an orthogonal set of axes and parallel to the a, b, and c^* axes respectively; this coordinate system

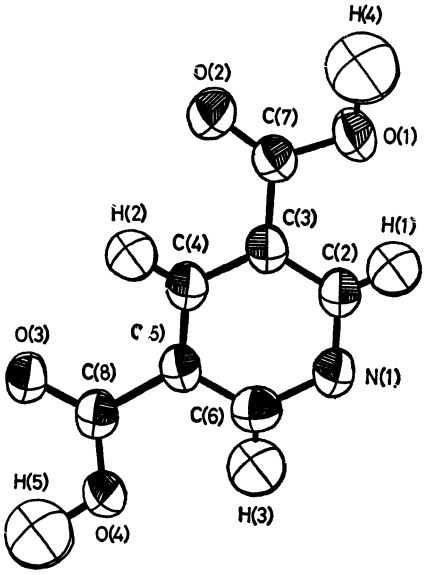

Fig. 3. The anisotropic thermal ellipsoids of non-hydrogen atoms and the isotropic thermal ellipsoids of hydrogen atoms. Ellipsoids are scaled to include 74% probability.

is used throughout this paper. The displacements of all the atoms from the planes are listed in Table 4.

Roughly speaking, the molecule in the crystal has the C_{2v} symmetry, as is shown in Fig. 2. The bond lengths and angles related by the C_{2v} symmetry are equal within the limits of experimental error except for

Table 4.

(1) The distances from the least-squares plane defined by twelve non-hydrogen atoms of a molecule

Atom	Deviation (Å)	Atom	Deviation (Å)
N (1)	0.051	O (2)	0.098
C (2)	0.031	O (3)	0.188
C (3)	0.000	O (4)	−0.229
C (4)	−0.013	H (1)	0.07
C (5)	0.011	H (2)	−0.05
C (6)	0.039	H (3)	0.05
C (7)	−0.005	H (4)	−0.02
C (8)	−0.006	H (5)	−0.15
O (1)	−0.120		

(2) The distances from the least-squares plane defined by the pyridine ring atoms

Atom	Deviation (Å)	Atom	Deviation (Å)
N (1)	0.000	O (2)	0.149
C (2)	0.001	O (3)	0.215
C (3)	0.000	O (4)	−0.251
C (4)	−0.002	H (1)	0.03
C (5)	0.002	H (2)	−0.02
C (6)	−0.002	H (3)	−0.01
C (7)	0.018	H (4)	0.01
C (8)	−0.005	H (5)	−0.17
O (1)	−0.111		

Table 5. The C–N–C bond angles, C–N and N···H bond lengths of several pyridine derivatives

Compound	C–N–C	N–C(1)	N–C(2)	N···H	Reference
Pyridine hydrochloride	128	1.32 Å	1.32 Å	*	a
α-pyridone	125.1	1.401	1.335	*	b
Quinolinic acid	125.1	1.350	1.324	0.89	c
Cinchomeronic acid	122.5	1.349	1.342	1.09	c
Picolinic acid hydrochloride	121	1.39	1.32	*	d
Pyridine hydrogen nitrate	120.4	1.375	1.333	*	e
Dinicotinic acid	119.8	1.345	1.339	1.29	f
Calcium dipicolinate	119.0	1.339	1.326	+	g
Strontium dipicolinate	118.8	1.335	1.335	+	h
Nicotinamide	118.4	1.370	1.336	*	i
Nicotinic acid	117.5	1.343	1.336	*	j
Picolinamide	117.4	1.348	1.335	+	k
Dipicolinic acid	116.8	1.338	1.336	2.17	l
Pyridine	116.7	1.340	1.340	+	m

a) P. C. Reart, *Acta Crystallogr.*, **15**, 427 (1962).
b) B. R. Penfold, *ibid.*, **6**, 591 (1953).
c) F. Takusagawa, K. Hirotsu, and A. Shimada, *ibid.*, **A28**, S15 (1972).
d) P. A. Laurent, *ibid.*, **18**, 799 (1965).
e) A. J. Serewicz, B. K. Robertson, and E. A. Meyers, *J. Phys. Chem.*, **69**, 1915 (1965).
f) This study.
g) G. Strahs and R. E. Dickerson, *Acta Crystallogr.*, **B24**, 571 (1968).
h) K. J. Palmwer, R. Y. Wong, and L. C. Lewis, *ibid.*, **B28**, 233 (1972).
i) W. B. Wright and G. S. D. King, *ibid.*, **7**, 283 (1954).
j) W. B. Wright and G. S. D. King, *ibid.*, **6**, 305 (1953).
k) T. Takano, Y. Sasada, and M. Kakudo, *ibid.*, **21**, 514 (1966).
l) F. Takusagawa, K. Hirotsu, and A. Shimada, This Bulletin **46**, 2020 (1973).
m) B. Bak, L. H. Nygaard, and J. R. Andersen, *J. Mol. Spectrosc.*, **2**, 361 (1958).
* The N···H distance was not determined.
\+ The corresponding N···H bond was not found.

those of the two carboxyl groups. The bond lengths in a pyridine ring are in good agreement with those pyridine itself, but the bond angles are not. The C-(2)–N(1)–C(6) bond angle is 119.8(2),° which lies between the pyridine[6] (116.8°) not protonated at the nitrogen atom and some pyridine derivatives[7–9] (~125°) protonated at the nitrogen atom. The C–N–C bond angles and C–N and N···H bond lengths of several pyridine derivatives are listed in Table 5. The C–N–C bond angle seems to be inversely proportional to the N···H distance, as is shown in Table 5.

Each carboxyl group consists of C–O(H) and C=O groups. The differences between two C–O(H) lengths, C(7)–O(1) and C(8)–O(4), and between two C=O bond lengths, C(7)–O(2) and C(8)–O(3), are 0.035(3) and −0.025(3) Å respectively; these differences are significant in view of their estimated standard deviations. The former difference may be explained by the increase in the double-bond character of the C(8)–O(4) group, which participates in a very short O···H···N hydrogen bond, as will be seen later. On the other hand, the latter difference may be due to the fact that the O(3) atom takes part in the hydrogen bond, while the O(2) atom does not, although there will be a decrease in the double-bond character in the C(8)–O(3) bond corresponding to the increase in this character in the C(8)–O(4) bond. A similar situation is observed also in quinolinic acid[9] and cinchomeronic acid.[9] Therefore, the longer C–O distance in the carbonyl group may be related to the participation of this group in the hydrogen bond. One carboxyl group (C(7)O(1)-O(2)H(4)) twists by 6.7° out of the plane of the pyridine ring, while the other twists by 12.1°.

Molecular Arrangement and Hydrogen-bond System. The crystal structure is shown in Figs. 4 and 5. The distances and angles of hydrogen bonds are listed in Table 6. The molecules lie approximately on the planes parallel to the (0 0 1) plane at $z=1/4$ and 3/4, with a spacing of 3.136 Å. The best plane through the carbon, nitrogen, and oxygen atoms of the 1 and 2 molecules, related to each other by the two-fold screw axis at $z=1/4$, is calculated by the least-squares analysis to be:

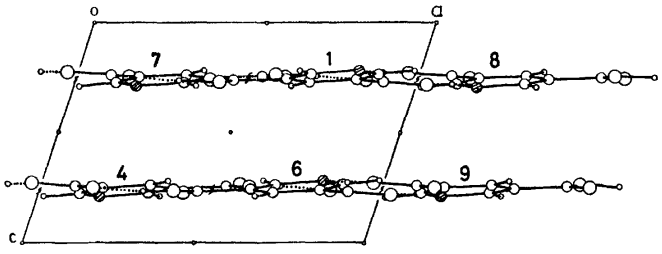

Fig. 4. A view of the crystal structure down the *b* axis. The hydrogen bonds are shown by broken lines. The numbers on pyridine rings correspond to those of the symmetry codes shown in Table 6.

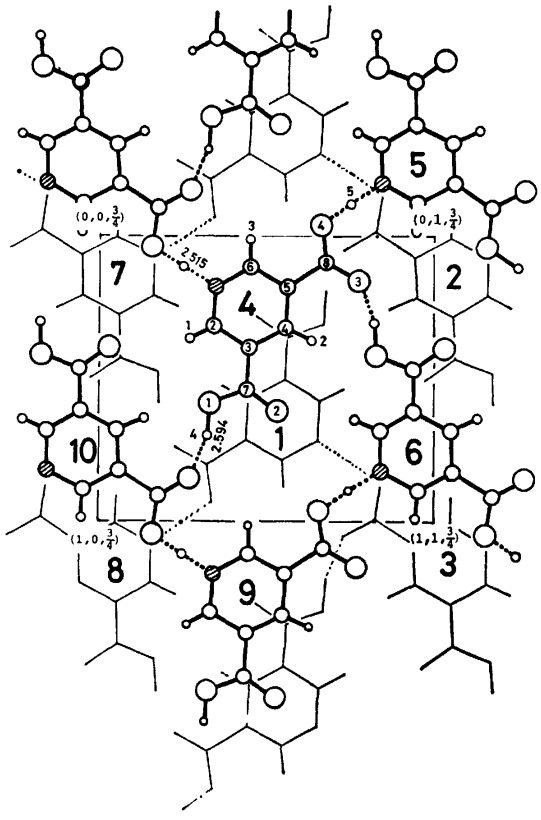

Fig. 5. A view of the crystal structure along the normal to the (001) plane, showing the relative orientation of the molecules in two adjacent layers parallel to the (001) plane. The hydrogen bonds are shown by broken lines. The numbers in pyridine rings correspond to those of the symmetry codes shown in Table 6.

$$0.0279X+0.0240Y+0.9939Z=1.8942.$$

The dihedral angle which it makes with the (0 0 1) plane is 2.1°. Figure 4 shows the crystal structure down the *b* axis. Figure 5 shows a view normal to the (0 0 1) plane and illustrates the relative orientation of the molecules in two neighboring layers. The upper layer of the molecules drawn with heavy lines in this figure involves the molecules on the plane at $z=3/4$.

Each molecule on the same plane is joined through two kinds of hydrogen bonds related by the two-fold screw axes, with four neighboring molecules, and forms a sheet parallel to the (0 0 1) plane. The sheets are related by the center of symmetry and are not linked by the hydrogen bond, but only by the van der Waals forces.

One carbonyl oxygen atom (O(3)) participates in a hydrogen bond (O(3)···H(4)–O(1); 2.594(3) Å), while the other (O(2)) does not. The nitrogen atom in a pyridine ring, however, takes part in a hydrogen bond (N(1)···H(5)···O(4); 2.515(3) Å), as in the crystals of nicotinic acid, dipicolinic acid, quinolinic acid, and cinchomeronic acid. This fact suggests that the O–H···N or $^{+}$N–H···O hydrogen bond is energetically more favored than the O–H···O hydrogen bond in these compounds.

In the O(4)···H(5)···N(1) hydrogen bond, the angle is 174(3)°, which indicates a straight hydrogen bond, and the distance between the O(4) and N(1) atoms is

6) B. Bak, L. H. Nygaard, and J. R. Andersen, *J. Mol. Spectrosc.*, **2**, 361 (1958).
7) P. C. Rerat, *Acta Crystallogr.*, **15**, 427 (1962).
8) B. R. Penfold, *ibid.*, **6**, 591 (1953).
9) F. Takusagawa, K. Hirotsu, and A. Shimada, *ibid.*, **A28**, S15 (1972).

Table 6. Hydrogen bond distances (Å) and angles (degree)

O——H ··· ···X	Symmetry	O···X	e.s.d.	O–H	e.s.d.	H···X	e.s.d.	Angle	e.s.d.
O(1)–H(4)···O(3)	(1, 1, 2)	2.594	0.003	1.09	0.04	1.54	0.04	163	3
O(4)–H(5)···N(1)	(1, 3, 3)	2.515	0.003	1.23	0.04	1.29	0.04	174	3

C——X ··· ···H	Symmetry	Angle	e.s.d.	C——X ··· ···O	Symmetry	Angle	e.s.d.
C(2)–N(1)···H(5)	(1, 1, 3)	119	2	C(2)–N(1)···O(4)	(1, 1, 3)	121.1	0.2
C(6)–N(1)···H(5)	(1, 1, 3)	120	2	C(6)–N(1)···O(4)	(1, 1, 3)	121.1	0.2
C(8)–O(3)···H(4)	(2, 2, 1)	137	1	C(8)–O(3)···O(1)	(2, 2, 1)	130.4	0.2

Symmetry 1=(x, y, z); 2=(1−x, 1/2+y, 1/2−z); 3=(2−x, 1/2+y, 1/2−z); 4=(1−x, 1−y, 1−z);
5=(−1+x, 3/2−y, 1/2+z); 6=(x, 3/2−y, 1/2+z); 7=(1−x, −1/2+y, 1/2−z);
8=(2−x, −1/2+y, 1/2−z); 9=(2−x, 1−y, 1−z); 10=(x, 1/2−y, 1/2+z)

2.515(3) Å, which is very short in the O–H···N type of hydrogen bond. The O(4)···H(5) and N(1)···H(5) bond distances are 1.23(4) and 1.29(4) Å, which are equal within the limits of experimental error. Therefore, this bond may be considered as an example of the single minimum hydrogen bond[16] of the O–H···N type of hydrogen bond. This may also be confirmed by the C(2)–N(1)–C(6) bond angle of 119.8(2)°.

Figure 6 shows the models proposed for two kinds of twins. In the twin(Fig. 6(a)) which has the directions of the *a* and *b* axes in common, the transition may take place across the (0 0 1) plane, since the molecules are arranged in layers closely parallel to this plane and since these layers are stacked together with a spacing of about 3.136 Å. On the other hand, the twin(Fig. 6(b)) which has the directions of the *b* and *c* axis in common may depend on the change in the torsional angle, O(3)–C(8)–O(4)–H(5). Such a twist causes only a little change in the angle and distance of the O(4)···H(5)···N(1) hydrogen bond. Furthermore, no abnormal approach between the intermolecular atoms is found in this twin model because of the layer structure. Therefore, the main reason for the existence of two kinds of twins may be the layer structure in this crystal. It is not easy to explain conclusively the relation between the twinning patterns and the pH of aqueous solutions on recrystallization, since it may be characterized by many factors. However, the formation of two types of twins seems to be related with the amounts of ⩾N, +⩾N–H, —O–H and —O⁻ on the crystal surfaces, which themselves depend on the pH of the aqueaus solution on recrystallization.

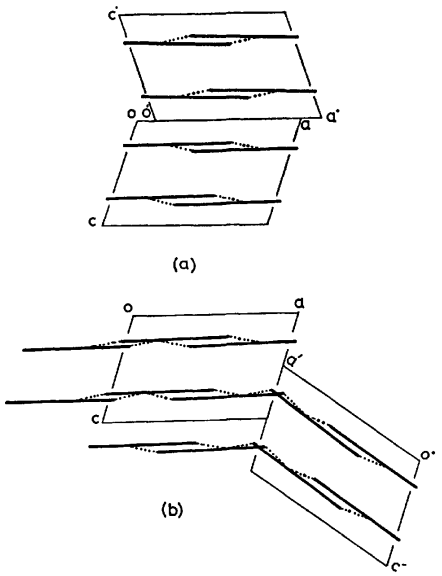

Fig. 6. The model proposed for two kinds of twins. A molecule is shown by a heavy line, and hydrogen bonds are shown by broken lines. (a): This twinning crystal has the directions of *a* and *b* axes in common, and it is obtained from an aqueous acidic solution. (b): This twinning crystal has the directions of *b* and *c* axes in common, and it is obtained from an aqueous solution. In both models, the origins, O and O′, have same value of *y* coordinate, *y*=0.

Computer Programs. All the calculations were performed on a FACOM 270-30 computer at the Computer Center of Osaka City University, using the following programs—RSLC-3 (cell constant),[10] RSSFR-3 (Fourier synthesis),[11] HBLS-IV (block diagonal least-squares refinement),[12] DAPH(bond length, bond angle and least-squares plane),[13] SCALE (film factor, Lp and layer scaling),[14] and TE-I(thermal ellipsoid).[15]

10) T. Sakurai, "The Universal Crystallographic Computing System (I)," edited by T. Sakurai, p. 18, The Crystallographic Society of Japan (1967).
11) T. Sakurai, *ibid.*, p. 45.
12) T. Ashida, *ibid.*, p. 65.
13) T. Ashida, *ibid.*, p. 76.
14) H. Yoshioka, K. Hirotsu, and F. Takusagawa, unpublished work.
15) F. Takusagawa, unpublished work.
16) The "single minimum hydrogen bond" means the hydrogen bond which has the single minimum potential function.

The Molecular and Crystal Structure of the Cyclic Pentamer of Formaldehyde, 1,3,5,7,9-Pentoxecane

Yozo CHATANI and Katsuki KITAHAMA*

Department of Polymer Science, Faculty of Science, Osaka University, Toyonaka, Osaka 560

(Received January 22, 1973)

The crystal structure of the cyclic pentamer of formaldehyde, 1,3,5,7,9-pentoxecane, has been determined by the X-ray diffraction method. The unit cell is orthorhombic, with $a=8.154$ Å, $b=10.673$ Å, $c=7.666$ Å. The space group is Pbcn, and there are four molecules per unit cell. The structure was refined by the block-diagonal least-squares method to a final discrepancy factor, R, of 0.049, using 712 reflections observed with an automatic four-circle single-crystal diffractometer. The molecules in the crystals are ten-membered rings with an exact C_2–2 symmetry; the torsion angles of the five independent C–O bonds are 72.9°, −118.7°, 84.2°, −123.4°, and 69.8°, and the two halves of the molecule are related by a twofold rotation axis. The averaged C–O bond length is 1.410 Å, and the averaged C–O–C and O–C–O bond angles are 115.6° and 111.8° respectively. The close intramolecular H···H distances are 2.17 Å and 2.20 Å.

In a previous paper,[1] the molecular and crystal structure of the cyclic hexamer of formaldehyde, 1,3,5,7,9,11-hexoxecane $(-CH_2-O-)_6$, was reported. The cyclic pentamer, 1,3,5,7,9-pentoxecane $(-CH_2-O-)_5$, is also of interest from the viewpoint of molecular conformation. To date, many investigations have been made with regard to the structure determination of ring compounds of the $(-X-)_m$ or $(-X-Y-)_m$ type. However, little is known of ten-membered ring compounds with such a sequence. Pentoxecane is also interesting with respect to the radiation-induced solid-state polymerization.[2,3] Pentoxecane undergoes a ring-opening polymerization in the crystalline state to form linear polyoxymethylene $(-CH_2-O-)_n$ under irradiation. The polymer resulting from the solid-state polymerization is highly crystalline, just as in the cases of trioxecane $(-CH_2-O-)_3$,[4-6] tetroxocane $(-CH_2-O-)_4$,[7] and hexoxecane $(-CH_2-O-)_6$.[1] The preferred orientations of the resultant polymer crystals are, however, characteristic for each cyclic oligomer. In the present paper, the molecular and crystal structure of pentoxecane will be reported, and the relationship between the crystal structure and the solid-state polymerization will be discussed briefly.

Experimental

The pentoxecane was obtained through the courtesy of Drs. Miyaka and Yamauchi of Mitsui-Toatsu Chemicals, Inc. The melting point of pentoxecane is 61.3 °C. Crystals were grown as rhombohedrons by the slow evaporation of a methanol solution. The crystals were found to sublime slowly when exposed to the atmosphere. To prevent the sublimation of the samples, single crystals were sealed in thin-walled Lindemann glass capillary tubes. The cell constants were determined from Weissenberg photographs and θ values measured with a single-crystal diffractometer.

Crystal data:

1,3,5,7,9-pentoxecane, $(-CH_2-O-)_5$

Molecular weight 150.1

Orthorhombic $a=8.154\pm0.005$ Å

$b=10.673\pm0.009$

$c=7.666\pm0.005$

Volume of the unit cell: $V=661.8$ Å^3

Density, calculated with $Z=4$: $D_x=1.494$ g/cm^3; measured: $D_m=1.49$ g/cm^3

Number of electrons per unit cell: $F(000)=320$

Absorption coefficient for $\lambda_{MoK\alpha}$ (=0.7107 Å): $\mu=1.62$ cm^{-1}.

The systematic absences of $0kl$ for k odd, of $h0l$ for l odd, and of $hk0$ for $h+k$ odd indicate that the space group is Pbcn.

Intensity measurements were performed using a Rigaku-Denki automatic four-circle single-crystal diffractometer with MoKα radiation. The crystal used for intensity measurements was $0.2\times0.2\times0.3$ mm^3 in size. The integrated intensities were measured for all reflections in the sphere of the radius $\sin\theta/\lambda<0.65$ Å^{-1}, using the θ—2θ (moving crystal, moving counter) technique. The procedures used in getting the observed structure factors were similar to those used in the case of hexoxecane.[1] A total of 749 independent reflections were examined, and 712 reflections were observed. No correction was made for absorption. In a previous paper,[2] the solid-state polymerization of pentoxecane by X- or γ-irradiation was reportod. The polymer yield depends upon the irradiation temperature. The present intensity measurements were performed at 16 °C, and, judging from the constancy of the intensities of three reference reflections measured every 25 reflections, such a polymerization was found to be suppressed during the measurements. Therefore, it was unnecessary to correct the observed structure factors for any decrease caused by polymerization.

Structure Determination

The space group Pbcn possesses eight general equivalent points. Since there are four molecules in the unit cell, the molecules themselves have one kind of twofold symmetry. The possible symmetry of the molecule which can possess in the space group Pbcn is either a center of symmetry or a twofold rotation

* Present address: Institute of Science and Industrial Research, Osaka University, Suita, Osaka.

1) Y. Chatani, T. Ohno, T. Yamauchi, and Y. Miyake, *J. Polym. Sci., Polym. Phys.*, **11**, 369 (1973).

2) Y. Chatani, K. Kitahama, H. Tadokoro, T. Yamauchi, and Y. Miyake, *J. Macromol. Sci.*, **B4**, 61 (1970).

3) M. Nishii, K. Hayashi, and S. Okamura, *J. Polym. Sci.*, **B7**, 891 (1969).

4) S. Okamura, K. Hayashi, and Y. Nakamura, *Isotopes Radiation*, **3**, 416 (1960).

5) K. Hayashi, M. Nishii, and S. Okamura, *J. Polym. Sci.*, **C4**, 839 (1963).

6) G. Carazzolo, S. Leghissa, and M. Mammi, *Makromol. Chem.*, **60**, 171 (1963).

7) Y. Chatani, T. Uchida, H. Tadokoro, K. Hayashi, M. Nishii, and S. Okamura, *J. Macromol. Sci.*, **B2**, 567 (1968).

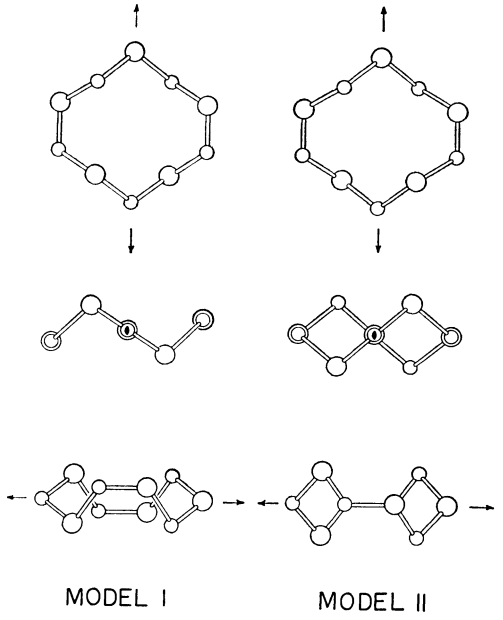

Fig. 1. Two models of a pentoxecane molecule.

axis. Since the ten-membered cyclic molecules of pentoxecane cannot have a center of symmetry, they must possess a twofold rotation axis. In the pentoxecane ring, the twofold rotation axis can pass through a carbon atom and an oxygen atom lying across the ring from each other. Two typical possible models which can satisfy the twofold rotation symmetry are shown in Fig. 1. The conformation of Model I is denoted by the sequence of $G\bar{S}CS\bar{G}\bar{G}SC\bar{S}G$, and Model II, by $\bar{G}S\bar{G}S\bar{G}\bar{G}S\bar{G}S\bar{G}$, or their enantiomers, C is a *cis*-form (the torsion angle is defined as 0°), G and S are a clockwise *gauche*-form and a *skew*-form respectively, and $\bar{G}$ and $\bar{S}$ are a counter-clockwise *gauche*-form and a *skew*-form respectively. Since the twofold rotation axis in the molecule coincides with the twofold rotation axis parallel to the *b* axis, the two models were selected by a comparison of the F_o and F_c of (*h*0*l*) reflections, varying the rotation angle of the molecule about the twofold rotation axis. Model I was easily excluded. Therefore Model II was refined three-dimensionally by a block-diagonal least-squares program of Dr. Ashida using a NEAC 2200 electronic computer at Osaka University. The five independent hydrogen atoms were revealed unambigously by a difference Fourier synthesis, as is shown in Fig. 2, the maxima being between 0.6 and 0.7 e/Å^3. The coordinates of these peaks were introduced into the refinement as hydrogen atoms and were given isotropic thermal factors. The weighting scheme used in the least-squares calculation was:

$$w = 0 \text{ for } F_o = 0$$
$$w = 0{\cdot}4 \text{ for } 0 < |F_o| \leq F_{min}$$
$$w = 1{\cdot}0 \text{ for } F_{min} < |F_o| \leq 4F_{min}$$
$$w = (4F_{min}/|F_o|)^2 \text{ for } |F_o| > 4F_{min}$$
$$F_{min} = 30 \text{ in the scale of Table 2.}$$

The atomic scattering factors used for carbon and

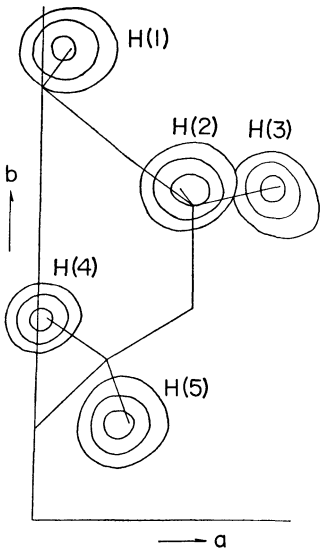

Fig. 2. Composite difference Fourier map. Contours are at intervals of 0.2 e/Å^3, begining at 0.2 e/Å^3.

oxygen were those[8] in the International Tables for X-ray Crystallography, Vol. III, while for hydrogen the bonded values of Stewart *et al.*[9] were used. A set of final structure factors for all the observed reflections shown in Table 2 was calculated on the basis of the final positional and thermal parameters shown in Table 1. The discrepancy factor, $R(= \Sigma(|F_o| - |F_c|)/\Sigma|F_o|)$, for the observed reflections was 0.049.

Results and Discussion

Molecular Structure and Thermal Motion. Figure 3 shows the molecular structure of pentoxecane. The ten-membered ring molecule has a C_2–2 symmetry; the twofold rotation axis passes through C(1) and O(3). The bond lengths, bond angles, and torsion

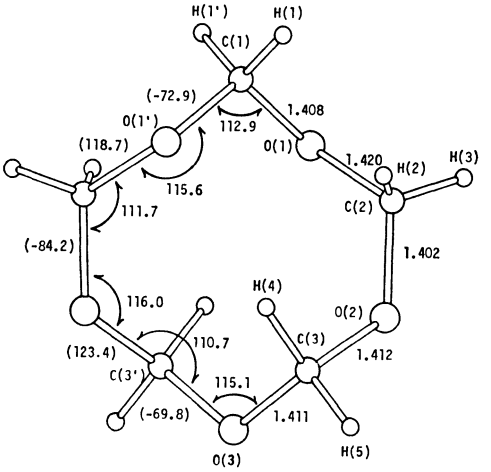

Fig. 3. Bond lengths (Å), bond angles (°), and torsion angles in parentheses (°) of pentoxecane molecule.

8) "International Tables for X-ray Crystallography," Vol. III, Kynoch Press, Birmingham (1962), p. 202.
9) R. F. Stewart, F. R. Davidson, and W. T. Simpson, *J. Chem. Phys.*, **42**, 3175 (1965).

TABLE 1. THE FINAL ATOMIC PARAMETERS AND THEIR ESTIMATED STANDARD DEVIATIONS

	x	y	z	$B_{ij}\times10^5$					
				$B_{11}(B)$	B_{22}	B_{33}	B_{12}	B_{13}	B_{23}
C(1)	0.5000	0.4968(2)	0.2500	1257(34)	671(18)	1481(41)	0	468(65)	0
O(1)	0.6290(1)	0.4239(1)	0.1820(2)	1139(18)	882(11)	1310(19)	99(23)	428(31)	14(24)
C(2)	0.7290(2)	0.3626(2)	0.3075(2)	1011(24)	892(17)	1719(33)	−166(33)	−180(48)	−238(38)
O(2)	0.7234(2)	0.2321(1)	0.2888(2)	1207(21)	874(12)	2063(27)	347(25)	−104(37)	−280(29)
C(3)	0.5910(2)	0.1710(2)	0.3716(2)	1529(29)	784(16)	1823(35)	59(38)	−865(57)	286(38)
O(3)	0.5000	0.1000(2)	0.2500	2019(38)	666(16)	2695(47)	0	−1814(72)	0
H(1)	0.543(2)	0.548(2)	0.346(2)	3.3(4)					
H(2)	0.695(2)	0.388(2)	0.428(2)	3.2(4)					
H(3)	0.843(3)	0.394(2)	0.278(3)	5.8(6)					
H(4)	0.516(2)	0.238(2)	0.434(2)	3.8(4)					
H(5)	0.637(2)	0.113(2)	0.456(3)	3.8(4)					

The anisotropic temperature factors are of the form $\exp[-(B_{11}h^2+B_{22}k^2+B_{33}l^2+B_{12}hk+B_{13}hl+B_{23}kl)]$. The isotropic temperature factors for hydrogen atoms are of the form $\exp(-B\sin^2\theta/\lambda^2)$ and are given in Å^2.

TABLE 2. THE OBSERVED AND THE FINAL CALCULATED STRUCTURE FACTORS ($\times10$)

H	K	F_o	F_c
		(L = 0)	
0	2	183	-191
0	4	204	-224
0	6	279	-304
0	8	86	88
0	10	7	2
0	12	84	100
1	1	207	203
1	3	574	603
1	5	27	-26
1	7	32	-27
1	9	4	-7
1	11	7	-8
1	13	32	38
2	0	270	-261
2	2	606	606
2	4	94	-79
2	6	148	150
2	8	99	-104
2	10	123	138
2	12	47	54
3	1	290	-279
3	3	104	108
3	5	412	427
3	7	99	103
3	9	42	50
3	11	22	-28
3	13	11	13
4	0	227	229
4	2	258	-254
4	4	194	191
4	6	18	19
4	8	254	269
4	10	4	3
4	12	31	-28
5	1	17	-18
5	3	53	-53
5	5	137	135
5	7	242	247
5	9	70	-69
5	11	24	22
6	0	94	-101
6	2	229	234
6	4	19	15
6	6	54	-53
6	10	85	83
7	1	77	77
7	3	43	44
7	5	101	107
7	7	91	-96
7	9	4	-1
8	0	196	202
8	2	60	61
8	4	20	-21
8	6	56	-57
8	8	20	17
9	1	58	60
9	3	16	22
9	5	38	-41
9	7	55	54
10	0	34	31
10	4	10	11
		(L = 1)	
0	2	194	190
0	4	485	484
0	6	189	-182
0	8	99	101
0	10	59	-62
0	12	33	-33
1	1	658	664
1	2	136	-127
1	3	404	386
1	5	56	51
1	6	128	-124
1	7	86	-81
1	8	45	46
1	9	84	-88
1	10	41	41
1	11	21	-25
1	13	47	42
2	1	191	195
2	2	518	-521
2	3	181	-171
2	4	159	-148
2	5	174	-177
2	6	297	294
2	7	49	52
2	8	75	-78
2	9	38	38
2	10	51	53
2	11	9	3
2	12	40	-37
2	13	14	16
3	1	284	-283
3	2	319	-309
3	3	14	10
3	4	19	16
3	5	150	-136
3	6	34	33
3	7	10	-11
3	8	54	-54
3	9	6	-1
3	10	56	55
3	11	63	61
3	13	35	33
4	1	2	-3
4	2	192	-174
4	3	24	-22
4	4	287	-287
4	5	44	-43
4	6	125	-128
4	7	65	64
4	8	227	228
4	9	22	-21
4	10	26	24
4	11	20	-18
4	12	16	13
5	1	145	150
5	3	75	75
5	5	126	-119
5	7	78	75
5	9	31	35
5	11	35	-34
6	1	132	-132
6	3	13	-9
6	5	78	77
6	7	44	46
6	9	175	179
7	4	6	4
7	5	52	52
7	9	81	-78
7	10	23	-22
8	1	74	-70
8	2	73	73
8	4	38	41
8	5	27	20
8	6	9	8
8	7	9	-9
8	8	5	8
9	1	136	134
9	2	10	7
9	3	10	16
9	4	39	-40
9	5	13	15
9	7	42	-38
10	2	40	-43
10	3	20	-21
		(L = 2)	
0	0	1208	1418
0	2	30	-19
0	4	27	-10
0	6	258	255
0	8	126	-117
0	10	24	-19
0	12	51	-52
1	0	424	-432
1	1	187	-188
1	2	440	433
1	3	227	-220
1	4	9	8
1	5	111	-112
1	6	140	-146
1	7	22	-30
1	8	109	-107
1	10	50	46
1	11	20	-14
1	12	15	12
1	13	38	-32
2	0	257	245
2	1	378	356
2	2	556	-552
2	3	168	-163
2	4	146	133
2	5	18	-13
2	6	91	-91
2	7	125	-123
2	8	38	44
2	9	74	-75
2	10	123	-126
2	11	48	48
2	12	36	-30
2	13	39	32
3	0	254	237
3	1	175	169
3	2	44	45
3	3	88	-92
3	4	13	-7
3	5	320	-317
3	6	219	-217
3	7	64	-68
3	8	72	70
3	9	45	-43
3	10	15	-10
3	11	20	22
3	12	24	-19
4	0	304	-306
4	1	44	45
4	2	151	154
4	3	140	-134
4	4	82	-82
4	5	11	9
4	6	27	-30
4	7	81	84
4	8	177	-178
4	9	56	-54
4	10	16	-14
4	11	16	18
4	12	3	1
5	0	288	-289
5	1	59	57
5	2	14	16
5	3	68	-68
5	4	23	22
5	5	88	-84
5	6	45	45
5	7	163	-161
5	8	10	11
5	9	24	26
5	10	34	31
5	11	6	-4
6	0	11	8
6	1	168	-172
6	2	154	-158
6	3	77	25
6	4	18	13
6	5	98	103
6	6	13	-15
6	7	3	3
6	8	19	22
6	9	32	36
6	10	69	-64
6	11	25	-21
7	0	42	38
7	1	46	-45
7	2	78	-81
7	3	66	-62
7	4	15	-17
7	5	70	-72
7	6	60	61
7	7	61	65
7	8	17	18
7	9	29	-22
8	0	157	-156
8	1	6	-1
8	2	39	-41
8	3	26	25
8	4	13	14
8	5	50	-51
8	6	24	25
8	7	23	24
8	8	19	-18
9	0	64	60
9	1	41	-41
9	2	11	9
9	3	22	-18
9	4	20	-20
9	5	21	17
10	0	10	-12
10	1	6	5
10	2	10	-10
10	3	29	29
		(L = 3)	
0	2	134	-136
0	4	33	31
0	6	30	29
0	8	152	-155
0	10	68	72
0	12	6	-1
1	1	16	-12
1	2	125	119
1	3	195	-187
1	4	83	80
1	5	109	-107
1	6	218	217
1	7	110	112
1	8	117	-118
1	9	18	20
1	10	60	-57
1	11	28	-27
1	12	18	-16
2	1	35	-41
2	2	122	117
2	3	366	362
2	4	159	159
2	5	202	205
2	6	174	-170
2	7	75	-74
2	9	86	-87
2	10	19	-17
2	11	20	-17
2	12	29	26
3	1	52	57
3	2	321	318
3	3	167	-158
3	4	60	62
3	5	80	76
3	6	74	-71
3	7	12	14
3	8	82	83
3	9	21	23
3	10	75	-76
3	11	32	-34
3	12	15	-8
4	1	82	82
4	2	158	155
4	3	37	-39
4	4	36	32
4	5	46	45
4	6	32	38
4	7	66	-68
4	8	87	-88
4	9	30	34
4	10	24	-22
4	11	16	17
4	12	5	5
5	1	176	-183
5	2	155	-156
5	3	26	25
5	4	105	-110
5	5	7	8
5	6	48	50
5	7	21	24
5	8	6	1
5	9	8	-11
5	10	31	31
6	1	145	-147
6	2	87	89
6	3	73	-74
6	4	28	-26
6	5	67	-72
6	6	48	-51
6	7	53	53
6	8	22	18
6	9	7	3
6	10	26	-20
7	1	29	27
7	2	51	-52
7	3	87	-94
7	4	27	-26
7	5	21	24
7	6	36	-33
7	7	26	-31
7	8	36	29
7	9	45	42
8	1	120	120
8	2	9	-6
8	3	5	2
8	5	8	-17
8	6	7	-2
8	7	8	-8
8	8	10	-7
9	1	58	-58
9	3	16	4
		(L = 4)	
0	0	173	176
0	2	36	39
0	4	118	125
0	6	137	-142
0	8	154	156
0	10	50	50
0	12	9	-4
1	0	149	151
1	1	5	0
1	2	339	-336
1	3	11	-11
1	4	89	91
1	5	199	204
1	6	82	79
1	7	98	103
1	8	137	137
1	9	47	-44
1	10	52	-54
1	11	28	26
1	12	26	-29
2	0	47	-49
2	1	209	-208
2	2	244	240
2	3	16	-20
2	4	58	-57
2	5	75	77
2	6	20	25
2	7	138	143
2	8	27	26
2	9	26	23
2	10	77	74
2	11	21	-17
2	12	11	7
3	0	414	-424
3	1	6	14
3	2	78	80
3	3	73	75
3	4	37	34
3	5	107	104
3	6	126	124
3	7	20	24
3	8	36	-33
3	9	23	21
3	10	24	25
3	11	4	-7
3	12	13	-7
4	0	286	296
4	1	27	29
4	2	15	-20
4	3	11	10
4	4	15	21
4	5	33	33
4	7	80	-76
4	8	34	35
4	9	31	26
4	10	23	23
4	11	8	4
5	0	236	247
5	1	13	-17
5	2	2	0
5	3	138	141
5	4	22	-19
5	5	7	2
5	6	75	-74
5	7	29	32
5	8	6	12
5	9	19	20
5	10	26	-31
6	0	105	106
6	1	141	148
6	2	51	51
6	3	17	-11
6	4	36	-37
6	5	100	-105
6	6	58	59
6	7	10	3
6	8	19	-15
6	9	40	-37
7	0	33	-31
7	1	10	-11
7	2	63	64
7	3	54	56
7	4	9	11
7	5	47	49
7	6	34	-27
7	7	9	1
7	8	41	-39
		(L = 5)	
0	2	101	-108
0	4	144	-143
0	6	26	20
0	8	104	103
0	10	5	-10
1	1	31	-29
1	3	92	-90
1	5	34	32
1	6	135	-134
1	7	60	-64
1	8	114	115
1	9	11	18
1	11	40	41
2	1	74	-71
2	2	8	10
2	3	179	-179
2	4	65	-64
2	5	36	-36
2	6	35	38
2	7	20	-24
2	8	44	47
2	9	70	73
2	10	10	6
2	11	36	32
3	1	70	71
3	2	70	-67
3	3	119	120
3	4	118	-122
3	5	13	13
3	6	83	82
3	7	4	-9
3	8	25	-25
3	9	28	-28
3	10	4	10
3	11	9	-2
4	1	133	-138
4	2	31	-30
4	3	51	49
4	4	91	92
4	5	18	21
4	6	28	27
4	8	18	-12
4	9	18	-19
5	1	102	107
5	2	134	138
5	3	45	47
5	4	50	57
5	5	21	20
5	6	41	-42
5	8	15	15
5	9	24	-23
6	0	31	-32
6	1	113	117
6	2	41	-42
6	3	29	26
6	4	7	11
6	5	38	46
6	6	12	10
7	1	31	-28
7	3	13	14
7	4	44	45
7	5	42	-43
7	6	17	20
8	1	63	-63
8	2	41	-40
8	3	5	-6
8	4	32	-32
8	5	20	-19
9	1	7	-8
9	2	21	-18
		(L = 6)	
0	0	67	74
0	2	20	23
0	4	93	-93
0	6	36	-41
0	8	67	-68
0	10	47	-45
1	0	87	-89
1	1	75	79
1	2	126	127
1	3	35	-40
1	4	52	-53
1	5	114	-114
1	6	19	27
1	7	88	-83
1	8	96	-94
1	10	27	24
2	0	111	-117
2	1	26	29
2	2	43	-46
2	3	67	68
2	4	24	28
2	5	48	-49
2	6	31	-33
2	7	71	-73
2	8	32	-33
2	9	33	24
2	10	23	-25
3	0	258	259
3	1	75	-77
3	2	95	-97
3	3	53	-53
3	4	24	-26
3	5	10	-9
3	6	15	-11
3	8	15	8
3	9	8	0
3	10	28	-25
4	0	149	-153
4	1	38	-38
4	2	81	-80
4	3	35	38
4	4	5	-9
4	5	39	-38
4	6	56	56
4	7	33	33
4	8	19	14
4	9	5	1
5	0	101	-101
5	1	37	-37
5	2	15	17
5	3	60	-64
5	4	14	-13
5	5	15	-16
5	6	40	41
5	7	19	21
6	0	58	-58
6	1	56	-57
6	2	32	-28
6	3	8	-7
6	4	10	13
6	5	66	65
6	6	23	-20
6	7	19	-15
7	0	14	8
7	1	17	11
7	2	15	-12
7	3	9	1
7	4	7	-2
7	5	46	-46
7	6	27	-20
8	0	28	26
8	1	25	26
8	3	30	-29
		(L = 7)	
0	2	171	175
0	4	56	58
0	6	22	-24
0	8	12	-12
1	1	2	0
1	2	41	-38
1	3	44	46
1	4	9	8
1	5	44	45
1	6	54	54
1	7	19	-17
1	8	49	-45
1	9	15	-12
2	1	18	15
2	2	31	29
2	5	26	-28
2	6	27	20
2	7	30	28
2	8	31	-30
2	9	21	-16
3	1	65	-69
3	3	88	-92
3	4	41	39
3	5	24	-23
3	6	40	-39
3	7	19	19
3	9	14	19
4	1	57	62
4	2	23	-22
4	3	16	-22
4	4	53	-51
4	5	12	-11
4	6	48	-54
4	7	4	-9
4	8	19	23
5	1	14	9
5	2	41	-37
5	3	52	-52
5	4	16	-21
5	5	50	-47
5	6	32	25
5	7	25	22
6	1	48	-53
6	2	17	-18
6	3	29	20
6	4	37	33
6	5	3	-8
6	7	25	20
7	3	22	15
		(L = 8)	
0	0	58	-61
0	4	42	41
0	6	79	80
1	0	66	62
1	1	46	-52
1	2	29	-31
1	3	50	55
1	4	28	25
1	5	44	48
1	6	39	-34
1	7	40	35
1	8	12	17
2	0	119	116
2	1	28	27
2	4	19	-19
2	5	19	-19
2	6	27	25
2	7	5	1
3	0	41	-37
3	1	68	66
3	2	44	42
3	3	21	19
3	4	16	-11
3	6	13	8
4	0	29	31
4	1	14	12
4	2	83	81
4	3	5	-2
4	4	14	14
4	5	5	2
4	7	47	-48
5	0	27	24
5	1	35	34
5	2	27	-26
5	3	12	10
5	4	16	15
6	0	12	14
6	1	6	-8
6	2	25	17
		(L = 9)	
0	2	92	-87
0	4	25	-21
1	2	8	8
1	3	20	-16
1	4	38	37
1	5	31	-26
2	2	32	29
2	3	11	13
2	4	17	18
2	5	15	18
3	1	29	28
3	2	20	17
3	3	34	35
3	4	24	25

Table 3. Molecular dimensions of pentoxecane

Bond lengths (Å)			
C(1)–O(1)	1.408(3)	C(1)–H(1)	0.98(2)
O(1)–C(2)	1.420(2)	C(2)–H(2)	1.00(2)
C(2)–O(2)	1.402(2)	C(2)–H(3)	1.01(2)
O(2)–C(3)	1.412(2)	C(3)–H(4)	1.05(2)
C(3)–O(3)	1.411(3)	C(3)–H(5)	0.97(2)
average	1.410		1.00
Bond angles (°)			
O(1')–C(1)–O(1)	112.9(2)	H(2)–C(2)–O(1)	110(1)
C(1)–O(1)–C(2)	115.6(2)	H(2)–C(2)–O(2)	112(1)
O(1)–C(2)–O(2)	111.7(2)	H(3)–C(2)–O(1)	103(2)
C(2)–O(2)–C(3)	116.0(2)	H(3)–C(2)–O(2)	110(2)
O(2)–C(3)–O(3)	110.7(2)	H(4)–C(3)–H(5)	110(2)
C(3)–O(3)–C(3')	115.1(2)	H(4)–C(3)–O(2)	110(1)
H(1)–C(1)–H(1')	113(2)	H(4)–C(3)–O(3)	111(1)
H(1)–C(1)–O(1)	109(1)	H(5)–C(3)–O(2)	107(1)
H(1')–C(1)–O(1)	107(1)	H(5)–C(3)–O(3)	108(1)
H(2)–C(2)–H(3)	112(2)		
Torsion angles (°)			
C(1)–O(1)	−72.9	O(2)–C(3)	123.4
O(1)–C(2)	118.7	C(3)–O(3)	−69.8
C(2)–O(2)	−84.2		
Intramolecular H···H distances (Å)			
H(2)···H(4)	2.17(3)	H(1)···H(2)	2.20(3)

Estimated standard deviations shown in parentheses refer to the last decimal positions.

angles derived from the final atomic parameters are listed in Table 3 and are also shown in Fig. 3. The rings have five independent C–O bonds, and their lengths range from 1.402 Å to 1.420 Å and are averaged to be 1.410 Å. The O–C–O bond angles range from 110.7° to 112.9° and are averaged to be 111.8°. The C–O–C bond angles range from 115.1° to 116.0° and are averaged to be 115.6°. The five independent torsion angles are −72.9°, 118.7°, −84.2°, 123.4°, and −69.8°, which indicate approximately either a *gauche*-form or a *skew*-form.

Table 4 shows the molecular dimensions of some cyclic oligomers of formaldehyde: trioxecane, pentoxecane and hexoxecane. In the trioxecane molecule, the O–C–O and C–O–C bond angles are close to the tetrahedral angle of 109.5°. The average C–O–C bond angles in both pentoxecane and hexoxecane are about 6° larger than the tetrahedral angle. In the hexoxecane molecule, the O–C–O bond angle is also 4.5° larger than the tetrahedral angle. Such large departures from the tetrahedral angle can be attributed to the effect of close H···H overlapping; the resultant close intramolecular H···H distances are 2.17 Å and 2.20 Å for pentoxecane, and 2.13 Å for hexoxecane.

Hendrickson[13] examined many possible molecular conformations of cyclodecane in terms of the strain energy: bond angle bending strain, torsional strain, and nonbonded interactions of hydrogen atoms. The conformation of the pentoxecane ring is similar to Model XXIX in his article. In the case of cyclodecane, however, he ignored Model XXIX, since the model is incapable of escaping serious nonbonded H···H interactions.

Table 5 lists the root mean square vibration amplitudes and the direction cosines of the principal axes of the thermal ellipsoids to the crystallographic *a*, *b*, and *c* axes (see Fig. 4). In the case of hexoxecane,[1] the rigid body approximation[14,15] was undertaken for the molecule of the $\bar{3}$ symmetry, but a reasonable result could not be obtained. In the cases of hexoxecane and also pentoxecane, the thermal ellipsoids suggest that there are considerable intramolecular motions, *i.e.*, torsional motions. Therefore, no corrections of the bond lengths and bond angles for thermal motions were made.

Crystal Structure. Two projections of the crystal structure of pentoxecane, viewed along the *c* and *b* axes, are shown in Fig. 5. Some close intermolecular atomic distances, less than 3.8 Å for the C···O pair and less than 4.2 Å for the C···C pair, are listed in Table 6. There are no abnormal distances between

Taele 4. Molecular dimensions[a] of cyclic oligomers of formaldehyde

	Trioxecane $(-CH_2-O-)_3$			Pentoxecane $(-CH_2-O-)_5$	Hexoxecane $(-CH_2-O-)_6$
Molecular symmetry	C_{3v}-3m			C_2-2	C_{3i}-$\bar{3}$
Method	X[b]	M[c]	ED[d]	X	X
C–O (Å)	1.421	1.411	1.411	1.410	1.411
C–H (Å)	1.07	1.09[e]	1.116	1.00	1.06
O–C–O (°)	109.6	111.2	111.0	111.8	114.0
C–O–C (°)	110.4	108.2	109.2	115.6	115.4
H–C–H (°)	114	109.5[e]	111.8	112	116
Ref.	(10)	(11)	(12)	This work	(1)

a) Average values of nonequivalent bond lengths and bond angles when there are nonequivalent values. b) X-ray diffraction. c) Microwave. d) Electron diffraction. e) Assumed value.

10) V. Busetti, A. Del Pra, and M. Mammi, *Acta Crystallogr.*, **B25**, 1191 (1969).
11) T. Oka, K. Tsuchiya, S. Iwata, and Y. Morino, This Bulletin, **37**, 4 (1964).
12) A. H. Clark and T. G. Hewitt, *J. Mol. Structure*, **9**, 33 (1971).
13) J. B. Hendrickson, *J. Amer. Chem. Soc.*, **86**, 4854 (1964).
14) D. W. Cruickshank, *Acta Crystallogr.*, **9**, 754 (1956).
15) V. Schomaker and K. N. Trueblood, *ibid.*, **23**, 1049 (1968).

Table 5. Temperature parameters (B_i in Å^2) and r.m.s. displacements (U_i in Å) along the principal axes of the thermal ellipsoids and the direction cosines of these axes with respect to the a, b, and c axes

	B_i	U_i	l	m	n	B[a)]
C(1)	2.82	0.189	0.7472	0.0000	−0.6645	
	3.06	0.197	0.0000	−1.0000	0.0000	3.29
	4.00	0.225	0.6645	0.0000	0.7473	
O(1)	2.51	0.178	0.7274	−0.0733	−0.6822	
	3.55	0.212	−0.6434	0.2728	−0.7153	3.37
	4.06	0.227	0.2386	0.9593	0.1513	
C(2)	2.57	0.180	0.9490	0.2370	0.2077	
	3.78	0.219	0.3136	−0.6444	−0.6974	3.60
	4.44	0.237	−0.0315	0.7270	−0.6859	
O(2)	2.87	0.191	0.8659	−0.4967	−0.0585	
	4.05	0.226	−0.4571	−0.7383	−0.4958	4.01
	5.12	0.255	−0.2031	−0.4560	0.8665	
C(3)	2.86	0.190	−0.6032	0.4983	−0.6229	
	3.75	0.218	−0.4768	−0.8512	−0.2192	3.97
	5.30	0.259	−0.6394	0.1648	0.7510	
O(3)	3.03	0.196	0.0000	1.0000	0.0000	
	3.53	0.212	−0.7772	0.0000	−0.6291	4.91
	8.17	0.322	−0.6291	0.0000	0.7772	

a) Isotropic temperature parameter equivalent to the given anisotropic temperature parameters.

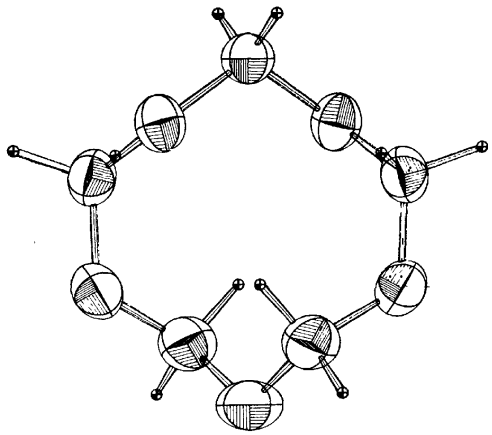

Fig. 4. Thermal ellipsoids of carbon and oxygen atoms in a pentoxecane molecule viewed along the c axis.

the molecules.

As has already been mentioned, the solid-state polymerization of pentoxecane by X- or γ-irradiation was successful. The single crystal habit of pentoxecane is retained at the completion of polymerization, and the orientation of the resultant polyoxymethylene crystallites is governed by the symmetry of the parent pentoxecane crystal. The polymer chains grow along the two face-diagonal axes, [110] and [$\bar{1}$10], which are equivalent to each other, as if the crystals were "twinned crystals." In addition to the crystals, a small amount of crystallites with another preferred orientation is formed, that is, the polymer chains are oriented along the [101] and [$\bar{1}$01] axes, which are equivalent to each other. The details of the orientation of polymer crystals have already been reported.[2)]

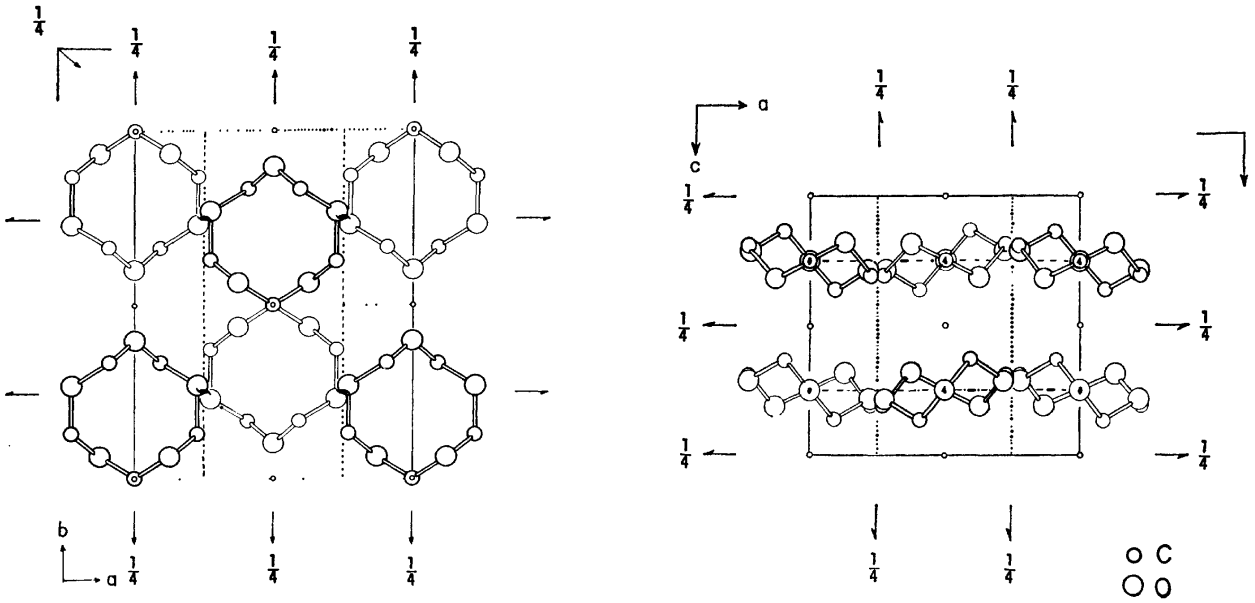

Fig. 5. Crystal structure of pentoxecane viewed along the c axis (left) and b axis (right).

Table 6. Intermolecular atomic distances less than 3.8 Å for C···O and 4.2 Å for C···C

C···O		C···C	
C(1, a)···O(2, e)	3.39 Å	C(2, a)···C(3, e)	3.64Å
C(2, a)···O(3, e)	3.39	C(3, a)···C(2, d)	3.67
C(3, a)···O(1, d)	3.45	C(1, a)···C(1, b)	3.83
C(1, a)···O(1, b)	3·58	C(3, a)···C(2, c)	3.86
C(3, a)···O(2, d)	3.69	C(1, a)···C(3, e)	3.93
C(2, a)···O(1, b)	3.75	C(2, a)···C(1, b)	4.15
O(1, a)···C(1, e)	3.78		

a: x, y, z; b: $x, 1-y, -\frac{1}{2}+z$; c: $-\frac{1}{2}+x, \frac{1}{2}-y, 1-z$; d: $1\frac{1}{2}-x, \frac{1}{2}-y, \frac{1}{2}+z$; e: $1\frac{1}{2}-x, \frac{1}{2}+y, z$

It has also been noted that the polymer formation can be detected by irradiation at 20 °C. The polymerization rate increases with the elevation of the irradiation temperature, and the maximum rate is found at about 50 °C. No polymer is obtained by irradiation above the melting point, 61.3 °C. In order to clarify such specificities of the solid-state polymerization, many physicochemical investigations are necessary.

The authors wish to thank Professor H. Tadokoro of Osaka University for his interest in the work and his constant encouragement. The thermal ellipsoids of the pentoxecane molecule were drawn with a plotter by the use of the universal crystallographic computation program system 5020 UNICS of the University of Tokyo.

BULLETIN OF THE CHEMICAL SOCIETY OF JAPAN, VOL. 46, 2305—2307 (1973)

Magnetic Susceptibilities of Solid Oxygen-Argon Mixtures

Yoshihiro MORI,* Akira SAKAKIBARA,** and Hiroo INOKUCHI

The Institute for Solid State Physics, The University of Tokyo, Roppongi, Tokyo 106

(Received February 3, 1973)

The magnetic susceptibility in solid oxygen-argon mixtures has been obtained as a function of the temperature from 12 K to the melting point. In case of the 95% O_2–5% Ar system, the behavior of the magnetic susceptibility was similar to that of pure oxygen except for some dynamical effects caused by the addition of argon to the oxygen lattices. In the composition range between 92% and 66% O_2, the appearance of a novel phase, δ, was observed from the magnetic susceptibility measurements; its temperature and concentration dependence was discussed qualitatively on the basis of the crystal structure.

The magnetic susceptibility of solid oxygen was first measured from 2 K to its melting point by Kanda *et al.*[1] Since then, the magnetic properties of solid oxygen have been studied by various methods, such as crystallographic analysis,[2] optical-absorption measurements in relation to magnon excitation,[3] and electronic 'double' transitions.[4]

It has been clarified through these studies that there exists an antiferromagnetic spin ordering over a long range in the lowest-temperature α phase; in this sample the crystal structure is monoclinic and nearly closed-packed in both [001] and [$\bar{2}$01] planes. On the other hand, in the higher-temperature phases, β (23.8—43.8 K) and γ (43.8—54.4 K), the order is only short range because of the nearest-neighbor interactions.

In the present study, the results of magnetic susceptibility measurements of oxygen-argon mixtures with oxygen contents between 66% and 95% will be reported and the effects of the addition of diamagnetic argon atoms will be discussed.

Experimental

The magnetic susceptibitily measurements were carried out from 12 K to the melting point in each of the oxygen-argon mixtures by the Faraday method, as has previously been described.[5] The magnetic field was set at about 9×10^3 Gauss throughout the measurements. The field strength was calibrated by measuring the susceptibility of sucrose, the mass susceptibility of which was taken to be -0.566×10^{-6} emu/g.

The preperation method and the thermal history of the sample were as follows. Gaseous mixtures of oxygen and argon in various ratios containing 5—10 mg of oxygen were condensed into a small quartz tube cooled at the temperature of liquid helium, and then the tube was sealed off. The quartz ampoule (5 mm in diameter and 15 mm in length) was suspended by a Pyrex glass string from the arm of a Saltorius Electrono Microbalance, cooled to about 80 K, and kept at this temperature for more than ten minutes in order to liquefy and mix the gases. This liquid mixture was then solidified at about 50 K. After this treatment, it was cooled to 12 K within less than 15 min.

The temperature was measured with an Au : Co–Cu

* Present address: Faculty of Pharmaceutical Sciences, Toyama University, Gofuku, Toyama.

** Faculty of Engineering Okayama University, Okayama.

1) E. Kanda, T. Haseda, and A. Otsubo, *Physica*, **20**, 131 (1954).

2) M. F. Collins, *Proc. Phys. Soc.* (London), **89**, 415 (1966). C. S. Barrett, L. Meyer, and J. Wasserman, J. Chem. Phys., **47**, 592 (1967).

3) T. G. Blocker, M. A. Kinch, and F. G. West, *Phys. Rev. Lett.*, **22**, 853 (1969). E. J. Wachtel and R. G. Wheler, *ibid.*, **24**, 233 (1970).

4) Yu. G. Litvinenko, V. V. Eremenko, and T. I. Garber *Phys. Stat. Sol.*, **30**, 49 (1968).

5) N. Ohigashi and H. Inokuchi, This Bulletin, **42**, 1212 (1969).

thermocouple placed below the ampoule. The temperature of the sample was calibrated by the phase-transition temperatures of pure solid oxygen and also by measuring several times the susceptibilities of the paramagnetic salts whose suscepitibilities are known, Mohr's salt ($Fe(NH_4)_2(SO_4)_2 \cdot 6H_2O$) and Tutton's salt ($Mn(NH_4)_2(SO_4)_2 \cdot 6H_2O$), under the same conditions.

Results and Discussion

Figure 1 shows the temperature dependence of the magnetic susceptibility at each oxygen molar ratio, corrected for the diamagnetism of the argon and the quartz ampoule.

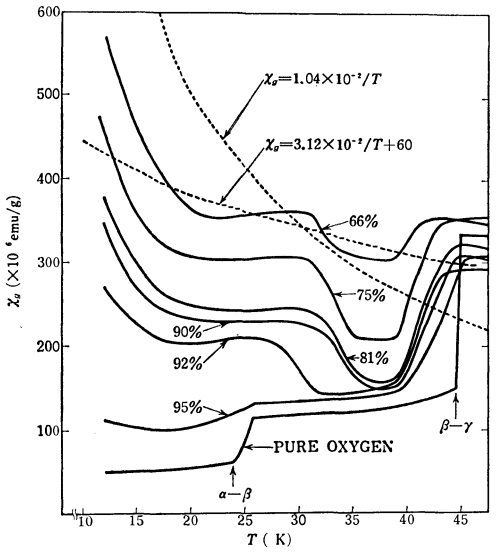

Fig. 1. The magnetic susceptibility of solid oxygen-argon systems.

In case of the 95% O_2, the behavior of the magnetic susceptibility was very similar to that of pure oxygen. This shows that the antiferromagnetic properties characteristic of each crystalline phase, α, β, and γ, of solid oxygen are not so much affected at these low concentrations of argon.

From the viewpoint of the dynamics of crystallization, however, this solid was found to behave differently from pure oxygen. The transformation temperatures from β to γ are lowered to about 40 K. The transformation process was also observed to be less discontinuous; an abrupt change in the susceptibility at each transition temperature, as in pure solid oxygen, was not observed in this mixture even at the slowest of temperature increases (1 °C/min), which was controlled by changing the vacuum in the Dewar vessel. Because of this experimental design, the susceptibility did not reach equilibrium during the transformation. These dynamical effects resulting from the addition of argon to the oxygen lattice have been previously observed in a determination of the oxygen-argon system by Barrett *et al.*,[6] and also through the measurement of the specific heat.[7]

On the other hand, with a further increase in the argon content, the magnetic susceptibilities showed some behavior very different from that of pure oxygen and the 95% O_2 mixture. They are consistent with an interesting phenomenon discovered by Barrett,[5] namely, that a novel homogeneous phase, 'δ', different from the phase of pure oxygen and pure argon, exists in the composition range between 55 and 80% O_2, while the monoclinic phase disappears. Furthermore, the upper limit of oxygen content at which the δ phase appears can be extended to 90% when the mixture is cooled from the γ phase down to the temperature of liquid hydrogen within less than an hour.

The stable-temperature region of this phase was estimated from the decrease in the susceptibility to be below 30—31 K for the 90%, 81%, 75%, and 66% oxygen mixture. In the case of the 92% O_2 and 8% Ar samples, a similar decrease in susceptibility was observed, but at a slightly lower temperature, about 26 K. These transformation temperatures do not agree in detail with those of the phase diagram.[6] According to this, the δ phase containing 80—90% O_2 is transformed to the β phase via a two-phase $\delta+\beta$ region at temperatures between 25 and 29 K, and that of 66—80% is transformed to the hexagonal closed-packed phase of argon + the β phase via the $\delta+\beta$ region at 29 K. This discrepancy may arise from the fact that the magnetic susceptibility measurements can not give such a sensitive indication of these complex transformation processes as X-ray diffraction analysis.

The temperature and concentration dependence of the susceptibility in the δ-phase region can be interpreted on the basis of the crystal structure. A possible structure of the δ phase was also determined by Barrett.[8] According to their work, unit cell has a body-centered cubic lattice with $a=13.23\pm0.02$ Å and $Z=64$, which is a super lattice of the γ structure

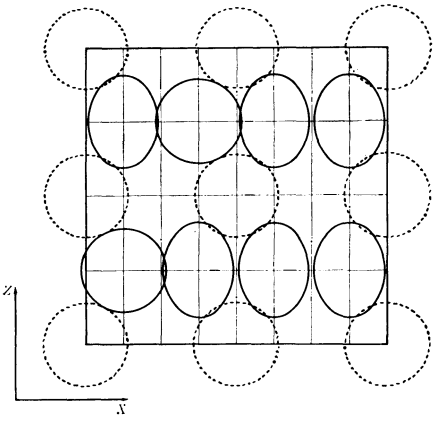

Fig. 2. The [010] plane of unit cell of the δ structure belonging to the space group I_{2_13}. The solid and dotted circles represent argon atoms with a diameter of 3.75 Å. The ellipses represent oxygen molecules with a major axis of 3.18Å.[10] The tilting of the molecular axis is postulated to be in this plane. The corner's argon represented by a dotted circle is displaced by 0.005, 0.005, 0.005 from each position along the threefold axis.

6) C. S. Barrett, L. Meyer, and J. Wasserman, *J. Chem. Phys.*, **44**, 998 (1966).

7) E. L. Pace and R. L. Bivens, *ibid.*, **53**, 748 (1970).

8) C. S. Barrett, T. H. Jordan, and L. Meyer, *ibid.*, **51**, 2941 (1969).

of pure oxygen, with $a=6.83\pm0.05$ Å and $Z=8$. The position of the argon atoms in the δ structure has not been exactly determined, but some plausible models have been suggested. One of them is illustrated in Fig. 2. In this model, the argon and oxygen molecules are placed in a periodic sequence as; $\cdots Ar,O_2,O_2,O_2\cdots$ in the rows across the middle of the cube faces denoted 'γ rows.' The distance between the oxygen molecules in a γ row is 3.31 Å, which is equal to the nearest-neighbor distance in β-O_2 and about 0.1 Å shorter than in γ-O_2. Therefore, we can expect that there exists a fairly strong antiferromagnetic exchange interaction between these three oxygen molecules $(O_2)_3$ in a γ row. Consequently, the total spin moment of this trimer of the form $(O_2)_3$ decreases and becomes one in the antiferromagnetic short-range ordered state.

The paramagnetic increase below about 20 K is dependent on the argon content and seems to obey a Curie-Wiess law. A qualitative interpretation can be given in terms of weak antiferromagnetic interactions between the corner or the body-center's oxygens and the trimer in a γ row. The exchange interaction for these oxygen molecules, separated by about 3.8 Å, estimated to be equal to or less than 2 K from the 'statistical' Weiss temperature obtained for oxygens dispersed into the f.c.c. lattice of argon.[9] If the argon ratio is increased, some of the sixteen oxygen molecules at the corner and body-center's sites are successively replaced by argon, that is, 0 for 81% O_2, 4 for 75% O_2 and 10 for 66% O_2, so that the exchange interaction is weakened. Furthermore, as the neighboring trimers are separated by more than 4.1 Å, the magnetic susceptibility increases, obeying a Curie-Weiss law with a nearly zero Weiss temperature and also a smaller total spin moment. This is represented in the limiting form, $\chi(\text{emu/g})=C'/T+\theta$, where θ is the Weiss temperature and where C' equals 1.043×10^4, that is, the value of 1/3 of 3.128×10^4 for a free oxygen molecule. A quantitative treatment, however, was not attempted because it was not possible to estimate the contributions of residual phases, such as the α and β phases of solid oxygen, and of oxygens randomly dispersed in the segregated argon matrix.

Some interesting phenomena due to δ-phase transformation have also been observed from magnetic susceptibility measurements in solid oxygen-fluorine systems. These results will be reported elsewhere.

9) T. G. Blocker, C. L. Simmons, and F. G. West, *J. Appl. Phys.*, **40**, 1154 (1969).
10) R. F. W. Bader, W. H. Henneker, and P. E. Cade, *J. Chem. Phys.*, **46**, 3341 (1967).

BULLETIN OF THE CHEMICAL SOCIETY OF JAPAN, VOL. 46, 2307—2311 (1973)

Thermoluminescence from the UV-Irradiated Solution of Triphenylmethane at Low Temperature

Naoto YAMAMOTO, Michio MATSUMURA, and Hiroshi TSUBOMURA

Department of Chemistry, Faculty of Engineering Science, Osaka University, Toyonaka, Osaka 560

(Received February 22, 1973)

Triphenylmethane, irradiated in the near ultraviolet region in a non-polar rigid medium at 77 K, showed thermoluminescence consisting of three bands, fluorescence and phosphorescence of triphenylmethane and fluorescence of triphenylmethyl radical. With the increase of solute concentration the yield of the emissions from triphenylmethane decreased while that of the emission from the radical increased. It was concluded that the emissions from triphenylmethane were due to the recombination between triphenylmethane cation and the photo-ejected electron, and that the fluorescence from the radical was mainly due to the electron transfer reaction between triphenylmethane cation and triphenylmethyl anion. Detailed emission processes inlcuding electron transfer and energy transfer processes were discussed.

Thermoluminescence from low temperature UV-irradiated solution of aromatics has been investigated by many authors.[1-4] It has been recognized that the luminescence in many cases is caused by recombination of the charged species generated by the photo-ionization of aromatic molecules. Gibbons *et al.*[3] found that the thermoluminescence from an irradiated solution of toluene comprises the fluorescence and the phosphorescence of toluene together with the fluorescence of the benzyl radical. The former two emissions were concluded to be caused by the recombination of the solvated electron with the toluene cation, while the mechanism for the last one was left untouched.

In this paper, we have investigated the thermoluminescences from triphenylmethane irradiated in non-polar organic rigid solutions and give an explanation for the emission mechanism.

Experimental

Commercial triphenylmethane was sublimed in vacuum. Purification of *N,N,N',N'*-tetramethyl-*p*-phenylenediamine

1) W. Meyer and A. C. Albrecht, *J. Phys. Chem.*, **66**, 1168 (1962).
2) M. Gauthier-Bodard and J. Bullot, *Ber. Bunsen. Phys. Chem.*, **72**, 348 (1968).
3) W. A. Gibbons, G. Porter, and M. I. Savadatti, *Nature*, **206**, 1355 (1965).
4) B. Brocklehurst, W. A. Gibbons, F. T. Lang, G. Porter, and M. I. Savadatti, *Trans. Faraday Soc.*, **62**, 1793 (1966).

(TMPD) was described previously.[5] Isopentane and methylcyclohexane were purified by passing through 1 m silica gel columns. Solutions of triphehylmethane in a 2 : 1 mixture of isopentane and methylcyclohexane (hereafter called MP) were deaerated by purging with nitrogen. Irradiation of the solution in the UV region was carried out at 77 K with a high pressure mercury lamp (250 W) through a Toshiba UV-D25 glass filter and an aqueous solution of 2.0 M nickel sulfate. Infrared light was obtained from the same lamp using a Toshiba VR-67 glass filter. The thermoluminescence from the irradiated solution was measured with a Shimadzu GF 16 monochromator and an RCA 1P28 photomultiplier. Details of the measurement are described elsewhere.[6] The absorption spectra were measured with a Cary Model 15 spectrophotometer.

Results

Change of the absorption spectrum of an MP solution of triphenylmethane by UV-irradiation is shown in Fig. 1. The bands lying in the range 25—35 kK and around 20 kK were in fairly good agreement with those of triphenylmethyl radical assigned by Adam and Weissman.[7] Formation of the triphenylmethyl radical was found to be proportional to the square of the intensity of UV-light from the absorption intensity measurement. It is therefore concluded that the radical is produced by a bi-photonic mechanism.[4,8] The irradiated solution showed weak luminescence on warming. A thermoluminescence spectrum is shown in Fig. 2. The band with maximum at 34.5 kK corresponds to the fluorescence of triphenylmethane, and that at 24.4 kK to the phosphorescence of the same

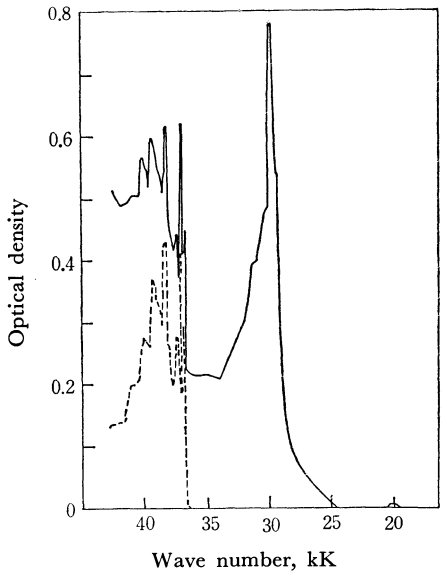

Fig. 1. Absorption Spectra of a 1.5×10^{-4} M MP solution of triphenylmethane at 77 K.
---- before irradiation
—— after irradiation for 10 min

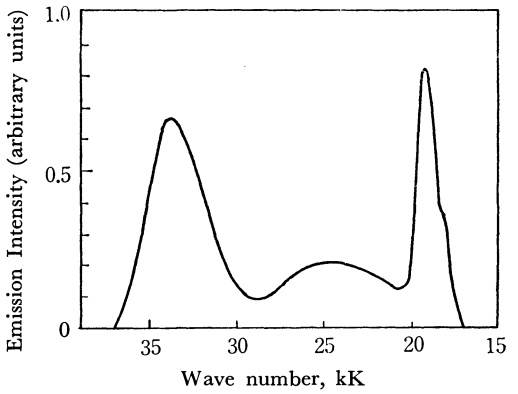

Fig. 2. Thermoluminescence spectrum from a 5×10^{-4} M solution of triphenylmethane irradiated for 10 min at 77 K.

molecule. The band at 19.4 kK agrees well in shape and position with the normal fluorescence of triphenylmethyl radical ($^2E\leftarrow{}^2A_2$ transition).[9]

The intensity of thermoluminescence was measured for each emission band as functions of time after the irradiated solution was taken out from the Dewar (Fig. 3). Curves (a) for fluorescence and (b) for phosphorescence of triphenylmethane are similar in shape, while curve (c) for fluorescence of the triphenylmethyl radical differs considerably, suggesting that the latter appears by a different mechanism from that for the emission of triphenylmethane. It was also found from simultaneous observation of the glow curves and the change of absorption with warming that the radical survives after the emission from the radical already fades out.

The emission intensities change markedly with experimental conditions such as concentration of the solution and UV-irradiation time. Figure 4 shows the emission yield (obtained by integrating the thermal

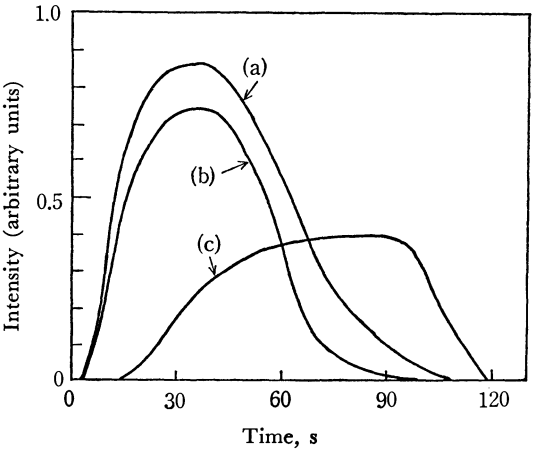

Fig. 3. Thermal glow curves for the irradiated 2.5×10^{-4} M solution of triphenylmethane. The irradiateon time was 5 min. The curves were obtained for the three bands corresponding to the fluorescence (a) and phosphorescence (b) of triphenylmethane and the fluorescence of triphenylmethyl radical (c), respectively.

5) T. Imura, N. Yamamoto, and H. Tsubomura, This Bulletin, **43**, 1607 (1970).
6) K. Yoshinaga, N. Yamamoto, and H. Tsubomura, *J. Luminescence*, **4**, 417 (1971); **6**, 179 (1973).
7) F. C. Adam and S. I. Weissman, *J. Amer. Chem. Soc.*, **80**, 2057 (1958).
8) H. Yamada, N. Nakashima, and H. Tsubomura, *J. Phys. Chem.*, **74**, 2897 (1970).
9) G. N. Lewis, D. Lipkin, and T. T. Magel, *J. Amer. Chem. Soc.*, **66**, 1579 (1944).

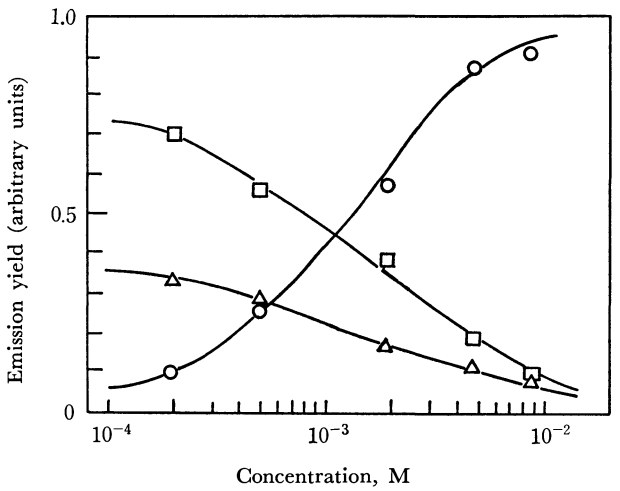

Fig. 4. Emission yields (see text) for the thermoluminescence from the irradiated MP solutions of triphenylmethane as a function of the triphenylmethane concentration. The yields were measured at the maxima for the fluorescence (-□-□-) and phosphorescence (-△-△-) of triphenylmethane and for the fluorescence of triphenylmethyl radical (-○-○-), respectively.

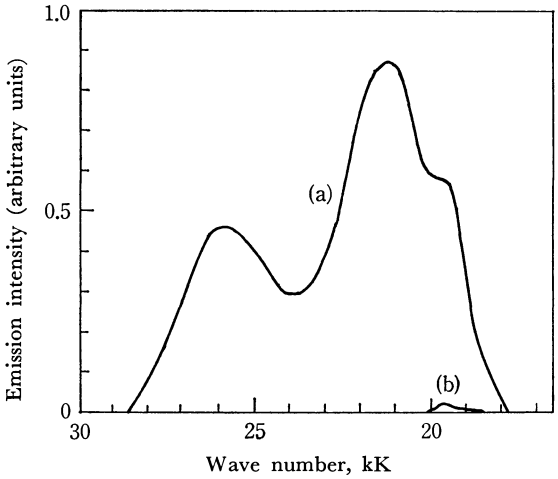

Fig. 5. Emission spectra for the thermoluminescence from the irradiated MP solutions.
(a), for a solution containing $1,5\times10^{-5}$ M TMPD and 7×10^{-3} M triphenylmethane;
(b), for a solution of 7×10^{-3} M triphenylmethane.

Table 1. Influence of IR-irradiation on the yield of thermoluminescence

Concentration of triphenylmethane 2.25×10^{-4} M
UV-irradiation time 10 min.
IR-irradiadiation time 30 sec.

	Emission yield (arbitrary units)		
	Fluorescene band of triphenyl-methane	Phosphore-scence band of triphenyl-methane	Fluorescence band of tri-phenylmethyl radical
Without IR-irradiation	337	184	106
With IR-irradiation	45	22	87

glow curve with time) for the three bands of the thermoluminescence against the concentration of the solute. Concentrated solutions (10^{-3}—10^{-2} M) absorbed almost all the UV-lights (the cell used was 13 mm thick) and therefore gave nearly constant amounts of triphenylmethyl radical in the media for the irradiation time of 10 min. For solutions with concentrations below 10^{-3} M, part of the light passes through the solution. Such solutions were irradiated until the yield of the radical became equal to that of the concentrated solutions. As is obvious from Fig. 4, the emission from triphenylmethane were strong at lower concentration and weak at higher concentration. On the other hand, the fluorescence from the radical, hardly observable at concentration of 2×10^{-4} M, became strong at concentration above 10^{-3} M.

No absorption band of triphenylmethane cation was found for the irradiated solution in the visible and near infrared region.[10]

We also measured the thermoluminescence for the MP rigid solution containing TMPD (1.5×10^{-5} M) and triphenylmethane (7×10^{-3} M). Strong thermoluminescence was observed and its spectrum was found to consist of three bands, *i.e.*, the fluorescence and phosphorescence of TMPD and the fluorescence of triphenylmethyl radical (Fig. 5, curve a). The fluorescence of triphenylmethyl radical was 11 times stronger in intensity than that obtained for an MP solution containing only 7×10^{-3} M triphenylmethane where the irradiation time was 5 min for both cases. For the irradiated TMPD-triphenylmethane solution, the TMPD cation and triphenylmethyl radical were proved to be present by absorption measurement, but no absorption band was found in the visible region ascribable to triphenylmethyl anion.[11]

The thermoluminescence was also studied for a UV-irradiated solution of triphenylmethane after being exposed to infrared light. The emissions from triphenylmethane became weak but the fluorescence from the radical was only slightly affected (Table 1).

Discussion

Emission Mechanism. It is evident from UV absorption spectra studies that the triphenylmethyl radical is formed in the UV-irradiated solution of triphenylmethane at 77 K. The radical is presumably formed by the following bi-photonic excitation.[4,8]

$$\phi_3CH \xrightarrow{h\nu_1} {}^3[\phi_3CH] \xrightarrow{h\nu_2} \phi_3C\cdot + H\cdot \qquad (1)$$

The ionization potential of triphenylmethane is 8.80 eV in the gas phase,[12] and its triplet state energy is 3.58 eV higher than that of the ground state. Therefore, if it is photo-ionized by the bi-photonic process as are many aromatics in the low temperature matrices,

$$\phi_3CH \xrightarrow{h\nu} {}^3[\phi_3CH] \xrightarrow{h\nu'} [\phi_3CH]^+ + e \qquad (2)$$

10) T. Shida and W. H. Hamill, *J. Chem. Phys.*, **44**, 2375 (1966).
11) K. K. Brandes, R. Suhrmann, and R. J. Gerdes, *J. Org. Chem.*, **32**, 741 (1967).
12) V. V. Sorokin, *Zh. Fiz. Khim.*, **40**, 2332 (1966).

the second step needs a photon energy equal to or higher than 5.2 eV in the gas phase. Due to polarization energy, the necessary energy for the second step in the matrix may be smaller. As the light source used in the present work has an energy distribution in the range 5.2—3.4 eV, such a photo-ionization is assumed to take place to a small extent, though we could not observe the absorption bands for the triphenylmethane cation.

The triphenylmethyl radical formed is expected to capture the electron ejected in the medium because of its large electron affinity.

$$e + \phi_3C\cdot \longrightarrow \phi_3C^- \quad (3)$$

The anion and other charged species frozen at 77 K become mobile when the solution is warmed. The triphenylmethane cation and the solvated electron will recombine causing emissions from triphenylmethane as follows:

$$\phi_3CH^+ + e_{solv} \longrightarrow {}^1\phi_3CH^* \text{ or } \phi_3CH^* \quad (4)$$

$${}^1\phi_3CH^* \longrightarrow \phi_3CH + h\nu_F \quad (5)$$

$${}^3\phi_3CH^* \longrightarrow \phi_3CH + h\nu_P \quad (6)$$

On the other hand, the triphenylmethyl anion will react with the triphenylmethyl cation and emit fluorescence of the triphenylmethyl radical as follows:

$$\phi_3CH^+ + \phi_3C^- \longrightarrow \phi_3CH + {}^2\phi_3C\cdot^* \quad (7)$$

$${}^2\phi_3C\cdot^* \longrightarrow \phi_3C\cdot + h\nu_F' \quad (8)$$

As the first excited doublet state of the radical is energetically the lowest of all the excited states of triphenylmethane and the radical formed, the fluorescence from it will prevail as the result of the electron transfer and energy transfer processes.

Variations in the intensities of the emission bands with concentration (Fig. 4) can be explained as follows. In dilute solutions, reactions (1) and (2) by irradiation occur uniformly in the cell, while in concentrated solutions they take place mostly near the surface of the irradiated side of the cell, the concentration of the triphenylmethyl radical thus becoming much higher at that part of the solution. As the concentration of the radical becomes higher, the ratio of the photo-ejected electrons captured by the radical compared with those trapped in the matrix become higher.[6,13] Consequently, as reactions (4), (5) and (6) are dominant so are the emissions from triphenylmethane at low concentrations, while as reactions (7) and (8) become dominant so do the emissions from the radical at high concentrations. This fits the trends of curves in Fig. 4.

For the case of TMPD-triphenylmethane solution, it is most probable that the electrons generated mainly by the photo-ejection from TMPD are captured by triphenylmethyl radicals, and the electron transfer reaction between TMPD cation and triphenylmethyl anion leads to the fluorescence from the radical. That the emissions from triphenylmethane were weakened by illumination in the infrared to a greater extent than the emission from the radical seems to result from the fact that the electron is bound by the radical more tightly than in the matrix (Table 1).

The emission from benzyl radical observed for the irradiated solution of toluene might be due to the reaction between benzyl anion and toluene cation.[3,14]

Electron transfer and energy transfer on recombination. We have concluded that the combination of triphenylmethane cation with triphenylmethyl anion leads to emission from the triphenylmethyl radical.

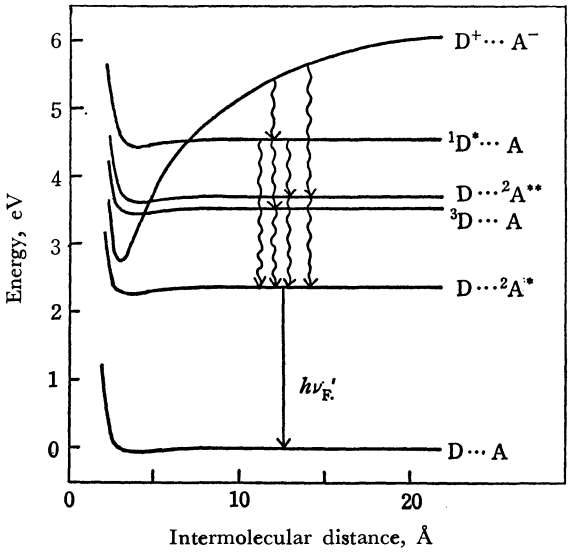

Fig. 6. The potential energy curves for the various states of a system made of triphenylmethane cation (D^+) and trimethyl radical anion (A^-).

The triphenylmethyl anions are expected to be distributed at fairly large distances (~100 Å)[13,15] from the triphenylmethane cations at 77 K. As the matrix is warmed, the anion is mobilized and is drawn near the cation by the Coulombic force along the $D^+\cdots A^-$ curve in Fig. 6. The velocity of the anion should be determined by the Coulombic force $e^2/\varepsilon r^2$, and the resisting force by $6\pi\eta bv$ according to the Stokes' law, where ε and η are respectively the dielectric constant and viscosity of the medium, and b and v the radius and velocity of the anion, respectively. Thus we have

$$v = e^2/6\pi\eta b\varepsilon r^2 \quad (9)$$

In order to estimate the distance between the ions at which the electron transfer reaction occurs at the maximum rate, it is necessary to derive the absolute value of the reaction rate as a function of the distance. The probability of the electron transfer from the anion to the cation P_{CT} is proportional to the amount of charge transfer interaction V_{CT}.

$$P_{CT} = 2|V_{CT}|/h \quad (10)$$

$$V_{CT} = \langle \Phi_f | H | \Phi_i \rangle \quad (11)$$

where Φ_i and Φ_f are, respectively, the wave functions for the initial and final states of the system and H is

13) N. Yamamoto, Y. Nakato, and H. Tsubomura, This Bulletin, **40**, 451 (1967).

14) B. Brocklehurst, R. D. Russell, and M. I. Savadatti, *Trans. Faraday Soc.*, **62**, 1129 (1966).

15) W. M. McClain and A. C. Albrecht, *J. Chem. Phys.*, **44**, 1594 (1966).

the total Hamiltonian. We roughly estimate the value of the right side of Eq. (11), using a simple model consisting of two carbon monocations C_A^+ and C_B^+ fixed at a distance of r and an electron. Assuming that the electron is initially localized on C_A^+ and transferred to C_B^+, the initial and the final electronic wave functions are the atomic orbitals of the each atom represented by Φ_A and Φ_B, respectively. In this case, the matrix element in Eq. (11) can be simply written as follows.

$$\langle \Phi_f | H | \Phi_i \rangle = \langle \Phi_B | H | \Phi_A \rangle \quad (12)$$

Assuming that it is proportional to the overlap integral of the orbitals, approximated to be proportional to $\exp(-3.07\times10^8 r)$, and taking the value of 2.4 eV for the element at $r=1.40$ Å, as suitable for the usual MO calculation of π-electron systems, we obtain

$$P_{CT} = 8.48 \times 10^{16} \exp(-3.07\times10^8 r) \quad (13)$$

By taking the probability of existence of unreacted ion-pair to be p, and assuming the initial distance between the cation and the anion to be very much greater than the distance at which the electron transfer reaction takes place predominantly, the extermination of the ion-pairs due to the electron transfer can be represented as a function of distance:

$$\begin{aligned} dp/dr &= -(P_{CT}/v)p \\ &= -6.94\times10^{36}\,\eta b\varepsilon r^2 \exp(-3.07\times10^8 r)p \end{aligned} \quad (14)$$

The most probable distance for the reaction corresponds to the distance making dp/dr the maximum. Hence, the following equation is obtained, taking $d^2p/dr^2=0$

$$\begin{aligned} &-(2-3.07\times10^8 r_{max})/r_{max}^3 \\ &= 6.94\times10^{36}\eta b\varepsilon \exp(-3.07\times10^8 r_{max}) \end{aligned} \quad (15)$$

It is found that the r_{max} determined from Eq. (15) is rather insensitive to η, b and ε. Saturated hydrocarbons at 77 K have viscosities of the order of 10^{12} P.[16] At the temperature of maximum thermoluminescence, the viscosity is definitely higher than 10^3 P. We calculated r_{max} using the values of 10^{12} and 10^3 P for the viscosity of the solvent. Taking 4.0 Å for b and 2.5 for ε, the distances obtained are 7.6 Å for $\eta=10^3$ P and 14.8 Å for $\eta=10^{12}$ P.

The primary electronic state thus formed by the electron transfer reaction, which should have a total energy equal to the CT state at that distance, may be such as D**···A, D···A** etc., where D** and A** are higher excited states of triphenylmethane and triphenylmethyl radical. The energy relaxation due to intra-molecular radiationless transitions is thought to be very quick. The inter-molecular energy transfer, such as transition from either ^{1}D* or ^{3}D* to ^{2}A*, depends strongly on the inter-molecular distance. Since the dipole-dipole transition from ^{1}D* to ^{2}A* is spin-allowed, this process should take place very effectively at the distances considered.[17] The transition from ^{3}D* to ^{2}A*, although it is spin-forbidden, seems also to be effective because the triplet state of D is long-lived at low temperatures. These radiationless processes are represented in Fig. 6 by the wave lines. The fluorescence from the radical observed is understandable as due to the electron transfer followed by energy transfer reactions (Fig. 6).

16) J. R. Lombardi, J. W. Raymonda, and A. C. Albrecht, *J. Chem. Phys.*, **40**, 1148 (1964).
17) D. L. Dexter, *ibid.*, **21**, 836 (1953).

BULLETIN OF THE CHEMICAL SOCIETY OF JAPAN, VOL. 46, 2311—2314 (1973)

Molecular Structure of Ethane. Comparison of the Structure Parameters of CH_3CD_3 in the Torsionally Excited State and in the Ground State

Takao IIJIMA

Department of Chemistry, Faculty of Science, Hokkaido University, Sapporo 060

(Received March 10, 1973)

The structure parameters of ethane have been re-examined by the use of the spectroscopic moments of inertia and the electron diffraction results, on the basis of the large amplitude theory for the torsional motion. The results have been applied to the CH_3CD_3-species in order to see whether or not the change of the moment of inertia in the torsionally excited state observed by Hirota and Matsumura is consistent with the theoretical prediction on the deformation of the molecular frame upon torsion proposed by Veillard. The conclusion has been affirmative. The elongation of the C–C distance by 0.0028 Å and the decrease of the HCH angle by 0.05° in the torsionally excited state as expected from the theoretical calculation have been found to be consistent with the experimental result of microwave spectroscopy.

According to several experimental results obtained by microwave spectroscopy[1–3] and a series of theoretical studies,[4–7] it seems that the torsional motion of molecules involves sizable deformations of the frame and/or the top. Meyer and Wilson[2] extensively investigated the rotational constants of torsionally excited states

1) P. Meakin, D. O. Harris, and E. Hirota, *J. Chem. Phys.*, **51**, 3775 (1969).
2) R. Meyer and E. B. Wilson, Jr., *ibid.*, **53**, 3969 (1970).
3) E. Hirota and C. Matsumura, *ibid.*, **55**, 981 (1971).
4) A. Veillard, *Chem. Phys. Lett.*, **3**, 128 (1969).
5) H. J. Monkhorst, *ibid.*, **3**, 289 (1969).
6) A. Veillard, *ibid.*, **3**, 565 (1969).
7) A. Veillard, *ibid.*, **4**, 51 (1969).

of ethyl formate and two other compounds. They concluded that observed changes of rotational constants upon torsional excitation could not be explained without allowing distortions of the molecular geometry upon torsion. An *ab-initio* molecular Hartree-Fock calculation of ethane was carried out by Veillard,[4] where the C–C distance and the HCH angle were optimized. The barrier hindering internal rotation was calculated to be 3.07 kcal/mol, which was very close to the experimental value 2.93 kcal/mol. The C–C distance of the eclipsed conformation was found to be longer than that of the staggered conformation by 0.019 Å, and the HCH angle was smaller by 0.34°. It was not necessary to vary the C–H distance.

In order to get experimental confirmation of this theoretical prediction, ethane is naturally the most suitable molecule. However, since ordinary ethane is inactive in microwave, the rotational constant of the torsionally excited state had not been available. Recently, Hirota and Matsumura[3] made successful observation of the microwave spectrum of CH_3CD_3 species and obtained the rotational constants of both the ground state and the torsionally excited state. The present study is an analysis of the structure parameters of ethane, especially for the purpose of seeing whether or not the theoretical calculation by Veillard is consistent with the experimental observation by Hirota and Matsumura. The conclusion of the present study is that they are consistent with each other. This is also to support the theoretical implication of Veillard's calculation that the electron correlation is not important in the barrier to internal rotation, contrary to the binding energy in which the effect of electron correlation (molecular correlation) is considerable.[8] The deformation of molecular geometry upon torsion is to give an additional correction in the structure determination by a joint use of spectroscopic and diffraction data, since the observed values of diffraction experiment are averaged quantities over torsionally excited state. The force constants determined by Nakagawa and Shimanouchi[9] were used throughout this work.

Analysis

Changes of the Structure Parameters between the Ground State and the First Excited State of Torsional Motion. On the basis of Veillard's calculation, the changes of the C–C distance and the HCH angle for different torsional states were estimated by assuming that the variation of the structure parameters follows the trigonometric function as that of the torsional potential, *viz.*,

$$\Delta r = \frac{c}{2}(1-\cos 3\phi) \qquad (1)$$

where c is 0.019 Å for the C–C distance and −0.34 Å for the HCH anlge, and ϕ is the torsional angle. The average value of Δr for the torsional state τ was evaluated by

$$\langle \Delta r \rangle_\tau = \frac{9}{4} c \langle \phi^2 \rangle_\tau \qquad (2)$$

where the $\langle \phi^2 \rangle$ was calculated by a harmonic approximation.

The values of $\langle \Delta r \rangle$ calculated by Eq. (2) are summarized in Table 1 for the ground state ($\tau=0$) and the first excited state ($\tau=1$). The thermal average values $\tau=T$ at the room temperature are also shown. A similar table for the HCH angle are shown also in the Table 1. From the values in Table 1, it is expected that the structure parameters of CH_3CD_3 for the first excited state of torsion is different from those of the ground state in such a way that the C–C distance is longer by 0.0028 Å and the HCH angle is smaller by 0.05°.

Table 1. Changes of the C–C distance and the HCH angle for different torsional states

	CH_3CH_3	CD_3CD_3	CH_3CD_3
$\langle \Delta r \rangle_0$	17(−31) [b]	12(−22)	14(−25)
$\langle \Delta r \rangle_1$	51(−92)	36(−65)	42(−76)
$\langle \Delta r \rangle_T$ [a]	27(−49)	26(−47)	25(−45)

a) Thermal average values at $T=288$ K
b) Values in the parentheses are the corresponding averages of the HCH angle in 10^{-3} degree units.

Even without the detailed analysis described in the following section, it can be seen that the b-axis moments of inertia I_b obtained by Hirota and Matsumura show a trend which is consistent with the estimation mentioned above. The increase in the C–C distance of 0.02% roughly corresponds to an increase in I_b of 0.04%. Observed value of I_b for the excited state is 0.03% as large as the I_b for the ground state (see Table 2).

Since the thermal average values $\langle \Delta r \rangle_T$ are almost equivalent for all the isotopic species, the isotope effect originating from the torsional distortion can not be expected to appear in r_g values obtained by electron diffraction. On the other hand, the small differences in $\langle \Delta r \rangle_0$ will be the isotope effect of this origin upon r_a^0 or r_z, *i.e.*, the zero-point average distances. More important is the difference between $\langle \Delta r \rangle_T$ and $\langle \Delta r \rangle_0$ which should be included in the correction of r_g to r_a^0 in the joint analysis of electron-diffraction and spectroscopic data on the basis of the zero-point average structure.[10]

Structure Parameters. The structure parameters of CH_3CH_3 and CD_3CD_3 were previously determined by Kuchitsu[10] by means of a joint use of electron diffraction data and spectroscopic moments of inertia. In his treatment, the torsional motion was regarded as a small-amplitude vibrational motion, which was valid since the torsional amplitudes of these molecules are not very large. In the present study, the structure parameters of h_6 and d_6-species were re-determined on the basis of the large amplitude theory for a molecule containing a single internal rotor,[11] simply in order to apply the obtained parameters to the torsionally excited state of CH_3CD_3 in which the small-amplitude approximation would probably fail. In fact the determined parameters of h_6 and d_6-species have shown

8) E. Clementi and H. Popkie, *J. Chem. Phys.*, **57**, 4870 (1972).
9) I. Nakagawa and T. Shimanouchi, *J. Mol. Spectrosc.*, **39**, 255 (1971).
10) K. Kuchitsu, *J. Chem. Phys.*, **49**, 4456 (1968).
11) T. Iijima and S. Tsuchiya, *J. Mol. Spectrosc.* **44**, 88 (1972).

Table 2. Moments of inertia of ethane (in amu. Å² units)

		I_0[f]	ΔI	I_z(SP)	I_z(ED)	I_z^{calcd}
CH_3CH_3	a	6.313[a] (12)[e]	0.040	6.353(20)	6.365(25)	6.348
	b	25.430[b] (3)	0.126	25.556(13)	25.513(34)	25.554
CD_3CD_3	a	12.569[a] (8)	0.059	12.628(18)	12.658(50)	12.632
	b	36.680[c] (6)	0.165	36.845(16)	36.785(67)	36.847
CD_3CH_3	a	—	0.051	—	—	9.490
	b	30.686[c]	0.142	30.828(10)	—	30.827
CD_3CH_3[g]	a	—	0.051	—	—	9.484
	b	30.790[d]	0.142	30.932(10)	—	30.921

a) Ref. 13, b) Ref. 14, c) Ref. 15, d) Ref. 3.
e) Values in the parentheses are the uncertainties as cited from Ref. 10, except for the uncertainties of I_z(SP) which were estimated in the present study.
f) Conversion factor 505531 Mc. amu. Å² was used. g) Torsionally excited state.

Table 3. Structure parameters of ethane[a] (in Å and degree units)

	I	II[b]		II	II[d]
	CH_3CH_3			CD_3CH_3	
C–C	1.5323	1.5323	C–C	1.5310	1.5338
C–H	1.1017	1.1017	C–H	1.1017	1.1017
HCH	107.51	107.30	C–D	1.0990	1.0990
	CD_3CD_3		HCH	107.30	107.25
C–C	1.5299	1.5299	DCD	107.35	107.30
C–D	1.0990	1.0990		Uncertainties[c]	
DCD	107.51	107.35	C–C ± 0.002, C–H(D) ± 0.002		
			HCH(DCD) ± 0.3°		

a) I; the r_α° parameters obtained from electron diffraction data. II; the best r_z-parameters.
b) The r_g-parameters consistent with the r_z-values of the set II are equivalent to the electron diffraction results of Ref. 17, except for the HCH and DCD angles or the non-bonded C···H and C···D distances, which are 2.196_4 Å for C···H and 2.190_9 Å for C···D.
c) To be applied to all the isotopic species. Note that these are uncertainties in the absolute values of the parameters and that the uncertainties in the relative scale are much smaller.
d) Torsionally excited state.

no significant discrepancy from those by Kuchitsu, if the difference in the operational definitions of the parameters is taken into account in the comparison.[12]

In Table 2 are listed the observed values of moments of inertia, the vibrational corrections calculated by the method reported elsewhere,[11,16] and the zero-point average moments of inertia I_z(SP). The moments of inertia calculated by the use of the r_α^0-parameters obtained from the electron diffraction result by Bartell and Higginbotham[17] are compared as I_z(ED). Although a trend that I_z(ED) was systematically larger than I_z(SP) by 0.02% was observed in the analysis by Kuchitsu, it is not seen in the present result. This is partly because of the correction for the torsional deformation included in the conversion of r_g into r_α^0.

A comparison of I_z(ED) and I_z(SP) suggests that a slight adjustment of HCH angle would lead to a set of parameters consistent with the I_z(SP). The values of I_z calculated by the adjusted parameters are listed in the column I_z^{calcd} of Table 2, while the values of the parameters are shown in Table 3.

The structure parameters for the ground state of CH_3CD_3 were then determined as follows. The C–C distance was set equal to the average of those of h_6 and d_6-species. The HCH and DCD angles were transferred from h_6 and d_6-species, respectively. The agreement of the calculated I_z^{calcd} with the observed I_z(SP) is satisfactory. For the torsionally excited state, the C–C distance and HCH (DCD) angle were varied according to the estimation described in the preceding section. The agreement of the calculated value of the moments of inertia with the observed is remarkable. It may be said that the theoretical prediction on the deformation of molecular frame upon torsion has been

12) The zero-point average structure in Ref. 10 is a representation of the atomic positions averaged over all zero-point motions including torsion, while the torsional motion is not included in the averaging in the present treatment. The effect of this difference appears mainly in the structure parameters related to hydrogen atoms.

13) D. E. Shaw and H. L. Welsh, *Can. J. Phys.*, **44**, 3823 (1967) and two preceding papers.

14) W. J. Lafferty and E. K. Plyler, *J. Chem. Phys.*, **37**, 2688 (1962).

15) H. C. Allen and E. K. Plyler, *ibid.*, **31**, 1062 (1959).

16) In order to reduce the off-diagonal term of the moments of inertia tensor in the kinetic energy Hamiltonian, the molecular-fixed coordinate-axes for h_6 and d_6-species were chosen in such a way that the torsion of an angle ϕ was represented by a rotation of $\phi/2$ of both ends in the opposite directions. For CH_3CD_3, the rotations of the two tops CH_3 and CD_3 were chosen to be inversely proportional to the moment of inertia of each top around the axis.

17) L. S. Bartell and H. K. Higginbotham, *J. Chem. Phys.*, **42**, 851 (1965).

given quantitative confirmation by experimental observation.

In the present analysis, the secondary isotope effect in the C–C distance was retained as originally reported in the electron diffraction study.[17] If this isotope effect is ignored and an average of the C–C distances in the h_6 and d_6-species is taken as the diffraction value, a slightly different set of structure parameters can be obtained, although the difference is of no significance. However, there would be no revision in the conclusion about the comparison of the ground state and the torsionally excited state of the CD_3CH_3 species.

As for the estimation of the uncertainties of the determined parameters, the present study has nothing to revise the values reported in Ref. 10, which are reproduced in Table 3. However, these are the uncertainties in the absolute values of the parameters, and the uncertainties in the relative scale, *i.e.*, the difference between the torsionally excited state and the ground state, are much smaller.

The author wishes to thank Professor Masao Kimura, Hokkaido University, for his encouragement. Numerical calculations were carried out on a FACOM 230—60 of the Hokkaido University Computing Center, and on a FACOM 270—20 of Professor Kimio Ohno's laboratory, to whom the author's thanks are also due.

BULLETIN OF THE CHEMICAL SOCIETY OF JAPAN, VOL. 46, 2314—2316 (1973)

Microwave Spectrum of Arsenic Trifluoride in the Excited Vibrational State

Toshio CHIKARAISHI and Eizi HIROTA

Department of Chemistry, Faculty of Science, Kyushu University, Higashi-ku, Fukuoka 812

(Received April 5, 1973)

The microwave spectrum of arsenic trifluoride was observed in the excited states of all the normal vibrations. The rotational constant at the equilibrium state was determined, and the equilibrium As–F distance was calculated to be 1.704_4 Å assuming the FAsF angle to be 95°58′. The *l*-type doubling constant, q_4, and the asymmetry parameter, η, of the As nuclear quadrupole coupling constant were determined in the $v_4=1$ to be 10.24 ± 0.02 MHz and $-0.00_5\pm0.01$, respectively.

Kisliuk and Geschwind[1] have measured the $J=2\leftarrow1$ transitions of arsenic trifluoride and have determined the ground-state rotational constant, the nuclear quadrupole coupling constant, and the vibration-rotation interaction constants, α_2^B and α_4^B, for a symmetric and a degenerate bending vibration, v_2 and v_4. Reichman and Overend[2] have analyzed the infrared v_1 band of arsenic trifluoride and determined the ground-state rotational constant and the α_1^B constant. Mirri[3] has obtained the force field of AsF_3 by the combined use of the vibrational frequencies and the centrifugal stretching and Coriolis' coupling constants. On the other hand, Konaka[4] and Konaka and Kimura[5] have determined the thermal-average distance, r_g(As—F), by gas-phase electron diffraction and has calculated the zero-point average distance, r_z(As—F). In the present work the microwave spectrum in the excited states of all the normal vibrations was observed to obtain the equilibrium structure of arsenic trifluoride. The *l*-type doubling transitions in the v_4 state were also observed to determine the *l*-type doubling constant and to examine the asymmetry of the quadrupole coupling constant of the As nucleus induced by the degenerate bending vibration, v_4.

Experimental

A sample of arsenic trifluoride was donated to us by the courtesy of Dr. S. Konaka of Department of Chemistry, Hokkaido University, and it was purified through vacuum distillation. The spectrometer used was of conventional Hughes-Wilson type with 120 kHz sine-wave and square-wave Stark modulators. The spectrum was recorded while pumping the sample through the cell because of decomposition of arsenic trifluoride in the waveguide.

Results

The $J=1\leftarrow0$ transitions in the ground vibrational state and four excited vibrational states, v_1, v_2, v_3,

TABLE 1. OBSERVED FREQUENCIES OF THE $J=1\leftarrow0$ TRANSITION OF AsF_3 (MHz)

State	Assignment	ν_{obsd}[a]	Δ[b]
Ground	$F=1/2\leftarrow3/2$	11 817.21	−0.03
	$5/2\leftarrow3/2$	11 770.15	0.05
	$3/2\leftarrow3/2$	11 711.14	−0.02
v_1	$F=1/2\leftarrow3/2$	11 807.54	−0.20
	$5/2\leftarrow3/2$	11 761.44	0.36
	$3/2\leftarrow3/2$	11 702.60	−0.16
v_2	$F=1/2\leftarrow3/2$	11 827.66	−0.19
	$5/2\leftarrow3/2$	11 781.04	0.34
	$3/2\leftarrow3/2$	11 721.60	−0.15
v_3	$F=1/2\leftarrow3/2$	—	—
	$5/2\leftarrow3/2$	11 740.92	−0.26
	$3/2\leftarrow3/2$	11 682.60	−0.01
$2v_2$	$F=1/2\leftarrow3/2$	11 837.70	−0.37
	$5/2\leftarrow3/2$	11 792.14	0.68
	$3/2\leftarrow3/2$	11 732.90	−0.30

a) Accuracy is ±0.1 MHz. b) Δ=obsd−calcd.

1) P. Kisliuk and S. Geschwind, *J. Chem. Phys.*, **21**, 828 (1953).
2) S. Reichman and J. Overend, *Spectrochim. Acta*, **26A**, 379 (1970).
3) A. M. Mirri, *J. Chem. Phys.*, **47**, 2823 (1967).
4) S. Konaka, This Bulletin, **43**, 3107 (1970).
5) S. Konaka and M. Kimura, *ibid.*, 1693 (1970).

Table 2. Molecular constants, B_v, α_v^B and eqQ, of AsF_3 (MHz)[a]

State	B_v	$(eqQ)_v$	α_v^B	
Ground	5879.15 ± 0.02	$-235.7_2\pm0.21$	—	
ν_1	$5874.7_1\pm0.13$	$-233._3\pm1.4$	$4.4_4\pm0.15$	(4.71)[b]
ν_2	$5884.4_5\pm0.12$	$-235._8\pm1.3$	$-5.2_9\pm0.14$	$(-5.\pm1.)$[c]
ν_3	$5864.5_2\pm0.11$	$-232._2\pm1.8$	$14.6_3\pm0.13$	
$2\nu_2$	$5889.9_1\pm0.24$	$-233._1\pm2.6$	$10.7_5\pm0.26$	
ν_4	5879.24[d]	$-235._7\pm1.7$[d]	-0.16_5[d,e]	(-0.16 ± 0.04)[c]

a) Errors are standard deviations. b) Ref. 2. c) Ref. 1. d) From the $J=5\leftarrow4$ transition. e) In calculating α_4^B the ground-state rotational constant of 5879.08 MHz (Table 4) is used, which is determined by using the transitions of $J=2\leftarrow1$ through $5\leftarrow4$.

and $2\nu_2$, were measured. The observed frequencies are listed in Table 1. The rotational constants and the nuclear quadrupole coupling constants were determined using the following equation, Eq. (1):

$$\nu = 2B_v(J+1)+\Delta W_Q^{(1)}, \quad (1)$$

where $\Delta W_Q^{(1)}$ is the first-order contribution of the quadrupole effect. The vibration-rotation interaction constants were calculated by $\alpha_v^B=B_0-B_v$. The molecular constants determined are listed in Table 2. The ν_4 spectra were not resolved from those of the ground state in the $J=1\leftarrow0$ transition, but a hyperfine component $F=11/2\leftarrow9/2$ of the $J=5\leftarrow4$, $K=3$ transition was observed at 58773.09 MHz, which was higher than the ground state line by 1.65 MHz, and thus the α_4^B constant was calculated to be -0.16_5 MHz. This is in good agreement with the value of Kisliuk and Geschwind.[1] On the other hand, the α_2^B constant is much improved in accuracy compared with that reported in Ref. 1. Using all the four α^B constants thus obtained the equilibrium rotational constant, B_e, was calculated to be 5893.20 ± 0.30 MHz.

Because both arsenic and fluorine nuclei have only one stable isotope, no isotopic species of arsenic trifluoride are available. It is known that the effect of the intramolecular vibrations on the bond angle is relatively small, and therefore, taking the zero-point average bond angle θ_z(FAsF), 95°58′, obtained by Konaka[4] as the equilibrium value, the equilibrium length was calculated to be r_e(As—F)$=1.704_4$ Å. If the error in the angle is assumed to be ±1°, that of the bond length is ±0.0013 Å, where the double signs should be taken in the same order.

The l-type doubling transitions in the ν_4 vibrational state were observed for $J=2\leftarrow1$ through $J=5\leftarrow4$. A general expression for the frequencies of the lower and upper doublet components is given for the $J+1\leftarrow J$ transition by [6-8]

$$\begin{aligned}\nu^{\pm} &= 2B_4(J+1)\pm q_4(J+1)+(eqQ)_{v_4=1}\\ &\times[\{3/[(J+1)(J+2)]-1\mp(1/2)\eta\}f(I,J+1,F_f)\\ &-\{3/[J(J+1)]-1\mp(1/2)\eta\}f(I,J,F_i)] \quad (2)\end{aligned}$$

where B_4 and q_4 denote the rotational constant and l-type doubling constant, respectively, in the $v_4=1$ state, η (referred to as the asymmetry parameter) the asymmetry in the electric field gradient induced at the arsenic nucleus by the ν_4 mode, and $f(I,J,F)$ Casimir's function. The frequencies of the $K=\pm1$, $l_4=\mp1$ component are given by

$$\begin{aligned}\nu_0 &= 2B_4(J+1)+(eqQ)_{v_4=1}[\{3/[(J+1)(J+2)]-1\}\\ &\times f(I,J+1,F_f)-\{3/[J(J+1)]-1\}f(I,J,F_i)] \quad (3)\end{aligned}$$

By using Eqs. (2) and (3) the following equation is derived.

$$\begin{aligned}\Delta\nu^{\pm} &= \nu^{\pm}-\nu_0\\ &= \pm q_4(J+1)\mp(1/2)\eta(eqQ)_{v_4=1}\\ &\times[f(I,J+1,F_f)-f(I,J,F_i)] \quad (4)\end{aligned}$$

The lines of the ground vibrational state and the $K=\pm1$, $l_4=\mp1$ components of the ν_4 vibrational state are overlapped with each other, except for a hyperfine component of the $J=5\leftarrow4$ transition mentioned above. The effect of the l-type resonance[9] has not been ob-

Table 3. Observed frequencies of the l-type doubling transitions in the ν_4 state (MHz)

$J+1\leftarrow J$	$F'\leftarrow F''$	ν^-_{obsd}[a]	ν^-_{calcd}[b]	$\Delta\nu^-$
$2\leftarrow1$	$7/2\leftarrow5/2$	23510.52	23510.61	−20.56
	$5/2\leftarrow5/2$	23481.21	23481.00	−20.41
	$5/2\leftarrow3/2$	23451.60	23451.69	−20.56
	$3/2\leftarrow3/2$	23472.77	23472.84	−20.43
	$3/2\leftarrow1/2$	23525.53	23525.60	−20.70
	$1/2\leftarrow1/2$	23555.0	23555.22	−20.70
$3\leftarrow2$	$9/2\leftarrow7/2$	35250.40	35250.34	−30.65
	$7/2\leftarrow5/2$	35235.36	35235.61	−30.96
	$5/2\leftarrow3/2$	35235.36	35235.15	−30.54
	$3/2\leftarrow1/2$	35250.40	23250.88	−30.23
$4\leftarrow3$	$11/2\leftarrow9/2$	—	46994.72	—
	$9/2\leftarrow7/2$	46988.25	46988.83	−41.54
	$7/2\leftarrow5/2$	46985.44	46985.75	−41.29
	$5/2\leftarrow3/2$	46991.10	46991.64	−41.52
$5\leftarrow4$	$13/2\leftarrow11/2$	58740.35	58739.78	−50.82
	$11/2\leftarrow9/2$	58737.01	58737.03	−51.22
	$9/2\leftarrow7/2$	58734.55	58734.41	−50.10
	$7/2\leftarrow5/2$	58737.01	58737.36	−51.56

a) Accuracy is ±0.1 MHz. b) Calculated by using the parameters in Table 4.

6) A. Javan, *Phys. Rev.*, **99**, 1302 (1955).
7) R. L. White, *J. Chem. Phys.*, **23**, 249 (1955).
8) J. F. Lotspeich, A. Javan, and A. Engelbrecht, *ibid.*, **31**, 633 (1959).
9) E. Hirota and Y. Morino, *J. Mol. Spectrosc.*, **33**, 460 (1970); E. Hirota, *ibid.*, **37**, 20 (1971); **38**, 195 (1971).

served definitely. In calculating $\Delta\nu^-$ the center frequencies ν_0 of the ν_4 state were estimated by fixing B_4 to 5879.24 MHz, which was obtained from the α_4^B constant and the ground-state B value of 5879.08 MHz, the latter being determined using the $J=2\leftarrow1$ to $5\leftarrow4$ transitions. The observed frequencies of the l-type doubling transitions and $\Delta\nu^-$ are listed in Table 3. The upper components ν^+ are overlapped by the ν_2 satellites and are not resolved clearly because of the broad line width. The frequencies of the l-type doubling transitions were fitted to Eqs. (2) and (4) by a least-squares method, where the centrifugal distortion in the ν_4 state was assumed to be the same as in the ground vibrational state. The constants thus obtained are shown in Table 4. The l-type doubling constant is 10.24±0.02 MHz. The value of the As nuclear quadrupole coupling constant in the ν_4 state was also listed in Table 4. The difference in the hyperfine structure pattern of the ground state and the ν_4 state is hardly noticeable, and electric field gradient at the arsenic nucleus remains almost unaffected by the excitation of the ν_4 vibration. The asymmetry parameter is zero within experimental error.

TABLE 4. MOLECULAR CONSTANTS OBTAINED FROM THE TRANSITIONS OF $J=2\leftarrow1$ TO $J=5\leftarrow4$ (in MHz except for η)[a]

	Present	Reference
Ground State		
B_0	5879.08±0.01	5878.97±0.002[b]
eqQ	-236.1_6 ±0.26	−236.23±0.005[b]
D_J	0.0069_9 ±0.00033	0.00462±0.00002[c]
D_{JK}	-0.0084_6 ±0.00094	−0.00618±0.00005[c]
$\nu_4=1$		
B_4	5879.24[d]	
eqQ	$-235._7$ ±1.7[e]	
q_4	10.24±0.02	
η	-0.00_5±0.01	

a) Errors are standard deviations. b) Ref. 1. c) Ref. 3.
d) Fixed. e) Obtained fixing B_4 to 5879.24 MHz.

The calculation in the present work was carried out at the Computation Center at Kyushu University.

BULLETIN OF THE CHEMICAL SOCIETY OF JAPAN, VOL. 46, 2316—2320 (1973)

Transmission of Substituent Effects through the Oxygen and Sulfur Atoms. IV. CNDO/2 Charge Distributions in Vinyl and Divinyl Ethers and Sulfides

Okitsugu KAJIMOTO, Masaru KOBAYASHI, and Takayuki FUENO

Department of Chemistry, Faculty of Engineering Science, Osaka University, Toyonaka, Osaka 560

(Received April 13, 1973)

Charge distributions in vinyl methyl and divinyl ethers and their sulfur homologs bearing a polar substituent at the *trans*-β position were calculated by the CNDO/2 method. It was found that the effect of substituents on charge distribution is transmitted primarily through the successive π-polarization of the ethylenic units involved. In the divinyl compounds, the sulfur atom on the spd basis is calculated to transmit the substituent effects more effectively than the oxygen atom. The greater transmission efficiency of the sulfur atom is interpreted in terms of the pπ-dπ-pπ conjugation.

The reaction constant ρ of the Hammett equation is a useful experimental probe into the mode and efficiency of the transmission of the electronic effects of substituents in aromatic side-chain reactions.[1,2] A systematic examination of the ρ-values often permits quantitative comparison of the transmission efficiencies of the atoms or groups which intervene between reaction center and substituents.[3]

In the preceding papers of this series,[4-6] we compared the roles of the oxygen (Y=O) and sulfur (Y=S) atoms in transmitting the effects of ring-substituents (X) to the properties of the side-chain groups (CH_2Z and CH=CHZ) in two types of compounds I and II:

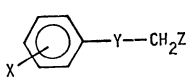

I (Y = O or S)

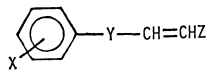

II (Y = O or S)

The properties investigated were the ^1H chemical shifts of the terminal hydrogen (Z=H),[4] the ^{13}C shifts of the aliphatic carbons (CH_2Z and CH=CHZ with Z=H),[5] and the ionization equilibrium constants of the carboxylic acids (Z=COOH).[6] It was found that, while in compounds I the sulfur atom is apparently a less efficient transmitter of the substituent effects than the oxygen atom, it becomes a more efficient transmitter in compounds II in which it is interposed between two unsaturated groups. The enhancement of the transmission efficiency of the sulfur atom was interpreted in terms of the pπ–dπ–pπ interaction, i.e., the "through-conjugative" contribution[7]

1) L. P. Hammett, "Physical Organic Chemistry," 2nd Ed. McGraw-Hill Book Company, New York, N. Y. (1970).
2) H. H. Jaffé, *J. Chem. Phys.*, **21**, 415 (1953).
3) S. H. Marcus, W. F. Reynolds, and S. I. Miller, *J. Org. Chem.*, **31**, 1872 (1966).
4) T. Fueno, O. Kajimoto, K. Izawa, and M. Masago, This Bulletin, **46**, 1418 (1973).
5) O. Kajimoto, M. Kobayashi, and T. Fueno, *ibid.*, **46**, 1422 (1973).
6) O. Kajimoto, M. Kobayashi, and T. Fueno, *ibid.*, **46**, 1425 (1973).
7) C. C. Price and S. Oae, "Sulfur Bonding," Ronald Press, New York, N. Y. (1962).

of the sulfur 3d-orbitals to the π-conjugation as can be represented by III.

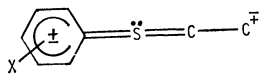

III

The purpose of the present paper is to rationalize the qualitative view stated above. Thus, we have undertaken to calculate the CNDO/2 charge distributions in various β-substituted derivatives of methyl vinyl (IV) and divinyl (V) ethers and their corresponding sulfur homologs, which may be regarded as the model compounds of I and II, respectively.

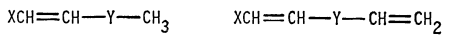

IV (Y = O or S) V (Y = O or S)

The results of calculation based on the spd basis set for the sulfur atom were found to be compatible with the substituent effects observed.

Method

Pople's CNDO/2 method[8] was used without modification. The sulfur atom was treated on both the sp and spd bases; the integral parameters were those determined by Santry and Segal.[9]

The molecular geometries and atomic numberings of IV and V are shown in Fig. 1. IV was assumed to be in the *s-cis* conformation[10] with the methyl C–H bonds directed as shown in Fig. 1, while V was assumed to have the *s-trans,s-trans* conformation which should apparently be the most stable planar form. In both IV and V, the β-substituent X was placed at a position *trans* to the atom Y. The substituents chosen for this study were the CH_3O, CH_3, H, F, and Cl atoms or groups. For the Cl atom, the 3d-orbitals were included throughout. All the necessary bond lengths were taken from the literature.[8]

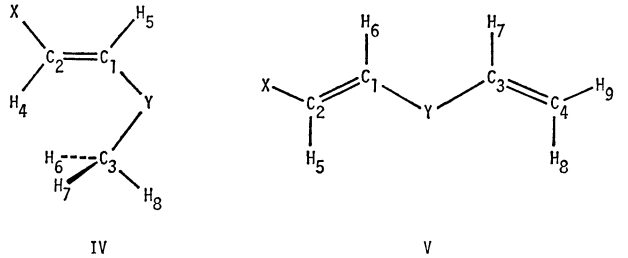

IV V

Fig. 1. Molecular geometries and atomic numberings of IV and V. The carbon atoms were assumed to have either sp^2 or sp^3 valence angles, and the CYC bond angles were assumed to be 110 and 105° for Y=O and Y=S, respectively.

Calculations were carried out on a NEAC 2200 computer at the Osaka University Computation Center. The outputs were required to be self-consistent to within 10^{-4} for all the atomic-orbital densities.

Results

The charge distributions calculated for the various derivatives of IV and V are summarized in Tables 1 and 2, respectively. The entries there are the net charge densities, both total and π, defined by

$$Q_r = n_r - q_r \quad (1)$$

where q_r is the pertinent electron density on atom r and where n_r is the number of its relevant valence electrons. The spd basis set was used for the sulfur atom, but, for the sake of comparison, calculations based on the sp basis were also carried out for divinyl sulfides. The results of the latter calculations are given in parentheses (Table 2).

Discussion

A. Charge distribution in Unsubstituted Compounds. Previous studies[3–5] on the ^1H and ^{13}C chemical shifts in ethers and sulfides have shown that an oxygen atom apparently behaves as a π-donor-σ-acceptor while a sulfur atom tends to act as a π,σ-acceptor. The view can readily be tested by analyzing the π and σ-charge densities on the oxygen and sulfur atoms. In Fig. 2, the amount of electronic charge transferred to or from these atoms in divinyl ether and sulfide are illustrated.[11] It can be seen that the oxygen atom strongly with-

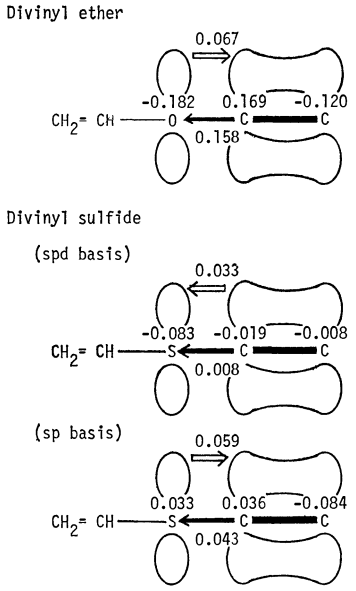

Fig. 2. Migration of the σ and π electronic charges from or to the oxygen or sulfur atom in divinyl ether and sulfide.

8) J. A. Pople and D. L. Beveridge, "Approximate Molecular Orbital Theory," McGraw-Hill Book Company, Inc., New York (1970).

9) D. P. Santry and G. A. Segal, *J. Chem. Phys.*, **47**, 158 (1967).

10) N. L. Owen and N. Sheppard, *Trans. Faraday Soc.*, **60**, 634 (1964).

11) The amount of electronic charge transferred *from* the pπ-orbital of the oxygen or sulfur atom *to* one of the ethylenic π-bonds can be obtained by dividing the π charge density Q_Y^π (Table 2) by 2. Likewise, one half the σ charge density on Y ($Q_Y^\sigma = Q_Y - Q_Y^\pi$) may be defined as the amount of the σ charge migration *from* Y *to* one of the olefinic groups.

TABLE 1. TOTAL AND π CHARGE DENSITIES ($\times 10^4$) IN SUBSTITUTED VINYL METHYL ETHERS AND SULFIDES (IV)

Position	Y=O					Y=S				
	CH_3O	CH_3	H	F	Cl	CH_3O	CH_3	H	F	Cl
					Total charge density					
C_1	721	1398	1637	940	1816	−1124	−416	−202	−982	−100
C_2	721	−10	−1305	1129	−512	1881	411	−67	2304	627
C_3	1388	1422	1429	1367	1394	−657	−629	−626	−676	−645
H_4	135	192	263	160	448	111	145	222	125	395
H_5	135	17	6	249	189	511	370	399	655	576
$H_{6,7}$	−116	−102	−81	−78	−38	270	283	313	316	354
H_8	−72	−86	−80	−9	5	370	365	382	429	444
Y	−1941	−2001	−1973	−1838	−1867	−926	−982	−853	−656	−645
					π-Charge density					
$C_1\pi$	−629	88	457	−210	781	−936	−229	172	−488	413
$C_2\pi$	−629	−869	−1189	−875	−1205	690	178	152	431	30
$Y\pi$	874	962	970	912	1061	−976	−805	−731	−882	−651

TABLE 2. TOTAL AND π CHARGE DENSITIES ($\times 10^4$) IN SUBSTITUTED DIVINYL ETHERS AND SULFIDES (V)

Position	Y=O					Y=S[a]				
	CH_3O	CH_3	H	F	Cl	CH_3O	CH_3	H	F	Cl
					Total charge density					
C_1	754	1439	1689	972	1860	−1111	−402	−189	−971	−82
						(−553)	(135)	(359)	(−370)	(506)
C_2	837	−649	−1204	1245	−425	1880	410	−77	2302	−616
						(1143)	(−334)	(−838)	(1547)	(−68)
C_3	1713	1698	1689	1699	1669	−166	−176	−189	−169	−189
						(383)	(370)	(359)	(368)	(339)
C_4	−1238	−1226	−1204	−1180	−1134	−120	−107	−77	−59	−13
						(−868)	(−853)	(−838)	(−820)	(−773)
H_5	161	231	313	192	490	85	130	213	103	388
						(17)	(68)	(139)	(37)	(321)
H_6	−9	−130	−138	107	32	444	295	322	581	491
						(199)	(66)	(68)	(317)	(247)
H_7	−156	−149	−138	−109	−97	294	303	322	350	363
						(53)	(59)	(68)	(93)	(108)
H_8	301	303	313	325	343	200	201	213	226	243
						(131)	(132)	(139)	(150)	(166)
H_9	238	239	250	276	295	129	130	148	175	194
						(100)	(101)	(111)	(135)	(155)
Y	−1817	−1856	−1818	−1736	−1741	−945	−969	−834	−720	−676
						(276)	(254)	(325)	(434)	(503)
					π-Charge density					
$C_1\pi$	−720	−12	370	−287	693	−928	−220	176	−481	425
						(−860)	(−127)	(248)	(−420)	(560)
$C_2\pi$	−491	−719	−1040	−747	−1061	690	451	156	428	33
						(−308)	(−545)	(−842)	(−566)	(−904)
$C_3\pi$	406	394	370	337	284	217	207	176	152	109
						(273)	(265)	(248)	(218)	(170)
$C_4\pi$	−1089	−1073	−1040	−994	−925	85	109	156	187	262
						(−887)	(−866)	(−842)	(−807)	(−732)
$Y\pi$	1253	1336	1339	1274	1410	−892	−729	−664	−820	−604
						(1111)	(1192)	(1188)	(1138)	(1284)

a) The data given in parentheses are those obtained by using the sp basis set for the sulfur atom.

draws σ-electron from the neighboring carbon atoms but donates π-electron to the ethylenic π-bond. On the other hand, the sulfur atom (spd) accepts a small fraction of electron from both the σ and π orbitals of ethylene. The π-electron-accepting property of the sulfur atom is ascribable to the participation of its 3d-orbitals in π-conjugation; the sulfur atom on the sp basis is predicted to be π-electron-donating, as can be seen in Fig. 2.

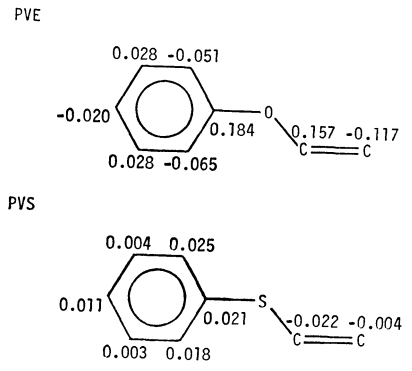

Fig. 3. The charge density distributions in phenyl vinyl ether (PVE) and sulfide (PVS).

Figure 3 shows the calculated total charge densities on the skeletal carbon atoms in phenyl vinyl ether (PVE) and sulfide (PVS). The charges in the vinyl moiety of these compounds are much the same as those in divinyl compounds. This endorses the validity of using the divinyl compounds as the model for PVE and PVS. In both types of compounds, the α-carbon atom of the sulfides are calculated to have a greater electron density than the β-carbon, in contrast to the greater electron density on the β-carbon in the unsaturated ethers.

The charge distributions shown in Fig. 3 are also to be compared with the ^{13}C chemical shift data presented previously.[5] In Fig. 4 the total electron densities q_τ of the various carbon atoms in PVE and PVS are plotted against the ^{13}C chemical shifts. For the purpose of comparison, the data of benzene[12] has also been plotted. The points for the PVS derivatives gather in the vicinity of the plot for benzene, while those for PVE's are spread in a relatively wide range of q_τ. The latter points are roughly fitted by a straight line with the slope of 175 ppm/electron, which is in fair agreement with the value 155 ppm/electron reported by Tokuhiro and Fraenkel[13] for azines.

B. Substituent Effects in Divinyl Ethers. The electronic effects of *trans*-β substituents on the charge distribution in divinyl ethers are expected to resemble those of *para* substituents in phenyl vinyl ethers. In Fig. 5, the π, σ, and total electron densities (q^π, q^σ, and q, respectively) on the α- and β-carbons of the various divinyl ether derivatives are plotted against the Hammett constants for *para* substituents, σ_p. Although the substituents studied are limited in number, it appears that all the calculated densities are linearly correlated with σ_p.

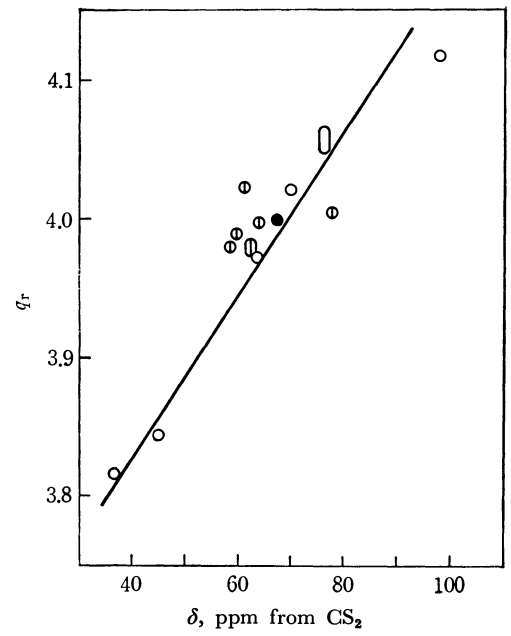

Fig. 4. Parallelism between the ^{13}C chemical shifts and the calculated total electron densities on carbon atoms of phenyl vinyl ether (PVE) and sulfide (PVS). ○, PVE; ⊖, PVS; ●, Benzene.

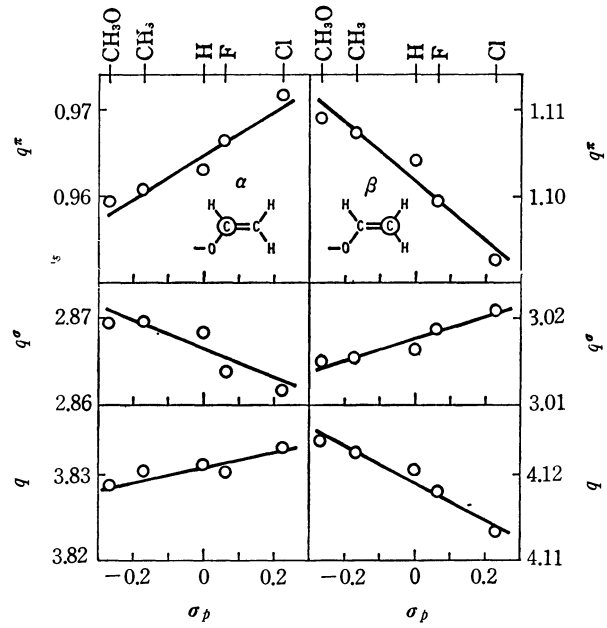

Fig. 5. The π, σ and total electron densities on the α- and β-carbons of substituted divinyl ethers.

The linear relationship shown in Fig. 5 are worthy of note in two important respects. First, the effects of substituents on the total electron density at the α- and β-carbons (q_α and q_β) are opposite in direction to each other; the electron-donating substituents tend to diminish q_α whereas they clearly enhance q_β. The results are in line with our previous observation that the ^{13}C chemical shifts, δ, of the α-carbon of PVE shows a Hammett-type dependence on ring substituents with a positive slope of $\rho_\alpha = 3.10\ \delta/\sigma$, in contrast to a "nor-

12) R. T. C. Brownlee and R. W. Taft, *J. Amer. Chem. Soc.*, **90**, 6537 (1968).

13) T. Tokuhiro and G. Fraenkel, *ibid.*, **91**, 5005 (1969).

mal" negative slope of $\rho_\beta = -4.84\ \delta/\sigma$ for the β-carbon.[5] A similar phenomenon, which was referred to as the "inverse" substituent effects, was observed for the γ- and δ-carbon atoms in *trans*-1-substituted-1,3-butadienes and rationalized in terms of the CNDO/2 total charge density.[14]

The second point which should be noted is that the substituent effects on the total electron density, q, is governed primarily by those on the π-electron density, q^π. The plots of the σ-electron density, q^σ, give slopes opposite in sign to those of q^π, and their dependence on substituents is relatively small. This would mean that, at least in the side-chain sp^2 carbons, any increase in q^π effected by substituents should be accompanied by a compensating decrease in q^σ which should, however, be overshadowed by the increase in q^π. In effect, therefore, the π-framework is considered to constitute a main route for the transmission of substituent effects in the case of unsaturated compounds. The electronic effect of substituents should thus be transmitted along the bonds through successive π-polarization of the ethylenic unit.[15] This in turn accounts for the inverse substituent effects as has been discussed in the last paragraph.

C. Transmission Efficiencies of the Oxygen and Sulfur Atoms. We now compare the efficiencies of the oxygen and sulfur atoms in transmitting the substituent effects. For this purpose, we will plot the total electron densities, $q_r(S)$, calculated for given positions (r) of the various derivatives of vinyl or divinyl sulfide against those obtained for the corresponding ethereal derivatives, $q_r(O)$. If such "O–S plots" are linear over the substituents studies, their slopes, *viz.*,

$$R_r = dq_r(S)/dq_r(O) \qquad (2)$$

may be regarded as a theoretical measure of the transmission efficiency of the sulfur atom relative to the oxygen atom.

Figure 6 shows the O–S plots for the terminal hydrogens H_8 and H_9 in vinyl methyl (IV) and divinyl compounds (V), respectively. The slope for the former hydrogen is $R_8=0.825$, indicating that the sulfur atom is a less efficient transmitter of substituent effects onto this particular hydrogen atom. By contrast, the *trans*-β hydrogen (H_9 of V in the spd approximation) has a slope of $R_9=1.139$, indicative of a greater transmission efficiency of the sulfur atom. It should be noted that the sulfur atom is calculated to be a less efficient transmitter ($R_9=0.956$) when its 3d-orbitals are left out of consideration (dashed line).

The O–S plots for the β-carbon atom in divinyl compounds are shown in Fig. 7. The slope is found to be $R_\beta=1.020$ when the spd basis set was used for the sulfur atom, while it is $R_\beta=0.885$ in the case of the sp approximation. Thus, the sulfur atom cannot be a more efficient transmitter of substituent effects than the oxygen atom, unless the 3d-orbitals of sulfur partake in the construction of the molecular orbitals.

In previous papers,[4-6] we demonstrated experimentally that the sulfur atom can transmit the substituent effects more efficiently than the oxygen atom, when it is interposed between two unsaturated groups. It was then inferred that the 3d-orbitals of the sulfur atom should play an essential and decisive role in this enhancement in the transmission efficiency. The theoretical results given in Figs. 6 and 7 are well in line with these experimental deductions. This reinforces our concept that the through-conjugative participation (III) of the sulfur 3d-orbitals in π-conjugation, *i.e.*, the $p\pi$–$d\pi$–$p\pi$ conjugation, is of distinct importance to the transmission of substituent effects in the compounds in which the sulfur atom is interposed between two unsaturated groups.[4,5]

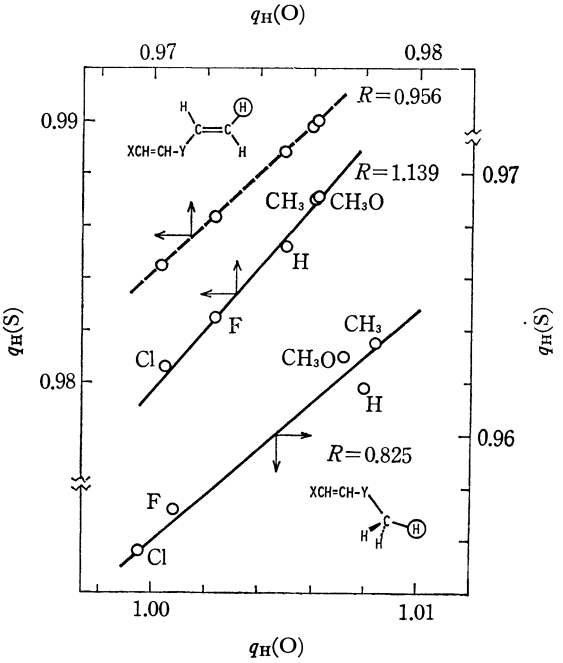

Fig. 6. "O-S plots" of the electron densities for the terminal hydrogens. R denotes the slope of each line. ——, spd basis; ----, sp basis.

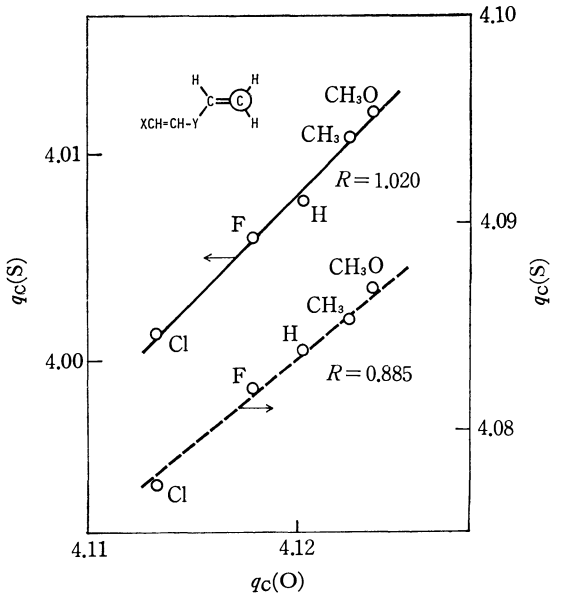

Fig. 7. "O-S plots" of the electron densities for the β-carbon atom. R denotes the slope. ——, spd basis; ----, sp basis.

14) O. Kajimoto and T. Fueno, *Tetrahedron Lett.*, **1972**, 3329.

15) The successive polarization of π-bondings is a well-known characteristics of conjugated molecules in general. The intervention of an oxygen atom does not affect this mode of transmission of the substituent effects.

Nuclear Quadrupole Effects in the Microwave Spectrum and Dipole Moment of Aniline*

Aritada HATTA,** Masao SUZUKI, and Kunio KOZIMA***

Laboratory of Molecular Spectroscopy, Tokyo Institute of Technology, Ookayama, Meguro-ku, Tokyo 152

(Received December 25, 1972)

The quadrupole hyperfine structure was resolved and analyzed for the vibrationally-ground state of the NH_2 species. The quadrupole coupling constants are: $\chi_{aa}=2.34$, $\chi_{bb}=1.86$, and $\chi_{cc}=-4.20$ MHz. The rotational constants obtained from the quadrupole corrected frequencies are as follows: $A=5617.67$, $B=2593.88$, and $C=1777.04$ MHz. The rotational constants of the ND_2 species in the vibrationally-ground state were also determined. By the use of the moments of inertia of both species, the non-planarity of this molecule was ascertained. The dipole moments of the NH_2 and the ND_2 species were determined to be 1.15 ± 0.02 D and 1.13 ± 0.01 D respectively.

In 1966 Lister and Tyler[1] reported their preliminary findings on the microwave spectra of aniline and its amino-monodeuterated species, and pointed out the non-planarity of the molecules. The detailed results have since been presented by Lister alone.[2] However, they did not observe the spectra due to the nuclear quadrupole coupling of nitrogen or those for the electric dipole moment.

In order to determine the value of the dipole moment, it seemed necessary to ascertain the effect of the ^{14}N quadrupole coupling on the spectra. For this purpose we have carried out this research.

Experimental

The microwave spectrometer used in this study was improved by adding a stabilized Klystron sweep system, since the longer time constants of 8~20 seconds were required to observe the hyperfine structure due to the ^{14}N quadrupole coupling. The measurements were made in the frequency range from 7.8- to 25-GHz at room temperature by using a 6-m absorption cell.

The sample of aniline, obtained from a commercial source, was purified by vacuum distillation before use. The amino-deuterated aniline, $C_6H_5ND_2$, was prepared by mixing the NH_2 species with D_2O. For measuring the spectrum of the ND_2 species, the waveguide was flushed several times with D_2O.

Results and Discussion

Only the a-type transitions were observed. As is shown in Table 1, the quadrupole hyperfine structures for the NH_2 species could be observed for some of the low-J R-branch transitions and all the Q-branch transitions of the vibrationally-ground state. The bracketed transitions in the table could not be well resolved. By using the transitions marked with asterisks in the table, the nuclear quadrupole coupling parameters, χ_{aa}, χ_{bb}, and χ_{cc}, were determined by a least-squares fitting according to the method of Bragg and Golden.[3] The quadrupole corrected frequencies, $\nu_{obsd}^{correct}$, were calculated by using these parameters. As the rigid-rotor approximation holds for these frequencies, the rotational constants, A, B, and C, were calculated from these frequencies by means of a least-squares fitting. The differences, Δ, between $\nu_{obsd}^{correct}$ and the frequencies calculated from the rotational constants, ν_{calcd}^{rigid}, are given in the last column of the table. It was ascertained that, for the bracketed transitions in the table, the splittings are within 0.3 MHz. The values of the rotational constants and those of χ_{gg} (g=a, b, or c) are listed in Table 2, where the a axis is nearly along the C–N bond and where the c axis is nearly perpendicular to the plane of the C_6H_5N fragment. The rotational constants obtained agreed very well with those reported by Lister and Tyler,[1] although their values were calculated from the high-J R-branch transition frequencies.

For the ND_2 species the low-J R-branch transition frequencies of the a-type in the vibrationally-ground state were also observed and assigned as shown in Table 3. By using the rigid-rotor approximation, the rotational constants were calculated by a least-squares fitting from the frequencies of the same transitions as those which are unresolved for the NH_2 species. The results are shown in Table 2.

By using a procedure similar to that of Kraitchman, and by choosing a z axis perpendicular to the plane of the C_6H_5N fragment, the z coordinate of the H or the D atom of the amino group was calculated to be 0.35 Å from the moments of inertia of the two species. The valency angle of $\angle$H–N–H and the angle between the C–N bond extended and the $\angle$H–N–H bisector were estimated as 112.3° and 38° respectively, by assuming only the N–H bond length to be 1.00 Å.

By using transition frequencies which are hardly affected at all by the ^{14}N quadrupole coupling, the dipole moments were measured for both the NH_2 and the ND_2 species. For the transitions used, the Stark energies are 10~20 times larger than the quadrupole coupling energies. Therefore, the Stark levels were calculated as in a strong-field case[4,5] and are those

* Presented in part at 23rd Annual Meeting of the Chemical Society of Japan, Tokyo, April, 1970.

** Present address: Department of Metal Processing, Faculty of Engineering, Tohoku University, Sendai.

*** To whom correspondence should be addressed. Present address: Faculty of Science and Engineering, Chuo University, Kasuga 1-chome, Bunkyo-ku, Tokyo 112.

1) D. G. Lister and J. K. Tyler, *Chem. Commun.*, **1966**, No. 6, 152.

2) D. G. Lister, Thesis, The University, Glasgow.

3) J. K. Bragg and S. Golden, *Phys. Rev.*, **75**, 735 (1949).

4) M. Mizushima, *J. Chem. Phys.*, **21**, 539 (1953).

5) W. Gordy and R. L. Cook, "Microwave Molecular Spectra," Interscience Publishers, New York (1970), Chapter 10.

TABLE 1. TRANSITION FREQUENCIES OF $C_6H_5NH_2$ IN THE VIBRATIONALLY-GROUND STATE (in MHz)

Transition $J' \leftarrow J$	Transition $F' \leftarrow F$	ν_{obsd} [a]	$\nu_{obsd} - \nu_{calcd}$	$\nu_{obsd}^{correct}$	Δ [b]
R-branch					
$2_{12} \leftarrow 1_{11}$	$3 \leftarrow 2$ } [c]	7924.80 [d]	0.02	7924.98	−0.01
	$1 \leftarrow 0$ }		−0.07		
	$2 \leftarrow 1$	7925.54 [d]	−0.03		
$2_{02} \leftarrow 1_{01}$	$3 \leftarrow 2$ }	8597.52	0.07	8597.6	0.1
	$2 \leftarrow 1$ }		−0.19		
	$1 \leftarrow 0$	8598.0	0.0		
	$2 \leftarrow 2$	8598.4	0.0		
$2_{11} \leftarrow 1_{10}$	$2 \leftarrow 2$	9558.	0.0	9558.66	−0.01
	$3 \leftarrow 2$	9558.57 [d]	−0.02		
	$2 \leftarrow 1$	9559.26 [d]	0.01		
	$1 \leftarrow 1$	9560.2	0.0		
$3_{13} \leftarrow 2_{12}$	$4 \leftarrow 3$ }	11804.06	0.12	—	
	$2 \leftarrow 1$ }		0.05		
	$3 \leftarrow 2$ }		−0.19		
$3_{03} \leftarrow 2_{02}$	$4 \leftarrow 3$ }	12563.08	0.09	—	
	$2 \leftarrow 1$ }		0.01		
	$3 \leftarrow 2$ }		−0.23		
$3_{22} \leftarrow 2_{21}$	$2 \leftarrow 1$	13112.2	0.0	13112.75	0.01
	$4 \leftarrow 3$	13112.57 [d]	−0.01		
	$3 \leftarrow 2$	13113.35 [d]	0.02		
$3_{21} \leftarrow 2_{20}$	$4 \leftarrow 3$	13662.30	0.00	13662.38	−0.01
	$3 \leftarrow 2$	13662.74	−0.02		
$3_{12} \leftarrow 2_{11}$	$2 \leftarrow 1$ }	14238.38	0.29	—	
	$4 \leftarrow 3$ }		0.08		
	$3 \leftarrow 2$ }		−0.17		
Q-branch					
$4_{13} \leftarrow 4_{14}$	$4 \leftarrow 4$	8055.43 [d]	0.04	8056.88	0.03
	$5 \leftarrow 5$	8057.40 [d]	0.02		
	$3 \leftarrow 3$	8057.87	−0.02		
$5_{14} \leftarrow 5_{15}$	$5 \leftarrow 5$	11821.12	−0.18	11822.52	−0.16
	$6 \leftarrow 6$	11823.08	−0.13		
$6_{15} \leftarrow 6_{16}$	$6 \leftarrow 6$	15945.65	−0.23	15946.90	−0.23
	$7 \leftarrow 7$ }	15947.50	−0.13		
	$5 \leftarrow 5$ }		−0.42		
$7_{25} \leftarrow 7_{26}$	$7 \leftarrow 7$	10637.68	0.00	10638.62	0.00
	$8 \leftarrow 8$ }	10639.07	0.06		
	$6 \leftarrow 6$ }		−0.13		
$8_{26} \leftarrow 8_{27}$	$8 \leftarrow 8$	14930.60	−0.12	14931.54	−0.12
	$9 \leftarrow 9$ }	14931.95	−0.11		
	$7 \leftarrow 7$ }		−0.28		
$9_{36} \leftarrow 9_{37}$	$9 \leftarrow 9$	8447.28	0.09	8447.94	0.09
	$10 \leftarrow 10$ }	8448.30	0.17		
	$8 \leftarrow 8$ }		0.06		
$10_{37} \leftarrow 10_{38}$	$10 \leftarrow 10$	12614.45	−0.15	12615.18	−0.14
	$11 \leftarrow 11$ }	12615.58	−0.06		
	$9 \leftarrow 9$ }		−0.16		

a) Maximum experimental uncertainties in frequency measurements are ±0.05 MHz for R-branches and ±0.1 MHz for Q-branches. b) $\Delta = \nu_{obsd}^{correct} - \nu_{calcd}^{rigid}$. c) Braces indicate unresolved lines. d) Quadrupole coupling constants were determined by using the differences of these transition frequencies.

Table 2. Rotational constants, principal moments of inertia, and quadrupole coupling constants of aniline in the vibrationally-ground state

$C_6H_5NH_2$	
$A=5617.67\pm0.15$ MHz	$I_a=89.962$ amu·Å^2
$B=2593.88\pm0.02$	$I_b=194.834$
$C=1777.04\pm0.02$	$I_c=284.391$
$\chi_{aa}=2.34\pm0.06$ MHz,	$\chi_{bb}=1.86\pm0.06$ MHz,
$\chi_{cc}=-4.20\pm0.06$ MHz	
$C_6H_5ND_2$	
$A=5521.15\pm1.90$ MHz	$I_a=91.534$ amu·Å^2
$B=2403.82\pm0.07$	$I_b=210.238$
$C=1679.01\pm0.07$	$I_c=300.996$

Conversion factor: 505375 amu·Å^2·MHz

Table 3. Transition frequencies of $C_6H_5ND_2$ in the vibrationally-ground state (in MHz)

Transition	ν_{obsd}[b]	$\nu_{obsd}-\nu_{calcd}$
$2_{02}\leftarrow 1_{01}$	8053.44	0.11
$2_{11}\leftarrow 1_{10}$	8890.34	−0.12
$3_{03}\leftarrow 2_{02}$[a]	11815.88	−0.11
$3_{13}\leftarrow 2_{12}$[a]	11095.90	0.12
$3_{12}\leftarrow 2_{11}$[a]	13259.20	0.05
$3_{22}\leftarrow 2_{21}$	12248.45	−0.03
$3_{21}\leftarrow 2_{20}$	12680.88	−0.10
$4_{04}\leftarrow 3_{03}$[a]	15339.89	−0.22
$4_{14}\leftarrow 3_{13}$[a]	14686.35	−0.02
$4_{13}\leftarrow 3_{12}$[a]	17520.57	0.14
$4_{23}\leftarrow 3_{22}$	16243.50	0.07
$4_{22}\leftarrow 3_{21}$[a]	17233.95	0.23
$4_{32}\leftarrow 3_{31}$	16526.87	0.23
$4_{31}\leftarrow 3_{30}$	16591.70	−0.09
$5_{05}\leftarrow 4_{04}$[a]	18693.14	0.12
$5_{14}\leftarrow 4_{13}$	21615.28	−0.03
$5_{24}\leftarrow 4_{23}$	20164.83	−0.22
$5_{23}\leftarrow 4_{22}$[a]	21878.79	−0.26
$5_{33}\leftarrow 4_{32}$	20698.94	0.41
$5_{32}\leftarrow 4_{31}$	20918.79	0.18
$5_{41}\leftarrow 4_{40}$	20670.53	0.21

a) Rotational constants were determined from these transition frequencies. b) Maximum experimental uncertainties in frequency measurements are ±0.2 MHz.

Table 4. Stark effect and dipole moments of aniline[a]

Transition	Shift MHz(kV/cm)$^{-2}$ Obsd	Calcd
$C_6H_5NH_2$		
$2_{02}\leftarrow 1_{01}$ $M_J=0$	−11.47±0.85	−11.75
$3_{12}\leftarrow 2_{11}$ $M_J=2$	−10.86±0.35	−10.54
$3_{13}\leftarrow 2_{12}$ $M_J=0$	−0.548±0.024	−0.503
$C_6H_5ND_2$		
$3_{12}\leftarrow 2_{11}$ $M_J=0$	−0.436±0.153	−0.523
$M_J=2$	−11.53±0.37	−11.52
$3_{03}\leftarrow 2_{02}$ $M_J=2$	3.67 ±0.39	3.68

Dipole moment $C_6H_5NH_2$	$C_6H_5ND_2$
$\mu_a^2=1.33\pm0.04$	$\mu_a^2=1.27\pm0.02$
$\mu=1.15\pm0.02$D	$\mu=1.13\pm0.01$D

a) Electric-field calibration was made with OCS for which $\mu=0.7152$ D.

determined for the asymmetric rotor without the quadrupole coupling effects. The value of the dipole moment of the NH_2 species agreed with that of the ND_2 species within the range of experimental uncertainty. As was expected, the component, μ_c, which is nearly perpendicular to the plane of the phenyl group, is zero for the NH_2 or the ND_2 species within the range of experimental uncertainty.

The value of the dipole moment of the NH_2 species is markedly different from that of 1.48 D obtained from the dielectric constant measurements at the temperature of 459 K in vapor.[6] It is certain that the value of this study is more accurate, for the difference between the values of the moment is probably due to the incorrect value of the sum of the atomic and the electric polarization as estimated from the molar refraction. The atomic polarization of this molecule may be anomalously large.

6) L. G. Groves and S. Sugden, *J. Chem. Soc.*, **1937**, 158.

The Photoconductivity of Poly(*N*-vinylcarbazole). III. Photoconductivity in a Sandwich-type Cell.[1)]

Kenichi Okamoto*, Shigekazu Kusabayashi* and Hiroshi Mikawa

Department of Applied Chemistry, Faculty of Engineering, Osaka University, Yamadakami, Suita, Osaka 565

(Received March 21, 1972)

Photoconductivity in a sandwich-type cell of a PVCz film was investigated in a high vacuum and in the air. A large photocurrent was observed in the π–π^* absorption region and a small photocurrent in the visible region. The former showed the following interesting points in its behavior. In low applied fields, no difference was found between the photoconductivity with positive-electrode illumination and that with negative-electrode illumination. In moderate or high fields, however, the photoconductivity with positive-electrode illumination was significantly different from that with negative-electrode illumination. The former showed a superlinear dependence on the applied field (consequently, $i_{ph}^{+} \gg i_{ph}^{-}$) and a spectral response coinciding with the absorption spectrum. This photoconductive behavior was explained by assuming the mechanism of carrier generation, namely, the field-assisted thermal dissociation of exciplexes and the detrapping of trapped carriers by singlet excitons. Carriers are supposed to migrate through the overlap of π-electrons of neighboring carbazyl rings in the same polymer chain.

Many investigations of the photoconductive properties of poly-*N*-vinylcarbazole (PVCz) have been reported in recent years.[2)] Most of them, however, have been carried out in the air. It is well known that ambient oxygen affects the photoconductive properties of molecular crystals.[3)] It is, therefore, necessary to investigate the photoconductive properties of PVCz in a high vacuum. In a previous paper the present authors reported on the photoconductivity in a surface-type cell, especially the effect of ambient oxygen on the photoconductivity and the effect of the pre-irradiation of UV light or γ-rays.[4)] In the present investigation the authors studied the photoconductivity in a sandwich-type cell of a fresh film of PVCz in a high vacuum (10^{-7} mmHg) as well as in the air.

Experimental

The method of preparing a sandwich-type cell of a PVCz film (area of electrode: 1 cm^2) and the method of electrical measurement were described in the previous paper.[5)] A 500W xenon lamp was used as the light source; it was monochromatized by a grating monochromator. The purity of the monochromatic light was 5–10 mμ in the half width; its intensity was changed by means of neutral filters. The light intensity was measured by means of a thermopile (Kipp and Zonen CA 1) or an actinometer by the use of potassium ferrioxalate. The following data were taken for a fresh cell which had stood for several hours in the dark under an applied DC voltage.

Results

Unless otherwise noted, the results were obtained in a high vacuum with freshly cast films 15 μ thick. Although an asymmetrical Metal-PVCz-Nesa sandwich-type cell was used for the following experiments, a symmetrical Au-PVCz-Au sandwich-type cell showed similar results.

Time Dependence of Photocurrent. The response curves of the photocurrent changed with both the applied voltage and the light wavelength. Representative response curves (Types A, B and C) are illustrated in Fig. 1. In low applied fields, the illumination with the weakly-absorbed light (λ>360 mμ) induced a photocurrent of the A type, while the illumination with the strongly-absorbed light (λ<360 mμ) induced that of the B type. In the latter case, the difference in magnitude between the peak and the steady-state photocurrents becomes smaller with an increase in the applied voltage. The photoresponse curve of the B type seems to be attributable to some effect of non-homogeneously-distributed space charges which are built up by the illumination with the strongly-absorbed light.

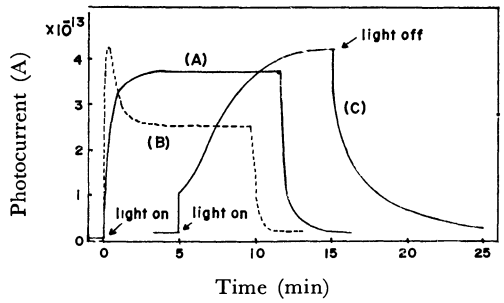

Fig. 1. Representative photoresponse curves in a PVCz sandwich-type cell (Types A, B and C).

In middle applied fields as large as 35000 V/cm, with negative-electrode illumination a photoresponse curve of the B type was observed only at 300—310 mμ. On the other hand, with positive-electrode illumination it was still observed at 270—340 mμ. In high applied fields as large as 150000 V/cm, every photoresponse curve, with one exception, belonged to the A type, and the response times of the rise and decay curves of the

* Present address; Department of Chemical Engineering, Faculty of Engineering, Yamaguchi University, Ube, Yamaguchi.

1) The experimental results in this paper were presented at the 18th annual meeting of the Society of Polymer Science, Japan Kyoto, May, 1969.

2) References (1)~(9) of part 1 of this series (see Ref. (4)).

3) S. Sakai, M. Yoshida, S. Tanaka, H. Mitsudo, and Y. Ooshika, *J. Phys. Chem. Solids*, **28**, 1913 (1967). I. Nakada a H. Kaiyoh, *J. Phys. Soc. Japan*, **17**, 93 (1962). A. Bree and L. E. Lyons, *J. Chem. Soc.*, **1960**, 5179.

4) K. Okamoto, S. Kusabayashi, and H. Mikawa, This Bulletin, **46**, 1948 (1973).

5) K. Okamoto, S. Kusabayashi, and H. Mikawa, *ibid.*, **46**, 1953 (1973).

photocurrent were too small to be measured by means of a vibrating-reed electrometer (below 1 sec). The illumination of 230—280 mμ or 350—370 mμ light on a positive electrode or of 350—360 mμ light on a negative electrode induced a photocurrent consisting of two components with different response times (C type), as is shown in Fig. 1. One has a very small response time (below 1 sec), and the other, a fairly large one (5—20 min). Similar behavior was observed in the decay part of this photocurrent. The subsequent re-illumination of the same light induced a photocurrent with the same behavior and also consisting of two components.

The results to be presented below were obtained for the steady-state values of the photocurrent, unless otherwise noted.

Voltage Dependence of Photocurrent. Figure 2 shows the voltage dependence of the photocurrent. In applied fields lower than 2000 V/cm the photocurrent was proportional to the applied voltage regardless of either the polarity of the illuminated electrode or the wavelength of the illuminating light, although some photocurrent (photovoltaic current) was observed without any applied voltage. In low fields the observed photocurrent apparently consists of both a photovoltaic current and a true photocurrent.

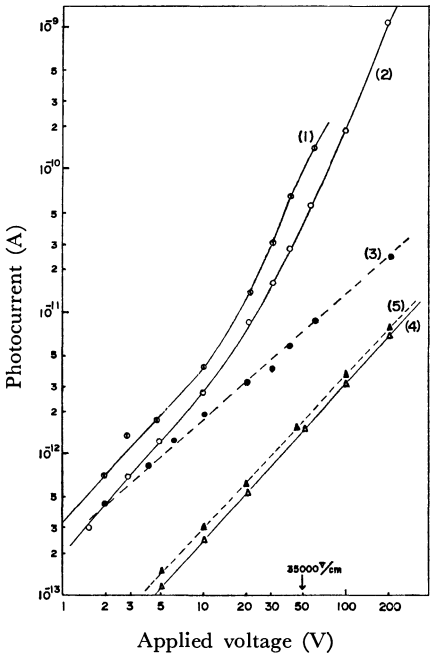

Fig. 2. Voltage dependence of photocurrent in an Ag-PVCz-Nesa sandwich-type cell. In high vacuum with nesa electrode illumination.
(1) peak value of i_{ph}^{+} at 330 mμ, (2) steady state value of i_{ph}^{+} at 330 mμ, (3) steady state value of i_{ph}^{-} at 330 mμ, (4) i_{ph}^{+} at 500 mμ, and (5) i_{ph}^{-} at 500 mμ.

In applied fields higher than about 7000 V/cm the voltage dependence of the photocurrent, however, varied with both the polarity of the illuminated electrode and the wavelength. In the case of negative-electrode illumination the photo-current (abbreviated to i_{ph}^{-}) was proportional to the applied voltage in every wavelength region over the whole range of voltage applied (0—150000 V/cm). On the other hand, in the case of positive electrode illumination the photocurrent (abbreviated to i_{ph}^{+}) changed with the n-th power of the applied voltage (n=1.4—2.0) in the UV region shorter than 360 mμ, although it was proportional to the applied voltage in the visible region longer than 360 mμ. It should be noted that the wavelength of 360 mμ corresponds to the absorption edge of a film 15 μ thick. The superlinearity of the photocurrent on the applied voltage was observed not only for the steady-state photocurrent, but also for the peak value of the photocurrent of the B type, as is shown by Curve (1) in Fig. 2. This voltage dependence of the photocurrent was not affected by the electrode materials, such as Au, Ag, Cu, Al, and nesa coating.

Light-intensity Dependence of Photocurrent. The photocurrent was always proportional to the light intensity (10^{12}—10^{14} photons/cm² s) regardless of the applied voltage, the wavelength (300—600 mμ), the polarity of the illuminated electrode, and the ambient oxygen, as is shown in Fig. 3. In a surface-type cell the photocurrent showed a linear dependence on the light intensity in a high vacuum and a sublinear dependence in the air. This lowering of the light-intensity dependence of the photocurrent was attributed to the introduction of some shallow hole trap levels by the air.[4] The effect of the hole trap levels due to oxygen molecules in the air may not be significant in a sandwich type cell.

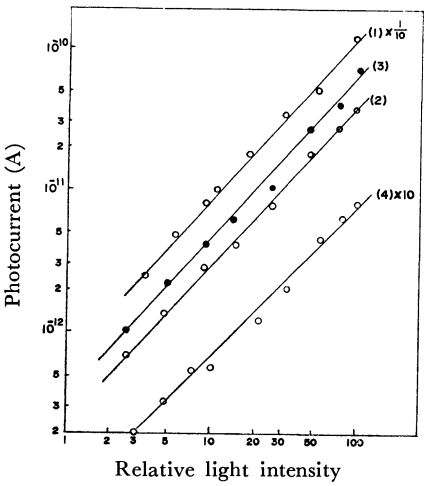

Fig. 3. Light intensity dependence of photocurrent in an Au-PVCz-Nesa sandwich-type cell. With positive Au electrode illumination.
(1) 350 mμ, 150000 V/cm in high vacuum; (2) 350 mμ, 35000 V/cm in high vacuum; (3) 350 mμ, 35000 V/cm in the air and (4) 450 mμ, 35000 V/cm in high vacuum.

Spectral Dependence of Photocurrent. The spectral dependence of the photocurrent shown in Figs. 4 and 8 was obtained by normalizing the observed photocurrent values to the values for the light intensity of 2×10^{13} photons/cm² s according to the light-intensity dependence. The spectral dependence of the photocurrent varied with the polarity of the illuminated electrode, the applied voltage, and the film thickness, but it was not affected by either air or the electrode materials. As is shown by the dotted line in Fig. 4,

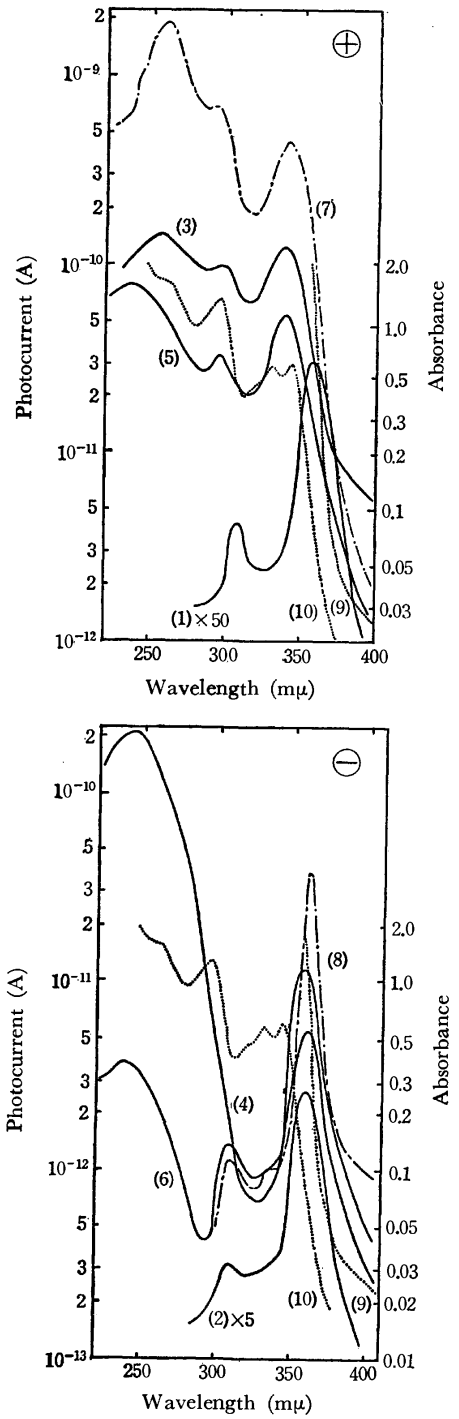

Fig. 4. Spectral dependence of photocurrent in an Au-PVCz-Nesa sandwich-type cell. Film thickness 15 μ. With positive Au electrode illumination; (1) 2 V (3) 50 V and (5) 50 V. With negative Au electrode illumination; (2) 2 V (4) 50 V and (6) 50 V. With positive nesa electrode illumination; (7) 200 V. With negative nesa electrode illumination; (8) 200 V. (1)~(4) and (7)~(8), in high vacuum. (5) and (6), in the air. (9) absorption spectrum of a PVCz film 15 μ thick. (10) absorption spectrum of a PVCz film about 1 μ thick.

the absorption spectrum of PVCz has its absorption maxima at 344.8, 331.8, 297, and 262.8 mμ and its absorption minima at 338, 312, and 282 mμ.

In low fields no difference was observed between i_{ph}^+ and i_{ph}^- either in magnitude or in the positions of the peaks and the minima. The photocurrent peaks were observed at 360, 310, and 250 mμ, and the photocurrent minima, at 330 and 290 mμ. This spectral dependence of the photocurrent corresponds inversely to the absorption spectrum except for the 250 mμ peak. This behavior is similar to that reported by Klöpffer *et al.*.[6] The 360-mμ photocurrent peak was observed at the absorption edge. The 330-mμ photocurrent minimum was observed in the region of the 344.8- and 331.8-mμ absorption peaks, which were unresolved in the photocurrent spectrum, probably because of both the fairly large half-width of the monochromatic light and the small difference in the extinction coefficients in this region.

In the middle applied fields as large as 35000 V/cm, a marked difference of photocurrent was observed both in magnitude and in the positions of the photocurrent peaks and minima, depending on whether the positive or the negative electrode was illuminated. With negative-electrode illumination the spectral dependence of the photocurrent was similar to the case of the low applied field; that is, it corresponded inversely to the absorption spectrum. With positive-electrode illumination, however, the photocurrent peaks shifted to a shorter wavelength and were observed at 340, 295—300 and 240—250 mμ, while the photocurrent minima were observed at 315 and 285 mμ. The spectral dependence of i_{ph}^+ thus corresponded just to the absorption spectrum. The magnitude of i_{ph}^+ in the UV region was 20—100 times larger than the corresponding value of i_{ph}^-. This is apparently attributable to the superlinear dependence of i_{ph}^+ on the applied voltage in the middle and high fields.

In the high fields as large as 150000 V/cm the spectral dependence of the photocurrent was the same as in the case of a middle applied field. The i_{ph}^+/i_{ph}^- ratio in the UV region was 70—500. This value of the ratio is 3—10 times larger than that in the middle applied fields. These results were obtained for a film 15 μ thick. As is shown in Fig. 8, in a thick film (0.5 mm thick) the 360 mμ photocurrent peak for the film 15 μ thick shifted to 370—380 mμ, which corresponds to the absorption edge of the thick film.

The above-mentioned spectral dependence of i_{ph}^+ is a new observation, one very different from those reported by others.[6]

In a high vacuum with a negative illuminated metal electrode a large photocurrent with no activation energy was observed in the region shorter than 300 mμ, as is shown by Curve (4) in Fig. 4. This is attributable to the photoemission current from the electrode metal into a high vacuum, independent of PVCz.

Temperature Dependence of Photocurrent. Figure 5 shows the temperature dependence of the photocurrent. Log i_{ph} *vs* $1/T$ plots gave straight lines over the whole temperature range (20—160 °C).

In a middle field, 35000 V/cm, the activation energy of the photocurrent (ΔE_{ph} in the equation: $i_{ph} \propto \exp(-\Delta E_{ph}/kT)$) was 0.07—0.15 eV in the visible

6) H. Bauser and W. Klöpffer, *Chem. Phys. Lett.*, **7**, 137 (1970); *Kolloid Z. Z. Polym.*, **241**, 1026 (1970). M. Hayashi, M. Kuroda, T. Imura, and A. Inami, *Kobunshikagaku*, **21**, 577 (1964).

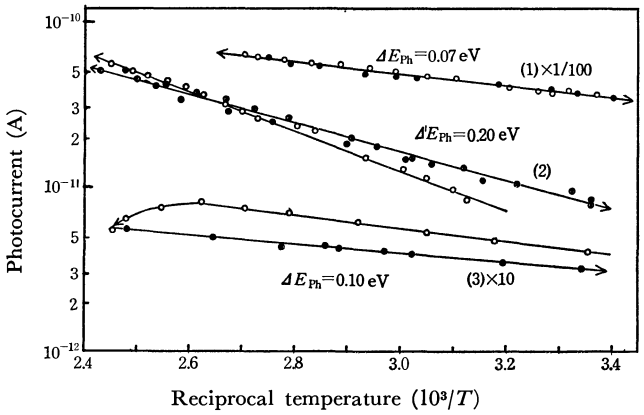

Fig. 5. Temperature dependence of photocurrent in an Au-PVCz-Nesa sandwich-type cell. With positive-electrode illumination in high vacuum.
(1) 350 mμ (Nesa), 150000 V/cm. (2) 360 mμ (Au), 35000 V/cm. (3) 450 mμ (Au), 35000 V/cm.
○; the first heating run. ●; the first cooling run. ⓘ; the second heating run.

region and 0.18—0.22 eV in the UV region. The latter is larger than the former by about 0.09 eV. In a high field, 150000 V/cm, ΔE_{ph} in the UV region was 0.07—0.10 eV, smaller by about 0.11 eV than the corresponding ΔE_{ph} value at 35000 V/cm.

There is no significant difference between the photoconductive properties mentioned above in a high vacuum and those in the air.

Photovoltaic Current. Even without applied voltage a fairly large photocurrent was observed in a short circuit, the spectral response of which is shown in Figs. 6(a) and (b). In the cell which had not been exposed to air after the evaporation of a metal electrode in a high vacuum, the photocurrent always flowed in the bulk from a metal electrode to a nesa electrode, regardless of whether the nesa or the metal electrode was illuminated. This photocurrent cannot be explained by the Dember effect, the difference in the carrier mobilities, but seems to be caused by a photovoltaic effect resulting from the contact interface between the electrode and the PVCz film. The authors called this photocurrent a "photovoltaic current."

The photovoltaic current is changed irreversibly by the introduction of air. In the air, with metal electrode illumination the photovoltaic current flowed in the bulk from a metal to a nesa electrode, as in the case of a high vacuum. With nesa electrode illumination, however, it flowed oppositely in the region shorter than 360 mμ, as is shown in Fig. 6(b). Furthermore, the photovoltaic current in the air was much smaller than that in high vacuum. When a cell exposed once to air after the evaporation of an electrode was put back into a high vacuum, the photovoltaic current was not restored to its original value.

It seems that the phenomena mentioned above can be interpreted by supposing that there is a large potential barrier at the interface between a metal electrode and a PVCz film, such as the well-known barrier in a metal—P type semiconductor system.[7] This potential barrier may determine the photovoltaic current in a high vacuum. The potential barrier is lowered by the

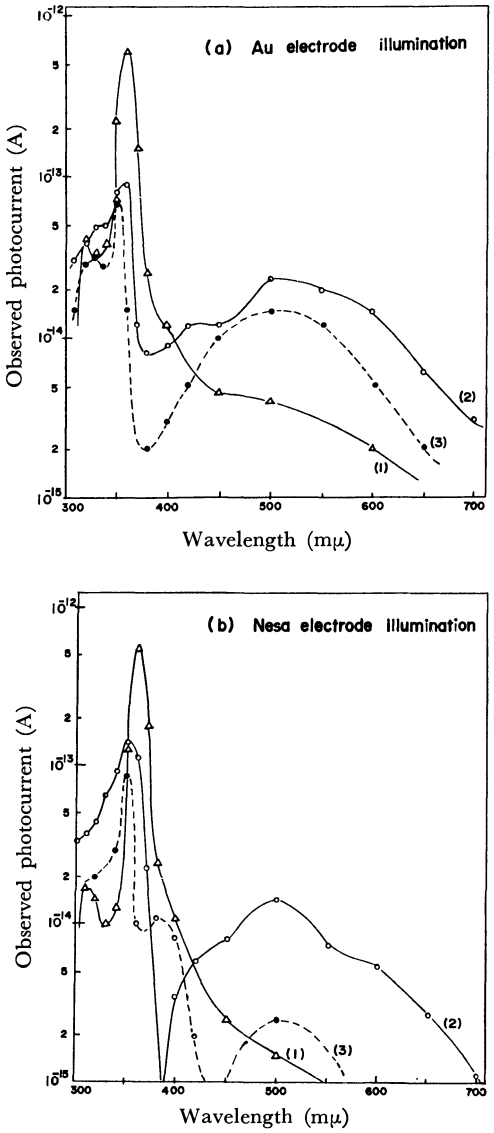

Fig. 6. Photovoltaic current in an Au-PVCz-Nesa sandwich-type cell.
(a) Au electrode illumination. The photovoltaic current always flows from Au to nesa in the bulk. (1) in high vacuum, for the cell which has not been exposed to air after the evaporation of an Au electrode. (2) in the air. (3) in high vacuum after exposing the cell to air.
(b) Nesa electrode illumination. (1) in high vacuum, the photovoltaic current flows from Au to nesa in the bulk. (2) in the air, from nesa to Au at λ<380 mμ and from Au to nesa at λ>400 mμ. (3) in high vacuum after exposing the cell to air, from nesa to Au at λ<420 mμ and from Au to nesa at λ>420 mμ.

air, as is observed in a metal—P type semiconductor system. If so, in the air the photovoltaic current seems to be determined mainly by the Dember effect.

Hole Injection into a PVCz Film from a Metal Electrode. The photoemission of holes from various metals (Au, Al and Cu) into a PVCz film has been observed by Lakatos *et al.*[8] Hole emission was observed also in an

7) L. E. Lyons, "Physics and Chemistry of the Organic Solid State," Vol. 1. ed. by D. Fox, M. M. Labes and A. Weissberger, Interscience Publishers, New York (1963), p. 788.
8) A. I. Lakatos and J. Mort, *Phys. Rev. Lett.*, **21**, 1444 (1968).

Au-PVCz-Nesa sandwich-type cell and was found to be significantly affected by the air. When a cell was not exposed to air after the evaporation of a gold electrode in a high vacuum, no photocurrent due to hole injection from the gold electrode was observed. The photocurrent in the visible and the near IR regions with the gold positive electrode showed values similar to those of the negative gold electrode as is shown in Fig. 7. If a cell was exposed to air after the evaporation of a gold electrode in a high vacuum, it showed a fairly large current due to hole emission both in the air and in a high vacuum; that is, the photocurrent in the visible and the near IR regions with the positive gold electrode increased significantly and was much larger than the photocurrent with the negative gold electrode, as shown in Fig. 7.

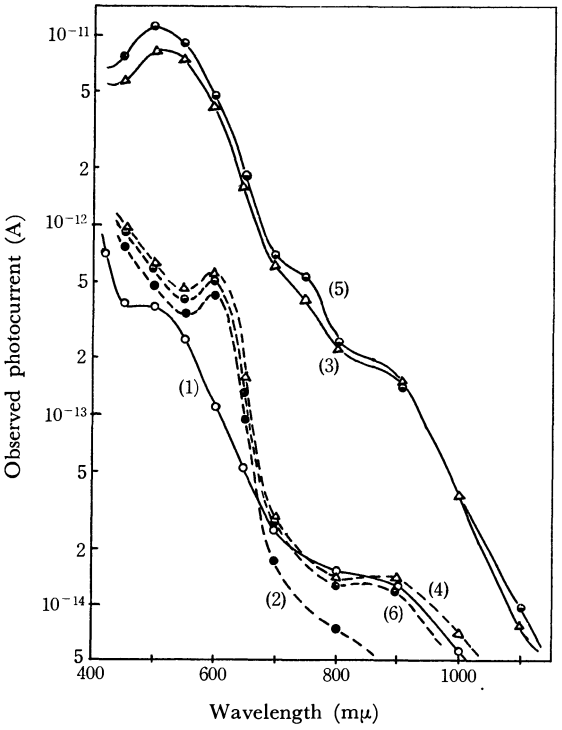

Fig. 7. Effect of air on photocurrent in the visible and the near IR regions in an Au-PVCz-Nesa sandwich-type cell.
With illuminated Au electrode biased positively (1, 3 and 5) or negatively (2, 4 and 6), under 35000 V/cm. (1) and (2); in high vacuum, for the cell which has not been exposed to air after the evaporation of an Au electrode. (3) and (4); in the air. (5) and (6); in high vacuum, for the cell having been exposed to air.

The above-mentioned effect of air on the hole emission current can probably be interpreted in terms of a decrease in the contact potential barrier, just as in the case of the photovoltaic current discussed above.

Effect of the Crystallinity on Photocurrent. Untreated PVCz has poor crystallinity, but the crystallinity was improved by appropriate heat-treatment.[9] The relation between the crystallinity and the photoconductivity was studied. The powder of the polymer was compressed to a disk (1 cm in diameter and 2—3 mm thick), which was then hot-pressed under various conditions to a film with varied crystallinity. Gold semitransparent electrodes were evaporated on both sides of the film. The photocurrent was measured for the Au-PVCz-Au sandwich-type cell thus obtained; it is shown in Fig. 8 and in Table 1. Judging from the crystalline peak at $2\theta=8°15'$[9,10] in the X-ray diffraction curves shown in Fig. 9, the I film is highly crystalline, while II is moderately and III, poorly so.

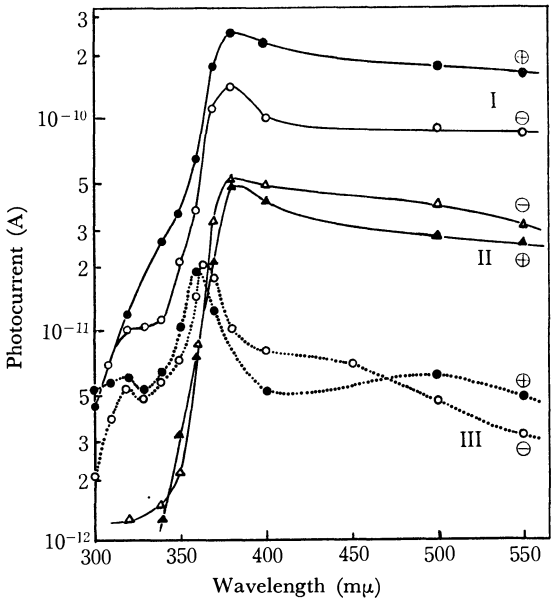

Fig. 8. Effect of the crystallinity of a PVCz film on photocurrent. In high vacuum, 8000 V/cm. ⊕; positive-electrode illumination, ⊖; negative-electrode illumination.
I, a film annealed under a hot-press (240° C, 150 kg/cm², 40 min), highly crystalline, 0.5 mm thick. II, a film annealed under a hot press (240 °C, 100 kg/cm², 15 min), moderately crystalline, 0.4 mm thick. III, a film cast from a benzene solution, poorly crystalline, 0.07 mm thick.

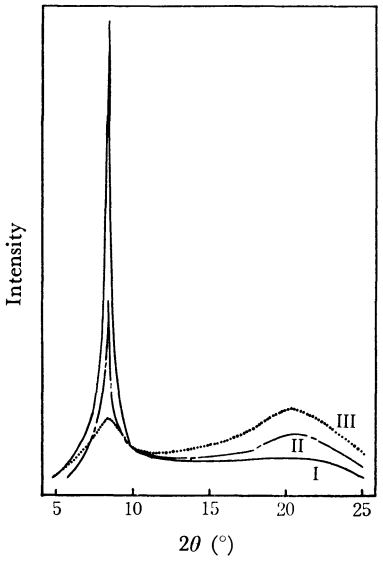

Fig. 9. X-ray diffraction patterns of PVCz films. I, II and III are the same films as described in Fig. 8 and Table 1.

9) A. Kimura, S. Yoshimoto, Y. Akana, H. Hirata, S. Kusabayashi, H. Mikawa, and N. Kasai, *J. Polym. Sci. A-2*, **8**, 643 (1970).

10) R. G. Crystal, *Macromolecules*, **4**, 379 (1971).

The magnitude of the photocurrent could not be compared directly in these three kinds of films because the spectral response curves changed slightly with the film thickness, as is shown in Fig. 8. As the red shift of the photocurrent peak in the longer wavelength π–π^* absorption region is mainly due to the change in the absorption edge of a film with the film thickness, the magnitude of the photocurrent maximum at this wavelength was compared in order to examine the correlation between the crystallinity and the photocurrent. As is shown in Table 1, the higher the crystallinity of a film, the larger the photocurrent.

Although the results shown in Table 1 may not be attributable to only the difference in crystallinity because of the effect of heat-treatment on the concentration of impurity in a film, they seem to suggest a correlation between the crystallinity and the photoconductivity. A similar correlation has been reported for the γ-ray induced current in polyethylene films.[11]

Table 1. Effect of the crystallinity of PVCz films on photocurrent

Film No.	Thickness (mm)	Crystallinity	Absorption edge (mμ)	Photocurrent[a] i_{ph}^+	Photocurrent[a] i_{ph}^-
III	0.5	very good	380	7.4	12.5
III	0.4	moderate	380	2.6	2.4
III	0.07	poor	360	1	1

a) Relative value of photocurrent at the peak wavelength, film III being a standard. Under 8000 V/cm in high vacuum.

Discussion

Sharp reported on the photoconductivity of *N*-isopropylcarbazole, a model compound of PVCz.[12] No photocurrent was observed in the π–π^* absorption region longer than 280 mμ, although some intrinsic photoconduction was observed in the region shorter than 280 mμ. Furthermore, i_{ph}^- was larger than i_{ph}^+. An acceptor such as picryl chloride does not sensitize the photocurrent and acts only as a trapping center for an electron, the majority carrier. It has also been reported that the photoconductivities of *N*-vinylcarbazole and some alkylcarbazoles are smaller than that of PVCz, and that the light in the lower π–π^* absorption region is not effective for photoconduction.[13]

As is shown in Fig. 4, PVCz shows, however, a large photocurrent both in the lower and higher π–π^* absorption regions as well as a small photocurrent in the visible region. Furthermore, i_{ph}^+ is much larger than i_{ph}^- in moderate and high applied fields and a hole is expected to be the majority carrier. These photoconductive properties of PVCz are thus in sharp contrast with the photoconductivity of the related compounds.

Carrier Generation. The photocurrent in the visible region must be due to the optical reexcitation of trapped carriers, as has been reported previously.[4] Now, we are interested in carrier generation in the π–π^* absorption region of PVCz.

We have found that PVCz, a fairly strong electron donor, interacts easily even with a very weak electron acceptor, such as dimethyl terephthalate or chloroform, to form a so-called exciplex.[14] This suggests the possibility of the existence of some impurity in a PVCz film, which can form an exciplex under UV illumination. As the singlet exciton created by the π–π^* absorption in PVCz covers many pendant carbazyl groups during its lifetime,[14,15] a fairly high exciplex-forming efficiency can be expected by the π–π^* excitation. The carrier generation *via* the exciplex may be considered.

$$D^* + A \rightarrow (D^+\cdots A^-)^* \rightarrow D^+ + A^-, \quad (1)$$

$$A^- + D \text{ or } D^* \rightarrow D^- + A, \quad (2)$$

where D is the ground state of PVCz; D*, a singlet excited state; A, an impurity with an electron accepting property, and A^-, an impurity anion (immobile). $(D^+\cdots A^-)^*$ are an exciplex, D^+ and D^- are ion radicals of PVCz (*i.e.*, mobile charge carriers). Equation (1) shows the ionization of an exciplex (ion pair) into a mobile carrier ion in a film. Equation (2) shows the excitation of an electron donor (A^-) thermally or by a singlet exciton. The excitations of trapped carriers and/or of acceptors by singlet excitons may also be considered.

$$\begin{aligned} M^+ + D^* &\rightarrow M + D^+, \\ M^- + D^* &\rightarrow M + D^-, \end{aligned} \quad (3)$$

where M^+ is a trapped hole or an acceptor, and M^-, a trapped electron or a donor. The detrapping of trapped carriers by singlet excitons has been examined in anthracene.[16]

The dissociation of an exciplex (or ion pair) has been discussed in connection with the photoconductivity in aromatic hydrocarbon crystals. The energy required for the separation of an ion pair is evaluated roughly as 0.5 eV for anthracene.[17] The dissociation of an ion pair in a molecular crystal will need a fairly large activation energy. It may usually be difficult for an exciplex to dissociate into free ions in a film with a low dielectric constant. This dissociation may, however, be possible under conditions which reduce the energy required for the separation of an ion pair,—for example, under a strong electric field, as has been proposed by Lyons.[18] The following two kinds of fields[19] may be considered as strong electric fields in a PVCz film: (a) the local field surrounding an ion already produced (or a trapped carrier), and (b) the field near the surface which may act as a part of a diffuse double layer.

In a PVCz sandwich-type cell both carriers are not

11) K. Yahagi and K. Shinohara, *J. Appl. Phys.*, **37**, 310 (1966).
12) J. H. Sharp, *J. Phys. Chem.*, **71**, 2587 (1967).
13) M. Lardon, E. Lell-Daller, and J. W. Weigl, *Mol. Cryst.* **2**, 241 (1967).
14) K. Okamoto, A. Yano, S. Kusabayashi, and H. Mikawa; The 24th Annual Meeting of the Chemical Society of Japan, Osaka, April, 1969. Preprint 1-142.
15) W. Klöpffer, *J. Chem. Phys.*, **50**, 2337 (1969).
16) M. Pope, J. Burgos and N. Wotherspoon, *Chem. Phys. Lett.*, **12**, 140 (1971).
17) F. Gutmann and L. E. Lyons, "Organic Semiconductors," John Wiley & Sons Inc., New York (1967), p. 349.
18) L. E. Lyons, *J. Chem. Soc.*, **1957**, 5001.
19) Ref. 17, p. 392.

replenished with a metal or a nesa electrode.[13,21,22] Both carriers must be discharged at each electrode according to the electroneutral condition. The magnitude of photocurrent will be limited by the smaller value of either the number of holes having reached a negative electrode through the bulk or the number of electrons having reached a positive electrode. For the understanding of the photoconductive behavior, it is important to know how this number changes with the applied voltage, the polarity of the illuminated electrode, or the wavelength of the illuminating light.

If the processes represented by Eqs. (1), (2) and (3) are supposed to be carrier generation processes in the UV region in a PVCz sandwich-type cell, the photoconductive behavior can be explained favorably as follows.

In low applied fields, the exciplex will dissociate into free ions only in the local field surrounding an ion (or a trapped carrier), because the field near the surface will be small. The carriers will also be created by Process (3). In a PVCz film, impurities, A, and trapped carriers (or acceptors) will exist not only at the surface layer but also in the bulk. In homogeneous carrier generation, (1) recombination of the carriers will occur with a lower probability because of the lower concentration of the carriers than that in the case of surface carrier generation; (2) both carriers migrate in the bulk and can contribute to the photocurrent, and (3) space charge effects will be smaller because of the relatively homogeneous distribution of trapped carriers. Therefore, in general, homogeneous carrier generation in the bulk seems to be favored rather than the generation at surface. With an increase in the absorption coefficient of a film, the illuminating light is absorbed only in the region near the surface and the favorable conditions in the homogeneous carrier generation gradually disappear. Therefore, the spectral response of the photocurrent corresponds inversely to the absorption spectrum and the photocurrent peak in the longer wavelength region shows a red shift with an increase in the film thickness, unless there is an additional condition favoring the surface carrier generation. There is no significant difference either in magnitude or in the spectral dependence between i_{ph}^+ and i_{ph}^- in low fields.

When a higher voltage is applied, the field near the surface becomes larger and may be supposed to be large enough to assist the thermal dissociation of an exciplex. With positive-electrode illumination, hole carriers generated will be swept away before recombining with the immobile A^- ion. A mobile electron is generated from an A^- ion by Process (2). Thus, the thermal dissociation of an exciplex assisted by the field near the surface may act as a primary carrier generation process. Therefore, with an increase in applied voltage, significantly more carriers are generated, more favorably in the vicinity of an illuminated positive electrode rather than in the bulk. Consequently the spectral response of the photocurrent corresponds to the absorption spectrum with positive-electrode illumination in moderate and high applied fields. During the migration in the bulk to the opposite negative electrode, the hole carriers are frequently trapped and gradually fill hole traps in the same manner as has been mentioned previously.[4] As a result of the hole traps being filled, the effective mobility of a hole may become larger. With positive-electrode illumination, the number of holes reaching the negative electrode will become significantly larger with the applied voltage;—i_{ph}^+ in the UV region has, therefore, a superlinear dependence on the applied field.

On the other hand, in the case of negative-electrode illumination, most of the hole carriers generated by the same process as in positive-electrode illumination remain near the surface, without discharging at a negative electrode, and recombine with the immobile A^- ion. With negative-electrode illumination, the thermal dissociation of an exciplex assisted by the field near the surface seems not to act as a carrier generation process and the bulk carrier generation seems to be predominant even above a middle applied field. The i_{ph}^- neither shows a superlinear dependence on the applied voltage nor a spectral response corresponding to the absorption spectrum, even in high applied fields.

Photoresponse Curves. With positive-electrode illumination, as the carriers are generated preferentially at the surface, some effect of space charges distributed nonhomogeneously in a film may be more significant than in the case of the negative-electrode illumination. For this reason, a photoresponse curve of the B type is observed with positive-electrode illumination by the UV light, even in middle applied fields.

In high applied fields, the B type is not observed and the C type as well as the A type is observed. This may be explained as follows. At a high applied voltage, the effective hole mobility increases with the filling of hole traps and finally becomes equal to the value of the hole mobility which would be observed in the absence of any traps. With this gradual increase in the effective hole mobility, the photocurrent gradually increases during the illumination. In high fields the homogeneous illumination gives a photoresponse curve of the C type in Fig. 1, while the nonhomogeneous illumination gives an A or C type.

Activation Energy of Photocurrent. As the photocurrent in the visible region is due to the optical reexcitation of the carriers trapped by deep trap levels,[4] no significant activation energy seems to be needed for the carrier generation. The activation energy, ΔE_{ph} (0.07—0.15 eV at 35000 V/cm), in the visible region seems to be the energy required for the carrier migration. In a middle field (35000 V/cm) ΔE_{ph} in the UV region is assumed to be the sum of the activation energy for carrier migration and that for carrier generation. The former is estimated to be less than the value of ΔE_{ph} in the visible region, because under UV illumination a steady-state Fermi level for the hole[20] is lowered much more than in the case of visible illumination. The latter may be the energy required for the field-assisted thermal dissociation of an exciplex. In a high field as large as 150000 V/cm, the value of ΔE_{ph} in the UV region was lowered by about 0.1 eV. This lowering of the ΔE_{ph} value may be due to the filling up of the hole traps mentioned above, and the ΔE_{ph} value observed in high fields may not be the

20) A. Rose, *RCA Rev.*, **1951**, 362. *Phys. Rev.*, **97**, 322 (1955).

energy required for the carrier migration, but only that required for the carrier generation. The energy required for the field-assisted thermal dissociation of an exciplex may, consequently, be estimated to be about 0.1 eV.

Comparison with Pulse Photoconductivity Data. The transient pulse photocurrent in a PVCz film has been reported on by Regensburger,[21] Szymanski,[22] and Pai.[23] Their results, which were obtained under high applied fields, agree with each other in the following two points. The efficiency of hole carrier generation increases significantly with an increase in the applied field; the hole carrier mobility also increases significantly with both the temperature and the applied field, suggesting that the hole carrier migration process involves the field-assisted thermally-activated jump. These results correspond to the finding of the superlinearity of the voltage dependence of i_{ph}^{+}, which was observed in the steady-state photocurrent in the present investigation. The activation energy for hole carrier generation obtained from the transient measurements is nearly the same as the value (about 0.1 eV) observed in the present steady-state measurements. The activation energy for hole carrier migration obtained from the transient measurement (0.36 eV[23] or 0.4—0.7 eV[21] in air) is much larger than that (about 0.1 eV at 35000 V/cm and nearly zero at 150000 V/cm) observed in the present investigation. This may be attributed to the fact that, under the steady-state conditions, most of the hole traps are filled by holes, while under the conditions of the transient measurements the hole traps remain empty during the experiment.

Carrier Migration. From the X-ray analysis,[9,10] NMR spectra[24,25] and electron diffraction[10] the structure of solid PVCz has been suggested to be as follows. The crystalline nature of PVCz is sensitive to heat treatment. In a specimen stretched under a hot-press, the crystalline diffraction peak at $2\theta=8°15'$ is sharp and strong and the amorphous peak shows an appreciable decrease in its intensity. Thus, an annealed or stretched film is crystalline and takes a pseudo-hexagonal packing structure of a rigid rod-like molecule, with a cross sectional diameter of about 12.6 Å with only a chain-to-chain order. This chain may have isotactic 3/1 and syndiotactic 2/1 helix parts in a stereo-block manner.

From the structure of solid PVCz, it seems most probable that carriers can move primarily along the chain from a carbazyl group to another adjacent carbazyl group, through the overlap of the π-electron systems of carbazyl rings in the same polymer chain. This carrier migration process is supported by the correlation between the crystallinity and the photocurrent and also strongly by the significant decrease in the photocurrent in the copolymers of *N*-vinylcarbazole with a small amount of another monomer, which severs the overlap of the π-electron systems of carbazyl rings in the same polymer chain, thereby significant hindering the migration of the carriers.[26]

The authors wish to acknowledge the financial support of the Fuji Photo Co. for this work.

21) P. J. Regensburger, *Photochem. Photobio.*, **8**, 429 (1968).
22) A. Szymanski and M. M. Labes, *J. Chem. Phys.*, **50**, 3568 (1969).
23) D. M. Pai, *ibid.*, **52**, 2285 (1970).
24) S. Yoshimoto, Y. Akana, A. Kimura, H. Hirata, S. Kusabayashi, and H. Mikawa, *Chem. Commun.*, **1969**, 987.
25) D. J. Williams, *Macromolecules*, **3**, 5602 (1970).
26) K. Okamoto, K. Kato, S. Kusabayashi, and H. Mikawa, This Bulletin, in press.

The Vibrational Assignments of Propyl Bromide and Its Two Asymmetrically-Deuterated Species

Michiro HAYASHI, Keiichi OHNO, and Hiromu MURATA

Department of Chemistry, Faculty of Science, Hiroshima University, Higashi-sendamachi, Hiroshima 730

(Received November 30, 1972)

The vibrational assignments of the observed spectra of propyl bromide and its two asymmetrically-deuterated species have been worked out. Since the two *gauche* isomers come not to be equivalent for the asymmetrically-deuterated species, the infrared bands of the *gauche* isomer can be expected to be split into doublets, while the bands of the *trans* isomer remain singlets. The observed infrared bands for the *gauche* isomer were actually the doublets for the C–Br stretching and two CH_2 rocking modes. The C–D stretching and deformation modes of the β-deuterated species were also in the expected spectral patterns. In order to confirm the vibrational assignments, the normal vibration calculation was carried out using a modified Urey-Bradley force field for the parent and two asymmetrically-deuterated species.

Brown and Sheppard[1] studied the rotational isomerism of propyl bromide using the infrared spectra in the liquid and crystalline states.

Komaki *et al.*[2] also studied the infrared and Raman spectra of this substance in relation to the rotational isomerism. They concluded that the *trans* and *gauche* isomers co-exist in the gaseous and liquid states, while only the *trans* isomer persists in the crystalline state. The conclusion as to the molecular forms of the isomers by Komaki *et al.* had been drawn on the basis of the normal vibration calculation and the vibrational product rule of the skeletal vibrations between isomers.

The molecular forms of the isomers have also been confirmed by Sarachman by means of microwave spectroscopy.[3]

McDevitt *et al.*[4] studied the far-infrared spectra of this substance. As for the vibrational assignments, they worked them out for only the skeletal and some CH_2 rocking vibrations.

Recently, Tanabe and Saëki[5] have worked out the vibrational assignments of propyl bromide and chloride on the basis of absorption intensity measurements. They have also carried out the normal vibration calculation in the local-symmetry force field.

In this paper, we will deal with vibrational assignments of propyl bromide based on a comparison of the spectra with those of its two asymmetrically-deuterated species and on the results of the normal vibration calculation. Our assignments of the spectra are almost the same as those by Tanabe and Saëki except for several points which will be discussed in the future.

For the determination of the molecular forms of the rotational isomers, the asymmetrically-deuterated species of the original molecule usually gives useful information. as Neu and Gwinn,[6] de Hemptinne,[7] and Bernstein *et al.*[8] have shown for the case of 1,2-dibromoethane.

For propyl bromide, since the two *gauche* isomers come not to be equivalent for asymmetrically-deuterated species, such as the CH_3CHDCH_2Br and CH_3CH_2-$CHDBr$ species, the infrared bands of the *gauche* isomer are expected to be split into doublets, while the bands of the *trans* isomer remain singlets.

In order to find the molecular forms for a molecule with a structure similar to propyl bromide, such as propyl mercaptan, it is useful to find which asymmetrically-deuterated species gives better splitting patterns of the spectra, thus making possible an easier discrimination of the results. This is the second purpose of the present investigation of propyl bromide and its asymmetrically-deuterated species.

Experimental

The sample of the parent propyl bromide used in the measurements was a commercial product purified by redistillation. The α-deuterated species, CH_3CH_2CHDBr, was prepared by a method similar to that used in the preparation of α-deuterated butyl alcohol;[9] that is, propionaldehyde was reduced to α-deuterated propyl alcohol by $LiAlD_4$ in ethyl ether, and the resultant alcohol was brominated by PBr_3. The β-deuterated species, CH_3CHDCH_2Br, was prepared by the addition of propylene and DBr, with benzoylperoxide as the catalyst.[10] The purities of the deuterated species were found to be better than 90% by both gas chromatography and a study of the infrared spectra.

The infrared spectra in the region from 200 to 4000 cm^{-1} were recorded with a Perkin-Elmer instrument (model 621). For the measurements in the crystalline state, the vapor of the sample was directly condensed on a CsI plate in a cell cooled with liquid nitrogen in a vacuum and was then annealed several times in order to keep the sample from reaching the supercooled liquid state.

Vibrational Assignment

As is shown in Fig. 1, for the parent species there are equivalent two *gauche* isomers, and they produce

1) J. K. Brown and N. Sheppard, *Trans. Faraday Soc.*, **50**, 535 (1954).
2) C. Komaki, I. Ichishima, K. Kuratani, T. Miyazawa, T. Shimanouchi, and S. Mizushima, This Bulletin, **28**, 330 (1955).
3) T. N. Sarachman, Smp. Mol. Struct. Spectr., 23rd, Sept. 1968, Columbus, Ohio, N7.
4) N. T. McDevitt, A. L. Rozek, F. F. Bentley, and A. D. Davidson, *J. Chem. Phys.*, **42**, 1173 (1965).
5) K. Tanabe and S. Saëki, Symposium on Molecular Structure, Sendai (1972), paper 5C20 and the private communication.
6) J. T. Neu and W. D. Gwinn, *J. Chem. Phys.*, **18**, 1642 (1950).
7) M. de Hemptinne, *Contrib. etude structure mol. Vol. commem Victore Henri*, 151 (1947/48).
8) H. J. Bernstein, A. D. E. Pullin, S. B. Rabinovitch, and N. R. Larson, *J. Chem. Phys.*, **20**, 1227 (1952).
9) A. Streitwieser, Jr., *J. Amer. Chem. Soc.*, **75**, 5014 (1953).
10) M. S. Kharasch, M. C. McNab, and F. R. Mayo, *ibid.*, **55**, 2531 (1933).

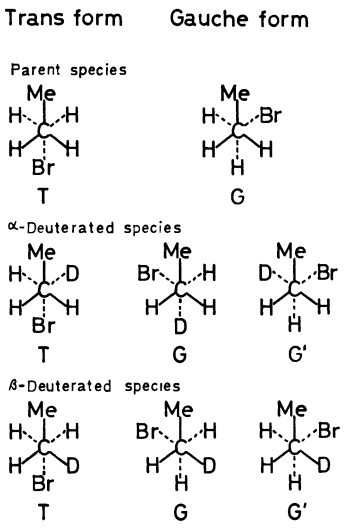

Fig. 1. Rotational isomers of propyl bromide and its asymmetrically-deuterated species.

two non-equivalent pairs of the four *gauche* forms if one of the hydrogens in the CH_2 groups is replaced by a deuterium, while the *trans* isomer produces two equivalent forms. Therefore, the infrared bands for the *gauche* isomers may be expected to be split into doublets for the asymmetrically-deutetrated species.

Spectra in the Region from 300 to 1000 cm^{-1}. In Fig. 2, the observed infrared spectra in the region from 300 to 1000 cm^{-1} are shown; the solid and the dotted lines indicate the spectra in the liquid and crystalline states respectively.

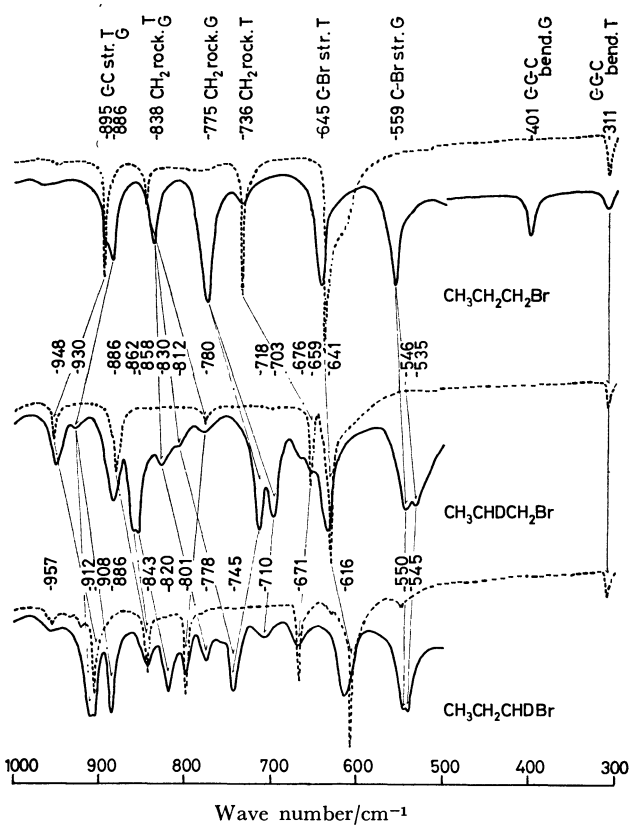

Fig. 2. Observed infrared spectra in the 300—1000 cm^{-1} region for the parent, β-deuterated, and α-deuterated species of propyl bromide. Solid and dotted lines indicate the spectra in the liquid and the crystalline states, respectively.

According to the reported vibrational assignments,[1,2] the strong infrared bands at 645 and 559 cm^{-1} of the parent species are the C–Br stretching vibrations for the *trans* and *gauche* isomers respectively. For the α- and β-deuterated species, the corresponding bands are found with nearly equal frequencies, and the band vanishing in the crystalline state appears to be a doublet, as is expected, while the band persisting in the crystalline state is a singlet.

As Shimanouchi and Suzuki[11] have already pointed out in their paper on dichloromethylene, upon asymmetrical deuteration the CH_2 rocking mode keeps its original mode, with relatively smaller modifications than the other hydrogen deformation modes. In the case of propyl bromide, the shifts of the CH_2 rocking modes are also expected to be relatively simple, though the shifts of the other vibrational modes between the parent and the deuterated species may be complicated.

For the parent species of propyl bromide, according to the reported assignments,[2] one of the two CH_2 rocking modes is the band at 736 cm^{-1} persisting in the crystalline state for the *trans* isomer and the band at 775 cm^{-1} appearing in the liquid state for the *gauche* isomer.

For the asymmetrically-deuterated species, there are two kinds of CH_2 rocking modes; they can be regarded as the CHD and CH_2 rocking modes, though a larger mutual mode mixing is expected. The CHD rocking mode is expected to be at a lower frequency than the CH_2 rocking mode.

For the β-deuterated species, the band at 659 cm^{-1} persisting in the crystalline state can be assigned to the CHD rocking mode for the *trans* isomers, which is a singlet. For the *gauche* isomer, the doublet around 710 cm^{-1} can be easily assigned to this mode.

For the α-deuterated species, the band at 671 cm^{-1} persisting in the crystalline state can be assigned to this mode for the *trans* isomer, which is a singlet. For the *gauche* isomer, although the band at 710 cm^{-1} appearing only in the liquid state can be easily assigned to one of components of the doublet of this mode, there are two possibilities for the other component of the doublet; that is, either the band at 710 cm^{-1} is the unsplit doublet or the band at 745 cm^{-1} appearing only in the liquid state is another component of the doublet.

Since the band at 710 cm^{-1} is too weak to be regarded as the unsplit doublet when comparison is made with the corresponding doublet of the β-deuterated species, the band at 745 cm^{-1} must be the component of the doublet with the band at 710 cm^{-1}. The present assignments are also supported by the result of the normal vibration calculations, as will be described later.

The doublet spacing for the *gauche* isomer of the α-deuterated species (35 cm^{-1}) is larger than that for the β-deuterated species (15 cm^{-1}), according to the

11) T. Shimanouchi and I. Suzuki, *J. Mol. Spectrosc.*, **8**, 222 (1962).

present assignments, in the same manner as the calculated spacings (the calculated spacings are 32 and 4 cm^{-1} respectively).

From the tendency found in the frequency separations between the two CH_2 rocking modes for a series of molecules with $-CH_2-CH_2-$ groups, as has already been reported,[12] the bands around 840 cm^{-1} for the parent species can be assigned to another CH_2 rocking mode, which corresponds to the CH_2 rocking mode for the deuterated species. The bands at 780 and 801 cm^{-1} for the β- and α-deuterated species respectively can be assigned to the corresponding CH_2 rocking mode for the *trans* isomer.

However, the assignment cannot be made immediately for the *gauche* isomer. For the β-deuterated species, there is no possible band if the corresponding mode for the *gauche* isomer is considered to have a lower frequency than that for the *trans* isomer, as is the case in the parent species. If bands at higher frequencies are permitted for this mode, there is a weak doublet around 820 cm^{-1} with a reasonable spacing for this mode.

For the α-deuterated species, there is a single band at a lower frequency than that for the *trans* isomer; in explaining this, there are three possibilities: 1) this band may be regarded as an unsplit doublet; 2) another component may overlap with the band at 745 cm^{-1}, which is assigned to the CHD rocking mode for the *gauche* isomer, and 3) this unknown component may have a higher frequency than that for the *trans* isomer.

In order to find the correct assignments in view of the above possibilities, the results of the normal vibration calculation are useful, as is shown in Tables 5—7.

From the calculation, the localization of the higher-frequency mode of two CH_2 rocking vibrations is found to be rather worse than that of the lower-frequency mode, though both of them are well localized from the other mode, as is to be expected. Furthermore, if the rocking modes for the *trans* and *gauche* isomers are designated as T and G respectively, they are possibly arrayed in the order of GTGT from higher to lower frequencies for the β-deuterated species, while for the α-deuterated species they are arrayed in the same order (TGGT) as that for the parent species.

Therefore, for the β-deuterated species, the doublet around 820 cm^{-1} can be assigned to this mode, while for the α-deuterated species, the band at 745 cm^{-1} can be regarded as containing one of the components of the doublet which has the band at 778 cm^{-1} as another component with reasonable spacing.

There are two C–C stretching modes for one isomer; one of them can be expected around 900 cm^{-1}. For the parent species, the bands at 895 and 886 cm^{-1} can be assigned to this mode for the *trans* and *gauche* isomers respectively.

For the deuterated species, one of the two CH_2 twisting modes, which should be more properly called a CD deformation mode,[11] can also be expected in the same region for the C–C stretching mode. In this region, there are two distinct bands in the crystalline state for both α- and β-deuterated species.

For the β-deuterated species, the bands at both 886 and 948 cm^{-1} persisting in the crystalline state accompany the bands in the liquid state on the lower-frequency side. The band accompanying the band at 886 cm^{-1} is a strong doublet with a small spacing, while the band accompanying the band at 948 cm^{-1} is a shoulder and seems to be a singlet.

According to the normal vibration calculation, the CD deformation mode should not only have a lower frequency for both the *trans* and *gauche* isomers, but should have a larger spacing of the doublet for the *gauche* isomer than that for the C–C stretching mode. Therefore, the band at 886 cm^{-1} and the doublet around 860 cm^{-1} can be assigned to the CD deformation mode for the *trans* and *gauche* isomers respectively, while the bands at 948 and 930 cm^{-1} can be assigned to the C–C stretching mode for the *trans* and *gauche* isomers respectively.

For the α-deuterated species, the calculation indicates that: 1) the C–C stretching mode has a higher frequency than the CD deformation mode; 2) both the C–C stretching and CD deformation modes have relatively large spacing of the doublet for the *gauche* isomer, and 3) one of the components of the doublet of the C–C stretching mode for the *gauche* isomer has a higher frequency than that for the *trans* isomer.

Taking the above results into account, for the *trans* isomer the bands at 843 and 908 cm^{-1} can be assigned to the CD deformation and the C–C stretching modes respectively. The band at 820 cm^{-1} can be assigned to one of the components of the doublet for the CD deformation mode for the *gauche* isomer, where the other component can be regarded to overlap the band at 843 cm^{-1} for the *trans* isomer. The band at 886 cm^{-1} assigned to the C–C stretching mode for the *gauche* isomer forms a doublet with a reasonable spacing and with a shoulder of the band at 908 cm^{-1} of the *trans* isomer.

Spectra in the Region from 1000 to 1200 cm^{-1}. In this region, one of the C–C stretching modes and two of the CH_3 rocking modes can be expected for one isomer. Actually, three bands exist, at 1022, 1036, and 1097 cm^{-1}, in the crystalline state for the parent species; they can be assigned to the C–C stretching mode, the CH_3 rocking mode belonging to the A″ species, and that belonging to the A′ species for the *trans* isomer respectively, taking into account the results of the calculation.

There are three corresponding bands, at 1017, 1064, and 1143 cm^{-1}, in the crystalline state for the β-deuterated species.

For the α-deuterated species, the band for the C–C stretching mode is at 1020 cm^{-1} in the crystalline state. However, the assignments cannot be made immediately for the two CH_3 rocking modes. As no other mode is possible in the expected region from 1000 to 1200 cm^{-1} for these two CH_3 rocking modes, some of the four bands appearing in the crystalline state are probably the modes in question. Among these

12) M. Hayashi, Y. Shiro, and H. Murata, This Bulletin, **39**, 112 (1966).

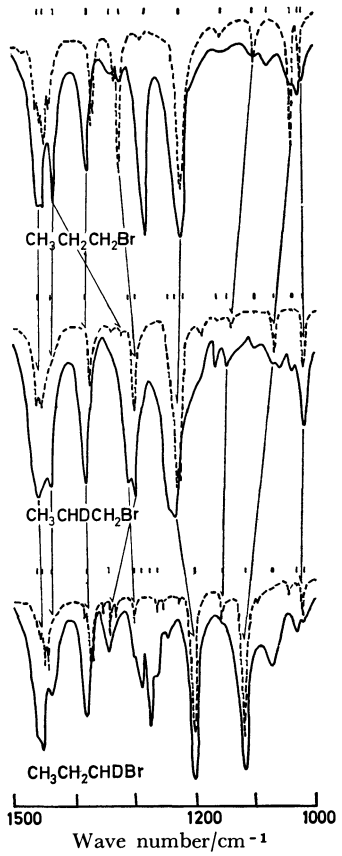

Fig. 3. Observed infrared spectra in the 1000—1500 cm^{-1} region for the parent, β-deuterated, and α-deuterated species of propyl bromide. Solid and dotted lines indicate the spectra in the liquid and the crystalline states, respectively.

four bands, the strongest band, at 1118 cm^{-1}, may be assigned to the CH_3 rocking mode corresponding to the strong band belonging to the A″ species for the parent species, though the difference between the calculated and observed frequencies seems to be a little large.

This assignment seems suspect because the band at 1118 cm^{-1} is too strong compared with the corresponding bands for the parent and the β-deuterated species. However, a similar strong band has also been found in this region for the monodeuterated ethyl bromide, CH_3CHDBr, reported by Bak *et al.*[13] Therefore, this may be a permissible assignment.

Another CH_3 rocking mode corresponding to the mode belonging to the A′ species for the parent species may be assigned to either the weak band at 1154 cm^{-1} or the band considered to overlap the band at 1118 cm^{-1}. There is no way to find which is correct, since the calculated frequency is probably not reliable. Therefore, we will tentatively assign the band at 1154 cm^{-1} to the CH_3 rocking mode.

For the *gauche* isomer, the tentative assignments for the C–C stretching and the two CH_3 rocking modes are shown in Tables 5—7; they have been made taking into account the results of the calculation and the assignments of the *trans* isomer.

Spectra in the Region from 1200 to 1500 cm^{-1}. In this region, there are nine CH_2 and CH_3 hydrogen deformation modes for one isomer.

For the deuterated species, since one of the CH_2 groups is replaced by a CHD group, when the results for $CHDCl_2$ described earlier are taken into account the set of CH_2 hydrogen deformation modes can be expected to change in their characteristic and to be more or less shifted to a lower-frequency side.

Among these shifted modes, the CHD rocking mode and the CD deformation mode originating from the CH_2 twisting mode have previously been assigned. The CHD scissoring mode and the CH deformation mode originating from the CH_2 wagging mode can be expected around 1290 and 1220 cm^{-1} respectively.

On the assignments of the spectra for the parent species, the potential energy distributions of the normal vibrations for propyl chloride calculated by Snyder and Schachtschneider[14] give a suitable point of reference, though they did not report any explicit assignments of the observed spectra.

The CH_2 wagging modes can be assigned to the strong bands at 1224 and 1326 cm^{-1} in the crystalline state for the *trans* isomer and to a strong band at 1282 cm^{-1} and a weak band at 1326 cm^{-1} in the liquid state for the *gauche* isomer.

As is shown in Table 5, judging from the calculated frequency it seems better to regard the CH_2Br wagging mode for the *gauche* isomer as overlapping the strong band at 1224 cm^{-1}. However, if this assignment is chosen, the intensity change of the band at 1282 cm^{-1} between the liquid state and the crystalline state cannot be understood unless the band for the CH_2 twisting mode exhibits a drastic intensity change between that for the *trans* isomer and that for the *gauche* isomer.

As for the two CH_2 twisting modes, since the spectra are expected to be weak and since, actually, no remarkable bands exist in the expected region, it is not easy to make any definite assignments. Therefore, the weak bands and the shoulders in this region are only tentatively assigned to these modes.

Only one band, at 1380 cm^{-1}, exists in the liquid state in the expected region for the CH_3 symmetric deformation mode; this band appears in the crystalline state at 1378 cm^{-1} as a doublet due to the crystalline field. As the difference in the molecular forms is considered to have a negligible influence on this mode, these may be regarded as overlapping bands due to the *trans* and *gauche* isomers.

Around 1440 cm^{-1}, there exist complicated bands which correspond to the CH_3 asymmetric deformation and CH_2 scissoring modes, where the lowest band at 1435 cm^{-1} existing in the liquid and crystalline states is probably one of the CH_2 scissoring modes due to both the *trans* and *gauche* isomers, in view of the finding on ethyl chloride reported by Miller and Kiviat.[15]

For the β-deuterated species, the strong bands at 1230 and 1295 cm^{-1} can be easily assigned to the CH_2 wagging mode and the CH deformation mode originating from the CHD wagging mode for the *trans* isomer.

13) B. Bak, D. H. Christensen, J. Møller, and S. Detoni, *Acta Chem. Scand.*, **12**, 2021 (1958).

14) R. G. Snyder and J. H. Schachtschneider, *J. Mol. Spectrosc.*, **30**, 290 (1969).

15) F. A. Miller and F. E. Kiviat, *Spectrochim. Acta*, **25A**, 1363 (1969).

For the *gauche* isomer, the CH_2 wagging mode and the CH deformation mode can be assigned to the bands at 1230, 1235, and 1308 cm^{-1}, taking into account the results of the calculation where the band at 1308 cm^{-1} is regarded as the overlapping band of two spectra due to two kinds of *gauche* isomers.

Since one of the CH_2 twisting modes (CD deformation mode) is shifted to the lower-frequency side around 900 cm^{-1}, there is one CH_2 twisting mode for one isomer which can be assigned to the shoulder at 1210 cm^{-1} for the *trans* isomer. For the *gauche* isomer, as the calculation indicates that only a slight frequency shift can be expected for the CH_2 twisting mode among the one *trans* isomer and the two kinds of *gauche* isomers, and as the lower-frequency side of the band at 1230 cm^{-1} seems to be too broad, the other weak band assigned to the CH_2 twisting mode may be considered to be hidden somewhere near the foot of the band.

Corresponding to the CH_2 scissoring mode at 1435 cm^{-1} for the parent species, either the band at 1319 or 1331 cm^{-1} in the crystalline state can be regarded as the CHD scissoring mode for the *trnas* isomer. Though there is no way to decide which is the correct assignment, the band at 1319 cm^{-1} may be considered to be preferable on the basis of the results of the calculation.

For the *gauche* isomer, since the band around 1295 cm^{-1} is too much weakened in the crystalline state, the band may consist of several overlapping bands due to the *gauche* isomer. Therefore, the CHD scissoring modes for the *gauche* isomers can be regarded as overlapped on this band.

For the α-deuterated species, the strong band at 1200 cm^{-1} can be easily assigned to the CH deformation mode originating from the CHD wagging mode for the *trans* isomer on the basis of a comparison of the spectra with those for CH_3CHDBr.

There are several weak bands in the crystalline state in the expected region for the higher-frequency CH_2 wagging mode. As the corresponding band at 1296 cm^{-1} for the β-deuterated species is also not very strong, the weak band can be assigned to this mode. However, in this region, the CHD scissoring and CH_2 twisting modes are expected, both of which are also expected to be weak. As the results of the calculation indicate that the CH_2 wagging mode has the highest frequency, while the CH_2 twisting mode has the lowest, if the relatively stronger bands are selected from the observed bands in this region, the bands at 1341, 1296 and 1260 cm^{-1} can be assigned to the CH_2 wagging, CHD scissoring, and CH_2 twisting modes respectively.

For the *gauche* isomer, though the assignments become more ambiguous than those for the *trans* isomer, the tentative assignments shown in Table 7 have been made taking into account the results of the calculation.

The assignments of the other modes, such as the CH_3 symmetric deformation, CH_2 scissoring, and CH_3 asymmetric deformation modes, are obtained from a comparison of the spectra with those for the other species.

Spectra for the C–H and C–D Stretching Modes. As is shown in Fig. 4, the C–H and C–D stretching vibrations are found in the regions around 2950 and 2200 cm^{-1} respectively.

A comparison of the spectra between the parent and deuterated species and between those in the liquid and crystalline states leads to the conclusion that the band at 2848 cm^{-1} is due to the β–CH_2 group of the *gauche* isomer, while the band at 3003 cm^{-1} is due to the α-CH_2 group of the *trans* isomer. For the β-deuterated species, one of the two C–H stretching modes of the β–CH_2 group is shifted to the region around 2200 cm^{-1} by replacing one of the hydrogens with a deuterium. The shifted bands consist of three bands; one of them (2197 cm^{-1}) persists in the crystalline state and can be assigned to the *trans* isomer, while the two other bands, which vanish in the crystalline state, can be assigned to the *gauche* isomer. Again, the spectra assigned to the *gauche* isomer are doublets, as is seen for the spectra below 900 cm^{-1}.

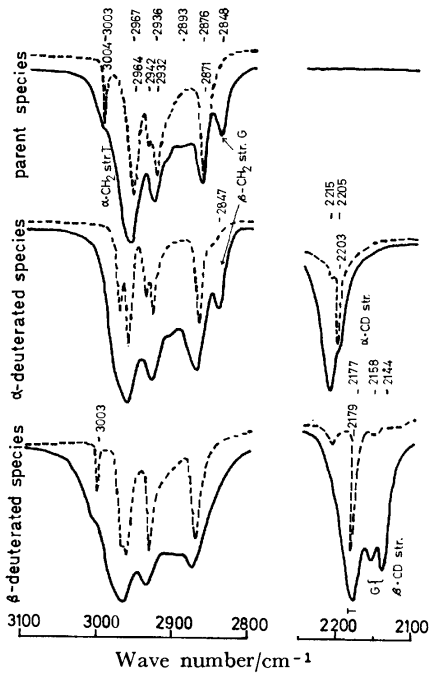

Fig. 4. Observed infrared spectra of the C-H and C-D stretching vibrations for the parent, α-deuterated, and β-deuterated species of propyl bromide. Solid and dotted lines indicate the spectra in the liquid and the crystalline states, respectively.

For the α-deuterated species, though the shifted bands are seen at 2215 and 2205 cm^{-1}, and though the band at 2215 cm^{-1} can be assigned to the *gauche* isomer, the band for the *gauche* isomer seems to be a singlet, although it may be an unresolved doublet with a smaller spacing.

Spectra in the Region below 550 cm⁻¹. As for the skeletal deformation and torsional modes, McDevitt *et al.*[4] have already reported the observed infrared and Raman spectra in the liquid state below 400 cm^{-1}, along with the assignments for the parent species. However, the assignments in Table 1 are very different from those reported by McDevitt *et al.*

They made their assignments on the basis of a comparison of the spectra of propyl chloride and bromide with those of isopropyl and *t*-butyl chlorides and bromides in the liquid state. Not only does this comparison of the spectra seem to us to be inadequate, but the lack of the spectra in the crystalline state leads to incorrect assignments for the rotational isomers.

Table 1. Infrared spectra of $CH_3CH_2CH_2Br$ (cm^{-1})[a]

Liquid	Int.	Crystal	Int.	Assignment	Liquid	Int.	Crystal	Int.	Assignment
133[b]				CH_2–CH_2 torsion T, G	1097	w	1100	w	CH_3 rock. A′ T
202[b]				C–C–Br bend. G	1152	w	1154	vw	
220[b]				C–C–Br bend. T, CH_3-C torsion T			1214 sh	ms	CH_2 twist. T, G
					1224	vs	1221	vs	CH_2 wag. T
273[b]				CH_3–C torsion G	1282	vs	1288	vw	CH_2 twist. T, G, CH_2 wag. G
311	vw	311	m	C–C–C bend. T	1326	w	1325	s	CH_2 wag. T, G
401	w	—		C–C–C bend. G	1238	w	1335	w	
559	s	—		C–Br str. G	1380	s	1365, 1370	ms	CH_3 sym. def. T, G
		623 sh	m		1435	s	1433, 1439	ms	CH_2 sci. T, G
645	s	637	vs	C–Br str. T			1447	ms	
736	m	737	s	CH_2 rock. T			1450 sh	ms	
775	s	—		CH_2 rock. G	1456	s	1456	ms	CH_3 asym. def. A′, A″ T, G
838	ms	—		CH_2 rook. G	1463	s	1463	ms	
		849, 851	w	CH_2 rock. T	2848	ms	—		CH_2C sym. str. G
886	ms	—		C–C str. G	2876	s	2871	s	C–H str. T, G
895	ms	893, 897	m	C–C str. T	2893 sh	s			
							2903 sh	m	
953	vvw	951	vw		2918 sh	s			
1022	m	1023	m	C–C str. T			2932	ms	
1028	m	—		C–C str. G	2936	vs	2942	s	
1036	m	1038	m	CH_3 rock. A″ T, G	2967	vs	2964	vs	
1078	w	—		CH_3 rock. A′ G	3003	ms	3004	m	CH_2Br antisym. str. T

a) Int.=intensity; s, m, w=strong, medium, weak; v=very; sh=shoulder; b=broad; T, G=*trans* form, *gauche* form.
b) Infrared frequencies were measured by McDevitt *et al.*, Ref. 4.

Table 2. Infrared spectra of CH_3CHDCH_2Br (cm^{-1})[a]

Liquid	Int.	Crystal	Int.	Assignment	Liquid	Int.	Crystal	Int.	Assignment
		310	m	C–C–C bend. T	1143	w	1138	mw	CH_3 rock. T, G
535	s	—		C–Br str. G	1157	vw	1157	w	
546	s	—			1191 sh	w	1187	m	
607	w	—			1210 sh	m	1224	vs	CH_2 twist. T, G
		616	m		1230	vs	1228	vs	CH_2 wag. T, G
641	s	633	vs	C–Br str. T	1235 sh	vs	—		CH_2 wag. G
659	m	659	s	CHD rock. T	1295	s	1295, 1299	s	CH def. T, CHD sci. G
676	m	—			1308	s	—		CH def. G
703	s	—		CHD rock. G			1319	w	CHD sci. T
718	s	—					1331	w	
780	w	780	w	CH_2 rock. T	1379	s	1366, 1369	s	CH_3 sym. def. T, G
812 sh	w	—		CH_2 rock. G	1437	s	—		CH_2 sci. T, G
830	m	—					1451	s	
858	s	—		CD def. G	1459	s	1462	s	CH_3 asym. def. T, G
862	s	—			2144	m	—		C–D str. G
886	s	882, 895	m	CD def. T	2158	m	—		
930	w	—		C–C str. G	2177	m	2179	m	C–D str. T
948	m	953	m	C–C str. T	2876	s	2872	m	CH_3 sym. str. T, G
		1009 sh	vw		2895 sh	s			C–H str. T, G
1017	s	1019	m	C–C str. T, G	2935	s	2932	s	
1036	m	—		CH_3 rock. G	2965	vs	2961, 2968	vs	
1053	m	—							
1064	m	1063	m	CH_3 rock. T					
1095	w	—		CH_3 rock. G	3003 sh	m	3003	mw	CH_2Br antisym. str. T

a) See footnote a) of Table 1.

TABLE 3. INFRARED SPECTRA OF CH_3CH_2CHDBr (cm^{-1})[a)]

Liquid	Int.	Crystal	Int.	Assignment	Liquid	Int.	Crystal	Int.	Assignment
		311	m	C-C-C bend. T	1154	vw	1154	w	CH_3 rock. T
545	s	—		C-Br str. G	1200	vs	1201	vs	CH def. T, G
550	s	550	vw				1206		
		555	vw				1223	w	
		596	w		1242	w	1249	w	
616	s	607	vs	C-Br str. T	1260	w	1260	w	CH_2 twist. T
		638	w		1272	s	—		CH_2 twist. G, CHD sci. G
671	w	669	s	CHD rock. T	1289	m	—		
710	w	—		CHD rock. G	1296	m	1300	w	CHD sci. T
745	s	—					1328	w	
759 b	w	—			1341	mw	1338	mw	CH_2 wag. T, G
778	m	—		CH_2 rock. G	1349 sh	w	1349	w	
801	m	799	s	CH_2 rock. T	1381	s	1366	m	CH_3 sym. def. T, G
		801					1370		
820	s	—		CD def. G			1382	w	
843	m	844	s	CD def. T, G	1435	m	—		CH_2 sci. T, G
886	s	—		C-C str. G	1455	s	1453	m	
908	s	907	s	C-C str. T			1457	m	CH_3 asym. def. T, G
912	s	—		C-C str. G	1461 sh	s	1465	mw	
		921	w		2205	m	2203	w	C-D str. T
957	w	954	w		2215	m	—		C-D str. G
1020 sh	w	1020	w	C-C str. T, G	2847	s	—		CH_2C sym. str. G
1027	w	—		C-C str. G	2875	vs	2873	s	C-H str. T, G
		1041	w		2910 sh	s			
1068	m	—		CH_3 rock. G	2934	vs	2934	s	
							2942		
1118	vs	1118	vs	CH_3 rock. T, G	2967	vs	2965	s	
							2975	vs	

a) See footnote a) of Table 1.

The incorrectness of their assignments can be clearly seen if their assignments for propyl chloride are compared with those reported by Komaki *et al.* and by Snyder *et al.*

The assignments in Table 1 have been obtained from a comparison of the spectra of propyl bromide with those of propyl chloride, both in the liquid and crystalline states, and have been confirmed from the normal vibration calculations to be described in the next section.

Normal Vibration Calculation

In order to confirm the vibrational assignments, a normal vibration study based on a modified Urey-Bradley force field has been carried out.

The bond lengths used in the calculation were transferred from those of ethyl bromide determined by microwave study by Flanagan and Pierce.[16] They were $r(C-Br)=1.950$, $r(C-C)=1.518$, $r(C-H)_{CH_3}=1.093$, and $r(C-H)_{CH_2}=1.087$ Å. On the other hand, all of the valency angles were assumed to be tetrahedral in disregard of the observed values. The internal symmetry coordinates were taken from those given in the papers by Takahashi[17] and by Clark.[18]

At first, the force constants were transferred from those for propane[19] and for ethyl bromide[20] in the simple Urey-Bradley force field; the force constants for ethyl bromide were obtained in order to fit the calculated frequencies to the observed frequencies for the parent ethyl bromide and its three deuterated species, CH_3CD_2Br, CD_3CH_2Br, and CD_3CD_2Br, by the least-squares technique.

The internal rotation force constant for the skeletal torsion was assumed to be the value obtained from the reported far-infrared band for the CH_3 torsion of ethyl chloride.[15] This value of the force constant corresponds to the barrier height of 3.49 kcal/mol. The force constant for the CH_3 torsion was assumed to be the value obtained from the barrier height of 2.77 kcal/mol. This barrier height is the average of the observed barrier height of the CH_3 group in the *trans* and the *gauche* isomers of propyl fluoride, as determined by means of microwave spectroscopy.[21]

However, the calculated frequencies could not reproduce the observed frequencies well enough, especially for the CH_2 deformation, C-Br stretching, and C-H stretching modes.

Therefore, the force field was modified as follows: 1) the *trans* and *gauche* coupling terms between the CH_3 and CH_2C groups and between the CH_2C and CH_2Br groups were added; 2) the C-H bond interac-

16) C. Flanagan and L. Pierce, *J. Chem. Phys.*, **38**, 2963 (1963).
17) H. Takahashi, *Nippon Kagaku Zasshi*, **82**, 1304 (1961).
18) E. A. Clark, *J. Chem. Phys.*, **45**, 1759 (1966).
19) H. Takahashi, *Nippon Kagaku Zasshi*, **83**, 978 (1962).
20) K. Ohno, to be published.
21) E. Hirota, *J. Chem. Phys.*, **37**, 283 (1962).

Table 4. Force constants for propyl bromide[a] ($F' = -0.1F$)

K(C–Br)	1.784	(1.874)[e]	$\kappa(CH_2Br)$	−0.032	(−0.047)
K(C–C)	2.695	(2.568)	$\kappa(CH_2C)$	−0.045	
K(C–H), CH_2Br	4.401	(4.499)	$\kappa(CH_3)$	−0.036	(−0.010)
K(C–H), CH_2C	4.115		$Y(CH_2–CH_2)$	0.109[b]	
K(C–H), CH_3	4.209	(4.229)	$Y(CH_2–CH_3)$	0.087[c]	
H(C–C–Br)	0.033		F(C···C···Br)	0.669	
H(C–C–H)	0.258		F(C···C···H)	0.406	
H(H–C–Br)	0.164	(0.192)	F(H···C···Br)	0.303	
H(H–C–H)	0.352		F(H···C···H)	0.250	
H(C–C–C)	0.275[d]		F(C···C···C)	0.335[d]	
$t(CH_3, CH_2)$	0.056		$g(CH_3, CH_2)$	−0.018	
$t(CH_2, CH_2)$	0.001		$g(CH_2, CH_2)$	−0.033	
			p(C–H)	−0.144	(−0.128)

a) The units of the force constants are in mdyn/Å for stretching, K; bending, H; repulsion, F; and bond interaction, p; and in mdyn·Å for intramolecular torsion, k; internal rotation, Y; *trans* coupling, t; and *gauche* coupling, g.
b) The value of Y is assumed from the barrier height of 3.49 kcal/mol.
c) The value of Y is assumed from the barrier height of 2.77 kcal/mol.
d) Force constants are transferred from propane, Ref. 19.
e) ( ) indicates the values for ethyl bromide.

Table 5. Observed and calculated frequencies of $CH_3CH_2CH_2Br$ (cm^{-1})

No.	Obsd	Calcd	P.E.D.[a]	No.	Obsd	Calcd	P.E.D.[a]
Trans form			A′ species	*Gauche* form			A species
1	2967	2953	CH_3 asym. str. (100)	1	3003	3005	CH_2Br antisym. str. (100)
2	2936	2944	CH_2Br sym. str. (98)	2	2967	2955	CH_3 asym. str. (92)
3	2876	2865	CH_3 sym. str. (70), CH_2C sym. str. (31)	3	2967	2953	CH_3 asym. str. (100)
				4	2936	2944	CH_2Br sym. str. (90)
4	2876	2883	CH_2C sym. str. (70), CH_3 sym. str. (31)	5	2936	2934	CH_2C antisym. str. (85)
				6	2876	2865	CH_3 sym. str. (71), CH_3 sym. str. (30)
5	1463	1475	CH_3 asym. def. (38), CH_2C sci. (34)	7	2848	2884	CH_2C sym. str. (70), CH_3 sym. str. (29)
6	1456	1461	CH_2Br sci. (27), CH_3 asym. def. (46)	8	1463	1472	CH_3 asym. def. (65)
7	1435	1429	CH_2C sci. (47), CH_2Br sci. (52)	9	1456	1465	CH_3 asym. def. (85)
8	1380	1384	CH_3 sym. def. (100)	10	1435	1453	CH_2Br sci. (49), CH_2C sci. (27)
9	1326	1323	CH_2C wag. (85)	11	1435	1443	CH_2C sci. (55), CH_2Br sci. (39)
10	1224	1231	CH_2Br wag. (100)	12	1380	1384	CH_3 sym. def. (100)
11	1097	1070	CH_3 rock. (40), C–C str. (31)	13	1326	1348	CH_2C wag. (65)
12	1022	1023	C–C str. (67)	14	1282	1286	CH_2C twist. (76)
13	895	909	C–C str. (46), CH_3 rock. (40)	15	1282	1226	CH_2Br wag. (65)
14	645	641	C–Br str. (82), C–C–C bend. (20)	16	1214	1204	CH_2Br twist. (67)
15	311	309	C–C–C bend. (54), C–Br str. (26)	17	1078	1065	CH_3 rock. (39)
16	220	216	C–C–Br bend. (90)	18	1036	1044	CH_3 rock. (43)
			A″ species	19	1028	1022	C–C str. (73)
17	3003	3005	CH_2Br antisym. str. (100)	20	886	901	C–C str. (54), CH_3 rock. (35)
18	2967	2955	CH_3 asym. str. (93)	21	838	830	CH_2C rock. (30), CH_2Br rock. (34), CH_3 rock. (23)
19	2936	2935	CH_2C antisym. str. (93)				
20	1456	1464	CH_3 asym. def. (87)	22	775	753	CH_2Br rock. (49), CH_2C rock. (33)
21	1288	1281	CH_2C twist. (78)				
22	1214	1222	CH_2Br twist. (78)	23	559	571	C–Br str. (97)
23	1036	1054	CH_3 rock. (48)	24	401	407	C–C–C bend. (61)
24	850	830	CH_2 C rock. (43), CH_2Br rock. (28), CH_3 rock. (27)	25	273	264	CH_3–C torsion (42), C–C–Br bend. (31)
25	736	738	CH_2Br rock. (46), CH_2C rock. (42)	26	202	189	C–C–Br bend. (35), CH_3–C torsion (52)
26	220	228	CH_3–C torsion (96)	27	133	95	CH_2–CH_2 torsion (75)
27	133	106	CH_2–CH_2 torsion (90)				

a) Potential energy distributions are shown in percent for the internal symmetry coordinates, where only contributions greater than 20% are included.

Table 6. Observed and calculated frequencies of CH_3CHDCH_2Br (cm^{-1})

No.	Obsd	Calcd	P.E.D.[a]
Trans form			A species
1	3003	3005	CH_2Br antisym. str. (100)
2	2965	2954	CH_3 asym. str. (100)
3	2965	2953	CH_3 asym. str. (100)
4	2935	2944	CH_2Br sym. str. (99)
5	2876	2909	CHC str. (97)
6	2876	2870	CH_3 sym. str. (99)
7	2177	2130	CDC str. (100)
8	1459	1467	CH_3 asym. def. (84)
9	1459	1464	CH_3 asym. def. (87)
10	1459	1448	CH_2Br sci. (95)
11	1379	1384	CH_3 sym. def. (100)
12	1295	1309	CHDC wag. (54), CHDC twist. (25)
13	1319	1299	CHDC sci. (75)
14	1230	1230	CH_2Br wag. (90)
15	1210	1208	CH_2Br twist. (79)
16	1143	1133	CH_3 rock. (24), CHDC twist. (29), C–C str. (32)
17	1064	1060	CH_3 rock. (44), C–C str. (29)
18	1017	1021	C–C str. (35), CH_3 rock. (39)
19	948	910	C–C str. (58), CH_3 rock. (28)
20	886	886	CHDC twist. (18), CHDC wag. (30)
21	780	789	CH_2Br rock. (54)
22	659	660	CHDC rock. (66)
23	641	640	C–Br str. (82)
24	310	307	C–C–C bend. (54), C–Br str. (26)
25	—	226	CH_3–C torsion (96)
26	—	212	C–C–Br bend. (88)
27	—	103	CH_2–CHD torsion (90)
Gauche form(G)			A species
1	3003	3004	CH_2Br antisym. str. (100)
2	2965	2954	CH_3 asym. str. (99)
3	2965	2953	CH_3 asym. str. (100)
4	2935	2943	CH_2Br sym. str. (100)
5	2876	2910	CHC str. (97)
6	2876	2870	CH_3 sym. str. (99)
7	2158	2130	CDC str. (100)
8	1459	1467	CH_3 asym. def. (85)
9	1459	1464	CH_3 asym. def. (87)
10	1437	1447	CH_2Br sci. (95)
11	1379	1384	CH_3 sym. def. (100)
12	1308	1337	CHDC wag. (44), CHDC twist. (21)
13	1295	1305	CHDC sci. (79)
14	1230	1220	CH_2Br wag. (68), C–C str. (28)
15	1210	1207	CH_2Br twist. (69)
16	1095	1130	CH_3 rook. (27), C–C str. (33), CHDC twist. (23)
17	1036	1042	CH_3 rock. (51)
18	1017	1015	C–C str. (40), CH_3 rock. (35)
19	930	904	C–C str. (50)
20	862	877	CHDC twist. (17), CHDC wag. (24), C–C str. (25)
21	812	792	CH_2Br rock. (58)
22	718	699	CHDC rock. (55)
23	546	563	C–Br str. (93)
24	—	400	C–C–C bend. (64)
25	—	254	CH_3–C torsion (52), C–C–Br bend. (27)
26	—	185	C–C–Br str. (41), CH_3–C torsion (44)
27	—	94	CH_2–CHD torsion (77)
Gauche form(G′)			A species
1	3003	3005	CH_2Br antisym. str. (100)
2	2965	2954	CH_3 asym. str. (100)
3	2965	2953	CH_3 asym. str. (100)
4	2935	2944	CH_2Br sym. str. (98)
5	2876	2909	CHC str. (95)
6	2876	2870	CH_3 sym. str. (98)
7	2144	2130	CDC str. (100)
8	1459	1467	CH_3 asym. def. (84)
9	1459	1464	CH_3 asym. def. (86)
10	1437	1448	CH_2Br sci. (93)
11	1379	1384	CH_3 sym. def. (100)
12	1308	1324	CHDC wag. (49), CHDC twist. (17)
13	1295	1295	CHDC sci. (89)
14	1235	1239	CH_2Br wag. (91)
15	1210	1209	CH_2Br twist. (69)
16	1143	1133	CH_3 rock. (24), C–C str. (40), CHDC twist. (27)
17	1053	1051	CH_3 rock. (49)
18	1017	1019	C–C str. (48), CH_3 rock. (36)
19	930	900	C–C str. (54), CH_3 rock. (33)
20	858	865	CHDC twist. (30), CHDC wag. (36)
21	830	803	CH_2Br rock. (68)
22	703	695	CHDC rock. (56)
23	535	550	C–Br str. (85)
24	—	404	C–C–C bend. (62)
25	—	256	CH_3–C torsion (49), C–C–Br bend. (28)
26	—	186	C–C–Br bend. (39), CH_3 torsion (47)
27	—	94	CH_2–CHD torsion (77)

a) See a) of Table 5. Potential energy distributions are shown in percent for the internal symmetry coordinates of $CH_3CH_2CH_2Br$. Though the designations of the CH and CD deformation modes are used in Tables 2—3 and in the text, in this table, the designations of the CHD wagging and twisting modes are used for the convenience of the comparison with the results for the parent species.

TABLE 7. OBSERVED AND CALCULATED FREQUENCIES OF CH_2CH_2CHDBr (cm^{-1})

No.	Obsd	Calcd	P.E.D.[a]
Trans form			A species
1	2967	2976	CHBr str. (99)
2	2967	2955	CH_3 asym. str. (93)
3	2967	2953	CH_3 asym. str. (100)
4	2934	2935	CH_2C antisym. str. (93)
5	2875	2865	CH_3 sym. str. (72), CH_2C sym. str. (29)
6	2875	2884	CH_2C sym. str. (71), CH_3 sym. str. (29)
7	2205	2177	CDBr str. (100)
8	1461	1471	CH_3 asym. def. (70)
9	1455	1464	CH_3 asym. def. (87)
10	1455	1449	CH_2C sci. (82)
11	1381	1384	CH_3 sym. def. (100)
12	1341	1327	CH_2C wag. (80)
13	1296	1295	CHDBr sci. (57)
14	1260	1274	CH_2C twist. (72)
15	1200	1214	CHDBr wag. (47), CHDBr twist. (33)
16	1154	1091	CH_3 rock. (32), C–C str. (20)
17	1118	1064	CH_3 rock. (46), C–C str. (28)
18	1020	1028	C–C str. (63)
19	909	936	C–C str. (37), CH_3 rock. (28)
20	843	866	CHDBr twist. (18), CHDBr wag. (17), CH_3 rock. (26), C–C str. (24)
21	801	795	CH_2C rock. (51), CH_3 rock. (23)
22	671	663	CHDBr rock. (65)
23	616	603	C–Br str. (63)
24	311	309	C–C–C bend. (53), C–Br str. (26)
25	—	226	CH_3–C torsion (95)
26	—	213	C–C–Br bend. (87)
27	—	104	CHD–CH_2 torsion (90)
Gauche form(G)			A species
1	2967	2976	CHBr str. (100)
2	2967	2955	CH_3 asym. str. (93)
3	2967	2953	CH_3 asym. str. (100)
4	2934	2935	CH_2C antisym. str. (93)
5	2875	2865	CH_3 sym. str. (72), CH_2C sym. str. (29)
6	2847	2884	CH_2C sym. str. (71), CH_3 sym. str. (29)
7	2215	2176	CDBr str. (100)
8	1461	1471	CH_3 asym. def. (71)
9	1455	1464	CH_3 asym. def. (87)
10	1435	1447	CH_2C sci. (84)
11	1381	1384	CH_3 sym. def. (100)
12	1341	1335	CH_2C wag. (79)
13	1289	1293	CHDBr sci. (67)
14	1289	1285	CH_2C twist. (61)
15	1200	1210	CHDBr wag. (40), CHDBr twist. (26)
16	1118	1104	CH_3 rock. (30), C–C–str. (41)
17	1068	1060	CH_3 rock. (44), CH_2C rock. (21)
18	1020	1023	C–C str. (73)
19	912	942	C–C str. (22), CH_3 rock. (50)
20	820	828	CHDBr twist. (20), CHDBr wag. (17), CH_2C rock. (26)
21	745	795	CH_2C rock. (29)
22	710	666	CHDBr rock. (74)
23	550	557	C–Br str. (93)
24	—	399	C–C–C bend. (56)
25	—	259	CH_3–C torsion (45), C–C–Br bend. (28)
26	—	188	C–C–Br bend. (37), CH_3–C torsion (49)
27	—	94	CHD–CH_2 torsion (76)
Gauche form(G′)			A species
1	2967	2975	CHBr str. (100)
2	2967	2955	CH_3 asym. str. (99)
3	2967	2953	CH_3 asym. str. (100)
4	2934	2935	CH_2C antisym. str. (99)
5	2875	2865	CH_3 sym. str. (73), CH_2C sym. str. (28)
6	2847	2884	CH_2C sym. str. (72), CH_3 sym. str. (29)
7	2215	2177	CDBr str. (100)
8	1461	1471	CH_3 asym. def. (72)
9	1455	1464	CH_3 asym. def. (87)
10	1435	1446	CH_2C sci. (86)
11	1381	1384	CH_3 sym. def. (100)
12	1341	1364	CH_2C wag. (57)
13	1272	1289	CH_2C twist. (54), CHDBr sci. (34)
14	1272	1268	CHDBr sci. (41), CH_2C twist. (32)
15	1200	1203	CHDBr wag. (46), CHDBr twist. (23)
16	1118	1092	CH_3 rock. (33), CHDBr twist.(21)
17	1068	1054	CH_3 rock. (24), C–C str. (39)
18	1027	1032	C–C str. (45), CH_3 rock. (36)
19	886	916	C–C str. (44), CHDBr twist. (22), CH_3 rock. (24)
20	843	861	CHDBr twist. (15), CHDBr wag (17), C–C str. (22), CH_3 rock. (27)
21	778	783	CH_2C rock. (50)
22	745	699	CHDBr rock. (69)
23	545	545	C–Br str. (90)
24	—	390	C–C–C bend. (55)
25	—	260	CH_3–C torsion (43), C–C–Br bend. (27)
26	—	188	C–C–Br bend. (36), CH_3–C torsion (50)
27	—	94	CHD–CH_2 torsion (77)

a) See a) of Table 6.

tion constants were introduced; 3) the C–H stretching force constants of the CH_2 groups were considered to be not necessarily equal for the CH_2C and CH_2Br groups, and 4) the stretching force constants of K(C–C) and K(C–Br), the bending force constant of H(H–C–Br), and the intramolecular torsions were also considered to be different from the values transferred from similar molecules.

These force constants were determined by the least-squares technique in order to reproduce the observed frequencies for the parent species. They are shown in Table 4, together with the other transferred force constants. The calculated and observed frequencies for the parent and two asymmetrically-deuterated species are given in Tables 5—7, together with the potential energy distributions. A good agreement has been obtained between the calculated and observed frequencies for the two deuterated species as well as for the parent species. Since the force constants were adjusted for the parent species, this agreement for the deuterated species is considered to indicate the reasonableness of the present assignments.

From the potential energy distributions, for the parent species larger mode mixings are obvious between the two CH_2 scissoring modes, between the C–C stretching and CH_3 rocking modes, and between the two CH_2 rocking modes.

Although the mode mixing has been found to be relatively large between two skeletal bending vibrations, as had been expected, the mode designations in the internal coordinates still seem to be valid for this molecule. Therefore, the designations of the C–C–C and C–C–Br bending modes are more adequate for the description of the actual modes of the vibrations than the designations of the symmetric and antisymmetric deformation modes of the two skeletal bendings.

22) S. Mizushima, T. Shimanouchi, K. Nakamura, M. Hayashi, and S. Tsuchiya, *J. Chem. Phys.*, **26**, 970 (1957).

Discussion

Mizushima *et al.*[22] pointed out that when a heavier atom or group, such as the halogen atom or the CH_3 group, occupies the position *trans* to the halogen atom, the stretching vibration of the carbon-halogen bond is observed at a higher frequency than in the other configurations.

This tendency is also found in the cases of the deuterated species and the parent species of propyl bromide. That is, the C–Br stretching vibrations for the *trans* isomers of the three isotopic species were always observed at higher frequencies than those for the *gauche* isomers. Furthermore, even for the two different *gauche* isomers of the α- and β-deuterated species, the C–Br stretching vibration appears at a higher frequency for the *gauche* isomers with the deuterium atom at the posittion *trans* to the bromine atom than that for the other, *gauche* isomer with its hydrogen atom at the posittion *trans* to the bromine atom.

As for the frequency splittings of the *gauche* isomers resulting from the asymmetrical deuteration, the bands in the range from 500 to 1000 cm^{-1} give more obvious patterns of the doublets than the bands in the other range. Although the spacings of the doublets for the CH_2 deformation modes are found to be larger, in general, for the α-deuterated species than for the β-deuterated species, the patterns of the doublets seem to be more distinct for the β-deuterated species than for the α-deuterated species. Therefore, the β-deuterated species may be preferable in the determination of the molecular forms of the rotational isomers for the $XCH_2CH_2CH_3$-type molecules.

The authors wish to express their thanks to Dr. Kazutoshi Tanabe and Dr. Shinnosuke Saëki of the Government Chemical Industrial Research Institute of Tokyo for their pre-publication information on their vibrational assignments.

Studies of the Preparation and Physical Properties of Multivalent Metal Condensed Phosphates. V.[1] The Grinding of Various Aluminum Phosphates

Mitsutomo TSUHAKO,* Itaru MOTOOKA,** and Masamitsu KOBAYASHI**

*Kobe Women's College of Pharmacy, Higashinada-ku, Kobe 658

**Department of Chemistry, Faculty of General Education, Kobe University, Nada-ku, Kobe 657

(Received December 1, 1972)

Changes in the structures of various aluminum phosphates as a result of grinding were studied by a variety of physical methods—X-ray analysis, DTA, TGA, infrared absorption spectroscopy and electron microphotography, and their acidic properties were investigated in order to obtain information on the surface activity of the compounds. The X-ray diffraction patterns indicated that the A, B, and C types of $Al_4(P_4O_{12})_3$ and $AlPO_4$ (Berlinite) did not become completely amorphous even after grinding for 72 hr; this shows that the crystal structures of these compounds were relatively stable to grinding. Substance K was structurally more fragile than the other aluminum phosphates ($Al_4(P_4O_{12})_3$, $AlPO_4$), becoming completely amorphous on being ground for 72 hr. On DTA and TGA, the ground aluminum phosphates exhibited an endothermic peak, accompanied by a weight loss due to the loss of adsorbed water in the vicinity of 100 °C. A further weight loss at higher temperatures was presumably due to dehydration caused by the condensation of P–OH. The amounts of acids on the ground aluminum phosphates were almost independent of the acid strength, which was around $+1.5$ (pK_a). The amounts of acids of the A, B, and C types and of $AlPO_4$ tended to increase slightly with the grinding time. The amount of acid of the K substance reached a maximum after 6 hrs' grinding but decreased slowly when grinding was continued for longer than 15 hr.

Grinding is known to cause changes in the structure, composition, and properties of substances.[2-6] The present authors have previously reported the formation conditions and the acidic properties of various aluminum phosphates.[7,8] The present paper will describe an investigation of the change in the structure and acidic properties of various aluminum phosphates on grinding.

Experimental

Apparatus and Method. An Ishikawa grinder, model AGA (agate mortar), was used; grinding was carried out at room temperature and at a relative humidity of 20~25%. X-Ray analysis was carried out with a Rigaku Denki Geigerflex X-ray diffractometer, using Ni filtered Cu$K\alpha$ radiation. Hitachi EPI-S2 and EPI-G2 spectrophotometers were used for the infrared spectroscopy, spectra being taken by means of a KBr tablet or on Nujol mulls. A Rigaku Denki differential thermogravimetric analyzer, 8002 HD, was used for the DTA and TGA. The method reported by Tanabe and his co-workers[9,10] was used for measuring the acidic properties of various aluminum phosphates. The amount of water was determined by both the Karl-Fischer method and TGA.

Preparation of Various Aluminum Phosphates. *1) $AlPO_4$ (Berlinite)*: Aluminum hydroxide (hydrargillite type) or γ-alumina and phosphoric acid were mixed to give a Al_2O_3/P_2O_5 (R) molar ratio of 1.0/1.0. The mixture was then dehydrated over a small flame with vigorous agitation to complete the reaction; the product was heated at 500 °C for 20 hr in a thermostated electric furnace to prepare the sample. The heated product was proved to be $AlPO_4$, Berlinite, by the X-ray diffraction method.

2) A, B, and C types of $Al_4(P_4O_{12})_3$: α-Alumina and ammonium dihydrogen phosphate were mixed thoroughly to give a molar ratio of R=1/3~1/4. The A type product was obtained by heating the mixture at 750 °C for 20 hr in an electric furnace; the B type, by heating it at 500~550 °C for 20 hr, and the C type, by heating it at 650~700 °C for 20 hr. The products were thoroughly washed with water to remove the excess phosphoric acid and dried at 80 °C for 20 hr. The X-ray diffraction patterns of the A, B, and C types of $Al_4(P_4O_{12})_3$ were identical with those of the respective ASTM cards.

3) K Substance (the substance which we tentatively designated previously as the K substance has characteristic X-diffraction peaks at $2\theta=11.2$, 18.0, 26.8°): α-Alumina and phosphoric acid were mixed to give a molar ratio of R=1/3~1/4. The mixture was heated at 300 °C for 20 hr and then treated in a manner similar to that described above.

Results and Discussion

1) Changes Caused by Grinding of the A, B, and C Types of $Al_4(P_4O_{12})_3$. As an example, Fig. 1 shows the changes in the X-ray diffraction pattern of the A type caused by grinding. It can be seen that the X-ray diffraction peaks become weaker with the grinding time, as the destruction of the crystal structure to give an amorphous form progresses. However, as the X-ray diffraction pattern indicates that the A type does not become completely amorphous even after grinding for 72 hr, it can be seen that the crystal structure of the A type is relatively more stable when ground than sodium phosphates.[2,3] Changes in the X-ray diffraction patterns of the B and C types are similar

1) Part IV, M. Tsuhako, I. Motooka, and M. Kobayashi, *Nippon Kagaku Zasshi*, **92**, 1136 (1971).
2) I. Motooka, G. Hashizume, and M. Kobayashi, *ibid.*, **87**, 255, (1966).
3) I. Motooka, G. Hashizume, and M. Kobayashi, *ibid.*, **87**, 953 (1966).
4) I. Motooka, G. Hashizume, and M. Kobayashi, *Kogyo Kagaku Zasshi*, **71**, 1512 (1968).
5) I. Motooka, G. Hashizume, and M. Kobayashi, This Bulletin, **40**, 2095 (1967).
6) I. Motooka, G. Hashizume, and M. Kobayashi, *ibid*, **41**, 2040 (1968).
7) M. Tsuhako, I. Motooka, and M. Kobayashi, *Nippon Kagaku Zasshi*, **92**, 318 (1971).
8) M. Tsuhako, I. Motooka, and M. Kobayashi, *ibid.*, **92**, 1131 (1971).
9) K. Tanabe and T. Takeshita, "San Enki Shokubai," Sangyo Tosho, Tokyo (1966), p. 159.
10) G. Matsuzaki, Y. Fukuda, T. Kobayashi, K. Kubo, and K. Tanabe, *Shokubai*, **11**, 210 (1969).

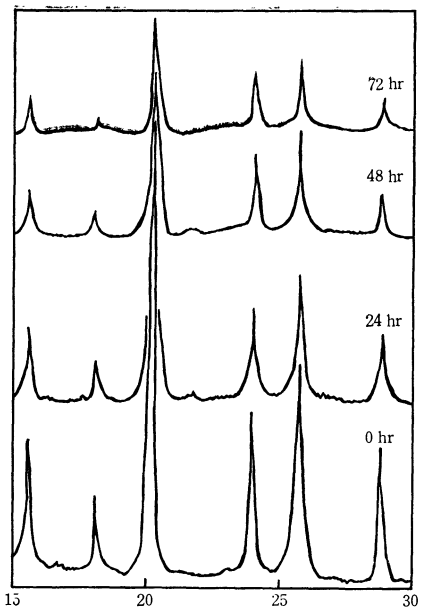

Degree, 2θ (°) Cu$K\alpha$ 40 KV—7 mA

Fig. 1. The changes in X-ray diffraction pattern of type A of $Al_4(P_4O_{12})_3$ on grinding.

to that with the A type, though the results indicate that the crystal structure of the B type breaks down somewhat more easily than those of the A and C types. The changes in the infrared absorption spectrum of the A type caused by grinding are shown in Fig. 2. Although the changes are not appreciable, a new absorption (shoulder) due to grinding appears near 940 cm^{-1}, corresponding to a P–OH bending absorption.[11,12] Since absorptions due to the stretching and bending of P–OH groups appear at 2500~3000 and near 900 cm^{-1} respectively, it is assumed that P–OH is formed by the cleavage of the P–O–P or P–O–Al linkages on grinding. The absorptions at 3400~3600 and near 1600 cm^{-1} increase with the grinding time, presumably because of the adsorption of water onto active sites formed by grinding.

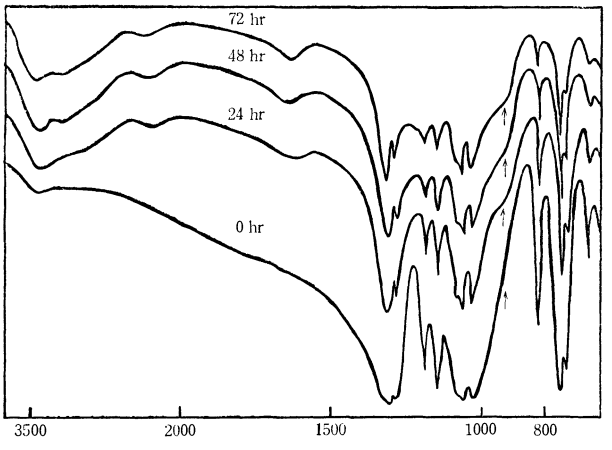

Wave number (cm^{-1})

Fig. 2. The changes in infrared absorption spectra of type A of $Al_4(P_4O_{12})_3$ on grinding.

2) *Changes Caused by Grinding of $AlPO_4$ (Berlinite).* Changes in the X-ray diffraction pattern and IRS of $AlPO_4$ on grinding show the same tendencies as those for the A, B, and C types. The X-ray diffraction pattern of $AlPO_4$ does not indicate a completely amorphous state even after having been ground for 72 hr, showing that the crystal structure is somewhat stable to grinding. A shoulder appears near 940 cm^{-1} in the IRS when the sample is ground for 48~72 hr, presumably because of the formation of P–OH by the cleavage of the P–O–Al linkage.

3) *Changes Caused by Grinding of the K Substance.* Changes in the X-ray diffraction pattern of the K substance on grinding are shown in Fig. 3. The change in structure to an amorphous form is greater than those of the A, B, and C types of $Al_4(P_4O_{12})_3$ and $AlPO_4$

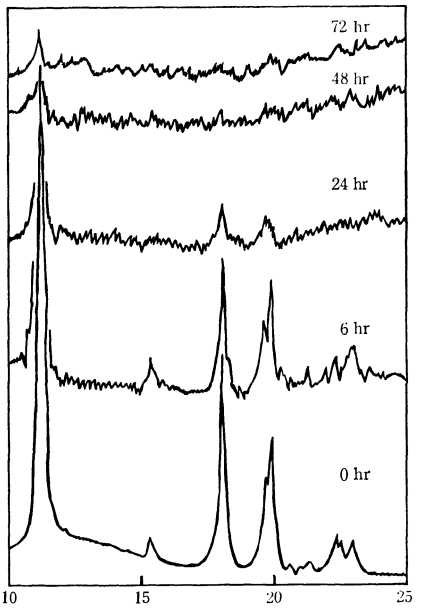

Degree, 2θ (°) Cu$K\alpha$ 40 KV—70 mA

Fig. 3. The changes in X-ray diffraction pattern of substance K on grinding.

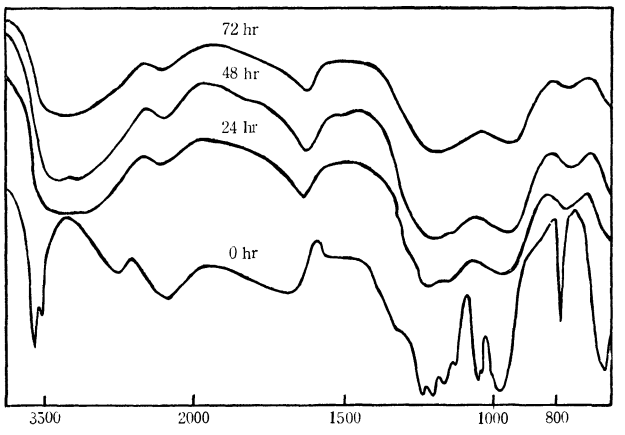

Wave number (cm^{-1})

Fig. 4. The changes in infrared absorption spectra of substance K on grinding.

11) D. E. C. Corbridge, *J. Appl. Chem.*, **6**, 456 (1956).
12) D. E. C. Corbridge and E. J. Lowe, *J. Chem. Soc.*, **1954**, 493, 4555.

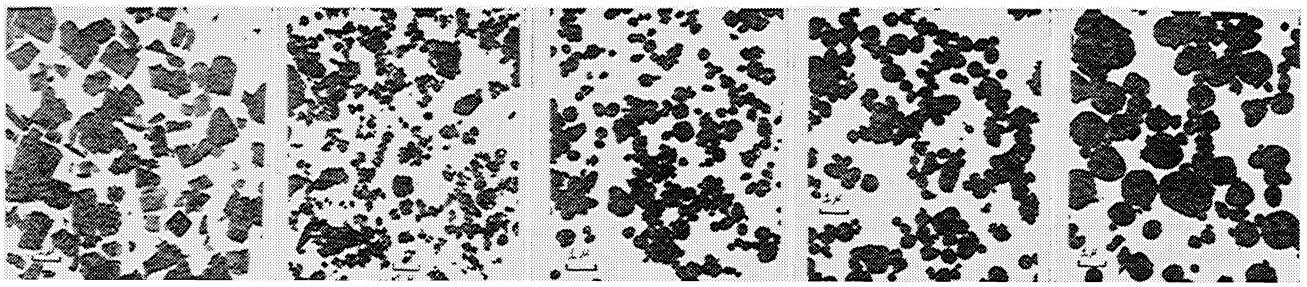

Fig. 5. Electron microphotographs of substance K; grinding time.
(a): Original, (b): 6 hr, (c): 15 hr, (d): 24 hr, (e): 72 hr.

(Berlinite), a completely amorphous form resulting after 72 hr's grinding. The crystal structure of the K substance is, therefore, more unstable than those of the A, B, and C types and $AlPO_4$. Fig. 4 shows the change in the IRS of the K substance on grinding. The K substance shows two sharp absorption peaks near 3600 cm^{-1} due to water of crystallization, and a broad absorption at 2600~2700 cm^{-1} due to P–OH. On grinding, the two sharp absorption peaks near 3600 cm^{-1} become smaller; the appearance of a broad absorption at a slightly lower wave number indicates that water of crystallization is released by the destruction of the crystal structure on grinding, and water molecules are adsorbed onto active sites of the surface of the ground K substance. Generally, water of crystallization is released when hydrated substances are ground, and their crystal structures break down easily.[4,13,14] The K substance contains water of crystallization and follows this general rule. It is, therefore, believed that the K substance is more unstable to grinding than the A, B, and C types and $AlPO_4$.

4) *Change in the Particle Size of the K Substance on Grinding.* The results of electron microphotography are shown in Fig. 5. It may be seen that particles of the K substance become very small after being ground for 6~15 hr. However, the particles gradually become larger again when grinding is continued for longer than 24 hr. This can be explained as resulting from the adsorption of moisture by the initially formed small-sized particles, leading to their subsequent agglomeration,[15] though this phenomenon is not seen with particles of the A, B, and C types or $AlPO_4$.

5) *Changes in the DTA and TGA of Various Aluminum Phosphates on Grinding.* Changes in the DTA and TGA of the K substance are shown in Fig. 6. The A, B, and C types and $AlPO_4$ show almost identical tendencies, an endothermic peak accompanied by weight loss due to the dehydration of adsorbed water around 100 °C. The endothermic peak and the weight loss increase with the grinding time, suggesting that the amount of water released increases with grinding.

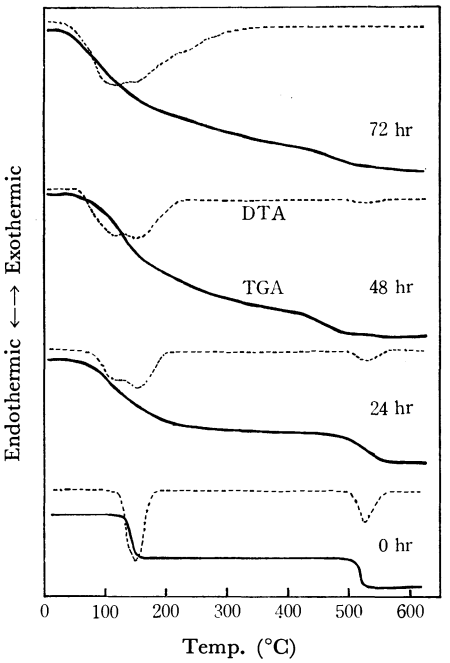

Fig. 6. The changes in DTA and TGA of substance K on grinding.

When the temperature is further increased, a further weight loss occurs, presumably because of dehydration caused by the condensation of the P–OH group. The unground K substance exhibits large endothermic peaks in the vicinity of 150~160 °C (the first endothermic peak, due to the dehydration of water of crystallization) and in the vicinity of 540 °C (the second endothermic peak, presumably due to the dehydration caused by the condensation of P–OH). However, the first endothermic peak becomes broader with an increase in the grinding time and overlaps with the endothermic peak due to the dehydration of adsorbed water, while the second endothermic peak gradually becomes smaller as the grinding time increases, and disappears almost completely after 48~72 hr's grinding. This again shows that the structure of the K substance is easily broken down by grinding. The changes in the water content on grinding are shown in Fig. 7, which shows the changes in the dehydration quantities of ground A, B, and C types, $AlPO_4$, and the K substance when they are heated to 650 °C. The K substance has a moisture content of about 16~17% in its original state, but the moisture content increases gradually with grinding.

13) I. B. Bleeker, *Chem. News*, **101**, 30 (1910).
14) Y. Arai, and T. Yasue, *Kogyo Kagaku, Zasshi*, **74**, 1343 (1971).
15) A similar tendency was observed when the surface area was measured by the BET method, though this point is being studied further because of problems in the measurement of the surface area of these aluminum phosphates.

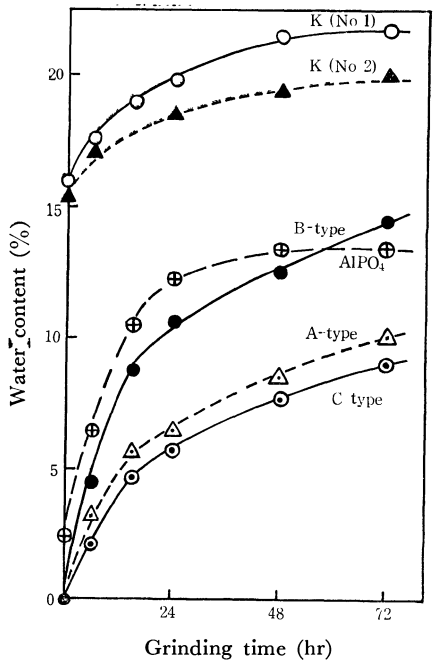

Fig. 7. The changes in water content of various aluminum phosphates on grinding.

The moisture contents of the A, B, and C types and $AlPO_4$ also increase gradually with grinding, and at a faster rate than for the K substance.

6) *Changes in the Acid Strength and Amounts of Acid of the A, B, and C Types of $Al_4(P_4O_{12})_3$ and $AlPO_4$ on Grinding.* The amounts of acid were not changed by the acid strength when the A, B, and C types and $AlPO_4$ were ground. The amounts of acid contained in unground samples of these aluminum phosphates are very small, but they increase slightly with the grinding time. It is considered that the increase in the amounts of acid is due to both the increase in surface area and the formation of P–OH by the cleavage of the P–O–P or P–O–Al linkages on grinding.

7) *Changes in the Acid Strength and Amount of Acid of the K Substance on Grinding.* As with the A, B, and C types and $AlPO_4$, almost no change in the amount of acid was observed upon a change in the acid strength when the K substance was ground. The amount of acid of the unground K substance is much larger than those of the A, B, and C types and $AlPO_4$. The changes in the amount of acid of the K substance on grinding are shown in Fig. 8. The amount of acid becomes very large when the sample is ground for 6 hr, but it gradually decreases with further grinding. This may be explained as follows. On grinding, the particles initially become smaller and the surface area of the sample increases, so there is an increase in the amount of acid per unit weight. However, upon more prolonged grinding the crystal structure breaks down and the agglomeration of the amorphous particles occurs, with a consequent decrease in the surface area and, hence, in the acidity of the K substance.

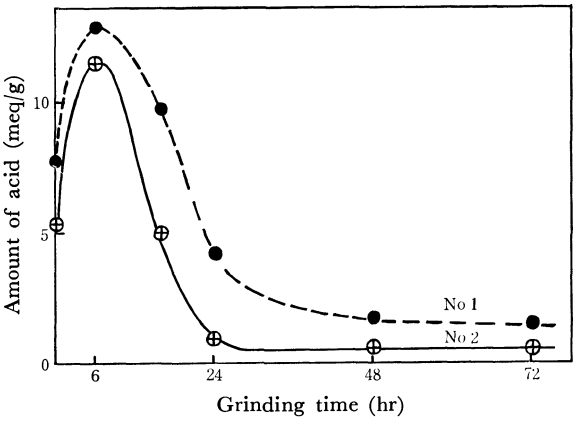

Fig. 8. The changes in amount of acid of substance K on grinding.
Amount of acid is the value at $pK_a = 1.5$

The authors are grateful to the Teikoku Kako Co., Ltd. for the measurement of the surface area, and the use of their electron microphotograph, and to Prof. T. Matsuo for his kind and valuable advice.

The Electron-scavenging Process in 3-Methylhexane Glass at 77 K Studied by ESR

Koichi OKA, Hideo YAMAZAKI, and Shoji SHIDA

Laboratory of Physical Chemistry, Tokyo Institute of Technology, Meguro-ku, Tokyo 152

(Received December 4, 1972)

The effect of various additives, *i.e.*, nitrous oxide, sulfur hexafluoride, methyl chloride, and sulfur dioxide, on the yield of the trapped electrons produced in the γ-irradiated 3-methylhexane (3MHX) glass at 77 K have been investigated by the ESR technique. The yields of the trapped electrons were reduced by the addition of all the solutes examined; the efficiency of electron scavenging was found to be in the order of $SF_6 > CH_3Cl > N_2O > SO_2$. The concentration dependence of the electron scavengers showed that the efficiency of the electron scavenging in the glassy state had values intermediate between those in the gas and liquid phases. The high efficiency observed in the glassy state suggests that the non-solvated electrons before being trapped move about rapidly in the glassy matrix as the form of quasi-free electrons. The ESR-power saturation of the trapped electrons was considerably reduced by the addition of N_2O; a possible mechanism of the relaxation of the ESR is proposed.

The electron-scavenging process is one of the most important problems in radiation chemistry. To examine this problem, physical methods, such as optical absorption measurement by means of pulse radiolysis,[1] ESR studies,[2,3] and luminescence measurement,[4] have been used as well as the chemical method of product analysis. A considerable number of experiments have been made on electron scavenging by chemical analysis in the gas[5,6] and the liquid phases;[7-9] however, there has been little work in the glassy state.[10] The main difficulties of the product analysis in the glassy state at low temperatures are the fact that the spatial distribution of solutes may be nonhomogeneous and the fact that the overall reactions are not isothermal. Therefore, the kinetic treatment based on the homogeneous distribution of reactants and on the isothermal condition is not applicable. The physical methods may still give some insight into this problem, though concerning the nature of the trapped electrons, the spatial distribution has been studied by photobleaching[11] and by the microwave-power saturation of ESR.[12,13] The structure of the trapped electrons has also been studied by means of pulse radiolysis[1,14] and by ESR.[3,15] However, little study has been done on the electrons before being trapped. These electrons should resemble those photo-released from the trapped states,[16] 'mobile electrons,' but they may be different in energy.

In the present work, ESR has been used to measure the trapped electrons in 3-methylhexane (3MHX) glass and to obtain information on the electrons before they were trapped by the scavenger technique. The energy of electron attachment has been said to be different in each electron scavenger[17-20] in the gas phase, so that the electrons are scavenged even in the solid phase. The ESR technique is expected to be useful for testing the efficiency of electron attachment in the solid phase. The electron scavengers (N_2O, SF_6 and CH_3Cl) used in the present work are well known, but SO_2 is not usually used in the gas and the liquid phases. In the present work, N_2O, one of the most important electron scavengers, has been studied in detail.[21] The trapped electrons decreased upon the addition of N_2O to the hydrocarbon matrix and also changed in their nature; the ESR-power saturation of the trapped electrons was remarkably reduced by the addition of N_2O.

Experimental

Pure-grade 3MHX (Aldrich Chemical Co.) was purified by passing it through an activated silica gel column; it was degassed by the freeze-pump method and stored in sodium-potassium alloy for more than a day before use. The gaseous materials, SF_6, CH_3Cl, N_2O and SO_2 (Matheson Co.) were

1) H. A. Gillis, N. W. Klassen, G. G. Teather, and K. H. Lokan, *Chem. Phys. Lett.*, **11**, 12, (1971); I. A. Taub and H. A. Gillis, *J. Amer. Chem. Soc.*, **91**, 6507 (1969); N. V. Klassen, H. A. Gillis, and G. G. Teather, Report of National Research Council of Canada, Division of Physics RXNR 2321 (1972).
2) D. R. Smith and J. J. Pieroni, *Can. J. Chem.*, **45**, 2723 (1967).
3) H. Yoshida and T. Higashimura, *ibid.*, **48**, 504 (1970).
4) K. Funabashi, C. Hebert, and J. L. Magee, *J. Phys. Chem.*, **75**, 3221 (1971); M. Magat, "Progress and Problems in Contemporary Radiation Chemistry," Prague, p. 423 (1971); A. C. Albrecht, *ibid.*, p. 331.
5) P. Ausloos, *Progs. React. Kinet.*, **5**, 113 (1969); W. J. Holtslander and G. R. Freeman, *J. Phys. Chem.*, **71**, 2562 (1967).
6) G. R. A. Johnson and J. M. Warman, *Trans. Faraday Soc.*, **61**, 1709 (1965).
7) G. Scholos and M. Simic, *Nature*, **202**, 895 (1964).
8) F. Williams, *J. Amer. Chem. Soc.*, **86**, 3954 (1964).
9) J. M. Warman, K.-D. Asmus, and R. H. Schuler, *Adavan. Chem. Ser.*, **82**, 25 (1968).
10) T. Wakayama, T. Kimura, T. Miyazaki, K. Fueki, and Z. Kuri, This Bulletin, **42**, 266 (1969); T. Sawai, Y. Shinozaki, and G. Meshitsuka, *ibid.*, **45**, 984 (1972).
11) W. H. Hamill, "Radical Ions," Ed. by E. T. Kaiser and L. Kevan, Wiley-Interscience, New York, (1968) p. 321.
12) K. Tsuji and F. Willaims, *Trans. Faraday Soc.*, **65**, 1718 (1969).
13) J. Zimbrick and L. Kevan, *J. Chem. Phys.*, **47**, 2364 (1967).
14) J. T. Richards and J. K. Thomas, *ibid.*, **53**, 218 (1970).
15) J. Lin, K. Tsuji and F. Williams, *J. Amer. Chem. Soc.*, **90**, 2766 (1968).
16) F. S. Dainton and G. A. Salmon, *Proc. Roy. Soc. Ser. A.* **285**, 319 (1965).
17) D. Rapp and D. D. Briglia, *J. Chem. Phys.*, **43**, 1480 (1965).
18) L. G. Christophorou and J. A. D. Stockdale, *ibid.*, **48**, 1956 (1968).
19) R. P. Blaunstein and L. G. Christophorou, *ibid.*, **49**, 1526 (1968).
20) D. A. Raelis and J. M. Goodibgs, *Can. J. Chem.*, **49**, 1571 (1971).
21) S. Sato, This Bulletin, **41**, 304 (1968).

commercially obtained and were used without purification.

In a mercury-free system, 3MHX was measured with a measuring capillary (2 mm i.d.), and the amounts of gaseous material added were determined by means of an oil manometer with a flask of a constant volume. The Ostwald absorption coefficients of various electron scavengers in liquid 3MHX at room temperature were used to determine the concentration of the solutes in 3MHX glass at 77 K. The samples were sealed in a Suprasil quartz ESR tube (3 and 5 mm, i.d.) and irradiated for 20 min—4 hr by ^{60}Co γ-rays at 77 K in the dark, at a dose rate of 0.8×10^{6} r/hr. After the irradiation, the ESR spectra of the samples were immediately measured in the dark by means of a JEP-1 X-band ESR spectrometer with a field modulation of 100 kHz. A multimode microwave cavity was used to determine the signal intensity by referring to a standard sample. After the initial measurement, bleaching experiments were performed with infrared light (>1000 nm) from a tungsten lamp through two Toshiba glass filters (V-B46 and IR-RIA).

In the saturation study the microwave power of ESR was measured by means of a thermistor power meter in the range of 0.01—10 mW. The magnetic field, H_1, of the microwaves in the cavity under the present operating conditions was given approximately by the following relationship: $H_1=2.0\times10^{-2}P^{1/2}$, where P is the microwave power in mW and where H_1 is that in gauss.[22] The power saturation curve was measured in the $1-10^{-3}$ mW range by the use of multimode microwave cavity at the modulation frequency of 100 kHz. The ratio of the saturation factor, Z, was directly measured from the signal-intensity ratio of the sample to a DPPH crystal, because the signal of the DPPH crystal was not entirely saturated under the conditions of the measurement.

Results

The ESR spectrum of γ-irradiated 3MHX glass is shown in Fig. 1. The singlet spectrum at the center is due to the trapped electrons (e_t^-) and is photobleached by the irradiation of infrared light. The remaining spectrum is due to a free radical. The line shape of e_t^- is close to a gaussian. The line width of e_t^- between the maximum slope is about 3.5±0.2 gauss and is broadened at a high microwave power. The singlet ESR spectrum of e_t^- was well resolved from that of the free radicals by photobleaching with infrared light. The microwave-power saturation of e_t^- was measured at various total doses. The experimental values coincide with the theoretical curves calculated by the saturation factor, as is shown in Fig. 2. With the irradiation doses between $(0.83-10)\times10^{19}$ eV/g, the saturation curve moves gradually to the side of a high microwave power at high total dose, but the curvature does not change.

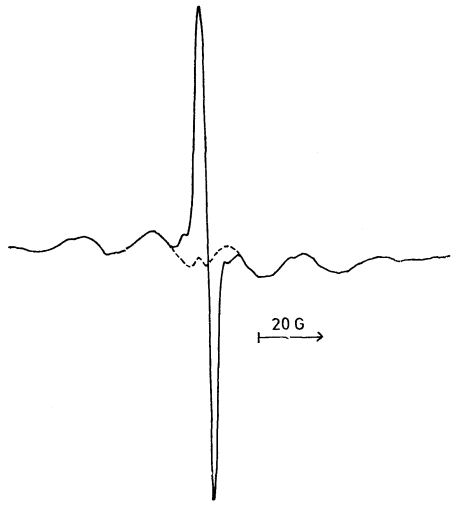

Fig. 1. ESR spectra of pure 3-methylhexane glass γ-irradiated to a dose of 9×10^{18} eV/g at 77 K. Solid curve; immediately after the irradiation, dotted curve; after the photobleaching by infrared light.

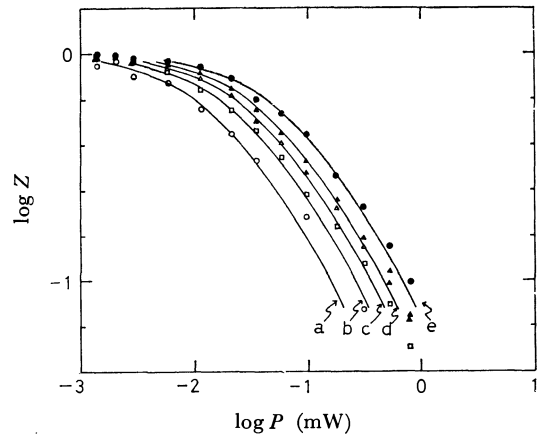

Fig. 2. Experimental values and theoretical curves of microwave-power saturation for e_t^- in 3-methylhexane glass at 77 K. The saturation factor, Z, is plotted as a function of microwave power, P, and the experimental values correspond to ○; 8.3×10^{18}, □; 17×10^{18}, △; 33×10^{18}, ▲; 50×10^{18}, ●; 10×10^{19} eV/g and the calculated curves correspond to a) $T_1=1.3\times10^{-2}$, b) 7.6×10^{-3}, c) 5.6×10^{-3}, d) 4.4×10^{-3}, e) 3.0×10^{-3} s.

A study was made of the scavenging of e_t^- in γ-irradiated 3MHX glass at 77 K as a function of the electron-scavenger concentration. It is well known that the electron scavengers reduce the formation of e_t^-. The signal intensity of e_t^- decreased rapidly with the concentration of SF_6 (Fig. 3) and disappeared completely at a relatively low concentration compared with the cases of the other electron scavengers. The addition of SF_6 did not alter the line shape of the e_t^- signal and did not produce any new signal. The

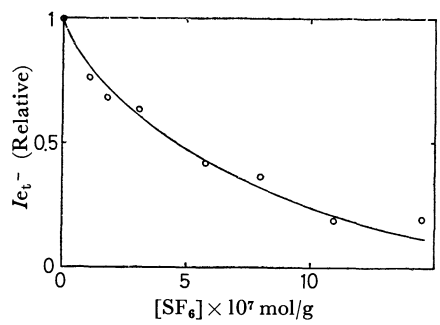

Fig. 3. Effect of addition of SF_6 on the relative signal intensity of e_t^- in 3-methylhexane glass at 77 K γ-irradiated to a dose of 2.0×10^{19} eV/g.

22) C. P. Poole, Jr., "Electron Spin Resonance," Interscience Publishers, New York (1967), p. 341.

microwave-power saturation curve of e_t^- shifted slightly to the side of the low power upon the addition of SF_6.

When N_2O was added, the signal intensity of e_t^- decreased at the low microwave power. At a high microwave power, the signal intensity of e_t^- increased with the concentration of N_2O and then decreased, as is shown in Fig. 4. The line shape and the width of the e_t^- signal did not change upon the addition of N_2O, and the signal could be photobleached by the infrared light at any concentration of N_2O. However, when N_2O was added, the microwave-power saturation curve shifted to the side of the high power and the shape of the saturation curve changed, as is shown in Fig. 5.

Figure 6 shows the ESR spectrum of γ-irradiated 3MHX glass containing CH_3Cl. The signal at the center is due to e_t^-, and the quartet signal, to CH_3. The microwave-power saturation curve of e_t^- did not shift upon the addition of CH_3Cl. After the photobleaching, the signal of e_t^- disappeared and that of

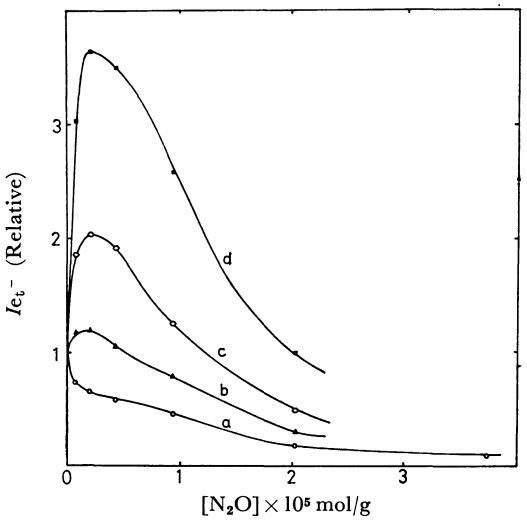

Fig. 4. Effect of addition of N_2O on the relative signal intensity of e_t^- for various microwave power in 3-methylhexane glass at 77 K γ-irradiated to a dose of 1.7×10^{19} eV/g: a) extrapolated value at the zero microwave power, b) 0.027 mW, c) 0.048 mW, d) 0.081 mW.

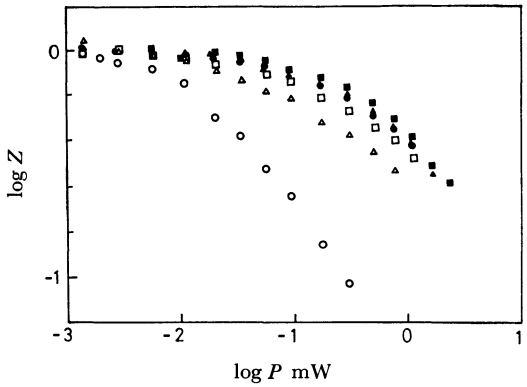

Fig. 5. Microwave-power saturation curve for e_t^-, plotting the saturation factor, Z, *versus* microwave power, P, in 3-methylhexane glass γ-irradiated to a dose of 1.7×10^{19} eV/g at 77 K: N_2O concentration of ○; 0×10^{-7}, △; 4.7×10^{-7}, □; 1.1×10^{-6}, ●; 2.2×10^{-6}, ▲; 4.7×10^{-6}, ■; 10×10^{-6} mol/g.

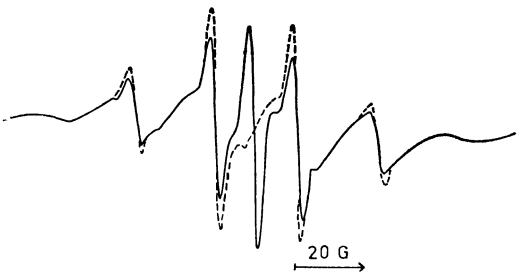

Fig. 6. ESR spectra of 3-methylhexane glass containing 3×10^{-6} mol/g CH_3Cl γ-irradiated to a dose of 9×10^{18} eV/g at 77 K. Solid curve; immediately after the irradiation, dotted curve; after the photobleaching by infrared light.

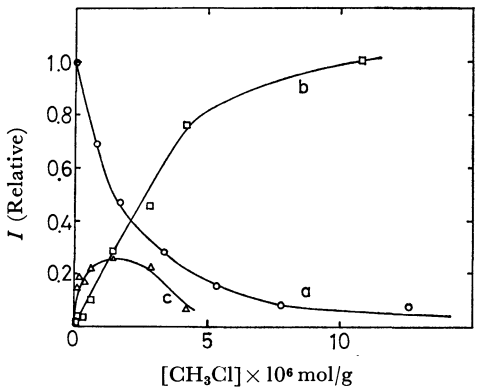

Fig. 7. Effect of addition of CH_3Cl on the relative signal intensity of e_t^- in 3-methylhexane glass γ-irradiated to a dose of 9×10^{18} eV/g at 77 K: a) e_t^-, b) CH_3, c) the increment of CH_3 by photobleaching.

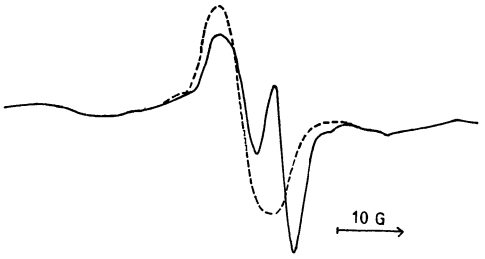

Fig. 8. ESR spectra of 3-methylhexane glass containing 5.4×10^{-6} mol/g SO_2 γ-irradiated to a dose of 9×10^{18} eV/g at 77 K. Solid curve; immediately after the irradiation, dotted curve; the photobleaching by infrared light.

CH_3 increased. As is shown in Fig. 7, the signal intensity of e_t^- decreased, while the quartet signal of CH_3 increased, with the concentration of $CHCl_3$, which underwent a dissociative electron attachment.

The ESR spectrum of γ-irradiated 3MHX glass containing SO_2 is shown in Fig. 8. A new singlet signal (g=2.007, ΔH_{msl}=8 gauss) appeared in the presence of SO_2, and the signal increased when the e_t^- was photobleached. The signal seems to be due to SO_2^-; the ESR signal of SO_2^- formed from the adsorbed SO_2 on MgO has been measured by another method.[23] The broad linewidth is probably due to the anisotropy of SO_2^-. Figure 9 shows that the signal

23) R. A. Schoonheydt and H. J. Lunsford, *J. Phys. Chem.*, **76**, 323 (1972).

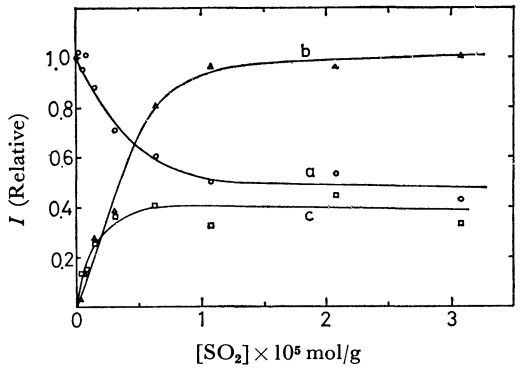

Fig. 9. Effect of addition of SO_2 on the relative signal intensity in 3-methylhexane glass γ-irradiated to a dose of 9×10^{18} eV/g at 77 K: a) e_t^-, b) SO_2^-, c) the increment of SO_2^- by photobleaching.

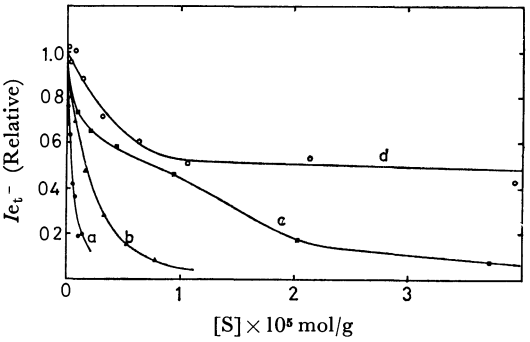

Fig. 10. Summary of the effect of addition of various electron scavenger on the relative signal intensity of e_t^-: a) SF_6, b) CH_3Cl, c) N_2O, d) SO_2.

intensity of e_t^- decreased, and that of SO_2^- increased, with the concentration of SO_2. Even at high concentrations of SO_2, the signal of e_t^- did not completely disappear.

The electron-scavenging studies of e_t^- in 3MHX by various electron scavengers are summarized in Fig. 10, which shows that the efficiency of electron scavenging obtained from the initial slope of the curves is in the order of $SF_6>CH_3Cl>N_2O>SO_2$ and that the curvature of each scavenger is different from all others.

Discussion

In the absence of electron scavengers, the liberated electrons are either recombined with parent cations or trapped by physical sites in the glassy matrix:

$$3MHX \rightsquigarrow 3MHX^+ + e^- \quad (1)$$

$$e^- + 3MHX^+ \xrightarrow{k_n} 3MHX \quad (2)$$

$$e^- + \text{physical site} \xrightarrow{k_t} e_t^- \quad (3)$$

where k_n and k_t are the rate constants of neutralization and of electron trapping. In the presence of the electron scavenger, S, a part of the electrons can be scavenged before the recombination or the trapping:

$$e^- + S \xrightarrow{k_s} S^- \quad (4)$$

where k_s is the rate constant of electron scavenging. The measurement was made only of the decrease in the trapped-electron yield by the addition of the scavengers in this experiment. The reaction of electron attachment competes with those of electron trapping and neutralization. If the reaction of the electron scavenging and the electron trapping are treated by homogeneous kinetics, the following equations are obtained:

$$G_0(e_t^-)/G(e_t^-) = 1 + (k_s/\tau)S \quad [1]$$

$$\tau = k_n[M^+] + k_t[T.S.] \quad [2]$$

where $G_0(e_t^-)$ is the G-value of e_t^- at zero scavenger concentration and where [T.S.] is the concentration of the physical trapping site. Because the ion pairs neutralize geminately, the local concentration of parent cations, $[M^+]$, is a dose-independent constant in Eqs. [1] and [2], it is expressed microscopically as a function of the distance between the electrons and the parent cations. The concentration of the physical trapping sites was estimated to be larger than 10^{-3} mol/l from the total dosage effects.[24] The relative rate constants of electron scavenging, k_s/τ, are obtained from the initial slope of the curves in Fig. 11, in which the plots for SF_6 and CH_3Cl are almost linear and in the curves for N_2O and SO_2 are concave downwards. The deviation of the plots from the straight line may be due to the fact that these reactions are not homogeneous. When k_s is very large, the concentration of scavengers can be relatively small in the measurement and the heterogeneity of the competition reaction may be ignored. The reciprocal concentration at which the yield of e_t^- decreases to a half, $1/S_{1/2}$, and the k_s/τ ratio are shown in Table 1. The values of k_s/τ and $1/S_{1/2}$ are the same sequences of series, and the $1/S_{1/2}$ ratio is almost ten times larger than k_s/τ. To express the efficiency of electron scavenging, the values of k_s/τ seem to be more adequate than that of $1/S_{1/2}$. The electron-scavenging efficiency of SF_6 in the liquid phase is found to be almost the same as that of N_2O by the measurement of the hydrogen depression,[25] because the electrons were solvated and the efficiencies were determined by a diffusion-controlled process. In the gas phase, the ratio of efficiencies between SF_6 and

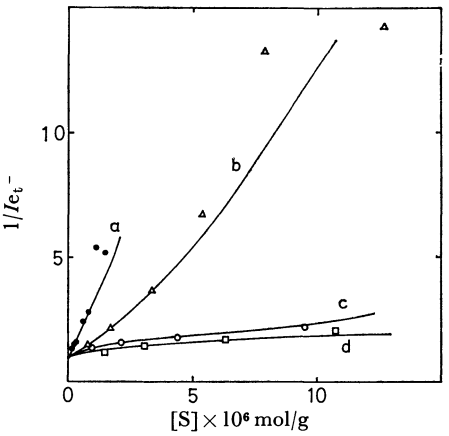

Fig. 11. The inverse of the relative signal intensity of e_t^- plotted *versus* the concentration of various electron scavenger: a) SF_6, b) CH_3Cl, c) N_2O, d) SO_2.

24) A. Ekstrom, R. Suenram, and J. E. Willard, *J. Phys. Chem.*, **74**, 1888 (1970).

Table 1.

	Solid[a]		Liquid	Gas		
	$1/S_{1/2}$ l/mol	k_s/τ l/mol	α[b] l/mol	$1/S_{1/2}$[c] l/mol	σ A²	$\int\sigma(E)dE$ A² eV
SF_6	2×10^3	2×10^2	18	$\geqq3\times10^8$	2.15[d]	
CH_3Cl	6×10^2	6×10	(5)		0.058[e]	1.54×10^{-3}[e]
N_2O	9×10	2×10	16	3×10^4	0.0978[e]	1.05×10^{-2}[e]
SO_2	—	10				

a) This work in 3MHX glass; b) From the measurement of hydrogen depression in liquid cyclohexane, α is equivalent to $1/S_{1/2}$ from Ref. 9; c) From the measurement of N_2 formation in gaseous propane by the addition of N_2O; d) Electron-attachment cross section by thermal electron from Ref. 17; e) Electron-attachment cross section by electrons of E_{max} from Refs. 17 and 19.

N_2O was measured[6] and found to be about 10^4 and the electron-attachment cross sections were measured directly by the methods of mass spectrometry for negative ions,[17-19] as is shown in Table 1. The electron scavenging in the glassy state seems to have an intermediate character between those in the gas and liquid phases with respect to the ratios and the absolute values of $1/S_{1/2}$. These experimental results indicate that, before being trapped, the electrons interact with a solvent weaker than the solvated electrons in the liquid phase.

The formations of SO_2^- and CH_3 were observed by the use of ESR in the presence of SO_2 and CH_3Cl. The electron scavengers, SO_2 and CH_3Cl, attach to the electrons produced by γ-irradiation or by photobleaching of e_t^-, and the negative ions or the free radicals appear by means of those reactions:

$$e_t^- \xrightarrow{h\nu} e^- \quad (5)$$

$$e^- + SO_2 \longrightarrow SO_2^- \quad (6)$$

$$e^- + CH_3Cl \longrightarrow CH_3 + Cl^- \quad (7)$$

On the other hand, the electron scavenging by SF_6 and N_2O produces no negative ions or free radicals. The solute, SF_6, attaches to the electrons as intermediate species:

$$e^- + SF_6 \longrightarrow [SF_6^-] \quad (8)$$

The pair of SF_6^- and the parent cation is unstable and is neutralized by electron jumps from the negative ions or by the migration of negative ions in the matrix. In the CH_3Cl solution, however, the dissociative electron attachment by CH_3Cl takes place,[26] and an ion pair of Cl^- and the parent cations forms near the CH_3 radicals by means of the cage effect of a glassy matrix. The ion pair must be unstable and must be neutralized to leave CH_3 radicals. In the experimental results of low-pressure mass spectrometry, SO_2 and N_2O attach dissociatively to electrons with some energy by the formation of O^-:

$$e^- + SO_2 \longrightarrow SO + O^- \quad (9)$$

$$e^- + N_2O \longrightarrow N_2 + O^- \quad (10)$$

The cage effect in glassy matrix disturbs the dissociative electron attachment of SO_2, and SO_2^- is formed. However, N_2O^- dissociates easily, and the parent cations are neutralized by O^- migration in the matrix. Therefore, no negative ion were trapped in the matrix by the addition of N_2O.

The energy distribution of electrons, $p(E, t)$, is the function of the electron energy, E, and the time, t. When the electrons are thermalized, the spatial distribution, $D(r)$, is the integrated product of the degradation factor, $R(E, r)$, and the initial energy distribution, $\int R(E, r)p(E, O)dE$, where r is the distance between electrons and the parent cations. If the electrons are trapped after a complete thermalization and if the concentration of trapping sites is very large, the portion of ionic species being trapped is the integrated product, $4\pi\int r^2D(r)\phi(r/r_t)dr$,[27] where $\phi(r/r_t)$ is the probalility of electron trapping, where r_t is $e^2/\varepsilon V_t$, where ε is the dielectric constant, and where V_t is the depth of the physical or chemical site. When r is larger than r_t, $\phi(r/r_t)$ can be expected to be large. The chemical site is usually deeper than the physical site. When the concentration of electron scavengers is small, the electron-scavenging efficiency, k_s, is proportional to the integrated cross section of electron attachment, $\int\sigma(E)P(E)Q(E)dE$, where $\sigma(E)$ is the cross section of electron-scavenging as a function of the electron energy, $p(E)=\int p(E, t)dt$ is the time-average distribution of electrons, and $Q(E)$ are the portions of electrons which should have been physically trapped in the absence of the electron scavengers. In a glassy matrix, $Q(E)$ will be small for the electrons near the thermal energy, because the electrons in the low-energy population will geminately recombine with the parent cation and will not contribute to the reaction with the scavengers. Therefore, $P(E)Q(E)$ in the glassy state will more likely be the energy distribution function in the gas phase than that in the liquid phase, where the collisional deactivation is easier than in the glassy state, so that energy is distributed only

25) P. P. Infelta and R. H. Schuler, *ibid.*, **76**, 987 (1972).

26) "Fundamental Processes in Radiation Chemistry," Ed. by J. E. Willard and P. Ausloos, New York, Interscience Publishers (1968), p. 620.

27) If the function, $\phi(r/r_t)$, is similar to Onsager's equation, Laplace transformation of yield of trapped species as a function of various scavengers, r_t, will be obtained as the function, $D(r)$. Assumption of Magee's process, other functions $P(E)$ and $p(E, t)$, can be written as function of $D(r)$.

near the thermal energy in the liquid phase. In the electron-scavenging process, it is important to know what percentage of the total ionization is trapped. By the ESR and photoabsorption methods, the *G*-value of electron trapping, $G(e_t^-)$, in 3MHX glass at 77 K is 0.9.[15] In the gas phase, however, the yield of ionization has been estimated from the *W*-value[28] to be 4. If the ionization efficiency is the same in the gas and solid phases, the portion of electrons being trapped in the 3MHX glass, $\int P(E)Q(E)dE = 4\pi\int r^2D(r)(r/r_t)dr$, is estimated to be 0.2 ($\simeq$0.9/4). Recently, however, the quasi-free electron model[29] has successfully been applied to the behavior of electrons in the condensed phase, so the electron-scavenging process should be reexamined from this point of view. In the gas phase, the cross section of electron attachment with scavengers has been measured as a function of the electron energy. For example, the electron energies for the maximum cross section, E_{max}, of SF_6, N_2O, and CH_3Cl are, respectively, 0.02,[17] 2.25,[18] and 0.02eV,[19] while the E_{max} of SO_2 has two values, 5 and 8 eV.[20] When E_{max} is small, for example, in the cases of SF_6 and CH_3Cl, k_s is reduced to being proportional to $\int\sigma(E)dE$, considering that $P(E)Q(E)$ is constant in the range of near-thermal energies, in contrast with the rapid change of $\sigma(E)$ in this region. Even at high concentrations, SO_2 can not scavenge a part of the electrons, because the $\sigma(E)$ of SO_2 is nearly zero at a small electron energy.

The saturation study of ESR also provides information on the structure of e_t^-. The rapid and fast passage and the nonadiabatic condition ($H_1/H_m\omega_m \ll \sqrt{T_1T_2}$, $\omega_m T_1 \gg 1$, $\gamma H_1^2 \ll \omega_m H_m$)[30] are given by the data of Tsuji and Williams[12]; T_1 is about $10^{-2}-10^{-3}$, T_2 is about $10^{-7}-10^{-8}$, $\sqrt{T_1T_2}$ is about $10^{-5}-10^{-6}$, the angular frequency of magnetic-field modulation, ω_m, is $2\pi\times10^5$, and the peak modulating magnetic field, H_m ,is about 1 gauss in this experiment, where H_1 is the component of the rotating magnetic field, perpendicular to the z-direction and where γ is the gyromagnetic ratio. The spin-lattice relaxation time, T_1, given by the equation of the saturation factor, $Z=(1+2\gamma H_1^2T_1/\pi H_m)^{-1}$,[30] is not accurate because of the error in H_1 values, but the relative values give useful information regarding the structure. The higher microwave-power saturation curve of e_t^- in pure 3MHX (Fig. 2) agrees with the equation of Z, and shift to a microwave power shows the decrease in T_1 with an increase in the total dose. However, the shift to the higher microwave power in Fig. 5 shows the decrease in T_1 with the concentration of N_2O. In addition to the shift, the shape of the saturation curve changes when N_2O is added. Because the variation in T_1 and T_2 values due to the addition of N_2O affects the conditions of the power-saturation measurement, a different type of equation for the saturation factor should be applied. The singlet signal of the trapped electrons produced by the addition of N_2O is different from that in pure 3MHX glass and has the following properties: 1) the signal has the same ESR linewidth at any concentration of N_2O and is photobleached by the infrared light much like the trapped electrons in pure 3MHX glass; 2) the signal disappears at a large concentration of N_2O; 3) in the presence of N_2O, the absorption spectrum shows a broad near-infrared band which shifts to a slightly shorter wavelength than that in pure 3MHX[31]; 4) no such shift of the absorption band or change in the ESR relaxation time can be observed in a polar matrix such as 2-methyltetrahydrofuran.[31] These phenomena must result from the formation of trapped electrons in a slightly different structure, and must not be due to negative species such as N_2O^-.

The spin-lattice relaxation mechanism is partly due to the spin-orbit coupling of the Van Vleck theory,[32] partly to the modulation of the spin-spin interaction by the lattice vibrations (Waller theory),[33] and partly to the cross relaxation by the spin-spin interaction.[34] The transition due to the spin-orbital interaction of the trapped electrons in pure 3MHX must be small; it has the same value for any sample, no matter the total dose, but the geometrical change in the structure of the trapping site should affect this value. When N_2O is added, the electrons may be trapped near the N_2O molecule and the field in the trapping sites appears to be perturbed by N_2O, so that the spin-orbit interaction increases. However, the spin-spin interaction is related to the overlapped area of the ESR spectra; therefore, the interaction of the e_t^-—e_t^- type is greater than that of the e_t^-—R (free radical) type. In the Waller mechanism, the e_t^-—e_t^- interaction may dominate the e_t^-—R interaction. The cross relaxation depends on the facts that the spins of R are in good contact with the lattice and that those of e_t^- are in poor contact. Therefore, the cross relaxation takes place *via* the spin-lattice relaxation of R by the mutual spin flip between e_t^- and R. At any rate, the spin-lattice relaxation increases with an increase in the concentrations of the spins due to the e^- and free radicals, whose concentrations are related to the total doses of irradiation. The addition of SF_6 decreases the concentrations of e_t^- and free radicals, and the rate of spin-lattice relaxation is decreased. When CH_3Cl is added, the concentration of e_t^- decreases and that of CH_3 increases, so that the decrease in the spin-lattice relaxation by the Waller mechanism of the (e_t^-—e_t^-) type will be partially compensated for by the increase in that of the (e_t^-—R) type caused by the cross relaxation. Therefore, the total amounts of spin-lattice interaction seem to be almost the same.

28) P. Alder and H. K. Bothe, *Z. Naturforch.*, **20** a, 1700 (1965).
29) K. Fueki, D. -F. Feng, and L. Kevan, *Chem. Phys. Lett.*, **13**, 616 (1972); H. T. Davis, L. D. Schmidt and R. M. Minday, *ibid.*, **13**, 413 (1972).
30) M. Weger, *Bell. System Tech. J.*, **39**, 1013 (1960).
31) Private communication from S. Sato; and S. Mizutani, Tokyo Institute of Technology Thesis for master's degree (1971).
32) J. H. Van Vleck, *J. Chem. Phys.*, **7**, 72 (1939).
33) I. Waller, *Z. Physik*, **79**, 370 (1932); J. H. Van Vleck, *Phys. Rev.*, **57**, 426 (1940).
34) N. Bleombergen, S. Shapiro, P. S. Pershan, and J. O. Artman, *ibid.*, **114**, 445 (1959).

Modified CNDO 2 Calculations of Ionization Potentials for Some Unsaturated Hydrocarbons

Koichi OHNO,* Tomohiko HIROOKA, Yoshiya HARADA, and Hiroo INOKUCHI

The Institute for Solid State Physics, The University of Tokyo, Roppongi, Tokyo 106

**College of General Education, The University of Tokyo, Komaba, Tokyo 153*

(Received December 16, 1972)

The orbital energies of several unsaturated hydrocarbon molecules have been calculated using a modified CNDO/2 method, with the electron repulsion integrals evaluated from Klopman's formula and the σ–π separation factor proposed by Tinland and Jaffé. The empirical parameters are determined to reproduce the observed ionization potentials for ethylene and benzene *via* Koopmans' theorem. The results are shown to agree well with the available experimental ionization potentials and with the assignments of the photoelectron spectra.

Photoelectron spectroscopy provides much information on the ionized states of molecules; not only are the adiabatic first ionization potentials and the higher ionization potentials determined by the measurement of the excess kinetic energies of photoelectrons,[1-7] but also information on the symmetry of ionized states can be obtained from the observed angular distribution of photoelectrons.[8] On the other hand, based upon Koopmans' theorem,[9] the development of molecular orbital methods made it possible to compare the observed vertical ionization potentials with the calculated orbital energies not only for π-electrons but for σ-electrons. They also enable us to compare the assignments of the electron energy levels expected from the observed angular distribution of photoelectrons with those derived from the symmetry of molecular orbitals. However, the methods have not been sufficient to give reasonable interpretation of the observed photoelectron spectra.

Although the all-electron *ab initio* methods have also been advanced, the calculations are time consuming and not always more reliable than the semi-empirical calculations.

In the present paper, we modified the CNDO method introduced by Pople *et al.*[10,11] and established a simpler and more reliable method for the assignment and prediction of photoelectron spectra of unsaturated hydrocarbon molecules.

Method and Parametrizations

The method used here is almost the same as the CNDO/2 method proposed by Pople and Segal;[11] the following semi-empirical parametrizations are taken.

(1) The electron repulsion integrals, γ_{AB}, are evaluated from Klopman's formula:[12]

$$\gamma_{AB} = e^2/\sqrt{R_{AB}^2 + G_{AB}^2}$$

and:

$$G_{AB} = \frac{e^2}{2}(\gamma_{AA}^{-1} + \gamma_{BB}^{-1})$$

where R_{AB} is the interatomic distance between A and B. For one-center repulsion integrals, the semi-empirical values are used:

for carbon atoms, $\gamma_{AA}(C) = 11.144$ eV,

and

for hydrogen atoms, $\gamma_{AA}(H) = 12.845$ eV.

(2) The resonance integrals, β_{AB}, are determined by the use of the following formula;

$$\beta_{AB} = \frac{\beta_A^\circ + \beta_B^\circ}{2} S_{AB},$$

where S_{AB} is the overlap integral between the two atomic orbitals. β_A° is an empirical parameter depending upon the kind of atom. For carbon atoms, we introduced another parameter, k, which is a σ–π separation factor proposed by Tinland[13] and Jaffé[14];

$$\beta^\circ(C\pi) = k\beta^\circ(C),$$
$$\beta^\circ(C\sigma) = \beta^\circ(C).$$

Now, we have three unknown empirical parameters, $\beta^\circ(H)$, $\beta^\circ(C)$, and k, for unsaturated hydrocarbon molecules. These parameters must be determined in order to reproduce the observed spectra. As the simplest parametrization, we chose the first three levels of ethylene, (πb_{1u}), (σb_{1g}), and (σa_g), and the first two levels of benzene, (πe_{1g}) and σe_{2g}), as the standards; they should be fitted to the first three observed ionization potentials of ethylene and the first two of benzene respectively.

The orbital energies of ethylene and benzene were calculated as a function of the unknown parameters, the ranges of the parameters, -10.0 eV$\geqq\beta^\circ(C)\geqq -14.0$ eV, -6.0 eV$\geqq\beta^\circ(H)\geqq -10.0$ eV, and $0.2\leqq$

1) M. I. Al-Joboury and D. W. Turner, *J. Chem. Soc.*, **1963**, 5141; **1964**, 4434.
2) D. C. Frost, C. A. McDowell, and D. A. Vroom, *Proc. Roy. Soc., Ser. A*, **296**, 566 (1967).
3) D. W. Turner, C. Baker, A. D. Baker, and C. R. Brundle, "Molecular Photoelectron Spectroscopy," John Wiley & Sons Ltd., London and New York (1970).
4) A. D. Baker, C. Baker, C. R. Brundle, and D. W. Turner, *Int. J. Mass Spec. Ion Phys.*, **1**, 285 (1968).
5) B. Jonsson and E. Lindholm, *Chem. Phys. Lett.*, **1**, 501 (1967).
6) J. H. D. Eland, *Int. J. Mass Spec. Ion Phys.*, **9**, 214 (1972).
7) F. Brogli and E. Heilbronner, *Helv. Chim. Acta.*, **55**, 1415 (1972).
8) T. A. Carlson and C. P. Anderson, *Chem. Phys., Lett.*, **10**, 561 (1971).
9) T. Koopmans, *Physica*, **1**, 104 (1933).
10) J. A. Pople, D. P. Santry, and G. A. Segal, *J. Chem. Phys.*, **41**, 2911 (1964).
11) J. A. Pople and G. A. Segal, *ibid.*, **43**, S136 (1965); **44**, 3289 (1966).
12) G. Klopman, *J. Amer. Chem. Soc.*, **87**, 3300 (1965).
13) B. Tinland, *Mol. Phys.*, **16**, 413 (1969).
14) J. D. Bene and H. H. Jaffé, *J. Chem. Phys.*, **48**, 1807 (1968).

$k \leqq 0.6$, the calculated orbital energies were arranged as (πb_{1u}), (σb_{1g}), (σa_g), (σb_{2u}), ··· for ethylene, and as (πe_{1g}), (σe_{2g}), (πa_{2u}), ··· for benzene, and no interchanges of the orders were found. Although the optimization was not completely carried out, a set of the following values for the parameters leads to satisfactory results with regard to the standard levels;

$$\beta^\circ(C) = -12.0\,eV, \quad \beta^\circ(H) = -7.0\,eV,$$

and $$k = 0.40.$$

With these parameters, the orbital energies of other unsaturated hydrocarbon molecules were calculated by means of a FACOM-270-20/30 Computer.

Results and Discussion

The parameter values determined in the previous section were used in the calculations of the orbital energies of ethylene, *trans* 1,3-butadiene, benzene, naphthalene, and azulene. Based upon Koopmans' theorem, the absolute values of the calculated orbital energies were compared with the (vertical) ionization potentials obtained from the available data of the photoelectron spectra, and also with the calculated values by Dewar[15] and others.[16-21] The results are shown in Tables 1—5. As can be seen in the tables, the calculated ionization potentials smaller than 16 eV agree, in general, with the observed values. Especially for ethylene and butadiene, our results seem much better than the MINDO calculations by Dewar. From the present results, it may be concluded that both of the first two levels for *trans* 1,3-butadiene are to be attributed to π-electrons, as has been previously reported.[22,23] Furthermore, we are encouraged by the fact that the assignment of the photoelectron spectra for benzene from the calculated orbital energies and their symmetries completely coincides with the recent assignment from the angular distribution data of the photoelectrons reported by Carlson and Anderson.[8] These assignments are not only consistent with the analysis of the vibrational structure by Turner;[3] they also agree with the order of the orbital energies predicted by Jonsson and Lindholm.[5] In addition, since the three lowest IP bands of naphthalene are sharp,[3,6,7] it seems reasonable to assign these bands to the three highest occupied π-orbitals, as assigned in Table 4. In the case of azulene, our calculation also explains the first three bands as π-excitations.

The general conclusion of our results is that the calculated π-electron ionization potentials are in comparatively good agreement with those obtained by the MINDO calculations, but that the calculated ionization potentials for σ-electrons are quite different from these obtained by MINDO. It seems that the introduction of the fairly small σ–π separation factor has led to appropriate separations between the σ-

TABLE 1. IONIZATION POTENTIALS OF ETHYLENE (in eV)

Obsd 4)	Calcd		
	This calcn	MINDO[15]	*ab initio*[16]
10.51	10.62 $\pi 1b_{1u}$	10.37 π	10.17 $\pi 1b_{1u}$
12.38	12.96 $1b_{1g}$	11.47	14.00 $1b_{1g}$
14.47	14.51 $3a_g$	11.65	15.81 $3a_g$
15.68	18.61 $1b_{2u}$	14.37	17.82 $1b_{2u}$
18.87	21.61 $2b_{3u}$	19.21	21.66 $2b_{3u}$
	29.54 $2a_g$	28.01	28.29 $2a_g$

TABLE 2. IONIZATION POTENTIALS OF BENZENE (in eV)

Obsd				Calcd			
a)	b)	c)	d)	This calcn	MINDO[15]	CNDO[17]	*ab initio*[18]
9.25	9.3	9.2, 9.5	πe_{1g}	9.77 πe_{1g}	9.54 π	9.4 πe_{1g}	10.31 πe_{1g}
11.49	11.4	11.6	e_{2g}	11.48 e_{2g}	10.07	9.8 e_{2g}	14.30 e_{2g}
11.7, 12.2	12.1	12.3	πa_{2u}	12.55 πa_{2u}	11.30	13.0 e_{1u}	14.64 πa_{2u}
13.8	13.8	14.0	e_{1u}	14.68 e_{1u}	12.29	13.8 b_{2u}	17.04 e_{1u}
14.7	14.7	14.8	b_{2u}	15.30 b_{2u}	12.49 π	14.3 b_{1u}	17.96 b_{2u}
15.4	15.4	15.4	b_{1u}	16.34 b_{1u}	14.80	15.2 πa_{2u}	18.33 b_{1u}
16.8	16.9	16.8	a_{1g}	20.93 a_{1g}	15.22	19.6 a_{1g}	20.16 a_{1g}
18.3, 19.9	19.2	19.0	e_{2g}	22.50 e_{2g}	19.24	20.1 e_{2g}	23.09 e_{2g}
				28.18 e_{1u}	26.05	24.8 e_{1u}	28.38 e_{1u}
				35.74 a_{1g}	32.75	31.2 a_{1g}	31.94 a_{1g}

a) Turner *et al.*[3] b) Jonsson and Lindholm.[5] c) Carlson and Anderson.[8] d) Assignment from Refs. 5 and 8.

15) M. J. S. Dewar and S. D. Worley, *J. Chem. Phys.*, **50**, 654 (1969).
16) J. M. Schulman, J. W. Moskowitz, and H. Hollister, *ibid.*, **46**, 2759 (1967).
17) P. A. Clark and J. L. Ragle, *ibid.*, **46**, 4235 (1967).
18) S. D. Peyerimhoff and R. J. Buenker, *Theoret. Chim. Acta* (Berl.), **19**, 1 (1970).
19) P. A. Clark, *J. Chem. Phys.*, **54**, 45 (1971).
20) R. J. Buenker and J. L. Whitten, *ibid.*, **49**, 5381 (1968).
21) R. J. Buenker and S. D. Peyerimhoff, *Chem. Phys. Lett.*, **3**, 37 (1969).
22) H. Kato, H. Konishi, H. Yamabe, and T. Yonezawa, This Bulletin, **40**, 2761 (1967).
23) J. H. D. Eland and L. J. Danby, *Z. Naturforsch.*, *A*, **23**, 355 (1968).

Table 3. Ionization potentials of *trans* 1,3-butadiene (in eV)

Obsd 3)	Calcd					
	This calcn		MINDO[15]	CNDO[19]	*ab initio*[20]	
9.08	9.78	πb_g	9.51 π	9.40 πb_g	9.78	πb_g
11.34	11.47	πa_u	10.30	10.00 a_g	13.01	πa_u
12.3	11.97	a_g	11.27	11.47 a_g	14.04	a_g
13.1	13.03	a_g	11.38 π	12.20 b_u	15.54	b_u
(14.0)	13.99	b_u	11.68	12.69 πa_u	15.68	a_g
15.2	16.85	b_u	13.47	14.90 b_u	18.03	b_u
18.0	17.63	a_g	13.72	16.33 a_g	18.14	a_g
19.4	21.42	b_u	18.00	19.30 a_g	21.17	b_u
20.2	22.18	a_g	19.58	19.71 b_u	22.89	a_g
	27.93	b_u	25.81	24.45 b_u	27.89	b_u
	31.92	a_g	30.36	27.62 a_g	30.30	a_g

Table 4. Ionization potentials of naphthalene (in eV)

Obsd 6, 7, 3)	Calcd			
	This calcn		MINDO[15]	*ab initio*[21]
8.12	9.21	$\pi 1a_u$	8.62 π	9.30 $\pi 1a_u$
8.91	9.48	$\pi 2b_{1u}$	9.30 π	10.20 $\pi 2b_{1u}$
10.08	10.49	$\pi 1b_{3g}$	9.37	11.84 $\pi 1b_{3g}$
10.85	10.62	$6b_{1g}$	9.86	13.51 $\pi 1b_{2g}$
11.05	10.83	$9a_g$	10.24	14.20 $9a_g$
11.35	11.56	$\pi 1b_{2g}$	10.32 π	14.41 $6b_{1g}$
11.90	12.43	$7b_{3u}$	11.21	15.43 $7b_{3u}$
12.5	13.13	$\pi 1b_{1u}$	11.31 π	15.66 $\pi 1b_{1u}$
13.5	13.52	$6b_{3u}$	11.62	16.57 $7b_{2u}$
13.7	13.62	$7b_{2u}$	11.63	17.15 $6b_{3u}$
14.45	14.56	$5b_{1g}$	12.00	17.26 $5b_{1g}$
15.9	15.25	$8a_g$	13.17 π	17.99 $8a_g$
16.25	15.77	$6b_{2u}$	13.19	18.19 $6b_{2u}$
	17.81	$4b_{1g}$	14.04	19.52 $7a_g$
	17.86	$7a_g$	14.65	20.25 $5b_{3u}$
	20.03	$5b_{3u}$	15.97	20.36 $4b_{1g}$
	22.90	$5b_{2u}$	18.93	23.15 $6a_g$
	23.37	$6a_g$	19.16	23.71 $5b_{2u}$
	23.39	$4b_{3u}$	19.99	24.11 $4b_{3u}$
	26.89	$3b_{1g}$	24.10	27.88 $3b_{1g}$
	27.76	$5a_g$	25.48	28.47 $5a_g$
	29.97	$4b_{2u}$	27.60	29.64 $4b_{2u}$
	33.89	$3b_{3u}$	30.21	31.16 $3b_{3u}$
	37.18	$4a_g$	34.23	33.00 $4a_g$

Table 5. Ionization potentials of azulene (in eV)

Obsd 6)	Calcd					
	This calcn		MINDO[15]		*ab initio*[21]	
7.42	8.59	$\pi 2a_2$	8.22 π		8.26	$\pi 2a_2$
8.52	9.04	$\pi 3b_1$	8.73 π		9.44	$\pi 3b_1$
10.0	10.71	$\pi 1a_2$	9.74		12.37	$\pi 1a_2$
11.0	11.18	$17a_1$	9.91		13.49	$\pi 2b_1$
11.35	11.38	$12b_2$	10.15		14.08	$17a_1$
12.5	11.55	$\pi 2b_1$	10.51		15.08	$12b_2$
13.2	11.94	$16a_1$	10.59 π		15.44	$\pi 1b_1$
14.5	12.46	$11b_2$	11.02		15.44	$11b_2$
15.7	13.03	$10b_2$	11.37 π		15.72	$16a_1$
	13.05	$\pi 1b_1$	11.46		16.28	$15a_1$
	13.56	$15a_1$	12.90 π		16.87	$10b_2$
	16.16	$14a_1$	12.93		18.24	$9b_2$
	16.32	$9b_2$	13.23		18.36	$14a_1$
	18.14	$13a_1$	14.65		19.56	$13a_1$
	18.20	$8b_2$	15.13		20.31	$8b_2$
	20.28	$12a_1$	16.07		21.20	$12a_1$
	21.86	$11a_1$	17.12		21.43	$11a_1$
	22.28	$7b_2$	19.60		24.06	$7b_2$
	24.29	$10a_1$	20.78		24.99	$10a_1$
	26.49	$6b_2$	23.68		27.05	$6b_2$
	27.98	$9a_1$	25.08		28.21	$9a_1$
	30.34	$5b_2$	27.97		30.02	$5b_2$
	33.49	$8a_1$	30.32		31.13	$8a_1$
	37.31	$7a_1$	33.72		32.84	$7a_1$

electron levels and the π-electron levels. Moreover, the parameters, β°(C) and β°(H), were adjusted to reproduce the shallow levels for ethylene and benzene; thus, it is natural that the present results are plausible for the ionization potentials smaller than about 16 eV. Although the physical meaning of the choice of the empirical parameters is not very clear, the present method may provide, as in the sense of the Pariser-Parr-Pople calculations for the electronic spectra of π-electron system, a complementary means for interpreting or predicting the photoelectron spectra of unsaturated hydrocarbon molecules.

Kinetic Studies of the Solvent Extraction of Metal Complexes. II. The Rate of the Extraction of Iron(III) with Thenoyltrifluoroacetone into Carbon Tetrachloride

Tatsuya SEKINE, Jun-ichi YUMIKURA, and Yū KOMATSU

Department of Chemistry, Science University of Tokyo, Kagurazaka, Shinjuku-ku, Tokyo 162

(Received January 18, 1973)

The rate of the solvent extraction of iron(III) in 4.0 M perchlorate ionic media with 2-thenoyltrifluoroacetone (TTA) into carbon tetrachloride has been measured under various conditions. The rate was found to be first order with respect to the concentration of iron(III) in the aqueous phase, first-order with respect to TTA in the organic phase, but independent and inversely first-order with respect to the hydrogen-ion concentration. From these results, it was concluded that the rate-determining step in this extraction is the formation of the first complex between the undissociated form, TTA(HA), and Fe^{3+} in the higher acid concentration range, but that the reaction between the anionic form, TTA(A^-), and Fe^{3+} also becomes a rate-determining step as the acid concentration decreases. It was also found that chloride ions accelerate the extraction; this was interpreted by more rapid reactions between TTA (in the both forms, HA and A^-) and an iron(III) chloride complex. From these results, the rate constants for the rate-determining reactions were calculated to be $K_{HA}=10^{0.57}$ M^{-1} min^{-1} and $K_A=10^{6.84}$ M^{-1} min^{-1} in 4.0 M(H, Na)ClO_4 at 25 °C by means of these equations: $-d[Fe^{3+}]/dt=K_{HA}[Fe^{3+}][HA]$ (where [HA] is the total concentration of both enol and keto forms of uncharged TTA in the aqueous phase) and $-d[Fe^{3+}]/dt=K_A[Fe^{3+}]\cdot[A^-]$. The $FeCl^{2+}$ species reacts with both HA and A^- more rapidly than does the Fe^{3+} species, and the rate constants of the reactions of the former are in both cases higher than those of the latter by a factor of 28.

It has been pointed out that the rate of the reaction of metal ions in aqueous solutions is low when the charge is larger and/or when the radius is small; this has been explained as being due to the slow substitution of the hydrated water on such ions with the reactant. As examples of these metal ions, Be^{2+}, Al^{3+} and other strongly-hydrolysing metal ions were cited by Eigen.[1] In the previous paper of the present series,[2] it was reported that the solvent extraction of beryllium(II) with 2-thenoyltrifluoroacetone(TTA) in carbon tetrachloride is extremely slow because of the slow formation of the first complex of this metal ion in the aqueous phase with a TTA anion. In the course of another experiment of the present laboratory,[3] it was found that the extraction of iron(III) with TTA in chloroform was rather slow. The slow extraction of iron(III) with TTA has been reported by Bolomey and Wish[4] and by Adin and Newman.[5] It has been reported by Dyrssen[6] that the extraction of iron(III) with β-isopropyltropolone(IPT) is slow; the rate of this IPT extraction was studied more quantitatively by McClellan and Menis.[7] The extraction of iron(III) with alkylphosphoric acid has been studied kinetically by several workers, as Coleman and Roddy summarized in their review.[8]

The present study has been undertaken in order to make quantitative measurements of the rate of iron(III) extraction with TTA and in order to clarify the details of the mechanism of this slow extraction. The organic phase used is carbon tetrachloride, and the aqueous phase employed is perchlorate ionic media, 4.0 M(H, Na)ClO_4, except in a few cases. This aqueous phase was chosen in order to use the equilibrium data obtained for this aqueous solution in Ref. 3 for the analysis of the results. Since it has been found that the rate of extraction is accelerated by the addition of the chloride ion,[5,8] this effect was also measured.

Experimental

Reagents. The stock solution of iron(III) was prepared as follows. A weighed amount of analytical-grade metallic iron was dissolved in warm perchloric acid; the mixture was then stored as the stock solution. A working solution containing 1.0×10^{-2} M iron(III), 1.0 M perchloric acid, and 3.0 M sodium perchlorate was prepared from the above stock solution. The TTA was obtained from Dojindo & Co. The sodium perchlorate was prepared from sodium carbonate and perchloric acid, and it was recrystallized three times from water. All of the other reagents were of a reagent grade.

Procedures. The details of the procedures are essentially the same as those described in the previous paper[2] except that the amount of the metal ion was determined by colorimetry in the present study. The aqueous phase was prepared so as to contain 1.0×10^{-3} M of iron(III), 4.0 M of the perchlorate ion, and various amounts of sodium and hydrogen-ions. Some experiments were also carried out in order to ascertain the effect of coexisting salt on the rate of extraction by changing the sodium perchlorate concentration. The organic phase was carbon tetrachloride containing TTA. The initial volume of each phase was always 5.0 ml. The two phases were placed in stoppered glass tubes (volume, 20 ml) and vigorously agitated at 25±0.3 °C. The shaking speed was chosen so as to be high enough that no acceleration of the rate of extraction was observed upon a further increase in the agitation speed; thus, the effects due to the transport of materials and to any interfacial re-

1) M. Eigen, *Pure Appl. Chem.* **6**, 97 (1963).
2) T. Sekine, Y. Koike, and Y. Komatsu, This Bulletin, **44**, 2907 (1971).
3) T. Sekine and T. Tetsuka, *ibid.*, **45**, 1620 (1972).
4) R. A. Bolomy and L. Wish, *J. Amer. Chem. Soc.*, **72**, 4488 (1950).
5) A. Adin and L. Newman, *J. Inorg. Nucl. Chem.*, **32**, 3321 (1970).
6) D. Dyssen, *Trans. Royal. Inst. Technol. Stockholm*, **1962**, 188.
7) B. E. McClellan and O. Menis, *Anal. Chem.*, **43**, 436 (1971).
8) C. F. Coleman and J. W. Roddy, "Solvent Extraction Review," Vol. 1, ed. by Y. Marcus, Marcel Dekker, New York (1971), p. 63.

action could be eliminated from consideration, as has been described in the previous paper.[2] After a certain interval, the two phases were centrifuged. A certain portion of the organic phase was pipetted out, and the content of the iron(III)–tris TTA chelate was determined by colorimetry. The absorption was determined at 500 nm; the molar extinction coefficient at this wavelength was found to be 3.7×10^3. It was found that Beer's law held, at least until a concentration of 2.0×10^{-4} M of the iron(III)–TTA chelate in carbon tetrachloride. The amount of aqueous iron(III) was estimated from the difference between the iron(III) concentration in the initial aqueous phase and that in the organic phase at equilibrium. The hydrogen-ion concentration was calculated from the amount of perchloric acid added.

Statistical

The rate of the extraction of Fe^{3+} ion with an acidic extractant, HA, may be written, in many cases, as follows:

$$-\frac{d[Fe^{3+}]}{dt} = k_0[Fe^{3+}]^a[HA]_{org}^b[H^+]^c \quad (1)$$

When the extractant and the hydrogen-ion are present in a large excess to iron(III), Eq. (1) can be written as follows:

$$-\frac{d[Fe^{3+}]}{dt} = q[Fe^{3+}]^a \quad (2)$$

Here, q is the multiplication of the rate constant, k_0, and the other two concentrations in Eq. (1), which are kept at certain values throughout a series of experiments. When the reaction order with respect to iron(III) is unity, as in the case of the present study, the following simplified statistical treatment is possible. Assuming that the value of a in Eq. (2) is unity, it can be written by integration as:

$$-\log[Fe^{3+}] = q't + C_0 \quad (3)$$

where C_0 is a constant and where q' is $q\times\log e$. Equation (3) shows that when a is unity, the $-\log[Fe^{3+}]$ *vs.* t plot should be a straight line with a slope of q'.

The reaction order with respect to the other two elements in Eq. (1) can be determined from the measurements when one of these two concentrations is kept at a certain value. For example, when the concentration of the hydrogen-ion is kept at h, the quantity, q_{HA}, can be written, in the first step, as follows:

$$\log q_{HA} = \log k_0h^c + b\log[HA]_{org} \quad (4)$$

As can be seen from Eq. (4), the reaction order with respect to the extractant, b, can be determined from the slope of the $\log q_{HA}$ *vs.* $\log[HA]_{org}$ plot.

Since the reaction order with respect to the hydrogen-ion, c, was found in the present study to change from minus one to zero upon an increase in the hydrogen-ion concentration, the following more general equation, containing a term in which the reaction order with respect to the hydrogen-ion concentration is zero, was employed:

$$-\frac{d[Fe^{3+}]}{dt} = k_0[Fe^{3+}][HA]_{org}^b(1+K_H[H^+]^{-1}) \quad (5)$$

On the other hand, when the concentration of the extractant is kept at a certain value, ha, the q_{H^+} quantity is obtained as:

$$\log q_{H^+} = \log k_0(ha)^b + \log(1+K_H[H^+]^{-1}) \quad (6)$$

Furthermore, since the addition of the chloride ion was found to accelerate the extraction, the following statistical treatment was made for this effect. Under the conditions where the concentrations of the extractant and hydrogen-ion are kept constant at h and ha, but where the aqueous phase contains a certain amount of the liquid, Cl^-, the rate may be represented by the following equation (the higher terms with respect to Cl^- are not given here and the b value is always unity in Eq. (6)):

$$-\frac{d[Fe^{3+}]}{dt} = q_L[Fe^{3+}] \quad (7)$$

where q_L is

$$\log q_L = \log k_0(ha)(1+K_Hh^{-1}) + \log(1+K_{Cl}[Cl^-]) \quad (8)$$

The constants in Eqs. (6) and (8) can be determined by a curve-fitting method.[2,9-11]

When the initial concentration of the extractant in the organic phase is denoted by $C_{HA(org)}$, the following equations are obtained if the volumes of the two phases are the same and if $[A^-]\ll C_{HA(org)}$:

$$K_a = [H^+][A^-][HA]^{-1} \quad (9)$$

$$K_d = [HA]_{org}[HA]^{-1} \quad (10)$$

$$C_{HA(org)} = [HA]_{org} + [HA] + [A^-] \quad (11)$$

$$[A^-] = C_{HA(org)}K_a(K_d+1)^{-1}[H^+]^{-1} \quad (12)$$

The values of these constants in the carbon tetrachloride–4.0 M (H, Na)ClO_4 system have been reported to be $\log K_a=-6.57$ and $\log K_d=1.93$.[2] Since $K_d\gg1$, and since, thus, $C_{HA}\simeq[HA]_{org}$, Eq. (12) can be written as:

$$[A^-] = [HA]_{org}K_aK_d^{-1}[H^+]^{-1} \quad (13)$$

Results

Iron(III) was always added initially to the aqueous phase. Since the data used for the analysis were only those obtained from the experiments in the early stage of extraction, the effect of the back extraction may be negligible.

Reaction Order with Respect to Fe^{3+}. In all the experiments, each of the $-\log[Fe^{3+}]$ *vs.* t plots always gave a staright line. Thus, as can be seen from Eq. (3), the reaction order with respect to iron(III) is always unity.

Reaction Order with Respect to TTA(HA). The rate of extraction was determined in the TTA concentration range between 0.05 M and 0.3 M and at the hydrogen-ion concentration of 1.0 M. The $\log q_{HA}$ *vs.* $\log[HA]_{org}$ plot is given in Fig. 1. As may be seen from the figure, the plot obtained is a straight ling with a slope of +1; thus, the rate of extraction was concluded to be proportional to the TTA concentration under these conditions.

9) L. G. Sillén, *Acta Chem. Scand.*, **10**, 186 (1956).
10) T. Sekine, M. Sakairi, and Y. Hasegawa, This Bulletin, **39**, 2141 (1966).
11) F. J. C. Rossotti and H. Rossotti, "The Determination of Stability Constants," McGraw-Hill, New York (1961).

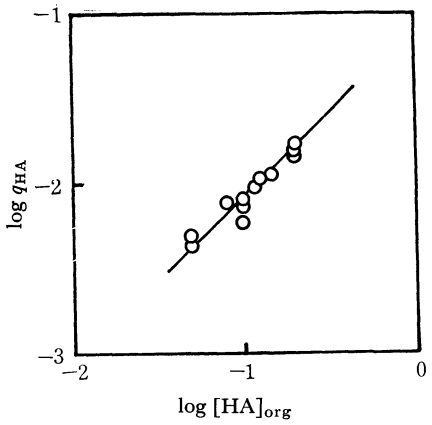

Fig. 1. Dependence of the rate of Fe(III) extraction on the TTA concentration in the organic phase (q_{HA} *cf.* Eq. (4)).

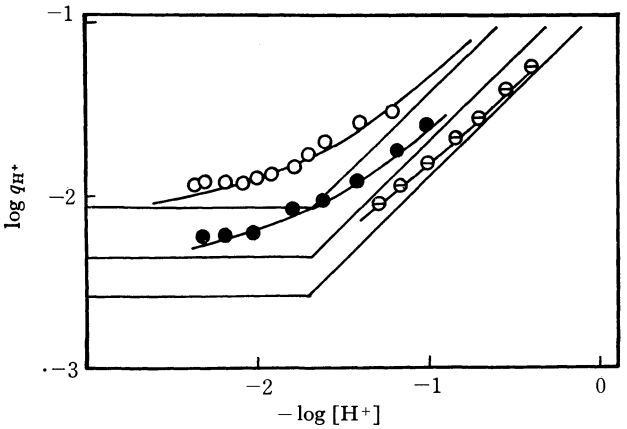

Fig. 2. Dependence of the rate of Fe(III) extraction on the hydrogen-ion concentration (q_{H^+} *cf.* Eq. (6)). ○: CCl_4 containing 0.2 M TTA, ●: CCl_4 containing 0.1 M TTA and ⊖: CCl_4 containing 0.05 M TTA. The two straight lines for each plot are the two asymptotes; $Y=\log k_0(ha)$ and $Y=\log k_0K_H(ha)$ $-\log[H^+]$, and the solid curve is calculated by introducing the rate constants in Table 1 into Eq. (6).

Reaction Order with Respect to H^+. The rate of extraction was determined in the range of hydrogen-ion concentrations from 2.0 M to 0.04 M and at the TTA concentrations of 0.05 M, 0.1 M, and 0.2 M. Figure 2 gives the log q_{H^+} *vs.* $-\log[H^+]$ plot. As may be seen from Fig. 2, the slope for the plot approaches zero in the lowest $-\log[H^+]$ region, but it increases with the increase in $-\log[H^+]$ until it approaches unity. From this fact, it was concluded that there are two mechanisms for the extraction and that they can be represented by Eq. (6).

The rate constants in the absence of chloride ions were determined from these results by the curve-fitting method; they are listed in Table 1(a).

Effect of the Chloride Ions. The rate was determined as a function of the chloride-ion concentration in the aqueous phase when the TTA concentration was 0.1 M and when the hydrogen-ion concentration was 1.0 M. Figure 3 gives the log q_L plot where L is Cl^-; the rate is accelerated by the chloride ion, and it becomes almost proportional to the chloride concentration in the higher range. The constant, K_{Cl}, in Eq. (8) was determined from this plot by the curve-fitting method; it is listed in Table 1.

Table 1. Summary of constants

(a) Constants for the equation:

$$-d[Fe^{3+}]/dt = k_0[Fe^{3+}][HA]_{org}(1+K_H[H^+]^{-1})(1+K_{Cl}[Cl^-])$$

$\log k_0 = -1.36$ $(M^{-1}\,min^{-1})$

$\log K_H = -0.30$ (M)

$\log K_{Cl} = 2.32$ (M^{-1})

(b) Reaction constants$(M^{-1}\,min^{-1})$ defined by Eqs. (14) and (15).[a)]

$\log K_{HA} = 0.57$

$\log K_A = 6.84$

$\log K_{HA-Cl} = 2.01$

$\log K_{A-Cl} = 8.28$

a) Rate constant for the reaction between Fe^{3+} and HA (K_{HA}) which has been computed by using the total concentration of HA in the aqueous phase, Fe^{3+} and A^-(K_A), $FeCl^{2+}$ and HA(K_{HA-Cl}), and $FeCl^{2+}$ and A^-(K_{A-Cl}).

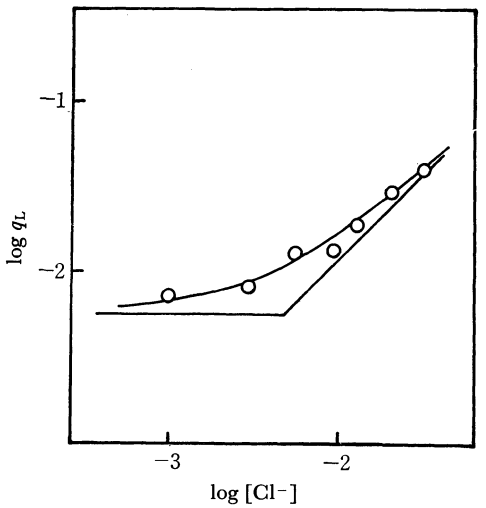

Fig. 3. Dependence of the rate of Fe(III) extraction on the chloride ion concentration. The straight lines are two asymptotes; $Y=\log C$ and $Y=\log CK_{Cl}+\log[Cl^-]$ where C is equal to $\log k_0(ha)(1+K_Hh^{-1})$ in which ha is 0.1 M and h is 1.0 M. The solid curve was obtained by introducing the constants in Table 1 into Eq. (8).

In order to consider the effect of the chloride ion on the rate of extraction further, the rate was determined with 0.1 M TTA in the organic phase in the presence of the chloride-ion at a certain concentration, 5×10^{-3} M, but in the presence of the hydrogen-ion at various concentrations. Figure 4 shows these results. As may be seen from Fig. 4, the addition of chloride always increases the rate by a factor of $10^{0.24}$. Thus, it can be concluded that both mechanisms, one independent of, and the other inversely first-order dependent on the hydrogen-ion, are affected by the chloride-ion in the same manner. From the amounts of the chloride complexes, $FeCl^{2+}$ and $FeCl_2^+$, in the aqueous phase, which were computed by using the stability constants in 4.0 M (H, Na)ClO_4,[3)] that is, $\log\beta_1=0.88$ and $\beta_2=0.80$, the rate constants for the extraction in the presence of chloride-ion were determined to be

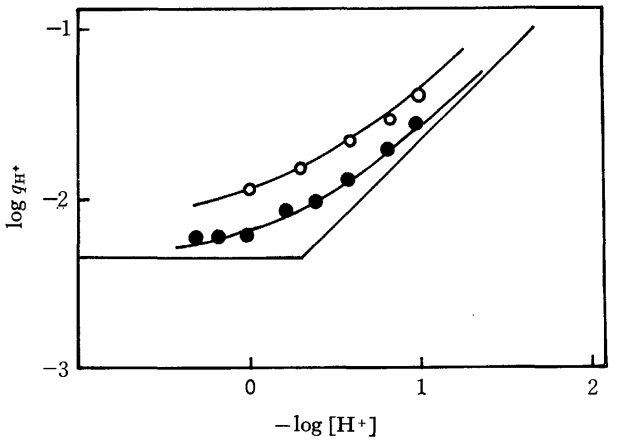

Fig. 4. Dependence of the rate of Fe(III) extraction on the hydrogen ion concentration in the presence of 5×10^{-3} M chloride-ion (○) and its absence (●) in the aqueous phase when the TTA concentration in the organic phase is 0.1 M. The two straight lines are the same as those given in Fig. 2. The curve for the full circle is $Y=\log k_0(ha)\,(1+K_H[H^+]^{-1})$ and that for the open circles is $Y=\log k_0(ha)(1+K_{Cl}[Cl^-]_a)(1+K_H[H^+]^{-1})$ in which ha is 0.1 M and $[Cl^-]_a$ is 5.0×10^{-3} M.

as listed in Table 1 (b).

Since the rate of the extraction of iron(III) with IPT has been reported to be dependent on the concentration of the coexisting sodium perchlorate,[7] the dependence of the rate on the sodium perchlorate concentration was also determined. The results are given in Table 2. As may be seen from the table, the rate is not very much affected by the change in the salt concentration.

Discussion

Since the rate of extraction is always first-order with respect to TTA, and zero and inversely first-order with respect to the hydrogen-ion, and since the effect of interfacial reaction is negligible in the present study, Eq. 5 may, by introducing Eq. (13), be written as:

$$-\frac{d[Fe^{3+}]}{dt}=K_{HA}[Fe^{3+}][HA]+K_A[Fe^{3+}][A^-] \quad (14)$$

where $K_{HA}=k_0K_d$ and where $K_A=k_0K_HK_dK_a^{-1}$. Equation (14) shows that the rate of extraction is controlled by two reactions, one between Fe^{3+} and HA and the other between Fe^{3+} and A^- in the aqueous phase.

Table 2. The effect of ionic strength adjusted by sodium perchlorate on the rate of extraction at two hydrogen ion concentrations (q_{H^+} *cf.* Eq. (6))

Ionic strength	log q_{H^+} at $[H^+]=1.0$ M	log q_{H^+} at $[H^+]=0.05$ M
4.0 M	−2.18	−1.32
3.0 M	−2.17	−1.28
1.0 M	−2.20	−1.22
0.1 M		−1.09

The effect of the chloride-ion can, then, be treated from Eqs. (8) and (14) and the stability constant of the $FeCl^{2+}$ species as follows:

$$-\frac{d[Fe^{3+}]}{dt}=K_{HA}[Fe^{3+}][HA]+K_A[Fe^{3+}][A^-]+K_{HA-Cl}[FeCl^{2+}][HA]+K_{A-Cl}[FeCl^{2+}][A^-] \quad (15)$$

where $K_{HA-Cl}=K_{HA}K_{Cl}\beta_1^{-1}$ and where $K_{A-Cl}=K_AK_{Cl}\beta_1^{-1}$.

By using the constants in Table 1(a) and these relations, the values of these constants were calculated to be as given in Table 1(b).

Adin and Newman[5] determined the rate of the extraction of iron(III) with TTA and reported that the TTA extraction of iron(III) takes place by way of two mechanisms; one is independent of, and the other is dependent on, $[H^+]^{-1}$. They also reported an acceleration of the extraction by the chloride-ion. These results are summarized in Table 3. Their results are similar to those obtained in the present study, although the solvent is different and the electrolyte concentration and the background cation are different. These authors, however, explained the inversely first-order dependence of the rate on the hydrogen-ion in terms of the hydrolysis of iron(III); in other words, they assumed that the $FeOH^{2+}$ species reacted with the HA-form TTA much faster than did the Fe^{3+} species, and they assumed that the $FeOH^{2+}$ species reacted much faster than the $FeCl^{2+}$ species. According to these authors, the $FeOH^{2+}$ species reacts with the HA-form TTA faster than does the Fe^{3+} species by a factor of 10^4.

Statistically, it is impossible to distinguish whether this inversely first-order dependence on the hydrogen-ion which has been observed in both the previous and the present studies is due to a $Fe^{3+}+A^-\rightarrow FeA^{2+}$ re-

Table 3. Previous work on the rate of iron(III) extraction with chelating extractants

Chelate	Organic phase	Aqueous phase	k ($M^{-1}min^{-1}$)	Ref.	Remarks
TTA (room temparature)	C_6H_6	—	—	4	Slow extraction at pH 4.5 but rapid back extraction
TTA (25 °C)	C_6H_6	1.0 M (H, Li)ClO_4	30	5	$Fe^{3+}+(HTTA)_{enol}\rightarrow FeTTA^{2+}+H^+$
			2.6×10^4		$FeOH^{2+}+(HTTA)_{enol}\rightarrow FeTTA^{2+}$
			1.2×10^3		$FeCl^{2+}+(HTTA)_{enol}\rightarrow FeTTA^{2+}+H^++Cl^-$
IPT (21±1 °C)	$CHCl_3$	1.0 M (H, Na)ClO_4 $[H^+]=1.0$	1.5×10^{10}	7	$Fe^{3+}+IPT^-\rightarrow Fe(IPT)^{2+}$ First-order dependence on $NaClO_4$ when its concentration is 1—4 M and zeroth-order dependence on H^+ in the range $[H^+]$ 1—5 M were also observed.

action or to a $FeOH^{2+}+HA \rightarrow FeA^{2+}+H_2O$ reaction. The present authors, however, believe that the former mechanism is dominant in the system studied in this paper, because, as may be seen from Fig. 4, the rate of extraction is always increased by the chloride-ion by a factor of $10^{0.24}$ at 5×10^{-3} M; that is, the increase is the same for lower $-\log[H^+]$ region, where the reactions between HA and the Fe^{3+} and $FeCl^{2+}$ species are dominant, and for the higher region, where the reactions between A^- and the Fe^{3+} and $FeCl^{2+}$ species are also dominant.

According to the viewpoint of previous authors,[5] the rate of extraction can be represented by:

$$-\frac{d[Fe^{3+}]}{dt}=k[HA]([Fe^{3+}]+K'[FeCl^{2+}]+K''[FeOH^{2+}])$$
$$=k[Fe^{3+}][HA](1+K'\beta_1[Cl^-]+K''K_h[H^+]^{-1}) \quad (16)$$

where $K_h=[FeOH^{2+}][H^+][Fe^{3+}]^{-1}$. Thus, when the chloride concentration is zero and a certain value, L_1, and when the concentration of the extractant in the aqueous phase was a certain value of ha_1, the rates may be represented by:

$$-\frac{d[Fe^{3+}]}{dt}=k(ha_1)[Fe^{3+}](1+K''K_h[H^+]^{-1}) \quad (17)$$

$$-\frac{d[Fe^{3+}]}{dt}=k(ha_1)[Fe^{3+}](1+K'\beta_1L_1+K''K_h[H^+]^{-1}) \quad (18)$$

From these equations, it is obvious that the ratio of the two rates, which can be obtained by dividing Eq. (18) by Eq. (17), changes with the change in the hydrogen-ion concentration; this is not observed in the results in Fig. 4.

Although the hydrolysis does not seem to be the reason for the inversely first-order dependence of the rate on the hydrogen-ion shown in Figs. 3 and 4, hydrolysis seems to accelerate the rate of extraction. Unfortunately, since the rate in the higher $-\log[H^+]$ region, where the effect can be expected, is too high to be measured accurately by the experimental method employed here, the quantitative relation between the rate and the degree of hydrolysis could not be determined.

The conclusion drawn in the present study is somewhat similar to that reported by McCllelan and Menis for the extraction of Fe^{3+} with IPT.[7] They described that the extraction is proportional to $[HIPT]_{org}$ and $[H^+]^{-1}$, and they explained these dependences in terms of the $Fe^{3+}+IPT^- \rightarrow FeIPT^{2+}$ reaction. At the same time, they described that the rate is independent of $[H^+]$ when it is from 1.0 M to 5.0 M, although they did not give any rate constant for this latter reaction. They also reported that the rate at 0.1 M $[H^+]$ shown a first-order dependence on the concentration of the coexisting sodium perchlorate. In the present study, however, the effect of the change in the sodium perchlorate concentration on the rate of TTA extraction was found to be only slight, as may be seen from Table 2.

The results in Table 1 can be compared with those obtained with regard to beryllium(II) TTA extraction from a 4.0 M sodium perchlorate solution into carbon tetrachloride.[2] The rate constant of the formation of the first beryllium(II)–TTA complex in 4.0 M sodium perchlorate, $-d[Be^{2+}]/dt=k[Be^{2+}][A^-]$, was obtained as $10^{4.3}$ M^{-1} min^{-1}, which is about one three-hundredth of the rate constant of the first iron(III)–TTA complex under the same conditions. It is remarkable that the rate of the TTA extraction of beryllium(II) is only slightly affected by the formation of $BeCl^+$ species. For example, when the chloride concentration in a 4.0 M Na(Cl, ClO_4) medium is 1.0 M, about 25% of the total beryllium(II) is assumed to be in the $BeCl^+$ and $BeCl_2$ forms ($\beta_1=10^{-0.85}$ and $\beta_2=10^{-0.70}$)[12], but the difference in the rate of the TTA complex formation in the presence of the 1.0 M chloride-ion from that in its absence is small (Fig. 4 in Ref. 2).

It is remarkable that the TTA anion reacts with the hydrated Fe^{3+} ion much faster than does the undissociated TTA. Since it is known that the enol-form TTA in the aqueous phase reacts with a metal ion much faster than does the keto-form, and since the concentration of the enol-form is only one-sixtieth of the keto-form,[13] we may reasonably assume that the rate constant for the reaction which actually takes place, $Fe^{3+}+HA(enol) \rightarrow FeA^{2+}+H^+$, is about $10^{2.4}$ (M^{-1} min^{-1}) (60 times the K_{HA} value in Table 1(b) and that the $Fe^{3+}A^- \rightarrow FeA^{2+}$ reaction is thus $10^{4.5}$ times faster than the reaction with the enol-form undissociated TTA.

The authors are grateful to Mr. Toshihiro Tetsuka of the present laboratory for his experimental aid and valuable discussions.

12) T. Sekine, Y. Komatsu, and M. Sakairi, This Bulletin, **44**, 1480 (1971).

13) J. C. Reid and M. Calvin, *J. Amer. Chem. Soc.*, **72**, 2948 (1950).

Variational Calculation of Atoms and Molecules by a Modified Hassé Method Using Hulthén Functions.[1] III. Long-range Interactions between Hydrogen Atom and Proton and between Two Hydrogen Atoms

Tokio YAMABE, Shingo ISHIMARU, and Kenichi FUKUI

Department of Hydrocarbon Chemistry, Kyoto University, Sakyo-ku, Kyoto 606

(Received February 2, 1973)

The variation method using the wave function of the modified Hassé form is applied to the problem of long-range interactions between hydrogen atom and proton and between two hydrogen atoms. The interaction energy is also related to the perturbation energy under the Unsöld approximation by the use of several pertinent approximations, and an "improved second-order Unsöld energy," which will be higher than the exact second-order perturbation energy, is newly proposed. The numerical results show that the present trial wave function is quite effective; particularly, at $R \gtrsim 10$ (a.u.), the dispersion energy between hydrogen atoms is better than that of Hirschfelder-Linnett, which might be the best variational result at a large nuclear separation. Furthermore, the importance of considering the degeneracy in treating the induction energy is numerically disclosed for an example of H–H$^+$ interaction. The coefficients in the asymptotic form of the dispersion energy between two hydrogen atoms are briefly discussed, and, finally, a new method for the calculation of the second-order energy is suggested.

It is desirable that an expression of the long-range interaction energy between atoms and molecules has the following properties: (1) the result is an upper or lower bound to the exact value, (2) it is given in a simple analytical closed form, and (3) it gives a reasonable asymptotic form when expanded in inverse powers of the nuclear separation, R. Many works have been devoted to obtaining an energy which satisfies the above conditions, particularly for such simple but essential systems as H—H$^+$, H—H and He—He. Among these, one of the most brilliant successes is the exact second-order perturbation energy, E_2, of H—H$^+$ obtained by Dalgarno and Lynn.[2] On the other hand, within the framework of the Unsöld approximation,[3] exact analytical expressions of the second-order perturbation energy, $\overline{E}_2$(Unsöld), which satisfies the latter two properties, have been derived by several authors[4,5] for the above molecular systems. Moreover, in our own previous paper,[6] the results of two hydrogen atoms and two helium atoms were examined and it was found that, at a large R value, the analytical formula gives an energy which is almost an upper bound to the exact one, if the absolute value of the energy in the ground state, E_0, of the isolated system, H_0, is applied to the average excitation energy, $\langle \Delta E \rangle_{\mathrm{Av}}$, in:

$$\overline{E}_2\,(\text{Unsöld}) = -\frac{(H_1^2)_{00} - (H_1)_{00}^2}{\langle \Delta E \rangle_{\mathrm{Av}}}, \qquad (1)$$

where H_1 is the non-expanded perturbation and where $(F)_{00}$ signifies the expectation value, $\langle \phi_0 | F | \phi_0 \rangle$, of the operator, F, concerning the unperturbed wave function of the ground state, ϕ_0. The charge overlap effect, which was extensively discussed by Kreak and Meath,[7] is automatically involved in $\overline{E}_2$(Unsöld). Therefore, considering that the Unsöld approximation corresponds to the following form for the first-order perturbation function:[8]

$$\phi_1 \sim AH_1\phi_0\,, \qquad (2)$$

the variational function including the above first-order wave function may be expected to give a fairly good interaction energy, especially at a large R value. Indeed, in order to get the result which is an upper bound and which, besides, includes the preferable properties at a large R value, the following variational function was employed in treating the problem of the long-range interaction between two atoms:[9]

$$\phi = (1 + AH_1)\phi_0. \qquad (3)$$

An approximate upper bound can thus be obtained, provided that $(H_1H_0H_1)_{00}$ and $(H_1^3)_{00}$ are small enough compared with $(H_1^2)_{00}$.

It has been pointed out by several authors,[10,11] however, that the variational function of Eq. (3) often gives unreasonable results for the perturbation energy; for example, if H_1 is the exact Coulombic interaction and if ϕ_0 is a 1s-like atomic orbital, $(H_1H_0H_1)_{00}$ and $(H_1^3)_{00}$ are infinite, as will be demonstrated in the case of H—H$^+$. To overcome this type of difficulty, the present authors[11] previously proposed a modified Hassé form and, in the atomic cases of hydrogen and helium, showed that the divergence of the above integrals can not only be easily removed, but that the variational function applied is quite effective. The wave function will be also favorable for the calculation of the long-range interaction energy, because the correction is mainly brought about for the exponentially decreasing terms and the asymptotic behavior through the third-order energy is retained.

1) Part II: Ref. 6.
2) A. Dalgarno and N. Lynn, *Proc. Phys. Soc. Ser. A*, **70**, 223 (1957).
3) A. Unsöld, *Z. Phys.*, **43**, 374 (1927).
4) G. M. Roe, *Phys. Rev.*, **88**, 659 (1952).
5) K. Fukui and T. Yamabe, *Intern. J. Quantum Chem.*, **2**, 359 (1968).
6) T. Yamabe, S. Ishimaru, and K. Fukui, This Bulletin, **45**, 1384 (1972).
7) H. Kreak and W. J. Meath, *J. Chem. Phys.*, **50**, 2289 (1969).
8) J. C. Slater and J. G. Kirkwood, *Phys. Rev.*, **37**, 686 (1931): H. R. Hassé, *Proc. Cambridge Phil. Soc.*, **27**, 66 (1931).
9) L. I. Shiff, "*Quantum Mechanics*", second ed., McGraw-Hill Book Co., New York (1955), p. 179.
10) B. Kirtman and M. L. Benston, *J. Chem. Phys.*, **46**, 472 (1967).
11) T. Yamabe, S. Ishimaru, and K. Fukui, This Bulletin, **43**, 2012 (1970).

Another type of variational function[12] usually involves ionic and polarization terms, and the effect of the electron exchange and the associated Laguerre function or the Slater-type orbital are often used for the radial part of the trial function. However, if the exact perturbation is applied in the calculation, this wave function gives only exponentially decreasing terms and a part of the correct asymptotic form, so the potential will be rather higher than the true one at a large nuclear separation.

Therefore, in the present article, we will investigate the long-range interaction energy by using the wave function of the modified Hassé form and by sorting the results into perturbation energies, which makes it possible to discuss the reliability of the Unsöld-type perturbation energy. Two cases of H—H$^+$ and H—H systems will be examined numerically.

The Variation Method Applied and Its Relation to the Perturbation Method

We assume the perturbation acting between two atoms to be the sum of the Coulombic interactions:

$$H_1 = \frac{Z_a Z_b}{R} - \sum_{j=1}^{n_a} \frac{Z_b}{r_{bj}} - \sum_{k=1}^{n_b} \frac{Z_a}{r_{ak}} + \sum_{j=1}^{n_a}\sum_{k=1}^{n_b} \frac{1}{r_{jk}} \tag{5}$$

where $n_{a(b)}$ is the number of electrons of the atom a(b) with a nuclear charge, $Z_{a(b)}$ and where $r_{bj(ak)}$ is the distance between the nucleus of the b(a) atom and the $j(k)$ electron belonging to the atom a(b) (all in atomic units). In order to remove the divergence difficulty mentioned in the introduction, we replace H_1 in Eq. (3) by the following function:[11]

$$\bar{H}_1 = \frac{Z_a Z_b}{R} - \sum_{j=1}^{n_a} \frac{Z_b(1-e^{-m_b r_{bj}})}{r_{bj}} - \sum_{k=1}^{n_b} \frac{Z_a(1-e^{-m_a r_{ak}})}{r_{ak}} + \sum_{j=1}^{n_a}\sum_{k=1}^{n_b} \frac{(1-e^{-k r_{jk}})}{r_{ik}}, \tag{6}$$

in which m_a, m_b, and k are supposed to be positive parameters, and use the variational function of the modified Hassé form:

$$\bar{\psi} = (1 + A\bar{H}_1)\phi_0 . \tag{7}$$

The upper bound, $\bar{E}$, of the total energy, E, of the perturbed system, H, is then obtained as follows:

$$\bar{E} = E_0 + E_1 + \frac{2A[(\bar{H}_1 H_1)_{00} - E_1(\bar{H}_1)_{00}] + A^2(\bar{H}_1(H_0 - E_0 + H_1 - E_1)\bar{H}_1)_{00}}{1 + 2A(\bar{H}_1)_{00} + A^2(\bar{H}_1^2)_{00}} \geqq E, \tag{8}$$

where $E_0 = (H_0)_{00}$ and $E_1 = (H_1)_{00}$. $\bar{E}$ is further classified into the second- and third-order perturbation energies by regarding $A\bar{H}_1\phi_0$ as the approximate first-order perturbation function, $\bar{\phi}_1$. That is, following the variation-perturbation theory, the upper bound, $\bar{E}_2$, of the second-order energy is given by:

$$\bar{E}_2 = 2\langle\bar{\phi}_1|H_1 - E_1|\phi_0\rangle + \langle\bar{\phi}_1|H_0 - E_0|\bar{\phi}_1\rangle \tag{9}$$

$$= 2A[(\bar{H}_1 H_1)_{00} - E_1(\bar{H}_1)_{00}] + A^2(\bar{H}_1(H_0 - E_0)\bar{H}_1)_{00} \tag{10}$$

$$= 2A[(\bar{H}_1 H_1)_{00} - E_1(\bar{H}_1)_{00}] + \frac{1}{2}A^2(\nabla H_1)_{00}^2 \geqq E_2, \tag{10'}$$

which gives the minimum:[13]

$$\bar{E}_2 = -\frac{[(\bar{H}_1 H_1)_{00} - E_1(\bar{H}_1)_{00}]^2}{(\bar{H}_1(H_0 - E_0)\bar{H}_1)_{00}} \geqq E_2 \tag{11}$$

when

$$A = -\frac{(\bar{H}_1 H_1)_{00} - E_1(\bar{H}_1)_{00}}{(\bar{H}_1(H_0 - E_0)\bar{H}_1)_{00}} . \tag{12}$$

The third-order energy is, approximately:

$$\bar{E}_3 = -2A\bar{E}_2(\bar{H}_1)_{00} + A^2(\bar{H}_1(H_1 - E_1)\bar{H}_1)_{00} . \tag{13}$$

The residue in $\bar{E}$, hence, consists of the fourth- and higher-order terms. At a large R value, the results of Eq. (8) can also be related to the perturbation energy with the Unsöld approximation by the use of several pertinent approximations; *i.e.*, we may put

$$(\bar{H}_1)_{00} \sim (H_1)_{00} \tag{14}$$

$$(\bar{H}_1^2)_{00} \sim (\bar{H}_1 H_1)_{00} \sim (H_1^2)_{00} , \tag{15}$$

because the discrepanicies between them are of the order of e^{-2R}. For instance, the relative magnitudes of these integrals in the case of H—H$^+$, which we will discuss in the next section, are presented in Table 1. The results show that these assumptions are reasonable. Moreover, considering that the denominator of Eq. (8) is almost unity,[6] and using the relations, $|E_0| \gg |E_1|$ and $(H_1^2)_{00} \gg (H_1)_{00}$, Eq. (8) can be approximated by:

$$\bar{E} \sim E_0 + E_1 + \frac{(H_1^2)_{00} - (H_1)_{00}^2}{E_0 - \Delta} \gtrsim E, \tag{16}$$

where

$$\Delta = \frac{(\bar{H}_1 H_0 \bar{H}_1)_{00} + (\bar{H}_1 H_1 \bar{H}_1)_{00}}{(H_1^2)_{00} - (H_1)_{00}^2} . \tag{17}$$

Equation (16) shows that, if the $E_0 - \Delta$ value is chosen as $-\langle\Delta E\rangle_{Av}$, Eq. (1) gives almost an upper bound. Δ is considered to be a correction depending on the R value and the variational parameters (in our previous derivation of the upper bound,[6] Δ was neglected). Ex-

TABLE 1. THE RELATIVE MAGNITUDES OF SEVERAL INTEGRALS IN THE CASE OF H–H$^+$ INTERACTION

R (a.u.)	m	$(\bar{H}_1)_{00}/(H_1)_{00}$	$(\bar{H}_1 H_1)_{00}/(H_1^2)_{00}$	$(\bar{H}_1^2)_{00}/(H_1^2)_{00}$	$(H_1)^2_{00}/(H_1^2)_{00}$
6.0	4.0	1.270	0.993	0.990	0.561×10^{-7}
8.0	4.3	1.251	1.000	0.999	0.604×10^{-10}
10.0	4.3	1.244	1.000	1.000	0.489×10^{-15}

12) L. O. Hirschfelder and J. Y. Linnett, *J. Chem. Phys.*, **18**, 130 (1950).

13) Dalgarno got an upper bound to E_2 using the function of the type of Eq. (2) in the perturbation-variation theory as follows:

$$-\frac{[(H_1^2)_{00} - (H_1)^2_{00}]^2}{(H_1(H_0 - E_0)H_1)_{00}} \gtrsim E_2 .$$

See A. Dalgarno, "Quantum Theory," Vol. 1, ed. by D. R. Bates, Academic Press Inc., New York (1961), p. 193.

panding $1/(E_0-\Delta)$ into the power series of Δ/E_0 and neglecting the higher-order terms than Δ/E_0, one obtains another expression:

$$\bar{E} \sim E_0 + E_1^+ + \frac{(H_1^2)_{00}-(H_1)_{00}^2}{E_0} + \frac{(\bar{H}_1H_0\bar{H}_1)_{00}+(\bar{H}_1H_1\bar{H}_1)_{00}}{E_0^2}. \quad (18)$$

Although $(\bar{H}_1H_1\bar{H}_1)_{00}/E_0^2$ in Eq. (18) is a part of the third-order energy, $(\bar{H}_1H_0\bar{H}_1)_{00}/E_0^2$ should be included in the second-order energy, as may be seen in Eq. (10). Indeed, under the same order of the approximation as the above, Eq. (10) gives:

$$\bar{E}_2 \sim \frac{(H_1^2)_{00}-(H_1)_{00}^2}{E_0} + \frac{(\bar{H}_1H_0\bar{H}_1)_{00}}{E_0^2} \gtrsim E_2, \quad (19)$$

which may be called "the improved second-order Unsöld energy" and which is plausible when compared with the modified form of the exact second-order energy given by Lennard-Jones:[14]

$$E_2 = \frac{(H_1^2)_{00}-(H_1)_{00}^2}{E_0} + \sum_i{}' \frac{(H_1)_{0i}E_0^i(H_1)_{i0}}{E_0(E_0-E_0^i)}, \quad (20)$$

where E_0^i is the i-th eigenvalue of H_0(*i.e.*, $H_0\phi_0^i=E_0^i\phi_0^i$ ($\phi_0^0=\phi_0$, $E_0^0=E_0$)) and where $\sum'$ means that the summation does not include the case of $i=0$. Equation (19) corresponds to the results obtained by replacing $E_0-E_0^i$ by $-\langle\Delta E\rangle_{Av}=E_0$ and by deleting the divergence difficulty. It should be noticed that the second-order energy of Eq. (1) with $\langle\Delta E\rangle_{Av}=-E_0$ differs from that of the (perturbation-) variation method by the amount of $(\bar{H}_1H_0\bar{H}_1)_{00}/E_0^2$, though the correction does not affect the first leading term of the asymptotic form of Eq. (1), as will be shown below.

H–H$^+$ Interaction

As the simplest example, let us first consider the interaction between a hydrogen atom with a nucleus, a, and a proton, b. The perturbation may be obtained from Eq. (5) as follows:

$$H_1 = \frac{1}{R} - \frac{1}{r_{b1}}. \quad (21)$$

If one applies the variational function of Eq. (3), with the 1s atomic orbital as the unperturbed wave function, the $(H_1^3)_{00}$ and $(\bar{H}_1H_0\bar{H}_1)_{00}$ appearing in the expression of the total energy become infinite because of the divergence of integrals:

$$(r_{b1}^{-3})_{00} = \lim_{\varepsilon\to 0} 4\left(-\log\varepsilon+1-\log 2\gamma+\frac{1}{2R}\right)e^{-2R} - \frac{2}{R} - 2e^{2R}Ei(-2R) + 2e^{-2R}Ei(2R), \quad (22)$$

$$(r_{b1}^{-4})_{00} = 4e^{-2R}\lim_{\varepsilon\to 0}\frac{1}{\varepsilon}, \quad (23)$$

where:

$$Ei(-x) = -\int_x^\infty \frac{e^{-t}}{t}dt, \quad Ei(x) = -\int_{-x}^\infty \frac{e^{-t}}{t}dt$$

and where $\log\gamma$ is the Euler constant, 0.5772156649···. However, if one uses the variational function of Eq. (7), in which $\bar{H}_1$ is, in the present example, given by:

$$\bar{H}_1 = \frac{1}{R} - \frac{1-e^{-mr_{b1}}}{r_{b1}}, \quad (24)$$

$(\bar{H}_1H_1\bar{H}_1)_{00}$ and $(\bar{H}_1H_0\bar{H}_1)_{00}$ become finite by the cancellation of singularities so long as m is finite. For large m values, these values are, respectively, approximated by:

$$(\bar{H}_1H_1\bar{H}_1)_{00} \sim -4e^{-2R}\log m \quad (25)$$

$$(\bar{H}_1H_0\bar{H}_1)_{00} \sim 4me^{-2R}, \quad (26)$$

which diverge to negative and positive infinity as $m\to\infty$.

Thus, the divergence characters are included in the exponentially decreasing terms, which can not be obtained unless exact calculations are performed. The conventional perturbation calculation with the Unsöld approximation[15] did not solve this problem since the perturbation is usually expanded in powers of R^{-1} and the exponentially decreasing terms are completely omitted. Nevertheless, the conventional calculation is considered to be reliable, because, according to our correction, the divergence character has been excluded and so exerts little influence on the part expressed in the inverse powers of R.[16]

Now, let us calculate the interaction energy, $\bar{E}-E_0$. All of the integrals in Eq. (8) can be written as follows:

$$(H_1)_{00} = \left(1+\frac{1}{R}\right)e^{-2R} \quad (27)$$

$$(\bar{H}_1)_{00} = (H_1)_{00} + \left(\frac{e^{-mr_{b1}}}{r_{b1}}\right)_{00} \quad (28)$$

$$(H_1^2)_{00} = \frac{1}{R^2} - \frac{2}{R}\left(\frac{1}{r_{b1}}\right)_{00} + \left(\frac{1}{r_{b1}^2}\right)_{00} \quad (29)$$

$$(\bar{H}_1H_1)_{00} = (H_1^2)_{00} + \frac{1}{R}\left(\frac{e^{-mr_{b1}}}{r_{b1}}\right)_{00} - \left(\frac{e^{-mr_{b1}}}{r_{b1}^2}\right)_{00} \quad (30)$$

$$(\bar{H}_1^2) = 2(\bar{H}_1H_1)_{00} - (H_1^2)_{00} + \left(\frac{e^{-2mr_{b1}}}{r_{b1}^2}\right)_{00} \quad (31)$$

$$(\nabla H_1)_{00}^2 = \left(\frac{[1-e^{-mr_{b1}}]^2}{r_{b1}^4}\right)_{00} - 2m\left(\frac{e^{-mr_{b1}}[1-e^{-mr_{b1}}]}{r_{b1}^3}\right)_{00} + m^2\left(\frac{e^{-2mr_{b1}}}{r_{b1}^2}\right)_{00} \quad (32)$$

14) J. E. Lennard-Jones, *Proc. Roy. Soc. Ser. A*, **129**, 598 (1930).

15) A. Dalgarno and J. T. Lewis, *Proc. Phys. Soc. Ser. A*, **69**, 57 (1956).

16) For example, assuming $r_{a1}<R$ and α is a constant not equal to zero,

$$\left(\frac{e^{-\alpha r_{b1}}}{r_{b1}^3}\right)_{00} = \sum_{l=0}^\infty\sum_{m=0}^\infty\sum_{n=0}^\infty (2l+1)\int \frac{r_{a1}^{m+n}}{\sqrt{r_{a1}\bar{R}}\,R^{m+n+2}} \times P_l(\cos\theta)\,P_m(\cos\theta)\,P_n(\cos\theta)\,I_{l+1/2}(\alpha r_{a1})\,K_{l+1/2}(\alpha R)\,\phi_0^2 d\tau$$
$$= \frac{2e^{-\alpha R}}{(\alpha R)^3}\left[\frac{\alpha^2}{(2-\alpha)^2}-\frac{\alpha^2}{(2+\alpha)^2}\right] + \frac{4e^{-\alpha R}}{(\alpha R)^4}\left[\frac{2\alpha^3}{(2+\alpha)^3}+\frac{2\alpha^3}{(2-\alpha)^3}+\frac{\alpha^2}{(2+\alpha)^2}-\frac{\alpha^2}{(2-\alpha)^2}\right] + \frac{16e^{-\alpha R}}{(\alpha R)^5}\left[\frac{\alpha^4}{(2-\alpha)^4}-\frac{\alpha^4}{(2+\alpha)^4}\right] + e^{-\alpha R}O([\alpha R]^{-6}),$$

where θ is the angle between r_{a1} and R and $I_\nu(z)$ and $K_\nu(z)$ are well-known Bessel functions of purely imaginary argument. This integral can be neglected for large R.

TABLE 2. THE INTERACTION ENERGIES BETWEEN HYDROGEN AND PROTON WITHOUT THE RESONANCE EFFECT (in a.u.)

R (a.u.)	The present result			Dalgarno and Lynn[a]
	m	A	$E-E_0$	
5.0	3.8	−2.350	-0.4712×10^{-2}	-0.462×10^{-2}
6.0	4.0	−2.183	-0.1980×10^{-2}	-0.206×10^{-2}
7.0	4.1	−2.088	-0.9743×10^{-3}	-0.105×10^{-2}
8.0	4.2	−2.042	-0.5414×10^{-3}	-0.595×10^{-3}
9.0	4.3	−2.020	-0.3278×10^{-3}	-0.365×10^{-3}
10.0	4.3	−2.009	-0.2111×10^{-3}	-0.235×10^{-3}

a) Ref. 17.

$$(\overline{H}_1H_1\overline{H}_1)_{00}=\frac{1}{R^3}-\frac{1}{R^2}[2(\overline{H}_1)_{00}+(H_1)_{00}]+\frac{1}{R}[2(\overline{H}_1H_1)_{00}+(\overline{H}_1^2)_{00}]-\left(\frac{[1-e^{-mr_{b1}}]^2}{r_{b1}^3}\right)_{00}. \quad (33)$$

The integrals on the right-hand sides are given in Appendix A. The interaction energies, optimized at each R value with respect to m, are listed in Table 2. The results are comparable with those obtained through the second-order perturbation energy under the Unsöld approximation and without the resonance effect.[17] That the values of m are finite means that the divergence difficulty is deleted and that, as expected, A approaches $1/E_0=-2.0$ at large R values.

Next, let us examine the second- and third-order perturbation energies in connection with the above variational calculation. At large enough R values, exponentially decreasing terms can be neglected and $(H_1^2)_{00}$ and $(\overline{H}_1H_0\overline{H}_1)_{00}$ can be simplified only to the parts which are the origin of the well-known expression of a power series of R^{-1}, namely:

$$(H_1^2)^{L}_{00}=-\frac{1}{R^2}+\left(1+\frac{1}{2R}\right)e^{-2R}Ei(2R)+\left(1-\frac{1}{2R}\right)e^{2R}Ei(-2R) \quad (34)$$

$$\sim\sum_{n=1}^{\infty}\frac{4(n+1)(2n)!}{(2R)^{2n+2}}, \quad (34')$$

$$(\overline{H}_1H_0\overline{H}_1)^{L}_{00}=\frac{1}{2R^2}+\left(\frac{1}{2}-\frac{3}{4R}\right)e^{-2R}Ei(2R)+\left(\frac{1}{2}+\frac{3}{4R}\right)e^{2R}Ei(-2R) \quad (35)$$

$$\sim\sum_{n=1}^{\infty}\frac{2n(2n+2)!}{(2R)^{2n+4}}. \quad (35')$$

From Eq. (1),

$$\overline{E}_2^{L}(\text{Unsöld})=-2(H_1^2)^{L}_{00} \quad (36)$$

and from Eq. (19),

$$\overline{E}_2^{L}=\frac{4}{R}\left[\frac{1}{R}-e^{-2R}Ei(2R)+e^{2R}Ei(-2R)\right]. \quad (37)$$

According to the results of Dalgarno and Lynn,[2] the exact second-order energy without exponentially decreasing terms is given by:

$$E_2^{L}=\frac{1}{R^2}\left[\frac{5}{2}-(R+1)^2e^{-2R}Ei(2R)-(R-1)^2e^{2R}Ei(-2R)\right]. \quad (38)$$

On expanding the exponential integrals, Eqs. (36)—(38) are reduced to:

$$\overline{E}_2^{L}(\text{Unsöld})\sim-\sum_{n=1}^{\infty}\frac{(n+1)(2n)!}{2^{2n-1}R^{2n+2}} \quad (36')$$

$$\overline{E}_2^{L}\sim-\sum_{n=1}^{\infty}\frac{2(2n)!}{2^{2n-1}R^{2n+2}} \quad (37')$$

$$E_2^{L}\sim-\sum_{n=1}^{\infty}\frac{(2n+1)(n+2)}{4n}\frac{(2n)!}{2^{2n-1}R^{2n+2}}. \quad (38')$$

From Eqs. (37′) and (38′), it may easily be seen that $\overline{E}_2^{L}$ is higher than E_2^{L} in all terms of the series, that is, that the relation of Eq. (19) is still kept for the non-exponentially decreasing terms:

$$\overline{E}_2^{L}>E_2^{L}. \quad (39)$$

$\overline{E}_2^{L}$(Unsöld) is, however, so only in the first term, probably because the higher multipole transition has a larger excitation energy than does the lowest dipole transition. The numerical results, presented in Table 3, show that the non-exponentially decreasing terms are negligible and that the expressions of $\overline{E}_2^{L}$(Unsölid)

TABLE 3. THE PERTURBATION ENERGIES BETWEEN HYDROGEN AND PROTON ESTIMATED BY SEVERAL METHODS (in a.u.)

R (a.u.)	E_1	$\overline{E}_2$(Unsöld)	$\overline{E}_2^{L}$(Unsöld)	$\overline{E}_2$	$\overline{E}_2^{L}$
5.0	0.5448×10^{-4}	-0.4153×10^{-2}	-0.4109×10^{-2}	-0.2639×10^{-2}	-0.3768×10^{-2}
6.0	0.7168×10^{-5}	-0.1833×10^{-2}	-0.1828×10^{-2}	-0.1569×10^{-2}	-0.1716×10^{-2}
7.0	0.9503×10^{-6}	-0.9358×10^{-3}	-0.9353×10^{-3}	-0.8761×10^{-3}	-0.8958×10^{-3}
8.0	0.1266×10^{-6}	-0.5307×10^{-3}	-0.5306×10^{-3}	-0.5120×10^{-3}	-0.5148×10^{-3}
9.0	0.1692×10^{-7}	-0.3246×10^{-3}	-0.3246×10^{-3}	-0.3170×10^{-3}	-0.3174×10^{-3}
10.0	0.2267×10^{-8}	-0.2101×10^{-3}	-0.2101×10^{-3}	-0.2064×10^{-3}	-0.2065×10^{-3}

R (a.u.)	E_2	E_2^{L}	$\overline{E}_3$	$\overline{E}_3^{L}$
5.0	-0.4093×10^{-2}	-0.4331×10^{-2}	-0.2179×10^{-2}	-0.7515×10^{-3}
6.0	-0.1929×10^{-2}	-0.1963×10^{-2}	-0.4271×10^{-3}	-0.2355×10^{-3}
7.0	-0.1008×10^{-3}	-0.1019×10^{-2}	-0.1008×10^{-3}	-0.7756×10^{-4}
8.0	-0.5829×10^{-3}	-0.5836×10^{-3}	-0.3013×10^{-4}	-0.2685×10^{-4}
9.0	-0.3590×10^{-3}	-0.3591×10^{-3}	-0.1103×10^{-4}	-0.1053×10^{-4}
10.0	-0.2333×10^{-3}	-0.2333×10^{-3}	-0.4722×10^{-5}	-0.4646×10^{-5}

17) A. Dalgarno and N. Lynn, *Proc. Phys. Soc. Ser. A*, **69**, 821 (1956).

Table 4. The interaction energies between two hydrogen atoms (in a.u.)

R (a.u.)	The present result				Hirschfelder and Linnett[a]
	m	k	A	$\overline{E}-E_0$	
6.0	3.5	2.9	−0.419	-0.1922×10^{-3}	-0.6367×10^{-3}
7.0	3.2	2.6	−0.553	-0.6774×10^{-4}	-0.1465×10^{-3}
8.0	3.1	2.5	−0.694	-0.2883×10^{-4}	-0.4000×10^{-4}
9.0	3.0	2.4	−0.819	-0.1400×10^{-4}	
10.0	2.9	2.4	−0.897	-0.7288×10^{-5}	-0.6980×10^{-5}
11.0	2.8	2.4	−0.935	-0.3993×10^{-5}	
12.0	2.8	2.4	−0.949	-0.2295×10^{-5}	-0.2013×10^{-5}

a) Ref. 12.

and $\overline{E}_2{}^{\mathrm{L}}$ are quite effective.

Similarly, the third-order energy in Eq. (18) is approximated by:

$$\overline{E}_3{}^{\mathrm{L}} = (\overline{H}_1H_1\overline{H}_1)^{\mathrm{L}}{}_{00}/E_0{}^2 = 4\left[\frac{2}{R}-\frac{2}{R^3}-\left(2-\frac{3}{R}-\frac{3}{2R^2}\right)e^{-2R}Ei(2R) + \left(2+\frac{3}{R}-\frac{3}{2R^2}\right)e^{2R}Ei(-2R)\right], \quad (40)$$

which is, in the form of a power series of R^{-1}:

$$\overline{E}_3{}^{\mathrm{L}} \sim -\sum_{n=1}^{\infty}\frac{n(n+2)(2n+2)\,!}{2^{2n+1}R^{2n+5}} \quad (41)$$

and which leads to the same result as that of Dalgarno and Lewis[15] except for the difference in the average energy. The numerical results are also listed in Table 3.

H–H Interaction

In the case of two hydrogen atoms, the perturbation is given by:

$$H_1 = \frac{1}{R}-\frac{1}{r_{b1}}-\frac{1}{r_{a2}}+\frac{1}{r_{12}}. \quad (42)$$

According to Eq. (6), $\overline{H}_1$ is written as follows:

$$\overline{H}_1 = \frac{1}{R}-\frac{1-e^{-mr_{b1}}}{r_{b1}}-\frac{1-e^{-mr_{a2}}}{r_{a2}}+\frac{1-e^{-kr_{12}}}{r_{12}}. \quad (43)$$

In Table 4, the interaction energy optimized with respect to m and k is shown, together with the best variational results for large separations calculated by Hirschfelder and Linnett[12] (HL) using the exact perturbation and the trial function, which consists of the 1s atomic orbital with a variable exponent and which is corrected by considering the ionic states, the polarization effect, and the electron exchange. As a matter of course, the values of HL are better than ours at $R\leqq8$, where the exchange effect plays an important role. However, at a longer distance, where only the Coulombic interaction is dominant, the present energy becomes lower than that of HL in spite of its simple expression.

In Table 5, the perturbation energies through the third-order are listed and the second-order perturbation energy is compared with the result previously obtained by the present authors.[6] The second-order energy of the Unsöld type approaches $\overline{E}_2$ at large R values; this is consistent with the previous observation.[6]

Following our calculation, the third-order energy, $\overline{E}_3$, is positive, while the asymptotic form[18] gives a negative value ($-3986\,R^{-11}$). The difference may be partly due to the fact that the present result includes the charge-overlap effect,[19] which is usually repulsive in the order of e^{-2R}, and partly to the fact that, in the calculation of $(\overline{H}_1H_1\overline{H}_1)_{00}$, we neglected the $-(e^{-kr_{12}}/r_{b1}r_{12}r_{a2})_{00}+(e^{-mr_{b1}}e^{-kr_{12}}/r_{b1}r_{12}r_{a2})_{00}$ terms, which are of the e^{-2R} order and which are totally negative (the $\overline{E}_3$ and $\overline{E}$ thus obtained are, accordingly, higher than the respective exact values). Therefore, it is not strange that $\overline{E}_3$ is positive for not sufficiently large nuclear distances.

For such large R values that the exponentially decreasing terms can be neglected, the non-exponentially decreasing terms of $(H_1{}^2)_{00}$, which are the same as those in $(\overline{H}_1H_1)_{00}$ and $(\overline{H}_1{}^2)_{00}$, were obtained in our previous paper[6] as follows:

$$(H_1{}^2)^{\mathrm{L}}{}_{00} = \frac{1}{R^2}-\frac{7}{12}+e^{2R}Ei(-2R)\left(\frac{11}{16R}-\frac{11}{8}-\frac{R}{2}+\frac{R^2}{6}\right) + e^{-2R}Ei(2R)\left(-\frac{11}{16R}-\frac{11}{8}+\frac{R}{2}+\frac{R^2}{6}\right). \quad (44)$$

Hence, $\overline{E}_2{}^{\mathrm{L}}$(Unsöld) is in the expanded form:

$$\overline{E}_2{}^{\mathrm{L}}(\text{Unsöld}) = \frac{1}{E_0}(H_1{}^2)^{\mathrm{L}}{}_{00} \sim -\frac{1}{3}\sum_{n=1}^{\infty}\frac{n(n+7)(2n+4)\,!}{(2n+3)(2R)^{2n+4}} \sim -\frac{6.0}{R^6}-\frac{135.0}{R^8}-\frac{3937.5}{R^{10}}-\cdots. \quad (45)$$

Moreover, the second-order perturbation energy of Pauling and Beach[20] is:

$$E_2{}^{\mathrm{L}} = -\frac{6.49903}{R^6}-\frac{124.399}{R^8}-\frac{3285.828}{R^{10}}-\cdots. \quad (46)$$

By comparing Eqs. (45) and (46), it may easily be seen that, as in the case of H–H$^+$, the Unsöld approxima-

18) Y. M. Chan and A. Dalgarno, *Mol. Phys.*, **14**, 101 (1968).

19) At $R=10$, for example, $e^{-2R}=0.2\times10^{-8}$ and $-3986\,R^{-11}=-4\times10^{-8}$. So the effect of the charge overlap will surpass that of the asymptotic form in the region $R<10$.

20) L. Pauling and J. Y. Beach, *Phys. Rev.*, **47**, 686 (1935).

TABLE 5. THE PERTURBATION ENERGIES BETWEEN TWO HYDROGEN ATOMS (in a.u.)

R (a.u.)	E_1	$\overline{E}_2$	$\overline{E}_2$ (Unsöld)[a]	$\overline{E}_3$
6.0	-0.5965×10^{-4}	-0.1534×10^{-3}	-0.4351×10^{-3}	0.2092×10^{-4}
7.0	-0.1052×10^{-4}	-0.6470×10^{-4}	-0.1251×10^{-3}	0.7469×10^{-5}
8.0	-0.1791×10^{-5}	-0.2965×10^{-4}	-0.4269×10^{-4}	0.2605×10^{-5}
9.0	-0.2972×10^{-6}	-0.1466×10^{-4}	-0.1737×10^{-4}	0.7513×10^{-6}
10.0	-0.4832×10^{-7}	-0.7443×10^{-5}	-0.8176×10^{-5}	0.2041×10^{-6}
11.0	-0.7727×10^{-8}	-0.4054×10^{-5}	-0.4282×10^{-5}	0.6946×10^{-7}
12.0	-0.1219×10^{-8}	-0.2333×10^{-5}	-0.2421×10^{-5}	0.3919×10^{-7}

a) Ref. 6.

TABLE 6. THE INTERACTION ENERGIES BETWEEN HYDROGEN AND PROTON WITH THE RESONANCE EFFECT (in a.u.)

R (a.u.)	The present result			Dalgarno and Lynn[a]	The exact value[b]
	m	A	$\overline{E}-E_0$		
2.0	2.5	−1.185	-0.9428×10^{-1}	-0.6591×10^{-1}	−0.1026
3.0	1.9	−1.442	-0.7479×10^{-1}	-0.6546×10^{-1}	-0.7756×10^{-1}
4.0	1.3	−1.797	-0.4506×10^{-1}	-0.4393×10^{-1}	-0.4608×10^{-1}
5.0	1.1	−2.103	-0.2398×10^{-1}	-0.2368×10^{-1}	-0.2442×10^{-1}
6.0	0.9	−2.326	-0.1169×10^{-1}	-0.1151×10^{-1}	-0.1197×10^{-1}
7.0	1.3	−2.250	-0.5416×10^{-2}	-0.5295×10^{-2}	-0.5595×10^{-2}
8.0	1.5	−2.200	-0.2455×10^{-2}	-0.2395×10^{-2}	-0.2570×10^{-2}
9.0	3.1	−2.136	-0.1126×10^{-2}	-0.1095×10^{-2}	-0.1195×10^{-2}
10.0	6.5	−2.092	-0.5388×10^{-3}	-0.5250×10^{-3}	-0.5800×10^{-3}

a) Ref. 17. b) Ref. 23.

tion with $\langle\Delta E\rangle_{Av}=-E_0$ tends to underestimate the coefficient of the first leading term, while overestimating those of the higher-order terms. Therefore, if one chooses the average excitation energy so that correct coefficient of R^{-6} may be obtained, the adjustment unfortunately increases errors in the coefficients of the second- and higher-order terms.[21] On the other hand, the correction terms, $(\overline{H}_1H_0\overline{H}_1)^L{}_{00}$, is:

$$(\overline{H}_1H_0\overline{H}_1)^L{}_{00}=\frac{5}{12}-\frac{1}{R^2}+e^{2R}Ei(-2R)\left(\frac{R^2}{6}+\frac{R}{2}-\frac{7}{8}-\frac{25}{16R}\right)+e^{-2R}Ei(2R)\left(\frac{R^2}{6}-\frac{R}{2}-\frac{7}{8}+\frac{25}{16R}\right), \quad (47)$$

which is written in the following power series:

$$(\overline{H}_1H_0\overline{H}_1)_{00}\sim\frac{2}{3}\sum_{n=1}^{\infty}\frac{n(n+1)(n+5)(2n+4)\,!}{(2R)^{2n+6}}. \quad (48)$$

Hence, from Eqs. (19), (44) and (47), $\overline{E}_2{}^L$ is obtained as follows:

$$\begin{aligned}\overline{E}_2{}^L&=\frac{1}{6}-\left(\frac{R^2}{3}-\frac{9}{4}-\frac{7}{8R}\right)e^{2R}Ei(-2R)-\left(\frac{R^2}{3}-\frac{9}{4}+\frac{7}{8R}\right)e^{-2R}Ei(2R)\\&\sim-4\sum_{n=1}^{\infty}\frac{n(n+3)(2n+2)\,!}{(2R)^{2n+4}}\\&\sim-\frac{6.0}{R^6}-\frac{112.5}{R^8}-\frac{2835.0}{R^{10}}-\cdots.\end{aligned} \quad (49)$$

Equation (49) gives the upper values for all orders of R^{-1}, as in the case of H–H$^+$.

Discussion

It has been stressed by several authors[7,15,22] that the major factor limiting the accuracy of the long-range interaction energy between the hydrogen atom and the proton is the neglect of the degeneracy arising from the identity of the nuclear fields. Therefore, let us now examine the energy, including the effect of the degeneracy. The wave function for the $1s\sigma_g$ is given by:

$$\overline{\phi}_{1s\sigma_g}=(1+P)(1+A\overline{H}_1)\phi_0 \quad (50)$$

where P is a usual projection operator which interchanges the two nuclei, a and b. Performing the integration analytically with some manipulations, and optimizing with respect to m in $\overline{H}_1$, the results shown in Table 6 are obtained. It is remarkable that the present result is, for all nuclear distances, superior to that calculated by Dalgarno and Lynn[17] by the use of a modification of a trial function given by HL for the H–H system. That there is a great discrepancy between the results in Tables 1 and 6 demonstrates the importance of considering the degeneracy particularly in treating the induction force, because, as has been mentioned above, the present dispersion energy for H–H, even without any exchange effect, is better than that of HL for $R\gtrsim10$.

It is of interest that Eq. (49) gives good coefficients when multiplied by the value of 6.499/6.0 so that the coefficient of the first leading term may become the

21) G. Starkschall and R. G. Gordon, *J. Chem. Phys.*, **56**, 2801 (1972).

22) H. Margenau, *Phys. Rev.*, **56**, 1000 (1939).

exact value; that is:

$$\frac{6.499}{6.0}\bar{E}_2^{\mathrm{L}} \sim \frac{6.499}{R^6} - \frac{121.9}{R^8} - \frac{3070.8}{R^{10}} - \cdots . \quad (51)$$

This coincidence implies the utility of the conditions in Eq. (19). However, the correction for the coefficient of R^{-6} should be essentially brought about by use of the sum in Eq. (20),[14] which corresponds to $(\bar{H}_1H_0\bar{H}_1)_{00}/E_0^2$ in the present treatment, whereas, as is shown in Eq. (48), $(\bar{H}_1H_0\bar{H}_1)_{00}/E_0^2$ does not include the term of R^{-6}, but begins with R^{-8}. The difference may be caused by the average energy approximation applied. Followingly, it seems more legitimate to correct the result of Eq. (45) by adding $-(\bar{H}_1H_0\bar{H}_1)_{00}/E_0\langle\Delta E\rangle_{\mathrm{Av}}$, in which $\langle\Delta E\rangle_{\mathrm{Av}}$ is adjusted so as to give the preferable coefficient of R^{-8}. Indeed, if the value of 2.122 is adopted for $\langle\Delta E\rangle_{\mathrm{Av}}$, the coefficients of R^{-8} and R^{-10} become 124.4 and 3417.9 respectively; the latter is better than the value, 3724, obtained by Starkschall and Gordon.[21]

Furthermore, one can easily improve the numerical accuracy by the combination of our method with that presented by Goodisman,[24] who also treated the divergence problem in the calculation of $(\bar{H}_1H_0\bar{H}_1)_{00}$. If the complete set of eigenfunctions $\{\phi_0{}^i\}$ of the unperturbed Hamiltonian H_0 is available, the following first-order variational function, $\bar{\phi}_1{}^{(n)}$, can be used instead of $\bar{\phi}_1$:

$$\bar{\phi}_1{}^{(n)} = A[\bar{H}_1\phi_0 - \sum_{i=1}^{n}\bar{V}_i\phi_0{}^i] - \sum_{i=1}^{n}\frac{V_i\phi_0{}^i}{\varepsilon_i}, \quad (52)$$

where:

$$V_i = \langle\phi_0{}^i|H_1|\phi_0\rangle \quad (53)$$

$$\bar{V}_i = \langle\phi_0{}^i|\bar{H}_1|\phi_0\rangle \quad (54)$$

$$\varepsilon_i = E_0{}^i - E_0 . \quad (55)$$

Substituting Eq. (52) into Eq. (9) gives:

$$\bar{E}_2{}^{(n)} = -\sum_{i=1}^{n}\frac{V_i{}^2}{\varepsilon_i} + 2A[(\bar{H}_1H_1)_{00} - E_1(\bar{H}_1)_{00} - \sum_{i=1}^{n}\bar{V}_iV_i] + A^2[(\bar{H}_1(H_0-E_0)\bar{H}_1)_{00} - \sum_{i=1}^{n}\varepsilon_i\bar{V}_i{}^2] \geqq E_2 . \quad (56)$$

which is reduced to Eq. (10) when the terms of the summation concerning i are omitted and to the exact value when $n=\infty$. Minimizing Eq. (56) with respect to A, one obtains:

$$\bar{E}_2{}^{(n)} = -\sum_{i=1}^{n}\frac{V_i{}^2}{\varepsilon_i} + \frac{[(\bar{H}_1H_1)_{00} - \sum_{i=1}^{n}\bar{V}_iV_i]^2}{\sum_{i=1}^{n}\varepsilon_i\bar{V}_i{}^2 - (\bar{H}_1(H_0-E_0)\bar{H}_1)_{00}} \geqq E_2 . \quad (57)$$

In the above equation, no divergence difficulty appears in the denominator. The improvement made possible by applying this expression is now under investigation in our laboratory.

23) D. R. Bates, K. Ledsham, and A. L. Stewart, *Phil. Trans. Roy. Soc., Ser A*, **246**, 215 (1953).
24) J. Goodisman, *J. Chem. Phys.*, **47**, 2707 (1967).

Appendix A. The basic integrals used in the case of H–H$^+$

$$(e^{-mr_{b1}})_{00} = \left[-I_2{}^- - \left(\frac{I_2{}^-}{2} + 2I_3{}^+\right)\frac{1}{R}\right]e^{-2R} + \left[\left(\frac{I_1{}^-}{2} + I_2{}^+\right) + \left(\frac{I_2{}^-}{2} + 2I_3{}^+\right)\frac{1}{R}\right]e^{-mR} \quad (A1)$$

$$\left(\frac{e^{-mr_{b1}}}{r_{b1}}\right)_{00} = \left[-I_1{}^- - \left(\frac{I_1{}^-}{2} + I_2{}^+\right)\frac{1}{R}\right]e^{-2R} + \left(\frac{I_1{}^-}{2} + I_2{}^+\right)\frac{e^{-mR}}{R} \quad (A2)$$

$$\left(\frac{e^{-mr_{b1}}}{r_{b1}{}^2}\right)_{00} = \left[-\log\left|\frac{m-2}{m+2}\right| - \left(I_1{}^+ + \frac{1}{2}\log\left|\frac{m-2}{m+2}\right|\right)\times\frac{1}{R}\right]e^{-2R} + \frac{I_1{}^+}{R}e^{-mR} + \left(1-\frac{1}{2R}\right)e^{2R}Ei(-[m+2]R) + \left(1+\frac{1}{2R}\right)e^{-2R}Ei(-[m-2]R) \quad (A3)$$

$$\left(\frac{e^{-mr_{b1}}}{r_{b1}{}^3}\right)_{00} = \left[-4\lim_{\varepsilon\to 0}\log\varepsilon\gamma + 4 - (m+2)\log(m+2) + (m-2)\log|m-2| + \left(2+\frac{m}{2}\log\left|\frac{m-2}{m+2}\right|\right)\frac{1}{R}\right]e^{-2R} - \frac{2}{R}e^{-mR} - \left(m+2-\frac{m}{2R}\right)e^{2R}Ei(-[m+2]R) - \left(m-2+\frac{m}{2R}\right)e^{-2R}Ei(-[m-2]R) \quad (A4)$$

$$\left(\frac{e^{-mr_{b1}}}{r_{b1}{}^4}\right)_{00} = \left[4\lim_{\varepsilon\to 0}\left(\frac{1}{\varepsilon} + m\log\varepsilon\gamma\right) - \frac{m}{R} - \left(6m + \frac{(m-2)^2}{2}\log|m-2| - \frac{(m+2)^2}{2}\log|m+2| - \frac{m^2-4}{4R}\log\left|\frac{m-2}{m+2}\right|\right]e^{-2R} + \frac{m}{R}e^{-mR} + \left[\frac{(m+2)^2}{2} - \frac{m^2-4}{4R}\right]e^{2R}Ei(-[m+2]R) + \left[\frac{(m-2)^2}{2} + \frac{m^2-4}{4R}\right]e^{-2R}Ei(-[m-2]R) , \quad (A5)$$

where

$$I_n{}^+ = \frac{1}{(m+2)^n} + \frac{1}{(m-2)^n}$$

and

$$I_n{}^- = \frac{1}{(m+2)^n} - \frac{1}{(m-2)^n} .$$

Appendix B. The additional integrals necessary in the case of H–H. Most integrals in the case of two hydrogen atoms are easily obtained by the use of the results in Appendix A repeatedly. Only the integrals below which appear in the third-order energy should be newly calculated:

$$(e^{2r_{b1}}Ei(-[m+2]r_{b1}) + e^{-2r_{b1}}Ei(-[m-2]r_{b1}))_{00} = \left[\left(\frac{1}{2}I_2{}^- - \frac{1}{4}I_1{}^+\right) + \frac{1}{R}\left(\frac{2}{3}I_3{}^+ - \frac{1}{4}I_1{}^+\right) - \frac{1}{8}\left(1+\frac{1}{R}\right)\log\left|\frac{m-2}{m+2}\right|\right]e^{-2R} + \left[\frac{I_1{}^+}{6}R - \left(\frac{1}{4}I_1{}^- + \frac{1}{6}I_2{}^+\right) - \left(\frac{2}{3}I_3{}^+ - \frac{1}{4}I_1{}^+\right)\frac{1}{R}\right]e^{-mR} + e^{2R}Ei(-[m+2]R)\left(\frac{R^2}{6} - \frac{R}{4} + \frac{1}{4} - \frac{1}{8R}\right)$$

$$+ e^{-2R}Ei(-[m-2]R)\left(\frac{R^2}{6}+\frac{R}{4}+\frac{1}{4}+\frac{1}{8R}\right) \quad (B1)$$

$$(e^{2r_{b1}}Ei(-[m+2]r_{b1}) - e^{-2r_{b1}}Ei(-[m-2]r_{b1}))_{00}$$
$$=\left[\left(\frac{1}{2}I_2^{+}+\frac{1}{4}I_1^{-}\right)+\frac{1}{R}\left(\frac{2}{3}I_3^{-}+\frac{1}{4}I_1^{-}+\frac{1}{2}I_2^{+}\right)\right]e^{-2R}$$
$$+\left[\frac{I_1^{-}}{6}R-\left(\frac{1}{4}I_1^{+}+\frac{1}{6}I_2^{-}\right)-\frac{1}{R}\left(\frac{2}{3}I_3^{-}+\frac{1}{4}I_1^{-}\right.\right.$$
$$\left.\left.+\frac{1}{2}I_2^{+}\right)\right]e^{-mR}+\frac{1}{4}e^{2R}Ei(-[m+2]R)\left(\frac{2}{3}R^2-R+\frac{1}{2}\right)$$
$$-\frac{1}{4}e^{-2R}Ei(-[m-2]R)\left(\frac{2}{3}R^2+R+\frac{1}{2}\right) \quad (B2)$$

$$\left(\frac{e^{2r_{b1}}Ei(-[m+2]r_{b1})+e^{-2r_{b1}}Ei(-[m-2]r_{b1})}{r_{b1}}\right)_{00}$$
$$=\left[I_1^{-}+\frac{1}{2R}\left(I_2^{+}+\frac{I_1^{-}}{2}\right)\right]e^{-2R}+\left[\frac{I_1^{+}}{2}-\frac{1}{2R}\left(I_2^{+}\right.\right.$$
$$\left.\left.+\frac{I_1^{-}}{2}\right)\right]e^{-mR}-\left(\frac{1}{4}-\frac{R}{2}\right)e^{2R}Ei(-[m+2]R)$$
$$+\left(\frac{1}{4}+\frac{R}{2}\right)e^{-2R}Ei(-[m-2]R) \quad (B3)$$

$$\left(\frac{e^{2r_{b1}}Ei(-[m+2]r_{b1})-e^{-2r_{b1}}Ei(-[m-2]r_{b1})}{r_{b1}}\right)_{00}$$
$$=\left[I_1^{+}+\frac{1}{2R}\left(I_2^{-}+\frac{3}{2}I_1^{+}\right)+\left(\frac{1}{2}+\frac{3}{8R}\right)\right.$$
$$\left.\times\log\left|\frac{m-2}{m+2}\right|\right]e^{-2R}+\left[\frac{I_1^{-}}{2}-\frac{1}{2R}\left(I_2^{-}+\frac{3}{2}I_1^{+}\right)\right]$$
$$\times e^{-mR}+e^{2R}Ei(-[m+2]R)\left(\frac{R}{2}-\frac{3}{4}+\frac{3}{8R}\right)$$
$$-e^{-2R}Ei(-[m-2]R)\left(\frac{R}{2}+\frac{3}{4}+\frac{3}{8R}\right) \quad (B4)$$

$$\left(\frac{e^{(2-k)r_{b1}}Ei(-[m+2]r_{b1})+e^{-(2+k)r_{b1}}Ei(-[m-2]r_{b1})}{r_{b1}}\right)_{00}$$
$$=\frac{1}{2}e^{-2R}\left[\frac{1}{k}\left(R-\frac{1}{k}+\frac{1}{2}\right)\log\left|\frac{m-2}{m+k-2}\right|\right.$$
$$-\frac{1}{4+k}\left(R+\frac{1}{4+k}+\frac{1}{2}\right)\log\left|\frac{m-2}{m+k+2}\right|-\frac{1}{k}\left(R+\frac{1}{k}\right.$$
$$\left.+\frac{1}{2}\right)\log\left|\frac{m+2}{m+k+2}\right|-\frac{1}{4-k}\left(R+\frac{1}{4-k}+\frac{1}{2}\right)$$
$$\times\log\left|\frac{m+2}{m+k-2}\right|-\frac{1}{k(m+k+2)}-\frac{1}{(4+k)(m+k+2)}$$
$$\left.-\frac{1}{k(m+k-2)}+\frac{1}{(4-k)(m+k-2)}\right]+\frac{1}{2}e^{-(m+k)R}$$
$$\times\left[\frac{1}{k(m+k+2)}+\frac{1}{(4+k)(m+k+2)}+\frac{1}{k(m+k-2)}\right.$$
$$\left.-\frac{1}{(4-k)(m+k-2)}\right]+\frac{1}{2}e^{(2-k)R}Ei(-[m+2]R)$$
$$\times\left[\frac{1}{k}\left(\frac{1}{k}+\frac{1}{2}\right)+\frac{1}{4-k}\left(\frac{1}{4-k}+\frac{1}{2}\right)\right]$$
$$+\frac{1}{2}e^{-(2+k)R}Ei(-[m-2]R)\left[\frac{1}{k}\left(\frac{1}{k}-\frac{1}{2}\right)\right.$$
$$\left.+\frac{1}{4+k}\left(\frac{1}{4+k}+\frac{1}{2}\right)\right]+\frac{1}{2}e^{2R}Ei(-[m+k+2]R)$$
$$\times\left[\frac{1}{k}\left(R-\frac{1}{k}-\frac{1}{2}\right)+\frac{1}{4+k}\left(R-\frac{1}{4+k}-\frac{1}{2}\right)\right]$$
$$+\frac{1}{2}e^{-2R}Ei(-[m+k-2]R)\left[\frac{1}{k}\left(R-\frac{1}{k}+\frac{1}{2}\right)\right.$$
$$\left.-\frac{1}{4-k}\left(R+\frac{1}{4-k}+\frac{1}{2}\right)\right] \quad (B5)$$

$$\left(\frac{e^{(2-k)r_{b1}}Ei(-[m+2]r_{b1})-e^{-(2+k)r_{b1}}Ei(-[m-2]r_{b1})}{{r_{b1}}^2}\right)_{00}$$
$$=\frac{e^{-2R}}{R}\left[\frac{1}{k}\log\left|\frac{m-2}{m+k-2}\right|+\frac{1}{4+k}\log\left|\frac{m-2}{m+k+2}\right|\right.$$
$$\left.-\frac{1}{k}\log\left|\frac{m+2}{m+k+2}\right|+\frac{1}{4-k}\log\left|\frac{m+2}{m+k-2}\right|\right]$$
$$+\frac{e^{(2-k)R}}{R}Ei(-[m+2]R)\left(\frac{1}{k}-\frac{1}{4-k}\right)-\frac{e^{-(2+k)R}}{R}$$
$$\times Ei(-[m-2]R)\left(\frac{1}{k}+\frac{1}{4+k}\right)-\frac{e^{2R}}{R}Ei(-[m+k+2]R)$$
$$\times\left(\frac{1}{k}+\frac{1}{4+k}\right)+\frac{e^{-2R}}{R}Ei(-[m+k-2]R)\left(\frac{1}{k}+\frac{1}{4-k}\right)$$
$$-\left(1-\frac{1}{2R}\right)X+\left(1+\frac{1}{2R}\right)e^{-2R}Y \quad (B6)$$

where

$$X=\int_R^{\infty}\frac{e^{-kx}}{x}[Ei(-[m+2]x) - e^{-4x}Ei(-[m-2]x)]dx$$
$$=\frac{e^{-(m+k)R}}{R}\sum_{n=1}^{\infty}\left[\frac{1}{(m-2)^n}-\frac{1}{(m+2)^n}\right]\frac{(-1)^{n+1}}{n}$$
$$\times\sum_{s=1}^{N}\frac{(-1)^{s+1}(n+s-1)\,!}{(m+k+2)^sR^{n+s-1}} \quad (B7)$$

in which N is the s that minimizing $(n+s-1)!/(m+k+2)^s \times R^{n+s-1}$, and where

$$Y=\int_0^R\frac{e^{-kx}}{x}[e^{4x}Ei(-[m+2]x) - Ei(-[m-2]x)]dx$$
$$-\int_0^R\frac{e^{-kx}}{x}[Ei(-[m+2]x) - e^{-4x}Ei(-[m-2]x)]dx$$
$$-X$$
$$=\log\gamma R\sum_{i=1}^{\infty}\frac{R^i}{i\,i!}[(-[k-4])^i - 2(-k)^i + (-[k+4])^i]$$
$$-\sum_{i=1}^{\infty}\frac{R^i}{i^2\,i!}[(-[k-4])^i - 2(-k)^i + (-[k+4])^i]$$
$$+\log|m+2|\sum_{i=1}^{\infty}\frac{R^i}{i\,i!}[(-[k-4])^i - (-k)^i]$$
$$-\log|m-2|\sum_{i=1}^{\infty}\frac{R^i}{i\,i!}[(-k)^i - (-[k+4])^i]$$
$$+\sum_{i=1}^{\infty}\frac{(-[k-4])^i-(-k)^i}{i\,!}R^i\sum_{j=1}^{\infty}\frac{(-[m+2])^jR^j}{j\,j!\,(i+j)}$$
$$-\sum_{i=1}^{\infty}\frac{(-k)^i-(-[k+4])^i}{i\,!}R^i\sum_{j=1}^{\infty}\frac{(-[m-2])^jR^j}{j\,j!\,(i+j)}$$
$$-X \quad (B8)$$

in which the infinite series are truncated so that they give necessary accuracy.

$$\left(\frac{e^{-mr_{b1}}e^{-kr_{a2}}}{r_{b1}r_{12}r_{a2}}\right)_{00}$$
$$=\frac{R^3}{2}\sum_{\tau=0}^{\infty}(2\tau+1)\left[W_{\tau}^{0}\left(1,1;\frac{R}{2}(2+k),\frac{R}{2}(2+m)\right)\right.$$
$$\left.\times G_{\tau}^{0}\left(0,\frac{R}{2}(2-k)\right)G_{\tau}^{0}\left(0,\frac{R}{2}(m-2)\right)\right.$$

$$
\begin{aligned}
&- W_\tau^0\left(1, 0; \frac{R}{2}(2+k), \frac{R}{2}(2+m)\right) \\
&\quad \times G_\tau^0\left(0, \frac{R}{2}(2-k)\right) G_\tau^0\left(1, \frac{R}{2}(m-2)\right) \\
&+ W_\tau^0\left(0, 1; \frac{R}{2}(2+k), \frac{R}{2}(2+m)\right) \\
&\quad \times G_\tau^0\left(1, \frac{R}{2}(2-k)\right) G_\tau^0\left(0, \frac{R}{2}(m-2)\right) \\
&- W_\tau^0\left(0, 0; \frac{R}{2}(2+k), \frac{R}{2}(2+m)\right) \\
&\quad \times G_\tau^0\left(1, \frac{R}{2}(2-k)\right) G_\tau^0\left(1, \frac{R}{2}(m-2)\right)\Bigg] \qquad \text{(B9)}
\end{aligned}
$$

where W_τ^0 and G_τ^0 refer to the notation of Ref. 25.

25) M. Kotani, A. Amemiya, E. Ishiguro, and T. Kimura, "Table of Molecular Integrals," 2nd ed., Maruzen Co., Tokyo (1963).

BULLETIN OF THE CHEMICAL SOCIETY OF JAPAN, VOL. 46, 2369—2372 (1973)

Distribution of Uranyl Nitrate between 1- or 2-Butanol and Aqueous Phases

Norio Yui, Yōichi Kurokawa, and Taketoshi Fujita

Department of Applied Science, Faculty of Engineering, Tohoku University, Aoba, Aramaki, Sendai 980

(Received February 2, 1973)

The distribution of uranyl nitrate between 1- or 2-butanol and aqueous phases and the effect of nitric acid or sodium nitrate on the distribution at 25 °C have been studied. Conductance measurements have been carried out for the butanol solutions of uranyl nitrate. It was found that high water content in the butanol phase gives rise to the dissociation of the salt. Semi-empirical relations hold for the distribution considering the dissociation of salt in the butanol phase. Observed and calculated slopes agree in the plots of distribution ratio *vs.* nitrate concentration. The results were discussed in comparison with distribution data in literature.

A study of the distribution of electrolyte between aqueous and organic phases provided a method of investigating the thermodynamic properties of organic solutions. However, such a study has been limited to organic solvents almost immiscible with water. Isomeric butanol has a moderate dielectric constant and is miscible with water to a greater extent. Thus, water seems to play an important role in the distribution. The extraction of uranyl nitrate was discussed in some detail.[1] In most cases, the electrolyte was considered to be completely dissociated in aqueous phase and completely associated in the organic phase. Previous conductance measurements on the 1-butanol phase containing alkali halides indicated that these salts were considerably dissociated.[2,3] A marked deviation from thermodynamic distribution ratio could occur depending upon the degree of association in the butanol phase. We investigated the equilibrium composition of alkali halide–1-butanol–water system. A semi-empirical treatment of the distribution of alkali halides was performed, assuming that these salts in the butanol phase are dissociated.[4] This study was undertaken to examine how far the above treatment is applicable to the distribution of uranyl nitrate between the butanol and aqueous phases.

Experimental

Materials. Uranyl nitrate hexahydrate, sodium nitrate, nitric acid, 2-butanol, and 1-butanol were of reagent grade and used without further purification.

Procedure. The electric equipment, conductance cell (flask type) and methods were essentially the same as before, except for the conductance bridge which was of a YOKOGAWA BV-Z-103B type.[2,3] A quartz flask type cell with lightly platinized electrodes was used. The cell constant was determined to be 0.1893 cm^{-1} with 0.1 M KCl. All measurements were carried out in a thermostat at 25±0.01 °C. The conductance of the solute was determined by subtracting the conductance of the solvent from that of the solution. Since the specific conductance of pure 1-butanol was 9.12×10^{-9} ($ohm^{-1}\cdot cm^{-1}$) at 25 °C, solvent correction in pure 1-butanol system was not necessary even for very dilute solution.

100 ml each of aqueous and butanol solutions were taken into a flask with a stopper, and shaken in a thermostat for a few hours. A portion of the solution was then taken from both phases for analysis. In the presence of nitric acid or sodium nitrate, the distribution equilibrium was established within half an hour. The initial concentration of uranyl nitrate in the aqueous phase ranged from 10^{-4} to 10^{-2} M, and that of nitric acid or sodium nitrate from 0.05 to 3 M.

Analysis. *Uranyl Ion*: The method was essentially the same as that reported.[5-7] A sample solution (1—5 ml) from each phase was evaporated to dryness below 80 °C to avoid loss of uranyl salt. A buffer solution of pH 5 and 0.1% solution of neothorin was added to the sample solution.

1) Y. Marcus and A. S. Kertes, "Ion Exchange and Solvent Extraction of Metal Complexes" Wiley-Interscience, New York (1969).

2) Y. Kurokawa and N. Yui, *Tech. Reports, Tohoku Univ.*, **37**, 153 (1972).

3) N. Yui, Y. Kurokawa, M. Sono, and T. Hiramoto, *Nippon Kagaku Zasshi*, **89**, 483 (1968). N. Yui, Y. Kurokawa, and M. Nakayama, This Bulletin, **46**, 1027 (1973).

4) N. Yui and Y. Kurokawa, *Nippon Kagaku Zasshi* **89**, 487 (1968).

5) S. Shibata and T. Matsumae, This Bulletin, **32**, 279 (1959).

6) E. Hesford and H. A. C. McKay, *Trans. Faraday Soc.*, **54**, 573 (1958).

7) B. G. W. Hollingshed, "Oxine and its Derivatives" Vol. II Oxine, Part 2, Butterworths, London (1954), p. 497.

The absorbance of the solution was then measured at 600 mμ against a reference solution.

Sodium Ion: This was analyzed by the potentiometric or EDTA method.[8] The former is as follows. The sample solution was passed through a resin column converted into hydrogen ion form. It was eluted by 2 M HCl. The effluent was evaporated to dryness to remove hydrochloric acid and the residue was dissolved in a small amount of water. The solution was analyzed for chloride by the potentiometric method.

Nitrate Ion: This was analyzed by spectrophotometry.[9]

Hydrogen Ion: This was titrated with sodium hydroxide solution using phenolphthalein as an indicator.

Solvent Composition: Equilibrium compositions in the absence of solute were determined by gas chromatography.[4]

Results and Discussion

Mutual solubilities of 1-butanol–water and 2-butanol–water systems are given in Table 1. Dielectric constant ε was estimated from the values for water and butanol assuming that ε of the mixtures is a linear function of the weight fraction as in the cases of ethanol–water mixture.[10] Both butanols are miscible with water and consequently both butanol phases have high dielectric constants.

Table 1. Mutual solubilities of 1-butanol–water and 2-butanol–water systems at 25 °C (wt %)

	1-Butanol–Water			2-Butanol–Water		
	Water	1-Butanol	ε	Water	2-Butanol	ε
Aqueous phase	92.7	7.3	73	80.5	19.5	67
Butanol phase	20.3	79.7	23	37.5	62.5	38

The conductance of uranyl nitrate $\Lambda(\text{ohm}^{-1}\cdot\text{cm}^2)$ in a few kinds of pure alcohol and 1-butanol–water(11.0 wt%) isgiven in Fig. 1, by means of the plots Λ *vs.* the square root of concentration. Conductance decreases in the order ethanol(24.3)>propanol(20.1)>1-butanol (17.1) over all concentrations, the order being in line with that of dielectric constant (given in parentheses). The plots show a marked deviation from linearity as in the case of LiI and NH_4I.[12] This indicates that uranyl nitrate behaves as a weak electrolyte. Addition of water to pure 1-butanol causes a large change in conductance. A sharp rise on approaching infinite dilution suggests a possibility of the following dissociation:

$$UO_2(NO_3)_2 = UO_2(NO_3)^+ + NO_3^- \quad (1)$$

However, concentrated uranyl nitrate solution might not be dissociated in pure 1-butanol. Association constants were not calculated because of a sharp increase in conductance at infinite dilutions. A plot by Shedlowsky's method is not linear for the 1-butanol–water (11 wt%) system. It seems that dissociation in two stages occurs to some extent. Trzebiatowska obtained an association constant of 1.44×10^4 in ethanol and concluded that covalency participates in uranyl nitrate from the very small Bjerrum parameter *a*.[11] However, interpretation of such an adjustable parameter is too uncertain to draw a clear conclusion.

Distribution of Uranyl Nitrate between 1- or 2-Butanol and Aqueous Phases. The results are shown in Fig. 2 with the plots $K_d(U)$ *vs.* $\log(NO_3^-)_a$. The distribution ratio of uranyl nitrate $K_d(U)$ is defined by $\Sigma(UO_2)_a/\Sigma(UO_2)_b$, where subscripts a and b refer to the aqueous and butanol phases, respectively. Curve III gives the distribution of uranyl nitrate between

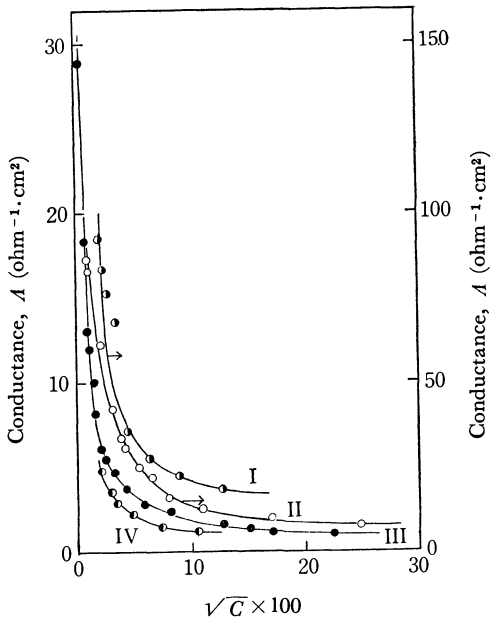

Fig. 1. Conductance Λ *vs.* square root of molarity.
I: in 1-BuOH–Water (11wt%), II: in EtOH[11], III: in PrOH[11], IV: in 1-BuOH

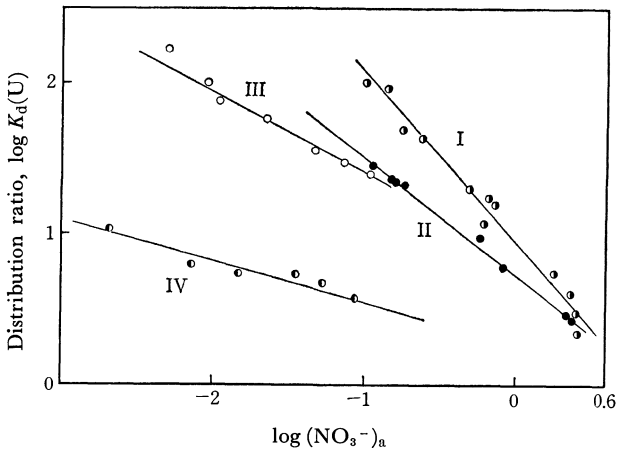

Fig. 2. Distribution ratio $K_d(U)$ *vs.* nitrate ion concentration in aqueous phase.
I: 1-BuOH–nitric acid solution, II: 1-BuOH–sondium nitrate solution, III: 1-BuOH–water, IV: 2-BuOH–water

8) B. Sen, *Z. Anal. Chem.*, **157**, 2 (1957).
9) T. Akisada, *Bunseki Kagaku*, **12**, 614 (1963).
10) H. S. Harned and B. B. Owen, "The Physical Chemistry of Electrolytic Solutions," Reinhold Publishing Co., (1964), p. 161.
11) J. Trzebiatowska and M. Chmielowska, *J. Inorg. Nucl. Chem.*, **20**, 106 (1961); **26**, 837 (1964); **28**, 1435 (1966).
12) H. Y. Venkatasetty and G. H. Brown, *J. Amer. Chem. Soc.*, **66**, 2075 (1962).
13) Y. Kurokawa and N. Yui, *Tech. Reports, Tōhoku Univ.*, **29**, 211 (1964).
14) H. A. C. McKay and A. R. Mathieson, *Trans. Faraday Soc.*, **47**, 428 (1951).
15) Ref. 1, p. 933.

1-butanol and aqueous phases, and curve IV that between 2-butanol and aqueous phases. The distribution showed the same trend as in the acids, namely it approaches a constant value at higher concentration.[13] This indicates that uranyl nitrate tends to be transferred into the butanol phase with increasing concentration. The ionization constants of uranyl nitrate were determined in various solvents by means of the Walden rule, a slight dissociation being found to take place. However, notable dissociation was found in 1-butanol.[14] Uranyl nitrate showed an appreciable conductivity in diethyl ether on being dissolved in the form of hexahydrate.[15] The relatively high water content in the butanol phase causes the dissociation of salt. Water content is 38 wt% in 2-butanol phase and 20 wt% in 1-butanol phase, causing an increase of conductance (Fig. 1). The first stage of dissociation might therefore occur in the butanol phase. $K_d(U)$ of the 1-butanol system is larger than that of the 2-butanol system over all concentrations. The difference is principally due to the difference in water contents. It seems that water plays the principal role in the distribution of uranyl nitrate. We assume that uranyl nitrate in both phases is dissociated into free ions as follows, the species extracted being the same over all concentrations:

$$(UO_2^{2+})_a + 2(NO_3^-)_a \overset{K}{\longleftrightarrow} (UO_2NO_3^+)_b + (NO_3^-)_b \quad (2)$$

$$K = \frac{[UO_2NO_3^+]_b[NO_3^-]_b}{[UO_2^{2+}]_a[NO_3^-]_a^2} \propto \frac{1}{K_d(U)^2(NO_3^-)_a} \quad (3)$$

If this is the case, the slope of the plot $K_d(U)$ *vs.* $\log(NO_3^-)_a$ should be -0.5 (Eq. 3). The observed values for 1-butanol and 2-butanol systems are about -0.5 and -0.3, respectively. The lower value for 2-butanol system might be due to the second stage dissociation because of high water content of the butanol phase, indicating that mixed species $UO_2NO_3^+$ and UO_2^{2+} are involved. In the case of the solvent extraction with a reagent such as TBP, the slope is -2.[16] Since no data are available concerning activity coefficients in this system, the activity is replaced by concentration.

Distribution of Uranyl Nitrate Coexisting with Nitric Acid or Sodium Nitrate. Use of a salting-out agent is common in solvent extraction. Nitrate is generally chosen for the extraction of uranyl nitrate.[17] Salting effects of nitric acid and sodium nitrate on the distribution of uranyl nitrate were investigated in the concentration range 0.06—3 M. The results are given in Fig. 2, in which curve I denotes the distribution of uranyl nitrate coexisting with nitric acid and curve II that with sodium nitrate. We see that the effect is enhanced. Distributions of nitric acid and sodium nitrate are given in Fig. 3 by means of logarithms of distribution ratio *vs.* solute concentration in aqueous phase. $K_d(H)$ is the distribution ratio of nitric acid defined by $(H^+)_a/(H^+)_b$ and $K_d(NO_3)$ is that of sodium nitrate by $(NO_3^-)_a/(NO_3^-)_b$, where (H^+) denotes the acid concentration and (NO_3^-) the sodium nitrate concentration in each phase. Nitric acid is extracted into butanol phase more than other mineral acids,

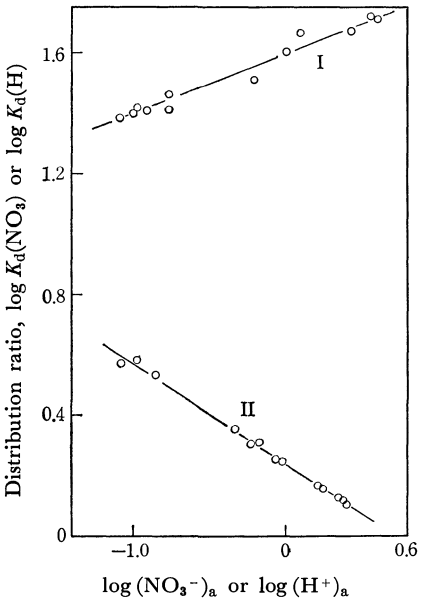

Fig. 3. Distribution ratio of sodium nitrate *vs.* nitrate ion in aqueous phase and that of nitric acid *vs.* acid in aqueous phase.
I: sodium nitrate, II: nitric acid

indicating its strong interaction with butanol. This may be ascribed to the weak electrolytic behavior and conspicuous covalent character of the acid.[18] Alcock *et al.* studied the extraction of mineral acids from an aqueous solution by TBP and showed that perchloric acid is a strong electrolyte in TBP, but not other acids.[19] In the case of nitric acid, a volume change occurred at the expense of the aqueous phase, apparently due to a much higher uptake of water by the butanol phase which certainly facilitates ionization. We assume that the first stage dissociation occurs in the butanol phase, the species extracted are the same and the concentration is represented in the observed one not in the activity. The following relation is obtained for the system coexisting with nitric acid.

$$K_d(U) \propto K_d(H) \cdot (NO_3)_a^{-1} \quad (4)$$

$K_d(H)$ is determined to be $K_d(H) \propto (NO_3)_a^{-0.3}$ from Fig. 3. By combining this relation and Eq. (4), a slope of -1.3 equal to the observed value is obtained. In the same way, the following relation can be obtained

$$K_d(U) \propto K_d(NO_3) \cdot (NO_3)_a^{-1} \quad (5)$$

Since $K_d(NO_3)$ is proportional to $(NO_3)_a^{0.2}$ (Fig. 3), the plot $K_d(U)$ *vs.* $(NO_3)_a$ yields a slope of -0.8 by combining this relation with Eq. (5). This is in good agreement with the observed slope -0.8. The degree of ionization of sodium nitrate in TBP is higher than that of uranyl nitrate at an equal solute concentration by an order of magnitude.[20] The ionization in the butanol phase would be still higher because of its high water content. We assumed that the solvent composition remains approximately constant inde-

16) K. Naito, This Bulletin, **33**, 363 (1960).
17) Ref. 1, p. 630.
18) R. M. Diamond and D. G. Tuck, "Progress in Inorganic Chemistry," ed. by E. A. Cotton, Interscience Publishers, New York (1960), p. 155.
19) K. Alcock, S. S. Grimley, T. V. Healy, J. Kennedy, and H. A. C. McKay, *Trans. Faraday Soc.*, **52**, 39 (1956).
20) Ref. 1, p. 704.

pendent of solute concentration. However, the observed phenomenon was more complicated and involved a change of solvent composition accompanied by the solute. Dielectric constant change in the butanol phase caused by solute and water and that in aqueous phase caused by the butanol salted out might affect the equilibrium to a great extent. The distribution of uranyl nitrate in the butanol–water system was given by Morrison and Freiser.[21] They treated the distribution in terms of complex formation in the butanol phase, but their results are not in line with ours. Good agreement was obtained between the observed and calculated slopes by a semi-empirical treatment. This might indicate that distribution is associated with the predominance of ion species in the butanol phase. At a higher concentration the treatment is probably no longer valid. Changes in solvation, association and solvent composition should be taken into consideration.

21) G. H. Morrison and H. Freiser, "Solvent Extraction in Analytical Chemistry," John Wiley & Sons, Inc. New York (1957), p. 65.

Thanks are due to Mr. K. Takada for his assitance in the experiments.

BULLETIN OF THE CHEMICAL SOCIETY OF JAPAN, VOL. 46, 2372—2380 (1973)

The Crystal Structure of Quinolinic Acid

Fusao TAKUSAGAWA, Ken HIROTSU, and Akira SHIMADA

Department of Chemistry, Faculty of Science, Osaka City University, Sugimoto-cho, Sumiyoshi-ku, Osaka 558

(Received February 8, 1973)

The crystal structure of quinolinic acid (2,3-pyridinedicarboxylic acid) has been determined by the method of X-ray diffraction. The crystal is monoclinic, with a space group of $P2_1/c$ and with cell dimensions of $a=7.421$, $b=12.729$, $c=7.850$ Å, and $\beta=116.96°$. The crystal structure was solved by the inspection of a Patterson map. The final R value was 6.78% for 1224 observed reflections. The quinolinic acid molecule takes the form of a zwitter ion in the crystal. The pyridine ring in the molecules shows a significant deformation from the C_{2v} symmetry of idealized geometry. The lengths of the two C–C bonds joining the carboxyl groups to the ring are longer than the normal value. There is an intramolecular hydrogen bond between the adjacent carboxyl groups. The bond lengths in the two C–O groups which participate in this intramolecular hydrogen bond are longer than those of the other two C–O groups. One of the two carbonyl oxygen atoms participates in a hydrogen bond, while the other is free from it. The molecules are arranged in layers closely parallel to the (0 1 0) plane. Each molecule on the same plane is hydrogen-bonded to form an endless chain along the a axis. These chains are packed by the van der Waals forces. The thermal diffuse scattering observed on Weissenberg photographs can be explained by this hydrogen-bond system.

This work is a part of series of O–H···N hydrogen bonding studied based on X-ray crystal structure analyses of some carboxylic acids with a pyridine ring. The O–H···N or $^+$N–H···O hydrogen bond has been found in all the crystals of dipicolinic acid,[1] dinicotinic acid,[2] and cinchomeronic acid[3] thus far studied, without exception. It seems that it would be of interest to elucidate the effect of a nitrogen atom in a pyridine ring on the hydrogen-bond formation in solids.

The melting point of a quinolinic acid crystal is the lowest of those of the six pyridine dicarboxylic acids, and this molecule has adjacent carboxyl groups. These facts suggest that there is some hydrogen bond which acts not between molecules, but within a molecule. Such an intramolecular hydrogen bond is known in 3,4-furandicarboxylic acid,[4] which has an aromatic five-membered ring. On the contrary, while the crystal structures of five carboxylic acids which have adjacent carboxyl groups substituted on a benzene ring(phthalic acid,[5] trimellitic acid,[6] hemimellitic acid,[7] pyromellitic acid,[8] and mellitic acid[9]) have previously been determined by the X-ray method, no intramolecular hydrogen bond between the adjacent carboxyl groups has been found in their crystal structures. If the geometrical configuration plays an important role in the formation of an intramolecular hydrogen bond between the adjacent carboxyl groups substituted on the aromatic six-membered ring, it may be impossible to form this type of hydrogen bond in crystal. In this regard, it will also be of interest to find out the mode of the hydrogen bond in this crystal.

Experimental

The crystals were obtained in the form of light yellow prisms by recrystallization from an aqueous solution. Weissenberg

1) F. Takusagawa, K. Hirotsu, and A. Shimada, This Bulletin, **46**, 2020 (1973).
2) F. Takusagawa, K. Hirotsu, and A. Shimada, This Bulletin, **46**, 2292 (1973).
3) F. Takusagawa, K. Hirotsu, and A. Shimada, *Acta Crystallogr.*, **A28**, S15 (1972).
4) D. E. Williams and R. E. Rundle, *J. Amer. Chem. Soc.*, **86**, 1660 (1964).
5) H. Jaggi, *Z. Kristallogr.*, **109**, 3 (1957).
6) F. Takusagawa, K. Hirotsu, and A. Shimada, This Bulletin, to be published.
7) F. Takusagawa, K. Hirotsu, and A. Shimada, This Bulletin, to be published.
8) F. Takusagawa, K. Hirotsu, and A. Shimada, This Bulletin, **44**, 1274 (1971).
9) S. F. Darlow, *Acta Crystallogr.*, **14**, 159 (1961).

Table 1. Crystal data for quinolinic acid

Molecular formula	$C_7H_5NO_4$
Molecular weight	167.12
Crystal size	$\sim 0.3\times0.3\times0.3$ mm
Crystal system	Monoclinic
Space group	$P2_1/c$
Cell dimensions;	
a	7.421±0.006 Å
b	12.729±0.008
c	7.850±0.008
β	116.96±0.08°
V	660.9±0.8 Å^3
Z	4
Density (calculated)	1.680 g/cm^3
Density (observed)	1.66
Radiation	Cu $K\alpha$(λ=1.5418 Å)
Linear absorption coefficient	14.17 cm^{-1}
Number of independent reflections	1371
The atom numbering	

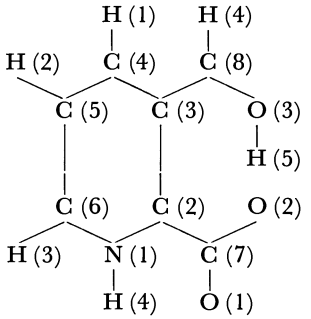

photographs showed the crystal to be monoclinic, with a space group of $P2_1/c$. The cell dimensions were measured from zero-layer Weissenberg photographs, which had been calibrated with superimposed Al powder lines. They are given, along with other crystal data, in Table 1. There are four molecules in a unit cell, corresponding to the density of 1.66 g/cm^3 observed by the flotation method. One of the crystals was in the shape of a sphere with the average diameter of 0.3 mm. The intensity data were collected for the 0—10 layers around the b axis and the 0—2 layers around the c axis by the use of the multiple-film equi-inclination integrating Weissenberg technique with Cu $K\alpha$ radiation. The intensities of the diffraction spots were estimated visually by comparison with intensity standard. Of the possible 1513 reflections within a Cu $K\alpha$ sphere, 1371 independent reflections were measured; 147 were too weak to be observed. The absorption coefficient is 14.17 cm^{-1} for Cu $K\alpha$ radiation, and no absorption correction was applied. Appreciable thermal diffuse scattering was observed along the directions of the b* and c* axes on Weissenberg photographs.

Structure Determination and Refinement

The crystal structure was solved by the inspection of a sharpened Patterson map which had been resolved enough to give the orientation and location of the molecules in the unit cell. The first postulated structure gave an R value of 41%, which decreased to 15% after three cycles of least-squares refinement with individual isotropic thermal factors. Since the 0 4 0 reflection seemed to have a strong extinction effect, this reflection was removed from the later refinements.

The coordinates and anisotropic thermal parameters were refined in a block-diagonal least-squares procedure, minimizing the function $\Sigma w(F_o-F_c)^2$, where:

$$w = 0.5 \text{ for } 0.5 \geqq |F_o|,$$

$$w = 1.0 \text{ for } 6.0 > |F_o| > 0.5 \text{ and}$$

$$w = 6.0/|F_o| \text{ for } |F_o| \geqq 6.0.$$

The atomic scattering factors used were those listed in the International Table for X-ray Crystallography for C, N and O atoms and the spherical scattering factors proposed by Stewart, Davidson, and Simpson[10] for the H atom. At the stage of R=9.6%, a difference Fourier map was computed, and from it the positions of the five hydrogen atoms were located (Fig. 1). With anisotropic thermal parameters for non-hydrogen atoms and isotropic thermal parameters for hydrogen atoms, the final R value was 6.78%, excluding unobserved reflections. The observed and calculated structure factors are listed in Table 2. The fractional coordinates and thermal parameters are listed in Table 3.

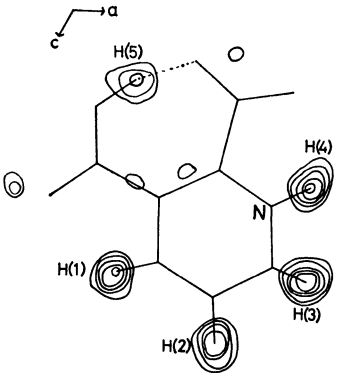

Fig. 1. A composite drawing of the electron density associated with the hydrogen atoms. The contours are at intervals of 0.1 e·Å^{-3}, beginning with the 0.2 e·Å^{-3} contour.

Results and Discussion

Molecular Structure. The bond lengths and angles are listed, along with their estimated standard deviations, in Table 4, and they are shown in Fig. 2. Figure 1 shows a difference Fourier map along the b axis, in which there is no high peak except those due to hydrogen atoms. Figure 3 shows the anisotropic thermal ellipsoids of the non-hydrogen atoms and the isotropic thermal ellipsoids of the hydrogen atoms. The net charges and π-bond orders calculated by the CNDO/2 method[11] are shown in Fig. 4.

10) R. F. Stewart, E. R. Davidson, and W. T. Simpson, *J. Chem. Phys.*, **42**, 3175 (1965).

11) J. A. Pople and D. L. Beveridge, "Approximate Molecular Orbital Theory," McGraw-Hill Book Co., New York (1970).

Table 2. The observed and calculated structure factors

F_o, F_c and DF have been multiplied by 10. The unobserved reflection is indicated by an asterisk. The reflection, for which the $|F_o-F_c|/|F_o|$ is larger than 0.3, is indicated by a plus sign.

L	FO	FC	DF	L	FO	FC	DF	L	FO	FC	DF	L	FO	FC	DF	L	FO	FC	DF	L	FO	FC	DF
H,K= 0 0				4 58 65	-6	-1 143 137	5	4 20 19	1	-1 196 191	4	-4 58 -59	1	-7 25 29	-3								
2 411	-388	-22		5 106	-102	-4	0 18 -20	1	5 18 -22	4	0 210 219	-9	-3 50 43	6	-6 42 43	-1								
4 32	38	-6		6 88	-87	-1	1 50 -46	-4	6 11 -9	-2	1 343 342	1	H,K= 0 4		-5 55 -58	2								
6 25	-22	-3		7 83	70	13	2 21 25	-3	H,K= 5 2		2 14 -12	-1	1 119	-119	0	-4 29 -25	-3							
8 41	39	1		8 52	44	8	H,K= 8 1		-9 16 17	0	3 243	-246	3	2 197	215	-18	-3 65 66	0						
H,K= 1 0				H,K= 2 1			-8 33 29	4	-8* 0 -5	5	4 49 47		2	3 55	-65	10	-2 329	358	-24					
-8 19	-20	0		-9 14	12	2	-7 26 -22	-3	-7 233 255	-21	5 114 113		0	4 27	-31	4	-1 8	-10	2					
-6 141	-148	6		-8 103	95	7	-6 35 29	6	-6 20 20	0	6 38 -34		-3	5 61	67	-6	0+ 15	-2	-12					
-4 60	67	-7		-7 19	21	-2	-5 82 69	12	-5 100 -100	0	7 53 50		3	6 30	27	3	1+ 15	8	7					
-2 21	-21	0		-6 30	31	-1	-4 30 -25	-5	-4 4 -5	0	H,K= 3 3			7 37	-39	1	2 19	18	0					
0 135	-138	2		-5 35	-34	0	-3 116 105	11	-3+ 15 -7	-8	-9* 0 6		-6	8 38	-40	1	3 18	14	3					
2 93	-91	-1		-4 265	-263	18	-2 41 32	8	-2 41 -43	2	-8 16 -13		-2	H,K= 1 4			H,K= 7 4							
4 65	-61	-4		-3 107	-103	-4	-1 9 9	0	-1 128 131	-3	-7 158 -163		4	-9 12	-12	0	-9 17	-15	-2					
6 126	-125	0		-2 316	360	-43	0 42 -44	2	0 36 31	4	-6 282 -283		1	-8+ 27	18	9	-8 71	75	-3					
8 67	65	2		-1 184	-181	-3	H,K= 9 1		1 23 22	1	-5 46 42		3	-7* 0	-10	10	-7* 0	7	-7					
H,K= 2 0				0 288	283	5	-7* 0 2	-2	2 30 -29	-1	-4 73 -64		-9	-6 95	97	-2	-6 25	-25	0					
-8 25	23	1		1 364	-380	16	-6 74 72	1	3 86 89	-2	-3 437 462		-25	-5 61	67	-6	-5* 0	-5	5					
-6+ 14	-8	-5		2 121	-108	-12	-5 20 18	1	4* 0 4	-4	-2 69 72		-3	-4+ 6	4	2	-4 144	-141	-3					
-4 231	-237	6		3 272	272	0	-4 78 -69	-8	5 62 61	1	-1 299	-286	-12	-3 30	-29	-1	-3 24	-21	-2					
-2 116	105	11		4 112	108	4	-3 53 -45	-8	H,K= 6 2		0 95 85		10	-2+ 21	-11	-9	-2 33	34	-1					
0 255	-265	9		5 116	-116	0	-2+ 8 2	6	-9* 0 -1	1	1 244	-235	-9	-1 49	-47	-2	-1 15	13	2					
2 111	131	-19		6 32	-2	-8	H,K= 0 2		-8 12 13	0	2 62 60		1	0 89	86	2	0 18	-18	0					
4 247	-265	18		7 49	-42	-6	0 17 -22	4	-7 37 -38	0	3 93 -91		-1	1 126	119	7	1 17	-15	-2					
6 61	51	10		H,K= 3 1			1 10 12	-1	-6 26 -25	0	4 282	-297	15	2 106	96	10	2 46	38	7					
H,K= 3 0				-9+ 15	8	7	2 9 -7	-1	-5 128 -129	0	5 24 -25		0	3 75	-76	0	H,K= 8 4							
-8 36	28	8		-8 50	-49	-1	3 573	-632	58	-4 47 46	0	6* 0 -5		5	4 38	32	5	-8+ 14	-6	-7					
-6 58	-60	1		-7 174	165	8	4 27 27	0	-3 249	-261	12	7+ 19 29		-10	5 37	35	1	-7* 0	-2	2					
-4 170	-146	-23		-6 282	-286	4	5 14 -14	0	-2 43 -39	-3	H,K= 4 3			6 101	106	-4	-6 130	-121	-9					
-2 83	-85	2		-5 81	-80	0	6 42 -46	4	-1 55 -55	0	-9 5 -6		0	7+ 9	13	-3	-5 32	30	1					
0 419	445	-25		-4 12	-11	0	7 142	142	0	0* 0 6	-6	-8 63	60	2	8 52	-50	-1	-4 76	-66	-10					
2 189	185	3		-3 492	-479	-12	8 12 15	-2	1 156	180	-23	-7 31 -36		4	H,K= 2 4			-3 35	-34	-1					
4 102	93	8		-2 106	-101	-5	H,K= 1 2		2* 0 10	-10	-6+ 18 -11		-6	-9 20	15	-4	-2 43	-41	-1					
6+ 9	5	3		-1 231	234	-2	-9+ 8 4	4	3 92 -84	-8	-5+ 9 -2		-6	-8 16	-13	-2	-1 15	11	4					
H,K= 4 0				0 156	157	0	-8* 0 1	-1	H,K= 7 2		-4 25 -24		-1	-7 26	-28	1	0 22	18	4					
-10 52	42	10		1 299	304	-4	-7 75 74	0	-9 25 28	-3	-3 109	-98	-11	-6 22	20	1	H,K= 9 4							
-8 176	-165	-11		2 79	76	3	-6 23 21	1	-8+ 11 6	4	-2 115	113	2	-5 14	-12	-2	-6 33	34	0					
-6 222	223	0		3 118	122	-4	-5 168	-174	6 -7 42 40	2	-1 173	171	1	-4 182	162	19	-5+ 15	8	6					
-4 103	91	11		4 352	-347	-5	-4* 39	-33	-5 -6* 0 -7	7	0+ 16	-8	-8	-3+ 7	-10	2	-4 15	-19	4					
-2 85	-90	4		5* 0	1	-1	-3 324	314	9 -5 95	96	0	1 54	-46	-7	-2 28	-24	-3	-3* 0	3	-3					
0 170	169	1		6* 0	7	-7	-2 46	45	0 -4* 0	1	0	2 24	20	3	-1 22	-27	5	H,K= 0	5						
2 144	-150	5		7 29	-33	3	-1 351	345	5 -3 86	-76	-10	3 21	-22	0	0 145	146	0	1 286	-260	-26					
4 37	-36	0		H,K= 4 1			0 110	106	4 -2+ 17	10	7	4 25	-24	0	1 24	-20	-4	2 74	77	-2					
6 71	68	3		-10 39	44	-5	1 582	-574	-7 -1+ 22	1	21	5 31	35	-4	2 76	-79	3	3 225	-205	-19					
H,K= 5 0				-9 16	-11	-4	2 95	-95	0 0* 0	-4	4	6 34	33	1	3 27	25	2	4 182	171	11					
-10 68	-62	-5		-8 105	98	6	3 129	119	9 1+ 13	-8	-5	H,K= 5 3			4 231	235	-3	5 76	77	-1					
-8 98	88	9		-7 82	85	-3	4 33	31	1 H,K= 6 2			-9 9	11	-1	5 35	-35	0	6 113	-121	8					
-6 72	-75	3		-6 59	-61	1	5 107	107	0 -8* 0	-8		8 27	-23	-3	6 54	-46	-8	7 14	-16	2					
-4 289	326	-36		-5 62	-55	-7	6+ 11	-2	-9 -7+ 21	27	-6	-7 104	-103	-1	7 10	7	2	8 22	22	0					
-2 31	25	5		-4 20	20	0	7+ 12	-6	-6 19	15	4	-6 138	133	4	H,K= 3 4			H,K= 1 5							
0 244	-253	9		-3 166	168	-2	8+ 9	0	-8 -5 29	31	-2	-5 21	21	0	-9+ 9	12	-3	-9* 0	7	-7					
2 116	122	-6		-2 138	139	0	H,K= 2 2		-4 19	-15	-4	-4 111	-111	0	-8 35	-34	-1	-8 26	-33	6					
4 18	21	-3		-1 172	-170	-2	-9 22	-19	-3 -3 74	-73	-1	-3 59	-56	-3	-7 18	-12	-5	-7 27	-28	0					
H,K= 6 0				0 41	-49	8	-8 15	-11	-3 -2 12	9	2	-2 150	141	8	-6 68	74	-5	-6 40	41	0					
-8 125	122	3		1 72	62	10	-7 11	-10	0 -1+ 17	-8	-9	-1 62	55	6	-5 19	16	2	-5 45	-45	0					
-6 47	-46	0		2 48	45	2	-6 10	9	1 0 11	-9	-2	0 5	4	1	-4 93	68	25	-4 101	-104	2					
-4 13	11	1		3 25	20	4	-5 203	221	-18 1+ 17	24	-6	1 67	-70	2	-3 19	14	5	-3 177	158	19					
-2 426	-415	-11		4+ 28	-20	-8	-4+ 3	4	-1 H,K= 9 2			2 93	103	-9	-2 104	96	7	-2 131	151	-20					
0 20	20	0		5 31	-29	-2	-3 279	-248	-30 -7 35	32	2	3 26	-20	-5	-1 88	90	-2	-1 44	-49	5					
2 30	-34	3		6 19	22	-3	-2 55	-48	-6 -6 16	13	3	4+ 26	-16	-9	0 354	-333	-20	0 60	-52	-7					
4 58	47	10		H,K= 5 1			-1 385	450	-64 -5 15	-10	-4	5 32	25	7	1 71	-73	2	1 216	212	4					
H,K= 7 0				-10 65	56	9	0+ 1 0	-1	-4* 0 1	-1	H,K= 6 3			2 155	-157	1	2 130	-123	-6					
-8 88	-93	4		-9 38	-30	-7	1 70 -75	5	-3 116	-103	-13	-9* 0 2		-2	3 54	60	-6	3 58	-52	-6					
-6 31	27	4		-8 18	-13	-4	2 27 29	-1	-2 9 -8	0		-8 54	52	1	4 78	-75	-2	4* 0	-6	6					
-4 168	164	3		-7 128	133	-5	3 77 92	-15	H,K= 0 3			-7 36	-40	4	5 25	-24	-1	5 70	64	6					
-2 49	-49	0		-6 136	138	-1	4 22 -19	-2	1 443	-432	-11	-6 144	-153	9	6* 0	-4	4	6 59	63	-3					
0 33	34	-1		-5 36	-32	-4	5 21 14	6	2 166	-163	-3	-5 81	84	-3	H,K= 4 4			7 42	-36	-5					
2 61	-47	-14		-4 114	-120	6	6 20 15	4	3 205	-191	-13	-4 143	-155	2	-9+ 19	-12	-6	8 31	-30	0					
H,K= 8 0				-3 58	58	0	7 56 48	7	4 241	-213	-27	-3 158	154	4	-8 129	128	0	H,K= 2 5							
-8* 0	0	0		-2 180	181	-1	H,K= 3 2		5 15	16	-1	-2 62	60	1	-7 7	7	0	-9* 0	0	0					
-6 148	137	10		-1 86	-90	3	-9 35	-28	-6 6 127	129	-1	-1 21	24	-3	-6 168	-186	18	-8 67	-64	-3					
-4 93	85	7		0+ 0	3	-2	-8+ 10	-5	-5 7+ 16	-10	-6	0+ 9	3	5	-5 21	25	-4	-7* 0	-7	7					
-2 49	44	4		1 66	75	-9	-7 244	-262	17 8 25	-26	1	1 88	96	-7	-4 80	-63	-17	-6 52	-63	10					
0 35	-27	-7		2 98	95	2	-6+ 0	-4	3 H,K= 1	3		2+ 10	15	-5	-3 79	-80	0	-5 34	-31	-3					
H,K= 9 0				3+ 19	10	8	-5 84	-88	3 -9 9	11	-2	3 87	-81	-5	-2 45	46	0	-4 212	201	11					
-6 41	-37	-3		4* 0	1	-1	-4+ 13	-8	-4 -8 39	49	-10	H,K= 7 3			-1 76	82	-6	-3 201	181	19					
-4 16	13	2		5+ 30	-17	-12	-3 335	-320	-15 -7 10	-9	-1	-9 55	54	1	0 118	-111	-6	-2 310	-295	-15					
-2 86	-71	-15		H,K= 6 1			-2* 0	3	-3 -6 45	-49	3	-8 40	44	-4	1 37	-45	8	-1 106	101	4					
H,K= 0 1				-9* 0	9	-9	-1 488	480	7 -5 43	-48	4	-7 13	10	3	2 132	130	2	0 123	-135	11					
1 518	496	22		-8 44	37	6	0 36	-36	0 -4 228	221	7	-6 50	-56	6	3 11	-13	2	1 159	171	-11					
2 113	-122	8		-7 36	35	0	1 244	-259	15 -3 174	170	3	-5 62	-61	0	4 11	12	-1	2 75	68	6					
3 254	250	4		-6 121	-131	10	2 42	45	-3 -2 389	-417	27	-4 186	183	2	5 24	26	-1	3 121	-132	10					
4 226	-266	40		-5 63	-68	4	3 228	-238	10 -1 290	287	2	-3 50	51	0	6 46	-52	5	4 80	-82	1					
5 58	-59	0		-4 191	-196	5	4 25	-29	4 0 402	393	9	-2 108	-98	-10	H,K= 5 4			5 77	76	0					
6 149	154	-5		-3 179	-188	8	5 48	-39	-8 1+ 11	3	8	-1 115	-112	-2	-9* 0	1	-1	6* 0	1	-1					
7 13	11	1		-2 49	42	7	6+ 13	5	7 2+ 23	-37	14	0 14	-16	1	-8 63	-63	0	7 28	26	2					
8 33	-27	-6		-1 34	-32	-1	7 61	-48	-12 3 63	59	3	1 26	26	0	-7 7	-7	0	H,K= 3 5							
H,K= 1 1				0 38	30	7	H,K= 4 2		4 82	88	-6	2+ 7	-2	-4	-6 45	40	4	-9 33	-28	-4					
-9 8	-6	0		1 78	-82	4	-9 52	52	0 5 86	83	2	H,K= 8 3			-5+ 24	17	7	-8 48	48	0					
-8 53	54	-1		2 18	-14	-3	-8+ 3	4	-1 6 55	-59	4	-8 18	19	0	-4 241	-237	-4	-7 116	-111	-5					
-7* 0	9	-9		3 95	83	11	-7* 0	0	0 7 69	-66	-3	-7 22	21	0	-3+ 19	-11	-7	-6 214	222	-7					
-6 67	-69	1		4 45	-55	9	-6* 0	0	0 8 31	32	0	-6 43	44	-1	-2 27	-23	-3	-5 85	81	3					
-5 77	80	-2		H,K= 7 1			-5 256	270	-14 H,K= 2 3			-5 47	-54	6	-1 72	-79	6	-4+ 14	6	7					
-4 226	222	4		-9 43	-40	-3	-4 17	-16	0 -9* 0	-10	10	-4 9	-8	-1	0 178	186	-7	-3 276	250	26					
-3 217	-229	11		-8 32	33	-1	-3 100	-89	-11 -8 91	92	0	-3 127	-113	-13	1 57	67	-10	-2 135	129	6					
-2 378	-366	-12		-7 37	-31	-5	-2 76	80	-3 -7 28	-31	3	-2* 0	0	0	2 88	-95	7	-1 58	-51	-6					
-1 149	-154	4		-6 49	-54	4	-1 147	-159	11 -6 27	-26	-1	-1* 0	3	-3	3 20	-18	-2	0 102	-98	-4					
0 240	241	-1		-5 67	63	4	0 28	-32	3 -5 98	100	-2	0+ 16	-24	7	4 17	-13	-3	1 234	-232	-1					
1 168	-180	12		-4 214	220	-5	1 15	12	3 -4 146	-147	1	H,K= 9 3			H,K= 6 4			2 47	-47	0					
2 105	85	19		-3 48	-44	-3	2* 0	0	0 -3 49	-48	0	-6 59	58	1	-9* 0	3	-3	3 133	-136	3					
3* 0	5	-5		-2 120	-116	-3	3 134	137	-3 -2 195	179	16	-5* 0	-7	7	-8 90	-95	4	4 278	266	11					

TABLE 2. (Continued)

L	FO	FC	DF	L	FO	FC	DF	L	FO	FC	DF	L	FO	FC	DF	L	FO	FC	DF	L	FO	FC	DF	L	FO	FC	DF
9	32	31	0	-8	18-	16	2	2	112	103	9	-6	30	35	-9	-8	43	47	-4	-4	14	12	1	-1	46	42	4
6*	0	-1	1	-7*	0	10	-10	3	141	130	10	-5	2*	28	0	-7	33	-31	-1	-9	18	-18	0	0*	0	5	-5
H,K=	4	5		-6*	0	-7	7	4	125	116	8	-4	89	-96	6	-6	33	-33	0	-2	73	71	1	1	42	40	1
-9	20	18	1	-5	144	-140	-4	5*	0	-2	2	-3	16	-13	-2	-5	47	46	0	-1	18	-19	1	2	26	-27	0
-8	93	-102	9	-4*	0	-4	4	6	86	-81	-5	-2	59	57	1	-4	38	34	4	0	26	28	-2	H,K=	6	10	
-7	103	-114	11	-3	78	73	5	7+	10	13	-3	-1	59	58	0	-3	58	-53	-4	1	27	28	0	-7	22	-25	2
-6	72	72	0	-2	58	58	0	8	20	19	0	0	14	16	0	-2	217	-236	19	2	32	35	-2	-6	24	-26	1
-4	40	-38	-1	-1	151	-167	15	H,K=	1	7		1	18	-18	0	-1*	0	0	0	5*	0	-4	4	-5	64	-62	-2
-3	133	-131	-2	0	17	16	1	-8	27	-30	3	H,K=	8	7		0	92	-22	0	H,K=	6	9		-4	51	51	0
-2	57	-62	5	1	26	20	5	-7	29	24	5	-6	42	-47	5	1	15	-14	-1	-7*	0	6	-6	-3	96	-108	12
-1	73	67	5	2	44	-49	4	-6	19	15	3	-5	33	27	6	2+	8	1	6	-6	63	-66	3	-2	40	-39	0
0+	4	-2	-1	3	49	-51	1	-5+	12	-4	-7	-4*	0	-1	1	H,K=	7	8		-5	10	-8	-1	-1	26	-24	-2
1	23	-18	-5	4	28	28	0	-4	121	-115	-5	-3	76	79	-3	-7*	0	0	0	-4	101	-103	1	0	10	7	2
2	28	-26	-1	5	15	-12	-3	-3	88	-91	3	-2	13	14	-1	-6	21	21	0	-3	101	-102	0	1	42	53	-10
3	40	-37	-2	6	25	-25	0	-2	255	223	32	-1+	12	5	6	-5*	0	5	-5	-2+	15	9	5	H,K=	7	10	
4*	0	2	-2	7	46	-43	-3	-1	178	-169	-8	H,K=	0	8		-4	89	94	-4	-1	37	-36	0	-6*	0	0	0
5	16	18	-2	H,K=	3	6		0	254	-270	16	0	766	796	-29	-3	28	24	4	0	13	-16	2	-5	35	37	-2
H,K=	5	5		-9	31	32	-1	1	29	28	0	1	68	75	-6	-2	12	-12	0	1	12	-16	3	-4*	0	3	-3
-9	35	34	0	-8	9	10	0	2	52	55	-2	2	24	-25	0	-1*	0	-5	5	2+	9	-5	-3	-3	57	-62	4
-8+	9	4	5	-7	175	172	2	3	57	-55	-2	3	55	55	0	0*	0	-1	1	H,K=	7	9		-2*	0	3	-3
-7	100	-108	7	-6+	20	6	14	4	64	-64	0	4+	36	22	13	H,K=	8	8		-6+	8	4	3	-1*	0	9	-9
-6	92	-91	0	-5	108	107	1	5	31	-29	-1	5	54	-52	-1	-6	73	81	-7	-5*	0	7	-7	H,K=	0	11	
-5	19	20	0	-4	20	20	0	6	22	19	2	6	30	-25	-4	-5	22	-27	4	-4	65	66	-1	1	86	-88	2
-4	50	45	4	-3	170	157	13	7	32	30	2	7	32	32	0	-4	34	34	0	-3	27	25	2	2	34	-31	-2
-3*	0	-5	5	-2*	0	2	-2	H,K=	2	7		H,K=	1	8		-3	32	31	0	-2	38	-36	-2	3	90	-82	-8
-2	137	-134	-3	-1	254	-250	-3	-8	58	-54	-3	-8	19	-14	-5	-2	32	32	0	-1	49	57	-8	4	68	-65	-3
-1	51	55	-3	0	45	41	3	-7	24	20	4	-7*	0	11	-11	H,K=	0	9		0	12	-13	1	5*	0	0	0
0	29	-20	-8	1	173	176	-3	-6	35	33	1	-6	23	-20	-2	0*	0	0	0	H,K=	0	10		6	44	45	0
1	51	-56	4	2	57	-60	3	-5	74	-74	0	-5	60	-56	-3	1	116	106	9	0+	15	10	4	H,K=	1	11	
2	60	-63	2	3	152	157	-5	-4	54	50	3	-4	89	-79	-9	2	48	-45	-2	1	97	-102	4	-7	26	-22	-3
3+	0	4	-3	4	54	51	2	-3	63	54	8	-3*	0	3	-3	3	108	108	0	2	29	-28	0	-6*	0	-4	4
4+	12	-7	-5	5	41	34	7	-2	58	-51	-7	-2	25	21	4	4	84	-89	-15	3	123	-123	0	-5+	26	18	7
H,K=	6	5		6	13	-11	-2	-1	111	-114	2	-1	36	31	5	5	43	-50	6	4	12	11	0	-4	48	42	6
-9	12	-13	0	H,K=	4	6		0	60	-68	7	0	25	-26	1	6	53	68	-14	5	2	2	0	-3	54	50	3
-8	23	-23	0	-9	30	-31	1	1	135	-137	1	1	72	-72	0	7	16	17	0	6	49	-52	3	-2	84	-74	-10
-7	15	-14	-1	-8*	0	-5	5	2	53	-54	1	2	90	-78	-12	H,K=	1	9		7	46	51	-5	-1	76	78	-1
-6	87	94	-7	-7	28	-25	-3	3	97	93	3	3	47	44	2	-8*	0	12	-12	H,K=	1	10		0	125	136	-10
-5	27	27	0	-6+	11	-3	-7	4	21	18	3	4*	0	0	0	-7	30	32	-2	-7	8	9	-1	1*	0	0	0
-4	156	167	-10	-5	176	-171	-4	5	70	-72	1	5	34	-31	-2	-6*	0	-10	10	-6	28	24	4	2	21	-16	-5
-3	156	160	-4	-4	16	16	0	6	26	24	1	6	69	-68	-1	-5*	0	11	-11	-5	16	-12	-4	3	22	22	0
-2	30	-23	-6	-3	101	96	4	H,K=	3	7		7	14	-16	1	-4	26	23	2	-4	14	-15	0	4	42	37	4
-1	46	46	0	-2	115	-120	4	-8	17	-16	-1	H,K=	2	8		-3	64	-62	-2	-3	34	33	0	5*	0	3	-3
0+	15	-10	-4	-1	48	51	-2	-7	103	103	0	-8*	0	0	0	-2	73	-57	-15	-2	36	34	1	H,K=	2	11	
1	32	38	-5	0	38	44	-5	-6	205	209	-3	-7	25	24	0	-1	23	25	-1	-1	109	106	2	-7*	0	-3	3
2	19	17	1	1+	10	-7	-3	-4	83	76	6	-6	36	-39	2	0	48	43	5	0	72	77	-4	-6	14	-10	-4
3	55	-56	1	2*	0	-5	5	-3	249	-229	-19	-5	25	20	4	1	105	-104	0	1	59	-61	1	-5	32	31	1
H,K=	7	5		3	84	-90	6	-2	109	-115	5	-4	75	-61	-13	2	69	67	1	2	53	-52	0	-4	34	-31	-3
-8	15	-17	2	4	36	-35	-1	-1	143	145	-1	-3	24	21	2	3	59	47	11	3	12	13	-1	-3	20	-16	-4
-7	26	27	-1	5*	0	-1	1	0	17	-13	-4	-2	38	-30	-7	4	16	-14	-1	4	19	17	1	-2	28	28	0
-6	18	21	-3	H,K=	5	6		1	123	129	-5	-1*	0	4	-4	7*	0	8	-8	5	42	38	4	-1	44	47	-2
-5	32	-29	-3	-9	20	-21	1	2	34	-31	-3	0	30	-28	-1	H,K=	2	9		6*	0	-2	2	0*	0	2	-2
-4	154	-153	0	-8*	0	8	-8	3	82	76	6	1	32	30	2	-8	33	31	1	H,K=	2	10		1	36	38	-2
-3*	0	-2	2	-7	150	-157	7	4	174	188	-13	2+	15	10	4	-7*	0	2	-2	-7*	0	-5	5	2	40	38	2
-2	86	81	5	-6	29	-31	2	5	14	15	-1	3*	0	-11	11	-6	44	48	-3	-6*	0	-6	6	3*	0	-4	4
-1	97	-106	9	-5	20	16	3	6	16	15	1	4	156	-165	8	-5	24	17	6	-5	70	68	1	4	30	-29	0
0	20	19	0	-4+	15	8	7	H,K=	4	7		5	31	30	1	-4	76	-74	-2	-4*	0	-2	2	5	32	35	-3
1	52	53	-1	-3*	0	2	-2	-9	14	13	1	6	30	29	1	-3	108	-113	4	-3+	22	15	6	H,K=	3	11	
2	26	-32	5	-2	70	73	-3	-8	31	-30	-1	H,K=	3	8		-2	156	146	10	-2	21	-21	0	-7	45	-49	3
H,K=	8	5		-1	82	-80	-2	-7	21	20	1	-8	38	37	1	-1	57	-54	-3	-1	34	34	0	-6	116	-122	6
-8*	0	-12	12	0	41	-40	-1	-6*	0	0	0	-7	11	13	-2	0	17	21	-3	0	22	-21	0	-5+	12	6	5
-7+	9	3	5	1	41	-41	0	-5	21	17	3	-6	70	-74	3	1	41	-43	2	1	13	-12	-1	-4	51	-48	-3
-6	19	-19	0	2	48	49	-1	-4	27	21	5	-5	31	-28	-3	2*	0	0	0	2	32	32	0	-3	86	78	8
-5	59	-55	-4	3	53	-59	5	-3	31	24	6	-4	28	21	7	3	30	30	0	3	14	13	1	-2	65	60	5
-4	30	28	1	4*	0	-7	7	-2	29	-28	-1	-3	15	-11	-4	4	33	32	1	4	13	-13	0	-1	49	-48	0
-3	66	-64	-1	H,K=	6	6		-1	81	-86	4	-2	99	-96	-2	5	37	-39	2	5	11	13	-1	0*	0	0	0
-2	46	-42	-3	-9	17	-15	-2	0	55	-48	-6	-1	63	-67	3	6	9	11	-2	6+	10	14	-4	1	66	-64	-2
-1	34	-29	-4	-8	24	-28	3	1*	0	-10	10	0	174	185	-10	H,K=	3	9		H,K=	3	10		2	19	15	3
0	29	36	-7	-7	36	34	2	2*	0	4	-4	1	44	41	2	-8	24	-27	2	-7	81	-90	8	3	55	-57	1
H,K=	9	5		-6	44	44	0	3	31	33	-1	2	95	95	0	-7	61	-61	0	-6*	0	-4	4	4	89	-103	14
-5	30	-34	3	-5	100	102	-1	4	14	15	0	3	53	-48	-4	-6	139	-141	2	-5	89	-85	-3	H,K=	4	11	
-4	46	48	-2	-4	80	-80	0	5	22	-27	4	4	46	43	2	-5	56	-52	-3	-4	22	-16	-6	-7	17	-19	1
H,K=	0	6		-3	178	184	-6	H,K=	5	7		5	22	21	0	-4	34	-31	-2	-3	68	-63	-5	-6	10	-13	2
0+	9	14	-4	-2	64	66	-2	-8	20	17	2	H,K=	4	8		-3	103	-101	-2	-2	16	-13	-2	-5	12	-10	-1
1	100	88	11	-1	45	42	2	-7	55	53	1	-8	65	-64	0	-2	55	-57	2	-1	89	83	5	-4*	0	-1	1
2	18	21	-2	0	13	-12	-1	-6	87	-84	-3	-7*	0	-1	1	-1*	0	-7	7	0+	11	-7	-4	-3*	0	-2	2
3	349	328	20	1	109	-114	4	-5*	0	1	-1	-6	110	117	-7	0	21	16	5	1	92	-91	-1	-2	16	-12	-4
4	37	-36	0	2	17	-16	0	-4	59	56	3	-5	17	-18	1	1	112	118	-5	2	22	15	6	-1	33	34	0
5	1	0	0	3	46	48	-1	-3*	0	10	-10	-4	43	32	10	2	14	11	2	3	87	-85	-1	0	51	50	0
6	82	81	0	H,K=	7	6		-2	88	-83	-4	-3	58	58	0	3	97	101	-3	4	36	-32	-4	1	26	26	0
7	93	-96	2	-8	11	-9	-1	-1*	0	7	-7	-2+	0	-1	0	4	139	-146	7	5	30	-26	-3	2*	0	-2	2
8	25	-26	0	-7	38	-39	1	0	20	-16	-4	-1	58	-58	0	5	31	-33	2	H,K=	4	10		3	26	-27	0
H,K=	1	6		-6	12	10	1	1	53	52	1	0	36	33	3	H,K=	4	9		-7	34	33	0	H,K=	5	11	
-8*	0	-7	2	-5	70	-67	-2	2	64	-68	3	1	43	41	1	-8	58	70	-11	-6*	0	8	-8	-7	23	-20	-2
-7	36	-37	0	-4	3	-3	0	3	14	11	2	2	83	-84	1	-7	88	90	-2	-5	81	77	4	-6	36	40	-4
-6	39	-36	-2	-3	86	79	7	4	20	20	0	3*	0	7	-7	-6	42	-38	-4	-4*	0	2	-2	-5*	0	-6	6
-5	87	73	14	-2	18	-14	-3	H,K=	6	7		4	23	18	4	-5	41	-33	-8	-3	78	-72	-6	-4	24	-22	-3
-4	46	43	3	-1	12	-12	0	-8	41	-47	5	H,K=	5	8		-4	21	20	1	-2	66	62	3	-3*	0	6	-6
-3	139	-128	-11	0*	0	3	-3	-7	22	19	2	-8	22	22	0	-3	58	53	5	-1+	12	5	6	-2	57	53	4
-2	61	-60	-1	1	12	14	-1	-6	108	122	-13	-7*	0	2	-2	-2*	0	1	-1	0	12	-12	0	-1	31	-27	-4
-1	203	*199	-3	H,K=	8	6		-5	58	-56	-1	-6*	0	0	0	-1*	0	-6	6	1*	0	4	-4	0	17	15	2
0	151	-146	-5	-7+	16	-22	5	-4	88	91	-3	-5+	14	-9	-5	0	45	44	1	2*	0	9	-9	1	32	-32	0
1	242	240	-4	-6	22	-25	2	-3	93	-96	2	-4	102	99	3	1*	0	0	0	3	44	50	-5	2	25	27	-2
2	122	128	-6	-5	23	-24	1	-2	53	-53	0	-3	22	19	3	2*	0	4	-4	4	24	24	0	H,K=	6	11	
3	46	-44	-2	-4	30	25	4	-1	35	-34	0	-2	24	21	3	3	43	42	1	H,K=	5	10		-6	64	-67	3
4	47	-44	-2	-3	54	54	0	0	22	23	0	-1	63	64	-1	4*	0	8	-8	-7	63	71	-7	-5	22	25	-2
5	80	-75	-4	-2	16	-15	-1	1	55	-63	7	0	78	-83	4	H,K=	5	9		-6	16	15	1	-4	43	-47	4
6*	0	4	-4	-1*	0	2	-2	2	36	-37	1	1	52	-54	2	-8*	0	-1	1	-5	33	29	3	-3	54	55	-1
7*	0	-5	5	H,K=	0	7		H,K=	7	7		2	50	51	0	-7	48	56	-8	-4*	0	-5	5	-2	27	29	-1
H,K=	2	6		-5+	0	-2	1	-8	33	-36	2	3	14	14	0	-6	48	45	2	-3*	0	7	-7	-1	34	32	1
-9	19	10	3	1	195	198	-2	-7	12	10	1	H,K=	6	8		-5+	21	-14	-6	-2	47	-46	-1	0	17	-20	3

Table 3. The final parameters and their estimated standard deviations (in parentheses)

The coordinates of the non-hydrogen atoms have been multiplied by 10^4; those of the hydrogen atoms, by 10^3. The anisotropic thermal parameters of non-hydrogen atoms are of the form $\exp[-(B_{11}h^2+B_{22}k^2+B_{33}l^2+B_{12}hk+B_{13}hl+B_{23}kl)]$, and have been multiplied by 10^4. For the hydrogen atoms, the values listed are isotropic thermal parameters $B(\text{A}^2)$.

Atom	x	y	z	$B(\text{Å}^2)$
N (1)	9366 (3)	1222 (2)	1061 (3)	—
C (2)	7353 (3)	1248 (2)	−36 (3)	—
C (3)	6118 (3)	1262 (2)	885 (3)	—
C (4)	7064 (3)	1226 (2)	2882 (3)	—
C (5)	9135 (4)	1217 (2)	3937 (3)	—
C (6)	10290 (3)	1221 (2)	2956 (3)	—
C (7)	6823 (4)	1213 (2)	−2183 (4)	—
C (8)	3827 (3)	1329 (2)	−73 (4)	—
O (1)	8242 (3)	1077 (2)	−2534 (3)	—
O (2)	5008 (3)	1351 (2)	−3382 (3)	—
O (3)	2872 (3)	1523 (2)	−1843 (3)	—
O (4)	2985 (3)	1189 (2)	944 (3)	—
H (1)	601 (4)	115 (2)	336 (4)	3.4 (0.6)
H (2)	984 (5)	126 (2)	536 (5)	4.6 (0.8)
H (3)	1155 (5)	119 (2)	331 (5)	4.2 (0.7)
H (4)	1010 (6)	120 (3)	43 (5)	5.0 (0.8)
H (5)	354 (6)	125 (3)	−266 (5)	5.4 (0.9)

Atom	B_{11}	B_{22}	B_{33}	B_{12}	B_{13}	B_{23}
N (1)	131 (4)	59 (2)	143 (4)	3 (4)	175 (7)	8 (4)
C (2)	150 (5)	41 (2)	127 (4)	0 (4)	155 (7)	4 (4)
C (3)	130 (5)	45 (2)	149 (4)	2 (4)	157 (8)	3 (4)
C (4)	140 (5)	56 (2)	143 (4)	3 (4)	176 (8)	2 (4)
C (5)	162 (5)	65 (2)	118 (4)	12 (5)	137 (8)	6 (4)
C (6)	106 (4)	71 (2)	145 (2)	5 (5)	114 (8)	6 (5)
C (7)	178 (6)	63 (2)	149 (5)	−10 (5)	203 (9)	−2 (5)
C (8)	129 (5)	54 (2)	170 (5)	−6 (4)	154 (8)	−12 (5)
O (1)	211 (5)	114 (2)	164 (4)	3 (5)	254 (7)	−10 (5)
O (2)	167 (4)	104 (2)	124 (4)	9 (4)	97 (6)	16 (4)
O (3)	130 (4)	121 (2)	165 (4)	21 (5)	116 (6)	33 (5)
O (4)	140 (4)	100 (2)	225 (5)	−9 (4)	244 (7)	1 (4)

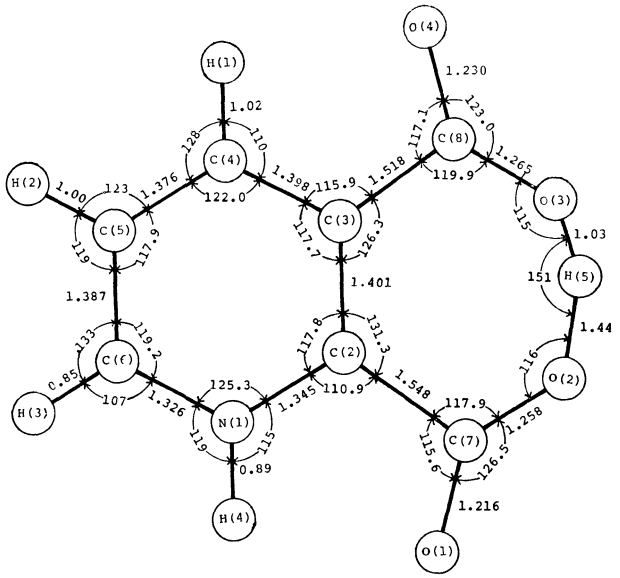

Fig. 2. Dimensions of quinolinic acid molecule.

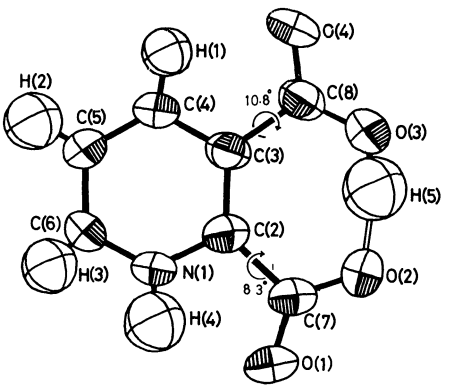

Fig. 3. The anisotropic thermal ellipsoids of non-hydrogen atoms and the isotropic thermal ellipsoids of hydrogen atoms. Ellipsoids are scaled to include 74% probability.

Table 4. Intramolecular bond lengths and angles

Bond	Length	e.s.d.	Bond	Angle	e.s.d.
N(1)-C(2)	1.345 Å	0.003 Å	C(2)-N(1)-C(6)	125.3°	0.2°
C(2)-C(3)	1.401	0.004	N(1)-C(2)-C(3)	117.8	0.2
C(3)-C(4)	1.398	0.004	N(1)-C(2)-C(7)	110.9	0.2
C(4)-C(4)	1.376	0.004	C(3)-C(2)-C(7)	131.3	0.2
C(5)-C(6)	1.387	0.004	C(2)-C(3)-C(4)	117.7	0.2
C(6)-N(1)	1.326	0.003	C(2)-C(3)-C(8)	126.3	0.2
C(2)-C(7)	1.548	0.004	C(4)-C(3)-C(8)	115.9	0.2
C(3)-C(8)	1.518	0.004	C(3)-C(4)-C(5)	122.0	0.2
C(7)-O(1)	1.216	0.004	C(4)-C(5)-C(6)	117.9	0.3
C(7)-O(2)	1.258	0.004	C(5)-C(6)-N(1)	119.2	0.3
C(8)-O(3)	1.265	0.004	C(2)-C(7)-O(1)	115.6	0.3
C(8)-O(4)	1.230	0.004	C(2)-C(7)-O(2)	117.9	0.2
C(4)-H(1)	1.02	0.03	O(1)-C(7)-O(2)	126.5	0.3
C(5)-H(2)	1.00	0.04	C(3)-C(8)-O(3)	119.9	0.3
C(6)-H(3)	0.85	0.04	C(3)-C(8)-O(4)	117.1	0.3
N(1)-H(4)	0.89	0.04	O(3)-C(8)-O(4)	123.0	0.3
O(2)-H(5)	1.44	0.04	H(1)-C(4)-C(3)	110	2
O(3)-H(5)	1.03	0.04	H(1)-C(4)-C(5)	128	2
			H(2)-C(5)-C(4)	123	2
			H(2)-C(5)-C(6)	119	2
			H(3)-C(6)-C(5)	133	3
			H(3)-C(6)-N(1)	107	3
			H(4)-N(1)-C(2)	115	3
			H(4)-N(1)-C(6)	119	3
			H(5)-O(2)-C(7)	116	2
			H(5)-O(3)-C(8)	115	2
			O(2)-H(5)-O(3)	151	4

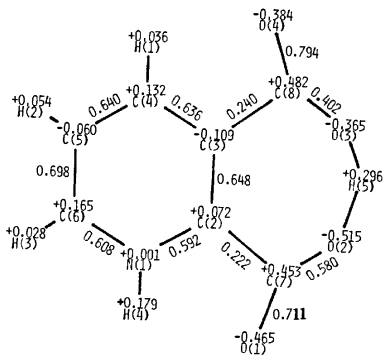

Fig. 4. The net charges and π-bond orders calculated by the CNDO/2 method.

The quinolinic acid molecule may be a mixture of the following two forms:

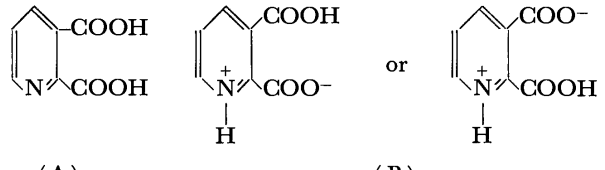

(A) (B)

However, the present study shows that the molecule takes the zwitter ion(B) in the crystal. The existence of the molecule in this form is quite evident from the assignment of a hydrogen atom in the difference Fourier map. It is also confirmed by the C(2)–N(1)–C(6) bond angle of 125.3(2)° and by the four C–O bond lengths of 1.216 (4), 1.258(4), 1.265(4), and 1.230(4) Å in the two carboxyl groups (the values in parentheses denote e.s.d.'s in their last digits).

The quinolinic acid molecule is approximately planar, with a maximum deviation of 0.242 Å. The pyridine ring is planar, the maximum deviation of a ring atom from the least-squares plane being 0.013 Å. The equations of the two planes through twelve non-hydrogen atoms of a molecule and six non-hydrogen atoms of a pyridine ring are:

$$0.0551X+0.9983Y+0.0215Z=1.8705 \quad \text{and}$$

$$0.0117X+0.9998Y+0.0156Z=1.6535$$

respectively, where X, Y, and Z are coordinates in Å referred to an orthogonal set of axes and parallel to the a, b, and c^* axes respectively. The displacements of all the atoms from these two planes are listed in Table 5.

The pyridine ring in the molecule shows a significant deformation from the C_{2v} symmetry of idealized geometry. The differences between the corresponding bond lengths, the N(1)–C(2) and N(1)–C(6), the C(2)–C(3) and C(5)–C(6), and the C(3)–C(4) and C(4)–C(5) bonds, are 0.019(3), 0.014(4), 0.022(4) Å respectively. The bond lengths of the side which has both carboxyl groups are longer than those of the other side. This difference may depend on the asymmetric substitution of two carboxyl groups, because no such difference has been found in dipicolinic acid[1] and

Table 5.

(1) The distances from the least-squares plane defined by twelve non-hydrogen atoms of a molecule.

Atom	Deviation(Å)	Atom	Deviation(Å)
N (1)	−0.061	O (1)	0.154
C (2)	−0·016	O (2)	−0.066
C (3)	0.021	O (3)	−0.190
C (4)	0.038	O (4)	0.242
C (5)	−0.031	H (1)	0.17
C (6)	−0.088	H (2)	0.11
C (7)	0.040	H (3)	0.10
C (8)	0.025	H (4)	−0.06
		H (5)	0.12

(2) The distances from the least-squares plane defined by the six non-hydrogen atoms of pyridine ring.

Atom	Deviation(Å)	Atom	Deviation(Å)
N (1)	0.009	O (1)	0.229
C (2)	0.002	O (2)	−0.086
C (3)	−0.012	O (3)	−0.297
C (4)	0.013	O (4)	0.108
C (5)	−0.001	H (1)	0.11
C (6)	−0.010	H (2)	−0.08
C (7)	0.065	H (3)	0.02
C (8)	−0.071	H (4)	0.04
		H (5)	0.05

dinicotinic acid,[2] in which two carboxyl groups are substituted symmetrically on the pyridine ring.

The lengths of the two C–C bonds joining the carboxyl groups to the ring are 1.548(4) and 1.518(4) Å, longer than the normal value(about 1.48~1.50 Å for sp^2—sp^2 bond); the difference between these two bond lengths, 0.030(4), is significant, judging from their estimated standard deviations. The two C–O bond lengths in each carboxyl group are slightly different from each other. In carbonyl groups, the difference between the C(7)–O(1) and C(8)–O(4) bond lengths, 0.014(4) Å, is due to the fact that the O(4) atom participates in the hydrogen bond, while the O(1) atom is free from it. Similar differences were also observed in dinicotinic acid[2] and cinchomeronic acid.[3] On the other hand, the C(7)–O(2) and C(8)–O(3) bond lengths, 1.258(4) and 1.265(4) Å, are equal within the limits of experimental errors. Their average value, 1.262 Å, is shorter than the normal bond length between the carbon and hydroxyl oxygen atom, and lies between the values of the C=O and C–O(H) bond lengths. The reason for these abnormal C–O(H) bond lengths is the formation of an intramolecular hydrogen bond which joins the O(2) and O(3) atoms at a very short distance, 2.399(3) Å. A similar tendency was observed in carboxyl groups of 3,4-furandicarboxylic acid.[4] The H(5) atom is bonded to the O(3) atom rather than to the O(2) atom in this analysis, corresponding to the slight difference between C–O distances related to these two oxygen atoms. In connection with this finding, it is desirable to locate the position of this hydrogen atom by neutron-diffraction study, since there has been a speculation that the hydrogen atom might be placed symmetrically between the oxygen atoms when they are joined by a short hydrogen bond. There is a good correlation between the π-bond orders and the observed bond lengths, as is shown in Fig. 4. The C(3)–C(2)–C(7) and C(2)–C(3)–C(8) bond angles deviate greatly from 120° due to the sp^2 hybridization of the C(2) and C(3) atoms. These deviations are caused by the formation of an intramolecular hydrogen bond. Both carboxyl groups are twisted by −8.3° (C(7)O(1)O(2)) and 10.8° (C(8)O(3)O(4)) out of the plane of the pyridine ring, as is shown in Fig. 3, so that the O(2) and O(3) atoms approach each other.

The intramolecular hydrogen bond between the adjacent carboxyl groups was found in 3,4-furandicarboxylic acid,[4] with an aromatic five-membered ring. However, the intramolecular hydrogen bond of this type has not thus far been found in the crystal structures of carboxylic acids with a benzene ring and another aromatic six-membered ring. From a geometrical point of view, the formation of the hydrogen bond of this type seems to be more difficult in the carboxylic acids with an aromatic six-membered ring than in those with a five-membered ring. Hence it may be noted that the hydrogen bond of this type has been found in the crystal of quinolinic acid, which has an aromatic six-membered ring.

Molecular Arrangement and Hydrogen-bond System. The crystal structure is shown in Figs. 5 and 6. The distances and angles of hydrogen bonds are listed in Table 6. The molecules are arranged in layers closely parallel to the (0 1 0) plane at $y=1/8$, 3/8, 5/8 and 7/8. These planes have a spacing of 3.182 Å. The dihedral angle which the best plane of a molecule makes with the (0 1 0) plane is 3.3°. Figure 5 is a view parallel to the (0 1 0) plane. Figure 6 is a view normal to the (0 1 0) plane and illustrates the relative orientation of the molecules in two neighboring layers. Figures 6(a) and 6(b) show the relation between the planes

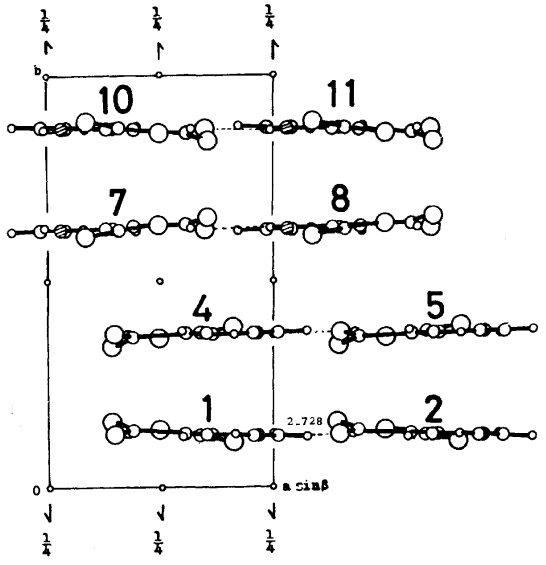

Fig. 5. A view of the crystal structure down the *c* axis. The hydrogen bonds are shown by broken lines.

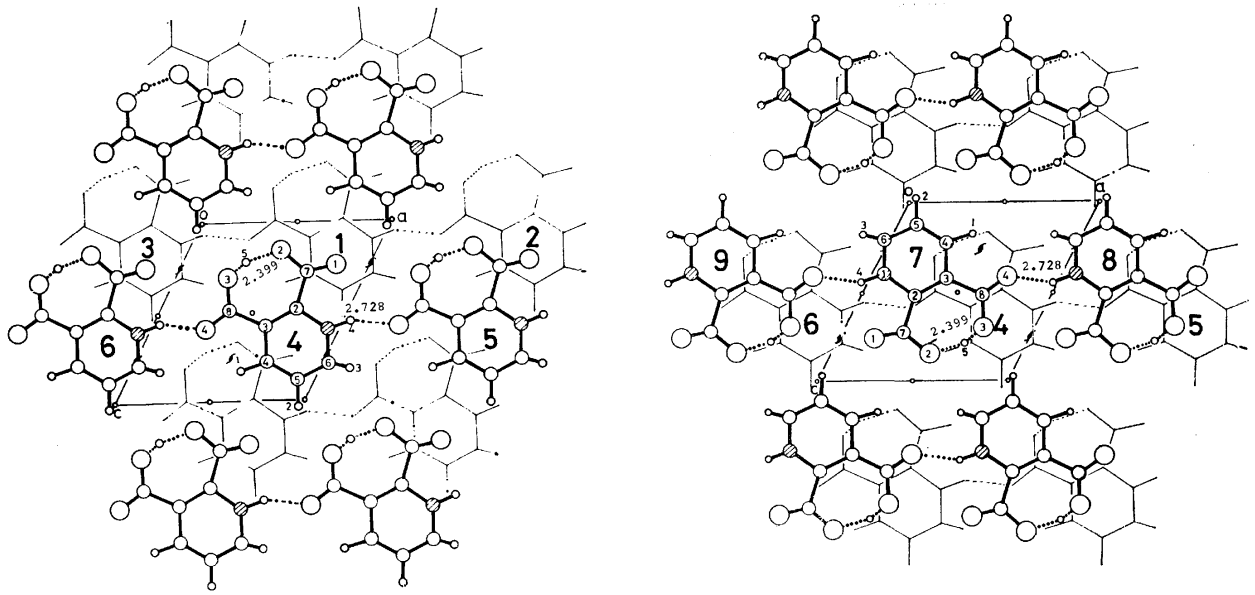

(a) (b)

Fig. 6. A view of the crystal structure down the b axis, showing the relative orientation of the molecules in two adjacent layers parallel to the (010) plane. (a): The relation between the planes at $y=1/8$ and 3/8 related by the c-glide at $y=1/4$. (b): The relation between the planes at $y=3/8$ and 5/8 related by the center of symmetry at $y=1/2$.

Table 6. Hydrogen bond distances(Å) and angles (degree)

X——H....O	Symmetry	X···O	e.s.d.	X-H	e.s.d.	H···O	e.s.d.	Angle	e.s.d.
N(1)-H(4)..O(4)	(1, 1, 2)	2.728	0.003	0.89	0.04	1.99	0.04	140	4
O(3)-H(5)..O(2)	(1, 1, 1)	2.399	0.003	1.03	0.04	1.44	0.04	151	4

C——O....X	Symmetry	Angle	e.s.d.
C(8)-O(4)..H(4)	(2, 2, 1)	133	4
C(8)-O(4)..N(1)	(2, 2, 1)	144.8	0.2
C(7)-O(2)..H(5)	(1, 1, 1)	116	2
C(7)-O(2)..O(3)	(1, 1, 1)	128.7	0.2

Symmetry 1 = (x, y, z)
2 = $(1+x, y, z)$
3 = $(-1+x, y, z)$
4 = $(x, 1/2-y, 1/2+z)$
5 = $(1+x, 1/2-y, 1/2+z)$
6 = $(-1+x, 1/2-y, 1/2+z)$
7 = $(1-x, 1/2+y, 1/2-z)$
8 = $(2-x, 1/2+y, 1/2-z)$
9 = $(-x, 1/2+y, 1/2-z)$
10 = $(1-x, 1-y, 1-z)$
11 = $(2-x, 1-y, 1-z)$
12 = $(-x, 1-y, 1-z)$

at $y=1/8$ and 3/8, and 3/8 and 5/8. In Figs. 5 and 6, the same numerals designate the same molecules. The symmetry codes of the molecules with these numbers are shown in Table 6.

Each molecule on the same plane is joined, through the N(1)-H(4)···O(4) hydrogen bond, with two neighboring molecules and forms an endless chain along the a axis. The carbonyl oxygen atom, O(4), participates in a hydrogen bond(O(4)···H(4)-N(1); 2.728(3) Å), while another atom (O(1)) is free from the hydrogen bond. Similar situations are observed also in nicotinic acid,[12] dinicotinic acid,[2] and cinchomeronic acid.[3] Those facts suggest that the O-H···N or $^+$N-H···O hydrogen bond is more energetically favored than the O-H···O hydrogen bond in solids.

There is no hydrogen bond between the chains on the same plane, those on the planes at $y=1/8$ and 3/8 related by the c-glide plane at $y=1/4$, and those on the planes at $y=3/8$ and 5/8 related by the center of symmetry at $y=1/2$. These chains are packed together only by the van der Waals forces. Therefore, there is an anisotropy of the bonding forces joining the molecules in this crystal. The appreciable thermal diffuse scattering along the directions of the b^* and c^* axes may be caused by this anisotropy of the bonding forces. Similar patterns were observed in dipicolinic acid monohydrate[1] and other crystals in which molecules are joined by this type of hydrogen bond.[13]

Computer Programs. All the calculations were performed on a FACOM 270-30 computer at the Computer Center of Osaka City University by the use

12) W. B. Wright and G. S. D. King, *Acta Crystallogr.*, **6**, 305 (1953).

13) J. L. Amorós and M. Amorós, "Molecular Crystals," John Wiley and Sons, Inc., New York (1968).

of the following programs—RSLG-3(cell constant),[14] RSSFR-3(Fourier synthesis),[15] HBLS-IV(block-diagonal least-squares refinement),[16] DAPH(bond length, bond angle and least-squares plane),[17] SCALE (film factor, Lp and layer scaling),[18] CNINDO(CNDO and INDO calculation),[11] and TE-I(thermal ellipsoid).[19]

This paper is dedicated to the late Dr. Walter C. Hamilton, who took an interest in the intramolecular hydrogen bond of this compound. The authors wish to express their thanks to Dr. Kichisuke Nishimoto of this faculty for his useful advice in the CNDO calculation.

14) T. Sakurai, "The Universal Crystallographic Computing System (I)," edited by T. Sakurai, The Crystallographic Society of Japan (1967) p. 18.
15) T. Sakurai, *ibid.*, p. 45.
16) T. Ashida, *ibid.*, p. 65.
17) T. Ashida, *ibid.*, p. 76.
18) H. Yoshioka, K. Hirotsu, and F. Takusagawa, Unpublished work.
19) F. Takusagawa, Unpublished work.

BULLETIN OF THE CHEMICAL SOCIETY OF JAPAN, VOL. 46, 2380—2387 (1973)

Studies on Intermolecular Complex Formation. III. Crystal Structure of Thymine-*N*,*N*-Diethylmelamine Complex Monohydrate

Chihiro TAMURA, Tadashi HATA, and Sadao SATO

The Central Research Laboratories of Sankyo Co., Ltd., Hiromachi, Shinagawa-ku, Tokyo 140

(Received February 14, 1973)

The crystal and molecular structure of the thymine-*N*,*N*-diethylmelamine complex monohydrate has been solved by means of the direct method. The crystals are monoclinic, with the space group of $P2_1/c$ and with $a=7.167$, $b=16.123$, $c=13.179$ Å, and $\beta=104.2°$. The final *R*-factor for 1612 reflections is 0.087. These two components are hydrogen-bonded by a NH···N and two NH···O bonds with distances of 2.881, 2.821, and 3.006 Å. The complex formation ability for thymine and uracil has also been tested for some other organic compounds with amino and nitrogen heterocycles.

Intermolecular interactions in crystalline fields have recently come into focus after Hoogsteen displayed some model complexes of DNA.[1] The pairing mechanism has been interpreted as being due to special features in the purine and pyrimidine structures, in which the atoms in these molecules are arranged in appropriate combinations of so-called "complementary hydrogen bond."[2-18] Such arrangements would have a bearing on the biological duplication mechanism. Subsequently, we have been trying to determine some role for the intermolecular complex formation between nucleotide bases and organic compounds.[19,20] It has been found that cytosine and adenine exhibit a rather strong affinity for many organic compounds, while thymine and/or uracil are less reactive and bind only with a few organic compounds that have a $-\underset{\displaystyle NH_2}{\underset{|}{C}}=N-\underset{\displaystyle NH_2}{\underset{|}{C}}=N-$ grouping or a few other basic groups. In this paper we wish to describe the crystal structure of the thymine–*N*,*N*-diethylmelamine monohydrate complex and the general ability of complex formation in some organic compounds that can produce a complex with thymine and/or uracil. The biological importance of the melamine molecule and its derivatives has already been discussed in several places.[21,22] These studies may make it possible to project an illustrative intermolecular spatial system.

1) K. Hoogsteen, *Acta Crystallogr.*, **12**, 822, (1959); **16**, 907 (1963).
2) H. M. Sobell, K. Tomita, and A. Rich, *Proc. Natl. Acad. Sci. U. S.*, **49**, 885 (1963).
3) F. S. Mathews and A. Rich, *J. Mol. Biol.*, **8**, 89 (1964).
4) A. E. V. Hashemeyer and H. Sobell, *Acta Crystallogr.*, **18**, 525 (1965); *ibid.*, **19**, 125 (1965).
5) L. L. Labana, H. M. Sobell, *Proc. Natl. Acad. Sci. U. S.*, **57**, 459 (1967).
6) H. M. Sobell, *J. Mol. Biol.*, **18**, 1 (1966).
7) E. J. O'Brien, *Acta Crystallogr.*, **23**, 92 (1967).
8) S. H. Kim and A. Rich, *Science*, **158**, 1046 (1967).
9) L. Katz, K. Tomita, and A. Rich, *J. Mol. Biol.*, **13**, 340 (1969).
10) T. D. Sakore and H. M. Sobell, *ibid.*, **43**, 77 (1969).
11) F. Mazza, H. M. Sobell, and G. Kartha, *ibid.*, **43**, 407 (1969).
12) T. D. Sakore, S. S. Tavale, and H. M. Sobell, *ibid.*, **43**, 361 (1969).
13) S. S. Tavale, T. D. Sakore, and H. M. Sobell, *ibid.*, **43**, 375 (1969).
14) T. D. Sakore, H. M. Sobell, F. Mazza, and G. Kartha, *ibid.*, **43**, 385 (1969).
15) D. Veot and A. Rich, *J. Amer. Chem. Soc.*, **91**, 3069 (1969).
16) S. H. Kim and A. Rich, *J. Mol. Biol.*, **42**, 87 (1969).
17) W. Saenger and D. Suck, *ibid.*, **60**, 87 (1971).
18) R. Chandross and A. Rich, *Biopolymers*, **10**, 1795 (1971).
19) C. Tamura, N. Sakurai, and S. Sato, This Bulletin, **44**, 1473 (1971).
20) C. Tamura, T. Hata, S. Sato, and N. Sakurai, *ibid.*, **45**, 3245 (1972).
21) G. R. Zins, *J. Pharmacol. Exp. Therap.*, **150**, 109 (1965).
22) H. Bruhin, X. Bühlmann, W. H. Hook, W. Hoyle, B. Orford, and W. Visches, *J. Pharm. Pharmacol.*, **21**, 423 (1969).

TABLE 1. STRUCTURE FACTOR DATA ($\times 10$) FOR THE OBSERVED REFLECTIONS

TABLE 1. (Continued)

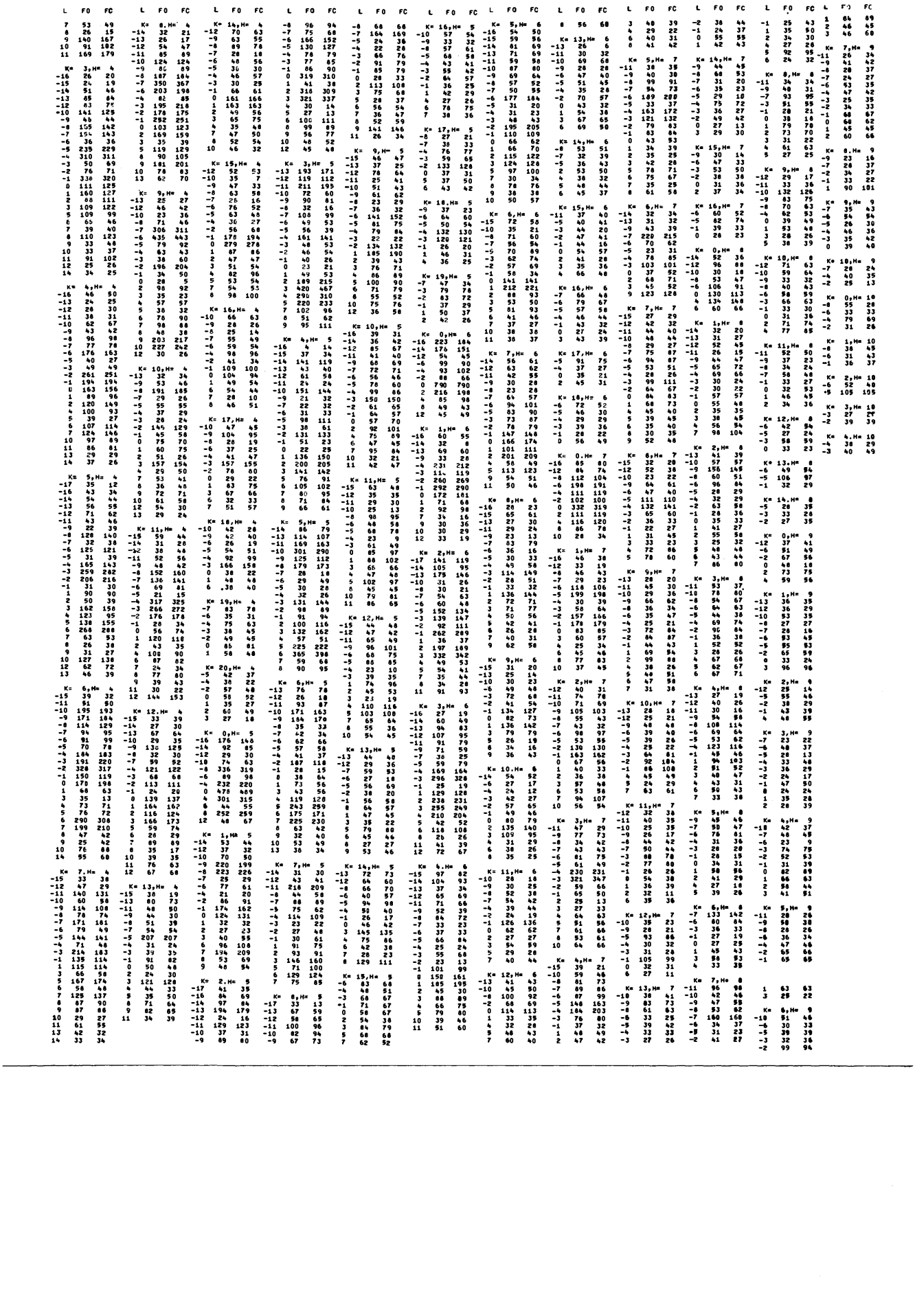

Experimental

Equivalent moles of nucleotide bases and some nitrogen heterocycles were dissolved in hot 70% aqueous ethanol, and then allowed to stand for several days in a refrigerator. The X-ray diffraction of the materials obtained and of each component were measured up to $2\theta=50°$ (Cu Kα) with a Rigaku model D6C diffractometer.

The single crystals of thymine–*N*,*N*-diethylmelamine thus obtained, which were suitable for X-ray analysis, were used for the intensity measurements. A crystal measuring $0.5\times0.3\times0.2$ mm was chosen for recording the crystal data and the intensities. Preliminary Weissenberg photographs showed that the crystals belong to the monoclinic system, with the space group of $P2_1/c$. The lattice parameters from the diffractometer are: $a=7.167(9)$, $b=16.123(18)$, $c=13.179(15)$ Å, $\beta=104.2(1)°$, $D_{obsd}=1.39$, and $D_{calcd}=1.44$ g/cm^3. The three-dimensional intensities were collected on a Rigaku Denki four-circle automatic diffractometer with a FACOM-R computer system up to a 2θ limit of 60° using Mo Kα radiation and the $2\theta/\theta$ scan mode at a scan speed of 2° min^{-1}. A crystal was mounted along the *a*-axis, and a total of 1612 independent reflections were collected. Three standard reflections were used to monitor the crystal stability during the measurement. The data were corrected for the usual Lorentz and polarization factors, but no corrections were made for absorption.

Structure Analysis and Refinement

The reiterative application of Sayre's equation[23] was used to determine the phases of 270 reflections having $E\geqq1.50$. Three reflections (1,2,−3; 1,3,−3; 3,14,0) were chosen for specifying the origin, and three other reflections (0,0,16; 0,0,3; 5,5,6), were denoted by the symbols A, B and C respectively. The B and C symbols were uniquely determined to be −A and A respectively by subsequent calculations. Then the structure was satisfactorily solved by an interpretation of the *E*-map based on these phases. The atomic parameters were refined by the method of least-squares, using the block-diagonal least-squares program. When the *R*-factor was reduced to 0.18, the difference synthesis was calculated in order to determine the positions of the hydrogen atoms; the six atoms attached to C(11) and C(13) were vague because of disorder. The final *R*-factor reached was 0.087 for the structure factors listed in Table 1. The atomic parameters are given in Tables 2, 3 (a), and 3 (b).

Table 2. Fractional atomic coordinates in thymine—*N*,*N*-diethylmelamine complex monohyrate

Atom	*x*/*a*	*y*/*b*	*z*/*c*
N (1)	0.2413	0.9612	0.1210
C (2)	0.2674	0.8827	0.2221
N (3)	0.3082	0.7341	0.2485
C (4)	0.3255	0.6529	0.1588
N (5)	0.3004	0.7143	0.0527
C (6)	0.2607	0.8669	0.0402
N (7)	0.2361	0.9381	−0.0659
N (8)	0.2501	0.9688	0.3085
N (9)	0.3911	0.9615	0.6868
C (10)	0.4744	1.0368	0.8682
C (11)	0.3855	1.0960	0.7857
C (12)	0.4360	1.0545	0.5953
C (13)	0.3631	1.1886	0.5557
N (14)	0.0926	0.9770	0.4310
C (15)	0.1288	1.1377	0.4535
N (16)	0.1573	1.1997	0.5644
C (17)	0.1503	1.0989	0.6507
C (18)	0.1151	0.9334	0.6321
C (19)	0.0864	0.8757	0.5175
O (20)	0.0483	0.7180	0.4931
O (21)	0.1365	1.2362	0.3774
W	0.0098	0.9488	0.1899
H (7A)	0.204	0.552	0.771
H (7B)	0.274	0.602	0.887
H (8A)	0.216	0.445	0.427
H (8B)	0.246	0.620	0.376
H (16)	0.191	0.313	0.594
H (17)	0.173	0.164	0.714
H (18)	0.120	0.416	0.717
H (20A)	0.021	0.675	0.411
H (20B)	0.055	0.628	0.581

Results and Discussion

Intermolecular Interactions and Hydrogen-bond Systems. The cytosine and adenine molecules have a strong tendency to bind with acidic organic compounds, especially with molecules containing a carboxylic acid moiety. However, few organic compounds can bind with thymine or uracil under these experimental conditions. In such circumstances, we have tried to un-

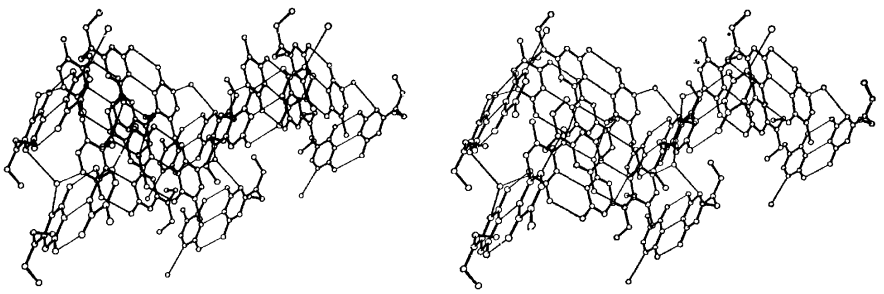

Fig. 1. Stereoscopic view of the packing and hydrogen bonding. Molecular bonds are drawn thick and hydrogen bonds thin.

23) D. Sayre, *Acta Crystallogr.*, **5**, 60 (1952).

TABLE 3(a). ANISOTROPIC THERMAL PARAMETERS IN THYMINE–*N*,*N*-DIETHYLMELAMINE COMPLEX MONOHYDRATE

The thermal parameters are given in the form

$$T = \exp[-(B_{11}h^2+B_{22}k^2+B_{33}l^2+2B_{12}hk+2B_{13}hl+2B_{23}kl)].$$

Atom	B_{11}	B_{22}	B_{33}	B_{12}	B_{13}	B_{23}
N (1)	0.00356	0.01109	0.00485	0.00081	0.00162	0.00021
C (2)	0.00326	0.01237	0.00448	−0.00025	0.00158	0.00043
N (3)	0.00335	0.01149	0.00435	0.00062	0.00155	0.00012
C (4)	0.00318	0.01402	0.00542	0.00077	0.00163	0.00013
N (5)	0.00353	0.01401	0.00439	0.00107	0.00133	−0.00108
C (6)	0.00277	0.01152	0.00450	0.00071	0.00097	0.00034
N (7)	0.00487	0.01332	0.00473	0.00112	0.00231	−0.00020
N (8)	0.00422	0.01475	0.00501	0.00021	0.00209	0.00069
N (9)	0.00649	0.02709	0.00912	−0.00394	0.00313	−0.00202
C (10)	0.00670	0.02456	0.01369	0.00013	0.00180	0.00063
C (11)	0.00672	0.02299	0.00962	−0.00329	0.00235	−0.00127
C (12)	0.01205	0.02420	0.01401	−0.00234	0.00253	−0.00085
C (13)	0.00601	0.04780	0.01340	−0.00072	0.00244	−0.00559
N (14)	0.00249	0.00944	0.00383	−0.00026	0.00119	−0.00029
C (15)	0.00224	0.00996	0.00345	0.00043	0.00101	−0.00010
N (16)	0.00336	0.01152	0.00377	−0.00002	0.00148	−0.00041
C (17)	0.00283	0.01233	0.00347	0.00044	0.00086	−0.00025
C (18)	0.00270	0.01055	0.00384	−0.00035	0.00137	0.00058
C (19)	0.00252	0.01150	0.00360	−0.00005	0.00109	−0.00000
O (20)	0.00423	0.01532	0.00652	0.00088	0.00159	−0.00058
O (21)	0.00338	0.01293	0.00436	−0.00077	0.00133	0.00058
W	0.00362	0.01530	0.00420	−0.00008	0.00076	−0.00032

TABLE 3(b). ISOTROPIC THERMAL PARAMETERS OF SOME HYDROGEN IN THYMINE–*N*,*N*-DIETHYLMELAMINE COMPLEX MONOHYDRATE

Atom	B_{iso}	Atom	B_{iso}	Atom	B_{iso}
H (7A)	5.64	H (8B)	3.99	H (18)	9.06
H (7B)	4.57	H (16)	2.36	H (20A)	4.76
H (8A)	4.20	H (17)	1.12	H (20B)	5.30

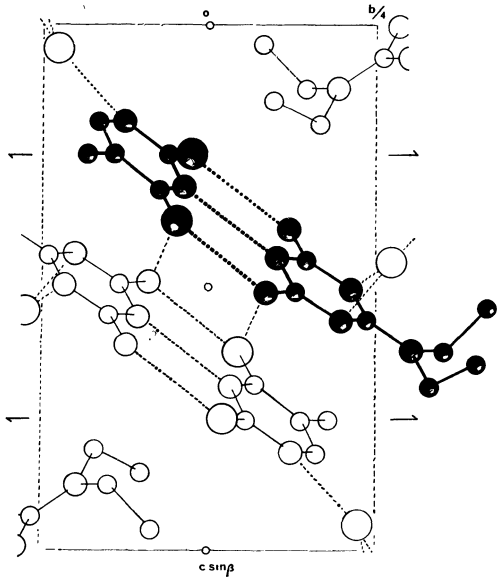

Fig. 2. Molecular packing and hydrogen bonding in thymine–*N*,*N*-diethylmelamine complex monohydrate.

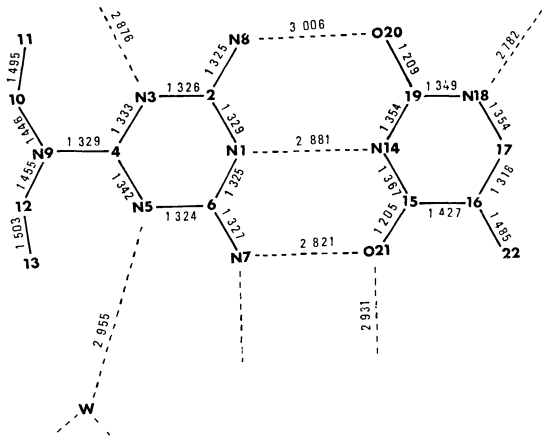

Fig. 3(a). Interatomic distances in thymine–*N*,*N*-diethylmelamine complex monohydrate.

TABLE 4. INTERMOLECULAR COMPLEX FORMATION BETWEEN SOME NITROGEN HETEROCYCLES AND NUCLEOTIDE BASES

	A	C	T	U
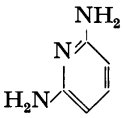 2,6-diamino-pyridine	−	−	−	−
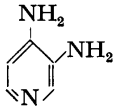 3,4-diamino-pyridine	−	−	−	−
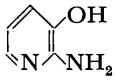 2-amino-3-hydroxy pyridine	−	−	−	−
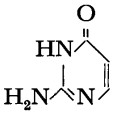 isocytosine	+	?	−	−
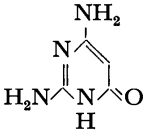 2,4-diamino-6-hydroxypyrimidine	−	+	+	+
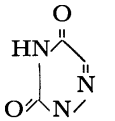 6-azauracil	+	−	−	−
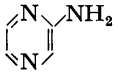 aminopyrazine	−	−	−	−
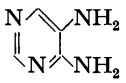 4,5-diamino-pyrimidine	−	−	−	−
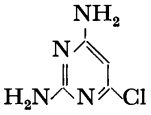 4-chloro-2,6-diaminopyrimidine	−	−	+	+
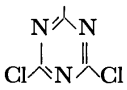 cyanuric chloride	+	+	−	−
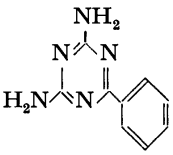 2,4-diamino-6-phenyl-5-triazine	+	+	−	+
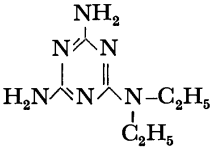 2,4,6-triamino *N,N*-diethyl-1,3,5-triazine	+	+	+	+

	A	C	T	U
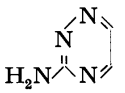 3-amino-1,2,4-triazine	−	−	−	−
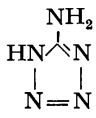 5-amino-tetrazole	−	−	−	−
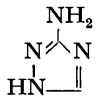 3-amino-1,2,4-triazole	−	−	−	−
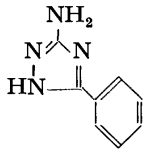 3-amino-5-phenyl-1,2,4-triazole	−	−	−	−
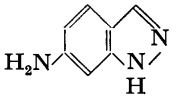 6-aminoindazole	−	−	−	−
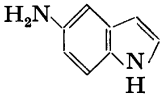 5-aminoindole	−	−	−	−
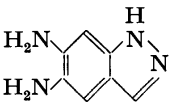 5,6-diamino-indazole	−	−	−	−
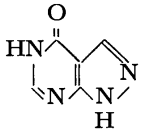 4-hydroxy pyrazolo-[3,4d]pyrimidine	+	−	−	−
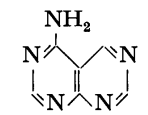 4-aminopyrimido [4,5d]pyrimidine	−	−	−	−
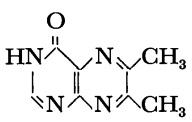 2-amino-6,7-dimethyl-4-hydroxypteridine	−	−	−	−
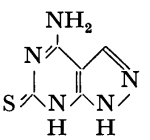 4-amino-6-mercapto pyrazolo[3,4d]-pyrimidine	−	−	−	−

cover some specific atomic arrangement or any molecule that can associate with thymine or uracil by means of hydrogen bonding. Table 4 shows the materials tested in this experiment. Some molecules with a number of exocyclic amino groups in combination with endocyclic –N= parts, especially in an arrangement which corresponds to a 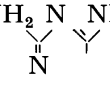 group, were found to be able to associate with these molecules. Therefore, combining this finding with the results for cytosine and adenine, it can be said that at least a partially molecular basicity or acidity plays an important role in binding the two components, presumably a so-called acid-and-base interaction. From this point of view, adenine, cytosine, thymine, and uracil can be classified into two groups; cytosine and adenine act as basic nucleotide bases which can bind with acidic components, such as carboxylic acids, while the other two are acidic nucleotide bases which can bind with basic components, such as melamine. However, the binding force is sometimes seriously affected by some other molecular

Table 5. Atomic distances of three hydrogen bonds

Components	Distances (Å)			Type	Ref.
9-Ethylguanine–1-methyl-5-bromocytosine	2.91	2.95	2.86	B	2)
Deoxyguanosine–5-bromodeoxycytidine	2.83	2.92	2.78	B	4)
1-Methyl-5-iodouracil–9-ethyl-2,6-diaminopurine	2.92	2.91	2.87	A	5)
1-Methylthymine–9-ethyl-2,6-diaminopurine	2.99	2.99	2.87	A	14)
1-Methyl-5-fluorouracil–9-ethyl-2,6-diaminopurine	2.89	2.88	2.81	A	18)
Isocytosine-isocytosine	2.904	2.908	2.861	B	37)
Cytosineacetic acid–cytosineacetic acid	2.790	2.823	2.790	B	36)
Cytosine–cytosine (trimer complex with resorcylic acid)	2.889	2.815	2.778	B	35)
Thymine–*N*,*N*-diethylmelamine	3.006	2.881	2.821	A	This work

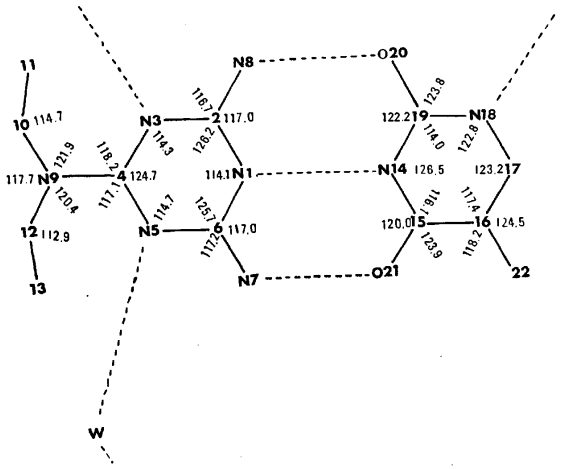

Fig. 3(b). Interbond angles in thymine-*N*,*N*-diethylmelamine complex monohydrate.

feature; thus, not all similar molecular structures can always bind with each other. The local atomic basicity or acidity may be considered to be appropriate for association at each specific site, but steric hindrance may be the determining factor in the formation of molecular complex crystals. Detailed molecular geometry can be evaluated only by X-ray analysis.

Description of the Crystal Structure. The crystal and molecular structure is shown in a stereographic plot in Fig. 1, while a projectional view along the *a*-axis is shown in Fig. 2. The thymine and melamine molecules are associated with each other mainly by means of two NH···O hydrogen bonds (2.821 and 3.006 Å) and one NH···N bond (2.881 Å). This hydrogen-bond system is defined as consisting of the specific nitrogen and oxygen atoms in both molecules, which form the tips of the capital letter "W"; two such molecules bind with each other, with both tops of the letter, thus forming three hydrogen bonds.

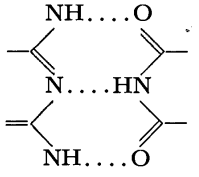

I (A)

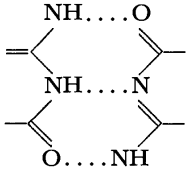

I (B)

There are several analogous three-hydrogen bond ystems, I(A) and I(B), which are summarized in

Table 6. Intermolecular atomic distances, less than 3.7 Å between the molecules

x, *y*, *z*		N (8) ·····O (21)	3.297
N (1) ·····N (14)	2.881	N (9) ·····C (16)	3.541
N (7) ·····O (21)	2.821	N (9) ·····C (17)	3.427
N (8) ·····O (20)	3.006	C (12)·····C (17)	3.584
N (18)·····W (23)	2.782	2−*x*, 1−*y*, 1−*z*	
1+*x*, *y*, *z*		N (7) ·····O (21)	2.931
N (7) ·····N (8)	3.380	−*x*, 1/2+*y*, 1/2−*z*	
O (22)·····O (20)	3.413	W (23)·····C (2)	3.507
C (21)·····N (8)	3.672	W (23)·····N (3)	2.876
C (21)·····O (20)	3.446	W (23)·····N (8)	3.186
1−*x*, −*y*, 1−*z*		W (23)·····C (10)	3.424
C (11)·····C (13)	3.696	W (23)·····C (11)	3.396
1−*x*, 1−*y*, 1−*z*		*x*, 1/2−*y*, 1/2+*z*	
N (1) ·····N (14)	3.394	C (10)·····C (19)	3.711
N (1) ·····C (15)	3.621	C (10)·····O (20)	3.539
N (1) ·····C (21)	3.633	C (11)·····C (19)	3.542
C (2) ·····N (14)	3.636	C (11)·····O (20)	3.506
C (2) ·····C (15)	3.351	1−*x*, 1/2+*y*, 1/2−*z*	
N (3) ·····C (15)	3.295	C (17)·····N (3)	3.658
N (3) ·····C (16)	3.477	C (17)·····C (4)	3.633
N (3) ·····C (21)	3.380	C (21)·····N (3)	3.632
C (4) ·····N (14)	3.668	C (21)·····N (8)	3.634
C (4) ·····C (15)	3.460	W (23)·····N (5)	2.955
C (4) ·····C (16)	3.395	W (23)·····C (6)	3.282
C (4) ·····C (17)	3.526	W (23)·····N (7)	3.272
N (5) ·····N (14)	3.424	W (23)·····C (13)	3.661
N (5) ·····N (18)	3.491	1+*x*, 1/2−*y*, 1/2+*z*	
N (5) ·····C (19)	3.332	C (13)·····N (8)	3.707
C (6) ·····N (14)	3.202	C (13)·····O (20)	3.437
C (6) ·····O (20)	3.626	*x*, 1/2−*y*, −1/2+*z*	
N (7) ·····N (8)	3.624	C (19)·····C (11)	3.542
N (7) ·····N (14)	3.630	O (20)·····C (10)	3.539
N (7) ·····C (19)	3.543	O (20)·····C (11)	3.506
N (7) ·····C (20)	3.318	−1+*x*, 1/2−*y*, −1/2+*z*	
		O (20)·····C (13)	3.437

Table 5. The molecular complexes of similar hydrogen-bonding arrangements have been reported by Sobell *et al.*[14] and Rich *et al.*[18] These facts suggest that an atomic arrangement such as that in I(A) is one of the fundamental combination schemes for binding among molecules. The paired-molecular complex formed in this manner is connected by the remaining

Table 7. Interatomic bond distances and angles in thymine–*N*,*N*-diethylmelamine monohydrate complex

N (1)–C (2)	1.329 Å	C (2)–N (1)–C (6)	114.1°
N (1)–C (6)	1.325	N (3)–C (2)–N (8)	116.7
C (2)–N (3)	1.326	N (1)–C (2)–N (3)	126.2
C (2)–N (8)	1.325	N (1)–C (2)–N (8)	117.0
N (3)–C (4)	1.333	C (2)–N (3)–C (4)	114.3
C (4)–N (5)	1.342	N (3)–C (4)–N (5)	124.7
C (4)–N (9)	1.329	N (3)–C (4)–N (9)	118.2
N (5)–C (6)	1.324	N (5)–C (4)–N (9)	117.1
C (6)–N (7)	1.327	C (4)–N (5)–C (6)	114.7
N (9)–C (10)	1.446	N (1)–C (6)–N (5)	125.7
N (9)–C (12)	1.455	N (5)–C (6)–N (7)	117.2
C (10)–C (11)	1.495	N (1)–C (6)–N (7)	117.0
C (12)–C (13)	1.503	C (4)–N (9)–N (10)	121.9
N (14)–C (15)	1.367	C (4)–N (9)–C (12)	120.4
N (14)–C (19)	1.355	C (10)–N (9)–C (12)	117.7
C (15)–C (16)	1.427	N (9)–C (10)–C (11)	114.7
C (16)–C (17)	1.318	N (9)–C (12)–C (13)	112.9
C (17)–N (18)	1.354	C (15)–N (14)–C (19)	126.5
N (18)–C (19)	1.349	N (14)–C (15)–C (16)	116.1
C (19)–O (20)	1.209	C (16)–C (15)–C (21)	123.9
C (16)–O (22)	1.485	N (14)–C (15)–C (21)	120.0
C (15)–C (21)	1.205	C (15)–C (16)–C (17)	117.4
		C (17)–C (16)–C (21)	124.5
		C (15)–C (16)–C (21)	118.2
		C (16)–C (17)–N (18)	123.2
		C (17)–N (18)–C (19)	122.8
		N (14)–C (19)–N (18)	114.0
		N (18)–C (19)–O (20)	123.8
		N (14)–C (19)–O (20)	122.2

NH···O hydrogen bond at a distance of 2.931 Å, and such units are stacked in such a way that they are parallel to the alternate (0, 1, 1, and 0,1,–1) crystallographic planes. One water molecule is associated by means of hydrogen bonds between these triazine-ring systems in the direction of the *a*-axis. The component molecules are almost coplanar, and the dihedral angle of both least-squares planes is 4.9°. Parallel sheets of the component molecules are separated from each other at an average spacing of 3.35 Å, since the maximum deviation between the atoms in some charge-transfer complexes is 3.26 Å.[24] Therefore, for the complex formation of this series, in some way the molecular stacking or van der Waals forces are second-order in importance. Sakurai *et al.*[25,26] reported some charge-transfer complexes between the molecules of thymine and quinone, which would imply that stacking forces between these hygroscopic moieties play an important role in the complex formation.

In the three-hydrogen-bond system the distances of the two bondings on the outside differ by about 0.2 Å even though *N*,*N*-diethylmelamine is a fairly symmetric molecule. It is hard to explain why hydrogen bonding between the atoms N(8) and O(20) is weak in such symmetrical three-hydrogen bonds. The other intermolecular atomic distances are shown in Table 6.

Table 8. Deviations of the atoms from the least-squares planes (Å)

N,*N*-Diethylmelamine		Thymine	
N (1)	−0.004	N (14)	−0.0141
C (2)	0.004	C (15)	−0.002
N (3)	−0.016	C (16)	−0.004
C (4)	0.000	C (17)	−0.012
N (5)	0.033	N (18)	−0.014
C (6)	−0.004	C (19)	0.003
N (8)	−0.009	O (20)	0.010
N (9)	−0.008	C (21)	0.024

Description of the Molecular Structure. The intramolecular atomic bond lengths and angles are shown in Figs. 3(a) and 3(b) and in Table 7. As was discussed earlier, the existence of a hydrogen atom attached to nitrogen may be indicated by its bond angle, in the manner of Singh;[27] the usual –NH– angle is 125°, while for –N= it is 116°. In this complex both components agree well with this hypothesis, since the mean C–N–C bond angle of melamine is 114.4° and that of thymine is 124.7°. The difference synthesis at the *R*-factor, 0.14, indicated that there are no protons around the triazine nitrogen hetero-atoms, while there are two protons attached to N(14) and N(18) in the thymine molecule. The bond lengths of the endocyclic part of thymine differ significantly from those found in the literature; *i.e.* the C=O distances of 1.209 and 1.205 Å are slightly shorter than those found in thymine monohydrate[28] (1.234 and 1.231), methylthymine[29] (1.237 and 1.214 Å) and uracil (1.230 and 1.241 Å). The mean bond length of all the N–C distances in *N*,*N*-diethylmelamine is 1.330 Å, and that in thymine is 1.356 Å. These values are slightly shorter than the expected values between 1.37 and 1.38 Å observed for uracil,[30] thymine monohydrate,[28] barbiturate derivatives,[31,32] but they are compatible with those in melamine[33] and purine,[34] with values from 1.34 to 1.35 Å. The deviations of atoms from each molecular plane are listed in Table 8.

24) A. W. Hanson, *ibid.*, **19**, 610 (1965).
25) T. Sakurai and M. Okunuki, *ibid.*, **B27**, 1445 (1971).
26) T. Sakurai and H. Tagawa, *ibid.*, **B27**, 1453 (1971).
27) C. Singh, *ibid.*, **19**, 861 (1965).
28) R. Gerdil, *ibid.*, **14**, 333 (1961).
29) K. Hoogsteen, *ibid.*, **16**, 28 (1963).
30) G. S. Parry, *ibid.*, **7**, 313 (1954).
31) W. Bolton, *ibid.*. **16**, 166 (1963).
32) D. Mootz and G. A. Jeffery, *ibid.*, **19** 717 (1965).
33) E. W. Hughes, *J. Amer. Chem. Soc.*, **63**, 1737 (1941).
34) D. G. Watson, R. M. Sweet, and R. E. Marsh, *Acta Crystallogr.*, **19**, 573 (1965).
35) to be published.
36) R. E. Marsh, R. Biersted and E. L. Eichhorn, *Acta Crystallogr.*, **15**, 310 (1962).
37) B. D. Sharma and J. F. McConnel, *ibid.*, **19**, 797 (1965).

Studies on Intermolecular Complex Formation. IV. Crystal Structure of Cytosine-Resorcylic acid 2 : 1 Complex monohydrate

Chihiro TAMURA, Sadao SATO, and Tadashi HATA

The Central Research Laboratories of Sankyo Co., Ltd., Hiromachi, Shinagawa-ku, Tokyo 140

(Received February 14, 1973)

The crystal and molecular structure of a cytosine and resorcylic acid complex monohydrate has been solved by the direct method. The molecular complex is formed by two moles of cytosine and one mole of resorcylic acid. The crystals are monoclinic, with a space group of $P2_1/n$, and with $a=8.335$, $b=20.605$, $c=10.159$ Å, and $\beta=95.5°$. The final R-factor for 1820 reflections is 0.100. Resorcylic acid is hydrogen-bonded to one of the cytosine molecules with one hydrogen bond, and to the two cytosine molecules with one hydrogen bond, and the two cytosine molecules are associated with three hydrogen bonds in a system similar to that of the guanine-cytosine hydrogen bond in the Watson-Crick model.

Recently the biological significance and drug activity of several molecular complexes have been investigated.[1-26] Since we surveyed a number of organic compounds interacting with nucleotide bases, some molecules with specific atomic constellations have been found to form complexes with cytosine and/or adenine.[25] Some of those complex structures have already been solved by means of single-crystal analysis. Herein we wish to describe the crystal structure of the resorcylic acid–cytosine monohydrate complex.

Experimental

Cytosine and resorcylic acid were dissolved in 70% aqueous ethanol at room temperature and crystallized as single crystals after the solution had been cooled in a refrigerator. The mass spectrometry of this complex revealed that both components were present. Preliminary oscillation and Weissenberg photographs showed that the crystals belong to the monoclinic system, space group of $P2_1/n$, and the density of the crystals was determined to be $1.34\,g\cdot cm^{-3}$ by the flotation method. The lattice parameters are $a=8.335$ (10), $b=20.605(18)$, $c=10.159(11)$ Å, and $\beta=95.5$ (1)°. The results of the elemental analysis and the calculation of the molecular weight from the cell constants and the measured density were compatible with a 2 : 1 molar ratio for cytosine and resorcylic acid with one water molecule.

Three-dimensional intensity data were collected on a Rigaku Denki auto-diffractometer up to a 2θ limit of 60°, using Mo Kα radiation with the $2\theta/\theta$ scanning mode at a scan speed of $2°\,min^{-1}$. The intensities were reduced to structure factors by correcting for the Lorentz-polarization factors using a program attached to this equipment. Because of the small size of the crystals, no corrections were made for absorption. The 1830 independent observed structure factors thus obtained were used for structure analysis.

Structure Analysis

The normalized structure factors, E, were calculated from the observed structure factors, F, which were put on an absolute scale by the use of Wilson's statistics.[27] A trial structure was obtained using the symbolic addition procedure. The reflections of 267 with $|E|$ values greater than 1.30 were obtained using the $\Sigma 2$ of Hauptman and Karle.[28] Three linear independent reflections (5,6,−6; 7,0,1; 0,5,2), each with a large number of interactions, were assigned to be +, three other reflections (1,15,5; 2,7,7; 7,1,2) were denoted by the symbols A, B, and C. After the symbolic addition procedure, the A, B, and C symbols are uniquely determined to be all −. A Fourier synthesis using these signs for the E-values showed over 38 large peaks. From a knowledge of the geometry of the molecules, the peaks corresponding to 27 atoms could easily be recognized. The initial structure factor calculations for the 27 atoms gave an R-factor of 0.38, with an isotropic temperature factor. After five cycles of block-diagonal least-squares refinements, the R-factor was reduced to 0.24. The remaining water molecules

1) K. Hoogsteen; *Acta Crystallogr.*, **12**, 822, (1959); *ibid.*, **16**, 907 (1963).
2) H. M. Sobell, K. Tomita, and A. Rich, *Proc. Natl. Acad. Sci. U. S.*, **49** 885 (1963).
3) F. S. Mathews and A. Rich, *J. Mol. Biol.*, **8**, 89 (1964).
4) A. E. V. Hashemeyer and H. Sobell, *Acta Crystallogr.*, **18**, 525 (1965).
5) A. E. V. Hashemeyer and H. Sobell, *ibid.*, **19**, 125 (1965).
6) L. L. Labana, H. M. Sobell, *Proc. Natl. Acad. Sci. U. S.*, **57**, 459 (1967).
7) H. M. Sobell, *J. Mol. Biol.*, **18**, 1 (1966).
8) E. J. O'Brien, *Acta Crystallogr.*, **23**, 92 (1967).
9) S. H. Kim and A. Rich, *Science*, **158**, 1046 (1967).
10) S. H. Kim, A. Rich, *Proc. Natl. Acad. Sci. U. S.*, **60**, 402 (1968).
11) E. Shefter, *J. Pharm. Sci.*, **57**, 1163 (1968).
12) K. Uehara, T. Mizoguchi, S. Hosomi, T. Fujiwara, and K. Tomita, *J. Biochem.*, **64**, 589 (1968).
13) E. Shefter, *Science*, **160**, 1351 (1968).
14) L. Katz, K. Tomita, and A. Rich, *J. Mol. Biol.*, **13**, 340 (1969).
15) T. D. Sakore and H. M. Sobell, *ibid.*, **43**, 77 (1969).
16) F. Mazza, H. M. Sobell and G. Kartha, *ibid.*, **43**, 407 (1969).
17) T. D. Sakore, S. S. Tavale, and H. M. Sobell, *ibid.*, **43**, 361 (1969).
18) S. S. Tavale, T. D. Sakore, and H. M. Sobell, *ibid.*, **43**, 375 (1969).
19) T. D. Sakore, H. M. Sobell, F. Mazza, and G. Kartha, *ibid.*, **43**, 385 (1969).
20) D. Voet and A. Rich, *J. Amer. Chem. Soc.*, **91**, 3069 (1969).
21) S. H. Kim and A. Rich, *J. Mol. Biol.*, **42**, 87 (1969).
22) W. Saenger and D. Suck, *ibid.*, **60**, 87 (1971).
23) H. S. Kim and G. A. Jaffrey, *Acta Crystallogr.*, **B27**, 1123 (1971).
24) R. Chandross and A. Rich, *Biopolymers*, **10**, 1795 (1971).
25) C. Tamura, N. Sakurai and S. Sato, This Bulletin, **44**, 1473 (1971).
26) C. Tamura, T. Hata, S. Sato, and N. Sakurai, *ibid.*, **45**, 3245 (1972).
27) A. J. C. Wilson, *Acta Crystallogr.*, **2**, 318 (1949).
28) H. Hauptman and J. Karle, *ibid.*, **6**, 136 (1953).

were found from the subsequent Fourier synthesis. Then difference synthesis was carried out in order to obtain the positions of the hydrogen atoms, which appeared satisfactorily on the map. The eight subsequent refinement cycles used the anisotropic temperature factor for C, N and O and the isotropic factor for H gave a final *R*-factor of 0.100 for all the observed reflections.

Table 1. Fractional atomic coordinates in cytosine–resorcylic acid (2:1) complex monohydrate

Atom	*x/a*	*y/b*	*z/c*
C (1)	−0.0718	0.2165	0.2923
C (2)	−0.1980	0.1835	0.2167
C (3)	−0.3507	0.1920	0.2570
C (4)	−0.3790	0.2311	0.3629
C (5)	−0.2545	0.2617	0.4284
C (6)	−0.1017	0.2573	0.3974
C (7)	−0.1633	0.1437	0.1010
O (8)	−0.0188	0.1361	0.0801
O (9)	−0.2803	0.1192	0.0307
O (10)	−0.4772	0.1602	0.1881
O (11)	0.0825	0.2100	0.2616
N (12)	0.4376	0.0077	−0.2265
C (13)	0.3088	−0.0174	−0.3041
N (14)	0.1579	−0.0070	−0.2691
C (15)	0.1375	0.0303	−0.1633
C (16)	0.2683	0.0580	−0.0844
C (17)	0.4158	0.0448	−0.1190
C (18)	0.3332	−0.0511	−0.4013
N (19)	−0.0107	0.0426	−0.1370
N (20)	−0.3622	−0.0960	−0.4579
C (21)	−0.2391	−0.0623	−0.3867
N (22)	−0.0884	−0.0719	−0.4261
C (23)	−0.0552	−0.1086	−0.5294
C (24)	−0.1874	−0.1435	−0.5995
C (25)	−0.3361	−0.1343	−0.5604
O (26)	−0.2616	−0.0274	−0.2936
N (27)	0.0901	−0.1135	−0.5596
W (28)	−0.2699	0.1634	−0.2403
H (4)	−0.486	0.238	0.383
H (5)	−0.247	0.282	0.510
H (6)	0.015	0.255	0.430
H (10)	−0.420	0.139	0.108
H (11)	0.078	0.188	0.200
A H (19)	−0.091	0.014	−0.166
B H (19)	−0.018	0.063	−0.054
H (16)	0.252	0.083	−0.017
H (17)	0.533	0.070	−0.098
H (12)	0.553	0.007	−0.323
A H (27)	0.171	−0.096	−0.499
B H (27)	0.112	−0.081	−0.591
H (24)	−0.176	−0.164	−0.676
H (25)	−0.436	−0.145	−0.606
H (20)	−0.466	−0.084	−0.429
H (22)	0.013	−0.058	−0.374
A W (28)	−0.243	0.195	−0.239
B W (28)	−0.271	0.159	−0.136

Results and Discussion

The final atomic parameters are given in Tables 1 and 2 and the corresponding structure factors, in Table 3. The bond lengths and angles are shown in Table 4, while Fig. 1 shows a diagram of the atomic notation. The crystal structure and hydrogen-bond system of the molecules are shown in Fig. 3, while a stereographic view is illustrated by the ORTEP plot in Fig. 2. Some important intermolecular atomic distances are listed in Table 5. The average estimated standard deviations for bond distances are: for C–C within 0.020 Å; for C–N and C–O within 0.013 Å; and for bond angles, 1.0° for all the heavy atoms.

Description of Crystal and Molecular Structure. As is shown in the stereographic plot (Fig. 2), two approximately coplanar cytosine (A and B) molecules are coupled to each other, with two NH···O (2.889, 2.778 Å) and one NH···N (2.815 Å) hydrogen bonds forming

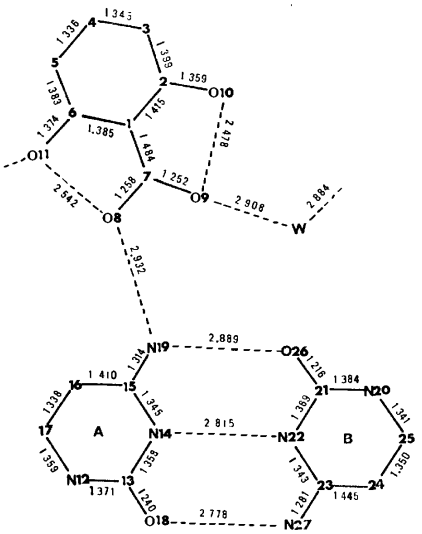

Fig. 1(a). Interatomic distances in cytosine-resorcylic acid (2 : 1) complex monohydrate.

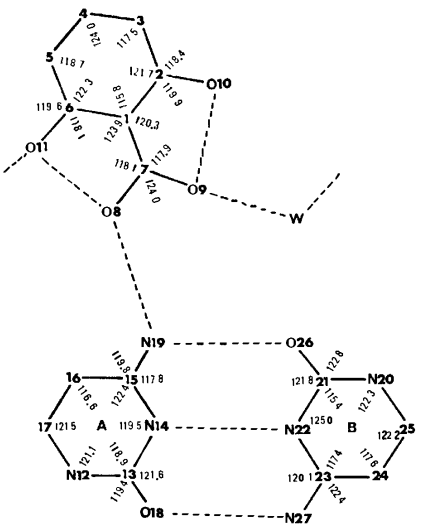

Fig. 1(b). Interbond angles in cytosine-resorcylic acid (2 : 1) complex monohydrate.

TABLE 2(a). ANISOTROPIC THERMAL PARAMETERS IN CYTOSINE-RESORCYLIC ACID (2:1) COMPLEX MONOHYDRATE
The thermal parameters are given in the form $T=\exp[-(B_{11}h^2+B_{22}k^2+B_{33}l^2+2B_{12}hk+2B_{13}hl+2B_{23}kl)]$.

Atom	B_{11}	B_{22}	B_{33}	B_{12}	B_{13}	B_{23}
C (1)	0.01679	0.00145	0.00928	0.00104	0.00311	0.00006
C (2)	0.01258	0.00158	0.00565	0.00033	0.00259	−0.00021
C (3)	0.01630	0.00181	0.00854	0.00089	0.00124	0.00054
C (4)	0.02185	0.00304	0.01423	0.00260	0.00921	0.00176
C (5)	0.02685	0.00222	0.01003	−0.00030	0.00570	0.00051
C (6)	0.02183	0.00245	0.01016	−0.00050	0.00438	−0.00064
C (7)	0.01521	0.00142	0.00740	−0.00055	0.00170	0.00059
O (8)	0.01787	0.00286	0.00938	−0.00128	0.00298	−0.00145
O (9)	0.01753	0.00273	0.00888	−0.00133	−0.00007	−0.00074
O (10)	0.01716	0.00371	0.01327	0.00047	0.00128	0.00168
O (11)	0.01831	0.00263	0.01141	−0.00195	0.00269	−0.00141
N (12)	0.00677	0.00184	0.00666	−0.00018	0.00039	−0.00062
C (13)	0.00928	0.00148	0.00689	−0.00035	0.00125	−0.00032
N (14)	0.00636	0.00143	0.00626	−0.00029	0.00041	−0.00063
C (15)	0.00877	0.00180	0.00513	0.00026	0.00057	0.00004
C (16)	0.01011	0.00220	0.00684	0.00070	0.00175	−0.00051
C (17)	0.01218	0.00189	0.00755	−0.00057	−0.00192	−0.00069
C (18)	0.00709	0.00195	0.00588	−0.00044	0.00100	−0.00075
N (19)	0.00760	0.00228	0.00627	−0.00076	0.00028	−0.00039
N (20)	0.00609	0.00223	0.00783	−0.00125	0.00075	−0.00112
C (21)	0.00886	0.00174	0.00649	−0.00006	0.00114	0.00009
N (22)	0.00784	0.00168	0.00414	−0.00007	0.00028	−0.00071
C (23)	0.00839	0.00137	0.00496	0.00042	0.00102	0.00015
C (24)	0.01184	0.00152	0.00656	0.00032	0.00091	−0.00054
C (25)	0.01001	0.00157	0.00648	−0.00033	−0.00055	−0.00066
O (26)	0.00859	0.00252	0.00884	−0.00003	0.00128	−0.00150
N (27)	0.00817	0.00179	0.00682	−0.00023	0.00072	0.00005
W (28)	0.02303	0.00306	0.01034	0.00141	0.00380	−0.00026

TABLE 2(b). ISOTROPIC THERMAL PARAMETERS OF HYDROGEN IN CYTOSINE-RESORCYLIC ACID (2:1) COMPLEX MONOHYDRATE

Atom	B_{iso}	Atom	B_{iso}	Atom	B_{iso}
H (4)	5.77	B H (19)	4.20	H (24)	4.70
H (5)	4.59	H (16)	3.08	H (25)	2.96
H (6)	9.09	H (17)	4.14	H (20)	3.06
H (10)	4.46	H (12)	10.08	H (22)	5.01
H (11)	5.30	A H (27)	6.74	A W (28)	1.48
A H (19)	4.82	B H (27)	3.31	B W (28)	7.51

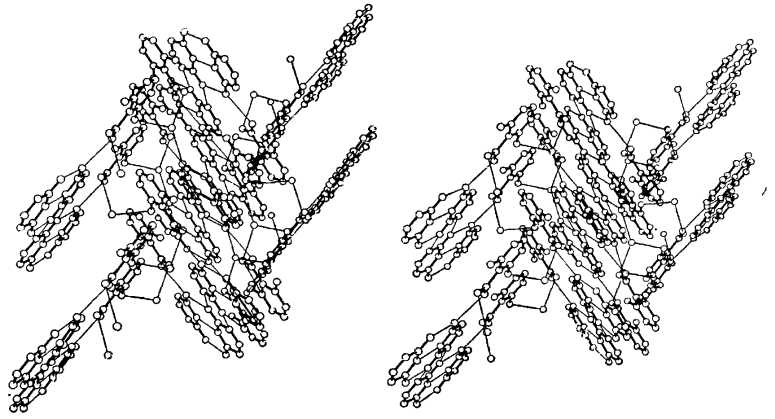

Fig. 2. Stereoscopic view of the packing and hydrogen bonding. Molecular bonds are drawn thick and hydrogen bonds thin.

TABLE 3. STRUCTURE FACTOR DATA (×10) FOR THE OBSERVED REFLECTIONS

L	FO	FC
K=	1, H=	0
1	368	374
2	232	265
3	294	308
4	217	244
6	165	184
7	326	329
8	96	106
K=	2, H=	0
1	642	639
2	145	168
3	91	90
4	315	332
5	160	149
6	64	84
8	73	33
9	117	115
10	82	38
11	111	82
K=	3, H=	0
2	120	132
3	201	240
4	241	250
5	295	255
6	234	241
7	269	246
8	90	80
9	145	136
K=	4, H=	0
1	545	592
2	1663	1642
3	463	440
5	203	203
8	153	178
9	97	113
K=	5, H=	0
1	551	574
2	2596	2628
3	320	287
4	514	496
5	229	237
8	293	290
9	88	130
K=	6, H=	0
1	644	644
2	1607	1590
3	597	602
4	595	583
5	409	407
7	110	79
9	94	79
K=	7, H=	0
0	20	0
1	387	411
2	637	648
3	172	169
4	85	68
7	71	56
K=	8, H=	0
1	347	310
2	441	447
3	90	87
4	119	196
6	63	32
7	103	100
8	136	157
9	182	196
11	86	88
K=	9, H=	0
1	242	230
3	340	309
4	616	624
5	360	333
6	76	41
7	93	65
9	20	32
10	77	84
11	84	108
K=	10, H=	0
1	84	82
2	384	370
3	450	449
4	957	948
6	152	144
10	125	154
K=	11, H=	0
1	339	307
2	125	116
3	144	130
4	738	714
5	156	136
6	138	97
7	102	93
9	102	86
K=	12, H=	0
1	79	72
2	237	240
3	271	286
4	135	193
5	154	161
10	19	12
K=	13, H=	0
2	95	103
3	148	142
4	96	68
6	82	129
7	116	138
K=	14, H=	0
2	82	111
5	90	102
6	162	230
7	181	172
10	83	77
K=	15, H=	0
0	15	0
2	103	115
3	176	166
4	224	196
6	382	413
K=	16, H=	0
1	236	242
2	137	141
5	83	109
6	205	220
K=	17, H=	0
2	72	98
5	119	122
6	76	104
7	141	124
K=	18, H=	0
4	109	88
K=	19, H=	0
1	95	86
2	78	69
8	124	151
K=	20, H=	0
1	77	82
2	15	38
5	112	102
6	83	95
9	18	28
K=	21, H=	0
3	90	83
7	81	82
8	139	134
9	15	27
K=	22, H=	0
5	104	62
K=	24, H=	0
1	84	64
4	13	30
K=	25, H=	0
1	103	78
K=	0, H=	1
-7	336	364
-5	391	391
-3	851	802
1	867	874
3	675	665
5	271	297
7	143	141
9	205	201
11	91	77
K=	1, H=	1
-12	88	60
-8	96	84
-7	332	311
-6	153	184
-5	413	388
-4	404	361
-2	225	215
0	343	357
1	70	55
2	845	844
3	173	178
6	85	73
7	137	138
9	160	172
K=	2, H=	1
-11	111	99
-9	94	88
-7	142	150
-4	992	959
-3	105	84
-2	173	169
0	143	156
1	116	121
2	763	750
3	614	630
4	217	211
5	110	99
6	63	28
8	137	135
K=	3, H=	1
-11	96	121
-9	85	107
-7	199	185
-6	391	408
-5	173	125
-3	263	251
-2	250	256
0	313	308
1	1064	1112
3	118	121
4	228	201
5	131	107
6	196	206
7	89	105
10	127	149
K=	4, H=	1
-11	91	102
-9	143	147
-8	103	67
-7	317	296
-6	319	311
-5	74	93
-4	250	254
-3	130	155
-2	446	447
0	1009	1039
1	524	527
2	483	454
3	245	232
4	97	75
5	136	135
6	81	84
7	136	149
9	131	143
11	79	53
K=	5, H=	1
-9	77	102
-8	81	88
-7	134	154
-6	189	190
-5	455	453
-4	386	392
0	306	281
1	1161	1137
2	530	522
3	442	445
4	160	147
5	106	114
7	123	133
K=	6, H=	1
-7	71	61
-6	186	153
-5	358	324
-4	118	142
-3	245	224
-2	536	498
0	354	348
1	493	536
2	124	148
3	168	161
4	155	176
5	134	168
6	81	101
11	84	66
12	79	58
K=	7, H=	1
-9	163	169
-5	374	367
-4	151	157
-3	163	196
-2	773	740
-2	637	740
2	236	220
3	320	299
4	522	514
5	222	253
6	65	112
7	192	183
8	186	183
K=	8, H=	1
-11	84	64
-9	116	131
-8	176	222
-6	165	180
-5	364	306
-4	198	212
-3	223	217
-2	110	102
0	177	159
1	300	320
2	185	136
3	123	163
4	86	118
6	135	135
8	296	292
9	68	41
11	123	91
K=	9, H=	1
-8	98	98
-7	84	87
-6	150	124
-5	199	175
-4	80	68
-3	242	273
0	288	289
2	160	177
4	381	391
5	226	217
7	86	83
8	95	62
K=	10, H=	1
-9	135	149
-8	79	78
-6	89	57
-4	70	75
-3	713	743
-2	630	623
1	188	200
2	159	171
3	723	716
4	349	347
5	15	14
7	126	112
9	89	95
11	94	79
K=	11, H=	1
-4	136	130
-3	215	198
-2	126	127
0	178	214
2	165	146
3	571	589
7	121	103
10	22	20
K=	12, H=	1
-7	71	72
-5	124	113
-4	78	31
-3	435	444
0	261	248
1	134	149
2	64	70
3	90	72
5	67	44
6	421	454
K=	13, H=	1
-10	119	115
-7	100	111
-4	145	167
-3	96	53
-2	84	88
0	188	157
1	119	77
3	86	130
4	182	155
5	203	209
6	286	262
8	17	14
12	83	66
K=	14, H=	1
-5	157	194
-3	233	217
-2	192	174
-2	190	174
1	98	115
2	123	99
3	156	182
6	23	16
K=	15, H=	1
-7	71	70
-5	98	106
0	135	129
5	456	454
6	180	202
11	108	97
12	90	45
K=	16, H=	1
-5	196	199
-4	110	125
-3	82	88
-2	106	101
1	76	102
3	125	133
4	85	119
5	236	263
6	86	88
K=	17, H=	1
-4	72	38
-3	187	182
0	101	99
2	136	151
3	210	201
4	211	217
5	173	207
6	89	49
11	92	62
K=	18, H=	1
-2	98	65
1	165	188
2	115	111
3	78	40
4	292	277
5	105	97
7	96	120
K=	19, H=	1
-6	87	57
1	94	106
3	123	131
4	164	153
7	109	99
K=	20, H=	1
-4	73	51
-2	15	19
0	105	89
3	109	104
7	107	131
8	127	141
K=	21, H=	1
0	104	126
3	76	86
7	127	153
K=	22, H=	1
-5	87	97
1	248	261
2	192	227
7	121	127
K=	23, H=	1
2	169	188
5	10	43
K=	24, H=	1
1	78	53
2	101	96
3	85	68
K=	25, H=	1
-7	19	44
1	123	116
K=	26, H=	1
3	108	74
4	12	19
K=	0, H=	2
-10	99	98
-6	337	333
-4	430	439
-2	322	318
0	477	510
2	379	424
4	94	57
8	106	54
10	280	311
K=	1, H=	2
-13	84	82
-8	163	152
-7	206	163
-5	72	89
-4	83	69
-3	426	428
-2	596	598
0	122	99
2	286	268
3	1164	1109
4	189	214
5	83	100
6	64	76
8	83	137
9	240	249
10	77	111
K=	2, H=	2
-12	88	87
-11	78	58
-8	112	76
-7	128	115
-6	71	66
-5	246	229
-4	173	156
-3	486	467
-2	108	115
0	264	221
1	184	164
2	355	376
3	158	151
4	118	111
5	319	375
6	119	143
7	77	92
8	131	124
9	345	374
10	277	307
11	176	215
12	94	81
K=	3, H=	2
-10	106	126
-8	126	89
-7	188	197
-5	299	272
-4	69	71
-2	193	178
0	198	178
1	281	264
2	270	249
3	591	578
4	295	273
5	430	420
6	117	151
8	175	166
9	292	300
10	145	147
11	238	268
K=	4, H=	2
-12	93	113
-5	253	220
-4	208	219
-2	71	81
1	1075	1014
2	154	156
3	104	84
5	221	206
7	90	99
8	416	429
9	110	101
10	74	45
11	118	140
K=	5, H=	2
-11	89	43
-7	97	76
-6	131	116
-5	270	255
-4	436	420
-3	101	120
-2	184	133
0	259	263
1	157	156
2	221	263
3	217	194
4	68	7
5	182	181
6	80	28
8	229	257
9	103	114
11	95	86
12	111	119
K=	6, H=	2
-11	109	114
-9	103	61
-8	134	141
-5	88	94
-4	306	299
-2	355	355
0	206	208
1	981	957
2	279	290
4	125	180
5	371	373
6	99	87
7	305	313
8	94	77
K=	7, H=	2
-9	73	21
-6	239	209
-5	111	123
-4	150	154
-3	410	404
0	422	427
1	706	678
2	138	122
4	227	231
5	154	140
7	597	619
8	191	199
13	129	134
K=	8, H=	2
-10	132	145
-9	117	117
-6	110	68
-3	246	232
0	115	103
1	453	436
2	203	190
5	235	228
6	268	252
7	196	170
8	190	198
9	51	41
11	82	54
13	106	112
K=	9, H=	2
-9	77	36
-7	76	127
-4	122	122
-3	159	175
0	204	213
1	354	367
2	142	116
3	141	154
4	195	208
6	483	501
7	148	163
8	156	155
K=	10, H=	2
-9	81	63
-6	129	88
-5	135	107
-4	153	137
-3	126	70
-2	163	195
0	164	184
1	102	102
3	171	172
6	288	313
7	193	213
9	127	119
K=	11, H=	2
-10	77	30
-9	110	115
-5	107	95
-3	120	92
0	79	78
1	101	87
2	140	161
3	254	271
5	245	235
6	156	187
8	98	99
K=	12, H=	2
-9	141	100
-8	110	108
-7	101	110
-6	120	123
-3	75	65
-2	264	240
0	96	85
1	93	57
5	529	559
7	102	88
12	109	57
K=	13, H=	2
-8	136	129
-7	101	96
-3	80	83
0	163	121
1	121	109
3	108	92
4	241	196
5	284	249
6	297	274
7	124	143
K=	14, H=	2
-8	102	129
-4	21	29
-2	276	255
0	81	56
1	127	107
2	108	116
4	388	414
5	17	24
6	94	87
8	17	39
9	138	122
10	23	16
K=	15, H=	2
-8	103	116
-4	101	73
4	270	277
5	182	183
7	143	129
8	21	8
K=	16, H=	2
-11	93	42
-7	88	93
-4	101	79
-3	234	248
0	163	142
3	204	201
4	130	138
7	111	93
K=	17, H=	2
-3	138	175
1	235	235
3	296	298
4	80	101
K=	18, H=	2
-11	109	44
-6	155	154
-3	124	149
0	76	88
1	115	121
2	129	127
3	201	219
4	158	143
5	84	107
K=	19, H=	2
-6	98	112
-5	104	104
-4	93	96
0	13	34
2	245	244
K=	20, H=	2
-9	116	66
-3	90	61
2	131	148
3	174	164
7	102	60
K=	21, H=	2
-5	109	113
2	110	126
K=	22, H=	2
1	186	171
3	135	137
K=	23, H=	2
-5	109	81
-3	95	105
1	130	109
K=	24, H=	2
-4	97	110
0	140	116
2	89	105
3	91	81
K=	25, H=	2
-6	56	34
0	107	106
1	94	76
K=	26, H=	2
0	84	57
K=	0, H=	3
-11	161	160
-7	260	277
-3	828	841
1	298	314
3	264	278
5	565	564
K=	1, H=	3
-10	86	75
-9	119	84
-7	74	66
-4	254	195
-3	439	428
-2	376	356
0	385	418
2	615	616
3	67	40
5	106	108
8	76	84
9	94	118
K=	2, H=	3
-11	134	142
-7	76	81
-6	90	53
-4	156	172
-3	308	287
-2	388	381
0	167	183
1	147	156
2	348	332
3	362	378
4	530	545
6	136	114
8	189	199
9	101	115
10	115	114
K=	3, H=	3
-12	84	49
-10	147	146
-8	118	110
-6	134	84
-4	388	382
-3	205	246
-2	63	37
0	60	8
1	68	54
2	116	116
3	123	137
4	440	427
5	97	124
6	125	129
7	85	90
8	86	40
10	213	237
K=	4, H=	3
-11	128	119
-8	106	73
-4	140	141
-2	475	452
0	67	82
1	249	269
2	249	248
3	240	235
4	392	411
5	78	78
6	206	202
8	106	119
11	76	54
K=	5, H=	3
-9	173	179
-6	71	85
-4	114	113
-3	256	253
-2	14	32
0	419	385
1	240	250
2	240	263
3	508	504
4	253	275
7	187	216
8	80	97
10	144	146
K=	6, H=	3
-11	106	98
-6	102	61
-5	515	515
-3	300	318
-2	180	200
1	390	411
2	452	458
3	170	148
4	215	218
5	191	211
6	182	179
10	82	71
11	130	150
K=	7, H=	3
-9	127	138
-6	90	106
-5	144	165
-4	227	222
0	393	395
2	476	438
3	129	145
8	219	228
11	87	55
K=	8, H=	3
-12	102	81
-9	174	167
-5	79	64
-4	164	178
-3	75	84
-2	98	79
0	68	85
1	197	197
2	339	309
3	74	89
6	109	105
7	94	122
8	138	124
K=	9, H=	3
-9	168	129
-6	0	193
-5	98	89
-3	83	77
-2	141	158
0	97	70
1	305	274
4	93	67
6	78	103
8	220	202
K=	10, H=	3
-8	101	105
-6	82	46
0	161	138
1	230	221
2	113	117
3	129	116
4	76	41
6	198	243
8	149	142
K=	11, H=	3
-10	75	14
-7	235	242
-3	71	66
0	329	307
1	414	408
2	139	151
5	80	59
6	234	200
9	114	116
K=	12, H=	3
-12	105	79
-10	76	19
-9	81	52
-6	190	201
-5	118	138
-3	157	146
-2	101	90
0	274	256
2	179	164
3	131	121
6	143	124
7	110	109
K=	13, H=	3
-7	213	216
-3	71	93
0	271	283
1	15	36
6	229	227
8	87	99
K=	14, H=	3
-7	162	104
-5	74	38
-1	115	82
2	79	38
6	190	177
K=	15, H=	3
-7	83	77
-5	127	124
-1	88	133
3	84	57
6	98	107
8	99	104
K=	16, H=	3
-7	108	96
-5	80	73
-2	110	107
-1	163	163
4	72	29
K=	17, H=	3
-10	85	49
-4	86	86
-3	89	98
-2	200	191
4	256	224
K=	18, H=	3
-9	95	57
-5	79	71
-4	74	55
-2	131	135
-1	77	38
2	86	61
3	96	79
4	136	136
K=	19, H=	3
-6	76	12
-5	133	121
-1	19	37
4	102	99
K=	20, H=	3
-10	146	119
-4	94	99
-3	115	117
4	110	102
5	90	83
K=	21, H=	3
-9	83	33
-2	20	37
K=	22, H=	3
-7	86	49
2	151	142
K=	23, H=	3
-6	22	15
-4	81	106
7	16	19
K=	0, H=	4
-10	186	224
-8	116	100
-6	68	90
-4	335	323
-2	225	193
0	88	74
2	342	389
4	324	324
6	121	94
K=	1, H=	4
-11	80	111
-7	274	299
-5	86	52
-4	240	204
-1	899	852
1	107	98
3	415	416
4	67	63
5	111	157
6	100	88
K=	2, H=	4
-10	86	81
-9	190	179
-8	176	145
-7	208	203
-6	78	112
-4	163	149
-3	454	435
-1	20	63
0	112	95
1	93	124
2	227	209
3	209	178
4	64	60
5	180	166
K=	3, H=	4
-10	53	48
-9	156	183
-8	179	187
-7	197	183
-6	119	151
-5	115	107
-4	96	105
-1	387	362
0	144	137
1	190	217
3	238	219
4	222	261
5	291	282
6	125	138
K=	4, H=	4
-9	129	110
-8	231	210
-7	126	125
-5	162	138
-4	15	56
-3	498	482
-1	308	297
0	177	186
1	120	57
3	212	237
4	77	83
5	110	126
6	8	35
7	89	42
11	79	63
K=	5, H=	4
-10	102	59
-9	257	262
-8	69	49
-5	149	176
-4	167	130
-3	401	425
0	213	212
1	572	572
4	211	223
5	111	96
6	121	112
7	81	96
K=	6, H=	4
-7	160	128
-6	158	189
-5	334	335
-3	381	390
-1	281	299
0	218	256
2	124	142
3	82	64
4	79	88
5	79	53
6	119	147
K=	7, H=	4
-10	155	105
-8	80	59
-7	158	160
-4	84	118
-3	82	93
-1	132	175
0	131	108
1	282	268
2	129	122
3	89	148
7	169	164
10	89	74
K=	8, H=	4
-11	107	80
-7	166	164
-4	106	131
-3	61	62
-1	98	70
0	104	97
1	371	356
2	128	151
4	82	87
7	108	129
K=	9, H=	4
-11	139	130
-7	131	149
-6	230	215
-5	101	86
-3	101	72
-1	119	122
0	359	333
1	86	93
3	129	127
7	99	132
10	92	69
K=	10, H=	4
-7	89	94
-6	225	218
-5	217	230
-4	212	230
-1	227	196
0	312	319
1	84	42
2	257	245
3	83	72
5	73	85
9	73	82
K=	11, H=	4
-11	93	43
-10	86	49
-5	275	307
1	156	188
4	71	49
8	141	135
9	95	89
10	13	37
K=	12, H=	4
-7	106	89
-5	92	86
-3	68	56
-1	158	161
3	90	60
8	73	25
9	153	152
K=	13, H=	4
-7	84	108
-6	74	67
-5	200	210
-1	124	101
1	118	121
2	131	128
3	72	91
8	77	92
K=	14, H=	4
-5	143	153
-4	129	137
-3	96	109
2	169	171
3	78	94
9	105	90
K=	15, H=	4
-7	89	109
-6	113	91
-4	138	124
-3	71	86
2	120	151
4	88	79
8	94	72
K=	16, H=	4
-3	87	89
2	110	132
6	73	58
7	126	127
K=	17, H=	4
-3	157	176
-1	95	94
1	94	65
3	87	82
6	98	80
7	76	79
K=	18, H=	4
-5	84	49
-3	92	73
0	114	67
K=	19, H=	4
-5	82	88
-3	116	136
6	10	37
K=	20, H=	4
-9	99	81
K=	22, H=	4
-1	118	107
0	77	51
5	112	119
K=	23, H=	4
-1	89	51
6	11	38
K=	24, H=	4
-1	79	67
K=	26, H=	4
3	98	70
K=	0, H=	5
-7	552	491
-5	158	170
-3	296	297
-1	759	739
1	131	112
9	97	70
K=	1, H=	5
-9	85	65
-8	467	495
-7	109	117
-6	68	64
-5	112	144
-4	150	152
-1	106	89
0	182	177
1	125	100
2	261	251
3	115	106
4	141	116
6	91	81
K=	2, H=	5
-10	120	145
-9	151	119
-8	353	338
-7	105	98
-5	125	149
-4	100	82
-3	83	71
-1	309	307
3	165	176
4	109	109
5	76	70
6	103	108
8	97	75
K=	3, H=	5
-10	251	243
-8	295	277
-5	184	185
-4	246	229
-3	127	129
-1	141	106
1	170	160
5	81	89
6	75	100
K=	4, H=	5
-10	253	272
-9	209	206
-7	129	145
-6	135	154
-5	134	107
-4	122	142
-3	208	218
-1	196	208
0	325	315
1	144	94
3	92	78
5	106	109
K=	5, H=	5
-13	81	31
-10	151	167
-9	127	77
-7	122	126
-6	241	245
-5	250	232
-3	278	286
-1	136	132
0	92	87
1	361	389
2	194	198
4	95	99
7	90	73
10	78	68
K=	6, H=	5
-9	95	72
-7	81	57
-6	592	583
-5	299	312
-1	79	85
0	491	491
1	191	205
3	88	23
7	81	43
K=	7, H=	5
-12	138	126
-7	152	135
-6	460	467
-4	130	130
-3	294	310
-1	0	4
0	82	75
1	268	259
3	79	35
4	142	134
7	75	67
10	85	76
K=	8, H=	5
-10	122	110
-9	102	112
-6	96	106
-5	140	102
-1	104	92
1	89	79
K=	9, H=	5
-12	166	163
-11	129	111
-7	18	42
-6	102	115
-5	243	236
-4	82	107
-3	99	77
-1	72	101
0	86	90
1	114	108
2	135	126
3	121	98
4	135	145
5	69	72
K=	10, H=	5
-12	112	95
-11	94	71
-7	94	112
-5	148	145
-4	307	311
-3	200	222
-1	107	130
2	204	227
3	131	146
5	126	135
8	20	28
11	109	77
K=	11, H=	5
-10	77	51
-5	94	98
-4	475	479
-3	219	215
1	112	91
2	169	191
3	148	170
5	69	73
8	109	77
K=	12, H=	5
-4	445	472
-1	137	151
2	202	233
3	97	112
K=	13, H=	5
-9	101	55
-5	131	127
-3	96	110
0	72	43
2	141	144
9	80	71
K=	14, H=	5
-8	105	89
-5	101	131
-3	188	212
0	76	48
9	104	89
K=	15, H=	5
-11	0	8
-6	74	53
-5	95	63
-1	150	161
3	128	123
5	89	105
9	106	116
K=	16, H=	5
-8	87	41
9	80	45
K=	17, H=	5
-8	81	64
5	98	59
K=	18, H=	5
-1	84	89
0	106	116
1	99	77
7	100	87
K=	19, H=	5
-9	83	44
-7	89	63
-6	131	114
7	105	70
K=	20, H=	5
7	145	134
K=	21, H=	5
0	188	215
1	108	75
5	12	8
6	18	40
K=	22, H=	5
0	150	158
6	18	53
K=	25, H=	5
-1	118	79
K=	0, H=	6
-8	84	104
-4	210	164
0	77	80
2	158	164
4	106	84
K=	1, H=	6
-9	92	66
-8	160	153
-4	40	33
-1	166	184
0	93	78
1	112	103
2	285	335
8	111	136
11	0	15
K=	2, H=	6
-9	0	14
-7	88	65
-3	103	86
-1	253	254
1	79	90
2	123	130
5	108	130
K=	3, H=	6
-12	85	68
-8	99	101
-7	14	39
-6	113	114
-1	191	220
0	157	155
1	321	325
2	94	84
3	87	111
4	147	141
5	91	82
7	167	167
K=	4, H=	6
0	152	138
1	181	197
2	8	8
3	124	104
4	114	133
6	110	108
K=	5, H=	6
-7	84	90
-6	101	103
-4	20	14
0	199	199
1	77	87
5	84	87
K=	6, H=	6
-12	53	40
-9	76	27
-6	154	148
-4	100	84
-1	162	122
0	290	320
1	107	64
2	73	39
3	124	114
6	80	84
7	134	114
8	76	52
K=	7, H=	6
-11	94	81
-7	107	115
-6	136	147
-5	147	125
-3	102	112
0	262	253
3	189	198
5	80	80
6	88	114
K=	8, H=	6
-12	55	32
-10	110	103
-7	124	110
-3	239	238
-1	161	126
0	99	82
1	126	88
6	139	134
7	115	110
K=	9, H=	6
-8	81	52
-6	118	89
-3	83	84
3	152	177
4	96	117
5	179	165
10	89	53
K=	10, H=	6
-9	121	83
-4	83	93
-3	144	125
-1	76	53
0	111	101
3	205	182
K=	11, H=	6
-10	92	49
-9	84	53
-5	132	102
-4	196	205
-3	109	124
-1	73	82
4	108	103
5	151	168
K=	12, H=	6
-11	59	58
-8	49	33
-5	246	246
-4	117	109
-3	116	80
-1	145	142
4	149	137
6	88	81
K=	13, H=	6
-11	112	95
-4	116	113
-3	94	81
2	74	66
5	157	170
K=	14, H=	6
-8	125	101
-5	96	88
3	93	104
7	16	26
K=	15, H=	6
-5	88	72
5	81	116
K=	16, H=	6
-8	53	40
-5	123	84
-4	170	199
-3	195	207
K=	17, H=	6
-4	222	225
2	88	98
3	79	79
5	10	42
7	100	81
K=	18, H=	6
-7	99	65
-6	117	94
-5	85	64
-3	174	182
0	135	140
1	111	112
K=	21, H=	6
-7	108	87
-1	100	120
K=	22, H=	6
-5	116	87
-1	154	160
0	128	146
1	91	74
K=	23, H=	6
2	8	39
K=	0, H=	7
-5	426	404
1	796	786
K=	1, H=	7
-6	89	83
-5	103	69
-3	97	114
0	127	120
1	335	324
2	504	504
3	122	144
4	101	105
8	114	124
K=	2, H=	7
-5	141	156
0	150	138
1	258	270
2	91	61
4	161	173
K=	3, H=	7
-8	118	96
-5	110	113
0	357	364
2	382	366
3	188	195
4	212	216
5	93	75
K=	4, H=	7
-3	125	122
-1	123	147
0	210	203
1	160	182
2	112	94
3	401	441
4	225	233
6	108	102
K=	5, H=	7
-9	56	39
-8	112	79
-7	227	185
-4	119	113
-3	252	267
-1	309	305
0	181	195
2	84	103
3	328	319
4	139	143
K=	6, H=	7
-7	102	105
-6	95	60
-3	137	98

TABLE 3. (Continued)

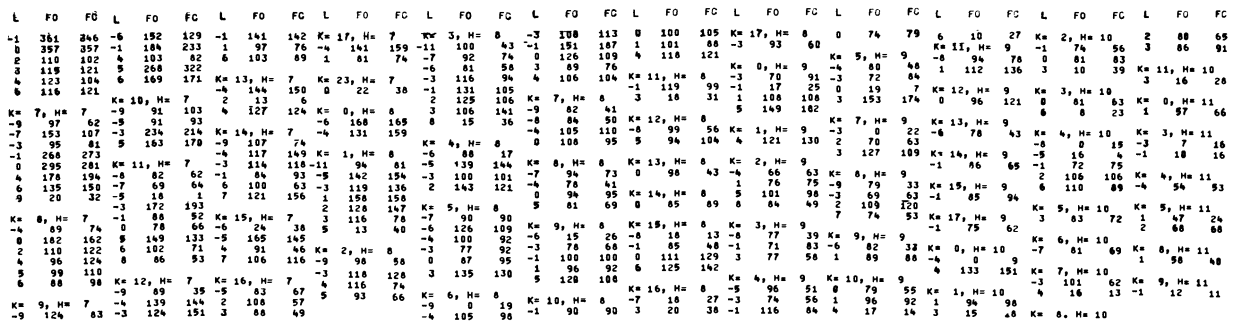

TABLE 4. INTERATOMIC BOND DISTANCES AND ANGLES IN CYTOSINE–RESORCYLIC ACID (2:1) COMPLEX MONOHYDRATE

C (1) - C (2)	1.415 Å	C (1) - C (2) - C (3)	121.7°
C (2) - C (3)	1.399	C (1) - C (2) - O (10)	119.9
C (3) - C (4)	1.345	C (3) - C (2) - O (10)	118.4
C (4) - C (5)	1.336	C (2) - C (1) - C (6)	115.8
C (5) - C (6)	1.383	C (6) - C (1) - C (7)	123.9
C (6) - C (1)	1.385	C (2) - C (1) - C (7)	120.3
C (1) - C (7)	1.484	C (1) - C (6) - C (5)	122.5
C (7) - O (8)	1.258	C (1) - C (6) - O (11)	118.1
C (7) - O (9)	1.252	C (5) - C (6) - O (11)	119.6
C (2) - O (10)	1.359	C (4) - C (5) - C (6)	118.7
C (6) - O (11)	1.374	C (3) - C (4) - C (5)	124.0
N (12) - C (13)	1.371	C (2) - C (3) - C (4)	117.5
C (13) - N (14)	1.357	C (1) - C (7) - O (9)	117.9
N (14) - C (15)	1.345	C (1) - C (7) - O (8)	118.1
C (15) - C (16)	1.410	O (8) - C (7) - O (9)	124.0
C (16) - C (17)	1.338	C (13) - N (12) - C (17)	121.1
C (17) - N (12)	1.359	N (12) - C (13) - N (14)	118.9
C (13) - O (18)	1.240	N (12) - C (13) - O (18)	119.4
C (15) - N (19)	1.341	N (14) - C (14) - O (18)	121.6
N (20) - C (21)	1.384	C (13) - N (14) - C (15)	119.5
C (21) - N (22)	1.369	N (14) - C (15) - C (16)	122.4
N (22) - C (23)	1.343	N (14) - C (15) - N (19)	117.8
C (23) - C (24)	1.445	C (16) - C (15) - N (19)	119.8
C (24) - C (25)	1.350	C (15) - C (16) - C (17)	116.6
C (25) - N (20)	1.341	C (16) - C (17) - N (12)	121.5
C (21) - O (26)	1.216	C (21) - N (20) - C (25)	122.3
C (23) - N (27)	1.281	N (20) - C (21) - N (22)	115.4
		N (20) - C (21) - O (26)	122.8
		N (22) - C (21) - O (26)	121.8
		C (21) - N (22) - O (26)	125.0
		N (22) - C (23) - C (24)	117.4
		N (22) - C (23) - N (27)	120.1
		C (24) - C (23) - N (27)	122.4
		C (23) - C (24) - C (25)	117.6
		C (24) - C (25) - N (20)	122.2

a pseudo-dimer, while to the amino group in one of the cytosines, A, the carboxylic acid group in resorcylic acid is bound by one hydrogen bond (2.932 Å). Further, these three molecules make a coplanar net-work. The other component, the water molecule, associates with the O(9) of the carboxyl and the O(11) of the phenolic groups of the neighboring resorcylic acid molecule in the crystal packing. These distances are 2.908 Å for O(9)···W and 2.884 Å for O(11)···W. There are two intramolecular hydrogen bonds at a distance of 2.478 for O(9)–O(10) and 2.542 Å for O(8)–O(11); these values agree well with the case of *o*-salicylic acid.[29,30] Although the amino groups of the two cytosine molecules, C(15)–N(19) of A and C(23)–N(27) of B, seem to have the same bond lengths, the values of the two molecules are significantly different; the values are 1.341 and 1.281 Å for A and B respectively. This significant shortening of the bond length in the B molecule can be attributed to the double-bond character in this specific portion. A few examples of the C=NH double bond lengths have been reported, *e.g.*, that in 1,3-dimethyl-4-imino-5-oxo-2-thione-imidazolidine is 1.25 Å.[31] The two cytosine molecules, A and B, are actually not identical, since B has no proton at N(22); A has a proton at the corresponding atom N(14), forming a cationic structure. This extra proton in the A molecule is the one which has migrated from the resorcylic acid proton. Furthermore, the bond lengths of the carboxyl groups are 1.258 Å for C(7)–O(8) and 1.252 Å for C(7)–O(9); these values correspond to the usual carboxyl acid anion structure observed in many aminoacids.[32] In the difference map, there are no hydrogen peaks around the carbonyl oxygen atoms. These facts indicate that the resorcylic component molecule is anionic. A similar phenomenon has been observed in the *N*-benzoyl glycine–cytosine complex, in which the proton from the acid moiety migrates to the base moiety. However, in the molecular complex of caffeine with 5-chlorosalcylic acid, the proton is retained in the acid moiety.[11] Thus far, no such anion-cation structure has been found for binding between a carboxylic acid and a basic compound. Interestingly, the cytosine B molecule is neutral and has no extra proton. Consequently, the actual nomenclature of this complex is cytosinyl-cation-cytosine-resorcylic acid anion-monohydrate.

The mean value of the C–N bonds in the cytosine-ring system is 1.359 Å which corresponds to those of

29) W. Cochran, *ibid.*, **6**, 260 (1953).
30) M. Sundaralingam and L. H. Jensen, *ibid.*, **18**, 1053 (1965).
31) T. Kinoshita, S. Sato, and C. Tamura, *Tetrahedron Lett.*, **1971**, 3695.
32) G. V. Gurskaya, "The Molecular Structure of Aminoacids (Translated from Russian)," Consultants Bureau, New York (1968).

Table 5. Intermolecular atomic distances, less than 3.7 Å between the molecules

x, y, z		C (18) .... O (26)	3.484
O (9) .... O (10)	2.478	$1-x, -y, -z$	
O (8) .... O (11)	2.542	O (17) .... C (17)	3.251
O (8) .... N (19)	2.932	$-x, -y, -1-z$	
O (8) .... W (28)	2.908	N (12) .... N (20)	3.687
N (14) .... N (22)	2.815	N (12) .... C (25)	3.443
N (18) .... N (27)	2.778	C (13) .... N (20)	3.422
N (19) .... O (26)	2.889	C (13) .... C (21)	3.542
$-x, -y, -z$		C (13) .... N (22)	3.647
C (2) .... N (22)	3.487	C (13) .... C (23)	3.658
C (2) .... C (23)	3.372	C (13) .... C (24)	3.576
C (2) .... N (27)	3.460	C (13) .... C (25)	4.432
C (1) .... C (13)	3.676	N (14) .... N (22)	3.495
C (1) .... N (14)	3.687	N (14) .... C (23)	3.203
C (1) .... C (18)	3.554	N (14) .... C (24)	3.394
C (6) .... C (13)	3.642	N (14) .... N (27)	3.574
C (6) .... C (18)	3.249	C (15) .... C (23)	3.522
C (4) .... N (27)	3.554	C (15) .... C (24)	3.407
C (3) .... C (23)	3.544	C (15) .... N (27)	3.664
C (3) .... N (27)	3.387	C (16) .... C (24)	3.668
C (7) .... C (13)	3.603	C (17) .... C (25)	3.747
C (7) .... N (14)	3.292	C (18) .... N (20)	3.371
C (7) .... C (15)	3.644	C (18) .... C (21)	3.223
O (9) .... N (14)	3.540	C (18) .... N (22)	3.602
O (9) .... C (15)	3.689	C (18) .... O (26)	3.496
O (8) .... N (12)	3.608	N (19) .... N (27)	3.417
O (8) .... C (13)	3.507	O (26) .... N (27)	3.620
O (8) .... N (14)	3.432	N (27) .... W (28)	2.832
O (8) .... C (15)	3.524	$-1-x, -y, -z$	
O (8) .... C (16)	3.693	O (11) .... N (20)	3.428
O (11) .... N (12)	3.495	$1/2+x, 1/2-y, 1/2+z$	
O (11) .... C (13)	3.421	C (2) .... W (28)	3.567
O (11) .... C (18)	3.268	C (3) .... O (11)	3.478
O (11) .... C (21)	3.503	C (3) .... W (28)	3.607
O (10) .... N (22)	3.299	O (10) .... W (28)	2.884
O (10) .... C (23)	3.455	$1/2+x, 1/2-y, -1/2+z$	
N (19) .... N (19)	3.280	O (9) .... C (4)	3.509
$1+x, y, z$		C (16) .... C (4)	3.722
N (12) .... N (20)	3.692	$-1/2+x, 1/2-y, 1/2+z$	
N (12) .... C (20)	3.582	C (4) .... O (9)	3.509
N (12) .... O (26)	2.758	C (4) .... C (16)	3.722
C (13) .... N (20)	3.661	$1/2+x, 1/2-y, -1/2+z$	
C (13) .... O (26)	3.578	O (11) .... C (4)	3.703
C (17) .... O (8)	3.216	O (11) .... C (16)	3.478
C (17) .... O (26)	3.675	W (28) .... C (2)	3.567
C (18) .... N (20)	2.813	W (28) .... C (3)	3.607
C (18) .... C (21)	3.561	W (28) .... O (10)	2.884
C (18) .... C (25)	3.742		

Table 6. Deviations of the atoms from the least-squares planes (Å)

Resorcilic acid		Cytosine (B)		Cytosine (A)	
C (1)	−0.004	N (12)	−0.001	N (20)	0.002
C (2)	−0.012	C (13)	0.013	C (21)	0.005
C (3)	−0.027	N (14)	−0.030	N (22)	−0.019
C (4)	−0.010	C (15)	−0.017	C (23)	0.010
C (5)	0.021	C (16)	0.005	C (24)	−0.012
C (6)	0.047	C (17)	−0.002	C (25)	0.005
C (7)	0.015	N (18)	0.010	O (26)	0.003
O (8)	−0.068	O (19)	0.022	N (27)	0.008
O (9)	0.108				
O (10)	−0.056				
O (11)	−0.015				

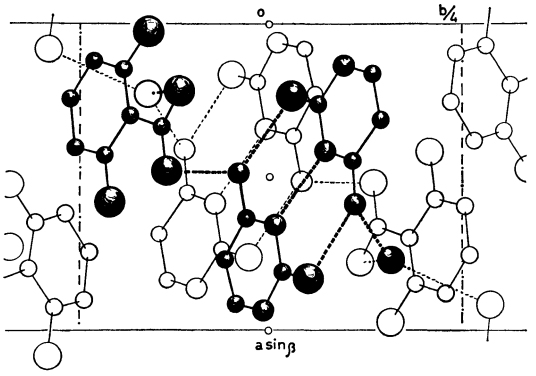

Fig. 3. The molecular packing and hydrogen bonding in cytosine–resorcylic acid (2 : 1) complex monohydrate viewed along the c-axis.

isocytosine,[33] thymine monohydrate,[34] uracil[35] barbituric acid,[36] and cytosine monohydrate[37] (1.354, 1.372, 1.361, 1.369 and 1.361 Å respectively), but which is slightly longer than those of the completely-conjugated systems of melamine,[34] pyrimidine[35] and purine[36] (1.343, 1.326, and 1.337 Å respectively). The bond lengths of C(16)–C(17), 1.338 Å, and C(24)–C(25), 1.350 Å, are clearly shorter than the fully-conjugated C=C double bond of 1.395 Å. The deviations of the atoms from each molecular plane are listed in Table 6; the inter-plane angles of the individual molecules are 7.23° for cytosine(A)–cytosine(B) and 5.14° for cytosine(B)–resorcylic acid.

A particularly interesting phenomenon in this analysis is the fact that the two cytosine molecules could form three hydrogen bonds in which they are bound to each other, with the formation of a pseudo-dimer of A and B. Such a hydrogen-bonding scheme resembles that of the guanine–cytosine three-hydrogen-bond system in the Watson-Crick model and its model complex.[2] Furthermore, it is reminiscent of the crystal structure of isocytosine[33] reported by McConell, in which tautomeric isomers of two cytosine molecules are bound by three hydrogen bonds. The present analysis of the complex is structurally different, but the

33) B. D. Sharma and J. F. McConnell, *Acta Crystallogr.*, **19**, 797 (1965).
34) R. Gerdil, *ibid.*, **14**, 333 (1961).
35) G. S. Parry, *ibid.*, **7**, 313 (1963).
36) W. Bolton, *ibid.*, **16**, 166 (1963).
37) G. A. Jeffrey and T. Kinoshita, *ibid.*, **16**, 20 (1963).
38) E. W. Hughs, *J. Amer. Chem. Soc.*, **63**, 1737 (1941).
39) P. J. Wheatley, *Acta Crystallogr.*, **13**, 80 (1960).
40) D. G. Watson, R. M. Sweet, and R. E. Marsh, *ibid.*, **19**, 573 (1965).
41) D. L. Barker and R. E. Marsh, *ibid.*, **17**, 1581 (1964).

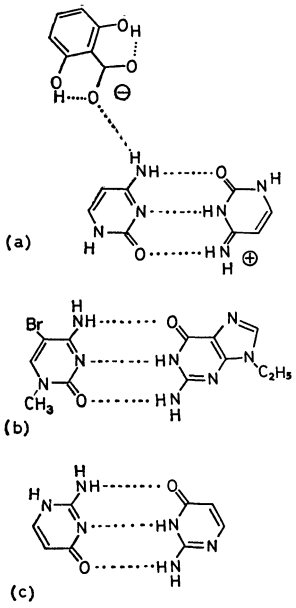

Fig. 4. Hydrogen bonding scheme of (a) present analysis, (b) 9-ethyl guanine[2] and (c) isocytosine[33].

combination scheme between these two molecules is very similar in manner when the proton is introduced from resorcylic acid, as is shown in Fig. 4. The crystal structures of cytosine and cytosine monohydrate have been determined to contain two hydrogen bonds which are of the 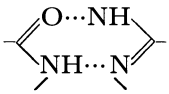 type; this has been established using NH···O and NH···N hydrogen bonds, as is shown in Figs. 5(a) and (b).[30] On the other hand, in crystals of cytosine-5-acetic acid (5-acetic-cytosine) and the

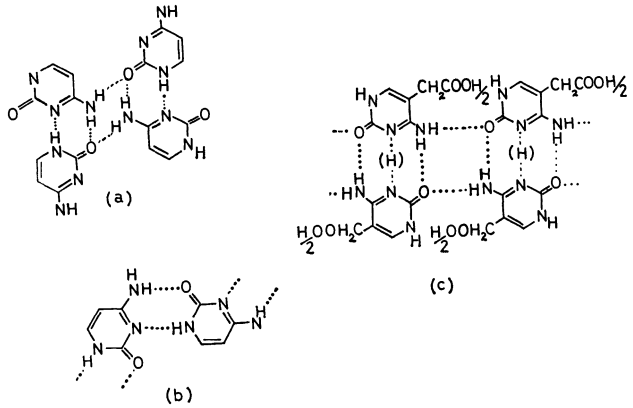

Fig. 5. Various hydrogen-bonding scheme in cytosine and its derivatives. (a) Cytosine[41] (b) cytosine monohydrate[37] (c) cytosine-5-acetic acid[42].

present complex which contain carboxylic acid moieties, the crystals form three hydrogen bonds (Fig. 5(c)).[42] These facts indicate that the change in the internal electronic states in the molecules is caused by a proton in the crystals involving a catalytic effect. The three-hydrogen-bond scheme resembles the Watson-Crick model between cytosine and guanine. In biological paths of RNA or DNA, the protonation of the bases may occur in many instances; thus, the cytosine–cytosine three-hydrogen-bond system might be said to be an interaction potentially important as a genetic proto-type in dynamic biological processes.

The authors are indebted to Miss Yuko Moriyama for her computational assistance.

42) R. E. Marsh, R. Bierstadt, and E. L. Eichhorn, *ibid.*, **15**, 310 (1962).

Optical and Magnetic Studies of $CuSeO_3 \cdot 2H_2O$ Based on the Refined Crystal Structure

Takeshi Asai and Ryôiti Kiriyama

Institute of Scientific and Industrial Research, Osaka University, Yamadakami, Suita, Osaka 565

(Received March 2, 1973)

Magnetic, IR and electronic spectral studies were made on $CuSeO_3 \cdot 2H_2O$, its crystal structure being refined. The IR band at 927 cm^{-1} was found to be due to a rocking vibration of a water molecule. The H-bonding scheme was suggested. The electronic spectrum shows a maximum of the d-d transition bands at *ca.* 14000 cm^{-1}. This was explained on the basis of a square pyramidal coordination of a Cu ion. Above 100 K the magnetic susceptibility obeys the Curie-Weiss law with $\theta = -92._6$ K and $\mu_{eff} = 2.00\,\beta_B$. At lower temperatures it shows a broad maximum at *ca.* 45 K, a sharp peak at $26._4$ K corresponding to T_N. The behaviour could be explained from the antiferromagnetic superexchange interactions of Cu cations through the σ-bonds of SeO_3^{2-} anions. The small anisotropy and the number of cations intermediated by each anion give rise to the 1-dimensional character. A linear Heisenberg model and the molecular field model gave J/k values of -33 and -31 K, respectively. The latter model also gave the observed ratio of $|\theta|/T_N$.

Magnetic properties of transition metal compounds have attracted the attention of many workers and studies have been carried out according to several different methods. The compounds studied can be classified into (a) those with highly anisotropic structures of a linear chain or a sheet arrangement of metal ions since the theories are expected to be phenomenologically applicable and (b) those in which the simple anions like halide or oxide anions coordinate to a metal atom since the quantum mechanics is useful for an explanation of the mechanism. They have given information on the nature of the chemical bond and the superexchange interaction. Studies on the compounds which belong to neither (a) or (b) do not seem to have been carried out. They are desirable because of their utility for testing the theories. The present study has been carried out with $CuSeO_3 \cdot 2H_2O$, the easiest system for application to the theory. The trigonal-pyramidal oxo-anion SeO_3^{2-} is potential to form MO's of both a σ- and a π-type character with metal cations. However, the nature of the bonds and the mechanism of magnetic interactions depend to a great extent on the conformation attained in the crystal lattice.

Experimental

Preparation. The hydrated sample was obtained by the usual method[1] and was confirmed by powder X-ray diffractometry[2] and also by chemical analysis of Cu content. A deuterated sample for IR study was obtained in a sealed tube at 120 °C with fully dried $CuSO_4$ and Na_2SeO_3 dissolved into D_2O. The powder X-ray diffraction pattern of the deuterate was the same as that of the hydrate.

IR and Electronic Spectra. IR spectra were recorded in the region 4000—400 cm^{-1} on a JASCO DS-402G spectrometer. Both KBr pellets and nujol mulls were employed. Diffuse reflectance spectra were obtained in the range 8250—35000 cm^{-1} with Hitachi EPU-2 and EPS-3T spectrometers with MgO as a standard. The spectra were recorded on a pure sample and one diluted with MgO to 80 wt.-%. Dilution was confirmed to have no effect on the position of absorption maxima.

Magnetic Measurement. Magnetic susceptibility was measured on powder samples by a Faraday balance. Temperatures were varied from 4 K to room temperature. $Co-Hg(SCN)_4$ was used as a reference substance of susceptibility.[3] Corrections were made for diamagnetism[4] but not for TIP.

Refinement of the Crystal Structure. The space group and lattice constants of Gattow[2] were confirmed; the space group is D_4^2–$P2_12_12_1$(No. 19) and lattice constants are $a = 6.664$, $b = 9.156$ and $c = 7.369(\pm 0.005)$ Å with $Z = 4$. Intensity data were collected using a Rigaku Denki four-circle X-ray diffractometer with a scintillation counter and Mo$K\alpha$ radiation. A total of 2311 reflections in two octants were measured within $\sin\theta/\lambda$ of 0.85. By averaging intensities of symmetry-related reflections in two octants,[5] intensities for 1347 independent reflections were obtained, of which 75 reflections had less than 2σ, the e.s.d. of $|F_o|$, and were taken to be zero. Intensities were corrected for Lorentz and polarization effects, but not for absorption and extinction effects. Dimensions of the crystal were $0.05 \times 0.08 \times 0.12$ mm^3; $\mu R = 1.19$.

Using atomic parameters of Gattow's analysis[2] and isotropic temperature factors of 1.0 for all atoms[6] as initial parameters, four cycles of the least-squares refinements were carried out. Anisotropic temperature factors were then introduced and four more cycles were repeated. Shifts of atomic parameters and temperature factors in the last cycle were less than 0.1 σ and 0.2 σ, respectively, with the exception of y-parameter of O_w1(0.14σ) and a temperature factor $B12$ of Cu(0.52σ). The final R-value ($R = \sum||F_o| - |F_c|| \sum|F_o|$) was 0.045 (0.038 excluding $|F_o| = 0$). In the earlier stages the weights were 1.0 for all reflections. In the later stages the following weights were used.

If $|F_o| \leqq 8.9$, $w = 0.25$,
if $|F_o| > 83.3$, $w = 1/|F_o|$,
and otherwise, $w = 1.0$.

1) Gmelins Handbuch der Anorganischen Chemie, Nr. 60, Cu, **B1**, 609 (1958).

2) G. Gattow, *Acta Crystallogr.*, **11**, 377 (1958).

3) B. N. Figgis and R. S. Nyholm, *J. Chem. Soc.*, **1958**, 4190.

4) P. W. Selwood, "Magnetochemistry," 2nd Ed., Interscience Publishers, New York (1956).

5) Since this space group lacks the center of symmetry, 2311 reflections were taken to be independent at first and refinements were performed including imaginary parts of the anomalous dispersion. The atomic parameters for the two sets of indexing were the same within the e. s. d., and their R values were 0.080 and 0.068. The difference in the intensities of I_{hkl} and $I_{h\bar{k}l}$ were therefore taken to be an error in measurement and the average values of I_{hkl} and $I_{h\bar{k}l}$ were used for the later work, which is reported here.

6) Only the atomic parameters were taken because of negative temperature factors.

Atomic scattering amplitudes used in these calculations were those of Cu^+, Se and O^-.[7] Corrections for the real parts of the anomalous dispersion were included. All calculations were performed with the aid of UNICS PROGRAM HBLS-IV and RSDA-4 on NEAC 2200/500 and 700 computers at the Computer Center, Osaka University.

Results and Discussion

IR Spectra. IR spectra of $CuSeO_3 \cdot 2H_2O$ and the dideuterate are shown in Fig. 1. The spectrum of the hydrate is in good agreement with that published by Sathianandan *et al.*[8] They assigned the band at 927 cm^{-1} to a bending vibration of Cu–O–Se. Since this band disappeared on deuteration, hydrogen atoms should take part in it. It can be assigned to a rocking vibrational mode of a water molecule. The corresponding band of a deuterate is not obvious because of its overlap with Se–O stretching bands. If we take a new band at 659 cm^{-1} as a rocking mode of D_2O, it gives 0.71 for the frequency ratio $\nu(D_2O)/\nu(H_2O)$, which is comparable to the observed ratios of $\nu(OD)/\nu(OH)$ and $\delta(D_2O)/\delta(H_2O)$ (0.73—0.74). Since the rocking vibration of a water of crystallization often appears at 800—700 cm^{-1},[9] this is a rare example of its appearing at a higher frequency.

Electronic Spectrum. The spectrum shown in Fig. 2 presents a broad *d-d* transition band at *ca.* 14000 cm^{-1} and an intense charge transfer band above 25000 cm^{-1}. The *d-d* transition band has a maximum at 13500 cm^{-1} and a shoulder at 10500 cm^{-1}. It is resolved into three components if we assume a Gaussian line shape with a common half width (Table 1).

A copper(II) cation is in an almost regular square pyramid composed of five oxygen atoms with a slight rhombic distortion (*vide post*). This configuration lacks the center of symmetry, explaining the high intensity of the absorption band. In this C_{2v} environment the 3*d* orbital levels are all split, three transitions being symmetry-allowed. The transition of $d_{x^2-y^2} \leftarrow d_{xy}$ is still forbidden, but the vibronic mechanism can bring forth the band of this transition.

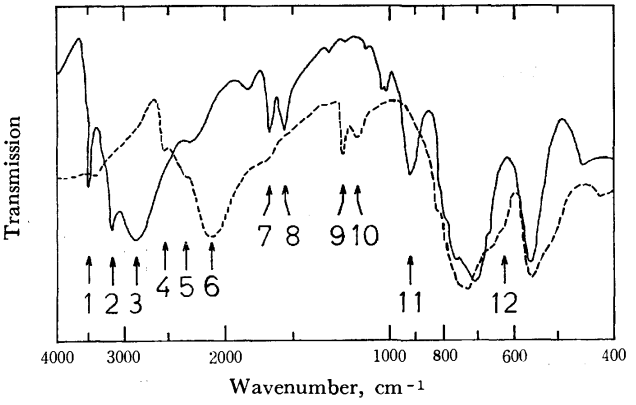

Fig. 1. Infrared spectra of $CuSeO_3 \cdot 2H_2O$ (——) and $CuSeO_3 \cdot 2D_2O$ (----). Bands attached with numbers are the vibrational modes involving H or D atoms.
1: ν_{OH}(3490 cm^{-1}), 2: ν_{OH}(3175 cm^{-1}), 3: ν_{OH}(2880 cm^{-1}), 4: ν_{OD}(2540 cm^{-1}), 5: ν_{OD}(2350 cm^{-1}), 6: ν_{OD}(2100 cm^{-1}), 7: δ_{HOH}(1650 cm^{-1}), 8: δ_{HOH}(1548 cm^{-1}), 9: δ_{DOD}(1215 cm^{-1}), 10: δ_{DOD}(1145 cm^{-1}), 11: $\nu_R(H_2O)$(927 cm^{-1}), 12: $\nu_R(D_2O)$(659 cm^{-1})

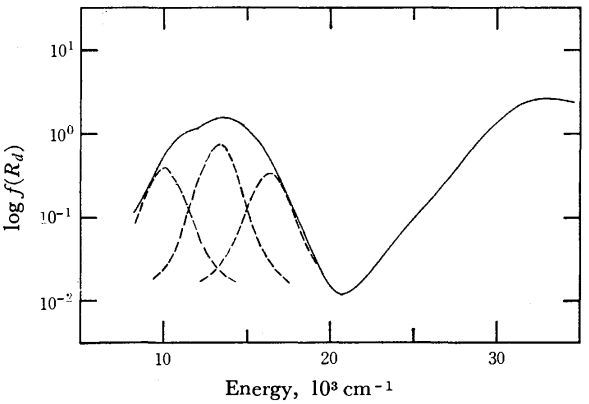

Fig. 2. Diffuse reflectance spectrum.
Observed (——) and resolved components (----).

Table 1. Resolution and assignment of the *d-d* transition bands

Energies (cm^{-1})	Relative intensity	Assignment[a]
10000	1.4	$^2A_1 \leftarrow {}^2A_2$
13200	1.7	$^2A_1 \leftarrow {}^2A_1'$
16300	1.3	$^2A_1 \leftarrow {}^2B_1, {}^2B_2$

a) Notations are given with an approximation of the C_{2v} point symmetry. A_1 and A_1' correspond to $d_{x^2-y^2}$ and d_{z^2} orbitals, respectively.

Since distortion is very small, it can be said that the energy difference between d_{xz} and d_{yz} orbitals is too small to be detected in the powder reflectance spectrum. Some polarized electronic spectra[10] show that this difference is less than 1500 cm^{-1} and that the transitions occur at 14200—16800 cm^{-1}. The component at 16300 cm^{-1} can therefore be assigned to the $d_{x^2-y^2} \leftarrow d_{xz}, d_{yz}$ transitions. This is also confirmed in the following estimation.

Copper(II) complexes in an environment of a tetragonally distorted octahedron of oxygen atoms give transitions of $d_{x^2-y^2} \leftarrow d_{z^2}$ in a wide range of energy. This energy was shown to be related to the axial Cu–O bond length.[11] Smith[12] succeeded in explaining the relationship from the molecular orbital formation between copper and ligand atoms and the electrostatic crystal field energy. His treatment was modified[12,13] for a square pyramidal coordination with the C_{4v}

7) IUCr, "International Tables for Crystallography," Vol. 3, Kynoch Press, Birmingham (1962).
8) K. Sathianandan, L. D. McCory and J. L. Margrave, *Spectrochim. Acta*, **20**, 957 (1964).
9) H. J. Prask and H. Boutin, *J. Chem. Phys.*, **45**, 699, 3284 (1966).
10) R. J. Dudley and B. J. Hathaway, *J. Chem. Soc. A*, **1970**, 1725; M. J. Bew, R. J. Dudley, R. J. Fereday, B. J. Hathaway and R. C. Slade, *ibid.*, **1971**, 1437; R. J. Dudley and B. J. Hathaway, *ibid.*, **1971**, 1442.
11) D. E. Billing, B. J. Hathaway and P. Nichols, *ibid.*, **1969**, 316.
12) D. W. Smith, *ibid.*, **1970**, 176.
13) C. E. Schäffer and C. K. Jørgensen, *Mol. Phys.*, **9**, 401 (1965); D. W. Smith, *J. Chem. Soc. A*, **1969**, 1708.

symmetry, giving the energies 12900, 11400 and 15100-17600 cm^{-1} for $d_{x^2-y^2} \leftarrow d_{z^2}$, $d_{x^2-y^2} \leftarrow d_{xy}$ and $d_{x^2-y^2} \leftarrow d_{xz}, d_{yz}$, respectively. These values are in good agreement with those of resolved components. π-bonding between copper and basal oxygen atoms were involved in this estimation. Since these quantities were treated only as parameters to fit the data by Smith, the agreement between resolved and estimated values does not necessarily mean the presence of the π-bonding. It might be negligible in this compound.

Refined Crystal Structure. The final atomic parameters, temperature factors and $|F_o|$'s and $|F_c|$'s are given in Tables 2, 3 and 4, respectively. The projection of the refined structure to the (100) plane is shown in Fig. 3. Interatomic distances and angles are given in Table 5.

The gross feature of the structure is the same as that of Gattow,[2] but significant shifts (0.06—0.15 Å) of oxygen atoms were found. Thus the selenium and copper atoms attain more regular coordinations.

The bond lengths and angles show that the copper atom is located in the square pyramid of oxygen atoms rather than in the distorted octahedron as stated by Gattow[2] and Handlovič[14] for the isomorphous $CuHPO_3 \cdot 2H_2O$. Four oxygen atoms forming the basal plane are planar, the deviations being within 0.030 Å. The copper atom is 0.137 Å above this plane as is often the case in the copper complexes of a square pyramidal configuration. Three interatomic distances (mean 1.952 Å) of basal Cu–O(SeO_3) bonds are the same within the e.s.d., but the basal Cu–O_w1 distance is significantly longer. The apical Cu–O_w2 distance became longer than that of Gattow's structure (2.27→2.323 Å), whereas the next-nearest oxygen atom O_w2' came closer than before (3.21→3.117 Å). In spite of the shortened Cu–O_w2' distance this oxygen atom should be excluded from coordination to the copper atom, not only because it is much longer than the longest one in the square pyramid but also because the copper atom has three next-nearest neighbours of uncoordinating Se atoms at 3.128—3.182 Å. This configuration is in good agreement with that of $CuHPO_3 \cdot 2H_2O$,[14] $Cu(NH_3)_4SO_4 \cdot H_2O$[15] and $Cu(NO_3)_2 \cdot CH_3NO_2$.[16]

A selenite anion forms a very slightly distorted trigonal pyramid. Its average dimensions are Se–O= 1.70_6, O–O=2.60_7 Å and O–Se–O=99.7° with the selenium atom 0.80_3 Å above the basal plane. These values are comparable to those of $ZnSeO_3 \cdot 2H_2O$,[17] $MgSeO_3 \cdot 6H_2O$,[18] H_2SeO_3,[19] $Na_3H(SeO_3)_2$[20] and $K_3H(SeO_3)_2$.[21] A selenite anion coordinates to three different copper atoms, with each oxygen atom towards a single copper atom, and connects the CuO_5 pyramids into a three-dimensional network.

No hydrogen atoms could be found in the analysis. However, consideration of interatomic distances and angles around O_w1 and O_w2 led to the sole probable scheme of hydrogen bonds of water molecules. A water molecule H_2O 1 may direct its hydrogen atoms towards O 1 and O 3 belonging to the two neighbouring CuO_5 pyramids and its negative dipole towards the copper atom (Table 5). The water molecule H_2O 2 has two copper neighbours. The angle Cu–O_w2–Cu' and also an electrostatic repulsion between hydrogen and copper atoms suggest a configuration in which two lone pairs direct towards two copper atoms and one hydrogen atom to O 2 atom belonging to another CuO_5 neighbour. Another hydrogen atom may be free from the hydrogen bonding or incorporated to

TABLE 2. POSITIONAL PARAMETERS

Values in parentheses are the e.s.d.'s in the last decimal.

Atom	x/a	y/b	z/c
Cu	0.4809(1)	0.6542(1)	0.2860(1)
Se	0.7287(1)	0.3911(1)	0.4573(1)
O 1	0.2556(7)	0.7812(5)	0.2283(6)
O 2	0.5288(6)	0.6137(5)	0.0295(6)
O 3	0.7335(7)	0.5594(5)	0.3561(6)
O_w 1	0.4489(7)	0.7155(5)	0.5425(7)
O_w 2	0.2921(8)	0.4415(6)	0.3100(8)

TABLE 3. TEMPERATURE FACTORS ($\times 10^4$) IN THE FORM OF $\exp\{-(B_{11}h^2+B_{22}k^2+B_{33}l^2+B_{12}hk+B_{13}hl+B_{23}kl)\}$

Values in parentheses are the e.s.d.'s in the last decimal.

Atom	B_{11}	B_{22}	B_{33}	B_{12}	B_{13}	B_{23}
Cu	55(1)	30(1)	34(1)	22(2)	0(2)	−2(1)
Se	42(1)	24(0)	29(1)	0(1)	2(1)	−2(1)
O 1	64(8)	41(4)	52(6)	39(10)	46(3)	28(8)
O 2	57(7)	45(4)	37(5)	7(11)	−1(12)	−5(9)
O 3	64(8)	29(4)	64(6)	11(10)	−25(13)	7(8)
O_w 1	92(9)	53(5)	47(6)	41(11)	−5(15)	−10(10)
O_w 2	94(10)	66(8)	85(8)	30(13)	9(17)	0(12)

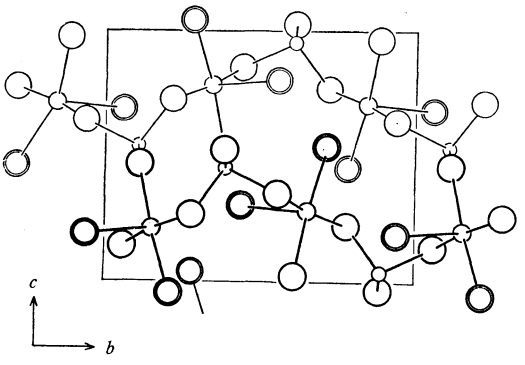

Fig. 3. Crystal structure of $CuSeO_3 \cdot 2H_2O$ projected to the (100) plane. The middle circle shows a Cu atom, the smallest one Se, the largest single one O(SeO_3) and the largest double one O(H_2O).

14) M. Handlovič, *Acta Crystallogr.*, **B25**, 227 (1969).
15) B. Morosin, *ibid.*, **B25**, 19 (1969).
16) B. Duffin and S. C. Wallwork, *ibid.*, **20**, 210 (1966).
17) V. F. Gladkova and Yu. D. Kondrashev, *Kristallografiya*, **9**, 190 (1964).
18) R. Weiss, J.-P. Wendling and D. Grandjean, *Acta Crystallogr.*, **20**, 563 (1966).
19) F. K. Larsen, M. S. Lehmann and I. Søtofte, *Acta Chem. Scand.*, **25**, 1233 (1971).
20) S. F. Kaplan, M. I. Kay and B. Morosin, *Ferroelectrics*, **1**, 31 (1970).
21) M. S. Lehmann and F. K. Larsen, *Acta Chem. Scand.*, **25**, 3859 (1971).

Table 4. Structure factors $3|F_o|$ and $3|F_c|$

K	|FO|	|FC|
H = 0	L = 0	
2	70	59
4	436	439
6	50	41
8	127	122
10	16	18
12	40	21
14	40	38
H = 1	L = 0	
1	300	294
2	345	344
3	156	147
4	218	219
5	238	240
6	67	70
7	29	28
8	142	137
9	195	192
10	15	16
11	32	36
12	76	77
13	88	90
14	50	50
15	50	46
H = 2	L = 0	
0	145	127
1	144	125
2	256	232
3	0	1
4	32	8
5	83	80
6	325	321
7	41	38
8	59	55
9	11	13
10	194	189
11	25	21
12	87	85
13	19	9
14	96	96
15	23	6
H = 3	L = 0	
1	287	276
2	403	402
3	232	226
4	101	93
5	146	138
6	144	138
7	17	9
8	53	53
9	131	128
10	15	16
11	21	0
12	0	15
13	38	38
14	42	37
15	44	40
H = 4	L = 0	
0	564	569
1	28	33
2	23	27
3	92	85
4	294	288
5	0	2
6	16	13
7	137	138
8	92	91
9	35	39
10	17	10
11	98	100
12	19	7
13	42	42
14	26	32
H = 5	L = 0	
1	122	114
2	13	8
3	20	10
4	144	137
5	175	168
6	21	22
7	65	63
8	152	151
9	141	140
10	56	54
11	39	40
12	89	90
13	85	87
H = 6	L = 0	
0	70	61
1	174	166
2	56	53
3	82	77
4	17	11
5	131	124
6	152	149
7	77	73
8	43	41
9	31	25
10	113	108
11	36	34
12	60	58
13	22	22
H = 7	L = 0	
1	144	137
2	219	205
3	132	125
4	0	1
5	46	46
6	124	116
7	36	28
8	23	10
9	25	20
10	31	22
11	32	20
12	39	34
H = 8	L = 0	
0	139	133
1	0	9
2	17	10
3	82	78
4	90	87
5	26	13
6	0	6
7	135	131
8	31	28
9	47	46
10	0	0
11	111	113
H = 9	L = 0	
1	17	15
2	78	73
3	38	40
4	51	52
5	43	46
6	60	55
7	63	61
8	92	92
9	57	63
H =10	L = 0	
0	0	16
1	102	100
2	0	1
3	75	72
4	0	3
5	84	81
6	41	37
7	47	50
H =11	L = 0	
1	42	38
2	81	77
3	44	46
H = 0	L = 1	
1	143	146
2	157	150
3	365	351
4	159	149
5	75	68
6	92	88
7	272	261
8	223	213
9	34	28
10	69	68
11	158	154
12	89	87
13	67	61
14	48	46
15	66	73
H = 1	L = 1	
0	336	350
1	116	121
2	305	311
3	112	104
4	212	211
5	108	103
6	261	263
7	82	78
8	147	146
9	0	10
10	140	139
11	52	47
12	116	120
13	23	25
14	24	27
15	22	9
H = 2	L = 1	
0	0	4
1	256	259
2	351	356
3	156	154
4	156	158
5	89	89
6	117	114
7	162	161
8	88	86
9	35	39
10	28	29
11	96	95
12	39	35
13	52	49
14	59	56
15	30	27
H = 3	L = 1	
0	144	147
1	113	109
2	193	187
3	70	64
4	155	154
5	140	137
6	240	238
7	91	91
8	112	109
9	85	83
10	112	110
11	80	80
12	112	112
13	55	56
14	39	29
H = 4	L = 1	
0	217	212
1	123	122
2	111	111
3	210	206
4	159	150
5	42	41
6	68	66
7	188	188
8	157	159
9	25	26
10	78	78
11	118	117
12	68	70
13	47	44
14	47	46
H = 5	L = 1	
0	235	231
1	171	172
2	214	205
3	75	72
4	121	120
5	142	136
6	142	137
7	25	22
8	89	89
9	57	59
10	80	85
11	18	12
12	70	67
13	25	25
H = 6	L = 1	
0	70	71
1	90	91
2	145	140
3	116	111
4	126	121
5	62	61
6	84	79
7	104	103
8	62	59
9	65	66
10	64	60
11	52	52
12	35	22
13	54	56
H = 7	L = 1	
0	20	18
1	111	112
2	72	69
3	50	47
4	44	46
5	128	127
6	100	97
7	57	54
8	47	47
9	97	95
10	50	51
11	62	60
12	59	58
H = 8	L = 1	
0	166	158
1	80	77
2	43	41
3	101	94
4	124	119
5	0	18
6	52	50
7	77	77
8	81	83
9	27	17
10	57	59
H = 9	L = 1	
0	85	85
1	111	115
2	65	63
3	48	46
4	42	40
5	108	108
6	42	41
7	20	17
8	33	16
9	55	59
H =10	L = 1	
0	70	69
1	0	14
2	32	32
3	48	46
4	65	65
5	36	30
6	50	49
7	56	49
H =11	L = 1	
0	0	17
1	66	66
2	23	17
3	26	31
H = 0	L = 2	
0	20	15
1	306	309
2	113	115
3	116	118
4	125	116
5	134	128
6	262	260
7	38	37
8	135	133
9	0	2
10	232	226
11	0	4
12	83	80
13	20	6
14	112	113
15	26	26
H = 1	L = 2	
0	210	210
1	260	264
2	171	177
3	96	96
4	153	155
5	272	275
6	135	134
7	82	81
8	152	151
9	117	114
10	70	73
11	66	68
12	58	54
13	60	71
14	60	60
15	47	47
H = 2	L = 2	
0	262	278
1	171	168
2	45	44
3	49	51
4	342	360
5	141	143
6	99	99
7	109	108
8	121	117
9	113	112
10	0	11
11	41	42
12	28	32
13	69	67
14	43	49
15	24	21
H = 3	L = 2	
0	193	194
1	149	150
2	70	73
3	68	70
4	184	188
5	189	185
6	53	49
7	33	31
8	172	172
9	123	128
10	70	70
11	54	50
12	87	88
13	78	83
14	53	52
H = 4	L = 2	
0	0	6
1	201	207
2	103	105
3	196	197
4	80	82
5	114	118
6	180	180
7	70	65
8	108	111
9	31	32
10	151	155
11	21	10
12	69	70
13	0	18
14	82	85
H = 5	L = 2	
0	76	77
1	166	167
2	196	197
3	135	135
4	53	54
5	162	162
6	140	136
7	124	122
8	38	32
9	53	48
10	51	53
11	58	60
12	21	24
13	28	31
H = 6	L = 2	
0	179	178
1	43	44
2	91	89
3	66	67
4	159	157
5	98	94
6	95	91
7	99	98
8	45	48
9	73	71
10	25	21
11	78	76
12	28	30
H = 7	L = 2	
0	112	107
1	72	72
2	38	36
3	69	70
4	117	113
5	76	74
6	75	71
7	53	52
8	98	97
9	72	72
10	44	48
11	39	39
H = 8	L = 2	
0	0	13
1	135	130
2	50	52
3	134	134
4	38	38
5	89	86
6	65	66
7	58	59
8	63	64
9	34	28
10	52	53
H = 9	L = 2	
0	0	1
1	61	63
2	118	116
3	82	84
4	0	12
5	45	40
6	74	77
7	75	80
8	37	25
9	24	8
H =10	L = 2	
0	42	41
1	0	4
2	63	65
3	56	50
4	40	32
5	36	38
6	50	52
H =11	L = 2	
0	41	39
1	49	44
2	41	46
H = 0	L = 3	
1	244	244
2	320	331
3	294	294
4	79	80
5	206	204
6	209	204
7	106	104
8	27	22
9	41	40
10	32	29
11	28	27
12	35	32
13	37	38
14	34	34
15	22	22
H = 1	L = 3	
0	200	194
1	125	128
2	266	274
3	237	245
4	168	169
5	51	50
6	157	158
7	170	172
8	90	90
9	73	74
10	97	95
11	86	85
12	70	71
13	61	61
14	52	48
15	50	48
H = 2	L = 3	
0	60	64
1	96	97
2	29	26
3	116	118
4	194	200
5	95	96
6	126	128
7	147	150
8	161	165
9	66	65
10	63	62
11	113	113
12	133	134
13	24	21
14	46	45
H = 3	L = 3	
0	218	221
1	183	185
2	203	215
3	230	239
4	164	168
5	117	116
6	125	126
7	145	147
8	38	41
9	0	13
10	40	41
11	61	56
12	45	41
13	28	32
14	0	9
H = 4	L = 3	
0	81	80
1	173	176
2	216	221
3	186	186
4	46	45
5	143	147
6	164	169
7	72	73
8	32	38
9	57	55
10	63	68
11	30	32
12	36	37
13	48	50
14	45	44
H = 5	L = 3	
0	16	11
1	43	41
2	102	107
3	96	99
4	87	93
5	70	69
6	119	118
7	96	97
8	98	101
9	100	100
10	95	96
11	68	73
12	70	70
13	64	63
H = 6	L = 3	
0	117	121
1	133	132
2	19	15
3	130	130
4	133	134
5	88	88
6	47	50
7	86	86
8	95	95
9	43	42
10	37	36
11	51	54
12	70	69
H = 7	L = 3	
0	130	131
1	116	116
2	92	94
3	122	123
4	111	112
5	99	97
6	53	57
7	55	55
8	46	46
9	53	52
10	9	6
11	21	16
H = 8	L = 3	
0	47	46
1	66	68
2	72	74
3	60	62
4	36	38
5	78	79
6	90	91
7	38	37
8	45	45
9	60	62
10	65	70
H = 9	L = 3	
0	45	48
1	50	50
2	22	24
3	14	15
4	56	57
5	70	73
6	57	59
7	36	31
8	50	58
H =10	L = 3	
0	78	83
1	78	81
2	0	5
3	69	71
4	68	72
5	55	59
6	0	9
H = 0	L = 4	
0	334	345
1	21	23
2	105	103
3	81	85
4	196	192
5	214	212
6	28	29
7	40	37
8	92	92
9	191	188
10	22	21
11	80	76
12	20	4
13	121	119
14	28	17
H = 1	L = 4	
0	262	262
1	227	233
2	157	161
3	90	92
4	222	225
5	168	166
6	96	97
7	20	15
8	116	116
9	113	116
10	85	86
11	37	39
12	43	46
13	37	41
14	68	70
H = 2	L = 4	
0	60	58
1	239	242
2	43	41
3	271	280
4	76	76
5	158	157
6	117	120
7	124	123
8	62	64
9	83	87
10	110	111
11	0	20
12	48	51
13	0	23
14	43	49
H = 3	L = 4	
0	112	112
1	127	130
2	200	204
3	109	112
4	149	156
5	89	92
6	125	129
7	95	98
8	87	88
9	86	85
10	102	104
11	82	82
12	37	32
13	28	21
14	80	80
H = 4	L = 4	
0	202	206
1	21	18
2	166	172
3	71	70
4	128	130
5	143	146
6	55	55
7	60	65
8	61	65
9	132	140
10	20	25
11	61	66
12	0	4
13	83	90
H = 5	L = 4	
0	180	186
1	141	145
2	0	15
3	102	100
4	154	155
5	131	128
6	18	10
7	55	57
8	95	95
9	84	88
10	32	36
11	25	25
12	41	39
13	52	52
H = 6	L = 4	
0	0	3
1	139	140
2	60	59
3	117	120
4	102	103
5	90	94
6	77	78
7	61	66
8	89	90
9	25	29
10	68	69
11	21	16
12	69	74
H = 7	L = 4	
0	0	3
1	51	48
2	107	110
3	92	92
4	38	39
5	22	20
6	80	80
7	96	102
8	37	37
9	32	32
10	68	74
11	74	79
H = 8	L = 4	
0	62	58
1	21	19
2	135	141
3	48	47
4	44	39
5	55	56
6	70	69
7	55	57
8	25	20
9	63	60
H = 9	L = 4	
0	57	59
1	65	66
2	34	37
3	71	79
4	63	66
5	43	49
6	30	32
7	67	57
8	47	49
H =10	L = 4	
0	0	4
1	60	57
2	33	39
3	38	42
4	54	59
5	31	34
H = 0	L = 5	
1	69	73
2	157	159
3	38	42
4	108	107
5	157	156
6	58	53
7	103	100
8	180	177
9	63	63
10	75	77
11	89	91
12	86	89
13	0	1
14	27	31
H = 1	L = 5	
0	107	108
1	205	208
2	73	69
3	257	263
4	120	120
5	40	38
6	57	58
7	173	173
8	45	44
9	76	75
10	26	33
11	91	89
12	21	18
13	61	62
14	24	8
H = 2	L = 5	
0	58	55
1	199	199
2	304	315
3	69	71
4	57	58
5	112	113
6	164	165
7	32	35
8	65	61
9	72	71
10	58	58
11	48	50
12	53	55
13	25	25
14	0	12
H = 3	L = 5	
0	0	2
1	170	167
2	23	22
3	192	198
4	32	26
5	46	48
6	77	74
7	162	165
8	64	66
9	79	79
10	75	73
11	95	101
12	39	40
13	57	60

TABLE 4. (Continued)

K	|FO|	|FC|
H = 4 L = 5		
0	83	81
1	87	91
2	113	115
3	54	57
4	113	113
5	129	129
6	61	62
7	81	82
8	125	126
9	56	56
10	50	55
11	66	73
12	57	65
13	21	19
H = 5 L = 5		
0	152	152
1	127	131
2	108	108
3	150	156
4	127	131
5	41	39
6	43	46
7	89	91
8	58	62
9	45	40
10	42	42
11	32	36
12	23	17
H = 6 L = 5		
0	74	71
1	112	113
2	152	155
3	44	44
4	37	34
5	102	104
6	73	76
7	29	26
8	37	40
9	96	102
10	58	59
11	39	34
H = 7 L = 5		
0	55	57
1	56	53
2	50	50
3	70	71
4	79	80
5	44	37
6	69	66
7	81	82
8	75	79
9	48	51
10	68	70
H = 8 L = 5		
0	79	80
1	78	78
2	41	44
3	60	65
4	75	78
5	77	77
6	44	40
7	45	43
8	52	50
9	45	48
H = 9 L = 5		
0	101	101
1	61	53
2	70	69
3	41	43
4	80	79
5	28	23
6	39	36
7	0	20
H =10 L = 5		
0	42	38
1	44	50
2	35	34
3	0	20
H = 0 L = 6		
0	0	17
1	235	238
2	55	54
3	226	229
4	12	11
5	146	142
6	33	32
7	117	114
8	0	14
9	48	46
10	0	0
11	19	9
12	0	7
13	0	5
H = 1 L = 6		
0	180	176
1	73	73
2	29	22
3	0	10
4	144	142
5	133	132
6	99	96
7	85	87
8	112	112
9	66	64
10	120	119
11	89	91
12	34	38
13	0	3
H = 2 L = 6		
0	26	26
1	87	88
2	87	87
3	26	26
4	15	16
5	164	165
6	74	70
7	96	95
8	19	19
9	212	212
10	34	38
11	43	41
12	0	16
13	113	115
H = 3 L = 6		
0	203	210
1	144	142
2	23	19
3	102	103
4	191	192
5	115	116
6	41	41
7	0	10
8	111	113
9	41	42
10	63	65
11	38	37
12	21	18
13	0	14
H = 4 L = 6		
0	22	19
1	166	166
2	36	39
3	167	171
4	43	45
5	88	92
6	24	24
7	76	75
8	82	88
9	41	41
10	33	32
11	0	6
12	54	53
H = 5 L = 6		
0	65	61
1	21	15
2	20	12
3	85	85
4	28	30
5	69	67
6	93	96
7	111	109
8	48	53
9	46	44
10	98	101
11	86	89
H = 6 L = 6		
0	0	7
1	40	40
2	161	161
3	31	26
4	18	13
5	88	90
6	107	112
7	33	37
8	0	7
9	104	112
10	27	31
H = 7 L = 6		
0	145	142
1	116	118
2	26	16
3	97	98
4	112	114
5	55	56
6	0	8
7	35	40
8	54	54
9	26	11
H = 8 L = 6		
0	0	13
1	55	55
2	24	28
3	72	71
4	60	61
5	30	27
6	29	23
7	28	21
8	83	89
H = 9 L = 6		
0	0	21
1	40	28
2	21	14
3	76	78
4	27	26
5	0	13
H = 0 L = 7		
1	70	68
2	160	161
3	19	25
4	68	66
5	144	140
6	93	88
7	86	79
8	85	83
9	61	62
10	44	44
11	80	76
12	61	61
H = 1 L = 7		
0	39	30
1	125	125
2	90	87
3	204	202
4	52	51
5	61	60
6	20	25
7	155	156
8	30	34
9	53	51
10	22	21
11	76	80
12	0	4
H = 2 L = 7		
0	32	28
1	180	181
2	172	175
3	88	88
4	88	90
5	103	99
6	138	136
7	18	10
8	69	68
9	56	56
10	47	49
11	32	37
12	78	75
H = 3 L = 7		
0	62	61
1	113	114
2	19	19
3	158	159
4	57	57
5	51	53
6	32	31
7	140	140
8	63	61
9	61	65
10	34	28
11	80	80
12	28	28
H = 4 L = 7		
0	71	68
1	56	55
2	113	111
3	25	26
4	73	74
5	118	118
6	81	82
7	66	64
8	59	60
9	55	58
10	40	33
11	62	63
H = 5 L = 7		
0	95	100
1	77	77
2	98	98
3	130	130
4	78	82
5	29	35
6	47	49
7	90	90
8	41	41
9	31	22
10	37	39
H = 6 L = 7		
0	42	43
1	108	108
2	85	86
3	57	62
4	31	33
5	82	88
6	77	79
7	0	11
8	38	42
9	71	74
H = 7 L = 7		
0	84	75
1	48	48
2	37	37
3	68	69
4	78	83
5	38	32
6	42	45
7	67	65
8	64	68
H = 8 L = 7		
0	67	68
1	49	47
2	40	38
3	32	28
4	61	61
5	65	73
6	51	51
H = 9 L = 7		
0	68	76
1	31	28
2	55	59
3	39	43
H = 0 L = 8		
0	125	123
1	32	27
2	21	9
3	84	81
4	92	89
5	140	135
6	26	21
7	60	57
8	36	40
9	103	103
10	24	26
11	50	48
H = 1 L = 8		
0	150	150
1	141	141
2	45	44
3	56	57
4	131	130
5	129	128
6	50	53
7	24	26
8	56	55
9	75	75
10	44	46
11	48	40
H = 2 L = 8		
0	42	43
1	186	184
2	38	42
3	163	161
4	70	67
5	113	109
6	61	60
7	78	78
8	48	51
9	27	27
10	50	49
11	0	10
H = 3 L = 8		
0	74	72
1	85	85
2	87	90
3	48	48
4	90	90
5	92	90
6	81	81
7	68	65
8	42	44
9	64	65
10	66	67
11	62	65
H = 4 L = 8		
0	79	77
1	22	24
2	86	89
3	57	62
4	70	69
5	96	97
6	49	47
7	57	57
8	30	33
9	75	81
10	26	24
H = 5 L = 8		
0	127	128
1	104	105
2	37	33
3	71	71
4	107	103
5	100	98
6	0	16
7	0	31
8	40	45
9	33	44
H = 6 L = 8		
0	22	19
1	96	98
2	29	24
3	81	83
4	63	65
5	61	65
6	46	48
7	55	57
8	71	72
H = 7 L = 8		
0	19	0
1	33	29
2	69	71
3	36	44
4	37	33
5	36	33
6	64	67
7	72	72
H = 8 L = 8		
0	33	16
1	0	15
2	88	92
3	42	40
4	26	29
H = 0 L = 9		
1	122	118
2	109	107
3	132	129
4	39	32
5	119	116
6	73	70
7	41	45
8	23	20
9	30	32
10	30	28
H = 1 L = 9		
0	31	28
1	66	65
2	84	85
3	103	101
4	46	43
5	29	23
6	87	85
7	97	95
8	58	55
9	61	56
10	60	43
H = 2 L = 9		
0	37	39
1	42	40
2	44	43
3	69	68
4	60	59
5	52	50
6	71	68
7	102	101
8	84	80
9	49	46
10	50	45
H = 3 L = 9		
0	64	63
1	110	106
2	99	100
3	109	105
4	47	44
5	48	44
6	93	91
7	83	83
8	0	16
9	28	18
10	25	17
H = 4 L = 9		
0	25	16
1	95	92
2	78	80
3	88	89
4	0	19
5	91	92
6	70	72
7	27	34
8	23	20
9	24	28
H = 5 L = 9		
0	26	23
1	18	10
2	31	27
3	47	47
4	49	50
5	52	52
6	52	52
7	55	56
8	65	65
H = 6 L = 9		
0	85	83
1	74	71
2	25	25
3	60	59
4	83	80
5	50	46
6	24	28
7	56	58
H = 7 L = 9		
0	61	60
1	79	79
2	63	67
3	62	65
4	47	48
H = 0 L =10		
0	73	71
1	69	69
2	33	32
3	85	83
4	53	47
5	30	22
6	100	97
7	40	42
8	44	43
9	0	2
H = 1 L =10		
0	63	64
1	111	107
2	53	55
3	42	45
4	33	37
5	110	106
6	53	52
7	39	40
8	44	43
9	62	61
H = 2 L =10		
0	147	145
1	24	19
2	32	32
3	22	25
4	120	119
5	46	47
6	29	21
7	53	53
8	43	45
H = 3 L =10		
0	86	86
1	87	87
2	0	5
3	25	28
4	67	64
5	89	89
6	23	16
7	28	28
8	66	67
H = 4 L =10		
0	41	48
1	71	69
2	29	31
3	87	84
4	39	41
5	38	35
6	72	74
7	46	41
H = 5 L =10		
0	0	11
1	78	75
2	76	76
3	46	46
4	22	18
5	69	67
6	65	63
H = 6 L =10		
0	95	90
1	35	22
2	61	62
3	34	34
4	57	61
H = 0 L =11		
1	30	23
2	37	41
3	69	66
4	54	48
5	0	3
6	17	22
7	111	104
H = 1 L =11		
0	72	70
1	36	36
2	106	104
3	58	54
4	57	57
5	20	11
6	72	73
7	30	26
H = 2 L =11		
0	0	12
1	106	103
2	82	83
3	61	59
4	23	23
5	58	60
6	39	43
H = 3 L =11		
0	57	52
1	0	6
2	64	65
3	24	24
4	50	50
5	45	43
6	62	64
H = 4 L =11		
0	82	82
1	27	25
2	35	31
3	55	50
4	61	60
5	0	7
H = 5 L =11		
0	46	53
1	58	57
2	86	85
H = 0 L =12		
0	166	163
1	34	30
2	0	10
3	39	35
4	117	112
H = 1 L =12		
0	0	25
1	67	66
2	52	52
3	33	32
4	44	44
H = 2 L =12		
0	0	13
1	33	29
2	46	41
3	27	26
H = 3 L =12		
0	33	27
1	66	70

a weak bent hydrogen bonding to H_2O 1. The situations of water molecules H_2O 1 and H_2O 2 belong to the D- and B-types, respectively, of Chidambaram *et al.*[22] The IR spectrum showed three ν_{OH} bands at 3490, 3175 and 2880 cm^{-1}, indicating three O–H···O distances of *ca.* 2.92, 2.77 and 2.69 Å.[23] These values are in good agreement with the observed ones for the scheme mentioned above. The hydrogen atoms seem to point to one of the lone pairs of the acceptor oxygen atoms.

Magnetic Susceptibility. The magnetic susceptibility and its reciprocal are plotted against temperature in Fig. 4. Above 100 K the Curie-Weiss law holds, giving a Weiss temperature θ of $-92._6$ K and a magnetic moment μ_{eff} of 2.00 β_B. At lower temperatures the susceptibility shows two maxima, one rounded and appearing at *ca.* 45 K and the other sharp and located at $26._4$ K. Below 10 K it seems to have a constant value. These features resemble those of $Cu(HCOO)_2 \cdot 4H_2O$,[24,25] a blue modification of $Cu(HCOO)_2$,[26] $Cu(C_4H_4N_2)Br_2$ and other similar compounds.[27] The broad maxima were explained to be due to the one- or two-dimensional magnetic interaction and the sharp maxima to the onset of the antiferromagnetic ordering of spins throughout the crystal at the Néel temperature T_N. Constant sus-

22) R. Chidambaram, A. Sequeira and S. K. Sikka, *J. Chem. Phys.*, **41**, 3616 (1964).

23) W. C. Hamilton and J. A. Ibers, "Hydrogen Bonding in Solids," Benjamin, New York, N. Y. (1968), p. 85.

24) R. B. Flippen and S. A. Friedberg, *J. Chem. Phys.*, **38**, 2652 (1963).

25) H. Kobayashi and T. Haseda, *J. Phys. Soc. Jap.*, **18**, 541 (1963).

26) M. Inoue and M. Kubo, *Inorg. Chem.*, **9**, 2310 (1970).

27) M. Inoue, *Nippon Kagaku Zasshi*, **92**, 1 (1971).

Table 5. Interatomic distances (Å) and angles (°) with their e.s.d.'s.
The subscript indicates symmetry operations given below to derive the atomic parameters.

1	x	y	z	5	$x-1/2$	$3/2-y$	$1-z$
2	$1/2-x$	$1-y$	$z+1/2$	6	$1-x$	$y-1/2$	$1/2-z$
3	$1/2-x$	$1-y$	$z-1/2$	7	$1-x$	$y-1/2$	$3/2-z$
4	$x+1/2$	$3/2-y$	$1-z$				

A. CuO_5 square pyramid

Cu–O 1	1.946(5)	O 1–Cu–O 2	91.61(19)
Cu–O 2	1.952(4)	O 2–Cu–O 3	91.75(19)
Cu–O 3	1.963(5)	O 3–Cu–O_w 1	88.08(20)
Cu–O_w 1	1.983(5)	O_w 1–Cu–O 1	87.49(20)
Cu–O_w 2	2.325(6)	O_w 2–Cu–O 1	95.72(20)
		O_w 2–Cu–O 2	90.17(19)
O 1–O 2	2.795(6)	O_w 2–Cu–O 3	94.22(19)
O 2–O 3	2.811(6)	O_w 2–Cu–O_w 1	96.11(20)
O 3–O_w 1	2.743(7)		
O_w 1–O 1	2.717(7)	O 1–O 2–O 3	87.96(18)
O_w 2–O 1	3.177(7)	O 2–O 3–O_w 1	90.06(20)
O_w 2–O 2	3.041(7)	O 3–O_w 1–O 1	90.94(21)
O_w 2–O 3	3.152(8)	O_w 1–O 1–O 2	90.94(20)
O_w 2–O_w 1	3.213(8)		
Cu–O_w 2_7	3.116(6)	O_w 2_1–Cu–O_w 2_7	170.76(17)

B. SeO_3^{2-} anion

Se–O 1	1.701(4)	O 1–Se–O 2	100.23(22)
Se–O 2	1.702(5)	O 2–Se–O 3	98.14(22)
Se–O 3	1.712(4)	O 3–Se–O 1	100.43(21)
O 1–O 2	2.611(6)	O 1–O 2–O 3	60.70(17)
O 2–O 3	2.580(6)	O 2–O 3–O 1	60.25(17)
O 3–O 1	2.623(6)	O 3–O 1–O 2	59.05(17)

C. Around O_w 1

O_w 1–O 1_4	2.652(7)	O 1_4–O_w 1–O 3_5	103.39(22)
O_w 1–O 3_5	2.620(7)	O 1_4–O_w 1–O_w 2_2	89.97(21)
O_w 1–O_w 2_2	2.921(8)	O 3_5–O_w 1–O_w 2_2	83.88(21)
		Cu_1–O_w 1–O 1_4	121.83(24)
		Cu_1–O_w 1–O 3_5	123.59(24)
		Cu_1–O_w 1–O_w 2_2	124.27(24)

D. Around O_w 2

O_w 2–O 2_2	2.729(7)	O 2_2–O_w 2–O_w 1_3	82.99(21)
O_w 2–O_w 1_3	2.921(8)	O 2_2–O_w 2–O 1_6	132.15(23)
O_w 2–O 1_6	3.364(8)	O_w 1_3–O_w 2–O 1_6	102.79(20)
		Cu_1–O_w 2–O 2_2	128.63(25)
		Cu_1–O_w 2–O_w 1_3	131.18(25)
		Cu_1–O_w 2–O 1_6	82.78(18)
		Cu_6–O_w 2–O 2_2	111.02(21)
		Cu_6–O_w 2–O_w 1_3	72.44(16)
		Cu_6–O_w 2–O 1_6	34.68(10)
		Cu_1–O_w 2–Cu_6	115.28(21)

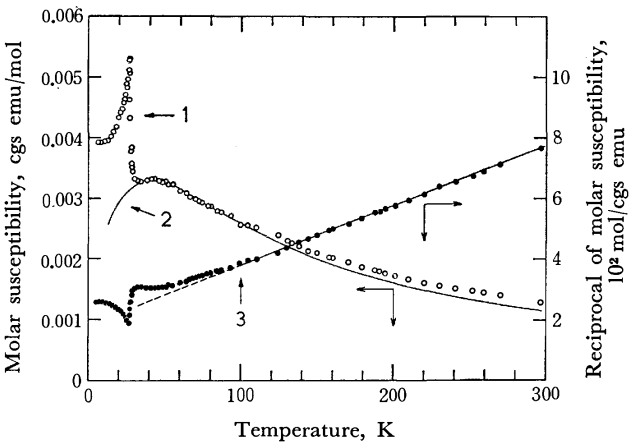

Fig. 4. Molar magnetic susceptibility and its reciprocal plotted against temperature.
1: Observed molar susceptibility, 2: calculated one for a linear Heisenberg spin system with $g=2.00$ and $J/k=-33$ K, 3: reciprocal of the observed one.

ceptibilities below T_N were observed, and in the case of $Cu(HCOO)_2\cdot 4H_2O$[25] the magnetization was measured to be 3% of the moment of a Cu(II) ion originating from the canting of the spins. The magnetic susceptibility of $CuSeO_3\cdot 2H_2O$ can also be explained in a similar manner.

The possible paths of superexchange interaction between magnetic ions were sought in the crystal structure. A linear path of Cu–H_2O···Cu along the crystallographic b axis is most apparent and a conformable path of magnetic interaction is known for $Cu(NH_3)_4SO_4\cdot H_2O$.[28] However, the interaction through an H_2O molecule is very weak as is evident from the small θ and J values found in $Cu(NH_3)_4SO_4\cdot H_2O$[28] and $CuSO_4\cdot 5H_2O$,[29] and cannot explain the observed maximum at high temperatures. The other paths should involve SeO_3^{2-} anions. Each SeO_3^{2-} anion combines three different CuO_5 square pyramids and forms a three-dimensional network. Interatomic distances and angles concerning three Se–O–Cu paths are almost the same. If these paths contribute equally to the magnetic interaction, $CuSeO_3\cdot 2H_2O$ should be a three-dimensional ferromagnet or antiferromagnet. As a matter of fact, a broad maximum of susceptibility characteristic of the one- or two-dimensional magnet is observed. There must, therefore, be a certain difference between the three paths of Cu–O–Se–O–Cu. The environments of three oxygen atoms of an SeO_3^{2-} anion are schematically projected along the pseudosymmetry axis of the anion in Fig. 5. These oxygen atoms are also a proton acceptor. Bond angles which are made by Se, Cu and a hydrogen-donor atoms are very close to 120° except O_w1_4–O 3_2–Cu_2. These values suggest that the orbitals of oxygen atoms are the sp^2 hybrid ones and that one of them is used for a σ-bond with the Se atom while the other two lone pairs are

28) S. Saito, *J. Phys. Soc. Jap.*, **26**, 1388 (1969); and references therein.
29) S. Wittekoek, T. O. Klassen and N. J. Poulis, *Physica*, **39**, 293 (1968); and references therein.

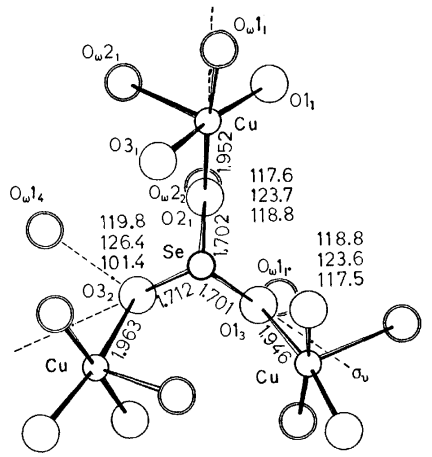

Fig. 5. Environment around an SeO_3^{2-} anion viewed along the pseudo-symmetry axis of the anion. Three numbers given for each oxygen atom of the anion are the angles of Se-O-Cu, Se-O-O(hydrogen donor) and Cu-O-O (hydrogen donor), respectively, in their order. Interatomic distances are given in Å and angles in degree.

directed towards Cu and a hydrogen-donor atoms. These sp^2 orbitals may extend within the plane normal to the basal plane of an anion and passing through the Se and O atoms, since in this conformation the oxygen atoms are bound most tightly to the Se atom by the additional formation of π-bonds. The p_π orbitals of oxygen atoms may then direct midway between the z- and x-(or y-) axes of Cu coordinate system and have only a negligible effect on the superexchange interaction between Cu atoms. The main paths of the superexchange interaction may thus involve an O–Se–O σ-bond, and the path Se–O–Cu may be weaker than the other two since the deviation of the Cu atom from the sp^2 lobus is the greatest for this oxygen atom (Fig. 5). The path Cu–O 1–Se–O 2–Cu···makes up a helical one-dimensional spin system along the crystallographic a axis. Though the difference between the three Se–O–Cu paths brings forth a linear magnetic system, the Se–O 3–Cu path may introduce a three-dimensional interaction between Cu(II) ions because the difference is not serious.

The magnetic susceptibility of $CuSeO_3 \cdot 2H_2O$ can be explained qualitatively on the refined crystal structure. Some of the parameters concerning the magnetic interactions were estimated phenomenologically. For a one-dimensional spin system there are two formalisms of magnetic susceptibility based on the Ising[30] and Heisenberg[31] spins. The Ising model could not explain the temperature dependence of the susceptibility above 30 K, while the Heisenberg model gave a fair agreement. The g and J/k values giving the best fit are 2.00 and -33 K, respectively (Fig. 4). On the other hand, the molecular field theory[32,33] gives the relationships among θ, T_N, and J values. If a single J value is assumed for three O–Se–O paths, the observed θ gives $J/k = -31$ K, agreeing excellently with the value obtained by the Heisenberg model. The results also show that the difference in magnitude of superexchange interactions is very small. The ratio $|\theta|/T_N$ was estimated to be 3.0 using the above J value, which is comparable with the observed one (3.5). The g value of 2.00 seems smaller for a Cu(II) compound and the difference between two J/k values appears too small to give the magnetic behaviour of a linear spin system. An explanation for this may be as follows. Since each SeO_3^{2-} anion intermediates three copper(II) ions antiferromagnetically, the spin at each copper(II) cation is required to be "up" by the Cu′–O 1–Se–O 3–Cu interaction and at the same time to be "down" by the Cu″–O 2–Se–O 3–Cu interaction. The two interactions may be almost cancelled to give the observed features. The treatment is only approximate and the individual values cannot be taken to be accurate. Agreement as a whole indicates that the explanation is adequate.

In this mechanism the σ-bonds play an important role for the superexchange interaction. In $Ba_2Cu(HCOO)_6 \cdot 4H_2O$[34] and a blue modification and a royal blue one of $Cu(HCOO)_2$[26] the σ-bonds of an $HCOO^-$ anion induce a ferromagnetic spin ordering and the π-bonds an antiferromagnetic one. If these schemes for formates are applied to the present system, $CuSeO_3 \cdot 2H_2O$ should be ferromagnetic, which is contrary to observation. In the nuclear spin-spin coupling in a high resolution NMR,[35] the sign of the multibond coupling is known largely to depend on the molecular conformation even in the saturated hydrocarbons, as well as on the number of intermediate bonds. It means that the spin-spin coupling of the magnetic ion depends on the species of the intervening oxo-anions and on their conformations in the crystal structure. In fact, the very simple model without any account for the conformation leads to the antiferromagnetic coupling of two Cu(II) spins through only the σ-bonds of SeO_3^{2-} anion. Thus, it is not astonishing that $CuSeO_3 \cdot 2H_2O$ shows antiferromagnetic behaviour without any superexchange interaction through π-bonds of the anion.

The authors wish to thank Prof. Y. Shimura and Dr. S. Kaizaki, Osaka University, for their help in the measurement of diffuse reflectance spectra.

30) G. F. Newell and E. W. Montroll, *Rev. Mod. Phys.*, **25**, 353 (1953).
31) J. C. Bonner and M. E. Fisher, *Phys. Rev.*, **135**, A640 (1964).
32) A. H. Morrish, "The Physical Principles of Magnetism," John Wiley, New York, N. Y. (1965), Chap. 8.
33) J. S. Smart, "Magnetism," Vol. 3, ed. by G. T. Rado and H. Suhl, Academic Press, New York, N. Y. (1963), p. 63.
34) J. M. Barbour, D. A. Morton-Blake and A. L. Porte, *J. Chem. Soc. A*, **1968**, 878.
35) M. Barfield and D. M. Grant, "Advances in Magnetic Resonance," Vol. 1, ed. by J. S. Waugh, Academic Press, New York, N. Y. (1966), p. 149.

A New Method for the Precise Measurement of the Polarographic Current and Its Application in Digital Polarography

Sadato SAKURAI, Hideko SHIRAI, and Eiji NIKI

Department of Industrial Chemistry, Faculty of Engineering, The University of Tokyo, Hongo, Tokyo 113

(Received October 31, 1972)

In order to increase polarographic precision and sensitivity, the oscillopolarographic current was digitized and stored in a 100-channel pulse-height analyzer (PHA) operated in the multi-scaler mode (MS mode). An oscillopolarograph which could sweep the DC potential rapidly was combined with the PHA. The digitized oscillopolarographic current was repeatedly stored in the PHA, so that the statistical noise was reduced and the signal-to-noise ratio of the oscillopolarographic current was increased. Also, the drift due to the change in the experimental conditions was removed effectively by shortening the measurement time. Therefore, precision was efficiently improved by means of accumulation. The relative deviation was 0.25% at the concentration of the 5×10^{-7} M cadmium ion. As an example of the application, trace amounts of copper, lead, and cadimum in 99.99% indium metal were analyzed.

Recent developments in electronics have resulted in various improvements of polarography, such as those of radio-frequency polarography and pulse polarography. Besides, digital accumulation and processing[1] have been introduced to permit a high rate of data collection and greater accuracy, resolution, and precision. A small computer[2] has been employed on-line in an electrochemical system to provide semi-automated polarographic measurements.

Recently several reports have been published concerned with the precise measurement of the polarographic current at a low concentration using an accumulator or a digital computer. Perone and Harrar *et al.*[3] applied a rapid potential sweep and thus repeatedly accumulated the polarographic current. The relative deviation of their result was 0.1% at the concentration of 1 mM and 1.3% at the concentration of 2×10^{-7} M. Matsuda and Tamamushi[4] reported that the long-term integration of diffusion currents was reasonably accurate even at concentrations as low as 10^{-6} M. Shults, Fisher and Schaap[5] demonstrated that a precision and accuracy of about 0.1% could be obtained by using the mode of comparative polarography and by measuring the difference between the diffusion currents of unknown and standard solutions. Lingane[6] measured the diffusion current up to 0.1% and integrated it over an exactly known time which covered 50 or more mercury drops.

The detection limit in square-wave polarography is about 10^{-8} M, restricted by the capillary effect. If the statistical noises arising from the power supply, the capillary effect, etc. are sufficiently reduced by means of accumulation, a sensitivity of more than 10^{-8} M can be expected.

In this experiment, the oscillopolarographic current was digitized and a train of pulses proportional in number to the current was accumulated in the PHA. The statistical noise decreases in proportion to $1/\sqrt{n}$, where n is the number of repeated samplings. The coefficient of the variation in the oscillopolarographic current was improved by the accumulation.

Experimental

General. A block diagram of the apparatus is shown in Fig. 1. The rapid DC potential sweep, on which the square-wave voltage is superimposed, is used; the alternating faradaic current is measured through the gate circuit, which is used to eliminate the charging current. After the alternating faradaic current is rectified, amplified, and converted into the voltage, the output voltage is changed into a train of pulses proportional in number to its voltage by using a digital voltmeter. The train of pulses is stored in the 100-channel PHA. The beginning of the channel scanning of the PHA is synchronized with the start of the potential sweep, so that each oscillopolarographic current in the same state of the mercury drops and at the same applied potential is repeatedly stored in the same channel of the PHA. Therefore, the channel advance corresponds to the potential sweep

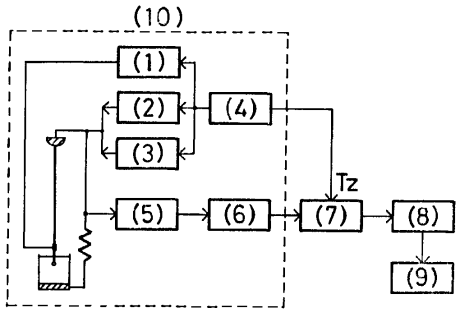

Fig. 1. The block diagram of the digital polarograph.
(1) Drop dislodger circuit, (2) Sweep potential generator, (3) Superimposed SW voltage generator, (4) Timing circuit, (5) Gate circuit, (6) Tuned rectifying detector, (7) Digital voltmeter, (8) Pulse height analyzer, (9) Digital printer, (10) Oscillopolarograph.
Tz is the start signal of the potential sweep.

1) G. Lauer and R. A. Osteryoung, *Anal. Chem.*, **38**, 1137 (1966). G. L. Booman, *ibid.*, **38**, 1141 (1966). G. Lauer, R. Anel, and F. C. Anson, *ibid.*, **39**, 765 (1967). K. Momoki, H. Sato, and H. Ogawa, *ibid.*, **39**, 1077 (1967). L. Ramaley and G. S. Wilson, *ibid.*, **42**, 606 (1970). R. G. Clem and W. W. Goldsworthy, *ibid.*, **43**, 918 (1971).

2) S. P. Perone, D. O. Jones, and W. F. Gutknecht, *ibid.*, **41**, 1155 (1969). G. P. Hicks, A. A. Eggert and E. C. Toren, *ibid.*, **42**, 729 (1970). W. F. Gutknecht and S. P. Perone, *ibid.*, **42**, 906 (1970). L. B. Sybrandt and S. P. Perone, *ibid.*, **43**, 382 (1971).

3) S. P. Perone, J. E. Harrar, F. B. Stephens, and R. E. Anderson, *ibid.*, **40**, 899 (1968).

4) K. Matsuda and R. Tamamushi, *This Bulletin*, **42**, 439 (1969).

5) W. D. Shults, D. J. Fisher, and W. B. Schaap, *Anal. Chem.*, **39**, 1379 (1967).

6) J. J. Lingane, *Anal. Chim. Acta.*, **44**, 411 (1969).

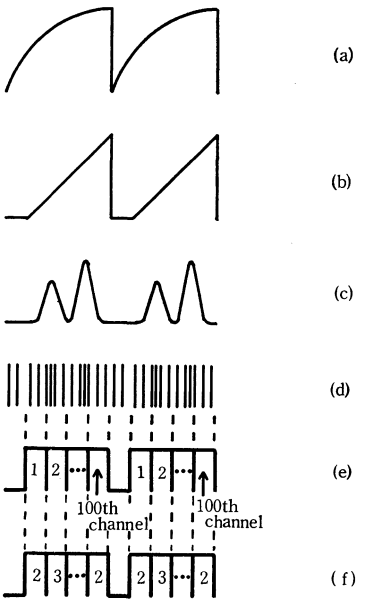

Fig. 2. The time sequence of the operation.
(a) Drop current, (b) Potential sweep, (c) Oscillographic SW polarogram, (d) Output of digital voltmeter, (e) The PHA has 100 channels., (f) Output of digital printer.

and the accumulated numbers of the pulses correspond to the oscillopolarographic current at a given value of the applied potential. The numbers of pulses stored in each channel of the PHA are printed out by a digital printer at the end of a predetermined number of scannings. The digital data thus obtained can be plotted as is shown in Fig. 5. The time sequence of the operation is shown in Fig. 2.

Instrumentation. *Oscillopolarograph (Yanagimoto digital polarograph PE 21)*: An oscillographic square-wave polarogram and an oscillographic direct-current polarogram can be measured. A mercury drop is detached by the drop dislodger, and the start time of the potential sweep is synchronized with the dislodgement of the mercury drop. The oscillopolarographic current is converted into voltages from 0 mV to +50 mV, which is proportional to its current.

Digital Voltmeter (Takeda Riken 6154 B digital voltmeter): In this experiment, the digital voltmeter is used as a voltage-to-frequency converter. The output voltage from the oscillopolarograph is introduced into the digital voltmeter and then converted into a train of pulses proportional in number to its voltage. This digital voltmeter converts the input voltage of 100 mV into the frequency of 10 kHz. The height of the output pulse from the digital voltmeter is 4 V, and the rise time of the pulse is about 1 μs.

Multichannel Pulse-height Analyzer: A Toshiba 100-channel PHA (EDS-34206) is connected to a plug-in unit M (type UE 730-007); thus, the measurement can be performed in the multi-scaler mode (MS mode). The train of pulses from the digital voltmeter is stored in the PHA from the lst channel to the 100th channel. In Fig. 3 the time sequence of the operation of the PHA is shown. The capacity of the PHA is (10^5-1)pulses/channel.

Experimental Conditions. In order to reduce the fluctuation of the current arising from the depleting effect,[7] which was caused by the fact that the concentration of the depolarizer in the vicinity of the electrode decreased during the electrolysis, the actual measurement was started after electrolysis over 10 mercury drops using the same potential

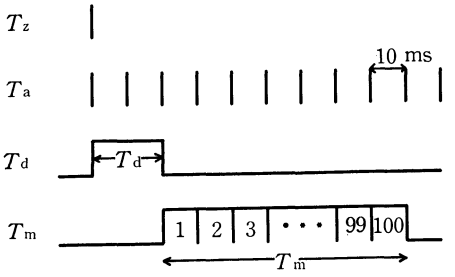

Fig. 3. The time sequence of the operation of the PHA.
T_z: The signal for the start of the measurement.
T_a: The signal for the channel advance.
T_d: The delay time of the scanning of the PHA.
T_m: The operating time of the PHA. When the sweep reaches the 100th channel, it goes back to the 1st channel and waits for the next T_z signal.
All the time of the PHA refers to the clock signal generated by a 1 M Hz Xtal oscillator.

sweep as the actual measurement. The decrease due to the depleting effect was most marked at the beginning of the electrolysis; it reached a constant value after 10 mercury drops.[7] Also, gelatin was added at 0.01% in order to decrease the variation in the current arising from the fluctuation of the solution. The temperature was controlled within ±0.01 °C by surrounding the cell with lagging material in order to limit the variation in the oscillopolarographic current due to temperature change within 0.015%. All the solutions were deoxygenated by passing pure nitrogen through for at least 10 min.

Results and Discussion

It is impossible to avoid the error arising from quantization when the train of pulses is sampled repeatedly at definite intervals. The relation between the coefficient of the variation and the number of repeated samplings is shown in Fig. 4. In the actual measurement, other statistical noises arising from the power supply, the capillary effect, etc. are added. In order to measure the oscillopolarographic current at a low concentration, the residual current had to be elimi-

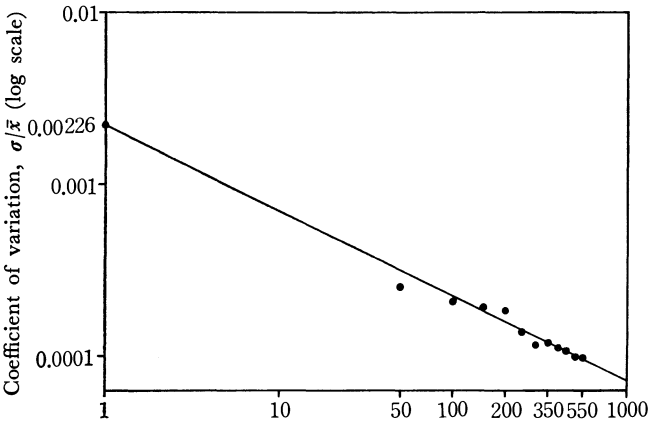

Fig. 4. The decrease of the coefficient of variation by accumulation.
Straight line: $\log \sigma/\bar{x} \propto -1/2 \log n$, n is the number of repeated sampling.
●: Experimental

7) E. Niki and H. Shirai, *Bunseki Kagaku*, **20**, 1022 (1971).

Table 1. The relation between the concentration of cadmium ion and the coefficient of variation of the oscillopolarographic current

Concn. (M)	Method	$\bar{x}$	σ	$\sigma/\bar{x}$	m (mg/s)	N
10^{-3}	DC	1171	1.10	0.0009	1.11	10
10^{-3}	SW	1996	1.05	0.0005	1.11	10
5×10^{-5}	SW	2774	2.68	0.0010	1.11	16
5×10^{-6}	SW	3015	5.59	0.0017	1.11	20
5×10^{-7}	SW	1308	3.32	0.0025	1.09	25

Concn.: Concentration, $\bar{x}$: The accumulated numbers of pulses which correspond to the height of the cadmium peak by oscillopolaography, σ: Standard deviation, $\sigma/\bar{x}$: The coefficient of variation, m: Mercury flow rate, N: The number of repeated sampling.

nated. At first, the solution of the supporting electrolyte was scanned and the digitized residual current was stored in the PHA, whose channels were related to the applied potential. Next, after changing the sign of the memory, the solution containing the supporting electrolyte plus the sample was scanned under the same conditions as in the first scan. Consequently, an oscillopolarogram in which the residual current had been subtracted could be obtained. Table 1 shows the precision of the current measurements on solutions containing various concentrations of the cadmium ion. The relative deviation was 0.05% at a concentration of the 1 mM cadmium ion; this value was obtained by integrating the oscillographic square-wave polarographic current over 10 mercury drops. The relative deviation was 0.25% at a concentration of the 5×10^{-7} M cadmium ion; this value was obtained by accumulating the oscillographic square-wave polarographic current over 25 mercury drops. It is evident that the statistical noise was reduced efficiently by accumulation. The change in the time constant of the square-wave oscillator, which changed the wave form of the superimposed SW voltage, had little effect on the precision of the current measurement (Table 2). The change in the amplitude of the superimposed SW voltage also had little effect on the precision of the current measurement (Table 3). Therefore, it is profitable to use the large amplitude of the superimposed SW voltage (30 mV), because the square-wave polarographic current is in proportion to the amplitude of the superimposed SW voltage. Table 4 indicates that the precision of the current measurement decreased as the rate of the potential sweep increased. Therefore, the sweep rate of 0.2 V/s was used in this experiment. As an example of application, trace amounts of copper, lead, and cadmium in 99.99% indium metal were analyzed. The indium metal was dissolved in concentrated nitric acid. The solution which contained the indium ion was heated until the indium nitrate had crystallized. The reduction potentials of the cadmium ion and the indium ion are

Table 2. The relation between the time constant of SW oscillator (SW Frequency-200 Hz) and the coefficient of variation

Sample 1 mM $CdSO_4$ in 1 M KCl

Time const. (ms)	$\bar{x}$	σ	$\sigma/\bar{x}$
110	2995	3.25	0.0011
210	2876	3.13	0.0011
310	2796	2.62	0.00094
410	2743	5.08	0.0019
510	2709	3.18	0.0012
610	2673	2.11	0.00079
710	2649	2.83	0.0011
810	2623	2.78	0.0011
910	2605	1.73	0.00067
1010	2572	3.30	0.0013

Table 3. The relation between the amplitude of the superimposed SW potential and the coefficient of variation

Sample 1 mM $CdSO_4$ in 1 M KCl

ΔE (mV)	$\bar{x}$	σ	$\sigma/\bar{x}$
1	2917	3.45	0.0012
2	1976	1.92	0.00097
5	2482	2.52	0.0010
10	2507	1.94	0.00077
20	2002	3.50	0.0017
30	2485	3.00	0.0012

ΔE: The amplitude of the superimposed SW potential.

Table 4. The relation between the rate of potential sweep and the coefficient of variation

Sample 1 mM $CdSO_4$ in 1 M KCl

Pot. (V)	R (V/s)	$\bar{x}$	σ	$\sigma/\bar{x}$
−0.439	0.1	3674	2.04	0.00065
	0.2	2981	2.33	0.00078
	0.3	2667	3.90	0.0015
−0.001	0.3	1745	3.11	0.0018
	0.5	1356	3.40	0.0025

Pot.: The initial potential (*vs.* Hg-pool), R: Sweep rate.

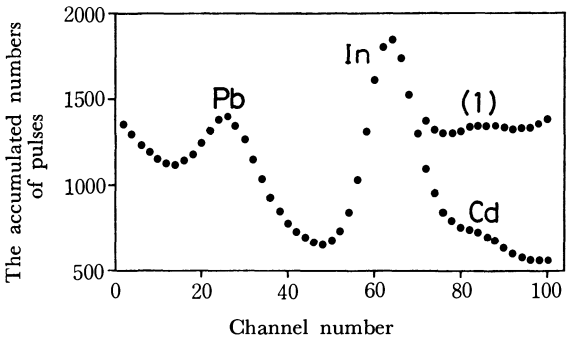

Fig. 5. The oscillographic SW polarogram of 1.5×10^{-7} M cadmium ion, 2×10^{-6} M lead ion and indium ion in 0.025 M $In(NO_3)_3$ and 1 M H_3PO_4.
$m=1.17$ mg/s, $T=21\pm0.01$ °C
Peak pot. (Pb^{2+}) = −0.402 V *vs.* SCE
Peak pot. (In^{3+}) = −0.530 V *vs.* SCE
Peak pot. (Cd^{2+}) = −0.594 V *vs.* SCE
(1): 0.025 M $In(NO_3)_3$ in 1 M H_3PO_4+0.54 M HNO_3
Peak pot. (In^{3+}) = −0.510 V *vs.* SCE
Peak pot. (Cd^{2+}) = −0.598 V *vs.* SCE

close together, and the waves overlap in almost all the supporting electrolytes. However, indium forms a complex with phosphate ions in phosphoric acid,[8] so the half-wave potential of the indium complex deviates from that of the indium ion. Fig. 5 shows an oscillographic square-wave polarogram of the cadmium ion, the lead ion, and the indium ion in 0.025 M indium nitrate plus 1 M phosphoric acid. The appearance of the indium peak may be attributed to the fact that the quantity of indium is so large that the complex formation can not mask the indium peak completely.

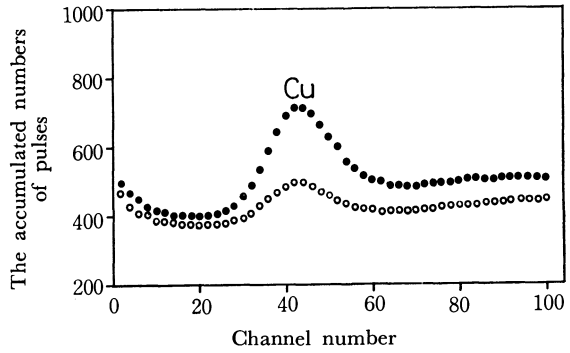

Fig. 6. The oscillographic SW polarogram of 8×10^{-7} M copper(I) ion and indium ion.
●: in 0.025 M $In(NO_3)_3$ and 1 M H_3PO_4
○: in 1 M H_3PO_4 only
$m=1.14$ mg/s, $T=21\pm0.01$ °C
Peak pot. (Cu^+) = +0.018 V *vs.* SCE

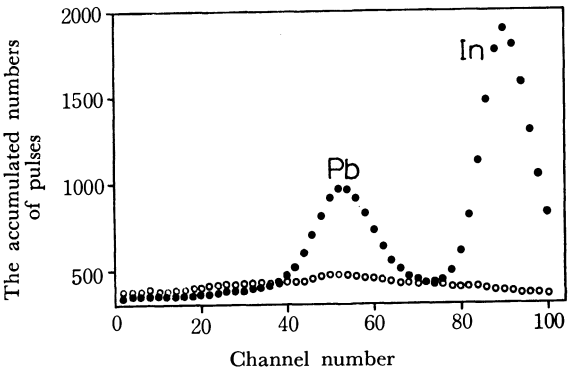

Fig. 7. The oscillographic SW polarogram of 2×10^{-6} M lead ion and indium ion.
●: in 0.025 M $In(NO_3)_3$ and 1 M H_3PO_4
○: in 1 M H_3PO_4 only
$m=1.16$ mg/s, $T=21\pm0.01$ °C
Peak pot. (Pb^{2+}) = −0.402 V *vs.* SCE

8) A. Holroyd and J. E. Salmon, *J. Chem. Soc.*, **1956**, 269.

However, if 0.54 M nitric acid is added, the cadmium peak appears distinctly (Fig. 5). The half-wave potentials of indium and cadmium differ by 63 mV in 1 M phosphoric acid, while the half-wave potentials differ by 88 mV in 1 M phosphoric acid plus 0.54 M nitric acid. In Figs. 6 and 7, oscillographic square-wave polarograms of the copper(I) ion and the lead ion in 0.025 M indium nitrate plus 1 M phosphoric acid are shown. The oscillographic square-wave polarograms of the supporting electrolyte are shown at the same time. It is obvious that very small amounts of the copper(I) ion and the lead ion are present in 1 M phosphoric acid. In Fig. 8 the relation between the accumulated numbers of the pulses and the concentrations of the cadmium ion is shown. Table 5 shows the quantitative analytical data of trace amounts of copper, lead, and cadmium in 99.99% indium metal.

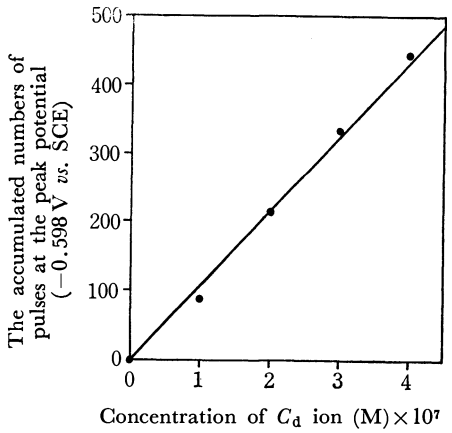

Fig. 8. The relation between the concentrations of cadmium ion and the accumulated numbers of pulses.

Table 5. The quantitative analytical data of trace amounts of copper, lead, and cadmium in 99.99% indium metal

Metal	Contents (ppm)
Cu	16
Pb	129
Cd	6

Conclusion

As has been indicated in the quantitative analysis of a trace amount of cadmium in indium metal, the precise measurement of 10^{-7} M could be performed in this experiment. If the statistical noise is decreased sufficiently, a sensitivity as high as 10^{-8} M or even higher can be expected in the near future.

Investigation on Low-spin Cobalt(II) Complexes. III. Structural, Optical and Magnetic Properties of Five-coordinate Complexes

Yuzo NISHIDA and Hideharu SHIMOHORI

Department of Chemistry, Faculty of Science, Kyushu University, Fukuoka 812

(Received December 18, 1972)

ESR and reflectance spectra of low-spin five-coordinate cobalt(II) complexes $[CoXdpe_2]Y$, where dpe represents 1,2-bis(diphenylphosphino)ethane and X,Y are Cl^-, Br^-, NCS^-, NO_3^- and ClO_4^- anions, were measured. From the results it was inferred that the structures of $[CoCldpe_2]ClO_4$ and $[CoBrdpe_2]ClO_4$ are distorted trigonal bipyramids whereas those $[CoNCSdpe_2]ClO_4$ and $[CoNO_3dpe_2]NO_3$ are square pyramids.

In the last few years several papers have appeared on the low-spin five-coordinate cobalt(II) complexes,[1-3] the syntheses, electronic spectra and magnetic data of which have increased. However, ESR data are considered to be most reliable for understanding the relation between structure, electronic spectrum and magnetic moment of these complexes. We measured the ESR and reflectance spectra of low-spin five-coordinate cobalt(II) complexes $[CoXdpe_2]Y$, where dpe represents 1,2-bis(diphenylphosphino)ethane and X,Y are Cl^-, Br^-, NCS^-, NO_3^- and ClO_4^- anions. From results we discussed their structural, optical and magnetic properties.

Experimental

1,2-bis(diphenylphosphino)ethane, dpe, was prepared by the method of Hewertson and Watson.[4]

$[CoXdpe_2]Y$ (X=Cl^-, Br^-, NCS^-, Y=ClO_4^- and X=NO_3^-, Y=NO_3^-) were prepared by the method of Sacco and Gorieri.[5] They reported a brown crystal for $[CoNCSdpe_2]ClO_4$ but we obtained a green one. (Found: C, 62.94; H, 5.18; N, 1.44. Calcd for $[CoNCSdpe_2]ClO_4$: C, 62.80; H, 4.78; N, 1.38) $[CoBrdpe_2]ClO_4 \cdot 2CHCl_3$ was obtained as a red prism by recrystallization of green $[CoBrdpe_2]ClO_4$ from a hot chloroform solution. (Found: C, 50.88; H, 4.10%. Calcd for $[CoBrdpe_2]ClO_4 \cdot 2CHCl_3$: C, 50.92; H, 3.96%).

The ESR spectra were measured with a JEOL ESR-apparatus model JES-MX-3X at various temperatures using X- and K-bands. Manganese(II) doped in MgO was used as a standard marker. The infrared spectra were recorded with a Hitachi EPI-S2 spectrophotometer in the region 4000~650 cm^{-1} on a KBr disk. The reflectance spectra were measured with a Hitachi EPS-3T recording photometer at room temperature.

Theoretical

For the five-coordinate metal complexes, the two geometries of the highest symmetry are (a) trigonal bipyramid(D_{3h}) and (b) square pyramid(C_{4v}). For (a) the chromophore has C_{3v} symmetry if the axial ligands are not the same and/or the metal lies in the plane of equatorial ligands. For (b) the chromophore naturally retains C_{4v} symmetry, even when the metal lies out of the plane of four basal ligands (it generally lies above it).

Splittings of 3d orbitals in both five-coordinate chromophores have been studied experimentally and theoretically.[6-8] Application of the angular overlap model to MX_5 chromophores of trigonal bipyramidal and square pyramidal geometries gives the pattern shown in Fig. 1 for the energy of antibonding "d" molecular orbital.[9] The crystal field model gives a similar pattern.

Since the electronic structure of a cobalt(II) ion is $3d^7$, low-spin trigonal bipyramidal cobalt(II) complexes should be more or less distorted from a perfect D_{3h} symmetry, because of the Jahn-Teller effect on the degenerate ground state.

The probable ground state of low-spin cobalt(II) complex with a distorted trigonal bipyramidal geometry

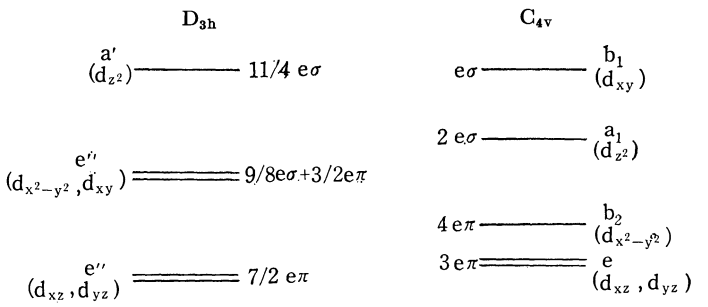

Fig. 1. The splittings of 3d orbitals in five-coordinate chromophores. (According to Jørgensen[9])

1) G. Dyer and D. W. Meek, *J. Amer. Chem. Soc.*, **89**, 3983 (1967).
2) J. P. Maher, *J. Chem. Soc., A*, **1968**, 2918.
3) F. Tsay, H. B. Gray, and J. Danon, *J. Chem. Phys.*, **54**, 3760 (1971).
4) H. Hewertson and H. R. Watson, *J. Chem. Soc.*, **1962**, 1490.
5) A. Sacco and F. Gorieri, *Gazz. Chim. Ital.*, **93**, 637 (1963).
6) C. Furlani, *Coord. Chem. Rev.*, **3**, 141 (1967).
7) M. Ciampolini, Structure and Bonding, **6**, 52 (1969).
8) P. L. Orioli, *Coord. Chem. Rev.*, **6**, 285 (1971).
9) C. K. Jørgensen, *J. Phys. Radium*, **26**, 825 (1965).

Table 1. Electronic repulsion energy of low-spin five-coordinate cobalt(II) complexes

$\|(z^2)^+(z^2)^-(xy)^+\|$	$3F_0-8F_2+33F_4$
$\|(z^2)^+(z^2)^-(x^2-y^2)^+\|$	$3F_0-8F_2+33F_4$
$\|(z^2)^+(z^2)^-(yz)^+\|$	$3F_0+7F_2-42F_4$
$\|(z^2)^+(z^2)^-(xz)^+\|$	$3F_0+7F_2-42F_4$
$\|(x^2-y^2)^+(x^2-y^2)^-(z^2)^+\|$	$3F_0-8F_2+33F_4$
$\|(x^2-y^2)^+(x^2-y^2)^-(xy)^+\|$	$3F_0+12F_2-67F_4$
$\|(x^2-y^2)^+(x^2-y^2)^-(yz)^+\|$	$3F_0-3F_2+8F_4$
$\|(x^2-y^2)^+(x^2-y^2)^-(xz)^+\|$	$3F_0-3F_2+8F_4$

is $(d_{z^2})^2(d_{x^2-y^2})^1$ or $(d_{z^2})^2(d_{xy})^1$, if we assume that in the d^3 configurations d_{z^2} remains the lowest orbital for the vacancies and consequently in a S=1/2 configuration is doubly occupied.

On the other hand in the case of a square pyramidal cobalt(II) complex, the predicted ground state is only $(d_{xy})^2(d_{z^2})^1$. No other states are likely for the ground state, even though the electronic repulsion energy is taken into account.

We calculated theoretical three g-values for both predicted ground states according to the methods given previously.[10] For a trigonal bipyramidal complex, we tentatively assumed the ground state to be $(d_{z^2})^2(d_{x^2-y^2})^1$, but found that the same results were also obtained for $(d_{z^2})^2(d_{xy})^1$.

1) The case where the ground state $(d_{z^2})^2(d_{x^2-y^2})^1$ is assumed.

By applying the spin-orbit interaction Hamiltonian $k\zeta ls$ to the zeroth-order Kramers doublet $(d_{z^2})^2(d_{x^2-y^2}^+)^1$ and $(d_{z^2})^2(d_{x^2-y^2}^-)^1$ as a perturbation, the ground state doublets are written by means of perturbation theory as follows.

$$\left.\begin{aligned}\Psi_a^+ &= N_a\{|(d_{z^2})^2(d_{x^2-y^2}^+)^1| - ika_1|(d_{z^2})^2(d_{xy}^+)^1| \\ &\quad + \frac{1}{2}ika_2|(d_{z^2})^2(d_{yz}^-)^1| - \frac{1}{2}ka_3|(d_{z^2})^2(d_{xz}^-)^1|\} \\ \Psi_a^- &= N_a\{|(d_{z^2})^2(d_{x^2-y^2}^-)^1| + ika_1|(d_{z^2})^2(d_{xy}^-)^1| \\ &\quad + \frac{1}{2}ika_2|(d_{z^2})^2(d_{yz}^+)^1| + \frac{1}{2}ka_3|(d_{z^2})^2(d_{xz}^+)^1|\}\end{aligned}\right\} \quad (1)$$

where N_a, ζ and k represent normalization constant, one-electron spin-orbit coupling constant for 3d orbitals and orbital reduction factor, respectively. Coefficients a_1, a_2 and a_3 denote $\zeta/\Delta[(x^2-y^2)-xy]$, $\zeta/\Delta[(x^2-y^2)-yz]$ and $\zeta/\Delta[(x^2-y^2)-xz]$, respectively, where $\Delta[(x^2-y^2)-xy]$ denotes the energy difference between the states $(d_{z^2})^2(d_{x^2-y^2})^1$ and $(d_{z^2})^2(d_{xy})^1$. Configurations which do not contribute to g-values were neglected. By means of the usual methods,[10] we obtain the following results in the first order.

$$\left.\begin{aligned}g_z &= 2N_a^2[1-4k^2a_1] \\ g_x &= 2N_a^2[1-k^2a_2] \\ g_y &= 2N_a^2[1-k^2a_3]\end{aligned}\right\} \quad (2)$$

This indicates that $g_z > g_x \approx g_y > 2$, since a_1, a_2 and a_3 have negative values.

2) The case where the ground state $(d_{xy})^2(d_{z^2})^1$ is assumed.

By the same procedure we obtained the perturbed ground state wave functions

$$\left.\begin{aligned}\Psi_b^+ &= N_b\left\{|(d_{xy})^2(d_{z^2}^+)^1| + \frac{\sqrt{3}}{2}ikb_1|(d_{xy})^2(d_{yz}^-)^1| \right. \\ &\quad \left. + \frac{\sqrt{3}}{2}ikb_2|(d_{xy})^2(d_{xz}^-)^1|\right\} \\ \Psi_b^- &= N_b\left\{|(d_{xy})^2(d_{z^2}^-)^1| + \frac{\sqrt{3}}{2}ikb_1|(d_{xy})^2(d_{yz}^+)^1| \right. \\ &\quad \left. - \frac{\sqrt{3}}{2}ikb_2|(d_{xy})^2(d_{xz}^+)^1|\right\}\end{aligned}\right\} \quad (3)$$

which include only terms which contribute to g-values. Three g-values are calculated as follows.

$$\left.\begin{aligned}g_z &= 2N_b^2 \\ g_x &= 2N_b^2[1-3k^2b_1] \\ g_y &= 2N_b^2[1-3k^2b_2]\end{aligned}\right\} \quad (4)$$

where N_b, b_1 and b_2 represent normalization constant, $\zeta/\Delta[z^2-yz]$ and $\zeta/\Delta[z^2-xz]$, respectively. g_z is shown to be nearly equal to 2, and g_x and g_y greater than 2.

It is thus predicted that the two possible geometries of low-spin five-coordinate cobalt(II) complexes can be discriminated by means of ESR spectroscopy.

Results and Discussion

Structures and ESR Spectra. Figure 2 shows the ESR spectra of polycrystalline samples of $[CoCldpe_2]ClO_4$ and $[CoNCSdpe_2]ClO_4$, obtained at room temperature using the K-band. For $[CoCldpe_2]ClO_4$, $g_\parallel=2.345$, $g_\perp=2.097$, for $[CoNCSdpe_2]ClO_4$, $g_\parallel=1.998$, $g_\perp=2.225$ are calculated according to the methods of Kneubühl[11] and Sands.[12] The ESR data $[CoXdpe_2]Y$ are summarized in Table 2. It is evident that the ESR patterns can be divided into two classes, (A) complexes with the relation $g_\parallel > g_\perp$ and (B) those with the relation $g_\parallel < g_\perp$.

We see from Eqs. (2) and (4) that the structures of (A) $[CoCldpe_2]ClO_4$ and $[CoBrdpe_2]ClO_4$ are distorted trigonal bipyramids, whereas those (B) $[CoNCSdpe_2]ClO_4$ and $[CoNO_3dpe_2]NO_3$ are square py-

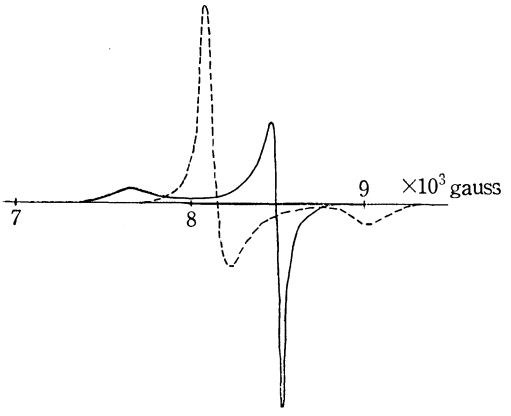

Fig. 2. ESR spectra of $[CoCldpe_2]ClO_4$ and $[CoNCSdpe_2]ClO_4$ polycrystalline samples at room temperature (K-band).

10) Y. Nishida and S. Kida, *This Bulletin*, **45**, 461 (1972); *Chem. Lett.*, **1973**, 57.

11) F. K. Kneubühl, *J. Chem. Phys.*, **33**, 1074 (1960).

12) R. H. Sands, *Phys. Rev.*, **99**, 1222 (1955).

Table 2. ESR data of low-spin five-coordinate cobalt(II) complexes [CoXdpe$_2$]Y

	$g_{\parallel}$		$g_{\perp}$
The powder samples by K-band at 295 K			
[CoCldpe$_2$]ClO$_4$	2.345		2.097
[CoNCSdpe$_2$]ClO$_4$	1.998		2.225
The powder samples by X-band at 295 K			
[CoCldpe$_2$]ClO$_4$	2.26		2.06
[CoBrdpe$_2$ClO$_4$	2.26		2.07
[CoNCSdpe$_2$]ClO$_4$	2.01		2.25
[CoNO$_3$dpe$_2$]	*		2.44
[CoBrdpe$_2$]ClO$_4$·2CHCl$_3$	1.99	2.19	2.27
The CH_2Cl_2 glasses by X-band at 150 K			
[CoCldpe$_2$]ClO$_4$	2.30		2.02
[CoBrdpe$_2$]ClO$_4$	2.27	2.11	2.04
[CoNCSdpe$_2$]ClO$_4$	2.03		2.28
[CoNO$_3$dpe$_2$]NO$_3$	2.00		2.34

* The precise $g_{\parallel}$ value can not be calculated because of the overlapping of two absorptions.

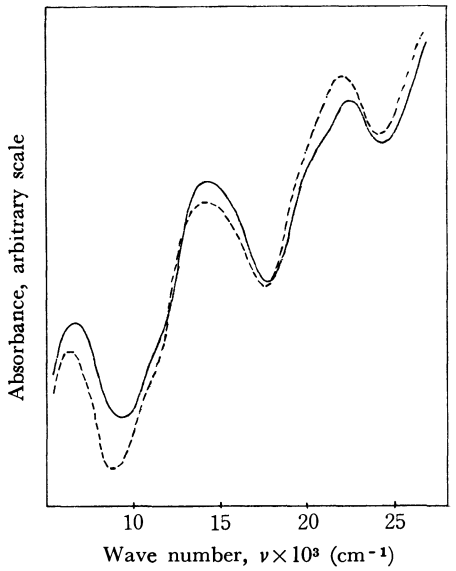

Fig. 3. Reflectance spectra of [CoCldpe$_2$]ClO$_4$ (——) and [CoBrdpe$_2$]ClO$_4$ (----).

ramids. This seems to be in line with the results of electronic spectra. The reflectance spectra of A and B complexes shown in Figs. 3 and 4, respectively, are seen to differ completely. The reflectance spectra of A complexes are very similar to the spectrum of [CoClQP]BPh$_4$,[13] whose structure has been determined by X-ray analysis[14] to be trigonal bipyramid, while those of B complexes are similar to that of [CoBrPNNP]BPh$_4$[15] with a square pyramidal geometry. A good agreement was observed between the results of ESR, electronic spectra and the structures of low-spin five-coordinate cobalt(II) complexes.

13) QP: tris(o-diphenylphosphinophenyl)phosphine, BPh_4^-: tetraphenylborate anion.

14) T. L. Blundell, H. M. Powell, and L. M. Venanzi, *Chem. Commun.*, **1967**, 763.

15) PNNP: tris(2-diphenylphosphinoethyl)amine, L. Sacconi and A. Dei, *J. Coord. Chem.*, **1**, 229 (1971).

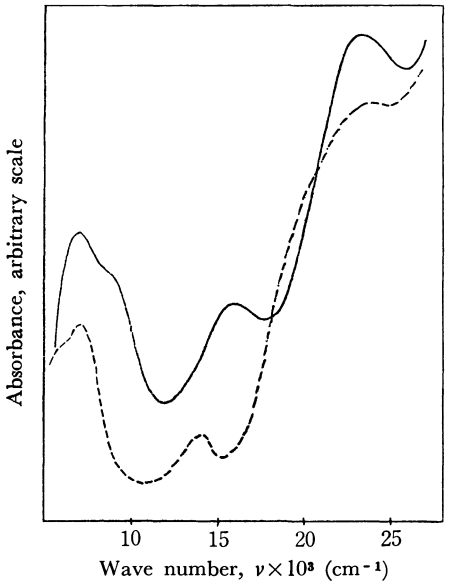

Fig. 4. Reflectance spectra of [CoNCSdpe$_2$]ClO$_4$ (——) and [CoNO$_3$dpe$_2$]NO$_3$ (----).

Although ESR studies of low-spin square pyramidal cobalt(II) complexes have been published, this is the first report on an ESR spectrum of a distorted trigonal bipyramidal cobalt(II) complex. Our ESR data of [CoCldpe$_2$]ClO$_4$ and [CoBrdpe$_2$]ClO$_4$ are similar to those of [CoCldpe$_2$]Cl and [CoBrdpe$_2$]Br, by Horrocks, Van Vecke and Hall,[16] who discussed them on the assumption that the ground state of the latter complexes is $(d_{xy})^2(d_{x^2-y^2})^1$.

Electronic Spectra. In order to interpret the electronic spectra A complexes, the energy difference between the d_{xy} and the $d_{x^2-y^2}$ orbitals, degenerate in the perfect D_{3h} symmetry should be determined. This can be estimated from the results of ESR spectra.

From Eq. (2) we obtain the following result for [CoCldpe$_2$]ClO$_4$.

$$8N_a^2k^2\zeta/\Delta[(x^2-y^2)-xy] \simeq 0.345$$

If we assume N_a^2, $k^2 \approx 1$ and use the value of free ion, $-515\ cm^{-1}$ for ζ, $\Delta[x^2-y^2)-xy]$ is calculated to be $11800\ cm^{-1}$. However, as it is known that k is reduced from unity in the metal complexes[17] and also ζ is reduced from free ion value, it is reasonable to assign the peak at $6500\ cm^{-1}$ and the shoulder at

Table 3. Selection rules for electric dipole

		a_1'	e'	e''
D_{3h} symmetry	a_1'	f	a	f
	e'	a	a	a
	e''	f	a	a
		b_1	a_1	b_2	e
C_{4v} symmetry	b_2	a	f	f	a
	a_1	f	a	f	a
	b_2	f	f	a	a
	e	a	a	a	a

a : allowed, f : forbidden

16) W. D. Horrocks, Jr, G. Van Vecke, and D-D. Hall, *Inorg. Chem.*, **6**, 694 (1967).

10000 cm^{-1} for the electronic transitions, $d_{xy} \rightarrow d_{x^2-y^2}$ and $d_{yz}, d_{xz} \rightarrow d_{x^2-y^2}$, respectively, on the basis of the results of ESR, the splittings of 3d orbitals and the selection rules of the electric dipole transition in D_{3h} symmetry (Table 3).

The electronic spectra of a low-spin trigonal bipyramidal nickel(II) complex show two peaks in the range 15000—25000 cm^{-1}. One peak of large intensity ($\log \varepsilon \sim 3$) in the lower energy region and the another peak of small intensity($\log \varepsilon \sim 2$) in the higher energy region have been assigned to the electronic transitions d_{xy}, $d_{x^2-y^2} \rightarrow d_{z^2}$ and d_{yz}, $d_{xz} \rightarrow d_{z^2}$, respectively.[18] This remarkable difference in the transition probability of two peaks can be explained in terms of selection rules for these electric dipole transitions (Table 3). Using the above results, two peaks at 14000 and 20000 cm^{-1} observed for A complexes can be assigned to the electronic transitions $d_{x^2-y^2} \rightarrow d_{z^2}$ and $d_{xy} \rightarrow d_{z^2}$, respectively. The energy difference between two peaks (14000 and 20000 cm^{-1}) is about 6000 cm^{-1}, which is consistent with the conclusion that the peak at 6500 cm^{-1} can be assigned to the electronic transition $d_{xy} \rightarrow d_{x^2-y^2}$. The peaks due to the electronic transitions $d_{yz}, d_{xz} \rightarrow d_{z^2}$ are observed at 23000 cm^{-1}. Our assignment is partially the same as that of Norgett *et al.*[19] for the complex $[CoNO_3QP]^+$, but they did not observe the electronic transition $d_{xy} \rightarrow d_{x^2-y^2}$.

In order to interpret the electronic spectra of B complexes, we used the results of the electronic spectra of square planar complex $[Codpe_2](ClO_4)_2$ and distorted octahedral complex $[Codgm_2(Ph_3P)_2]$,[20] since the assumed ground state of the latter two complexes is $(d_{xy})^2(d_{z^2})^1$.[21] The absorption peak due to the electronic transition $d_{z^2} \rightarrow d_{xy}$ is observed at 22000 cm^{-1} and 10500 cm^{-1} for $[Codpe_2](ClO_4)_2$ and $[Codgm_2(Ph_3P)_2]$, respectively. It is therefore reasonable to assign the peaks at 16000 cm^{-1} of $[CoNCSdpe_2]ClO_4$ and 14000 cm^{-1} of $[CoNO_3dpe_2]NO_3$ to the electronic transition $d_{z^2} \rightarrow d_{xy}$. Other peaks at 7000, 9000 and 23000 cm^{-1} of $[CoNCSdpe_2]ClO_4$ are assigned to the electronic transitions $d_{yz}, d_{xz} \rightarrow d_{z^2}$, $d_{x^2-y^2} \rightarrow d_{z^2}$ and $d_{yz}, d_{xz}, d_{x^2-y^2} \rightarrow d_{xy}$, respectively. The intensities of these peaks are also elucidated in terms of selection rules of electric dipole transitions in C_{4v} symmetry (Table 3).

Novel Configurational Change. We found a novel configurational change by adduct formation of chloroform for the complex $[CoBrdpe_2]ClO_4$. From the results of ESR and electronic spectra, the structure of green $[CoBrdpe_2]ClO_4$ is assumed to be a distorted trigonal bipyramid. When this green complex was recrystallized from a hot chloroform solution, red prisms were obtained. The result of elemental analysis is compatible with that of the adduct of chloroform of the parent complex $[CoBrdpe_2]ClO_4 \cdot 2CHCl_3$. The results of infrared spectra of the green and the red complexes also support the empirical formula. Two molecules of chloroform of the red complex can be removed at 110 °C in a vacuum, the color turning green. The ESR and reflectance spectra are shown in Figs. 5 and 6, respectively. It is estimated that the structure of the red complex is a distorted square pyramid and ground state is $(d_{xy})^2(d_{z^2})^1$, since the reflectance spectrum is quite similar to the spectra of B complexes and the ESR spectrum shows a small in-plane anisotropy.

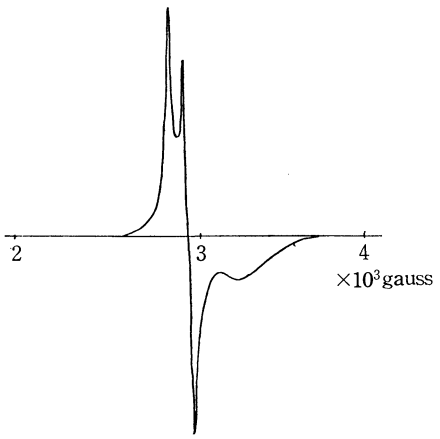

Fig. 5. ESR spectrum of $[CoBrdpe_2]ClO_4 \cdot 2CHCl_3$ polycrystalline sample at room temperature (X-band).

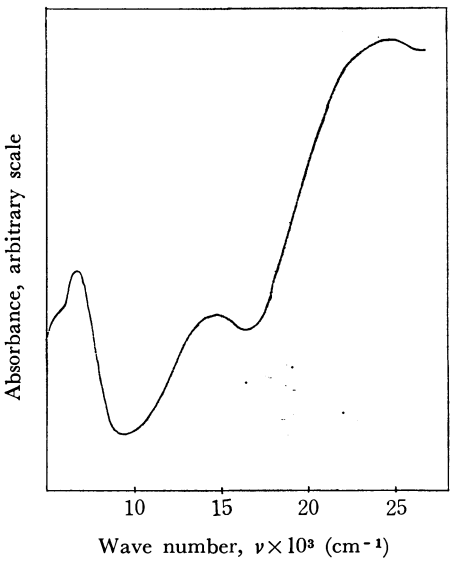

Fig. 6. Reflectance spectrum of $[CoBrdpe_2]ClO_4 \cdot 2CHCl_3$.

ESR Spectra of Glasses. The ESR spectra of $[CoCldpe_2]ClO_4$, $[CoNCSdpe_2]ClO_4$ and $[CoNO_3dpe_2]NO_3$ in CH_2Cl_2 glasses at 150 K are similar to those of polycrystalline samples. However, the situation differs for $[CoBrdpe_2]ClO_4$. The ESR spectrum of green $[CoBrdpe_2]ClO_4$ in CH_2Cl_2 glass at 150 K shows a typical rhombic symmetry, very similar to that of red $[CoBrdpe_2]ClO_4 \cdot 2CHCl_3$ in CH_2Cl_2 glass at 150 K (Fig. 7). This might be attributed to the existence of both, the trigonal bipyramid and the square pyramid in a solution.

17) M. Gerloch and J. R. Miller, *Progr. Inorg. Chem.*, **10**, 1 (1968).
18) O. St. C. Headley, R. S. Nyholm, C. A. McAuliffe, L. Sindellari, M. L. Tobe, and L. M. Venanzi, *Inorg. Chim. Acta.*, **4**, 93 (1970).
19) M. J. Norgett, L. H. M. Thornley, and L. M. Venanzi, *J. Chem. Soc., A*, **1967**, 540.
20) dgm: dimethylglyoximato anion, Ph_3P: triphenylphosphine, G. N. Schrauzer and R. J. Windgassen, *Chem. Ber.*, **99**, 602 (1966).
21) Y. Nishida, unpublished work.

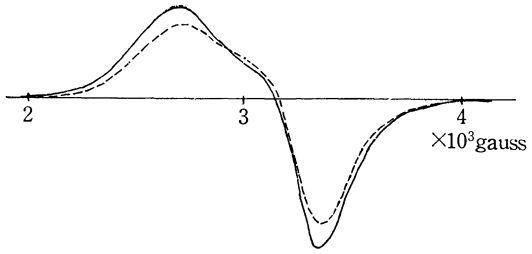

Fig. 7. ESR spectra of $[CoBrdpe_2]ClO_4$ (——) and $[CoBrdpe_2]ClO_4 \cdot 2CHCl_3$ in CH_2Cl_2 glasses at 150 K (X-band).

Magnetic Moments. The magnetic moments of these low-spin five-coordinate cobalt(II) complexes $[CoXdpe_2]Y$ fluctuate in the range 2.0—2.3 B.M., which is lower than that of square planar complexes, and higher than that of the octahedral complexes.[10] This can be elucidated according to the equation of Van Vleck, using the results of ESR and electronic spectra.

Conclusion

It was confirmed that two possible geometries, the trigonal bipyramid and the square pyramid, of low-spin five-coordinate cobalt(II) complexes can be discriminated by means of ESR spectroscopy.

The electronic spectra of both geometries have been characterized by means of ESR spectra and selection rules for electric dipole transitions. The absorption peak due to the electronic transition $d_{xy} \rightarrow d_{x^2-y^2}$ of a trigonal bipyramidal complex has been identified from the result of an ESR spectrum.

Acknowledgment: We wish to express our sincere thanks to Professor S. Kida for his valuable discussion. We also thank Professor S. Misumi and Dr. T. Isobe for use of the ESR apparatus and Professor Y. Murakami and Dr. Y. Matsuda for ESR measurement by the K-band.

BULLETIN OF THE CHEMICAL SOCIETY OF JAPAN, VOL. 46, 2410—2416 (1973)

Metal Complexes Containing Six-membered Chelate Rings. III. Preparation and Structure of Mono- and Bis(2,4-Pentanediamine)cobalt(III) Complexes Containing Acetylacetonate or Oxalate Ion[1]

Fujio Mizukami, Haruko Ito, Junnosuke Fujita, and Kazuo Saito

Department of Chemistry, Faculty of Science, Tohoku University, Aoba, Aramaki, Sendai 980

(Received December 18, 1972)

New cobalt(III) complexes $[Co(acac)_2(2,4\text{-ptn})]^+$, $[Co(acac)(2,4\text{-ptn})_2]^{2+}$ and $[Co(ox)(2,4\text{-ptn})_2]^+$ have been synthesized, resolved into optical isomers and their structures determined; 2,4-ptn=optically active (*RR* and *SS*) and *meso* (*RS*) 2,4-pentanediamine, acac=acetylacetonate ion, ox=oxalate ion. The patterns of circular dichroism spectra of these complexes in the first absorption band region are very similar to those of the corresponding α-diamine cobalt(III) complexes.

Kawaguchi *et al.*[2] recently determined the absolute configuration of $(-)_{589}$-$[Co(acac)(tn)_2]^{2+}$ (tn=trimethylenediamine) as *Δ*. This complex shows a main circular dichroism (CD) band with positive sign in the first absorption band region. The result agrees with that of a number of chiral complexes of cobalt(III) containing such five-membered chelate rings as ethylenediamine (en). The CD curve of *Δ*-$[Co(tn)_3]^{3+}$ is known to differ greatly from that of *Δ*-$[Co(en)_3]^{3+}$ in the first absorption band region.[3] Mason[4] proposed a new regional rule for a metal complex to account for such a difference. We have reported[1] that the *tris*-cobalt(III) complexes of *meso*(*RS*)- and optically active (*RR* or *SS*)-2,4-pentanediamine showed CD curves differing from those of both $[Co(en)_3]^{3+}$ and $[Co(tn)_3]^{3+}$, while the optically active 2,4-pentanediamine chelate gave vicinal contribution to the CD similar to that of the optically active propylenediamine (pn) chelate. In order to elucidate the optical activity of metal complexes, therefore, it is desirable to accumulate CD data on those complexes containing six-membered chelates.

This paper deals with preparation of optically active cobalt(III) complexes containing 2,4-pentanediamine and acetylacetonate or oxalate ion and their stereochemistry on the basis of CD and pmr spectra.

Experimental

Optically active-(*RR* and *SS*) and *meso*-(*RS*) 2,4-pentanediamine were synthesized according to the method reported previously.[5]

Δ-$(-)_{546}$-$[Co(acac)_2(RR\text{-}2,4\text{-}ptn)](ClO_4)$. This was synthesized according to a method similar to that for the cor-

1) Part II of this series, F. Mizukami, H. Ito, J. Fujita, and K. Saito, This Bulletin, **45**, 2129 (1972).

2) H. Kawaguchi, K. Matsumoto, H. Kuroya, and S. Kawaguchi, *Chem. Lett.*, **1972**, 125.

3) F. Woldbye, *Rec. Chem. Progr.*, **24**, 197 (1963). P. G. Beddoe and S. F. Mason, *Inorg. Nucl. Chem. Lett.*, **4**, 433 (1968). J. R. Gollogly and C. J. Hawkins, *Chem. Commun.*, **1968**, 689. R. R. Judkins and D. J. Royer, *Inorg. Nucl. Chem. Lett.*, **6**, 305 (1970). P. G. Beddoe, M. J. Hardings, S. F. Mason, and B. J. Peart, *Chem. Commun.*, **1971**, 1283.

4) S. F. Mason, *J. Chem. Soc., A*, **1971**, 667.

5) F. Mizukami, H. Ito, J. Fujita, and K. Saito, This Bulletin, **44**, 3051 (1971).

responding ethylenediamine complex.[6] Charcoal (1.5 g) and *RR*-2,4-pentanediamine (0.66 g) were added to a 20% aqueous methanol solution (80 ml) of $Na[Co(acac)_2(NO_2)_2]\cdot 5H_2O$[7] (3 g) with stirring at room temperature. After 20 min, the charcoal was filtered off and washed with 10 ml of water. The filtrate and washings were combined, and then evaporated to about 35 ml at about 50 °C under reduced pressure. The solution was passed through a column containing cation exchanger Dowex 1-X4 in sodium form. The column was washed with water to remove tris(acetylacetonato)cobalt(III). At this stage the column gave two separated bands, violet and red ($[Co(acac)(RR\text{-}2,4\text{-}ptn)_2]^{2+}$). The violet band was eluted with 0.3 M sodium perchlorate solution, but the two diastereoisomers did not separate in the column. Thus, each fraction was checked by its CD and absorption spectrum. Fractions showing similar spectral data were collected, and evaporated under reduced pressure. Crystals thus obtained were recrystallized fractionally from water until the CD exhibited a constant curve. Less soluble crystals seemed to be a pseudo-racemate of Δ and Λ isomers, and only the more soluble $(-)_{546}$-isomer was obtained as pure optically active diastereoisomer, its yield appearing to be greater (>60%) than that of the other.

Found: C, 39.01; H, 6.14; N, 5.95%. Calcd for $C_{15}H_{28}N_2O_8CoCl$: C, 39.27; H, 6.15; N, 6.11%.

Δ-$(-)_{589}$-[Co(acac)(RR-2,4-ptn)$_2$](ClO$_4$)$_2$. To an aqueous solution (25 ml) of *trans*-$[CoCl_2(RR\text{-}2,4\text{-}ptn)_2]ClO_4$[1] (1 g) was added sodium acetylacetonate (0.28 g). The solution was stirred for half an hour at 60 °C, and cooled to room temperature. A red powder was precipitated by addition of sodium perchlorate (5 g) in 3 ml of water, filtered off and air dried. More complex was obtained by evaporating the filtrate in a desiccator over diphosphorus pentoxide under reduced pressure. Total yield: 1.2 g (93%). The crude complex was a mixture of Δ and Λ diastereoisomers, and separated into optical isomers by fractional recrystallization from water. Pure $(-)_{589}$-isomer (0.7 g) was obtained, but $(+)_{589}$-isomer was always accompanied by a small amount of $(-)_{589}$-isomer. The pmr spectrum of the crude complex showed that the $(-)_{589}$-isomer was obtained in much greater yield (>75%) than the $(+)_{589}$-isomer.

Found: C, 31.98; H, 6.28; N, 9.94%. Calcd for $C_{15}H_{35}N_4O_{10}CoCl_2$: C, 32.10; H, 6.29; N, 9.98%.

Δ,Λ-[Co(acac)$_2$(RS-2,4-ptn)](ClO$_4$). To a 20% aqueous ethanol solution (125 ml) of $Na[Co(acac)_2(NO_2)_2]\cdot 5H_2O$ (5 g) were added 2.5 g of charcoal and 1 g of *RS*-2,4-pentanediamine. The solution was stirred for 15 min at room temperature, and the charcoal was then filtered off and washed with 30 ml of water. The filtrate and washings were combined, and 35 g of sodium perchlorate in 30 ml of water was added. After a while, a red powder ($[Co(acac)(RS\text{-}2,4\text{-}ptn)_2](ClO_4)_2$) precipitated was filtered off. To the filtrate was added more sodium perchlorate (35 g). On cooling the solution at 0 °C for 1.5 hr, more $[Co(acac)(RS\text{-}2,4\text{-}ptn)_2](ClO_4)_2$ was precipitated almost completely, and then filtered off. The filtrate was cooled again at 0 °C for 5 hr. Purple crystals thus formed were filtered off, and recrystallized from hot ethanol. Yield: 1.3 g.

Found: C, 39.01; H, 6.34; N, 6.40%. Calcd for $C_{15}H_{28}N_2O_8CoCl$: C, 39.27; H, 6.15; N, 6.11%.

Λ-$(+)_{546}$-[Co(acac)$_2$(RS-2,4-ptn)]$^+$. Δ,Λ-$[Co(acac)_2(RS\text{-}2,4\text{-}ptn)](ClO_4)$ (1 g) and sodium hydrogendibenzoyltartrate (0.45 g) (2 : 1 mole ratio) were dissolved in 100 ml of water with stirring at about 80 °C. The solution was cooled gradually to room temperature. A purple powder was precipitated, filtered off, washed with a small amount of water and air dried. (0.7 g). This was dissolved in an appropriate amount of ethanol containing an excess mole of silver perchlorate. The silver hydrogen dibenzoyltartrate was filtered off, and the filtrate was evaporated to dryness. The residue was dissolved again in a small amount of water, and filtered. The filtrate was gradually evaporated to remove less soluble racemic perchlorate which was filtered off occasionally. Evaporation was continued until the ratio of $\Delta\varepsilon$ and ε values of the filtrate became constant. From the final filtrate, more soluble optically active perchlorate was obtained crystalline but it was contaminated with silver perchlorate which could not be removed completely. Thus the quantitative CD curve of this isomer was determined with the aid of the ε values of the racemate.

Δ,Λ-[Co(acac)(RS-2,4-ptn)$_2$](ClO$_4$)$_2\cdot H_2O$. To a suspension of *trans*-$[CoCl_2(RS\text{-}2,4\text{-}ptn)_2]Cl$ (5 g) in 50 ml of water was added an aqueous solution (50 ml) of sodium acetylacetonate (2 g), and this was warmed at 70 °C for 2 hr. After cooling, the solution was filtered and excess sodium perchlorate was added to the filtrate. Red crystals were precipitated, filtered off and recrystallized from water (75 °C). The complex thus obtained was assigned tentatively to *cis-cis* isomer of three possible geometrical isomers. Attempts to resolve this complex into optical isomers with sodium hydrogendibenzoyltartrate were only partially successful.

Found: C, 31.02; H, 6.91; N, 9.36%. Calcd for $C_{15}H_{37}N_4O_{13}CoCl_2$: C, 31.10; H, 6.44; N, 9.67%.

trans-cis-*Δ,Λ-[Co(ox)(RS-2,4-ptn)$_2$]Cl·2H$_2$O (less soluble isomer in water).* A solution of $[Co(NO_2)_2(RS\text{-}2,4\text{-}ptn)_2]NO_2$[8] (2.2 g) and oxalic acid (2 g) in 70 ml of water was warmed at 60—70 °C for 1 hr. To this was added 10 ml of concentrated hydrochloric acid dropwise over a period of 2 hr with warming at 60—70 °C, which was then cooled to room temperature. Pink flakes were filtered off, washed with a small amount of water and ethanol, and air dried. Yield: 1 g. This complex is hardly soluble in water. The other geometrical isomer, *cis-cis*-$[Co(ox)(RS\text{-}2,4\text{-}ptn)_2]Cl$ was highly soluble in water and was obtained from the filtrate.

Found: C, 33.75; H, 7.62; N, 13.25%. Calcd for $C_{12}H_{32}N_4O_6CoCl$: C, 34.09; H, 7.63; N, 13.25%.

Δ-$(-)_{510}$- and Λ-$(+)_{510}$-trans-cis-[Co(ox)(RS-2,4-ptn)$_2$]ClO$_4\cdot 2H_2O$. To a suspension of Δ,Λ-*trans-cis*-$[Co(ox)(RS\text{-}2,4\text{-}ptn)_2]Cl\cdot 2H_2O$ (0.8 g) in 50 ml of water was added silver nitrate (0.3 g) with stirring. After 30 min, silver chloride was filtered off, and washed with 50 ml of water. The filtrate and washings were combined, and stirred with sodium hydrogendibenzoyltartrate (0.38 g) for 2 hr at 60 °C. A pink powder was precipitated upon cooling at room temperature and filtered off to give crude dibenzoyltartrate salt of $(-)_{510}$-isomer (0.6 g). The filtrate was stored to obtain $(+)_{510}$-isomer. The crude dibenzoyltartrate was converted into perchlorate by treating with 99% acetic acid saturated with magnesium perchlorate. The crude perchlorate of $(-)_{510}$-isomer was recrystallized from water fractionally until the CD showed a constant curve. The pure optically active perchlorate is much more soluble in water than the racemate. The filtrate free of pink powder was stirred with an excess of anion exchanger Dowex 1-X4 in

6) L. J. Boucher and J. C. Bailar, Jr., *J. Inorg. Nucl. Chem.* **27**, 1093 (1965). L. J. Boucher, *Inorg. Chem.*, **6**, 2162 (1967).

7) A. Rosenheim and A. Garfunkel, *Ber.*, **44**, 1865 (1911).

8) C. J. Dippel and F. M. Jaeger, *Rec. Trav. Chim.*, **50**, 525 (1931).

perchlorate form for 4 hr at room temperature. The anion exchanger was filtered off, and washed with a small amount of water. The filtrate and washings were combined, evaporated to 40 ml at 55 °C under reduced pressure and filtered to remove less soluble racemate. Crystals were obtained fractionally from the filtrate by evaporation in a vacuum desiccator over diphosphorus pentoxide. Each fraction was checked by its CD, and pure perchlorate salt of $(+)_{510}$-isomer was obtained by repeating such fractional recrystallization.

Found: C, 29.85; H, 6.47; N, 11.78%. Calcd for $C_{12}H_{32}N_4O_{10}CoCl$: C, 29.61; H, 6.59; N, 11.51%.

*cis-cis-Δ,Λ-[Co(ox)(*RS*-2,4-ptn)$_2$]Cl·6H$_2$O (more soluble isomer in water).* A suspension of *trans*-[$CoCl_2$(*RS*-2,4-ptn)$_2$]Cl (6 g) and oxalic acid (2.1 g) in 110 ml of water was warmed at 70 °C for 2.5 hr and cooled to room temperature. A mixture of *cis-cis*- and *trans-cis*-isomer was obtained, and separated by recrystallization from 50 ml of hot water. More soluble *cis-cis*-isomer was condensed in the filtrate, and crystallized by evaporation in a vacuum desiccator over diphosphorus pentoxide. A pure complex was obtained by recrystallizing from hot water. Yield: *cis-cis*-isomer 7.2 g. *trans-cis*-isomer 0.3 g.

Found: C, 29.14; H, 7.48; N, 11.39%. Calcd for $C_{12}H_{40}N_4O_{10}CoCl$: C, 29.13; H, 8.15; N, 11.32%.

*Δ-(+)$_{510}$- and Λ-(−)$_{510}$-cis-cis-[Co(ox)(*RS*-2,4-ptn)$_2$]-ClO$_4$·4H$_2$O.* To a solution of *Δ,Λ-cis-cis*-[Co(ox)(*RS*-2,4-ptn)$_2$]Cl·6H$_2$O (1 g) in 50 ml of water was added sodium hydrogendibenzoyltartrate (0.44 g) in 20 ml of water. The solution was stirred for 2 hr at 60 °C. A red powder was precipitated upon cooling at room temperature and filtered off. The powder was crude dibenzoyltartrate of $(+)_{510}$-isomer, and converted into perchlorate as in the case for the *trans-cis*-isomer. The filtrate was stirred with anion exchanger Dowex 1-X4 in perchlorate form (3 g) for 4 hr at room temperature. The anion exchanger was filtered off and washed with a small amount of water. The filtrate and washings were combined, and crystallized fractionally by evaporation of the solution in a vacuum desiccator over diphosphorus pentoxide. Fractions which exhibited similar CD were combined and recrystallized from water until the CD of $(-)_{510}$-isomer became constant.

Found: C, 27.99; H, 6.86; N, 10.50%. Calcd for $C_{12}H_{36}N_4O_{12}CoCl$: C, 27.57; H, 6.94; N, 10.72%.

*Λ-(+)$_{546}$-[Co(ox)(*SS*-2,4-ptn)$_2$]ClO$_4$.* A solution of *trans*-[$CoCl_2$(*SS*-2,4-ptn)$_2$]ClO_4 (1 g) and oxalic acid (0.5 g) in 30 ml of water was warmed at 65 °C for 2 hr, and evaporated to dryness at 50 °C under reduced pressure. The residue, a mixture of *Δ* and *Λ* isomer, was separated into diastereoisomers by fractional recrystallization from water. Both isomers were very soluble in water, only less soluble *Λ*-isomer with a constant CD being obtained crystalline.

Found: C, 30.55; H, 6.14; N, 12.19%. Calcd for $C_{12}H_{30}N_4O_9CoCl$: C, 30.75; H, 6.45; N, 11.95%.

Measurements. Visible and ultraviolet absorption spectra were recorded with a Hitachi 124 recording spectrophotometer. The CD curves were recorded with a Model ORD/UV-5 spectrophotometer of JASCO with its CD attachment. PMR spectra in D_2O and in a mixed solvent of D_2O and pyridine were obtained with a Varian T-60 spectrometer using Na-TMS as internal standard. All the measurements were carried out at room temperature.

9) R. J. York, W. D. Bonds, Jr., B. P. Cotsoradis, and R. D. Archer, *Inorg. Chem.*, **8**, 789 (1969). S. H. Laurie, *J. Chem. Soc. Dalton*, **1972**, 573.

Results and Discussion

Structure of the Complexes. A pair of diastereoisomers *Δ* and *Λ* are possible for the complexes [Co(acac)$_2$(*RR*-2,4-ptn)]$^+$ and [Co(acac)(*RR*-2,4-ptn)$_2$]$^{2+}$. However, only one pure isomer was obtained for each complex. Purity can be checked by pmr spectra, since the pairs of isomers are not enantiomeric with each other and the stereochemical environments of the protons on the chelate rings may differ for the two diastereoisomers.

Figure 1a shows the pmr spectrum of $(-)_{546}$-[Co(acac)$_2$(*RR*-2,4-ptn)]$^+$ in D_2O. A sharp doublet at 1.2 ppm, a doublet at 2.2 ppm and a singlet at 5.8 ppm are assigned to the methyl signal of the diamine chelate,[1] two kinds of methyl signals Me_1 and Me_2 (Fig. 2b) and the methylene signal of the acetylacetonato chelate,[9] respectively. The appearance of a single doublet of the methyl signal on the diamine chelate may indicate that the complex ion has C_2 symmetry, and that the diamine chelate takes a *λ*-skew boat conformation with two equatorial methyl groups (Fig. 2b). The pmr spectrum of unresolved [Co(acac)$_2$(*RR*-2,4-ptn)]$^+$ is more complex than that of the $(-)_{546}$-isomer, and reveals itself as a mixture of the two diastereoisomers (Fig. 1b).

A similar difference is seen between $(-)_{546}$-[Co(acac)(*RR*-2,4-ptn)$_2$]$^{2+}$ and a mixture of the two diastereoisomers. Each diastereoisomer should have two kinds of methyl groups Me_1 and Me_2 in the diamine chelate, whenever the chelates are in a *λ*-skew boat conformation (Fig. 2g). However, the spectrum of the $(-)_{546}$-isomer at 60 MHz shows no such presence (Fig. 3a). This might be due to the small difference in chemical shift between Me_1 and Me_2. A mixture of the two diastereoisomers gives a quartet signal due to the methyl groups of the diamine chelates. The mole ratio of the two isomers can be determined by the intensity of each peak (Fig. 3b).

[Co(acac)$_2$(*RS*-2,4-ptn)]$^+$ has no symmetry element except C_1, even thought the *RS*-2,4-pentanediamine chelate takes a fixed chair conformation with two equa-

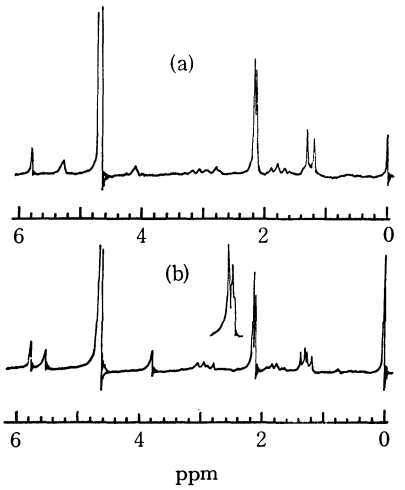

Fig. 1. a) PMR spectra of *Δ*(−)$_{546}$-[Co(acac)$_2$(*RR*-2,4-ptn)]$^+$, b) *Δ,Λ*-[Co(acac)$_2$(*RR*-2,4-ptn)]$^+$ in D_2O.

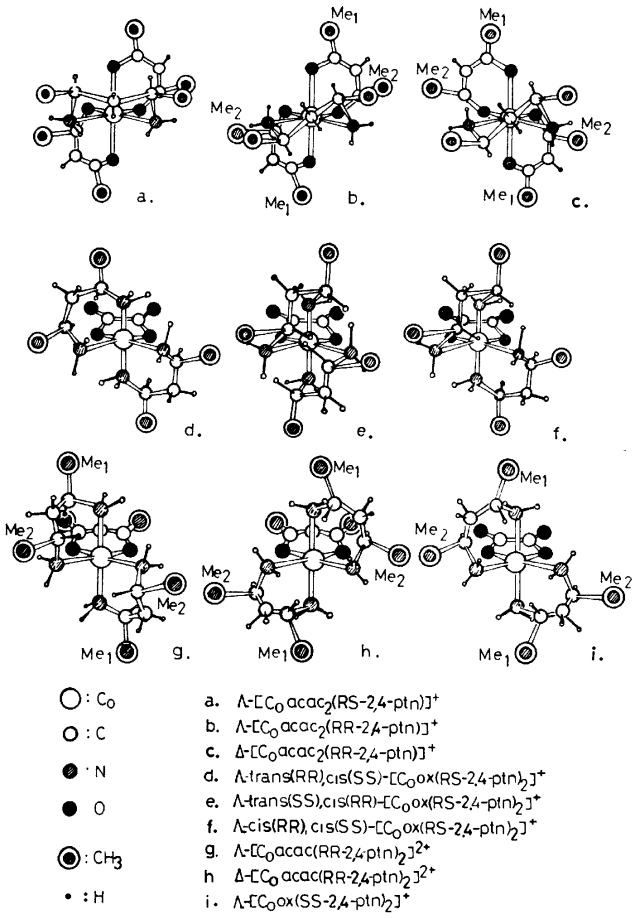

Fig. 2. Schematic structures of $[Co(AA)_{2,1}(2,4\text{-ptn})_{1,2}]$ (AA =acac$^-$, ox^{2-}).

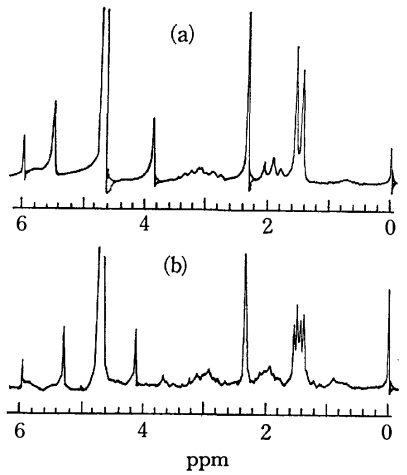

Fig. 3. PMR spectra of a) $\Delta(-)_{589}$-$[Co(acac)(RR\text{-}2,4\text{-ptn})_2]^{2+}$, b) Δ,Λ-$[Co(acac)(RR\text{-}2,4\text{-ptn})_2]^{2+}$ in D_2O.

torial methyl groups.[10] Therefore, the two methyl groups of the diamine chelate and the four methyl and the two methyne groups of the acetylacetonato chelates should all be in different environments. However, the pmr spectrum of the complex shows such a clear difference only on the methyne signal (Fig. 4a).

For the complexes of the type $[Co(AA)(RS\text{-}2,4\text{-ptn})_2]$ (AA=acac$^-$, ox^{2-}), three geometrical isomers can exist with respect to the location of the asymmetric carbon atoms of the diamine. These isomers are designated as *cis(RR)cis(SS)*, *trans(RR)cis(SS)* and *trans(SS)cis(RR)* (Fig. 2d, e, f). Each geometrical isomer has two optical isomers Δ and Λ, Of these six isomers, an enantiomeric pair, *Λ-trans(SS)cis(RR)* and *Δ-trans(RR)cis(SS)*, seems to have steric hindrance between the diamine chelates (Fig. 2e). Accordingly, two enantiomeric pairs, *Λ-cis(RR)cis(SS)* and *Δ-cis(SS)cis(RR)*, and *Λ-trans(RR)cis(SS)* and *Δ-trans(SS)-cis(RR)*, may be formed.

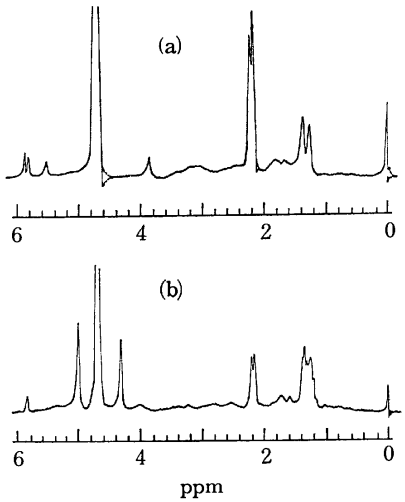

Fig. 4. PMR spectra of a) $\Delta\Lambda$-$[Co(acac)_2(RS\text{-}2,4\text{-ptn})]^+$, b) Δ,Λ-$[Co(acac)(RS\text{-}2,4\text{-ptn})_2]^{2+}$ in D_2O.

We have obtained two geometrical isomers of racemic $[Co(ox)(RS\text{-}2,4\text{-ptn})_2]^+$, *cis-cis*(more soluble isomer in water) and *trans-cis*(less soluble isomer in water) isomer, and resolved them into optical isomers.

For $[Co(acac)(RS\text{-}2,4\text{-ptn})_2]^{2+}$, only a *cis-cis* geometrical isomer has been obtained, its optical resolution being only partially successful (see Experimental).

Since the *RS*-2,4-pentanediamine chelate would be in a chair conformation, the symmetries of *cis-cis* and *trans-cis* isomers are C_1 and C_2, respectively (Fig. 2). Thus the former has four unequivalent methyl groups and the latter two kinds of methyl groups on the diamine chelate. We see from Fig. 5b that the pmr spectrum of *Λ*-$(+)_{510}$-*cis(RR)cis(SS)*-$[Co(ox)(RS\text{-}2,4\text{-ptn})_2]^+$ in a mixed solvent of pyridine and D_2O (1 : 4 in volume) clearly exhibits an octet signal due to the methyl groups of the diamine, although the *Λ*-$(+)_{510}$-*trans(RR)cis(SS)*-$[Co(ox)(RS\text{-}2,4\text{-ptn})_2]^+$ gives a triplet signal which seems to be an accidental overlapping of two doublet signals (Fig. 5a). Thus we can determine the geometrical structure of the isomers by pmr spectra. A mixed solvent of pyridine and D_2O is more effective for the present complexes than D_2O, since it makes the difference in chemical shifts of the unequivalent methyl groups greater. The pmr spectrum of *Λ*-$(+)_{510}$-*trans(RR)cis(SS)*-$[Co(ox)(RS\text{-}2,4\text{-ptn})_2]^+$ in D_2O shows only a doublet methyl signal (Fig. 5c).

The only isomer of $[Co(acac)(RS\text{-}2,4\text{-ptn})_2]^{2+}$ we obtained can be assigned to the *cis-cis* structure, since its pmr spectrum shows two kinds of methyl signals for

10) T. G. Appleton and J. R. Hall, *Inorg. Chem.*, **9**, 1807 (1970).

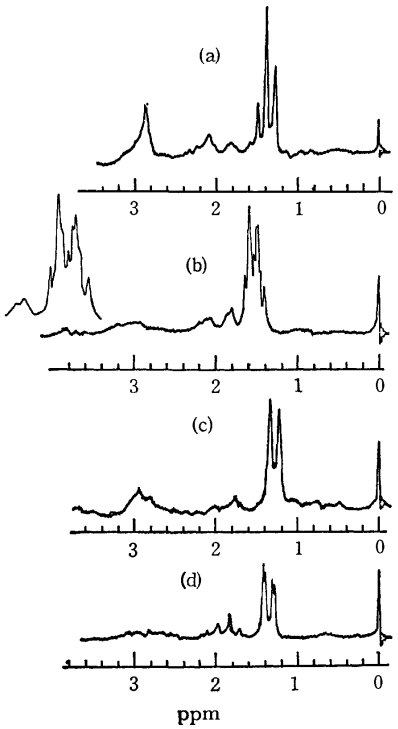

Fig. 5. PMR spectra of a) $\Lambda(+)_{510}$-*trans*(*RR*)*cis*(*SS*)-[Co(ox)(*RS*-2,4-ptn)$_2$]$^+$ in D_2O-pyridine mixed solvent, b) $\Lambda(+)_{510}$-*cis*(*RR*)*cis*(*SS*)-[Co(ox)2,4-ptn)$_2$]$^+$ in D_2O-pyridine mixed solvent, c) $\Lambda(+)_{510}$-*trans*(*RR*)*cis*(*SS*)-[Co(ox)(*RS*-2,4-ptn)$_2$]$^+$ in D_2O, d) $\Lambda(+)_{546}$- or Δ,Λ-[Co(ox)(*SS*-2,4-ptn)$_2$[$^+$ in D_2O.

the acetylacetonato chelate (Fig. 4b).

[Co(ox)(*SS*-2,4-ptn)$_2$]$^+$ gives a pair of diastereoisomers, Δ and Λ. However, the pmr spectrum of Λ-isomer at 60 MHz is almost the same as that of a diastereoisomeric mixture Δ and Λ, no detectable chemical shift difference being observed in the methyl signals (Fig. 5d).

CD Spectra. The absorption and CD spectra of the optical isomers we prepared are shown in Figs.

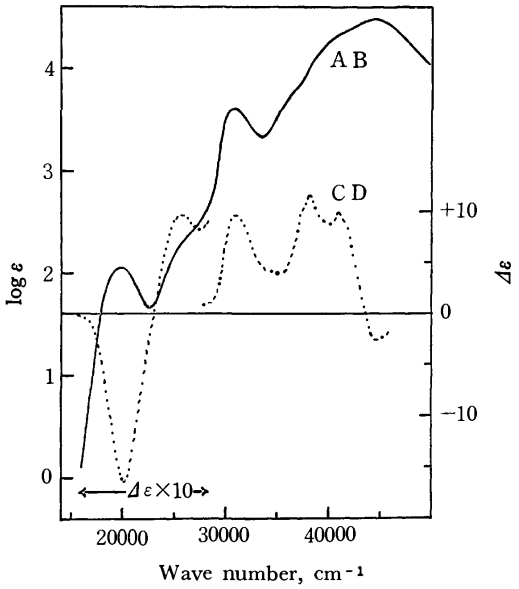

Fig. 6. Absorption (AB) and CD spectra of $\Lambda(-)_{589}$-[Co(acac)(*RR*-2,4-ptn)$_2$]$^{2+}$ in water.

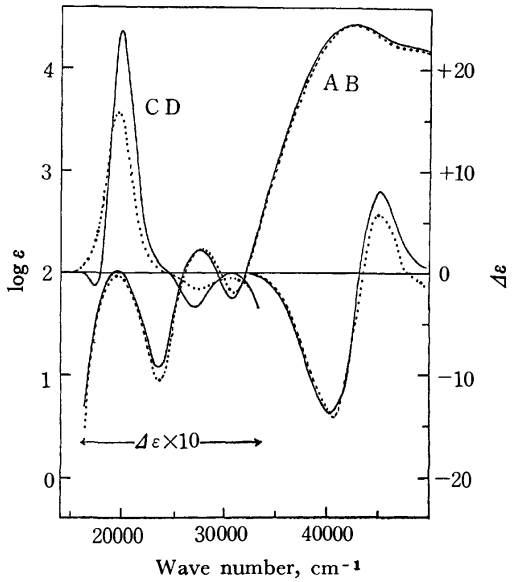

Fig. 7. Absorption (AB) and CD spectra of (——) $\Lambda(+)_{510}$-*trans*(*RR*)*cis*(*SS*)-[Co(ox)(*RS*-2,4-ptn)$_2$]$^+$, (·····) $\Lambda(+)_{510}$-*cis*(*RR*)*cis*(*SS*)-[Co(ox)(*RS*-2,4-ptn)$_2$]$^+$ in water.

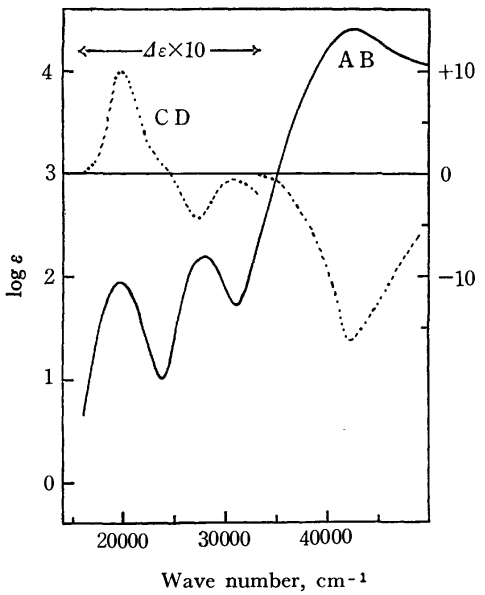

Fig. 8. Absorption (AB) and CD spectra of $\Lambda(+)_{546}$-[Co(ox)(*SS*-2,4-ptn)$_2$]$^+$ in water.

6—9 and their numerical data in Table 1. Assignment of the absolute configurations of the complexes was made by comparison of their CD patterns in the first absorption band region with those of the related complexes of known absolute configuration.

The CD curve of Λ-[Co(en)$_3$]$^{3+}$ [11] (five-membered chelate) differs greatly from that of Λ-[Co(tn)$_3$]$^{3+}$ [12] (six-membered chelate) in the first absorption band region.[3] The main CD band of the former is strong and has positive sign (+1.89), while that of the latter is very weak and has negative sign (−0.14). On the

11) Y. Saito, K. Nakatsu, M. Shiro, and H. Kuroya, This Bulletin, **30**, 795 (1957).

12) Y. Saito, T. Nomura, and F. Marumo, *ibid.*, **41**, 530 (1968).

TABLE 1. NUMERICAL DATA OF ABSORPTION (AB) AND CIRCULAR DICHROISM (CD) ν IN $10^3\,cm^{-1}$, ($\log\varepsilon$) AND ($\varepsilon_l-\varepsilon_r$)

Complex	AB	CD
$\Lambda(+)_{546}$-[Co(acac)$_2$(*RS*-2,4-ptn)]ClO_4	18.62 (2.08)	17.30 (−1.41)
		19.42 (+3.66)
	ca. 25.3 (*ca.* 2.4)	25.00 (−3.03)
	31.00 (3.81)	30.30 (−51.79)
$\Lambda(-)_{546}$-[Co(acac)$_2$(*RR*-2,4-ptn)]ClO_4	18.52 (2.08)	17.33 (+1.28)
		19.42 (−2.78)
	ca. 25.3 (*ca.* 2.5)	25.13 (+2.15)
	30.96 (3.82)	30.58 (+30.63)
		35.97 (+3.50)
	ca. 40.7 (*ca.* 4.4)	39.37 (−44.50)
	44.05 (4.49)	46.30 (+12.00)
$\Lambda(-)_{589}$-[Co(acac)(*RR*-2,4-pin)$_2$]$(ClO_4)_2$	19.80 (2.06)	20.08 (−1.64)
	ca. 26.0 (*ca.* 2.3)	25.84 (+0.96)
	30.86 (3.61)	30.96 (+9·63)
		38.17 (+11.72)
	ca. 41.0 (*ca.* 4.3)	40.98 (+9.98)
	44.44 (4.48)	44.64 (−2.74)
$\Lambda(+)_{510}$-*trans*(*RR*)*cis*(*SS*)[Co(ox)(*RS*-2,4-ptn)$_2$]$ClO_4\cdot 2H_2O$	19.61 (2.01)	17.39 (−0.13)
		19.88 (+2.36)
	27.62 (2.22)	27.03 (−0.34)
	42.55 (4.43)	40.32 (−13.75)
		45.05 (+8.13)
$\Lambda(+)_{510}$-*cis*(*RR*)*cis*(*SS*)[Co(ox)*RS*-2,4-ptn)$_2$]ClO_4-$4H_2O$	19.61 (1.96)	19.65 (+1.57)
	27.86 (2.23)	27.40 (−0.16)
	42.55 (4.42)	40.65 (−14.13)
		45.05 (+5.78)
$\Lambda(+)_{546}$-[Co(ox)(*SS*-2,4-ptn)$_2$]ClO_4	19.72 (1.94)	19.84 (+1.00)
	27.93 (2.19)	27.17 (−0.44)
	42.74 (4.40)	42.37 (−16.16)

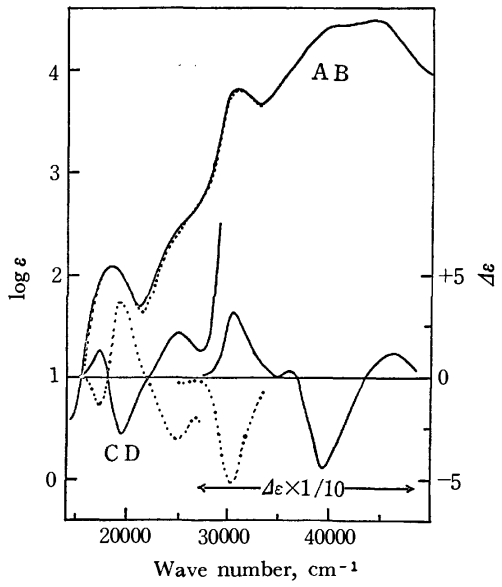

Fig. 9. Absorption (AB) and CD spectra of (——) $\Lambda(-)_{546}$-[Co(acac)$_2$(*RR*-2,4-ptn)]$^+$, (·····) $\Lambda(+)_{546}$-[Co(acac)$_2$(*RS*-2,4-ptn)]$^+$ in water.

other hand, Λ-[Co(*RR*-2,4-ptn)$_3$]$^{3+}$ [13] and Δ-[Co(*RR*-2,4-ptn)$_3$]$^{3+}$ [14] give a single CD band with positive and negative signs, respectively,[1] in agreement with the sign of the main CD band of [Co(en)$_3$]$^{3+}$. However, the CD magnitudes of these two diastereoisomers differ greatly (Λ-isomer: +2.69; Δ-isomer: −0.55), even when the vicinal contribution of the optically active *RR*-2,4-pentanediamine chelate is taken into account.[1] Thus, the CD spectra of tris-β-diamine complexes differ more or less from those of tris-α-diamine complexes.

On the other hand, the CD spectrum of Δ-(b)$_{589}$-[Co(acac)(tn)$_2$]$^{2+}$ whose absolute configuration was determined by the X-ray method[2] is very similar to that of the corresponding ethylenediamine complex, [Co(acac)(en)$_2$]$^{2+}$. Although the absolute configuration of the latter is assigned on the basis of its CD sign in the first absorption band region,[15] such a similarity suggests that a difference in the CD between six-membered and five-membered diamine complexes is not so marked for the present bis-type complex as in the tris-type complex. (−)$_{589}$-[Co(acac)(*RR*-2,4-ptn)$_2$]$^{2+}$ gives a CD curve very similar to that of Δ-[Co-

13) A. Kobayashi, F. Marumo, Y. Saito, J. Fujita, and F. Mizukami, *Inorg. Nucl. Chem. Lett.*, **7**, 777 (1971).

14) A. Kobayashi, F. Marumo, and Y. Saito, presented at the 22nd Symposium on Coordination Chemistry, Osaka, Japan (1972).

15) A. J. McCaffery, S. F. Mason, and B. J. Norman, *J. Chem. Soc.*, **1965**, 5094.

(acac)(tn)$_2$]$^{2+}$ in the entire region, and can be safely assigned to Δ configuration (Fig. 6). For [Co(acac)-(*RS*-2,4-ptn)$_2$]$^{2+}$, complete optical resolution was not achieved, but the complex shows a CD pattern similar to that of the corresponding RR-2,4-pentanediamine complex.

No report has been published on the absolute configuration of any oxalato-bis-α-diamine complex by the X-ray method.[16] However, such a configuration may be assigned without ambiguity on the basis of the CD sign in the first absorption band region, since the CD is usually very similar to that of [Co(en)$_3$]$^{3+}$. Stereospecifically formed Λ-oxalato-bis-diamine type complexes give a main CD band with the positive sign in this region.[17] The main CD bands of both $(+)_{510}$-*cis-cis* and $(+)_{510}$-*trans-cis* isomers of [Co(ox)(*RS*-2,4-ptn)$_2$]$^+$ are positive and almost enantiomeric with those of Δ-[Co(ox)(α-diamine)$_2$]$^+$ (α-diamine=en, R-pn) (Fig. 7).[15] Therefore, the $(+)_{510}$- and $(+)_{510}$-isomers can be assigned to *Λ-cis(RR)cis(SS)* and *Λ-trans(RR)-cis(SS)* structure, respectively. The *Λ-cis(RR)cis(SS)* isomer has one positive CD band, while the *Λ-trans-(RR)cis(SS)* isomer has one very weak negative and one strong positive band from longer to shorter wave length, but the origin of this difference is unknown.

In a similar way, less soluble $(+)_{546}$-isomer of [Co-(ox)(*SS*-2,4-ptn)$_2$]$^+$ is assigned to Λ configuration (Fig. 8). The CD spectrum of $(-)_{546}$-[Co(acac)$_2$(*RR*-2,4-ptn)]$^+$ is shown in Fig. 9. It is almost enantiomeric with the spectra of $(+)_{546}$-[Co(acac)$_2$(en)]$^+$ [18] and $(+)_{546}$-[Co(acac)$_2$(NH$_3$)$_2$]$^+$ [18] which are assigned to Λ configuration from the sign of their CD in the first absorption band region.[19] Therefore, $(-)_{546}$-[Co-(acac)$_2$(*RR*-2,4-ptn)]$^+$ can be assigned to Δ configuration. $(+)_{546}$-[Co(acac)$_2$(*RS*-2,4-ptn)]$^+$ gives a CD curve enantiomeric with that of $(-)_{546}$-[Co(acac)$_2$-(*RR*-2,4-ptn)]$^+$, and is assigned to Λ configuration (Fig. 9). Thus, the CD spectra of bis-acetylacetonato-β-diamine cobalt(III) complexes are essentially the same as those of the corresponding ethylenediamine complexes.

All the results lead to the conclusion that the mono- and bis-β-diamine complexes of the types given in this paper show CD spectra similar to those of the corresponding α-diamine complexes, and their absolute configuration may be assigned on the basis of their CD sign in the first absorption band region as well as the α-diamine complexes.

It is to be noted that the assignment of structures for the present bis-diamine complexes on the basis of pmr and CD spectra is consistent with that deduced from the studies with molecular models; the smaller the steric interaction among chelate rings in a complex, the greater the formation of a diastereoisomer. For example, the steric interaction for the Δ-$(-)_{589}$-isomer of [Co(acac)(*RR*-2,4-ptn)$_2$]$^{2+}$ seems to be smaller than that for the Λ-isomer, and the former is always formed to a much greater extent than the latter.

We are grateful to the Ministry of Education for a Grant-in-aid for studies on optically active complexes.

16) $(-)_D$-[Co(ox)(en)$_2$]$^+$ has been assigned to Δ configuration by the X-ray analysis. T. Aoki, K. Matsumoto, S. Ooi, and H. Kuroya, This Bulletin, **46**, 159 (1973).

17) T. Hattori, M. Saburi, and S. Yoshikawa, presented at the 21st Symposium on Coordination Chemistry, Nagoya, Japan (1971). F. Mizukami, to be published.

18) L. J. Boucher, *Inorg. Chem.*, **9**, 1202 (1970); *Inorg. Chim. Acta*, **6**, 29 (1972).

19) The absolute configuration of these two complexes seems to be Δ from comparison of the CD spectra of some [CoN_2O_4] type complexes. However, the absolute configuration is not discussed here.

Racemization and Isotopic Exchange of Tris(acetylacetonato)silicon(IV) Perchlorate in Organic Solvents

Tomoaki INOUE and Kazuo SAITO

Department of Chemistry, Faculty of Science, Tohoku University, Aoba, Aramaki, Sendai 980

(Received 26 December 1972)

Racemization of trisacetylacetonatosilicon(IV) ions and their isotopic exchange reaction with acetylacetone-^{14}C (Hacac) have been studied in tetrachloroethane (TCE) and acetonitrile (AN). No solvolysis takes place at least below 60 °C, and the racemization rate R is expressed as follows: $R=$[complex] $(k_1+k_2$[acid]) (in TCE) and $R=$[complex] $(k_3+k_4$[base]) (in AN). The rate constants and activation parameters at 50 °C are as follows: rate constants, 4.79×10^{-6} s^{-1}, 1.35×10^{-4} M^{-1} s^{-1}, 3.87×10^{-5} s^{-1} and 1.19×10^{-1} M^{-1} s^{-1}, activation enthalpy ($\Delta H^{\neq}$/kcal mol^{-1}) 31.6±0.1, 29.3±1.9, 25.7±0.2 and *ca.* 18, and activation entropy ($\Delta S^{\neq}$/cal mol^{-1} K^{-1}) 14.6, 14.2, 0.53, −5.75, respectively, for k_1, k_2 (for trichloroacetic acid), k_3 and k_4 (for 2,6-lutidine). No isotopic exchange is observed within 6 hr at 60 °C in the solvents. The racemization should proceed intra-molecularly and presumably *via* an intermediate of coordination 5 with one of the ligands as unidentate.

Dynamic properties of β-diketonato complexes of metal ions have been studied from various viewpoints. Geometrical isomerization of the complexes with asymmetric β-diketones was studied mainly by measuring their NMR signals.[1] Trisacetylacetonato- and trisbenzoylacetonatocobalt(III) were partly resolved and their racemization and geometrical isomerization discussed in detail.[2] All the work was centered around intra-molecular rearrangement of the complexes. We have conducted kinetic studies of isotopic exchange of some acetylacetonato complexes of typical and transition metal ions, and discussed the intermolecular course of reaction in organic solvents.[3,4] Since these studies have been limited to those of chargeless complex species, we thought it desirable to extend the studies to silicon(IV) which gives univalent cationic complex with three β-diketonato ligands.

Silicon(IV) compounds with tetrahedral structure have been studied extensively, but much less is known about those with co-ordination number six. Phthalocyaninato,[5] tropolonato[6] and β-diketonato[7] complexes were synthesized and their structures discussed. However, reaction kinetics has been studied only with the tris-β-diketonatosilicon(IV) ion.

Dhar, Doron and Kirschner[8] first resolved trisacetylacetonatosilicon(IV) $[Si(acac)_3]^+$ and studied its hydrolysis, methanolysis and racemization. They concluded that the loss of optical activity is mainly due to solvolysis.[9] Pearson, Edgington and Basolo considered an S_N2 displacement mechanism for the base hydrolysis.[10] From the difference in the rates of loss of optical activity and the hydrolysis, participation of intrinsic racemization was suggested.[9] Muetterties and Wright studied the base hydrolysis of a similar complex with dibenzoylmethane $[Si(dbm)_3]^+$ in ^{18}O-labelled water, and suggested nucleophilic attack of hydroxide ions on the carbon atom adjacent to the coordinated oxygen.[11]

We found that $[Si(acac)_3]^+$ undergoes racemization in carefully dehydrated organic solvents without being involved in other reactions such as hydrolysis, and studied the reaction kinetics of the non-catalyzed and acid- or base-catalyzed reaction path in 1,1,2,2-tetrachloroethane (TCE) and acetonitrile (AN). The result has been compared with that of intermolecular isotopic exchange of the complex with ^{14}C-labelled acetylacetone, and the mechanisms of racemization discussed.

Experimental

Materials. *Preparation and Resolution of the Complex*: Trisacetylacetonatosilicon(IV) hydrogen dichloride $[Si(acac)_3]Cl\cdot HCl$ was prepared by Dilthey's method[12] and resolved by Dhar *et al*'s method[8] with slight modification. Crystals of hydrogen-dibenzoyl-*d*-tartrate salt of this complex $(-)_D$-$[Si(acac)_3]$-$(-)_D$-$C_{18}H_{13}O_8$ were filtered off from the aqueous solution, and the crystals of $(+)_D$-$[Si(acac)_3]$-ClO_4 precipitated with sodium perchlorate from the filtrate. The resolution was partial but the racemization rate was independent of the degree of resolution. $(-)_D$-$[Si(acac)_3]\cdot C_{18}H_{13}O_8$ was converted into $(-)_D$-$[Si(acac)_3]ClO_4$ with the anion exchange resin Dowex 1-X8 by the batch method. $(+)_D$-$[Si(acac)_3]ClO_4$ was recrystallized from chloroform solution with ether and used for the kinetic runs. This complex is stable for several months in dry air below 15 °C, and for 2 weeks at *ca.* 30 °C. The perchlorate is soluble in nitriles, ketones, carboxylic acids, alcohols, and some haloalkanes, but insoluble in ethers, hydrocarbons and water. The dibenzoyltartrates are very stable, and soluble in carboxylic acids, some alcohols and haloalkanes, but insoluble in ethers, hydrocarbons and water.

$(+)_D$-Enantiomer of this complex assigned to Λ configuration on the basis of Larsen's treatment.[13] The $\Delta\varepsilon$ of the

1) J. J. Fortman and R. E. Sievers, *Inorg. Chem.*, **6**, 2022 (1967). J. G. Gordon, II, and R. H. Holm, *J. Amer. Chem. Soc.*, **92**, 5319 (1970); J. R. Hatchison, J. G. Gordon, II, and R. H. Holm, *Inorg. Chem.*, **10**, 1004 (1971).

2) R. C. Fay, A. Y. Girgis and U. Klabunde, *J. Amer. Chem. Soc.*, **92**, 7056 (1970); A. Y. Girgis and R. C. Fay, *ibid.*, **92**, 7061 (1970).

3) K. Saito and K. Masuda, This Bulletin, **41**, 384 (1968).

4) *Idem*, *ibid*, **43**, 119 (1970).

5) R. D. Joyner and M. E. Kenney, *Inorg. Chem.*, **1**, 236 (1962).

6) E. L. Muetterties and C. M. Wright, *J. Amer. Chem. Soc.*, **86**, 5132 (1964).

7) R. M. Pike, *Coord. Chem. Rev.*, **2**, 163 (1967).

8) S. K. Dhar, V. Doron, and S. Kirschner, *J. Amer. Chem. Soc.*, **80**, 753 (1958).

9) *Idem*, *ibid.*, **81**, 6372 (1959).

10) R. G. Pearson, D. N. Edgington, and F. Basolo, *ibid.*, **84**, 3233 (1962).

11) E. L. Muetterties and C. M. Wright, *J. Amer. Chem. Soc.*, **87**, 21 (1965).

12) W. Dilthey, *Ber.*, **36**, 923 (1903).

circular dichroism (CD) of $\Delta(-)_D$-[Si(acac)$_3$]-(−)$_D$-$C_{18}H_{13}O_8$ and $\Lambda(+)_D$-[Si(acac)$_3$]ClO_4 were −162 and +180 at 302 and 304 nm at 25 °C, respectively. The specific rotation was +866° for the Λ-[Si(acac)$_3$]ClO_4 at the D-line at 25 °C.

Solvents: 1,1,2,2-Tetrachloroethane (TCE) was dehydrated with anhydrous calcium sulfate in a dry box and gently distilled. The procedure was repeated three times; the product contained 0.001 M water. Careless procedure gives rise to the increase in water content. Acetonitrile was refluxed with diphosphorus pentoxide and distilled. The procedure was repeated and finally distilled with potassium carbonate. The product contained 0.002 M water. Anhydrous calcium sulfate was also useful for its dehydration. Acetophenone was dehydrated with calcium sulfate and distilled under a reduced pressure. The water content was 0.002 M.

Other Reagents: Pyridine and its derivatives were dehydrated with anhydrous calcium sulfate and distilled. The water content was less than 0.01 M. Trichloroacetic acid was sublimed *in vacuo*. The labelled acetylacetone was prepared by Miss Kazuyo Masuda.[3)]

Experimental Procedure. Racemization: The optically active perchlorate (≃0.1 g) was dissolved in the solvent (25 ml) in a dried vessel in a dry box. Whenever necessary, a given volume of the acid or the base solution was added to make the concentration 0.001 to 0.1 M. The product was sealed in five small test tubes. They were placed in a thermostat (±0.02 °C) and picked up one by one at proper intervals. They were cooled in a mixture of table salt and ice, and the optical rotation measured at the Na–D line. They were then diluted and the u.v. absorption examined. The runs were carried out in the temperature range 30—60 °C.

The rate constant was calculated by the equation

$$k_{obsd} = [\ln(\alpha_0/\alpha_t)]/2t \quad (1)$$

where α_0 and α_t are the optical rotations at time zero and t, respectively.

Isotopic Exchange Kinetics: The complex (0.04—0.08 g) and acetylacetone-^{14}C (0.01—0.02 g) were dissolved in TCE or AN in a long-necked flask in a dry box and kept in a thermostat (60±0.02 °C). Aliquots were withdrawn at appropriate intervals, and poured into cooled diethylether. The complex precipitated at once free from Hacac, filtered off with a small piece of filter paper, washed with diethylether and dried *in vacuo*. The β-activity of the precipitate (10 mg) on the paper was counted with a 2π gas flow counter with Q-gas.

Apparatus. A JASCO DIP-SL polarimeter and a Hitachi 124 spectrometer were used for the measurement of optical rotation and u.v. absorption spectrum, respectively. JASCO model ORD/UV-5 was used for recording the circular dichroism spectrum. Aloka FC-1E counter was used for the β-activity counting of ^{14}C. The water content was measured by the Karl Fischer method.

Results

The Kinetic Formula in TCE. The change in absorbance at 305 nm and optical rotation at the Na–D line of the reaction mixture are shown in Fig. 1. The constant absorbance indicates the absence of decomposition of the complex. Hence the decrease in optical rotation should be due to racemization of the complex. The dependence of k_{obsd} on the complex concentration is illustrated in Fig. 2. The rate constant remains unchanged in the range 0.005—0.05 M and the racemization rate is given by

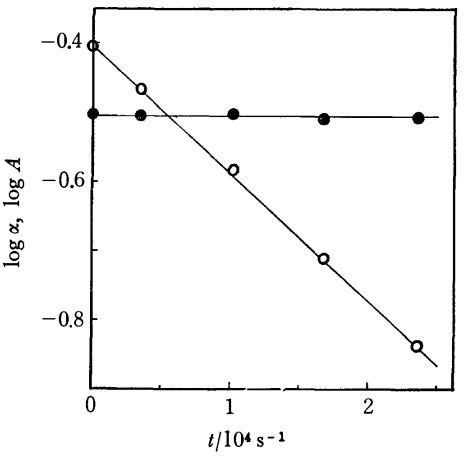

Fig. 1. Change of optical rotation at Na-D line and absorption spectrum at 305 nm in TCE. (● absorption, ○ rotation)

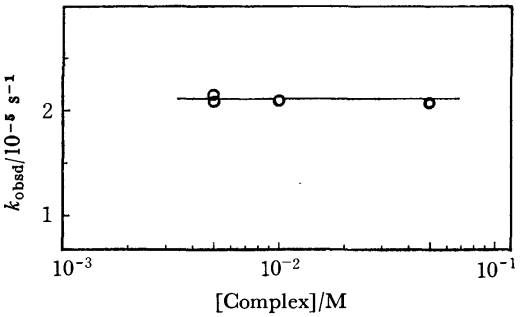

Fig. 2. Influence of the complex concentration upon k_{obsd} in TCE.

$$R - k_{obsd}[\text{complex}] \quad (2)$$

Free acetylacetone gave no effect on the rate of racemization (Fig. 3). The racemization is catalyzed by trichloroacetic acid as shown in Fig. 4. The straight lines have intercepts, which coincide with k_{obsd} values obtained in the absence of acid at the given temperature. Weaker acids do not give catalytic action. Hence k_{obsd} is given by

$$k_{obsd} = k_1 + k_2[\text{trichloroacetic acid}] \quad (3)$$

The results are summarized in Table 1. The catalytic action of trichloroacetic acid is reckoned as acid catalysis for the following reason. When equimolar

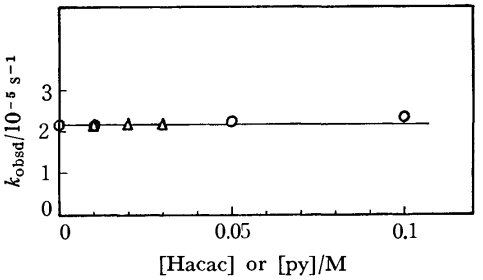

Fig. 3. Influence of concentration of free Hacac and pyridine in TCE. (△ Hacac, ○ pyridine)

13) E. Larsen, S. F. Mason, and G. H. Searle, *Acta Chem. Scand.*, **20**, 191 (1966).

Table 1. Rate constants and activation parameters

t °C	TCE		AN		Acetophenone
	k_1/s^{-1}	$k_2/M^{-1}s^{-1}$	k_3/s^{-1}	$k_4/M^{-1}s^{-1}$ a)	k_5/s^{-1}
30 b)			2.63×10^{-6}	1.66×10^{-2}	
40	9.50×10^{-7}	3.55×10^{-5}	1.08×10^{-5}		7.20×10^{-6}
50	4.79×10^{-6}	1.35×10^{-4}	3.87×10^{-5}	1.19×10^{-1}	2.85×10^{-5}
60	2.12×10^{-5}	6.23×10^{-4}	1.37×10^{-4}		1.19×10^{-4}
$\Delta H^{\neq}$ c)	31.6±0.1	29.3±1.9	25.7±0.2	18.5	28.7
$\Delta S^{\neq}$ d)	14.6	14.2	0.53	−5.75	8.93

a) k_4 for 2,6-lutidine, b) ±0.05 °C, c) kcal mol^{-1} at 50 °C, d) cal mol^{-1} K^{-1} at 50 °C.

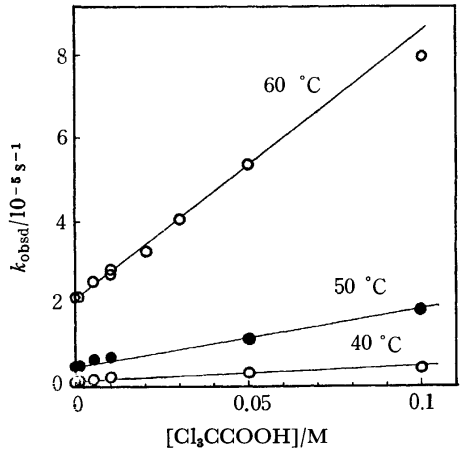

Fig. 4. Influence of concentration of trichloroacetic acid in TCE.

amounts of trichloroacetic acid and pyridine were added to the TCE solution, the k_{obsd} decreased as compared with that in the presence of trichloroacetic acid alone. On the other hand, the electric conductivity of the equimolar mixture was greater than those of pure solutions of trichloroacetic acid and pyridine in TCE. This fact shows that the dissociation of trichloroacetic acid was facilitated by the addition of pyridine. If the trichloroacetate anion had been the catalyzing species, the equimolar mixture should have exhibited greater catalytic activity. Hence, the proton seems to be the catalyzing species.

The fact that pyridine shows catalytic activity in AN (see below) but not in TCE can be interpreted by considering that pyridine is capable of forming hydrogen bonding with TCE[14] and does not behave as a base in this solvent.

No isotopic exchange was observed within 6 hr at 60 °C regardless of the presence or the absence of trichloroacetic acid.

In Acetonitrile. Plots of the rotation and the absorbance *vs.* time disclosed that racemization is not involved in decomposition of the complex. Independence of the rate constant of the concentrations of the complex and of free acetylacetone indicates that a relationship similar to Eq. (2) also holds in this solvent. Water in the concentration range 0.002—0.01 M and trichloroacetic acid gave no influence upon the rate of racemization. The racemization is catalyzed by bases such as strychnine, 2,6-lutidine, γ-picoline, pyridine and pyridine *N*-oxide, the extent decreasing in this order. The catalytic activity of pyridine was quenched by the addition of an equimolar amount of trichloroacetic acid, and the acceleration seems to be due to the base catalysis. The plot of k_{obsd} values *vs.* the concentrations of these bases gave straight lines with intercepts, which coincide with the k_{obsd} values in the absence of the bases (Fig. 5). Thus the rate constant is given by

$$\text{Rate} = k_{obsd}[\text{complex}] = [\text{complex}](k_3 + k_4[\text{base}]) \quad (4)$$

The data are listed in Tables 1 and 2. The k_4 values are not sufficiently reproducible and the plots gave different gradients according to the batch of a given base, although the intercepts were always equal. It

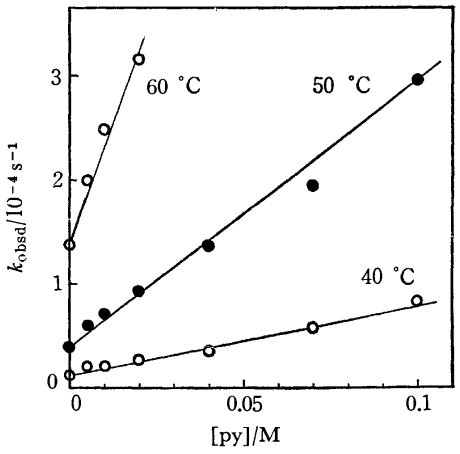

Fig. 5. Influence of pyridine concentration upon k_{obsd} in AN.

Table 2. Approximate k_4 values for some bases at 30 °C

Base	pK_a a)	$k_4/M^{-1}s^{-1}$
Strychnine	8.0	2×10
2,6-Lutidine	6.58	2×10^{-2}
γ-Picoline	6.02	2×10^{-3}
Pyridine	5.17	1.5×10^{-4}
Pyridine *N*-oxide	0.56 b)	2×10^{-4} c)
4-Cyanopyridine	1.86	0

a) at 25 °C, b) at 23 °C, c) at 50 °C.

14) H. Götz, E. Heilbronner, A. R. Katritzky, and R. A. Jones, *Helv. Chim. Acta.*, **44**, 387 (1961); G. R. Wiley and S. I. Mitler, *J. Amer. Chem. Soc.*, **94**, 3287 (1972).

appears as if some unidentified compounds in the pyridine bases give catalytic action on top of that of the bases themselves. Hence only approximate values of k_4 are listed in Table 2. Nevertheless, they increase with increase in basicity of the bases. There was no influence of water and trichloroacetic acid upon the rate.

No appreciable isotopic exchange was observed within 20 hr at 60 °C both in the absence and the presence of bases.

In Acetophenone. The results are given in Table 1. No influence was observed in the presence of different amounts of water and free acetylacetone.

Discussion

All experimental results are summarized in Table 1. The absence of isotopic exchange clearly indicates that the racemization takes place *via* an intramolecular mechanism. Since no net chemical reaction is involved during the course of racemization, some kind of twisting mechanism should be operating.

Intra-molecular racemization can proceed either with or without break of one of the metal-oxygen bonds between silicon(IV) and acetylacetonate. The latter mechanism maintaining coordination number 6 was interpreted by Ray and Dutt[15] and by Bailar[16] in slightly different ways. However, racemization of $[Si(acac)_3]^+$ is subject to acid catalysis in TCE and to base catalysis in AN. Such catalytic actions are more easily understood by considering an intermediate with coordination number 5, because twist mechanism without bond break will be less sensitive towards acid and base catalysis.

An intermediate with coordination number 5 can be either trigonal bipyramid or square pyramid but should have a plane of symmetry with the unidentate ligand at the apical position. When one of the bonds of a ligand is broken, a trigonal bipyramidal intermediate seems to be easily formed without involving drastic intra-molecular rearrangement. (Fig. 6) On the other hand, if a square pyramidal intermediate were to be formed, the intra-molecular rearrangement would be more substantial and require bigger enthalpy of activation. Stability of trigonal bipyramidal and square pyramidal structure was compared both theoretically and experimentally by several authors.[17] It seems that

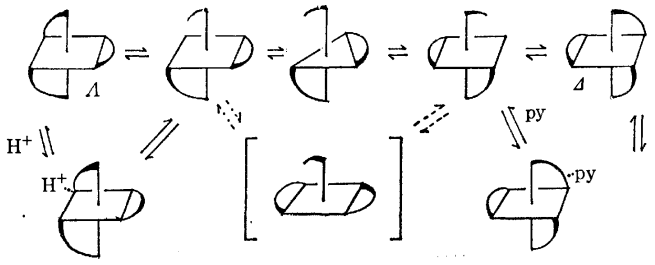

Fig. 6. Plausible mechanism of racemization.

15) P. C. Ray and N. K. Dutt, *J. Indian Chem. Soc.*, **20**, 81 (1943).
16) J. C. Bailar, Jr., *J. Inorg. Nucl. Chem.*, **8**, 165 (1958).

former is energetically more favorable although the energy difference does not appear very big. This does not necessarily imply that the energy barrier to be overcome is also small; however, we are inclined to presume the trigonal bipyramidal intermediate to be more feasible.

Two possible rate-determining steps can be encountered whenever an intermediate with coordination number 5 is involved. One is to assume that the bond breaks to give the intermediate as rate-determining step and the intra-molecular rearrangement proceeds fast. An alternative is to regard that one of the bonds of a given ligand breaks and forms quickly and the intra-molecular rearrangement to be the rate-determining step. So far as the intermediate has trigonal bipyramidal structure, the intra-molecular rearrangement will not require big enthalpy, and we can presume that the break of the first bond of one of the ligands will be the rate-determining step. From kinetic studies in ^{18}O-labelled water, Muetterties and Wright[11] suggested that the rate-determining step for the aquation of $[Si(dbm)_3]^+$ is the break of one of the ligands facilitated by the attack of water upon the carbonyl carbon. This is in line with our result, although the reaction environment differs.

If the break of one of the bonds of a ligand were the rate-determining step, the acid and base catalysis should be understood in such a way that acid or base will affect the metal ligand bond to facilitate its break. Such an action will give lower $\Delta H^{\neq}$ values as compared with those in the absence of catalysis. The $\Delta H^{\neq}$ values for k_1 and k_2 path are 31.6±0.1 and 29.3±1.9 kcal per mole, respectively. Although the difference is only slightly bigger than the experimental error, acid catalysis can be understood as to facilitate the bond break at the rate-determining step. The difference in $\Delta H^{\neq}$ values in the presence and the absence of base catalysis is more marked, although the experimental error must be bigger. Primary and secondary amines change the absorption spectrum of the reaction mixture and seem to bring about net chemical reaction. As Table 2 shows, there is an overall trend that the greater the basicity of a given pyridine base, the greater the catalytic activity with smaller $\Delta H^{\neq}$ and $\Delta S^{\neq}$ values. This may suggest that the base catalysis operates bimolecularly. The possible attack can take place on either the central silicon or the ligand. Bulky molecules such as *l*-strychnine and 2,6-lutidine give remarkable catalytic action, and the attack upon silicon is less likely. Optically active *l*-strychnine catalyzed both Δ- and Λ-complex equally.

In the absence of catalytic action, the racemization proceeds faster in AN(and acetophenone) than in TCE. Such a solvent effect could be understood by considering that AN, as a weak base, gives more marked solvation than TCE, and facilitates the break of the Si–O bond in the rate-determining step.

Thanks are due to Ministry of Education for Grant in Aid.

17) R. J. Gillespie, *J. Chem. Soc.*, **1963**, 4672; J. Zemann, *Z. Anorg. Allgem. Chem.*, **324**, 241 (1963); L. Sacconi, *Pure Appl. Chem.*, **17**, 95 (1968).

Heterocyclic Azomethine Compounds and Their Reduction Products as Analytical Reagents. I. Syntheses and Acid Dissociation Constants of Picolinaldehyde 2-Hydroxyanil and Its Derivatives and Their Reactions with Metal Ions

Makoto OTOMO and Kazunobu KODAMA

Department of Synthetic Chemistry, Nagoya Institute of Technology, Showa-ku, Nagoya 466

(Received December 20, 1972)

Picolinaldehyde 2-hydroxyanil and its methyl, chloro and nitro derivatives at the 5-position of benzene nucleus were synthesized for the purpose of investigating their applicability as an analytical reagent. The acid dissociation constants were determined by means of potentiometric titration in aqueous dioxane of various concentrations. It was found that the basicity of donor atoms of the parent compound increases with the introduction of a methyl group and decreases with that of a chloro or nitro group. The three compounds other than the nitro derivative are light-colored and react with many divalent metal ions in slightly basic media to form strongly colored chelates, which can be extracted into organic solvents such as partially halogenated hydrocarbons. The distribution coefficients of the three compounds between chloroform and water were also determined spectrophotometrically, that of the chloro derivative being the largest.

The analytical use of heterocyclic azo compounds in color forming reactions with metal ions is very familiar. 2-Pyridylazo compounds, which are strongly colored and have a hydroxy group in *ortho*-position to the azo group, have been proved to be very useful as spectrophotometric reagents and also as metal indicators. However, in spite of the easiness of preparation, only a limited number of azomethine analogs have been used analytically. It is important to note that the stability constants of some metal chelates with picolinaldehyde 2-hydroxyanil are of the same order of magnitudes as those of 4-(2-pyridylazo)-resorcinol.[1] Both compounds have three donor groups capable of coordinating to metals and act as a terdentate ligand. 2-(2-pyridylazo)phenyl (*o*-PAP) also reacts with many metal ions over a wide range of pH to form strongly colored chelates.[2] A series of azomethines represented by the general formula(1) have been synthesized and their applicability to the spectrophotometric determination of copper(II) examined.[3] However, no attempt seems to

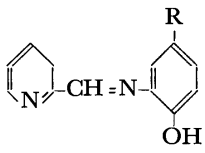

R=H, CH_3, Cl, C_6H_5

(1)

have been made so far to elucidate the stability of the chelates formed. Picolinaldehyde 2-mercaptoanil, a thio analog of picolinaldehyde 2-hydroxyanil, shows a marked selectivity towards metals which form brightly colored insoluble sulfides.[4] Some azomethine derivatives of 8-hydroxyquinoline have also been synthesized.[5]

We have synthesized four azomethine compounds, picolinaldehyde 2-hydroxyanil (I), -2-hydroxy-5-methylanil(II), -2-hydroxy-5-chloroanil(III) and -2-hydroxy-5-nitroanil(IV), in order to study quantitatively the effects of substituents at the 5-position of the benzene nucleus on the acid dissociation constants and the stability of metal chelates, and to obtain information on their applicability as an analytical reagent. It is found that the basicity of the imino and pyridine nitrogens, as well as of the phenolic oxygen, is greatly affected by the introduction of an electron-releasing or -withdrawing group into the ring. These compounds except for (IV) may be conveniently used as an extractive spectrophotometric reagent for some divalent metal ions.

Experimental

Preparations. Compound (I) is prepared as follows: To a solution of 10 g of *o*-aminophenol (purified by sublimation) in 80 ml ethanol is added a solution of 11 g of freshly distilled picolinaldehyde in 20 ml ethanol. The mixture is kept at 60—70 °C for 2 hr, and the ethanol is evaporated under reduced pressure. The resulting brown residue is recrystallized from ligroin to give 10 g of pale yellow-orange needle-like crystals.

The other azomethine compounds are prepared similarly from substituted *o*-aminophenols. The melting points and analytical data of the synthesized compounds together with the IR data are given in Table 1.

Sodium perchlorate is prepared by neutralization of a sodium carbonate solution with perchloric acid, followed by shaking with 1-(2-pyridylazo)-2-naphthol (PAN) in benzene to remove heavy metals which may be present and concentrating the aqueous phase until bulk of sodium perchlorate has crystallized out. The crystals are collected and recrystallized from water.

Apparatus. A model HM-6A pH meter (Toa Dempa Co., Ltd.) equipped with a combination electrode, type GC-125, is calibrated at pH 6.88 and 4.01 with standard buffer solutions (Toa Dempa Co., Ltd.). The pH meter readings are corrected according to the method described by van Uitert and Haas.[6] A Hitachi model 181 spectrophotometer

1) W. J. Geary, G. Nickless and F. H. Pollard, *Anal. Chim. Acta*, **26**, 575 (1962); *ibid.*, **27**, 71 (1962).

2) F. H. Pollard, G. Nickless and R. G. Anderson, *Talanta*, **13**, 725 (1966).

3) K. Isagai and K. Isagai, *Nippon Kagaku Zasshi*, **88**, 1292 (1967); *Bunseki Kagaku*, **17**, 171 (1968).

4) R. G. Anderson and G. Nickless, *Proc. Soc. Anal. Chem.*, **3**, 149 (1966).

5) T. Hata and T. Uno, This Bulletin, **45**, 477 (1972).

6) L. G. van Uitert and C. G. Haas, *J. Amer. Chem. Soc.*, **75**, 451 (1953).

Table 1. Azomethine compounds synthesized

Compound	Mp (°C)[a]	Formula	Analysis (%) Found	Calcd	IR(CH=N) band (cm^{-1})
I	108	$C_{12}H_{10}ON_2$	C 72.68	72.71	1627
			H 5.01	5.09	
			N 14.21	14.13	
II	104	$C_{13}H_{12}ON_2$	C 73.56	73.57	1623
			H 5.72	5.70	
			N 13.20	13.20	
III	138	$C_{12}H_9ON_2Cl$	C 62.15	61.95	1627
			H 4.05	3.90	
			N 12.05	12.04	
IV	200	$C_{12}H_9O_3N_3$	C 59.14	59.25	1621
			H 3.63	3.73	
			N 17.14	17.28	

a) Although all the melting points are uncorrected, the reported values for I, II, and III in Refs. 1 and 3 seem to be too low.

and a Hitachi model 124 double-beam spectrophotometer are used for measurement of absorbance in quartz cells of 10 mm pathlength.

Determination of Acid Dissociation Constants. Since all the azomethine compounds synthesized are almost insoluble in water, potentiometric titration is carried out in aqueous dioxane of various concentrations. A solution containing the sodium salt of each ligand (5×10^{-3} M) and sodium perchlorate (0.1 M) is titrated with 0.2 M perchloric acid at 25±0.1 °C under CO_2-free nitrogen atmosphere.

Determination of Distribution Coefficients. The distribution coefficients of the three compounds other than (IV) are determined spectrophotometrically. Extraction is carried out in a 50 ml centrifuging tube fitted with a glass stopper. A 10 ml portion of 0.1 M sodium perchlorate solution containing appropriate amounts of sodium hydroxide is vigorously shaken with 10 ml each of 1×10^{-3} M reagent in chloroform for 10 min at 25±0.5 °C. After equilibration, the pH of the aqueous phase is determined, and the absorbance of the organic phase is then measured at the absorption maximum, 358 nm for (I), 370 nm for (II), or 367 nm for (III).

Results and Discussion

Acid Dissociation Constants. The acid dissociation constants of the four compounds are determined in aqueous dioxane of various concentrations. The potentiometric titration curves in 50 v/v% aqueous dioxane are shown in Fig. 1. Each titration curve exhibits only one pH inflection at $a=1$. This shows that the dissociation of proton from the phenolic oxygen occurs independently in the alkaline region, whereas the dissociation of protons from the pyridine and azomethine nitrogens overlaps in the acidic region:

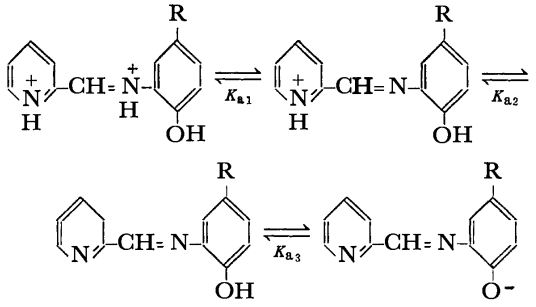

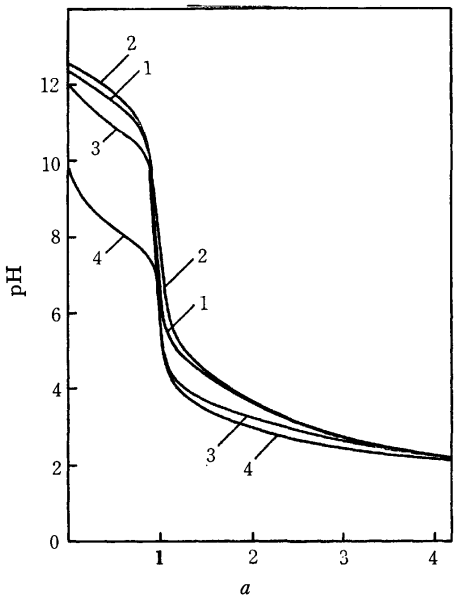

Fig. 1. Potentiometric titration curves of the azomethine compounds in 50 v/v% aqueous dioxane solution, $\mu=0.1$, 25 °C; abscissa a represents mol of acid added per mol of ligand (sodium salt).
Curve 1. Picolinaldehyde 2-hydroxyanil
2. Picolinaldehyde 2-hydroxy-5-methylanil
3. Picolinaldehyde 2-hydroxy-5-chloroanil
4. Picolinaldehyde 2-hydroxy-5-nitroanil

The acid dissociation constants are calculated as follows. For dissociation of a tribasic ligand acid, we have the relation[7]

$$R[H^+]^3 + (R-1)K_{a1}[H^+]^2 + (R-2)K_{a1}K_{a2}[H^+] + (R-3)K_{a1}K_{a2}K_{a3} = 0 \quad (1)$$

where $R=\{(3-a)C_L+[H^+]-[OH^-]\}/C_L$, C_L is the concentration of the ligand, and a the degree of neutralization. Since pK_{a1} and pK_{a2} are obviously close in magnitude whereas pK_{a3} is much larger, values for the first two dissociation constants are obtained conveniently by transforming Eq. (1) into the linear forms

$$\frac{(1-R)[H^+]}{R-2} = \frac{R[H^+]^2}{R-2}\cdot\frac{1}{K_{a1}} + K_{a2} \quad (2)$$

and

$$\frac{2-R}{R[H^+]^2} = \frac{R-1}{R[H^+]}\cdot\frac{1}{K_{a2}} + \frac{1}{K_{a1}K_{a2}} \quad (3)$$

and solving them to obtain K_{a1} and K_{a2} as the reciprocals of the calculated slopes. The value of K_{a3} is calculated from the approximate equation, $K_{a3}=(R-2)[H^+]/(3-R)$.

The plots of pK_{a1}, pK_{a2}, or pK_{a3} thus obtained *vs.* the mole fraction of dioxane, n_2, are linear in every case. The values of pK_{a1} and pK_{a2} decrease and that of pK_{a3} increases with increasing mole fraction of dioxane. These are summarized in Table 2. The value of pK_{a1} for (II) can not be estimated since hydrolysis takes place below pH 4. The acid dissociation constants of (I) in 50 v/v% aqueous dioxane agree well with the values reported by Geary, Nickless and Pollard ($pK_{a1}=3.05$, $pK_{a2}=4.45$ and $pK_{a3}=11.80$[1]).

7) H. Irving and J. J. R. F. da Silva, *J. Chem. Soc.*, **1963**, 448.

Table 2. Acid dissociation constants of the azomethine compounds
At 25 °C, $\mu=0.1$

Compound	pK_{a1}	pK_{a2}	pK_{a3}
(I)	$3.69-3.62n_2$	$4.80-2.47n_2$	$9.99+8.68n_2$
(II)	—	$5.03-2.82n_2$	$10.31+8.22n_2$
(III)	$3.43-3.56n_2$	$4.08-3.33n_2$	$9.52+8.05n_2$
(IV)	$2.81-4.37n_2$	$3.98-3.97n_2$	$7.12+6.49n_2$

It can be seen from Table 2 that the basicity of the donor atoms of the parent compound (I) is increased by the introduction of an electron-releasing group into the benzene ring and *vice versa* by the introduction of an electron-withdrawing group. As may be expected, the basicity of (II) is the highest. A good linear relationship holds between the pK_{a3} values for these compounds and the Hammett σ_p values for the benzene series.[8] The value of pK_{a2} may be ascribed to the dissociation of the –NH= group of pyridine nucleus.[9] The pK_{a2} and pK_{a3} values for (I) and (II) are higher than those of the corresponding azo compounds, *o*-PAP[4] and 2-(2-pyridylazo)-4-methylphenol (PAC),[10] respectively. This means that one would expect metal complexes of (I) and (II) to be more stable than those of *o*-PAP and PAC, respectively. The pK_{a2} and pK_{a3} values for (II) are also higher than those of 2-(2-thiazolylazo)-4-methylphenol (TAC).[11]

Distribution Coefficients. In the range of pH investigated (9.90—11.80), the following equation might hold for reagent extraction.

$$\log D_L = \log K_{DL} - \log(K_{a3}/[H^+]+1) \quad (4)$$

where D_L is the distribution ratio. The value of the distribution coefficient K_{DL} for a given compounds is obtained from Eq. (4). The results are given in Table 3. It is apparent that the log K_{DL} value varies with the substituent in the order $Cl>CH_3>H$ ($\gg NO_2$). These compounds show weak flluorescence in chloroform.

Table 3. Distribution coefficients of the azomethine compounds
At 25 °C, $\mu=0.1$

Compound	log K_{DL}
(I)	1.53±0.04
(II)	2.18±0.06
(III)	2.38±0.04

Reaction with Metal Ions. Many metal ions react with the synthesized compounds in the neutral or slightly basic region to give orange to orange-red color. Of these only divalent metal ions form chelates extractable into organic solvent such as chloroform, 1,2-dichloroethane, and *o*-dichlorobenzene, suggesting that uncharged 1 : 2 metal-ligand chelates are extracted. It is noteworthy that the extracted metal chelates are red to reddish violet in color, fairly differing from those observed in an aqueous dioxane solution; *e.g.*, the nickel(II) chelate of (I) in 20 v/v % aqueous dioxane at pH 9.3 has an absorption maximum at about 455 nm, while the peak of the chloroform extract is located at 529 nm. Metal chelates of (IV), however, can not be extracted into any organic solvent examined, although a potentiometric titration curve of a mixture of nickel(II) and (IV) in 50 v/v % aqueous dioxane with a standard sodium hydroxide solution clearly shows a 1 : 2 metal-ligand complex being formed. The absorption maxima and the apparent molar absorptivities of the divalent-metal chelates extracted into chloroform are given in Table 4. The spectrum of each chelate shows a broad, intense band well separated from that of the reagent, the shift being larger than 100 nm. The band for a metal shifts toward longer wavelength in the order $CH_3>Cl>H$.

Cadmium(II) and zinc(II) are found to form the most strongly colored chelates with these compounds. The cobalt(II) chelates change in color from red to violet during the course of extraction with chloroform

Table 4. Spectral properties of the metal chelates extracted into chloroform
Total metal concentration: 2.0×10^{-5} M
Total ligand concentration: 2.5×10^{-4} M

Metal	(I)			(II)			(III)		
	λ_{max} (nm)	$\varepsilon_{max}\times10^{-4}$ (l/mol·cm)	pH	λ_{max} (nm)	$\varepsilon_{max}\times10^{-4}$ (l/mol·cm)	pH	λ_{max} (nm)	$\varepsilon_{max}\times10^{-4}$ (l/mol·cm)	pH
Mn(II)	500	2.2	8.9	520	1.9	9.0	512	2.3	8.8
Co(II)	493	1.7	8.9				505	2.1	8.8
Ni(II)	520	2.2	8.9	540	2.0	9.2	532	2.1	8.6
Cu(II)	515	1.3	8.9	535	1.2	9.9	530	1.4	8.7
Zn(II)	500	2.6	8.9	518	2.2	7.2	513	2.3	8.7
Cd(II)	500	2.5	8.9	518	2.1	8.7	512	2.3	8.6
Hg(II)	502	~2	8.9	521	~2	8.7	515	~2	8.6
Pb(II)	475	0.68	8.9				480	0.60	8.6
UO_2(II)	450	0.81	8.9	472	1.3	6.4			

8) H. H. Jaffé, *Chem. Revs.*, **53**, 191 (1953).
9) S. J. Angyal and C. L. Angyal, *J. Chem. Soc.*, **1952**, 1461.
10) G. Nakagawa and H. Wada, *Nippon Kagaku Zasshi*, **83**, 1098 (1962).
11) G. Nakagawa and H. Wada, *ibid.*, **85**, 202 (1964).

in a slightly basic solution, a precipitate appearing on the boundary of the two phases even in the presence of perchlorate ion. The reaction of nickel(II) with these compounds proceeds rapidly at the pH given in Table 4 and the chelates formed can be readily extracted into chloroform. However, the rate decreases markedly with decrease in pH of the solution. The comparatively lower molar absorptivities of the copper(II) chelates give rise to structural interest. The results imply that the azomethine compounds may be useful as a reagent for extractive spectrophotometric analysis of zinc(II), cadmium(II) and mercury(II). Their behaviors which are similar to those of *o*-PAP and PAR, suggest that these compounds act as a terdentate ligand toward metals to form two five-membered chelate rings.

We are grateful to The Asahi Glass Foundation for the Contribution to Industrial Technology for the financial support.

BULLETIN OF THE CHEMICAL SOCIETY OF JAPAN, VOL. 46, 2424—2428 (1973)

The Crystal Structure of $(-)_{589}$-Acetylacetonatobis(trimethylenediamine)cobalt(III) Arsenic(V) (+)-Tartrate Monohydrate

Keiji MATSUMOTO, Hiroshi KAWAGUCHI,* Hisao KUROYA, and Shinichi KAWAGUCHI

Department of Chemistry, Faculty of Science, Osaka City University, Sumiyoshi-ku, Osaka 558

(Received January 8, 1973)

The crystal structure of $(-)_{589}$-[Co acac tn_2][As-(+)-tart]$_2\cdot H_2O$ has been determined by the X-ray diffraction method. The crystals are monoclinic, with lattice constants of $a=12.02(1)$ Å, $b=13.73(2)$ Å, $c=9.02(1)$ Å, and $\beta=107.4(3)°$, and with the space group of $P2_1$, containing two formula units in a cell. The structure was determined by the application of Patterson and Fourier techniques and was refined by the least-squares method to an R factor of 10.4%. The absolute configuration of $(-)_{589}$-[Co acac tn_2]$^{2+}$ can be denoted as Δ. The two Co-tn chelate rings assume the chair form, and the Co-acac chelate ring is almost planar. The geometry of [As-(+)-tart]$_2^{2-}$ is identical with that of [Sb-(+)-tart]$_2^{2-}$.

Several investigations have been made regarding the assignment of the CD spectrum of $\Delta(+)_{589}$-[Co tn_3]$^{3+}$ in the region of the octahedral T_{1g} absorption. Those who studied the solution spectra of the complex have identified the negative CD peak in the lower frequency as the E_a component.[1-3] On the other hand, Judkins and Royer indicate that the E_a component has a positive CD peak in the shorter wavelength region,[4] and they support the distortion theories.[5-7]

According to Mason *et al.*,[8] the single CD peak of $(-)_{589}$-[Co acac tn_2]$^{2+}$ in the visible region has the same negative sign as the E_a component of the parent trigonal complex, $\Delta(+)_{589}$-[Co tn_3]$^{3+}$. If the absolute configuration of $(-)_{589}$-[Co acac tn_2]$^{2+}$ is determined, it will be possible to assign the E_a component of $\Delta(+)_{589}$-[Co tn_3]$^{3+}$ on the basis of Mason's rule.[8] Therefore, we carried out the crystal-structure determination of $(-)_{589}$-[Co acac tn_2][As-(+)-tart]$_2\cdot H_2O$ by the X-ray method. A preliminary report of this work has been published.[9]

Experimental

The brownish-yellow, plate-like crystals of $(-)_{589}$-[Co-acac tn_2]][As-(+)-tart]$_2\cdot H_2O$ were prepared by Hiroshi Kawaguchi and Shinichi Kawaguchi. Using Ni$K\alpha$ radiation, the unit-cell dimensions were obtained from a least-squares treatment of 29 θ-values on $0kl$ and $h0l$ Weissenberg photographs calibrated with aluminum powder ($a=4.0494$ Å). The systematic absences of $0k0$ for k odd suggest that the space group is $P2_1$ or $P2_1/m$. However, since the compound is optically-active, $P2_1$ was chosen. The crystal data are as follows:

monoclinic
$a=12.02(0.01)$Å
$b=13.73(0.02)$Å
$c=9.02(0.01)$Å
$\beta=107.4(0.3)°$
space group $P2_1$
$Z=2(D_m=1.79, D_c=1.79$ g.cm$^{-3})$
μ(Ni$K\alpha$)$=54.4$ cm^{-1}

Multiple-film, equi-inclination Weissenberg photographs were taken for the 0—7 and 0—6 layers about the b and a axes with Ni$K\alpha$ radiation ($\lambda=1.6591$ Å). For both sets of films, prismatic specimens ($\sim 0.1\times 0.2\times 0.5$ mm) were used. The intensities were estimated by visual comparison with the calibrated intensity scales. After correction for the ususl

* Present adress: Faculty of Literature and Science, Kochi University, Asakura, Kochi.

1) J. R. Gollogly and C. J. Hawkins, *Chem. Commun.*, **1968**, 689.

2) P. G. Beddoe and S. F. Mason, *Inorg. Nucl. Chem. Lett.*, **4**, 433 (1968).

3) F. Woldbye, ORD of transition metal complexes, European Research Office, U. S. Army, Frankfurt a. M. (1959); *Record of Chemical Progress*, **24**, 197 (1963).

4) R. R. Judkins and C. J. Royer, *Inorg. Nucl. Chem. Lett.*, **6**, 305 (1970).

5) A. G. Karipides and T. S. Piper, *J. Chem. Phys.*, **40**, 674 (1964).

6) A. D. Liehr, *J. Phys. Chem.*, **68**, 665 (1964).

7) M. Shinada, *J. Phys. Soc. Japan*, **19**, 1607 (1964).

8) A. J. McCaffery, S. F. Mason, and B. J. Norman, *J. Chem. Soc.*, **1965**, 5094.

9) H. Kawaguchi, K. Matsumoto, H. Kuroya, and S. Kawaguchi, *Chem. Lett.*, **1972**, 125.

Lp factor and the spot shape,[10] the structure amplitudes were placed on a common arbitrary scale by internal correlation. A total of 2241 independent reflections were collected, but 454 of these were too weak to be observed. Therefore, they were assumed to be zero. No correction for absorption was applied.

Determination of the Crystal Structure

The initial coordinates of the cobalt and two arsenic atoms were deduced from a three-dimensional Patterson function. A three-dimensional Fourier synthesis phased on these heavy atoms revealed the positions of nine light atoms of the complex cation and five oxygen atoms of tartrate anions. Three cycles of refinement were carried out for the positional and thermal parameters by the least-squares method, and the resulting parameters were used to compute a Fourier function, which gave the probable positions of the three chelate rings around the cobalt atom, but not those of all the atoms of tartrate ions. The subsequent Fourier synthesis phased on these atoms showed the coordinates of all the remaining non-hydrogen atoms. The three cycles of block-diagonal least-squares refinement yielded an R factor of 12.5%, isotropic temperature factors being used for all the atoms. Three more cycles of refinement, in which anisotropic temperature factors were applied for the three heavy atoms, reduced the R factor to 10.4% for 1787 observed reflections. The following weighting scheme was employed:

$w=0.3$ for $F_0<12.2$

$w=1.0$ for $12.2\leq F_0\leq 93.5$

$w=93.5/F_0$ for $F_0>93.5$

Throughout the refinement, atomic scattering factors taken from the International Tables for X-ray Crystallography[11] were used. A difference Fourier synthesis obtained at this stage did not show any peaks attributable to hydrogen atoms. The final atomic coordinates and thermal parameters are given in Table 1. The observed and calculated structure factors are preserved by the Chemical Society of Japan.[12]

The absolute structure of the crystal was assigned on the basis of the known configuration of the (+)-tartrate ion,[13] and was found to correspond to the inversed set of the atomic coordinates given in Table 1; the Δ configuration has been assigned to the complex cation on the basis of the present X-ray study.

Discussion

The crystal consists of the $(-)_{589}$-[Co acac tn_2]$^{2+}$ cations, the [As-(+)-tart]$_2^{2-}$ anions, and water molecules, which are held together by N–H···O and O–H···O hydrogen bonds. Projections of the absolute structures viewed along b and c axes are presented in Figs. 1 and 2 respectively. Possible hydrogen bonds are summarized in Table 2. All the hydrogen atoms of N(3) and N(4) and one of the hydrogen atoms linked to N(1) and N(2) participate in the N–H···O hydrogen bonds. The interatomic distance between O(H_2O) and O(10) is 3.10 Å, and that between O(H_2O) and O(4), 2.86 Å. The O(4)–O(H_2O)–O(10) angle is

Table 1. Final atomic coordinates[a] and temperature factors with standard deviations in parentheses

Atom	x/a	y/b	z/c	B
As(1)	0.1609(2)	0.0000	0.0395(3)	b)
As(2)	0.1270(2)	−0.0408(3)	0.5402(3)	b)
Co	0.3142(3)	0.4810(4)	0.7276(4)	b)
N(1)	0.192(1)	0.467(2)	0.525(2)	3.7(4)
N(2)	0.446(2)	0.434(2)	0.652(2)	3.9(4)
C(1)	0.223(2)	0.473(3)	0.374(3)	4.9(6)
C(2)	0.328(3)	0.406(3)	0.382(3)	5.1(7)
C(3)	0.443(2)	0.447(3)	0.485(3)	5.1(6)
N(3)	0.191(2)	0.509(2)	0.829(2)	4.2(4)
N(4)	0.346(2)	0.619(2)	0.690(2)	3.9(5)
C(4)	0.208(3)	0.597(3)	0.931(3)	5.3(7)
C(5)	0.216(3)	0.691(3)	0.843(4)	6.9(9)
C(6)	0.340(3)	0.690(3)	0.815(3)	5.3(7)
O(1)	0.285(1)	0.348(1)	0.755(2)	3.7(4)
O(2)	0.429(1)	0.496(1)	0.921(2)	3.4(3)
C(7)	0.293(3)	0.192(3)	0.883(4)	5.7(8)
C(8)	0.331(2)	0.296(2)	0.880(3)	3.7(5)
C(9)	0.413(2)	0.334(3)	1.009(3)	4.5(6)
C(10)	0.456(2)	0.424(2)	1.023(3)	3.3(5)
C(11)	0.553(2)	0.461(3)	1.170(3)	5.1(6)
O(3)	0.331(2)	0.035(1)	0.178(2)	4.7(4)
O(4)	0.414(2)	0.153(2)	0.345(2)	5.5(5)
O(5)	0.118(2)	0.083(1)	0.172(2)	4.2(6)
O(6)	0.233(2)	0.032(2)	0.487(2)	5.2(4)
O(7)	0.023(2)	0.081(2)	0.481(2)	5.5(5)
O(8)	0.044(2)	0.239(2)	0.425(3)	6.4(5)
C(12)	0.329(2)	0.109(2)	0.263(3)	3.5(5
C(13)	0.207(2)	0.142(2)	0.271(3)	4.1(6)
C(14)	0.207(3)	0.134(2)	0.434(3)	4.4(6)
C(15)	0.079(3)	0.155(3)	0.445(3)	5.4(7)
O(9)	0.767(2)	0.348(2)	0.471(2)	5.3(5)
O(10)	0.769(2)	0.212(2)	0.614(3)	6.9(6)
O(11)	0.963(2)	0.417(2)	0.649(2)	4.3(4)
O(12)	0.810(2)	0.391(2)	0.851(2)	4.5(4)
O(13)	1.118(2)	0.339(2)	0.994(2)	5.5(5)
O(14)	1.007(2)	0.462(2)	1.023(2)	4.5(4)
C(16)	0.811(3)	0.289(3)	0.587(3)	5.3(7)
C(17)	0.930(3)	0.321(3)	0.698(3)	4.7(6)
C(18)	0.908(2)	0.331(2)	0.835(3)	3.6(5)
C(19)	1.019(2)	0.375(2)	0.967(4)	4.3(6)
H_2O	0.521(2)	0.225(2)	0.652(3)	8.2(7)

a) This atomic coordinate set corresponds to the mirror image of the absolute crystal structure.

b) Anisotropic thermal parameters ($\times 10^4$) are given below. Temperature factors are of the form: $\exp[(-h^2B_{11}+k^2B_{22}+l^2B_{33}+hkB_{12}+hlB_{13}+klB_{23})]$.

Atom	B_{11}	B_{22}	B_{33}	B_{12}	B_{13}	B_{23}
As(1)	64(2)	70(2)	110(3)	−3(4)	40(4)	3(5)
As(2)	68(2)	79(2)	114(4)	−4(4)	29(4)	9(6)
Co	50(3)	70(4)	86(5)	−7(7)	20(6)	8(8)

10) D. C. Philips, *Acta Crystallogr.*, **7**, 746 (1954).

11) "International Tables for X-ray Crystallography," Vol. III, Kynoch Press, Birmingham (1962), pp. 201.

12) The complete data of the F_0-F_c table are kept as Document No. 7314 at the office of the Bulletin of the Chemical Society of Japan. A copy may be secured by citing the document number.

13) J. M. Bijvoet, A. J. van Bommel, and A. F. Peerdeman, *Nature*, **168**, 271 (1951).

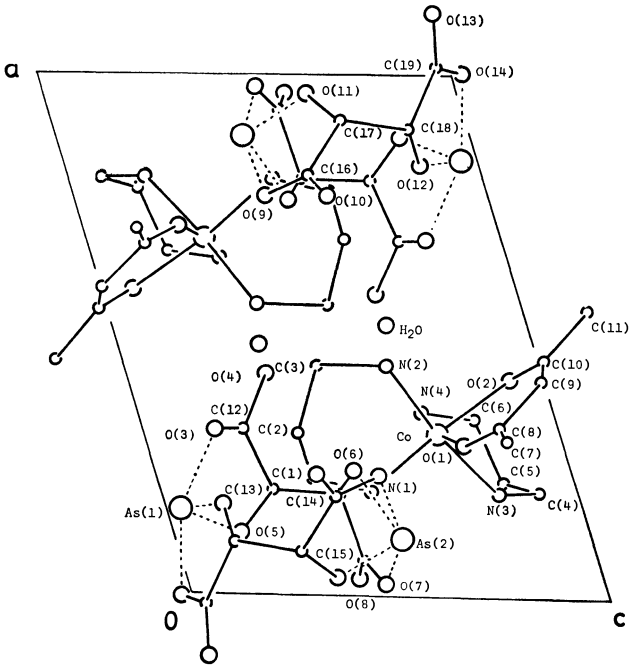

Fig. 1. Projection of the absolute structure of $(-)_{589}$-[Co acac tn_2][As-(+)-tart]H_2O along the *b* axis.

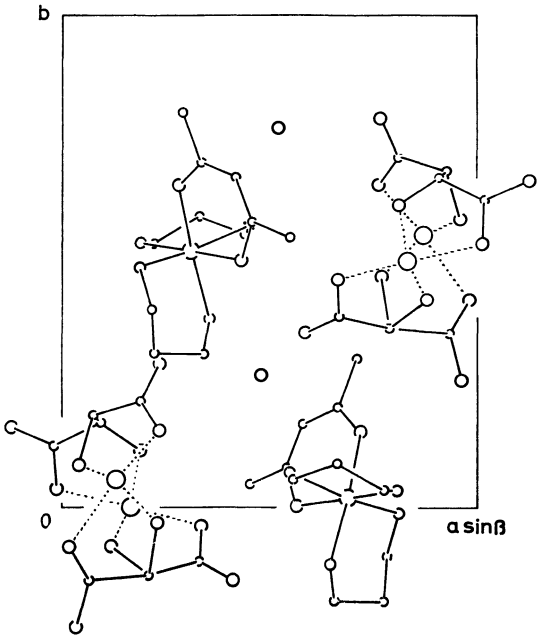

Fig. 2. The *c* projection of the absolute structure.

92°. Therefore, both hydrogen atoms of the water molecule seem to take part in the O–H···O hydrogen-bond formation.

A perspective view of the complex cation is shown in Fig. 3. The cobalt atom is octahedrally coordinated by the four nitrogen atoms of the two trimethylenediamine molecules and the two oxygen atoms in the enolate chelate of acetylacetone. The complex cation has no two-fold axis, in contrast with the case of the $(-)_{589}$-$[Co(NCS)_2tn_2]^+$ complex.[14]

14) K. Matsumoto, M. Yonezawa, H. Kuroya, H. Kawaguchi, and S. Kawaguchi, This Bulletin, **43**, 1269 (1970).

Table 2. Possible hydrogen bonds

N	O	N···O	H···O	Angle around H
N (1) I	O (7) II	3.00 Å	2.02 Å	158°
N (2) I	H_2O I	3.01	2.06	152
N (3) I	O (11) III	3.01	2.23	131
N (3) I	O (13) III	3.04	2.05	160
N (4) I	O (10) IV	2.96	1.99	156
N (4) I	O (4) IV	3.03	2.01	170
O	O	O···O		
H_2O I	O (4) I	2.86		
H_2O I	O (10) I	3.10		

I x, y, z II $-x, 1/2+y, 1-z$
III $1-x, y, z$ IV $1-x, 1/2+y, 1-z$

The positions of the hydrogen atoms were computed on the assumption that the $>NH_2$ groups have the tetrahedral geometry and the N–H bond distances are 1.03 Å.

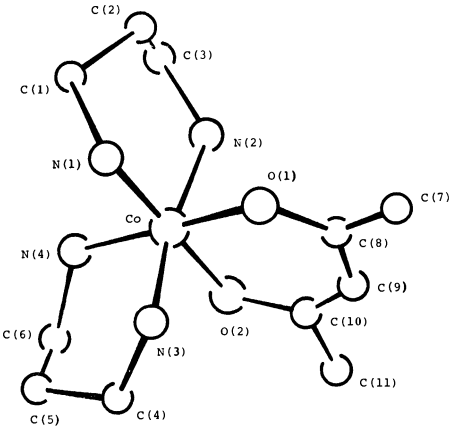

Fig. 3. Perspective view of the complex cation.

It was previously indicated that the rotational strengths of the E_a transitions of $\Lambda(-)_{589}$-[Co en_3]$^{3+}$ and $\Lambda(+)_{589}$-[Co tn_3]$^{3+}$ are negative in sign,[1-3] that the $(-)_{589}$-[Co acac en_2]$^{2+}$ complex shows a single CD band with a negative sign in the visible region, and that it is mainly derived from the dominant E_a component of $(-)_{589}$-[Co en_3].[3+ 8] On this basis, the $(-)_{589}$-[Co acac en_2]$^{2+}$ complex was concluded to have the Λ configuration.[8] Likewise, the Cotton effect of $(-)_{589}$-[Co acac tn_2]$^{2+}$ in the first-absorption-band region is negative in sign (Fig. 4), suggesting that the Λ configuration should be assigned to it; actually, this has been found to be the case. Thus, the spectral assignment for $(+)_{589}$-[Co tn_3]$^{3+}$ made by several workers[1-3] is quite compatible with the results of the present X-ray study.

However, Judkins and Royer identified the positive CD band of $\Lambda(+)_{589}$-[Co tn_3]$^{3+}$ in the region of the octahedral T_{1g} transition as E_a component.[4] If their assignment of the CD peak is correct, the Λ configuration should be given to $(-)_{589}$-[Co acac tn_2]$^{2+}$; this is inconsistent with our result. Piper's model for optical activity is not supported in this case, either.[15]

15) K. R. Butler and M. R. Snow, *Chem. Commun.*, **1971**, 550; K. Matsumoto and H. Kuroya, This Bulletin, **45**, 1755 (1972).

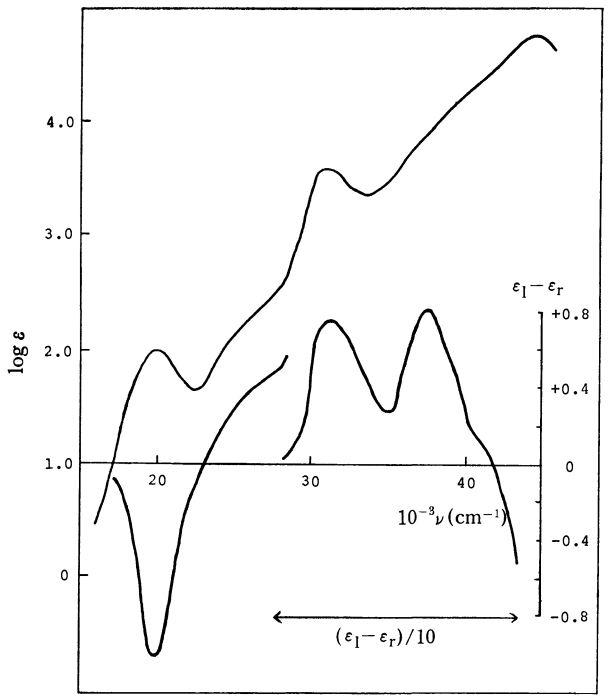

Fig. 4. Absorption and circular dichroism spectra of $(-)_{589}$-[Co acac tn_2]$^{2+}$ in water.

Recent conformational analyses of the chelate ring formed by trimethylenediamine (tn) provide an interesting basis for the interpretation of the CD spectrum of $(+)_{589}$-[Co tn_3]$^{3+}$. Those who computed its conformational preference derived significantly different results from one another,[16-18] but they all joined in suggesting that the energy difference between the tris-chair form and the tris-lel-skew-boat form is quite small. It seems that, in soluton, a conformational equilibrium involving significant amount of two or more conformers prevails, as has been pointed out by Woldbye.[18,19] This is possibly the case with $\Delta(-)_{589}$-[Co acac tn_2]$^{2+}$, whose CD spectrum shows a single negative peak in the visible region. Though such a conformational equilibrium is to be expected in solution, the absolute configuration of $\Delta(-)_{589}$-[Co acac tn_2]$^{2+}$ was found to be related to that of $\Delta(+)_{589}$-[Co tn_3]$^{3+}$ in terms of Mason's rule.[8] Therefore, the CD spectrum of $\Delta(+)_{589}$-[Co tn_3]$^{3+}$ in water should have a negative peak in the region of $A_{1g}\rightarrow E_a$ transition.[20]

The two six-membered diamine chelate rings of $(-)_{589}$-[Co acac tn_2]$^{2+}$ assume the chair form in the crystal. The coordination angles in both chelate rings are 96°, slightly larger than those (94°) found in $(-)_{589}$-[Co tn_3]$^{3+}$.[21] The Co-acac chelate ring is almost planar, the maximum deviation from the best

Table 3. Bond distances and angles with their estimated standard deviations in parentheses

Co-N (1)	1.98 (2) Å	As (2)-O (11)	1.82 (2)	N (1)-Co-N (2)	96 (1)°	O (9)-As (2)-O (11)	85 (1)°
Co-N (2)	2.01 (2)	O (3)-C (12)	1.28 (3)	N (3)-Co-N (4)	96 (1)	As (2)-O (6)-C (14)	121 (2)
Co-N (3)	2.00 (3)	O (4)-C (12)	1.23 (4)	Co-N (1)-C (1)	121 (2)	As (2)-O (7)-C (15)	112 (2)
Co-N (4)	1.98 (2)	C (12)-C (13)	1.55 (4)	Co-N (2)-C (3)	121 (2)	As (2)-O (9)-C (16)	113 (2)
N (1)-C (1)	1.52 (4)	O (5)-C (13)	1.42 (3)	Co-N (3)-C (4)	117 (2)	As (2)-O (11)-C (17)	115 (2)
N (2)-C (3)	1.50 (4)	C (13)-C (14)	1.48 (4)	Co-N (4)-C (6)	116 (2)	O (3)-C (12)-O (4)	126 (3)
N (3)-C (4)	1.50 (4)	O (6)-C (14)	1.49 (4)	N (1)-C (1)-C (2)	110 (3)	O (3)-C (12)-C (13)	117 (2)
N (4)-C (6)	1.51 (4)	C (14)-C (15)	1.58 (5)	N (2)-C (3)-C (2)	109 (3)	O (4)-C (12)-C (13)	118 (2)
C (1)-C (2)	1.55 (5)	O (7)-C (15)	1.31 (4)	N (3)-C (4)-C (5)	112 (3)	C (12)-C (13)-C (14)	108 (2)
C (2)-C (3)	1.52 (5)	O (8)-C (15)	1.23 (4)	N (4)-C (6)-C (5)	113 (3)	C (12)-C (13)-O (5)	111 (2)
C (4)-C (5)	1.53 (5)	O (9)-C (16)	1.31 (4)	C (1)-C (2)-C (3)	113 (3)	O (5)-C (13)-C (14)	111 (2)
C (5)-C (6)	1.58 (5)	O (10)-C (16)	1.22 (4)	C (4)-C (5)-C (6)	107 (3)	C (13)-C (14)-O (6)	109 (2)
Co-O (1)	1.89 (2)	C (16)-C (17)	1.54 (5)	O (1)-Co-O (2)	96 (2)	C (13)-C (14)-C (15)	110 (3)
Co-O (2)	1.88 (2)	O (11)-C (17)	1.48 (4)	Co-O (1)-C (8)	127 (2)	O (6)-C (14)-C (15)	106 (3)
O (1)-C (8)	1.31 (3)	C (17)-C (18)	1.54 (4)	Co-O (2)-C (10)	121 (2)	C (14)-C (15)-O (8)	117 (3)
O (2)-C (10)	1.33 (3)	O (12)-C (18)	1.42 (3)	O (1)-C (8)-C (9)	122 (3)	C (14)-C (15)-O (7)	117 (3)
C (7)-C (8)	1.50 (4)	C (18)-C (19)	1.53 (4)	O (2)-C (10)-C (9)	129 (3)	O (7)-C (15)-O (8)	126 (3)
C (8)-C (9)	1.39 (4)	O (13)-C (19)	1.23 (4)	O (1)-C (8)-C (7)	119 (3)	O (9)-C (16)-O (10)	127 (3)
C (9)-C (10)	1.33 (4)	O (14)-C (19)	1.32 (4)	O (2)-C (10)-C (11)	108 (2)	O (9)-C (16)-C (17)	115 (3)
C (10)-C (11)	1.57 (4)			C (7)-C (8)-C (9)	119 (3)	O (10)-C (16)-C (17)	119 (3)
				C (9)-C (10)-C (11)	123 (3)	C (16)-C (17)-O (11)	110 (2)
				C (8)-C (9)-C (10)	126 (3)	C (16)-C (17)-C (18)	104 (2)
As (1)-O (3(	2.11 (2)			O (3)-As (1)-O (5)	84 (1)	O (11)-C (17)-C (18)	110 (2)
As (1)-O (5)	1.83 (3)			O (12)-As (1)-O (14)	87 (1)	C (17)-C (18)-O (12)	112 (2)
As (1)-O (12)	1.77 (2)			As (1)-O (3)-O (12)	110 (2)	C (17)-C (18)-C (19)	106 (2)
As (1)-O (14)	1.99 (2)			As (1)-O (5)-C (13)	117 (2)	O (12)-C (18)-C (19)	110 (2)
As (2)-O (6)	1.79 (2)			As (1)-O (12)-C (18)	117 (2)	C (18)-C (19)-O (13)	125 (3)
As (2)-O (7)	2.06 (2)			As (1)-O (14)-C (19)	111 (2)	C (18)-C (19)-O (14)	115 (3)
As (2)-O (9)	2.01 (2)			O (6)-As (2)-O (7)	85 (1)	O (13)-C (19)-O (14)	120 (3)

16) R. J. Geue and M. R. Snow, *J. Chem. Soc.*, *A*, **1971**, 2981.
17) J. R. Gollogly and C. J. Hawkins, *Inorg. Chem.*, **11**, 156 (1972).
18) S. R. Niketić and F. Woldbye, *Acta Chem. Scand.*, in press.
19) P. G. Beddoe, M. J. Harding, S. F. Mason, and B. J. Peart, *Chem. Commun.*, **1971**, 1283.
20) K. R. Butler and M. R. Snow, *Inorg. Chem.*, **10**, 1838 (1971).
21) T. Nomura, F. Marumo, and Y. Saito, This Bulletin, **42**, 1016 (1969).

plane being 0.08 Å. The average Co–O bond distance is 1.89 Å, and the O–Co–O angle is 96°. The important bond distances and angles within the complex cation and anion are listed in Table 3.

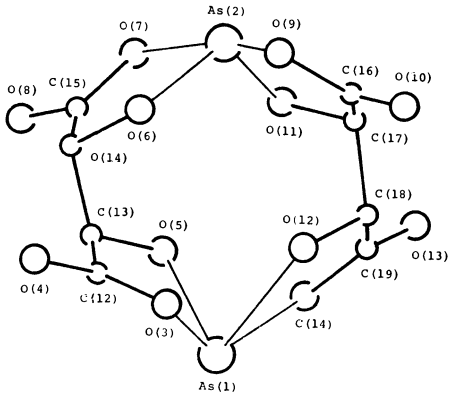

Fig. 5. Coordination about the two arsenic atoms.

A perspective view of $[As\text{-}(+)\text{-}tart]_2^{2-}$ is given in Fig. 5. The shape of the complex anion is identical with that of $[Sb\text{-}(+)\text{-}tart]_2^{2-}$.[14,22] The dimeric structure is built up of the two tetradentate tartrate ions and the two arsenic atoms. Two kinds of As–O distances are found, as in the case of $[Sb\text{-}(+)\text{-}tart]_2^{2-}$; one, As–O(alcoholic), is 1.80 Å, and the other, As–O (carboxylic), 2.04 Å.

The authors wish to express their thanks to Mr. Ken Hirotsu and Mr. Masayuki Hinamoto, who adapted the HBLS-4 and the RSSFR-3 computer programs to the FACOM 270-30 computer at Osaka City University. This research was aided in part by a Scientific Research Grant from the Ministry of Education, to which also the authors' thanks are due.

22) R. E. Tapscott, R. L. Belford, and I. C. Paul, *Coord. Chem. Rev.*, **4**, 323 (1969); J. G. Forrest and C. K. Prout, *J. Chem. Soc., A*, **1967**, 1312.

BULLETIN OF THE CHEMICAL SOCIETY OF JAPAN, VOL. 46, 2428—2430 (1973)

Absorption Band in the Near-Ultraviolet Region Observed for Binuclear Copper(II) Complexes

Sigeo KIDA, Yuzo NISHIDA, and Masatomi SAKAMOTO

Department of Chemistry, Faculty of Science, Kyushu University, Hakozaki, Fukuoka 812

(Received December 28, 1972)

Elucidation of the origin of near-ultraviolet absorption believed to be characteristic of binuclear copper(II) complexes was attempted. The absorption was attributed to charge transfer transitions from nonbonding orbitals of bridging oxygen atoms to the vacant metal *d*-orbital. Appearance of the band in the near-ultraviolet region was interpreted in terms of the red-shift due to the decreasing *s*-character of the nonbonding orbitals enforced by the steric requirement of the complex. On this basis, the spectra of dialkoxo- or dihydroxo- bridged complexes and of copper alkanoates can consistently be explained.

It is well-known that copper(II) alkanoates of a binuclear structure always show an absorption at about 27 kK.[1] A number of investigations have been carried out for the origin of this absorption,[2~7] but the results are still in considerable controversies. A relatively intense absorption band ($\varepsilon=1\sim3\times10^3$) was observed at about 28 kK for many binuclear copper(II) complexes bridged by two alkoxo groups.[8] It was assumed that the band is characteristic of the binuclear structure.

By making use of CD and absorption spectra, we have tried to give a detailed explanation of the origin of the near-ultraviolet bands believed to be characteristic of the binuclear structures of both the copper(II) acetate- and the μ-dialkoxo- types.

Experimental

Optically active N-(3-hydroxypropyl)-(−)1,2-propanediamine $NH_2CH(CH_3)CH_2NH(CH_2)_3OH$ (=pn-prol) and its copper(II) complex $[Cu_2(pn\text{-}prol')_2](ClO_4)_2$ were prepared by the method reported,[8] where pn-prol′ represents deprotonated anion of pn-prol.

The CD and absorption spectra were measured with a JASCO ORD-UV/5 optical rotatory dispersion recorder with a CD attachment. Absorption measurements were carried out over the temperature range 24~−32 °C with a Hitachi EPS-2 spectrometer, a special device being used for temperature control.

Discussion

$[Cu_2(pn\text{-}prol')_2]^{2+}$ has the structural formula as shown in Fig. 1. Its CD and absorption (AB) spectra in methanol are shown in Fig. 2. The band at 28.2 kK is a typical absorption considered to be characteristic of binuclear structure. This band increases in intensity with the lowering of temperature (Fig. 2),

1) S. Yamada, H. Nakamura and R. Tsuchida, This Bulletin, **30**, 953 (1957). *ibid.*, **31**, 303 (1958).
2) B. N. Figgis and R. L. Martin, *J. Chem. Soc.*, **1957**, 3837.
3) R. L. Martin and A. Whithey, *ibid.*, **1958**, 1394.
4) S. Kida, Y. Nakashima, Y. Morimoto, K. Niimi, and S. Yamada, This Bulletin, **37**, 549 (1964).
5) A. E. Hansen and C. J. Ballhausen, *Trans. Faraday Soc.*, **61**, 631 (1965).
6) L. Dubicki and R. L. Martin, *Inorg. Chem.*, **5**, 2203 (1966).
7) L. Dubicki, *Aust. J. Chem.*, **25**, 1141 (1972).
8) Y. Ishimura, Y. Nonaka, Y. Nishida, and S. Kida, submitted to this Bulletin.

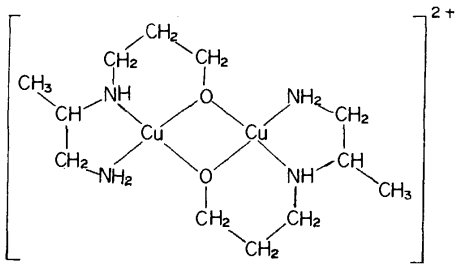

Fig. 1. Structural formula of $[Cu_2(pn\text{-}prol')_2]^{2+}$.

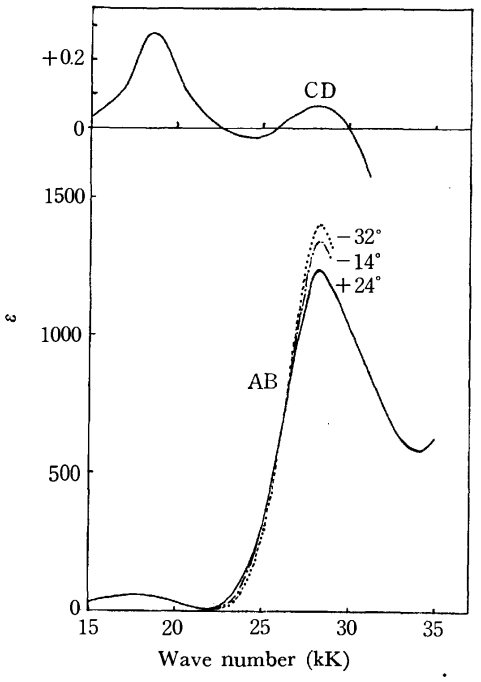

Fig. 2. Absorption and CD spectra of $[Cu_2(pn\text{-}etol')_2](ClO_4)_2$ in methanol.

indicating that it is due to the transition from the ground singlet state. A positive CD band was observed at nearly the same position, and a negative CD band relatively small intensity at 24.8 kK. The temperature dependence of this band could not be confirmed because of experimental difficulty.

Since $[Cu\ pn_2](ClO_4)_2$ has no CD band in the region 23~30 kK,[9] both CD bands are unlikely to be due to d-d transitions and are most probably attributable to charge transfer transitions from the nonbonding orbitals of bridging oxygen atoms to the empty copper d-orbitals.

Although the structure of this compound has not been determined, its skeltal structure can be analogized in high probability with that of $[Cu_2(aca\text{-}prol')_2]$, in which two copper ions, all the coordinating atoms and two carbon atoms bonded with bridging oxygen are practically coplanar, where aca-prol′=$^-OC(CH_3)$-$CHCHC(CH_3)NCH_2CH_2CH_2O^-$.[10] Thus nonbonding orbitals on the oxygen atoms, denoted by p_z and p_π', should be pure 2p-orbitals normal to the coordination plane. The CT-transitions will, therefore, occur from $p_+(=p_\pi+p_\pi')$ or $p_-(=p_\pi-p_\pi')$ to $d_+(=d_{x^2-y^2}+d_{x^2-y^2}')$ or $d_-(=d_{x^2-y^2}-d_{x^2-y^2})$, where p_+, p_-, d_+ and d_- indicate bonding (+) and antibonding (−)-orbitals with respect to the p_π-p_π' and the $d_{x^2-y^2}$·$d_{x^2-y^2}'$ interactions, respectively. However, the transition to the d_+ orbital can not be the origin of the band at 28.2 kK, because the band is attributable to the transition only from the ground singlet state, as demonstrated by measurements of the spectra. This would be understood more easily in terms of electron-formulism, *i.e.*, the possible singlet-singlet CT transitions would be from the $(d_-)^\alpha(d_-)^\beta$ state to the $(d_-)^\alpha(p_-)^\beta$ and the $(d_-)^\alpha(p_+)^\beta$ states, where α and β refer to $m_s=+1/2$ and $-1/2$ respectively; no transitions from the low-lying excited states could be compatible with the fact that the intensity of the band increases with lowering of temperature. Since p_+ and p_- are bonding and antibonding with respect to the p_π-p_π' interaction, the $p_+\leftrightarrow d_-$ and the $p_-\leftrightarrow d_-$ transitions may be assigned to the band at 28.2 and 24.8 kK, respectively. The energy difference between the two bands may be compatible with the energy of the p_π-p_π' interaction considered from the estimated distance 2.3 Å.[10]

Irreducible representations under various symmetries are shown in Table 1 for the p_+, p_- and d_- orbitals together with the direct products of those orbitals. In C_2-symmetry both electric- and magnetic-dipole transitions are allowed for $p_+\leftrightarrow d_-$ and $p_-\leftrightarrow d_-$ transitions, but in D_{2h}-symmetry no electric-dipole transition is allowed for both transitions. In C_{2h}-symmetry, which is a fairly good approximation for the compound, electric-dipole transition is allowed for only the $p_+\leftrightarrow d_-$ transition. Thus, it is clear that assignment of the 28.2 kK band to the $p_+\leftrightarrow d_-$ transition best elucidates the observed intensity ($1\sim3\times10^3$). Accordingly, the $p_-\leftrightarrow d_-$ transition may be assigned to the band at 24.8 kK, since p^+ and p_- are bonding and antibonding with respect to the $p_\pi\cdot p_\pi'$ interaction. The energy difference between the two bands may be compatible with the energy of the p_π-p_π' interaction considered from the estimated O–O distance 2.3 Å.[10] This assignment is also consistent with the fact that the absorption at 24.8 kK is so weak as to be hidden by the lower part of the intense band at 28.2 kK, and that CD intensity of the latter band is very small relative to AB intensity. However, it is safer not to form a final

Table 1. Irreducible representations of p_+, p_- and d_- orbitals and selection rules for the transition between these orbitals under various symmetries

	D_{2h}	C_{2h}	C
$p_+=p_\pi+p_\pi'$	b_{1u}	a_u	a
$p_-=p_\pi-p_\pi'$	b_{3g}	b_g	b
$d_-=d_{x^2-y^2}-d_{x^2-y^2}'$	b_{1g}	a_g	a
$p_+\leftrightarrow d_-$	$a_u(---)$	$a_u(z)$	$a(z, R_z)$
$p_-\leftrightarrow d_-$	$b_{2g}(R_y)$	$b_g(R_xR_y)$	$b(x, y, R_xR_y)$

x, y and z in ( ) denote "allowed for electric-dipole transition of x, y and z-polarization," respectively, and R_x, R_y, R_z in ( ) denote "allowed for magnetic-dipole transition of x, y and z-polarization," respectively.

9) Y. Nishida and S. Kida, *ibid.*, **43**, 3814 (1970).

10) J. A. Bertland and J. A. Kelly, *Inorg. Chim. Acta.*, **4**, 203 (1970).

conclusion for the origin of the 24.8 kK band until the temperature dependence of the CD band is confirmed, though the present assumption is in harmony with Dubicki's observation of single-crystal spectra of copper(II) acetate.[7]

It is well-known that electronegativity of a nonbonding electron-pair on an oxygen atom is highly dependent on the degree of hybridization of 2s and 2p orbitals. For the present complex, the nonbonding orbital on the oxygen atom can be regarded to be a practically pure $2p_z$ orbital. Accordingly, the CT bands shift to the near-ultraviolet region, as characteristic bands of the binuclear structure. This could be interpreted as follows. In the case of a simple coordination of alkoxo or hydroxo group, the two nonbonding electron pairs should have a considerable *s*-character as has been proved for free water and some similar molecules,[11,12] so that CT bands are observed at a relatively high frequency region. On the other hand, in the case where oxygen atoms function as a bridge in a binuclear complex, the oxygen atoms may be forced to form sp^2 hydridized σ-bonds by steric requirement, leaving p_z-orbital as a nonbonding orbital. Thus the CT band appears in a relatively lower frequency region, frequently showing a distinct peak.

Thus it follows that even in the case of a mononuclear complex an absorption band similar to that observed for binuclear complexes can appear at the near-ultraviolet region, granted that nonbonding orbitals on negatively charged oxygen (or nitrogen) atoms are of mainly *p*-character. In fact, some bis(β-diketonato) copper(II) complexes show a shoulder at 25.8 kK.[13]

Copper(II) Alkanoates. Recently Dubicki measured single-crystal spectra over the temperature range 287~4.2 K and found that the near-ultraviolet spectrum of copper(II) acetate consists of two bands at 27.8 and 30.8 kK, polarized parallel and perpendicular to copper-copper axis, respectively, the two bands being identified as singlet-singlet transitions from the fact that their intensities increase with lowering of temperature. Dubicki assigned these bands to the CT transitions $b_{2u}(p_y) \leftrightarrow b_{1g}(d_{x^2-y^2})$ and $e_g(p_x) \leftrightarrow b_{2u}(d_{x^2-y^2})$, where $b_{2u}(p_y)$ and $e_g(p_x)$ are nonbonding ligand molecular orbitals composed of out-of-plane and in-plane (with respect to the $-C\begin{smallmatrix}O-Cu-\\ \vdots \\ O-Cu-\end{smallmatrix}$ plane) oxygen 2p-orbitals, respectively. However, our conclusion on the elucidation of near-ultraviolet spectra of copper(II) acetate, though being the same as Dubicki's in attributing the band to the CT transitions from nonbonding oxygen orbitals to vacant metal d-orbitals, differs in that only p_x (out-of-plane) orbitals are taken into consideration as the orbitals from which an electron transfers. The in-plane nonbonding orbital (p_y) is regarded as a sp^2-hybridized orbitals, whose energy is much lower than that of the out-of-plane p-orbitals and is thus neglected.

Thus, the bands at 27.8 and 30.8 kK should be assigned to some transitions from the out-of-plane π-orbitals to the metal d-(b_{2u}) orbital. Judging from the observed intensities ($\varepsilon > 100$), the absorptions are not likely to be symmetry-allowed ones.

It should be noted that the appearance of CT bands in such a relatively low-frequency region can also be interpreted in terms of a high *p*-character of the nonbonding orbitals of the negatively charged oxygen atoms.

Possibility of Double Excitations. The possibility of double excitation of d–d transitions for copper(II) acetate and other binuclear metal complexes has been pointed out.[5,14,15] Dubicki could not ignore this possibility, though his discussion appeared in favor of the CT-transition origin.[7] However, in the case of chromium(II) acetate it seems improbable that the double excitations are the origin of the near-ultraviolet bands (ν_{max}=29.2 and 30.8 kK),[4] apart from the problem of absorption intensity, because any combination of the d–d transitions which are most probably distributed within the range 17~25 kK could not account for the observed frequencies 29.2 and 30.8 kK. Similar relations are observed in the case of μ-dialkoxodicopper(II) complexes, *i.e.*, frequencies of the near-ultraviolet bands (~28 kK) are too low to be assigned to some combinations of the d–d transitions (15~18 kK).[18] These facts imply that the near-ultraviolet band is better interpreted in terms of CT transitions than double excitations of d–d transitions at least for the binuclear copper(II) complexes discussed in this paper.

11) J. E. Lennard-Jones and J. A. Pople, *Proc. Roy. Soc., Ser. A*, **202**, 166 (1950).
12) J. A. Pople, *ibid.*, **202**, 323 (1950).
13) J. Ferguson, *J. Chem. Phys.*, **34**, 1609 (1961).
14) H. J. Schugar, G. R. Rossman, C. G. Barraclough, and H. G. Gray, *J. Amer. Chem. Soc.*, **94**, 2683 (1972).
15) L. Dubicki and P. Day, *Inorg. Chem.*, **11**, 1868 (1972).

Studies of the Ruthenium(III) Complex. V. Aquation and Anation Reactions of Halogenoacetatopentaammineruthenium(III) Complexes in Aqueous Solutions

Akira OHYOSHI, Satoshi SHIDA, Shuichi IZUCHI, Futoshi KITAGAWA, and Katsutoshi OHKUBO

Department of Industrial Chemistry, Faculty of Engineering, Kumamoto University, Kumamoto 860

(Received January 10, 1973)

The kinetics of aquation and anation reaction have been studied with pentaammineruthenium(III) complexes containing halogenoacetates (fluoro-, monochloro-, dichloro-, trichloro-, bromo-, and iodoacetates). It has been found that the aquation reaction proceeds through two kinds of paths, *i.e.* the acid-catalysed path and the acid-uncatalysed path, except the cases of dichloro- and trichloroacetate complexes. The aquations of dichloro- and trichloroacetate complexes are not catalysed by a proton because these ligand acids are strong acids. The equilibrium constants between $[RuH_2O(NH_3)_5]^{3+}$ and $[RuO_2CRX(NH_3)_5]^{2+}$ (O_2CRX=halogenoacetate), K_{eq}, were calculated from the anation and aquation rate constants. The k_{aq} and K_{eq} values for the fluoro-, chloro-, dichloro-, trichloro-, bromo-, and iodoacetatocomplexes are, respectively: k_{aq}, 10×10^{-5}, 7.5×10^{-5}, 19.1×10^{-5}, 49.0×10^{-5}, 6.8×10^{-5} and 6.7×10^{-5} sec^{-1}; K_{eq}, 5.2×10^{-3}, 3.6×10^{-3}, 9.0×10^{-3}, 23×10^{-3}, 3.5×10^{-3}, and 3.3×10^{-3} M, at 60 °C. The free energy plot, log k_{aq} *vs.* log K_{eq}, gave a straight line with a gradient of 1.0. It has been concluded that the acid-uncatalysed reaction proceeds via a S_N1 mechanism, while the acid-catalysed reaction seems to take place with a S_N2 mechanism. Some remarks have been made on the molecular interaction between the complex and the acid catalyst.

In a previous paper we reported on the kinetics of acid-hydrolysis for carboxylatopentaammineruthenium-(III) complexes.[1] It was found that one of the reaction paths, *i.e.*, the acid-uncatalysed one, proceeded through a dissociative mechanism; however, the mechanism for the acid-catalysed path was not clear. We have now extended the study to obtain further information concerning the reaction mechanism. Thus, the aquation and anation rate constants were measured, and the reaction mechanisms were discussed on the basis of the free-energy relationship.[2]

Experimental

Materials. All the chemicals used were of a reagent grade. Twice-distilled water was used in all kinetic runs. The ionic strength and the acidity of the reaction solution were adjusted with *p*-toluenesulphonic acid and its sodium salt.

Chloropentaammineruthenium (III) chloride was prepared by the method of Allen *et al.*[3),4)] from ruthenium trichloride and hydrazine hydrate.

Found: H, 5.08; N, 23.75%. Calcd for $[RuCl(NH_3)_5]Cl_2$: H, 5.19; N, 23.98%.

Aquopentaammineruthenium(III) perchlorate was prepared by the method of Endicott and Taube.[5)]

Found: H, 3.20; N, 13.74%. Calcd for $[Ru(H_2O)(NH_3)_5](ClO_4)_3$: H, 3.42; N, 13.94%.

Halogenoacetatopentaammineruthenium(III) perchlorates were prepared by the method of Stritar and Taube[6)] from chloropentaammineruthenium chloride, a halogenoacetate buffer solution, and a zinc amalgam.

Found: C, 5.06; H, 3.40; N, 15.00%. Calcd for $[RuO_2CCH_2F(NH_3)_5](ClO_4)_2$: C, 5.19; H, 3.68; N, 15.15%.

Found: C, 4.77; H, 3.50; N, 14.86%. Calcd for $[RuO_2CCH_2Cl(NH_3)_5](ClO_4)_2$: C, 5.02; H, 3.59; N, 14.63%.

Found: C, 4.73; H, 3.18; N, 13.73%. Calcd for $[RuO_2CCHCl_2(NH_3)_5](ClO_4)_2$: C, 4.68; H, 3.12; N, 13.65%.

Found: C, 4.58; H, 2.86; N, 12.83%. Calcd for $[RuO_2CCCl_3(NH_3)_5](ClO_4)_2$: C, 4.39; H, 2.74; N, 12.79%.

Found: C, 4.40; H, 3.08; N, 13.14%. Calcd for $[RuO_2CCH_2Br(NH_3)_5](ClO_4)_2$: C, 4.59; H, 3.25; N, 13.38%.

Found: C, 4.30; H, 2.85; N, 12.17%. Calcd for $[RuO_2CCH_2I(NH_3)_5](ClO_4)_2$: C, 4.21; H, 2.98; N, 12.28%.

Kinetic Runs. The aquation rate was measured spectrophotometically as previously has been described.[1)]

The rate of anation is expressed by the ordinary second-order rate formula:

$$dx/dt = k_{an}(a-x)(b-x) - k_{aq}x \quad (1)$$

where x is the concentration of the $[RuO_2CRX(NH_3)_5]^{2+}$ ion at time t, and where a and b are the initial concentrations of $[RuH_2O(NH_3)_5]^{3+}$ and the halogenoacetate ion respectively. The last is known from the formal concentration and the acid dissociation constant under the given conditions. When the value of a is negligibly small as compared with b, Eq. (1) can be integrated to give;

$$\ln[(x_\infty - x)/x_\infty] = -(k_{aq} + bk_{an})t \quad (2)$$

where the suffix ∞ denotes the equilibrated state. When the anation is measured by a spectrophotometric method, Eq. (2) is replaced by;

$$\ln[(A_\infty - A_t)/(A_\infty - A_0)] = -(k_{aq} + bk_{an})t \quad (3)$$

where A_0, A_t, and A_∞ are the extinctions of the reaction mixture in the initial state, at time t, and in the final state respectively. By plotting $\log(A-A_t)$ vs. t, the apparent rate constant, k_{obs}, can be obtained. The equilibrium quotient, K_{eq}, was calculated from the value of k_{aq} and k_{an}.

Results and Discussion

Aquation Reactions. The pseudo first-order rate constants, k_{obs}, for the aquation of complexes were measured at different hydrogen-ion concentrations of the reaction solution. As is illustrated in Fig. 1, the plots of k_{obs} *vs.* the hydrogen-ion concentration gave straight lines for all the complexes. The observed rate constant, k_{obs}, can be expressed by Eq. (4);

1) A. Ohyoshi, A. Jyo, and N. Shin, This Bulletin, **45**, 2121 (1972).
2) C. H. Langford, *Inorg. Chem.*, **4**, 265 (1965).
3) A. D. Allen, F. Bottomley, R. O. Harris, V. P. Reinsalu, and C. V. Senoff, *J. Amer. Chem. Soc.*, **89**, 5595 (1967).
4) A. D. Allen and C. V. Senoff, *Can. J. Chem.*, **45**, 1337 (1967).
5) J. F. Endicott and H. Taube, *J. Amer. Chem. Soc.*, **84**. 4984 (1962).
6) J. A. Stritar and H. Taube, *Inorg. Chem.* **8**, 2281 (1969).

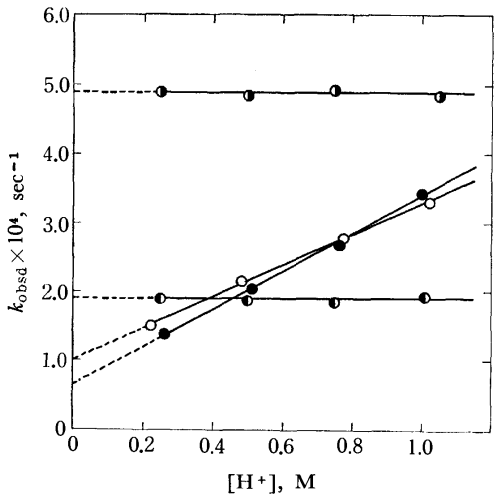

Fig. 1. Relationship between k_{obs} of aquation reaction and the hydrogen-ion concentration. (60 °C, $\mu=1.0$)
○ fluoroacetato-, ● iodoacetato-, ◐ dichloroacetato-, ◑ trichloroacetato- complex.

$$k_{obs} = k_{H_2O} + k_H[H^+] \quad (4)$$

where k_{H_2O} is the acid-independent rate constant and where k_H is the acid-dependent rate constant. In the cases of dichloro- and trichloro-acetatocomplexes, the contribution of the k_H path in Eq. (4) was negligible compared with the k_{H_2O} path; therefore, the rate constant of aquation, k_{aq} could be approximated as equal to k_{H_2O}. The calculated k_{H_2O} and k_H values are listed in Table 1, together with the pK_a values of the ligand acids.

Table 1. Rate constants of acid-catalysed and uncatalyzed paths in the aquation reaction of halogenoacetatopentaammineruthenium(III) complexes at $\mu=1.0$

Complexes	temp. °C	pK_a [a] (35 °C)	$k_{H_2O} \times 10^4$, sec^{-1}	$k_H \times 10^4$, M^{-1} sec^{-1}
Fluoroacetato-	40.1	2.624	0.1	0.25
	50.0		0.28	0.82
	60.0		1.0	2.3
	70.0		1.4	7.9
Chloroacetato-	40.0	2.90	0.05	0.44
	50.3		0.17	1.41
	59.8		0.75	2.50
	70.4		1.48	8.4
Bromoacetato-	40.3	2.94	0.10	0.50
	50.0		0.14	1.45
	60.0		0.68	2.6
	69.5		1.7	8.5
Iodoacetato-	40.2	3.21	0.04	0.86
	49.6		0.13	1.50
	60.2		0.67	2.7
	71.8		1.4	8.7
Dichloroacetato-	60.0	1.32	1.91	—
Trichloroacetato-	60.1	0.70	4.90	—

a) These values obtained from Ref. 7.

The rates of aquation increase with an increase in the ionic strength. Applying the Brønsted-Bjerrum-Christiansen formulation[8] (Eq. 5), the dependence of the ionic strength on the k_H value was investigated.

$$\ln k_H = \ln k_{H,0} + \frac{2AZ_1Z_2\sqrt{\mu}}{1+B\sqrt{\mu}} \quad (5)$$

where k_H is the acid-dependent rate constant, $k_{H,0}$ is the same for infinite dilution, Z_1 and Z_2 are the charges on the two reactants, μ is the ionic strength, A is a constant equal to 0.509 for water at 25 °C, and the B constant is of the order of the magnitude of unity.

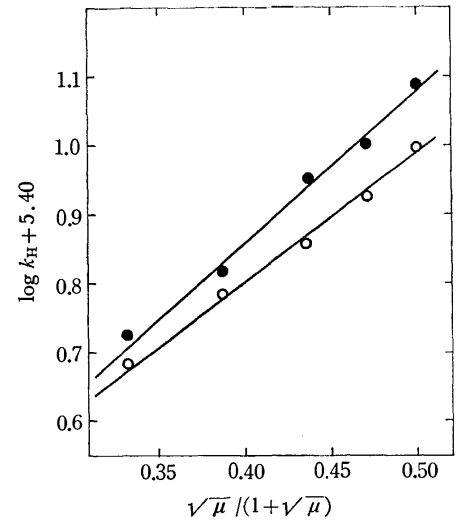

Fig. 2. Relationship between the acid-catalysed rate constant k_H and the ionic strength of the solution. (60 °C, [H$^+$]=0.025 M)
○ Fluoroacetato complex, ● Iodoacetato complex
temp: 60 °C, [H$^+$]=0.025 M

Figure 2 shows the relationship; between the k_H values and μ according to the simplified equation, Equation (5). Since the present experiment was carried out at $\mu=1.0$, this relationship is not sufficiently reliable; however, the slopes of the straight lines in Fig. 2 are both nearly +2, and these facts suffice to show the role of the proton at the transition state in the acid-dependent path. These results show that the aquation rate of the complex is dependent on the hydrogen-ion concentration and that the two reaction paths are involved in the reaction. This can be expressed by Eq. (6) for one path and by Eqs. (7) and (8) for the other path:

$$[(NH_3)_5Ru\text{–}O\overset{\overset{O}{\|}}{C}RX]^{2+} + H_2O \xrightarrow{k_6} [(NH_3)_5RuOH_2]^{3+} + RXCO_2^- \quad (6)$$

$$[(NH_3)_5Ru\text{–}O\overset{\overset{O}{\|}}{C}RX]^{2+} + H^+ \xrightarrow{K_h} [(NH_3)_5Ru\text{–}O\overset{\overset{OH}{|}}{C}RX]^{3+} \quad (7)$$

7) G. Kortüm, W. Vogel, and K. Andrussow, "Dissociation Constants of Organic Acid in Aqueous Solution," Butterworths, London (1961), p. 291—295.

8) F. Basolo and R. G. Pearson, "Mechanisms of Inorganic Reactions", 2nd ed., John Wiley and Sons Inc., New York (1967), p. 34.

$$[(NH_3)_5Ru\text{-}\overset{OH}{\overset{|}{O}}CRX]^{3+} + H_2O \xrightarrow{k_8}$$
$$[(NH_3)_5RuOH_2]^{3+} + RXCO_2^- + H^+ \quad (8)$$

The rate constant of the uncatalysed path (Eq. (6)), k_6 corresponds to k_{aq}. Equations (7) and (8) indicate the acid-catalysed path, the rate constant, k_H, of which can be expressed by Equation (9);

$$k_H = k_8 K_h \quad (9)$$

This relationship for the hydrolysis of similar complexes of Co(III), Rh(III), and Ir(III) has previously been reported.[9-13]

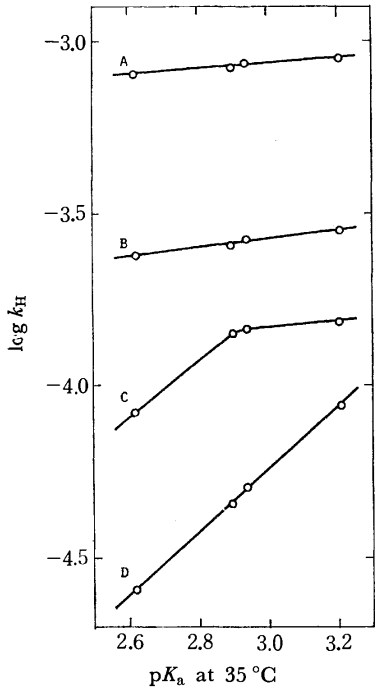

Fig. 3. Relationship between k_H of aquation reactions and pK_a of the ligand acids.
A: 70 °C, B: 60 °C, C: 50 °C, D: 40 °C

As is shown in Fig. 3, the plot of log k_H *vs.* the pK_a value of the ligand acid gives a straight line, with a gradient almost unity at lower reaction temperatures, while the gradient is about zero at higher temperatures, therefore, the weak acid seems to behave as the strong acid. The smaller k_H values of fluoroacetatocomplex compared to these of the iodoacetatocomplex (Table 1) may be due to the smaller tendency of forming a protonated intermediate shown by Eq. (7); that is, the electrostatic effect of the halogen atom is reflected in the constant, K_h, of Eq. (7), which is important in determining the k_H values.

Some remarks should be made here on the molecular interaction between carboxylatopentaammineruthenium(III) complexes ($(NH_3)_5RuOC(=O)R^{2+}$) and the acid catalyst, H^+. Three distinctive modes of interaction can be allowed in view of the orbital symmetry and orbital energies of the two species:

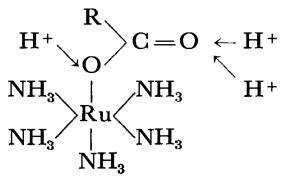

Ru-O=2.5 Å; Ru-N=2.23 Å; N-H=1.031 Å; C-O=1.28—1.43 Å, ∠RuOC=105°; ∠OCO=122.4—130°

The preliminary calculations of the all-valence-shell-electron extended Hückel MO on the above interacting system of $(NH_3)_5RuOC(=O)R^{2+}$—H^+ [14] have demonstrated that the most plausible interaction of the H^+ catalyst occurs predominantly in the direction of the orbital expansion of the nonbonding lone-pair 2p-orbital on the oxygen atom of the Ru–O bond in terms of the weakening of the Ru–O; in the case of $(NH_3)_5$-$RuOC(-O)H^{2+}$, the bond population of Ru–O (0.085) is lessened to 0.073 by the electrophilic attack of the H^+ catalyst (H^+—$0 \gtrsim 0.97$ Å).

It is worthy of emphasis that the single C–O bond is not weakened by the attack of the catalyst and that, in some measure, the solvent of H_2O participates in the weakening of the Ru–O bond; the details of this will be discussed precisely in a succeeding paper.

As is shown in Table 1, an antiparallel relationship is found between the k_{H_2O} values and the pK_a values of the halogenocarboxylic acids. Similar results were obtained for the carboxylato-[9] and amino acido-[13] pentaamminecobalt(III), and analogous ruthenium-(III) complexes.[1] These results indicate that the aquation takes place via the S_N1 (lim) mechanism because the rupture of the metal-ligand bond depends on the bond strength predicted by the pK_a of the carboxylic acids.

Anation Reactions and the Free-Energy Relationship. The anation reaction of aquopentaammineruthenium (III) complexes with halogenoacetate ions may be written as;

$$[RuH_2O(NH_3)_5]^{3+} + RXCOO^-$$
$$\rightleftarrows [RuO_2CRX(NH_3)_5]^{2+} + H_2O \quad (10)$$

and the rate constant, k_{obs}, may be expressed by the following equation;

$$k_{obs} = k_{aq} + k_{an}[RXCOO^-] \quad (11)$$

The k_{an} is obtained from the slope of the linear plot of k_{obs} vs. $[RXCOO^-]$, as is shown in Fig. 4. The equilibrium quotient, K_{eq}, is expressed by:

$$K_{eq} = k_{aq}/k_{an} \quad (12)$$

The values of k_{an} and K_{eq} are listed in Table 3.

9) F. Basolo, J. G. Bergmann, and R. G. Pearson, *J. Phys. Chem.*, **56**, 22 (1952).
10) F. Monacelli, F. Basolo, and R. G. Pearson, *J. Inorg. Nucl. Chem.*, **24**, 1241 (1962).
11) K. Kuroda, *Nippon Kagaku Zasshi*, **82**, 572 (1961).
12) K. Ogino, T. Murakami, and K. Saito, This Bulletin, 41, 1615 (1968).
13) T. Murakami, K. Ogino, H. Kobayashi, H. Yamazaki, and K. Saito, *ibid.*, **44**, 120 (1971).
14) The Coulomb integrals for the s, p, and d orbitals of Ru were taken to be −9.00 eV, −7.00 eV, and −12.00 eV respectively, on the basis of L. L. Lohr, Jr., and W. N. Lipscomb, *Inorg. Chem.*, **3**, 22 (1964), and those for the s and p orbitals of the other atoms were supplied by J. Hinze and H. H. Jaffè, *J. Amer. Chem. Soc.*, **84**, 540 (1962).

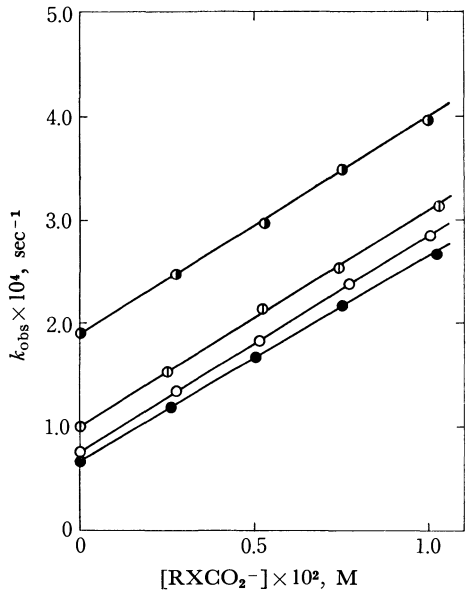

Fig. 4. Relationship between the k_{obs} of anation reaction and the concentration of halogenoacetate ion. (60 °C, μ=0.1)
● iodoacetato-, ○ chloroacetato-, ⓘ fluoroacetato, ◑ dichloroacetato-complex

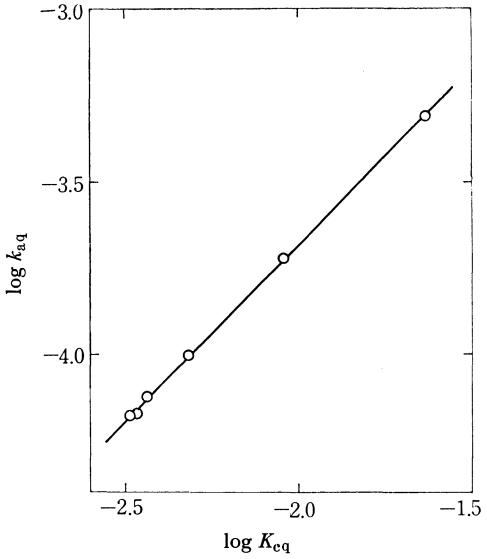

Fig. 5. Linear free energy relationship between the equilibrium quotient K_{eq} and the rate constant for aquation, k_{aq}.
Least-squares equation $\log k_{aq} = -1.63+1.02 \log K_{eq}$

Table 2. Rate constants of aquation and anation, and equilibrium quotients of aquation-anation reactions of halogenoacetatopentaammineruthenium(III) complexes

Complexes	$k_{an}\times10^2$, $M^{-1}sec^{-1}$	$k_{aq}\times10^5$, sec^{-1}	$K_{eq}\times10^3$, M
Fluoroacetato-	2.1	10	4.8
Chloroacetato-	2.1	7.5	3.6
Bromoacetato-	1.9	6.8	3.5
Iodoacetato-	2.0	6.7	3.3
Dichloroacetato-	2.1	19.1	9.0
Trichloroacetato-	2.1	49.1	23

Langford[2], Haim[15] and Murakami *et al.*[13] examined the linear free-energy relationship between the equilibrium quotient and the rate constant for aquation reactions of various acidopentaamminecobalt(III) complexes and obtained a gradient unity in their log-log plot;

$$\Delta \ln k_{aq} = \alpha \Delta \ln K_{eq} \qquad (13)$$

This value suggests a similarity between the transition state and the product. When this value is unity, the state of the ligand is the same as that in the product.

A similar plot of our results for the halogenoacetatopentaammineruthenium(III) complexes is shown in Fig. 5. An apparent α value of 1.0 is obtained from the gradient of the straight line. Thus, it can be concluded that the halogenoacetate ligand in the transition state for the aquation reaction is very similar to solvated anions; that is, the aquation reaction proceeds by the S_N1 mechanism.

Haim[15] gives Eq. (14) in discussing the relation between k_{aq} and K_{eq} for the auqations of the pentaammine series of cobalt(III) complexes:

$$\log k_{aq} = \log k_x K_0 - \log K_{eq} \qquad (14)$$

where K_0 is the ion-pair or outer-sphere complex formation constant between the aquopentaammine ion and the incoming ligand, and k_x, the inner sphere-outer sphere interchange velocity of the ion pair.

In the present study, a similar discussion is possible for the anation and aquation mechanisms. Since $K_{eq}=K_0k_x/k_{aq}$, the gradient of 1.0 in the $\log k_{aq}$ *vs.* $\log K_{eq}$ plot (Fig. 5) implies that the first term on the right-hand side of Equation (14) is independent of the nature of the incoming ligand, $RXCO_2^-$, in Reaction (10). The $\log k_xK_0$ term will be constant if the individual values of k_x and K_0 remain constant as the ligand $RXCO_2^-$ is varied. Since the value of K_0 is determined by the charge of the ligand, Langford's linear correlation for the $RXCOO^-$ ligands implies that the values of k_x are independent of the nature of the ligand. As is shown in Table 2, the observed rate constants for various anation reactions are practically the same; that is, there is little assistance by the incoming ligand in the outer sphere-inner sphere interchange reaction. In other words, this interchange is the rate-determining step for the anation reaction.

15) A. Haim, *Inorg. Chem.*, **9**, 426 (1970).

Kinetic Studies of Thermal Decomposition Reactions of Amminechromium(III) Complexes in Solid State.

Kenzo NAGASE and Nobuyuki TANAKA*

College of General Education, Tohoku University, Kawauchi, Sendai 980

Department of Chemistry, Faculty of Science, Tohoku University, Aoba, Aramaki, Sendai 980

(Received January 22, 1973)

Kinetics of the thermal decomposition reactions of $[Cr(NH_3)_6]X_3$ (X=Br, I and NCS) and $[Cr(NCS)(NH_3)_5](NCS)_2$ in solid state were studied by the manometric method. The rate constants, activation energies and activation entropies of the substitution reactions of outer-sphere anions for coordinated ammonia molecules were presented, and possible reaction mechanisms were discussed.

It is well-known that the decomposition of chromium(III) complexes having volatile ligands such as ammonia, water and ethylenediamine is initiated by substitution of an outer-sphere anion for ligand; for example, $[Cr(NH_3)_6]Cl_3$ liberates ammonia to form $[CrCl(NH_3)_5]Cl_2$.[1,2] This behavior differs entirely from that of many cobalt(III) complexes of which the decomposition is initiated by electron transfer from a ligand or an outer-sphere anion to a central metal ion.[3,4]

Investigations on these substitution reactions of chromium(III) complexes have been reported, but the mechanisms are not clear. This might be attributed to the lack of kinetic measurements. There are a few works on kinetic measurements: Wendlandt and Bear[5] obtained isothermal kinetic data for the deaquation of $[Cr(H_2O)(NH_3)_5]X_3$ (X=Cl, Br, I and NO_3), and Tanaka and Nagase[2] those for deammonation of $[Cr(NH_3)_6]Cl_3$, $[CrCl(NH_3)_5]Cl_2$ and *cis*-$[CrCl_2(NH_3)_4]Cl$. Tsuchiya and his coworkers also obtained kinetic data for the deaquation of $[Cr(H_2O)(NH_3)_5]X_3$ (X=Cl, Br, I, NO_3, SO_3 and SO_4) from the DTG and DTA curves.

We have studied kinetics of the thermal decomposition of $[Cr(NH_3)_6]X_3$ (X=Br, I and NCS) and $[Cr(NCS)(NH_3)_5](NCS)_2$ by the manometric method, and discussed the mechanisms on the basis of kinetic data.

Experimental

Apparatus and Procedure. Pressure-time curves were obtained by the apparatus described previously.[3] Details of the procedure were reported.[2]

A Hitachi EPI-2G infrared spectrophotometer and a Hitachi EPS-3T spectrophotometer equipped with a standard integrating sphere attachment were used for the measurements of the infrared absorption spectra and diffuse reflectance spectra, respectively.

Materials. The complexes $[Cr(NH_3)_6]Cl_3$[7] and $[Cr(H_2O)(NH_3)_5]Cl_3$[8] were prepared according to literature. $[Cr(NH_3)_6]Br_3$ and $[Cr(NH_3)_6]I_3$ were obtained by adding HBr and HI, respectively, to the aqueous solution of $[Cr(NH_3)_6]Cl_3$. $[Cr(NCS)(NH_3)_5](NCS)_2$ was prepared by a modified Werner's method.[9] A mixture of 15 g of $[Cr(H_2O)(NH_3)_5]Cl_3$ and 20 g of KNCS was dissolved in a solution of 10 ml of glacial acetic acid in 50 ml of water. The filtrate was cooled and orange crystals were separated by filtration. For the preparation of $[CrI(NH_3)_5]I_2$, the solution containing $[Cr(H_2O)(NH_3)_5]Cl_3$ and HI was heated on a water bath until purple crystals were separated. $[Cr(NH_3)_6](NCS)_3$ was prepared as follows: the mixture of $[Cr(NH_3)_6]Cl_3$ and methanol saturated with KNCS was left standing overnight at room temperature, and filtered off. The yellow filtrate was evaporated until crystals of $[Cr(NH_3)_6](NCS)_3$ were separated.

Results

Hexamminechromium(III) bromide loses one mole of ammonia to form $[CrBr(NH_3)_5]Br_2$ as shown by

$$[Cr(NH_3)_6]Br_3 \longrightarrow [CrBr(NH_3)_5]Br_2 + NH_3 \quad (1)$$

Pressure-time curves of $[Cr(NH_3)_6]Br_3$ in the temperature range of 213 to 232 °C are given in Fig. 1. Reaction (1) proceeded essentially according to a

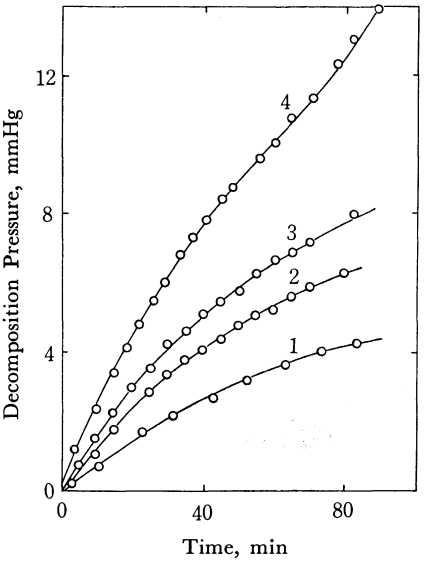

Fig. 1. Pressure-time curves of $[Cr(NH_3)_6]Br_3$ at (1) 213, (2) 221, (3) 225 and (4) 232°C.

1) W. W. Wendlandt and J. P. Smith, "The Thermal Properties of Transition-Metal Ammine Complexes", Elsevier, Amsterdam, 1967.
2) N. Tanaka and K. Nagase, This Bulletin, **42**, 2854 (1969).
3) N. Tanaka and K. Nagase, *ibid.*, **40**, 546 (1967).
4) N. Tanaka, K. Nagase, and S. Nagakura, *ibid.*, **41**, 1143 (1968).
5) W. W. Wendlandt and J. L. Bear, *J. Inorg. Nucl. Chem.*, **26**, 531 (1964).
6) R. Tsuchiya, Y. Kaji, A. Uehara, and E. Kyuno, This *Bulletin*, **42**, *1881 (1969)*.
7) M. Mori, *Nippon Kagaku Zasshi*, **74**, 253 (1953).
8) M. Mori, *ibid.*, **74**, *255 (1953)*.
9) A. Werner and J. von Halben, *Ber.*, **39**, 2668 (1906).

first-order rate equation, but deammonation was suppressed by the increase of decomposition pressure. In the case of $[Cr(NH_3)_6]Cl_3$ the deammonation proceeded almost independently of the decomposition pressure.[2] On the pressure-time curve, there is an inflection point at 232 °C, indicating that the reaction

$$[CrBr(NH_3)_5]Br_2 \longrightarrow [CrBr_3(NH_3)_3] + 2NH_3$$

follows Reaction (1). In fact, the sample heated at 232 °C for 90 min was confirmed to be a mixture of $[CrBr(NH_3)_5]Br_2$ and $[CrBr_3(NH_3)_3]$ from its infrared and reflectance spectra. The infrared spectrum also showed the formation of a small amount of ammonium bromide.

When $[Cr(NH_3)_6]Br_3$ was heated at 230 °C in a vacuum (the system was continuously evacuated with a rotary pump), the main product was not $[CrBr_3(NH_3)_3]$ but chromium nitride. This shows that $[CrBr_3(NH_3)_3]$ is stable above 230 °C in the presence of free ammonia. This was also observed for $[CrCl_3(NH_3)_3]$. In the case of iodide complex, $[CrI_3(NH_3)_3]$ could not be obtained even when the sample was heated in the presence of free ammoria, $[CrI(NH_3)_5]I_2$ only being obtained by heating the sample in a sealed capillary tube.

Plots of $\log(1-x)$ *versus* time are given in Fig. 2, where x denotes fractional decomposition. The kinetic parameters for Reaction (1) are given in Table 2.

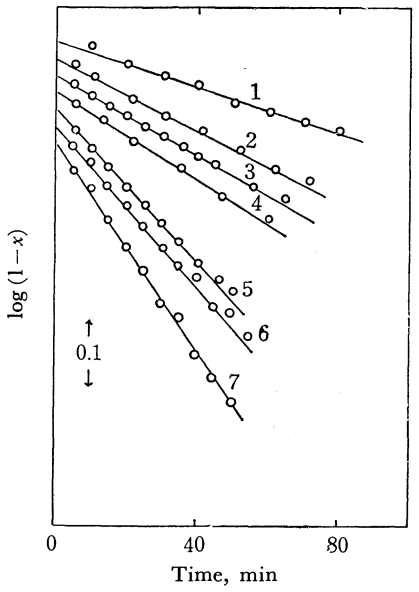

Fig. 2. Plots of a first-order rate equation for $[Cr(NH_3)_6]Br_3$ at (1) 210, (2) 213, (3) 215, (4) 217, (5) 219, (6) 221 and (7) 225 °C.

When hexamminechromium(III) iodide was heated in an inert gas atmosphere or in a vacuum, the complex decomposed to chromium nitride. The reaction is represented by

$$[Cr(NH_3)_6]I_3 \longrightarrow CrN + 3NH_4I + 2NH_3 \quad (2)$$

It proceeded essentially according to a first-order rate equation, but decomposition was suppressed by the increase of decomposition pressure, as seen for the bromide complex. The first-order rate constants of Reaction (2) were determined by the measurement of initial rates. The activation parameters obtained are given in Table 2.

The order of the thermal stabilities of the hexamminechromium(III) halides heated under the conditions of manometric measurement is as follows:

$$[Cr[NH_3)_6]Cl_3 < [Cr(NH_3)_6]Br < [Cr(NH_3)_6]I_3$$

This differs from that of the thermal stabilities reported by Wendlandt and Chou.[10] The order they obtained from the temperature of initial mass-loss in the air is as follows:

$$[Cr(NH_3)_6]I_3 < [Cr(NH_3)_6]Cl_3 < [Cr(NH_3)_6]Br_3$$
$$(190°C) \qquad (200°C) \qquad (250°C)$$

By heating $[Cr(NH_3)_6]I_3$ in the air, free iodine was observed which is considered to be formed by the reaction of the iodide ion and the oxygen in air.

$[CrI(NH_3)_5]I_2$ was obtained almost quantitatively when $[Cr(NH_3)_6]I_3$ was heated in a sealed capillary tube, in which the decomposition pressure became very high and the whole system was maintained at a furnace temperature. The infrared absorption peaks of the product are given in Table 1, together with those of $[Cr(NH_3)_6]I_3$ and $[CrI(NH_3)_5]I_2$.

Table 1. Wave numbers of the product,[a] $[Cr(NH_3)_6]I_3$ and $[CrI(NH_3)_5]I_2$

	$\delta_d(NH_3)$	$\delta_s(NH_3)$	$\rho_r(NH_3)$
Product	1586	1292	746
$[Cr(NH_3)_6]I_3$	1595	1307	738
$[CrI(NH_3)_5]I_2$	1587	1292	747

a) The product was obtained by heating $[Cr(NH_3)_6]I_3$ at 225 °C for 24 hr in a sealed capillary tube.

Kinetic runs of hexamminechromium(III) thiocyanate in a temperature range of 99 to 116 °C are given in Fig. 3, where α denotes the mole ratio of free ammonia to chromium(III) complex. The reaction is represented by

$$[Cr(NH_3)_6](NCS)_3 \longrightarrow [Cr(NCS)_3(NH_3)_3] + 3NH_3 \quad (3)$$

It proceeded almost independent of the pressure of free ammonia, obeying the Prout-Tompkins equation, $dx/dt=kx(1-x)$, where x denotes fractional decompo-

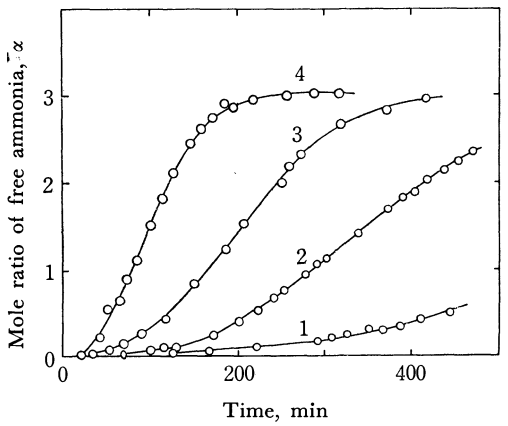

Fig. 3. Kinetic runs of $[Cr(NH_3)_6](NCS)_3$ at (1) 99, (2) 106, (3) 110 and (4) 116°C.

10) W. W. Wendlandt and C. Y. Chou, *J. Inorg. Nucl. Chem.*, **26**, 943 (1964).

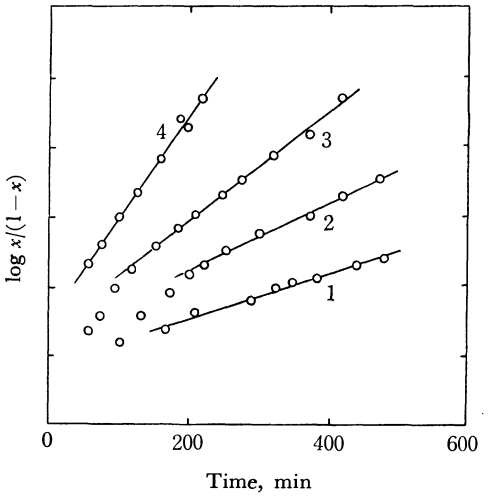

Fig. 4. Plots of $\log x/(1-x)$ versus time of $[Cr(NH_3)_6](NCS)_3$ at (1) 99, (2) 106, (3) 110 and (4) 116 °C.

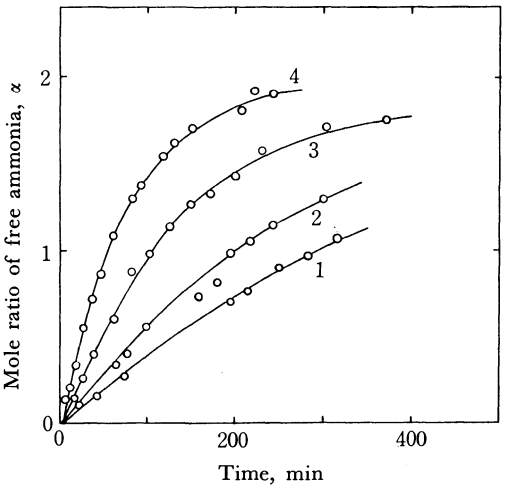

Fig. 5. Kinetic runs of $[Cr(NCS)(NH_3)_5](NCS)_2$ at (1) 91, (2) 94, (3) 101.5 and (4) 105.5 °C.

sition. Plots of $\log [x/(1-x)]$ *versus* time are given in Fig. 4, from which the second-order rate constants were determined. The kinetic parameters of Reaction (3) are given in Table 2.

Kinetic runs of $[Cr(NCS)(NH_3)_5](NCS)_2$ in the temperature range 91—105.5 °C are given in Fig. 5. The reaction is represented by

$$[Cr(NCS)(NH_3)_5](NCS)_2 \longrightarrow [Cr(NCS)_3(NH_3)_3] + 2NH_3 \quad (4)$$

This obeys a first-order rate equation although this complex contains thiocyanate ions as in the case of $[Cr(NH_3)_6](NCS)_3$. The kinetic parameters are given in Table 2.

Discussion

Kinetic parameters of amminechromium(III) complexes are given in Table 2. The data of $[Cr(NH_3)_6]Cl_3$, $[CrCl(NH_3)_5]Cl_2$ and *cis*-$[CrCl_2(NH_3)_4]Cl$[2] are also given for the sake of comparison. For $[Cr(NH_3)_6]I_3$, the substituted complexes such as $[CrI(NH_3)_5]I_2$ and $[CrI_3(NH_3)_3]$ could not be obtained under the conditions for manometric measurement, but $[CrI(NH_3)_5]I_2$ was obtained by heating $[Cr(NH_3)_6]I_3$ in a sealed capillary tube. This indicates that the reactions including a partial equilibrium such as

$$[Cr(NH_3)_6]I_3 \longrightarrow [CrI(NH_3)_5]I_2 + NH_3$$
$$[CrI(NH_3)_5]I_2 \rightleftharpoons CrN + NH_3 + 3NH_4I$$

may take place in the case of the iodide complex; the formation of the triammine complex, as seen for $[Cr(NH_3)_6]X_3$ (X=Cl, Br and NCS), is considered to be small because of the steric hindrance, *i.e.*, an iodide ion is too large to form $[CrI_3(NH_3)_3]$.

Thus, it is supposed that the decomposition of all the complexes listed in Table 2 is essentially initiated by substitution of an outer-sphere anion for a coordinated ammonia.

For the hexamminechromium(III) complexes, the order of temperature at which the rate constant is equal to 1×10^{-5} sec^{-1} is as follows:

$$[Cr(NH_3)_6](NCS)_3 \underset{(77°C)}{<} [Cr(NH_3)_6]Cl_3 \underset{(156°C)}{<} [Cr(NH_3)_6]Br_3 \underset{(184°C)}{<} [Cr(NH_3)_6]I_3 \underset{(194°C)}{}$$

It should be noted that the stability of the complexes depends strongly on an outer-sphere ion. The order is quite different from that of the hexamminecobalt(III) complexes whose decomposition is initiated by electron transfer from an outer-sphere anion to a central cobalt(III).[3]

Two types of mechanism are considered for the substitution reaction which includes the replacement of a ligand, dissociation (S_N1) and displacement (S_N2). S_N1 *mechanism*:

$$[Cr(NH_3)_6]X_3 \rightleftharpoons \underset{\text{five coordination}}{[Cr(NH_3)_5]X_3} + NH_3 \longrightarrow [CrX(NH_3)_5]X_2 + NH_3$$

Table 2. Kinetic parameters of the substitution reactions of amminechromium(III) complexes in solid state

Reaction	$k\times10^5$, sec^{-1} (t, °C)	E_a kcal/mol	$\Delta S^{\neq}$ e. u.
$[Cr(NH_3)_6]Cl_3 \rightarrow [CrCl(NH_3)_5]Cl_2+NH_3$	2.97 (170)	30	−12
$[Cr(NH_3)_6]Br_3 \rightarrow [CrBr(NH_3)_5]Br_2+NH_3$	2.16 (192)	43	12
$[Cr(NH_3)_6]I_3 \rightarrow CrN+3NH_4I+2NH_3$	3.0 (204)	49	18
$[Cr(NH_3)_6](NCS)_3 \rightarrow [Cr(NCS)_3(NH_3)_3]+3NH_3$	10.7 (99)	28	−3
$[CrCl(NH_3)_5]Cl_2 \rightarrow [CrCl_2(NH_3)_4]Cl+NH_3$	1.70 (191)	38	1
$[Cr(NCS)(NH_3)_5](NCS)_2 \rightarrow [Cr(NCS)_3(NH_3)_3]+2NH_3$	1.45 (85)	36	15
cis-$[CrCl_2(NH_3)_4]Cl \rightarrow$ *cis, cis*-$[CrCl_3(NH_3)_3]+NH_3$	11.0 (136)	31	−2

S_N2 *mechanism*:

$$[Cr(NH_3)_6]X_3 \rightleftharpoons [CrX(NH_3)_6]X_2 \longrightarrow$$
seven coordination
$$[CrX(NH_3)_5]X_2 + NH_3$$

In the case of S_N1, the rate of deammonation is almost independent of the size of an outer-sphere anion and decreases with the increase of the pressure of free ammonia, while in the case of S_N2, the rate depends strongly on the size of an outer-sphere anion. From the equation

$$\Delta H^{\neq} = \Delta H_1^{\neq} - \Delta H_2^{\neq},$$

where $\Delta H_1^{\neq}$ and $\Delta H_2^{\neq}$ are the enthalpies of activation for bond breaking and bond making, respectively, it is supposed that activation energy of S_N1 is larger than that of S_N2. Moreover, the reaction of S_N1 is considered to have larger entropy of activation from the freedom of the activated complex.

Although it is impossible to assign the reaction of all the complexes listed in Table 2, $[Cr(NH_3)_6]Br_3$ and $[Cr(NH_3)_6]I_3$ might belong to S_N1 and $[Cr(NH_3)_6]Cl_3$ to S_N2 from their kinetic behavior. The reason that $[Cr(NH_3)_6](NCS)_3$ decomposed at the lowest temperature may be due to the fact that the nitrogen atom coordinated directly to chromium(III) is the smallest in size.

The authors wish to thank the Ministry of Education for the financial support granted this research.

BULLETIN OF THE CHEMICAL SOCIETY OF JAPAN, VOL. 46, 2438—2443 (1973)

Metal Chelates of Aromatic *o,o'*-Dihydroxyazo Compounds. I. The Fluorescence Properties of the Metal Chelates of *o,o'*-Dihydroxyazobenzene and Their Use in Fluorometry

Keizō Hiraki

Department of Chemistry, Faculty of Science and Technology, Kinki University, Kowakae, Higashi-Osaka 577

(Received November 2, 1972)

As fluorometric reagents for the determination of Al, Ga, In, *etc.*, 11 derivatives of *o,o'*-dihydroxyazobenzene were examined in an attempt to determine the most desirable structure of azo compounds. *o,p,o'*-Trihydroxyazobenzene type compounds were more sensitive than *o,o'*-dihydroxyazobenzene; CH_3O-group substitution at the *para* position was also efficient. The SO_3H substitution increased, whereas the Cl substitution decreased the fluorescence of metal complexes, and the CH_3-substituted compound did not form fluorescent metal complexes because of its low solubility in water and because of the steric hindrance. Superchrome Garnet Y and Lumogallion seemed to be excellent fluorometric reagents for Al and Ga; 2-(2,4-dihydroxyphenylazo)-1-hydroxybenzene and 3-(2-hydroxy-4-methoxyphenylazo)-4-hydroxybenzene sulfonic acid were also useful. Therefore, the several conditions for the fluorometric determination of Al and Ga with those compounds were also investigated.

It has been recognized that some azo compounds can be used as fluorometric reagents for aluminum, gallium, and other metal ions. Pontachrome Blue Black R[1] and Eriochrome Red B[2] are widely used for the determination of aluminum, while Lumogallion[3,4] is one of the most sensitive fluorometric reagents for aluminum and gallium and has been employed for the determination of aluminum in sea water.[5] However, few systematic investigations of the usefulness of azo compounds for the fluorometry of metal ions have yet been performed.

Freeman and White[6,7] studied the relationship between the structures of several *o,o'*-dihydroxyazo compounds and the fluorescent characteristics of the metal complexes. However, they did not observe any general regularity, because the fluorescence properties were obtained in an aqueous solution in some cases and in a dimethylformamide solution in other cases, and because the pH of the solution was not always the optimum for the fluorescence.

In this paper, the usefulness of *o,o'*-dihydroxyazo compounds in the fluorometric determination of aluminum and gallium will be discussed. *o,o'*-Dihydroxyazobenzene was chosen as the basic azo compound; ten substituted compounds, in which –OH, $-OCH_3$, $-SO_3H$, –Cl, and/or $-CH_3$ groups were substituted for hydrogen atoms at the *ortho*, *meta*, and *para* positions of azobenzen, were synthesized. Among these compounds, Superchrome Garnet Y,[8] Mordant Blue 31,[9] and Lumogalliion[3] had previously been reported on. The fluorescence measurements were done in an aqueous medium to avoid the complication of the operation and to make the comparison easy, and the usefulness of these azo compounds for the fluorometry was ex-

1) M. Ishibashi, T. Shigematsu, and Y. Nishikawa, *Bunseki Kagaku*, **6**, 568 (1957).
2) Y. Nishikawa, K. Hiraki, and K. Morishige, *J. Facul. Sci. Technol., Kinki Univ.*, **2**, 15 (1967).
3) Y. Nishikawa, K. Hiraki, K. Morishige, and T. Shigematsu, *Bunseki Kagaku*, **16**, 692 (1967).
4) Y. Nishikawa, K. Hiraki, K. Morishige, A. Tsuchiyama, and T. Shigematsu, *ibid.*, **17**, 1092 (1968).
5) T. Shigematsu, Y. Nishikawa, K. Hiraki, and N. Nagano, *ibid.*, **19**, 551 (1970).
6) C. Donald, J. Freeman, and C. E. White, *J. Amer. Chem. Soc.*, **78**, 2678 (1956).
7) C. E. White and G. G. Guilbault, eds., "Fluorescence," Marcel Dekker, New York (1967), p. 275.
8) K. Hiraki, This Bulletin, **45**, 1395 (1972).
9) K. Hiraki, *ibid.*, **45**, 789 (1972).

amined under the optimum analytical conditions.

Reagent and Apparatus

Synthesis of Azo Compounds. The eleven azo compounds used in this investigation are shown in Table 1. These azo compounds were synthesized by the usual diazotization and coupling, and were precipitated from an aqueous solution by adding concentrated hydrochloric acid. The products thus obtained were purified by repeated recrystallizations from 6M hydrochloric acid or an ethanol solution, and were then dried at room temperature on silica gel in a desiccator.

Azo Compound Solutions. A definite weight of each of the azo compounds was dissolved in redistilled water or purified ethanol, and then the solution was diluted to give a 0.1—0.01% solution.

Standard Solutions of Aluminum, Gallium, Scandium, and Indium. The stock solution of aluminum was prepared by dissolving 1.6803 g of aluminum in water containing 5 ml of concentrated hydrochloric acid, and by then diluting the solution to 100 ml. The stock solution was diluted with water to make a standard solution containing 1.00 μg aluminum per ml. The stock solutions of gallium, scandium, and indium were prepared by dissolving 99.99, 99.9, and 99.99% pure oxides respectively with 6M hydrochloric acid; the standard solutions were obtained by the subsequent suitable dilution of the stock solutions.

Rhodamine B Solution. 0.1 g of Rhodamine B was dissolved in water, and then the solution was diluted to 100 ml. The stock solution was diluted with water to make a solution containing 0.168 μg Rhodamine B

Table 1. Chemical formulae of o,o'-dihydroxyazo compounds

Compd. No.	o,o'-Dihydroxyazo compound		Diazonium component	Coupling component
I	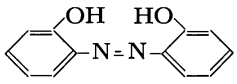	2-(2-hydroxyphenylazo)-1-hydroxybenzene	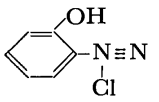	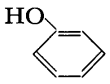
II	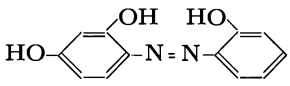	2-(2,4-dihydroxyphenylazo)-1-hydroxybenzene	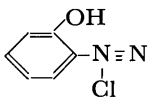	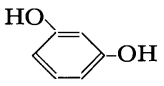
III	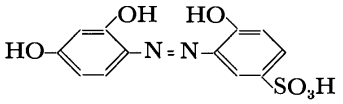	3-(2,4-dihydroxyphenylazo)-4-hydroxybenzenesulfonic acid	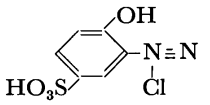	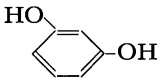
IV	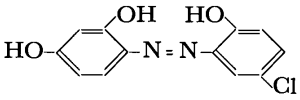	2-(2,4-dihydroxyphenylazo)-1-hydroxy-4-chlorobenzene	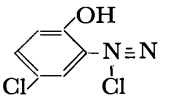	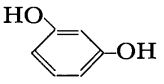
V	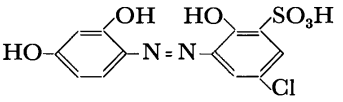	3 (2,4-dihydroxyphenylazo)-2-hydroxy-5-chlorobenzenesulfonic acid	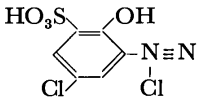	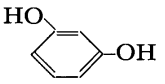
VI	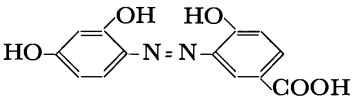	3-(2,4-dihydroxyphenylazo)-4-hydroxybenzenecarboxylic acid	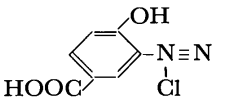	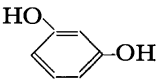
VII	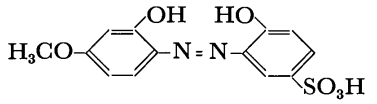	3-(2-hydroxy-4-methoxyphenylazo)-4-hydroxybenzenesulfonic acid	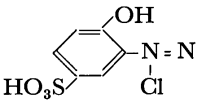	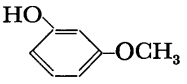
VIII	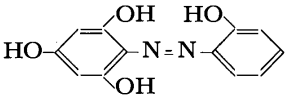	2-(2,4,6-trihydroxyphenylazo)-1-hydroxybenzene	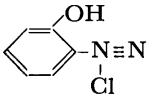	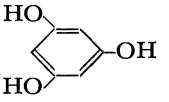
IX	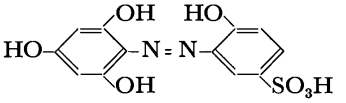	3-(2,4,6-trihydroxyphenylazo)-4-hydroxybenzenesulfonic acid	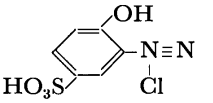	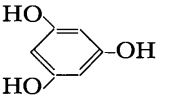
X	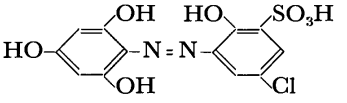	3-(2,4,6-trihydroxyphenylazo)-2-hydroxy-5-chlorobenzenesulfonic acid	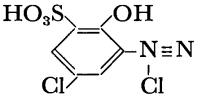	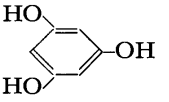
XI	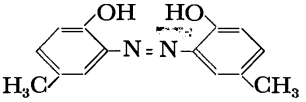	3-(2-hydroxy-5-methylphenylazo)-4-hydroxy-1-methylbenzene	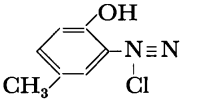	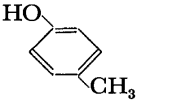

per ml; this solution was employed as the reference fluorescence standard in adjusting the sensitivity of the instrument.

All the other chemicals used were the analytical grade. Ethanol, hydrochloric acid, and ammonia were distilled until they did not show fluorescence.

Apparatus. The spectrofluorometric measurements were made with a Hitachi spectrophotometer, Model EPU-2A, equipped with a Hitachi fluorometric attachment, Model G-3 (exciting source : 150 W Xenon lamp). A Hitachi-Horiba glass electrode pH meter, Model M-5, was used for the pH measurements.

Experimental

The general procedure was as follows. To 15—20 ml of a sample solution containing appropriate amounts of metal ions such as aluminum, gallium, scandium, *etc.*, a certain quantity of a 0.1—0.01% azo compound solution and 2 ml of a 20% ammonium acetate solution or a 20% ammonium chloride solution are added. The pH value is adjusted to a desired one with a dilute hydrochloric acid solution or an ammonia solution, after with the solution is diluted to 25 ml with water. If the reaction is slow, the solution is kept at 50—80 °C for 10 min before the final dilution. The fluorescence intensity is measured at the optimum-excitation and maximum-emission wavelengths, using a Rhodamine B solution as the reference standard.[10]

Results and Discussion

Fluorescence Properties of Metal-o,o'-dihydroxyazo Compounds. Table II summarized the fluorescence behavior of several metal complexes with the *o,o'*-dihydroxyazo compounds synthesized in the present work. As may be seen in the table, metal complexes with Compounds II, III, IV, V, and VII show intense fluorescence, but the complexes with Compounds VIII, IX, X, and XI are weakly fluorescent or non-fluorescent. Compound VI, which is a carboxyl-substituted product, can not be practically used in the fluorometry, because the reagent itself has a strong fluorescence.

The fluorescence intensities of the aluminum complexes obtained under the optimum conditions increase in this order: Compound IV<II=VII<V<III. The weaker fluorescence of the Compound II complex may result from its low solubility in water. The sulfo-substituted compound III forms a strong fluorescent complex, but this reagent fluorescences remarkably. On the other hand, chloro substitution decreases the fluorescence intensity of the complex because of the electron-withdrawing property of chlorine atom. The chloro- and sulfo-substituted compound V, also called Lumogallion, is a very useful and accurate fluorometric reagent for trace amounts of aluminum. This may be the result of the fact that the fluorescence of the aluminum complex decreases a little, while the blank fluorescence decreases markedly, in comparison with Compound III.

Freeman and White pointed out that the fluorescence intensity increased in the presence of an additional hydroxyl group or a methoxyl group on the position *para* to the azo group in *o,o'*-dihydroxyazobenzene. In the order of sensitivity presented above, Compound VII was less sensitive than Compound V. However,

Table 2. Optimum fluorescence conditions of various metal-*o,o'*-dihydroxyazo compound complexes

Compound No.	Ion	$\lambda_{Excitation,\ max.}$ (nm)	$\lambda_{Emission,\ max.}$ (nm)	pH	Standing time	Metal to ligand ratio	Fluorescence intensity[a]
I	—	—	—	—	—	—	—
II	Al	365, 480	568	5.0	5 min, room temp	1 : 1	83.5
	Ga	365, 485	575	3.0	5 min, room temp	1 : 1	11.0
	Sc	480	580	6.5	5 min, room temp		1.3
	Mg	480	560	12.0	5 min, room temp		0.5
III	Al	365, 485	562	5.5	10 min, 80 °C	1 : 1	195.0
	Ga	365, 485	570	3.0	5 min, room temp	1 : 1	25.5
	Sc	482	580	6.0	5 min, room temp		0.8
	In	480	570	5.0	5 min, room temp		0.3
IV	Al	365, 485	576	6.3	10 min, 50 °C	1 : 1	15.3
	Ga	365, 485	580	3.5	5 min, room temp		1.5
V	Al	365, 485	576	5.0	10 min, 80 °C	1 : 1	135.0
	Ga	365, 485	580	3.0	10 min, 80 °C	1 : 1	24.3
VI	—	—	—	—	—	—	—
VII	Al	495	570	4.0	5 min, room temp		81.6
	Ga	500	570	3.5	5 min, room temp		2.7
VIII	—	—	—	—	—	—	—
IX	—	—	—	—	—	—	—
X	—	—	—	—	—	—	—
XI	—	—	—	—	—	—	—

a) Fluorescence intensity was obtained on 1 μg of metal ions. Fluorometer was set at 60 div. with 0.168 μg Rhodamine B/ml standard solution. Longer excitation wavelength was selected.

10) The fluorescence spectra were not corrected, since the present research was done mainly for analytical purposes.

this comparison was made principally for analytical purposes. The sensitivity of the fluorometer was set in such a manner that the fluorescence intensity of the Rhodamine B reference standard gave a definite reading (60 division) under several optimum conditions for every complex. The optimum excitation wavelength and the maximum emission wavelength of the aluminum-Compound VII complex (λ_{ex} : 495 nm, λ_{em} : 570 nm) are somewhat different from those of the Compound-V complex (λ_{ex} : 485 nm, λ_{em} : 576 nm) and of the other complexes (λ_{ex} : 480—485 nm, λ_{em}: 560—580 nm). The Rhodamine B standard shows a higher fluorescence intensity under the measuring condition for the Compound VII complex; accordingly, the sensitivity of the instrument is reduced. When the sensitivity of the instrument is kept constant, the stronger fluorescence of the aluminum complex occurs in the order of V<VII<III.

On the gallium complexes, the effect of the substituent group is similar, but the fluorescence intensity is much weaker than that of the aluminum complexes.

Compounds II and III also form fluorescent complexes with scandium, indium, and magnesium, but their fluorescence is too weak to use for the fluorometry of scandium, indium, and magnesium.

Compound I, VIII, IX, X, and XI do not form fluorescent complexes. Compound I is hardly soluble in water, although the reagent forms fluorescent aluminum and gallium complexes in an alcoholic medium. The water-solubility of Compound XI is also very low, so the fluorescence intensity is reduced. In the case of Compounds VIII, IX, and X, the reasons for the non-fluorescence are not clear.

The excitation and the emission spectra of these complexes are shown in Figs. 1, 2, 3, and 4. The excitation spectra are very similar in shape except in the cases of Compound VII complexes. On the other hand, the emission spectra of the complexes with the same compound are deformed in a certain manner by

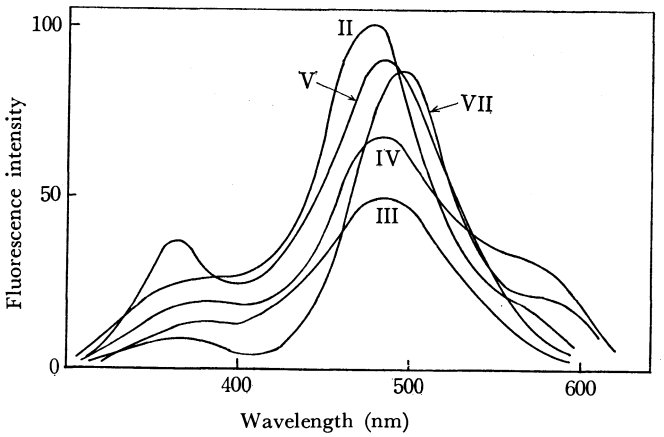

Fig. 1. Excitation spectra of aluminum complexes with *o,o'*-dihydroxyazo compounds.
II: Compound II (*cf.* Table 1, first column), emission monochromator set at 568 nm; III: Compound III, emission monochromator set at 562 nm; IV: Compound IV, emission monochromator set at 576 nm; V: Compound V, emission monochromator set at 576 nm; VII: Compound VII, emission monochromator set at 570 nm

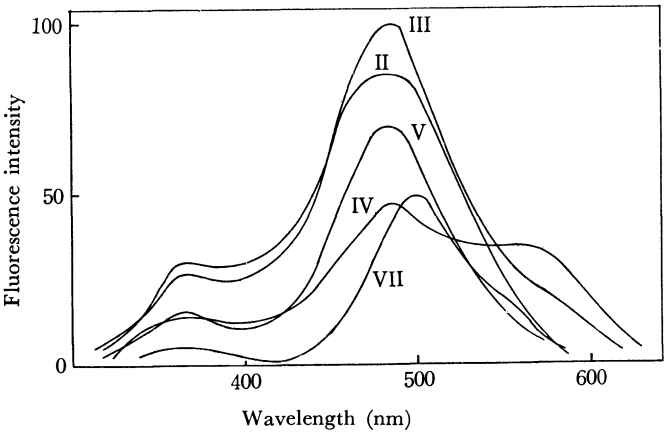

Fig. 2. Excitation spectra of gallium complexes with *o,o'*-dihydroxyazo compounds.
II: Compound II (*cf.* Table I, first column), emission monochromator set at 575 nm; III: Compound III, emission monochromator set at 570 nm; IV: Compound IV, emission monochromator set at 580 nm; V: Compound V, emission monochromator set at 580 nm; VII: Compound VII, emission monochromator set at 570 nm

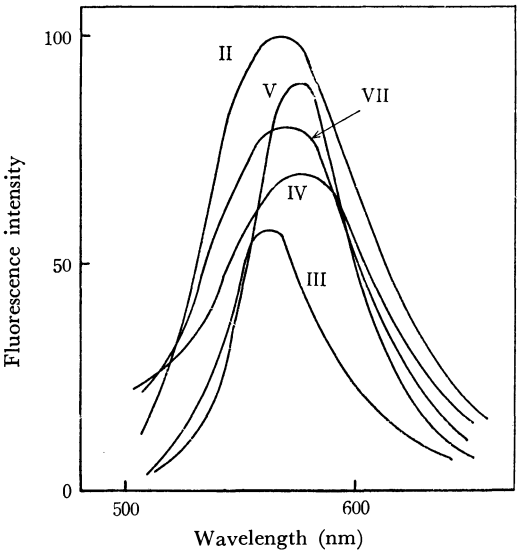

Fig. 3. Emission spectra of aluminum complexes with *o,o'*-dihydroxyazo compounds.
II: Compound II (*cf.* Table I, first column), excitation monochromator set at 480 nm; III: Compound III, excitation monochromator set at 485 nm; IV: Compound IV, excitation monochromator set at 485 nm; V: Compound V, excitation monochromator set at 485 nm; VII: Compound VII, excitation monochromator set at 495 nm

a change in the central metal ions. For example, the emission maximum of the gallium complex shifts to a slightly longer wavelength than that of the aluminum complex.

Fluorometric Determination of Aluminum and Gallium with 2-(2,4-Dihydroxyphenylazo)-1-hydroxybenzene (Compound II) and 3-(2-hydroxy-4-methoxyphenylazo)-4-hydroxybenzene Sulfonic Acid (Compound VII). As has been considered above, Compound III (Superchrome Garnet Y) and Compound V (Lumogallion) are excellent reagents; Compound II and Compound VII

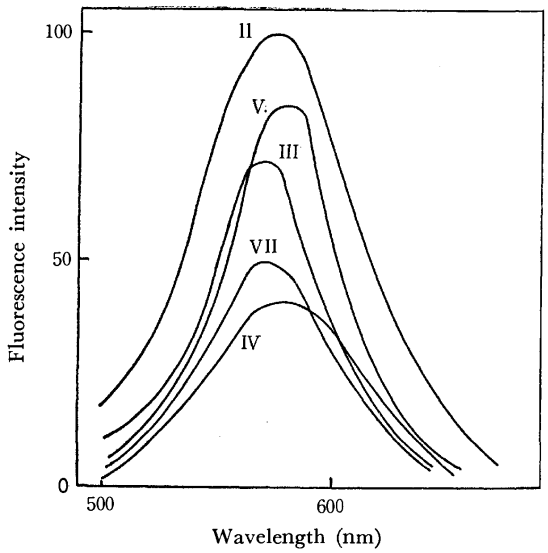

Fig. 4. Emission spectra of gallium complexes with *o,o'*-dihydroxyazo compounds.
II: Compound II (*cf.* Table I, first colum), excitation monochromator set at 485 nm; III: Compound III, excitation monochromator set at 485 nm; IV: Compound IV, excitation monochromator set at 485 nm; V: Compound V, excitation monochromator set at 485 nm; VII: Compound VII, excitation monochromator set at 500 nm

also seem to be useful for the fluorometric determination of aluminum and gallium. Analytical methods using Superchrome Garnet Y and Lumogallion were previously reported; in the present research, the procedures with the latter two reagents were studied.

(a) Effect of Standing Time: The fluorescence of these complexes developed fully within a few minutes after the preparation of the solutions, and it is stable for 2 hr at least.

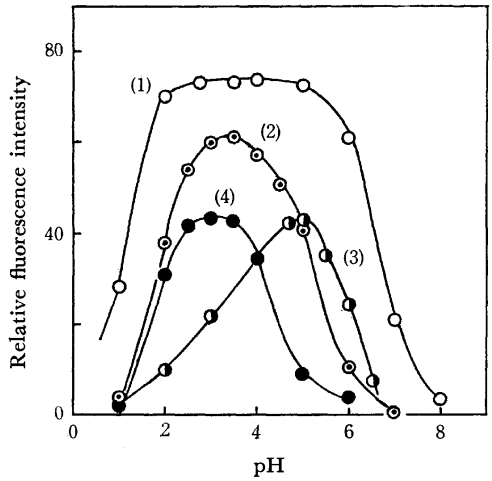

Fig. 5. Effect of pH of solution on fluorescence intensity.
(1) Al complex with compound VII, Al 1.0 μg, 495 nm/570 nm, 50 div. *vs.* 0.168 μg Rhodamine B/ml standard solution; (2) Ga complex with compound VII, Ga 10 μg, 500 nm/570 nm, 100 div. *vs.* 0.168 μg Rhodamine B/ml standard solution; (3) Al complex with compound II, Al 1.0 μg, 480 nm/568 nm, 30 div. *vs.* 0.168 μg Rhodamine B/ml standard solution; (4) Ga complex with compound II, Ga 5.0 μg, 485 nm/575 nm, 40 div. *vs.* 0.168 μg Rhodamine B/ml standard solution

(b) Effect of pH: The effect of the pH on the fluorescence intensities of metal complexes is shown in Fig. 5. The aluminum-Compound VII complex shows its maximum fluorescence in the pH range from 2.7 to 5; the gallium complex, at pH 3.5, the aluminum-Compound II complex, at pH 5, and the gallium complex, near pH 3.

(c) Effect of the Reagent Concentration: Various amounts of the reagent were added to solutions containing an adequate amount of aluminum (2 μg for Compound II and 1 μg for Compound VII) or 10 μg of gallium, after which the fluorescence intensity was measured at the optimum pH. The results, shown in Fig. 6, indicate that 1 ml of a 0.1% Compound VII solution is required for up to 1 μg of aluminum in 25 ml, and 3 ml, for 10 μg of gallium, while 0.5 ml and 0.8 ml of a 0.01% Compound II solution are desirable for 0.05—2 μg of aluminum and 0.5—12 μg of gallium respectively.

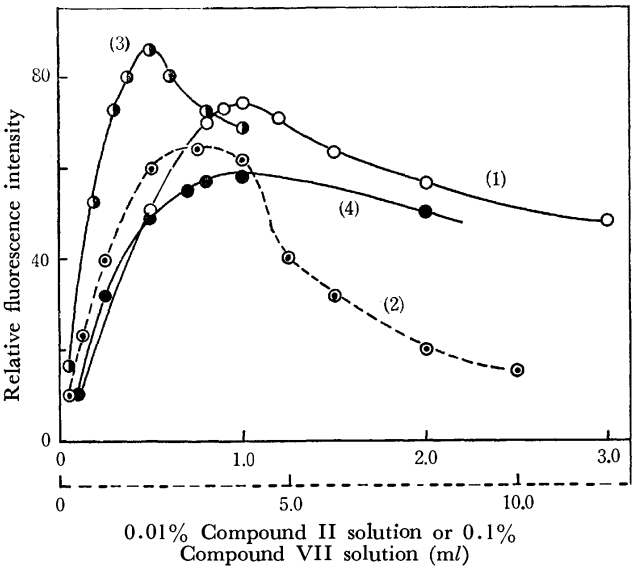

Fig. 6. Effect of reagent concentration.
(1) Al Complex with Compound VII, Al 1.0 μg, 495 nm/570 nm, 50 div. *vs.* 0.168 μg Rhodamine B/ml standard solution; (2) Ga complex with Compound VII, Ga 10 μg, 500 nm/570 nm, 100 div. *vs.* 0.168 μg Rhodamine B/ml standard solution; (3) Al complex with Compound II, Al 2.0 μg, 480 nm/568 nm, 30 div. *vs.* 0.168 μg Rhodamine B/ml standard solution; (4) Ga complex with Compound II, Ga 10 μg, 485 nm/575 nm, 40 div. *vs.* 0.168 μg Rhodamine B/ml standard solution

(d) Calibration Curves: Figure 7 presents the calibration curves for the fluorometric determinations of aluminum and gallium with Compound II and Compound VII; these curves were obtained under the above conditions. The sensitivity of the fluorometer was regulated by setting the fluorescence of the standard Rhodamine B solution (0.168 μg/ml) at a certain reading (40—100 division).

Linear relationships are observed between the fluorescence intensity and the metal-ion concentration; the determinable ranges, within an average error of 3 per cent, are 0.05—1 μg Al/25 ml and 0.5—12 μg Ga/25 ml with Compound II, and 0.05—2 μg Al/25 ml and 2—20 μg Ga/25 ml with Compound VII.

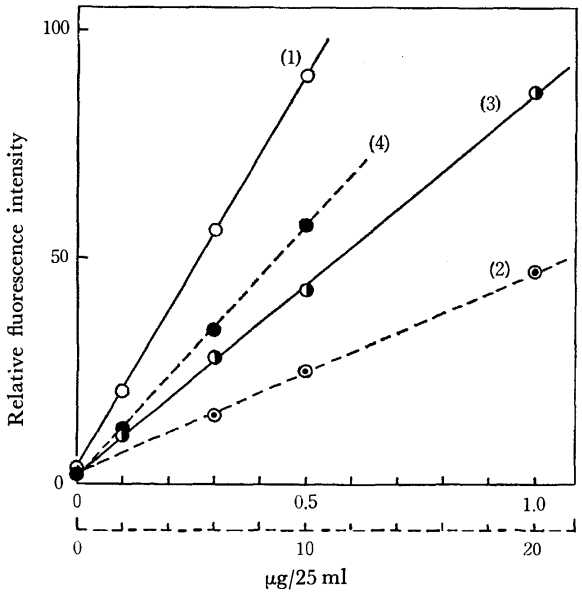

Fig. 7. Calibration curves for aluminum and gallium.
(1): Al-Compound VII system, 495 nm/570 nm, 100 div. *vs.* 0.168 μg Rhodamine B/ml standard solution; (2): Ga-Compound VII system, 500 nm/570 nm, 50 div. *vs.* 0.168 μg Rhodamine B/ml standard solution; (3): Al-Compound II system, 480 nm/568 nm, 60 div. *vs.* 0.168 μg Rhodamine B/ml standard solution; (4): Ga-Compound II system, 485 nm/575 nm, 40 div. *vs.* 0.168 μg Rhodamine B/ml standard solution.

(e) Effects of Diverse Ions: The interference of foreign ions was studied. The following metal ions diminish the fluorescence and give a negative error; in the aluminum-Compound II system, tenfold amounts of cobalt(II), copper(II), iron(III), gallium(III), zirconium(IV), vanadium(V), and chromium(VI); in the aluminum-Compound VII system, hundredfold amounts of cobalt(II), copper(II), nickel(II), tin(II), iron(III), gallium(III), thallium(III), zirconium(IV), titanium(III), vanadium(V), and chromium(VI); for the gallium-Compound II complex, sixfold amounts of copper(II), iron(III), vanadium(V), and molybdenum(VI); and for the gallium-Compound VII complex, twofold amounts of cobalt(II), copper(II), iron (III), and vanadium(V), and fivefold amounts of tin-(II), nickel(III), thallium(III), and chromium(VI).

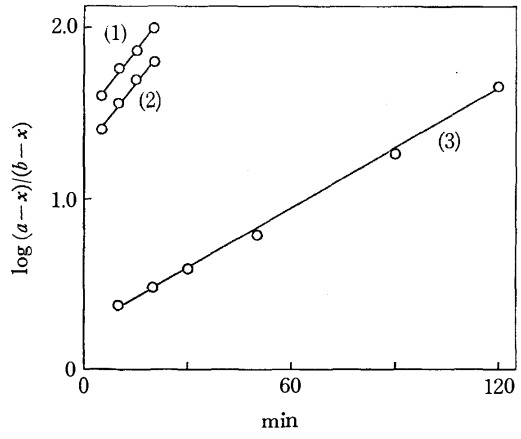

Fig. 8. Kinetics of chelate formation as indicated by fluorescence.
a is initial concentration of aluminum, *b* is initial concentration of compound II, and *x* is concentration of chelate as indicated by fluorescence (at 15 °C).
(1) *a*: 50 μmol, *b*: 5 μmol; (2) *a*: 5 μmol, *b*: 50 μmol; (3) *a*: 5 μmol, *b*: 5 μmol

The aluminum ion gives a positive error in the determination of gallium.

(f) Determination of the Metal-to-Ligand Ratio: Although the existence of the 1 : 1 complex was expected, it could not be confirmed fluorometrically either by the mole-ratio method or by the continuous-variation method. Therefore, the kinetic method was used (reaction temperature—15 °C). Figure 8 shows that the formation of the aluminum-Compound II complex follows the second-order kinetics; this may support the above expected composition. Similar results were obtained in the aluminum-Compound VII, gallium-Compound II, and gallium-Compound VII systems; therefore, the complexes may be said to have the same composition as those of the complexes with Compounds III and V.

The author wishes to express his appreciation to Professor Tsunenobu Shigematsu (Institute for Chemical Research, Kyoto University), Professor Yasuharu Nishikawa (Faculty of Science and Technology, Kinki University), and Professor Masayuki Tabushi (Tohoku Women's College) for their kind advice and suggestions throughout the investigation.

The Infrared Spectra and Normal Coordinate Treatments of X_3M–$Mn(CO)_5$ (X=Cl, Br, and I; M=Si, Ge, and Sn). II.[1]

Satoru ONAKA

Department of Chemistry, Nagoya Institute of Technology, Showa-ku, Nagoya 466

(Received November 27, 1972)

The infrared absorption spectra (2200—50 cm^{-1}) have been measured for four metal-metal bonded molecules, Cl_3Si–$Mn(CO)_5$, Cl_3Ge–$Mn(CO)_5$, Br_3Ge–$Mn(CO)_5$, and I_3Sn–$Mn(CO)_5$. Vibrational normal coordinate analyses have been made for each of these molecules on the basis of a modified Urey-Bradley force-field. The calculated frequencies agree closely with validly-assigned frequencies. The metal-metal stretching force constant, K(M–Mn), or the F-matrix element, f(M–Mn), varies with the halogen atom, and increases as the electronegativity of X increases. The force constant, K(M–Mn), or f(M–Mn) depends also on the IVb metal atom, and increases in the order of: $K(Si\text{–}Mn) \geqq K(Ge\text{–}Mn) > K(Sn\text{–}Mn)$, or $f(Si\text{–}Mn) \geqq f(Ge\text{–}Mn) > f(Sn\text{–}Mn)$. However, there is no clear relationship between the electronegativity of M and the K(M–Mn) or (M–Mn). These dependences of K(M–Mn) or f(M–Mn) on X and M are discussed, along with the bonding implications of the M–Mn bonds, on the basis of the sets of the force constants, or the sets of the F-matrix elements, and are interpreted in terms of the predominant σ-bonding framework of the M–Mn bonds.

The nature of metal-metal bonding between a transition metal and a main-Group IV b metal has been studied by a number of spectroscopic techniques, such as IR, NMR, NQR, the Mössbauer effect, *etc.*[1-13]; the common interest of these studies is to clarify the effect of the component-metal atoms or the substituents of the component metal atoms on the nature and/or the strengths of metal–metal bondings in question. Among these techniques, vibrational analyses are quite useful in evaluating the extent of the metal–metal interaction in terms of the force constants. According to a recent report on vibrational analyses by Risen *et al.*,[2b] the metal–metal bond strength in X_3M–$Co(CO)_4$ (M=Ge and Sn, X=Cl, Br, and I) increases linearly with the electronegativity of X and the M–Co bond is predominantly σ in character. In Part I of the present series of studies of metal–metal bondings,[1] the present author studied the effect of L on the Sn–Mn bonding nature for L_3Sn–$Mn(CO)_5$ (L=Cl, Br, and CH_3) and obtained similar result–that the Sn–Mn strength is strongly affected by the electronegativity of L on the tin atom, and that the π-interaction between the Sn and Mn of Cl_3Sn–$Mn(CO)_5$ is more pronounced than that of $(CH_3)_3Sn$–$Mn(CO)_5$.

The present study was undertaken in order to clarify the effects of the Component IV b metal atom and the electronegativity of the X in X_3M group on the M–Mn bonding nature, and in order to facilitate interpretations of Raman-[14] and IR-[15] intensity studies of a series of X_3M–$Mn(CO)_5$ (X=Cl, Br, and I; M=Si, Ge, and Sn) compounds by making vibrational analyses.

Experimental

All the compounds were prepared by the methods in the literatures.[16-21] The purity of the samples was checked by elemental analysis and by IR spectra. The infrared spectra in the CO stretching region were measured with a Jasco model IR-G spectrophotometer in a hexane solution, using a NaCl liquid cell (0.1 mm). The spectra were calibrated by making use of gaseous DCl by means of a superposition method. The Nujol mull samples were also examined with a Hitachi EPI-L spectrophotometer and a FIS-3 double-beam vacuum spectrophotometer in the region from 50 to 700 cm^{-1}. The results are summarized in Table 1 and Figs. 1 and 2.

Spectral Assignments

The molecular structure of Br_3Ge–$Mn(CO)_5$ has been determined by electron-diffraction analysis;[22] its molecular geometry is quite similar to those of $(CH_3)_3Sn$–

1) Part I. S. Onaka, This Bulletin, **44**, 2135 (1971).
2) a) K. L. Watters, J. N. Brittain, and W. M. Risen, Jr., *Inorg. Chem.*, **8**, 1347 (1969). b) K. L. Watters, W. M. Butler, and W. M. Risen, Jr., *ibid.*, **10**, 1970 (1971).
3) S. Onaka, T. Miyamoto, and Y. Sasaki, This Bulletin, **44**, 1851 (1971).
4) T. L. Brown, P. A. Edwards, C. B. Harris, and J. L. Kirsh, *Inorg. Chem.*, **8**, 763 (1969).
5) D. D. Spencer, J. L. Kirsh, and T. L. Brown, *ibid.*, **9**, 235 (1970).
6) Y. Kume, D. Nakamura, M. Kubo, and S. Onaka, *J. Magn. Resonance*, **10**, 58 (1973).
7) S. Onaka, Y. Sasaki, and H. Sano, This Bulletin, **44**, 726 (1971).
8) S. Onaka and H. Sano, *ibid.*, **45**, 1271 (1972).
9) S. Ichiba, M. Katada, and H. Negita, *ibid.*, **45**, 1679 (1972).
10) "Chemical Applications of Mössbauer Spectroscopy", ed. by V. I. Goldanskii and R. H. Herber, Academic Press, New York (1968).
11) E. A. Gilinskaya, "Crystallophymiya" Vol. 7, Itogi Nauki, Moskwa (1971).
12) M. I. Bruce, "Advances in Organometallic Chemistry" Vol. 6, Ed. by F. G. A. Stone and R. West, Academic Press, New York (1968).
13) D. J. Cardin, S. A. Keppie, M. F. Lappert, and M. R. Litzow, *J. Chem. Soc., A*, **1971**, 2262.
14) S. Onaka, to be published.
15) S. Onaka, to be published.
16) S. Onaka, *Nippon Kagaku Kaishi*, **10**, 1978 (1972).
17) W. Jetz, P. B. Simons, J. A. J. Thompson, and W. A. G. Graham, *Inorg. Chem.*, **5**, 2217 (1966).
18) W. Jetz and W. A. G. Graham, *J. Amer. Chem. Soc.*, **89**, 2273 (1967).
19) H. C. Clark, J. D. Cotton, and J. H. Tsai, *Inorg. Chem.*, **5**, 1582 (1966).
20) D. Seyferth, H. P. Hofmann, R. Burton, and J. F. Helling, *ibid.*, **1**, 227 (1962).
21) A. N. Nesmeyanov, K. N. Anisimov, N. E. Kolobova, and A. B. Antonova, *Iz. Akad. Nauk SSSR*, **1966**, 160.
22) N. I. Gaptochenko, N. V. Alekseev, A. B. Antonova, K. N. Anisimov, N. E. Kolobova, I. A. Ronova, and Yu, T. Struchkov, *J. Organometal. Chem.*, **23**, 525 (1970).

TABLE 1. OBSERVED INFRARED SPECTRA, VIBRATIONAL ASSIGNMENTS, AND CALCULATED FREQUENCIES

Observed frequency, cm^{-1}	Intensity	Calculated frequency, cm^{-1}	Assignments	Approximate vibrational modes
		$Cl_3Si-Mn(CO)_5$		
2124	w	2123	S_5	CO str.
2036	vs	2036	S_4, S_{19}	CO str.
660	sh	651	S_{13}	MnCO def.
650	vs	648	S_{27}	MnCO def.
		570	S_{28}	MnCO def.
542	m	539	S_{16}	MnCO def.
515	m	507	S_{20}	SiCl str.
497	m			
460	w	461	$S_7 + S_8$	SiCl str. + SiMn str.
		459	S_{18}	MnC str.
412	w	411	$S_1 + S_7$	MnC str. + SiCl str.
400	w	403	S_2	MnC str.
291	s	291	$S_8 + S_9$	SiMn str. + ClSiCl def.
201	w			
180	s	188	S_{21}	ClSiCl def.
140	m	144	$S_{10} + S_9$	CMnC, CMnSi def. + ClSiCl def.
120	w	125	$S_{25} + S_{23}$	CMnC, CMnSi def. + CMnC def.
		112	S_{24}	CMnC, CMnSi def.
		85	$S_9 + S_{10}$	ClSiCl def. + CMnC, CMnSi def.
		81	$S_{25} + S_{23}$	CMnC, CMnSi def. + CMnC def.
		$Cl_3Ge-Mn(CO)_5$		
2128	w	2128	S_5	CO str.
2048	vs	2049	S_{19}	CO str.
2038	s	2038	S_4	CO str.
655	sh	654	S_{13}	MnCO def.
633	vs	637	$S_{26} + S_{27}$	MnCO def.
535	vw	539	S_{16}	MnCO def.
451	vs	452	S_{18}	MnC str.
411	vw	410	S_1	MnC str.
398	m	398	S_2	MnC str.
371	vs	373	S_{20}	ClGe str.
		366	S_7	
231	m	231	S_8	GeMn str.
164	m	163	S_{21}	ClGeCl def.
126	m	132	S_9	ClGeCl def.
		125	$S_{23} + S_{25}$	CMnC def.
112	vw	111	S_{24}	CMnC def.
96	vw	91	S_{11}	CMnC, CMnGe def.
		83	S_9	ClGeCl def.
		77	S_{25}	CMnC, CMnGe def.
		$Br_3Ge-Mn(CO)_5$		
2126	w	2126	S_5	CO str.
2047	vs	2047	S_{19}	CO str.
2036	s	2036	S_4	CO str.
655	s	654	S_{13}	MnCO def.
631	vs	634	$S_{26} + S_{27}$	MnCO def.
555	vw, br	562	S_{27}	MnCO def.
535	vw	539	S_{16}	MnCO def.
449	vs	448	S_{18}	MnC str.
		404	S_1	MnC str.
394	vw	396	S_2	MnC str.
373	w			
290	s	292	S_{20}	BrGe str.
275	vs	259	S_7	BrGe str.
190	w	190	S_8	GeMn str.
132	w	125	S_{23}	CMnC def.

Table 1 (continued)

Observed frequency, cm^{-1}	Intensity	Calculated frequency, cm^{-1}	Assignment	Approximate vibrational modes
120	br, vw	120	$S_{10} + S_9$	CMnC, CMnGe def. + BrGeBr def.
		115	$S_{24} + S_{21}$	CMnC, CMnGe def. + BrGeBr def.
98	w	103	S_{21}	BrGeBr def.
		71	S_{25}	CMnC, CMnGe def.
		62	S_9	BrGeBr def.
		I_3Sn-$Mn(CO)_5$		
2117	m	2118	S_5	CO str.
2042	vs	2041	S_{19}	CO str.
2035	s	2035	S_4	CO str.
645	s	647	S_{13}	MnCO def.
630	vs	636	$S_{26} + S_{27}$	MnCO def.
545	w	545	S_{16}	MnCO def.
493	vw			
452	s	452	S_{18}	MnC str.
410	vw	409	S_1	MnC str.
394	m	398	S_2	MnC str.
204	vs	206	S_{20}	ISn str.
192	vs	184	S_7	ISn str.
155	m	155	S_8	SnMn str.
		124	$S_{23} + S_{24}$	CMnC, CMnSn def.
118	m	111	$S_{24} + S_{23}$	CMnC, CMnSn def.
		99	S_9	ISnI def.
		86	S_{21}	ISnI def.
70	m	67	$S_{24} + S_{21}$	CMnC, CMnSn def. + ISnI def.

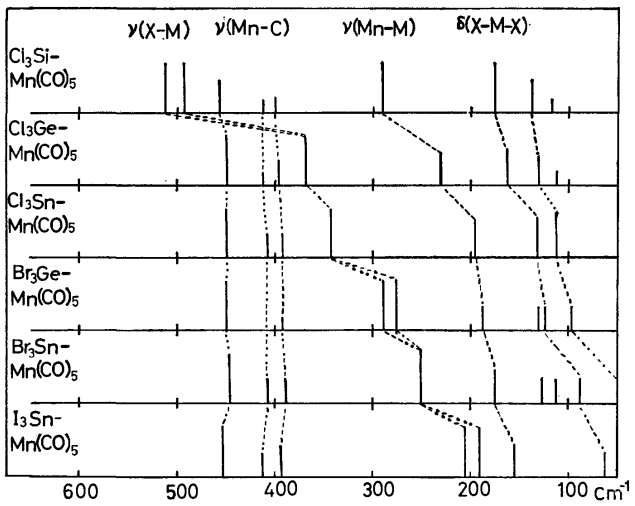

Fig. 1. Correlation diagram of observed ν(X-M), ν(Mn-C), ν(Mn-M), and δ(X-M-X) modes for X_3M-$Mn(CO)_5$.

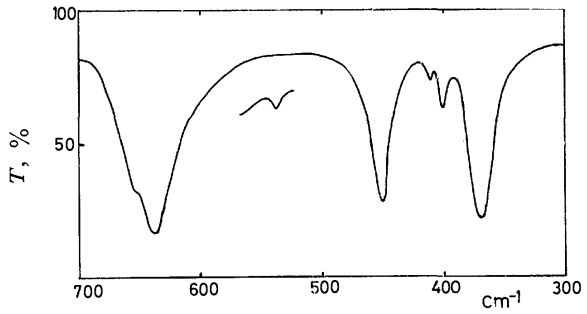

Fig. 2a. Typical spectrum of X_3M-$Mn(CO)_5$: Cl_3Ge-$Mn(CO)_5$.

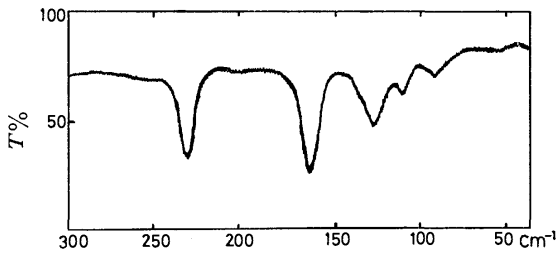

Fig. 2b. Typical spectrum of X_3M-$Mn(CO)_5$: Cl_3Ge-$Mn(CO)_5$.

$Mn(CO)_5$[23] and $(C_6H_5)_3Sn$–$Mn(CO)_5$[24] (the structures of the latter two compounds were determined by X-ray analyses). According to these reports, the local symmetry around the tin or germanium atom is C_{3v}, while that of the manganese atom is C_{4v}. Similar local symmetries are assumed for I_3Sn–$Mn(CO)_5$, Cl_3Ge–$Mn(CO)_5$, and Cl_3Si–$Mn(CO)_5$ because of the close resemblance of their vibrational spectra and physical and chemical properties to those of Br_3Ge–$Mn(CO)_5$, $(CH_3)_3Sn$–$Mn(CO)_5$, and $(C_6H_5)_3Sn$–$Mn(CO)_5$. In the vibrational analysis, these molecules can be regarded as a symmetric-top molecules, and the vibrational representation is $\Gamma_{vib}=15A_1+2A_2+11E$. This re-

23) R. F. Bryan, *J. Chem. Soc., A*, **1968**, 696.
24) H. P. Weber and R. F. Bryan, *Acta Crystallogr.*, **22**, 822 (1967).

Table 2. Symmetries of vibrational modes for X_3M–$Mn(CO)_5$ (C_{3v})

CO str. $3A_1 + E$
MnCO def. $3A_1 + A_2 + 3E$
MnC str. $3A_1 + E$
MX str. $A_1 + E$
M–Mn str. A_1
MX_3 def. $A_1 + E$
X–M–Mn def. E
CMnC def. $A_1 + E$
CMnC, C–Mn–M def. $2A_1 + 2E$
Torsion A_2

presentation is spanned by symmetrically complete sets of symmetry coordinates, as is detailed in Table 2 for X_3M–$Mn(CO)_5$ molecules. Among the fifteen symmetry coordinates involving C–O stretching, Mn–C stretching, and Mn–C–O deformation vibrations, three C–O stretching, three Mn–C stretching, and four Mn–C–O deformation vibrations can be expected, on the basis of many studies of $LMn(CO)_5$ compounds and previous work on L_3Sn–$Mn(CO)_5$, to be observed above 390 cm^{-1} for each of these molecules of the C_{4v} local symmetry around the manganese atom. Table 1 and Fig. 1 show that the vibrational spectra of Cl_3Ge–$Mn(CO)_5$, Br_3Ge–$Mn(CO)_5$, and I_3Sn–$Mn(CO)_5$ above 390 cm^{-1} are almost identical with one another, and that they are nearly identical with the spectra reported earlier for Cl_3Sn–$Mn(CO)_5$ and Br_3Sn–$Mn(CO)_5$. Therefore, all the bands observed above 390 cm^{-1} are considered to be mainly due to the vibrations of the $Mn(CO)_5$ moiety, and the same assignments of the observed bands as those given previously for Cl_3Sn–$Mn(CO)_5$ and Br_3Sn–$Mn(CO)_5$ are made for Cl_3Ge–$Mn(CO)_5$, Br_3Ge–$Mn(CO)_5$, and I_3Sn–$Mn(CO)_5$. In the spectral region of 150—390 cm^{-1}, three fundamentals which are mainly M–X (A_1+E) and Mn–M (A_1) stretching vibrations can be expected for Cl_3Ge–$Mn(CO)_5$, Br_3Ge–$Mn(CO)_5$, and I_3Sn–$Mn(CO)_5$. Br_3Ge–$Mn(CO)_5$ and I_3Sn–$Mn(CO)_5$ show broad, intense absorptions at 275 and 192 cm^{-1} respectively, with shoulders occur at frequencies higher by 10—20 cm^{-1} than those of the strong bands; these bands are assignable to the Br–Ge and I–Sn stretching vibrations respectively.[16] The spectrum of Cl_3Ge–$Mn(CO)_5$, however, shows a broad, intense absorption at 371 cm^{-1} which is assignable to Ge–Cl stretching vibrations[2a]; the A_1 and E fundamentals of Ge–Cl stretching modes are expected to be overlapped in this spectrum. The spectra of Cl_3Ge–$Mn(CO)_5$ and I_3Sn–$Mn(CO)_5$ display bands with medium intensities at 231 and 155 cm^{-1} respectively. These bands are assigned mainly to Ge–Mn and Sn–Mn stretching vibrations.[2a,16] The spectrum of Br_3Ge–$Mn(CO)_5$, however, shows a weak bands at 190 cm^{-1}; this absorption is assigned mainly to the Ge–Mn stretching vibration of this molecule. The vibrational modes, which are chiefly the X–M–X deformation vibrations and the skeletal C–Mn–C, M–Mn–C, and X–M–Mn deformations, are expected to occur below 150 cm^{-1} for the Cl_3Ge–$Mn(CO)_5$, Br_3Ge–$Mn(CO)_5$, and I_3Sn–$Mn(CO)_5$ molecules. The X–M–X deformation vibrations of Cl_3Ge–$Mn(CO)_5$ are observed at 164 and 126 cm^{-1}; those of Br_3Ge–$Mn(CO)_5$ are observed at 132, 120, and 98 cm^{-1}, and that of I_3Sn–$Mn(CO)_5$ is observed at 70 cm^{-1}.[2] Most of the skeletal C–Mn–C, M–Mn–C, and X–M–Mn deformation vibrations escape detection for these molecules.

As for Cl_3Si–$Mn(CO)_5$, however, the infrared spectrum is quite different from those of X_3Ge–$Mn(CO)_5$ and X_3Sn–$Mn(CO)_5$ in the spectral region above 400 cm^{-1}; that is, only two peaks are observed in the CO stretching region (the E and A_1 (axial) modes are expected to be overlapped) and additional bands with medium intensities are observed at 515 and 497 cm^{-1} in the middle frequency region, besides the Mn–C–O deformation and Mn–C stretching vibrations. According to previous papers on $(CH_3)_nSiCl_{4-n}$[25] and Cl_3Si–$Co(CO)_4$[2a] and the present normal coordinate analysis, these bands are assignable mainly to the Si–Cl stretching vibrations of the E mode (the E mode is supposed to split into two peaks). In the low frequency region, strong bands are observed at 291 and 180 cm^{-1}, and bands with medium to weak intensities are observed at 201, 140, and 120 cm^{-1}. The strong peak at 291 cm^{-1} is assigned mainly to the Si–Mn stretching vibration, while the peaks observed at 180 and 140 cm^{-1} are assigned mainly to $SiCl_3$ deformations.[2a] The bands at 120 cm^{-1} is assigned mainly to C–Mn–C skeletal bending motions, on the basis of the normal coordinate analysis of this molecule.

All the vibrational assignments are presented in Table 1.

Normal Coordinate Analysis

The frequency calculations were carried out on the basis of Wilson's GF matrix method[26] by making use of a modified Urey-Bradley force field.[27] The symmetry and the internal coordinates used were the same as those previously described.[1] The interatomic distances for the $Mn(CO)_5$ moiety used in the calculations were those found in the X-ray analyses of $(CH_3)_3Sn$–$Mn(CO)_5$[23] and $(C_6H_5)_3Sn$–$Mn(CO)_5$.[24] The values of the bond lengths, r(M–X), were taken from the values in Cl_3Si–$Co(CO)_4$,[28] Br_3Ge–$Mn(CO)_5$,[22] and X_4M.[29] The Mn–M bond distances were those found in the structural analyses of Cl_3Si–$Co(CO)_4$,[28] Br_3Ge–$Mn(CO)_5$,[22] and R_3Sn–$Mn(CO)_5$[23,24]: r(Si–Mn) is 2.25 Å, r(Ge–Mn) is 2.44 Å, and r(Sn–Mn) 2.67 Å. Since the trial calculation of Cl_3Sn–$Mn(CO)_5$ revealed that an error of *ca.* 0.17 Å in estimating the r(Sn–Mn) distance causes only negligible changes in the K(Sn–Mn) and other force constants,[30] the use of these metal–metal bond lengths may be

25) A. L. Smith, *J. Chem. Phys.*, **21**, 1997 (1953).
26) E. B. Wilson, *ibid.*, **9**, 76 (1941).
27) I. Nakagawa and T. Shimanouchi, *Spectrochim. Acta*, **22**, 759 (1966).
28) W. T. Robinson and J. A. Ibers, *Inorg. Chem.*, **6**, 1208 (1967).
29) R. J. H. Clark and C. J. Willis, *ibid.*, **10**, 1118 (1971).
30) S. Onaka, unpublished data.

seen to provide a better basis for normal coordinate analyses.

Above 400 cm^{-1}, the infrared spectra of these molecules are almost identical with those of $Cl_3Sn-Mn(CO)_5$, $Br_3Sn-Mn(CO)_5$, and $(CH_3)_3Sn-Mn(CO)_5$. This agreement is strong evidence that the molecular force fields for the $Mn(CO)_5$ moiety are nearly identical, and so the initial force fields were assumed to be identical with those of $L_3Sn-Mn(CO)_5$ in all the four present molecules. Actually, the calculated frequencies closely agree with the observed frequencies above 400 cm^{-1} throughout the $X_3M-Mn(CO)_5$ series of molecules without causing any serious alterations in that portion of the force-field elements which concern the vibrational modes of the $Mn(CO)_5$ moiety. The initial force constants for the MX_3 groups were taken from the MX_4, LMX_3,[31,32] and $X_3Sn-Mn(CO)_5$[1] molecules, while the reasonable starting values of K(M–Mn) was obtained from the K(Sn–Mn) of $Cl_3Sn-Mn(CO)_5$.[1] The initial force-field elements, such as H(MnMX), F(C···M), F(X···Mn), and Y(M–Mn), were transferred from the force constants of $X_3Sn-Mn(CO)_5$ (X stands for Cl and Br).[1] The force constants were adjusted so as to get the best fit of the calculated frequencies with the observed frequencies, with reference to the Jacobian matrix elements. The numerical calculations were carried out by the use of a HITAC 5020 E of the Computation Center of the University of Tokyo; the programs, BGLZ and LSMB, were set up in the laboratory of Professor Takehiko Shimanouchi.

Results

The final sets of the force constants and the F-matrix elements, f(M–Mn), are presented in Table 3, along with those of $Cl_3Sn-Mn(CO)_5$ and $Br_3Sn-Mn(CO)_5$, which are obtained in a previous work.[1] The symbols and the suffixes have the same meanings as have previously been described.[1]

The eigenvectors obtained show that the vibrational modes associated with the M–Mn stretching vibration are extensively coupled with other vibrational modes, especially with the C–Mn–C deformations, X–M and Mn–C stretching and/or X–M–X deformation vibrations. The purities of the vibrational modes of the M–Mn stretching vibrations are evaluated from the potential energy distribution to the M–Mn stretching coordinate (PED). As is shown in Table 4, the vibrational purities of the M–Mn stretching motions in $Cl_3Si-Mn(CO)_5$ and $I_3Sn-Mn(CO)_5$ are significantly low, and a considerable degree of the contribution of the Cl–Si–Cl deformation and C–Mn–C deformation vibrations to the Si–Mn and Sn–Mn stretching vibrations respectively is observed. The separation of the Mn–M stretching motion from other motions increases in accordance with the increase in the mass of M for $Cl_3M-Mn(CO)_5$, while the purity of the Mn–M

TABLE 3. FORCE CONSTANTS AND F-MATRIX ELEMENT, f(M–Mn), IN md/Å

	$Cl_3Si-Mn(CO)_5$	$Cl_3Ge-Mn(CO)_5$	$Cl_3Sn-Mn(CO)_5$	$Br_3Ge-Mn(CO)_5$	$Br_3Sn-Mn(CO)_5$	$I_3Sn-Mn(CO)_5$
K_a(MnC)	2.0	1.78	1.8	1.78	1.8	1.90
K_e(MnC)	2.32	2.25	2.2	2.22	2.2	2.25
K_a(CO)	16.75	16.85	16.9	16.82	16.85	16.77
K_e(CO)	17.07	17.25	17.23	17.22	17.20	17.09
K(SMMn)	1.30	1.23	1.0	0.85	0.82	0.41
K(MX)	1.85	0.65	1.8	1.52	1.39	1.2
H(XMX)	0.06	0.036	0.06	0.01	0.04	0.01
H(MnMX)	0.02	0.02	0.02	0.02	0.02	0.01
H_e(CMnC)	0.15	0.15	0.15	0.15	0.15	0.15
H_a(CMnC)	0.15	0.15	0.15	0.15	0.15	0.15
H(CMnM)	0.10	0.10	0.10	0.10	0.10	0.10
H_i(MnCO)	0.80	0.80	0.80	0.80	0.80	0.82
H_o(MnCO)	0.85	0.87	0.85	0.88	0.85	0.85
H_a(MnCO)	0.90	0.83	0.86	0.81	0.83	0.80
F(X···X)	0.32	0.32	0.12	0.32	0.12	0.32
F(Mn···X)	0.02	0.02	0.05	0.02	0.05	0.05
F_a(C···C)	0.01	0.01	0.01	0.01	0.01	0.01
F_e(C···C)	0.01	0.01	0.01	0.01	0.01	0.01
F(C···M)	0.01	0.01	0.01	0.01	0.01	0.01
Y(Mn–M)*	0.005	0.005	0.005	0.005	0.005	0.005
P(MC, CO)	0.50	0.50	0.50	0.50	0.50	0.50
P(MC, MC)	0.40	0.40	0.40	0.40	0.40	0.40
P_t(CO, CO)	0.38	0.32	0.30	0.32	0.30	0.30
P_c(CO, CO)	0.17	0.17	0.17	0.17	0.17	0.17
f(M–Mn)	1.36	1.30	1.13	0.91	0.95	0.53

* md Å

31) Y. Kakiuchi, This Bulletin, **26**, 260 (1953).

32) T. Shimanouchi, *J. Chem. Phys.*, **17**, 245, 734, 848 (1949).

Table 4. Potential energy distribution matrix in M–Mn stretching vibration

Approximate vibrational modes	$(PED)_{ij}$					
	Cl_3Si–$Mn(CO)_5$	Cl_3Ge–$Mn(CO)_5$	Cl_3Sn–$Mn(CO)_5$	Br_3Ge–$Mn(CO)_5$	Br_3Sn–$Mn(CO)_5$	I_3Sn–$Mn(CO)_5$
S_1 Mn–C str.	11	13	11	7	8	5
S_7 M–X	16			11	16	4
S_8 M–Mn str.	44	67	68	54	46	36
S_9 X–M–X def.	18	15	5	7		
S_{10} C–Mn–C def.		4	14	12	22	45
S_{13} Mn–C–O def.			4	3	5	9

$$(PED)_{ij} = \frac{(L_{ij})^2 \cdot (F_S)_{ii}}{\lambda_j} \times 100$$

stretching motion decreases with the increase in the mass of X in X_3M, as is expected.

Discussion

The principal objective of the present study is to clarify the variation in the force constants, K(M–Mn), K(Mn–C), K(C–O), and so on, and the F-Matrix elements, f(M–Mn), f(Mn–C), and f(C–O), as the metal atom, M, and the halogen atom, X, are replaced by X_3M–$Mn(CO)_5$ molecules. The effect of the X in the X_3M group on these force constants and on f(M–Mn) is exhibited in Table 3 for X_3Sn–$Mn(CO)_5$ (X stands for Cl, Br, and I) and X_3Ge–$Mn(CO)_5$ (X stands for Cl and Br); the K(M–Mn) and the f(M–Mn) values fall in the order of: chloride>bromide (>iodide). That is, the values of K(M–Mn) and f(M–Mn) increase with the increase in the electronegativity of X; especially for X_3Sn–$Mn(CO)_5$, there is a nearly linear relationship between the K(Sn–Mn) or f(Sn–Mn) values and the electronegativity of X, though the values of K(Mn–C) and K(C–O) or f(Mn–C) and f(C–O) remain almost constant in responce to the change in X.[33] The electron-withdrawing ability of the SnX_3 group is expected to increase in accordance with the increase in the electronegativity difference between halogen and tin atoms. This expectation is substantiated by the previous NQR study of X_3Sn–$Mn(CO)_5$; *i.e.*, the halogen NQR study of X_3Sn–$Mn(CO)_5$ has shown that the ionic character (%) of tin–halogen bonds in X_3Sn–$Mn(CO)_5$ falls in the order of: Sn–Cl>Sn–Br>Sn–I,[6] and a good linear relationship exists, as is shown in Fig. 3, between the f(Sn–Mn) or the K(Sn–Mn) values and the ionic character of the Sn–X bond, thus providing evidence that the electron-withdrawing ability of the SnX_3 group is in the order of: $Cl_3Sn>Br_3Sn>I_3Sn$.

In the previous work on L_3Sn–$Mn(CO)_5$,[1] the present author has studied the effect of the substituent, L, on the Sn–Mn bonding nature on the basis of the sets of force constants, K(Sn–Mn), K(Mn–C), and K(C–O); he there concluded that the π-interaction between the tin and manganese atoms of $(CH_3)_3Sn$–

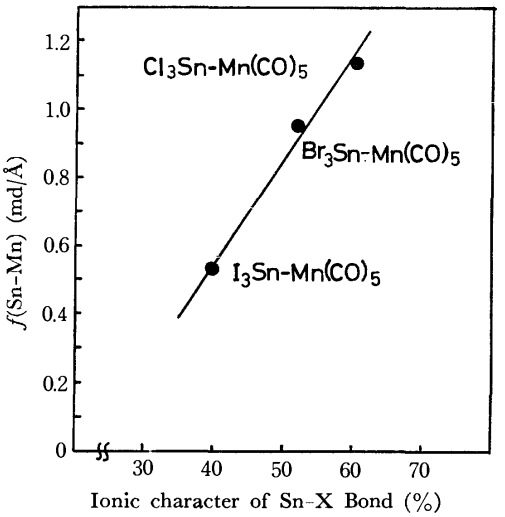

Fig. 3. The relationship between the f(Sn-Mn) and the ionic character of the Sn-X bond.

$Mn(CO)_5$ is weaker than those of X_3Sn–$Mn(CO)_5$ (X=Cl and Br), since not only K(Sn–Mn) but also K(Mn–C) and K(C–O) are changed by the substitution of L from X to CH_3. For the present X_3Sn–$Mn(CO)_5$ and X_3Ge–$Mn(CO)_5$ molecules, it seems that the σ-characters in the Ge–Mn and Sn–Mn bondings predominantly increase with the increase in the electronegativity of X, because the change in X causes no notable amount of variation in K(M–C) and K(C–O) or in f(Mn–C) and f(C–O) in spite of the pronounced dependence of K(M–Mn) or f(M–Mn) on the electronegativity of X (the f(Sn–Mn) of Cl_3Sn–$Mn(CO)_5$ is roughly twice that of I_3Sn–$Mn(CO)_5$). Watters *et al.* have studied X_3M–$Co(CO)_4$ (X=Cl, Br, and I; M=Ge and Sn) by IR and found that the K(Co–M) value decreases monotonously with the decrease in the electronegativity of X, while K(Co–C) and K(C–O) are kept constant.[2b] They have interpreted this similar finding in terms of the difference of the σ-framework of the Co–M bond based on the molecular σ-bonding systems.

Now, let us investigate the effect of M on the M–Mn bondings. As is shown in Table 3, the values of K(M–Mn) or f(M–Mn) increase in accord with the variation in the metal atom, M, from Sn to Si for the corresponding halogen compounds, though the K(Mn–C) and

33) As the manner of the changes in f(Mn–C) and f(C–O) toward the substitution of X or M is quite similar to those of K(Mn–C) and K(C–O), the values of f(Mn–C) and the f(C–O) were eliminated from the Table.

K(C–O) or f(Mn–C) and f(C–O) values remain almost constant.[34] However, there is no clear relationship between the electronegativity of M and the force constant, K(M–Mn) or f(Mn–M). By comparing the sets of force constants, K(M–Mn), K(Mn–C), and K(C–O), or the sets of F-matrix elements, f(M–Mn), f(Mn–C), and f(C–O), it can reasonably be concluded, on the basis of above discussions, that the π-characters in the Si–Mn and Ge–Mn bonds are in the same order as that in the Sn–Mn bond, and that the σ-character of the M–Mn bond is, if anything, primarily responsible for the order of M–Mn bond strength, $f(\text{Si–Mn}) \geqq f(\text{Ge–Mn}) > f(\text{Sn–Mn})$.

34) Although the numerical value of f(Sn–Mn) in Br_3Sn–Mn$(CO)_5$ is slightly larger than that of Br_3Ge–Mn$(CO)_5$, this difference cannot be regarded as significant.

The author wishes to express his deep gratitude to Professor Tastuo Miyazawa for his kind permission to use the far-infrared spectrophotometers.

BULLETIN OF THE CHEMICAL SOCIETY OF JAPAN, VOL. 46, 2450—2453 (1973)

Kinetic Studies of the Nickel Phthalate Complex Formation in Solution by the Pressure-jump Method

Shoji HARADA, Hideyuki TANABE, and Tatsuya YASUNAGA

Department of Chemistry, Faculty of Science, Hiroshima University, Higashisenda-machi, Hiroshima 730

(Received December 22, 1972)

The rate constants of the complex formation and the dissociation of the nickel phthalate (*o*-phthalate) complex have been determined by the pressure-jump method. The thermodynamic parameters of the reaction were obtained from studies at various temperatures between 10 and 30 °C. Upon a comparison of the data on the nickel complexes of the succinate, adipate, maleate, and phthalate, no systematic relationship between the nature of the ligands and the kinetic values has been found; this can be ascribed to the monodentated form of these complexes. The rate-determining step is the loss of the water molecule from the inner-coordination sphere of the nickel ion when the monodentated complex is formed.

Although the equilibrium properties of the nickel dicarboxylate complexes[1] have been well studied, relatively few systematic kinetic studies have been carried out. The development of the relaxation techniques[2] has, however, made it possible to study these fast reactions kinetically. In many of these studies of the complex formation reactions, the relaxation effect has been ascribed to one of the reactions of the step-by-step mechanism proposed by Eigen *et al.*[2] When the nickel complex of the bidentate ligand is formed, two inner-coordinated waters should be replaced by the ligand. Therefore, the mechanism of the bidentated chelate complex formation through the outer-sphere complex and the monodentated complex has usually been proposed. If the complex is stable as a chelate, the rate-determining step can be discussed by two different theories. Nancollas and Sutin[3] and Cavasino[4] have thought that the first bond formation between the nickel ion and the ligand is the rate-determining step. On the other hand, Hoffmann *et al.*[5-8] have considered that the chelate-ring closure is the rate-determining step and have calculated the rate constants of each reaction of the step-by-step mechanism. Nevertheless, if the complex is stable as a monodentated form rather than as a chelate, the same treatment as that carried out in the nickel maleate complex formation[9] will be applied.

The present study was undertaken in an attempt to confirm if one of these theories can be applied to the nickel phthalate complex formation. Another purpose has been to ascertain the ligand effects on the kinetic values of the nickel dicarboxylate complexes where the ligand has a pair of the carboxylate group maintained by the C–C single bond, and the C–C double bond, and the aromatic ring.

Experimental

All of the chemicals used were of a reagent grade. The nickel phthalate solution was prepared by mixing a stoichiometric amount of $NiSO_4$ with phthalic acid. Titration with a solution of $Ba(OH)_2$ was done until all the sulfate ions had precipitated out as insoluble $BaSO_4$. The solid $BaSO_4$ was then removed by filtration. The titration of the solution to pH 6.5 yielded a solution with most of the ligands in the dissociated form. The concentration of the nickel phthalate was determined by dimethylglyoxime titration. The solution to be studied was prepared by the dilution of the standard solution to the desired concentration.

1) L. G. Sillén and A. E. Martell, "Stability Constants of Metal-Ion Complexes," Special Publication No. 17, The Chemical Society, London, (1964).

2) M. Eigen and L. De Maeyer, "Technique of Organic Chemistry," Vol. VIII, 2nd ed., S. L. Friess, E. S. Lewis, and A. Weissberger, Ed., Interscience Publishers, Inc., New York, N. Y., Part 2, (1963).

3) G. H. Nancollas and N. Sutin, *Inorg. Chem.*, **3**, 360 (1964).

4) F. P. Cavasino, *J. Phys. Chem.*, **69**, 4380 (1965).

5) U. Nickel, H. Hoffmann and W. Jaenicke, *Ber. Bunsenges. Physik. Chem.*, **72**, 526 (1968).

6) H. Hoffman and U. Nickel, *ibid.*, **72**, 1096 (1968).

7) H. Hoffmann, *ibid.*, **73**, 432 (1969).

8) H. Hoffmann and E. Yeager, *ibid.*, **74**, 641 (1970).

9) S. Harada and T. Yasunaga, This Bulletin, **46**, 502 (1973).

The pressure-jump method with a conductivity readout has been described in considerable detail elsewhere.[10] The time constant of the apparatus was 100 μsec. A small improvement was made by placing a solenoid valve at the gas inlet of the pressure-jump cell. This improvement has resulted not only in making the experiments easier, but also in increasing the signal-to-noise ratio with the improvement of cutting off the entering of the useless gas after the metal diaphragm burst. Because of the use of the conductivity readout, no buffering or supporting electrolytes were added, and so the ionic strength of the solution was varied arbitrarily. In order to determine the kinetic parameters of the reaction, a series of experiments was run covering the concentration range from 0.00051 to 0.051 M of the nickel phthalate and the temperature range from 10 to 30 °C. The relaxation times quoted are the mean values of several runs.

Results

In all the nickel phthalate solutions, the relaxation spectrum was characterised by a single relaxation time. A representative relaxation spectrum is shown in Fig. 1. The experimental conditions and the observed relaxation times at 25 °C are shown in Table 1. In the present studies, the complex formation reaction may be expressed as follows:

$$M^{2+} + L^{2-} \underset{k_d}{\overset{k_f}{\rightleftharpoons}} ML \qquad (1)$$

where M^{2+} is the metal ion, L^{2-} is the ligand, ML is the complex, and k_f and k_d are the rate constants of the complex formation and the dissociation at zero ionic strength respectively. For such a mechanism, the rate constants are related to the relaxation time, τ, by the following equation:

$$1/\tau = k_f\gamma_{\pm}^2(C_M+C_L) + k_d \qquad (2)$$

where $\gamma_{\pm}$ is the mean activity coefficient of the free ions at a finite ionic strength, and where C_M and C_L are the ionic concentrations of the metal ion and the ligand respectively. As may be seen from Eq. (2), the plot of $1/\tau$ against $\gamma_{\pm}^2(C_M+C_L)$ gives k_f and k_d from the slope and the intercept of the line respectively. Such a plot requires the stability constant, K $(=k_f/k_d)$, if we are to calculate the ionic concentrations. Unfortunately, however, an appropriate K was not available, so the values of k_f, k_d, and K were obtained in the following way.

As the first approximation, a value of K which had been estimated from the literature value[11] was used to calculate the ionic concentrations. The activity coefficients of the ions were calculated by the use of the Kielland equation.[12] Then, the $1/\tau$ values were plotted against $\gamma_{\pm}^2(C_M+C_L)$. Here, the ratio between

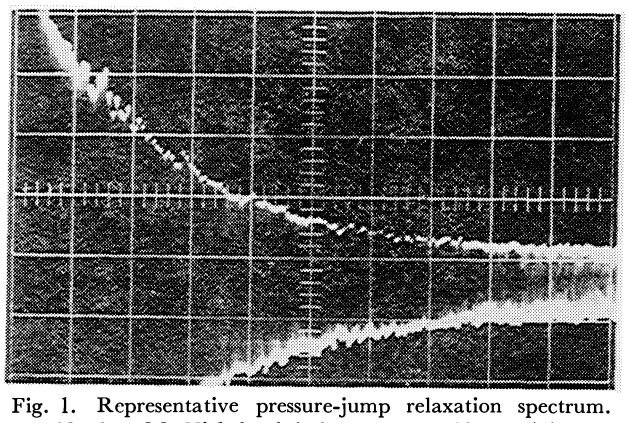

Fig. 1. Representative pressure-jump relaxation spectrum. 4.08×10^{-3} M Nickel phthalate; sweep 200 μsec/div. at 20°C.

Table 1. Relaxation times and experimental conditions for the nickel phthalate system at 25°C

C_0[a] (10^{-4} M)	C_{NiPh} (10^{-4} M)	$C_{Ni}=C_{Ph}$ (10^{-4} M)	μ (10^{-4})	$\gamma_{\pm}$	$1/\tau$ (10^3 sec^{-1})
5.1	0.6	4.6	18.4	0.83	3.1
10.2	1.7	8.5	34.0	0.78	3.3
20.4	5.4	15.0	60.0	0.73	3.6
40.8	15.4	25.4	102	0.68	4.2
61.2	27.4	33.8	135	0.64	4.4
102	54.4	47.6	190	0.60	4.8
204	130	73.7	295	0.55	5.3
306	212	94.0	376	0.52	5.7
408	297	111	445	0.50	6.1
510	384	126	506	0.48	6.4

a) C_0 refers to the total stoichiometric concentrations of the nickel phthalate.

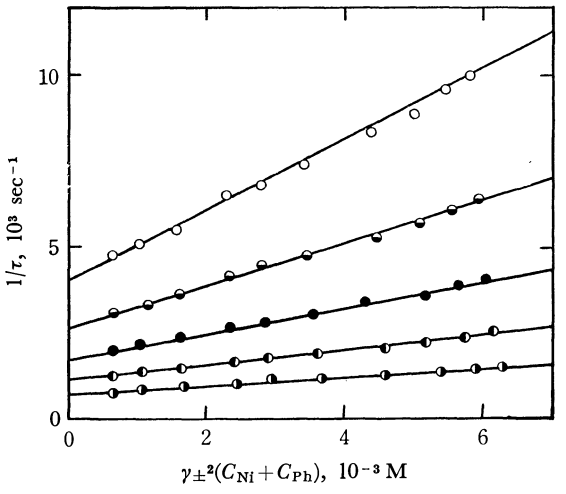

Fig. 2. $1/\tau$ *vs.* $\gamma_{\pm}^2(C_{Ni}+C_{Ph})$ plot at 10°C (◑), 15°C (◐), 20 °C (●), 25 °C (◒), and 30 °C (○).

Table 2. The formation and dissociation rate constants and the stability constants of the nickel phthalate ($\mu\rightarrow0$)

t (°C)	k_f (M^{-1} sec^{-1})	k_d (sec^{-1})	K (M^{-1})
10	1.2×10^5	0.7×10^3	1.8×10^2
15	2.2×10^5	1.1×10^3	2.0×10^2
20	3.7×10^5	1.7×10^3	2.2×10^2
25	6.3×10^5	2.6×10^3	2.4×10^2
30	10.4×10^5	4.0×10^3	2.6×10^2

10) S. Harada, K. Amidaiji, and T. Yasunaga, *ibid.*, **45**, 1752 (1972).
11) M. Yasuda, K. Yamasaki, and H. Ohtaki, *ibid.*, **33**, 1067 (1960).
12) J. Kielland, *J. Amer. Chem. Soc.*, **59**, 1675 (1937).

k_f and k_d should coincide with the first estimated K value. The above procedures were repeated until a constant K value was obtained. The final results at each temperature are shown in Fig. 2. The values of the ionic concentrations, the ionic strengths, and the mean activity coefficients in Table 1 are referred to the final result at 25 °C. The rates and the stability constants obtained at various temperatures are given in Table 2.

The Arrhenius energies of activation, $\Delta E_f^{\neq}$ and $\Delta E_d^{\neq}$, were obtained from the plot of log k_f and log k_d respectively against $1/T$. Other thermodynamic parameters of the complex formation. *i.e.*, the entropy of activation, $\Delta S_f^{\neq}$, the enthalpy of activation, $\Delta H_f^{\neq}$, and the free energy of activation, $\Delta G_f^{\neq}$, were calculated from the following equations; they are listed in Table 3:

$$\log A = \log\frac{eRT}{Nh} + \frac{\Delta S_f^{\neq}}{2.3R} \quad (3)$$

$$\Delta H_f^{\neq} = \Delta E_f^{\neq} - RT \quad (4)$$

$$\Delta G_f^{\neq} = \Delta H_f^{\neq} - T\Delta S_f^{\neq} \quad (5)$$

where A is the frequency factor.

Discussion

The stability constants in Table 4 show that the oxalate, malonate, and malate ligands make very stable five- or six-membered chelate complexes, coordinating their carboxyl group or hydroxyl group to the nickel ion. Meanwhile, the succinate, adipate, maleate, and phthalate ligands make much less stable complexes. A definite difference can also be seen in the complex dissociation rate constant. Since the complexes in the former group are stable as chelates, the characteristics of the ligands, *e.g.*, the carbon number and the substituted groups, may be reflected very much in the stabilities and the dissociation rate constants of the complexes. In the latter group, on the other hand, the dissociation rate constants nearly all have the same value, $(2\sim4)\times10^3$ sec^{-1}, and the differences between the ligands are very small compared to the case of the former group. Moreover, the values are very close to the complex dissociation rate constants, $k_{d'}$ reported by Hoffmann *et al.*:[5-7]

$$Ni(H_2O)_5L \xrightarrow{k_{d'}} Ni(H_2O)_6^{2+} + L^{2-}. \quad (6)$$

These facts imply that the complex is plausible as a monodentated form rather than as a chelate.

The generally accepted mechanism for the complex-formation reactions is a step-by-step mechanism proposed by Eigen *et al.*[2] The scheme may be represented as follows:

$$\underset{\text{(I)}}{M^{2+} + L^{2-}} \overset{K_0}{\rightleftharpoons} \underset{\text{(II)}}{M^{2+}\cdots\overset{H}{\underset{H}{O}}\cdots L^{2-}} \underset{k_{-2}}{\overset{k_1}{\rightleftharpoons}} \underset{\text{(III)}}{M^{+} - L^{-}} \underset{k_{-2}}{\overset{k_2}{\rightleftharpoons}} \underset{\text{(IV)}}{ML} \quad (7)$$

where (I) is the free ion, (II) is the outer-sphere complex, (III) is the monodentated complex, (IV) is the bidentated chelate complex, and K_0 is the outer-sphere complex formation constant. If the complex is considered to be very stable as a chelate, the overall rate constants are related to the rate constants of each step in Reaction (7) as follows:

$$k_f = K_0 k_1\left(\frac{k_2}{k_2+k_{-1}}\right) \quad (8)$$

Table 3. Kinetic data of the nickel phthalate complex formation at 25 °C ($\mu\rightarrow0$)

K, M^{-1}	2.4×10^2
k_f, M^{-1} sec^{-1}	6.3×10^5
k_d, sec^{-1}	2.6×10^3
$E_f^{\neq}$, kcal mol^{-1}	18
$E_d^{\neq}$, kcal mol^{-1}	15
$\Delta G_f^{\neq}$, kcal mol^{-1}	11
$\Delta H_f^{\neq}$, kcal mol^{-1}	18
$\Delta S_f^{\neq}$, cal deg^{-1} mol^{-1}	27
K_0, M^{-1}	25
k_1, sec^{-1}	2.5×10^4

Table 4. Rates and stability constants of the nickel dicarboxylate complexes at 25 °C

Ligand	k_f (M^{-1} sec^{-1})	k_d (sec^{-1})	K (M^{-1})	μ	Reference
Oxalate	7.4×10^4	3.6	2.1×10^4	0.1	3
	5.2×10^5	3.6	1.4×10^5	—	7
	—	—	2.0×10^5	0.1	1
Malonate	7.0×10^4	44	1.6×10^3	0.1	4
	4.2×10^5	35	1.2×10^4	→0	15[a]
	—	—	1.6×10^3	0.1	11
Succinate	5.8×10^5	4×10^3	2.1×10^2	→0	15[a]
	—	—	40	0.1	11
Adipate	8.5×10^5	4×10^3	2.1×10^2	—	7
	—	—	40	0.1	11
Maleate	8.4×10^5	2.1×10^3	4×10^2	→0	9
	—	—	1.0×10^2	0.1	11
Phthalate	6.3×10^5	2.6×10^3	2.4×10^2	→0	This work
Malate	5.6×10^5	17	3×10^4	→0	10

a) The reported rate constants at 20 °C were converted to the value at 25 °C.

$$k_d = k_{-1}\left(\frac{k_{-2}}{k_2+k_{-1}}\right) \quad (9)$$

If a further assumption is made that the first bond formation between the nickel ion and the phthalate ligand is the rate-determining step, Eq. (9) becomes:

$$k_d = k_{-1}\cdot\frac{k_{-2}}{k_2}. \quad (10)$$

This equation shows that if the complex is a stable chelate, *i.e.*, $k_{-2}/k_2 \ll 1$, k_{-1} will be much larger than 10^4 sec^{-1}. This is implausible as a value of k_{-1}. On the other hand, Hoffmann *et al.*[5-8] determined all of the rate constants in Reaction (7) on the assumptions that K_0k_1 is the same for all the nickel dicarboxylates and is equal to the k_d of the adipate, and that k_{-1} can be assumed from the linear correlation between k_{-1} and the basicity of the carboxylate group. If we try to apply the same procedures to the nickel phthalate system, the rate constants will be given as follows: $K_0k_1=8.5\times10^5$ M^{-1} sec^{-1}, $k_{-1}=4\times10^3$ sec^{-1}, $k_2=1.1\times10^4$ sec^{-1}, and $k_{-2}=1.0\times10^4$ sec^{-1} at 25 °C. The result that k_2 is nearly equal to k_{-2}, however, means that the monodentated complex and the chelate complex are present in comparable concentrations; hence, it is in conflict with the above assumption that the chelate complex is very stable.

The stability constant, K, is given by this equation:

$$K = K_0 + K_0K_1 + K_0K_1K_2 \quad (11)$$

where K_0 can be calculated by the Fuoss equation[13] to be 25 M^{-1} at $\mu=0$, and where $K_1=k_1/k_{-1}$ and $K_2=k_2/k_{-2}$. On the assumptions that k_1 is equal to the water-exchange rate constant on the nickel ion,[14] 2.7×10^4 sec^{-1}, and that k_{-1} is found to be 4×10^3 sec^{-1} from the Hoffmann relationship between k_{-1} and the basicity of the ligand, K_1 can be calculated to be about 7. Therefore, Eq. (11) can be rewritten as:

$$K = 25(1+7+7K_2) \quad (12)$$

If the complex is stable as a chelate, *i.e.*, $K_2 \gg 1$; then, K will become much larger than 2×10^2 M^{-1}. In the nickel phthalate system, however, the stability constant obtained is 2.4×10^2 M^{-1}; this means that $K_2<1$, *i.e.*, that the monodentated complex is more stable than the chelate complex. In most of the previous studies of the nickel dicarboxylate complex-formation reactions, the concentration of the monodentated complex has been assumed to be negligibly small in comparison with those of the free ions and the chelate complex, but this assumption can not be properly applied to the nickel phthalate system, just as in the nickel maleate system.[8]

If we assume that the concentration of the chelate complex is negligibly small in comparison with that of the monodentated species, Reaction (7) can be simplified to the following mechanism:

$$\underset{\text{(I)}}{Ni^{2+} + Ph^{2-}} \overset{K_0}{\rightleftharpoons} \underset{\text{(II)}}{Ni^{2+}\cdot\overset{H}{\underset{H}{O}}\,Ph^{2-}} \underset{k_{-1}}{\overset{k_1}{\rightleftharpoons}} \underset{\text{(II)}}{Ni^{+} - Ph^{-}} \quad (13)$$

where Ph^{2-} means the phthalate ion. Taking into account the facts that the formation and the dissociation of the outer-sphere complex are very fast and that $K_0\gamma_{\pm}^2(C_{Ni}+C_{Ph})$ is much smaller than unity, the relaxation time of the rate-determining step of Reaction (13) is given by the equation:

$$1/\tau = K_0k_1\gamma_{\pm}^2(C_{Ni}+C_{Ph}) + k_{-1}. \quad (14)$$

Since the concentration of the outer-sphere complex is small, the overall stability constant is given as follows:

$$K = K_0\cdot\frac{k_1}{k_{-1}} = \frac{k_f}{k_d} \quad (15)$$

By comparing Eq. (14) with Eq. (2), the following equations were obtained:

$$k_f = K_0k_1 \quad (16)$$

$$k_d = k_{-1} \quad (17)$$

With the values of k_f and K_0, k_1 was calculated to be 2.5×10^4 sec^{-1}; this value is very close to the water-exchange rate constant on the nickel ion. Moreover, k_{-1}, which is equal to k_d, is equal to the value estimated from Hoffmann's rule and the basicity of the ligand. These good coincidences of the rate constants suggest that the above discussion is correct and that the complex is stable as a monodentated form rather than as a chelate in the case of the nickel phthalate. The rate-determining step of the complex formation is the loss of the water molecule from the inner-sphere of the nickel ion when the monodentated complex is formed.

In addition to the nickel phthalate, pressure-jump studies were also carried out on the nickel complexes of the isophthalate and the terephthalate ligands; however, no relaxation effect was observed in these solutions. This is the same tendency as that observed in the maleate complex and the fumarate complex, where the relaxation effect was observed only in the former solution. From these facts, it may be concluded that the second carboxyl group is not coordinated directly to the nickel ion, but is indispensable in stabilizing the monodentated complex in the nickel complexes of the phthalate and the maleate ligands.

One of the purposes of the present studies has been to ascertain the ligand effect of the seven-membered nickel dicarboxylate complexes. The results obtained above show no systematic relationship between the natures of the ligands and the kinetic values. This may be ascribed to the characteristics of the monodentated form of these complexes.

13) R. M. Fuoss, *J. Amer. Chem. Soc.*, **80**, 5059 (1958).
14) T. J. Swift and R. E. Connick, *J. Chem. Phys.*, **37**, 307 (1962).
15) J. L. Bear and C. T. Lin, *J. Phys. Chem.*, **72**, 2026 (1968).

The Liquid Membranes of the Thiocyanate Ion-Sensitive Electrode

Nobuhiko ISHIBASHI and Kenyu KINA

Department of Applied Analytical Chemistry, Faculty of Engineering, Kyushu University, Higashi-ku, Hakozaki, Fukuoka 812

(Received January 29, 1973)

Ion-selective electrode membranes responsive to the thiocyanate ion were prepared by using ion-association extraction systems. A crystal violet or tetraphenylarsonium cation was used as an ion exchange-site in the liquid nitrobenzene membrane. The liquid membrane electrode exhibits an ideal Nernstian response to the thiocyanate ion down to 10^{-5} *M*. The selectivity of the liquid membrane largely depends on the extractability of the diverse anion into nitrobenzene. The order of the selectivity coefficients, K_j, is as follows:

$$ClO_4^- > IO_4^- > SCN^- > I^- > ClO_3^- > NO_3^- > Br^- > BrO_3^- > Cl^-$$

High selectivities for thiocyanate over SO_4^{2-}, $H_2PO_4^-$, Cl^-, BrO_3^-, and Br^- were observed. The membrane potential is independent of the pH variation in the region from pH 2 to 12.

In recent years many kinds of selective ion-sensitive electrodes have been developed as analytical sensors which are capable of determining the activities of objective ions selectively.

Commercial thiocyanate-sensitive electrodes are usually prepared by using a compacted polycrystalline membrane of silver thiocyanate or a mixture of it with silver sulfide. A bromide-sensitive electrode with a AgBr membrane was also used as a thiocyanate-sensitive electrade,[1] since the thiocyanate ion reacts with a AgBr membrane to form a thin film of insoluble AgSCN on the membrane surface.

Hirsh and Protoch have found that the perchlorate ion-selective electrode of the liquid-membrane type is sensitive to perrhenate and thiocyanate ions; they performed the titration of thiocyanate with mercuric nitrate using this perchlorate ion-selective electrode.[2]

In this work, the thiocyanate-sensitive liquid membranes were prepared by using ion-association extraction systems, and the performance of the liquid membranes was studied.

Experimental

Apparatus and Chemicals. The measurements of the membrane potential were made with a Takeda Riken electrometer, TR-8651. The conductance of the liquid membrane was measured at 25 °C by the use of a Yanagimoto conductivity outfit, MY–7. The crystal violet and tetraphenylarsonium chloride were obtained from the Kishida Kagaku Co. and Wako Pure Chemicals Co. respectively. The thiocyanate stock solution was prepared by dissolving reagent-grade sodium thiocyanate in deionized water and was then standardized titrimetrically by the Volhard method. This stock solution was diluted to the desired concentration.

Preparation of the Liquid Membrane. Both the crystal violet and the tetraphenylarsonium ion were used as anion-exchange sites. By such a large, singly-charged cation, the thiocyanate ion can be extracted into nitrobenzene. The crystal-violet membrane was prepared by extraction with crystal-violet dyestuff in the following manner.

One hundred ml of a 1×10^{-3} M sodium thiocyanate solution and 100 ml of an equimolar crystal-violet solution were transferred into a separating funnel. The resulting aqueous solution was shaken with 100 ml of nitrobenzene for 60 min. The organic phase which was thus separated from the aqueous phase was shaken again with 100 ml of the 1×10^{-3} M sodium thiocyanate solution in order to purify it. After the phase separation had been completed, the organic solution was filtered through a dry filter paper in order to remove droplets of water; it was then diluted to 1×10^{-4} M with nitrobenzene when used as a thiocyanate-sensitive liquid membrane.

The thiocyanate ion was precipitated as white needles from an aqueous solution using the tetraphenylarsonium ion. The tetraphenylarsonium membrane was prepared by dissolving the precipitate in nitrobenzene.

Measurement of the Liquid Membrane Potential. The electromotive force of the following concentration cell was measured by means of the electrometer in order to evaluate the membrane performance:

$$+ \quad \underbrace{\text{SCE/Reference solution/organic liquid membrane/}}_{\text{(Electrode)}} \quad \text{Sample solution/SCE} \quad -$$

The cell assembly was the same as that described elsewhere.[3] The reference solution and the sample solution were separated in the lower part of a U-shaped glass tube by the use of a liquid membrane such as a nitrobenzene solution of tetraphenylarsonium thiocyanate.

Results and Discussion

Membrane Potential. Figure 1 shows the effect of the concentration of the membrane solute on the membrane potential. An increase in the concentration

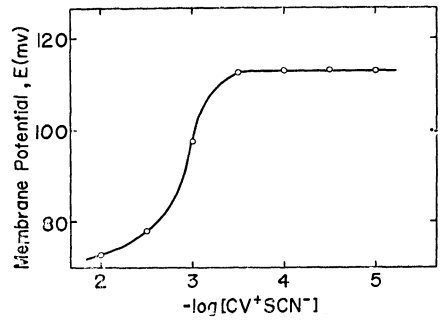

Fig. 1. Effect of membrane site concentration (15 °C).
Reference solution: 1×10^{-3} M NaSCN
Sample solution: 1×10^{-5} M NaSCN
CV^+: Crystal violet

1) R. A. Durst (Editor), *Ion-selective electrodes*, N. B. S. Spec. Publ. 384, U. S. Printing office, Washington (1970).

2) R. F. Hirsch and J. D. Protoch, *Anal. Lett.*, **2**, 295 (1969).

3) N. Ishibashi and H. Kohara, *ibid.*, **4**, 785 (1971).

of the membrane solute beyond about $10^{-3.5}$ M causes a drop in the membrane potential. This is probably due to the elution of the membrane solute on an adjacent aqueous solution. Hence, a dilute organic solution is preferable as the liquid membrane. However, the electrical resistance of the membrane increases with a decrease in the concentration of the membrane solute, and the membrane potential tends to become unstable. Consequently, 1×10^{-4} M was used as the membrane concentration throughout the study.

The membrane potential can be expressed by the following equation:

$$E = (RT/F)\ \ln\ (a'_{SCN}/a''_{SCN}) \qquad (1)$$

where a'_{SCN} and a''_{SCN} denote the thiocyante activities of the reference solution and the sample solution respectively. As the reference solution, we used a 1×10^{-3} M aqueous sodium thiocyante solution. Fig. 2 shows the electrode response to the sample solution at varying concentrations; the figure shows that an ideal Nernstian relationship of the potential against the logarithmic activity of the thiocyanate ion holds down to 10^{-5} M of the sodium thiocyanate solution. No difference was found in the linearity range of the electrode responses between the crystal-violet membrane and the tetraphenylarsonium membrane.

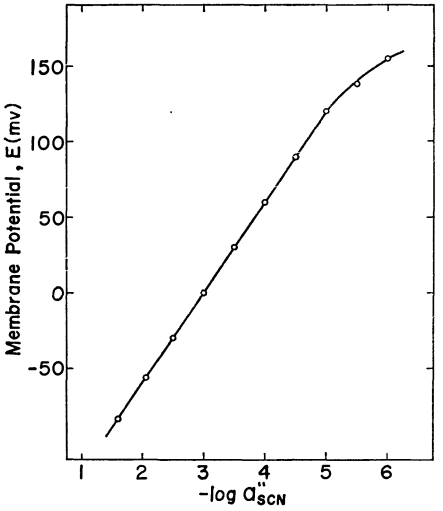

Fig. 2. Electrode response to aqueous NaSCN solution (26°C).
Reference solution: 1×10^{-3} M NaSCN
Membrane solvent: Nitrobenzene

Electrode Response as a Function of the pH. The pH effect on the membrane potential is given in Fig. 3. The pH adjustment was made by the addition of sodium hydroxide or sulfuric acid. The variation in pH has no effect on the membrane potential over the range from pH 2.5 to 12. The crystal-violet membrane showed a somewhat larger decrease of the membrane potential below pH 2 than did the tetraphenylarsonium membrane. The potential decrease in the crystal-violet membrane electrode below pH 2 may be attributed to the conversion of the crystal-violet to its acidic form and to the change in the liquid-junction potential between an agar salt bridge and the sample solution.

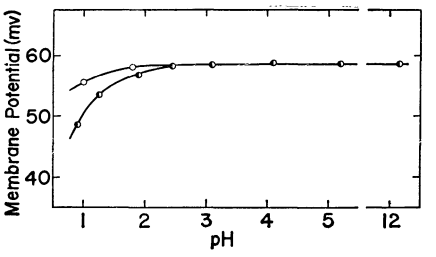

Fig. 3. Electrode response as a function of pH (15°C).
Reference solution: 1×10^{-3} M NaSCN
Sample solution: 1×10^{-4} NaSCN
-○- Tetraphenylarsonium membrane
-◐- Crystal violet membrane

The tetraphenylarsonium membrane is affected only by the variation in the liquid-junction potential.

Electrode Response in the Presence of Diverse Anions. The electrode response in the presence of an interfering ion is empirically given by the following equation[4]:

$$E = \text{constant} - 2.303\,RT/F\ \log\ (a''_{SCN} + K_j(a_j'')^{1/z}) \qquad (2)$$

where K_j is the selectivity coefficient of j-ion for the thiocyante electrode and where z is the charge of the j-ion. As can be seen from Fig. 4, the electrode potential is depressed by the presence of diverse ions. A large value of K_j corresponds to a remarkable change in the membrane potential.

The selectivity coefficients can be obtained by the measurement of the membrane potentials in both the presence and absence of diverse ions. The observed values of K_j are listed in Table 1 with respect to the crystal-violet membrane. From the K_j values, the order of interference is found to be:

$ClO_4^- > IO_4^- > I^- > ClO_3^- > NO_3^- > Br^- > BrO_3^- > Cl^-$,
$H_2PO_4^-$, $CH_3CO_2^-$, SO_4^{2-}

The tetraphenylarsonium membrane gave the same selectivity coefficient, K_j. It can be said that the se-

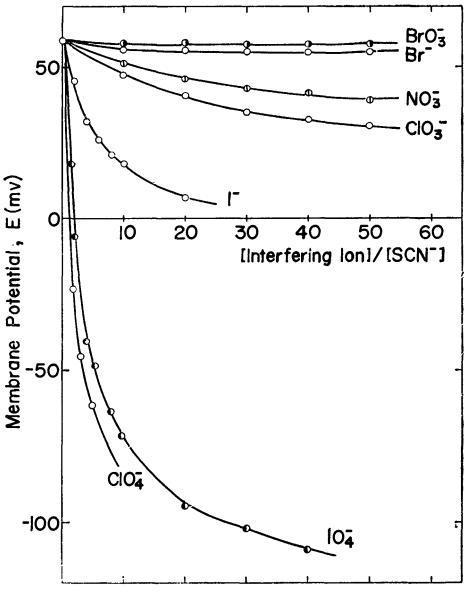

Fig. 4. Electrode response in the presence of interfering anion.

[4] J. W. Ross, *Science*, **156**, 1378 (1967).

Table 1. Selectivity coefficients of thiocyanate-sensitive liquid membrane electrode (exchange-site: crystal violet)

Anion	K_j	Anions	K_j
ClO_4^-	12.0	Br^-	0.006
IO_4^-	6.7	BrO_3^-	0.002
SCN^-	1.0	Cl^-	$<10^{-4}$
I^-	0.34	$H_2PO_4^-$	$<10^{-4}$
ClO_3^-	0.05	$CH_3CO_2^-$	$<10^{-4}$
NO_3^-	0.03	SO_4^{2-}	$<10^{-4}$

quence of selectivity is independent of the site species in nitrobenzene. The electrode has higher selectivities for the thiocyanate ion over bromide and chloride ions than does the solid-state electrode.[1] From the conductivity measurement of the liquid membrane, it was found that the site and its counter anion in nitrobenzene were in an almost complete dissociation.

According to Eisenman's theoretical treatment[5] of the membrane potential, the selectivity of the electrode with a liquid membrane is determined by the relative partition coefficient and the mobilities between the objective ion and the competitive ion in a limiting case of a complete dissociation. The sequence of K_j values in Table 1 is consistent with the ease of the extraction of the anions into the organic solvent.[6] Hence, the observed selectivity order qualitatively supports Eisenman's theoretical prediction, since there is no large difference among the ionic mobilities.

The authors wish to thank the Ministry of Education for its grant-in-aid.

5) F. Conti and G. Eisenman, *Biophys. J.*, **6**, 227 (1966).
6) N. A. Gibson and D. C. Weatherburn, *Anal. Chim. Acta*, **58**, 159 (1972).

BULLETIN OF THE CHEMICAL SOCIETY OF JAPAN, VOL. 46, 2456—2459 (1973)

The pH-dependent Variation of the Absorption and Circular Dichroism Spectra in Some Ternary Mixed Complexes of Copper(II) Containing Diethylenetriamine and Optically Active Amino Acids

Tasuku MURAKAMI, Tsunenori NOZAWA, and Masahiro HATANO

Chemical Research Institute of Non-aqueous Solutions, Tohoku University, Sendai 980

(Received February 8, 1973)

The absorption and circular dichroism(CD) spectra of some ternary mixed complexes of copper(II) with diethylenetriamine(dien) and various optically active α-amino acids have been measured in an aqueous solution at various pH values. The amino acid may coordinate to one of the planar positions, with its carboxylate or amino group as a unidentate ligand, in a neutral or a very high pH region. On the other hand, from the red shift of the d–d absorption band and the augmentation of the visible CD magnitude, it seems reasonable to expect that a large portion of the amino acid will form a chelate ring with an axial ligation in the pertinent pH region.

In general, coordination compounds of copper(II) typically consist of four nearby donor atoms arranged approximately in a plane about the metal ion, with the possibility of one or two more distant axial donors. The effect of the axial ligation on the spectral feature of copper(II) complexes has been investigated by many workers,[1–4] and it has been clarified that the stronger ligation to the copper ion along the tetragonal axis causes the d–d absorption band to shift to a lower energy and the intensity of the band to increase appreciably. However, little attention has been paid to the formation of the chelate ring containing an axial ligation in an aqueous solution, probably because of the instability of the chelate. Wellman *et al.*[5] detected the axial chelation of potential tridentate α-amino acids by optical rotatory dispersion. Recently, such an axial chelation has been confirmed by Martin and his co-workers.[6]

In a previous communication,[7] we reported that the copper(II) complex of L-alaninamide with dien has its amide nitrogen coordinated to the copper(II) ion at the axial position. Recently, Aiba *et al.*[8] have reported that when diamine or amino acid is added to an aqueous solution of $[Cu(dien)(H_2O)]^{2+}$, the d–d absorption band shifts to a much longer wavelength; this phenomenon suggests the formation of a sort of five-coordinated complex. In this study, we wish to report the pH-dependent variations of the CD magnitude and of the d–d absorption observed in the ternary mixed complexes of copper(II) with dien and various optically active α-amino acids; such knowledge will help to clarify the axial interaction between donor

1) J. Bjerrum, C. J. Ballhausen, and C. K. Jørgensen, *Acta Chem. Scand.*, **8**, 1275 (1954).
2) R. L. Belford, M. Calvin, and G. Belford, *J. Chem. Phys.*, **26**, 1165 (1957).
3) L. L. Funck and T. R. Ortolano, *Inorg. Chem.*, **7**, 567 (1968).
4) A. A. G. Tomlinson and B. J. Hathaway, *J. Chem. Soc., A*, **1968**, 1685 (1968).
5) K. M. Wellman, T. G. Mecca, W. Mungall, and C. R. Hare, *J. Amer. Chem. Soc.*, **90**, 905 (1968).
6) E. W. Wilson, Jr., M. H. Kasperian, and R. B. Martin, *ibid.*, **92**, 5365 (1970).
7) T. Murakami, T. Nozawa, and M. Hatano, *ibid.*, **92**, 5768 (1970).
8) H. Aiba, A. Yokoyama, and H. Tanaka, presented at the 26th annual meetings of Chemical Society of Japan held in Hiratsuka, April, 1972.

groups and the copper ion in aqueous solutions.

Experimental

Complex Formations and Measurements. Each solution of the ternary mixed complexes for the spectral observation was prepared by mixing equimolar aliquots of stock solutions of copper(II) nitrate, dien, and amino acids, whose equivalent weights has been checked by titration. The concentrations used here varied over the range from 1.5×10^{-3} to 6.0×10^{-2} M. To follow the same solution with a change in pH, additional drops of 0.1 or 1.0 M NaOH were added. The measurements of the pH of the solutions were performed with a Toa-Dempa HM-8 or Hitachi-Horiba M-5 pH meter.

The following optically active α-amino acids were used: L-alanine(abbreviated to L-alaH), L-valine(L-valH), L-proline(L-proH), and D-phenylglycine(D-phglyH). The D-phenylglycine was supplied by the Ajinomoto Co., Ltd. The CD curves in the region from 400 to 1000 nm were obtained by means of a JASCO J-20A spectropolarimeter at room temperature. The absorption measurements were made on a Hitachi EPS-3T spectrophotometer at room temperature.

Results and Discussion

Some typical absorption spectra observed here for the ternary mixed complexes of dien and α-amino acid are shown in Fig. 1. At pH 6.3, the absorption exhibits a maximum at about 16400 cm^{-1} with ε(molar absorptivity)$\sim$78, a value which almost coincides with that of $[Cu(dien)(H_2O)]^{2+}$. Titration experiments predict that the amino group of the amino acid may be protonated in the neutral pH region in these systems.[9] Consequently, the predominant species in the neutral pH region seem to be those involving dien and an amino acid, which may coordinate to the copper(II) ion only with its carboxylate end as a unidentate ligand. As the pH of the solution is raised, the absorptivity on the lower wavenumber side of the visible absorption band becomes appreciably high and the band, as a whole, shifts to the lower wavenumber side. This spectral feature is nearly identical with those observed in the formation of the five-coordinated complexes, such as $[Cu(NH_3)_5]^{2+}$[10] and $[Cu(dien)(diamine)]^{2+}$.[8]

Figures 2—5 show the variation in the CD spectra of the mixed complexes with the pH values in solution. Each of the mixed complexes except for the L-proline complex exhibits two extrema, at about 13000 and 17000 cm^{-1} in the neutral pH region. As the pH is increased, both of the two CD components become

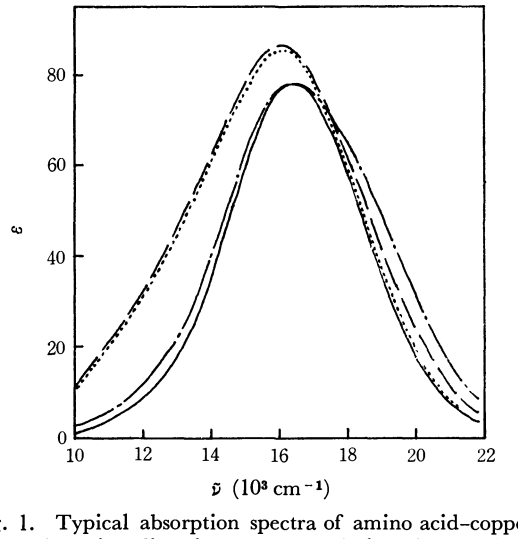

Fig. 1. Typical absorption spectra of amino acid–copper(II) complex with dien in aqueous solution (L-valine); concentration of complex is *ca.* 6×10^{-2} M.
—— pH 6.3, ----- pH 8.4
—— pH 10.5, —— pH 11.9

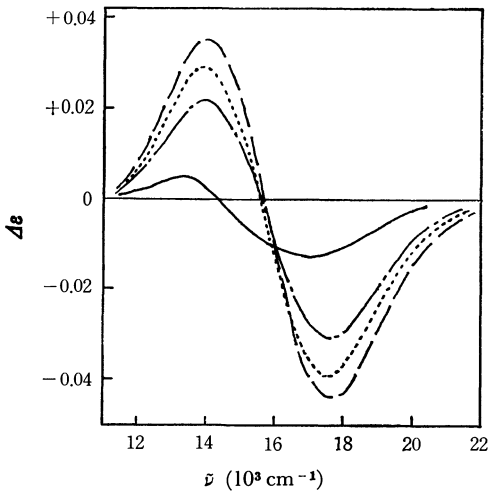

Fig. 2. CD spectra of L-alanine–copper(II) complex with dien in aqueous solution; concentration of complex is *ca.* 6×10^{-2} M.
—— pH 6.7, ----- pH 8.4
—— pH 10.1, —— pH 11.3

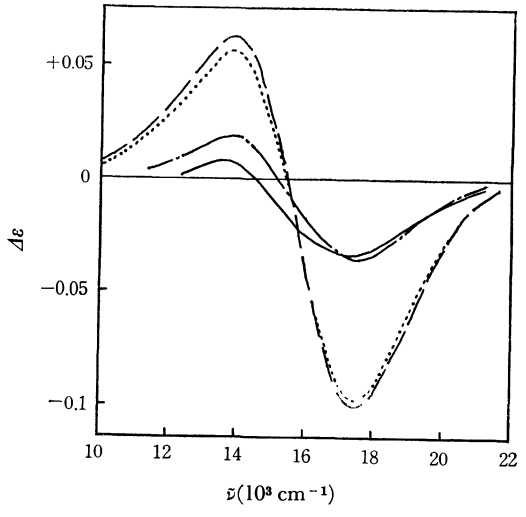

Fig. 3. CD spectra of L-valine–copper(II) complex with dien in aqueous solution; concentration of complex is *ca.* 6×10^{-2} M.
—— pH 6.3, ----- pH 8.4
—— pH 10.5, —— pH 11.9

9) Unpublished experiments performed in this laboratory.

10) F. A. Cotton and G. Wilkinson, "Advanced Inorganic Chemistry," 2nd Ed., Interscience Publishers, New York (1966) p. 906.

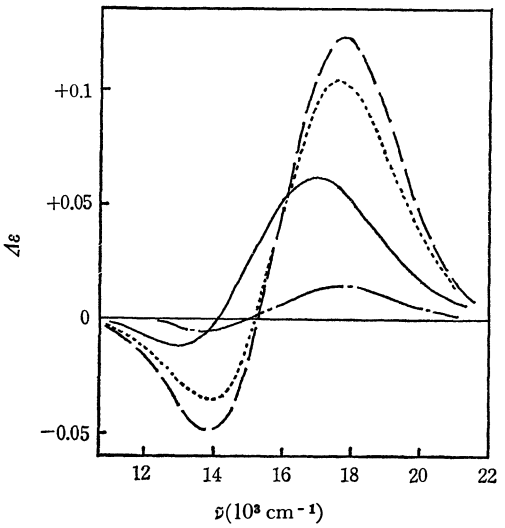

Fig. 4. CD spectra of D-phenylglycine-copper(II) complex with dien in aqueous solution; concentration of complex is *ca.* 6×10^{-2} M.
—— pH 6.7, ----- pH 8.4
—— pH 10.5, —— pH 12.0

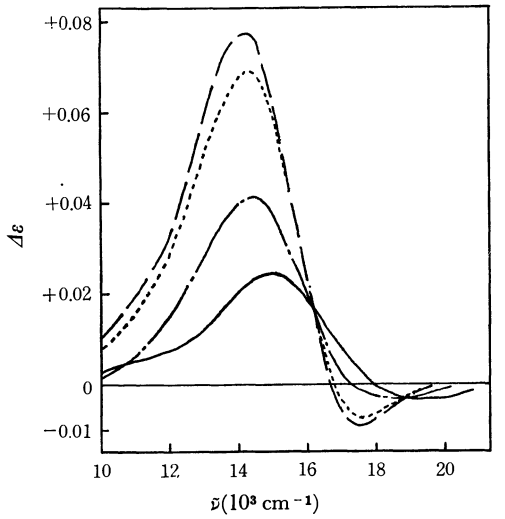

Fig. 5. CD spectra of L-proline-copper(II) complex with dien in aqueous solution; concentration of complex is *ca.* 6×10^{-2} M.
—— pH 7.1, ----- pH 8.8
—— pH 10.2, —— pH 12.0

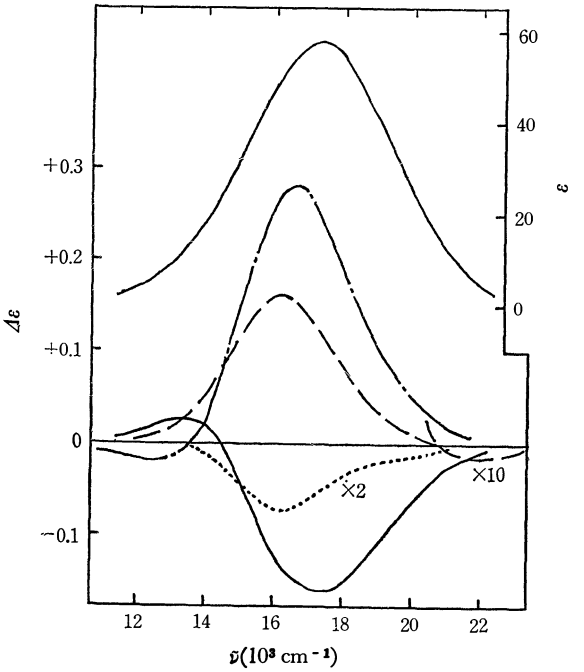

Fig. 6. Absorption and CD spectra of [Cu(en)(am)]-type complexes in aqueous solution.
—— L-valine, ----- L-alanine
—— L-proline, —— D-phenylglycine

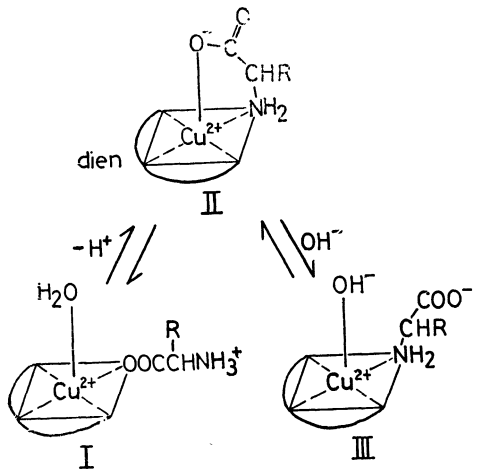

Fig. 7. Proposed equilibrium scheme for the ternary mixed complexes of copper(II) with dien and amino acids in aqueous solution.

very intense.[11] Therefore, the $\Delta\varepsilon$ values of the two components are comparable to those of complexes with optically active amino acids chelated in the square plane about the copper(II) ion, such as $[Cu(L\text{-am})_2]$ and $[Cu(en)(L\text{-am})]^+$ (see Refs. 12 and 13, and Fig. 6). However, as the pH is increased further, the intensities of the CD bands revert to those in the low pH region.

These profiles of the absorption and CD spectra in the mixed complexes can be reasonably explained by assuming the equilibrium scheme shown in Fig. 7. In the present mixed complexes, dien should occupy three coordination positions in the square plane about the copper(II) ion; then the amino acid cannot form a chelate ring in the plane. Therefore, the amino acid would coordinate to the copper(II) ion, with its carboxylate end as a unidentate ligand, in the neutral pH region(species I). In the higher pH region suitable for the deprotonation of the protonated amino group, it is anticipated that a large portion of the amino acid will form a chelate ring with an axial coordination, that is, an axial chelation(five-coordinated species II). Such a chelate formation appears to be a more plausible elucidation for the red shift of the absorption band and

11) When L-lactic acid, which coordinates to copper(II) ion with its carboxylate group as a unidentate ligand, was used instead of the amino acid, the similar spectral behaviors could not be observed. The absorptivity at only higher wavenumber side increases with increase of pH, and the observed CD magnitude remains much small ($\Delta\varepsilon\sim+0.005$).

12) T. Yasui, This Bulletin, **38**, 1746 (1965).

the augmentation of the CD magnitudes. For the following two reasons, the amino group of amino acid instead of the carboxylate group seems to coordinate in the plane, as is illustrated in the five-coordinated species II. The first reason is the tendency of the copper(II) ion to coordinate to strong donor groups in the square plane. The second reason is the labile character of the copper(II) ion, which makes an exchange of ligand groups in the coordination plane possible. As the pH in solution is increased so as to make the concentration of the hydroxide ion comparable to that of the complex ion, a large portion of the carboxylate group at the axial position may be displaced by the hydroxide ion (species III).

The CD curves for the mixed complexes increase in magnitude with an increase in the concentration of complexes. For example, the $\Delta\varepsilon$ values of the higher wave number component in the L-alanine complex are -0.030, -0.045, and -0.055 at about pH 10, corresponding to the concentrations of 1.5×10^{-3}, 1.5×10^{-2}, and 6×10^{-2} M respectively. The concentration dependence seems to be evidence for the preceding scheme that the hydroxide ion would displace the carboxylate group in an axial position, that is, for the (II) $\rightleftharpoons$(III) equilibrium shown in Fig. 7. There seem to be fewer species with other five-coordinated structures in the solution. We say this because, if the amino acids in the ternary mixed complexes, [Cu(dien)(L-am)]$^+$, would chelate in the square plane, we could expect that the CD spectral features would be very similar to those for [Cu(en)(L-am)]$^+$-type complexes. However, this does not seem to be the case.

So far as the donor atoms in the square plane about the copper(II) ion are concerned, when [Cu(N_3O)] is converted to [Cu(N_4)], such as in (I)$\rightarrow$(II) in Fig. 7, the absorption spectrum should shift to a higher wavenumber. However, the difference in the absorption maxima, $\tilde{\nu}_{max}$, for [Cu(N_3O)]- and [Cu(N_4)]-type complexes is not very much— *e.g.*, 16400 cm^{-1} for [Cu(dien)(H_2O)]$^{2+}$ and 16700 cm^{-1} for [Cu(dien)(RNH_2)]$^{2+}$ (R=CH_3– or CH_3CH_2–).[8] In addition, the axial ligation may play a role in shifting the absorption band to a lower wavenumber. Therefore, the more the five-coordinated species(II) are formed in solution, the lower the observed absorption shifts.

Most L-amino acid copper(II) complexes of the [Cu(L-am)$_2$]- and [Cu(en)(L-am)]$^+$-type, except for the L-proline complexes, exhibit a negative main CD band in the higher wavenumber region, with a much smaller positive component at lower wavenumbers.[12,13] The present mixed complexes also exhibit similar CD curves in the neutral or very high pH regions. In both pH regions, L-amino acid coordinates with its carboxylate or amino group as a unidentate ligand. Thus, the unidentate L-amino acids impose a dominant negative CD curve in the d–d band of the copper(II) ion as well as in the case of the chelated L-amino acids. This seems also to be the case with the observed CD cuvres for amino acid complexes of cobalt(III) in aqueous solutions.[14] In the pH region where the five-coordinated species(II) may be formed, the CD magnitude of the lower wavenumber component becomes comparable to that of the higher wavenumber component. Therefore, the chelation containing an axial position seems responsible for the increase in the $\Delta\varepsilon$ of the lower wave number component in particular.

We wish to thank Professor Kazuo Saito and Dr. Junnosuke Fujita for their valuable comments. We wish also to acknowledge the help of the Ajinomoto Co., Ltd., in supplying many amino acids. This research was supported in part by a grant from the Ministry of Education.

13) C. J. Hawkins and C. L. Wong, *Aust. J. Chem.*, **23**, 2237 (1970).

14) T. Yasui, J. Hidaka, and Y. Shimura, This Bulletin, **39**, 2417 (1966).

A Kinetic Study of the Ligand Substitution Reaction of Tetramethylenediaminetetraacetatocobaltate(II) with Trimethylenediaminetetraacetate

Hiroshi OGINO, Toshiyuki WATANABE, Jong-Jae CHUNG,* and Nobuyuki TANAKA

Department of Chemistry, Faculty, of Science, Tohoku University, Aoba, Aramaki, Sendai 980

(Received February 26, 1973)

The kinetics of the ligand substitution reaction of tetramethylenediaminetetraacetatocobaltate(II) (cobalt(II)–TDTA) with trimethylenediaminetetraacetate (TRDTA) was investigated by two different polarographic methods. The kinetic data at pH 4.9 to 5.6 were obtained by means of a conventional method in which the reaction was initiated by the mixing of two reactant solutions and was followed polarographically. However, this method could not be applied to solutions with pH values lower than 4.9, for the rate of the reaction is immeasurably fast in such a low pH region. The kinetic data at pH values down to 3.7 were obtained by analyses of the polarographic current which was observed in solutions containing TRDTA and the substitution-inert cobalt(III)–TDTA complex. From these data, it was found that the reaction proceeds through four simultaneous reaction paths, two paths of which are the nucleophilic substitution reactions, while the others are the dissociation reactions of cobalt(II)–TDTA complex ions.

In this paper, the kinetics of the ligand substitution reaction of tetramethylenediaminetetraacetatocobaltate(II) (cobalt(II)–TDTA)[1] with trimethylenediaminetetraacetate (TRDTA) will be studied by the polarographic method. The kinetics of this reaction cannot be investigated by the methods which are usually applied to many other systems. For example, the nuclear magnetic resonance method cannot be applied to this system, for cobalt(II) ions are paramagnetic. As the spectral data of cobalt(II)–TDTA and cobalt(II)–TRDTA are essentially identical, the spectrophotometric method cannot be applied to this reaction either. It will be shown in this paper that polarography provides very useful methods for the kinetic study of this reaction. The results obtained in this work will be compared with the related ones reported previously.[2,3]

Experimental

Reagents. The trimethylenediaminetetraacetic acid (H_4trdta)[4], tetramethylenediaminetetraacetic acid (H_4tdta),[5] and potassium tetramethylenediaminetetraacetatocobaltate(III) (K[Cotdta]·$3H_2O$)[5] were prepared and recrystallized by methods described previously. The preparation and standardization of a solution of cobalt(II) nitrate,[6] disodium dihydrogen trimethylenediaminetetraacetate(Na_2H_2trdta)[7] and disodium dihydrogen tetramethylenediaminetetraacetate (Na_2H_2tdta)[3] were done in ways reported in the literature. All the other chemicals were of an analytical-reagent grade and were used without further purification.

Kinetic Measurement and Apparatus. It has been reported that cobalt(II)–TRDTA shows a polarographic one-electron oxidation wave, with a half-wave potential of +0.05 V *vs.* SCE, in an acetate buffer–potassium nitrate solution.[8] TRDTA, TDTA, and cobalt(II)–TDTA do not show any polarographic waves under these experimental conditions. The kinetic measurements were made by two different methods, both utilizing the anodic wave of cobalt(II)–TRDTA; these methods were designated as Methods A and B.

In Method A, which is a conventional one, the reaction was initiated by the addition of a known amount of cobalt(II)–TDTA solution to an acetate buffer-potassium nitrate solution containing TRDTA in a large excess; the rate of the reaction was measured by following the increase in the anodic current due to the formation of cobalt(II)-TRDTA at +0.15 V *vs.* SCE. The overall reaction of TRDTA with cobalt(II)–TDTA is expressed by Eq. (1):

$$\left\{\begin{matrix}CoY^{2-}\\ \downuparrows\\ CoHY^{-}\end{matrix}\right\} + \left\{\begin{matrix}Z^{4-}\\ \downuparrows\\ HZ^{3-}\\ \downuparrows\\ \vdots\\ \downuparrows\\ H_4Z\end{matrix}\right\} \underset{k^-}{\overset{k^+}{\rightleftharpoons}} \left\{\begin{matrix}CoZ^{2-}\\ \downuparrows\\ CoHZ^{-}\end{matrix}\right\} + \left\{\begin{matrix}Y^{4-}\\ \downuparrows\\ HY^{3-}\\ \downuparrows\\ \vdots\\ \downuparrows\\ H_4Y\end{matrix}\right\} \quad (1)$$

where Y^{4-} and Z^{4-} mean quadridentate TDTA and TRDTA anions respectively; $CoHY^-$ and $CoHZ^-$, hydrogen complexes of cobalt(II)-TDTA and -TRDTA respectively, and k^+ and k^-, the rate constants for the forward and the backward reactions. Under these experimental conditions, the backward reaction can be neglected; therefore, the reaction studied can be treated as a pseudo first-order reaction:

$$\text{Rate} = k^+_{obs}[CoY]_{app} \quad (2)$$

where:

$$[CoY]_{app} = [CoY^{2-}] + [CoHY^-]$$

and where k^+_{obs} means a pseudo-first-order rate constant. Solving the rate law in essentially the same way as has been reported previously,[2] the equation:

$$\log \frac{\bar{\imath}_e}{\bar{\imath}_e - \bar{\imath}} = \frac{1}{2.303} k^+_{obs}\, t \quad (3)$$

was obtained, where $\bar{\imath}$ and $\bar{\imath}_e$ denote the current at time

---

* Present address: Kyung-Pook National University, Korea.

1) The general formula of the ligands in this paper is:

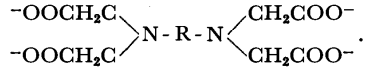

The abbreviated names of the ligands are:
TDTA (R=$CH_2CH_2CH_2CH_2$), TRDTA (R=$CH_2CH_2CH_2$), EDTA (R=CH_2CH_2), PDTA (R=$CH_2CH(CH_3)$), and *meso*-BDTA (R=$CH(CH_3)CH(CH_3)$).

2) H. Ogino and N. Tanaka, This Bulletin, **40**, 857 (1967). In that paper, 2.303 in Eqs. (7) and (10) should read 1/2.303. The values of k^+ were calculated with the correct equations.

3) H. Ogino, T. Baba and N. Tanaka, *ibid.*, **42**, 1578 (1969).

4) N. Tanaka and H. Ogino, *ibid.*, **37**, 877 (1964).

5) H. Ogino, S. Kobayashi and N. Tanaka, *ibid.*, **43**, 97 (1970).

6) N. Tanaka and H. Ogino, *ibid.*, **38**, 439 (1965).

7) H. Ogino, *ibid.*, **38**, 771 (1965).

8) N. Tanaka and H. Ogino, *ibid.*, **38**, 1054 (1965).

t and at an infinite time respectively. The values of k^{+}_{obs} were calculated from Eq. (3). The measurements were made in solutions at an ionic strength of 0.2 (KNO_3) and in the pH range from 4.9 to 5.6. All the polarograms were recorded by means of a Yanagimoto PB-4 pen-recording polarograph, using a dropping mercury electrode (DME) which had an m value of 1.16 mg sec^{-1} and a drop time t_d of 6.55 sec in a deaerated 0.1 M acetate buffer–0.1 M potassium nitrate solution containing 0.005% gelatin at 25 °C, −0.50 V *vs.* SCE, and a mercury height of 60 cm.

Method B consists of analyses of the polarographic kinetic current which was observed in solutions containing TRDTA and the substitution-inert cobalt(III)-TDTA complex. The current-time curves during the life of a mercury drop were recorded by means of a Rikendenshi SP-J1 recorder with a DC-201 preamplifier. The DME used had an m value of 1.87 mg sec^{-1} and a t_d value of 4.84 sec in a deaerated 0.1 M potassium nitrate solution containing 0.005% gelatin at 25 °C, −1.0 V *vs.* SCE, and a mercury height of 50 cm. The ionic strength employed was 0.5 (KNO_3), and the pH range was from 3.7 to 4.6.

All the measurements were carried out at 25 °C. Gelatin was added as a maximum suppressor in a concentration of 0.005%. The pH of the solutions was measured with a Hitachi-Horiba F-5 pH meter.

Results

Results Obtained by Method A. The values of k^{+}_{obs} were found to be a linear function of the initial concentration of TRDTA, $[Z]_0$, and of the hydrogen ion concentration, as is shown in Fig. 1, provided that all other experimental conditions were kept constant. Under these experimental conditions, the predominant species of TRDTA was H_2Z^{2-}.[9] On the basis of the above results, the reaction of cobalt(II)-TDTA with TRDTA was considered to proceed through the following four simultaneous reaction paths:

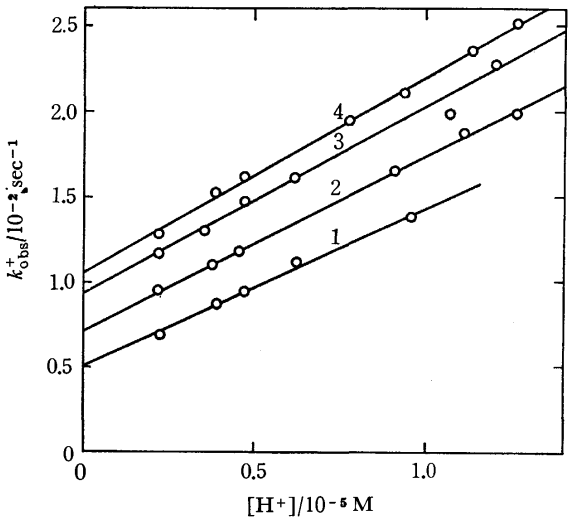

Fig. 1. The value of k^{+}_{obs} as a function of the hydrogen ion concentration at ionic strength 0.2 (KNO_3) and 25 °C containing 0.2 mM cobalt(II)-TDTA, 0.1 M acetate buffer and 0.005% gelatin. Initial concentrations of TRDTA, $[Z]_0$, are: 4 mM (1), 6 mM (2), 8 mM (3), and 10 mM (4).

$$CoY^{2-} + H_2Z^{2-} \overset{k^{CoY}_{H_2Z}}{\rightleftharpoons} CoZ^{2-} + H_2Y^{2-} \quad (4)$$

$$CoHY^{-} + H_2Z^{2-} \overset{k^{CoHY}_{H_2Z}}{\longrightarrow} CoHZ^{-} + H_2Y^{2-} \quad (5)$$

$$CoY^{2-} \overset{k^{CoY}}{\rightleftharpoons} Co^{2+} + Y^{4-} \quad (6)$$

$$CoY^{2-} + H^{+} \overset{k^{CoY}_{H}}{\rightleftharpoons} Co^{2+} + HY^{3-} \quad (7)$$

On the basis of the reaction mechanism, the following equation was derived:

$$k^{+}_{obs} = k^{CoY}_{H_2Z}[H_2Z^{2-}] + k^{CoHY}_{H_2Z}K^{H}_{CoHY}[H^+][H_2Z^{2-}] + k^{CoY} + k^{CoY}_{H}[H^+] = k^{CoY}_{H_2Z}\frac{[H^+]^2}{\alpha_{Z(H)}K_3K_4}[Z]_f + k^{CoHY}_{H_2Z}K^{H}_{CoHY}\frac{[H^+]^3}{\alpha_{Z(H)}K_3K_4}[Z]_f + k^{CoY} + k^{CoY}_{H}[H^+] \quad (8)$$

where:

$$\alpha_{Z(H)} = 1 + \frac{[H^+]}{K_4} + \frac{[H^+]^2}{K_3K_4} + \frac{[H^+]^3}{K_2K_3K_4} + \frac{[H^+]^4}{K_1K_2K_3K_4}$$

$$K^{H}_{CoHY} = \frac{[CoHY^-]}{[CoY^{2-}][H^+]}$$

K_1, K_2, K_3, and K_4 are the acid dissociation constants of H_4Z,[9] and $[Z]_f$ means the total concentration of the uncomplexed ligand, Z. In the pH range of the present experiment, the value of $\alpha_{Z(H)}$ was practically identical with $[H^+]^2/K_3K_4$.[10] Since TRDTA was present in a large excess, $[Z]_f$ was almost the same as its initial concentration, $[Z]_0$, during the reaction process; therefore, Eq. (8) can be rewritten as:

$$k^{+}_{obs} = (k^{CoY} + k^{CoY}_{H_2Z}[Z]_0) + (k^{CoY}_{H} + k^{CoHY}_{H_2Z}K^{H}_{CoHY}[Z]_0)[H^+] \quad (9)$$

Equation (9) clearly indicates that the plots of the values of the intercepts and slopes of the straight lines shown in Fig. 1 against $[Z]_0$ should yield linear relations. They are reproduced in Fig. 2. Each rate constant given in Eq. (9) was determined from the values of the intercepts and the slopes of the straight lines shown in Fig. 2; all are given in Table 2.

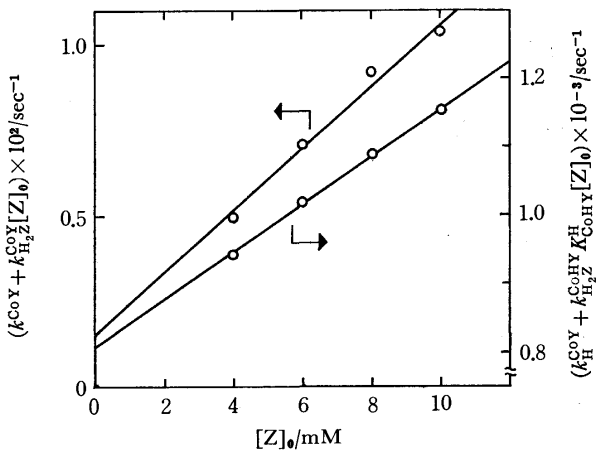

Fig. 2. The plots of $(k^{CoY}_{H} + k^{CoHY}_{H_2Z}K^{H}_{CoHY}[Z]_0)$ and $(k^{CoY} + k^{CoY}_{H_2Z}[Z]_0)$ against $[Z]_0$ at ionic strength 0.2 and 25 °C containing 0.2 mM cobalt(II)-TDTA, 0.1 M acetate buffer and 0.005% gelatin.

9) G. Anderegg, *Helv. Chim. Acta*, **47**, 1801 (1964).

10) The error of this assumption is less than 0.5%.

Results Obtained by Method B. The cobalt(III)-TDTA ion gives a limiting diffusion current corresponding to a one-electron reduction which starts at a more positive potential than the dissolution of mercury. The addition of TRDTA causes a decrease in the limiting current at the potential range more positive than about −0.1 V *vs.* SCE, as is shown in Fig. 3.

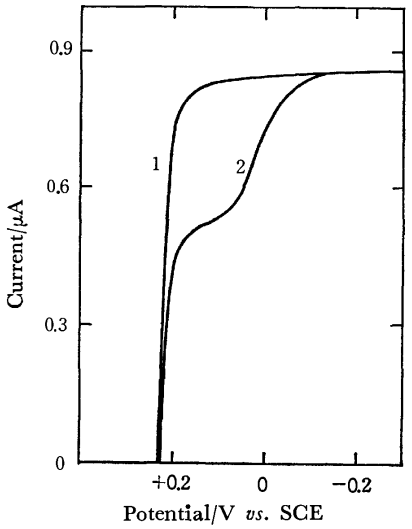

Fig. 3. Polarograms of 0.4 mM cobalt(III)-TDTA in the presence of 40 mM TDTA (curve 1) and 40 mM TDTA +4 mM TRDTA (curve 2) in solutions of ionic strength 0.5 (KNO_3) and pH 3.74 containing 80 mM acetate buffer and 0.005% gelatin.

Table 1. Dependence of the value i_k (at $t=t_d$) on the mercury height

Mercury height/cm	40.7	51.0	60.8
$i_k/\mu A$ (at $t=t_d$)	0.25_5	0.26_1	0.26_0

Measurements were made under the following conditions: 0.4 mM cobalt(III)-TDTA, 8 mM TRDTA, 32 mM TDTA, 80 mM acetate buffer and 0.005% gelatin at ionic strength 0.5 (KNO_3), pH 3.79 and 25 °C. The applied potential was +0.13 V *vs.* SCE.

The value of the instantaneous current at $t=t_d$ corresponding to the decrease in the limiting current, which was denoted as i_k, was found to be independent of the mercury height of DME. This is shown in Table 1, which reveals that i_k is a kinetic current. These phenomena can be interpreted by means of the following equations:

$$\text{Co(III)-TDTA} + e \longrightarrow \text{Co(II)-TDTA} \quad (10a)$$

$$\text{Co(II)-TDTA} + \text{TRDTA} \rightleftharpoons \text{Co(II)-TRDTA} + \text{TDTA} \quad (10b)$$

$$\text{Co(II)-TRDTA} \longrightarrow \text{Co(III)-TRDTA} + e \quad (10c)$$

The electrode process expressed by Eqs. (10a) to (10c) is the so-called ECE mechanism (electrochemical-chemical-electrochemical mechanism), which has previously been treated theoretically.[11] If the concentrations of TDTA and TRDTA are in excess over that of cobalt(II)-TDTA, the substitution reaction (10b) can be expressed as a pseudo first-order reaction:

$$\text{Co(II)-TDTA} \underset{l_b}{\overset{l_f}{\rightleftharpoons}} \text{Co(II)-TRDTA} \quad (11)$$

where l_f and l_b mean the rate constants for the forward and the backward reactions respectively. The apparent equilibrium constant of Reaction (11), K, is given as:

$$K = \frac{l_f}{l_b} = \frac{[\text{Co(II)-TRDTA}]}{[\text{Co(II)-TDTA}]} = \frac{K_{CoZ}[Z^{4-}]}{K_{CoY}[Y^{4-}]} = \frac{\alpha_{Y(H)}K_{CoZ}[Z]_f}{\alpha_{Z(H)}K_{CoY}[Y]_f} \quad (12)$$

where K_{CoY} and K_{CoZ} denote the stability constants for the cobalt(II)-TDTA and cobalt(II)-TRDTA complexes respectively. The value of $(\alpha_{Y(H)}\ K_{CoZ})/(\alpha_{Z(H)}\ K_{CoY})$ was polarographically determined in this work to be $11._8$. The value of K given in Eq. (12) was kept larger than unity by adjusting the concentrations of TDTA and TRDTA. For this condition, the following equation has been derived[11]:

For $K>1$:

$$\left|\frac{i_k}{i_d}\right| = \frac{K}{K-1}\left\{1-\exp(-lt)-2\theta\exp(-K^2\theta^2)\int_\theta^{K\theta}\exp(\lambda^2)d\lambda\right\} \quad (13)$$

where:

$$l = l_f + l_b$$

$$\theta = \sqrt{\frac{lt}{K^2-1}}$$

and where the symbol i_d indicates the diffusion current observed in the absence of Reaction (10b). In this method, the word "current," denoted by i_k or i_d, means an instantaneous current observed four seconds after the beginning of the mercury-drop growth. The rate constants, l_f and l_b, can be determined from Eq. (13) by using the value of $|i_k/i_d|$, which is obtained experimentally.

The pH dependence of the l_f values at various initial concentrations of TRDTA, $[Z]_0$, was also examined, as is shown in Fig. 4; the figure reveals that l_f is a first-

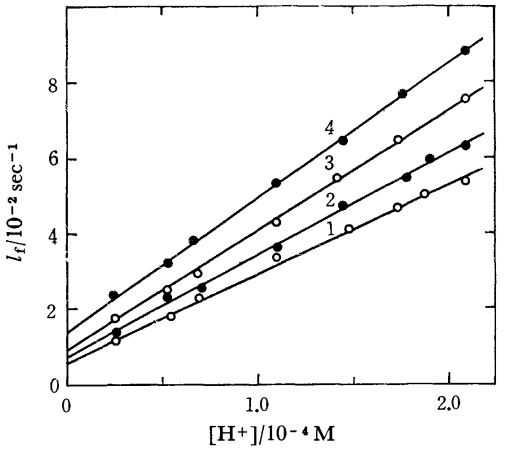

Fig. 4. The value of l_f as a function of the hydrogen ion concentration at ionic strength 0.5 (KNO_3) and 25 °C containing 0.4 mM cobalt(III)-TDTA, 24 mM TDTA, 80 mM acetate buffer and 0.005% gelatin.
Initial concentrations of TRDTA are: 4 mM (1), 6 mM (2), 8 mM (3), and 10 mM (4).

11) K. Ogino (née Ebata) and N. Tanaka, This Bulletin, **39**, 2672 (1966).

TABLE 2. RATE CONSTANTS OBTAINED BY METHODS A AND B AT 25 °C

Reaction	Rate constant	
	Method A (μ=0.2)	Method B (μ=0.5)
$CoY^{2-} + H_2Z^{2-} \xrightarrow{k^{CoY}_{H_2Z}} CoZ^{2-} + H_2Y^{2-}$	8.9×10^{-1} M^{-1} sec^{-1}	4×10^{-1} M^{-1} sec^{-1}
$CoHY^{-} + H_2Z^{2-} \xrightarrow{k^{CoHY}_{H_2Z}} CoHZ^{-} + H_2Y^{2-}$	$3.5\times10^{4}/K^{H}_{CoHY}$ M^{-1} sec^{-1}	$2.3\times10^{4}/K^{H}_{CoHY}$ M^{-1} sec^{-1}
$CoY^{2-} \xrightarrow{k^{CoY}} Co^{2+} + Y^{4-}$	1.5×10^{-3} sec^{-1}	6×10^{-3} sec^{-1}
$CoY^{2-} + H^{+} \xrightarrow{k^{CoY}_{H}} Co^{2+} + HY^{3-}$	8.1×10^{2} M^{-1} sec^{-1}	$1._3\times10^{2}$ M^{-1} sec^{-1}

order function with respect to both the hydrogen ion concentration and $[Z]_0$. These experimental results are understandable by assuming the same four reaction paths as Eqs. (4) to (7) for Reaction (10b), resulting in the same equation as in the case of Eq. (9)[12]:

$$l_f = (k^{CoY} + k^{CoY}_{H_2Z}[Z]_0) + (k^{CoY}_{H} + k^{CoHY}_{H_2Z}K^{H}_{CoHY}[Z]_0)[H^+] \quad (14)$$

Each rate constant was obtained in the same way as in Method A, on the basis of Fig. 4 and Eq. (14). The results are summarized in Table 2.

Discussion

It was revealed that the reaction of cobalt(II)-TDTA with TRDTA proceeds through four simultaneous reaction paths in the pH range from 3.7 to 5.6; these reaction paths consist of two nucleophilic ligand substitution reactions and two dissociation reactions of cobalt(II)-TDTA. The values of rate constants obtained by the two different methods are, as a whole, in good agreement with each other.

It should be noted that, in a lower pH range, reactions other than (4) to (7), such as:

$$CoY^{2-} + H_3Z^{-} \underset{}{\overset{k^{CoY}_{H_3Z}}{\rightleftharpoons}} CoZ^{2-} + H_3Y^{-} \quad (15)$$

$$CoHY^{-} + H_3Z^{-} \underset{}{\overset{k^{CoHY}_{H_3Z}}{\rightleftharpoons}} CoHZ^{-} + H_3Y^{-} \quad (16)$$

may proceed. However, since the concentration of H_3Z^- is less than 6% of $[Z]_f$ even at pH 3.7, and since the values of $k^{CoY}_{H_3Z}$ and $k^{CoHY}_{H_3Z}$ seem to be smaller than those of $k^{CoY}_{H_2Z}$ and $k^{CoHY}_{H_2Z}$ respectively,[13] it seems reasonable to neglect the contributions of Reactions (15) and (16) to the total reaction.

The dissociation rate constants of cobalt(II)-TDTA and some related complexes are summarized in Table 3. These data show that the cobalt(II)-TDTA complex dissociates easier than the other complexes shown in Table 3. This may be due to the instability of the seven-membered diamine chelate ring which is present in the cobalt(II)-TDTA complex.

TABLE 3. DISSOCIATION RATE CONSTANTS

Ligand (L)	μ	k^{CoL}/sec^{-1}	k^{CoL}_{H}/(M^{-1} sec^{-1})	Ref.
EDTA	0.2	$<5\times10^{-4}$	3×10	2[a]
TRDTA	0.2	$<5\times10^{-3}$	5×10^{2}	2[a]
TDTA	0.2	1.5×10^{-3}	8.1×10^{2}	This work[a]
	0.5	6×10^{-3}	$1._3\times10^{2}$	This work[b]
meso-BDTA	0.2	—	5.1	3[a]
PDTA	0.2	—	4.3	3[a]

a) Method A, b) Method B.

TABLE 4. COMPARISON BETWEEN THE OBSERVED AND THE CALCULATED VALUES OF $(k^{Cotdta}_{H}/k^{CoL}_{H})$

Observed	Calculated
$\frac{k^{Cotdta}_{H}}{k^{Cbtrdta}_{H}} = \begin{cases}1._6 \text{ (Method A)}\\ 0.2_6 \text{ (Method B)}\end{cases}$	$\frac{K_{Cotrdta}}{K_{Cotdta}} = 0.69_5$[a]
$\frac{k^{Cotdta}_{H}}{k^{Coedta}_{H}} = \begin{cases}2._7\times10 \text{ (Method A)}\\ 4._3 \text{ (Method B)}\end{cases}$	$\frac{K_{Coedta}}{K_{Cotdta}} = 4._5$[b] or $1._2\times10$[c]

a) This value was determined in this work polarographically. b) Obtained in this work. c) From Ref. 9.

Table 4 compares the ratios of the observed rate constants, k^{CoY}_{H}/k^{CoL}_{H}, and the estimated ones which were calculated on the basis of the method proposed by Bydalek and Margerum.[15] Since TDTA is very similar to EDTA and TRDTA, the k^{CoY}_{H}/k^{CoL}_{H} ratio can be expected to be approximately the same as the reverse ratio of the stability constant, K_{CoL}/K_{CoY}, as has been shown in previous paper.[2,3] The observed ratios are practically identical with the calculated ones.

In Method A, it is necessary to stir and homogenize the solution for at least 5 to 10 seconds when the reaction is initiated. Therefore, it is desirable to measure the reaction which has a longer half-life than 40—50 seconds when DME is used. In this work, the rate of the reaction increases with the decrease in the pH of the solution. The kinetic measurements were not done in the pH range lower than 4.9 by Method A, for the rate of the reaction is immeasurably fast in this pH range. On the other hand, Method B, based on the

12) In this study, it is assumed that $\alpha_{Z(H)}$ is equal to $[H^+]^2/K_3K_4$. The contribution of terms other than $[H^+]^2/K_3K_4$ to $\alpha_{Z(H)}$ is 6% at pH 3.7, and decreases with an increase in the pH to reach 0.7% at pH 4.6.

13) In many kinds of multidentate-ligand substitution reactions, such as $ML+L' \rightleftarrows ML'+L$, which have thus far been investigated, the rate constants decrease in this order: $k^{ML}_{L'} > k^{ML}_{HL'} > k^{ML}_{H_2L'}$. This indicates that a reaction rate decreases with an increase in the extent of the protonation of an attacking ligand.[14] Therefore, it is reasonable to assume that the value of $k^{CoY}_{H_3Z}$ in the Co(II)-TDTA-TRDTA system is much less than that of $k^{CoY}_{H_2Z}$.

14) For instance, M. Kodama, C. Sasaki, and M. Murata, This Bulletin, **41**, 1333 (1968); M. Kodama, *ibid.*, **42**, 2532 (1969).

15) T. J. Bydalek and D. W. Margerum, *Inorg. Chem.*, **2**, 678 (1963).

ECE mechanism, is quite useful for such a fast reaction as long as the following conditions are fulfilled; that is, the rates of the electrode reactions (10a) and (10c) are much faster than the chemical reaction (10b). This indicates that the measurement can be performed even in a pH range lower than 4.9 by utilizing this method.

There seems to be no example of the application of the electrode process, followed by chemical and electrochemical reactions (ECE mechanism), to the multidentate-ligand substitution reaction. In this study, the kinetic treatment over a wider pH range could be carried out by utilizing Method B together with Method A, and it was confirmed that Method B is applicable to the kinetic study of the multidentate-ligand substitution reactions.

The authors wish to thank the Ministry of Education for the financial support granted for this research.

BULLETIN OF THE CHEMICAL SOCIETY OF JAPAN, VOL. 46, 2464—2467 (1973)

Binuclear Metal Complexes. VII.[1] Preparation and Properties of Binuclear Copper(II) and Nickel(II) Complexes of Hydrogen-bridged Macrocycles[2]

Hisashi Okawa, Tadashi Tokii,* Yoneichiro Muto,* and Sigeo Kida
Department of Chemistry, Faculty of Science, Kyushu University, Hakozaki, Fukuoka 812
**Department of Chemistry, Saga University, Saga 814*

(Received April 23, 1973)

Two types of binuclear copper(II) and nickel(II) complexes, OK-3(H), 3(H)-M_2 and [OK-m, 3(H)-M_2]ClO_4 (m=2 or 3), have been synthesized, where OK-3(H),3(H) is a macrocycle composed of two 2,6-diformyl-4-methylphenol and four hydroxylamine, and OK-m,3(H) is a macrocycle composed of two 2,6-diformyl-4-methylphenol, one diamine (ethylene diamine (m=2) or 1,3-diaminopropane (m=3)), and two hydroxylamine. It was found that a very strong antiferromagnetic exchange interaction is operating between two copper(II) ions for OK-3(H), 3(H)-Cu_2 and [OK-2,3(H)-Cu_2]ClO_4. The complex [OK-2,3(H)-Ni_2]ClO_4.DMF was found to be a novel-type binuclear nickel(II) complex, in which one nickel(II) ion is diamagnetic and the other is paramagnetic.

In the preceding paper of this series, Okawa and Kida[3] synthesized some binuclear copper(II) and nickel(II) complexes of the macrocycles formulated in Fig. 1. In this paper we report two types of binuclear copper(II) and nickel(II) complexes of new hydrogen-bridged macrocycles (Fig. 2).

The macrocycles were prepared by the combination of 2,6-diformyl-4-methylphenol, hydroxylamine and diamines. The complexes of the macrocycle composed of two 2,6-diformyl-4-methylphenol and four hydroxylamine are abbreviated to OK-3(H), 3(H)-M_2, in which imino nitrogens are connected by two O···H···O bridges. The complexes of the macrocycle composed of two 2,6-diformyl-4-methylphenol, one diamine and two hydroxylamine are abbreviated to [OK-m, 3(H)-M_2]$^+$, where imino nitrogens are connected by one alkylene (ethylene (m=2) or 1,3-propylene(m=3)) chain and one O···H···O bridge.

The structures and properties of the complexes were studied from elemental analyses, infrared and visible spectra, mass spectrum, molar conductivities, and cryomagnetic measurements.

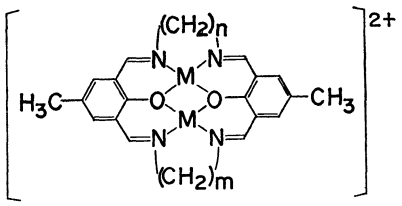

Fig. 1.

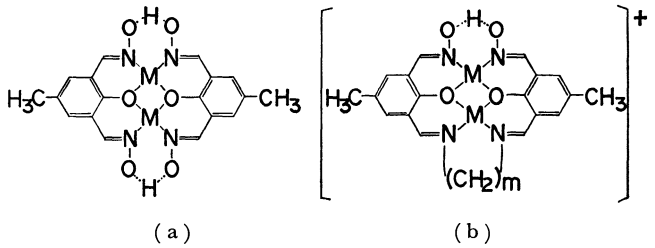

(a) (b)

Fig. 2. Structures of (a) OK-3(H),3(H)-M_2 and (b) [OK-m, 3(H)-M_2]$^+$ complexes.

Experimental

Syntheses. *OK-3(H),3(H)-Cu_2*: A solution of 2,6-diformyl-4-methylphenol (330 mg), hydroxylamine hydrochloride (278 mg), and copper(II) acetate monohydrate (400 mg) in 50 % ethanol (100 ml) was neutralized with an aqueous solution of sodium hydroxide (160 mg) to give a dark green precipitate. It was collected and thoroughly washed with hot pyridine.

Found: C, 41.96; H, 3.10; N, 10.49%. Calcd for $C_{18}H_{16}N_4O_6Cu_2$: C, 42.27; H, 3.15; N, 10.95%.

OK-3(H),3(H)-Ni_2·$3H_2O$. To a green solution of 2,6-diformyl-4-methylphenol (330 mg), hydroxylamine hydro-

1) Part VI: H. Okawa, T. Tokii, Y. Nonaka, Y. Muto, and S. Kida, This Bulletin, **46**, 1462 (1973).

2) This work was presented at the 22nd synposium on Coordination Chemistry, Osaka, November 8, 1972.

3) H. Okawa and S. Kida, This Bulletin, **45**, 1759 (1972).

chloride (278 mg) and nickel(II) chloride hexahydrate (475 mg) in 50% ethanol (100 ml), a 10% aqueous solution of sodium hydroxide was added until the solution was neutralized. Soon yellow crystalline powder separated out. It was collected and washed with water.

Found: C, 39.11; H, 3.68; N, 10.13%. Calcd for $C_{18}H_{22}N_4O_9Ni_2$: C, 38.90; H, 3.99; N, 10.01%.

[OK-2,3(H)-Cu$_2$]ClO$_4$. *N,N'*-Ethylenebis(3-formyl-5-methylsalicylaldimino)copper(II)[3] (828 mg), hydroxylamine hydrochloride (278 mg), and copper(II) perchlorate hexahydrate (741 mg) were dissolved in methanol (100 ml). To the clean solution was added dropwise an aqueous solution of sodium hydroxide (160 mg) to give brown prisms. They were collected and washed with ethanol.

Found: C, 39.97; H, 3.46; N, 9.50; Cu, 20.76%. Calcd for $C_{20}H_{19}N_4O_8ClCu_2$: C, 39.65; H, 3.16; N, 9.25; Cu, 20.97%.

[OK-3,3(H)-Cu$_2$]ClO$_4$·H$_2$O. *N,N'-1,3*-Propylenebis(3-formyl-5-methylsalicylaldimino)copper(II)[3] (214 mg), hydroxylamine hydrochloride (70 mg), and copper(II) perchlorate hexahydrate (182 mg) were dissolved in 70% methanol, and were stirred at 50 °C for 3 hr. When the reaction mixture was cooled, dark green prisms separated out. They were collected and recrystallized from methanol.

Found: C, 39.17; H, 4.11; N, 9.22%. Calcd for $C_{21}H_{23}N_4O_9ClCu_2$: C, 39.54; H, 3.63; N, 8.78%.

[OK-2,3(H)-Ni$_2$]ClO$_4$·DMF. *N,N'*-Ethylenebis(3-formyl-5-methylsalicylaldimino)nickel(II)[3] (705 mg), hydroxylamine hydrochloride, (208.5 mg), and nickel(II) perchlorate hexahydrate (384 mg) were dissolved in *N,N*-dimethylformamide (200 ml). To this solution an aqueous solution of sodium hydroxide (180 mg) was added. The reaction mixture was refluxed for 4 hr and concentrated to 30 ml to give orange prisms.

Found: C, 41.70; H, 3.91; N, 10.27%. Calcd for $C_{23}H_{26}N_5O_9ClNi_2$: C, 41.27; H, 3.92; N, 10.46%.

Measurements. Infrared spectra were measured with a Hitachi 215 grating spectrophotometer on a KBr disk. Electronic spectra were measured with a Hitachi EPS-3T recording spectrophotometer. Magnetic susceptibilities were determined by the Gouy method over the range from liquid nitrogen to room temperature. Effective magnetic moments were calculated from the equation

$$\mu_{eff} = 2.83\sqrt{(\chi_A - N\alpha)T},$$

where Pascal's constants were used for correction of diamagnetism. The temperature independent paramagnetism, $N\alpha$, for a nickel(II) ion was estimated to be 193×10^{-6} c.g.s./mol.[4] Molar conductivities were measured in absolute methanol solution (*ca.* 10^{-3} mol) at 25 °C.

Results and Discussion

OK-3(H),3(H)-M$_2$ complexes. Some main infrared absorption bands, ligand field bands and magnetic moments at room temperature of OK-3(H), 3(H)-Cu$_2$ and OK-3(H),3(H)-Ni$_2$·3H$_2$O are given in Table 1.

The band at 1610 cm^{-1} can be assigned to the C=N stretching vibration. The broad band observed in the region 1750—1740 cm^{-1} appears to be similar in its origin to the bands found for Ni(DMG)$_2$[5] and [Co(DMG)$_2$XY]$^{-1}$ (X, Y=Cl$^-$, Br$^-$, NO$_2^-$ or H$_2$O)[6] (DMG=dimethylglyoximate anion), where each of the band was assigned to a strongly hydrogen-bonded OH-vibration. The mass spectrum of OK-3(H),3(H)-Cu$_2$ showed two signals at m/e=510 and 512; these are well corresponding to the molecular ion (mol wt=511.43). Recently we also found two peaks due to the molecular ion for a binuclear copper(II) complexes.[1] The appearance of two (or three) molecular ion peaks, therefore, characteristic of a binuclear copper(II) complex, since naturally occurring copper is composed of ^{63}Cu(69.09%) and ^{65}Cu(30.91%). Judging from these facts we concluded that the complexes possess a binuclear structure constructed with the macrocycle containing hydrogen-bridges shown in Fig. 2a.

The complex OK-3(H),3(H)-Cu$_2$ is practically insoluble even in the solvents of high donar-ability such as pyridine and *N,N*-dimethylformamide. The complex is stable in cold concentrated hydrochloric acid, sulfuric acid, and sodium hydroxide solution. The magnetic moment of the complex at room temperature is subnormal (0.59 B.M.). Its magnetic susceptibility was measured over a temperature range 77—300 K (Fig. 3). Although a deviation was found below 120 K owing to a small amount of paramagnetic impurity, the experimental data are well explained on the basis of the Bleaney-Bowers equation[7]

Table 1. Properties of OK-3(H), 3(H)-M$_2$, and [OK-m, 3(H)-M$_2$]$^+$ complexes

	IR (cm^{-1})				Λ[a]	d-d bands (kK)		μ_{eff} (B.M.)
	O···H···O	C=N	C=O	ClO$_4^-$		solid	methanol	
OK-3(H), 3(H)-Cu$_2$	1750	1610				14.9	—[b]	0.59
OK-3(H), 3(H)-Ni$_2$·3H$_2$O	1740	1610				—[c]	—[b]	2.87
[OK-2,3(H)-Cu$_2$]ClO$_4$	1760	1635 1628		1110—1080	—[b]	20—15.4	—[b]	0.59
[OK-3,3(H)-Cu$_2$]ClO$_4$·H$_2$O	1770	1637 1629		1110—1080	109	15.6	16.4(110) 14.3 (93)	0.61
[OK-2,3(H)-Ni$_2$]ClO$_4$·DMF	1780	1680 1622	1635	1110—1060	95	—[c]	20—16.7	2.25 (3.31)[d]

a) Molar conductivity (Ω^{-1}cm^{2}mol^{-1}). b) Hardly soluble in methanol. c) Given in Fig. 4. d) This moment is obtained by assuming that one nickel(II) ion is diamagnetic.

4) Ballhousen, "Introduction to Ligand Field Theory," McGraw-Hill Book Company, Inc. (1962), p. 142.
5) R. E. Rundle and M. Parasol, *J. Chem. Phys.*, **20**, 1487 (1952).
6) J. Fujita, A. Nakahara, and R. Tsuchida, *ibid.*, **23**, 1541 (1955).
7) B. Bleaney and K. D. Bowers, *Proc. Roy. Soc. Ser A*, **214**, 451 (1952).

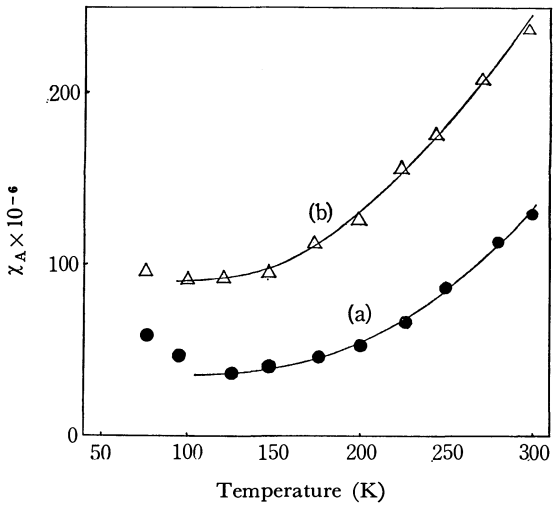

Fig. 3. Variation of molar susceptibility with temperature of (a) OK-3(H), 3(H)-Cu_2, and (b) [OK-2, 3(H)-Cu_2]ClO_4.

$$\chi_A = \frac{Ng^2\beta^2}{3kT}\left[1+\frac{1}{3}\exp(-2J/kT)\right]^{-1} + N\alpha,$$

in which each simbol means the general meaning. By the best fit of the experimental χ_A values to the equation, $-2J$, g, and $N\alpha$ were evaluated to be 870 cm^{-1}, 2.20, and 36×10^{-6} e.s.u./mol respectively. This large $-2J$ value indicates a very strong antiferromagnetic exchange interaction between the copper(II) ions. Generally the more planar the geometry around the copper(II) ion is, the larger the spin-exchange interaction between the copper(II) ions becomes.[8-10]

The reflectance spectrum of OK-3(H),3(H)-Ni_2·$3H_2O$ in Fig. 4 clearly indicates that the geometry around the nickel(II) ion is practically octahedral. The magnetic moment at room temperature is 2.84 B. M., that is slightly lower value compared with most octahedral nickel(II) complexes. The magnetic susceptibility of the complex obeys the Curie-Weiss law (Fig. 5a). The Weiss constant was determined to be -77 K, indicating an antiferromagnetic exchange inter-

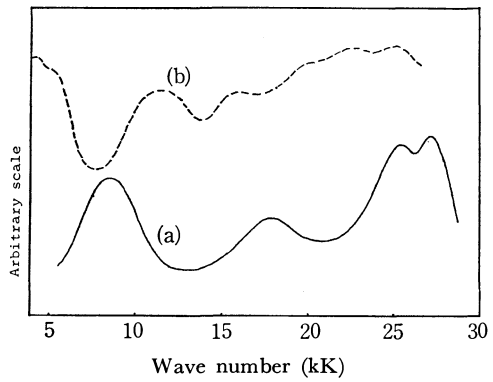

Fig. 4. Reflectance spectra of (a) OK-3(H), 3(H)-Ni_2·$3H_2O$, and (b) [OK-2, 3(H)-Ni_2]ClO_4·DMF.

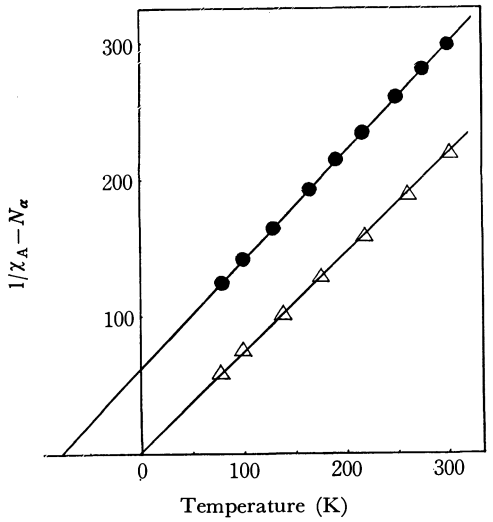

Fig. 5. Plots of the inverse susceptibilities of (a) OK-3(H), 3(H)-Ni_2·$3H_2O$, and (b) [OK-2, 3(H)-Ni_2]ClO_4·DMF per nickel atom as a function of temperature. In the latter case one nickel(II) ion is assumed to be diamagnetic.

action between a pair of nickel(II) ions.

Pilkington and Robson[11] reported that the μ_{eff} value for $LCu_2(ClO_4)_2$·$2H_2O$ (=[OK-3,3-Cu_2]$(ClO_4)_2$·$2H_2O$) was 0.58 B.M. at room temperature and the Weiss constant for LNi_2Cl_2·$2H_2O$ (=[OK-3,3-Ni_2]-Cl_2·$2H_2O$) was -125 K.

[OK-m,3(H)-M_2]$^+$ Complexes. The properties of [OK-m,3(H)-M_2]$^+$ complexes are given in Table 1. Since in the infrared spectra a band due to the O···H···O bond was observed in the region 1780—1760 cm^{-1}, the complexes were assumed to have a binuclear structure of the macrocycle formulated in Fig. 2b. Two bands in the region 1640—1620 cm^{-1} were attributed to the C=N stretching vibrations. This is consistent with the fact that there are two non-equivalent azomethine groups in [OK-m,3(H)-M_2]$^+$ complexes. The broad, strong band near 1110—1070 cm^{-1} was assigned to perchlorate ion.[12] In [OK-2,3(H)-Ni_2]ClO_4·DMF a shoulder was observed at 1635 cm^{-1}, which might be assigned to the $\nu_{C=O}$ mode of coordinated *N,N*-dimethylformamide.

The molar conductivities for [OK-3,3(H)-Cu_2]-ClO_4·H_2O and [OK-2,3(H)-Ni_2]ClO_4·DMF in absolute methanol at 25 °C clearly indicate that they are 1 : 1 electrolytes.

The reflectance spectrum of [OK-2,3(H)-Cu_2]ClO_4 possesses a very broad band around 20—15.5 kK. Similar spectrum was found for [OK-2,3-Cu_2]Cl_2.[3] The broadening of the band will be caused by the superposition of the d–d transition bands of the copper(II) ions, whose geometries are different from each other. The electronic spectrum of [OK-3,3(H)-Cu_2]-ClO_4·H_2O is similar to that of [OK-3,3-Cu_2]Cl_2·H_2O.[3] The splitting of the d–d band (16.4 and 14.3 kK) in methanol has been attributed to the fact[11] that the solvent molecule coordinates to the copper(II) ion to

8) H. Okawa, M. Honda, and S. Kida, *Chem. Lett.*, **1972**, 1027.

9) Y. Muto, K. Kato, H. B. Jonassen, and L. J. Cusachs, This Bulletin, **42**, 417 (1969).

10) M. Kato, Y. Muto, H. B. Jonassen, K. Imai, K. Katsuki, and S. Ikegami, *ibid.*, **42**, 2555 (1969).

11) N. F. Pilkington and R. Robson, *Aust. J. Chem.*, **23**, 2225 (1970).

12) B. J. Hathaway and A. E. Underhill, *J. Chem. Soc.*, **1961**, 3091.

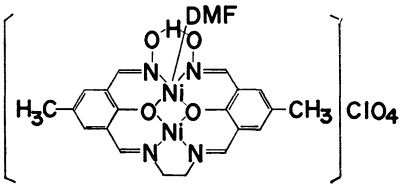

Fig. 6. The probable structure of [OK-2,3(H)-Ni_2]ClO_4·DMF.

form five- or six-coordinate complex.

The magnetic moment for [OK-2,3(H)-Cu_2]ClO_4 at room temperature was very low (0.59 B.M.). Its magnetic susceptibility was measured at various temperatures (Fig. 3b). The χ_A values obeyed the Bleaney-Bower's equation and the magnetic parameters obtained are $-2J=725\ cm^{-1}$, $g=2.10$, and $N\alpha=90\times10^{-6}$ c.g.s./mol.

The reflectance spectrum of [OK-2,3(H)-Ni_2]ClO_4·DMF given in Fig. 4b is markedly complicated; it differs from any of the spectra for octahedral,[13,14] planar,[13,14] and tetrahedral[15] nickel(II) complexes. Since it is evident from infrared spectral data that the strong intramolecular hydrogen-bond is present and that *N,N*-dimethylformamide coordinates to the nickel(II) ion, a tetragonal-pyramidal, five-coordinate structure is naturally assigned to the present complex. Recently many spectroscopic investigations of five-coordinate nickel(II) complexes have been reported,[14,16,17] and it is now well known that most low-spin tetragonal-pyramidal nickel(II) complexes have d–d bands in the region 10—20 kK.[16-18] On the other hand, high-spin, tetragonal-pyramidal nickel(II) complexes show d-d bands in the region 25—5 kK.[16,17] Judging from these facts at least one of the two nickel(II) ions in the complex seems to keep a high-spin, tetragonal-pyramidal geometry. In fact its magnetic moment at room temperature was 2.25 B.M. per nickel atom, indicating the presence of a paramagnetic nickel(II) ion. The relatively small magnetic moment of the complex will be explained in terms of (i) antiferromagnetic exchange interaction between a pair of paramagnetic nickel(II) ions or (ii) a binuclear system composed of one paramagnetic and one diamagnetic nickel(II) ions.

In order to clarify this magnetic phenomenon the magnetic susceptibility was measured at various temperatures (Fig. 5b). Since this complex obeys the Curie-Weiss law and its Weiss constant is very small ($\theta=-2$ K), it is evident that the relatively low magnetic moment is attributed to the novel binuclear system containing one high-spin and one low-spin nickel(II) ions. There are only few reports upon the complexes composed of paramagnetic and diamagnetic nickel(II) ions.[19] The reflectance spectrum given in Fig. 4b, therefore, can be interpreted as the superposition of the spectra of low-spin planar and high-spin tetragonal-pyramidal nickel(II) ions. The solution spectrum in methanol, however, was very simplified and showed a broad band around 15—20 kK. This spectrum resembles that of [OK-2,3-Ni_2]-Cl_2.[3] This fact indicates that in methanol solution the complex is coordinated with neither *N,N*-dimethylformamide nor methanol molecule, and keeps the planar structure.

It is known that *N,N'*-ethylenebis(salicylaldimino)-nickel(II) retains the planar structure in polar solvents such as pyridine.[20] In addition to this Okawa and Kida[3] reported that *N,N'*-ethylenebis(3-formyl-5-methylsalicylaldimino)nickel(II) and OK-2,3-Ni did not add pyridine and *N,N*-dimethylformamide. Therefore, in the present case, it is evident that *N,N*-dimethylformamide molecule coordinates to the nickel(II) ion in the 6–6–6 condensed ring system involving hydrogen-bridge, but not to the nickel(II) ion in the rigid 6–5–6 condensed ring system. Here, it is to be noted that no apical coordination takes place in any polar solvents in the case of [OK-2,3-Ni_2]Cl_2,[3] which has the same ring-system as [OK-2,3(H)-Ni_2]ClO_4·DMF, except that two imino nitrogens are connected with 1,3-propylene bridge instead of –O···H···O– bridge.

13) S. Yamada, *Coord. Chem. Rev.*, **1**, 415 (1966).
14) L. Sacconi, *ibid.*, **1**, 192 (1966).
15) L. Sacconi, *ibid.*, **1**, 126 (1966).
16) C. Furlani, *ibid.*, **3**, 141 (1968).
17) M. Ciampolini, *Structure and Bonding*, **6**, 52 (1969).
18) E. K. Barefield and D. H. Busch, *Inorg. Chem.*, **10**, 1216 (1971).
19) M. Kondo and M. Kubo, *J. Phys. Chem.*, **61**, 1648 (1957).
20) H. C. Clark and A. L. Odell, *J. Chem. Soc.*, **1955**, 3431.

The Chemical Structure of Glass of the $NaPO_3$–Sb_2O_4 System

Makoto WATANABE

Department of Industrial Chemistry, Chubu Institute of Technology, Matsumoto-cho, Kasugai-shi, Aichi 487

(Received January 22, 1973)

Glassy substances of the $NaPO_3$–Sb_2O_4 system with P/Sb ratios in the range from 5.0 to 300 were prepared by heating a mixture of $NaPO_3$ glass and Sb_2O_4 at 1000 °C and by then rapidly quenching the melt of the mixture. From the results of the colorimetric determination and the average degree of polymerization of the condensed phosphates, it has been found that the chain length of the phosphates increases with an increase in the P/Sb ratio. When the glass was treated with water, antimony trioxide was deposited. By using these results, a theoretical treatment for the average degree of polymerization of condensed phosphates has been made and it has been concluded that there are P–O–Sb linkages in the glass of the $NaPO_3$–Sb_2O_4 system.

Phosphate glasses containing oxoacid anions of some elements other than phosphorus have attracted the interest of many investigators. In our previous papers,[1,2] we reported the chemical structure of sodium phosphate glass containing antimony tri- or pentoxide. In the present paper, we will examine the structural framework of sodium phosphate glass containing antimony tetroxide by using the same method as in the previous papers.

Experimental

Materials and Procedure. Sodium phosphate glass was prepared by heating monosodium orthophosphate in a platinum crucible at 1000 °C for 3 hr and by then quenching the resulting melt by placing the crucible in ice water. Antimony tetroxide was made by heating antimony trioxide at 800 °C until a constant weight was reached. The increase in the mass was very close to the calculated value of the oxidation of antimony trioxide to tetroxide (98.3%). Glassy products were obtained by heating mixture of the $NaPO_3$–Sb_2O_4 system with P/Sb ratios in the range from 5.0 to 300 in a platinum crucible at 1000 °C for 2 hr and by then quenching the melts rapidly by placing the crucible in ice water. The distribution and the average degree of the polymerization of phosphate species contained in the glasses were measured by using the same method as in the previous papers.[1,2]

Results and Discussion

The ignition loss of a mixture of the $NaPO_3$–Sb_2O_4 system was very close to the calculated value of the reduction of antimony tetroxide to trioxide. When the glassy substances were treated with an alkaline solution, a white substance was deposited; the deposit gave only X-ray diffraction patterns of antimony trioxide. It can be concluded from the results that the valence of antimony in the glasses may be three. The glassy substances are colorless and transparent, and give no X-ray diffraction patterns. The phosphates present in the aqueous solution of the glassy products were separated by paper chromatography and were then determined colorimetrically. As Table 1 shows, the quantities of ortho-, pyro-, and triphosphates decrease with an increase in the P/Sb ratio, while those of higher polyphosphates increase. The quantities of tri- and tetrametaphosphates are very small throughout the full range of P/Sb ratios.

Table 1. Distribution of phosphates of the $NaPO_3$–Sb_2O_4 system with P/Sb ratios of 5.0—300

	Phosphate (P%)					
P/Sb	Ortho	Pyro	Tri	Trimeta	Tetrameta	Higher
5.0	10.6	34.2	10.5	3.7	2.9	38.1
7.0	9.9	15.0	7.7	3.1	3.0	61.3
10	2.1	7.0	5.3	4.9	2.4	78.3
15	1.5	6.4	3.4	3.5	3.8	81.4
20	1.3	5.5	3.3	4.0	3.1	82.8
30	1.3	5.2	3.3	3.6	1.6	85.0
50	1.0	4.1	2.1	4.7	1.7	86.4
80	1.1	1.8	2.9	4.0	1.2	89.0
100	0.9	1.2	2.8	4.0	2.7	88.4
150				3.6	3.7	92.7
200				2.9	3.3	93.8
300				2.8	1.2	96.0

The average degree of polymerization of $NaPO_3$ glass was about 100, while that of the phosphates contained in the glassy products, which was also measured by the pH titration method increases with an increase in the P/Sb ratio, as may clearly be seen in Fig. 1, it can be concluded that sodium phosphate glass may react with antimony oxide to form the P–O–Sb linkage and the valence of the antimony may be reduced to three under these conditions. The

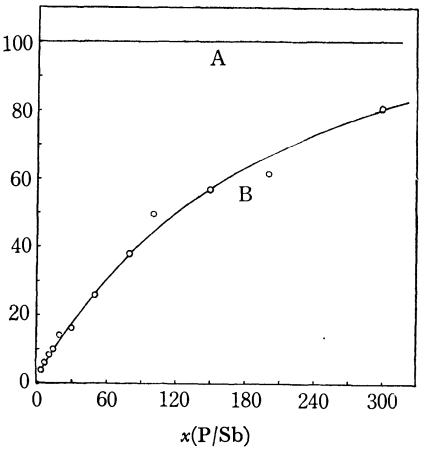

Fig. 1. Variation of average chain length of polyphosphates.
A: Sodium phosphate glass
B: Experimental values of the $NaPO_3$–Sb_2O_4 system

1) M. Watanabe, K. Tanabe, T. Takahara, and T. Yamada, This Bulletin, **44**, 712 (1971).
2) M. Watanabe and M. Kato, *ibid.*, **45**, 1058 (1972).

P–O–Sb linkage may be very much less stable than the P–O–P linkage. Therefore, the P–O–Sb linkage may be rapidly hydrolyzed to produce phosphate ions and antimony trioxide in an aqueous solution.

By using these results as a basis, a theoretical treatment for the average degree of polymerization of the phosphates present in the glassy products can be made. The theory has already been described in previous papers.[1,2] A summary of the theory is as follows. The valence of antimony present in the glasses is considered to be three, and there are three possible types of structures containing P–O–Sb linkages. If x, y, and z are the numbers of phosphorus atoms, P–O–Sb linkages, and Sb–O$^-$ linkages per atom of antimony respectively, the average chain length, $\bar{n}$, of the polyphosphates produced by the hydrolysis of P–O–Sb linkages is given by Eq. (1):

$$(\bar{n}+2)/\bar{n} = (x+y-z)/x \qquad (1)$$

The values calculated by using this equation are listed in Column I of Table 2. When x is larger than 30,

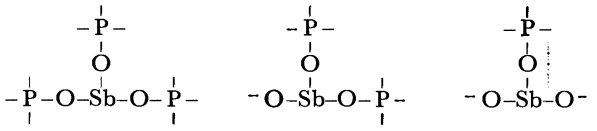

Structure A Structure B Structure C

even the calculated values of $\bar{n}$ based on Structure A are larger than the measured ones. Considering other factors which shorten the chain length of the phosphates present in the glasses, for example, the branching points and impurities, Eq. (1) is modified into Eq. (2):

$$(\bar{n}+2)/\bar{n} = (x+y-z+fx)/x \qquad (2)$$

where f is the factor shortening the chain length of the polyphosphate and is given with respect to an atom of phosphorus. As may clearly be seen in Column II of Table 2, when the f factor is arbitrarily set at 0.015, the calculated values of $\bar{n}$ based on Structure A are very close to the measured ones throughout the range of P/Sb ratios from 5.0 to 300. From these results, it may reasonably be concluded that the structural framework of the glasses of the $NaPO_3$–Sb_2O_4 system with P/Sb ratios larger than 5.0 is Structure A.

Table 2. Average chain length of polyphosphates of the $NaPO_3$–Sb_2O_4 system

		Column I $\bar{n}$ calcd by Eq. (1) Structure			Column II $\bar{n}$ calcd by Eq. (2) (f=0.015) Structure		
x (P/Sb)	$\bar{n}$ Found	A ($y=3$, $z=0$)	B ($y=2$, $z=1$)	C ($y=1$, $z=2$)	A ($y=3$, $z=0$)	B ($y=2$, $z=1$)	C ($y=1$, $z=2$)
5.0	4.1	3.3	10	—	3.3	9.3	—
7.0	5.8	4.7	14	—	4.5	13	—
10	8.8	6.7	20	—	6.3	17	—
15	9.7	10	30	—	9.3	25	—
20	14	13	40	—	12	31	—
30	16	20	60	—	17	41	—
50	26	33	100	—	27	57	∞
80	38	53	160	—	38	73	800
100	50	67	200	—	45	80	400
150	57	100	300	—	57	92	240
200	62	133	400	—	67	100	200
300	81	200	600	—	80	109	171

According to the results described in this paper and in the previous papers,[1,2] when the P/Sb ratio is larger than 5.0, antimony tetr- and pentoxides are reduced to trioxide and the trioxide reacts with $NaPO_3$ glass to form Structure A at 1000 °C. The values of the f factors of the $NaPO_3$–Sb_2O_3 and –Sb_2O_5 systems were 0.02 and 0.01 respectively. The difference in the value of the factor between these systems may be caused by the quantities of impurities contained in the antimony oxides and/or the experimental conditions—for example, the cooling speed of the melts. The f factor of the pure sodium phosphate glass ranges from 0.025 to 0.01, depending on the conditions of the preparation.

Photochemical Reduction of *p*-Quinones with Hydrogen Donors Studied by CIDNP Technique[1,2]

Kazuhiro MARUYAMA, Tetsuo OTSUKI, Akio TAKUWA, and Seiichi ARAKAWA
Department of Chemistry, Faculty of Science, Kyoto University, Kyoto 606
(Received September 29, 1972)

Photo-reduction of *p*-benzoquinone, 1,4-naphthoquinone, and their methyl- or chloro-derivatives has been investigated by means of CIDNP technique. Strongly polarized PMR signals due to unstable reaction intermediates, *p*-quinones, and hydroquinones were observed during the course of reaction. Structures of the unstable reaction intermediates, none of which accumulated as reaction products, were determined, their polarized PMR signals being compared with those of the unstable reaction intermediates resulting from the deuterated substrates. From these results, a reaction scheme for these photo-reduction was proposed.

Photo-reduction of *p*-benzoquinone or chloranil in the presence of hydrogen donors is well known.[3-5] However, no systematic studies or details of the reaction mechanism have been published.

According to Moore and Waters,[3] chloranil reacted with *p*-xylene to form 2,3,5,6-tetrachloro-4-(4-methylbenzyloxy)-phenol. A similar compound was isolated in the photochemical reaction of chloranil with tetralin.[6] Chemically induced dynamic nuclear polarization (CIDNP) technique affords an effective method for investigating unstable active intermediates as well as stable products produced through radical mechanism even in a very small amount.

A preliminary examination revealed that *p*-benzoquinone and its methyl- or chloro-derivatives dissolved in a suitable solvent are photochemically reduced in the presence of hydrogen donors; *i.e.*, xanthene, 9,10-dihydroanthracene, fluorene, or diphenylmethane, to give hydroquinone, quinhydrone, and/or their methyl- and chloro-derivatives. During the course of photo-reductions, strongly polarized PMR signals due to stable reaction products; *i.e.*, hydroquinones, unstable reaction intermediates, as well as *p*-benzoquinones could be observed.

Photo-reduction of *p*-benzoquinone, 1,4-naphthoquinone, and their methyl- or chloro-derivatives by several types of hydrogen donors was investigated by means of CIDNP technique, and stable photo-reduction products were also investigated in macro scale in the photochemical reaction. Emphasis is laid on the photochemical reaction of *p*-quinones with xanthene.

Results and Discussion

Using the NMR probe shown in Fig. 1 we examined the process of photochemical reaction of *p*-quinones with hydrogen donors *in situ* by NMR spectrometer. Carbon tetrachloride and acetone-d_6 were used as solvents. Light was introduced into the probe from the upper side through a hole, reflected by a mirror. A 500 W high-pressure mercury arc lamp was used.

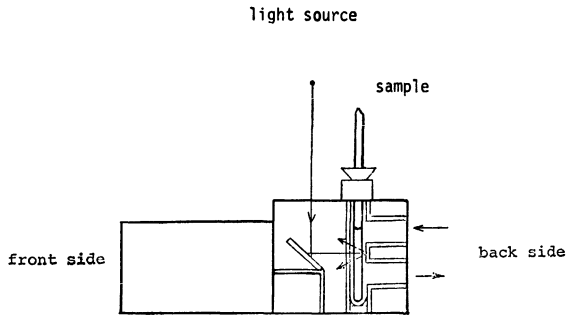

Fig. 1. NMR probe for irradiation.

Structures of the *p*-quinones and types of hydrogen donors are shown in the following.

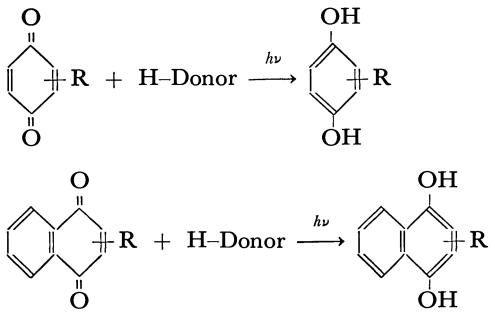

R: H, CH_3, $(CH_3)_2$, $(CH_3)_3$, $(CH_3)_4$, Cl, $(Cl)_2$, $(Cl)_3$ *etc.*

H–Donor: Xanthene, 9,10-Dihydroanthracene, Fluorene, Ether, Alkylaromatics.

Figure 2 shows PMR spectra observed in the reaction of *p*-benzoquinone with xanthene. Spectra (a), (b), and (c) correspond respectively to the PMR spectra observed before irradiation, during the course of irradiation, and after a longer irradiation. Comparing (b) with (a) we find newly appearing strong polarized signals (indicated by arrows). However, when irradiation is stopped they disappear completely with the exception of signal 1 within a few seconds. Since spectrum (c) is obtained after a long photochemical reaction, signal 1 is due to benzene ring protons of hydroquinone which is a stable product. Thus, emission polarized signal 1 in (b) can be assigned to benzene ring protons of hydroquinone. Actually, hydroquinone and bixanthyl are the only stable reaction

1) This work was presented at the International Symposium "Organic Chemistry in Excited State," held at Reading, England, July 24th, 1972.
2) Photochemical Reaction of Quinones X. Previous report of this series; *Chem. Lett.*, **1972**, 131.
3) A. Schönberg and A. Mustafa, *J. Chem. Soc.*, **1945**, 657.
4) A. Schönberg and A. Mustafa, *ibid.*, **1944**, 67.
5) R. F. Moore and W. A. Waters, *ibid.*, **1953**, 3405.
6) A. Schönberg, G. O. Schenck, and D-A. Neumüller "Preparative Organic Photochemistry," Springer (1968), p. 182.

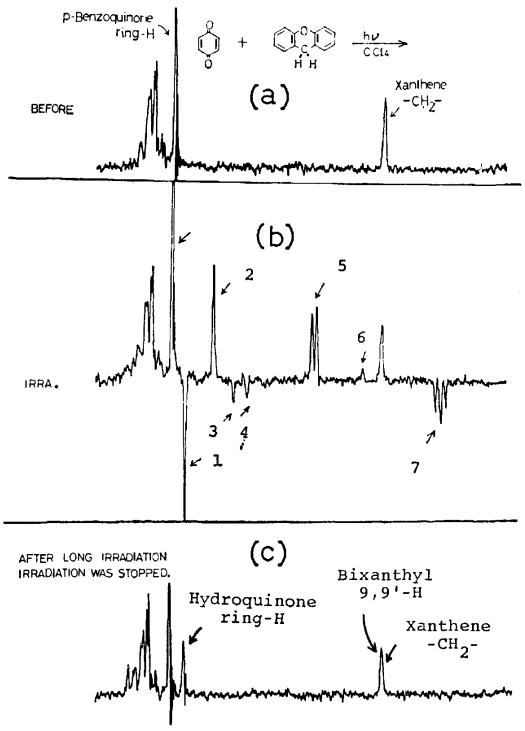

Fig. 2. PMR spectra observed in the photochemical reaction of *p*-benzoquinone with xanthene (solvent: CCl_4, 22 °C). (a): before irradiation, (b): during irradiation, (c): after long irradiation (in this case irradiation was stopped)

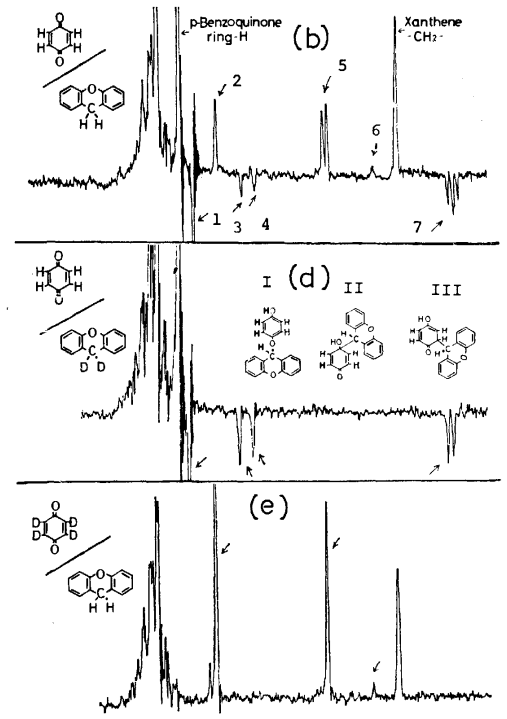

Fig. 3. PMR spectra observed in the photochemical reaction of *p*-benzoquinone with xanthene (solvent: CCl_4, 22 °C).
(b): during irradiation, reaction of *p*-benzoquinone with xanthene
(d): during irradiation, reaction of *p*-benzoquinone with deuterated xanthene
(e): during irradiation, reaction of deuterated *p*-benzoquinone with xanthene

products. Bixanthyl gives no polarized PMR signal.[7] None of the unstable intermediates giving the polarized PMR signals [signals 2,3,4,5,6, and 7 in (b)] accumulate in the reaction system.

For the purpose of obtaining information on their structure we have used deuterated xanthene in 9-methylene group and deuterated *p*-benzoquinone (Fig. 3). Spectrum (b) is observed in the reaction of non-deuterated *p*-benzoquinone with xanthene, (d) in that of non-deuterated *p*-benzoquinone with deuterated xanthene, and (e) in that of deuterated *p*-benzoquinone with non-deuterated xanthene. Three absorption polarized signals 2, 5, and 6 appearing in (b) disappear in (d). Thus, we can conclude that they are based on methine proton of xanthene moiety of the active intermediates. On the other hand, signal 7 changes to doublet from triplet (double doublet). Further, comparing (e) with (b), three emission polarized signals 3, 4, and 7 disappear and the absorption polarized signal 5 changes to singlet from doublet. From the results we may assign three structures ([I], [II], and [III]) to the unstable intermediates. Absorption polarized signal 2 might be due to methine proton of xanthene moiety in [I] and emission polarized signals 3 and 4 to two pair protons of hydroquinone moiety in [I]. These two emission polarized signals might be the right half of the AX-type signal and we can not observe the left half hidden behind the other larger signals of aromatic ring protons. Ab-

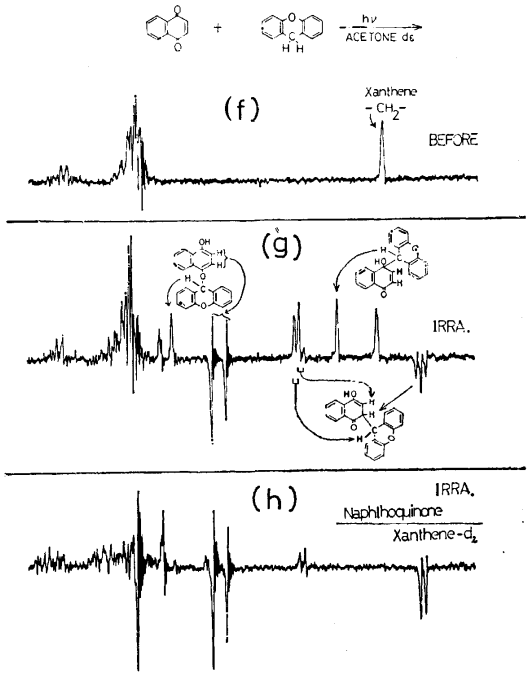

Fig. 4. PMR spectra observed in the photochemical reaction of 1,4-naphthoquinone with xanthene (solvent: CCl_4, 22 °C).
(f): before irradiation, (g): during irradiation,
(h): during irradiation, but with use of deuterated xanthene

7) We could not observe the polarized PMR signal in the combination reaction of two symmetrical radicals. G. L. Closs and A. D. Trifunac, *J. Amer. Chem. Soc.*, **92**, 2183, 2186 (1970); R. Kaptein and L. J. Oosterhoff, *Chem. Phys. Lett.*, **4**, 195, 214 (1969).

sorption polarized signal 5 may be assigned to methine proton of xanthene moiety in [III] and emission polarized signal 7 to methine proton of *p*-benzoquinone moiety in [III]. Rather weak absorption polarized signal 6 may be due to methine proton of xanthene moiety in [II]. Assignment of signal 6 to [II] can be deduced from a comparison of the polarized PMR signal observed in the photochemical reaction of anthraquinone with xanthene. In this case a sole strongly polarized absorption signal in the corresponding chemical shift region to signal 6 could be observed.[8] The assignments can be further supported by comparison of these results with those observed in the reaction of 1,4-naphthoquinone with xanthene (Fig. 4). PMR spectra (f), (g), and (h) were obtained in the photochemical reaction of 1,4-naphthoquinone with xanthene, (f) being observed before irradiation, and (g) during the course of irradiation. (h) was also observed during the course of irradiation, but in the reaction of 1,4-naphthoquinone with deuterated xanthene in the 9-methylene group. We see that (g) has quite the same pattern of signals as (b) (Fig. 2). Thus, we may assign the three structures described in (g) to the unstable intermediates. As in the photochemical reaction of *p*-benzoquinone, none of these intermediates accumulates in the reaction system, and we obtain only 1,4-dihydroxynaphthalene and bixanthyl as stable products.

Since only the products which are produced through radical mechanism can give such a polarized PMR signal, photochemical reduction process of *p*-quinones by xanthene can be summarized as follows. Photo-excited *p*-benzoquinone, probably in the triplet state, abstracts hydrogen atom from xanthene and forms

Possible structure of unstable intermediates

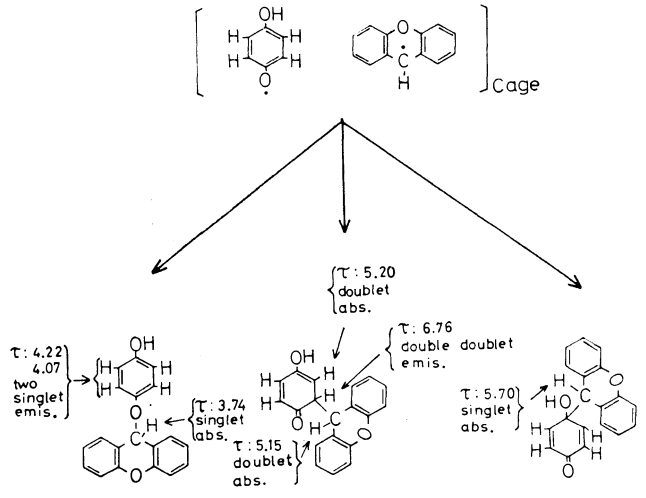

Reaction Scheme 1.

Possible structure of unstable intermediates

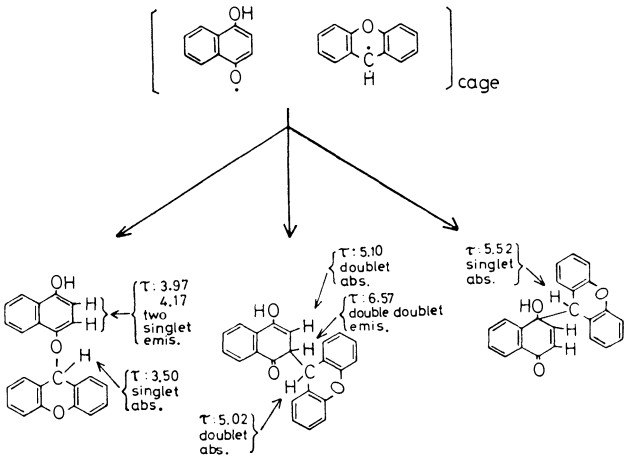

Reaction Scheme 2.

semiquinone radical and xanthyl radical in a solvent cage. These two radicals may combine in the solvent cage to form three unstable intermediates which finally decompose to solvent separated semiquinone radical and xanthyl radical (Reaction Schemes 1 and 2). Analogous examples which can be observed in photochemical reactions of methyl- or chloro-substituted *p*-quinones are shown in Figs. 5—8. From the PMR spectra observed in the reaction of 2,5-dimethyl-*p*-benzoquinone with xanthene (Fig. 5), we see that PMR signals in the chemical shift region of methyl proton undergo a strong nuclear spin polarization also. When the sample was irradiated in a NMR probe the corresponding numbers of polarized PMR signals 5, 6, 7, and 9 (Fig. 5 (b)) to methyl groups of stable or unstable products could be observed. Thus, the emission polarized signal 5 corresponds to methyl protons of 2,5-dimethylhydroquinone. Methyl protons of quinone themselves also show emission polarized signal. A more typical example of similar phenomena can be found in Fig. 6 (b) (signal 8) and Fig. 7 (b) (signal 8). The other three or more absorption polarized PMR signals 6, 7, and 9 (Fig. 5 (b)) can be observed in the

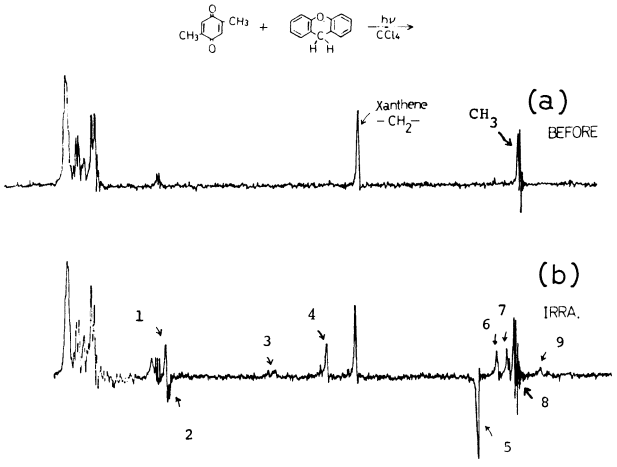

Fig. 5. PMR spectra observed in the photochemical reaction of 2,5-dimethyl-*p*-benzoquinone with xanthene (solvent; CCl_4, 22 °C).
(a): before irradiation, (b): during irradiation

8) From a consideration of their structures, [I], [II], and [III] should be so stable as to be isolated, but none of them accumulated in the photochemical reaction examined. Because of the higher polarity of the solvents used the unstable intermediates might be forced to decompose giving two radicals. In fact we were able to isolate the adducts which might be derived from similar reaction intermediates in the photochemical reaction of 2,3-dichloro- or 2,3-dibromo-1,4-naphthoquinone with xanthene dissolved in cold benzene.

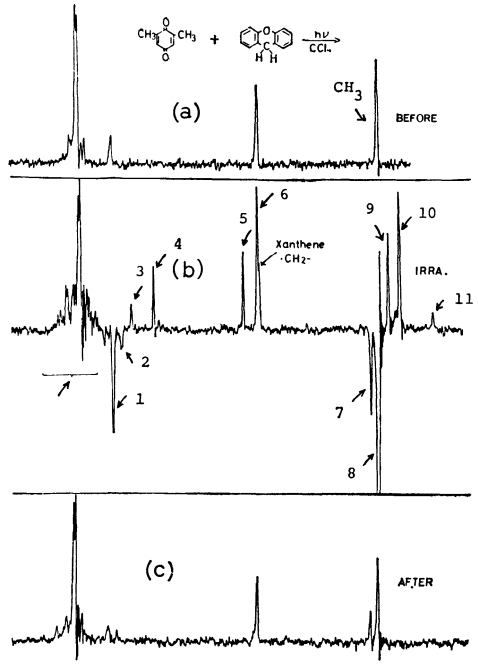

Fig. 6, PMR spectra observed in the photochemical reaction of 2,6-dimethyl-p-benzoquinone with xanthene (solvent; CCl_4, 22 °C).
(a): before irradiation, (b): during irradiation,
(c): after long irradiation (in this case irradiation was stopped)

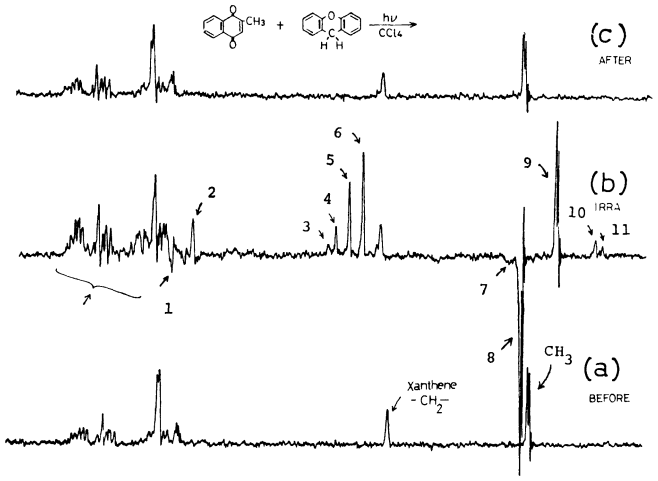

Fig. 7. PMR spectra observed in the photochemical reaction of 2-methyl-1,4-naphthoquinone with xanthene (solvent; CCl_4, 22 °C).
(a): before irradiation, (b): during irradiation,
(c): soon after irradiation (in this case irradiation was stopped)

methyl group region. The signals should be due to methyl protons of the unstable intermediates.

The emission polarized signal 1 in Fig. 6 (b) of the polarized PMR signals observed in the photochemical reaction of 2,6-dimethyl-p-benzoquinone with xanthene is due to the ring protons of quinone. The absorption polarized signals 3, 4, 5, and 6 in Fig. 6 (b) can be assigned to the unstable intermediates. They may be due to the methine proton of xanthene moiety having structures in which xanthene moiety attaches to the oxygen atom or carbonyl carbon. One of the two

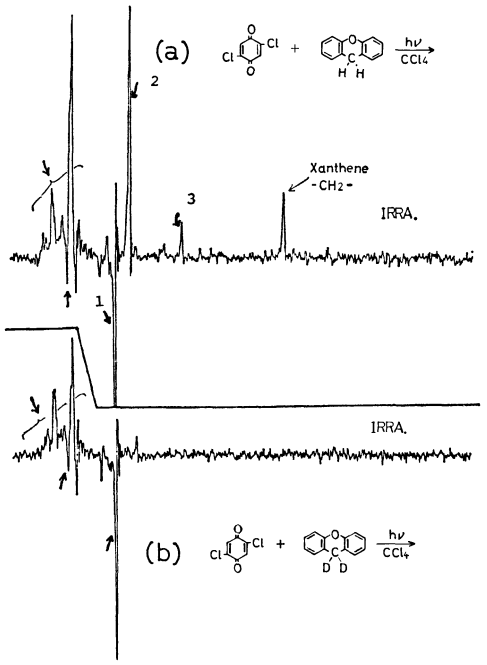

Fig. 8. PMR spectra observed in the photochemical reaction of 2,5-dichloro-p-benzoquinone with xanthene (solvent: CCl_4, 22 °C).
(a): during irradiation, (b): during irradiation, but with use of deuterated xanthene

emission polarized signals (signal 7 in Fig. 6 (b)] in methyl proton region corresponds to methyl group of 2,6-dimethylhydroquinone and the other (signal 8) to the methyl groups of quinone itself. The other three or the more absorption polarized signals 9, 10, and 11 (Fig. 6 (b)) are due to the methyl protons of the unstable intermediates. In Fig. 7 we find a quite analogous example in the photochemical reaction of 2-methyl-1,4-naphthoquinone with xanthene. Several groups of strongly polarized PMR signals containing the strong emission polarized signal 8 due to methyl protons of quinone can be observed. They correspond to the ring proton, the methine proton, and the methyl proton of quinone or xanthene moieties in methyl substituted hydroquinone or in unstable intermediates [signal 7 to CH_3 of hydroquinone, and signals 9, 10, 11 to CH_3's of unstable intermediates]. PMR spectra observed in the photochemical reaction of 2,5-dichloro-p-benzoquinone with xanthene are shown in Fig. 8. Both spectra (a) and (b) are observed during the course of irradiation, (b) being of the deuterated xanthene case. Thus, absorption polarized signals in (a) (signals 2 and 3) are assigned to methine proton of xanthene moiety of unstable active intermediates. Emission polarized signal 1 is due to the ring proton of 2,5-dichlorohydroquinone produced as a stable product.

We can thus decide the attaching position of xanthene moiety to p-quinone moiety to form the unstable intermediates. The positions are indicated by arrows as follows.

For example, 2-methyl-p-benzoquinone forms five unstable intermediates. It is interesting that almost all the possible intermediates having a different structure can be found.

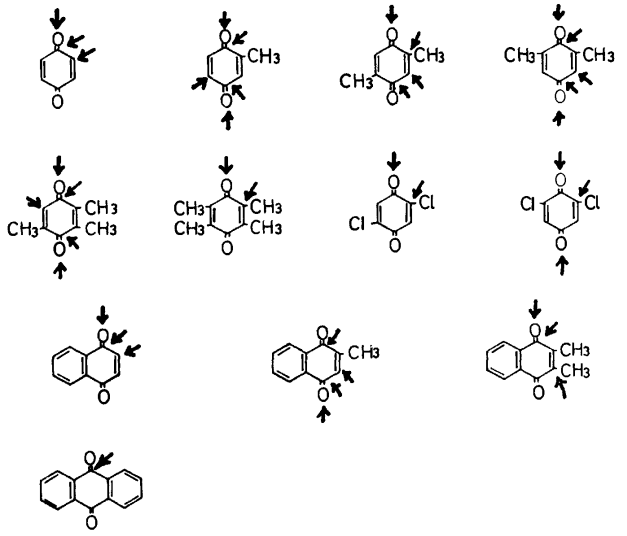

p-Quinone as a starting material, hydroquinone as stable product, and unstable intermediates can give the polarized PMR signal. However, no bixanthyl as the other stable reaction product and no xanthene as the other starting material in the photochemical reaction can give any polarized PMR signal. The photochemical reaction of *p*-quinones with xanthene in carbon tetrachloride or acetone is quite clean and gives only hydroquinones and bixanthyl as the stable reaction products. The photochemical reactions of *p*-quinones with xanthene can be formulated as follows.

$$Q[^0S] \xrightarrow{h\nu} Q[^1S] \longrightarrow Q[T]$$

$$Q[T] + R\text{-}H \longrightarrow [R\text{-}H\cdots Q] \longrightarrow [R\cdot,\cdot QH]_{cage}$$

$$R\text{-}H + Q \longleftarrow$$

$$[R\cdot,\cdot QH]_{cage} \rightarrow \underline{[\text{Unstable Intermediates}]} \rightarrow \cdot QH + R\cdot$$

$$2\cdot QH \longrightarrow \underline{Q} + \underline{QH_2} \qquad \downarrow$$

$$R-R$$

Q: *p*-Benzoquinones.
R-H···Q: Transition state.
·QH: Semiquinone Radicals.
QH_2: Hydroquinones.
The compounds underlined show the polarized signals.

The compounds underlined can show the polarized PMR signals. We can observe analogous polarized PMR signals in the photochemical reaction of *p*-quinones with the other hydrogen donors described above.

Experimental

Materials. Commercial *p*-quinones of guaranteed grade were purified by recrystallization or by sublimation.

TABLE 1. MELTING POINTS OF *p*-QUINONES

p-Quinones	Mp (°C)
p-Benzoquinone	111
2-Methyl-*p*-benzoquinone	66[a]
2,5-Dimethyl-*p*-benzoquinone	123—124[a]
2,6-Dimethyl-*p*-benzoquinone	71[a]
2,3,5-Trimethyl-*p*-benzoquinone	28[a]
2,3,5,6-Tetramethyl-*p*-benzoquinone	111—112
2,5-Dichloro-*p*-benzoquinone	161—162
2,6-Dichloro-*p*-benzoquinone	119
1,4-Naphthoquinone	125—126
2-Methylnaphthoquinone	104—105
Anthraquinone	286 (sub)[b]

a) Synthesized. b) Sublimed.

When not available, they were synthesized by oxidation of the corresponding phenols with Fremy's salt.[9]

CIDNP Examination. A typical CINDP examination of the photochemical reaction is as follows: a suitable amount of *p*-quinone ($\sim 10^{-2}$—10^{-3} M) and xanthene were dissolved (or suspended) in suitable solvents such as carbon tetrachloride, acetone-d_6, or benzene-d_6[10] in a NMR sample tube made of usual glass.

The sample was irradiated by a 500 W high pressure mercury arc lamp and PMR spectra were observed before, during, and after irradiation. A 60 MHz NMR spectrometer manufactured by JEOL was used.

Products. Photochemical reactions of *p*-quinones with xanthene are so smooth and clean that hydroquinones produced are in general separated out in the sample tube within a few minutes. The same photochemical reactions were examined in a macro scale using a test tube as reaction vessel. The sample was irradiated by a 400W high pressure mercury arc lamp through 10 cm thick of water layer. When the color of *p*-quinone had faded completely, the volume of the sample was reduced to 2~3 ml, and hydroquinone and bixanthyl were separated by short Florisil (100~200 mesh) column. Melting points of hydroquinones produced were: hydroquinone, 170 °C; 2-methylhydroquinone, 126—127 °C; 2,5-dimethylhydroquinone, 217 °C; 2,6-dimethylhydroquinone, 149—151 °C; 2,3,5-trimethylhydroquinone, 168—170 °C; 2,3,5,6-tetramethylhydroquinone, 233 °C; 2,5-dichlorohydroquinone, 170 °C; 2,6-dichlorohydroquinone, 164 °C; 1,4-dihydroxynaphthalene, 173 °C; 2-methyl-1,4-dihydroxynaphthalene, (decn. < 100 °C). Melting point of bixanthyl, 208—209 °C.

9) H. J. Teuber and G. Staiger, *Chem. Ber.*, **88**, 802 (1955); H. J. Teuber and H. H. Dietz, *Angew. Chem. Internat. Edn.*, **4**, 871 (1965).

10) Photochemical reactions of *p*-quinone with xanthene are so fast that the solvents do not interfere with the photochemical reactions.

Structural Studies of Tryptophan Metabolites by X-ray Diffraction Method. I. The Crystal and Molecular Structure of 5-Hydroxy-DL-Tryptophan

Akio WAKAHARA, Masaru KIDO, Takaji FUJIWARA, and Ken-ichi TOMITA

Faculty of Pharmaceutical Sciences, Osaka University, Toneyama, Toyonaka, Osaka 560

(Received December 18, 1972)

5-Hydroxy-DL-tryptophan was crystallized from a methanol solution in the monoclinic space group C2/c, with cell-dimensions of $a=16.765$, $b=5.892$, $c=20.887$ Å, and $\beta=92.06°$. The molecular structure and stereoconfiguration have been elucidated by the direct method for non-primitive space group. A Fourier map, calculated with the largest 198 normalized structure factors as Fourier coefficients, revealed the whole structure which was refined by the least-squares method. The molecule is a zwitterion as in the crystal structure of amino acids, each amino nitrogen atom having an extra proton. The indole ring plane forms a dihedral angle of 40° with that formed by an acid group. With respect to the conformation about the C(α)–C(β) bond, the orientation of C(β)–C(γ) bond is *trans* with respect to the C(α)–COO$^-$. The molecules are arranged in double layers parallel to the *ab*-plane. The layer by polar groups is held together by a series of hydrogen bonds in a three-dimensional network, and by non-polar groups in the other layer, indole rings being stacked by van der Waals forces. The D- and L-forms of 5-hydroxytryptophan are hydrogen-bonded into two types of dimer related by the center of symmetry, one through N–H···O, and the other through O–H···O hydrogen bonding.

5-Hydroxytryptophan (5-HTP) was found as a precursor of 5-hydroxytryptamine (serotonin) in a metabolic pathway of tryptophan.[1-3] In animal tissues 5-HTP is decarboxylated to serotonin,[4] a similar reaction being observed between tryptophan and tryptamine.[5] Bell and Fellows have isolated 5-HTP as a free plant amino acid from seeds of *Griffonia simplicifolia*.[6] X-ray structure determination of tryptophan has been made by several authors because of its biochemical importance. With the exception of tryptophan hydrochloride,[7] their attempts did not succeed due to the difficulty of obtaining a good single crystal.[8-10] The pharmacological action of 5-HTP is also of interest, because of the fact that 5-HTP has excellent radiation protective ability.[11-13] Sano recently showed that 5-HTP is most effective for medical treatment of endogenous depression.[14] As a part of a programme of studies on the crystal and molecular structures of tryptophan metabolites, we performed the structure analysis on 5-hydroxy-DL-tryptophan. A preliminary result has been reported.[15] Refinement based on the three-dimensional photographic data has now been completed.

Experimental

5-Hydroxy-DL-tryptophan (Sigma Chemical Co.) was dissolved in methanol at room temperature and kept at 5 °C. Crystals were very thin colourless laths elongated parallel to the b-axis. Recrystallization of the commercial sample was extremely difficult. The crystal used for the determination of unit-cell parameters and for the collection of intensity data had dimensions of the order $0.03\times0.06\times0.75$ mm. Approximate lattice parameters were determined from oscillation and Weissenberg photographs taken around the b-axis, and were later refined by the precise measurement of the 2θ angles for 8 reflections on a Rigaku Denki manual four circle diffractometer. The systematic extinctions showed that the space group was either C2/c or Cc. From the distribution of the normalized structure magnitudes, a centro-

TABLE 1. CRYSTAL DATA OF 5-HYDROXY-DL-TRYPTOPHAN

$C_{11}H_{12}N_2O_3$, M.W. 220.23
colorless and transparent needles, Monoclinic
$a=16.765(9)$, $b=5.892(4)$, $c=20.887(9)$ Å
$\beta=92.06(4)°$
$V=2074.2$ Å^3, $Z=8$, $F(000)=928$
μ(for CuKα) $=10.0$ cm^{-1}
$D_m=1.405$ g/cm^3, $D_x=1.408$ g/cm^3
Absent spectra; (kkl) : $h+k=2n+1$
$(h0l)$: $l=2n+1$
Space group; C2/c

TABLE 2. STATISTICAL AVERAGES

	Experimental	Centrosymmetric	Noncentrosymmetric
$\langle\|E\|\rangle$	0.733	0.798	0.886
$\langle\|E^2-1\|\rangle$	0.962	0.968	0.736
$\langle\|E\|^2\rangle$	1.000	1.000	1.000

1) S. Udenfriend, C. T. Clark, and E. Titus, *J. Amer. Chem. Soc.*, **75**, 501 (1953).
2) C. Mitoma, H. Weissbach, and S. Udenfriend, *Nature*, **175**, 994 (1955).
3) S. Udenfriend, E. Titus, H. Weissbach, and R. E. Peterson, *J. Biol. Chem.*, **219**, 335 (1956).
4) C. T. Clark, H. Weissbach, and S. Udenfriend, *J. Biol. Chem.*, **210**, 139 (1954).
5) H. Weissbach, W. King, A. Sjoerdsma, and S. Udenfriend, *J. Biol. Chem.*, **234**, 81 (1959).
6) E. A. Bell and L. E. Fellows, *Nature*, **210**, 529 (1966).
7) T. Takigawa, T. Ashida, Y. Sasada, and M. Kakudo, This Bulletin, **39**, 2369 (1966).
8) B. Dawson and A. Mathieson, *Acta Crystallogr.*, **4**, 475 (1951).
9) B. Khawas and G. S. R. Krishna Murti, *Indian J. Phys.*, **42**, 175 (1968).
10) B. Khawas and G. S. R. Krishna Murti, *Acta Crystallogr.*, **B25**, 1006 (1969).
11) S. Kobayashi, W. Nakamura, and H. Eto, *Int. J. Radiat. Biol.*, **11(5)**, 505 (1966).
12) Z. Deanovic and Z. Supek, *Iugoslav. Physiol. Pharmacol. Acta*, **3(2)**, 137 (1967).
13) H. Langendorff, M. Langendorff, and C. Streffer, *Strahlentherapie*, **135**, 452 (1968).
14) I. Sano, *Münch. Med. Wschr.*, **114(40)**, 1713 (1972).
15) A. Wakahara, M. Kido, T. Fujiwara, and K. Tomita, *Tetrahedron Lett.*, **1970**, 3003.

symmetric space group C2/c was chosen as the correct space group. The crystal and physical data are given in Table 1. Intensity data were recorded on equi-inclination Weissenberg films of *h0l* to *h4l* zones, for a crystal rotating about the b-axis, using Cu$K\alpha$ radiation. Intensities were estimated visually by comparison with a calibrated film strip. These were corrected for spot size, Lorentz and polarization factors. Intensity data of 1084 non-zero reflections were then adjusted to the absolute scale and normalized structure factor E, and $\sum_2$ lists were computed. The statistical averages in Table 2 confirm that the crystal is centro-symmetric.

Determination and Refinement of the Structure

Phases for 5-hydroxy-DL-tryptophan were determined by means of the symbolic addition procedure by Hauptman and Karle. To specify the origin for non-primitive space group C2/c, two structure factors of large magnitude having linearly independent vectors were assigned as having positive signs.[16] Three other reflections whose signs were specified by symbols a, b, and c were chosen among reflections with many $\sum_2$ interactions. This starting set is shown in Table 3. By hand calculation, the phases of additional 193 reflections were determined in terms of the starting signs and letters. The three dimensional E-map, computed with the assignments a=b=c=−, revealed high peaks corresponding to each atom in the molecule.

TABLE 3. STARTING SET FOR SYMBOLIC ADDITION PROCEDURE

h	k	l	Phase	$\|E\|$
3	3	17	+	2.88
8	2	−17	+	2.84
1	3	16	a	4.23
8	2	−14	b	3.61
7	1	−18	c	2.93

The map has no spurious peaks of density greater than that of the 16 non-hydrogen atoms. None of the phases was subsequently found to be incorrect when compared with the phase corresponding to the fully refined structure. The positional coordinates of the sixteen atoms as selected from the E-map were subjected to the structure factor calculation and the three-dimensional Fourier synthesis. At this stage, the discrepancy factor $R=\sum||F_o|-|F_c||/\sum|F_o|$ was 0.32. The structure was refined by successive Fourier syntheses and least-squares method based on only the observed non-zero reflections; using the isotropic thermal parameters for all the nonhydrogen atoms, the R index converged to 0.20 after 5 cycles. The difference synthesis was then computed to obtain the hydrogen atoms. The peaks of the twelve hydrogen atoms clearly appeared on this map, where their heights are within the range 0.3—0.8 e.Å^{-3}. It was confirmed that the molecule of 5-hydroxy-DL-tryptophan exists as a zwitterionic form in crystalline state. The block-diagonal approximation was used for the least-squares refinement. This refinement proceeded including these hydrogen atoms and applying the anisotropic temperature factors for nonhydrogen atoms. Since the shifts in the positional parameters in the final cycle were less than one tenth of the estimated standard deviations, the refinement was terminated at this stage. It was thought that the unfavorable shape of the crystal resulted in a rather high R factor of 0.119. Observed and calculated structure factors from the last cycle are given in Table 4, and the atomic coordinates and thermal parameters with their estimated standard deviations in Table 5. Overall isotropic temperature factor for hydrogen atoms was also refined, the final value being 2.2 Å^2. A difference Fourier map synthesized with the phases by only heavy atom contributions and the final electron density map for the heavy atoms are illustrated in Fig. 1.

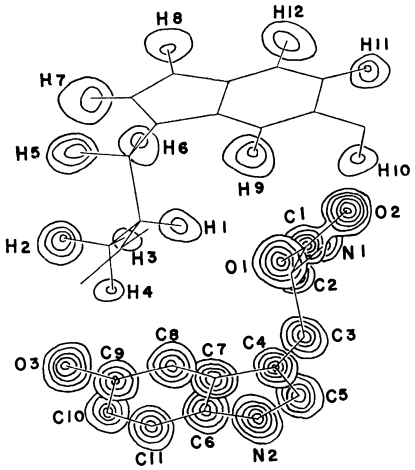

Fig. 1. Superimposed three-dimensional electron-density distribution for the heavy atoms (the lower half) and the hydrogen atoms (the upper half), viewed along the b-axis; contours at intervals of 2 e.Å^{-3} for the heavy atoms, and 0.2 e.Å^{-3} for the hydrogen atoms.

All the numerical calculations were carried out on an NEAC 2200-500 computer of this University, a HITAC 5020 E in the computing center, the University of Tokyo, and a FACOM 230-60 in the data processing center, Kyoto University, using the programs written by Dr. Tamaichi Ashida and by the authors.

Description and Discussion of the Structure

Bond Lengths and Angles. The bond distances and valency angles in the molecule are shown in Fig. 2; the average standard deviations are about 0.012 Å for bonds and 0.8° for angles. The average of six C–C bond lengths in the six-membered ring is 1.382 Å, while that of C–N bonds in the five-membered ring is 1.384 Å. The C(10)—C(11) bond (1.352 Å) is significantly shorter than the mean value taken from other indole derivatives, such a short distance being found only in 5-methoxy-(*N*,*N*)-dimethyltryptamine hydrochloride (1.360 Å).[17] As expected, the molecule is a zwitterion, with an amino nitrogen atom accepting a proton from an acid group and assuming the tetrahedral configuration C–NH_3^+. The value

16) H. Hauptman and J. Karle, *Acta Crystallogr.*, **12**, 93 (1959).

17) G. Falkenberg and D. Carlström, *ibid.*, **B27**, 411 (1971).

TABLE 4. OBSERVED AND CALCULATED STRUCTURE AMPLITUDES FOR 5-HYDROXY-DL-TRYPTOPHAN

The columns in each group headed by the values of h and k give l, $10|F_o|$, and $10|F_c|$.

L	FO	FC	L	FO	FC	L	FO	FC	L	FO	FC	L	FO	FC	L	FO	FC	L	FO	FC	L	FO	FC	L	FO	FC
H,K=	0	0	8	49	-49	0	95	-86	6	11	9	5	35	-33	2	4	-4	16	93	-96	12	41	-56	-3	4	-4	-2	28	-22
4	41	-34	10	18	-22	1	8	7	8	8	7	6	54	45	3	32	-25	17	45	-42	15	36	-32	-4	25	-27	-3	19	-19
6	283	320	18	45	-33	2	6	-7	12	28	26	7	21	27	4	44	48	18	14	18	18	13	-8	-5	9	-10	-4	12	17
8	88	82	-2	7	6	3	23	-25	14	13	11	8	65	64	6	18	-17	19	30	25	21	7	-8	-13	3	-2	-5	30	-33
10	48	41	-4	30	26	4	41	-44	15	30	27	9	67	-60	7	35	-42	21	10	13	-1	13	-12	H,K=	19	3	-6	28	-22
12	59	-52	-6	26	-23	5	62	-69	16	14	10	10	64	-59	8	13	-16	22	66	-71	-2	26	25	0	6	-7	-8	35	-27
14	33	27	-12	36	-25	7	22	-22	21	23	23	11	33	-30	10	14	-18	23	15	-20	-3	9	-12	1	11	-12	-10	45	45
16	61	-56	-14	43	37	8	30	-29	-1	13	-10	12	71	60	11	18	19	-1	11	5	-4	21	-17	2	6	-8	-11	22	-18
18	39	30	-18	37	-29	9	35	-37	-2	30	-25	13	33	34	13	16	-18	-2	6	-5	-5	26	26	3	6	-6	-12	24	-17
20	43	40	H,K=	14	0	10	29	-28	-3	35	-29	14	52	45	14	37	-31	-3	67	59	-6	62	55	4	11	12	-15	14	12
22	15	-15	0	40	-42	11	49	-54	-4	21	-19	15	37	-33	15	35	25	-4	79	-76	-7	27	-28	5	11	-11	-16	12	10
26	13	18	2	32	29	12	15	18	-5	21	-19	16	57	-57	16	59	-52	-6	66	-52	-8	49	-59	-1	9	-7	-18	33	-28
H,K=	2	0	4	58	68	13	33	-26	-7	23	20	18	21	-21	17	24	19	-14	38	29	-9	13	-17	-5	7	-9	-20	2	2
0	78	-92	6	61	-59	19	20	-17	-8	17	15	19	24	22	19	20	-17	-8	43	-30	-10	34	-31	H,K=	0	4	H,K=	8	4
2	98	107	10	37	36	20	20	19	-10	41	-35	24	37	-40	20	10	-6	-9	58	50	-11	31	28	2	20	22	0	25	-22
4	87	99	12	43	-40	23	22	30	-13	39	34	-1	17	-14	21	27	25	-10	28	-19	-12	15	12	4	8	10	1	19	-19
6	30	-20	14	34	-35	-1	21	-15	-14	19	16	-2	38	-31	22	16	-15	-11	15	11	-13	10	-11	5	9	4	2	6	8
8	65	63	-2	29	28	-2	43	-44	-15	24	24	-3	48	-45	23	13	12	-12	46	-35	-14	62	-63	6	19	-14	3	15	-9
10	21	13	-8	68	-70	-3	6	-7	-18	23	22	-4	131	-135	-1	14	16	-13	24	16	-16	36	-33	7	37	-35	4	27	26
12	70	61	-10	64	-65	-4	46	42	-20	21	-24	-5	74	-66	-2	68	73	-14	52	-42	-17	11	15	8	21	21	5	12	14
14	55	43	-12	40	30	-5	7	8	-23	12	-14	-6	92	-86	-3	32	-25	-18	23	-16	-18	34	-16	9	19	-20	6	28	-28
16	39	37	-14	64	-59	-7	8	-9	H,K=	13	1	-7	9	10	-4	17	-19	-23	19	-26	-19	12	-7	10	28	25	7	10	13
18	18	18	-16	64	-71	-8	24	-14	0	47	51	-8	57	51	-6	68	-64	-24	23	-23	-21	22	24	11	29	23	8	21	21
24	29	29	H,K=	16	0	-9	34	-29	1	32	-25	-10	54	-40	-7	15	15	H,K=	3	3	H,K=	9	3	12	41	-40	12	10	-3
-2	104	111	0	38	28	-10	56	-62	2	43	-40	-11	42	-43	-8	36	-35	0	44	-44	0	15	12	13	8	6	16	25	-16
-4	51	-46	2	39	35	-11	28	-19	3	18	15	-12	41	-39	-9	11	-10	1	10	-13	1	8	5	14	14	13	17	23	-22
-6	97	-89	4	38	-39	-12	35	32	4	37	-29	-13	9	11	-10	14	-14	2	29	26	3	28	28	15	31	-26	18	3	5
-8	24	21	8	18	22	-13	16	-14	5	39	-31	-14	28	24	-11	52	55	3	17	12	4	44	-50	18	18	-14	-1	15	18
-10	48	-39	-2	37	-34	-14	16	17	7	33	-30	-15	22	21	-12	28	-24	4	15	-11	7	14	17	19	32	26	-2	48	56
-12	74	-61	-12	16	-15	-15	24	-26	9	14	17	-16	35	38	-14	91	-101	5	10	-13	9	26	21	20	33	40	-3	29	-28
-14	82	-83	H,K=	18	0	-16	63	-60	10	19	-19	-17	11	12	-15	36	-33	6	22	21	10	28	-28	21	6	-6	-4	17	-17
-18	35	36	2	21	17	-17	28	-24	12	45	-53	-18	33	38	-16	21	-22	7	10	-12	11	13	-16	H,K=	2	4	-5	57	-61
-20	49	-54	-4	29	22	-20	37	-30	13	25	-24	-23	20	17	-17	58	61	8	19	15	16	24	-22	0	12	5	-6	21	-20
-24	33	31	-6	31	23	-26	41	-42	14	17	19	-24	19	18	-19	16	15	9	32	28	17	20	-17	1	19	12	-8	43	43
H,K=	4	0	-8	42	33	H,K=	7	1	18	23	-25	-25	21	30	-20	34	-33	10	17	16	18	13	-13	2	38	45	-9	11	-10
0	209	-235	-10	14	14	0	42	36	-1	55	-56	H,K=	4	2	-21	29	-32	11	41	35	-1	10	-14	3	33	-40	-11	32	-32
2	206	-219	-14	22	20	1	65	71	-2	12	-13	0	8	7	-23	13	17	12	47	41	-2	32	-24	5	38	-43	-12	29	21
4	87	-102	H,K=	20	0	2	11	9	-4	26	-25	1	45	41	H,K=	10	2	13	31	-26	-3	12	-14	6	14	-14	-13	14	-12
6	123	-149	0	13	10	3	46	-46	-6	35	32	2	37	32	0	28	-19	14	30	20	-4	60	-64	7	28	24	-17	17	19
8	116	-130	-6	38	37	4	38	-35	-7	35	-28	3	2	1	2	25	19	15	41	35	-5	35	-39	8	2	1	-18	31	37
10	88	-97	H,K=	1	1	6	72	-82	-8	19	-20	4	43	41	3	19	-17	16	13	14	-6	35	-30	9	9	-9	-15	8	-7
12	51	-49	1	59	-67	8	40	39	-9	19	-20	6	42	51	4	16	-16	17	57	53	-8	26	22	10	3	-2	-20	16	14
14	9	6	2	61	65	9	51	-56	-15	24	-21	8	42	47	5	9	-10	19	37	-36	-9	36	-36	11	11	-11	H,K=	10	4
-4	76	-60	3	231	216	10	14	17	-18	32	-39	9	36	-35	6	30	-37	23	29	28	-10	59	-62	13	25	21	0	13	-16
-6	51	-38	4	198	208	12	49	-54	-21	27	-30	10	28	26	8	15	-17	24	5	-8	-11	65	-73	14	28	-20	1	17	21
-8	61	44	5	49	50	14	13	-13	H,K=	15	1	11	42	-36	18	25	-22	-1	56	-60	-12	55	-60	15	28	22	2	16	10
-16	25	19	6	187	-193	15	31	-30	1	24	20	12	19	18	-2	34	-28	-2	85	-99	-16	16	-20	17	24	21	3	12	11
-18	40	-33	7	62	-51	18	28	28	3	19	-24	14	37	32	-4	15	-12	-3	8	9	-17	37	-36	19	16	-19	4	37	36
-20	54	-54	8	13	-15	22	32	-37	6	19	14	15	35	-26	-5	37	36	-4	6	-2	-18	14	-15	20	32	-37	5	23	-20
-22	32	-30	9	75	70	24	32	32	7	30	34	16	57	53	-6	17	20	-5	34	24	-22	10	9	21	8	7	6	8	9
-26	23	-24	10	129	109	-1	40	30	8	20	20	17	45	-34	-7	36	39	-6	27	-17	H,K=	11	3	22	26	34	10	32	38
H,K=	6	0	12	56	-56	-2	43	-42	9	13	-18	20	26	-22	-9	31	24	-7	31	-25	0	31	-30	-1	28	-29	11	8	-5
2	109	-122	13	31	-23	-3	10	9	10	23	-26	22	33	34	-10	37	-33	-8	33	-23	1	26	-26	-2	13	6	12	40	32
4	64	-67	14	22	-17	-4	37	-30	13	21	17	23	25	-34	-11	22	21	-9	2	-1	4	32	-31	-3	25	-23	13	13	-17
8	41	-31	15	31	-26	-5	134	120	15	15	-14	24	27	27	-13	41	44	-10	5	8	5	21	24	-4	16	12	15	26	-19
10	50	-50	16	12	-18	-6	40	34	16	23	-25	-1	42	39	-16	29	-26	-11	12	16	6	30	-35	-5	30	26	16	20	12
12	73	-85	17	23	-16	-7	47	45	17	16	-20	-2	3	2	-22	19	-21	-13	24	26	7	26	-33	-6	27	20	-1	45	-47
16	21	13	20	20	16	-8	9	-8	-1	14	-11	-3	51	45	H,K=	12	2	-14	52	49	9	16	-20	-7	37	32	-3	15	15
18	64	-47	21	27	-38	-10	19	18	-2	58	59	-4	29	25	0	30	-34	-16	59	63	10	26	-25	-8	41	31	-4	8	6
20	22	-16	25	23	27	-11	54	56	-3	24	-32	-5	54	45	1	10	10	-17	11	-12	11	14	18	-9	20	15	-5	29	23
-2	81	79	-1	38	-33	-12	33	-24	-5	19	-19	-6	44	38	7	27	27	-18	11	11	12	8	-8	-10	6	2	-6	12	-14
-4	85	82	-2	30	24	-13	19	18	-6	58	-60	-8	7	8	8	43	-45	-20	34	29	13	30	-21	-11	15	15	-7	48	-48
-6	78	-70	-3	161	147	-14	31	28	-7	19	-20	-9	31	27	9	22	23	-22	29	36	14	11	11	-13	31	19	-8	8	-9
-8	75	65	-4	54	-49	-15	6	-7	-8	36	32	-10	23	21	15	35	28	-23	7	-5	15	12	-15	-15	24	25	-10	16	14
-10	84	92	-5	49	-42	-16	23	24	-11	27	-24	-12	46	43	16	15	15	H,K=	5	3	-2	20	-15	-16	14	14	-11	11	-9
-12	27	-24	-6	138	139	-18	71	-71	-12	27	-27	-13	22	-24	17	14	-16	1	45	-47	-3	14	20	-17	14	11	-15	18	-17
-14	26	20	-7	85	-87	-20	42	49	-13	18	-18	-14	34	35	18	9	11	2	54	53	-4	15	18	-18	22	20	-16	13	17
-16	49	-40	-8	58	-58	-21	18	19	H,K=	17	1	-15	7	6	-3	15	-17	3	33	-32	-6	10	13	-20	13	-11	-17	17	-23
-18	28	-21	-9	14	12	-22	36	38	10	16	-16	-16	64	66	-4	81	95	4	33	34	-7	46	-43	-22	11	-12	-18	23	28
-22	67	-72	-10	33	-31	-23	21	-28	12	20	15	-18	21	25	-9	14	-13	5	13	12	-8	37	39	H,K=	4	4	-19	26	28
-24	28	29	-11	9	10	-24	27	-37	-14	13	-15	-19	17	-21	-10	57	58	6	11	10	-13	39	-39	0	9	8	H,K=	12	4
H,K=	8	0	-12	63	71	H,K=	9	1	-15	15	18	-22	42	46	-11	12	-10	7	9	11	-14	34	32	1	23	-24	1	4	1
0	19	14	-13	34	-27	0	44	41	H,K=	19	1	-25	16	-16	-12	15	14	8	11	11	H,K=	13	3	2	32	-37	3	9	-12
2	53	44	-14	47	-44	1	35	-33	1	11	12	H,K=	6	2	-14	26	21	10	24	28	0	19	19	4	23	-25	4	23	-24
4	4	4	-15	33	-27	2	39	40	2	14	-14	0	99	99	-17	19	-18	13	49	36	1	32	29	5	28	32	5	25	26
6	68	70	-17	37	30	3	28	27	3	11	13	1	43	38	-19	22	-18	14	55	-43	2	25	-28	6	26	27	-1	45	47
8	68	66	-18	34	31	5	28	29	4	3	-2	2	34	30	H,K=	14	2	15	22	19	3	11	12	7	31	-35	-2	45	-46
12	82	89	-20	32	27	6	22	14	5	15	15	3	43	36	1	37	-47	16	53	47	4	17	18	9	19	18	-3	11	12
14	19	16	-21	19	-22	7	14	-13	8	11	-14	4	36	32	15	28	-24	17	28	-23	6	17	20	10	44	-56	-8	33	-31
16	24	-22	-25	13	15	8	24	18	-1	16	22	5	20	-19	-1	24	-23	18	30	26	8	22	-18	11	53	48	-10	23	-23
18	44	41	-26	26	31	9	16	17	-3	11	11	6	78	103	-2	26	23	19	28	24	-1	25	27	12	17	13	-12	9	5
-2	38	-30	H,K=	3	1	10	38	40	-5	16	13	7	16	15	-3	16	18	20	24	24	-2	39	38	13	33	-25	-13	25	-32
-6	21	16	0	19	-17	11	27	30	-7	15	17	8	12	-8	-5	45	-56	21	15	15	-4	32	30	14	37	33	-14	12	14
-8	76	-70	1	34	26	12	13	14	-10	18	19	9	22	23	-6	33	37	22	17	17	-5	34	30	15	11	10	-15	7	3
-10	21	15	2	50	48	13	13	16	H,K=	1	1	17	42	34	-7	41	-45	-1	17	15	-6	11	14	16	14	-16	-16	20	-25
-12	81	78	3	51	48	14	24	-20	-4	16	21	18	21	-16	-9	24	23	-2	26	21	-7	45	43	17	29	25	-17	14	12
-14	50	-39	4	12	12	15	19	18	H,K=	0	2	20	33	33	-11	20	-18	-3	32	-26	18	15	17	-3	9	1	H,K=	14	4
-16	62	50	5	34	29	16	24	18	2	90	-98	21	34	-32	-12	39	46	-4	91	91	-10	47	52	-4	31	-25	1	13	13
-20	60	55	7	38	35	17	20	13	3	101	93	23	20	23	-13	19	-17	-5	41	-38	-11	8	6	-5	32	25	10	26	-14
-24	36	-39	8	38	-39	19	23	18	4	88	-80	-1	23	-19	-18	15	-18	-6	40	30	-12	15	-13	-6	27	27	11	8	-5
H,K=	10	0	10	9	7	20	17	-16	5	31	25	-2	75	75	H,K=	16	2	-7	11	10	-13	33	31	-9	6	4	12	20	-12
0	61	-57	11	13	-11	22	16	21	6	70	-63	-3	45	40	13	19	-17	-8	23	14	-16	26	30	-10	34	-31	-1	19	18
4	58	51	12	42	35	-1	42	34	7	33	-29	-4	61	53	-2	33	-37	-9	10	-6	-18	36	-40	-11	52	49	-3	16	15
6	13	12	16	8	7	-3	58	58	8	56	-51	-5	13	-12	-4	16	-17	-10	23	14	H,K=	15	3	-12	8	11	-4	9	10
10	46	46	17	18	-15	-4	30	-28	9	139	136	-6	22	-24	-5	21	17	-11	16	18	0	16	14	-13	13	15	-5	14	14
12	50	54	20	20	-19	-7	43	41	10	53	49	-7	34	-27	H,K=	18	2	-12	48	51	1	32	33	-17	23	15	-7	14	15
14	28	25	26	22	-23	-8	44	43	11	39	34	-8	12	-13	0	15	-14	-13	32	34	6	24	20	-20	32	-41	-8	22	-20
18	17	12	-1	17	15	-9	58	59	12	75	-74	-9	25	22	1	18	19	-14	53	51	7	22	21	-21	6	-8	-12	8	6
20	31	24	-2	71	-77	-10	11	7	13	46	-43	-10	45	39	-1	11	14	-17	16	20	8	24	22	-22	16	-13	-13	11	11
-2	36	-29	-3	31	30	-11	17	14	14	54	-54	-11	49	-46	-2	21	-24	-18	18	19	-5	22	19	H,K=	6	4	-14	18	-20
-4	34	-23	-4	29	24	-15	31	21	15	61	54	-12	28	-28	-5	18	20	-19	40	41	-6	11	-9	1	15	14	-15	9	-15
-6	29	-23	-5	60	-60	-16	37	32	16	7	7	+13	52	-51	H,K=	1	3	-24	11	10	-9	14	16	2	49	-54	H,K=	16	4
-8	9	-11	-6	77	77	-17	30	25	18	31	-25	-15	16	16	1	33	-37	H,K=	7	3	-10	3	3	3	17	16	0	10	15
-10	45	34	-7	57	-46	-18	42	35	19	34	-28	-16	31	-23	2	17	-15	0	74	81	-12	18	17	4	35	-35	7	16	-14
-12	29	25	-8	11	10	-19	39	-34	20	16	-21	-17	37	-35	3	18	12	1	30	23	-13	12	-15	5	16	-18	-2	15	17
-14	21	20	-9	43	-36	-20	13	-11	21	11	13	-18	8	-7	4	55	48	2	20	17	-14	15	-18	6	11	16	-12	11	-8
-16	72	81	-10	45	-37	-23	29	36	22	36	-34	-19	33	-26	5	19	-18	4	40	43	H,K=	17	3	7	27	35	H,K=	18	4
-18	53	54	-11	82	-87	-24	15	16	25	7	-7	-21	22	22	6	11	-13	5	23	24	0	9	-7	8	38	-43	1	18	-19
-22	35	42	-13	35	-36	H,K=	11	+1	H,K=	2	2	-22	20	-21	7	7	-9	6	5	-10	1	22	-21	9	35	45	-2	10	-10
-24	9	14	-14	36	33	0	18	-15	0	51	-46	-23	9	-12	9	26	-23	7	12	10	2	9	-10	10	12	-12	-5	11	-10
H,K=	12	0	-15	24	-22	1	40	-35	1	36	-32	-24	26	26	10	8	6	8	23	23	3	11	-10	13	11	9			
2	33	-33	-17	46	-45	2	15	18	2	5	-3	H,K=	8	2	11	45	-40	9	13	-12	7	17	-17	14	16	-14			
4	24	22	-22	19	-24	3	32	-26	3	53	-57	0	37	-29	12	46	42	10	31	37	9	7	-9	15	11	12			
6	46	43	H,K=	5	1	5	11	-7	4	47	-47	1	42	-45	13	45	42	11	26	30	-2	22	-19	20	10	13			

of 1.491 Å for the C(2)—N(1) bond length is in good agreement with the average value, C–N$^+$ = 1.487 Å, for α-amino acids.[18] In the ionized carboxyl group, the two C–O distances differ significantly, and C(1)–O(2) bond length (1.283 Å) is somewhat longer than that usually observed in many COO$^-$ groups. This might be explained by the fact that the O(2) atom is an acceptor of two short hydrogen bondings. The angle C(α)–C(β)–C(γ) is significantly larger than the tetrahedral value, the value 114.9° being very close to a mean angle of 114° of the examined 27 compounds.[19]

Planarity of the Molecule. As far as tryptophan derivatives are concerned, the conformation of a molecule as a whole can be well described in the two

18) R. E. Marsh and J. Donohue, *Advan. Protein Chem.*, **22**, 235 (1967).

19) G. N. Ramachandran and A. V. Lakshminarayanan, *Biopolymers*, **4**, 495 (1966).

Table 5. Fractional coordinates and thermal parameters with standard deviations ($\times 10^4$)
The anisotropic temperature factors are in the form of $\exp[-(B_{11}h^2+B_{22}k^2+B_{33}l^2+B_{12}hk+B_{13}hl+B_{23}kl)]$.

Atom	x	y	z	B_{11}	B_{22}	B_{33}	B_{12}	B_{13}	B_{23}
C (1)	0.3793 (4)	0.7124 (15)	0.0032 (3)	0.0014 (3)	0.0079 (33)	0.0005 (1)	−0.0025 (14)	0.0004 (3)	0.0016 (10)
C (2)	0.3568 (5)	0.4858 (15)	0.0339 (3)	0.0021 (3)	0.0074 (33)	0.0004 (1)	−0.0002 (15)	0.0012 (3)	−0.0016 (10)
C (3)	0.3744 (4)	0.4831 (14)	0.1049 (3)	0.0018 (3)	0.0068 (32)	0.0001 (1)	−0.0007 (15)	0.0006 (3)	−0.0011 (9)
C (4)	0.3348 (5)	0.3021 (14)	0.1396 (3)	0.0024 (3)	0.0050 (33)	0.0001 (1)	0.0035 (15)	0.0005 (3)	−0.0015 (9)
C (5)	0.3683 (5)	0.1148 (15)	0.1690 (3)	0.0021 (3)	0.0091 (35)	0.0007 (2)	0.0007 (16)	0.0011 (4)	−0.0012 (11)
C (6)	0.2372 (5)	0.0880 (15)	0.1843 (3)	0.0028 (3)	0.0059 (33)	0.0001 (1)	−0.0006 (15)	0.0008 (3)	0.0015 (9)
C (7)	0.2500 (4)	0.2876 (14)	0.1484 (3)	0.0020 (3)	0.0042 (31)	0.0000 (1)	0.0020 (14)	0.0003 (3)	0.0011 (9)
C (8)	0.1874 (4)	0.4281 (15)	0.1321 (3)	0.0014 (3)	0.0112 (34)	0.0001 (1)	0.0012 (14)	0.0001 (3)	0.0001 (9)
C (9)	0.1116 (5)	0.3623 (16)	0.1472 (3)	0.0016 (3)	0.0153 (36)	0.0004 (1)	0.0008 (15)	0.0005 (3)	0.0025 (11)
C (10)	0.1007 (5)	0.1628 (16)	0.1823 (3)	0.0019 (3)	0.0143 (38)	0.0006 (2)	−0.0033 (16)	0.0004 (3)	0.0037 (11)
C (11)	0.1615 (5)	0.0241 (17)	0.2008 (3)	0.0029 (4)	0.0196 (40)	0.0004 (1)	−0.0072 (19)	0.0011 (4)	−0.0004 (11)
N (1)	0.4011 (4)	0.2985 (13)	0.0030 (3)	0.0036 (3)	0.0097 (29)	0.0003 (1)	−0.0009 (15)	0.0012 (3)	0.0024 (9)
N (2)	0.3100 (4)	−0.0154 (14)	0.1968 (3)	0.0032 (3)	0.0135 (31)	0.0006 (1)	0.0047 (15)	0.0018 (3)	0.0017 (10)
O (1)	0.3426 (4)	0.8794 (12)	0.0217 (3)	0.0039 (3)	0.0157 (28)	0.0015 (2)	−0.0008 (14)	0.0020 (3)	0.0008 (10)
O (2)	0.4358 (3)	0.7093 (10)	−0.0366 (3)	0.0022 (2)	0.0103 (24)	0.0013 (1)	0.0019 (11)	0.0027 (3)	0.0047 (9)
O (3)	0.0447 (3)	0.4804 (14)	0.1291 (3)	0.0015 (2)	0.0460 (35)	0.0015 (2)	0.0043 (14)	0.0017 (3)	0.0123 (12)
H (1)	0.290	0.460	0.022						
H (2)	0.464	0.290	0.019						
H (3)	0.379	0.159	0.019						
H (4)	0.412	0.432	−0.026						
H (5)	0.441	0.460	0.111						
H (6)	0.357	0.639	0.122	Final thermal parameter for hydrogen atoms: overall isotropic; 2.2 Å^2					
H (7)	0.429	0.076	0.172						
H (8)	0.319	−0.161	0.224						
H (9)	0.199	0.580	0.104						
H (10)	0.050	0.600	0.096						
H (11)	0.041	0.124	0.193						
H (12)	0.152	−0.133	0.228						

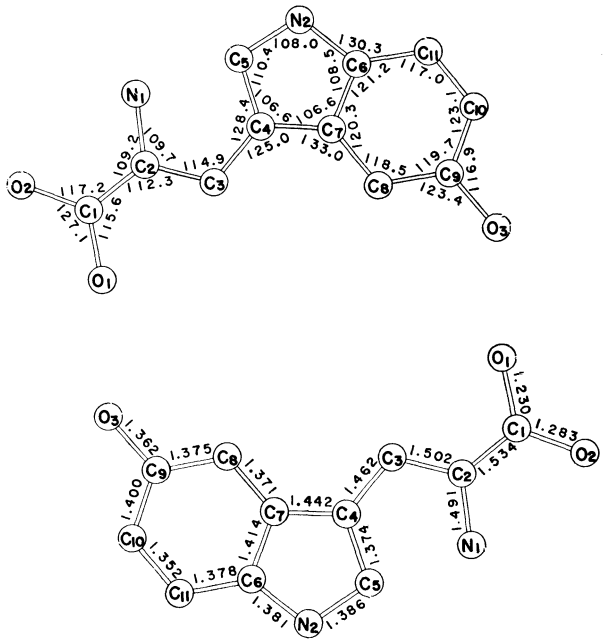

Fig. 2. Bond distances and angles of 5-hydroxy-DL-tryptophan. The standard deviation for the bond lengths ranges between 0.011 and 0.013Å. The standard error for the angles is approximately 0.8°.

planes which consist of the indole ring and the acid group. The equations of the least-squares planes are: for the indole ring, $0.0846X+0.5114Y+0.8552Z=3.8776$ and for the carboxyl group with α-carbon, $0.6536X+0.1469Y+0.7425Z=4.8350$ in rectangular Ångstrom space. These two planes form a dihedral angle of 40.1°, which is considerably differing from 70.6° in L-tryptophan hydrochloride.[7] This is attributed to the difference in conformation of the ionized carboxyl group. The deviations of the individual atoms from the best planes are given in Table 6. It is concluded that nine atoms of indole ring and C(β) atom are almost in a plane within the limit of experimental error.

Table 6. Deviations (Å) of atoms from the best plane

Indole group		Acid group	
Atom	Distance	Atom	Distance
C (4)	0.009	O (1)	−0.005
C (5)	0.003	O (2)	−0.005
N (2)	−0.017	C (1)	0.013
C (6)	−0.001	C (2)	−0.003
C (7)	0.017		
C (8)	−0.028	*N (1)	0.137
C (9)	0.009	*C (3)	−1.260
C (10)	0.003		
C (11)	0.005		
*O (3)	0.070		
*C (3)	0.025		
*C (2)	1.305		
*H (10)	0.290		

* Excluded from the least-squares calculations. The mean deviation from the indole ring is 0.010 Å and that from the acid group 0.007 Å.

However, the O(3) atom of the hydroxyl group is 0.07 Å out of the plane as found in serotonin picrate monohydrate.[20] The amino nitrogen atom is 0.137 Å, being displaced from the acid plane as in α-amino acid, the N(1)–C(2) bond forming an angle of 5.4° with this plane.

Molecular Conformation. As shown in Fig. 3, in the present molecule, the C(β)–C(γ) bond lies at *trans* position to the C(α)–COO^- bond and *gauche* to the C(α)–NH_3^+ bond. Similar conformations have been observed in glycyl-L-tryptophan dihydrate[21] and DL-tryptophan formate.[22] On the other hand, L-tryptophan hydrochloride occurs in a different conformation, and the orientation of C(β)–C(γ) bond moves to *gauche* position with respect to both the C(α)–COOH and C(α)–NH_3^+. In the case of tryptophan, Ramachandran and Lakshminarayanan pointed out that C(γ) atom should take I or III position in Fig. 3.[19] Some torsion angles are given in Table 7.

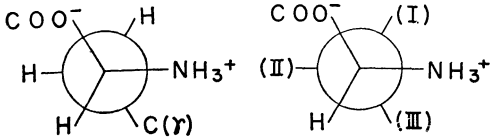

Fig. 3. Newman projections about C(α)–C(β) bond.

Table 7. Torsion angles

C(5)–C(4)–C(3)–C(2)	±110.7°
C(4)–C(3)–C(2)–C(1)	±163.6°
C(4)–C(3)–C(2)–N(1)	± 74.8°
C(10)–C(9)–O(3)–H(10)	±165.9°

Two Modes of Dimers. An interesting aspect of this crystal structure is the hydrogen-bonding scheme. The D- and L-forms of 5-hydroxytryptophan are hydrogen-bonded into two types of dimers related by center of symmetry. Molecule (A) is an original molecule whose coordinates are given in Table 5. Two molecules (A) and (B) or (A) and (C) form DL-dimer in solid state. The A-B type of dimer is a typical cyclic dimer[23] joined through O(3)–H(10)···O(2) hydrogen bonding (2.688 Å). Another type (A-C dimer) is a nonplanar dimer[23] linked together by an N(1)–H(2)···O(2) hydrogen bridge (2.798 Å). This hydrogen-bonded dimer has been found in the crystal structure of DL-valine.[24] Judging from the distances of the hydrogen bonds and the molecular packing in crystals, we suppose that A-B dimers are originally formed in solution and then the crystallization is performed by A-C dimerization.

20) U. Thewalt and C. E. Bugg, *Acta Crystallogr.*, **B28**, 82 (1972).
21) R. A. Pasternak, *ibid.*, **9**, 341 (1956).
22) E. Bye, A. Mostad, and C. Römming, to be published in *Acta Chem. Scand.* (1973).
23) G. C. Pimentel and A. L. McClellan, "The Hydrogen Bond," ed. by L. Pauling, W. H. Freeman and Company, San Francisco and London (1960), p. 100.
24) M. Mallikarjunan and S. T. Rao, *Acta Crystallogr.*, **B25**, 296 (1969).

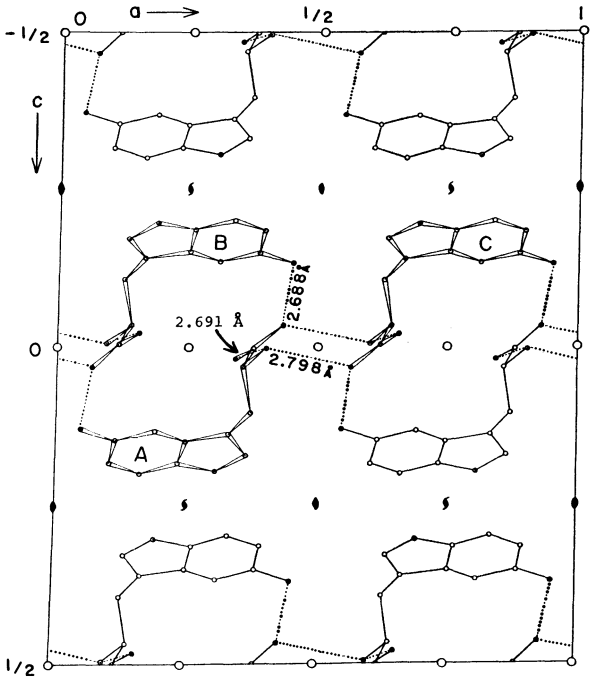

Fig. 4. Molecular packing of 5-hydroxy-DL-tryptophan as seen along the b-axis. The dotted lines show hydrogen bonds.

Packing of the Molecules. The packing in the structure is illustrated in Fig. 4. The molecules are arranged in double layers parallel to (001), and connected through hydrogen bondings described above. The third hydrogen bond of 2.691 Å is observed between the N(1) atom and the O(1) atom (Table 8). By this linkage along b-axis, dimers are connected into an infinite three-dimensional network. It is of considerable interest that the nitrogen atom of the indole ring is not involved in any hydrogen bonds, and nonpolar indole planes are stacked by van der Waals forces. All the intermolecular contacts of less than 3.5 Å between pairs of non-hydrogen atoms are summarized in Table 8. All the atoms other than C(2), C(3), C(4), C(6), and C(7) have one or more intermolecular neighbors within 3.5 Å. Unusually close contact (3.201 Å) is found between C(5) and O(3) of the adjacent molecule. The distance of H(7)···O(3) is 2.24 Å and the C(5)–H(7)–O(3) angle is 153±6°. This might suggest that this short contact arises from hydrogen bonding of the C–H···O type described by Sutor.[25] This work was partly supported by a research grant from the Ministry of Education.

TABLE 8. INTERMOLECULAR DISTANCES LESS THAN 3.5 Å

(a) Hydrogen bonds

Donor	Acceptor	Distance	Angle formed by carbon atom-Donor-Acceptor
O(3)–H(10)	O(2) on (B)	2.688 Å	115.3°
N(1)–H(2)	O(2) on (C)	2.798	113.7°
N(1)–H(3)	O(1) on (D)	2.691	115.2°

(b) Other distances

Atom cn (A)	Atom	Distance
O(1)	C(8) (B)	3.425 Å
O(2)	C(9) (B)	3.494
N(1)	C(1) (D)	3.473
C(5)	O(1) (D)	3.390
N(1)	C(8) (E)	3.412
N(1)	C(9) (E)	3.277
O(3)	C(5) (F)	3.201
C(11)	N(2) (G)	3.477
C(10)	N(2) (G)	3.456

Symmetry code;				
	(A)	x	y	z
	(B)	$1/2-x$	$3/2-y$	$-z$
	(C)	$1-x$	$1-y$	$-z$
	(D)	x	$-1+y$	z
	(E)	$1/2-x$	$1/2-y$	$-z$
	(F)	$-1/2+x$	$1/2+y$	z
	(G)	$1/2-x$	$1/2+y$	$1/2-z$

25) D. J. Sutor, *J. Chem. Soc.*, **1963**, 1105.

Structural Studies of Tryptophan Metabolites by X-ray Diffraction Method. II. The Crystal and Molecular Structure of Tryptamine Hydrochloride

Akio WAKAHARA, Takaji FUJIWARA, and Ken-ichi TOMITA

Faculty of Pharmaceutical Sciences, Osaka University, Toneyama, Toyonaka, Osaka 560

(Received December 18, 1972)

The crystal structure of tryptamine hydrochloride has been solved by the application of the symbolic addition method, and refined by successive Fourier syntheses and least-squares procedures. The crystals are orthorhombic, space group Pbca, with lattice parameters $a=8.545$, $b=10.025$ and $c=24.252$ Å. All the positions of hydrogen atoms were found in the difference Fourier map and included in the refinement. The ethylamine side chain bound to the indole ring is in a folded configuration as found in the crystal structure of serotonin picrate monohydrate. A weakly basic nitrogen atom of the indole ring takes part in the hydrogen bonding with the adjacent ion. Every chloride ion behaves as an acceptor for four hydrogen bonds. This is in line with the absence of any marked cleavage where indole rings are packed together to form a pleated sheet and a three-dimensional network structure is essentially stabilized by the hydrogen bond formation.

Tryptamine, a tryptophan metabolite, was first isolated from shoots and flowers of *Acacia* species.[1] A significant biological implication of this compound lies in its role as starting material for the biosynthesis of alkaloids containing an indole ring. It has been also reported to have anti-radiation ability[2-4] as well as serotonin and 5-hydroxytryptophan. In order to study the correlation between the molecular structure and its pharmacodynamic action, it is necessary to elucidate the stereoconfiguration of the molecule. In the course of studies on tryptamine hydrochloride, we found that the aminoethyl side chain of this molecule is in folded configuration.[5] Extended conformation was reported in the case of a serotonin-creatinine sulphate complex.[6] The same folded configuration was found in the crystal structure of serotonin picrate monohydrate.[7] The present paper gives a more detailed account of the methods and the results of analysis. The structure is compared with that of other tryptophan metabolites, some structural features of radiation protective agents being described.

Experimental

Crystals were prepared by slow evaporation from an aqueous solution, and obtained as transparent yellow prismatic crystals. Preliminary rotation and Weissenberg photographs showed them to be orthorhombic, the space group being uniquely determined as Pbca from the absent spectra. The unit-cell dimensions were finally determined with a Rigaku Denki manual four-circle diffractometer at room temperature. Melting point of this crystal measured with a DSC (differential scanning calorimeter) is in agreement with the reference value.[8] The density was measured by the flotation method in a benzene-carbon tetrachloride mixture. It was confirmed that no solvent of crystallization is contained in the crystal, the result coinciding with DSC results. The physical and crystal data obtained are given in Table 1.

TABLE 1. CRYSTAL DATA OF TRYPTAMINE HYDROCHLORIDE

$C_{10}H_{12}N_2 \cdot HCl$, M.W. 196.68, mp 256—257°C	
Yellowish prism-shaped crystals. Orthorhombic	
$a=8.545(9)$, $b=10.025(8)$, $c=24.252(16)$ Å	
$V=2077.5$ Å^3, $Z=8$, $F(000)=832$	
Absorption coefficient for X-rays ($\lambda=1.5418$ Å):	
$\mu=29.2$ cm^{-1}, $D_m=1.261$ g·cm^{-3}, $D_x=1.258$ g·cm^{-3}	
Absent spectra	$(0kl)$: $k=2n+1$
	$(h0l)$: $l=2n+1$
	$(hk0)$: $h=2n+1$
Space group; Pbca	

Intensities of 875 independent non-zero reflections were measured visually on equi-inclination Weissenberg photographs of 0 to 7th layers around the b-axis, with the use of Ni-filtered Cu$K\alpha$ radiation. Corrections were made for the Lorentz-polarization factors and spot-shape. No absorption effect was taken into account, since the crystal used was sufficiently small. The data were then adjusted to the absolute scale by means of Wilson's method. The overall temperature factor obtained at this stage was 3.35 Å^2. The SIGMA program was utilized to list the E-values and $\sum_2$ relationships with their probabilities.

Determination and Refinement of Structure

The structure of tryptamine hydrochloride was successfully solved by using the direct method. Reflections with $|E|>1.3$ were selected, five of them being given a sign or a letter symbol as follows.

h	k	l	phase	$\|E\|$
2	2	3	+	3.11
5	4	16	+	2.77
2	5	14	+	2.69
5	2	3	A	2.81
6	4	8	B	3.10

Application of $\sum_1$ formula to reflection (446) indicated that it has a positive sign of 88% probability. It is also included in the initial starting set. The sign

1) E. P. White, *New Zealand J. Sci. Tech.*, **25B**, 137 (1944).
2) H. Langendorff and R. Koch, *Strahlentherapie*, **98**, 245 (1955).
3) P. Alexander and Z. M. Bacq, *Radiat. Res.*, **2**, 292 (1955).
4) I. I. Sapezhinskii and N. M. Emanuel, *Dokl. Akad. Nauk. SSSR*, **132**, 1441 (1960).
5) A. Wakahara, T. Fujiwara, and K. Tomita, *Tetrahedron Lett.*, **1970**, 4999.
6) I. L. Karle, K. S. Dragonette, and S. A. Brenner, *Acta Crystallogr.*, **19**, 713 (1965).
7) U. Thewalt and C. E. Bugg, *ibid.*, **B28**, 82 (1972).
8) A. H. Jackson and A. E. Smith, *J. Chem. Soc.*, **1965**, 3498.

relations between a number of reflections strongly suggested A=B=+. At the end of the process the phases of 157 independent reflections were determined, and a Fourier synthesis was calculated with normalized structure factors as the coefficients (*E*-map). The three dimensional *E*-map showed the sites of all 13 atoms of this molecule. Another 20 spurious peaks of the same height as that of light atoms appeared. The indole ring plane enables us to distinguish true peaks from false ones. The structure was refined by the block-diagonal-matrix least-squares method, first with isotropic thermal parameters and then with anisotropic temperature factors. The estimated parameters of hydrogen atoms were computed in such a way as to give bond angles as close to trigonal or tetrahedral as possible. The distances were assumed to be 1.08 Å for C–H, 1.01 Å for N–H, and 0.97 Å for O–H. The amino nitrogen atom had to be the protonated form, and three hydrogen atoms were placed on it. This nitrogen atom has three chloride neighbors at reasonable hydrogen-bonding distances and angles. Thus, three hydrogen atoms were placed at proper positions on the N···Cl⁻ line. In order to check the expected positions of hydrogen atoms, a difference Fourier synthesis was prepared and all the hydrogen peaks were obtained near the calculated positions as shown in Fig. 1. This may indicate the correctness of the assumed positions of hydrogen atoms and the assignment of hydrogen bonding system. More refinement cycles were performed, which included refinement of the positional and overall isotropic thermal parameters of the hydrogen atoms. Refinement was stopped when parameter shifts were less than one fourth of their standard deviations, giving an *R* value of 0.094. The N–H and C–H bond lengths are in the ranges 0.99—1.11 Å and 1.03—1.17 Å, respectively. The final electron density map is shown in Fig. 2. The final observed and calculated structure factor amplitudes are given in Table 2 and final atomic positional and thermal parameters in Table 3. The scattering factors used throughout the refinement were taken from *International Tables for X-ray Crystallography* (1962). All calculations were done on an NEAC 2200—500 of this University, using programs written by T. Ashida and the authors.

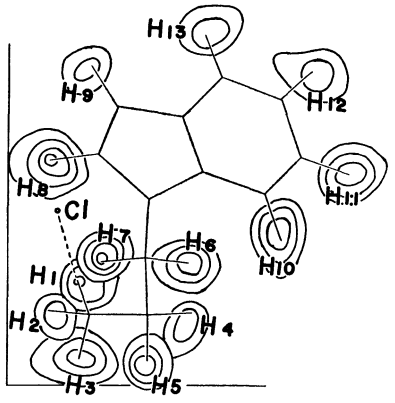

Fig. 1. The location of hydrogen atoms from a three-dimensional difference Fourier map. Contours from 0.2 e.Å^{-3} at intervals of 0.2 e.Å^{-3}.

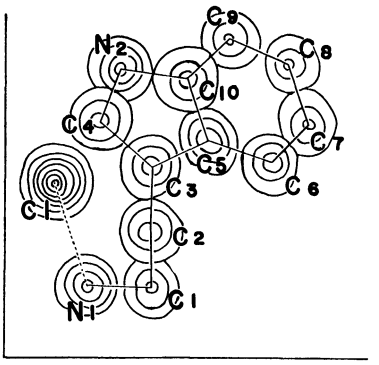

Fig. 2. A composite drawing of the final electron density map, viewed along a-axis. Contour intervals of 2.0 e.Å^{-3} for light atoms and 4.0 e.Å^{-3} for the chloride ion, the first contour begins at 2.0 e.Å^{-3}.

Description and Discussion of the Structure

Molecular Dimensions. The bond lengths and angles are shown in Fig. 3 and Table 4 together with those of the other tryptophan metabolites. The numbering of other metabolites corresponds to that of tryptamine in Fig. 3. We see some interesting structural features of radiation protective agents containing indole ring (indicated with asterisk in Table 4). The C(3)–C(4) bond, 1.342—1.387 Å, is apparently shorter than a normal aromatic C–C bond (1.395 Å). The corresponding bond of four radiation protectors is longer than that of other indole derivatives, and is compatible to 1.381 Å of yohimbane hydrobromide[9] and 1.395 Å of reserpine.[10] On the other hand, the C(2)–C(3) distance of the protector is slightly shorter than that of the other related compounds. The corresponding length of yohimbane and reserpine is 1.489 Å and 1.444 Å, respectively. It is of biological in-

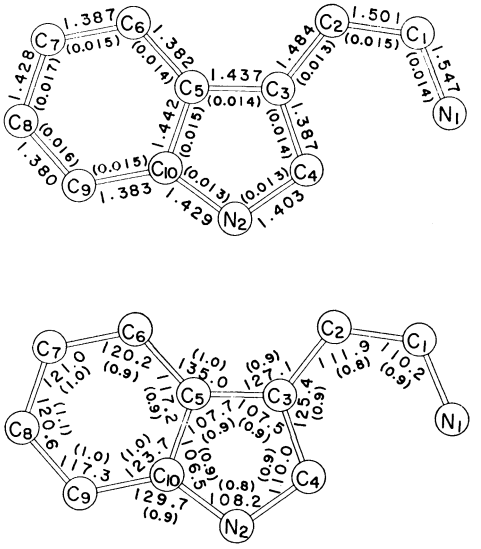

Fig. 3. Bond lengths (Å) and valency angles (°). The standard deviations are given in parentheses.

9) J. P. Fennessey and W. Nowacki, *Z. Kristallogr.*, **131**, 342 (1970).

10) I. L. Karle and J. Karle, *Acta Crystallogr.*, **B24**, 81 (1968).

TABLE 2. THE OBSERVED AND THE FINAL CALCULATED STRUCTURE FACTORS

L	FO	FC	L	FO	FC	L	FO	FC	L	FO	FC	L	FO	FC	L	FO	FC	L	FO	FC	L	FO	FC	L	FO	FC
H,K=	0	0	1	117	111	12	16	-15	11	66	-61	24	22	25	13	22	-22	12	27	-34	9	30	28	8	45	-40
4	123	-121	2	124	-120	14	37	-38	13	20	-22	25	27	-25	15	29	-35	14	20	-25	11	35	-30	11	38	-36
6	233	-241	3	233	-268	H,K=	9	1	17	20	-22	27	13	-13	16	40	-40	H,K=	9	4	16	36	33	13	41	-38
8	19	-19	5	19	-20	1	27	29	18	30	33	28	8	-9	17	20	-16	6	12	-15	20	9	-12	14	17	16
10	173	-174	6	114	96	3	21	23	21	29	29	H,K=	4	3	18	30	-31	8	12	-16	H,K=	8	5	15	21	-17
12	79	-80	8	93	97	6	30	-32	H,K=	6	2	0	8	10	20	35	-39	H,K=	10	4	0	30	-32	H,K=	8	6
14	124	-116	9	42	39	8	58	-51	0	48	-42	1	21	17	22	25	-25	5	15	16	4	24	-25	0	24	-24
16	33	-30	10	40	-35	15	17	-21	2	49	-41	2	19	20	25	21	20	H,K=	1	5	6	17	-15	1	10	-14
18	40	39	11	73	71	H,K=	10	1	3	47	-40	3	64	70	H,K=	2	4	1	39	-39	8	26	33	2	35	-36
20	20	-17	12	20	20	0	54	-54	4	16	16	4	142	-163	0	68	-71	2	16	6	10	34	34	8	29	30
24	51	50	13	122	119	3	22	-24	5	65	-58	5	118	118	1	40	-39	3	68	78	11	34	35	9	36	-35
26	66	58	14	50	46	5	36	-37	7	95	-92	7	27	33	2	28	23	6	67	-77	14	22	21	10	10	6
28	27	25	15	17	-19	H,K=	0	2	9	84	-81	8	76	82	3	6	-2	8	69	-79	16	10	13	H,K=	9	6
H,K=	1	0	17	45	-36	2	143	-144	12	42	36	9	74	62	4	127	118	9	49	-56	H,K=	9	5	9	25	25
2	74	-64	18	65	-56	3	44	38	13	20	23	10	44	41	5	53	-48	10	12	11	4	24	25	H,K=	1	7
4	20	-24	20	99	-89	4	34	38	17	46	48	11	57	58	6	63	64	12	29	-27	6	23	28	1	91	-99
6	370	-371	24	28	30	5	146	-148	19	44	43	12	16	16	7	63	-61	15	15	16	10	14	17	2	9	9
8	196	-196	H,K=	2	1	6	62	-65	23	13	15	13	10	9	8	49	-46	16	37	39	12	24	24	4	28	-37
10	25	-22	0	384	331	7	176	-179	H,K=	7	2	15	19	-20	9	26	-29	18	21	28	H,K=	0	6	5	29	27
12	50	51	1	136	-146	8	23	16	1	57	-48	16	27	27	10	72	-68	19	12	-8	2	106	104	9	26	27
14	25	-25	2	87	98	9	149	-160	2	10	-11	17	43	-40	14	33	-29	20	16	19	3	25	28	10	58	63
16	62	55	3	289	279	10	41	-45	3	37	-38	19	45	-47	15	19	18	22	30	24	4	84	96	11	34	31
18	65	66	4	108	-96	11	96	-113	5	23	-24	21	34	-30	16	33	-34	26	9	-13	5	26	27	14	38	-36
20	82	82	5	143	130	12	101	120	6	35	26	22	30	-30	17	24	25	H,K=	2	5	7	51	52	15	27	27
22	13	13	6	46	38	13	21	20	8	23	23	23	41	-34	18	33	-39	0	91	-89	8	76	-83	H,K=	2	7
30	12	-12	7	141	132	14	44	50	11	51	60	H,K=	5	3	19	27	-28	1	36	33	9	65	69	0	32	-26
H,K=	2	0	8	54	50	15	35	37	13	54	61	1	45	40	22	33	36	2	36	-32	10	68	-78	1	18	16
0	196	212	9	18	-20	16	13	-14	15	37	31	2	47	43	23	33	35	3	7	-5	11	71	70	2	21	19
2	8	6	10	15	-20	17	75	86	17	22	23	3	40	42	26	13	12	4	82	-86	12	26	-31	3	74	64
4	219	-256	11	28	32	18	29	-33	23	16	-17	4	78	74	H,K=	3	4	6	33	-29	13	41	-40	4	28	28
6	87	-80	12	122	-106	19	52	53	H,K=	8	2	5	19	17	1	34	33	8	29	24	14	36	-41	5	92	77
8	36	-33	13	55	-49	21	31	33	0	19	20	6	15	15	3	39	-29	9	37	-41	16	20	19	6	29	26
10	65	61	14	140	-120	23	70	65	1	13	-16	7	36	31	4	32	28	10	42	42	17	36	-40	7	62	54
12	91	81	15	22	-22	29	18	-14	3	24	24	8	59	-59	5	58	-49	12	59	60	18	21	-23	8	57	-50
14	112	109	16	21	-17	H,K=	1	2	5	43	37	9	26	-22	6	84	75	14	87	104	19	46	-45	9	54	53
18	41	36	17	24	-25	1	102	-87	7	20	19	10	46	37	7	40	42	15	36	45	21	32	-33	13	32	-31
22	52	-50	21	28	-27	2	31	-26	11	45	45	11	44	-37	8	22	-21	16	16	20	H,K=	1	6	14	33	28
26	13	-9	23	24	-21	3	185	-219	14	26	-31	12	25	27	10	75	-77	22	21	-24	1	66	63	16	26	-25
H,K=	3	0	26	33	42	4	64	62	17	14	-14	13	51	-48	12	46	-51	23	11	13	2	64	-57	17	20	-22
2	10	9	H,K=	3	1	5	35	-32	19	23	-23	15	39	-39	16	41	40	24	41	-40	3	74	67	19	34	-38
4	51	49	1	168	147	6	110	114	H,K=	9	2	16	20	-19	17	6	-4	H,K=	3	5	4	71	-61	H,K=	3	7
6	74	-69	2	87	-87	7	14	-15	3	28	28	17	20	-21	H,K=	4	4	1	42	-34	6	43	-39	1	23	25
8	42	-42	3	28	29	8	57	56	H,K=	10	2	20	21	-23	0	32	-27	2	122	129	8	59	-60	2	30	-30
10	80	71	6	189	-226	9	60	56	4	12	-10	25	19	20	1	8	10	4	113	113	9	29	-30	3	89	93
12	95	85	8	120	-127	10	47	-47	6	5	4	H,K=	6	3	2	32	31	5	16	14	10	26	-22	4	34	-38
14	16	-17	9	50	-52	11	93	92	H,K=	1	3	0	30	23	3	6	-3	6	76	85	11	51	-52	5	31	24
16	53	-43	10	37	-31	13	103	109	1	170	201	3	30	-31	5	28	30	8	49	47	12	32	-37	6	29	31
18	44	44	11	30	-28	15	57	56	2	7	-6	6	18	-17	6	72	61	10	58	58	13	24	-30	8	12	-10
22	36	-37	12	27	-24	17	61	59	3	95	92	7	48	-50	7	69	-69	11	17	-19	14	29	30	11	66	-77
24	43	-45	13	19	-19	23	33	-34	4	61	60	8	41	40	8	27	-25	12	37	35	15	25	-27	12	22	-22
28	20	24	15	63	-54	25	33	-34	5	80	-67	14	25	-23	9	25	-25	14	49	-48	16	36	36	13	55	-61
H,K=	4	0	16	60	56	29	12	-11	6	26	-27	H,K=	7	3	10	20	-24	16	45	-45	17	30	-30	15	28	-29
0	29	-35	17	73	-73	H,K=	2	2	7	33	-28	2	20	19	12	32	-32	17	32	31	18	16	19	17	22	-23
2	36	-31	18	25	31	0	229	204	9	124	-108	4	45	47	13	20	22	18	28	-27	H,K=	2	6	21	19	20
4	58	-50	19	25	25	1	48	-43	11	50	-52	8	35	-40	14	24	-24	19	12	-12	0	67	-68	24	10	7
6	13	14	20	29	27	2	43	44	12	18	17	11	26	-28	17	32	30	20	39	-38	2	12	-12	H,K=	4	7
8	36	-33	22	29	31	3	290	307	14	35	35	12	24	24	H,K=	5	4	22	29	-26	3	97	-83	0	23	30
10	58	53	23	35	38	4	130	-121	18	28	-28	13	20	-18	1	10	-10	23	15	-18	5	46	-42	1	18	16
12	70	69	H,K=	4	1	5	118	115	20	83	-81	14	30	-29	2	49	-43	H,K=	4	5	6	28	-29	2	37	-34
14	77	70	0	182	-167	6	32	29	22	28	23	15	21	-21	3	57	-52	0	107	112	7	46	-43	4	14	17
16	57	-60	2	60	-55	7	39	40	24	21	23	H,K=	8	3	5	39	-34	1	12	16	8	15	18	5	64	-61
26	11	-14	3	41	-31	8	23	-24	25	26	27	0	20	-22	7	40	40	2	80	72	9	20	-22	6	12	-13
28	19	-20	4	106	-106	9	32	33	27	18	18	2	21	21	8	78	-71	3	20	17	11	22	22	7	31	-34
H,K=	5	0	5	28	24	11	13	15	29	8	6	3	30	-32	9	23	19	4	67	73	14	29	30	8	53	-59
4	57	58	7	66	-68	12	22	17	H,K=	2	3	5	44	-55	10	56	-58	5	21	20	16	50	-52	11	44	-45
6	51	58	8	90	90	15	24	-24	0	108	107	7	20	-24	11	29	30	6	24	19	H,K=	3	6	14	26	26
8	69	75	9	70	-82	16	36	-40	1	34	-31	8	20	-20	12	55	-58	7	8	7	2	30	31	15	28	27
10	17	18	10	60	64	19	67	-58	2	74	63	9	20	-22	13	12	16	8	92	-101	3	23	-18	17	40	39
12	55	53	11	62	-70	H,K=	3	2	3	76	-63	19	13	17	14	35	39	9	19	-18	H,K=	4	6	19	22	27
14	20	-24	12	48	50	1	136	116	4	39	-37	H,K=	9	3	16	63	68	10	78	-88	0	87	-73	21	20	21
16	61	-64	14	32	37	2	19	17	5	141	-148	1	41	-46	18	13	12	12	26	-20	3	63	-53	24	4	-8
20	39	-40	17	62	62	3	18	19	6	28	26	2	20	-21	23	9	-11	15	39	36	7	17	-19	H,K=	5	7
22	24	-30	19	46	56	4	96	78	7	59	-57	3	31	-38	H,K=	6	4	16	35	-39	8	26	27	1	66	-55
24	20	-22	H,K=	5	1	5	85	-80	9	132	-139	8	33	-37	0	56	-52	18	47	-34	9	19	-19	3	26	-26
26	13	17	1	47	-41	6	37	34	10	33	-32	11	26	34	2	51	-50	19	21	-20	16	20	22	7	13	14
H,K=	6	0	2	50	41	7	17	15	12	25	-24	13	19	19	3	56	58	22	35	31	17	28	30	9	16	13
0	101	107	3	64	-59	8	51	-45	13	15	16	H,K=	10	3	4	57	-59	H,K=	5	5	H,K=	5	6	11	9	10
2	23	22	4	65	62	9	80	-71	14	19	-21	0	29	-32	5	81	81	2	57	-58	1	35	-34	13	11	12
4	68	68	5	23	20	10	42	-44	15	62	50	10	18	20	8	86	85	5	16	-14	2	82	63	15	44	37
6	36	34	6	54	54	15	25	22	16	17	-16	H,K=	0	4	10	35	41	6	10	-10	3	71	-57	H,K=	6	7
8	45	-43	7	17	-20	18	29	28	17	36	33	3	78	74	11	35	39	7	44	43	6	18	23	1	15	14
10	48	-43	9	17	14	H,K=	4	2	19	69	62	4	48	-53	14	12	17	8	62	-68	7	12	8	2	18	-17
12	24	-18	10	31	35	0	17	18	22	20	18	5	56	48	15	18	-22	10	44	-43	8	12	13	3	11	10
14	108	-96	11	45	44	1	19	19	23	20	18	8	79	76	16	40	42	11	21	-21	9	39	34	4	27	27
16	52	-56	13	48	50	2	30	29	26	26	25	9	72	70	18	29	30	12	17	-19	10	33	34	5	21	21
20	13	17	20	28	-27	3	118	105	H,K=	3	3	10	22	24	21	19	-17	13	39	-41	11	26	25	7	14	15
22	33	34	H,K=	6	1	4	64	-63	1	61	-62	11	58	57	22	39	-38	16	40	38	18	26	-25	12	9	-9
24	34	37	0	14	15	5	122	110	2	97	-106	12	137	136	H,K=	7	4	18	24	21	23	7	-8	H,K=	7	7
H,K=	7	0	1	21	-21	6	45	41	3	154	-156	14	74	67	1	12	14	22	19	20	H,K=	6	6	3	17	-15
2	66	-73	5	45	38	7	52	-45	4	43	42	16	42	41	2	71	64	24	16	20	0	8	5	10	9	-7
4	39	-45	8	40	38	8	20	-21	5	44	-43	17	33	-31	3	26	29	H,K=	6	5	1	27	-25	H,K=	8	7
6	95	-104	11	30	-31	9	21	22	6	87	-77	18	37	-37	4	35	37	0	23	26	2	16	15	3	24	21
8	35	-36	13	20	-20	10	23	25	7	24	25	19	86	-80	6	58	57	1	55	47	3	37	31	5	28	32
10	21	-19	14	34	-32	11	14	16	8	48	-46	21	41	-41	10	31	34	2	16	-19	4	41	47	8	4	-4
16	21	24	15	17	-19	12	10	-15	9	21	20	22	36	-30	11	22	-21	3	11	-12	5	87	72	13	11	-10
18	19	23	17	28	29	15	34	-30	10	69	-64	23	36	36	13	19	-20	5	12	16	6	29	38	H,K=	9	7
20	23	26	23	14	-14	16	28	-29	11	103	103	26	26	-25	15	23	-22	6	24	-27	7	37	34	1	25	26
22	19	22	H,K=	7	1	18	25	27	12	12	12	H,K=	1	4	16	28	-28	7	43	-36	10	48	-45	2	20	-18
H,K=	8	0	2	30	29	19	27	-26	13	86	80	1	87	87	17	15	-16	8	12	-8	12	40	-37	3	27	24
0	82	-87	4	40	39	H,K=	5	2	14	26	26	2	161	143	21	19	19	10	25	-20	13	12	-17			
2	42	-48	11	42	40	1	113	112	15	63	52	3	53	44	H,K=	8	4	12	22	22	14	24	-21			
12	57	62	H,K=	8	1	3	97	98	16	59	67	4	79	85	0	53	52	14	27	22	20	15	13			
20	18	19	0	24	24	4	28	31	17	55	47	5	14	14	1	18	-17	16	21	23	22	17	22			
H,K=	9	0	1	26	-28	5	56	-53	20	24	-26	6	125	148	4	22	30	H,K=	7	5	H,K=	7	6			
2	27	-29	2	26	28	6	28	-26	21	28	-33	8	50	54	7	26	-26	2	60	-52	1	34	28			
8	36	36	7	37	34	8	51	-49	22	20	19	10	28	36	9	48	-48	7	12	14	4	33	-32			
H,K=	1	1	9	23	24	9	86	-80	23	33	-33	11	65	-72	10	21	-24	8	35	-38	6	17	-16			

terest that N(1), C(1) and C(2) atoms of the side chain of tryptamine, and C(3)–C(4) bond of an indole ring take part in the formation of a nonplanar six-membered ring of the alkaloids, yohimbane and reserpine. In the comparison of C(3)–C(4) and C(2)–C(3) bond lengths, we included three more indole derivatives, skatole[11] (1.34 and 1.50 Å), glycyl-L-tryptophan[12] (1.338 and 1.534 Å) and 5-methoxy-dimethyltryptamine[13] (1.365 and 1.509 Å) which had been determined by X-ray analysis. The molecular mechanism of the radiation protective action of these compounds containing an indole ring is still obscure, but the facts mentioned above indicate that the mechanism may be to some

11) A. W. Hanson, *ibid.*, **17**, 559 (1964).

12) R. A. Pasternak, *ibid.*, **9**, 341 (1956).

13) G. Falkenberg and D. Carlström, *ibid.*, **B27**, 411 (1971).

Table 3. Final positional coordinates and thermal parameters with their standard deviations ($\times 10^4$)
Anisotropic thermal parameters are in the form of $\exp[-(B_{11}h^2+B_{22}k^2+B_{33}l^2+B_{12}hk+B_{13}hl+B_{23}kl)]$.

Atom	x	y	z	B_{11}	B_{22}	B_{33}	B_{12}	B_{13}	B_{23}
Cl	0.1715 (3)	0.6462 (3)	0.0394 (1)	0.0118 (3)	0.0081 (3)	0.0019 (0)	−0.0002 (6)	−0.0025 (2)	−0.0003 (2)
N(1)	0.4492 (8)	0.8548 (9)	0.0646 (3)	0.0091 (11)	0.0126 (13)	0.0019 (2)	0.0026 (20)	0.0006 (7)	−0.0054 (8)
N(2)	0.4851 (9)	0.4124 (7)	0.0908 (3)	0.0152 (13)	0.0039 (11)	0.0019 (2)	0.0090 (18)	−0.0029 (8)	−0.0009 (6)
C(1)	0.5584 (11)	0.8604 (11)	0.1155 (3)	0.0197 (18)	0.0152 (17)	0.0006 (1)	−0.0251 (30)	0.0004 (8)	0.0002 (8)
C(2)	0.6687 (10)	0.7437 (9)	0.1152 (4)	0.0104 (12)	0.0035 (12)	0.0022 (2)	0.0002 (21)	−0.0007 (9)	0.0014 (7)
C(3)	0.5841 (9)	0.6147 (9)	0.1172 (3)	0.0066 (11)	0.0097 (14)	0.0011 (1)	0.0027 (18)	0.0002 (7)	0.0017 (7)
C(4)	0.5750 (9)	0.5229 (10)	0.0745 (4)	0.0074 (12)	0.0106 (15)	0.0020 (2)	0.0028 (20)	−0.0022 (8)	−0.0020 (9)
C(5)	0.4960 (9)	0.5616 (10)	0.1629 (3)	0.0076 (11)	0.0120 (15)	0.0010 (1)	0.0050 (21)	−0.0003 (7)	0.0017 (7)
C(6)	0.4573 (9)	0.6068 (9)	0.2150 (4)	0.0099 (13)	0.0035 (13)	0.0022 (2)	0.0036 (19)	−0.0014 (8)	0.0010 (7)
C(7)	0.3646 (10)	0.5292 (12)	0.2493 (4)	0.0099 (14)	0.0168 (18)	0.0020 (2)	0.0044 (24)	0.0006 (9)	0.0031 (11)
C(8)	0.3033 (12)	0.4042 (12)	0.2310 (4)	0.0145 (18)	0.0166 (20)	0.0025 (2)	0.0002 (29)	0.0017 (10)	0.0063 (11)
C(9)	0.3381 (10)	0.3564 (10)	0.1790 (4)	0.0096 (12)	0.0071 (14)	0.0026 (2)	−0.0017 (22)	−0.0002 (9)	0.0037 (9)
C(10)	0.4302 (9)	0.4359 (11)	0.1456 (4)	0.0086 (12)	0.0109 (15)	0.0018 (2)	0.0045 (22)	−0.0014 (8)	0.0016 (9)
H(1)	0.363	0.793	0.056						
H(2)	0.522	0.863	0.031						
H(3)	0.401	0.956	0.054						
H(4)	0.499	0.866	0.152						
H(5)	0.635	0.950	0.117						
H(6)	0.737	0.763	0.149						
H(7)	0.734	0.753	0.079	Final thermal parameter for hydrogen atoms: Overall isotropic; 3.3 Å^2					
H(8)	0.616	0.540	0.033						
H(9)	0.461	0.340	0.065						
H(10)	0.504	0.703	0.232						
H(11)	0.339	0.555	0.291						
H(12)	0.239	0.348	0.260						
H(13)	0.294	0.249	0.165						

Table 4. The molecular dimensions of tryptophan metabolites

	a*	b*	c*	d*	e	f	g
(A) Bond lengths (in Å)							
N(1)–C(1)	1.547	1.491	1.486	1.51	1.505	1.492	
C(1)–C(2)	1.501	1.502	1.513	1.53	1.539	1.532	
C(2)–C(3)	1.484	1.462	1.494	1.48	1.530	1.500	1.514
C(3)–C(4)	1.387	1.374	1.369	1.38	1.344	1.350	1.342
C(3)–C(5)	1.437	1.442	1.439	1.47	1.451	1.435	1.470
C(4)–N(2)	1.403	1.386	1.362	1.39	1.377	1.371	1.401
C(10)–N(2)	1.429	1.381	1.370	1.39	1.391	1.370	1.385
C(5)–C(10)	1.442	1.414	1.407	1.40	1.382	1.412	1.407
C(5)–C(6)	1.382	1.371	1.403	1.41	1.412	1.393	1.434
C(6)–C(7)	1.387	1.375	1.370	1.42	1.397	1.379	1.409
C(7)–C(8)	1.428	1.400	1.401	1.38	1.386	1.400	1.396
C(8)–C(9)	1.380	1.352	1.375	1.40	1.399	1.368	1.409
C(9)–C(10)	1.383	1.378	1.392	1.43	1.400	1.390	1.422
(B) Valency angles (in degree)							
N(1)–C(1)–C(2)	110.2	109.7	110.9	108	109.7	111.4	
C(1)–C(2)–C(3)	111.9	114.9	114.7	108	114.2	112.5	114.7
C(2)–C(3)–C(4)	125.4	128.4	127.8	131	128.0	125.8	127.2
C(2)–C(3)–C(5)	127.1	125.0	126.4	125	126.5	127.5	125.2
C(4)–C(3)–C(5)	107.5	106.6	105.7	104	105.5	106.6	107.1
C(3)–C(4)–N(2)	110.0	110.4	110.7	113	111.5	110.5	110.3
C(4)–N(2)–C(10)	108.2	108.0	108.8	106	107.4	108.7	108.2
N(2)–C(10)–C(5)	106.5	108.5	107.8	110	107.8	107.5	108.2
N(2)–C(10)–C(9)	129.7	130.3	130.8	128	129.0	130.8	128.2
C(5)–C(10)–C(9)	123.7	121.2	121.4	122	123.2	122.0	123.5
C(3)–C(5)–C(10)	107.7	106.6	106.9	107	107.7	106.8	106.1
C(6)–C(5)–C(10)	117.2	120.3	119.3	121	121.1	119.2	119.8
C(3)–C(5)–C(6)	135.0	133.0	133.7	132	131.2	134.2	134.1
C(5)–C(6)–C(7)	120.2	118.5	118.6	117	114.6	118.7	116.7
C(6)–C(7)–C(8)	121.0	119.7	121.7	122	124.8	121.2	122.2
C(7)–C(8)–C(9)	120.6	123.1	120.5	122	119.7	121.8	122.5
C(8)–C(9)–C(10)	117.3	117.0	118.4	116	116.4	117.7	115.2

a) Tryptamine hydrochloride, this work, b) 5-Hydroxy-DL-trypophan[14], c) Serotonin picrate monohydrate[7], d) Serotonin-creatinine sulfate complex[6], e) L-Tryptophan hydrochloride[15], f) DL-Tryptophan formate[16], g) 3-Indolylacetic acid[17]. * Radiation protective agents.

extent due to the difference in the localization of electron density distribution or the difference in the resonance structure of a five-membered ring of radiation protective agents compared with other indole derivatives.[18–20] The mean C–C distance in the benzene ring of tryptamine hydrochloride is 1.400 Å, while that of a pyrrole ring 1.422 Å. In all indole compounds, the C(3)–C(5) bond is evidently longer than the standard aromatic C–C bond.

Configuration. Aminoethyl side chain is in a folded configuration. The orientation of the C(2)–C(3) bond is *gauche* with respect to C(1)–NH_3^+ bond, and the torsion angles as defined by Klyne and Prelog[21] are −60.6° (*syn-clinal*) and +110.9° (*anti-clinal*) for the atoms N(1)–C(1)–C(2)–C(3) and C(1)–C(2)–C(3)–C(4), respectively. From conformational studies on tryptamine derivatives applying normal stereochemical rules, Chothia and Pauling proposed two possible values, 180° (*anti-periplanar*) and ±60° (*syn-clinal*), for the former torsion angle, and 0° (*syn-periplanar*) and ±90° (center of *clinal* region) for the latter one.[22] The configurations of 5-hydroxytryptophan and serotonin picrate resemble that of tryptamine. On the other hand, *anti-periplanar* conformation about C(1)–C(2) bond was observed in a serotonin-creatinine sulfate complex (+172.5°) and 5-methoxy-*N*,*N*-dimethyltryptamine hydrochloride (+179.2°). The best plane was computed for the atoms in the indole

14) Preceding paper; A. Wakahara, M. Kido, T. Fujiwara, and K. Tomita, This Bulletin, **46**, 2475 (1973).
15) T. Takigawa, T. Ashida, Y. Sasada, and M. Kakudo, *ibid.*, **39**, 2369 (1966).
16) E. Bye, A. Mostad, and C. Römming, *Acta Chem. Scand.*, **25**, 364 (1971).
17) I. L. Karle, K. Britts, and P. Gum, *Acta Crystallogr.*, **17**, 496 (1964).
18) A. Szent-Gyorgyi and I. Isenberg, *Proc. Nat. Acad. Sci. Wash.*, **46**, 1334 (1960).
19) J. P. Green and J. P. Malrieu, *ibid.*, **54**, 659 (1965).
20) R. Foster and C. A. Fyfe, *J. Chem. Soc., B*, **1966**, 926.
21) W. Klyne and V. Prelog, *Experientia*, **16**, 521 (1960).
22) C. Chothia and P. Pauling, *Proc. Nat. Acad. Sci. Wash.*, **63**, 1063 (1969).

Table 5. Distances of atoms from the least-squares plane through the indole ring (in Å)

Atom	Distance	Atom	Distance
C(3)	0.003	C(4)	0.013
C(5)	−0.022	C(6)	0.006
C(7)	−0.002	C(8)	0.009
C(9)	−0.004	C(10)	0.008
N(2)	−0.009	C(2)[a]	0.024
C(1)[a]	1.324	N(1)[a]	2.498

a) Excluded from calculation of the plane.

ring and expressed by the equation, $0.8146X-0.4580Y+0.3559Z=2.2578$ in rectangular coordinates in Ångstrom. The indole part of tryptamine molecule is planar, the mean deviation of the atoms from this plane being 0.008 Å and the maximum deviations are +0.0125 and −0.0217 Å for the atoms C(4) and C(5), respectively. The individual deviations of the atoms from this least-squares plane are given in Table 5. The plane formed by N(1), C(1) and C(2) atoms makes a dihedral angle of 83.9° with that of the indole plane. The corresponding angle in serotonin-creatinine sulfate is 12.6°.

The Molecular Environment. The crystal structure viewed along a-axis is given in Fig. 4 and intermolecular distances less than 3.75 Å including hydrogen bonds in Table 6. The side chains of tryptamine are in a folded configuration, and the packing is dominated by a three-dimensional network of hydrogen bonds. The three hydrogen atoms attached to an amino nitrogen atom form three hydrogen bondings with adjacent chloride ions. These three chloride atoms are approximately at three vertices of a regular tetrahedron centered at the N(1) atom, with the C(1) atom directed toward the fourth vertex, the average N–H···Cl

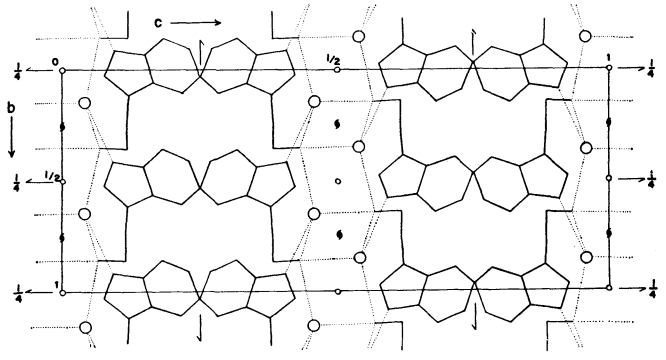

Fig. 4. The crystal structure of tryptamine hydrochloride projected along a-axis.

Table 6. Intermolecular short contacts less than 3.75 Å

Symmetrycode			
Original molecule	x	y	z
(A)	$-1/2+x$	$3/2-y$	$-z$
(B)	$1/2-x$	$-1/2+y$	z
(C)	$1/2-x$	$1/2+y$	z
(D)	$1/2+x$	y	$1/2-z$
(E)	$1-x$	$-1/2+y$	$1/2-z$
(F)	$3/2-x$	$-1/2+y$	z

(a) Hydrogen bonds

Donor	Acceptor (Original molecule)	Distance	Angle of C-Donor-Acceptor
Original N(1)–H(1)	Cl	3.221 Å	128.2°
(A) N(1)–H(2)	Cl	3.157	105.9
(B) N(1)–H(3)	Cl	3.158	108.5
(C) N(2)–H(9)	Cl	3.235	111.0

(b) Other short contacts

Atom (i)	Atom (j)	Distance (d_{ij})
C(9)	N(1) (B)	3.705 Å
C(9)	C(1) (B)	3.722
C(9)	C(6) (B)	3.659
C(8)	C(6) (B)	3.742
C(6)	C(7) (D)	3.671
C(7)	C(1) (E)	3.748
N(2)	C(2) (F)	3.459
C(4)	C(2) (F)	3.688
C(4)	C(1) (F)	3.668

distance being 3.179 Å. Another hydrogen bond is found between the N(2) atom of indole ring and chloride ion, whose distance is 3.235 Å. As a whole, each chloride atom links with the four neighboring tryptamine cations. N(1)–H···Cl hydrogen bonds form infinite columns around the center of symmetry or along the screw axes, and molecules are arranged in a double layered system parallel to *ab*-plane. In the polar part of the molecules, the hydrogen bond formation is substantial to stabilize the molecular packing. The indole rings are packed by van der Waals forces into the non-polar layer. Unusual short contacts are not observed (Table 6).

The authors wish to thank Drs S. Kobayashi and W. Nakamura, National Institute of Radiological Sciences, Chiba, for discussions and interest throughout the course of this investigation. The work was partly supported by a research grant from the Ministry of Education

Photochemical Reaction of Diaryl Thioketones in Ethereal Solutions. A Stable Transient Free-Radical

Noboru KITO and Atsuyoshi OHNO

Sagami Chemical Research Center, Nishiohnuma, Sagamihara-shi, Kanagawa 229

(Received February 1, 1973)

Photochemical reactions of thiobenzophenone and its 4,4′-dimethoxy derivative in ethereal solutions such as tetrahydrofuran and diethyl ether have been studied by means of product analyses and ESR spectroscopy. It was found that the reaction involves quite stable transient free-radicals of the type $Ar_2\dot{C}SR$. The efficiency of free-radical trapping by diaryl thioketones and the reaction mechanism are discussed.

Photo-excited thiobenzophenone abstracts the hydrogen atom from an appropriate solvent through its n,π* triplet state, giving diphenylsulfhydrylmethyl radical.[1,2] The primary process of the reaction is similar to that of benzophenone[3] but products differ to a great extent. In order to obtain further insight into the photo-reaction of thiobenzophenone, we have studied ESR spectroscopy of the transient free-radicals in ethereal solutions. The results are given in this paper. Several studies have been made on detection and positive indication by ESR spectroscopy of transient free-radical species produced by continuous photo-irradiation.[4]

Thiobenzophenone is a good scavenger for free carbon-radicals.[5] The results of the present study also give a direct evidence for the mechanism of scavenging reactions and suggest the availability of thiobenzophenone as a spin-trapping agent.

Results and Discussion

Products. Irradiation with light (>300 nm) on thiobenzophenone in tetrahydrofuran (THF) afforded **1**, **2**, and **3** in 3.1, 35.2, and 54.5% yields, respectively. A similar reaction in diethyl ether gave **1**, **4**, and **5** in 3.6, 37.4, and 52.0% yields, respectively. Their structures were confirmed by spectral and elemental analyses. It was confirmed that no rearrangement from **3** to **2** and from **5** to **4** or *vice versa* took place under the reaction conditions. Compounds **2** and **4** were apparently resulted in by the (in-cage) combination of diphenylsulfhydrylmethyl, **6a**, and the solvent-derived free-radicals, **8**,[1] while **3** and **5** were formed by the reaction of solvent-derived free-radicals with thiobenzophenone, a potential molecular-type scavenger toward carbon-radicals.[5,6] Thus, the analyses of products suggest that the reaction involves three transient free-radicals, **6a**, **7a**, and **8**.

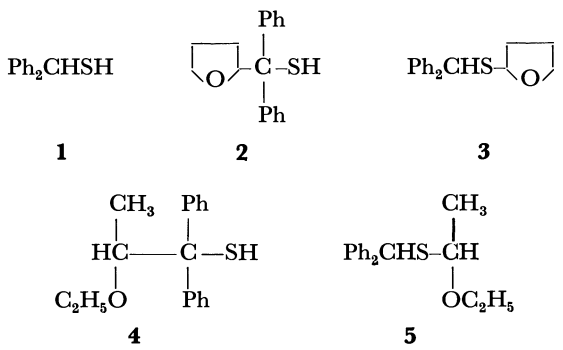

1 **2** **3**

4 **5**

$Ar_2\dot{C}$–SH $Ar_2\dot{C}$–SR

6a: Ar=C_6H_5– **7a**: Ar=C_6H_5–

6b: Ar=4-$CH_3OC_6H_4$– **7b**: Ar=4-$CH_3OC_6H_4$–

(RH=solvent molecule)

8a

8b

ESR Spectroscopy. The ESR spectrum obtained by continuous photo-irradiation on THF solution of thiobenzophenone at 25 °C is shown in Fig. 1a.

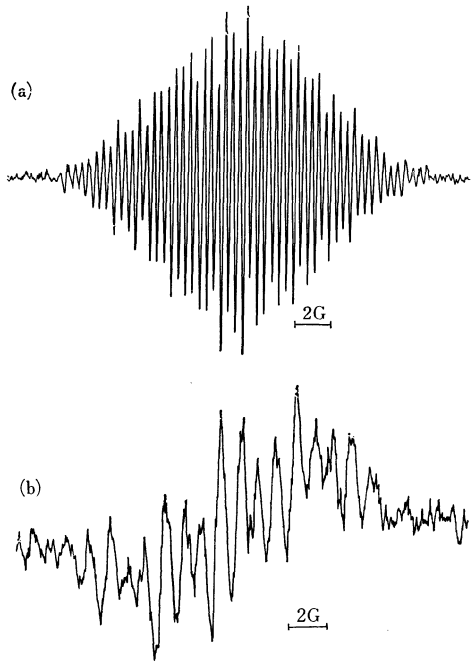

Fig. 1. Observed ESR spectra of **7a** in (a) THF and (b) MTHF.

1) A. Ohno and N. Kito, *Int. J. Sulfur Chem., A*, **1**, 26 (1971).
2) D. R. Kemp and P. de Mayo, *Chem. Commun.*, **1972**, 233.
3) G. Porter and F. Wilkinson, *Trans. Faraday Soc.*, **57**, 1685 (1961).
4) a) P. B. Ayscough and R. Wilson, *J. Chem. Soc.*, **1963**, 5412; b) P. B. Ayscough, E. P. Sargent, and R. Wilson, *ibid.*, **1963**, 5418; c) R. Wilson, *J. Chem. Soc. B*, **1968**, 84; d) R. L. Ward, *J. Chem. Phys.*, **38**, 2588 (1963); e) R. Wilson, *Can. J. Chem.*, **44**, 551 (1966).
5) G. Tsuchihashi, M. Yamauchi, and A. Ohno, This Bulletin, **43**, 968 (1970).
6) A. Ohno, Y. Ohnishi, M. Fukuyama, and G. Tsuchihashi, *J. Amer. Chem. Soc.*, **90**, 7038 (1968).

Table 1. Hyperfine splitting constants and g-values for photo-paramagnetic diaryl thioketones-THF system

Starting Thioketone	A_o	A_m	A_p	A_{OCH_3}	$A_{\alpha H}$	g-Value
$(C_6H_5)_2C{=}S$	2.71	0.77	3.10	—	1.16	2.0051
$(4\text{-}CH_3OC_6H_4)_2C{=}S$	2.45	0.70	—	0.35	1.05	2.0053

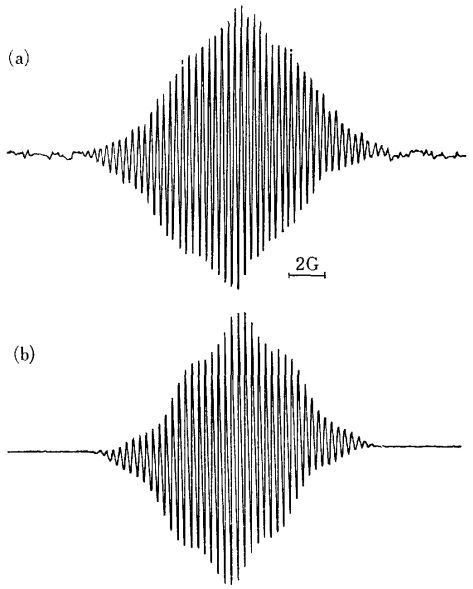

Fig. 2. (a) Observed and (b) calculated ESR spectra of **7b** in THF.

The observed spectra accord well with their computer-simulated ones[7] using the splitting constants, listed in Table 1, with a line width of 192 mG (Fig. 2). They are spectra of neither **8a**[8] nor thioketyls,[9,10] and must be those of **6** or **7**.

When the photo-reaction was carried out in 2-methyltetrahydrofuran (MTHF), the recorded spectrum distinctly showed the absence of double-splittings (Fig. 1b). Figure 3 shows the ESR spectrum of photo-irradiated thiobenzophenone in diethyl ether. The doublet-splittings of 1.12 gauss observed here are again absent when the reaction is carried out in di-

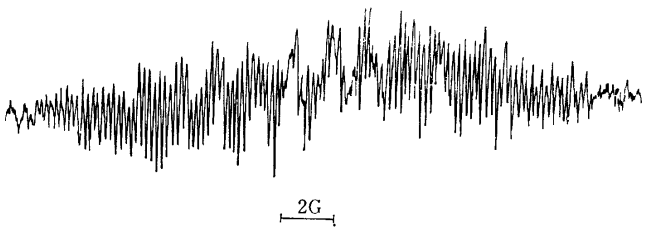

Fig. 3. Observed ESR spectrum of **7a** in diethyl ether.

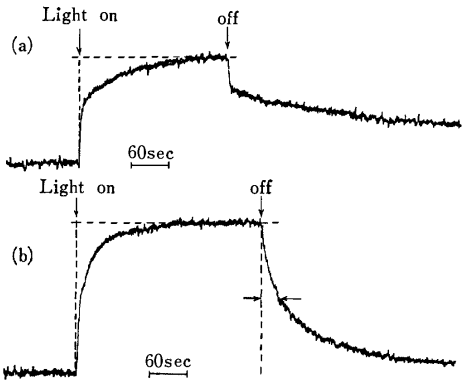

Fig. 4. The change of the intensities of ESR spectra due to the transient free-radicals during the photolyses of (a) thiobenzophenone (10.833 mM) and (b) 4,4'-dimethoxythiobenzophenone (10.173 mM) in THF at 25°C. The spectra were recorded with modulation width of 20 gauss and with response time of 0.1 sec.

isopropyl ether. These results indicate unequivocally that the free-radicals detected on the spectrometer are not **6** but **7**.

It is noteworthy that **7** is a quite stable free-radical. From the decay-curves (Fig. 4), half-lives of **7a** and **7b** (RH=THF) in THF at 25 °C are calculated to be 90 and 29 sec, respectively. Since these values are independent of initial concentrations of diaryl thioketones and irradiation time, the kinetics of the decay is of first-order in **7**. Formation of such a long-lived composite free-radical may make thiobenzophenone a useful reagent for spin-trapping.

Another paramagnetic species is detected from the reaction of thiobenzophenone (Fig. 4a). This accumulates rapidly when the light is turned on and decays instantaneously when it is shut off. We believe that this short-lived species is **6a**. If this were due to **8a**, the absence of such a phenomenon in Fig. 4b cannot be rationalized: since **7b** is less stable than **7a** under experimental conditions, the trapping of **8a** by 4,4'-dimethoxythiobenzophenone should be less effective than that by thiobenzophenone.[11] Thus, both **6a** and **7a** are more stable (or less reactive) than **6b** and **7b**, respectively. The substituent effect observed here is a general trend for the stability of benzyl-type free-radicals.[12]

Thus the mechanism of the photochemical reaction of diaryl thioketones in ethereal solutions is as follows:

$$Ar_2C{=}S \xrightarrow{h\nu} \longrightarrow {}^3(Ar_2C{=}S)_{n,\pi^*}$$

$${}^3(Ar_2C{=}S)_{n,\pi^*} + RH \longrightarrow Ar_2\dot{C}\text{-}SH + R\cdot$$

$$Ar_2\dot{C}\text{-}SH + R\cdot \longrightarrow Ar_2C\begin{matrix}R\\SH\end{matrix}$$

$$Ar_2\dot{C}\text{-}SH + RH \longrightarrow Ar_2CHSH + R\cdot$$

7) The computer program for the simulation of spectra was supplied by The Shionogi Research Laboratory. We wish to express our cordial thanks to Dr. K. Nishikida. The program was run by IBM 360 System.

8) A. J. Dobbs, B. C. Gilbert, and R. O. C. Norman, *Chem. Commun.*, **1969**, 1353.

9) H. C. Heller, *J. Amer. Chem. Soc.*, **89**, 4288 (1967).

10) E. G. Janzen and C. M. DuBose, Jr., *J. Phys. Chem.*, **70**, 3372 (1966).

11) G. Tsuchihashi, M. Ohnishi, and A. Ohno, Abstract of papers, 4th Symposium on Organosulfur Chemistry, Gifu City, Gifu, 1970, pp 8—10.

12) a) C. Walling, E. R. Briggs, K. B. Walfstirn, and F. R. Mayo, *J. Amer. Chem. Soc.*, **70**, 1537 (1948); b) M. Imoto, M. Kinoshita, and M. Nishigaki, *Makromol. Chem.*, **86**, 217 (1965).

$$Ar_2C{=}S + R\cdot \longrightarrow Ar_2\dot{C}{-}SR$$

$$Ar_2\dot{C}{-}SR + RH \longrightarrow Ar_2CHSR + R\cdot$$

Since the last two processes constitute a chain reaction, they suggest the possibility that the half-lives of the free-radicals do not necessarily mean the *true* values. However, we believe they are almost true, if not completely so. The concentration of **8a** is too low to be detected, indicating immediate trapping of **8a** by thiobenzophenone. Therefore, if the hydrogen-abstraction by **7** is a fast process, its steady-state concentration may also be too low to be detected after the light is shut off.

Experimental

Materials. Thiobenzophenone was prepared as reported previously.[1] 4,4'-Dimethoxythiobenzophenone was similarly prepared from the corresponding ketone in 88% yield. The thioketone was recrystallized twice from ethanol-chloroform mixture: mp 117—118 °C (lit,[13] mp 116—118 °C).

Solvents were refluxed over calcium hydride under a 50 cm column packed with helics for several days and fractionally distilled. The second distillation was performed just before use over sodium wire after being refluxed for a few hours.

Spectrometry. A 0.25—0.50 M solution of a thioketone placed in a 10 mm o.d. glass tube connected with 1.5—2.0 mm o.d. quartz tube was thoroughly degassed by the usual thawing and freezing method and sealed in a high vacuum (10^{-6} torr). The light from a 100W high-pressure mercury lamp was focused on the sample in the microwave cavity of the ESR spectrometer. The spectra of photochemically generated transient free-radicals were recorded at 25±0.3 °C (room temperature) with a X-band JES-ME-IX type spectrometer (Japan Electron Optics Laboratory Co. Ltd.) with 100 KHz field modulation. In order to obtain well resolved spectra, it was necessary to adjust concentrations of the solution and find the right moment of irradiation with respect to life-time of free-radicals.

Photochemical Reaction of Thiobenzophenone in THF. Prior to the reaction, slow stream of argon gas was passed for 30 min through the THF (60 m*l*) solution of thiobenzophenone (613 mg, 2.59 mmol) in a Pyrex vessel. Irradiation with light from a 400W high-pressure mercury lamp (principal wavelength: 315 and 366 nm) was continued until complete decolorization of the thioketone (19 hr) took place at the temperature of running water. After excess solvent was removed, the residue was chromatographed on a column of silica-gel with elution by a mixture of *n*-hexane and benzene. The following compounds were isolated (mg, % yield, *n*-hexane : benzene ratio): diphenylmethanethiol (**1**) (16, 3.1, 2 : 8), diphenyltetrahydro-2-furylmethanethiol (**2**) (246, 35.2, 3:7), and benzhydryl tetrahydro-2-furyl sulfide (**3**) (381, 54.5, 4 : 6).

2: NMR(δ from TMS, CCl_4) 1.48—2.01 (m, 4H), 2.28 (s, 1H), 3.63—3.97 (m, 2H), 4.65—4.93 (m, 1H), and 7.02—7.55 (m, 10H); mass spectrum (*m/e*) 270 (M^+), 236, 200, 199, 198 (Ph_2CS^+, base), 165, 121, and 71; Found: C, 75.48; H, 6.60; S, 11.80%. Calcd for $C_{17}H_{18}OS$: C, 75.53; H, 6.71; S, 11.84%.

3: NMR(δ from TMS, CCl_4) 1.49—2.30(m, 4H), 3.71—4.17(m, 2H), 4.85—5.03(m, 1H), and 7.04—7.56(m, 10H), mass spectrum (*m/e*) 270 (M^+), 168, 167 (Ph_2CH^+, base), 166, 165, 151, 105, 77, and 71; Found: 75.41; H, 6.58; S, 11.81%. Calcd for $C_{17}H_{18}OS$: C, 75.53; H, 6.71; S, 11.84%.

Photochemical Reaction of Thiobenzophenone in Diethyl Ether. An ether solution (60 ml) of thiobenzophenone (580 mg, 2.93 mmol) was similarly irradiated for 30 hr. Separation on a column chromatography gave the following compounds (mg, % yield, *n*-hexane : benzene ratio): diphenylmethanethiol (**1**) (21, 3.6, 2 : 8), 1,1-diphenyl-2-ethoxypropanethiol (**4**) (298, 37.4, 3 : 7), and benzhydryl 1-ethoxyethyl sulfide (**5**) (412, 52.0, 4 : 6).

4: NMR(δ from TMS, CCl_4) 1.11 (d, 3H), 1.13 (t, 3H), 2.53 (s, 1H), 3.52 (q-q, 2H), 4.24 (q, 1H), and 7.03—7.54(m, 10H); mass spectrum (*m/e*) 272 (M^+), 238, 200, 199, 198 (Ph_2CS^+, base), 167, 165, 121, 105, and 73; Found: C, 74.81; H, 7.41; S, 11.70%. Calcd for $C_{17}H_{20}OS$: C, 74.97; H, 7.40; S, 11.75%.

5: NMR(δ from TMS, CCl_4) 1.10 (t, 3H), 1.47 (d, 3H), 3.48 (q-q, 2H), 4.50 (q, 1H), 5.23 (s, 1H), and 7.03—7.47 (m, 10H); mass spectrum (*m/e*) 272 (M^+), 236, 168, 167 (Ph_2CH^+, base), 166, 165, 105, 77, 73; Found: C, 74.79; H, 7.35; S, 11.72%. Calcd for $C_{17}H_{20}OS$: C, 74.97; H, 7.40; S, 11.75%.

13) R. M. Elofson, L. A. Baker, F. F. Gadallah, and R. A. Sikstrom, *J. Org. Chem.*, **29**, 1355 (1964).

Palladium-Catalyzed Coupling Reaction of Aromatic Compounds

Hataaki YOSHIMOTO and Hiroshi ITATANI

Ube Industries, Ltd., Polymer Research Laboratory, Goi, Ichihara-shi, Chiba 290

(Received February 19, 1973)

The oxidative coupling reaction of aromatic compounds proceeds catalytically with palladium salt under oxygen pressure. Yields and isomer distributions are attributed to the reaction variables such as temperature, additives, and the nature of the substituent on a benzene ring. Naphthalene was converted mainly into 1-substituted products and *o*-xylene into 4-substituted products. The coupling of diphenyl ether afforded diphenylene oxide with coupling dimers. An intramolecular two stage dehydrogenation process is proposed.

Palladium compounds have recently attracted much attention from the viewpoint of synthetic organic chemistry and theoretical interest.[1] Van Helden and Verberg[2] reported on the oxidative coupling of benzene derivatives by palladium chloride and sodium acetate in acetic acid solution. Subsequent studies by Davidson and Triggs[3] showed no precipitation of metallic palladium under oxygen pressure. No coupling proceed catalytically since excess acetic acid existed in the reaction system. We have reported[4] on the palladium-catalyzed coupling reaction of styrene with benzene under oxygen pressure in the absence of acetic acid. This paper gives a detailed description of the palladium-catalyzed coupling of aromatic compounds.[5]

Results

Coupling of Alkylbenzenes. Coupling of toluene gave six isomers, 2,2'-, 2,3'-, 2,4'-, 3,3'-, 3,4'-, and 4,4'-dimethylbiphenyls. Yields and isomer distributions of bitolyls at several temperatures are given in Table 1. *Meta*-substituted bitolyls were major products and the yield of *ortho*-substituted bitolyls increased with increasing temperature. However, the system of palladium chloride and sodium acetate[6] accelerated the formation of *ortho*-substituted bitolyls with decreasing temperature. The difference may be due to the reaction process. The former is a catalytic reaction whereas the latter is stoichiometric, precipitating palladium black during the course of reaction. Methyl group shows a high degree of steric effect on the coupling. Namely, yields of biaryls at 150 °C were 7500, 5700, 4100, 400, and zero percent from toluene, *o*-xylene, *m*-xylene, *p*-xylene, and mesitylene as starting material, respectively. The coupling product of *o*-xylene consisted of 1% of 2,3,2',3'-, 24% of 2,3,3',4'-, and 75% of 3,4,3',4'-tetramethylbiphenyls, whereas that of naphthalene contained 43% of 1,1'-, 50% of 1,2'-, and 7% of 2,2'-binaphthyls. The former is contributed by steric requirement and the latter by electronic factor.

Table 1. Yield and isomer distribution of dimethylbiphenyl[a]

Reation		Compositions (%)						
Temp. °C	Press. kg/cm²	2,2'	2,3'	2,4'	3,3'	3,4'	4,4'	yield[c] (%)
120	50	2	12	8	31	36	11	1840
150	50	2	13	10	28	35	12	5140
180	50	2	19	13	24	30	12	2270
120	13	2	17	13	28	31	9	480
150[b]	50	2	12	8	32	34	12	7500

a) Carried out with $Pd(OAc)_2$ (0.5 mmol) and toluene (50 ml).
b) Acetylacetone (0.5 mmol) was added.
c) Based on $Pd(OAc)_2$ used.

Table 2. Effect of palladium compounds on coupling of toluene[a]

Pd compound	Bitolyl yield %[b]
$Pd(OAc)_2$	5140
$Pd(OAc)_2$ + acetylacetone	7400
$Pd(acac)_2$	5400
$Pd(OAc)_2(PPh_3)_2$	1700
$Pd(PPh_3)_4$	310
$PdCl_2$ + KOAc (1 : 5)	200

a) Carried out with Pd compound (0.5 mmole), toluene (50 ml).
b) Based on Pd compound used.

Table 3. Effect of β-diketone on coupling of dimethyl phthalate[a]

β-Diketone	Biaryl yield %[b]
Acetylacetone	5200
Benzoylacetone	3600
Trifluoroacetylacetone	3070
Ethyl acetoacetate	3000
——	2130
Acetoacetanilide	1570
Salicylaldehyde	500

a) Carried out with $Pd(OAc)_2$ (1 mmol), β-diketone (1 mmol), dimethyl phthalate (100 ml) and O_2-N_2 (1 : 1) (50 kg/cm²) at 150°C for 6 hr.
b) Based on $Pd(OAc)_2$ used.

1) a) R. Huttel, *Synthesis*, **1970**, 225; b) E. W. Stern, "Catalysis Reviews," Vol. 1, ed. by H. Heinemann, Marcel Dekker, Inc., New York, N. Y. (1968), p, 73. c) J. Tsuji, "Advances in Organic Chemistry," vol. 6, ed. by E. C. Taylor, and H. Wynberg, Interscience Publishers, New York, N. Y. (1969), p. 109.
2) R. van Helden and G. Verberg, *Rec. Trav. Chim. Pays-Bas*, **84**, 1263 (1965).
3) J. M. Davidson and C. Triggs, *Chem. Ind.* (London), **1966**, 457; **1967**, 1361; *J. Chem. Soc., A*, **1968**, 1324; 1331.
4) a) H. Itatani, M. Matsuda, and H. Yoshimoto, Japan 92041 (1968); 33687 (1969). b) I. Moritani, Y. Fujiwara, S. Teranishi, H. Itatani, and M. Matsuda, Symposium on Homogeneous Catalytic Reactions Involving Palladium, American Chemical Society, Minneapolis Meeting, April, 1969, B. 172.
5) H. Itatani and H. Yoshimoto, *Chem. Ind.* (London), **1971**, 674.
6) M. O. Unger and R. A. Fouty, *J. Org. Chem.*, **34**, 18 (1969).

Effect of Palladium Compounds. Various palladium compounds can be used as catalyst (Table 2). Palladium acetylacetonate as well as palladium acetate are effective catalysts. Tetrakis(triphenylphosphine)palladium shows lower activity, precipitating palladium metal during the course of reaction.

Effect of Additives. Addition of an equimolar amount of acetylacetone to palladium acetate increased the yield of the coupling products (Tables 1 and 2). The influence of several β-diketones on the yield of bitolyl is shown in Table 3. Acetylacetone highly activated palladium acetate for the coupling.

Effect of Reaction Variables. Increase in oxygen pressures increases the yields of coupling products but not pressure above 25 kg/cm^2. Under 50 kg/cm^2 of the mixture of nitrogen and oxygen (1 : 1), use of less than 10 mmol/l of palladium acetate is recommended since the overall yield of biaryls does not increase in the presence of excess palladium acetate. Addition of solvent to this system remarkably decreased the yield of coupling products. However, mesitylene or butyl acetate can be applied in as little an amount as possible for the coupling of high melting compounds such as anthracene, phenanthrene, and acenaphthene.

Coupling of Diphenyl Ether. Diphenyl ether was considerably converted into diphenylene oxide, an intramolecular coupling product, with dimerized products. However, the reaction of diphenylmethane involved a small amount of fluorene, an intramolecular coupling product, with dibenzylbiphenyl, benzophenone, and fluorenone. The coupling of anisole gave dimethoxybiphenyl containing only 2% of *ortho*-disubstituted isomer (Table 4).

Table 4. Coupling of diphenyl ether and the related derivatives[a]

Aromatic compound	Products	Yield %[b]
Diphenyl ether	Diphenylene oxide	3080
	Dimers of diphenyl ether	4610
Diphenylmethane	Fluorene	340
	Dimers of diphenylmethane	5010
	Benzophenone	4120
	Fluorenone	230
Anisole[c]	Dimethoxybiphenyl[d]	740

a) Carried out with $Pd(OAc)_2$ (0.15 mmol), acetylacetone (0.15 mmol), aromatic compound (15 ml).
b) Based on $Pd(OAc)_2$ used.
c) Reaction temperature, 120°C.
d) The compositions are 2,2'- 2%, 2,3'- 10%, 2,4'- 21%, 3,3'- 17%, 3,4'- 29%, 4,4'- 21%.

Discussion

Davidson and Triggs[3] proposed an intermolecular coupling process of σ-phenylpalladium(II) complex on the basis of isolation of palladium(I) complex and measurement of kinetic isotope effect. Unger and Fouty[6] suggested the intramolecular reaction through a diarylpalladium(II) complex for explaining the isomer distribution of bitolyls.

Under oxygen pressure in the absence of acetic acid the coupling reaction is catalytic and thus the yield of biaryl was greatly enhanced. In this system, palladium remaining in the solution can be reoxidized to its active oxidation state by the action of molecular oxygen.

Oxygen adduct complex $Pd(PPh_3)_2O_2$[7,8] takes part in the oxidation of the coordinating triphenylphosphine to triphenylphosphine oxide. Stern[9] explained the mechanism by assuming that the oxygen adduct palladium(0) complex serves to abstract hydrogen from aromatic nucleus and concurrently changes to a σ-arylpalladium(II) complex. By applying this mechanism, the overall process for the palladium-catalyzed coupling can be represented as follows.

$$PdX_2 + 2RH \longrightarrow R\text{-}Pd\text{-}R + 2HX$$
$$R\text{-}Pd\text{-}R \longrightarrow R\text{-}R + Pd$$
$$Pd + O_2 + RH \longrightarrow R\text{-}Pd\text{-}OOH$$
$$R\text{-}Pd\text{-}OOH + acacH \longrightarrow R\text{-}Pd\text{-}acac + HOOH$$
$$R\text{-}Pd\text{-}acac + RH \longrightarrow R\text{-}Pd\text{-}R + acacH$$

where RH denotes an aromatic compound, and acacH acetylacetone. The key step of the mechanism is a reoxidation of palladium(0) with molecular oxygen. The effect of addition of acetylacetone to this system may be explained by assuming the formation of a stable *cis*-diaryl palladium complex which is active on subsequent coupling in analogy with *cis*-hydroxo-olefin complex[1b] known in the Wacker process.

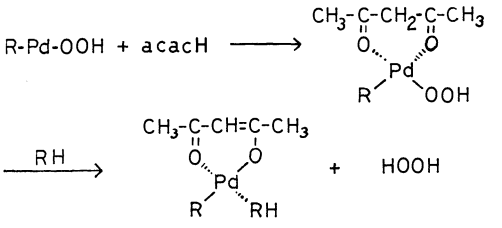

The two stage coupling mechanism was proposed based on the primary isotope effects[10] in the competitive coupling between benzene and benzene-d_6 and also the characteristic isomer distributions of biaryls.

Isomer distribution of the coupling products changes remarkably with the substituent. The coupling of *o*-xylene is attributed to steric effect of methyl group while naphthalene is influenced by polar effect. The

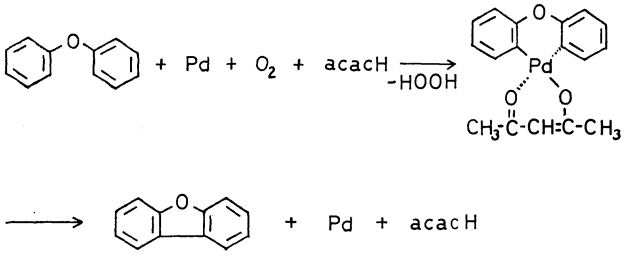

7) G. Wilke, H. Schott, and P. Heimbach, *Angew. Chem.*, **79**, 62 (1967); *Angew. Chem. Int. Ed. Engl.*, **6**, 92 (1967).
8) S. Takahashi, K. Sonogashira, and N. Hagihara, *Nippon Kagaku Zasshi*, **87**, 610 (1966).
9) E. W. Stern, "Transition Metals in Homogeneous Catalysis," ed. by G. N. Schrauzer, Marcel Dekker, Inc., New York, N. Y. (1971), p. 93.
10) M. Kashima, H. Yoshimoto, and H. Itatani, *J. Catal.*, **29**, 92 (1973).

reaction of diphenyl ether affords an intramolecular ring closure which is facilitated *via* a stable transition state of a six π electron system, whereas the reaction of diphenylmethane does not favor a ring formation.

The possibility exists that biphenyl formation may involve homolytic substitution of phenyl radical.[11] However, it is well-known that a radical can not exist in the presence of oxygen. The presence of excess 2,6-di-*tert*-butyl-*p*-cresol does not influence the coupling at all. Thus the reaction mechanism involving free radicals is unlikely.

In contrast to the Wacker process and acetoxylation of olefins, the palladium-catalyzed oxidative coupling is markedly inhibited in the presence of mineral acid, polar solvent, sodium acetate, lithium chloride, and some metal ions. The coupling process favors the simple system consisting of palladium acetate and aromatic compounds under oxygen pressure. For prevention of explosion, oxygen should be diluted with an inert gas.

Experimental

Palladium acetate,[12] palladium acetylacetonate[13] and tetrakis(triphenylphosphine)palladium[8] were prepared according to literatures. Palladium chloride (Nippon Engelhald Co.) and a gaseous mixture of oxygen and nitrogen (1 : 1) (Nippon Sanso Co.) were used. Benzene, toluene, and *o*-xylene were distilled before use. Other chemicals were reagent grade and were used without further purification.

Bis(triphenylphosphine)palladium Acetate. To a stirred solution of palladium acetate (0.224 g) in ether (25 ml) was added a solution of triphenylphosphine (0.786 g) in ether (25 ml). After stirring at room temperature for 1 hr, yellow precipitates formed were collected, washed with ether and dried, mp 118—120 °C. Found: C, 64.77; H, 4.99%. Calcd for $C_{40}H_{36}O_4P_2Pd$: C, 64.14; H, 4.84%.

General Procedure. In a glass vessel (250 ml) were placed palladium acetate, acetylacetone, aromatic compound and some additives when necessary. The glass vessel was inserted into a stainless steel autoclave (300 ml) and subjected to a pressure of 50 kg/cm^2 with a gaseous mixture of oxygen and nitrogen (1 : 1) at room temperature. The autoclave was heated at 150 °C for 4 hr with shaking 35 times per minute. After cooling, the filtrate was analyzed with a Shimadzu GC 4APT gas chromatograph on silicone SE 30 (20% on Diasolid, 1 m long) and Apiezon L (5% on Diasolid, 2 m long) columns using helium as a carrier gas. Products were identified with authentic samples by glc and also by comparison of their melting points (if isolated), IR and mass spectra.[14]

Coupling Reaction of Diphenyl Ether. The reaction was carried out in an autoclave (100 ml). The resulting products were analyzed by glc (SE 30 column). Stilbene was used as an internal standard for diphenylene oxide, and pyrene was used for the coupling dimers. The fraction boiling at 200—240 °C/1 mmHg was collected from the reaction mixture. The mass spectrum shows the molecular ion at *m/e* 338 which is consistent with the dimer of diphenyl ether.

Coupling of Naphthalene. A mixture of naphthalene (50 g), palladium acetate (0.112 g), and acetylacetone (0.050 g) was shaken at 150 °C for 4 hr. The resulting solution was analyzed by glc (SE 30 column) at 240 °C. Triphenylethylene was used as an internal standard. Binaphthyl was obtained in 4500% yield based on palladium acetate used. The composition was shown to be 43% of 1,1′-, 50% of 1,2′-, and 7% of 2,2′-binaphthyls. After removal of naphthalene by distillation, the residue was chromatographed over alumina using benzene as a solvent. Evaporation of benzene gave 6.9 g of crude binaphthyls which was extracted with hot methanol (110 ml) to afford 1,1′-binaphthyl (1.4 g) having mp 157—158 °C. After recrystallization from ethanol, mass spectroscopy showed the molecular ion 254 identical with 1,1′-binaphthyl. The residue was again treated with a mixture of benzene (25 ml) and ethanol (75 ml). The undissolved material (0.3 g) was collected by filtration. Recrystallization from benzene gave 2,2′-binaphthyl mp 182—183 °C. Mass spectroscopy showed the molecular ion to be identical with 2,2′-binaphthyl. 1,2′-Binaphthyl was identified by comparison of glc retention time with that of an authentic specimen prepared from 2-tetralone and 1-bromonaphthalene according to the modified procedure by M. Orchin[15] for the synthesis of 2-ethylbiphenyl.

11) O. C. Dermer and M. T. Edmison, *Chem. Rev.*, **57**, 77 (1957).
12) T. A. Stephenson, S. M. Morehouse, A. R. Powell, J. P. Heffer, and G. Wilkinson, *J. Chem. Soc.*, **1965**, 3632.
13) A. A. Grinberg, L. K. Simonova, *Zh. Prikl. Khim.*, **26**, 880 (1953); *Chem. Abstr.*, **47**, 11060 g (1953).
14) H. Itatani and H. Yoshimoto, *J. Org. Chem.*, **38**, 76 (1973).
15) M. Orchin, *J. Amer. Chem. Soc.*, **68**, 571 (1946).

Studies on Carbamoylation Reactions of Polyethylenimine and Its Low Molecular Weight Analogues with Cyanate Ions

Tsuneo Okubo and Norio Ise

Department of Polymer Chemistry, Faculty of Engineering, Kyoto University, Sakyo-ku, Kyoto 606

(Received February 22, 1973)

Carbamoylation reaction of ions of polyethylenimine and its low molecular weight analogues, *i.e.*, ethylenediamine, triethylenetetramine, and tetraethylenepentamine, with cyanate ions are investigated in the presence of simple-, micelle-, and poly-electrolytes and in their absence. The rate constants are practically independent of the valency of the cations and are much larger than that previously found for the ammonium cyanate reaction. Both of the activation enthalpy and entropy decrease with increasing valency of the cations. Added electrolytes are found to decelerate the reactions. The reactions of polycations are retarded more strongly by simple cations than by catalyst polycations, whereas those of simple cations are decelerated more effectively by polycations than by simple cations. The kinetic data are discussed thermodynamically in terms of the Brönsted theory and the activity coefficients of the reactant ions. The interaction parameters between reactant electrolyte and added electrolyte are also derived thermodynamically and discussed.

Interionic reactions in the presence of various electrolytes are interesting from the biological point of view and have been studied by many researchers (For a convenient review, see Ref. 1). In a previous paper,[2] we studied quantitatively the catalytic influence of polyelectrolytes for the ionic reaction between oppositely charged ionic species shown in Eq. 1, and also the electrostatic interactions between ions of polyelectrolytes and those of simple electrolytes.

$$NH_4^+ + OCN^- = (NH_2)_2CO \qquad (1)$$

In this paper we obtain quantitative information on ionic reactions between ionic species of various charge types. For this purpose, the carbamoylation reactions of ethylenediamine, triethylenetetramine, tetraethylenepentamine and polyethylenimine with cyanate ions shown in Eqs. (2), (3), (4) and (5) are studied.

$$\overset{+}{N}H_3\text{–}CH_2\text{–}CH_2\text{–}\overset{+}{N}H_3 + 2OCN^- = \underset{\displaystyle CONH_2}{\overset{\displaystyle |}{NH}}\text{–}CH_2\text{–}CH_2\text{–}\underset{\displaystyle CONH_2}{\overset{\displaystyle |}{NH}} \qquad (2)$$

$$\overset{+}{N}H_3\text{–}(\text{–}CH_2\text{–}CH_2\text{–}\overset{+}{N}H_2\text{–})\text{–}H + 4OCN^- = \underset{\displaystyle CONH_2}{\overset{\displaystyle |}{NH}}\text{–}(\text{–}CH_2\text{–}CH_2\text{–}\underset{\displaystyle CONH_2}{\overset{\displaystyle |}{N}}\text{–})_3\text{–}H \qquad (3)$$

$$\overset{+}{N}H_3\text{–}(\text{–}CH_2\text{–}CH_2\text{–}\overset{+}{N}H_2\text{–})_4\text{–}H + 5OCN^- = \underset{\displaystyle CONH_2}{\overset{\displaystyle |}{NH}}\text{–}(\text{–}CH_2\text{–}CH_2\text{–}\underset{\displaystyle CONH_2}{\overset{\displaystyle |}{N}}\text{–})_4\text{–}H \qquad (4)$$

$$\text{–}(\text{–}CH_2\text{–}CH_2\text{–}\overset{+}{N}H_2\text{–})_n\text{–} + nOCN^- = \text{–}(\text{–}CH_2\text{–}CH_2\text{–}\underset{\displaystyle CONH_2}{\overset{\displaystyle |}{N}}\text{–})_n\text{–} \qquad (5)$$

The reactions (2) through (5) are simple reactions like reaction (1). After mixing silver cyanate with aqueous solutions of hydrochlorides of polyethylenimine and its low molecular weight analogues, the precipitate of silver chloride can be isolated from the reaction system. We obtain solutions containing reactant ions only, which is convenient for quantitative investigations. Since all the reactions (2) through (5) proceed between ionic species of unlike charges, the measurement of the electrical resistance of the reaction system offers a convenient and accurate technique for monitoring the reaction.

Experimental

Materials. The details of the preparation of silver cyanate were described earlier.[2] Polyethylenimine (PEI) was furnished by the Dow Chemicals Co., Michigan (Montrek 12). A molecular weight of 4500 was obtained from viscosity determination using an equation proposed by Jones, Langsjoen, Neumann and Zomlefer.[3] Dilute aqueous solutions of PEI were purified by passing them through columns of cation and anion exchange resins. The concentration of PEI was determined by a conductometric method. The fraction of tertiary amino groups was measured by acetylation to be 0.25.

The tertiary amino groups of PEI do not react with cyanate ions. The reaction velocity was determined from the conductance at very low conversions of the reaction in our experiments. The tertiary amines, which are partly responsible for the conductance, were therefore dealt with as reactant ions, in addition to the primary and secondary amino groups. The hydrochloride of PEI (PEI·HCl) was prepared by partial neutralization of PEI solution with HCl (degree of neutralization = 0.92) to prevent the hydrolysis of the PEI salt. Ethylenediamine (ED), triethylenetetramine (TT), and tetraethylenepentamine (TP) were purified by distillation or recrystallization.[4] These bases were partially neutralized with HCl; the degrees of neutralization of ED, TT and TP were 0.77, 0.72, and 0.70, respectively. Sodium polyacrylate (NaPAA) was a product of the Toa Gosei Chemicals Co., Nagoya, Japan. The weight average degree of polymerization was 640. Dilute solutions of NaPAA were converted to the acid form by passing them through ion-exchange resin columns. Completeness of the conversion was assured by checking the atomic absorption spectrum of the solution for sodium ions. A copolymer of diethyldiallylammonium chloride and sulfur dioxide (DECS) was kindly

1) N. Ise, *Fortschr. Hochpolym. Forsh.*, **7**, 536 (1970).
2) T. Okubo and N. Ise, *Proc. Roy. Soc.*, **A327**, 413 (1972).
3) G. D. Jones, A. Langsjoen, M. M. C. Neumann, and J. Zomlefer, *J. Org. Chem.*, **9**, 125 (1944).
4) N. Ise and T. Okubo, *J. Phys. Chem.*, **70**, 2400 (1966).

donated by the Nitto Spinning Co., Koriyama, Japan.[5] Sodium chloride, calcium chloride, and cetyltrimethylammonium bromide (CTABr) were guaranteed reagents.

Kinetic Measurements. A conductometric method was applied to the determination of the reaction rate.[6] The details of the experiments were described earlier.[2] The reactant solutions of ED·OCN, TT·OCN, TP·OCN and PEI·OCN were prepared by mixing hydrochloride solutions of the bases with silver cyanate. In all reaction mixtures, silver chloride, a by-product, was completely removed by filtration. Removal was checked by measuring the concentration of remaining silver chloride using an atomic absorption spectrophotometer. Thus, the filtrate is believed to contain reactant ions only. A cell of the Jones and Ballinger type (cell constant=7.64 cm^{-1}) was used together with a Wheatstone bridge.[8] The maximum experimental error of the resistance was $\pm 0.1\%$. Kinetic measurements were carried out at 30, 40, and 50 °C and within 1% conversion. The error of our measurements was at the highest 3% of the reaction rate. The pH values of the reaction solution were between 5.5 and 7.5 during the reaction.

Results and Discussion

The second-order rate constants k_2 of the carbamoylation reactions are compiled in Table 1. The magnitude of k_2 was about the same for the four reactants studied, whereas it was 20 to 100 fold larger than that for the ammonium cyanate–urea conversion.[9] As is seen from the Table, the k_2 value decreases with increasing concentration and this tendency becomes more distinct with increasing valency of the reactant cations.

Table 1. The second-order rate constants for reactions of ED·OCN, TT·OCN, TP·OCN and PEI·OCN

Reactant	Concentration ($mol \cdot l^{-1}$)	k_2($l \cdot mol^{-1} \cdot min^{-1}$)		
		30°C	40°C	50°C
ED·OCN	0.00766	0.816	—	—
	0.00957	0.830	1.78	3.27
	0.0139	0.709	1.63	—
	0.0184	0.638	1.43	—
	0.0232	0.632	1.43	—
	0.0312	0.592	1.27	—
	0.0411	0.588	1.19	—
	0.0822	0.514	—	—
TT·OCN	0.00425	1.270	—	—
	0.00890	0.955	2.08	3.76
	0.0142	0.706	1.71	—
	0.0171	0.712	1.47	—
	0.0213	0.592	1.38	—
	0.0282	0.526	1.14	—
	0.0366	0.489	0.96	—
	0.0784	0.261	—	—
TP·OCN	0.00417	1.341	2.63	—
	0.00872	0.964	1.60	2.85
	0.0140	0.721	1.23	—
	0.0167	0.701	1.12	—
	0.0209	0.559	1.03	—
	0.0277	0.465	0.836	—
	0.0360	0.390	0.706	—
	0.0780	0.208	—	—
PEI·OCN	0.00766	1.37	—	—
	0.00957	1.15	1.64	2.80
	0.0139	0.536	1.31	—
	0.0184	0.572	0.889	—
	0.0232	0.457	0.904	—
	0.0312	0.442	0.882	—
	0.0411	0.315	0.582	—
	0.0822	0.196	—	—

Table 2. Thermodynamic quantities for reactions of NH_4OCN, ED·OCN, TT·OCN, TP·OCN, and PEI·OCN at 40 °C

Reactant[a]	$\Delta G^{\neq}$ ($kcal \cdot mol^{-1}$)	$\Delta H^{\neq}$ ($kcal \cdot mol^{-1}$)	$\Delta S^{\neq}$ ($cal \cdot deg^{-1} \cdot mol^{-1}$)
NH_4OCN[b]	23.6	22.9	−2
ED·OCN	20.6	12.9	−24.6
TT·OCN	20.5	12.8	−24.6
TP·OCN	20.6	10.1	−33.7
PEI·OCN	20.6	8.0	−40.2

a) Concentrations of the reactants are 0.00957, 0.00890, 0.00872 and 0.00957 $mol \cdot l^{-1}$ for ED·OCN, TT·OCN TP·OCN and PEI·OCN, respectively.
b) Okubo and Ise, Ref. 2.

5) S. Harada and K. Arai, *Makromolek. Chem.*, **107**, 78 (1967).

6) It is clearly shown that the conductance method can give the "correct" rate constant of the carbamoylation reaction, even when the side reaction, especially carbonate formation (Eq. (A)) proposed by Wyatt and Kornberg exists.[7] If the carbonate really formed, the rate constant, k, from the conductance method is given by Eq. (B).

$$OCN^- + 2H_2O = HCO_3^- + NH_3 \quad (A)$$

$$\frac{-d\{[NH_4^+]+[OCN^-]+[HCO_3^-]\}}{2dt} = k\left\{\frac{[NH_4^+]+[OCN^-]+[HCO_3^-]}{2}\right\} \quad (B)$$

when the equivalent conductances of NH_4^+, OCN^- and HCO_3^- are approximately equal to each other and when the $[H^+]$ and $[OH^-]$ are negligible, *i.e.*, $[NH_4^+]=a-x$, $[OCN^-]=a-x-y$ and $[HCO_3^-]=[NH_3]=y$, where the notations a, x, and y are the same as those given in Ref. 7, Eq. (B) becomes

$$-\frac{d[NH_4^+]}{dt} = k[NH_4^+]^2 \quad (C)$$

Eq. (C) clearly shows that k obtained from the conductance is apparently "correct". Furthermore, it can be easily shown that the k from the conductance correlates with the rate constant of carbamoylation at infinite dilute, k_{u_0} by Eq. (D).

$$k = k_{u_0} f_1^2 \left(\frac{a-x-y}{a-x}\right) \approx k_{u_0} f_1^2 \quad \text{at} \quad t \approx 0 \quad (D)$$

where f_1 is the activity coefficient of 1-valent ions. For the details of the derivation of Eqs. (C) and (D), the readers should consult the work of Wyatt and Kornberg. Thus, the conductance method is conveninent for the rate determination of the carbamoylation reaction.

7) P. A. H. Wyatt and H. L. Kornberg, *Trans. Faraday Soc.*, **48**, 454 (1952).

8) J. Jones and M. Ballinger, *J. Amer. Chem. Soc.*, **53**, 411 (1931).

9) J. C. Warner and E. L. Warrick, *ibid.*, **57**, 1491 (1935).

For example, the k_2 value of ED·OCN decreases by 40 percent with a ten-fold increase in the reactant concentration, whereas that of PEI decreases more than 80 percent. A quantitative explanation for the decreasing tendency will be described later.

The free energy ($\Delta G^{\ddagger}$), enthalpy ($\Delta H^{\ddagger}$), and entropy ($\Delta S^{\ddagger}$) of activation of the carbamoylation reactions are listed in Table 2. These parameters for the ammonium cyanate–urea conversion are also given in the Table from the previous publication.[2] The $\Delta G^{\ddagger}$ values of the carbamoylation reactions studied in the present work are constant within experimental error, being smaller than that for the NH_4OCN reaction. The $\Delta H^{\ddagger}$ values decrease sharply with increasing valency of the reactant cations. The electrostatic attractive forces between cations and anions become stronger with increasing valency and may decrease the activation energy. As is clearly shown in Table 2, $\Delta S^{\ddagger}$ decreases with increasing valency of the cations. The $\Delta S^{\ddagger}$ value is much smaller than that for the NH_4^+—OCN^- reaction. According to our previous study on the partial molal volume,[10,11] the PEI cation is hydrated electrostrictionally by two water molecules per repeating unit at the full degree of neutralization. On the other hand the ammonium ion is reported to be hydrated by three water molecules from compressibility measurement.[12] If these values are correct, the NH_4^+—OCN^- reaction should have larger $\Delta S^{\ddagger}$ than the polycation reaction. In addition to the dehydration factor, the local accumulation of OCN^- in the vicinity of the polycation by strong electrostatic attractive forces would result in small $\Delta S^{\ddagger}$ values for the PEI^+—OCN^- reaction.

The second-order rate constant for a reaction between ions can be represented as follows by Brönsted,[13,14]

$$k_2 = k_{2o}\gamma_+\gamma_-/\gamma_X \tag{6}$$

where γ_+ denotes the single-ion activity coefficient of the amino groups of the macroion, and γ_- the single-ion activity coefficient of the cyanate anions. X indicates the activated complex. The reference value, k_{2o}, is a limiting velocity constant at zero concentration of the reactant ions. For convenience, we discuss the rate constant by using a reference constant k_2^* which is the rate constant at 0.01 equiv. l^{-1} without foreign salt. The constant k_2^* is correlated with k_{2o} by the equation

$$k_2^* = k_{2o}\gamma_+^*\gamma_-^*/\gamma_X^* \tag{7}$$

where γ_+^*, γ_-^* and γ_X^* are the single-ion activity coefficients of the species indicated by the suffix at the reference concentration. From Eqs. (6) and (7) the following equation is derivable.

$$\log(k_2/k_2^*) = 2\log(\gamma_\pm/\gamma_\pm^*) - \log(\gamma_X/\gamma_X^*) \tag{8}$$

where $\gamma_\pm$ and $\gamma_\pm^*$ are the mean activity coefficients of the reactive groups which are related to the single-ion activity coefficients γ_+, γ_-, γ_+^* and γ_-^* by Eqs. (9) and (10) (see for example, Ref. 15)

$$\gamma_\pm^2 = \gamma_+\cdot\gamma_- \tag{9}$$

$$\gamma_\pm^{*2} = \gamma_+^*\cdot\gamma_-^* \tag{10}$$

The first and second terms of the right-hand side of Eq. (8) denote the changes of the activity coefficients of the reactant ion and activated complex, respectively, in going from the specified state to the reference state.

At this point we wish to try to estimate the activity coefficients of the reactant ions from the kinetic parameter, k_2, using Eq. (8). In the case of interionic reactions between ions of unlike signs and of the same valence (NH_4^+ and OCN^-, for example), the activated complex is considered to be neutral. The second term of the right-hand side of Eq. (8), therefore, can be safely neglected, compared to the first term, because the activity coefficients of neutral molecules are not so sensitive to changes in ionic concentration. In the present case, (Eqs. (2) to (5)), on the other hand, the complex is not neutral except in the final stage of the reaction. However, it is still expected that the second term of the right-hand side of Eq. (8) is much smaller than the first term. Thus we neglect the second term and obtain:

$$\log(k_2/k_2^*) = 2\log(\gamma_\pm/\gamma_\pm^*) \tag{11}$$

It should be noted here that γ is the single-ion activity coefficient of the amino groups of the macroion, and not that of the macroion (to be denoted as $\gamma_{\alpha+}$). The mean activity coefficient of polyelectrolyte ($\gamma_{\alpha\pm}$) is given by the following equation.

$$\gamma_{\alpha\pm}^{\alpha+1} = \gamma_{\alpha+}\cdot\gamma_-^{\alpha} \tag{12}$$

where the effective valency of the macroions is α. Physicochemical measurements such as e.m.f. measurement give $\gamma_{\alpha\pm}$, not $\gamma_\pm$. Thus, the relation between $\gamma_{\alpha+}$ and γ_+ must be given to complete the discussion of the mean activity coefficients of the reaction systems. The chemical potential of the macrocations, $\mu_{\alpha+}$, is given by the sum of the chemical potentials of the reactive group i (the amino groups in the present case), μ_{+i},

$$\mu_{\alpha+} = \sum_{i=1}^{\alpha}\mu_{+i} \tag{13}$$

We assume here that the value of μ_{+i} is not dependent on the location of the group on the cation chain. Then we obtain,

$$\mu_{\alpha+} = \alpha\mu_+ \tag{14}$$

From Eq. (15) we have

$$\gamma_{\alpha+} = \gamma_+^{\alpha} \tag{15}$$

The relation between k_2 and $\gamma_{\alpha\pm}$, is therefore, given by

$$\log(\gamma_{\alpha\pm}/\gamma_{\alpha\pm}^*) = \frac{\alpha}{\alpha+1}\log(k_2/k_2^*) \tag{16}$$

By using Eq. (16), the mean activity coefficients of ED·OCN, TT·OCN, TP·OCN and PEI·OCN in aqueous media were calculated from the observed kinetic data (Fig. 1). The α value equals to Z[D.N.], where, Z and [D.N.] are the valency of reactive cation and the degree of neutralization, respectively. The α values of ED·OCN, TT·OCN, TP·OCN and PEI·OCN were 1.5, 2.9, 3.5 and 96.3, respectively. The

10) N. Ise and T. Okubo, *J. Amer. Chem. Soc.*, **90**, 4527 (1968).
11) N. Ise and T. Okubo, *Kobunshi Kagaku* **27**, 193 (1970).
12) J. F. Hinton and E. S. Amis, *Chem. Rev.*, **71**, 627 (1971).
13) J. N. Brönsted, *Z. Phys. Chem.*, **102**, 169 (1922).
14) J. N. Brönsted, *ibid.*, **115**, 337 (1925).

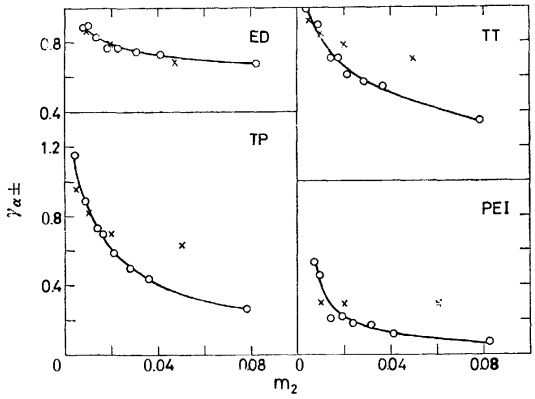

Fig. 1. $\gamma_{\alpha\pm}$ calculated from the kinetic data at 30 °C.
○: from the kinetic data
×: from e.m.f. measurements for hydrochlorides (Ise and Okubo, Ref. 4)

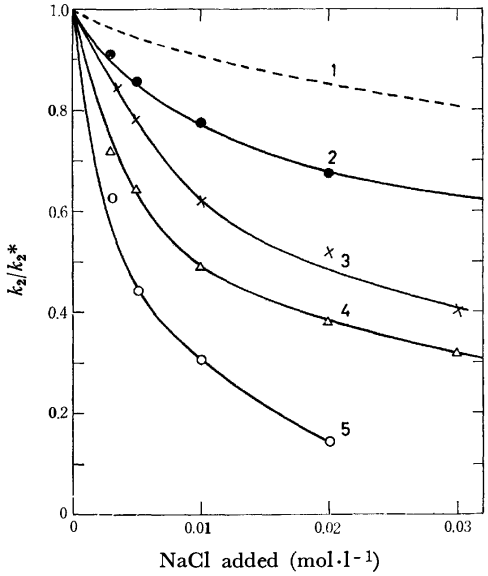

Fig. 2. Decelerating effect of NaCl at 30 °C.
[Reactant]=0.01 mol·l^{-1}
Curve 1: NH_4OCN 2: ED·OCN 3: TT·OCN
4: TP·OCN 5: PEI·OCN

$\gamma_{\alpha\pm}^*$ values at 0.01 mol·l^{-1} were taken from the literature.[4] For comparison, the values of $\gamma_{\alpha\pm}$ from the e.m.f. measurements of the hydrochlorides, *i.e.*, ED·HCl, TT·HCl, TP·HCl and PEI·HCl are also given in the figure.[4] The $\gamma_{\alpha\pm}$ value of ED·OCN coincides with that of ED·HCl very well. The agreement between the $\gamma_{\alpha\pm}$ values of the cyanate and hydrochloride, however, becomes less satisfactory with increasing valency of the cations. This may be due to the fact that μ_{+i} depends for higher valence cations on the location of the reactive group i. Furthermore, the agreement is not good at higher concentrations, perhaps due to the specificity of the anions. Qualitatively, however, the concentration dependence of $\gamma_{\alpha\pm}$ derived from the kinetic data is satisfactory compared with that from the electrochemical measurements.

15) R. A. Robinson and R. H. Stokes, "Electrolyte Solutions," 2nd Ed., Butterworths, London (1959), Chapt. 2.

Now we turn to the catalytic action of added salts on the carbamoylation reactions. Figure 2 shows the decelerating effect of sodium chloride on the ED·OCN, TT·OCN, TP·OCN and PEI·OCN reactions. The data for NH_4·OCN by Warner and Warrick[9] are also given for comparison. The quantity k_2^* denotes the rate constant at $t=0$, at a reactant concentration of 0.01 mol·l^{-1} in the absence of the added salt. As is clearly seen from the Figure, the reactions of the higher valence cations with cyanate anions are retarded more effectively with sodium chloride than those of the lower valence cations.

Let us next discuss the interactions between reactant electrolyte and catalyst salt more quantitatively. For this purpose, it is convenient to use the interaction parameter, β_{23}, defined by Eq. (17).[16]

$$\beta_{23} = (1+\alpha)\partial \ln \gamma_{\alpha\pm}/\partial m_3 \qquad (17)$$

were $\gamma_{\alpha\pm}$ and m_3 denote the mean activity coefficient of the reactant electrolyte and the concentration of sodium chloride, respectively. The β_{23} values obtained from the kinetic data by the use of Eq. (16) are compiled in Table 3. The negative value of β_{23} suggests that the interactions between the reactant electrolyte and the salt are electrostatic (see Refs. 17 and 18). The value of β_{23} increases with increasing concentration of sodium chloride, suggesting a weakening of the electrostatic forces with addition of sodium chloride. As is clearly seen, the magnitude of β_{23} increases strikingly with increasing valency of the reactant cations.

Table 3. Interaction parameter β_{23}
Component 2 : ED·OCN, TT·OCN, PEI·OCN
Component 3 : NaCl

m_3 (mol·l^{-1})	β_{23}			
	ED·OCN	TT·OCN	TP·OCN	PEI·OCN
0.003	−46.6	−151	−326	−11700
0.005	−38.5	−132	−192	−9100
0.01	−29.4	−84	−119	−8000
0.02	−14.7	−63	−93	−6000
0.03	—	−64	−89	—

The dependence of β_{23} on the valency of the reactant cations implies the following. The higher the valency of the reactant cations, the more strongly they attract chloride ions which in turn prevent the cyanate ions from approaching the reactant cations. This shielding effect of the chloride ions becomes greater as the reactant cations are more highly charged.

The catalytic action of a polyelectrolyte on the carbamoylation reactions of ED·OCN, TT·OCN, TP·OCN and PEI·OCN is portrayed in Fig. 3. The decelerating efficiency of DECS was about the same for all of the carbamoylation reactions studied, in contrast to the action of sodium chloride. This suggests that the interactions between the catalyst polyelectrolyte (*i.e.*, DECS) and reactant electrolyte (2–1, 4–1, 5–1,

16) G. Scatchard, *J. Amer. Chem. Soc.*, **68**, 2315 (1946).
17) T. Okubo, N. Ise, and F. Matsui, *ibid.*, **89**, 3697 (1967).
18) F. Matsui, N. Ise, and T. Okubo, *Polym. J.*, **1**, 64 (1970).

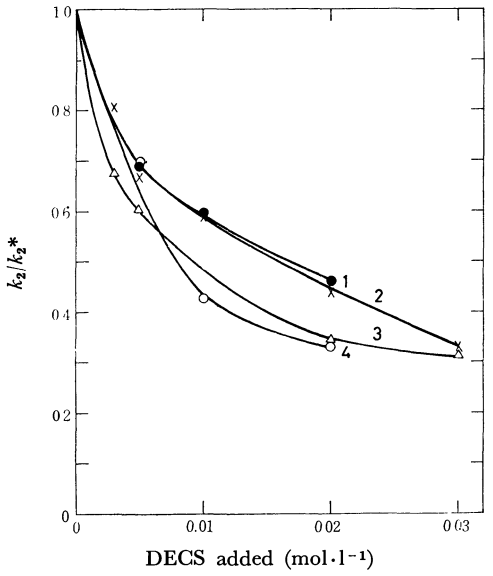

Fig. 3. Decelerating effect of DECS at 30 °C.
[Reactant]=0.01 mol·l^{-1}
Curve 1: ED·OCN 2: TT·OCN
3: TP·OCN 4: PEI·OCN

100–1 valence types) are relatively similar in spite of the large range in the cation valency. The valency of the DECS cations (degree of polymerization about 2000) is much higher than the valencies of the reactant cations (2∼100). The attractive forces between the DECS cations and the cyanate anions, therefore, are much stronger than those between the reactant cations of various valencies and Cl^-. Thus, the difference in the strength of the interactions between the reactant cations and Cl^- may not strongly affect the retarding effects by the DECS cations.

The retarding influences of simple-, micelle-, and polyelectrolytes on the carbamoylation reactions of ED·OCN and PEI·OCN are compared in Table 4. For ED·OCN, the catalytic effect was the weakest for calcium chloride and increased in the order:

$$CaCl_2 < NaCl < CTABr < DECS < NaPAA \quad (19)$$

On the other hand, the retarding effect on the PEI·OCN reaction was in the order:

$$DECS < CTABr < NaCl < CaCl_2 \quad (20)$$

Generally speaking, the retarding action of the added salt is strong when the valencies of reactant cations and salt cations differ greatly from each other. These results are accounted for as follows. The fact that CTABr and DECS are more effective retarders than sodium chloride and calcium chloride in the ED·OCN reaction can be understood if we consider that these macrocations attract cyanate ions more strongly than Na^+ and Ca^{2+}. Sodium chloride is more effective than calcium chloride since the concentration of the chloride ions, which we recall do not favor the approach of cyanate ions to ED cations, is lower in the presence of Ca^{2+} than in the case of Na^+. The ED cations are less effectively shielded by calcium chloride than by sodium chloride, so that the ED·OCN reaction is decelerated less strongly by the former than by the latter.

For the PEI·OCN reaction, the situation is also interpretable by similar considerations. The chloride ion concentration around the PEI cations should be lower in the presence of DECS and CTABr cations than in the case of Na^+ and Ca^{2+} as a result of the attractive interaction between the macrocations and chloride ions, and of the very strong repulsive interaction between the macrocations and PEI cations. Thus, DECS and CTABr are not strong retarders in the PEI·OCN reaction. This situation is consistent with the activity data for the ternary systems, water–polyelectrolyte(2)–salt(3),[1,18] indicating that addition of low molecular weight salts as the third component 3 produces more efficient shielding effect on the polyelectrolyte (component 2) than that of another polyelectroylte (component 3). We have no reasonable explanation for the higher efficiency of calcium chloride as compared to sodium chloride. In summary, we state that the reactions of polycations are more effectively decelerated by coexisting simple cations than by catalyst polycations, whereas reactions of simple cations are retarded more strongly by polycations than by simple cations.

Table 4. Decelerating effect of various salts on the ED·OCN and PEI·OCN reactions at 30 °C
[Reactant]=[Added salt]=0.01 mol·l^{-1}

Added salt	k_2/k_2^*	
	ED·OCN	PEI·OCN
NaCl	0.77	0.31
$CaCl_2$	0.93	0.25
CTABr	0.58	0.36
DECS	0.60	0.43
NaPAA	0.12	—

The authors express their thanks to Drs. W. N. Vanderkooi and J. C. Moore of the Dow Chemical Co., Midland, Mich., and to Dr. S. Harada of the Nitto Spinning Co., Koriyama, Japan, for kindly furnishing polyethylenimine and copolymer of diethyldiallylammonium chloride and sulfur dioxide, respectively.

Studies on the Synthesis of Furan Compounds. XXX.[1] Syntheses and Steric Configurations of 3-(5-Nitro-2-furyl)-2-(5-bromo-2-furyl)acrylic Acid and Its Related Compounds[2]

Ichiro HIRAO, Yasuhiko KATO, and Shiro KOZAKURA

Laboratory of Organic Synthesis, Department of Industrial Chemistry, Kyushu Institute of Technology, Tobata-ku, Kita-Kyushu 804

(Received March 1, 1973)

cis- and *trans*- 3-(5-Nitro-2-furyl)-2-(5-bromo-2-furyl)acrylic acids (II and III) and their functional derivatives have been synthesized in connection with the syntheses and steric configurations of 3-(5-nitro-2-furyl)-2-(5-bromo-2-furyl)acrylonitrile and its related compounds. The treatment of *cis*-3-(5-nitro-2-furyl)-2-(2-furyl)-acrylic acid (I) with bromine in refluxing carbon tetrachloride afforded a 1 : 1 mixture of II and III in quantitative yield. II and III afforded methyl (IV and VI) and ethyl (V and VII) esters, *via* each acid chloride (VIII or IX) by treatment with methanol and ethanol, respectively. Similarly, *cis*- and *trans*- 3-(5-nitro-2-furyl)-2-(5-bromo-2-furyl)acrylamides (X and XI) were obtained by treatment of VIII and IX with dry ammonia in benzene. Isomerization was observed in the conversion of X into *trans*-3-(5-nitro-2-furyl)-2-(5-bromo-2-furyl)-acrylonitrile (XII) upon treatment with phosphoryl chloride, while XI maintained its configuration under similar conditions to afford XII. On the other hand, *cis*-acid and esters (II, IV, and V) were converted into the corresponding *trans* isomers (III, VI, and VII) respectively, by treatment with hydrazine hydrate in refluxing methanol. II was confirmed to be isomerized to III by heating with hydrochloric acid or by irradiation with ultraviolet light (406 mμ). The structures and configurations of these compounds were discussed on the basis of their IR and NMR spectra.

cis-3-(5-Nitro-2-furyl)-2-(5-bromo-2-furyl)acrylonitrile has been prepared by bromination of both *cis*- and *trans*- 3-(5-nitro-2-furyl)-2-(2-furyl)acrylonitriles.[3] It could not be hydrolyzed to *cis*-3-(5-nitro-2-furyl)-2-(5-bromo-2-furyl)acrylic acid (II) by heating with 36% hydrochloric acid for 12 hr. Thus, bromination of 3-(5-nitro-2-furyl)-2-(2-furyl)acrylic acid has been carried out with the purpose of preparing II as a raw material in connection with the antibacterial properties of nitrofuran derivatives.[4-11] The present paper deals with the syntheses, steric configurations, and configurational interconversions of *cis*- and *trans*-3-(5-nitro-2-furyl)-2-(5-bromo-2-furyl)acrylic acids and their related compounds.

Results and Discussion

A mixture of *cis*- (II) and *trans*-3-(5-nitro-2-furyl)-2-(5-bromo-2-furyl)acrylic acid (III) was obtained quantitatively by treatment of *cis*-3-(5-nitro-2-furyl)-2-(2-furyl)acrylic acid (I) with an equimolar amount of bromine in refluxing carbon tetrachloride. It was confirmed to be a 1 : 1 mixture of II (48.9%) and III (51.1%) by NMR analysis, from which II and III were isolated in a 29.8% and a 33.1% yield, respectively, by fractional crystallization from aqueous methanol. In the IR spectra, a C=O stretching absorption appeared at 1690 cm^{-1} in II and at 1710 cm^{-1} in III. The NMR spectra of II and III revealed an olefinic proton signal at δ 7.39 and 6.88, respectively, indicating that the olefinic proton and COOH group are on one side of the ethylene double bond in the molecule of II. Methyl (IV and VI) and ethyl (V and VII) esters were obtained respectively by heating II and III with thionyl

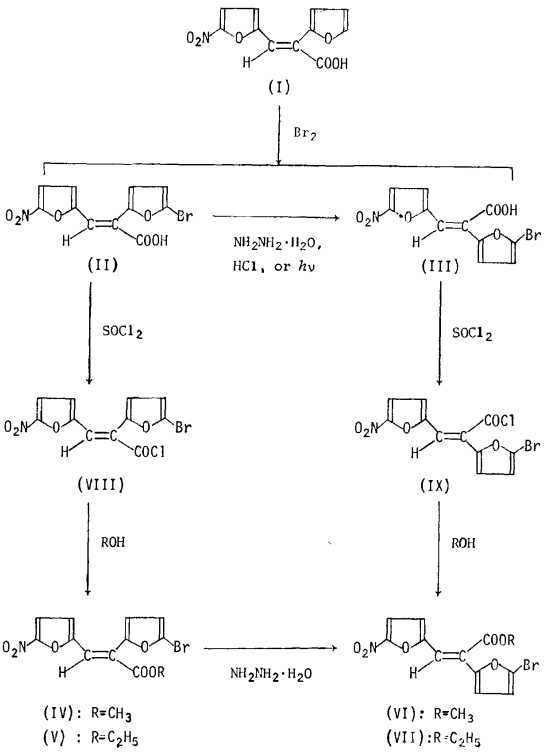

Scheme 1.

1) Part XXIX of this series: I. Hirao, Y. Kato, Y. Fukano, and S. Yanai, This Bulletin, **46**, 1826 (1973).

2) Presented at the 27th Annual Meeting of the Chemical Society of Japan, Nagoya, October 13, 1972.

3) Y. Kato, T. Kuboyama, and I. Hirao, This Bulletin, **45**, 3165 (1972).

4) I. Hirao and Y. Kato, *Nippon Kagaku Zasshi*, **85**, 693 (1964); **86**, 633 (1965).

5) Y. Kato, Y. Hara, and I. Hirao, *ibid.*, **86**, 957 (1965).

6) Y. Kato and I. Hirao, *ibid.*, **87**, 1336 (1966).

7) I. Hirao, *ibid.*, **88**, 574 (1967); **89**, 713 (1968).

8) Y. Kato, H. Nakajima, and I. Hirao, *ibid.*, **89**, 955 (1968).

9) Y. Kato, This Bulletin, **44**, 489 (1971).

10) I. Hirao, Y. Kato, and T. Hirota, *ibid.*, **44**, 1923 (1971).

11) I. Hirao and Y. Kato, *ibid.*, **44**, 3136 (1971).

chloride in benzene and treating the resulting acid chlorides (VIII and IX) with methanol or ethanol. These esters were confirmed to retain the steric configuration of each mother acid by a comparison of the NMR spectra of IV and V with those of VI and VII. The olefinic proton signals in IV and V shifted to lower magnetic field than those in VI and VII; this suggests that IV and V are *cis*, and VI and VII are *trans*. In the IR spectra, *cis* esters also exhibited a C=O stretching absorption band at lower frequencies than the corresponding *trans* ester. In a comparison with the IR spectrum of IX, the *cis*-configuration of VIII was suggested by a shift to lower frequencies of the C=O stretching band to be similar to the relation observed between *cis* and *trans* forms of the acid and ester.

When VIII was treated with dry ammonia in benzene at room temperature, *cis*-3-(5-nitro-2-furyl)-2-(5-bromo-2-furyl)acryl amide (X) was obtained. Similarly, IX and ammonia produced *trans*-acrylamide (XI) in a good yield, indicating that the configurational interconversion did not take place in the reaction with ammonia under the conditions employed. Isomerization was observed in the dehydration reaction of X. On treatment with hot phosphoryl chloride, X afforded *trans*-3-(5-nitro-2-furyl)-2-(5-bromo-2-furyl)acrylonitrile (XII) as the main product, along with *cis*-acrylonitrile (XIII).[3] While XI maintained its *trans*-configuration giving rise to XII, a part of XI was changed the configuration to produce XIII. The structures of X and XI were supported by their IR and NMR spectra (see Experimental). The *trans*-configuration of XII is clearly shown by comparing its IR and NMR spectra with those of III and XIII.

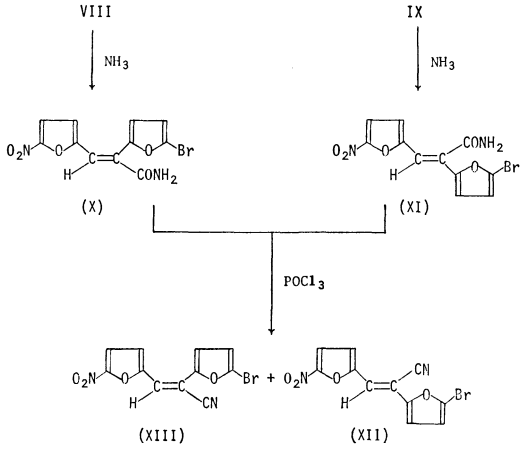

Scheme 2.

When refluxed with 3/2 equimolar of hydrazine hydrate in methanol for 2 hr, 55% of II, 70% of IV, and 73% of V were respectively converted into III, VI, and VII. Similarly, 64% and 60% of II was isomerized to III on being heated with an equimolar amount of hydrochloric acid in methanol for 1.5 hr and by irradiation with UV light (406 mμ) for 25 hr. The conversion ratio was estimated on the basis of UV or NMR analysis.

Experimental

All the melting points are uncorrected. Elemental analyses were carried out with a Yanagimoto CHN Corder, MT-2 type. The IR spectra were taken on a JASCO IRA-2 grating infrared spectrophotometer by the KBr-disk method. The band positions are expressed in wave number, cm^{-1}. The UV spectra were performed on a Shimadzu photoelectric spectrophotometer, Model QV-50. UV-light irradiation and analyses were also carried out with the same apparatus. The NMR spectra were determined with a Japan Electron Optics Lab. JNM-C-60HL spectrometer. All the spectra were measured in DMSO-d_6 with a concentration of 2 mol% at 60 MHz, with HMDS as an internal reference; the chemical shifts are expressed in δ-values.

cis- *and* trans- *3-(5-Nitro-2-furyl)-2-(5-bromo-2-furyl)acrylic Acid (II and III).* A solution of bromine (50 g, 310 mmol) in carbon tetrachloride (100 ml) was slowly added to a stirred, warmed (70 °C) suspension of I (74.7 g, 300 mmol) in carbon tetrachloride (500 ml). The resulting mixture was then refluxed for 2 hr. After cooling, the precipitated product was filtered, washed with carbon tetrachloride (200 ml), and dried. Thus, 97.6 g (99.2%) of monobromo compound was obtained as brown-colored powder; mp 140—151 °C. The product was determined to be a mixture of II and III with the ratio of 48.9 : 51.1 by a comparison of NMR signal intensities. Fractional crystallization from methanol containing 20% of water afforded 29.3 g (29.8%) of II, 32.6 g (33.1%) of III, and 26.4 g of the recovered mixed-acid.

cis Acid (II); small orange needles, mp 187—189 °C. UV λ_{max}^{MeOH} mμ (ε): 227 (19400), 310 (11200), and 404 (11900). IR: 1690 (C=O). NMR (at 24 °C): 6.69 (d, 1H, J=3.8 Hz, bromofuran ring C_4–H), 6.83 (d, 1H, J=3.8 Hz, bromofuran ring C_3–H), 7.06 (d, 1H, J=4.1 Hz, nitrofuran ring C_3–H), 7.39 (s, 1H, olefinic proton), and 7.65 (d, 1H, J=4.1 Hz, nitrofuran ring C_4–H). Found: C, 40.60; H, 1.85; N, 4.26%. Calcd for $C_{11}H_6NO_6Br$: C, 40.24; H, 1.83; N, 4.27%.

trans Acid (III); brown granules; mp 175 °C. UV λ_{max}^{MeOH} mμ (ε): 305 (16400) and 406 (25100). IR: 1710 (C=O). NMR (at 24 °C): 6.69 (s, 2H, bromofuran ring C_3–H and C_4–H), 6.88 (s, 1H, olefinic proton), 6.96 (d, J=4.1 Hz, nitrofuran ring C_3–H), and 7.65 (d, 1H, J=4.1 Hz, nitrofuran ring C_4–H). Found: C, 40.16; H, 1.76; N, 4.11%. Calcd: the same value as II above.

cis- *and* trans- *3-(5-Nitro-2-furyl)-2-(5-bromo-2-furyl)acryloyl Chloride (VIII and IX).* A mixture of II or III (each 9.54 g, 30 mmol), thionyl chloride (3.6 g, 30 mmol), *N,N*-dimethylformamide (2 g) and dry benzene (300 ml) was stirred at 70 °C for 3 hr. The resulting solution was brought to dryness *in vacuo* and the residual acid chloride was washed with dry ether (50 ml). The crude chlorides were used in the subsequent experiments without further purification.

cis Acid chloride (VIII); brown powder, mp 137—139 °C. Yield: 9.8 g (97%). IR: 1740 (C=O).

trans Acid chloride (IX); brown powder, mp 97—100 °C. Yield: 9.6 g (95%). IR: 1790 (C=O).

Preparation of Esters (IV, V, VI and VII). VIII or or IX (each 3.4 g, 10 mmol) was dissolved in alcohol (10—20 ml) and the resulting solution was left standing at room temperature for a day. The precipitated product was filtered and recrystallized from alcohols to give pure esters.

cis Methyl ester (IV); brown plates (from methanol), mp 117—119 °C. Yield: 2.8 g (82%). IR: 1715 (C=O).

NMR (at 62 °C): 3.83 (s, 3H, O–CH_3), 6.72 (d, 1H, J=3.8 Hz, bromofuran ring C_4–H), 6.87 (d, 1H, J=3.8 Hz, bromofuran ring C_3–H), 7.09 (d, 1H, J=4.1 Hz, nitrofuran ring C_3–H), 7.44 (s, 1H, olefinic proton), and 7.64 (d, 1H, J=4.1 Hz, nitrofuran ring C_4–H). Found: C, 42.35; H, 2.68; N, 4.01%. Calcd for $C_{12}H_8NO_6Br$: C, 42.11; H, 2.38; N, 4.01%.

trans Methyl ester (V); ocherous needles (methanol), mp 106—107 °C. Yield: 2.5 g (73%). IR: 1720 (C=O). NMR (at 24 °C): 3.95 (s, 3H, O–CH_3), 6.73 (s, 2H, bromofuran ring C_3–H and C_4–H), 7.01 (s, 1H, olefinic proton), 7.03 (d, 1H, J=4.1 Hz, nitrofuran ring C_3–H), and 7.65 (d, 1H, J=4.1 Hz, nitrofuran ring C_4–H). Found: C, 42.02; H, 2.37; N, 4.02%. Calcd: the same value as IV above.

cis Ethyl ester (IV); ocherous needles (ethanol), mp 80—81 °C. Yield: 3.2 g (90%). IR: 1715 (C=O). NMR (at 62 °C): 1.31 (t, 3H, J=7.5 Hz, C–CH_3), 4.30 (q, 2H, J=7.5 Hz, O–CH_2–C), 6.73 (d, 1H, J=3.8 Hz, bromofuran ring C_4–H), 6.89 (d, 1H, J=3.8 Hz, bromofuran ring C_3–H), 7.09 (d, 1H, J=4.1 Hz, nitrofuran ring C_3–H), 7.43 (s, 1H, olefinic proton), and 7.64 (d, 1H, J=4.1 Hz, nitrofuran ring C_4–H). Found: C, 43.52; H, 2.51; N, 3.83%. Calcd for $C_{13}H_{11}NO_6Br$: C, 43.82; H, 2.81; N, 3.93%.

trans Ethyl ester (VII); brown cylinders (ethanol), mp 114—115 °C. Yield: 3 g (84.3%). IR: 1720 (C=O). NMR (at 75 °C): 1.31 (t, 3H, J=7.5 Hz, C–CH_3), 4.45 (q, 2H, J=7.5 Hz, O–CH_2–C), 6.73 (s, 2H, bromofuran ring C_3–H and C_4–H), 7.01 (s, 1H, olefinic proton), 7.03 (d, 1H, J=4.1 Hz, nitrofuran ring C_3–H), and 7.65 (d, 1H, J=4.1 Hz, nitrofuran ring C_4–H). Found C, 43.51; H, 2.84; N, 3.99%. Calcd: the same value as VI above.

cis- *and* trans- *3-(5-Nitro-2-furyl)-2-(5-bromo-2-furyl)acrylamide (X and XI).* To a stirred solution of VIII or IX (each 7 g, 20 mmol) in dry benzene (300 ml) was introduced dry ammonia. During the reaction, the temperature was kept below 30 °C. The resulting reaction mixture was filtered and the product was washed with water (200 ml) and then dried. Recrystallization from methanol afforded pure amides.

cis Amide (X); yellow needles, mp 181 °C. Yield: 6 g (81.5%). IR: 3350, 3160 (NH_2), and 1652 (C=O). NMR (at 24 °C): 6.73 (d, 1H, J=3.8 Hz, bromofuran ring C_4–H), 6.85 (d, 1H, J=3.8 Hz, bromofuran ring C_3–H), 6.95 (d, 1H, J=4.1 Hz, nitrofuran ring C_3–H), *ca.* 7.68 (broad s, 2H, NH_2), and 7.68 (d, 1H, J=4.1 Hz, nitrofuran ring C_4–H). Found: C, 40.65; H, 2.32; N, 8.22%. Calcd for $C_{11}H_7N_2O_5Br$: C, 40.37; H, 2.14; N, 8.56%.

trans Amide (XI): ocherous needles, mp 173—174 °C. Yield: 5.3 g (78%). IR: 3425—3040 (NH_2 and furan ring C–H) and 1661 (C=O). NMR (at 24 °C): 6.70 (d, 1H, J=3.8 Hz, bromofuran ring C_4–H), 6.72 (s, 1H, olefinic proton), 6.82 (d, 1H, J=3.8 Hz, bromofuran ring C_3–H), 6.93 (d, 1H, J=4.1 Hz, nitrofuran ring C_3–H), 7.72 (d, 1H, J=4.1 Hz, nitrofuran ring C_4–H), 7.83 (broad s, 1H, NH), and 8.20 (broad s, 1H, NH). Found: C, 40.20; H, 2.46; N, 8.35%. Calcd: the same value as X above.

cis- *and* trans- *3-(5-Nitro-2-furyl)-2-(5-bromo-2-furyl)acrylonitrile (XIII and XII).* A mixture of X or XI (each 3.3 g, 10 mmol), phosphoryl chloride (40—50 ml) and *N,N*-dimethylaniline (2 drops) was heated at 50—60 °C for 45 min. After cooling, the resulting mixture was poured into crushed ice with agitation. The solidified product was collected, washed with water, and dried. This was identified as a mixture of XII and XIII (63—65 : 37—35) by its NMR spectrum. Yield, 2.6—2.3 g (84—74%); mp 184—189 °C. The mixture was fractionally crystallized from methanol to afford 0.66 g (21.2%) of XII and 0.08 g (2.6%) of XIII.

trans Nitrile (XII); yellow powder, mp 164—166 °C. IR: 2230 (C≡N). NMR (at 97 °C): 6.77 (d, 2H, J= 3.8 Hz, bromofuran ring C_3–H and C_4–H), 7.23 (d, 1H, J= 4.1 Hz, nitrofuran ring C_3–H), 7.25 (s, 1H, olefinic proton), 7.64 (d, 1H, J=4.1 Hz, nitrofuran ring C_4–H). Found: C, 42.58; H, 1.61; N, 9.25%. Calcd for $C_{11}H_5N_2O_4Br$: C, 42.72; H, 1.62; N, 9.06%.

cis Nitrile (XIII); orange-red powder, mp 216 °C, undepressed on admixture with the authentic sample.[3] NMR (at 111 °C): 6.72 (d, 1H, J=3.8 Hz, bromfouran ring C_4–H), 6.90 (d, 1H, J=3.8 Hz, bromofuran ring C_3–H), 7.28 (d, 1H, J=4.1 Hz, nitrofuran ring C_3–H), 7.52 (s, 1H, olefinic proton), and 7.64 (d, 1H, J=4.1 Hz, nitrofuran ring C_4–H).

Conversion of II, IV, and V into III, VI, and VII. By Hydrazine Hydrate: A mixture of II, IV, or V (each 5 mmol), 80% hydrazine hydrate (0.47 g, 7.5 mmol), and methanol (100 ml) was stirred under reflux for 2 hr. The resulting solution was brought to dryness *in vacuo* and the residue was washed with water and then dried. A part of the residue was dissolved in DMSO-d_6 and the component ratio was determined by NMR. II was converted into III in 55% yield, IV into VI in 70%, and V into VII in 73%.

By Hydrochloric Acid: A mixture of II (1.64 g, 5 mmol), 36% hydrochloric acid (0.5 g), and methanol (100 ml) was refluxed for 1.5 hr. The resulting solution was brought to dryness *in vacuo*. Work-up as above afforded 64% of the conversion.

By UV-light Irradiation: A methanolic solution of II (10 μg/ml) was irradiated in a quartz cell with ultraviolet light (406 mμ) at room temperature for 25 hr. The conversion ratio was determined by the change of absorbance at 406 mμ. 60% of II was converted into III.

Oxidation of *p*-Tolyl Triphenylmethylhydrazo Sulfone[1]

Minoru KOJIMA, Nobumasa KAMIGATA, Hiroshi MINATO, and Michio KOBAYASHI

Department of Chemistry, Faculty of Science, Tokyo Metropolitan University, Fukazawa, Setagaya, Tokyo 158

(Received March 10, 1973)

In order to synthesize and study the decomposition of *p*-tolyl triphenylmethylazo sulfone, *p*-tolyl triphenylmethylhydrazo sulfone was oxidized by various oxidizing agents. Although it was oxidized fairly easily by mercury(II) oxide or potassium permanganate, the azo compound formed was unstable and decomposed immediately with evolution of nitrogen. The main products were *p*-tolyl triphenylmethyl sulfone and *p*-tolyl *p'*-benzhydrylphenyl sulfone; both are ascribable to the recombination of *p*-toluenesulfonyl and triphenylmethyl radicals.

Aryl arylazo sulfones yield aryl and arenesulfonyl radicals upon irradiation of light[2] or upon thermolyses in neutral or basic media.[3,4] They yield aryl cations when they are decomposed in acidic media.[5,6]

All the azosulfones studied so far by various investigators are aryl azosulfones, and the decompositions of alkyl azosulfones have not been investigated yet. In an attempt to understand the chemistry of alkyl azosulfones, the synthesis of *p*-tolyl triphenylmethylazo sulfone(I) has been investigated. I is expected to decompose at fairly low temperatures, since both the trityl and *p*-tosyl radicals are resonance-stabilized radicals.

Results and Discussion

Aryl triphenylmethylazo sulfones are not described in the literature. In order to synthesize I, oxidation of *p*-tolyl triphenylmethylhydrazo sulfone (II) was attempted.

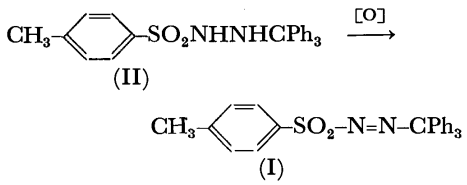

(II) (I)

Although II was oxidized fairly easily by such oxidizing agents as yellow mercury(II) oxide, manganese(IV) oxide, potassium permanganate or bromine, nitrogen was evolved simultaneously, and I could not be isolated.

Oxidation with mercury(II) oxide in benzene did not take place appreciably at room temperature, but proceeded smoothly at the boiling point of the solvent. When the products were subjected to column chromatography on Florisil, the main product was triphenylmethyl alcohol(III) (75% yield). When the oxidation was carried out in air, triphenylmethyl peroxide (IV) was found in 20 mol% yield. Under nitrogen, formation of IV was suppressed, and triphenylmethane (V) was found in 1.5 mol% yield. Mercury(II) *p*-toluenesulfonate precipitated and amounted to 20 mol%. Almost no *p*-toluenesulfinate was contained in the salt which precipitated. When *p*-toluenesulfinic acid was treated with mercury(II) oxide in benzene, the main product was mercury(II) *p*-toluenesulfinate and very little mercury(II) *p*-toluenesulfonate was found; this finding shows that the mercury(II) *p*-toluenesulfonate formed upon oxidation of II is not ascribable to the oxidation of *p*-toluenesulfinic acid which is a possible intermediate.

When the products of oxidation of II with mercury(II) oxide in benzene were not subjected to column chromatography but separated by recrystallizations, the yield of III was only 35% and *p*-tolyl triphenylmethyl sulfonte(VI) was found in 50% yield. A separate experiment showed that on a Florisil, alumina or silica gel column VI was quantitatively converted to III (another main product was *p*-toluenesulfonic acid). Therefore, VI must be one of the main products of oxidation of II in benzene.

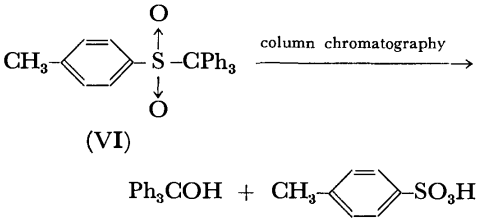

(VI) (III)

Since aryl arylazo sulfones undergo heterolysis in acidic media and homolysis in neutral or basic media, it is possible that the decomposition of I produced by oxidation of II is influenced by *p*-toluenesulfonic acid formed as a product. Therefore, II was oxidized with mercury(II) oxide in benzene in the presence of triethylamine (1.5 mol/mol of II). The products isolated by column chromatography were III (44 mol%), V (22 mol%), *p*-benzhydrylphenyl *p'*-tolyl sulfone (VII) (24 mol%) and triethylammonium *p*-toluenesulfonate (23 mol%). These products are quite different from those found in the absence of triethylamine.

When II was oxidized by mercury(II) oxide in pyridine, the oxidation proceeds even at about 30 °C. Nitrogen was evolved in an almost quantitative yield, and the products isolated by column chromatography were III (42—47 mol%), V (7—8 mol%), and VII (25—30 mol%). When the oxidation was carried out in air, IV was found in a small yield (3.6 mol%) in addition to the products described above. When the oxidation products were analyzed by NMR

1) Organic Sulfur Compounds. Part XLI.
2) M. Kobayashi, S. Fujii, and H. Minato, This Bulletin, **45**, 2039 (1972).
3) M. Kobayashi, H. Minato, M. Kojima, and N. Kamigata, *ibid.*, **44**, 2501 (1971).
4) M. Kojima, H. Minato, and M. Kobayashi, *ibid.*, **45**, 2032 (1972).
5) M. Kobayashi, H. Minato, and N. Kobori, *ibid.*, **43**, 219 (1970).
6) N. Kamigata, M. Kobayashi, and H. Minato, *ibid.*, **45**, 2047 (1972).

before the column-chromatographic separation, VI and VII were found in 20 and 30 mol% yields, respectively. Therefore, about a half of the total yield of III (after the column chromatography) is ascribable to the hydrolysis of VI during the chromatography, but the other half must have been formed as such directly by the oxidation of II. Since VI does not isomerize to VII even when VI was treated with pyridine, VII must be a primary reaction product.

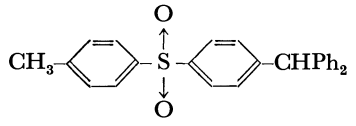

(VII)

When powdery MgO was used as a base instead of an amine, VI was formed in 50—65% yield and the yield of VII was only 2 mol%. Other products were V (1.5 mol%) and IV (oxidation in air) (10 mol%).

In the oxidation in benzene, no products ascribed to the reactions with benzene were found under varied conditions.

When II was oxidized with potassium permanganate in acetonitrile, oxidation proceeded smoothly and nitrogen was evolved almost quantitatively. The products were III (65 mol%), VI (trace) and an unidentified sulfone (30 wt%; the IR spectrum resembles that of VII but its NMR spectrum does not show the methine proton).

When II was oxidized with manganese(IV) oxide in acetonitrile, oxidation proceeded slowly at room temperature, and it took 10 days before the evolution of nitrogen ceased (70 mol%). The reaction mixture was extracted with an $NaHCO_3$ solution. *p*-Toluenesulfonic acid (49 mol%) was obtained from the aqueous extract, and the evaporation of the organic layer gave almost pure III. The yields of the sulfones (VI or VII) were negligibly small.

Oxidation of II with bromine in acetonitrile proceeded rapidly at room temperature with evolution of nitrogen (90 mol%). When the reaction mixture was diluted with water, extracted with chloroform and the extract was evaporated, almost pure III was obtained. No sulfone (VI or VII) was found.

The experimental results described above show that II can readily be oxidized to I but I is very unstable and decomposes with evolution of nitrogen.

Formation of IV shows that triphenylmethyl radical was present and the decomposition of I is homolytic. Sulfone VI is formed by the combination of triphenylmethyl and *p*-tosyl radicals. Since triphenylmethyl radicals are fairly stable, they diffuse out of solvent cage, and form IV upon reaction with oxygen. Part of triphenylmethyl radicals are further oxidized by excess oxidizing agent to III. Part of *p*-tosyl radicals are further oxidized by excess oxidizing agents to *p*-tosyloxy radicals, and then to *p*-toluenesulfonic acid.

Bromine is known to be an efficient radical-scavenger, as exemplified by the efficient trapping of α-cyanoisopropyl radical by bromine in the decomposition of azoisobutyronitrile. Therefore, when II was oxidized with bromine, all the triphenylmethyl radicals were probably converted to triphenylmethyl bromide, which was then hydrolyzed to III. *p*-Tosyl radicals were probably converted to *p*-tosyl bromide, which was then hydrolyzed to *p*-toluenesulfonic acid.

The absence of the products ascribed to the reactions with benzene can be explained in terms of the small reactivity of the resonance-stabilized triphenylmethyl and *p*-toluenesulfonyl radicals. The arenesulfonyl radicals produced by the decomposition of arenesulfonyl iodides did not react with aromatic solvents.[7] Part of the arenesulfonyl radicals formed by the photolysis of aryl α-disulfones attacked aromatic solvents, but the yields of the aromatic substitution products were low.[8]

The oxidation of *N,N'*-diarenesulfonylhydrazine gave the corresponding diimide, which immediately decomposed. The main products were α-disulfone (by recombination in cage), thiolsulfonate and sulfonic acid.[9]

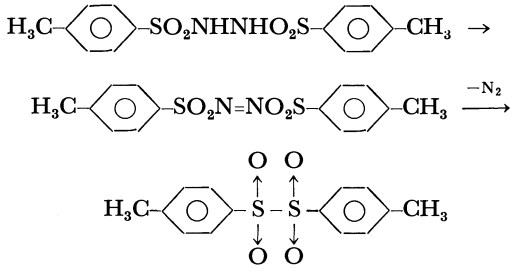

Arenesulfonyl radicals formed in this system also did not react with solvent molecules (benzene, tetrachloroethylene, anisole, *etc*).

The oxidation of II with HgO in the presence of base yielded VII. Formation of VII can be explained by addition of *p*-tosyl radical at a *para* position of triphenylmethyl radical.

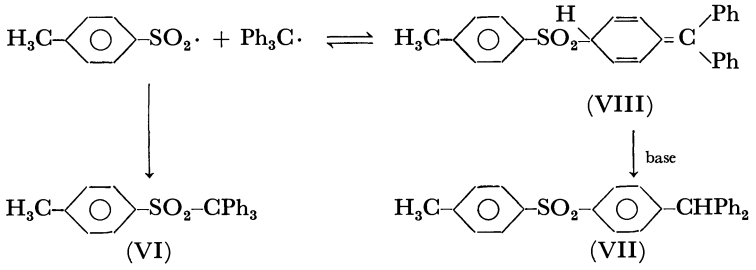

7) C. M. M. da Silva Correa, A. S. Lindsay, and W. A. Waters, *J. Chem. Soc., C*, **1968**, 1872; C. M. M. da Silva Correa, and W. A. Waters, *ibid.*, **1968**, 1874, 1880.

8) M. Kobayashi, K. Tanaka, and H. Minato, This Bulletin, **45**, 2906 (1972).

9) Y. Kohara, M. Kobayashi, and H. Minato, *ibid.*, **43**, 2933 (1970).

VII is formed only when a strong base is present. These finding can be rationalized by assuming that the formation of VIII is reversible and VIII is converted to VII by prototropy catalyzed by base. In the absence of base, VIII redissociates to triphenylmethyl and *p*-tosyl radicals, which recombine and form VI. Formation of VIII from triphenylmethyl and *p*-tosyl radicals is analogous to the formation of the Gomberg trityl(IX) from two triphenylmethyl radicals.[10] It is known that IX isomerizes to X with a basic catalyst.[11]

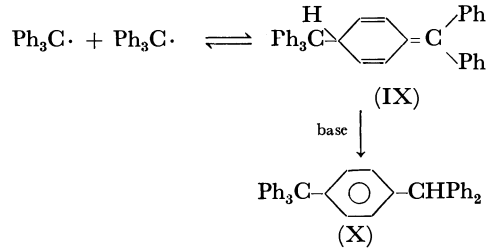

Formation of much triphenylmethane in the HgO-oxidation of II in the presence of triethylamine could be ascribed to abstraction of hydrogen of the amine with triphenylmethyl radical. However, a separate experiment showed that in the presence of a strong base II is converted to triphenylmethane, *p*-toluenesulfinic acid and nitrogen. Therefore, this base-catalyzed decomposition of II appears to be the better explanation for the formation of triphenylmethane in the HgO-base-oxidation of II.

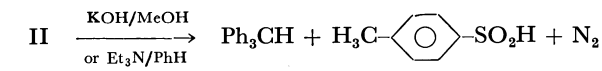

When such stronger oxidizing agents as manganese (IV) oxide were used, the radical pair formed by the decomposition of I were probably further oxidized on the surface of the solid oxidizing agents, and therefore no sulfones were found.

Experimental

Materials. Pyridine and triethylamine were purified by the usual procedures. Yellow mercury(II) oxide was used as received. Manganese(IV) oxide was that used for elemental analyses.

Synthesis of p-*Tolyl Triphenylmethylhydrazo Sulfone(II).* Triphenylmethyl chloride (2.8 g) was added to a chloroform (60 ml) solution of *p*-tosylhydrazine (2.8 g). After 2 hr refluxing, the *p*-tosylhydrazine hydrochloride which precipitated was filtered, and the filtrate was evaporated. Recrystallization of the residue from ethanol gave pure II; mp 136 °C (decomp); yield, 1.6 g (37%). IR, 1160, 1308, 1325 (S–O), 3230, 3280 (N–H) cm^{-1}. NMR, δ, 2.45(s), 4.10(b), 4.95(s), 7.20(m). Found: C, 72.66; H, 5.47%. Calcd for $C_{26}H_{24}O_2N_2S$: C, 72.87; H, 5.64%.

Oxidation of II. The results are summarized in Table 1. Typical examples are shown below.

a) Oxidation of II with HgO in Benzene. A mixture of II (1.290 g, 3.0 mmol), yellow mercury(II) oxide (0.683 g, 3.16 mmol), anhydrous sodium sulfate (1.2 g) and benzene (50 ml) was stirred with a magnetic stirrer at 70 °C. The yellow color of mercury(II) oxide disappeared, and nitrogen was evolved. The mixture was filtered, and the filtrate was evaporated. Crystallization of the residue from benzene–ether yielded crystals of VI (0.618 g, 1.55 mmol; mp 171 °C (lit, 173 °C)) first, and then those of III (0.273 g, 1.05 mmol; mp 160—161 °C(lit, 164.2 °C). They were identified by their IR and NMR spectra.

Table 1. Products of oxidation of $TsNHNHCPh_3$ with HgO

Run	Reactants (mmol)		Solvent	Others	Separation method
	$TsNHNHCPh_3$	HgO			
1	3.00	3.16	PhH	—	Recryst. from Et_2O–PhH
2	6.10	30	PhH	Et_3N 10 mmol	Florisil column
3	4.96	10.2	Py	—	Florisil column
4	5.71	6.95	Py	under N_2	Florisil column
5	5.32	6.35	Py	—	Florisil column
6	2.18	2.18	PhH	MgO 21.8 mmol under N_2	Florisil column
7	2.00	4.80	PhH	—	Florisil column

Run	Products, mmol (mol%)						
	TsOH	Ph_3CH	$(Ph_3CO)_2$	Ph_3COH	$TsCPh_3$	$TsC_6H_4CHPh_2$	Unknown sulfone
1	—	—	—	1.05(35.0)	1.55(51.7)	—	—
2	1.43(23.4)	1.35(22.0)	—	2.74(45.7)	(a)	1.5 (23.4)	—
3	—	—	0.18(7.2)	2.16(43.4)	(a)	1.5 (30.2)	23.5 wt%
4	—	0.46(8.0)	—	2.7 (47.2)	(a)	1.41(24.8)	20.4 wt%
5	—	0.38(7.1)	0.15(5.6)	2.23(42.0)	(20) b)	1.68(31.6)	(10) b)
6	—	0.33(1.5)	0.11(9.7)	1.43(66.1)	—	—	—
7	—	—	0.23(22)	1.52(76.0)	—	—	—

a) Hydrolyzed during chromatography. b) Determined by NMR.

10) H. Lankamp, W. Th. Nanta, and C. MacLean, *Tetrahedron Lett.*, **1968**, 249.

11) R. D. Guthrie and G. R. Weisman, *Chem. Commun.*, **1969**, 1316.

b) Oxidation of II with HgO in the Presence of Triethylamine. Triethylamine (1.0 g, 10 mmol) and mercury(II) oxide (6.487 g, 30.0 mmol) were added to a benzene solution (100 ml) of II (2.609 g, 6.10 mmol), and the mixture was refluxed for 2 hr. It was filtered, and the filtrate was washed with water, dried and then concentrated. Florisil column chromatography of the residue yielded V (0.328 g, 1.35 mmol), III (0.712 g, 2.74 mmol) and VII (0.600 g, 1.5 mmol). The addition of S-benzylisothiourea hydrochloride to the aqueous washings gave crystals of *p*-toluenesulfonate (0.483 g, 1.43 mmol). VII, mp 158 °C; IR; 1150, 1300, 1320 cm^{-1}(S–O); NMR($CDCl_3$), δ, 2.36(s, 3H), 5.55(s, 1H), 6.95~7.89 (m, 18 H); Found: C, 78.19; H, 5.58; S, 8.72%. Calcd for $C_{26}H_{22}O_2S$: C, 78.37; H, 5.57; S, 8.05%.

c) Oxidation of II with HgO in Pyridine. A mixture of II (3.420 g, 8.0 mmol), pyridine (40 ml) and mercury(II) oxide (2.07 g, 9.6 mmol) was stirred at 60—70 °C. After the evolution of gas ceased, the mixture was filtered, and the pyridine was removed by vacuum distillation of the filtrate. The residue was found to contain VI and VII in a 7 : 10 ratio from its NMR spectrum($CDCl_3$). When the residue was subjected to Florisil column chromatography, V (7.1 mol%), IV (2.8 mol%), III (42 mol%), and VII (32 mol%) were isolated. Therefore, the amount of VI present before the chromatography can be calculated as 22 mol% ($32 \times 7/10$).

Reaction between II and Triethylamine. A mixture of II (0.838 g, 1.96 mmoles), triethylamine (1.0 g) and benzene (50 ml) was refluxed for 18 hr. When it was washed with aq Na_2CO_3 and the organic layer was concentrated, V was obtained; 0.460 g, 1.91 mmoles (98 mol%). When the aqueous layer was concentrated and S-benzylisothiourea hydrochloride was added, *p*-toluenesulfinate salt was obtained; 0.423 g, 1.31 mmol.

BULLETIN OF THE CHEMICAL SOCIETY OF JAPAN, VOL. 46, 2504—2511 (1973)

Photochemical Reactions of Enamino Ketones[1)]

Kazutoshi YAMADA, Takeo KONAKAHARA, and Hirotada IIDA

Department of Synthetic Chemistry, Faculty of Engineering, Chiba University, Yayoicho, Chiba 280

(Received February 21, 1973)

Photochemical reactions of *N*-aryl enamino ketones including one enone system and one divinylamine system in the molecule were examined. Photochemical behaviours of *N*-aryl enamino ketones differed for the tertiary and secondary amines involved. While 5,5-dimethyl-3-(*N*-methylanilino)cyclohex-2-en-1-one gave an oxidative cyclization product, 3-anilino-5,5-dimethyl-cyclohex-2-en-1-one gave two major products and a minor one. One of the major products was characterized as 3,3-dimethyl-5-hydroxy-3,4-dihydro-1-benzazocines by their elemental analyses and spectroscopic properties. The compounds showed 6π system pseudo aromaticity in their NMR spectra. The temperature-dependent NMR signals for *gem*-dimethyl protons were due to the flapping of the 8-membered ring. The reduction product with diborane was identified as 1,2,3,4,5,6-hexahydro-1-benzazocine by comparison with an authentic sample. The other major product was a ketene adduct and the minor product, a lactone.

N-Aryl enamino ketones involve both a conjugated enone and a divinylamine system in the molecules. Molecular rearrangement reactions of conjugated enones such as cyclohexenones are known as those of cyclohexadienones.[2)] Divinylamines are isoelectronic with pentadienyl anion. The former was reported to give similar cyclization products.[3)] Linschitz and Grellmann[4)] obtained carbazole derivatives on irradiation of *N*-substituted diphenylamines. Chapman and his co-workers[5)] reported on the nonoxidative photocyclization of *N*-methylaniline enamines to give *trans*-hexahydrocarbazoles. However, all the reactions were of *N*-substituted tertiary amines and we could find no report of photoreactions of *N*-unsubstituted secondary enamines, except for that of diphenylamine which is converted into carbazole with a considerable number of side reactions.[4)] Enamino ketones including these two functional groups are also of importance as intermediates in organic syntheses,[6)] and various investigations have been reported.[7-10)] Photoreactions

1) Preliminary report: K. Yamada, T. Konakahara, S. Ishihara, H. Kanamori, T. Itoh, K. Kimura, and H. Iida, *Tetrahedron Lett.*, **1972**, 2513.

2) W. A. Noyes, Jr., G. S. Hammond, and J. N. Pitts, Jr., "Advances in Photochemistry," John Wiley & Sons, New York, London (1963).

3) A. Schönberg, G. O. Schenk, O. A. Neumüller, "Preparative Organic Photochemistry," 2nd Edn., Springer-Verlag New York Inc. (1968), p. 138.

4) a) K.-H. Grellmann, G. M. Sherman, and H. Linschitz, *J. Amer. Chem. Soc.*, **85**, 1881 (1963); H. Linschitz and K.-H. Grellmann, *ibid.*, **86**, 303 (1964); b) Groen *et al.* reported photocyclization of phenylthioethenes to give a "normal" and an "abnormal" product in low yields (S. H. Groen, R. M. Kellog, J. Buter, and H. Wynberg, *J. Org. Chem.*, **33**, 2218 (1968)).

5) O. L. Chapman, G. L. Eian, *J. Amer. Chem. Soc.*, **90**, 5329 (1968); O. L. Chapman, G. L. Eian, A. Bloom, and J. Clardy, *ibid.*, **93**, 2918 (1971).

6) a) M. Regitz and H. Schwall, *Ann. Chem.*, **728**, 99 (1969); b) R. J. Friary, R. W. Frank, J. F. Tobin, *Chem. Commun.*, **1970**, 283, c) A. G. Cook, "Enamines: Synthesis, Structure, and Reactions," Marcel Dekker, New York and London (1969).

7) For example: A. I. Meyers, A. H. Reine, and R. Gault, *J. Org. Chem.*, **34**, 698 (1969); and references cited therein.

8) a) J. Freimanis, I. Mazeika, *Tero. Eksp. Khim.*, **4**, 601 (1968); *Chem. Abstr.*, **71**, 2865a (1969); b) J. Freimanis, *Zh. Org. Khim.*, 1067 (1967); *Chem. Abstr.*, **68**, 68348d (1968); c) J. Freimanis, J. Stradins, and I. Kravis, *Zh. Obshch. Chim.*, **39**, 631 (1969); *Chem. Abstr.*, **71**, 35474a (1969).

9) C. Kashima, M. Yamamoto, and N. Sugiyama, *J. Chem. Soc., C*, **1969**, 111.

10) J. V. Greenhill, *J. Chem. Soc., B*, **1969**, 299.

of this type of compound, however, have been investigated only for the photocycloaddition of lycopodine derivatives with allene[11a] or methyl methacrylate,[11b] the photodimerization of 1-methylthymine,[12] photoreduction of kynuric acid with sodium sulfite,[13] and the photoisomerization of 1,2-diphenyl-6-methyl-2,3-dihydro-4-pyridone.[14]

In this paper we wish to report photocyclization reactions of *N*-aryl enamino ketones.[1] Irradiation of 3-(*N*-methylanilino)-5,5-dimethylcyclohex-2-en-1-one in nitrogen-saturated ether gave 2,3-dihydro-2,2,9-trimethylcarbazol-4(1*H*)-one in good yields. No corresponding product was obtained on irradiation of an *N*-unsubstituted 3-anilinccyclohex-2-en-1-one derivative in benzene solution. This compound gave two major and one minor products. One of the major products was characterized as 3,3-dimethyl-5-hydroxy-3,4-dihydro-1-benzazocine by its spectroscopic properties. The reactions of five *N*-unsubstituted enamino ketones (Scheme I) were investigated. The enamino ketones were prepared by the condensation of cyclohexane-1,3-diones with the corresponding anilines in the presence of a trace amount of concentrated sulfuric acid or *p*-toluenesulfonic acid in toluene (see Experimental).

Results and Discussion

Preparation of Enamino Ketones. The enamino ketones (**3** and **4**) were prepared from aniline derivatives (**1**) and 5,5-dimethylcyclohexane-1,3-dione or cyclohexane-1,3-dione (**2**) in the presence of sulfuric acid or *p*-toluenesulfonic acid by azeotropic distillation employing a Dean-Stark trap. The enamino ketones (**4c** and **4b**) were prepared by methylation of the hydroxyl derivatives with diazomethane. Ketones (**3** and **4**) are illustrated in Scheme 1 (for the yields and physical data see Experimental). Their spectral data are in line with the expected structures.

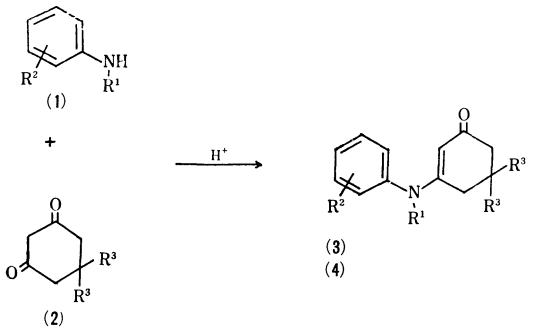

(**3**) $R^1=CH_3$, $R^2=H$, $R^3=CH_3$

(**4**) **a**, $R^1=R^2=H$, $R^3=CH_3$
b, $R^1=H$, $R^2=3'$-Cl, $R^3=CH_3$
c, $R^1=H$, $R^2=4'$-OCH_3, $R^3=CH_3$
d, $R^1=H$, $R^2=3'$-OCH_3, $R^3=CH_3$
e, $R^1=R^2=R^3=H$

Scheme 1.

Irradiation of 3-(N-Methylanilino)-5,5-dimethylcyclohex-2-en-1-one. Irradiation of 3-(*N*-methylanilino)-5,5-dimethylcyclohex-2-en-1-one (**3**) in ether (5.5×10^{-3} M) with a 450-W Pyrex-jacketed immersion lamp (>3000 Å) under nitrogen gave a major product together with a minor one. The major product (mp 137—138 °C, yield, 38%) isolated after the evaporation of ether and crystallization from *n*-hexane–benzene (4 : 1), was identified as 2,3-dihydro-2,2,9-trimethylcarbazol-4(1*H*)-one (**7**) by comparison of spectroscopic properties with a known sample.[15] A benzene solution of **3** was also irradiated to give the same product. Attempted isolation of the minor product by column chromatography on silica gel was not successful. The photoproduct, which may be a nonoxidative hexahydrocarbazole intermediate, could not be identified or isolated, since it was unstable under these conditions. The oxidative photochemical cyclization can be considered as an electrocyclic reaction of a divinylamine. Its excited-state (probably n,π^* triplet[16]) closure should take a conrotatory course according to the Woodward-Hoffmann rule.[5,17] The initially formed dipolar ion intermediate (**5**) analogous to the observed one in oxidative photocyclization of diphenylamine,[4] seemed to give a final product through two possible reaction paths (Scheme 2).

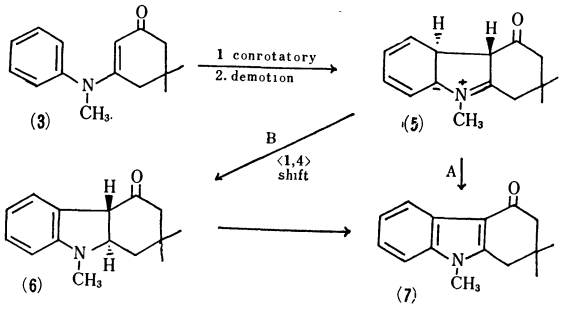

Scheme 2.

Path A gives the final product directly by oxidation with the residual air in the flask or elimination of two hydrogen atoms due to enolization; path B involves a *trans*-hexahydrocarbazole intermediate (**6**) formed by a thermal, suprafacial<1,4>sigmatropic shift of a hydrogen atom.

In order to examine the molecular orbital implication of this reaction, the bond orders (p_{rs}), frontier densities (f_r), and superdelocalizabilities (S_r) were

11) a) K. Wiesner, I. Jirkovsky, M. Fishman, and C. A. J. Williams. *Tetrahedron Lett.*, **1967**, 1523; b) Z. Koblicova and K. Wiesner, *ibid.*, **1967**, 2563, and analogous reaction was reported by Cantrell (T. S. Cantrell, *Tetrahedron*, **27**, 1227 (1971)).

12) N. J. Turro, G. S. Hammond, J. N. Pitts, and D. Valentine, "Annual Survey of Photochemistry," Vol. 1, Wiley-Interscience, New York, London, Sydony and Toronto (1969), p. 147.

13) T. Tokuyama, S. Senoh, T. Sakan, K. S. Brown, Jr., and B. Witkop, *J. Amer. Chem. Soc.*, **89**, 1017 (1969).

14) C. Kashima, M. Yamamoto, Y. Sato, and N. Sugiyama, This Bulletin, **42**, 3596 (1969).

15) W. Sucrow, E. Wiese, *Chem. Ber.*, **103**, 1767 (1970).

16) The photoreaction of enamino ketone (**3**) carried out with a low-pressure mercury arc lamp, filtered with a quartz plate (2537 Å), gave the same photoproducts as those obtained with a high-pressure mercury arc lamp but in a lower yield (**7**, 13%). Benzene was employed as the solvent, and the minor product was not isolated.

17) R. B. Woodward and R. Hoffmann, "The Conservation of Orbital Symmetry," Verlag Chemie, GmbH, Academic Press Inc., New York (1970).

calculated for 3-(*N*-methylanilino)-5,5-dimethylcyclohex-2-en-1-one (**3**), and the values compared with experimental results. The usual parameters[18] were used in the calculations. The bond orders in the ground state and in the first excited state between C–3 and C–7 are calculated as follows:

	G	n,π^*	π,π^*
P_{37}	0.0861	0.0785	−0.0540

S_r values for radical reaction are also illustrated in Fig. 1. Since the P_{37} value for the n,π^* excited state is larger than that of π,π^*, the photoreaction occurs more favorably through the former state. This is in good agreement with experimental facts.[16] The S_r and f_r values for radical reaction at C–3 and C–7 indicate that these positions are more reactive than the others.

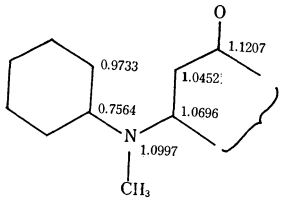

Fig. 1.

$S_r^{(R)}$ values of the enamino ketone (**3**)

Irradiation of 3-Anilino-5,5-dimethylcyclohex-2-en-1-one. For the irradiation of 3-anilino-5,5-dimethylcyclohex-2-en-1-ones (**4**), a benzene solution was employed because of lower solubility of enamine ketones (**4**) in ether. The solution of **4** was irradiated for 0.5 to 2 hours under the same conditions as for **3** to give two major products (**8** and **10**) and a minor one (**11**) (Scheme 3). Yields of **8a**—**e** are summarized in Table 1. In the case of (**4b**) the tlc R_f values (silica gel, benzene–ethyl acetate 9 : 1) were 0.81, 0.68, and 0.54, respectively. One of the two major products with a R_f value 0.68, **8b**, was characterized as 7-chloro-3,3-dimethyl-5-hydroxy-3,4-dihydro-1-benzazocine by its elemental analysis and physical properties. Elemental analysis and high resolution mass spectrum indicate the molecular formula $C_{13}H_{14}NOCl$, formed by elimination of methylene group from the starting material (**4b**). The molecular formula involves one oxygen atom, but the IR spectrum showed a carbonyl band at 1698 cm^{-1} and a hydroxy-absorption at 3324 cm^{-1}. This coexistence of the carbonyl and a hydroxy-absorption indicates the presence of a keto-enol equilibrium (Scheme 3). Measurements of IR spectra of **8b** in various solvents showed a remarkable change in the ratio $D(\nu_{OH})/D(\nu_{C=O})$ of the absorbance for the two absorption bands (Table 2). This indicates that solvation in polar solvents stabilizes the enol form giving rise to an increase of the ratio $D(\nu_{OH})/D(\nu_{C=O})$. This is also supported by the fact that only absorption due to enol form at 3170 cm^{-1} and 1198 cm^{-1} was observed in tetrahydrofuran solution highly diluted with carbon tetrachloride.

TABLE 1. SUMMARY OF YIELDS OF (**8**)

Compound	Conversion (%)	Yield (%)
8a	25	14
8b	19	12
8c	25	20
8d	90	17
8e	4	3

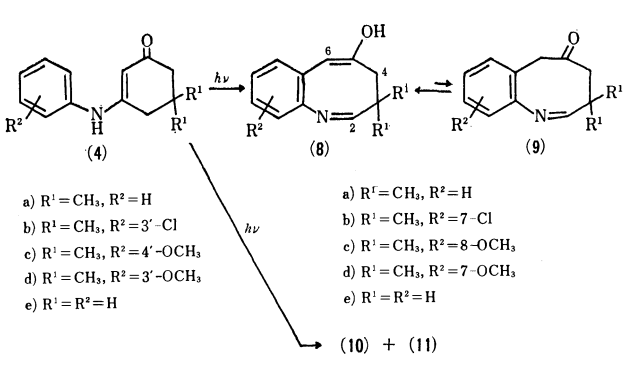

Scheme 3.

TABLE 2. SUMMARY OF IR SPECTRAL DATA OF **8b** IN VARIOUS SOLVENTS

Solvent	ν_{OH} (cm^{-1})	$\nu_{C=O}$ (cm^{-1})	$\nu_{C=N}$ (cm^{-1})	ν_{C-O} (cm^{-1})	$D(\nu_{OH})/D(\nu_{C=O})$
KBr	3324	1698	1630	1200	0.4
CCl_4	3200	1713	1640	1200	1.0
Dioxane	3175	1713	1632	1198	2.0
THF[a]	3170	1713	1632	1198	2.7
CCl_4[b]	3170	—	—	1198	—

a) THF: tetrahydrofuran.
b) THF solution **8b** was highly diluted with CCl_4. Only the absorption bands at 3170 (strong) and 1198 cm^{-1} (medium) were observed.

The absorption bands at 1382, 1367, and 1215 cm^{-1} indicate the presence of *gem*-dimethyl group. This was further supported in the NMR by the presence of a signal at $\delta(CCl_4, TMS)$ 1.28 (singlet, 6H) and by the absence of a signal assignable to a methine proton in the range δ 2—5 (Table 3). The mass spectrum showed a fragment ion peak ($C_{12}H_{11}NOCl$, 220.0400, base) formed by elimination of methyl radical from the molecular ion ($C_{13}H_{14}NOCl$, 235.0743) with a "flat-topped metastable" ion (m^*=206), indicating the presence of a *gem*-dimethyl group (Scheme 4-1).[18,19] A broad NMR signal at δ 6.18 (1H) exchangeable with deuterium oxide and a singlet-like signal at δ 6.98 (1H) were assigned to the enolic hydroxyl proton at C–5 and vinyl proton at C–6, respectively. An aryl substitution of the vinyl group shifts the *gem*-proton signal downfield to the range δ 6—8.5 compared with that of alkyl substituted one (δ *ca.* 5.5) because of deshielding by the ring. The IR spectra of **8a** and **8e** (753 and 694 cm^{-1}; 753 and 692 cm^{-1}) and their NMR spectra indicate the presence of an *ortho*-

18) a) L. E. Orgel, T. L. Cottrel, W. Dick, and Sutton, *Trans. Faraday Soc.*, **47**, 113 (1951); b) A. Streitwieser, Jr. and P. M. Nair, "Conference of Hyperconjugation," Pergamon Press, London (1959).
19) F. W. McLafferty, "Mass Spectrometry of Organic Ions," Academic Press, New York, London (1963), p. 641.

Table 3. Summary of NMR spectral data of (**8**)[a]

Compd.	Position										
	2	3	4	5-OH[c]	6	7	8	9	10	R^1	R^2
8a[b]	6.56 (s, 1H)	—	2.33 (s, 2H)	6.17 (bs, 1H)	7.10 (s, 1H)	7.37 (m, 1H)	6.99[f] (t, d, 2H)		7.37 (m, 1H)	1.28 (s, 6H)	—
8b	6.37 (s, 1H)	—	2.24 (s, 2H)	6.22 (bs, 1H)	6.98 (s-l[e], 1H)	—	6.8[g] (d, d, 1H) or 6.82[h] (d, d, 1H)	7.13[i] (d, d, 1H)	6.82[h] (d, d, 1H) or 6.8[g] (d, d, 1H)	1.82 (s, 6H)	—
8c	6.19 (s, 1H)	—	2.22 (s, 2H)	5.82 (bs, 1H)	6.77 or 6.85 (s-l, 1H)	6.85 or 6.77 (s-l, 1H)	—	6.92[j] (d, d, 1H)	6.72[k] (d, 1H)	1.25 (s, 6H)	3.71 (s, 3H)
8d[b]	6.52 (s, 1H)	—	2.30 (s, 2H)	6.11 (bs, 1H)	6.57 (s-l, 1H)	—	6.61[l] or 6.47 (d, d, 1H)	7.20[m] (t, 1H)	6.47[l] or 6.61 (d, d, 1H)	1.28 (s, 6H)	3.79 (s, 3H)
	6.59[d,n] (t, 1H)	2.62[d,o] (t, d, 2H)	2.37[p] (t, 2H)	6.18 (bs, 1H)	7.02 (s, 1H)	7.18 (m, 1H)	6.80 (m, 2H)		7.18 (m, 1H)	—	—

a) Values (100 MHz in CCl_4), b) In $CDCl_3$, c) Disappeared with the addition of D_2O, d) Demonstrated by double resonance, e) s-l; singlet-like, f) $J_{ortho}=7.5$, $J_{meta}=2.4$ Hz, g) $J_{ortho}=7$, $J_{meta}=ca.$ 7.5 Hz, h) $J_{ortho}=8.7$, $J_{meta}=ca.$ 2.5 Hz, i) $J_{ortho}=8.7$, $J_{ortho}=7$ Hz, j) $J_{9,10}=8$, $J_{7,9}=3$ Hz, k) $J_{9,10}=8$ Hz, l) $J_{8,9}=8$, $J_{8,10}=3$ Hz, m) $J_{8,9}=J_{9,10}=8$ Hz, n) $J_{2,3}=3.0$ Hz, o) $J_{3,4}=4.5$, $J_{2,3}=3.0$ Hz, p) $J_{3,4}=4.5$ Hz.

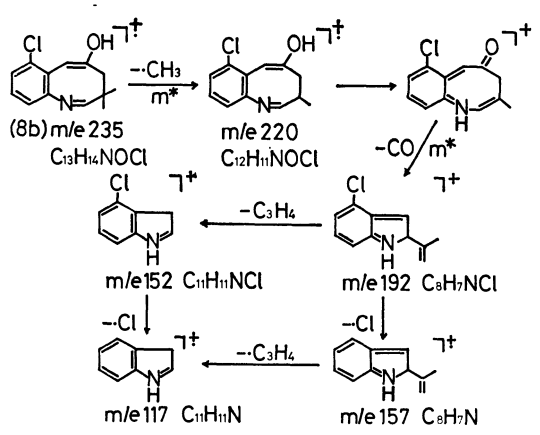

Scheme 4-1.

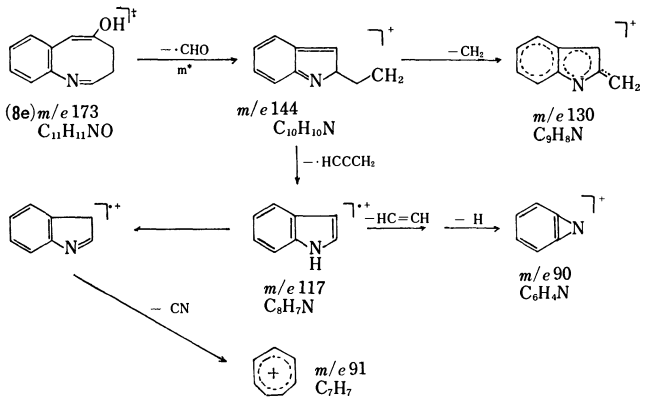

Scheme 4-2.

disubstituted phenylene group. The latter showed AA'BB' patterns. The spectroscopic data showed 1,2,3-trisubstitution of **8b** and **8d**, and those of **8c** 1,2,4-trisubstitution (see Experimental and Table 3). A strong C–N stretching absorption at 1295 cm^{-1} and a C=N stretching absorption at 1630 cm^{-1} in the IR spectrum of **8b** suggested the presence of an anil system. This was also supported by an NMR signal at δ 6.37 (singlet, 1H) (see Tables 2 and 3). The singlet signal indicated that the carbon adjacent to the anil group was quaternary. The corresponding signal of **8e** at δ 6.59 was a one-proton triplet (J=3.0 Hz), coupled with a two-proton triplet signal at δ 2.62 (J=4.5 and 3.0 Hz) for the methylene protons. The coupling was demonstrated by the double resonance. A two-proton triplet at δ 2.3 (J=4.5 Hz) of **8e**, coupled with the methylene described above, corresponded to a two-proton singlet at δ 2.24 of **8b**.[20,21]

Structure **8** including a dihydroazocine ring, can now be written. Its UV spectrum showed more reasonable absorption maxima (λ_{max} (EtOH) 257 (ε 15800) and 305.5 nm (7010)) for the chromophores compared with those of the related compounds (styrene, λ_{max} (EtOH) 244 (ε 12000) and 282 nm (500); *ortho*-aminostyrene, λ_{max} 240 (ε 10000) and 332 nm (1600); diethylketone-anil, λ_{max} 250 (ε 12000) and 300 nm (2000); 2-methoxyazocine, λ_{max} (isooctane) 214 (ε 8750) and 305 nm (350)).

The mass spectrum of **8b** showed three intense peaks (except isotopic peaks due to ^{37}Cl) at *m/e* 235 (molecular ion $M^{+\cdot}$ peak, 40.5% of base), 220 (base), and 192 (40.2% of base) with some weak peaks (Scheme 4-1). The empirical formula of each fragment ion was determined by means of high-resolution mass spectrometry (see Experimental).

The structure was confirmed by the fact that reduction of **8e** with diborane in tetrahydrofuran gave a product identical with authentic 1,2,3,4,5,6-hexahydro-1-benzazocine (**21**), which was prepared from benzo-2-cycloheptenone oxime (Scheme 5).

20) No signals assignable to ring-juncture hydrogens for one of the tautomeric isomers, 3,4-dihydro-3,3-dimethylcyclopent[*b*]-indolin-1(2*H*)-one, were found, which were found at δ 3.5 (multiplet) in the spectrum of 1*b*,4-dimethyl derivative.[21]

21) The NMR spectral data were kindly supplied by Prof. Dr. Yoshio Ban (Hokkaido University).

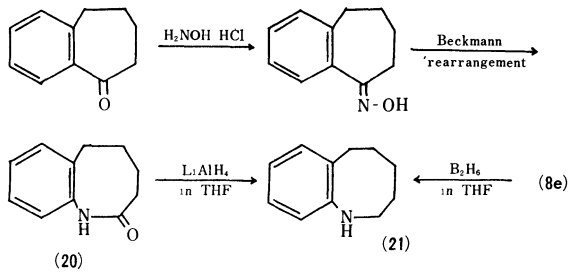

Scheme 5.

Eu(dpm)$_3$-induced shifts in the NMR were used for obtaining information on the conformation of **8b**. The shift-values ($\Delta Eu=\delta_{Eu}-\delta_0$) for the *gem*-dimethyl were 0.93 and 1.01 ppm (in CCl_4) and 1.16 ppm for methylene. The former methyl signal was assignable as *endo*, and the latter as *exo* (Formula **22**). The temperature-dependent NMR signal for the *gem*-dimethyl of **8b** may be considered to be due to the 8-membered ring-flapping of **22**: half height width $b_{1/2}$ 1.25 Hz at 36 °C; 1.75 Hz at −10 °C; 3.65 Hz at −20 °C; 4.90 Hz at −30 °C. The stability of the compounds, the downfield-shifts of signals for protons at 2- and 6-positions, and the stability of the enol-form can be

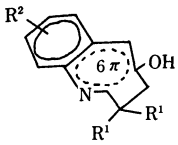

(**22**)

attributed to the 6π system pseudo aromaticity. The spectra (UV, IR, NMR, and mass) of other derivatives prepared from (**4a**—**e**) were in accord with the structures (**8a**—**e**). A possible reaction path is illustrated in Scheme VI. The higher yield of **4a**—**d** than of **4e** is considered to be due to the stabilization of the radical or charge at the *tertiary* center of (**23a**—**d**, $R^1=CH_3$).

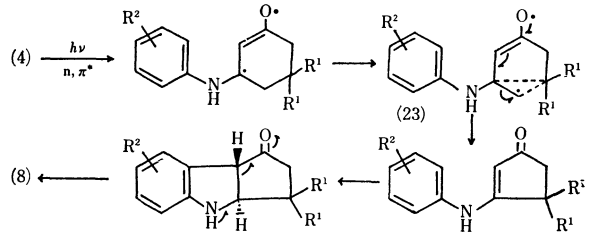

Scheme 6.

Irradiation of hydroxyl derivatives of the enamino ketone (**4**, $R^1=CH_3$, $R^2=3'$ -and 4'-OH) in benzene gave rise to less destruction of the starting material, isolation of traces of similar photoproducts not being possible.

The other major product (**10**) was ketene adduct and the minor one (**11**) a lactone (see Experimental).

Experimental

All melting points and boiling points are uncorrected. Melting points were measured with a Yanagimoto micro melting point apparatus. Ultraviolet spectra were recorded on a Hitachi EPS-3T spectrophotometer. Infrared spectra were recorded on Model IR-G and IR-S (Japan spectroscopic Co., Ltd.) spectrometers. NMR spectra were recorded with JNM 4H-100, Hitachi H-60 and Varian HA-100D high resolution spectrometers for solutions in deuteriochloroform, carbon tetrachloride, or methanol-d_4. The temperature-dependent NMR spectra were measured on a Varian A-60D in a deuteriochloroform solution at −30, −20, −10, and 36 °C. Chemical shifts are reported in δ (internal tetramethylsilane). The mass spectra were obtained with Hitachi RMU-6E (for normal mass spectra), JMS-OlSG (Japan Electron Optics Lab., for high resolution mass spectra), and CEC11OB (for high resolution mass spectra) mass spectrometers at 70 eV. Elemental analyses were performed at the Institute of Physical and Chemical Research.

*Preparation of Enamino Ketones (**3**) and (**4a**).* 5,5-Dimethyl-3-(*N*-methylanilino)cyclohex-2-en-1-one (**3**) and 3-anilino-5,5-dimethylcyclohex-2-en-1-one (**4a**) were prepared from 5,5-dimethylcyclohexane-1,3-dione[22] and anilines (*N*-methylaniline and aniline) in the presence of sulfuric acid by azeotropic distillation with toluene; **3**: mp 80 °C (lit,[9] 84 °C), M^+ 229; **3a**: mp 184—185 °C (lit,[9] 181 °C).

*3-(3'-Chloroanilino)-5,5-dimethylcyclohex-2-en-1-one (**4b**).* *m*-Chloroaniline (1.96 g, 0.015 mol), 5,5-dimethylcyclohexane-1,3-dione (2.14 g, 0.015 mol) and toluene (300 ml) were refluxed in the presence of sulfuric acid in a flask equipped with a Dean-Stark trap for 6 hr. The reaction mixture was treated by the usual method to give 3.34 g (87.0%) of the pure enamino ketone: mp 153 °C (from benzene); UV λ_{max}(EtOH) 230 (ε 8790), 315 nm (24200); IR (KBr) 3100, 1590, 780, and 715 cm^{-1}; NMR ($CDCl_3$, 60 MHz) 6.84—7.35 (m, 5, aromatic and N-H), 5.52 (s, 1, vinyl), 2.32 (s, 2, methylene-4), 2.18 (s, 1, methylene-6), and 1.08 (s, 6); mass spectrum (70 eV) *m/e* (rel. intensity) 251 (27), 249 (81; M^+), 234 (21), 232 (34), 221 (10), 206 (14), 195 (34), 194 (42), 193 (100), 192 (95), 178 (9), 167 (12), 166 (22), 165 (24), 164 (43), 152 (10), 130 (44), 127 (11), 126 (12), 111 (17), 76 (12), 68(28).

Found: C, 67.42; H, 6.60%. Calcd for $C_{15}H_{16}NOCl$: C, 67.32; H, 6.47%.

*5,5-Dimethyl-3-(4'-hydroxyanilino)cyclohex-2-en-1-one (**4**, $R^1=H$, $R^2=4'$-OH, $R^3=CH_3$).* *p*-Aminophenol (1.0 g, 0.01 mol), 5,5-dimethylcyclohexane-1,3-dione (1.4 g, 0.01 mol), and toluene (200 ml) were heated for 4 hr under the same conditions as for **4b**. The resulting solid product was filtered, and washed with cold water. Recrystallization from ethanol gave 0.88 g (37%) of the enamino ketone; mp 227—230 °C; UV λ_{max}(EtOH) 304 nm (ε 17100), mass spectrum *m/e* 231 (M^+).

*5,5-Dimethyl-3-(4'-methoxyanilino)cyclohex-2-en-1-one (**4c**).* To a solution diazomethane[23] in 500 ml of ether, generated from nitrosomethylurea (6.2 g, 0.06 mol), was added 5,5-dimethyl-3-(4'-hydroxyanilino)cyclohex-2-en-1-one (4.10 g, 0.018 mol) in 100 ml of ethanol, allowed to stand overnight in an ice-box. Tlc indicated the presence of the starting material and the product (silica gel with benzene–ethyl acetate 1 : 1, R_f value 0.7 and 0.6, respectively). This was recrystallized from ethyl acetate to give 1.17 g (34%) of the pure enamino ketone (colorless needles): mp 194 °C (lit,[24] 189—190 °C); UV λ_{max} (EtOH) 314 nm (ε 19700); IR (KBr) 3370, 3150, 1610, and 1550 cm^{-1}; NMR methanol-d_4, 100 MHz) δ 7.08 and 6.89 (AA'MM' pattern,

22) R. L. Shriner and H. R. Todd, "Organic Syntheses," Coll. Vol. II, (1943), p. 200.
23) F. Arndt, *ibid.*, p. 165.
24) M. Regitz and H. Schwall, *Ann. Chem.*, **728**, 99 (1969).

4, $J_{AM}=J_{A'M'}=8$ Hz, aromatic), 5.28 (s, 1, vinyl), 3.75 (s, 3, $-OCH_3$), 2.38 (s, 2, methylene-4), 2.16 (s, 2, methylene-6), and 1.08 (s, 6, *gem*-dimethyl); instead of the N–H proton signal, increase of the OH signal (δ 4.75) of methanol was observed; mass spectrum (70 eV) *m/e* (rel. intensity) 246 (20), 245 (100), 230 (10), 228 (26), 217 (13), 202 (12), 190 (16), 189 (88), 175 (10), 174 (71), 160 (10), 146 (12), 123 (12), 122 (23), 108 (11).

*5,5-Dimethyl-3-(3'-hydroxyanilino)cyclohex-2-en-1-one (**4**, $R^1=H$, $R^2=3'$-OH, $R^3=CH_3$).* Prepared from 5,5-dimethylcyclohexane-1,3-dione (1.4 g, 0.01 mol) and *m*-aminophenol (1.0 g, 0.01 mol) as yellow prisms (from ethanol, 41%): mp 246 °C; UV λ_{max} (EtOH) 314 nm (ε 25500); mass spectrum (70 eV) *m/e* 231 (M^+).

Found: C, 72.28; H, 7.42; N, 5.97%. Calcd for $C_{14}H_{17}NO_2$: C, 72.70; H, 7.41; N, 6.06%.

*5,5-Dimethyl-3-(3'-methoxyanilino)cyclohex-2-en-1-one (**4d**).* Prepared by methylation of 5,5-dimethyl-3-(3'-hydroxyanilino)cyclohex-2-en-1-one (**2**, $R^1=H$, $R^2=3'$-OH, $R^3=CH_3$) with diazomethane as light yellow needles (from benzene, 73.2%): mp 118 °C; UV λ_{max} (EtOH) 314 nm (ε 20400), λ_{max} (acidic EtOH) 301 nm (ε 17700); IR (KBr) 3425, 3245, 1605, and 1583 cm^{-1}; NMR ($CDCl_3$, 100 MHz) 7.2 (m, 1, aromatic proton-2'), 7.1 (broad, 1, N–H), 6.68 (m, 3, aromatic), 5.57 (s, 1, vinyl), 3.72 (s, 3, $-OCH_3$), 2.32 (s, 2, methylene-4), 2.15 (s, 2, methylene-6), and 1.05 (s, 6, *gem*-dimethyl); mass spectrum (70 eV) *m/e* (rel. intensity) 245 (98, M^+), 228 (49), 217 (9), 202 (13), 189 (83), 174 (17), 160 (100), 146 (28), 130 (27), 122 (10), 117 (11), 107 (11) 92 (18), 83 (14), 77 (25).

Found: C, 73.67; H, 7.97; N, 5.52%. Calcd for $C_{15}H_{19}NO_2$: C, 73.47; H, 7.76; N, 5.71%.

*3-Anilinocyclohex-2-en-1-one (**4e**).* Aniline (4.3 g, 0.046 mol), cyclohexane-1,3-dione (5 g, 0.045 mol) and toluene (600 ml) were heated for 5 hr under the same conditions as for **4b**. The product was recrystallized from benzene–ethyl acetate to give 6.36 g (76%) of the pure enamino ketone (**4e**) (colorless prisms): mp 182 °C (lit,[25] 179—181 °C); UV λ_{max} (EtOH) 225 (ε 6650) and 309 nm (18700); IR (KBr) 3245, 1590, 1570, 1530, 750, and 706 cm^{-1}; NMR ($CDCl_3$, 100 MHz) 7.0—7.7 (m, 6, aromatic and N–H), 5.53 (s, 1, vinyl), 2.49 (t, 2, $J_{4.5}=6$ Hz, methylene-4), 2.3 (t, 2, $J_{6.5}=6$ Hz, methylene-6), and 1.96 (p, 2, $J_{5,4}=J_{5,6}=6$ Hz, methylene-5), mass spectrum (70 eV) *m/e* (rel. intensity) 188 (13), 187 (77, M^+), 186 (18), 170 (26), 160(13), 159 (100), 158 (50), 144 (14), 131 (22), 130 (54), 117 (9), 93 (23), 92 (35), 85 (11), 77 (36).

Irradiation of Enamino Ketones. All n,π^* irradiations were carried out in a flask equipped with a Pyrex-jacketed immersion lamp at its center. An Ushio Type UM-452 450-W mercury lamp was used as the light source. π,π^* Irradiations were also carried out in the same manner with a quartz-jacketed immersion lamp (Ushio Type ULI-8BQ 80-W). For the sake of complete dissolution the enamino ketones were agitated in ether or benzene for 30 min with a magnetic stirring bar. Agitation and bubbling of dry nitrogen were continued during the course of preparation of the solution and irradiation. The progress of reaction was monitored by tlc.

*Irradiation of 5,5-Dimethyl-3-(N-methylanilino)cyclohex-2-en-1-one (**3**) in Ether with High Pressure Mercury Arc Lamp.* A solution of enamino ketone (**3**) (500 mg, 2.18 mmol) was irradiated in 750 ml of ether (5.5×10^{-3} M) for 4 hr. Tlc (silica gel) revealed a decrease in the amount of starting material and the presence of one major product and one minor one. Evaporation of the solvent *in vacuo* at room temperature left an oily residue. The product soluble in *n*-hexane was separated to give 75 mg of 2,3-dihydro-2,2,9-trimethylcarbazol-4(1*H*)-one (**7**) (conversion 40%,[24] yield 38%). Recrystallization from *n*-hexane–benzene (4 : 1) gave 41 mg of light-yellow needles: mp 137—138 °C; mass spectrum (70 eV) *m/e* (rel. intensity) 227 (86, M^+), 171 (100, $M-C_4H_8$), 143 (52, $M-C_4H_8-CO$)), 128 (10, C_9H_6N), 115 (15, C_8H_5N).

Isolation of the minor product by column chromatography on silica gel was not possible.

*Irradiation of 5,5-Dimethyl-3-(N-methylanilino)cyclohex-2-en-1-one (**3**) in Benzene with High Pressure Mercury Arc Lamp.* A solution of enamino ketone (**3**) (200 mg, 0.87 mmol) was irradiated in 20 ml of benzene (4.4×10^{-2} M) for 8 hr. Tlc (silica gel) of the product mixture showed the presence of same two products as in the case of irradiation in ether.

*Irradiation of 5,5-Dimethyl-3-(N-methylanilino)cyclohex-2-en-1-one (**3**) in Benzene with Low Pressure Mercury Arc Lamp.* A solution of enamino ketone (**3**) (200 mg, 0.87 mmol) was irradiated in 20 ml of benzene (4.4×10^{-2} M) for 16 hr at *ca.* 10 °C with a low pressure mercury arc lamp. Tlc (silica gel) of the product mixture showed the presence of the same two products as in the case of irradiation with high pressure mercury arc lamp. Column chromatography on silica gel (0.05—0.20 mm, E. Merck) in *n*-hexane containing increasing amount of benzene gave 25 mg of the carbazole (**7**) (13%).

*Irradiation of 3-Anilino-5,5-dimethylcyclohex-2-en-1-one (**4a**).* Four grams of enamino ketone (**4a**) was divided into five 800 mg portions, and each portion was dissolved in 2 l of benzene (2.3×10^{-1} M). After irradiation for 2 hr, the solvent was evaporated to 10 ml *in vacuo* below 30 °C. The resulting light-brown crystals and the starting material (compared with standard material by tlc) were separated by decantation and the mother liquor was evaporated to give 160 mg of the photoproducts. They were composed of 3,3-dimethyl-5-hydroxy-3,4-dihydro-1-benzazocine (**8a**) (one of the two major products), ketene adduct (**10a**), lactone (**11a**) (minor product), and polymerized products (tlc analysis on silica gel; R_f values 0.73, 0.83, 0.69, and 0.0, respectively; benzene–ethyl acetate 4 : 1). The combined mother liquor of five portions (820 mg) were chromatographed over silica gel eluted with *n*-hexane–benzene. The first band gave **10a** recrystallized from *n*-hexane as light-yellow crystals, 11%): mp 177—178 °C, UV λ_{max} (EtOH) 271.5 nm (ε 45600); IR (KBr) 3360, 1630, 1600, 1530, 1500, 750, and 700 cm^{-1}; NMR ($CDCl_3$, 100 MHz) 7.24 (m, 10), 6.10—6.70 (m, 3), 2.35 (q, 1), 1.35 (d, 3), and 1.32 (s, 3); mass spectrum (70 eV, high resolution) *m/e* 304 ($C_{20}H_{20}N_2O$ (M^+, obsd. 304.1575 mu, error from calculated value -0.0030 mu), 289 $C_{19}H_{17}N_2O$ ($M-CH_3$. 289.1339, -0.0029), 261 $C_{18}H_{17}N_2$ ($M-CH_3+CO$), 261.1391, -0.0017), 212 $C_{14}H_{14}NO$ ($M-(CH_3+C_5H_3N)$, 212.1075, -0.0015), 197 $C_{13}H_{11}NO$ ($M-(CH_3+C_5H_3N+CH_3)$, 197.0841, 0.0013), 184 ($C_{13}H_{14}N$ ($M-(CH_3+CO+C_5H_3N)$, 184.1124, $+0.0045$), 169 ($C_{11}H_7NO$ ($M-(CH_3+C_5H_3N+CH_3+C_2H_4)$, 169.0528, -0.0079), 155 $C_{11}H_{12}$ ($M-(CH_3+CO+C_5H_3N+C_2H_2N)$, 144.0940, -0.0056), 118 C_9H_{10} ($M-(CH_3+CO+C_5H_3N+C_2H_2N+C_2H_2)$, 118.0748, -0.0037).

The second band gave 3,3-dimethyl-5-hydroxy-3,4-dihydro-1-benzazocine (**8a**): mp 70—73 °C (light-yellow needles from *n*-hexane), UV λ_{max} (EtOH) 229 (ε 10400) (Sh), 252.5 16200), 306 (4800, sh), and 315 nm (5100); IR (KBr) 3320 (OH), 1708 (C=O), 1630 (C=N), 1385, 1365, 1297 (Ar–N), 1215, 1182, 753, and 694 cm^{-1}; NMR: summarized

25) 300 mg of the starting material was recovered from the residue (insoluble to *n*-hexane).

in Table 3; mass spectrum (70 eV) *m/e* 201 (M^+), 186 ($M-CH_3$), 158 ($M-(CH_3+CO)$), 118 ($M-(CH_3+CO+C_3H_4)$), 77 (C_6H_5).

Found: C, 77.58; H, 7.51; N, 6.96%. Calcd for $C_{13}H_{15}NO$: C, 77.61; H, 7.46; N, 6.97%'

The third band gave a trace of **11a**: mp 100—101 °C (colorless); UV λ_{max} (EtOH) 270.5 nm (ε 27100); mass spectrum (70 eV) *m/e* 229 (M^+).

*Irradiation of 3-(3'-Chloroanilino)-5,5-dimethylcyclohex-2-en-1-one (**4b**).* Enamino ketone (**4b**) (2.11 g, 8.6 mmol) was divided in to three portions, each portion being dissolved in 2 l of benzene. In one case, 702.55 mg was dissolved in 2 l of benzene (1.4×10^{-3} M). The solution was irradiated for 30 min and then concentrated to 10 ml *in vacuo* below 30 °C. Removal of the starting material by the same method as that for **4a** left an oily product. Column chromatography of the combined oily products (409 mg) on silica gel (30 g) in *n*-hexane containing an increasing amount of benzene gave 42 mg of **10b** (24%), 21 mg, of **8b**, and 16 mg of **11b** (9% isolated). **10b**: mp 156 °C (yellow needles from *n*-hexene); UV λ_{max} (EtOH) 274.6 (ε 41960) and 349.5 nm (510): IR (KBr) 3340, 1630, 1599, 1525, 1485, 783, and 700 cm^{-1}; NMR ($CDCl_3$, 60 MHz) 7.22 (s, 2), 6.76—7.15 (m, 6), 6.3—6.7 (broad, 3), and 1.37 (s, 6); mass spectrum (70 eV, high resolution) *m/e* 372 $C_{20}H_{18}N_2OCl_2$ (M^+, obsd. 372.0732 mu, error −0.0065), 357 $C_{19}H_{15}N_2OCl_2$ ($M-CH_3$, 357.0519, −0.0041), 322 ($C_{19}H_{15}N_2OCl$ ($M-(CH_3+Cl)$, 322.0838, −0.0036), 246 $C_{14}H_{13}NOCl$ ($M-(CH_3+Cl+C_5H_2N)$, 246.0667. −0.0019), 231 $C_{13}H_{10}NOCl$ ((*m/e* 246)−CH_3, 231.0467, +0.0016), 218 ($C_{13}H_{13}NCl$ ((*m/e* 246)−CO, 218.0689, −0.0049), 211 $C_{14}H_{13}NO$ ((*m/e* 246)−Cl, 211.0976, −0.0023), 182 $C_{13}H_{12}N$ ((*m/e* 246) NO ((*m/e* 246)−Cl, 211.0976, −0.0023), 182 $C_{13}H_{12}N$ ((*m/e* 211)−CHO, 182.0920, −0.0051), 167 $C_{12}H_9N$ (167.0692, −0.0046), 152 $C_{11}H_6N$ (152.0576, +0.0076).

7-Chloro-3,3-dimethyl-5-hydroxy-3,4-dihydro-1-benzazocine (**8b**) was obtained from the second band: mp 104.5—105 °C (colorless needles from *n*-hexane); UV λ_{max} (EtOH) 257 (ε 15800) and 305.5 nm (7010); IR (KBr) 3324 (strong, OH), 1698 (strong, C=O), 1630 (strong, C=N), 1382, 1367, 1295 (strong, Ar–N), 1215, 1200, and 830 cm^{-1} (strong), and also see Table II; NMR; summarized in Table 3; mass spectrum (70 eV, high resolution) *m/e* 235 $C_{13}H_{14}NOCl$ (M^+, obs. 235.0743, error −0.0021), 220 $C_{12}H_{11}NOCl$ (220.0400, −0.0129), 192 $C_{11}H_{11}NCl$ (192.0434, −0.0146), 157 $C_{11}H_{11}N$ (152.0227, −0.0040), 117 C_8H_7N (117.0570, −0.0009), observed metastable peaks: 235→220 *m**=206 (calcd 206.0) "flat-topped", 220→192 *m**=168 (calcd 167.6) "flat-topped" (Scheme 4–1).

Found: C, 66.41; H, 6.17%. Calcd for $C_{13}H_{14}NOCl$: C, 66.38; H, 5.96%.

The third band gave **11b**: mp 98 °C (from *n*-hexane); UV λ_{max} (EtOH) 274 nm (ε 20000); NMR ($CDCl_3$, 60 MHz) 6.17—7.22(m, 6), 2.26 (broad d, 2), and 1.24 (t, 6); mass spectrum 70 eV) *m/e* 263 (M^+).

Found: C, 63.73; H, 5.40%. Calcd for $C_{14}H_{14}NO_2Cl$: C, 63.75; H, 5.31%.

*Irradiation of 5,5-Dimethyl-3-(4'-methoxyanilino)cyclohex-2-en-1-one (**4c**).* Four grams of enamino ketone (**4c**) were divided into ten portions. Each portion (400 mg) was added to 2 l. of benzene (0.82×10^{-3} M). The solution was irradiated for 4 hr at room temperature and evaporated to 10 ml. This was treated in the same way as for **4a**. 990 mg of the photoproducts were obtained from the combined mother liquor. Column chromatography on silica gel (45 g) in *n*-hexane containing an increasing amount of benzene gave 16.0 mg of 3,3-dimethyl-5-hydroxy-8-methoxy-3,4-dihydro-1-benzazocine (**8c**). This was recrystallized from *n*-hexane for analysis: mp 93—94 °C (light-yellow needles); UV λ_{max} (EtOH) 252 (ε 11700) and 316 nm (2900); IR (KBr) 3350 (strong, OH), 1705 (C=O), 1630 (C=N), 1390, 1369, 1300 (Ar–N), and 1180 cm^{-1}; NMR; summarized in Table 3; mass spectrum (70 eV) *m/e* (rel. intensity) 232 (11), 231 (65, M^+), 217 (17), 216 (100), 189 (6), 188 (38), 173 (5).

Found: C, 72.64; H, 7.44; N, 6.01%. Calcd for $C_{14}H_{17}NO_2$: C, 72.70; H, 7.41; N, 6.06%.

*Irradiation of 5,5-Dimethyl-3-(3'-methoxyanilino)cyclohex-2-en-1-one (**4d**).* Enamino ketone (**4d**) (1.26 g, 5.1 mmol) was added to 2 l of benzene (2.6×10^{-3} M). The solution was irradiated for 4 hr at room temperature and evaporated to 10 ml. After separation of the starting material, the products (1.12 g) were chromatographed on silica gel (50 g) in *n*-hexane containing an increasing amount of benzene to give 12.5 mg of 3,3-dimethyl-5-hydroxy-7-methoxy-3,4-dihydro-1-benzazocine (**8d**) (17%). This was recrystallized from petroleum ether for analysis: mp 84 °C (colorless needles); UV λ_{max} (EtOH) 215 (ε 19000), 252 (10700), and 299.5 nm (3700); IR (KBr) 3340 (strong, OH), 1706 (C=O), 1634 (C=N), 1381, 1365, 1300 (Ar–N), 1218 and 1200 cm^{-1}; NMR; summarized in Table 3; mass spectrum (70 eV) *m/e* (rel intensity) 232 (8), 231 (45, M^+), 217 (17), 216 (100), 189 (7), 188 (45), 173 (5), 148 (6), 77 (11).

Found: C, 72.83; H, 7.56%. Calcd for $C_{14}H_{17}NO_2$: C, 72.70; H, 7.41%.

*Irradiation of 3-Anilinocyclohex-2-en-1-one (**4e**).* Enamino ketone (**4e**) (5.41 g, 29 mmol) was divided into ten portions, and each portion was irradiated for 2 hr in 2 l of benzene (1.45×10^{-3} M). From the combined reaction mixture was recovered 5.20 g of the starting material. A mixture of the photoproducts (210 mg, conversion 3.9%) was chromatographed on silica gel (35 g) in *n*-hexane containing an increasing amount of benzene. Only the second band was isolated to give 5-hydroxy-3,4-dihydro-1-benzazocine (**8e**) (6.25 mg, 3%); mp 101—102.5 °C (yellow needles from *n*-hexane); UV λ_{max} (EtOH) 227 (ε 6700, sh), 254 (11000), 302 (3100, sh), and 313 nm (3400); IR (KBr) 3330 (strong, OH), 1697 (strong, CO=), 1635 (strong, C=N), 1282 (Ar–NO, 753, and 692 cm^{-1}; NMR; summarized in Table 3; mass spectrum (70 eV, high resolution) *m/e* 173 $C_{11}H_{11}NO$ (M^+, obsd. 173.0844 mu. error +0.003 mu), 144 $C_{10}H_{10}N$ (144.0797 −0.0016), 130 C_9H_8N (130.0646, −0.0011), 117 (C_8H_7N (117.0609, +0.0030), 91 C_7H_7 (91.0528, −0.0020), 90 C_6H_4N (90.0429, +0.0085) (see Scheme IV–2).

Cinnamylidenemalonic Acid. This was quantitatively prepared from cinnamaldehyde and malonic acid according to the procedure of Stuart:[27] mp 208—209 °C (decomp., yellow needles, lit, 208 °C decomp.); UV λ_{max} (EtOH) 236 (ε 3900) and 330 nm (14800).

δ-Phenylvaleric Acid. This was obtained by reduction of cinnamylidenemalonic acid with the Raney nickel followed by decarboxylation according to the reported procedure;[28] yield 80%: mp 57.0—58.8 °C(lit,[29] 58—59 °C); UV λ_{max} (EtOH) 238 (ε 72), 244 (95), 249 (136), 254.2 (183), 255.5 (181), 259.8 (213), 261.9 (215), 264.9 (165), and 268.7 nm (171).

Benzo-2-cycloheptenone. The cyclization procedure[26] in phosphoric acid–phosphorus pentoxide was employed. Yield 79%, bp 123—124 °C/6 mmHg (lit,[26] 90~93 °C/1 mmHg);

26) R. C. Gilmore and W. J. Horton, *J. Amer. Chem. Soc.*, **73**, 1411 (1951).
27) C. M. Stuart, *J. Chem. Soc.*, **49**, 365 (1886).
28) J. W. Cook, R. Philip, and A. R. Somerville, *J. Chem. Soc.*, **1948**, 164.

The Prins Reaction of Cyclooctene and Cyclododecene

Akira UCHIDA, Toyohiro MAEDA, and Sumio MATSUDA

Department of Petroleum Chemistry, Faculty of Engineering, Osaka University, Yamadakami, Suita 565

(Received August 12, 1972)

The reaction products of the sulfuric acid-catalyzed condensation of cyclooctene or cyclododecene with formaldehyde in acetic acid at 40 °C were investigated. The reaction of cyclooctene gave a mixture of 4,5-hexamethylene-1,3-dioxane, 2-cyclooctenylmethyl acetate, and 1-acetoxy-2-acetoxymethylcyclooctane, while the reaction of cyclododecene gave a mixture of cyclic ethers; one was identified as 3-oxabicyclo[10,3,0]-6-pentadecene, and the others were estimated to be 15-acetoxy-3-oxabicyclo[9,3,1]pentadecane and 12,17-dioxatricyclo[13,3,0,$0^{10.14}$]-2-octadecene.

The condensation of cyclopentene or cyclohexene with formaldehyde in the presence of acid-catalysts, Prins reaction, has been the subject of several investigations,[1-5] and the mechanism of the acid-catalyzed reaction of cyclohexene in acetic acid has been studied quite extensively.[2-5] However, the acid-catalyzed condensation of medium-sized cyclic olefins with formaldehyde is almost unknown.

In this report, the sulfuric acid-catalyzed condensation of cyclooctene or cyclododecene with formaldehyde in acetic acid was investigated.

Results and Discussion

Reaction of Cyclooctene. Cyclooctene was treated with a 1.4-fold molar amount of paraformaldehyde in acetic acid in the presence of sulfuric acid. The reaction gave roughly two fractions. The glpc of the lower-boiling fraction indicated that it consisted of two components, I and IIa, and its IR spectrum demonstrated the presence of an ester group and an ether group in it. By the hydrolysis of the fraction with Claisen alkali, IIa was converted into 2-cyclooctenylmethanol (IIb), while I stayed unchanged. Compounds I and IIb were isolated by column chromatography on alumina. In the IR spectrum of I, the absorption of the ether group was observed at 1150—1030 cm^{-1} but no absorption of the ester group. On the NMR spectrum, there was a quartet at τ 5.1—5.6; this was attributed to the methylene protons adjacent to two oxygen atoms. On the basis of the elementary analysis and the spectroscopic properties of I, compound I was confirmed to be 4,5-hexamethylene-1,3-dioxane.

Compound IIa was isolated from the lower-boiling fraction by preparative glpc or by column chromatography on silica gel. The IR spectrum of IIa indicated the presence of an acetoxy group and a double bond in IIa. The position of the double bond was determined by a comparison of the NMR spectra of IIa and its hydrogenation product (III). The signals in the NMR spectrum of IIa at τ 7.5—7.9, which corresponded to 3H and to the allylic protons, disappeared in that of III. Thus, the double bond was assumed to be adjacent to the tertiary carbon atom. On the basis of the spectroscopic properties of IIa and IIb, they were identified as 2-cyclooctenylmethyl acetate and 2-cyclooctenylmethanol respectively.

The higher-boiling fraction was identified as 1-acetoxy-2-acetoxymethylcyclooctane (IVa). Compound IVa had the typical IR absorption of the acetoxy group at 1710 and 1220 cm^{-1}. In its NMR spectrum, two sharp signals of acetoxy protons at τ 8.80 and 8.10, and two multiplets of methyne and methylene protons at τ 5.3—5.0 and 6.4—6.1, were observed.

To determine the structure IVa was hydrolyzed with Claisen alkali to IVb (X=H); IVb was compared with authentic 2-hydroxymethylcyclooctan-1-ol prepared from cyclooctanone. The spectroscopic data and the glpc-retention times of the two compounds were identical. Thus, IVa was confirmed to be 1-acetoxy-2-acetoxymethylcyclooctane.

On the basis of the glpc of the crude reaction product, the product was found to contain 5 wt% of I, 20 wt% of IIa, 65 wt% of IVa, and 10 wt% of unknown substances.

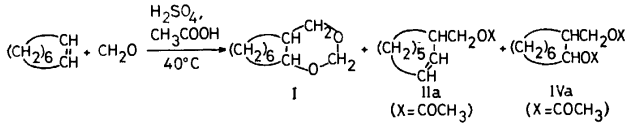

Reaction of Cyclododecene. The reaction of cyclododecene with a 1.4-fold molar amount of paraformaldehyde in acetic acid in the presence of sulfuric acid was attempted. The fractional distillation of the reaction product gave, roughly, two fractions. The glpc indicated that the lower-boiling fraction consisted of V and that the higher-boiling fraction was a mixture of VIa and VII.

Compound V showed the typical IR absorption of ether group at 1050 and 1020 cm^{-1}, and the NMR signals at τ 6.0—6.4 and 6.5—7.0 were attributed to the oxygen-linked methylene protons. To determine the relative position of the double bond in V, compound V was hydrogenated to VIII and the NMR spectra of V and VIII were compared with each other. The proton counts of allylic protons at τ 7.5—8.2, which disappeared after the hydrogenation of V, were less than 4H; this suggested that the double bond was not flanked by two methylene group, but was, rather, situated adjacent to the tertiary carbon atom. To clarify

1) R. P. Stapp and J. C. Randall, *J. Org. Chem.*, **35**, 2948 (1970).

2) J. Matti, *Bull. Soc. Chim. Fr.*, 4 **51**, 974 (1932); S. Olsen and H. Padberg, *Z. Naturforsch.*, **1**, 448 (1946); S. Olsen, *ibid.*, **1**, 671 (1946); S. Olsen, *Angew. Chem.*, **59**, 32 (1947).

3) A. T. Blomquist and J. Wolinsky, *J. Amer. Chem., Soc.*, **79**, 6025 (1957).

4) L. J. Dolby, *J. Org. Chem.*, **27**, 2971 (1962).

5) E. Smissman and R. A. Mode, *J. Amer, Chem, Soc.*, **79**, 3447 (1957).

whether compound V had a 3,4-disubstituted tetrahydrofuran ring or a 3,4,5-trisubstituted tetrahydropyran ring, the ether ring in VIII was cleaved with hydrogen iodide and the resultant diiodomethyl compound was treated with lithium aluminum hydride to give IX. Compound IX demonstrated spectroscopic properties and glpc-retention times identical with those of authentic 1,2-dimethylcyclododecane prepared from 2-methyl-2-carbethoxycyclododecanone.

On the basis of the spectroscopic properties of V, VIII, and IX, and from these observations, they were identified as 3-oxabicyclo[10,3,0]-6-pentadecene (V), 3-oxabicyclo[10,3,0]pentadecane (VIII), and 1,2-dimethylcyclododecane (IX) respectively.

Compound VIa was isolated by a preparative glpc of the higher-boiling fraction. On the basis of the elementary analysis and the mass spectrum VIa was determined to be $C_{16}H_{28}O_3$. The IR and NMR spectra of VIa indicated the presence of an acetoxy group and an ether ring in it. To determine the size of the ether ring in VIa, VIa was converted to the tosylate, which was then treated with lithium aluminum hydride to give X.

If compound VIa had the 3,4-disubstituted tetrahydrofuran ring, X might be identical with VIII. Although the elementary analysis and mass spectra of VIII and X were identical, their IR and NMR spectra or their glpc-retention times were different. This obviates the presence of a 3,4-disubstituted tetrahydrofuran moiety in VIa.

Though there was no experimental evidence for the presence of a 3,4,5-trisubstituted tetrahydropyran ring in VI, it seemed reasonable to assume that VIa was 15-acetoxy-3-oxabicyclo[9,3,1]pentadecane, because no other ether ring could be formed from the mechanistic considerations and because such a 3,4,5-trisubstituted tetrahydropyran derivative had previously been obtained by the Prins reaction of cyclohexene.[3,4] Similarly, on the basis of the elementary analysis and mass spectrum compound VII was estimated to be $C_{16}H_{26}O_2$. The IR and NMR spectra justified the presence of two ether rings and a double bond in VII. The allylic protons in VII, which were estimated by a comparison of the NMR spectrum of VII with that of the product of the hydrogenation of VII, amounted to 3H; this suggested that the double bond was adjacent to the tertiary carbon atom. On the basis of the experimental results described here, the relative positions of the two ether rings and, thus, the structure of VII could not be elucidated. However, because no product derived from the carbonium ion formed by a hydride shift was found in any other product described in this paper, the migration of the carbonium-ion center seemed unlikely; it seemed, rather, reasonable to assume that the two ether rings were adjacent to each other. On the basis of these considerations, it was decided that compound VII was 12,17-dioxatricyclo[13,3,0,$0^{10,14}$]-2-octadecene.

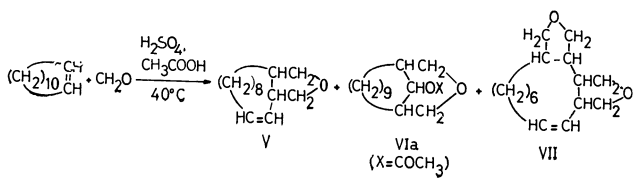

The glpc of the reaction product indicated that the product contained 40 wt% of V, 20 wt% of VIa, 30 wt% of VII, and 10 wt% of unknown substances.

Experimental

All of the mps and bps are uncorrected. The IR spectra were recorded on a Hitachi EPI-G2 type grating infrared spectrometer, and the NMR spectra were taken on a JNM-3H-60 (60 MHz) NMR spectrometer (Japan Electron Optics Lab.) with tetramethylsilane as the internal standard. The chemical shifts (τ) were followed by the splitting patterns (s, singlet; d, doublet; t, triplet; m, multiplet) and the relative strengths. For the analyses by glpc, was used a GC-4B type Shimadzu Seisakusho gas chromatograph with a column 2.5 mm i.d. and 2 m in length; this column contained polyethylene glycol 20 M (20%) on Celite 545.

The paraformaldehyde, acetic acid, and sulfuric acid were used as received. The cyclooctene and the cyclododecene (a mixture of *ca.* 45% of the *cis*- and *ca.* 55% of the *trans*-isomer) received from Wako Chemicals were fractionally distilled. The cyclooctanone and cyclododecanone were prepared by the hydroboration of the corresponding olefins, followed by oxidation with hydrogen peroxide.

Prins Reaction of Cyclooctene. To stirred suspension of 24.0 g (0.64 mol) of paraformaldehyde in 92 ml of acetic acid and 15.5 ml of concentrated sulfuric acid, was added gradually a mixture of 50 g (0.46 mol) of cyclooctene and 41 ml of acetic acid at 40 °C; the solution was then stirred for additional 2 hr. After the addition of 100 ml of water and 50 ml of ether, the mixture was transferred to a separatory funnel. The water layer was removed and the organic layer was washed several times with a saturated aqueous sodium bicarbonate solution and twice with water, and then dried over anhydrous magnesium sulfate. The ether was removed *in vacuo*, and the residual oil was fractionally distilled; Fraction 1 (0.8 g, bp 31 °C/15 mmHg), Fraction 2 (14.9 g, bp 76—77 °C/0.4 mmHg), Fraction 3 (21.5 g, bp 110—120 °C/0.4 mmHg), and a residue.

Fraction 1 was identified as the starting olefin.

Hydrolysis of Fraction 2. A solution of 10 g of Fraction 2 in Claisen alkali (10 g of potassium hydroxide in 31.2 ml of methanol and 8 ml of water) was refluxed for an hour, after which the reaction mixture was worked up; 7.4 g of a hydrolyzed product (bp 90—93 °C/0.4 mmHg) was thus obtained. This substance was separated into benzene eluate and methanol eluate by column chromatography on alumina.

The removal of the solvent from the benzene eluate yielded 4,5-hexamethylene-1,3-dioxane; bp 70—71 °C/0.5 mm Hg; IR (neat) 1150, 1080, 1040, 1030 cm^{-1} (CH_2–O–CH_2–O–CH); NMR (CCl_4) τ 5.1—5.6 (q, 2H, O–C$\underline{H}_2$–O), 6.2—6.6 (m, 3H, CH–C$\underline{H}_2$–O+C$\underline{H}$–O), 7.5—9.0 (m, 13H, other $\underline{H}$); MS (*m/e*) 170 (3), 140 (24), 122 (100); Found: C, 70.36; H, 10.94%; Calcd for $C_{10}H_{18}O_2$: C, 70.54; H, 10.66%; mol. wt., 170.24.

The removal of the solvent from the methanol eluate left 2-cyclooctenylmethanol (IIb); NMR (CCl_4) τ 4.3—4.6 (m, 2H, C$\underline{H}$=C$\underline{H}$), 6.5—6.9 (m, 3H, –C$\underline{H}_2$–O$\underline{H}$), 7.8—8.6 (m, 11H, other $\underline{H}$); Found: C, 76.56; H, 11.84%. Calcd for

6) A. P. Krapcho, J. Diamanti, C. Cayen, and R. Bingham, "Organic Synthesis," Vol. 47 (1967), p. 22.

$C_9H_{16}O$: C, 77.09; H, 11.50%.

2-Cyclooctenylmethyl acetate (IIa) was isolated by preparative glpc or by column chromatography; IR (neat) 1720, 1220 cm^{-1} (CH_3COO), 1650 cm^{-1} (C=C); NMR (CCl_4) τ 4.2—4.7 (m, 2H, CH=CH), 6.1—6.4 (m, 2H, $-CH_2-O$), 7.5—7.9 (m, 3H, $CH_2-CH=CH-CH$), 7.9—8.1 (s, 3H, CH_3COO), 8.1—8.9 (m, 8H, other H); MS (*m/e*) 182 (3), 140 (3), 122 (100), 107 (77); mol. wt. for $C_{11}H_{18}O_2$, 182.25.

Fraction 3 was confirmed to be 1-acetoxy-2-acetoxymethylcyclooctane (IVa); IR (neat) 1710, 1220 cm^{-1} (CH_3COO); NMR (CCl_4) τ 5.0—5.3 (broad m, 1H, CH–OCOCH$_3$), 6.1—6.4 (m, 3H, $CH_2-OCOCH_3$+CH–CH_2–), 7.8—9.0 (m, 19H, CH_3CO (s×2)+other H); MS (*m/e*) 212 (8), 199 (2), 182 (10), 164 (13), 154 (14), 140 (100); mol. wt. for $C_{13}H_{22}O_4$, 242.31.

Hydrogenation of IIa to III. In a 200 ml Erlenmeyer flask, were placed a Raney-Ni catalyst (prepared from 5.0 g of Ni–Al alloy (20%)), 50 ml of ethanol, and 5.0 g of IIa. The mixture was stirred with a magnetic stirrer, after which hydrogen was bubbled through it for 1 hr. The catalyst was then removed from the reaction product by filtration.

The removal of the ethanol from the filtrate yielded cyclooctylmethyl acetate (III); IR (neat) 1730, 1230 cm^{-1} (CH_3COO); NMR (CCl_4) τ 6.2—6.3 (d, 2H, CH_2-O), 8.0 (s, 3H, CH_3CO), 8.2—9.0 (m, 15H, other H); MS (*m/e*) 184 (3), 124 (18), 96 (100), 82 (37); Found: C, 64.59; H, 9.32%. Calcd for $C_{11}H_{20}O_2$: C, 64.44; H, 9.16%; mol. wt., 184.27.

Hydrolysis of IVa. When compound IVa was hydrolyzed with Claisen alkali, 2-cyclooctenylmethanol was obtained; IR (neat) 3300, 1020 cm^{-1} (CH); NMR (CCl_4) τ 5.5—5.8 (m, 2H, OH), 5.8—6.3 (m, 1H, CH–OH), 6.3—6.9 (m, 2H, $-CH_2-OH$), 7.8—9.0 (m, 13H, other H); MS (*m/e*) 156 (8), 140 (64), 122 (100); glpc-retention time (220 °C, 67 ml-H_2/min), 11.4 min; Found: C, 68.02; H, 11.60%. Calcd for $C_9H_{18}O_2$: C, 68.31; H, 11.47%; mol. wt., 158.32.

Synthesis of IVb. 2-Carbethoxycyclooctanone[6] was treated with lithium aluminum hydride in tetrahydrofuran. The subsequent work-up of the reaction product yielded authentic IVb. The glpc-retention time and the spectroscopic properties of the authentic sample were identical with those of IVb.

Prins Reaction of Cyclododecene. To a stirred suspension of 9.2 g of paraformaldehyde (0.25 mol) in 35.0 ml of acetic acid and 6.1 ml of concentrated sulfuric acid, was added gradually a mixture of 30.0 g of cyclododecene (0.18 mol), 10.0 ml of acetic acid, and 8.0 ml of ether at 40 °C, after which the mixture was stirred for additional 2 hr. The subsequent work-up of the reaction product yielded 14.2 g of Fraction 1 (bp 53—56 °C/0.5 mmHg), 6.7 g of Fraction 2 (bp 103—105 °C/0.5 mmHg), 11.3 g of Fraction 3 (bp 140—150 °C/0.5 mmHg), and a residue.

Fraction 1 was identified as cyclododecene by glpc and its IR spectrum.

Fraction 2 was identified as 3-oxabicyclo[10,3,0]-6-pentadecene (V); IR (neat) 1050, 1020 cm^{-1} (CH_2-O-CH_2); NMR (CCl_4) τ 4.5—4.9 (m, 2H, CH=CH), 6.0—6.4 (m, 2H, OCH_2), 6.5—7.0 (m, 2H, OCH_2), 7.5—8.2 (m, 4H, allyl H+tertiary H), 8.2—9.5 (m, 14H, other H); MS (*m/e*) 208 (100), 177 (8), 165 (6); mol. wt. for $C_{14}H_{24}O$, 208.33.

Fraction 3 was treated with Claisen alkali, and the resultant oil was separated into the ether eluate and the methanol eluate by column chromatography on alumina. The removal of the solvent from the ether eluate left 12,17-dioxatricyclo-[13,3,0,$0^{10,14}$]-2-octadecene (VII); mp 92—95 °C (methanol); IR (KBr) 1060, 1050 cm^{-1} (CH_2-O-CH_2), 980 cm^{-1} (C=C); NMR (CCl_4) τ 4.4—4.8 (m, 2H, CH=CH), 6.0—7.0 (m, 8H, CH_2-O-CH_2), 7.2—7.9 (m, 3H, allyl H), 7.9—9.4 (m, 13H, other H); MS (*m/e*) 250 (100), 219 (22), 209 (27); Found: C, 76.57; H, 10.69%. Calcd for $C_{16}H_{26}O_2$: C, 76.75; H, 10.47%; mol. wt., 250.23. From the ethanol eluate, a mixture of 3-oxabicyclo[9,3,1]pentadecan-15-ol (VIb, X=H) (*ca.* 67%) and VII (*ca.* 33%) was obtained; NMR (CCl_4) τ 4.4—4.8 (m, CH=CH), 5.8 (m, CH_2-O-CH_2+CH–$OCOCH_3$), 7.3—9.3 (m, OH, which disappeared upon deuterium exchange+other H).

15-Acetoxy-3-oxabicyclo[9,3,1]pentadecane (VIa) was isolated by the preparative glpc of Fraction 3; IR (neat) 1720, 1230 cm^{-1} (CH_3COO), 1060, 1020 cm^{-1} (CH_2-O-CH_2); NMR (CCl_4) τ 5.0—5.3 (m, 1H, CH–$OCOCH_3$), 6.4—6.6 (m, 4H, CH_2-O-CH_2), 8.0—9.0 (m, 23H, CH_3COO (s)+other H); MS (*m/e*) 268 (3), 250 (3), 226 (4), 208 (100); Found: C, 71.61; H, 10.53%. Calcd for $C_{16}H_{28}O_3$: C, 71.60; H, 10.52%; mol. wt., 268.38.

Hydrogenation of V to VIII. The Raney-Ni catalyst prepared from 3.0 g of Ni–Al alloy was used for the hydrogenation of V in 50 ml of ethanol. The subsequent work-up of the product yielded 5.0 g of 3-oxabicyclo[10,3,0]pentadecane (VIII); bp 110—115 °C/2 mmHg; IR (neat) 1110, 1060 cm^{-1} (CH_2-O-CH_2); NMR (CCl_4) τ 6.1—6.9 (q×2, 4H, CH_2-O-CH_2), 7.7—8.2 (m, 2H, CH), 8.2—9.0 (m, 20H, other H); MS (*m/e*) 210 (9), 209 (6), 208 (14), 179 (10), 149 (10), 135 (17), 121 (17), 109 (16), 95 (56), 82 (100); glpc-retention time (230 °C, 47 ml-H_2/min), 44.0 min; Found: C, 79.44; H, 12.65%. Calcd for $C_{14}H_{26}O$: C, 79.93; H, 12.46%.

Conversion of VIII to 1,2-Dimethylcyclododecane (IX). A mixture of 3.0 g of VIII and 25 ml of an aqueous solution of hydrogen iodide (47%) was refluxed for 3 hr. After the subsequent addition of water to the reaction mixture, the product was extracted with three 50-ml portions of ether. The ethereal extract was dried over anhydrous magnesium sulfate. To the stirred suspension of 1.7 g of lithium aluminum hydride in 70 ml of tetrahydrofuran, was added the ethereal extract, and then the mixture was refluxed for 3 hr. The lithium aluminum hydride remaining in the reaction mixture, was decomposed by addition of water, and the resultant solution was filtered. The filtrate was washed with sulfuric acid and water, and dried over anhydrous magnesium sulfate. The ether was removed from the filtrate, and the residual oil was separated into an *n*-hexane eluate and an ether eluate by column chromatography on alumina. From the *n*-hexane eluate, 0.8 g of 1,2-dimethylcyclododecane (IX) was obtained, while from the ether eluate, 1.0 g of VIII was recovered. IX; IR (neat) 2900, 2850, 1440, 720 cm^{-1} (alkane); NMR (CCl_4) τ 8.2—9.0 (m, 22H, H on ring), 9.0—9.4 (m, 6H, CH_3); MS (*m/e*) 196 (100), 182 (10), 168 (32), 139 (36); glpc-retention time (180 °C, 44 ml-H_2/min), 37.0 min; Found: C, 85.34; H, 14.37%. Calcd for $C_{14}H_{28}$: C, 85.63; H, 14.37%; mol. wt., 196.36.

Conversion of VIb to 3-oxabicyclo[9,3,1]pentadecane (X). To a stirred solution of 14.3 g of *p*-toluenesulfonyl chloride in 20 ml of pyridine, which had been cooled in an ice-water bath, was added a solution of 4.0 g of a mixture of VIb (*ca.* 67%) and VII (*ca.* 33%) in 20 ml of pyridine. The reaction mixture was warmed to room temperature and stirred for an additional 15 hr. After the addition of 150 ml of water to the reaction mixture, the product was extracted with ether. The ethereal extract was washed with a 6 M hydrogen chloride solution, a saturated aqueous sodium carbonate solution, and water, and dried over anhydrous sodium sulfate. The resultant ether solution was added slowly to a suspension of 1.3 g of lithium aluminum hydride in 70 ml of tetrahydrofuran. When the resultant mixture was worked up and the less volatile VII was removed by distillation to

yield X; IR (neat) 1080 cm^{-1} (CH_2–O–CH_2); NMR (CCl_4) τ 6.0—7.0 (m, 4H, $C\underline{H}_2$–O–$C\underline{H}_2$), 7.6—9.3 (m, 22H, other H); MS (*m/e*) 210 (9), 209 (9), 208 (17), 179 (9), 135 (17), 121 (22), 109 (39), 95 (69), 82 (100); glpc-retention time (230 °C, 47 ml-H_2/min), 46.5 min; Found: C, 80.15; H, 12.58%. Calcd for $C_{14}H_{26}O$: C, 79.93; H, 12.46%; mol. wt., 210.35.

Hydrogenation of VII. A solution of 5.0 g of VII in 30 ml of ethanol was treated with a Raney-Ni catalyst (from 5.0 g of Ni–Al alloy) in a hydrogen stream at atmospheric pressure; the subsequent work-up of the reaction product yielded 5.0 g of 12,17-dioxatricyclo[13,3,0,$0^{10,14}$]pentadecane; IR (neat) 1060, 1050 cm^{-1} (CH_2–O–CH_2); NMR (CCl_4) τ 6.0—7.2 (m, 8H, $C\underline{H}_2$–CH_2), 7.7—7.9 (m, 1H, H on ring), 7.9—9.2 (m, 19H, other H).

Synthesis of IX. To a solution of 9.3 g of 2-methyl-2-carbethoxycyclododecanone[6] in 20 ml of ethanol, was added 70 ml of 6 M hydrogen chloride solution, after which the mixture was refluxed for 90 hr. The reaction product was then worked up, and 3.1 g of 2-methylcyclododecanone (XII) (bp 85—90 °C/3 mmHg) was thus obtained.

In a 300-ml, four-necked flask fitted with a mechanical stirrer, dropping funnel, a reflux condenser, and a gas-inlet tube, and flushed with nitrogen, were placed 9.8 ml of *n*-butyllithium (15%) in *n*-hexane (0.10 mol) and 40 ml of ether. The solution was stirred vigorously, and then was added 5.5 g of methyltriphenylphosphonium bromide (0.02 mol) and then 3.0 g of XII (0.015 mol). The mixture was subsequently refluxed for 12 hr. When the reaction mixture was worked up, 0.5 g of 2-methyl-1-methylenecyclododecane (XIII) (bp 75—78 °C/2 mmHg) was obtained. A solution of 1.0 g of XIII in 20 ml of ethanol was treated with a Raney-Ni catalyst (from 2.0 g of Ni–Al alloy) in a hydrogen stream at atmospheric pressure; the subsequent work-up of the product yielded 1.0 g of 1,2-dimethylcyclododecane (bp 48—49 °C/25 mmHg). The spectroscopic properties and the glpc-retention time were identical with those described for IX.

BULLETIN OF THE CHEMICAL SOCIETY OF JAPAN, VOL. 46, 2515—2519 (1973)

The Synthesis and The Configuration of 3-Aminotetrahydrothiophene-3-carboxylic Acids

Minoru HATANAKA and Toshiyasu ISHIMARU

The Institute of Scientific and Industrial Research, Osaka University, Yamadakami, Suita, Osaka 565

(Received September 25, 1972)

Several monomethylsubstituted 3-aminotetrahydrothiophene-3-carboxylic acids have been synthesized from the corresponding 3-ketotetrahydrothiophenes by the Strecker and the Bucherer-Bergs syntheses. In each case, the former synthesis leads to one stereoisomer, and the latter, to the opposite stereoisomer. The configurations of 3-amino-2-methyltetrahydrothiophene-3-carboxylic acids have been determined by a study of the NMR spectra; the others have been estimated on the basis of these results. The configurations do not contradict those first assigned to the alkyl substituted 1-amino-1-cyclohexanecarboxylic acids.

The anticancer activity of 1-amino-1-cyclopentanecarboxylic acid (**1**) was first described by Connors *et al.*,[1] and since then several alicyclic α-amino acids have been synthesized from their biological point of view.[2] This paper will deal with the syntheses of 3-aminotetrahydrothiophene-3-carboxylic acids as heterocyclic analogs of **1**. Our interest in these compounds also arises from the fact that some derivatives of DL-α-methylcysteine (**2**) and DL-α-methylethionine (**3**) promote tumor growth.[3]

Munday[4] and Brimelow *et al.*[5] reported that alkylsubstituted cyclohexanones yield, stereospecifically, different isomers of the corresponding α-amino acids, depending on the method of preparation (*i. e.*, the Strecker and the Bucherer-Bergs syntheses). Although their configurations were first assigned by Munday[4] to be **4** for the Strecker products and **5** for the Bucherer products, Cremlyn *et al.*[6] recently reported the opposite assignment. Thus, the configurational assignment remains equivocal because of the absence of conclusive proof.

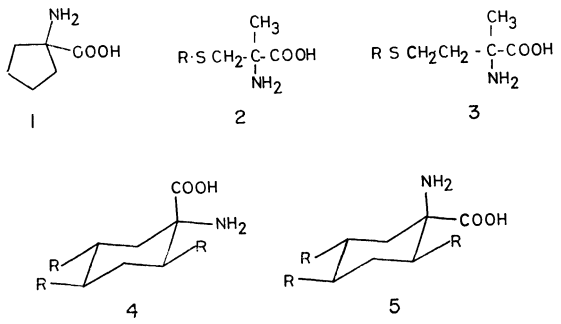

We attempted both the Strecker and the Bucherer-Bergs syntheses for monomethylsubstituted 3-ketotetrahydrothiophenes. The elucidation of the stereoisomerisms of the two methods in this series is another

1) T. A. Connors and L. A. Elson, *Biochem. Pharmacol.*, **1**, 239 (1958).

2) T. A. Connors, L. A. Elson, A. Haddow, and W. C. J. Ross, *ibid.*, **5**, 108 (1960); A. B. Mauger and W. C. J. Ross, *ibid.*, **11**, 847 (1962); S. Aaronson and B. Bensky, *ibid.*, **11**, 983 (1962); P. Tailleur and L. Berlinguet, *Can. J. Chem.*, **40**, 2214 (1962).

3) G. E. W. Wolstenholme and C. M. O'Connor (Editors). "Ciba Foundation Symposium on Amino Acids and Peptides with Antimetabolic Activity," (1958), p. 99.

4) L. Munday, *J. Chem. Soc.*, **1961**, 4372.

5) H. C. Brimelow, H. C. Carrington, C. H. Vasey, and W. S. Waring, *ibid.*, **1962**, 2789.

6) R. J. W. Cremlyn and M. Chisholm, *J. Chem. Soc., C*, **1967**, 2269; R. J. W. Cremlyn, R. M. Ellam, and T. K. Mitra, *Indian J. Chem.*, **8**, 219 (1970); *J. Chem. Soc., C*, **1971**, 1647.

purpose of the present paper.

Results and Discussion

Synthesis. The starting materials, 2-, 4-, and 5-methyl-3-ketotetrahydrothiophenes (**6b–d**, Table 1), were prepared in good yields by means of a modification of the method used by Woodward *et al.*[7] for the synthesis of 3-ketotetrahydrothiophene (**6a**) (Scheme 1).

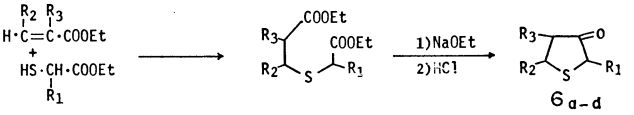

Scheme 1.

TABLE 1. 3-KETOTETRAHYDROTHIOPHENES

No	Compound			Bp °C/mmHg	Yield[a] %	IR[b] $\nu_{C=O}$
	R_1	R_2	R_3			
6a	H	H	H	73—75/16[c]	72[c]	1738
6b	CH_3	H	H	77—84/18	85	1737
6c	H	CH_3	H	77—82/17	77.5	1737
6d	H	H	CH_3	69—70/15	75	1740

a) Based on the mole of ethyl thioglycolate or ethyl thiolactate. b) All spectra were measured in liquid film state. c) Ref. 7: bp 74.5 °C/15 mmHg; 30% yield.

The Strecker reaction with 3-ketotetrahydrothiophene (**6a**) gave a 45% yield of 3-aminotetrahydrothiophene-3-carboxylic acid (**7**), in which case the hydrolysis of the intermediate amino nitrile was conducted by heating it with refluxing 20% hydrochloric acid for 12 hours. However, in the Strecker reaction with the 4-methyl ketone (**6d**) the hydrolysis of the amino nitrile (**8**) under similar conditions produced mainly the corresponding amide; prolonged heating for 2 days was required to give the amino acid (**9**). This resistance to hydrolysis seems to be attributable to the steric effect of the adjacent 4-methyl group. The Bucherer-Bergs reaction with the 4-methyl ketone (**6d**) afforded a 74% yield of the hydantoin (**10**) which was then hydrolyzed by heating with aqueous alkali in an autoclave at 180 °C for 30 hours to produce the amino acid (**11**).

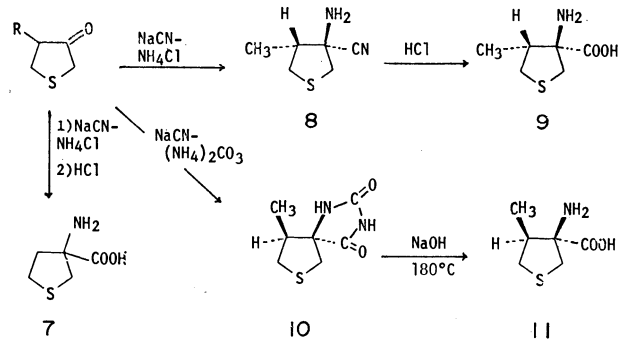

Scheme 2.

The resulting amino acids (**9** and **11**) were indistinguishable from each other by their melting points or by their R_f values upon paper chromatography, but the NMR spectra (Table 2) of their hydrochlorides were obviously different, especially in the signals due to the 4-methyl protons; **9** showed at 1.05 ppm and **11** at 1.15 ppm. Thus, it is apparent that the Strecker product **9** (called the α-form) and the Bucherer product **11** (the β-form) are stereoisomers.

Although the 2-methyl ketone (**6b**) similarly yielded the α-isomer (**13b**) *via* the Strecker reaction, the Bucherer reaction with **6b** followed by the alkaline cleavage of the resulting hydantoin (**14b**) gave a mixture (1 : 1 ratio, on the basis of the signals of the 2-methyl protons in its NMR spectrum) of the isomeric amino acids (**13b** and **15b**). Comparable results were also obtained in the case of the 5-methyl ketone (**6c**); the Strecker reaction gave the α-isomer (**13c**) while the Bucherer reaction produced a 1 : 1 mixture of **13c** and **15c**. This implies that the alkali-induced epimerization of the 2-methyl or the 5-methyl group, occupying the carbon atom adjacent to the sulfur atom, took place *via* carbanion formation during the hydrolysis of the hydantoin. The NMR spectra of the hydantoins (**14b** and **14c**) displayed sharp doublets due to the methyl protons at 1.08 and 1.28 ppm respectively, indicating that they are single isomers. Indeed, when Strecker's amino nitrile (**12b**) was treated with ammonium carbonate, the resulting hydantoin (**18**) was proved by a comparison of the NMR spectra to be isomeric with Bucherer's (**14b**). Therefore, the milder hydrolysis developed by Yamada *et al.*[8] was used for the Bucherer hydantoins (**14b** and **14c**); they were treated with *p*-toluenesulfonyl chloride to form the monotosylates (**16**). The treatment of **16** with cold aqueous alkali followed by the heating of the resulting hydantoic acids (**17**) with 10% hydrochloric acid afforded the desired amino acids (β-isomers), **15b** and **15c** respectively. These amino acids displayed NMR spectra different from those of the corresponding Strecker amino acids (Table 2).

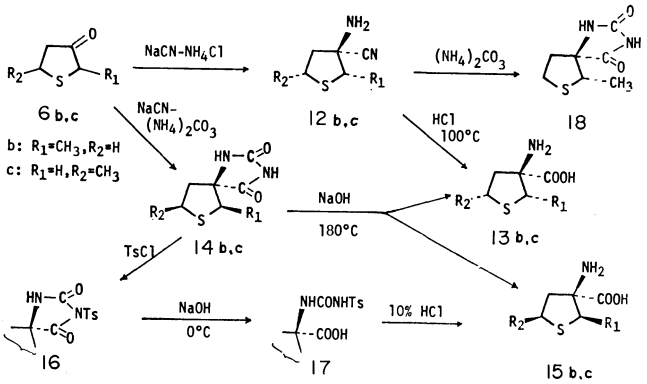

Scheme 3.

In all cases, the stereospecificities of both methods were determined to be >90% on the basis of the signals of the methyl protons in the NMR spectra of the crude products.

7) R. B. Woodward and R. H. Eastman, *J. Amer. Chem. Soc.*, **68**, 2229 (1946).

8) K. Hiroi, K. Achiwa, and S. Yamada, *Chem. Pharm. Bull.* (Tokyo), **16**, 444 (1968).

Table 2. 3-Aminotetrahydrothiophene-3-carboxylic acids

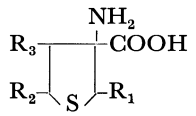

Compound			Strecker product					Bucherer product				
R_1	R_2	R_3	No	Mp[a] °C	R_f[b]	NMR[c] δ	Yield[d] %	No	Mp[a] °C	R_f[b]	NMR[c] δ	Yield[e] %
H	H	H	**7**	286.5—287.5(d)	0.35		45					
CH_3	H	H	**13b**	319—320(sub)	0.47	1.35	41.5	**15b**	256—257(d)	0.49	1.30	33.5
H	CH_3	H	**13c**	261—262(d)	0.54	1.45	36	**15c**	259—260(d)	0.54	1.40	15
H	H	CH_3	**9**	281—282(sub)	0.46	1.05	42	**11**	281—282(sub)	0.44	1.15	62

a) All melting points (capillary) are uncorrected. The symbols in parentheses show: d, decompose; sub, sublime. b) R_f values on paper chromatography; the solvent, *n*-butanol: acetic acid: water (4:1:1). c) Chemical shifts of the methyl protons of the hydrochlorides of these amino acids (in D_2O, at 60 MHz). d) Based on the corresponding 3-ketotetrahydrothiophenes. e) Based on the corresponding hydantoins.

Table 3. Chemical shifts of 2-protons and 2-methyl protons in the derivatives of 2-methyl amino acids (**13b** and **15b**) (60 MHz)

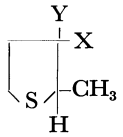

Compound		Concn mg/ml	Solvent	Strecker product		Bucherer product	
X	Y			2-CH_3	2-H	2-CH_3	2-H
NH_3^+Cl	COOH	10	D_2O	1.35	3.68	1.30	4.05
NH_2	$COOCH_3$	7	$CDCl_3$	1.18	3.23	1.19	3.79
NH_2	CH_2OH	7	$CDCl_3$	1.24	3.15	1.23	3.29

The values are in ppm (δ) relative to internal tetramethylsilane.

Configurational Assignment. As has been described above, the amino nitriles (**8** and **12b**) strongly resisted toward hydrolysis. This suggests that the nitrile groups in the Strecker amino nitriles are located *cis* to the methyl groups. Strong support for this assignment is obtained from the studies of the NMR spectra of the 2-methyl amino acids.

For comparison, the 2-methyl amino acids (**13b** and **15b**) were converted to amino esters by treatment with thionyl chloride in methanol, and subsequently to amino alcohols by lithium aluminum hydride reduction. The chemical shifts of the 2-protons and the 2-methyl protons (they appear in the AX_3 pattern) of these compounds are given in Table 3.

In the cases of both the amino acids and the amino esters, the signals due to the 2-protons of the Bucherer products appear at a field lower by 0.37 and 0.56 ppm respectively than those for the Strecker products. It is known that, in a rigid ring system (*e.g.*, a three-membered ring and a rigid bicyclic system such as bicyclo[2,2,2]octane), a carboxyl substituent causes resonances due to the *cis*-vicinal protons to appear downfield of those due to the *trans*-vicinal protons.[9] Also, in the case of a five-membered ring, such an effect has recently been observed.[10] Consequently, our results indicate that the 2-protons are located *cis* to the carboxyl groups in the Bucherer products and *trans* in the Strecker products. In agreement with this assignment, a comparison of the signals of the 2-protons of the amino esters with those for the amino alcohols shows little difference in the case of the Strecker products, but the signal of the amino alcohol shifts 0.5 ppm to a higher field in the case of the Bucherer products.

As a result, the carboxyl group is introduced from the more hindered side of the starting ketone (**6b**) in the Strecker reaction and oppositely from the less hindered side in the Bucherer reaction. Therefore, in the cases of the 4-methyl and the 5-methyl amino acids also it seems to be reasonable to say that the carboxyl groups in the Strecker products are *cis* to the methyl groups, while they are *trans* in the Bucherer products.

These stereochemical results of both reactions are consistent with Munday's conclusion as to the alkyl amino-cyclohexane-carboxylic acids.

9) L. M. Jackman, "Application of Nuclear Magnetic Resonance Spectroscopy in Organic Chemistry," 2 Ed., Pergamon, London (1969), pp. 227—237.

10) K. Horikawa and S. Masuyama, This Bulletin, **43**, 551 (1970); T. Matsumoto, T. Okabe, and K. Fukui, *Chem. Lett.*, **1972**, 29.

Experimental

All the melting points are uncorrected. The IR spectra were measured on a JASCO Model IR-S Spectrometer. The NMR spectra were obtained on a 60 MHz Hitachi R-20 Spectrometer, using tetramethylsilane as the internal standard.

3-Ketotetrahydrothiophenes. A modification of the method of Woodward *et al.*[7] for the preparation of 3-ketotetrahydrothiophene (**6a**) was used for the compounds listed in Table 1; this method, in our hands, gave good yields of these compounds. The preparation of *2-methyl-3-ketotetrahydrothiophene (**6b**)* will be described as an example. To a stirred solution of ethyl thiolactate (53.6 g, 0.4 mol) containing piperidine (0.5 ml), methyl acrylate (38 g, 0.44 mol) was slowly added, while the mixture was maintained at 40—50 °C by occasional cooling. During the reaction, more piperidine (0.5 ml) was added. After the addition of methyl acrylate was complete, the mixture was warmed at 50 °C for 10 min, and then washed with ice water and dried over $MgSO_4$. A mixture of sodium ethoxide [prepared from sodium (11 g) and anhydrous ethanol (30 ml)] in dry benzene (400 ml) was heated at 75—80 °C and a solution of the above Michael-addition product in dry benzene (200 ml) was slowly added over a 1.5-h period. The temperature was then raised to 80—90 °C and the azeotropic mixture (150 ml) of benzene–ethanol was distilled. After cooling, 10% hydrochloric acid (200 ml) was added. The benzene layer was washed with water, dried over $MgSO_4$, and evaporated *in vacuo*. The remaining residue of the Dieckmann product was refluxed with methanol (800 ml) and 20% hydrochloric acid (200 ml) for 4 h. The mixture was cooled in an ice bath, neutralized with a 20% sodium hydroxide solution, and then extracted with methylene chloride (3×100 ml). Drying over $MgSO_4$, the evaporation of the solvent, and the distillation of the residue gave a colorless liquid (39.4 g, 85%); bp 77—84 °C/18 mmHg.

*3-Aminotetrahydrothiophene-3-carboxylic Acid (**7**).* A solution of 3-ketotetrahydrothiophene (6.4 g, 0.063 mol) in methanol (30 ml) was added to a solution of ammonium chloride (8.9 g) and sodium cyanide (7.5 g) in concentrated ammonium hydroxide (51 ml). The mixture was cooled in an ice-salt bath, saturated with ammonia gas, and then shaken at room temperature for 2 days in a tightly sealed bottle. The mixture was diluted with water (100 ml) and extracted with ether (3×50 ml). The extract was washed with water, dried over K_2CO_3, and evaporated *in vacuo*. The remaining residue of the amino nitrile was refluxed with 20% hydrochloric acid (40 ml) for 12 h. After the subsequent evaporation of the solvent *in vacuo*, the residue was dissolved in water (30 ml) and the solution was decolorized with charcoal and again evaporated to dryness *in vacuo*. The resultant solids were extracted with ethanol. After filtration, pyridine was added to the cold filtrate and the mixture was allowed to stand overnight in the refrigerator. The white precipitate was collected by filtration, yielding the amino acid (**7**) (4.6 g, 45%), which was subsequently purified by recrystallization from water. Mp 286.5—287.5 °C (decomp.).

Found: C, 36.34; H, 6.95; N, 8.40%. Calcd for $C_5H_9NO_2S \cdot H_2O$: C, 36.35; H, 6.71; N, 8.47%.

*3-Amino-5-methyltetrahydrothiophene-3-carboxylic Acid (α-Isomer, **13c**).* By the procedure described for **7**, this was prepared from **6c** (5.8 g, 0.05 mol), yielding 2.9 g (36%). Mp 261—262 °C (decomp.).

Found: C, 45.02; H, 7.37; N, 8.95%. Calcd for $C_6H_{11}NO_2S$: C, 44.70; H, 6.87; N, 8.68%.

*3-Amino-4-methyltetrahydrothiophene-3-carboxylic Acid (α-Isomer, **9**).* This was prepared from **6d** (11.6 g, 0.1 mol) by a procedure virtually identical with that described for **7**, but the hydrolysis of the resulting amino nitrile (**8**) to the amino acid (**9**) required heating with 20% hydrochloric acid for 2 days, thus yielding 6.8 g (42%). Mp 281—282 °C (decomp.).

Found: C, 43.26; H, 7.21; N, 8.07%. Calcd for $C_6H_{11}NO_2S \cdot 1/3H_2O$: C, 43.09; H, 7.03; N, 8.37%.

*3-Amino-2-methyltetrahydrothiophene-3-carboxylic Acid (α-Isomer, **13b**).* By the procedure described for **9**, this was prepared from **6b** (11.6 g, 0.1 mol), yielding 6.7 g (41.5%). Mp 319—320 °C (sublime).

Found: C, 44.68; H, 7.21; N, 8.26%. Calcd for $C_6H_{11}NO_2S$: C, 44.70; H, 6.87; N, 8.68%.

*Bucherer Hydantoins, **10**, **14b** and **14c** (β-Isomers).* The usual method was used for the preparation of all the Bucherer hydantoins listed in Table 4. The preparation of *4-methyltetrahydrothiophene-3*-spiro-*5'-hydantoin* (**10**) will be described as an example. A mixture of **6d** (9.2 g, 0.0793 mol), ammonium carbonate (24 g), and 60% aqueous ethanol (130 ml) was warmed at 50 °C; a solution of sodium cyanide (4.1 g) in water (20 ml) was added with stirring. The reaction mixture was stirred at 50—60 °C for 3 h, and then at 85 °C for 1 h. After concentration to 70 ml *in vacuo*, the solution was acidified to pH 6 by the addition of 20% hydrochloric acid and then allowed to stand overnight at 5 °C. The precipitate was collected by filtration and re-

Table 4. Properties of hydantoins

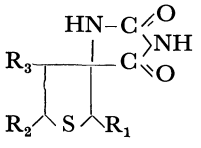

No	Compound			Mp, °C	Yield, %	NMR[a] (Assignment)
	R_1	R_2	R_3			
10	H	H	CH_3	173.5—175	74	0.96, d (4-CH_3)
14c	H	CH_3	H	240—243	72	1.28, d (5-CH_3)
14b	CH_3	H	H	172.5—176	61	1.08, d (2-CH_3) 3.60, q (2-H)
18[b]	CH_3	H	H	180—181.5	35	1.16, d (2-CH_3) 3.40, q (2-H)

a) Measured in DMSO-d_6. Symbols show: d, doublet; q, quartet. b) Prepared from **6b** *via* the amino nitrile (**12b**).

crystallized from aqueous ethanol, yielding 10.9 g (74%).

Found: C, 45.21; H, 5.02; N, 15.15; S, 17.25%. Calcd for $C_7H_{10}N_2O_2S$: C, 45.12; H, 5.40; N, 15.03; S, 17.20%.

*2-Methyltetrahydrothiophene-3-*spiro*-5'-hydantoin(α-Isomer, **18**).* The amino nitrile (**12b**) [prepared from **6b** (3.22 g, 0.0278 mol) *via* the Strecker route] was added to a stirred mixture of ammonium carbonate (8.5 g) and 60% aqueous ethanol (45 ml); the mixture was then stirred at 55—60 °C for 3 h, and subsequently at 85 °C for 1 h. The evaporation of the ethanol, the acidification (to pH 6) of the residue, and the filtration of the precipitate gave the crude hydantoin. Pure **18** was obtained by dissolving it in a 1M sodium hydroxide solution (30 ml); the solution was washed with ethyl acetate and adjusted to pH 6 with 20% hydrochloric acid. The precipitate was collected by filtration, washed with 40% aqueous ethanol, and dried *in vacuo*. Yield 1.82 g (35%).

Found: C, 45.00; H, 5.43; N, 15.12%. Calcd for $C_7H_{10}N_2O_2S$: C, 45.12; H, 5.40; N, 15.03%.

*3-Amino-4-methyltetrahydrothiophene-3-carboxylic Acid (β-Isomer, **11**).* A solution of **10** (10.5 g, 0.0565 mol) in a 1 M sodium hydroxide solution (60 ml) was heated in an autoclave at 180 °C for 30 h, and then decolorized with charcoal and evaporated to dryness *in vacuo*. The residue was suspended in ethanol (50 ml), and lactic acid (6 g) was added. The mixture was stirred at room temperature for 1 h, and then allowed to stand overnight in the refrigerator. The precipitate was collected by centrifuge. The product was purified by dissolving it in 5% ammonium hydroxide (50 ml), and the solution was decolorized with charcoal and concentrated to 10 ml *in vacuo*. The white crystals were collected by filtration, yielding 5.6 g (62%). Mp 281—282 °C (sublime).

Found: C, 44.46; H, 7.03; N, 8.99%. Calcd for $C_6H_{11}NO_2S$: C, 44.70; H, 6.87; N, 8.68%.

*3-Amino-2-methyltetrahydrothiophene-3-carboxylic Acid (β-Isomer, **15b**).* This was prepared by the use of the method of Yamada *et al.*[8] A solution of tosyl chloride (19 g, 0.1 mol) in acetone (50 ml) was slowly added over a period of 6 h to a stirred solution of **14b** (9 g, 0.484 mol) in acetone (150 ml), while the mixture was maintained at pH 9—10 by the dropwise addition of a 1 M potassium hydroxide solution (210 ml). The mixture was then stirred for additional 10 h. The acetone was evaporated *in vacuo* and the precipitate was collected by filtration. The filtrate was acidified with acetic acid and extracted with ethyl acetate. After the evaporation of the ethyl acetate, the residue was combined with the precipitate and the mixture was stirred with 1 M aqueous sodium hydroxide (100 ml) at 0—10 °C for 5 h. The insoluble material was filtered and the filtrate was acidified with 20% hydrochloric acid. The white precipitate of the hydantoic acid (**11**) was collected by filtration and heated with 10% hydrochloric acid (100 ml) at 90—98 °C for 3 h. The mixture was then allowed to stand overnight in the refrigerator. The precipitate was filtered and the filtrate was evaporated to dryness *in vacuo*. The residue was dissolved in ethanol (50 ml), and after the addition of pyridine, the solution was left overnight at 5 °C. The white precipitate was collected by filtration and dried *in vacuo*. Yield 2.6 g (33.4%). Mp 256—257 °C (decomp.).

Found: C, 38.33; H, 7.06; N, 7.47%. Calcd for $C_6H_{11}NO_2S \cdot 3/2\ H_2O$: C, 38.28; H, 7.49; N, 7.44%.

*3-Amino-5-methyltetrahydrothiophene-3-carboxylic Acid (β-Isomer, **15c**).* By the procedure described for **15b**, this was prepared from **14c** (15% yield). Mp 259—260 °C (decomp.).

Found: C, 42.05; H, 7.53; N, 8.17%. Calcd for $C_6H_{11}NO_2S \cdot 1/2\ H_2O$: C, 42.33; H, 7.10; N, 8.22%.

Methyl 3-Amino-2-methyltetrahydrothiophene-3-carboxylate (β-Isomer). A slurry of **15b** (4.28 g, 0.0266 mol) in anhydrous methanol (15 ml) was treated at 0 °C with thionyl chloride (3.3 ml). The mixture was refluxed for 3 h, and then evaporated to dryness *in vacuo*. The residue was shaken for 30 min with dry chloroform (50 ml) saturated with ammonia gas. After filtration, the filtrate was evaporated *in vacuo*. The oily residue was purified through a neutral alumina column with benzene, yielding the amino ester (3.84 g, 82.5%). Tlc indicated the presence of a single component. IR (liquid film): 3300 (NH), 1730 (C=O) cm^{-1}. NMR ($CDCl_3$): see Table 3.

Methyl 3-Amino-2-methyltetrahydrothiophene-3-carboxylate (α-Isomer). By the procedure described above, this was prepared from **13b** (2.36 g, 0.0146 mol), yielding 1.75 g (68%). IR (liquid film): 3300 (NH). 1730 (C=O) cm^{-1}. NMR ($CDCl_3$): see Table 3.

3-Amino-3-hydroxymethyl-2-methyltetrahydrothiophene (β-Isomer). A solution of 3.75 g (0.0212 mol) of the amino ester (β-isomer) in anhydrous tetrahydrofuran (20 ml) was slowly added to an ice-cooled slurry of lithium aluminum hydride (1.2 g, 0.0315 mol) in anhydrous ether (150 ml). The mixture was stirred at room temperature for 2 days and then decomposed with water (3 ml). A 10% sodium hydroxide solution (32 ml) was then added and the aqueous layer was extracted with chloroform containing ethanol. The combined organic layers were dried over $MgSO_4$ and evaporated *in vacuo*. The remaining residue of the amino alcohol was purified through a neutral alumina column with benzene to give a colorless liquid (3.01 g, 96%). Tlc indicated the presence of a single component. IR (liquid film): 3250 (OH, NH) cm^{-1}. NMR ($CDCl_3$): see Table 3.

3-Amino-3-hydroxymethyl-2-methyltetrahydrothiophene (α-Isomer). By the procedure described above, this was prepared from 1.75 g (0.01 mol) of the amino ester (α-isomer), yielding 1.02 g (70%). IR (liquid film): 3250 (OH, NH) cm^{-1}. NMR ($CDCl_3$): see Table 3.

The authors wish to thank Mr. Takuzo Fujino for his microanalysis and Mr. Yoshio Takai for his measurement of the NMR spectra.

Syntheses of Isomaltose, Isomaltotetraose, and Isomaltooctaose

Shinkiti KOTO, Tetsuo UCHIDA, and Shonosuke ZEN

School of Pharmaceutical Sciences, Kitasato University, Shirokane, Minato-ku, Tokyo 108

(Received September 27, 1972)

Ethyl 2,3,4-tri-*O*-benzyl-6-*O*-*p*-nitrobenzoyl-1-thio-α-D-glucopyranoside (I–1) was brominated and subsequently condensed with a deacylated derivative of I–1 in nitromethane in the presence of 2,6-lutidine to give ethyl 2,2′,3,3′,4,4′-hexa-*O*-benzyl-6′-*O*-*p*-nitrobenzoyl-1-thio-α-isomaltoside (I–2) in a 92% yield. These processes were repeated on I–2 to give the blocked tetrasaccharide (I–4) in a 49% yield. Finally, the octasaccharide (I–8) was synthesized in an 11% yield by one more repetition of this reaction cycle. The blocked glycosides, I–2, I–4, and I–8, gave isomaltose, isomaltotetraose, and isomaltooctaose respectively after the sequence of unblocking processes: bromolysis, hydrolysis, methanolysis, and hydrogenolysis.

In synthetic carbohydrate chemistry, it has long been one of the major tasks to synthesize oligosaccharides.[1,2] Since Helferich's gentiobiose synthesis,[3] very many oligosaccharides of various types have been synthesized by all sorts of methods.

At present, there are three general methods for oligosaccharide synthesis: the original and the modified Koenigs-Knorr method,[1,2,4] Kochetkov's ortho ester method,[5] and Lemieux's glycal method.[6] Until recently, however, the fundamental course for the synthesis of relatively higher members of oligosaccharide does not seem to have been laid out or checked, although there were some early investigations.[7] Quite recently, Fréchet and Schuerch started their investigations of the step-by-step oligosaccharide synthesis on polymer support[8] and recorded the synthesis of some higher homologs in excellent yields.[9]

This paper will deal with an approach to the synthesis of the higher oligosaccharide, as in our first program: a series of syntheses of isomaltose,[10] isomaltotetraose, and isomaltooctaose by a systematic repeating scheme in which the condensation between blocks of oligosaccharide was performed as is outlined in Chart 1.[11]

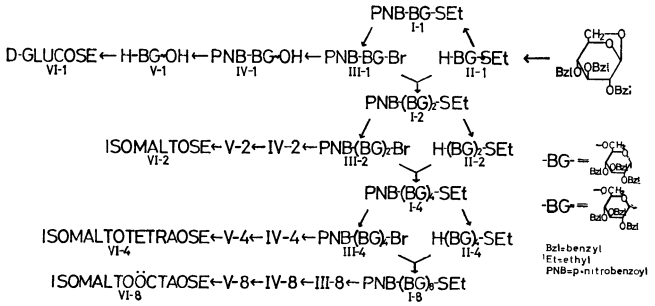

Chart 1.

The anhydro ring of the tri-*O*-benzyl derivative of levoglucosan[12] was cleaved with ethanethiol in the presence of zinc chloride to give the starting ethyl 2,3,4-tri-*O*-benzyl-1-thio-α-D-glucopyranoside (II–1) in a 40% yield. This compound was then converted into the desired *p*-nitrobenzoate (I–1) and also 3,5-dinitrobenzoate (Ia–1) in the usual fashion. I–1 was then bromolyzed by Weygand's method[13] to generate 2,3,4-tri-*O*-benzyl-6-*O*-*p*-nitrobenzyl-α-D-glucopyranoside[14] (III–1) quantitatively.

Throughout this study, glycosidations were carried out by the so-called modified Koenigs-Knorr reaction.[1,2] The choice of the condensing reagent is important for the propagation of the glycoside chain up to a higher degree. 2,6-Lutidine[5] was selected since it is able to form a homogeneous reaction mixture without any activity toward the thio group and without any formation of water during the condensation. As for the solvent, nitromethane might be best for the glycosidation, because of its high polarity to ionize the glycosyl bromide as well as its excellent solvency to various organic materials.

The α-bromide (III–1) was condensed with II–1

1) R. W. Bailey and J. P. Pridham, *Adv. Carbohyd. Chem.*, **17**, 121 (1962); J. H. Pazur, "The Carbohydrates, Chemistry and Biochemistry," Vol. IIA, Academic Press, New York (1970), p. 69.
2) R. J. Ferrier, *Fortschr. Chem. Forsch.*, **14**, 389 (1970).
3) B. Helferich and W. Klein, *Ann. Chem.*, **450**, 219 (1926).
4) W. Koenigs and E. Knorr, *Ber.*, **34**, 957 (1901).
5) N. K. Kochetkov, A. J. Kholin, and A. F. Bochkov, *Tetrahedron*, **23**, 693 (1967).
6) R. U. Lemieux, R. Suemitsu, and S. W. Gunner, *Can. J. Chem.*, **46**, 1040 (1968); R. U. Lemieux, Y. Ito, K. James, and T. L. Nagabhushan, *Can. J. Chem.*, **51**, 7 (1973).
7) B. Helferich and R. Goots, *Ber.*, **64**, 109 (1931).
8) J. M. Frechét and C. Schuerch, *J. Amer. Chem. Soc.*, **93**, 492 (1971); *ibid.*, **94**, 604 (1972).
9) J. M. Frechét and Schuerch, *Carbohyd. Res.*, **22**, 399 (1972).
10) B. Lindberg, *Acta Chem. Scand.*, **3**, 1355 (1949); M. L. Wolfrom, A. O. Pittet, and I. C. Gillam, *Proc. Natl. Acad. Sci. U. S.*, **47**, 700 (1961).
11) S. Koto, T. Uchida, and S. Zen, *Chem. Lett.*, **1972**, 1049. Recently the synthesis of gentiohexaose by block condensation has been recorded by K. Takiura *et al.*, *Chem. Pharm. Bull.* (Tokyo), **20**, 438 (1972).
12) G. Zémplen, Z. Csüros, and S. Angyal, *Ber.*, **70**, 1848 (1937).
13) F. Weygand and H. Ziemann, *Ann. Chem.*, **657**, 179 (1962).
14) T. Ishikawa and H. G. Fletcher, Jr., *J. Org. Chem.*, **34**, 563 (1969).

in the above reaction system to give the blocked α-linked disaccharide (I–2) in a yield of over 90%. The oily I–2 was characterized as a deacylated crystalline compound, ethyl 2,2′,3,3′,4,4′-hexa-*O*-benzyl-1-thio-α-isomaltoside (II–2). When an analogous condensation was carried out by the use of Ia–1, the yield was about 50%.

I–2 was subjected to this sequence of unblocking processes: (1) bromolysis to split off the ethylthio group, giving a bromide (III–2); (2) hydrolysis to regenerate the hydroxyl group on the head; (3) methanolysis to remove the acyl group on the tail, and (4) catalytic hydrogenolysis to remove the benzyl groups of the body, giving isomaltose. II–2 was also bromolyzed, hydrolyzed, and hydrogenolyzed to give isomaltose.

The bromide (III–2) was condensed with II–2 to give the α-linked tetrasaccharide (I–4) in about 50% yield. The degree of polymerization was confirmed by PMR spectrum. I–4 was unblocked to give isomaltotetraose and was partially unblocked into the deacylated compound (II–4).

The connection of the tetrasaccharide blocks, II–4 and III–4, which had been derived from I–4 by bromolysis, gave the α-linked octasaccharide (I–8) in about 10% yield. The degree of polymerization was confirmed by PMR spectrum. The unblocking processes of I–8 gave isomaltooctaose (VI–8).

The synthesized blocked oligosaccharides, I–2, I–4, and I–8, had an α-linked structure, which was confirmed by their $[M]_D$ values within the range of experimental error as well as by PMR. In their PMR spectra, a doublet of an anomeric proton on the head appeared around 5.4 (J=5 Hz), whereas a signal of an internal anomeric proton(s) was observed around 5.0 (J=3 Hz). The very crucial problem of the propagation of the mixing of glycoside linkages by the formation of the undesired anomer at each condensation step, if any, may by overcome by the purification of the blocked glycosides, such as the I's of II's, before and/or after each condensation.

Turvey and Whelan[15] have investigated the partial hydrolyzate of a *Leuconostoc mesenteroides* dextran and found a linear correlation between the values of $[M]_D$ or R_M and the degree of polymerization (*D.P.*). It was found that all the values of the $[M]_D$'s and R_M's of the synthesized free oligosaccharides had a good linearity to the degree of polymerization (Figs. 1 and 2). In addition the $[M]_D$ values of the blocked oligosaccharides, I, II, IV, and V, also had good correlations to the degree of polymerization, although the ratios of the anomers of IV and V were not determined.

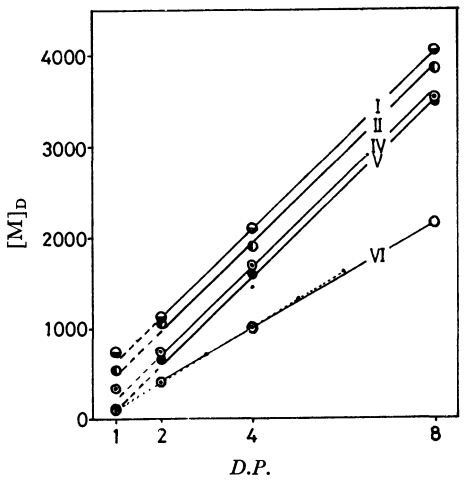

Fig. 1. Relations between *D.P.* and $[M]_D$.
····· Plotted by Turvey and Whelan

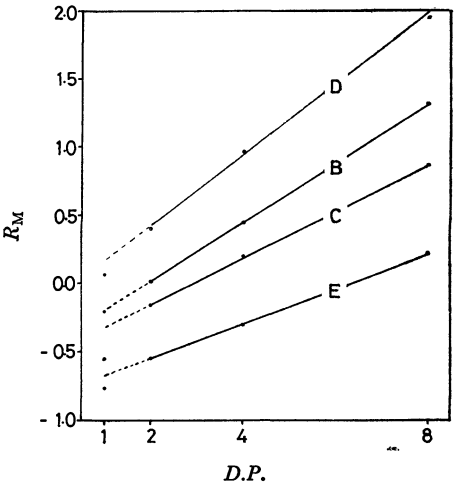

Fig. 2. Relations between *D.P.* and R_M.

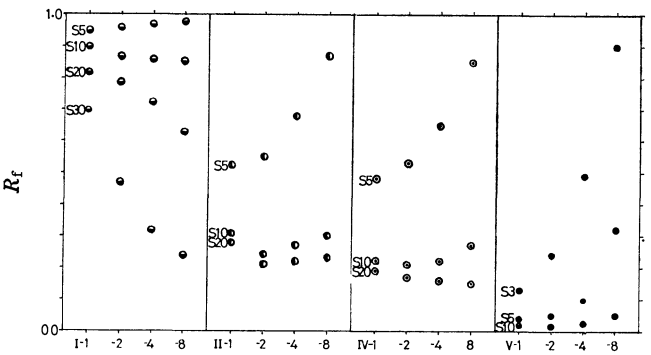

Fig. 3. Relations between *D.P.* and R_f of tlc.

The values of the R_f's in the tlc of the homolog had some correlation to the degree of polymerization (Fig. 3). The R_f's of II, IV, and V, all of which have hydroxy group(s), had roughly an inverse correlation to the degree of polymerization or the molecular size: the ratios of the occupancy of the polar group in the blocked oligosaccharide decrease as the molecular size increases.

Experimental

General Procedures. (1) The solvent systems used for the tlc (silica gel No. 7731, Merck; 10% sulfuric acid spray) and for the column chromatography over silica gel (Kanto Chemical Co.) were as follows: benzene : 2-butanone= (S40) 40 : 1, (S30) 30 : 1, (S20) 20 : 1 (S15) 15 : 1, (S10) 10 : 1, (S7) 7 : 1, (S5) 5 : 1, (S4) 4 : 1, and S(3) 3 : 1, by volume.

(2) The solvent systems used for the paper chromato-

15) J. R. Turvey and W. J. Whelan, *Biochem. J.*, **67**, 49 (1957).

graphy (Toyo filter paper No. 525, unless otherwise stated; ascending development as high as 35 cm at 25 °C; aniline hydrogenphthalate spray) and the column chromatography over cellulose powder (Toyo Roshi Co.,; 100—200 mesh) were as follows: (A) *n*-butanol : acetic acid : water=4 : 1 : 5, (B) *n*-propanol : ethyl acetate : water=6 : 1 : 3, (C) *n*-propanol : nitromethane : water=5 : 2 : 3, (D) *n*-butanol : pyridine : water=6 : 4 : 3, and (E) *n*-propanol : ethyl acetate : water=3 : 1 : 3, by volume.

(3) The melting point was determined by means of a Yanagimoto micromelting point apparatus; uncorrected values are given. The specific rotation was measured in a 1-dm tube by means of an Atago Polux apparatus. The IR spectrum was determined by means of a JASCO IRA-1 infrared spectrometer. The PMR spectrum was measured by means of a Varian S-60T spectrometer in $CDCl_3$, with TMS as the internal standard, unless otherwise mentioned. The elemental analysis was effected by means of a Perkin-Elmer Model 240 Elemental Analyzed apparatus.

(4) The bromolysis was performed by treatment with a bromine solution (Br : petroleum ether=1 : 25, by volume; prepared just before use) in ether (occasionally containing dioxane) at 25 °C for 5 min in a dark place. The bromolyzed mixture was evaporated below 20 °C and then dried at 40 °C. Three co-evaporation with toluene at 40 °C gave a hard yellowish syrup. These operations were performed as quickly as possible, using an oil pump (35 l/min).

Ethyl 2,3,4-Tri-O-benzyl-1-thio-α-glucopyranoside (II-1). A mixture of tri-*O*-benzyl-levoglucosan[12] (7.13 g), zinc chloride (2.08 g), and ethanethiol (35.7 ml) was stirred for 1.5 hr at 25 °C and then poured into iced aqueous sodium bicarbonate. The benzene extract was chromatographed with the S20 solvent to give II-1 after the elution of the unchanged material (1.35 g). Crystallization with *n*-hexane gave colorless needles (3.10 g; 47%); mp 61—63.5 °C, $[\alpha]_D^{25}$ +111° (*c* 1.8, $CHCl_3$). The PMR spectrum contained diagnostic signals of the thioethyl group at δ 1.27 (a triplet; CH_3-) and at δ 2.54 (a quartet; -CH_2-). A doublet of the anomeric proton appeared at δ 5.38, J=5.0 Hz.

Found: C, 70.07; H, 6.88%. Calcd for $C_{29}H_{34}O_5S$: C, 70.42; H, 6.93%.

Ethyl 2,3,4-Tri-O-benzyl-6-O-p-nitrobenzoyl-1-thio-α-D-glucopyranoside (I-1). II-1 (2.00 g) was treated with *p*-nitrobenzoyl chloride (1.23 g) in pyridine (10 ml) at 25 °C overnight. After the hydrolysis of the excess chloride, the benzene extract was chromatographed with the S40 solvent and crystallized with ethanol to give I-1 (2.32 g; 89%); mp 91—92 °C, $[\alpha]_D^{25}$ +116° (*c* 1.0, $CHCl_3$). The IR spectrum (film) showed characteristic bands of the ester group at 1729 cm^{-1} and of the nitro group at 1530 and 1350 cm^{-1}. The PMR spectrum showed the presence of three benzyl groups (δ 7.1~7.5) and one thioethyl group per *p*-nitrobenzoyl group (quasi-quartet, centered at δ 8.18) in I-1.

Found: C, 67.35; H, 5.83; N, 2.06%. Calcd for $C_{36}H_{37}NO_8S$: C, 67.17; H, 5.79; N, 2.18%.

Ethyl 2,3,4-Tri-O-benzyl-6-O-(3,5-dinitrobenzoyl)-1-thio-α-D-glucopyranoside (Ia-1). II-1 (200 mg) was treated with 3,5-dinitrobenzoyl chloride (140 mg) in pyridine (1.0 ml) overnight. After working-up as above, crystallization with diisopropyl ether gave Ia-1 (261 mg; 93%); mp 123—126 °C, $[\alpha]_D^{25}$ +110° (*c* 1.4, $CHCl_3$). The IR spectrum (KBr) had characteristic bands of an ester group at 1725 cm^{-1} and of the nitro group at 1545 and 1348 cm^{-1}. The PMR spectrum showed the presence of three benzyl groups per 3,5-dinitrobenzoyl group (δ 9.0—9.3) in Ia-1.

Found: C, 62.90; H, 5.35; N, 3.84%. Calcd for $C_{36}H_{36}N_2O_{11}S$: C, 62.78; H, 5.27; N, 4.07%.

Ethyl 2,2',3,3',4,4'-Hexa-O-benzyl-6'-O-p-nitrobenzoyl-1-thio-α-isomaltoside (I-2). From I-1. I-1 (0.87 g) was treated with a bromine solution (2.2 ml) in diethyl ether (14 ml) to give a bromide, III-1, $[\alpha]_D^{25}$ +127° (*c* 2.9, $CHCl_3$),[14] which was then condensed with II-1 (0.87 g) in nitromethane (6.0 ml) containing 2,6-lutidine (0.16 ml) for 20 hr. Subsequent chromatography with the S40 solvent gave a homogenous oil of I-2 (1.34 g; 92%), $[\alpha]_D^{25}$ +105° (*c* 2.0 $CHCl_3$). The PMR spectrum showed the presence of six benzyl groups and one thioethyl group per *p*-nitrobenzoyl group in I-2.

Found: C, 69.25; H, 7.22; N, 1.27%. Calcd for $C_{63}H_{65}NO_{13}S$: C, 70.30; H, 6.09; N, 1.30%.

Ethyl 2,2',3,3',4,4'-Hexa-O-benzyl-1-thio-α-isomaltoside (II-2). I-2 (1.32 g) was methanolyzed with dilute sodium methoxide (0.15 M; 20 ml) at 50 °C for 2 hr. Subsequent chromatography with the S20 solvent and crystallization with *n*-hexane gave colorless needles of II-2 (0.96 g; 84%); mp 98—100 °C, $[\alpha]_D^{25}$ +114° (*c* 1.1, $CHCl_3$). The IR(KBr) and PMR spectra indicated the absence of the *p*-nitrobenzoyl group. A couple of doublets of H-1 and H'-1 appeared at δ 5.41, J=4.5 Hz and at δ 5.08, J=4.0 Hz respectively.

Found: C, 72.65; H, 7.02%. Calcd for $C_{56}H_{62}O_{10}S$: C, 72.54; H, 6.74%.

From Ia-1. Ia-1 (100 mg) was bromolyzed in diethyl ether (1.6 ml) with a bromine solution (0.25 ml) to give a bromide, which was then condensed with II-2 (100 mg) in nitromethane (0.97 ml) in the presence of 2,6-lutidine (0.025 ml). Subsequent chromatography with the S40 solvent gave an amorphous disaccharide (76 mg; 47%), which was then methanolyzed with dilute sodium methoxide to give II-2 (52 mg; 39% from Ia-1). Admixture with the above II-2 showed no depression.

Isomaltose (VI-2). From I-2. I-2 (0.14 g) was bromolyzed with the bromine solution (0.22 ml) in diethyl ether (1.5 ml) and then stirred in moist dioxane (10%-H_2O; 10 ml) containing silver carbonate (0.2 g) at room temperature for 1 hr, followed by chromatography with the S15 solvent to give IV-2 (0.084 g; 63%), $[\alpha]_D^{25}$ +72° (*c* 0.5, $CHCl_3$). IV-2 (100 mg) was dissolved in dioxane (1 ml), treated with dilute sodium methoxide (0.15 M; 5 ml), and then chromatographed with the S5 solvent to give V-2 (77 mg; 90%), $[\alpha]_D^{25}$ +73° (*c* 0.5, $CHCl_3$). V-2 (67 mg) was hydrogenolyzed in moist methanol (initial, 2%-H_2O—final, 50%-H_2O), containing five drops of acetic acid over palladium black (20 mg×2)) to give a glass of VI-2 (18 mg; 69%), $[\alpha]_D^{25}$ +126° (*c* 0.8, H_2O)), which was identified with the authentic isomaltose by paper chromatography (Toyo filter paper No. 50; solvents, A, B, and D), as well as by a comparison with β-octa-*O*-*p*-nitro-benzoate[16] (mp 199—201 °C, $[\alpha]_D^{25}$ +97° (*c* 1.4, $CHCl_3$)), using the results of elemental analysis, a mixed-melting point determination, the specific rotation, IR(KBr), PMR, and the R_f's of tlc.

From II-2. II-2 (0.50 g) was bromolyzed in diethyl ether (5 ml) with the bromine solution (0.77 ml), hydrolyzed in moist dioxane (10%-H_2O; 10 ml) in the presence of silver carbonate (140 mg) for 2 hr, and then chromatographed with the S7 solvent to give V-2 (0.23 g; 48%). V-2 (117 mg) was hydrogenolyzed to give VI-2 (35 mg; 77%), which was identified with authentic isomaltose by paper chromatography (Toyo filter paper No. 50; solvents, A, B, and D), and also by comparison of β-octa-*O*-*p*-nitrobenzoate.[16]

16) *Cf.* E. M. Montgomery, F. B. Weakley, and G. E. Hilbert, *J. Amer. Chem. Soc.*, **71**, 1682 (1949). The octa-*O*-*p*-nitrobenzoate prepared from the authentic isomaltose according to their directions melted at 200—202 °C and had $[\alpha]_D^{25}$ +99° (*c* 1.0, $CHCl_3$) (Found: C, 52.90; H, 2.95; N, 7.17%).

Ethyl Dodeca-O-benzyl-terminal-6-O-p-nitrobenzoyl-terminal-1-thio-α-isomaltotetraoside (I-4). I-2 (0.95 g) in diethyl ether (14 ml) was treated with a bromine solution (1.41 ml) to give sirupy III-2, which was then condensed with II-2 (0.95 g) in nitromethane (8 ml) containing 2,6-lutidine (0.10 ml) for 2 days. A crude mixture was chromatographed with the S40 solvent to give a homogenous oil of I-4 (0.84 g; 59%), $[\alpha]_D^{25}$ +108° (*c* 1.0, $CHCl_3$) as the main product. The PMR spectrum showed the presence of 12 benzyl groups and one thioethyl group per *p*-nitrobenzoyl group in I-4.

Ethyl Dodeca-O-benzyl-terminal-1-thio-α-isomaltotetraoside (II-4). I-4 (85 mg) was dissolved in a mixture of methanol (20 ml) and dioxane (5 ml) and treated with dilute sodium methoxide (1.5 M; 0.25 ml) at 50 °C for 2 hr. The mixture was chromatographed with the S15 solvent to give II-4 (77 mg; 98%), $[\alpha]_D^{25}$ +106° (*c* 1.0, $CHCl_3$). The PMR spectrum had no signal of the *p*-nitrobenzoyl group.

Isomaltotetraose (VI-4). I-4 (60 mg) in diethyl ether (1.0 ml) containing dioxane (0.05 ml) was treated with a a bromine solution (0.057 ml) to give 66 mg of II-4, which was then stirred in moist dioxane (13%-H_2O; 4 ml) with silver carbonate (50 mg) for 1 hr. Subsequent chromatography with the S15 solvent gave IV-4 (38 mg; 65%), $[\alpha]_D^{25}$ +91° (*c* 1.0, $CHCl_3$), which was then methanolyzed in methanol (20 ml) containing dioxane (1 ml) with dilute sodium methoxide (1.5 M; 0.25 ml) and chromatographed with the S7 solvent to give V-4 (26 mg; 74%), $[\alpha]_D^{25}$ +91° (*c* 1.0, $CHCl_3$). V-4 (19 mg) was hydrogenolyzed in a mixed solvent of dioxane, methanol, and water (3+1+1 ml, initial→1+1+6 ml, final, containing 5 drops of acetic acid) to give a hygroscopic glass of VI-4 (4.5 mg; 63%), $[\alpha]_D^{25}$ +148° (*c* 0.5, H_2O); it was identified with the authentic isomaltotetraose by paper chromatography with the B, C, and D solvents, as well as by a comparison with β-tetradeca-*O*-benzoate[17] (mp 140.5—145.5 °C, $[\alpha]_D^{25}$ +169° (*c* 0.3, $CHCl_3$)), using the results of elemental analysis, a mixed-melting point determination, IR (KBr), and the R_f's of tlc.

Ethyl Tetracosa-O-benzyl-terminal-6-O-p-nitrobenzoyl-terminal-1-thio-α-isomaltooctaoside (I-8). I-4 (213 mg) was treated in diethyl ether (3.1 ml) containing dioxane (0.4 ml) with a bromine solution (0.16 ml) to give III-4, to which was then added a solution of II-4 (213 mg) in nitromethane (2.0 ml) containing 2,6-lutidine (0.013 ml). After one week, the mixture was chromatographed with the S30 solvent to give I-8 (45 mg; 11%), $[\alpha]_D^{25}$ +110° (*c* 1.1, $CHCl_3$) as the main product. The PMR spectrum showed the presence of 24 benzyl groups per *p*-nitro-benzoyl-group in I-8.

Ethyl Tetracosa-O-benzyl-terminal-1-thio-α-isomaltooctaoside (II-8). I-8 (10 mg) was treated in a mixed solvent of methanol (10 ml) and dioxane (1 ml) with dilute sodium methoxide (1.5 M; 0.15 ml) for 2 hr at 50 °C. Subsequent chromatography with the S20 solvent gave II-8 (8.3 mg; 86%), $[\alpha]_D^{25}$ +110° (*c* 0.8, $CHCl_3$). The IR spectrum (film) showed no absorption of the *p*-nitrobenzoyl group.

Isomaltooctaose (VI-8). I-8 (31.6 mg) was dissolved in a mixed solvent of diethyl ether (0.5 ml) and dioxane (0.1 ml) and then treated with a bromine solution (0.03 ml) to give III-8, which was then stirred in moist dioxane (14%-H_2O; 7 ml) with silver carbonate for 2 hr and chromatographed with the S20 solvent to give IV-8 (17.4 mg; 56%), $[\alpha]_D^{25}$ +99° (*c* 0.5, $CHCl_3$). IV-8 (11 mg) was treated in a mixed solvent of methanol (20 ml) and dioxane (5 ml) with dilute sodium methoxide (1.5 M; 0.25 ml) and chromatographed with the S15 solvent to give V-8 (9.8 mg; 93%), $[\alpha]_D^{25}$ +102° (*c* 0.3, $CHCl_3$).[18] V-8 (8.0 mg) was hydrogenolyzed in a mixed solvent of dioxane, methanol, and water (5+1+0.5 ml, initial→2+0.5+4 ml, final; containing five drops of acetic acid) over palladium balck (10 mg×5) to give a glass of VI-8 (1.8 mg; 59%), $[\alpha]_D^{25}$ +165° (*c* 0.2, H_2O), which had the same R_f values as the eighth spot of the partial hydrolyzate of Dextran T10 (Pharmacia Fine Chemicals Co.), developed with the B and C solvents.

17) *Cf.* Ref. 15; the preparation of the tetradeca-*O*-benzoate from the authentic isomaltotetraose according to their directions gave only an amorphous product (mp 142—146 °C, $[\alpha]_D^{25}$ +164° (*c* 0.9, $CHCl_3$) (Found: C, 68.60; H, 4.58%).

18) *Cf.* E. R. Ruckel and C. Schuerch, *J. Org. Chem.*, **31**, 2233 (1966). The reported value for the blocked polysaccharide with $\overline{DP}_n$=9 is $[\alpha]_D^{25}$ +109° ($CHCl_3$).

Electrochemical Fluorination of Diols and Heterocyclic Compounds[1]

Takashi ABE, Shunji NAGASE, and Hajime BABA

Government Industrial Research Institute, Nagoya, Hirate-machi, Kita-ku, Nagoya 462

(Received November 16, 1972)

Electrochemical fluorination of diols ($HO-CH_2-CH_2-)_2X$ ($X=CH_2$, O, S, NH, NCH_3, NC_2H_5) afforded the corresponding perfluoro-heterocyclic compounds together with the cleaved products as a result of cyclization. Perfluoro-*p*-dioxane, a new compound having boiling point at 22.5—23.0 °C, was obtained from diethylene glycol. Electrochemical fluorination of heterocyclic compounds such as tetrahydropyran, *p*-dioxane, *p*-thioxane and morpholine was carried out and the results were compared with those obtained with diols.

Upon electrochemical fluorination, the formation of five- or six-membered perfluoro-heterocyclic compounds has been known to take place from the straight chain starting material containing a sufficient number of carbon atoms and hetero atom in proper position.[2-4]

We studied the electrochemical fluorination of such diols as 1,3-propanediol and 1,4-butanediol in order to obtain perfluoromalonic acid and perfluorosuccinic acid, respectively.[5,6] From 1,4-butanediol, perfluorotetrahydrofuran, formed as a result of cyclization, was obtained as the main product. It seems of interest to investigate the electrochemical fluorination of the compounds having two functional groups in order to obtain perfluoro-heterocyclic compounds.

The aim of this work is to examine the ring formation upon electrochemical fluorination of the compounds of the type $(HO-CH_2-CH_2-)_2X$ [$X=CH_2$(I), O(II), S(III), NH(IV), NCH_3(V), NC_2H_5(VI)], comparing the yields with those obtained from the fluorination of corresponding heterocyclic compounds and also to discuss the reaction mechanism. No detailed study has been reported on the fluorination of diols containing hetero atom, while the heterocyclic compounds dealt with in the present work were familiar starting material for the fluorination in electrochemical process.[4,7] As expected ring formed products, $\overline{CF_2CF_2CF_2CF_2CF_2O}$ (XI) was formed from I, $\overline{CF_2CF_2OCF_2CF_2O}$ (XII) from II, $\overline{CF_2CF_2OCF_2CF_2}SF_4$ (XIII) from III, $\overline{CF_2CF_2OCF_2CF_2}NF$ (XVI) from IV, $\overline{CF_2CF_2OCF_2CF_2}NCF_3$ (XV) from V and $\overline{CF_2CF_2OCF_2CF_2}NC_2F_5$ (XVI) from VI, respectively.

Experimental

Materials and Apparatus. All reagents except *p*-thioxane[8] were commercial products and used after purification when necessary. The purity of anhydrous hydrogen fluoride was higher than 99.5%.

All the features of the apparatus (capacity of the electrolytic cell, 1 l; electrodes, Ni plates; effective anodic surface area, 9.2 dm^2) and the procedures were essentially the same as described previously.[5,9,10]

General Procedures. In order to compare the results with those obtained in each experiment, the conditions for fluorination were made to be the same; the electrolysis was carried out by batch (0.34 mol%), and cell temperatures and anodic current density were adjusted to 5—6 °C and 2.7 A/dm^2. The most important setting condition was the amount of electricity passed, *i.e.*, reaction time. Electrolysis was continued until the theoretical amount of electricity required to complete the reaction had passed. This was based on the amount of current assumed to be required to form fluorine which would react with the starting material. Taking an example in III (X=S), the following equation is available.

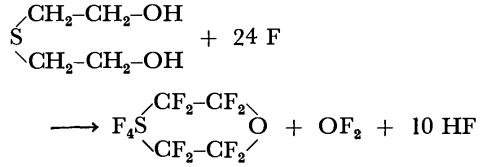

Thus 4.8 Faraday (128.7 A hr) is required to fluorinate 0.20 mol of the starting material. The value of yield (mol %) of six-membered perfluoro-cyclic ether should coincide with that of the current efficiency of the six-membered perfluoro-cyclic ether by the above equation.

As a typical example, the procedures for the fluorination of pentamethylene-1,5-diol (I) will be described. Anhydrous hydrogen fluoride (about 1 l) was introduced into the cell. Prior to fluorination, electrolysis was carried out in order to remove a trace of impurity until the voltage rose to 6.5 V. The sample (20.8 g) of I was introduced into the cell, and electrolysis was carried out with an anodic current density of 2.7 A/dm^2, at a cell voltage of 4.8—6.1 V, and

1) This paper is designated Part 1 of a series "Studies on the Cyclization upon Electrochemical Fluorination."

2) E. A. Kauck and J. H. Simons, U. S. 2644823 (1953); Saline Ludwigsshalle A. G., Ger. 1069639 (1959); Minnesota Mining and Manufacturing Co., Brit. 1007288 (1965); W. Blöchl, Fr. 1436269 (1966).

3) J. A. Young, T. C. Simmons, and F. W. Hoffmann, *J. Amer. Chem. Soc.*, **78**, 5637 (1956); J. A. Young and R. D. Dresdner, *ibid.*, **80**, 1889 (1958).

4) F. W. Hoffmann, T. C. Simmons, R. B. Beck, H. V. Holler, T. Katz, R. J. Koshar, E. R. Larsen, J. E. Mulvaney, F. E. Rogers, B. Singleton, and R. S. Sparks, *ibid.*, **79**, 3424 (1957).

5) S. Nagase, T. Abe, and H. Baba, This Bulletin, **41**, 1921 (1968).

6) Actually perfluorosuccinoyl fluoride was the product, and was easily led to perfluorosuccinic acid by subsequent hydrolysis.

7) a) Minnesota Mining and Manufacturing Co., U. S. 2594272 (1952); b) Minnesota Mining and Manufacturing Co., U. S. 2500388 (1950); c) R. D. Dresdner and J. A. Young, *J. Amer. Chem. Soc.*, **81**, 574 (1959); d) T. C. Simmons, F. W. Hoffmann, R. B. Beck, H. V. Holler, T. Katz, R. J. Koshar, E. R. Larsen, J. E. Mulvaney, K. E. Paulson, F. E. Rogers, B. Singleton, and R. S. Sparks, *ibid.*, **79**, 3429 (1957): R. E. Banks and E. D. Burling, *J. Chem. Soc.*, **1965**, 6081.

8) E. Fromm and B. Ungar, *Ber.*, **56**, 2288 (1923).

9) T. Abe, S. Nagase, and K. Kodaira, This Bulletin, **43**, 957 (1970).

10) T. Abe, S. Nagase, K. Kodaira, and H. Baba, *ibid.*, **43**, 1812 (1970).

a cell temperature of 5—6 °C. Electrolysis was conducted for 130.0 A hr (Theoretical; 128.7 A hr).

Gases evolving from the cell were passed through a reflux condenser kept at −25 °C, over NaF pellets and perfluorocarboxylic acid fluoride absorber[11] (a couple of polyethylene bottles containing water), and then bubbled through an alkaline solution of sodium sulfite containing a small amount of potassium iodide in series of Ichinose gas washers in order to eliminate oxygen difluoride, and finally collected in traps immersed in liquid nitrogen. After electrolysis, the solution drained from the cell was checked, none of perfluorinated compounds being found.[12]

The reaction products (12.9 g) condensed in cold traps were subjected to low temperature distillation and separated into three fractions. Each fraction was subsequently analysed by glc (column; silica gel, Kel F #3 30% on Chromosorb PAW, carrier; He). Compounds in Fractions 1, 2 and 3 were as follows. Fraction 1 (bp∼−77.9 °C, 0.8 g): CF_4,[13] C_2F_6, CHF_3, Fraction 2 (bp −77.8∼−56.5 °C, 1.5 g): C_3F_8, C_2HF_5, CF_3OCF_3, $CF_3OC_2F_5$, Fraction 3 (bp −56.4 °C∼r.t., 10.6 g): $\overline{CF_2CF_2CF_2CF_2CF_2O}$ (XI), $\overline{CF(CF_3)CF_2CF_2CF_2O}$, $\overline{CF_2CF_2CF_2CF_2O}$, C_3F_8, $CF_3OC_2F_5$, n-C_4F_{10}, n-C_5F_{12}. The first two compounds (XI, $\overline{CF(CF_3)CF_2CF_2CF_2O}$) were separated by repetitive glc and were analysed by IR, ^{19}F-NMR, Mass, and fluorine determination.

Results and Discussion

The reaction conditions for the fluorination of diols and heterocyclic compounds are given in Tables 1 and 2, respectively. The results obtained are summarized in Table 3.

We see that the formation of six-membered heterocyclic compounds were observed from corresponding diols, and their yields from diols and also from the fluorination products of heterocyclic compounds were significantly affected by the hetero atom.

Typical features of the fluorination products were observed in the fluorination of I and II. A considerable amount of the five-membered perfluoro-heterocyclic compounds ($\overline{CF(CF_3)CF_2CF_2CF_2O}$ and $\overline{CF_2CF_2CF_2CF_2O}$ from I, $\overline{CF_2OCF_2CF_2O}$ from II) was obtained as well as the expected six-membered compounds (XI from I and XII from II, respectively).

Similarly, ring contraction was observed in the fluorination of tetrahydropyran (VII) and *p*-dioxane (VIII). Thus ring expansion was expected to occur and an attempt was made to obtain XI by the fluorination of 2-methyltetrahydrofuran. When 2-methyltetrahydrofuran was subjected to electrochemical fluorination (reaction conditions: sample, 0.20 mol; anodic current density, 2.7 A/dm²; electricity passed, 102.6 A hr; cell voltage, 4.8—5.1 V; cell temp., 5—6 °C), the product (29.4 g) mainly consisted of perfluoro-

Table 1. Conditions for the fluorination of diols
Anodic current density, 2.7 A/dm²; cell temp., 5—6 °C; sample fed, 0.20 mol: general formula of the sample, $(HO\text{-}CH_2\text{-}CH_2\text{-})_2X$ (X represents a substituent).

Sample X	Cell voltage (V)	Electricity passed (A hr)	Products obtained (g)
CH_2 (I)	4.8—6.1	130.0	12.9
O (II)	4.8—5.1	102.2	4.3
S (III)	4.7—5.5	129.5	20.0
NH (IV)	4.9—5.3	117.6	8.6
NCH_3 (V)	4.9—5.3	137.5	12.7
NC_2H_5 (VI)	5.1—5.4	159.6	14.4

11) The products in perfluorocarboxylic acid fluoride absorber were worked up in almost the same way as reported.[5] Perfluoroglutaric acid obtained was converted into silver salt prior to analysis because of its strong hygroscopic character. The perfluorocarboxylic acids obtained were as follows. Silver perfluoroglutarate (0.5 g); mono-basic acid sodium salt (4.6 g) [sodium trifluoroacetate (7 wt%), sodium perfluoropropionate (7), sodium perfluorobutyrate (19), sodium perfluorovalerate (67)].

12) No perfluorinated products were found in the cell drainings throughout experiments.

13) Arranged in the order of decrease in product composition (wt%).

Table 2. Conditions for the fluorination of heterocyclic compounds
Anodic current density, 2.7 A/dm²; cell temp., 5—6 °C; sample fed, 0.20 mol

Sample	Cell voltage (V)	Electricity passed (A. hr)	Products obtained (g)
tetrahydropyran (VII)	4.7—4.9	104.8	18.1
p-dioxane (VIII)	5.1—5.3	83.0	14.9
p-thioxane (IX)	5.6—6.6	107.5	27.1
morpholine (X)	4.9—5.1	93.8	17.0

Table 3. Results with the flourination of diols and heterocyclic compounds

Sample	Perfluoro-heterocyclic compound Yield (mol%)
I	XI (6.2),[a] $\overline{CF(CF_3)CF_2CF_2CF_2O}$ (4.3),[b] $\overline{CF_2CF_2CF_2CF_2O}$ (4.7)
II	XII (trace), $\overline{CF_2OCF_2CF_2O}$ (1.3)
III	XIII (1.3), $\overline{CF_2CF_2CF_2CF_2O}$ (0.8)
IV	XIV (0.1)
V	XV (2.7)
VI	XVI (7.1),[c] XV (1.1)
VII	XI (16.0), $\overline{CF(CF_3)CF_2CF_2CF_2O}$ (7.0), $\overline{CF_2CF_2CF_2CF_2O}$ (2.0)
VIII	XII (3.0), $\overline{CF_2OCF_2CF_2O}$ (1.0)
IX	XIII (9.7)
X	XIV (0.4)

a) Bp 32.0 °C (reported 32 °C).[7a] Found: F, 70.7%. Calcd: F, 71.3%.
b) Bp 26.5—27.0 °C. Found: F, 70.5%. Calcd: F, 71.3%.
c) Bp 67.6 °C. Found: F, 70.3%. Calcd: F, 70.8%.

2-methyltetrahydrofuran, and XI produced as a result of the ring isomerization. The yields of the two compounds were 36.1% and 8.5%, respectively.

Perfluoro-*p*-dioxane[14] (XII) was produced as the ring formed product from II, and also the fluorination product of VIII, though the electrochemical fluorination of VIII yielded only perfluoro-1,2-dimethoxyethane as a cleaved product.[7b]

Fluorination of IV afforded a trace of perfluoromorpholine (XIV), which was obtained also in poor yield from morpholine (X). However, when *N*-alkyldiethanolamines (V and VI) were subjected to electrochemical fluorination, the production of an increased amount of the ring formed products (perfluoro-*N*-alkylmorpholines, XV and XVI) was observed as compared with that from IV.[15]

Mechanism. For the formation of perfluoroheterocyclic compounds from diols, there seems to be two conceivable mechanisms operating simultaneously during the course of electrochemical fluorination. One involves cyclization *via* oxonium compound followed by dehydration (Path A), and the other involves cyclization by radicals formed on the carbon chain of the same molecule (Path B). It is well-known that oxonium compounds are formed when alcohols and ethers are dissolved in anhydrous hydrogen fluoride.[16] In the case of pentamethylene-1,5-diol (I), oxonium compound (XVII) is formed when I is dissolved in anhydrous hydrogen fluoride, XVIIa and XVIIb being then formed by dehydration followed by isomerization. Formation of tetrahydropyran including a trace of methyltetrahydrofuran from I in hydrogen fluoride was ascertained in the following experiment, and it is strongly suggested that this type of cyclization (Path A) could occur: 5 g of I was added to 50 ml anhydrous hydrogen fluoride in a 300 ml flask made of poly(chlorotrifluoroethylene), fitted with a reflux condenser (−25 °C). After being left standing 2 hr at room temperature, the solution was diluted with water (200 ml) extracted with ether, the ethereal solution (about 300 ml) being then neutralized by alkaline solution. After removing ether by distillation, the distillation residue (0.5 g) was analysed by glc (column; Carbowax 4000 20% on Celite 545, carrier; He). glc analysis showed the presence of tetrahydropyran (major) and trace of 2-methyltetrahydrofuran.

On the other hand, fluoro-alcohol (XVIII) carrying fluorine atom in α position, which is considered to be formed during the course of electrochemical fluorination of primary alcohol, eliminates hydrogen fluoride and changes into acid fluoride (XIX). The acid fluoride thus obtained may proceed to perfluorocarboxylic acid fluorides[11] (perfluoroglutaryl fluoride, perfluorovaleryl fluoride and other degradaded perfluoroacid fluorides), but part of it (XIX) may be subjected to radical attack by the carbon radical of

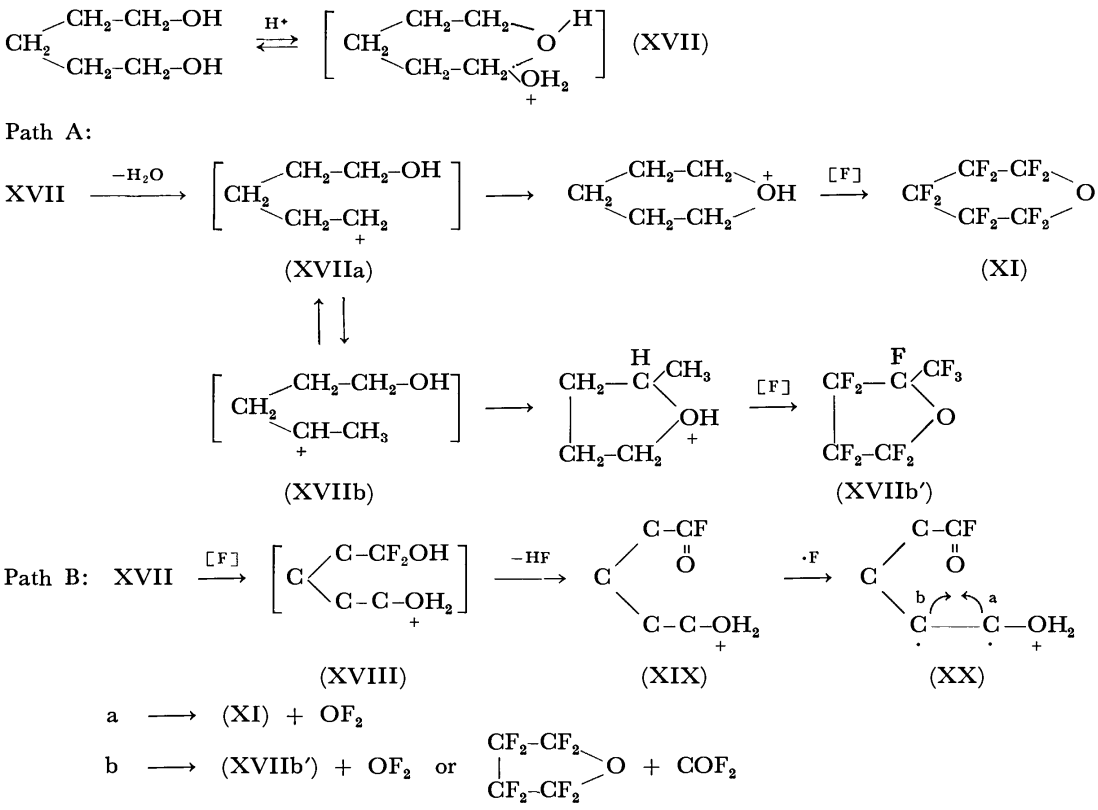

14) Bp 22.5—23.0 °C. ^{19}F-NMR (chemical shift from external CF_3COOH); 10.7 ppm (singlet, CF_2). On the other hand, perfluoro-1,2-dimethoxyethane had a bp of 9.0—10.0 °C (reported 13 °C). ^{19}F-NMR; −20.5 ppm (triplet, CF_3), 14.2 ppm (quartet, CF_2).

15) Alkylamines give the corresponding perfluoroalkylamines in the best yield in the case of tertiary amines. *Cf. e. g.*, E. A. Kauck and J. H. Simmons, U. S. 2616927 (1952); Brit. 666733 (1952).

16) See for example, "The Chemistry of Non-Aqueous Solvents," Vol. II, ed. by J. J. Lagowski, Academic Press Inc., New York (1967), p. 81; "Protonated Heteroaliphatic Compounds," by G. A. Olah and A. M. White, *Chem. Rev.*, **70**, 561 (1970).

the same molecule resulting from the hydrogen abstraction by fluorine radical creating the bond in either way, B-a or -b.

Accordingly, Path A may be the first step in the reaction, while Path B may occur during the course of electrochemical fluorination. The usual poor yield of the ring formed products from diols which contain a hetero atom may be explained to be due to an undesirable influence of the protonated hetero atom on the stability of the carbonium ion formed (XVIIIa, XVIIb) and also an easier fission of the bond of the carbon-hetero atom.

The authors wish to express their sincere thanks to Mr. S. Fujii for the ^{19}F-NMR experiment, Mr. K. Kodaira for the Mass measurements, and Dr. K. Inukai of this Institute for his interest in this work.

BULLETIN OF THE CHEMICAL SOCIETY OF JAPAN, VOL. 46, 2527—2534 (1973)

Intramolecular Interaction between the Phenol and the Indole Chromophores

Takashi TAMAKI

Research Institute for Polymers and Textiles, Kanagawa-ku, Yokohama 221

(Received February 1, 1973)

The singlet-energy transfer from the phenol to the indole chromophores occurs intramolecularly, with a high efficiency, in the compounds containing these chromophores joined by the methylene and the amide groups. The total emission spectra of the compounds consisted only of those from the indole chromophore, neither the fluorescence nor the phosphorescence of the phenol chromophore contributing to them, and the excitation spectra of the fluorescence were similar to the absorption spectra. The quantitative analysis of the fluorescence-polarization spectra suggested that the ^1L_b transition of the indole chromophore was excited in the energy transfer. The intramolecular interactions between these chromophores in the ground and excited states are discussed.

The fluorescence yield of the protein is very low compared with the contribution to be expected from the constituents of the aromatic amino acids.[1-4] Weber and Rosenheck[5] have suggested that the phenolic hydroxide of the tyrosine residue is hydrogen-bonded to the neighboring carboxylate moieties in the excited state, thus resulting in the non-fluorescent phenolate ion. Cowgill[6] has proposed the hypothesis that the peptide bond enhances the vibrational deactivation of the aromatic ring. The combined action of these effects may be responsible for the reduction of the fluorescence quantum yield of the protein.[7]

The fluorescence of the protein containing the tryptophane residue is the only one attributable to the residue, neither the phenylalanine residue nor the tyrosine residue having any detectable fluorescence. The excitation spectra of the fluorescence indicate the excitation-energy transfer from the tyrosine to the tryptophane residues in some proteins,[8-10] though no such sensitization of any tryptophanyl fluorescence by the tyrosine residue has been observed in other proteins.[1,11] The excitation-energy transfer seems reasonable from the viewpoint of the energy-level sequence of the aromatic amino acids: Phe<Tyr<Trp<Tyr^-; it is primarily due to the long-range dipole-dipole interaction, the theory of which has been developed by Förster.[12]

The measurements of the fluorescence of the compounds which contain the phenol and/or the indole chromophores provide convenient information for studying the fluorescence of the protein. A number of reports have been published concerning the quantum yield,[13-17] the lifetime,[18,19] and the peak position[20-23] of the fluorescence and the intramolecular[10] and intermolecular energy transfer.[24]

In this experiment, a series of compounds, I—VI, containing the phenol or its methyl ether, and the indole chromophores joined by the methylene groups and the amide group were prepared, and the intramolecular interaction between these chromophores was studied in

1) F. W. J. Teale, *Biochem. J.*, **76**, 381 (1960).
2) G. Weber, *Nature*, **190**, 27 (1961).
3) J. A. Gally and G. M. Edelman, *Biochim. Biophys. Acta*, **60**, 499 (1962).
4) I. A. Vladimirov and E. A. Burshtein, *Biophysics* (Engl. Transl.), **5**, 455 (1960).
5) G. Weber and K. Rosenheck, *Biopolym. Symp. No. 1*, 333 (1964).
6) R. W. Cowgill, *Biochim. Biophys. Acta*, **200**, 18 (1970).
7) S. V. Konev, "Fluorescence and Phosphorescence of Proteins and Nucleic Acids," Plenum Press, New York, N. Y. (1967).
8) I. Weinryb and R. F. Steiner, *Biochemistry*, **9**, 135 (1970).
9) J. A. D'Anna, Jr. and G. Tollin, *ibid.*, **10**, 57 (1971).
10) J. W. Longworth, *Photochem. Photobiol.*, **7**, 587 (1968).
11) L. Augenstein and J. Nag-Chaudhuri, *Nature*, **203**, 1145 (1964).
12) Th. Förster, *Rad. Res., Supp.*, **2**, 326 (1960).
13) A. White, *Biochem. J.*, **71**, 217 (1959).
14) J. Feitelson, *J. Phys. Chem.*, **68**, 391 (1964).
15) E. P. Kirby and R. F. Steiner, *ibid.*, **74**, 4480 (1970).
16) R. W. Cowgill, *Biochim. Biophys. Acta*, **133**, 6 (1967).
17) R. W. Cowgill, *ibid.*, **109**, 536 (1965).
18) E. Leroy, H. Lami, and G. Laustriat, *Photochem. Photobiol.*, **12**, 411 (1971).
19) W. B. De Lauder and Ph. Wahl, *Biochim. Biophys. Acta*, **243**, 153 (1971).
20) N. Mataga, Y. Torihashi, and K. Ezumi, *Theor. Chim. Acta*, **2**, 158 (1964).
21) J. Eisinger and G. Navon, *J. Chem. Phys.*, **50**, 2069 (1969).
22) M. S. Walker, T. W. Bednar, and R. Lumry, *J. Chem. Phys.*, **45**, 3445 (1966).
23) J. W. Longworth, *Photochem. Photobiol.*, **12**, 29 (1970).
24) G. Weber, *Biochem. J.*, **75**, 335 (1960).

some detail on the basis of the fluorescence and the phosphorescence measurements.

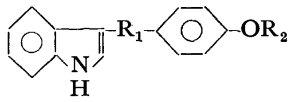

I; $R_1=CH_2CH_2$, $R_2=CH_3$
II; $R_1=CH_2CH_2CH_2$, $R_2=CH_3$
III; $R_1=CH_2CH_2CH_2$, $R_2=H$
IV; $R_1=CH_2CONHCH_2$, $R_2=CH_3$
V; $R_1=CH_2CONHCH_2$, $R_2=H$
VI; $R_1=CH_2CH_2NHCOCH_2CH_2$, $R_2=CH_3$

Recently, the intramolecular energy transfer has been investigated in several donor-acceptor pairs combined by methylene groups.[25] Schnepp and Levy[26] have observed that the efficiency of the singlet-energy transfer from the naphthalene to the anthracene groups is comparable to that of the donor fluorescence, and they have considered a Förster-type mechanism for the transfer. Lamola *et al.*[27] have found that the singlet excitation is transferred from the naphthalene to the benzophenone chromophores with a high, but not total, efficiency, and that the triplet-energy transfer from the latter to the former chromophores occurs with a total efficiency, which the exchange mechanism can account for. The fluorescence from the intramolecular exciplex formed in this pair has also been reported.[28]

Experimental

*1-(3-Indolyl)-2-(*p*-methoxyphenyl)ethane (I).* The ethereal solution of indolylmagnesium iodide was prepared according to the procedure described by Baker.[29] Into 16.5 g of *p*-methoxyphenylethylbromide in ether, we stirred a solution of the Grignard compound of indole (9 g of indole). The reaction mixture was then gently refluxed for about 3 hr. The Grignard compound was decomposed with ice and ammonium chloride, and the compound was extracted with ether. The residue from the ether extract was recrystallized from benzene; mp 113—114 °C.

Found: C, 81.06; H, 6.47; N, 5.24%. Calcd for $C_{17}H_{17}NO$: C, 81.24; H, 6.82; N, 5.57%.

*1-(3-Indolyl)-3-(*p*-methoxyphenyl)propane (II).* This compound was prepared by a procedure analogous to that of 1-(3-indolyl)-2-(*p*-methoxyphenyl)ethane, using a Grignard compound of indole and 3-(*p*-methoxyphenyl)propylbromide in ether. The compound was recrystallized from benzene; mp 80—82 °C.

Found: C, 81.51; H, 7.51; N, 5.14%. Calcd for $C_{18}H_{19}NO$: C, 81.48; H, 7.22; N, 5.28%.

β-(3-Indolyl)vinyl p*-methoxyphenyl Ketone.* To 5.5 g of indole-3-aldehyde and 18 g of sodium hydroxide in water–ethanol (20—15 ml), we added 7.1 g of *p*-methoxyacetophenone. The reaction mixture was then stirred for 8 hr at 60 °C to give a red solution. The solution was concentrated, and the residue was solidified. The compound was subsequently washed with water and recrystallized from benzene; mp 169—173 °C.

Found: C, 78.46; H, 5.31; N, 4.59%. Calcd for $C_{18}H_{15}NO_2$: C, 77.96; H, 5.45; N, 5.05%.

2-(3-Indolyl)ethyl p*-methoxyphenyl Ketone.* The ethanol solution of 5 g of β-(3-indolyl)vinyl *p*-methoxyphenyl ketone was reduced with hydrogen at 10 atmospheres in the presence of Raney nickel at 55 °C for 30 min.[30] The product was collected and recrystallized from ethanol; mp 132 °C.

Found: C, 77.79; H, 6.10; N, 5.17%. Calcd for $C_{18}H_{17}NO_2$: C, 77.39; H, 6.13; N, 5.01%.

*1-(3-Indolyl)-3-(*p*-hydroxyphenyl)propane (III).* According to a modification of the Wolf-Kishner reduction,[31] the carbonyl group of 2-(3-indolyl)ethyl *p*-methoxyphenyl ketone was reduced and its methoxy group was simultaneously demethylated. A paste product was thus obtained, and the compound was repeatedly recrystallized from a water-acetone mixture; mp 108—110 °C.

Found: C, 82.15; H, 6.51; N, 5.34%. Calcd for $C_{17}H_{17}NO$: C, 81.24; H, 6.82; N, 5.57%.

N-p-*Methoxybenzyl-3-indolylacetamide (IV),* N-p-*Hydroxybenzyl-3-indolylacetamide (V), and* N-*2-(3-Indolyl)ethyl-2-(*p*-methoxyphenyl)propionamide (VI).* These compounds were prepared by the method using carbodiimide.[32] The reaction mixture including the corresponding acid and amide components, and *N,N*-dicyclohexylcarbodiimide in acetonitrile was stirred overnight over ice. The filtered solution was evaporated, and the products were recrystallized from benzene.

IV: mp 107—109 °C.

Found: C, 73.02; H, 6.18; N, 9.31%. Calcd for $C_{18}H_{18}N_2O_2$: C, 73.45; H, 6.16; N, 9.52%.

V: mp 184—186 °C.

Found: C, 73.02; H, 5.58; N, 9.67%. Calcd for $C_{17}H_{16}N_2O_2$: C, 72.84; H, 5.75; N, 9.99%.

VI: mp 90—91 °C.

Found: C, 74.93; H, 6.70; N, 8.28%. Calcd for $C_{20}H_{22}N_2O_2$: C, 74.51; H, 6.88; N, 8.69%.

Measurements. The emission and the fluorescence excitation spectra were measured by means of a Hitachi spectrophotofluorometer, Model MPF-2A. The excitation spectra were obtained at 20 per cent of the absorption of the peak maxima, so they could be compared with the absorption spectra.

The efficiency of the energy transfer of the singlet excitation from the phenol or its methyl ether to the indole chromophores, Φ_t, was calculated according to the following considerations.

The fluorescence intensity, $F_N(\lambda)$, of the compounds on excitation at λ nm is represented by this equation:

$$F_N(\lambda) = Q_N \cdot [A_{In}(\lambda) + A_{Ph}(\lambda) \cdot \Phi_t] \quad (1)$$

where Q_N is the fluorescence quantum yield and where A_{In} and A_{Ph} are the quanta absorbed by the indole moiety and the phenol or its methyl ether moiety respectively. It seems reasonable that A_{In} is equal to that of the model compound containing only the indole chromophore: 3-methylindole for I, II, and III; indole-3-acetamide for IV and V, and *N*-acetyltryptamine for VI; it also seems reasonable that A_{Ph} is equal to that of the model compound containing only the phenol or its methyl ether chromophore: *p*-methylanisole for I and II; *p*-cresol for III; *N*-acetyl-*p*-methoxyphenylethylamine for IV; *p*-hydroxyphenylethylamine for V, and *p*-methoxyphenylpropionamide for VI. On these assump-

25) A. A. Lamola, "Energy Transfer and Organic Photochemistry," John Wiley and Sons, New York (1969), p. 20.
26) O. Schnepp and M. Levy, *J. Amer. Chem. Soc.*, **84**, 172 (1962).
27) A. A. Lamola, P. A. Leermakers, G. W. Byers, and G. S. Hammond, *ibid.*, **87**, 2322 (1965).
28) D. Breen and R. A. Keller, *ibid.*, **90**, 1935 (1968).
29) J. W. Baker, *J. Chem. Soc.*, **1940**, 458.
30) B. R. Baker, *J. Org. Chem.*, **65**, 1572 (1943).
31) Huang-Minlon, *ibid.*, **68**, 2487 (1946).
32) E. Schröder and K. Lübke, "*The Peptides* (Engl. Transl.)," vol. 1, Academic Press, New York (1965), p. 108.

tions, the ratio of $F_N(\lambda)$ to the fluorescence intensity of the model compound, $F_{In}(\lambda)$, may be represented by an equation in which

$$F_N(\lambda)/F_{In}(\lambda) = \beta \cdot [\{\Phi_t \cdot A_{Ph}(\lambda)/A_{In}(\lambda)\} + 1] \quad (2)$$

β is the ratio of the fluorescence quantum yields. In Eq. (2), the value of Φ_t can be calculated from the measurements of $F(\lambda)$, $A(\lambda)$, and β.

In the study of the temperature dependence of the fluorescence intensity, a quartz tube (3 mm in diameter) containing the sample in EPA was cooled in the temperature of liquid nitrogen and then left in a Dewar flask at room temperature during the course of the measurement. The temperature was monitored by means of a copper-constantan thermocouple injected into the sample tube; it increased monotonously at the average rate of 2.5 °C per minute from −120 to 20 °C.

In order to avoid the depolarization due to the Brownian movement, the fluorescence-polarization spectra were measured at −70 °C in a propylene glycol solution, which forms a rigid glass at that temperature.

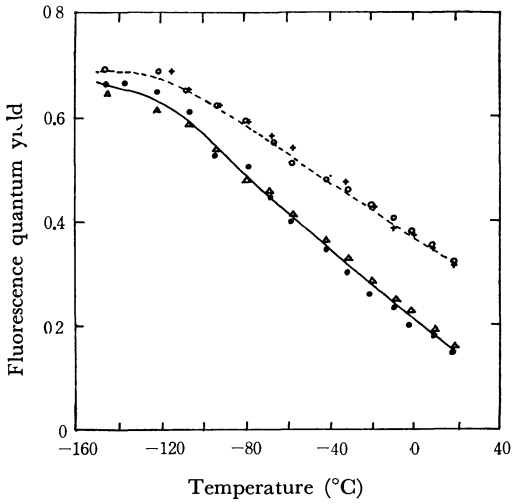

Fig. 2. The temperature dependence of the fluorescence intensities of (+) 3-methylindole, I (○), II (●), and III (△) in EPA.

Results

The total emission spectra of 3-methylindole, *p*-cresol, and an equimolar mixture of them in EPA at 77 K are shown in Fig. 1a. The 0–0 fluorescent emission band of 3-methylindole is located at a longer wavelength than that of *p*-cresol, as in the case of the phosphorescence. The emission spectrum of *p*-methylanisole was analogous to that of *p*-cresol. The excitation wavelength is 280 nm, at which the ratio of the number of the quanta absorbed by 3-methylindole and *p*-cresol is about 1 : 0.3. The emission spectrum of the equimolar (2×10^{-5} M) mixture is superimposed on those of the constituents, as is seen in Fig. 1a.

The total emission spectrum of I at 77 K is shown in Fig. 1b. The spectra of both the fluorescence and the phosphorescence are very similar to those of 3-methylindole. None of the emission from the anisole moiety can be seen in Fig. 1b. This confirms that the excitation energy is transferred from the phenol chromophore to the indole chromophore with a high efficiency. The shapes of the emission spectra of the other compounds were also very similar to that of 3-methylindole, except for the slight blue shift in the spectra of IV, V, and VI, which contain amide groups. The ratio of the intensities of the fluorescence to the phosphorescence of these compounds was little different from that of 3-methylindole.

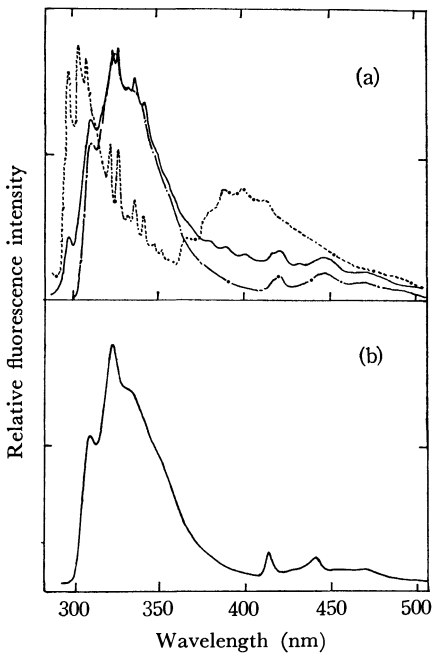

Fig. 1. The total emission spectra in EPA at 77 K, (a): (dotted line) *p*-cresol, (broken line) 3-methylindole, and (solid line) their equimolar (2×10^{-5} M) mixture. (b): I.

The fluorescence characteristics at room temperature in ethanol and in dioxane are listed in Table 1. The positions of the fluorescence peaks are shifted to longer wavelengths in ethanol, the absorption spectra undergoing a very small shift. The pronounced red shift of the fluorescence of indole and its derivatives induced by the polar solvent has been suggested as resulting from the reorientation of the surrounding solvent molecules in the excited state,[20,21] or, alternatively, from the formation of the exciplex with the solvent molecules.[22,23]

The fluorescence spectra of the compounds containing the amide groups (IV, V, and VI) are shifted to somewhat shorter wavelengths than that of 3-methylindole, as is shown in Table 1. These compounds also indicate a slight blue shift in the absorption spectra; they have the same Stokes shift as 3-methylindole. The fluorescence yields of these compounds are low in ethanol, whereas they approach the normal level in dioxane (Table 1). Cowgill[16] has also observed the low fluorescence yields of the tryptophanyl and the tyrosyl derivatives in a polar solvent that can solvate the carbonyl group by hydrogen-bonding.

The fluorescence yields of II and III are about half as high as those of 3-methylindole and I at room temperature, irrespective of the existence of oxygen molecules and of the polarizability of the solvent, as is demonstrated in Table 1. However, the former recover to the same level as the latter at low temperatures (Fig. 2).

Table 1. Relative quantum yields and wavelength maxima of the fluorescence in ethanol and dioxane which are in air and flushed with argon gas

Compound	in Ethanol			in Dioxane		
	Fluorescence Maximum (nm)	Relative Quantum yield		Fluorescence Maxmium (nm)	Relative Quantum yield	
		in Air	Ar		in Air	Ar
3-Methylindole	350	3.3_5	4.8	335	3.4	4.0
I	350	3.4	4.8	335	3.6	4.3
II	350	1.6	2.0	335	1.6	2.0
III	350	2.0_5	2.6	335	1.8_5	2.3
3-Acetamidoindole	345	2.7	3.4_5	333	3.4	4.0
IV	345	2.8_5	3.6	333	3.4_5	4.2
V	345	2.8	3.8	333	3.6	4.3
VI	348	3.0	4.2_5	335	3.1_5	3.9

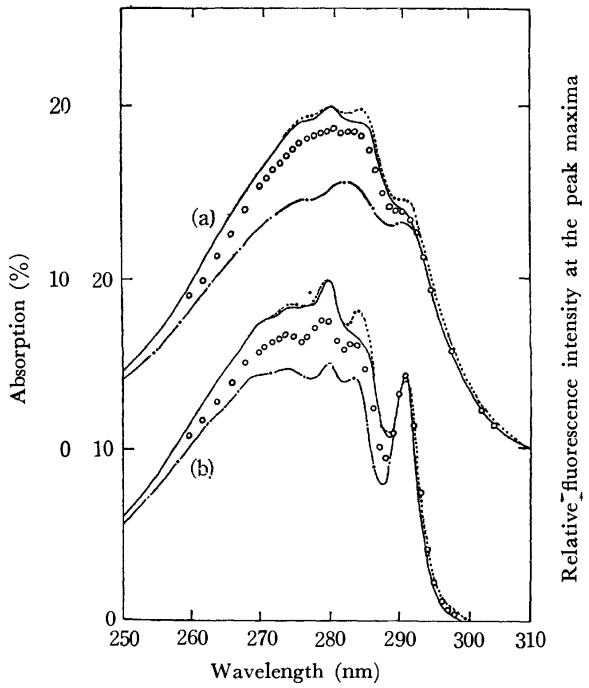

Fig. 3. The absorption and the fluorescence excitation spectra of I (a) in ethanol, and (b) in methylcyclohexane: (dotted line) the absorption spectrum, and (○) the excitation spectrum. The absorption spectra of (broken line) 3-methylindole, and (solid line) the equimolar mixture of 3-methylindole and *p*-methylanisole. The spectra except for that of 3-methylindole were obtained at 20 per cent of the absorption of the peak maxima.

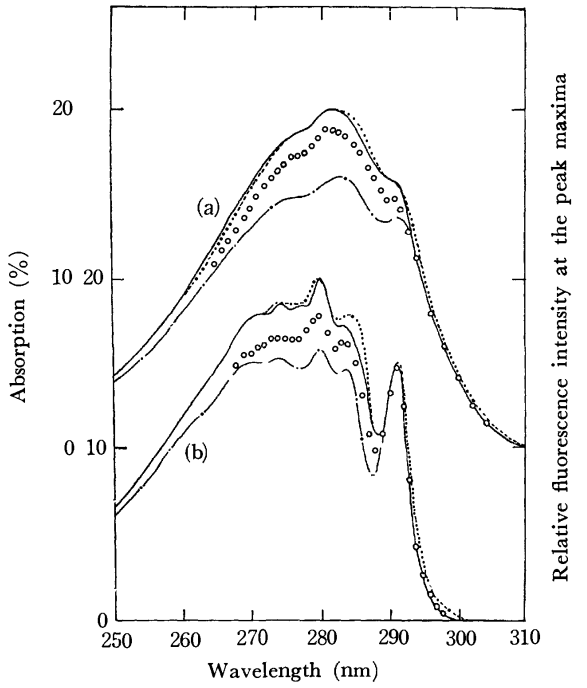

Fig. 4. The absorption and the fluorescence excitation spectra of III (a) in ethanol, and (b) in methylcyclohexane: (dotted line) the absorption spectrum, and (○) the excitation spectrum. The absorption spectra of (broken line) 3-methylindole, and (solid line) the equimolar mixture of 3-methylindole and *p*-cresol. The conditions are the same as those in Fig. 3.

As may be seen in Fig. 2, the fluorescence yields decrease upon an increase in the temperature, the shapes of the fluorescence spectra remaining unaltered. It is known that the nonradiative deactivation process of the indole derivatives is temperature-dependent.[3] From the slope of the straight line obtained by plotting $\log(1/Q_N-1)$ *vs.* the reciprocal of the absolute temperature,[15] the value of the activation energy of the process in I was evaluated to be 2.5 kcal/mol, which was equal to that of 3-methylindole. The fluorescence yields of II and III depend more strongly upon the temperature than do those of 3-methylindole and I (Fig. 2).

The absorption spectra of the compounds and the equimolar mixtures of the model compounds containing the indole chromophore or the phenol (anisole) chromophore alone are shown in Figs. 3—7. The absorption spectra of the compounds show a distinct spectral distortion compared with those of an equimolar mixture of the model compounds, as may be seen in the figures. The spectral difference is more predominant in methylcyclohexane than in ethanol. The absorption spectra of IV, V, and VI in methylcyclohexane were not available because of the poor solubility. The results obtained for II were very similar to those for I.

The fluorescence-excitation spectra are also illu-

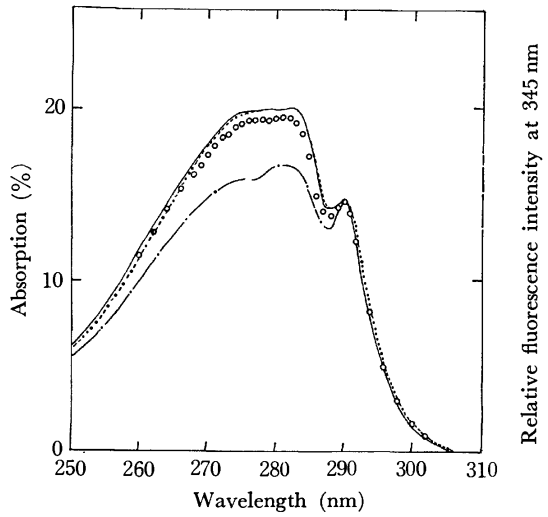

Fig. 5. The absorption spectra of (dotted line) IV, (broken line) 3-acetamidoindole, and (solid line) the equimolar mixture of 3-acetamidoindole and *N*-acety-*p*-methoxyphenethylamine, and (○) the fluorescence excitation spectrum of IV in ethanol. The conditions are the same as those in Fig. 3.

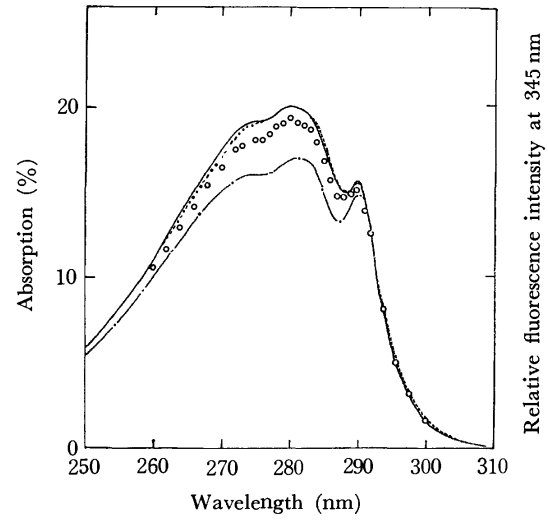

Fig. 6. The absorption spectra of (dotted line) V, (broken line) 3-acetamidoindole, and (solid line) the equimolar mixture of 3-acetamidoindole and *p*-hydroxyphenethylamine, and (○) the florescence excitation spectrum of V in ethanol. The conditions are the same as those in Fig. 3.

strated in Figs. 3—7. They are normalized to the absorption spectra of the equimolar mixtures of the model compounds on the long wavelength edge, in which the incident light is absorbed only by the indole chromophore. They are similar to the absorption spectra of the compounds rather than to those of the equimolar mixtures of the model compounds. However, the excitation spectra never reach the same level as the absorption spectra at wavelengths shorter than 290 nm, where the absorption spectra of the two chromophores overlap.

The values of the efficiencies of the singlet-excitation-energy transfer, Φ_t, which vary from 0.36 to 0.78, are listed in Table 2; they were calculated using Eq. (2). They seem to be subject to experimental error pri-

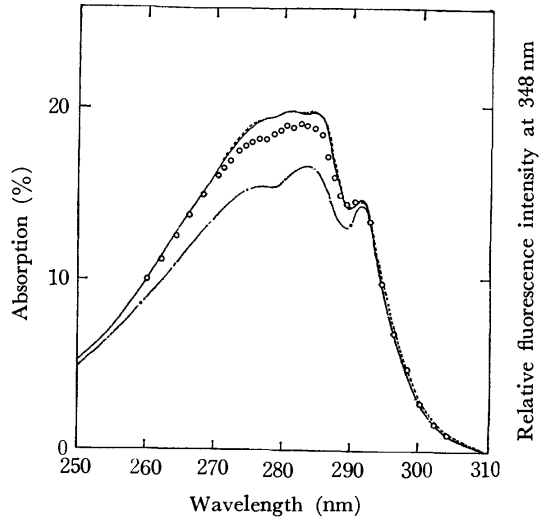

Fig. 7. The absorption spectra of (dotted line) VI, broken line) *N*-acetyltryptamine, and (solid line) the equimolar mixture of *N*-acetyltryptamine and *p*-methoxyphenylpropionamide, and (○) the fluorescence excitation spectrum of VI in ethanol. The conditions are the same as those in Fig. 3.

Table 2. Efficiencies of the intramolecular energy transfer from the phenol to the indole chromophores

Compound	Φ_t in Ethanol	Φ_t in Methylcyclohexane
I	0.63	0.46
II	0.60	0.49
III	0.48	0.36
IV	0.69	—
V	0.56	—
VI	0.78	—

marily because of our neglect of the small spectral differences between the absorption spectra of the compounds and the equimolar mixtures of the model compounds in the long-wavelength band.

The spectra of the fluorescence-excitation polarization in propylene glycol at −70 °C are shown in

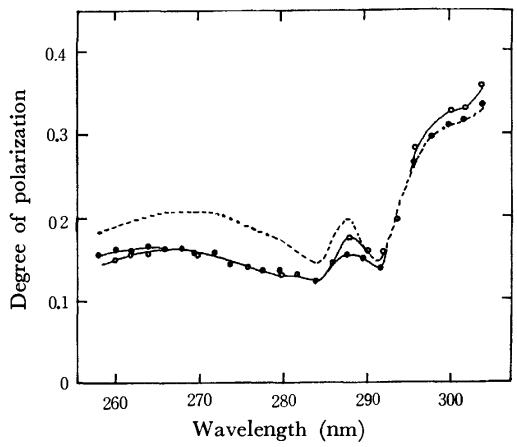

Fig. 8. The fluorescence-polarization spectra in propylene glycol at −70 °C: (dotted line) 3-methylindole, (-○-) I, and (-●-) III. The fluorescence was measured at 360 nm.

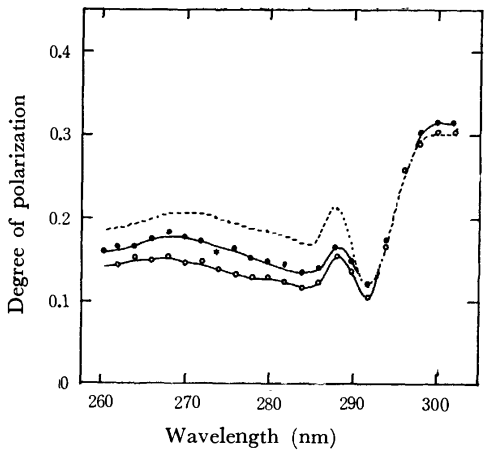

Fig. 9. The fluorescence-polarization spectra in propylene glycol at −70 °C: (dotted line) 3-acetamidoindole, (-○-) IV, and (-●-) V. The fluorescence was measured at 340 nm.

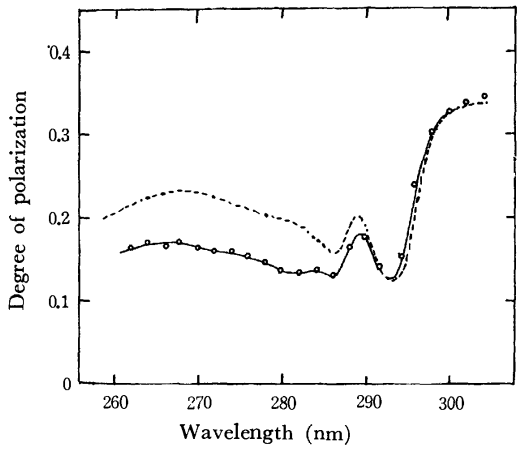

Fig. 10. The fluorescence-polarization spectra in propylene glycol at −70 °C: (dotted line) *N*-acetyltryptamine, and (-○-) VI. The fluorescence was measured at 360 nm.

Figs. 8—10. The spectrum of I exhibits an intense depolarization in wavelengths shorter than 290 nm, while it agrees well with the spectrum of 3-methylindole above 290 nm, as is shown in Fig. 8. The results for II were the same as those for I, and similar results were also obtained for the other compounds (Fig. 8—10).

Discussion

In the near ultraviolet spectra of indole and its derivatives, the ^1L_a and the ^1L_b electronic transition bands overlap strongly.[33-35] It is observed that the ^1L_a transition band is more sensitive to perturbation by solute-solvent interaction than is the ^1L_b transition band. Konev[7] and Strickland *et al.*[34] presented evidence that, on the addition of a drop of butanol to indole and 3-methylindole in hexane, the ^1L_a bands undergo a large red shift and broadening, while the ^1L_b bands undergo only a minor change. The spectral changes are believed to be due to the formation of a hydrogen bond, which severely affects the ^1L_a transition, the moment of which passes through the imino group, but which scarcely at all affects the ^1L_b transition, which is almost perpendicular to the ^1L_a transition.

From the facts that the distortion of the absorption spectra of I—VI is pronounced in the bands to which the absorption of the phenol group contributes little, and is obviously predominant in a non-polar solvent (Fig. 3-7), it may be said to be due to the change in the ^1L_a band of the indole chromophore, a change which is induced by weak intramolecular hydrogen bonding to the phenolic oxygen or the π orbitals of the phenol ring.[36,37] On the other hand, it has been pointed out that the absorption spectra of the adjacent chromophores close to each other differ from the sum of those of the constituents in the peak position and the intensity, mainly because of long-range exciton interaction.[27] The ^1L_b band as well as the ^1L_a band may be expected to change as a result of such interaction.

The low fluorescence yields of II and III at room temperature are anomalous (Table 1 and Fig. 2). The reduction of the population of the singlet state in II and III due to the low probability of the intramolecular energy transfer, due to the enhancement of the intersystem crossing, and due to the photochemical reaction may be excluded, since the efficiencies of the intramolecular energy transfer in II and III were as high as those in other compounds (Table 2), since the ratios of the fluorescence to the phosphorescence of II and III were the same as that of 3-methylindole, and since no detectable absorption change could be observed after irradiation for the fluorescence measurement. Therefore, it may be inferred that the molecular configuration of II and III, in which the two aromatic rings are joined by three methylene groups, is responsible for the fluorescence quenching.

Hirayama's $n=3$ rule states that the aromatic ring pairs combined with three methylene groups have a face-to-face parallel configuration and are likely to form an intramolecular excimer or exciplex as a result of the strong overlap of the two π orbitals.[38] Recently, the temperature dependence of the excimer formation in 1,3-dinaphthylpropane was reported.[39] The disappearance of the excimer emission at low temperature was interpreted in terms of rotation barriers in the methylene chain joining the naphthalene nuclei.

From the fact that the fluorescence yields of II and III approach that of 3-methylindole at low temperatures (Fig. 2), it may be suggested that the quenching of the monomer fluorescence at room temperature has its origin in the formation of the intramolecular com-

33) P.- S. Song and W. E. Kurtin, *J. Amer. Chem. Soc.*, **91**, 4892 (1969).
34) E. H. Strickland, J. Horwitz, and C. Billups, *Biochemistry*, **9**, 4914 (1970).
35) Y. Yamamoto and J. Tanaka, This Bulletin, **45**, 1362 (1972).
36) E. H. Strickland, C. Billups, and E. Kay, *Biochemistry*, **11**, 3657 (1972).
37) M. G. Reinnecke, H. W. Johnson, Jr., and J. F. Sebastian, *J. Amer. Chem. Soc.*, **91**, 3817 (1969).
38) F. Hirayama, *J. Chem. Phys.*, **42**, 3163 (1965).
39) E. A. Chandross and C. J. Dempster, *J. Amer. Chem. Soc.*, **92**, 3586 (1970).

plex between the indole group in the excited state and the phenol group in the ground state.

The efficiencies of the energy transfer from the phenol to the indole chromophores in the compounds containing the amide group (IV, V, and VI) remain as high as in the other compounds (Table 2), whereas it has been suggested that the peptide group enhances the internal conversion of the phenol chromophore.[16] On the other hand, there is no evidence that *N*,*N*-dimethylacetamide reduces the efficiencies of the fluorescence or of the intramolecular energy transfer in the compounds containing the phenol chromophore (III and V), although the amide compound intermolecularly quenches the fluorescence of phenol by forming a hydrogen bond.[17] These results indicate that the rate constant of the energy transfer is much greater than those of the radiationless deactivation and of the diffusion-controlled bimolecular encounter.

According to the theory of resonance-energy transfer developed by Förster,[12] the critical radius, R_0, that is, the distance at which the probability of the energy transfer is 50 percent, can be calculated from the experimental parameters. The values of R_0 calculated for the energy transfer from *p*-cresol or *p*-methylanisole to 3-methylindole both in ethanol and in methylcyclohexane are listed in Table 3. The results that the value of R_0 are larger in ethanol (26 and 29 Å for *p*-cresol, and *p*-methylanisole respectively) than in methylcyclohexane (22 and 25 Å) are mainly the result of the more intense overlap integrals and fluorescence yields of the donor molecules in ethanol than in methylcyclohexane. They may agree with the results that the efficiencies of the intramolecular energy transfer are larger in ethanol than in methylcyclohexane, as is shown in Table 2.

Table 3. Calculated critical radii for the resonance energy transfer from *p*-cresol or its methyl ether to 3-methylindole in ethanol and in methylcyclohexane

Donor	Solvent	R_0[a] (Å)
p-Cresol	Ethanol	26
p-Cresol	Methylcyclohexane	22
p-Methylanisole	Ethanol	29
p-Methylanisole	Methylcyclohexane	25

a) The quantum yields of the donor fluorescence were evaluated using that of *p*-cresol which is 0.23 in water.[16] The random orientation of the donor and the acceptor molecules was assumed.

However, it has been suggested that the intramolecular singlet-excitation transfer must be totally efficient in a compound in which the donor-acceptor chromophores are less than ten angstroms apart.[40] The experimental difficulties are responsible for the low transfer efficiencies, as is calculated in Table 2. Higher values might be obtained if the slight spectral distortion in the long-wavelength band could be taken into account.

The depolarization of the fluorescence of the compounds in propylene glycol (Fig. 8—10) may be quantitatively analyzed using the equation formulated by Weber:[41]

$$1/P - 1/3 = [\sum f_i/(1/P_i - 1/3)]^{-1} \quad (3)$$

where P is the degree of the polarization, P_i is that of the ith molecule, and f_i is the fraction of the fluorescence intensity of the ith molecule to the total fluorescence intensity. Now, two types of fluorescence are considered: one ($i=0$) is the fluorescence from the molecule in which the incident quanta are absorbed directly by the indole chromophore, and the other ($i=1$) is the fluorescence from the molecule in which the phenol chromophore is initially excited and the excitation energy is intramolecularly transferred to the indole chromophore. The further sequence of i can be disregarded, since the probability of the reverse transfer of the excitation energy is very low because of the small overlap integral.

Therefore, f_0 and f_1 are represented by the equation: $f_0=A_{\mathrm{In}}/(A_{\mathrm{In}}+\Phi_t\cdot A_{\mathrm{Ph}})$; $f_1=\Phi_t\cdot A_{\mathrm{Ph}}/(A_{\mathrm{In}}+\Phi_t\cdot A_{\mathrm{Ph}})$. The values of P_1, as calculated assuming that Φ_t is 100 percent and substituting the values of P of the model compounds containing only the indole chromophore for the values of P_0, are listed in Table 4. It is remarkable that P_1 indicates the negative polarization on the excitation near 270 nm. This can be expected if the emitting oscillator differs from the exciting one and if $\cos^2\theta<1/3$ is satisfied, where θ is the relative orientation angle.[42]

Table 4. Polarization of the fluorescence on excitation at 270 nm in propylene glycol at −70 °C

Compound	f_0	f_1	P	P_0	P_1[d]
I	0.76	0.24	0.15	0.20[a]	−0.02
II	0.76	0.24	0.16	0.20[a]	0.00
III	0.82	0.18	0.15_5	0.20[a]	-0.07_5
IV	0.80	0.20	0.15	0.21[b]	−0.13
V	0.84	0.16	0.17	0.21[b]	-0.02_5
VI	0.81	0.19	0.16	0.22[c]	−0.12

a) 3-Methylindole. b) 3-Acetamidoindole. c) *N*-Acetyltryptamine. d) Calculated using Eq. (3).

Since the relative orientation of the exciting oscillator in the phenol ring and the emitting one in the indole ring cannot remain unaltered because of the flexibility of the methylene groups combining the two chromophores, the negative polarization cannot be caused by intramolecular energy transfer, which may induce the depolarization of the fluorescence. Therefore, the result may be interpreted on the assumption that the excitation energy absorbed by the phenol group is transferred to the ^1L_b transition oscillator of the indole group, and that it is internally converted to that of the ^1L_a, which is perpendicular to the former and which is known to emit fluorescence in the polar solvent.[33]

These conclusions agree well with the results described by Weber,[24] who observed a small but doubtless negative polarization of indole in the presence of a

40) L. Stryer and R. P. Haugland, *Proc. Nat. Acad. Sci. U. S.*, **58**, 719 (1967).

41) G. Weber, *Biochem. J.*, **51**, 145 (1952).

42) F. Perrin, *Ann. Phys.*, **12**, 169 (1929).

large amount of phenol.

The overlap integral of the donor fluorescence and the acceptor absorption spectra, and the relative orientation of the two electronic transition moments, are critical in the intermolecular and intramolecular energy transfers. It is difficult to expect that the ^1L_b transition moment would take an especially favorable orientation in such energy transfers. On the other hand, the ^1L_b band may overlap more strongly with the phenolic fluorescence than the ^1L_a band, since the former is located in the long-wavelength absorption bands of the indole moiety. Thus, the activity of the ^1L_b transition in the energy transfer may be interpreted in terms of the overlap integral factor rather than in terms of the orientation factor.

BULLETIN OF THE CHEMICAL SOCIETY OF JAPAN, VOL. 46, 2534—2537 (1973)

Anodic Ring Opening Reaction of 2-Methoxy-1-cyclopentene-1-carboxylic Acids

Sigeru TORII, Hideo TANAKA, Tokio FUKUOKA, and Shukuo HIRAI
Department of Industrial Chemistry, Okayama University, Okayama 700

(Received February 12, 1973)

Electrolysis of 2-methoxy-1-cyclopentene-1-carboxylic acids **2** and **12a** gave α,β- or β,γ-ring opening products **4**, **5a**, **7a**, and **15**. Electrolysis of **2** without separation of anode and cathode compartments gave **6a** in a notable yield. **6a** is expected to be formed by the reduction of a key intermediate **8**, which can be rationalized by leading to **4** and **5**. The results from the anodic oxidation of **12** suggest that the C=C double bond function of **12** was initially oxidized giving **14** followed by discharge of the carboxylate anion to afford **15**. A possible mechanism for the anodic reaction of **2** and **12** has been discussed.

During the course of a study on the anodic oxidation of α,β-unsaturated carboxylic acids,[1a-d] it was found that the anodic reaction of α-methoxy-γ,γ-dimethylaconic acid in protic solvents gives lactone carbonate[1c] and the electrolysis of 5-substituted 2-furoic acids affords α,β-unsaturated butenolides along with the ring opening products.[1b,d] In both cases, the C=C double bond functions were initially oxidized to afford dimethoxy derivatives followed by further two electron oxidation of the carboxyl group.

Our interest in the anodic reaction of α,β-unsaturated carboxylic acids led us to investigate the oxidation of substituted cyclic α,β-unsaturated carboxylic acids. We wish here to report on the α,β- and β,γ-ring cleavage reactions of β-methoxy-α,β-unsaturated carboxylic acids (**2** and **12a**) by electrolysis.

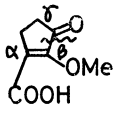

2

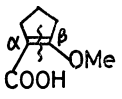

12a

Compound **2** obtained by hydrolysis of readily available ethyl ester **1a**[2] was electrolyzed in methanol containing a drop of concentrated sulfuric acid using one or two compartment cells fitted with platinium foil electrodes under a constant current.

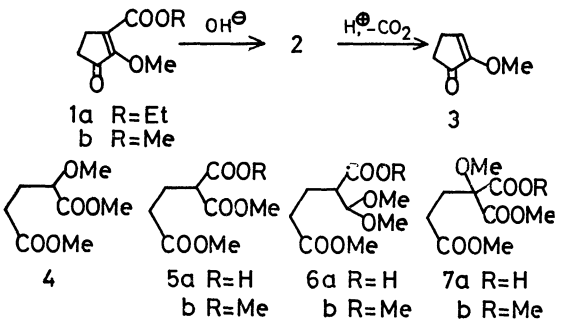

In Experiment 1 (Table 1), the major products were **3**[3] and **4**.[4]

In Experiment 2, a prominent portion of acidic component was obtained together with **3** and **4** when electrolysis was interrupted at an early stage. On being treated with diazomethane the acidic products could be converted into methyl esters **1b**, **7**, and a small amount of minor products. However, when a cell without separation of the electrolysis compartments was used, compounds **5b**,[5] **6b**, and **7b** were isolated after esterification (Experiment 3). Details of experimental conditions along with the results are given in Table 1. Identification of products **3**, **4**, **5b**, **6b**, and **7b** were carried out by their spectral data and microanalyses (see Experimental).

Mechanistic consideration suggests that the electrolysis of **2** (Scheme 1), would give rise to a cationic

1) a) A. Takeda, S. Torii, and H. Oka, *Memoirs of School of Eng., Okayama Univ.*, **3**, 107 (1968); b) S. Torii, H. Tanaka, H. Ogo, and S. Yamasita, This Bulletin, **44**, 1079 (1971); c) S. Torii, T. Furuta, T. Miyaoka, H. Sako, H. Tanaka, and K. Uneyama, *ibid.*, **44**, 2258 (1971); d) S. Torii, H. Tanaka, and T. Okamoto, *ibid.*, **45**, 2783 (1972).

2) O. T. Schmidt and R. Eckert, *Ann.*, **618**, 71 (1958).

3) K. Bernauer, *ibid.*, **588**, 230 (1954); R. M. Acheson, *J. Chem. Soc.*, **1956**, 4232.

4) A. S. Matthews, W. G. Overend, F. Shafizaden, and M. Stacey, *ibid.*, **1955**, 2511; A. J. Birch, J. H. Birkinshaw, P. Chaplen, L. Mo, A. H. Manchanda, A. Pelter, and M. M. Riano, *Aust. J. Chem.*, **22**, 1933 (1969).

5) F. L. M. Pattison, R. L. Buchanan, and F. H. Dean, *Can. J. Chem.*, **43**, 1700 (1965); K. Schank and N. Moell, *Chem. Ber.*, **102**, 71 (1969).

intermediate **C**, which is expected to be formed from either radical intermediate **A** or **B** by one electron oxidation. On the other hand, most of our attempts to isolate a trimethoxy derivative **9** expected to be formed from the intermediate **C** with subsequent reaction with methanol failed. However, the formation of **4**, **5a**, **6a**, and **7a** *via* **8** reveals that the cation **C** would be attacked by a solvent leading to the cleavage of β,γ-bond of the intermediate **C**. Because of the high chemical instability under the acidic work-up conditions **8** was hydrolyzed rapidly to give **5a**. The formation of **8** *in situ* was also demonstrated by the isolation of **6b** as a result of reduction of the double bond when electrolysis was carried out in one compartment cell (Experiment 3).

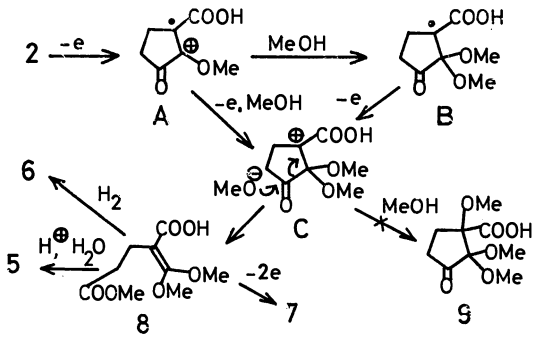

Scheme 1.

Conversion of **8** into **4** *via* **5a** and **7a** might be also explained as follows (Scheme 2). Most of the ortho ester intermediates **9**, **10**, and **11** would be readily hydrolyzed to **4**, **5a**, and **7a** under acidic conditions, *in situ* or during after treatment.

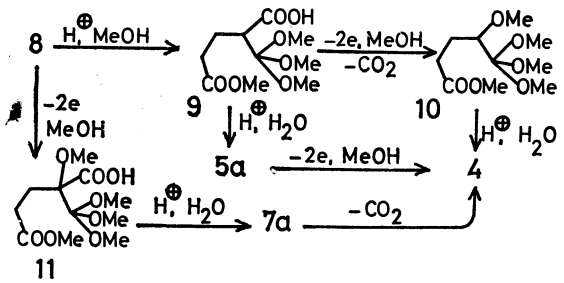

Scheme 2

Formation of **3** from **2** could be rationalized as the result of acid-catalyzed decarboxylation, since stirring of **2** in methanol containing a drop of concentrated sulfuric acid provided **3** in a moderate yield. The presence of an appreciable amount of **3** in the earlier stage of electrolysis of **2** suggests that the anodic oxidation of **3** would afford **4** as follows. Actually, electrolysis of **3** under the same conditions as in Experiment 1 (Table 1) gave **4** in 57% yield.

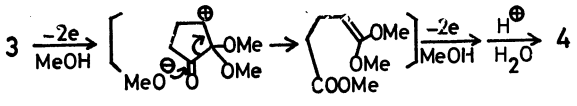

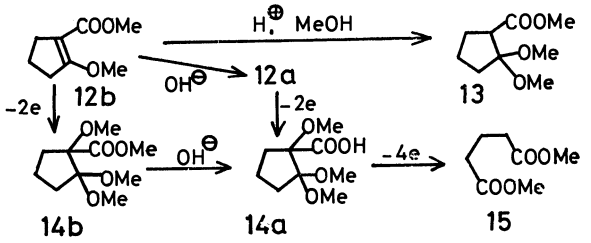

Scheme 3.

In order to compare the electrochemical nature of **2** with that of its analogous compound, electrolysis of the acid **12a** prepared by hydrolysis of **12b**[6] was attempted. The reaction conditions and the results are listed in Table 1. As a major product, methyl glutarate **15** was isolated from the neutral product including several minor constituents. On the other hand, electrolysis of **12b** gave **13** and **14b** without producing other notable products. It is clear that the acetal ester **13** was derived from **12b** by acid-catalyzed solvation with methanol (Scheme 3). After hydrolysis of **14b** with aqueous potassium hydroxide, electrolysis of the alkaline solution in acetonitrile gave rise to the ring opening of **14a** to give **15**. These results reveal that **14a** should be precursors of **15** in the case of anodic oxidation of **12a**.

It is considered that the differences in the products resulting from electrolyses of **2** and **12** are apparently consistent with the intrinsic chemical nature of the postulated intermediate **C** and the electrochemical behavior of **14a**.

Experimental[7]

Electrolysis. Procedure A. The cell used was a water-jacketed beaker, 3.2 cm or 5.5 cm in diameter, 10 cm high, fitted with a gas lead pipe, a thermometer, and magnetic stirrer. The electrodes were two platinum foils (1.5×2.0 cm^2) about 1 mm apart from each other. The current was controlled manually, its direction being changed every 30 sec by means of a commutator. The reaction temperature was controlled by cooling externally with circulating water.

Procedure B. Electrolysis was carried out with two platinium foil electrodes (1.5×2.0 cm^2) under a constant current. The cell used consists of two compartments separated by a glas-filter.[1]

2-Methoxy-3-oxo-1-cyclopentene-1-carboxylic Acid (2). A solution of ethyl 2-methoxy-3-oxo-1-cyclopentene-1-carboxylate(**1a**),[2] (1.00 g), Na_2CO_3 (1.00 g), and water (25 ml) was stirred for 24 hr at room temperature. The aqueous solution was washed with ether, neutralized with dilute HCl, and

6) F. Lacasa, J. Pascual, and L. V. Arco, *Anales real soc. espãn. fis. y guin.*, **52B**, 549 (1956); *Chem. Abstr.*, **51**, 5711 (1957); R. Mayer and B. Gebhardt, *Chem. Ber.*, **93**, 1212 (1960).

7) Preparative and analytical glpc were performed with a a partially modified Yanagimoto GCG-550T type apparatus using a column packed with 10% coated SE-30 Silicone grease on Celite 545, 80/100 mesh, 3 m long (4 ϕ), carrier gas H_2 at 120 °C or 140 °C. All melting and boiling points are uncorrected. Infrared spectra were determined with a Hitachi EPI/S2 spectrophotometer. NMR spectra were obtained on a Japan Electron Optics Laboratory Spectrometer (JNM-C-60) in deuterochloroform with TMS as an internal reference. Microanalyses were carried out by Miss M. Harada.

Table 1. Electrolytic conditions and results for compounds **2**, **12a**, **12b** and **14**

Experiment[a]		1	2	3	4	5	6
Substrate		**2**	**2**	**2**	**12a**	**12b**	**14**
(g)		1.00	1.00	0.96	0.50	4.00	0.20
Supporting	H_2SO_4 (mg)	70	70	70	—	—	—
Electrolyte	$LiClO_4$ (g)	6.0	6.0	—	0.50	2.00	—
	1 M-KOH (ml)	—	—	—	—	—	10
Solvent	MeOH	130	130	40	30	120	—
(ml)	MeCN	—	—	—	—	—	30
Current	(A)	0.25	0.25	0.25	1.00	0.70	0.80
Terminal voltage	(V)	11.5—18.5	19.5—28.0	8.5—12.0	14.5—15.5	8.2	12.0
Temperature	(°C)	10.0—12.0	11.5—13.5	11.0—12.0	26.0	26.0	19.0—20.3
Time	(hr)	5.5	2.75	5.75	2.0	14	0.5
Product (g)							
Neutral component		0.90	0.70	0.43	0.31	3.95	0.08
Acidic component		trace	0.23	0.38	0.07	trace	0.05
Neutral component[b]	(%)						
3		17.0	30.0	6.0	—	—	—
4		72.0	13.0	72.0	—	—	—
15		—	—	—	59.2	—	76.0
2-Methoxycarbonylcyclopentanone		—	—	—	—	6.0	—
13		—	—	—	—	43.0	—
14b		—	—	—	—	24.0	—
12b (Recovered)		—	—	—	—	9.0	—
Acidic component[b,c]	(%)						
5b		—	—	23.0	—	—	—
6b		—	—	53.0	—	—	—
7b		—	47.0	15.0	—	—	—
1b (Recovered)		—	26.0	—	—	—	—

a) Experiments 3, 4, 5, and 6 were carried out without separation of anode and cathode compartments.
b) The product abundances calculated are based on the peak area of glpc.
c) Isolated acidic products were treated with diazomethane before analysis.

extracted with chloroform. The extract was washed with water and dried(Na_2SO_4). Evaporation of the solvent gave 0.49 g of **2**, mp 148.5—149.5 °C (Benzene); IR (Nujol) 3450—2200, 1709 (COOH), 1672 (C=O), 1614 (C=C) cm^{-1}; NMR ($CDCl_3$) δ 2.39—2.90 (m, 4H), 4.27 (s, 3H, CH_3O), 8.81 (s, 1H, COOH).

Found: C, 53.83; H, 5.03%. Calcd for $C_7H_8O_4$: C, 53.85; H, 5.16%.

Electrolysis of **2**. *(Procedure B).* A mixture of lithium perchlorate (6.00 g) and concd H_2SO_4 (70 mg) in MeOH (130 ml) was poured into the anode and cathode compartments. The carboxylic acid **2**(1.00 g) was charged in the anode compartment and electrolyzed under a constant current (0.25 A) at 10—12 °C for 1.5 hr. The anode solution was concentrated by suction and taken up in chloroform. The solution was washed with water followed by aqueous $NaHCO_3$ and dried (Na_2SO_4). Removal of the solvent gave a crude liquid (0.90 g). The constituent of the oil was elucidated by glpc as shown in Table, Exp. 1. The major component **4**[4] was isolated by preparative glpc: IR (Neat) 2845 (CH_3-O), 1741 (C=O) cm^{-1}; NMR ($CDCl_3$) δ 1.80—2.20 (m, 2H, CH_2), 2.30—2.60 (m, 2H, CH_2CO), 3.39 (s, 3H, CH_3O), 3.68 (s, 3H, CH_3OOC), 3.77 (s, 3H, CH_3OOC), 3.92 (m, 1H, CH). Microanalyses gave correct results.

The spectral data of **3**[3] (minor product) isolated by preparative glpc are as follows: IR (Neat) 3098 (HC=C), 1715 (C=O), 1631 (C=C) cm^{-1}; NMR ($CDCl_3$) δ 2.98 (broad, 4H, CH_2), 3.76 (s, 3H, CH_3O), 6.39 (t, J=2.5 Hz, HC=C).

(Procedure A). A mixture of **2** (0.96 g) in MeOH (40 ml) containing H_2SO_4 (*ca.* 70 mg) was electrolyzed (Table 1, Exp. 3). The mixture was concentrated under reduced pressure and the residue was taken up in chloroform. The solution was washed successively with water, aqueous $NaHCO_3$, and water, and then dried (Na_2SO_4). Removal of the solvent gave an oil (0.43 g), whose glpc results are shown in Table 1 (Exp. 3). Components **3** and **4** were isolated by preparative glpc from the oil. Spectral data of **3** and **4** were identical with those of the corresponding authentic samples.

The aqueous alkaline solution was acidified with dilute HCl to pH 3—4 and extracted with chloroform. The extracts were washed with water and dried (Na_2SO_4). Removal of the solvent gave the acidic material as an oil (0.38 g). By treating with diazomethane, the acidic fraction was converted into the corresponding methyl esters, whose glpc results[8a] showed the presence of three major compounds: **5b** (Peak area 23%, R_t 8.2 min), **6b** (53%, 9.6 min), and **7b** (15%, 14.2 min) along with several minor peaks (total 9%). The major products **5b**, **6b**, and **7b** were isolated by preparative glpc.

Compound **5b**[5]: IR (Neat) 2850 (CH_3O), 1740 (C=O) cm^{-1}; NMR ($CDCl_3$) δ 2.00—2.60 (m, 4H, CH_2), 3.51 (t, 1H, CH), 3.70 (s, 3H, CH_3OOC), 3.78 (s, 6H, CH_3OOC).

8) a) Carrier gas flow rate: 35 ml/min at 140 °C. b) 20 ml/min at 140 °C.

Compound **6b**: IR (Neat) 2840 (CH_3O), 1741 (C=O) cm^{-1}; NMR ($CDCl_3$) δ 1.80—2.80 (m, 5H), 3.42 (s, 6H, gem CH_3O), 3.73 (s, 3H, CH_3OOC), 3.76 (s, 3H, CH_3OOC), 4.58 (d, J=7.5 Hz, 1H, CH).

Found: C, 51.56; H, 7.75%. Calcd for $C_{10}H_{18}O_6$: C, 51.27; H, 7.75%. Compound **7b**: IR (Neat) 2880 (CH_3O), 1745 (C=O) cm^{-1}; NMR ($CDCl_3$) δ 2.44 (s, 4H, CH_2), 3.43 (s, 3H, CH_3O), 3.73 (s, 3H, CH_3OOC), 3.86 (s, 6H, CH_3-OOC).

Found: C, 48.76; H, 6.60%. Calcd for $C_{10}H_{16}O_7$: C, 48.39; H, 6.50%.

*2-Methoxy-2-cyclopentenone (**3**).* A solution of **2** (0.50 g) in MeOH (40 ml) containing a drop of concd H_2SO_4 was stirred for 5.5 hr 11—13 °C. After removal of the solvent, the residue was taken up in chloroform. The solution was washed with water and aqueous $NaHCO_3$ and dried (Na_2SO_4). Removal of the solvent gave an oil (91 mg), whose glpc[8b] results showed the presence of two major components: **3** (Peak area 70%, R_t 4.3 min), unknown (30%, 6.0 min). Isolation of **3** was carried out by preparative glpc, its structure being confirmed by comparison with the spectral data of an authentic sample.[3]

*Electrolysis of 2-Methoxy-1-cyclopentenone (**3**). (Procedure B).* A mixture of lithium perchlorate (6.00 g) in MeOH containing concd H_2SO_4 (70 mg) was poured into both compartments. In the anode compartment **3** (0.20 g) was charged and electrolyzed under a constant current of 0.25 A at 10.0—11.0 °C for 2.0 hr with stirring. The solution of the anode compartment was then worked up as described above to give a crude oil (230 mg), which was chromatographed on 5 g of silica gel (Wakogel C-200) with AcOEt–Benzene (1 : 5) to give a clean oil (144 mg). Glpc analysis of the oil showed the presence of methyl 2-methoxyglutarate (**4**) (79%). Analytical specimen of **4** was obtained by preparative glpc. IR and NMR spectra of **4** were identical with those of an authentic sample.

*2-Methoxy-1-cyclopentene-1-carboxylic Acid (**12a**).* A mixture of **12b** (10 g),[6] K_2CO_3 (10 g), and water (35 ml) was stirred for 8 hr at room temperature. The resulting solution was cooled to 10 °C and acidified with dilute HCl to pH 6.0—6.5 and extracted with chloroform. The extracts were washed with water and dried (Na_2SO_4). Concentration of the solution gave crude **12a**, 4.5 g (49.4%), mp 148—148.3 °C (Benzene); IR (Nujol) 2600 (COOH), 1670, 1640, 1610, 1600 (C=O, C=C) cm^{-1}; NMR ($CDCl_3$) δ 1.95 (m, 2H, CH_2), 2.40—2.90 (m, 4H, CH_2), 3.89 (s, 3H, CH_3O), 9.57 (s, 1H, COOH).

Found: C, 59.43; H, 7.07%. Calcd for $C_7H_{10}O_3$: C, 59.14; H, 7.09%.

*Electrolysis of 2-Methoxy-1-cyclopentene-1-carboxylic Acid (**12a**). (Procedure A).* A mixture of **12a** (0.50 g) and lithium perchlorate (0.50 g) in MeOH was electrolyzed (Table 1, Exp. 4). The reaction mixture was concentrated *in vacuo* and the residue was taken up in chloroform. The solution was worked up in the usual manner. Removal of the solvent gave an oil (0.31 g), whose glpc results (Table 1) showed the presence of dimethyl glutarate (59.2%) as a major component isolated by preparative glpc.

*Electrolysis of Methyl 2-Methoxy-1-cyclopentene-1-carboxylate (**12b**). (Procedure A).* A mixture of **12b** (4.00 g) and lithium perchlorate (2.00 g) in MeOH (120 ml) was electrolyzed (Table 1, Exp. 5). The mixture was worked up in the usual manner to give an oil (3.95 g), whose glpc results[8] showed the presence of four major components: methyl 2-cyclopentanone-1-carboxylate (Peak area 6%, R_t 4.3 min), **13** (43%, 6.0 min), recovered **12b** (9%, 7.8 min), and **14b** (24%, 10.6 min) along with several minor compounds (18%). The major products were isolated by preparative glpc or by preparative tlc. The structural assignments of methyl 2-cyclopentanone-1-carboxylate, **12b**, and **13** were carried out by comparing their spectral data with those of the corresponding authentic specimen. The physical data of **14b** together with microanalyses are as follows: IR (Neat) 2845 (CH_3O), 1737 (C=O) cm^{-1}; NMR ($CDCl_3$) δ 1.50—2.50 (m, 6H, CH_2), 3.24 (s, 6H, CH_3O), 3.39 (s, 3H, CH_3O), 3.78 (s, 3H, CH_3OOC).

Found: C, 55.04; H, 8.30%. Calcd for $C_{10}H_{18}O_5$: C, 55.03; H, 8.31%.

*Electrolysis of 1,2,2-Trimethoxycyclopentane-1-carboxylic Acid (**14a**). (Procedure A).* A solution of **14b** (215 mg, purity 70%) obtained in the above procedure in 1 M aqueous KOH (1.26 ml) was stirred for 25 hr at room temperature. To this solution was added a mixed solution of acetonitrile (30 ml) and water (10 ml). The mixture was electrolyzed, reaction conditions and results being given in Table 1, Exp. 6.

*Methyl 2,2-Dimethoxycyclopentane-1-carboxylate (**13**).* A mixture of **12b** (0.50 g) and a drop of concd H_2SO_4 in MeOH (30 ml) was stirred at room temperature for 1 hr. The resulting solution was concentrated and taken up in chloroform. The solution was washed with water and dried (Na_2SO_4). Evaporation of the solvent gave an oil (0.31 g), consisting of two components (**13** and **12b**) as elucidated by glpc[8b]: **13** (Peak area 89%, R_t 6.0 min) and recovered **12b** (8%, 7.8 min). Both compounds isolated by preparative glpc were confirmed by comparison with authentic sepcimens.

Synthetic Studies of Carbohydrate Derivatives with Photochemical Reactions. IX.[1] The Photochemical Addition of 1,3-Dioxolane to Several Enoses

Kazuo MATSUURA, Kazunari NISHIYAMA, Koh YAMADA, Younosuke ARAKI, and Yoshiharu ISHIDO

Department of Chemistry, Faculty of Science, Tokyo Institute of Technology, O-okayama, Meguro-ku, Tokyo 152

(Received February 24, 1973)

The photochemical addition reactions of 1,3-dioxolane to enoses with an endocyclic or exocyclic double bond, such as 3,4,6-tri-*O*-acetyl-D-glucal, 2,3,4,6-tetra-*O*-acetyl-2-hydroxy-D-glucal, methyl 4,6-di-*O*-acetyl-2,3-dideoxy-α-D-*erythro*-hex-2-enopyranoside, and methyl 5-deoxy-2,3-*O*-isopropylidene-β-D-*erythro*-pent-4-enofuranoside, were studied. It was found that the addition of 1,3-dioxolane to the enoses proceeds with great ease, thus affording the corresponding 1,3-dioxolan-2-yl derivatives in excellent yields, and with a considerable regiospecificity and stereoselectivity. The reactions of tetrahydrofuran with the enoses were also studied.

In this series of investigations, the photochemical reaction of sugar derivatives has been studied mainly from a synthetic standpoint of view.[2] Rosenthal and Elad[3] have reported that an acetone-sensitized photochemical addition of 1,3-dioxolane to a terminal olefinic compound affords 2-substituted dioxolane derivatives as the main products, plus its 4-substituted isomers as the minor products. This reaction has also been shown to be applicable to enoses; *i. e.*, 5,6-dideoxy-1,2-*O*-isopropylidene-α-D-*xylo*-hex-5-enofuranose and 3-deoxy-1,2; 5,6-di-*O*-isopropylidene-3-methylene-α-D-*ribo*-hexfuranose, which have a terminal and an exocyclic double bond respectively, thus giving the corresponding equimolar adducts with 1,3-dioxolane in 45 and 55% yields respectively.[4]

In the field of carbohydrate chemistry, it is now an essential problem to obtain an excellent method of synthesizing sugar derivatives with a branched-aldehyde structure; such derivatives can conceivably be derived from such a photochemical addition of 1,3-dioxolane to enoses involving an endocyclic double bond, followed by acid-catalyzed hydrolysis under mild conditions, since the functional group can be converted into a hydroxymethyl group by reduction or into a heterocyclic structure by an appropriate set of reactions, *etc.* In a previous paper,[2a] the present authors briefly reported on the acetone-sensitized photochemical addition of 1,3-dioxolane to 3,4,6-tri-*O*-acetyl-D-glucal (**1**) and 2,3,4,6-tetra-*O*-acetyl-2-hydroxy-D-glucal (**2**); in that study, though, the final structural determination was not achieved. The photochemical additions of **1**, **2**, methyl 4,6-di-*O*-acetyl-2,3-dideoxy-α-D-*erythro*-hex-2-enopyranoside (**3**), and methyl 5-deoxy-2,3-*O*-isopropylidene-β-D-*erythro*-pent-4-enofuranoside (**4**) will be described in this article.

Results and Discussion

An acetone-sensitized photochemical addition of 1,3-dioxolane to **1** was carried out by irradiating it with a high-pressure mercury lamp in 1,3-dioxolane under a nitrogen atmosphere. The subsequent chromatographic separation of the sirup obtained by the concentration of the reaction mixture on a column of silica gel afforded 4,5,7-tri-*O*-acetyl-2,6-anhydro-3-deoxy-D-*arabino*-L-*glycero*-heptose ethylene acetal (**5**) and 4,5,7-tri-*O*-acetyl-2,6-anhydro-3-deoxy-D-*arabino*-D-*glycero*-heptose ethylene acetal (**6**) in 37 and 37% yields respectively, along with 5,6,8-tri-*O*-acetyl-3,7-anhydro-1,4-dideoxy-2-*C*-methyl-D-*arabino*-D-*glycero*-octitol (**7**)[2f] (24% yield). **7** was produced by the nucleophilic

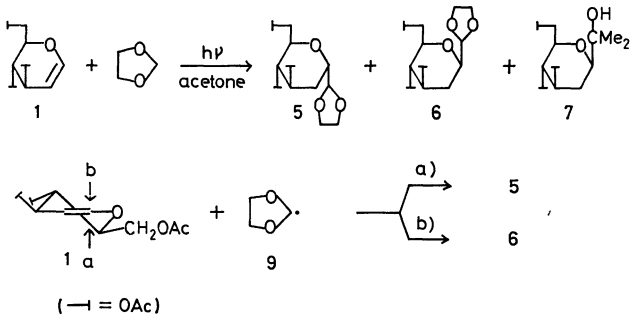

attack of the 2-propanol-2-yl radical (**8**), which had been formed from acetone by the abstraction of a hydrogen atom from 1,3-dioxolane, on the C-1 of **1**. The structural assignments of **5** and **6** were made on the basis of their NMR data, shown in Table 1. In the spectrum of **5**, the signals of H-2, H-3a, and H-3e are observed as multiplets at δ 4.01, 1.79, and 2.22 ppm respectively, while $J_{2,3a}$, $J_{2,3e}$, and $J_{3a,3e}$ have been determined to be 6.0, 4.0, and 14.0 Hz respectively. In the spectrum of **6**, on the other hand, the signals of H-2, H-3a, and H-3e are observed at δ 3.56 as an octet, and those at 1.61 and 2.19 ppm, as multiplets, while $J_{2,3a}$, $J_{2,3e}$, and $J_{3a,3e}$ were determined to be 11.5, 2.2, and 11.5 Hz respectively. The 1,3-dioxolan-2-yl groups at C-2 in **5** and **6** were concluded to be in axial and equatorial orientations respectively, on the basis of the above assignments for H-2s in **5** and **6** being in equatorial and axial orientations respectively. Consequently, the photochemical addition of 1,3-dioxolan-2-yl radical (**9**) to **1** can conceivably

1) Part VIII: K. Matsuura, Y. Araki, and Y. Ishido, This Bulletin, **46**, 2261 (1973).

2) a) K. Matsuura, S. Maeda, Y. Araki, Y. Ishido, and A. Murai, *Tetrahedron Lett.*, **1970**, 2869; b) K. Matsuura, S. Maeda, Y. Araki, and Y. Ishido, This Bulletin, **44**, 292 (1971); c) K. Matsuura, Y. Araki, and Y. Ishido, *ibid.*, **45**, 3496 (1972); d) K. Matsuura, Y. Araki, Y. Ishido, and S. Sato, *Chem. Lett.*, **1972**, 849; e) K. Matsuura, Y. Araki, Y. Ishido, and M. Kainosho, *ibid.*, **1972**, 853; f) K. Matsuura, Y. Araki, Y. Ishido, K. Kushida, and A. Murai, *Carbohyd. Res.*, in press; g) Y. Araki, K. Matsuura, Y. Ishido, and K. Kushida, *Chem. Lett.*, **1973**, 383.

3) I. Rosenthal and D. Elad, *J. Org. Chem.*, **33**, 805 (1968), and the preceding papers.

4) J. S. Jewell and W. A. Szareck, *Tetrahedron Lett.*, **1969**, 43.

Table 1. NMR spectral data of **5**, **6**, **10**, and **11**

Protons	Chemical shifts in δ value			
	5	**6**	**10**	**11**
H-1	5.01	4.88	5.01	5.04
H-2	4.01	3.56	3.57	3.58
H-3a	1.79	1.61	—	5.0—5.3
H-3e	2.22	2.19	5.66	—
H-4	5.31	4.85—5.1	5.11	5.09
H-5	4.90		5.35	5.0—5.3
H-6	3.8—4.4	3.6	3.73	3.6—3.7
H-7,7′		4.06, 4.25	4.2—4.4	4.15—4.4
O-$(CH_2)_2$-O	3.8—4.1	3.8—4.1	3.8—4.1	3.8—4.1
O-$COCH_3$	2.02, 2.04, 2.07	2.01, 2.02, 2.06	2.00, 2.06, 2.12, 2.17 (ax.)	2.03, 2.06, 2.07, 2.10
Coupling constants in Hz				
H-1—H-2	4.0	3.6	5.8	3.0
H-2—H-3a	6.0	11.5	—	9.1
H-2—H-3e	4.0	2.2	1.3	—
H-3a—H-3e	14.0	11.5	—	—
H-3a—H-4	9.5	11.5	—	9.2
H-3e—H-4	5.0	3.0	3.2	—
H-4—H-5	8.0		9.8	9.2
H-5—H-6			9.8	
H-6—H-7		4.5	2.4	
H-6—H-7′		2.5	4.9	
H-7—H-7′		12.0	12.2	

These data were obtained in $CDCl_3$ by the use of tetramethylsilane as the internal standard.

take place regiospecifically at the C-1 of **1** from both the α- and β- sides of the 1-enopyranosyl ring, without any configurational selectivity, thus giving **5** and **6** in a relative ratio of 1 : 1.

The treatment of **2** under similar conditions afforded 3,4,5,7-tetra-*O*-acetyl-2,6-anhydro-D-*glycero*-D-*talo*-heptose ethylene acetal (**10**) and 3,4,5,7-tetra-*O*-acetyl-2,6-anhydro-D-*glycero*-D-*gulo*-heptose ethylene acetal

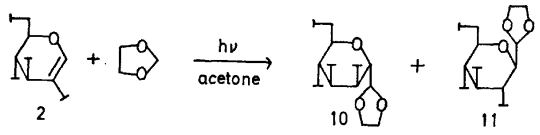

+ other 3 Products

(**11**) in 17 and 42% yields respectively. Much as in the previous reaction, three products, which are the adducts with **8**, were concomitantly afforded in this case.[5] The NMR spectral evidence for the structural determination of **10** and **11** is demonstrated in Table 1. In the spectrum of **10**, the signals of H-2 and H-3 are observed at δ 3.57 (quartet) and 5.66 (quartet) ppm respectively, and $J_{2,3}$ and $J_{3,4}$ were determined to be 1.3 and 3.2 Hz respectively. Moreover, only one of the four acetyl signals is observed at δ 2.17 ppm. In the spectrum of **11**, on the other hand, the signal of H-2 is observed at δ 3.58 (quartet) ppm, $J_{2,3}$ and $J_{3,4}$ were determined to be 9.1 and 9.2 Hz respectively, and all the acetyl signals are observed in the equatorial region. In **10**, the 1,3-dioxolan-2-yl group and the *O*-acetyl group are concluded to occupy the axial orientation at C-2 and C-3 respectively. In **11**, on the other hand, they are in the equatorial orientation at C-2 and C-3 respectively. The addition of the **9** radical may take place on the C-1 of **2** from the α- and β-sides of the 2-hydroxy-1-enopyranosyl ring, thus giving **10** and **11** respectively; this reaction was thus established to involve the *cis*-addition-type mechanism.

Subsequently, the photochemical addition of 1,3-dioxolane to **3** and **4** respectively under the irradiation of a low-pressure mercury lamp was investigated.[6]

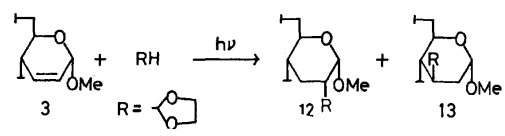

Table 2. NMR spectral data of **12** and **13**

Protons	Chemical shifts in δ value **12**	Peotons	**13**
H-1	4.77	H-1	4.80
H-2	2.1	H-2a	1.68
H-3a	2.1	H-2e	1.96
H-3e	1.9	H-3	2.42
H-4	4.99	H-4	5.01
H-5	3.9	H-5	3.9
H-6	4.13	H-6	4.03
H-6′	4.22	H-6′	4.25
H-2′	4.97	H-3′	4.75
O-$(CH_2)_2$-O	3.8—4.1	O-$(CH_2)_2$-O	3.8—4.1
O-CH_3	3.40	O-CH_3	3.37
O-$COCH_3$	2.04, 2.08	O-$COCH_3$	2.04, 2.08
Coupling constants in Hz			
H-1—H-2	4.0	H-1—H-2a	3.3
H-2—H-2′	6.0	H-1—H-2e	1.5
H-3a—H-4	9.0	H-2a—H-2e	14.0
H-3e—H-4	5.3	H-2a—H-3	12.6
H-4—H-5	9.0	H-2e—H-3	4.3
H-5—H-6	3.5	H-3—H-3′	4.8
H-5—H-6′	5.2	H-3—H-4	10.5
H-6—H-6′	11.8	H-4—H-5	10.5
		H-5—H-6	5.5
		H-5—H-6′	2.8
		H-6—H-6′	12.5

These data were determined in $CDCl_3$ by the use of tetramethylsilane as the internal standard.

5) Gas Chromatographic examination elucidated the relative ratio of the three products to be 1 : 2 : 1, and the major product to be 4,5,6,8-tetra-*O*-acetyl-3,7-anhydro-1-deoxy-2-*C*-methyl-D-*glycero*-D-*gulo*-octitol. Details with respect to these results will be published elsewhere.

6) It is natural and advantageous to irradiate the reaction mixture with a low pressure mercury lamp in the absence of acetone as the photosensitizer on account of the concomitant formation of the adduct with acetone, by which the yield of the expected product is directly affected, when the reaction was carried out under the irradiation of a high pressure mercury lamp in the presence of acetone. However, the irradiation of **1** or **2** in pure 1,3-dioxolane afforded no product and resulted in the complete recovery of the corresponding starting materials.

The irradiation of **3** afforded methyl 4,6-di-*O*-acetyl-2,3-dideoxy-2-*C*-(1,3-dioxolan-2-yl)-α-D-*erythro*-D-*glycero*-hexopyranoside (**12**) and methyl 4,6-di-*O*-acetyl-2,3-dideoxy-3-*C*-(1,3-dioxolan-2-yl)-α-D-*arabino*-hexopyranoside (**13**) in 39 and 39% yields respectively. The structural determination of **12** and **13** was accomplished by the use of their NMR spectral data (Table 2). In the spectrum of **12**, H-2, H-3a, and H-3e signals are observed at δ *ca.* 2.1 (multiplet), *ca.* 2.1 (multiplet), and *ca.* 1.9 (multiplet) ppm respectively, and $J_{1,2}$ is found to be 4.0 Hz. In the spectrum of **13**, on the other hand, H-2a, H-2e, and H-3 signals are observed at δ 1.68, 1.96, and 2.42 ppm respectively, and $J_{2a,3}$, $J_{2e,3}$, and $J_{3,4}$ are found to be 12.6, 4.3, and 10.5 Hz respectively. On the basis of this evidence, **12** and **13** were concluded to involve a 1,3-dioxolan-2-yl group at C-2 and C-3 respectively in equatorial orientations. It can thus be stated that this reaction affords the thermodynamically more stable stereoisomers selectively in a relative ratio of 1 : 1, since no product with an axial substituent is formed.

Incidentally, similar products could be obtained by carrying out the irradiation with a high-pressure mercury lamp in the presence of acetone as the photosensitizer. However, the reaction was inevitably accompanied by the formation of methyl 4,6-di-*O*-acetyl-2,3-dideoxy-2-*C*-(1-hydroxy-1-methylethyl)-α-D-*erythro*-D-*glycero*-hexopyranoside, which had previously been shown to be formed by the addition of the **8** resulting from acetone to **3**,[2d] in a 10% yield.

The irradiation of **4** with a low-pressure mercury lamp under the conditions employed for **3** was, on the other hand, found by tlc and glc to afford at least six products.

Among these products, only methyl 5-deoxy-2,3-*O*-isopropylidene-β-D-*ribo*-hex-dialdofuranoside 6-ethylene acetal (**14**) was isolated in a 10% yield from the reaction mixture. The structure of **14** was confirmed by its NMR spectral data (Table 3). Such a formation of several products in this case, in contrast with the cases of the other enoses employed in the present study, may be due to the high reactivity of the exocyclic double bond, as is generally accepted,[7] and also to a potential photoisomerization of the photoaddition product once formed.[8]

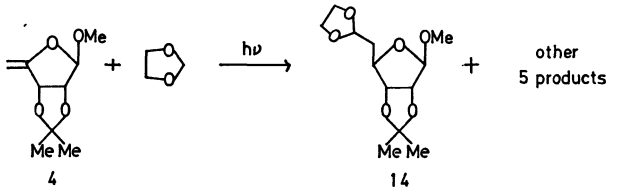

The photochemical addition of 1,3-dioxolane to the enoses, as far as it has been examined, may be summarized as follows:

1) In the reaction of such enoses as **1**, the addition takes place regiospecifically at C-1 from both the α- and β-sides of the 1-enopyranosyl ring, thus giving the corresponding equimolar adducts, such as **5** and **6** in high yields in a relative ratio of 1 : 1. In the reaction of such enoses as **2**, which have a substituent at their C-2 position, on the other hand, the preferential formation of an isomer such as **11**, which is thermodynamically more stable than a configurational isomer such as **10**, is observed. 2) In the reaction of such 2-enoses as **3**, isomers with thermodynamically stable (*i. e.*, equatorial) substituents, such as **12** and **13**, are produced, although no regioselectivity is observed. 3) The reaction of 4-enoses involving an exocyclic double bond such as **4** proceeds with great ease in comparison with those of the other enoses, although such a reaction lacks regio- and stereoselectivity. 4) On the basis of the results obtained by the reaction of **2**, it can be considered that these reactions proceed in part at least by means of a *cis*-addition mechanism.

In addition to the photochemical addition reaction of 1,3-dioxolane, similar photochemical addition of tetrahydrofuran(THF) to enoses was investigated in view of the reactivity of 1,3-dioxolane, the location of the 2-yl radical of which is established by the adjacent two oxygen atoms.

The irradiation of **3** in THF by means of a low-pressure mercury lamp gave methyl 4,6-di-*O*-acetyl-2,3-dideoxy-3-*C*-(2-tetrahydrofuranyl)-α-D-*arabino*-hexopyranoside (**15**) and methyl 4,6-di-*O*-acetyl-2,3-dideoxy-2-*C*-(2-tetrahydrofuranyl)-α-D-*erythro*-D-*glycero*-hexopyranoside (**16**) in 15 and 32% yields respectively. In this case, 44% of the starting material was recovered. The structure of **15** and **16** were confirmed by com-

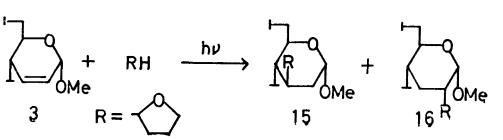

Table 3. NMR spectral data of **14**

Chemical shifts		Coupling constants	
Protons	δ value	Protons	Hz
H-1	4.86	H-1—H-2	0
H-2	4.54	H-2—H-3	6.0
H-3	4.66	H-3—H-4	3.5
H-4	4.11	H-4—H-5(5′)	7.0
H-5,5′	2.11	H-5(5′)—H-6	5.0
H-6	5.05		
O-$(CH_2)_2$-O	3.94[a]		
O-CH_3	3.31		
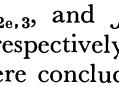	1.32, 1.45		

These data were obtained in $CDCl_3$ by the use of tetramethylsilane as the internal standard.

a) These signals appeared centering in the vicinity of this chemical shift.

7) Exocyclic double bonds have generally accepted to have higher reactivities than endocyclic double bonds in the free radical addition reaction of thio radicals to double bonds; *cf.* M. Fukuyama, "Yuhriki-no-Kagaku (Chemistry of Free Radicals)," ed. by H. Sakurai and K. Tokumaru, Nanko-do, Tokyo (1967), p. 219.

8) D. Elad and R. D. Youssefyeh, *Tetrahedron Lett.*, **1963**, 2189: in this paper, acetone-induced photoisomerization of 2-substituted 1,3-dioxolanes into the corresponding esters has been reported.

paring their NMR spectra with those of **13** and **12** respectively (*cf.* Table 1).

In the photochemical addition of **4** in place of **3**, the formation of at least five products and the recovery of no starting material were detected by tlc and glc, although their structures could not be determined. **1** was, moreover, recovered quantitatively by treating it under the same conditions. Furthermore, the irradiation of **2** in THF in the presence of acetone as the photosensitizer was carried out by means of a high-pressure mercury lamp to give a mixture of two products, **17a** and **17b**(1 : 1), in a 27% yield.[9] The NMR spectra of these products showed that all the acetyl groups are in an equatorial orientation, and the integration curve demonstrated that these are the corresponding equimolar adducts of **2** with THF, which may correspond to two of the three structures shown in Fig. 1, although their structures could not be confirmed. On the basis of these results, the order of the reactivity of the enoses to THF may be concluded to be (**4**>) **3**>**2**(>**1**).

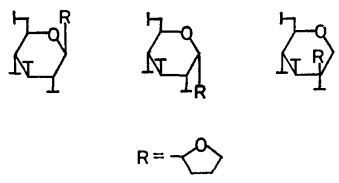

Fig. 1.

In contrast with the cyclic ethers described above, the reactivity of tetrahydropyran was found to be remarkably lower; it gave only a trace of products[10] in reactions with **2** and **3** respectively, and they were recovered almost quantitatively.

Moreover, an acyclic ether such as diethyl ether gave no product at all in spite of a variety of examinations with respect to the potential dependence on the concentration, the effect of the variation in the photosensitizer(such as acetone, 2-butanone, acetophenone, or benzophenone), and irradiation by means of a low-pressure mercury lamp or a high-pressure one in the presence of photosensitizers in reactions with the enoses.

It may thus be concluded with respect to the reactivity of the ethers employed herein that:

1,3-Dioxolane>THF>THP>Diethyl Ether

Experimental

The solvents used for the experiment were purified in the usual manner prior to use. Irradiations were carried out with a high-pressure mercury lamp (450 W) of Ushio Electric, Inc., in a Pyrex-glass tube at a distance of about 5 cm, or with a low-pressure mercury lamp (30 W) of Riko Kagaku Co., Ltd., in a quartz test tube, and with one (6 W) of Ushio Electric, Inc., under a nitrogen atmosphere at room temperature. The tlc's were carried out by the use of Wakogel B-5, and the solvent system of benzene–methanol (9 : 1 v/v) was used for the development. The NMR spectra were taken with a Varian HA-100 apparatus in deuterochloroform using tetramethylsilane as the internal standard. The glc data were obtained with a Hitachi K-53 model; Column: 10% SE-30 on Chromosorb W (60—80 mesh); carrier gas: nitrogen under 1.5 Atm unless otherwise noticed; oven temperature: 200 °C, and injection temperature: 300 °C. The mass spectra were taken with a Hitachi RMU 6E model spectrometer.

4,5,7-Tri-O-*acetyl-2,6-anhydro-3-deoxy*-D-*arabino*-L-glycero-*heptose Ethylene Acetal* (**5**) *and 4,5,7-Tri*-O-*acetyl-2,6-anhydro-3-deoxy*-D-arabino-D-glycero-*heptose Ethylene Acetal* (**6**): A solution of 3,4,6-tri-*O*-acetyl-D-glucal (**1**) (1.00 g) in a solvent system composed of acetone (2 ml) and 1,3-dioxolane (10 ml) was irradiated by means of a high-pressure mercury lamp for 73 hr, after which the reaction mixture was concentrated *in vacuo*.

The residual sirup was chromatographed on a column of silica gel (Mallinckrodt Silica Gel, 100-mesh) by the use of a solvent system of benzene–acetone, whose relative content ratio was changed in turn to 99 : 1 (800 ml), 98 : 2 (800 ml). and 97 : 3 (800 ml) v/v for the elution. **5** (500 mg, 37%), **6** (500 mg, 37%), and 5,6,8-tri-*O*-acetyl-3,7-anhydro-1,4-dideoxy-2-*C*-methyl-D-*arabino*-D-*glycero*-octitol (**7**) (255 mg, 21%) were eluted out in turn separately. The retention volumes of **1**, **5**, **6**, and **7** in glc were 1, 4.4, 4.6, and 2.5 respectively. The specific rotations of these products were as follows; **5**: $[\alpha]_D^{22}$ +28.0° (*c* 1.0, Me_2CO), **6**: $[\alpha]_D^{22}$ +8.0° (*c* 1.0, Me_2CO). Found: C, 52.39 (**5**), and 52.08 (**6**); H, 6.71 (**5**) and 6.60 (**6**)%. Calcd for $C_{15}H_{22}O_9$: C, 52.02; H, 6.40%. The NMR data of **5** and **6** are demonstrated in Table 1.

3,4,5,7-Tetra-O-*acetyl-2,6-anhydro*-D-glycero-D-talo-*heptose Ethylene Acetal* (**10**) *and 3,4,5,7-Tetra*-O-*acetyl-2,6-anhydro*-D-glycero-D-gulo-*heptose Ethylene Acetal* (**11**). A solution of 2,3,4,6-tetra-*O*-acetyl-2-hydroxy-D-glucal (**2**) (1.00 g) in a solvent system composed of acetone (2 ml) and 1,3-dioxolane (10 ml) was irradiated by means of a high-pressure mercury lamp for 54 hr, after which the reaction mixture was concentrated *in vacuo*. The resultant sirup was chromatographed on a column of silica gel by the use of a solvent system of benzene–acetone, whose relative content ratio was changed in turn to 96.5 : 3.5 (1000 ml), 96 : 4 (800 ml), 95 : 5 (800 ml), and acetone (100 ml) v/v, for the elution; this afforded **10** (210 mg, 17%), **11** (510 mg, 42%), and three by-products[5] (equimolar adducts of **2** with acetone, 225 mg, 19%). The retention volumes of **2**, **10**, **11**, and the by-products in glc were, respectively, 2.1, 7.7, 8.1, 3.7, 4.4, and 5.0. Mass spectrum of **11**: *m/e*=404 (M^+), 344[$(M-60)^+$], and 331 [$(M-73)^+$]. Specific rotations: **10**: $[\alpha]_D^{22}$ +22.3° (*c* 1.0, Me_2CO), **11**: $[\alpha]_D^{22}$ −2.0° (*c* 1.0, Me_2CO). Found: C, 50.52 (**10**) and 51.01 (**11**): H, 6.04 (**10**) and 6.04 (**11**)%. Calcd for $C_{17}H_{24}O_{11}$: C, 50.49; H, 5.98%. The NMR data of these products are shown in Table 1.

Methyl 4,6-Di-O-*acetyl-2,3-dideoxy-2*-C-*(1,3-dioxolan-2-yl)*-α-D-erythro-D-glycero-*hexopyranoside* (**12**) *and Methyl 4,6-Di*-O-*acetyl-2,3-dideoxy-3*-C-*(1,3-dioxolan-2-yl)*-α-D-arabino-*hexopyranoside* (**13**). A) A solution of methyl 4,6-di-*O*-acetyl-2,3-dideoxy-α-D-*erythro*-hex-2-enopyranoside (**3**) (1.00 g) in 1,3-dioxolane (25 ml) was irradiated by means of a low-pressure mercury lamp (30 W) for 115 hr, after which the reaction mixture was concentrated *in vacuo*. The residual sirup was chromatographed on a column of silica gel by the use of a solvent system of benzene–acetone, whose relative content ratio was changed in turn to 99 : 1 (1000 ml), 98 : 2 (500 ml), 97 : 3 (500 ml), 9 : 1 (200 ml) v/v, for the elution; this afforded **3** (115 mg, 12% recovery), **12** (510 mg, 39%),

9) Two peaks corresponding to **17a** and **17b** were detected in glc with retention volumes of 8.3 and 8.9, respectively, and their chromatographic separation has not yet been accomplished.

10) The amounts of the corresponding products in the reaction with **2** or **3** were determined as less than 10% yields by means of glc.

and **13** (510 mg, 39%). The retention volumes of **3**, **12**, and **13** in glc were, respectively, 0.8, 2.2, and 2.2. The specific rotations of **12** and **13** were $[\alpha]_D^{22}$ +84.5° (*c* 1.0, Me_2CO) and $[\alpha]_D^{22}$ +55.7° (*c* 1.0, Me_2CO) respectively. Found: C, 52.62 (**12**) and 52.91 (**13**): H, 7.05 (**12**) and 7.12 (**13**)%. Calcd for $C_{14}H_{22}O_8$: C, 52.82; H, 6.97%. The NMR spectral data of these products are shown in Table 2. B) A similar treatment of **3** (1.00 g) in a solvent composed of 1,3-dioxolane (9 ml) and acetone (1 ml) under irradiation with a high-pressure mercury lamp (450 W) for 14 hr, and a similar chromatographic treatment of the sirup obtained by the concentration of the reaction mixture, afforded **12** (420 mg, 32%) and **13** (410 mg, 31%), in addition to methyl 4,6-di-*O*-acetyl-2,3-dideoxy-2-*C*-(1-hydroxy-1-methylethyl)-α-D-*erythro*-D-*glycero*-hexopyranoside[2d] (60 mg, 10%).

*Methyl 5-Deoxy-2,3-O-isopropylidene-β-D-ribo-hexo-dialdofuranoside 6-Ethylene Acetal (**14**).* A solution of methyl 5-deoxy-2,3-*O*-isopropylidene-β-D-*erythro*-pent-4-enofuranoside (**4**) (1.00 g) in 1,3-dioxolane (180 ml) was irradiated by means of a low-pressure mercury lamp (6 W) for 51 hr, after which the reaction mixture was concentrated *in vacuo*. The residual sirup was chromatographed on a column of silica gel by the use of a solvent system of benzene–acetone, whose relative content ratio was changed in turn to 99 : 1 (1000 ml), 98 : 2 (500 ml), and 97 : 3 (500 ml), for the elution, thus affording **14** (140 mg, 10%). Its retention volume in glc was 5.4 with reference to that of **4** (1.0) under 0.8 Atm of nitrogen gas. $[\alpha]_D^{22}$ −70.8° (*c* 1.0, Me_2CO). Found: C, 55.78; H, 7.53%. Calcd for $C_{12}H_{20}O_6$: C, 55.37; H, 7.75%. The NMR data of this product are shown in Table 3.

*Methyl 4,6-Di-O-acetyl-2,3-dideoxy-3-C-(2-tetrahydrofuranyl)-α-D-arabino-hexopyranoside (**15**) and Methyl 4,6-Di-O-acetyl-2,3-dideoxy-2-C-(2-tetrahydrofuranyl)-α-D-erythro-D-glycero-hexopyranoside (**16**).* A solution of **3** (0.500 g) in THF (25 ml) was irradiated by means of a low-pressure mercury lamp (30 W) for 210 hr, after which the reaction mixture was concentrated *in vacuo*. The residual sirup was chromatographed on a column of silica gel by the use of a solvent system of benzene–acetone (98 : 2 v/v, 1000 ml) for the elution, thus affording **3** (220 mg, 44% recovery), **15** (95 mg, 15%), and **16** (205 mg, 32%). The retention volumes of **15** and **16** in glc were 3.2 and 3.4 respectively. The specific rotations of **15** and **16** were as follows: $[\alpha]_D^{22}$ +78.5 (*c* 1.0, Me_2CO) and +66.1° (*c* 1.0, Me_2CO) respectively. The NMR spectral data of **15** and **16** are almost superimposable with those of **13** and **12** respectively, except that the singals of the tetrahydrofuranyl-ring protons are observed at δ *ca.* 1.8—2.0 (4H) and 3.8—4.0 (3H) ppm in both cases. Moreover, these were concluded, on the basis of the relative ratios of the integration curves of their NMR spectra, to be equimolar adducts of **2** with THF.

*Irradiation of 2,3,4,6-Tetra-O-acetyl-2-hydroxy-D-glucal (**2**) in Tetrahydrofuran–Acetone with a High-pressure Mercury Lamp.* A solution of **2** (1.00 g) in a solvent system composed of tetrahydrofuran (22.5 ml) and acetone (2.5 ml) was irradiated with a high-pressure mercury lamp for 150 hr, after which the reaction mixture was concentrated *in vacuo*. The residual sirup was chromatographed on a column of silica gel by the use of the solvent system of benzene–acetone, whose relative content ratio was changed in turn to 97 : 3 (1500 ml) and 91 : 9 (1000 ml) v/v for the elution, thus affording **2** (110 mg, 11% recovery), a mixture of the corresponding equimolar adducts **17a** and **17b** (330 mg, 27%), and the same three by-products (equimolar adducts of **2** with acetone,[5] 460 mg, 40%) as have been described in the second example of this section.

The authors are grateful to Mr. Katsuhiko Kushida, Nippon Electric Varian, and Mr. Asao Murai, Central Research Lab., Ajinomoto Co., Inc., for the NMR and mass spectral determinations respectively, and also to the members of the Laboratory of Organic Elemental Analysis, Tokyo Institute of Technology, for the elemental analyses.

Crystal and Molecular Structure of ω-Amino Acids, ω-Aminosulfonic Acids and Their Derivatives. V. Crystal and Molecular Structure of γ-Guanidino Propane Sulfonic Acid

Yang Bae KIM,* Akio WAKAHARA, Takaji FUJIWARA, and Ken-ichi TOMITA

Faculty of Pharmaceutical Sciences, Osaka University, Toneyama, Toyonaka, Osaka 560

(Received March 8, 1973)

The crystal structure of γ-guanidino propane sulfonic acid was determined by the symbolic addition method with X-ray intensity data on a diffractometer and refined by the least-squares method to an *R*-value 0.069 for 1963 reflections. The crystals were monoclinic, space group $P2_1/c$, $Z=8$, with $a=10.080$, $b=8.013$, $c=19.716$ Å and $\beta=98.17°$. Two independent molecules in the asymmetric unit both have a zwitterionic form, $(NH_2)_2^+$-$CNHCH_2CH_2CH_2SO_3^-$. There are two forms, *trans* zigzag and *cis* ones, which are linked by N(1)H···O hydrogen bonds. The molecules are held together in the crystal by a three-dimensional network of NH···O hydrogen bonds.

γ-Guanidino propane sulfonic acid (GGPSA) is a guanidyl derivative of 3-amino propane sulfonic acid, homotaurine, which has strong activity towards the behavior of neurones when applied extracellularly.[1] Short-chain ω-guanidino acids and homotaurine also depress cortical responses.[2-3] Tsunoo *et al.* reported that homotaurine and γ-amino-β-hydroxy propane sulfonic acid (GABOPSA) act to lower blood pressure, and GGPSA and γ-guanidino-β-hydroxy propane sulfonic acid (GGBOPSA) acts to depress the lowering of blood pressure.[4]

It is of interest to investigate systematically the molecular structure of such compounds and elucidate the relationship between the molecular conformations and their physiological actions.

We previously reported the crystal data of GGBOPSA, GGPSA and γ-guanidino-β-hydroxybutyric acid (GGBOBA),[5] and the molecular and crystal structure of GGBOPSA.[6]

In this paper, we describe a detailed molecular and crystal structure of γ-guanidino propane sulfonic acid (GGPSA) and compare it with that of ω-amino sulfonic acids and amino acid containing guanidyl group, L-arginine.[7]

Experimental

The compound was recrystallized from an aqueous solution as colorless, transparent prismatic crystals.

Crystallographic Measurement. The space group was determined from Weissenberg and precession photographs, and lattice costants were obtained from precise measurement of the 2θ angles for 9 reflections on a diffractometer with Cu*K*α radiation. Density was measured by the flotation method in a mixture of ethylene dibromide and acetonitrile.

Table 1. Crystal data

Molecular formula; $C_4H_{11}N_3O_3S$. M.W. 181.2,	
Colorless transparent prism, Monoclinic system	
$a = 10.080(3)$ Å	$b = 8.013(8)$ Å
$c = 19.716(1)$ Å	$\beta = 98.17(3)°$
Volume of unit cell,	1576.3 Å^3
Density (by flotation)	1.518 g/cm^3
Density (calculated)	1.522 g/cm^3
$Z = 8$	F(000) = 768
Absent spectra; $h0l$ when $l = 2n + 1$	
$0k0$ when $k = 2n + 1$	
Space group; $P2_1/c$ with two independent molecules in an asymmetric unit.	

The crystal data are listed in Table 1.

Three-dimensional intensity data were collected on a computer controlled four-circle diffractometer (Rigaku Denki Co. Ltd.) with Ni-filtered Cu*K*α radiation using a crystal mounted about the *b*-axis. A total of 1963 independent reflections limited within $\sin\theta/\lambda<0.53$ Å^{-1} was scanned by a ω-2θ technique at a scan speed of 4° per minute. During the course of data collection, the intensities for three standard reflections 020, 006, and 500 were measured every 50 reflections in order to check the stability of the electronics or the damage on crystal lattice. All the reflections were recorded and corrected for usual Lorentz and polarization effects, no absorption correction being made.

Structure Determination and Refinement. An approximate scale and the over-all temperature factor were calculated by Wilson's method. The structure determination was tried at first by a heavy atom procedure, but there was some trouble in interpreting the Patterson function owing to too many large peaks. Failing in this, we tried to determine the structure by means of the symbolic addition method proposed by Karle and Karle.

Normalized structure factor, $|E|$, and $\sum_2$ lists ($|E|\geqq1.5$, probability greater than 97%) were calculated by the program "SIGMA" written by T. Ashida. Three-dimensional *E*-maps of 8 possible cases were calculated from the sign relations between four symbols A to D, for 145 reflections. One of them gave the positions of two sulfur atoms reasonably coincident with the corresponding coordinates in the Patterson function. The positions of all the non-hydrogen atoms were found by the following Fourier synthesis with phases of only two heavy atoms. An *R*-index, $\sum||F_o|-|F_c||/\sum|F_o|$, was reduced from 0.32 to 0.27 by successive syntheses with

* Present address: College of Pharmacy, Seoul National University, Seoul, Korea.

1) D. R. Curtis and J. C. Watkins, *J. Neurochem.*, **6**, 117 (1960).
2) D. P. Purpura, M. Girado, and H. Grundfest, *Science*, **127**, 1179 (1958).
3) D. R. Curtis and J. C. Watkins, *Nature*, **191**, 1010 (1961).
4) S. Tsunoo, K. Horisaka, H. Tanaka, T. Chida, S. Nakajima, and Z. Fukai, *J. Showa Med. Assoc.*, **30**, 521 (1970).
5) Y. B. Kim, A. Wakahara, T. Fujiwara, and K. Tomita, *Chem. Lett.*, **1972**, 891.
6) Y. B. Kim, A. Wakahara, T. Fujiwara, and K. Tomita, This Bulletin, **46**, 2194 (1973).
7) I. L. Karle and J. Karle, *Acta Crystallogr.*, **17**, 835 (1964).

a constant over-all temperature factor. Refinement was carried out for all reflections by the block-diagonal least-squares procedure with unit weight. The R-index was reduced to 0.14 with isotropic temperature factors for all non-hydrogen atoms and decreased further with anisotropic temperature factors to 0.11. In this state, a calculated difference Fourier synthesis (Fig. 1) revealed the locations of all the twenty-two hydrogen atoms. They were included in the final least-squares cycles with anisotropic temperature factors for non-hydrogen atoms and isotropic one for hydrogen atoms. The final R-value was 0.069. The observed and calculated structure factors for each reflection are listed in Table 2.

Calculations were carried out on an NEAC 2200—700 computer, this University, and a FACOM 230—60 computer, University of Kyoto. The scattering factors were taken from

TABLE 2. OBSERVED AND CALCULATED STRUCTURE FACTORS[a)]

K	Fo	Fc
H.L=	0	0
2	252	-277
4	18	20
6	92	-94
8	66	68
H.L=	0	1
1	68	67
2	293	355
3	151	-151
4	39	43
5	19	19
6	52	-48
7	4	6
8	9	-12
H,L=	0	2
1	59	-56
2	252	-279
3	14	-11
4	162	160
5	41	-38
6	40	-38
7	19	22
8	7	-9
H.L=	0	3
1	60	56
2	107	-107
3	20	-19
4	39	37
5	22	-21
6	69	69
7	27	27
8	19	24
H,L=	0	4
0	221	243
1	109	-112
2	198	-205
3	96	95
4	95	90
5	77	-79
6	27	-22
7	12	12
8	48	54
H,L=	0	5
1	85	-84
2	46	-39
3	66	63
4	15	-12
5	68	71
6	44	-47
7	58	-57
8	16	17
H,L=	0	6
0	102	96
1	219	-237
2	186	-188
3	58	55
4	113	107
5	24	-25
6	67	-68
7	59	59
8	2	-3
H.L=	0	7
1	71	69
2	40	36
3	8	-8
4	16	17
5	23	-22
6	19	-17
7	8	3
H.L=	0	8
0	65	-64
1	29	11
2	58	59
3	157	150
4	65	61
5	84	-82
6	7	8
7	5	-5
H,L=	0	9
1	105	-101
2	19	-14
3	61	58
4	26	25
5	28	28
6	9	-11
7	40	-41
H,L=	0	10
0	22	-8
1	100	-98
2	78	-69
3	46	42
4	28	-26
5	11	10
6	12	12
7	31	32
H,L=	0	11
1	63	58
2	4	0
3	49	-46
4	17	-12
5	4	-2
6	29	-28
7	27	27
H,L=	0	12
0	9	-6
1	15	-13
2	84	82
3	57	52
4	27	-27
5	64	-59
6	7	8
H,L=	0	13
1	25	-21
2	26	-24
3	8	4
4	11	9
5	8	7
6	4	4
H,L=	0	14
0	41	-36
1	4	3
2	43	42
3	44	-43
4	61	-61
5	31	33
6	29	29
H,L=	0	15
1	16	15
3	12	-13
4	3	-1

K	Fo	Fc
5	9	11
H,L=	0	16
0	54	-52
1	5	2
2	61	62
3	31	-33
4	4	-1
5	19	21
H,L=	0	17
1	8	-8
2	51	-49
3	24	-25
4	39	39
H,L=	0	18
0	18	-18
1	23	23
2	11	10
3	27	-28
4	65	-67
H.L=	0	19
1	19	19
2	26	28
3	4	-5
H,L=	0	20
0	23	-23
1	47	50
2	9	-11
H,L=	1	0
0	42	-44
1	22	20
2	42	-44
3	21	-27
4	62	-65
5	103	103
6	48	50
7	27	-24
8	10	-9
H.L=	1	1
1	109	107
2	27	-28
3	11	12
4	3	-5
5	19	-18
6	62	-63
7	51	53
8	2	-5
H.L=	1	2
0	34	-25
1	170	176
2	124	124
3	84	-80
4	62	-57
5	50	52
6	20	20
7	55	-57
8	12	-15
H,L=	1	3
1	55	-51
2	46	-48
3	54	-53
4	22	17
5	72	-76
6	6	-9
7	13	14
H.L=	1	4
0	203	218
1	60	57
2	45	28
3	6	-8
4	38	-37
5	52	50
6	16	-12
7	33	-33
8	27	29
H,L=	1	5
1	17	18
2	47	50
3	7	7
4	7	-8
5	9	9
6	24	-23
7	12	16
8	33	31
H,L=	1	6
0	96	-96
1	73	74
2	78	76
3	110	-103
4	16	13
5	19	17
6	53	-57
7	28	-29
8	13	-12
H,L=	1	7
1	63	-62
2	13	12
3	30	27
4	45	43
5	35	-35
6	67	68
7	8	5
H,L=	1	8
0	107	-104
1	27	30
2	23	-15
3	61	-62
4	3	-1
5	23	20
6	20	21
7	16	-16
H,L=	1	9
1	20	19
2	4	-2
3	50	49
4	36	-35
5	30	30
6	54	-50
7	14	-13
H,L=	1	10
0	18	-15
1	22	-27
2	37	-34
3	19	20
4	80	73
5	10	-12
6	39	-37
7	8	10
H,L=	1	11
1	13	-11
2	11	10

K	Fo	Fc
3	47	-49
4	11	-12
5	3	1
6	18	18
7	12	-13
H.L=	1	12
0	4	5
1	89	87
2	44	39
3	36	33
4	7	-7
5	37	-35
6	9	-8
H,L=	1	13
1	23	-20
2	59	58
3	64	62
4	6	4
5	19	20
6	15	-13
H.L=	1	14
0	55	-55
1	88	-86
2	26	-24
3	24	23
4	7	4
5	4	5
6	10	-9
H,L=	1	15
1	38	38
2	21	-22
3	58	-57
4	12	12
5	14	-15
H,L=	1	16
0	20	-19
1	30	-31
2	22	20
3	79	81
4	18	17
5	39	-40
H,L=	1	17
1	29	-29
2	77	-79
3	29	27
4	4	-5
H,L=	1	18
0	38	45
1	81	-92
2	45	43
3	16	-17
H,L=	1	19
1	25	23
2	38	35
H,L=	1	20
0	78	-77
1	37	-41
H,L=	2	0
0	42	-45
1	360	-448
2	115	120
3	5	-4
4	94	-94
5	16	-14
6	21	-22
7	53	58
8	29	-31
H,L=	2	1
1	189	197
2	112	108
3	76	-77
4	111	112
5	37	-34
6	5	7
7	12	11
H.L=	2	2
0	136	-141
1	101	101
2	74	-76
3	161	169
4	59	59
5	102	-102
6	66	70
7	13	-15
8	6	-4
H.L=	2	3
1	81	-90
2	8	6
3	69	77
4	62	-72
5	63	73
6	3	-1
7	31	-41
8	3	-3
H,L=	2	4
0	91	-197
1	79	-135
2	30	39
3	49	63
4	73	-119
5	4	2
6	40	40
7	51	53
8	13	-11
H,L=	2	5
1	73	69
2	37	38
3	66	-63
4	42	-43
5	26	-26
6	39	-40
7	36	35
8	6	5
H,L=	2	6
0	8	-5
1	5	-3
2	172	171
3	63	59
4	58	-52
5	44	-41
6	42	41
7	8	-10
H,L=	2	7
1	28	28
2	32	-32
3	64	-61
4	2	-3
5	2	0
6	21	21
7	16	-15

K	Fo	Fc
H,L=	2	8
0	102	98
1	35	-32
2	13	9
3	24	23
4	117	-114
5	12	14
6	24	24
7	13	-13
H,L=	2	9
1	45	39
2	80	78
3	40	-37
4	20	18
5	19	22
6	19	-18
7	5	6
H,L=	2	10
0	120	-121
1	12	-11
2	54	54
3	22	-20
4	12	16
5	14	13
6	46	45
7	15	-16
H,L=	2	11
1	18	-18
2	88	-84
3	25	-24
4	21	-23
5	18	18
6	47	49
H,L=	2	12
0	38	35
1	44	41
2	15	11
3	56	-56
4	78	-72
5	13	14
6	1	-4
H,L=	2	13
1	5	-4
2	85	83
3	39	37
4	14	13
5	8	8
6	45	-45
H.L=	2	14
0	87	-83
1	13	-12
2	10	5
3	10	-8
4	91	91
5	20	20
H.L=	2	15
1	11	-10
2	49	-48
3	9	-4
4	13	13
5	5	-2
H,L=	2	16
0	12	17
1	56	57
2	23	-26
3	10	-10
H,L=	2	17
1	21	-21
2	15	17
3	43	43
4	6	4
H,L=	2	18
0	15	14
1	23	-22
2	26	-25
3	35	-36
H.L=	2	19
1	23	24
2	24	-25
H,L=	3	0
0	61	66
1	31	-26
2	66	-69
3	18	-21
4	95	93
5	1	1
6	53	-51
7	1	0
8	11	10
H.L=	3	1
1	85	-82
2	68	-70
3	35	-36
4	24	-25
5	14	-14
6	69	72
7	4	-3
8	18	-17
H,L=	3	2
0	218	230
1	113	-112
2	78	-78
3	12	-9
4	39	39
5	25	-23
6	35	-35
7	35	36
8	37	39
H.L=	3	3
1	23	19
2	50	49
3	54	49
4	43	-44
5	14	-13
6	20	20
7	12	12
H,L=	3	4
0	130	-143
1	134	-140
2	32	27
3	55	52
4	43	44
5	37	-39
6	18	-20
7	14	16
H,L=	3	5
1	32	-41
2	39	-47
3	9	-10
4	28	27

K	Fo	Fc
5	20	-18
6	38	40
7	21	22
H,L=	3	6
0	107	105
1	111	-105
2	81	-77
3	106	105
4	5	3
5	80	-80
6	16	-16
7	20	19
H.L=	3	7
1	35	32
2	65	66
3	57	55
4	4	2
5	35	35
6	23	-23
7	31	-30
H,L=	3	8
0	108	-105
1	135	-132
2	11	-8
3	70	66
4	5	-3
5	2	0
6	33	35
7	38	39
H,L=	3	9
1	38	32
2	43	-41
3	70	-64
4	33	-35
5	71	-69
6	1	0
7	60	60
H.L=	3	10
0	31	26
1	3	-1
2	96	96
3	110	107
4	71	-71
5	73	-70
6	17	16
H.L=	3	11
1	24	-21
2	8	5
3	40	41
4	7	6
5	13	9
6	6	-8
H,L=	3	12
0	3	2
1	67	-69
2	27	26
3	5	4
4	57	-54
5	14	-13
6	4	5
H,L=	3	13
1	14	13
2	63	60
3	11	-11
4	6	-5
5	37	-36
H,L=	3	14
0	162	-164
1	34	34
2	90	88
3	15	14
4	7	-4
5	22	-20
H.L=	3	15
1	37	-34
2	50	-48
3	62	60
4	14	-16
H,L=	3	16
0	41	-40
1	23	20
2	51	50
3	27	-25
4	54	-54
H,L=	3	17
1	41	-40
2	39	39
3	26	25
H,L=	3	18
0	70	-72
1	10	9
2	50	49
H,L=	4	0
0	113	114
1	71	75
2	7	3
3	38	-38
4	33	33
5	4	-3
6	9	-8
7	31	-32
H.L=	4	1
1	49	58
2	5	-5
3	18	22
4	41	41
5	37	-34
6	5	8
7	8	-8
H,L=	4	2
0	16	16
1	16	11
2	76	-71
3	63	56
4	72	-68
5	57	59
6	14	11
7	26	-24
H,L=	4	3
1	26	-22
2	23	25
3	4	3
4	17	-14
5	6	4
6	40	-37
7	21	20
H,L=	4	4
0	14	5
1	19	22
2	9	2

K	Fo	Fc
3	86	-84
4	112	112
5	60	61
6	30	-31
7	20	-22
H.L=	4	5
1	65	-62
2	144	-140
3	2	-1
4	10	2
5	13	-11
6	55	53
7	4	1
H,L=	4	6
0	121	127
1	39	-31
2	51	-49
3	78	-74
4	12	-8
5	38	36
6	48	-51
7	22	-21
H.L=	4	7
1	8	6
2	22	26
3	26	27
4	27	33
5	4	-4
7	6	-8
H,L=	4	8
0	21	-15
1	13	13
2	13	-13
3	63	-60
4	72	71
5	37	36
6	22	-20
H,L=	4	9
1	17	19
2	16	-14
3	6	-11
4	17	14
5	16	-15
6	13	13
H.L=	4	10
0	54	51
1	75	73
2	105	-103
3	24	25
4	34	32
5	2	-6
6	19	-19
H.L=	4	11
1	26	-26
2	14	12
3	13	12
4	22	-17
5	45	47
6	15	-14
H,L=	4	12
0	98	98
1	5	-2
2	38	-39
3	49	-48
4	29	28
5	5	1
H,L=	4	13
1	59	58
2	53	51
3	52	-51
4	25	-23
5	45	-46
H,L=	4	14
0	4	2
1	84	86
2	23	-23
3	48	51
4	24	25
H,L=	4	15
1	31	-31
2	9	-10
3	37	37
4	5	-4
H.L=	4	16
0	67	66
1	50	-54
2	30	-28
3	2	1
H,L=	4	17
1	12	13
2	7	9
H,L=	4	18
0	13	-13
H,L=	5	0
0	74	-69
1	29	-27
2	54	51
3	76	71
4	41	-42
5	83	-82
6	29	30
7	27	28
H,L=	5	1
1	48	-43
2	55	52
3	100	94
4	6	-8
5	18	13
6	39	-41
7	14	-15
H,L=	5	2
0	155	-161
1	45	-43
2	79	75
3	10	-7
4	7	-6
5	15	-15
6	25	22
7	18	20
H,L=	5	3
1	33	34
2	25	22
3	35	-37
4	19	-18
5	36	-35
6	19	19
7	3	-3
H,L=	5	4
0	89	-104
1	108	118

K	Fo	Fc
2	84	82
3	43	48
4	47	-50
5	28	-28
6	17	19
7	2	-5
H.L=	5	5
1	48	-39
2	4	1
3	98	92
4	23	-20
5	21	19
6	16	18
7	6	-4
H,L=	5	6
0	147	-145
1	51	-50
2	130	128
3	50	-47
4	121	-120
5	44	40
6	39	37
H,L=	5	7
1	34	30
2	15	17
3	48	-42
5	47	-46
6	19	-18
H,L=	5	8
0	102	-105
1	90	82
2	83	75
3	29	-23
5	42	42
6	35	35
H.L=	5	9
1	20	-19
2	89	-89
3	4	-5
4	24	-25
5	40	39
6	63	62
H,L=	5	10
0	40	39
1	43	41
2	59	58
3	94	-92
4	110	-111
5	34	34
H,L=	5	11
1	6	5
2	80	83
3	28	-28
5	2	-1
H,L=	5	12
0	92	-103
1	69	72
2	40	42
3	66	-61
4	6	6
5	22	19
H,L=	5	13
1	34	34
2	20	-19
3	11	-11
4	5	-4
H,L=	5	14
0	23	21
1	96	93
2	20	-21
3	29	-27
4	33	-32
H.L=	5	15
1	21	-20
2	35	35
3	4	-2
H.L=	5	16
0	7	0
1	26	25
2	4	4
H,L=	6	0
0	106	98
1	26	-20
2	59	-55
3	32	-31
4	31	-26
5	6	-4
6	43	-43
H.L=	6	1
1	37	32
2	82	81
3	2	3
4	25	-20
6	3	-2
H,L=	6	2
0	13	10
1	19	14
2	39	-40
3	21	19
4	98	106
5	6	-6
6	26	-27
H,L=	6	3
1	27	-27
2	8	2
3	24	-29
4	31	-36
5	27	28
6	19	20
H,L=	6	4
0	1	1
1	14	-11
2	34	-32
3	63	65
4	34	32
5	86	-82
6	27	-30
H,L=	6	5
1	53	-53
2	43	39
3	43	41
4	15	-11
5	44	42
6	5	0
H,L=	6	6
0	7	-2
1	110	-105
2	1	-2
3	3	2
4	42	42

K	Fo	Fc
5	27	-26
6	19	-19
H.L=	6	7
1	73	70
3	54	-50
4	14	15
6	6	5
H,L=	6	8
0	33	31
1	22	-26
2	58	-56
3	99	100
4	4	-1
5	41	-39
H,L=	6	9
1	9	6
2	9	-12
3	5	-4
4	8	-2
5	36	37
H,L=	6	10
0	7	9
1	80	-83
2	27	26
3	46	43
4	25	-28
5	2	-2
H,L=	6	11
1	5	-2
2	22	-19
3	41	-42
4	6	6
H,L=	6	12
0	6	-3
1	66	-65
2	6	4
3	19	23
4	11	-9
H,L=	6	13
1	27	25
2	32	-33
3	21	-20
H,L=	6	14
0	22	24
1	22	-21
2	21	19
H,L=	6	15
1	17	-16
H,L=	7	0
0	23	21
1	49	42
2	18	16
3	77	-76
4	75	-71
5	46	42
6	50	48
H,L=	7	1
1	46	43
2	74	70
3	73	-69
4	52	-49
5	34	-32
H,L=	7	2
0	40	-41
1	70	66
2	28	30
3	5	9
4	3	-5
5	15	-16
6	10	9
H,L=	7	3
1	11	7
2	39	-36
3	18	22
4	13	-15
5	24	23
6	17	18
H,L=	7	4
0	42	47
1	23	25
2	6	2
3	28	-33
4	34	-34
5	34	36
H,L=	7	5
1	24	-25
2	63	59
3	15	-12
4	20	-15
5	19	19
H,L=	7	6
0	43	-41
1	38	38
2	10	-9
3	71	-65
4	71	64
5	36	33
H,L=	7	7
1	11	10
2	46	-41
3	11	6
4	3	-1
5	10	-9
H,L=	7	8
0	44	36
1	25	22
2	24	-18
3	12	13
4	7	5
H,L=	7	9
1	47	-45
2	21	16
3	19	18
4	19	19
H.L=	7	10
0	21	22
1	17	-18
2	36	-33
3	55	-54
4	44	41
H,L=	7	11
1	53	53
2	8	-11
3	19	-22
H,L=	7	12
0	40	39
1	37	36
2	52	-49
H,L=	7	13
1	24	-22

K	Fo	Fc
H.L=	8	0
0	23	33
1	89	-114
2	31	-36
3	23	26
4	25	27
5	32	-36
H,L=	8	1
1	49	64
2	2	-4
3	46	-51
4	15	12
5	14	-16
H,L=	8	2
0	2	-2
1	32	-30
2	6	-4
3	129	121
4	32	-29
5	58	-52
H.L=	8	3
1	25	-24
3	3	-1
4	16	15
5	32	28
H,L=	8	4
0	12	15
1	50	-48
2	23	21
3	10	9
4	28	-30
5	17	-20
H,L=	8	5
1	19	15
2	13	17
3	19	-15
H,L=	8	6
0	86	-84
1	14	-15
2	37	35
3	19	21
4	18	-13
H,L=	8	7
1	3	0
2	56	-53
3	33	33
4	23	21
H,L=	8	8
0	8	-11
1	18	-20
2	46	46
H,L=	8	9
1	8	-10
2	10	11
3	13	-11
H,L=	8	10
0	33	-47
1	39	41
2	14	16
H,L=	8	11
1	22	-22
H,L=	9	0
0	11	18
1	11	-20
2	38	-35
3	28	-26
4	55	51
H.L=	9	1
1	24	23
2	49	-45
3	17	-17
4	5	2
H,L=	9	2
0	53	52
1	39	41
2	18	-17
3	13	-12
4	16	-16
H,L=	9	3
1	23	-19
2	49	48
3	22	19
H,L=	9	4
0	23	-20
1	12	-11
2	7	-7
3	5	3
H,L=	9	5
1	16	16
2	6	-9
3	11	-11
H,L=	9	6
1	9	10
2	12	-12
H,L=	9	7
1	10	-12
2	8	9
H,L=	9	8
0	3	2
1	12	-11
H,L=	10	0
0	77	-78
1	9	8
2	39	37
H,L=	10	1
1	2	3
2	35	-34
H,L=	10	2
1	15	20
2	45	47
H.L=	10	3
1	9	-12
H,L=	10	4
0	31	-43
1	3	7
H,L=	1	-1
1	61	-56
2	59	-60
3	23	24
4	61	65
5	21	22
6	23	-25
7	23	-23
8	3	1
H,L=	1	-2
0	55	-49
1	128	123
2	64	-61
3	63	-57
4	22	-23

K	Fo	Fc
5	48	48
6	51	54
7	77	-79
8	23	-25
H.L=	1	-3
1	136	131
2	140	-137
3	20	13
4	82	80
5	9	-5
6	24	23
7	23	23
8	3	-3
H,L=	1	-4
0	192	-198
1	122	-120
2	82	75
3	143	-135
4	6	-3
5	93	92
6	55	52
7	8	-3
8	52	-55
H,L=	1	-5
1	151	-146
2	27	-26
3	65	60
4	80	76
6	27	-24
7	43	-45
8	7	6
H.L=	1	-6
0	50	49
1	41	44
2	110	108
3	60	-57
4	78	-70
5	46	-46
6	11	10
7	7	3
8	21	-24
H,L=	1	-7
1	34	34
2	98	-92
3	12	-10
4	61	-60
6	35	36
7	43	45
H,L=	1	-8
0	150	-150
1	122	112
2	26	-19
3	41	-40
4	8	-7
5	38	36
6	50	50
7	29	29
H.L=	1	-9
1	20	-17
2	119	120
3	28	-28
4	24	24
6	44	-43
7	16	-18
H.L=	1	-10
0	110	105
1	21	-20
2	62	58
3	88	83
4	79	-78
5	78	-77
6	24	22
7	14	15
H.L=	1	-11
1	24	23
2	12	-14
3	21	22
4	15	16
5	14	-15
6	2	-1
7	15	16
H.L=	1	-12
0	45	-48
1	37	35
2	34	36
3	46	41
4	27	24
5	37	-38
6	17	-17
H,L=	1	-13
1	29	-29
2	58	57
3	15	-14
4	63	-64
5	14	-13
6	35	-38
H.L=	1	-14
0	32	29
1	38	-34
2	29	-24
3	30	29
4	14	-13
5	10	-8
6	20	21
H.L=	1	-15
0	8	-7
2	63	-63
3	52	50
4	22	20
5	33	34
H,L=	1	-16
0	77	-85
1	38	-44
2	49	-50
3	77	80
4	64	65
5	56	-59
H,L=	1	-17
1	29	30
2	58	63
3	20	-19
4	16	16
H,L=	1	-18
0	87	121
1	36	-47
2	9	-8
3	48	-44
4	17	-14
H,L=	1	-19
1	17	-15

K	Fo	Fc
2	47	-43
3	6	7
H,L=	1	-20
0	43	45
1	9	-9
2	56	-56
H,L=	2	-1
1	179	-178
2	179	-176
3	116	119
4	9	9
5	20	22
6	6	-3
7	11	-13
8	22	20
H,L=	2	-2
0	88	84
1	146	-140
2	41	38
3	67	70
4	56	49
5	56	-55
6	7	6
7	20	17
8	22	20
H,L=	2	-3
1	7	-8
2	175	-174
3	53	-50
4	35	34
5	17	-9
6	47	47
7	5	-4
8	16	-14
H,L=	2	-4
0	96	-87
1	147	-145
2	153	-149
3	33	30
4	111	105
5	6	10
6	53	-53
7	25	24
8	10	-9
H,L=	2	-5
1	15	15
2	67	62
3	8	4
4	87	89
5	9	9
6	100	-98
7	7	-8
8	16	15
H,L=	2	-6
0	233	238
1	131	-134
2	54	42
3	109	104
4	31	-31
5	39	-37
6	42	-42
7	18	18
8	49	49
H,L=	2	-7
1	57	-49
2	79	-81
3	18	14
4	34	32
5	10	10
6	13	11
7	27	-26
H,L=	2	-8
0	64	58
1	181	169
2	141	-133
3	35	34
4	135	133
5	45	-40
6	64	-65
7	12	-12
H,L=	2	-9
1	73	69
2	74	69
3	90	-84
4	41	-40
5	29	31
6	84	-88
7	2	0
H,L=	2	-10
0	131	130
1	9	13
2	107	-105
3	33	-31
4	44	44
5	39	39
6	21	22
7	5	1
H,L=	2	-11
1	24	-24
2	13	-14
3	2	-1
4	65	63
5	50	49
6	14	-17
7	35	-36
H,L=	2	-12
0	65	64
1	63	59
2	103	-100
3	11	-7
4	36	30
5	6	-3
6	40	-39
H,L=	2	-13
1	66	64
2	48	-47
3	36	-37
5	19	18
6	11	12
H,L=	2	-14
0	38	36
1	48	49
2	46	-47
3	108	-109
4	61	62
5	66	67
6	8	-5
H,L=	2	-15
1	12	-12
2	38	37

K	Fo	Fc
3	8	-6
4	26	26
5	7	8
H,L=	2	-16
0	86	82
1	65	65
2	6	-2
3	59	-59
4	41	-43
5	3	1
H,L=	2	-17
1	19	20
2	53	-51
3	46	-49
4	5	-2
H,L=	2	-18
0	9	11
1	37	34
2	5	-4
3	41	-42
4	42	42
H,L=	2	-19
1	19	-21
2	31	30
3	2	1
H,L=	2	-20
0	7	-9
1	53	54
2	10	13
H,L=	3	-1
1	18	22
2	61	68
3	33	35
4	25	-23
5	34	-32
6	23	-23
7	53	57
8	6	-8
H,L=	3	-2
0	66	65
1	21	-18
2	13	7
3	44	37
4	58	-56
5	57	59
6	37	-37
7	2	-5
8	50	54
H,L=	3	-3
1	91	-86
2	47	-50
3	75	69
4	7	-5
5	49	-46
6	39	41
7	16	-14
8	15	-16
H,L=	3	-4
0	117	-113
1	150	145
2	11	4
3	8	6
4	125	114
5	1	-1
6	46	-45
7	58	-59
8	6	4
H.L=	3	-5
1	53	50
2	156	150
3	88	81
4	15	-15
5	56	-54
6	45	-48
7	15	25
H.L=	3	-6
0	54	-55
1	97	97
2	101	100
3	115	-114
4	56	-52
5	54	57
6	20	-19
7	15	-17
H,L=	3	-7
1	135	-138
2	65	-64
3	47	52
4	32	-37
5	20	21
6	3	-6
7	13	-14
H,L=	3	-8
0	205	-200
1	66	63
2	18	4
3	24	25
4	20	16
5	3	-1
6	50	50
7	43	-48
H,L=	3	-9
1	98	92
2	21	17
3	8	5
4	51	50
5	18	-17
6	12	-12
7	27	29
H,L=	3	-10
0	115	-117
1	18	16
2	83	78
3	115	-114
4	81	-81
5	80	78
6	34	35
7	25	-24
H,L=	3	-11
1	24	-23
2	18	16
3	2	0
4	30	28
6	3	3
7	5	-6
H,L=	3	-12
0	41	38
1	27	27
2	124	123
3	45	-47

TABLE 2. (continued)

K	Fo	Fc	K	Fo	Fc	K	Fo	Fc	K	Fo	Fc	K	Fo	Fc	K	Fo	Fc	K	Fo	Fc	K	Fo	Fc	K	Fo	Fc	K	Fo	Fc
4	125	-125	2	73	-66	4	15	16	2	23	-22	3	14	-15	5	24	-22	2	32	-27	1	23	22	1	51	-51	5	45	42	2	26	-26	2	4	4
5	10	-7	3	29	-26	5	35	-36	3	45	44	4	56	-57	H,L=	5	-16	3	4	5	2	40	-40	2	36	-50	H,L=	8	-2	3	31	30	3	22	-19
6	51	55	4	5	1	6	17	17	H,L=	4	-19	5	6	4	0	19	-20	4	61	58	4	5	-4	3	15	-18	0	84	79	4	7	4	H,L=	9	-9
H,L=	3	-13	5	37	39	7	40	42	1	27	25	6	17	-16	1	45	40	5	8	7	H,L=	6	-16	4	5	6	1	62	-53	H,L=	8	-12	2	28	28
1	44	48	6	18	17	H,L=	4	-10	2	7	-10	7	48	51	2	5	-7	6	3	3	0	91	-110	5	10	10	2	54	-49	0	11	-11	3	25	-24
2	100	-102	7	9	-10	0	62	-58	H,L=	4	-20	H,L=	5	-8	3	50	-48	H,L=	6	-7	1	13	12	6	47	47	3	75	71	1	32	32	H,L=	9	-10
3	79	-82	H,L=	4	-3	1	117	-113	0	48	48	0	99	100	4	22	24	1	67	63	2	43	44	H,L=	7	-8	4	14	-15	2	25	-23	0	6	-4
4	25	28	1	90	-84	2	11	-7	1	44	-45	1	118	110	H,L=	5	-17	2	45	40	3	7	-9	0	68	-70	5	64	-61	3	3	-1	1	31	30
6	6	7	2	7	-3	3	88	87	H,L=	5	-1	2	84	-80	1	12	-12	3	49	-47	H,L=	6	-17	1	75	-71	H,L=	8	-3	H,L=	8	-13	2	13	12
H,L=	3	-14	3	82	78	4	18	16	1	44	-40	3	1	2	2	25	21	4	30	31	2	56	57	2	52	51	1	15	16	1	5	-4	3	39	-32
0	85	-99	4	14	-15	5	28	-30	2	16	-16	4	9	8	3	25	26	5	6	-3	3	8	7	3	32	32	2	62	-57	2	27	30	H,L=	9	-11
1	60	-66	5	36	34	6	7	5	3	28	-24	5	48	50	H,L=	5	-18	6	38	-36	H,L=	6	-18	4	20	21	3	39	-39	3	13	-10	1	6	1
2	72	70	6	32	-36	H,L=	4	-11	5	27	-25	6	10	-10	0	22	22	H,L=	6	-8	0	22	19	5	10	-13	4	10	7	H,L=	8	-14	2	11	12
3	3	0	7	30	-30	1	21	22	6	44	44	H,L=	5	-5	1	46	44	0	6	5	1	4	-6	H,L=	7	-9	5	4	-3	0	14	16	H,L=	9	-12
4	38	-40	H,L=	4	-4	2	60	61	7	25	24	1	15	-13	2	42	43	1	11	10	2	22	18	1	8	-6	H,L=	8	-4	1	4	4	0	4	2
5	49	48	0	63	-60	3	5	-7	H,L=	5	-2	2	2	3	3	33	-32	2	25	-26	H,L=	7	-1	2	20	22	0	59	54	2	21	-19	1	32	32
6	36	36	1	15	-10	4	2	0	0	6	-7	3	14	12	H,L=	5	-19	3	88	-88	1	2	-2	3	9	11	1	126	-118	H,L=	8	-15	2	10	7
H,L=	3	-15	2	19	22	5	33	-35	1	28	-28	4	9	-10	1	8	8	4	34	-34	2	14	14	4	14	-14	2	55	-52	1	11	-11	H,L=	9	-13
1	51	-49	3	108	110	6	47	-49	2	39	-38	5	28	-29	2	40	-39	5	50	54	3	3	-2	5	9	8	3	30	29	2	1	0	1	7	-6
2	17	15	4	21	18	H,L=	4	-12	3	34	-30	6	7	7	H,L=	6	-1	6	6	3	4	27	-27	H,L=	7	-10	4	103	96	H,L=	9	-1	H,L=	10	-1
3	14	11	5	77	-78	0	108	105	4	61	62	H,L=	5	-10	1	7	-11	H,L=	6	-9	5	40	38	0	34	31	5	16	-14	1	15	-12	1	23	23
4	1	1	6	47	47	1	86	-79	5	10	6	0	22	17	2	49	-66	1	46	-42	6	17	16	1	14	-10	H,L=	8	-5	2	10	-5	2	4	5
5	5	5	H,L=	4	-5	2	23	21	6	14	-16	1	103	97	3	14	-15	2	27	-21	H,L=	7	-2	2	15	14	1	33	-28	3	23	-22	H,L=	10	-2
H,L=	3	-16	1	45	43	3	44	40	7	33	33	2	74	-68	5	19	25	3	49	49	0	52	-46	3	49	43	2	24	23	4	21	21	0	30	-30
0	89	-88	2	24	20	4	54	-56	H,L=	5	-3	3	2	-2	6	27	33	4	5	-1	1	19	17	4	54	-48	3	5	6	H,L=	9	-2	1	43	-47
1	59	59	3	19	17	6	3	2	1	4	-2	4	72	66	H,L=	6	-2	5	31	27	2	35	34	5	4	0	4	6	-4	0	53	52	2	45	47
2	94	95	4	9	9	H,L=	4	-13	2	19	17	5	7	4	0	36	66	6	13	8	3	55	53	H,L=	9	-11	5	16	17	1	4	0	H,L=	10	-3
3	42	38	5	61	-62	1	46	-42	3	56	59	6	20	-20	1	7	4	H,L=	6	-10	4	43	-44	1	29	1	H,L=	8	-6	2	14	-15	1	15	-19
4	97	-97	6	33	35	2	82	-83	4	12	-9	H,L=	5	-11	2	26	-21	0	26	-21	5	50	50	2	43	42	0	102	109	3	40	-43	2	20	-25
5	2	0	7	31	32	3	30	27	5	25	26	1	74	72	3	15	14	1	115	114	6	47	47	H,L=	7	-12	1	33	-37	4	3	1	H,L=	10	-4
H,L=	3	-17	H,L=	4	-6	4	21	22	6	7	-6	2	49	48	4	85	81	2	51	44	H,L=	7	-3	0	35	-33	2	73	-73	H,L=	9	-3	0	62	-83
1	55	52	0	142	-138	5	22	23	H,L=	5	-4	3	11	10	5	8	-11	3	60	-57	1	7	7	1	52	-51	3	53	51	1	15	-18	1	9	-12
2	5	-2	1	18	-16	6	14	15	0	59	81	4	15	7	6	33	-35	4	27	-27	2	20	16	2	24	24	1	21	25	2	28	-34	2	29	41
3	5	-3	2	12	-4	H,L=	4	-14	1	8	-11	5	19	-21	7	26	-25	5	20	19	3	18	-17	3	18	15	5	18	-17	3	34	33	H,L=	10	-5
4	10	10	3	85	-83	0	88	-85	2	22	-26	6	11	-13	H,L=	6	-3	6	44	46	4	6	4	4	5	-2	H,L=	8	-7	4	6	4	2	2	-4
H,L=	3	-18	4	13	3	1	67	-70	3	43	54	H,L=	5	-12	1	29	23	H,L=	6	-11	5	15	-12	H,L=	7	-13	1	9	6	H,L=	9	-4	H,L=	10	-6
0	74	-72	5	16	15	2	41	-41	4	11	-14	0	79	76	2	39	41	1	34	34	H,L=	7	-4	1	10	8	2	29	-33	0	11	16	0	58	-57
1	37	-32	6	11	-11	3	142	143	5	26	-29	1	13	12	3	46	-47	2	44	-42	0	108	-102	2	21	17	3	14	17	1	56	79	1	60	-57
2	39	38	7	41	42	4	54	54	6	16	-19	2	64	-66	4	12	-10	3	62	-62	1	12	-7	3	4	1	4	14	-14	2	12	-13	2	54	49
3	20	21	H,L=	4	-7	5	60	-59	7	7	8	3	108	-102	5	33	-32	4	23	24	2	59	55	4	13	-12	5	16	-16	3	3	-5	H,L=	10	-7
4	20	-20	1	43	-42	H,L=	4	-15	H,L=	5	-5	4	20	19	6	34	-33	5	17	-17	3	10	9	H,L=	7	-14	H,L=	8	-8	4	12	16	1	27	-23
H,L=	3	-19	2	92	92	1	67	66	1	16	26	5	59	56	7	29	31	H,L=	6	-12	4	28	-24	0	26	25	0	23	31	H,L=	9	-5	2	19	17
1	9	-3	3	60	62	2	19	19	2	6	-11	6	44	-47	H,L=	6	-4	0	54	-46	5	10	6	2	32	-34	1	4	-2	1	37	55	H,L=	10	-8
2	5	5	4	32	-36	3	7	-7	3	39	-32	H,L=	5	-13	0	66	66	1	37	-40	6	23	22	3	9	9	2	35	-39	2	1	-1	0	22	20
3	18	-18	5	21	22	4	26	27	4	11	13	1	87	-81	1	59	56	2	17	13	H,L=	7	-5	4	7	8	3	17	17	3	39	-37	1	23	-20
H,L=	3	-20	6	6	-5	5	22	-22	5	67	-68	2	57	-54	2	41	-39	3	79	-75	1	23	24	H,L=	7	-15	4	58	66	4	9	-3	2	5	-4
0	32	-31	7	13	-15	H,L=	4	-16	6	22	23	3	69	66	3	62	-59	4	7	9	2	42	46	1	34	-36	5	15	-20	4	6	7	H,L=	10	-9
1	55	-54	H,L=	4	-8	0	44	45	7	7	8	4	13	9	4	47	-48	5	54	52	3	52	49	2	6	6	H,L=	8	-9	0	24	20	1	17	15
2	30	30	0	139	172	1	112	-114	H,L=	5	-6	5	14	-16	5	91	91	H,L=	6	-13	4	24	-31	3	4	4	1	14	20	1	6	-5	H,L=	10	-10
H,L=	4	-1	1	35	-44	2	19	-22	0	180	167	H,L=	5	-14	6	8	-7	1	52	-49	5	12	-11	H,L=	7	-16	2	45	46	2	43	-38	0	8	-13
1	13	12	2	44	49	3	19	-14	1	0	0	0	82	-77	H,L=	6	-5	2	16	13	6	15	15	0	14	-14	3	19	-19	3	84	-75			
2	56	54	3	59	70	4	25	25	2	56	-49	1	75	72	1	12	-9	3	34	36	H,L=	7	-6	1	45	48	4	16	-16	4	13	10			
3	21	-21	4	66	-73	H,L=	4	-17	3	56	-49	2	39	37	2	35	-37	4	3	5	0	39	-48	2	13	-12	H,L=	8	-10	H,L=	9	-7			
4	40	-38	5	78	-98	1	68	-63	4	59	57	3	69	-70	3	24	25	5	31	32	1	28	-26	H,L=	7	-17	0	110	108	1	43	-40			
5	9	-7	6	19	22	2	27	-28	5	41	-41	4	42	40	4	4	-3	H,L=	6	-14	2	53	58	1	34	40	1	15	-18	2	12	10			
6	7	4	7	13	14	3	39	37	6	54	-55	5	22	24	5	19	16	1	71	71	3	31	-33	H,L=	8	-1	2	102	-98	3	56	48			
7	22	20	H,L=	4	-9	4	17	16	7	30	29	H,L=	5	-15	6	17	20	2	72	67	4	62	-67	1	24	-19	3	4	0	4	4	0			
H,L=	4	-2	1	7	10	H,L=	4	-18	H,L=	5	-7	1	14	-17	H,L=	6	-6	3	14	11	5	33	-34	2	30	29	4	30	29	H,L=	9	-8			
0	8	-12	2	113	-104	0	4	-4	1	24	-18	3	23	23	0	9	-5	4	76	-73	6	26	30	3	13	10	H,L=	8	-11	0	27	-22			
1	16	10	3	75	-69	1	11	-16	2	21	23	4	6	-3	1	102	93	H,L=	6	-15	H,L=	7	-7	4	15	12	1	15	-16	1	113	105			

a) Six reflections, 021, 022, 210, 204, 214, and 244, were excluded from the least-squares refinement probably because of the high extinction effect.

the International Tables for X-Ray Crystallography.[8]

Results and Discussion

The final atomic parameters are given in Table 3, together with their estimated standard deviations. As shown in Fig. 1, there are two molecules (A and B) in an asymmetric unit and one hydrogen atom of a sulfonate group is protonated to the nitrogen atom of a guanidyl group. Thus, the two molecules of GGPSA occur in zwitterionic forms, $(NH_2)_2{}^+CNHCH_2CH_2CH_2SO_3{}^-$, as in the case of GGBOPSA,[6] L-arginine dihydrate,[7] γ-aminobutyric acid (GABA),[9] γ-amino-β-hydroxybutyric acid (GABOB),[10] taurine,[11,12] homotaurine[13] and γ-guanidinobutyric acid hydrochloride (GGBA·HCl).[14]

Bond Distances and Angles. The interatomic distances and angles are listed in Table 4 together with their standard deviations. The bond lengths and angles of the two molecules are similar and acceptable as a whole. However, the length for C(A2)–(A3) (1.523 Å) is shorter than that for C(B2)–C(B3) (1.552 Å), which may be due to the difference in C(3)–N(1) distance.

In the sulfonate group, the averages of three S–O distances, three O–S–O angles and three O–S–C(1) angles are 1.457 Å, 112.3° and 106.5° (molecule A) and 1.456 Å, 112.4° and 106.3° (molecule B), respectively. These values are very similar to those of other compounds containing a sulfonate group; GGBOPSA,[6] taurine[11,12] and homotariune.[13] The deviations of angles around the sulfur atom from tetrahedral angles are probably duc to the van der Waals repulsion by the short contacts of O–O distances which are averaged to be 2.42 Å in both molecules as in the case of GGBOPSA.[6]

In the guanidyl group, the three C–N distances of

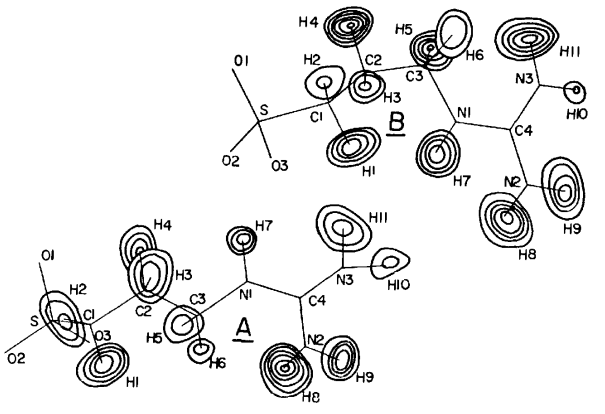

Fig. 1. Difference Fourier map of GGPSA. Contours are drawn at intervals of 0.1 e.Å^{-3}, starting with the contour of 0.3 e.Å^{-3}.

8) "International Tables for X-Ray Crystallography," Vol. 3, Kynoch Press, England (1962).

9) K. Tomita, T. Fujiwara, and H. Higashi, *Jap. J. Brain Physiol.*, **111**, 111 (1971).

10) K. Tomita, M. Harada, and T. Fujiwara, This Bulletin, to be published.

11) H. H. Sutherland and D. W. Young, *Acta Crystallogr.*, **16**, 897 (1963).

12) Y. Okaya, *ibid.*, **21**, 726 (1966).

13) S. Ueoka, T. Fujiwara, and K. Tomita, This Bulletin, **45**, 3634 (1972).

14) T. Maeda, T. Fujiwara, and K. Tomita, *ibid.*, **45**, 3628 (1972).

Table 3. Final positional and thermal parameters (estimated standard deviations in parentheses)

Anisotropic temperature factors are expressed in the form

$\exp\{-(B_{11}h^2 + B_{22}k^2 + B_{33}l^2 + B_{12}hk + B_{13}hl + B_{23}kl)\}$.

Atom	x	y	z	B_{11} or B	B_{22}	B_{33}	B_{12}	B_{13}	B_{23}
S (A)	0.6591(2)	0.2493(2)	0.0329(1)	0.0050(2)	0.0094(3)	0.0009(1)	0.0015(4)	0.0013(2)	0.0001(2)
O (A1)	0.5224(5)	0.2271(7)	−0.0002(3)	0.0055(5)	0.0170(10)	0.0018(2)	−0.0015(12)	−0.0012(4)	−0.0014(6)
O (A2)	0.7518(5)	0.2695(7)	−0.0175(2)	0.0071(5)	0.0189(10)	0.0011(2)	0.0003(12)	0.0029(4)	−0.0004(6)
O (A3)	0.7043(5)	0.1203(6)	0.0828(3)	0.0117(7)	0.0106(9)	0.0016(2)	0.0089(12)	0.0031(5)	0.0021(6)
C (A1)	0.6671(8)	0.4430(9)	0.0771(4)	0.0132(10)	0.0082(12)	0.0015(2)	−0.0006(18)	0.0030(7)	0.0003(8)
C (A2)	0.5716(8)	0.4550(10)	0.1312(4)	0.0109(9)	0.0132(14)	0.0014(2)	0.0012(19)	0.0023(7)	−0.0000(9)
C (A3)	0.6286(7)	0.3759(10)	0.1993(4)	0.0089(9)	0.0169(15)	0.0015(2)	0.0045(19)	0.0033(7)	0.0016(9)
C (A4)	0.5682(7)	0.3673(9)	0.3170(4)	0.0063(8)	0.0100(12)	0.0018(2)	−0.0018(16)	0.0009(6)	−0.0002(8)
N (A1)	0.5354(6)	0.4008(8)	0.2490(3)	0.0090(8)	0.0153(12)	0.0012(2)	0.0028(15)	0.0014(6)	0.0011(7)
N (A2)	0.6806(6)	0.2876(8)	0.3387(3)	0.0089(7)	0.0152(12)	0.0007(2)	0.0064(15)	0.0010(5)	−0.0009(7)
N (A3)	0.4878(7)	0.4198(8)	0.3591(3)	0.0116(8)	0.0159(12)	0.0017(2)	0.0073(17)	0.0045(6)	−0.0004(8)
S (B)	0.1650(2)	0.3698(3)	0.2202(1)	0.0073(2)	0.0117(3)	0.0008(1)	−0.0026(4)	0.0012(2)	−0.0003(2)
O (B1)	0.0457(5)	0.4103(7)	0.1738(3)	0.0101(6)	0.0180(11)	0.0012(2)	0.0059(13)	−0.0003(5)	−0.0010(6)
O (B2)	0.2479(5)	0.2401(7)	0.1940(3)	0.0109(7)	0.0213(12)	0.0014(2)	0.0078(14)	0.0038(5)	−0.0014(7)
O (B3)	0.2469(6)	0.5144(7)	0.2426(3)	0.0143(7)	0.0150(10)	0.0018(2)	−0.0145(14)	0.0023(5)	0.0001(7)
C (B1)	0.1172(7)	0.2847(9)	0.2967(3)	0.0085(8)	0.0109(12)	0.0010(2)	−0.0009(16)	0.0030(6)	0.0001(8)
C (B2)	0.0264(7)	0.4057(9)	0.3294(3)	0.0074(8)	0.0120(13)	0.0012(2)	−0.0013(16)	0.0023(6)	0.0007(8)
C (B3)	0.0023(7)	0.3407(9)	0.4008(3)	0.0071(8)	0.0117(13)	0.0013(2)	−0.0016(16)	0.0012(6)	0.0014(8)
C (B4)	0.1391(7)	0.2976(8)	0.5124(4)	0.0072(8)	0.0095(12)	0.0015(2)	−0.0034(15)	0.0026(6)	−0.0003(8)
N (B1)	0.1261(5)	0.3517(7)	0.4472(3)	0.0068(6)	0.0115(10)	0.0011(2)	−0.0024(13)	0.0007(5)	0.0009(7)
N (B2)	0.2571(6)	0.3107(8)	0.5516(3)	0.0066(7)	0.0205(13)	0.0010(2)	−0.0030(15)	0.0012(5)	0.0013(8)
N (B3)	0.0357(6)	0.2282(8)	0.5360(3)	0.0072(7)	0.0168(12)	0.0013(2)	−0.0055(15)	0.0014(5)	0.0037(7)
H (A1)	0.761	0.456	0.103	1.612					
H (A2)	0.647	0.530	0.043	3.878					
H (A3)	0.560	0.566	0.139	4.052					
H (A4)	0.481	0.419	0.113	1.778					
H (A5)	0.660	0.252	0.187	4.183					
H (A6)	0.713	0.443	0.212	3.959					
H (A7)	0.454	0.446	0.236	2.049					
H (A8)	0.713	0.211	0.312	2.159					
H (A9)	0.700	0.274	0.380	1.990					
H (A10)	0.480	0.405	0.405	5.576					
H (A11)	0.392	0.485	0.348	5.346					
H (B1)	0.207	0.256	0.329	1.327					
H (B2)	0.055	0.145	0.284	8.076					
H (B3)	0.067	0.517	0.339	3.020					
H (B4)	−0.063	0.420	0.301	1.953					
H (B5)	−0.025	0.220	0.401	1.972					
H (B6)	−0.079	0.428	0.416	3.804					
H (B7)	0.209	0.431	0.437	1.958					
H (B8)	0.338	0.329	0.539	2.543					
H (B9)	0.266	0.299	0.591	3.230					
H (B10)	0.042	0.174	0.582	2.719					
H (B11)	−0.061	0.229	0.523	3.543					

Table 4. Bond lengths (Å) and angles (°) of GGPSA (estimated standard deviations listed in parentheses)

	A	B		A	B
S-O(1)	1.449(5)	1.441(5)	O(1)-S-O(2)	111.4(3)	113.6(4)
S-O(2)	1.466(5)	1.472(6)	O(1)-S-O(3)	113.8(3)	113.6(4)
S-O(3)	1.455(5)	1.455(6)	O(2)-S-O(3)	111.6(3)	110.0(4)
S-C(1)	1.777(8)	1.781(7)	C(1)-S-O(1)	107.6(4)	108.8(4)
C(1)-C(2)	1.538(11)	1.537(9)	C(1)-S-O(2)	104.3(4)	105.2(4)
C(2)-C(3)	1.523(11)	1.552(10)	C(1)-S-O(3)	107.5(4)	105.0(4)
C(3)-N(1)	1.464(10)	1.443(9)	S-C(1)-C(2)	113.9(6)	111.3(5)
C(4)-N(1)	1.360(9)	1.345(8)	C(1)-C(2)-C(3)	113.0(7)	110.4(6)
C(4)-N(2)	1.318(9)	1.327(9)	C(2)-C(3)-N(1)	109.7(6)	108.8(6)
C(4)-N(3)	1.310(9)	1.323(9)	C(3)-N(1)-C(4)	122.9(6)	123.1(6)
			N(1)-C(4)-N(2)	119.6(7)	119.3(6)
			N(1)-C(4)-N(3)	118.4(7)	119.8(6)
			N(2)-C(4)-N(3)	122.0(7)	120.9(7)

each molecule have normal values. Separations of the guanidyl group from the backbone, *i. e.*, C(3)–N(1) distance, are 1.464 Å (A) and 1.443 Å (B), and are very similar to those of GGBOPSA (1.456 Å), γ-guanidinobutyric acid hydrochloride (GGBA·HCl) (1.477 Å[14]) and L-arginine dihydrate (1.471 Å[7]). The three N–C(4)–N angles are 119.6°, 122.0° and 122.0 118.4° (A) and 119.3°, 120.9° and 119.8° (B). C(4)–N distances are averaged to be 1.329 Å and 1.332 Å for A and B, respectively, indicating to that they have somewhat double bond character. Calculation by Pauling's method[15] indicates that the double bond characters of C(4)–N(1), C(4)–N(2), and C(4)–N(3) bonds are approximately 24%, 37%, and 39% for A, and 29%, 35%, and 36% for B, whereas the corresponding values for GGBOPSA[6] and GGBA·HCl[14] are 32%, 25%, and 43%, and 35%, 29%, and 36%, respectively.

The C–H and N–H distances are within the ranges 0.91 Å—1.29 Å and 0.77 Å—1.09 Å, respectively.

Conformation. Conformations of the two molecules are of great interest, those around C(1)–C(2) and C(2)–C(3) being *gauche-trans* in molecule A, and *trans-gauche* in molecule B (Fig. 2). GGBOPSA,[6] GABA·HCl,[9] GABOB,[10] homotaurine[13] and GGBA·HCl[14] showed *trans-trans* conformations, and GABA[16] a *gauche-trans* form similar to molecule A. The *trans-gauche* conformation of molecule B, however, is a rare one in the derivatives of γ-amino acid and γ-guanidino acid so far investigated. Conformations of the sulfonate group around S–C(1), took the most stabilized forms (Fig. 2).

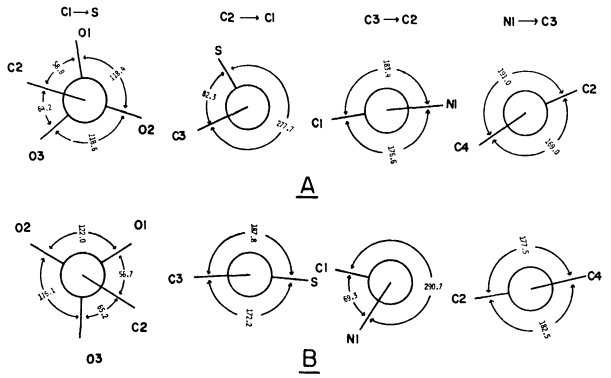

Fig. 2. Newman projection of atoms around four bonds. The arrow indicates the bond direction viewing down from front to back of paper.

The torsion angles around C(3)–N(1) are 169.0° (A) and 177.5° (B), which mean roughly a *trans* conformation similar to that of GGBOPSA[6] and L-arginine dihydrate.[7]

Planarity. The guanidyl groups are essentially planar in both molecules. Equations of the least-squares plane of each molecule through the atoms N(1)–C(4)–N(2)–N(3) and deviations of individual atoms from the corresponding plane are listed in Table 5. The planarity of guanidyl groups in GGPSA is in good agreement with that of GGBOPSA,[6] L-arginine dihydrate[7] and of GGBA·HCl.[14]

The dihedral angles between the plane of a guanidyl group and that passing through C(1)–C(2)–C(3) are 12.95° in molecule A, and 69.87° in molecule B. The corresponding angle of GGBOPSA is 27.4°. Molecule A therefore, has a value nearer that of GGBOPSA, since both have *trans zigzag* conformations.

Crystal Structure. Distances and angles of hydrogen bonds are listed in Table 6. All feasible hydrogen atoms in the molecule are utilized to form hydrogen bonds, the molecules being held together by a three-dimensional network of NH···O hydrogen bonds (Fig. 3).

In molecule A, the guanidyl group is connected with five neighboring molecules by seven hydrogen bonds and the sulfonate group performs the role as an acceptor of six hydrogen bonds. The distances of N(A1) to O(B2) and to O(B3) are 3.215 Å and 3.033 Å, respectively, and the N(A1)–H(A7) bond is directed to bisect these two directions. The distances of N(A3) to O(B3) of the original molecule and to O(A3) of a neighboring molecule translated by operation of (x, $0.5-y$, $0.5+z$) are 3.188 Å and 2.876 Å, respectively, the N(A3)–H(A11) bond bisecting the two directions. Thus, the H(A7) and H(A11) atoms are considered to contribute to form bifurcated hydrogen bonds.

15) L. Pauling, "The Nature of the Chemical Bond," 3rd. ed., Ithaca, Cornell University Press (1960).

16) K. Tomita, H. Higashi, and T. Fujiwara, This Bulletin, **46**, 2199 (1973).

TABLE 5. EQUATIONS OF LEAST-SQUARES PLANES AND DEVIATIONS OF INDIVIDUAL ATOMS FROM THE PLANES OF GUANIDYL GROUPS IN GGPSA

	Equations[a)]	Deviations of atoms in Å			
		N (1)	C (4)	N (2)	N (3)
GGPSA (A)	$-0.48255X-0.86818Y-0.11577Z=-5.61564$	−0.0028	+0.0089	−0.0031	−0.0030
GGPSA (B)	$0.31393X-0.89952Y-0.30382Z=-5.18435$	+0.0031	−0.0093	+0.0031	+0.0031

a) X, Y, and Z are orthogonal coordinates in Å parallel to a, b, and c^*.

TABLE 6. HYDROGEN BOND LENGTHS AND ANGLES OF GGPSA

Bond lengths		Bond angles	
N(A1)-H(A7)·····O(B2) (I)	3.215 Å	C(A3)-N(A1)-O(B2) (I)	110.7°
N(A1)-H(A7)·····O(B3) (I)	3.033 Å	C(A4)-N(A1)-O(B2) (I)	109.5°
N(A2)-H(A8)·····O(B3) (II)	2.869 Å	C(A3)-N(A1)-O(B3) (I)	135.7°
N(A2)-H(A9)·····O(A2) (III)	2.861 Å	C(A4)-N(A1)-O(B3) (I)	101.4°
N(A3)-H(A10) ···O(A1) (III)	2.987 Å	C(A4)-N(A2)-O(B3) (II)	117.6°
N(A3)-H(A11) ···O(A3) (IV)	2.876 Å	C(A4)-N(A2)-O(A2) (III)	118.9°
N(A3)-H(A11) ···O(B3) (I)	3.188 Å	C(A4)-N(A3)-O(A1) (III)	139.6°
		C(A4)-N(A3)-O(B3) (I)	95.5°
		C(A4)-N(A3)-O(A3) (IV)	160.8°
N(B1)-H(B7)·····O(A3) (IV)	2.862 Å	C(B3)-N(B1)-O(A3) (IV)	113.8°
N(B2)-H(B8)·····O(A1) (III)	3.011 Å	C(B4)-N(B1)-O(A3) (IV)	117.4°
N(B2)-H(B9)·····O(B2) (III)	2.852 Å	C(B4)-N(B2)-O(A1) (III)	124.1°
N(B3)-H(B10) ···O(B1) (III)	2.922 Å	C(B4)-N(B2)-O(B2) (III)	114.2°
N(B3)-H(B11) ···O(A2) (V)	2.906 Å	C(B4)-N(B3)-O(B1) (III)	124.2°
		C(B4)-N(B3)-O(A2) (V)	130.8°

(I) (x, y, z); (II) $(x, -0.5-y, 0.5+z)$; (III) $(x, 0.5-y, -0.5+z)$; (IV) $(x, 0.5-y, 0.5+z)$; (V) $(-1+x, 0.5-y, -0.5+z)$

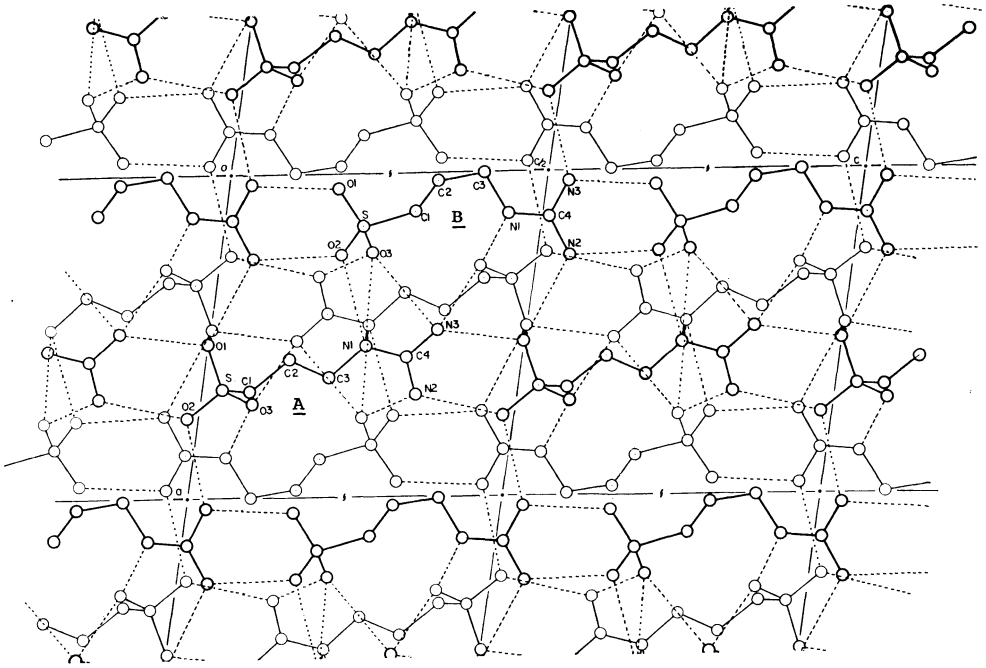

Fig. 3. The crystal structure projected along b-axis.

In molecule B, the guanidyl group is connected with four neighboring molecules by five hydrogen bonds, the sulfonate group fulfilling the role as an acceptor of six hydrogen bonds.

On the other hand, the guanidyl group of GGBOPSA[6] is connected with three neighboring molecules by six hydrogen bonds, and the sulfonate group performs the role of an acceptor of five hydrogen bonds and the N(2)–H bond is bifurcated to O(2) and O(4) of (2-x, 1-y, 1-z).

Homotaurine molecules are jointed to each other with three NH···O hydrogen bonds to form a three-dimensional network, and there are three NH···O intermolecular and one intramolecular hydrogen bonds in taurine.

The intermolecular contacts between adjacemt molecules are kept by normal van der Waals distances.

We wish to thank Prof. S. Tsunoo and Dr. K. Horisaka, Showa Medical School, for valuable adivce and for supply of the sample. This work was partly supported by a research grant from the Ministry of Education.

BULLETIN OF THE CHEMICAL SOCIETY OF JAPAN, VOL. 46, 2549—2559 (1973)

Effects of *N*-Acyl- and *N*-*s*-Triazinyl Groups on the Rearrangement of *S*-(*s*-Triazinyl)-2-aminothiophenols and *O*-(*s*-Triazinyl)-2-aminophenols

Takeo SHIOJIMA, Toshio KURODA, Sohei OHKAWA, Yasushi HASEGAWA, and Kohji MATSUI

Department of Chemistry, Faculty of Engineering, Gunma University, Tenjincho, Kiryu, Gunma 376

(Received March 20, 1973)

S-*s*-Triazinyl-2-aminothiophenols (I) containing methoxyl and/or dimethylamino groups in the *s*-triazine nucleus gave disulfides of *N*-*s*-triazinyl-2-aminothiophenols upon the S→N migration of the *s*-triazinyl group in the presence of acid; the rate of S→N migration was slow compared to that of the O→N migration of the corresponding *O*-*s*-triazinyl-2-aminophenol. On acylation or *s*-triazinylation, *S*-dimethoxy-*s*-triazinyl-2-aminothiophenol (I-1) and *O*-dimethoxy-*s*-triazinyl-2-aminophenol (II-1) gave *N*-acyl-*N*-*s*-triazinyl- or *N*,*N*-bis (*s*-triazinyl) derivatives upon the S→N or O→N migration of the *s*-triazinyl group. However, *S*-dimethylaminomethoxy-*s*-triazinyl-2-aminothiophenol (I-2), *S*-bis[(dimethylamino)-*s*-triazinyl]-2-aminothiophenol (I-3) and the corresponding derivatives of *o*-aminophenol gave *N*-acyl- or *N*-*s*-triazinyl derivatives, wihtout any migration of the *s*-triazinyl group, by acylation or *s*-triazinylation. The facility of the rearrangement of these *N*,*S*-bis-(*s*-triazinyl)-2-aminothiophenols and *N*,*O*-bis(*s*-triazinyl)-2-aminophenols depended not only upon the substituents in *S*- or *O*-*s*-triazine nucleus, but also upon the substituents in the *N*-*s*-triazine nucleus; the substituents in the *N*-*s*-triazine nucleus of strong electron-attracting and of strong electron-donating substances were not appropriate for the rearrangement in the presence of alkali to give disulfides of *N*-*s*-triazinyl-2-aminothiophenols (III-I) or *N*-*s*-triazinyl-2-aminophenols (III-II).

In previous papers,[1] we have reported that *O*-*s*-triazinyl-2-aminophenols rearrange in protic solvents or photochemically[2] to give the corresponding *N*-*s*-triazinyl-2-aminophenols.

It has been known that not only *O*-aryl-2-aminophenols, but also their *N*-acyl derivatives,[3] undergo the rearrangement of the *O*-aryl groups. Similarly, many *S*-aryl derivatives of *o*-aminothiophenol, their *N*-acyl derivatives,[4] and other related compounds, such as 2-acetamido-2′-nitrodiphenylsulfoxide,[5] 2-acetamido-2′-nitrodiphenylsulfone[4-1] or *o*-*N*-alkylamino sulfides, have been known to rearrange to yield the *N*-nitrophenyl derivatives or the derivatives of phenothiazine.[6] Recently, rearrangements of *s*-triazinyl groups have been reported in the reactions of 1-acylamino- or 1-*s*-triazinylamino-8-hydroxynaphthalene-3,6-disulfonic acid[7] and 3-hydroxy-2-naphthanilide with chloro-*s*-triazines.[8] However, in these papers the effect of *N*-acyl and *N*-triazinyl groups on the rearrangement of the *s*-triazinyl group, and their function in that rearrangement have not been mentioned. This paper will report on the S→N and O→N rearrangement of the *s*-triazinyl group of *S*-*s*-triazinyl-2-aminothiophenols, *N*-acyl, or *N*-*s*-triazinyl derivatives of *S*-*s*-triazinyl-2-aminothiophenols and *O*-*s*-triazinyl-2-aminophenols; the effects of *N*-acyl and *N*-*s*-triazinyl groups and their function in the rearrangement will also be discussed.

1) a) T. Harayama, K. Okada, S. Sekiguchi, and K. Matsui, *J. Heterocycl. Chem.*, **7**, 981 (1970). b) N. Maeno, T. Itagaki, S. Uno, and K. Matsui, This Bulletin, **45**, 3133 (1972).

2) K. Matsui, N. Maeno, S. Suzuki, H. Shizuka, and T. Morita, *Tetrahedron Lett.*, **1970**, 1467.

3) K. C. Roberts and C. G. M. deWorms, *J. Chem. Soc.*, **1934**, **727**; K. C. Roberts and C. G. M. deWorms, *ibid.*, **1935**, 1309.

4) a) W. J. Evans and S. Smiles, *ibid.*, **1935**, 181. b) K. J. Farrington and W. K. Warburton, *Aust. J. Chem.*, **9**, 480 (1956). c) C. F. Witht and S. Smiles, *J. Chem. Soc.*, **1935**, 340.

5) A. Levi, L. A. Warren, and S. Smiles, *ibid.*, **1933**, 1490.

6) W. E. Truce, E. M. Kreider, and W. W. Brand, "The Smiles and Related Rearrangements of Aromatic Systems," Organic Reactions, Vol. 18, John Wiley & Sons, Inc., (1970) p. 117; K. Fujii, *J. Pharm. Soc. Jap.*, **77**, 3 (1957).

7) R. Budziarek, *Chem. Commun.*, **1968**, 1427; *J. Chem. Soc., C*, **1971**, 74.

8) R. Budziarek and P. Hampson, *ibid.*, **1971**, 1167.

Results and Discussion

S-s-Triazinyl-2-aminothiophenols and *O-s*-triazinyl-2-aminophenols[1b] of the following general formulas were synthesized for this work:

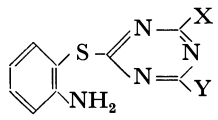

(I)

(1) X=Y=-OCH_3
(2) X=-OCH_3, Y=-$N(CH_3)_2$
(3) X=Y=-$N(CH_3)_2$

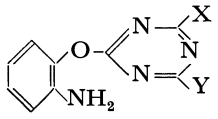

(II)

S→N Rearrangement of the s-*Triazinyl Group of* S-s-*Triazinyl-2-aminothiophenols (I-1∼3).* In contrast to the cases of *O-s*-triazinyl-2-aminophenols,[1] the (I) compounds could be easily prepared by treating *o*-aminothiophenol with the corresponding chloro-*s*-triazines in the presence of sodium hydroxide; the success in preparing the (I) compounds by this method is considered to be due to the facts that the nucleophilic reactivity of the thiophenoxide anion is much larger than that of the phenoxide anion[9] and that the rate of the rearrangement of *S-s*-triazinyl-2-aminothiophenols is much slower than that of *O-s*-triazinyl-2-aminophenols in an alkaline solution. Table 1 lists the compounds obtained.

Generally, *S-s*-triazinyl-2-aminothiophenols are much more inactive to rearrangement than the corresponding *O-s*-triazinyl-2-aminophenols. For example, (I-1) could be stored for a long period and scarcely no rearrangement was observed even in an alkaline solution. However, (II-1) gave *N-s*-triazinyl-2-aminophenol upon storage in the laboratory in a solid state. This difference in the facility of the rearrangement agreed with the difference in mobility between -SAr and -OAr as leaving groups in the nucleophilic substitution reactions with amine; the mobility order is known as -OAr>-SAr.[10] However, (I-1) readily gave a disulfide of *N*-(4,6-dimethoxy-*s*-triazin-2-yl)-2-aminothiophenol (III-I-1) when a dilute solution (0.5 g/100 ml acetone) was treated with a small amount of hydrochloric acid, while when a concentrated solution

Table 1. *S-s*-Triazinyl-2-aminothiophenols

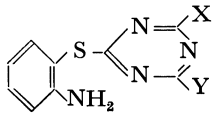

	X	Y	Yield (%)	Mp (°C)	Solvent for recrystallization		Anal (%) Found	Anal (%) Calcd
(I-1)	OCH_3	OCH_3	95	121—122	Benzene-ligroin	C	50.26	49.98
						H	4.84	4.58
(I-2)	OCH_3	$N(CH_3)_2$	60	102—103	Benzene-ligroin	C	52.34	51.97
						H	5.54	5.45
(I-3)	$N(CH_3)_2$	$N(CH_3)_2$	42	76.5—77.5	Petroleum ether	C	53.71	53.77
						H	6.27	6.25

Table 2. Disulfides of *N-s*-triazinyl-2-aminothiophenols

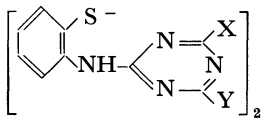

	X	Y	Yield (%)		Mp (°C)	Solvent for recrystallization	M. W.[c] Found	M. W.[c] Calcd		Anal (%) Found	Anal (%) Calcd
(III-I-1)	OCH_3	OCH_3	93[a]	—[b]	159—160	Methanol	540	527	C	50.54	50.18
									H	4.16	4.21
(III-I-2)	OCH_3	$N(CH_3)_2$	87	95	190—191	Benzene-ligroin	—	—	C	52.40	52.16
									H	5.47	5.11
(III-I-3)	$N(CH_3)_2$	$N(CH_3)_2$	80	95	184—185	Benzene-ligroin	587	579	C	54.14	53.96
									H	6.08	5.92

a) Yields of disulfides after standing for 24 hr in acetone in the presence of hydrochloric acid (1×10^{-2} mol/l) at room temperature.
b) Yields of disulfides after heating at 200 °C for 5 hr.
c) Measured by the method of Rast.

9) R. G. Pearson, H. Sobel, and J. Songstad, *J. Amer. Chem. Soc.*, **90**, 319 (1969); R. G. Pearson and J. Songstad, *ibid.*, **89**, 1827 (1968).

10) L. Bartolotti, and A. Cerniani, *Chem. Abstr.*, **50**, 15182e, (1956).

(20 g/100 ml) was used, (III-I-1), *N,N*-bis(*s*-triazinyl)-2-aminothiophenol (IV-I-1-8) and *o*-aminothiophenol were obtained, indicating that an intermolecular migration of the *s*-triazinyl group took place.

Compounds (I-2) and (I-3) are more inactive than (I-1) to the rearrangement, as may be expected; however, they also gave disulfides of the corresponding *N*-*s*-triazinyl-2-aminothiophenols when treated with an acid or when heated above their melting points. The disulfides of *N*-*s*-triazinyl-2-aminothiophenols thus obtained are listed in Table 2.

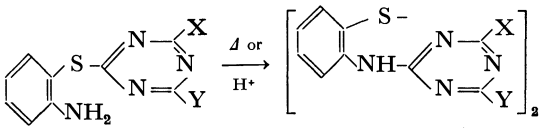

(I) (III-I)

Rearrangement of the S- *or* O-s-*Triazinyl Group during the Reactions of* S-*Dimethoxy*-s-*triazinyl*-2-*aminothiophenol (I-1) and* O-*Dimethoxy*-s-*triazinyl*-2-*aminophenol (II-1) with Acylating or* s-*Triazinylating Reagents. (a) Reaction of* S-*(4,6-Dimethoxy*-s-*triazin*-2-*yl)*-2-*aminothiophenol (I-1)*: When I-1 was treated with 2-chloro-4,6-dimethoxy-*s*-triazine in acetone under nearly neutral conditions by adding sodium carbonate, *N,N*-bis(*s*-triazinyl)-2-aminothiophenol (IV-I-1-8) was obtained as the main product instead of the expected *N,S*-bis(*s*-triazinyl)-2-aminothiophenol. A similar migration of the *S*-*s*-triazinyl group during the reaction was observed when I-1 was treated with acetic anhydride, benzoyl chloride, cyanuric chloride, or ethyl chloroformate. I-1 reacted readily with phenyl isocyanate (at room temperature) or phenyl isothiocyanate (at 60 °C) in benzene to give *N*-*s*-triazinyl-*N*-phenyl-

Table 3. *N*-Acyl-*N*-*s*-triazinyl- and *N,N*-bis(*s*-triazinyl)-2-aminothiophenols and 2-aminophenols

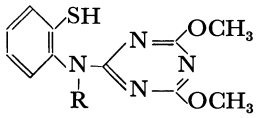

	R	Yield (%)	Mp (°C)	Solvent for recrystallization		Anal (%) Found	Calcd
(IV-I-1-1)	$COCH_3$	85	137—138	Benzene	C	51.10	50.99
					H	4.32	4.57
(IV-I-1-2)	COC_6H_5	87	138—139	Benzene-ligroin	C	58.23	58.68
					H	4.07	4.38
(IV-I-1-3)	$CONHC_6H_5$	95	170—171	Benzene	C	56.50	56.24
					H	4.53	4.72
(IV-I-1-4)	$CSNHC_6H_5$	95	167	Benzene	C	54.54	54.53
					H	4.25	4.32
(IV-I-1-5)	$COCH_2COCH_3$	54	134—135	Benzene-ligroin	C	51.83	51.72
					H	4.72	4.64
(IV-I-1-6)	$COOCH_2CH_3$	74	105—106	Ethanol	C	49.85	49.99
					H	4.55	4.79
(IV-I-1-7)	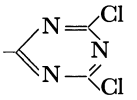	97	155—156	Benzene	C	40.75	41.03
					H	2.70	2.69
(IV-I-1-8)	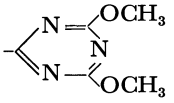	82	175—176	Benzene-ligroin	C	47.92	47.63
					H	4.49	4.26
(IV-I-1-9)	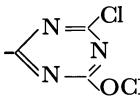	75	146.5—147.0	Benzene	N	24.12	24.04
(IV-I-1-10)	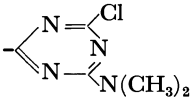	90	168.5	Benzene-ligroin	N	26.76	26.62

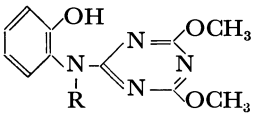

(IV-II-1-1)	$COCH_3$	70	133—134	Ligroin	C	54.06	53.79
					H	5.10	4.86
(IV-II-1-2)	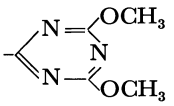	81	132—133	Benzene	C	49.32	49.61
					H	4.46	4.39

carbamoyl- or *N*-*s*-triazinyl-*N*-phenylthiocarbamoyl-2-aminothiophenol in a good yield. I-1 also reacted with diketene upon heating under reflux in xylene to give *N*-acetoacetyl-*N*-dimethoxy-*s*-triazinyl-2-aminothiophenol. Thus, *N*-acyl- and *N*-*s*-triazinyl-*S*-dimethoxy-*s*-triazinyl-2-aminothiophenols were not obtained in these cases. However, in the reaction of I-1 with acrylonitrile (heated in dioxane in the presence of Triton B) or 2,4-dinitrofluorobenzene (in the presence of triethylamine), merely an *N*-substituted product (V-I-1-1～V-I-1-2) was obtained, without any rearrangement in any case.

Table 3 lists the compounds thus obtained.

(b) Reaction of O-(4,6-Dimethoxy-s-triazin-2-yl)-2-aminophenol (II-1): A similar rearrangement was observed in the reaction of II-1 with 2-chloro-4,6-dimethoxy-*s*-triazine or acetic anhydride, which gave *N*,*N*-bis(*s*-triazinyl)-2-aminophenol or *N*-acetyl-*N*-*s*-triazinyl-2-aminophenol.

In most of these cases (except the case of diketene), (I-1) and (II-1) are stable under the reaction conditions and scarcely no formation of the rearranged product [(III-I) or (III-II)] was observed when the acylating or *s*-triazinylating reagents were absent. From these results, a process involving the intermediary formation of *N*-*s*-triazinyl-2-aminothiophenol or *N*-*s*-triazinyl-2-aminophenol (III) is not considered for these reactions; the reactions are, assumed to proceed by means of a preferential acylation or *s*-triazinylation of the amino group, followed by a rearrangement giving the end products. This assumption is supported by thin-layer chromatograms of the reaction mixture; for example, in the reaction of II-1 with acetic anhydride in the presence of triethylamine, no spot of *N*-*s*-triazinyl-2-aminophenol (III-II-1) was observed at any time during the course of the reaction (developed on a silica gel layer; developing solvent, chloroform–benzene–ligroin–methanol=15 : 5 : 5 : 5 by volume). A short time after the reaction components were mixed, however, a new, unidentified spot appeared, followed by a spot of *N*-acetyl-*N*-*s*-triazinyl-2-aminophenol (IV-II-1-1). The latter increased gradually with the reaction time; however, the unidentified spot [probably attributable to *N*-acetyl-*O*-*s*-triazinyl-2-aminophenol (V-II-1-1)] was small and remained almost constant throughout the course of the reaction until it disappeared at last.

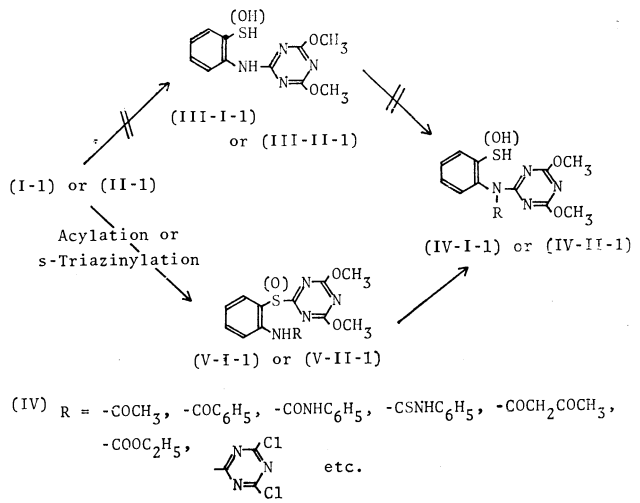

(IV) R = $-COCH_3$, $-COC_6H_5$, $-CONHC_6H_5$, $-CSNHC_6H_5$, $-COCH_2COCH_3$, $-COOC_2H_5$, etc.

In contrast to the case of I-1, II-1 gave merely *N*-dimethoxy-*s*-triazinyl-2-aminophenol when heated with diketene in xylene or when heated with acrylonitrile. Because of the slow S→N migration, the reaction of (I-1) is assumed to proceed by means of a preferential reaction at the amino group, followed by the rearrangement giving the end product. On the other hand, (II-1) rearranges rapidly upon mere heating; therefore, in the case of II-1 the rearrangement is considered to take place in preference to the reaction of the amino group with the reagent, because the preformed *N*-*s*-triazinyl-2-aminophenol is inert to the attack by diketene or acrylonitrile under the present reaction conditions.

From the results, it is obvious that the introduction of the acyl or *s*-triazinyl group into the amino group very much facilitates the S→N or O→N migration of the *S*- or *O*-dimethoxy-*s*-triazinyl group. Generally, the nucleophilic reactivities of NH-*s*-triazinyl and NH-acyl groups are known to be low. Thus, the rate of the rearrangement of *N*-acyl-*O*-(2,4-dinitrophenyl)-2-aminophenols is much slower than that of the parent aminoether in the absence of alkali.[3] Therefore, it is unlikely that the ready rearrangement of intermediary *N*-acyl or *N*-*s*-triazinyl derivatives (V) merely proceeds by means of a general nucleophilic attack by the NH-acyl or NH-*s*-triazinyl group. However, a process involving the formation of a reactive anion by the abstraction of a proton from the NH-acyl- or NH-*s*-triazinyl group is also unlikely, for, in most of these cases, the acylation and *s*-triazinylation were carried out under nearly neutral conditions; in certain cases, as in the reaction of I-1 with phenyl isocyanate, even though the reactions were carried out without the addition of any base, the rearrangement took place very readily. Consequently, it may be considered that the presence of an acidic –NH– hydrogen atom resulting from the introduction of an acyl or *s*-triazinyl group is important for the ready rearrangement, and that the difference in effect of introducing an acyl group between the nitrophenyl (retardation) and *s*-triazinyl (acceleration) derivatives is attributable to the presence or absence of a ring nitrogen atom in the migrating aryl nucleus. From these considerations, it seems reasonable to assume that the ready rearrangement of *N*-acyl or *N*-*s*-triazinyl derivatives of I-1 and II-1 proceeds by intramolecular four-center electrophilic-nucleophilic processes, as is shown below:

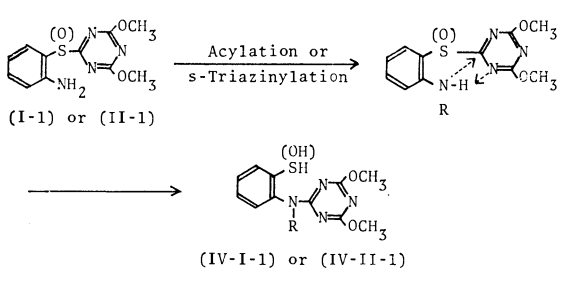

R = Acyl- or s-Triazinyl Group

From the viewpoint of this assumption, it may be considered that the -NH- group of the 2,4-dinitrophenyl derivative is more favorable for the protonation-like process than are the ordinary NH-acyl groups; however, its nucleophilic reactivity is assumed to be too low to attack the *s*-triazine ring carbon. An opposite situation holds for the *N*-β-cyanoethyl derivative.

Reactions of S-*(2-Dimethylamino-4-methoxy-*s*-triazin-2-yl)-2-aminothiophenol (I-2),* O-*(2-Dimethylamino-4-methoxy-*s*-triazin-2-yl)-2-aminophenol (II-2),* S-[*2,4-Bis-(dimethylamino)-*s*-triazin-2-yl]-2-aminothiophenol (I-3), and* O-[*2,4-Bis(dimethylamino)-*s*-triazin-2-yl)-2-aminophenol (II-2) with Acylating or* s-*Triazinylating Reagents, and the Migration of the* s-*Triazinyl Group of* N,S-*Bis(*s-*triazinyl)-2-aminothiophenols and* N,O-*Bis(*s-*triazinyl)-2-aminophenols.* When I-2 or II-2 was treated with acetic anhydride, phenyl isocyanate, benzoyl chloride, ethyl chloroformate, cyanuric chloride, 2,4-dichloro-6-methoxy-*s*-triazine, or 2,4-dichloro-6-methyl-*s*-triazine in manners similar to those described above, an *N*-acyl- or *N-s*-triazinyl-derivative was obtained in every case, without any migration of the *S*- or *O*-triazinyl group. Tables 4 and 5 list the compounds, (V-I-2) and (V-II-2), thus obtained. Similar results were also obtained in the reactions of I-3 and II-3 with acylating or *s*-triazinylating reagents; Tables 6 and 7 list the compounds, (V-I-3) and (V-II-3), thus obtained.

When *N*-chloro-*s*-triazinyl-*O-s*-triazinyl-2-aminophenols [(V-II-2-5)～(V-II-2-7) and (V-II-3-8)～(V-II-3-10)] and *N*-chloro-*s*-triazinyl-*S-s*-triazinyl-2-aminothiophenols [(V-I-2-4)～(V-I-2-6) and (V-1-3-5)

Table 4. *N*-Acyl-*S-s*-triazinyl- and *N,S*-bis(*s*-triazinyl)-2-aminothiophenols (V-I-2)

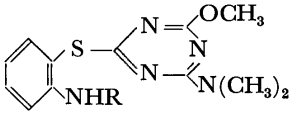

	R	Yield (%)	Mp (°C)	Solvent for recrystallization		Anal (%) Found	Calcd
(V-I-2-1)	$COCH_3$	91	146—146.5	Benzene–ligroin	C	52.34	52.65
					H	5.32	5.36
(V-I-2-2)	COC_6H_5	84	147—148	Benzene–ligroin	C	60.21	59.83
					H	5.22	5.03
(V-I-2-3)	$CONHC_6H_5$	84	201—220	Dioxane	C	57.27	57.57
					H	5.21	5.07

R =

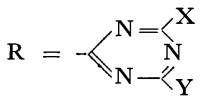

	X	Y					
(V-I-2-4)	Cl	Cl	95	176.5	Benzene	C	42.03	42.37
						H	3.55	3.33
(V-I-2-5)	Cl	OCH_3	90	144	Benzene–ligroin	C	46.01	45.67
						H	4.37	4.07
(V-I-2-6)	Cl	CH_3	95	158—159	Benzene–ligroin	C	47.12	47.46
						H	4.08	4.23
(V-I-2-7)	Cl	$N(CH_3)_2$	91	190—191	Benzene	N	29.14	28.84
(V-I-2-8)	CH_3	OCH_3	83	119—120	Benzene–ligroin	N	27.71	27.98
(V-I-2-9)	OCH_3	$N(CH_3)_2$	84	141—142	Benzene–ligroin	C	50.54	50.34
						H	5.39	5.40
(V-I-2-10)	CH_3	$N(CH_3)_2$	97	167—168	Benzene–ligroin	N	30.15	30.48
(V-I-2-11)	$N(CH_3)_2$	$N(CH_3)_2$	93	148—149	Benzene–ligroin	C	51.49	51.57
						H	6.29	5.92

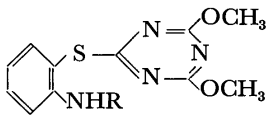

	R						
(V-I-1-1)	$C_6H_3(NO_2)_2$-(2,4-)	30	231—232	Monochlorobenzene	C	47.60	47.44
					H	3.01	3.28
(V-I-1-2)	CH_2CH_2CN	60	106—107	Ethanol	C	52.15	52.38
					H	5.04	4.76

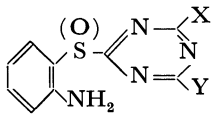
(I) or (II)

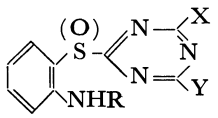
(V-I) or (V-II)

(V-I-2), (V-II-2), X=-OCH_3, Y=-$N(CH_3)_2$

(V-I-3), (V-II-3), X=Y=-$N(CH_3)_2$

R=-$COCH_3$, -COC_6H_5, -$CONHC_6H_5$, -$COOC_2H_5$,

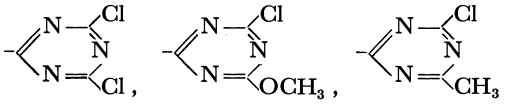

~(V-I-3-7)] were treated with dimethylamine, one or two chlorine atoms were replaced by a dimethylamino group, depending upon the amounts of dimethylamine used and the reaction temperature; the migration of the *O*- or *S*-*s*-triazinyl group was not observed in any case. However, in the reaction with sodium methoxide, not only the replacement of the chlorine atom, but also the migration of the *s*-triazinyl group, took place. For example, V-II-2-5 reacted with an equimolar amount of sodium methoxide to give V-II-2-6. However, with more than two equivalents of sodium methoxide V-II-2-5 gave *N*-(4-dimethylamino-6-methoxy-*s*-triazin-2-yl)-2-aminophenol (III-II-2) under the O→N

Table 5. *N*-Acyl-*O*-*s*-triazinyl- and *N*,*O*-bis(*s*-triazinyl)-2-aminophenols (V-II-2)

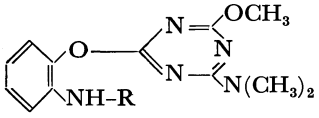

	R	Yield (%)	Mp (°C)	Solvent for recrystallization		Anal (%) Found	Calcd
(V-II-2-1)	$COCH_3$	76	175—176	Benzene	C	55.25	55.43
					H	5.78	5.65
					N	23.06	23.09
(V-II-2-2)	$CONHC_6H_5$	92	168—169	Benzene	C	60.35	59.99
					H	5.51	5.30
					N	22.40	22.09
(V-II-2-3)	COC_6H_5	63	110—111	Benzene-ligroin	C	62.79	62.45
					H	5.50	5.24
					N	19.30	19.16
(V-II-2-4)	$COOC_2H_5$	88	88— 89	Benzene-methanol	C	53.85	54.04
					H	6.05	5.75
					N	21.04	21.00

R = 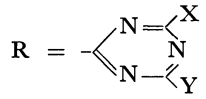

	X	Y					
(V-II-2-5)	Cl	Cl	95	136—137	Benzene-petroleum ether	C	44.41	44.02
						H	3.70	3.45
						N	27.66	27.38
(V-II-2-6)	Cl	OCH_3	75	99—100	Methanol	C	47.75	47.47
						H	4.55	4.23
						N	27.36	27.68
(V-II-2-7)	Cl	CH_3	91	147—148	Benzene	C	49.07	49.43
						H	4.63	4.41
						N	28.57	28.82
(V-II-2-8)	Cl	$N(CH_3)_2$	86	166—167	Benzene-ligroin	C	49.12	48.87
						H	5.05	4.82
						N	30.51	30.17
(V-II-2-9)	$N(CH_3)_2$	$N(CH_3)_2$	70	160—161	Benzene	C	53.88	53.51
						H	6.45	6.14
						N	32.87	32.49
(V-II-2-10)	OCH_3	$N(CH_3)_2$	95	142—143	Benzene	C	51.95	52.29
						H	5.83	5.61
						N	30.84	30.49
(V-II-2-11)	CH_3	$N(CH_3)_2$	95	165—166	Acetone	C	54.81	54.40
						H	6.05	5.83
						N	31.61	31.72

rearrangement and the cleavage of one of the *s*-triazinyl groups. III-II-2 was also obtained from V-II-2-7 when it was treated with more than one equivalent of sodium methoxide. Similarly, V-II-3-8 gave V-II-3-9 or III-II-3 when treated with one or more than two equivalents of sodium methoxide. However, when V-II-3-8 was treated with one and a half equivalents of sodium methoxide, even though the reaction mixture was slightly acidic at the end of the reaction, instead of an intermediary *N*-[bis(dimethylamino)-*s*-triazinyl]-*N*-(chloromethoxy-*s*-triazinyl)-2-aminophenol (IV-II-3)′ or *O*-[bis(dimethylamino)-*s*-triazinyl]-*N*-(dimethoxy-*s*-triazinyl)-2-aminophenol (V-II-3)′, the rearranged product of the latter (IV-II-3), which gave III-II-3 in the presence of alkali, was obtained, together with III-II-3. Thus, it is obvious that the reaction of V-II-2-5 or V-II-3-8 with sodium methoxide proceeds by means of a preferential replacement of the chlorine atoms by methoxyl groups, followed by the O→N migration of the *O*-*s*-triazinyl group to give IV-II-2 or IV-II-3, which gave the end product by a cleavage of the dimethoxy-*s*-triazinyl group, as is shown below.

Compound (V-II-3-10), however, unlike V-II-2-7 or V-II-3-9, gave only a replaced product when

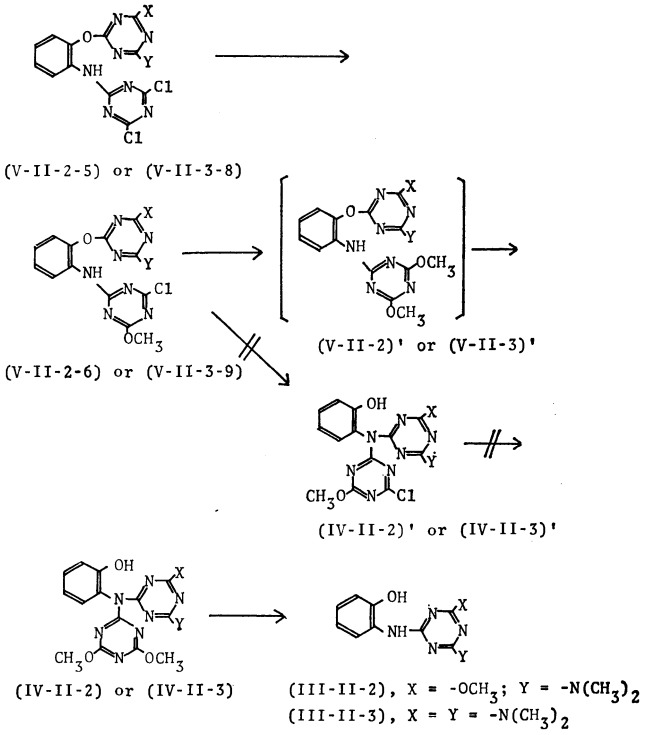

TABLE 6. *N*-ACYL-*S*-*s*-TRIAZINYL- AND *N*,*S*-BIS(*s*-TRIAZINYL)-2-AMINOTHIOPHENOLS (V-I-3)

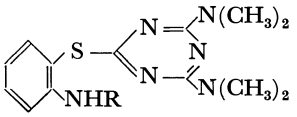

	R	Yield (%)	Mp (°C)	Solvent for recrystallization	Anal (%)	Found	Calcd
(V-I-3-1)	$COCH_3$	72	138.5—139.5	Ligroin	C	54.22	54.20
					H	5.94	6.06
(V-I-3-2)	$CONHC_6H_5$	95	186	Benzene	C	58.96	58.66
					H	5.85	5.66
(V-I-3-3)	$CSNHC_6H_5$	62	170—170.5	Benzene	C	56.26	56.44
					H	5.52	5.45
(V-I-3-4)	$C_6H_3(NO_2)_2$(2,4-)	87	193.5—194.0	Benzene	C	50.24	49.99
					H	4.93	4.42

R = 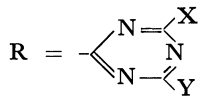

	X	Y					
(V-I-3-5)	Cl	Cl	95	170—171	Benzene-ligroin	C	44.33	44.38
						H	4.02	3.96
(V-I-3-6)	Cl	OCH_3	—	161.5	Benzene-ligroin	C	47.17	47.06
						H	5.00	4.65
(V-I-3-7)	Cl	CH_3	—	174.5	Benzene-ligroin	C	48.72	48.86
						H	5.09	4.82
(V-I-3-8)	OCH_3	OCH_3	90	152—153.5	Benzene-ligroin	N	29.68	29.35
(V-I-3-9)	Cl	$N(CH_3)_2$	—	195—196	Benzene-ligroin	N	31.36	31.33
(V-I-3-10)	CH_3	OCH_3	—	177—178	Benzene-ligroin	N	30.60	30.48
(V-I-3-11)	OCH_3	$N(CH_3)_2$	—	181—181.5	Benzene-ligroin	C	52.07	51.57
						H	6.20	5.92
(V-I-3-12)	CH_3	$N(CH_3)_2$	—	172.5—173	Benzene-ligroin	C	53.18	53.50
						H	5.26	4.98
(V-I-3-13)	$N(CH_3)_2$	$N(CH_3)_2$	—	169.5—170.5	Benzene-ligroin	C	52.35	52.72
						H	6.23	6.42

TABLE 7. *N*-ACYL-*O*-*s*-TRIAZINYL- AND *N*,*O*-BIS(*s*-TRIAZINYL)-AMINOPHENOLS (V-II-3)

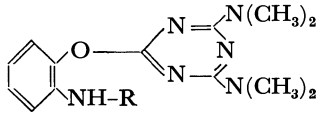

	R	Yield (%)	Mp (°C)	Solvent for recrystallization		Anal (%) Found	Calcd
(V-II-3-1)	$COCH_3$	95	203—204	Benzene	C	57.00	56.95
					H	6.70	6.37
					N	26.33	26.57
(V-II-3-2)	$CONHC_6H_5$	93	218—219	Dioxane	C	60.90	61.05
					H	5.93	5.89
					N	24.75	24.92
(V-II-3-3)	COC_6H_5	74	121—122	Benzene-ligroin	C	63.77	63.47
					H	6.05	5.86
					N	22.38	22.21
(V-II-3-4)	$CSNHC_6H_5$	49	162	Dioxane	C	58.95	58.66
					H	5.93	5.66
					N	24.06	23.94
(V-II-3-5)	$COOC_2H_5$	95	113—114	Methanol	C	55.80	55.48
					H	6.64	6.40
					N	24.06	24.26
(V-II-3-6)	$C_6H_3(NO_2)_2$(2,4-)	95	145—146	Benzene-ligroin	N	25.01	25.44
(V-II-3-7)	CH_2CH_2CN	31	132—133	Benzene-ligroin	C	58.95	58.70
					H	6.58	6.47
					N	30.30	29.95

R = 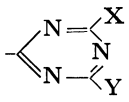

	X	Y					
(V-II-3-8)	Cl	Cl	95	164—165	Benzene-ligroin	C	45.89	45.52
						H	4.16	4.06
(V-II-3-9)	Cl	OCH_3	95	102—103	Methanol	C	48.87	48.87
						H	4.64	4.82
(V-II-3-10)	Cl	CH_3	95	103—104	Methanol	C	51.05	50.81
						H	5.23	5.02
(V-II-3-11)	CH_3	OCH_3	88	134—135	Benzene	C	54.22	54.41
						H	5.82	5.79
(V-II-3-12)	Cl	$N(CH_3)_2$	95	187—188	Benzene	C	50.34	50.20
						H	5.47	5.34
(V-II-3-13)	$N(CH_3)_2$	$N(CH_3)_2$	82	182—183	Benzene	C	54.61	54.65
						H	6.85	6.60
(V-II-3-14)	OCH_3	$N(CH_3)_2$	95	142—143	Benzene-ligroin	C	53.75	53.51
						H	6.30	6.14
						N	32.80	32.84
(V-II-3-15)	CH_3	$N(CH_3)_2$	95	165—166	Benzene	C	55.71	55.61
						H	6.26	6.34

treated with sodium methoxide. Similarly, III-I-2 was obtained in the reaction of V-I-2-4 with sodium methoxide; however, V-I-3-5 gave merely a replaced product upon treatment with an excess of sodium methoxide. Thus, although, because of the ready rearrangement *N*-dimethoxy-*s*-triazinyl derivatives of V-I-1～2 and V-II-1～3 types could not be obtained, *N*,*S*- and *N*,*O*-bis(*s*-triazinyl) derivatives of V-I-2～3 and V-II-2～3 types containing such substituents as -Cl, -Cl; -Cl, $-OCH_3$; -Cl, $-CH_3$; -Cl, $-N(CH_3)_2$; $-OCH_3$, $-CH_3$; $-OCH_3$, $-N(CH_3)_2$; $-N(CH_3)_2$, $-N(CH_3)_2$, and $-CH_3$, $-N(CH_3)_2$ in the *N*-*s*-triazine nucleus were prepared as fairly stable compounds, as Tables 4, 5, 6, and 7 show. From these results it has become clear that the facility of the rearrangement of *N*,*S*-bis(*s*-triazinyl)-2-aminothiophenols

Table 8. Rearrangement of *N*,*O*-bis(*s*-triazinyl)-2-aminophenols and *N*,*S*-bis(*s*-triazinyl)-2-aminothiophenols in the presence of sodium hydroxide in acetone

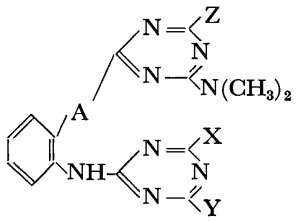

X	Y	$\sigma_m X+\sigma_m Y$[a]	A =	-O-		-S-	
			Z =	$-OCH_3$,	$-N(CH_3)_2$	$-OCH_3$,	$-N(CH_3)_2$
Cl	OCH_3	+0.488		×[1]	×[2]	×[3]	×[3]
Cl	CH_3	+0.304		○	○	×	×
OCH_3	OCH_3	+0.230		●	●	●	○
Cl	$N(CH_3)_2$	+0.162		○	—	○	○
CH_3	OCH_3	+0.049		●	○	○	○
OCH_3	$N(CH_3)_2$	−0.096		×	○	×	×
CH_3	$N(CH_3)_2$	−0.280		×	×	×	×
$N(CH_3)_2$	$N(CH_3)_2$	−0.422		×	×	×	×

a) Effect attributable to substituents in the *N*-*s*-triazine nucleus can be expressed by $\sigma_m X+\sigma_m Y$.[13]
1), 2) and 3); Results obtained after standing for 5 hr at room temperature, after standing for 24 hr at room temperature and after standing for 5 hr at 60°C, respectively.
○ indicates a formation of the rearranged product.
× indicates a failure of the rearrangement.
● indicates that the compound was not obtained owing to the rearrangement during the synthesis.

and *N*,*O*-bis(s-triazinyl)-2-aminophenols depends not only upon the substituents in the *S*- or *O*-*s*-triazine nucleus, but also upon the substituents in the *N*-*s*-triazine nucleus; however, no simple relation such as holds in the case of the substituents in the *O*-*s*-triazine nuclues[1b] was observed between the facility of the rearrangement and the substituents in the *N*-*s*-triazine nucleus. As will be mentioned later, some of the compounds, V-I-2∼3 and V-II-2∼3, rearrange in the presence of alkali (*cf.* Table 8). However, these results suggest that the ready rearrangement during the methoxydechlorination proceeds in a manner similar to that mentioned before by means of intramolecular four-center electrophilic-nucleophilic processes, and that, in these cases, the presence of alkali is necessary not for the rearrangement, but for the hydrolytic fission of the *s*-triazinyl group.

Migration of the S- *and* O-s-*Triazinyl Groups of* N-*Acyl*-S-s-*triazinyl*-, N,S-*Bis(*s-*triazinyl)-2-aminothiophenols, and* N-*Acyl*-O-s-*triazinyl*-, N,O-*Bis(*s-*triazinyl)-2-aminophenols in the Presence of Alkali.* The compounds listed in Tables 4∼7 are stable in a neutral or acidic solution. However, in the presence of sodium hydroxide some of these compounds give III-I or (III-II) upon the S→N or O→N migration of the *S*- or *O*-*s*-triazinyl group and the subsequent hydrolytic fission of the acyl group or one of the *s*-triazinyl groups, while *N*-2,4-dinitrophenyl and *N*-*β*-cyanoethyl derivatives of V-I-3 and V-II-3 types fail to give the rearranged products even in the presence of alkali. The results are shown in Table 8.

In the reaction of *N*-acyl derivatives of V-II-2 and (V-II-3) types in the presence of alkali, anions formed by the dissociation of the NH- groups were confirmed to be reactive species, as will be discussed in a subsequent paper;[11] similar reactive species may be assumed in the rearrangement of *N*,*O*-bis(*s*-triazinyl)-2-aminophenols and the corresponding derivatives of 2-aminothiophenol in the presence of alkali. It has been established, from the results on *N*-substituted *o*-amino sulfides and *o*-amino sulfones,[4a,5] that the proper balance of acidity and nucleophilicity of an attacking group is important for the rearrangement in the presence of alkali. However, in these cases it is assumed that a simple relation between acidity and nucleophilicity does not hold among the compounds used, because there is no similarity in the *N*-substituents. Therefore, it may be better to use as *N*-*s*-triazinyl groups a series of *N*-substituents of the same kind in order to make clear the importance of the proper balance mentioned above.

From Table 8 it is obvious that a good correlation holds between the substituents in the *N*-*s*-triazine nucleus ($\sigma_m X+\sigma_m Y$)[12] and the reactivity. Substituents in the *N*-*s*-triazine nucleus of strong electron-attracting or strong electron-donating substances were not appropriate for the rearrangement; this suggests that the balance between the acidity of the NH- group and the nucleophilicity of the anion is important. The failure of the rearrangement of derivatives containing strong electron-attracting substituents may be attributed to the low nuclepohilic reactivities of their anions, while the derivatives containing strong electron-donating substituents are assumed to be too weakly

11) T. Shiojima, Y. Hashida, and K. Matsui, submitted to this Bulletin.
12) Y. Fukushima, N. Nohara, Y. Hashida, S. Sekiguchi, and K. Matsui, This Bulletin, **44**, 794 (1971). Y. Fukushima, Y. Hashida, and K. Matsui, *Nippon Kagaku Kaishi*, **1972**, 629.

acidic to provide a sufficient concentration of reactive anions under the present reaction conditions.

Experimental

All the melting points are uncorrected.

The infrared spectra were measured in potassium bromide discs on a Jasco D-301 spectrophotometer. The NMR spectra were recorded on a Varian A-60D spectrometer. The elemental analyses were performed in the Micro-analytical Center of Gunma University.

The identification of the reaction products was performed by means of their NMR and infrared spectra, by elemental analyses, by molecular-weight determinations, by studying the solubility in an alkaline solution, by the color reaction of the -SH or -OH group, and by mixed-melting-point tests with an authentic sample.

Materials. S-s-*Triazinyl-2-aminothiophenols (I-1~3).* S-*(4,6-Dimethoxy-s-triazin-2-yl)-2-aminothiophenol (I-1)*: A solution of 2.5 g (0.02 mol) of *o*-aminothiophenol in 10 ml of a 10% sodium hydroxide solution was stirred, drop by drop, into a solution of 3.5 g (0.02 mol) of 2-chloro-4,6-dimethoxy-*s*-triazine in 30 ml of acetone at room temperature. Stirring was continued for 2 hr at 30 °C, and then the solution was poured into 200 ml of ice water. The precipitate was then filtered and dried. IR (KBr) cm^{-1}, (NH_2) 3440, 3400; (*s*-triazine) 810. NMR ($CDCl_3$), δ 3.90 (s, 6H), 4.18 (s, 2H), 7.30 (m, 4H).

S-*(4-Dimethylamino-6-methoxy-s-triazin-2-yl)-2-aminothiophenol I-2*: The I-2 compound was prepared in a manner similar to that described above by treating *o*-aminothiophenol with 2,4-dichloro-6-methoxy-*s*-triazine, followed by treatment with dimethylamine. IR (KBr) cm^{-1}, (NH_2) 3300, 3190; (*s*-triazine) 790. NMR (DMSO-d_6), δ 2.95 (s, 6H), 3.90 (s, 3H), 5.00 (s, 2H), 7.03(m, 4H).

S-[*4,6-Bis(dimethylamino)-s-triazin-2-yl*]-*aminothiophenol (I-3)*: A solution of 5.0 g (0.04 mol) of *o*-aminothiophenol in 20 ml of a 10% sodium hydroxide solution was stirred, drop by drop, into a solution of 8.0 g (0.04 mol) of 2-chloro-4,6-bis(dimethylamino)-*s*-triazine in 30 ml of dioxane; then the mixture was refluxed with stirring for 12 hr and poured into 200 ml of ice water. The oily precipitate was extracted with benzene, the benzene layer was washed with a sodium hydroxide solution and evaporated *in vacuo*, and the residue was collected. IR (KBr) cm^{-1}, (NH_2), 3400, 3310, (*s*-triazine) 795. NMR (DMSO-d_6), δ 2.95 (s, 12H), 5.20 (s, 2H), 7.00 (m, 4H).

Rearrangement of I in the Presence of Acid. A typical run is the case of *S*-(dimethoxy-*s*-triazinyl)-2-aminothiophenol (I-1). To a solution of 0.5 g of I-1 in 100 ml of acetone, we added 3 drops of concd. hydrochloric acid at room temperature. After it had stood for 24 hr at room temperature, the mixture was poured into ice water and neutralized with sodium carbonate; the precipitate thus formed was filtered and dried. IR(KBr) cm^{-1}; (NH) 3380. NMR (DMSO-d_6), δ 3.85 (s, 6H), 7.60(m, 4H), 9.65 (s, 1H).

Reactions of S-s-*Triazinyl-2-aminothiophenols (I) or* O-s-*Triazinyl-2-aminophenols (II) with Acylating or* s-*Triazinylating Reagents.* Some typical runs are noted below.

i) Reaction of I-1 with Acetic Anhydride to give N-*(Acetyl)*-N-*(dimethoxy-s-triazinyl)-2-aminothiopheonl (IV-I-1-1).* To a stirred solution of 2.6 g (0.01 mol) of I-1 and 6 ml of triethylamine in 50 ml of acetone, we added 2.0 g (0.02 mol) of acetic anhydride at room temperature. After it had stood for 5 hr, the mixture was poured into 200 ml of ice water, and the precipitate thus formed was filtered and dried. NMR (DMSO-d_6), δ 2.04 (s, 3H), 3.85 (s, 6H), 7.50 (m, 4H), 9.38 (s, 1H).

ii) Reaction of I-1 with Benzoyl Chloride to give N-*(Benzoyl)*-N-*(dimethoxy-s-triazinyl)-2-aminothiophenol (IV-I-1-2).* To a stirred mixture of 2.6 g (0.10 mol) of I-1, 30 ml of acetone, and 1.7 g (0.01 mol) of benzoyl chloride, 12 ml of a 5% sodium hydroxide solution was added, drop by drop, while the reaction mixture was kept at a nearly neutral condition at room temperature. After stirring for 5 hr, the mixture was poured into 200 ml of ice water, and the precipitate thus obtained was filtered and dried. NMR (DMSO-d_6), δ 3.85 (s, 6H), 7.70 (m, 9H), 9.55 (s, 1H).

iii) Reaction of I-1 with Cyanuric Chloride to give N-*(Dichloro-s-triazinyl)*-N-*(dimethoxy-s-triazinyl)-2-aminothiophenol (IV-I-1-7).* To a stirred solution of 2.6 g (0.01 mol) of I-1 in 50 ml of acetone, we added 1.8 g (0.01 mol) of cyanuric chloride, a 10 ml portion of a 1 N solution of sodium carbonate was then added, drop by drop, at 0 °C. After it had been stirred for 1 hr, the reaction mixture was poured into 300 ml of ice water, and the precipitate thus formed was filtered and dried. NMR (DMSO-d_6), δ 3.75 (s, 6H), 7.55 (m, 4H), 10.87 (s, 1H).

iv) Reaction of I-1 with Phenyl Isocyanate to give N-*(Dimethoxy-s-triazinyl)*-N-*(phenylcarbamoyl)-2-aminothiophenol (IV-I-1-3).* To a stirred solution of 2.6 g (0.01 mol) of I-1 in 100 ml of benzene, we added 1.2 g (0.01 mol) of phenyl isocyanate at room temperature. After it had been stirred for 3 hr, the precipitate thus formed was filtered and dried. NMR (DMSO-d_6) δ 3.83 (s, 6H), 7.35 (m, 9H), 8.23 (s, 1H), 9.35 (s, 1H).

v) Reaction of II-2 with Phenyl Isocyanate to give N-*(Phenylcarbamoyl)*-O-*(4-dimethylamino-6-methoxy-s-triazin-2-yl)-2-aminophenol (V-II-2-1).* To a solution of 2.6 g (0.01 mol) of (II-2) in 50 ml of benzene, we added 1.2 g (0.01 mol) of phenyl isocyanate at room temperature. After the mixture had been stirred for 5 hr, the precipitate thus formed was filtered and dried. NMR (DMSO-d_6), δ 3.10 (d, 6H), 3.83 (s, 3H), 7.30 (m, 9H), 8.14 (s, 1H), 9.13 (s, 1H).

vi) Reaction of II-2 with 2,4-Dichloro-6-methoxy-s-triazine to give N-*(4-Chloro-6-methoxy-s-triazin-2-yl)*-O-*(4-dimethylamino-6-methoxy-s-triazin-2-yl)-2-aminophenol (V-II-2-6).* To a stirred solution of 2.6 g (0.01 mol) of II-2 and 1.8 g (0.01 mol) of 2,4-dichloro-6-methoxy-*s*-triazine in 100 ml of acetone, we added a solution of 1.0 g (0.012 mol) of sodium bicarbonate in 30 ml of water, drop by drop, at room temperature. After having been stirred for 2 hr, the reaction mixture was poured into 300 ml of ice water; the precipitate thus formed was then filtered and dried. NMR (DMSO-d_6), δ 3.10 (d, 6H), 3.85 (s, 3H), 3.90(s, 3H), 7.40(m, 4H), 10.10(s, 1H).

vii) Reaction of II-3 with 2,4-Dinitrofluorobenzene to yield N-*(Dinitrophenyl)*-O-[*4,6-bis(dimethylamino)-s-triazin-2-yl*]-*2-aminophenol (V-II-3-6).* To a stirred solution of 2.7 g (0.01 mol) of II-3 and 1.0 g (0.01 mol) of triethylamine in 100 ml of benzene, we added 1.8 g (0.01 mol) of 2,4-dinitrofluorobenzene at room temperature. After the mixture had been stirred at room temperature for 8 hr, the benzene was distilled off *in vacuo*; the residue was then washed with water and filtered. NMR (DMSO-d_6), δ 2.99 (s, 12H), 7.40 (m, 7H), 9.91 (s, 1H).

viii) Reaction of II-3 with Ethyl Chloroformate to give N-*Ethoxycarbonyl)*-O-[*4,6-bis(dimethylamino)-s-triazin-2-yl*]-*2-aminophenol (V-II-3-5).* To a mixture of 2.7 g (0.01 mol) (I-3), 1.5 g (0.018 mol) of sodium bicarbonate, and 30 ml of water in 100 ml of acetone, we added a solution of 2.0 g (0.018 mol) of ethyl chloroformate in 50 ml of acetone at room temperature. After having been stirred, for 5 hr at room temperature, the reaction mixture was poured into 500 ml of ice water, and the precipitate thus formed was

filtered and dried. NMR (DMSO-d_6), δ 1.19 (t, 3H), 2.99 (s, 12H), 4.09 (q, 2H), 7.15 (m, 4H), 8.60 (s, 1H).

Reactions of N-*(Chloro-*s*-triazinyl)*-S-*(*s*-triazinyl)-2-amino thiophenols and* N-*(Chloro-*s*-triazinyl)*-O-*(*s*-triazinyl)-2-aminophenols with Neucleophiles.* Some typical runs will be shown in the case of *N*-(4,6-dichloro-*s*-triazin-2-yl)-*O*-[4,6-bis(dimethylamino)-*s*-triazin-2-yl]-2-aminophenol (V-II-3-8).

i) Reaction of V-II-3-8 with Dimethylamine to give N-*(4-Chloro-6-dimethylamino-*s*-triazin-2-yl)*-O-*[4,6-bis(dimethylamino)-*s*-triazin-2-yl]-2-aminophtnol (V-II-3-12).* To a solution of 2.1 g (0.005 mol) of V-II-3-8 in 100 ml of acetone, we added 1.2 ml (0.01 mol) of a 40% dimethylamine solution at 0 °C. After having been stirred for 3 hr at 0 °C, the reaction mixture was poured into 300 ml of ice water; the precipitate thus formed was then filtered and dried. NMR (DMSO-d_6), δ 2.98 (s, 18H), 7.30(m, 4H), 8.60(s, 1H). When the reaction was carried out using 2.5 ml of a 40% dimethylamine solution at 50 °C, the reaction product was V-II-3-13.

ii) Reaction of V-II-3-8 with Sodium Methoxide. ii-a) Reaction of V-II-3-8 with Sodium Methoxide in a Molar Ratio of 1 : 1 to give N-*(4-Chloro-6-methoxy-*s*-triazin-2-yl)*-O-*[4,6-bis(dimethylamino)-*s*-triazin-2-yl]-2-aminophenol (V-II-3-9).* To a mixture of 2.1 g (0.005 ml) of V-II-3-8 in 100 ml of methanol, we added 5 ml of a 1 N methanolic sodium methoxide solution at 0 °C. After it had stood for 1 night, the reaction mixture was poured into 300 ml of ice water. The precipitate thus formed was filtered and dried. (This compound was also obtained by the condensation of I-3 with 2,4-dichloro-6-methoxy-*s*-triazine). NMR (DMSO-d_6), δ 2.85 (s, 12H), 3.85 (s, 3H), 7.40 (m, 4H), 10.10 (s, 1H).

ii-b) When the Above-mentioned reaction was carried out using 15 ml of a sodium methoxide solution, *N*-[4,6-bis-(dimethylamino)-*s*-triazin-2-yl]-2-aminophenol (mp 185—186 °C)[1b] (III-II-3) (yield, 95%) and dimethylcyanuric acid[13] (yield, 82%) were obtained. However, in the reaction of V-II-3-8 with sodium methoxide in a molar ratio of 1 : 1.5, two rearranged products were obtained. One was *N*-[4,6-bis(dimethylamino)-*s*-triazin-2-yl]-2-aminophenol (yield, 33%), and the other was found to be *N*-(4,6-dimethoxy-*s*-triazin-2-yl)-*N*-[4,6-bis(dimethylamino)-*s*-triazin-2-yl]-2-aminophenol. (Mp 95—97 °C, recrystallized from cyclohexane), (yield, 36%). Found: C, 52.66; H, 5.83; N, 30.32%. Calcd for $C_{18}H_{23}N_9O_3$: C, 52.29; H, 5.61; N, 30.49%. NMR (DMSO-d_6), δ 2.97 (s, 12H), 3.83 (s, 6H), 7.55 (m, 4H), 8.98 (s, 1H).

Rearrangement of N,S-*Bis(*s*-triazinyl)-2-aminothiophenols (V-I) and* N,O-*Bis(*s*-triazinyl)-2-aminophenols (V-II) in the Presence of Sodium Hydroxide.* To a solution of 0.2 g of a *N,S-* or *N,O*-bis(*s*-triazinyl) derivative in 30 ml of acetone, we added 3 ml of a 0.5 N sodium hydroxide solution. After having stood (at room temperature in the case of V-II, and at 60 °C in the case of V-I) the reaction mixture was developed on a silica gel layer, using a mixture of benzene and acetone (6 : 1 by volume) as the developing solvent. From the thin-layer chromatogram thus obtained, the rearranged product was eluted with ethanol and thus identified.

13) A. W. Hofmann, *Ber.*, **19**, 2067 (1886), K. H. Slotta, R. Tschesche, *ibid.*, **60**, 303 (1927).

BULLETIN OF THE CHEMICAL SOCIETY OF JAPAN, VOL. 46, 2559—2562 (1973)

Reactions of Diphenylphosphinothioyl Isothiocyanate and Related Compounds with Some Nucleophiles and Carbodiimides

Iwao Ojima,* Kin-ya Akiba, and Naoki Inamoto

Department of Chemistry, Faculty of Science, The University of Tokyo, Hongo, Tokyo 113

(Received March 23, 1973)

Diphenylphosphinothioyl isothiocyanate (**1**) reacted with alcohols, water and diphenylphosphinothioic acid to give the esters and anhydride of diphenylphosphinothioic acid by substitution reaction on the phosphorus atom, but reacted with amines by addition to the isothiocyanate group to afford diphenylphosphinothioylthioureas or their ammonium salts. Diphenylphosphine and *p*-toluenethiol, however, did not react with **1**. On the contrary, diphenylphosphinothioyl isocyanate underwent only addition reaction with water, amine and thiol. Isothiocyanate (**1**) and *p*-toluenesulfonyl isothiocyanate were found to undergo 1,2-cycloaddition reaction with carbodiimides across the C=S bond to produce 1,3-thiazetidine derivatives.

Diphenylphosphinothioyl isothiocyanate (**1**) is an ambident substrate and has two reaction sites on phosphorus and carbon atoms.

This paper describes the reaction sites of **1** in the reactions with some nucleophiles and carbodiimides. Nucleophiles used were water, alcohols diphenylphosphinothioic acid (**2**), amines, diphenylphosphine and *p*-toluenethiol. Reactions of **1** with **2**[1] and diethylamine[2] have been reported. The results of these reactions are summarized in Scheme 1.

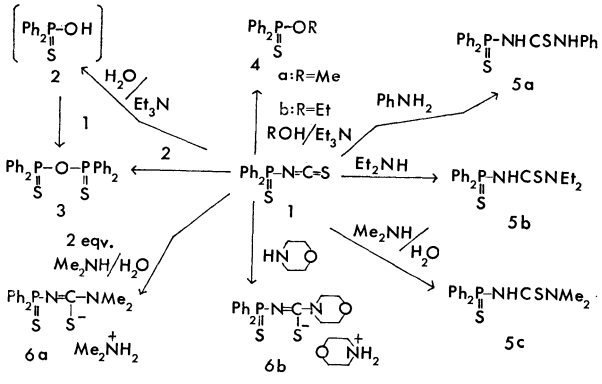

Scheme 1.

* Present address: Sagami Chemical Research Center, Nishi-onuma, Sagamihara, Kanagawa 229.

1) I. Ojima, K. Akiba, and N. Inamoto, This Bulletin, **42**, 2975 (1969).

2) I. Ojima, T. Onishi, T. Iwamoto, N. Inamoto, and K. Tamaru, *ibid.*, **44**, 2150 (1971).

It is remarkable that nucleophiles, the center of which is oxygen, attack selectively the phosphorus atom of **1** in the presence of triethylamine. This is attributable to formation of strong P–O bond in the substitution reaction.

The amines added to the carbon atom of the isothiocyanate group to give diphenylphosphinothioylthioureas (**5**) in quantitative yields, whereas diphenylamine did not react with **1** even when reaction temperature was raised up to 120 °C, because of its low nucleophilicity. Thioureas (**5**) can act as bidentate ligands.[2]

The reaction with 40% aqueous dimethylamine shows that the addition reaction with the amine predominates over the substitution reaction with water.

Attack of amines on the phosphorus atom has been reported in the case of diethoxyphosphoryl isothiocyanate.[3]

$$(EtO)_2P(O)-NHCSNR_2 \xleftarrow{R_2NH} (EtO)_2P(O)-NCS \xrightarrow{2R_2NH} (EtO)_2P(O)NR_2$$

In the case of **1**, however, the reactions with two equivalents of dimethylamine or morpholine provided ammonium salts (**6**), no substitution being observed under the present reaction conditions, though a formation of P–N bond by decomposition of **6** is possible.[4]

$$Ph_2P(S)-N(R_2N)-C(S^{\ominus})R_2\overset{\oplus}{N}H_2 \xrightarrow[in\ vacuo]{80-100\,^{\circ}C} Ph_2P(S)NR_2 + R_2\overset{\oplus}{N}H_2\overset{\ominus}{S}CN$$

6

It is curious that diphenylphosphine and *p*-toluenethiol, strong nucleophiles, react not with **1** but with ordinary isothiocyanates.[1,5]

The IR spectrum of **1** displays a strong band at 1960 cm^{-1} (–N=C=S). The value is considerably low as compared with that of ordinary isothiocyanates (2020—2100 cm^{-1}). This phenomenon would be interpreted by a large contribution of a canonical structure (**1′**).

$$>P(S)-N=C=S \longleftrightarrow >P=N-\overset{\oplus}{C}=S \overset{\ominus}{S} \longleftrightarrow \textit{etc.}$$

1 **1′**

The large contribution of **1′** increases the reactivity of the carbon atom of **1** toward nucleophiles, and also the hardness[6] of the carbon atom. The reaction with soft bases, diphenylphosphine and *p*-toluenethiol, may therefore become difficult.

In contrast with the reactions of **1**, diphenylphosphinothioyl isocyanate (**7**) reacted with water and diethylamine to give aminodiphenylphosphine sulfide (**8**) and 1,1-diethyl-3-diphenylphosphinothioylurea (**9**), respectively, no nucleophilic attack on the phosphorus atom being observed. Addition of *p*-toluenethiol to **7** produced a monothiocarbamate (**10**). This is attributable to a higher reactivity of the isocyanate group.

$$[Ph_2P(S)-NHCO_2H] \xrightarrow{-CO_2} Ph_2P(S)-NH_2 \quad (\mathbf{8})$$

$$[Ph_2P(S)-NHCO_2H] \xleftarrow{H_2O} Ph_2P-N=C=O \ (\mathbf{7}) \xrightarrow{Et_2NH} Ph_2P(S)-NHCONEt_2 \quad (\mathbf{9})$$

$$Ph_2P-N=C=O \ (\mathbf{7}) \xrightarrow{p\text{-}MeC_6H_4SH} Ph_2P(S)-NHCOSC_6H_4Me\text{-}p \quad (\mathbf{10})$$

If the contribution of **1′** is large, **1** should undergo 1,4-cycloaddition like thioacyl isothiocyanate.[7] Reactions of **1** with carbodiimides were performed from this standpoint.[8]

When an equimolar mixture of **1** and dicyclohexylcarbodiimide was heated, the adduct (**11a**) was obtained in a nearly quantitative yield. The IR spectrum showed a very strong band at 1640 cm^{-1} (C=N), and the UV spectrum displayed absorption maxima at 223 (log ε 4.81) and 260 nm (sh., log ε 4.23).

$$R^1-N=C=S + R^2-N=C=N-R^2 \rightarrow R^1-N=C(-S-)(-N(-R^2)-)-C=N-R^2$$

1 $R^1=Ph_2P(S)$
14 $R^1=p\text{-}MeC_6H_4SO_2$

11

a : $R^1=Ph_2P(S)$, $R^2=c\text{-}C_6H_{11}$
b : $R^1=Ph_2P(S)$, $R^2=i\text{-}Pr$
c : $R^1=p\text{-}MeC_6H_4SO_2$, $R^2=c\text{-}C_6H_{11}$

12

13

a : $R^1=Ph_2P(S)$, $R^2=c\text{-}C_6H_{11}$
b : $R^1=p\text{-}NO_2C_6H_4$, $R^2=c\text{-}C_6H_{11}$
c : $R^1=p\text{-}MeC_6H_4SO_2$, $R^2=o\text{-}MeC_6H_4$
d : $R^1=p\text{-}NO_2C_6H_4$, $R^2=i\text{-}Pr$
e : $R^1=MeSO_2$, $R^2=Ph$

The spectral data confirm that **11a** is a new 1,3-thiazetidine derivative, and not a 1,3-diazetidine derivative (**13a**) or a 1,4-cycloadduct (**12**), because the strong absorption band at 223 nm is too short to be assigned to the π–π^* transition of a C=S bond[9] and no absorption band caused by n–π^* transition could be detected. Furthermore, **11a** did not catalyse the

3) A. Schmidpeter and K. Stoll, *Angew. Chem.*, **79**, 242 (1967).
4) A. Schmidpeter and H. Groeger, *Chem. Ber.*, **100**, 3052 (1967).
5) For example, K. Issleib and G. Harzfeld, *Chem. Ber.*, **97**, 3430 (1964).
6) R. G. Pearson and J. Songstad, *J. Amer. Chem. Soc.*, **89**, 1827 (1967).
7) J. Goerdeler and H. Schenk, *Chem. Ber.*, **98**, 3831 (1965).
8) Preliminary report: I. Ojima and N. Inamoto, *Chem. Commun.*, **1970**, 1629.
9) K. Hirayama, "Handbook of Ultraviolet and Visible Spectra of Organic Compounds," Plenum Press, New York, (1967), p. 87.

decomposition of sodium azide by iodine (Feigl test),[10] indicating the absence of a C=S group.

The reaction of **1** with diisopropylcarbodiimide gave a similar adduct (**11b**).

Ulrich and Sayigh[11] reported that the 1,2-cycloaddition of carbodiimide and isothiocyanate having electron-withdrawing group always gives 1,3-diazetidine derivative (**13**). *p*-Toluenesulfonyl isothiocyanate (**14**) ($\nu_{N=C=S}$ 1890 cm^{-1}) was allowed to react with dicyclohexylcarbodiimide under conditions similar to those used by Ulrich *et al.* Adduct (**11c**), which also gave a negative Feigl test, was obtained in a nearly quantitative yield.

Comparison of the C=N stretching vibrations (1620—1640 cm^{-1}) of 1,3-thiazetidines (**11**) with those of **13** reported by Ulrich and Sayigh[11] also suggests that the adducts (**13**) are 1,3-thiazetidines (see Table 1). Recent work by Ulrich *et al.*[12] supports our results.[8]

Table 1. C=N stretching vibrations of 1,3-thiazetidines (**11**) and "1,3-diazetidines (**13**)" reported by Ulrich *et al.*[11]

	R^1	R^2	$\nu_{C=N}$ (cm^{-1})
11a	$Ph_2P(S)$	*c*-C_6H_{11}	1640
11b	$Ph_2P(S)$	*i*-Pr	1630
11c	*p*-$MeC_6H_4SO_2$	*c*-C_6H_{11}	1620
"**13b**"	*p*-$NO_2C_6H_4$	*c*-C_6H_{11}	1655
"**13c**"	*p*-$MeC_6H_4SO_2$	*o*-MeC_6H_4	1600
"**13d**"	*p*-$NO_2C_6H_4$	*i*-Pr	1655
"**13e**"	$MeSO_2$	Ph	1615

These results show that the cycloaddition of the isothiocyanates having electron-withdrawing group and carbodiimides occurs across the C=S bond of the isothiocyanate to give 1,3-thiazetidines, and not across the C=N bond to give 1,3-diazetidines.

Experimental

All melting and boiling points are uncorrected. IR, UV, NMR and Mass spectra were measured with Hitachi Model EPI-G2, Hitachi Model EPS-3, JEOL-C-60H, and Hitachi Model RMU-6D spectrometers, respectively.

Materials. Diphenylphosphinothioyl isothiocyanate (**1**) was prepared from diphenylphosphinothioyl chloride and ammonium thiocyanate, mp 48—49 °C (lit,[4] 48 °C). *p*-Toluenesulfonyl isothiocyanate (**14**) was prepared from potassium *N*-(*p*-toluenesulfonyl)dithiocarbamate[13] and thionyl chloride, bp 114—118 °C/0.5 mmHg (lit,[14] 115—125 °C/0.65 mmHg).

*Preparation of Diphenylphosphinothioyl Isocyanate (**7**).* A mixture of potassium cyanate (10.0 g, 0.12 mol) and diphenylphosphinothioyl chloride (25.3 g, 0.10 mol) in 400 ml of acetonitrile was stirred at room temperature for 24 hr, and filtered. The filtrate was evaporated and the residue was treated with petroleum ether to give colorless crystals of **7** in an almost quantitative yield. Mp 42—43 °C, IR (Nujol): 2240 cm^{-1} (–N=C=O).

Found: C, 59.97; H, 4.08; N, 5.33; S, 12.62%. Calcd for $C_{13}H_{10}NOPS$: C, 60.23; H, 3.89; N, 5.40; S, 12.37%.

*Reaction of **1** with Water.* A solution of **1** (0.5 g, 1.8 mmol) and water (1 g, 55 mmol) in 100 ml of acetone was heated in the presence of a few drops of triethylamine under reflux for 5 hr. After the solvent was removed, the residue was recrystallized from benzene to give diphenylphosphinothioic anhydride (**3**) in a quantitative yield, mp 197—198 °C (lit,[15] 197—198 °C).

*Reaction of **1** with Ethanol and Methanol.* A solution of **1** (0.75 g, 2.6 mmol) in 100 ml of ethanol was heated under reflux in the presence of a few drops of triethylamine for 2 hr. After the solvent was removed, the residue was dissolved in petroleum ether and recrystallized to give ethyl diphenylphosphinothioate (**4b**) in a quantitative yield, mp 38—39 °C (lit,[16] 42—43 °C). The IR spectrum is identical with that of an authentic sample.

In a similar reaction with methanol, **4a** was obtained in a quantitative yield, mp 83—85 °C (lit,[16] 84.5—85.5 °C).

*Reaction of **1** with Aniline.* Aniline (0.53 g, 5.7 mmol) and **1** (1.5 g, 5.6 mmol) were mixed without solvent and an exothermic reaction occurred. The mixture was then heated at 80—90 °C for a few minutes. White crystals thus obtained were recrystallized from dichloromethane or ethanol to give 3-diphenylphosphinothioyl-1-phenylthiourea (**5a**) in a nearly quantitative yield, mp 143—145 °C.

Found: C, 61.85; H, 4.62; N, 7.38; S, 16.90%. Calcd for $C_{19}H_{17}N_2PS_2$: C, 61.96; H, 4.62; N, 7.62; S, 17.39%.

*Reaction of **1** with Aqueous Dimethylamine.* 40% aqueous dimethylamine (1.0 g, 8.9 mmol) and **1** (3.0 g, 10.9 mmol) were mixed. After an exothermic reaction subsided, the solvent was removed under reduced pressure. The residue was washed with ether to give 1,1-dimethyl-3-diphenylphosphinothioylthiourea (**5c**) in an almost quantitative yield, mp 94—96 °C (lit,[4] 95.5—96 °C).

Use of two equivalents of 40% aqueous dimethylamine gave the corresponding dimethylammonium salt (**6a**).[2]

*Reaction of **1** with Morpholine.* A mixture of morpholine (1.8 g, 20.7 mmol) and **1** (2.8 g, 10.1 mmol) in 50 ml of ether was stirred at room temperature. An exothermic reaction occurred to give ammonium salt (**6b**) in a quantitative yield, mp 135—138 °C (from ethanol).

Found: C, 56.06; H, 6.03; N, 9.41; S, 14.51%. Calcd for $C_{21}H_{28}N_3O_2PS_2$: C, 56.12; H, 6.24; N, 9.35; S, 14.25%.

Equimolar mixture of morpholine and **1** also produced **6b**. No free thiourea derivative could be obtained.

*Reaction of **7** with Water.* A solution of **7** (0.50 g, 1.93 mmol) and 2 ml of water in 50 ml of acetone was heated under reflux for 2 hr. The mixture was allowed to stand overnight at room temperature to afford aminodiphenylphosphine sulfide (**8**) in an almost quantitative yield, mp 99—101 °C (lit,[17] 102—104 °C).

10) F. Feigl, "Spot Tests in Organic Analysis," Fifth Eng. Ed., Elsevier Pub. Co., Amsterdam, (1956), pp. 228—233.

11) H. Ulrich and A. A. R. Sayigh, *Angew. Chem.*, **77**, 545 (1965); H. Ulrich, "Cycloaddition Reactions of Heterocumulenes," Academic Press, New York, (1967), pp. 233—235.

12) H. Ulrich, B. Tucker, and A. A. R. Sayigh, *J. Amer. Chem. Soc.*, **94**, 3484 (1972).

13) K. Hartke, *Arch. Pharm.*, **299**, 174 (1966); *Chem. Abstr.*, **64**, 15783e (1966).

14) Farbenfabriken Bayer A. -G. (by K. Dickore and E. Kuehle), Ger. 1,183,492, Dec. 17, 1964; *Chem. Abstr.*, **62**, 7691c (1965).

15) T. R. Hopkins and P. W. Vogel, *J. Amer. Chem. Soc.*, **78**, 4447 (1956).

16) T. A. Mastryukova, T. A. Melent'eva, and M. I. Kabachnik, *Zh. Obshch. Khim.*, **35**, 1197 (1965); *Chem. Abstr.*, **63**, 11605f (1965).

17) I. N. Zhmurova, I. Yu. Voitsekhovskaya, and A. V. Kirsanov, *Zh. Obshch. Khim.*, **29**, 2083 (1959); *Chem. Abstr.*, **54**, 8681h (1960).

Reaction of **7** *with Diethylamine.* Diethylamine (0.40 g, 5.5 mmol) was added to **7** (1.1 g, 4.25 mmol) without solvent and heated at 50—60 °C for 5 min. Crystals thus produced were recrystallized from cyclohexane to give 1,1-diethyl-3-diphenylphosphinothioylurea (**9**) in a nearly quantitative yield, mp 128—130 °C. IR (Nujol): 3150 (NH) and 1625 cm^{-1} (C=O).

Found: C, 61.41; H, 6.15; N, 8.39; S, 9.51%. Calcd for $C_{17}H_{21}N_2OPS$: C, 61.44; H, 6.33; N, 8.44; S, 9.64%.

Reaction of **7** *with* p-*Toluenethiol.* A mixture of **7** (0.5 g, 1.9 mmol) and *p*-toluenethiol (0.25 g, 2.0 mmol) was heated at 50 °C for one hour without solvent. The resulting solid was recrystallized from benzene-petroleum ether to give *S-p*-tolyl *N*-(diphenylphosphinothioyl)monothiocarbamate (**10**) in a nearly quantitative yield, mp 94—96 °C (dec); IR (Nujol): 3350 sh, 3180 (NH), and 1695 cm^{-1} (C=O).

Found: C, 62.86; H, 4.69; N, 3.51; S, 16.93%. Calcd for $C_{20}H_{18}NOPS_2$: C, 62.64; H, 4.73; N, 3.65; S, 16.72%.

Reaction of **1** *with Dicyclohexylcarbodiimide.* A solution of **1** (0.55 g, 2.0 mmol) and carbodiimide (0.414 g, 2.01 mmol) in 100 ml of dry cyclohexane was heated under reflux for 30 min. After the solvent had been removed, the residue was recrystallized from petroleum ether to give the adduct (**11a**) in a quantitative yield, mp 120—122 °C. IR (Nujol): 1640 cm^{-1} (C=N); $\lambda_{max}^{c\text{-}C_6H_{12}}$: 223 (log ε 4.81) and 260 sh nm (log ε 4.23); MS: *m/e* 481 (M^+, 9%) and 217 (Ph_2PS^+, 100).

Found: C, 64.52; H, 6.41; N, 8.05; S, 13.61%. Calcd for $C_{26}H_{32}N_3PS_2$: C, 64.86; H, 6.65; N, 8.73; S, 13.31%.

When a mixture of **1** and the carbodiimide was heated at 90—95 °C for a few minutes, the adduct (**11a**) was also obtained in a quantitative yield.

Reaction of **1** *with Diisopropylcarbodiimide.* A mixture of **1** (0.577 g, 2.02 mmol) and carbodiimide (0.279 g, 2.21 mmol) was heated without solvent for 2 hr. An oily product was obtained in a nearly quantitative yield. Since the distillation resulted in decomposition, column chromatography on silica gel using petroleum ether was performed to obtain colorless oil (**11b**). IR (neat): 1630 cm^{-1} (C=N).

Found: C, 59.65; H, 5.98; N, 10.63; S, 16.12%. Calcd for $C_{20}H_{24}N_3PS_2$: C, 59.83; H, 6.02; N, 10.46; S, 15.97%.

Reaction of p-*Toluenesulfonyl Isothiocyanate (***14***) with Dicyclohexylcarbodiimide.* A mixture of **14** (1.0 g, 4.72 mmol) and carbodiimide (1.0 g, 4.86 mmol) was heated at 80 °C for 30 min. The resulting solid was recrystallized from petroleum ether to give the adduct (**11c**) in a quantitative yield, mp 144—146 °C. IR (Nujol): 1620 cm^{-1} (C=N); $\lambda_{max}^{c\text{-}C_6H_{12}}$: 229 sh (log ε 4.43), 235 sh (4.50), 248 (4.55), and 262 sh nm (4.46).

BULLETIN OF THE CHEMICAL SOCIETY OF JAPAN, VOL. 46, 2562—2564 (1973)

Synthesis of Carbocyclic Adenosine Analogs: 9-(2′,3′,4′,5′-Tetrahydroxycyclopentyl)adenines[1]

Tetsuo SUAMI, Shigeru NISHIYAMA, Kinichi TADANO, and Frieder W. LICHTENTHALER[2]

Department of Applied Chemistry, Faculty of Engineering, Keio University, Hiyoshi, Yokohama 223

(Received March 30, 1973)

The synthesis of five 9-(2′,3′,4′,5′-tetrahydroxycyclopentyl)adenines with 1,2,4/3,5- (**2a**), 1,2,3/4,5- (**2b**), 1,4,5/2,3- (**2c**), 1,4/2,3,5- (**2e**) and all-*cis* configuration (**2d**) are described, by amination of 4-amino-5-nitro-6-chloropyrimidine with the respective 5-aminocyclopentanetetrols (**3a**—**e**), followed by reduction of the nitro group and cyclization with formamide.

Preliminary antifungal properties are reported.

Nucleoside analogs, in which the ribofuranosyl moiety is replaced by the hydrolytically and enzymatically more stable cyclopentane ring, have attained much interest in the past decade[1,3–8], its main stimulus stemming from their possible function as antimetabolites or nucleoside substitutes in nucleic acid metabolism. This allurement was enhanced by the isolation of aristeromycin (**1**), with promising antibacterial and antifungal properties, from natural sources,[5] which, nevertheless, was preceded by a chemical synthesis of the DL-form of **1**.[4]

Since it has been demonstrated in the case of a carbocyclic puromycin analog, that the lack of the ring-*O*-function and the hydroxymethyl group in the ribofuranosyl moiety are not detrimental for bioactivity,[8] it appeared of interest to biologically evaluate adenosine analogs of type **2**, in which the ribofuranose portion is replaced by a tetrahydroxycyclopentane system.

The present report describes the synthesis of five of these 9-(2′,3′,4′,5′-tetrahydroxycyclopentyl)adenines (**2a**—**e**), *i. e.* products that—with respect to the C-2′ and C-3′ arrangement of the OH-groups in adenosine—resemble the *ribo*-configuration (**2a** and **2b**), as well as the *xylo*-(**2a**, **2e**), *lyxo*- (**2d**) and *arabino*-forms (**2b**, **2c**), the latter being conceivably of main interest in view of the antiviral activity of 9-(β-D-arabinofura-

1) Nucleoside Analogs III. Part II: T. Suami, Y. Sakota, N. Karimoto, N. Takoi, and Y. Tsukamoto, This Bulletin, **44**, 1695 (1971).

2) On leave of absence from Institute für Organische Chemie, Technische Hochschule, Darmstadt, Germany.

3) K. C. Murdock and R. B. Angier, *J. Amer. Chem. Soc.*, **84**, 3748, 3758 (1962).

4) Y. F. Shealy and J. D. Clayton, *ibid.*, **88**, 3885 (1966); **91**, 3075 (1969).

5) H. Yamamoto, T. Kusaka, M. Shibata, T. Kishi, M. Muroi, and K. Mizuno, Jap. 23596 (Appl. Dec. 19, 1966); *J. Antibio.* (Tokyo) *Ser. A*, **21**, 255 (1968); T. Kishi, M. Muroi, T. Kusaka, M. Nishikawa, K. Kamiya, and K. Mizuno, *Chem. Commun.*, **1967**, 852; *Chem. Pharm. Bull.*, **20**, 940 (1972).

6) H. J. Schaeffer and R. Vince, *J. Pharm. Sci.*, **11**, 15 (1968).

7) T. Suami, Y. Sato, Y. Fukai, and Y. Sakota, *J. Heterocycl. Chem.*, **6**, 663 (1969).

8) S. Daluge and R. Vince, *J. Med. Chem.*, **15**, 171 (1972).

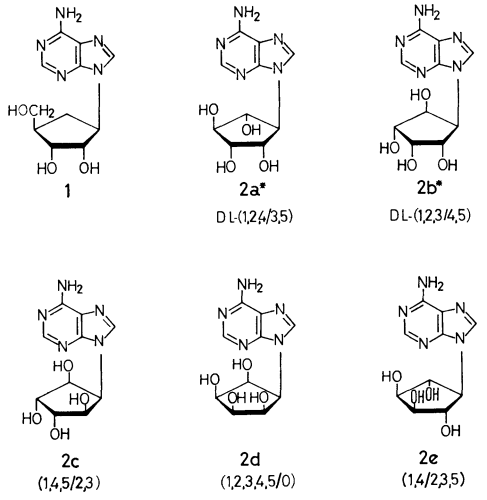

Scheme 1.

*) Formulae **2a** and **2b** depict only one enantiomer of the respective racemate.

nosyl)adenine.[9]

Since methods are available for the stepwise *de novo* construction of the purine base from a cycloalkylamino function,[1,6-8] the principal problem was the preparation of the respective 5-aminocyclopentanetetrols. All ten theoretically possible isomers being known now in the form of their pentaacetyl derivatives,[10] the more readily accessible compounds **3a**—**e**[10-12] were subjected to complete deacetylation with hydrochloric acid to afford the respective aminotetrols **4a**—

Table 1. Aminotetrols, **4a**—**e**

Compd.	Mp (°C)	Yield (%) of crude product	Anal (%) C	H	N
			40.26	7.43	9.39[a]
4a	185—186 (dec)	89	40.51	7.19	9.19
4b	sirup	95	—	—	—
4c	114—118	54	40.24	7.29	9.27
4d	sirup	93	—	—	—
4e	159—161	77	40.59	7.25	9.38

a) Calcd for $C_5H_{11}NO_4$

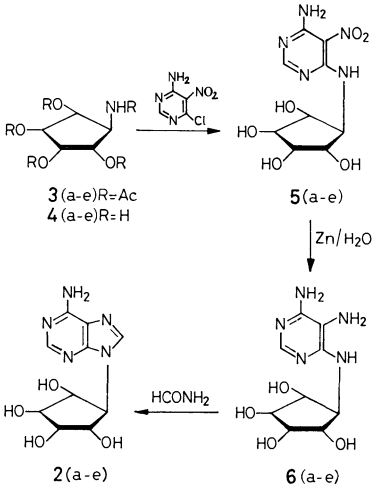

Configurations of Series

a = 1,2,4/3,5 (DL)
b = 1,2,3/4,5 (DL)
c = 1,4,5/2,3 (meso)
d = 1,2,3,4,5/0 (meso)
e = 1,4/2,3,5 (meso)

Table 2. Tetrahydroxycyclopentylamino derivatives, **5a**—**e**

Compd.	Mp (°C) (dec)	Yield (%) of crude product	Anal (%) C	H	N
			37.63	4.56	24.20[a]
5a	266—271	61	37.73	4.42	24.20
5b	247—248	94	37.89	4.41	24.45
5c	263—264	77	37.56	4.61	24.01
5d	240—243	81	37.76	4.45	24.47
5e	250—253	80	37.60	4.31	24.75

a) Calcd for $C_9H_{13}N_5O_6$

e (Table 1). By condensation with 4-amino-5-nitro-6-chloropyrimidine, they were converted into the corresponding 6-tetrahydroxycyclopentylamino derivatives **5a**—**e**, each obtained in crystalline form and quite acceptable yields (Table 2). The next step, reduction of the nitro group, was carried out by using zinc dust as the reductant in boiling water, affording the crude

Table 3. Tetrahydroxycyclopentyladenines, **2a**—**e**

Compd.	Configuration	Mp (°C)	Yield (%)	Anal (%) C	H	N	λ_{max} in nm ($\varepsilon \times 10^3$) pH 1 (0.1M HCl)	pH 7 (H_2O)	pH 13 (0.5% NaOH)
				44.94	4.90	26.21[a]			
2a	1,2,4/3,5	268—270 (dec)	39	45.01	4.85	26.10	259 (23)	261 (21)	261 (19)
2b	1,2,3/4,5	263—264 (dec)	36	44.70	4.71	25.88	259 (9)	260 (17)	263 (16)
2c	1,4,5/2,3	330	30	45.02	4.69	25.98	260 (7)	260 (7)	260 (11)
2d	1,2,3,4,5/0	263—267 (dec)	11	45.10	4.86	26.00	261 (12)	260 (14)	260 (14)
2e	1,4/2,3,5	270—275 (dec)	22	45.24	4.84	25.96	259 (15)	261 (15)	261 (15)

a) Calcd for $C_{10}H_{13}N_5O_4$

9) G. J. Dixon, R. W. Sidwell, F. A. Miller, and B. J. Sloan, *Antimicrobial Agents Chemother.*, 172 **1968** and preceding papers; C. Shipman, Jr., S. H. Smith, and J. C. Drach, *Proc. Natl. Acad. Sci. U. S. A.*, **69**, 1753 (1972); D. Pavan-Langston and C. H. Dohlman, *Amer. J. Ophthalmol.*, **74**, 81 (1972).

10) T. Suami, K. Tadano, S. Nishiyama, and F. W. Lichtenthaler, *J. Org. Chem.*, **38**, (1973) in press.

11) T. Suami, Y. Sakota, K. Tadano, and S. Nishiyama, This Bulletin, **44**, 2222 (1971).

12) R. Ahluwalia, S. J. Angyal, and B. M. Luttrell, *Aust. J. Chem.*, **23**, 1819 (1970).

triaminopyrimidines **6a**—**e** in yields above 70%. Without further purification, they were cyclized by refluxing in formamide to give the title compounds, adenine analogs **2a**—**e** (Table 3), featuring the UV absorption characteristics at pH 1, 7 and 13, required for 9-substituted adenine derivatives.[13]

The antiviral properties of compounds **2a**—**e** are being evaluated. With respect to antifungal activity, **2e** showed an inhibition value of 34% against *piricularia oryzae* (strain Kita No. 373), whilst the pentahydroxycyclohexyl-adenines of *scyllo* and *myo*-2 configuration[1] exhibited values of 30 and 41% respectively, in this systems.

Experimental[14]

Melting points were determined in capillary tubes and uncorrected. UV spectral measurements were effected with a Hitachi EPS-2 instrument. Since preparative procedures employed varied only slightly within the different stereoisomers (a—e series, respectively), general procedures are given exclusively.

*5-Amino-1,2,3,4-cyclopentanetetrols (**4a**—**e**) by Deacetylation of Their Pentaacetates.* The respective tetra-*O*-acetyl-5-acetamido-1,2,3,4-cyclopentanetetrol (**3a**,[10] **3b**,[10] **3c**,[11] **3d**[11] and **3e**,[12] 1.0—1.3 g portions) was refluxed in 6 M hydrochloric acid (10 ml) for 1.5—2.0 h and subsequently evaporated *in vacuo*. The residue was taken up in water and triturated with Amberlite IRA-400 for removal of chloride ions. Charcoal treatment and evaporation to dryness yielded a crystalline residue in the case of **4a**, **4c** and **4e**, which was filtered with ethanol to give the crude products, that were directly used for the ensuing reaction. For analytical samples, small amounts were recrystallized from ethanol giving the data in Table 1. The aminotetrols **4b** and **4d** resisted crystallization from the usual solvents. Their sirups were used for further reactions.

*4-Amino-5-nitro-6-(2′,3′,4′,5′-tetrahydroxycyclopentyl)aminopyrimidines (**5a**—**e**).* The crude aminotetrols (**4a**—**e**), as obtained above (500 mg portions), and 4-amino-5-nitro-6-chloropyrimidine[15] (590 mg, 1.05 mol) were refluxed for 8 h in 2-menthoxyethanol (50 ml) containing 3 ml of triethylamine. On allowing the reaction mixture to cool to ambient temperature, crystallization occurred in the case of **5a**, **5d** and **5e**. The crystals were filtered off to give the crude products used for further experiments. In the cases (**5b** and **5c**), the reaction mixture was evaporated *in vacuo*, followed by crystallization of the residue with a small amount of water (**5b**) or by extraction with ethyl acetate (**5c**), to give the crude products. Small samples of each were recrystallized from water to give the data in Table 2.

*4,5-Diamino-6-(2′,3′,4′,5′-tetrahydroxycyclopentyl)aminopyrimidines (**6a**—**e**).* The respective nitropyrimidines **5a**—**e**, as obtained above (600—700 mg portions), were added to a boiling suspension of 15 g of zinc powder in 150 ml of water with vigorous stirring, and the heating was continued for 8 h. The reaction mixture was filtered whilst still hot. On cooling to ambient temperature, crystallization occurred in all cases except **6b**, which required prior concentration to a small volume. Filtration and drying *in vacuo* gave the crude products, used for the subsequent cyclization, as pale yellow crystals except for **6d**, obtained as an amorphous solid; **6a** (mp 255—258 °C, dec; 85%), **6b** (mp 181—187 °C, dec; 72%), **6c** (mp 151—155 °C; 89%), **6d** (mp 200—210 °C, dec; 98%) and **6e** (mp 260—265 °C, dec; 74%).

*9-(2′,3′,4′,5′-Tetrahydroxycyclopentyl)adenines (**2a**—**e**).* The respective triaminopyrimidines **6a**—**e** (400—500 mg portions) were refluxed in formamide (10—20 ml) for 30—60 min, whereafter the mixture was taken to dryness *in vacuo*. The residue was triturated with water or ethanol to give the crude product, which was recrystallized from water, involving charcoal treatment, to give the analytically pure products of Table 3.

The authors wish to express their appreciation to the Japan Ministry of Education for supporting this investigation and to the Japan Society for the Promotion of Science for granting a Visiting Professorship (to F. W. L.). They are also indebted to Mr. Yukio Sakota for assistance in some experiments.

13) R. K. Robins, K. J. Dille, C. H. Willits, and B. E. Christensen, *J. Amer. Chem. Soc.*, **75**, 263 (1953).

14) For elemental analyses we are indebted to Mr. Saburo Nakada of this department.

15) W. R. Boon, W. G. M. Jones, and G. R. Ramage, *J. Chem. Soc.*, **1951**, 99.

Syntheses of Decadiendiyndials and Tetradecatetraendiyndials and Intramolecular Cyclization of Former Dialdehydes

Ryonosuke MUNEYUKI, Mamoru MORIMOTO, Motomu TANAKA, Tsutomu KATAKAMI, Takayoshi KASHITANI, Masahiko IYODA, and Masazumi NAKAGAWA

Department of Chemistry, Faculty of Science, Osaka University, Toyonaka, Osaka 560

(Received May 1, 1973)

Substituted 2,8-decadien-4,6-diyndials (I, II and III) were synthesized by the oxidative coupling of corresponding substituted pentenynals (VII and XIII) or acetal (XI). It was found that decadiendiyndials (I, II and III) give readily dihydrofuranylidene derivatives (X, XIV and XXV) by the addition of methanol followed by intramolecular cyclization. Thermal reaction of dialdehyde (I, II, and III) afforded difuranylacetylene derivatives (IX, XXI and XXII). 5-Phenyl-2,4-heptadien-6-ynal (XXXII) was prepared from 3-phenyl-2-penten-4-ynal (VIII) or its acetal (XI) by a modified Wittig reaction or by the condensation of ethyl vinyl ether. Oxidative Coupling of XXXII or 5-*t*-butyl-2,4-heptadien-6-ynal afforded 5,10-diphenyl- (XXIX) or 5,10-di-*t*-butyl-2,4,10,12-tetradecatetraen-6,8-diyndial (XXX) which showed no tendency for intramolecular cyclization.

During the course of studies on the syntheses of dehydroannulenes, we have investigated the syntheses of substituted decadiendiyndials (I, II and III) and tetradecatetraendiyndials (XXIX and XXX) which seemed to be potential precursors of dehydroannulenes.

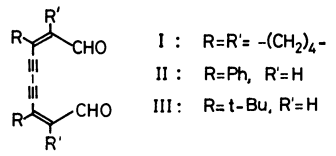

It was found that the dialdehydes (I, II and III) give readily difuranylacetylene derivatives (IX, XXI and XXII) by thermal reaction and dihydrofuranylidene derivatives (X, XIV and XXV) by nucleophilic addition of methanol followed by intramolecular cyclization.

Synthesis. Bis-tetramethylene derivative (I) could be obtained by the reaction sequence outlined in Scheme 1. Acetylenic alcohol (V) obtained by ethynylation of 2-alkoxymethylenecyclohexanone (IV)[1] was treated with cupric acetate in pyridine[2] (the Eglinton's method) to yield hexadiyndiol (VI). Hydrolysis of VI afforded dialdehyde (I). I was also prepared by the Eglinton's oxidative coupling of 1-ethynyl-2-formylcyclohexene[1] (VII) in the presence or absence of methanol. However, the oxidative coupling of 3-phenyl-2-penten-4-ynal (VIII)[3] in the presence of

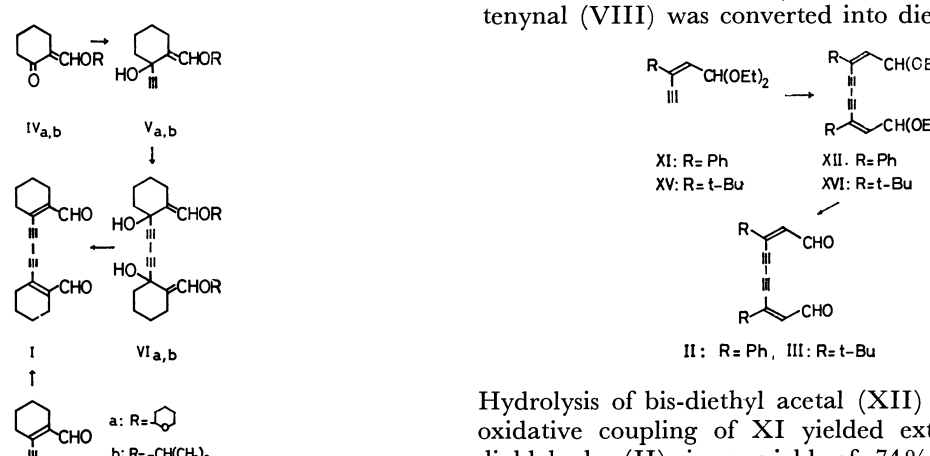

Scheme 1.

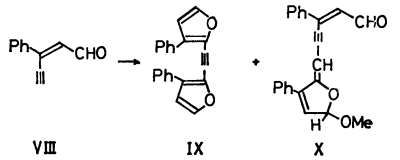

methanol resulted in the formation of bis(3-phenyl-2-furanyl)acetylene (IX, 13%) and dihydrofuranylidene derivative (X, 41%). In the absence of methanol, IX was obtained in a yield of 30.5%. Phenylpentenynal (VIII) was converted into diethyl acetal (XI).

Hydrolysis of bis-diethyl acetal (XII) obtained by the oxidative coupling of XI yielded extremely unstable dialdehyde (II) in a yield of 74%. Formation of appreciable amount of IX was observed when II was allowed to stand for 2 days at room temperature. The Eglinton's reaction of *t*-butylpentenynal (XIII)[4] in the absence of methanol at a low temperature (15—20 °C) afforded dialdehyde (III). However, the re-

1) a) W. S. Johnson and H. Posvic, *J. Amer. Chem. Soc.*, **69**, 1361 (1947); b) R. B. Woodward and W. H. McLamore, *ibid.*, **71**, 379 (1949); c) A. S. Dreiding and S. N. Nickel, *ibid.*, **76**, 3965 (1954); d) P. Schiess and H. L. Chia, *Helv. Chim. Acta*, **53**, 485 (1970); e) G. M. Pilling and F. Sondheimer, *J. Amer. Chem. Soc.*, **93**, 1970 (1971).

2) G. Eglinton and A. R. Galbraith, *J. Chem. Soc.*, **1959**, 889.

3) K. Fukui, T. Okamoto, and M. Nakagawa, *Tetrahedron Lett.*, **1971**, 3121.

4) T. Katakami, S. Tomita, K. Fukui, and M. Nakagawa, *Chem. Lett.*, **1972**, 225.

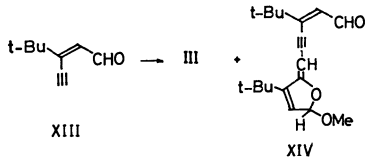

XIII XIV

action performed in the presence of methanol gave a mixture of III and dihydrofuranylidene derivative (XIV). NMR spectroscopy revealed that the mixture consists of 50% of III and 10—15% of XIV. III could be obtained by the hydrolysis of bis-diethyl acetal (XVI) which was prepared by the oxidative coupling of diethyl acetal (XV).[5]

Dialdehyde (XVIII) could not be obtained by the Eglinton's reaction of methylpentenynal (XVII)[6] in the presence of methanol, but the UV spectrum of the product (λ_{max}^{EtOH} 247, 285, 357 nm) was found to be similar with that of X. Attempts to prepare XVIII from diacetylenic glycol (XX) obtained by the Glaser reaction of XIX[6] gave fruitless results owing to sluggish anionotropic rearrangement.

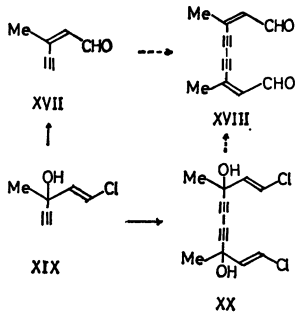

XVII XVIII XIX XX

Thermal Cyclization of Dialdehydes (I, II and III). Formation of bis(2-furanyl)acetylene derivatives (IX, XXI and XXII) was observed on heating solutions of dialdehydes (II, III and I) in organic solvents. The results are summarized in Table 1. This results indicate that the formation of IX in the oxidative coupling of phenylpentenynal (VIII) is attributable to a secondary reaction of initially formed dialdehyde (II). The possibility of catalytic action of cupric acetate in pyridine for the cyclization reaction could be excluded by the experiments performed in benzene or ether containing cupric acetate and pyridine (see Experimental). Intramolecular cyclization of acetylenic compounds containing oxygen function has been well-known.[7] However, the formation of difuranylacetylene derivatives (IX, XXI and XXII) from II, III and I seems to be symmetry-allowed thermal process.

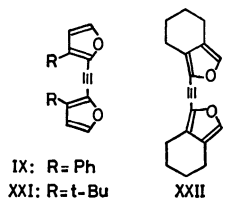

IX: R=Ph
XXI: R=t-Bu XXII

TABLE 1. FORMATION OF DIFURANYLACETYLENES

Dialdehyde	Solvent	Temperature (°C)	Reaction period (hr)	Yield (%)
I	xylene	120	5	XXII 57
II	benzene	50	8	IX 86
III	benzene	60	20	XXI 82
III	pyridine	60	6.5	XXI 54[a]

a) Low yield of XXI can be attributed to gradual decomposition of III in pyridine.

It is to be noted that the mass spectral patterns of II and III were found to be similar to those of IX and XXI indicating facile formation of difuranyl derivatives from II and III prior to the fragmentation.

Formation of Dihydrofuranylidene Derivatives (X, XIV and XXV). The formation of dihydrofuranylidene derivatives (X or XIV) by the Eglinton's oxidative coupling of pentenynals (VIII or XIII) in the presence of methanol can be regarded as a result of secondary reaction of initially formed dialdehydes (II or III), *i. e.*, addition of methanol to carbonyl carbon of dialdehyde forms hemiacetal (XXIII), and nucleophilic attack of oxygen atom of hemiacetal (XXIII) to acetylenic carbon atom gives rise to dihydrofuranylidene compound (XXIV). Because the cyclization reaction did not proceed without pyridine, it is evident that pyridine has a role of proton acceptor.

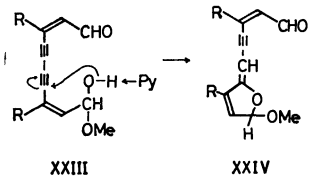

XXIII XXIV

In the case of dialdehyde (I), no cyclization took place by pyridine–methanol. However, treatment of I in ether with sodium methoxide–methanol at 0 °C afforded dihydrofuranylidene derivative (XXV). Dihydrofuranylidene derivative (XXV) could be separated into *cis*-(XXVa) and *trans*-isomers (XXVb) on chromatography on silica gel.

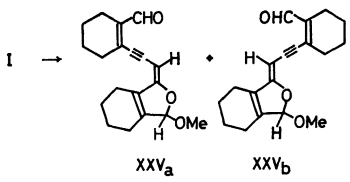

XXV$_a$ XXV$_b$

It is to be noted that acetylenic compounds with analogous dihydrofuranylidene system (XXVIa, XXVIb and XXVII) have been found in naturally occurring poly-ynes.[8] An intramolecular cyclization of ketoalcohol (XXVIII) in biogenetic path way to form XXVII has been postulated by Bohlmann and Florenz.[9]

5) M. Iyoda, H. Miyazaki, and M. Nakagawa, *Chem. Commun.*, **1972**, 431.
6) I. Heilbrom, E. R. H. Jones, and M. Julia, *J. Chem. Soc.*, **1949**, 1430.
7) *E. g.*, F. Toda and M. Nakagawa, This Bulletin, **32**, 514 (1959); **33**, 1287 (1960); W. Ried, *Angew. Chem.*, **70**, 273 (1958).
8) F. Bohlmann, P. Herbst, C. Arndt, H. Schonowsky, and H. Gleinig, *Chem. Ber.*, **94**, 3193 (1961).
9) F. Bohlmann and G. Florenz, *ibid.*, **99**, 990 (1966).

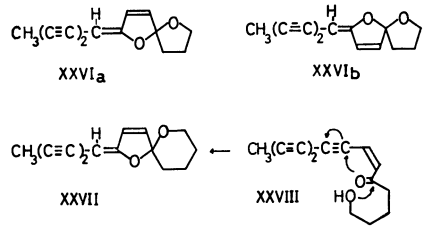

Syntheses of Tetradecatetraendiyndials (XXIX and XXX). Facile intramolecular cyclization observed in decadiendiyndials (I, II and III) can be attributed to the proximate position of oxygen atom of formyl group to acetylenic carbon atom favorable for the formation of stable five-membered ring which is caused by the *cis*-configuration of ethylenic linkage with respect to acetylene and formyl functions. We have prepared diphenyl- (XXIX) and di-*t*-butyltetradecatetraendiyndials (XXX). Expectedly intramolecular cyclization could not be observed in these dialdehydes (XXIX and XXX).

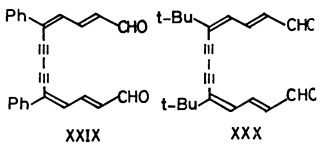

Phenylheptadienynal (XXXII) was prepared by different two routes. Phenylpentenynal (VIII)[3] was treated with diethyl 2-(cyclohexylimino)ethylphosphonate carbanion[10] and the product (XXXI) was hydrolyzed to yield XXXII in a yield of 51%. Condensation of ethyl vinyl ether in the presence of boron trifluoride[11] with acetal (XI) derived from VIII afforded ethoxy acetal (XXXIII) which gave XXXII

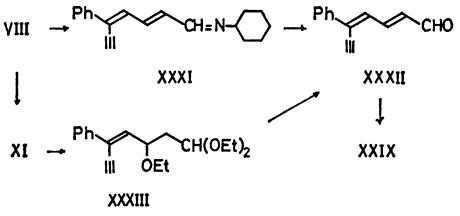

on treatment with hydrochloric acid in tetrahydrofuran. Oxidative coupling of XXXII by the Eglinton's method yielded XXIX in a high yield. Di-*t*-butyltetradecatetraendiyndial (XXX) was obtained similarly from 5-*t*-butyl-2,4-heptadien-6-ynal.[6] Quite recently the preparation of 4,5 : 10,11-bis(tetramethylene)-2,4,10,12-tetradecatetraen-6,8-diyndial, a vinylog of I, was reported by Yamamoto and Sondheimer.[12]

Experimental

All the melting points are not corrected. The UV and IR spectra were obtained on a Hitachi EPS-3T and a Hitachi EPI-2 spectrophotometers, respectively. Shoulder was indicated by an asterisk. The NMR and mass spectra were obtained on a Varian A-60 (internal standard, TMS) and a Hitachi RM-50 (ionization energy, 70 eV) spectrometers, respectively. Chemical shifts are recorded in τ-unit. Silica gel (Merck, Kieselgel 60) and alumina (Merck, act. II–III) were used in the chromatography.

2-Tetrahydropyranoxymethylenecyclohexanone (IVa). 2-Hydroxymethylenecyclohexanone (105.6 g, 0.84 mol) was added over 40-min period to freshly distilled pure 2,3-dihydropyran (84 g, 1.0 mol) containing few drops of phosphoryl chloride under stirring and cooling with running water. After being kept overnight at room temperature, the mixture was stirred for 3 hr at 30 °C and then mixed with ether (150 ml), washed successively with saturated sodium carbonate and sodium chloride solutions. IVa was obtained as a colorless liquid, bp 117—130 °C/6×10^{-4} mmHg, 43.5 g (24.7%), IR (neat): 1670, 1660*, 1590, 1195, 1110, 1075, 1035 cm^{-1}.

Found: C, 67.69; H, 8.58%. Calcd for $C_{12}H_{18}O_3$: C, 68.53; H, 8.63%.

1-Ethynyl-2-tetrahydropyranoxymethylenecyclohexanol (Va). To a suspension of lithium acetylide [from acetylene and lithiumamide (lithium 1.89 g, 0.275 g-atom)] in liquid ammonia (300 ml) was added over a period of 30 min a solution of IVa (52.5 g, 0.25 mol) in ether (100 ml). After the mixture had been stirred for 3.5 hr, the ammonia was allowed to evaporate. The residue was mixed with a saturated solution of ammonium chloride and extracted with ether. The extract was worked up by the usual way. Va was obtained as a viscous liquid, bp 142—144 °C/10^{-3} mmHg, 43.15 g (73.0%).

Found: C, 70.72; H, 8.57%. Calcd for $C_{14}H_{20}O_3$: C, 71.16; H, 8.53%.

1-Ethynyl-2-isopropoxymethylenecyclohexanol (Vb). The reaction of 2-isopropoxymethylenecyclohexanone (IVb)[1] with lithium acetylide in liquid ammonia by the procedure used in Va afforded Vb in a yield of 60% as a colorless liquid, bp 76.1—77.0 °C/4×10^{-3} mmHg, n_D^{20} 1.4936.

Found: C, 73.50; H, 9.25%. Calcd for $C_{12}H_{18}O_2$: C, 74.19; H, 9.34%.

2-Ethynyl-1-cyclohexenecarboxaldehyde (VII). To a stirred solution of Va (20 g) in tetrahydrofuran (250 ml) was added 10% aqueous sulfuric acid (35 ml). After being kept at room temperature overnight, the reaction mixture was washed successively with saturated sodium chloride, 10% sodium carbonate and saturated sodium chloride solutions, and dried. Evaporation of the solvent under reduced pressure afforded faint brown crystals, 7.3 g (64%). Vacuum sublimation of the crystals yielded pure VII, mp 50—51 °C [lit. 52—53 °C[13]; 49.5—50 °C[1e]].

Found: C, 80.17; H, 7.51%. Calcd for $C_9H_{10}O$: C, 80.56; H, 7.51%.

Bis(2-formyl-1-cyclohexenyl)-1,3-butadiyne (I). *1) From Va*: A solution of Va (43.0 g, 0.182 mol) in pyridine (150 ml) was added to a mixture of cupric acetate monohydrate (120 g) and pyridine (900 ml). After being stirred overnight at room temperature, the mixture was stirred at 40 °C for 7 hr. Insoluble material was removed by filtration and washed thoroughly with ether. The combined filtrate and washings were concentrated under reduced pressure (bath temp. below 80 °C). The residue was dissolved in ether. After being washed 4 times with saturated sodium chloride solution and dried, the solvent was removed under reduced pressure to give crude VIa. Crude VIa was dis-

10) W. Nagata and Y. Hayase, *J. Chem. Soc., C*, **1969**, 460.

11) R. Rüegg, M. Montavon, G. Ryser, G. Saucy, U. Schwiter, and O. Isler, *Helv. Chim. Acta*, **42**, 854 (1959).

12) K. Yamamoto and F. Sondheimer, *Angew. Chem.*, **85**, 41 (1973).

13) P. Schiess, H. L. Chia, and Chr. Seeter, *Tetrahedron Lett.*, **1968**, 5747.

solved in a mixture of sulfuric acid (10 ml), water (90 ml) and tetrahydrofuran (900 ml) and the mixture was allowed to stand at room temperature for 22 hr. After being stirred for 1.5 hr at 50 °C, the reaction mixture was worked up by the usual way. The oily residue (29.5 g) obtained by evaporating the solvent *in vacuo* was chilled in a dry ice-acetone bath to result in crystallization. The crystals were filtered and recrystallized from benzine to give pure I, pale yellow crystals, 5.4 g, mp 89.0—90.5 °C; UV: $\lambda_{max}^{95\%EtOH}$ (ε) 205.5 (22150), 231* (10050), 238.5 (13470), 258* (12300), 270 (14550), 290 (15900), 317 (15800), 334(16800), 358(12400) nm, IR (KBr-disk): 1670 (C=O), 1580 (C=C) cm^{-1}, NMR ($CDCl_3$): −0.12 (s, 2H, CHO), 7.62 (m, 8H, allylic CH_2), 8.32 (m, 8H, non-allylic CH_2), Mass (*m/e*): 266 (M^+), 239 (M–29).

Found: C, 80.91; H, 6.95%. Calcd for $C_{18}H_{18}O_2$: C, 81.17; H, 6.81%.

The mother liquors were chromatographed on alumina to yield second crop of I.

2) From VII. a) Oxidative Coupling in the Presence of Methanol: A solution of VII (200 mg, 1.49 mmol) in pyridine (2 ml) was added to a mixture of cupric acetate monohydrate (1.00 g, 5.01 mmol), pyridine (5 ml) and methanol (3 ml). After being stirred for 2 hr at 16 °C, the reaction mixture was poured onto 3 M hydrochloric acid (50 ml) and extracted with ether (20 ml×3). The extract, after being washed and dried, was evaporated under reduced pressure. The crystals thus obtained was chromatographed on alumina. Elution with *n*-hexane–benzene (1 : 1) and benzene afforded pure I, 171 mg (86%).

b) Oxidative Coupling in the Absence of Methanol: To a mixture of cupric acetate monohydrate (1.00 g, 5.01 mmol) and pyridine (7 ml) was added a solution of VII (200 mg, 1.49 mmol) in ether (3 ml). After being stirred for 6 hr at 16 °C, the reaction mixture was worked up to give I, 183 mg (92%).

3-Phenyl-2-penten-4-ynal Diethyl Acetal (XI). A solution of *p*-toluenesulfonic acid monohydrate (0.385 g, 2.02 mmol) in ethanol (2 ml) was added to a mixture of VIII[3] (3.852 g, 24.7 mmol) and ethyl orthoformate (13.25 g, 89.4 mmol). After being stirred for 24 hr at room temperature, the reaction mixture was chilled in an ice-bath and then poured onto ice-water containing sodium hydrogen carbonate, and extracted with ether. The extract, after being washed and dried (potassium carbonate), was concentrated under reduced pressure. The residue was distilled *in vacuo* to yield XI, 4.948 g (87%), bp 93—96 °C/0.005 mmHg, Mass (*m/e*): 230 (M^+), IR (CCl_4): 3321 (C≡CH), 2090 (–C≡C–), 1615 (C=C), 1000—1150 (C–O–C) cm^{-1}. NMR (CCl_4): 2.31—2.82 (m, 5H, phenyl), 3.62 (d, J=7.5 Hz, 1H, olefinic), 4.60 (d, J=7.5 Hz, 1H, acetal), 6.38 (q, J=7.0 Hz, 2H, CH_2), 6.42 (q, J=7.0 Hz, 2H, CH_2), 6.70 (s, 1H, C≡CH), 8.82 (t, J=7.0 Hz, 6H, CH_3).

Elemental analysis gave unsatisfactory result owing to extremely unstable nature of XI to hydrolysis.

3,8-Diphenyl-2,8-decadien-4,6-diyndial (II). To a solution of XI (327 mg, 1.42 mmol) in ether (3 ml) was added a mixture of cupric acetate monohydrate (566 mg, 2.83 mmol), pyridine (6 ml) and ether (2 ml). The mixture was stirred at 15 °C for 17 hr and then poured onto 3 M hydrochloric acid (49 ml), and extracted with ether (20 ml×4). The extract was washed successively with water, saturated solutions of sodium hydrogen carbonate and sodium chloride, and evaporated under reduced pressure. The residue (XII) containing water was mixed with 20% aqueous acetic acid (5 ml) and the mixture was stirred for 15 min at room temperature. The reaction mixture containing light brown crystals was mixed with water (40 ml) and extracted with dichloromethane (30 ml×4). The extract, after being washed and dried, was concentrated under reduced pressure to yield crystals. Chromatography of the crystals on silica gel followed by elution with carbon tetrachloride containing 10—20% dichloromethane afforded pure II, yellow crystals, 163 mg (74%), mp 119.4—120.3 °C, Mass (*m/e*): 310 (M^+), IR (KBr-disk): 2850, 2740 (CHO), 2135 (–C≡C–), 1668 C=O), 1581, 1560 (C=C) cm^{-1}, NMR ($CDCl_3$): −0.27 (d, J=8.0 Hz, 2H, CHO), 2.01—2.68 (m, 10H, phenyl), 3.07 (d, J=8.0 Hz, 2H, olefinic).

Found: C, 84.86; H, 4.57%. Calcd for $C_{22}H_{14}O_2$: C, 85.14; H, 4.55%.

Bis(3-phenyl-2-furanyl)acetylene (IX). A solution of II (93 mg, 0.30 mol) in benzene (4 ml) was kept at 50 °C for 8 hr. The reaction mixture was concentrated unduer reduced pressure and chromatographed on alumina. Elution with carbon tetrachloride–20% dichloromethane afforded IX, colorless crystals, 81 mg (86%), mp 131.5—131.8 °C (from benzene–*n*-hexane), Mass (*m/e*): 310 (M^+), IR (KBr-disk): 3140, 3215 (furan CH), 892 (furan) cm^{-1}, NMR ($CDCl_3$): 2.50 cd, J=2.0 Hz, 2H, α–H of furan), 2.10—2.87 (m, 10H, phenyl), 3.76 (d, J=2.0 Hz, 2H, β–H of furan), UV: λ_{max}^{EtOH} (ε) 231.5, (32900), 258.5* (14800), 342.5 (17500) nm.

Found: 84.84; H, 4.52%. Calcd for $C_{22}H_{14}O_2$: C, 85.14; H, 4.55%.

6-(5-Methoxy-3-phenyl-2-dihydrofuranylidene)-3-phenyl-2-penten-4-ynal (X). a) In the Presence of Pyridine and Methanol: A solution of II (83 mg, 0.26 mmol) in pyridine (5 ml) and methanol (8 ml) was stirred for 2 hr at 30 °C, and then the mixture was poured onto 3 M hydrochloric acid (40 ml). The mixture was extracted with dichloromethane (30 ml×4). The extract, after being washed and dried, was concentrated under reduced pressure. Brownish oily residue was chromatographed on silica gel and eluted with benzene to yield X as pale brown oil, 78 mg (85%), Mass (*m/e*): 342 (M^+), IR (neat): 2180 (–C≡C–), 1662 (C=O), 1620 (C=C) cm^{-1}. The NMR spectrum of X showed complexes pattern owing to the presence of *cis*- and *trans*-isomers.

A solution of 2,4-dinitrophenylhydrazine (97 mg, 0.49 mmol) and phosphoric acid (1.2 ml) in ethanol (0.8 ml) was added to a solution of X (47 mg, 0.13 mmol) in ethanol (8 ml) and the mixture was stirred for 15 hr at room temperature. Red crystals deposited were washed thoroughly with benzene. Red crystals obtained by evaporating the washings under reduced pressure were chromatographed on silica gel. Elution with benzene afforded pure 2,4-dinitrophenylhydrazone of X red crystals, mp 208.4—209.8 °C, 58 mg (81%).

Found: C, 66.61; H, 4.22; N, 10.51%. Calcd for $C_{22}H_{22}N_4O_6$: C, 66.66; H, 4.24; N, 10.27%.

b) In the Absence of Pyridine: A solution of II (108 mg, 0.34 mmol) in methanol (10 ml) and ether (5 ml) was stirred for 28 hr at 30 °C. Brown oily residue obtained by evaporating the solvent was chromatographed on silica gel, and eluted with benzene. IX (39 mg, 36%) was obtained from early fractions and the following fractions afforded II (28 mg, 26%) and then X (35 mg, 29%).

Oxidative Coupling of Phenylpentenynal (VIII). a) In the Presence of Methanol. A solution of VIII[3] (1.00 g, 6.4 mmol) in pyridine (10 ml) and methanol (10 ml) was added to a mixture of cupric acetate monohydrate (5.00 mg, 0.025 mol), pyridine (30 ml) and methanol (10 ml). After being stirred for 30 min at room temperature, the mixture was poured onto 3 M hydrochloric acid (200 ml) and extracted with benzene. The extract was washed successively with water, saturated sodium hydrogen carbonate and sodium

chloride solutions and dried. Chromatography of the residue obtained by evaporating the extract afforded IX, 127 mg (13%) and X, 449 mg (41%).

b) In the Absence of Methanol. To an ice-cooled so-solution of cupric acetate monohydrate (2.00 g, 0.010 mol) in pyridine (20 ml) was added a solution of VIII (1.00 g, 0.0064 mol) in ether (15 ml). After the mixture had been stirred for 12 hr at 15—20 °C, ice-cooled 3 M hydrochloric acid (100 ml) was added and the mixture was extracted with dichloromethane (30 ml×3). The extract, after being washed and dried, was concentrated under reduced pressure. The residue was chromatographed on alumina. The fractions eluted with carbon tetrachloride containing 10—20% of dichloromethane afforded IX (303 mg, 30.5%).

3,8-Di-t-butyl-2,8-decadien-4,6-diyndial (III). a) From XIII: A solution of XIII (945 mg, 6.94 mmol) in ether (12 ml) was added to a mixture of cupric acetate monohydrate (2.10 g, 10.5 mmol) and pyridine (20 ml) and the mixture was stirred for 24 hr at 15—20 °C. The reaction mixture was poured onto 3 M hydrochloric acid (110 ml) and extracted with ether (40 ml×3). The extract was worked up by the usual way. Crude crystals obtained were chromatographed on alumina. Elution with benzene yielded pure III, mp 83.3—84.5 °C (from benzene-*n*-hexane), pale yellow needles, 765 mg (80%), Mass (*m/e*): 270 (M^+), IR (KBr-disk): 2115 (–C≡C–), 1681 (C=O), 1574 (C=C) cm^{-1}; NMR ($CDCl_3$): −0.09 (d, J=7.5 Hz, 2H, CHO), 3.61 (d, J=7.5 Hz, 2H, olefinic), 8.74 (s, 18H, *t*-Bu), UV: λ_{max}^{EtOH} (ε) 224.5* (13200), 232.0 (14400), 253.5 (13200), 264.5 (14300), 280.0 (14100), 303.5* (10500), 322.0 (12200), 343.5 (8300) nm.

Found: C, 80.14; H, 8.20%. Calcd for $C_{18}H_{22}O_2$: C, 79.96; H, 8.20%.

b) From XV: To a stirred mixture of cupric acetate monohydrate (50 g) and pyridine (300 ml) was added a solution of XV[5] (9.50 g, 0.045 mol) in pyridine (50 ml) at 50 °C and the mixture was stirred for 2 hr at the same temperature. The cooled reaction mixture was poured onto a mixture of cracked ice and dilute hydrochloric acid, and extracted with ether. The extract, after being washed and dried, was concentrated under reduced pressure to give crude XVI [NMR (CCl_4): 3.19 (d, J=7.0 Hz, 2H, olefinic), 4.86 (d, J=7.0 Hz, 2H, acetal), 6.44 (q, J=7.0 Hz, 4H, CH_2), 6.49 (q, J=7.0 Hz, 4H, CH_2), 8.82 (t, J=7.0 Hz, 12H, CH_3), 8.82 (s, 18H, *t*-Bu)]. Crude XVI was mixed with acetic acid (250 ml) and water (80 ml). After being stirred for 30 min, the mixture was worked up by the usual way and chromatographed on alumina to yield pure III, 6.6 g (55% based on XV).

Oxidative Coupling of XIII in the Presence of Methanol. A mixture of XIII (500 mg, 3.64 mmol), cupric acetate monohydrate (1.706 g, 8.54 mmol), pyridine (15 ml) and methanol (11 ml) was stirred for 22 hr at room temperature. The reaction mixture was worked up by the usual way to give brownish crystals. The crystals were chromatographed on alumina and eluted with benzene. A mixture of III and 6-(5-methoxy-3-*t*-butyl-2-dihydrofuranylidene)-3-*t*-2-penten-4-ynal (XIV was obtained by evaporating the benzene eluate. The approximate composition of the mixture could be estimated to be III, 250 mg (50%) and XIV, 70—75 mg (10—15%) by an NMR spectroscopy.

Oxidative Coupling of 1-Chloro-3-methyl-1-penten-4-yn-3-ol (XIX). A mixture of XIX[6] (2.7 g, 0.0207 mol), methanol (20 ml), cuprous chloride (0.3 g), ammonium chloride (1.7 g) and one drop of concentrated hydrochloric acid was stirred vigorously for 3.5 hr under a slightly elevated pressure of oxygen. Insoluble material was removed by filtration and washed with methanol. The combined filtrate and washings were concentrated under reduced pressure and the residue was extracted with ether. The extract was washed with 5% hydrochloric acid and water, successively, and dried. The residue obtained by evaporating the solvent was chromaotgraphed on alumina. Elution with benzene afforded 1,10-dichloro-3,8-dimethyl-1,9-decadien-4,6-diyn-3,8-diol (XX), colorless crystals, mp 65—70 °C, IR (Nujol mull): 3350, 3090, 3000, 2950, 2880, 2160, 1630, 1485, 1450, 1375, 930, 825 cm^{-1}, NMR (CCl_4): 3.47 (d, J=13.4 Hz, 2H, H^1), 4.00 (d, J=13.4 Hz, 2H, H^2), 6.60 (s, 2H, OH), 8.40 (s, 6H, CH_3).

Found: C, 55.03; H, 4.58; Cl, 27.15%. Calcd for $C_{12}H_{12}O_2Cl_2$: C, 55.62; H, 4.67; Cl, 27.39%.

Treatment of XIX with cupric acetate-pyridine resulted in recovery of the starting material.

Bis(3-t-butyl-2-furanyl)acetylene (XXI). a) Thermal Cyclization in the Absence of Pyridine. A solution of III (82 mg, 0.3 mmol) in benzene (4 ml) was stirred for 20 hr at 60 °C. Concentration of the reaction mixture under reduced pressure afforded yellow crystals (81 mg) which were chromatographed on alumina and eluted with *n*-hexane containing 20—30% of benzene. Evaporation of the eluate yielded XXI, pale yellow crystals, 68 mg (82%), mp 42.0—42.6 °C (from ether-*n*-hexane), Mass (*m/e*): 270 (M^+), IR (KBr-disk): 3130 (furan C–H), 1585 (C=C), 890 (furan) cm^{-1}, NMR ($CDCl_3$): 2.69 (d, J=2.0 Hz, 2H, α–H of furan), 3.62 (d, J=2.0 Hz, 2H, β–H of furan), 8.64 (s, 18H, *t*-Bu), UV: λ_{max}^{EtOH} (ε) 253.0 (16200), 296.0* (19700), 300.5 (20100), 318.5* (12600) nm.

Found: C, 80.20; H, 8.27%. Calcd for $C_{18}H_{22}O_2$: C, 79.96; H, 8.20%.

Bis(3,4-tetramethylene-2-furanyl)acetylene (XXII). a) Cyclization at 120 °C. A solution of I (112 mg) in *p*-xylene (5 ml) was kept at 120 °C for 5 hr. Crystals obtained by removing the solvent under reduced pressure was chromatographed on alumina (5 g). Elution with *n*-hexane–benzene (1 : 1) afforded XXII, colorless crystals, mp 146—147 °C (from benzine), 64 mg (57%), Mass (*m/e*): 266 (M^+, base peak), IR (KBr-disk): 2170 (–C≡C–), 1547 (C=C), 1505 (C=C) cm^{-1}, NMR ($CDCl_3$): 2.87 (s, 2H, α–H of furan), 7.43 (m, 8H, allylic CH_2), 8.29 (m, 8H, non-allylic CH_2).

Found: C, 81.02; H, 6.88%. Calcd for $C_{18}H_{18}O_2$: C, 81.17; H, 6.81%.

b) Cyclization at 60 °C. A solution of I (104.5 mg) in benzene (5 ml) was heated to 60 °C for 2 hr. Chromatography on alumina (3 g) of the reaction mixture yielded XXII, 1.9 mg (1.8%) and recovered I, 76.9 mg (73.6%).

Cyclization of III in the Presence of Cupric Acetate and Pyridine. To a mixture of cupric acetate monohydrate (184 mg, 0.92 mmol) and pyridine (4 ml) maintained at 60±2 °C was added a solution of III (198 mg, 0.73 mmol) in benzene (10 ml). The mixture was stirred in nitrogen atmosphere at the same temperature for 5 hr, then poured onto 3 M hydrochloric acid (30 ml) and extracted with ether (30 ml×3). The extract was washed and dried. A mixture of light brown crystals and liquid obtained by evaporating the extract was chromatographed on alumina and eluted with *n*-hexane containing 20% of benzene to yield XXI, 91 mg (46%). The results of reactions performed under different conditions are summarized in Table 2.

cis- and trans-1-(2-Formylcyclohexenyl)-3-(3,4-tetramethylene-5-methoxy-2-dihydrofuranylidene)-1-propyne (XXVa and XXVb). To an ice-cooled solution of I (186 mg, 0.698 mmol) in ether (10 ml) was added 1 M solution of sodium methoxide in methanol (2 ml). After being stirred for 30 min at the same temperature, the mixture was mixed with 3 M hydro-

TABLE 2. FORMATION OF XXI IN THE PRESENCE OF CUPRIC ACETATE

Temp. °C	II (mg)	$Cu(OAc)_2 \cdot H_2O$ (mg)	Solvent (ml)	Reaction time (hr)	XXI (mg) (%)
40	221	250	pyridine 4 + benzene 10	24	92 (41)
50	193	409	pyridine 4 + ether 3	24	109 (56)

chloric acid (1 ml) and extracted with ether (20 ml). The extract, after being washed and dried, was concentrated under reduced pressure. Brownish yellow oily residue was chromatographed on silica gel to yield a mixture of XXVa and XXVb (187 mg, 90%). The mixture was re-chromatographed on silica gel. Elution with benzene resulted in the separation of isomers. XXVa was obtained from early fractions, yellow crystals, mp 115.6—116.2 °C (from benzene-methanol), Mass (*m/e*): 298 (M^+), 267 (M–31), 266 (M–32), IR (KBr-disk): 2160 (–C C–), 1670 (C=O), 1626 (C=C), 1580 (C=C) cm^{-1}, NMR ($CDCl_3$): −0.10 (s, 1H, CHO), 4.26 (s, 1H, hemiacetal), 4.80 (s, 1H, olefinic), 6.58 (s, 3H, OCH_3), 7.25—8.00 (m, 8H, allylic CH_2), 8.29 (m, 8H, non-allylic CH_2), UV: λ_{max}^{EtOH} (ε) 249* (10900), 256 (11200), 286.5 (8750), 360 (20500) nm.

Found: C, 76.33; H, 7.44%. Calcd for $C_{19}H_{22}O_3$: C, 76.48; H, 7.43%.

Evaporation of the following benzene eluates afforded XXVb, yellow crystals, mp 91.5—93.0 °C (from methanol), Mass (*m/e*): 298 (M^+), IR (KBr-disk): 2175 (–C≡C–), 1663 (C=O), 1626 (C=C), 1578 (C=C) cm^{-1}, NMR ($CDCl_3$): −0.27 (s, 1H, CHO), 4.18 (s, 1H, hemiacetal), 5.33 (s, 1H, olefinic), 6.50 (s, 3H, OCH_3), 7.40—8.00 (m, 8H, allylic CH_2), 8.29 (m, 8H, non-allylic CH_2).

Found: C, 75.86; H, 7.42%. Calcd for $C_{19}H_{22}O_3$: C, 76.48; H, 7.43%.

XXVa and XXVb showed closely related mass, IR and UV spectra. However, marked difference of chemical shifts of olefinic protons between XXVa (4.80) and XXVb (5.33) was observed. The structure of XXVa was assigned to the isomer with low τ-value, because the olefinic proton in XXVa is dishielded by the magnetic anisotropy of oxygen atom of dihydrofuran ring.

5-Phenyl-2,4-heptadien-6-ynal (XXXII). a) By the Modified Wittig Reaction: Sodium hydride dispersion in mineral oil (50%, 1.84 g, 0.383 mol) was washed under nitrogen atmosphere with petroleum ether (3 ml×4). The sodium hydride, after being dried *in vacuo*, was mixed with tetrahydrofuran (10 ml) and a solution of diethyl 2-(cyclohexylimino)ethylphosphonate[10] (10.0 g, 0.0383 mol) in the same solvent (30 ml) was added under ice-cooling and the mixture was stirred for 15 min. A solution of VIII (2.00 g, 0.0128 mol) in the same solvent (15 ml) was then added at −15 °C. The mixture was stirred at −10——15 °C for 15 hr, then poured onto ice-water, and extracted with ether (30 ml×3). After being washed and dried, the extract was evaporated under reduced pressure to yield a crude mixture containing XXXI, dark brown oil, 8.07 g. The material was dissolved in benzene (60 ml) and mixed with 1% aqueous solution of oxalic acid (180 ml). After being stirred for 15 hr at 20—25 °C, the organic layer was separated and the aqueous layer was extracted with dichloromethane (20 ml×2). The combined organic layer was washed and dried. The residue obtained by evaporating the solvent was chromatographed on silica gel. Elution with carbon tetrachloride and dichloromethane afforded XXXII, yellow crystals (from carbon tetrachloride–methanol), mp 69.5—70.3 °C, 1.18 g (51%), IR ($CHCl_3$): 3300 (≡C–H), 2085, 2710 (CHO), 1686 (C=O), 1608 (C=C) cm^{-1}, NMR (CCl_4): 0.33 (d, J=7.5 Hz, 1H, CHO), 2.06—2.95 (m, 8H, phenyl and olefinic), 3.75 (dd, J=7.5 and 15 Hz, α-position of CHO), 6.32 (s, 1H, ≡C–H).

Found: C, 85.73; H, 5.48%. Calcd for $C_{13}H_{10}O$: C, 85.69; H, 5.53%.

b) By the Isler's Method: A solution of borontrifluoride etherate (72 mg) in benzene (1 ml) was added to a solution of acetal (XI, 16.98 g, 0.0737 mol) in the same solvent (23 ml). at 40 °C and a solution of ethyl vinyl ether (6.233 g, 0.0864 mol) in the same solvent (10 ml) was slowly added at 40—45 °C. The mixture was kept at the same temperature for 4 hr and then allowed to cool on standing. Finely powdered potassium carbonate was added to the mixture. The filtrate was concentrated under reduced pressure to give crude XXXIII, brown oil, 22.68 g. A mixture of crude XXXIII, tetrahydrofuran (187 ml) and 3 M hydrochloric acid (125 ml) was vigorously stirred at 25 °C for 48 hr. The reaction mixture was extracted with ether. The extract, after being washed and dried, was concentrated under reduced pressure. Oily residue containing crystals was purified by a chromatography on silica gel to yield pure XXXII, 8.168 g (61% based on XI).

5,10-Diphenyl-2,4,10,12-tetradecatetraen-6,8-diyndial (XXIX). To a mixture of XXXII (740 mg, 4.07 mmol), methanol (5 ml) and pyridine (5 ml) was added a solution of cupric acetate monohydrate (3.50 g) in methanol (25 ml) and pyridine (25 ml). After being stirred for 3 hr at 25 °C, the mixture was chilled on an ice-bath, mixed with 3 M hydrochloric acid, and extracted with chloroform (30 ml×3). The extract, after being washed and dried, was concentrated under reduced pressure. The residue was chromatographed on silica gel (30 g) and eluted with carbon tetrachloride–dichloromethane to yield XXIX, yellow crystals, 691 mg (94%). The crystals dissolved in benzene was passed through a short column of alumina. Concentration of the filtrate afforded pure XXIX, orange yellow crystals, mp *ca.* 155 °C (decom.) (from benzene–cyclohexane), IR ($CHCl_3$): 1677 (C=O), 1603 (C=C) cm^{-1}, NMR ($CDCl_3$): 0.31 (d, J=8.0 Hz, 2H, CHO), 1.93—2.78 (m, 16H, phenyl and olefinic), 3.58 (dd, J=8.0 Hz and 15 Hz, 2H, olefinic H^2).

Found: C, 86.56; H, 4.98%. Calcd for $C_{26}H_{18}O_2$: C, 86.16; H, 5.01%.

5,10-Di-t-butyl-2,4,10,12-tetradecatetraen-6,8-diyndial (XXX). A solution of 5-*t*-butyl-2,4-heptadien-6-ynal[5] (1.20 g, 7.4 mmol) in pyridine (10 ml) and methanol (10 ml) was added to a mixture of cupric acetate monohydrate (5.00 g), pyridine (40 ml) and methanol (40 ml). After being kept at 25 °C for 21 hr, the reaction mixture was worked by up by the way used for XXIX. Crude yellow crystals thus obtained were chromatographed on alumina to yield pure XXX, 1.01 g (85%), yellow crystals, mp 154.4—155.7 °C (from benzene–*n*-hexane), IR (KBr-disk): 2745 (CHO), 2230 (–C≡C–), 1677 (C=O), 1604 (C=C) cm^{-1}, NMR ($CDCl_3$): 0.29 (d, J=8.0 Hz, 2H, CHO), 2.39 (dd, J=11 Hz and 15 Hz, 2H, H^3, H^{12}), 3.30 (d, J=11 Hz, 2H, H^4, H^{11}), 3.67 (dd, J=8.0 Hz and 15 Hz, 2H, H^2, H^{13}), 8.73 (s, 18H, *t*-Bu).

Found: C, 81.91; H, 8.17%. Calcd for $C_{22}H_{26}O_2$: C, 81.95; H, 8.13%.

Chemical Evidence for the Existence of pπ-dπ Interaction between the Unsaturated Bond and the Sulfur Atom in Allyl and Vinyl Sulfide Systems[1)]

Iwao OJIMA and Kiyosi KONDO*

Sagami Chemical Research Center, Nishi-Onuma, Sagamihara 229

(Received January 26, 1973)

Chemical evidence for the activation of double bonds by the use of 3d orbitals of the sulfur atom was observed in the reaction of allyl benzyl sulfide and phenyl vinyl sulfide with diazomethane. Similar supporting evidence was also obtained in the reaction of acetophenone tosylhydrazone with allyl benzyl sulfide in the presence of sodium methoxide at 150 °C. It was found that there should not be any important role of the oxygen atom of allyl benzyl ether in directing the orientation of the 1,3-dipolarophile.

It is well known that the thermal cycloaddition of diazoalkanes to the simple non-conjugated olefins is a very slow and difficult process.[2,3)] Thus, nowadays the thermal or photochemical formation of cyclopropanes from diazoalkanes and non-conjugated olefins is believed to be a carbenic process.[4)] Certain diazoalkanes bearing an allylthio-substituent have, however, been found to undergo a ready intramolecular cycloaddition to produce pyrazolines, which were thereafter further transformed into cyclopropanes under the same reaction conditions.[5)] 1-Phenyl-3-thiabicyclo[3.1.0]hexane (**1**) was obtained by the thermal decomposition at 150 °C, or by the photolysis at 10 °C, of α-(allylthio)acetophenone tosylhydrazone (**2**) in the presence of sodium methoxide. The carbenic process could be observed in this α-allylthio system when the photolysis was carried out at −70 °C; this process afforded an entirely different product, **3**.[6)] Thus, the formation of **1** may mean that an intramolecular cycloaddition of the diazoalkane moiety to the double bond of the allylthio group and a subsequent elimination of molecular nitrogen really do occur under the present reaction conditions. Conclusive evidence for the intramolecular thermal cycloaddition of the diazoalkane was observed when 4-allylthio-4-methylpentan-2-one tosylhydrazone (**4**) was used as a substrate. Thus, the bicyclic pyrazoline, **5**, was actually isolated in the thermal decomposition of **4** in the presence of sodium methoxide; the pyrazoline, **5**, was then further converted to the 3-thiabicyclo[4.1.0]heptane, **6**, by irradiation.[5)] These facts seem to indicate that the intramolecular thermal cycloaddition is a ready process even at 10 °C and that the subsequent elimination of nitrogen is also an effective process under the photolytic conditions. The high efficiency of the intramolecular cycloaddition to the isolated double bond may be partly due to some kind of activating effect of the sulfur atom in the molecule as well as to the *intramolecular* nature of the reaction.

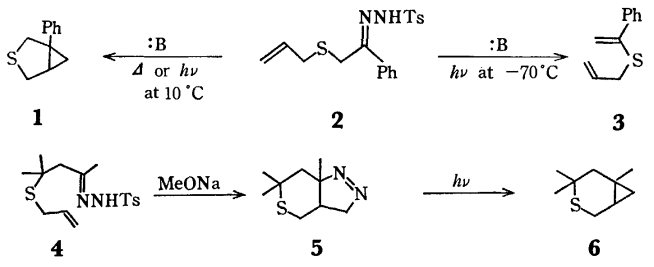

Scheme 1.

In order to clarify the activating effect of the sulfur atom, *intermolecular* cycloadditions of diazoalkanes to allyl sulfide and vinyl sulfide systems were investigated. This paper will deal with the evidence for the existence of pπ–dπ interaction between the sulfur atom and the unsaturated bond.

Results and Discussion

Acetophenone tosylhydrazone was thermally decomposed in the presence of an equivalent of sodium methoxide and two equivalents of allyl benzyl sulfide in diglyme at 150 °C. The products were separated by column chromatography on silica gel to give 1-(benzylthio)methyl-2-methyl-2-phenylcyclopropane (**9**) in a 28% yield (**9a**/**9b**=29/71). The formation of the cyclopropane, **9**, can be accounted for either by the attack of a carbene intermediate on the olefin or by the 1,3-dipolar cycloaddition of phenylmethyldiazomethane to the unsaturated bond, followed by the loss of a nitrogen molecule. The former possibility seems to be less likely, for recent investigations have shown that the reaction of allylic sulfides with carbene or carbenoid species appears to involve mainly a [2.3]sigmatropic rearrangement of the intermediately-formed allyl sulfonium ylides.[7)] Moreover, in the above system, the generated carbene is prone to be converted to acetophenone azine or styrene smoothly.[8)] Though the reaction mixture was carefully examined, the sulfide, **7**, could not be detected in the product.

These considerations lead us to speculate that the cyclopropanes (**9a** and **7b**) were formed through the pyrazoline (**8a** or **8b**), and that subsequently the

* To whom correspondence should be addressed.

1) A part of this work was reported in preliminary form: K. Kondo and I. Ojima, *Chem. Lett.*, **1972**, 771.

2) R. Huisgen, R. Grashey, and J. Sauer in "The Chemistry of Alkenes," ed. S. Patai, Interscience, New York (1964), pp. 830—831.

3) H. Paul, I. Lange and A. Kausmann, *Chem. Ber.*, **98**, 1789 (1965).

4) W. Kirmse, "Carbene Chemistry," Academic Press, New York (1964).

5) K. Kondo and I. Ojima, *Chem. Commun.*, **1972**, 63.

6) K. Kondo and I. Ojima, *ibid.*, **1972**, 62.

7) For example, W. Kirmse, and M. Kapps, *Chem. Ber.*, **101**, 994, 1004 (1968); W. Ando, T. Yagihara, S. Tozune, and T. Migita, *J. Amer. Chem. Soc.*, **91**, 2786 (1969); W. Ando, T. Yagihara, S. Tozune, I. Imai, J. Suzuki, T. Toyama, S. Nakaido, and T. Migita, *J. Org. Chem.*, **37**, 1721 (1972).

8) C. G. Overberger and J-P. Anselme, *ibid.*, **29**, 1188 (1964).

molecular nitrogen was eliminated, as is shown in Scheme 2. The observed ratio of the **9a** and **7b** isomers seems to reflect the relative degree of their thermodynamic stabilities, supporting the intermediacy of the 1,3-diradical produced by the thermal fragmentation of **8** under the present reaction conditions.[5,9]

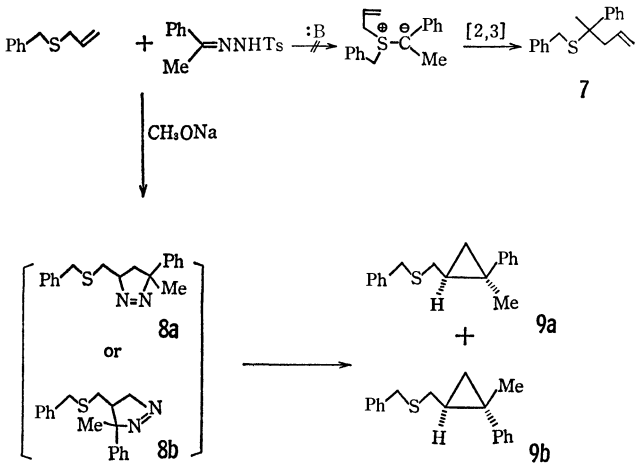

Scheme 2.

In order to elucidate the orientational effect of hetero atoms in the allylic systems, the thermal reactions of allyl benzyl sulfide and allyl benzyl ether with diazomethane were examined. Thus, allyl benzyl sulfide was allowed to react with diazomethane in ether at room temperature for a week in a sealed tube. The reaction mixture was then purified by column chromatography on silica gel to give 3-(benzylthio)-methyl-Δ^1-pyrazoline (**10**) in a 79% yield; this substance subsequently afforded a cyclopropane derivative, **11**, on irradiation with a high-pressure mercury lamp. The structure of the pyrazoline **10** was determined by studing its NMR spectrum. The NMR spectrum of the pyrazoline displayed three multiplets, at τ 8.80 (1H), at τ 8.40 (1H), and in the τ 6.18—5.35 (3H) region. The former two can be assigned to the resonance of non-equivalent H^b methylene protons, and the latter, to that of the H^a methine proton and of H^c methylene protons.[10] If the structure of the pyrazoline is 4-benzylthiomethyl-Δ^1-pyrazoline (**12**), H^a protons should appear as a double AB quartet (4H) in the region near τ 6.00, and the H^b proton, as a multiplet (1H) in a higher field (see the Experimental section for the case of **13b**). Thus, the structure of the pyrazoline obtained can be assigned to 3-(benzylthio)methyl-Δ^1-pyrazoline (**10**).

In contrast with the observed specific orientation in the case of the allyl sulfide system, the reaction of allyl benzyl ether with diazomethane under similar conditions afforded a mixture of two Δ^1-pyrazolines, **13a** and **13b** (**13a**/**13b**=67/33), in a 74.5% yield. These pyrazolines could fortunately be separated and purified by column chromatography on silica gel, and their structures were established by means of their NMR spectra. The fact that two different adducts were obtained in the case of allyl benzyl ether implies that

9) I. Ojima and K. Kondo, to be published.

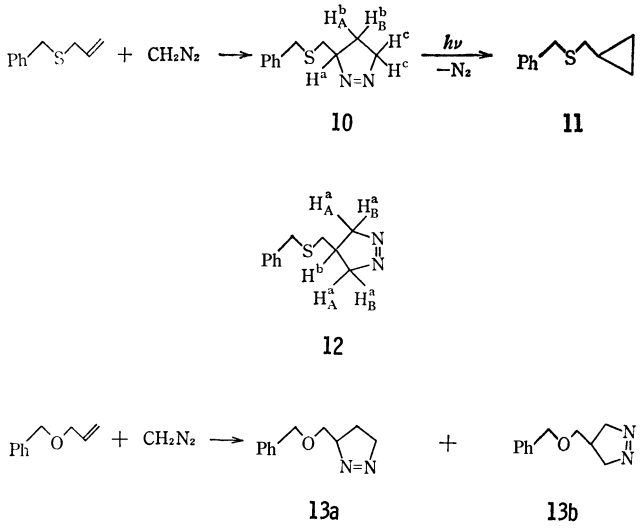

Scheme 3.

the oxygen atom plays no important role in directing the orientation of the 1,3-dipolarophile.

It has recently been suggested that the through-space $p\pi$–$d\pi$ conjugation between the double bond and the sulfur atom is operative in the reactions of allyl aryl sulfones with diazomethane.[11] The exclusive nucleophilic attack of diazomethane on the terminal carbon found in the present investigation appears to provide chemical evidence for the existence of homoallylic $p\pi$–$d\pi$ conjugation even in the case of a simple allyl sulfide system.

A similar activating effect of the hetero atom on the double bond can also be expected to emerge in the case of vinyl sulfides. Both vinyl ethers and sulfides are known to be electron-rich olefins because of the contributing structures, such as **14A** and **15A**. Thus, these compounds can easily be hydrolyzed under acidic conditions.[12] It is also known, however, that the sulfur atom has the ability to stabilize a carbanion on the α-position using its 3d orbitals.[13]

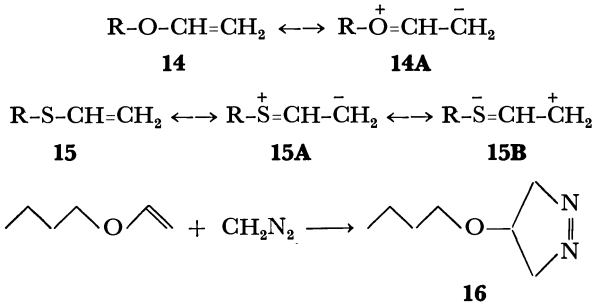

Scheme 4.

10) R. J. Crawfod, A. Mishra, and R. J. Dummel, *J. Amer. Chem. Soc.*, **88**, 3959 (1966).

11) V. N. Mikhailova and A. D. Bulat, *J. Org. Chem. USSR*, **3**, 1597 (1967) (in English); *Chem. Abstr.*, **68**, 12897q

12) L. Brandsma and J. F. Arens in "The Chemistry of the Ether Linkage" ed. S. Patai, Interscience, New York, p. 568.

13) For example, R. B. Woodward and R. H. Eastman, *J. Amer. Chem. Soc.*, **68**, 2229 (1946); W. J. Brehm and T. Levenson, *ibid.*, **76**, 5389 (1954); D. S. Tarbell and W. E. Lovett, *ibid.*, **78**, 2259 (1956); W. E. Parham and R. F. Motter, *ibid.*, **81**, 2146 (1959).

Thus, the contribution of another resonance structure, **15B**, also seems to be important in determining the character of the double bond in a vinyl sulfide, but no such effect of the sulfur atom in withdrawing electrons in such a way has been observed in cycloaddition reactions. D'yakonov has reported that the reaction of *n*-butyl vinyl ether with diazomethane produced 4-butoxy-Δ^1-pyrazoline (**16**).[14] This result is apparently consistent with the importance of the **14A** resonance structure.

Phenyl vinyl sulfide was allowed to react with an excess of diazomethane in ether at room temperature in a sealed tube for a week to give 3-phenylthio-Δ^1-pyrazoline (**17**) in a 40.4% yield; no formation of 4-phenylthio-Δ^1-pyrazoline (**18**) could be observed. This finding is to be expected in view of the predominant contribution of the canonical structure, **15B**, in preference to that of **15A**, to the resonance hybrid of the sulfide, and it well corresponds to the case of vinyl sulfones.[15]

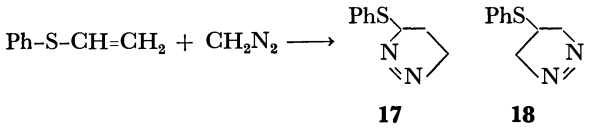

17 **18**

Scheme 5.

It is sufficient to note at this point that both nucleophilic and electrophilic attacks on allyl and vinyl sulfides tend to occur at the terminal carbon. Such a versatile character of the olefinic sulfides seems to be associated with the large polarizability of the molecule due to the participation of the 3d orbitals of a sulfur atom.

Experimental

Measurements. The melting points and boiling points are uncorrected. The infrared spectra were recorded on a Hitachi-Perkin-Elmer Model 337 Infracord or a Hitachi EPI-G3 spectrophotometer, using samples as neat liquids or KBr disks or Nujol mulls. The nuclear magnetic resonance spectra were obtained by the use of a Varian HA-100 or Hitachi R20-B spectrometer, using TMS as the internal standard. The mass spectra were measured by means of a Hitachi RMU-6E spectrometer at 70 eV. Photolyses were carried out using a 450-W high-pressure mercury lamp (Ushio Electric Inc.).

Materials. The allyl benzyl sulfide,[16] and allyl benzyl ether[17] were prepared according to the reported method. The phenyl vinyl sulfide[18] was prepared from β-chloroethyl phenyl sulfide[19] by treatment with potassium hydroxide in ethanol. The acetophenone tosylhydrazone was prepared by the condensation of acetophenone and tosylhydrazide; mp 148—150 °C (lit,[20] 147.5—150 °C).

Thermal Decomposition of Acetophenone Tosylhydrazone in Allyl Benzyl Sulfide in the Presence of Sodium Methoxide. In 50 ml of diglyme, 1.64 g (10.0 mmol) of allyl benzyl suifide and 1.44 g (5.0 mmol) of acetophenone tosylhydrazone and 300 mg of sodium methoxide were dissolved. The mixture was heated in an oil bath at 150 °C for 1 hr. After the precipitated sodium *p*-toluenesulfinate had then been filtered off, the filtrate was distilled under reduced pressure to remove the solvent. The residue was submitted to column chromatography on silica, using *n*-hexane as the eluent; 1-(benzylthio)methyl-2-methyl-2-phenylcyclopropane (**9**) (375 mg, 28% yield) was thus obtained. The isomer ratio of the cyclopropane, **9**, was determined to be *cis*(**9a**)/*trans* (**9b**)=29/71 by glpc analysis, using 20% SE-30 on chromosorb W at 200 °C.

9: NMR(CCl_4): **9a**: τ 9.30—8.60 (m, H^b+H^c), 8.73 (s, H^a), 8.06 (octet, H^d, $J_{dd}=12$ Hz, $J_{cd}=6$ and 8 Hz), 6.51 (s, H^e, and 3.00—2.65 (m, Ph).

9b: τ 9.05—8.60 (m, H^b+H^c), 8.72 (s, H^a), 7.52 (octet, H^d, $J_{dd}=13$ Hz, $J_{cd}=6$ and 7 Hz), 6.36 (s, H^e), 2.95—2.65 (m, Ph).

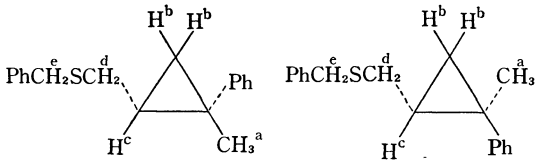

9a **9b**

Mass (*m/e*): 268 (M^+, 13.8), 227 (48.8), 177 (13.8), 145 (100), 131 (26.2), 91 (91.3), and 77 (20.0).

Found: C, 80.32; H, 7.28; S, 12.03%. Calcd for $C_{18}H_{20}S$: C, 80.54; H, 7.51; S, 11.95%.

Reaction of Allyl Bnezyl Sulfide with Diazomethane. A mixture of 1.64 g (10 mmol) of allyl benzyl suifide and an excess of diazomethane in 50 ml of ether, which had been prepared from 10 g of *N*-nitroso-*N*-methylurea and aqueous sodium hydroxide, was sealed in a glass tube and stirred for a week at 15 °C. After the solvent and excess diazomethane had then been evaporated, the residue was submitted to column chromatography on silica. The unreacted allyl benzyl sulfide was eluted by the use of *n*-hexane-benzene, and the 3-(benzylthio)methyl-Δ^1-pyrazoline (**10**) was eluted by the use of chloroform (1.62 g, 78.7%).

10: NMR (CCl_4): τ 9.05—8.64 (m, $H_A{}^b$), 8.58—8.18 (m, $H_B{}^b$), 7.25 (octet, H^e, $J_{ee}=14$ Hz, $J_{ea}=5$ and 7 Hz), 6.37 (s, H^d), 6.18—5.35 (m, H^a+H^c), and 3.00—2.65 (m, Ph).

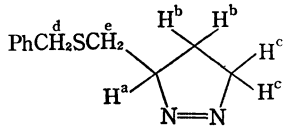

Mass (*m/e*): 206 (M^+, 4.1), 178 (M^+-N_2, 3.5), 137 (3.5), 122 (13.5), 91 (100), 83 (51.4), and 69 (16.2).

Found: C, 64.09; H, 6.67; S, 15.58%. Calcd for $C_{11}H_{14}N_2S$: C, 64.04; H, 6.84; S, 15.54%.

Reaction of Allyl Benzyl Ether with Diazomethane. A mixture of 1.58 g (10.7 mmol) of allyl benzyl ether and an excess of diazomethane in 50 ml of ether, which had been prepared from 10 g of *N*-nitroso-*N*-methylurea and aqueous sodium hydroxide in ether, was stirred at 15 °C for a week

14) I. A. D'yakonov, *Zh. Obshch. Khim.*, **17**, 67, (1947): *Chem. Abstr.*, **42**, 902 (1948).
15) W. E. Parham, F. D. Blake, and D. R. Theissen, *J. Org. Chem.*, **27**, 2415 (1962).
16) H. J. Backer and G. J. de Jong, *Rec. Trav. Chim. Pays-Bas*, **67**, 889 (1948).
17) R. H. Baker, K. H. Cornell, and M. J. Cron, *J. Amer. Chem. Soc.*, **70**, 1490 (1948).
18) F. Montanari, *Boll. Sci. Fac. Chim. Ind. Bologna*, **14**, 55 (1956): *Chem. Abstr.*, 51, 5723b.
19) G. M. Bennett and W. A. Berry, *J. Chem. Soc.*, **1927**, 1666.
20) D. Farnum, *J. Org. Chem.*, **28**, 870 (1963).

in a sealed glass tube. The excess diazomethane and ether were then removed, and the residual reaction mixture was chromatographed on silica. From the *n*-hexane–benzene eluates, unreacted allyl benzyl ether was recovered, and 3-benzylthiomethyl-Δ^1-pyrazoline (**13a**) and 4-(benzylthio)-methyl-Δ^1-pyrazoline (**13b**) were eluted in this order by the use of benzene–chloroform (1.51 g, 74.5%). The ratio of the pyrazoline, **13a**/**13b**, was determined to be 67/33 on the basis of the following NMR spectra.

13a: NMR (CCl_4): τ 8.80—8.30 (m, H^b), 6.24 (octet, H^e, $J_{ea}=4$ Hz, $J_{ee}=10$ Hz), 5.95—5.40 (m, H^a+H^e), 5.61 (s, H^d), and 2.84 (s, Ph).

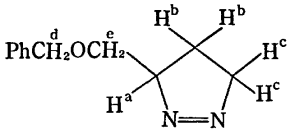

IR (neat): 1550 cm^{-1} ($\nu_{N=N}$). There is no absorption in the 3100—3500 cm^{-1} region because of the isomerization of **13a** to Δ^2-pyrazoline.

Mass (*m/e*): 190 (M^+ 1.2), 107 (7.2), 91 (100), 77 (4.8), and 69 (7.2).

Found: C, 69.28; H, 7.60%. Calcd for $C_{11}H_{14}N_2O$: C, 69.45; H, 7.42%.

13b: NMR (CCl_4): τ 7.83 (septet, H^b, $J_{ab}=J_{bc}=6$ Hz), 6.96 (d, H^c, $J_{bc}=6$ Hz), 5.84 (d, H^a, $J_{ab}=6$ Hz), 5.68 (s, H^d), and 2.84 (s, Ph).

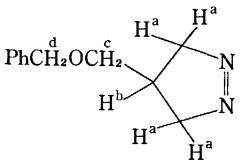

IR (neat): 1550 cm^{-1} ($\nu_{N=N}$). There is no absorption in the 3100—3500 cm^{-1} region, because of the isomerization of **13a** to Δ^2-pyrazoline.

Mass (*m/e*): 190 (M^+, 2.5), 108 (11.9), 107 (13.5), 91 (100), 77 (8.5), and 69 (17.0). Found: C, 69.24; H, 7.35%. Calcd for $C_{11}H_{14}N_2O$: C, 69.45; H, 7.42%.

*Photolysis of 3-(Benzylthio)methyl-Δ^1-pyrazoline (**10**).* The pyrazoline **10** (412 mg, 2.0 mmol) was dissolved in 20 ml of monoglyme in a quartz photolysis vessel, after which the solution was irradiated for 3 hr. During irradiation, the vessel was cooled with an air stream and the reaction temperature was maintained at room temperature. After the solvent had been evaporated, the reaction mixture was submitted to column chromatography on silica. Benzylthiomethylcyclopropane (**11**) was obtained from a *n*-hexane–benzene eluate (92.5 mg, 26%).

11: NMR (CCl_4): τ 9.65—9.35 (m, $H_A{}^a$), 9.35—8.95 (m, $H_B{}^a$), 8.85—8.60 (m, H^b), 7.76 (d, H^c, $J_{bc}=7$ Hz), 6.39 (s, H^d), and 2.96—2.65 (m, Ph).

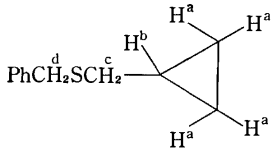

Mass (*m/e*): 178 (M^+, 22.2), 137 (11.1), 122 (31.9), 91 (100), and 87 (18.1).

Found: C, 73.94; H, 7.80; S, 18.94%. Calcd for $C_{11}H_{14}S$: C, 74.10; H, 7.91; S, 17.98%.

Reaction of Phenyl Vinyl Sulfide with Diazomethane. A mixture of 1.36 g (10 mmol) of phenyl vinyl sulfide and an excess of diazomethane in 50 ml of ether, which had been prepared from 10 g of *N*-nitroso-*N*-methylurea and aqueous sodium hydroxide in ether, was stirred at 15 °C for a week in a sealed glass tube. A small amount of a polymerization product of phenyl vinyl sulfide was precipitated in the solution during that time. After the polymer had been filtered off and the excess diazomethane and ether had been evaporated, the residue was chromatographed on silica. From a chloroform eluate, 720 mg (40.4%) of 3-(phenylthio)-Δ^1-pyrazoline (**17**), bp 84 °C/0.55 mmHg, were obtained.

17: NMR (CCl_4): τ 8.80—8.35 (m, $H_A{}^b$), 8.25—7.80 (m, $H_B{}^b$), 6.25—5.55 (m, H^a), 4.60—4.35 (m, H^e), and 2.85—2.40 (m, Ph). IR (neat): 1540 cm^{-1} ($\nu_{N=N}$). Mass

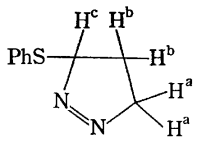

(*m/e*): 178 (M^+, 4.2), 150 (6.3), 110 (100), 109 (31), 77 (14.1), 68 (33.8), 41 (19.7), and 39 (15.5). Found: C, 60.93; H, 5.40; S, 18.29%. Calcd for $C_9H_{10}N_2S$: C, 60.64; H, 5.65; S, 17.99%.

The authors wish to express their thanks to the Kawakami Memorial Foundation for its partial support of this research.

An X-Ray Study of Coal Tar Pitch

Minoru SHIRAISHI and Kazuo KOBAYASHI

National Research Institute for Pollution and Resources, Kawaguchi, Saitama 332

(Received September 27, 1972)

The diffuse X-ray scattering from coal tar pitch has been investigated by using Fourier transformation for the 002 band and Diamond's least-squares method for the 11 band. From the results of this investigation, the layers were found to be stacked parallel to each other, partly in groups of 8—9 layers, the average number of the layers being 2.46. The distribution of the layer size showed a peak at the diameter of 8.4—10 Å, the average layer size was 8.9 Å, which corresponded to 25 atoms per layer.

It has been known that the properties of synthetic carbon depend largely on the structure of the starting materials and also on the condition of heating up to about 600 °C. However, not only the mechanism of the pyrolysis of the starting materials, but also the physical features of starting materials, have not yet been clarified. Therefore, it is valuable to clarify the structure of pitch from the viewpoint of the utilization of pitch as the starting material for synthetic carbon.

It has been known that the fundamental structure of coal tar pitch consists of various sizes of aromatic-ring systems.[1,2] However, the X-ray diffraction pattern of coal tar pitch shows only a small, diffuse scattering, corresponding to the 002, 100, and 110 reflections of graphite. The analysis of such diffuse scattering as is shown in coal and coal tar pitch is painstaking and difficult in the selection of its method.

In the present paper, the Fourier transformation, which Hirsch[3] used first and which Diamond[4] developed for the analysis of coal, was applied to the analysis of the 002 band of pitch. Moreover, Diamond's method[4,5] was used for the analysis of the 11 band of pitch. The size of the aromatic layer and the thickness of the aromatic layer stacking were estimated by using those methods.

Experimental

Sample. The sample was coal tar pitch which had already been treated at 390 °C. Table 1 shows some properties of the pitch used.

TABLE 1. SOME PROPERTIES OF PITCH USED

Ultimate analysis	C	92.1%
	H	4.5%
Specific gravity		1.31
Softening point		82.2 °C
Temperature of processing		390 °C

Experimental Procedure. The X-ray scattering was measured for a powdered sample using a diffractometer, a scintillation counter, a pulse-height analyser, and Cu$K\alpha$ radiation. Monochromation was carried out with balanced filters of Ni and Co.

The X-ray intensity was measured in two ranges, $0.01 \leqq s \leqq 0.44$ and $0.66 \leqq s \leqq 0.96$ Å^{-1} ($s = 2\sin\theta/\lambda$). The same experimental conditions of the slit system and of the electric power of the X-ray tube were adopted for both ranges of s.

The intensity of X-rays in the high-angle range ($0.66 \leqq s \leqq 0.96$ Å^{-1}) was measured by point counting or a fixed time method using the balanced filters. The intensity curve in the high-angle range was obtained by plotting the average value of two or more measurements. In the low-angle range ($0.01 \leqq s \leqq 0.44$ Å^{-1}), the X-ray intensity was recorded by a scanning method.

The observed intensity was then corrected for polarization, absorption, and geometrical factors. The absorption factor, $A(\theta)$, was obtained from Milberg's equation:[6]

$$A(\theta) = 1 - \frac{1}{\alpha}(1 - e^{-\alpha}) \tag{1}$$

$$\alpha = 2\rho'\left(\frac{\mu}{\rho}\right)\cdot A \cdot \mathrm{cosec}2\theta$$

with $A = 0.1614$ cm, $\rho' = 0.7$ g/cm^3, and $\mu/\rho = 4.60$ cm^2/g, where ρ' is the bulk density of the sample, where μ/ρ is the mass absorption coefficient for Cu$K\alpha$ and where A is the breadth of the X-ray beam.

Diamond's Method. The analysis derived by Diamond[4,5] was used for the 11 band, in which a linear combination of theoretical intensity curves from small layers of different sizes and from amorphous carbon atoms was fitted to the experimental curve over the range from 0.66 to 0.96 Å^{-1} by the method of least-squares. By means of a matrix transformation, the distribution, λ_i, in proportion by weight of the material, in each of the specified-layer-size groups, which are 5.8, 8.4, 10, 15, 20, and 30 Å in diameter, and of the amorphous atom, is derived by means of the following equation:

$$\lambda_i = \sum_j h_{ij} I_j \tag{2}$$

where h_{ij} is an element of the matrix calculated theoretically and where I_j is the observed intensity. The average layer diameter, $\bar{L}$, is defined by the relation:

$$\bar{L} = \sum_i' \lambda_i L_i / \sum_i' \lambda_i \tag{3}$$

where L_i is the specified layer size and where the prime denotes the omission of the term for amorphous carbon atoms. The relation between the layer size, L, and the number, N, of atoms in the layer of that size is given by the equation:

$$L = 2.5\sqrt{N/2} \tag{4}$$

Fourier Transformation. In the region of $s \leqq 0.40$ Å^{-1}, the main diffraction pattern is the 002 band, which is inter-

1) S. Otani and A. Yokoyama, This Bulletin, **42**, 1417 (1969).
2) The Coal Tar Data Book, 2nd Edition, The Coal Tar Research Association, Percy Lund, Humpheries & Co., London (1965).
3) P. B. Hirsch, *Proc. Roy. Soc. Ser., A*, **226**, 143 (1954).
4) R. Diamond, Ph. D. Dissertation, University of Cambridge, (1956), *Phil. Trans. Roy. Soc. London*, **A 252**, 193 (1959).
5) R. Diamond, *Acta Crystallogr.*, **10**, 359 (1957); **11**, 129 (1958).
6) M. E. Milberg, *J. Appl. Phys.*, **29**, 64 (1958).

preted by analogy with pure carbons as being due to the stacking of parallel layers. The scattering curve was analyzed by the Fourier transformation method of Hirsch[3] and Diamond.[4] The Fourier transform of the following form:

$$P(u) = 2\int_0^\infty \frac{I_{002}}{f^2}\cos 2\pi us\,ds \qquad (5)$$

gives the probability of finding a layer at a distance of u along the normal to a given layer. In Eq. (5), I_{002} is the intensity of the 002 band, f is the atomic scattering factor for the carbon atom, and s is the reciprocal distance. The interlayer spacing, d, was obtained from the periodicity in the transform $P(u)$. This function can be used to determine stacking distribution using the second differences of the peak weights above a smooth background curve following the minima in $P(u)$, in the manner of Hirsch.[3] If $P(n)$ is the weight of the nth peak from the origin in the transform, the probability, $f(n)$, that a given stack contains n layers ($n \geqq 2$) is given by the following equation:

$$f(n) = P(n) - 2P(n+1) + P(n+2) \qquad (6)$$

The following procedure was used to determine I_{002}. The experimentally-observed intensity was corrected for geometrical, polarization, and absorption factors. The intensity of I_{obs} in absolute units was obtained by dividing the above corrected intensity by the value of $\sum\lambda$ determined by Diamond's method. The Compton scattering was subtracted from I_{obs} in order to obtain the coherent scattering, I_{coh}. The Breit-Dirac recoil factor to the 2/3 power was considered to be correct for the Compton scattering. The minimum value of I_{coh}/f^2 in the neighourhood of $s=0.40$ Å^{-1} was subtracted from I_{coh}/f^2 in the region of $s \leqq 0.44$ Å^{-1}. I_{002} was estimated as the product of the above difference and s:[7]

$$I_{002} = s\cdot\left(\frac{I_{coh}}{f^2} - A\right) \qquad (7)$$

$$A = (I_{coh}/f^2)_{s\fallingdotseq 0.4}$$

Results

002 Band. In Fig. 1 the observed X-ray intensity, I_{obs}, is plotted in the range of s values smaller than 0.44 Å^{-1}. Fig. 1 shows that the corrected intensity of the 002 band reaches 55 electron units at $s \approx 0.29$ Å^{-1}. The intensity curve of the 002 band, I_{002}, obtained by Eq. (7), is given against s in Fig. 2.

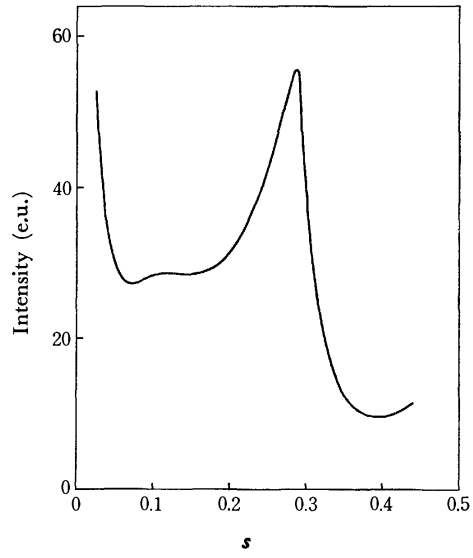

Fig. 1. X-ray intensity curve of coal tar pitch in low angle range.

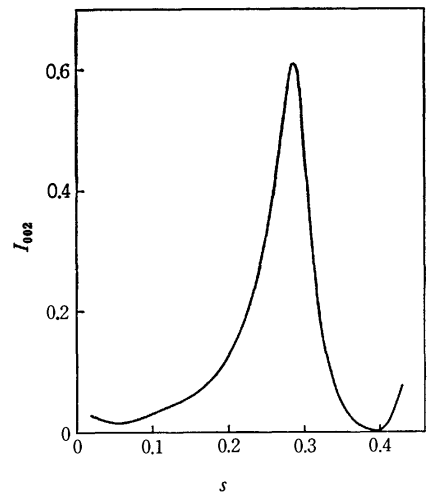

Fig. 2. X-ray intensity curve for 002 band of coal tar pitch.

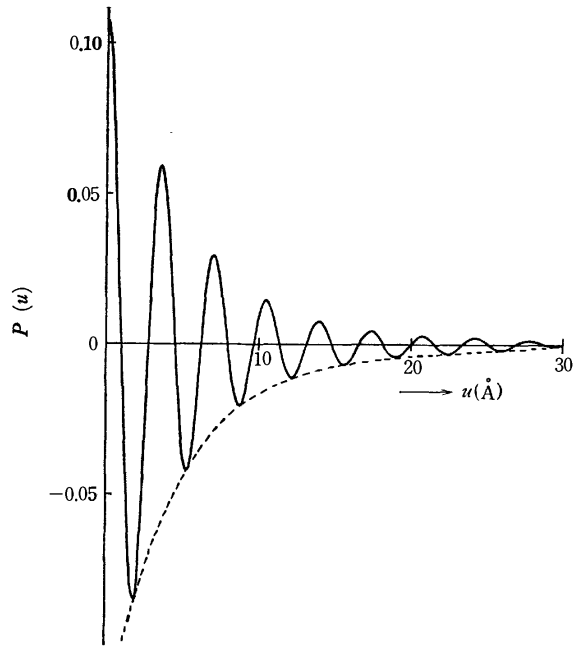

Fig. 3. Fourier transform of I_{002}.

The integration in Eq. (5) was replaced by a summation over the range from $s=0.01$ to $s=0.40$ corresponding to the minimum intensity of I_{002}. The results of the transform for coal tar pitch are shown in Fig. 3. The amplitude of oscillation is observed up to the 9th peak from the point of origin. The number of 9 corresponds to the maximum number of layers which may be considered to be packed parallel to each other at nearly equal distances. (Table 2)

A histogram of the stacking of the layers is given in Fig. 4. The layers per stack were observed up to 9 layers, but the fraction of stacks containing 8 and 9 layers was not obtained because $P(10)$ and $P(11)$ in Eq. (6) were unknown. Apart from the singly-occurring layers, the most frequently occurring groups contain two (55 wt%) or three (26 wt%) layers in the pitch

7) W. Ruland, *Carbon*, **2**, 365 (1965).

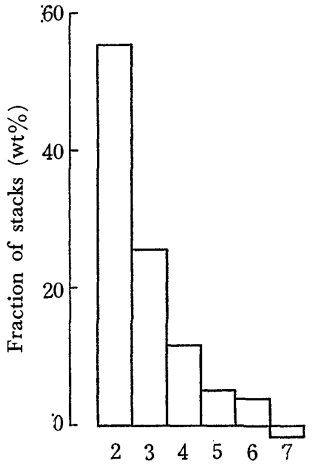

Fig. 4. Histogram of stack heights in coal tar pitch.

Table 2. Structural parameters of pitch used

Interlayer spacing	d	3.44 Å
Average number of layers per stack	$\bar{n}$	2.46
Thickness of stack	L_c	8.45 Å
Average layer size	$\bar{L}$	8.87 Å
Average number of atoms per layer	$\bar{N}$	25.2

used. The interlayer spacing, d, the average thickness of layer stack, L_c, and the average number of layers per stack other than the single layer, $\bar{n}$, are given in Table 2.

It is interesting to note that the interlayer spacing (3.44 Å) is equal to that in the non-graphitic carbons[8] and slightly smaller than that derived from the peak in Fig. 2.

11 Band. The X-ray intensity curve in electron units, obtained by dividing the collected X-ray intensity by $\Sigma\lambda_i$, is shown in Fig. 5 over a range extending from $s=0.66$ to 0.96 Å^{-1}. As is shown in Fig. 5, the intensity of the 11 band is weak in comparison with

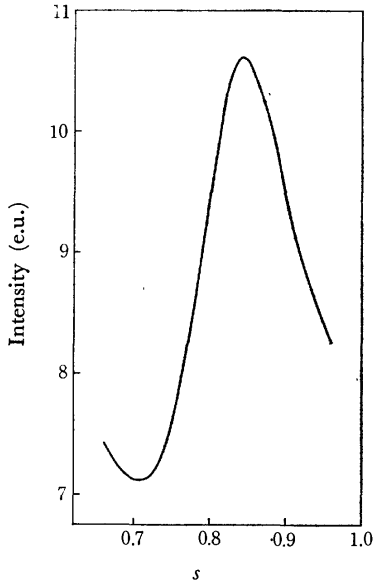

Fig. 5. X-ray intensity curve of coal tar pitch in high angle range.

8) R. E. Franklin, *Acta Crystallogr.*, **4**, 253 (1951).

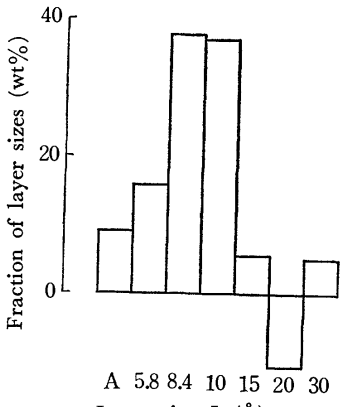

Fig. 6. Layer size histogram for coal tar pitch. The size group A is amorphous (single) carbon atoms.

the background scattering. The peak has a value of about 10.7 e.u.

A layer-size histogram of the coal tar pitch is given in Fig. 6. The fraction of amorphous matter is about 9%, and the fractions of the layer size in 8.4 and 10 Å are 38% and 37% respectively. The fraction of the layer size in 20 Å shows a minus value. The average layer size was 8.87 Å, and the number of carbon atoms per layer, $\bar{N}$, was 25.2.

Discussion

The transform, $P(u)=2\int(I_{002}/f^2)\cos 2\pi us ds$, is in principle the most general way for estimating the stacking distribution. There is a problem, however, in the determination of I_{002}. Diamond[4] derived two transforms as follows:

$$P_1(u) = 2\int\frac{s^2I}{f^2}\cos 2\pi us ds \tag{8}$$

and

$$P_2(u) = 2\int\frac{I}{f^2}\cos 2\pi us ds \tag{9}$$

The first gives the probability of finding a layer at a distance of u along the normal to a given layer; it thus represents a projection of the density of the interatomic vectors to the normal to the layers at any given point in the specimen. The second function corresponds to a projection of the density of the interatomic vectors along an arbitrary radius with random orientation.

Franklin[9] and Diamond[4] considered that the function, s^2I/f^2, in Eq. (8) was the best plot for the evaluation of the 002 reflection and the stacking distribution determined. However, when an undistorted profile is desired, an sI/f^2 plot is preferable to an s^2I/f^2.[7] Therefore, Eq. (7) was adopted for the best evaluation of the 002 reflection in this paper.

On the other hand, Fig. 1 shows a weak peak of $s\approx 0.1$ Å^{-1}, the existence of which implies that there may be a variation in the density in this region. There are two possible explanations of the variation in density.[3,10] First, the spacing of the peak may be due to some repeat distance of the structure; secondly, the peak may be due to the internal structure of the unit, which, for ex-

9) R. E. Franklin, *Acta Crystallogr.*, **3**, 107 (1950).

10) J. K. Brown and P. B. Hirsch, *Nature*, **175**, 229 (1955).

Table 3. Properties of pitch used by van krevelen and by cartz

Van Krevelen			Cartz		
Ultimate analysis	C	92.7%	Interlayer spacing	d	3.53 Å
	H	4.4%	Average number of layers per stack	$\bar{n}$	1.59 Å[a]
Aromaticity	f_a	0.89	Average layer size	$\overline{L}$	7.0 Å
Number of aromatic carbon atoms	C_{ar}	27	Average number of atoms per layer	$\overline{N}$	15.7

a) Included single layers

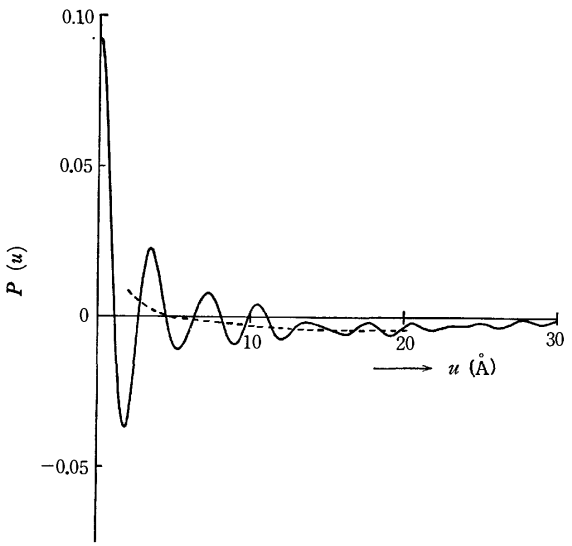

Fig. 7. Fourier transform of I_{coh}/f^2.

ample, has a greater than average density in its core and a less than average density in its peripheral regions. Therefore, the transform, $P_2(u)$, in Eq. (9) of this pitch was tried. As is shown in Fig. 7, there appear about five rapid oscillations due to the layers, but no maximum of the slow modulation of the transform appears. (The modulation is a dotted curve on Fig. 7) Accordingly, although Fig. 1 shows a peculiar region of $s \approx 0.1$, a distinct order with a distance of *ca.* 10 Å is not observed in this pitch from an analysis of the Fourier transformation.

Cartz[11] has examined a specimen of pitch for which structural parameters had been determined by Van Krevelen, using the statistical structure analysis. (Table 3). The carbon and hydrogen contents of the coal tar pitch used in the present experiment are nearly equal to those of the sample used by Van Krevelen and Cartz. However, the histograms of the stacking of the layers and the layer sizes are different in shape. Although the histogram of the layer size obtained by Diamond's method contains a negative term and does not give directly the true proportion of layers of the sizes indicated, the comparison with the shape of the histogram is more significant[4] and the average layer size, $\overline{L}$, is quite accurate.[12] Since C_{ar} stands for the average number of aromatic carbon atoms per cluster unit, the value of C_{ar} is compared with the number of atoms in a coherently-diffracting layer as deduced from X-ray data, $\overline{N}$. The average number of atoms per layers (25.2) in this pitch is found to be larger than the result, $\overline{N}$, by Cartz and slightly smaller than that, C_{ar} obtained by Van Krevelen.

Since the layers deduced from the high-angle diffraction pattern are diffracted effectively coherently in the 11 and the 20 region, all that may be said about the average layer size, $\overline{L}$, is that it represents the lower limit of the actual size of the imperfect sheet and the upper limit of the size of the perfect region of the layer. Therefore, the average layer size, $\overline{L}$, cannot necessarily be identified with the aromatic molecule as determined by statistical structural analysis. Notwithstanding the above reservation, the average number of atoms per layer, $\overline{N}$, is rather closer to the number of aromatic carbon atoms, C_{ar}, obtained by the statistical structural analysis than the $\overline{N}$ obtained by Cartz using X-ray analysis. The above discussion indicates that the average layer size, $\overline{L}$, obtained in this pitch is smaller than the aromatic molecule in this pitch.

On the other hand, the number of layers in the stacks were obtained from the area under the peaks of the Fourier transform by a second difference method. The proportion of single layers can not, however, be derived by the same method, since the origin peak in the transform is not accurate. In view of the height of the minima in the experimental curve, it seems that an appreciable proportion of the layers are unassociated.

Conclusion

On the basis of the results of the present experiments, the aromatic layers of the coal tar pitch used can be said to be distributed mostly at layer sizes of 8.4—10 Å. The average layer size which diffracts effectively coherently had a diameter of 8.9 Å and contained 25 atoms per layer. It was found that such aromatic layers stacked parallel to each other up to 8—9 layers. The average number of layer stacking was 2.46, excluding an isolated single layer and the interlayer spacing was 3.44 Å.

Therefore, it can be concluded that the crystallite size of the coal tar pitch was 8.9 Å in diameter and 8.5 Å in thickness.

The authors wish to thank Dr. S. Toyoda for countless discussions and a thorough review of the paper, and Dr. K. Ouchi, Dr. T. Yamakawa and Dr. Y. Sanada for much encouragement and many suggestions.

11) L. Cartz and P. B. Hirsch, *Phil. Trans. Roy. Soc.* (London), **A252**, 557 (1960).
12) M. Shiraishi and K. Kobayashi, *Nippon Kagaku Kaishi*, **1972**, 1135.

NOTES

BULLETIN OF THE CHEMICAL SOCIETY OF JAPAN, VOL. 46, 2579—2580 (1973)

The Simulation Analysis of Dipeptide Hydrolysis Catalyzed by Divalent Metal Ions

Katsutoshi OHKUBO and Hiroyuki SAKAMOTO

Department of Synthetic Chemistry, Faculty of Engineering, Kumamoto University, Kurokami, Kumamoto 860

(Received June 7, 1972)

Some quantitative studies of the kinetics of peptide hydrolysis in the presence of metal ions have been hitherto recorded, and such divalent metal ions (M^{2+}) as Co(II)[1] and Cu(II)[2,3] have been pronounced as effective catalysts for the following reactions of dipeptide (A–B) hydrolysis:

$$\text{A–B}^{\pm} \underset{k_{-1}}{\overset{k_1}{\rightleftharpoons}} \text{A}\frown\text{B} \underset{k_{-2}}{\overset{k_2}{\rightleftharpoons}} \text{B–A}^{\pm} \quad (1)$$

$$\text{A–B}^{\pm}(\text{or B–A}^{\pm}) \rightleftharpoons \text{A–B}^{-}(\text{or B–A}^{-}) + \text{H}^{+} \quad (2)$$

$$\text{A–B}^{-}(\text{or B–A}^{-}) + \text{M}^{2+} \rightleftharpoons \text{A–B}\text{---}\text{M}^{+}(\text{or B–A}\text{---}\text{M}^{+}) \quad (3)$$

$$\text{A–B}\text{---}\text{M}^{+}(\text{or B–A}\text{—}\text{M}^{+}) \underset{\text{H}_2\text{O}}{\overset{K}{\rightleftharpoons}} \text{M}^{2+} + \text{A} + \text{B} \quad (4)$$

where A⌒B denotes the dioxopiperazine intermediate. Recently, Long *et al.*[4,5] have noted that the rate of glycyl-glycine hydrolysis is directly proportional to the concentrations of Co(II), Ni(II), Zn(II), and/or Mn(II) over the pH range of 3.8—6.0.

In the present paper, the simulation analysis was performed on the rate of dipeptide hydrolysis catalyzed by Zn(II), Co(II), and/or Ni(II) by means of a computer technique based on the kinetic method;[6] also the mechanism for the divalent metal ion-catalyzed dipeptide hydrolysis will be briefly discussed on the basis of ASMO-SCF and extended Hückel MO calculations.[7]

Results and Discussion

Let us first discuss the simulation results on Zn(II)-catalyzed hydrolyses of dipeptides; glycyl-L-leucine (G–L), glycyl-L-alanine (G–A), and glycyl-glycine (G–G). As can be seen from Fig. 1, the time conversions of the dipeptide concentrations calculated with the rate constants listed in Table 1 were satisfactorily in accordance with those[5] obtained experimentally. In the absence of the Zn(II) ion, only the acid H^+ (pH 5.6) accelerates a little the rate of G–L hydrolysis.

In regard to the cleavage of peptide bond in G–L G–A, and G–G, the order of the bond fission caused by the Zn(II) ion, G–G>G–A>G–L, was not directly related to that of the bond populations of their peptide bonds (G–G=1.036; G–A=1.035; G–L=1.035); this may be ascribed to the difference in the steric hindrances of the substituents (R_1 and R_2) in $H_3\overset{+}{N}CH(R_1)C(=O)NHCH(R_2)CO_2^-$ to the interaction of the Zn(II) ion.

Next, let us discuss the rate constant, k, of Reaction (3) in G–G hydrolysis with Zn(II), Co(II), and/or Ni(II). Fig. 2 shows the k values obtained experimentally[4] (k_{obsd}) and those calculated (k_{calcd}) by means of Arrhenius and activated complex theories on the basis of least-squares error analysis. Both the k_{obsd} and k_{calcd} values were found to be identical within the limits of technical error. As may be seen from Fig. 2, the Zn(II) ion seems to be predominant as a catalyst for the G–G hydrolysis. This distinctive catalytic nature of the Zn(II) ion is well reflected in the distinctive kinetic data of the Zn(II) ion (see Table 2).

Finally, the mechanism for the metal ion-catalyzed hydrolysis will be briefly discussed. The electronic structure of G–G in a weak acid solution, $H_3\overset{+}{N}CH_2C$-

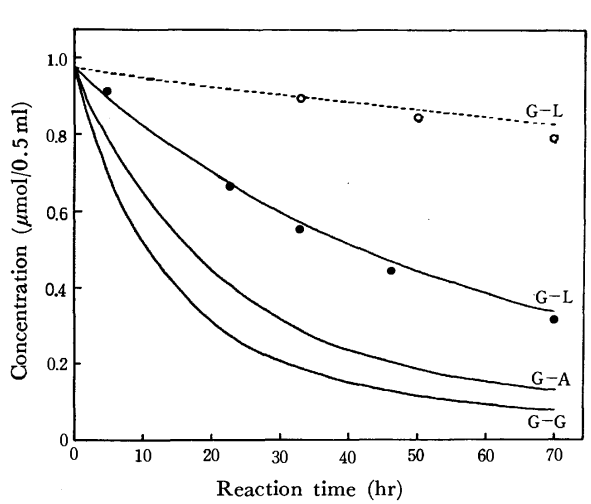

Fig. 1. Plots of dipeptide concentrations *vs.* reaction time in Zn(II) ion-catalyzed hydrolysis at 95 °C in pH 5.6. (dotted curve: absence of Zn(II); solid curve: presence of 0.04 M Zn(II); ○ and ●: experimental data cited from Ref. 5)

1) L. Lawrence and W. J. Moore, *J. Amer. Chem. Soc.*, **73**, 151 (1951).

2) I. J. Grant and R. W. Hay, *Aust. J. Chem.*, **18**, 1189 (1965).

3) M. M. Jones, T. J. Cook, and S. Brammer, *J. Inorg. Nucl. Chem.*, **28**, 1265 (1966).

4) D. A. Long, T. G. Truscott, J. R. Cronin, and R. G. Lee, *Trans. Faraday Soc.*, **67**, 1094 (1971).

5) J. R. Cronin, D. A. Long, and T. G. Truscott, *ibid.*, **67**, 2096 (1971).

6) K. Ohkubo and T. Hashimoto, This Bulletin, **45**, 3350 (1972).

7) The calculation details of the ASMO–SCF and the extended Hückel methods respectively have been described in the following references: R. Hoffmann, *J. Chem. Phys.*, **39**, 1397 (1963); *ibid.*, **40**, 2474 (1964) and T. Yonezawa, H. Konishi, and H. Kato, This Bulletin, **42**, 933 (1967). The Coulomb integrals of the C, N, and O atoms were taken from J. Hinze and H. H. Jaffé, *J. Amer. Chem. Soc.*, **85**, 540 (1963), except for that of the oxygen 2p-orbital (−15.85 eV).

TABLE 1. SECOND-ORDER RATE CONSTANTS[a] USED FOR THE SIMULATIONS OF THE REACTION OF GLYCINE-CONTAINING DIPEPTIDES AND DIOXOPIPERAZINES IN THE PRESENCE OF 0.04 M Zn(II) ION AT pH 5.6 AND 95 °C

Dipeptide	$10^3 k_1$	$10^3 k_{-1}$	$10^3 k_2$	$10^3 k_{-2}$	$10^3 k_{overall}$[b]	$10^3 k'_{overall}$[c]
G-G	17.5	12.5	17.5	12.5	11.8	11.8
G-A	11.25	4.0	6.25	3.0	6.25	7.25
G-L	3.75 (0.04)	1.5 (0.004)	4.5 (0.03)	1.5 (0.005)	3.25 (0.002)	3.25 (0.002)

a) Strictly speaking, these second-order rate constants can be represented by $k'(H^+)$, wherein k' denotes third order rate constants. The values in parentheses indicate the rate constants for G-L hydrolysis in the absence of Zn(II).
b) The rate constant for the reaction, $A-B\pm+M^{2+}+H_2O\rightarrow$products.
c) The rate constant for the reaction, $B-A\pm+M^{2+}+H_2O\rightarrow$products.

TABLE 2. KINETIC DATA FOR THE REACTION OF DIVALENT METAL ION-CATALYZED G-G HYDROLYSIS

G-G—M^+ + H_2O → products

Metal ion	Experimental[c] A[a]	Experimental[c] $\Delta S^{\neq}$ (cal/mol·K)	Experimental[c] $\Delta H^{\neq}$ (kcal/mol)	Computer A[a]	Computer E[b] (kcal)	Computer $\Delta S^{\neq}$ (cal/mol·K)	Computer $\Delta H^{\neq}$ (kcal/mol)
Co(II)	5.79×10^{26}	+62	53	$(8.273\pm0.903)\times10^{26}$	54.01±0.08	+61.21±0.21	53.27±0.08
Ni(II)	5.30×10^{24}	+52	50	$(1.118\pm0.159)\times10^{25}$	51.30±0.10	+53.65±0.28	50.56±0.10
Zn(II)	9.93×10^{10}	−10	25	$(6.046\pm0.293)\times10^{10}$	25.42±0.03	−11.52±0.09	24.68±0.03

a) Frequency factor, b) Activation energy, c) Cited from Ref. 4.

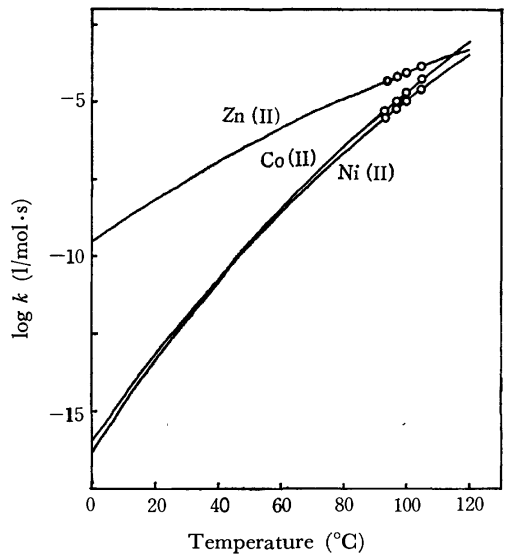

Fig. 2. Plots of log k *vs.* temperature in glycyl-glycine hydrolysis catalyzed by divalent metal ions. (O:experimental data cited from Ref. 4)

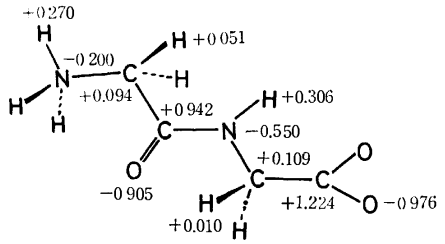

Fig. 3. Electronic structure of G-G in weak acid solution.

(=O)$NHCH_2CO_2^-$, is[8] presented in Fig. 3 by the use of the formal charges calculated by the ASMO-SCF method: the highest occupied (HO) MO of G–G± is strongly localized by the nonbonding lone-pair oxygen 2p-orbital of the CO_2^- group. Bearing in mind that the divalent metal ion behaves as an electron acceptor against G–G±, an assumed complex, A–B···M^+ (or B–A···M^+), in Eqs. (2) and (3) may be represented by the following interacting system:

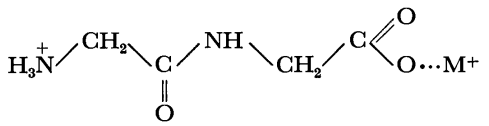

The distinctive nature of the Zn(II) ion mentioned above may be the result of the low-lying, lowest-unoccupied (LU) AO level of the Zn(II) ion; In view of the orbital energies of the LU AOs of the metal ions (−9.39 eV[9] for the Zn(II) p-orbital; −7.86 eV[9] for the Co(II) d-orbital; −7.633 eV[9] for the Ni(II) d-orbital) and the HOMO of the nonbonding lone-pair 2p-orbital of oxygen (−10.50 eV) in the terminal CO_2^- group, it seems from the energetic point of view[10] that the Zn(II) ion may interact easily and strongly with G–G± in the above interacting system. Therefore, the nucleophilic attacking of the H_2O molecule on the more positively-charged carbonyl carbon in the peptide bond may be expected in the case of G–G—Zn^+.

8) With regard to the geometry of glycyl-glycine (Zwitterion), see L. E. Sutton, ed., "Interatomic Distances," The Chemical Society, London (1958).

9) C. E. Moore, "Atomic Energy Levels," Natl. Bur. Std. Circ., No. 467 (1958), Vols. 1, 2, and 3.

10) In an aqueous solution, the divalent metal ion may react with dipeptides as an aquo-complex involving a fixed number of water molecules.[11] Therefore, we should take into consideration the lability order of aquo-complexes in the water substitution with the dipeptide. In this respect, the lability order, Zn(II)≫Co(II)>Ni(II),[12] and/or the order of the rates in water-molecule exchange, Co(II)≧Ni(II),[13] are closely related to that of the rates in the dipeptide hydrolyses by the divalent metal ions.

11) H. Taube, "Progress in Stereochemistry," Butterworths, Washington, D. C. (1962), Vol. 3, p. 95.

12) G. Geier, *Bunsenges. Phys. Chem.*, **69**, 617 (1965).

13) T. J. Swift and R. E. Connick, *J. Chem. Phys.*, **37**, 307 (1962).

BULLETIN OF THE CHEMICAL SOCIETY OF JAPAN, VOL. 46, 2581—2582 (1973)

CNDO/2 Calculation of the Valence Electron Contribution to the Intermolecular Potential of Some Ground State Closed Shell Molecules

Masao HASHIMOTO and Taro ISOBE

The Chemical Research Institute of Non-Aqueous Solutions, Tohoku University, Sendai 980

(Received August 4, 1972)

The empirical or semiempirical theories of intermolecular forces seem to be able to yield satisfactory results for the problem of the stability of solids and for that of conformation of polymers, but in the quatitative calculation of the interaction energy they have more or less been clouded by ambiguous parameters or factors. This is also the result of the artificial distinction between a long- and a short-range force in the usual calculations of the interaction energy in the region of the van der Waals minimum. Thus, it is necessary now to seek a method by which these forces can be unified.

The possibility that a molecular orbital theory could yield an attractive interaction between two closed-shell atoms or molecules has often been discussed.[1] A careful CI calculation for He···He was done recently[2] using very elaborate multiconfigurational wavefunctions, and successful result was thus obtained. However, it is doubtful that this method can be practically applied to larger systems.

The energy of interaction, $U(M\cdots M)$, is generally defined as follows:

$$U(M\cdots M) = E(M\cdots M) - 2E(M) \quad (1)$$

where M is a molecule or an atom and where $M\cdots M$ is a dimer.

Assuming that intermolecular bonding is mainly brought about by an overlap between two molecular orbitals, we will calculate $U(M\cdots M)$ by means of the CNDO/2 SCF MO method[3] and will study the applicability of this method to the molecular-interaction problem by considering the contribution to the lattice energy of the molecular crystal.

The molecules treated in the present work are N_2, C_2H_2, and CO_2, which form crystals belonging to Pa3 space group, and C_2H_4, which forms a crystal belonging to the $P2_1/n$ space group.

Theoretical

Dimer Orbitals and Energies Obtained by the CNDO/2 Method. In this work, the dimer can be treated as one species, and there is essentially no difference between the intermolecular bond and the intramolecular bond so long as the LCAO MO approximation is used. The dimer orbitals and energies can, then, be obtained in the usual way, like the monomer orbital, from the following matrix elements:

$$F_{rr} = -\frac{1}{2}(I_r+A_r) + \left[(P_{AA}-Z_A) - \frac{1}{2}(P_{rr}-1)\right]\gamma_{AA} + \sum_{B(\neq A)}(P_{BB}-Z_B)\gamma_{AB} \quad \text{(orbital } r \text{ on atom } A) \quad (2)$$

$$F_{rs} = \frac{1}{2}S_{rs}(\beta_A+\beta_B) - \frac{1}{2}P_{rs}\gamma_{AB} \quad (r \text{ on } A,\ s \text{ on } B). \quad (3)$$

The total electronic energy of the dimer is expressed as follows:

$$E_{\text{elec}} = \frac{1}{2}\sum_{r,s} P_{rs}(H_{rs}+F_{rs}). \quad (4)$$

The Coulombic repulsion energy between cores is as follows:

$$E_{\text{core}} = \sum_{A\neq B} Z_A Z_B / R_{AB}. \quad (5)$$

The total dimer energy, $E(M\cdots M)$, is, therefore:

$$E_{\text{total}} = E_{\text{elec}} + E_{\text{core}}. \quad (6)$$

The intermolecular interaction energy is, then:

$$U(M\cdots M) = E_{\text{total}}(M\cdots M) - 2E_{\text{total}}(M). \quad (7)$$

The pair interaction energy (7) was summed over all the pairs in the crystal, assuming the pairwise additivity of the intermolecular forces. One half of the above sum was compared with the experimental heat of sublimation.

The assumption of the pairwise additivity is based upon the finding[4] that, in the system of He_3, the non-additive contribution in the neighbourhood of the van der Waals minimum is negligible.

Modification of Slater Atomic Functions at Larger Value. Simple Slater atomic orbitals are usually used for the calculation of the electronic states of molecules; they are expressed, for example, as follows:

$$\chi_{2p_z} = (\alpha^5/\pi)^{1/2}\exp(-\alpha r) r\cos\theta \quad (8)$$

χ in (8) gives a satisfactorily correct charge distribution when r is small, but it gives incorrect results when r becomes large.

One of the atomic functions accurate also in the region of large r values is the linear combination of (8) with different orbital exponent α's:

$$\chi'_{2p_z} = r\cos\theta\sum a_i(\alpha_i^5/\pi)^{1/2}\exp(-\alpha_i r) \quad (9)$$

The coefficients, a_i's, and orbital exponents, α_i's, have been determined by the Hartree–Fock–Roothan Method by Clementi.[5] In the present paper the above types of Clementi's atomic orbitals will be used as basic functions, unless otherwise stated.

The CNDO/2 parametrization was done as usual[3] except for the use of Slater's μ-values; the FORTRAN program for CNDO/2 written by Kikuchi[6] was modified so as to be applicable to Clementi's AO basis.

1) R. G. Gordon and Y. S. Kim, *J. Chem. Phys.*, **56**, 3122 (1972).
2) H. F. Schafer III, D. R. McLaughlin, F. E. Harris, and B. J. Alder, *Phys. Rev. Letts.*, **24**, 1469 (1970).
3) J. A. Pople and D. L. Beveridge, "Approximate Molecular Orbital Theory", McGraw-Hill (1970).
4) O. A. Novaro and V. Beltran-Lopez, *J. Chem. Phys.*, **56**, 815 (1972).
5) E. Clementi, *IBM J. Res. Develop.*, **9**, 2 (1965); *ibid.*, *supplement*, "Tables of Atomic Functions".
6) O. Kikuchi, "Molecular Orbital Method—Practical Use by Computer", A Series of Monographs Modern Trends in Chemistry, No. 6, Kodansha, Tokyo (1971).

In the present work, μ-values appear, for example, as α_i in (9).

All the numerical calculations were done on a NEAC-2200 model 700 computer system at the Computer Center of Tohoku University.

Results and Discussion

Figures 1 and 2 indicate the dependency of the $U(M\cdots M)$ of C_2H_4 on the intermolecular distance, R, when the two molecules have a parallel and perpendicular configuration respectively.

The summation of (7) over all the pairs of molecules in the crystal was approximated by that over the nearest and the second-nearest neighbour molecules,

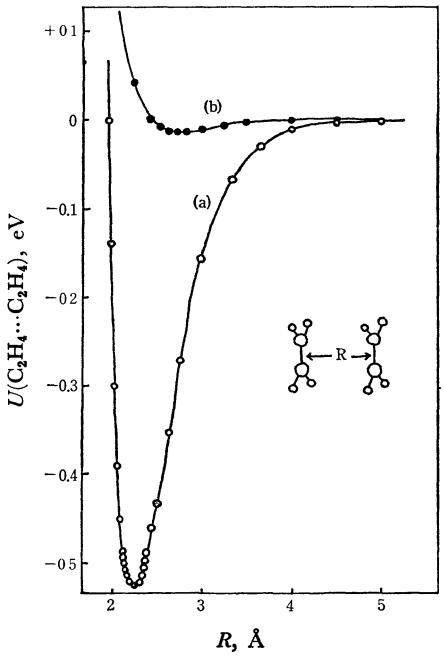

Fig. 1. The dependency of $U(M\cdots M)$ of C_2H_4 on intermolecular distance R when the two molecules have a parallel configuration.
(a) using Clementi's AO; (b) using simple Slater's AO.

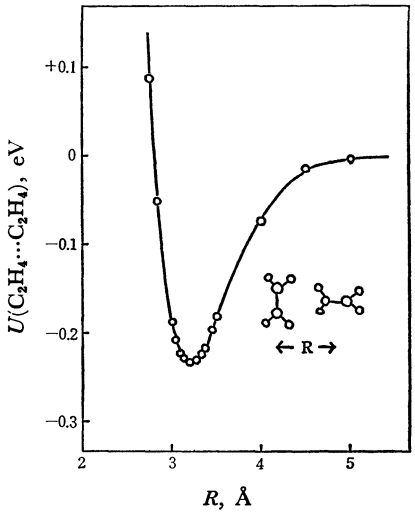

Fig. 2. The dependency of $U(M\cdots M)$ of C_2H_4 on intermolecular distance R when the two molecules have a perpendicular configuration (using Clementi's AO).

Table 1.[a)]

M	$1/2\sum U(M\cdots M)$	heat of Sublimation (obs.)
N_2	−0.06480	−0.07164[12)]
C_2H_2	−0.24834	−0.23851[13)]
C_2H_4	−0.11360	−0.18213[14)]
CO_2	−0.28465	−0.28621[15)]

a) In electron volt, error ±0.00025

since the third-nearest neighbour molecules in the crystal are from 11.1 to 19.4 Å away from the central molecule and in this region the $U(M\cdots M)$ might be negligible, as may be seen from Figs. 1(a) and 2. More or less similar situations are observed for the other crystals.

In Table 1, the experimental heat of sublimation, which does not include the zero-point energy, and a half of the calculated interaction energy summed over the nearest and the second-nerarest neighbour molecules in the crystals are compared. The consistency seems to be quite good.

In Fig. 1 the $U(M\cdots M)$ (a) calculated by using Clementi's AO is compared with that (b) calculated using the simple Slater AO.

The overlap integrals among the simple Slater AOs are very small and negligible in the region of the intermolecular distances. However they become effective if Clementi's AOs are used.

To show the partial reliability of the present work, we wish to cite two example: 1) Many authors have examined the refinement of Bunn's crystal structure for ethylene,[7)] and it is known today to have $P2_1/n$ space group.[8)] If the $\sum U(M\cdots M)$ of C_2H_4 is calculated for Bunn's structure, it becomes +3.37 eV and is strongly repulsive. This does not explain the formation of the stable crystal. 2) The lower-temperature form of the crystalline acetylene has already been suggested to be Cmca.[9,10)] The present calculation of $\sum U(M\cdots M)$ of C_2H_2 for the Cmca structure is −0.51456 eV, surely lower that of the high-temperature form, −0.49668 eV.

Furthermore, the *staggered* configuration of CH_3OH molecule was found to have an energy lower by 0.04486 eV or 1.03 kcal/mole than the *eclipsed* configuration. This is in good agreement with the experimental value of 1.07 kcal/mole.[11)]

The authors wish to thank Dr. Enrico Clementi of the IBM Research Laboratory for his kind offer of the table of atomic functions.

7) C. N. Bunn, *Trans. Faraday Soc.*, **40**, 23 (1944).
8) S. M. Blumenfeld, P. Reddy, and H. L. Welsh, *Can. J. Phys.*, **48**, 513 (1970).
9) M. Ito, T. Yokoyama, and M. Suzuki, *Spectrochim. Acta*, **26A**, 695 (1970).
10) M. Hashimoto M. Hashimoto, and T. Isobe, This Bulletin, **44**, 649 (1971).
11) C. C. Lin and J. D. Swalen, *Rev. Mod. Phys.*, **31**, 841 (1959).
12) B. L. Kohin, *J. Chem. Phys.*, **33**. 882 (1960).
13) D. McIntosh, *J. Phys. Chem.*, **11**, 306 (1907).
14) C. J. Egan and J. D. Kemp, *J. Amer. Chem. Soc.*, **59**, 1264 (1937).
15) H. Sponer and M. Bruch-Willstatter, *J. Chem. Phys.*, **5**, 745 (1937).

BULLETIN OF THE CHEMICAL SOCIETY OF JAPAN, VOL. 46, 2583—2584 (1973)

Circular Dichroic Evidence for the Cholesteric Phase in Solid Films of Poly-γ-methyl-glutamate

Taro TACHIBANA and Etsuko ODA

Chemical Laboratory, Ochanomizu University, Otsuka, Bunkyo-ku, Tokyo 112

(Received October 21, 1972)

Concentrated solutions of synthetic polypeptides are known to have a cholesteric liquid crystal structure.[1] Samulski and Tobolsky[2] presented evidences for such a structure in solid films of poly-γ-benzyl-L-glutamate (PBLG) made by casting from solution. The structure in the solid films was inferred from swelling and birefringence studies and X-ray observation. Thus, if the solid films in which the periodicity is comparable to the wavelength of light can be prepared, it is reasonable to expect them to show the cholesteric colors, since the cholesteric liquid crystal exhibits selective reflection of circularly polarized light. Such an example has been reported[3] only for a concentrated solution of poly-γ-ethyl-glutamate in ethyl acetate.

Recently a patent[4] was published in which it was described that solid films with iridescent colors were obtained from poly-γ-methyl-D(or L)-glutamate (PMDG or PMLG). In order to confirm our presumption that the colors are due to cholesteric color, we have performed circular dichroic studies with colored films.

Experimental

Concentrated solutions (24 wt%) of PMDG and PMLG (D. P., *ca* 230) in 1,2-dichloroethane (provided from Central Research Laboratories, Ajinomoto Co., Inc.)[5] were used after being diluted to 8 weight percent with the same solvent. A small amount of the solution was spread as thin films on the surface of a plate glass, rubbed in one direction with a glass rod. The solvent was then allowed to evaporate freely in air at room temperature. After being dried completely, thin solid films were formed on the glass surface. They were then stripped off the glass surface by introducing the film-covered glass plates into water. Solid films 10 to 30 micron thick were preferred for the optical study. Although they were more or less opaque and colorless for transmitted light, they assumed a uniform reflection color varying from blue to red depending on the angle of view and incidence. The color depended also on the initial concentration of solution and the evaporation rate; when the rate was slower, the color was displaced from blue to red when viewed at a certain angle.

Samples with uniform thickness and area suitable for measuring the circular dichroism were cut out from the films and mounted on a holder with a window, 6 mm×6 mm. Circular dichroism was measured by using a JASCO Automatic Recording Spectropolarimeter Model J-10. Unless otherwise stated, incident light was cast at right angle to the sample film.

Results and Discussion

As expected, circular dichroism (CD) was observed for the sample films reflecting blue to red light. Typical circular dichroic curves for a PMDG film are illustrated in Fig. 1, where the CD (ordinate) is

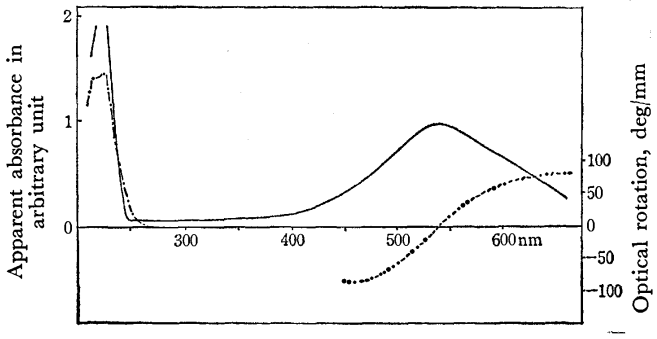

Fig. 1. Circular dichroism (——) and optical dispersion (····) of solid films (20 μ thick) of PMDG.
Line (-·-·-) shows a CD curve of dilute solution (0.04 wt%) of PMDG in 1,2-dichloroethane.

expressed as the apparent absorbance of the left circularly polarized light minus that of the right one. The CD curve exhibited a large band with a peak in the region 450—650 nm and a small band with a peak in the region 220—230 nm. The latter band, also observed for the solutions of PMDG in chloroform, was the same as the CD band which has been attributed to the n–π* transition in the α-helix of PMDG molecules.[6] The 450—650 band is due to selective reflection of circularly polarized light of one sense in that wavelength region, since no absorption is found here for the solution. Since the apparent absorbance is actually due to the reflection, it is concluded from Fig. 1 that the PMDG films reflect selectively the left circularly polarized light. On the other hand, the PMLG films were found to give the CD curve of the opposite sense. The result indicates the presence of a cholesteric liquid crystal structure in the solid films of PMDG or PMLG.

Liquid crystals in the cholesteric phase are well-known to form a macroscopic helical structure. Polarizing microscope examination showed that the birefringence of the film of PMDG or PMLG is optically negative and the optical axis is almost normal to the

1) C. Robinson, *Trans. Faraday Soc.*, **52**, 571 (1956).

2) E. T. Samulski and A. V. Tobolsky, *Nature*, **216**, 997 (1967); *Pure Appl. Chem.*, **23**, 145 (1970).

3) C. Robinson, *Mol. Cryst.*, **1**, 467 (1966).

4) N. Okuda, S. Mori, Y. Takagi, and Y. Takeda, Japanese, No. 5154 (1970).

5) PMG was prepared by ring-opening polymerization of γ-methyl-glutamate NCA in 1,2-dichloroethane using *N,N*-dimethylethylenediamine as initiator (S. Mori and N. Iwatsuki, private communication).

6) G. Holzwarth and P. Doty, *J. Amer. Chem. Soc.*, **87**, 218 (1965).

film surface, *i.e.* the axis of the macrohelix is almost vertical to the film surface. Thus, for normal incidence, the pitch p of the macrohelix is inferred from the equation[7] $\lambda_m = n \cdot p$, where λ_m is the wavelength of the maximum reflection and n is the average refractive index. The value for λ_m was obtained from the peak of the CD curve and n was experimentally estimated as about 1.4. For a sample which showed the CD curve of Fig. 1, the pitch was estimated as 350 nm by using $\lambda_m = 500$ nm and $n = 1.4$.

The helical sense can be deduced from the sense of the circularly polarization of the reflected light or from the sign of the optical rotatory dispersion; a left-handed helical structure reflects left circularly polarized light and it shows negative optical rotation on the short wavelength side of the reflection band[7,8,9,10]. Figure 1 shows that the PMDG films reflect left circularly polarized light and that they show negative optical rotation at the short wavelength side of the inversion. It is thus concluded that the PMDG films have a left-handed macrohelix. For the PMLG films a right-handed macrohelix was found. Since the molecular helix (α-helix) of PMDG (or PMLG) is known to be left-handed (or right-handed), this result indicates that the sense of the macrohelix is the same as that of the molecular helix of each enantiomer.

The dependence of the reflection on the angle of incidence was also measured. The wavelength peak was compared with the value calculated by Fergason's formula[11] which gives the wavelength of maximum reflection as a function of the angle of incidence and of reflection for cholesteric liquid crystal. The observed value of the peak was in good agreement with the value calculated by assuming that the reflection planes are placed parellel to the film surface. This shows that the reflection planes of the cholesteric phase are parallel to the film surface, being consistent with the result of the polarizing microscope examination.

The cholesteric structure of the films was so heat-resistant that it was not destroyed until near the decomposition temperature of this polymer.

The colors of the solid films of PMDG were found to change reversibly by absorbing organic vapor such as chloroform or benzene. With the progress of absorption, the color turned red, becoming finally faint. Corresponding to the visual color change, the peak of the CD curve shifted to longer wavelength region. This indicates the increase of the pitch of the macrohelix by absorbing organic vapor between the planes in which the molecules lie, since the change of the refractive index is not so sensitive in this case.

Colored films were not obtained from a racemic mixture of PMDG and PMLG. Among polyglutamate esters, PBLG is also reported to form a solid film with a cholesteric structure,[2] but it did not exhibit cholesteric color. Formation of the solid film with cholesteric color was most favorable from solutions of PMDG or PMLG which was prepared according to the method in Ref. (5). This explanation is still not clear.

The result we presented has a new significance for the observation[12] that the light reflected from certain iridescent beetles is also circularly polarized, suggesting the presence of a cholesteric structure in their cuticles.

7) Hl. de Vries, *Acta Crystallogr.*, **4**, 219 (1951).
8) S. Chandrasekhar and K. N. S. Rao, *ibid.*, **A24**, 445 (1968).
9) M. Aihara and H. Inaba, *Opt. Commun.*, **3**, 77 (1971).
10) Here it should be noted that confusion occurs regarding the sense of circular polarization in the literature. For example, according to Conners' paper (*J. Opt. Soc. Amer.*, **58**, 875 (1968)), a right-handed helix reflects left circularly polarized light. Then, he adopted a definition contrary to the normal usage for the sense of circularly polarized light.
11) J. L. Fergason, *Mol. Cryst.*, **1**, 293 (1966).
12) A. C. Neville and S. Caveney, *Biol. Rev. Cambridge Phil. Soc.*, **44**, 531 (1969).

BULLETIN OF THE CHEMICAL SOCIETY OF JAPAN, VOL. 46, 2584—2586 (1973)

Studies on Microcapsules. XV. Electrophoretic Behavior of Carboxylated Polyphthalamide Microcapsules Containing Aqueous Solutions of Polyelectrolytes

Motoharu SHIBA, Suiichi TOMIOKA, and Tamotsu KONDO*

Research Laboratory, Chugai Pharmaceutical Co., Ltd., Toshima-ku, Tokyo 171

** Faculty of Pharmaceutical Science, Scinence University of Tokyo, Shinjuku-ku, Tokyo 162*

(Received November 24, 1972)

In an earlier paper of this series,[1] we reported that polyphthalamide microcapsules containing aqueous solution of anionic or cationic polyelectrolytes move towards the anode or cathode in an electric field according to the sign of charge on the encapsulated polyelectrolyte though the microcapsule membrane itself has no charge at all. Polyphthalamide microcapsules containing amphionic polyelectrolyte migrate either to the anode or to the cathode depending on the pH of the medium, showing the existence of an isoelectric point. All these findings indicated that the direction of electrophoresis of microcapsules containing aqueous solution of polyelectrolyte is determined by the sign of electric charge on the encapsulated polyelectrolyte.

However, if a certain portion of encapsulated polyelectrolyte molecules is supposed to have been chemically incorporated into the microcapsule membrane during the microencapsulation to give the membrane an electric charge, the direction in which microcap-

1) M. Shiba, Y. Kawano, S. Tomioka, M. Koishi, and T. Kondo, *Kolloid-Z. Z. Polym.*, **249**, 1056 (1971).

sules move in an electric field does not necessarily reflect the sign of charge on the encapsulated polyelectrolyte. Thus, for example, polyphthalamide microcapsules containing aqueous solution of bovine serum albumin migrated to the anode even at a lower pH than that of the isoelectric point of the protein.[2] This was interpreted as follows: A portion of the encapsulated bovine serum albumin molecules participates in the interfacial polycondensation reaction between diamine and acid dichloride, giving the membrane a negative charge since the protein has many amino groups reactive with acid dichloride and the charge on the encapsulated, unreacted protein molecules is screened by the charge of outer surface of microcapsule membrane.

The present study is aimed at confirming the dependence of the net charge of aqueous microcapsules containing polyelectrolyte upon the surface charge of their membrane. Poly-L-lysine phthalamide microcapsules containing aqueous solution of polyelectrolytes were prepared and their electrophoretic mobilities were determined at various hydrogen ion concentrations. The aqueous carboxylated polyphthalamide microcapsules containing polyelectrolyte are superior to the above-mentioned polyphthalamide microcapsules containing aqueous solution of bovine serum albumin in that the charge can be safely assumed to be uniformly distributed in the membrane since it consists of a single component and a free choice of polyelectrolyte to be encapsulated can be made.

Experimental

Materials. The polyelectrolytes were sodium heparinate (Daiichi Chemical Medicine Ind. Co., Tokyo) and 2-methyl-5-vinylpyridine–methyl acrylate–methacrylic acid copolymer (abbreviated hereafter as MPM) (Tanabe Pharmaceutical Co., Ltd., Osaka). Polyvinylpyrrolidone (PVP) was also used as electrically neutral polymer to be encapsulated.

L-Lysine of the highest purity available (Ajinomoto Co., Ltd., Tokyo) was used.

Preparation of Microcapsules. Poly-L-lysine phthalamide (PLPA) microcapsules containing aqueous polyelectrolyte solution were prepared by the same procedure as in a previous work.[3]

Measurements of Electrophoretic Mobilities. Electrophoretic mobility measurements on the carboxylated polyphthalamide microcapsules containing polyelectrolyte solution were carried out at room temperature in a quartz flat microelectrophoretic cell. For each measurement 40 microcapsules were timed in each direction to eliminate the polarization effect of the electrodes. The dispersion media were HCl-CH_3COONa (pH 2—3), acetate (pH 3—6), and phosphate (pH 6—8) buffers, the ionic strength of which was maintained at 1×10^{-1} or 2×10^{-3} with NaCl.

The samples for electrophoretic measurement were prepared by pipetting a few drops of the microcapsule suspension into a large volume of the dispersion media.

In view of the size of microcapsules (about 3 μm in diameter) and the ionic strength of the dispersion media (2×10^{-3} and higher), mobilities were converted into zeta-potentials ζ by means of the simple Smoluchowski equation

$$\zeta = \frac{4\pi\eta v}{D}$$

where v is the mobility, η and D are the viscosity and dielectric constants, respectively, of dispersion medium.

Results and Discussion

In Fig. 1 is shown the variation of the zeta-potential with the pH of the medium for PLPA microcapsules containing aqueous solution of PVP and for those containing aqueous solution of sodium heparinate. The electrophoretic behavior of PLPA microcapsules con-

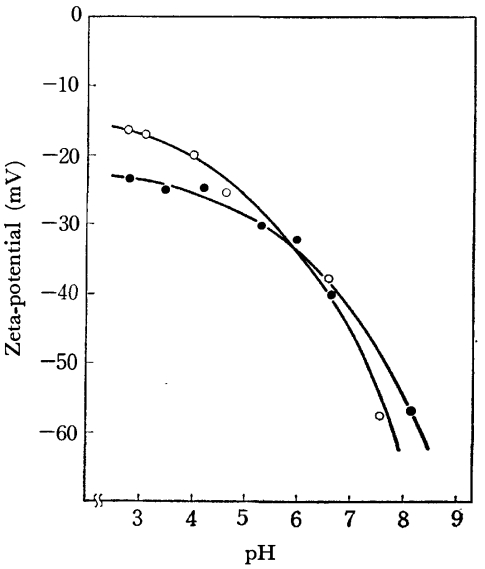

Fig. 1. Zeta-potential of carboxylated microcapsules containing 0.5% polymer solution as a function pH at an ionic strength of 2×10^{-3}. PVP, —○—, sodium heparinate, —●—.

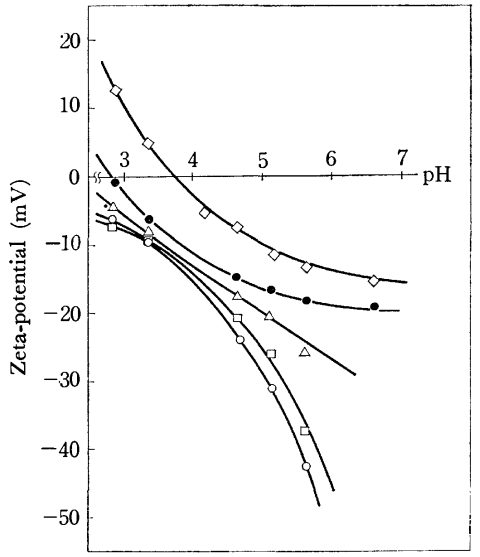

Fig. 2. Zeta-potential of carboxylated microcapsules containing MPM solution as a function of pH at an ionic strength of 1×10^{-2}. Concentration of MPM: —○— 0%; —□— 0.1%; —△— 0.3%; —●— 0.5%; —◇— 1.0%.

2) M. Shiba, Y. Kawano, S. Tomioka, M. Koishi, and T. Kondo, This Bulletin, **44**, 2911 (1971).

3) Y. Shigeri, M. Tomizawa, K. Takahashi, M. Koishi, and T. Kondo, *Can. J. Chem.*, **49**, 3623 (1971).

taining PVP was almost the same as that of those containing no polymer.[3] This is reasonable because PVP is electrically neutral and the zeta-potential of PLPA microcapsules is, therefore, determined solely by the charge of microcapsule membrane. In contrast, sodium heparinate seems to play an important role in determining the zeta-potential of PLPA microcapsules at low pH. Since the dissociation of carboxyl groups of PLPA should decrease with increasing hydrogen ion concentration, screening of the charge of the polyelectrolyte by the microcapsule membrane would be less significant with the lowering of pH of the medium. At high pH, the zeta-potential of PLPA microcapsules containing the polyelectrolyte was slightly less negative than that of those containing PVP. This may be due to the higher counter ion concentration near the membrane surface.

Figure 2 gives the plot of the zeta-potential against the pH of the medium for PLPA microcapsules containing aqueous solution of MPM, an amphionic polyelectrolyte having an isoelectric point at pH 4. The zeta-potential varied with both pH of the medium and the concentration of MPM. At low concentrations of MPM, PLPA microcapsules migrated to the anode independent of pH. When the microcapsules contained high concentrations of MPM, the direction in which they moved in an electric field reversed at low pH, while they still migrated towards the anode at high pH. This may result from the fact that some of MPM molecules are absorbed on the inner surface of microcapsule membrane to give it a positive charge which surpasses the negative charge of the outer membrane surface at low pH. We see from the figure that an increase in the concentration of MPM gives rise to a decrease in the absolute value of the zeta-potential of negatively charged PLPA microcapsules. The decrease in the zeta-potential may be caused by the increasing concentration of counter ions liberated from the encapsulated polyelectrolyte molecules.

BULLETIN OF THE CHEMICAL SOCIETY OF JAPAN, VOL. 46, 2586—2587 (1973)

ESR of Hot Ions: Ni(I) Complex Ions Produced in Ni(II) Complexes by γ-Irradiation

Chikara AMANO, Tokuko WATANABE, and Shizuo FUJIWARA

Department of Chemistry, Faculty of Science, The University of Tokyo, Hongo, Bunkyo-ku, Tokyo 113

(Received December 6, 1972)

X- or γ-Irradiation has been shown to produce in solids metal ions with uncommon valence and geometrical configuration.[1-4] In this paper a report is given on the ESR spectra of monovalent nickel complex ions with the $3d^9$ electron configuration and a discussion on the electronic state of the Ni(I) complex ions in terms of observed g-values.

Forty-six Ni(II) complexes were synthesized by standard methods (Table 1).[5] Nickel(II) chloride hexahydrate, the starting material, was purified by an anion exchange method to remove a trace of cobaltous and cupric ions. The polycrystalline complexes ($\sim$100 mg) were γ-irradiated at room temperature with a γ-ray dosage of 1×10^7 R with dose rate of 5×10^5 R/h, and at 77 K with a γ-ray dosage of 1×10^6 R with dose rate of 5×10^4 R/h. ESR spectra were recorded at 77 K on a JEOL 3BSX spectrometer.

Of the forty-six complexes examined, nine gave strong signals upon γ-irradiation (Table 2). Other complexes gave only weak absorptions at $g\sim2$ probably due to radicals produced from ligand molecules.

γ-Irradiated $[Ni(en)(H_2O)_4]SO_4\cdot H_2O$, $[Ni(en)_2(H_2O)_2](ClO_4)_2$, $[Ni(l\text{-ala})_2(H_2O)_2]2H_2O$, and $[Ni(succinimde)_2(H_2O)_4]4H_2O$ give broad ESR absorptions (line width$\sim$100 G) of an approximately axial pattern. The other complexes in Table 2 shows several narrower absorptions. It is to be noted that in both these cases relatively large g-shifts ($\Delta g=0.2$—0.3) are observed, suggesting that the paramagnetic centers produced upon γ-irradiation are due to nickel ions. In the case of irradiated $[Ni(en)(H_2O)_4]SO_4\cdot H_2O$, $[Ni(en)_2(H_2O)_2](ClO_4)_2$ and $[Ni(l\text{-ala})_2(H_2O)_2]\text{-}2H_2O$, it is observed that $g_{\parallel}>g_{\perp}>2$, which is expected for a d^9 electron configuration with tetragonally elongated octahedral symmetry (ground state $^2B_{1g}$). According to ligand field theory a d^7 electron configuration in the ground state $^2B_{1g}$ is also consistent with this observation. However, as far as we know, complex ions

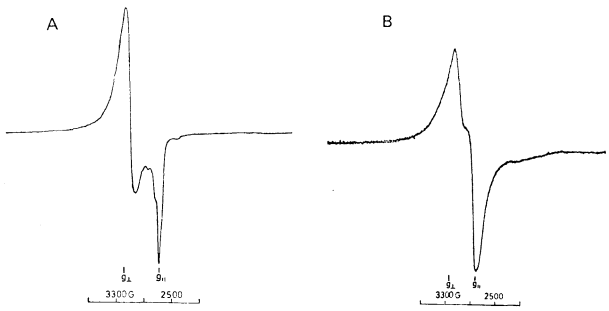

Fig. 1. A. ESR spectrum of $[Ni(en)(H_2O)_4]^+$ produced in γ-irradiated polycrystalline $[Ni(en)(H_2O)_4]SO_4\cdot H_2O$.
B. ESR spectrum of $[Ni(l\text{-ala})_2(H_2O)_2]^-$ produced in γ-irradiated polycrystalline $[Ni(l\text{-ala})_2(H_2O)_2]2H_2O$.

1) D. A. Morton-Blake, *J. Phys. Chem.*, **74**, 1508 (1970).
2) S. Fujiwara, T. Watanabe, and H. Tadano, *J. Coord. Chem.*, **1**, 196 (1971).
3) T. Krigas and M. T. Rogers, *J. Chem. Phys.*, **54**, 4796 (1971).
4) J. Isoya and S. Fujiwara, This Bulletin, **45**, 2182 (1972).
5) Gmelins Handbuch der Anorganischen Chemie, System-Nummer (1969) p. 57.

Table 1. γ-Irradiated Ni(II) complexes

A. $[Ni(NH_3)_6]Cl_2$, $[Ni(NH_3)_6](ClO_4)_2$, $[Ni(en)_3]Cl_2\cdot 2H_2O$, $[Ni(en)_3]SO_4$, $[Ni(en)_3](ClO_4)_2\cdot 1/2\,H_2O$, $Ni(N_2H_4)_3SO_4$, $Ni(N_2H_4)_3Cl_2$, $Ni(N_2H_4)_3(NO_3)_2$

B. $[Ni(NH_3)_4(NCS)_2]$, $[Ni(en)_2(H_2O)_2](NO_3)_2$, $[Ni(en)_2(H_2O)_2](ClO_4)_2$, $[Ni(en)(H_2O)_4](NO_3)_2$, $[Ni(en)(H_2O)_4]SO_4\cdot H_2O$, $Ni(N_2H_4)_2Cl_2$, $Ni(N_2H_4)_2SO_4\cdot 3H_2O$, $Ni(py)_2Cl_2$, $Ni(py)_4Cl_2$, $Ni(py)_2(H_2O)_2(NO_2)_2$, $Ni(py)_2(H_2O)_2SO_4$, $[Ni(dipy)(H_2O)_4]SO_4\cdot 2H_2O$, $[Ni(gly)_2(H_2O)_2]$, $[Ni(l\text{-}ala)_2(H_2O)_2]2H_2O$, $[Ni(C_7H_5O_2)_2(H_2O)_2]$, $[Ni(C_5H_7O_2)_2(H_2O)_2]$, $[Ni(C_9H_6NO)_2(H_2O)_2]$, $[Ni(C_{10}H_8NO)_2(H_2O)_2]$, $[Ni(C_9H_4NOBr_2)_2(H_2O)_2]$, $Ni(C_9H_7N)_2Cl_2$, $Ni(iso\text{-}C_9H_7N)_4Cl_2$, $[Ni(C_{10}H_9O_2)_2(H_2O)_2]$, $Ni(C_3H_5NO_2)_2\cdot 8H_2O$, $[Ni(C_7H_7NO_2)_2(H_2O)_2]$

C. $K_2[Ni(CN)_4]H_2O$, $Na_2[Ni(CN)_4]\cdot 3H_2O$, $[Ni(C_4H_7N_2O_2)_2]$, $[Ni(C_7H_6NO_2)_2]$, $[Ni(C_7H_6NO)_2]$, $[Ni(C_8H_8NO)_2]$, $[Ni(C_9H_{10}NO)_2]$, $[Ni(C_{10}H_{12}NO)_2]$, $[Ni(C_2H_3OS_2)_2]$, $[Ni(C_3H_5OS_2)_2]$, $[Ni(C_3H_6NS_2)_2]$, $[Ni(C_6H_6N_2O)_2]$

D. $[Ni(C_7H_5O_2)_2]$, $[Ni(C_9H_6NO)_2]$

en=ethylenediamine, N_2H_4=hydrazine, py=pyridine, dipy=α,α'-dipyridyl, gly$^-$=glycinate, l-ala$^-$=l-alaninate, $C_7H_5O_2^-$=salicylaldehyde anion, $C_5H_7O_2^-$=acetylacetonate, $C_9H_6NO^-$=8-hydroxyquinolinate, $C_{10}H_8NO^-$=2-methyl-8-hydroxyquinolinate, $C_9H_4NOBr_2^-$=5,7-dibromo-8-hydroxyquinolinate, $C_9H_7N^-$=quinolinate, iso-$C_9H_7N^-$=isoquinolinate, $C_{10}H_9O_2^-$=benzoylacetonate, $C_3H_5NO_2^-$=succinimide anion, $C_7H_7NO_2^-$=o-aminobenzoate, $C_4H_7N_2O_2^-$=dimethylglyoximate, $C_7H_6NO_2^-$=salicylaldoxime anion, $C_7H_6NO^-$=salicylaldimine anion, $C_8H_8NO^-$=N-methylsalicylaldimine anion, $C_9H_{10}NO^-$=N-ethylsalicylaldimine anion, $C_{10}H_{12}NO^-$=N-propylsalicylaldimine anion, $C_2H_3OS_2^-$=methylxanthogenate, $C_3H_5OS_2^-$=ethylxanthogenate, $C_3H_6NS_2^-$=dimethyldithiocarbamate, $C_6H_6N_2O^-$=picolinamide anion

Table 2. ESR parameters of Ni(I) complex ions

Complex ions	Matrices	$g_\parallel$	$g_\perp$	Ref.
$[Ni(en)(H_2O)_4]^+$	$[Ni(en)(H_2O)_4]SO_4\cdot H_2O$	2.434±0.005	2.080±0.005	
$[Ni(en)_2(H_2O)_2]^+$	$[Ni(en)_2(H_2O)_2](ClO_4)_2$	2.275±0.005	2.039±0.005	
$[Ni(l\text{-}ala)_2(H_2O)_2]^-$	$[Ni(l\text{-}ala)_2(H_2O)_2]2H_2O$	2.309±0.005	2.037±0.005	
$[Ni(C_3H_5NO_2)_2(H_2O)_4]^-$	$[Ni(C_3H_5NO_2)_2(H_2O)_4]4H_2O$	2.012±0.005	2.364±0.005	
$[Ni(CN)_4]^{3-}$	$K_2[Ni(CN)_4]H_2O$	2.298±0.002[b]		
$[Ni(CN)_4]^{3-}$	$Na_2[Ni(CN)_4]3H_2O$	2.271±0.002[b]		
$[Ni(C_2H_3OS_2)_2]^-$	$[Ni(C_2H_3OS_2)_2]$	2.300±0.003[b]		
$[Ni(C_3H_5OS_2)_2]^-$	$[Ni(C_3H_5OS_2)_2]$	2.278±0.003[b]		
$[Ni(C_3H_6NS_2)]^-$	$[Ni(C_3H_6NS_2)_2]$			
$[Ni(en)(H_2O)_4]^+$	EG–H_2O[a]	2.359±0.002	2.072±0.002	10)
$[Ni(en)_2(H_2O)_2]^+$	EG–H_2O	2.282±0.002	2.068±0.002	10)
$[Ni(CN)_4]^{3-}$	EG–H_2O	2.131±0.002	2.030±0.002	10)
$[Ni(C_2H_3OS_2)_2]^-$	Xylene	2.282±0.002	2.076±0.002	10)
$[Ni(C_3H_5OS_2)_2]^-$	Xylene	2.280±0.002	2.074±0.002	10)

a) Ethyleneglycol: water=2 : 1 v/v. b) g-value for the most intense line.

with the d^7 electron configuration always give the relation $g_\perp > g_\parallel \sim 2$.[6-9] Therefore it may be concluded that in the above complexes, monovalent nickel complex ions are produced through reduction of Ni(II) complexes by γ-irradiation. On the other hand, in irradiated $[Ni(succinimide)_2(H_2O)_4]4H_2O$ we find $g_\perp > g_\parallel \sim 2$, which is expected for d^9 ions with tetragonally compressed octahedral symmetry (ground state $^2A_{1g}$).

Each of the remaining five complexes in Table 2 gives several absorptions which are most likely due to Ni(I) complex ions from their relatively large g-shifts, such shifts being due to heavy atoms, *i.e.* nickel ions in the present case. A preliminary investigation on a single crystal of $Na_2[Ni(CN)_4]3H_2O$ shows that the number of paramagnetic species is greater than that of inequivalent sites in the host crystal. In X-irradiated nickel(II) acetate tetrahydrate, Morton-Blake observed seven monovalent nickel complex ions with different g-values.[1]

It should be noted that for $[Ni(en)(H_2O)_4]^+$ and $[Ni(CN)_4]^{3-}$ g-values observed in the lattice of the host complexes are considerably larger than in rigid solutions (Table 2). This suggests that the structure of the Ni(I) complex ions is different in these two matrices. The yield of the Ni(I) species produced by γ-irradiation is strongly dependent on the counter ions and crystal structure of the complexes. ESR spectra of Ni(I) can be observed in irradiated $[Ni(en)(H_2O)_4]SO_4\cdot H_2O$ and $[Ni(en)_2(H_2O)_2](ClO_4)_2$, but not in $[Ni(en)(H_2O)_4](NO_3)_2$ and $[Ni(en)_2(H_2O)_2](NO_3)_2$. In the latter two complexes the yield of paramagnetic species, if exist at all, should be lower at least by two orders of magnitude.

We would like to thank Mr. Shingo Katsura, γ-ray Irradiation Center, for his assistance, and also Dr. Yoji Arata for helpful discussions and remarks in the preparation of this paper.

6) S. Geschwind and J. P. Rameika, *J. Appl. Phys.*, **33**, 721 (1961).
7) U. Höchli and K. A. Müller, *Phys. Rev. Lett.*, **12**, 730 (1964).
8) R. Lacroix, U. Höchli and K. A. Müller, *Helv. Phys. Acta*, **37**, 627 (1964).
9) U. Höchli, K. A. Müller, and P. Wysling, *Phys. Lett.*, **15**, 5 (1965).
10) C. Amano and S. Fujiwara, This Bulletin, **46**, 1379 (1973).

BULLETIN OF THE CHEMICAL SOCIETY OF JAPAN, VOL. 46, 2588—2589 (1973)

The Structure of Ordered β V_2D as Determined by Means of the Deuteron Magnetic Resonance

Keikichi NAKAMURA

National Research Institute for Metals, Nakameguro, Meguro-ku, Tokyo 153

(Received December 26, 1972)

According to the V–D phase diagram,[1,2] there are three types of ordered phases: β V_2D, $\delta(\alpha'')$, and $\gamma(\alpha''')$ V_4D_3. The β form is body-centered tetragonal, with $c_0/a_0 \simeq 1.1$, and it is stable up to +140 °C. The δ and γ forms are pseudocubic and stable from −60 to −120 and below −120 °C respectively.

We have measured the deuteron magnetic resonance of the V–D system over wide ranges of the deuterium concentration and the temperature. The results confirm the published V–D phase diagram.[1,2] The deuteron quadrupole coupling constants have been measured as 68.6±1.2 KHz (R.T.) for β V_2D and 37.5±0.4 KHz (−130 °C) for γ V_3D_4. The asymmetry parameters were approximately zero for both forms. These values agree well with the recent NMR results.[3] The observed deuteron quadrupole coupling constants and the asymmetry parameter of δ, γ V_4D_3 are approximetely the same as those for β Nb_4D_3. In view of this fact and the similarity of neutron diffraction pattern between γ V_4D_3 and β Nb_4D_3,[4] it may be assumed that the deuteriums in γ V_4D_3 occupy tetrahedral intersticies such as those in the β Nb_4D_3.

The deuteron quadrupole coupling constant of β V_2D is roughly twice those of γ V_4D_3, β Nb_4D_3,[5] and β Ta_2D[6,7]. The c_0/a_0 ratio of β V_2D is about 1.1, which is different from the pseudocubic character of the other forms, — e.g., 1.008 for Ta_2D. In spite of the relatively large lattice expansion along the c axis, the asymmetry parameter is approximately zero. This is comparable to that of β Ta_2D ($\eta \simeq 0.24$).[6,7] These considerations clearly indicate the site of deuterium in β V_2D. Firstly, the EFG of the site must be symmetry with respect to the c axis. Secondly, the deuterium must repel the two nearest-neighboring vanadium atoms along the c axis so as to deform the cubic cell to tetragonal. Thirdly, the V–D distance in this form must be shorter than that in γ V_4D_3. The only possible site which satisfies the above three conditions is the octahedral site (o-site), whose EFG is symmetric with respect to the c axis.

Next, let us determine the ordered deuterium arrangement in β V_2D. Consider that there are n deuterium atoms and $6n$ o-sites in a ordered V_2D unit cell. However, it is necessary to consider only $2n$ o-sites because of their symmetry with respect to the c axis. Thus, the problem can be reduced to a manner of selecting n o-sites from $2n$ o-sites.

Consider a linear array of vanadium atoms with a spacing of c_0 along the c axis. The o-sites are at the middle of the V–V axis, standing in a line with the same spacing of vanadium:

-V-O-V-O-V-O-V-O-V-O-V-O-V-O-V-

If a deuterium atom occupies an o-site, it would displace the two nearest-neighboring vanadium atoms by $\pm z$. Consequently, it becames geometrically difficult for deuterium to occupy the two nearest-neighboring o-sites and the array of deuterium atoms will be:

-V-D-V-E-V-D-V-E-V-D-V-E-V-D-V-E-V-D-V-E-V-

where E means that the site is empty. A translation of the above one-dimensional lattice points by $\pm 1/2$ 1/2 1/2 determine the array of atoms on the next side. Thus, we obtain a three-dimensional arrangement of deuterium, as is shown in Fig. 1. This structure is

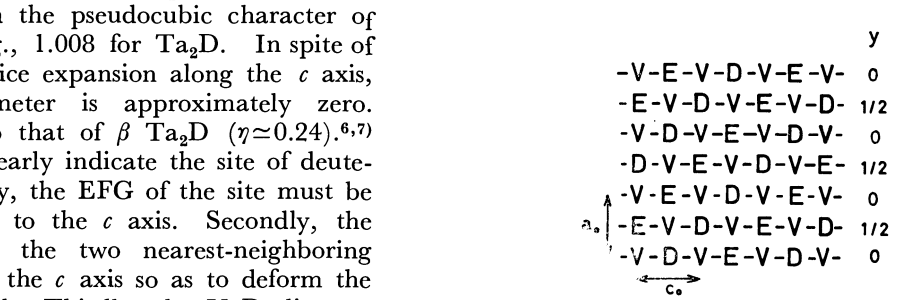

Fig. 1. Three-dimensional arrangement of β V_2D, a projection onto (010) plane.

consistent with the results of a recent neutron diffraction study[8] except for the existence of a small proportion of tetrahedral occupation in that study.

It should be noted that there are $4n$ tetrahedral sites (t-sites) whose EFG is symmetric with respect to the c axis. Therefore, the occupation of these t-sites by deuterium may not be negligible. However, at high temperatures, this effect does not change the principal axis directions and the asymmetry parameter of the EFG, but changes only the principal value of the EFG.

1) H. Asano, T. Yamaguchi, and M. Hirabayashi, Preprint of the 70th Meeting of the Japan Institute of Metals, p. 79 (1972), *Phys. Stat. Sol.* (*a*), **15**, 267 (1973).

2) D. G. Westlake and M. H. Muller, Preprint of the International Meeting on Hydrogen in Metals, Jülich, p. 66 (1972).

3) R. R. Arons, H. G. Bohn, and H. Lütgemeir, *ibid.*, p. 66.

4) V. A. Somenkov, M. G. Zemylyanov, M. E. Kost, N. A. Chernoplekov, and A. A. Chertkov, *Soviet Physics-Doklady*, **13**, 669 (1969).

5) K. Nakamura, This Bulletin, **46**, 2028 (1973).

6) B. Pedersen and D. D. Slotfeld-Ellingsen, *J. Less Common Metals*, **23**, 223 (1971).

7) K. Nakamura, This Bulletin, **45**, 3356 (1972).

8) V. A. Somenkov, I. R. Entin, A. Yu. Cherryakov, S. Sh. Shil'shtein and A. A. Chertkov. Soviet Physics-Solid State, 13, 2178 (1972).

Table 1.

$K\times10^{-8}$ cm	$\lvert(eq)_{tet}\rvert/\lvert(eq)_{oct}\rvert$
1.8	0.412
1.5	0.449
1.0	0.511

Thus, from the temperature dependence of the deuteron quadrupole coupling constant, we can, in principle, determine the proportion of the *t*-occupation of the deuterium. It has been shown that about 5% of deuterium atoms are in the *t*-sites.[8] Since the sign of the EFG of the *t*-site is the reverse that of the *o*-site, the following simple relation may be hold:

$$[(e^2qQ/h)^{\beta}_{oct}\times0.95]-[(e^2qQ/h)^{\beta}_{tet}\times0.05]=(e^2qQ/h)_{\beta}=68.6\text{ KHz (R.T.)}$$

where $(e^2qQ/h)^{\beta}_{oct}$ and $(e^2qQ/h)^{\beta}_{oct}$ are the quadrupole coupling constants for the *o*- and *t*-sites of the tetragonal β V_2D respectively. With the $(e^2qQ/h)^{\beta}_{tet}\simeq(e^2qQ/h)_T=37.5$ KHz approximation, $(e^2qQ/h)^{\beta}_{tet}$ is calculated to be 74.2 KHz, larger by about 10.8% than the observed value.

It is of interest to compare the experimental quadrupole coupling constant ratio $(e^2qQ/h)_T/(e^2qQ/h)^{\beta}_{oct}\simeq0.5$ with that calculated from the simple electrostatic model used in the previous paper.[7] With a_0 3.00 Å and c_0 3.1 Å for β V_2D (*o*-site) and with $a_0=3.16$ Å for γ V_4D_3 (*t*-site), the calculated ratio for three values of the screening constant is shown in Table 1. A comparison of the values in the table with the experimental one shows that $K=1.1\times10^8$ cm^{-1} is suitable in this case. However, it has elsewhere been shown[7] that a value of $K=1.8\times10^8$ cm^{-1} is most suitable for the Ta-D system if the charge on the Ta ion is 5. Thus, the discrepancy in the K value seems to indicate the limit of the application of the electrostatic model to the high-concentration interstitial systems.

The author wishes to express his deep gratitude to professor Shizuo Fujiwara and Dr. Ichiro Morimoto for their helpful advice and encouragement.

BULLETIN OF THE CHEMICAL SOCIETY OF JAPAN, VOL. 46, 2589—2590 (1973)

Model Complexes of Catalyzers for Asymmetric Hydrogenation. I. Crystal Structure of β-Cyanoethyl(D(−)-*erythro*-1,2-diphenyl-2-hydroxyethylamine)bis(dimethylglyoximato)cobalt

Yuji OHASHI, Yoshio SASADA, Yasuhisa TASHIRO, Yoshiaki OHGO, Seiji TAKEUCHI, and Juji YOSHIMURA

Laboratory of Chemistry for Natural Products, Tokyo Institute of Technology, Ookayama, Meguro-ku, Tokyo 152

(Received December 28, 1972)

It has recently been shown that the complexes of bis(dimethylglyoximato)cobalt(II) and optically active amine (abbreviated to $Co(DMG)_2$-amine) catalyze asymmetric hydrogenation of olefins, α-diketones and α-keto carboxylic esters.[1-5] Optical yields vary with the amine and solvent. From chemical consideration and CD and NMR spectra, these complexes seem to have a structure[5] as shown in Fig. 1. The $Co(DMG)_2$ plane is twisted by hydrogen bonding between one of the oxygen atoms of DMG and the hydroxyl group of amine. The direction of this twist is determined by the absolute configuration of the optically active amine. Asymmetry around the cobalt atom caused by the twisted plane is transferred to the products at a certain stage of catalytic reaction. The present work has been undertaken to examine this hypothesis and to give a structural explanation to the mechanism of asymmetric hydrogenation.

The crystal structure of the title compound $C_{25}H_{33}N_6O_5Co$ was determined by X-ray method. Crystal data; $M=556.51$, monoclinic with $a=13.31$, $b=8.84$, $c=23.90$ Å, $\beta=108.0°$, $V=2673.2$ Å^3, $Z=4$. The density calculated is 1.37 g/cm^3, while that measured by flotation is 1.38 g/cm^3. Systematic absence of reflections is $0k0$ for $k=2n+1$, the space group being $P2_1$. The molecular arrangement, however, seems to have an approximate $P2_1/c$ symmetry because $h0l$ reflections are very weak for $l=2n+1$. A total of 2127 independent reflections were collected on Weissenberg photographs using Cu$K\alpha$ radiation. Intensities were measured visually. Correction for Lorentz and polarization factors was applied as usual but not that for absorption.

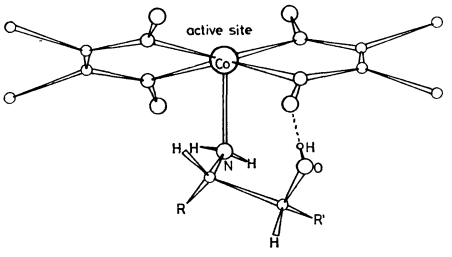

Fig. 1.

1) Y. Ohgo, S. Takeuchi, and J. Yoshimura, This Bulletin, **44**, 583 (1971).

2) Y. Ohgo, S. Takeuchi, and J. Yoshimura, Presented at the 19th Symposium on Organometallic Chemistry, October, 1971, Preprints p. 55.

3) S. Takeuchi, Y. Ohgo, and J. Yoshimura, Presented at the 25th Annual Meeting of Chemical Society of Japan, October, 1971. Preprints p. 410.

4) Y. Ohgo, Y. Natori, and J. Yoshimura, Presented at the 26th Annual Meeting of Chemical Society of Japan, April, 1972. Preprints p. 1010.

5) S. Takeuchi, Thesis, Tokyo Institute of Technology (1972).

At first an approximate $P2_1/c$ symmetry was tentatively assumed. Atomic positions were easily obtained by the heavy atom method and refined by block-diagonal least-squares. After three cycles of the least-squares, an electron density was calculated, where the peaks for the amine were broader and lower than those of the others. This suggests that in the two crystallographically independent complexes the β-cyanoethyl and the $Co(DMG)_2$ groups are related almost strictly by a c-glide plane, but not the amine ligands. Thus a trial structure based on $P2_1$ was constructed, in which the atomic parameters of the former two groups were taken from the refinement based on $P2_1/c$, those of the optically active amine being obtained by resolving the average structure. Further refinement was carried out by block-diagonal least-squares. Anisotropic temperature factors were taken into account for the cobalt atom and all other atoms were constrained to isotropic motion. The final R factor was 0.14. The estimated standard deviations of bond distances and angles are 0.02—0.04 Å and 2—3°, respectively.

Structures of two crystallographically independent complexes are identical to each other within standard deviations. Figure 2 shows one of these complexes

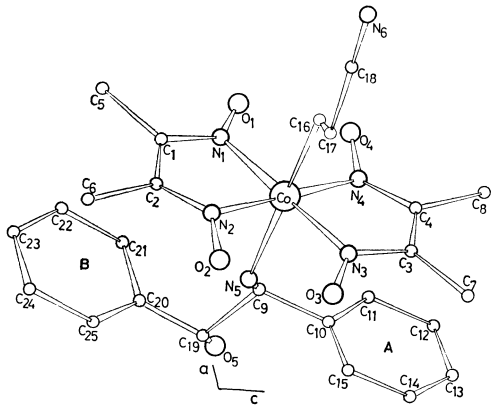

Fig. 2.

projected along the b axis. The $Co(DMG)_2$ groups are planar within standard deviations except for the methyl groups. Two methyl groups above the two benzene rings are slightly shifted upward to avoid short contact with the benzene rings. Figure 3 shows the complex viewed along N(1)—N(2). The plane of $Co(DMG)_2$ except the methyl groups makes angles of 13° and 15° with the benzene ring A and B, respectively. The distances from the centers of the rings to the $Co(DMG)_2$ plane are 3.59 Å for A and 3.91 Å for B. The average Co–N distance and N–Co–N

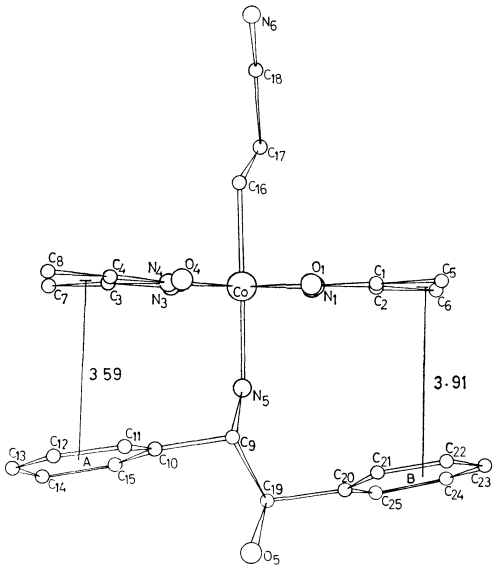

Fig. 3.

angle for the equatorial ligands are 1.89 Å and 82°, respectively. The axial Co–N distance is 2.08 Å and the Co–C distance is 2.04 Å. These distances and angles are close to those of alkyl cobaloxime.[6] The axial Co–N and Co–C bonds make angles of 84° and 85° with the $Co(DMG)_2$ plane, respectively. The other distances and angles also agree with the values published.

As to the conformation of amine, O(5) and N(5) atoms are *trans* as shown in Fig. 3. Thus contrary to expectation, there is no hydrogen bonding between the oxygen atom of DMG and the hydroxyl group of amine. The hydroxyl group does not make any hydrogen bonding with neighbouring complexes.

Any distance between non-bonded atoms, within the complex and between neighbouring ones, is not abnormally shorter than the usual van der Waals contact.

The structure of the complex obtained here is different from the assumed structure shown in Fig. 1. However, it does not seem that the mechanism of asymmetric induction could be revealed with the present structure, since the asymmetry of amine would have no effect on active site of the cobalt atom. An alternative explanation might be as follows. The complex coordinated by the amine of *gauche* conformation probably exists in solution, which might catalyze asymmetric hydrogenation.

6) P. G. Lenhert, *Chem. Commun.* **1967**, 980.

BULLETIN OF THE CHEMICAL SOCIETY OF JAPAN, VOL. 46, 2591 (1973)

ESR and Optical Spectra of Ion Radicals of Some Triptycene Derivatives

Fumio TANAKA and Noboru MATAGA

Department of Chemistry, Faculty of Engineering Science, Osaka University, Toyonaka, Osaka 560

(Received December 28, 1972)

It is important to study the delocalization interactions between the groups when a molecule contains two or more π-electronic groups separated by saturated chemical bonds. The mechanisms of CT (charge transfer) complex formation and of electron transfer reaction are cases closely connected with this problem. Hillier and Rice[1] studied theoretically the electronic state of *para*-cyclophane anion radicals and predicted appearance of a charge resonance band at 9000 cm^{-1} when the distance between the two molecular plane is *ca.* 3A. Ishitani and Nagakura[2] measured the optical and ESR spectra of 2,2'-*para*-cyclophane anion and showed that the absorption band at 760 nm could be interpreted as a charge resonance spectrum. If the two π-electronic systems are different, it might be possible, by means of ESR and optical measurements of the ion radicals, to examine directly the extent of the charge transfer in the ground state and the appearance of the CT band for a definite separation between the π-electronic groups. We have conducted such studies for 1,4-quinone triptycene anion (I) and dimethoxytriptycene cation (II).

Synthesized and purified samples of triptycene derivatives (supplied by Dr. F. Ogura of this University) were used without further purification. I was produced by reduction of corresponding molecule with metallic potassium in THF or DME solution. II was prepared by dissolving the molecule in concd sulfuric acid.

Optical absorption spectra were measured with Cary 14 and Cary 15 spectrophotometers. The ESR spectra were recorded with a JES-3BX spectrometer using X-band.

The absorption spectra of I in DME were almost the same as those of *p*-benzoquinone anion radical in the same solvent. No new absorption band which might be attributed to the interaction between the *p*-benzoquinone group and other parts of I was found in the spectra of I. We come across quite similar circumstances in the case of II, *viz.* absorption bands which correspond to the 437 nm and 282 nm bands of 1,4-dimethoxybenzene cation radical can be observed, but none due to the interaction between the dimethoxybenzene cation group and the other groups. Thus, the excess electron in I and the positive hole in II seem to be fairly well localized at quinone and dimethoxybenzene groups, respectively.

The same conclusion has been reached also from the ESR measurements. The ESR spectra of both I and II show no hfs due to the delocalization interaction between the component groups, *viz.*, the spectra of I shows the hfs due to the two protons in the quinone group, and the hfs constants of II are very close to the corresponding ones[3] of *cis*-form 1,4-dimethoxybenzene cation radical. In the case of free 1,4-dimethoxybenzene cation radical, both *cis*- and *trans*-isomers can exist in solution.[3] However, the 1,4-dimethoxybenzene group in II take only the *cis*-form owing to the barrier due to the bridge-head proton.

The fact that there are no significant intramolecular delocalization effects in the case of the above ion radicals may be of some interest from the viewpoint of the electronic structures of ions and molecular complexes in solution. According to recent experimental and theoretical studies,[4] it has become clear that the electronic structure of many TCNB (1,2,4,5-tetracyanobenzene) complexes with various aromatic hydrocarbons in the S_1 state can be considered to be a contact ion-pair with no significant delocalization interaction between the component TCNB anion and hydrocarbon cation. In the case of the TCNB complex in the S_1 state, quantum chemical calculations indicate clearly that it has a symmetrical overlapping structure where the intermolecular overlap integral is very small and the ion-pair structure may be stabilized strongly by solvation.[4] The intermolecular overlap integrals between the constituent groups of I and II may be rather small in view of their geometrical structure. On the other hand, the delocalization interaction between two identical aromatic groups is sufficiently strong for the "fast transfer" of the excess electron to occur when they are separated by one or two methylene groups.[5,6] In the case of I and II, we are concerned with the charge transfer between different groups, where the trapping of the excess electron or the positive hole at one group occurs very easily. The trapping may be facilitated by strong solvation of the ion radical groups.

1) I. H. Hillier and S. A. Rice, *J. Chem. Phys.*, **45**, 4639 (1966).
2) A. Ishitani and S. Nagakura, *Mol. Phys.* **12**, 1 (1967).
3) W. F. Forbes and P. D. Sullivan, *Can. J. Chem.*, **44**, 1501 (1966).
4) H. Masuhara and N. Mataga, *Z. Phys. Chem.* N. F., **80**, 113 (1972); H. Masuhara, N. Tsujino and N. Mataga, This Bulletin, in press.
5) H. M. McConnell, *J. Chem. Phys.*, **35**, 58 (1961); J. E. Harriman and A. H. Maki, *ibid.*, **39**, 778 (1963).
6) In the case of dibenzotriptycene anion, the odd electron is delocalized completely over two naphthalene groups.

BULLETIN OF THE CHEMICAL SOCIETY OF JAPAN, VOL. 46, 2592—2593 (1973)

The Catalytic Oxidation of Hydrogen on Zirconium Dioxide

Takuya HAMAMURA, Yoshito ONISHI, and Yasuo IIZUKA*

Department of Chemistry, Faculty of Industrial Arts, Kyoto Technical University, Matsugasaki, Sakyo-ku, Kyoto 606

(Received January 24, 1972)

The previous paper was concerned with the catalytic oxidation of carbon monoxide on zirconium dioxide.[1] The experimental results were there compared with those for anatase and rutile[2~5] in order to examine the correlation between zirconium dioxide and titanium dioxide with respect to their catalytic actions. It was found that the reaction mechanism could be explained in entirely the same manner as that on titanium dioxide.

The oxidation mechanism of hydrogen on titanium dioxide was extremely analogous to that of carbon monoxide,[4] and titanium and zirconium belong to the same group in the periodic table. Therefore, the oxidation mechanism of hydrogen on zirconium dioxide can also be expected to be similar to that of carbon monoxide.

Experimental

Two kinds of samples of ZrO_2-1 (3.8 m^2/g) and ZrO_2-2 (1.0 m^2/g) used in the previous experiment were again employed.[1] The apparatus, procedure, and method of pretreatment of the catalysts used were essentially the same as before.[2] The reaction rate was measured by using a mixed gas with a composition of $H_2/O_2=2/1$ in the temperature range of 450—600 °C and under pressures of 10^{-1}—10^{-3} mmHg.

Results and Discussion

The oxidation rate of hydrogen on zirconium dioxide was nearly of the first order with respect to P_{H_2} and was independent of P_{O_2}. Consequently, the reaction rate can be expressed by the following equation:

$$d(H_2O)/dt = k \cdot P_{H_2} \quad (1)$$

where k is a constant. The Arrhenius plots of k on ZrO_2-1 and -2 are given in Fig. 1, together with those on anatase and rutile.[4] The ZrO_2-1 and -2 show almost the same values in their catalytic activities. The activation energy of zirconium dioxide is the value of 22.6 kcal/mol, intermediate between anatase, 29.2 kcal/mol, and rutile, 17.8 kcal/mol.

When instead of a mixture of H_2 and O_2, hydrogen, at a pressure of about 10^{-2} mmHg, was introduced into the reaction system, it reacted with the surface oxygen of the catalyst and the water vapor thus formed was caught in the trap. The rate of the formation of water was found to be proportional to P_{H_2}:

$$d(H_2O)/dt = k_{H_2} \cdot P_{H_2} \quad (2)$$

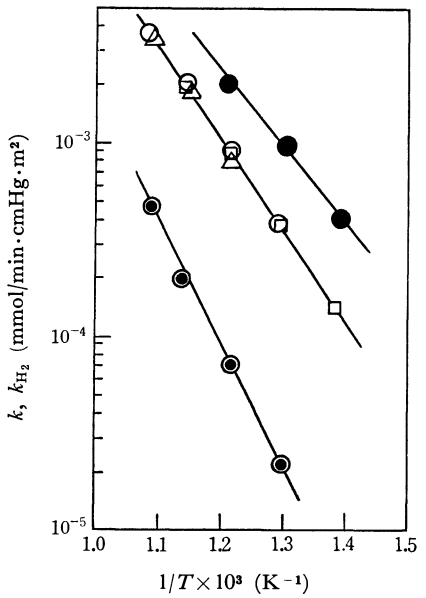

Fig. 1. Effect of temperature on the reaction rate constant.
□: ZrO_2-1 ○: ZrO_2-2 ◉: Anatase ●: Rutile

where k_{H_2} is the reduction rate constant of zirconium dioxide by hydrogen. The Arrhenius plots of k_{H_2} on ZrO_2-1 are shown in Fig. 1 by the mark △. It is obvious that k_{H_2} agrees with k. It was reported in the preceding paper that the oxygen-uptake rate of the reduced zirconium dioxide was much faster than the reduction rate of zirconium dioxide.[1]

From all these results, the mechanism of the oxidation of hydrogen on zirconium dioxide can be expressed as follows. The reaction consists of the following two steps;

$$H_2(g) + O(s) \xrightarrow{A} H_2O(g) + (s) \quad (3)$$

$$(s) + 1/2\,O_2(g) \longrightarrow O(s) \quad (4)$$

where O(s) refers to the surface oxygen of the catalyst and (s) the oxygen defect on the surface. Step (4) is much faster than Step (3), so the overall reaction rate is proportional to P_{H_2}. This reaction mechanism is extremely analogous to that of the oxidation of carbon monoxide.

The activation energies of the oxidations of carbon monoxide and hydrogen on anatase, rutile, and zir-

Table 1. Activation energies for the oxidations of CO and H_2 and those for the thermal desorption of surface oxygen from the catalysts (kcal/mol)

Catalysts	Oxidation of CO	Oxidation of H_2	Thermal desorption of surface oxygen
Anatase	16.0	29.2	57.8
Rutile	6.7	17.8	38.4
ZrO_2	12.5	22.6	44.0

* Present address: Asahi Glass Co., Ltd., Ichihara, Chiba

1) T. Hamamura, Y. Onishi, and Y. Iizuka, This Bulletin, **45**, 1288 (1972).
2) Y. Onishi and T. Hamamura, *ibid.*, **43**, 996 (1970).
3) Y. Onishi, *ibid.*, **44**, 1460 (1971).
4) Y. Onishi, *ibid.*, **44**, 912 (1971).

conium dioxide are summarized in Table 1, together with the activation energies of the thermal desorption of the surface oxygen from these three catalysts.[1,2,4,5] The values of activation energies in each column of Table 1 decrease in this order: anatase, zirconium dioxide, and rutile. These facts suggest that the activation energies of the two oxidation reactions are connected with the bond strength between the surface oxygen and the catalyst surface.

The authors wish to express their deep thanks to Professor Yasuro Nakazawa and Professor Masayoshi Ihara of Kyoto Technical University for their kind advices and discussions.

5) Y. Onishi and T. Hamamura, *Memoirs of the Faculty of Industrial Arts, Kyoto Technical University, Science and Technology*, **19**, 44 (1970).

BULLETIN OF THE CHEMICAL SOCIETY OF JAPAN, VOL. 46, 2593—2594 (1973)

Elimination Reactions of Propylene Chlorohydrins over Solid Acids

Yasuhide ANJU, Isao MOCHIDA*, Akio KATO, and Tetsuro SEIYAMA
Department of Applied Chemistry, Faculty of Engineering, Kyushu University, Fukuoka 812
(Received August 31, 1972)

In a previous paper, the elimination reactions of ethylene chlorohydrins over solid acids, solid bases, and metals supported by silica gel were investigated and the reaction mechanism was discussed.[1] In the present paper, the elimination reactions of propylene chlorohydrins over solid acids are studied in order to elucidate the effect of the methyl group on the reactivities and in order to examine the validity of the mechanism proposed for the reaction of ethylene chlorohydrin.

Experimental

Silica–alumina and alumina were described in a previous paper.[2] 2-Chloro-1-propanol(I) and 1-chloro-2-propanol (II) were separated from commercial 1-chloro-2-propanol (Tokyo Kasei Co., E. P. grade; *ca.* 20% 2-chloro-1-propanol) by gas chromatography with a PEG column. The reaction rates were measured by the microcatalytic gas-chromatographic technique at 300°.[1-3] Hydrogen gas was used as the carrier. TCP (4 m, 60°) and Tween 80 (2 m, 80°) were used in a column in the reaction of 1-chloro-2-propanol and 2-chloro-1-propanol respectively. The conversions were reproduced from a pulse to a pulse, indicating that the elimination reactions of propylene chlorohydrins over the solid acid were catalytic.

Results and Discussion

The Reactivities of Propylene Chlorohydrins. The elimination reactions of propylene chlorohydrins on silica–alumina and alumina are summarized as follows:

Reactant	Catalyst	Product	Eliminated group
$CH_3CHClCH_2OH$ (I)	SiO_2-Al_2O_3	CH_3CH_2CHO	HCl
		CH_2=$CHCH_2OH$	
	Al_2O_3	CH_3CH_2CHO	HCl
		CH_2=$CHCH_2OH$	

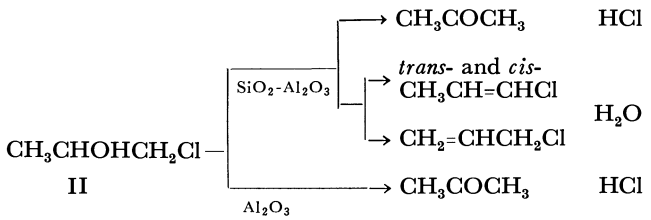

where allyl alcohol was not detected. The reaction rates are shown in Table 1, together with the elimination rates of some related reactants for the sake of comparison.[1,3] The dehydrochlorination reactivities of these reagents on both catalysts are summarized as follows:

$$\underset{\text{Cl OH}}{\text{CH}_3\text{CH–CH}_2} \gg \underset{\text{OH Cl}}{\text{CH}_3\text{CH–CH}_2} \simeq \underset{\text{OH Cl}}{\text{CH}_2\text{–CH}_2} \gg \underset{\text{Cl Cl}}{\text{CH}_3\text{CH–CH}_2}$$

(primary-chlorine elimination)

The dehydration reactivities on silica–alumina were:

$$\underset{\text{OH Cl}}{\text{CH}_3\text{CH–CH}_2} \gg \underset{\text{Cl OH}}{\text{CH}_3\text{CHCH}_2} \simeq \underset{\text{Cl OH}}{\text{CH}_2\text{–CH}_2}$$

It should be noted that alumina did not show any dehydration activity for 1-chloro-2-propanol(II). Over silica–alumina, the dehydrochlorination of 1,2-dichloropropane gave the same reaction products as the dehydration of 1-chloro-2-propanol(II). The product distributions of the two reactants are compared in Table 2, where the same tendency is observed on silica–alumina.

The Reaction Mechanism. 1) *Silica–Alumina*: The authors have proposed a carbonium-ion mechanism for the dehydrochlorination of ethylene chlorohydrin on silica–alumina in a previous paper:[1]

$$\text{CH}_2\text{OHCH}_2\text{Cl} \xrightarrow{-\text{Cl}^-} \text{CH}_2\text{OHCH}_2^+ \xrightarrow{-\text{H}^+} \text{CHOH=CH}_2 \longrightarrow \text{CH}_3\text{CHO}$$

* Research Institute of Industrial Science, Kyushu University.

1) I. Mochida, Y. Anju, A. Kato, and T. Seiyama, This Bulletin, **45**, 1635 (1972).

2) I. Mochida, Y. Anju, H. Yamamoto, A. Kato, and T. Seiyama *ibid.*, **44**, 3305 (1971).

3) I. Mochida, Y. Anju, A. Kato, and T. Seiyama, *ibid.*, **43**, 2245 (1970).

Table 1. The rate of elimination reaction at 300°C (ml/g min)

Reaction	Catalyst: Silica-alumina –HCl	Silica-alumina $-H_2O$	Alumina –HCl	Alumina $-H_2O$
Reactant				
$CH_3CHClCH_2OH$ (I)	11300	0	15000	0
$CH_3CHOHCH_2Cl$ (II)	870	1390	5000	0
CH_2ClCH_2OH[a]	1100	0	3300	0
$CH_3CHClCH_2Cl$[b]				
→ $CH_3CH{=}CHCl$ / $CH_2{=}CHCH_2Cl$	950	—	220	—
→ $CH_3CCl{=}CH_2$	0	—	30	—
$CH_3CHOHCH_2OH$	—	0	—	1
CH_2ClCH_2Cl[a]	3.2	—	14.2	—

a) Ref. 1. b) Ref. 3.

Table 2. The product distribution of the reaction:

$$CH_3CHXCH_2Cl \begin{cases} \nearrow CH_3CH{=}CHCl + HX & (X=Cl \text{ or } OH) \\ \searrow CH_2{=}CHCH_2Cl + HX & (X=Cl \text{ or } OH) \end{cases}$$

Catalyst	Ratio: Allyl chloride / 1-Chloropropylene (X=OH)	Allyl chloride / 1-Chloropropylene (X=OH)	*trans*-1-Chloropropylene / *cis*-1-Chloropropylene (X=OH)	*trans*-1-Chloropropylene / *cis*-1-Chloropropylene (X=Cl)
Silica-alumina	1.10	0.61	0.25	0.14
Alumina	—	0.18	—	0.024

where the carbonium-ion formation may be the rate-determining step. The reactivity order above shown can be understood in terms of the stability order of carbonium-ion intermadiates: $CH_3\overset{+}{C}HCH_2OH \gg \overset{+}{C}H_2CHOHCH_3 \simeq \overset{+}{C}H_2CH_2OH > \overset{+}{C}H_2CHClCH_3$ and $CH_3\overset{+}{C}HCH_2Cl \gg CH_3CH_2Cl\overset{+}{C}H_2 \simeq CH_2Cl\overset{+}{C}H_2$. The lack of any dehydration reaction of 2-chloro-1-propanol(I) on silica–alumina may also be understood by this mechanism. To understand the two series of reactivity orders, $CH_3CHClCH_2OH > CH_3CHCl$-$CH_2Cl$ (the secondary chlorine elimination) and CH_3-$CHOHCH_2Cl \gg CH_3CHClCH_2Cl$ (the primary chlorine elimination) which are due to the effects of the β-substituent, the strong adsorption ability of the hydroxyl group onto the solid acid may have to be taken into account in addition to the stability of the carbonium ion as has been described in the previous paper.[1]

The product distributions can also be understood by the carbonium-ion mechanism as follows. It may be natural that the product distributions in the dehydration of 1-chloro-2-propanol(II) and the dehydrochlorination of 1,2-dichloropropane are similar for the same carbonium ion ($CH_3\overset{+}{C}HCH_2Cl$) can be assumed as the intermediate for both reactions. Taking into account the steric hindrace as indicated by Tominaga *et al.*,[4] and the nonstereospecificity of the carbonium-ion mechanism in the dehydrohalogenation on solid acids,[5] the highly preferential formation of *cis*-1-chloropropylene may be explained by the interaction between the eliminating anion and proton to be abstracted;

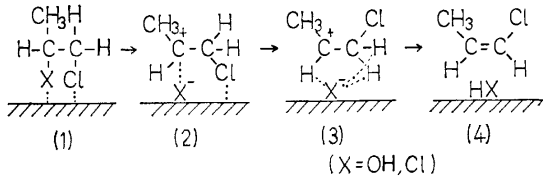

The chlorine atom and the hydroxyl group may interact with surface acid sites at the initial stage (1), and then the carbonium ion may be formed by the abstraction of the hydroxyl group (2) because dehydration is now considered. The abstracted anion may interact with the hydrogen to be eliminated, resulting in methyl and Cl groups in a *cis*-position to each other (3). The subsequent cleavage of β-hydrogen results in the *cis*-olefin.

Alumina: The facts that no dehydration of 1-chloro-2-propanol occurred on alumina in spite of the secondary position of the hydroxyl group and that alumina had a greater activity for the dehydrochlorinations of halohydrins than silica–alumina indicate the characteristics of alumina as a catalyst. The former fact can not be explained by the carbonium-ion mechanism. We assume that the elimination reaction on alumina proceeds through a concerted mechanism.[2,6] It has been reported that the chlorine atom is more easily removed than the hydroxyl group in the S_N2 reaction.[7] The higher reactivity of chlorine may be true if the C–X bond still exists in the intermediate. This mechanism corresponds to the concerted one in the elimination reaction. The higher dehydrochlorination activity of alumina may be partly due to this mechanism.

4) H. Tominaga, T. Nakamura, H. Arai, and T. Kunugi, *Kogyo Kagaku Zasshi*, **74**, 199 (1971).
5) P. Andreu, S. S. Zerain, and H. Noller, *An. Quim.*, **55**, 141 (1969).
6) H. Knozinger, H. Buhl, and K. Kochloefl, *J. Catal.*, **24**, 57 (1972) H. Noller, P. Andreu, and M. Hunger, *Angew. Chem. Int. Ed. Engl.*, **10**, 172 (1971).
7) E. S. Gould, "Mechanism and Structure in Organic Chemistry", Henry Holt and Company, (1959), p. 261.

BULLETIN OF THE CHEMICAL SOCIETY OF JAPAN, VOL. 46, 2595—2596 (1973)

The Crystal Structure of Rb(TCNQ)-II

Ichimin SHIROTANI and Hayao KOBAYASHI*

The Institute for Solid State Physics, The University of Tokyo, Roppongi, Minato-ku, Tokyo 106

**Department of Chemistry, Faculty of Science, Toho University, Narashino, Chiba 275*

(Received January 24, 1973)

X-Ray studies of several TCNQ salts have revealed that the planar TCNQ molecules are stacked face-to-face to form columns in most of these crystal structures. The infinite columns hitherto reported consist of tetradic, triadic, diadic, and monadic units of TCNQ molecules.[1-6]

Rb(TCNQ) is polymorphic at room temperature.[7,8] The crystals of Rb(TCNQ)-I are monoclinic. The $TCNQ^-$ radical ions form columns contructed from diadic units of $TCNQ^-$. The crystal structure of Rb(TCNQ)-II will be reported in this paper.

Experimental

The dark purple crystal of Rb(TCNQ)-II was kindly supplied by Sakai. The cell dimensions were determined from Weissenberg photographs. The shape of the crystal used for the collection of the intensity data was approximate parallelepiped, with a maximum dimension of 0.3 mm. Equi-inclination Weissenberg photographs were taken around the c axis up to the third layer with Cu$K\alpha$ radiation ($\lambda=1.5418$ Å); the multiple film technique was used. In all, 811 reflections were observed. The intensities were estimated visually by comparison with a standard film strip and were converted to $|F(hkl)|$ by applying the usual Lorentz, polarization, and shape corrections.

The crystal data of Rb(TCNQ)-II are: $Rb^+(C_{12}H_4N_4)^-$, F.W. 290, triclinic, $a=9.914\pm0.001$, $b=7.196\pm0.003$, $c=3.390\pm0.002$ Å, $\alpha=92.70\pm0.10$, $\beta=86.22\pm0.11$, $\gamma=97.73\pm0.07$, $v=275.20$Å^3, $D_x=1.757$, $Z=1$, space group $P\bar{1}$, $F(000)=137$

Determination of the Structure and Discussion

The space group $P\bar{1}$ was assumed tentatively and was then indeed verified at a later stage of the refinement. The trial structure was readily deduced from the three-dimensional Patterson synthesis. The atomic parameters were refined anisotropically by the block-diagonal least-squares method. The calculated positions of all the hydrogen atoms were included. The weighting scheme adopted was; $w=1$ for $F>3.5$ and $w=0.2$ for $F<3.5$. The final R value was 0.130.

The final positional and thermal prameters are given

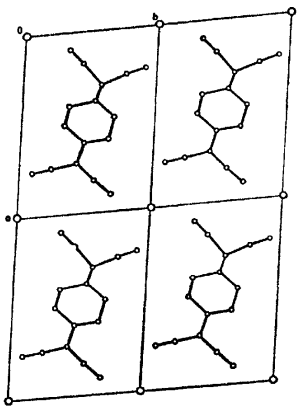

Fig. 1a. Projection of the structure along the b axis.

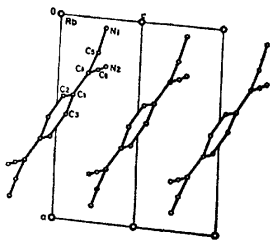

Fig. 1b. Projection of the structure along the c axis.

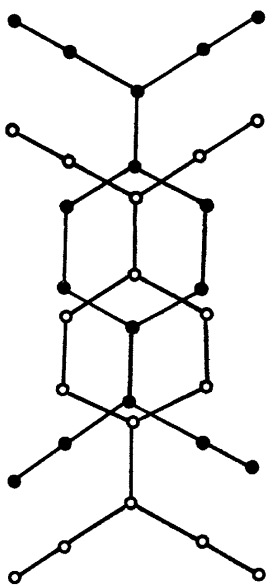

Fig. 2. Nearest neighbour overlap of $TCNQ^-$.

1) C. J. Fritchie and P. Arthur, *Acta Crystallogr.*, **21**, 139 (1966) C. J. Fritchie, *ibid.*, **20**, 892 (1966).

2) H. Kobayashi, Y. Ohashi, F. Marumo, and Y. Saito, *ibid.*, **B26**, 459 (1970); H. Kobayashi, F. Marumo, and Y. Saito, *ibid.*, **B27**, 374 (1971).

3) T. Sandaresan and S. C. Wallwork, *ibid.*, **B28**, 491, 1163, 2474, 3065 (1972).

4) A. T. McPhail, G. M. Semeniuk, and D. B. Chesnut, *J. Chem. Soc., A*, **1971**, 2174.

5) A. W. Hanson, *Acta Crystallogr.*, **B24**, 768 (1968).

6) P. Goldstein, K. Seff, and K. N. Trueblood, *ibid.*, **B24**, 778 (1968).

7) N. Sakai, I. Shirotani, and S. Minomura, This Bulletin, **45**, 3314, 3321 (1972).

8) J. G. Vegter, T. Hiba, and J. Kommander, *Chem. Phys. Lett.*, **3**, 427 (1969).

Table 1. The final atomic parameters and their estimated standard deviations
Temperature factor $=\exp[-(h^2B_{11}+k^2B_{22}+l^2B_{33}+2hkB_{12}+2hlB_{13}+2klB_{23})]\times 10^4$

ATOM	X	Y	Z	B_{11}	B_{22}	B_{33}	B_{12}	B_{13}	B_{23}
Rb	0	0	0	80	124	260	33	72	36
	0	0	0	4	6	21	4	6	8
N(1)	905	3108	5373	116	123	677	31	113	−38
	21	25	50	28	43	178	29	55	66
N(2)	2410	9136	5693	95	150	1014	47	123	−18
	21	27	58	27	45	213	29	60	76
C(1)	3880	5349	1898	84	65	497	23	121	−26
	23	27	55	27	40	178	27	54	63
C(2)	3986	3509	763	66	150	722	38	101	−14
	23	31	62	29	53	214	32	60	80
C(3)	4883	6887	1053	98	120	724	261	147	12
	25	31	64	32	51	212	33	65	80
C(4)	2746	5814	3680	93	71	695	23	107	28
	24	28	61	30	43	206	29	61	72
C(5)	1732	4331	4724	105	114	871	33	130	−127
	25	31	66	33	52	241	34	71	84
C(6)	2562	7614	4837	60	165	681	31	35	1
	22	32	62	28	56	209	31	59	81

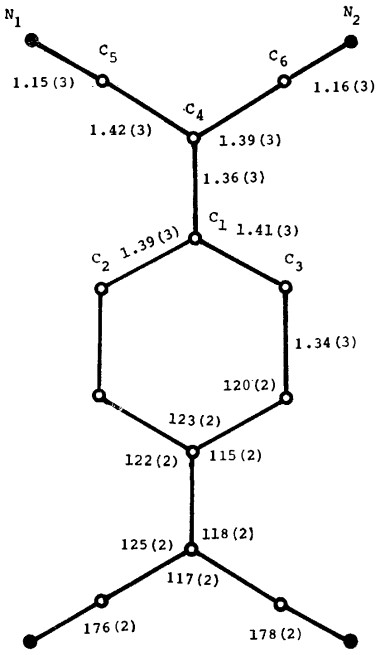

Fig. 3. Bond lengths (Å) and angles (°) with their standard deviations (in parenthses).

in Table 1. The observed and calculated structure factors are given in Table 2.[9] The structure within one unit cell is shown in Figs. la and 1b as viewed along the c axis and the b axis respectively. $TCNQ^-$ ions are stacked in a plane-to-plane manner and form columns of monadic units. This columnar structure is very similar to those found in the crystals of *N*-methylphenazinium(TCNQ).[1] The inter-planar spacing of TCNQ is 3.43 Å. The mode of overlapping is illustrated in Fig. 2. This type of overlapping has been observed in various TCNQ salts.[1-6] The bond lengths and angles of the $TCNQ^-$ are shown in Fig. 3. These values show that the $TCNQ^-$ ion has a quinoid character. It is known that crystals of Rb-(TCNQ)-I have monoclinic symmetry and that $TCNQ^-$ ions are stacked face-to-face to form columns of diadic units of $TCNQ^-$. Within a column, two different intermolecular spacings, 3.159 and 3.484 Å, appear alternately.[10]

Table 3. The pysical properties of both Rb(TCNQ)

	Rb(TCNQ)-II	Rb(TCNQ)-I
Electrical resistivity Ω cm (R. T.)	10^2	10^5
Activation energy eV	0.16∼0.19	0.53∼0.41 below the transition point 0.37∼0.28 above the transition point
Transition temperature K	230	374
The electrical anomalies at high pressure Kbar	unobservable	1, 3.5
Absorption peaks cm^{-1}	6250 16250, 26380	8500 15750, 26500

The physical properties of both Rb(TCNQ) substances are summarized in Table 3.[7] The resistivity of Rb(TCNQ)-I is about 10^3 times that of Rb(TCNQ)-II. The near-infrared absorption band of salt-II, which is due to the inter-radical charge transfer in the crystal, shifted toward a longer length than that of salt-I. The difference in the physical properties may arise from the difference in the columnar structures.

The authors are grateful to professor Saito for his interest in this study and his kind advice. They are also indebted to Dr. Sakai for kindly supplying the crystals of Rb(TCNQ).

9) Table 2 is kept by the office of the Chemical Society of Japan (Document No. 7313).

10) A. Hoekstra, T. Sopieder, and A. Vos, *Acta Crystallogr.*, **B28**, 14 (1972).

BULLETIN OF THE CHEMICAL SOCIETY OF JAPAN, VOL. 46, 2597—2598 (1973)

Polymerization of Methyl Methacrylate with the Chlorocarbonylbis-(triphenylphosphine)rhodium(I)-Organic Halides System[1)]

Noriyuki KAMEDA and Noriko ITAGAKI

Department of Chemistry, Faculty of Science and Engineering, Nihon University, Narashinodai, Funabashi, Chiba 275

(Received May 8, 1972)

Recently it has been reported that zero-valent transition-metal complexes conjugated with organic halides act as effective radical initiators of methyl methacrylate (MMA).[2,3)] Bamford and his co-workers[2)] found that metal carbonyls in the presence of organic halides can initiate the free-radical polymerization of MMA and that the polymers thus obtained are more stereospecific than those obtained in the usual free-radical polymerization. In this case, the valency, state of metal appears to play an important role in the free-radical initiation of MMA.

In a previous paper,[4)] we reported that some low-valent metal complex, *trans*-$PtHCl\{P(C_2H_5)_3\}_2$ (Pt complex) and the alkyl halide system can serve as radical initiators of MMA and styrene. Chlorocarbonylbis(triphenylphosphine)rhodium(I) (Rh complex) has been known as hydrogenation catalysts of ethylene and acetylene,[5)] and in the presence of organic halides they may serve much like the Pt complex in initiating the polymerization of MMA.

This paper will describe the results of the polymerization of MMA with a system composed of the Rh complex and organic halides, and also the results of kinetic studies of the polymerization with the system composed of the Rh complex and carbon tetrachloride.

Experimental

Methyl methacrylate (MMA) was purified by an ordinary method and was stored in a refrigerator until use.

The organic halides were purified by distillation or recrystallization.

Chlorocarbonylbis(triphenylphosphine)rhodium (I) (Rh complex) was synthesized according to the method in the literature[6)] and then purified by recrystallization from a benzene solution. It had an mp of 194—196 °C (lit,[6)] 195—197 °C).

The other reagents were purified by ordinary methods.

The polymerization was carried out in a sealed glass tube (30 ml) containing a given amount of the Rh complex (18 mg) dissolved in benzene (5 ml); MMA (5 ml) and the required amount of organic halides (solution=3 ml; solid=3 g) were placed in it, and then the air in the tube was replaced with nitrogen before sealing. Polymerization was carried out in a tube in a thermostat maintained at a given temperature. After polymerization, the contents of the tube were poured into a large amount of methanol in order to precipitate the polymer. The conversion was calculated from the weight of the dried polymer thus obtained.

The number-average molecular weight ($\bar{M}_n$) of the resulting polymers was calculated from the intrinsic viscosity, [η], in chloroform at 25 °C according to the following equation[7)]:

$$[\eta] = 3.4 \times 10^{-5}\bar{M}_n^{0.83}.$$

The rate of polymerization (R_p) was measured by the dilatometric method, using a dilatometer with a capacity of 10 ml as the reaction vessel. The Rh complex was weighed and placed in the reaction vessel, and then benzene was added. After the Rh complex had been solved, the atmosphere of the apparatus was replaced with nitrogen and the reaction vessel was filled with a known amount of MMA and carbon tetrachloride. The dilatometer was placed in a constant-temperature bath, and the rate of contraction in volume was followed up by the use of a cathetometer.

Results and Discussion

Effect of Organic Halides. The results of the polymerization of MMA with the Rh complex in the presence of various kinds of organic halides (carbon tetrachloride, carbon tetrabromide, chloroform, bromoform, iodoform, methylene chloride, hexachloroethane, chlorobenzene, and benzyl chloride) at 60 °C for 7 hr. The initiating activity of the halides was shown only by carbon tetrachloride and carbon tetrabromide, the polymer yields of which were 30.8% ($\bar{M}_n=6.4\times10^4$) and 9.0% ($\bar{M}_n=2.6\times10^4$) respectively. The nuclear magnetic resonance spectra of poly(methyl methacrylate) obtained with these initi-

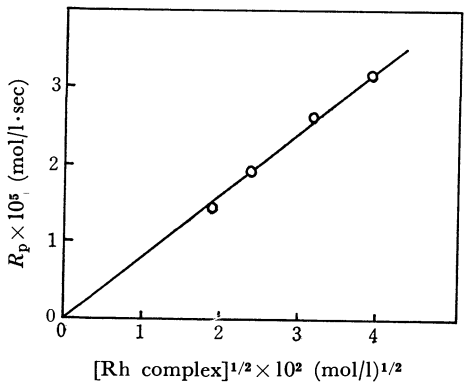

Fig. 1. Relationship between R_p and the concentration of Rh complex: [MMA]=4.65 mol/l, [Carbon tetrachloride]=2.05 mol/l, in benzene at 50 °C.

1) Presented in part at the 26th (April, 1972) Meeting of the Chemical Society of Japan.

2) C. H. Bamford and C. A. Finch, *Trans. Faraday Soc.*, **59**, 118, 548 (1963).

3) C. H. Bamford, G. C. Eastmond, and K. Hargreaves, *Trans. Faraday Soc.*, **64**, 175 (1968).

4) N. Kameda, Y. Imamura, and M. Takeda, *Kogyo Kagaku Zasshi*, **71**, 612 (1968).

5) L. Vaska and R. E. Rhodes, *J. Amer. Chem. Soc.*, **87**, 4970 (1965).

6) D. Evans, J. A. Osborn and G. Wilkinson, "Inorganic Syntheses," Coll. Vol. 11, 99 (1968).

7) S. N. Chinai, J. D. Matlack, A. L. Resnick, and R. J. Samuels, *J. Polym. Sci.*, **17**, 391 (1955).

ator systems showed that its tacticity was similar to that obtained with the conventional radical polymerized poly(methyl methacrylate). No polymer was obtained by the use of the Rh complex alone.

Kinetic Studies of the Polymerization with the System of the Rh complex and Carbon Tetrachloride. Figure 1 shows the relationship between the R_p and the concentration of the Rh complex at constant concentrations of both MMA and carbon tetrachloride.

From this figure, the rate was found to be proportional to the square root of the concentration of the Rh complex. The plots of R_p against the concentration of carbon tetrachloride at constant concentrations of both the Rh complex and MMA are shown in Fig. 2, in which the rate is indicated to be proportional to the square root of the concentration of carbon tetrachloride. The square-root dependence of the concentration of carbon tetrachloride on the rate was observed only in the concentration range lower than 5×10^{-3} mol/l. When the concentration of carbon tetrachloride becomes higher than this, the rate becomes constant and independent of the concentration of carbon tetrachloride.

Figure 3 shows the relationship between the R_p and the concentration of MMA at constant concentrations of both the Rh complex and carbon tetrachloride. From this figure, it is clear that the rate is proportional

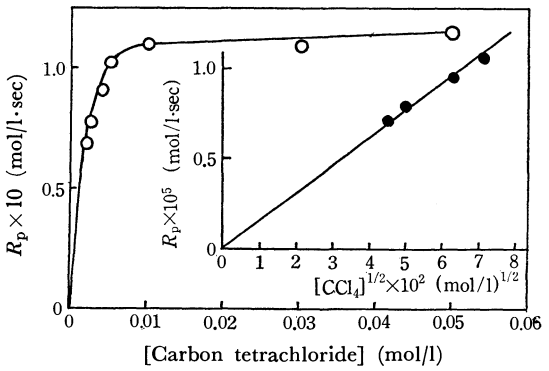

Fig. 2. Relationship between R_p and the concentration of carbon tetrachloride: [MMA]=4.65 mol/l, [Rh complex] $=10^{-3}$ mol/l, in benzene at 50 °C.

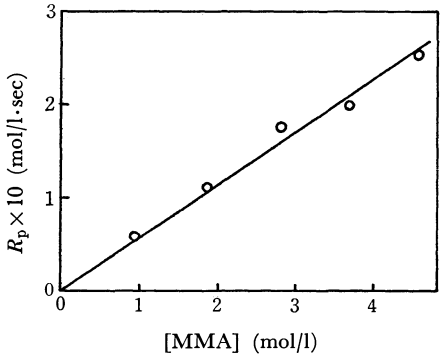

Fig. 3. Relationship between R_p and the concentration of MMA: [Rh complex] $=10^{-3}$ mol/l, [Carbon tetrachloride] =2.05 mol/l, in benzene at 50 °C.

to the concentration of MMA. This finding indicates that MMA does not participate in the initiation of the radical production.

Effect of Radical Inhibitor. The effects of several radical inhibitors on the polymerization with the system of the Rh complex and carbon tetrachloride were investigated. α,α-Diphenyl-β-picrylhydrazyl (5×10^{-3} mol/l) and *p*-benzoquinone (5×10^{-3} mol/l) inhibit the polymerization.

Mechanism of MMA Polymerization with the Rh Complex and the Organic Halids System. The results on the polymerization kinetics and on the radical inhibitor, indicate that the polymerization of MMA with the Rh complex and carbon tetrachloride proceeds through a radical mechanism. From the fact that the rate of polymerization is proportional to the square root of the concentration of the Rh complex and of carbon tetrachloride, it can be presumed that free radicals are produced by the reaction of the Rh complex and carbon tetrachloride. These free radical are considered to be trichloromethy radicals, because of the fact that hexachloroethane is found by gas-chromatographic analysis. Trichlorocarbonylbis(triphenylphosphine)rhodium(III) was also found from the infrared spectra in the reaction of the Rh complex and carbon tetrachloride at 60 °C for 3 hr.

Further investigation is required for the elucidation of the mechanism of the Rh complex reaction.

BULLETIN OF THE CHEMICAL SOCIETY OF JAPAN, VOL. 46, 2599—2600 (1973)

The Polymerization of Vinyl Monomers in the Presence of Surface-active Agents. V. The Copolymerization of Methyl Methacrylate with Styrene

Yoshikazu ARITA, Shinsaku SHIRAISHI, Manabu SENŌ, and Teruzo ASAHARA
Institute of Industrial Science, University of Tokyo, Roppongi, Minato-ku, Tokyo 106

(Received November 30, 1972)

In the previous papers of this series, we have reported the polymerization of methyl methacrylate (MMA)[1,2] and styrene (St)[3] in the presence of a surface-active agent in an aqueous medium without any ordinary initiators. The polymerization reactions were considered to proceed via a radical mechanism, because the polymerizations were inhibited by the addition of hydroquinone or diphenylpicrylhydrazyl and also by passing air continuously into the reaction system during the reaction period. In this paper we will present the results of the copolymerization of MMA with St; we attempted this in order to confirm that the present reaction proceeds *via* a radical mechanism and also to ascertain some particular aspects of this reaction system if possible.

Experimental

Materials. MMA and St were purified by ordinary procedures and were stored in a refrigerator until use. The sodium tetrapropylenebenzenesulfonate(ABS from the Lion Fat & Oil Co.) was purified by recrystallization from aqueous acetone.

Copolymerization. The copolymerization of MMA with St was carried out in a manner similar to that described in a previous paper.[2]

Characterization of the Copolymers. The composition of the copolymers was determined by the IR technique. The calibration curve for the quantitative analysis was prepared by measuring the intensity of the C=O absorption at 1725 cm^{-1} of 1% chloroform solutions of mixtures of poly(MMA) and poly(St) in various ratios by using a cell 0.268 mm thick. The curve was expressed by this equation:

$$\log (I_0/I) = 0.61[C]$$

where I_0 is the percentage transmission of the solvent only, where I is that of the solution, and where [C] is the concentration of the MMA component in copolymers (g/100 ml of a chloroform solution).

The composition of the copolymers was also determined by elementary analyses, which gave the same results as obtained by the IR techniques afore-mentioned.

The NMR spectra were measured at 34 °C with 3% solutions in carbon tetrachloride using a Hitachi-Perkin Elmer R-20A Spectrometer working at 60 MHz, with tetramethylsilane as the internal standard.

Results and Discussion

The copolymerization of St(M_1) with MMA(M_2) has been widely investigated, and the monomer reactivity ratios have been reported to be $r_1=0.52$ and $r_2=0.46$ for a bulk polymerization at 60 °C,[4] $r_1=0.54$ and $r_2=0.42$ for a solution polymerization in benzene at 60 °C,[5] and $r_1=0.56$ and $r_2=0.50$ for an emulsion polymerization at 35 °C.[6] In the present report, the copolymerization of St with MMA in the presence of ABS without any ordinary initiators will be examined. The results are summarized in Table 1. As is shown in Table 1, the rate of the copolymerization of St with MMA is much smaller than that of the polymerization of MMA. This phenomenon has also been observed in the usual radical copolymerization of St with MMA. Therefore, the propagation reaction may proceed in the same way as the usual radical copolymerization, though the initiation reaction may be different from usual in the point of the necessity for the micelles to be formed in our present polymerization system.

TABLE 1. COPOLYMERIZATION OF MMA WITH St

MMA/St[a]	Conversion (%)	$[\eta]$[b]
∞	52.3	8.20
4.00	19.9	5.09
2.33	16.3	3.70
1.50	16.4	3.87
1.00	14.4	3.87
0.67	11.1	3.87
0.43	22.5	4.20
0.25	13.9	3.85
0	15.3	4.85

a) Reactant mole ratio. b) In benzene solution at 30°C. Water 100 g, ABS 1 g, comonomer 0.1 mol, at 80°C, 2 hr, under nitrogen atmosphere.

The polymers obtained were fractionated by precipitation from a 2% benzene solution by ethanol; all of the polymers in the solution precipitated out in the precipitation range (volume ratio of the precipitant to the polymer solution) of 0.9 to 1.2, which indicated that the polymer was exclusively the copolymer of the two monomer components.[7] The dependence of the composition of the copolymers on initial ratio of monomers was examined. The composition of the resulting copolymers was determined by the IR technique using the calibration equation described above. The copolymer composition curve

1) T. Asahara, M. Senō, S. Shiraishi, and Y. Arita, This Bulletin, **43**, 3895 (1970).
2) T. Asahara, M. Senō, S. Shiraishi, and Y. Arita, *ibid.*, **45**, 2862 (1972).
3) T. Asahara, M. Senō, S. Shiraishi, and Y. Arita, *ibid.*, **46**, 249 (1973).
4) F. M. Lewis, C. Walling, W. Cummings, E. R. Briggs, and F. R. Mayo, *J. Amer. Chem. Soc.*, **70**, 1519 (1948).
5) C. C. Price and J. G. Walsh, *J. Polym. Sci.*, **6**, 239 (1951).
6) F. T. Wall, T. E. Florin, and C. J. Delbeq, *J. Amer. Chem. Soc.*, **72**, 4769 (1950).
7) K. Tomioka and Y. Shinohara, *Kobunshi Kagaku*, **21**, 83 (1964).

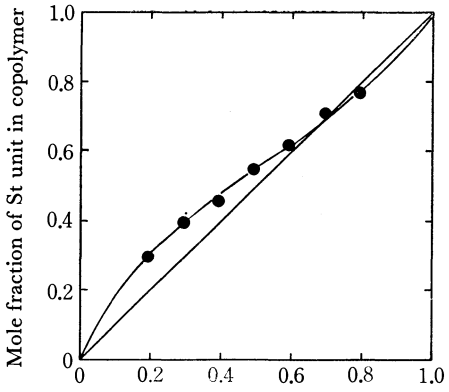

Fig. 1. Copolymerization of MMA with St, Copolymer composition curve.
Water 100 g, ABS 1 g, comonomer 0.1 mol, 80 °C, 2 hr, under nitrogen atmosphere.

thus obtained is shown in Fig. 1.

The apparent monomer reactivity ratios (mrr) were calculated to be $r_1=0.71\pm0.03$ and $r_2=0.40\pm0.03$ by Mayo and Lewis' intersection method. These values were very different from Mayo's data.

According to Wall's investigation into the solubility of St and MMA in water,[6] we calculated the monomer ratios in the oil phase in the present system and corrected the copolymer composition curve and reactivity ratio. The corrected values were $r_1=0.61\pm0.03$ and $r_2=0.48\pm0.03$, which apparently approached Mayo's data. The values were still slightly different from the usual mrr, but it is considered that these values show that the copolymerization proceeds *via* a radical mechanism.

8) K. Ito and Y. Yamashita, *J. Polym. Sci., Part B*, **3**, 625 (1965).

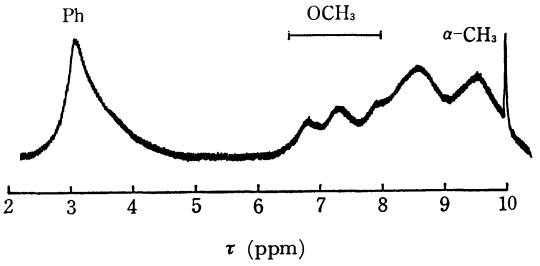

Fig. 2. NMR spectrum of MMA-St cooplymer of reactant mole ratio 1.0 at 60 MHz, at 34 °C in CCl_4 solution.

The NMR spectrum of the copolymer gave results similar to those of Yamashita's investigation.[8] As is shown in Fig. 2, the α-methyl proton resonance of the MMA unit appears at 9.2—9.1 ppm and the methoxy proton resonance is resolved into three peaks, which is a characteristic feature of the copolymers of St and MMA formed through a radical mechanism.

The results presented above and those of the previous reports[1,2,3] definitely confirmed that the polymerization of our reaction system proceeds *via* a radical mechanism. It was also clarified that, in the emulsion copolymerization, the mrr of each monomer component obtained by the usual copolymerization technique must be modified by considering their solubility parameters, especially the distribution coefficient.

BULLETIN OF THE CHEMICAL SOCIETY OF JAPAN, VOL. 46, 2600—2602 (1973)

Rearrangement of 2-Aryloxybenzazoles

Takeshi NAGAI, Yoshiaki FUKUSHIMA, Toshio KURODA, Hiroshi SHIMIZU, Shizen SEKIGUCHI, and Kohji MATSUI

Department of Synthetic Chemistry, Gunma University, Tenjincho, Kiryu, Gunma 376

(Received January 22, 1973)

O-Acylphenols are known to undergo rearrangement in the presence of Lewis acid[1] or photochemically[2] to give *o*- and/or *p*-acylphenols. Similarly, aryloxy-*s*-triazines give *o*- and/or *p*-hydroxyaryl-*s*-triazines on irradiation.[3] However, aryloxy-*s*-triazines containing 2-amino groups undergo rearrangement to give o-hydroxyarylamino-*s*-triazines in protic solvents in the dark[4] or on irradiation with ultraviolet light in aprotic solvents.[5] This paper reports on the rearrangement of 2-aryloxybenzazoles (benzoxazole, benzothiazole, and benzimidazole).

Preparation of 2-Aryloxybenzazoles. 2-Aryloxybenzazoles having the following general formula were synthesized by the condensation of 2-chlorobenzazoles with the corresponding phenolates. 2-(2-Aminophenoxy)benzothiazole was obtained by the hydrogenation of the corresponding nitro compound. In the hydrogenation of 2-(2-nitrophenoxy)benzoxazole, however, 2-(2-hydroxyanilino)benzoxazole was obtained as the main product instead of 2-(2-aminophenoxy)benzoxazole. 2-Aryloxybenzazoles thus obtained are listed in Table 1.

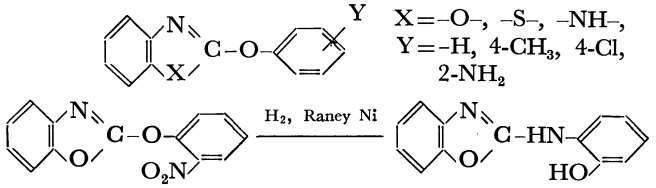

1) For example, A. H. Blatt, "The Fries Reaction," Organic Reactions, Vol. 1, John Wiley and Sons, Inc., New York, N. Y. (1942), p. 342.

2) a) J. C. Anderson and C. B. Reese, *Proc. Chem. Soc.*, **1960**, 217; *J. Chem. Soc.*, **1963**, 1781; b) H. Kobsa, *J. Org. Chem.*, **27**, 2293 (1962).

3) H. Shizuka, T. Kanai, T. Morita, Y. Ohto, and K. Matsui, *Tetrahedron*, **27**, 4021 (1971).

4) T. Harayama, K. Okada, S. Sekiguchi, and K. Matsui, *J. Heterocycl. Chem.*, **7**, 981 (1970); N. Maeno, T. Itagaki, S. Uno, and K. Matsui, This Bulletin, **45**, 3133 (1972).

5) a) K. Matsui, N. Maeno, S. Suzuki, H. Shizuka, and T. Morita, *Tetrahedron. Lett.*, **17**, 1467 (1970); (b) H. Shizuka, N. Maeno, and K. Matsui, *Mol. Photochem.*, **4**, 335 (1972).

Table 1. 2-Aryloxybenzazoles

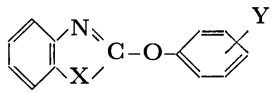

X	Y	Mp (°C)	Recrystn. Solvent
O	H	57— 57.5 (56)[a]	Ethanol
O	4-CH_3	62— 63	Ligroin
O	2-NO_2	142—143.5	Acetone–water
O	4-Cl	101—101.5	Ligroin
S	H	51— 52	Petroleum ether
S	4-CH_3	40	Petroleum ether
S	4-Cl	81	Ethanol
S	2-NO_2	108	Ethanol
S	2-NH_2	86— 87	Benzene–ligroin
NH	H	228—229 (222—223)[b]	Ethanol
NH	4-CH_3	259—260	Dioxane

a) P. Seidel, *J. Prakt. Chem.*, **42**, 455 (1890); b) T. Seki, M. Sasajima, and Y. Watanabe, *Yakugaku Zasshi*, **85**, 962 (1965).

Table 2. 2-(Hydroxyaryl)benzazoles

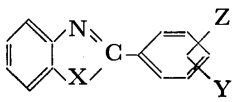

X	Y	Z	Yield (%)	Mp (°C)	Recrystn. Solvent
O	H	2-OH	14	125—126 (122—123)[a]	Acetone
		4-OH	31	252—253 (250)[b]	Ethanol
O	5-CH_3	2-OH	30	134—135	Ligroin
O	H	2-NH_2	20	106—107	Acetone
		4-NH_2	25	172—174 (169—170)[c]	Acetone–water
S	H	2-OH	28.5	123—124 (129)[d]	Ethanol
		4-OH	28.5	220—222 (228—229)[e]	Ethanol
S	5-CH_3	2-OH	53	123—124	Ethanol
S	5-Cl	2-OH	19	157—158	Ethanol
NH	H	2-OH	15	243—244 (238—239)[f]	Ethanol
		4-OH	21	278—279 (277—278)[g]	Acetone
NH	5-CH_3	2-OH	11	259—260	Benzene

a) S. Skrap and M. Moser, *Ber.* **55**, 1089 (1922); b) R. Passerini, *J. Chem. Soc.*, **1954**, 2260; c) F. F. Stephens and J. D. Bower, *ibid.*, **1949**, 2971; d) A. W. Hofmannn, *Ber.*, **13**, 1237 (1880); e) M. T. Bogert and H. B. Corbitt, *J. Amer. Chem. Soc.*, **48**, 783 (1926); f) H. Hüber, *Ann.*, **210**, 345 (1881); g) J. Sawlewicz and Z. Sznigir, *Acta Pol. Pharm.*, **18**, 1 (1961); *Chem. Abstr.*, **55**, 27277h (1961).

Rearrangement in the Dark. 2-Aryloxybenzazoles (*ca.* 5.0 g) were heated at 150 °C for 24 hr in nitrobenzene (300 ml) with aluminum chloride in a 1 : 1 molar ratio, but no 2-(hydroxyaryl)benzazoles, Fries rearranged products, were producd. Failure of rearrangement in these cases is attributed to the preferential coordination of aluminium chloride to the ring nitrogen atom instead of the aryloxy oxygen. By heating at 200 °C for 5 hr, no reaction took place in 2-aryloxy-benzoxazoles or -benzthiazoles, 2-aryloxybenzimidazoles being decomposed with cleavage of phenol. However, 2-(2-aminophenoxy)benzthiazole underwent rearrangement slowly in methanol or ethanol to give 2-(2-hydroxyanilino)benzthiazole, a Smiles rearranged product, although it did not react in such aprotic solvents as benzene, cyclohexane, carbon tetrachloride, and butyl ether. The Smiles rearrangement of 2-(2-aminophenoxy)benzthiazole took place readily in the presence of a small amount of hydrochloric acid to give a rearranged product quantitatively; the catalytic effect by acid is attributable to the lowering of electron-density of the ring carbon atoms by the protonation at the ring nitrogen atom. Thus, the formation of 2-(2-hydroxyanilino)benzoxazole by hydrogenation of 2-(2-nitrophenoxy)benzoxazole indicates the ready O→N migration of the 2-benzoxazolyl group of preformed 2-(2-aminophenoxy)benzoxazole.

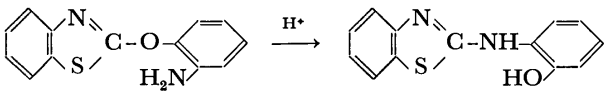

Photo-rearrangement of 2-Aryloxybenzazoles. Irradiation of 2-aryloxybenzazoles (*ca.* 5.0 g) in cyclohexane or ethanol (300 ml) with low pressure mercury lamp gave 2-(2- and/or 4-hydroxyphenyl)benzazoles.[6] The photo-rearranged products thus obtained are listed in Table 2. However, under similar conditions

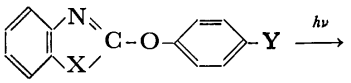

Y=-H, -CH_3, -Cl

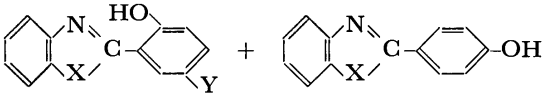

Y=-H, -CH_3, -Cl Y=-H

2-anilinobenzazoles gave no rearranged 2-(2- or 4-aminophenyl)benzazoles. On the other hand, when 2-(2-aminophenoxy)benzthiazole was irradiated in cyclohexane, no 2-(2-aminohydroxyphenyl)benzthiazole, a photo-Fries rearranged product, was obtained, but 2-(2-hydroxyanilino)benzthiazole, a photo-Smiles rearranged product, was obtained in a good yield.

Quantum Yields for the Product Formation from 2-Aryloxybenzazoles. The quantum yields of the product for

6) In the photo-rearrangement of 2-aryloxybenzazoles, several by-products other than rearranged ones were produced (see Experimental). For example, 12 hr's irradiation of 5 g of 2-(4-chlorophenoxy)benzoxazole in 300 ml of ethanol gave 2-(5-chloro-2-hydroxyphenyl)benzoxazole (11%), benzoxazole (1%), *p*-chlorophenol (27%), benzoxazolone (30%), and 2-ethoxybenzoxazole (<1%). In this paper discussion is restricted to rearranged products.

mation from 2-aryloxybenzazoles were measured. The values obtained in ethanol are as follows: 0.084 for 2-(4-methylphenoxy)benzoxazole, 0.025 for 2-(4-methylphenoxy)benzthiazole, and 0.15 for 2-(4-methylphenoxy)benzimidazole. The quantum yields of the product formation from 2-(4-methylphenoxy)benzoxazole at 2537 Å did not change with concentration ($<\sim 7\times10^{-3}$ mol/l) and irradiation time (2~9 min) in the presence of piperylene as a triplet quencher ($10^{-4}\sim 2\times10^{-2}$ mol/l). Similar results were also obtained with 2-(4-methylphenoxy)benzthiazole and -benzimidazole. The results are in line with the general photo-Fries-rearrangement involving the intramolecular process *via* the lowest excited singlet state.

Experimental

Preparation of 2-Aryloxybenzazoles. 2-Aryloxybenzazoles were prepared by the condensation of 2-chlorobenzazoles with the equimolar corresponding phenolates. Typical procedures are described in the case of 2-(4-methylphenoxy)-, 2-phenoxy-benzthiazoles and 2-phenoxybenzoxazole.

2-(4-Methylphenoxy)benzthiazole. After 17 g (0.100 mol) of 2-chlorobenzthiazole and 17.4 g (0.133 mol) of sodium *p*-methylphenoxide in 50 ml of *p*-methylphenol had been heated at 130 °C for 24 hr, the mixture was poured into a large amount of aqueous sodium hydroxide solution. After the mixture had been extracted with benzene, the benzene solution was concentrated and the residue was distilled under reduced pressure (bp 178—178.5 °C/3 mmHg) and recrystallized from ethanol. 2-Phenoxybenzthiazole (bp 178—180 °C/8 mmHg) was prepared by a similar method.

2-Phenoxybenzoxazole. After 15.3 g (0.100 mol) of 2-chlorobenzoxazole and 17.4 g (0.15 mol) of sodium phenoxide in 50 ml of phenol had been heated at 120 °C for 20 hr, the mixture was poured into a large amount of aqueous sodium hydroxide solution and filtered out. The precipitate was recrystallized from ethanol. Other aryloxybenzazoles except for the above-mentioned three aryloxybenzazoles were prepared by similar methods.

Hydrogenation of 2-(2-Nitrophenoxy)benzoxazole: A mixture containing 50 ml of dioxane, 5 g (0.020 mol) of 2-(2-nitrophenoxy)benzoxazole, and 3 g of Raney Nickel was stirred for 12 hr under a pressure of 120 kg/cm² of hydrogen at room temperature. After the catalyst had been removed by filtration and the solvent evaporated, the residue was dissolved in 200 ml of 3% aqueous sodium hydroxide. After filtration the filtrate was neutralized with dilute hydrochloric acid, filtered, and dried to give 3.5 g (80%) of crude 2-(2-hydroxyanilino)benzoxazole. Recrystallzation from ethanol–water gave an analytical sample, mp 176—177 °C. Found: C, 68.72; H, 4.28%. Calcd for $C_{13}H_{10}O_2N_2$: C, 69.01; H, 4.46%.

Smiles and Photo-Smiles Rearrangements of 2-(2-Aminophenoxy)-benzthiazole (2APB): To a solution of 0.5 g (0.002 mol) of 2APB in 10 ml of acetone or ethanol was added a small amount of concd hydrochloric acid (*ca.* 0.08 g). After the mixture had been allowed to stand at room temperature for 2 days (for Smiles rearrangement) or 21 days (for photo-Smiles rearrangement), it was poured into 50 ml of ice-water, filtered, and dried. Recrystallization from benzene gave 2-(2-hydroxyanilino)benzthiazole quantitatively, mp 178.5—179 °C; NMR (DMSO-d_6) τ 0.2(s, OH), 1.7(s, NH). Found: C, 64.70; H, 4.46%. Calcd for $C_{13}H_{10}ON_2S$: C, 64.66; H, 4.16%.

After a solution of 5 g (0.02 mol) of 2APB in 300 ml of ethanol had been irradiated at room temperature with a low pressure mercury lamp (30W) for 7 days, the solvent was distilled off, and the residue was dissolved in 300 ml of benzene. The benzene solution was extracted with 200 ml of 4% sodium hydroxide solution. The aqueous solution was neutralized with hydrochloric acid and extracted with 200 ml of benzene. Column chromatography and recrystallization of the former benzene solution afforded 3.6 g of 2APB and 0.4 g (28.9%, based on the reacted 2APB) of benzthiazolone, and 0.7 g (50%, based on the reacted 2APB) of 2-(2-hydroxyanilino)benzthiazole from the latter benzene solution.

Photo-rearrangement and Actinometry: A low pressure mercury lamp was used as the 2537 Å radiation source with a Vycor glass filter. Irradiation was continued for 7 to 10 days. Actinometry was carried out with a ferric oxalate solution,[7] throughly degassed on a high vacuum line by the freeze-pump-thaw method.

Structural assignments of all products were performed by means of NMR, IR, UV, MS and elemental analyses. The results of the elemental analysis of all new products were within the experimental error.

7) C. G. Hatchard and C. A. Parker, *Proc. Roy. Soc. Ser. A*, **235**, 518 (1956).

BULLETIN OF THE CHEMICAL SOCIETY OF JAPAN, VOL. 46, 2602—2604 (1973)

Fluorescence Lifetime of Pyrene in Different Solvents

Akira NAKAJIMA

Division of Chemistry, Research Institute of Applied Electricity, Hokkaido University, Sapporo 060

(Received March 12, 1973)

As has been reported in a previous paper,[1] the forbidden components in the vibrational structures of the absorption and fluorescence spectra of aromatic hydrocarbons are markedly enhanced in very polar solvents. These intensity enhancements have been shown to be well correlated with the dielectric property of the solvent. It is known that the radiative lifetime of the fluorescence can be estimated using the theoretical relation[2-4] from the integral of the corresponding absorption spectrum. Experimentally it is determined from the observed fluorescence lifetime and quantum yield.[2] It is supposed that the intensity enhancements by solvents may be accompanied by a decrease in the radiative lifetime. Under these circumstances, it is of interest to study the applicability of the relation

1) A. Nakajima, This Bulletin, **44**, 3272 (1971).

2) J. B. Birks, "Photophysics of Aromatic Molecules," Wiley-Interscience, London (1970).

3) S. J. Strickler and R. A. Berg, *J. Chem. Phys.*, **37**, 79 (1962).

4) J. B. Birks, *Proc. Roy. Soc., Ser. A*, **275**, 135 (1963).

Table 1. Fluorescence lifetimes (τ) of pyrene in three solvents

Excitation	τ (ns)		
	Air-gap discharge	Ruby laser	
Concentration	9.7×10^{-6} M	9.7×10^{-6} M	1.07×10^{-4} M
Cyclohexane	408± 5	338± 9	369±11
1,2-Dichloroethane	202± 3	170±12	187± 4
Dimethyl sulfoxide	275±11	233± 8	238± 6

and the change in the radiative rate.

In this work, the fluorescence lifetimes were measured at various vibronic bands in three representative solvents, and the radiative rate constants calculated from the observed lifetimes and quantum yields were compared with those estimated from the integrated absorption spectra. In addition, on the basis of the constancy of the fluorescence lifetimes over the vibronic band system, it was confirmed that there was no appreciable specific interaction between the solute and solvent molecules.

Experimental

The fluorescence lifetimes were measured by excitation with the frequency-doubled light pulses from a Q-switched ruby laser (a duration of ~20 ns, 3472 Å) and with the UV light pulses from an air-gap discharge (a duration of ~10 ns). An about 2% mesh filter was used for attenuation of the strong exciting laser light. The fluorescence emission was detected with a Hamamatsu TV R-446 photomultiplier through a Hitachi G-3 grating monochromator. The slit width of the monochromator was less than 3 mμ for the laser excitation and 10 to 30 mμ for the discharge excitation. The fluorescence decay curves were displayed on an Iwasaki SS-112 synchroscope and photographed. The lifetimes were estimated from the photographs, the analyses of which gave most part of errors of about 10 ns.

The fluorescence spectra were measured with a Hitachi MPF-2A spectrofluorometer. The absolute quantum yields of pyrene fluorescence in various solvents were calculated assuming the value of 0.65[5] in a degassed cyclohexane solution from the relative yields, which were evaluated from the areas under the corrected fluorescence spectra.

The concentrations of the solutions were 9.7×10^{-6} and 1.07×10^{-4} M. The solutions used were thoroughly deaerated by the usual method of freeze-pump-thaw cycles.

Pyrene was purified by recrystallization, zone-refining, and vacuum sublimation. Super-special grade cyclohexane, G. R. grade 1,2-dichloroethane, and spectroscopic grade dimethyl sulfoxide were used without further purification. The purities of pyrene and these solvents were checked by measuring the fluorescence and excitation spectra.

Results and Discussion

Since there are two kinds of components, solvent-sensitive and insensitive, in the vibronic band system, the possibility can be considered that the fluorescence decay times might be different between these components in various solvents. Thus, the lifetimes of pyrene fluorescence were measured at several vibrational band peaks in three solvents of different polarities. Table 1 gives the fluorescence lifetimes averaged over the vibronic band system with the maximum deviations. As seen from Table 1, the lifetimes measured by the laser excitation were appreciably shorter than those measured by the discharge excitation. This phenomenon may be much related to the bimolecular decay process due to the interaction between the excited molecules found by excitation at a high photon density.[6,7] In fact, a slight deviation from the single exponential curve could be observed in the initial time region. In cyclohexane and 1,2-dichloroethane by the laser excitation, the lifetimes in 1.07×10^{-4} M solutions are about 10% longer than those in 9.7×10^{-6} M solutions. This may be caused by the dissociation of excimers formed in a small amount due to the low viscosity of these solvents and the somewhat high concentration of the solutions. Weak excimer emission was actually observed in 1.07×10^{-4} M cyclohexane solutions.

In view of the considerable errors in the decay time analysis, the lifetimes given in Table 1 should be regarded as taking almost the same values in the whole region of the fluorescence spectrum in each solvent. If the solvent-enhanced bands are assumed to arise from some species such as a specifically solvated solute molecule or more unlikely, a complex formed between the solute and solvent molecules, the lifetimes observed at the solvent-sensitive bands might differ from those observed at the solvent-insensitive bands. However, the constant lifetimes obtained over the whole vibronic band system indicate the participation of a single species responsible for both these bands, in accord with the conclusions derived from the fluorescence spectra by excitation at different wavelengths and the excitation spectra by monitoring at various vibrational bands.

Since the intensities of the forbidden bands change in various solvents, the corresponding changes in the radiative rate can be expected. In general, the radiative rate constant, k_0, can be calculated from the observed fluorescence lifetime, τ, and the quantum yield, η, by the following relation:[2]

$$k_0 = \eta/\tau . \tag{1}$$

On the other hand, k_0 can also be estimated from the absorption spectrum of the first electronic transition by the well-known equation:[2-4]

$$k_0 = 2.88 \times 10^{-9} n^2 \bar{\nu}_0^2 \int \varepsilon d\bar{\nu} , \tag{2}$$

where ε is the molar extinction coefficient and n is the

5) J. B. Birks, D. J. Dyson, and I. H. Munro, *Proc. Roy. Soc., Ser. A*, **275**, 575 (1963).
6) H. Masuhara and N. Mataga, *Chem. Phys. Lett.*, **7**, 417 (1970).
7) T. Kobayashi, K. Yoshihara, and S. Nagakura, *Mol. Phys.*, **21**, 573 (1971).

Table 2. Radiative rate constants (k_0) estimated by Eqs. (1) and (2)

Solvent	k_0 (s^{-1})	
	(1)	(2)
Cyclohexane	1.6×10^6	1.9×10^6
1,2-Dichloroethane	1.8×10^6	2.1×10^6
Dimethyl sulfoxide	2.0×10^6	2.6×10^6

refractive index of the solvent. $\bar{\nu}_0$ was taken to be the wave number of the 0–0 band. This simplified formula[2] was used in view of the accuracy of the present results.

In Table 2, the values of the radiative rate constants evaluated by Eqs. (1) and (2) are given. In spite of the large errors inherent to the evaluations, the agreement between the values obtained by these two different methods is good. Though the applicability of Eq. (2) to weak or forbidden transitions may be questionable,[3] it can be well employed for an order estimation, including the cases of enhancements by solvents.

As seen from Table 2, the k_0 values increase appreciably on going from cyclohexane to dimethyl sulfoxide, corresponding to the enhancements of the forbidden bands with the increase in the solvent polarity. In a highly polar solvent, the contribution of the forbidden components to the vibronic band system can be comparable to that of the vibronically allowed components, indicating that the intermolecular perturbation by solvent can become as important as the intramolecular perturbation due to vibronic coupling.

BULLETIN OF THE CHEMICAL SOCIETY OF JAPAN, VOL. 46, 2604—2605 (1973)

Rapid and Sensitive Atomic-Absorption Determination of Arsenic by Arsine–Argon–Hydrogen Flame System with the Use of a Zinc Powder Tablet as Reductant

Yuroku YAMAMOTO, Takahiro KUMAMARU, Yasuhisa HAYASHI, and Toshihiko KAMADA*

Department of Chemistry, Faculty of Science, Hiroshima University, Hiroshima 730

**Department of Hygiene, Faculty of Medicine, Hiroshima University, Hiroshima 730*

(Received November 20, 1972)

Determination of arsenic in trace amount is often necessary in connection with pollution. Accuracy of the determination of arsenic can be fairly enhanced by introduction of arsenic as arsine gas into argon-hydrogen flame.[1–4] Chu *et al.*[5] have recently described a flameless atomic-absorption spectrophotometric method for arsenic determination involving chemical conversion of arsenic into arsine. We showed that antimony and selenium can be rapidly determined by introducing stibine or hydrogen selenide gas into argon-hydrogen flame.[6,7]

This paper deals with a method for the rapid, sensitive and accurate determination of arsenic by atomic-absorption spectrophotometry in combination with the argon-hydrogen system. Arsine was rapidly evolved from arsenic(III) or aresenic(V) solutions by reduction with zinc powder tablets, stannous chloride and potassium iodide. With the combined use of these reagents, both optimum hydrochloric acidity and interference of diverse ions in the reduction process could be reduced to a considerable extent.

Experimental

Reagents. All solutions were prepared with Chemicals of analytical reagent grade and deionized water, the aqueous solutions being stored in polyethylene bottles.

Standard Arsenic(III) Solutions: Prepared by dissolving 1.320 g of diarsenic trioxide (As_2O_3) in 10 ml of water containing 4 g of sodium hydroxide, and diluting it to 1000 ml with water. An aliquot of this solution was diluted with water to give a concentration of 0.2 ppm immediately before use.

Standard Arsenic(V) Solution: Prepared by dissolving 2.403 g of potassium dihydrogen arsenate in water and diluting it to 1000 ml with water. An aliquot of this solution was diluted with water to give a concentration 0.2 ppm immediately before use.

Stannous Chloride Solution: Prepared by dissolving stannous chloride dihydrate in 10 M hydrochloric acid to give a concentration of 10%(w/v).

Potassium Iodide Solution: Prepared by dissolving potassium iodide in water to give a concentration of 40% (w/v).

Zinc Tablets 50 g of arsenic-free zinc powder (200 mesh), 4 g of kaolin powder, and 10 ml of water were mixed in a mortar to make a paste. This was moulded into small tablets, 8 mm in diameter, 3 mm in thickness and about 0.5 g in weight, and dried in an electric oven.

Apparatus. The atomic-absorption was measured with a Nippon Jarrell-Ash Model AA-1 EW atomic-absorption spectrophotometer equipped with a Westinghouse arsenic hollow cathode lamp. The apparatus used for generation and collection of arsine was the same as that reported.[6,7]

Recommended procedure: Transfer into a reaction bottle a sample solution less than 20 ml in total volume and

1) W. Holak, *Anal. Chem.*, **41**, 1712 (1969).
2) E. F. Dalton and A. J. Malanoski, *At. Abs. Newslett.*, **10**, 92 (1971).
3) F. J. Fernandez and D. C. Manning, *ibid.*, **10**, 36 (1971).
4) D. C. Manning, *ibid.*, **10**, 123 (1971).
5) R. C. Chu, G. P. Barron, and P. A. W. Baugarner, *Anal. Chem.*, **44**, 1476 (1972).
6) Y. Yamamoto, T. Kumamaru, Y. Hayashi, and R. Tsujino, *Anal. Lett.*, **5**, 419 (1972).
7) Y. Yamamoto, T. Kumamaru, Y. Hayashi, and M. Kanke, *ibid.*, **5**, 717 (1972).

containing not more than 1 μg of arsenic. Add 2 ml of 12 M hydrochloric acid, 1 ml of the potassium iodide solution and 2 ml of the stannous chloride solution. Dilute the mixture to 25 ml with water. Swirl the solution to mix thoroughly and stand it at room temperature for 15—30 min. After adding two zinc tablets, immediately connect the reaction bottle to the collection unit and allow the reaction to take place for 90 sec at room temperature by agitating the mixture with a magnetic stirrer. Turn the four-way stopcock to "sweep" forcing the hydrogen and arsine into the burner mixing chamber, and also introducing argon into the system to sweep the gases into the flame. Simultaneously record the absorption signal on a recorder. Finally return the stopcock to "bypass".

The working conditions are: wavelength 1937 Å, slit-width 0.10 mm, lamp current 15 mA. Flow rates of gases for a standard 10-cm slot burner: argon 8.0 l/min (1.5 kg/cm²G), hydrogen 7.0 l/min (0.4 kg/cm²G) using air-acetylene regulator system, respectively, auxiliary argon 4.0 l/min (2.0 kg/cm²G).

Results and Discussion

In the conventional method for arsenic determination by colorimetry, granular zinc metal is used as the reducing agent. Evolution of arsine has to be continued for about half an hour because the reaction proceeds gradually. Holak[1] used granular zinc for arsine generation and collected the arsine by freezing in a liquid nitrogen trap. It was then introduced into an air-acetylene flame after being brought to room temperature and swept with nitrogen. The procedure required considerable time. It was found[2–4] that it is not necessary to wait for the reaction to complete since almost all the hydrides are formed during the early period of the reaction when smaller granular zinc (20 mesh) is used. We have reported[6,7] that zinc powder tablets are effective for rapid and quantitative evolution of stibine and hydrogen selenide.

We also found that the use of the zinc tablets together with stannous chloride and potassium iodide considerably accelerate the reduction even in a lower acidic medium. Conditions were investigated for the quantitative production of arsine by use of a mixture of reagents.

The mechanism of the conversion of trivalent and pentavalent arsenic into arsine appears to be very complicated. It is therefore of interest to investigate the role of potassium iodide and stannous chloride in the overall reduction process. It is known[8] that both potassium iodide and stannous chloride are highly effective not only for the complete reduction of arsenic from the pentavalent to the trivalent state, but also for the suppression of the interference of diverse metal ions in the overall reduction process. A potassium iodide solution (0—3.0 ml) and a stannous chloride solution (0—6.0 ml) were added respectively to arsenic(III) and arsenic(V) solutions, each containing 1.0 μg of arsenic with a final acidity of 2 M. It was found that potassium iodide and stannous chloride enhanced to a great extent the recovery of arsenic as arsine from the trivalent state (KI with 0.8% $SnCl_2$, 4-fold; $SnCl_2$ with 1.6% KI, 3-fold) when at least 0.3 ml of the potassium iodide and 0.5 ml of the stannous chloride solutions were added. Thus the potassium iodide or stannous chloride concentration was usually kept at 1.6% or 0.8%. As a result, the same values in the atomic-absorption signal were obtained when evolution of arsine took place either from trivalent arsenic or pentavalent arsenic state.

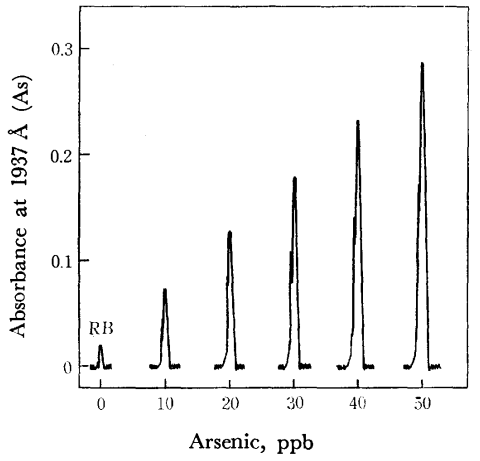

Fig. 1. Absorption signal *vs.* concentration of arsenic. (RB is a reagent blank)

The optimum range of acidity was about 1.5—2.5 M in hydrochloric acid. Addition of at least one zinc tablet was enough to obtain a highest and constant recovery of arsenic as arsine.

After addition of the reagents no distinct evolution took place appreciably for a few seconds, during which time we could connect the reaction bottle to the gas collection unit without any loss of arsine. Arsine was vigorously generated by grinding the tablets by agitating the mixture with a magnetic stirrer. A constant and maximum sharp signal was obtained for only one minute gas sampling. The calibration curve was constructed by the procedure described above by use of arsenic(III) standard solution. An example is shown in Fig. 1. An appreciable value of absorbance is observed in the reagent blank. This can be attributed to the arsenic contained in the zinc tablets as impurities. The same results were obtained by using the arsenic(V) solution as a standard. The sensitivity for 1% absorption of the signal was estimated to be 0.001 ppm of arsenic and the linearity of absorption *vs.* concentration was good over the range 0.01—0.05 ppm. The precision was estimated to be 3% from the results of ten solutions with 1 μg of arsenic. The effect of diverse cations on the reduction process was studied using a solution containing 1.0 μg of arsenic(III). The following ions did not interfere at the 250 ppm level: chromium(III), manganese(II), iron(III), aluminium, cobalt(II), nickel(II), copper(II), zinc, silver, cadmium, mercury(II), sodium, potassium, magnesium, and calcium. The maximum permissible amount of the other ions was as follows: lead and antimony(III) 10 ppm, selenium 0.4 ppm.

The authors thank Mr. R. Tsujino, Nippon Jarrell-Ash Co. Ltd., for his assistance in the device of the apparatus for the evolution of arsine.

8) E. B. Sandell, "Colorimetric Determination of Traces of Metals," 3rd ed., Interscience, New York (1959), p. 289.

BULLETIN OF THE CHEMICAL SOCIETY OF JAPAN, VOL. 46, 2606—2607 (1973)

The Crystal and Molecular Structure of *trans*-2,2′-Dichloroazobenzene

Masayuki KOMEYAMA*, Shunzo YAMAMOTO, Norio NISHIMURA, and Shigeo HASEGAWA
Department of Chemistry, Faculty of Science, Okayama University, Tsushima, Okayama 700

(Received February 2, 1973)

In a previous paper,[1] the dipole moment and spectral data of substituted azobenzenes have been presented. The dipole moment and the intensity of the π–π^* band are apparently reduced by the introduction of methyl groups into ortho position with respect to azo group. This has been interpreted as due to the reduced conjugation by the twisting of the molecule. In this connection, it became desirable to obtain information about the molecular structure of 2,2′-disubstituted azobenzene in crystal. Recently, the crystal and molecular structures of 4,4′-disubstituted azobenzenes were determined and it was found that the molecules are nearly planar.[2-4] However, for 2,2′-disubstituted ones, no such information is available as yet. This paper presents the three-dimentional X-ray structure analysis of 2,2′-dichloroazobenzene.

Experimental

2,2′-Dichloroazobenzene was prepared from *o*-chloroaniline,[5] and recrystallized by slow evaporation from a benzene–ligroin solution. The compound crystallized as red plates having a predominant (001) face.

Crystal data: $C_{12}H_8N_2Cl_2$; M=251.1; mp=138—139 °C, monoclinic, a=13.651(8), b=3.946(8), c=11.626(4) Å, β=114.40(3)°, U=570.4 Å^3, D_m=1.47, D_x=1.46 g cm^{-3}, Z=2. Absorption coefficient for Cu$K\alpha$; μ=48.8 cm^{-1}. F(000)=256.

Absent spectra: $h0l$ when h is odd and $0k0$ when k is odd. Space group is $P2_1/a$.

Using Cu$K\alpha$ radiation, multiple-film equi-inclination Weissenberg photographs were taken for the layers from $0kl$ to $9kl$ and from $h0l$ to $h2l$. A total of 995 independent non-zero reflections was recorded. The intensities were estimated visually. After Lorentz, polarization and spot-shape corrections were made, the intensities of various layers were adjusted to the same relative scale by making use of all the common reflections. The relative values were converted to an absolute scale by Wilson's method. No corrections were applied for absorption and extinction effects.

Structure Determination

In the space group $P2_1/a$, four is the minimum number of asymmetric units necessary to fulfill the symmetry operation, while there are only two molecules in the unit cell. Hence it must be that the molecules themselves are centrosymmetric, and occupy the position of a center of symmetry of the cell.

Approximate x,y,z parameters for all non-hydrogen atoms were easily determined from a three-dimensional Patterson map. The structure was refined by the block-diagonal least-squares method[6] with isotropic thermal parameters to an R value of 0.17 and with anisotropic ones to the R of 0.10. The difference Fourier synthesis showed the locations of all the four hydrogen atoms. Furthermore, six cycles of calculation were made with anisotropic thermal parameters for the non-hydrogen atoms and with isotropic thermal parameters (initially set at B=3.5 Å^2) for the hydrogen atoms using unit weight for all the observed reflections. The final R index was 0.087 for all the observed reflections. The final positional and thermal parameters are given in Table 1. The numerical calculations were performed with the aid of a HITAC 5020E computer of the Computer Center of the University of Tokyo, a FACOM 230—60 computer of the Data Processing Center of Kyoto University. The atomic scattering factors were taken from Ref. (7).

Results and Discussion

The bond lengths and angles are shown in Fig. 1. The average C–C bond length in the benzene ring is 1.389 Å. The bond angles in benzene ring range from 118.6 to 121.4°. The other bond lengths and angles are listed in Table 2, together with the corresponding bond lengths and angles of azobenzene and other related compounds. As shown in Table 2, the N=N, N–C and C–Cl bond lengths and the N=N–C

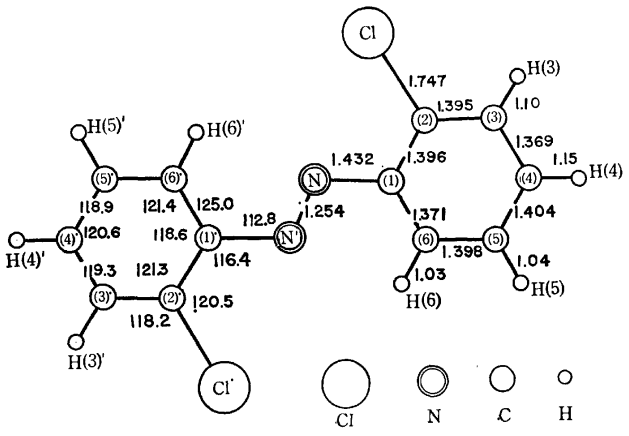

Fig. 1. Bond lengths and angles. Estimated standard deviations are 0.007—0.010 Å for lengths not involving H, 0.07 Å for C–H lengths and 0.5—0.7° for angles not involving H.

* Present address: Okayama Plant, Kuraray Co. Ltd., 1-3 Kaigan-dori, Okayama

1) S. Yamamoto, N. Nishimura, and S. Hasegawa, This Bulletin, 44, 2018 (1971).
2) A. G. Amit and H. Hope, *Acta Chem. Scand.*, **20**, 835 (1966).
3) C. J. Brown, *Acta Crystallogr.*, **21**, 153 (1966).
4) H. Hope and D. Victor, *ibid.*, **B25**, 1849 (1969).
5) F. Meyer and E. Trampedach, *Ann. Chem.*, **320**, 129 (1902).
6) Y. Okaya and T. Ashida, HBLS IV. The Universal Crystallographic Computing System (I), p. 65, The Crystallographic Society of Japan (1967).

TABLE 1. FINAL FRACTIONAL ATOMIC COORDINATES AND THEIR ESTIMATED STANDARD DEVIATIONS FOR THE ATOMS IN ASYMMETRIC UNIT, AND ISOTROPIC THERMAL PARAMETERS FOR HYDROGEN ATOMS

	x	y	z	B_{iso}		x	y	z	B_{iso}
C(1)	0.1202(5)	−0.0415(16)	0.1391(5)		N	0.0093(4)	0.0129(15)	0.0573(4)	
C(2)	0.1516(5)	0.0436(15)	0.2659(5)		Cl	0.0591(1)	0.2175(5)	0.3176(1)	
C(3)	0.2571(5)	−0.0052(18)	0.3545(5)		H(3)	0.280(5)	0.068(17)	0.453(6)	1.0(14)
C(4)	0.3307(5)	−0.1447(18)	0.3165(6)		H(4)	0.419(5)	−0.207(18)	0.382(6)	1.3(14)
C(5)	0.3012(5)	−0.2333(19)	0.1896(6)		H(5)	0.353(5)	−0.328(16)	0.152(5)	0.6(12)
C(6)	0 1949(5)	−0.1817(17)	0.1029(5)		H(6)	0.175(5)	−0.260(17)	0.011(6)	1.6(14)

ANISOTROPIC THERMAL PARAMETERS[a)] AND ESTIMATED STANDARD DEVIATIONS ($\times 10^4$) FOR THE NON-HYDROGEN ATOMS

	B_{11}	B_{22}	B_{33}	B_{12}	B_{13}	B_{23}
C(1)	47(4)	443(41)	55(5)	−9(22)	43(7)	32(23)
C(2)	50(4)	368(39)	67(5)	−9(21)	62(8)	−13(24)
C(3)	50(4)	591(48)	52(5)	−27(24)	25(7)	45(26)
C(4)	53(4)	564(48)	79(6)	−23(25)	44(8)	63(29)
C(5)	58(4)	597(50)	81(6)	52(27)	55(8)	79(31)
C(6)	57(4)	543(46)	59(5)	14(25)	46(8)	41(26)
N	50(3)	593(40)	52(4)	12(20)	36(6)	−20(22)
Cl	53(1)	717(13)	62(1)	−10(7)	54(2)	−118(7)

a) Anisotropic temperature factors are of the form $\exp(-h^2B_{11}-k^2B_{22}-l^2B_{33}-hkB_{12}-hlB_{13}-klB_{23})$.

TABLE 2. COMPARISON OF THE BOND LENGTHS AND ANGLES BETWEEN THIS COMPOUND AND RELATED COMPOUNDS

	N=N	N-C	C-Cl	N-N-C	N-C(1)-C(6)	N-C(1)-C(2)
This compound	1.254 Å	1.432 Å	1.747 Å	112.8°	125.0°	116.4°
Azobenzene[9]	1.243	1.443	—	113.6	124.1	115.5
4,4'-Dimethyl-azobenzene[9]	1.244	1.433	—	113.8	128.8	112.6
4,4'-Dibromo-azobenzene[9]	1.276	1.528	—	112.2	125.6	114.7
4,4'-Dichloro-azobenzene[9]	1.252	1.443	1.737	112.6	125.9	114.2
N-5-Chloro-salicylideneaniline[8]	—	1.419	1.755	—	124.3	116.1
2-Chloro-*N*-salicylideneaniline[10]	—	1.421	1.737	—	121.2	120.2

TABLE 3. DEVIATION (Å) OF ATOM FROM PLANE (1) AND (2)

	Plane(1)	Plane(2)		Plane(1)	Plane(2)
C(1)	−0.017*	0.000*	C(6)	−0.001*	0.277
C(2)	−0.003*	−0.249	N	0.013*	0.000*
C(3)	−0.002*	−0.247	N'	−0.232	0.000*
C(4)	0.010*	0.029	Cl	0.001*	−0.585
C(5)	0.000*	0.286			

Least-squares plane is determined by the atoms with asterisk.
Dihedral angle between the two plane is 12.8°.
The numbering of each atom is the same as that in Fig. 1.

TABLE 4. INTERMOLECULAR CONTACTS

Atom	Neighbour atom	Distance	Atom	Neighbour atom	Distance
(1) I···II			(4) II···IV		
C(4)	Cl	3.54 Å	H(3)	H(3)	2.55 Å
H(4)	Cl	3.02	H(3)	C(3)	3.01
(2) I···III			Cl	H(3)	3.00
Cl	H(3)	3.00	(5) III···IV		
H(3)	H(3)	2.55	Cl	H(4)	3.08
H(3)	C(3)	3.01	Cl	H(5)	3.08
(3) I···V					
Cl	Cl	3.95			
Cl	C(2)	3.63			

Perpendicular distance from benzene ring (I) to benzene ring (V) is 3.62 Å

Key for position of molecules
I: x, y, z; II: $1/2+x$, $1/2-y$, z; III: $1/2-x$, $1/2+y$, $1-z$; IV: $1-x$, $-y$, $1-z$; V: x, $1+y$, z

and N–C–C (*cis* and *trans* relative to the central double bond) bond angles are well consistent with the corresponding values of the related compounds.

The intramolecular distance between Cl and N atoms (2.98 Å) is considerably shorter than the sum of the van der Waals radii of Cl and N atoms (3.3 Å). Hence the steric repulsion between these two atoms must exist. As mentioned above, however, the bond lengths and angles are hardly affected by the introduction of Cl atom into *ortho* position with respect to azo group.

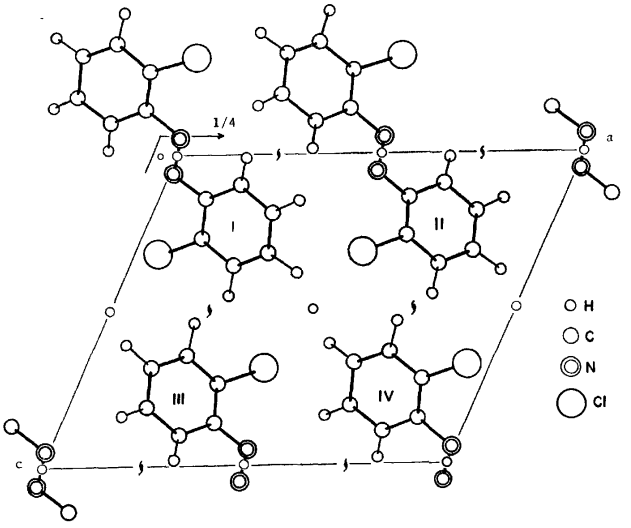

Fig. 2. The projection of the crystal structure along the b-axis.
Key for molecules I: x, y, z; II: $1/2+x$, $1/2-y$, z; III: $1/2-x$, $1/2+y$, $1-z$, IV: $1-x$, $-y$, $1-z$.

As shown in Table 3, the benzene ring including N and Cl atoms is planar within 0.02 Å. This plane (plane 1) makes a dihedral angle of 12.8° with the N=N–C plane (plane 2). From the inspection of Table 3, it can be concluded that the dihedral angle between these two planes is the twisting angle of the benzene ring around the N–C bond. As mentioned in the section of structure determination, this compound has the center of symmetry. The two benzene rings must be symmetrically twisted around the azo group. This is in accord with the previous suggestion that the molecule is twisted in the same manner. The cause of the twist has already been discussed in some detail.[1)]

The mode of packing of the molecules in the crystal can be seen in Fig. 2. The short intermolecular contacts are summarized in Table 4. They show the normal van der Waals interaction.

The authors wish to express their deep gratitude to Professor Masao Haisa and Mr. Setsuo Kashino for their kind guidance and valuable adivce.

7) H. P. Hanson, F. Herman, J. D. Lea, and S. Skillman, *Acta Crystallogr.*, **17**, 1040 (1964).
8) C. J. Brown, *ibid.*, **21**, 146 (1966).
9) J. Bregman, L. Leiserwitz, and G. M. J. Schmidt, *J. Chem. Soc.*, **1964** 2068.
10) J. Bregman, L. Leiserwitz, and K. Osaki, *ibid.*, **1964** 2086.

BULLETIN OF THE CHEMICAL SOCIETY OF JAPAN, VOL. 46, 2608—2609 (1973)

Derivatives of 1,2-Dithiole-3-thione. II. Thermal Rearrangement of Iminothiocarbonyl Compounds.

Seizo TAMAGAKI, Keishi SAKAKI, and Shigeru OAE

Department of Applied Chemistry, Faculty of Engineering, Osaka City University, Sugimoto-cho, Sumiyoshi-ku, Osaka 558

(Received February 20, 1973)

The synthesis[1] and cyclization mechanism[2] of thiocarbonyl ylides have recently attracted considerable attention. A solution of thiourea in chloroform reacts rapidly and exothermically with 2,2-dicyano-3,3-bis-(trifluoromethyl)oxirane, giving dicyanomethylene sulfonium dicyanomethylide in a high yield.[3] Certain thiocarbonyl compounds have been found to give the olefins by a similar treatment. The initial step of the reaction seems to be the formation of ylides, which collapses to a three-membered ring, giving rise to expulsion of sulfur to afford the final product.

We have synthesized the terminal *N*-analog of thiocarbonyl ylide for the first time and found it to undergo similar rearrangement. This report deals with the nature of the thermal rearrangement of thiocarbonyl imines(B).[4]

Results and Discussion

When trithione(A) was treated with chloramine-B or corresponding substituted chloramines in methanol, thiocarbonyl imines(B) were obtained as red-colored precipitates in nearly quantitative yields.

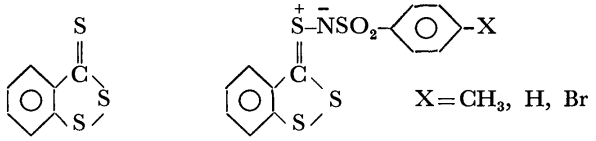

(A) (B)

When compound(B) (X=H) thus obtained was heated by refluxing in various solvents or kept standing at room temperature for a month without solvent, the rearranged imine (*N*-benzenesulfonyl-1,2-benzodithiole-3-imine)(C) was obtained. The analytical data are summarized in Table 1.

In order to clarify the mechanism of rearrangement we carried out kinetic measurements at about 60 °C. The rate of the rearrangement was followed by the disappearance of the absorption band due to thiocarbonylimine, appearing at 472—506 nm. In every case the reaction follows first-order kinetics. The relevant data are collected in Tables 2 and 3.

The marked change in rate with solvents indicates that the reaction rate sequence is not parallel at all with the ordinary polarity scale such as dielectric constant or dipole-moment. Instead, a relatively better correlationship can be found with $1/\lambda_{max}$ for the thiocarbonyl imine itself (Fig. 1). Accordingly, it should be pointed out that rearrangement involves a transition structure like the state of photoexcitation in

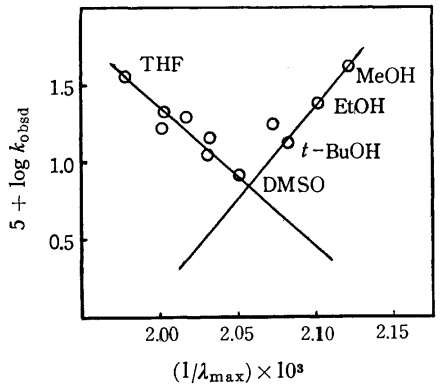

Fig. 1. Plot of log k_{obsd} *vs.* $1/\lambda_{max}$.

Table 1. Products analysis

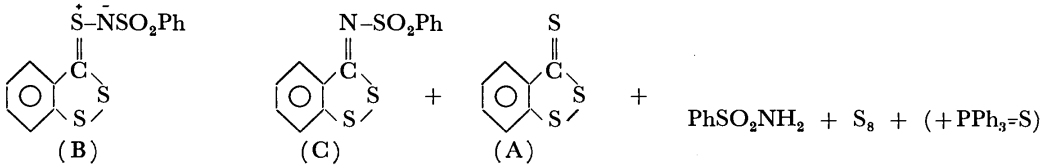

(B) (C) (A)

Solvent	Yield (%)				
Neat	86.2	8.1	6.1		
CH_3CN	85.5	8.1			
MeOH	31.9	67.5	67.5	31.9	
(CH_3CN)	(74.9)	(20.8)			(72.5)

Parenthesis indicates the reaction carried out in the presence of an equimolar quantity of triphenyl phosphine.

1) E. B. Knott, *J. Chem. Soc.* **1955**, 916. B. H. Freeman, S. G. Harris, B. W. Kennedy, and D. Lloyd, *Chem. Commun.*, **1972**, 912.

2) H. H. J. MacDonald and R. J. Crawford, *Can. J. Chem.*, **50**, 428 (1972). R. B. Woodward and R. Hoffmann, *Angew. Chem. Int. Ed. Engl.*, **8**, 1475 (1969). R. M. Kellogg, S. Wassenaar, and J. Buter, *Tetrahedron Lett.*, **1970**, 4689.

3) W. J. Middleton, *J. Org. Chem.*, **31**, 3731 (1966).

4) Derivatives of 1,2-dithiole-3-thione. I. S. Tamagaki and S. Oae, *Tetrahedron Lett.*, **1972**, 1159.

which the charge-separation initially existing completely disappears due to the charge-transfer photoexcitation.[5] The significant increasing change in entropies of activation on going from the reaction in THF to that in CH_3CN also implies that the extent of desolvation on proceeding from the initial state to the transition state is larger in the latter solvent. We can thus conclude that the rearrangement takes place through the initial ring closure to a three-membered thiaziridine ring, followed by the loss of sulfur. The following mechanism would be fully compatible with the negative ρ-value, *i.e.*, -0.56 (Table 3).

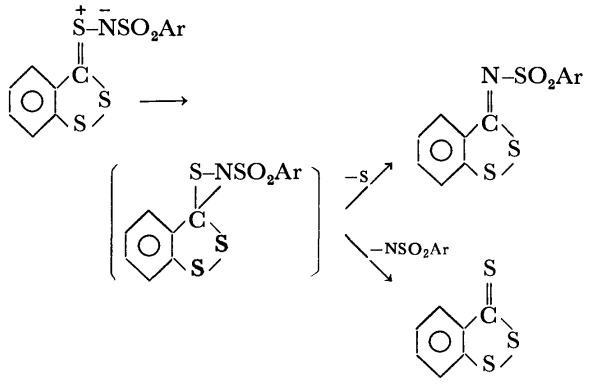

As for the reaction in protic solvents we see that the plot (Fig. 1) against solvent such scale as either $1/\lambda_{max}$ or E_T (not given here) displays a behavior essentially different from that of the reaction in aprotic solvents. The reaction is facilitated in more polar alcohols. The lower value of activation energy of 11 kcal/mol as compared with that in aprotic solvents (20 kcal/mol) would support the view that the reaction is brought by nucleophilic interaction of the oxygen atom of alcohol with the tetravalent sulfur atom of thiocarbonyl imine, giving a relatively large charge-separation. The slightly positive rho value of $+0.13$ also supports this.

Experimental

Products. The thermal reaction was carried out by the following procedure. Thiocarbonylimine (339 mg, 1.0 mmol) was heated in various solvents or in neat until thiocarbonyl imine disappeared. The solvent was then evaporated *in vacuo* and the residual crystals were dissolved in a small amount of $CHCl_3$. The residue was chromatographed on silica gel using benzenel. The rearranged product obtained was purified by recrystallization from benzene. The yields of products are given in Table 1.

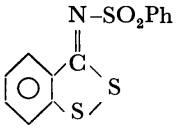

Mp 176—177 °C, elemental analysis: Found: C, 50.65; H, 2.73; N, 4.55%. Calcd for $C_{13}H_9O_2NS_3$: C, 50.88; H, 2.93; N, 4.56%.

Kinetics. Thiocarbonyl imine (1.5 mg) was dissolved in 50 ml solvent. The solution was kept at 60.1 °C in a thermostat. Every ten minutes 3 ml of the solution was pipetted out and poured into the UV cell which was cooled previously in order to stop the reaction. The reaction rate was obtained by determining the intensity of UV spectra due to thiocarbonyl imine (493 mn in CH_3CN). The results are collected in Table 2.

Table 2. Kinetic data for thermal rearrangement of thiocarbonyl imine (B) at 60.1 °C

Solvent	λ_{max} (nm)[a]	$10^4 k$, sec^{-1}
THF	506	3.28
DCE	500	1.52
Pyridine	499	2.05
$CHCl_3$	496	1.80
CH_3CN	493	1.08
CH_3NO_2	492	1.38
DMSO	488	0.78
n-BuOH	483	1.80
t-BuOH	480	1.29
EtOH	476	3.27
MeOH	472	3.90

a) The absorption band of thiocarbonyl imine in various solvents. DCE: dichloroethane.

Table 3. Effect of temperature and substituent at 60.1 °C

Solvent	E_a, kcal/mol	$\Delta S^{\neq}$, e.u.	Rho value
CH_3CN	23.8	3.8	-0.56
THF	20.2	-5.8	
MeOH	11.2	-46.1	$+0.13$

5) E. M. Kosower, *J. Amer. Chem. Soc.*, **80**, 3253, 3267 (1958).

BULLETIN OF THE CHEMICAL SOCIETY OF JAPAN, VOL. 46, 2610 (1973)

The Oxidation of α- and β-Methylstyrenes by Manganese(III) Acetate

Akira KASAHARA, Ryu-ichi SAITO, and Taeko IZUMI

Department of Applied Chemistry, Faculty of Engineering, Yamagata University, Yonezawa, Yamagata 992

(Received January 26, 1973)

Earlier studies established that, in acetic acid at 135 °C, α-methylstyrene (I) and β-methylstyrene (II) reacted with manganese(III) acetate to give lactone (III and IV),[1] which could also be obtained with the same reactions in refluxing acetic acid–acetic anhydride.[2] Heiba *et al*[1] suggested that the $\cdot CH_2COOH$ radical is produced directly by the thermolysis of the complex and that the great selectivity of $\cdot CH_2COOH$ radical toward addition to the olefin over allylic hydrogen abstraction leads to high yields of lactones. On the other hand, Gilmore and Mellor[3] reported that, in the presence of potassium bromide, cyclohexene reacts with manganese(III) acetate at 70 °C in acetic acid, thus leading to the formation of cyclohexenyl acetate as the major product. The finding that the potassium bromide-catalyzed oxidation of cyclohexene proceeded *via* allylic hydrogen atom abstraction led us to examine the reactions of I and II under similar conditions.

At 80 °C in acetic acid, I reacted slowly with manganese(III) acetate, but the addition of potassium bromide led a rapid reaction and to the formation of β-phenylallyl acetate (V) as the major product (70%); no evidence for any lactone formation was obtained. Using this same set of conditions, from II cinnamyl acetate (VI) (62%) and α-phenylallyl acetate (VII) (10%) were obtained. These results indicate that potassium bromid-catalyzed oxidation of allylic olefin by manganese(III) acetate proceeds *via* allylic hydrogen abstraction rather than *via* $\cdot CH_2COOH$ radical addition to the olefin.

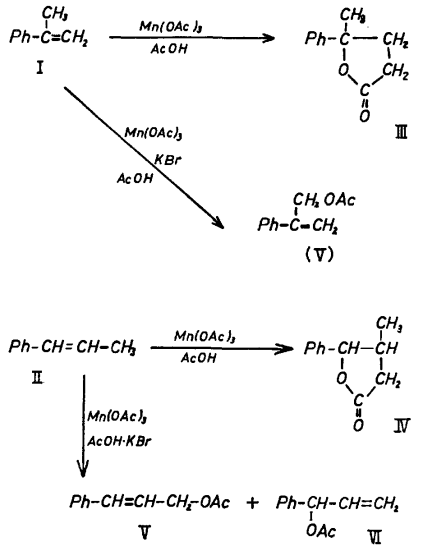

Fig. 1.

Experimental

Manganese(III) acetate was prepared by a modification of Christiansen's procedure.[3,4] β-Phenylallyl acetate (V) was prepared from α-methylstyrene by selenium dioxide oxidation;[5] bp 115—117 °C/7 mmHg (lit.[5] 112—113 °C/5 mmHg). Cinnamyl acetate (VI) was synthesized by esterifying cinnamyl alcohol with acetic anhydride (bp 124 °C/5 mmHg (lit.[6] bp 113 °C/2.4 mmHg)), while α-phenylallyl acetate (VII) was prepared by the esterification of the alcohol (from acrolein and phenylmagnesium bromide) with acetic anhydride (bp 106 °C/6 mmHg (lit.[6] bp 92 °C/2 mmHg)). Gas-chromatographic analyses were carried out on a column, silicon SE 30 (5% on celite), 1 m at 100 °C, with a Hitachi K-53 gas-chromatograph.

Oxidation of α-Methylstyrene (I). Manganese(III) acetate (5.0 g) in acetic acid (60 ml) was heated at 80 °C under nitrogen. To the stirred solution we then added I (1.2 g) and potassium bromide (0.25 g), and the solution was maintained at 80 °C until the color disappeared (*ca.* 6 hr). The reaction mixture was added to 500 ml of ether, which was then extracted four times with ice water. The ether layer was dried over anhydrous magnesium sulfate, filtered, and stripped on a rotary evaporator. The residual oil was distilled under reduced pressure, and the distillate was purified by gas-chromatography and identified as V (70% yields) by comparing the retention time on the gas-chromatogram and the infrared and NMR spectra with those of an authentic sample.

Oxidation of β-Methylstyrene (II). The oxidation of II was carried out in the manner described for I. On work-up, the reaction products contained VI (62% yields) and VII (10% yields), the infrared and NMR spectra and the retention time of which were identical with those of an authentic sample.

1) E. I. Heiba, R. M. Dessau, and W. J. Koehl, Jr., *J. Amer. Chem. Soc.*, **90**, 5905 (1968).
2) J. B. Bush, Jr., and H. Finkbeiner, *ibid.*, **90**, 5904 (1968).
3) J. R. Gilmore and J. M. Mellor, *J. Chem. Soc.*, **1971**, 2355.
4) O. T. Chistiansen, *Z. Anorg. Chem.*, **27**, 325 (1901).
5) L. F. Hatch and T. L. Patton, *J. Amer. Chem. Soc.*, **76**, 2705 (1954).
6) Z. Rappoport, S. Winstein, and W. G. Young, *ibid.*, **94**, 2320 (1972).

BULLETIN OF THE CHEMICAL SOCIETY OF JAPAN, VOL. 46, 2611—2612 (1973)

The Synthesis of the Salts of L-Aspartic Anhydride with Alkylsulfuric Acid and Their Use in the Preparation of Aspartylphenylalanine Methyl Ester

Yasuo ARIYOSHI, Tetsuo YAMATANI, and Yohko ADACHI

Central Research Laboratories, Ajinomoto Co., Inc., Suzuki-cho, Kawasaki-ku, Kawasaki 210

(Received January 25, 1973)

In our previous paper,[1] α-L-aspartyl-L-phenylalanine methyl ester (α-APM), which has a sweet taste,[2] has been conveniently prepared by the condensation of L-aspartic anhydride hydrochloride with methyl L-phenylalaninate, followed by the separation of α-APM from a mixture of α- and β-APM. In the present paper, we will describe the synthesis of the salts of L-aspartic anhydride with alkylsulfuric acid and their use in the preparation of α-APM.

By bringing L-aspartic acid into contact with an excess molar amount of concentrated sulfuric acid in ethyl acetate, we obtained L-aspartic acid sulfate, which, on dehydration with two molecular equivalents of acetic anhydride in ethyl acetate, gave the corresponding anhydride (I). Although the anhydride (I) could not be isolated, its structure was assumed to be the salt of L-aspartic anhydride with mixed acetic-sulfuric anhydride (I). The treatment of the anhydride (I) with an equimolar amount of an alcohol, such as methanol, 2-propanol, or cyclohexanol, gave the salts of L-aspartic anhydride with alkylsulfuric acid (II) (Table 1). The reaction of the anhydride (I) with an alcohol took place exclusively at the sulfuric acid moiety of I. The results of the elemental analyses of the reaction products agreed with the values calculated for the anhydrides (II) (Table 1). All of the salts of L-aspartic anhydride with alkylsulfuric acid were practically stable and were used successfully in the preparation of α-APM. In order to increase the formation of the desired α-isomer, the reaction conditions, such as the temperature, the solvent effects, and the molar ratios of both reactants, were investigated. It was found that the reaction could be effected by adding carbon dioxide, by employing an excess of methyl L-phenylalaninate, and by conducting it at a low temperature.

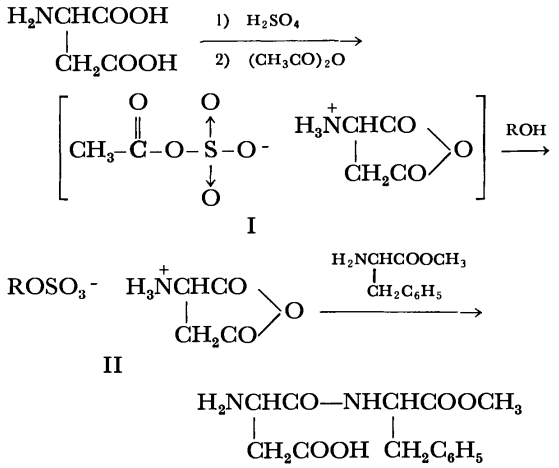

The treatment of L-aspartic anhydride isopropylsulfate with 4 molecular equivalents of methyl L-phenylalaninate in the presence of carbon dioxide in ethylene dichloride at −20 °C gave a mixture of α- and β-APM, from which α-APM was isolated in a 45% yield by separation through its hydrochloride salt, followed by neutralization and subsequent column chromatography.

Experimental

All the melting points are uncorrected. The determination of α- and β-APM by paper electrophoresis was carried out according to the method described in a previous paper.[3] The IR spectra were recorded in Nujol mull with a Jasco IR-S spectrometer. The NMR spectra were obtained with a Varian T-60 spectrometer at 60 MHz; the chemical shifts are given from sodium 2,2-dimethyl-2-silapentane-5-sulfonate, used as the internal reference.

L-Aspartic Acid Sulfate. A mixture of L-aspartic acid (60 g), concentrated sulfuric acid (52.5 ml), and ethyl acetate (200 ml) was stirred for 48 hr at room temperature. The crystals were then collected by filtration and dried *in vacuo* over phosphorus pentoxide; yield, 99 g (95%), mp 151—152 °C. Found: C, 20.59; H, 3.87; N, 6.00; S, 13.71%. Calcd for $C_4H_7O_4N \cdot H_2SO_4$: C, 20.78; H, 3.80; N, 6.06; S, 13.85%.

The Salts of L-Aspartic Anhydride with Alkylsulfuric Acid. In a typical procedure (No 1 in Table 1), a mixture of L-aspartic acid sulfate (11.55 g), ethyl acetate (10 ml), acetic

TABLE 1. THE SALTS OF L-ASPARTIC ANHYDRIDE WITH ALKYLSULFURIC ACID(II)

No.	R	Yield (%)	Mp °C	Found (%)				Calcd (%)				IR cm^{-1}	
				C	H	N	S	C	H	N	S		
1	CH_3–	93	105—109[a]	26.13	4.24	6.13	13.91	26.43	3.96	6.17	14.10	1820	1890
2	$(CH_3)_2CH$–	82	98—101.5	32.64	5.32	5.23	12.42	32.94	5.10	5.49	12.55	1800	1885
3	C_6H_{11}–	90	95—100[b]	40.52	5.94	4.80	10.84	40.68	5.76	4.75	10.85	1810	1890

a) Partly melted at 96°C. b) Partly melted at 67°C.

1) Y. Ariyoshi, T. Yamatani, N. Uchiyama, Y. Adachi, and N. Sato, This Bulletin, **46**, 1893 (1973).

2) R. H. Mazur, J. M. Schlatter, and A. H. Goldkamp, *J. Amer. Chem. Soc.*, **91**, 2684 (1969).

3) Y. Ariyoshi and N. Sato, This Bulletin, **45**, 942 (1972).

anhydride (12.8 g), and concentrated sulfuric acid (0.5 g) was stirred for 4 hr at room temperature. Anhydrous methanol (24 ml) was then added to the solution with stirring and cooling in an ice-bath. After stirring for 30 min in an ice-bath, the crystals thus formed were collected by filtration, washed with anhydrous ethyl acetate, and dried *in vacuo* over phosphorus pentoxide and sodium hydroxide pellets; yield, 10.5 g (93%); $[\alpha]_D^{26}$ +15.3° (*c* 2, 6 M HCl); NMR (D_2O, DSS): δ 3.22(d, 2H, J=5.5 Hz), 3.80(s, 3H), 4.50 (t, 1H, J=5.5 Hz).

The data are given in Table 1.

Synthesis of α-APM. Carbon dioxide (8.8 g) was introduced into a solution of methyl L-phenylalaninate (71.6 g) in ethylene dichloride (750 ml) containing 8 ml of methanol at −10 °C. To the stirred solution, L-aspartic anhydride isopropylsulfate (22.7 g) was added, portion by portion, at −20 °C. After stirring for 30 min at this temperature, hot water (300 ml, 70—80 °C) and sodium carbonate (6.3 g) were successively added to the solution. After the removal of the excess of methyl L-phenylalaninate by two extractions with 150-ml portions of ethylene dichloride, the aqueous layer was acidified to pH 3 with dilute hydrochloric acid. The solution was found to contain 20.3 g (61%) of α-APM and 5.8 g (19%) of β-APM by paper electrophoresis. The solution was concentrated *in vacuo* to 135 ml and kept in a refrigerator overnight to give crystals (α-APM·HCl, 20 g, 55%), which were then dissolved in water (150 ml). The solution was adjusted to pH 4.8 with a 5% aqueous sodium carbonate solution while being stirred at 50 °C, and then it was kept in a refrigerator overnight to give crystals (α-APM, 14 g, 46%). The crystals were dissolved in water (500 ml) and passed through a column (1×20 cm) of Dowex 1×4 (acetate form) while being maintained at 45 °C, and then the column was washed with water (20 ml). The eluate and washings were concentrated *in vacuo* to give α-APM, which was recrystallized from water; yield, 12.6 g (42%); mp 235—236 °C (decomp.); $[\alpha]_D^{26}$ +31.5° (*c* 1, acetic acid). lit,[1] mp 235—236 °C; $[\alpha]_D$ +32° (*c*, 1, acetic acid); lit,[2] mp 190 °C and 246—247 °C. lit,[4] mp 245—247 °C. Found: C, 55.46; H, 6.24; N, 8.96%. Calcd for $C_{14}H_{18}O_5N_2 \cdot 1/2H_2O$: C, 55.44; H, 6.31; N, 9.24%.

4) J. M. Davey, A. H. Laird, and J. S. Morley, *J. Chem. Soc.*, *C*, **1966**, 555.

The Photoconductivity of Poly(*N*-vinylcarbazole). V.[1] The Doping Effects of Various Materials on the Photoconductivity[2]

Kenichi OKAMOTO,* Shigekazu KUSABAYASHI,* and Hiroshi MIKAWA

Department of Applied Chemistry, Faculty of Engineering, Osaka University, Yamadakami, Suita, Osaka 565

(Received June 21, 1972)

The photoconductivity and fluorescence spectra of poly(*N*-vinylcarbazole) (PVCz) films doped with various materials were investigated. The photoconductive properties of doped films may be grouped into three classes according to the kind of dopant. The doping of an electron donor, such as tetramethyl-*p*-phenylenediamine and 1,5-diaminonaphthalene, reduced the photocurrent in all the wavelength regions by a factor of 10^2 to 10^4 because of the hole-trapping effect of the dopant molecule. The exciplex formed between the donor and PVCz does not seem to contribute to the photocurrent. The doping of an acceptor, such as TCNE and dimethyl terephthalate, on the other hand, enhanced the photocurrent. The field-assisted thermal dissociation of an excited CT complex formed between PVCz and an acceptor seems to be a carrier generation process. The doping of anthracene or perylene quenched the fluorescence of PVCz by a factor of 10 to 30 and reduced the photocurrent in the UV region by a factor of 2 to 7, while it enhanced the photocurrent in the absorption region of the dopant.

In their previous papers[1,3] the present authors have examined the photoconductivity of PVCz and explained it by assuming that the carriers were generated through the field-assisted thermal dissociation of an exciplex formed with a fairly good efficiency between PVCz and some impurity with an electron-accepting ability, and also through the detrapping of trapped carriers by singlet excitons, and that the carriers migrated through the overlap of the π-electrons of the neighboring carbazyl rings in the same polymer chain.

In the present paper the doping effects of various materials on the photoconductivity and the fluorescence spectra of PVCz were examined.

Experimental

Materials. *PVCz*: The preparation of PVCz was described in a previous paper.[3]

Carbazole: A commercial product was subjected to a Diels-Alder reaction with maleic anhydride in order to remove a trace of anthracene[4], and was then purified by repeated recrystallizations from *o*-dichlorobenzene and subsequently from acetone.

Anthracene: A commercial product of a scintillation grade was recrystallized three times from benzene.

Perylene, Tetracyanoethylene (TCNE) and Dimethyl terephthalate (DMTP): Commercial products were recrystallized two or three times from benzene and subsequently sublimed *in vacuo*.

*Tetramethyl-*p*-phenylenediamine (TMPD) and 1,5-Diaminonaphthalene (DAN)*: A commercial product of the HCl salt was reprecipitated twice from an aqueous solution of ammonia and then recrystallized three times from *n*-hexane or benzene under a nitrogen stream.

p-*Nitroaniline (PNA)*: A commercial product was recrystallized three times from methanol. The solvents were purified by the ordinary method.

Measurements. Doped films were prepared by casting a 5 wt% benzene solution of PVCz with a certain amount of a dopant onto a quartz plate in a manner similar to that described previously.[3] The films of the following doping amounts were used in the measurements: carbazole 2.0 mol% (per carbazole unit in PVCz), anthracene 3.0 mol%, perylene 1.4 mol%, TMPD 1.8 mol%, DAN 2.7 mol%, TCNE 1.8 mol%, DMTP 1.8 mol%, and PNA 1.9 mol%. The thickness of the films was about 15 μ for the electrical measurements and about 1—2 μ for the fluorescence measurements. The preparation of a sandwich-type cell of a film (area of electrode, 1 cm^2) and the electrical measurement were carried out in a manner similar to that described previously.[3] The ESR spectrum of PVCz powder doped with TCNE (8 mol%) was also measured under illumination with UV or visible light from a 500 W superhigh pressure Hg lamp as well as in the dark.

Results

Dark Conductivity. Carbazole, anthracene, perylene, DMTP, TMPD, and PNA did not have any significant effect on the conductive properties (the magnitude of the dark current, the voltage dependence, and the activation energy) of a PVCz film in the dark.[5]

On the other hand, the doping of DAN or TCNE changed the conductive properties. The dark current for a film doped with DAN was much smaller than that of an undoped film by a factor of ten to a hundred. It was ohmic over the applied fields (0—100000 V/cm). Its activation energy (ΔE_d in the $i_d \propto \exp(-\Delta E_d/kT)$ equation) was 0.9 eV below 100 °C and 1.5 eV above 100 °C, as is shown in Table 1. The former value is similar to that of an undoped film, while the latter is considerably larger. The doping of TCNE enhanced the dark current by a factor of several hundreds to a thousand and lowered the value of ΔE_d (0.8 eV) a little.

Shape of the Photoresponse. The doping of carbazole, anthracene, perylene, or PNA did not have any effect on the photoresponse behavior. The films doped with these materials showed photoresponse curves

* Present address: Department of Chemical Engineering, Faculty of Engineering, Yamaguchi University, Ube, Yamaguchi.

1) Part IV of this series, K. Okamoto, K. Kato, K. Murao, S. Kusabayashi, and H. Mikawa, This Bulletin, **46**, 2883 (1973).

2) A part of the experimental results in this paper was presented at the 26th Symposium of the Society of Electrophotography of Japan, Osaka, November, 1970.

3) K. Okamoto, S. Kusabayashi, and H. Mikawa, Part III of this series, This Bulletin, **46**, 2324 (1973).

4) K. Kihara, T. Ishii, Y. Suzuki, and T. Takeuchi, *Kogyo Kagaku Zasshi*, **73**, 2632 (1970).

5) K. Okamoto, S. Kusabayashi, and H. Mikawa, Part II of this series, This Bulletin, **46**, 1953 (1973).

Table 1. Activation energies of photo and dark conductivities

Doping material	ΔE_d (eV)	ΔE_{ph} (eV)	Wavelength of illuminating light (mμ)
Carbazole	1.1	0.17	350
Anthracene	1.1	0.14	360
		0.13	380
Perylene	1.0	0.12	350
		0.15	440
TMPD	0.93—1.2	0.24 (below 80 °C)	360
		0.50 (80—140°C)	360
DAN	0.9 (below 100 °C)	0.25 (below 100 °C)	350
	1.3—1.6 (100—140 °C)	0.44 (100—140 °C)	350
TCNE	0.82	0.22	350
		0.24	550
DMTP	1.0—1.1	0.19 (below 90 °C)	350
		0.33 (90—160°C)	350
PNA	—	0.23	360
		0.25	430
Undoped	1.0—1.3	0.13—0.22	UV
		0.07—0.16	Visible

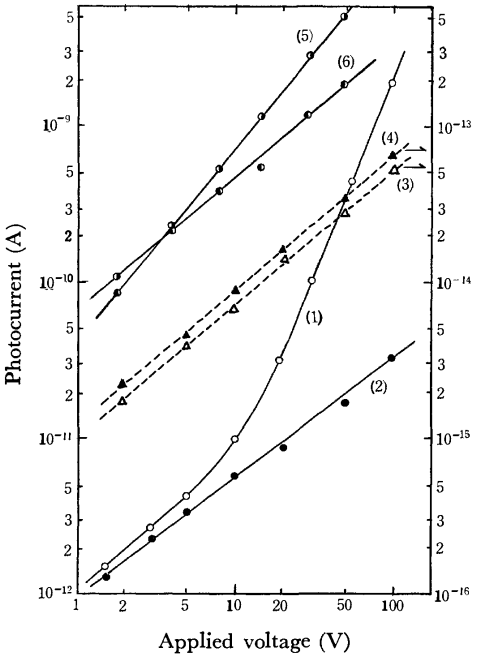

Fig. 1. Voltage dependence of photocurrent in doped films at 20 °C in high vacuum.
(1) perylene, i^+_{ph}, 350 mμ; (2) perylene, i^-_{ph}, 350 mμ; (3)DAN, i^+_{ph}, 360 mμ; (4) DAN, i^-_{ph}, 360 mμ; (5) TCNE, i^+_{ph}, 350 mμ, and (6) TCNE, i^+_{ph}, 550 mμ.

similar to those observed in an undoped film.

The doping of DMTP did not have any effect in the photoresponse behavior when a negative electrode was illuminated (this photocurrent is abbreviated to i^-_{ph}) or when a positive electrode was illuminated by the light of longer wavelength than 360 mμ, but it caused a considerable space charge effect on the photocurrent when a positive electrode was illuminated by UV light (this photocurrent is abbreviated to i^+_{ph}). i^+_{ph} in the region shorter than 360 mμ reached a peak value soon after light-on and decreased slowly with time until it leveled off to a steady-state value after 10—40 min. The steady-state value was much smaller than the peak value, especially when the light of the wavelength corresponding to the absorption peak was used. This difference between the peak and the steady values was quite large as compared with the case of an undoped film.

In a film doped with TCNE or DAN, the normal photoresponse curve (A type in the previous paper[3]) was observed at every wavelength irrespective of the polarity of the illuminated electrode.

Light-intensity Dependence of the Photocurrent. In every doped film except TCNE, the photocurrent was found to be proportional to the light intensity, irrespective of both the polarity of an illuminated electrode and the wavelength of light. This is the same as the case of a PVCz film. In a film doped with TCNE, the photocurrent was found to be proportional to the 0.8-th power of the light intensity.

Voltage Dependence of the Photocurrent. In films with dopants other than TMPD and DAN, the photocurrent showed a voltage dependence similar to that observed in an undoped film, as is shown in Fig. 1. In applied fields higher than 15000 V/cm, i^+_{ph} was proportional to the n-th power of the applied voltage (n=1.4—2.0) in the UV region shorter than 360 mμ, although it was proportional to the applied voltage in the visible region. The i^+_{ph} in applied fields lower than 15000 V/cm and the i^-_{ph} were proportional to the applied voltage, irrespective of the wavelength of light. In these films i^+_{ph} was larger than i^-_{ph} in high fields, although they were roughly equal to each other in low applied fields. This behavior is similar to the case of an undoped film.

On the other hand, in a film doped with TMPD or DAN both i^+_{ph} and i^-_{ph} were proportional to the applied voltage over the whole voltage region, and the super-linear dependence of i^+_{ph} in the high-field region was not observed. There was no significant difference in magnitude between i^+_{ph} and i^-_{ph} in these films, as is shown in Fig. 2(b). It should be noted that these dopants are fairly strong electron donors.

Spectral Dependence of the Photocurrent. The spectral dependence of the photocurrent in the doped films shown in Figs. 2(a—d) was obtained by normalizing the observed photocurrent values to the values for the light intensity of 2×10^{13} photons/cm^2 s according to the light-intensity dependence. The photocurrent values in Fig. 2 were obtained from the cells which showed the representative values of photocurrent among several cells. The magnitudes of the photocurrents in Figs. 2 can be compared directly with each other. The dopants are grouped according to both their spectral dependence and the magnitudes of the photocurrents. Figures 2(a—d) also show the absorption spectra of the undoped and doped films used in the photoconductivity measurements. No new absorption

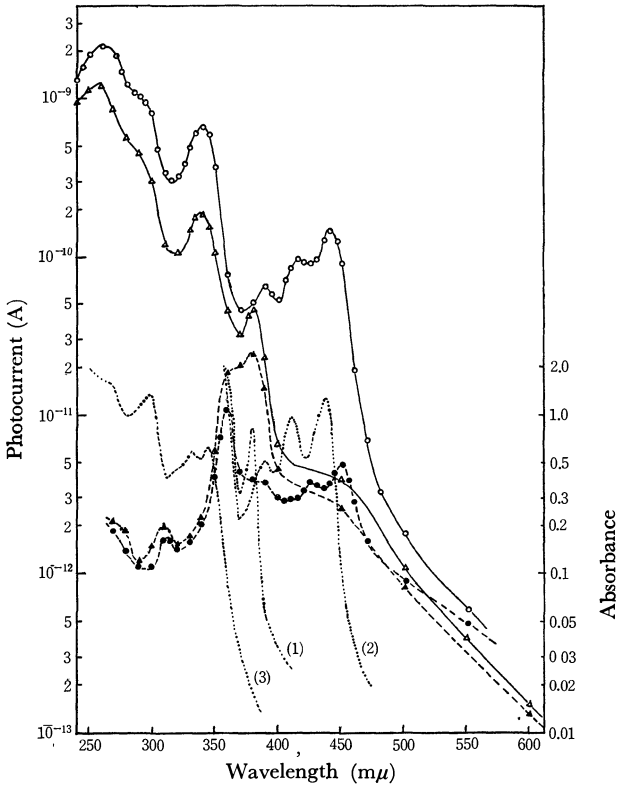

Fig. 2(a). Spectral dependence of photocurrent in a sandwich-type cell of a PVCz film doped with anthracene or perylene under 35000 V/cm in high vacuum at 20° C.
Film doped with anthracene; —△— for i^+_{ph}, and ---▲--- for i^-_{ph}.
Film doped with perylene; —○— for i^+_{ph}, and ---●--- for i^-_{ph}.
The absorption spectra of the PVCz films are given by the dotted lines. (1) doped with anthracene, (2) doped with perylene, and (3) an undoped film 1 μ thick (This spectrum is given in order to show the π—π^* bands of PVCz).

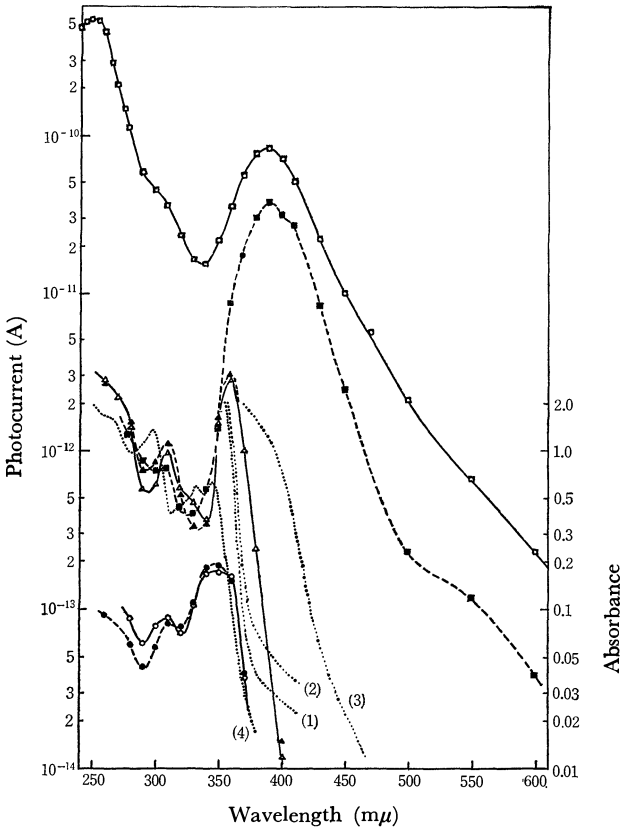

Fig. 2(b). Spectral dependence of photocurrent in a sandwich-type cell of a PVCz film doped with TMPD, DAN, or PNA under 35000 V/cm in high vacuum at 20 °C.
Film doped with TMPD; —△— for i^+_{ph}, and ---▲--- for i^-_{ph}.
Film doped with DAN; —○— for i^+_{ph}, and ---●--- for i^-_{ph}.
Film doped with PNA; —□— for i^+_{ph}, and ---■--- for i^-_{ph}.
The absorption spectra of the PVCz films are given by the dotted lines. (1) doped with TMPD, (2) doped with DAN, (3) doped with PNA, and (4) an undoped film 1 μ thick.

band was observed in the doped films except in the case of TCNE. The film doped with TCNE shows the charge-transfer (CT) absorption bands, as is well known.[6]

Group A. Carbazole, anthracene, and perylene belong to this group. The spectral dependence of the photocurrent is almost the same as that observed in an undoped film, as is shown in Figs. 2(a) and (c). The spectral dependence of i^+_{ph} corresponds to the absorption spectrum, while that of i^-_{ph} corresponds inversely to it. In the film doped with anthracene or perylene, new photocurrent peaks are observed in the absorption region of the dopant. This sensitized photocurrent in the film doped with perylene showed a spectral dependence similar to that in the π-π^* absorption bands of PVCz. The doping of carbazole hardly changed the magnitude of the photocurrent at all in any of the wavelength regions. The doping of anthracene or perylene reduced the photocurrent in the absorption region of PVCz by a factor of 2 to 7, while it enhanced the photocurrent in the lowest absorption band of the dopant by factors of 10 for i^+_{ph} and 2—3 for i^-_{ph}.

Group B. TMPD, DAN, and PNA belong to this group. As is shown in Fig. 2(b), both i^+_{ph} and i^-_{ph} showed the same spectral dependence, one which corresponded rather inversely to the absorption spectrum, and both were significantly reduced in magnitude by doping.

In a film doped with TMPD or DAN, both i^+_{ph} and i^-_{ph} significantly decreased in all the wavelengthr egions. The decrease in the photocurrent was 1/1000—1/10000 for i^+_{ph} or 1/30—1/300 for i^-_{ph} in the case of DAN, while it was 1/100—1/10000 or 1/5—1/20 in the case of TMPD, respectively. Thus, i^+_{ph} decreased much more than i^-_{ph}; hence, i^+_{ph} was almost equal to i^-_{ph} in magnitude in all the wavelength regions. It is very interesting that the photocurrent decreased by a factor of 10^2—10^4 by the doping of small amount (1—3 mol%) of TMPD or DAN.

In a film doped with PNA, the photocurrent in the absorption region of PVCz decreased by a factor of 10—100 for i^+_{ph} and by one of 5—10 for i^-_{ph}. The value of i^+_{ph} was, however, still larger than i^-_{ph}, although the i^+_{ph}/i^-_{ph} ratio in the UV region (4—30 in this case) was considerably smaller than the corresponding ratio of an undoped film (50—500). In a film doped with

6) H. Meier, W. Albrecht, and U. Tschirwitz, *Ber. Bunsenges. Physik. Chem.*, **73**, 795 (1969).
7) J. Tanaka, This Bulletin, **36**, 833 (1963).

PNA, the incident light of wavelength shorter than 385 mμ was absorbed almost completely. Consequently, a photocurrent peak was not observed at 360 mμ, but at 390 mμ. In the wavelength region from 380 mμ to about 500 mμ, the photocurrent was a little larger than that of an undoped film.

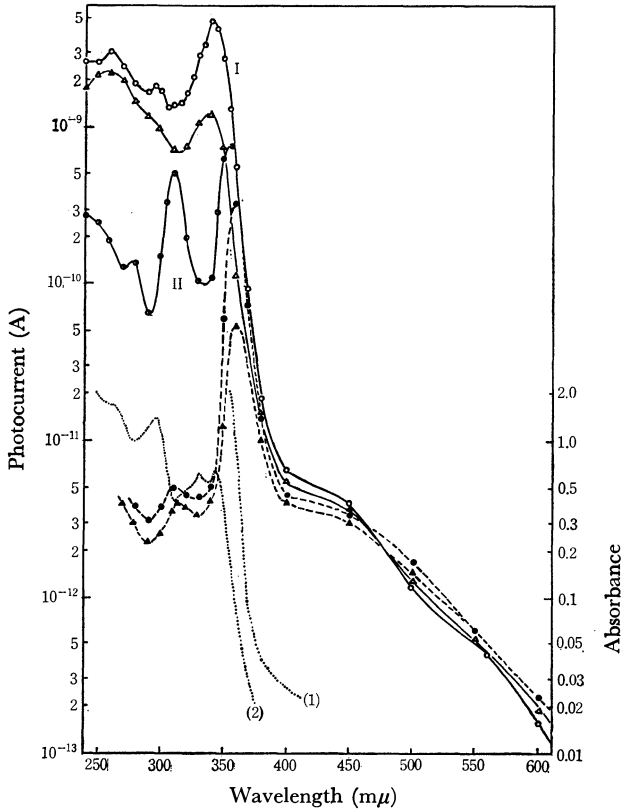

Fig. 2(c). Spectral dependence of photocurrent in a sandwich-type cell of both a PVCz film and a PVCz film doped with DMTP under 35000 V/cm in high vacuum at 20 °C.
PVCz; —△— for i_{ph}^{+}, and ---▲--- for i_{ph}^{-}.
Film doped with DMTP; the curves I and II for i_{ph}^{+} (see the text) and ---●---for i_{ph}^{-}.
The absorption spectra of the PVCz films are given by the dotted lines. (1) doped with DMTP and (2) an undoped film 1 μ thick.

Group C. DMTP belongs to this group. In a film doped with DMTP the spectral dependence of i_{ph}^{-} was almost the same as that observed in an undoped film. The spectral dependence of i_{ph}^{+}, however, changed with the measurement conditions, as is shown in Fig. 2(c), because of a considerable space charge effect. In Fig. 2(c) Curve I shows the spectral dependence of i_{ph}^{+} measured under conditions which make the space-charge effect as small as possible. In order to release space charges formed by the previous UV illumination, the visible light of wavelengths longer than 400 mμ was used for a long time in each case before UV light was used for the measurement. Curve II shows the spectral dependence of i_{ph}^{+} measured after space charges were built up by the preillumination of the UV light of wavelengths shorter than 330 mμ. In Curve I the spectral dependence was similar to that of an undoped film, and the magnitude of i_{ph}^{+} in the UV region was considerably larger than the magnitude of i_{ph}^{+} in an undoped film; that is, the chemical sensitization of the photocurrent was observed. On the other hand, in Curve II the spectral dependence corresponded inversely to the absorption spectrum, and the magnitude of i_{ph}^{+} in the UV region, especially at the absorption peaks, was considerably smaller than that of an undoped film.

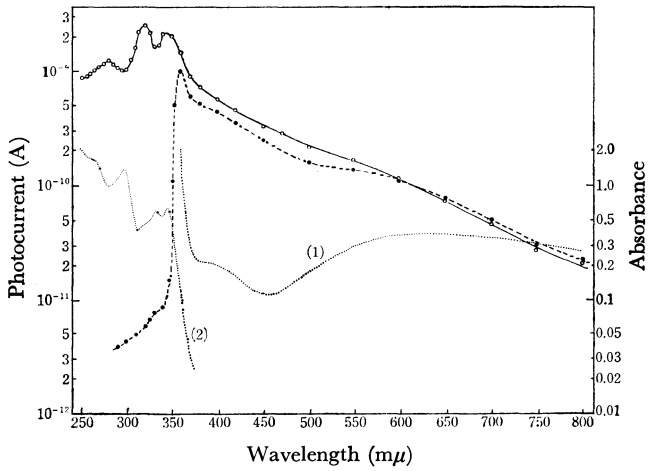

Fig. 2(d). Spectral dependence of photocurrent in a sandwich-type cell of a PVCz film doped with TCNE under 35000 V/cm in high vacuum at 20 °C.
—○— for i_{ph}^{+}, and ---●--- for i_{ph}^{-}.
The absorption spectra of the PVCz films are given by the dotted lines. (1) doped with TCNE and (2) an undoped film 1 μ thick.

Group D. TCNE belongs to this group. The peaks of i_{ph}^{+} were observed at 340 and 320 mμ, and the minima, at 330 and 295 mμ, as is shown in Fig. 2(d). The i_{ph}^{-} showed only a peak at 360 mμ and showed neither a clear peak nor a minimum in the wavelength region shorter than 350 mμ. The doping of TCNE enhanced both i_{ph}^{+} and i_{ph}^{-} a little in the UV region and significantly in the visible region. The degree of increase in the photocurrent in the UV region was 10—20 fold at 360 mμ, 3—4 fold at 350 mμ, and 2 fold at 330 mμ. Thus, the doping of TCNE caused not only the spectral sensitization, but also the chemical sensitization of the photocurrent.

Activation Energy of Photocurrent. The activation energies of the photocurrent (ΔE_{ph}) in doped films are listed in Table 1. In a film doped with carbazole, anthracene, or perylene, the value of ΔE_{ph} (0.15—0.20 eV) was almost the same as that observed in an undoped film. In a film doped with PNA, or TCNE, the value of ΔE_{ph} was 0.2—0.3 eV, a little larger than that of an undoped film. In a film doped with TMPD, DAN, or DMTP, the photocurrent showed clearly different temperature dependences in the high- and low-temperature ranges, as is shown in Fig. 3. In these films, ΔE_{ph} was 0.19—0.25 eV in the low-temperature range and 0.35—0.50 eV in the high-temperature range, the latter being fairly large. Although the values of ΔE_{ph} mentioned above were the values for the photocurrent in the absorption region of PVCz, similar values of ΔE_{ph} were also obtained for the spectrally-sensitized photocurrent.

Fluorescence Spectra of the Doped Films. Information

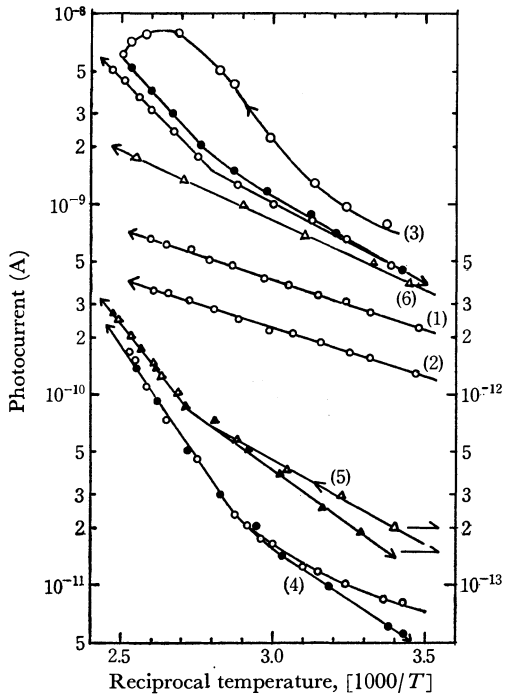

Fig. 3. Temperature dependence of photocurrent in a sandwich-type cell of the doped PVCz films under 35000 V/cm with positive electrode illumination in high vacuum. (1) perylene, 350 mμ, (2) perylene, 440 mμ, (3) DMTP, 360 mμ, (4) TMPD, 360 mμ, (5) DAN, 350 mμ, and (6) undoped, 350 mμ.

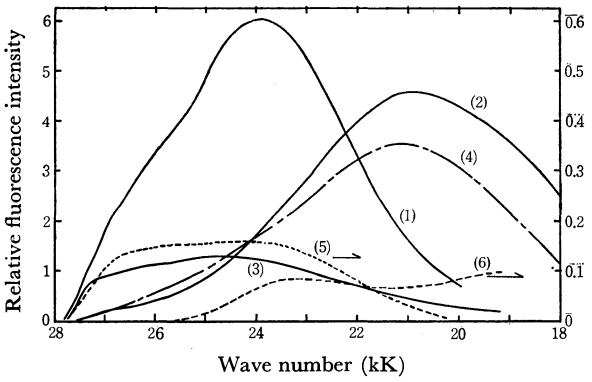

Fig. 4. Fluorescence spectra of the doped PVCz films. Excitation wavelength; 313 or 334 mμ, film thickness; 1 μ, atmosphere; air. (1) undoped, (2) doped with DMTP, (3) DAN, (4) TMPD, (5) TCNE, and (6) PNA.

concerning the electronic interaction between PVCz and a dopant molecule is necessary for understanding the photoconductive properties in doped films, so the fluorescence spectra of doped films excited by 313 or 334 mμ light were measured; they are shown in Fig. 4.

In a film doped with carbazole, the fluorescence spectrum was the same as that of an undoped film, no significant quenching of fluorescence being observed. When PVCz was doped with anthracene or perylene, energy transfer occurred from the excited singlet state of a carbazole chromophor of PVCz to the dopant molecule,[8] and the fluorescence of PVCz was significantly quenched and much fluorescence was emitted by the dopant. For instance, in films doped with 0.3 or 1.4 mol% of perylene the fluorescence of PVCz was quenched by a factor of 6 or 15 respectively.

The fluorescence of perylene in three films with the same doping amount was examined by directly exciting a perylene molecule with 405 mμ light. The films examined were a PVCz film, an *N*-vinylcarbazole (VCz)–vinyl acetate copolymer (VCz 81 mol%) film, and a polystyrene film. The relative intensities of the total fluorescence emission of perylene were as follows: a polystyrene film, 1.0; a VCz-vinyl acetate copolymer film, 0.92, and a PVCz film, 0.82. Thus, the intensity of the total fluorescence emission of perylene doped in a PVCz film is a little smaller than that in a polystyrene film. There may be some interaction between the excited molecule of perylene and a PVCz molecule.

In a film doped with TCNE or DAN, the fluorescence of PVCz was quenched by a factor of 30 in the case of TCNE or by one of 5 in the case of DAN, and no new emission band was observed. In a film doped with TMPD, DMTP, or PNA, the fluorescence of PVCz was quenched by a factor of from 10 to 100 and a new broad emission band was observed at about 21000 cm^{-1}. TMPD being a strong electron donor, the fluorescence of an exciplex between TMPD and perylene[9] or α-methylnaphthalene[10] has been observed in the same wavelength region. The new broad emission band may, therefore, be attributed to the fluorescence of the exciplex. The quenching of the fluorescence of PVCz in a film doped with DAN seems to be due to a similar process. A new broad emission band at about 21000 cm^{-1} in a film doped with DMTP may be attributed to the fluorescence of an exciplex. A similar emission band has been reported in the PVCz–DMTP system in solution.[11] In a film doped with PNA, the fluorescence of PVCz was quenched almost completely and a new weak emission band was observed in the visible region. As the ionization potential of gaseous PNA is 8.85 eV,[12] it is probable that PNA acts as a weak electron acceptor to PVCz. The new emission band may be due to the formation of an exciplex.

Discussion

It is useful to know the relative energy levels of the highest occupied and the lowest unoccupied π molecular orbitals of both the dopants and PVCz in understanding the photo and dark conductivities of the doped films. The dopants used in the present study are molecules with many π electrons, the gaseous ionization potentials of which have been measured by various methods.[12] These values of ionization potential were

8) K. Okamoto, A. Yano, S. Kusabayashi, and H. Mikawa, The 24th Annual Meeting of the Chemical Society of Japan, Osaka, April, 1970, Preprint 1-142; W. Klöpffer, *J. Chem. Phys.*, **50**, 2337 (1969).

9) H. Leonhardt and A. Weller, *Ber. Bunsenges. Physik. Chem.*, **67**, 791 (1963).

10) N. Yamamoto, Y. Nakato, and H. Tsubomura, This Bulletin, **40**, 451 (1967).

11) Y. Yamamoto, K. Tanaka, T. Omiti, M. Ooka, and T. Nishijima, The first Symposium on Charge Transfer Complex, Nagoya, June, 1969, Preprint p. 105.

12) F. Gutmann and L. E. Lyons, "Organic Semiconductors," John Wiely & Sons, Inc., New York (1967), p. 669.

used as a measure of the highest occupied π molecular orbital. The energy level of the lowest unoccupied π molecular orbital was estimated from the energy of the lowest absorption band, which may be attributed to the transition from the highest occupied to the lowest unoccupied π molecular orbitals except in the case of PNA. The lowest absorption band of PNA is due to the intramolecular CT band.[7] The energy levels of both dopants and PVCz thus obtained are shown in Fig. 5. From Fig. 5, the dopants used in this study may be grouped into three categories: donor, acceptor, and neutral. The photoconductive properties and fluorescence spectra of doped films may also be classified into these three groups.

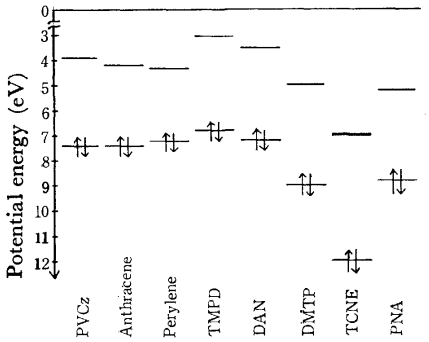

Fig. 5. Relative energy levels of the highest occupied and the lowest unoccupied π molecular orbitals of the dopant molecules and of PVCz.

Donors (TMPD and DAN). Films doped with these donors are characterized by the following three points; a significant decrease in the photocurrents ($i^+_{ph}=i^-_{ph}$) in all the wavelength regions, the disappearance of the superlinear dependence of i^+_{ph} on the applied voltage, and a large activation energy of the photocurrent in the high-temperature range.

As the formation of an exciplex $(PVCz^-\cdots D^+)^*$ is clear from the fluorescence spectra, the following Eqs., (1) and (2), are conceivable as carrier generation processes.

$$PVCz^* + D \longrightarrow (PVCz^-\cdots D^+)^* \longrightarrow PVCz^- + D^+ \quad (1)$$

$$D^+ + PVCz\ (\text{or } PVCz^*) \longrightarrow D + PVCz^+ \quad (2)$$

where D is a donor molecule; $(PVCz^-\cdots D^+)^*$, an exciplex; D^+, an immobile cation of a donor, and $PVCz^-$ and $PVCz^+$, ion radicals of PVCz (*i.e.*, mobile charge carriers). Equation (1) shows the ionization of an exciplex into a mobile carrier. Equation (2) shows the excitation of an electron from PVCz (or PVCz*) to an electron acceptor, D^+. A similar process has been presented in order to explain the photoconductive properties of a PVCz film,[3] although in that case PVCz acts as an electron donor. In the present case, excited PVCz molecules acting as electron acceptors, these processes do not seem to occur, judging from the significant decrease in the photocurrent in the doped films. This may be due to the ease of recombination between $PVCz^-$ and D^+ in Eq. (1), probably because of the small electron mobility in PVCz films. If so, the formation of an exciplex may have only the effect of decreasing the efficiency of the extrinsic carrier generation through the reduction of the life-time of the excited singlet state of PVCz.

Figure 5 suggests that the highest occupied π molecular orbital of a donor may act as a hole trap level and may reduce the effective hole mobility significantly. Both the increase in the ΔE_{ph} value and the disappearance of the superlinear dependence of i^+_{ph} on the applied voltage can be explained in terms of this hole trapping effect of a donor.

Acceptors (TCNE, DMTP, and PNA). In a film doped with TCNE, a sensitization of the photocurrent was observed in the absorption region of PVCz as well as in the CT absorption region. The apparent quantum yield of the photocurrent was determined as the ratio of the number of electrons flowing in the external circuit to the number of the photons absorbed by the film. It was in the order of 10^{-3}—10^{-2} at the CT bands and in that of $\sim 10^{-4}$ in the UV region. The former is much higher than the latter. The carrier generation *via* the excited CT state, such as that presented by the following equations, seems to contribute considerably to the photocurrent:

$$PVCz^* + TCNE \longrightarrow (PVCz^+\cdots TCNE^-)^*$$

$$(PVCz\cdots TCNE) \xrightarrow{h\nu_{CT}} \downarrow \quad (3)$$

$$PVCz^+ + TCNE^-$$

$$TCNE^- + PVCz^* \longrightarrow TCNE + PVCz^- \quad (4)$$

The film doped with TCNE showed an ESR signal even in the dark. This ESR signal was enhanced a little by illumination both with UV light and with visible light. The ESR signal must be due to the radical ion of TCNE or PVCz. This supports the carrier generation represented by Eqs. (3) and (4).

Although the doping of DMTP had no effect on the photocurrent in the visible region, a significant influence was observed on the photocurrent in the absorption region of PVCz. Both the peak photocurrent and the steady-state photocurrent in the UV region measured under the conditions which made the space charge effect as small as possible were fairly sensitized by doped DMTP; there was no influence on the other properties of the photocurrent, such as the large value of the i^+_{ph}/i^-_{ph} ratio, the spectral dependence, and the superlinearity of i^+_{ph} on the applied voltage. It is clear from the fluorescence spectrum that, in this film, the exciplex $(PVCz^+\cdots DMTP^-)^*$ is formed with a good efficiency by the UV light illumination in spite of the small concentration of DMTP. The exciplex thus formed seems to be responsible for the chemical sensitization of the photocurrent. The field-assisted thermal dissociation of the exciplex $(PVCz^+\cdots A^-)^*$ assumed in the previous paper as an extrinsic carrier generation mechanism in a PVCz film must be a primary carrier generation process under UV illumination in this doped film. This is represented by the following Eqs., (5) and (6):

$$PVCz^* + DMTP \longrightarrow (PVCz^+\cdots DMTP^-)^* \longrightarrow PVCz^+ + DMTP^- \quad (5)$$

$$PVCz^* + DMTP^- \longrightarrow PVCz^- + DMTP \quad (6)$$

In the PNA doped film the photocurrent (i^{+}_{ph}) decreased significantly in the UV region, although the exciplex seemed to be formed. Although the reason for this is not clear, it is conceivable that this can be attributed to the effect of the product of the hydrogen abstracting reaction of PNA[13] or to the presence of a small amount of an impurity such as *p*-diaminobenzene, a strong donor, in PNA.

Neutral Materials (Carbazole, Anthracene, and Perylene). Doping of carbazole had no effect on either the photocurrent or the fluorescence spectrum of PVCz.

In a film doped with anthracene or perylene (doping amount, 1—3 mol%), the fluorescence of PVCz was quenched by a factor of from 10 to 30, while the photocurrent in the absorption region of PVCz decreased by a factor of from 2 to 7. Judging from the quenching of the fluorescence of PVCz, the lifetime of the singlet exciton of PVCz and, consequently, the number of the carbazole rings covered with the singlet exciton during its lifetime may be estimated to decrease by a factor of from 10 to 30 as compared with the case of the undoped film. Therefore, in the doped film the efficiency of extrinsic carrier generation will decrease by the same factor. The decrease in the photocurrent in the absorption region of PVCz was, however, much smaller than the decrease presumed from the degree of the fluorescence quenching. This may be due to the contribution of carrier generation through the excited state of the dopant molecule.

In the doped film, the sensitized photocurrent was observed in the proper absorption region of anthracene or perylene. The apparent quantum yield of this photocurrent was from a tenth to a fifth of that of the photocurrent in the proper absorption region in a PVCz film (the quantum yield of PVCz in this region is, for instance, 1×10^{-4} for i^{+}_{ph} at 330 mμ under 35000 V/cm in the film of 15 μ thick). Some interaction between the dopant molecule in the excited state and PVCz in the ground state, which is probable from the fluorescence spectra mentioned above, may be responsible for the photocurrent sensitized spectrally with anthracene or perylene.

Doped anthracene or perylene may be expected from Fig. 5 to act as a hole trap center It has been reported that, in an anthracene single crystal doped with tetracene, the dopant molecule acts as a hole trap center.[14] Such a trapping effect by the dopant was not, however, observed in the film doped with anthracene or perylene.

The authors wish to thank the Fuji Photo Film Co. for its financial support of this work.

13) I. Ichikawa and K. Kimura, Symposium on Molecular Structure, Kyoto, 1971, Preprint p. 215.

14) K. Oyama and I. Nakada, *J. Phys. Soc. Japan*, **24**, 792 (1968); D. C. Hoestery and G. M. Letson, *J. Phys. Chem. Solids*, **24**, 1609 (1963).

BULLETIN OF THE CHEMICAL SOCIETY OF JAPAN, VOL. 46, 2619—2625 (1973)

Some Doping Effects on the Semiconducting Properties of Gd_2CuO_4

Tadao KENJO and Seishi YAJIMA

The Oarai Branch, The Research Institute for Iron, Steel and Other Metals, Tohoku University, Oarai, Ibaraki 311-13

(Received August 28, 1972)

Some doping effects on the semiconducting properties of the Gd_2CuO_4 compound were investigated. The ZrO_2 or ThO_2 (0.5 mol%) lowered the resistivity of the Gd_2CuO_4 at room temperature by a factor of 10^4. The thermoelectric powers of the same samples were negative. These were explained as being due to the Cu^+ ions formed by the dopants. The CaO dopant lowered the resistivity by a factor of ten and converted the sign of the thermoelectric power from negative to positive. The resistivity of the BaO-doped samples increased with an increase in the dopant concentration up to 0.5 mol%, and decreased with an increase in the dopant concentration in the concentration region lower than that. This suggested that the dopant of BaO was less effective on the resistivity-lowering than was the CaO. The samples doped with the ZrO_2 and CaO simultaneously gave a trend similar to those doped with the BaO in the concentration dependence of the resistivity. Silver oxide and indium oxide were also employed as dopants, but no doping effects were observed on either resistivity or the lattice parameters.

The Ln_2CuO_4 compounds (Ln=Gd, Sm, Nd, and Pr) are semiconductive, and their resistivities increase with an increase in the atomic number of Ln.[1] It has been suggested that the most important electron-carriers come from cuprous cations, Cu^+, probably formed by a thermal decomposition of cupric cations, Cu^{2+}.[1] The trend for the resistivities to increase with an increase in the atomic number of Ln was explained as being due to: (1) a variation in the number of the donor centers or (2) a variation in the activation energy.[1] However, it is not known which factor is more important.

As is well known, some dopants introduce donor

1) T. Kenjo and S. Yajima, This Bulletin, **46**, 1329 (1973).

centers.[2,3,5,6] If the dopants do not change the activation energy very greatly, any electrical effects due to the dopants can be ascribed to the first case. The X-ray diffraction data indicated that the lattice parameters for the Gd_2CuO_4 did not shift with doping, suggesting no variation in the activation energy. Therefore, the comparison of the doped to undoped Ln_2CuO_4 in the semiconducting properties may give an answer to the above problem.

Dopants usually lower the resistivity. Therefore, the most marked doping effect can be expected for the compound whose resistivity is the greatest. Since the Gd_2CuO_4 showed the greatest resistivity in the Ln_2CuO_4 series, it was chosen as the compound to be doped.

Donor centers are formed when the valence of the dopant is greater than that of the site.[2,3,5,6] Zirconium oxide, ZrO_2, and thorium oxide, ThO_2, were chosen as dopants which could be expected to occupy the Gd^{3+} sites, because they are chemically similar to the rare earth oxides.

Acceptor centers will be formed by dopants whose valences are smaller than those of the site. The most probable acceptor centers in this case are the Cu^{3+} or the Gd^{4+} cations. Since both of them are unstable and are not well known, it would be of interest to see if doped divalent cations lower the resistivity of the Gd_2CuO_4. Alkaline earth oxides are most suitable for the above purpose, because they are chemically similar to Gd_2O_3 and because they are expected to occupy the Gd^{3+} sites. Barium oxide, BaO, and calcium oxide, CaO, were employed as the dopants here.

Silver oxide, Ag_2O, and indium oxide, In_2O_3, were expected to occupy the Cu^{2+} sites and to form acceptor and donor centers respectively. They were also used as dopants.

Experimental

Reagents and Materials. An aqueous solution of $Gd(NO_3)_3$ was prepared by dissolving Gd_2O_3 (Nippon Yttrium Co., Ltd., 99.9%) in nitric acid (Wako Pure Chemical Co., Ltd., GR grade). The maximum contents of the impurities contained in the Gd_2O_3 used were Fe_2O_3, 10 ppm; CuO, 10 ppm; CaO, 30 ppm; ZrO_2, 10 ppm and ThO_2, 10 ppm.[7] An aqueous solution of $Cu(NO_3)_2$ was prepared by dissolving GR-grade $Cu(NO_3)_2 \cdot 3H_2O$. The maximum contents of the impurities contained in the $Cu(NO_3)_2$ used were; Fe, 30 ppm; Zn, 50 ppm; Ni, 40 ppm; Ba, 20 ppm; Ca, 4.5 ppm; Zr, 10 ppm, and Th, not detected.[8] The aqueous solutions of the nitrates of Zr, Ag, and Th were prepared by dissolving GR-grade $ZrO(NO_3)_2$, $AgNO_3$, and $Th(NO_3)_4$ respectively. The aqueous solutions of $Ca(NO_3)_2$, $Ba(NO_3)_2$, and $In(NO_3)_3$ were obtained by dissolving GR-grade $CaCO_3$, $BaCO_3$, and EP-grade In_2O_3 respectively in nitric acid. The concentration of the $AgNO_3$ solution was determined gravimetrically. The concentrations of the other solutions were determined chelatometrically against a standard EDTA solution.

Procedure. The samples were prepared by the same method as in a previous work.[1] Aliquot portions of $Gd(NO_3)_3$, $Cu(NO_3)_2$, and the nitrate of the dopants were mixed, and a sodium hydroxide solution (1M) was stirred in. After the mixture had stood overnight, filtering-washing was repeated until no sodium ion was detected in the filtrate by the flame test. The mixed hydroxides thus obtained were dried at 120 °C and preheated at 750 °C for 4 hr in air. The lumped oxide mixtures were milled, pressed into 15-mmϕ pellets, and heated at 1000 °C for 15 hr in air. The pellets thus obtained were removed from the furnace and cooled to room temperature. These samples thus obtained were cut into rods 12—13 mm long and 3—4 mm thick for the electrical measurements. The resistivity was measured by the 4-probe method using Du Pont No. 4622 Conductive Silver Coating Materials. The thermoelectric power was measured by means of the method of the previous work.[1] The bulk densities of the samples thus obtained were essentially the same as those of the undoped Gd_2CuO_4.

Results

The concentrations of the dopants are expressed as a mol% of the dopants against the total moles of the Gd_2CuO_4 and the dopants used. The signs for the values of the thermoelectric power are the same as in the previous work, being positive for a *p*-type and negative for an *n*-type.

Figures 1, 2, 3, and 4 show the data for the ZrO_2- or ThO_2-doped Gd_2CuO_4. As will be described in a later section, the mole ratio of raw oxide mixtures was: Gd_2O_3: CuO: $ZrO_2 = 1-x : 1 : x$. The sample containing 5 mol% ZrO_2 gave only the X-ray diffraction pattern of the Gd_2CuO_4 phase, while the ZrO_2 phase was found for the sample containing 10 mol% ZrO_2. This indicated that the solubility of ZrO_2 in Gd_2CuO_4 was between 5 and 10 mol%.

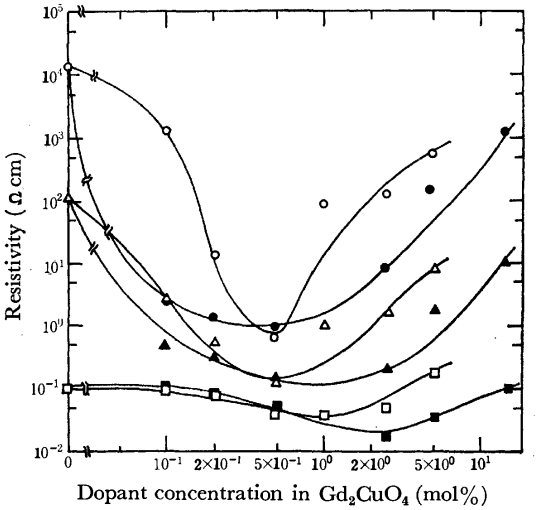

Fig. 1. Variation of resistivity with dopant concentration in Gd_2CuO_4.
○: room temperature for ZrO_2-doping, △: 200 °C for ZrO_2-doping, □: 800 °C for ZrO_2-doping, ●: room temperature for ThO_2-doping, ▲: 200 °C for ThO_2-doping, ■: 800 °C for ThO_2-doping.

2) G. H. Jonker, *Philips Research Reports*, **24**, 1 (1969).
3) T. Kawaguchi, "Handotai no Kagaku," Maruzen Co., (1971), p. 56.
4) R. W. G. Wyckoff, "Crystal Structures," Vol. 3, Interscience Publishers, New York, N.Y. (1965) p. 68.
5) Stephan P. Mittof, "Progress in Ceramic Science," Vol. 4, edited by J. E. Burke, Pergamon Press, p. 217.
6) O. Kubaschewski and B. E. Hopkins, "Oxidation of Metals and Alloys," Butterworths, London (1967), p. 15.
7) Private communication, Nippon Yttrium Co., Ltd.
8) Private communication, Kanto Chemical Co., Ltd.

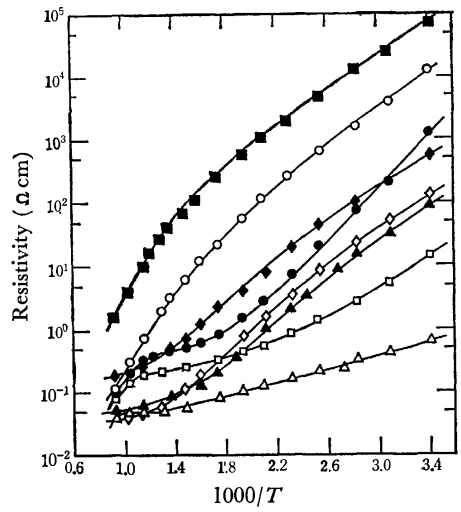

Fig. 2. Temperature dependence of resistivity for ZrO_2-doped Gd_2CuO_4.
○: undoped Gd_2CuO_4, ●: 0.1 mol%, □: 0.2 mol%, △: 0.5 mol%, ▲: 1 mol%, ◇: 2.5 mol%, ◆: 5.0 mol%, ■: less dense specimen of undoped Gd_2CuO_4

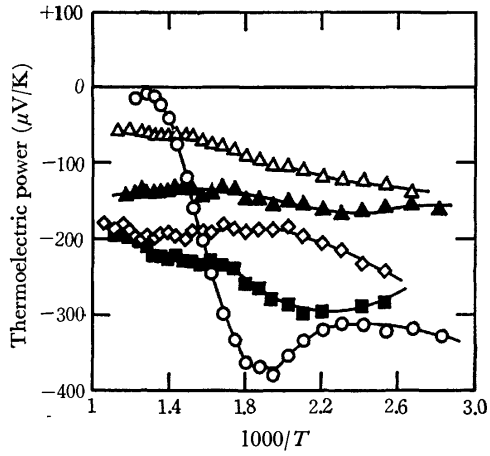

Fig. 3. Temperature dependence of thermoelectric power for ThO_2- or ZrO_2-doped Gd_2CuO_4.
○: undoped Gd_2CuO_4, ◇: 0.5 mol% ThO_2, △: 15 mol% ThO_2, ■: 0.5 mol% ZrO_2, ▲: 5 mol% ZrO_2.

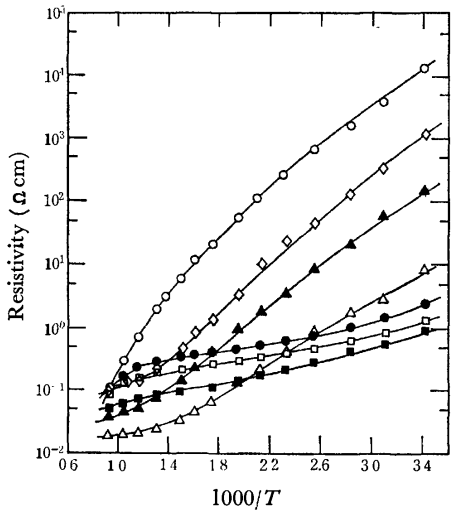

Fig. 4. Temperature dependence of resistivity for ThO_2-doped Gd_2CuO_4.
○: undoped Gd_2CuO_4, ●: 0.1 mol%, □: 0.2 mol%, ■: 0.5 mol%, △: 2.5 mol%, ▲: 5 mol%, ◇: 15 mol%.

The resistivity, ρ, particularly at room temperature, decreases with an increase in the concentration of ZrO_2 up to 0.5 mol%. Beyond this concentration, however, the resistivity increases with an increase in the concentration of ZrO_2 (Fig. 1). Figure 2 shows the temperature dependence of the resistivity for the various contents of ZrO_2. The resistivity-lowering due to the dopant is the most marked at room temperature. The log ρ *vs.* $1/T$ plots for the samples of $x<0.5$ mol% show shoulders in the high-temperature region. As is indicated by the black squares in Fig. 2, the resistivity of the less dense specimen is ten times that of the denser one (open circles); the bulk density of the former is 0.64 of the theoretical value, while that of the latter is 0.90 of the same value. The curves for the two specimens are parallel. Figure 3 indicates that the ZrO_2-doped Gd_2CuO_4 are *n*-type semiconductors.

The solubility of ThO_2 in the Gd_2CuO_4 was between 15 and 20 mol%. The ThO_2-doped samples are similar to the ZrO_2-doped ones in the dependence of the resistivity on the dopant concentration and in the thermoelectric power data; the resistivity is at a minimum at 0.5 mol% ThO_2, and the thermoelectric power is negative.

Figures 5, 6, and 7 give the data for the CaO- or BaO-doped Gd_2CuO_4. The solubility of CaO in the Gd_2CuO_4 was between 1 and 5 mol%. Figure 5 shows that the resistivity decreases with an increase in the dopant concentration, but not so markedly as in the case of the ZrO_2- or ThO_2-doping. The log ρ *vs.* $1/T$ plots (Fig. 6) indicate that the ρ values for the CaO-doped samples, as well as their slopes, approach those for the undoped Gd_2CuO_4 in the high-temperature region. Figure 7 shows that the thermoelectric

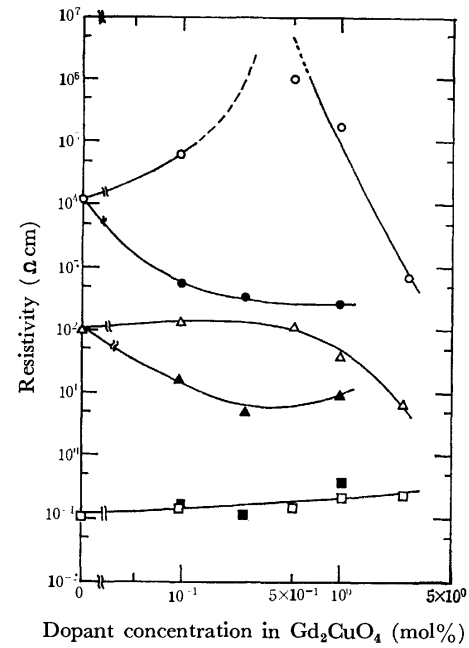

Fig. 5. Variation of resistivity with dopant concentration in Gd_2CuO_4.
○: room temperature for BaO, △: 200 °C for BaO-doping, □: 800 °C for BaO-doping, ●: room temperature for CaO-doping, ▲: 200 °C for CaO-doping, ■: 800 °C for CaO-doping.

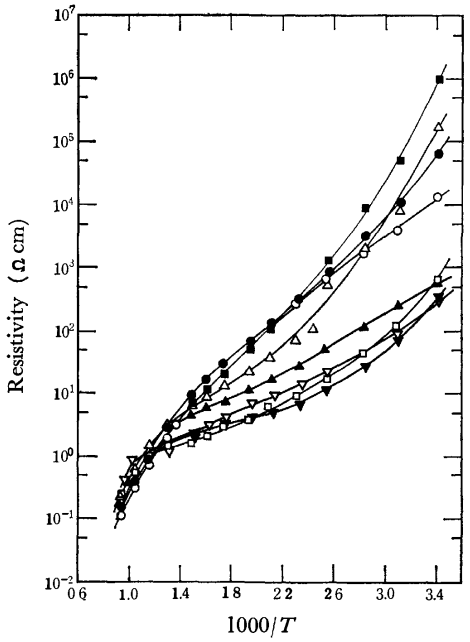

Fig. 6. Temperature dependence of resistivity for BaO- or CaO-doped Gd_2CuO_4.
○: undoped Gd_2CuO_4, ●: 0.1 mol% BaO, ■: 0.5 mol% BaO, △: 1 mol% BaO, □: 2.5 mol% BaO, ▲: 0.1 mol% CaO, ▲: 0.25 mol% CaO, △: 1 mol% CaO.

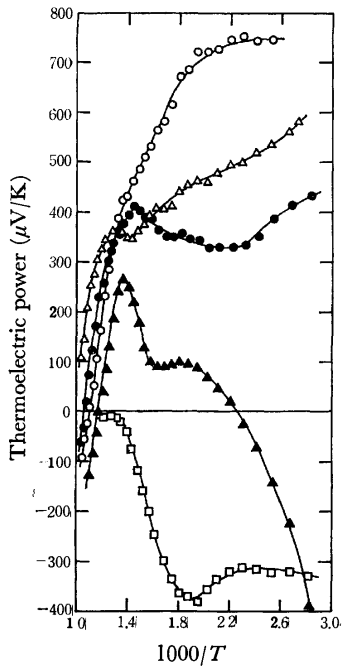

Fig. 7. Temperature dependence of thermoelectric power for CaO- or BaO-doped Gd_2CuO_4.
□: undoped Gd_2CuO_4, ○: 0.25 mol% CaO, △: 1 mol% CaO, ▲: 0.5 mol% BaO, ●: 2.5 mol% BaO.

power was changed from negative to positive values by doping the CaO.

The solubility of BaO in the Gd_2CuO_4 was between 2.5 and 5 mol%. The plots of the resistivity *vs.* the dopant concentration (Fig. 5) show the maximum resistivity value at 0.5 mol% BaO. Figure 6, showing the temperature dependence of the resistivity, is similar to the plots for the CaO-doped samples. The samples containing large amounts of BaO give positive thermoelectric powers, except in the high-temperature region (Fig. 7). The sample containing 0.5 mol% BaO, the resistivity of which is the maximum (Fig. 5), changes its sign of the thermoelectric power at 180 and 580 °C.

Figures 8, 9, and 10 show the data for the Gd_2CuO_4 doped both with ZrO_2 and with CaO simultaneously with a constant total mole value of the ZrO_2 and CaO.

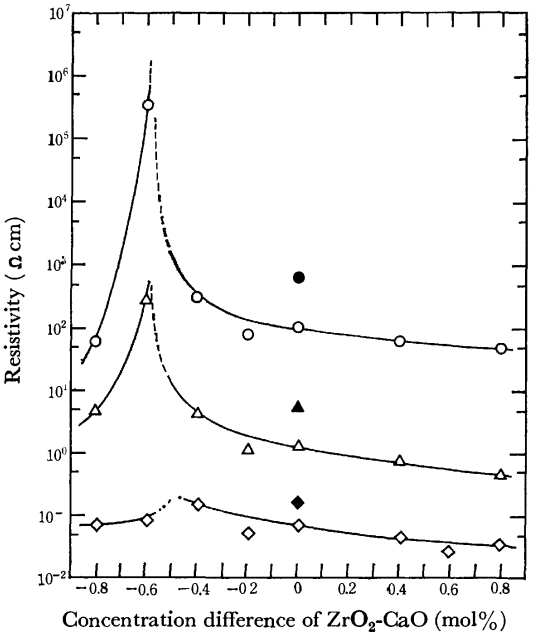

Fig. 8. Variation of resistivity with concentration difference, ZrO_2-CaO, in Gd_2CuO_4.
○: room temperature for ZrO_2+CaO=1 mol%, △: 200 °C for ZrO_2+CaO=1 mol%, ◇: 800 °C for ZrO_2+CaO=1 mol%, ●: room temperature for ZrO_2+CaO=10 mol%, ▲: 200 °C for ZrO_2+CaO=10 mol%, ◆: 800 °C for ZrO_2+CaO=10 mol%.

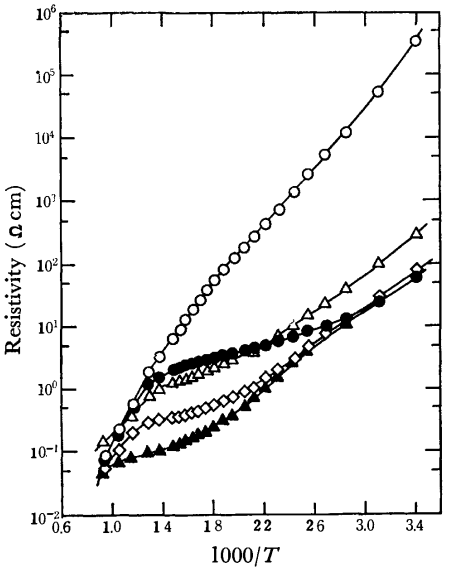

Fig. 9. Temperature dependence of resistivity for ZrO_2- and CaO-doped Gd_2CuO_4.
●: ZrO_2=0.1 mol%, CaO=0.9 mol%, ○: ZrO_2=0.2 mol%, CaO=0.8 mol%, △: ZrO_2=0.3 mol%, CaO=0.7 mol%, ◇: ZrO_2=0.4 mol%, CaO=0.6 mol%, ▲: ZrO_2=0.7 mol%, CaO=0.3% mol%.

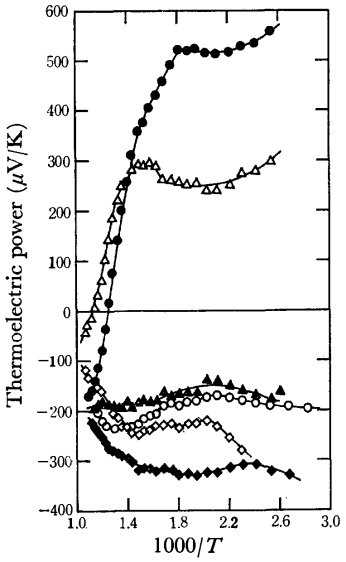

Fig. 10. Temperature dependence of thermoelectric power for ZrO_2- and CaO-doped Gd_2CuO_4.
△: ZrO_2= 0.1 mol%, CaO=0.9 mol%, ●: ZrO_2=0.2 mol%, CaO=0.8 mol%, ◇: ZrO_2=0.3 mol%, CaO=0.7 mol%, ◆: ZrO_2=0.4 mol%, CaO=0.6 mol%, ○: ZrO_2= 0.5 mol%, CaO=0.5 mol%, ▲: ZrO_2=0.6 mol%, CaO= 0.4 mol%.

Figure 8 shows the dependence of the resistivity on the composition of ZrO_2–CaO in mol%. The ρ value is at its maximum at the concentrations of 0.2 and 0.8 mol% of ZrO_2 and CaO respectively. The CaO- and ZrO_2-rich samples show essentially the same trend as the CaO-doped and ZrO_2-doped samples respectively in the temperature dependence of their resistivities.

Discussion

The lattice sites occupied by a dopant can be estimated by the use of an X-ray diffractometer when the dopant concentration is higher than its sensitivity limit. When the ZrO_2, for example, is doped, the mole ratio of the raw oxide mixtures, $CuO: Gd_2O_3: ZrO_2$, is $1: 1-x: x$ or $1-x: 1: x$, where x is the dopant concentration. The former ratio is used when the ZrO_2 is expected to occupy the Gd^{3+} sites; the dopant in the latter case is expected to occupy the Cu^{2+} sites. If the ZrO_2 occupies the Gd^{3+} sites, the ZrO_2 phase will be found in the samples prepared in the latter fashion. If the ZrO_2 occupies the Cu^{2+} sites, the same phase will be found in the former samples. The X-ray diffraction data indicated that ZrO_2 phase was present in the samples when $CuO: Gd_2O_3: ZrO_2 = 1-x: 1: x$, and that no ZrO_2 phase was present when $CuO: Gd_2O_3: ZrO_2 = 1: 1-x: x$; $x<0.1$ for both cases. Consequently, the doped ZrO_2 or the ThO_2 was found to occupy the Gd^{3+} sites in the concentration region of $0.1>x>0.05$.

The X-ray diffraction data described above still leave two problems: (1) it is not known which sites are occupied by the dopants in the $x<0.05$ concentration region, and (2) a small amount of the ZrO_2 or ThO_2 may be present in the Cu^{2+} sites, although an X-ray diffractometer does not detect them. It is difficult to give a clear answer to the above problems, but the following assumptions may be made: (1) the ZrO_2 or ThO_2 occupies the Gd^{3+} sites also in the $x<0.05$ concentration region, and (2) the fraction of the Cu^{2+} sites which might be occupied by the dopants is so small that the electrical effects due to them are negligibly small. The above two assumptions seem reasonable, because the sites occupied by the dopants are unlikely to depend upon the dopant concentration, and because the ZrO_2 or ThO_2 is chemically more similar to Gd_2O_3 than to CuO.

The doped Gd_2CuO_4 decreases in its resistivity with an increase in the concentration of ZrO_2 up to 0.5 mol%. This suggests the presence of donor centers. The doped Zr^{4+} cations occupy the Gd^{3+} sites and may be initially reduced to Zr^{3+} cations to minimize the strain energy due to the oxygen vacancies, but the Zr^{3+} cations formed, if they were fixed at the sites, do not act as donor centers because they are on the Gd^{3+} sites, where an appreciable electron-overlapping cannot be expected.[1] The Cu^+ ions, on the other hand, seem to be more probable donor centers, because they are on the Cu^{2+} sites, where an electron-overlapping *can* be expected.[1] The Cu^+ ions are formed by the reduction of the Cu^{2+} ions while the Zr^{3+} ions are oxidized to Zr^{4+} ions—that is, $Cu^{2+}+Zr^{3+}=Cu^+ + Zr^{4+}$. This reaction is an electron-transfer from the Zr^{3+} to Cu^{2+} ions, and results in excess positive and negative charges at the Zr^{4+} and Cu^+ ion respectively. It is electrostatically unstable. However, the electrostatic energy needed for the electron-transfer is compensated for by the energy difference between the Cu^+ formation and the excitation of the Zr^{3+} to the Zr^{4+} ion, because the Cu^+ ion seems to be more stable than the Zr^{3+} ion.

The increase in the resistivity with the increase in the concentration of ZrO_2 beyond 0.5 mol% is unexpected. An increase in the resistivity is usually ascribable to a decrease in the number of carriers or to a decrease in the mobility.[3,5,6] In this case, however, a decrease in the number of carriers is not likely, because such a doping effect as would decrease the number of carriers cannot be expected. A decrease in the mobility is not likely either, although the mobility might be lowered because of the electron scattering by the lattice vacancies. Therefore, some changes in the grain boundary are more likely to be causes of the above fact. As can be seen in Fig. 2, the less dense specimen is greater than the denser one in its resistivity, while the slopes in the log ρ *vs.* $1/T$ plots are the same. This is simply because the less dense sample is smaller than the denser one in the contacting area of the grains. The ZrO_2 dopant, on the other hand, enhances not only the resistivity but also the slopes of the plots. Therefore, a decrease in the contacting area of the grains, which is one of the changes in the grain boundary, is not a cause of the increase in the resistivity with the increase in the concentration of ZrO_2. Another possible change in the grain boundary would be a deposit of some insulators on the grain boundary. A small amount of ZrO_2, for example, one too small

to be detected by an X-ray diffractometer, might increase both the resistivity and the activation energy of the samples.

The previous work[1] revealed that the resistivity of Ln_2CuO_4 decreases with a decrease in the atomic number of Ln. This fact was explained as being due to: (1) a variation in the activation energy, or (2) a variation in the number of the donor centers formed by the thermal decomposition of the Cu^{2+} to the Cu^{+} ions. However, it is not known which factor is the more important. The activation energy corresponds to the energy gaps between the split 3d-electron energy levels of the Cu^{2+} ions, which are affected by the ligand-field strength at the Cu^{2+} sites.[1] The ligand-field strength is determined by the distance between the Cu^{2+} ions and the closest neighbors. Since no change is indicated in the lattice parameters of the doped Gd_2CuO_4, the distance described above may also be unchanged by doping. On the basis of the above discussion and the X-ray diffraction data, it seems reasonable to assume that the ligand-field strength at the Cu^{2+} sites is unchanged by doping; therefore, the doping method varies the number of donor centers without a great variation in the activation energy. The activation energy is related to the thermoelectric power by this equation: $\alpha \propto -E/T$, for the Maxwell distribution, where α is the thermoelectric power; E, the activation energy, and T, the temperature.[1,3] Therefore, the dopants are expected to lower the resistivity without a great variation in the thermoelectric power. In fact, Fig. 2 shows that the Gd_2CuO_4 doped with 0.5 mol% ZrO_2 is lower than the Pr_2CuO_4[1] in its resistivity, while the former is greater than the latter in its thermoelectric power. The $\alpha \propto -E/T$ relationship is applied to the data for the Ln_2CuO_4 compounds. If the trend for the resistivity of the Ln_2CuO_4 to decrease with a decrease in the atomic number of Ln was simply due to an increase in the number of donor centers, and not to a variation in the activation energy, the thermoelectric powers of the Ln_2CuO_4 compounds would not depend upon the atomic number of Ln. However, their thermoelectric powers increase with an increase in the atomic number of Ln,[1] suggesting that the above trend is ascribable to an increase in the activation energy. The X-ray diffraction data seem to support this suggestion; the lattice parameter of the tetragonal Ln_2CuO_4, c/a, increases with a decrease in the atomic number of Ln.[1,4]

Figure 5 shows that the resistivity decreases with an increase in the concentration of CaO, suggesting a formation of acceptor centers. It has been suggested on the basis of the X-ray diffraction results that the doped Ca^{2+} or Ba^{2+} ions occupy the Gd^{3+} sites. If they occupy the Gd^{3+} sites without oxygen vacancies, the doped alkaline earth cations would be forced to be in a trivalent state. Trivalent alkaline earth cations, however, are very unstable. The Cu^{2+} ions, on the other hand, seem to be more readily oxidized to Cu^{3+} ions, although the Cu^{3+} ions may still be unstable. As in the case of the Cu^{+} formation, the formation of the Cu^{3+} ions is an electron transfer from the Cu^{2+} ions to the Ca^{3+} ions which might be initially formed. This electron-transfer is again electrostatically unstable. The electrostatic energy needed for the electron-transfer may be compensated for by the energy difference between the formation of the divalent alkaline earth cations and the excitation of the Cu^{2+} to Cu^{3+} ions. The Cu^{3+} ions would not be very stable, so many acceptor centers cannot be expected to be formed. This may be one of the reasons why the CaO-doping is not so effective on the resistivity-lowering as the ZrO_2- or ThO_2-doping. The presence of the acceptor centers is directly suggested by the positive thermoelectric power (Fig. 7).

The number of acceptor centers formed at a given dopant concentration is such a number as will minimize the total energy of the strain due to the oxygen vacancies and that of the excitation of the Cu^{2+} to Cu^{3+} ions. The strain energy may be made smaller by doping larger cations. Therefore, the number of acceptor centers formed at a given dopant concentration can be made smaller by doping larger cations. The experimental results for the BaO-doped Gd_2CuO_4 show the expected behavior (Figs. 5—7). The resistivity increases with an increase in the dopant concentration in the concentration region of $x<0.5$ mol%. The sample doped with 0.5 mol% BaO shows a medium trend between the undoped and 2.5 mol% BaO-doped samples in the temperature dependence of the thermoelectric power. These data suggest that the donor centers initially formed by the thermal decomposition are recombined with the acceptor centers formed by doping the BaO, and that the former still number more than the latter. In concentration region of $x<0.5$ mol%, the CaO-doped samples are p-type semiconductors and decrease in resistivity with an increase in the concentration of the CaO. These results indicate that the BaO dopant at a given concentration produces a smaller number of acceptor centers than the CaO dopant. In the concentration region of $x>0.5$ mol%, the BaO-doped samples behave much like the CaO-doped ones; the resistivity decreases with an increase in the concentration of BaO, and the thermoelectric power is positive, over the temperature range investigated. These facts suggest that the acceptor centers number more than the donor centers in this concentration region.

The recombination of the donors with the acceptors can be made by doping the ZrO_2 and CaO simultaneously. Since the donor centers consist of Cu^{+} ions formed by the ZrO_2-doping and those formed by the thermal decomposition of the Cu^{2+} ions, the dopant concentration where the resistivity is at its maximum will shift to a CaO-rich composition because of the donor centers formed by the thermal decomposition. Figure 8 shows the expected results; the maximum resistivity can be seen at CaO=0.8 mol% and ZrO_2= 0.2 mol%. The thermoelectric power data correspond to the resistivity data; the sign is changed at the same concentration.

On the basis of the series of data shown in Figs. 5 to 10, it can be concluded that the most important donor centers in the Ln_2CuO_4 compounds are the Cu^{+} ions formed by the thermal decomposition of the Cu^{2+}

ions.

An attempt to dope Ag_2O and In_2O_3 was unsuccessful. This failure may be partly due to too great a difference in the ionic radii between the Cu^{2+} ion and either the Ag^+ or the In^{3+} ion ($Cu^{2+}=0.72$ Å, $Ag^+=0.97$ Å, and $In^{3+}=0.81$ Å) and partly to too small a latitude of the Cu^{2+} site for the ionic size. This may be related to the covalent nature of the Cu–O bonds.

BULLETIN OF THE CHEMICAL SOCIETY OF JAPAN, VOL. 46, 2625—2629 (1973)

Kinetic Study of Triplet-Triplet Energy Transfer in Fluid Solution by Means of Laser Pulse Photolysis[1)]

Takeshi TAKEMURA, Hiroaki BABA, and Masahisa FUJITA

Division of Chemistry, Research Institute of Applied Electricity, Hokkaido University, Sapporo 060

(Received September 26, 1972)

The kinetics of triplet-triplet (T-T) energy transfer in fluid solution has been studied by means of laser pulse photolysis with acetophenone as the energy donor and naphthalene as the acceptor. Decay curves of phosphorescence of the donor and rise-and-decay curves of sensitized T-T absorption of the acceptor were obtained. These were analyzed to determine the unimolecular and bimolecular rate constants (denoted by k_1 and k_2 respectively) for the deactivation processes of the triplet state of donor or acceptor and the rate constant (k_t) for the T-T energy transfer. In isooctane at room temperature these rate constants were found to be: $k_1=0.67\times10^6$ sec^{-1} and $k_2=2.0\times10^{10}$ M^{-1} sec^{-1} for acetophenone, $k_2'=1.6\times10^{10}$ M^{-1} sec^{-1} for naphthalene, and $k_t=1.0\times10^{10}$ M^{-1} sec^{-1}. The k_t value obtained from the donor phosphorescence is in good agreement with that from the acceptor T-T absorption. The experimental results suggest that T-T transfer and T-T annihilation processes are not strictly diffusion-controlled.

Triplet-triplet (T-T) energy transfer between molecules in fluid solution has been extensively investigated since the work of Bäckström and Sandros.[2-9)] It is generally believed that, when the transfer is exothermic by at least 3 kcal/mol, the transfer rate is nearly equal to the encounter frequency predicted by the Debye equation for diffusion-controlled kinetics, provided that the solvent viscosities are greater than 3 cP.[5)]

On the other hand, Nordin and Strong pointed out on the basis of computational analysis that an energy difference greater than 3 kcal/mol between donor and acceptor triplet states does not necessarily lead to diffusion-controlled quenching.[6)] Wagner and Kochevar also indicated that the triplet energy transfer is not totally diffusion-controlled in solvents of low viscosity.[7)]

T–T energy transfer has so far been studied through spectroscopic and photochemical experiments performed by either steady excitation or the usual flash photolysis method in which the flash duration is of the order of microseconds.[10,11)] Such a duration is too long for direct observation of the T–T transfer process in fluid solution.

In an attempt to obtain detailed information on energy transfer and other rate processes associated with the donor and acceptor triplet states, we re-examined T–T energy transfer in solution by using a frequency-doubled ruby laser with a pulse duration of 25 nsec. Acetophenone was chosen as the energy donor and naphthalene as the acceptor, and isooctane was used as a solvent of low viscosity. We utilized the fact that acetophenone shows a phosphorescence emission of appreciable intensity even in a fluid solution, provided that the solvent is fully degassed. In this way we were able to measure both the phosphorescence of the donor and the sensitized T–T absorption of the acceptor, and hence it was possible to investigate the dynamic behavior of the donor and acceptor triplet species simultaneously.

Experimental

Reagents were obtained from Wako Pure Chemical Industries, Osaka. Acetophenone was purified by high-vacuum distillation. Spectro-grade isooctane was used without further purification. Sample solutions consisted of acetophenone of a constant concentration (1.0×10^{-2} M) and naphthalene of varying concentrations ($\sim10^{-4}$ M), with isooctane as the solvent. Each solutions was degassed repeatedly by freeze-thaw cycles until the phosphorescence intensity of acetophe-

1) Presented at the Symposium on Molecular Structure held by the Chemical Society of Japan at the Kyoto Hall, Kyoto, Oct. 16, 1971.

2) J. B. Birks, "Photophysics of Aromatic Molecules," Wiley Interscience, New York (1970).

3) C. A. Parker, "Photoluminescence of Solutions," Elsevier Publishing Company, Amsterdam (1968).

4) H. L. J. Bäckström and K. Sandros, *Acta Chim. Scand.*, **14**, 48 (1960).

5) K. Sandros and H. L. J. Bäckström, *ibid.*, **16**, 958 (1962).

6) S. Nordin and R. L. Strong, *Chem. Phys. Lett.*, **2**, 429 (1968).

7) P. J. Wagner and I. Kochevar, *J. Amer. Chem. Soc.*, **90**, 2232 (1968).

8) H. Baessler, G. Vaubell, and H. Kallman, *J. Chem. Phys.*, **53**, 370 (1970).

9) R. B. Cundall, G. E. Evans, and E. J. Laud, *J. Phys. Chem.*, **73**, 3982 (1969).

10) G. Porter and F. Wilkinson, *Proc. Roy Soc., Ser. A*, **264**, 1 (1961).

11) A. Yekta and N. J. Turro, *Mol. Photochem.*, **3**, 307 (1972).

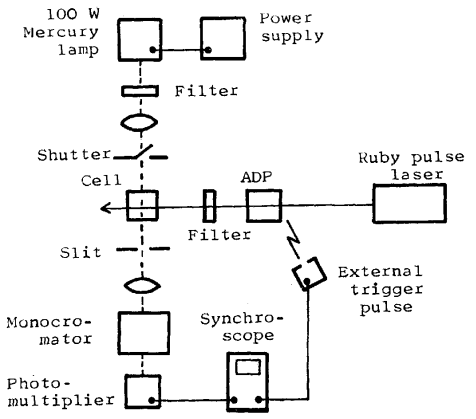

Fig. 1. Diagrammatic representation of the apparatus for laser pulse photolysis.

none reached a maximum.

Phosphorescence spectra were measured at room temperature with a Hitachi MPF-2A fluorescence spectrophotometer.

The apparatus for laser pulse photolysis is schematically shown in Fig. 1. A Japan Electron Optics Laboratory JLS-R3A giant pulse ruby laser with a peak output of 150 MW and pulse width of 25 nsec was used. The sample in a 10-mm square quartz cell was excited by the second harmonic (347 mμ) of the ruby laser generated by an ADP crystal. It should be noted that only the donor molecule of acetophenone absorbs at 347 mμ. To observe the rise and decay of T–T absorption, light from a 100-W extra-high pressure mercury lamp was passed through the cell at right angles to the laser beam, dispersed by a grating monochromator, and was then detected by an RCA 1P28 photomultiplier and an Iwasaki 100 MHz oscilloscope. In order to measure the phosphorescence decay, the emission from the solution excited by the frequency-doubled laser pulse was detected instead of the light from the mercury lamp (Fig. 1).

The exciting pulse of the second harmonic had an energy of 4×10^{-7} einstein/pulse, which was reproducible within an error of ±10 %. Since the principal source of error is the variation in energy of the pulse, the overall experimental error may safely be assumed to be ±20 %.

Most of the measurements were made with the above-mentioned exciting pulse (hereafter called normal- or high-intensity pulse). For certain purposes, we used an exciting pulse whose energy was reduced to 1 % of the energy of the normal-intensity pulse by means of a suitable system of glass filters (hereafter called low-intensity pulse).

The donor phosphorescence was observed at 420 mμ, and the acceptor T–T absorption at 410 mμ, unless otherwise stated. All the emission and absorption measurements were made at room temperature (about 20 °C).

Results and Discussion

Kinetic Scheme. Creation and degradation of triplet states in fluid solution involving intermolecular triplet-triplet energy transfer may be expressed by the following mechanisms:

$$^1D \longrightarrow {}^3D^* \qquad (1a)$$

$$^3D^* \xrightarrow{k_1} {}^1D \qquad (1b)$$

$$^3D^* + {}^3D^* \xrightarrow{k_2} {}^1D^* + {}^1D \qquad (1c)$$

$$^3D^* + {}^1A \xrightarrow{k_t} {}^1D + {}^3A^* \qquad (1d)$$

$$^3A^* \xrightarrow{k_1'} {}^1A \qquad (1e)$$

$$^3A^* + {}^3A^* \xrightarrow{k_2'} {}^1A^* + {}^1A \qquad (1f)$$

where ^1D, $^3D^*$ and ^1A, $^3A^*$ represent the ground and triplet states of donor (D) and acceptor (A), respectively; k_1 or k_1' is the sum of the rate constants for all unimolecular decay processes including both radiative and nonradiative transitions; k_2 or k_2' is the bimolecular rate constant for T–T annihilation, and k_t is that for T–T energy transfer. The formation of the triplet excited dimer can be neglected, since it has only a small rate constant[12] and does not appreciably contribute to the triplet decay.

The rate equations for the donor-acceptor system after pulse excitation are given by

$$-\frac{d[^3D^*]}{dt} = (k_1+k_2[^3D^*] + k_t[^1A])[^3D^*] \qquad (2)$$

$$\frac{d[^3A^*]}{dt} = k_t[^1A][^3D^*] - (k_1'+k_2'[^3A^*])[^3A^*] \qquad (3)$$

Although these equations cannot be solved exactly, we can determine the rate parameters if we choose appropriate experimental conditions.

Rate Constants Derived from the Donor Phosphorescence. The phosphorescence spectrum of acetophenone in isooctane at room temperature is similar in location and shape to the spectrum of that in a rigid-glass solution at low temperature (Fig. 2).[13]

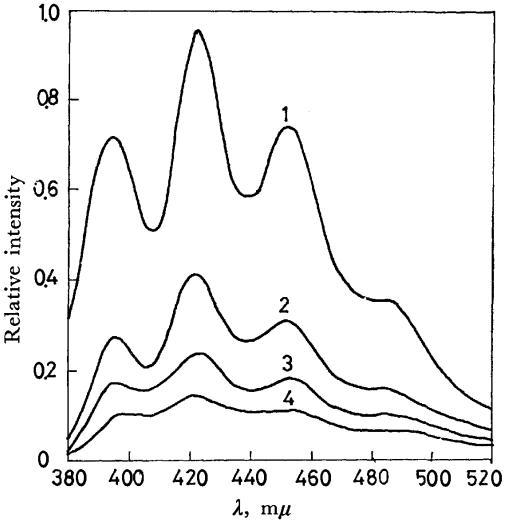

Fig. 2. Phosphorescence spectra of acetophenone–naphthalene system obtained by steady excitation at 340 mμ in isooctane. The concentrations of naphthalene: (1) 0; (2) 0.8×10^{-4}; (3) 2.0×10^{-4}; (4) 4.0×10^{-4} M.

When the acetophenone–naphthalene system was excited at 347 mμ by the normal-intensity pulse, the phosphorescence of the donor generally showed non-exponential decay. On the other hand, excitation by the low-intensity pulse led to a phosphorescence decay curve which was exponential within the limit of experimental errors. These observations indicate that the importance of the term involving k_2 on the right hand side of Eq. (2) largely depends upon the intensity of the exciting light.

12) J. Langelaar, G. Jansen, R. P. H. Rettschnick, and G. J. Hoytink, *Chem. Phys. Lett.*, **12**, 86 (1971).

13) W. D. K. Clark, A. D. Litt, and C. Steel, *J. Amer. Chem. Soc.*, **91**, 5413 (1969).

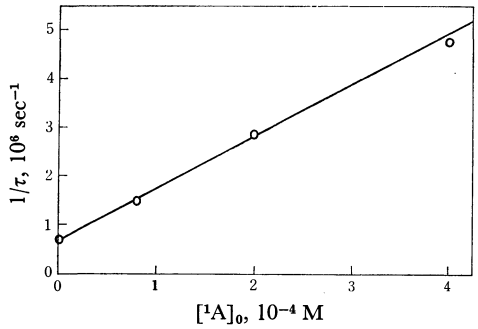

Fig. 3. Plot of $1/\tau$ *vs.* $[^1A]_0$ for acetophenone–naphthalene system in isooctane.

The phosphorescence lifetime τ as obtained from the decay curve corresponding to the low-intensity pulse decreases with increase in the amount of naphthalene added as an acceptor. The plot of $1/\tau$ against the initial acceptor concentration $[^1A]_0$ is found to be linear within the limit of experimental errors (Fig. 3). With the low-intensity pulse, the term involving k_2 can be neglected in Eq. (2), and $[^1A]=[^1A]_0-[^3A^*]$ can be replaced by $[^1A]_0$, so that $1/\tau$ is expressed as

$$1/\tau = k_1 + k_t[^1A]_0$$

The linear relation in Fig. 3 can thus be understood. From the intercept and slope of the straight line, we at once obtain

$$k_1 = 0.67\times 10^6 \text{ sec}^{-1}$$
$$k_t = 1.1\times 10^{10} \text{ M}^{-1}\cdot\text{sec}^{-1}$$

In the case of the normal-intensity pulse, the term neglected before should be included, but Eq. (2) should be simplified at the instant of pulse excitation, that is, at $t=0$. Thus, if the phosphorescence intensity of the donor is denoted by I, Eq. (2) can be written in the form:

$$-\left[\frac{1}{I}\frac{dI}{dt}\right]_{t=0} = k_1 + k_2[^3D^*]_0 + k_t[^1A]_0 \qquad (4)$$

where $[^3D^*]_0$ is the concentration of the initially produced triplet state of the donor, *i.e.* $[^3D^*]$ at $t=0$.

Figure 4 shows a plot of $-[(1/I)(dI/dt)]_{t=0}$ against $[^1A]_0$, which gives a straight line as expected from Eq. (4). From the intercept of the line, we obtain $k_1+k_2[^3D^*]_0=2.5\times 10^6$ sec^{-1}. It will be shown later that $[^3D^*]_0=0.90\times 10^{-4}$ M. Thus, recalling that $k_1=0.67\times 10^6$ sec^{-1}, we obtain

$$k_2 = 2.0\times 10^{10} \text{ M}^{-1}\cdot\text{sec}^{-1}$$

Further, from the slope of the straight line, we obtain

$$k_t = 0.90\times 10^{10} \text{ M}^{-1}\cdot\text{sec}^{-1}$$

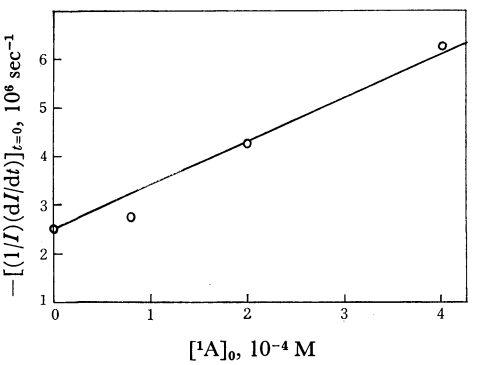

Fig. 4. Plot of $-[(1/I)(dI/dt)]_{t=0}$ *vs.* $[^1A]_0$ for acetophenone–naphthalene system in isooctane.

We here refer to spectral data resulting from the steady excitation on the usual spectrophotometer. The intensity of the phosphorescence spectrum of acetophenone, obtained by steady excitation at 340 mμ, decreases with the increasing amount of naphthalene (Fig. 2). The phosphorescence quenching is interpreted to be due to the T–T energy transfer from acetophenone to naphthalene.

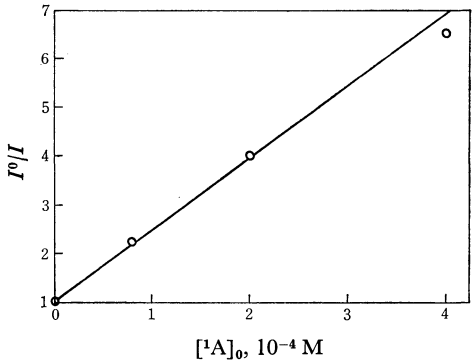

Fig. 5. Stern-Volmer plot for the quenching of phosphorescence of acetophenone by naphthalene in isooctane.

A Stern-Volmer plot for the quenching of acetophenone phosphorescence is given in Fig. 5. The plot is linear as expected. In the case of steady excitation, T–T annihilation can be disregarded on account of the low intensity of exciting light. Consequently, the following equation of Stern-Volmer type is obtained by reference to Eq. (2):

$$I^0/I = 1 + k_t[^1A]_0/k_1 \qquad (5)$$

where I^0 and I are the steady intensities of the donor phosphorescence in the absence and presence of the acceptor, respectively. From the slope of the straight line in Fig. 5, $k_t/k_1=1.5\times 10^4$ M^{-1} is obtained; hence, by use of the known value of k_1, it follows that

$$k_t = 1.0\times 10^{10} \text{ M}^{-1}\cdot\text{sec}^{-1}$$

Rate Constants Derived from the Acceptor T–T Absorption. Figure 6 represents typical examples showing the time behavior of the transient absorption at 410 mμ obtained for a mixture of acetophenone and naphthalene in isooctane by excitation with a normal-intensity laser pulse. The intensity of absorption first rises rapidly, reaches a maximum or a peak, and then decays rather slowly. The maximum intensity value increases with the amount of naphthalene, provided that the concentration of acetophenone is kept constant.

We made a series of measurements, changing the wavelength at which the transient absorption was monitored, and plotted the absorption intensity at a definite time after the pulse excitation as a function of the monitoring wavelength. The resulting spectrum agreed well with the T–T absorption spectrum of naphthalene in literature. No transient absorption could be detected from a solution of acetophenone

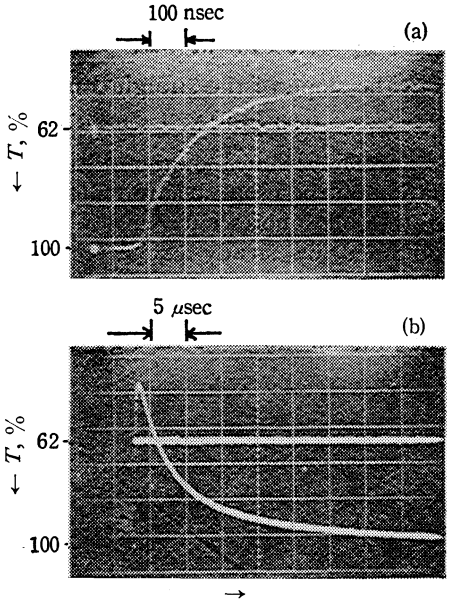

Fig. 6. Rise and decay of the sensitized T–T absorption of naphthalene. (a) rise curve; (b) rise-and-decay curve. $[^1A]_0=2.0\times10^{-4}$ M.

alone or of naphthalene alone in isooctane under the present experimental conditions.

The foregoing observations clearly indicate that the transient absorption as given in Fig. 6 is due to the T–T transition in triplet naphthalene molecules produced by T–T energy transfer in which acetophenone acts as a donor and naphthalene as an acceptor. We note that the wavelength of 410 mμ corresponds to a peak in the T–T absorption spectrum of naphthalene.

The absorbance for the transient T–T absorption at a particular wavelength, *i.e.* 410 mμ in the present experiment, will be denoted by A_b, or by $A_b(t)$ when it is desirable to show explicitly that the absorbance is a function of time. There is, of course, the following relation between A_b and $[^3A^*]$:

$$[^3A^*] = A_b/\varepsilon l \qquad (6)$$

where ε and l are the molar extinction coefficient for the T–T absorption of acceptor and the effective absorbing path length, respectively.

Let us denote the time at which the peak occurs in the $A_b(t)$ curve by t_p. Then, at any time t later than t_p by at least three microseconds, the decay curve of $A_b(t)$ is represented by the following relation between $[^3A^*]$ and t:

$$1/[^3A^*] = k_2't + C \qquad (7)$$

where C is a constant. At the time under consideration $[^3D^*]$ is so small that the first term on the right-hand side of Eq. (3) can be neglected; k_1' also is negligible because of its relatively small magnitude.[12] Equation (3) is thus simplified to give Eq. (7).

A plot of $1/[^3A^*]$ against t is shown in Fig. 7. The values of $[^3A^*]$ were derived on the basis of Eq. (6) from experimental data for A_b; the ε value at 410 mμ was taken to be 1.4×10^4,[14] and l was estimated to be

14) S. G. Hadley and R. A. Keller, *J. Phys. Chem.*, **73**, 4356 (1969).

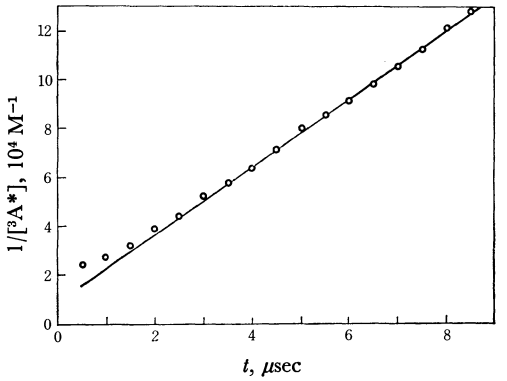

Fig. 7. Plot of $1/[^3A^*]$ *vs.* t for acetophenone–naphthalene system in isooctane. $[^1A]_0=2.0\times10^{-4}$ M.

0.7 cm. We see that the relation of $1/[^3A^*]$ to t can be satisfactorily expressed in the form of Eq. (7) for $t>3$ μsec. From the slope of the straight line we obtain

$$k_2' = 1.6\times10^{10}\ \mathrm{M^{-1}\cdot sec^{-1}}.$$

Let us consider the rate of rise of absorbance at the instant of excitation (*cf.* Fig. 6a). At $t=0$, Eq. (3) becomes

$$\left[\frac{d[^3A^*]}{dt}\right]_{t=0} = k_t[^1A]_0[^3D^*]_0 \qquad (8)$$

Therefore, a plot of the initial slope of the $[^3A^*]-t$ curve, $(d[^3A^*]/dt)_{t=0}$, against the initial acceptor concentration, $[^1A]_0$, should yield a straight line with a slope of $k_t[^3D^*]_0$. This is valid as may be seen in Fig. 8. As will be shown later, $[^3D]_0$ is evaluated as 0.90×10^{-4} M. Hence, from the slope of the straight line, we obtain

$$k_t = 1.0\times10^{10}\ \mathrm{M^{-1}\cdot sec^{-1}}$$

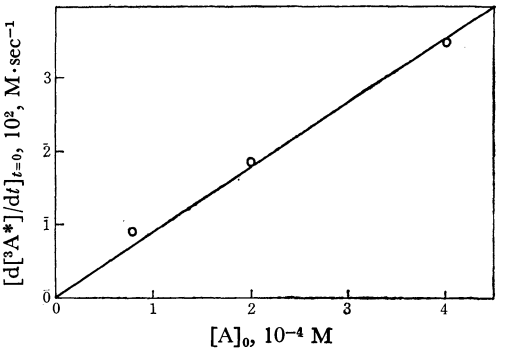

Fig. 8. Plot of $[d[^3A^*]/dt]_{t=0}$ *vs.* $[^1A]_0$ for acetophenone–naphthalene system in isooctane.

This is in good agreement with the k_t values derived from the data on donor phosphorescence.

Evaluation of $[^3D^*]_0$. The initial concentration of the donor triplet $[^3D^*]_0$ immediately after the excitation with the normal- or high-intensity laser pulse is important in determining rate parameters.

The experiments related to Figs. 4 and 8 were carried out under the same conditions with respect to the intensity of exciting pulse. According to the definition of t_p, we have $d[^3A^*]/dt=0$ at $t=t_p$. Thus by neglecting the term of k_1' it follows from Eq. (3) that

TABLE 1. RATE CONSTANTS OF VARIOUS PROCESSES OF TRIPLET ENERGY DEACTIVATION AND TRANSFER FOR ACETOPHENONE–NAPHTHALENE PAIR IN ISOOCTANE AT ROOM TEMPERATURE

Observation	$k_1\times10^{-6}$ sec^{-1}	$k_2\times10^{-10}$ $M^{-1}\cdot sec^{-1}$	$k'_2\times10^{-10}$ $M^{-1}\cdot sec^{-1}$	$k_t\times10^{-10}$ $M^{-1}\cdot sec^{-1}$	α
Donor phosphorescence (steady excitation)				1.0	0.76
Donor phosphorescence (laser pulse excitation)	0.67	2.0		1.1	0.83
				0.9	0.61
T–T absorption of A (laser pulse excitation)			1.6	1.0	0.76

$$[^3D^*]_{t_p} = k_2'[^3A^*]^2_{t_p}/k_t[^1A]_{t_p} \quad (9)$$

The values for rate constants k_2' and k_t have already been obtained without the knowledge of $[^3D^*]_0$, $[^1A]_{t_p}$ being equal to $[^1A]_0-[^3A^*]_{t_p}$. For $[^1A]_0=2.0\times10^{-4}$ M, $[^3A^*]_{t_p}$ is found to be 0.39×10^{-4} M from the A_b value at t_p. Hence $[^3D^*]_{t_p}$ is determined to be 0.15×10^{-4} M from Eq. (9). On the other hand, the ratio between $[^3D^*]_{t_p}$ and $[^3D^*]_0$ can be obtained by use of the decay curve of the donor phosphorescence. Thus, for $[^1A]_0=2.0\times10^{-4}$ M, we find that $[^3D^*]_{t_p}/[^3D^*]_0=0.17\pm0.02$. This along with the value of $[^3D^*]_{t_p}$ leads to

$$[^3D^*]_0 = 0.90\times10^{-4}\ M$$

Considerations on the Values of Rate Constants. The rate constants determined by various procedures are summarized in Table 1. It is obvious that the values of k_t obtained from the donor phosphorescence caused by steady or laser-pulse excitation and from the sensitized acceptor T–T absorption caused by laser-pulse excitation are in good agreement within the limit of experimental errors. This indicates that the behavior of triplet states in less viscous solvents can be satisfactorily described by the reaction scheme given in Eq. (1).

The triplet-triplet energy transfer process given in Eq. (1d) can be represented by a more detailed mechanism involving an encounter complex:

$$^3D^* + {}^1A \underset{\overleftarrow{k}}{\overset{\overrightarrow{k}}{\rightleftharpoons}} [^3D^*\ldots{}^1A] \xrightarrow{k_{et}} {}^1D + {}^3A^*$$
$$\text{(I)} \qquad\qquad \text{(II)}$$

Process (I) corresponds to the encounter of a donor molecule in the excited triplet state and an acceptor molecule in the ground state. Process (II) represents the energy transfer from the donor to the acceptor in the encounter complex. It can then be shown that k_t in Eq. (1d) is expressed as

$$k_t = \alpha\vec{k} \quad (10)$$

with

$$\alpha = k_{et}/(\overleftarrow{k}+k_{et})$$

The encounter between donor and acceptor molecules can be regarded as a diffusion-controlled process. Thus, if the Debye equation is applicable to such a process, the rate constant $\vec{k}$ is given by

$$\vec{k} \equiv k_{dif} = \frac{8RT}{3000\eta} \quad (11)$$

Using the $\vec{k}$ value obtained from this equation and the observed k_t values, α is calculated to be less than unity from Eq. (10), as is shown in Table 1.

The fact that the parameter α is less than unity leads to the view that the overall energy-transfer process as given by Eq. (1d) is not diffusion-controlled in a strict sense. Because of the assumptions involved in the evaluation of k_{dif}, too much reliance cannot be placed on the value of α. However, in our recent experiments on the temperature dependence of T–T energy transfer for acetophenone–1,4-dibromonaphthalene pair in isooctane, it was found that the value of α decreases with the decreasing solvent viscosity caused by the rise in temperature; for example, $\alpha(0\ ^\circ C)=0.57$ and $\alpha(65\ ^\circ C)=0.26$. This shows the value of k_{et} to be comparable to that of $\overleftarrow{k}$ and thus gives evidence in favor of the above-mentioned view.

A similar result is also obtained for the T–T bimolecular annihilation process: when the values of k_2 and k_2' described before are compared with twice the diffusion-controlled rate constant k_{dif} evaluated from Eq. (11), it can be seen that k_2 and k_2' are about seven-tenths as large as $2k_{dif}$. This factor 0.7 corresponds to the parameter α given in Eq. (10), and is comparable to the values of α shown in Table 1.

Studies of the DNA–Acridine Complexes. I. Fluorescence Depolarization

Yukio KUBOTA

Department of Chemistry, Yamaguchi University, Yamaguchi 753

(Received December 15, 1972)

The motion of the DNA–acridine complexes in solution was studied by the fluorescence depolarization method. Five derivatives of 3,6-diaminoacridine were used in order to investigate the effect of amino substituion on the depolarization results. A linear relation between the reciprocal polarization ($1/P$) and T/η was obtained by varying the temperature of a native DNA–acridine solution. The limiting polarization (P_0) and the mean rotational relaxation time (ρ_h) of the complex were evaluated from these data. The ρ_h value of the complex (30—50 nsec) was much larger than the value of free acridine in water, but it was much too small to correspond to the rotation of the whole DNA molecule. Further, it was found that the values of P_0 and ρ_h for 3,6-bis(diethylamino)-acridine are much smaller than those for other acridines. This may result from some steric hindrance of the binding by bulky diethylamino groups.

The interaction of aminoacridines and their derivatives with DNA has been extensively studied by various techniques. Interest in this topic has been stimulated by the biological activity of the acridines and by their structural similarity to carcinogens, such as polycyclic hydrocarbons and benzacridines. At present, it is generally accepted that acridine molecules bind to DNA to form two types of complexes; one (Complex I) results from the acridine-acridine interaction on the outside of the DNA helix at low values of the molar ratio of nucleotides to acridine molecules (N/A),[1,2] while the other (Complex II) occurs at high N/A values, where the acridine-nucleotide interaction is involved.[3] Lerman[4,5] proposed that, in Complex II, acridine molecules are intercalated in a sandwich-like way between adjacent base pairs in the double-stranded helix. Evidence in support of this model includes the data of viscosity,[4] the chemical reactivity of bound acridines,[6] polarized fluorescence,[5] sensitized fluorescence,[7] *etc.* On the other hand, Peacocke and his co-workes[8,9] proposed a modified intercalation model in order to interpret the effects of denaturation and the ionic strength on the interaction of acridines with DNA. In this model, the positively-charged nitrogen of the acridine ring associates closely with the negatively-charged phosphate group of DNA, and the flat acridine ring is inserted between adjacent bases on the same polynucleotide chain. In both models, the structure of acridine derivatives can be expected to influence their binding to DNA. Therefore, it is important to study the effect of the acridine structure on the interaction between acridines and DNA by using various acridine derivatives and various techniques.

In the present study, the DNA–acridine complexes were investigated by the fluorescence depolarization method,[10–13] using five derivatives of 3,6-diaminoacridine. The aims of this study are: (1) to obtain some information on the characteristics of the complex related to the rotation or internal motion of the bound acridine and (2) to reveal the relation between these properties and the structure of 3,6-amino groups.

Experimental

Materials. A highly-polymerized calf thymus DNA was purchased from the Worthington Biochemical Corporation. The concentration of DNA was determined spectrophotometrically at 259 nm, with an extinction coefficient per molar DNA phosphate ($\varepsilon_P=6600$). The hyperchromicity was 35% at room temperature and at an ionic strength of 0.01; this means that the DNA used was native. The thermal denaturation of DNA was performed by heating the DNA solutions for 20 min in boiling water and by then rapidly cooling them in ice water.

Acridine orange (AO) and proflavine (PF) were obtained from Chroma and British Drug Houses respectively. 3,6-Bis(methylamino)acridine ($Ac[NHMe]_2$), 3,6-bis(ethylamino)acridine ($Ac[NHEt]_2$), and 3,6-bis(diethylamino)-acridine ($Ac[NEt_2]_2$) were prepared according to the method described by Albert.[14] These acridines were purified by repeated recrystallizations and by chromatography.

Measurements. The solutions of the complexes were made up in a 0.005 M phosphate buffer (ionic strength of 0.01) at pH 6.8. This low ionic strength was used to minimize the amount of unbound acridine molecules. The acridine concentrations were $(1—2.5)\times10^{-6}$ M.

The absorption spectra were measured with a Shimadzu MPS-50L spectrophotometer.

The fluorescence spectra and polarization were measured with a Hitachi MPF-2A spectrophotofluorometer, with a pair of Polacoat dichroic filters as the polarizer and the analyzer. With the incident beam vertically polarized, the degree of polarization (P) is given by:[15,16]

1) D. F. Bradley and M. K. Wolf, *Proc. Nat. Acad. Sci. U.S.*, **45**, 944 (1959).
2) A. L. Stone and D. F. Bradley, *J. Amer. Chem. Soc.*, **83**, 3627 (1961).
3) A. R. Peacocke and J. N. H. Skerrett, *Trans. Faraday Soc.*, **52**, 261 (1956).
4) L. S. Lerman, *J. Mol. Biol.*, **3**, 18 (1961).
5) L. S. Lerman, *Proc. Nat. Acad. Sci. U.S.*, **49**, 94 (1963).
6) L. S. Lerman, *J. Mol. Biol.*, **10**, 367 (1964).
7) G. Weill and M. Calvin, *Biopolymers*, **1**, 401 (1963).
8) D. S. Drummond, V. F. W. Simpson-Gildmeister, and A. R. Peacocke, *ibid.*, **3**, 135 (1965).
9) N. J. Pritchard, A. Blake, and A. R. Peacocke, *Nature*, **212**, 1360 (1966).
10) F. Perrin, *J. Phys. Radium*, **7**, 390 (1926).
11) G. Weber, *Biochem. J.*, **51**, 145, 155 (1952).
12) G. Weber, *Advan. Protein Chem.*, **8**, 415 (1953).
13) R. F. Steiner and A. J. McAlister, *J. Polym. Sci.*, **24**, 105 (1957).
14) A. Albert, "The Acridines," Second Edition, St. Martin's Press, New York (1966), and the other papers cited therein.
15) T. Azumi and S. P. McGlynn, *J. Chem. Phys.*, **37**, 2413 (1962).
16) R. F. Chen and R. L. Bowman, *Science*, **147**, 1729 (1965).

$$P = \frac{I_{VV} - GI_{VH}}{I_{VV} + GI_{VH}} \quad (1)$$

where I_{VV} and I_{VH} are the measured fluorescence intensities with the analyzer vertically and horizontally oriented; the correction factor, $G = I_{HV}/I_{HH}$, is obtained with the incident beam horizontally polarized.

The fluorescence lifetimes were measured by means of a JASCO FL-10 phase fluorometer equipped with a 500-W xenon lamp and a CT-20P prism monochromator; the cut-off color and interference filters were used to select appropriate emission bands. The arrangement was similar to the one described in detail in an earlier paper.[17] The light emerging from the monochromator was modulated at a frequency of 13.56 MHz. The phase shifts of the fluorescent samples were measured by comparison with the phase shift of light scattered from a colloidal solution of silica.[18]

The measurements of the flow dichroism were carried out at 25 °C by the use of a Shimadzu QV-50 spectrophotometer equipped with an attachment. The datails of the theory and the experiment procedures have previously been reported by Wada and Kozawa.[19]

All the measurements except those of the flow dichroism were made at temperatures from 10 to 70 °C.

Results and Discussion

A typical fluorescence polarization spectrum is shown for the DNA–Ac[NHMe]$_2$ complex in Fig. 1. No change in the P value was observed at the wavelengths from 400 to 490 nm; this indicates that only one electronic transition exists in this wavelength region.[7,20] The other complexes gave similar polarization spectra. Therefore, the complexes were excited in this wavelength region. Further, no significant change in the P value was observed at N/A values higher than *ca.* 100. Our equilibrium dialysis and absorption data[21] showed that almost all the acridine molecules are bound to DNA at a high N/A value and even at elevated temperature up to 65 °C. Accordingly, the value of P at a sufficiently high N/A value can be expected to reflect the rotational characteristics of the unit to which

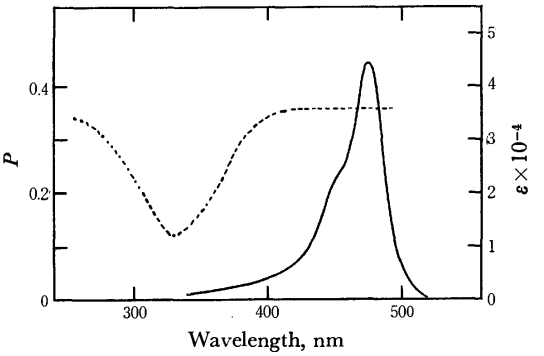

Fig. 1. Fluorescence polarization (·····) and absorption (——) spectra of a native DNA–Ac[NHMe]$_2$ complex at 25 °C. Ac[NHMe]$_2$: 2.2×10^{-6} M, N/A: 240

17) A. Müller, R. Lumry, and H. Kokubun, *Rev. Sci. Instrum.*, **36**, 1214 (1965).
18) Dupont Colloidal Silica, "Ludox" AS.
19) A. Wada and S. Kozawa, *J. Polym. Sci.*, **A2**, 853 (1964).
20) V. Zanker, *Z. Phys. Chem. N. F.*, **2**, 52 (1954).
21) Y. Kubota, Y. Eguchi, K. Hashimoto, and Y. Fujisaki, unpublished results.

Table 1. Polarization of the DNA-acridine complexes at 25 °C

Actridine	Native DNA		Denatured DNA	
	N/A	P	N/A	P
PF	270	0.34_2	300	0.27_4
AO	260	0.34_5	240	0.27_6
Ac[NHMe]$_2$	240	0.35_7	270	0.28_1
Ac[NHEt]$_2$	260	0.35_4		
Ac[NEt$_2$]$_2$	240	0.32_3		

an acridine molecule is attached. The polarization of the complex at 25 °C is tabulated in Table 1. At every temperature investigated, the value of P in the case of denatured DNA was lower than that in the case of native DNA, and the value of P for Ac[NEt$_2$]$_2$ was smaller than those for other acridines.

For plane-polarized exciting light, the Perrin equation[10] relates the value of P to the molecular characteristics on the assumption that the molecule undergoing the Brownian rotation is spherical:

$$1/P - 1/3 = (1/P_0 - 1/3)(1 + RT\tau/\eta V) \quad (2)$$

where P_0 is the limiting value of P when $T/\eta = 0$; R, the gas constant; T, the absolute temperature; τ, the lifetime of fluorescence; η, the viscosity of the solvent, and V, the molar volume of the rotating molecule. The rotational relaxation time of this molecule (ρ_0) equals $3V\eta/RT$. If the molecule is ellipsoidal in shape the expression for P is given by:[11-13]

$$1/P - 1/3 = (1/P_0 - 1/3)(1 + 3\tau/\rho_h) \quad (3)$$

where $\rho_h = 3\eta V_e/RT$ is the harmonic mean of the three principal rotational relaxation times and where V_e is the effective hydrodynamic volume of the molecule.

If V and τ are constant, both equations predict a linear relation between $1/P$ and T/η, and the rotational relaxation time can be calculated by the determination of the slope (β) of such a plot:

$$\rho_h = 3(1/P_0 - 1/3)/(\beta \times T/\eta) \quad (4)$$

If V changes with the temperature, or if two or more rotational units of distinctly different volumes are present, deviations from linearity are to be expected.[11]

Figures 2 and 3 show some results of the plots of $1/P$ against T/η; η was assumed to be that of water and was interpolated from the values given in the literature.[22] For all the native DNA-acridine complexes studied in this work, there exists a linear relation between $1/P$ and T/η over the temperature range from 10 to *ca.* 60 °C. However, there is an abrupt increase in the value of $1/P$ above *ca.* 60 °C; this implies that the bound acridine now reflects the new rotational unit associated with the denaturation of DNA. The $1/P$ *vs.* T/η curves of the complexes are similar in shape to those reported by Anufrieva *et al.*[23] for DNA–AO complexes and by Ellerton *et al.*[24] for DNA–PF complexes. However, all the P values of Anufrieva

22) "Kagaku Binran (Kisohen II)," Maruzen, Tokyo (1966), p. 505.
23) E. V. Anufrieva, M. V. Vol'kenshtein, and T. V. Sheveleva, *Biofizika*, **7**, 554 (1962).
24) N. F. Ellerton and I. Isenberg, *Biopolymers*, **8**, 767 (1969).

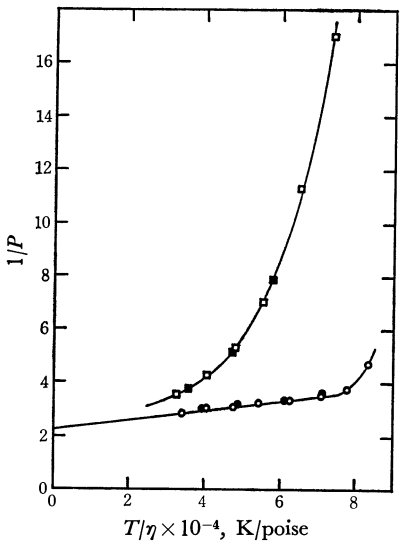

Eig. 2. Plots of $1/P$ *vs.* T/η for DNA–Ac[NHMc]$_2$ complexes.
Ac[NHMe]$_2$: 2.2×10^{-6} M
○ ●: native DNA (N/A=240)
□ ■: denatured DNA (N/A=270)
Symbols of ○ and □ denote data obtained on heating the solution, while those of ● and ■ denote data obtained on cooling the solution; the same notation is used in Fig. 3.

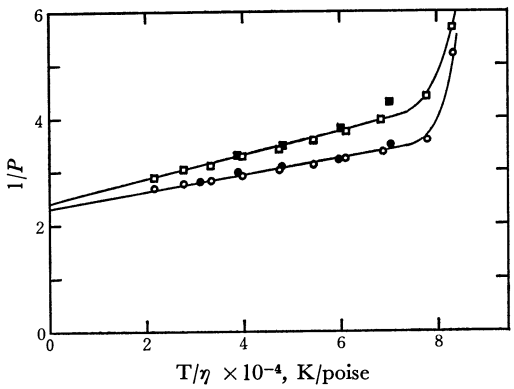

Fig. 3. Plots of $1/P$ *vs.* T/η for native DNA–Ac[NHEt]$_2$ and native DNA–Ac[NEt$_2$]$_2$ complexes.
○ ●: Ac[NHEt]$_2$ (2.0×10^{-6} M, N/A=260)
□ ■: Ac[NEt$_2$]$_2$ (2.2×10^{-6} M, N/A=240)

et al. are much lower than ours and those of Ellerton *et al.*

On the other hand, the value of P in the case of denatured DNA remarkably decreased with an increase in the temperature. As may be seen in Fig. 2, the plots of $1/P$ *vs.* T/η showed a marked departure from linearity. This phenomenon is probably due to the structural change in denatured DNA resulting from the collapse of the double-helical regions at elevated temperatures.[25]

The results obtained on cooling the solutions of the complexes from the maximum temperature (69 °C in all systems) are shown in Figs. 2 and 3. The temperature effects were in general reversible between 10 and 69 °C; a further elevation of the maximum temperature led to an irreversibility of the temperature

25) A. M. Michelson, "The Chemistry of Nucleosides and Nucleotides," Academic Press, New York (1963), p. 444.

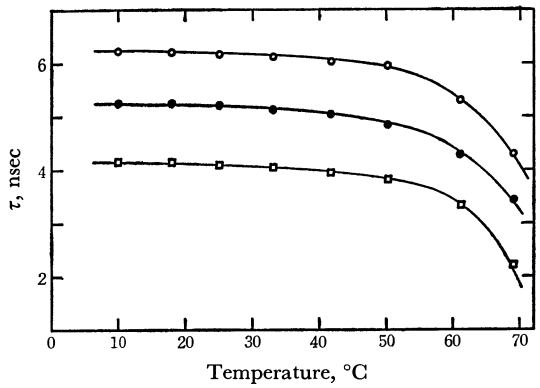

Fig. 4. The variation of fluorescence lifetimes (τ's) with temperature.
○: native DNA–PF (N/A=270)
●: native DNA–AO (N/A=260)
□: native DNA–Ac[NEt$_2$]$_2$ (N/A=240)

effects. This implies that, under the present experiment conditions, the tertiary structure of native DNA is not significantly lost as the polarization of the bound acridine is altered.

Next, the fluorescence lifetimes of the complexes were measured under each of the experimental conditions in order to ascertain the proper values for use in calculating the rotational relaxation times. Figure 4 shows the dependence of the fluorescence lifetimes on the temperature for the DNA–PF, DNA–AO, and DNA–Ac[NEt$_2$]$_2$ complexes. The value of τ for each complex declines very slowly with the temperature up to *ca.* 60 °C, but it sharply decreases above *ca.* 60 °C; this temperature coincides with the temperature at which the value of P rapidly decreases. Similar results were obtained in the cases of Ac[NHMe]$_2$ and Ac[NHEt]$_2$. Since almost all acridine molecules are bound to DNA under the present experiment conditions, the decrease of τ above *ca.* 60 °C may be ascribed to a certain change in the binding site associated with the denaturation of DNA. Further studies of the variation in τ with the temperature are in progress.

Table 2. Depolarization results at 25 °C

Acridine	N/A	τ (nsec)	P_0	ρ_h (nsec)
PF	470	6.1	0.43_5	$52._6$
	270	6.1	0.43_9	$52._0$
AO	930	5.2	0.44_4	$47._9$
	260	5.2	0.44_0	$48._4$
Ac[NHMe]$_2$	420	4.0	0.44_2	$47._9$
	240	4.0	0.43_9	$48._3$
Ac[NHEt]$_2$	260	4.0	0.43_5	$45._4$
Ac[NEt$_2$]$_2$	240	4.0_5	0.42_0	$32._1$

Because of the small variation in the value of τ below *ca.* 60 °C, the mean rotational relaxation times were evaluated by Eq. (4), using an average value of τ for each system and the slope of the linear portion of the $1/P$ *vs.* T/η plots. The calculated values are summarized in Table 2. The depolarization results in Table 2 show that: (1) the values of P_0 and ρ_h are independent of N/A, (2) the value of ρ_h is of almost the same order of magnitude except for Ac[NEt$_2$]$_2$,

(3) the value of ρ_h for $Ac[NEt_2]_2$ is much smaller than those for the other acridines, and (4) the value of P_0 for $Ac[NEt_2]_2$ is also lower than those for the others.

The ρ_h value of the bound acridine (30—50 nsec) is much larger than the value for the free acridine in water (a few tenths of 1 nsec), but it is much too small to correspond to the rotation of the whole DNA molecule.[26] Since almost all acridine molecules are bound and are very fara part under the present experimental conditions (high N/A value and low ionic strength), any depolarization due to the free acridine or energy transfer between bound acridine molecules may be ruled out. Furthermore, it has previously been shown[27] that the rate constant of an intercalation reaction between native DNA and PF is about 10^4—10^2 sec^{-1}; therefore, the dissociation of the bound acridine could not occur during the lifetime of the excited state (4—6 nsec).

From the measurements of the nanosecond anisotropy, Wahl *et al.*[28] determined the rotational relaxation time of DNA–ethidium bromide (EB) in water to be 28 nsec; this value is also much too small for the rotation of the whole DNA molecule. Wahl *et al.* proposed that the depolarization is due either to a restricted motion of the EB molecule in its binding site on DNA, without any motion of the DNA, or to a local deformation motion of the DNA, and they showed that the latter is the only likely hypothesis that fits the restraints of the intercalation model.[4,29]

On the other hand, studies of the fluorescence quenching[30] and equilibrium dialysis[31] of the DNA-acridine complexes showed that the binding constants of PF, AO, $Ac[NHMe]_2$, and $Ac[NHEt]_2$ are of the same order of magnitude, while that of $Ac[NEt_2]_2$ is much smaller than those of the others. This suggsets that the bulky diethylamino groups produce some steric hindrance of the binding.

Table 3. Flow dichroism at 25 °C[a]

Acridine	λ_{max}[b] (nm)	$B(\alpha)$[c] at λ_{max}
PF	462	−0.84
AO	502	−0.82
$Ac[NHMe]_2$	475	−0.84
$Ac[NHEt]_2$	476	−0.82
$Ac[NEt_2]_2$	508	−0.70

a) The molar concentration of DNA phosphate (M_P) is 1.38×10^{-3} M_P. $N/A=15$ to 50.
b) The maximum wavelength of absorption spectrum of the complex in the visible region.
c) The reduced dichroism at a perfect orientation. The value of $B(\alpha)$ was obtained according to the method described by Wada.[32]

In view of these findings, the depolarization results of $Ac[NEt_2]_2$ in Table 2 can be interpreted to show that the $Ac[NEt_2]_2$ molecule, when intercalated between base pairs, leads to a larger local change in the DNA helix and, hence, a larger local deformation motion than the other acridines. If this is the case, some difference in the orientation of the bound acridines can be expected to occur between $Ac[NEt_2]_2$ and the others. In practice, preliminary results on flow dichroism reveal that the magnitude of the dichroism for the DNA–$Ac[NEt_2]_2$ complex is much smaller than those for the other complexes (see Table 3). Further studies by flow techniques are now in progress to clarify the orientation of the bound acridines; the results will be presented in a subsequent paper.

This work was supported in part by a Grant for Scientific Research by the Ministry of Education.

26) P. K. Callis and N. Davidson, *Biopolymers*, **7**, 335 (1969).
27) H. J. Li and D. M. Crothers, *J. Mol. Biol.*, **39**, 461 (1969).
28) Ph. Wahl, J. Paoletti, and J. B. Le Pecq, *Proc. Nat. Acad. Sci. U.S.*, **65**, 417 (1970).
29) W. Fuller and M. J. Waring, *Ber. Bunsenges. Physik. Chem.*, **68**, 805 (1964).
30) G. Löber and G. Achtert, *Biopolymers*, **8**, 595 (1969).
31) Preliminary results at ionic strength of 0.01 and at 25 °C revealed that the binding constant of $Ac[NEt_2]_2$ is the order of 10^5 M^{-1}, while those of other acridines the order of 10^6 M^{-1}.
32) A. Wada, *Biopolymers*, **2**, 361 (1964).

Near-infrared Spectroscopic Studies of the States of Water in Lyotropic Liquid Crystals

Masuo AIZAWA and Shuichi SUZUKI

Research Laboratory of Resources Utilization, Tokyo Institute of Technology, Ookayama, Meguro-ku, Tokyo 152

(Received December 21, 1972)

The states of water in lyotropic liquid crystals of the polyoxyethylene–nonylphenylether and water system were investigated by means of near-infrared spectroscopic measurements. The states of water were classified into nonbonded, singly-hydrogen-bonded, and doubly-hydrogen-bonded states, and their relative concentrations were calculated from the intensities of the combination bands of $2\nu_1+\nu_3$ and $\nu_1+\nu_2+\nu_3$ in the temperature range from 25 to 50 °C. An increase in the hydrogen-bonded water species was found for the liquid crystal. Furthermore, the nonbonded and singly-hydrogen-bonded water species decreased, while the doubly-hydrogen-bonded water species increased in the liquid crystal structure, as compared with ordinary water. The structural properties of the liquid crystal are discussed.

Liquid crystalline structures may be prepared thermally from one component (thermotropic systems) or by the treatment of certain compounds with a controlled amount of water or other polar solvent (lyotropic systems). Lyotropic liquid crystals are strongly birefringent and may vary in texture from a turbid free-flowing fluid to a waxy substance or clear gel. A solvent is responsible for the formation of the lyotropic liquid crystals. Especially in the biological system, water plays an important role in the formation of the lyotropic liquid crystals.[1] The states of water in lyotropic liquid crystals, however, have not yet been clarified. We reported previously that the states of water involved in macromolecular gels should be classified into at least three groups, because most of the so-called free water has been found to be fairly restricted.[2-4] The present investigation was undertaken in order to determine the states of water in the lyotropic liquid crystals.

Various measurements, such as infrared and Raman spectroscopy, NMR, X-ray diffraction, and dielectric relaxation measurements, have been used in the studies of the structure of water. These methods have also been extended to aqueous solutions, and a number of structural models have been postulated for liquid water.[5] These models are generally classified into multi-state models and uniform-state models. For both a multi-state model and a uniform-state model, the degree of association of water has been the main subject of study. The vibrational spectroscopic investigation is effective, because it is extremely sensitive to the strength and extent of hydrogen bonding. The frequency of OH stretching vibrations is known to decrease in a regular manner with the strength of the hydrogen bonding. Therefore, Raman or infrared fundamental, overtone, and combination bands, which involve OH stretching, may serve as a probe of hydrogen bonding. As has been pointed out by Falk,[6] the frequencies of bending vibrations increase upon hydrogen bonding, but the shifts are much smaller, and, hence, somewhat less useful as a structural probe. As the combination bands involving OH stretching have been used successfully in quantitative investigations of the hydrogen bonding of water,[7-11] near-infrared spectroscopic analysis was carried out in this work.

The combination of nonionic surfactants and water being a typical example of how the lyotropic liquid crystals are formed, the polyoxyethylene–nonylphenylether and water system is used in this investigation. The water molecules are presumed to be strictly restricted in the lyotropic liquid crystal, because polyoxyethylene–nonylphenylether may be highly ordered and their hydrophilic sites may be hydrated. In view of the hydrogen-bonding association, the states of water in a lyotropic liquid crystal can be classified into three states: the nonbonded, singly-hydrogen-bonded, and doubly-hydrogen-bonded states. The concentrations of the nonbonded, singly-hydrogen-bonded, and doubly-hydrogen-bonded water species were calculated for this system by near-infrared spectrum analysis in the 900—1300 nm region.

Experimental

Materials. The polyoxyethylene–nonylphenylether was supplied by the Kao Atlas Co., Ltd. The average polymerisation degree of the oxyethylene residue is 13.2. This nonionic surfactant is denoted as C_9Ph_{13} in this paper.

Near-infrared Spectra. The spectra were recorded with a Shimazu SV-50A spectrophotometer. All the measurements were made with water or an aqueous solution in a 1-cm cell and with an empty cell in the reference beam. Temperature control for the sample and the reference cells was achieved with circulating water at a fixed temperature.

1) J. L. Fergason and G. H. Brown, *J. Amer. Oil Chem. Soc.*, **45**, 120 (1968); G. T. Stewart, *Mol. Cryst. Liq. Cryst.*, **7**, 75 (1969).
2) J. Mizuguchi, M. Takahashi, and M. Aizawa, *Nippon Kagaku Zasshi*, **91**, 723, 961 (1970).
3) M. Aizawa and S. Suzuki, This Bulletin, **44**, 2967 (1971).
4) M. Aizawa, J. Mizuguchi, S. Suzuki, S. Hayashi, T. Suzuki, N. Mitomo, and H. Toyama, *ibid.*, **45**, 3031 (1972).
5) D. Eisenberg and W. Kauzmann, "The Structure and Properties of Water," Oxford Univ. Press, London (1969), p. 254.
6) M. Falk and T. A. Ford, *Can. J. Chem.*, **44**, 1699 (1966).
7) K. Buijs and G. R. Choppin, *J. Chem. Phys.*, **39**, 2035 (1963).
8) G. R. Choppin and K. Buijs, *ibid.*, **39**, 2042 (1963).
9) O. D. Bonner and G. B. Woolsey, *J. Phys. Chem.*, **72**, 899 (1968).
10) O. D. Bonner, and G. B. Woolsey, *ibid.*, **72**, 2512 (1968).
11) G. R. Choppin and J. R. Downey, Jr., *J. Chem. Phys.*, **56**, 5899 (1972).

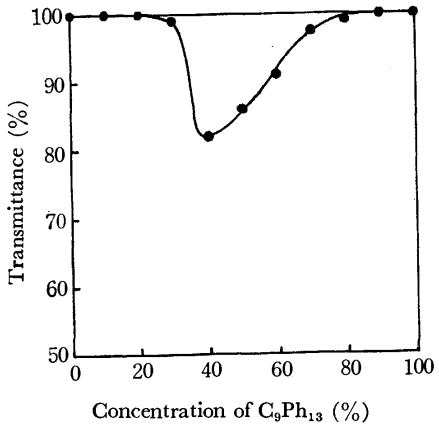

Fig. 1. Concentration dependence of transmittance at 900 nm.

Results

Near-infrared Spectra of Water in Lyotropic Liquid Crystals. Polyoxyethylene–nonylphenylether (C_9Ph_{13}) is known to form a smectic liquid crystal with less than approximately 75% of water. The transmittance measured at 900 nm in this experiment is shown in Fig. 1 for various C_9Ph_{13} contents. The transmittance becomes poor in the concentration range from 40 to 60% of C_9Ph_{13}. In the above concentration range, these mixtures form a gel at room temperature. The rheological properties of these mixtures have been reported elsewhere.[8]

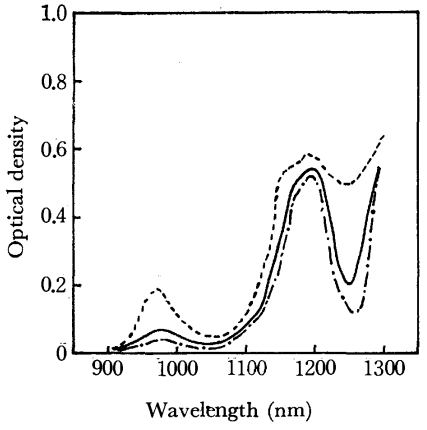

Fig. 2. Spectra of water in liquid crystals containing 60% (——), 80% (—·—) of C_9Ph_{13}, and pure water (·····) at 25 °C.

The near-infrared spectra of water in liquid crystals containing 60 and 80% of C_9Ph_{13} at 25 °C are presented in Fig. 2. The spectrum of pure water is illustrated as a reference. As has been reported by Buijs and Choppin,[7] the absorption band at 977 nm can be assigned to the combination band of $2\nu_1+\nu_3$, and the bands at 1160 and 1200 nm, to that of $\nu_1+\nu_2+\nu_3$, where ν_1 (symmetric stretching), ν_2 (bending), and ν_3 (asymmetric stretching) are the fundamental vibrations. As for the bands around 1200 nm, the three peaks at 1160, 1200, and 1250 nm were assigned to the bands of the water species involving 0, 1, and 2 hydrogen bondings respectively.[7] As the temperature is raised, the bands have been observed to become sharper and to shift toward the blue, so as to approach a constant wavelength asymptotically. On the contrary, the formation of hydrogen bonding is known to shift the water bands toward the red.[9–10]

As is shown in Fig. 2, the peak of $2\nu_1+\nu_3$ in the lyotropic liquid crystals was observed to shift to a longer wavelength compared with that of ordinary water. In addition, the peak height at 1160 nm attributed to the monomeric water species is suppressed. These spectra suggest that the monomeric water species decrease in the liquid crystals. The association degree of water in the liquid crystals was surveyed by the quantitative analysis of both the $2\nu_1+\nu_3$ and $\nu_1+\nu_2+\nu_3$ bands.

Hydrogen Bonding of Water in the Liquid Crystal. The band of $2\nu_1+\nu_3$ was analysed in order to estimate the association degree of water. As has been described above, the band of $2\nu_1+\nu_3$ can be expected to shift to a longer wavelength in the liquid crystals because of the decrease in monomeric water species.

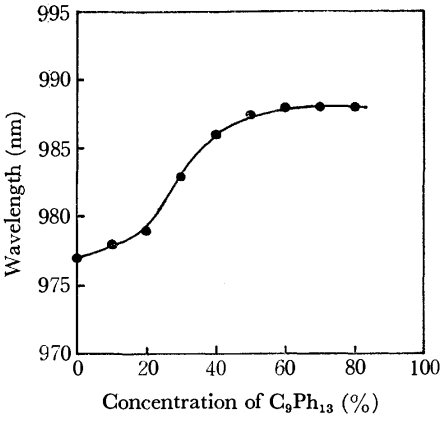

Fig. 3. Concentration dependence of the wavelength at $2\nu_1+\nu_3$ band.

The concentration dependence of the $2\nu_1+\nu_3$ band is shown in Fig. 3. The maximum of the $2\nu_1+\nu_3$ band shifts to a longer wavelength with an increase in the C_9Ph_{13} concentration, reaching approximately 988 nm. This indicates that the association degree of water increases in the liquid crystals in which the C_9Ph_{13} concentration is more than approximately 30%.

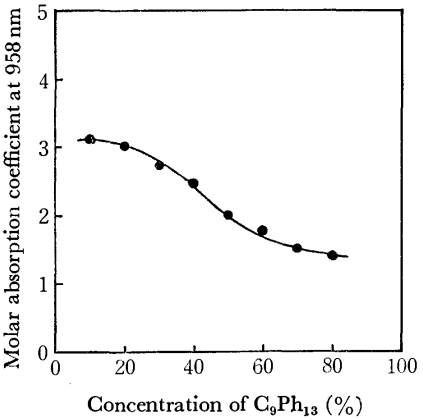

Fig. 4. Molar absorption coefficients at 958 nm for various concentrations of C_9Ph_{13}.

As the characteristic band for liquid monomeric water has been reported to be 958 nm, the absorbance at 958 nm may serve as a measure of the amount of liquid monomeric water. If the hydrogen-bonding association increases in the liquid crystals, the molar absorption coefficient at 958 nm can be expected to decrease in the liquid crystals. In Fig. 4, the molar absorption coefficient at 958 nm is shown for various concentrations of C_9Ph_{13} at 25 °C. A marked suppression of the molar absorption coefficient at 958 nm was observed in the liquid-crystal phase. Thus, it is reasonable to state that most of the monomeric water species disappear because of the strong interaction between C_9Ph_{13} and water in the liquid crystals.

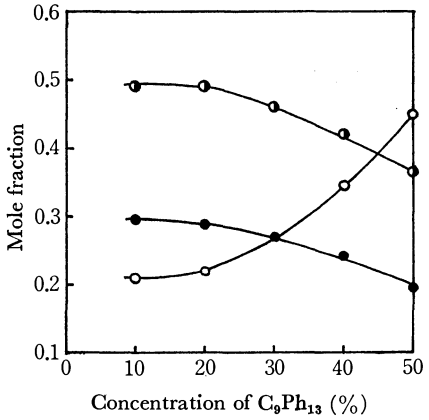

Fig. 5. Mole fractions of nonbonded (—●—), singly-bonded (—◑—), and doubly-bonded (—○—) water species in various concentrations of C_9Ph_{13}.

The relative amounts of nonbonded, singly-bonded, and doubly-bonded water species can be calculated according to the method of Buijs and Choppin.[7] In Fig. 5, C_0, C_1, and C_2, which are the relative concentrations of nonbonded, singly-bonded, and doulby-bonded water species respectively, are presented for various C_9Ph_{13} concentrations at 25 °C.

A baseline in the range from 1100 to 1300 nm was constructed so as to deduct the contribution of the strong band of water at 1447 nm and the sharp band of C_9Ph_{13} at 1200 nm. The baseline was calculated from a sum of the exponentials, $A=A_1e^{d_1(\lambda-\lambda_0)}+A_2e^{d_2(\lambda-\lambda_0)}$, for the band at 1447 nm[7] and by multiplying the observed molar absorption coefficients of C_9Ph_{13} at 1160, 1200, and 1250 nm with the molar concentration of the liquid crystals. The molar absorption coefficients of C_9Ph_{13} were then determined in the temperature range surveyed. The influence of the band at 980 nm was disregarded. The quantitative correction becomes difficult in the concentrated liquid crystals because of the marked disturbance by the band of C_9Ph_{13}. Therefore, C_0, C_1, and C_2 were calculated in the concentration range from 0 to 50% of C_9Ph_{13}.

As was expected, not only C_0 but also C_1 decreases with an increase in the C_9Ph_{13} concentration. A decrease in C_0 and C_1 was observed in the liquid crystals containing more than 30% of C_9Ph_{13}. In contrast with C_0 and C_1, an increase in C_2 was found in the above liquid crystals. Thus, most of the water in the liquid crystals is singly- or doubly-hydrogen-bonded and the monomeric water species are reduced compared with ordinary water. An increase in the doubly-bonded water species is characteristic in this system.

Temperature Effect on the States of Water in the Liquid Crystal. The physicochemical properties, such as the viscosity and birefringence of the liquid crystal, show a drastic change at approximately 40 °C. Such a drastic change may be caused by the structural change in the liquid crystal. Therefore, the states of water can be expected to show anomalous changes accompanying the above changes.

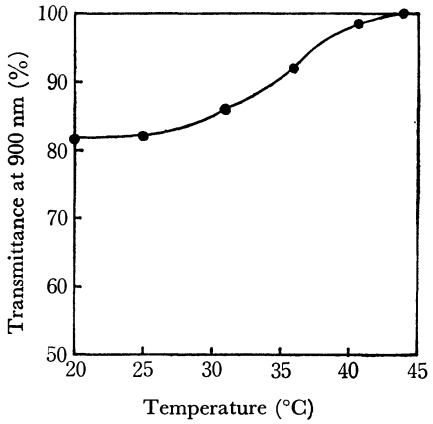

Fig. 6. Temperature dependence of transmittance at 900 nm for the liquid crystal containing 40% of C_9Ph_{13}.

The transimittance at 900 nm is a suitable measure for following the structural transition of the liquid crystal. The temperature dependence of the transmittance at 900 nm is shown in Fig. 6 for the liquid crystal containing 40% of C_9Ph_{13}. Though this liquid crystal shows a poor transmittance at room temperature, it gives excellent transparency above approximately 40 °C. A kind of structural transition may occur around this temperature.

If such a structural transition is caused by dehydration, the relative concentration of the monomeric water species, C_0, will increase. The temperature effect on the relative concentrations of nonbonded, singly-bonded, and doubly-bonded water species is shown in Fig. 7

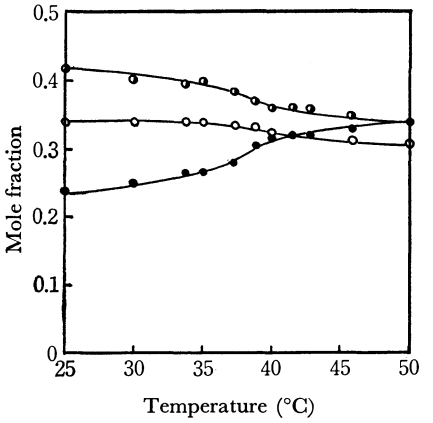

Fig. 7. Temperature dependence of mole fractions of nonbonded (—●—), singly-bonded (—◑—), and doubly-bonded (—○—) water species in the liquid crystal containing 40% of C_9Ph_{13}.

for the liquid crystal containing 40% of C_9Ph_{13}. The relative concentration of the nonbonded water species, C_0, increases gradually with an increase in the temperature. Accompanying the temperature dependence of C_0, the relative concentrations of the singly-bonded and doubly-bonded water species, C_1 and C_2, decrease with an increase in the temperature. These changes indicate that a marked dehydration of C_9Ph_{13} occurs with the structural transition in this temperature range.

Discussion

The spectrum analysis of the combination bands, $2\nu_1+\nu_3$ and $\nu_1+\nu_2+\nu_3$, has revealed that the degree of hydrogen-bond association increases in the lyotropic liquid crystals compared with ordinary water. For instance, in the liquid crystal containing 50% of C_9Ph_{13}, only 18% of the water is nonbonded, whereas approximately 32% of the water is nonbonded in ordinary water at 25 °C. In addition, the relative concentration of the doubly-hydrogen-bonded water species exceeds that of the singly-hydrogen-bonded ones in the liquid crystal. Such an increased degree of hydrogen-bond association, especially doubly-hydrogen-bond association, may be closely related to the mechanism of the liquid-crystal formation.

One of the possible explanations for the increase in the doubly-hydrogen-bonded water species is the hydration to the ether bonds of the polyoxyethylene chain. Each hydrogen atom of water can be linked with the oxygen atom of an ether bond in the polyoxyethylene chain. Water molecules may be bridged between two polyoxyethylene chains by hydrogen bonding. Gel formation may be caused by such a water bridge. This explanation is supported by the temperature dependence of the concentration of the doubly-hydrogen-bonded water species. The hydrogen bonds dissociate markedly around 40 °C, at which temperature the gel recovers fluidity. Moreover, it has been reported that this liquid crystal changes its birefringence from positive to negative with a phase transition of the liquid crystal at approximately 40 °C.[9] Therefore dehydration is thought to occur around 40 °C and to give fluidity.

The C_9Ph_{13} and water system is known to form smectic liquid crystals. The molecules in the smectic structure may be arranged in neat rows within individual layers or the molecules within a layer may be randomly distributed. The orientation of the C_9Ph_{13} and water molecules, however, cannot be determined by this method. The mobility and orientation of water molecules in lyotropic liquid crystals are now under investigation.

12) S. Kuroiwa, *Kogyo Kagaku Zasshi*, **63**, 1384 (1960).
13) S. Kuroiwa, *ibid.*, **70**, 2103 (1967).

BULLETIN OF THE CHEMICAL SOCIETY OF JAPAN, VOL. 46, 2637—2642 (1973)

Emission Spectra of Benzene, Toluene, and Xylenes by Controlled Electron Impact

Teiichiro OGAWA, Masaharu TSUJI, Minoru TOYODA, and Nobuhiko ISHIBASHI

Faculty of Engineering, Kyushu Unviersity, Hakozaki, Fukuoka 812

(Received January 11, 1973)

The emission spectra of gaseous aromatic hydrocarbons under electron impact excitation (60—300 eV) were measured in the 220—450 nm region at very low pressures. A characteristic band was observed in all cases in the 240—340 nm region; this band was assigned to the transition from the lowest excited singlet state to the electronic ground state. Photoemissions from the fragment species, such as H (Balmer series) and CH (A→X, B→X), were also observed. The excited species were concluded, from the relations of the emission intensities to the electron-beam current and to the gas pressure, to be produced by one-electron processes. The relative intensity and the vibrational structure of the observed spectra were examined and compared with those of the fluorescence spectra produced by photo-excitation.

The electric discharge method has been one of the most effective ways of studying excited molecules and their emission spectra. Although the methods are very useful in the detection of unstable species, however, the complicated character of the discharge is a major obstacle for any detailed analysis of the mechanism of fragmentation and excitation of the species concerned. The ideal way to produce excited molecules by means of electrons is, in this respect, the crossed electron and molecular-beam method,[1] in which the photoemission of excited species can be obtained at very low pressures, where the effect of molecular collision is greatly reduced and the energy of electrons can be controlled. However, the disadvantage of this method is the low intensity of photoemission. Although recent developments in instrumentation have made the study of smaller molecules feasible, little has been done on complicated organic molecules.

Extensive studies have been carried out in recent years on the excited species of the aromatic hydrocarbons. The fluorescence spectra in the gas phase

1) T. Horie, T. Nagura, and M. Otsuka, *J. Phys. Soc. Jap.*, **11**, 1157 (1956).

at low pressures have been observed for benzene,[2-5] toluene,[5,6] and other aromatic molecules.[5] Electron impact is an effective alternate method for exciting molecules at low pressures in the gas phase. The spectroscopic investigation of the electron-molecule collisions of these molecules would not only give the emission spectra by a different excitation method, but would also reveal the mechanism of the collision and fragmentation.

The emission spectra of fragment species of methane and chlorinated methanes[7] and methanol[8] under electron impact excitation have been reported. The emission spectra of benzene by controlled electron impact have been measured in the 240—300 nm region, and the lifetime of the $^1B_{2u}$ state has been studied.[9] The emission spectra of toluene and anisole[10] and of xylenes[11] in the 250—450 nm region obtained by this method have also been communicated by the present authors. In the present report, detailed results on benzene, toluene, and xylenes will be described and the relationship between the emission spectra obtained by the controlled electron impact method and the fluorescence spectra obtained by photo-excitation will be discussed.

Experimental

The sample vapor was crossed so as to collide with an electron beam in a chamber, as is shown schematically in Fig. 1. The cell was made of glass and was about 4.5 cm in diameter and about 40 cm in length. The electron was emitted from a tungsten filament (a), was accelerated by three electrodes (c, d, e), and was introduced into the collision chamber through a slit (2×15 mm) in the center of one of the electrodes (c). Two electromagnets (h) were placed so as to collimate the electron beam. The voltages of the two electrodes in the collision chamber (b, c) were set equal for the quantitative measurements. After being purified in a vacuum line (j) by repeated freezing and pumping, the sample was jetted into the collision chamber through a nozzle 0.1—1.0 mm in diameter (g). The chamber was evacuated (i) continuously to a high vacuum; a Penning gauge attached to the chamber indicated a pressure of the order of 10^{-4}—10^{-5} mmHg during the electron-impact measurements. The actual pressure in the impact region was expected to be higher than the value indicated and smaller than 10^{-2} mmHg. The sample vapor was excited by the collision with the electron, and the photoemission was observed through a quartz window (f). An electron beam of 10—1000 μA at 60—300 eV was used for the excitation. The energy distribution of the incident electron was not measured;

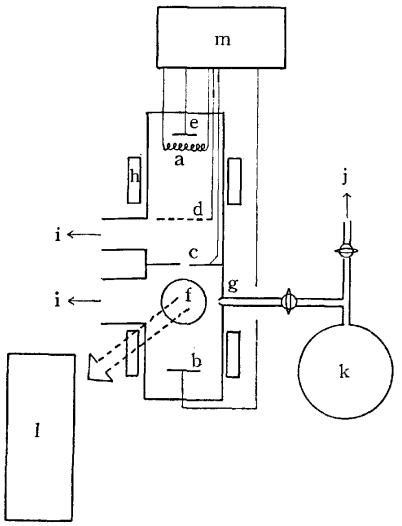

Fig. 1. Schematic diagram of the collision chamber. Controlled electron beam was introduced through a slit (c) and sample vapor was jetted through a nozzle (g). Photoemission at the collision region was observed through a quartz window (f). (a) tungsten filament, (b) electron target, (c) electrode with a slit in its center, (d) electrode, (e) electrode, (f) quartz window, (g) nozzle, 0.1—1.0 mm in diameter, (h) electromagnet, (i) to diffusion pump, (j) to vacuum line for the sample preparation, (k) gas reservoir to store sample vapor before use, (l) monochromator, (m) power supply.

however, it is expected to be no less than the voltage used for heating the filament (6—9 V).

The fluorescence spectra under photon-excitation were taken by the use of a standard quartz cell (10×10 mm) placed just in front of the entrance slit. The sample vapor in the cell was irradiated with a Hamamatsu TV L299 low-pressure mercury lamp.

The spectra were obtained with a Jarrell-Ash JE25 monochromator equipped with two 1200 groove/mm gratings blazed for 300 and 600 nm, and it had a reciprocal dispersion of about 33 Å/mm. The photons were detected photoelectrically with an EMI 9558QB photomultiplier and a Burr-Brown 3421J OP amplifier. The wavelength was calibrated by means of a low-pressure mercury lamp. The further details of the apparatus have been described elsewhere.[12]

All the compounds used were of a JIS specially pure reagent grade and were obtained from either Wako Pure Chemical Ind. or the Kishida Chemical Co.

Results and Discussion

A typical emission spectrum of benzene by electron impact is shown in Fig. 2. The impact voltage was 200 V and the electron-beam current was 1 mA in this measurement. The bands in the 250—300 nm region agreed well with those of Smith[9] and were assigned to the vibronic band of the forbidden $^1B_{2u}$—$^1A_{1g}$ transition. The transitions from vibrationally-excited states of the upper electronic level such as $6_1^0 1_0^2$ [13] (255 nm) and $6_1^0 1_0^1$ (260 nm) are quite intense.

2) M. Nishikawa and P. K. Ludwig, *J. Chem. Phys.*, **52**, 107 (1970).
3) C. S. Parmenter and M. W. Schuyler, *ibid.*, **52**, 5366 (1970).
4) H. F. Kemper and M. Stockburger, *ibid.*, **53**, 268 (1970).
5) J. M. Blondeau and M. Stockburger, *Ber. Bunsenges. Phys. Chem.*, **75**, 450 (1971).
6) C. S. Burton and W. A. Noyes, Jr., *J. Chem. Phys.*, **49**, 1705 (1968).
7) T. Ogawa, I. Fujita, M. Hatada, and K. Hirota, This Bulletin, **44**, 659 (1971).
8) I. Fujita, M. Hatada, T. Ogawa, and K. Hirota, *ibid.*, **44**, 1751 (1971).
9) W. H. Smith, *J. Chem. Phys.*, **54**, 4169 (1971).
10) T. Ogawa, M. Tsuji, M. Toyoda, and N. Ishibashi, *Chem. Lett.*, **1972**, 233.
11) T. Ogawa, M. Tsuji, M. Toyoda, and N. Ishibashi, *ibid.*, **1972**, 1157.
12) T. Ogawa, M. Toyoda, M. Tsuji, and N. Ishibashi, *Technology Repts. Kyushu Univ.*, **45**, 427 (1972).
13) When a certain normal mode m is involved in an electronic transition, the notation m_k^i shows that there is a transition from the ith vibrational level m^i in the upper electronic state to the kth vibrational level m_k in the ground electronic state. J. H. Callomon, T. M. Dunn, and I. M. Mills, *Phil. Trans. Roy. Soc.* (London), **A259**, 499 (1966).

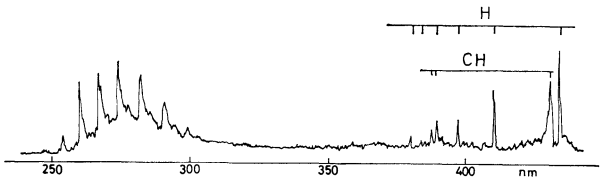

Fig. 2. Emission spectrum of benzene by electron impact. 200 V impact at 1 mA.

Balmer series of the hydrogen atom and the $B^2\Sigma^- - X^2\Pi$ transition and the $A^2\Delta - X^2\Pi$ transition of the CH radical were found in the 370—440 nm region. The Swan system of C_2 and Schüler's T spectrum of $C_4H_2^+$ were also observed in the 430—550 nm region.

The fluorescence spectra of benzene in the gas phase were taken at various excitation wavelengths; several different resonance spectra have been reported at such a low pressure as 0.2 mmHg, where collisional deactivation is not complete.[4,5] A comparison of those spectra with the present spectrum under electron-impact excitation reveals several points of interest. The equilibrated fluorescence[4] (the emission spectra of 0.2 mmHg benzene with 40 mmHg hexane, in which the Boltzmann equilibrium is established in the $^1B_{2u}$ state) shows no remarkable band above 267 nm, whereas the present spectrum has a strong band head at 261 nm ($6_1^0 1_0^1$). Since the pressure in the impact chamber was very low in the present study, molecular collisions were not so frequent that photoemission from vibrationally excited states was observed. The resonance spectra excited by irradiation with a monochromatic light[4,5] consist of only a few strong progressions and appear to be simpler than the present spectrum. This finding is probably connected with the facts that the excitation energy of the electron impact is higher and the energy distribution of the electron beam is broader than those in the case of the photon excitation with a monochromatic light. The variation in impact voltage between 60—300 V did not, however, induce any remarkable change in the appearance of the spectrum under the resolution of the spectrometer used. It seems

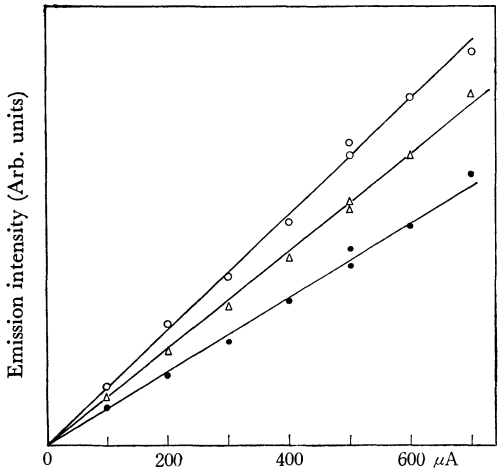

Fig. 3. Dependence of photoemission intensity on the electron beam current. Emission of excited benzene molecules at the impact voltage of 150 V.
○: $6_1^0 1_1^0$ band, △: $6_1^0 1_0^0$ band, ●: $6_1^0 1_0^1$ band.

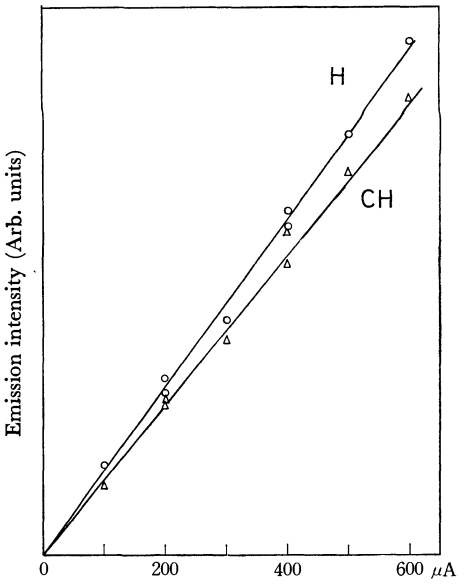

Fig. 4. Dependence of photoemission intensity on the electron beam current. Emission of fragment species at the impact voltage of 150 V.
○: atomic hydrogen, △: CH radical.

that the molecule received enough excess energies even when excited with electrons of 60 V; a similar emission spectrum was observed upon excitation by electrons with higher energies.

The dependence of the emission intensity on the electron-beam current was measured; the results are shown in Figs. 3 and 4. The intensities of the photoemission of the excited parent species of benzene and of the fragment species (H and CH) were proportional to the electron-beam current. Thus, the excitation of a π electron of benzene is concluded to be a one-electron process, as is that of fluorobenzene.[14] The fragmentations of benzene to H and to CH are also concluded

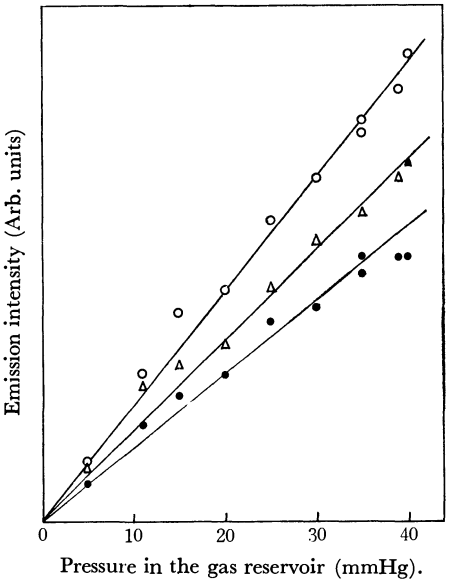

Fig. 5. Dependence of photoemission intensity on the gas pressure in the gas reservoir. Emission of excited benzene molecules. Impact voltage 200 V; electron beam current 70 μA.
○: $6_1^0 1_1^0$ band, △: $6_1^0 1_0^0$ band, ●: $6_1^0 1_0^1$ band.

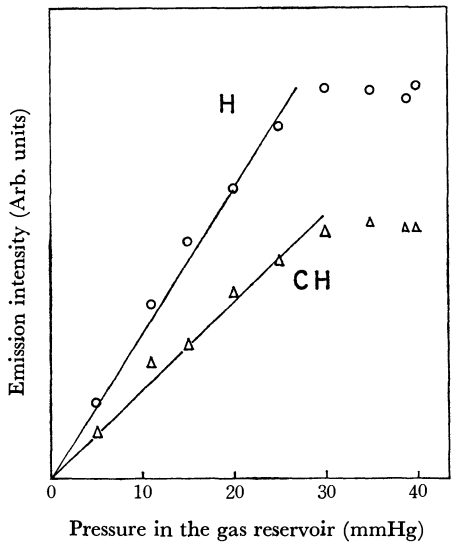

Fig. 6. Dependence of photoemission intensity on the gas pressure in the gas reservoir. Emission of fragment species. Impact voltage 200 V; electron beam current 70 μA.
○: atomic hydrogen, △: CH radical.

to be one-electron processes; an identical conclusion has previously been obtained in the case of methane.[7]

The relationship between the emission intensity and the gas pressure in the gas reservoir was also measured in the case of benzene; the results are shown in Figs. 5 and 6. The intensities of the photoemission of the excited parent species and of the fragment species (H and CH) were found to be proportional to the gas pressure in the gas reservoir. The gas pressure in the gas reservoir can be expected to be proportional to the pressure in the impact region since the gas is jetted through a small nozzle; this presumption was confirmed in the case of nitrogen by measuring the pressure in the impact chamber. This finding indicates that intermolecular quenching processes by collisions are not important.

The proportionality between the emission intensity and the amount of electrons and molecules mentioned above is also found in the photoemission of various molecules.[7,14] This result seems to indicate that the excitation and the fragmentation take place through one-electron processes, such as;

$$X \xrightarrow{\text{electron}} X^* \qquad (1)$$

$$X \xrightarrow{\text{electron}} X^{**} \begin{cases} \xrightarrow{\text{fast}} X^* \\ \xrightarrow{\text{fast}} H^*, CH^* \cdots \end{cases} \qquad (2)$$

where X stands for benzene, where * indicates the lower electronically excited state from which the photoemission was observed, and where ** indicates highly excited states, which are probably some kinds of superexcited states.[15] Although the relative importance of the two processes, (1) and (2), could not be determined in the present study, the observation of the Balmer series of hydrogen implies the importance of the second process, since the excitation energy of a typical line of this series (12—13 eV) is more than the typical ionization potential of aromatic hydrocarbons (*ca.* 9 eV). The role and the importance of the superexcited states have also been discussed in the case of the electron impact of CH_4[16] and in the field of radiation chemistry[15] and mass spectrometry.[17]

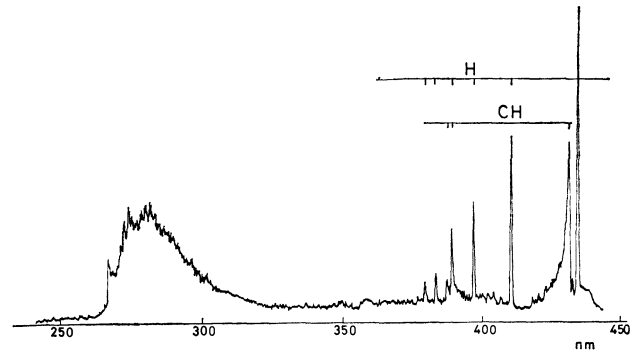

Fig. 7. Emission spectrum of toluene by electron impact. 300 V impact at 1 mA.

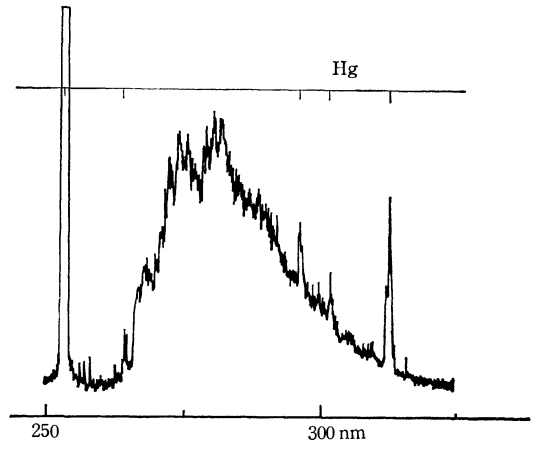

Fig. 8. Emission spectrum of toluene under photon excitation by a low-pressure mercury lamp (2537 Å). vapor pressure, about 10 mmHg.

A typical emission spectrum of toluene under electron-impact excitation is shown in Fig. 7, and that under photon excitation in Fig. 8. A characteristic band was observed in the 270—320 nm region, and the band in Fig. 7 is very similar to that in Fig. 8. The photoemission of H and CH was also observed in the case of electron impact. Since the symmetry of the molecule is C_{2v} for toluene, the 0—0 transition (267 nm) is allowed, unlike the case in benzene. The characteristic band of toluene is located in a longer wavelength region than that of benzene. This band is broader than that of benzene; however, several fine structures between 267—300 nm could be observed above the non-resolved background.

The fluorescence spectra of toluene in the gas phase were observed at 0.1 mmHg[5] and at 20 mmHg.[6] The location and the shape of the present spectrum

14) T. Ogawa, M. Tsuji, M. Toyoda, and N. Ishibashi, This Bulletin, **46**, 1063 (1973).
15) R. L. Platzman, *Radiation Res.*, **17**, 419 (1962).
16) D. A. Vroom and F. J. de Heer, *J. Chem. Phys.*, **50**, 573 (1969).
17) K. Hirota, *Nippon Kagaku Zasshi*, **89**, 327 (1968); **91**, 585 (1970).

under electron-impact excitation are similar to those of the latter, as is shown in Fig. 8. The most striking features of the former experiment are the loss of structure and the increase in the fraction of the background as the excitation energy is increased to higher vibronic levels. Blondeau and Stockburger[5] concluded that vibrational rearrangement dominated at higher vibrational levels and that discrete bands no longer were observable. Their spectrum excited at 932 cm^{-1} above the 0—0 level almost lost its vibrational progression. On the other hand, the present spectrum keeps some of its vibrational features even when the molecule is excited at 200 V. This finding is noteworthy, since the pressure in the impact chamber of the present study is extremely low. However, a detailed comparison of their spectra with the emission spectra obtained by electron impact would require a further improvement in the resolution of the present spectra. The fluorescence spectrum of toluene in solution[18] was found to correspond well to the emission spectrum obtained by electron impact.

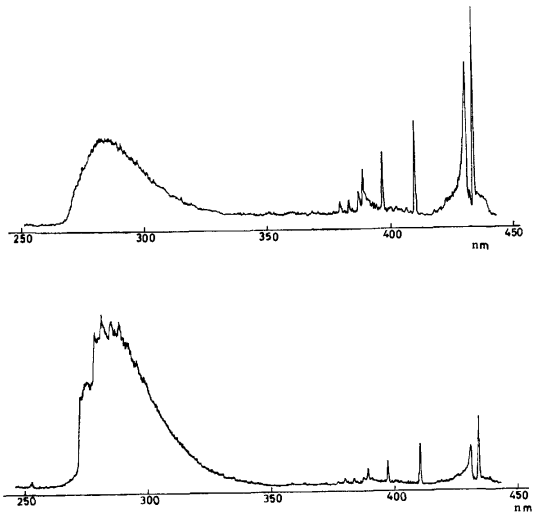

Fig. 9. Emission spectra of xylenes by electron impact.
Top; *o*-xylene, 300 V impact at 1 mA.
Bottom; *p*-xylene, 200 V impact at 1 mA.

Typical emission spectra of xylenes under electron-impact excitation in the 250—450 nm region are shown in Fig. 9. The spectrum of *m*-xylene is similar to that of *o*-xylene. A characteristic band is observed in the 270—340 nm region in all cases, though its location and the vibrational structures differ from each other. Thus, such aromatic molecules as benzene, toluene, xylenes, cumene,[19] and cymene[19] show a characteristic band in this region, and it may well be concluded that this band is a feature common to all aromatic hydrocarbons. The fluorescence spectra of aromatic hydrocarbons in dilute solutions[18] were found to correspond well to the emission spectra by electron impact for various molecules. Thus, all the characteristic bands observed in the present study were assigned to the transition from the lowest excited singlet state to the electronic ground state, as in the case of the fluorescence spectra. Although the energy of the electrons in the present study is much larger than that of the photons in the fluorescence study, the spectra under electron-impact excitation are in many cases similar to those under photon-impact excitation. This is superficially correlative to the fact that the electron-impact (energy-loss) spectra are closely related to the photoabsorption spectra of the same molecules.[20]

The spectrum of *p*-xylene has more vibrational structures and is less diffuse than that of *o*-xylene. This difference in the appearance of the spectra of the two molecules was also observed in the fluorescence in the gas phase[5] and in solution.[18] The relative intensities of the bands of the parent species over the hydrogen Balmer series are also remarkably different in the two spectra, as is shown in Fig. 9. (The cross sections for the formation of excited hydrogen atoms are reported to be almost the same for the different hydrocarbons.[16]) The fluorescence yield of *p*-xylene has been reported to be larger than those of *o*- and *m*-xylenes.[21] It can be concluded that molecules with higher symmetry have sharper and stronger bands than those with less symmetry in the emission spectra obtained by electron impact, just as in the fluorescence. In molecules with high symmetry, there are less vibrational modes which may interact with the electronic level than in those with low symmetry. The more complicated structure and the higher intensity of the emission band of *p*-xylene are probably to be ascribed to the difference in this vibronic interaction. The de-

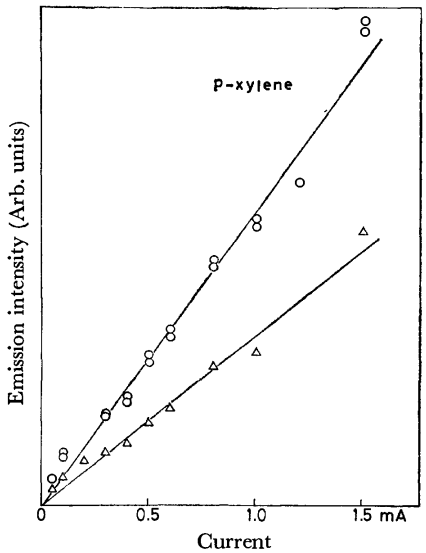

Fig. 10. Dependence of photoemission intensity on the electron beam current. Emission of excited *p*-xylene molecules at the impact voltage of 300 V.
○: features at 286, 302, and 312 nm (Since these three features have almost equal intensities, these are shown on the identical line).
△: feature at 277 nm.

18) I.S. Berlman, "Handbook of Fluorescence Spectra of Aromatic Molecules," Academic Press, N. Y. (1971).
19) T. Ogawa, M. Tsuji, M. Toyoda, and N. Ishibashi, unpublished.
20) E. N. Lassettre, A. Skerbele, M. A. Dillon, and K. J. Ross, *J. Chem. Phys.*, **48**, 5066 (1968).
21) W. A. Noyes Jr. and D. A. Harter, *J. Phys. Chem.*, **75**, 2741 (1971).

pendence of the intensity of the photoemission of *p*-xylene on the electron-beam current was measured. The four features of the band of the parent species at 277, 286, 302, and 312 nm showed a linear relationship, as is shown in Fig. 10. This linear relationship indicates that the excitation of a π electron of *p*-xylene is a one-electron process. The identical relationship was also observed for the photoemission of the hydrogen atom and the CH radical just as in the case of benzene.

In the emission spectra under electron-impact excitation, the photoemission from the small fragments of large molecules was usually observed more easily than that from the large parents themselves. It seems likely that larger species have more freedom of motion and of fragmentation and that non-radiative processes become more predominant. The aromatic molecules are exceptional molecules in that the excited large parent species give intense photoemission. The intensities of the photoemission of all the species mentioned above were found to be proportional to the electron-beam current and to the gas pressure. These results indicate that intermolecular quenching processes by collisions are unimportant and that superexcited states may be involved in the excitation.[14]

The few examples which have been discussed in this paper show that the electron-impact method is a useful one for studying electronic excited states. Further research with a higher resolution would reveal even more details on the mechanism of the excitation.

The authors wish to thank Professor Emeritus Kozo Hirota of Osaka University for his interest and encouragement, and Professors Tadao Horie and Tsuruji Iwai and Dr. Seiji Tsurubuchi of Osaka University for their advice on the design of the collision chamber. We also wish to thank Mr. Taketoshi Sonoda for his technical assistance. This work was supported by funds of the Ministry of Education (General research C, 1972)

BULLETIN OF THE CHEMICAL SOCIETY OF JAPAN, VOL. 46, 2642—2646 (1973)

A Theoretical Consideration of the Electron-scavenging Process in Liquid Hydrocarbons. IV. Integral Transforms in the Prescribed Diffusion Approximation

Hideo YAMAZAKI and Kyoji SHINSAKA

Laboratory of Physical Chemistry, Tokyo Institute of Technology, Meguro-ku, Tokyo 152

(Received January 26, 1973)

The relations of the integral transforms and the integral form between various distribution functions have been discussed in the prescribed diffusion approximation for the Smoluchowski equation. The initial electron distribution from the central-ion cluster in a spur or a track, $\omega(r, 0)$; the time dependence of the central value of the electron distribution, $\omega(0, t)$; the time dependence of the space-averaged electron concentration, $N(t)$, after pulse irradiation, and the scavenger-concentration dependence of the relative G-value of electron scavenging, $G_s(k_sC_s)$, as a function of the scavenger concentration, C_s, and the rate constant, k_s, are shown to be connected by this diagram of the Laplace transforms and the integral form:

$$\begin{array}{ccc} \omega(0, t) & \xleftarrow[\text{Laplace transform}]{} & \omega(r, 0) \\ \text{Integral form} \downarrow & & \\ N(t) & \xrightarrow[\text{Laplace transform}]{} & G_s(k_sC_s) \end{array}$$

By the use of this relation, the various distribution functions are evaluated from the generalized Gaussian initial distribution. The square-root relationship of the $G_s(k_sC_s)$ to the scavenger concentration is discussed.

The experimental and theoretical approaches to the electron-recombination process in the radiolysis of hydrocarbons have indicated that the various quantities measured are interconnected. Hummel[1] and Schuler[2] proposed that the scavenger-concentration dependence of the G-value for electron scavenging was connected with the time dependence of the charged species after pulse radiolysis by means of a Laplace transform. Recently, Mozumder[3] extended the prescribed diffusion approximation of the Smoluchowski equation to the multiple-ion spur, blob, and track. He obtained various relationships, namely, the time dependence of the concentration of the charged species after pulse irradiation as well as the G-value of electron scavenging, as functions of the scavenger concentration, using the initial Gaussian distribution of the thermalized electrons. Sato and Oka[4] and Tachiya[5] obtained the relation between the G-value of electron scavenging and the initial spatial distribution of the thermalized electrons by ignoring the effect of diffusion. In a

1) A. Hummel, *J. Chem. Phys.*, **49**, 4840 (1968).
2) S. J. Rzad, P. P. Infelta, J. M. Warman, and R. H. Schuler, *ibid.*, **52**, 3971 (1970).
3) Mozumder, *ibid.*, **55**, 3020 (1971): **55**, 3026 (1971).
4) S. Sato and T. Oka, This Bulletin, **44**, 856 (1971).
5) M. Tachiya, *J. Chem. Phys.*, **56**, 6269 (1972).

previous paper,[6] in which the diffusion term of the Smoluchowski equation was neglected, the present authors showed a square-type flow chart of interconnection by means of Laplace transforms among four characteristic functions, the initial spatial distribution of thermalized electrons, the scavenger-concentration dependence of the relative G-value of electron recombination, the time dependence of the electron concentration after pulse irradiation, and the life-time spectrum of the decay of the electron concentration after pulse irradiation. In this paper it will be shown that a similar square diagram of the flow chart of the characteristic functions is present in the prescribed diffusion approximation of the Smoluchowski equation. Various explicit expressions of the characteristic functions for the generalized Gaussian distribution of the thermalized electrons will be given using these relations of the integral transforms in the flow chart.

Theory

The Extended Form of the Smoluchowski Equation and its Prescribed Diffusion Approximation. The extended form of the Smoluchowski equation[7] for the time-dependent spatial distribution of electrons without any electron scavenger in spherical geometry or in cylindrical geometry is expressed by:

$$\frac{\partial C}{\partial t} = D(1/r^n)\frac{\partial}{\partial r}\left(r^n\frac{\partial C}{\partial r}\right) + \frac{u}{r^n}\frac{\partial}{\partial r}\left(r^n C\frac{\partial \psi}{\partial r}\right) \quad (1)$$

($n=2$, spherical geometry; $n=1$, cylindrical geometry),

where $C(r, t)$ is the distribution function, D is the diffusion constant, u is the mobility, and ψ is the static electric potential.

The electric-field strength is given thus for spherical geometry:

$$F_n = \frac{e\partial\psi(r,t)}{\partial r} = -e^2(N^+(r,t) - N(r,t))/\varepsilon r^2 \quad (2)$$

and thus for cylindrical geometry:

$$F_n = \frac{e\partial\psi(r,t)}{\partial r} = -2e^2(N^+(r,t) - N(r,t))/\varepsilon r \quad (3)$$

where the plus sign of the superscript denotes quantities for positive ions, ε is the dielectric constant, and $N^+(r, t)$ and $N(r, t)$ are given by:

$$N^+(r,t) = \int_0^r C^+(r,t)\mathrm{d}v \quad (4)$$

and:

$$N(r,t) = \int_0^r C(r,t)\mathrm{d}v \quad (5)$$

where $\mathrm{d}v$ is a volume element. For the sake of simplicity it is assumed that the positive ions are localized at the origin or in the z-axis:

$$C^+(r,t) = N(t)\delta(r) \quad (6)$$

where $\delta(r)$ means the Delta function of r; the prescribed diffusion approximation is used for the distribution of electrons:

$$C(r,t) = N(t)\omega(r,t) \quad (7)$$

where $\omega(r, t)$ is a solution for the corresponding diffusion equation. Equations (2) and (3) may then be rewritten as:

$$F_n = \frac{e\partial\psi(r,t)}{\partial r} = -e^2N(t)\left(1-\int_0^r\omega(r,t)\mathrm{d}v\right)\Big/\varepsilon r^2, \quad (8)$$

$$(\mathrm{d}v = 4\pi r^2\mathrm{d}r)$$

and:

$$F_n = \frac{e\partial\psi(r,t)}{\partial r} = -2e^2N(t)\left(1-\int_0^r\omega(r,t)\mathrm{d}v\right)\Big/\varepsilon r, \quad (9)$$

$$(\mathrm{d}v = 2\pi r\mathrm{d}r)$$

According to the analysis of Mozumder,[3] the electron decay by recombination is to be expressed in terms of the central value of the electron distribution, $\omega(0, t)$, for spherical and for cylindrical geometry:

$$\frac{N(t)}{N(0)} = 1\Big/\left[1+4\pi Dr_cN(0)\int_0^t\omega(0,t)\mathrm{d}t\right] \quad (10)$$

where $N(0)$ is the initial number of electrons in a spur or in a unit length of track and where $r_c(=e^2/\varepsilon kT)$ is the Onsager length. The details of the more general calculation for evaluating Eq. (10) are given in the Appendix. Inversely, the central value, $\omega(0, t)$, in a spur or in a track is given by the electron-decay function for recombination:

$$\omega(0,t) = \frac{\mathrm{d}}{\mathrm{d}t}\left\{\frac{1}{4\pi Dr_c}\left(\frac{1}{N(t)}-\frac{1}{N(0)}\right)\right\} \quad (11)$$

Relations of Laplace Transforms. Since $\omega(r, t)$ is the solution of a diffusion equation, the central values of distributions in a spherical spur and in a cylindrical track are expressed in terms of the initial distribution:

$$\omega(0,t) = \frac{4\pi}{(2\sqrt{\pi Dt})^3}\int_0^\infty \exp(-r^2/4Dt)\omega(r,0)r^2dr \quad (12)$$

and:

$$\omega(0,t) = \frac{2\pi}{(2\sqrt{\pi Dt})^2}\int_0^\infty \exp(-r^2/4Dt)\omega(r,0)r\mathrm{d}r \quad (13)$$

The relation between the initial distribution and the central value of distribution in spherical geometry can be conveniently described by the Laplace transform:

$$\omega(0, 1/4D\tau)\sqrt{\pi}/2\sqrt{\tau}^3 = \int_0^\infty \exp(-\xi\tau)\omega(\sqrt{\xi}, 0)\sqrt{\xi}\,\mathrm{d}\xi \quad (14)$$

and:

$$\omega(\sqrt{\xi}, 0)\sqrt{\xi} = \frac{1}{2\pi i}\int_{c-i\infty}^{c+i\infty}\omega(0, 1/4D\tau)\frac{\sqrt{\pi}}{2\sqrt{\tau}^3}\exp(\xi\tau)\mathrm{d}\tau \quad (15)$$

where τ and ξ are the substitutions of $1/4Dt$ and r^2 respectively, and where c is taken as having a larger real value than the conversion axis. Similarly, the Laplace transforms in cylindrical geometry are:

$$\omega(0, 1/4D\tau)/\tau = \int_0^\infty \exp(-\xi\tau)\omega(\sqrt{\xi}, 0)\mathrm{d}\xi \quad (16)$$

and:

$$\omega(\sqrt{\xi}, 0) = \frac{1}{2\pi i}\int_{c-i\infty}^{c+i\infty}\omega(0, 1/4D\tau)\frac{1}{\tau}\exp(\xi\tau)\mathrm{d}\tau \quad (17)$$

According to Hummel,[1] Schuler,[2] and Mozumder,[3] the G-value, G_s, of electron scavenging is expressed by the Laplace transform of $N(t)/N(0)$:*1

6) H. Yamazaki and K. Shinsaka, This Bulletin, **45**, 1335 (1972).

7) H. Yamazaki and K. Shinsaka, *ibid.*, **43**, 2713 (1970).

*1) In a previous paper,[6] the relative G-value of the electron recombination was used instead of $G_s(\beta)$, that of electron scavenging.

$$G_s(\beta) = \beta\int_0^\infty N(t)/N(0)\exp(-\beta t)\mathrm{d}t \quad (18)$$

where β is the product of the rate constant, k_s, of the electron scavenging and the scavenger concentration, C_s. Using the inverse Laplace transform, $N(t)/N(0)$ is given by:

$$N(t)/N(0) = \frac{1}{2\pi i}\int_{c-i\infty}^{c+i\infty}\frac{G_s(\beta)}{\beta}\exp(\beta t)\mathrm{d}\beta \quad (19)$$

As a summary of these transforms of the four characteristic functions, the following flow chart of the transformations is given by Fig. 1. A similar flow chart of the linear response of the four characteristic functions was given in a previous paper[6] using the potential control approximation.

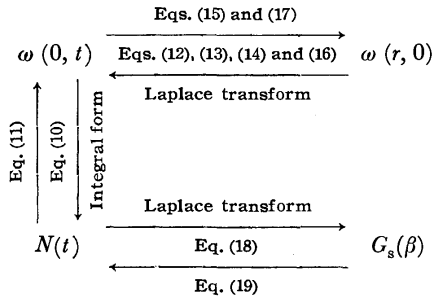

Fig. 1. Flow chart of Laplace trasform and integral form of the four characteristic functions: $\omega(r, 0)$, $\omega(0, t)$, $N(t)$ and $G_s(\beta)$.

Examples of Distribution Functions. To evaluate the explicit form of the four characteristic functions, a generalized Gaussian distribution for the thermalized electrons in the spherical spur will be considered:

$$\omega(r, 0) = A_m r^m \exp(-r^2/b^2) \quad (20)$$

where A_m is a normalization constant and where b is a constant of the spread of the distribution:

$$A_m = 1\Big/\int_0^\infty 4\pi r^{m+2}\exp(-r^2/b^2)\mathrm{d}r \quad (21)$$

Similarly, the initial distribution in cylindrical geometry is expressed by Eq. (20) with the normalization constant of:

$$A_m = 1\Big/\int_0^\infty 2\pi r^{m+1}\exp(-r^2/b^2)\mathrm{d}r \quad (22)$$

By using Eqs. (12), (13), (14), and (16), the central values in the distribution of electron can be obtained for spherical and cylindrical geometries:

$$\omega(0, t) = (4Dt)^{m/2}/\{\pi^{3/2}(4Dt+b^2)^{(m+3)/2}\} \quad (23)$$

and:

$$\omega(0, t) = (4Dt)^{m/2}/\{\pi(4Dt+b^2)^{(m+2)/2}\} \quad (24)$$

By means of Eq. (10) the time dependence of the concentration in spherical geometry is expressed in terms of the incomplete beta function:

$$\frac{N(t)}{N(0)} = 1\Big/\left\{1+\frac{r_c N(0)}{b}B\left(\frac{1}{2}, \frac{m+2}{2}; \frac{4Dt}{b^2}\right)\right\} \quad (25)$$

where the incomplete beta function is defined by:

$$B(p, q; x) = \int_0^x \frac{x^{q-1}}{(1+x)^{p+q}}\mathrm{d}x \quad (26)$$

By the use of the Laplace transform, Eq. (18), the G-value of electron scavenging is obtained:

$$G_s(\beta) = \beta\int_0^\infty 1\Big/\left\{1+\frac{r_c N(0)}{b}B\left(\frac{1}{2}, \frac{m+2}{2}; \frac{4Dt}{b^2}\right)\right\} \times \exp(-\beta t)\mathrm{d}t \quad (27)$$

For dilute concentrations of a scavenger, $G_s(\beta)$ can be expanded as the power series of β for the Gaussian distribution ($m=0$):

$$G(\beta) = \frac{1}{1+K} + \frac{\sqrt{\beta}\,K\sqrt{\pi}}{\sqrt{\alpha}(1+K)^2}\{\exp(\beta/\alpha)\,Erfc(\sqrt{\beta/\alpha})\} - \frac{\beta K^2}{\alpha(1+K)^3}[\exp(\beta/\alpha)\,Ei\{-(\beta/\alpha)\}] \quad (28)$$

where $Erfc$ and Ei are the error function and the exponential integral function,[8]*2) and where K and α denote $2r_cN(0)/(\sqrt{b\pi})$ and $4D/b^2$ respectively. The leading term in the low concentration of the scavenger is $\beta^{1/2}$, which corresponds to the square-root dependence proved by various experiments. The coefficient of the $\beta^{1/2}$ term is:

$$\frac{K\sqrt{\pi}}{\sqrt{\alpha}(1+K)^2} = \frac{r_c N(0)}{\sqrt{D}(1+2r_cN(0)/\sqrt{\pi}\,b)^2} \quad (29)$$

which corresponds to α in Schuler's expression.[2]*3)

Similarly, in cylindrical geometry $N(t)/N(0)$ is given for the Gaussian distribution ($m=0$) for the thermalized electrons by:

$$N(t)/N(0) = 1/\{1+r_cN(0)\ln(1+4Dt/b^2)\} \quad (30)$$

$G_s(\beta)$ is evaluated by[8] means of the Laplace transform:

$$G_s(\beta) = \beta\int_0^\infty\{1-r_cN(0)\ln(1+\alpha t)+r_c^2N^2(0) \times(\ln(1+\alpha t))^2\cdots\}\exp(-\beta t)\mathrm{d}t = 1-\exp(\beta/\alpha)\,Ei(-(\beta/\alpha))+\cdots \quad (31)$$

Therefore, the square-root law does not hold for the electron-recombination process with the Gaussian distribution of thermalized electrons in the cylindrical track. After a long interval, however, the cylindrical track is converted to the 'isolated' ion-pair geometry after recombination in the track. Therefore, the final state can be expressed by the spherical coordinate and

8) For example, H. Beteman, "Table of Integral Transforms. I," McGraw-Hill Book Co., New York (1954).

*2) The error function and exponential integral function are given by:

$$Erfc(x) = \frac{2}{\sqrt{\pi}}\int_x^\infty\exp(-v^2)\mathrm{d}v$$

and:

$$-Ei(-x)\int_x^\infty\exp(-v)/v\mathrm{d}v$$

*3) In Schuler's expression[2], $G_s(\beta)$ can be written as:

$$G_s(\beta) = g_{fl} + g_{gl}\{\sqrt{\alpha\beta/k_s}/(1-\sqrt{\alpha\beta/k_s})\}$$

where g_{fl} and g_{gl} are the relative G-values of free electrons and of geminate electrons:

$$g_{fl} = G_{fl}/(G_{fl}+G_{gl})$$

and:

$$g_{gl} = G_{gl}/(G_{fl}+G_{gl})$$

Schuler's expression can be expanded in the series of β:

$$G_s(\beta) = g_{fl} + g_{gl}\sqrt{\alpha\beta/k_s} + \cdots$$

From Eq. (28), the coefficients of the first and second terms are found to be:

$$g_{fl} = 1/(1+K)$$

and:

$$g_{gl}\sqrt{\alpha/k_s} = \frac{r_cN(0)}{\sqrt{D}(1+2r_cN(0)/\sqrt{\pi}\,b)^2}$$

the square-root law is valid.[3] The contribution of the spherical spurs to the whole process of recombination can be estimated by the factor of $\sigma(=1/\{(2r_cG_i)\text{-}(-dE/dx)\})$, where r_c is the Onsager radius, G_i is the G-value of the total ionization, and $(-dE/dx)$ is the average LET in the radiation track. For example, the α beam of 20 Mev and the ^{4+}N beam of 80 Mev, which are used for the study of the LET effect in hydrocarbons,[9] the factor σ, is evaluated as 2×10^{-2} and 4×10^{-3} respectively, assuming that G_i is 3 and r_c is 100 Å. Therefore, the contribution of the square-root dependence is negligibly small in these cases.

In this paper, the integral transforms in the prescribed diffusion approximation have been discussed. The prescribed diffusion approximation, one of the most common approximations, has been used since the initial stage of the development of the theroy of radiation chemistry. However, the real importance of the integral transforms is that the transforms can also be applied to the other forms of approximation.[5,10-12] On the other hand, in their preliminary stages of development these approximations should be considered as of equal importance.

The authors wish to thank Professor Shoji Shida and Dr. Shin Sato of Tokyo Institute of Technology and Dr. Kenji Fueki of Nagoya University for reading the preliminary manuscript of this paper and for their helpfull discussions, and Miss Toshiko Kitagawa for typing the manuscripts of this series.

Appendix

Introduction of a Finite Reaction Radius. It is reasonable to consider the finite radius, r_0, of the reaction between central-ion clusters and the surrounding electrons, because to consider ion clusters as a point or an axis is not a realistic view of the models, as has been discussed in connection with other approximations,[10,13] and the origin of coordinate is a singular point of the Smoluchowski equation. The solution of the diffusion equation, $\partial v/\partial t = D\Delta^2 v + \delta(r-r')\delta(t)$, is given by,[14]

$$v(r,t) = \frac{1}{8(\pi Dt)^{3/2}} \exp\{-(r-r')^2/4Dt\} \qquad \text{(A-1)}$$

If the reaction radius, r_0, is used, then the value, $\omega(r_0, t)$, at the reaction radius can be used instead of the central value, $\omega(0, t)$. In spherical coordinates, $\omega(r_0, t)$ can be expressed by the initial distribution, $\omega(r, 0)$, by using the super position of the solutions of Eq. (A-1) outside of the ion cluster*4):

$$\omega(r_0,t) = \frac{2\pi}{(2\sqrt{\pi Dt})^3}\int_{r_0}^{\infty}\int_0^{\pi} \exp(-d^2/4Dt)\omega(r,0)r^2 dr \sin\theta d\theta \qquad \text{(A-2)}$$

where d is the distance between the ion and the electron:

$$d^2 = r^2 + r_0^2 - 2rr_0\cos\theta \qquad \text{(A-3)}$$

Similarly, in the cylindrical geometry of a track in cylindrical coordinates, $\omega(r_0, t)$ is given by:

$$\omega(r_0,t) = \frac{1}{(2\sqrt{\pi Dt})^2}\int_{r_0}^{\infty}\int_0^{2\pi} \exp(-d^2/4Dt)\omega(r,0)r dr d\theta \qquad \text{(A-4)}$$

After integration, Eqs. (A-2) and (A-4) are transformed to:

$$\omega(r_0,t) = \frac{2\pi}{(2\sqrt{\pi Dt})^3}\exp(-r_0^2/4Dt)\int_{r_0}^{\infty}\exp(-r^2/4Dt) \times\omega(r,0)r^2\frac{2Dt}{rr_0}\left\{\exp\left(\frac{rr_0}{2Dt}\right)-\exp\left(-\frac{rr_0}{2Dt}\right)\right\}dr$$
$$= \frac{1}{\sqrt{\pi Dt}}\exp(-r_0/4Dt)\int_{r_0}^{\infty}\exp(-r^2/4Dt) \times\omega(r,0)\frac{r}{r_0}\sinh\left(\frac{rr_0}{2Dt}\right)dr \qquad \text{(A-5)}$$

and

$$\omega(r_0,t) = \frac{1}{4Dt}\exp(-r_0^2/4Dt)\int_{r_0}^{\infty}\exp(-r^2/4Dt) \times\omega(r,0)I_0\left(\frac{rr_0}{2Dt}\right)r dr \qquad \text{(A-6)}$$

where I_0 denotes the modified Bessel function. For the outside of the ion cluster ($r>r_0$), $N^+(r, t)$ and $N(r, t)$ can be expressed by:

$$N^+(r,t) = N^+(t) \qquad \text{(A-7)}$$

and
$$N(r,t) = N(t)\Delta + N(t)\int_{r_0}^{r} 4\pi\omega(r,t)r^2 dr \qquad \text{(A-8)}$$

or
$$N(r,t) = N(t)\Delta + N(t)\int_{r_0}^{r} 2\pi\omega(r,t)r dr$$

where Δ is a correction factor of the electron probability in the ion cluster and is given by:

$$\Delta = 4\pi\int_0^{r_0}\omega(r,t)r^2 dr \qquad \text{(A-9)}$$

or
$$\Delta = 2\pi\int_0^{r_0}\omega(r,t)r dr$$

Then, by the use of Eqs. (2) and (3), Eqs. (8) and (9) can be corrected by:

$$\frac{\partial\psi}{\partial r} = -\frac{e}{\varepsilon r^2}N(t)\left\{1-\Delta-\int_{r_0}^{r}\omega(r_1,t)4\pi r_1^2 dr_1\right\} \qquad \text{(A-10)}$$

in the spherical geometry and:

$$\frac{\partial\psi}{\partial r} = -\frac{2e}{\varepsilon r}N(t)\left\{1-\Delta-\int_{r_0}^{r}\omega(r_1,t)2\pi r_1 dr_1\right\} \qquad \text{(A-11)}$$

in the cylindrical geometry. Considering that $\omega(r, t)$ is a solution of the diffusion equation:

$$\frac{\partial\omega(r,t)}{\partial t} = \frac{D}{r^n}\frac{\partial}{\partial r}\left(r^n\frac{\partial\omega}{\partial r}\right) \qquad \text{(A-12)}$$

where $n=1$ for the cylindrical geometry and $n=2$ for the spherical geometry, the Smoluchowski equation can be expressed by:

$$\frac{dN(t)}{dt}\omega(r,t) = -\frac{N(t)u}{r^2}\frac{\partial}{\partial r}\left\{\omega(r,t)\frac{e}{\varepsilon}N(t) \times\left(1-\Delta-\int_{r_0}^{r}\omega(r_1,t)4\pi r_1^2 dr_1\right)\right\} \qquad \text{(A-13)}$$

9) M. Matsui, T. Karasawa, and M. Imamura, The 15th Conference of Radiation Chemistry at Osaka, Oct. (1972).
10) H. Yamazaki and K. Shinsaka, This Bulletin, **44**, 2611 (1971).
11) G. C. Abell and A. Mozmder, *J. Chem. Phys.*, **56**, 4079 (1972).
12) G. C. Abell, A. Mozmder, and J. L. Magee, *ibid.*, **56**, 5422 (1972).
13) M. G. Robinson and G. R. Freeman, *ibid.*, **55**, 5644 (1971).
14) For example, H. S. Carslaw, and J. C. Jaeger, "Conduction of Heat in Solids," Clarendon Press, Oxford (1959), p. 256.

*4) It is possible to use the solution of the diffusion equation with the boundary condition:

$$(\partial\omega(r,t)/\partial r)_{r=r_0} = 0$$

in the prescribed diffusion approximation. In this case, however, the solution assumes a more complicated expression, so, for the sake of simplicity, the present solutions for the diffusion equation were used instead.

in the spherical geometry and:

$$\frac{dN(t)}{dt}\omega(r,t) = -\frac{N(t)u}{r}\frac{\partial}{\partial r}\left\{\omega(r_1,t)\frac{2e}{\varepsilon}N(t) \times\left(1-\Delta-\int_{r_0}^{r}\omega(r_1,t)2\pi r_1 dr_1\right)\right\} \quad \text{(A-14)}$$

in the cylindrical geometry.

By integration outside of the ion cluster, Eqs. (A-13) and (A-14) become:

$$\frac{d}{dt}\left(\frac{1}{N(t)}\right) = \left\{4\pi u\Big/\left(4\pi\int_{r_0}^{\infty}\omega(r_1,t)r_1^2 dr_1\right)\right\} \times\left\{\omega(r_0,t)\frac{e}{\varepsilon}(1-\Delta)\right\} = 4\pi ue\omega(r_0,t)/\varepsilon \quad \text{(A-15)}$$

and:

$$\frac{d}{dt}\left(\frac{1}{N(t)}\right) = \left\{2\pi u\Big/\left(2\pi\int_{r_0}^{\infty}\omega(r_1,t)r_1 dr_1\right)\right\} \times\left\{\omega(r_0,t)\frac{2e}{\varepsilon}(1-\Delta)\right\} = 4\pi ue\omega(r_0,t)/\varepsilon \quad \text{(A-16)}$$

After integration over time, Eqs. (A-15) and (A-16) are transformed to the same expression for both the spherical and cylindrical geometries. $N(t)$ can be obtained from $\omega(r_0, t)$ instead of $\omega(0.\, t)$:

$$\frac{N(t)}{N(0)} = \frac{1}{1+4\pi Dr_c N(0)\int_0^t \omega(r_0,t_1)dt_1} \quad \text{(A-17)}$$

If r_0 is converged to zero, Eq. (A-17) is reduced to Eq. (10).

BULLETIN OF THE CHEMICAL SOCIETY OF JAPAN, VOL. 46, 2646—2650 (1973)

Mechanism of Hydrogenolysis. III. Thermal Hydrogen Exchange and Demethylation of Toluene-2-d_1, -3-d_1, and -4-d_1

Yoshiki SATO and Akira AMANO

Department of Applied Chemistry, Faculty of Engineering, Tohoku University, Aoba, Aramaki, Sendai 980

(Received February 5, 1973)

Rates of gas phase thermal hydrogen exchange and hydrogenolytic demethylation of toluene-2-d_1, -3-d_1, and -4-d_1 are evaluated using flow apparatus at temperatures 675—750 °C in the presence of a large excess molecular hydrogen. Both the exchange and the demethylation obey three-halves order rate law indicating the chain mechanism carried by hydrogen atom, the former being found slightly faster than the latter. Rate parameters of the two reactions taking place concurrently are then correlated with the extended Hückel superdelocalizability values appropriate to methylcyclohexadienyl transient formation. Overall applicability of the dynamic index as a measure of reactivity of deuteriotoluenes toward hydrogen atom attack is taken as an additional support for the generally accepted chain mechanism whose rate-determining step consists of electroneutral hydrogen atom addition to aromatic nucleus.

Gas phase demethylation of a series of methyl substituted benzenes in a stream of a large excess hydrogen has been a subject of numerous investigations.[1] General features of the reaction including product distribution and kinetic behavior can be accounted for by the free radical chain mechanism in which the following atomic cracking process (*reaction a*) assumes the rate-controlling role.[2]

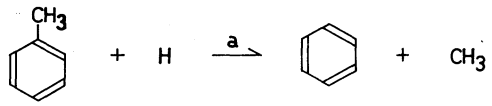

The process may be looked upon as consisting of the addition of attacking hydrogen atom to the phenyl carbon adjacent to methyl group followed by the elimination of methyl radical through the intermediary formation of methylcyclohexadienyl radical.

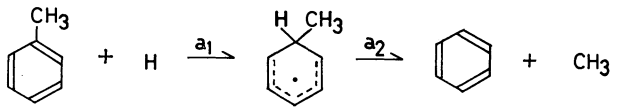

It has been shown that the rate of the consecutive sequence described above is determined by addition (*reaction* a_1).[3] Attempts had hitherto been made to correlate either the atom localization energy[4] or the maximum free valence[5] with observed free radical addition rate constants, showing that these *static reactivity indices* were in limited practical use. However, the ease with which the key reaction proceeds could be predicted by the modified superdelocalizability values, the *dynamic reactivity index* $S_r(R)$ proposed by Fukui

1) a) H. Matsui, A. Amano, and H. Tokuhisa, *Bull. Jap. Petrol. Inst.*, **1**, 67 (1959); S. Masamune, A. Amano, and H. Tokuhisa, *Tech. Reports Tohoku Univ.* (Japan), **25**,(1) 27 (1960); S. Masamune, M. Uchiyama, and H. Tokuhisa, *ibid.*, **25**(1), 39 (1960). b) A. Amano, M. Uchiyama, Y. Sato, H. Tominaga, H. Arai, and T. Kunugi, This Bulletin, **43**, 3653 (1970).

2) A. Amano, H. Tominaga, and H. Tokuhisa, *Bull. Jap. Petrol. Inst.*, **7**, 59 (1965); S. W. Benson and R. Shaw, *J. Chem. Phys.*, **47**, 4052 (1967).

3) H. Tominaga, H. Arai, T. Kunugi, A. Amano, M. Uchiyama, and Y. Sato, This Bulletin, **43**, 3658 (1970).

4) F. H. Burkitt, C. A. Coulson, and H. C. Longuet-Higgins, *Trans. Faraday Soc.*, **47**, 553 (1951).

5) B. Pullman, *J. Chim. Phys.*, **55**, 790 (1958).

et al.[6] of the ring carbon atom at which the addition-elimination takes place.[1]

The extended Hückel calculation on toluene, however, gives the values of $S_r(R)$ which indicate that phenyl hydrogen is more susceptible to substitution than methyl group upon hydrogen atom attack. A qualitative evidence for this has been provided by Burr *et al.* in their study on the pyrolysis of deuterium laveled toluene.[7] Isotopic distribution in the product observed can only be explained on the assumption that hydrogen-deuterium exchange is slightly faster than demethylation.

In the present work, rate of hydrogen-deuterium exchange relative to that of demethylation has been evaluated using toluene-2-d_1, -3-d_1, and -4-d_1 as reactants. Results are then correlated with the relevant $S_r(R)$ values. In so doing, we expect to extend the applicability of the concept of the superdelocalizability to radical substitutions and also to provide an additional support for the mechanism of hydrogenolysis. Some characteristic features of the key reaction are envisaged during the course of the present approach and will also be reported.

Experimental

Toluene-2-d_1, -3-d_1 and -4-d_1 were prepared by the methods of Fukuda *et al.*[8] and Weldon *et al.*[9] with minor modifications from *o*-chloro, *m*-bromo and *p*-bromo derivatives of toluene, respectively. Gas chromatographic analysis revealed that the synthetic materials purified through conventional distillation consisted of more than 99.8 mol% toluene fraction accompanied by a trace amount of ether. Infrared absorption spectra were in good agreement with those of toluene-d_1's reported by Turkevich *et al.*[10] and by Tiers.[11] The synthetic materials were passed through a reaction vessel and the fraction collected as unreacted toluene was used in the subsequent rate measurements. Cylinder hydrogen, 99.9 mol% purity as analyzed by mass-spectrometry, was used after conventional purification.

Rates of the reaction of each toluene-d_1 were measured by a flow apparatus specially designed for sufficient accuracy in both temperature and residence time. Details of the apparatus and procedures were described elsewhere.[12]

Liquid products were introduced into a gas chromatographic apparatus with a 3 *m*-Apiezon Grease L packed column for analysis of total isotopic benzenes. A Perkin-Elmer 337 Infrared Spectrometer, equipped with KBr optics and effective slit width of approximately 25 microns, was then used to analyze toluene fraction for deuterium distribution at wave lengths 21.62, 21.93, 22.10 and 22.12 mμ for toluene, toluene-2-d_1, toluene-3-d_1 and toluene-4-d_1, respectively.

Results and Discussion

Stoichiometry. Liquid products from each of the three isomeric toluene-d_1's mainly consisted of benzene, benzene-d_1 and toluene together with unreacted toluene-d_1. No intramolecular migration of deuterium in toluene-d_1 was detected. Hydrocarbons of higher molecular weight were also present, but they did not amount to more than a few percent of toluene-d_1 reacted. The gas phase thermal reaction of toluene-d_1 thus consists of simultaneous hydrogenolytic demethylation (*reactions b* and *b'*) and hydrogen-deuterium exchange (*reactions c* and *c'*).

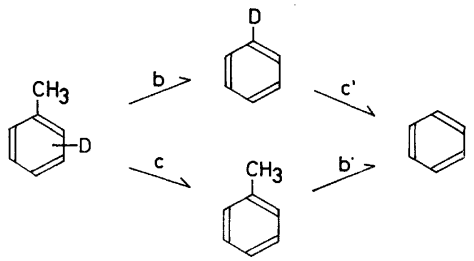

Kinetics. The results of the rate measurements for both demethylation and exchange of toluene-2-d_1, toluene-3-d_1, and toluene-4-d_1 are listed in Tables 1, 2, and 3, respectively. They exhibit validity of the overall

Table 1. Rates of demethylation and exchange of toluene-2-d_1

Temp. (°C)	H_2/reactant (mol/mol)	Residence time (s)	Conversion (mol %)		Three-halves order rate constant[a] ($l^{1/2}$ mol$^{-1/2}$ s^{-1})	
			demethylation	exchange	demethylation	exchange
675.0	5.00	8.33	3.68	10.00	0.0458	0.0827
	4.97	4.20	2.00	9.97		
700.0	5.05	10.90	10.40	16.00		
	5.03	8.18	7.91	10.73		
	5.06	5.44	5.33	8.78	0.1039	0.1510
	5.08	4.08	4.13	6.56		
	5.34	1.96	1.97	2.44		
725.3	5.10	3.97	7.38	9.86	0.1983	0.2560
750.2	5.17	1.93	6.90	8.27	0.3836	0.4877
	5.04	1.32	4.90	7.56		

a) Evaluated by the least-squares method for three-halves order plots of the relevant data.

6) H. Kato, K. Morokuma, T. Yonezawa, and K. Fukui, This Bulletin, **38**, 1749 (1965).
7) J. G. Burr, R. A. Meyer, and J. D. Strong, *J. Amer. Chem. Soc.*, **86**, 3846 (1964).
8) T. Fukuda and T. Kusama, *Nihon Kagaku Zasshi*, **76**, 28 (1955).
9) L. H. P. Weldon and C. L. Wilson, *J. Chem. Soc.*, **1946**, 235.
10) J. Turkevich, H. A. McKenzie, L. Friedman, and R. Spurr, *J. Amer. Chem. Soc.*, **71**, 4045 (1949).
11) G. V. D. Tiers, *J. Chem. Phys.*, **19**, 1072 (1951).
12) A. Amano, O. Horie, Y. Sato, and T. Katayose, *J. Jap. Petrol. Inst.*, **15**, 125 (1972).

TABLE 2. RATES OF DEMETHYLATION AND EXCHANGE OF TOLUENE-3-d_1

Temp. (°C)	H_2/reactant (mol/mol)	Residence time (s)	Conversion (mol %)		Three-halves order rate constant[a] ($l^{1/2}$ $mol^{-1/2}$ s^{-1})	
			demethylation	exchange	demethylation	exchange
677.1	5.00	8.33	3.87	4.95	0.0475	0.0613
700.7	4.97	10.84	7.95	11.50		
	5.01	8.10	6.68	8.77	0.0841	0.1174
	5.03	5.40	4.71	5.81		
	5.02	2.05	1.84	2.40		
724.6	4.92	4.03	7.09	7.94		
	4.96	2.02	3.65	4.33	0.1881	0.2146
	5.20	1.31	2.45	2.81		
750.8	5.14	2.55	9.43	10.50		
	5.09	1.94	7.26	9.24	0.4006	0.4874
	5.13	1.29	4.88	6.86		

a) Evaluated by the least-squares method for three-halves order plots of the relevant data.

TABLE 3. RATES OF DEMETHYLATION AND EXCHANGE OF TOLUENE-4-d_1

Temp. (°C)	H_2/reactant (mol/mol)	Residence time (s)	Conversion (mol %)		Three-halves order rate constant[a] ($l^{1/2}$ $mol^{-1/2}$ s^{-1})	
			demethylation	exchange	demethylation	exchange
676.3	5.06	8.30	3.54	4.19		
	5.05	5.56	2.51	3.05	0.0439	0.0516
	5.01	2.11	0.95	—		
700.4	5.07	8.05	6.48	8.51		
	5.17	5.29	4.24	5.02		
	5.12	4.04	3.66	—	0.0855	0.1048
	5.17	2.69	2.37	—		
	5.19	1.35	1.05	—		
725.6	4.95	3.94	5.82	6.70		
	5.01	1.97	3.01	—	0.1574	0.1764
	5.13	1.30	1.95	—		
750.6	5.09	1.93	6.49	7.52	0.3523	0.3935
	5.10	1.30	4.23	4.78		

a) Evaluated by the least-squares method for three-halves order plots of the relevant data.

TABLE 4. OBSERVED ACTIVATION ENERGIES, A-FACTORS AND RATES OF EXCHANGE RELATIVE TO THOSE OF DEMETHYLATION AT 700 °C

Reactant	Demethylation		Exchange		Relative rate
	E (kcal/mol)	log A	E (kcal/mol)	log A	
Toluene-2-d_1	54.0	11.12	45.0	9.27	1.45
Toluene-3-d_1	52.9	10.85	49.1	10.12	1.32
Toluene-4-d_1	53.6	10.95	51.5	10.55	1.22

three-halves order rate law for exchange (*reaction c*) as well as demethylation (*reaction b*), kinetics of the latter being in accord with those of methylbenzenes.[1] The values of $k_{1.5}$'s are then fitted into the Arrhenius formulation giving rise to the values of A-factor and activation energy (Table 4). The rate of exchange relative to that of demethylation at 700 °C, at which experiments have been carried out, is also given. The kinetic parameters of demethylation observed for three isomeric toluene-d_1's are in good agreement within error limits with each other and also with those of toluene.[12]

Kinetic Isotope Effects. Neither the secondary kinetic isotope effect nor the effect exerted by deuterium atom at different positions toward thermal demethylation has been detected. This is not surprising in view of the negligibly small effect caused by the introduction of deuterium in place of hydrogen on the electronic structure of the ring carbon atom at which substitution takes place. A similar conclusion was drawn for electrophilic nitration[13] and also for radical alkylation[14] of benzene.

Mechanism of Hydrogen-Deuterium Exchange. A similarity in demethylation (*reaction b*) and exchange (*reaction c*) with respect to the reaction order as well

13) W. M. Lauer and W. E. Noland, *J. Amer. Chem. Soc.*, **75**, 3689 (1953).

14) E. L. Eliel, Z. Welvart, and S. H. Wilen, *J. Org. Chem.*, **23**, 1821 (1958).

as the values of kinetic parameters indicates that these two reactions proceed through similar pathways. Since the key reaction in the free radical chain of the demethylation is the atomic cracking (*reaction a*), the corresponding version of the exchange would be as follows.

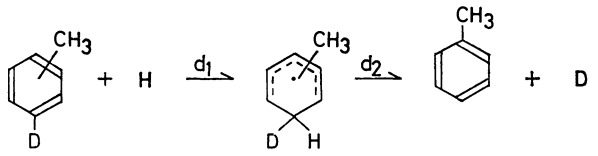

The transient structure may be looked upon as methylcyclohexadienyl radical possessing sp^3-hybridized carbon atom which links both incoming hydrogen and outgoing deuterium. It is thus expected that the rate of *reaction d* is influenced by methyl substituent according to its position relative to deuterium in the same molecule, just as in the case of polymethylbenzenes where the demethylation rate is affected by other methyl substituents. The effect exerted by the methyl group upon *reaction d* may be conveniently correlated with $S_r(R)$ proved to be an appropriate reactivity index for the demethylation.[1b] Details of the definition and evaluation of the superdelocalizability values have been described.[1b] In executing the computation, it is assumed that molecular geometry of toluene-d_1 is identical with that of toluene and the valence state ionization potential of deuterium atom is taken to be equal to that of hydrogen. A slight alteration in the values of these structural parameters does not affect the final results in any significant amount. As an example, 10% change in the ionization potential produces uncertainty in the fifth digit of the final $S_r(R)$ values. The results of the extended Hückel calculation are summarized in Table 5. The linear relation obtained for the plots

Table 5. Reactivity indices of toluene by extended Hückel method

Position	Modified superdelocalizability			Atomic bond population
	$S_r(R)$	$S_r(E)$	$S_r(N)$	
1	0.4029	0.2749	0.5309	0.7744
2	0.4149	0.3255	0.5044	0.8243
3	0.4125	0.2836	0.5414	0.8276
4	0.4086	0.3246	0.4926	0.8276

of logarithmic rates of the exchange relative to that of demethylation at 700 °C *vs.* the values of $S_r(R)$ are given in Fig. 1. Other superdelocalizability values, *i.e.* $S_r(E)$ and $S_r(N)$, and also atomic bond population (Table 5), show no linearity with the observed reactivity ratios. This can be taken as an additional support not only for our mechanistic interpretation of the exchange reaction, but also for the use of $S_r(R)$ as reactivity index for thermal substitutions in general. The best explanation so far for the factor influencing the reactivity of atomic cracking (*reactions* a_1 and d_1) is found in the mechanism assuming electroneutral hydrogen atom attack and rehybridization of sp^2 ring carbon atom to the sp^3-state in a concerted manner.

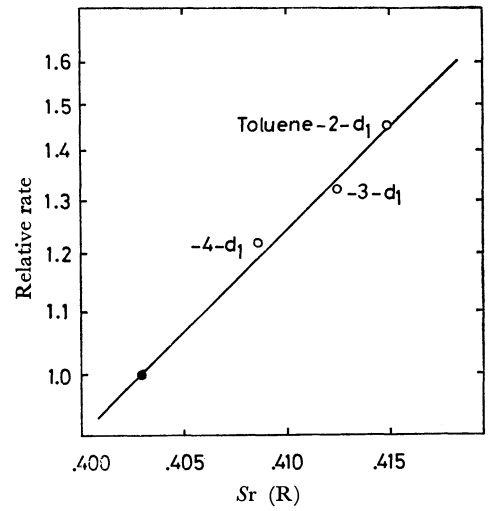

Fig. 1. Correlation between observed relative reactivity and modified superdelocalizability. ●: Demethylation, ○: Exchange.

Hydrogen Atom Addition to Aromatics and Olefins. Gas phase reactions of hydrogen atom with a series of mono-substituted benzenes have been investigated using pulse-radiolytic technique.[15] The results indicate that the addition took place to form cyclohexadienyl-type transients, the latter presumably decomposing to benzene at higher temperatures.[16] The rate of the adduct formation was found to obey the Hammett rule with slightly negative ρ-values (−0.7——0.8). These results suggest that the attacking hydrogen atom could be more conveniently classified as electrophilic reagent. However, according to the theoretical implications of the Hammett rule, ρ-values are by far the more sensitive towards ionic substitutions and are not suitable for classifying reactions consistently.[17] In fact, the data available for radical alkylation of benzene give ρ-values in the range from −1.0 to +1.0. The radiolytic reactions might involve substrates with electrons populated at energy states higher than those usually encountered in thermal reactions. It is therefore possible in the former that the attacking hydrogen atom tends to be more electrophilic.

In this connection, it is interesting to refer to results reported on reactions of hydrogen atom with olefins. According to Cvetanović,[18] the lack of parallelism between hydrogen atom and electrophilic oxygen atom in the rates of addition to a series of olefins was taken as an evidence for support of the electroneutral nature of the former. In spite of the above, hydrogen atom addition to propene, but-1-ene and isobutene has been reported as being somewhat electrophilic, based on the parallelism between the values of $S_r(E)$ and the observed overall rates of the hydrogenolysis.[19] Electronic be-

15) M. Anbar, D. Meyerstein, and P. Neta, *Nature*, **209**, 1348 (1966); M. C. Sauer, Jr. and I. Mani, *J. Phys. Chem.*, **74**, 59 (1970).
16) A. Amano, O. Horie, and N. H. Hanh, *Chemistry Letters*, **1972**, 917.
17) T. Tsuruta, T. Fueno, and J. Furukawa, *Bull. Inst. Chem. Res.*, Kyoto Univ., **34**, 214 (1956).
18) R. J. Cvetanović, "Advances in Photochemistry," Vol. 1, p. 115, Interscience, New York, 1963.
19) H. Tominaga, H. Arai, K. A. Moghul, N. Takahashi, and T. Kunugi, *Kogyo Kagaku Zasshi*, **74**, 371 (1971).

TABLE 6. THERMOCHEMICAL DATA OF THE RELEVANT SPECIES AT 700 °C

Species	ΔH_f (kcal/mol)
	44.64
	43.18
H·	55.48
CH_3·	41.81
	82.52
	80.55
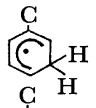	81.51
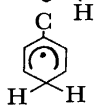	80.87

havior of the hydrogen atom toward addition should therefore be reckonned as still controversial.

Comparison between Exchange and Demethylation. In agreement with the qualitative result obtained by Burr *et al.*,[7] we found that exchange (*reaction d*) was faster than demethylation (*reaction a*) by a factor of about 1.3. The converse would most probably be the case if elimination (*reactions* a_2 and d_2) played the rate-controlling role in the overall substitution, since *reaction* d_2 is more endothermic than *reaction* a_2 by about 14 kcal/mol. Our estimated ΔH_f values at 700 °C, based on thermochemical data (Table 6) are −16.1 and approximately −18 kcal/mol for the rate-controlling *reactions* a_1 and d_1, respectively. These values are in accord with the present results, and indicate, on the basis of LFER concept, that the tranistion-state structures for both *reactions* a_1 and d_1 resemble cyclohexadienyl transient.

According to the mechanistic analysis given quite independently by Benson *et al.* in their study of the pyrolysis of 1,3-cyclohexadiene in the presence of benzene and toluene,[20] *reaction* a_1 was found to be faster than the addition of hydrogen atom to benzene-d_6 (*reaction* e_1) by a factor of 1.5.

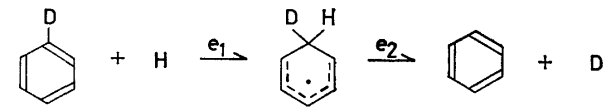

Reactivity ratio of *reactions* a_1 and e_1 in the range 0.3—0.7 has, however, been obtained on the hydrogen-deuterium exchange of benzene-d_1 both in the presence and in the absence of toluene. If we assume the latter ratio, the rates are in the order $d_1 > e_1 > a_1$. This coincides with what is expected from the calculated values of $S_r(R)$.

20) S. W. Benson and R. Shaw, *J. Amer. Chem. Soc.*, **89**, 5351 (1967).

Simulation Analysis of the Acid-catalyzed Hydrolysis of Carboxylatopentammineruthenium(III) Complexes

Katsutoshi OHKUBO, Hiroyuki SAKAMOTO, Futoshi KITAGAWA, and Akira OHYOSHI

Faculty of Engineering, Kumamoto University, Kurokami, Kumamoto 860

(Received February 5, 1973)

The mechanism of the acid-catalyzed hydrolysis of $(NH_3)_5RuO_2CR^{2+}$ (R=H, CH_3, C_2H_5, $(CH_3)_2CH$, CH_2OH, and/or CH_2NH_2) has been established by the trapezoidal simulation analyses with a computer. The proposed reaction sequences of S_N1 combined with S_N2 mechanisms involving a quasi-stable intermediate $(NH_3)_5Ru^{3+}$ have proved to be plausible, and the kinetic parameters (rate constants, $\Delta H^{\neq}$, $\Delta S^{\neq}$, *etc.*) have been given for all of the elementary reactions. The aquation rate has been determined by the solvent-assisted, heterolytic dissociation of $(NH_3)_5RuO_2CR^{2+}$ and follows this order: formato>acetato>propionato>isobutyrato>glycolato>glycinato.

In the previous paper,[1] the acid hydrolyses of alkyl-, hydroxyl-, and/or amino-substituted-carboxylatopentaammineruthenium(III) complexes ($(NH_3)_5RuO_2CR^{2+}$) have been proved to proceed in the pseudo first-order fashion:

$$(NH_3)_5RuO_2CR^{2+} + H_2O \xrightarrow[k_{obs}]{H^+} (NH_3)_5RuOH_2^{3+} + RCO_2^- \quad (1)$$

The pseudo first-order rate constant, k_{obsd}, can be represented by the acid-dependent and acid-independent rate constants, k_H and k_d respectively, with a good analytic fit:[1]

$$k_{obs} = k_H[H^+] + k_d \quad (2)$$

The kinetic relationship of Eq. (2) has also been established in the aquation of pentaammine-amino acid cobalt(III) complexes.[2,3] The mechanism of such an aquation reaction has been interpreted, in terms of the reaction paths involving the protonated complex, as:

$$(NH_3)_5MOC(=O)R^{n+} + H^+ \overset{K}{\rightleftharpoons} (NH_3)_5MOC(-OH)R^{(n+1)+} \quad (3)$$

$$(NH_3)_5MOC(-OH)R^{(n+1)+} + H_2O \xrightarrow{k} (NH_3)_5MOH_2^{(n+1)+} + RCO_2^- + H^+ \quad (4)$$

where M denotes the central transition metal.

The aquation mechanism, however, has not yet been strictly established, since Reactions (3) and (4) cannot well explain the kinetic expression of Eq. (2).[4]

The present study was undertaken in order to elucidate the mechanism of the acid-catalyzed hydrolysis of $(NH_3)_5RuO_2CR^{2+}$ (R=H, CH_3, C_2H_5, $(CH_3)_2CH$, CH_2OH, and/or CH_2NH_2) using the technique of computer simulation.

Simulation Results and Discussion

Elementary Reactions of Aquation. In view of the kinetic relationship expressed by Eq. (2), Reaction (1) may be considered to consist of the following two reaction paths involving a quasi-stable intermediate of $(NH_3)_5Ru^{3+}$ (*i.e.*, acid-catalyzed S_N2 and acid-independent S_N1 reactions):

$$(NH_3)_5RuO_2CR^{2+} \xrightarrow[k_H]{H^+} (NH_3)_5Ru^{3+} + RCO_2^- \quad (5)$$

$$(NH_3)_5RuO_2CR^{2+} \xrightarrow{k_d} (NH_3)_5Ru^{3+} + RCO_2^- \quad (6)$$

$$(NH_3)_5Ru^{3+} + H_2O \underset{k_e}{\overset{k_{H_2O}}{\rightleftharpoons}} (NH_3)_5RuOH_2^{3+} \quad (7)$$

The corresponding differential terms (rate equations) derived from Eqs. (5)—(7) are:

$$d[(NH_3)_5RuO_2CR^{2+}]/dt = -d[RCO_2^-]/dt = -(k_H[H^+]+k_d)[(NH_3)_5RuO_2CR^{2+}] \quad (8)$$

$$d[(NH_3)_5Ru^{3+}]/dt = (k_H[H^+]+k_d)[(NH_3)_5RuO_2CR^{2+}] + k_e[(NH_3)_5RuOH_2^{3+}] - k'_{H_2O}[(NH_3)_5Ru^{3+}] \quad (9)$$

$$d[(NH_3)_5RuOH_2^{3+}]/dt = k'_{H_2O}[(NH_3)_5Ru^{3+}] - k_e[(NH_3)_5RuOH_2^{3+}] \quad (10)$$

where k_{H_2O}' stands for the pseudo first-order rate constant derived from $k_{H_2O}[H_2O]$. Assuming the stationary-state for the concentration of $(NH_3)_5Ru^{3+}$, Eq. (2) can be reproduced as:

$$-d[(NH_3)_5RuO_2CR^{2+}]/dt = d[(NH_3)_5RuOH_2^{3+}]/dt = \{k_H[H^+]+k_d\}[(NH_3)_5RuO_2CR^{3+}] \quad (11)$$

Some remarks on Reactions (5) and (6) should be made here in connection with the molecular interaction between $(NH_3)_5RuO_2CR^{2+}$ and H^+ and/or the H_2O solvent. From the results of the extended Hückel MO calculations of the above interacting systems, the most plausible interactions of H^+ and H_2O with $(NH_3)_5RuO_2CR^{2+}$ occur, respectively, in the direction of the orbital expansion of the nonbonding lone-pair 2p-orbital on the oxygen atom of the Ru–O bond and in that of the lowest-unoccupied, antibonding dp-σ orbital on the Ru–O bond axis, which leads to a weakening of the Ru–O.[5] The acid-catalyzed and the solvent-assisted dissociation processes (reactions (5) and (6) respectively) are energetically comparable with the heterolytic cleavage of the Ru–O (see the $\Delta H^{\neq}$ values in Table 2). It is worthy of emphasis that the constants

1) A. Ohyoshi, A. Jyo, and N. Shin, This Bulletin, **45**, 2121 (1972).

2) K. Ogino, T. Murakami, and K. Saito, *ibid.*, **41**, 1615 (1968).

3) T. Murakami, K. Ogino, H. Kobayashi, H. Yamasaki, and K. Saito, *ibid.*, **44**, 120 (1971).

4) The present extensive study corrects and unveils some discrepancies in the aquation mechanism proposed previously in Ref. 1.

5) The discussions referred to in the remarks made above will be developed in detail in a succeeding paper.

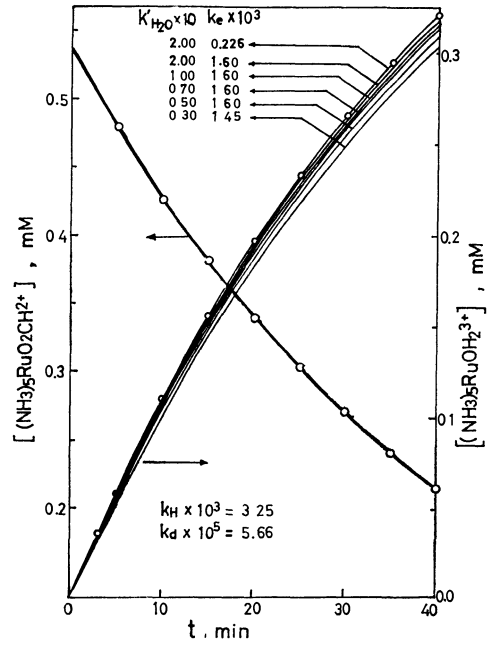

Fig. 1. Variations in time conversions of $[(NH_3)_5RuO_2CH^{2+}]$ and $[(NH_3)_5RuOH_2^{3+}]$ with various sets of values of k_H, k_d, k'_{H_2O}, and k_e at 61°C: $[(NH_3)_5RuO_2CH^{2+}]_i=0.536$ mM; $[H^+]=0.1$ M; $\mu=0.1$.
——: Simulation, ○: Experiment

of k_H and k_d seem to be pseudo rate constants, *i.e.*, $k_H'[H_2O]$ and $k_d'[H_2O]$ respectively.

Determination of the Rate Constants. We will determine the rate constants of the elementary reactions expressed by Eqs. (5)—(7) on the basis of the simulation analysis. Figure 1 indicates the dependence of the time conversions of $[(NH_3)_5RuO_2CR^{2+}]$ and $[(NH_3)_5RuOH_2^{3+}]$ upon various values of k_H, k_d, $k_{H,O}'$, and k_e for the formato-complex. The values of k_H and k_d obtained experimentally[1] for the formato-complex show a good analytic fit, while the best values of $k_{H,O}'$ and k_e were found to be 2.00×10^{-1} M^{-1} s^{-1} and 2.26×10^{-4} s^{-1} respectively; the latter k_e value was obtained

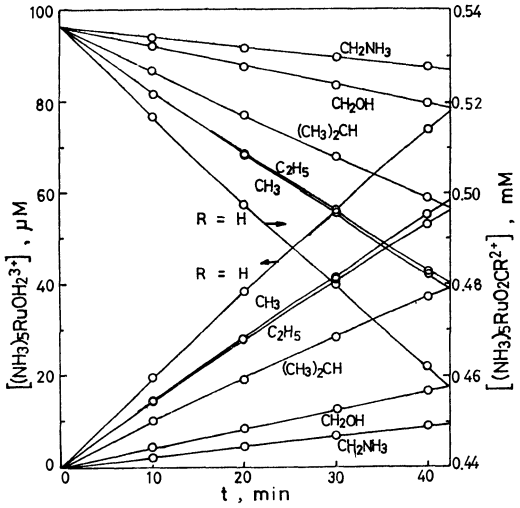

Fig. 2. Simulated time-conversions of $[(NH_3)_5RuO_2CR^{2+}]$ and $[(NH_3)_5RuOH_2^{3+}]$ *vs.* experimental ones: $[(NH_3)_5RuO_2CR^{2+}]_i=0.536$ mM; $[H^+]=0.1$ M; $\mu=0.1$; $T=40$ °C.
——: Simulation, ○: Experiment

from the anation studies[6] of $(NH_3)_5RuOH_2^{3+}$ under the same reaction conditions. The validity of the above values of $k_{H,O}'$, k_e, k_H, and k_d will be tested in the acid hydrolysis of $(NH_3)_5RuO_2CR^{2+}$, where R denotes an alkyl group. As can be seen from Fig. 2, the simulated time conversions of $[(NH_3)_5RuO_2CR^{2+}]$ and $[(NH_3)_5RuOH_2^{3+}]$ are in satisfactory accordance with the experimental values. Table 1 shows the values of k_{obsd}, k_H, k_d, $k_{H,O}'$, and k_e in the Arrhenius-type equations, which were determined by a further simulation analysis of the complex-hydrolyses in the acid solution ($[H^+]=0.025$—0.1 M) at the temperatures of 40, 50, and 70 °C under the condition of $\mu=0.1$. As may be seen from Table 1, the relationship shown by Eq. (2) is completely accounted for.[7]

Reaction Sequences. Now, let us discuss the validity of the reaction schemes represented by Eqs. (5)—(7). From the rate equations of Eqs. (8)—(10), the time-dependence of the [reactant], the [intermediate], and/or the [product] can be reproduced by the non-steady-state analysis:

$$[(NH_3)_5RuO_2CR^{2+}] = [(NH_3)_5RuO_2CR^{2+}]_i e^{-\lambda_1 t} \quad (12)$$

$$[(NH_3)_5Ru^{3+}] = [(NH_3)_5RuO_2CR^{2+}]_i[(1-e^{-\lambda_1 t}) - k'_{H,O}(e^{-\lambda_1 t}-e^{-\lambda_1 t})/(\lambda_2-\lambda_1) - (e^{-\lambda_1 t}-1)/\lambda_2] \quad (13)$$

$$[(NH_3)_5RuOH_2^{3+}] = k'_{H,O}[(NH_3)_5RuO_2CR^{2+}]_i \times [(e^{\lambda_2}-e^{\lambda_1})/(\lambda_2-\lambda_1) - (e^{\lambda_2}-1)/\lambda_2] \quad (14)$$

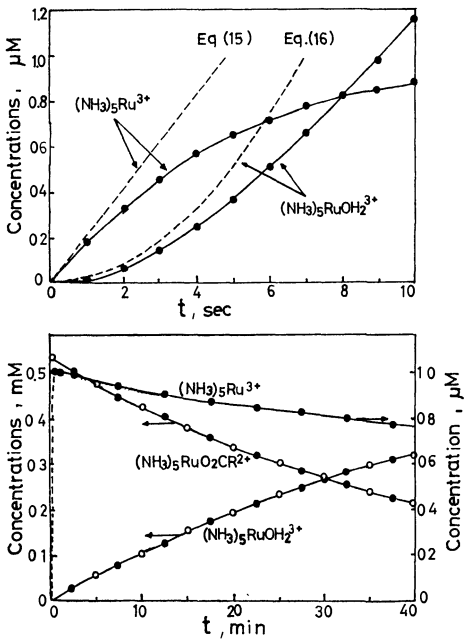

Fig. 3. Time conversions of $[(NH_3)_5RuO_2CR^{2+}]$, $[(NH_3)_5Ru^{3+}]$, and $[(NH_3)_5RuOH_2^{3+}]$ for formato-complex. (Reaction conditions were the same ones in Fig. 1.)
○: from experiments; ●: from Eqs. (12)—(14); —: from simulations

6) A. Ohyoshi, S. Shida, S. Izuchi, F. Kitagawa, and K. Ohkubo, This Bulletin, **46**, 2431 (1973).

7) Strictly speaking, Eq. (2) can be adopted at $t\gtrsim20$ s (see Fig. 3). At $t\gtrsim20$ s, the stationary-state treatment for [intermediate] is possible. In Table 1, the relative errors of the sum of $k_H[H^+]$ and k_d values against k_{obsd} ones (*viz.* $(k_{obsd}-(k_H[H^+]k_d))/k_{obsd}\times100\%$) fall in the range of 0.06—1.15% except in the cases of the propionate- and glycinate-complexes (below 4.60 and 7.45% respectively).

Table 1. The rate constants for the acid-catalyzed hydrolyses of $(NH_3)_5RuO_2CR^{2+}$

$(NH_3)_5RuO_2CR^{2+}$ (R)	Over-all reaction k_{obsd} s^{-1}	Reaction (5) k_H $M^{-1}s^{-1}$	Reaction (6) k_d s^{-1}
H	$5.757\times10^{8}e^{-18580/RT}$	$2.493\times10^{9}e^{-18130/RT}$	$2.277\times10^{10}e^{-21820/RT}$
CH_3	$2.198\times10^{10}e^{-21060/RT}$	$1.361\times10^{10}e^{-18700/RT}$	$2.000\times10^{10}e^{-24790/RT}$
C_2H_5	$8.061\times10^{10}e^{-21800/RT}$	$5.016\times10^{9}e^{-19490/RT}$	$9.723\times10^{15}e^{-30290/RT}$
$(CH_3)_2CH$	$1.547\times10^{11}e^{-22440/RT}$	$2.643\times10^{10}e^{-20180/RT}$	$5.127\times10^{12}e^{-25360/RT}$
CH_2OH	$1.154\times10^{11}e^{-22850/RT}$	$2.491\times10^{11}e^{-22220/RT}$	$1.797\times10^{11}e^{-23940/RT}$
CH_2NH_2	$3.823\times10^{12}e^{-25430/RT}$	$4.970\times10^{17}e^{-33290/RT}$	$1.919\times10^{12}e^{-25020/RT}$

For Reaction (7), $k'_{H_2O}=4.678e^{-2094/RT}$ and $k_e=6.999e^{-6869/RT}$ s^{-1}.

Table 2. The kinetic parameters of activation for the acid-catalyzed hydrolyses of $(NH_3)_5RuO_2CR^{2+}$

$(NH_3)_5RuO_2CR^{2+}$ (R)	Over-all reaction		Reaction (5)		Reaction (6)	
	$\Delta H^{\ddagger}$ (kcal/mol)	$-\Delta S^{\ddagger}$ (eu)	$\Delta H^{\ddagger}$ (kcal/mol)	$-\Delta S^{\ddagger}$ (eu)	$\Delta H^{\ddagger}$ (kcal/mol)	$-\Delta S$ (eu)
H	17.92±0.12	20.67±0.35	17.48±0.02	17.73±0.05	20.18±0.92	14.86±2.79
CH_3	20.42±0.05	13.40±0.15	18.05±0.29	14.37±0.11	24.14±0.05	4.43±0.14
C_2H_5	21.15±0.20	10.91±0.61	18.84±0.04	16.53±0.89	29.64±0.14	12.40±0.44
$(CH_3)_2CH$	21.84±0.19	9.61±0.58	19.52±0.29	13.23±0.87	24.70±0.01	2.57±0.02
CH_2OH	22.20±0.05	10.14±0.14	21.56±0.31	8.81±0.92	23.33±0.44	9.66±1.32
CH_2NH_2	24.75±0.12	3.23±0.37	32.62±0.82	−18.9±2.58	24.34±0.05	4.58±0.15

For Reaction (7), Forward: $\Delta H^{\ddagger}=1.44\pm0.05$kcal/mol; $-\Delta S^{\ddagger}=57.67\pm0.02$ e.u.
Backward: $\Delta H^{\ddagger}=6.22\pm0.00$ kcal/mol; $-\Delta S^{\ddagger}=56.87\pm0.01$ e.u.

where $\lambda_1=k_H[H^+]+k_d$, $\lambda_2=k_{H,O}'+k_e$, and the subscript i=initial state. As Fig. 3 indicates, the time conversions of the [component] calculated from Eqs. (12)—(14) are in complete agreement with those obtained from the experimental and simulation results. It may be deduced, therefore, that the acid-catalyzed hydrolysis of $(NH_3)_2RuO_2CR^{2+}$ proceeds *via* the reaction sequences proposed (Eqs. (5)—(7)).

Remark should be here made on the concentration-change of components produced during the initial short stage of the reaction. From Eqs. (13)—(14), the [component] values may be approximated as:

$$[(NH_3)_5Ru^{3+}] \approx k'_{H,O}[(NH_3)_5RuO_2CR^{2+}]_i\times\lambda_1 t \quad (15)$$

$$[(NH_3)_5RuOH_2^{3+}] \approx k'_{H,O}[(NH_3)_5RuO_2CR^{2+}]_i\times\lambda_1 t^2/2 \quad (16)$$

As can be seen from Fig. 3, Eqs. (15) and (16) reproduce the reaction for at least 1.0 s after the start of the reaction. Moreover, the initial rates of the formation or consumption of the components, $r_i[C]$, can be represented by extended analysis[8] in the case of a formato-complex:

$$r_i[(NH_3)_5RuO_2CR^{2+}] \approx -1.53\times10^{-3}[(NH_3)_5RuO_2CR^{2+}]_i^{0.975}[H^+]_i^{0.699} \text{ M/s}$$

$$r_i[(NH_3)_5Ru^{3+}] \approx 3.12\times10^{-4}[(NH_3)_5RuO_2CR^{2+}]_i^{1.000}[H^+]_i^{0.702} \text{ M/s}$$

$$r_i[(NH_3)_5RuOH_2^{3+}] \approx 1.57\times10^{-3}[(NH_3)_5RuO_2CR^{2+}]_i^{1.000}[H^+]_i^{0.704} \text{ M/s}$$

Kinetic Parameters of Activation for Elementary Reactions. Mention should be made here of the enthalpy and entropy of activation, $\Delta H^{\ddagger}$ and $\Delta S^{\ddagger}$, for each elementary reaction. Using the rate constants listed in Table 1, the least-squares calculations of $\Delta H^{\ddagger}$ and $\Delta S^{\ddagger}$ values were performed by means of a computer. Table 2 shows the $\Delta H^{\ddagger}$ and $\Delta S^{\ddagger}$ values for all the elementary reactions. Judging from the $\Delta H^{\ddagger}$ values in Table 2, the reaction step of Eq. (6) may be said to determine the over-all reaction rate, except in the case of the glycinato-complex; the reaction rates follow this order: formato>acetato>propionato>isobutyrato>glycolato >glycinato.

Procedure of Simulation

The procedure of non-steady-state simulation will now be interpreted briefly. According to the trapezoidal simulation method,[9] the series of increments ($D(i)$, $i=1$—4) may be defined by the following terms on the basis of Eqs. (5)—(7):

$$D(1) = k_H[H^+][(NH_3)_5RuO_2CR^{2+}]dt$$

$$D(2) = k_d[(NH_3)_5RuO_2CR^{2+}]dt$$

$$D(3) = k_{H,O}[H_2O][(NH_3)_5Ru^{3+}]dt = k'_{H,O}[(NH_3)_5Ru_2^{3+}]dt$$

$$D(4) = k_e[(NH_3)_5RuOH_2^{3+}]dt$$

According to the rate equations of Eqs. (8)—(10), we obtain:

$$D[(NH_3)_5RuO_2CR^{2+}]_{av} = -D(1)_{av} - D(2)_{av}$$

$$D[RCO_2^-]_{av} = D(1)_{av} + D(2)_{av}$$

$$D[(NH_3)_5Ru^{3+}]_{av} = D(1)_{av} + D(2)_{av} - D(3)_{av} + D(4)_{av}$$

$$D[(NH_3)_5RuOH_2^{3+}]_{av} = D(3)_{av} - D(4)_{av}$$

where the average increments, D_{av}, are evaluated from $(D_t+D_{t+dt})/2$, by the use of the increments at the reaction times of t and $t+dt$, as D_t and D_{t+dt} respec-

8) The analytical method was similar to that described in detail in Ref. 9.

9) K. Ohkubo and T. Hashimoto, This Bulletin, **45**, 3350 (1972).

tively.

The desired concentrations of the components, C (reactant, intermediate, and product), $[C]_t$, at the reaction time, t, can be calculated by:

$$[C]_t = [C]_i + \sum^{n} D[C]_{av} \qquad (ndt = t)$$

where $[C]_i$ and $D[C]_{av}$ are, respectively, the initial concentration of the component, C, and the over-all increment (or decrement) changing with t. In this paper, the $[C]_t$ values were evaluated every 0.1 s (in the case of the initial short stage of the reaction, dt=0.02 s).

BULLETIN OF THE CHEMICAL SOCIETY OF JAPAN, VOL. 46, 2654—2659 (1973)

Emission Processes in Cadmium Photosensitization

Shigeru TSUNASHIMA, Tsutomu TOYONO, and Shin SATO

Department of Applied Physics, Tokyo Institute of Technology, Ookayama, Meguro-ku, Tokyo 152

(Received February 15, 1973)

The possibility of the cadmium-photosensitized luminescence of NH_3, CO_2, CO, and CH_4 was examined at 250 °C. In the case of NH_3, a very strong band emission was observed at 432 nm, with a band width of about 100 nm. The sensitized luminescence of NH_3 was attributed to the emission from an excited complex between triplet cadmium and NH_3. In the case of CH_4, a weak emission was observed at about 420 nm. In the cases of CO_2, CO, and N_2, however, no positive evidence of the sensitized luminescence was obtained. From the pressure dependence of the quenching of the 326.1 nm resonance line, the efficiencies of CO_2, CO, NH_3, and N_2 for quenching the triplet cadmium atoms were estimated to be 0.16, 0.03, 3.3×10^{-4}, and 4.9×10^{-5}, respectively, the efficiencies of *cis*-2-butene being assumed to be unity.

In spite of there having been many investigations of the mercury photosensitization, there have been only a few investigations of the cadmium photosensitization.[1] Since the nature of the $Cd(^3P_1)$ atoms is similar to that of the $Hg(^3P_1)$ atoms except for the amount of available excitation energy, a comparison of the two photosensitized reactions will give further information about the detailed mechanism of photosensitization.

It is known that the triplet mercury atoms cause: (a) an electronic energy transfer to molecules which have low-lying triplet states, such as olefins, aromatics, and ketones; (b) a hydrogen-atom abstraction reaction with paraffins, and (c) the conversion of the electronic energy to a luminescence emission.[1-4] Since Penzes, Strausz, and Gunning reported that CH_4, NH_3, and H_2O give a mercury-photosensitized luminescence in the spectral regions of 240—280, 290—400, and 254—320 nm respectively, many investigations of the mercury-photosensitized luminescence have been made with NH_3, H_2O, amines, alcohols, and rare gases by Gunning *et al.*,[2] Phillips *et al.*,[3] and Callear *et al.*[4] Phillips *et al.* attributed the sensitized luminescence to an excited complex between the $Hg(^3P_0)$ atom and a substrate.[3]

In the cadmium photosensitization, processes similar to (a) and (b) have been shown to occur in the reactions of olefins, acetylene, benzene, ketones, and hydrogen.[5] A process similar to (c) was recently reported to occur in the cadmium-photosensitized reactions of NH_3.[6] By analogy with the Hg–NH_3 system, Phillips *et al.* assigned the observed band emission at 430 nm to the emission from an excited complex between $Cd(^3P_0)$ and NH_3.[6]

The present paper will report the results of an independently-undertaken study of the cadmium-photosensitized luminescence and of the quenching for the 326.1 nm resonance line, using NH_3, CH_4, CO, CO_2, and N_2 as the substrates.

Experimental

Apparatus. A diagram of the experimental arrangement is shown in Fig. 1. The light source used was a home-made, U-shaped cadmium lamp (50 cm long and 8 mm o.d.) made of Pyrex; the emitted light was longer than 300 nm. The cylindrical quartz reaction cell was 20 mm in diameter and 50 cm long, with two flat planes. To minimize the intensity of the reflected light on the cell wall, several black-painted aluminum plates were inserted vertically between the lamp and the cell. The cell, the lamp, and the plates were kept in an electric furnace at 250 ± 1 °C. The light

1) J. G. Calvert and J. N. Pitts, Jr., "Photochemistry," John Wiley and Sons, Inc., New York, 1965.

2) S. Penzes, O. P. Strause, and H. E. Gunning, *J. Chem. Phys.*, **45**, 2322 (1966); H. E. Gunning, S. Penzes, H. S. Sandhu, and O. P. Strausz, *J. Amer. Chem. Soc.*, **91**, 7684 (1969).

3) C. G. Freeman, M. J. McEvan, R. F. C. Claridge, and L. F. Phillips, *Chem. Phys. Lett.*, **5**, 555 (1970); **6**, 482 (1970); **8**, 226 (1971); **9**, 578 (1971), *Trans. Faraday Soc.*, **66**, 2974 (1970); **67**, 67, 2004, 2565 (1971); R. H. Newman, C. G. Freeman, M. J. McEvan, R. F. C. Claridge, and L. F. Phillips, *ibid.*, **66**, 2827 (1970), **67**, 1360 (1971).

4) A. B. Callear and J. McGurk, *Chem. Phys. Lett.*, **7**, 491 (1970); J. Koskikallio, A. B. Callear, and J. H. Conner, *ibid.*, **8**, 467 (1971); A. B. Callear and J. H. Conner, *ibid.*, **13**, 245 (1972).

5) S. Tsunashima and S. Sato, This Bulletin, **40**, 2987 (1967), **41**, 284, 2281 (1968); S. Tsunashima, S. Hirokami, and S. Sato, *Can. J. Chem.*, **46**, 995 (1968); S. Tsunashima, S. Satoh, and S. Sato, This Bulletin, **42**, 329, 1531 (1969); S. Sato, C. Takahashi, and S. Tsunashima, *ibid.*, **43**, 1319 (1970); S. Tsunashima, O. Ohsawa, C. Takahashi, and S. Sato, *ibid.*, **45**, 83 (1973).

6) P. D. Morten, C. G. Freeman, M. J. McEvan, R. F. C. Claridge, and L. F. Phillips, *Chem. Phys. Lett.*, **16**, 148 (1972).

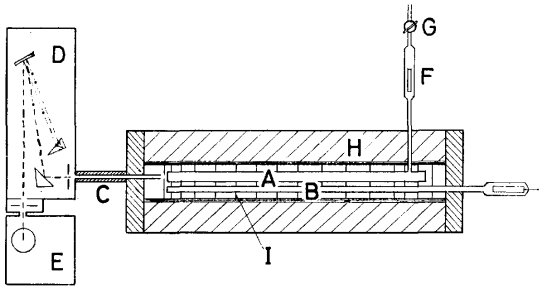

Fig. 1. Experimental system for studying the sensitized emission. A. Quartz Reaction Cell; B. Pyrex Cd Lamp; C. Light Guide; D. Monochromator; E. Photomultiplier; F. Cd Stopper; G. Stop-cock to Vacuum System; H. Furnace; I. Aluminum Plates.

from the cell was detected by means of an 1P28 photomultiplier tube through a light guide and a monochromator. The light guide used was a black-painted porcelain tube 5 mm in i.d. and 30 cm long. The monochromator and the photomultiplier used was a Hitachi Photoelectric Spectrophotometer, model EPU-2A. The emission intensity was measured by means of the photometer of the spectrophotometer and was recorded on a Yokokawa Laboratory Recorder, Type 3043. The reaction cell, containing a few pieces of cadmium metal, was connected to a mercury-free vacuum system through a cadmium stopper, which prevented the cadmium vapor from escaping from the cell. The glass tube between the furnace and the cadmium stopper was heated at about 290 °C by means of an electric heating tape in order to avoid the deposit of cadmium vapor. Some deposits of cadmium were, however, found on the tube at the insulator of the furnace. The pressure of the gas was measured by means of a W & T model 62-075 pressure gauge supplied by the Nagano Keiki Co.

A few experiments on the cadmium-photosensitized decomposition of NH_3 were carried out using a cell 5 cm long and 5 cm in diameter. The experimental details have previously been described.[5]

Materials. The cadmium metal used was high-purity cadmium (99.9999%) manufactured by the Osaka Asahi Metal Co. Pure-grade NH_3, CO_2, and *cis*-2-butene (Takachiho Shoji Co.) were used after degassing at the temperature of liquid nitrogen. Pure-Grade CH_4 and CO (Takachiho Shoji Co.) were used after having been passed through a trap at the temperature of liquid nitrogen. Pure-grade N_2 (Suzuki Shokan Co.) was used after having been passed through a molecular sieve trap at -110 °C.

The light intensity absorbed by cadmium was measured by using the cadmium-photosensitized *cis-trans* isomerization of *cis*-2-butene, assuming the quantum yield of the *trans*-isomer formation to be 0.5.[5] A typical light intensity absorbed in the cell used in the emission study was 6.8 ± 0.4 μEinstein min^{-1}.

Results

Emission Spectrum. When the empty cell only was illuminated by means of the cadmium lamp, line spectra were observed at 326, 340, 347, 361, 468, 480, and 509 nm with the entrance slit of 0.04 mm. These line spectra coincided with the emission spectra of the lamp used. These line spectra may be due to the scattered light on the cell wall. An attempt to minimize the intensity of the scattered light was unsuccessful.

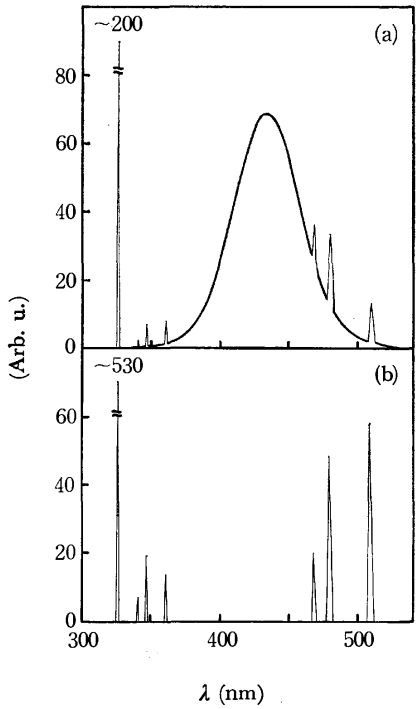

Fig. 2. Observed emission intensity distributions in the presence of 31 Torr of NH_3 (a) and in the absence of NH_3 (b); entrance slit is 0.04 mm and the spectra are not corrected for the sensitivity of the photomultiplier.

In the presence of the cadmium vapor in the cell at 250 °C and *ca.* 4.8×10^{-3} Torr, the intensity of the 326 nm emission increased, but those of the other lines remained almost constant.[7] When 31 Torr of NH_3 was added, as is shown in Fig. 2, the 326 nm line was quenched and a new band emission, with a band width of about 100 nm, was observed at 432 nm. Such a new band emission could not be observed when NH_3 alone was illuminated by the cadmium lamp. When CO_2, CO, or N_2 was the added gas, no emission other than the scattered light was observed in the 300—550 nm region, even when the entrance slit was opened up to 0.8 mm. In the case of CH_4, a very weak emission was observed at about 420 nm. The intensity at 420 nm was about 600 times less than that observed in the case of NH_3. The emission at 420 nm was very faint and decreased with the increase in the irradiation time. A similar tendency was also observed in the intensity at the 326 nm line. Beacuse of the low emission intensity and the large irradiation time dependence, no further study of the case of CH_4 was performed.

Pressure Dependence on the Emission in the NH_3–Cd System. In the case of NH_3, the profile of the band emission at 432 nm was almost the same at 3.0, 31, and 47 Torr, while the intensity at 432 nm increased

7) "C. R. C. Handbook of Chemistry and Physics," **50**, D167 (1969—1970).

Table 1. Irradiation time dependence of the emissions at 326.1 and 432 nm in the presence of 63.5 Torr of NH_3.

Irradiation time (min)	Relative Emission Intensity	
	326.1 nm	432 nm
0	(1.00)	(1.00)
1.0	0.942	0.940
2.0	0.878	0.881
3.0	0.825	0.823
5.0	0.720	0.710
8.0	0.562	0.566
10.0	0.485	0.490
14.0	0.372	0.368

Table 2. Products in the cadmium-photosensitized decomposition of NH_3 at 250 °C.

Pressure (Torr)	Absorbed Light Intensity (μEinstein)	Quantum Yield	
		H_2	N_2
52.5[a]	14.6	0.024	0.007
52.5[a]	40.7	0.032	0.009
76.4[b]	14.6	0.039	0.012
79.6[c]	440	0.212	0.053
92.6[b]	14.6	0.037	0.008
96.6[c]	1100	0.079	0.019

a) cell volume 86 ml, light intensity 0.194 μEinstein min^{-1}.
b) cell volume 95 ml, light intensity 0.194 μEinstein min^{-1}.
c) cell volume 160 ml, light intensity 6.8 μEinstein min^{-1}.

with the increase in pressure. As is shown in Table 1, the intensity at 432 nm decreased with the increase in the irradiation time. The rate of the decrease increased with the increase in pressure. The emission intensities at 432 nm extraporated to zero irradiation time are plotted in Fig. 3. In this case, the entrance slit of the monochromator was kept at 0.05 mm; this corresponds to the band width of about 0.7 nm at 432 nm.

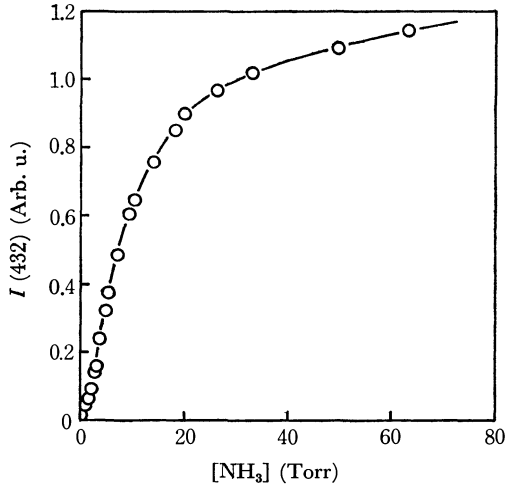

Fig. 3. The emission intensity at 432 nm as a function of NH_3 pressure.

Decomposition of NH_3. After the irradiation of NH_3 in the presence of the cadmium vapor with the cadmium lamp, hydrogen and nitrogen were observed as the decomposition products. We were unsuccessful in trying to detect hydrazine, a possible reaction product, using a gas chromatograph. The relative yield of hydrogen and nitrogen was 3.7 ± 0.8. The apparent quantum yields of the product formation are listed in Table 2.

Quenching of the 326.1 nm Resonance Line. The efficiencies of N_2, NH_3, CO, and CO_2 in quenching the triplet cadmium were studied using the quenching of the 326.1 nm resonance line. The emission intensities at 326.1 nm were measured as a function of the pressure. In order to obtain a good reproducibility, the intensities were measured with a low sensitivity of the photomultiplier and with an entrance slit of 0.5 mm, which corresponds to the band width of 4 nm.

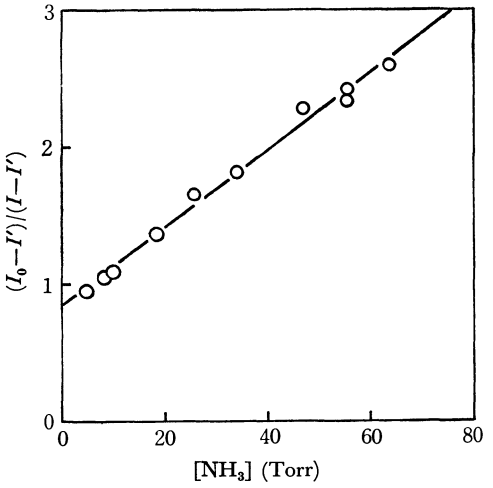

Fig. 4. Stern-Volmer plots of NH_3 for quenching 326.1 nm resonance line.

A typical plot of $(I_0-I')/(I-I')$ against the pressure is shown in Fig. 4, where I_0 and I are the emission intensities at 326.1 nm in the absence and in the presence of a quencher gas respectively. I' is the scattered light intensity at 326.1 nm. On the assumption that 140 Torr of CO quenches the triplet cadmium completely, I' was estimated to be 0.91% of the I_0. In the case of N_2, CO, or CO_2 as the quencher gas, no irradiation time dependence of the emission intensity was observed. In the case of NH_3, however, the intensity decreased with the increase in the irradiation time, as was observed in the case of the 432 nm emission. The irradiation time dependences in both cases agreed well, as is shown in Table 1. In this case, the value of the initial emission intensity was estimated by an extrapolation of the observed intensity to zero irradiation time.

As is shown in Fig. 4, a straight line was obtained. From the intercept and the slope of the straight line, the half-quenching pressure was estimated to be the intercept divided by the slope. The values of the intercept and of the half-quenching pressure are listed in Table 3.

Table 3. Half-quenching pressures and intercepts of Stern-Volmer plots for quenching 326.1 nm resonance line at 250 °C.

Quencher	Intercept	Half-quenching Pressure (Torr)
N_2	0.96±0.01	220 ±3
NH_3	0.85±0.03	29.8 ±1.4
CO	0.84±0.22	0.34 ±0.09
CO_2	0.55±0.27	0.060±0.030

Discussion

Emitting Species in the Cadmium-photosensitized Emission of NH_3. In the case of the vacuum ultraviolet photolysis of NH_3, it has been shown that the NH and NH_2 radicals formed emit their fluorescence at about 324 and 400—600 nm respectively.[8,9] In the case of the cadmium photosensitization, the available energy is only 87.7 kcal mol^{-1}, which is comparable to the N–H bond energy of NH_3 (103 kcal mol^{-1})[10] if the CdH formation is taken into account. The $NH_3 \rightarrow NH + H_2$ (ΔH=89.7 kcal mol^{-1})[9] reaction is energetically impossible in the cadmium photosensitization. When an excited NH_2 radical is assumed to emit the 432 nm band emission, it is necessary to assume the reexcitation of the NH_2 radical by the direct absorption of light and/or the energy transfer from triplet cadmium. A mechanism which includes these processes fails to explain the pressure dependence of the observed emission intensities. The assumption that the emitting species was CdH, which is a possible reaction intermediate in the cadmium-photosensitized reactions of NH_3 and CH_4, was also excluded for the same reason.

In the case of mercury photosensitization, the 350 nm band emission has been attributed to the emission from the complex between the $Hg(^3P_0)$ atom and the NH_3 molecule.[3] Phillips *et al.*, using a phase-modulation method, found a band emission at 430 nm in the cadmium-photosensitized reactions of NH_3.[6] By analogy with the Hg–NH_3 system, they attributed the emitting species to a complex between $Cd(^3P_0)$ and NH_3.[6]

Pressure Dependence of the NH_3 Emission. The pressure dependence of the emission intensity at 432 nm, shown in Fig. 3, was not completely explained by the mechanism proposed by Phillips *et al.*[6] In their mechanism, it was assumed that there were bimolecular and termolecular reactions between $Cd(^3P_0)$ and NH_3 involved in the formation of the complex.[6]

One of the mechanisms which can explain the observed pressure dependence of the emission is shown below:

$$Cd + h\nu(326.1) \longrightarrow Cd(^3P_1) \qquad k_a \qquad (1)$$

$$Cd(^3P_1) \longrightarrow Cd + h\nu(326.1) \qquad k_0 \qquad (2)$$

$$Cd(^3P_1) + A \longrightarrow CdA^{*\prime} \qquad \alpha k_q \qquad (3)$$

$$\longrightarrow \text{other reactions} \qquad (1-\alpha)k_q \qquad (4)$$

$$CdA^{*\prime} + A \longrightarrow CdA^* + A \qquad k_s \qquad (5)$$

$$CdA^{*\prime} \longrightarrow Cd + A \qquad k_d \qquad (6)$$

$$CdA^* \longrightarrow Cd + A + h\nu' \qquad k_f \qquad (7)$$

$$CdA^* + A \longrightarrow Cd + 2A \qquad k_m \qquad (8)$$

Here, $CdA^{*\prime}$ and CdA^* represent, respectively, an unstabilized and a stabilized complex between the triplet cadmium and NH_3. NH_3 is denoted as A. In this mechanism, it is assumed that the unstabilized complex does not radiate the emission. It is also assumed that the $Cd(^3P_1)$ atoms are responsible for the formation of the complex, because the participation of $Cd(^3P_0)$ in the cadmium photosensitization has not been established.[1] If, however, the $Cd(^3P_0)$ is responsible for the complex formation, Reaction (3) should be replaced by Reactions (9) and (10):

$$Cd(^3P_1) + A \longrightarrow Cd(^3P_0) + A \qquad \alpha k_q \qquad (9)$$

$$Cd(^3P_0) + A \longrightarrow CdA^{*\prime} \qquad (10)$$

The steady-state treatment of the above mechanism gives the following relation:

$$1/I = (1+k_0/k_q[A])(1+k_d/k_s[A])(1+k_m[A]/k_f)/\alpha I_a. \qquad (I)$$

Here, I represents the total emission intensity arising from the stabilized complex. Since the emission profile was almost the same at all pressures examined, the observed emission intensity at 432 nm ($I(432)$) may be proportional to the total emission intensity (I) *i.e.*, $I(432)=cI$. The proportional factor, c, may depend on the geometry of the apparatus and on the sensitivity of the photomultiplier used. At the pressures high enough for $(1+k_d/k_s[A])\approx 1$, Eq. (I) can be reduced to this form:

$$1/I(432)(1+k_0/k_q[A]) = (1+k_m[A]/k_f)/c\alpha I_a. \qquad (II)$$

Assuming a value of k_0/k_q equal to the half-quenching pressure of NH_3 (Table 3), the left-hand side of Eq. (II) is plotted against the pressure of NH_3 in Fig. 5. As is shown in Fig. 5, a straight line was obtained in the high-pressure region. At the pressures low enough for $(1+k_m[A]/k_f)\approx 1$, Eq. (I) can be reduced to this form:

$$1/I(432)(1+k_0/k_q[A]) = (1+k_d/k_s[A])/c\alpha I_a. \qquad (III)$$

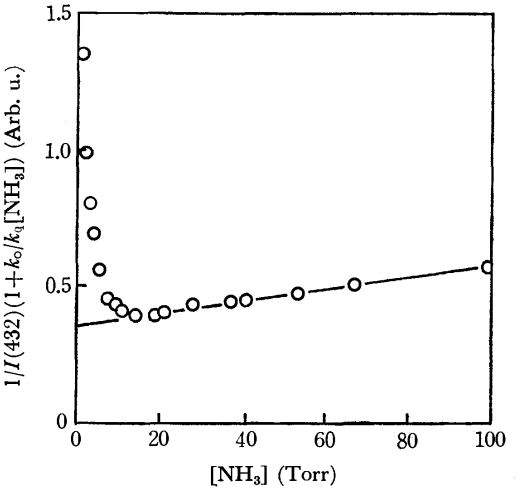

Fig. 5. The plots of $1/I(432)(1+k_0/k_q[A])$ as a function of NH_3 pressure.

8) K. H. Becker and K. H. Werge, *Z. Naturforsch.*, **18a**, 600 (1963).

9) H. Okabe and M. Lenzi, *J. Chem. Phys.*, **47**, 5241 (1967).

10) "C. R. C. Handbook of Chemistry and Physics," **50**, F163 (1969—1970).

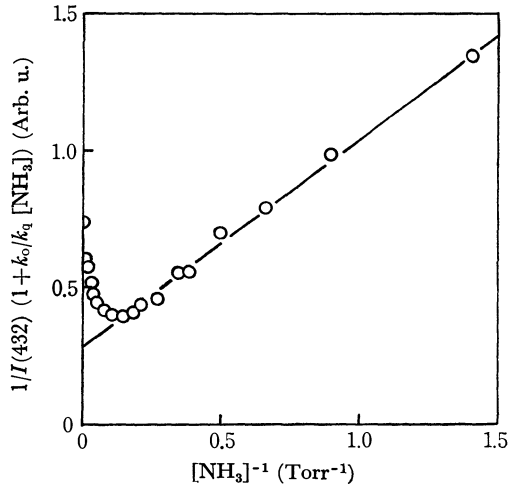

Fig. 6. The plots of $1/I(432)(1+k_o/k_q[A])$ as a function of reciprocal of NH_3 pressure.

The left-hand side of Eq. (III) is plotted against the reciprocal of the pressures in Fig. 6. As is shown in Fig. 6, the plots show a straight line in the low-pressure region. The intercepts of the straight lines coincided with each other within the limits of experimental error. From the intercepts and the slopes of the straight lines, the values of k_m/k_f and k_d/k_s were calculated to be $(1.2\pm0.2)\times10^{-2}$ Torr^{-1} and 2.8 ± 0.2 Torr respectively.

Assuming the cross section of 9 Å^2 for Reactions (5) and (8),[11] which corresponds to $k_m=k_s=1.4\times10^{11}$ l mol^{-1} s^{-1} at 250 °C, the lifetimes of the unstabilized complex and the stabilized complex were calculated to be 8.2×10^{-8} and 2.9×10^{-9} s respectively. The finding that the lifetime of the unstabilized complex is longer than that of the stabilized complex seems somewhat strange. It may, however, be explained by one of the following chains of reasoning: (a) If the total spin is conserved during Reactions (3) or (10), the unstabilized complex, CdA*', should be in a triplet state. Because the lifetime of $\sim10^{-9}$ s is a typical value for a fluorescence emission, the stabilized complex, CdA*, may be in an excited singlet state. Generally, an excited singlet state has a shorter lifetime than an excited triplet state. The difference in the spin multiplicity might explain the estimated shorter lifetime of the stabilized complex. (b) If the following reactions are considered to occur in the mechanism:

$$CdA^* + A \longrightarrow Cd + 2A \qquad k_m' \qquad (8)$$

$$\longrightarrow CdA_2^* \qquad k_m \qquad (11)$$

$$CdA_2^* \longrightarrow CdA^* + A \qquad (12)$$

where CdA_2^* represents a dimer complex between the triplet cadmium atom and two NH_3 molecules, the value of k_m should be smaller than that of k_s. A small value of k_m gives a large value for the lifetime. If k_m'/k_m is larger than 30, the lifetime of the stabilized complex should be longer than 9×10^{-8} s.

Effects of Decomposition Products. The formations of hydrogen and nitrogen in the cadmium-photosensitized reactions of NH_3 may be explained in terms of the following reactions:

$$Cd + h\nu(326.1) \longrightarrow Cd(^3P_1) \qquad (1)$$

$$Cd(^3P_1) \longrightarrow Cd + h\nu(326.1) \qquad (2)$$

$$Cd(^3P_1) + NH_3 \longrightarrow CdH + NH_2 \qquad (13)$$

$$CdH \longrightarrow Cd + H \qquad (14)$$

$$H + NH_3 \longrightarrow H_2 + NH_2 \qquad (15)$$

$$2NH_2 \longrightarrow NH + NH_3 \qquad (16)$$

$$2NH \longrightarrow H_2 + N_2 \qquad (17)$$

The CdH formation is assumed because of the small excitation energy of the triplet cadmium. The reactions of NH and NH_2 radicals are still in question, because the reaction of the hydrogen atom and hydrazine, one of the products, is considered to explain the formation of nitrogen and hydrogen in the mercury-photosensitized decomposition of NH_3.[12]

As will be shown later, the efficiency of hydrogen in quenching the triplet cadmium is about 2×10^3 times that of NH_3. One of the products, hydrogen, will compete with NH_3 in quenching the triplet cadmium, even in the presence of 0.05% of NH_3.

$$Cd(^3P_1) + H_2 \longrightarrow CdH + H \qquad (18)$$

$$\longrightarrow Cd + H_2 \qquad (19)$$

Here, again the CdH formation is assumed.[5] If Reaction (18) is included in the mechanism, the apparent quantum yield of the decomposition should increase with the increase in the irradiation time, while the observed emission intensities at 326.1 and 432 nm should decrease at the same rate. These effects explain well the results shown in Tables 1 and 2.

Using the values of the quantum yield and the half-quenching pressure of NH_3, it was estimated that Reaction (13) accounts for only about 2% of the quenching for the triplet cadmium. This value is about one order of magnitude smaller than that obtained in the mercury photosensitization, in which the available excitation energy is much higher than that in the cadmium photosensitization.[12]

Quenching of the 326.1 nm Resonance Line. In the usual Stern-Volmer plots, the intercept of the straight line is expected to be unity. The intercept obtained here, however, was less than unity for every case examined (Table 3 and Fig. 4). Similar results were obtained by Phillips *et al.* in the mercury-photosensitized luminescence of NH_3.[4] They explained the deviation from unity in terms of the effect of the Lorentz broadening of the resonance line; *i.e.*, the absorbed light intensity increases with the increase in the pressure.[3] To check this possibility in the present study, the Lorentz breadth and the Doppler breadth of the resonance line were compared using the following equations:[13]

$$\Delta\nu_D = 2\nu_0(\sqrt{2R\ln 2}/c)\sqrt{T/M} \qquad (IV)$$

$$\Delta\nu_L = 2\sigma_L^2 N\sqrt{2RT/\pi\mu} \qquad (V)$$

11) "C. R. C. Handbook of Chemistry and Physics," **50**, F151 (1969—1970).

12) C. C. McDonald and H. E. Gunning, *J. Chem. Phys.*, **23**, 532 (1955); S. Takamuku and R. A. Back, *Can. J. Chem.*, **42**, 1426 (1964); M. Z. Hoffman, M. Goldmaster, and R. L. Damour, *J. Chem. Phys.*, **47**, 2195 (1967).

13) A. C. G. Mitchell and M. W. Zemansky, "Resonance Radiation and Excited Atoms," Cambridge University Press, London (1934), p. 99, 170.

Here, $\Delta\nu_D$ and $\Delta\nu_L$ are, respectively, the Doppler breadth and the Lorentz breadth for the resonance line. ν_0 and σ_L^2 are, respectively, the frequency of the resonance line and the effective cross-section for the Lorentz broadening. R, T, M, μ, and N are the gas constant, the temperature, the mass, the reduced mass, and the number of foreign gas molecules in 1 cm^3 respectively. The Doppler breadth of the 326.1 nm resonance line was estimated to be $1.4\times10^9\ s^{-1}$ at 250 °C. The Lorentz breadth was $6.4\times10^8\ s^{-1}$ at 250 °C in the presence of 100 Torr of NH_3, assuming the cross-section for the Lorentz broadening to be 40 $Å^2$. That is, the effect of the Lorentz broadening may be ignored in the present study.

Bender observed in his study of the quenching for the cadmium resonance line, that the absorbed light intensity in the evacuated system was lower than that in the presence of a quencher gas.[14] He explained this in terms of the low vapor pressure of cadmium; *i.e.*, in the evacuated system, the faster distillation of the vapor to the colder part of the apparatus causes a lowering of the vapor pressure.[14] As was mentioned in the Experimental section, the deposit of cadmium was observed in this study. If this effect is operative in the present study, the absorbed light intensity in the evacuated system should be smaller than that expected in the presence of a quencher gas. Even in the presence of 0.1 Torr of a quencher, the mean free path of cadmium is expected to be about two orders of magnitude smaller than that in the evacuated system, in which the pressure may be smaller than the vapor pressure of cadmium (4.8×10^{-3} Torr).[7] This effect may explain the small value of the intercept shown in Table 3.

The relative quenching efficiencies of CO_2 and H_2 have been estimated to be, respectively, 0.16 and 0.8 times that of *cis*-2-butene.[5] Using these values and the values of the half-quenching pressure (Table 3), the efficiencies of H_2, CO_2, CO, NH_3, and N_2 in quenching the triplet cadmium were estimated to be 0.8, 0.16, 0.03, 3.3×10^{-4}, and 4.9×10^{-5} respectively, when the efficiency of *cis*-2-butene was assumed to be unity. The order of the efficiencies obtained is in good agreement with that obtained by Lipson and Mitchell and by Steacie and LeRoy.[15,16] The values of NH_3 and N_2 are, however, much smaller than those obtained by them. This deviation may be mainly due to the presence of a small amount of impurities and/or decomposition products which can quench the triplet cadmium efficiently, such as hydrogen.

14) P. Bender, *Phys. Rev.*, **36**, 1535 (1930).

15) H. C. Lipson and A. C. G. Mitchell, *ibid.*, **48**, 625 (1935).

16) E. W. R. Steacie and D. J. LeRoy, *J. Chem. Phys.*, **11**, 164 (1943).

BULLETIN OF THE CHEMICAL SOCIETY OF JAPAN, VOL. 46, 2659—2662 (1973)

Relationship between Self-Diffusion and Interdiffusion in Gaseous Systems

Hiromasa HIRAKAWA, Yoshinobu KAMEI, Masayasu SUGISAKI, and Yasumichi OISHI

Department of Nuclear Engineering, Faculty of Engineernig, Kyushu University, Fukuoka 812

(Received February 20, 1973)

Self-diffusion coefficients of oxygen and interdiffusion coefficients were measured for the O_2–He system at 25 °C under 760 Torr. The interdiffusion coefficients obtained were compared with theoretical values calculated by the kinetic theory and by Darken's phenomenological theory. The phenomenological equation was tested in comparison with the kinetic theory by making use of the results and the data reported by other investigators. A criterion determining the magnitude or error of the phenomenological equation was given.

The interrelation between self-diffusion[1] and interdiffusion coefficients for gaseous systems has been described by rigorous kinetic theory. However, calculation has been successful only for dilute gaseous systems, the kinetic theory failing to describe satisfactorily the interdiffusion for condensed systems in terms of self-diffusion coefficients. So far the data of interdiffusion have been analyzed only by means of the phenomenological equation. Darken[2] introduced the concept of intrinsic diffusion flux density for the respective components to explain the Kirkendall effect observed in the interdiffusion of a metallic alloy system and derived a phenomenological equation. This has been widely applied in the analysis of interdiffusion in binary metallic systems. Essentially the same equation was also derived by Hartley and Crank[3] and tested by many

1) "Self-diffusion coefficient" is defined as the diffusion coefficient for diffusion in a homogeneous system where no chemical concentration gradient exists. The term is used for the diffusion coefficient not only in a pure system of single component but also in a homogeneous multicomponent system. Thus, the effective diffusion coefficient defined by the kinetic theory and the intradiffusion coefficient defined by Albright and Mills (*J. Phys. Chem.*, **69**, 3120 (1965)) and McCarty and Mason (*Phys. Fluids*, **3**, 908 (1960)) are included in the present definition.

2) L. S. Darken, *Trans. AIME*, **175**, 184 (1948).

3) G. S. Hartley and J. Crank, *Trans. Faraday Soc.*, **45**, 801 (1949).

authors for various organic binary solutions. The simple form of Darken's equation has the advantage that it can be easily extended to diffusion in the systems of more than two components. An extension to the ternary system has been made for a Ne^{20}–Ne^{22}–CO_2 system with satisfactory results.[4] The Kirkendall effect has also been observed in the interdiffusion in gaseous systems.[5] In Darken's equation the diffusion flux density relative to the external frame is given as a sum of the intrinsic diffusion flux density and the mass flow term. The intrinsic diffusion coefficients are assumed to be equal to the self-diffusion coefficients for the ideal systems, and the interdiffusion coefficient is given by

$$D_{AB} = N_B D_A^* + N_A D_B^* \quad (1)$$

where D_{AB} is the interdiffusion coefficient, N mole fraction, D^* the self-diffusion coefficients, and subscripts A and B refer to components A and B, respectively.

McCarty and Mason[6] and Miller and Carman[7] examined the validity of Darken's equation for the interdiffusion in gaseous systems and found that Eq. (1) was less accurate than the following equation derived from the kinetic theory.

$$\frac{1}{D_A^*} = \frac{N_A}{D_{A^*A}} + \frac{N_B}{D_{AB}} \quad (2)$$

McCarty and Mason further pointed out that Eq. (1) is consistent with Eq. (2) only in the case

$$\frac{D_{AB}^2}{D_{A^*A} D_{B^*B}} = 1. \quad (3)$$

Deviation of the ratio from unity can be a measure for the error resulting from application of the phenomenological equation to a gaseous system for which the kinetic theory holds.

In the present paper, the criterion by means of $D^2_{AB}/D_{A^*A}D_{B^*B}$ has been transformed into mass and potential terms. Thus the magnitude of a possible error coming from the phenomenological equation when applied to an actual system can be estimated with thermodynamic data without knowing the self-diffusion and interdiffusion coefficients. The derived criterion was tested with various binary systems. Necessary self-diffusion coefficients and interdiffusion coefficients were measured by a conventional diaphragm-cell method.

Experimental

Experiments were carried out by means of a Ney-Armistead type[8] diaphragm-cell technique. The cell constant was determined by using the self-diffusion coefficient of carbon dioxide determined by Winn[9] as a standard. The details of the apparatus have been described elsewhere[4].

Commercial helium gas and oxygen gas both of 99.99% purity (Osaka Sanso Co., Japan) were used without further purification. The isotope ratios of these gases were of natural abundance. The O^{18}-enriched oxygen gas was obtained from O^{18}-enriched water by electrolysis. CO_2 gas was O^{18}-enriched with the use of exchange reaction between $CO^{16}O^{16}$ and 5% O^{18}-enriched oxygen on the surface of a red-hot iron wire. Gas mixtures of O_2 and He having the required compositions were prepared in separate storage vessels, transferred into the diffusion cells by means of a Toepler pump, and a diffusion run was then performed. In the measurements of self-diffusion coefficients of O_2 in binary mixtures of O_2 and He, both sides of the diffusion couple were made to have the same chemical composition and one side enriched with O^{18}. For measurements of interdiffusion coefficients the composition difference between the diffusion couple was taken to be approximately 0.2 mole fraction of He. In all experiments the denser gas mixture was placed in the lower cell. Measurements were carried out at 25 ± 0.5 °C under 760 Torr.

The compositions of the binary mixtures of O_2 and He and the isotope ratios of $^{16}O_2$ and $^{17}O_2$ were determined with a mass spectrometer.

Results

Self-diffusion coefficients of O_2 in the binary system of O_2 and He were measured for several compositions. The results are summarized in Table 1. Interdiffusion coefficients for the binary system of O_2 and He were also measured for three compositions. The results are summarized in Table 2. The reciprocals of these diffusion coefficients are plotted as a function of the mole fraction of He in Fig. 1. Equation (2) shows that the reciprocal of the self-diffusion coefficient of one component in a binary system is dependent linearly upon its mole fraction, if the interdiffusion coefficient is independent of composition. The relation holds in the results for O_2 (Fig. 1). The self-diffusion coefficients of He in the binary system of O_2 and He (chain line) were estimated from Eq. (2) by using the value of the self-diffusion coefficient of He in the pure He system D_{B^*B},[10] where the self-diffusion coefficient of He for

TABLE 1. SELF-DIFFUSION COEFFICIENTS OF O_2 FOR THE O_2–He BINARY SYSTEMS

Mole fraction of He	D_A^*
0.000	0.199
0.201	0.236
0.444	0.304
0.606	0.359
0.750	0.443
0.900	0.547

TABLE 2. INTERDIFFUSION COEFFICIENTS FOR THE O_2–He SYSTEM

Mole fraction of He	D_{AB}
0.504	0.682
0.696	0.747
0.898	0.778

4) Y. Oishi, M. Sugisaki, Y. Kamei, and Y. Shono, This Bulletin, **45**, 2984 (1972).
5) E. J. Hellund, *Phys. Rev.*, **57**, 737 (1940). L. Miller and P. C. Carman, *Nature*, **186**, 594 (1960). K. P. McCarty and E. A. Mason, *Phys. Fluids*, **3**, 908 (1960).
6) K. P. McCarty and E. A. Mason, *ibid.*, **3**, 908 (1960).
7) L. Miller and P. C. Carman, *Trans. Faraday Soc.*, **57**, 2143 (1961).
8) E. P. Ney and F. C. Armistead, *Phys. Rev.*, **71**, 14 (1947).
9) E. B. Winn, *ibid.*, **80**, 1024 (1950).
10) The value extrapolated for 25 °C from the data by P. J. Bendt, *Phys. Rev.*, **110**, 85 (1958).

Table 3. Comparison of $(m_A+m_B)/2\sqrt{m_Am_B}$ with the experimental value $(D_{AB})^2/(D_{AA}D_{BB})$

A	B	T[°C]	D_{AB}	D_{AA}	D_{BB}	$(D_{AB})^2/(D_{AA}D_{BB})$	Ω	$(m_A+m_B)/2\sqrt{m_Am_B}$
He	— N_2	25	0.687[a]	1.57[f]	0.212[h]	1.42	0.931	1.51
He	— O_2	25	0.729[a]	1.57[f]	0.232[h]	1.46	1.00	1.59
					(0.202)[j]	(1.68)		
He	— Ar	25	0.729[a]	1.57[f]	0.178[h]	1.90	1.03	1.74
He	— CO_2	25	0.612[a]	1.57[f]	0.113[h]	2.11	0.994	1.81
H_2	— N_2	0	0.674[b]	1.29[b]	0.185[h]	1.90	0.967	2.00
H_2	— CH_4	0	0.625[b]	1.29[b]	0.206[h]	1.47	1.03	1.59
H_2	— O_2	0	0.697[b]	1.29[b]	0.187[h]	2.01	0.999	2.12
H_2	— CO	0	0.651[b]	1.29[b]	0.190[g]	1.73	0.962	2.00
H_2	— CO_2	0	0.550[b]	1.29[b]	0.0970[i]	2.42	1.01	2.44
CO	— O_2	0	0.185[c]	0.190[g]	0.187[h]	0.96	0.999	1.00
CO	— N_2	0	0.192[b]	0.190[g]	0.185[h]	1.05	1.00	1.00
CO	— CO_2	0	0.137[b]	0.190[g]	0.0970[f]	1.02	1.07	1.03
CO	— Ne	25	0.259[d]	0.113[h]	0.516[h]	1.15	0.980	1.08
CO_2	— N_2	25	0.158[c]	0.113[h]	0.212[h]	1.04	1.04	1.03
CO_2	— CH_4	0	0.153[b]	0.0970[f]	0.206[h]	1.17	0.998	1.13
N_2	— O_2	0	0.181[c]	0.185[h]	0.187[h]	0.95	0.999	1.00
Xe	— Ar	0	0.0962[e]	0.0480[e]	0.156[h]	1.24	0.977	1.18

$$\Omega=\frac{\sigma_{AA}^2W_{AA}^{(1)}\ \sigma_{BB}^2W_{BB}^{(1)}}{(\sigma_{AB}^2W_{AB}^{(1)})^2}$$

a) S. L. Seager, L. R. Geertson, and J. C. Giddings, *J. Chem. Eng. Data*, **8**, 168 (1963).
b) "American Institute of Physics Handbook" (1957).
c) N. H. Chen and D. F. Othmer, *J. Chem. Eng. Data*, **7**, 37 (1962).
d) J. D. Breetveld, R. DiPippo, and J. Kestine, *J. Chem. Phys.*, **45**, 124 (1966); from mixture viscosity.
e) I. Amdure and T. F. Schatzki, *J. Chem. Phys.*, **27**, 1049 (1957).
f) The value extrapolated for 25 °C from the data by P. J. Bendt, *Phys. Rev.*, **110**, 85 (1958).
g) S. Weissman, *J. Chem. Phys.*, **40**, 3397 (1964).
h) E. B. Winn, *Phys. Rev.*, **80**, 1024 (1950).
i) I. Amdure, J. W. Irvine, Jr., E. A. Mason, and J. Ross, *J. Chem. Phys.*, **20**, 436 (1952).
j) Present experimental result.

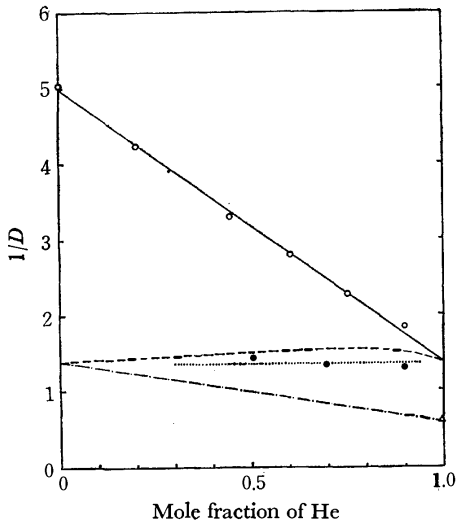

Fig. 1. Reciprocal of diffusion coefficients for the O_2–He system; ○, experimental self-diffusion coefficients of O_2; ●, experimental interdiffusion coefficients; ·-·-·, estimated self-diffusion coefficients of He; △, experimental value by Bendt[9]; ——, theoretical interdiffusion coefficients by the phenomenological equation; ·····, theoretical interdiffusion coefficients by the kinetic theory.

zero mole fraction of He should be equal to the interdiffusion coefficient for the same composition.

The value of the interdiffusion coefficient D_{AB} calculated by Eq. (2) is 0.721, which agrees closely with the average of our values, 0.736. Seager *et al.*[11] and Wasik *et al.*[12] also reported the values, 0.729, 0.736, respectively. The interdiffusion coefficients for the O_2–He system were calculated by the kinetic theory for cases in which the various data[13] of potential parameters were available. The calculation gives a maximum 0.751 and minimum 0.708. The average value, shown in Fig. 1 by a dotted line, agrees well with the experimental results. For the sake of comparison, the results obtained by Eq. (1) are also shown (broken line), maximum deviation from experimental result being approximately 14.7%. This deviation should be attributed to the approximation made in the derivation of Darken's equation.

Discussion

A Criterion for Comparison of the Phenomenological Equation with the Kinetic Theory. For the case where the rigorous kinetic theory is valid, the applicability of Eq. (1) can be tested by whether the ratio $D^2_{AB}/$

11) S. L. Seager, L. R. Geertson, and J. C. Giddings, *J. Chem. Eng. Data*, **8**, 168 (1963).
12) S. P. Wasik and K. E. McCulloh, *J. Res. Nat. Bur. Std.*, **73A**(2), 207 (1969).
13) The potential parameters were obtained according to the combining rule from the force constants data determined by viscosity and 2nd virial coefficients measurements at various temperatures (see also Ref. (15)).

$(D_A{}^*{}_A D_B{}^*{}_B)$ is unity or not, as mentioned by McCarty and Mason. For the O_2–He system at 25 °C, we obtain

$$\frac{D_{AB}^2}{D_A{}^*{}_A D_B{}^*{}_B} = \frac{(0.729)^2}{(0.199)(1.69)} = 1.57$$

The deviation from unity may be taken as a measure for the deviation of the interdiffusion coefficient obtained by the phenomenological equation from the correct value, the square root of 1.57 indicating the deviation.

This criterion can be further simplified and rewritten by use of the rigorous kinetic theory. In order to simplify the derivation, we let $D_A{}^*{}_A$ and $D_B{}^*{}_B$ equal to D_{AA} and D_{BB} respectively. The interdiffusion coefficient D_{ij} is then expressed as follows:[14]

$$D_{ij} = 0.00092916 \frac{T^{3/2}\sqrt{(m_i+m_j)/m_i m_j}}{P\sigma_{ij}^2 W_{ij}^{(1)}(1:\varepsilon_{ij}/kT)} \text{ [cm}^2\text{/s]} \qquad (4)$$

where P is pressure [atm], T temperature [K], σ_{ij} and ε_{ij} the potential parameters, m_i and m_j molecular masses, and $W_{ij}^{(1)}$ $(1:\varepsilon_{ij}/kT)$ the term associated with the collision integral. Thus, we obtain

$$\frac{D_{AB}^2}{D_{AA}D_{BB}} = \frac{(m_A+m_B)}{2\sqrt{m_A m_B}}\left[\frac{\sigma_{AA}^2 W_{AA}^{(1)}\sigma_{BB}^2 W_{BB}^{(1)}}{(\sigma_{AB}^2 W_{AB}^{(1)})^2}\right] \qquad (5)$$

Values of $D^2{}_{AB}/D_{AA}D_{BB}$ for various systems were calculated by use of experimental data and compared with $(m_A+m_B)/2\sqrt{m_A m_B}$. Some of the examples are listed in Table 3. It is noted that the values of Ω,[15] *i.e.* the term in the brackets in Eq. (5) are close to unity, so $D^2{}_{AB}/D_{AA}D_{BB}$ may be approximated to $(m_A+m_B)/2\sqrt{m_A m_B}$, if a few percent error is allowed. Thus the discrepancy of the phenomenloogical equation from Eq. (2) is ascribed mostly to the deviation of $(m_A+m_B)/2\sqrt{m_A m_B}$ from unity.

14) J. O. Hirschfelder, R. B. Bird, and E. L. Spotz, *Chem. Rev.*, **44**, 205 (1949); *J. Chem. Phys.*, **16**, 968 (1948).

15) The values of Ω were calculated for various systems on the basis of the Lennard-Jones (12: 6) potential model by means of a computer. The potential parameters σ_{ij} and ε_{ij} in all combinations were calculated according to the combining rules:

$$\sigma_{ij} = \frac{1}{2}(\sigma_{ii}+\sigma_{jj})$$

$$\varepsilon_{ij} = \sqrt{\varepsilon_{ii}\cdot\varepsilon_{jj}}$$

from the force constants listed in the Appendix of "Molecular Theory of Gases and Liquids" (J. O. Hirschfelder, C. F. Curtiss and R. B. Bird, John Willy & Sons, Inc., New York, 1964).

BULLETIN OF THE CHEMICAL SOCIETY OF JAPAN, VOL. 46, 2662—2664 (1973)

Charge Transfer in Acetonitrile-Halogen Complexes

Hisao NEGITA, Kaoru SHIBATA, Yoshihiro FURUKAWA, and Koji YAMADA

Department of Chemistry, Faculty of Science, Hiroshima University, Hiroshima 730

(Received February 26, 1973)

The charge transfer in acetonitrile-halogen complexes was examined by means of the nuclear quadrupole resonances resulting from the relevant nuclei. ^{14}N NQR parameters ($|e^2Qq|=3.6000$ MHz and $\eta=0.0183$) and ^{35}Cl NQR parameters ($|e^2Qq|=107.44$ and 108.50 MHz) were obtained for the acetonitrile-chlorine complex, whereas ^{14}N NQR parameters ($|e^2Qq|=3.5439$ MHz and $\eta=0.0043$) and a ^{81}Br NQR parameter ($|e^2Qq|=640.52$ MHz) were obtained for the acetonitrile-bromine complex. From these parameters, the charged states of the nitrogen, chlorine, and bromine atoms in these charge-transfer complexes were calculated by means of the Townes and Dailey theory. In the case of the acetonitrile-bromine complex, the charge loss at the nitrogen atom was not equal to the gain at the bromine atom, as long as the charge was assumed to be transferred only to the p-orbital of the latter. This discrepancy was explained by assuming some d-hybridization at the bromine atom. The charged states of the nitrogen atoms in these complexes were qualitatively in good agreement with the electron affinities of the chlorine and bromine molecules. Moreover, the temperature dependences of the ^{14}N and ^{81}Br nuclear quadrupole coupling constants in the acetonitrile-bromine complex were investigated in the range from -196 to -60 °C.

The charge-transfer (CT) complexes of nitriles or amines with halogens have been investigated by various spectroscopic methods. The NQR method is particularly useful for investigating the charge distribution in the CT complexes. However, NQR data have been reported only on the halogen atoms in electron acceptors. Therefore, we planned to examine ^{14}N NQR in some weak CT complexes, including the CT complexes of acetonitrile with the chlorine and bromine molecules. The crystal structure of the acetonitrile-bromine complex was recently determined to be as is shown in Fig. 1.[1] The open and shaded circles represent atoms at $y=0$ and $y=\pm 1/2$ respectively. The intramolecular bonds are represented by the solid lines, while the intermolecular bonds are represented by the broken lines. The distance between the nitrogen and bromine atoms in the acetonitrile-bromine complex is shorter by 0.61 Å than the sum of their van der Waals radii. Therefore, it may be considered that there is a weak interaction between the acetonitrile and bromine molecules. A similar intermolecular interaction may be expected to exist between the acetonitrile and chlorine molecules.

1) K. M. Marstokk and K. O. Strømme, *Acta Crystallogr.*, **B24**, 713 (1968).

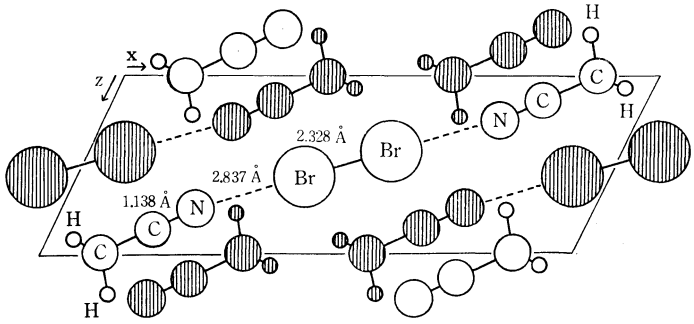

Fig. 1. The crystal structure of the acetonitrile-bromine complex.

Experimental

The ^{14}N NQR spectra of these CT complexes were obtained by the use of a frequency-modulated spectrometer described previously,[2] whereas the ^{35}Cl and ^{81}Br NQR spectra of these CT complexes were obtained by the use of a superregenerative spectrometer. The resonance frequencies were measured by means of two heterodyne-type frequency meters, BC-221 and TS-175C/U, whose frequencies were checked by means of a frequency counter, TR-5578, of the Takeda Riken Co. The measurements were carried out at the temperature of liquid nitrogen, but the studies of the temperature dependences were performed by blowing the vapour of the liquid nitrogen from a Dewar bottle. The temperatures were measured by the use of a thermocouple.

Preparation of the Acetonitrile-chlorine Complex. Gaseous chlorine was generated by the reaction of hydrogen chloride with manganese dioxide, and was liquefied by the use of a mixture of acetone and dry ice as the coolant. Then acetonitrile obtained from commercial sources was mixed with liquid chlorine in the mol ratio of 2: 1 at about −70 °C.

Preparation of the Acetonitrile-bromine Complex. Commercial acetonitrile was mixed with commercial bromine in the mol ratio of 2: 1 at about −40 °C.

Results and Discussion

Generally a pair of ^{14}N NQR frequencies, ν_I and ν_{II}, are observed as follows:

$$\nu_I = |e^2Qq|(3-\eta)/4, \quad (1)$$

$$\nu_{II} = |e^2Qq|(3+\eta)/4. \quad (2)$$

On the other hand, the ^{35}Cl or ^{81}Br NQR frequency, ν_0, is obtained according to the following equation:

$$\nu_0 = |e^2Qq|(1+\eta^2/3)^{1/2}/2, \quad (3)$$

where $|e^2Qq|$ and η are the quadrupole coupling constant and the asymmetry parameter respectively. Our sample of the acetonitrile-chlorine complex revealed a pair of ^{14}N resonance lines and two ^{35}Cl resonance lines, with an intensity ratio of about 5: 3, as is shown in Fig. 2. We attributed the resonance line of 53.72 MHz to the ^{35}Cl nuclei in the CT complex, and that of 54.25 MHz, to the ^{35}Cl nuclei in the non-reacted chlorine molecules. The acetonitrile-bromine complex showed a pair of ^{14}N resonance lines and a ^{81}Br resonance line, as is shown in Fig. 2. The ^{14}N nuclear quadrupole coupling constant in the acetonitrile-bromine complex is lower than that in the acetonitrile-chlorine complex. This seems to suggest that the interaction between the nitrogen and bromine atoms is stronger than that between the nitrogen and chlorine atoms in the CT complexes. The quadrupole coupling constants and asymmetry parameters derived by substituting these resonance frequencies into Eqs. (1), (2), and (3) are listed in Table 1.

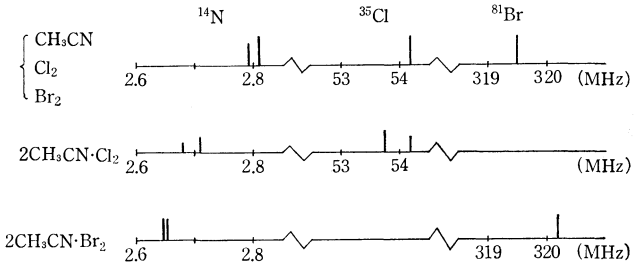

Fig. 2. NQR absorption lines in acetonitrile-halogen complexes.

The orbitals at the nitrogen atom or halogen atoms have the general form listed in Table 2, where the value of s is 0.5 in the case of the nitrogen atom[3] and 0 in the cases of the halogen atoms. The occupation numbers of these orbitals at the nitrogen atom in acetonitrile are denoted by a, a, b, and 2, whereas those in the CT complexes denoted by a, a, b', and x. The quadrupole coupling constant has been related to

Table 1. NQR parameters in acetonitrile-halogen complexes

Complex		ν (MHz)	$\lvert e^2Qq\rvert$ (MHz)	η (%)
$2CH_3CN\cdot Cl_2$	^{14}N	2.6835;2.7165	3.6000	1.83
	^{35}Cl	53.72 54.25	107.44 108.50	—
$2CH_3CN\cdot Br_2$	^{14}N	2.6541;2.6618	3.5439	0.43
	^{81}Br	320.26	640.52	—

2) H. Negita, M. Hayashi, and T. Okada, *J. Sci. Hiroshima Univ., Ser. A*, **35**, 85 (1971).

3) E. A. C. Lucken, "Nuclear Quadrupole Coupling Constants," Academic Press, London and New York (1969), p. 227.

Table 2. Orbitals and their occupation numbers at the nitrogen atom

Orbital	Occupation number[a]	
$\varphi_1=\chi_{P_x}$	a	(a)
$\varphi_2=\chi_{P_y}$	a	(a)
$\varphi_3=\sqrt{s}\,\chi_s+\sqrt{1-s}\,\chi_{P_z}$	b	(b')
$\varphi_4=\sqrt{1-s}\,\chi_s-\sqrt{s}\,\chi_{P_z}$	2	(x)

a) The numbers in the parentheses are those in the complex.

the occupation numbers of p-orbitals (N_x, N_y, and N_z) by Townes and Dailey:[4]

$$|e^2Qq/e^2Qq_p| = N_z - (N_x+N_y)/2, \quad (4)$$

where $|e^2Qq_p|$ is the quadrupole coupling constant produced by one p-electron in the outmost occupied shell. From Table 2, the N_x, N_y, and N_z values of the nitrogen atom in an acetonitrile molecule are found to be a, a, and $(b+2)/2$ respectively, while those in the CT complexes are found to be a, a, and $(b'+x)/2$ respectively. Therefore, the electron number transferred from the nitrogen atom, δ, is shown by the following equation:

$$\delta = (b+2) - (b'+x)$$
$$= 2(|e^2Qq_{compound}| - |e^2Qq_{complex}|)/|e^2Qq_p|. \quad (5)$$

The electron numbers transferred to the halogen atoms are calculated from their coupling constants. The $|e^2Qq_p|$ values of the nitrogen, chlorine, and bromine atoms are 10, 109.74,[5] and 643.03 MHz[6] respectively.

Table 3. The values of δ in acetonitrile-halogen complexes

Complex	Value of δ	
	Nitrogen	Halogen
$2CH_3CN\cdot Cl_2$	+0.028	−0.021
$2CH_3CN\cdot Br_2$	+0.029	−0.004

Table 3 lists these values of δ in the CT complexes. In spite of the rough approximations, the values of δ at the nitrogen and chlorine atoms in the acetonitrile-chlorine complex are complementary. However, the value of δ at the bromine atom in the acetonitrile-bromine complex is about one-seventh of that at the nitrogen atom. This discrepancy can be interpreted by theorizing that a part of the charge transferred from the nitrogen atom enters the d_{z^2}-orbital of the bromine atom, which has less effect on the coupling constant than the p_z-orbital. This interpretation is along the same lines as that for the bromine molecular crystal, where the d-orbital of the atom has been taken by Kojima *et al.*,[7] to be used for the intramolecular bond. The recently-reported values of the electron affinities of the chlorine and bromine molecules are 2.52±0.17 and 2.87±0.14 eV respectively,[8] these values are parallel with the values of δ at the nitrogen atoms. According to the crystal structure of the acetonitrile-bromine complex, the bromine-bromine length, 2.328 Å, is longer than that observed in the free molecule, 2.284 Å.[1] This indicates that the negatively-charged bromine atoms repel each other.

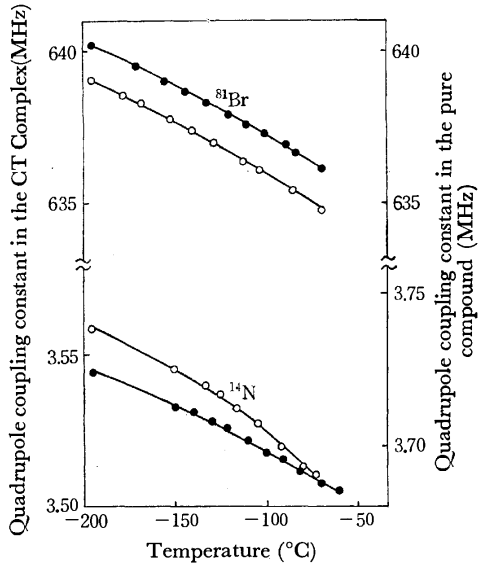

Fig. 3. The temperature dependences of ^{14}N and ^{81}Br quadrupole coupling constants in acetonitrile (○), bromine (○), and acetonitrile-bromine complex (●).

The temperature dependences of the ^{14}N and ^{81}Br quadrupole coupling constants in acetonitrile, bromine, and the acetonitrile-bromine complex are shown in Fig. 3. No phase transition is observed in the range from −196 to −60 °C. The temperature dependence of the ^{14}N quadrupole coupling constant in the CT complex is smaller than that in acetonitrile. Therefore, we see that the vibration of an acetonitrile molecule in the CT complex is suppressed by the interaction with the bromine atom. On the other hand, the temperature dependence of the ^{81}Br quadrupole coupling constant in the CT complex is nearly the same as that in solid bromine. This suggests that the bromine molecule interacts with its neighboring molecules to some extent, even in the molecular crystal, as is to be expected from its crystal structure.[9]

4) C. H. Townes and B. P. Dailey, *J. Chem. Phys.*, **17**, 782 (1949).
5) V. Jaccarino and J. G. King, *Phys. Rev.*, **83**, 471 (1951).
6) J. G. King and V. Jaccarino, *ibid.*, **94**, 1610 (1954).
7) S. Kojima, K. Tsukada, A. Shimauchi, and Y. Hinaga, *J. Phys. Soc. Jap.*, **9**, 795 (1954).
8) J. J. DeCorpo and J. L. Franklin, *J. Chem. Phys.*, **54**, 1885 (1971).
9) J. Donohue and S. H. Goodman, *Acta Crystallogr.*, **18**, 568 (1965).

Variations of Heat of Immersion of Ferric Oxyhydroxides in Water with Structural Changes by Heating

Tatsuo ISHIKAWA and Katsuya INOUYE

Department of Chemistry, Faculty of Science, Chiba University, Chiba 280

(Received March 1, 1973)

The relationship between the activity of ferric oxyhydroxides (α-, β-, and γ-FeOOH) and structural changes has been investigated by determining the heat of immersion in H_2O and H_2O vapor adsorption. For each ferric oxyhydroxide, the monolayer capacity of H_2O adsorption and the heat of immersion decreased with the progress of transformation into α-Fe_2O_3. Above the transformation temperature the heat of immersion increased with the outgassing temperature. The heat of immersion of α-Fe_2O_3 obtained by outgassing each ferric oxyhydroxide at 400 and 500 °C increased with the accompanying increase in crystallite size. β-FeOOH showed higher heat of immersion and larger monolayer capacity per unit surface area than other ferric oxyhydroxides. It is presumed that the higher heat of immersion and larger monolayer capacity observed for β-FeOOH are ascribed to micropores in β-FeOOH crystals produced by the removal of molecular water originally contained.

Although ferric oxyhydroxides and oxides are commonly known as significant corrosion products of iron, the surface property in view of the structure of these compounds still remains unclarified. The surface activity of ferric oxyhydroxide, for instance, is expected to vary with the degree of its structural transformation into other compounds. Jurinak[1] reported that the adsorptive activity of α-FeOOH to H_2O suddenly decreases at the transformation temperature into α-Fe_2O_3. The present authors have studied the SO_2 adsorption on ferric oxyhydroxides[2] and ferric oxides at various outgassing temperatures[3] in order to show that β-FeOOH chemisorbs a larger amount of SO_2 than other ferric oxyhydroxides and that the amount of chemisorbed SO_2 by each ferric oxyhydroxide, regarded as a measure of reactivity, decreases with the progress of transformation into α-Fe_2O_3.

It appears that a knowledge of the interaction between H_2O and ferric oxyhydroxides is essential to understand the surface properties of ferric oxyhydroxides as main corrosion products of iron. Several investigators[4-6] have suggested that the surface activity of ferric oxides, evaluated by the heat of immersion in water and H_2O vapor adsorption, depends upon the temperature of heat treatment and the number of hydroxyl groups on the surfaces of resulting ferric oxides. We found that the heat of immersion of ferric oxides of different particle size (50 to 650 Å in diameter) is independent of particle size.[7] However, there has been no investigation into the change of heat of immersion of ferric oxyhydroxides with structural transformation. In the present work, the heat of immersion in water and H_2O adsorption isotherms are determined and discussed for α-, β-, and γ-ferric oxyhydroxides with outgassing at various temperatures up to 500 °C in order to confirm the change of activity towards H_2O with the structural changes.

Experimental

Materials. The preparation of ferric oxyhydroxides has been described in detail[3]. α-FeOOH(α-1) was prepared by the hydrolysis of 0.1 M ferric oxalate solution at 100 °C with the initial pH 6.6. More crystalline α-FeOOH(α-2) was obtained by the hydrolysis of ferric sulfate solution at 50 °C with the adjusted pH 13.6. β-FeOOH(β-1) prepared by hydrolysing 0.1 M ferric chloride solution containing urea at 100 °C is more crystalline than other β-FeOOH(β-2) obtained by heating 0.1 M ferric chloride solution at 75 °C. Crystalline γ-FeOOH(γ-1) was prepared by the oxidation of ferrous hydroxide suspension with $NaNO_3$, and amorphous γ-FeOOH(γ-2) by the oxidation of ferrous sulfate solution in the presence of $Na_2S_2O_3$.

Procedure. The heat of immersion in water was measured at 30.0 °C by means of a twin-type microcalorimeter (Oyodenki Kenkyujo, CM-204S) consisting of a pair of calorimeters, one of them being the reference. Prior to the immersion experiments, approximately 200—300 mg of the sample was heated up to 110, 150, 200, 300, 400, and 500 °C at a heating rate of 8 °C/min in a glass ampule under 10^{-5} Torr and outgassed for 5 hr at each temperature. After outgassing, the glass ampule was sealed off in a vacuum and set in the calorimeter. When the calorimeter attained thermal equilibrium, the ampule was broken in order to immerse the sample in water.

The water adsorption experiment was performed gravimetrically at 30.0 °C by means of a quartz spring balance.

The surface area of the sample was determined by a conventional volumetric method by nitrogen adsorption according to the BET method. The pretreatment of the sample in the H_2O adsorption and surface area determinations was identical to that in the heat of immersion measurement.

The X-ray diffraction patterns were obtained by the powder method with a diffractometer (Rigaku Denki Co., 2001) by use of Mn-filtered Fe$K\alpha$ at 30 kV and 10 mA.

Results and Discussion

The X-ray diffraction patterns of ferric oxyhydroxides are shown in Fig. 1.

The changes of X-ray diffraction patterns of α-2, β-1, and γ-1 with outgassing at various temperatures

1) J. J. Jurinak, *J. Colloid Sci.*, **19**, 477 (1964).
2) T. Ishikawa and K. Inouye, *Nippon Kagaku Zasshi*, **91**, 935 (1970).
3) T. Ishikawa and K. Inouye, This Bulletin, **45**, 2350 (1972).
4) F. H. Healey, J. J. Chessick, and A. V. Fraioli, *J. Phys. Chem.*, **60**, 1001 (1956).
5) A. C. Zettlemoyer and E. McCafferty, *Z. Phys. Chem.*, **64**, 41 (1969).
6) Y. Nakahara, *Kogyo Kagaku Zasshi*, **74**, 1061 (1971).
7) T. Ishikawa, M. Okamoto, Y. Itō, and K. Inouye, *Nippon Kagaku Kaishi*, **1972**, 1751.

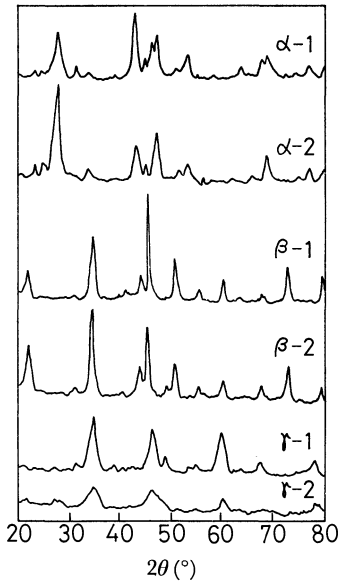

Fig. 1. X-ray diffraction patterns of ferric oxyhydroxides.

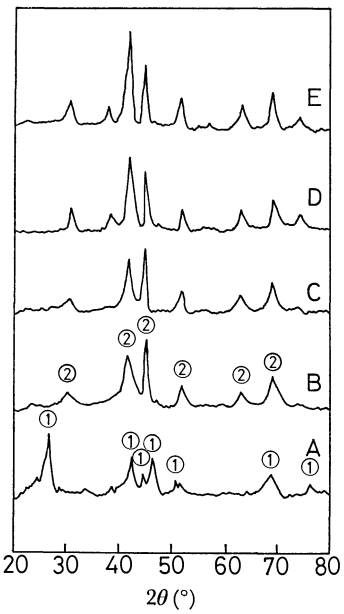

Fig. 2. X-ray diffraction patterns of α-2 at various outgassing temperatures: ①, α-FeOOH; ②, α-Fe_2O_3; A, 150 °C; B, 200 °C; C, 300 °C; D, 400 °C; E, 500 °C.

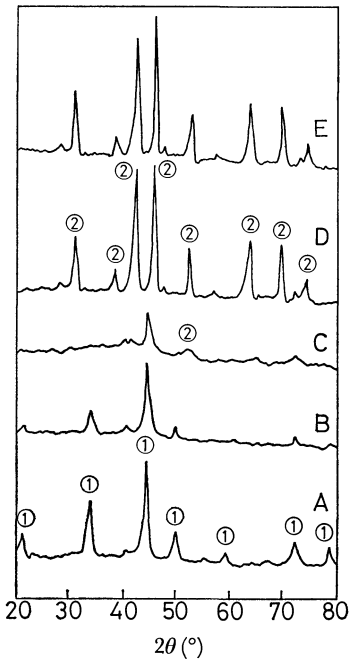

Fig. 3. X-ray diffration patterns of β-1 at various outgassing temperatures: ①, β-FeOOH; ②, α-Fe_2O_3; A, 150 °C; B, 200 °C; C, 300 °C; D, 400 °C; E, 500 °C.

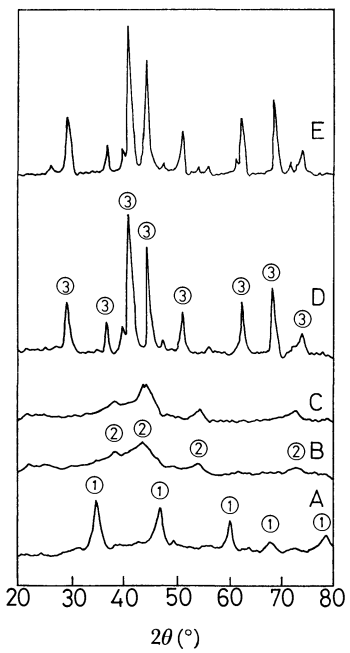

Fig. 4. X-ray diffraction patterns of γ-1 at various outgassing temperatures: ①, γ-FeOOH; ②, γ-Fe_2O_3; ③, α-Fe_2O_3; A, 150 °C; B, 200 °C; C, 300 °C; D, 400 °C; E, 500 °C.

are shown in Figs. 2, 3, and 4 respectively, illustrating the mode of transformation of each ferric oxyhydroxide into α-Fe_2O_3 at particular temperature ranges. α-FeOOH is transformed into α-Fe_2O_3 at 200 °C. β-FeOOH changes to an amorphous mixture, composed of β-FeOOH and α-Fe_2O_3, in the temperature range 200—300 °C, and is further transformed into the crystalline α-Fe_2O_3 above 400 °C. γ-FeOOH is transformed into γ-Fe_2O_3 at 200 °C and is converted into crystalline α-Fe_2O_3 at 400 °C. These results show that all ferric oxyhydroxides are transformed into α-Fe_2O_3 above 400 °C.

The weight loss accompanying the change of ferric oxyhydroxide to α-Fe_2O_3 is 10% corresponding to the dehydration formula; $2FeOOH \rightarrow Fe_2O_3 + H_2O$. To obtain the variations of weight loss with outgassing temperature (Fig. 5), the samples were subjected to heat treatment in the same manner as those in the H_2O adsorption and the heat of immersion measurements. For α-2 and γ-1, the weight loss increases with the rise of temperature up to 200 or 300 °C, followed by almost constant weight above 300 °C. The total weight loss at 500 °C corresponds to 11.2 and 12.8% for γ-1 and α-2, respectively. These values are somewhat larger than the theoretical value (10%), because of the dehydration of adsorbed water and the "bound"

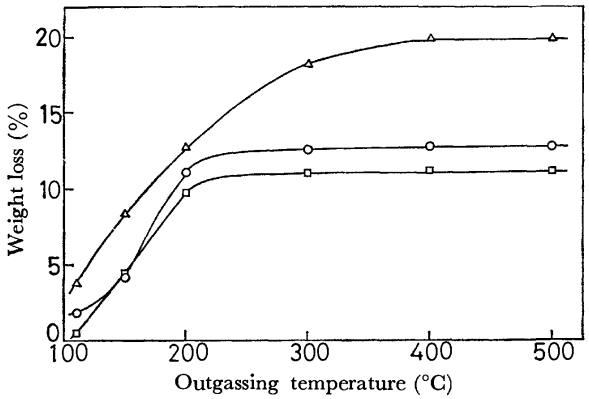

Fig. 5. Relation between weight loss and outgassing temperature: ○, α-2; △, β-1; □, γ-1.

water supposedly contained in the ferric oxyhydroxide crystals.[8] Although the X-ray diffraction patterns obtained for these samples (α-2 and γ-1) remain almost unchanged up to 150 °C, an approximate 4.5% weight loss is observed. This indicates that α-2 and γ-1 are partially transformed into amorphous ferric oxide below 150 °C. On the other hand, the weight loss of β-1 increases with the rise in outagssing temperature up to 400 °C, reaching a total weight loss of 20% at 500 °C. This large weight loss is due to the removal of chlorine and molecular water originally contained in β-FeOOH crystals.[3]

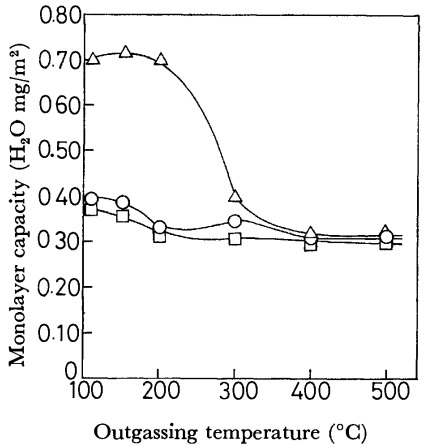

Fig. 6. Effect of outgassing temperature on monolayer adsorption capacity: ○, α-2; △, β-1; □, γ-1.

H_2O adsorption isotherm is the BET-II type for each sample. The monolayer capacity (A_m) of H_2O adsorption per unit BET surface area, calculated from the N_2 adsorption isotherm, is shown in Fig. 6 as a function of outgassing temperature. The A_m values of α-2 and γ-1 decrease with the rise in temperature up to 200 °C and become nearly constant above 400 °C, whereas A_m of β-1 below 200 °C is considerably high but decreases abruptly in the temperature range 200—300 °C. Above 400 °C, where transformation into α-Fe_2O_3 occurs, the A_m value of β-1 becomes equal to that of α-2 and γ-1. The large A_m of β-FeOOH seems to be

8) G. Okamoto, R. Furuichi, and N. Sato, *Electrochim. Acta*, **12**, 1287 (1967).

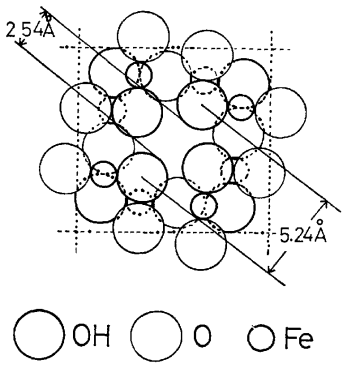

Fig. 7. Projection of the crystal structure of β-FeOOH on (001). β-FeOOH has a tetragonal lattice with the following unit cell dimensions: $a=b=10.48$ Å, $c=3.02$ Å.

due to the formation of micropores in crystals with the release of molecular water by outgassing. The crystal structure of β-FeOOH proposed by Mackay[9] has micropores parallel to c-axis as shown in Fig. 7. The diameter of these micropores is estimated to be 2.54 Å from the effective diameter of the hydroxyl group (1.35 Å) and the distance between hydroxyl groups (5.24 Å). On the other hand, the diameter of N_2 molecule and H_2O molecule is 3.5 and 2.5 Å, respectively. H_2O molecule has a strong dipole moment, whereas N_2 molecule has only a quadrupole moment. Thus, it is plausible that the micropores are more accessible to H_2O molecules than to N_2 molecules. According to X-ray diffraction results (Fig. 3) in which the β-FeOOH crystal turns into an amorphous state in the temperature range 200—300 °C, the decrease in A_m of β-FeOOH in the course of outgassing below 300 °C seems to be due to the destruction of β-FeOOH structure having the micropores.

The decrease in A_m of α-FeOOH or γ-FeOOH below 200 °C might be attributed mainly to the removal of surface hydroxyl groups. The heat of immersion (ΔH_I) per unit surface area of α-FeOOH is shown in Fig. 8 against outgassing temperature. The decrease in ΔH_I below 150 °C is considered to be due to the removal of the hydroxyl groups acting as hydrophilic sites on the ferric oxyhydroxide surface. In contrast

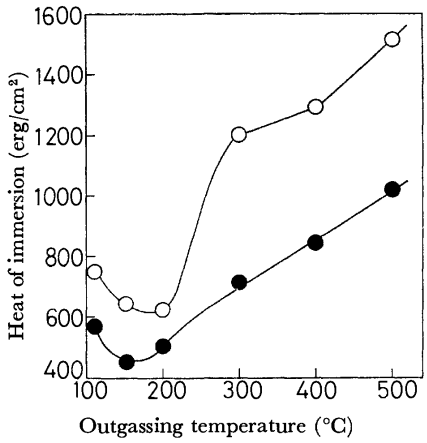

Fig. 8. Effect of outgassing temperature on the heat of immersion of α-FeOOH: ○, α-1; ●, α-2.

9) A. L. Mackay, *Miner. Mag.*, **32**, 545 (1960).

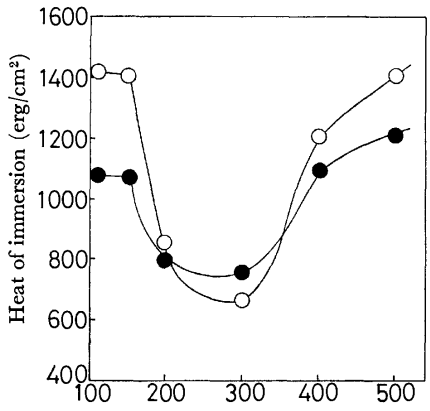

Fig. 9. Effect of outgassing temperature on the heat of immersion of β-FeOOH; ○, β-1, ●, β-2.

to this, the increase in ΔH_I above 200 °C seems to be caused by rehydration of the α-Fe_2O_3 surface, the dehydrated surface being readily rehydrated to be covered again with hydroxyl groups during the immersion process in water.[5] γ-FeOOH shows the same tendency as α-FeOOH. As illustrated in Fig. 9, β-FeOOH shows a larger ΔH_I than that of other ferric oxyhydroxides below 150 °C, the ΔH_I value falling sharply in the temperature range 150—200 °C. Above 300 °C, ΔH_I increases with temperature probably by surface rehydration as with other ferric oxyhydroxides.

It is apparent that α-Fe_2O_3 samples obtained by outgassing α-2, β-1, and γ-1 at 400 and 500 °C were almost completely dehydrated, since they show a constant weight loss above 400 °C as shown in Fig. 5. The heat of immersion (ΔH_I) for these samples therefore includes the heat evolved with the rehydration of dehydrated α-Fe_2O_3 surface. The heat of rehydration depends upon the stability of the oxygen bridge such as $-Fe\langle\overset{O}{O}\rangle Fe-$ which is formed on dehydration. The stability of the oxygen bridge is considered to be related to the crystallinity of α-Fe_2O_3. The crystallite size as a measure of crystallinity was calculated by the Scherrer equation for the α-Fe_2O_3 (104) pattern at 2θ of 41.9° in X-ray diffraction diagrams. ΔH_I was plotted against crystallite size (Fig. 10) to show that it increases with increase in crystallite size. This could be explained by assuming that the oxygen bridge of less crystalline α-Fe_2O_3 is so unstable as to be rehydrated with evolution of less heat than that of more crystalline α-Fe_2O_3.

The large ΔH_I of β-FeOOH below 150 °C (Fig. 9)

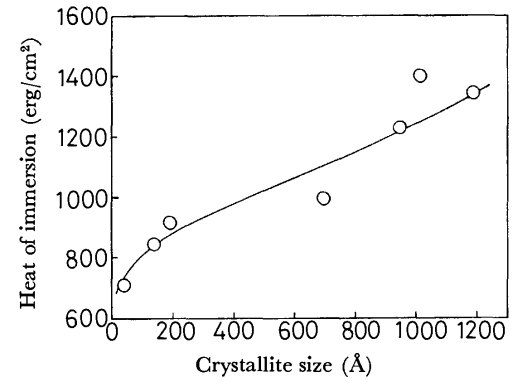

Fig. 10. Relation between crystallite size and the heat of immersion.

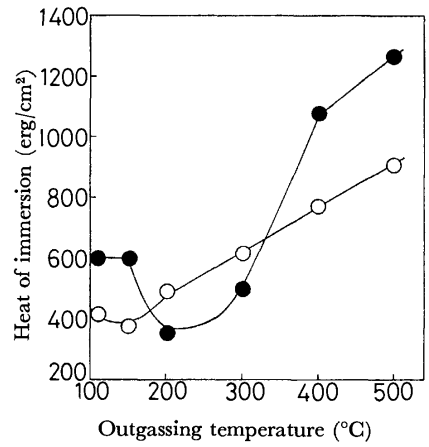

Fig. 11. The heat of immersion per unit H_2O surface area: ○, α-2; ●, β-1.

seems to be associated with the microporous structure of β-FeOOH. The depression of ΔH_I in the temperature range 150—200 °C is caused by the destruction of the microporous structure of β-FeOOH. The heat of immersion in water, per unit surface area obtained by N_2 adsorption, shows a large value caused by the existence of the micropores into which H_2O molecules are adsorbed more easily than N_2 molecules. To exclude the micropore effect on the heat of immersion, calculation based on the surface area estimated from H_2O adsorption, using 10.6 Å for the sectional area of an adsorbed water molecule, was attempted. However, β-FeOOH still showed a higher heat of immersion than other ferric oxyhydroxides up to 150 °C (Fig. 11). It is concluded, therefore, that β-FeOOH is more reactive to H_2O as compared with other ferric oxyhydroxides.

The Crystal Structure of Cinchomeronic Acid

Fusao TAKUSAGAWA, Ken HIROTSU, and Akira SHIMADA

Department of Chemistry, Faculty of Science, Osaka City University, Sugimoto-cho, Sumiyoshi-ku, Osaka 558

(Received March 2, 1973)

The crystal structure of cinchomeronic acid (3,4-pyridinedicarboxylic acid) has been determined by the method of X-ray diffraction. The crystals are orthorhombic, with a space group of $P2_12_12_1$, and with cell dimensions of $a=11.211$, $b=11.206$, and $c=5.285$ Å. The structure was determined by the method of symbolic addition. The final R value was 5.90% for 828 observed reflections. The molecule takes the form of a zwitter ion in the crystal. The pyridine ring has, approximately, the C_{2v} symmetry. One carboxyl group consists of C=O and C–O(H) groups, while the other consists of two C···O groups. These carboxyl groups twist out of the plane of a pyridine ring by 39.6° and 73.0° respectively. The hydrogen bonds are in the forms of two spirals around the two-fold screw axes parallel to the c axis, thus linking the molecules three-dimensionally. There are four molecules per turn of the spiral along the c axis. The carbonyl oxygen atom O(2) is free from the hydrogen bond, while the nitrogen atom N(1) in the pyridine ring participates in it. The relations between the C–N–C bond angle of the pyridine ring and the N···H distance, and also between the net charge on the nitrogen atom calculated by the "complete neglect of differential overlap" (CNDO) method and the O···N distance for a hydrogen bond are discussed in connection with five pyridine-carboxylic acids.

This work is a part of series of O–H···N hydrogen bonding studies by means of X-ray crystal structure analyses of some carboxylic acids based on a pyridine ring. In the course of this study, some interesting features have been revealed in connection with the form of a molecule as well as with the type of hydrogen-bond formation. Thus, the nicotinic acid[1] and dipicolinic acid[2] molecules took a neutral form, while the quinolinic acid[3] molecule took the form of a zwitter ion. The dinicotinic acid[4] molecule was intermediate between the above two forms. Such a problem does not occur in carboxylic acids based on a benzene ring, since they do not involve a nitrogen atom, which can also take part in a hydrogen bond. Moreover, the relation among the molecular forms (neutral or intermediate or zwitter ion), the positions of the substituted carboxyl groups and the hydrogen-bonding system has not been established in the crystal structures studied hitherto. In this sense, it seemed that it would be of interest to elucidate the effect of a nitrogen atom in a pyridine ring on the hydrogen-bond formation in solids. The cinchomeronic acid molecule in the present study can take three forms—neutral, intermediate and zwitter ions, and it has the same framework and isoelectronic structure as phthalic acid[5] and quinolinic acid. It is also of interest to study the intramolecular hydrogen bond between adjacent carboxyl groups, because it has already been found in the crystals of quinolinic acid, but not in those of phthalic acid.

Experimental

The crystals were obtained in the form of colorless prisms by recrystallization from an aqueous solution. Weissenberg photographs showed the crystal to be orthorhombic, with the space group $P2_12_12_1$. The unit cell dimensions were measured from zero-layer Weissenberg photographs, which were calibrated with superimposed Al powder lines. The crystal data are given in Table 1. Using a spherically shaped crystal with an average diameter of 0.4 mm, the intensity data were collected for the 0—5 layers around the c axis and for the 0—2 layers around the b axis by the use of a multiple-film equi-inclination integrating Weissenberg technique, with Cu$K\alpha$ radiation. The intensities were estimated visually by comparison with an intensity standard. Of the possible 922 reflections within the Cu$K\alpha$ sphere, 848 independent reflections were measured; 20 were too weak to be observed. No absorption and extinction corrections were applied.

TABLE 1. CRYSTAL DATA FOR CINCHOMERONIC ACID

Molecular formula	$C_7H_5NO_4$
Molecular weight	167.12
Crystal size	~0.4×0.4×0.4 mm
Crystal system	Orthorhombic
Space group	$P2_12_12_1$
Cell dimensions;	
a	11.211±0.006 Å
b	11.206±0.004
c	5.285±0.003
V	664.0±0.6 Å^3
Z	4
Density(calculated)	1.672 g/cm^3
Density(observed)	1.65
Radiation	Cu$K\alpha$ ($\lambda=1.5418$ Å)
Linear absorption coefficient	13.95 cm^{-1}
Number of independent reflections	848
Atom numbering	

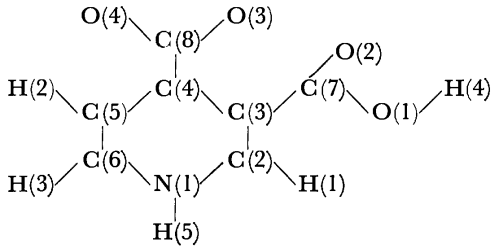

1) W. B. Wright and G. S. D. King, *Acta Crystallogr.*, **6**, 305 (1953).
2) F. Takusagawa, K. Hirotsu, and A. Shimada, This Bulletin, **46**, 2020 (1973).
3) F. Takusagawa, K. Hirotsu, and A. Shimada, This Bulletin, **46**, 2372 (1973).
4) F. Takusagawa, K. Hirotsu, and A. Shimada, This Bulletin, **46**, 2292 (1973).
5) H. Jaggi, *Z. Kristallogr.*, **109**, 3 (1957).

Structure Determination and Refinement

The crystal structure was solved easily by the symbolic addition method. The first postulated structure gave an R value of 41%; this decreased to 17% after three cycles of least-squares refinements with individual isotropic thermal parameters.

Anisotropic thermal parameters were then introduced, and the block-diagonal least-squares refinement was

Table 2. The observed and calculated structure factors

F_o, F_c and DF have been multiplied by 10.
The unobserved reflection is indicated by an asterisk. The reflection with
$|F_o - F_c| / |F_o|$ larger than 0.3 is indicated by a plus sign.

K	FO	FC	DF	K	FO	FC	DF	K	FO	FC	DF	K	FO	FC	DF	K	FO	FC	DF	K	FO	FC	DF	K	FO	FC	DF
H=L= 0	0			3	16	16	0	6	81	86	-5	1	27	28	0	3	175	171	3	4	22	26	-4	1	101	106	-4
2	291	280	10	4	141	152	-10	7	110	112	-1	2	105	106	0	4	152	149	3	5	58	57	0	2	200	192	7
4	485	490	-5	5	170	167	2	8	41	49	-7	3	21	18	3	5	203	211	-7	6	33	28	4	3	99	101	-1
6	84	87	-2	6	99	100	-1	9	55	58	-2	4	13	15	-1	6	225	221	4	7	40	36	3	4	42	42	0
8	316	312	3	7	55	54	1	10	36	40	-4	5	53	59	-5	7	45	52	-7	8*	0	3	-3	5	81	81	0
10	17	17	0	8	97	90	7	11	7	9	-1	6	54	56	-1	8	36	42	-5	9	9	10	-1	6	65	67	-1
12	55	61	-5	9	48	46	2	12	27	29	-2	7	109	98	11	9	80	82	-1	10	61	55	5	7	23	24	-1
14	12	12	0	10	81	74	6	13	15	16	-1	8	32	32	0	10	116	112	3	H=L= 10		2		8	64	65	0
H=L= 1	0			11*	0	1	-1	14	26	23	3	9	37	36	0	11	33	32	0	0	60	62	-2	9	29	26	2
1	118	121	-3	12	18	22	-4	H=L= 2		1		10	46	46	0	12	39	40	0	1	132	122	9	10	51	51	0
2	74	77	-2	H=L= 8		0		0	413	389	24	11	42	38	3	13	60	54	6	2	17	19	-1	11	5	5	0
3	47	60	-12	0	137	137	0	1	818	757	61	H=L= 9		1		H=L= 3		2		3	37	40	-3	12	18	13	4
4	599	583	15	1	60	66	-5	2	471	465	5	0	24	26	-1	0	5	7	-1	4	47	51	-4	H=L= 5		3	
5	29	33	-3	2	32	33	-1	3	275	271	4	1	84	82	2	1	256	246	10	5	31	31	0	0	15	17	-2
6	97	106	-8	3	13	13	0	4	118	120	-2	2	82	83	-1	2	301	280	21	6	54	50	4	1	86	85	1
7	157	146	11	4*	0	4	-4	5	122	129	-7	3	152	147	4	3	311	297	14	7	75	71	3	2	62	61	0
8*	0	3	-3	5	114	118	-4	6	31	37	-5	4	82	86	-4	4	46	48	-2	8	19	20	-1	3	41	44	-3
9	21	22	0	6	57	54	2	7	191	193	-2	5	40	45	-4	5	135	134	1	9	23	23	0	4	54	59	-5
10	12	15	-3	7	28	29	-1	8	77	78	-1	6	128	119	8	6	38	43	-5	H=L= 11		2		5	100	94	5
11	8	9	-1	8	36	34	1	9	67	69	-1	7	24	25	-1	7	248	240	8	0	22	24	-1	6	32	30	1
12	13	13	0	9	53	49	3	10	83	82	1	8	5	5	0	8	17	20	-2	1	24	29	-4	7	54	56	-1
13	51	54	-2	10	22	20	2	11	83	81	2	9	42	43	0	9	39	41	-2	2	55	54	0	8	57	58	-1
14	20	23	-2	11	24	27	-2	12	14	13	0	10	38	39	0	10	49	48	0	3	29	28	1	9	82	74	8
H=L= 2	0			H=L= 9		0		13	20	21	0	H=L= 10		1		11	22	22	0	4	46	48	-1	10	27	25	2
0	280	277	2	1	93	88	4	14	34	35	0	0	128	118	10	12	19	22	-2	5	32	30	2	11	15	11	4
1	342	334	7	2	18	21	-2	H=L= 3		1		1	154	153	0	13	41	35	5	6*	0	2	-2	H=L= 6		3	
2	508	550	-41	3	31	27	4	0	164	155	8	2	70	73	-2	H=L= 4		2		7	41	42	0	0	63	62	0
3	256	263	-6	4	178	167	10	1	377	346	30	3	30	33	-3	0	333	319	14	8	7	9	-2	1	114	120	-6
4	27	33	-6	5	28	27	0	2	249	250	0	4	27	33	-5	1	83	85	-2	H=L= 12		2		2	101	100	1
5	23	25	-1	6	22	19	3	3	487	460	26	5	50	54	-4	2	204	202	2	0	64	59	4	3	213	207	6
6	161	165	-4	7	94	83	10	4	36	39	-3	6	26	29	-3	3	97	104	-6	1	11	12	-1	4	137	143	-6
7	95	97	-1	8	50	43	6	5	144	155	-10	7	95	81	13	4	119	120	0	2	18	20	-2	5	10	9	0
8	106	110	-4	9	55	48	6	6	159	163	-4	8	24	25	0	5	136	138	-1	3	50	49	1	6	14	17	-2
9	59	61	-1	10	37	33	4	7	89	104	-14	9	21	19	2	6	49	52	-2	4	10	8	2	7	12	10	2
10	53	49	3	11	69	63	6	8	54	60	-6	10	22	19	2	7	103	103	0	5	38	41	-2	8	53	53	0
11*	0	0	0	H=L= 10		0		9	82	84	-1	H=L= 11		1		8	98	103	-5	6	22	20	2	9*	0	5	-5
12	82	84	-1	0	39	43	-3	10	57	59	-1	0	43	40	2	9	55	61	-6	H=L= 13		2		10	27	23	3
13	27	30	-3	1	84	83	0	11	50	48	2	1	40	41	-1	10	50	49	0	0+	2	1	1	11	32	28	4
14	11	13	-2	2*	0	4	-4	12	37	37	0	2	49	46	2	11	32	27	4	1	8	11	-2	H=L= 7		3	
H=L= 3	0			3	95	94	0	13	18	19	0	3	48	45	2	12	21	24	-2	2	15	15	0	0	178	182	-4
1	76	81	-5	4	37	39	-2	H=L= 4		1		4	7	8	0	13	25	23	1	3	27	27	0	1	90	92	-2
2+	11	14	-3	5	31	30	0	0	19	21	-2	5	22	29	0	H=L= 5		2		4	46	48	-2	2	66	65	0
3	123	119	4	6	73	67	6	1	149	158	-8	6	17	21	-3	0	56	62	-5	H=L= 0		3		3	60	62	-1
4	386	406	-20	7*	0	2	-2	2	518	502	15	7	30	29	0	1	222	218	4	0+	0	0	0	4	92	88	4
5	280	274	6	8	20	22	-1	3	210	207	3	8	14	13	0	2	94	104	-9	1	137	147	-9	5	100	105	-5
6	133	118	15	9	26	22	4	4	109	104	4	9*	0	17	-17	3	87	92	-5	2	129	124	5	6	30	27	3
7	166	156	9	10	74	61	13	5	21	22	0	H=L= 12		1		4	122	116	5	3	65	64	0	7	26	26	0
8	140	144	-3	H=L= 11		0		6	99	115	-15	0	20	19	0	5	85	85	0	4	142	137	4	8	72	70	2
9	90	91	0	1	58	56	2	7	84	84	0	1	87	89	-1	6	24	27	-2	5	124	117	6	9	13	11	1
10*	0	4	-4	2	106	102	3	8	114	127	-12	2	14	17	-2	7	20	21	-1	6	264	254	9	10	7	8	0
11	2	2	0	3	21	23	-2	9	48	51	-2	3	47	51	-3	8	86	83	2	7	104	102	1	H=L= 8		3	
12	26	27	0	4	134	128	6	10	112	108	3	4	30	30	0	9	120	109	10	8	68	66	1	0	60	64	-4
13	13	14	-1	5	31	28	3	11	41	45	-3	5	22	22	0	10	41	40	1	9	91	90	1	1	116	119	-3
14	22	24	-2	6*	0	0	0	12	9	10	-1	6	32	32	0	11	18	15	2	10	34	31	3	2	54	56	-2
H=L= 4	0			7*	0	1	-1	13	37	34	3	7	33	27	5	12	42	41	0	11	38	34	4	3	28	34	-6
0	96	93	3	8+	7	4	3	H=L= 5		1		H=L= 13		1		H=L= 6		2		12	11	11	0	4	96	91	5
1	65	73	-7	9	35	32	2	0	28	30	-2	0	58	52	5	0	148	157	-8	H=L= 1		3		5	79	81	-1
2	28	28	0	H=L= 12		0		1	91	94	-3	1	15	19	-4	1	22	16	5	0	212	239	-27	6	58	55	3
3	45	50	-4	0	120	114	6	2	161	172	-10	2	10	11	-1	2	134	137	-3	1	94	103	-8	7	41	43	-1
4	13	14	-1	1	30	31	0	3	47	52	-4	3	56	51	4	3	182	199	-16	2	44	40	4	8	36	36	0
5	60	58	2	2	60	58	1	4	158	160	-2	4	5	5	0	4	88	93	-4	3	155	157	-2	9	28	29	0
6	92	96	-4	3	96	92	4	5	138	139	0	5	11	11	0	5	46	52	-6	4	59	57	1	10	25	29	-4
7	74	68	5	4	12	11	1	6	125	135	-10	H=L= 14		1		6	96	97	0	5	90	96	-5	H=L= 9		3	
8	35	41	-6	5	17	16	1	7	79	84	-5	0	5	5	0	7	38	40	-1	6	120	129	-8	0	66	71	-4
9	37	39	-2	6	52	47	5	8	81	84	-2	1	10	13	-2	8	38	38	0	7	107	111	-4	1	86	77	8
10	29	28	1	7	27	29	-1	9	20	23	-3	2	18	20	-2	9	41	42	-1	8	128	131	-2	2	61	58	3
11	28	28	0	H=L= 13		0		10	39	43	-4	H=L= 0		2		10	11	14	-2	9	99	105	-5	3	92	96	-3
12	7	6	0	1	13	9	3	11	26	27	0	0+	37	60	-23	11	41	39	1	10	101	95	5	4	48	48	0
13	30	36	-5	2	45	43	2	12+	10	13	-3	1+	10	17	-6	12	35	28	6	11	82	78	3	5	27	27	0
H=L= 5	0			3	6	4	1	13	38	34	4	2	293	303	-9	H=L= 7		2		12	23	20	3	6	52	53	0
1	27	25	2	4	56	58	-1	H=L= 6		1		3	255	237	17	0	67	72	-4	H=L= 2		3		7	29	25	4
2	210	191	18	5	9	7	2	0	118	126	-8	4	162	144	17	1	76	87	-11	0	211	218	-6	8	31	29	1
3	22	29	-6	6	7	7	0	1	170	179	-8	5+	10	6	4	2	67	73	-5	1	190	184	5	9	18	20	-1
4	133	127	5	H=L= 14		0		2	90	104	-14	6	274	258	15	3	37	35	2	2	74	66	8	H=L= 10		3	
5	138	142	-3	0	1	1	0	3	40	43	-2	7	37	36	1	4	21	21	0	3	103	95	8	0	22	25	-2
6	38	39	0	1	10	10	0	4	84	92	-7	8	11	9	1	5	69	71	-2	4	223	224	0	1	77	70	6
7	134	141	-6	2	29	27	1	5	91	96	-5	9	35	38	-2	6	83	83	0	5	93	102	-8	2	44	44	0
8	161	153	7	H=L= 0		1		6	61	70	-9	10	35	35	0	7	22	21	1	6	74	71	2	3	36	35	0
9	73	78	-4	0+	1	0	1	7	33	35	-1	11	155	142	12	8	21	19	2	7	112	119	-6	4	90	76	13
10	36	39	-3	1	199	184	15	8	89	89	0	12	75	69	5	9	29	27	1	8	75	76	-1	5	26	25	0
11	18	23	-4	2	491	452	39	9	103	103	0	13	14	15	-1	10	63	58	5	9	20	21	0	6	31	31	0
12	33	33	0	3	263	248	14	10	31	32	0	H=L= 1		2		11+	10	13	-3	10	42	42	0	7	32	30	2
13	41	42	-1	4	410	398	12	11	17	17	0	0	89	97	-8	H=L= 8		2		11	16	13	2	8	7	6	1
H=L= 6	0			5	67	76	-9	12	3	3	0	1	344	323	20	0	219	214	4	12	51	49	1	H=L= 11		3	
0	252	242	10	6	127	126	0	H=L= 7		1		2	240	218	21	1	119	120	-1	H=L= 3		3		0	82	74	8
1	289	282	7	7	77	91	-13	0	20	18	1	3	185	178	7	2	95	98	-2	0	119	129	-10	1	23	25	-1
2	45	48	-2	8	90	94	-3	1	51	61	-9	4	242	249	-7	3	78	76	1	1	111	112	-1	2	30	27	3
3	230	221	9	9	13	9	4	2	136	144	-8	5	98	98	0	4	73	81	-7	2	107	100	6	3	10	10	0
4	94	88	6	10	118	126	-8	3	123	136	-13	6	47	44	3	5	108	110	-1	3	154	159	-5	4	56	50	5
5*	0	5	-5	11	92	93	0	4	52	54	-1	7	93	96	-3	6	132	124	7	4	49	51	-1	5	21	22	0
6	54	57	-2	12	29	32	-3	5	46	53	-6	8	94	97	-3	7	27	32	-5	5	59	59	0	6	30	25	5
7	77	72	4	13	46	49	-2	6	127	122	4	9	52	56	-4	8*	0	4	-4	6	57	59	-1	H=L= 12		3	
8	67	67	0	14	35	35	0	7	118	120	-2	10	107	116	-8	9	2	3	0	7	102	104	-1	0	21	22	-1
9	141	156	-14	H=L= 1		1		8	26	29	-2	11	22	24	-1	10	24	19	4	8	50	50	0	1	19	19	0
10	52	52	0	0	208	203	5	9	87	87	0	12	31	31	0	11	7	5	2	9	70	67	2	2	26	25	1
11	33	33	0	1	377	347	30	10	58	58	0	13	7	8	-1	H=L= 9		2		10+	18	23	-5	3	29	21	8
12	52	51	0	2	171	196	-25	11	61	55	6	H=L= 2		2		0	145	140	4	11	31	29	1	4	30	26	4
H=L= 7	0			3	627	577	49	12	24	23	1	0	6	6	0	1	62	69	-7	12	51	48	2	H=L= 13		3	
1	270	257	13	4	31	36	-4	H=L= 8		1		1	244	263	-18	2	116	119	-3	H=L= 4		3		0*	0	7	-7
2	70	70	0	5	290	284	6	0	19	19	0	2	85	87	-1	3	20	22	-2	0	101	111	-9	H=L= 0		4	

Table 2 (Continued)

K	FO	FC	DF	K	FO	FC	DF	K	FO	FC	DF	K	FO	FC	DF	K	FO	FC	DF	K	FO	FC	DF	K	FO	FC	DF
0	162	179	-17	8	21	24	-2	4	36	36	0	4	40	43	-3	7*	10	7	3	8	35	34	1	2	16	17	0
1	62	71	-8	9	22	28	-5	5	24	20	3	5	26	29	-2	8	4	5	-1	9	18	19	0	3	17	21	-4
2	28	36	-8	10	11	12	0	6	42	43	-1	6	44	37	6	9*	0	3	-3	H=L=	4	5		4	13	12	1
3	168	153	14	11	14	14	0	7	70	69	1	7	25	25	0	H=L=	1	5		0	39	36	2	5	14	14	0
4	122	106	16	H=L=	3	4		8*	0	3	-3	8	25	32	-7	0	88	88	0	1	75	77	-2	6	65	64	1
5	153	167	-14	0	13	15	-2	9	23	23	0	H=L=	9	4		1	109	103	6	2	110	100	9	H=L=	8	5	
6	147	138	9	1	88	91	-2	10	62	57	4	0	14	16	-2	2	70	53	17	3	76	72	3	0	75	76	-1
7	20	17	2	2	70	72	-1	H=L=	6	4		1	33	39	-5	3	23	19	3	4	42	45	-3	1	29	30	0
8	44	43	1	3	89	85	4	0	202	205	-3	2	26	30	-3	4	15	14	1	5	29	35	-6	2	39	43	-3
9	30	33	-2	4	53	54	-1	1	63	60	3	3	27	29	-2	5	102	96	5	6	29	27	2	3	20	21	-1
10	52	50	1	5	94	96	-2	2	35	34	0	4	43	43	0	6	42	39	2	7	65	69	-4	4	16	20	-3
11	9	11	-1	6	58	62	-3	3	102	102	0	5*	11	14	-3	7	36	34	2	8	22	20	2	5	24	26	-1
H=L=	1	4		7	122	114	8	4	54	63	-9	6	15	18	-3	8	17	14	3	H=L=	5	5		H=L=	9	5	
0	106	114	-7	8	17	16	0	5	13	13	0	7	14	15	-1	9	36	38	-1	0	9	10	-1	0	48	53	-4
1	110	104	5	9	32	28	3	6	76	78	-2	H=L=	10	4		H=L=	2	5		1	28	26	1	1	22	23	0
2	119	109	10	10	55	52	2	7	36	36	0	0	9	10	0	0	33	29	4	2	37	40	-2	2	31	37	-6
3	74	70	4	11	20	23	-3	8	46	41	4	1	33	33	0	1*	23	14	9	3	76	84	-8	3	29	28	1
4	20	20	0	H=L=	4	4		9	50	46	4	2	12	11	1	2	89	79	9	4	14	13	1				
5	189	156	33	0	29	30	0	H=L=	7	4		3	50	54	-4	3	131	129	1	5	2	2	0				
6	71	66	4	1	68	78	-9	0	104	110	-5	4	27	27	0	4	115	113	2	6	18	20	-2				
7	98	97	1	2	105	113	-8	1	32	34	-1	5	39	43	-3	5	52	55	-3	7	27	27	0				
8	19	16	2	3	140	124	15	2	67	72	-5	H=L=	11	4		6	33	34	0	8	36	40	-4				
9	38	44	-6	4	128	121	6	3	26	30	-3	0*	0	0	0	7	17	20	-2	H=L=	6	5					
10	34	36	-1	5	41	40	1	4	166	154	12	1	38	43	-4	8	37	32	5	0	48	48	0				
11	15	16	0	6	90	83	7	5	37	38	0	2	28	32	-4	9	26	23	2	1	47	51	-3				
H=L=	2	4		7	37	36	1	6	39	41	-1	3	16	17	-1	H=L=	3	5		2	30	34	-4				
0*	5	0	5	8	19	18	1	7	23	25	-1	H=L=	0	5		0	69	72	-3	3	25	30	-5				
1	47	50	-2	9	29	29	0	8	30	28	2	0*	0	0	0	1	106	102	4	4	39	41	-2				
2	156	132	23	10	20	15	5	9	26	27	-1	1	66	63	3	2	20	19	0	5	5	3	1				
3	45	45	0	H=L=	5	4		H=L=	8	4		2	114	102	11	3	109	97	12	6	9	11	-1				
4	37	36	0	0	41	47	-6	0	28	33	-5	3	21	16	4	4	141	138	3	7*	16	24	-7				
5	105	111	-6	1	97	99	-1	1	48	50	-1	4	38	39	-1	5	36	40	-4	H=L=	7	5					
6	37	44	-7	2	156	146	10	2	28	31	-2	5	112	112	0	6	51	63	-12	0	29	26	2				
7	65	57	7	3	98	97	1	3	47	60	-12	6	16	19	-3	7	35	34	0	1*	7	4	2				

TABLE 3. THE FINAL PARAMETERS AND THEIR ESTIMATED STANDARD DEVIATIONS (in parentheses).

The coordinates of the non-hydrogen atoms have been multiplied by 10^4; those of the hydrogen atoms, by 10^3. The anisotropic thermal parameters of non-hydrogen atoms are of the form $\exp[-(B_{11}h^2+B_{22}k^2+B_{33}l^2+B_{12}hk+B_{13}hl+B_{23}kl)]$, and have been multiplied by 10^4. For the hydrogen atoms, the values listed are isotropic thermal parameters B(Å^2).

Atom	x	y	z	B
N(1)	2012(3)	1974(3)	5763(6)	—
C(2)	2673(3)	1531(3)	7646(7)	—
C(3)	3608(3)	2173(3)	8622(6)	—
C(4)	3825(3)	3324(3)	7660(6)	—
C(5)	3111(3)	3764(3)	5762(7)	—
C(6)	2208(3)	3067(4)	4776(8)	—
C(7)	4465(3)	1601(3)	10438(7)	—
C(8)	4798(3)	4117(3)	8733(7)	—
O(1)	3944(2)	917(2)	12118(5)	—
O(2)	5521(2)	1762(3)	10265(6)	—
O(3)	5699(2)	4317(2)	7423(5)	—
O(4)	4562(3)	4551(3)	10835(6)	—
H(1)	251(3)	72(3)	826(7)	3.1(0.9)
H(2)	326(3)	457(4)	508(9)	4.2(1.0)
H(3)	161(4)	334(4)	336(10)	5.1(1.1)
H(4)	459(3)	43(3)	1259(8)	3.6(0.9)
H(5)	136(5)	150(5)	461(12)	7.9(1.6)

Atom	B_{11}	B_{22}	B_{33}	B_{12}	B_{13}	B_{23}
N(1)	68(2)	75(2)	264(12)	9(4)	−49(9)	−77(10)
C(2)	64(2)	65(2)	273(13)	12(4)	−1(11)	−27(11)
C(3)	66(2)	60(2)	177(11)	12(4)	−1(9)	−21(9)
C(4)	64(2)	59(2)	187(11)	7(4)	15(9)	−23(9)
C(5)	79(3)	72(3)	232(13)	10(5)	−2(11)	32(11)
C(6)	74(3)	87(3)	258(14)	32(5)	−57(11)	−12(12)
C(7)	68(3)	58(2)	197(12)	−14(4)	−33(10)	6(9)
C(8)	67(3)	52(2)	249(13)	2(4)	7(10)	−10(10)
O(1)	74(2)	75(2)	215(9)	13(4)	4(8)	60(8)
O(2)	66(2)	97(2)	326(11)	−22(4)	−46(8)	112(9)
O(3)	81(2)	77(2)	263(10)	−29(4)	82(9)	−47(8)
O(4)	90(2)	109(3)	317(12)	−62(5)	83(10)	−191(11)

continued to reduce the R value to 8.1%. At this stage of refinement, a difference Fourier map was computed, from which the positions of the five hydrogen atoms were located (Fig. 1). There was no significant peak on this map except those due to hydrogen atoms. With anisotropic thermal parameters for non-hydrogen atoms and isotropic thermal parameters for hydrogen atoms, the final R value was 5.90%, excluding un-

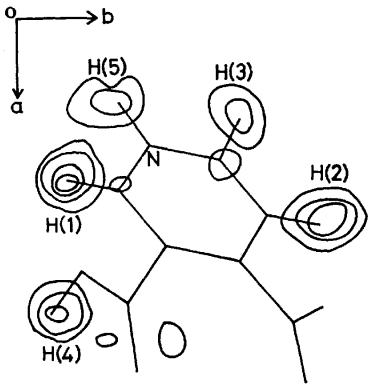

Fig. 1. A composite drawing of the electron density associated with the hydrogen atoms. The contours at intervals of 0.1 e·Å^{-3}, beginning with 0.2 e·Å^{-3} contour.

observed reflections. The $\sum w(F_o-F_c)^2$ function was minimized, where:

$$w = 0.5 \text{ for } |F_o| \leqq 0.5,$$
$$w = 1.0 \text{ for } 0.5 < |F_o| < 6.0 \text{ and}$$
$$w = 6.0/|F_o| \text{ for } 6.0 \leqq |F_o|.$$

The atomic scattering factors used were those listed in the International Table for X-ray Crystallography for C, N, and O atoms and the spherical scattering factors proposed by Stewart, Davidson, and Simpson[6] for H atom. The observed and calculated structure factors are listed in Table 2. The fractional coordinates and thermal parameters are listed, along with their estimated standard deviations, in Table 3.

Table 4. Bond lengths (Å) and bond angles (degree)

Bond	Length	e.s.d.	Bond	Angle	e.s.d.
N(1)–C(2)	1.336	0.005	C(2)–N(1)–C(6)	122.3	0.3
C(2)–C(3)	1.372	0.005	N(1)–C(2)–C(3)	120.6	0.4
C(3)–C(4)	1.406	0.005	C(2)–C(3)–C(4)	118.6	0.3
C(4)–C(5)	1.377	0.005	C(2)–C(3)–C(7)	120.4	0.3
C(5)–C(6)	1.381	0.006	C(4)–C(3)–C(7)	120.7	0.3
C(6)–N(1)	1.349	0.005	(C3)–C(4)–C(5)	119.4	0.3
C(3)–C(7)	1.502	0.005	C(3)–C(4)–C(8)	121.9	0.3
C(4)–C(8)	1.516	0.005	C(5)–C(4)–C(8)	118.7	0.3
C(7)–O(1)	1.310	0.004	C(4)–C(5)–C(6)	120.0	0.4
C(7)–O(2)	1.201	0.005	C(5)–C(6)–N(1)	119.4	0.4
C(8)–O(3)	1.245	0.004	C(3)–C(7)–O(1)	113.4	0.3
C(8)–O(4)	1.241	0.005	C(3)–C(7)–O(2)	121.2	0.3
C(2)–H(1)	0.98	0.04	O(1)–C(7)–O(2)	125.4	0.3
C(5)–H(2)	0.99	0.05	C(4)–C(8)–O(3)	118.9	0.3
C(6)–H(3)	1.05	0.05	C(4)–C(8)–O(4)	114.2	0.3
O(1)–H(4)	0.94	0.05	O(3)–C(8)–O(4)	126.9	0.4
N(1)–H(5)	1.09	0.06	H(1)–C(2)–N(1)	119	3
			H(1)–C(2)–C(3)	120	3
			H(2)–C(5)–C(4)	120	3
			H(2)–C(5)–C(6)	120	3
			H(3)–C(6)–C(5)	125	3
			H(3)–C(6)–N(1)	116	3
			H(4)–O(1)–C(7)	100	3
			H(5)–N(1)–C(6)	131	3
			H(5)–N(1)–C(6)	105	3

6) R. F. Stewart, E. R. Davidson, and W. T. Simpson, *J. Chem. Phys.*, **42**, 3175 (1965).

Results and Discussion

Molecular Structure. The bond lengths and angles are listed, along with their estimated standard deviations, in Table 4; they are shown in Fig. 2. Figure 3 shows the anisotropic thermal ellipsoids of the non-hydrogen atoms and the isotropic thermal ellipsoids of the hydrogen atoms. The ellipsoids are scaled to include a 74% probability.

The cinchomeronic acid molecule can take the three forms shown below and two intermediate forms between the neutral molecule (A) and the zwitter ions ((B) or (C)).

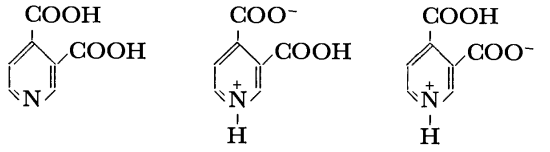

(A) Neutral molecule (B) Zwitter ion (C) Zwitter ion

The present study has revealed that the molecule takes the form of the zwitter ion (B) in the crystal. This is

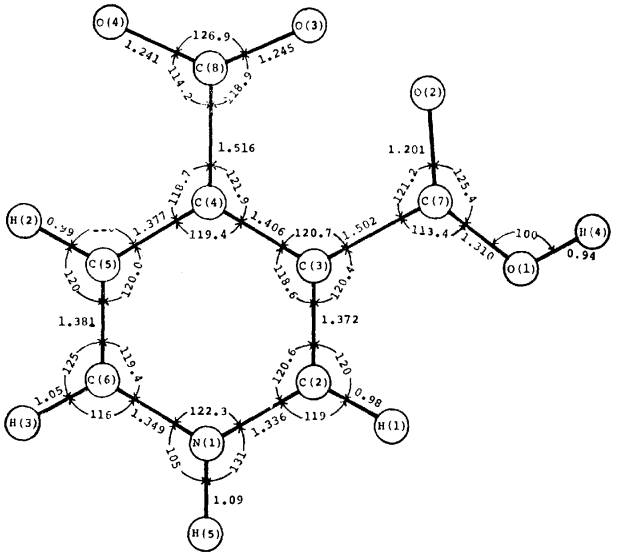

Fig. 2. Dimensions of cinchomeronic acid molecule.

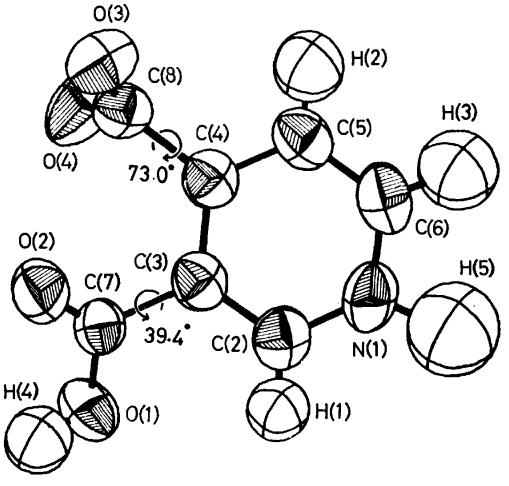

Fig. 3. The anisotropic thermal ellipsoids of non-hydrogen atoms and the isotropic thermal ellipsoids of hydrogen atoms. Ellipsoids are scaled to include a 74% probability.

evident from the position of the hydrogen atom in the difference Fourier map. It is also confirmed by the C(2)–N(1)–C(6) bond angle, 122.3(3)°, and the C(8)–O(3) and C(8)–O(4) bond lengths, 1.245(4) and 1.241(5) Å respectively (the values in parentheses denote the e.s.d.'s in the last digits).

The pyridine ring is essentially planar. The equation of the least-squares plane through six non-hydrogen atoms of the pyridine ring is:

$$0.6248X - 0.3913Y - 0.6756Z = -1.5159,$$

where X, Y, and Z are coordinates in Å along the a, b, and c axes respectively. The maximum deviation of the ring atom from this plane is 0.013 Å. The displacements of all the atoms from the plane are listed in Table 5.

Table 5. The distances from the least-squares plane defined by the six non-hydrogen atoms of the pyridine ring

Atom	Deviation(Å)	Atom	Deviation(Å)
N(1)	0.002	O(1)	−0.450
C(2)	−0.013	O(2)	0.946
C(3)	0.012	O(3)	0.965
C(4)	0.001	O(4)	−1.153
C(5)	−0.013	H(1)	0.01
C(6)	0.013	H(2)	−0.02
C(7)	0.215	H(3)	−0.02
C(8)	−0.047	H(4)	0.05
		H(5)	0.16

The differences in the corresponding bond lengths and angles of a pyridine ring, the N(1)–C(2) and N(1)–C(6), the C(2)–C(3) and C(6)–C(5), the C(3)–C(4) and C(5)–C(4) bond lengths, the N(1)–C(2)–C(3) and N(1)–C(6)–C(5), and the C(2)–C(3)–C(4) and C(6)–C(5)–C(4) bond angles, are −0.013(5), −0.009(5), 0.019(5) Å, 1.2(4)° and −1.4(3)°. These values show that the pyridine ring has, approximately, the C_{2v} symmetry in the molecule. The slight deviations from C_{2v} symmetry may be due to the substitution of a carboxyl group in the β-position.

In the carboxyl group (C(7)O(1)O(2)H(4)), each C–O bond length is clearly different from the others. Hence, this group consists of C=O and C–O(H) groups. On the other hand, the C(8)–O(3) and C(8)–O(4) bond lengths in another carboxyl group, 1.245(4) and 1.241(5) Å, are equal within the limits of experimental error. This fact suggests that the hydrogen atom moves from the oxygen atom O(4) to the nitrogen atom N(1) of a pyridine ring. The C(7)–O(2) bond length is the shortest of the four C–O bond lengths. This can be explained by the fact that only the O(2) atom does not participate in a hydrogen bond. Similar situations have been observed in dinicotinic acid and quinolinic acid. The difference between the C(3)–C(7) and C(4)–C(8) bond lengths, 0.014(5) Å, lies on the borderline of significance in relation to their estimated standard deviations. A similar tendency has been observed in quinolinic acid. These differences may be caused by the formation of a zwitter ion.

There is no intramolecular hydrogen bond between the adjacent carboxyl groups. The carboxyl groups twist by 39.6° (C(7)O(1)O(2)) and 73.0° (C(8)O(3)-O(4)) out of the plane of the pyridine ring, as is shown in Fig. 3, so that the repulsion between the oxygen atoms is reduced by the twists of the C–C bonds.

Molecular Arrangement and Hydrogen-bond System. The crystal structure is shown in Figs. 4 and 5. The distances and angles of hydrogen bonds are listed in Table 6. The hydrogen bonding system is shown in Fig. 6. In Figs. 4, 5, and 6, the same numbers designate the same molecules. The symmetry codes corresponding to these molecules are shown in Table 6.

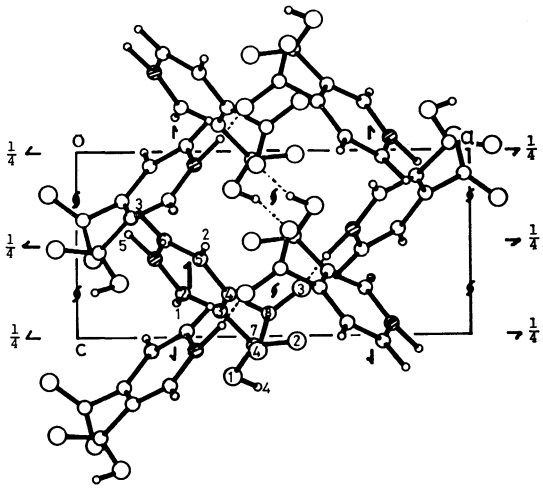

Fig. 4. A view of the crystal structure down the b axis. The hydrogen bonds are shown by broken lines.

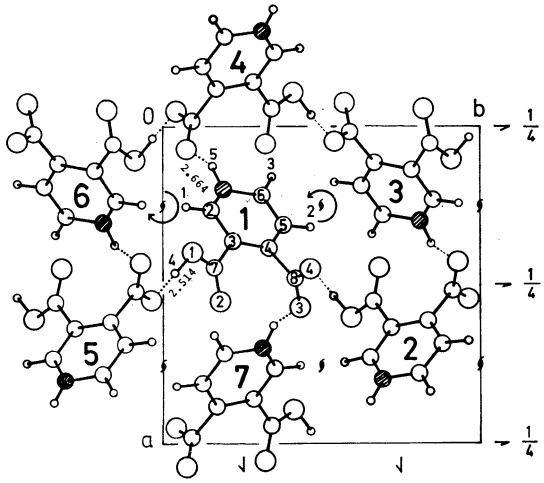

Fig. 5. A view of the crystal structure down the c axis. The hydrogen bonds are shown by broken lines. The ↻ signs around two-fold screw axes indicate the directions of spirals.

The hydrogen bonds are found in two spiral forms around the two-fold screw axes parallel to the c axis, thus linking the molecules three-dimensionally. There are four molecules per turn of spiral along the c axis. The carbonyl oxygen atom O(2) is free from the hydrogen bond, while the nitrogen atom N(1) in a pyridine ring participates in it. This is a remarkable feature of the crystal structures of carboxylic acids with a pyridine ring. This situation has been found in all crystal structures of pyridinecarboxylic acids deter-

Table 6. Hydrogen bond distances (Å) and angles (degree)

X——H·····O	Symmetry	X···O	e.s.d.	X—H	e.s.d.	H···O	e.s.d.	Angle	e.s.d.
O(1)–H(4)···O(4)	(1, 1, 5)	2.514	0.004	0.94	0.05	1.60	0.05	162	5
N(1)–H(5)···O(3)	(1, 1, 4)	2.664	0.004	1.09	0.06	1.59	0.06	166	5
C——O·····Y	Symmetry	Angle	e.s.d.						
C(8)–O(4)···H(4)	(5, 5, 1)	132	2						
C(8)–O(4)···O(1)	(5, 5, 1)	131.0	0.1						
C(8)–O(3)···H(5)	(4, 4, 1)	130	2						
C(8)–O(3)···N(1)	(4, 4, 1)	134.6	0.2						

Symmetry code

1=(x, y, z)	5=(1−x, −1/2+y, 5/2−z)
2=(1−x, 1/2+y, 5/2−z)	6=(1/2−x, −y, 3/2+z)
3=(1/2−x, 1−y, 3/2+z)	7=(1/2+x, 1/2−y, 1−z)
4=(−1/2+x, 1/2−y, 4−z)	8=(x, y, 3+z)

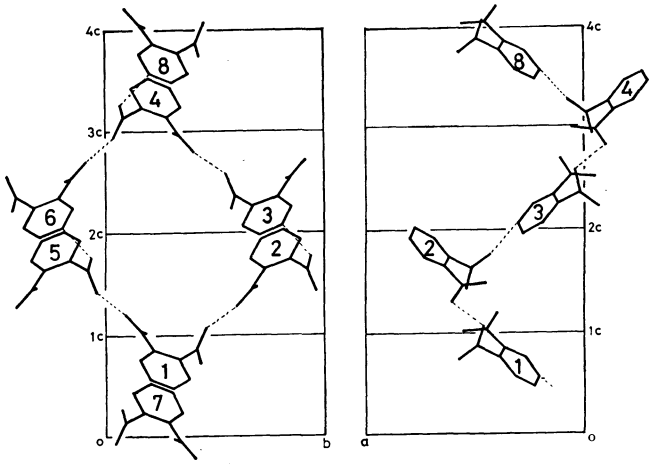

Fig. 6. The hydrogen bonding system.
(a): A view of the spiral down the a axis.
(b): A view of the spiral down the b axis.

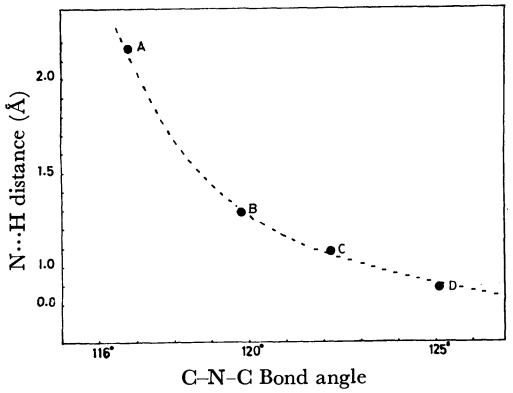

Fig. 7. The relation between the C–N–C bond angle of pyridine ring and the N···H distance for hydrogen bond.
A: Dipicolinic acid (Ref. 2); B: Dinicotinic acid (Ref. 4); C: Cinchomeronic acid (This study); D: Quinolinic acid (Ref. 3).

mined by the X-ray method except for that of one hydrate.

Figure 7 shows the relation between the C–N–C bond angle of a pyridine ring and the N···H distance for a hydrogen bond about four pyridine-dicarboxylic acids. There is a clear correlation between them. This result is an example of the change in electronic

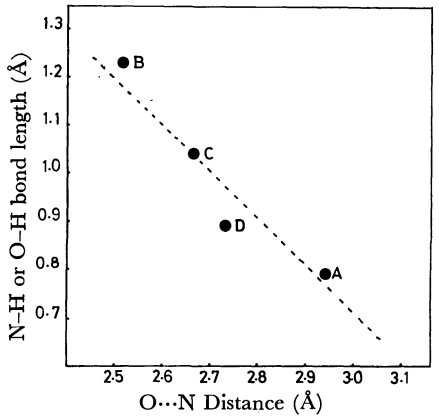

Fig. 8. The variation of the bond length in proton donor group with the O···N distance for hydrogen bond. A, B, C, and D are the same compounds as listed in Fig. 7.

structure in a nitrogen atom corresponding to the variation in interaction between the nitrogen and hydrogen atoms in the hydrogen bond. When the N···H distance is long, as in dipicolinic acid, the nitrogen atom acts as a proton acceptor and gives a C–N–C bond angle similar to that of pyridine[7] itself. On the other hand, the protonated nitrogen atom can be regarded as a proton donor in the case of a short N–H distance, as in quinolinic acid and cinchomeronic acid; it gives a larger C–N–C bond angle than that of pyridine itself in relation to the change in the electronic structure in a nitrogen atom. The situation lies between these two cases in dinicotinic acid. Figure 8 gives the variation in the bond length in a proton donor group with the O···N distance for a hydrogen bond. It may be seen that the stronger interaction occurs between the hydrogen and proton acceptor atoms in the case of the shorter hydrogen bond. Hence, the hydrogen bonds between the nitrogen and oxygen atoms in pyridine-dicarboxylic acids may be classified in terms of the O···N distance in to the following three forms:

(1) O–H···N: long hydrogen bond (longer than 2.75 Å)
(2) $\bar{O}$···H–$\overset{+}{N}$: middle hydrogen bond (2.60—2.75 Å)

7) B. Bak, L. H. Nygaard, and J. R. Andersen, *J. Mol. Spectrosc.*, **2**, 361 (1958).

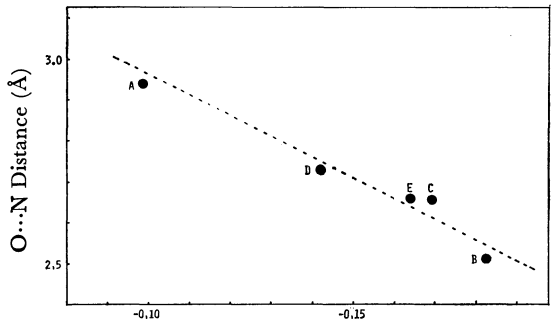

Fig. 9. The relation between the net charge on nitrogen atom calculated by the CNDO method and the O···N distance for hydrogen bond. A, B, C, and D are the same compounds listed in Fig. 7.
E: Nicotinic acid (Ref. 1)

(3) O–H–N: short hydrogen bond (shorter than 2.60 Å)

Using the neutral structures of several pyridinecarboxylic acids, the net charges on the nitrogen atoms were calculated by the use of the "complete neglect of differential overlap" (CNDO) method. They are plotted against the O···N distances in Fig. 9. There is a good linear relation between the calculated net charges on the nitrogen atoms and the observed O···N distances for hydrogen bonds. If this relation can be applied to the O···N hydrogen bonds of other pyridinecarboxylic acids, the O···N distances can be easily predicted by the calculation of the net charges on nitrogen atoms. In conclusion, the strength of the hydrogen bond increases with an increase in the net charge on a nitrogen atom. Moreover, the molecular form may depend on the change in the net charge on a nitrogen atom corresponding to the positions of substituted carboxyl groups.

Computer Programs. All the calculations were performed on a FACOM 270-30 computer at the Computer Center of Osaka City University by the use of the following programs—RSLC-3 (cell constant),[8] RSSFR-3 (Fourier synthesis),[9] HBLS-IV (block-diagonal least-squares refinement),[10] DAPH (bond length, bond angle and least-squares plane),[11] SCALE (film factor, Lp and layer scaling,)[12] TE-I (thermal ellipsoid),[13] CNINDO (CNDO and INDO calculations),[14] and PHASE-I, II, III (symbolic addition).[15]

The authors wish to express their thanks to Dr. Kichisuke Nishimoto of this faculty for his useful advice in the CNDO calculation.

8) T. Sakurai, The Universal Crystallographic Computing System (I) edited by T. Sakurai, p. 18, The Crystallographic Society of Japan, 1967.
9) T. Sakurai, *ibid.*, p. 45.
10) T. Ashida, *ibid.*, p. 65.
11) T. Ashida, *ibid.*, p. 76.
12) H. Yoshioka, K. Hirotsu, and F. Takusagawa, Unpublished work.
13) F. Takusagawa, Unpublished work.
14) F. Takusagawa, Unpublished work.
15) K. Nakatsu and K. Hirotsu, Unpublished work.

BULLETIN OF THE CHEMICAL SOCIETY OF JAPAN, VOL. 46, 2675—2683 (1973)

X-Ray Analysis of the Domain Structure of the 1:1 Complex of Carbazole–TCNQ

Hayao KOBAYASHI

Department of Chemistry, Faculty of Science, Toho University, Narashino, Chiba 275

(Received March 22, 1973)

The crystal structure of the 1:1 complex of carbazole–TCNQ was investigated by X-ray diffraction. Analysis of sharp spots and diffuse streaks in the diffraction patterns revealed that the crystal is composed of an ordered domain and a disordered one. The ordered domain is made up from two types of ordered molecular arrangements, whereas the disordered one consists of a one-dimensionally disordered structure. The structures of the two ordered domains are closely related with each other. They both contain mixed stack columns of alternating carbazole and TCNQ usually observed in charge transfer (CT) complexes. The existence of various types of domain structures as shown by diffraction patterns of many crystals grown from acetone, acetonitrile and tetrahydrofuran solutions can be interpreted in terms of the combinations of ordered and disordered domains. No CT band appears in the visible absorption spectra of the acetone solution of carbazole–TCNQ, whereas the spectra of the powdered crystals show a CT band at about 18000 cm^{-1}. The calculation of SCF-MO-CI of the system of the carbazole–TCNQ pair indicates a weak CT interaction.

Charge transfer (CT) complexes containing carbazole, a weak electron donor, do not seem to have been investigated much, no structural study ever having been reported. The crystal structure of the 1:1 complex of carbazole and 7,7,8,8-tetracyanoquinodimethane (TCNQ) has been determined. The domain structure

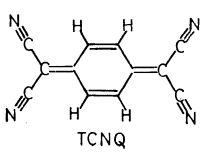

of carbazole–TCNQ, the analysis of diffuse streaks and the spectroscopic study are reported in this paper.

Experimental

The crystals of carbazole–TCNQ were grown by a diffusion method, acetone solution of both compoments being used. The crystal is hardly soluble and black, needle-like crystals could be easily obtained after a few days. Elemental analysis shows that the crystal is the 1:1 complex of carbazole–TCNQ. Found: C, 77.9; N, 18.9; H, 3.3%. Calcd for carbazole–TCNQ (1:1): C, 77.6; N, 18.9; H, 3.5%.

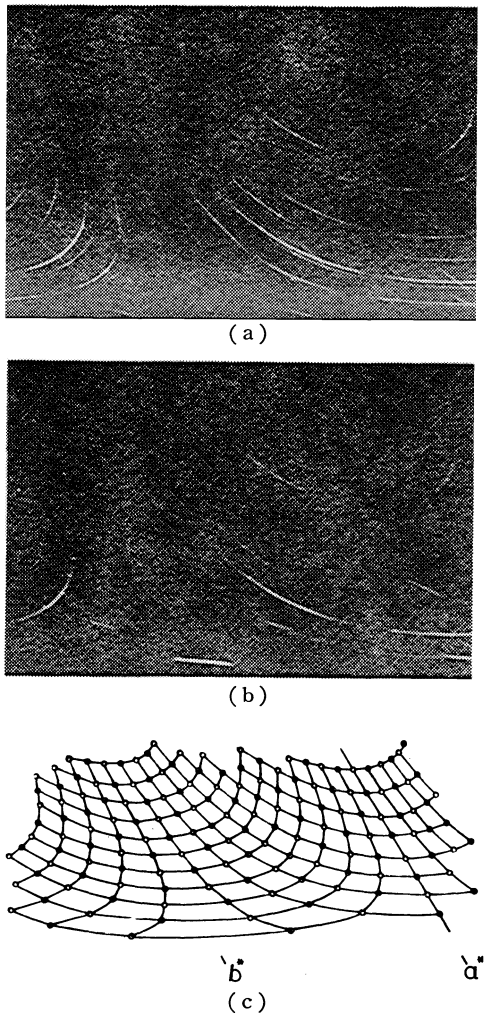

Fig. 1. Weissenberg photographs.
(a) (ξ, η, 1/2), (b) (ξ, η, 3/2), (c) Distribution of sharp spots observed in the photographs (a) and (b). The open circles and filled circles represent the two different groups IIIa and IIIb in Table 2.

Weissenberg photographs are shown in Fig. 1. Oscillation photographs of axes c and a show sharp layer lines and intermediate layer lines with diffuse streaks. Disregarding the layer lines accompanying diffuse streaks, all the spots can be indexed with respect to the orthorhombic unit cell with dimensions listed in Table 1. The diffuse streaks occur parallel to b^*. Distributions of the diffuse streaks are summarized in Table 2. In the half-integral layer lines, the sharp spots appear along the diffuse streaks at intervals of b^*. Closer examination revealed that these spots deviate slightly up and below alternately with respect to the streaks.

TABLE 1. CRYSTALLOGRAPHIC DATA OF THE AVERAGE STRUCTURE OF CARBAZOLE–TCNQ

Carbazole–TCNQ	Formula $C_{12}H_9N \cdot C_{12}H_4N_4$
Orthorhombic	Space group Immm
$a=10.751\pm0.010$ Å	F.W.$=371.4$ g/cm^3
$b=12.944\pm0.020$	d_m $=1.340$ g/cm^3 (flotation method)
$c=3.339\pm0.015$	d_x $=1.328$ g/cm^3
$U=464.6$ Å^3	Z $=1$

TABLE 2. SUMMARY OF REFLECTIONS
The Miller indices refer to the unit cell listed in Table 1. h, k, l, n and m indicate integral number; η may take non-integral values.

	a^*	b^*	c^*		
I	h	k	l	$h+k+l=2n$	sharp spots
II	$h/2$	η	l	$h=2n+1$, $l=2m+1$	streaks
IIIa	$h'/2$	k	$l'^*/2$	$h'=2n'+1$, $(h'+l')/2+k=2m'$, $l'=2n''+1$	sharp spots
IIIb	$h'/2$	k	$l'/2$	$h'=2n'+1$, $(h'+l')/2+k=2m'+1$, $l'=2n''+1$	sharp spots

a) h', l', n', n'', and m' indicate that they differ slightly from integer, *viz.*, the spots of groups IIIa and IIIb deviate slightly from the center of the streaks (group II).

The intensity data were collected with multiple-film equi-inclination Weissenberg photographs with Cu$K\alpha$ radiation. The intensities were estimated visually with a standard film strip and converted into $|F(hkl)|$ by applying the Lorentz-polarization and shape corrections.

Results and Discussion

Determination of the Average Structure. If the half-integral layer lines with diffuse streaks are neglected, the unit cell (Table 1) is of the average structure of a disordered crystal. In view of the planar structures of the component molecules, the space group Immm was assumed. The body centered lattice containing only one formula unit indicates that each lattice point is occupied by carbazole and TCNQ with equal prob-

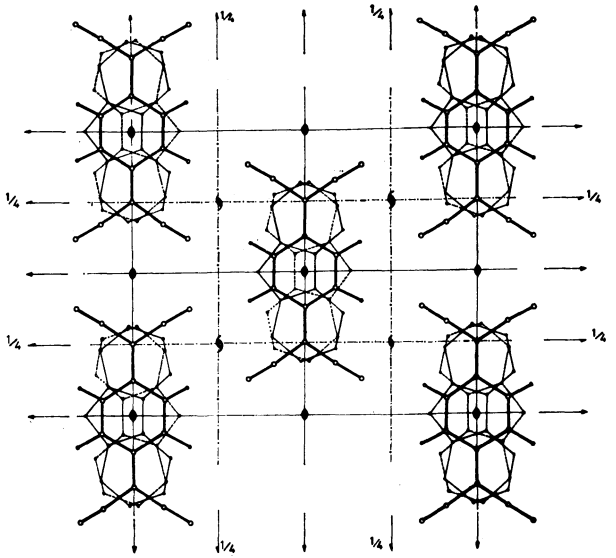

Fig. 2. Projection of the average structure along the c axis.

TABLE 3. FINAL ATOMIC PARAMETERS ($\times 10^4$) AND THEIR ESTIMATED STANDARED DEVIATIONS

The B_{ij}'s are defined by:

$$\exp\left[-(B_{11}h^2+B_{22}k^2+B_{33}l^2+2B_{12}hk+2B_{13}hl+2B_{23}kl)\right].$$

	x	y	z	B_{11}	B_{22}	B_{12}	B_{13}	B_{23}	B_{23}
				Carbazole					
C1	701(29)	0	0	129(48)	344(57)	170(159)	0	0	0
C2	1263(21)	1006(22)	0	128(34)	248(33)	1938(351)	−7(29)	0	0
C3	2412(27)	971(19)	0	270(41)	152(23)	1811(325)	−59(29)	0	0
C4	3106(42)	0	0	106(45)	204(43)	4315(937)	0	0	0
N1	0	1358(43)	0	192(73)	180(57)	70(280)	0	0	0
				TCNQ					
C5	622(17)	925(15)	0	138(32)	91(15)	2273(327)	−38(17)	0	0
C6	1258(30)	0	0	124(44)	111(26)	3541(754)	0	0	0
C7	2565(35)	0	0	275(56)	95(21)	457(226)	0	0	0
C8	3301(18)	878(13)	0	146(26)	77(12)	925(185)	16(17)	0	0
N2	3841(18)	1654(13)	0	193(14)	104(14)	2325(293)	24(18)	0	0

TABLE 4. OBSERVED AND CALCULATED STRUTURE FACTORS

The reflections belong to those of group I (Table 2).

H	K	L	FO	FC
0	2	0	119.5	116.2
0	6	0	2.7	6.6
0	10	0	20.0	18.7
0	16	0	3.4	2.6
1	3	0	30.2	29.4
1	7	0	3.0	2.2
1	11	0	1.0	0.6
2	2	0	42.1	33.3
2	6	0	3.5	4.1
2	10	0	6.6	5.1
2	14	0	1.1	1.5
3	1	0	45.8	39.6
3	5	0	10.5	7.0
3	9	0	1.7	2.8
3	15	0	2.7	2.1
4	2	0	3.3	2.7
4	6	0	7.1	8.5
4	12	0	3.5	3.9
5	3	0	35.9	34.2
5	7	0	9.2	7.8
5	11	0	2.8	4.2
6	2	0	2.6	3.8
6	6	0	3.3	2.0
6	12	0	1.8	0.9
7	3	0	2.7	5.2
7	7	0	4.8	3.7
8	2	0	4.1	5.6
8	6	0	8.0	7.5
9	5	0	1.4	2.9
10	6	0	1.4	4.1
10	10	0	3.3	2.0
12	0	0	1.3	1.6
0	3	1	9.0	9.1
0	7	1	2.4	3.6
0	11	1	16.0	16.3
0	15	1	3.4	2.3
1	2	1	32.1	34.4
1	6	1	12.0	13.2
1	10	1	5.5	5.2
2	3	1	13.0	16.6
2	11	1	3.3	3.6
3	0	1	41.1	39.8
3	4	1	10.3	13.1
3	8	1	2.2	3.3
4	1	1	13.3	15.1
0	4	0	54.7	53.6
0	8	0	6.4	8.1
0	12	0	16.1	14.9
1	1	0	68.7	58.7
1	5	0	25.0	26.0
1	9	0	13.3	13.9
2	0	0	39.8	34.0
2	4	0	11.5	9.7
2	8	0	3.0	3.8
2	12	0	1.9	2.9
2	16	0	1.3	0.1
3	3	0	14.5	15.3
3	7	0	2.9	2.3
3	11	0	2.1	5.7
4	0	0	44.5	40.2
4	4	0	8.6	9.6
4	8	0	5.2	5.1
5	1	0	31.8	31.6
5	5	0	5.5	7.3
5	9	0	4.5	6.9
6	0	0	12.3	9.9
6	4	0	2.1	3.0
6	8	0	1.8	1.4
7	1	0	1.4	4.3
7	5	0	6.9	7.8
7	11	0	1.5	2.3
8	4	0	1.2	3.1
9	3	0	1.2	2.2
10	2	0	1.9	1.6
10	8	0	1.5	0.9
11	1	0	1.9	5.7
0	1	1	172.3	175.7
0	5	1	20.7	23.6
0	9	1	10.1	10.6
0	13	1	4.7	5.5
1	0	1	32.4	35.6
1	4	1	1.6	3.0
1	8	1	6.8	9.4
2	1	1	17.3	21.8
2	9	1	4.6	4.6
2	15	1	1.0	0.6
3	2	1	5.4	5.4
3	6	1	2.6	2.0
3	14	1	1.1	0.2
4	3	1	8.9	11.7
4	5	1	2.1	2.6
4	11	1	2.1	2.4
5	2	1	26.3	28.3
5	6	1	9.5	11.1
5	12	1	1.2	2.6
6	3	1	1.0	3.2
6	9	1	1.3	0.0
7	4	1	3.4	5.5
7	8	1	1.5	1.1
8	1	1	1.0	0.3
8	5	1	4.2	3.1
9	0	1	1.3	2.0
10	1	1	0.9	1.8
11	0	1	1.3	5.0
12	1	1	0.8	0.6
0	2	2	29.9	29.3
0	6	2	3.5	2.8
0	10	2	10.6	8.8
1	1	2	15.6	14.6
1	5	2	5.7	4.5
1	9	2	4.8	4.6
2	0	2	6.0	6.6
2	4	2	2.4	3.5
2	10	2	2.8	3.4
3	1	2	9.7	14.6
3	5	2	2.8	5.3
4	0	2	7.8	5.3
4	4	2	1.0	2.5
4	8	2	1.6	3.2
5	1	2	10.0	9.3
5	5	2	1.5	2.3
5	9	2	2.0	2.2
6	0	2	3.5	2.9
6	4	2	1.2	4.9
6	8	2	1.0	0.1
7	5	2	2.8	2.5
8	2	2	1.5	2.8
8	6	2	3.3	3.6
11	1	2	1.2	2.1
0	5	3	4.8	3.3
0	11	3	5.8	4.0
1	2	3	4.7	4.2
1	6	3	1.6	1.3
0	0	4	14.0	13.2
1	1	4	3.9	4.1
4	9	1	2.9	4.6
5	0	1	14.9	17.5
5	4	1	8.1	10.0
5	10	1	4.0	5.2
6	1	1	4.6	5.9
6	5	1	2.8	4.1
7	0	1	1.5	5.5
7	6	1	4.5	4.8
7	10	1	1.3	1.7
8	3	1	1.4	5.9
8	7	1	3.1	5.2
9	6	1	1.1	2.2
10	3	1	1.1	0.1
10	9	1	1.9	1.8
0	0	2	83.1	80.4
0	4	2	11.8	13.8
0	8	2	4.0	4.4
0	12	2	8.8	6.9
1	3	2	4.6	6.5
1	7	2	0.7	1.9
1	11	2	1.1	0.6
2	2	2	6.5	8.9
2	8	2	1.6	1.0
2	12	2	1.4	2.2
3	3	2	2.3	5.4
3	7	2	1.6	1.6
4	2	2	1.1	2.0
4	6	2	0.5	0.4
4	12	2	2.0	1.4
5	3	2	9.9	11.5
5	7	2	2.8	4.2
5	11	2	2.3	2.3
6	2	2	1.8	3.5
6	6	2	5.1	2.8
7	3	2	1.1	0.0
7	7	2	2.5	1.6
8	4	2	1.3	1.3
10	2	2	1.2	1.2
0	1	3	29.2	24.6
0	9	3	3.8	3.6
1	0	3	8.0	7.7
1	4	3	1.4	0.2
1	10	3	1.7	0.0
0	2	4	6.9	6.0

ability. The average structure thus deduced was refined with the block-diagonal least-squares method. The final R-value was 0.15. The weighting scheme adopted was: $w=1$, for $|F_o|\geq 3.0$ and $w=0.2$ for $|F_o|<3.0$, for all the 179 observed reflections belonging to group I of the reflection (Table 2). The positional and thermal parameters are given in Table 3. The observed and calculated structure factors are compared in Table 4.

The structure within one unit cell as viewed along axis c is shown in Fig. 2. Each lattice point is occupied by carbazole and TCNQ with equal probability. The site symmetry of the lattice point is mmm(D_{2h}), the apparent molecular structures of each component molecules thus being D_{2h}. The orientation of carbazole should be disordered since it has no such high symmetry. The molecule is assumed to take one of two alternative orientations with equal probability (Fig. 2). The bond lengths and angles are shown in Fig. 3. The mean bond lengths are: C–C (TCNQ), 1.37; C–N, 1.16; C–C (carbazole), 1.37; C–N, 1.43 Å. The standard deviations of each bond length and angle are about 0.05 Å and 4°, respectively.

Interpretation of Diffuse Streaks. Consider a lattice

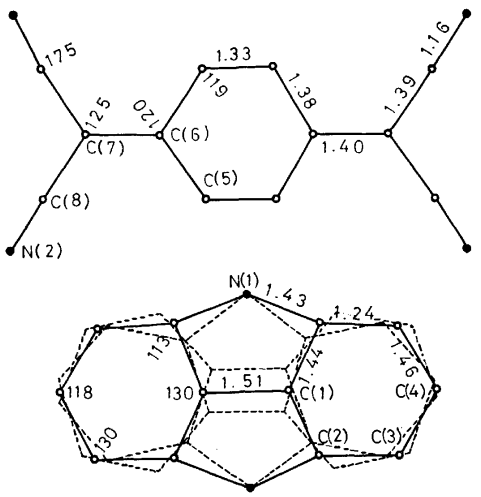

Fig. 3. Bond lengths (Å) and angles (°).
The broken line indicates the two alternative structure of carbazole.

having the same lattice constants as the average structure. Each lattice point can be occupied by TCNQ or carbazole, carbazole having two alternative orientations. Let us introduce $n_j(1-n_j)m_j$ and $(1-n_j)(1-m_j)$ to represent the probability that j-th lattice point is occupied by T, C^+, and C^- respectively, where T denotes TCNQ and C^+ and C^- are the carbazole with the polar axis parallel to the $\boldsymbol{b}$ direction and $-\boldsymbol{b}$ direction, respectively (Fig. 4a).

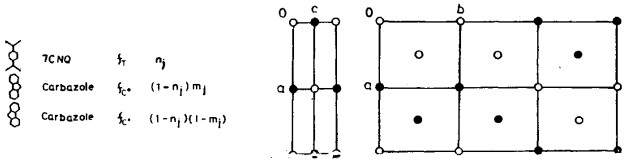

4a 4b(i) 4b(ii)

Fig. 4. (a) The occupancy probabilities of the lattice points. (b) Schematic drawing of the arrangement of TCNQ and carbazole. (i) indicates that the molecular arrangement is ordered in the a—c layer and (ii) shows an example of the stacking disorder along the b-direction.
The open circles and filled circles represent carbazole and TCNQ molecules, respectively.

The structure factor of this lattice is given by

$$F(\boldsymbol{k}) = \sum_j (n_j f_T + (1-n_j)m_j f_{C^+} + (1-n_j)(1-m_j)f_{C^-}) \exp(i\boldsymbol{k}\cdot\boldsymbol{R}_j), \quad (1)$$

where f is the molecular structure factor, $\boldsymbol{R}_j$ is the lattice vector of j-th lattice point and $\boldsymbol{k}$ is the scattering vector. The corresponding intensity is given by

$$I(\boldsymbol{k}) = |\langle F(\boldsymbol{k})\rangle|^2$$

Neglecting the correlation between n_j and $m_{j'}$ (the correlation between the position of TCNQ and the orientation of carbazole), we have

$$I(\boldsymbol{k}) = |\sum_j (\langle n\rangle f_T + (1-\langle n\rangle)\langle m\rangle f_{C^+} + (1-\langle n\rangle)(1-\langle m\rangle)f_{C^-}) \times e^{i\boldsymbol{k}\cdot\boldsymbol{R}_j}|^2 + |(f_T - \langle m\rangle f_{C^+} - (1-\langle m\rangle)f_{C^-}|^2 \sum_{jj'} \chi^T(j,j') \times e^{i\boldsymbol{k}\cdot(\boldsymbol{R}_j-\boldsymbol{R}_{j'})} + |f_{C^+} - f_{C^-}|^2 \sum_{jj'} \langle (1-n_j)(1-n_{j'})\rangle \times \chi^C(j,j') e^{i\boldsymbol{k}\cdot(\boldsymbol{R}_j-\boldsymbol{R}_{j'})}, \quad (2)$$

where $\langle\ \rangle$ indicates the statistical average and $\chi^T(j,j')$ and $\chi^C(j,j')$ are correlation functions expressed as

$$\chi^T(j,j') = \langle (n_j - \langle n\rangle)(n_{j'} - \langle n\rangle)\rangle$$

and

$$\chi^C(j,j') = \langle (m_j - \langle m\rangle)(m_{j'} - \langle m\rangle)\rangle \quad (3)$$

The intensity formula is composed of the following terms:

$$I = I_B + I_D^1 + I_D^2$$

where

$$I_B = |\sum_j (\langle n\rangle f_T + (1-\langle n\rangle)\langle m\rangle f_{C^+} + (1-\langle n\rangle)(1-\langle m\rangle)f_{C^-}) e^{i\boldsymbol{k}\cdot\boldsymbol{R}_j}|^2$$

$$I_D^1 = |(f_T - \langle m\rangle f_{C^+} - (1-\langle m\rangle)f_{C^-}|^2 \sum_{jj'} \chi^T(j,j') e^{i\boldsymbol{k}\cdot(\boldsymbol{R}_j-\boldsymbol{R}_{j'})}$$

and

$$I_D^2 = |(f_{C^+} - f_{C^-})|^2 \sum_{jj'} \langle (1-n_j)(1-n_{j'})\rangle \chi^C(j,j') e^{i\boldsymbol{k}\cdot(\boldsymbol{R}_j-\boldsymbol{R}_{j'})} \quad (4)$$

(1) I_B can be interpreted as the intensity of X-ray diffraction by the crystal with average structure. When $\langle n\rangle = 1/2$, $\langle m\rangle = 1/2$ (TCNQ and carbazole occupy each lattice point with equal probability, the orientation of carbazole being disordered), I_B gives the intensities of sharp spots in the integral layer lines (group I in Table 2) and can be written as

$$I_B = |\sum_j (f_T + (f_{C^+} + f_{C^-})/2)/2 \times e^{i\boldsymbol{k}\cdot\boldsymbol{R}_j}|^2$$

This intensity equation is the same as that used for the analysis of average structure.

(2) The second term I_D^1 involves the correlation function of TCNQ. Here, we take the average structure (Fig. 4b) in which the following assumptions were made.

1) The molecular arrangement of TCNQ and carbazole is ordered in each a-c layer.

2) The adjacent layers have no correlation irrespective of the molecular arrangement in the first a-c layer. Every lattice point in the second layer is occupied by TCNQ and carbazole with equal probability.

The correlation function $\chi^T(j,j')$ has non-zero value $(\pm 1/4)$ when the positions of the two lattice points j and j' are in the same a-c layer, and zero when they are not:

$$\chi^T(j,j') = \begin{cases} 1/4 \cdots n_1 + n_3 = 2m, & n_2 = 0 \\ -1/4 \cdots n_1 + n_3 = 2m+1, & n_2 = 0 \\ 0 \cdots n_2 \neq 0 \end{cases}$$

This means that the molecular arrangements in the a-c layer is ordered and no correlation exists between different layers. The adjacent layers are related with each other by the translational vector $(\boldsymbol{a}+\boldsymbol{b}+\boldsymbol{c})/2$. Thus we have $\boldsymbol{R}_j - \boldsymbol{R}_{j'} = n_1\boldsymbol{a} + n_2\boldsymbol{b}' + n_3\boldsymbol{c}$, where $\boldsymbol{b}' = (\boldsymbol{a}+\boldsymbol{b}+\boldsymbol{c})/2$. Judging from the molecular arrangement in the body centered lattice of the average structure, this type of stacking disorder is very liekly to occur in this crystal. With the use of Eq. (4) and the above values of $\chi^T(j,j')$, I_D^1 is written as follows.

$$I_D^1(\xi\boldsymbol{a}^*, \eta\boldsymbol{b}^*, \zeta\boldsymbol{c}^*) = \begin{cases} N^2|f_T - (f_{C^+} + f_{C^-})/2|^2/4 & \\ \quad \cdots \xi = n + 1/2,\ \zeta = m + 1/2 & (5) \\ 0 \quad \cdots \xi \neq n + 1/2 \text{ or } \zeta \neq m + 1/2 & \end{cases}$$

where N is the number of lattice points in the layer.

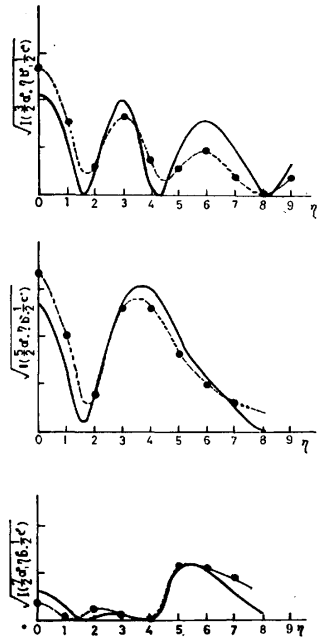

Fig. 5. The observed (solid lines) and calculated (broken lines) intensities of the streaks.

Equation (5) shows that the diffuse streaks appear in the diffraction patterns at the same positions as observed experimentally. The intensity along these streaks varies slowly according to the value of $|f^{T}-(f_{C^+}+f_{C^-})/2|^2$, some of which are shown in Fig. 5. The calculated value of $I_D{}^1$ agrees well with the visually estimated intensity of streaks.

(3) The third term $I_D{}^2$ depends on the correlation function involving the orientation of carbazole. The orientation of carbazole may be random in this disordered structure. Thus the correlation function $\chi^C(j,j')$ can be written as

$$\chi^C(j,j') = \delta_{jj'}/4 \qquad (6)$$

We obtain the equation for $I_D{}^2$ as follows:

$$I_D{}^2 = N|f_{C^+}-f_{C^-}|^2/8 \qquad (7)$$

From Eq. (7), we easily see that $I_D{}^2$ is not important because it indicates the faint scattering widely spread around the origin of the reciprocal lattice.

From the analysis of I_B, $I_D{}^1$, and $I_D{}^2$, we may say that the model of one-dimensionally disordered structure gives a fairly good explanation of the observed X-ray patterns.

Figures 2 and 4b show that the mixed stacks of carbazole and TCNQ exist along axis *c* like many other structures of CT complexes. The intermolecular distance between donor and acceptor molecules is 3.34 Å. The mode of overlapping can be considered to be the ring-external type observed in other CT complexes and radical salts of TCNQ.[1]

Interpretation of Sharp Reflections along the Streaks.
The diffuse streaks appear along the b^* direction, which indicate the stacking disorder along axis *b*.

1) H. Kobayashi, F. Marumo, and Y. Saito, *Acta Crystallogr.*, **B27**, 373 (1971); C. J. Fritchie, *ibid.*, **20**, 892 (1966); A. W. Hanson, *ibid.*, **19**, 610 (1965); R. M. Williams and S. C. Wallwork, *ibid.*, **B24**, 168 (1968).

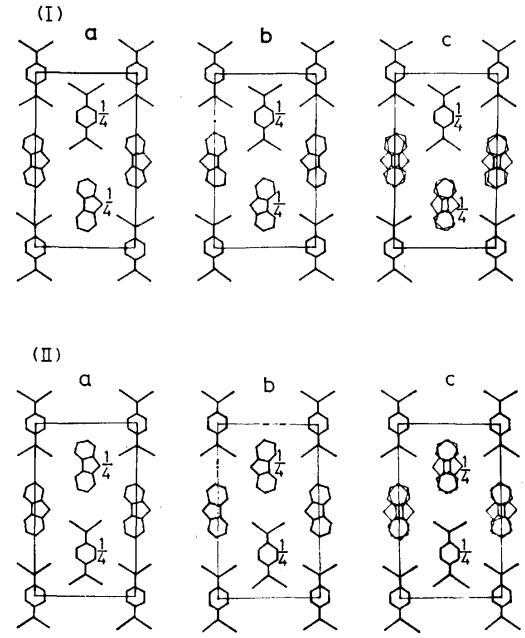

Fig. 6. The candidates of the ordered structures.

Table 5. Reflections diffracted from the ordered structures

The Bragg indices refer to the unit cell listed in Table 1.

l	*k*	*h*	*h*
		I[a]	II
0	$2n$	$2m$	$2m$
	$2n+1$	$2m+1$	$2m+1$
1/2	$2n$	$2m+3/2$	$2m+1/2$
	$2n+1$	$2m+1/2$	$2m+3/2$
1	$2n$	$2m+1$	$2m+1$
	$2n+1$	$2m$	$2m$
3/2	$2n$	$2m+1/2$	$2m+3/2$
	$2n+1$	$2m+3/2$	$2m+1/2$

a) Reflections correspond to those diffracted from structures Ia, Ib, and Ic.

Moreover, associated sharp spots do not lie exactly on the diffuse streaks but deviate slightly alternately from them. Thus the crystal seems to be not nuiform but composed of ordered and disordered domains.

Possible ordered structures are shown in Fig. 6. Six kinds of structures denoted by Ia, Ib, Ic, IIa, IIb, and IIc exist. The lattice spacings are twice those of average structure along directions *a* and *c*. Owing to the characteristic arrangement of molecules, additional and specific absence appears in X-ray diffraction patterns. They are summarized in Table 5 in terms of the basis vectors *a*, *b*, and *c* of average structure. The reflections from structure groups I and II correspond to those of groups IIIa and IIIb, respectively (Tables 2 and 5 and Fig. 1c). Specific features of these structures are as follows:

(1) Structures Ia and IIa are mirror images of each other, as likewise are Ib and IIb, and Ic and IIc.

(2) Ia, Ib, IIa, and IIb are polar due to the ordered orientation of carbazole molecules, while the lattices Ic and IIc are nonpolar due to disordered orientation.

(3) There are twofold axes along b. The lattices therefore might be monoclinic.

If the structures shown in Fig. 6 have rectangular unit cells, the sharp spots would be on the diffuse streaks. In order to explain the observed deviations, the structures should have monoclinic symmetry. It may be quite natural to assume that if the angles β of the unit cells of groups I and II (Fig. 6) are a little less or more than 90° the change in angles β of structures I and II would be equal in magnitude but opposite in sign, since the two structures are related to each other by the mirror planes perpendicular to axis a. If the structures of groups I and II are twinned submicroscopically by the mirror planes parallel to the b-c plane, the sharp spots may satisfy the specific extinction rules (Table 5), deviating alternately from the streaks.

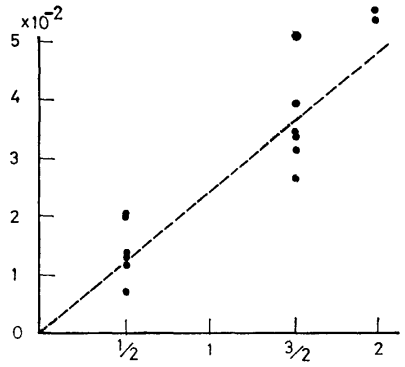

Fig. 7. The magnitude of the deviation of the spots from the streaks.
The numbers on the *abscissa* indicate the layer lines around axis c and those on the *ordinate* are $2|\Delta d|/d$, where d is the distance between two neighboring spots measured along axis a^*.

As shown in Fig. 7, the spots deviate more largely from the streaks in higher layer lines. Some elongated spots in the Weissenberg film of the upper layer around axis c split into two spots. A similar situation was observed for axis a. The magnitude of the change of β is about 0.2°. The crystal symmetry is reduced from Immm to C2 (or C2/m). The relationship between these cells is shown in Fig. 8. The lattice constants of

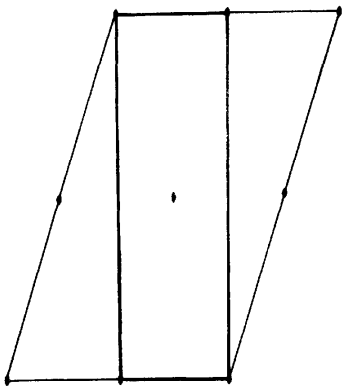

Fig. 8. The relationship between the cells of Immm and C2. The small change of β is neglected in this figure.

monoclinic cell are: $a=11.27$, $b=12.94$, $c=6.78$ Å, $\beta=107.4°$ and $Z=2$.

Using atomic parameters of the average structure and the models of ordered structures shown in Fig. 5, a comparison of the calculated and observed structure factors was made only for strong reflections ($h/2$, k, $1/2$) (Table 2) owing to difficulty in the visual estimation of the intensity of the spots in the streaks. R-value is about 0.19 (Table 6). The difference between models (Ia and IIc) is comparatively small. Thus no refinement was performed.

Description of the Domain Structure. The crystal of carbazole–TCNQ is hardly soluble in acetone, acetonitrile or tetrahydrofuran. The black needles precipitate when the acetone solutions of the components are mixed. From the fact that most non-ionic CT complexes of TCNQ are very soluble and the CT spectrum appears in the visible region, precipitation of black crystals seems to indicate that carbazole–TCNQ is a complex of ionic type, where the CT interaction between donor and acceptor is very strong. However, this is not cosistent with the fact that the CT interaction is very weak, since the visible spectrum of the acetone solution of carbazole–TCNQ closely resembles that of TCNQ (only one strong absorption maximum appears at 4000 Å) with no CT absorption. This fact indicates that the crystal structure of carbazole–TCNQ has somewhat unusual features.

The ordered domain composed of structures Ia, IIa,

TABLE 6. COMPARISON OF THE OBSERVED AND CALCULATED STRUCTURE FACTORS
Reflections belong to groups IIIa and IIIb (Table 2).

h ×2	k	l ×2	F_o	F_c	h ×2	k	l ×2	F_o	F_c	h ×2	k	l ×2	F_o	F_c
1	10	1	5.76	3.49	1	11	1	5.46	4.69	1	12	1	5.62	3.94
3	0	1	17.58	27.33	3	1	1	9.59	15.46	3	2	1	7.06	6.82
3	3	1	14.34	16.36	3	5	1	8.01	5.53	3	6	1	11.29	9.63
3	7	1	6.63	4.31	5	0	1	29.33	34.84	5	1	1	15.31	20.84
5	2	1	11.29	7.76	5	3	1	25.87	26.96	5	4	1	31.17	26.75
5	5	1	16.06	16.76	5	6	1	10.62	8.74	5	7	1	6.95	5.98
5	8	1	5.71	4.90	7	0	1	8.90	3.29	7	5	1	12.22	11.86
7	6	1	10.11	11.41	7	7	1	7.70	5.98	9	0	1	8.10	9.53
9	3	1	6.78	5.50	9	4	1	10.11	8.48	9	5	1	7.06	8.04
13	0	1	7.33	7.07	13	3	1	5.78	5.52	15	4	1	7.77	9.47
15	5	1	12.57	11.59	15	6	1	9.11	9.93	15	7	1	6.38	5.66
17	4	1	5.18	6.05										

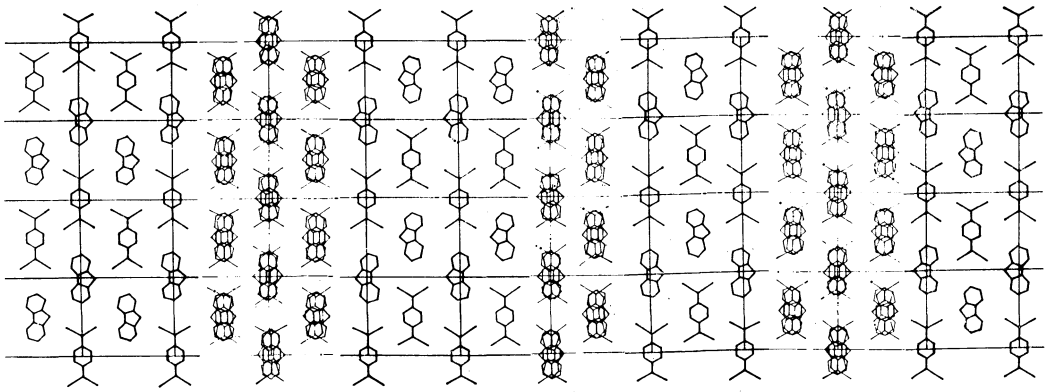

Fig. 9. Schematic drawing of the domain structure.

Ib and IIb has dipole moment along the b and $-b$ directions, respectively. On the other hand, the one-dimensionally disordered structure is non-polar. Thus, an adequate combination of these structures might interpret the appearance of the domain structure. Such a model seems to be stable because it resembles the well-known domain structures of ferromagnetic or ferroelectric substances. The most plausible structure may be that shown in Fig. 9. This structure indicates the strong interaction between domains with positive polarity and those with negative polarity, the domains with opposite polarities tending to gather together.

The crystal should contain an equal amount of positive and negative domains. However, it is difficult to estimate the ratios Ia/Ib and IIa/IIb. The thickness of random domain seems to be larger than that found in ferroelectrics or ferromagnetics, the intensity of the streaks being fairly strong. The space group of the ordered domain is C2.

The domain structure consisting of non-polar structures Ic and IIc can also explain the features of X-ray diffraction patterns. In this case, the ordered domain closely resembles the crystal structure of *N*-methylphenothiazine–TCNQ.[2] The orientation of an *N*-methylphenothiazine molecule is disordered like the carbazole molecule. Both structures contain mixed stacking columns of donors and acceptors. In spite of the assumed similarity of molecular arrangements, the properties of both complexes differ, *viz.*, *N*-methylphenothiazine–TCNQ is very soluble and the solution is strongly colored. This indicates that the non-polar domain dose not seem to be possible. The structure of polar domain structure seems to be confirmed by the appearance of various types of domain structures.

Absorption Spectra of the Crystal of Carbazole–TCNQ. The visible absorption spectrum of the solution of carbazole–TCNQ is similar to that of TCNQ. It is of interest that the CT band appears in the spectrum of a powdered sample (Fig. 10). The SCF-MO's of carbazole–TCNQ complex was calculated by assuming a complex as a single π-conjugated system using the semiempirical parameters.

The two center resonance integral is estimated by using the equation

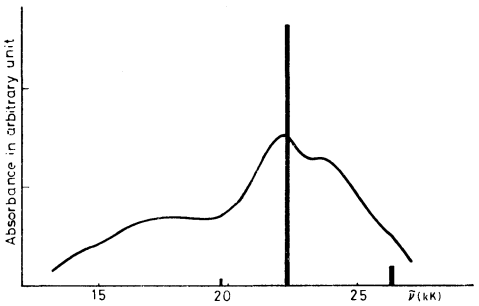

	Assignment		Character of transitions				
		$\bar{\nu}$(kK)	$(DD)_m$	$(AA)_m$	$(DA)_m$	$(AD)_m$	f
(1)	19.70	CT(D→A)	0.026	0.016	0.950	0.000	0.005
(2)	22.55	LE(A*)	0.014	0.905	0.051	0.030	1.985
(3)	26.05	CT(D→A)	0.024	0.066	0.906	0.002	0.136
(4)	29.60	CT(D→A) + LE(A*)	0.018	0.293	0.674	0.007	0.070
(5)	31.95	LE(A*)	0.013	0.877	0.073	0.023	0.018

Fig. 10. Absorption spectra of the powdered samples of carbazole–TCNQ and calculated results of SCF-MO-CI.

$$\beta_{\mu\nu} = -\kappa S_{\mu\nu}(I_\mu + I_\nu)/2$$

where $S_{\mu\nu}$ is overlap integral calculated by use of the Slater atomic orbitals, I_μ (I_ν) is ionization potential of the μ-th (ν-th) atom and κ is assumed to be 0.85 when μ and ν belong to the same molecule and 2.0 when they belong to different molecules. The two-center repulsion integral $\gamma_{\mu\nu}$ is evaluated according to the Nishimoto-Mataga method. Semiempirical constants I_μ and $\gamma_{\mu\nu}$ are the same as those given in Ref. 3 ($I_p(C^+)=11.16$, $I_p(N^+)=14.12$, $I_p(N^{++})=26.70$, $\gamma_{C^+C^+}=11.13$, $\gamma_{N^+N^+}=12.34$, $\gamma_{N^{++}N^{++}}=17.44$ eV). The relative arrangement of the constituent molecules is taken as shown in Fig. 2. After five cycles of SCF-MO calculation, the CI calculation was carried out with the lowest 25 singly-excited configulations. Characterization of transition was made according to the method described in Ref. 3.

The results are summarized in Fig. 10. Agreement between the calculated transitions and observed spectra is not satisfactory. The broad peak at about 18 kK, which cannot be observed in the spectra of component molecules, may be regarded as the CT absorption.

2) H. Kobayashi, This Bulletin, to be published.

3) T. Ohta, H. Kuroda, and T. L. Kunii, *Theor. Chim. Acta*, **19**, 167 (1970).

The strong peak at 22.5 kK can be assigned to the local excitation of TCNQ. The amount of charge transferred from carbazole to TCNQ is calculated to be 0.05 e. The small value seems to correspond to the weak interaction.

Various Types of Domain Structure. Since the crystal is made up from a combination of ordered

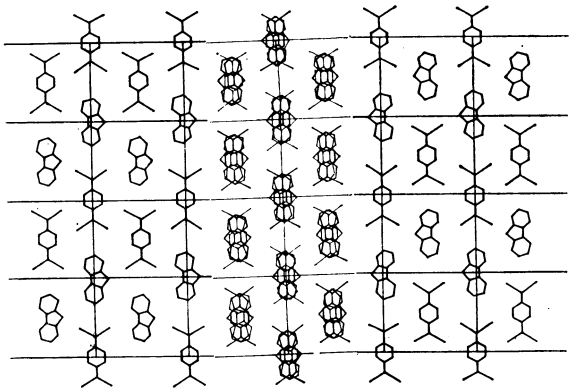

Fig. 11 (a)

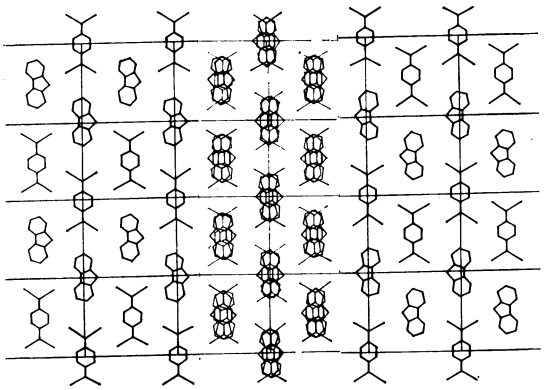

Fig. 11 (b)

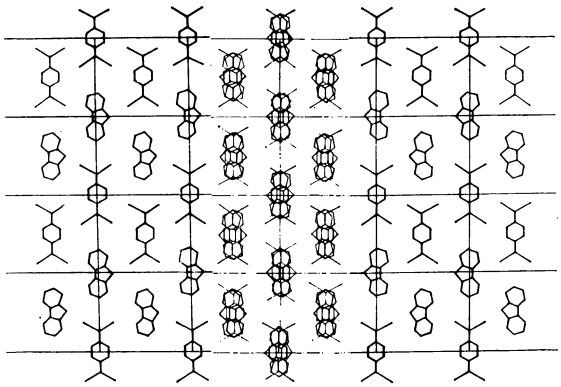

Fig. 11 (c)

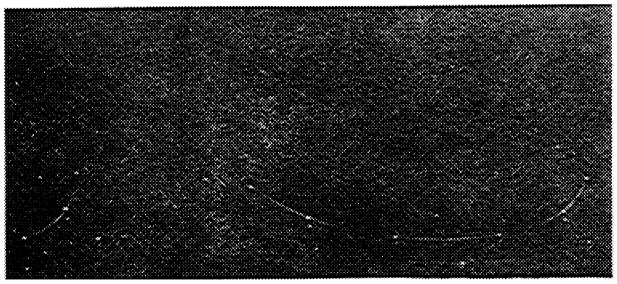

Fig. 11 (c′)

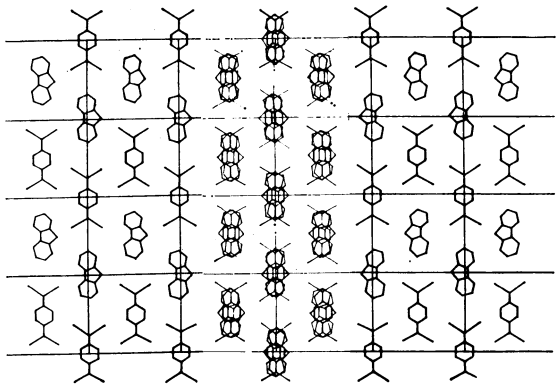

Fig. 11 (d)

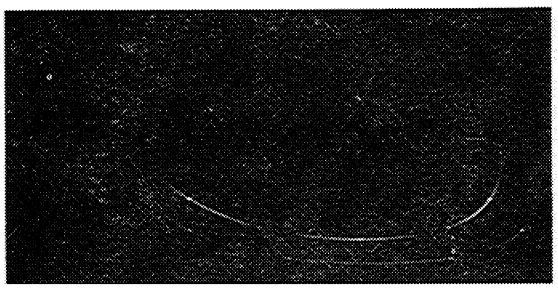

Fig. 11 (d′)

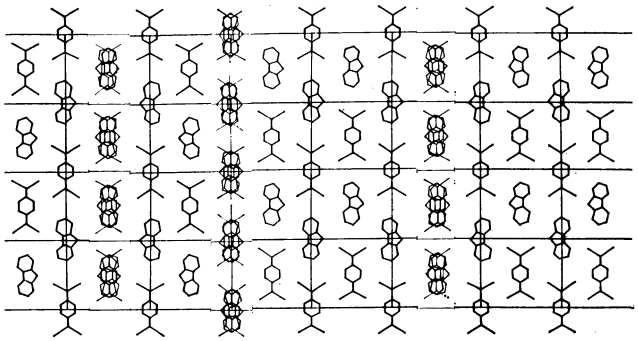

Fig. 11 (e)

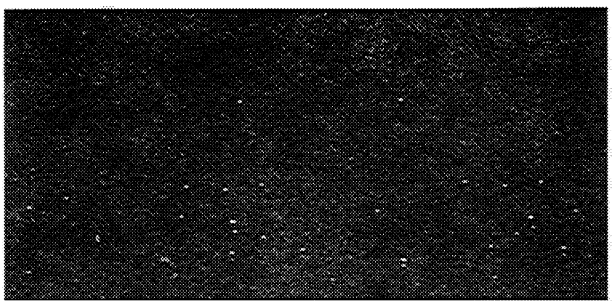

Fig. 11 (e′)

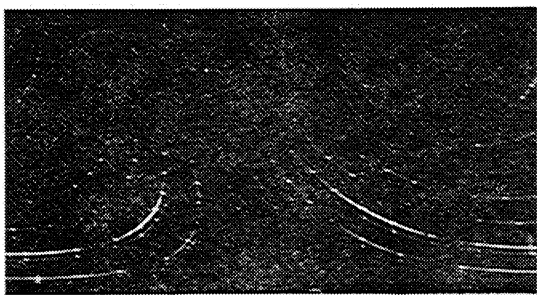

Fig. 11 (f)

(g)

Fig. 11. Various types of diffraction patterns and the corresponding domain structures.

and disordered structures, various types of crystals may appear according to the mode of combination. We examined the X-ray diffraction patterns of crystals grown from solvents such as acetone, acetonitrile and tetrahydrofuran, and found many types of patterns, but no solvent effect.

As judged from the X-ray diffraction patterns, the domain structure seems to be formed according to the following conditions:

From the necessity to cancel the polarity of the crystal, there should be equal amounts of positive and negative structures. The thickness of the domain wall will differ to some extent with the sample, since the non-polar structure seems to be less important in view of the stability of the crystalline state.

Type I: The structure composed of Ia, Ib, IIa, IIb and random structure (Fig. 9) gives the X-ray diffraction patterns shown in Fig. 1. The same patterns can also be observed from structures Ia, IIb and random structure (Fig. 11a) or of Ib, IIa and random structure (Fig. 11b). Thus we can not decide from the diffraction patterns which structure is realized in the crystal. All of the three structures might coexist.

Type II: The structure composed of Ia, Ib and random structure (Fig. 11c) gives the X-ray pattern shown in Fig. 11c′, that consisting of IIa, IIb and random structure (Fig. 11d) gives the X-ray pattern shown in Fig. 11d′. The order component of both structures bear twin relationship with each other and patterns are closely related. It may be interesting that the synthesis of Figs. 11c′ and 11d′ gives the same pattern as that of Fig. 1a. Concerning the ordered domain, both structures are made up of the half components of the structure shown in Fig. 9. This is the reason why the number of spots in Figs. 11c′ and 11d′ is a half of those in Fig. 1a.

Type III: Some crystals give diffraction patterns with very faint streaks as shown in Fig. 11e′. The corresponding crystal will be constructed from the regions of Ia and Ib, small amount of IIa and IIb and a very little of random domain (Fig. 11e).

Type IV: There seems to be a domain wall of one-dimensionally disordered structure, in which some inter-layer correlation exists, since in some films the apparent diffuse maxima are observed between sharp spots as shown in Fig. 11f. This type of diffuse maxima has been extensively discussed.[4]

Type V: It may be easily recognized that the sharp spots appear at the positions of the diffuse maxima described in type IV, if the inter-layer correlation becomes complete. Figure 11g shows that the above situation is realized in some crystals. In this case there exist some domain walls whose lattice constant b is twice as large as that of the average structure.

Similar types of X-ray diffraction patterns were reported for the crystals of *o*-chlorobenzamide.[5]

An attempt was made to prepare crystals with a completely polarized structure, which might have similar physical properties to the so-called electret. Silver-paste was coated on both sides of the wall of a 10 mm diam. glass tube, a voltage of 500 V being applied between them. Crystals were prepared by the diffusion method in this tube, but the experiment was not successful, the crystals precipitated appearing to be similar to those obtained before. The results seems to indicate that the stability due to interaction between the polar domains overcomes the stability due to the effect of an external electric field.

The author would like to express his sincere thanks to Prof. Yoshihiko Saito for his keen interest and encouragement. He is also grateful to Prof. Takaaki Danno for his encouragement and to Dr. Ichimin Shirotani for the experiment of visible absorption spectra.

4) A. J. C. Willson, *Acta Crystallogr.*, **2**, 245 (1949); H. Jagodginski, *ibid.*, **2**, 201 (1949); *ibid.*, **2**, 208 (1949).

5) K. Sakurai, Y. Takaki, and Y. Kato, 9th International Congress of Crystallography, Kyoto (1972), Collected Abstracts, p. 211.

Solubilization Behavior of the Surfactant–Polyethylene Glycol Complex in Relation to the Degree of Polymerization

Fumikatsu TOKIWA and Kaoru TSUJII

Research Laboratories, Kao Soap Company, 2-1-3 Bunka, Sumida-ku, Tokyo 131

(Received March 22, 1973)

The solubilization behavior of the complexes composed of a surfactant and polyethylene glycol (PEG) toward an oil-soluble dye, Yellow OB, has been studied in relation to the degree of polymerization, *n*, of PEG. The solubilizing powers of the anionic surfactants, sodium dodecyl sulfate and sodium *p*-octylbenzene sulfonate, become greater on the addition of PEG, the extent depending on *n*. They increase as *n* increases. It is proposed that there are at least two different types of complexes, *i.e.*, "oligomeric" and "polymeric" PEG–surfactant complexes. The boundary between the oligomeric and polymeric PEG's is estimated to be around an *n* value of 10—15. With an oligomeric PEG–surfactant complex, the solubilization of Yellow OB would occur mainly in the hydrocarbon part of the surfactant micelle. With a polymeric PEG–surfactant complex, on the other hand, the solubilization would take place in the region of a complex rich in PEG. Electrical-conductivity and absorption-spectral data on the complexes are also included in this paper.

When a surfactant is mixed with a polymer in an aqueous solution, a kind of complex is formed by the binding of the surfactant molecules onto the polymer molecule.[1-9] The physicochemical properties of the respective components are, in general, changed by the formation of this complex. For example, the solubilizing power of the surfactant becomes greater on the addition of the polymer.[1,2,8,9] However, the mechanism of the increase in the solubilizing power by the polymer–surfactnat complex formation has not yet been elucidated. The dependence of this complex formation on the degree of polymerization of the polymer is also not well understood.

In the present work, the solubilization behavior of polymer–surfactant complexes toward an oil-soluble dye, Yellow OB, has been studied in relation to the degree of polymerization of the polymer, using two anionic surfactants and polyethylene glycols with different degrees of polymerization. Discussion has also been made of the mechanism of the solubilization of Yellow OB by the complexes composed of the surfactant and polyethylene glycol.

Experimental

Materials. The samples of sodium dodecyl sulfate (abbreviated to $NaC_{12}S$) and sodium *p*-octylbenzene sulfonate (abbreviated to $NaC_8\phi S$) were the same as those used in previous experiments.[10,11] The polyethylene glycols (abbreviated to PEG) were of a reagent grade and had been purified by ion-exchange with Amberite IR-120 and IRA-410.[12] The average degrees of polymerization, *n*, of these PEG samples were 2, 3, 5, 9, 14, 20, 35, 91, and 136; these figures were determined from their hydroxyl values. The Yellow OB used as a solubilizate was of a reagent grade; it had been obtained from Wako Pure Chemicals Co. and recrystallized twice from an ethanol–water mixture (80/20).

Solubilization. The stock solution of a surfactant containing 1.0% PEG was prepared. A sample solution of the desired concentration was made up volumetrically by the dilution of the stock solution with the 1.0% PEG solution. The solubilization of Yellow OB was carried out in a water bath at 30 ± 0.1 °C for 65 hours to attain equilibrium, a method described elsewhere[10] being employed. The amount of the solubilized dye was determined by optical-density measurements at a wavelength of 445 mμ with a Shimadzu Model AQV-50 spectrophotometer.

Electrical Conductivity. A sample solution was prepared by the procedure described above. The conductivity measurements were made with a Toa Electronics Model CM-1DB conductometer at 25 ± 0.01 °C. The observed values were checked by measuring the conductivities of standard solutions of potassium chloride.

Absorption Spectra. The spectral measurements were performed with the above spectrophotometer at room temperature (about 25 °C).

Results and Discussion

In Fig. 1, the amounts of solubilized Yellow OB, *A*, in the presence of PEG with different *n* values are plotted against the concentration, *C*, of $NaC_8\phi S$, the concentration of PEG being kept constant at 1.0%. The *A vs. C* curves similar to those shown in Fig. 1 were obtained for the $NaC_{12}S$–PEG complex. As may be seen in this figure, there is a linear relation between *A* and *C*. The solubilizing power of the PEG–$NaC_8\phi S$ complex, which corresponds to the slope of each *A vs. C* curve, increases as the degree of polymerization of PEG, *n*, increases. Further, the concentration of $NaC_8\phi S$ at which the solubilization sets in shifts to a lower concentration with an increase in the *n*.

Mechanism of the Solubilization of Yellow OB by the Polymer–Surfactant Complex. When a polymer is mixed with a surfactant in an aqueous solution, a

1) S. Saito, *Kolloid Z.*, **154**, 19 (1957).
2) S. Saito, *ibid.*, **158**, 120 (1958).
3) T. Isemura and A. Imanishi, *J. Polymer Sci.*, **33**, 337 (1958).
4) C. Botre, F. DeMartiis, and M. Solinas, *J. Phys. Chem.*, **68**, 3624 (1964).
5) M. N. Jones, *J. Colloid Interface Sci.*, **23**, 36 (1967).
6) K. E. Lewis and C. P. Robinson, *ibid.*, **32**, 539 (1970).
7) M. L. Fishman and F. R. Eirich, *J. Phys. Chem.*, **75**, 3135 (1971).
8) H. Lange, *Kolloid-Z. Z. Polymere*, **243**, 101 (1971).
9) H. Arai, M. Murata, and K. Shinoda, *J. Colloid Interface Sci.*, **37**, 223 (1971).
10) F. Tokiwa, *J. Phys. Chem.*, **72**, 1214 (1968).
11) F. Tokiwa and K. Tsujii, *ibid.*, **75**, 3560 (1971).
12) I. Maruta, *Nippon Kagaku Zasshi*, **83**, 782 (1962).

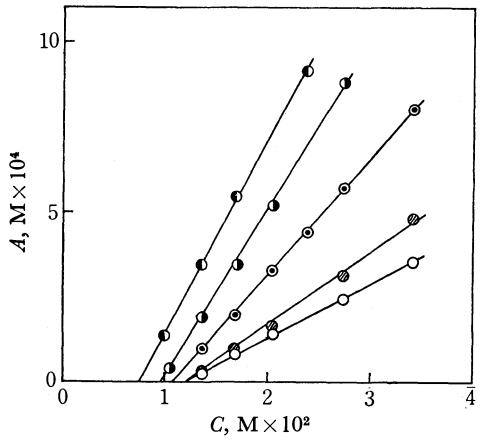

Fig. 1. The curves of the amount of solubilized Yellow OB *vs.* the concentration of $NaC_8\phi S$ in the presence of PEG: ○, $NaC_8\phi S$ alone; ◍, PEG-5; ⊙, PEG-14; ◑, PEG-35; ◐, PEG-136. The curves in the presence of PEG-2,3,9,20, or 91 are not shown here. The number written after PEG expresses the average degree of polymerization.

polymer–surfactant complex is formed by binding the surfactant molecules onto the long chain of the polymer molecule.[1-9] Further, it has been imagined that the binding of the surfactant molecules is not uniform along the polymer chain, but discrete, forming clusters or aggregates on it in such a manner as in micelle formation.[1,2,7-9] If this is the case, Yellow OB should be solubilized in these clusters. Such a solubilization mechanism in the complex is apparently analogous to that in the micelle of the surfactant alone. However, this mechanism itself can not account for such high solubilizing powers of the PEG–$NaC_8\phi S$ complex, as may be seen in Fig. 1.

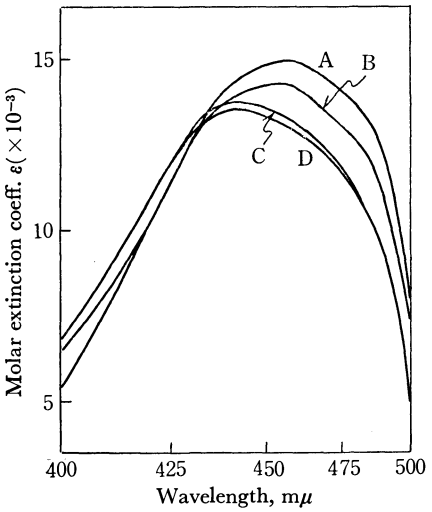

Fig. 2. The absorption spectra of Yellow OB in PEG alone (curve A), and in the aqueous solution of $NaC_8\phi S$ (curve D), $NaC_8\phi S$–PEG-5 (curve C) or $NaC_8\phi S$–PEG-136 (curve B) at 1.0% $NaC_8\phi S$ and PEG concentration.

Figure 2 shows the absorption spectra of Yellow OB in PEG alone as well as in aqueous solutions of $NaC_8\phi S$, $NaC_8\phi S$–PEG-5, and $NaC_8\phi S$–PEG-136. The spectra with $NaC_{12}S$ and $NaC_{12}S$–PEG are almost the same as those shown in Fig. 2, though not specifically shown. With the $NaC_8\phi S$–PEG-136 complex, the shape of the Yellow OB spectrum and its absorption maximum, λ_m, are very similar to those observed with PEG alone. With the $NaC_8\phi S$–PEG-5 complex, on the other hand, the spectrum closely resembles the spectrum in the $NaC_8\phi S$ solution. These results indicate that the solubilization behavior of $NaC_8\phi S$–PEG-136 toward Yellow OB is different from that of $NaC_8\phi S$–PEG-5. In the former case, the solubilization seems to occur in the PEG atmosphere of the complex, while in the latter case, it occurs mainly in the hydrocarbon part of the $NaC_8\phi S$ micelle. The results also suggest that there are at least two different types of complexes, that is, the "polymeric" PEG–$NaC_8\phi S$ complex and the "oligomeric" PEG–$NaC_8\phi S$ complex.

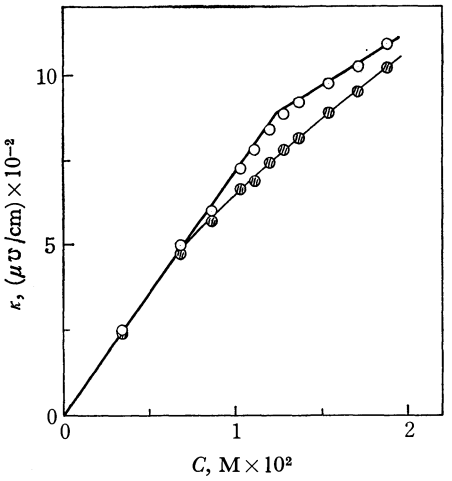

Fig. 3. The electrical conductivity *vs.* concentration curves for $NaC_8\phi S$ in the absence and presence of PEG: ○, $NaC_8\phi S$–PEG-5; ◍, $NaC_8\phi S$–PEG-136. The bold line indicates the curve for $NaC_8\phi S$ alone.

Figure 3 shows the conductivity *vs.* concentration curves for $NaC_8\phi S$ in the absence and in the presence of PEG. There is no difference between the curves for $NaC_8\phi S$ alone (bold line) and $NaC_8\phi S$–PEG-5 (open circle), while the curve for $NaC_8\phi S$–PEG-136 is different from that for $NaC_8\phi S$–PEG-5. This gives another piece of evidence for the existence of the two types of complexes.

To explain the solubilizing power of the complex being much greater than that of the surfactant micelle alone, we here propose new models of the polymer–surfactant complex, different from the model hitherto accepted,[1,2,7-9] based on the above spectral and conductivity data. The following models seem to be plausible for this explanation. The PEG polymer in the form of a random coil would be bound by the surfactant molecules with the hydrophilic group orientating to the aqueous phase; this model is analogous to the structure of polysoaps or proteins in an aqueous solution.[13,14] Probably, the solubilization of Yellow OB may take place in the region of a complex rich in PEG. The PEG itself is a very good solvent for this

13) T. Nakagawa and H. Inoue, *Kolloid-Z. Z. Polymere*, **195**, 93 (1964).
14) C. C. Bigelow, *J. Theoret. Biol.*, **16**, 187 (1967).

dye. An increase in solubilization on the addition of PEG can thus be explained by this mechanism. On the other hand, the PEG oligomer is gathered on the surface of the surfactant micelle in such a manner that polar substances, such as glycerol and dimethylphthalate, are adsorbed on the surface of the micelle.[15,16]

Boundary between Oligomer and Polymer in Complex Formation. The radius of a randam-coil polymer in solution, *i.e.*, the radius of gyration, is proportional to $n^{1/2}$ when the excluded volume effect of the polymer is negligible[17] and where n is the degree of polymerization of the polymer. This condition may be satisfied in the present case.[18] Thus, the average volume of the polymer coil will be proportional to $n^{3/2}$.

It seems reasonable to assume that the solubilization capacity of the polymeric PEG–surfactant complex is proportional to the volume of the polymer coil, provided that the solubilization of Yellow OB occurs in the region of this polymer coil, as has been already described. Thus, the solubilizing power of the complex is expected to be proportional to $n^{1/2}$, since the number of the polymer molecules is inversely proportional to n at a constant weight concentration.

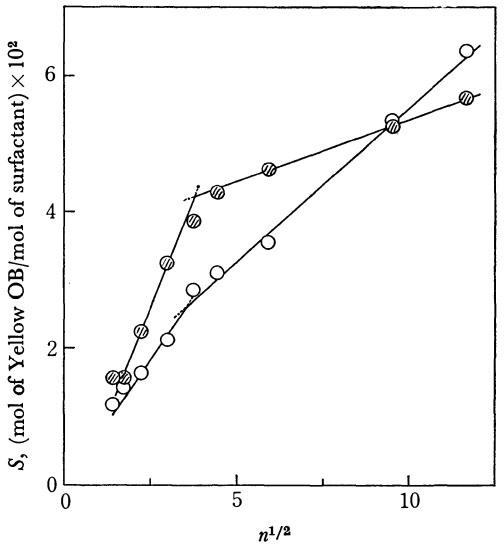

Fig. 4. The solubilizing power of surfactant–PEG-n complex plotted against $n^{1/2}$; ○, $NaC_{12}S$–PEG-n; ◍, $NaC_8\phi S$–PEG-n.

In Fig. 4, the solubilizing power, S, of the $NaC_8\phi S$–PEG complex, obtained from the slope of the straight line shown in Fig. 1, is plotted against $n^{1/2}$. This figure also includes the S *vs.* $n^{1/2}$ plot for the $NaC_{12}S$–PEG complex. In both cases, it should be noted that there is an inflection point around $n=10$—15. This point or region may be interpreted as a boundary between the two different types of polymer–surfactant complexes, or as a transition from oligomeric to polymeric PEG.

According to the thermodynamics of micelle formation, the following equation may be written:[19]

$$\mu_M^\circ = \mu_m^\circ + RT \ln C_O \qquad (1)$$

where μ_M° and μ_m° are the standard chemical potentials of a surfactant in the micelle phase and in the monomer phase respectively, and where C_O is the critical micelle concentration of the surfactant. Analogously to Eq. (1), we may write this equation:

$$\mu_c^\circ = \mu_m^\circ + RT \ln C_C \qquad (2)$$

for the formation of the polymer-surfactant complex. Here, μ_c° refers to the standard chemical potential of the surfactant in the complex phase, and C_C is the surfactant concentration of complex formation at which the solubilization begins. Eliminating μ_m° from Eqs. (1) and (2), we obtain:

$$\mu_c^\circ - \mu_M^\circ = RT \ln (C_C/C_O) \qquad (3)$$

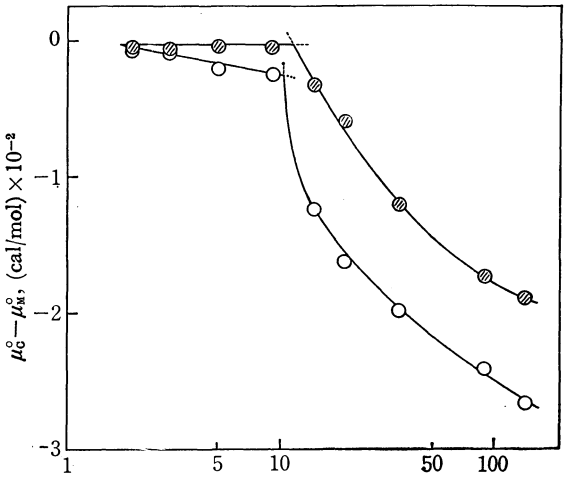

Fig. 5. The value of $(\mu_c^\circ - \mu_M^\circ)$ plotted against n: ○, $NaC_{12}S$–PEG-n: ◍, $NaC_8\phi S$–PEG-n.

The value of $(\mu_c^\circ - \mu_M^\circ)$ calculated from C_C and C_O by means of Eq. (3) is plotted against n in Fig. 5. The curves of $(\mu_c^\circ - \mu_M^\circ)$ *vs.* n for both the $NaC_8\phi S$–PEG and $NaC_{12}S$–PEG complexes have an inflection at $n=10$—15. In the oligomeric region, the value of $(\mu_c^\circ - \mu_M^\circ)$ is nearly independent of n and μ_c° is equal to μ_M°, which suggests that the complex formation takes place simultaneously with, or just after, the micelle formation. In the polymeric region, on the other hand, the value of $(\mu_c^\circ - \mu_M^\circ)$ decreases with the increase in n. This implies that the complex becomes more stable as n increases. Probably, these results could be explained as showing that the surfactant molecules are bound more easily onto the PEG polymer with a larger n because of the lower electrical repulsion of their ionic heads on the complex surface.

15) K. Shinoda, T. Nakagawa, T. Isemura, and B. Tamamushi, "Colloidal Surfactants," Academic Press, New York (1963), p. 140.
16) P. H. Elworthy, A. T. Florence, and C. B., Macfarlane, "Solubilization by Surface Active Agents," Chapman and Hall, London (1968), p. 68.
17) B. P. Flory, "Principles of Polymer Chemistry," Cornell University Press, New York (1953), Chap. 10.
18) F. E. Bailey, Jr., and J. V. Koleske, "Nonionic Surfactants," ed. by M. J. Schick, Marcel Dekker, New York (1967), p. 815.
19) p. 51 in Ref. 16.

The Contact-term Contributions to Lanthanide-induced ^{13}C Paramagnetic Shifts in Acridine, Quinoline, and Isoquinoline

Masatoshi HIRAYAMA and Yoshiaki HANYU*

Department of Chemistry, Faculty of Science, Ibaraki University, Bunkyo, Mito 310
**Naka Works, Hitachi Co., Ltd., Katsuta, Ibaraki 312*

(Received March 23, 1973)

^1H and ^{13}C paramagnetic shifts induced by $Eu(DPM)_3$ and $Pr(DPM)_3$ in acridine, quinoline, and isoquinoline in CCl_4 are observed. It has been found that, while the ^1H shifts can be interpreted solely in terms of a pseudo-contact interaction, there is a much larger contact-term contribution to ^{13}C shifts induced by $Eu(DPM)_3$ than by $Pr(DPM)_3$ in these compounds; this contribution to the ^{13}C shifts cannot be explained by a simple combination of σ- and π-contact terms.

Since the discovery by Hinckley[1] that the dipyridine adduct of europium(III) tris(dipivalomethanate), Eu(DPM)$_3$, produces large and stereo-specific chemical shifts in the NMR spectrum of cholesterol, numerous communications reporting work with lanthanide-shift reagents of this type have appeared. While the action of these shift reagents is generally attributed to a through-space dipolar interaction,[2,3] it has recently been reported that abnormal shift values are observed for atoms (^{14}N) co-ordinated to the lanthanide ion[4] and for ^{13}C and ^1H nuclei close to the co-ordinating atom in some aliphatic compounds.[5] Johnson *et al.* have reported that abnormal relative ^1H shift patterns are observed for substituted pyridine *N*-oxides and anilines with some lanthanide complexes, and that the shift patterns for these substrates with $Eu(FOD)_3$ are characteristic of a contact interaction attributed to the π-spin density.[6] For pyridine derivatives, several workers have observed ^1H shifts induced by $Ln(DPM)_3$ and $Ln(FOD)_3$ (Ln=lanthanide ion).[3,7-9] These shifts were interpreted approximately in terms of a pseudo-contact interaction by all these authors[3,7,8] except for Mackie *et al.*,[9] who showed that a contact mechanism made the major contribution to the observed shifts induced by $Eu(DPM)_3$ in γ-picoline. The large ^1H isotropic shifts observed in the complexes of Pr^{3+} and Nd^{3+} (nitrates and perchlorates) with some pyridine derivatives were interpreted as originating from both contact and pseudo-contact terms of nearly equal magnitudes, but of opposite signs.[10] Also for quinoline, the observed ^1H shifts induced by some lanthanide chelates, $Ln(DPM)_3$, could be explained approximately by a pseudo-contact term.[7,11] Huber *et al.* tentatively took account of the contact-term contribution through π-bonding by using the Hückel spin distribution of the quinoline anion radical; they obtained better predicted values, but the agreement was not good.[11]

On the other hand, we have previously reported that the observed ^{13}C paramagnetic shifts induced by two lanthanide chelates, $Ln(DPM)_3$ and $Ln(FOD)_3$, in pyridine and β-picoline include a large contact term which does not arise through π-bonding.[8] Thus, further data on the ^{13}C shifts are required for the interpretation of a spin-delocalization mechanism in such a system. We wish to report here on the ^{13}C shifts induced by $Eu(DPM)_3$ and $Pr(DPM)_3$ in acridine, quinoline, and isoquinoline, discussing the contact-shift patterns in these ligand compounds.

Experimental

Quinoline and isoquinoline were purified by vacuum distillation, and acridine, by recrystallization from ethanol. CCl_4 was used as the solvent. $Eu(DPM)_3$ and $Pr(DPM)_3$ were obtained from Dojindo Co., Ltd., Research Laboratories, and were dried before use. Particular care was taken for all the substrates used to ensure anhydrous conditions, since the observed shifts are very sensitive to traces of moisture. The solutions were *ca.* 1.1 M in acridine and *ca.* 1.4 M in quinoline and isoquinoline for ^{13}C, and *ca.* 0.6 M for ^1H. The amount of the lanthanide complex was continuously varied up to a complex-substrate molar ratio of 0.2.

The ^{13}C spectra were recorded at 22.63 MHz with a Hitachi R-22 spectrometer with an R-228 proton wide-band decoupler and an A-1600A signal-averaging analyzer at a probe temperature of 35 °C, and the ^1H spectra, with a Hitachi R-20A spectrometer at 60 MHz at a probe temperature of 34 °C, both spectrometers operating in the frequency-swept mode.

Results and Discussion

The observed ^1H and ^{13}C shifts for these compounds

1) C. C. Hinckley, *J. Amer. Chem. Soc.*, **91**, 5160 (1969).
2) Sometimes referred to as a pseudo-contact interaction.
3) W. DeW. Horrocks, Jr., J. P. Sipe, III, *J. Amer. Chem. Soc.*, **93**, 6800 (1971).
4) It is considered that a large contact-term contribution is included in the lanthanide-induced shift of the ^{14}N resonance of pyridine, from the experimental fact that a shift ratio $S(Yb)/S(Eu)$ in the ^{14}N resonance[20] disagrees largely with those in the proton resonances in pyridine.[7]
5) J. Briggs, F. A. Hart, G. P. Moss, and E. W. Randall, *Chem. Commun.*, **1971**, 364; J. Briggs, F. A. Hart, and G. P. Moss, *ibid.*, **1970**, 1506; R. J. Cushley, D. R. Anderson, and S. R. Lipsky, *ibid.*, **1972**, 636; M. Kainosho, K. Ajisaka, and K. Tori, *Chem. Lett.*, **1972**, 1061.
6) B. F. G. Johnson, J. Lewis, P. McArdle, and J. R. Norton, *Chem. Commun.*, **1972**, 535.
7) J. Reuben and J. S. Leigh, Jr., *J. Amer. Chem. Soc.*, **94**, 2789 (1972).
8) M. Hirayama, E. Edakawa, and Y. Hanyu, *Chem. Commun.*, **1972**, 1343.
9) R. K. Mackie and T. M. Shepherd, *Org. Magn. Resonance*, **4**, 557 (1972).
10) E. R. Birnbaum and T. Moeller, *J. Amer. Chem. Soc.*, **91**, 7274 (1969).
11) H. Huber and C. Pascual, *Helv. Chim. Acta*, **54**, 913 (1971).

Table 1. Comparisons of the observed lanthanide-induced shifts and the pseudo-contact contributions

Compound	Position	S_{obsd} (Eu)[a]	S_{obsd} (Pr)[a]	$\frac{S_{obsd}(Eu)}{S_{obsd}(Pr)}$	S_{pcs} (Eu)[c]	S_{pcs} (Pr)[c]
Acridine	1H	−20.1	+56.1	−0.36	−20.91	+55.38
	2H	− 3.1	+ 6.5	−0.48	− 1.51	+ 6.75
	3H	− 3.1	+ 6.5	−0.48	− 2.52	+ 6.75
	4H	− 4.3	+ 8.8	−0.49	− 4.16	+ 9.59
	10H	− 6.2	+ 9.3	−0.67	− 5.42	+12.07
	1C	−40.7	+47.0	−0.87	−16.88	+37.28
	2C	− 6.0	+ 8.5	−0.71	− 5.67	+14.91
	3C	− 4.8	+ 8.0	−0.60	− 4.54	+10.65
	4C	−12.2	+13.5	−0.90	− 6.05	+13.14
	10C	−18.7	+13.0	−1.44	−11.47	+17.75
	11C	+ 2.3	+13.0	+0.18	−10.84	+22.01
	12C	−38.0	+49.5	−0.77	−23.06	+43.67
Quinoline	2H	−27.0	+61.6	−0.44	−25.68	+57.25
	3H	− 8.1	+18.2	−0.45	− 9.84	+21.94
	4H	− 8.6	+14.2	−0.61	− 7.92	+17.65
	5H	− 6.2	+ 9.8	−0.63	− 6.02	+13.42
	6H	− 4.5	+ 8.4	−0.54	− 3.84	+ 8.57
	7H	− 3.2	+ 8.4	−0.38	− 2.63	+ 5.86
	8H	−23.1	+52.6	−0.44	−24.19	+53.93
	2C	−85.0	+94.0	−0.90	−31.12	+69.40
	3C	− 5.5	+27.3	−0.20	−15.64	+34.87
	4C	−21 0	+24.7	−0.85	−12.47	+27.79
	5C	− 8.5	+16.0	−0.53	− 8.55	+19.05
	6C	− 8.5	+11.3	−0.75	− 6.61	+14.73
	7C	−15.0	+20.7	−0.72	− 8.25	+18.40
	8C	−45.0	+54.0	−0.83	−22.78	+50.78
	9C	−39.5	+70.7	−0.56	−31.12	+69.40
	10C	+ 2.5	+33.0[b]	+0.08[b]	−15.64	+34.87
Isoquinoline	1H	−39.5	+72.3	−0.55	−41.02	+71.01
	3H	−43.7	+71.6	−0.61	−41.02	+71.01
	4H	−14.0	+25.4	−0.55	−15.71	+27.19
	5H	− 8.8	+14.1	−0.62	− 8.76	+15.16
	6H	− 5.2	+ 8.6	−0.60	− 5.60	+ 9.69
	7H	− 5.2	+ 8.6	−0.60	− 5.41	+ 9.36
	8H	− 8.8	+14.1	−0.62	− 9.94	+17.14
	1C	−93.6	+102.5	−0.91	−60.46	+104.67
	3C	−80.5	+99.8	−0.81	−60.46	+104.67
	4C	+ 1.7	+27.5	+0.06	−26.65	+46.13
	5C	− 4.7	+10.7	−0.44	−11.28	+19.52
	6C	−11.0	+10.4	−1.06	− 8.06	+13.95
	7C	− 1.7	+ 9.4	−0.18	− 8.25	+14.28
	8C	−11.0	+12.6	−0.87	−13.38	+23.16
	9C	+10.9	+22.8	+0.48	−26.65	+46.13
	10C	−29.0	+25.2	−1.15	−21.73	+37.62

a) S is the lanthanide-induced shift in ppm obtained by linear extrapolation to a complex-substrate ratio of 1.0. Negative signs designate shifts to lower field.
b) The large errors may be involved in these values, owing to the weak intensities of spectral lines.
c) The pseudo-contact contributions.

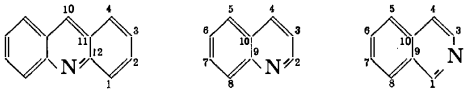

are listed in Table 1.[12] The spectral assignments made by Pugmire *et al.*[13] were used here, those for ^1H being quite consistent with those made from the observed splitting patterns. On the assumption that

12) In the course of this work, ^{13}C lanthanide-induced shift data for quinoline have been reported, which are quite similar to our data. See, A. A. Chalmers and K. G. R. Pachler, *Tetrahedron Lett.*, **1972**, 4033.

13) R. J. Pugmire, D. M. Grant, M. J. Robins, and R. K. Robins, *J. Amer. Chem. Soc.*, **91**, 6381 (1969).

the geometries of the adducts of $Eu(DPM)_3$ and $Pr(DPM)_3$ are identical, the $S_{obsd}(Eu)/S_{obsd}(Pr)$ ratio should be constant over all the positions in a ligand substrate if both $S_{obsd}(Eu)$ and $S_{obsd}(Pr)$ arise only from a pseudo-contact interaction. Table 1 shows that while the ratios for ^1H are approximately constant, those for ^{13}C are quite variable, and, furthermore, that the shifts of ^{13}C in the β-position to nitrogen (β-^{13}C) induced by $Eu(DPM)_3$ are positive in all three substrates (they are negative, but very small in the 3 position of quinoline). Thus, it is apparent from the present data that the contact-term contributions to the ^1H shifts by both $Eu(DPM)_3$ and $Pr(DPM)_3$ are very small, while those to the ^{13}C shifts are much larger when affected by $Eu(DPM)_3$ than by $Pr(DPM)_3$; this is consistent with the result for pyridine[8] with respect to the dependence of the contact-term contribution on a lanthanide chelate.

It has been recently found that this kind of lanthanide chelate adduct is not axially symmetric;[14] consequently, information is not obtainable concerning the location of its principal magnetic axis.[15] Therefore, the use of the so-called geometric factor $(3\cos^2\theta-1)/r^3$ in the calculation of pseudo-contact shifts, as is commonly done, is essentially inappropriate.[16] However, in the present estimation of a relative pseudo-contact term, this approximation is adopted, because such an approximation of an axial symmetry has successfully been used for a number of systems by many workers. Calculations done while changing the N–Eu(Pr) distance led to a good agreement of the relative geometric factors (R) with the relative observed ^1H shifts obtained with both $Pr(DPM)_3$ and $Eu(DPM)_3$ at 4.5 Å[17] for acridine, at 3.6 Å for quinoline, and at 3.0 Å for isoquinoline.[18] For ^{13}C, the agreement is, however, not good, particularly with $Eu(DPM)_3$. These results substantiate the above expectation that ^1H shifts can be approximately explained only with a pseudo-contact interaction.[19] Therefore, a proportionality constant (A) fitting $S_{pcs}(^1H)=A\times R$ to $S_{obsd}(^1H)$, was calculated by the least-squares technique. On the reasonable assumption that $S_{obsd}=S_{pcs}+S_{cs}$, the S_{cs} values for ^1H and ^{13}C were estimated as the differences in the S_{obsd} values and the S_{pcs} values calculated by using the A values. Hence, the S_{cs} values for ^1H should be small. The calculated results are listed in Table 2 only for $Eu(DPM)_3$ for a reason to be given below.

Since the S_{cs} values of ^{13}C induced by $Pr(DPM)_3$ are relatively small, these magnitudes are extremely sensitive to even small variations in A and to the molecular geometry of the ligand substrate; consequently,

Table 2. Comparisons of the contact contributions and the relative calculated contact terms

Compound	Position	$S_{cs}(Eu)$[a]	R_π[b]	R'_π[c]	R_σ[d]
Acridine	1H	+ 0.82	+ 0.18	+0.16	
	2H	− 1.59	+ 0.18	+0.07	
	3H	− 0.58	− 0.14	−0.04	
	4H	− 0.14	+ 0.29	+0.15	
	10H	− 0.78	+ 0.62	+0.25	
	1C	−23.82	− 1.00	−1.00	
	2C	− 0.33	− 0.99	−0.16	
	3C	− 0.26	+ 2.01	+0.74	
	4C	− 6.15	− 2.17	−0.96	
	10C	− 7.23	− 3.87	−1.49	
	11C	+13.14	+ 1.92	+0.63	
	12C	−14.94	+ 1.93	+1.66	
Quinoline	2H	− 1.32	+ 1.00	+0.07	−1.39
	3H	+ 1.74	+ 0.03	+0.06	−0.39
	4H	− 0.68	+ 2.31	+0.34	−0.35
	5H	− 0.18	+ 1.51	+0.32	−0.25
	6H	− 0.66	+ 0.10	+0.10	+0.03
	7H	− 0.57	+ 0.49	+0.08	−0.04
	8H	+ 1.09	+ 1.15	+0.34	-0.00_3
	2C	−53.88	+ 1.00	+1.00	+1.00
	3C	+10.14	+ 7.79	+0.56	−2.09
	4C	− 8.53	−15.12	−2.09	+0.50
	5C	+ 0.05	−10.00	−1.90	−0.06
	6C	− 1.89	+ 4.09	+0.30	−0.13
	7C	− 6.75	+ 0.01	+0.57	+0.19
	8C	−22.22	− 6.46	−2.02	−0.98
	9C	− 8.38	+ 7.90	+1.91	+0.39
	10C	+18.14	+10.72	+1.91	−1.52
Isoquinoline	1H	+ 1.52	+ 0.26	+0.27	−1.11
	3H	− 2.68	− 0.02	+0.06	−0.97
	4H	+ 1.71	+ 0.16	+0.32	−0.31
	5H	− 0.04	+ 0.14	+0.30	+0.02
	6H	+ 0.40	+ 0.07	+0.10	−0.02
	7H	+ 0.21	0	+0.03	−0.04
	8H	+ 1.14	+ 0.20	+0.30	−0.03
	1C	−33.14	− 1.00	−1.00	+1.00
	3C	−20.04	+ 0.71	+0.22	+0.54
	4C	+28.35	− 1.11	−1.95	−1.21
	5C	+ 6.58	− 0.77	−1.71	−0.22
	6C	− 2.94	− 0.10	+0.14	+0.12
	7C	+ 6.55	+ 0.65	+0.74	−0.18
	8C	+ 2.38	− 1.33	−1.91	−0.04
	9C	+37.55	+ 1.26	+1.55	−1.59
	10C	− 7.27	+ 0.77	+1.57	+0.27

a) The contact contributions, $S_{obsd}-S_{pcs}$.
b) The relative π-contact terms estimated from a spin-density distribution of the anion radical.
c) The relative π-contact terms estimated from a spin-density distribution of the cation radical.
d) The relative σ-contact terms, Ref. 21.

14) W. DeW. Horrocks, Jr., J. P. Sipe, III, and J. R. Luber, *ibid.*, **93**, 5258 (1971); R. E. Cramer and K. Seff, *Chem. Commun.*, **1972**, 400.
15) C. L. Honeybourne, *Tetrahedron Lett.*, **1972**, 1095.
16) G. N. La Mar, W. DeW. Horrocks, Jr., and L. C. Allen, *J. Chem. Phys.*, **41**, 2126 (1964).
17) For $Eu(DPM)_3$, a further better agreement was obtained with 3.8 Å.
18) This Ln–N distance for quinoline is approximately equal to those by Reuben *et al.* and Huber *et al.*, and that for isoquinoline is also quite similar to that by Huber *et al.*
19) Such a lack of the contact contribution in ^1H shifts is consistent with the results due to Reuben *et al.*[7] and Huber *et al.*,[11] but is inconsistent with the consideration on the γ-picoline–$Eu(DPM)_3$ system due to Mackie *et al.*[9] This may be attributed to that they have not taken account of the difference of a pseudo-contact shift contribution between γ-picoline and 2,4,6-trimethylpyridine arising from the difference of N–Eu distances based on steric hindrance. Relatively large contact shifts observed by Birnbaum *et al.* for some lanthanide complexes may be ascribed to a very short Ln–N distance.[10]

the intrinsic pattern of ^{13}C contact shifts was difficult to identify for the three ligand compounds. However, those induced by $Eu(DPM)_3$ are not greatly dependent on these parameters; hence, a pattern mode with marked features was commonly found for the three ligands; the patterns are downfield for α- and γ-^{13}C, and for the ^{13}C nearest to the Eu ion in the adjacent ring, and upfield for β-^{13}C, the contact-term contributions being comparatively small in the other positions. The spin-density distributions obtained from these contact shift patterns are shown in Fig. 1. It can thus

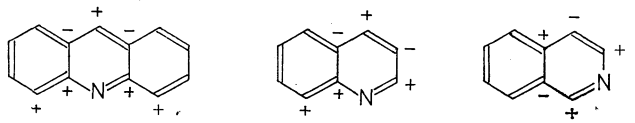

Fig. 1. The spin-density distributions induced by $Eu(DPM)_3$.

be assumed from the sign alternation in the pyridine ring that a negative spin induced by the Eu ion onto the nitrogen atom is transmitted through σ-bonds by means of a spin-polarization mechanism. Although this assumption is consistent with the observed large upfield shift of the ^{14}N resonance line induced by $Eu(DPM)_3$,[20] the sign alternation is opposite to that observed for the quinoline- and isoquinoline-$Ni(AcAc)_2$ systems, where the σ-contact shift term has already been shown to be the main contributor to the paramagnetic shifts.[21] Furthermore, the large positive spin density at C-1 in acridine and C-8 in quinoline cannot yet be reasonably explained.

Then, assuming that the contact shift term arises only through π-bonds (S_π), the relative π-contact terms (R_π) were tentatively estimated. First, the hyperfine splitting constants, a^C and a^H, were calculated from McLachlan's spin distribution[22] in the anion radicals of these compounds by using the approximation that the bonding orbital formed between an f-orbital on Eu containing an unpaired electron and a π^*-MO of a ligand substrate may be regarded as the π^*-MO itself. The following values for σ-π interaction parameters in the McConnell and the Karplus-Fraenkel equations[23] were used:

$Q^H_{CH}=-23.0$ G in the equation, $a^H=Q^H_{CH}\rho^\pi_C$;

$Q^C_{CN}=4.0$ G, $Q^C_{NC}=-20.5$ G,[24] and the generally-used values for S^C, $Q^C_{CC'}$, $Q^C_{C'C}$, and Q^C_{CH} in the equation,

$$a^C=(S^C+\sum_i Q^C_{CX_i})\rho^\pi+\sum_i Q^C_{X_iC}\rho^\pi_i.$$

Secondly, the R_π values were estimated from the contact-shift equation and the relation $\gamma_H/\gamma_C=ca.\ 4$. The calculated results are listed in Table 2. An attempt was also made to estimate the ^{13}C shifts from the spin-density distribution of the cation radical (Table 2). It is apparent from Table 2 that the ^{13}C contact shifts can be explained neither by a π-contact interaction nor by a suitable combination of σ- and π-contact terms. Although the spin-transfer mechanism is still under investigation, together with the diamagnetic induction effect, we assume that a positive spin induced directly by the Eu ion to α-^{13}C and the ^{13}C nearest to the Eu ion contributes to the ^{13}C paramagentic shift induced by $Eu(DPM)_3$.

20) M. Witanowski, L. Stefaniak, H. Januszewski, and Z. W. Wolkowski, *Tetrahedron Lett.*, **1971**, 1653.
21) I. Morishima, K. Okada, and T. Yonezawa, *J. Amer. Chem. Soc.*, **94**, 1425 (1972).
22) A. D. McLachlan, *Mol. Phys.*, **3**, 233 (1960).
23) M. Karplus and G. K. Fraenkel, *J. Chem. Phys.*, **35**, 1312 (1961).
24) A. H. Maki and E. W. Stone, *ibid.*, **39**, 1653 (1963).

The Microwave Spectrum and Quadrupole Coupling Constant Tensor of Bromomethylsilane

Michiro HAYASHI and Kazunori KUWADA

Department of Chemistry, Faculty of Science, Hiroshima University, Higashi-sendamachi, Hiroshima 730

(Received March 26, 1973)

The microwave spectra of four isotopic species of bromomethylsilane have been measured, *viz.*, the ^{79}Br and ^{81}Br species of $BrCH_2SiH_3$ and $BrCH_2SiD_3$. The observed rotational constants have been well explained by a model of which the structural parameters have been transferred from the corresponding parameters determined for ethylbromide and chloromethylsilane. The principal quadrupole coupling constants have been determined through the analysis of the first- and second-order effects of quadrupole coupling on the hyperfine structure of the observed spectra. It was concluded, within the experimental error, that the quadrupole coupling constants tensor of this molecule has the cylindrical symmetry around the largest principal axis, the direction of which coincides approximately with the C–Br internuclear line.

The microwave spectra of ethyl chloride and chloromethylsilane had been investigated by Schwendeman and Jacobs.[1,2] Their works were concerned with the r_s structure, the quadrupole coupling constants and the barrier to the internal rotation of these molecules. Wagner, Dailey, and Solimene[3] had investigated the microwave spectrum of ethyl bromide in relation to the diagonal components of the quadrupole coupling constant tensor referred to the principal inertial axes of the molecule.

Flanagan and Pierce[4] had reinvestigated the microwave spectrum of ethylbromide in order to determine the r_s structure, the barrier to the internal rotation and the quadrupole coupling constant tensor. They had found that in the limit of the first-order quadrupole coupling theory certain transitions show anomalous hyperfine splittings which are removed when the second-order quadrupole coupling effects are considered.

The present work is concerned with the investigation of the microwave spectrum of the ^{79}Br and ^{81}Br species of $BeCH_2SiH_3$ and $BrCH_2SiD_3$.

The approximate molecular structure had been estimated from the observed rotational constants and the quadrupole coupling tensor has been determined from the hyperfine splittings of the spectra. One of our interests on bromomethylsilane was on the barrier height of the internal rotation. Lowe and Parr[5] had estimated the barrier of this molecule to be roughly equal to that for chloromethylsilane (2550 cal/mol) by their semi-empirical theory. However, our preliminary calculations had indicated that the splittings of the spectra due to the internal rotation in the ground and first excited torsional states may be much smaller ($<$0.3 MHz) than the resolving power of our instrument for the transitions with $J<15$ if the barrier is higher than about 2000 cal/mol. As no spectra had actually been observed with the splitting due to the internal rotation, the barrier height cannot be determined at present.

Experimental

The samples of bromomethylsilane and its deuterated species were prepared by the reaction of $SiBr_4$ and diazomethane in ethylether and by the reduction of the resultant $BrCH_2SiBr_3$ with $LiAlH_4$ or $LiAlD_4$ in *n*-butylether.[6]

The microwave spectra of the samples were measured in the region from 8500 to 36000 MHz with conventional sinusoidal and square wave Stark modulation spectrometers at the temperature of dry ice.

Spectra and Analysis

Bromomethylsilane is a slightly asymmetric prolate top molecule with a plane of symmetry perpendicular to the largest moment of inertia. Both "a" and "b" type transitions have been observed. Both ^{79}Br and ^{81}Br have nuclear spin of 3/2, so that for each transition of every species, there are four comparatively intense hyperfine components except for the low J transitions, under the rule of $\Delta F=\Delta J$.

As is shown in Tables 1 and 6, these quartets exhibit more or less asymmetry of the splittings. Since the first-order perturbation theory predicts that for the transitions having $J>3$ the four hyperfine components will appear as two doublets with the equal splitting, the observed asymmetry of the splittings suggests that the perturbation treatment should be extended at least up to the second-order in the analysis of the quadrupole coupling effect.

For the quadrupole coupling tensor in the principal inertial axes system, χ_{ab} is alone the non-zero off-diagonal element from the molecular symmetry. The second-order effects on the hyperfine structure of the spectra, therefore, depend mainly on $|\chi_{ab}|$ when at least one of the energy levels of the transitions is in near degeneracy with the other levels. Since $|\chi_{ab}|$ is estimated to be relatively large, the rotational states within about 30000 MHz can affect with each other beyond the experimental error. Since the second-order perturbation sums relating to χ_{ab} contain the matrix element of $\Phi_{za}\Phi_{zb}$, the sums vanish unless the direct

1) R. H. Schwendeman and G. D. Jacobs, *J. Chem. Phys.*, **36**, 1245 (1962).
2) R. H. Schwendeman and G. D. Jacobs, *ibid.*, **36**, 1251 (1962).
3) R. S. Wagner, B. P. Dailey, and N. Solimene, *ibid.*, **26**, 1593 (1957).
4) C. Flanagan and L. Pierce, *ibid.*, **38**, 2963 (1963).
5) J. P. Lowe and R. G. Parr, *ibid.*, **44**, 3001 (1966).
6) D. Seyferth and E. G. Rochow, *ibid.*, **77**, 907 (1955).

TABLE 1. THE COMPARISON OF THE OBSERVED AND CALCULATED FREQUENCIES OF HYPERFINE COMPONENTS OF BROMOMETHYLSILANE IN MHz

Transition[a]	$^{79}BrCH_2SiH_3$					$^{81}BrCH_2SiH_3$				
		$(\nu-\nu_0)$[b]					$(\nu-\nu_0)$[b]			
	Obsd	Obsd	Calcd	Contribution (1)[c]	Contribution (2)[d]	Obsd	Obsd	Calcd	Contribution (1)[c]	Contribution (2)[d]
$3_{12}\leftarrow3_{03}$	18334.41	19.96	20.55	17.45	3.11	18429.47	16.71	16.60	14.57	2.03
	18380.71	−33.74	−32.74	−34.89	1.93	18384.91	−27.85	−27.83	−29.13	1.30
	18406.54	−7.91	−6.28	−10.47	4.18	18406.54	−6.22	−6.11	−8.74	2.63
	—	—	43.41	41.87	1.54	—	—	36.00	34.96	1.04
$4_{13}\leftarrow4_{04}$	18711.80	13.45	13.33	16.07	−2.74	18704.52	11.54	11.35	13.42	−2.07
	18673.27	−25.08	−25.29	−28.13	2.84	18671.45	−21.53	−21.67	−23.49	1.82
	18681.86	−16.49	−16.34	−12.63	−3.71	18679.31	−13.67	−13.41	−10.55	−2.86
	18734.79	36.44	36.60	31.57	5.03	18722.55	29.57	29.65	26.37	3.28
$5_{14}\leftarrow5_{05}$	19073.05	14.66	14.54	15.54	−1.00	19059.81	12.10	12.25	12.98	−0.72
	19030.73	−27.66	−27.61	−24.86	−2.75	19024.83	−22.88	−22.84	−20.76	−2.08
	19042.87	−15.52	−15.62	−13.47	−2.16	19035.75	−11.96	−12.81	−11.25	−1.57
	19080.99	22.60	22.78	26.93	−4.15	19066.68	18.97	19.36	22.49	−3.13
$6_{15}\leftarrow6_{06}$	19512.01	14.81	14.78	15.40	−0.62	19492.27	12.43	12.41	12.86	−0.45
	19472.99	−24.21	−24.20	−23.10	−1.10	19459.71	−20.13	−20.08	−19.29	−0.79
	19481.81	−15.39	−15.37	−14.00	−1.37	19467.24	−12.60	−12.66	−11.69	−0.97
	19519.93	22.73	22.73	24.50	−1.77	19499.01	19.17	19.19	20.46	−1.26
$7_{16}\leftarrow7_{07}$	20033.14	15.12	15.02	15.48	−0.46	20005.30	12.67	12.60	12.92	−0.32
	19995.14	−22.88	−22.88	−22.11	−0.77	19973.64	−18.99	−19.01	−18.46	−0.55
	20003.77	−14.25	−14.19	−14.46	0.27	19980.84	−11.79	−11.71	−12.07	0.36
	20040.79	22.77	22.79	23.13	−0.34	20011.82	19.19	19.19	19.31	−0.12
$8_{17}\leftarrow8_{08}$	20640.42	15.34	15.34	15.69	−0.35	20602.95	12.92	12.84	13.09	−0.25
	20602.95	−22.13	−22.21	−21.57	−0.64	20571.79	−18.24	−18.46	−18.01	−0.45
	20609.78	−15.30	−15.18	−14.90	−0.28	20577.39	−12.64	−12.63	−12.44	−0.19
	20646.81	21.73	21.70	22.36	−0.65	20608.41	18.38	18.20	18.66	−0.46
$9_{18}\leftarrow9_{09}$	21338.39	15.72	15.70	15.99	−0.29	21289.90	13.20	13.14	13.34	−0.21
	21300.73	−21.94	−21.93	−21.32	−0.61	21258.51	−18.19	−18.22	−17.79	−0.42
	21307.03	−15.64	−15.57	−15.36	−0.21	21263.67	−13.03	−12.98	−12.82	−0.16
	21344.05	21.38	21.34	21.95	−0.61	21294.54	17.84	17.88	18.32	−0.43
$10_{19}\leftarrow10_{010}$	22131.85	15.79	16.11	16.36	−0.25	22070.61	13.48	13.47	13.65	−0.18
	22093.98	−22.08	−21.95	−21.27	−0.68	22038.97	−18.16	−18.21	−17.74	−0.47
	22099.76	−16.30	−16.11	−15.84	−0.26	22043.69	−13.44	−13.40	−13.22	−0.19
	22136.94	20.88	21.02	21.78	−0.77	22074.75	17.62	17.65	18.18	−0.53
$11_{110}\leftarrow11_{011}$	23028.05	17.29	16.56	16.78	−0.22	22950.59	14.00	13.84	14.00	−0.16
	22987.66	−23.10	−22.42	−21.36	−1.06	22918.02	−18.57	−18.50	−17.81	−0.69
	22993.48	−17.28	−16.65	−16.35	−0.30	22922.58	−14.01	−13.84	−13.63	−0.21
	23031.88	21.12	20.51	21.78	−1.27	22953.98	17.39	17.35	18.18	−0.83
$4_{04}\leftarrow3_{03}$	16644.48	−2.73	−2.76	−2.76	0.00	16517.03	−2.32	−2.30	−2.30	0.00
	16642.55	−4.66	−4.51	−2.29	−2.12	16516.00	−3.35	−3.33	−1.92	−1.42
	16653.25	6.04	6.12	7.46	−1.34	16524.71	5.36	5.26	6.22	−0.96
	16650.73	3.52	3.34	6.99	−3.66	16522.80	3.45	3.48	5.83	−2.36
$4_{14}\leftarrow3_{13}$	16369.91	−5.89	−5.88	−5.99	0.11	16246.92	−4.86	−4.92	−4.99	0.08
	16378.38	2.58	2.59	2.61	−0.02	16253.90	2.12	2.16	2.18	−0.01
	16386.34	10.54	10.51	10.54	−0.03	16260.57	8.79	8.78	8.80	−0.02
	—	—	1.81	1.94	−0.14	—	—	1.53	1.63	−0.10
$4_{13}\leftarrow3_{12}$	16921.83	−9.89	−9.98	−4.13	−5.85	16792.27	−7.57	−7.54	−3.44	−4.10
	16934.98	3.26	3.16	4.47	−1.31	16802.63	2.79	2.83	3.73	−0.90
	16927.67	−4.05	−3.94	5.30	−9.24	16797.68	−2.16	−2.04	4.41	−6.45
	16928.17	−3.55	−3.47	−3.30	−0.17	16796.85	−2.99	−2.88	−2.76	−0.12
$5_{05}\leftarrow4_{04}$	20800.79	−2.29	−2.03	−2.03	0.00	20641.42	−1.80	−1.69	−1.69	0.00
	20807.42	4.34	4.43	−1.44	5.87	20646.20	2.98	2.91	−1.21	4.12
	20808.12	5.04	5.13	4.29	0.84	20647.39	4.17	4.15	3.57	0.57
	20814.94	11.86	12.67	3.70	8.96	20652.63	9.41	9.35	3.09	6.26
$5_{15}\leftarrow4_{14}$	20464.36	−3.79	−3.63	−3.85	0.22	20310.08	−3.07	−3.06	−3.21	0.15
	20468.73	0.58	0.65	0.54	0.11	20313.64	0.49	0.53	0.45	0.08
	20474.39	6.24	6.14	6.36	−0.22	20318.30	5.15	5.15	5.31	−0.16
	20470.09	1.94	1.82	1.98	−0.16	20314.76	1.61	1.54	1.65	−0.11

TABLE 1. (Continued)

$5_{14}\leftarrow4_{13}$	21162.11	−1.04	−0.82	−2.56	1.74					
	21165.12	1.97	2.11	1.83	0.28					
	21169.23	6.08	5.85	3.45	2.39					
	21162.11	−1.04	−0.72	−0.94	−0.22					
$6_{06}\leftarrow5_{05}$	24952.65	−1.51	−1.61	−1.61	0.00	24761.56	−1.31	−1.34	−1.34	0.00
	24951.65	−2.51	−2.64	−0.91	−1.73	24760.77	−2.10	−2.10	−0.76	−1.34
	24956.56	2.40	2.48	2.88	−0.40	24765.01	2.14	2.10	2.40	−0.30
	24953.52	−0.64	−0.51	2.18	−2.69	24762.59	−0.28	−0.26	1.82	−2.08
$6_{16}\leftarrow5_{15}$	24556.48	−2.71	−2.65	−2.69	0.04	24371.09	−2.16	−2.22	−2.24	0.03
	24559.07	−0.12	−0.11	−0.09	−0.01	24373.21	−0.04	−0.09	−0.08	−0.01
	24563.31	4.12	4.08	4.19	−0.12	24376.63	3.38	3.42	3.50	−0.08
	24560.69	1.50	1.54	1.60	−0.06	24374.52	1.27	1.30	1.34	−0.04
$6_{15}\leftarrow5_{14}$	25391.72	−1.43	−1.37	−1.75	0.38	25193.99	−1.17	−1.18	−1.46	0.28
	25394.02	0.87	0.77	0.85	−0.08	25195.85	0.69	0.66	0.71	−0.05
	25395.82	2.67	2.74	2.35	0.39	25197.39	2.23	2.25	1.95	0.30
	25392.61	−0.54	−0.57	−0.26	−0.31	25194.72	−0.44	−0.43	−0.22	−0.21
$8_{08}\leftarrow7_{17}$	17122.92	8.56	8.50	8.50	−0.01	16836.45	7.13	7.13	7.13	−0.00
	17100.76	−13.60	−13.61	−14.16	0.55	16817.82	−11.50	−11.47	−11.86	0.39
	17108.01	−6.35	−6.31	−7.35	1.03	16823.79	−5.53	−5.57	−6.16	0.60
	17131.09	16.73	16.75	15.31	1.44	16843.05	13.73	13.75	12.83	0.92
$9_{09}\leftarrow8_{18}$	21761.49	8.97	8.94	8.95	−0.01	21437.00	7.38	7.50	7.50	−0.00
	21739.01	−13.51	−13.43	−13.91	0.48	21418.32	−11.30	−11.32	−11.66	0.34
	21744.02	−8.50	−8.48	−8.08	−0.40	21422.58	−7.04	−7.07	−6.78	−0.29
	21767.67	15.15	15.06	14.77	0.29	21442.25	12.63	12.58	12.38	0.20
$10_{010}\leftarrow9_{19}$	26440.09	9.16	9.14	9.15	−0.01	26077.84	7.67	7.67	7.68	−0.00
	26417.84	−13.09	−13.06	−13.52	0.98	26059.19	−10.98	−11.01	−11.34	0.32
	26422.30	−8.63	−8.62	−8.49	−0.13	26062.99	−7.18	−7.22	−7.12	−0.10
	26445.53	14.60	14.63	14.18	0.45	26082.31	12.14	12.20	11.89	0.31

Transition[a]	$^{79}BrCH_2SiD_3$					$^{81}BrCH_2SiD_3$				
	Obsd	Obsd	Calcd	$(\nu-\nu_0)$[b] Contribution		Obsd	Obsd	Calcd	$(\nu-\nu_0)$[b] Contribution	
				(1)[c]	(2)[d]				(1)[c]	(2)[d]
$4_{13}\leftarrow4_{04}$	15126.24	14.68	14.80	16.41	−1.61	15123.00	12.28	12.50	13.66	−1.16
	15066.55	−45.01	−45.66	−28.72	−16.94	15069.32	−41.40	−41.62	−23.91	−17.71
	—	—	−20.14	−12.90	−7.24	—	—	−17.38	−10.74	−6.65
	15116.68	5.12	4.87	32.24	−27.37	15109.51	−1.21	−1.82	26.84	−28.66
$5_{14}\leftarrow5_{05}$	15421.53	15.09	15.07	15.94	−0.87	15413.79	12.70	12.66	13.27	−0.62
	15379.32	−27.12	−27.25	−25.51	−1.74	15378.64	−22.45	−22.49	−21.24	−1.25
	15390.88	−15.56	−15.74	−13.82	−1.93	15388.16	−12.93	−12.87	−11.50	−1.36
	15431.52	25.08	24.89	27.63	−2.74	15422.16	21.07	21.04	23.01	−1.97
$6_{15}\leftarrow6_{06}$	15781.36	15.27	15.25	15.85	−0.60	15767.70	12.58	12.77	13.20	−0.42
	15741.12	−24.97	−24.80	−23.78	−1.02	15734.56	−20.56	−20.52	−19.80	−0.73
	15746.79	−19.30	−19.26	−14.41	−4.85	15741.12	−14.00	−14.25	−12.00	−2.25
	15787.63	21.54	21.15	25.22	−4.07	15774.11	18.99	18.93	21.00	−2.07
$7_{16}\leftarrow7_{07}$	16208.53	15.53	15.51	15.97	−0.46	16188.14	12.97	12.97	13.30	−0.33
	16169.51	−23.49	−23.62	−22.81	−0.81	16155.66	−19.51	−19.56	−18.99	−0.57
	16177.64	−15.36	−15.28	−14.92	−0.37	16162.46	−12.71	−12.67	−12.42	−0.25
	16216.01	23.01	23.03	23.87	−0.84	16194.48	19.31	19.29	19.87	−0.58
$8_{17}\leftarrow8_{08}$	16706.60	15.84	15.84	16.22	−0.38	16678.09	13.23	13.23	13.50	−0.22
	16667.80	−22.96	−23.07	−23.30	−0.77	16645.71	−19.15	−19.10	−18.56	−0.54
	16675.06	−15.70	−15.69	−15.41	−0.28	16651.85	−13.01	−13.04	−12.82	−0.21
	16713.03	22.27	22.31	23.11	−0.80	16683.60	18.74	18.67	19.24	−0.56
$9_{18}\leftarrow9_{09}$	17279.11	16.17	16.24	16.55	−0.31	17241.21	13.53	13.56	13.78	−0.22
	17240.09	−22.85	−22.96	−22.07	−0.89	17208.83	−18.85	−18.97	−18.37	−0.60
	17246.69	−16.25	−16.24	−15.90	−0.34	17214.20	−13.48	−13.47	−13.24	−0.24
	17284.64	21.70	21.69	22.72	−1.03	17245.82	18.14	18.21	18.91	−0.70
$10_{19}\leftarrow10_{010}$	17930.44	16.68	16.68	16.95	−0.27	17881.53	13.90	13.92	14.11	−0.19
	17890.16	−23.60	−23.73	−22.04	−1.69	17848.26	−19.37	−19.40	−18.34	−1.06

TABLE 1. (Continued)

	17896.94	−16.82	−16.81	−16.42	−0.39	17853.73	−13.90	−13.93	−13.66	−0.27
	17934.25	20.49	20.51	22.58	−2.06	17885.11	17.48	17.49	18.78	−1.29
$11_{110}\leftarrow 11_{011}$	18664.89	17.06	17.16	17.41	−0.24	18603.36	14.11	14.31	14.48	−0.17
	18627.66	−20.17	−20.24	−22.15	1.91	18572.80	−16.45	−16.64	−18.43	1.79
	18630.46	−17.37	−17.19	−16.95	−0.24	18574.96	−14.29	−14.30	−14.10	−0.16
	18672.87	25.04	24.90	22.61	2.29	18610.20	20.95	20.95	18.80	2.15
$4_{04}\leftarrow 3_{03}$	15239.76	−2.61	−2.71	−2.71	0.00	15118.74	−2.09	−2.25	−2.25	0.00
	15257.33	14.96	16.25	−2.22	18.47	—	—	16.90	−1.85	18.74
	15254.05	11.68	11.98	7.31	4.67	15131.39	10.56	10.82	6.06	4.75
	15279.93	37.56	37.11	6.82	30.29	—	—	36.28	5.66	30.62
$4_{14}\leftarrow 3_{13}$	15013.37	−6.21	−5.80	−5.91	0.11					
	15021.57	1.99	2.38	2.51	−0.13					
	15030.44	10.86	10.40	10.47	−0.07					
	15021.57	1.99	1.73	2.05	−0.33					
$4_{13}\leftarrow 3_{12}$						15359.31	9.23	13.11	−3.30	16.41
						15358.15	8.07	7.94	3.68	4.26
						15383.43	33.35	30.84	4.16	26.68
						15347.59	−2.49	−3.08	−2.83	−0.25
$5_{05}\leftarrow 4_{04}$	19044.65	−2.38	−2.00	−2.00	0.00	18894.62	−2.49	−1.66	−1.66	0.00
	19033.63	−13.40	−16.49	−1.39	−15.11	18881.03	−16.08	−17.55	−1.15	−16.39
	19046.89	−0.14	−0.26	4.31	−4.48	18895.57	−1.54	−1.16	3.49	−4.65
	19023.57	−23.46	−21.33	3.59	−24.93	—	—	−23.92	2.99	−26.90
$5_{15}\leftarrow 4_{14}$	18768.83	−3.65	−3.57	−3.80	0.24	18623.04	−3.11	−2.99	−3.16	0.17
	18772.99	0.51	0.59	0.50	0.10	18626.53	0.38	0.48	0.41	0.07
	18778.54	6.06	6.03	6.32	−0.28	18631.30	5.15	5.05	5.25	−0.19
	18774.37	1.89	1.81	2.02	−0.21	18627.80	1.65	1.53	1.68	−0.14
$5_{14}\leftarrow 4_{13}$	19340.03	−1.67	−1.73	−2.47	0.75	19185.46	−1.61	−1.50	−2.05	0.55
	19343.71	2.01	1.92	1.83	0.08	19188.64	1.57	1.59	1.52	0.07
	19345.97	4.27	4.13	3.29	0.84	19190.58	3.51	3.36	2.72	0.63
	19340.03	−1.67	−1.31	−1.10	−0.30	19185.95	−1.12	−1.05	−0.85	−0.21
$6_{06}\leftarrow 5_{05}$	22846.83	−1.56	−1.60	−1.60	0.00	22666.98	−1.25	−1.32	−1.32	0.00
	22846.83	−1.56	−1.59	−0.86	−0.73	22666.98	−1.25	−1.25	−0.72	−0.54
	22850.91	2.52	2.60	2.84	−0.23	22670.38	2.15	2.18	2.35	−0.17
	22849.31	0.92	0.90	2.10	−1.20	22669.13	0.90	0.87	1.74	−0.88
$6_{16}\leftarrow 5_{15}$	22522.29	−2.73	−2.65	−2.66	0.01	22347.25	−2.17	−2.20	−2.21	0.01
	22524.91	−0.11	−0.15	−0.11	−0.04	22349.33	−0.09	−0.13	−0.10	−0.03
	22528.67	3.65	3.56	4.16	−0.60	22352.50	3.08	3.09	3.46	−0.37
	22526.23	1.21	1.28	1.61	−0.34	22350.49	1.07	1.14	1.34	−0.21
$6_{15}\leftarrow 5_{14}$	23206.52	−1.41	−1.42	−1.69	0.27	23021.05	−1.18	−1.21	−1.40	0.19
	23208.81	0.88	0.86	0.87	−0.01	23022.95	0.72	0.72	0.72	−0.01
	23206.68	−1.25	−0.91	2.24	−3.15	23022.95	0.72	0.81	1.86	−1.05
	23205.39	−2.54	−2.85	−0.32	−2.53	23021.05	−1.18	−1.25	−0.27	−0.98
$7_{07}\leftarrow 6_{16}$	13278.84	8.19	8.22	8.20	0.02	13043.14	6.91	6.88	6.87	0.02
	13256.58	−14.07	−14.12	−14.84	0.71	13024.39	−11.84	−11.90	−12.40	0.50
	13264.77	−5.88	−5.86	−6.57	0.70	13031.10	−5.13	−5.06	−5.50	0.44
	13288.45	17.80	17.85	16.47	1.38	13050.88	14.65	14.70	13.76	0.94
$8_{08}\leftarrow 7_{17}$	17442.08	8.93	8.96	8.97	−0.01	17171.53	7.53	7.50	7.51	−0.01
	17418.91	−14.24	−14.18	−14.78	0.60	17152.10	−11.90	−11.94	−12.36	0.42
	17424.80	−8.35	−8.32	−7.79	−0.53	17157.05	−6.95	−6.91	−6.53	−0.39
	17449.55	16.40	16.33	15.96	0.37	17177.55	13.55	13.59	13.34	0.25
$9_{09}\leftarrow 8_{18}$	21642.25	9.40	9.38	9.39	−0.01	21336.62	7.83	7.86	7.86	−0.01
	21618.86	−13.99	−13.92	−14.49	0.57	21317.07	−11.72	−11.72	−12.12	0.40
	21624.13	−8.72	−8.67	−8.51	−0.16	21321.58	−7.21	−7.24	−7.13	−0.11
	21648.85	16.00	15.95	15.37	0.58	21342.02	13.23	13.25	12.85	0.40

a) The frequencies of the hyperfine components of the transitions are shown in the order of $F'\leftarrow F=(J'+3/2\leftarrow J+3/2)$, $(J'+1/2\leftarrow J+1/2)$, $(J'-1/2\leftarrow J-1/2)$, $(J'-3/2\leftarrow J-3/2)$ where J' and J indicate the rotational quantum number of the higher and lower energy levels of the transition, respectively. The dash indicates that the component of the quartet is actually either completely obscured by the other spectra or defectively resolved from the other spectra.

b) The frequency difference of the hyperfine component (ν) and the hypothetical unsplit frequency (ν_0) of the transition.

c) The contribution to $\nu-\nu_0$ from the first-order theory.

d) The contribution to $\nu-\nu_0$ from the second-order theory.

Table 2. Hypothetical unsplit frequencies (ν_0) of bromomethylsilane in MHz

Transition	$^{79}BrCH_2SiH_3$	$^{81}BrCH_2SiH_3$	$^{79}BrCH_2SiHD_3$	$^{81}BrCH_2SiD_3$
$3_{12}\leftarrow 3_{03}$	18414.45 (0.32)[a]	18412.76 (−0.15)		
$4_{13}\leftarrow 4_{04}$	18698.35 (−0.21)	18692.98 (−0.16)	15111.56 (0.05)	15110.72 (0.06)
$5_{14}\leftarrow 5_{05}$	19058.39 (−0.23)	19047.71 (−0.08)	15406.44 (−0.11)	15401.09 (−0.07)
$6_{15}\leftarrow 6_{06}$	19497.20 (−0.06)	19479.84 (0.07)	15766.09 (0.04)	15755.12 (0.09)
$7_{16}\leftarrow 7_{07}$	20018.02 (−0.00)	19992.63 (0.14)	16193.00 (0.04)	16175.17 (0.01)
$8_{17}\leftarrow 8_{08}$	20625.08 (0.10)	20590.03 (0.10)	16690.76 (0.11)	16664.86 (0.05)
$9_{18}\leftarrow 9_{09}$	21322.67 (−0.02)	21276.70 (0.19)	17262.94 (0.04)	17227.68 (0.02)
$10_{19}\leftarrow 10_{010}$	22116.06 (−0.07)	22057.13 (0.06)	17913.76 (−0.07)	17867.63 (−0.07)
$11_{110}\leftarrow 11_{011}$	23010.76 (0.11)	22936.59 (−0.24)	18647.83 (−0.07)	18589.25 (−0.02)
$4_{04}\leftarrow 3_{03}$	16647.21 (−0.25)	16519.35 (−0.24)	15242.37 (0.71)	15120.83 (−0.33)
$4_{14}\leftarrow 3_{13}$	16375.80 (−0.10)	16251.78 (−0.09)	15019.56 (0.25)	
$4_{13}\leftarrow 3_{12}$	16931.72 (−0.17)	16799.84 (0.03)		15350.08 (−0.56)
$5_{05}\leftarrow 4_{04}$	20803.08 (0.10)	20643.22 (−0.09)	19047.03 (0.17)	18897.11 (0.72)
$5_{15}\leftarrow 4_{14}$	20468.15 (0.07)	20313.15 (0.07)	18772.48 (−0.23)	18626.15 (−0.01)
$5_{14}\leftarrow 4_{13}$	21163.15 (0.11)		19341.70 (−0.19)	19187.07 (0.20)
$6_{06}\leftarrow 5_{05}$	24954.16 (−0.12)	24762.87 (−0.07)	22848.39 (−0.18)	22668.23 (−0.04)
$6_{16}\leftarrow 5_{15}$	24559.19 (0.12)	24373.25 (0.12)	22525.02 (−0.11)	22349.42 (0.05)
$6_{15}\leftarrow 5_{14}$	25393.15 (0.23)	25195.16 (0.25)	23207.93 (0.28)	23022.23 (−0.01)
$7_{07}\leftarrow 6_{16}$			13270.65 (−0.00)	13036.23 (0.12)
$8_{08}\leftarrow 7_{17}$	17114.36 (−0.04)	16829.32 (0.00)	17433.15 (0.04)	17164.00 (0.04)
$9_{09}\leftarrow 8_{18}$	21752.52 (−0.01)	21429.62 (−0.07)	21632.85 (−0.01)	21328.79 (−0.09)
$10_{010}\leftarrow 9_{19}$	26430.93 (−0.02)	26070.17 (0.00)		

a) Obsd−Calcd

Table 3. Rotational constants (MHz) and moments of inertia[a] (amu·Å^2) for bromomethylsilane

	$^{79}BrCH_2SiH_3$		$^{81}BrCH_2SiH_3$		$^{79}BrCH_2SiD_3$		$^{81}BrCH_2SiD_3$	
	Obsd	Uncertainty[b]	Obsd	Uncertainty[b]	Obsd	Uncertainty[b]	Obsd	Uncertainty[b]
A	20075.59	0.49	20064.50	0.43	16440.09	0.45	16432.87	0.34
B	2151.50	0.02	2134.48	0.02	1963.01	0.02	1947.07	0.02
C	2012.49	0.03	1997.49	0.02	1849.16	0.02	1834.91	0.02
D_J[c]	0.0017	0.0003	0.0017	0.0003	0.0012	0.0004	0.0010	0.0003
	Obsd	Calcd	Obsd	Calcd	Obsd	Calcd	Obsd	Calcd
I_a	25.1814	25.1896	25.1953	25.2030	30.7499	30.7462	30.7634	30.7591
I_b	234.9668	236.1919	236.8404	238.0784	257.5285	258.9107	259.6368	261.0310
I_c	251.1968	252.1968	253.0831	254.0957	273.3841	274.4483	275.5072	276.5805
$I_a+I_b-I_c$	8.9514	9.1847	8.9525	9.1857	14.8943	15.2087	14.8929	15.2097

a) Conversion factor; 505531 MHz·amu·Å^2.
b) The uncertainty is calculated only from 2.5 times the standard deviation of the hypothetical unsplit frequencies to fit in with the modified rigid rotor expression.
c) The coefficient of the $[J(J+1)]^2$ term, see the text.

Table 4. The comparison of structural parameters

	$BrCH_2SiH_3$[a]	$ClCH_2SiH_3$[b]		$BrCH_2CH_3$[c]	$ClCH_2CH_3$[d]
r(SiC) (Å)	1.889	1.889	r(CC) (Å)	1.518	1.520
r(CX) (Å)	1.950	1.788	r(CX) (Å)	1.950	1.788
r(CH) (Å)	1.096	1.096	r(CH)CH_2 (Å)	1.087	1.089
r(SiH) (Å)	1.477	1.477	r(CH)CH_3 (Å)	1.093	1.091
α(SiCX)	109°18′	109°18′	α(CCX)	111°2′	111°2′
α(HSiH)	110°36′	110°36′	α(HCH)CH_3	108°52′	108°31′
α(HCH)	107°30′	107°30′	α(HCH)CH_2	109°54′	109°12′
α(SiCH)	109°18′	109°18′	α(CH_3CH)	105°25′	106°35′

a) This work, b) Footnote 2, c) Footnote 4, d) Footnote 1.

TABLE 5. QUADRUPOLE COUPLING CONSTANTS[a)]

		$^{79}BrCH_2SiH_3$		$^{81}BrCH_2SiH_3$		$^{79}BrCH_2SiD_3$		$^{81}BrCH_2SiD_3$	
χ_{aa}	(MHz)	339.6	(10.6)	283.2	(8.0)	332.0	(17.6)	275.5	(13.3)
$\eta\chi_{aa}$[b)]	(MHz)	244.8	(2.4)	204.6	(1.7)	254.1	(3.1)	211.9	(2.2)
χ_{ab}	(MHz)	381.4	(10.6)	319.1	(10.1)	399.1	(11.1)	332.6	(13.7)
χ_{zz}	(MHz)	573.7	(1.1)	479.5	(2.8)	586.6	(3.9)	488.3	(1.9)
χ_{xx}	(MHz)	−281.6	(18.3)	−235.6	(15.6)	−293.5	(31.8)	−244.6	(23.0)
χ_{yy}	(MHz)	−292.2	(6.5)	−243.9	(4.8)	−293.1	(10.3)	−243.7	(7.8)
η_{bond}[c)]		0.0185	(0.043)	0.0174	(0.043)	−0.0008	(0.072)	−0.0017	(0.063)
θ_{za}[d)]		31°33′	(40′)	31°36′	(41′)	32°32′	(1°5′)	32°36′	(56′)
θ[e)]		31°57′		31°55′		32°33′		32°30′	
$\chi_{zz}^{79}/\chi_{zz}^{81}$[f)]		1.1965				1.2014			

a) a, b, and c designate the principal intertial axes and z, x, and y designate the principal axes of the χ tensor. The figure in the parentheses indicates the uncertainty calculated from the standard deviation of the splittings.
b) $\eta=(\chi_{bb}-\chi_{cc})/\chi_{aa}$
c) $\eta_{bond}=(\chi_{xx}-\chi_{yy})/\chi_{zz}$
d) θ_{za} is the angle between the "a" inertial axis of the molecule and the "z" principal axis of the χ tensor.
e) θ is the angle between the "a" inertial axis and the C–Br internuclear line.
f) The reported ratio of the quadrupole moments of ^{79}Br and ^{81}Br is 1.19707.

TABLE 6. THE OBSERVED AND CALCULATED ASYMMETRY OF THE SPLITTINGS IN MHz[a)]

Transition	$^{79}BrCH_2SiH_3$			$^{81}BrCH_2SiH_3$			$^{79}BrCH_2SiD_3$			$^{81}BrCH_2SiD_3$		
	Obsd	Calcd total	Calcd one level[b)]	Obsd	Calcd total	Calcd one level[b)]	Obsd	Calcd total	Calcd one level[b)]	Obsd	Calcd total	Calcd one level[b)]
$3_{12}\leftarrow3_{03}$	−2.38[c)]	−3.82	−5.38	−2.19[c)]	−2.31	−3.57						
$4_{13}\leftarrow4_{04}$	14.40	14.32	13.96	10.17	10.03	10.12	−37.27[c)]	−35.45	−30.72	−42.71[c)]	−38.57	−32.60
$5_{14}\leftarrow5_{05}$	−4.20	−3.74	−4.13	−4.05	−2.92	−3.31	−1.57	−1.68	−1.50	−1.15	−1.24	−1.08
$6_{15}\leftarrow6_{06}$	−0.90	−0.87	−0.89	−0.79	−0.64	−0.68	0.60	0.35	−0.54	−0.15	−0.14	0.38
$7_{16}\leftarrow7_{07}$	−0.93	−0.92	−0.39	−0.68	−0.70	−0.29	−0.65	−0.82	−0.28	−0.46	−0.57	−0.19
$8_{17}\leftarrow8_{08}$	−0.44	−0.66	−0.22	−0.14	−0.46	−0.16	−0.83	−0.94	−0.17	−0.63	−0.62	−0.12
$9_{18}\leftarrow9_{09}$	−0.64	−0.70	−0.14	−0.52	−0.49	−0.10	−1.07	−1.27	−0.11	−0.76	−0.84	−0.08
$10_{19}\leftarrow10_{010}$	−0.69	−0.93	−0.10	−0.58	−0.63	−0.07	−2.97	−3.09	−0.08	−1.89	−1.89	−0.06
$11_{110}\leftarrow11_{011}$	−1.99	−1.80	−0.07	−1.17	−1.15	−0.05	5.18	4.69	−0.06	4.68	4.26	−0.04
$4_{04}\leftarrow3_{03}$	−4.45	−4.53	−5.38	−2.94	−2.96	−3.57	43.45	44.09	37.38	—	44.61	37.14
$4_{14}\leftarrow3_{13}$	−0.18[c)]	−0.23	0.00	−0.11[c)]	−0.16	0.00	−0.67	−0.49	0.00			
$4_{13}\leftarrow3_{12}$	13.65	13.62	13.96	9.53	9.53	10.12				−37.00	−39.09	−32.60
$5_{05}\leftarrow4_{04}$	13.45	13.99	13.96	10.02	9.80	10.12	−34.34	−35.56	−30.72	−36.29[c)]	−38.65	−32.60
$5_{15}\leftarrow4_{14}$	0.07	−0.04	0.00	0.02	−0.03	0.00	−0.01	−0.07	0.00	−0.01	−0.05	0.00
$5_{14}\leftarrow4_{13}$	−4.11	−4.07	−4.13				−1.45	−1.80	−1.50	−1.45	−1.32	−1.08
$6_{06}\leftarrow5_{05}$	−4.04	−4.03	−4.13	−3.21	−3.12	−3.31	−1.25	−1.70	−1.50	−1.25	−1.25	−1.08
$6_{16}\leftarrow5_{15}$	−0.03	0.00	0.00	0.01	−0.00	0.00	0.18	0.21	0.00	0.07	0.13	0.00
$6_{15}\leftarrow5_{14}$	−0.91	−1.16	−0.89	−0.81	−0.84	−0.68	0.90	0.34	−0.54	0.00	−0.13	−0.38
$7_{07}\leftarrow6_{16}$							1.03	1.37	1.14	1.03	0.98	0.79
$8_{08}\leftarrow7_{17}$	0.92	0.97	1.01	0.63	0.72	0.75	1.58	1.52	0.87	1.07	1.07	0.60
$9_{09}\leftarrow8_{18}$	1.17	1.17	0.79	0.99	0.82	0.59	1.33	1.32	0.70	0.89	0.92	0.48
$10_{010}\leftarrow9_{19}$	0.98	1.04	0.66	0.67	0.73	0.48						

a) The definition of the asymmetry of the splittings is in Eq. (1) in the text.
b) The contribution of $\delta\nu$ from a pair of levels in near degeneracy using the formula given in Eq. (2) in the text.
c) For these transitions, since one of the components of the quartets is obscured by the other spectra, the calculated frequency is used instead of the observed one for this component.

product of the representation of the two rotational states is equal to that of $\Phi_{za}\Phi_{zb}$. Then, the direct product of the representations of the states which are able to couple with each other should be belonging to the B_c species of the four group. Therefore, the number of the rotational states having the second-order quadrupole effects is much restricted.

Since the molecule is too close to the symmetric top, the transitions having $K_{-1}>1$ become to be weak and furthermore, the K degeneracy makes the hyperfine structure analysis of the observed spectra too complicated. Therefore, the measurements were not extended to these transitions. From the observed quartets, the analysis was performed by the following procedures.

First, rough values of the rotational constants were determined by fitting the averaged frequencies of the components for each quartet to the rigid rotor expression.

Second, the asymmetry of the splitting was defined for each quartet as:

$$\delta\nu = \nu(J'+1/2\leftarrow J+1/2) + \nu(J'-3/2\leftarrow J-3/2) - \nu(J'+3/2\leftarrow J+3/2) - \nu(J'-1/2\leftarrow J-1/2) \quad (1)$$
$$= a\chi_{ab}^2 + b\chi_{aa}^2 + c\eta\chi_{aa}^2 + d\eta^2\chi_{aa}^2$$

where $\nu(J'+1/2\leftarrow J+1/2)$ indicates a component of a quartet having $F'=J'+1/2$ and $F=J+1/2$ for the higher and lower levels of the transition, respectively, and so on, and a, b, c, and d are the constants depending on the structure and the type of the transition.

Then, χ_{ab} was obtained taking average of the χ_{ab} values derived from the observed $\delta\nu$ for each quartet.

Third, the observed quartets were corrected by subtracting the contributions of the χ_{ab} terms and the hypothetical quartet patterns due to the first-order quadrupole coupling effects were obtained from which the values of χ_{aa} and $\eta(=(\chi_{bb}-\chi_{cc})/\chi_{aa})$ were determined by the least-squares technique.

Fourth, the unperturbed frequencies for the transitions were calculated by fitting the calculated frequencies of the components of the quartets including both the first- and second-order contributions with the observed.

Fifth, by the least-squares technique the rotational constants were recalculated by fitting the obtained unperturbed frequencies to the rigid rotor expression modified by the term of $-D_J[J(J+1)]^2$ of the centrifugal distortion.

The procedures were repeated until the self-consistent results were obtained. For some of the transitions small χ_{aa}^2, $\eta\chi_{aa}^2$, and $\eta^2\chi_{aa}^2$ contributions were also included in the second-order perturbation corrections. The results are shown in Tables 1, 2, 3, and 5.

Discussion

Structure. Since the observed rotational constants of a sufficient number of the isotopic species are not available, the r_s structure of the molecule cannot be obtained at present. However, when the structural parameters for this molecule are assumed to be equal to those of chloromethylsilane except r(C–Br) which is taken to be equal to that of ethylbromide, the calculated moments of inertia reproduce the observed ones within the deviation of 0.6%.

As is shown in Table 4, the structural parameters of the skeleton of ethyl chloride and bromide are found to be essentially identical except r(C–Br), while r(C–Cl) is found to be identical for ethyl chloride and chloromethylsilane. Then, it is not surprising that the above set of the structural parameters for bromomethylsilane gives an excellent agreement between the calculated and the observed moments of inertia. Therefore, this structure may be proposed as the best structure of bromomethylsilane at present.

Quadrupole Coupling Tensor. As both diagonal and off-diagonal elements of the χ tensor in the inertial principal axis system are obtained, the own principal values and the own principal axis system of the χ tensor can easily be evaluated by diagonalization. As is shown in Table 5 the asymmetry parameter η_{bond} $(=(\chi_{xx}-\chi_{yy})/\chi_{zz})$ around the axis of the largest principal value χ_{zz} is close to zero so that the charge distribution is approximately axially symmetric about the z axis within the limit of the experimental error for all of the isotopic species. The angle θ_{za} which is the angle between the z axis and the "a" inertial principal axis, is also shown and compared with the angle θ which is the angle between the C–Br internuclear line and the "a" axis calculated from the structure mentioned above. The discrepancies between θ_{za} and θ are within about 30′ and the two angles can be regarded as essentially identical.

Then, it can be concluded that the C–Br bond in this molecule seems not to be bent within the limit of the experimental error.

The magnitude of the largest principal quadrupole coupling constant χ_{zz} can be related to the ionic character of the bond.

If the d and the double-bond characters of the bond orbital are neglected, the ionic character i is found by the equation:

$$i = (1-s^2) - (\chi_{zz}/\chi_{at})$$

where s is the s character of the bond orbital and may be taken to be $s^2=0.15$. $\chi_{at}=eQq_{at}$ is the quadrupole coupling constant of the atom and is taken to be $+769.76$ MHz[7] for ^{79}Br. Then, the ionicity of the C–Br bond in bromomethylsilane is calculated to be 10%, while that for ethyl bromide is calculated to be 14%.

The ratio of the quadrupole moments between ^{79}Br and ^{81}Br are found to be 1.1965 and 1.2014 for $BrCH_2SiH_3$ and $BrCH_2SiD_3$, respectively, which give an excellent agreement with the reported value (1.19707).[8]

Asymmetry of the Splittings. As already was mentioned, the asymmetry of the splittings has been removed when the second-order quadrupole coupling effects are considered. Since bromomethylsilane is so nearly a symmetric top, the calculation of the second-order quadrupole effects can be much simplified. Furthermore, near degeneracy of the energy levels occurs usually only in a pair of the levels having relatively low J and $K_{-1}=0$ or 1, that is, the levels $J_{1,J-1}$ and J_{0J} are in near degeneracy with $(J+1)_{0,J+1}$ and $(J-1)_{1,J-2}$, respectively.

Therefore, the asymmetry of the splittings $\delta\nu$ defined in Eq. (1) for these low transitions can be approximately expressed as the following formula without a serious error in comparison with the experimental error.

$$\begin{aligned}
\delta\nu &= [\delta\nu_1(J)-\delta\nu_2(J)]\chi_{ab}^2 && \text{for } J_{1,J-1}\leftarrow J_{0J}\\
\delta\nu &= [\delta\nu_2(J)-\delta\nu_2(J-1)]\chi_{ab}^2 && \text{for } J_{0J}\leftarrow(J-1)_{0,J-1}\\
\delta\nu &= 0 && \text{for } J_{1J}\leftarrow(J-1)_{1,J-1}\\
\delta\nu &= [\delta\nu_1(J)-\delta\nu_1(J-1)]\chi_{ab}^2 && \text{for } J_{1,J-1}\leftarrow(J-1)_{1,J-2}\\
\delta\nu &= [\delta\nu_2(J)]\chi_{ab}^2 && \text{for } J_{0J}\leftarrow(J-1)_{1,J-1}
\end{aligned} \quad (2)$$

where

$$\delta\nu_1(J) = \left[\frac{12(J+2)-J^2(2J+1)(2J+5)-(J+2)^2(2J-1)(2J+3)}{24J(J+1)(2J+1)(2J+3)\Delta E_1(J)}\right] \quad (3)$$

$$\Delta E_1(J) = \left[A-\frac{1}{2}(B+C)\right]\left[1+\frac{J(J+1)}{2}b_p\right] - 2(J+1)\left(\frac{B+C}{2}\right) \quad (4)$$

7) T. M. Sugden and C. N. Kenney, "Microwave Spectroscopy of Gases," Van Nostrand Co., London (1965), p. 121.

8) C. H. Townes and A. L. Schawlow, "Microwave Spectroscopy," McGraw-Hill Book Co., New York (1955), p. 645.

and $\delta\nu_2$ can be obtained by replacing J with $J-1$ and $\Delta E_2(J)=-\Delta E_1(J-1)$. As is shown in Table 6, the calculated $\delta\nu$ by the formula (2) which is labeled as "one level", gives a large portion of the total $\delta\nu$ of the transitions with $J<6$ for every isotopic species so that we may neglect the other contributions. However, the contribution becomes smaller as J increases except $J_{0J}\leftarrow(J-1)_{1,J-1}$ where this is still large even for the transitions with $J>6$.

Since the dependence on the molecular asymmetry is completely neglected for the matrix elements of $\Phi_{za}\Phi_{zb}$ on the derivation of Eq. (2), the above formula will be invalid if the molecular asymmetry increases. However, we believe, these will be useful for the molecules having Ray's asymmetry parameter $|\kappa|>0.90$.

BULLETIN OF THE CHEMICAL SOCIETY OF JAPAN, VOL. 46, 2698—2701 (1973)

Charge Transfer Interaction between the Cation Radicals of Some Aromatic Diamines and Triethylamine

Tadayoshi SAKATA, Toshihiro OKAI,* Hiroaki SUGIMOTO,** and Hiroshi TSUBOMURA

Department of Chemistry, Faculty of Engineering Science, Osaka University, Toyonaka, Osaka 560

(Received March 27, 1973)

Electronic spectra of the cation radicals of some aromatic diamines in triethylamine were found to differ remarkably from those in other solvents such as ether or alcohol as regards (1) swelling of the absorption at around 25000 cm^{-1}, (2) broadening of the first band system and (3) red shift of the same system. It was concluded that these phenomena are due to the charge transfer interaction between cation radicals and triethylamine.

Dimerization of organic ion radicals in solutions has been extensively studied.[1-6] An anion radical (A^-) or a cation radical (D^+) dimerizes easily in the solution and a new absorption band due to the charge transfer (CT) between the two half-occupied orbitals of component radicals appears in the long wavelength region. The local excitation bands of the component radicals are also influenced largely by dimerization.

Recently the existence of a complex formed between an organic molecule (D) and its cation radical (D^+) has been found and studied extensively by γ radiolysis.[7-10] In this case also, a new absorption band due to charge resonance interaction appears in the visible or near infrared region.

From this $D^+\cdots D$ type complex a $D^+\cdots D'$ type one would be expected, D' being a different molecule from D. However, no report seems to have been made so far. Since such a complex would be of importance as an intermediate in reactions of cation radicals, we have attempted to find it.

Experimental

Preparation of Materials. Commercial *p*-phenylenediamine(PPD) was recrystallized in benzene and sublimed *in vacuo*. Commercial *N,N*-dimethyl-*p*-phenylenediamine (DMPD) and *N,N*-diethyl-*p*-phenylenediamine(DEPD) were purified by use of the vacuum line technique.

An aqueous solution of commercial *N,N,N',N'*-tetramethyl-*p*-phenylenediamine(TMPD) dihydrochloride was treated with 28% ammonia. The precipitate obtained was dried and sublimed several times *in vacuo*. Triethylamine(TEA), tri-*n*-propylamine(TNPA) and tri-*n*-butylamine(TNBA) were dried over pellets of potassium hydroxide for a day and fractionally distilled in a stream of nitrogen under reduced pressure.

Procedure. Solutions of the aromatic diamines in aliphatic amines, ethanol and EPA were degassed in 15 mm diam. quartz cells by the freeze-pump-thaw technique and sealed. These solutions were cooled in a quartz Dewar with liquid nitrogen and irradiated with a 250 W high pressure mercury lamp through a Toshiba glass filter UV D2, passing 300—400 nm light, to produce the cation radicals of the aromatic diamines. These UV-irradiated samples were then illuminated in the visible and near infrared region, longer than 500 nm, through a Toshiba glass filter V-052 or V-G54 in order to remove absorption due to the solvated electron.[11,12]

The electronic absorption spectra were recorded with a Shimadzu Multipurpose Recording Spectrophotometer MPS-50L.

* Present address: Nippon Paint Co., Ltd., Osaka.

** Present address: Central Research Laboratory, Sumitomo Chem. Co., Ltd., Takatsuki, Osaka.

1) K. H. Hausser, *Z. Naturforsch.*, **11a**, 20 (1956).

2) K. H. Hausser and J. N. Murrell, *J. Chem. Phys.*, **27**, 500 (1957).

3) K. Uemura, S. Nakayama, Y. Seo, K. Suzuki, and Y. Ooshika, This Bulletin, **39**, 1348 (1966); A. Kawamori, A. Honda, N. Joo, K. Suzuki, and Y. Ooshika, *J. Chem. Phys.*, **44**, 4363 (1966).

4) R. H. Boyd and W. D. Phillips, *J. Chem. Phys.*, **43**, 2927 (1965).

5) M. Itoh, This Bulletin, **45**, 1947 (1972).

6) K. Kimura, T. Yamazaki, and S. Katsumata, *J. Phys. Chem.*, **75**, 1768 (1971).

7) B. Badger and B. Brocklehurst, *Trans. Faraday Soc.*, **65**, 2576, 2582, 2588 (1969).

8) I. C. Lewis and L. S. Singer, *J. Chem. Phys.*, **43**, 2712 (1965).

9) A. Kira, S. Arai, and M. Imamura, *ibid.*, **54**, 4890 (1971).

10) T. Shida and S. Iwata, *ibid.*, **56**, 2858 (1972).

11) K. Kimura, S. Katsumata, and K. Sawada, *J. Phys. Chem.*, **76**, 639 (1972).

12) A. Egawa, K. Kimura, and H. Tsubomura, This Bulletin, **43**, 944 (1970).

Results

Electronic absorption spectra of the cation radicals formed by UV-irradiation of PPD and its derivatives in the rigid glasses of TEA and EPA at 77 K are shown in Figs. 1—4. Curves a and b show the absorption of the irradiated solutions in EPA and TEA, respectively, and curves c give their differences.[13] Change of spectra from EPA solutions to TEA solutions can be characterized as follows.

1. Swelling of the absorption at around 25000 cm^{-1}, attributable to a new band as shown by curve c.
2. Broadening of the first longest wavelength band system of the cation.
3. Red shift of the same system.

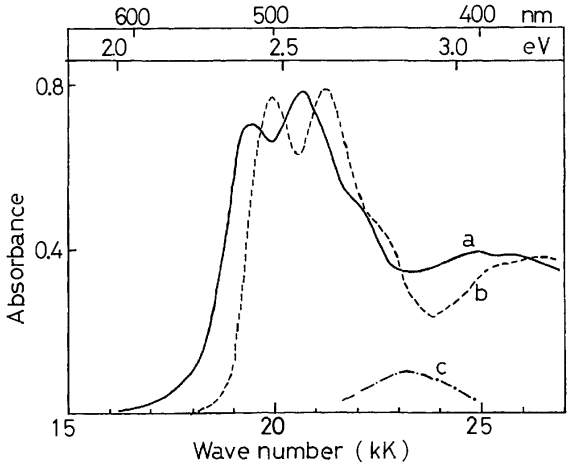

Fig. 1. The visible absorption spectra of the cation radical of *p*-phenylenediamine: a, in TEA; b, in EPA; c, a−b, the difference between a and b.

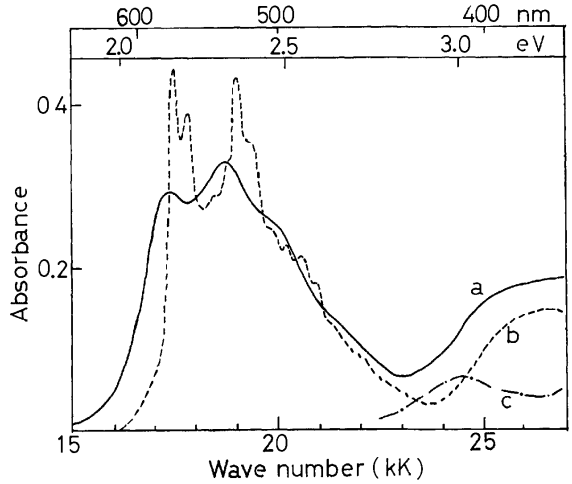

Fig. 2. The visible absorption spectra of the cation radical of *N,N*-dimethyl-*p*-phenylenediamine: a, in TEA; b, in EPA; c, a−b.

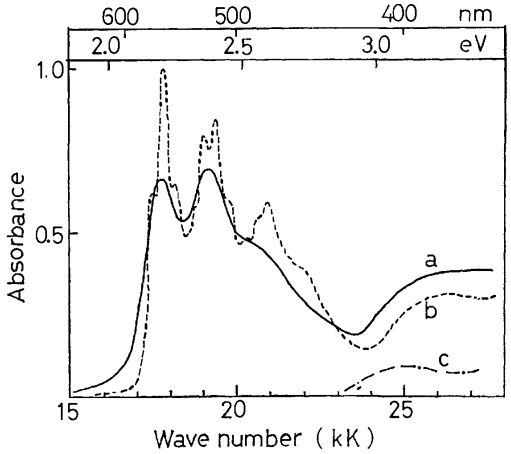

Fig. 3. The visible absorption spectra of the cation radical of *N,N*-diethyl-*p*-phenylenediamine: a, in TEA; b, in EPA; c, a−b.

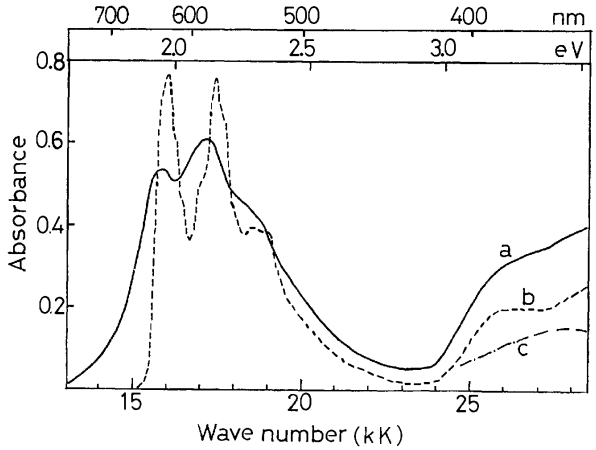

Fig. 4. The visible absorption spectra of the cation radical of *N,N,N',N'*-tetramethyl-*p*-phenylenediamine: a, in TEA; b, in EPA; c, a−b.

Table 1. Peak positions and half band widths of the first band system of the cation radical of *N,N,N',N'*-tetramethyl-*p*-phenylenediamine in various solvents at 77 K

Solvent	Width, cm^{-1}	λ_{max}, nm	
TEA	4600	585	635
TNPA	4000	582	632
TNBA	4400	578	632
EtOH	3300	575	625
EA[a)]	3300	573	623
EPA[b)]	3300	576	620
EP[c)]	3100	573	625

a) Ethyl ether (1): Ethyl alcohol (1).
b) Ethyl ether (5): Isopentane (5): Ethyl alcohol (2).
c) Ethyl ether (1): Isopentane (1).

In Table 1, are given the peak positions and the half widths of the first band system for TMPD cation radical in various solvents at 77 K, for the purpose of

Table 2. Peak position of the new band observed in TEA and calculated values of $E_{CT}{}^{v}$ and $E_{CT}{}^{a}$

D	Transition energy at the maximum of the new band, eV	$E_{CT}{}^{v}$, eV	$E_{CT}{}^{a}$, eV
PPD	2.9	2.33	1.46
DMPD	3.0	2.69	1.74
DEPD	3.1	2.79	1.92
TMPD	3.5	2.89	2.00

13) As the red shift of the first band system of PPD^{+} in TEA is especially strong, we obtained curve c for this case by shifting curve b to longer wavelength so that the positions of its vibronic bands agreed with those of curve a, and then subtracting the shifted curve b from a.

relating them with the nature of the solvent. The maximum wavelengths of the observed new absorption (curves c, Figs. 1—4) are summarized in Table 2.

Discussion

We see from Table 1 that the first band system of the cation radical in EA, EPA, and EP shows a tendency to become sharper and shift slightly to shorter wavelength with decreasing polarity of solvents. Since aliphatic amines are less polar than EPA, a sharpening of the band shape along with the blue shift is expected in amine solutions. The results are contrary to this expectation (Table 1 and Figs. 1—4), and it seems most likely that they can only be explained by taking the CT interaction between the cation radical and the aliphatic amine into account. In connection with this, the new absorption bands as shown by curves c, in Figs. 1—4 are most probably assigned to the CT bands, with the cation radical as acceptor and triethylamine as donor. These assignments are quantitatively verified as shown below.

By assuming weak CT interactions, the vertical CT energy ($E_{CT}{}^{v}$) from an aliphatic amine (D′) as an electron donor to a cation radical (D^+) as an electron acceptor can be expressed by

$$E_{CT}{}^{v} = I_p{}^{v}(D') - E_A{}^{v}(D^+) + P(D\cdots D'^+) - P(D^+\cdots D') \quad (1)$$

where $I_p{}^{v}$ and $E_A{}^{v}$ are vertical ionization potential and vertical electron affinity, respectively. $P(D^+\cdots D')$ represents the static polarization energy in the ground state of the complex, and $P(D\cdots D'^+)$ the electronic polarization energy in the excited CT state. The polarization energy can be estimated approximately using Born's equation $P=-(1-1/\varepsilon)e^2/2r_0$, where r_0 is the effective radius of an ion and ε the dielectric constant of the medium. The static dielectric constant of triethylamine at 77 K can be estimated to be $\varepsilon_{77K}=3.6$.[14] The dielectric constant in the visible region is calculated to be $\varepsilon_{op}=1.96$ using the refractive index $n^{20°C}=1.40$ at the sodium D-line.[16] When the effective radii for triethylamine and the cation radicals of the aromatic diamines are assumed to be both 3.3 Å, the polarization energy in Eq. (1) is calculated to be

$$P(D\cdots D'^+) - P(D^+\cdots D') = (1/\varepsilon_{op}-1/\varepsilon)e^2/2r_0 = 0.7 \text{ eV}.$$

The relation between the ionization potential of a neutral molecule and the electron affinity of its cation radical is schematically given in Fig. 5. As a rough approximation, we assume that

$$I_p{}^{v}(D) - I_p{}^{a}(D) \cong I_p{}^{a}(D) - E_A{}^{v}(D^+) \quad (2)$$

Superscripts v and a are abbreviations of "vertical" and "adiabatic", respectively. The $I_p{}^{v}$'s and $I_p{}^{a}$'s of DMPD

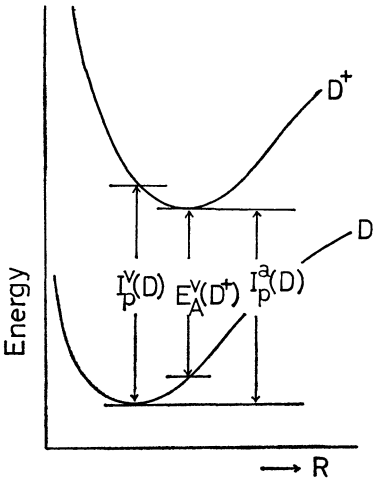

Fig. 5. Schematic energy curves for D and the cation D^+ against a generalized coordinate R for the molecular structure.

and TMPD were measured by Nakato *et al.*[17] The ionization potentials of PPD and DEPD can be estimated from the peak positions of the CT bands of the CT complexes formed between these aromatic diamines and 1,3,5-trinitrobenzene.[18] The results are shown in Table 3.

The theoretically expected values of E_{CT}, using 7.84 eV as the $I_p{}^{v}$ for triethylamine[19] are shown in

Table 3. Ionization potentials of aromatic diamines and electron affinities of their cation radicals

D	$I_p{}^{v}$ (D), eV	$I_p{}^{a}$ (D), eV	$E_A{}^{v}$ (D^+), eV
PPD	7.27	6.74[a]	6.21
DMPD	6.97	6.46	5.95
DEPD	6.81	6.28[a]	5.75
TMPD	6.75	6.20	5.65

a) Estimated by subtracting 0.53 eV from $I_p{}^{v}$. 0.53 eV is the avarage value of $I_p{}^{v}-I_p{}^{a}$ for DMPD and TMPD.

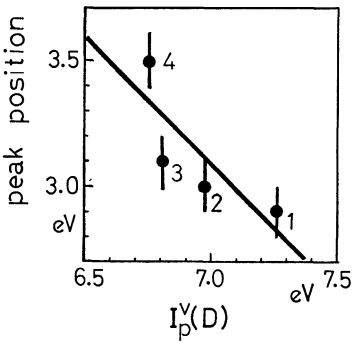

Fig. 6. Plot of the transition energies for the new bands of the cation radicals of: (1) *p*-phenylenediamine; (2) *N,N*-dimethyl-*p*-phenylenediamine; (3) *N,N*-diethyl-*p*-phenylenediamine; (4) *N,N,N′,N′*-tetramethyl-*p*-phenylenediamine, in the rigid glass of triethylamine at 77 K against their ionization potentials.

14) Assuming an approximate equation $\varepsilon_T{}'=\varepsilon_T-\alpha(T'-T)$ with $\alpha=5.2\times10^{-3}$ deg^{-1} and $\varepsilon_{298\,K}=2.42$, we obtain 3.6 as $\varepsilon_{77\,K}$[15]. Here, the value of α for triethylamine is taken to be equal to that for trimethylamine, since the former is not known.[15]

15) A. A. Maryott and E. R. Smith, Table of Dielectric Constants of Pure Liquids, National Bureau of Standards Circular 514 (Issued Aug. 10, 1951).

16) J.A. Riddick and W.B. Bunger, "Organic Solvents," third edition, John Wiley & Sons, New York (1970), p. 439.

17) Y. Nakato, M. Ozaki, A. Egawa, and H. Tsubomura, *Chem. Phys. Lett.*, **9**, 615 (1971).

18) The peak positions in carbon tetrachloride were measured to be 505, 578, 625, and 645 nm for PPD, DMPD, DEPD, and TMPD, respectively.

19) a) M. I. Al-Joboury and D. W. Turner, *J. Chem. Soc.*, **1964**, 4434. b) D. W. Turner, *Advan. Mass. Spectrom.*, **4**, 755 (1968).

Table 2, together with the observed values for the new bands. The agreement between calculated and observed values is fairly good. Taking account of errors in the calculation, the measured new bands can be ascribed to the CT bands.

The relation between the ionization potentials of the aromatic diamines and the peak positions of the new bands is shown in Fig. 6. The solid line in this figure is drawn with a gradient of -1, in accordance with Eq. (1). Four measured points are seen to lie fairly well on this line.

Table 4. Peak position of the new band for $TMPD^+$ in three aliphatic amines and ionization potentials of the amines

D′	Energy at the maximum of the new band, eV	I_p^v (D′), eV	I_p^a (D′), eV
TEA	3.49	7.84	7.50[a)]
TNPA	3.44		7.23[a)]
TNBA	3.26		

a) K. Watanabe and J. R. Mottle, *J. Chem. Phys.*, **26**, 1773 (1957).

The behavior of the new band for $TMPD^+$ in some aliphatic amines was examined, the result being given in Table 4. The energy at the maximum of the new band was found to become lower, the lower the ionization potential of the aliphatic amines, as expected theoretically from Eq. (1). The magnitude of the shift seems reasonable, although the exact data of ionization potential of these aliphatic amines are not available. These results strongly support our assertion that the new bands originate from charge transfer from triethylamine to the cation radicals.

The remarkable broadening of the first band system of the cation in TEA compared with that in EPA may be explained as follows. The minimum charge transfer energy, that is, the adiabatic charge transfer energy E_{CT}^a, can be obtained by substituting $I_p^a(D')$ and $E_A^a(D^+)$ for $I_p^v(D')$ and $E_A^v(D^+)$, respectively, in Eq. (1). The result is shown in Table 2. Here 7.50 eV was used as the value of I_p^v for TEA.[20] As is seen in this table, E_{CT}^a is smaller than E_{CT}^v by 6000—7000 cm^{-1}. Accordingly, it is most probable that the first band system of the cation radicals lies entirely in the region of the lower vibronic part of the CT state. These lower vibronic CT states may be considered to be pseudocontinuous and optically forbidden. They interact with the vibronic states of the first system of D^+ to broaden their band shape.[21,22] Similarly the red shift of the absorption peak of the first system of the cation radicals might be explained by the interaction with the CT states.

20) F. I. Vilesov, *USP Fiz. Nauk*, **81**, 669 (1963).
21) A. Nitzan and J. Jortner, *Chem. Phys. Lett.*, **11**, 458 (1971).
22) M. L. Goldberger and K. M. Watson, "Collision Theory," John Wiley & Sons, New York (1964).

BULLETIN OF THE CHEMICAL SOCIETY OF JAPAN, VOL. 46, 2701—2708 (1973)

An Experimental Study of Gibbs-Donnan Membrane Equilibria Across Permselective Membranes Which Involve the Ions of Strong Inorganic Electrolytes*

Reita TAMAMUSHI

National Institute of Arthritis, Metabolism, and Digestive Diseases, National Institutes of Health, Bethesda, Md. 20014, U.S.A.

*The Institute of Physical and Chemical Research, Wako-shi, Saitama, Japan***

(Received March 29, 1973)

The Donnan membrane equilibria arising across permselective collodion matrix membranes were studied both by a static and a flow method in systems which contain only simple strong electrolytes at relatively high concentrations, up to 0.4 equiv/l. Experimental details of the flow method and its advantage in studying the ion activity behavior are presented. From the measurements of equilibrium concentrations and Donnan membrane potentials the ratios of ion activity coefficients were calculated for the following pairs of electrolytes in mixed solutions: sodium chloride–sodium nitrate, sodium sulfate–ammonium sulfate, potassium oxalate–ammonium sulfate, and potassium oxalate–ammonium oxalate. The experiments prove the feasibility of determining the ratios of ion activity coefficients in mixed solutions at concentrations where other methods lose their usefulness.

After the theory of the Gibbs-Donnan equilibrium was developed by Donnan in 1911[1] extensive studies were carried out experimentally to test this theory.[2] These studies, however, were for a long time restricted

* The experimental work reported in this paper was carried out in 1952—1953, while the author worked at the National Institute of Arthritis, Metabolism, and Digestive Diseases, supported by a travel grant under the Fulbright Act.

** Permanent address of the author.

1) F. G. Donnan, *Z. Elektrochem.*, **17**, 572 (1911).

2) For example: (a) F. G. Donnan and A. J. Allmand, *J. Chem. Soc.*, **105**, 1941 (1914); (b) E. Hückel, *Kolloid-Z.*, Erganzungsband zu Band XXXVI (Zsigmondy Festschrift), s. 204 (1925); (c) T. R. Bolam, "The Donnan Equilibria and Their Application to Chemical, Physiological and Technical Processes," G. Bell and Sons, London (1932).

to systems containing colloidal, semicolloidal or relatively large ions like the ferrocyanide ion as the non-diffusible species. Donnan stated quite early, in 1924,[3] that "an accurate experimental study of the equilibria produced by ionically semipermeable membranes may prove to be of value in the investigation of ionic activity coefficients" of strong inorganic electrolytes. For several decades, however, studies of this type remained impossible until "permselective" membranes of extreme ionic selectivity were developed by Sollner and collaborators[4-7] by means of which Gregor and Sollner in 1945[6,7] demonstrated the feasibility of studying membrane equilibria in systems with solutions containing only the ions of the simple strong inorganic electrolytes. Shortly thereafter Sollner[8] showed explicitly how to investigate the activity behavior of individual ions in mixed solutions by the use of permselective membranes. In later years the properties of the permselective collodion matrix membranes have been greatly improved,[9-11] and more precise measurements of membrane equilibria at higher concentrations thus became feasible. It hardly needs to be mentioned that one may use for such studies, more or less conveniently, any of the various types of permselective ion exchanger membranes which have been described by numerous investigators during the last twenty years[12,13] provided their ionic selectivity is sufficiently high. Recently the Donnan membrane equilibrium across commercial permselective membranes was used by Wallace[14] for the determination of dissociation (or stability) constants of some inorganic electrolytes in aqueous solutions.

The results to be presented below show that the method suggested by Sollner[8] is very promising when applied to the experimental determination of activity coefficients in mixed solutions at concentrations where current theories cannot be tested by other methods. This general approach to the study of membrane equilibria and membrane potentials has assumed increasing interest in recent years in view of the advent of the liquid ion exchanger membranes[15-22] and the observation reported by Shean and Sollner[17] that such membranes, if properly constituted, show virtually zero leakage of the nominally impermeable ion even in systems with electrolyte solutions up to several molar. This latter observation and the possibilities it opens up have prompted the author to publish the present paper at this time.

Theoretical

Though the Donnan equilibrium is discussed to some extent in many textbooks of physical chemistry, it is necessary to recapitulate here some of its essential features which must be clearly understood in the present context.

Let us consider a system, System I, of two solutions 1 and 2 which are separated by an ideally cation-permeable membrane, $|\leftarrow\oplus\rightarrow|$. For the sake of simplicity, solutions 1 and 2 are assumed to contain uni-univalent strong electrolytes A^+X^- and B^+X^-, respectively, at different concentrations c_1 and c_2. The two solutions are at the same temperature, but not necessarily at the same pressure. The initial state of the system is represented by the scheme:

$$\begin{array}{l|c|l} [A^+] = c_1 & & [B^+] = c_2 \\ [X^-] = c_1 & \leftarrow\oplus\rightarrow & [X^-] = c_2 \\ \text{Solution 1} & & \text{Solution 2} \end{array} \qquad \text{(System I, initial state)}$$

The ionic exchanges of permeable cations A^+ and B^+ across the membrane must proceed in such a way that the electrical neutrality is satisfied in the bulk of both solutions 1 and 2. The semi-permeable nature of the membrane results in an unequal ionic distribution and an electric potential difference between the two solutions at the equilibrium state:

$$\begin{array}{l|c|l} [A^+] = c_1 - x & & [A^+] = x \\ [B^+] = x & \leftarrow\oplus\rightarrow & [B^+] = c_2 - x \\ [X^-] = c_1 & & [X^-] = c_2 \\ \text{Solution 1} & & \text{Solution 2} \end{array} \qquad \text{(System I, equilibrium state)}$$

Membranes commonly available are more or less permeable to water, and the equilibrium regarding water between the two solution phases should be considered as well as the equilibrium with respect to the permeable ions. Thus the conditions for membrane

3) F. G. Donnan, *Chem. Rev.*, **1**, 73 (1924).
4) C. W. Carr and K. Sollner, *J. Gen. Physiol.*, **28**, 119 (1940); H. P. Gregor and K. Sollner, *J. Phys. Chem.*, **50**, 53, 470 (1946); **51**, 299 (1947).
5) (a) C. W. Carr, H. P. Gregor, and K. Sollner, *J. Gen. Physiol.*, **28**, 179 (1945); (b) H. P. Gregor and K. Sollner, *J. Phys. Chem.*, **50**, 88 (1946); (c) K. Sollner and H. P. Gregor, *J. Phys. Colloid Chem.*, **54**, 325, 330 (1950).
6) H. P. Gregor, Ph. D. Thesis., Minneapolis, 1945.
7) K. Sollner and H. P. Gregor, *J. Amer. Chem. Soc.*, **67**, 346 (1945).
8) K. Sollner, *ibid.*, **68**, 156 (1946).
9) R. Neihof, *J. Phys. Chem.*, **58**, 916 (1954).
10) M. H. Gottlieb, R. Neihof, and K. Sollner, *J. Phys. Chem.*, **61**, 154 (1957); M. Lewis and K. Sollner, *J. Electrochem. Soc.*, **106**, 347 (1959).
11) (a) K. Sollner, *J. Phys. Chem.*, **49**, 47, 171, 265 (1945); (b) *J. Electrochem. Soc.*, **97**, 139C (1950); (c) *Ann. N. Y. Acad. Sci.*, **57**, 177 (1953); (d) *J. Macromol. Sci. Chem.*, **A3**, 1 (1969).
12) F. Helfferich, "Ion Exchange," McGraw-Hill Book Co., New York (1962).
13) N. Lakschminarayanaiah, *Chem. Rev.*, **65**, 491 (1965); "Transport Phenomena in Membranes," Academic Press, New York (1969).
14) R. M. Wallace, *J. Phys. Chem.*, **70**, 3922 (1966); **71**, 1271 (1967).
15) C. Botrè and G. Scibona, *Ann. Chim.* (Rome), **52**, 1199 (1962).
16) K. Sollner and G. M. Shean, *J. Amer. Chem. Soc.*, **86**, 1901 (1964).
17) G. M. Shean and K. Sollner, *Ann. N. Y. Acad. Sci.*, **137**, 759 (1966).
18) O. D. Bonner and D. C. Lunner, *J. Phys. Chem.*, **70**, 1140 (1966).
19) K. Sollner, *Ann. N. Y. Acad. Sci.*, **148**, 154 (1968).
20) G. Eisenman, *Anal. Chem.*, **40**, 310 (1968).
21) F. Conti and G. Eisenman, *Biophys. J.*, **6**, 227 (1966); J. L. Walker, Jr. and G. Eisenman, *ibid.*, **6**, 513 (1966).
22) K. Sollner, "The Basic Electrochemistry of Liquid Membranes" in "Diffusion Processes, Proceedings of the Thomas Graham Memorial Symposium, Univ. of Strathclyde," ed. by J. N. Sherwood, A. V. Chadwick, W. M. Muir, and F. L. Swinton, Gordon and Breach, London, New York, and Paris (1971).

equilibrium of system I are given by a following set of equations:[23,24]
for permeable cations A^+ and B^+,

$$\mu_{A^+}^{\circ(1)} + RT\ln a_{A^+}^{(1)} + F\phi^{(1)} = \mu_{A^+}^{\circ(2)} + RT\ln a_{A^+}^{(2)} + F\phi^{(2)} \quad (1a)$$

$$\mu_{B^+}^{\circ(1)} + RT\ln a_{B^+}^{(1)} + F\phi^{(1)} = \mu_{B^+}^{\circ(2)} + RT\ln a_{B^+}^{(2)} + F\phi^{(2)} \quad (1b)$$

for water,

$$\mu_{H_2O}^{\circ(1)} + RT\ln a_{H_2O}^{(1)} = \mu_{H_2O}^{\circ(2)} + RT\ln a_{H_2O}^{(2)} \quad (2)$$

The equalities between the chemical potentials between the two solutions do not hold for the anions X^-, that is

$$\mu_{X^-}^{\circ(1)} + RT\ln a_{X^-}^{(1)} - F\phi^{(1)} \neq \mu_{X^-}^{\circ(2)} + RT\ln a_{X^-}^{(2)} - F\phi^{(2)} \quad (3)$$

where μ_i° and a_i are the standard chemical potential and the activity, respectively, of the species i in the solutions specified by superscripts (1) and (2), $\phi^{(1)}$ and $\phi^{(2)}$ are the electric potentials of solutions 1 and 2, and the other symbols have their usual meaning.

The Donnan membrane potential is determined by the condition that, at the equilibrium, the work associated with the transfer of permeable cations should be counterbalanced by the electrical energy due to the potential difference between the two solutions. From Eqs. (1a) and (1b) we obtain,

$$E = \phi^{(2)} - \phi^{(1)} = \frac{RT}{F}\ln\frac{a_{A^+}^{(1)}}{a_{A^+}^{(2)}} + \frac{1}{F}(\mu_{A^+}^{\circ(1)} - \mu_{A^+}^{\circ(2)}) = \frac{RT}{F}\ln\frac{a_{B^+}^{(1)}}{a_{B^+}^{(2)}} + \frac{1}{F}(\mu_{B^+}^{\circ(1)} - \mu_{B^+}^{\circ(2)}) \quad (4)$$

for the Donnan membrane potential E, and

$$\frac{a_{A^+}^{(1)}}{a_{A^+}^{(2)}}\exp\left\{\frac{1}{RT}(\mu_{A^+}^{\circ(1)} - \mu_{A^+}^{\circ(2)})\right\} = \frac{a_{B^+}^{(1)}}{a_{B^+}^{(2)}}\exp\left\{\frac{1}{RT}(\mu_{B^+}^{\circ(1)} - \mu_{B^+}^{\circ(2)})\right\} \quad (5)$$

for the activity ratios of the permeable cations at the equilibrium.

The equilibrium condition for water, Eq. (2), will generally reslut in a pressure difference between the two solutions, which is called the osmotic pressure difference. Under the presence of the osmotic pressure difference, the standard chemical potential of the permeable cation in solution 1 is not equal to that in solution 2, *i.e.* $\mu_{A^+}^{\circ(1)} \neq \mu_{A^+}^{\circ(2)}$ and $\mu_{B^+}^{\circ(1)} \neq \mu_{B^+}^{\circ(2)}$. Such a difference in the standard chemical potentials due to the osmotic pressure difference, however, has been proved both theoretically and experimentally to be very small, and can be neglected in many cases, provided that the solutions are not too concentrated.[25] Experimentally, the osmotic pressure difference can be eliminated by adding a proper amount of impermeable neutral species to the solution of a lower concentration.[7]

Under such conditions the following relations can be used in place of Eqs. (4) and (5) for the membrane equilibrium with a sufficiently high accuracy: for the Donnan membrane potential,

$$E = \frac{RT}{F}\ln\frac{a_{A^+}^{(1)}}{a_{A^+}^{(2)}} = \frac{RT}{F}\ln\frac{a_{B^+}^{(1)}}{a_{B^+}^{(2)}} \quad (6)$$

and for the Donnan activity ratio,

$$\frac{a_{A^+}^{(1)}}{a_{A^+}^{(2)}} = \frac{a_{B^+}^{(1)}}{a_{B^+}^{(2)}} \text{ or } \frac{c_{A^+}^{(1)}}{c_{A^+}^{(2)}}\frac{\gamma_{A^+}^{(1)}}{\gamma_{A^+}^{(2)}} = \frac{c_{B^+}^{(1)}}{c_{B^+}^{(2)}}\frac{\gamma_{B^+}^{(1)}}{\gamma_{B^+}^{(2)}} \quad (7)$$

where c is the equilibrium concentration and γ the activity coefficient. In a particular case when the ratios of activity coefficients, $\gamma^{(1)}/\gamma^{(2)}$, are the same for A^+ and B^+ in the pairs of solutions 1 and 2, Eq. (7) and the condition of electrical neutrality give the simplified original formula of Donnan,[1,2c]

$$\frac{c_{A^+}^{(1)}}{c_{A^+}^{(2)}} = \frac{c_{B^+}^{(1)}}{c_{B^+}^{(2)}} = \frac{c_{X^-}^{(1)}}{c_{X^-}^{(2)}} \quad (8)$$

which refers to analytical concentrations rather than activities.

All the equations mentioned above have been derived by assuming the ideal permselectivity of membranes against cations and anions. Actual membranes, however, are not strictly ideal in their ionic selectivity, and show some leakage of nominally impermeable ions although this leakage is extremely small in the case of good permselective membranes. Such a small leak will not affect the equilibrium conditions for permeable ions seriously, and Eqs. (6) and (7) can be satisfied with a reasonably high accuracy, provided that the exchange rate of nominally impermeable ions across the membrane is very much lower than that of permeable ions.

These theoretical considerations lead to a useful conclusion as follows:[8]
(i) Measurements of equilibrium concentrations of permeable ions in the two solutions give the information on the ratios of their activity coefficients in mixed electrolyte solutions: *i.e.* from Eq. (7) we obtain,

$$\frac{\gamma_{A^+}^{(1)}}{\gamma_{A^+}^{(2)}}\frac{\gamma_{B^+}^{(2)}}{\gamma_{B^+}^{(1)}} = \frac{c_{B^+}^{(1)}}{c_{B^+}^{(2)}}\frac{c_{A^+}^{(2)}}{c_{A^+}^{(1)}} \quad (9)$$

The left-hand side of Eq. (9) is directly calculated from the analytical concentrations of permeable ions at the equilibrium without introducing any further assumptions, and therefore its accuracy is determined only by the accuracy of the concentration determination. If one of the two solutions, say solution 2, is sufficiently dilute so that ionic activity coefficients or their ratios are known by some theoretical means, the ratio of activity coefficients of the permeable cations in the other solution, solution 1, can be calculated.
(ii) Concomitant measurements of equilibrium concentrations and the Donnan membrane potential enable us to calculate the ratios of activity coefficients of permeable ions in solutions 1 and 2: *i.e.* from Eqs. (6) and (7) we obtain,

$$\frac{\gamma_{A^+}^{(1)}}{\gamma_{A^+}^{(2)}} = \frac{c_{A^+}^{(2)}}{c_{A^+}^{(1)}}\exp\left(\frac{EF}{RT}\right), \quad \frac{\gamma_{B^+}^{(1)}}{\gamma_{B^+}^{(2)}} = \frac{c_{B^+}^{(2)}}{c_{B^+}^{(1)}}\exp\left(\frac{EF}{RT}\right) \quad (10)$$

The activity coefficients of each permeable ion in one of the two solutions can be determined provided that the ionic activity coefficients in the other solution are available.

The Donnan membrane potential is usually measured

23) E. A. Guggenheim, "Thermodynamics," North-Holland Publishing Company, Amsterdam (1967), Chap. 1.42, 8.07, and 8.08.
24) R. Haase, "Thermodynamics of Irreversible Processes," Addison-Wesley Publishing Company, Reading, Mass. (1969), Chap. 1-20.
25) N. Kameyama, *Phil. Mag.*, **50**, 849 (1925). See also Ref. 2c, pp. 25—26 and Ref. 23, Chap. 8.08.

with a cell, saturated calomel electrode/saturated KCl bridge/solution 1/membrane/solution 2/saturated KCl bridge/saturated calomel electrode. The electromotive force of such a cell involves the liquid junction potentials at the junctions between the KCl bridges and the solutions. Therefore, the accuracy of the ionic activity coefficients determined by Eq. (10) is affected by the accuracy of correcting the measured electromotive force for the liquid junction potentials.

This method of determining ionic activity coefficients in mixed solutions is not exclusively restricted to such a simple system as mentioned above, but can be equally applied to membrane equilibria which may involve any desired combination of uni-univalent and uni-multivalent electrolytes, if the membranes are properly selected.

Experimental

In studying Donnan membrane equilibria with simple electrolytes it is important to use membranes with the following properties: (i) a very high degree of ionic selectivity towards cations over anions or *vice versa*, (ii) sufficiently high rates of exchange of permeable ions across the membrane so that the system can reach the equilibrium state within a reasonable period of time, and (iii) low water permeability. The requirement for membranes to fulfill the last two conditions is somewhat antagonistic. The ohmic resistance of membranes is an indication of the rates of ion exchange and water movement across the membranes; membranes of lower resistance which allow higher rates of ion exchange, tend to show higher water permeability.

By far the most suitable porous membranes for the experimental study of Donnan membrane equilibria with simple electrolytes are the permselective collodion matrix membranes developed by Sollner and collaborators, particularly the exclusively cation-permeable sulfonated polystyrene collodion membranes and the exclusively anion-permeable protamine collodion membranes,[26] which show excellent ionic selectivities.[4,5,9-11] Moreover their ion exchange capacity per cm^2 is very low, a decided advantage in many experimental situations. The information available on these permselective membranes with respect to their ionic selectivity, the rate of exchange of permeable ions across them, the water permeability, *etc.* makes it possible to select membranes with a suitable combination of the properties mentioned earlier.

Permselective sulfonated polystyrene collodion membranes were prepared by the dissolution method described by Neihof,[9] and permselective protamine collodion membranes by the adsorption method.[5] The membranes were test-tube-shaped (25×100 mm) and mounted on glass collars. They were tested for (a) their ohmic resistance in 0.1 M KCl, (b) their ionic selectivity, and (c) their water permeability. Membranes with resistances of several tens ohm cm^2 were considered to be most suitable. The membrane concentration potential of a concentration cell, such as 0.4 M KCl/membrane/0.2 M KCl, is a good measure of the ionic selectivity. We selected the membranes which showed the membrane concentration potential in agreement with the theoretical maximum value within 0.5 mV.

In studying Donnan membrane equilibria the most important experimental consideration is that the rate of exchange of permeable ions across the membrane should be very much faster than the rate of leakage of nominally impermeable ions. Typical results given in Table 1, which is reproduced from a paper by Sollner,[11c] clearly show that the leak of anions, particularly that of bivalent anions, is practically negligible with membranes of the type used here.

The water permeability of membranes was measured by a method similar to that used by Neihof.[27] The test-tube-shaped membrane was tied to a glass collar which was fitted with a rubber stopper carrying a micro-measuring-pipette. The membrane was filled with 30 ml of 0.1 M KCl and immersed in a beaker containing 60 ml of distilled water. The increase in the volume of the inside solution was read by the micro-measuring-pipette at given intervals. The average rate of water movement under these conditions amounted only to 0.03—0.04 ml per 100 cm^2 of membrane area per hour.

Protamine collodion membranes have properties similar but slightly inferior to those of sulfonated polystyrene collodion membranes.

TABLE 1. RATES OF CATION EXCHANGE AND ANION LEAK ACROSS TWO CATION-PERMEABLE SULFONATED POLYSTYRENE COLLODION MEMBRANES USED IN THE STUDY OF DONNAN MEMBRANE EQUILIBRIA[a]

Resistance of membrane in 0.1 M KCl	Original solutions		Cation exchange after 1 hr	Anion leak after 1 hr	Cation exchange after 4 hr	Anion leak after 4 hr
	Solution 1 (inside)	Solution 2 (outside)				
Ohm cm^2	equiv/l	equiv/l	per cent of possible exchange	per cent of actual cation exchange	per cent of possible exchange	per cent of actual cation exchange
60	0.1 NH_4Cl	0.1 $LiNO_3$	35.0	not detectable	83.0	<0.5
90	0.1 NH_4Cl	0.1 $LiNO_3$	29.0	not detectable	68.5	<0.5
60	0.1 $(NH_4)_2C_2O_4$	0.1 Li_2SO_4	35.0	not detectable	79.5	<0.05
90	0.1 $(NH_4)_2C_2O_4$	0.1 Li_2SO_4	29.5	not detectable	73.0	<0.05

a) The data were reproduced from Table 5 in Ref. 11c.

26) After completion of this work new anion-permeable membranes of better properties than old protamine collodion membranes were developed by Sollner and collaborators (see Ref. 10).

27) Ref. 9. See also K. Sollner and I. Abrams, *J. Gen. Physiol.* **24**, 1 (1940).

The ion distribution between two solutions separated by a membrane at the equilibrium was determined by the following two methods, one being called "static", and the other, "flow" or "dynamic" method. The latter is expected to be more suitable than the former for the systems of greater concentration ratios of impermeable ions and for the study of the activity behavior.

In the static method, the inside of a test-tube-shaped membrane was filled with 30 ml of one electrolyte (solution 1), and the membrane was immersed in a larger test tube containing 60 ml of the other electrolyte (solution 2). The membrane was equilibrated with the solutions to be examined prior to each experiment. Both solutions were stirred by passing purified nitrogen or air through the solution. After the membrane equilibrium had been attained, the solutions were analyzed for every ion involved.

Before each experimental run, a preliminary kinetic study was made to determine the time required to establish the equilibrium. Figure 1 shows an example of the kinetic study with a cation-permeable sulfonated polystyrene collodion membrane for the systems of potassium oxalate–ammonium oxalate and potassium oxalate–ammonium sulfate. In all our present systems the equilibrium was reached well within 15 hr.

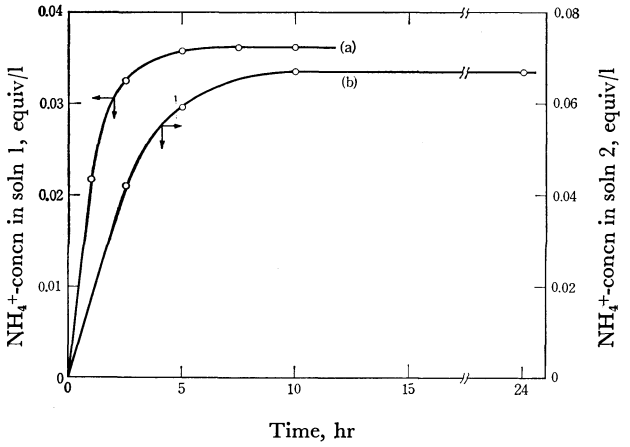

Fig. 1. Exchange of ammonium ions across a permselective cation-permeable sulfonated polystyrene collodion membrane in the course of approach to the membrane equilibrium by the static method. Initial state: (a), 0.200 M $K_2C_2O_4$ (soln 1) |←⊕→| 0.0100 M $(NH_4)_2C_2O_4$ (soln 2); (b), 0.100 M $(NH_4)_2SO_4$ (soln 1) |←⊕→| 0.100 M $K_2C_2O_4$ (soln 2). Volume of solution: soln 1/soln 2=30 ml/60 ml.

In studying the activity of ions by means of Donnan membrane equilibria, it is desirable to keep the composition of one of the two solutions practically unchanged during equilibration with the other solution. Theoretically this can be done by making the volume of the reference solution infinitely larger than that of the test solution.[8] The above-mentioned requirement is effectively satisfied by the *flow method*, that is, by running a large quantity of the reference solution (usually the more dilute solution) at a given constant rate by the outside of a test-tube-shaped membrane which contains the solution to be examined. By this method it is not necessary to determine analytically the equilibrium concentrations of ions in the reference solution; also, it makes it possible to use a very dilute reference solution and to study Donnan equilibria at large concentration ratios of impermeable ions. Furthermore, the flow method has the advantage that the approach to equilibrium can be checked by withdrawing a small amount of inside solution for analyses at given intervals; the change in the volume of the inside solution does not affect the equilibrium since the composition of the outside solution remains at the original, nominal level throughout.

In the present study, the initial volume of the inside solution (solution 1) was 25 ml, and about 60 l of the reference solution (solution 2) was run continuously by the outside of the membrane within about one week. The osmotic water movement across the membrane was compensated by adding a proper amount of impermeable neutral species, sucrose or glucose, to solution 2.[28] Both solutions were stirred by the gentle stream of purified nitrogen or air. A known quantity (1 ml) of the inside solution was pipetted out at given intervals, and analysed for the permeable ions in order to follow the kinetics of the ion exchange and to determine the equilibrium concentrations. The equilibrium was checked by running parallel the same experiments starting from both sides of the equilibrium with a common reference solution. Figure 2 shows a typical example of the kinetic approach to the equilibrium by the flow method, where the method was applied to the system containing potassium and ammonium oxalates. When the concentration ratio of impermeable ion was greater than 20, at least four days were required for the system to attain the equilibrium state.

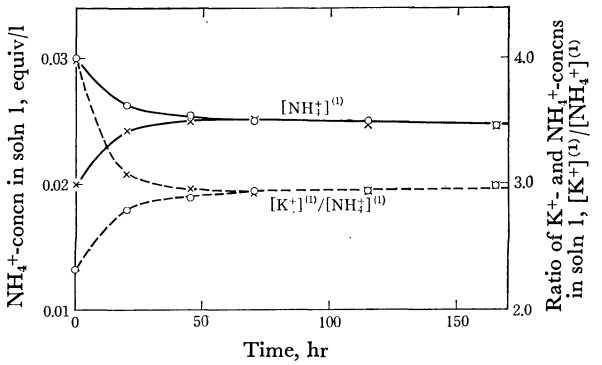

Fig. 2. Exchange of permeable ions, NH_4^+ and K^+, across permselective cation-permeable sulfonated polystyrene collodion membranes in the course of approach to the membrane equilibrium by the flow method. Initial state: solution 1, 0.0350 M $K_2C_2O_4$+0.0150 M $(NH_4)_2C_2O_4$ (-○-) and 0.0400 M $K_2C_2O_4$+0.0100 M $(NH_4)_2C_2O_4$ (-×-); common reference solution 2, 0.000750 M $K_2C_2O_4$+0.000250 M $(NH_4)_2C_2O_4$+0.120 M glucose. Solid lines represent the change in the NH_4^+-concentration in solution 1, and broken lines the change in the concentration ratio $[K^+]^{(1)}/[NH_4^+]^{(1)}$.

The membrane potential at the equilibrium was measured at 25.00±0.05 °C by constructing a conventional electrical cell with two saturated calomel electrodes.[5c] The contribution of liquid junction potentials was estimated by using Henderson's equation and ionic mobility data. The accuracy of the membrane potential thus obtained is considered to be ±0.5 mV in most cases.

28) The addition of impermeable neutral species to the less concentrated solution is a convenient and effective method of eliminating the osmotic water movement across the membrane. This method, however, has a drawback that the activity coefficients of the ions to be studied may or may not be influenced by the presence of some foreign materials. In the study of activity coefficients it will be better to use another method of compensating the effect of the osmotic water movement by blowing appropriately dried air at the proper rate through the more concentrated solution to keep its volume constant. Refer to R. Neihof and K. Sollner, *J. Phys. Chem.*, **61**, 159 (1957).

The concentrations of sodium and potassium ions were determined gravimetrically by the following method. A known volume of the sample solution was evaporated to dryness in order to remove ammonium salts present in the solution. Then the sodium or potassium salts were changed to the sulfate form by a conventional method using a proper amount of sulfuric acid. The sodium or potassium concentrations of the original solution were computed from the weight of the sulfate salts. Ammonium ions were determined by the micro-Kjeldahl method, chloride ions by the Volhard method, and oxalate ions were titrated with a standard potassium permanganate solution in acidic media. The accuracy of these analyses was better than ±0.5% except for concentrations below 0.05 equiv/l.

Results and Discussion

The results of seven typical experiments on Donnan membrane equilibria across permselective membranes, five obtained by the static method and two by the flow method, are given in the self-explanatory Tables 2, 3, and 4. Table 5 summarizes the ratios of activity coefficients of the permeable ions in mixed electrolyte solutions as calculated from the Donnan membrane equilibrium data (Tables 2—4) according to Eqs. (9) and (10).

From these results the following information is obtained with respect to the activity coefficients of the

Table 2. Donnan membrane equilibria across anion-permeable protamine collodion membrane determined by the static method at 25 °C

Volume of solution: solution 1/solution 2=30 ml/60 ml.

Exp.	Solute	Initial state: Concentration (equiv/l)		Equilibrium state: Concentration (equiv/l)		Concentration ratio Soln 1/Soln 2
		Soln 1	Soln 2	Soln 1	Soln 2	
I	Cl^-	0.05000	—	0.0365 ±0.0002	0.00753 ±0.00005	4.85±0.06
	NO_3^-	—	0.01000	0.0137[a]	0.00287[a]	4.77
	Na^+	0.05000	0.01000	0.0502 ±0.0001	0.0104 ±0.0001	4.83±0.06
II	Cl^-	0.1000	—	0.0842 ±0.0003	0.00867 ±0.00005	9.71±0.10
	NO_3^-	—	0.01000	0.0147[a]	0.00153[a]	9.61
	Na^+	0.1000	0.01000	0.0989 ±0.0001	0.0102 ±0.0001	9.69±0.10

a) Calculated by difference.

Table 3. Donnan membrane equilibria across cation-permeable sulfonated polystyrene collodion membrane determined by the static method at 25 °C

Volume of solution: solution 1/solution 2=30 ml/60 ml.

Exp.	Solute	Initial state: Concentration (equiv/l)		Equilibrium state: Concentration (equiv/l)		Concentration ratio, (1)/(2)	Membrane potential[c] (mV)	Donnan activity ratio, (1)/(2)[d]
		Soln 1	Soln 2	Soln 1	Soln 2			
III	K^+	—	0.2000	0.135 ±0.001	0.134 ±0.001	1.01±0.01	−0.6±0.2	0.98 ±0.02
	NH_4^+	0.2000	—	0.0670 ±0.0003	0.0676 ±0.0003	0.99±0.01		
	$C_2O_4^{2-}$	—	0.2000	0.000 ±0.0005	0.202 ±0.001	1.00[b]		
	SO_4^{2-}	0.2000	—	0.202[a]	0.000			
IV	Na^+	0.4000	—	0.362 ±0.001	0.0187 ±0.0001	19.4±0.2	66.2±0.5	13.1 ±0.3
	NH_4^+	—	0.02000	0.0366 ±0.0002	0.00180 ±0.00002	20.3±0.2		
	SO_4^{2-}	0.4000	0.02000	0.399[a]	0.0205[a]	19.5		
V	K^+	0.4000	—	0.358 ±0.001	0.0185 ±0.0001	19.4±0.2	66.0±0.5	13.1 ±0.3
	NH_4^+	—	0.02000	0.0362 ±0.0002	0.00178 ±0.00002	20.3±0.2		
	$C_2O_4^{2-}$	0.4000	0.02000	0.394 ±0.001	0.0203 ±0.0001	19.4±0.2		

a) Calculated as the sum of the cation concentrations.
b) Concentration ratio of impermeable anions in solution 1 and in solution 2.
c) Sign refers to solution 2.
d) Calculated from the membrane potential by Eq. (6).

TABLE 4. DONNAN MEMBRANE EQUILIBRIA ACROSS CATION-PERMEABLE SULFONATED POLYSTYRENE COLLODION MEMBRANE DETERMINED BY THE FLOW METHOD AT 25 °C

In each case the equilibrium was determined by running two experiments A and B starting from the opposite sides of the equilibrium, two similar membranes and a common reference solution 2 being used.

Exp.	Solute	Initial state: Concentration (equiv/l) Soln 1 A	Soln 1 B	Soln 2	Equilibrium state: Concentration in solution 1 (equiv/l) A	B	Concentration ratio,[b] (1)/(2)	Membrane potential[c] (mV)	Donnan activity ratio,[d] (1)/(2)
VI	K^+	0.1500	0.1700	0.00800	0.153 ±0.001	0.156 ±0.001	19.3±0.2	64.4±0.5	12.5±0.3
	NH_4^+	0.0500	0.0300	0.00200	0.0397 ±0.0001	0.0404 ±0.0001	20.1±0.2		
	$C_2O_4^{2-}$	0.2000	0.2000	0.01000	0.193[a]	0.196[a]	19.5±0.2		
	sucrose	—	—	0.205	—	—	—		
VII	K^+	0.0800	0.0700	0.00150	0.0730 ±0.0005	0.0730 ±0.0005	48.7±0.7	88.6±0.5	31.4±0.5
	NH_4^+	0.0200	0.0300	0.000500	0.0245 ±0.0001	0.0245 ±0.0001	49.0±0.7		
	$C_2O_4^{2-}$	0.1000	0.1000	0.00200	0.0975[a]	0.0975[a]	48.8		
	glucose	—	—	0.120	—	—	—		

a) Calculated as the sum of the cation concentration.
b) Average of experiments A and B.
c) Sign refers to suoltion 2.
d) Calculated from the membrane potential by Eq. (6).

TABLE 5. RATIOS OF ACTIVITY COEFFICIENTS OF THE PERMEABLE IONS IN MIXED ELECTROLYTE SOLUTIONS CALCULATED FROM THE DONNAN MEMBRANE EQUILIBRIUM DATA AT 25 °C

Exp.	Solute[a]	Composition of solutions: Concentration (equiv/l) Solution 1	Solution 2	Ratios of activity coefficients of permeable ions, i and j: $\gamma_i^{(1)}/\gamma_i^{(2)}$[b]	$\gamma_j^{(1)}/\gamma_j^{(2)}$[b]	$\{\gamma_i^{(1)}/\gamma_i^{(2)}\}/\{\gamma_j^{(1)}/\gamma_j^{(2)}\}$[c]
I	NaCl	0.0365	0.00753	—	—	1.01±0.02
	$NaNO_3$	0.0137	0.00287			(i=NO_3^-, j=Cl^-)
	c_t	0.0502	0.0104			
II	NaCl	0.0842	0.00867	—	—	1.01±0.02
	$NaNO_3$	0.0147	0.00153			(i=NO_3^-, j=Cl^-)
	c_t	0.0989	0.0102			
III	K_2SO_4	0.135	—	0.99±0.02	0.97±0.02	1.02±0.02
	$K_2C_2O_4$	—	0.134	(i=NH_4^+)	(j=K^+)	(i=NH_4^+, j=K^+)
	$(NH_4)_2SO_4$	0.0670	—			
	$(NH_4)_2C_2O_4$	—	0.0676			
	c_t	0.202	0.202			
IV	Na_2SO_4	0.362	0.0187	0.65±0.02	0.68±0.02	0.96±0.02
	$(NH_4)_2SO_4$	0.0366	0.00180	(i=NH_4^+)	(j=Na^+)	(i=NH_4^+, j=Na^+)
	c_t	0.399	0.0205			
V	$K_2C_2O_4$	0.358	0.0185	0.65±0.02	0.68±0.02	0.96±0.02
	$(NH_4)_2C_2O_4$	0.0362	0.00178	(i=NH_4^+)	(j=K^+)	(i=NH_4^+, j=K^+)
	c_t	0.394	0.0203			
VI	$K_2C_2O_4$	0.155	0.00800	0.62±0.02	0.65±0.02	0.96±0.02
	$(NH_4)_2C_2O_4$	0.0400	0.00200	(i=NH_4^+)	(j=K^+)	(i=NH_4^+, j=K^+)
	sucrose	none	0.205			
	c_t	0.195	0.0100			
VII	$K_2C_2O_4$	0.0730	0.00150	0.64±0.02	0.65±0.02	0.99±0.03
	$(NH_4)_2C_2O_4$	0.0245	0.000500	(i=NH_4^+)	(j=K^+)	(i=NH_4^+, j=K^+)
	glucose	none	0.120			
	c_t	0.0975	0.00200			

a) c_t: total concentration of nominally impermeable ions (the value being identical with the total electrolyte concentration).
b) Calculated by Eq. (10).
c) Calculated by Eq. (9).

permeable ions:
(i) In the sodium chloride–sodium nitrate systems with anion-permeable membranes (Experiments I and II), the constancy of the equilibrium concentration ratios as given by the original Donnan equation (8) is satisfied within the limit of experimental errors, which proves the almost identical behavior of the activity coefficients for chloride and nitrate ions in the solutions examined.
(ii) Experiment III shows that Eq. (8) is satisfied and the equilibrium concentration ratio is practically equal to the Donnan activity ratio in the ammonium sulfate–potassium oxalate system of the same anion concentration. This result shows that the activity coefficients of potassium and ammonium ions are not much affected by the change of anions from sulfate to oxalate.
(iii) In the potassium oxalate–ammonium oxalate system (Experiment VII), Eq. (8) is also satisfied with a reasonable accuracy, but the equilibrium concentration ratio is appreciably larger than the Donnan activity ratio. This means that the activity coefficients of potassium and ammonium ions in oxalate solutions decrease in a similar manner with increasing oxalate concentration from 0.002 to 0.1 equiv/l.
(iv) In Experiments IV—VI the constancy of the equilibrium concentration ratios is not fulfilled. The results given in Table 5 suggest that the activity coefficients of ammonium ion are slightly smaller than those of potassium and sodium ions in oxalate or sulfate solutions of concentrations higher than about 0.2 equiv/l.

The present study clearly demonstrates that the method proposed by Sollner[8] is quite feasible to the investigation of ionic activity coefficients in mixed electrolyte solutions on the basis of the Donnan membrane equilibrium. It was verified that the flow method has the following advantages over the static method when used in the study of the Donnan membrane equilibria: (i) a solution of a fixed composition can be used as the reference in a series of experiment, because the composition of the reference solution can be kept unchanged throughout the course to the equilibrium; and (ii) very dilute reference solutions can be employed in the determination of ionic activity coefficients in more concentrated solutions; this is of practical importance because with very dilute reference solutions the influence of any leakage of the membrane is minimized.

In principle, the Donnan membrane equilibrium is not restricted to the systems containing only strong electrolytes, but can equally be applied to any system involving partially dissociated electrolytes and neutral substances as well. With further developments of membranes of various types, porous or liquid, with ever increasing ionic selectivity and specificity, a large area will be opened up for the experimental study of ionic activity behavior in solutions of any desired composition and concentration. The studies along this line should be of interest not only in physical chemistry but also in colloid and biological chemistry.

This study was suggested by Dr. K. Sollner, Chief of the Section on Electrochemistry and Colloid Physics, National Institute of Arthritis, Metabolism, and Digestive Diseases, and carried out under his guidance. The author wishes to express his heartfelt thanks to Dr. Sollner for his valuable advice, critical discussions, and continual encouragement.

BULLETIN OF THE CHEMICAL SOCIETY OF JAPAN, VOL. 46, 2708—2711 (1973)

Conformation of Poly(*S*-benzyl-L-cysteine) in Solution

Hiroshi MAEDA, Takashi INOUE, Masa-aki TSUNODA, and Shoichi IKEDA
Department of Chemistry, Faculty of Science, Nagoya University, Chikusa-ku, Nagoya 464
(Received April 3, 1973)

Conformation of poly(*S*-benzyl-L-cysteine) was investigated by measurements of optical rotatory dispersion, infrared absorption and viscosity in dichloroacetic acid (DCA)–chloroform mixtures. Transition from random coil to the β-structure was confirmed to occur when DCA content of the solvent was reduced below 40% (v/v). Both dispersion parameters a_0 and b_0 increased as the polymers were transformed into the β-structure. Viscosity of the polymer solution changed only slightly with accompanying the transition. This was interpreted in terms of the formation of intramolecular β-structure. In the region where the β-structure was dominant both optical rotatory parameters and viscosity were independent of solvent composition. Such behavior has been rarely observed in the β-coil transition of other polypeptides. The β-structure of poly(*S*-benzyl-L-cysteine) was shown to be more stable than that of poly(*O*-benzyl-L-serine) as referred to respective random coil conformations.

Early studies on the β-structure in solution were mostly carried out in organic solvent systems for the purpose of detecting the β-structure in solution for the polypeptides which had been confirmed to be in this conformation in solid state. Short chain poly(γ-benzyl-L-glutamate)[1-5] and polymers of the derivatives of

1) P. Doty, A. Holtzer, J. H. Bradbury, and E. R. Blout, *J. Amer. Chem. Soc.*, **76**, 4493 (1954).
2) E. R. Blout and A, Asadourian, *ibid.*, **78**, 955 (1956).
3) A. Wada, M. Tsuboi, and E. Konishi, *J. Phys. Chem.*, **65**, 1119 (1961).
4) S. Ikeda and T. Imae, *Biopolymers*, **11**, 493 (1972).
5) T. Imae and S. Ikeda, *ibid.*, **11**, 509 (1972).

serine,[6-8] cysteine,[9-12] and threonine[13] have been shown experimentally to assume the β-structure in solution under suitable conditions (solvent composition, polymer concentration, temperature, *etc.*).

Those studies were also aimed at deducing experimentally the optical rotatory properties of the β-structure. It was commonly found that the increase in dextrorotation due to the formation of the β-structure as compared with the random coil conformation.[1-3,5-13] However, different results have been obtained about the Moffitt-Yang parameter b_0.[14,15] The parameter increased in many cases,[3,6-8,10-13] but it remained constant in others.[9,12] The extent of increase in b_0 was not unique, being fairly large in some cases[3,7] and small in others.[6,8,10-12] The different behavior of the change in b_0 has not been clarified so far.

With recent development in the preparation of protolytic polypeptides capable of forming the β-structure,[16-18] it has become possible to make various approaches to a study of the β-structure in solution. Nevertheless, the importance of its study in organic media is by no means reduced, since the β-structure in both organic solvents and aqueous media can not be assumed *a priori* to be identical. This is partly supported by the significant role assigned to the hydrophobic interaction in the β-structure in aqueous media.[19]

In the present study, the β-random coil transition of poly(*S*-benzyl-L-cysteine) was investigated in a mixed solvent system of dichloroacetic acid (DCA)–chloroform. The polymer was chosen because it has a less polar side chain than that of other polypeptides forming the β-structure,[1-13] and also because a comparison of the β-structures of serine and cysteine derivatives will be best attained, when polymers of their benzyl esters are compared.

The conformation of the present polypeptide in solid state was previously shown to be of β-structure.[20,21]

Experimental

Materials. *S*-Benzyl-L-cysteine was prepared according to the literatures.[22,22] *S*-Benzyl-*N*-carboxy-L-cysteine anhydride was synthesized as usual. Mp 109—110 °C. Polymerization was carried out in dichloromethane using sodium methoxide as an initiator. Polymer solutions were prepared by dissolving a weighed amount of the polymer into a mixed solvent prepared in advance.

Optical Rotatory Dispersion (ORD). The rotatory dispersion was measured on a JASCO ORD/UV 5 spectropolarimeter using a 1 cm cell at 25 °C. The wavelength region examined was 300 to 550 nm. Polymer concentration c was about 0.5 g/dl unless otherwise stated. The results were analyzed in terms of the Moffitt-Yang equation,[14,15]

$$[m'] = [3/(n^2+2)][\alpha](M_0/100)$$
$$= a_0\lambda_0^2/(\lambda^2-\lambda_0^2) + b_0\lambda_0^4/(\lambda^2-\lambda_0^2)^2$$

Additivity of the term $[3/(n^2+2)]$ was assumed for different solvent compositions.

Viscosity. Viscosity was measured at 25.0 °C using Ubbelohde type viscometers. Flow times of the solvents were larger than 100 s. Reduced viscosity was measured in the concentration range below 1 g/dl and plotted against c. Intrinsic viscosity $[\eta]$ and Huggins' constant k' were obtained from the intercept and slope of the plot, where k' was defined as $(1/[\eta]^2)\mathrm{d}(\eta_{sp}/c)/\mathrm{d}c$.

Infrared Spectra. Infrared spectra were recorded on a JASCO DS 402-G spectrophotometer at 25 °C. For determination of the spectra in solution, a cell with potassium bromide windows was used.

Results and Discussion

Solubility and Its Change with Time. Solubility of the sample D1119 in both DCA and chloroform was very low (less than 0.5 g/dl at 25 °C), but a mixture of the two liquids was found to serve as a solvent. Solutions with polymer concentration of about 0.5 g/dl were obtained when the DCA content was 4—80% (v/v). However, the solubility was found to change considerably after storage of the sample for about a year in a desiccator over P_2O_5. The range of DCA content giving solutions of the aged sample to the same concentration was reduced to 15—80%. Various measurements were then made on the aged sample. Almost the same results were obtained but quantitative agreement was not attained for some properties. The aged sample was designated D1119A and treated as a different sample.

Low solubility in DCA has been reported on the β-structure of polypeptides with nonpolar side chains, such as polyglycine I, poly-L-alanine, and poly-L-valine.[24] Thus similar behavior found in the present polymer might be attributed to the relatively nonpolar side chains involved.

6) G. D. Fasman and E. R. Blout, *J. Amer. Chem. Soc.*, **82**, 2262 (1960).
7) E. M. Bradbury, A. Elliott, and W. E. Hanby, *J. Mol. Biol.*, **5**, 487 (1962).
8) K. Imahori and I. Yahara, "Biopolymers Symposia," No. 1, 421 (1964).
9) B. S. Harrap and I. W. Stapleton, *Biochim. Biophys. Acta*, **75**, 31 (1963).
10) S. Ikeda, H. Maeda, and T. Isemura, *J. Mol. Biol.*, **10**, 223 (1964).
11) E. V. Anufrieva, I. A. Bolotina, B. Z. Volchek, N. G. Illarionova, V. I. Kalichevich, O. Z. Korotkina, Yu. V. Mitin, O. B. Ptitsyn, A. V. Purkina, and V. E. Eskin, *Biofizika*, **6**, 918 (1965).
12) K. Kamashima *J. Phys. Soc. Jap.*, **21**, 178 (1966).
13) S. Kubota, S. Sugai, and J. Noguchi, *Biopolymers*, **6**, 1311 (1968).
14) W. Moffitt and J. T. Yang, *Proc. Nat'l. Acad. Sci. U. S.*, **42**, 596 (1956).
15) W. Moffitt, *ibid.*, **42**, 736 (1956); W. Moffitt, *J. Chem. Phys.*, **25**, 467 (1956).
16) N. G. Illarionova, I. A. Bolotina, B. Z. Volchek, V. I. Kalichevich, Yu. V. Mitin, O. B. Ptitsyn, and A. V. Purkina, *Biofizika*, **11**, 762 (1966).
17) S. Ikeda, *Biopolymers*, **5**, 359 (1967).
18) H. Maeda and S. Ikeda, *ibid.*, **10**, 1635 (1971).
19) H. Maeda and S. Ikeda, *ibid.*, **10**, 2525 (1971).
20) E. R. Blout, C. deLoze, S. M. Bloom, and G. D. Fasman, *J. Amer. Chem. Soc.*, **82**, 3787 (1960).
21) R. D. B. Fraser, B. S. Harrap, T. P. MacRae, F. H. C. Stewart, and E. Suzuki, *J. Mol. Biol.*, **14**, 423 (1965).
22) J. Wood and V. duVigneaud, *J. Biol. Chem.*, **130**, 109 (1939).
23) M. Frankel, D. Gertner, H. Jacobson, and A. Zilkha, *J. Chem. Soc.*, **1960**, 1390.
24) C. H. Bamford, A. Elliott, and W. E. Hanby, "Synthetic Polypeptides," Academic Press, New York (1956).

Conformation of the Polymer in Solid State. Infrared spectra of the polymer in solid films cast from DCA–chloroform solutions showed amide I band at 1629 and 1694 cm^{-1} and amide II band at 1520 cm^{-1}. Thus the β-structure with antiparallel arrangement of adjacent chains can be assigned to the conformation of the polymer in solid state, which is consistent with previous results.[20,21]

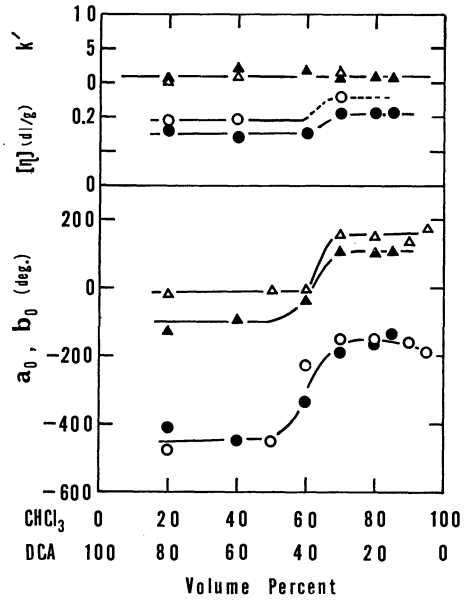

Fig. 1. Solution properties as a function of solvent composition. Polymer concentration: 0.5 g/dl. 25 °C. Circles: a_0 and intrinsic viscosity [η]. Triangles: b_0 and Huggins' constant k'. Open marks refer to D1119 and filled ones to D1119A.

Conformation of the Polymer in DCA–Chloroform Mixtures. The optical rotations of all polymer solutions were levorotatory everywhere in the wavelength region examined. The values of a_0 and b_0 are plotted in Fig. 1 against solvent composition. In the solvents of high DCA content (greater than about 50%) the dispersion is characterized by constant values of b_0 which are about zero for D1119 and −100° for D1119A. On further reduction of DCA content, b_0 begins to increase up to about 150 and 100°, respectively, indicating a conformational transition. The transition seems to be complete when DCA content reaches 30% or less, since no further change in b_0 is observed. Another parameter a_0 is also shown to increase around this region (DCA 30—50%) and to reach an almost constant value. A difference in the two samples is not detectable in the case of a_0.

Infrared spectra of the sample D1119 in solutions of low DCA content are given in Fig. 2. The difference spectra were obtained by subtracting the spectra of solvent from those of the solution. The amide I band splits into two peaks, one at 1630 cm^{-1} and the other at 1695 cm^{-1}. The results demonstrate that the conformation of the polymer in the solution is the β-structure with antiparallel arrangement of adjacent chains. Thus we can reasonably interpret the rotatory behavior in terms of the transition between random coil and β-structure.

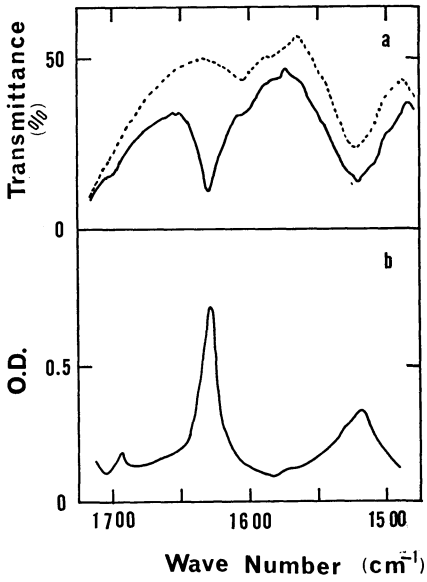

Fig. 2. Infrared spectra of the polymer solution. Sample: D1119. Solvent composition: DCA 5%–$CHCl_3$ 95% (v/v). Polymer concentration: 1 g/dl. Cell length: 200 μ.
(a) Spectra of the solution (solid line). Spectra of the solvent (broken line).
(b) Difference spectra of the polymer in solution.

Values of both intrinsic viscosity and Huggins' constant are also shown in Fig. 1. In the composition range where rotatory property changes sharply (DCA 30—40%), a slight but definite change in intrinsic viscosity occurs. Since the conformational transition from random coil to β-structure is confirmed to occur in this solvent composition range, the observed change in viscosity can be regarded to correspond to the transition. Contrary to the drastic changes in rotatory property, which is considered to reflect both the conformational change and the effect of polarity of the environment of chromophores, viscosity shows no such large change accompanying the transition. Since viscosity represents over-all shape and dimension of polymer chains and the effect of association as well, the results obtained strongly suggests that the β-structure of the present polymer is formed intramolecularly and that the association of polymers does not play a significant role in the formation of the β-structure. Huggins' constant also shows no appreciable change accompanying the transition, which has been known to be a measure of interparticle hydrodynamic interaction. It should be noted that changes in both intrinsic viscosity and Huggins' constant are many times larger than those obtained in the present study if association of polymers is essential for the formation of the β-structure.[10]

We can obtain the change in b_0 accompanying the transition to be about 150° (from 0 to +150°) or 200° (from −100 to +100°). This large change in b_0 is similar to that of poly(*O*-benzyl-L-serine),[7] these polypeptides differing from others in this respect. On the other hand, the increase in a_0 accompanying the transition is about 300° (from −450 to −150°), which is smaller than any other reported values for the coil to β transition. Generally, two contributions to a_0

should be taken into account, one from conformation-dependent optical activity and the other from environmental effect for chromophores. Since more peptide groups are considered to be solvated with DCA in the intramolecular β-structure than in the intermolecular one, the observed small increase in a_0 may be a support for the intramolecular β-structure of the present polymer.

Effect of Polymer Concentration. Effect of polymer concentration was examined using the sample E1119 at three values of c, 0.490, 0.802, and 1.173 g/dl, in the solvent of DCA content 5%. The values of b_0 were found to be constant (180—190°) and those of a_0 to slightly decrease with concentration. That rotatory properties are independent of polymer concentration also supports the assignment of the intramolecular β-structure.

Stability of the β-Structure. Comparison of the stability of the β-structure of the present polymer with that of poly(*O*-benzyl-L-serine)[7] becomes possible since temperature and solvent system (DCA–chloroform) are identical. If we assume that the β-structures of both polypeptides are molecularly dispersed, we can compare the stability in a quantitative manner, following the reasoning by Auer and Doty.[25] The composition where the midpoint of transition is located is about 10% DCA in the case of poly(*O*-benzyl-L-serine). This is considerably smaller than the value of about 35% DCA in the present polymer. Hence the difference in stability amounts to 2.303 RT log (35/10).[25] This demonstrates that the relative stability of the β-structure as referred to the random coil is larger by about 760 cal per mole of residue than that of the corresponding serine polymer. Since the chain length (as judged from intrinsic viscosity in DCA) and concentration of the two polymers were almost the same in the two experiments, the observed difference would be explained in terms of the difference between sulfur atom and oxygen atom involved in the respective side chains. It should be noted that association of polymers was not necessarily ruled out in the formation of the β-structure of poly(*O*-benzyl-L-serine), because viscosity was not measured.[7] Thus, if association was significant for the β-structure of poly(*O*-benzyl-L-serine), the estimated figure for the difference in stability becomes meaningless.

It should be emphasized that in the present system both optical rotatory parameters and viscosity were independent of solvent composition when the β-structure became dominant. Such behavior has been rarely reported for the β-coil transition.

25) H. E. Auer and P. Doty, *Biochemistry*, **5**, 1716 (1966).

BULLETIN OF THE CHEMICAL SOCIETY OF JAPAN, VOL. 46, 2711—2715 (1973)

Counterion Effect on the Titration Behavior of Poly(maleic acid)

Nobuhiko MUTO, Tsuyoshi KOMATSU, and Tsurutaro NAKAGAWA

Department of Polymer Science, Faculty of Science, Hokkaido University, Sapporo 060

(Received April 10, 1973)

The potentiometric titration of poly(maleic acid) (PMaA) in aqueous solutions containing alkali metal salts and a tetramethylammonium salt was carried out at 25 °C, and the effect of the counterions on the titration behavior of PMaA was examined in detail. The acidity of the primary carboxylic groups of PMaA increases in the order of $(CH_3)_4N^+ < Li^+ < Na^+ < K^+$, whereas that of the secondary carboxylic groups increases with the decrease in the crystallographical radius of the counterions, in agreement with the results for ordinary polycarboxylic acids. The order of $K^+ > Na^+ > Li^+$ for the binding strength to the primary carboxylate groups of PMaA is interpreted in terms of the radius of the hydrated cations; it can be attributed to the stable ring structure of the monoanion of the maleic acid residue, resulting from the hydrogen bonding between two adjacent carboxylate groups.

It is well known that the titration behavior of weak polyelectrolytes is remarkably affected by the nature of the counterions. This can be ascribed to the polyion-counterion interaction caused by the high electrostatic potential around the macroions. Gregor *et al.*[1,2] investigated the effect of alkali metal ions and tetraalkylammonium ions on the titration behavior of poly(acrylic acid) and poly(methacrylic acid), and demonstrated that the acidity of those polymonocarboxylic acids decreases with the increase in the counterion size; that is, the alkali metal ions are bound to the polyanions in the order of $Li^+ > Na^+ > K^+$. Similar phenomena have been observed in connection with the viscosity,[3] the conductivity,[3,4] and the counterion activity[5] in such polyelectrolyte systems.

As for polydicarboxylic acids, several studies have been performed on counterion binding with maleic

1) H. P. Gregor and M. Frederick, *J. Polymer Sci.*, **23**, 451 (1957).
2) I. Kagawa and H. P. Gregor, *ibid.*, **23**, 477 (1957).
3) H. P. Gregor, D. H. Gold, and M. Frederick, *ibid.*, **23**, 467 (1957).
4) K. Tamaki, M. Ozaki, M. Ogiwara, and I. Takemura, *Nippon Kagaku Zasshi*, **88**, 711 (1967).
5) I. Kagawa and K. Katsuura, *J. Polymer Sci.*, **17**, 365 (1955).

acid copolymers,[6-9] though few papers have described the effect of alkali metal ions in detail. Recently, homopolymers of maleic anhydride have been prepared by the use of γ-irradiation[10] and radical initiators,[10-12] and the titration behavior of their hydrolysis products in added salt-free solutions has been briefly reported.[10,13] The counterion effect on the behavior, however, has still not been adequately examined.

The present authors have synthesized a homopolymer of maleic anhydride by radical polymerization in acetic anhydride and have carried out the potentiometric titrations of the hydrolysis product, namely, poly(maleic acid) (PMaA), in aqueous solutions containing added salts. The present study will deal with the effects of alkali metal ions (Li^+, Na^+, and K^+) and the tetramethylammonium ion on the titration behavior of PMaA. Especially, the binding of the alkali metal ions to the primary carboxylate groups of PMaA will be discussed.

Experimental

The PMaA sample was prepared by reference to the procedure of Lang *et al.*[10] as follows. Maleic anhydride was polymerized in an acetic anhydride solution containing 50 wt% monomer and 3 wt% α,α'-azobisisobutyronitrile at 80 °C for 48 hr. The reaction mixture thus became a deep purple color.[10] From the reaction solution diluted with methyl ethyl ketone, the polymer was separated by precipitation in toluene. The poly(maleic anhydride) was purified by reprecipitation and dried *in vacuo* at 60 °C. The product retained a slight purple tint.[10,12] Found: C, 47.03; H, 3.67; N, 1.23%. Calcd for $(C_4H_2O_3)_n$: C, 48.92; H, 2.20%. The molecular weight of the poly(maleic anhydride) was determined by means of vapor-pressure osmometry to be 2500. The intrinsic viscosity, $[\eta]$, in acetophenone was 0.082 dl/g at 25.0 °C. The anhydride polymer was hydrolyzed in water at 80—90 °C for 6 hr. The PMaA solution was standardized potentiometrically and stored in a polyethylene container at 5 °C.

The titrants, NaOH and $Ba(OH)_2$ solutions, were prepared so as to be carbonate-free. As added neutral salts, the nitrates of lithium, sodium, and potassium, and tetramethylammonium chloride were used. All the chemicals used were of a guaranteed reagent grade. The maleic and acetic anhydrides were purified by distillation. All the aqueous solutions were prepared by the use of deionized water.

The pH values were measured by the aid of a Yokogawa KPH-51A pH meter, with Toa Denpa HG-4005 glass and HC-205 calomel electrodes separated by a saturated KCl-agar salt bridge. The titrations were performed in a special titration vessel maintained at 25.0 °C under a nitrogen atmosphere. It was found that the acid-base equilibrium was not immediately attained in the region around and beyond the half-neutralization point of PMaA. Similar phenomena have been observed in the cases of other polyacids.[14,15] In this region, the solutions were stirred for 15 min—1 hr after each addition of a certain amount of the base, until the pH readings were ascertained to be constant; then the titrations were resumed. The repeated-titration curves were reproducible to within ± 0.01 pH unit.

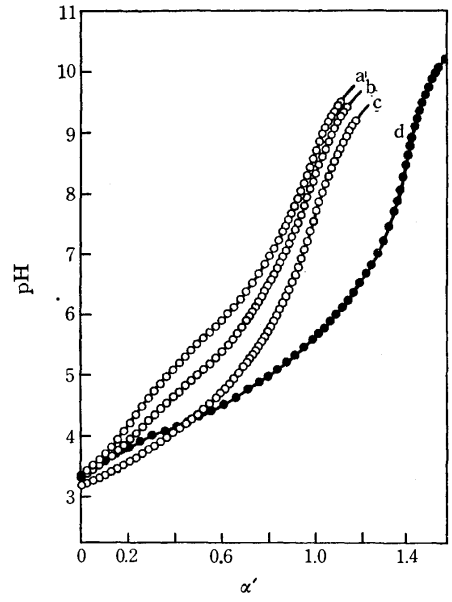

Fig. 1. The pH titration curves of 3.88×10^{-3} N PMaA (in the primary carboxylic groups) with NaOH in water (a), in 0.01 mol/l $NaNO_3$ (b), in 0.1 mol/l $NaNO_3$ (c), and with $Ba(OH)_2$ in water (d).

Results and Discussion

Figure 1 shows the pH titration curves of PMaA with NaOH and $Ba(OH)_2$ in water or in the presence of $NaNO_3$, where α' is the degree of the neutralization of the primary carboxylic groups of PMaA. Each titration curve with NaOH (open circles) has an inflection point at the same degree of neutralization ($\alpha'=1.0$), which corresponds to the equivalent point of the primary carboxylic groups, regardless of the ionic strength. It has been found that the carboxylic groups of PMaA as well as those of the ethylene–maleic acid copolymer[6] dissociate in two distinct steps.[10,13] The titration curve with $Ba(OH)_2$ (solid circles) had the end point for the total (primary and secondary) carboxylic groups at $\alpha'=1.4$. This indicates that, in the present PMaA sample, part of the secondary carboxylic groups (60%) are lost or are turned into some nonionic forms by side reactions in the course of the polymerization; as a result, there are many single carboxylic groups besides vicinal ones derived from the anhydride units. This finding is similar to that of Braun *et al.*,[12] who carried out the radical homopolymerization of maleic anhydride in organic solvents.

Figure 2 illustrates the titration curves of PMaA with

6) B. J. Felber, E. M. Hodnett, and N. Purdie, *J. Phys. Chem.*, **72**, 2496 (1968).
7) B. J. Felber and N. Purdie, *ibid.*, **75**, 1136 (1971).
8) A. J. Begala and U. P. Strauss, *ibid.*, **76**, 254 (1972).
9) C. Tondre and R. Zana, *ibid.*, **76**, 3451 (1972).
10) J. L. Lang, W. A. Pavelich, and H. D. Clarey, *J. Polymer Sci., Sec. A*, **1**, 1123 (1963).
11) R. M. Joshi, *Makromol. Chem.*, **53**, 33 (1962).
12) D. Braun, I. A. A. El Sayed, and J. Pomakis, *ibid.*, **224**, 249 (1969).
13) I. Sakurada, Y. Sakaguchi, S. Hōrin, and H. Uehara, *Kobunshi Kagaku*, **27**, 74 (1970).
14) H. P. Gregor, L. B. Luttinger, and E. M. Loeble, *J. Phys. Chem.*, **59**, 34 (1955).
15) N. Muto, T. Komatsu, and T. Nakagawa, *Nippon Kagaku Zasshi*, **92**, 43 (1971).

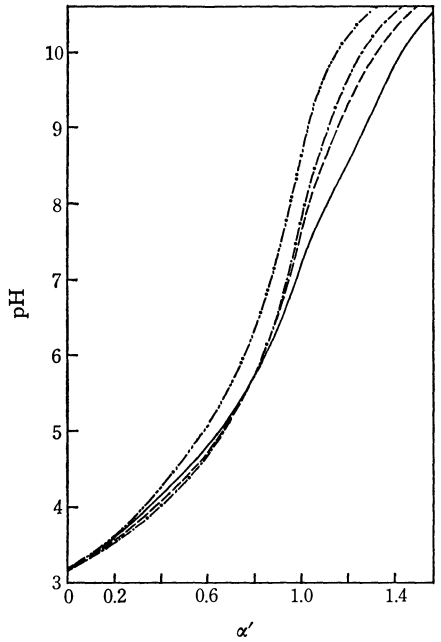

Fig. 2. The pH titration curves of 3.88×10^{-3} N PMaA with NaOH in 0.1 mol/l $LiNO_3$ (——), $NaNO_3$ (------), KNO_3 (-·-·-), and $(CH_3)_4NCl$ (·····).

NaOH in 0.1 mol/l solutions of four kinds of 1-1 salts. The first equivalent point is independent of the sort of added salt as well. Since, in these titrations, the added salt concentration (0.1 mol/l) is much higher than that of polyacid (*ca.* 10^{-3} N primary carboxylic groups), the dissociation behavior of PMaA must be substantially influenced by the cations of added salts, in spite of the use of NaOH as a titrant in all cases.

The effect of the four kinds of cations in the first dissociation step seems to differ from that in the second one. In the second dissociation step ($\alpha'\geq1.0$), the pH values at a given α' decrease in the order of $(CH_3)_4N^+>K^+>Na^+>Li^+$, in agreement with the cases of ordinary polycarboxylic acids.[1] On the other hand, in the first dissociation step a peculiar effect of the alkali metal ions is observed; that is, the pH values at a given α' decrease in the order of: $(CH_3)_4N^+>Li^+>Na^+>K^+$ in the region of $\alpha'\leq0.8$. It has been found that, in the titrations of the ethylene–maleic acid copolymer with KOH and $(CH_3)_4NOH$,[6] the pH values decrease in the order of: $(CH_3)_4N^+>K^+$ over the whole range of α'. This fact indicates that the potassium ion is bound to the polymer in a certain way.[6] Lang *et al.*[10] carried out similar titrations of PMaA with LiOH, NaOH, KOH, and $(CH_3)_4NOH$, but they made no reference to the specific effect of the alkali metal ions in the first dissociation step.

In order to characterize this counterion effect, the apparent acid-dissociation constants (K) were calculated from the titration curves according to this equation:

$$pK = pH + \log\frac{1-\alpha}{\alpha} \qquad (1)$$

where α is the degree of dissociation of the primary carboxylic groups of PMaA. The α values were determined from the electroneutrality condition in acidic solutions;

$$\alpha = \frac{[NaOH]+[H^+]}{[A_t]} = \alpha' + \frac{[H^+]}{[A_t]} \qquad (2)$$

where $[A_t]$ represents the total concentration of the primary carboxylic groups; the $[H^+]$ values were calculated from the measured pH values, with a correction for the activity coefficient ($\gamma_{H^+}=0.83$ at the ionic strength of 0.1[16]). It is well known that the apparent dissociation constant for weak polyacids continuously decreases with the increase in α. This effect is connected with the increasing difficulty in the removal of

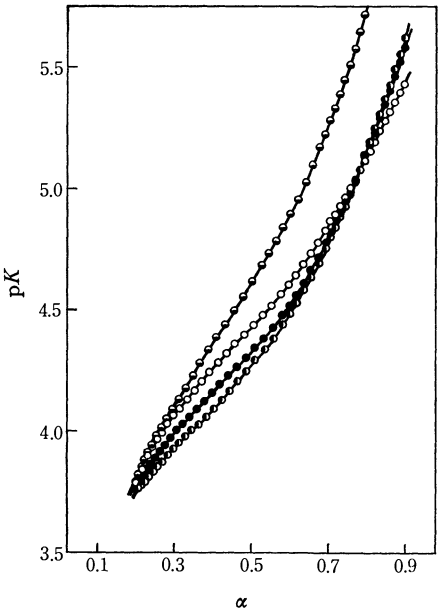

Fig. 3. The dependence of pK on α, calculated from the curves in Fig. 2. ○: $LiNO_3$, ●: $NaNO_3$, ◐: KNO_3, and ◒: $(CH_3)_4NCl$.

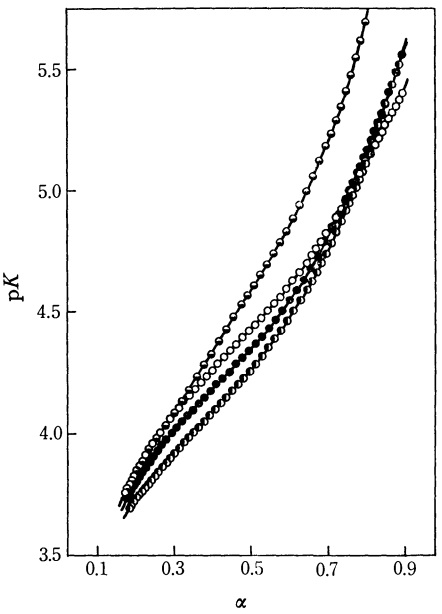

Fig. 4. The pK *vs.* α curves of 5.82×10^{-3} N PMaA with NaOH in 0.1 mol/l $LiNO_3$ (○), $NaNO_3$ (●), KNO_3 (◐), and $(CH_3)_4NCl$ (◒).

16) J. Kielland, *J. Amer. Chem. Soc.*, **59**, 1675 (1937).

protons from polyions with the increase in the charge on a polymer chain.[17]

Figures 3 and 4 show the pK *vs.* α curves. The latter was obtained at a polyacid concentration higher by 50% than the former. The curves with the same added salt are virtually superposed on each other, irrespective of the polymer concentration. In the case of poly(acrylic acid),[18] it has been found that the pK_{av} (pK at α=0.5) values at the same ionic strength are, in fact, constant over the concentration range of 10^{-3}—10^{-1} N polyacid.

Table 1. The pK_{av} values of the primary carboxylic groups of PMaA in 0.1 mol/l added salts

Counterion	Polyacid concentration[a]	
	3.88 mN	5.82 mN
$(CH_3)_4N^+$	4.61	4.59
Li^+	4.43	4.43
Na^+	4.33	4.35
K^+	4.27	4.27

a) In the primary carboxylic groups.

It is noticeable that, in the region of $\alpha \leq 0.8$, the pK values at a given α decrease in the order of: $(CH_3)_4N^+ > Li^+ > Na^+ > K^+$, and that the p$K$ curves in the presence of the alkali metal ions deviate most from each other in the region of $0.4 \leq \alpha \leq 0.5$. Table 1 summarizes the pK_{av} values of the primary carboxylic groups determined in Figs. 3 and 4. The differences in pK_{av} with the alkali metal ions (0.06—0.10 pK unit) are sufficiently larger than the estimated uncertainty on pK (0.02), not to mention the differences in the effect between the $(CH_3)_4N^+$ ion and the others. In such a case, the extent of the lowering in the pK or the increment in acidity gives a measure of the interaction between carboxylic groups and counterions.

On the basis of the assumption that no $(CH_3)_4N^+$ ions are bound to carboxylate groups in the PMaA–$(CH_3)_4NCl$ system, the degree of binding (θ) of the alkali metal ions (M^+) with the primary carboxylate groups (A^-) was calculated from the titration curves. The θ is defined by the equation:

$$\theta = \frac{[MA]}{[A_t]} = \frac{[A_t]-[HA]-[A^-]}{[A_t]} \qquad (3)$$

where [HA] and [A^-] are the concentrations of the undissociated and dissociated primary carboxylic groups respectively, and where [MA] is that of the primary carboxylate groups bound to the alkali metal ions. In Eq. (3), [HA] is found to be:

$$\begin{aligned}[HA] &= [A_t] - [NaOH] - [H^+] \\ &= [A_t](1-\alpha') - [H^+] \end{aligned} \qquad (4)$$

from the conservation and electroneutrality conditions. The [A^-] values in the 0.1 mol/l MNO_3 solutions are determined by the use of the reference curve for the 0.1 mol/l $(CH_3)_4NCl$ solution (Fig. 5). After the determination of the (pH+log[HA]) values for the 0.1 mol/l MNO_3 solutions at the same concentration of PMaA, the appropriate [A^-] concentrations in the MNO_3 solutions can be found in the reference graph. The scheme with the reference curve has been devised by Mandel *et al.*;[19] their method of calculation for the formation curves of metal-polyacid complexes from the titration curves is a modification of the method proposed by Gregor *et al.*[14]

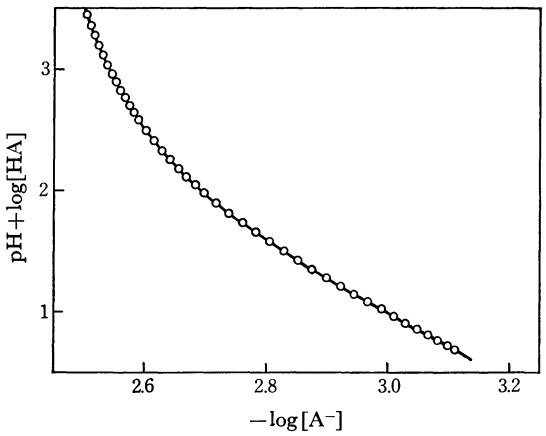

Fig. 5. The reference plot of 3.88×10^{-3} N PMaA in 0.1 mol/l $(CH_3)_4NCl$, for calculation of θ.

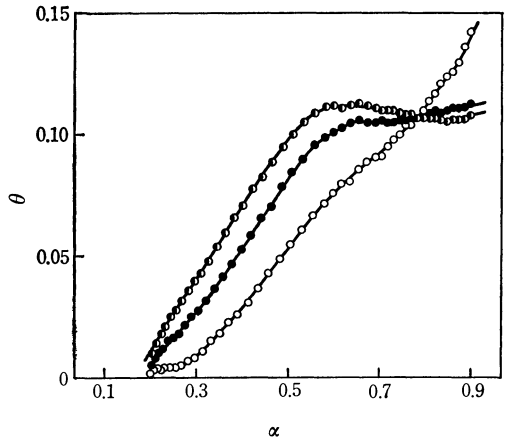

Fig. 6. The dependence of θ on α, calculated from the curves in Fig. 2. ○: Li^+, ●: Na^+, and ◐: K^+.

The dependence of θ on α is shown in Fig. 6. In the region of $\alpha \leq 0.8$, the binding strength was in the order of $K^+ > Na^+ > Li^+$, whereas in the region of $\alpha \geq 0.8$ the order was reversed. With the increase in α, the θ values in the cases of the K^+ and Na^+ ions were saturated so as to be practically constant (0.10—0.11) in the region of $\alpha \geq 0.5$. On the other hand, the θ values for Li^+ ions monotonously increased with α and grew much higher than those for other ions beyond α=0.8. Since, in the present PMaA sample, the equivalent point of the total carboxylic groups was found at α'=1.4, roughly half of the total carboxylic groups are dissociated at the above-mentioned point of α=0.8. That is to say, the dissociation behavior in the region of

17) J. Th. G. Overbeek, *Bull. Soc. Chim. Belges*, **57**, 252 (1948).
18) J. V. McLaren, J. D. Watts, and A. Gilbert, *J. Polymer Sci., Ser. C*, **16**, 1903 (1967).
19) M. Mandel and J. C. Leyte, *ibid., Ser. A*, **2**, 2883 (1964).

$\alpha \leq 0.8$ may be influenced predominantly by the typical primary carboxylic groups in the maleic acid residues, and then in the region of the larger α values the single and the secondary carboxylic groups may dissociate. Thus, the present results indicate that the mode of the binding of the alkali metal ions to the primary carboxylate groups of PMaA differs from that to the secondary and the single carboxylate groups.

The binding order of $Li^+ > Na^+ > K^+$ with the secondary carboxylate groups of PMaA (Fig. 2) agrees with the results for ordinary polymonocarboxylates[1,3,4] and for the secondary carboxylate groups of maleic acid copolymers.[8] The latter were obtained in connection with dilatometric studies of the binding of Li^+ and K^+ ions to the carboxylate groups in 0.2 mol/l $(CH_3)_4NCl$ solutions.[8] The results can be explained in terms of the crystallographical ionic radius of alkali metals;[2] that is, the smallest Li^+ ion is bound to the largest extent.

It is noteworthy that the binding strength of the alkali metal ions to the primary carboxylate groups is in the order of: $K^+ > Na^+ > Li^+$. In general, the binding strength of ion pairs increases with the decrease in a certain ionic-size parameter as far as the same valence type is concerned. The order of the binding strength with the primary carboxylate groups can, therefore, be interpreted in terms of the radii of the *hydrated* alkali metal ions, which increase in the order of: $K^+ < Na^+ < Li^+$. In other words, in the first dissociation step of PMaA the so-called solvent-separated ion pairs between hydrated cations and carboxylate groups are predominant, not the so-called contact ion pairs interpreted in terms of the crystallographical ionic radii of the counterions.[2]

It can be presumed that the specific counterion binding to the primary carboxylate groups results from the peculiar structure of the maleic acid polymers, in which the local density of ionizable groups on the main polymer chain is much higher than that in ordinary polycarboxylic acids; hence, the interaction between neighboring groups must be considerable. Recently, Strauss *et al.* measured by dilatometry the volume changes associated with the binding of the hydrogen ion to the anions of maleic acid copolymers in 0.2 mol/l $(CH_3)_4NCl$ solutions,[8] and pointed out that the monoanion of the maleic acid residue has the following structure:

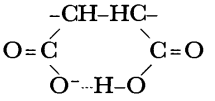

involving cooperative hydrogen bonding by two adjacent carboxylate groups.[8,20] Felber *et al.*,[7] who measured the heats of the protonation of the ethylene–maleic acid copolymer, have proposed the same structure in the first ionization process, too. In a monomeric maleic acid molecule, the intramolecular hydrogen bond of the hydrogen maleate anion has been confirmed.[21,22]

It is considered that, in the first dissociation step of PMaA, the monoanion of the maleic acid residue probably has a stable ring structure resulting from the hydrogen bond, in which a single electronic charge is distributed by resonance over a wide range. Therefore, the primary carboxylate groups, which would be bound to the alkali metal ions by nature, are more tightly bound to the protons of the secondary carboxylic groups. The present findings that hydrated alkali metal ions are more loosely bound to the primary carboxylate groups can be attributed to such a chelation of a proton with two adjacent carboxylate groups. In the second dissociation step, the intramolecular hydrogen bond almost disappears; hence, the contact ion pairs between alkali metal ions and carboxylate groups become predominant.

Finally, the potentiometric titration method has been found to be very useful in detecting such subtle differences in the modes of short-range interaction as the binding of counterions to polyelectrolytes. Similar studies will be performed on the titration behavior of other dicarboxylic acid polymers.

The authors wish to thank Professor Mitsuru Nagasawa of Nagoya University for generously supplying valuable unpublished data on PMaA and Associate Professor Seiichi Tokura of their own department for affording the facilities for the use of a vapor-pressure osmometer. The present work has been supported in part by a Grant for Scientific Research from the Ministry of Education.

20) A. W. Schultz and U. P. Strauss, *J. Phys. Chem.*, **76**, 1767 (1972).
21) S. Nagakura, *J. Chim. Phys.*, **61**, 217 (1964).
22) J. J. Christensen, R. M. Izatt, and L. D. Hansen, *J. Amer. Chem. Soc.*, **89**, 213 (1967).

Solvent Effect in Electron Spin Resonance Spectra and Electrochemical Reaction of Substituted Nitrobenzene Anion Radicals

Taitiro FUJINAGA, Yasuo DEGUCHI, and Kisaburo UMEMOTO*

Department of Chemistry, Faculty of Science, Kyoto University, Sakyo-ku, Kyoto 606

(Received October 5, 1972)

In order to examine the effect of solvents on the hyperfine splittings of anion radical the electron spin resonance spectra of substituted nitrobenzene anion radicals were studied. The effect of hydroxylic solvent is enhanced when the nitro group is forced out of the plane of the benzene ring due to the steric influence of the bulky functional group at the *ortho* position. The effect is reduced when the nitro group forms intramolecular hydrogen bond with the hydroxyl group at the *ortho* position. A model for the solvent effect considering the hindered rotation of the nitro group in the radical molecule caused by the formation of intermolecular hydrogen bond with solvent is found to be reasonable from a molecular orbital calculation, taking account of changes in molecular orbital parameters resulting from hydroxylic solvation. The shifts in polarographic half wave potentials with the solvent system as well as the dehalogenation reaction in the course of electrochemical reduction of halonitrobenzenes is interpreted by means of the model.

Several investigators have studied the solvent effect in electron spin resonance (ESR) spectra of organic anion radicals.[1-12] It is well-known that the hyperfine splittings in ESR spectra are influenced by the solvent characteristics as well as the species which interact with the radical in solution. The nitrogen coupling constant of di-*para*-anisyl nitric oxide increases with the increase of the dielectric constant of the solvent, the effect being remarkably enhanced in hydroxylic solvents such as water and alcohols.[2] The solvent effects of substituted nitrobenzene anion radicals were studied extensively by Adams and his co-workers[3-5] and summarized by Kitagawa;[6] the nitrogen coupling constant a^N of nitrobenzene anion radical produced electrochemically in aprotic solvents increases rapidly with the addition of a small amount of water. The effect is remarkable when the nitro group is sterically hindered. The presence of alkali metal cations also increases the a^N of *p*-chloronitrobenzene anion radical.[7] Theoretical studies of the dependency of the hyperfine splittings in ESR spectra on the solvent characteristics were undertaken by Reiger and Fraenkel[8] and Gendell *et al.*[9] on the assumption that the charge in the functional group is affected by the presence of localized complexes between the solvent and the functional group of the radical. Since then MO calculations have been recognized to be useful for the interpretation of the complicated phenomena observed in ESR spectra.[10-12] We have examined the solvent effect in ESR spectra as well as the electrochemical reduction of substituted nitrobenzene by MO calculation in order to clarify the nature of the solvent effect.

Experimental

All the nitro compounds, such as nitrobenzene, nitrophenol, 2-nitroresorcinol, nitrotoluene, nitroanisole, and halonitrobenzenes, were of G. R. grade and purified by recrystallization from benzene when necessary. Tetra-*n*-propyl ammonium perchlorate was prepared by adding perchloric acid to tetra-*n*-propyl ammonium hydroxide and purified by recrystallization from hot acetonitrile-water mixture. *N,N'*-Dimethylformamide (DMF) was dried over anhydrous potassium carbonate for a few days and then distilled twice taking the fraction boiling at 151—153 °C. Acetonitrile (ACN) was dried over anhydrous phosphorus pentoxide and the fraction distilled at 80—81 °C was used. The anion radicals were prepared by electrolytic reduction in DMF-water or ACN-water mixture containing 2×10^{-3} M nitro compound and 0.1 M tetra-*n*-propyl ammonium perchlorate. The cell and technique are described in detail elsewhere.[13-15] The coupling constants were calibrated with the splittings of nitrosodisulphonate anion.

Results and Discussion

Solvent Effect in ESR Spectra. The coupling constants of fluoronitrobenzene anion radicals in DMF-water mixture are given in Table 1. Assignments of the coupling constants to specific nuclei were made in accordance with Hückel MO calculation and INDO

* Present address: Department of Pure and Applied Sciences, College of General Education, University of Tokyo, Meguro-ku, Tokyo.

1) Y. Deguchi, This Bulletin, **35**, 260 (1962).
2) K. Umemoto, Y. Deguchi, and H. Takaki, *ibid.*, **36**, 560 (1963).
3) L. H. Piette, P. Ludwig, and R. N. Adams, *J. Amer. Chem. Soc.*, **83**, 3909 (1961); **84**, 4212 (1962).
4) P. Ludwig, T. Layloff, and R. N. Adams, *ibid.*, **86**, 4568 (1964).
5) J. Q. Chambers, T. Layloff, and R. N. Adams, *J. Phys. Chem.*, **68**, 661 (1964).
6) T. Kitagawa, *Rev. Polarog.* (Kyoto), **12**, 11 (1964).
7) T. Kitagawa, T. Layloff, and R. N. Adams, *Anal. Chem.*, **36**, 925 (1964).
8) P. H. Rieger and G. K. Fraenkel, *J. Chem. Phys.*, **37**, 2811 (1962).
9) J. Gendell, J. H. Freed, and G. K. Fraenkel, *ibid.*, **37**, 2832 (1962).
10) W. M. Gulick, Jr., and D. H. Geske, *J. Amer. Chem. Soc.*, **87**, 4049 (1965).
11) W. M. Gulick, Jr., W. E. Geiger, Jr., and D. H. Geske, *ibid.*, **90**, 4218 (1968).
12) D. H. Geske, J. L. Ragle, M. A. Bambenek, and A. L. Balch, *ibid.*, **86**, 987 (1964).
13) K. Umemoto, Y. Deguchi, and T. Fujinaga, This Bulletin, **36**, 1539 (1963).
14) T. Fujinaga, Y. Deguchi, and K. Umemoto, *ibid.*, **37**, **822** (1964).
15) K. Umemoto, *ibid.*, **40**., 1058 (1967).

TABLE 1. COUPLING CONSTANTS OF FLUORONITROBENZENE ANION RADICALS IN DMF–WATER MIXTURE (IN gauss)

		Water content (%)					
		0[a)]	5	10	20	50	90
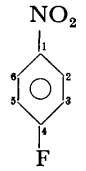	a^N	9.95	11.37	12.01	12.53	13.59	14.34
	$a_2^H = a_6^H$	3.56	3.49	3.49	3.46	3.44	3.48
	$a_3^H = a_5^H$	1.12	1.11	1.12	1.12	1.12	1.12
	a^F	8.55	8.16	8.05	8.05	8.05	8.06
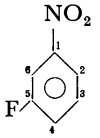	a^N	8.86	10.04	10.67	11.30	12.36	13.27
	a_2^H	2.99	2.89	2.92	2.92	2.92	2.92
	a_3^H	0.97	1.02	1.02	1.05	1.08	1.12
	a_4^H	3.43	3.31	3.30	3.32	3.30	3.32
	a_6^H	3.22	3.32	3.30	3.32	3.30	3.32
	a^F	4.02	3.89	3.82	3.74	3.62	3.62
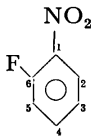	a^N	9.29	10.72	11.23	12.14	13.46	14.59
	a_2^H	3.64	3.60	3.52	3.49	3.37	3.45
	$a_3^H = a_5^H$	1.05	1.08	1.09	1.09	1.09	1.12
	a_4^H	4.34	4.04	3.88	3.76	3.47	3.45
	a^F	6.67	6.75	6.62	6.66	6.52	6.45

a) Assignments of the coupling constants to specific nuclei were made in accord with our Hückel MO calculation for *o*, *p*-isomers and with the INDO MO calculation[16] of Pople *et al.* for *m*-isomer.

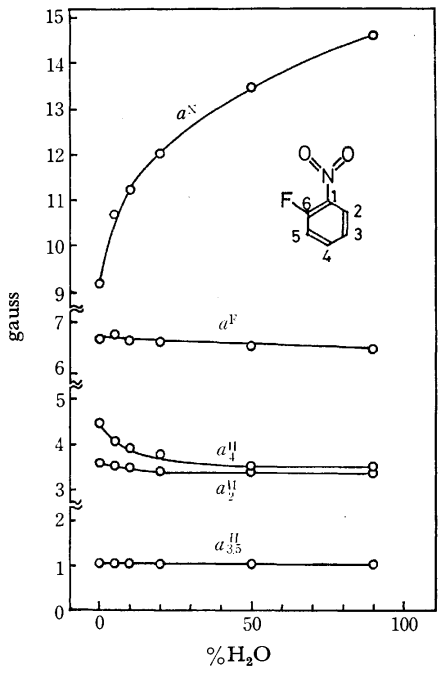

Fig. 1. Hyperfine coupling constants of *o*-fluoronitrobenzene anion radical shown as a function of water content in DMF–water mixture.

MO methods.[16] The graphical shifts in coupling constants of nitrogen, proton, and fluorine nuclei of *o*-fluoronitrobenzene anion radical are shown in Fig. 1 as a function of water content. Similar shifts in a^N of some other substituted nitrobenzene anion radicals are summarized in Figs. 2a and 2b. We see that a^N increases with the increase of water content, the splittings of nuclei at *meta* and *ortho* positions showing little change. The figures present an excellent comparison. In the case of fluoronitrobenzene, nitroanisole, and nitrotoluene (Fig. 2a), the shifts in a^N of *ortho* isomers are greater than those of *meta* or *para* isomers, and the shift in a^N of a radical with a bulkier substituent at the *ortho* position is remarkably enhanced with the increase of the water content. In the case of *o*-nitrophenol anion radical which forms an intramolecular hydrogen bond[13] (Fig. 2b), the shift in a^N is smaller than in the case of *para* and *meta* isomers. The shift in a^N of 2-nitroresorsinol anion radical which forms two intramolecular hydrogen bonds[4] is much smaller. These observations are in good accord with the following general aspects of the solvent effect of substituted nitrobenzene anion radicals:[4] i) When the nitro group forms intramolecular hydrogen bonds the solvent effect is impeded as the nitro group is rendered to be a weaker proton acceptor. ii) When the nitro group forms a localized complex with solvent molecules and is sterically hindered by the substituent at the *ortho* position in such a way as to be twisted out of plane of the benzene ring, the solvent effect is much more effective than in the unhindered cases. The second model is based on the fact that a substituted nitrobenzene anion radical having a sterically hindered nitro group has a larger nitrogen splitting and smaller ring proton splittings than unhindered substituted nitrobenzene anion radicals.[17] In general, the nitro group of *ortho* substituted nitrobenzene is known to be sensitive to the steric influence of the substituent at the *ortho* position and the twisting effect is operative in some cases, *e.g.*, in the case of *o*-nitrotoluene the twisted angle of the nitro group has been

16) J. A. Pople and D. L. Beveridge, "Approximate Molecular Orbital Theory," McGraw-Hill Book Co., New York (1970) Chap. 4; J.A. Pople, D.L. Beveridge, and P.A. Dobosh, *J. Amer. Chem. Soc.*, **90**, 4201 (1968).

17) D. H. Geske and J. L. Ragle, *J. Amer. Chem. Soc.*, **83**, 3532 (1961).

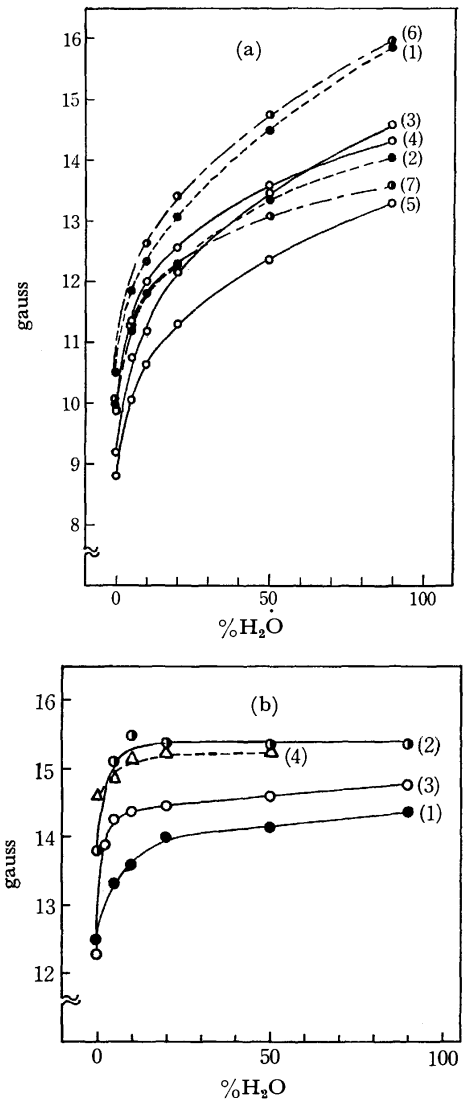

Fig. 2. Nitrogen coupling constants of substituted nitrobenzene anion radicals shown as the function of water content.

(a): In DMF–water mixture
1: *o*-nitrotoluene
2: *p*-nitrotoluene
3: *o*-fluoronitrobenzene
4: *p*-fluoronitrobenzene
5: *m*-fluoronitrobenzene
6: *o*-nitroanisole
7: *m*-nitroanisole

(b): In ACN–water mixture
1: *o*-nitrophenol
2: *p*-nitrophenol
3: *m*-nitrophenol
4: 2-nitroresorcinol

estimated to be 34°.[18] The chlorine atom is suggested to be about as effective as a methyl group with regard to its steric influence on an adjacent nitro group.[4] The fluorine atom is certainly less effective than chlorine atom. Nonetheless, if hydrogen bond complex is formed the nitro group should be dislocated to accommodate the added bulky group. This situation should be reflected in the observed extra sensitivity of the splittings (Table 1).[19]

In order to verify the applicability of the model of solvent effect, the Hückel MO calculation was performed for *o*-fluoronitrobenzene anion radical by taking account of the following two factors[8,12,20] i) The oxygen Coulomb integral α_0 of the nitro group increases as a result of hydroxylic solvation since the oxygen atom in the nitro group becomes more electronegative by forming intermolecular hydrogen bonds with solvents, ii) the resonance integral β_{CN} between the nitro group and the benzene ring decreases when the conjugation between the nitro group and the benzene ring is reduced by twisting of the nitro group. The calculated distribution of the unpaired electron spin densities of *o*-fluoronitrobenzene anion radical is summarized in Table 2. By using these densities the calculated hyperfine coupling constants were obtained from the relations

$$a^N = A\rho^N - B\rho^O \quad (1)$$

$$a_i^H = Q\rho_i^C \quad (2)$$

where ρ^N and ρ^O denote the electron spin densities on nitrogen and oxygen atoms, respectively, and ρ_i^C denotes the spin density on the i-th carbon atom to which the i-th hydrogen atom is bonded. A, B, and Q are constants. Equation (1) was given by Rieger and Fraenkel. They gave $A=99$ and $B=71$ gausses as values which fit their experimental nitrogen splittings.[8] Equation (2) was given by McConnel,[21] Q being estimated to be -30 gauss for hydrocarbon anion radicals.[22] The values of a^N and a_i^H obtained from Eqs. (1) and (2) by using our spin densities did not agree with the experimental results. However, the calculated results may still be used for studying the relative magnitude of the observed shift in splittings. The calculated shifts in a^N, a_2^H, and a_4^H with the increase of the Coulomb integral of the oxygen atom α_0 are graphically shown in Fig. 3a and those with the decrease of the resonance integral β_{CN} in Fig. 3b. The origin of the curves were so chosen that the calculated results might coincide with the experimental results. The calculated shifts in a^N and a_4^H with the increase of α_0 qualitatively correlates with the experimental results, namely a^N increases and a_4^H decreases (Figs. 1 and 3a). However, the change in the observed a_4^H was not reproduced by calculation, a more evident contradiction being shown for a_2^H which was found to show a slight increase by calculation and a slight decrease by experiment. On the other hand, the calculated shift in a^N, a_2^H, and a_4^H with the decrease of β_{CN} is qualitatively correlated with the experimental results; a^N increases and both a_2^H and a_4^H decrease. However, the relative magnitudes of the changes in a_2^H and a_4^H were calculated to be comparable. The experiment indicated that the magnitude of the change in a_4^H is greater than that in a_2^H. Hence, neither the increase of α_0 nor the decrease of β_{CN} reflects precisely the nature of the solvent effect by itself. However, the

18) B. M. Wepster, "Progress in Stereochemistry," Vol. 2, ed. by W. Klyne and P. B. D. de la Mare, Butterworths, London (1958) p. 110.

19) The out-of-plane bending of the nitro group, the other possibility of steric effect, seems to be less probable, since the ring nuclei splittings were observed to be affected by the solvent system (*cf.* Refs. 4 and 17).

20) T. Yonezawa, C. Nagata, H. Kato, A. Imamura, and K. Morokuma, "Ryoshi Kagaku Nyumon," (Introduction to Quantum Chemistry) Kagakudojin, Kyoto (1963) Chap. 2; see also Chap. 4 in Ref. 23.

21) H. M. McConnel, *J. Chem. Phys.*, **24**, 633, 764 (1956).

22) A. Carrington, *Quart. Rev.*, **17**, 67 (1963).

Table 2. Calculated energy level of the lowest vacant orbital m and π electron density $(c_r^{L.v})^2$ of *o*-fluoronitrobenzene

	$y=1.0$			$x=1.0$			
	$x=1.0$	$x=1.2$	$x=1.4$	$y=0.8$	$y=0.6$	$y=0.4$	$y=0.2$
m[a)]	−0.3153	−0.2458	−0.1825	−0.3415	−0.3678	−0.3912	−0.4080
O	0.1815	0.1661	0.1501	0.1982	0.2155	0.2321	0.2450
N	0.3140	0.3472	0.3760	0.3567	0.4032	0.4492	0.4857
1	0.0132	0.0066	0.0025	0.0124	0.0100	0.0060	0.0019
2	0.0993	0.1008	0.1027	0.0747	0.0496	0.0256	0.0071
3	0.0002	0.0000	0.0001	0.0003	0.0003	0.0002	0.0001
4	0.1024	0.1013	0.1017	0.0783	0.0526	0.0275	0.0077
5	0.0073	0.0057	0.0045	0.0061	0.0044	0.0025	0.0007
6	0.0859	0.0899	0.0941	0.0641	0.0420	0.0214	0.0059
F	0.0147	0.0163	0.0181	0.0108	0.0069	0.0034	0.0009

a) $\alpha+m\beta$ is the energy level of the lowest vacant orbital in units of the standard α and β in the Hückel MO calculation. MO parameters are as follows (see also Refs. 14 and 20).

$\underset{\alpha+0.1\beta}{C}\overset{\beta_{CN}}{-}\underset{\alpha+\beta}{N}\begin{matrix}\overset{\beta}{\diagup}O\\ \underset{\alpha_O}{\diagdown}O\end{matrix}$, $\alpha_O=\alpha+x\beta$, $\beta_{CN}=y\beta$, $\underset{\alpha+0.2\beta}{C}-\underset{\alpha+2.1\beta}{F}$

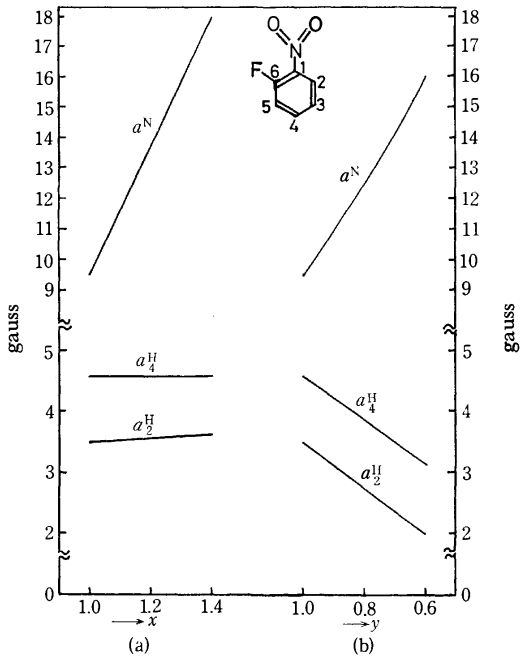

Fig. 3. (a) Calculated hyperfine coupling constants shown as a function of oxygen Coulomb integral parameter x: $\alpha_O=\alpha+x\beta$, $\beta_{CN}=\beta$.
(b) Calculated hyperfine coupling constants shown as a function of resonance integral parameter y between the nitro group and the benzene ring: $\alpha_O=\alpha+\beta$, $\beta_{CN}=y\beta$.

experimental results can be reproduced by combining both effects: A larger shift in a_4^H than a_2^H is expected by combining the two results (Figs. 3a and 3b). The expectation agrees very well with the experimental results. Thus, for the solvent effect the following model seems to be reasonable; the nitro group of the *o*-fluoronitrobenzene anion radical is strongly solvated with water, the solvated nitro group being simultaneously twisted out of the plane of the benzene ring. The model of solvent effect was first suggested by Ludwig *et al.*[4] as the most likely for *ortho* substituted nitrobenzene anion radicals based on the results of MO calculation for nitrobenzene anion radical given by Rieger and Fraenkel. The reason why the model of the solvent effect given by Ludwig *et al.* is acceptable, although their model was not derived from a precise MO calculation for *ortho* substituted nitrobenzene anion radical itself but for the unsubstituted nitrobenzene anion radical, can be understood as follows. For the shift in splittings, the MO calculation made by Rieger and Fraenkel and by us for both nitrobenzene and *o*-fluoronitrobenzene give similar results. Both a^N and a_2^H increase with the increase of α_O, while a^N increases and a_2^H as well as a_4^H decrease with the decrease of β_{CN}, indicating that the tendency of the shift in splittings with the variation of α_O and β_{CN} is insensitive to the species of the substituent as well as the position of the substitution. It is also expected that the results (Figs. 3a and 3b) can be applied to *meta* or *para* mono substituted nitrobenzene anion radicals. Thus, the experimental results where the relative magnitudes of the shift in splittings of mono substituted nitrobenzene anion radicals are in the order *ortho*>*meta*>*para* isomers, can be attributed to the steric influence of the substituent on the nitro group.

Solvent Effect in Polarographic Half-Wave Potentials. It is known that a correlation exists between polarographic half-wave potential $E_{1/2}$ and the energy of the lowest vacant orbital m such as[23]

$$-E_{1/2} = -bm + c \qquad (3)$$

where m is the energy in unit of β, b and c are both constants. The values $b=3.0$ and $c=1.0$ were obtained as values which fit our experimental results. Half-wave potentials calculated from Eq. (3) as well as the experimental results are given in Table 3. Comparison of the calculated values with the experimental values indicates that there are three characteristic cases. Firstly, for fluoronitrobenzene, in which little steric effect is expected, the calculated values correlate very

23) A. Streitwieser, Jr., "Molecular Orbital Theory for Organic Chemists," John Wiley & Sons, Inc., New York, London (1961) Chap. 7; see also Chap. 3 in Ref. 20.

Table 3. Half-wave potentials $E_{1/2}$ and energies of the lowest vacant orbitals m of substituted nitrobenzenes

	$-m$[a]	$-E_{1/2}$ V vs. SCE	
		calcd	obsd
o-fluoronitrobenzene	0.315	1.05	1.05
m-fluoronitrobenzene	0.2964	0.99	0.97
p-fluoronitrobenzene	0.3174	1.06	1.07
o-chloronitrobenzene	0.3074	1.02	1.06
m-chloronitrobenzene	0.2962	0.99	0.93
p-chloronitrobenzene	0.3085	1.03	0.99
o-nitrotoluene	0.2974	0.998	1.26[c]
m-nitrotoluene	0.2959	0.992	1.18[c]
p-nitrotoluene	0.2975	1.00	1.20[c]
o-nitrophenol	0.3403	1.12	0.83
m-nitrophenol	0.2970	0.99	1.08
p-nitrophenol	0.3461	1.14	1.12

a) MO parameters are the same as those used in previous works (Refs. 13 and 14).
b) Data in DMF cited in Ref. 24.
c) Data in ACN cited in Ref. 12.

well with the experimental results *viz.*, the order of the half-wave potential is *meta*>*ortho*>*para* isomers. Secondly, for chloronitrobenzene and nitrotoluene, in which steric hindrance of the nitro group is expected for *ortho* isomers, experimental results show that the order of the half-wave potential is *meta*>*para*>*ortho* isomers, while calculation shows it to be *meta*>*ortho*>*para* isomers. Thirdly, for nitrophenol, in which intramolecular hydrogen bond is expected for *ortho* isomers, experimental results show the order to be *ortho*>*meta*>*para* isomers, and calculation *meta*>*ortho*>*para* isomers. As is evident from the calculated values of m (Table 2), the energy level of the lowest vacant orbital falls with the increase of α_0 while it is enhanced with the decrease of β_{CN}. Thus, when hindered rotation of the nitro group is expected to be operative the half-wave potential will shift to more negative, resulting in a potential series of *meta*>*para*>*ortho* isomers. On the other hand, when intramolecular hydrogen bond is expected the half-wave potential will shift to less negative, resulting in a potential series of *ortho*>*meta*>*para* isomers. The expectation agrees very well with the experimental results of nitrotoluene, chloronitrobenzene and nitrophenol.

The half-wave potentials of halonitrobenzenes were reported to shift to less negative with increasing the concentration of water in DMF.[24] The shift in half-wave potentials of *ortho*, *meta*, and *para* isomers, at 20 per cent water content, were found to be 0.17 V, 0.17 V, 0.18 V, respectively, for fluoronitrobenzene and 0.17 V, 0.17 V, 0.19 V, respectively, for chloronitrobenzene and 0.14 V, 0.16 V, 0.18 V, respectively, for bromonitrobenzene and 0.14 V, 0.14 V, 0.17 V, respectively, for iodonitrobenzene, indicating that the relative magnitude of the shift in half-wave potential is generally in the order *ortho*<*meta*<*para* isomers. It is now evident that the hindered rotation of the nitro group resulting from the hydroxylic solvation will make the half-wave potential shift to more negative, while the hydroxylic solvation alone will make it shift to less negative. Thus, the slightest shift in half-wave potentials of *ortho* isomers and the most pronounced shift for *para* isomers with the increase of water concentration would be understood.

Solvent Effect in Electrochemical Reduction of Halonitrobenzene. The electrochemical reduction of mono substituted halonitrobenzene has been studied by ESR spectroscopy as well as by voltammetry, attention being paid to the elimination of the halogen atom. The chlorine atom of *o*-chloronitrobenzene and the bromine atom of *o*-bromonitrobenzene were eliminated by electrolytic reduction at mercury pool cathode and the ESR spectrum of nitrobenzene anion radical was observed.[14,24-26] When phenol or water was added as proton donors the elimination of the halogen atom was impeded. A survey of the proposed reaction mechanism for the elimination of the halogen atom of halonitrobenzene indicates that two electrons should be involved in this reaction.[24] Thus, the dehalogenation reaction at the electrode is shown schematically as follows by taking *o*-bromonitrobenzene as an example

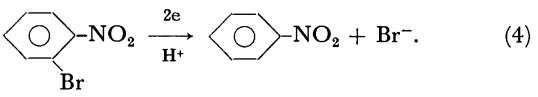

(4)

The process is considered to be a kind of electrophilic aromatic substitution reaction. The following transition state is acceptable in view of the fact that the aromatic substitution reaction under consideration proceeds following the electrochemical reduction

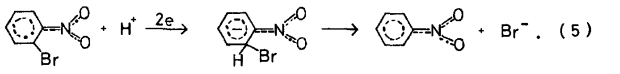

(I) (II) (III) (5)

The reactivity of the aromatic substitution reaction was studied by Fukui and his co-workers, and an index called the frontier electron density or superdelocalizability correlated with the stability of the transition state similar to the state (II) has been proved to be useful for elucidating the reactivity of the aromatic substitution.[27] The frontier electron density of the reaction under consideration is the electron density of the lowest vacant orbital of halonitrobenzene. It is formulated as $f_r^N=2(C_r^{lv})^2$. This index is reduced in magnitude (Table 2) with the reduction of the conjugation between the nitro group and the benzene ring. Thus, the dehalogenation reaction should be expected to be impeded as increasing the strong hydro-

24) T. Fujinaga, T. Arai, and C. Kitazawa, *Nippon Kagaku Zasshi*, **85**, 811 (1964); T. Fujinaga, K. Izutsu, K. Umemoto, T. Arai, and K. Takaoka, *ibid.*, **89**, 105 (1968); T. Fujinaga, K. Umemoto, and T. Arai, *Denki Kagaku*, **34**, 135 (1966).
25) T. Kitagawa and R. Nakashima, *Rev. Polarog.* (Kyoto), **13**, 115 (1966).
26) T. Kitagawa, T. Layloff, and R. N. Adams, *Anal. Chem.*, **35**, 1086 (1963).
27) Chap. 5 in Ref. 19 and Chap. 11 in Ref. 23.

xylic solvation.[28] The expectation is well correlated with experimental observation. A similar decrease of reactivity of the halogen atom of halonitrobenzene due to the hindered rotation of the nitro group has been summarized by Hammond and Hawthone;[29] the reactivity against piperidine decreases when the nitro group is sterically hindered. In conclusion, this model will constitute a major physical picture of solvent effect although it may not be conclusive, in so far as rigorous synthetic investigations by various experimental methods are still insufficient.

The authors express their thanks to Profs. Kenichi Fukui and Teijiro Yonezawa and laboratory members for their suggestions and cooperation in carrying out the molecular robital calculation. Thanks are also due to Prof. Toshio Arai for his discussion on the dehalogenation reaction.

28) The frontier electron density as well as the superdelocalizability indicate that the most reactive position of *ortho* substituted nitrovenzene anion radical is not *ortho* but *para* position. No sample reactions are known to verify this. Our present interest is to know how the reactivity of the ring substitution reaction changes with the value of β_{CN}, irrespective of the reaction position.

29) G. K. S. Hammond and M. F. Hawthone, "Steric Effect in Organic Chemistry," ed. by M. S. Newman, John Wiley & Sons, Inc., New York, London (1956) Chap. 3.

BULLETIN OF THE CHEMICAL SOCIETY OF JAPAN, VOL. 46, 2721—2723 (1973)

Studies on Fragment Ion Distribution and Reactions with the Use of a Charge Spectrometer. IV. Dependence of Cross Sections of Some Ion-Molecule Reactions on the Kinetic Energy of Ions

Toshio NAGATANI, Kenji YOSHIHARA, and Takanobu SHIOKAWA

Department of Chemistry, Faculty of Science, Tohoku University, Aoba, Aramaki, Sendai 980

(Received January 9, 1973)

Cross sections of methylamine and methanol for ion-molecule reactions with various rare gases have been studied by means of a charge spectrometer used as a double mass spectrometer. The results differed from those predicted by the Gioumousis-Stevenson theory. The difference was most pronounced for helium ion, the lightest ion.

It was reported by Field, Franklin, and Lampe[1] and also by Gioumousis and Stevenson[2] that the cross section of the ion-molecule reaction was inversely proportional to the square root of the kinetic energy of ions. Their argument was based on the theory of ion-induced dipole interaction. However, interpretation of the results by such a model is not always simple. The reaction cross section is predominantly determined by the collision cross section in gas kinetics when the energy of ions increases.[3]

The present report deals with the specific features of the reaction cross sections of methylamine and of methanol for various ions of rare gases.

Expreimental

Details of the charge spectrometer which also served as a double mass spectrometer of a perpendicular type were reported elsewhere.[4,5] The procedure was modified by applying a different electric field gradient. The primary ions of 10^{-13}—10^{-12} A were introduced into the source volume filled with target gases. The maximum pressure of the gases was 1.0×10^{-5} Torr. The reaction products in the source volume were abstracted into the analyzer system by the action of the installed lenses and measured with an electron multiplier of 16 stages.

An example of the mass spectrum of methylamine bombarded with Xe^+ with energy of 8.0 eV is shown in Fig. 1. We see that there are two series of product ions: one with mass-charge ratio of an integer produced through collision complex formation (open bars); the other with non-integer

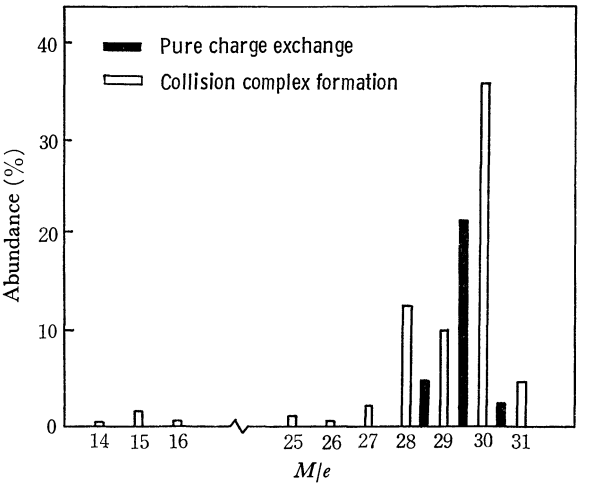

Fig. 1. Mass spectrum of methylamine bombarded with X^+.

1) F. H. Field, J. L. Franklin, and F. W. Lampe, *J. Amer. Chem. Soc.*, **79**, 2419 (1957).

2) G. Gioumousis and D. P. Stevenson, *J. Chem. Phys.*, **29**, 294 (1958).

3) D. A. Kubose and W. H. Hamill, *J. Amer. Chem. Soc.*, **85**, 125 (1963).

4) T. Shiokawa, K. Yoshihara, M. Yagi, T. Omori, H. Kaji, M. Hiraga, T. Nagatani, and Y. Takita, *Shitsuryo Bunseki*, **18**, 1230 (1970).

5) T. Nagatani, K. Yoshihara, and T. Shiokawa, *ibid.*, **20**, 97 (1972).

values of mass-charge ratio produced by pure charge exchange (closed bars). Since kinetic energy is transferred to the product in the complex formation, the apparent m/e ratio of the same fragment ion appears in the higher position as compared with that derived from pure charge exchange. Thus, the ions of the m/e ratio (30.5), (29.5), and (28.5) are considered to be the products by pure exchange whose net m/e ratios are (31), (30), and (29), respectively. The intensity of the ions caused by the charge exchange is 28.5% for the total ionization (Fig. 1). The same treatment is applicable to the other gases.

Results and Discussion

The ions abstracted into the analyzer system are classified as follows.

1) Primary ions,

a) having unchanged kinetic energy without interaction with target gases.

b) having altered kinetic energy by interaction with target gas molecules, *i.e.* inelastic scattering.

2) Stripping reaction products,

$$A^+ + B_1B_2 \longrightarrow AB_1^+ + B_2$$

where A^+ is the primary ion, B_1B_2 denotes the target molecule composed of parts B_1 and B_2, and AB_1^+ is the stripping reaction product.

3) Product ions formed through complex formation,

$$A^+ + B_1B_2 \longrightarrow [A-B_1B_2]^+ \longrightarrow B_1^+ + B_2 + A$$
$$\text{or } B_1 + B_2^+ + A \text{ etc.}$$

4) Product ions formed by charge exchange,

$$A^+ + B_1B_2 \longrightarrow A + B_1B_2^+$$

This is often accompanied by dissociation reactions.

$$A^+ + B_1B_2 \longrightarrow A + B_1B_2^+$$
$$B_1B_2^+ \longrightarrow B_1^+ + B_2$$
$$\text{or } B_1 + B_2^+$$

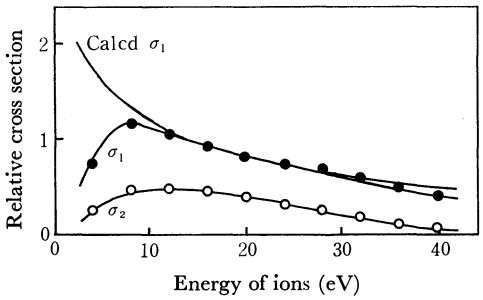

Fig. 2. Two kinds of cross sections of methylamine bombarded with Xe^+.

We defined the reaction cross section σ_1 according to complex formation and σ_2 according to charge exchange. The intensity of the stripping reaction products is very small and can be neglected. The relations of σ_1 and σ_2 with energy are shown in Fig. 2 which corresponds to the experiment of methylamine bombarded with Xe^+. The error of each experimental point does not exceed 20%. The calculated values are obtained by application of the Gioumousis-Stevenson's theory of inverse-square-root dependence of kinetic energy. Experimental values of σ_1 fit the calculated values in the range 12.0—32.0 eV. The charge exchange cross section σ_2 shows a somewhat different inclination from that of σ_1. Increase of σ_1 in the very low energy region implies that fragmentation increases as translational energy carried into the methylamine molecule from the xenon ion increases and the activated complex highly excited in its vibrational states increases.

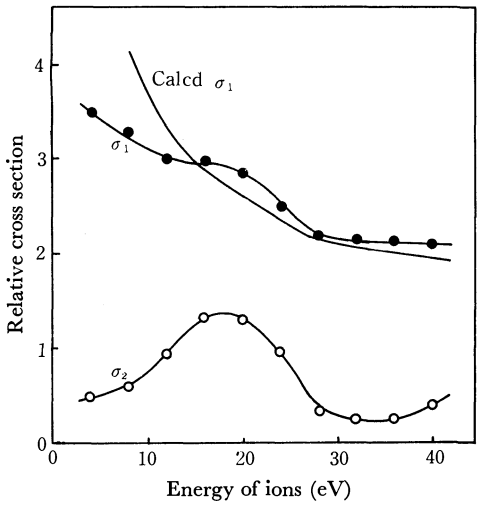

Fig. 3. Two kinds of cross sections of methanol bombarded with Xe^+.

The results for methanol are plotted in Fig. 3. The calculated values for σ_1 according to the Gioumousis-Stevenson's theory can nearly account for the experimental values in the range 16.0—36.0 eV. It seems that the inverse-square-root dependence of the cross section on ion energy fits the energy range below 40 eV irrespective of ions. The trend of σ_2 for methanol differs from that of σ_1. It has a maximum at 16.0—20.0 eV. For both systems the fragment ions which contribute to σ_2 include the same ionic species of the approximately same relative intensity.[6,7] This shows that the separation of σ_2 from σ_1 is quite good.

However, when Ar^+ is introduced into the source volume as the primary ion, there is a large difference

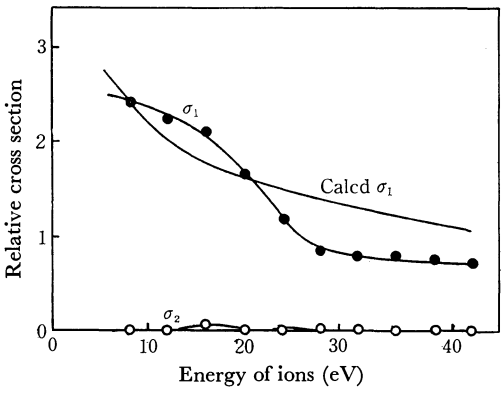

Fig 4. Ionization cross sections of methylamine bombarded with Ar^+.

6) T. Nagatani, K. Yoshihara, and T. Shiokawa, This Bulletin, **46**, 1306 (1973).

7) T. Nagatani, K. Yoshihara, and T. Shiokawa, *ibid.*, **46**, 1450 (1973).

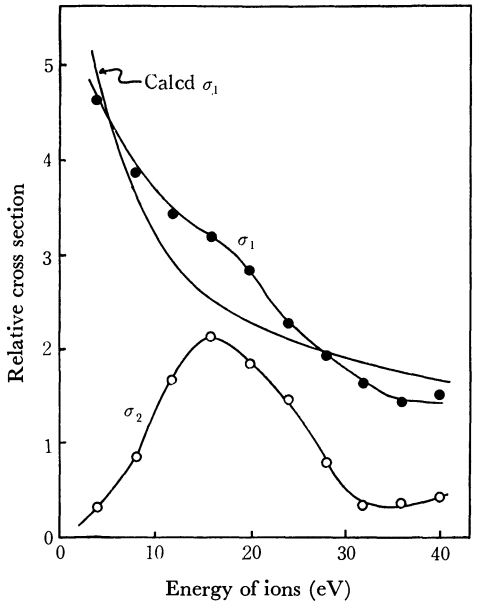

Fig. 5. Ionization cross sections of methanol bombarded with Ar^+.

between the systems of methylamine and methanol (Figs. 4 and 5). For the primary ion whose recombination energy is about 15 eV, the ratio σ_2/σ_1 is very small in methylamine. When translational energies of primary ions increase to 100—200 eV, σ_2 becomes 10% for σ_1, and negligible for the ions of 2 keV. The trend of σ_1 in 30—40 eV fits the calculated value.

σ_1 in the methanol system is in good accordance with the calculated value (Fig. 5). However, σ_2 has a maximum at about 16 eV. At this energy σ_2 contributes 40.1% of the total ionization cross section.

σ_2 is small for the primary ions of He^+. It is negligibly small in methylamine (Fig. 6). Similar results for methanol are shown in Fig. 7. The calculated values of σ_1 for methylamine and for methanol using the Gioumousis-Stevenson's theory largely differ from the experimental ones. Replacement of inverse-square-root dependence by inversely proportional dependence does not essentially change the situation. These discrepancies suggest some factors other than induced dipole interaction. In this connection recent reports by Koski and his co-workers are of interest.[8-11] Their

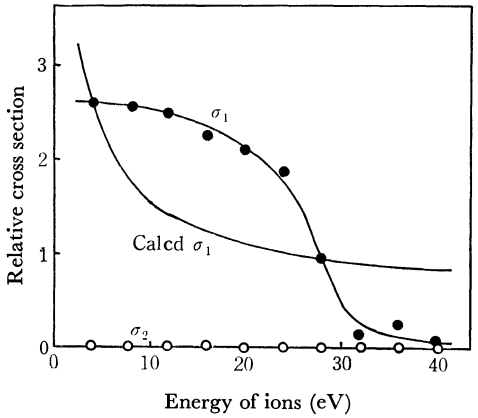

Fig. 6. Ionization cross sections of methylamine bombarded with He^+.

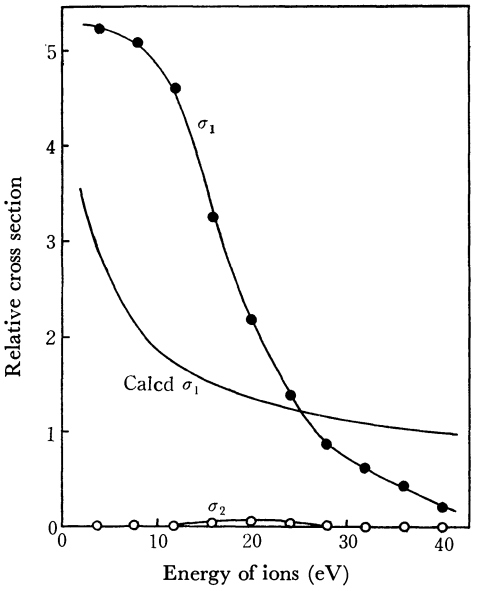

Fig. 7. Ionization cross sections of methanol bombarded with He^+.

results show that complicated factors are included in determining the formation of ionic species in the reaction of C^+ with hydrocarbons. However, it is not easy to understand why in the case of the lightest rare gas ion the deviation from the Gioumousis-Stevenson's theory is most pronounced. It is possible that the energy carried into the activated complex through the collision is not kept in vibronic states or that the contributed energy is limited through the collision which resembles an elastic one.

The authors thank Mr. Hiraga for his kind help in the operation of the double mass spectrometer.

8) R. C. C. Lao, R. W. Rozett, and W. S. Koski, *J. Chem. Phys.*, **49**, 4202 (1968).
9) P. S. Wilson, R. W. Rozett, and W. S. Koski, *ibid.*, **52**, 5321 (1970).
10) P. S. Wilson, R. W. Rozett, and W. S. Koski, *ibid.*, **53**, 1276 (1970).
11) P. S. Wilson, R. W. Rozett, and W. S. Koski, *ibid.*, **53**, 3494 (1970).

The Magnetic Properties of Manganese(II) Phthalocyanine

Hirokazu MIYOSHI, Hiroaki OHYA-NISHIGUCHI, and Yasuo DEGUCHI*

Department of Chemistry, Faculty of Science, Kyoto University, Kyoto 606

**College of Liberal Arts and Science, Kyoto University, Kyoto 606*

(Received January 11, 1973)

The magnetic transition from the ferro- to the para-magnetic state of manganese(II) phthalocyanine ($C_{32}H_{16}N_8Mn$) has been observed by measurements of the magnetic susceptibility, the magnetization and the proton magnetic resonance in the low-temperature range. The positive Weiss constants were obtained from the static susceptibility measurements and the proton magnetic measurements. Moreover, the magnetic-field dependences of the experimental results were found in the low-temperature range. All of those findings confirm the ferromagnetic behavior of this substance in the lower-temperature region. From the measurements of the frequency shift in the resonant circuit of the proton magnetic resonance apparatus, the transition temperature was determined to be 8.6 K. A possible mechanism of long-range ordering was also discussed on the basis of the crystal structure of this substance.

The phthalocyanines are interesting organo-metallic compounds which have been extensively studied for their semiconductive and photoconductive properties. Moreover, most of the transition-metal phthalocyanines are known to be paramagnetic; some of them have been studied in terms of their electronic structures by the electron spin resonance[1-4] or magnetostatic methods.[5]

The magnetic behaviors[6] of transition-metal phthalocyanines have been investigated in the temperature range above 77 K; the results obey the Curie-Weiss law, with mostly negative Weiss constants, thus implying the existence of large zero-field splittings or of antiferromagnetic exchange interactions among molecules. So far we know, most reports of the magnetic properties have been concentrated upon an investigation of the electronic structures of the molecule. However, the investigations of the magnetic properties themselves, especially from a viewpoint of the magnetic-phase transition, are still not well-established.

The magnetic properties of manganese (II) phthalocyanine (hereafter abbreviated as PcMn) are of considerable interest. This substance obeys the Curie-Weiss law in the high-temperature range, and its Weiss constant has a positive sign, unlike those of the other metal-phthalocyanines. The magnetic susceptibilities of PcMn have been measured by Lever,[6] who found the positive Weiss constant to be 6 K. Recently, Mitra and his co-workers[7] measured the magnetic susceptibilities and anisotropies of PcMn over quite a wide temperature range (1.7—300 K) and reported the existence of the ferromagnetic interaction among molecules; they added some speculations about the spin state of the molecule that a divalent-manganese ion might have at $s=3/2$. However no detailed discussion of the occurrence of the magnetic ordering has been made so far.

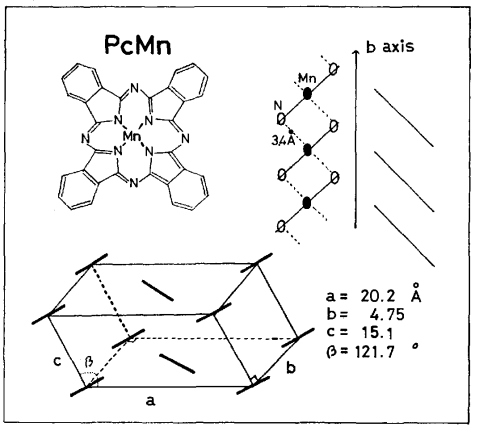

Fig. 1. Molecular and schematic crystal structures of manganese(II) phthalocyanine ($C_{32}H_{16}N_8Mn$). The molecular plane is approximately normal to the ab-plane.

We have studied the magnetic properties of PcMn in more detail and obtained affirmative evidence for the occurrence of the magnetic-phase transition of PcMn.

Experimental

PcMn was prepared by the method of Linstead *et al.*[8] The product was extracted with α-chloronaphthalene and then sublimed in an atmosphere of pure nitrogen at the temperature of 550 °C. The single crystals grown by sublimation were ground and powdered. Found: C, 67.54; H, 2.76; N, 19.19%. Calcd: C, 67.7; H, 2.8; N, 19.7%.

All the measurements were carried out in the microcrystalline state. The measurements of the static (dc) susceptibility and the temperature dependence of the magnetization were performed on powder samples of about 10—50 mg between 1.8 and 77 K in the magnetic fields of 0.82, 1.12, 1.88, 7.0, 8.3, and 10.2 KOe, by means of a magnetic torsion balance described elsewhere.[9] The temperatures of the samples were measured with a carbon resister

1) D. J. E. Ingram and J. E. Bennett, *Discuss. Faraday Soc.*, **19**, 140 (1955).
2) J. F. Gibson, D. J. E. Ingram, and D. Schonland, *ibid.*, **26**, 72 (1958).
3) S. E. Harrison and J. M. Assour, *J. Chem. Phys.*, **40**, 365 (1964).
4) J. M. Assour and S. E. Harrison, *Phys. Rev.*, **136**, A1368 (1964).
5) R. L. Martin and S. Mitra, *Chem. Phys. Lett.*, **3**, 183 (1969); *Inorg. Chem.*, **9**, 182 (1970).
6) A. B. P. Lever, *J. Chem. Soc.*, **1965**, 1821.
7) C. G. Barraclough, R. L. Martin, and S. Mitra, *J. Chem. Phys.*, **53**, 1638 (1970).
8) P. A. Barret, C. E. Dent, and R. P. Linstead, *J. Chem. Soc.*, **1936**, 1719.
9) M. Mekata, *J. Phys. Soc. Jap.*, **17**, 796 (1962).

and an AuCo–Cu thermocouple calibrated by measuring not only the magnetic susceptibility of Mn-Tutton salt, but also the vapor pressures of liquid helium, liquid hydrogen, and liquid nitrogen. Moreover, the susceptibility measurements were made by means of a Hartshorn bridge between 13.8 and 20.2 K in the temperature region attainable by the pumping out of liquid hydrogen. The temperature was determined from the known susceptibility of the standard sample, $Cr(NH_3)_6Cl_3$, and from the vapor pressures of liquid hydrogen.

The proton NMR absorption spectra were observed between 10.8 and 20 K using the usual Pound-Watkins-type oscillator with a 80 Hz field modulation and a field sweep. The oscillator coil with a sample tube was directly immersed in liquid hydrogen. The temperatures were measured with a calibrated carbon resister and by means of the vapor pressure of liquid hydrogen. The proton NMR absorption of liquid hydrogen was used as a standard for the estimation of the absorption line-shift. The magnetic field was calibrated by means of the proton absorption of H_2O.

Results

Magnetic Suscetibility. The diamagnetic correction was within the range of experimental error at low temperatures.[10] The results of the dc susceptibility measurements in the field of 10.2 KOe obey the Curie-Weiss law between 30 and 77 K; thus, a positive Weiss constant, 18.4 K, was obtained, one which agrees almost entirely with those reported by Mitra *et al.* From the slope of the $1/\chi_M$ *vs.* T plots, we obtained a g-value of 2.25, assuming that $s=3/2$ (the effective moment, $\mu_{eff}=4.36\ \mu_B$). At temperatures below about 20 K, the molar susceptibility deviates from the Curie-Weiss law and reaches a constant maximum value below 7 K; this behavior is dependent on the magnetic-field strength.

Avoiding the effect of an extensive magnetic field, as will be discussed later, the ac susceptibilities were also measured in the temperature range between 13.7 and 20.2 K.

The results precisely obey the Curie-Weiss law for $s=3/2$ and $g=2.93$ in this temperature range, in contrast with the results of the dc susceptibilities, and they show a positive Weiss constant of 9.0 K.

Magnetization. The field dependence of the magnetization was measured at the temperatures of 4.2, 11.1, and 20.3 K, as is shown in Fig. 2. At 20.3 K, the magnetizations are linearly dependent on the magnetic field as the usual paramagnetic substance, but at 11.1 K they deviate from a linear dependence and at 4.2 K they become larger. We have rewritten the data in relation with σ^2 to H/σ in Fig. 3. It is also worth-while to notice that, in Fig. 2, the value of the saturation magnetization extrapolated from the value at 4.2 K is much smaller than the value calculated using $s=3/2$ and $g=2$. The temperature dependence of the magnetization at several constant fields between 0.84 KOe and 10.2 KOe is shown in Fig. 4. The dependence of the magnetization on the magnetic-field strength is then found, as in the usual ferro-magnetic substances.

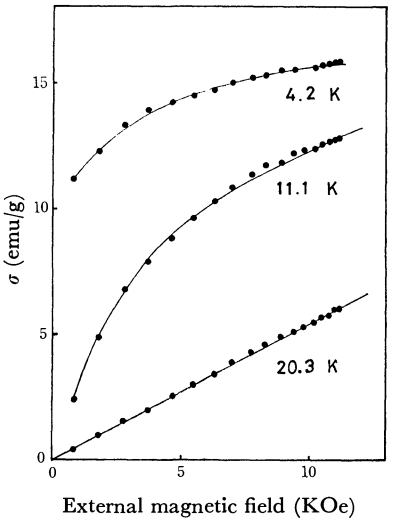

Fig. 2. Magnetization curves at 20.3, 11.1, and 4.2K.

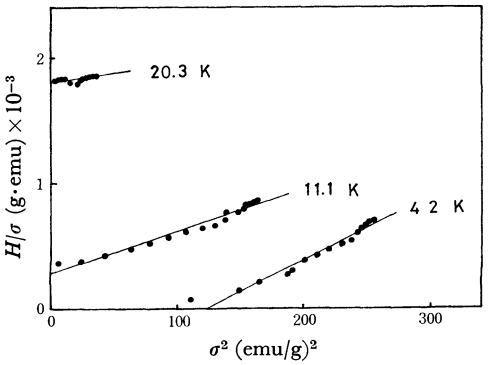

Fig. 3. H/σ *vs.* σ^2 plots of the magnetization curve at 20.3, 11.1, and 4.2 K.

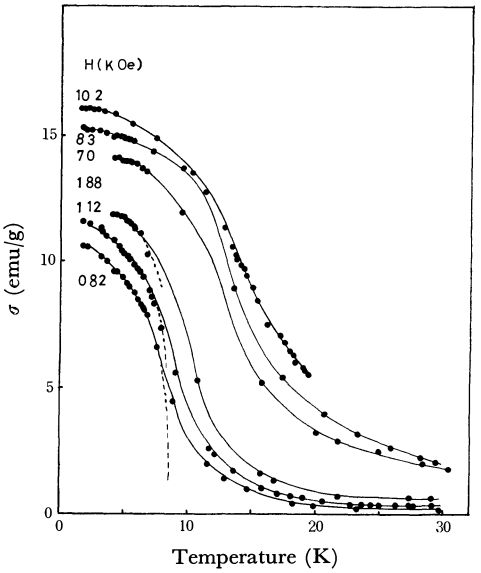

Fig. 4. Temperature dependences of the magnetization at the field of 0.82, 1.12, 1.88, 7.0, 8.3, and 10.2 KOe.

Proton Magnetic Resonance. The proton magnetic resonance (PMR) measurements were carried out at the frequencies of 18 and 12 MHz. In the first, when measured at the frequency of 18 MHz and the tem-

10) C. G. Barraclough, R. L. Martin, and S. Mitra, *J. Chem. Phys.*, **55**, 1426 (1971).

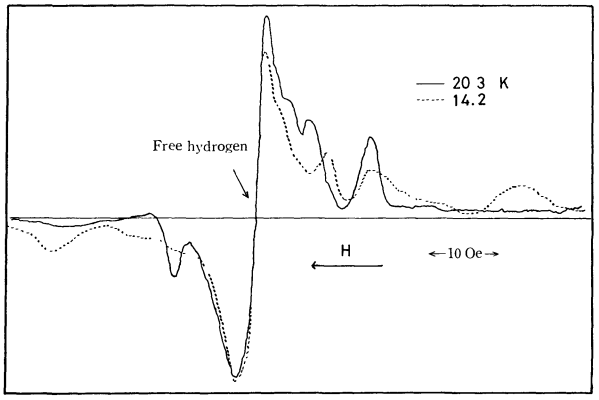

Fig. 5. PMR spectra of the polycrystalline sample at 20.3 and 14.2 K at 12 MHz. In the figure, *free hydrogen* means a free proton absorption of the coolant.

perature of liquid helium (4.2 K), no signals could be observed by sweeping the magnetic field between 500 Oe and 12 KOe. In the second, when measured between 10.8 and 20 K, a temperature range attainable by the pumping out of liquid hydrogen, several absorption lines were observed, as is shown in Fig. 5, where the absorption of the hydrogen molecule used as a coolant is superimposed upon them. We could confirm at least four lines, three in the lower field and one in the higher field. These signals can not be interpreted by the model of the two different proton sites in the molecule, but they may be attributed to the different local fields caused by the magnetic short-range ordering effect at the individual proton sites. We are now engaged in clarifying this point further. The shifts of the higher- and lower-field absorptions were measured from the position of that of the hydrogen molecule; the reciprocals of the shifts are plotted as a function of the temperature in Fig. 6. At 12 MHz, the results are linearly proportional to the temperature between 14 and 20.2 K. The straight line intersects the abscissa displaying the temperature of 9.6 K. Similarly, at 18 MHz, the reciprocal shifts are linear to the temperature between 15 and 20.2 K and intersect the abscissa at the same point, 9.6 K. However, the deviation from the linearity appears at a higher tem-

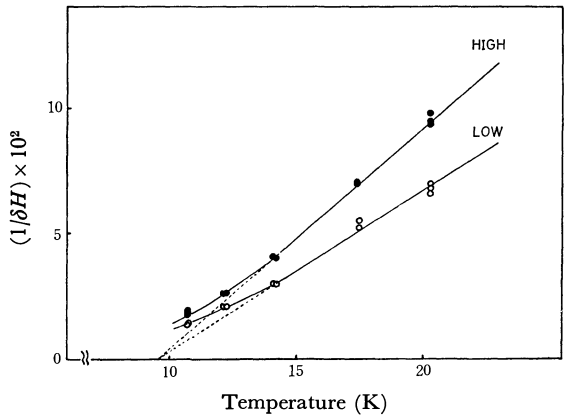

Fig. 6. Reciprocals of the PMR line shifts ($1/\delta H$) as a function of temperature at 12 MHz. HIGH and LOW mean higher and lower portions of the spectrum, as shown in Fig. 5, respectively.

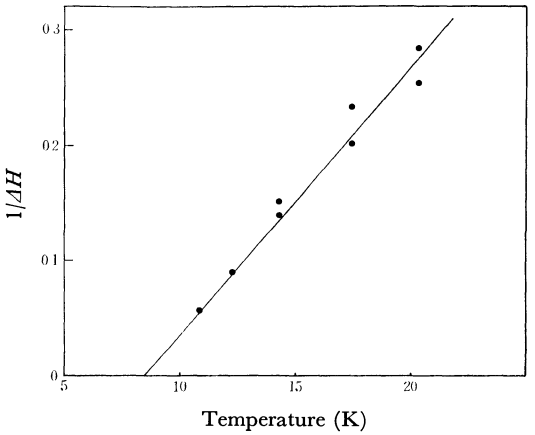

Fig. 7. Reciprocal PMR line-width ($1/\Delta H$) of the lower portion in Fig. 5 as a function of temperature.

perature, 15 K, and is much larger than that at 12 MHz.

The reciprocal line-width of the lower portion at 12 MHz is also shown as a function of the temperature in Fig. 7. The reciprocal PMR line-widths are linearly proportional to the temperature between 10.8 and 20.2 K.

To determine the transition temperature more accurately,[11] a powdered sample was placed in the coil of an oscillator used for PMR, and the relative ac susceptibilities (detected as a frequency shift in the resonant circuit) in a zero field and at 8 KOe were measured as a function of the temperature from 4.2 to 30 K. A typical measurement is shown in Fig. 8. The frequency shift in the zero field reaches a maximum around 9.2 K, but the point of intersection of the two gradients on the upper and the lower sides of the maximum is 8.6 K; this is regarded as the magnetic transition temperature. The shift at about 8 KOe also shows a broad maximum, but the transition point is obscured by the influence of the magnetic field.

Ferromagnetic Resonance. In order to investigate the magnetic-ordered state of PcMn, ferromagnetic resonance measurements using an X-band ESR spectrometer were carried out in both powder and needle-like

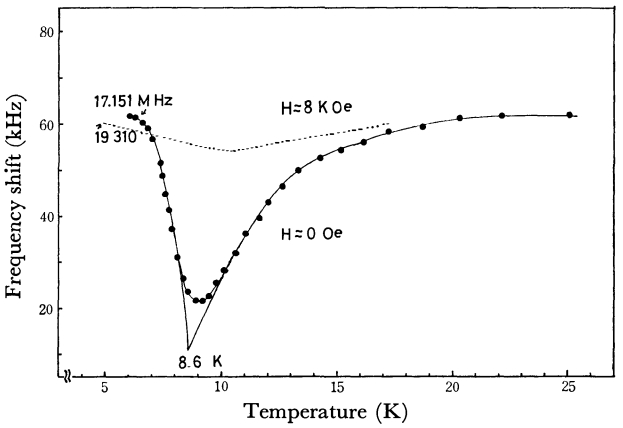

Fig. 8. Frequency shift (relative ac susceptibility) as a function of temperature.

11) H. H. Wickman, A. M. Trozzolo, H. J. Williams, G. W. Hull, and F. R. Merritt, *Phys. Rev.*, **155**, 563 (1967).

single crystal samples at 4.2 and 77 K with fields up to 25 KOe. Assuming the obtained needle-like crystal to be an infinitely elongated cylinder in order to calculate its demagnetization factor, and estimating the saturation magnetization (M_0) as 1.7β/ion (*cf.* Fig. 2), we calculated the resonance frequency (ω) of PcMn based upon Kittel's resonance conditions[12] and concluded that the deviation from the usual resonant field should be much smaller than 10^3 Oe ($\omega/\gamma = H + 2\pi M_0$, $2\pi M_0 \ll 10^3$ Oe). However, we observed only one weak absorption with $g \approx 2.0$, the line-width ≈ 6 Oe; they seemed to be a free-radical resonance characteristic of most of the phthalocyanine compounds reported by Assour and Harrison.[13]

Discussion

The Weiss constant derived from ac susceptibility measurements in the temperature range between 13.7 and 20.4 K has a positive value, 10 K; this suggests the existence of ferromagnetic interaction between molecules. As is well known,[14] when there is an applied magnetic field the ferromagnetic substance retains its magnetization in the vicinity of the Curie temperature. Thus, near the Curie temperature, the various magnetic properties of the ferromagnetic substance will be influenced by the applied magnetic field and, hence, the Curie temperature will be obscured. As is shown in Fig. 4, the dc susceptibility and the magnetization in the low-temperature range are dependent on the magnetic-field strength; the higher the magnetic field, the more gradually the magnetzation decreases when the temperature is raised, as is characteristic of the usual ferromagnetic substances (that is, as has been stated above, the influence of the magnetic field obscures the transition temperature from the para-magnetic state to the ferro-magnetic state). From the microscopic point of view, the results of PMR measurements between 10.8 and 20.2 K support the existence of a positive Weiss constant as well as the influence of the magnetic field, as will be shown below. The paramagnetic shift is proportional to the mean value, $\langle S_z \rangle$, of the electron-spin component and, consequently, to the bulk magnetic susceptibility of the sample. The Weiss constants obtained from the temperature variations of the paramagnetic shifts at 12 MHz and at 18 MHz are both 9.6 K; this is consistent with the results of the bulk ac susceptibility. The deviation from the Curie-Weiss law is larger at 18 MHz than at 12 MHz, indicating the influence of the magnetic field on the shifts. The positive Weiss constants obtained from the microscopic PMR measurements as well as from the bulk dc and ac susceptibility measurements, and the magnetic-field dependences of experimental results, all confirm the ferromagnetic behavior of this substance in the lower-temperature region.

Now, let us turn to the determination of the Curie temperature (T_c) of PcMn, in which spontaneous magnetization occurs. In Fig. 3, H/σ is plotted against σ^2. From the thermodynamic description[14] of the magnetization of a ferro-magnetic material, $H/\sigma = A + B\sigma^2$, where the coefficients, A and B, are the functions of the temperature. The Curie temperature (T_c) can be determined from the temperature at which the coefficient $A=0$. Taking this relation into account, it is evident that T_c exists between 4.2 and 11.1 K. As is shown in Fig. 2, the saturation magnetization (σ_s) extrapolated from the data at 4.2 K is 17.0 G cm^3/g, much smaller than the theoretically-estimated value, (29.5 G cm^3/g calculated from $s=3/2$ and $g=2.0$). Using the relation that $\sigma_s M = Ng\langle\mu\rangle$ on the assumption of $g=2.0$, the obtained average moment, $\langle\mu\rangle$, is 1.7 Bohr magneton. This value is about half the total spin value (3 Bohr magneton) expected from $s=3/2$. The temperature dependence of the magnetization in the magnetic field of 0.82 KOe suggests that the Curie temperature exists between 8 and 10 K, as is shown in Fig. 4.

The transition temperature was determined more accurately by relative ac susceptibility measurements using a PMR oscillator. In Fig. 8, the transition temperature is identified as 8.6 K on the basis of these data; this is consistent with the Weiss constants obtained by different methods of measurements. Similarly, as has already been mentioned, a remarkable magnetic-field dependence can be noticed, so that the transition temperature is obscured in the high magnetic field of 8 KOe. This is another piece of evidences for the ferromagnetic behavior of PcMn.

The reciprocal PMR line-width tends to broaden rapidly as the temperature is decreased, and it seems to diverge at T'_c (8.5 K), as may be extrapolated from Fig. 7. This temperature (T'_c) is surprisingly in agreement with the Curie temperature obtained above. So far we do not have a sufficient theoretical elucidation of the linewidth variation of PMR. However, provided that the divergence of the linewidth may be attributed to the onset of the long-range ordering of electron spins, we can recognize the coincidence of T'_c with T_c, because the rapid broadening of the line-width is the result of the critical fluctuation of spins in the neighborhood of the transition temperature.

From the experimental facts presented above, one may conclude that PcMn is the first example of a ferromagnet among the organo-metallic compounds and that its Curie temperature is 8.6 K.

A Possible Mechanism of Long-range Ordering. The above discussion has concentrated upon the magnetic properties. Now, let us briefly discuss the possible mechanism of long-range ordering. The crystal structure of PcMn is isomorphous with nickel(II) phthalocyanine,[15] whose structure is well known. As is shown in Fig. 1, the molecules are square planar ones stacked along the short monoclinic b axis of the crystal and the distance between these nearest molecules is 3.4 Å, which provides a possible pathway for magnetic ex-

12) C. Kittel, "Introduction to Solid State Physics," 3rd edition, J. Wiley & Sons., New York (1966), p. 525.

13) J. M. Assour and S. E. Harrison, *J. Phys. Chem.*, **68**, 872 (1964).

14) K. P. Belov; "Magnetic Transition," translated by W. H. Furry, Chaps. II and III, Consulants Bereau, New York (1961).

15) J. M. Robertson, *J. Chem. Soc.*, **1935**, 615; **1937**, 219.

change interaction between electron spins. The unit cell contains two nonequivalent molecules with parameters of (0, 0, 0) and (1/2, 1/2, 0). The axes of symmetry of a couple of molecules in the unit cell are almost at right angles, and both of them are equally inclined to the ac plane by an approximate angle of 45°.

Therefore, PcMn may form a magnetic chain different from the three-dimensionally-interacting spin system, and the exchange coupling between the next-nearest-neighbor spins in different chains (that is, between the different sites) is much weaker than that between nearest-neighbor spins in the same chain (between the equivalent ions along the b-axis). Possible pathways for superexchange between nearest-neighbor spins in the same chain were considered by S. Mitra *et al.*[7] It is well known theoretically[16] that the isolated magnetic linear chains do not have any magnetic-phase transition, but, in the presence of a small interaction between chains, there occurs a magnetic transition to the long-range ordered state in the lower-temperature region. Considering the discussion of PcCu based on ESR measurements,[4] there is a possibility for PcMn to go into a long-range ordered state, since the interaction between chains cannot be neglected. On the other hand, a reported speculation[7] on the electronic structure has suggested the existence of the zero-field splitting of the ground state, which may dominate the spin structure of the ordered state. Perhaps, the small value of saturation magnetization in Fig. 2 and the absence of any absorption signals of ESR and PMR measurements at 4.2 K suggests the canted ferromagnetism of PcMn. At any rate, for the discussion of the finer mechanism of the ferromagnetic interaction and the spin structure of the ordered state, it would be necessary to know which interaction is more dominant and what type of exchange is involved. Study along this line is now under way.

The authors wish to acknowledge their helpful discussions with Professor Mamoru Mekata, Dr. Yoshitami Ajiro and their other collaborators in the laboratory. They are also grateful to Professor Ikuji Tsujikawa and Dr. Hanako Kobayashi for offering them a chance to use the Hartshorn bridge apparatus. They also wish to thank Professor Natsu Ueda and Dr. Takashi Kobayashi for their helpful advice on the preparation of the manganese(II) phthalocyanine.

16) L. Onsager, *Phys. Rev.*, **65**, 117 (1944); H. E. Stanley and T. A. Kaplan, *Phys, Rev. Lett.*, **17**, 913 (1966).

BULLETIN OF THE CHEMICAL SOCIETY OF JAPAN, VOL. 46, 2728—2734 (1973)

The Magnetic Properties of Verdazyl Free Radicals. III.[1] The Anomalous Magnetic Behavior of Symmetrical Triphenylverdazyl

Nagao AZUMA,* Jun YAMAUCHI,** Kazuo MUKAI,*** Hiroaki OHYA-NISHIGUCHI,* and Yasuo DEGUCHI*

*Department of Chemistry, Faculty of Science, Kyoto University, Sakyo-ku, Kyoto 606
**The Institute for Chemical Research, Kyoto University, Uji, Kyoto 611
***Department of Chemistry, Faculty of Science, Ehime University, Matsuyama, Ehime 790

(Received February 7, 1973)

The static magnetic susceptibility and the ESR spectra from 1.6 to 300 K have been measured on a powder sample of the titled free radical. The broad maximum in the susceptibility which indicates an antiferromagnetic interaction has been observed at 6.9 K. The broadening of the ESR absorption line and the shift of the *g*-value have been found in the temperature region below T_{max}, in which the susceptibility reached its round maximum. There appeared anomalies in the slope of the susceptibility, the linewidth, and the *g*-value *versus* temperature curves in the vicinity of 1.7 K. These anomalies may imply a magnetic-phase transition from the short-range ordered state to the long-range ordered state at about 1.7 K. The existence of a ferromagnetic interaction between the magnetic chains in the triphenylverdazyl radical solid is discussed on the basis of the susceptibility, the spin distribution, and the crystal structure. It is understood qualitatively that the radical with a negative spin density has a latent ferromagnetic interaction in or between the magnetic chains, and that the obsrevation of this interaction greatly depends upon the molecular and crystal structure.

At a low temperature a number of free radical solids exhibit broad maxima in their susceptibilities which indicate an antiferromagnetic interaction between unpaired electrons in the radicals. In the case of neutral organic radicals, the magnetic behavior has been explained on the basis of magnetic linear chain models, where the linear Heisenberg and the one-dimensional Ising models have been commonly employed. On the other hand, all the organic free radicals show practically isotropic *g*-values very close to the free electron value. This implies a small spin-orbit interaction due to the quenching of the orbital angular momentum; as a result, one may take into account an isotropic exchange inter-

1) Part I: K. Mukai, N. Azuma, and K. Ishizu, This Bulletin, **43**, 3618 (1970).

action and a smaller magnetic dipolar one in order to interpret the magnetic data. Therefore, the appropriate model for discussing the magnetic behavior of free radicals may not be of the Ising-type with extremely anisotropic spins, but the Heisenberg model, with the isotropic exchange interaction; this model is employed in the present case. The one-dimensionality of the magnetic structure in the free radical solids may be acceptable, firstly, because the low symmetry of the crystal structure,[2-5] which, in turn, results in the small coordination number, z, of the unpaired electrons, where the linear chain $z=2$, and secondly, because of the uniaxial angular dependence of the $p_z\pi$-orbitals occupied by the unpaired electrons. In fact, we have found neither two- nor three-dimensional magnetic lattice in any organic radical solid, although Duffy *et al.*[6] proposed a magnetic quadratic-layered structure for di-*p*-anisyl nitroxide (DANO) in accordance with the crystal quadratic layer sub-lattice, which consists of molecular centers,[3] but with no regard for the angular dependence of the orbitals.[7]

It is well known theoretically[8] that the isolated magnetic linear chains do not show any sharp magnetic phase transition, but, a rather broad maximum susceptibility, and that, in the presence of a small interaction between the chains, the phase transition from a short-range ordered state to a long-range ordered state may occur. This magnetic phase transition has thus far been considered to be found in the complex of 1,3-bisdiphenylene-2-phenylallyl with benzene (BDPA-*Bz*)[7,9,10] and in 1,3-bisdiphenylene-2-*p*-chlorophenylallyl (*p*-Cl-BDPA).[7,11] The present paper will deal with 1,3,5-triphenylverdazyl (TPV), the magnetic measurements of which show the possible existence of the long-range ordering and whose crystal structure has been determined recently.[2]

If the crystal structure is known, one can carry out more detailed experiments to study minutely the magnetism of the radical solid. Unfortunately, the crystal structure of neither BDPA-*Bz* nor *p*-Cl-BDPA has been solved. It is also of much interest to relate the magnetic properties of radicals to their crystal structures and to examine the exchange interaction mechanism. In this paper we would like to describe the magnetic behavior of the titled radical and discuss the magnetism of TPV from the standpoints of exchange interaction, spin density, and the crystal structure. In the last section of discussion, the magnetism of the galvinoxyl radical will be discussed from the present point of view.

Experimental

The sample was prepared by the method of Kuhn and Trischmann and was purified a few times through recrystallization from a mixture of acetone and methanol.[12] The melting point, which ranged from 142.0 to 142.5 °C, was found to agree well with the value in the literature. The results of the elementary analysis for carbon, hydrogen, and nitrogen were in good accord with the calculated values (Found: C, 76.43; H, 5.52; N, 17.94%.) The ESR spectrum in 2-methyltetrahydrofuran (2-MeTHF) *in vacuo* appeared in nine lines, with a line separation of 5.8 Gauss which can be assigned as the hyperfine coupling constant of four nearly equivalent nitrogen nuclei, and which is close to the value measured in a benzene solution and reported in the literature.

The magnetic susceptibilities from 1.6 to 300 K were measured on powder samples prepared independently in a heterogeneous magnetic field up to 8.8 kOe by means of a magnetic torsion balance described elsewhere.[13] The temperatures were determined using a calibrated AuCo-Cu thermocouple and a carbon resister. Manganese Tutton salt was used for the calibration of the thermometers as well as the product of the magnitude times the gradient of the magnetic field.

The ESR absorption spectra were observed on powder samples from 1.7 to 4.2 K and at the temperature of liquid nitrogen and at room temperature using a JES-ME-type spectrometer with an 80 Hz-field modulation. The temperatures were determined by means of the vapor pressures of liquid helium. An aqueous solution of peroxylamine disulfonate was used as the standard for the estimation of the g-value at room temperature. Mn^{2+} in MgO was taken as the second standard for the g-value measurement at lower temperatures and as a field-calibrating material.

Results

Susceptibility. The data have been corrected for the diamagnetic contribution using Pascal's constants.[14] The absolute molar susceptibility, χ_M, corrected for diamagnetism, complies with Curie-Weiss law with a negative Weiss constant, $\theta=-8$ K, in the higher-temperature region. The susceptibility, however, deviates from the Curie-Weiss law at lower temperatures, and it shows a broad maximum with a value of $\chi_{max}=203\times10^{-4}$ emu/mol at a temperature of $T_{max}=6.9$ K. When the temperature is lowered further, the susceptibility decreases comparatively slowly towards a minimum and then, as is shown in Fig. 1, unexpectedly increases again just after passing through the minimum point at $T_n=1.7$ K, where a discontinuity in the slope of the susceptibility is observed. The finite susceptibility at 0 K is roughly estimated as to be equal to $\chi_{T=0}=170\times10^{-4}$ emu/mol by the extrapolation of the χ_M *versus* T curve between the T_{max} and T_n temperatures. The radical concentration, as determined from the susceptibility in the temperature region above

2) D. E. Williams, *J. Amer. Chem. Soc.*, **91**, 1243 (1969); preprint (to appear in *Acta Crystallogr.*).
3) A. W. Hanson, *Acta Crystallogr.*, **6**, 32 (1953).
4) D. E. Williams, *Mol. Phys.*, **16**, 145 (1969).
5) J. Lajzerowicz-Bonneteau, *Acta Crystallogr.*, **B24**, 196 (1968); D. E. Williams, *J. Amer. Chem. Soc.*, **89**, 4280 (1967).
6) W. Duffy, Jr., D. L. Strandburg, and J. E. Deck, *Phys. Rev.*, **183**, 2218 (1969).
7) J. Yamauchi, This Bulletin, **44**, 2301 (1971).
8) L. Onsager, *Phys. Rev.*, **65**, 117 (1944); H. E. Stanley and T. A. Kaplan, *Phys. Rev. Lett.*, **17**, 913 (1966).
9) W. O. Hamilton and G. E. Pake, *J. Chem. Phys.*, **39**, 2694 (1963).
10) W. Duffy, Jr., J. F. Dubach, P. A. Pianetta, J. F. Deck, D. L. Strandburg, and A. R. Miedema, *ibid.*, **56**, 2555 (1972).
11) J. Yamauchi, K. Adachi, and Y. Deguchi, *Chem. Lett.*, **1972**, 733 (1972); *J. Phys. Soc. Jap.*, **35**, 443 (1973).
12) R. Kuhn and H. Trischmann, *Monatsh. Chem.*, **95**, 457 (1964).
13) M. Mekata, *J. Phys. Soc. Jap.*, **17**, 796 (1962).
14) P. W. Selwood, "Magnetochemistry," Interscience Publisher, New York (1956).

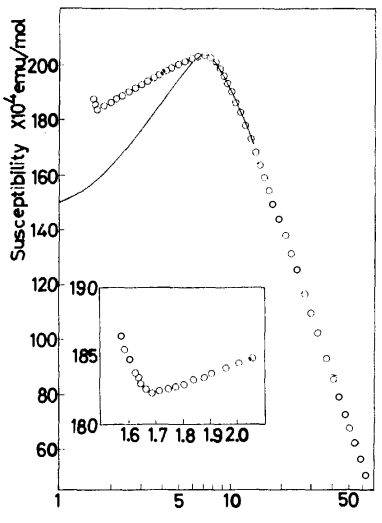

Fig. 1. Magnetic molar susceptibility of TPV.
Solid line represents the theoretical susceptibility calculated by the linear Heisenberg model. The inset shows the susceptibility at temperatures below 2 K.

77 K, was found to be 100% within the limit of experimental error. The reproducibility of the data was confirmed by comparing them with the data of samples prepared independently.

ESR. The ESR absorption spectrum shows a single line with an exchange-narrowed Lorentzian shape. In the higher-temperature region above T_{max}, the g-value was found to be practically isotropic, close to the free electron value and independent of the temperature. However, the g-value rapidly increases because of the anisotropic contribution in the lower-temperature region below T_{max}. The estimated g-value *versus* temperature curve is shown in Fig. 2. The temperature-dependent g-value of the another verdazyl radical, which exhibits a broad maximum susceptibility at *circa* 12 K but which is subjected to no long-range ordering in the available temperature range, is shown in the same figure for the sake of comparison.[15] The linewidth, which was taken to be the peak-to-peak linewidth (ΔH_p) of the first derivative of the resonance spectrum, probably starts to increase rapidly as the temperature is decreased below about T_{max}. The increase becomes more rapid as the temperatures approach

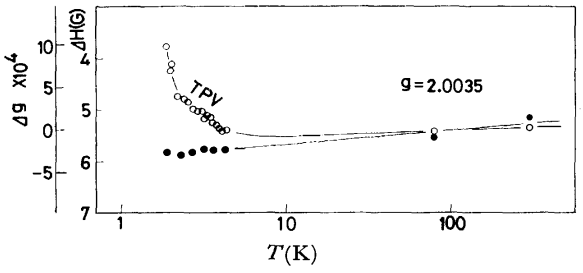

Fig. 2. Temperature dependent g-value of TPV.
ΔH stands for the shift of resonance field from the standard resonance field of Mn^{2+} in MgO (Gauss). Solid circles represent the g-value of the referred sample.

15) unpublished data.

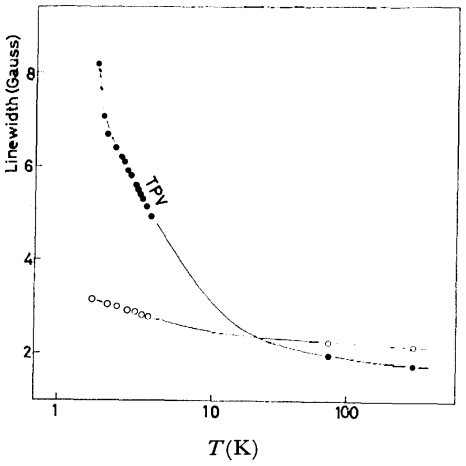

Fig. 3. Linewidth of TPV.
Open circles stand for the linewidth of the referred sample.

$T_n = 1.7$ K, which may be closely related to the increase in the g-value. The temperature dependences of the linewidths of TPV and the aforementioned radical are compared in Fig. 3.

Discussion

Susceptibility. One of the features of the susceptibility is, as may be seen in Fig. 1, that a finite susceptibility at 0 K seems to be left; this suggests a Heisenberg-type linear exchange interaction between unpaired electrons. This agrees well with the isotropic character of the g-factor. Therefore, the suceptibility may be described with neither Ising models[16,17] nor an exchange-coupled model.[18]

Therefore, we considered the linear Heisenberg model with isotropic exchange interaction, following the numerical calculation made by Bonner and Fisher.[19] The procedure of estimating the susceptibility has been described elsewhere.[7] The susceptibility gives an excellent fit to the value observed using $J/k = -5.4$ K, without any extra parameter such as a purity factor, in the temperature region above 6 K. However, the observed susceptibility deviates upwards from the theoretical value as the temperature is decreased below T_{max}. The value of $\chi_{max}/\chi_{T=0}$, being independent of the J parameter, is actually 1.2, while the theory predicts 1.45. On the other hand, the Weiss constant of -8 K, which agrees well with the value measured preliminarily in the temperature range above 77 K,[20] is larger in its absolute value than the theoretical one of 0.78 T_{max}, in contrast with the case of the product of T_{max} times χ_{max} 0.141 and 0.140 emu K/mol for the theoretical and observed values respectively. These two relationships are also independent of the J parameter.

16) J. W. Stout and R. C. Chisholm, *J. Chem. Phys.*, **36**, 979 (1962).
17) M. Inoue, *Nippon Kagaku Zasshi*, **92**, 1 (1971).
18) B. Bleaney and K. D. Bowers, *Proc. Roy. Soc., Ser. A*, **214**, 451 (1952).
19) J. C. Bonner and M. E. Fisher, *Phys. Rev.*, **135**, A640 (1964).
20) R. Kuhn. F. A. Neugebauer, and H. Trischmann, *Monatsh. Chem.*, **97**, 525 (1966).

Two coexistent interactions may make possible an interpretation of this feature. One of them rules predominantly and antiferromagnetically over the magnetism in the higher-temperature region and behaves one-dimensionally; the other is weaker than the former and is negligible in the higher-temperature region, but its latent ferromagnetic nature to tie up chain with chain is significant at temperatures below T_{max}. When the ferromagnetic contribution is adequately subtracted from the observed susceptibility, T_{max} may be shifted towards a higher temperature; the value of $|\theta|/T_{max}$ may then decrease to the theoretical value. One might suspect that the low-temperature discrepancy could be attributed to radical impurities, such as a defect in the crystal structure or a terminal spin contribution in the magnetic chain. However, the sample with a lower radical concentration (92%) shows a susceptibility quite similar to that of the pure sample except for the slight decrease in T_{max} (6.6 K), while a pure sample prepared independently gives an excellent agreement with the data of the other pure sample. Thus, the impurity contribution can not explain the discrepancy. Even if a two-dimensional antiferromagnetic model is taken into account, this low-temperature residual susceptibility may also be almost unchanged, although for the two-dimensional Heisenberg antiferromagnet neither an exact nor appropriate solution reliable at tempreatures below $|J|/k$ is yet known.

The presence of the interchain magnetic interaction accounts for the magnetic-phase transition from the short-range ordered state to the long-range ordered state, a transition which is inferred from the discontinuity in the slope of the susceptibility and the anomalies in the linewidth and g-value curves in the vicinity of 1.7 K.

ESR. Recently, Nagata *et al.* reported the short-range-order effects on the g-values in the Heisenberg linear chain antiferromagnets containing Mn^{2+} ion ($S=5/2$).[21] By introducing a small magnetic dipolar interaction and single-ion D-term, both of a uniaxial symmetry referred to the linear-chain direction, they classically estimated the simple relations between the anisotropies of the g-value and the susceptibility. The relationships were as follows:

$$\Delta g_{//}/g = (\chi_{//}-\chi_{\perp})/\chi_{//}, \quad (1)$$

$$\Delta g_{\perp}/g = (\chi_{\perp}-\chi_{//})/(2\chi_{\perp}). \quad (2)$$

When we assume the following relation for the powder sample:

$$\Delta g_{iso} = (\Delta g_{//}+2\Delta g_{\perp})/3, \quad (3)$$

then Eqs. (1) and (2) give this expression:

$$(1/g)\Delta g_{iso} = -(\chi_{//}-\chi_{\perp})^2/(3\chi_{//}\chi_{\perp}). \quad (4)$$

Eq. (4) indicates that, under their conditions, the g-value observed on the powder sample decreases with a decrease in the temperature if the anisotropic susceptibility is produced. We would like, however, to suggest that the essential part of Eqs. (1)—(4) lies in neither the sign nor the exact amplitude of the g-value shift, but in their suggestion that the anisotropic g-value reflects the anisotropy in susceptibility. Therefore, in comparison with the two curves shown in Fig. 2, the low-temperature g-value shift of TPV can be attributed to the susceptibility anisotropy in its solid. The striking shift in the temperature region below 2 K may imply the evolution of a severe change in the spin system in the vicinity of that temperature and may provide additional evidence of the phase transition at any temperature below 2 K. The sign of the g-value shift of TPV has to be subjected to an intense examination, together with the anisotropy in the susceptibility.

Although no appropriate theory for the linewidth of free radicals has been established, one of the present authors has previously reported the temperature dependence of the ESR absorption linewidth on a number of free radicals.[7] He found that the short-range ordering, remarkably developed near T_{max}, can be observed on the increase in the ESR linewidth, because the line broadening corresponds to an increase in the correlation time of the exchange motion due to the magnetic short-range ordering. In the present case, the line broadening probably starts to increase significantly at a higher temperature than what would be expected from T_{max} in view of the other data published.[7] This may be attributed to the precocious short-range ordering and may provide another support for the interchain ferromagnetic interaction derived from the susceptibility measurements. The broadening-out of the resonance line in the temperature region below 2 K may also be associated with the onset of the magnetic-phase transition in the neighborhood of that temperature, since, as the phase-transition temperature is approached, the increased spin-spin correlation results in the decreased exchange-narrowing of the linewidth.

Spin Distribution in the Molecule. The magnetic properties of free radicals with a delocalized unpaired electron may be greatly affected by the spin distribution. The proton NMR spectrum of TPV in a solution has exhibited well-resolved absorption lines.[22] Using the simple form of the McConnell relationship:[23]

$$a_i = -Q\rho_i, \quad Q = 23.7 \text{ Gauss},[24]$$

where a_i is the isotropic hyperfine splitting of the ith proton and where ρ_i is the spin density on the adjacent carbon atom, the spin densities on the carbon atoms were estimated, they are listed in Table 1. The McLachlan spin densities have been calculated and give a good agreement with the observed nitrogen hyperfine splitting of TPV.[23] Only the spin densities on the atoms with no adjacent hydrogen atom are also listed in the same table, because the McLachlan spin densities on aromatic rings do not always reproduce the proton splittings. The spin distribution in the table, together with the crystal structure to be considered in the next paragraph, will be discussed in connection with the magnetic structure of TPV.

Crystal Structure. According to the detailed crystallographic data which have been kindly supplied by

21) K. Nagata and Y. Tazuke, *J. Phys. Soc. Jap.*, **32**, 337 (1972); K. Nagata, Y. Tazuke, and K. Tsushima, *ibid.*, **32**, 1486 (1972).

22) P. Kopf, K. Morokuma, and R. Kreilick, *J. Chem. Phys.*, **54**, 105 (1971).

23) H. M. McConnell, *ibid.*, **24**, 764 (1956).

24) P. H. H. Fischer, *Tetrahedron*, **23**, 1939 (1967).

Table 1. Spin distribution

Position[a)]	Density
N1, N5	0.1944
N2, N4	0.2040
C3	—[b)]
C6	−0.0461
C7, C13	−0.0345
C8, C12, C14, C18	0.0473
C9, C11, C15, C17, C20, C24	−0.0179
C10, C16	0.0505
C19	0.0032
C21, C23	0.0067
C22	−0.0131

a) Numbering system is shown in Fig. 4.
b) The spin density is omitted in view of its small value for the sake of simplicity.

Williams prior to publication,[2] the molecule of TPV has no symmetry element in its crystalline state, although those of the other two symmetrical verdazyls possess a mirror plane.[25] The small twist angles about the bonds connecting the *sym*-tetrazyl ring with the aromatic rings attached to the nitrogens are observed in all three of the verdazyls, while the respective *C*-phenyl ring is almost coplanar with the plane defined by the four nitrogens. The atomic deviation of all the aromatic ring carbons from the plane of the nitrogens is comparatively small for all the radicals. There is no essential difference among the molecular geometries of the three radicals, so that the molecules of the symmetrical verdazyls seem to be subjected mainly to intramolecular requirements or to steric and electronic effects. Therefore, it may be acceptable to assume that the electronic configuration as well as the molecular structure of TPV in its solid state are similar to those in solution, except for the effect of the largest exchange force in the crystal. The molecular structure and the numbering system of TPV are shown in Fig. 4.

The crystals of TPV belong to the orthorhombic system, with the space group of $P2_12_12_1$ and with these lattice parameters; $a=18.467$, $b=9.854$, and $c=8.965$ Å. Figure 5 shows the mutual arrangement of the molecules; the numbers are used to show the molecular positions. The number of the intermolecular approaches less than 4.0 Å from the **1** molecule to those at the other positions is 58, 39 vectors of which direct to the molecules at the **1′**, **2**, and **2′** positions. The other 19 approaches are randomly distributed on the other five molecules and include neither N···N nor C···N contact. The 39 intermolecular approaches are listed in Table 2. For each molecule four planes are defined—three phenyl-ring planes and the plane of the four nitrogens. C6 is assumed to be positioned on the nitrogen plane. The dihedral angle between the planes including the two atoms being examined into the interatomic distance is shown in the third column of the same table. The angle defined by an interatomic vector and the corresponding plane in the **1** molecule is listed in the fourth column of the table.

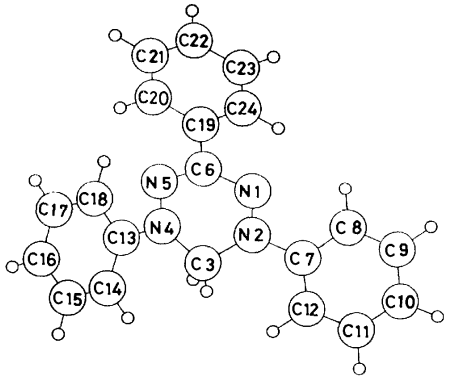

Fig. 4. Molecular structure and numbering system of TVP. C and N represent carbon and nitrogen atom, respectively. Small circles stand for hydrogen atoms.

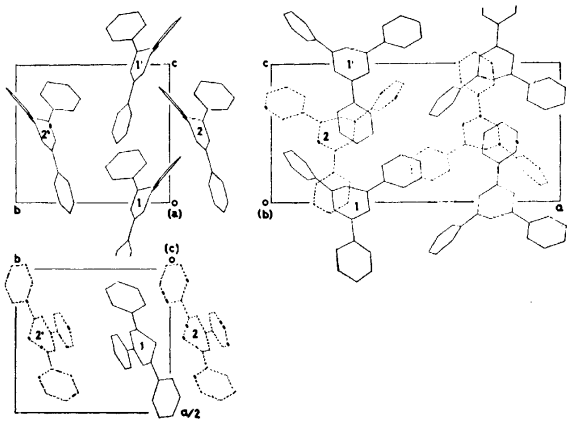

Fig. 5. Molecular packing of TPV.
(a), (b), and (c) correspond to the projections along the a-, b-, and c-axis, respectively. Numbers represent the molecular positions.

Exchange Interaction and Spin Densities. It is also important to discuss the relation between the signs of the apparent exchange integral and the spin density, because a problem may occur in certain solids of free radicals with a delocalized unpaired electron. Let us consider the following p-orbital exchange scheme:

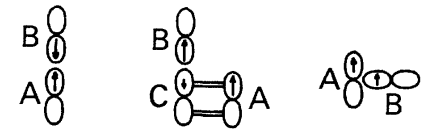

Case I corresponds to the general situation; that is, two p-orbitals on different molecules overlap with each other in the *z*-direction. In this case the favorable spin orientation is antiparallel or J_{AB} is negative, because of the evolution of a small covalent bond. Case II illustrates the arrangement of the orbitals in the solid, which was referred to as a certain solid. The A and C orbitals belong to one molecule, and B, to the neighboring molecule. When the down-spin on the C orbital is polarized by the up-spin on the A orbital, the former spin can be related to the negative spin density. The overlap integral of the B and C orbitals results in a negative exchange integral, J_{BC}, so that a positive J_{AB} may be observed. This mechanism is one way to explain the totally parallel spin

25) unpublished data.

orientation or the ferromagnetic interaction between unpaired electrons. Case III shows another variation of the orbital arrangement. The exchange integral in this case is positive but very small, because of the mutual orthogonality of the orbitals.[26,27] The magnitude of the apparent exchange interaction of these scheme may be proportional to the triple product of the spin densities on the two atoms concerned with the overalp and the corresponding exchange integral. This relation of the signs of the exchange integral and the spin densities is summarized and extended to a many-center problem by the following Hamiltonian:[26]

$$H^{AB} = -\mathbf{S}^{A}\mathbf{S}^{B}\sum_{ij} J_{ij}^{AB}\rho_i^{A}\rho_j^{B}, \qquad (6)$$

where $\mathbf{S}^{A}$ and $\mathbf{S}^{B}$ are the total spins on Molecules A and B and where ρ_i^{A} and ρ_j^{B} are the π-spin densities on the i and j atoms of Molecules A and B. When the sum in Eq. (6) is positive, the apparent exchange interaction is ferromagnetic. The negative sign of the sum corresponds to an antiferromagnetic exchange interaction between unpaired electrons.

$$H^{AB} = -J_{AB}\mathbf{S}^{A}\mathbf{S}^{B} \qquad (7)$$

When Eq. (6) is compared with Eq. (7), which corresponds to the Hamiltonian for the ordinary two-spin problem, then the sum in Eq. (6) can be named as the apparent exchange integral for a many-center problem.

Possible Magnetic Structure. The intermolecular distances less than 6.0 Å and the aforementioned angles were calculated in order to picture the magnetic structure of the TPV radical solid. Assuming that J_{ij}^{AB} is simply proportional to the inverse of the interatomic distance (d) alone and that the negative unity for d=1 Å, Eq. (6) was applied to the data of the interatomic distance less than 4.0 Å and the corresponding spin densities listed in Table 1. The results are shown in Table 2, where the values in the fifth and sixth columns have been multiplied by 10^5.

The molecules in the possible magnetic chain are related with each other by a twofold screw axis parallel to the c-axis. In this chain, the numbers of the intermolecular distances less than 4.0 Å from the atoms in the asymmetric unit molecule (Position **1**) to atoms in the nearest-neighboring (Position **2**) and the next nearest-neighboring (Position **1'**) molecules are 15 and 14 respectively; this is an interesting situation. The sum in Eq. (6) is negative for the nearest-neighboring molecule, while that for the next nearest-neighbor is positive, within the limits of the aforementioned broad assumption. The negative sign of the former sum indicates an antiferromagnetic interaction between the unpaired electrons, while the positive sign of the latter sum suggests a ferromagnetic interaction. However, these results may not indicate a competitive intrachain exchange interaction, but, rather, a cooperative totally antiferromagnetic interaction in the magnetic linear chain. It is suspected that the sum for the nearest-neighbor is estimated more highly than the sum for the next nearest-neighbor, taking account of the angular dependence of the exchange integral, J_{ij}^{AB}. The angle between the two orbitals may be inferred from the angles in the third and fourth columns of Table 2. We thus presume that the cooperative mechanism or the contribution of the second nearest-neighbor is too significant to neglect in this radical solid.

The number of the intermolecular approaches less than 4.0 Å associated with the nearest-neighboring molecule in the adjacent magnetic chain is 10, and the sum of these data gives a positive sign, which indicates

Table 2. Intermolecular distances (Å) and angles (degree), and the summation in Eq. (6)

Atoms	d	Dihedral angle	Direction angle	$\rho_i^{A}\rho_j^{B}$	$J_{ij}^{AB}\rho_i^{A}\rho_j^{B}$
From Molecule **1** *to Molecule* **2**					
C3–C6	3.93				
C3–C19	3.72				
C3–C20	3.80				
C11–C13	3.76	78.2	18.8	62.5	−16.6
C11–C18	3.80	78.2	0.5	−84.6	22.5
C12–N4	3.91	104.3	21.0	965.0	−246.5
C12–N5	3.60	104.3	4.8	920.0	−255.5
C12–C13	3.99	78.2	18.2	−163.2	40.9
C14–N1	3.42	104.3	16.4	920.0	−269.0
C14–N2	3.81	104.3	1.5	965.0	−253.0
C14–C6	3.79	104.3	32.9	−218.0	57.5
C14–C24	3.90	111.5	53.5	−84.7	21.7
C15–N1	3.68	104.3	32.6	−348.0	94.6
C15–N2	3.89	104.3	13.7	−365.0	93.9
C15–C7	3.94	97.3	3.0	61.8	−15.7
			Sum	2630.8	−725.2
From Molecule **1** *to Molecule* **1'**					
N2–C22	3.68	7.5	53.4	−267.0	72.5
C3–C22	3.82				
N4–C22	3.86	7.5	49.5	−267.0	69.2
C7–C22	3.59	42.9	84.9	45.2	−12.6
C7–C22	3.54	42.9	72.9	−23.1	6.5
C8–C22	3.92	42.9	65.9	−62.0	15.8
C8–C23	3.66	42.9	67.8	31.6	−8.6
C9–C23	3.79	42.9	63.4	−12.0	3.2
C10–C23	3.81	42.9	62.7	33.8	−8.9
C11–C23	3.68	42.9	66.6	−12.0	3.3
C12–C22	3.91	42.9	66.9	−62.0	15.9
C12–C23	3.57	42.9	72.3	31.6	−8.8
C13–C21	3.78	33.5	73.1	−23.1	6.1
C14–C21	3.68	33.5	80.7	31.6	−8.6
			Sum	−554.4	145.0
From Molecule **1** *to Molecule* **2'**					
N1–C22	3.89	39.6	53.5	−254.5	65.5
N1–C23	3.74	39.6	72.2	130.3	−34.9
C8–C19	3.90	68.5	42.3	15.1	−3.9
C8–C20	3.79	68.5	22.5	−84.6	22.4
C8–C21	3.73	68.5	6.1	31.7	−8.5
C8–C22	3.78	68.5	7.2	−62.0	16.4
C8–C23	3.85	68.5	24.8	31.7	−8.2
C8–C24	3.93	68.5	43.5	−84.6	21.6
C9–C20	3.79	68.5	22.5	32.1	−8.5
C24–C22	3.95	32.3	54.8	23.4	−5.9
			Sum	−221.4	56.0

a) Meanings of the figures are given in the text.

26) H. M. McConnell, *J. Chem. Phys.*, **39**, 1910 (1963).
27) J. Kanamori, *J. Phys. Chem. Solids*, **10**, 87 (1959).

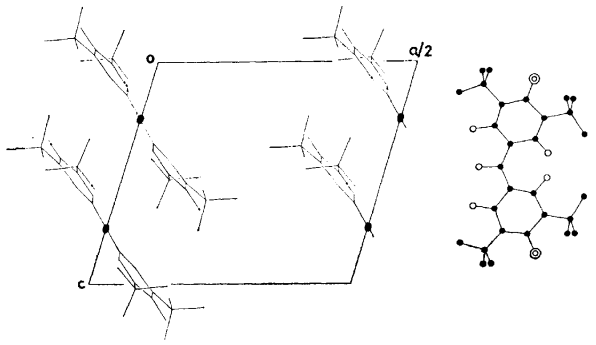

Fig. 6. Molecular packing and molecular structure of galvinoxyl radical. Solid ovals represent the diad axes. Solid circles stand for carbon atoms and doubled circles for oxygen atoms. Open circles represent hydrogen atoms. The methyl hydrogens in *tert*-butyl groups are not drawn.

a ferromagnetic interchain interaction. Thus, the intrachain antiferromagnetic and interchain ferromagnetic interactions inferred from the susceptibility measurement are qualitatively confirmed on the basis of the spin distribution and the crystal structure.

Galvinoxyl Radical. In order to confirm our proposal regarding the ferromagnetic interaction, let us consider the galvinoxyl radical solid, the susceptibility of which follows the Curie-Weiss law with a positive Weiss constant of 11 K above 83 K.[28] The crystal system of the radical solid is monoclinic, with a space group of C2/c, and with the cell dimensions of $a=23.78$, $b=10.87$, $c=10.69$ Å, and $\beta=106.6$ degrees.[4] Figure 6 shows the molecular packing, where the a-axis is drawn up to the half way mark. The molecule has a diad axis through the C–H bond in the methine group; this molecular twofold axis coincides with the crystallographic diad axis. The dihedral angel between the planes of the radical halves is 17 degrees. In Fig. 6, two methine carbons on the a-plane are positioned at (0.0, 0.03668, 0.25) and (0.0, −0.03668, 0.75); the other two methine carbons have the coordinates (0.5, 0.53668, 0.25) and (0.5, 0.46332, 0.75) respectively. Therefore, it can be said that this radical solid has a typical linear-chain magnetic structure along the c-axis, without any significant interchain interaction; therfore the above-mentioned susceptibility data may give information about its intrachain interaction alone. Within the chain, the intermolecular vectors which make angles from 70 to 90° (taken as an acute angle) with the phenyl plane and shorter than 5.0 Å were collected; the number of the vectors was 24. The spin densities were taken from Refs. 29 and 30. A procedure similar to that in the last section gives a positive sign for the sum in Eq. (6). Therefore, the comparatively large positive Weiss constant of 11 K may correspond to the ferromagnetic interaction caused by the overlap of a positive-spin-density-radical part with the negative-spin-density one in the neighboring molecule. It is interesting to notice that the qualitative magnetic behavior of two radical solids can be explained using Eq. (6).

28) K. Mukai, This Bulletin, **42**, 40 (1969).
29) B. Hakasson, *Acta Chem. Scand.*, **17**, 2281 (1963).
30) G. R. Luckhurst, *Mol. Phys.*, **11**, 205 (1966).

Summary

The experimental results may be summarized as follows:
1) The susceptibility of TPV is well described by the linear Heisenberg model in the temperature region above 6 K, but deviates upwards from the theoretical one with a decrease in the temperature below 6 K and then exhibits a discontinuity in its slope at 1.7 K. The parameters derived from the susceptibility are $\theta=-8$ K, $T_{max}=6.9$ K, $\chi_{max}=203\times10^{-4}$ emu/mol, and $J/k=-5.4$ K. 2) The ESR absorption linewidth, which is associated with the correlation time of the exchange motion, increases in the vicinity of T_{max} and broadens rapidly with a decrease in the temperature below 2 K. The temperature dependence of the g-value, which reflects the anisotropy in the susceptibility, is similar to that of the linewidth.

To summarize our interpretation of the results:
1) This radical solid may belong to the linear antiferromagnetic Heisenberg magnet, with a considerable ferromagnetic interaction between the chains. The discontinuing susceptibility at 1.7 K may imply a magnetic long-range ordering caused by the interchain ferromagnetic coupling. The pronounced increases in both the linewidth and the g-value below 2 K may be attributed to the critical fluctuation of electron spins in the neighborhood of the transition temperature. 2) The magnetic structure has been discussed on the basis of the spin distribution on the single molecule and the crystal structure. The possible linear chain is parallel to the c-axis, which is the shortest of the three orthorhombic axes. In this chain, the contribution of the second nearest-neighbor is significant and this is a ferromagnetic interaction which is cooperative with the antiferromagnetic one between the adjacent spins. The interchain interaction derived by our calculating procedure is ferromagnetic. 3) This magnetic structure can account for the qualitative experimental results of TPV. The method employed in the case of TPV was applied to the galvinoxyl radical solid and its positive Weiss constant of 11 K was attributed to the intrachain ferromagnetic interaction.

The authors would like to acknowledge the continuing guidance and encouragement of Professors Hideo Takaki and Mamoru Mekata of Kyoto University and Professor Kazuhiko Ishizu of Ehime University. They are also deeply indebted to Professor Yoshihiko Saito of the University of Tokyo for his helpful advice and for the use of considerable facilities in the determination of the crystal structures of the verdazyl radicals under consideration. They also thank Professor D. E. Williams of Louisville University, who supplied a preprint about the crystal structure of TPV and allowed them to reproduce the crystallographic figures of TPV and galvinoxyl radicals.

Interaction of Bovine Serum Albumin with Detergent Cations

Shoji KANESHINA, Mitsuru TANAKA,* Tatsuhiko KONDO,
Tomoaki MIZUNO, and Koichiro AOKI**

Department of Applied Chemistry, Faculty of Engineering, Tokushima University, Minamijōsanjima-chō, Tokushima 770

(Received February 19, 1973)

The binding isotherms of bovine serum albumin (BSA) with cationic detergents, decyltrimethylammonium bromide, dodecyltrimethylammonium bromide, and tetradecyltrimethylammonium bromide have been determined at temperatures 8 and 25 °C for pH 6.8. The isotherms have also been determined at pH 3.0 and 25 °C. The effect of KBr on the binding of dodecyltrimethylammonium bromide to BSA has been examined at 25 °C for pH 6.8. The results obtained are as follows. (a) The average number of detergent cations bound, $\bar{\nu}$, increased with the increase in the length of hydrocarbon chain, (b) the standard free energy changes $-\Delta G°$, calculated from the intrinsic association constants K, were comparable with the cohesive energy change when one methylene group is transferred from the aqueous phase to the hydrocarbon environment on micellization, (c) values of $\bar{\nu}$ at pH 3.0 differ only slightly from those at pH 6.8 in a wider range of detergent concentration, and (d) the presence of the salt shifted the binding isotherms to the lower detergent concentrations. These results are discussed as regards the nature of micellization of detergents.

Various studies have been made[1-5] on the interaction of serum albumin with anionic detergents but only a few[3,6-8] on cationic detergents.[9] So far it is known that the initial binding of anionic detergents to bovine serum albumin (BSA) involves 11 equivalent sites which do not interact, and that at higher levels of binding, at neutral pH, three stoichiometric complexes can be distinguished having the respective compositions AD_m, AD_n, and AD_{2n} (A: BSA, D: detergent anion, $m=11$, and $n=38$). Examination of the binding of different charged, cationic detergents to BSA will contribute significantly to elucidate whether the binding is attributed to the hydrophobic interaction or the electrostatic interaction. We have studied the effects of hydrocarbon chain length, pH, and added salt on the binding of cationic detergents to BSA by the method of equilibrium dialysis to elucidate the mechanism of interaction. The results obtained are compared with those of the binding of anionic detergents. The cationic detergents used are decyltrimethylammonium bromide (DeTAB), dodecyltrimethylammonium bromide (DTAB), and tetradecyltrimethylammonium bromide (TTAB).

Experimental

Materials. DeTAB, DTAB, and TTAB, prepared by the reaction of the corresponding alkylbromides with trimethylamine,[10] were purified by recrystallization from acetone. Alkylbromides used for the preparation of the cationic detergents were gas chromatographically pure. All the detergents prepared gave correct elemental analyses.

A solution of BSA (Armour, Lot. CK5010 and PK4471), after storage at 2—5 °C and pH 2 for 2 days was centrifuged and filtered to remove lipid contaminants.[4] The solution was dialyzed against distilled water and finally against the buffer solution of desired pH.

Equilibrium Dialysis. Detergent binding measurements were carried out by the method of equilibrium dialysis at 8(±0.01) and 25(±0.01) °C in phosphate buffer of ionic strength 0.1 and pH 6.8 and also at 25 °C in citrate buffer of ionic strength 0.1 and pH 3.0. Visking tubing for dialysis was heated for 3 hr in the saturated solution of $NaHCO_3$ near boiling point and rinsed thoroughly with distilled water to remove impurities. The tubing treated was then stored in distilled water at 2—5 °C. Bags were filled with 5 ml of *ca.* 1% protein solution in buffer and suspended in 10 ml of the same buffer for 3 days (at 25 °C) or 4 days (at 8 °C) with occasional shaking. The detergent was placed outside the dialysis bag. The amount bound to BSA was calculated by determining concentrations of detergent in the outside solution before and after the dialysis. A blank correction was made for the adsorption of detergent to the bag when no protein was present. The concentration of cationic detergent was determined by a spectrophotometric dye method.[11] The complex of orange II-detergent cation was extracted by chloroform and the optical density of the chloroform solution was determined at 485 mμ using a Hitachi 101 spectrophotometer. The protein concentration was determined from optical density measurements at 279 mμ; $E_{1\%}^{1cm}$ was assumed to be 6.67 for BSA at this wavelength.[4]

Critical Micelle Concentration (CMC). The CMC's of cationic detergents were determined by the surface tension method using the stalagmometer at 25(±0.01) °C. The values of CMC in aqueous solution of DeTAB, DTAB, and TTAB were 64.45, 15.54, and 4.01 mmol/kg-H_2O, respectively.

Results and Discussion

Binding Isotherms. The binding isotherms at

* Present address: Department of Chemistry, Faculty of Science, Fukuoka University, Nanakuma, Nishi-ku, Fukuoka
** Present address: Department of Synthetic Chemistry, Faculty of Engineering, Gifu University, Kagamigahara, Gifu

1) F. W. Putnam and H. Neurath, *J. Biol. Chem.*, **159**. 195 (1945).
2) F. Karush and M. Sonenberg, *J. Amer. Chem. Soc.*, **71**, 1369 (1949).
3) K. Aoki, *ibid.*, **80**, 4904 (1958).
4) R. V. Decker and J. F. Foster, *Biochemistry*, **5**, 1242 (1966).
5) J. A. Reynolds, S. Herbert, H. Polet, and J. Steinhardt, *ibid.*, **6**, 937 (1967).
6) J. F. Foster and J. T. Yang, *J. Amer. Chem. Soc.*, **76**, 1015 (1954).
7) A. V. Few, R. H. Ottewill, and H. C. Parreira, *Biochem. Biophys. Acta*, **18**, 136 (1955).
8) D. Jercher and H. Scheurer, *Z. Naturforsch.*, **86**, 541 (1953).
9) C. Tanford, *Advan. Protein Chem.*, **23**, 214 (1968).
10) A. B. Scott and H. V. Tartar, *J. Amer. Chem. Soc.*, **65**, 692 (1943).
11) A. V. Few and R. H. Ottewill, *J. Colloid Sci.*, **11**, 34 (1956).

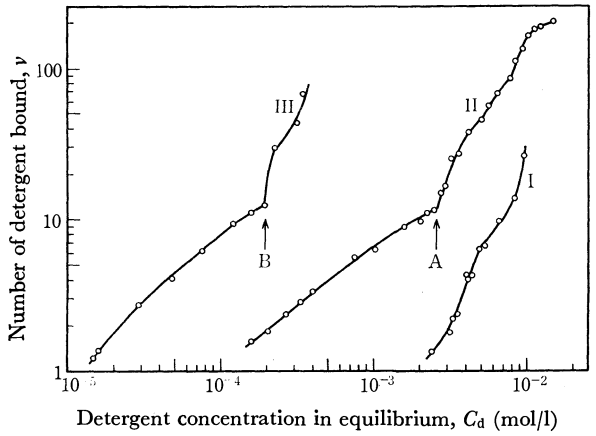

Fig. 1. Binding isotherms for cationic detergents and BSA at 25 °C and pH 6.8 (ionic strength 0.1). I: DeTAB, II: DTAB, and III: TTAB.

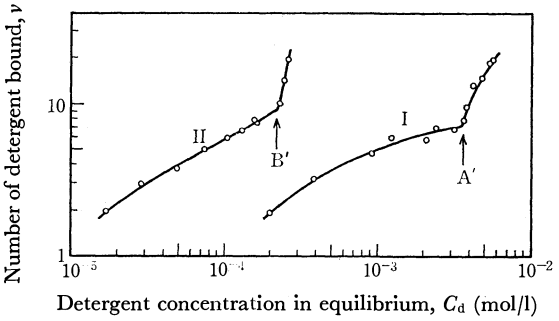

Fig. 2. Binding isotherms for cationic detergents and BSA at 8 °C and pH 6.8 (ionic strength 0.1). I: DTAB and II: TTAB.

pH 6.8 and 25 °C for three detergents are shown in Fig. 1. The shape of isotherm for DeTAB differs from that for others. The binding isotherms at 8 °C and pH 6.8 for DTAB and TTAB are shown in Fig. 2. At each temperature, the longer the hydrocarbon chain of detergents, the lower the concentration of free detergent in equilibrium. The slope of binding isotherm for DTAB and TTAB changes at 25 °C at points A and B (in Fig. 1) at which the number of bound detergent $\bar{\nu}$ is 12 and 13 for DTAB and TTAB, respectively. The slope of isotherm changes at 8 °C also at A′ and B′ (in Fig. 2) at which $\bar{\nu}=8$ and $\bar{\nu}=10$ for DTAB and TTAB, respectively. The concentration at A is the same as that at which several zones appear suddenly in the pattern of acrylamide-gel electrophoresis for this system.[12]

It is known that a cationic detergent, dodecylpyridinium bromide, as well as anionic detergents, forms the AD_m type complex with horse serum albumin.[3] It is seen in Figs. 1 and 2 that such a complex is formed at points A, B, A′, and B′, and that changes in conformation of the protein occurs in the region where $\bar{\nu}$ is larger than that at A or B, and the steepening of the isotherm begins. It was observed by using acrylamide-gel electrophoresis that the complex AD_{11} of sodium dodecylsulfate (SDS) prevented heat denaturation but the complex formed at point A did not prevent denaturation but rather promoted it.[13] Markus *et al.*[14] stated that the protective effect by SDS against urea denaturation of BSA is due to cross-links formed by the detergent anions between groups of nonpolar residues (presumably located in crevices formed by the folding of the peptide chain) and positively charged lysine residues. The mechanism of binding by Markus *et al.* is not applicable to the present system since no protection against denaturation occurs.[13] Thus, it is expected that the site on BSA for DTAB binding differs from that for SDS binding.

Thermodynamic Parameters. If the binding sites on protein are equivalent and non-interacting, the binding of detergents to protein is known to follow the equation[15]

$$\frac{1}{\bar{\nu}} = \frac{1}{Kn}\frac{1}{C_d} + \frac{1}{n} \qquad (1)$$

where $\bar{\nu}$ is the average number of moles of detergent cation bound per mole of protein, K the intrinsic association constant of each site for the detergent, n the total number of sites having an association constant K, and C_d the free detergent concentration in equilibrium. Plots of $1/\bar{\nu}$ *vs.* $1/C_d$ lie on a straight line for DTAB and TTAB in the region $\bar{\nu}<ca.$ 10. The intercept and slope of these lines for DTAB and TTAB give $1/n$ and $1/Kn$, respectively. The reciprocal plot for DeTAB, however, is not satisfactorily linear. The values of n and K thus obtained for DTAB and TTAB are given in Table 1 together with the standard free energy change calculated by the relation $\Delta G^\circ = -RT \ln K$. The values for anionic detergents by other workers are also included in Table 1 for comparison. The association constant K for cationic detergents increases with the increase in length of hydrocarbon tail and is lower than that for the corresponding alkylsulfates. The value of n increases with the increase in length of hydrocarbon tail at a constant temperature.

TABLE 1. ASSOCIATION CONSTANTS K, AFFINITIES $-\Delta G^\circ$, AND NUMBERS OF BINDING SITES FOR DETERGENTS ON BSAn

Detergent	K	$-\Delta G^\circ$ (kcal/mol)	n	Temp. °C	Ref.
$C_{12}H_{25}N(CH_3)_3Br$	1.6×10^3	4.1	8	8	
	4.5×10^2	3.6	22	25	
$C_{14}H_{29}N(CH_3)_3Br$	1.2×10^4	5.3	10	8	
	3.1×10^3	4.8	33	25	
$C_8H_{17}SO_4Na$	0.6×10^6	7.3	4—5	2	5
$C_{10}H_{21}SO_4Na$	1.4×10^6	7.8	5—6	2	5
$C_{12}H_{25}SO_4Na$	1.2×10^6	7.7	8—9	2	5
$C_{14}H_{29}SO_4Na$	1.0×10^6	7.5	10—11	2	5
$C_8H_{17}SO_4Na$	0.4×10^4	4.5	6	2	2
$C_{10}H_{21}SO_4Na$	3.4×10^4	5.7	8	2	2
$C_{12}H_{25}SO_4Na$	1.8×10^5	6.6	10	2	2

12) K. Aoki and S. Kaneshina, *Yukagaku*, **19**, 972 (1970).

13) K. Aoki, K. Hiramatsu, K. Kimura, S. Kaneshina, Y. Nakamura, and K. Sato, *Bull. Inst. Chem. Res., Kyoto Univ.*, **47**, 274 (1969).

14) G. Markus, R. V. Love, and F. C. Wissler, *J. Biol. Chem.*, **239**, 3687 (1964).

15) C. Tanford, "Physical Chemistry of Macromolecules," Wiley, New York, N. Y., (1963), p. 526.

The n value at 8 °C is in fair agreement with the number of detergents bound at points A′ and B′ in Fig. 2. The value of n at 25 °C, however, is far larger than $\bar{\nu}$ at A and B in Fig. 1.

The difference in values of $-\Delta G°$ for DTAB and TTAB can be attributed to the difference in the length of hydrocarbon tail. The difference in the standard free energy change thus calculated gives 1.0 kT per methylene group at two temperatures. The values for alkylsulfate, calculated from the data by Karush and Sonenberg,[2] was found to be 0.96 kT. These values are comparable with the cohesive energy change 1.0—1.2 kT[16] when one methylene group is transferred from the aqueous medium to the hydrocarbon environment on micellization of various detergents.

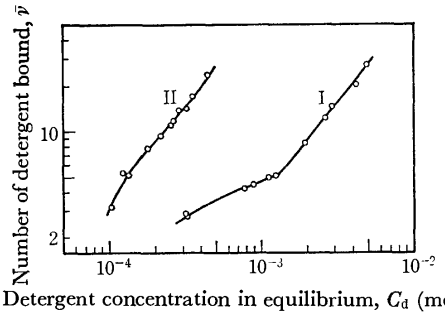

Fig. 3. Binding isotherms for cationic detergents and BSA at 25 °C and pH 3.0 (ionic strength 0.1). I: DTAB and II: TTAB.

Effect of pH. Equilibrium dialysis was carried out at more alkaline pH than the isoelectric point of BSA. If the pH of solution turns more acidic than that of isoelectric point, the net charge of BSA changes from negative to positive. Thus, if the binding is assumed to be electrostatic, the number of detergent cations bound should decrease remarkably at the acid pH. Isotherms of BSA with DTAB and TTAB at pH 3.0 are shown in Fig. 3. Comparing Fig. 3 with Fig. 1, we see that the difference in $\bar{\nu}$ between isotherms at pH 6.8 and 3.0 is not remarkable. The reversible expansion of BSA which occurs at below pH 3.5[17] would expose both sites for electrostatic binding and hydrophobic binding. However, the number of bound detergent cations did not change remarkably with pH. Thus, the interaction of BSA with detergent cations appears to be hydrophobic rather than electrostatic.

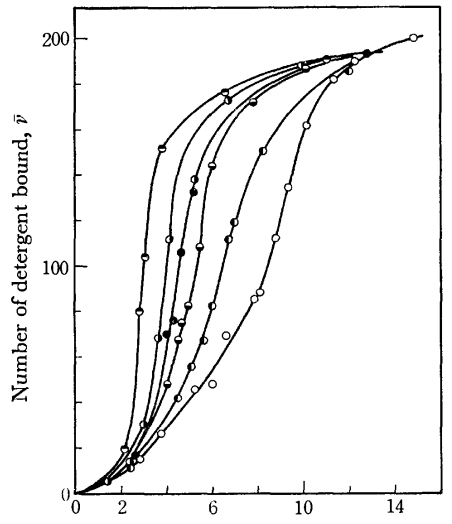

Fig. 4. Effect of KBr on the binding of DTAB to BSA at 25 °C and pH 6.8 (ionic strength 0.1). Concentrations of KBr; 0 (○), 0.02 (◐), 0.04 (◒), 0.06 (●), 0.10 (◑), and 0.15 (◓) mol/l.

Table 2. Effect of KBr on the CMC of DTAB in phosphate buffer (ionic strength 0.1, pH 6.8) at 25 °C

Concn of KBr (mol/l)	CMC $\times 10^3$ (mol/l)
0	12.2
0.02	8.6
0.04	6.6
0.06	5.3
0.10	4.0
0.15	3.2

Effect of Added Salt. The interaction of BSA with detergents at higher concentration is as follows. The binding isotherms of BSA with DTAB, obtained at various concentrations of added KBr, are shown in Fig. 4. In the range 0.02—0.15 mol/l, the increase in concentration of KBr shifts the isotherm toward the lower concentration of DTAB in equilibrium, *viz.*, the concentration of detergent at which a particular number of bound detergent cations lowers as the concentration of salt increases. This tendency is in line with the fact

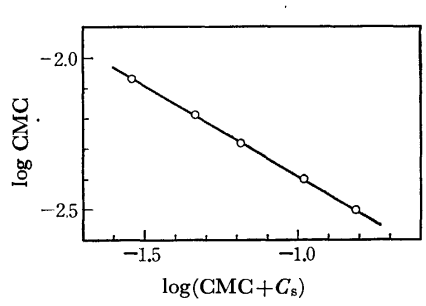

Fig. 5. Effect of KBr concentration on the CMC of DTAB in phosphate buffer (pH 6.8, ionic strength 0.1) at 25 °C.

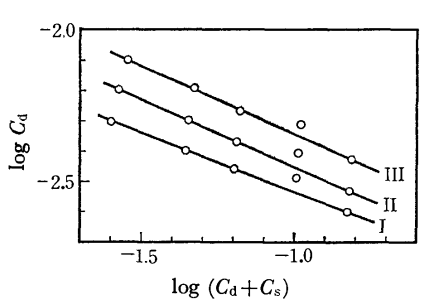

Fig. 6. Plots of log C_d *vs.* log (C_d+C_s) at constant $\bar{\nu}$. I: $\bar{\nu}$ = 50, II: $\bar{\nu}$ = 100, and III: $\bar{\nu}$ = 150.

16) J. N. Phillips, *Trans. Faraday Soc.*, **51**, 561 (1955). K. Shinoda, T. Nakagawa, B. Tamamushi, and T. Isemura, "Colloidal Surfactants" Academic Press, New York, N. Y., (1963), p. 42.

17) C. Tanford, *Proc. Iowa Acad. Sci.*, **59**, 206 (1952). G. Scatchard, *Am. Scientist*, **40**, 61 (1952).

that the added salt lowers the CMC of detergents. The effect of added KBr on the CMC of DTAB in the phosphate buffer solution is presented in Table 2. The CMC of detergent is related to the concentration of added salt C_s by the relation[18]

$$\log \mathrm{CMC} = a - b \log (\mathrm{CMC} + C_s) \qquad (2)$$

where a and b are constants. Data in Table 2 satisfy Eq. (2) as is shown in Fig. 5. If we assume that the binding of DTAB to BSA is governed by the same force as in the micelle formation, CMC in Eq. (2) can be replaced by the concentration of detergent in equilibrium C_d at a constant $\bar{\nu}$. The plot of log C_d *vs.* log (C_d+C_s) at a constant $\bar{\nu}$, for example $\bar{\nu}=50$, 100, and 150, falls on a straight line (Fig. 6).

In conclusion, the nature of the binding of alkyltrimethylammonium bromides with BSA is very similar to that of micelle formation of detergent. In the micelle formation of ionic detergent, hydrophobic interaction plays a predominant role. From the analogy to micelle formation, the cationic detergent-BSA interaction is hydrophobic in nature in the ranges of $\bar{\nu}$ and concentration of detergent in this experiment.

18) K. Shinoda, T. Nakagawa, B. Tamamushi, and T. Isemura, "Colloidal Surfactants" Academic Press, New York, N. Y., (1963), p. 58.

BULLETIN OF THE CHEMICAL SOCIETY OF JAPAN, VOL. 46, 2738—2741 (1973)

Ultrasonic and Thermodynamic Studies on the Aqueous Solutions of Tetramethylurea

Katsutaka SASAKI and Kiyoshi ARAKAWA

Research Institute of Applied Electricity, Hokkaido University, Sapporo 060

(Received February 27, 1973)

Ultrasonic absorption and sound velocity were measured for aqueous solutions of tetramethylurea at temperatures 10—30 °C. Excess compressibility and partial molar volume were obtained. The curves for the concentration dependence of density, viscosity, and absorption show a maximum at about 60 vol% (20 mol%). The excess compressibility curve shows a minimum at the same concentration. It is concluded that a molecular complex of the molar ratio 4: 1 (water: tetramethylurea) linked with hydrogen-bonds is formed at 20 mol%. In a dilute solution (below 4 mol%), the magnitude of ultrasonic absorption of tetramethylurea solutions is equal to that of 1,3-dimethylurea solutions, but is less than that of 1,3-diethylurea solutions. The tetramethylurea–water interaction is of a similar nature to that between 1,3-dimethylurea and water in a dilute solution.

From the results of our ultrasonic studies on the effects of guanidine hydrochloride, urea and its alkyl derivatives upon the structure of water, it was concluded that guanidine hydrochloride and urea molecules behave as a structure breaker for liquid water.[1-3]

Recently, Subramanian *et al.*[4] have shown from NMR and specific heat capacity data on aqueous solutions of urea and its derivatives that the relative decreasing order of structure making propensities (in water) is tetramethylurea>1,3-dimethylurea>urea, and they stated to have reached the same conclusion as ours. However, they have misinterpreted our study, for we made no mention of the aqueous solutions of tetramethylurea in our report.[2] Finer *et al.*[5] pointed out that the results of proton chemical shift studies on aqueous solutions of urea strongly disagree with that by Subramanian *et al.*[4] Therefore, the conclusion on the order of structure making propensities given by Subramanian *et al.* is doubtful.

In the present paper we report on ultrasonic studies on aqueous solutions of tetramethylurea with an intention to investigate alkyl group–water interactions, and compare it with the results for 1,3-dimethylurea and 1,3-diethylurea solutions. Despite the usefulness of the material as a good solvent for many organic substances, physicochemical studies on tetramethylurea solutions are very few.[6] Tetramethylurea is one of the few urea derivatives which is liquid at room temperatures and acts only as a hydrogen bond acceptor without an ability as a proton donor. We discuss in this paper the solute-solvent interactions in tetramethylurea solutions.

Experimental

Measurements of sound velocity and absorption coefficient were carried out by an ultrasonic pulse technique. The apparatus and procedure of measurements were already described.[7] The absorption coefficient was determined in the frequency range 15—45 MHz. Temperature range was 10—30 °C, the accuracy being within ±0.1 °C. The sound

1) K. Arakawa and N. Takenaka, This Bulletin, **40**, 2739 (1967).
2) K. Sasaki and K. Arakawa, *ibid.*, **42**, 2485 (1969).
3) K. Arakawa, N. Takenaka, and K. Sasaki, *ibid.*, **43**, 636 (1970).
4) S. Subramanian, T. S. Sarma, D. Balasubramanian, and J. C. Ahluwalia, *J. Phys. Chem.*, **75**, 815 (1971).
5) E. G. Finer, F. Franks, and M. J. Tait, *J. Amer. Chem. Soc.*, **94**, 4424 (1972).
6) A. Lüttringhause and H. W. Dirksen, *Angew. Chem. internat. edt.*, **3**, 260 (1964)
7) K. Arakawa and N. Takenaka, This Bulletin, **40**, 2063 (1967).

velocity was measured at 5 MHz.

Tetramethylurea (Aldlich Co. Ltd., USA) was used after being refluxed with calcium hydride under nitrogen atmosphere and distilled at 10 mmHg. Density of aqueous solutions was measured with an Ostwald type pycnometer at 20 °C, and partial molar volume was calculated. Viscosity coefficients for the solutions were measured with an Ostwald type viscometer (flow time for pure water, 270 s at 20 °C).

Results

Sound Velocity and Compressibility. The accuracy of sound velocity was within ±1 m/s. The values obtained are plotted against concentration (vol%) in Fig. 1. The density data at 20 °C are shown in Fig. 2. Excess compressibility $(V\kappa_s)_{\text{excess}}$ is defined by

$$(V\kappa_s)_{\text{excess}} = (V\kappa_s) - (x_1V_1\kappa_{s,1} + x_2V_2\kappa_{s,2}) \quad (8)^{8)}$$

where V, V_1, and V_2 are molar volume of solution, solvent, and solute, respectively, κ_s, $\kappa_{s,1}$, and $\kappa_{s,2}$, adiabatic compressibility of solution, solvent, and solute, respectively, and x_1 and x_2, mole fraction of solvent and solute, respectively. The results are plotted against concentration (mol%) in Fig. 3. We see that the excess compressibility curve has a minimum at about

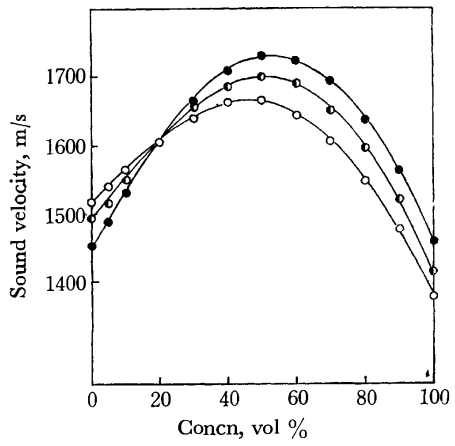

Fig. 1. Sound velocity for tetramethylurea solutions.
●: 10 °C, ◐: 20 °C, ○: 30 °C

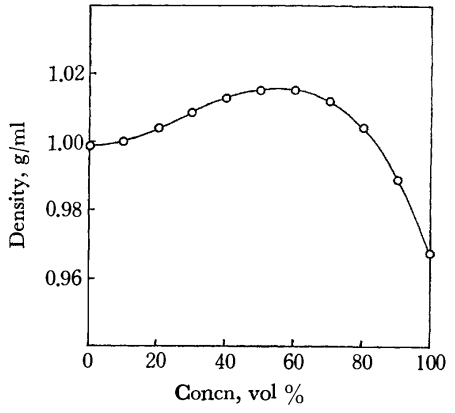

Fig. 2. Concentration dependence of density for tetramethylurea solutions at 20 °C.

8) The definition of excess compressibility from Eq. (1) is identical with that given previously. O. Kiyohara and K. Arakawa, This Bulletin, **44**, 1224 (1971).

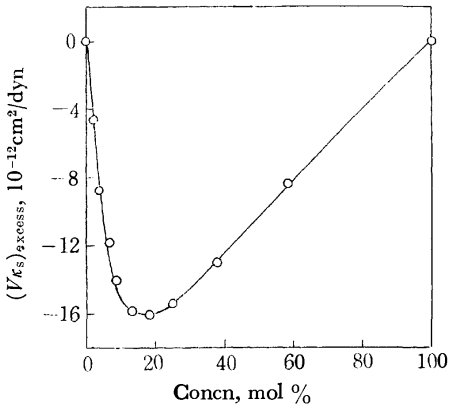

Fig. 3. Concentration dependence of excess compressibility for tetramethylurea solutions at 20 °C.

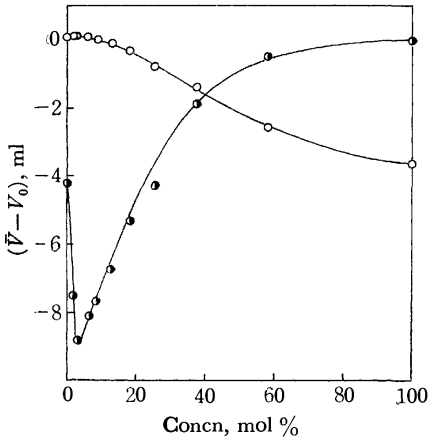

Fig. 4. Partial molar volume for tetramethylurea solutions at 20 °C.
○: water, ◑: tetramethylurea

20 mol%. The partial molar volume obtained from density data is given in Fig. 4. The partial molar volume of solute rapidly decreases up to about 4 mol% (20 vol%) while that of solvent water increases only slightly. Sound velocity *vs.* concentration curves at various temperatures intersect at about 20 vol% (4 mol%) (Fig. 1).

Ultrasonic Absorption and Viscosity. The data of ultrasonic absorption are reproducible within ±2%. The α/f^2 *vs.* concentration curves (α, absorption coefficient and f, frequency) are given in Fig. 5. The magnitude of absorption increases slowly up to about 20 vol% (4 mol%), and rapidly from 20 to about 60 vol%.

Viscosity coefficients were measured in order to obtain classical absorption. The results are given in Fig. 6. The classical absorption is given by

$$(\alpha/f^2)_{\text{class.}} = \frac{8\pi^2\eta}{3\rho V^3} \quad (2)$$

where ρ is density, V sound velocity and η viscosity coefficient. The structural absorption is given by

$$(\alpha/f^2)_{\text{struct.}} = (\alpha/f^2)_{\text{obsd.}} - (\alpha/f^2)_{\text{class.}} \quad (3)$$

The results at 20 °C as compared with the data of observed and classical absorption are given in Fig. 7. The increase of observed absorption is primarily at-

tributed to the structural absorption. The magnitude of absorption on the solutions of low concentration is compared with that of 1,3-dimethylurea and 1,3-diethylurea solutions (Fig. 8). The absorption is equal in magnitude to that of 1,3-dimethylurea solutions in the same region of concentration.

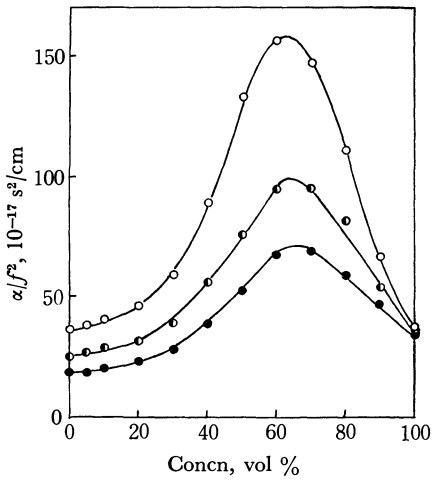

Fig. 5. Ultrasonic absorption (35 MHz) for tetramethylurea solutions.
○: 10 °C, ◐: 20 °C, ●: 30 °C

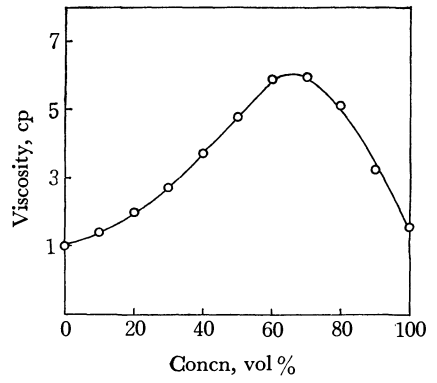

Fig. 6. Concentration dependence of viscosity for tetramethylurea solutions at 20 °C.

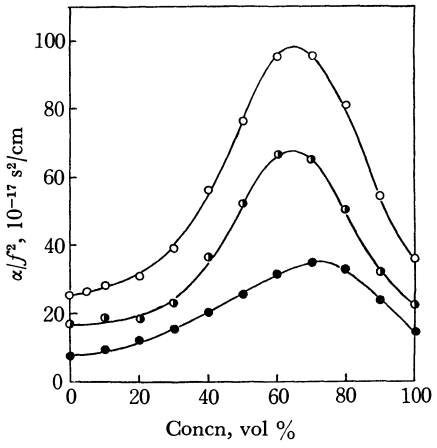

Fig. 7. Concentration dependence of ultrasonic absorption (35 MHz) for tetramethylurea solutions at 20 °C.
○: observed absorption, ◑: structural absorption, ●: classical absorption

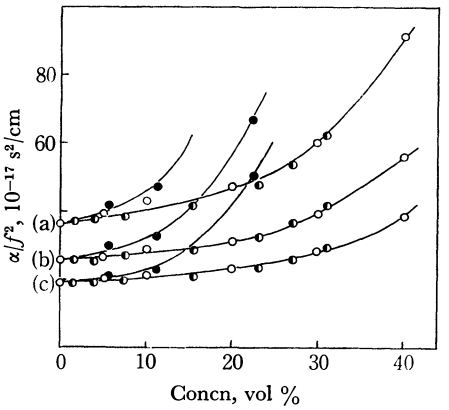

Fig. 8. Ultrasonic absorption for the solutions of alkyl derivatives. (a): 10 °C, (b): 20 °C, (c): 30 °C.
○: tetramethylurea, ◐: 1,3-dimethylurea, ●: 1,3-diethylurea

Discussion

Alkyl Group–Water Interaction. All curves intersect nearly at a point at about 20 vol% (4 mol%) (Fig. 1). An intersection point in a family of sound velocity *vs.* concentration curves at different temperatures appears in various aqueous systems.[9,10] The concentration at the crossing point (Fig. 1) corresponds to that of the sharp minimum of partial molar volume curve of solute (Fig. 4). The partial molar volume of solvent increases only slightly up to about this concentration. Below the concentration of 20 vol% (4 mol%), solute molecules might enter the cavities of water structure causing no conceivable rearrangement of the structure of water. This is due to the cooperative nature of structure formation in liquid water.[3] Since the magnitude of α/f^2 for pure tetramethylurea dose not differ much from that of pure water (Fig. 5), substitution of tetramethylurea molecules for solvent molecules in aqueous solutions causes no appreciable change in α/f^2 for solutions in a dilute region.

From a comparison of the magnitude of α/f^2 for tetramethylurea, 1,3-dimethylurea and 1,3-diethylurea solutions (Fig. 8), we can discuss alkyl group–water interactions. It is seen that the magnitude of absorption for tetramethylurea solutions is equal to that of 1,3-dimethylurea solutions, while the magnitude of α/f^2 for 1,3-diethylurea solutions is fairly larger. 1,3-Diethylurea molecules behave as a structure former on the structure of water.[2] The rapid increase of α/f^2 with concentration for 1,3-diethylurea solutions is ascribed to the structure formation around ethyl groups of solute molecules in water. In tetramethylurea and 1,3-dimethylurea solutions the situation is different.

Barone *et al.*[11] pointed out that from a spectroscopic study the structure forming ability of tetramethylurea in liquid water was stronger than that of 1,3-dimethlyurea and 1,3-diethylurea. However, the low "structure

9) R. Parshad, *J. Acoust. Soc. Amer.*, **20**, 66 (1948).
10) G. W. Willard, *ibid.*, **12**, 438 (1940).
11) G. Barone, E. Rizzo, and V. Vitagliano, *J. Phys. Chem.*, **74**, 2230 (1970).

temperature" [12,13] of tetramethylurea they gave should be ascribed to some other source, since their measurements were carried out in a higher concentration region. Study on iceberg formation should be made in a relatively dilute concentration region in order to avoid the effect from other factors of solute–solvent interactions.

The difference in α/f^2 *vs.* concentration curves (Fig. 8) is thus attributed to the difference between the behavior of the methyl group and ethyl group in water. The van der Waals radius of methyl group given by Pauling is about 2.0 Å.[14] The value is not much larger than that of water molecule,[14,15] and the methyl group seems to rotate nearly free from the absence of steric hindrance in water. Thus, the tetramethylurea-water interaction is found to be essentially similar to that of 1,3-dimethylurea solutions in low concentrations. This is in agreement with the result of viscosity increment (coefficient B) for solutions of tetramethylurea, 1,3-dimethylurea and 1,3-diethylurea by Herskovits *et al.*[16] The present result seems to be in line with that of the gas solubility study by Wetlaufer *et al.*[17]

Formation of Tetramethylurea Hydrate. The concentration of maximum density is found at about 60 vol% (18.5 mol%) (Fig. 2). The excess compressibility curve has a minimum at about 20 mol% (Fig. 3). It is thus expected that a tetramethylurea hydrate is formed. A maximum of α/f^2 was found at 63 vol% (20.4 mol%) at each temperature (Fig. 5) and a maximum of viscosity coefficient at 64 vol% (21.1 mol%) (Fig. 6).

Lüttringhause and Dirksen[6] proposed from density measurements that a molecular complex is formed with the molar ratio 6: 1 (water: tetramethylurea). However, we see a maximum or a minimum at a concentration of about 20 mol% in each curve for density, compressibility, ultrasonic absorption and viscosity coefficient. This corresponds to the molar ratio 4: 1 (solvent: solute). Tetramethylurea acts only as a hydrogen-bond acceptor, since all hydrogens of amide nitrogen are substituted by the CH_3 groups. Thus, it is tentatively assumed that tetramethylurea tetrahydrates are formed in aqueous solutions by hydrogen bonding. From the temperature dependence of maximum values of absorption, the apparent activation energy was calculated to be 6.9 kcal/mol. This value seems to be adequate for the tetrahydrate formation. The increase of observed absorption is mainly due to the increase of structural absorption (Fig. 7). Thus, we can conclude that the maximum value of ultrasonic absorption at 60 vol% is ascribed to the presence of tetrahydrate.

The authors wish to thank Mr. Nobuo Takenaka for his cooperation in this study.

12) J. D. Bernal and R. H. Fowler, *J. Chem. Phys.*, **1**, 515(1933).
13) R. A. Robinson and R. H. Stokes, "Electrolyte Solutions", Butterworths and Co. Ltd., London, (1959), p. 309.
14) L. Pauling, "The Nature of the Chemical Bond", 3rd., Cornell University, (1961), p. 260.
15) J. Morgan and B. E. Warren, *J. Chem. Phys.*, **6**, 666 (1938).
16) T. T. Herskovits, H. Jaillet, and A. T. DeSena, *J. Biol. Chem.*, **245**, 6511 (1970).
17) D. B. Wetlaufer, S. K. Malik, C. Stoller, and R. L. Coffin, *J. Amer. Chem. Soc.*, **86**, 508 (1964).

BULLETIN OF THE CHEMICAL SOCIETY OF JAPAN, VOL. 46, 2741—2744 (1973)

Kinetic Studies of Photosensitized Oxidation through Semioxidized Eosine in an Aqueous Solution

Yoshiharu USUI and Haru ENOKIDO*

Department of Chemistry, Ibaraki University, Mito 310

(Received April 5, 1973)

The rate constant for an electron transfer reaction between triplet eosine and potassium tris(oxalato)cobaltate-(III) was estimated. The experimental results from flash photolysis indicate that a transient semioxidized eosine exists in a free state. When a substrate was added to the deaerated eosine and complex solution at an optimum concentration, the original dye was restored by electron transfer from a substrate to the semioxidized eosine, sensitized oxidation occurring efficiently. Choosing indole and its derivatives as a substrate, we have obtained the elementary rate constants of the eosine recovery process.

In a previous paper it was reported that semioxidized eosine (E^+) produced by electron transfer from triplet eosine to potassium tris(oxalato)cobaltate(III) ($K_3[Co(C_2O_4)_3]$) might exist as a free radical in a degassed aqueous solution and the reactivity of E^+ for leucofluorescein was discussed on the basis of a comparison with its transient complex forms such as $E^+\cdots O_2^-$ and $E^+\cdots E^-$.[1)]

This paper shows kinetically the occurrence of eosine sensitized oxidation with a high efficiency in this deaerated solution, where original eosine could be reproduced through a semioxidized form *via* an electron transfer with a substrate. Since the sensitization cycles

* Japan Automobile Research Institute, Yatabe-machi, Ibaraki

1) Y. Usui, C. Iwanaga, and M. Koizumi, This Bulletin, **42**, 1231 (1969).

are not disturbed by the unreactive species of cobaltous and oxalate ions aquated from unstable potassium tris-(oxalato)cobaltate(II) in a neutral solution, the mechanism is expected to be determined as the simple scheme by the retarding effect of a substrate on the eosine bleaching rate.

Including the case of a coupled formation of E^+ and E^- by D–D mechanism,[2] this sensitized oxidation pattern through the path of the semioxidized form may be significant as compared with the classical photodynamic action in which oxygen needs to take the major role of substrate oxidation.[3]

Experimental

Purification of materials except substrates and most of the experimental procedures were similar to those described previously. All substrate reagents (Tokyo Kasei G.R.); indole, 3-methylindole, and L-tryptophan *etc.* were used without further purification. All the reactions were carried out at 25.0 °C.

Results and Discussion

Reaction Mechanism of Photooxidation of Eosine by Potassium Tris(oxalato)cobaltate(III). In flash photolysis of the deaerated eosine and complex aqueous solution, three main maxima of a transient species appeared at 408 nm (semireduced form, E^-), 460 nm (semioxidized form, E^+) and 580 nm (eosine triplet, E^T). E^- was slightly accompanied by D–D mechanism.[2] The lifetime of E^+ is considerably longer (~1 ms) than that in a plain aqueous solution, where the decay is expressed as the recombination of E^+ and E^- to restore original eosine.[4] When cobalt complex (C) is added in order of magnitude greater than 10^{-4} M, E^+ could be produced by the reaction of $E^T+C \longrightarrow E^+ + C^-$, a destructive bleaching of eosine occurring with high quantum yield.

A competitive effect of the complex concentration on the decay of E^T is shown in Fig. 1. Putting $k_s = k_d^{\circ} + k_D^s[D]$, the pseudo-first order rate constant (k) is written as

$$k = k_d^{\circ} + k_D^s[D] + k_c^s[C] = k_s + k_c^s[C]$$

where k_d°, k_D^s, and k_c^s ($=k_c^r + k_c^d$) are the rate constants on triplet eosine for a unimolecular decay, D–D interaction and a reaction with the complex, respectively. From the slope in Fig. 1, we get the k_c^s value as 9.2×10^6 M^{-1} sec^{-1}.

To clarify the genuine rate of an electron transfer from E^T to C by a steady-light illumination experiment, the quantum yield (Φ) of eosine bleaching was determined from the slope of a plot $\ln(e^E-1)$ *vs.* time (E is optical density). A linear relationship in the reciprocal plots ($1/\Phi$ *vs.* $1/[C]_0$) holds in the dilute concentration region of the complex lower than 1×10^{-3} M (Fig. 2). A deviation at higher concentration seems to be related with the effect of ionic strength and/or the reaction in an excited singlet state of eosine with the complex. Thus, the reaction scheme can be written as follows.

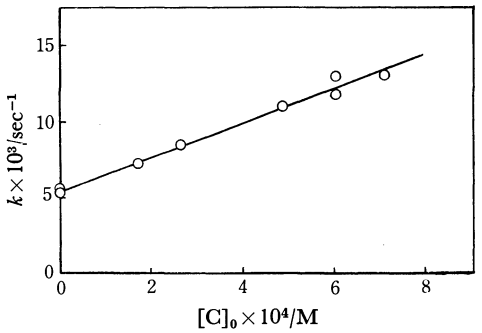

Fig. 1. Dependence of triplet eosine decay constant on $K_3[Co(C_2O_4)_3]$ concentration. ($[E]=1.0\times10^{-5}$M)

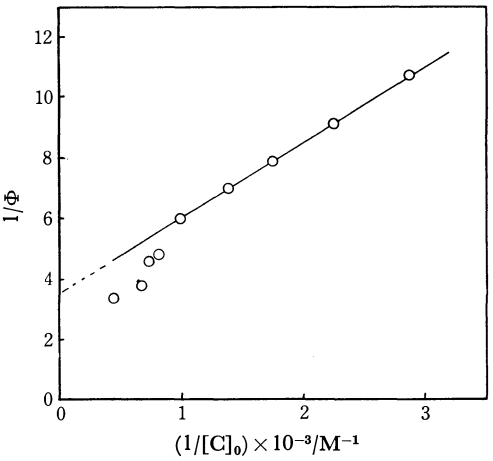

Fig. 2. Plots of $1/\Phi$ against $[K_3(Co(C_2O_4)_3)]_0^{-1}$. pH=7.0, $[E]=1.0\times10^{-5}$M.

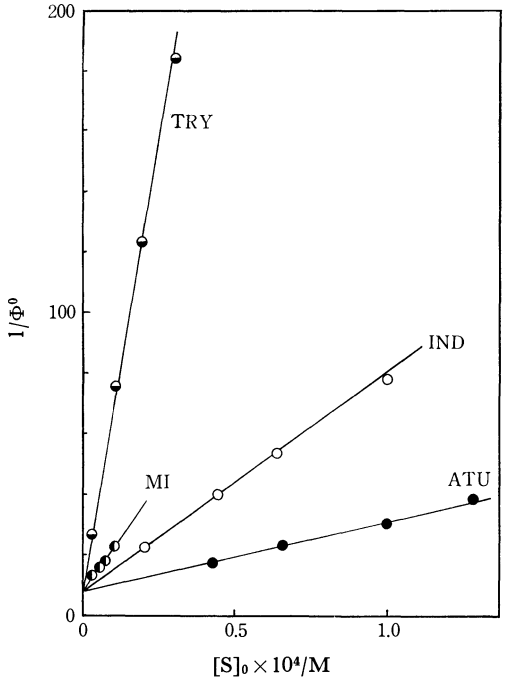

Fig. 3. Plots of $1/\Phi^0$ against substrate concentration.
—●—: Allylthiourea (ATU), —○—: Indole (IND),
—◐—: 3-Methylindole (MI), —◒—: L-Tryptophan (TRY)

2) Y. Usui and M. Koizumi, *Mol. Photochem.*, **4**, 57 (1972).
3) L. I. Grossweiner, *Photochem. and Photobiol.*, **10**, 183 (1969).

$$\begin{aligned}
&(1)\quad E \xrightarrow{h\nu} E^* \longrightarrow E^T && \phi_{st}I_{ab}\\
&(2)\quad E^T \longrightarrow E && k_d^{\circ}\\
&(3)\quad E^T + E \longrightarrow 2E \text{ (and } E^+ + E^-) && k_D^{s}\\
&(4)\quad E^T + C \longrightarrow E^+ + C^- && k_c^{r}\\
&\qquad\quad \longrightarrow E + C && k_c^{d} \Big\} k_c^{s}\\
&(5)\quad E^+ \longrightarrow \text{Decomposition} && k_+
\end{aligned}$$

$$\Phi = \frac{\phi_{st}k_c^{r}[C]}{k_s + k_c^{s}[C]} \qquad (I)$$

ϕ_{st} and k_s are known to be 0.64 and 4.5×10^3 sec^{-1} ($[E]_0=1.0\times10^{-5}$ M), respectively.[4,5] From an intercept and slope of the line in Fig. 2, the values of $\phi_{st}k_c^{r}/k_c^{s}$ and k_s/k_c^{s} were evaluated respectively as 0.2 and 0.71×10^{-3} M, in which the latter value coincides with the value 0.60×10^{-3} M obtained independently from the slope and interception in Fig. 1. Substituting ϕ_{st} and k_c^{s} values into $\phi_{st}k_c^{r}/k_c^{s}$, we get the genuine rate constant k_c^{r} to be 3.2×10^9 M^{-1} sec^{-1}. Thus the efficiency of an electron transfer between eosine triplet and the complex is roughly estimated to be one third.

Photosensitized Oxidation of Added Substrates. It was confirmed by flash photolysis that the rate constant for the reaction $E^+ + FH_2 \longrightarrow E + FH + H^+$ was of the order of magnitude of 10^9 M^{-1} sec^{-1} (FH_2, leucofluorescein)[1], and the reformation behavior of eosine was observed on the transient spectral change when phenanthroline and indole *etc.* were added.

Keeping the concentration of substrates and the complex as 50 μM and 1.0 mM, respectively (the competitive reaction of substrates with triplet eosine is neglected), we carried out semiquantitative survey for the retarding effect on quantum yield of eosine bleaching. Quite a large effect was obtained in the case of hydroquinone and indole-type substrates (Table 1).

It is noticeable that in the flash experiment of direct photoionization of a tryptophan alkaline solution,[6] the formation quantum yield (0.12) for a tryptophane radical cation was roughly of the same magnitude as its value listed in Table 1. By comparing the light energy (102 kcal) of maximum absorption wavelength which yields the same quantity of a tryptophan radical cation, its gain in energy is about two times higher in the eosine sensitization (55 kcal) than in the case of direct photoionization. From the viewpoint of a photoinactivation of aqueous lysozyme in which electron ejection from the essential tryptophan residues could inactivate the enzyme,[6] indole and its derivatives are taken as substrates for a kinetic treatment in the sensitized oxidation.

Kinetic Treatment of Photosensitized Oxidation of Several Substrates (S). From the above results, we see that the phenomenon could be interpreted by introducing following eosine recovery process in addition to the scheme (1) to (5);

$$\begin{aligned}
&(6)\quad E^+ + S \longrightarrow E + S^+ && k_+^{s}\\
&(7)\quad S^+ \longrightarrow \text{Decomposition}
\end{aligned}$$

Table 1. Relative recovery effect to bleaching eosine on the quantum yield (Φ°)[a]

Substrate	Φ°	$(\Phi_n^\circ-\Phi^\circ)/\Phi_n^\circ$
Leucofluorescein	0	1.00
Hydroquinone	0	1.00
L-Tryptophan	0.003	0.99
3-Methylindole	0.010	0.93
Indole	0.025	0.85
Phenylalanine	0.044	0.64
Trimethylamine	0.050	0.62
Allylthiourea	0.067	0.49
EDTA	0.070	0.47
Histidine	0.031	0.82
Imidazole	~0.17	~0
Adenine	~0.14	~0
none	0.13 (Φ_n°)	—

a) [Eosine]=10 μM, [Substrate]=50 μM, $[Co(OX)_3^{3-}]$=1.0 mM 25.0 °C, pH=7.0

Table 2. Rate constants for reaction (6)

Substrate	k_+^{s} M^{-1} sec^{-1}
L-Tryptophan	6.4×10^{8} [a]
3-Methylindole	1.9×10^{8}
Indole	7.3×10^{7}
Allylthiourea	2.0×10^{7}

a) pH=6.27

The eosine bleaching reaction was found to occur with a good linear relationship between $\ln(e^E-1)$ and time at the initial stage of a constant substrate concentration. Thus under conditions when reaction (4) predominates greatly over the reaction between E^T and S, the concentration dependence of the quantum yield of eosine bleaching in an initial stage (Φ^0) on a substrate is expressed as follows.

$$\Phi^\circ = \phi_{st}\frac{k_c^{r}[C]_o}{k_s+k_c^{s}[C]_o}\frac{k_+}{k_++k_+^{s}[S]_o} \qquad (II)$$

Figure 3 shows a linear relationship between the reciprocals of Φ° and initial substrate concentration $[S]_0$ as is expected from Eq. (II). Putting $[C]_0$= 1.0 mM, $k_s=4.5\times10^3$ sec^{-1} and $\phi_{st}=0.64$, we obtain

$$\frac{1}{\Phi^\circ} = 7.5\left(1+\frac{k_+^{s}}{k_+}[S]_o\right) \qquad (III)$$

From a flash experiment, we get k_+ as 1×10^3 sec^{-1} by analysing the decay of free semioxidized eosine as a first order.[1] Thus the rate constant k_+^{s} of reaction (6) for several substrates could be obtained from Eq. (III) and Fig. 3. The results are listed in Table 2. The k_+^{s} value for L-tryptophan is in good agreement with the value obtained in the flash photolysis experiment by Kepka and Grossweiner.[7] It seems that E^+ (and E^-) produced *via* D–D mechanism may exist freely during millisecond after flash irradiation.

4) T. Ohno, S. Kato, and M. Koizumi, This Bulletin, **39**, 232 (1966). V. Kashe and L. Lindqvist, *Photochem. and Photobiol.*, **4**, 923 (1965); E. F. Zwicker and L. I. Grossweiner, *J. Phys. Chem.*, **67**, 549 (1963).

5) M. Nemoto, H. Kokubun, and M. Koizumi, This Bulletin, **42**, 1223 (1969).

6) L. I. Grossweiner and Y. Usui, *Photochem. and Photobiol.*, **11**, 53 (1970), **13**, 195 (1971).

7) A. G. Kepka and L. I. Grossweiner, *ibid.*, **14**, 621 (1971).

Although it could be noted that all the compounds sensitized by eosine have lower ionization potential than that of eosine, investigations on k_+^s value should be extended to other combinations of sensitizer and substrate.

The authors wish to express their hearty thanks to Professor Masao Koizumi, Tohoku University, for his helpful discussion and encouragement, and to Miss Michiko Ohsawa who carried out a part of the experimental work. This work was supported in part by a grant (Y.U) from the Ministry of Education.

BULLETIN OF THE CHEMICAL SOCIETY OF JAPAN, VOL. 46, 2744—2747 (1973)

Studies of Photochemical Reactions Using Organic Photosensitizers. III. Direct Photolysis and Biacetyl-photosensitized Decomposition of Azopropanes

Shigeru YAMASHITA, Kuniyasu OKUMURA, and Teruo HAYAKAWA

Department of Chemistry, Faculty of Liberal Arts and Sciences, University of Osaka Prefecture, Mozu-Umemachi, Sakai, Osaka 591

(Received April 16, 1973)

The direct photolyses in the two wavelength regions and the biacetyl-photosensitized decomposition have been studied for 1,1′-azo-*n*-propane and 2,2′-azo-isopropane. The value of k_d/k_c, the ratio of the disproportionation rate to the combination rate of free radicals, has been found to be slighlty dependent on the exciting wavelength as for *n*-propyl and isopropyl radicals. The higher the exciting energies, the larger the ratio k_d/k_c. From the quenching study of biacetyl phosphorescence, it was found that the energy of the excited biacetyl molecule was transferred to the azopropane molecule at every collision.

The disproportionation and combination of alkyl radicals have been the object of many investigations. In the preceding work on the photodecomposition of vinyl iodide in the gas phase,[1] we found the slight energy dependence of k_d/k_c, the ratio of the rate of disproportionation to that of combination reactions of vinyl radicals as in the case of CH_3S radicals.[2]

In the present work, we have carried out the direct photolyses in the two wavelength regions and the biacetyl-photosensitized decomposition of 1,1′-azo-*n*-propane and 2,2′-azo-isopropane in order to study the energy dependence of the *n*-propyl and isopropyl radicals produced. The effect of the excess energy of *n*-propyl and isopropyl radicals on the ratio of k_d/k_c has been examined.

The photosensitizer, biacetyl, has been used for exciting azopropane to an excited state lower than the excited states caused by direct absorption in the UV-range or by mercury-photosensitization.

In the preceding papers of this series[3,4] we reported the benzene-photosensitized photolysis of nitrous oxide and the biacetyl-photosensitized photolysis of dimethylnitrosoamine, where the reactants were excited to the triplet states lying in the lower level comparing with the excited singlet states produced by direct absorption.

Since the lowest triplet level of biacetyl has been known to be 56 kcal/mol,[5] the *n*-propyl and isopropyl radicals produced by the biacetyl-sensitized photolyses of the corresponding azopropanes should have much less excess energy compared with the case of direct photolyses.

The phosphorescence of biacetyl was found to be quenched effectively[6] by azoalkanes indicating high efficiency of energy transfer from the biacetyl molecule in the triplet state to azoalkane molecules.

Experimental

Azo-*n*-propane and azo-isopropane were obtained from Merck Sharp and Dohme of Canada Ltd. and were purified by vacuum distillation and stored at low temperature in the dark. The absorption spectra of azo-*n*-propane and azo-isopropane in the vapor phase are shown in Fig. 1.

The apparatus was similar to that of the previous work[1] and a high intensity light source, USH-500D high pressure mercury lamp manufactured by Ushio Electric Co., was used for the sake of the predominance of radical-radical reactions with high concentration of the free radicals excluding radical-molecule reactions.[1,7]

For the direct photolysis, Toshiba UV-35 and UV-29 filters were used. When UV-35 was used, 366 nm line of the mercury lamp was almost exclusively effective for the photolyses of both azo-*n*-propane and azo-isopropane. By use of UV-29 filter, about ten percent contribution from 334 nm line was estimated for the excitation of azo-*n*-propane

1) S. Yamashita, S. Noguchi, and T. Hayakawa, This Bulletin, **45**, 659 (1972).

2) A. Jones, S. Yamashita, and F. P. Lossing, *Can. J. Chem.*, **46**, 833 (1968); S. Yamashita and F. P. Lossing, *ibid.*, **46**, 2925 (1968).

3) S. Yamashita, K. Adachi, and T. Hayakawa, This Bulletin, **43**, 2332 (1970).

4) S. Yamashita and T. Hayakawa, "Proceeding of the International Conference on Mass Spectroscopy", Kyoto (1969), p. 1113.

5) H. Ishikawa and W. A. Noyes, Jr., *J. Amer. Chem. Soc.*, **84**, 1502 (1962); G. N. Lewis and M. Kasha, *ibid.*, **66**, 2100 (1944).

6) R. E. Rebbert and P. Ausloos, *ibid.*, **87**, 1847 (1965).

7) J. O. Terry and J. H. Futrell, *Can. J. Chem.*, **45**, 2317 (1967).

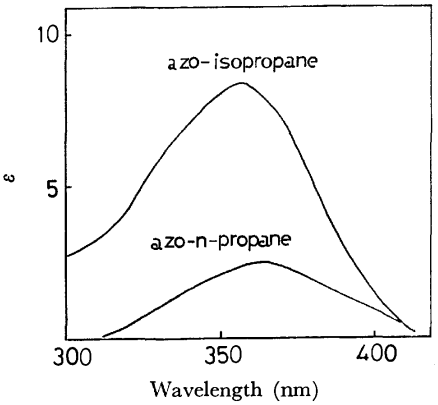

Fig. 1. Absorption spectra of azo-isopropane and azo-*n*-propane.

and about thirty percent contribution from 302, 313, and 334 nm lines for the excitation of azo-isopropane. Highly monochromatic light was not available to excite the reactants because high intensity of the light source was necessary for high concentration of free radicals. All of the runs were carried out at room temperature in the dark room. Before the analysis of the reaction products, unreacted azopropanes were condensed by a cold trap cooled at −20 °C. The separated products were analyzed by a gas chromatograph using a column packed with dimethylsulfolane on alumina, and by a Hitachi RMU-5 mass spectrometer when necessary. The emission measurements for quenching were carried out in the dark room. The exciting light was 436 nm line of a mercury lamp and the phosphorescence emitted by biacetyl in the absence and presence of azopropanes was measured by a grating monochromator and 1P28 photomultiplier with TR-8651 electrometer of Takeda Riken Ind. Co. Ltd.

Results and Discussion

The reaction products obtained were N_2, C_3H_8, C_3H_6, and C_6H_{14} in the direct photolysis and biacetyl-sensitized photolysis of both azopropanes. The product hexane was *n*-hexane in the photolysis of 1,1′-azo-*n*-propane and 2,3-dimethylbutane from 2,2′-azo-isopropane, respectively. In all of the runs, the amounts of C_3H_8 and C_3H_6 were found to be equimolar.

Under high light intensity conditions of this work, the reaction scheme may be rather simplified as following because radical-molecule reactions can be neglected due to the high concentration of the free radicals.

For the direct photolysis, the reaction scheme may be proposed as follows:

$$C_3H_7N_2C_3H_7 + h\nu \longrightarrow C_3H_7N_2C_3H_7^* \quad (1)$$

$$C_3H_7N_2C_3H_7^* \longrightarrow N_2 + C_3H_7\cdot + C_3H_7\cdot \quad (2)$$

$$C_3H_7\cdot + C_3H_7\cdot \xrightarrow{k_d} C_3H_8 + C_3H_6 \quad (3)$$

$$C_3H_7\cdot + C_3H_7\cdot \xrightarrow{k_c} C_6H_{14} \quad (4)$$

For the biacetyl-sensitized photolysis, the following processes seem to produce propyl radicals:

$$B + h\nu' \longrightarrow B^* \longrightarrow B^{**} \quad (5)$$

$$B^{**} + C_3H_7N_2C_3H_7 \longrightarrow B + C_3H_7N_2C_3H_7^{**} \quad (6)$$

$$C_3H_7N_2C_3H_7^{**} \longrightarrow C_3H_7\cdot + C_3H_7\cdot + N_2 \quad (7)$$

here, B means biacetyl and the symbols *, ** denote excited singlet and triplet states, respectively. According to the reaction scheme shown above, equimolar amounts of C_3H_8 and C_3H_6 should be produced, which is supported by the experimental results obtained.

The amount of CO and C_2H_6 were found to be negligible in the biacetyl-photosensitized reaction, meaning that the side reactions of the biacetyl photodecomposition could be left out of account probably because of the extremely large quenching cross section for biacetyl by azopropanes as described later.

Since the greaseless system was not available in the present work, complete separation of hexane has not been achieved. The corrected value of the rate of hexane formation was estimated by the difference $[N_2]-[C_3H_8]$ assuming a material balance between the products as described in the photolysis of 2,2′-azo-isobutane.[8] This procedure for the estimation of hexanes was found reasonable by a blank test and by the fact that the ratio between the direct photolysis products was in good agreement with the results of the greaseless system work reported by Terry and Futrell[7] when the wavelength range for excitation was arranged similar to their conditions.

Table 1. Photolysis of azo-isopropane
Illumination time: 2∼10 min

Filter	Pressure (Torr)	Products (micromole)				k_d/k_c
		N_2	C_3H_8	C_3H_6	C_6H_{14}	
UV-29	20.15	54.50	22.16	21.92	32.34	0.685
	20.18	43.62	18.13	18.30	26.49	0.712
	19.86	25.96	10.77	10.94	15.19	0.709
	20.11	13.96	5.60	5.57	8.36	0.671
UV-35	19.65	46.48	18.00	17.64	28.48	0.631
	19.98	36.40	13.92	15.48	22.48	0.619
	19.95	30.58	11.72	12.31	18.86	0.621
	19.62	21.09	8.22	8.63	12.87	0.639

Table 1 shows the results of the direct photolysis of azo-isopropane using UV-29 and UV-35 filters. The value of k_d/k_c was obtained by taking the ratio $[C_3H_8]/\{[N_2]-[C_3H_8]\}$ equal to $[C_3H_8]/[C_6H_{14}]$ assuming a material balance as described above. Table 2 shows the results of the direct photolysis of azo-*n*-propane.

The amounts of the photolysis products were found to be proportional to the illumination time, which

Table 2. Photolysis of azo-*n*-propane
Illumination time: 2∼10 min

Filter	Pressure (Torr)	Products (micromole)				k_d/k_c
		N_2	C_3H_8	C_3H_6	C_6H_{14}	
UV-29	22.20	9.89	1.23	1.12	8.66	0.143
	20.01	14.89	1.89	1.78	12.92	0.146
UV-35	20.60	25.02	2.80	2.80	22.22	0.126
	20.60	19.48	2.15	2.10	16.33	0.124
	20.10	9.74	1.06	1.03	8.68	0.122
	20.25	27.31	3.01	3.19	24.30	0.124
	20.40	32.00	3.51	3.74	28.49	0.123

8) D. G. L. James and R. D. Suart, *Trans. Faraday Soc.*, **65**, 175 (1969).

TABLE 3. BIACETYL-SENSITIZED PHOTOLYSIS OF AZO-ISOPROPANE

Filter: Toshiba VY-43.
Illumination time: 10~20min

Reactant pressure (Torr)	Biacetyl pressure (Torr)	Products (micromole)				k_d/k_c
		N_2	C_3H_8	C_3H_6	C_6H_{14}	
19.91	27.30	1.75	0.44	0.42	1.33	0.33
19.57	26.80	2.17	0.43	0.48	1.69	0.25
20.28	25.00	0.87	0.17	0.17	0.70	0.24

TABLE 4. BIACETYL-SENSITIZED PHOTOLYSIS OF AZO-*n*-PROPANE

Filter: Toshiba VY-43.
Illumination time: 10~20 min

Reactant pressure (Torr)	Biacetyl pressure (Torr)	Products (micromole)				k_d/k_c
		N_2	C_3H_8	C_3H_6	C_6H_{14}	
20.65	30.58	0.602	0.033	0.033	0.569	0.07
12.98	22.95	1.041	0.046	0.046	0.995	0.05
16.14	22.86	1.014	0.034	0.034	0.980	0.04

means that all the reaction products were produced in the primary process, not in the secondary process.

Tables 3 and 4 show the results of the biacetyl-photosensitized decomposition of azo-isopropane and azo-*n*-propane, respectively. The quantum yields of N_2 formation were obtained for the direct photolysis by UV-35 and for biacetyl-photosensitization, as shown in Table 5. The quantum yields by biacetyl-photosensitization are about one tenth smaller than that by the direct photolysis.

Figure 2 shows the phosphorescence spectrum of biacetyl vapor in the absence and presence of quenchers. Ausloos and Rebbert reported much higher

TABLE 5. QUANTUMM YIELDS OF N_2 FORMATION OBTAINED BY DIFFERENT EXCITATIONS

Reactants	Direct photolysis with UV-35 (366 nm)	Biacetyl-photosensitization
Azo-isopropane	0.66±0.04	0.08±0.02
Azo-*n*-propane	0.98±0.14	0.06±0.01

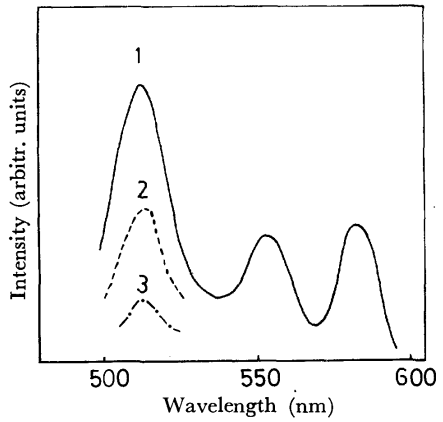

Fig. 2. Phosphorescence of biacetyl vapor (20 Torr, 20 °C). Curve 1: pure biacetyl, Curve 2: with 0.038 Torr O_2, Curve 3: with 3.7×10^{-4} Torr azo-isopropane.

cross sections of azomethane and azoethane than that of oxygen for quenching the phosphorescence of biacetyl.[6] In the present work azo-isopropane was found to have higher cross section than azomethane for quenching the phosphorescence of biacetyl. From the Stern-Volmer plot of the quenching experiments, the quenching rate constant k_q was found to be 3×10^{11} l mol^{-1} s^{-1}, equivalent to the value of the effective collisional cross section σ_Q^2 of 45×10^{-16} cm^2 taking the lifetime of the excited triplet biacetyl molecule to be 10^{-3} s.[9] The value of the quenching rate constant k_q suggests that the excited biacetyl molecule is quenched at every collision with azopropane molecule meaning high efficiency of energy transfer from excited biacetyl to reactant azopropane.

Rather low quantum yield of the azopropane decomposition in the case of the biacetyl-sensitized photolysis, in spite of the high efficiency of energy transfer from excited biacetyl to reactant azopropane, shows that excited azopropane produced by biacetyl-photosensitization is more easily deactivated than by the direct photolysis.

TABLE 6. DEPENDENCE OF THE RATIO k_d/k_c ON THE EXCITATION ENERGIES FOR THE PRODUCTION OF PROPYL RADICALS

Reactant	Excitation condition	Excitation energy (kcal/mol)	k_d/k_c
Azo-isopropane	Direct photolysis (UV-29 filter)	78~95	0.69
	Direct photolysis (UV-35 filter)	78	0.63
	Biacetyl-photosensitization	56	0.27
Azo-*n*-propane	Direct photolysis (UV-29 filter)	78~95	0.15
	Direct photolysis (UV-35 filter)	78	0.12
	Biacetyl-photosensitization	56	0.05

Table 6 summarizes the k_d/k_c values obtained with different excitation energies. The ratio k_d/k_c increases with increasing excitation energies for both azo-isopropane and azo-*n*-propane, which means that k_d/k_c increases with the increment of the excess energies carried by propyl radicals produced by photolysis. This tendency agrees with the results obtained in the case of CH_2=CH·[1] and CH_3S·[2] radicals produced by the photolyses.

The processes (2) and (7) forming two propyl radicals and one nitrogen molecule may be composed of two successive one-bond fission steps:

$$C_3H_7N_2C_3H_7^* \text{ (or } C_3H_7N_2C_3H_7^{**}) \longrightarrow C_3H_7N_2 + C_3H_7 \quad (8)$$

and succeedingly

$$C_3H_7N_2 \longrightarrow C_3H_7 + N_2 \quad (9)$$

Such two-step mechanism was previously confirmed

9) H. L. J. Backström and K. Sandros, *Acta Chem. Scand.*, **14**, 48 (1960).

in the case of the direct photolysis of azo-*n*-propane by illumination of the molecular flow of the reactant in the ion source of a mass spectrometer.[10]

The excess energies carried by propyl radicals were estimated in the case of azo-isopropane since the dissociation energy of the C–N bond of azo-isopropane has been found to be about 33 kcal/mol.[11] From the value of the C–N bond dissociation energy of azo-isopropane and other thermochemical data, the upper limit of the excess energy of the isopropyl radical may be estimated to be 28 kcal/mol for the direct photolysis with UV-35 and 14 kcal/mol for biacetyl-photosensitization. Table 6 shows, anyway, the higher the excitation energies, the larger the excess energies carried by propyl radicals resulting in the increment of k_d/k_c values. The considerably small k_d/k_c values obtained in the biacetyl-photosensitization might suggest the effect of the spin-multiplicity difference besides the energy dependence of k_d/k_c.

Since the effect of the addition of *n*-butane as third body to the reaction system was found almost insignificant, it was inferred that the hot propyl radicals produced by the highly intense illumination reacted each other before thermalization in accord with the suggestion given by Thynne.[12]

It may be said that the disproportionation reaction of free radicals is a kind of inter-radical hydrogen-atom abstraction in the transition state.[13,14] From this viewpoint the increment of the k_d/k_c values with increasing excitation energies seems to be understandable since the feasibility of hydrogen-atom abstraction by the free radicals increases with the increment of the excitation energies used for photochemical free radical formation.[15,16]

10) S. Yamashita and T. Hayakawa, This Bulletin, **46**, 2290 (1973).
11) B. G. Gowenlock, J. R. Majer, and D. R. Snelling, *Trans. Faraday Soc.*, **58**, 670 (1962).
12) J. C. J. Thynne, *Proc. Chem. Soc.*, **1961**, 68.
13) J. N. Bradley, *J. Chem. Phys.*, **35**, 748 (1961).
14) R. J. McNeal, *ibid.*, **40**, 108 (1964).
15) P. C. Kobrinsky and R. M. Martin, *ibid.*, **48**, 5728 (1968).
16) J. M. White, R. L. Johnson, Jr., and D. Bacon, *ibid.*, **52**, 5212 (1970).

BULLETIN OF THE CHEMICAL SOCIETY OF JAPAN, VOL. 46, 2747—2751 (1973)

Crystal Structure and Absolute Configuration of (−)-2,2′-Bisbromomethyl-1,1′-binaphthyl

Kazuaki HARATA and Jiro TANAKA

Department of Chemistry, Faculty of Science, Nagoya University, Chikusa-ku, Nagoya 464

(Received April 25, 1973)

Crystals of (−)-2,2′-bisbromomethyl-1,1′-binaphthyl have been subjected to crystal structure analysis in order to determine the absolute configuration of optically active 1,1′-binaphthyl derivatives. The crystals are orthorhombic, space group $P2_12_12_1$ with $Z=4$ and the lattice constants are; $a=10.360$, $b=13.052$, $c=13.178$ Å. The structure was solved by the heavy atom method and the final R index was 0.064. The absolute configuration was determined as (*S*)-configuration by utilizing the anomalous dispersion effect of bromine atom.

The absolute configuration of optically active substituted 1,1′-binaphthyl molecules is of great interest since the molecule has a C_2 symmetry and the rotational strength is very large in spite of simple chromophore structure. The chemical investigations revealed that the rotation around the 1,1′-single bond is restricted when the 2,2′-positions are substituted by the bulky groups.[1,2] Correlation of the absolute configuration with the optical activity of substituted binaphthyls will be important in developing the theory of the optical activity of coupled chromophore systems. The present investigation was undertaken to find the absolute configuration of one of the simplest hindered binaphthyls. The molecular structure and the absolute configuration will be discussed with a reference to the results of binaphthyl[3] and (+)-2,2′-dihydroxy-1,1′-bisnaphthalene-3,3′-dicarboxylic acid dimethyl ester.[4]

Experimental

Optically active (−)-1,1′-bisnaphthalene-2,2′-dicarboxylic acid was prepared according to the method of Hall and Turner[1] and the resolution was performed by successive recrystallization of diastereoisomer with quinine until the value of optical rotation gave an agreement with the reported one. The acid groups were reduced to hydroxymethyl groups and then transformed into bromomethyl groups. The configurations were retained throughout these reactions and it was confirmed by the CD spectral measurement.

The crystals used for crystallographic study were colorless thick plates or transparent prisms obtained from methylethylketone solution. The density was measured by the flotation method. The lattice constants were refined by a least-squares method using twelve reflections on Hilger-Watt four circle diffractometer with Cu$K\alpha$ radiation ($\lambda=1.5418$ Å).

1) D. M. Hall and E. E. Turner, *J. Chem. Soc.*, **1955**, 1242.
2) K. Mislow, *Angew. Chem.*, **70**, 683 (1958).
3) K. A. Kern and J. M. Robertson, *J. Chem. Soc.* (*B*), **1969**, 1146.
4) H. Akimoto and Y. Iitaka, *Acta Crystallogr.*, **B25**, 1941 (1969).

Crystal Data

(*S*)-(−)-2,2′-bisbromomethyl-1,1′-binaphthyl, $C_{22}H_{16}Br_2$, Mol. Wt. 440.2, orthorhombic,

$a=10.360\pm0.002$, $b=13.052\pm0.001$, $c=13.187\pm0.001$ Å

$D_m=1.625$, $D_c=1.639\ g\cdot cm^{-3}$, $Z=4$;

Absent spectra, $h00$, $0k0$, and $00l$ when h, k, or l is odd. Space group, $P2_12_12_1$. The intensity data were collected on the diffractometer using Cu–$K\alpha$ radiation and 2083 independent non-zero reflections were obtained.

Determination of the Structure

From the Patterson map the positions of bromine atom were determined and all of 22 carbon atoms were revealed from an electron density map calculated by the heavy atom method. Positional and thermal parameters were refined by the block-diagonal least-squares method. In the calculation of the structure factors, the anomalous dispersion effect was taken into account. The final R index was 0.064 for 1607 observed reflections with $|F_o|>3\sigma$. The atomic parameters with standard deviations are listed in Table 1, and observed and calculated structure factors are given in Table 2. Least-squares planes of naphthyl groups and the deviations of atoms from these planes are shown in Table 4. Atomic scattering factors were taken from the International Tables for X-ray Crystallography.[5]

TABLE 1. FINAL ATOMIC PARAMETERS WITH THEIR STANDARD DEVIATIONS

(1) THE ATOMIC COORDINATES

	x	y	z		x	y	z
Br	0.7492(2)	0.7294(1)	0.2718(1)	Br′	0.9705(2)	0.4481(1)	0.5063(1)
C(1)	0.8271(13)	0.4525(12)	0.2248(10)	C(1′)	0.9664(15)	0.4823(10)	0.2255(11)
C(2)	0.7383(17)	0.5111(10)	0.2793(10)	C(2′)	0.1834(15)	0.4810(11)	0.2950(13)
C(3)	0.6053(15)	0.4823(13)	0.2713(12)	C(3′)	0.0543(13)	0.4493(10)	0.2964(10)
C(4)	0.5627(15)	0.3923(20)	0.2190(13)	C(4′)	0.2259(14)	0.5446(12)	0.2206(13)
C(5)	0.6124(18)	0.2525(13)	0.1103(13)	C(5′)	0.1878(19)	0.6460(12)	0.0613(14)
C(6)	0.6956(20)	0.1868(14)	0.0584(13)	C(6′)	0.1033(18)	0.6772(12)	0.9873(14)
C(7)	0.8362(19)	0.2156(12)	0.0625(12)	C(7′)	0.9759(20)	0.6471(11)	0.9893(13)
C(8)	0.8777(16)	0.3030(11)	0.1188(12)	C(8′)	0.9215(17)	0.5844(12)	0.0679(11)
C(9)	0.7883(14)	0.3649(10)	0.1668(18)	C(9′)	0.0110(15)	0.5498(11)	0.1439(10)
C(10)	0.6518(15)	0.3402(11)	0.1649(12)	C(10′)	0.1421(16)	0.5786(11)	0.1423(11)
C(11)	0.7778(16)	0.5984(10)	0.3420(11)	C(11′)	0.0119(17)	0.3701(12)	0.3768(12)

(2) THE TEMPERATURE FACTORS

The temperature factors are expressed in the form: $T=\exp(-(\beta_{11}h^2+\beta_{22}k^2+\beta_{33}l^2+\beta_{12}hk+\beta_{13}hl+\beta_{23}kl))$

	β_{11}	β_{22}	β_{33}	β_{12}	β_{13}	β_{23}
Br	0.0148(2)	0.0055(1)	0.0065(1)	0.0036(4)	0.0024(3)	0.0025(2)
C(1)	0.0068(14)	0.0062(9)	0.0038(8)	0.0002(22)	0.0012(19)	0.0033(17)
C(2)	0.0082(15)	0.0059(9)	0.0031(8)	0.0015(23)	0.0013(23)	0.0017(14)
C(3)	0.0080(16)	0.0095(14)	0.0055(10)	0.0052(26)	0.0017(23)	0.0076(21)
C(4)	0.0088(18)	0.0067(11)	0.0071(12)	−0.0005(25)	0.0006(26)	0.0026(21)
C(5)	0.0136(23)	0.0065(12)	0.0069(12)	−0.0052(30)	−0.0055(29)	0.0025(20)
C(6)	0.0178(28)	0.0082(13)	0.0056(11)	−0.0023(34)	−0.0031(31)	0.0021(21)
C(7)	0.0173(25)	0.0044(9)	0.0053(10)	0.0028(29)	0.0007(28)	0.0012(17)
C(8)	0.0109(19)	0.0047(9)	0.0055(10)	0.0014(24)	0.0020(25)	−0.0010(17)
C(9)	0.0081(17)	0.0039(8)	0.0045(9)	−0.0024(20)	−0.0007(20)	0.0003(14)
C(10)	0.0080(17)	0.0046(9)	0.0061(11)	−0.0011(22)	−0.0000(24)	0.0032(16)
C(11)	0.0121(22)	0.0037(8)	0.0052(10)	0.0023(24)	0.0050(24)	0.0005(15)
Br′	0.0121(2)	0.0068(1)	0.0045(1)	0.0030(3)	0.0009(3)	0.0009(2)
C(1′)	0.0085(16)	0.0048(9)	0.0045(9)	−0.0015(21)	0.0030(24)	0.0013(15)
C(2′)	0.0080(16)	0.0054(10)	0.0072(12)	−0.0012(23)	−0.0010(25)	−0.0011(18)
C(3′)	0.0075(15)	0.0042(8)	0.0043(8)	−0.0008(21)	0.0013(19)	0.0009(15)
C(4′)	0.0068(17)	0.0064(10)	0.0077(12)	0.0008(24)	0.0004(24)	−0.0025(20)
C(5′)	0.0152(24)	0.0053(10)	0.0086(14)	0.0002(28)	0.0131(32)	−0.0002(20)
C(6′)	0.0160(24)	0.0060(10)	0.0069(12)	0.0015(28)	0.0076(34)	−0.0006(21)
C(7′)	0.0228(28)	0.0047(9)	0.0043(9)	0.0062(30)	0.0027(34)	−0.0005(16)
C(8′)	0.0136(21)	0.0063(11)	0.0032(8)	0.0037(27)	0.0018(23)	−0.0009(15)
C(9′)	0.0108(18)	0.0046(8)	0.0026(7)	0.0013(25)	0.0023(19)	0.0015(14)
C(10′)	0.0107(18)	0.0052(10)	0.0046(10)	−0.0007(24)	0.0029(24)	−0.0023(16)
C(11′)	0.0131(22)	0.0060(10)	0.0045(9)	0.0058(28)	0.0030(25)	0.0017(16)

5) "International Tables for X-ray Crystallography," The Kynoch Press, Birmingham, (1968), Vol. III, pp. 201, 213.

TABLE 2. OBSERVED AND CALCULATED SRTUCTURE FACTORS

L	FO	FC	L	FO	FC	L	FO	FC	L	FO	FC	L	FO	FC	L	FO	FC	L	FO	FC	L	FO	FC
H,K= 0 0			3	24	24	1	123	136	9	22	23	4	69	67	5	17	16	3	32	35	2	64	66	2	24	23
			4	20	22	2	101	96	10	7	5	5	60	56	6	15	14	4	18	20	3	28	30	3	25	21
			5	4	6	3	167	165	11	16	16	6	68	66	7	12	12	5	46	47	4	28	27	4	42	39
			6	29	29	4	26	22	12	7	4	7	20	19	8	22	22	6	37	39	5	84	83	5	17	15
			7	18	19	5	81	77	H,K= 1 11			8	15	15	H,K= 2 15			7	18	20	6	43	41	6	24	23
2	81	81	8	14	13	6	15	15	0	37	35	9	30	29	1	13	11	8	10	9	7	11	6	7	9	8
4	208	208	10	28	27	7	60	57	1	34	34	10	11	11	2	9	10	9	27	28	8	34	32	8	44	41
6	25	24	11	7	7	8	15	15	2	30	29	15	9	9	3	2	7	10	16	16	9	59	58	14	8	9
8	99	95	12	17	18	9	32	31	3	27	25	H,K= 2 5			H,K= 3 0			11	15	16	10	28	29	H,K= 5 1		
H,K= 0 1			H,K= 0 10			10	15	14	4	34	32	0	19	21	1	13	13	12	5	9	11	6	6	0	79	81
1	12	13	0	60	60	11	35	35	5	22	20	1	71	75	2	87	83	13	9	10	12	18	18	1	99	94
2	36	43	1	28	26	12	18	20	6	9	8	2	27	27	3	8	9	H,K= 3 8			13	23	25	2	50	46
3	152	144	2	29	26	13	7	7	7	16	14	3	46	43	4	43	44	0	21	20	14	8	8	3	55	50
4	22	21	3	35	33	14	16	18	8	17	17	4	28	30	5	28	26	1	6	4	H,K= 4 4			4	64	58
5	10	7	4	45	41	15	11	15	9	16	16	5	83	84	6	77	73	2	16	15	0	60	62	5	47	44
6	7	1	5	33	33	H,K= 1 4			11	12	12	6	42	42	7	33	29	3	19	20	1	42	42	6	35	34
7	95	93	6	39	37	0	82	90	H,K= 1 12			7	8	7	8	65	59	4	30	28	2	53	53	7	37	35
8	30	31	7	13	14	1	15	17	0	10	11	8	35	35	9	11	9	5	10	10	3	21	24	8	33	32
13	9	11	8	23	24	2	92	97	1	8	8	9	59	60	10	53	52	6	11	11	4	76	75	9	24	22
14	13	15	9	9	7	3	50	46	2	17	15	10	26	25	11	17	15	7	25	24	5	9	7	10	19	17
15	22	26	10	23	24	4	137	135	3	14	14	11	8	9	12	19	19	8	22	24	14	9	12	11	18	18
H,K= 0 2			12	9	11	5	19	18	4	19	18	12	16	18	13	11	10	9	8	8	H,K= 4 5			12	17	19
0	51	56	H,K= 0 11			6	93	91	5	16	14	13	30	33	14	14	19	10	13	14	0	27	30	13	4	6
1	6	6	1	26	24	7	12	12	6	15	12	14	10	11	15	10	12	11	17	19	1	49	50	14	14	17
2	34	42	3	22	20	8	60	60	7	23	21	H,K= 2 6			H,K= 3 1			12	14	16	2	51	54	H,K= 5 2		
3	44	41	4	12	11	9	24	24	8	11	10	0	15	15	0	56	55	13	7	9	3	65	68	0	41	41
8	26	25	5	10	8	10	61	62	9	9	7	1	53	55	1	147	144	H,K= 3 9			4	33	34	1	56	51
9	15	13	6	9	8	11	5	5	10	9	10	2	64	66	2	60	57	0	60	60	5	9	11	2	42	39
10	44	42	11	4	3	12	34	35	H,K= 1 13			3	69	69	3	114	108	1	38	39	10	22	23	3	59	56
11	17	16	H,K= 0 12			13	9	10	0	27	25	4	27	27	4	63	59	2	18	16	11	31	32	4	34	32
12	16	17	0	22	20	14	20	22	1	15	13	5	41	40	5	69	66	3	37	38	12	16	17	5	15	13
13	4	3	1	38	34	15	3	4	2	28	26	6	31	31	6	17	17	4	45	44	14	7	9	6	38	36
14	24	26	2	14	13	H,K= 1 5			3	12	11	7	28	29	7	63	59	5	40	38	H,K= 4 6			7	43	44
15	8	8	3	28	25	0	28	30	4	24	23	8	13	13	8	24	24	6	12	13	0	46	47	8	28	25
H,K= 0 3			4	18	16	1	67	72	H,K= 1 14			9	26	26	9	52	49	7	12	11	1	66	65	9	7	7
1	166	190	5	29	30	2	76	75	0	26	25	14	3	4	10	21	20	8	25	25	2	27	29	10	29	28
2	3	2	6	10	9	3	40	43	1	6	7	H,K= 2 7			11	21	19	9	19	18	3	33	35	11	21	21
3	42	39	7	17	16	4	40	37	2	16	16	0	35	35	12	12	15	10	4	1	4	41	41	12	9	10
H,K= 0 4			8	16	14	5	34	36	3	10	9	1	40	42	13	16	17	11	12	12	5	30	30	13	7	10
0	103	114	9	9	8	6	41	40	4	13	12	2	39	41	14	9	12	12	12	13	6	8	10	14	9	12
1	29	34	10	5	5	7	2	3	5	13	15	3	62	63	15	9	11	H,K= 3 10			7	17	19	H,K= 5 3		
2	111	113	H,K= 0 13			8	34	34	6	12	11	4	17	16	H,K= 3 2			5	32	32	8	15	15	0	6	3
3	96	92	1	22	22	9	23	24	H,K= 1 15			5	18	17	0	57	63	6	18	17	9	28	29	1	53	56
4	117	118	3	9	7	14	7	10	0	16	15	6	19	18	1	43	37	7	19	20	10	8	4	2	33	36
5	77	77	4	14	12	H,K= 1 6			1	5	7	7	50	50	2	60	55	8	8	9	H,K= 4 7			3	62	60
6	65	63	5	18	18	0	85	84	2	15	15	8	22	21	3	23	21	H,K= 3 11			0	34	33	4	4	5
7	40	39	6	18	18	1	20	18	3	11	11	9	8	9	4	35	35	0	23	21	1	35	37	5	44	44
8	37	36	7	13	14	2	59	62	4	8	10	H,K= 2 8			5	37	33	1	21	18	2	39	36	6	34	34
9	25	28	8	15	17	3	39	39	H,K= 2 0			0	73	73	6	42	39	2	48	46	3	11	8	7	32	30
10	14	15	H,K= 0 14			4	97	96	0	23	25	1	59	56	7	16	12	3	16	14	4	26	27	8	18	16
11	12	14	0	6	4	5	30	30	1	59	58	2	9	9	8	44	43	4	12	12	5	44	42	10	15	16
12	8	9	1	21	21	6	49	48	2	228	238	3	37	40	9	14	14	5	23	22	6	23	24	11	14	14
13	17	17	2	3	2	7	36	39	3	50	47	4	53	53	10	33	30	6	30	30	7	8	10	H,K= 5 4		
14	12	13	3	15	13	8	34	33	4	10	8	5	33	33	11	13	14	7	9	9	8	26	27	0	32	33
15	11	14	4	3	1	9	42	42	5	20	19	6	36	39	12	21	23	H,K= 3 12			9	23	22	1	43	46
H,K= 0 5			5	8	7	10	42	43	6	134	124	7	22	22	13	21	24	0	16	15	10	12	14	2	38	39
1	60	63	6	9	5	11	27	29	7	72	63	8	23	24	14	11	12	1	18	17	11	9	9	3	51	50
2	26	29	7	12	11	12	22	22	8	65	59	9	20	20	15	7	5	2	15	14	12	17	18	4	36	37
3	50	52	H,K= 0 15			13	9	7	9	5	5	10	17	19	H,K= 3 3			H,K= 3 13			13	16	17	5	37	37
4	12	11	1	13	10	14	16	17	10	62	58	11	7	8	0	57	60	0	27	24	H,K= 4 8			6	32	30
5	51	46	2	6	7	H,K= 1 7			11	19	18	12	13	13	1	85	89	1	17	15	0	12	11	7	17	18
6	71	67	3	8	6	0	45	45	12	23	24	13	11	12	2	23	18	2	23	24	H,K= 4 9			8	41	40
7	96	94	4	7	9	1	67	67	13	8	8	H,K= 2 9			3	72	64	3	10	10	0	4	1	9	29	30
8	35	34	H,K= 1 0			2	32	32	14	15	16	0	12	12	4	70	64	H,K= 3 15			1	17	17	10	28	29
9	10	10	1	72	68	3	64	66	15	1	5	1	12	12	5	78	76	0	13	15	2	18	14	11	8	9
10	12	14	2	20	19	4	49	49	H,K= 2 1			2	17	17	6	18	18	1	13	12	3	18	15	12	20	22
11	51	52	3	26	16	5	61	60	0	20	21	3	9	7	7	40	38	2	7	7	4	12	14	13	18	21
12	23	25	4	80	71	6	30	31	1	119	117	4	35	36	8	32	31	H,K= 4 0			5	17	17	H,K= 5 5		
13	9	9	5	46	39	7	24	22	2	44	41	5	30	28	9	22	21	0	146	151	6	15	17	0	15	19
H,K= 0 6			6	44	42	8	25	25	3	31	30	6	37	35	10	8	7	1	32	33	7	26	25	1	48	47
0	63	63	7	28	26	9	28	28	4	21	19	7	9	10	11	22	21	2	49	42	8	10	11	2	37	35
1	60	60	8	54	52	10	21	22	5	88	82	8	40	42	H,K= 3 4			3	52	50	9	5	5	3	30	30
2	21	25	9	20	21	11	20	22	6	28	29	9	20	21	0	62	66	4	130	125	10	23	24	4	40	40
3	17	17	10	46	45	12	9	9	7	18	18	10	15	16	1	58	62	5	54	54	11	10	11	5	34	37
4	25	28	11	21	22	13	11	15	8	20	18	11	5	2	2	67	68	6	18	15	H,K= 4 10			6	30	30
5	38	36	12	35	36	14	8	10	9	50	49	12	21	23	3	60	59	7	42	41	0	38	38	7	8	8
6	11	8	13	32	34	H,K= 1 8			10	22	21	H,K= 2 10			4	69	68	8	55	53	1	40	35	8	3	3
8	23	24	14	18	19	0	36	36	11	21	21	0	31	30	5	13	13	9	39	37	2	17	18	9	10	11
9	31	30	15	10	10	1	11	10	H,K= 2 2			1	52	49	6	58	57	10	18	18	3	39	37	10	8	9
10	5	6	H,K= 1 1			2	16	17	0	157	197	2	51	48	7	43	43	11	20	21	4	27	26	11	12	12
11	2	0	0	55	66	3	13	13	1	68	61	3	37	36	8	57	55	H,K= 4 1			5	25	24	12	7	8
13	11	9	1	92	91	4	25	23	2	33	31	4	20	18	9	3	5	0	11	13	6	18	17	13	4	3
14	13	14	2	59	54	5	18	21	3	46	44	5	33	31	10	46	46	1	30	30	7	27	28	H,K= 5 6		
H,K= 0 7			3	175	170	6	29	31	4	132	123	6	39	39	11	27	27	2	28	28	8	16	17	0	33	32
1	69	66	4	41	37	7	7	8	5	33	28	7	25	25	12	21	23	3	36	31	9	10	9	1	24	25
2	4	1	5	107	102	8	21	22	6	10	6	8	25	26	13	5	5	4	14	13	10	13	15	2	24	24
3	15	16	6	18	16	9	26	28	7	54	48	9	10	9	14	15	16	5	44	43	H,K= 4 11			3	39	38
4	16	18	7	79	72	10	22	22	8	56	55	10	10	12	H,K= 3 5			6	36	31	2	5	7	4	50	50
5	82	86	8	25	24	11	15	16	9	6	1	11	4	4	0	34	37	7	58	53	3	7	4	5	10	11
6	31	30	9	52	49	12	14	13	10	19	17	H,K= 2 11			1	64	65	8	17	16	4	17	16	6	19	19
7	12	13	10	9	8	13	12	15	11	11	11	3	14	13	2	22	23	9	17	18	5	8	8	7	47	49
8	20	22	11	48	46	H,K= 1 9			12	20	21	4	10	9	3	45	44	10	13	11	10	11	11	8	24	24
9	47	50	12	16	16	0	52	52	13	11	12	5	26	26	4	61	60	11	34	33	H,K= 4 12			9	6	5
10	7	9	13	8	8	1	36	34	14	17	21	6	15	15	5	21	24	12	12	12	0	23	21	10	15	16
11	10	8	14	10	10	2	62	59	H,K= 2 3			7	6	5	6	25	26	13	17	17	1	23	22	11	24	26
12	15	17	15	15	19	3	43	40	0	14	17	8	2	6	7	30	30	14	10	9	2	13	10	12	16	16
13	20	22	H,K= 1 2			4	34	32	1	90	91	9	12	14	8	17	13	H,K= 4 2			3	23	23	H,K= 5 7		
H,K= 0 8			0	15	16	5	42	40	2	36	35	10	19	18	9	5	7	0	22	19	4	4	5	0	50	52
0	19	18	1	64	63	6	32	31	3	79	75	H,K= 2 12			10	13	13	1	50	50	5	16	17	1	32	31
1	79	78	2	40	38	7	21	22	4	12	10	0	20	19	H,K= 3 6			2	115	114	H,K= 4 13			2	17	19
2	87	88	3	108	98	8	13	11	5	12	12	1	20	19	0	35	36	3	48	45	0	5	7	11	9	12
3	49	48	4	66	64	9	22	23	6	31	30	2	14	14	1	27	27	4	23	21	1	19	19	12	14	17
4	17	19	5	36	37	10	9	10	7	118	112	3	26	23	2	62	62	5	44	41	2	19	18	H,K= 5 8		
5	29	26	6	72	69	11	22	23	8	44	41	4	8	6	3	19	17	6	74	70	3	7	5	0	14	16
6	49	51	7	14	12	12	5	6	9	2	6	5	20	20	4	65	65	7	28	27	4	11	12	1	27	28
7	16	16	8	64	60	H,K= 1 10			10	12	12	6	23	20	5	48	48	8	17	16	5	14	14	2	11	8
8	22	22	9	15	13	0	12	10	11	56	55	7	13	14	6	55	53	9	24	23	6	14	15	3	9	9
9	5	4	10	50	48	1	7	9	12	19	18	8	13	10	7	11	14	10	30	29	7	6	5	4	16	13
10	12	14	11	19	19	2	8	8	14	9	7	9	7	0	12	22	24	11	15	15	H,K= 4 14			5	26	28
11	15	18	12	18	17	3	25	24	15	19	23	H,K= 2 13			13	15	19	12	16	17	1	15	15	6	22	23
12	18	19	13	16	17	4	8	9	H,K= 2 4			0	22	21	14	11	13	13	12	12	2	4	5	7	2	5
13	3	3	14	14	16	5	27	28	0	65	70	1	20	19	H,K= 3 7			14	9	8	3	15	17	8	9	10
H,K= 0 9			15	9	11	6	13	12	1	32	32	2	7	4	0	21	23	H,K= 4 3			4	5	4	9	15	15
1	16	15	H,K= 1 3			7	29	30	2	87	92	3	11	10	1	53	52	0	8	5	H,K= 5 0			10	13	13
2	38	35	0	19	22	8	12	13	3	32	29	4	17	15	2	68	67	1	42	40	1	59	55	11	5	5

Table 2. Continued

L	FO	FC	L	FO	FC	L	FO	FC	L	FO	FC	L	FO	FC	L	FO	FC	L	FO	FC	L	FO	FC
12	7	3	1	14	13	1	24	23	H=K= 6			3	32	32	3	9	10	6	26	27	2	13	13	H=K= 10		
H=K= 5			2	16	12	2	44	45	4	10	8	4	21	22	4	7	5	7	15	15	3	16	16	7	10	11
0	29	30	3	20	20	3	1	4	6	14	18	5	31	30	5	5	7	H=K= 8			4	12	10	8	5	5
1	15	13	4	19	19	4	45	45	7	3	2	6	23	22	6	7	7	0	11	11	5	5	6	9	9	9
2	69	69	5	36	33	5	34	31	8	10	10	11	8	7	7	8	10	1	24	26	6	12	13	H=K= 10		2
3	30	28	6	13	13	6	29	27	H=K= 6		12	H=K= 7		4	H=K= 8		0	2	14	15	7	12	10	0	7	6
4	8	7	7	14	13	7	9	9	0	17	12	0	19	19	0	32	32	3	25	26	8	8	7	1	17	18
5	21	18	8	10	8	8	40	42	1	13	17	1	24	23	1	31	31	4	4	5	9	4	2	2	20	19
6	37	36	9	32	32	9	21	20	2	10	9	2	11	11	2	24	21	5	10	12	10	10	11	3	9	9
7	10	13	10	15	15	10	24	26	3	14	18	3	44	43	H=K= 8		1	6	8	9	H=K= 9		4	4	5	6
8	11	13	11	24	24	12	12	16	4	3	5	4	31	29	2	14	14	7	8	4	0	20	23	5	12	13
9	9	10	12	12	13	H=K= 6		6	5	8	10	5	15	16	3	27	28	8	3	6	1	23	25	6	9	9
10	13	16	13	7	11	0	32	36	H=K= 6		13	H=K= 7		5	4	9	7	9	5	6	2	11	12	7	10	12
11	8	12	H=K= 6		2	1	29	31	2	9	8	0	29	32	5	18	17	H=K= 8		8	H=K= 9		5	8	0	4
H=K= 5		10	0	58	62	2	30	27	3	3	6	1	22	21	6	6	8	0	14	11	0	23	25	9	4	7
0	9	9	1	38	40	3	39	43	4	12	14	2	18	22	7	30	28	1	21	21	1	13	11	H=K= 10		3
1	20	20	2	34	33	4	16	14	H=K= 7		0	3	30	28	8	10	10	2	11	10	2	17	17	0	20	20
2	15	14	3	48	45	H=K= 6		7	4	38	39	4	19	21	9	14	15	3	20	18	3	14	15	1	8	7
3	12	12	4	49	46	0	31	31	5	2	2	5	15	13	H=K= 8		2	4	12	11	4	5	7	2	9	11
4	9	10	5	29	28	1	14	14	6	56	55	6	18	17	0	28	30	5	12	13	5	14	13	3	4	1
5	18	17	6	15	13	2	8	10	7	19	19	7	17	19	1	36	37	6	9	10	6	8	9	4	13	13
6	2	2	7	40	39	3	33	31	12	10	14	H=K= 7		6	2	34	32	7	13	18	9	7	7	H=K= 10		4
7	14	15	8	34	36	4	32	31	13	4	7	4	8	9	3	37	37	H=K= 8		10	H=K= 9		6	0	10	11
8	12	12	9	19	18	5	7	7	H=K= 7		1	5	21	24	4	24	21	0	5	5	0	15	14	1	9	11
9	12	16	10	5	5	6	15	14	0	26	25	6	16	14	5	16	16	1	15	22	1	12	13	2	11	10
10	3	2	11	20	19	7	25	25	1	46	42	7	12	12	6	18	17	2	1	1	2	11	11	3	5	6
H=K= 5		11	12	6	5	8	17	18	2	53	48	1	35	36	7	22	21	3	8	18	3	25	25	4	8	8
0	28	27	13	8	13	9	9	9	3	40	39	2	11	11	H=K= 8		3	H=K= 9		0	4	6	8	5	8	7
1	11	10	H=K= 6		3	10	14	17	4	43	41	3	25	25	0	25	29	2	6	8	5	9	9	6	8	7
H=K= 5		12	0	31	33	11	14	16	5	31	33	8	5	5	1	16	18	4	17	18	H=K= 9		7	8	3	5
1	8	10	1	23	20	H=K= 6		8	6	37	37	9	18	20	2	25	25	5	18	19	0	13	12	H=K= 10		5
2	5	4	2	38	40	0	29	28	7	5	4	10	10	11	3	22	18	6	11	13	1	14	13	0	16	19
3	16	16	3	26	27	1	36	35	8	32	31	11	9	6	4	24	25	H=K= 9		1	3	14	13	1	1	5
4	7	7	4	42	41	2	19	17	9	2	4	H=K= 7		7	5	10	9	0	29	29	4	15	16	2	17	14
5	2	6	5	15	13	3	24	24	10	20	20	0	4	3	6	20	21	1	22	20	6	2	6	3	10	10
6	9	8	6	28	29	4	20	17	11	11	12	1	18	17	7	7	7	2	22	20	7	4	5	4	13	15
7	16	19	7	51	51	5	23	22	12	13	17	2	32	32	8	20	20	3	20	19	8	9	11	5	4	3
H=K= 5		13	8	20	20	6	8	11	13	6	5	3	24	26	9	21	19	4	33	32	H=K= 9		8	6	10	12
2	19	20	9	17	17	7	19	21	H=K= 7		2	4	3	7	11	12	16	5	22	21	0	7	7	7	9	10
3	7	9	10	19	17	8	10	9	0	7	4	5	15	13	H=K= 8		4	6	18	16	1	13	12	H=K= 10		8
4	9	9	11	19	20	H=K= 6		9	1	29	28	6	20	22	0	33	33	7	3	7	2	9	9	0	1	1
5	9	10	12	12	14	4	12	12	2	10	11	7	7	7	1	9	9	8	12	14	3	4	6	1	10	14
H=K= 6		0	13	3	6	5	8	8	3	34	31	8	6	5	2	22	22	9	7	7	4	7	9	2	8	7
0	12	17	H=K= 6		4	6	8	9	4	5	6	9	2	3	3	16	17	10	12	16	5	8	10	H=K= 11		0
1	43	45	0	33	35	7	9	9	5	26	26	10	13	15	4	20	22	H=K= 9		2	6	9	12	6	0	3
2	87	83	1	22	23	H=K= 6		10	6	9	9	H=K= 7		9	5	7	8	3	25	24	7	4	3	H=K= 11		1
3	61	56	2	46	46	0	11	14	7	22	21	0	52	48	6	15	15	4	4	6	H=K= 10		0	0	6	9
4	34	32	3	21	21	1	30	29	8	7	6	1	7	7	7	11	11	5	15	14	0	22	20	1	13	12
5	31	29	4	20	18	2	16	15	9	20	19	2	8	6	8	9	10	6	18	15	1	22	21	H=K= 11		2
6	54	51	5	9	8	3	33	35	10	10	11	7	5	5	H=K= 8		5	7	9	11	2	15	16	6	5	3
7	29	28	6	27	25	4	7	6	11	12	12	8	17	21	0	43	47	8	5	5	3	16	14	H=K= 11		3
8	6	3	7	18	19	5	21	20	12	11	14	9	2	0	1	14	16	9	6	8	4	20	20	0	10	12
9	22	20	8	11	10	6	12	13	H=K= 7		3	H=K= 7		10	2	24	24	10	12	14	5	17	18	H=K= 11		7
10	8	6	9	14	16	7	12	14	0	28	31	0	5	3	3	14	15	H=K= 9		3	7	8	11	1	6	5
H=K= 6		1	H=K= 6		5	8	5	8	1	29	29	1	13	11	4	22	21	0	8	6	8	3	4	2	11	11
0	6	9	0	40	42	9	13	14	2	16	17	2	2	3	5	10	11	1	16	18	9	8	9			

Table 3. A comparison of calculated and observed intensity ratios of the Friedel's pair

h	k	l	$I_c(hkl)/I_c(\bar{h}\bar{k}\bar{l})$	$I_o(hkl)/I_o(hkl)$
1	3	13	0.63	0.89
2	4	10	0.67	0.77
2	13	2	1.72	2.60
3	1	6	1.78	1.35
4	4	5	0.67	0.74
4	7	3	1.58	1.61
7	2	10	1.61	1.21
5	8	2	0.46	0.91
7	2	6	0.46	0.70
8	1	4	1.58	1.16

Absolute Configuration

The absolute configuration of (−)-2,2′-bisbromomethyl-1,1′-binaphthyl was determined by the Bijvoet method using the values of $\Delta f' = -0.9$ and $\Delta f'' = 1.5$ for bromine atom.[5] A comparison of calculated and observed intensity ratios for hkl and $\bar{h}\bar{k}\bar{l}$ reflections is shown in Table 3 and the coordinates given in Table 1 are shown to be the correct ones in the right-handed coordinate system. Thus the absolute configuration can be designated as (S). All figures are drawn with the correct absolute configuration.

Results and Discussion

The present analysis showed that the absolute configuration of (−)-2,2′-bisbromomethyl-1,1′-binaphthyl is (S)-configuration. The chemical studies on (−)-2,2′-dihydroxymethyl-1,1′-binaphthyl and (−)-1,1′-bisnaphthalene-2,2′-dicarboxylic acid showed that the configurations were retained, so that all these related molecules have (S)-configuration. This result is in good agreement with the chemical correlation studies on substituted binaphthyls[2,6] and the X-ray study of Akimoto and Iitaka[4] on (+)-2,2′-dihydroxy-1,1′-bis-

Table 4. Least-squares planes and the deviation of atoms from the planes

The planes are of the form $AX+BX+CZ+P=0$, where X,Y,Z are coordinates measured along three cell edges in Å unit.

Naphthyl group I $0.113X-0.569Y+0.814Z+0.034=0$		Naphthyl group II $0.222X+0.801Y+0.556Z+6.771=0$	
C(1)	−0.02Å	C(1′)	0.00Å
C(2)	0.03	C(2′)	−0.03
C(3)	0.00	C(3′)	0.00
C(4)	0.02	C(4′)	0.02
C(5)	−0.01	C(5′)	0.00
C(6)	0.02	C(6′)	−0.02
C(7)	0.01	C(7′)	0.00
C(8)	0.01	C(8′)	0.02
C(9)	−0.03	C(9′)	0.01
C(10)	−0.03	C(10′)	0.00
C(11)	0.10	C(11′)	0.17

6) H. Akimoto, T. Shioiri, Y. Iitaka, and S. Yamada, *Tetrahedron Lett.* **1968**, 97.

Table 5. Comparison of bond lengths and angles

Molecule	Bond length between C(1) and C(1′)	Twist angle between two planes
1,1′-Binaphthyl[3]	1.475Å	68°
(+)-2,2′-Dihydroxy-1,1′-bisnaphthalene-3,3′-dicarboxylic acid dimethyl ester[4]	1.49Å	76.6°
(−)-2,2′-Bisbromomethyl-1,1′-binaphthyl	1.50Å	91.6°

naphthalene-3,3′-dicarboxylic acid dimethyl ester, which was shown as (*R*)-configuration.

The naphthyl groups are nearly planar (Table 4). One naphthyl group is twisted against the other one with an angle of 91.6°. The values for other related molecules are listed in Table 5. It is interesting that the present molecule exhibits the largest twist angle, which may be related to the steric repulsion of bulky substituents such as bromomethyl group.

The bond lengths and angles are shown in Figs. 1 and 2. The bond length between C(1) and C(1′) is close to the normal single bond like those in other related molecules, and the resonance effect may not be significant. The projection of molecules onto the crystallographic planes are illustrated in Figs. 3 and 4 with interatomic distances.

The absolute configuration determined as (*S*)-configuration will be used for the chiro-optical study of (−)-binaphthyl derivatives.

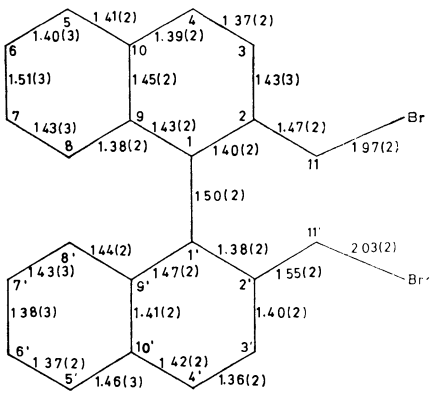

Fig. 1. Bond lengths (Å) with standard deviations.

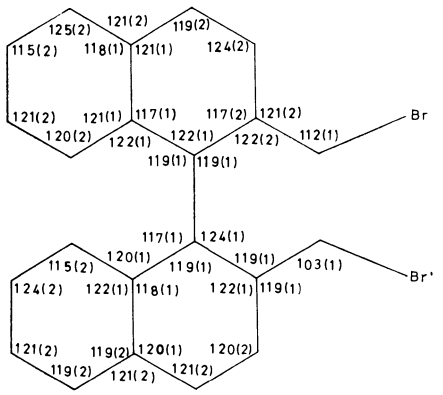

Fig. 2. Bond angles (degree) with standard deviations.

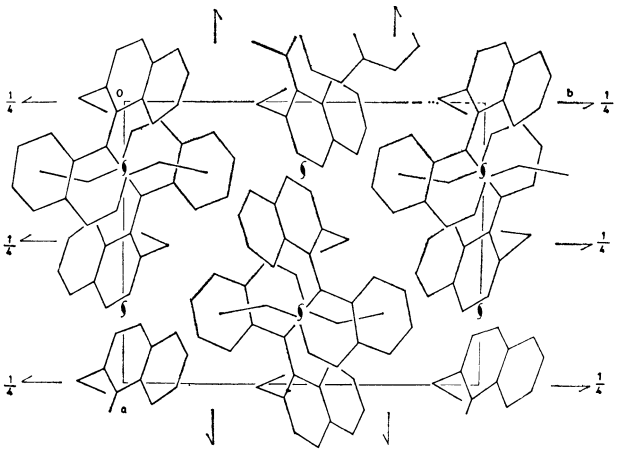

Fig. 3. Projection of the crystal structure along the c-axis.

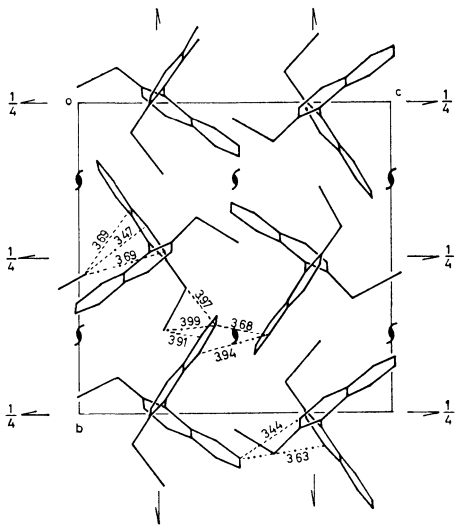

Fig. 4. Projection of the crystal structure along the a-axis.

The authors thank to Dr. Noriyoshi Sakabe in this laboratory for many helpful discussions. All calculations were carried out at the Computation Center of Nagoya University, using the programs of UNICS.[7]

7) "UNICS. A Universal Crystallographic Computation System," The Crystallographic Society of Japan, Tokyo (1967).

Infrared Absorption Intensities of Torsion-Rotation Transitions of Molecules with Symmetric Internal Rotor

Hiromu SUGETA and Tatsuo MIYAZAWA

Institute for Protein Research, Osaka University, Yamada-kami, Suita, Osaka 565

(Received June 5, 1973)

The infrared absorption intensities of torsion-rotation transitions were theoretically derived on the basis of torsion-rotation interactions of molecules with symmetric internal rotor. The theoretical intensities depend upon molecular structure parameters and molecular dipole moment. Implications of the present theory are discussed on absolute intensities, orientations of dipole transition moment, band types (A, B, or C), and deuteration effects on absorption intensities of methyl torsional transitions. For propylene oxide and propylene sulfide, the far infrared spectra of the gaseous state were measured, and the experimental absorption intensities of methyl torsional vibrations were compared with theoretical intensities.

A number of investigations on internal-rotation barriers of symmetric internal rotors ($-CH_3$, $-SiH_3$, $-CF_3$ *etc.*) have been carried out by the microwave spectroscopy[1] and far-infrared spectroscopy.[2] Far infrared bands due to torsional vibrations often exhibit complicated contours due to torsion-rotation interactions.[2] For detailed analyses of torsional bands, it is necessary to elucidate the effects of torsion-rotation interactions not only on energy levels but also on absorption intensities of torsion-rotation transitions. The effects of these interactions on energy levels have been extensively studied for analysing microwave spectra of molecules with symmetric internal rotors.[3] In the present study, the infrared absorption intensities of torsion-rotation transitions have been worked out, taking account of torsion-rotation interactions.

Torsion-Rotation Wave Functions

The model used in the present study consists of a rigid frame and a symmetric internal rotor that performs torsional motion with respect to the frame. With the principal-axis-method, the Hamiltonian (H) for this model is given by[3]

$$H = H_r + H_t + H_{tr} \tag{1}$$

where H_r and H_t are the rotational and torsional Hamiltonian, respectively, and H_{tr} is the Hamiltonian for the torsion-rotation interactions. These Hamiltonians may be written as,

$$H_r = AP_a^2 + BP_b^2 + CP_c^2 + F\mathscr{P}^2 \tag{2}$$

$$H_t = Fp_\alpha^2 + V(\alpha) \tag{3}$$

$$H_{tr} = -F(p_\alpha\mathscr{P} + \mathscr{P}p_\alpha) = -2Fp_\alpha\mathscr{P} \tag{4}$$

and

$$A = \hbar^2/2I_a \text{ etc} \tag{5}$$

$$F = \hbar^2/2rI_\alpha \tag{6}$$

$$r = 1 - \sum\lambda_g^2 I_\alpha/I_g \quad (g=a, b, \text{ or } c) \tag{7}$$

where I_g is the principal moment of inertia of the entire molecule, I_α is the moment of inertia of the internal rotor about its symmetry axis, λ_g is the direction cosine between the principal axis (g) and the internal-rotation axis. P_g is the component of the total angular momentum (in unit of $\hbar$) along the principal axis g,

$$\tilde{P} = [P_a\ P_b\ P_c] \tag{8}$$

p_α is the angular momentum of the internal rotor along its symmetry axis and $V(\alpha)$ is the potential energy for the internal-rotation. The angular momentum $\mathscr{P}$ in Eqs. (2) and (4) is given as

$$\mathscr{P} = \sum_g(\lambda_g I_\alpha/I_g)P_g = \boldsymbol{\rho}\cdot\boldsymbol{P} \tag{9}$$

where

$$\tilde{\boldsymbol{\rho}} = [\lambda_a I_\alpha/I_a\ \lambda_b I_\alpha/I_b\ \lambda_c I_\alpha/I_c] \tag{10}$$

In the present study, the torsion-rotation interaction H_{tr} [Eq. (4)] is treated as the perturbation term. The eigenvalues and wave functions of the rotational Hamiltonian H_r [Eq. (2)] are denoted as E_r and $|r\rangle$, respectively. The eigenvalues and wave functions of the torsional Hamiltonian H_t [Eq. (3)] are denoted as $E_{v\sigma}$ and $|v\sigma\rangle$, respectively, where v is the torsional quantum number and σ is the symmetry index ($\sigma=0$ for A and $\sigma=\pm1$ for E species). The unperturbed wave function is constructed as the product of the torsional and rotational parts, $|v\sigma\rangle|r\rangle$ and the matrix elements of the perturbation H_{tr} is given by

$$\begin{aligned}\langle r_2|\langle v_2\sigma_2|H_{tr}|v_1\sigma_1\rangle|r_1\rangle &= -2F\langle r_2|\langle v_2\sigma_2|p_\alpha\mathscr{P}|v_1\sigma_1\rangle|r_1\rangle \\ &= -2F\delta_{\sigma_1\sigma_1}\langle v_2\sigma_2|p_\alpha|v_1\sigma_1\rangle\langle r_2|\mathscr{P}|r_1\rangle\end{aligned} \tag{11}$$

Accordingly, with the first-order perturbation theory, the perturbed wave functions $|v\sigma,r\rangle$ are given by

$$|v\sigma, r\rangle = |v\sigma\rangle|r\rangle - 2F\sum_{v'}{}'\sum_{r'}\frac{\langle v'\sigma|p_\alpha|v\sigma\rangle\langle r'|\mathscr{P}|r\rangle}{(E_{v\sigma}+E_r)-(E_{v'\sigma}+E_{r'})}|v'\sigma\rangle|r'\rangle \tag{12}$$

Neglecting the rotational energy differences ($E_r - E_{r'}$) as compared with the torsional energy differences ($E_{v\sigma} - E_{v'\sigma}$), Eq. (12) may be rewritten as

$$|v\sigma, r\rangle = |v\sigma\rangle|r\rangle - 2F\left[\sum_{v'}{}'\frac{\langle v'\sigma|p_\alpha|v\sigma\rangle}{E_{v\sigma}-E_{v'\sigma}}|v'\sigma\rangle\right][\sum_{r'}\langle r'|\mathscr{P}|r\rangle|r'\rangle] \tag{13}$$

1) W. Gordy and R. L. Cook, "Microwave Molecular Spectra", Interscience Publishers, New York, N. Y. (1970), Chap. 12, p. 423; J. E. Wollrab, "Rotational Spectra and Molecular Structure", Academic Press, New York, N. Y. (1967), Chap. 6, p. 145.

2) K. D. Möller and W. G. Rothschild, "Far-Infrared Spectroscopy", Wiley-Interscience, New York, N. Y. (1971), Chap. 8, p. 256; A. Finch, P. N. Gates, K. Radcliffe, F. N. Dickson, and F. F. Bentley, "Chemical Applications of Far Infrared Spectroscopy", Academic Press, New York, N. Y. (1970), Chap. 4, p. 78.

3) C. C. Lin and J. D. Swalen, *Rev. Mod. Phys.*, **31**, 841 (1959); D. R. Herschbach, *J. Chem. Phys.*, **31**, 91 (1959).

Line Strength of Torsion-Rotation Transition

The absorption intensity (I) for the transition between states A and B is given by[4]

$$I = \frac{n}{z}\frac{8\pi^3\nu_{AB}}{3hc}[\exp(-E_A/kT)-\exp(-E_B/kT)]S_{AB} \quad (14)$$

where n is the number of molecules per unit volume, z is the partition function, E_A and E_B are the energy of the states A and B, respectively. ν_{AB} is the transition frequency

$$\nu_{AB} = (E_B-E_A)/h \quad (15)$$

and S_{AB} is the line strength given by

$$S_{AB} = \sum_a\sum_b|\langle b|\bar{\mu}|a\rangle|^2 = 3\sum_a\sum_b|\langle b|\bar{\mu}_F|a\rangle|^2 \quad (16)$$

where a and b denote individual degenerate substates of A and B, respectively, $\bar{\mu}$ is the electric dipole moment operator in the space-fixed coordinate system, and $\bar{\mu}_F$ is the F component. The component $\bar{\mu}_F$ is related to the molecule-fixed dipole moment operator μ_g by the direction cosine Φ_{Fg} between the space-fixed F axis and molecule-fixed g axis,

$$\bar{\mu}_F = \Phi_F\cdot\boldsymbol{\mu} = \sum_g\Phi_{Fg}\mu_g \quad (17)$$

$$\tilde{\Phi}_F = [\Phi_{Fa}\ \Phi_{Fb}\ \Phi_{Fc}] \quad (18)$$

$$\tilde{\mu} = [\mu_a\ \mu_b\ \mu_c] \quad (19)$$

In general, the molecule-fixed dipole moment μ_g depends only upon vibrational coordinates whereas the direction cosines Φ_{Fg} depend only upon rotational coordinates. For a molecule with a rigid frame and a symmetric internal rotor, then, the transition moment for the unperturbed wave functions $|v\sigma\rangle|r\rangle$ may be written as

$$\begin{aligned}\langle r_2|\langle v_2\sigma_2|\bar{\mu}_F|v_1\sigma_1\rangle|r_1\rangle &= \langle v_2\sigma_2|\boldsymbol{\mu}|v_1\sigma_1\rangle\cdot\langle r_2|\Phi_F|r_1\rangle \\ &= \sum_g\langle v_2\sigma_2|\mu_g|v_1\sigma_1\rangle\langle r_2|\Phi_{Fg}|r_1\rangle \quad (20)\end{aligned}$$

Furthermore, with the present model, the molecule-fixed dipole moment $\boldsymbol{\mu}$ in Eq. (20) is independent of the internal rotation and is equal to the permanent dipole moment $\boldsymbol{\mu}^\circ$.

$$\tilde{\mu} = \tilde{\mu}^\circ = [\mu_a^\circ\ \mu_b^\circ\ \mu_c^\circ] \quad (21)$$

Accordingly, for unperturbed wave functions,

$$\langle v_2\sigma_2|\mu_g|v_1\sigma_1\rangle = \mu_g^\circ\langle v_2\sigma_2|v_1\sigma_1\rangle = \mu_g^\circ\delta_{v_1v_1}\delta_{\sigma_1\sigma_1} \quad (22)$$

and Eq. (20) may be rewritten as,

$$\begin{aligned}\langle r_2|\langle v_2\sigma_2|\bar{\mu}_F|v_1\sigma_1\rangle|r_1\rangle &= \langle r_2|\langle v_2\sigma_2|\boldsymbol{\mu}^\circ\cdot\Phi_F|v_1\sigma_1\rangle|r_1\rangle \\ &= \delta_{v_1v_1}\delta_{\sigma_1\sigma_1}\boldsymbol{\mu}^\circ\cdot\langle r_2|\Phi_F|r_1\rangle \\ &= \delta_{v_1v_1}\delta_{\sigma_1\sigma_1}\langle r_2|\bar{\mu}_F|r_1\rangle \quad (23)\end{aligned}$$

The matrix element of the transition moment for $|v_2\sigma_2,r_2\rangle\leftarrow|v_1\sigma_1,r_1\rangle$ is now derived from the perturbed wave function $|v\sigma,r\rangle$ [Eq. (13)] and the transition moment for unperturbed wave functions $|v\sigma\rangle|r\rangle$ [Eq. 23)].

$$\begin{aligned}\langle v_2\sigma_2, r_2|\bar{\mu}_F|v_1\sigma_1, r_1\rangle &= \langle r_2|\langle v_2\sigma_2|\bar{\mu}_F|v_1\sigma_1\rangle|r_1\rangle \\ &\quad -2F\sum_v{}'\sum_r\frac{\langle v_2\sigma_2|p_\alpha|v\sigma_2\rangle}{E_{v_1\sigma_1}-E_{v\sigma_1}}\langle r_2|\mathscr{P}|r\rangle\langle r|\langle v\sigma_2|\bar{\mu}_F|v_1\sigma_1\rangle|r_1\rangle \\ &\quad -2F\sum_v{}'\sum_r\langle r_2|\langle v_2\sigma_2|\bar{\mu}_F|v\sigma_1\rangle|r\rangle\langle r|\mathscr{P}|r_1\rangle\frac{\langle v\sigma_1|p_\alpha|v_1\sigma_1\rangle}{E_{v_1\sigma_1}-E_{v\sigma_1}} \\ &= \delta_{v_1v_1}\delta_{\sigma_1\sigma_1}\langle r_2|\bar{\mu}_F|r_1\rangle \\ &\quad -2F\sum_v{}'\sum_r\frac{\langle v_2\sigma_2|p_\alpha|v\sigma_2\rangle}{E_{v_1\sigma_1}-E_{v\sigma_1}}\langle r_2|\mathscr{P}|r\rangle\delta_{vv_1}\delta_{\sigma_1\sigma_1}\langle r|\bar{\mu}_F|r_1\rangle \\ &\quad -2F\sum_v{}'\sum_r\delta_{v_1v}\delta_{\sigma_1\sigma_1}\langle r_2|\bar{\mu}_F|r\rangle\langle r|\mathscr{P}|r_1\rangle\frac{\langle v\sigma_1|p_\alpha|v_1\sigma_1\rangle}{E_{v_1\sigma_1}-E_{v\sigma_1}} \quad (24)\end{aligned}$$

Here only for $\sigma_1=\sigma_2(=\sigma)$, the transition moments are nonvanishing. Furthermore, for torsion-rotation transitions ($v_1\neq v_2$), Eq. (24) may be rewritten as,

$$\begin{aligned}\langle v_2\sigma, r_2|\bar{\mu}_F|v_1\sigma, r_1\rangle &= -2F\sum_r\left[\frac{\langle v_2\sigma|p_\alpha|v_1\sigma\rangle}{E_{v_1\sigma}-E_{v_1\sigma}}\langle r_2|\mathscr{P}|r\rangle\langle r|\bar{\mu}_F|r_1\rangle\right. \\ &\quad \left.+\langle r_2|\bar{\mu}_F|r\rangle\langle r|\mathscr{P}|r_1\rangle\frac{\langle v_2\sigma|p_\alpha|v_1\sigma\rangle}{E_{v_1\sigma}-E_{v_1\sigma}}\right] \\ &= 2F\frac{\langle v_2\sigma|p_\alpha|v_1\sigma\rangle}{E_{v_1\sigma}-E_{v_1\sigma}}\langle r_2|\bar{\mu}_F\mathscr{P}-\mathscr{P}\bar{\mu}_F|r_1\rangle \\ &= 2F\frac{\langle v_2\sigma|p_\alpha|v_1\sigma\rangle}{E_{v_1\sigma}-E_{v_1\sigma}}\langle r_2|[\bar{\mu}_F,\mathscr{P}]|r_1\rangle \quad (25)\end{aligned}$$

The commutation $[\bar{\mu}_F,\mathscr{P}]$ in Eq. (25) may be derived from the commutation relations between the angular momentum P_g (g=x, y, or z) and the direction cosines Φ_{Fg},[5]

$$[\Phi_{Fx}, P_x] = \Phi_{Fx}P_x - P_x\Phi_{Fx} = 0 \quad (26)$$

$$[\Phi_{Fx}, P_y] = [P_x, \Phi_{Fy}] = -i\Phi_{Fz}\ \textit{etc.} \quad (27)$$

From Eqs. (9), (17), and (21),

$$\begin{aligned}[\bar{\mu}_F, \mathscr{P}] &= [(\boldsymbol{\mu}^\circ\cdot\boldsymbol{\Phi}_F), (\boldsymbol{\rho}\cdot\boldsymbol{P})] \\ &= [(\mu_x^\circ\Phi_{Fx}+\mu_y^\circ\Phi_{Fy}+\mu_z^\circ\Phi_{Fz}), (\rho_xP_x+\rho_yP_y+\rho_zP_z)] \\ &= -i\{(\mu_y^\circ\rho_z-\mu_z^\circ\rho_y)\Phi_{Fx}+(\mu_z^\circ\rho_x-\mu_x^\circ\rho_z)\Phi_{Fy} \\ &\quad +(\mu_x^\circ\rho_y-\mu_y^\circ\rho_x)\Phi_{Fz}\} \\ &= -i(\boldsymbol{\mu}^\circ\times\boldsymbol{\rho})\cdot\boldsymbol{\Phi}_F \quad (28)\end{aligned}$$

Substituting Eq. (28) into Eq. (25), the transition moment is finally expressed as the product of the vibrational part and rotational part.

$$\begin{aligned}\langle v_2\sigma, r_2|\bar{\mu}_F|v_1\sigma, r_1\rangle &= \left\{-2iF\frac{\langle v_2\sigma|p_\alpha|v_1\sigma\rangle}{E_{v_1\sigma}-E_{v_1\sigma}}(\boldsymbol{\mu}^\circ\times\boldsymbol{\rho})\right\}\cdot\{\langle r_2|\Phi_F|r_1\rangle\} \quad (29) \\ &\qquad\text{[vibration]} \qquad\qquad \text{[rotation]}\end{aligned}$$

Absorption Intensity of Torsional Band

The vibrational part of the transition moment may be used for deriving the integrated absorption intensity of the torsional band. Thus, the molar absorption intensity of the torsional transitions $|v+1,\sigma\rangle\leftarrow|v,\sigma\rangle$ is given by

$$I_{v,\sigma;\,v+1,\sigma} = \frac{N}{z}\frac{8\pi^3}{3h^2c}[\exp(-E_{v,\sigma}/kT)-\exp(-E_{v+1,\sigma}/kT)] \times 4F^2|\boldsymbol{\mu}^\circ\times\boldsymbol{\rho}|^2\frac{|\langle v_2\sigma|p_\alpha|v_1\sigma\rangle|^2}{E_{v+1,\sigma}-E_{v,\sigma}} \quad (30)$$

4) B. L. Crawford, Jr. and H. L. Dinsmore, *J. Chem. Phys.*, **18**, 983 (1950).

5) P. C. Cross, R. M. Hainer, and G. W. King, *ibid.*, **12**, 210 (1944).

where N is the Avogadro number. The integrated absorption intensity of the torsional fundamental band is given by

$$\int_{\text{band}} \alpha(\nu)\mathrm{d}\nu = \sum_{v,\sigma} I_{v+1,\sigma;\, v,\sigma} \tag{31}$$

where $\alpha(\nu)$ is the molar absorption coefficient for the absorption frequency ν.

For a high barrier case (see Appendix I), the energy levels $E_{v\sigma}$ and the integrals $\langle v+1,\sigma|p_a|v,\sigma\rangle$ are almost independent of the symmetry index σ, and from Eqs. (A3), (A7), and (A8),

$$|\langle v+1|p_a|v\rangle|^2 = (N/2)^2[(v+1)s^{1/2}/2][1-(v+1)/2s^{1/2}] \tag{32}$$

$$E_{v+1}-E_v = (N/2)^2F[2s^{1/2}][1-(v+1)/2s^{1/2}] \tag{33}$$

so that

$$\frac{|\langle v+1|p_a|v\rangle|^2}{E_{v+1}-E_v} = (v+1)/4F \tag{34}$$

Substituting Eq. (34) into Eq. (30),

$$I_{v,v+1} = \frac{N}{z}\frac{8\pi^3}{3h^2c}[\exp(-E_v/kT)-\exp(-E_{v+1}/kT)] \times|\boldsymbol{\mu}^\circ\times\boldsymbol{\rho}|^2F(v+1) \tag{35}$$

Finally, with the harmonic oscillator approximation for energy levels, the integrated absorption intensity of the torsional band is obtained by substituting Eq. (35) into Eq. (31),

$$\int_{\text{band}} \alpha(\nu)\mathrm{d}\nu \cong (8\pi^3N/3h^2c)F|\boldsymbol{\mu}^\circ\times\boldsymbol{\rho}|^2 \tag{36}$$

Discussion

Absolute Absorption Intensity. By the use of Eq. (30) [or (35)] and (31) [or (36)], the integrated intensity of the torsional band may be calculated from molecular structure parameters and molecular dipole moment. The theoretical intensity value is also useful for estimating the path length and sample pressure required for absorption measurements.

The absorption intensity is proportional to $F|\boldsymbol{\mu}^\circ\times\boldsymbol{\rho}|^2$ as shown in Eq. (30). Accordingly, the fundamental transition is forbidden for molecules in which the dipole moment $\boldsymbol{\mu}^\circ$ and the $\boldsymbol{\rho}$ vector are parallel to each other, for examples for CH_3–CX_3, CH_3–NO_2 *etc.* On the other hand, if the dipole moment $\boldsymbol{\mu}^\circ$ is nearly perpendicular to the $\boldsymbol{\rho}$ vector, the absorption intensity is strong. For a simple example, if the dipole moment is parallel to the a axis ($\mu^\circ=\mu^\circ_a$, $\mu^\circ_b=\mu^\circ_c=0$) and the symmetry axis of the internal rotor is parallel to the b axis ($\lambda_a=\lambda_c=0$, $\rho_a=\rho_c=0$, $\lambda_b=1$, $\rho_b=I_a/I_b$), the absolute intensity of the torsional band is given by

$$\int_{\text{band}} \alpha(\nu)\mathrm{d}\nu = \frac{8\pi^3N}{3h^2c}\frac{h^2I_b}{8\pi^2I_a(I_b-I_a)}\left(\mu^\circ\frac{I_a}{I_b}\right)^2 = (N\pi/3c)(\mu^\circ)^2I_a/I_b(I_b-I_a) \tag{37}$$

Thus, for this simple case, the absorption intensity is nearly proportional to the inversed square of the moment of inertia (I_b) of the entire molecule. In general, the absorption intensity of torsional vibrations is expected to be weaker for a molecule with a larger (heavier) frame than for a molecule with a smaller (lighter) frame.

As an experimental proof of the present intensity theory, the far infrared bands due to methyl torsional vibrations were studied. The far infrared spectra of propylene oxide CH_3–$\underset{\backslash O /}{CH}$–$CH_2$ and propylene sulfide CH_3–$\underset{\backslash S /}{CH}$–$CH_2$ have been reported previously by Fateley and Miller.[6] In the present study, however, the absorption intensities of the torsional bands of these molecules were remeasured with a Hitachi FIS-3 Far Infrared Spectrophotometer. It is experimentally difficult to determine the absolute values of the absorption intensities in the far infrared region. Therefore, the absorption intensities of these two molecules were measured with the same spectral conditions and were found to be 0.9_7 and 0.2_0 $cm^{-2}\cdot atm^{-1}$ for propylene oxide and sulfide, respectively, at 300 K. On the other hand, the theoretical intensity was treated with Eqs. (30) and (31) and the intensity values were calculated as 1.76 and 0.45 $cm^{-2}\cdot atm^{-1}$ for propylene oxide and sulfide, respectively, at 300 K, from the structure parameters and dipole moments as determined by the analyses of microwave spectra.[7,8] The experimental ratio of the absorption intensities of propylene oxide and sulfide is $4._9$: 1, in good agreement with the theoretical intensity ratio of 3.9: 1.

The theoretical intensity of propylene oxide and sulfide was also treated with the harmonic oscillator approximation [Eq. (36)]. Although the barriers were not extremely high ($s=\sim69$ for oxide and ~89 for sulfide), the calculated intensity values of 2.03 and 0.47 agreed fairly well (especially for sulfide) with the intensity values calculated with Eqs. (30) and (31).

Orientation of Transition Moment. The band envelopes of absorption bands depend upon the direction of the transition dipole moment. The direction of the transition moment for the torsional vibration of the present model is given by the vector product of $\boldsymbol{\mu}^\circ\times\boldsymbol{\rho}$. This vector product is useful for predicting the type of the torsional bands of asymmetric-top molecules, since otherwise the direction of the transition dipole moment may not be determined from the molecular symmetry.

The molecules of propylene oxide and sulfide belong to the point group C_1 and the direction of the transition moment can not be determined from their molecular symmetry. However, from the present theory, the intensity ratio of the A, B, and C type transitions is calculated as 3: 18: 100 for propylene oxide and as 1: 16: 100 for propylene sulfide and accordingly both molecules are expected to exhibit prominent C-type band envelopes with sharp Q branches. In fact, as shown in Fig. 1, the far infrared spectra of propylene oxide and propylene sulfide exhibit Q-branch series primarily due to the C-type transitions.

Deuteration Effect of Methyl Group. The deuteration of a methyl group reduces the F value to about one half but approximately doubles the $\boldsymbol{\rho}$ vector.

6) W. G. Fateley and F. A. Miller, *Spectrochim. Acta*, **19**, 611 (1963).

7) J. D. Swalen and D. R. Herschbach, *J. Chem. Phys.*, **27**, 100 (1957).

8) S. S. Butcher, *ibid.*, **38**, 2310 (1963).

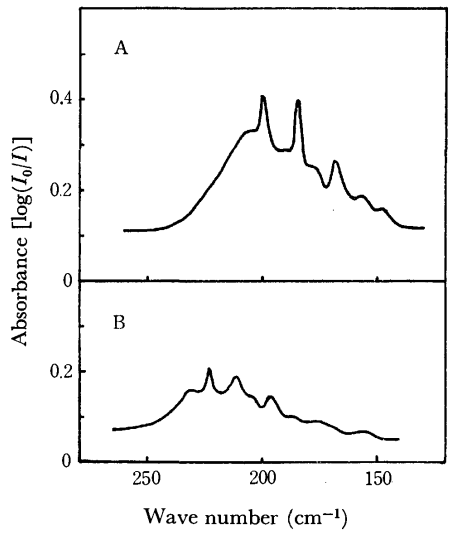

Fig. 1. Far infrared spectra of propylene oxide (path length of 4.9 m and sample pressure of 50 Torr) [A] and propylene sulfide (path length of 4.9 m and sample pressure of 96 Torr) [B].

Accordingly, the value of $F|\boldsymbol{\mu}^\circ \times \boldsymbol{\rho}|^2$ is increased nearly twice by the deuteration of the methyl group. For the simple example of Eq. (37), the absolute intensity of the torsional band is nearly proportional to I_α, the moment of inertia of the internal rotor, so that the intensity is nearly doubled on the deuteration of the methyl group. It is interesting to remark that the absorption intensities of the torsional vibration of the methyl group is expected to increase whereas the absorption intensities of the C–H stretching vibrations are decreased on deuteration of the methyl group. In fact, for ethyl fluoride, the absorption intensity of the torsional vibration of the methyl group was found to increase on deuteration of the methyl group.[9]

Appendix I High Barrier Approximation

The Hamiltonian and the wave equation for the internal rotation with the N-fold symmetry may be written as

$$H = Fp_\alpha^2 + V_N(1-\cos N\alpha)/2 \quad [p_\alpha = -i(\mathrm{d}/\mathrm{d}\alpha)] \tag{A1}$$

$$H\Psi_{v\sigma}(\alpha) = E_{v\sigma}\Psi_{v\sigma}(\alpha) \tag{A2}$$

where $E_{v\sigma}$ and $\Psi_{v\sigma}(\alpha)$ are the energy and wave function of the $v\sigma$ state (v: torsional quantum number, σ: symmetry index). Equations (A1) and (A2) may be transformed into a reduced form by the following transformations,

$$H = (N/2)^2 F\eta$$

$$p_\alpha = (N/2)p_x \quad [p_x = -i(\mathrm{d}/\mathrm{d}x)]$$

$$V_N = (N/2)^2 Fs$$

$$N\alpha = 2x$$

$$\Psi_{v\sigma}(\alpha) = \Phi_{v\sigma}(x)$$

$$E_{v\sigma} = (N/2)^2 F b_{v\sigma} \tag{A3}$$

$$\eta = p_x^2 + s(1-\cos 2x)/2 \tag{A4}$$

$$\eta\Phi_{v\sigma}(x) = b_{v\sigma}\Phi_{v\sigma}(x) \tag{A5}$$

For a high barrier case ($s \gg 1$), Eq. (A4) may be expanded in the power series of x.

$$\eta = p_x^2 + sx^2 - (1/3)sx^4 + (2/45)sx^6 - \cdots \tag{A6}$$

Equation (A6) may be treated as a perturbed harmonic oscillator Hamiltonian. The eigenvalues b_v for $b_v \ll s$ are derived by the second-order perturbation theory.

$$b_v = s^{1/2}(2v+1) - (1/2^3)[(2v+1)^2+1] - (1/2^6)s^{-1/2}(2v+1)[(2v+1)^2+3] \tag{A7}$$

The matrix elements of p_x, p_x^2, x, and x^2 are given, through first-order, as follows.

$$\langle v+1|p_x|v\rangle = is^{1/4}[(v+1)/2]^{1/2}[1-(1/4)s^{-1/2}(v+1)]$$

$$\langle v+3|p_x|v\rangle = -i(1/8)s^{-1/4}[(v+1)(v+2)(v+3)/2]^{1/2}$$

$$\langle v|p_x|v'\rangle = -\langle v'|p_x|v\rangle \tag{A8}$$

$$\langle v|p_x^2|v\rangle = (1/2)s^{1/2}(2v+1) - (1/8)[(2v+1)^2+1]$$

$$\langle v+2|p_x^2|v\rangle = -(1/2)s^{1/2}[(v+1)(v+2)]^{1/2} \times [1-(1/8)s^{-1/2}(2v+3)]$$

$$\langle v+4|p_x^2|v\rangle = (1/8)[(v+1)(v+2)(v+3)(v+4)]^{1/2}$$

$$\langle v|p_x^2|v'\rangle = \langle v'|p_x^2|v\rangle \tag{A9}$$

$$\langle v+1|x|v\rangle = s^{-1/4}[(v+1)/2]^{1/2}[1+(1/4)s^{-1/2}(v+1)]$$

$$\langle v+3|x|v\rangle = -(1/24)s^{-3/4}[(v+1)(v+2)(v+3)/2]^{1/2}$$

$$\langle v|x|v'\rangle = \langle v'|x|v\rangle \tag{A10}$$

$$\langle v|x^2|v\rangle = (1/2)s^{-1/2}(2v+1) + (1/8s)[(2v+1)^2+1]$$

$$\langle v+2|x^2|v\rangle = (1/2)s^{-1/2}[(v+1)(v+2)]^{1/2} \times [1+(5/24)s^{-1/2}(2v+3)]$$

$$\langle v+4|x^2|v\rangle = -(1/24s)[(v+1)(v+2)(v+3)(v+4)]^{1/2}$$

$$\langle v|x^2|v'\rangle = \langle v'|x^2|v\rangle \tag{A11}$$

9) H. Sugeta, Y. Adachi, and T. Miyazawa, The 28th Annual Meeting of the Chemical Society of Japan (1973), 2P05, p. 335.

Studies on the Interactions of 1-Substituted 2,4-Dinitrobenzenes with Hydroxide Ion in Aqueous Dimethyl Sulfoxide by Means of the Rapid Scan Spectrophototometer

Yoshinori HASEGAWA and Takehiro ABE

College of General Education, Tohoku University, Kawauchi, Sendai 980

(Received April 20, 1973)

The initial interactions of *m*-dinitrobenzene, 2,4-dinitroanisole, 2,4-dinitrofluorobenzene, and 2,4-dinitrochlorobenzene with hydroxide ion in aqueous dimethyl sulfoxide were studied with a rapid scan spectrophotometer. In all the cases, the first transient colored-species assigned to 1-hydroxy-3-substituted-2,6-dinitrocyclohexadienates were observed at initial stages before the formations of the second colored-species having the π-electronic structures of 1,3-dinitropentadienyl anion were complete.

In the interactions of aromatic polynitro compounds with nucleophiles, many transient colored-species have been detected by NMR and visible spectroscopies before the appearances of the thermodynamically stable colored-species.[1] No example has been reported of the initial transient colored-species formed from 1-X-2,4-dinitrobenzenes (X=H, CH_3O, halogeno) and bases.

An attempt has, therefore, been made to pursue the changes of the visible absorption spectra of the dimethyl sulfoxide (DMSO) solutions of *m*-dinitrobenzene, 2,4-dinitroanisole, 2,4-dinitrofluorobenzene, and 2,4-dinitrochlorobenzene in the presence of hydroxide ion.[2]

Experimental

All the dinitrobenzenes used were available commercially and were purified by recrystallization or by distillation. DMSO was dried with calcium hydride and fractionated under reduced pressure.

Electronic absorption spectra at various stages of a reaction path in solution were measured with a Hitachi rapid scan spectrophotometer RSP-2. The apparatus was equipped with an automatically controlled mixing cell, and could operate for the use of the continuous flow method. The mixing cell having the path length of 1.0 cm was roughly controlled at 25 °C by means of a thermocirculator. In the wavelength range from 220 to 700 nm it took 150 msec to record a spectrum on a memoriscope. The possible error in determining absorption positions with the spectrophotometer was estimated to be within 5 nm from the comparison between the spectra of the same solution, the one being recorded by the rapid scan spectrophotometer and the other being measured by a Hitachi recording spectrophotometer EPS-3.

The DMSO solutions subjected to the spectral measurements contained 2 or 10% (by volume) water. The DMSO solutions containing the corresponding amounts of water in the absence of both the dinitrobenzenes and sodium hydroxide were used as references.

Results

The spectral changes observed are shown in Figs. 1—4. In all the cases, the first colored-species having

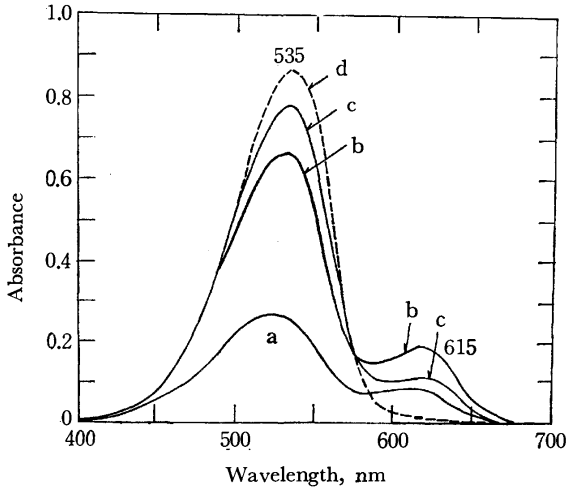

Fig. 1. Spectra observed with the DMSO solution containing *m*-dinitrobenzene (3.2×10^{-5} mol/l), sodium hydroxide (2.3×10^{-3} mol/l) and water (2% by volume). Times measured after the mixing: a, 19 msec; b, *ca.* 1/3 sec; c, 2 sec; d, 10 sec.

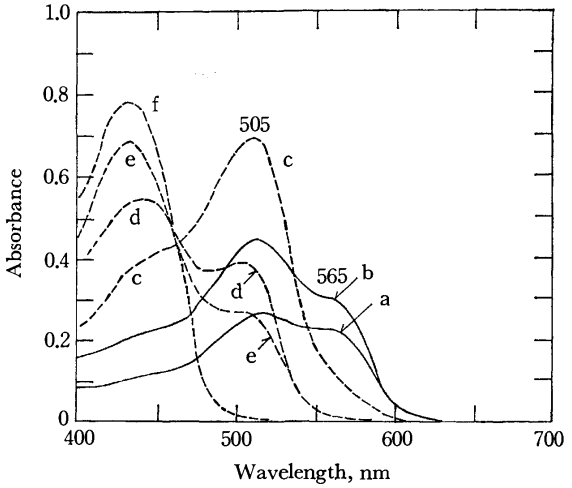

Fig. 2. Spectra observed with the DMSO solution containing 2,4-dinitroanisole (4.8×10^{-5} mol/l), sodium hydroxide (2.3×10^{-3} mol/l) and water (2% by volume). Times measured after the mixing; a, *ca.* 1/3 sec; b, 1 sec; c, 5 sec; d, 2 min; e, 4 min; f, 25 min.

1) For the recent reviews and references see: (a) M. J. Strauss, *Chem. Rev.*, **70**, 667 (1970); b) J. G. Tillett, *Ann. Rept. Progr. Chem. B* (Chem. Soc. London), **67**, 63 (1970); c) F. Millot, J. Morel, and F. Terrier, *C. A. Acad. Sci. Paris, Ser. C*, **274**, 23 (1972); d) M. R. Crampton and H. A. Khan, *J. Chem. Soc. Perkin Trans.* II, **1972**, 733. e) F. Terrier, F. Millot, and R. Schaal, *ibid.*, **1972**, 1192. f) F. Terrier, A. P. Chatrousse and R. Schaal, *J. Org. Chem.*, **37**, 3010 (1972); g) M. R. Crampton, M. A. El Ghariani, and H. A. Khan, *Tetrahedron*, **28**, 3299 (1972); h) M. P. Simonnin, M. J. Lecourt, F. Terrier, and C. A. Dearing, *Can. J. Chem.*, **50**, 3558 (1972).

2) This paper was reported in a preliminary form: Y. Hasegawa and T. Abe, *Chem. Lett.*, **1972**, 985.

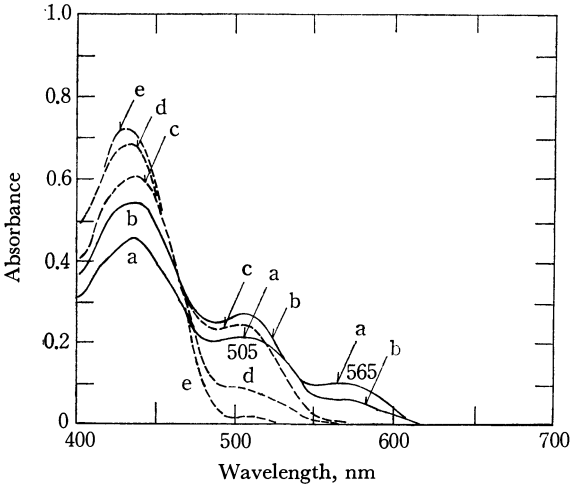

Fig. 3. Spectra observed with the DMSO solution containing 2,4-dinitrofluorobenzene (4.8×10^{-5}mol/l), sodium hydroxide (2.3×10^{-3}mol/l), and water (2% by volume). Times measured after the mixing: a, *ca.* 1/3 sec; b, 5 sec; c, 30 sec; d, 5 min; e, 12 min.

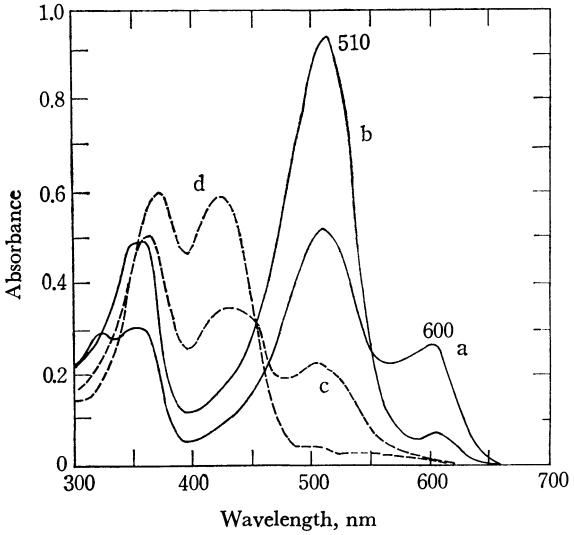

Fig. 4. Spectra observed with the DMSO solution containing 2,4-dinitrochlorobenzene (4.9×10^{-5}mol/l), sodium hydroxide (1.7×10^{-2}mol/l), and water (10% by volume). Times measured after the mixing: a, *ca.* 1/3 sec; b, 10 sec; c, 2 min; d, 8 min.

absorption bands in the range of 550—650 nm appeared at the initial stages and disappeared within several seconds after mixings. After the complete disappearances of the first colored-species, the second colored-species having bands at around 500 nm remained and gradually disappeared. As the peaks of the second colored-species decreased in intensity, the intensities of bands at 375 and 430 nm increased except the case of *m*-dinitrobenzene. The bands at 375 and 430 nm are due to 2,4-dinitrophenoxide ion, because the same alkaline solution of 2,4-dinitrophenol in DMSO containing 2% (by volume) water showed bands at 375 and 430 nm. The reaction product of 2,4-dinitrophenoxide ion agreed with the results of Bowden and Cook.[3] The peak intensity at 535 nm in Fig. 1 decreased very slowly after thermal equilibrium had been reached.

Discussion

From the analogy with the interactions of 2,4-dinitro-6-Y-anisoles (Y=F, Cl, CF_3, CN) with methoxide ion,[1e,4-6] the possible structures of the colored species are restricted to the following types **1**—**3**. This is supported by the theoretical calculations leading to the prediction that the stablization energies of 1,3- and 1,5-dinitropentadienyl anions (1.736 and 1.111 eV, respectively) are considerably great compared with that (0.004 eV) of 2,4-dinitropentadienyl anion.[7] The colored-species of the types **2** and **3** are expected to show absorption bands at the same range, because they have the similar π-electronic systems of 1,3-dinitropentadienyl anion.

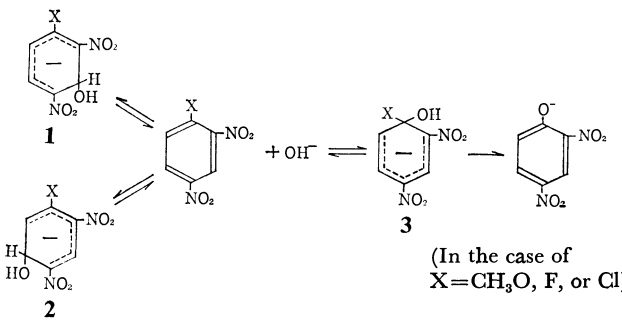

It has been known from visible and NMR spectroscopies that the methoxide complexes having the π-electronic structures of 1,3- and 1,5-dinitropentadienyl anions in media rich in DMSO show longer-wavelength bands at the ranges of *ca.* 505 nm and of 585—640 nm, respectively.[1,4-6] Accordingly, the first and second colored-species may be assigned, respectively, to the structure of the type **1** and to what has the same π-electronic structure with 1,3-dinitropentadienyl anion. According to Crampton,[8] the first colored-species should be the kinetically controlled products and the second colored-species should be thermodynamically more stable.

It is known from Figs. 1—4 that the substituents such as CH_3O, F, and Cl shift the band of the first colored-species of 1-hydroxy-2,6-dinitrocyclohexadienate (X=H in **1**) to the blue.

From the comparison with the band (λ_{max}=505 nm) of the methoxide complex of 2,4-dinitroanisole, having the established structure of 1,1-dimethoxy-2,4-dinitrocyclohexadienate,[1a] the band of the second colored-species formed from 2,4-dinitroanisole may be due to the similar structure **3** (X=CH_3O).

According to Crampton *et al.*,[1g] the second colored-species formed from 2,4-dinitro-fluorobenzene and

3) K. Bowden and R. S. Cook, *J. Chem. Soc. B*, **1971**, 1771.

4) F. Millot and F. Terrier, *Bull. Soc. Chim. France*, **1969**, 2692.
5) F. Terrier and M. P. Simonnin, *ibid.*, **1971**, 677.
6) F. Terrier, J. C. Hallé and M. P. Simonnin, *Org. Magn. Resonance*, **3**, 361 (1971).
7) H. Hosoya, S. Hosoya and S. Nagakura, *Theoret. chim. Acta*, **12**, 117 (1968).
8) M. R. Crampton, *Advan. Phys. Org. Chem.*, **7**, 211 (1969).

-chlorobenzene should be ascribed to the structures of the type **2** (X=F, Cl), since they have reported that the additions of bases occur not at the carbons carrying chlorines but at the 3-positions in picryl chloride and in 2,6-dinitrochlorobenzene derivatives.

Recently, from ESR studies Bellobono *et al.*[9] reported that the stable colored-species formed from *m*-dinitrobenzene and methoxide ion in DMSO containing 2% (by volume) methanol was the anion-radical of *m*-dinitrobenzene. However, the second colored-species formed from *m*-dinitrobenzene may be assigned to the structure **3** (X=H), because the band shape of the second colored-species in Fig. 1 does not resemble that of the 530-nm band of the *m*-dinitrobenzene anion-radical with a distinct vibrational structure.[10] Moreover, the anion-radical shows bands at 385 and 415 nm.[10] As mentioned by Crampton,[8] the anion-radical is probably a minor product.

9) I. R. Bellobono, A. Gamba, G. Sala, and M. Tampieri, *J. Amer. Chem. Soc.*, **94**, 5781 (1972).

10) T. Shida and S. Iwata, *J. Phys. Chem.*, **75**, 2591 (1971).

BULLETIN OF THE CHEMICAL SOCIETY OF JAPAN, VOL. 46, 2758—2761 (1973)

A Study of Complex Formation by the Cation Exchange Method. Bivalent Metal Complexes with Univalent Anions

Emiko OHYOSHI*

Department of Chemistry, Faculty of Science, Kumamoto University, Kurokami, Kumamoto 860

(Received November 13, 1972)

An attempt was made to estimate the amount of the cationic complex MA^+ adsorbed on a cation exchanger. This method is based on the fact that the ratio of the distribution coefficients of M^{2+} and MA^+ should vary with the ionic strength of the medium. The Ni(II) acetate system studied by Fronaeus has been reexamined. The results show that the distribution coefficient of $NiAc^+$ (Ac=acetate) is negligible compared with that of Ni^{2+} upon the variation of the ionic strength from 0.2 to 1.0. It was found that Fronaeus overestimated the distribution coefficient of $NiAc^+$ and that this caused the value of β_2 to be much greater. In conclusion, the two functions, φ_1 and f, introduced by Fronaeus could not be determined with high accuracy; for the stability constants obtained by Fronaeus's method, they must be confirmed by conducting the experiment at a different ionic strength.

The cation exchange resin has been widely used for the study of complex formation. In cases where the reaction $M^{2+}+A^-=MA^+$ or $M^{3+}+A^-=MA^{2+}$ occurs, it is difficult to estimate the amounts of them adsorbed on the resion. Fronaeus proposed a method to analyze the data under such conditions and used it to study the acetate complexes of Ni(II)[1] and Ce(III)[2] and the thiocyanate complexes of Ni(II).[3] In these investigations, he estimated an appreciable amount of the cationic complex to be adsorbed on the resin. On the other hand, it has been demonstrated, by means of acetate labelled with tritium and with ^{14}C, that the cationic species of Co(II) and Mn(II) acetate complexes are not taken up by the cation exchanger.[4] If Fronaeus overestimated the distribution coefficient of the cationic complex of Ni(II) acetate, the evaluation of the stability constants would also be higher.

In this study, we attempted to ascertain the extent of the adsorption of a cationic complex, MA^+, experimentally. Although M^{2+} and MA^+ were both adsorbed on the resin, the change in the ionic strength of the medium should have different effects on their distribution coefficients depending on the different ionic charges. From this, we can conclude whether the extent of the adsorption of MA^+ is appreciable or negligible. This method was applied to study the Ni(II) acetate system, and the results were compared with those obtained by Fronaeus's method.

Estimation of the Amount of MA^+ Adsorbed on a Cation Exchanger. When a cation exchange resin, NaR, is added to a solution involving a free metal ion, M^{2+}, and the complexes MA^+, MA_2, $\cdots$, MA_n^{2-n}, the following exchange equilibria are established:

$$M^{2+} + 2NaR = MR_2 + 2Na^+ \quad (1)$$

$$MA^+ + NaR = MAR + Na^+ \quad (2)$$

The distribution coefficients of M^{2+} and MA^+, l_0 and l_1, can be expressed as:

$$l_0 = [MR_2]/[M^{2+}] = k_0[NaR]^2/[Na^+]^2$$

$$l_1 = [MAR]/[MA^+] = k_1[NaR]/[Na^+]$$

where k_0 and k_1 are the equilibrium quotients of Reactions (1) and (2). The distribution of the metal, M(II), between resin and solution is given as:

$$\varphi = \frac{l_0(1+l_1'[A^-])}{1+\sum\beta_j[A^-]^j} \quad (3)$$

where $l_1'=l_1\beta_1/l_0$ and $\beta_j=[MA_j^{2-j}]/([M^{2+}][A^-]^j)$. For the determination of β_j under such conditions, Fronaeus[1] introduced two functions, φ_1 and f:

* Present address: Kurokami Radioisotope Laboratory, Kumamoto University, Kumamoto.

1) S. Fronaeus, *Acta Chem. Scand.*, **6**, 1200 (1952).
2) S. Fronaeus, *Svensk Kem. Tidskr.*, **65**, 19 (1953).
3) S. Fronaeus, *Acta Chem. Scand.*, **7**, 21 (1953).
4) N. C. Li, W. M. Westfall, A. Lindenbaum, J. M. White and J. Schubert, *J. Amer. Chem. Soc.*, **79**, 5864 (1957).

$$\varphi_1 = (l_0/\varphi - 1)/[A^-] \quad (4)$$

$$\varphi_1^0 = \lim_{[A^-]=0} \varphi_1 = \beta_1 - l_1'$$

$$f = [(l_0/\varphi)\{(\beta_1 - l_1')[A^-] - 1\} + 1]/[A^-]^2$$

$$= \beta_1\varphi_1 - \sum_{j=2}^{n} \beta_j [A^-]^{j-2} \quad (5)$$

At relatively small values of $[A^-]$, the following relation between the differences can be given:

$$\Delta f = \beta_1 \Delta\varphi_1 - \beta_3 \Delta[A^-] \quad (6)$$

β_1 can be obtained graphically from Eq. (6); β_2, $\beta_3 \cdots \beta_n$ can also be obtained from Eq. (5).

This method has been widely used in the study of complex formation containing cationic species. However, the evaluation of l_1/l_0 seems to be generally large, considering the differences in the ionic charge and in the size of M^{2+} and MA^+, *e.g.*, $l_1/l_0=0.78$ for the Mn(II) chloride system at $\mu=0.69$.[5] In this case, the value of k_1 is estimated to be greater than that of k_0. If l_1/l_0 is overestimated, all of the formation constants of complexes β_1, β_2, $\cdots$, β_n would also be overestimated. As may be seen from Eq. (4), the function φ_1 comes to involve a large error as $[A^-]$ approaches 0 where $l_0/\varphi \simeq 1$. The value of $\beta_1 - l_1'$ obtained from the extrapolation of φ_1 to $[A^-]=0$ must also be uncertain. Since this value affects the function f, reliable values for β_1, β_2, $\cdots$, β_n can not be expected by means of the functions φ_1 and f.

The use of the function $1/\varphi$, whose accuracy is much greater than that of φ_1 at small values of $[A^-]$, may be more feasible for the analysis of the data.

$$\frac{1}{\varphi} = \frac{1}{l_0} \frac{1 + \sum \beta_j [A^-]^j}{1 + l_1'[A^-]} \quad (7)$$

Differentiating $1/\varphi$ and assuming that the terms greater than $[A^-]^2$ can be neglected at small values of $[A^-]$, we obtain:

$$\frac{d(1/\varphi)}{d[A^-]} \simeq \frac{1}{l_0} \frac{(\beta_1 - l_1') + 2\beta_2[A^-]}{1 + 2l_1'[A^-]} \quad (8)$$

This equation shows that when l_1' can not be neglected, a plot of $1/\varphi$ *vs.* $[A^-]$ at small values of $[A^-]$ gives a curve the slope of which decreases ($\beta_2/l_1' < \beta_1 - l_1'$) or increases ($\beta_2/l_1' > \beta_1 - l_1'$) with an increase in $[A^-]$. On the other hand, if the plot gives a straight line and if the intercept agrees with the value of $1/l_0$ obtained experimentally, it can generally be concluded that l_1' can be neglected and that the slope corresponds to β_1/l_0. Though it is rare, an apparent linear relation between $1/\varphi$ and $[A^-]$ will be given when $\beta_2/l_1' \simeq \beta_1 - l_1'$. In this case, the slope corresponds to $(\beta_1 - l_1')/l_0$. However, we can readily distinguish between the two cases. The linear relation can be settled at any concentration of Na^+ in the former case, while it can not be expected in the latter since the value of β_2/l_1' becomes smaller of greater than that of $\beta_1 - l_1'$ at a different Na^+ concentration.

The term $\beta_1 - l_1'$, which can be obtained from the slope of the $1/\varphi$ plot *vs.* $[A^-]$ at $[A^-]=0$ (see Eq. (8)), is expressed by:

$$\beta_1 - l_1' = \beta_1\{(1 - k_1[Na^+]/(k_0[NaR])\} \quad (9)$$

When $[Na^+] \gg [M^{2+}]$ and $[NaR] \gg [MR]$, we obtain:

$$\beta_1 - l_1' = \beta_1(1 - K[Na^+]) \quad (10)$$

where K is nearly constant. The β_1 varying with the ionic strength can be estimated by the change in the activity coefficient of M^{2+}, γ. The relation expressed by:

$$\beta_1 = \gamma\beta_{1(a)}/\gamma_{(a)} \quad (11)$$

where $\beta_{1(a)}$ and $\gamma_{(a)}$ are β_1 and γ at a fixed ionic strength of a. By substituting this equation to Eq. (10), we obtain:

$$\gamma_{(a)}(\beta_1 - l_1')/\gamma = \beta_{1(a)}(1 - K[Na^+]) \quad (12)$$

When the values of $(\beta_1 - l_1')\gamma_{(a)}/\gamma$ decrease with an increase in $[Na^+]$, a linear relation can be obtained in a range where K is practically constant. From the slope, the magnitude of $K[Na^+]$, that is, l_1/l_0, can be estimated. On the other hand, the values remain essentially constant; in other words, the decrease in $\beta_1 - l_1'$ with an increase in the ionic strength is the same as that caused by the decrease in the activity of M^{2+}, the ratio l_1/l_0 is very small in comparison with unity, and l_1' can practically be neglected.

Experimental

Materials. A stock solution of Ni(II) was prepared by dissolving $NiCl_2 \cdot 6H_2O$ in 1.0 M $NaClO_4$ to obtain the concentration of 0.01 M. The solution involving 1.0 M CH_3COONa and 1.0 M CH_3COOH was diluted with 1.0 M $NaClO_4$ to produce various acetate concentrations at $\mu=1.0$. In a similar manner, acetate soltuions at other ionic strengths (0.2—0.5) were prepared. All the chemicals used were of a G.R. grade. For the cation exchanger, Dowex 50W-X8 (100—200 mesh) in the sodium form was used.

Procedures. The ion-exchange experiments were carried out as follows. The solutions (10 ml) made up from the stock solution of Ni(II) (1.0 ml) and the solutions in varying acetate concentrations (9.0 ml) were shaken with portions of dry resin (0.2—0.5 g) in 20 ml glass vials with stoppers for 8 hr at 25 °C. Then the amount of Ni(II) in each supernatant was determined by EDTA titration, using murexide as the indicator. The distribution coefficient, φ, was calculated as follows:

$$\varphi = \frac{\text{mmol of Ni(II) in the resin/mass of dry resin (g)}}{\text{mmol of Ni(II) in the soln./vol. of soln. (ml)}}$$

Results and Discussion

Measurements of l_0. Fronaeus reported that the distribution coefficient of Ni(II) is dependent on the concentration of NiR_2, though it is kept very small in comparison with the exchange capacity. He concluded that Ni^{2+} ions are not as free as Na^+ ions in the resin phase, but are partly coordinated to groups fixed at the exchanger. Thus, he corrected the φ values to that at a constant value of [NiR], 10^{-2} mmol/g, for the calculation of the formation constants of Ni(II) acetate complexes. It is important to know whether or not the exchange reaction between the Ni^{2+} ion and NaR is reversible. In the case of a reversible reaction involving a minute amount of M^{2+} compared with $[Na^+]$ and [NaR], the value of l_0 should remain

5) D. F. C. Morris and E. L. Short, *J. Chem. Soc.*, **1961**, 5148.

Table 1. Effect of variation in the mass of resin on l_0 of Ni(II), pH=4.5, μ=1.0, volume of soln.=10.0 ml

Mass of resin (g)	l_0
0.200	15.6
0.300	16.5
0.400	16.0
0.500	15.8

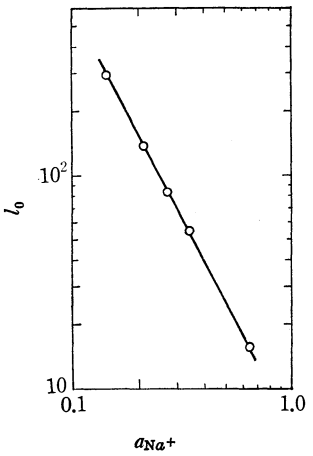

Fig. 1. Relationship between l_0 of Ni(II) and the activity of Na^+ ion.

unchanged with a varying mass of resin, and a linear relation whose slope is 2 should be obtained between log l_0 and the log of the activity of Na^+. To examine the reversivility, we measured l_0 as a function of the mass of the resin and the concentration of Na^+ in the solution. As is shown in Table 1 and Fig. 1, the value of l_0 remains practically constant with the variation in the mass of resin from 0.2 to 0.5 g, and the plot of log l_0 *vs.* the log of the activity of Na^+ yields a straight line with the slope of 2. From these results, the reversible exchange reaction between the Ni^{2+} ion and the exchanger, NaR, could be confirmed.

The Ni(II) Acetate System. The Ni(II) acetate complexes were studied by the cation exchange method. Figure 2 shows the realtion between $1/\varphi$ and [Ac^-] at the same ionic strength as that used by Fronaeus (μ=1.0). At the values of [Ac^-] examined, a linear relation is obtained and the intercept of the line agrees well with the value of $1/l_0$ obtained experimentally. This indicates either that l_1' is negligible or that β_1-l_1' is nearly equal to β_2/l_1. To know the magnitude of l_1', the experiments were carried out at the Na^+ concentrations of 0.2, 0.3, 0.4, and 0.5. The results are shown in Fig. 3, where $1/\varphi$ is plotted *vs.* [Ac^-]. All of the plots yield a good linearity, and the intercept of each line agrees well with the values of $1/l_0$ obtained at the corresponding concentration of Na^+. From this, we can conclude that l_1' is negligible at an ionic strength of less than 1, since it is unreasonable to say that the relation $\beta_1-l_1'\simeq\beta_2/l_1'$ is settled at any concentration of Na^+. The values for β_1-l_1' are given as 6.5, 5.9, 5.6, and 5.5 from the slopes of the straight lines at μ=0.2, 0.3, 0.4, and 0.5. In Eq. (12), when we take the fixed ionic strength as 0.2, the values of $\gamma_{(0.2)}$ $(\beta_1-l_1')/\gamma$ at μ=0.2, 0.3, 0.4, 0.5, and 1.0 were calculated to be 6.5, 6.7, 6.7, 6.8, and 6.0 by the estimation of the activity coefficient of Ni^{2+} from the formula of Davies:[6] $\log\gamma_i=-0.5Z_i^2\sqrt{\mu}/(1+\sqrt{\mu})+0.1Z_i^2\mu$, where Z_i=2. These values seem to be essentially the same, considering that the γ values were calculated from an approxinate formula. That is, the extent of the decrease in β_1-l_1' with an increase in the ionic strength is nearly equal to that caused by the decrease in the activity of Ni^{2+}. The acetate complex of Ni(II), $NiAc^+$, like those of Co(II) and Mn(II),[4] is not taken up by the cation exchanger to any appreciable extent. Thus, the values of β_1 at μ=0.2, 0.3, 0.4, 0.5, and 1.0 were obtained as 6.5, 5.9, 5.6, 5.5, and 5.2. The values for β_2 could not be determined exactly in the range of low concentrations of Ac^- studied. Fronaeus reported that β_1=4.7 and β_2=18 at μ=1.0. Although the value of β_1 is in fair agreement with our results, the value of β_2 appears to be too large. If such a high value is given for β_2, the slope of the lines in Fig. 3 must be increased with an increase of [Ac^-], even at small values of [Ac^-]. This large value of β_2 is caused by the estimation of l_1' as 1.9.

The value of 6.5 at μ=0.2 obtained for β_1 in this study is larger than that of 2.6 determined by polaro-

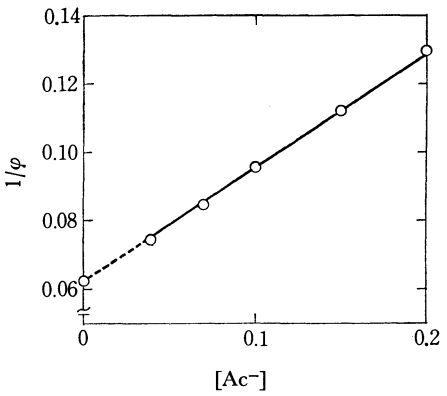

Fig. 2. A plot of $1/\varphi$ *vs.* [Ac^-] for Ni(II) acetate system at μ=1.0.

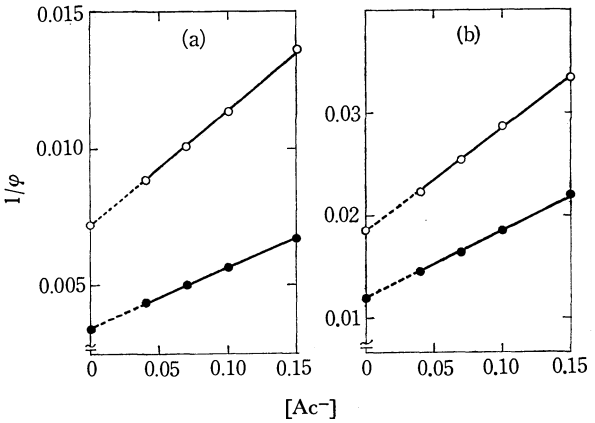

Fig. 3. Plots of $1/\varphi$ *vs.* [Ac^-] for Ni(II) acetate system at various ionic strengths; (a) μ=0.2 —●—, μ=0.3 —○—, (b) μ=0.4 —●—, μ=0.5 —○—.

6) C. W. Davies, *J. Chem. Soc.*, **1938**, 2093.
7) N. Tanaka and K. Kato, This Bulletin, **32**, 516 (1959).

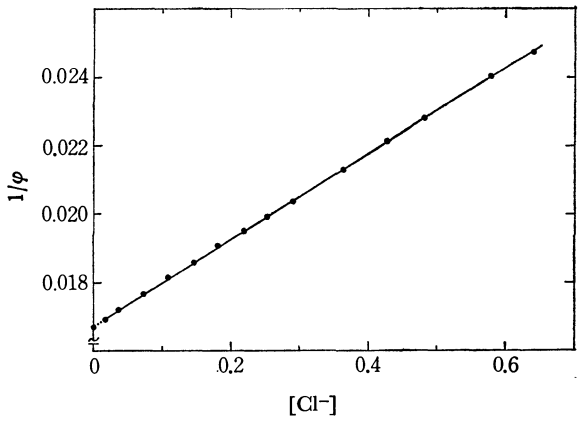

Fig. 4. A plot of $1/\varphi$ *vs.* [Cl⁻] for Mn(II) chloride system.[5]

graphy[7] at the same ionic strength. However, this value of 2.6 seems to be rather small in comparison with the value of 10 determined at $\mu=0.1$ by potentiometry.[8]

Mn(II) Chloride System. The study of Mn(II) chloride complexes by Fronaeus's method[5] appears to be a similar example of overestimating l_1'. Morris and Short estimated l_1' to be 2.98 and determined the formation constants, β_1, β_2, and β_3, to be 3.85, 1.80, and 0.44 at $\mu=0.691$. These values are comparable to those of the Fe(III) chloride complexes.[9] For the calculation of the function, φ_1, from which the value of β_1-l_1' was obtained, they used the value of l_0 obtained experimentally. As is shown in Fig. 4, when we try to plot the function $1/\varphi$ against [Cl⁻], a good linearity is yielded over the range of [Cl⁻] investigated and the intercept of the line agrees with the value of $1/l_0$ within the limits of experimental error ($\pm 0.5\%$). Assuming that $l_1'\simeq 0$, β_1 is obtained as 0.75. This value is close to that of 1.1 obtained by polarography.[10] It is noted that the evaluation of β_1-l_1' by Fronaeus's method is much affected by the value of l_0 adopted; that is, β_1-l_1' is greatly varied with a minute change in l_0.

In conclusion, when l_1' is estimated by Fronaeus's method to be appreciable, it is necessary to confirm the results by an experiment at a different ionic strength.

8) M. Yasuda, K. Yamasaki, and H. Ohtaki, *ibid.*, **33**, 1067 (1960).

9) E. Rabinowitch and W. H. Stockmayer, *J. Amer. Chem. Soc.*, **64**, 345 (1942).

10) S. Tribalat and J. M. Caldero, *C. R. Acad. Sci. Paris.*, **255**, 925 (1962).

BULLETIN OF THE CHEMICAL SOCIETY OF JAPAN, VOL. 46, 2761—2765 (1973)

Distribution of Alkali Metal Picrates between Water and Methyl Isobutyl Ketone

Tadashi IWACHIDO

College of Liberal Arts, Okayama University, Tsushima, Okayama 700

(Received December 8, 1972)

As regards the distribution of alkali metal picrates between water and methyl isobutyl ketone, distribution ratios of alkali metals and acid species were determined in the pH range 1.5—8.5. The extraction curves are almost the same for each alkali metal. Association constants of the picrates and the dissociation constant of picric acid in the organic phase were determined conductometrically. The association constants of picrates in the aqueous phase were determined with distribution coefficients by means of a solvent extraction method. The results obtained show that the picrates exist mainly in a dissociated form in both phases, whereas picric acid exists in a weakly dissociated form in the organic phase. The extractability of picrates is discussed on the basis of the extraction parameter proposed and compared with that of the nitrobenzene system.

The results obtained from the previous study on the distribution of alkali metal picrates between aqueous and nitrobenzene phases[1] can be summarized as follows. The extractability of alkali metal picrates can be represented in terms of the extraction parameter $D^{MR}K_a^{MR}/K_o^{MR}$, where K_a^{MR} and K_o^{MR} denote the association constants of the picrates in the aqueous and the organic phases, respectively, and D^{MR} denotes the distribution coefficient. The parameter can also be a good measure of the solvent. Since picrates are strong electrolytes, the ratio D^{MR}/K_o^{MR} is expected to increase with the ionizing power of solvent, giving rise to enhanced extractability.

Acetone and methyl ethyl ketone are known to be ionizing solvents for picrates stronger than nitrobenzene.[2,3] However, they are not suitable for extraction because of their high miscibility with water. Methyl isobutyl ketone (MIBK) was chosen, since it is a dipolar aprotic solvent with high ionizing power yet immiscible with water.

Association constants show that MIBK functions as an ionizing solvent with levelling property, in contrast to the differentiating property of nitrobenzene. The

1) T. Iwachido, This Bulletin, **45**, 432 (1972).

2) M. B. Reynolds and C. A. Kraus, *J. Amer. Chem. Soc.*, **70**, 1709 (1948).

3) C. W. Davies, "Ion Association", Butterworths, London (1962) p. 96.

levelling property, commonly observed in acetone and methyl ethyl ketone, becomes conspicuous with the addition of water, which reflects on the extractability of alkali metals. Discussion is made on the basis of equilibrium constants.

Experimental

Reagents. Alkali metal picrates were recrystallized from water except for lithium salt (from an alcohol-water mixture). Sodium and lithium picrates were determined to be monohydrate by measuring the weight loss on heating under reduced pressure. The solvent was purified in the usual way: MIBK previously treated with potassium permanganate was washed with an aqueous solution of sodium carbonate and distilled. The distillate was dried over anhydrous sodium sulfate for two days and distilled again.

Citric acid-citrate buffers (0.01 M) and phosphoric acid-phosphate buffers (0.01 M) were used to adjust the pH of the solutions to pH 2.5—5.5 and pH 6—8, respectively. Strongly acidic solutions (pH below 2.5) were prepared with hydrochloric acid. A series of buffer solutions were prepared with five kinds of alkali metals. All the aqueous solutions were previously saturated with MIBK and all the MIBK solutions with water, in order to avoid volume change on mixing.

Extraction. Dependence of distribution ratios of alkali metals and the acid species on pH was investigated as follows: 10 ml of a 0.01 M buffer solution and 10 ml of a 1×10^{-4} M aqueous alkali metal picrate solution were transferred to a 50 ml centrifuge tube equipped with a stopper. 20 ml of MIBK was then added. The resulting mixture was shaken for two hours at 25 °C. The distribution coefficients and association constants (in the aqueous phase) were determined by modifying the above procedures: 10 ml of an aqueous solution of alkali metal picrate (1×10^{-4} M) was mixed with 10 ml of a buffer solution containing an alkali metal of the same kind to various concentrations (up to 10^{-2} M). The resulting solution was then treated as before.

Determination of Alkali Metals and the Acid Species. After equilibration the alkali metals in the organic phase were determined with an atomic absorption spectrophotometer (Nippon Jarrell Ash, Type AA-1). The acid species in the aqueous phase was determined spectrophotometrically (Hitachi Ltd., Type 124) by using matched 50 mm cells at 355 nm, at which the absorption of dissolved MIBK is negligible.

The pH of an aqueous solution saturated with MIBK was measured with a pH meter in the usual way. The MIBK dissolved increased the pH value less than 0.02 unit in each case.

Conductance Measurements in the Organic Phase. Conductances of alkali metal picrates in dry and wet (water-saturated) MIBK solutions were measured with a conductometer (Ando Electric Co. Ltd., Universal Bridge, LCR-10). The solution was kept at 25±0.005 °C by circulating thermostated water around the vessel equipped with platinized platinum electrodes and a copper-constantan thermocouple. Specific conductances of the dry and wet solvents were 0.2 and 1.0 $\mu\Omega^{-1}$ cm^{-1}, respectively. Conductivities of the solutions of 0.5×10^{-4}—7×10^{-4} M were measured by a dilution method with a weighing buret.

Theoretical

The equilibria for the picric acid and alkali metal picrates, denoted by HR and MR, respectively, can be written as follows:

1) Dissociation of Picric Acid:

$$HR \rightleftarrows H^+ + R^- \qquad K_a^{HR} = \frac{[H^+]_a[R^-]_a}{[HR]_a} \tag{1}$$

$$K_o^{HR} = \frac{[H^+]_o[R^-]_o}{[HR]_o} \tag{2}$$

2) Association of Alkali Metal Picrates:

$$M^+ + R^- \rightleftarrows MR \qquad K_a^{MR} = \frac{[MR]_a}{[M^+]_a[R^-]_a} \tag{3}$$

$$K_o^{MR} = \frac{[MR]_o}{[M^+]_o[R^-]_o} \tag{4}$$

3) Distribution of the Acid and the Picrates:

$$D^{HR} = \frac{[HR]_o}{[HR]_a} \tag{5}$$

$$D^{MR} = \frac{[MR]_o}{[MR]_a} \tag{6}$$

Subscripts a and o refer to aqueous and organic phases, respectively; molar concentrations are given in brackets.

i) Association Constants in the Organic Phase K_o^{MR}. Association constants of the picrates in MIBK solutions were determined by the method of Shedlovsky.[4] Conductance Λ is related to the concentration of electrolyte C by the equation

$$\frac{1}{\Lambda S} = \frac{1}{\Lambda_\infty} + \frac{K_o^{MR}C\Lambda S f_o^2}{\Lambda_\infty^2} \qquad S \equiv \left[\frac{Z}{2}+\sqrt{1+\left(\frac{Z}{2}\right)^2}\right]^2$$

$$Z = \frac{\alpha\sqrt{C\Lambda}}{\Lambda_\infty^{3/2}} \tag{7}$$

where Λ_∞ refers to the limiting conductance; f to the mean activity coefficient, and α to the Onsager coefficient.

ii) Association Constants in the Aqueous Phase K_a^{MR} and Distribution Coefficients D^{MR}. The distribution ratio of the acid species in a sufficiently alkaline solution can be written as

$$q^R = \frac{[MR]_o+[R^-]_o}{[MR]_a+[R^-]_a} \tag{8}$$

Combination of Eqs. (3), (4), (6), and (8) leads to the following equation:

$$\frac{Y}{q^R} = \frac{1}{D^{MR}} + \frac{1}{D^{MR}K_a^{MR}f_a^2[M^+]_a} \tag{9}$$

$$Y = \frac{\sqrt{0.25+C_oK_o^{MR}f_o^2}+0.5}{C_oK_o^{MR}f_o^2} + 1$$

The values of the mean activity coefficient in both aqueous and MIBK solutions were approximated by the Debye-Hückel limiting law

$$-\log f^2 = \frac{3.6494\times10^6\sqrt{I}}{(\varepsilon T)^{3/2}} \tag{10}$$

where I denotes the ionic strength.

iii) Distribution of Acid Species. At equilibrium the distribution ratio of the acid species between the two phases can generally be written as

$$q^R = \frac{[HR]_o+[MR]_o+[R^-]_o}{[HR]_a+[MR]_a+[R^-]_a} \tag{11}$$

4) T. Shedlovsky, *J. Franklin Inst.*, **225**, 739 (1938).

Substitution of the equilibrium constants defined by Eqs. (1)—(6) into Eq. (11) gives

$$q^{R} = D^{HR}\frac{1+\left\{\left(1+\frac{1}{K_o^{MR}[M^+]_o}\right)D^{MR}K_a^{MR}[M^+]_a\right\}\frac{K_a^{HR}}{D^{HR}[H^+]_a}}{1+(1+K_a^{MR}[M^+]_a)\frac{K_a^{HR}}{[H^+]_a}} \quad (12)$$

iv) Distribution of Alkali Metals. The distribution of alkali metals can also be written as

$$q^{M} = \frac{[MR]_o+[M^+]_o}{[MR]_a+[M^+]_a} \quad (13)$$

Total concentrations of the acid species C^R and alkali metals C^M are represented as

$$C^R = [HR]_a + [HR]_o + [MR]_a + [MR]_o + [R^-]_a + [R^-]_o \quad (14)$$

$$C^M = [MR]_a + [MR]_o + [M^+]_a + [M^+]_o \quad (15)$$

The electroneutrality condition in the organic phase is expressed by

$$[R^-]_o = [M^+]_o + [H^+]_o \quad (16)$$

Combining Eqs. (14), (15), and (16) and solving for $[R^-]_a$ gives

$$\frac{1}{[R^-]_a} = \frac{1+\frac{(1+D^{HR})}{K_a^{HR}}[H^+]_a}{C^R-C^M+[M^+]_a-[H^+]_o} \quad (17)$$

On the other hand, rearrangement of Eq. (13) gives

$$q^{M} = \frac{[MR]_o\left(1+\frac{1}{K_o^{MR}[R^-]_o}\right)}{[MR]_a\left(1+\frac{1}{K_a^{MR}[R^-]_a}\right)} \quad (18)$$

Substitution of Eq. (17) into Eq. (18) gives the useful expression

$$q^{M} = D^{MR}\frac{\left\{1+\frac{1}{K_o^{MR}([M^+]_o+[H^+]_o)}\right\}}{\left\{1+\frac{1+(1+D^{HR})[H^+]_a/K_a^{HR}}{K_a^{MR}(C^R-C^M+[M^+]_a-[H^+]_o)}\right\}} \quad (19)$$

It should be noted that all the experiments were carried out under conditions where the value of C^M is about 100 times that of C^R.

Results and Discussion

Equilibria Involved in the Extraction System. Fundamental equilibria are shown by Eqs. (1)—(6). MIBK is a solvating solvent like water, but little is known about the solvates of the picrates both in wet MIBK solution and MIBK-saturated aqueous solution. The solvates in both phases are represented by the simplest symbols. The equilibrium constants obtained should be distinguished from those defined in a pure medium.

Interactions between alkali metal cations and the citrate anions added as buffers should be considered. The values of the ion-pair formation constants of the alkali metal citrates obtained by Rechnitz and Zamochnick[5] are 6.8, 5.0, 3.9, 3.1, and 2.1, in going from lithium to cesium at constant initial metal and citric acid concentration of 0.1 M and pH 8.3. The values are about a quarter of those of respective picrates. Under the present experimental conditions, however, the influence of the citrate ions are negligible below pH 5.5, when the acid dissociation constant of citric acid ($pK_3=6.396$)[6] is taken into account.

The dissociation constant of picric acid in the wet MIBK solution is determined conductometrically to be 3.00×10^{-5}. This indicates that the dissociation of the acid can no longer be neglected as compared with other equilibria. This is quite different from the case of the nitrobenzene system. Introduction of the acid dissociation complicates theoretical treatments, but without this the extraction curve especially the acidic parts can not be explained.

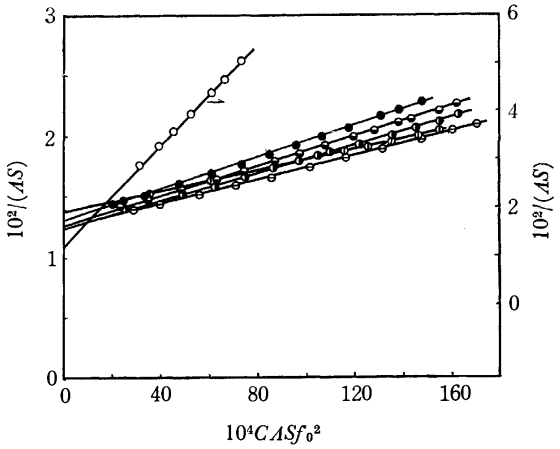

Fig. 1. Shedlovsky plot of the alkali metal picrates in wet MIBK ○: H-Pic, ◐: Li-Pic, ●: Na-Pic, ◒: K-Pic, ◑: Rb-Pic, ⊖: Cs-Pic.

Association Constants K_0^{MR}. Conductance measurements were carried out with dry and wet MIBK solutions. A plot of Λ *vs.* $C^{1/2}$ gives a curve characteristic of a weak electrolyte. The value of Λ_∞ evaluated graphically is used for the first Shedlovsky plot. The data required for the plot are given in Table 1. The reciprocal of the intercept on $1/(\Lambda S)$-axis gives the second approximation for Λ_∞. The Shedlovsky plot is repeated until Λ_∞ gives a constant value. The final plots are shown in Fig. 1, the values of Λ_∞ and K_0^{MR} being determined simultaneously (Table 2).

The levelling property of MIBK is reflected on the limiting conductances and all the equilibrium constants as seen from Table 2. The water added emphasizes the property. The strong levelling power of water has

Table 1. Dielectric constant (ε), viscosity (η), and specific gravity (SG) at 25 °C

Medium	ε	η (cP)	SG
Dry MIBK	12.66	0.546	0.79515
Wet MIBK	13.63	0.5766	0.79918
Water	78.54		
Water (MIBK satd.)	75.73		

5) G. A. Rechnitz and S. B. Zamochnick, *Talanta*, **11**, 1061 (1964).

6) R. G. Bates and G. D. Pinching, *J. Amer. Chem. Soc.*, **71**, 1274 (1949).

TABLE 2. CONSTANTS OBTAINED WITH THE MIBK SYSTEM

Comp.	Soln.	Λ_∞	K_0^{MR}	K_a^{MR}	D^{MR}	$K_a^{MR}D^{MR}/K_0^{MR}$ I	$1+A/[M]_a$ II	q^M_{calc} $(I\times II)^{1/2}$	q^M_{meas}	q^R_{calc} I/q^M_{calc}	q^R_{meas}
H-Pic	Dry										
	Wet	80.68	0.000030	0.381	500						
Li-Pic	Dry	76.10	80100								
	Wet	73.46	2390	30	0.19	0.0024	0.00609	0.0038	0.00386	0.63	0.634
Na-Pic	Dry	83.86	36100								
	Wet	78.08	4120	18	0.38	0.0017	0.00656	0.0033	0.00334	0.52	0.510
K-Pic	Dry	81.85	11700								
	Wet	79.80	3930	13	1.00	0.0033	0.00557	0.0043	0.00431	0.77	0.783
Rb-Pic	Dry	82.06	9140								
	Wet	80.29	3700	13	0.83	0.0029	0.00565	0.0040	0.00411	0.73	0.726
Cs-Pic	Dry	83.02	8350								
	Wet	81.22	3330	15	0.71	0.0032	0.00573	0.0043	0.00421	0.74	0.729

TABLE 3. CONSTANTS OBTAINED WITH THE NITROBENZENE SYSTEM[a)]

Comp.		Λ_∞	K_0^{MR}	K_a^{MR}	D^{MR}	$(K_a^{MR}D^{MR}/K_0^{MR})^{1/2}$	q^M_{meas}
H-Pic	Wet		3.47×10^{-8}	0.381	427		
Li-Pic	Wet		6.31×10^{5}	13.5	8.9×10^{-4}	0	
Na-Pic	Dry	33.9	30200				
	Wet	31.9	4680	24.0	0.0028	0.0038	0.0035
K-Pic	Dry	34.7	1150				
	Wet	40.3	832	43.7	0.014	0.027	0.025
Rb-Pic	Dry	35.1	646				
	Wet	40.7	447	87.1	0.022	0.066	0.061
Cs-Pic	Dry	36.4	646				
	Wet	40.4	269	117	0.068	0.17	0.18

a) taken from Refs. 1 and 8.

also been observed in the nitrobenzene system (Table 3). Association of the picrates in dry MIBK solutions is only a case that shows a definite correlation with the sizes of the cations concerned, though not so conspicuous as in the nitrobenzene system.

With dry ketones (acetone, methyl ethyl ketone, and MIBK), the $1/\varepsilon$ law is verified. The distance of closest approach is calculated to be about 4 Å on the basis of the theory by Denison and Ramsey.[7)] This suggests that the main factor in determining the extent of the ion association is an electrostatic force.

Distribution Coefficients D^{MR} and Association Constants K_a^{MR}. Measurements of these constants were carried out under conditions in which aqueous solutions were sufficiently alkaline (pH about 7.5) not to allow the presence of HR. A plot of Y/q^R *vs.* $1/(f_a^2[M^+]_a)$ shows a straight line in accordance with theoretical requirements (Fig. 2). The values of the intercept on the ordinate are so close to zero that the values of K_a^{MR} and D^{MR} are less accurate than those obtained with the nitrobenzene system.

For sodium picrate the value of K_a^{MR} is also determined potentiometrically to be about 20 by using a sodium-sensitive glass electrode. The value is in fair agreement with that given in Table 3, indicating the validity of the present method.

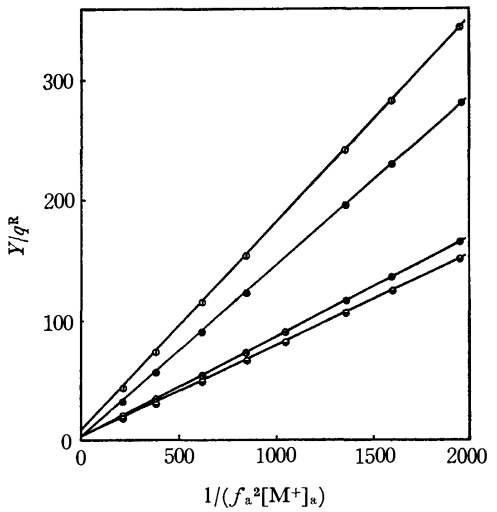

Fig. 2. The plot of Y/q^R *vs.* $1/(f_a^2[M^+]_a)$
The symbols used are the same as those in Fig. 1.

The D^{MR} values obtained show that MIBK dissolves larger quantities of the picrates than nitrobenzene. It is also shown that MIBK acts as a levelling solvent for the distribution and association of the picrates.

The value of D^{HR} is evaluated in such a way that the q^M and q^R curves calculated for five kinds of picrates

7) J. T. Denison and J. B. Ramsey, *J. Amer. Chem. Soc.*, **77**, 2615 (1955).
8) M. Yamane, T. Iwachido, and K. Tôei, This Bulletin, **44**, 745 (1971).

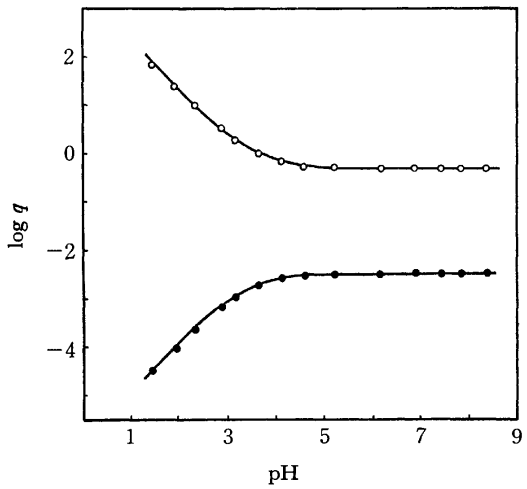

Fig. 3. The distribution of sodium picrate
○: q^R, ●: q^M

fit the observed ones. The best fit (Fig. 3, solid lines) is attained by choosing the value of 500, which is comparable to that obtained with the nitrobenzene system.

A value of 0.381[9] obtained in pure water is chosen for K_a^{HR} by neglecting a possible effect of the MIBK dissolved.

Distribution of Alkali Metals q^M. A typical plot of log q^M *vs.* pH for sodium picrate is shown in Fig. 3 by solid circles. The curves for the other picrates are not shown, since they were almost the same. The q^M and q^R values in Table 2 can serve as a measure of the slight differences in the curves among the picrates.

Appearance of a horizontal line can be explained by means of Eq. (19) as follows: When the aqueous solution is kept sufficiently alkaline, Eq. (19) can be rearranged into the following by neglecting $[H^+]_o$ and the terms containing $[H^+]_a$

$$q^M = D^{MR}\frac{\left([M^+]_o+\frac{1}{K_o^{MR}}\right)}{\left\{[M^+]_a+\frac{1}{K_a^{MR}}\left(1+\frac{D^{HR}}{K_a^{HR}}[H^+]_a+A\right)\right\}}\frac{[M^+]_a}{[M^+]_o}\left(1+\frac{A}{[M^+]_a}\right) \qquad (20)$$

$$C^R - C^M = A$$

This is further simplified to

$$(q^M)^2 = \frac{D^{MR}K_a^{MR}}{K_o^{MR}}\left(1+\frac{A}{[M^+]_a}\right) \qquad (21)$$

where $[M^+]_a/[M^+]_o$ is approximated by $1/q^M$. The concentrations of alkali metals remain practically constant over the whole pH range studied, since the concentrations of the picrates are much smaller than those of the alkali metals added as buffers. The values of q^M, therefore, become constant.

In the acidic region, on the other hand, circumstances are not so simple as in the alkaline region, since the term $[H^+]_o$ can not be neglected. Since no direct method for determining the $[H^+]_o$ values is known, the values are calculated from the pH:

$$[H^+]_o = \frac{K_o^{HR}K_o^{MR}D^{HR}[M^+]_o}{K_a^{HR}K_a^{MR}D^{MR}[M^+]_a}[H^+]_a \qquad (22)$$

Introduction of this term makes it difficult to estimate a simple relationship between the values of log q^M and pH, as has been shown in the nitrobenzene system.

Distribution of the Acid Species q^R. The dependence of the distribution ratio upon pH is calculated from Eq. (12). This equation can be simplified under sufficiently alkaline conditions as

$$q^R = \frac{D^{MR}K_a^{MR}}{K_o^{MR}}\left(K_o^{MR}[M^+]_a+\frac{1}{q^M}\right) \qquad (23)$$

This is further simplified to

$$q^R = \frac{D^{MR}K_a^{MR}}{K_o^{MR}}\cdot\frac{1}{q^M} \qquad (24)$$

showing that q^R values are independent of pH. The equation also shows that the q^M values are smaller than the q^R values by a factor of $(1+A/[M^+]_a)$. When the initial concentrations of C^M and C^R are equal ($A=0$), the values of q^M and q^R become the same, as in the nitrobenzene system.

In the acidic region, on the other hand, the q^R values vary almost linearly with pH, though the slope is slightly smaller than -1.

It has been comfirmed that the distribution of the picrates can be explained by means of six kinds of equilibria. The validity of such treatments may be proved indirectly by the fact that the K_a^{MR} value obtained with sodium picrate agrees well with that determined potentiometrically. No successful application to the mutual separation of alkali metals can be expected for the MIBK system because of its high levelling property.

The author wishes to express his gratitude to Professor Kyoji Tôei for his guidance throughout the course of this work. The work was supported in part by a grant from the Ministry of Education.

9) H. v. Halban and M. Seiler, *Helv. Chim. Acta*, **21**, 385 (1938).

ESR of Copper(II) Complexes in Magnetically Non-dilute Crystals. I. Single Crystals of Bis(L-alaninato)copper(II)

Hiroshi YOKOI and Shigeru OHSAWA*

Chemical Research Institute of Non-aqueous Solutions, Tohoku University, Katahira, Sendai 980

(Received January 11, 1973)

Single-crystal ESR studies have been carried out on bis(L-alaninato)copper(II). Only one symmetric absorption peak has been obtained in any direction of the magnetic field, regardless of the fact that there are two molecules per unit cell. The principal values and the directions of the principal axes of the g tensor have been determined, and a correlation between those components of the g tensor and the crystal structure has been confirmed on the basis of the effect of the spin-exchange interaction between the dissimilar copper(II) ions. The absorption linewidths have been examined in order to estimate the spin-exchange energy.

In general, it is not easy to determine the g values reflecting the local copper(II)-ion environment for the magnetically non-dilute crystals or polycrystals of copper(II) complexes with polymolecular unit cells if there is an appreciable spin-exchange interaction between the dissimilar copper(II) ions.[1-5] However, the estimation of the molecular g values from the crystal g values for the crystals of chemically-complicated chelate complexes with polymolecular unit cells is occasionally desired.[6] Single crystals of bis(L-alaninato)copper(II), which have two molecules per unit cell, showed only one symmetric ESR absorption line in any direction of the magnetic field. The purpose of this paper is to present the ESR findings on undiluted single crystals in connection with the crystal structure and spin-exchange interaction between dissimilar copper(II) ions.

Experimental

Single crystals of bis(L-alaninato)copper(II) were obtained from an aqueous solution by slow evaporation. The crystals

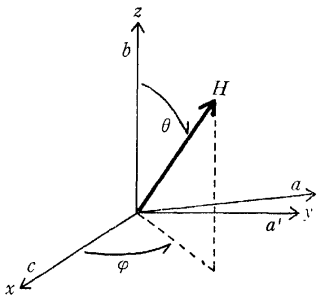

Fig. 1. A right-hand coordinate system fixed in monoclinic crystals (a', b, and c are the mutually perpendicular axes).

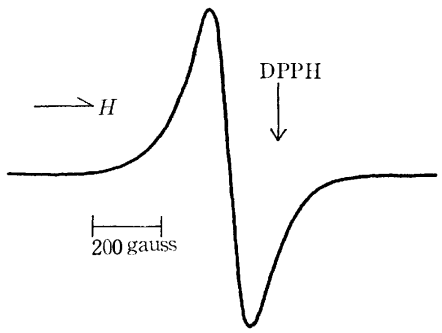

Fig. 2. The single crystal ESR spectrum of bis(L-alaninato)-copper(II) at $\theta=0°$ and $\varphi=0°$(X-band, at room temperature).

were optically identified by the use of a Stoe two-circle goniometer by measuring their interfacial angles. The crystals used in the ESR measurements were mounted on the end of a glass rod in various orientations by means of the goniometer. The ESR spectra were obtained at room temperature about each of three mutually perpendicular axes by rotation at 10 ° intervals, using a Hitachi X-band ESR spectrometer, Model-4001, equipped with a 100 kHz field modulation unit. The field was calibrated with an NMR probe and then with a benzene solution of vanadyl acetylacetonate.

Results

Crystals of bis(L-alaninato)copper(II) are monoclinic, with a bimolecular unit with these dimensions: $a=9.24\pm0.04$, $b=5.05\pm0.02$, $c=9.59\pm0.04$ Å, and $\beta=95.2\pm0.3°$. The space group is $P2_1(C_2^2)$.[7] A right-hand system is chosen in the crystals, as is shown in Fig. 1. Only one symmetric ESR absorption peak was observed in any direction of the magnetic field. One of the observed ESR spectra is shown in Fig. 2. All the rotation data of ESR measurements are shown in Figs. 3 and 4. The rotation data concerning the g values were fitted by the least-squares method to expressions of the type given by Schonland,[8] diagonalization then giving the eigenvalues and vectors for the g tensor.

The calculated direction angles for several molecular axes are given in Table 1. The principal values for the g tensor are also given in the table, together with the direction angles for the principal axes. The prin-

* Present address: Tokyo Shibaura Electric Co., Ltd., Komukai, Kawasaki.

1) A. Abragam and B. Bleaney, "Electron Paramagnetic Resonance of Transition Ions," Clarendon Press, Oxford (1970), p. 509.

2) G. F. Kokoszka and G. Gordon, "Technique of Inorganic Chemistry." Vol. VII, ed. by H. B. Jonassen and A. Weissberger, Interscience Publ., New York (1967), P. 226, and the references therein.

3) H. Abe, K. Ono, I. Hayashi, J. Shimada, and K. Iwanaga, *J. Phys. Soc. Jap.*, **9**, 814 (1954).

4) H. Abe and K. Ono, *ibid.*, **11**, 947 (1956).

5) I. M. Procter, B. J. Hathaway, and P. Nicholls, *J. Chem. Soc. A*, **1968**, 1678.

6) B. J. Hathaway and D. E. Billing, *Coordin. Chem. Rev.*, **5**, 143 (1970).

7) A. Dijkstra, *Acta Crystallogr.*, **20**, 588 (1966).

8) D. S. Schonland, *Proc. Phys. Soc.*, **73**, 788 (1959).

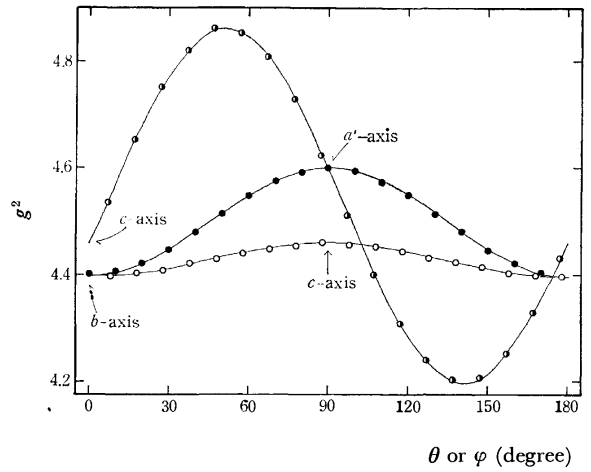

Fig. 3. The angular variance of g^2.
○: H in the bc plane, ●: H in the $a'b$ plane, ◑: H in the $a'c$ plane (the solid lines represent the calculated curves).

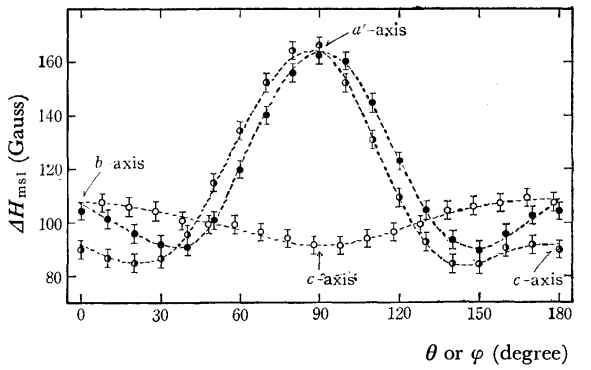

Fig. 4. The angular variance of ΔH_{msl} (the symbols are referred to in Fig. 3).

Table 1. The principal g values[a] and the direction cosines[b] for the principal g axes and some molecular axes

Direction	$\cos\theta_x$[c]	$\cos\theta_y$	$\cos\theta_z$
Cu-N(1)[d]	0.3256	−0.6956	−0.6404
Cu-O(1)	0.8059	−0.2656	−0.5292
⊥Cu-N-O(1)	0.5414	0.6925	0.4769
Cu-N(2)[d]	−0.3256	0.6956	−0.6404
Cu-O(2)	−0.8059	0.2656	−0.5292
⊥Cu-N-O(2)	−0.5414	−0.6925	0.4769
Internal bisector between the two ⊥ axes above	0.6159	0.7878	0
External bisector between the two ⊥ axes above	0	0	1.0
g_1=2.049	−0.7776	0.6288	0
g_2=2.096	0	0	1.0
g_3=2.203	0.6288	0.7776	0

a) Experimental errors in g factors were ±0.002. b) Experimental errors in θs were ±1.5°. c) θ_x, θ_y, and θ_z are the angles between the indicated directions and the x, y, and z axes respectively shown in Fig. 1. d) Two molecules in an unit cell are designated by the numbers 1 and 2. N and O represent the directly coordinating atoms.

cipal g values obtained in this work agree with those determined from the powder K-band ESR spectrum by the use of the approximation of Kneubühl.[9,10]

Discussion

When there are two types of copper(II) ions with different g values, g_a and g_b respectively ($\Delta g=|g_a-g_b|$), the observed ESR line shape will depend on whether the spin-exchange energy, $2J$, is greater or smaller than $\Delta g\beta H$. If $2J>\Delta g\beta H$, only one absorption peak is to be expected, because of the unifying effect of the exchange interaction.[1-4,6] Let us now consider the case of a unit cell containing only two sets of crystallographically-non-equivalent axial molecules ($g_{//}$ and $g_\perp$). Let the two principal axes of the molecules be inclined at the 2γ angle. In the case of $2J>(g_{//}-g_\perp)\beta H$, the following three principal g values ($g_1\leq g_2\leq g_3$) are given as the crystal g values:[4]

$$g_1 = g_\perp \quad (1)$$

$$g_2 = \sqrt{g_\perp^2+(g_{//}^2-g_\perp^2)\sin^2\gamma} \quad (2)$$

$$g_3 = \sqrt{g_\perp^2+(g_{//}^2-g_\perp^2)\cos^2\gamma} \quad (3)$$

where the axes of g_2 and g_3 are directed to the external and internal bisectors respectively of the axes normal to two sets of crystallographically-non-equivalent molecular planes, and where the g_1 axis is perpendicular to both the g_2 and g_3 axes.

It is characteristic of the crystals of bis(L-alaninato)-copper(II) that the direction angles of the g_3 axis are in close agreement with those of the above-mentioned internal bisector, whereas those of the g_2 axis coincide with those of the external bisector, as is shown in Table 1. These experimental facts can be clearly understood from Eqs. (1)—(3). On the assumption of an axial symmetry in the molecular g values for this complex in crystals, we can determine a $g_{//}$ value which minimizes the equation of $(g_2^{ob}-g_2^{calc})^2+(g_3^{ob}-g_3^{calc})^2$, where g^{ob} represents the observed g value, and g^{calc}, the g value calculated from Eqs. (2) and (3). This $g_{//}$ value was determined to be 2.247_0 using $g_\perp=2.049_0$ and $\gamma=28°29'$, where the γ value is half the angle between the two above-mentioned molecular planes. Then, the calculated g values were found to be as follows:

$$g_2^{calc} = 2.095_7 \text{ and } g_3^{calc} = 2.203_5$$

These calculated crystal g values agree with those listed in Table 1 within the limits of experimental error. The assumption of an axial symmetry in the molecular g values for this complex in crystals contradicts a suggestion previously reported.[9] From the point of view of chemical constitution, it had been considered that the local copper(II)-ion environment of bis(amino acidato)copper(II) complexes is rhombically distorted. However, a nearly axial symmetry in the molecular g values for this complex in crystals seems to be highly probable, since there is a satisfactory agreement between the calculated and experimentally-

9) H. Yokoi, M. Sai, T. Isobe, and S. Ohsawa, This Bulletin, **45**, 2189 (1972).
10) F. K. Kneubühl, *J. Chem. Phys.*, **33**, 1074 (1960).

determined g values, as has been mentioned above, since various bis(amino acidato)copper(II) complexes in magnetically-diluted crystals have been reported to be of an axial symmetry in the g values[11] and since it is considered that the alanine complex in crystals is not largely different from that in an aqueous solution in either the g values or the visible absorption energy; $g_{//}=2.264$, $g_{\perp}=2.056$, and $\lambda_{max}=617$ (nm) in aqueous-methanolic solutions, whereas the above-assumed molecular g values and $\lambda_{max}=590$ (nm) in crystals.[9]

The approximate spin-exchange energy can be estimated from the observed linewidth and the calculated dipolar width using the following equations:[12]

$$\Delta H = \frac{6.67(\Delta H^{d})^{2}}{H_{ex}} \tag{4}$$

$$H_{ex} = \sqrt{2.83}\frac{J}{g\beta}\sqrt{S(S+1)} \tag{5}$$

where ΔH and ΔH^{d} are the observed half-width and the dipolar half-width respectively, and where H_{ex} is the exchange energy between the copper(II) ions expressed in the units of the magnetic field. It is assumed in Eqs. (4) and (5) that J is the value of the isotropic exchange interaction. ΔH^{d} can be calculated from the second moment, $\langle \Delta H^{2} \rangle$, assuming that the line shape is of Gaussian form:

$$\Delta H^{d} = 2.35\sqrt{\langle \Delta H^{2} \rangle} = 2.35\left[\frac{3}{4}\mu^{2}\sum_{i,j}\frac{(3\cos\theta_{ij}-1)^{2}}{r_{ij}^{6}}\right]^{1/2} \tag{6}$$

Table 2. Estimation of the J value

Direction of H	g	ΔH_{msl} (gauss)	ΔH^{d}_{msl} (gauss)	J (cm^{-1})
$a' // H$	2.143	164	344	0.33
$b // H$	2.096	108	364	0.55
$c // H$	2.110	92	293	0.42

where μ is the magnetic moment, where r_{ij} is the distance between the copper ions i and j, and where θ_{ij} is the angle between r_{ij} and the static magnetic field. Instead of ΔH, the separation between the points of the maximum and minimum slopes, ΔH_{msl}, was used for all the calculations, with an appropriate correction. The results are summarized in Table 2. The estimated J values in the table slightly differ with different directions of H. The reason for this may be that Eqs. (4) and (5) are approximate equations for the present case, since they are valid only when the g tensor is isotropic,[1,12] and that the effect of hyperfine coupling on the linewidth is neglected in these equations.[12] It is expected that the actual J value in the crystals of bis(L-alaninato)copper(II) is slightly larger than those listed in Table 2 because of the broadening effect of the hyperfine structure, and that this effect becomes more profound with g in the indicated directions of H in the table. In conclusion, J is of the order of 0.5 cm^{-1} for this complex in crystals.

The authors are grateful to Professor Taro Isobe for his encouragement throughout this work; they also wish to thank Mr. Makoto Chikira for his helpful advice.

11) H. A. Kuska and M. T. Rogers, *J. Chem. Phys.*, **43**, 1744 (1965); H. C. Allen, Jr., M. I. Mandrioli, and J. W. Becker, *ibid.*, **56**, 997 (1972); M. Fujimoto and Y. Tomkiewicz, *ibid.*, **56**, 749 (1972).

12) J. H. Van Vleck, *Phys. Rev.*, **74**, 1168 (1948); C, J. Gorter and J. H. Van Vleck, *ibid.*, **72**, 1128 (1947); P. W. Anderson and P. R. Weiss, *Rev. Mod. Phys.*, **25**, 269 (1953).

The Electrochemical Behavior of the Low-valent Transition Metal Complexes. II. Iron(0)-2,2′-Bipyridine Complexes

Akira MISONO, Yasuzo UCHIDA, Masanobu HIDAI, Takamichi YAMAGISHI, and Hironori KAGEYAMA

Department of Industrial Chemistry, Faculty of Engineering, The University of Tokyo, Hongo, Bunkyo-ku, Tokyo 113

(Received February 7, 1973)

The electroreduction reaction of the zero-valent iron-2,2′-bipyridine complexes ($Fe(bipy)_2$ and $Fe(bipy)_3$) was studied in a hexamethylphosphoric triamide solution by polarography and ESR measurements. In the polarography, $Fe(bipy)_2$ was first reduced at a very less negative potential ($E_{1/2} = -0.76$ V *vs.* Hg pool) than the first wave potential of free bipyridine (-2.37 V *vs.* Hg pool). In the presence of excess bipyridine, $Fe(bipy)_2$ was first reduced at -1.10 V *vs.* Hg pool corresponding to the second reduction step of the solution of $Fe(bipy)_2$. The visible spectra of the solution of $Fe(bipy)_2$ in the presence of excess bipyridine was different from that of the solution of $Fe(bipy)_2$ only. The signal with hyperfine structure attributable to the anion radical of bipyridine was observed by means of ESR analysis of the solution electrolyzed at the potential corresponding to the second reduction step. From these results, it was concluded that $[Fe(bipy)(HMPT)_m]$ was reduced at the first step, and $[Fe(bipy)_2(HMPT)]$ was reduced at the second.

Although many electrochemical studies on high-valent transition metal complexes have been reported,[1,2] only a few studies on the electrochemical behavior of low-valent transition metal complexes have been carried out. It seemed that it would be interesting to perform a study of the electrochemical behavior of low-valent transition metal complexes in relation to evaluation of the charge distribution and the stability of the reduced complexes.

In a previous paper,[3] we reported a study on the electrochemical behavior of the low-valent nickel-2,2′-bipyridine complexes. In this paper, the electrochemical study on the zero-valent iron-2,2′-bipyridine complexes will be described.

Experimental

Materials. Hexamethylphosphoric triamide (HMPT) used as solvent was refluxed over calcium hydride for several hours and was then fractionally distilled under a reduced nitrogen pressure. Tetra-*n*-butylammonium perchlorate (TBAP) was prepared by the published method.[3] 2,2′-Bipyridine was used as purchased, mp 69.5—70.0 °C.

The examined complexes were bis(2,2′-bipyridine)iron(0) ($Fe(bipy)_2$), and tris(2,2′-bipyridine)iron(0) ($Fe(bipy)_3$). $Fe(bipy)_2$ was obtained by heating a benzene solution of diethylbis(2,2′-bipyridine)iron(II) ($Et_2Fe(bipy)_2$) at 50 °C for several hours.[4] $Fe(bipy)_3$ was obtained by decomposing $Et_2Fe(bipy)_2$ in the presence of excess bipyridine at 50 °C for several hours.[4] Tris(2,2′-bipyridine)iron(II) perchlorate ($[Fe(bipy)_3](ClO_4)_2$) was prepared according to the method of Nyholm *et al.*[5]

Apparatus and Procedure. The polarographic analysis was performed using an H-type cell. The cathode and the anode were a dropping mercury and a mercury pool, respectively. The concentration of the complexes was generally 5.0×10^{-3} mol/l, while that of TBAP was 2.0×10^{-1} mol/l. The polarograph used was a Yanagimoto Model PB-105. For the ESR analysis, an electrolytic cell as shown in the previous paper[3] was used. The ESR spectra were recorded on a JEOL Model JS-3BS-X Spectrometer. The visible spectra of the complex solution were measured using a Shimadzu Model MPS-50L Spectrophotometer. All operations were handled under nitrogen purified by activated copper.

Results and Discussion

Polarographic Results on the Complexes. The complex $Fe(bipy)_2$ is stable in non-polar solvents such as benzene and tetrahydrofuran, but it is unstable in polar solvents such as 1,2-dimethoxyethane, acetonitrile, and HMPT. The color of the HMPT solution of $Fe(bipy)_2$ changed from brown to violet, and lastly a yellow precipitate was produced under nitrogen at room temperature within a few hours. Therefore the polarographic measurement of the complexes was performed quickly. The polarographic results on the complexes are shown in Table 1.

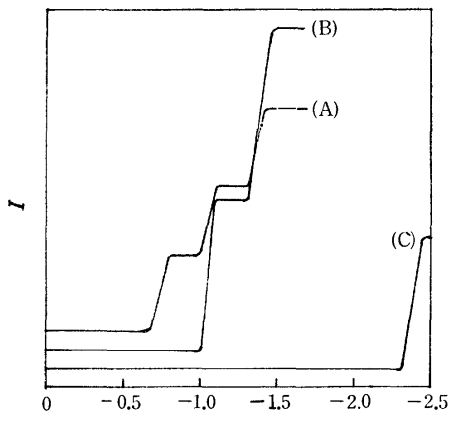

Fig. 1. Polarogram of $Fe(bipy)_2$ in the presence of bipyridine. (A): $Fe(bipy)_2$, (B): Addition of 10-fold molar amount of bipyridine, (C): Free bipyridine.

1) N. Tanaka, and Y. Sato, *Inorg. Nucl. Chem. Lett.*, **2**, 359 (1966); *ibid.*, **4**, 487 (1968); Y. Sato, and N. Tanaka, This Bulletin, **42**, 1021 (1969); *ibid.*, **41**, 2059, 2064 (1968).

2) N. Tanaka, and Y. Sato, *Electrochim. Acta*, **13**, 335 (1968).

3) A. Misono, Y. Uchida, Y. Yamagishi, and H. Kageyama, This Bulletin, **45**, 1438 (1972).

4) A. Yamamoto, K. Morifuji, S. Ikeda, T. Saito, Y. Uchida, and A. Misono, *J. Amer. Chem. Soc.*, **90**, 1878 (1968).

5) F. H. Burstall, and R. S. Nyholm, *J. Chem. Soc.*, **1952**, 3570.

Table 1. Polarographic results on the complexes

Complex	$E_{1/2}(1)$[b]	$E_{1/2}(2)$[b]	$E_{1/2}(3)$[b]	Wave height ratio
$Fe(bipy)_2$	−0.76	−1.08	−1.40	1.0 : 0.9 : 1.0
$Fe(bipy)_2$ + bipy[a]	−1.10	−1.41		1.0 : 0.9
$Fe(bipy)_3$	−1.89			
$[Fe(bipy)_3](ClO_4)_2$	−1.29	−1.53	−1.85	1.0 : 1.0 : 1.0
	(−1.34)[c]	(−1.55)[c]	(−1.89)[c]	
Free bipyridine	−2.37	−2.80		1.0 : 0.7

Conditions: cathode, a dropping mercury electrode; anode, a mercury electrode; solvent, hexamethylphosphoric triamide; concentration of the complex, 5.0×10^{-3} mol/l; supporting electrolyte, $(n\text{-}C_4H_9)_4N^+ClO_4^-$ (TBAP); concentration of TBAP, 2.0×10^{-1} mol/l.
a) $Fe(bipy)_2$: bipy=1.0: 10 (molar ratio) b) Potential *versus* Hg pool c) Ref. 2.

The first half-wave potential ($E_{1/2}(1)$) of $Fe(bipy)_2$ appeared at a far less negative potential (−0.76 V *vs.* Hg pool) than $E_1/_2(1)$ of free bipyridine. The reduction step of the complex was less reversible, but the electron to be transferred was supposed to be one from the slope of the reduction wave. The ratio of the heights of the first and the second waves was 1.0: 0.9, and the slope of the second wave indicates a one-electron transfer in the second as well as in the first.

When a 10-fold molar amount of bipyridine was added to the complex solution, the decomposition of the complex was suppressed, and the first wave appeared at −1.10 V *vs.* Hg pool corresponding to the second reduction step of the solution of $Fe(bipy)_2$ as shown in Fig. 1. The second wave appeared at −1.41 V *vs.* Hg pool corresponding to the third reduction step of the solution of $Fe(bipy)_2$. The addition of bipyridine increased the height of the second and the third waves of the solution of $Fe(bipy)_2$ only. Furthermore these waves became reversible as their height was increased by the addition of bipyridine as shown in Table 2. The change in the height and reversibility of the second and the third waves suggests that added bipyridine takes part in these reduction steps.

Table 2. Effect of addition of bipyridine on the second reduction wave of $Fe(bipy)_2$ in HMPT

Molar ratio		Relative wave height[a]	Slope (mV)[b]
bipy/$Fe(bipy)_2$	0	—	91.2
bipy/$Fe(bipy)_2$	10	2.2	73.4
bipy/$Fe(bipy)_2$	100	4.0	65.0

Conditions: cathode, a dropping mercury; anode, a mercury pool; concentration of the complex, 5.0×10^{-3} mol/l; concentration of TBAP, 2.0×10^{-1} mol/l.
a) The ratio of the height of the first wave in the presence of excess bipyridine to the height of the second wave in the absence of bipyridine b) Value in the log-plot analysis

The reduction waves of the solution of $Fe(bipy)_2$ at a considerably negative potential could not be successfully observed because of the disturbance in the wave shapes. The reduction wave of free bipyridine was observed after the wave in which the complex was considered to take part. After a prolonged reduction of the complex solution at about −2.0 V *vs.* Hg pool, the color of the solution faded and the resulting polarogram showed only the reduction waves of free bipyridine. These results may be attributable to the instability of the reduced species in spite of the presence of a large amount of bipyridine.

The Visible Spectra of the Complex Solutions. The complex $Fe(bipy)_2$ is very slightly soluble in benzene, to give a blue-violet colored solution. This intense color is considered to be due to the charge transfer between the central metal atom and the ligand molecule.[6] However $Fe(bipy)_2$ was readily soluble in HMPT, to give a brown colored solution, and then decomposed into a yellow precipitate within a few hours under nitrogen at room temperature.

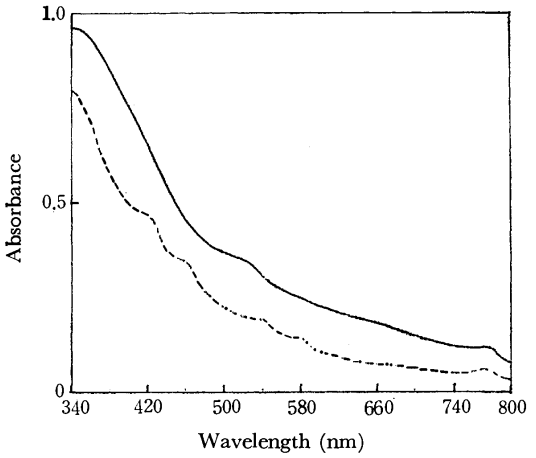

Fig. 2. The visible spectra of $Fe(bipy)_2$–HMPT solution.
——: $Fe(bipy)_2$ in HMPT
-----: $Fe(bipy)_2$+10-fold molar amount of bipyridine in HMPT.

When excess bipyridine was added to the complex solution, the visible spectrum of the solution is different from that of the solution of $Fe(bipy)_2$ in the absence of bipyridine. These spectra are shown in Fig. 2.

When $Et_2Fe(bipy)_2$, $Fe(bipy)_2$, and $Fe(bipy)_3$ were used as the catalysts for the oligomerization of butadiene(BD), the reaction intermediate is considered to be $[Fe(bipy)(BD)_2]$.[4] HMPT with a donor- and an acceptor-level can also coordinate to a low-valent transition metals. It is therefore reasonable to consider that the coordinated bipyridine is replaced by HMPT, and $[Fe(bipy)(HMPT)_m]$ (m=1, 2, or 3) is produced in an HMPT solution.

$Fe(bipy)_3$ is very slightly soluble and stable in ben-

6) Y. Kaizu, T. Yazaki, Y. Torii, and H. Kobayashi, This Bulletin, **43**, 2068 (1970).

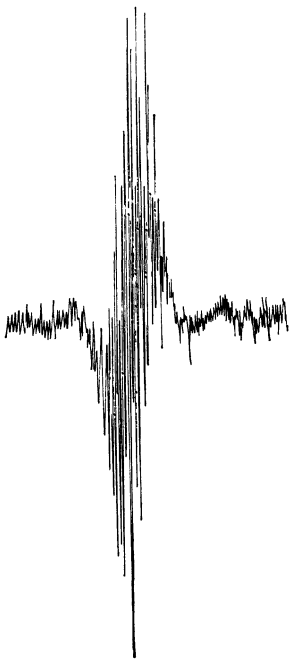

Fig. 3. ESR signal in the electrolysis of $Fe(bipy)_2$ at -1.30 V *vs.* Ag wire (*g*-value, 2.002_5).

zene and HMPT, to give a dark brown colored solution. The visible spectrum of the solution of $Fe(bipy)_3$ did not change by the addition of bipyridine.

ESR Measurements. In the electrolysis of $Fe(bipy)_2$ in HMPT at the potential sufficiently negative to cause the first reduction step, no ESR signal was observed. However in the electrolysis at the potential corresponding to the second reduction step, the ESR signal with hyperfine structure attributable to the anion radical of 2,2′-bipyridine[7] was observed. This signal was stable in HMPT and was observed to be overlapped with another signal with an ill-defined structure. The observed signal is shown in Fig. 3. The similar signal was observed in the electrolysis of the nickel(0)-2,2′-bipyridine complexes in HMPT at the potential corresponding to the second reduction step.[3]

Taking into account the polarographic results at the second reduction step, it was concluded that the anion radical of bipyridine was formed by the dissociation of the species produced at the second reduction step.

Reaction Mechanism in the Electrolysis of $Fe(bipy)_2$. Taking into account the polarographic results and the visible spectra of the solution of $Fe(bipy)_2$, the following equilibrium in HMPT is proposed.

$$[Fe(bipy)_2(HMPT)] \overset{HMPT}{\rightleftharpoons} [Fe(bipy)(HMPT)_m] + bipy$$

As a mechnism of the electro-reduction of $Fe(bipy)_2$ in HMPT, the following mechanism is proposed.

$$\begin{array}{ccc}
[Fe(bipy)_2(HMPT)] & \overset{-bipy}{\underset{+bipy}{\rightleftharpoons}} & [Fe(bipy)(HMPT)_m] \\
-e^- \uparrow\downarrow +e^- \text{ 2nd step} & \swarrow\ -[bipy]^- & -e^- \uparrow\downarrow +e^- \text{ 1st step} \\
[Fe(bipy)_2(HMPT)]^- & \overset{-bipy}{\underset{+bipy}{\rightleftharpoons}} & [Fe(bipy)(HMPT)_m]^- \\
-e^- \uparrow\downarrow +e^- \text{ 3rd step} & & -e^- \uparrow\downarrow +e^- \\
[Fe(bipy)_2(HMPT)]^{2-} & \overset{-bipy}{\underset{+bipy}{\rightleftharpoons}} & [Fe(bipy)(HMPT)_m]^{2-}
\end{array}$$

The complex $Fe(bipy)_2$ is unstable and gave a disturbed polarogram, from which no clear-cut information was obtained, but it showed more reduction waves at a potential more negative than the third reduction step, so a reduction state more than the third reduction state may be expected. Tris(2,2′-bipyridine)chromium(0) has previously been reported to be reduced to the hexa-anion stage, $Ca_3[Cr(bipy)_3]\cdot 7NH_3$.[8]

The Electroreduction Reaction of $Fe(bipy)_3$ in HMPT. Tanaka *et al.*[2,9] reported that in the electroreduction of $[Fe(bipy)_3](ClO_4)_2$ in acetonitrile, the following mechanism has been proposed.

$$[Fe(bipy)_3]^{2+} + e^- \rightleftharpoons [Fe(bipy)_3]^+ \qquad E_{1/2} = -1.34 \text{ V } vs. \text{ SCE}$$

$$[Fe(bipy)_3]^+ + e^- \rightleftharpoons [Fe(bipy)_3]^0 \qquad E_{1/2} = -1.55 \text{ V } vs. \text{ SCE}$$

$$[Fe(bipy)_3]^0 + e^- \rightleftharpoons [Fe(bipy)_3]^- \qquad E_{1/2} = -1.89 \text{ V } vs. \text{ SCE}$$

The first wave potential of $Fe(bipy)_3$ in HMPT appeared at -1.89 V *vs.* Hg pool. The visible spectrum of the solution of $Fe(bipy)_3$ is similar to that in benzene, and it did not change by the addition of free bipyridine. From the above results, the analogous reaction mechanism was proposed in the electrolysis of $Fe(bipy)_3$ in HMPT.

$$Fe(bipy)_3 + e^- \rightleftharpoons [Fe(bipy)_3]^-$$

7) N. Maki, T. Hirano, and S. Musha, *ibid.*, **36**, 756 (1963).
8) S. Herzog, U. Grimm, and W. Waichenbauer, *Z. Chem.*, **7**, 355 (1967).
9) N. Tanaka, T. Ogata, and N. Niizuma, The 18th Symposium on Polarography and Electric Analysis, Preprint p. 11, Tokyo (1972).

Ion-selective Electrodes Sensitive to Some Organic Compounds Used as Drugs

Kenyu KINA, Nobuko MAEKAWA, and Nobuhiko ISHIBASHI

Department of Applied Analytical Chemistry, Faculty of Engineering, Kyushu University Higashi-ku, Hakozaki, Fukuoka 812

(Received February 23, 1973)

Drug ion-selective electrodes with a liquid membrane have been developed which are sensitive to methacholine, neostigmine, *N*-1-methyl nicotinamide, diphenhydramine, vitamin B_1, vitamin B_6, *p*-aminosalicylic acid (PAS), and salicylic acid. Crystal violet or ferroin-compound cations and dipicrylamine or tetraphenylborate anions were used as the ion-exchange sites in the liquid membrane. Each liquid membrane was prepared by using the solvent-extraction method and exhibited an appropriate Nernstian response to the respective ion down to 10^{-4} or to 10^{-5} M. The electrode performances, including the selectivity coefficients, are summarized in Table 1.

In a previous paper vitamin-sensitive electrodes based on the solvent extraction of the protonated vitamin cation have been reported on.[1] Among other drugs, we found many ionic and water-soluble organic compounds. For example, methacholine chloride, neostigmine bromide, and *N*-1-methyl nicotinamide chloride are water-soluble salts of quarternary ammonium or pyridinum cations. Diphenhydramine, vitamin B_1, and B_6 are present as protonated cations in an acidic aqueous solution from pH 3 to 5. From the acid-dissociation constants of *p*-aminosalicylic acid and salicylic acid, it can easily be understood that they are present as singly-charged anions in the pH range from 6 to 11. These organic ions can be extracted with the ionic extractant into an organic solvent such as 1,2-dichloroethane or nitrobenzene; the resulting organic solution is useful as a "liquid membrane" for the corresponding ion-selective electrode.

This paper will describe the performance of the electrodes sensitive to some organic compounds used as drugs.

Experimental

Chemicals and Liquid-membrane Solutions. The crystal violet (CV) and the dipicrylamine (Hexyl) were obtained from the Kishida Kagaku Co. The sodium tetraphenylborate (TPB), *o*-phenanthroline (Phen), and bathophenanthroline (Bphen) were obtained from the Dojindo Co., Ltd. The objective drugs were obtained from the Kishida Kagaku Co. or the Tokyo Kasei Co.

The liquid membranes of the electrodes were prepared by using the ion-association extraction method.[1]

As the extractant of a drug cation, sodium tetraphenylborate or dipicrylamine was used, whereas the crystal violet cation or the ferroin compound (the iron chelate of *o*-phenanthroline or bathophenanthroline) was used as the extractant of the drug anion. Nitrobenzene (NB) or 1,2-dichloroethane (DCE) was used as the membrane solvent; the concentration of the liquid membrane was 1×10^{-4} M.

Evaluation of the Electrode Performance. Either a U-shaped glass tube or an Orion liquid-membrane barrel was used for the drug ion-sensitive electrode.

The selectivity and sensitivity of the drug ion-selective electrode were estimated by measuring the electromotive force of the following concentration cell:

+SCE/Reference solution (′)/Organic liquid membrane/Sample solution (″)/SCE−

The reference solution and sample solution were separated by means of the liquid membrane in the lower part of a U-shaped glass tube. The details of the cell assembly have been described in earlier papers.[2]

An Orion liquid-membrane barrel equipped with a Milliporefilter solvinert membrane (Pore size 0.25 micron) was used for the dynamic response and potentiometric titration studies. The outer chamber of the barrel was filled with the "liquid membrane." The internal reference chamber was filled with a corresponding drug-ion solution.

The measurements of the membrane potential were made by means of a Takeda Riken electrometer, TR-8651. The dynamic response of the electrode was recorded with a National Pen Recorder (Model VP-653A).

Results and Discussion

Response of the Electrode. The electrode potential in the presence of an interfering ion is empirically given by:

$$E = \text{Constant} + (2.303RT/nF)\log(A_i'' + K_j(A_j'')^{n/z}) \quad (1)$$

where n and z are the charges of the i and j-ions respectively and where K_j is the selectivity coefficient of the j-ion for the i-ion-sensitive electrode. As the reference solution we used a 1×10^{-3} M solution of the objective drug ion. The A_i'' and A_j'' activities in Equation (1) were approximated by the use of the molar concentration, because the dilute solution was used. The selectivity coefficient was determined by using the separate-solution method.[3] The observed electrode performance is summarized in Table 1. Methacholine and neostigmine electrodes are most sensitive, having useful response ranges up to 1×10^{-6} M. This suggests that methacholine and neostigmine cations are well extractable into the organic solvent, because the electrode of the higher extractable ion is usually more sensitive.[4]

The sequence of selectivity coefficients is consistent with the order of the extractability of the ion into the

1) N. Ishibashi, K. Kina, and N. Maekawa, *Chem. Lett.* **1973**, 119.

2) N. Ishibashi and H. Kohara, *Anal. Lett.* **4**, 785 (1971).

3) G. J. Moody and J. D. R. Thomas, "Selective Ion Sensitive Electrode," Merrow Pub. Co. Ltd., Watford, Herfordshire, England (1971), p. 12.

4) N. Ishibashi and K. Kina, This Bulletin, **46**, 2454 (1973).

Table 1. Performance of the drug ion-sensitive electrodes

Electrode	Solvent	Exchange site	Slope, $-$mV/log C[a]	Useful range	Selectivity coefficient, K_j
Methacholine	NB	Hexyl	-59	10^{-1}—10^{-6} M (pH 4—10)	$V.B_1$ 0.0017, TEA[b] 28, $K^+ < 10^{-4}$ Benzethonium 19, Neostigmine 5
Neostigmine	NB	TPB, Hexyl	-60	10^{-1}—10^{-5} M (pH 4—10)	TEA 0.61, Methacholine 0.16, N-1-methyl nicotinamide 0.004
	DCE	TPB	-60	10^{-1}—10^{-6} M (pH 4—10)	TEA 1.4, Methacholine 0.13, N-1-methyl nicotinamide 0.005
N-1-methyl-nicotinamide	NB	Hexyl	-60	10^{-1}—10^{-5} M (pH 4—10)	Na^+ 1×10^{-4}, K^+ 4.2×10^{-3}, NH_4^+ 1.3×10^{-3}, TEA 2.4×10^{2}, Methacholine 42.7
Diphen-hydramine	NB	Hexyl	-59	10^{-1}—10^{-5} M (pH 3—5)	Na^+ 1.9×10^{-5}, $K^+ < 10^{-4}$; $NH_4^+ < 10^{-4}$, TEA 0.04, Methacholine 0.02, Neostigmine 0.05
Vitamin B_1	DCE	TPB	-30	10^{-1}—10^{-5} M (pH 3—5)	$Na^+ < 10^{-4}$, $K^+ < 10^{-4}$, NH_4^+ 1×10^{-4}, $V.B_6$ 70
Vitamin B_6	NB	Hexyl	-57	10^{-1}—10^{-5} M (pH 3—5)	$Na^+ < 10^{-4}$, $K^+ < 2.5\times10^{-2}$, NH_4^+ 8×10^{-3}, $V.B_1$ 1×10^{-1}
p-Amino-salicylic acid (PAS)	NB	CV $Fe(Bphen)_3$	60	10^{-1}—10^{-5} M (pH 6—10)	Salicylic acid 30, Benzoic acid 9×10^{-2}, *p*-Aminobenzoic acid 8×10^{-2}, Phthalic acid 1×10^{-1}, Isophthalic acid 2×10^{-4}, Terephthalic acid 1×10^{-3}, Br^- 0.53, NO_3^- 3.7, Cl^- 0.012
	DCE	CV	60	10^{-1}—10^{-5} M (pH 6—10)	Br^- 1.05, NO_3^- 6.6
Salicylic acid	NB	CV, $Fe(phen)_3$ $Fe(Bphen)_3$	60	10^{-1}—10^{-5} M (pH 6—10)	$Cl^- < 10^{-4}$, I^- 1.03, *p*-Aminobenzoic acid $< 10^{-4}$

a) C denotes the molar concentration of drug ion. b) TEA denotes tetraethylammonium ion.

organic solvent.[5] Among the coexisting competitive ions, the easily extractable ion produces a large interference. Salicylic acid interferes remarkably with the performance of the *p*-aminosalicylic acid-sensitive electrode. This reflects a decreased extractability of *p*-aminosalicylic acid resulting from its hydrophilic amino group.

According to Eisenman's theoretical prediction of the liquid membrane potential,[6] the selectivity of the electrode depends entirely on the membrane solvent rather than on the particular exchange-site species in the limiting case of the complete dissociation in a liquid membrane. The ion-pair complex in the nitrobenzene membrane may be completely dissociated, because nitrobenzene has a relatively high dielectric constant and because the concentration of the ion pair is sufficiently dilute.[4]

As can be seen in the cases of the neostigmine-, *p*-aminosalicylic acid-, and salicylic acid-sensitive electrodes in Table 1, no difference in either the selectivity or the sensitivity was found among different exchange sites when nitrobenzene was used as the membrane solvent. The 1,2-dichloroethane membrane gives a selectivity quite different from that of the nitrobenzene membrane. Hence, the observed selectivity coefficients qualitatively support Eisenman's expectation.

Dynamic Response and Potentiometric Titration. The dynamic response was evaluated on the methacholine ion-sensitive electrode by exposing the electrode to a rapid change of methacholine-ion concentration from 10^{-5} to 10^{-3} M. The solution was agitated with a magnetic stirrer.

The electrode potential changed rapidly, and the resulting constant potential was obtained within one second, although the response time depends on the efficiency of the solution mixing. Such a rapid response is, in practice, sufficiently useful for performing the potentiometric titration. The methacholine ion-selective electrode was used in the potentiometric titration of methacholine chloride by using the sodium tetraphenylborate solution as a titrant. The end point of the potentiometric titration agreed well with that of the argentimetric titration of the chloride ion. As has been mentioned above, the several drug ion-selective electrodes have comparatively good analytical responses from the view points of sensitivity and selectivity.

These drug ion-selective electrodes, therefore, could be used in the analyses of mixed pharmaceutical preparations.

5) N. Ishibashi, K. Kohara, and N. Uemura, *Bunseki Kagaku* (Japan Analyst), **21**, 1072 (1972).

6) R. A. Durst ed., "Ion-selective Electrodes," N. B. S. Spec. Publ. 384, U. S. Printing Office, Washington (1970), p. 5.

This work was financially supported in part by a grant for Scientific Research form the Ministry of Education.

Kinetics and Mechanisms of the Reactions of Ce(IV) and Co(III) with Variamine Blue, [*N*-(*p*-Methoxyphenyl)phenylenediamine], in Aqueous Perchlorate Media

Taira IMAMURA and Masatoshi FUJIMOTO

Department of Chemistry, Faculty of Science, Hokkaido University, Sapporo 060

(Received March 31, 1973)

The kinetics of the non-complementary reactions of Ce(IV) and Co(III) with Variamine Blue perchlorate were studied under nitrogen atmosphere in aqueous perchlorate media of ionic strength $\mu=2.0$ M. The iminoquinone form of Variamine Blue was spectrophotometrically followed at 550 nm by stopped-flow technique. The rate constants of the stepwise reaction, $M^{n+}+(V.B.)\underset{k_r}{\overset{k_\alpha}{\rightleftharpoons}}M^{(n-1)+}+(V.B.)_{sox}$, $M^{n+}+(V.B.)_{sox}\xrightarrow{k_\beta}M^{(n-1)+}+(V.B.)_{ox}+2H^+$ were evaluated at 25 °C to be $k_\alpha=1.7\times10^5$ and $k_\beta=2.4\times10^5$ M^{-1} sec^{-1} for Ce^{4+} and $k_\alpha=1.35\times10^4$ and $k_\beta=1.53\times10^4$ M^{-1} sec^{-1} at [H]=1.0 M for Co^{3+}. The rates of Ce^{4+} were not affected by [H]. The [H]-dependence of k_α and k_β for Co^{3+} gives the mechanism $Co^{3+}_{aq}+B\underset{k_1}{\rightleftharpoons}$product, $CoOH^{2+}_{aq}+B\xrightarrow{k_2}$product, $Co^{3+}_{aq}\overset{K_h}{\rightleftharpoons}CoOH^{2+}_{aq}+H^+$, with $k_2\simeq10^7$ M^{-1} sec^{-1}, suggesting an outer-sphere mechanism for the electron transfer with $CoOH^{2+}$.

In preceding reports we discussed the reactions of Variamine Blue (abbr. V.B.) with iron(III) and thallium(III), in which the formation of the iminoquinone form of V.B. was treated as a two-setp reaction for iron(III)[1] and as a one-step reaction for thallium-(III).[2]

The question has been raised whether the two-step scheme is essential in the non-complementary reaction of V.B. with other metal ions in high oxidation states such as cerium(IV) and cobalt(III). The redox reaction rates of cobalt(III) are generally slower than those predicted from its high redox potential.[3] In the present paper the reactions of V.B. with aquo ions, cerium(IV) and cobalt(III) are reported.

Experimental

Materials. Deionized water was distilled with an all-joint Pyrex apparatus. Purified sodium perchlorate[4] was used to maintain the ionic strength at 2.0 M.

Cerium(IV) and cobalt(III) perchlorates were prepared by electrolytic oxidation from cerium(III) and cobalt(II) perchlorates, respectively. The current was kept constant at *ca.* 100 mA. The concentration of cerium(IV) was estimated by indirect spectrophotometric measurements of iron-(III) formed in the reaction with iron(II) perchlorate, with [$\varepsilon^{Fe(III)}_{260\,nm}=(2.88\pm0.33)\times10^3$].[5] Cobalt(III) was also determined similarly at 260 nm or directly at 605 nm with [$\varepsilon^{Co(III)}_{605\,nm}=35.5\pm1$].[6] The concentrations of cobalt(III) determined by the two spectrophotometric measurements agreed with each other within experimental error.

Cerium(III) perchlorate was prepared from cerium(III) carbonate and perchloric acid. Cobalt(II) perchlorate was prepared by heating cobalt(II) chloride with a slight excess of perchloric acid and made free from chloride by repeated recrystallization.

Commercial Variamine Blue hydrochloride often becomes a faint blue-color by air-oxidation or photochemical reaction. Dilute solution of Variamine Blue, for example, *ca.* 10^{-3} M, was colorless for 1—2 days but gradually turned bluish accompanied by precipitate formation.

Variamine Blue perchlorate was prepared from commercial V.B. hydrochloride.[7] 0.1 g V.B. and 0.04 g sodium dithionite were dissolved in hot water. The solution was shaken with 0.15 g active carbon and filtered. The filtrate was mixed with 5 ml saturated sodium perchlorate solution and cooled for *ca.* 1 hr in a refrigerator. The silky crystalline precipitate was filtered and washed with cold water and dried *in vacuo*. The elemental analyses of a commercial Variamine Blue hydrochloride and the prepared Variamine Blue perchlorate are given in Table 1.

Table 1. Elemental analyses of variamine blue specimens

Specimen		C(%)	H(%)	N(%)	Cl(%)
Commercial V.B. hydrochloride	Found	60.4	5.80	10.93	15.71
	Calcd for $C_{13}H_{15}ON_2Cl$	62.2	6.03	11.17	14.14
Prepared V.B. perchlorate	Found	49.35	4.56	8.70	
	Calcd for $C_{13}H_{15}O_5N_2Cl$	49.61	4.80	8.90	

Kinetics. Yanagimoto SPS-1 stopped-flow apparatus with a 4-jet mixing chamber and a 10 mm optical cell was used for kinetic measurements. The reservoirs of the stopped-flow apparatus were thermostated by circulating water from a thermostat. Purified nitrogen gas was passed through the reservoirs of the solutions in the course of measurements. The changes in absorbance were followed on the storage-screen of an oscilloscope.

The reactions of V.B. with cerium(IV) and cobalt(III) were studied in the hydrogen-ion concentration range 0.2—2.0 M since these ions are very unstable in low acid region. The reactions were followed at 550 nm, the absorption maximum of $(V.B.)_{ox}$, the iminoquinone form of V.B., in the presence of a large excess of metal ions.

1) T. Imamura and M. Fujimoto, This Bulletin, **45**, 438 (1972).
2) T. Imamura and M. Fujimoto, *ibid.*, **45**, 442 (1972).
3) D. A. Johnson and A. G. Sharpe, *J. Chem. Soc.*, **1964**, 3490.
4) Y. Kawai, T. Takahashi, K. Hayashi, T. Imamura, H. Nakayama, and M. Fujimoto, This Bulletin, **45**, 1417 (1972).
5) R. Bastian, R. Weberling, and F. Palilia, *Anal. Chem.*, **28**, 459 (1956); C. F. Wells and G. Davies, *J. Chem. Soc. A*, **1967**, 1858.
6) G. Davies and B. Warnovist, *Coord. Chem. Rev.*, **5**, 349 (1970).
7) L. Erdey, E. Zalay, and E. Bodor, *Acta Chim. Acad. Sci. Hung.*, **12**, 251 (1957).

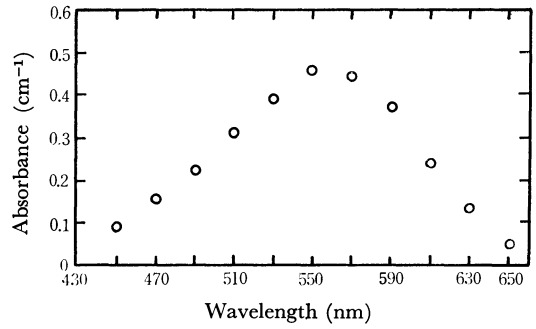

Fig. 1. Absorbance-wavelength plots at equilibrium of the initial fast reaction of V.B. with cobalt(III) measured by stopped-flow technique.
$[Co(III)]_0=2.6\times10^{-3}$M, $[V.B.]_0=2.5\times10^{-5}$M, [H]=0.5M, μ=2.0 and 25 °C.

Results

The rapid initial increase in absorbance at 550 nm was followed by a comparatively slow decrease.[8] Figure 1 shows the absorbance-wavelength plots at the end of the initial increase in absorbance measured by stopped-flow technique. No shift of absorption maximum at 550 nm was observed. The rates of increase in absorbances observed at any wavelengths in the visible range did not differ from each other.

Chloride ions did not affect the rate of increase in absorbance at 550 nm.

As shown in Figs. 2 and 3, the absorbances at 550 nm increase linearly with the initial concentrations of V.B., the half-life of reaction being independent of $[V.B.]_0$ under the experimental conditions. The rate also does not obey the pseudo-first-order rate law even in the presence of a large excess of metal ions as observed in the reaction of V.B. with iron(III).

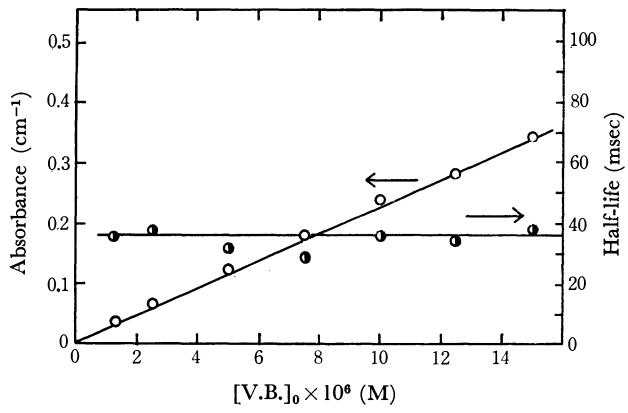

Fig. 2. Absorbance (550 nm) and half-life *vs.* initial concentration of V.B. plots in the reaction with cerium(IV).
$[Ce(IV)]=2.14\times10^{-4}$M, [H]=0.5M, μ=2.0 and 25 °C.

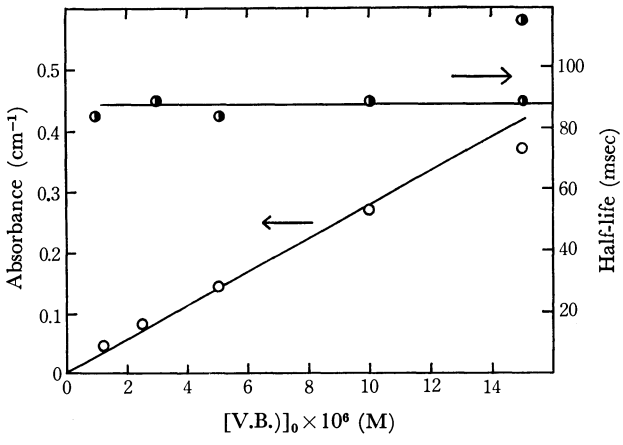

Fig. 3. Absorbance (550 nm) and half-life *vs.* initial concentration of V.B. plots in the reaction with cobalt(III).
$[Co(III)]=1.33\times10^{-3}$M, [H]=1.0M, μ=2.0 and 25 °C.

8) The slow decrease in absorbance suggests a subsequent redox reaction of the iminoquinone form of Variamine Blue with the oxidants, color fading being accelerated by the metal ions.

Discussion

The reactions of V.B. with Ce^{4+} and Co^{3+} are interpreted as a two-step mechanism:

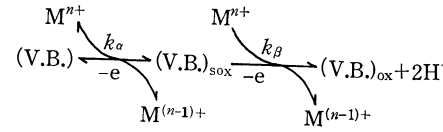

(1)

The values of rate constants for Ce^{4+} are evaluated by the equation in the preceding paper[1] to be $k_\alpha=1.7\times10^5$ and $k_\beta=2.4\times10^5$ $M^{-1}sec^{-1}$ at 25 °C and μ=2.0. The rates were not affected by hydrogen-ion concentrations. This suggests that the reaction proceeds *via* inner-sphere mechanism.

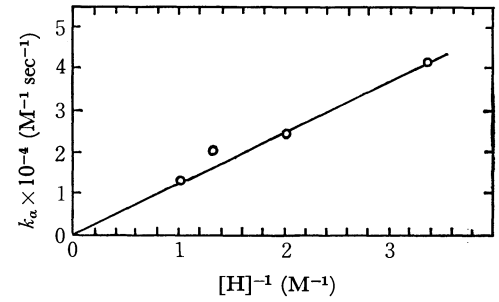

Fig. 4. Rate constant k_α *vs.* $[H]^{-1}$ plots in the reaction of V.B. with cobalt(III).

For the reaction of V.B. with Co^{3+}, the values of k_α and k_β are calculated to be 1.35×10^4 and 1.53×10^4 $M^{-1}sec^{-1}$, respectively, at 25 °C, μ=2.0 and [H]=1.0. The rate constants k_α and k_β are inversely proportional to hydrogen-ion concentration (Fig. 4). The observed second-order rate constants at each step suggest the expression to be

$$k_{obs} = k_1 + k_2K_h/[H], \quad (2)$$

corresponding to the reactions[9]

$$Co_{aq}^{3+} + B \overset{k_1}{\rightleftharpoons} \text{product} \quad (3)$$

9) The reactions can proceed *via* either path of the two indistinguishable reactions;

$CoOH^{2+}$ + protonated V.B. → product (6)

or

Co^{3+} + unprotonated V.B. → product. (7)

However, in the high acidity range the protonated form of Variamine Blue seems to be predominant.

$$CoOH_{aq}^{2+} + B \overset{k_2}{\rightleftharpoons} \text{product} \quad (4)$$

$$Co_{aq}^{3+} \overset{K_h}{\rightleftharpoons} CoOH_{aq}^{2+} + H^+ \quad (5)$$

where B is the species of Variamine Blue in the reaction. The type of rate law is common to many reactions of Co^{3+}. It should be noted that (2) is a special case of the general rate law

$$k_{obs} = (k_1 + k_2K_h/[H])/(1 + K_h/[H]) \quad (8)$$

for $K_h \ll [H]$ as fulfilled under experimental conditions. From the slope of k_α *vs.* $[H]^{-1}$-plot in Fig. 4, the value of k_2 was estimated to be in the order of magnitude of $10^7\ M^{-1}\,sec^{-1}$ using the value $K_h = (2 \pm 1) \times 10^{-3}$ M.[10] The rapid reaction of cobalt(III) with V.B. is most likely to be of an outer-sphere mechanism as in the reactions of Co^{3+} with hydroquinone or iodide.[6] The concentrations of $(V.B.)_{ox}$ calculated from the values of k_α and k_β are plotted as a function of time in Figs. 5 and 6. The concentrations agree with the ones observed in the course of reaction.

Increase in absorbance at 550 nm in the reactions

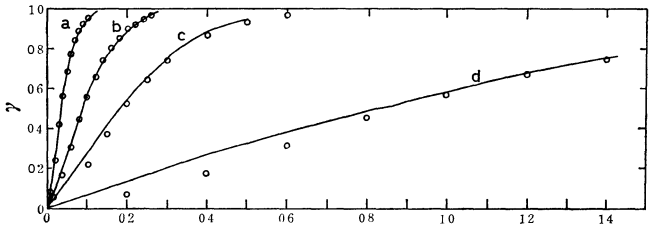

Fig. 5. Calculated concentration of $(V.B.)_{ox}$ in the reaction with cerium(IV). Solid lines show the observed concentration of $(V.B.)_{ox}$.
○ indicates the concentration of $(V.B.)_{ox}$ calculated with the values $k_\alpha = 1.69 \times 10^5$ and $k_\beta = 2.36 \times 10^5\ M^{-1}sec^{-1}$. $[V.B.]_0 = 5.0 \times 10^{-6}$ M, $[H] = 0.5$ M, 25 °C and (a) $[Ce(IV)]_0 = 8.54 \times 10^{-4}$, (b) 4.27×10^{-4}, (c) 2.14×10^{-4}, and (d) 8.54×10^{-5} M. $\gamma = [(V.B.)_{ox}]/[(V.B.)]_0$.

10) D. R. Rosseinsky, *Nature*, **216**, 791 (1967).

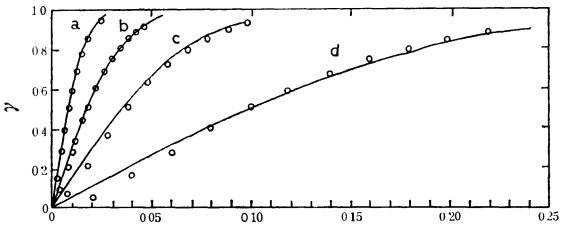

Fig. 6. Calculated concentration of $(V.B.)_{ox}$ in the reaction with cobalt(III). Solid lines show the observed concentration of $(V.B.)_{ox}$.
○ indicates the concentration of $(V.B.)_{ox}$ calculated with the values $k_\alpha = 1.35 \times 10^4$ and $k_\beta = 1.53 \times 10^4\ M^{-1}sec^{-1}$. $[V.B.]_0 = 5.0 \times 10^{-6}$ M, $[H] = 1.0$ M, 25 °C and (a) $[Co(III)]_0 = 2.78 \times 10^{-3}$, (b) 1.11×10^{-3}, (c) 5.05×10^{-4}, and (d) 1.11×10^{-4} M. $\gamma = [(V.B.)_{ox}]/[(V.B.)]_0$.

with cerium(IV) and cobalt(III) was about 15—20% larger than that measured in the reaction of commercial Variamine Blue with iron(III). The difference in absorbance exceeds the experimental error ±10%.

The fact that the absorbance at 600—650 nm increases in the reaction of V.B. with iron(III)[11] in low concentrations suggests the possibility of the presence of some polymeric species of V.B.[12] which is rather stable against iron(III). The extra increase in absorbance at 550 nm observed in the reaction with cerium(IV) and cobalt(III) would be ascribed to a further reaction of these polymeric forms or to some subreactions of V.B. with the metal ions owing to their very high redox potentials.

The present work was supported in part by a grant-in-aid for Scientific Research from the Ministry of Education.

11) T. Imamura, Dissertation, Hokkaido University, 1972, p. 28.
12) L. Erdey, I. Bauzas, and K. Vigh, *Talanta*, **1**, 377 (1958); L. Erdey, T. Meisel, B. Mohos, and F. Tudos, *ibid.*, **14**, 1477 (1964).

Isotopic Exchange Kinetics between Dibenzoylmethane-^{14}C and Its Tris-type Complex with Aluminium(III) in Tetrahydrofuran

Kazuyo MATSUZAWA (née MASUDA) and Kazuo SAITO

Department of Chemistry, Faculty of Science, Tohoku University, Aoba, Aramaki, Sendai 980

(Received May 2, 1973)

Isotopic exchange kinetics between [Al(dbm)$_3$] and Hdbm-^{14}C (dbm$^-$, anion of dibenzoylmethane in enol form) has been studied in tetrahydrofuran (THF) at 30 to 55 °C. During several half lives the McKay plot gives straight lines, the AB spectrum remaining unchanged. The rate is very small in the absence of catalysts, and accelerated by water and trichloroacetic acid, but not by weak acids and pyridine. The rate is expressed by

$$R = [\text{complex}](k_2[H_2O] + k_3'[\text{acid}] + k_3[\text{acid}][H_2O])$$

The Arrhenius plots of k_2, k_3', and k_3 give an equal $\Delta H^{\neq}$ value 25.6 kcal/mol. It appears one of the ligands is present as unidentate in the intermediate state, and the break of the remaining bond is the rate-determining step.

As an extension of our previous kinetic studies of isotopic exchange between acetylacetone-^{14}C (Hacac) and trisacetylacetonatoaluminium(III) ([Al(acac)$_3$]),[1] we have examined the isotopic exchange kinetics between the corresponding dibenzoylmethane (Hdbm) complex, in order to find the influence of a more basic ligand upon the kinetic formula and rate. Because of the smaller solubility of [Al(dbm)$_3$] in various organic solvents, the rate was precisely studied only in tetrahydrofuran (THF).

Experimental

Materials. *The Labelled Ligand*: Acetic acid-^{14}C imported from Radiochemical Centre, Ammersham, England, was converted into acetophenone in benzene by the Friedel-Crafts reaction, and treated with ethyl benzoate (Claisen condensation) to give Hdbm. The product with a specific activity *ca.* 10 μCi per mg was diluted with commercial Hdbm before use to obtain samples with a specific activity *ca.* 0.5 μCi per mg.

The Complex: Dibenzoylmethane (5 g) in ethanol (25 ml) was treated with aluminium chloride hexahydrate (1.5 g) in water (5 ml) and sodium acetate (3 g) in water (5 ml) to give crude [Al(dbm)$_3$] (4 g). The product was dissolved in THF (50 ml) and precipitated with a large amount of petroleum ether. The purity of these products were confirmed by elemental analysis and UV spectroscopy. Trichloroacetic acid and THF were purified as mentioned before.[1]

Kinetic Runs. The complex in THF (0.01 to 0.1 M) was mixed with Hdbm in THF (0.01 to 0.3 M) in a thermostat (total volume 10 to 15 ml) and portions (1 to 2 ml) were withdrawn into chilled petroleum ether (*ca.* 15 ml) at appropriate intervals. The complex was precipitated instantaneously in fine crystals, which were filtered off with a piece of filter paper and dried at 80 °C. A known amount of the precipitate (3 to 10 mg) was dissolved in anisole containing *p*-terphenyl and POPOP as wave length shifters and submitted to scintillation counting. The results were calculated by McKay's formula to obtain R values under various conditions.

Measurements. The counting rate was measured with an automatic apparatus from Nuclear Chicago. The AB spectra were recorded with a Hitachi 124 Double Beam Spectrometer. Karl Fischer titration was employed for the determination of water.

1) K. Saito and K. Masuda, This Bulletin, **43**, 119 (1970).

Results

The influence of the complex concentration upon R was examined as in Ref. 1, and a similar diagram to Fig. 1 of Ref. 1 was obtained. The influence of water content is shown in Fig. 1 at 30, 40, and 50 °C. The straight lines pass the origin, so that the k_0 values are expressed by

$$R = k_0[\text{complex}] = k_2[\text{complex}][H_2O] \quad (1)$$

Trichloroacetic acid catalyses the exchange reaction. The extent depends on the concentration of water at a given concentration of acid. Figure 2 shows that the lines have intercepts. When the concentration of trichloroacetic acid was increased at a given concentration of water, the k_0 values increase linearly in a low acid concentration range and then the gradient decreases as the acid concentration increases. (Fig. 3) Hence the overall formula is written for low acid concentration region as Eq. (2).

$$R = [\text{complex}](k_2[H_2O] + k_3'[\text{acid}] + k_3[\text{acid}][H_2O]) \quad (2)$$

The k_3 and the k_3' values are known from the gradients

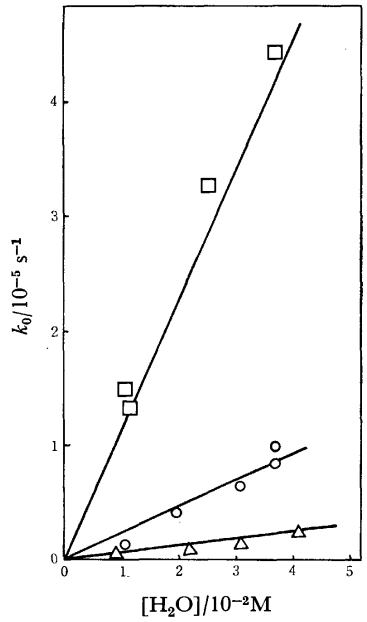

Fig. 1. Influence of water concentration at various temperatures.
(—△— 30 °C, —○— 40 °C, —□— 50 °C, [Hdbm] = 0.050 M)

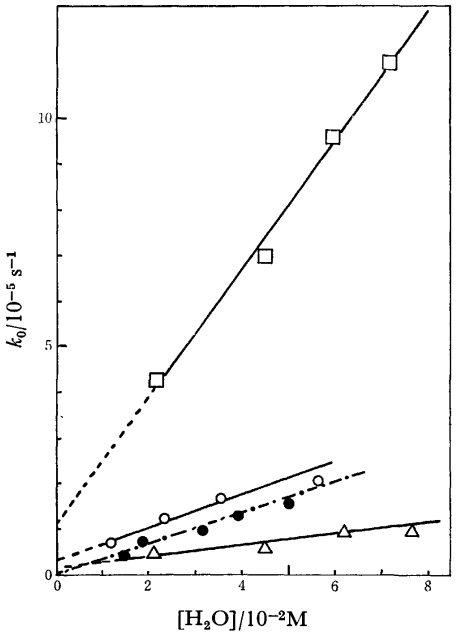

Fig. 2. Influence of water concentration in the presence of trichloroacetic acid at various temperatures.
(—△— 30 °C, —○— and —●— 40 °C, —□— 50 °C; open marks [acid]=0.0286 M, full marks [acid]=0.0021 M; [Hdbm]=0.050 M)

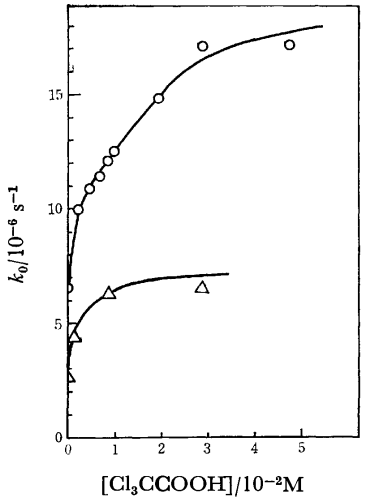

Fig. 3. Influence of concentration of trichloroacetic acid in the presence of known amounts of water.
(—△— 30 °C, [H$_2$O]=0.046 M; —○— 40 °C, [H$_2$O]=0.035 M; [Hdbm]=0.050 M)

and the intercepts of Fig. 2, respectively. Weaker acids such as *m*-toluic do not give acid catalysis. Pyridine has no influence on the exchange rate.

There is a very slight influence of the concentration of Hdbm upon the rate at given water concentrations, as shown in Fig. 4, in which $k_0/[H_2O]$ is plotted against [Hdbm]. The change in $k_0/[H_2O]$ is very small unless a large amount of Hdbm is added. The values of k's in Table 1 are those at [Hdbm]=0.05 M, and are very near to the intercepts of diagrams in Fig. 4.

Arrhenius plots of k_2, k_3', and k_3 at 30, 40, 50, and 55 °C gave parallel lines and the activation enthalpies were known to be 25.6±0.2 kcal/mol for all the terms. The k_0 values were converted into those at 25 °C and

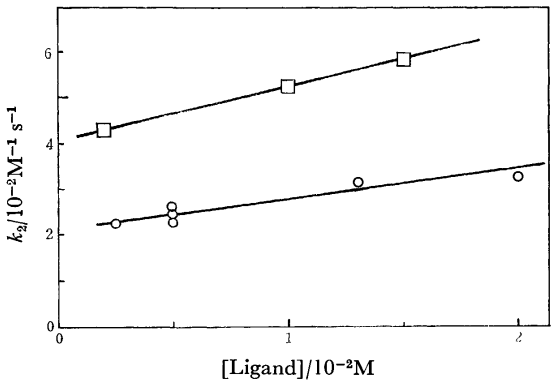

Fig. 4. Influence of concentration of free ligand.
(—○— 40 °C, [H$_2$O]=0.010 M; —□— 50 °C, [H$_2$O]=0.018 M)

TABLE 1. RATE CONSTANTS AND ACTIVATION PARAMETERS FOR THE ISOTOPIC EXCHANGE OF [Al(acac)$_3$] AND [Al(dbm)$_3$]
(in THF, k's converted into those at 25 °C)

	[Al(acac)$_3$]	[Al(dbm)$_3$]
k_1/s^{-1}	1.0×10^{-6}	≃0
k_2/M^{-1}s^{-1}	3.3×10^{-4}	3.2×10^{-5}
k_3'/M^{-1}s^{-1}	1.6×10^{-4} a)	2.0×10^{-5}
k_3/M^{-2}s^{-1}	2.0×10^{-2} b)	9.1×10^{-4} c)
$\Delta H^{\neq}$/kcal·mol^{-1} d)	21.4	25.6
$\Delta S^{\neq}$/cal·K^{-1}mol^{-1} e)	−7.8	−1.8

a) k_1' in Ref. 1 b) k_2' in Ref. 1. c) at [Cl$_3$CCOOH]=0.0286 M. d) equal for all the reaction paths e) for k_0 at [H$_2$O]=0.015 M in the absence of acid.

the k's tabulated in Table 1 together with those for the exchange reaction between [Al(acac)$_3$] and Hacac-^{14}C.[1]

Discussion

Since the absorption spectrum does not change during kinetic runs and McKay plots give straight lines, it is clear that the isotopic exchange takes place without involving net chemical change. It is remarkable that the exchange is very slow in the absence of water and acid. Except this the rate formula is very similar to that for [Al(acac)$_3$], although the figures are smaller by *ca.* one order than those for [Al(acac)$_3$]. Another marked feature for the present case is that the $\Delta H^{\neq}$ values are the same for all the reaction paths within experimental error. This fact is again very similar to that for [Al(acac)$_3$], although the value itself is bigger than that for [Al(dbm)$_3$].

We consider that the rate-determining step for the three reaction paths are equal. Fig. 5 gives the plausible reaction mechanism. Although the observed k values for each-term in Eq. (2) consist of more than one constant as seen in Fig. 5, the biggest and the most remarkable contribution should come from the k's at the rate-determining step. The equality of observed $\Delta H^{\neq}$ values can be ascribed to the equality of activation enthalpies for the k's. The capital K's indicate equilibrium constants for the given stages, and small k's rate constants at the rate-determining steps. The complex must be in rapid equilibrium with an intermediate

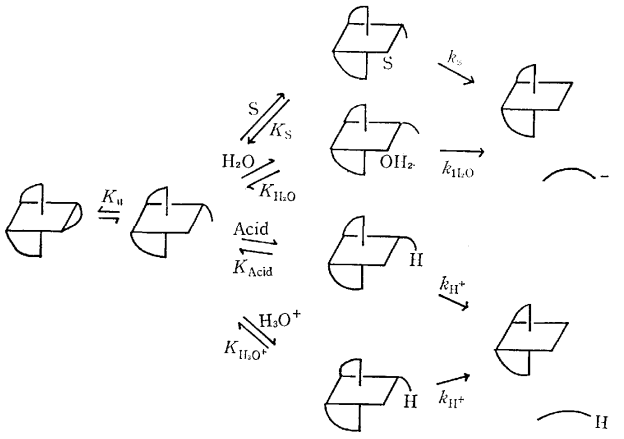

Fig. 5. Probable reaction mechanism.
(arc-like curves represent dbm$^-$; S, solvent molecule)

form, which has one of the ligands as unidentate. The break of its remaining bond is reckoned as the rate-determining step.

The catalytic action of water will be accounted for by considering that it occupies the vacant coordination site to retard the recombination of the free end of unidentate ligand. Hence k_2 is written as Eq. (3).

$$k_2 = k_{H_2O}K_uK_{H_2O} \quad (3)$$

The k_3' and the k_3 path seem to represent acid catalysis with different proton carriers. In the k_3' path, the acid itself will act as proton carrier and the following equation holds.

$$k_3' = k_{H^+}K_uK_{acid} \quad (4)$$

Addition of proton on the free end of unidentate ligand will make its recombination more difficult and increase the probability of break of the remaining bond. In the k_3 path, proton will be transferred to water according to Eq. (5) and k_3 is expressed by Eq. (6).

$$Cl_3CCOOH + H_2O \overset{K_{hdx}}{\rightleftharpoons} H_3O^+ + Cl_3CCOO^- \quad (5)$$

$$k_3 = k_{H^+}K_uK_{H_3O^+}[H_3O^+] \quad (6)$$

A characteristic feature in the present study is that the influence of acid concentration tends to show saturation. (Fig. 3) This trend is interpreted in two ways. If Eq. (5) reaches saturation in the given concentration range, further increase in acid concentration will not increase the $[H_3O^+]$. On the other hand, if all the free end of unidentate ligand were protonated, *i.e.* equilibrium $K_{H_3O^+}$ reaches saturation, further increase in $[H_3O^+]$ would not affect the rate.

Whenever HX is a weak acid, the H_3O^+ concentration is expressed by $(K_{hdx}[acid][H_2O])^{1/2}$ from Eq. (5). If so, square root of the acid concentration should have to be plotted on the abcissa in Fig. 2. Although K_{hdx} of trichloroacetic acid is not known in THF, it is a strong acid in water with a pK_a value 0.635 at 25 °C. When the acid is extremely strong, $[H_3O^+]$ is equal to acid concentration in the presence of excess of water, and equal to water concentration in the presence of excessive acid. Figure 3 gives straight lines when the acid concentration is small as compared with water concentration, and the curves approach saturated values with increase in acid concentration. Such a saturation is observed, however, before the acid concentration overwhelms the water concentration, and fails to be seen in Fig. 2. Thus we tend to consider that the saturation may be due to saturation of $K_{H_3O^+}$. Trisacetylacetonatoaluminium(III) did not exhibit such a saturation presumably owing to the smaller $K_{H_3O^+}$ value. The fact that ordinary organic acids fail to give acid catalysis is presumably because their K_{acid} and K_{hdx} values are not big enough to bring about effective protonation upon the free end.

As seen in Eqs. (3), (4), and (6), k_2, k_3', and k_3 involve various factors. The pK_a values of Hacac and Hdbm are not known in THF, but they are *ca.* 11 and 13 respectively at 25 °C in water. The smaller k's for $[Al(dbm)_3]$ than for $[Al(acac)_3]$ are understood by considering that the stronger Lewis base dbm$^-$ gives much smaller k_{H_2O} and k_{H^+} values than acac$^-$ does, and the bigger K_{acid} and $K_{H_3O^+}$ values are overwhelmed. The greater ΔH^* of $[Al(dbm)_3]$ than $[Al(acac)_3]$ is also thus accounted for. Absence of k_1 path for $[Al(dbm)_3]$ is similarly interpreted, too. Further, the effective charge of aluminium ions in $[Al(dbm)_3]$ will be smaller owing to the coordination of more basic dbm$^-$ and the equilibrium constant K_S (coordination of solvent molecule on the vacant site) would be smaller.

Another characteristics in the present kinetic study is that increase in the concentration of ligand increases the exchange rate, although the extent is very small. Such an influence was also seen in the exchange between $[Co(acac)_3]$ and Hacac-^{14}C in toluene and anisole.[2] If Hdbm attacks the vacant coordination site of the intermediate as rate-determining step, increase in Hdbm concentration will increase the rate of exchange. However, the gradients of lines in Fig. 4 are very small, and the contribution of ligand concentration is appreciable only at a high concentration range. The k_2 values at the ligand concentration 0.05 M are very near to that at null ligand concentration, and was not included in the main kinetic formula. If Hdbm behaved as an acid and gave proton to the free end of the unidentate ligand in the intermediate, a similar kinetic result would be obtained. This is not probable, however, because a stronger acid, *m*-toluic acid, does not exhibit acid catalysis. Further, $[Al(acac)_3]$ failed to show such a tendency. If acid catalysis were operating, a stronger acid, Hacac, should give a bigger influence on a more labile $[Al(acac)_3]$. Hence the effect in Fig. 4 should be due to the nucleophilic attack of Hdbm upon the complex, probably in the intermediate state. The basicity of Hdbm must be bigger than Hacac even in the protonated state.

Thus all the differences in kinetics between $[Al(dbm)_3]$ and $[Al(acac)_3]$ are understood by taking the difference in basicity of the ligands into account. Our present results seem to support and reinforce the reaction mechanism postulated in Ref. 1, that the complex is in rapid equilibrium with an intermediate with one of the ligands as unidentate and break of the remaining Al–O bond is the rate-determining step.

We thank Nishina Memorial Foundation for financial support.

2) K. Saito and M. Murakami, This Bulletin., **45**, 2472 (1972).

Catalysis of Manganese Salts in the Autoxidation of Cyclohexanone

Yoshio KAMIYA and Masayoshi KOTAKE

Department of Reaction Chemistry, Faculty of Engineering, University of Tokyo, Hongo, Tokyo 113

(Received May 25, 1973)

The rate of oxidation of cyclohexanone catalyzed by manganese salt increases remarkably in the presence of acetic acid, and is about one hundred times as high as the limiting rate of oxidation $k_p^2(RH)^2/2k_t$. However, manganese concentration does not affect the rate of oxidation much in a wide range. The oxidation of cyclohexanone by manganic ion should be the rate determining step, since the rate of oxidation, which is of first order in cyclohexanone but independent of manganous ion, corresponds to the rate of oxygen absorption of cyclohexanone with the same manganese concentration. The oxidation of cyclohexanone by manganic ion seems to proceed through enol intermediates, since the rate of oxidation increases in the presence of alkali acetates. The rate equation including enolization step and the subsequent oxidation of enol intermediate with manganic ion agrees with the experimental results. A remarkable synergistic effect of metal salts was observed in a mixture of manganese and cobalt. The oxidation products were also analyzed and discussed.

Although the autoxidation of cyclohexanone is an important process for the production of adipic acid and has been studied by many workers,[1] the role of metal catalysts in the autoxidation reaction is still not clear. The oxidation of cyclohexanone by metal ions was studied by Rocek and Riehl,[2] Best *et al.*[3] and Littler.[4,5] It was found that oxidation by V(V), Co(III), Ce(IV), and Mn(III) proceeds through direct oxidation, but that by Hg(II), Mn(VII), Tl(III), and Br_2 through enol intermediate.

The metal-catalyzed autoxidation of cyclohexanone shows a complicated behavior. (1) The rate of oxidation in an acidic solvent is much higher than that in a neutral one. (2) Although manganese salt is not so effective catalyst in acetic acid solution as cobalt salt, it shows the highest catalytic activity in the oxidation of cyclohexanone. (3) When a metal catalyst is used as a decomposer of hydroperoxide, the rate of oxidation of hydrocarbons does not exceed the limiting rate $k_p^2(RH)^2/2k_t$,[6] but that of cyclohexanone catalyzed by cobalt and manganese in acetic acid far exceeds the value of $k_p^2(RH)^2/2k_t$, where k_p and k_t represent the propagation and termination rate constants, respectively.

In a previous paper,[7] it was shown that the rate-determining step of the cobalt-catalyzed autoxidation of cyclohexanone in acetic acid is the oxidation of cyclohexanone by cobaltic ion. We have studied the effect of manganese catalyst on the autoxidation of cyclohexanone, since catalysis by manganese salt greatly differs from that by cobalt salt.

Experimental

Cyclohexanone was fractionally distilled and kept in a brown glass bottle and in nitrogen atmosphere. Acetic acid was distilled in the presence of potassium permanganate and acetic anhydride.

Manganic Acetate.[8] A mixture of manganous acetate (303 g) and glacial acetic acid (4.4 kg) was boiled under reflux for 2 hr. Potassium permanganate (68.2 g) was then added, the mixture being stirred under reflux for 45 min and then allowed to cool while water (750 ml) was added dropwise. The crude $Mn(OAc)_3 \cdot 2H_2O$ was recrystallized from a mixture of glacial acetic acid and water.

Oxidation of Cyclohexanone by Manganic Acetate in Nitrogen Atmosphere. The reaction vessel, a *ca.* 60 ml flask with two necks, one at the top and the other at the side of the flask, was connected through a tygon tube to a vacuum line and a nitrogen reservoir. The solution was frozen with a dry ice-acetone solution and degassed repeatedly in the usual way, and the vessel was filled with nitrogen. After thermal equilibrium had been obtained, samples were withdrawn through the side neck at appropriate intervals under current of nitrogen. The volume of each sample was 5 ml. Determination of manganic acetate was carried out by potentiometric titration using ceric sulfate after adding an excess amount of ferrous ammonium sulfate.

Determination of Reaction Products. Cyclohexanone was oxidized under vigorous agitation in a three necked flask with oxygen inlet and outlet, and the oxidation products were analyzed by gas chromatography with a 3 m column of diethyleneglycol adipate after esterification with diazomethane. After cooling of outlet gas, carbon dioxide was absorbed by passing through an aqueous solution of sodium hydroxide and titrated.

The oxygen absorption apparatus has been described elsewhere.[6]

Results and Discussion

Rate of Oxidation of Cyclohexanone. The steady rate of oxidation of neat cyclohexanone catalyzed by manganese decanoate as a function of catalyst concentration is given in Fig. 1. The rate of oxidation is of the order 0.7—0.8 with respect to manganese concentration and exceeds a little the limiting rate of

1) a) Fr. P. 1243571, Brit. P. 941662, Australian P. 61570. b) H. Masuda, K. Kobayashi, and N. Ohta, *Kogyo Kagaku Zasshi*, c) M. Ogawa, *ibid.*, **71**, 147 (1968). d) M. Ogawa, M. Kusunoki, and N. Kitabatake, *ibid.*, **70**, 1670 (1967).

2) J. A. Rocek and Sr. A. Riehl, *J. Org. Chem.*, **32**, 3569 (1967).

3) P. A. Best, J. S. Littler, and W. A. Waters, *J. Chem. Soc*, **1962**, 822.

4) J. S. Littler, *ibid.*, **1962**, 827.

5) J. S. Littler, *ibid.*, **1962**, 822.

6) a) Y. Kamiya, S. Beaton, F. A. Lafortune, and K. U. Ingold, *Can. J. Chem.*, **41**, 2020 (1963). b) Y. Kamiya, S. Beaton, F. A. Lafortune, and K. U. Ingold, *ibid.*, **41**, 2034 (1963). c) Y. Kamiya and K. U. Ingold, *ibid.*, **42**, 1027 (1964).

7) Y. Kamiya, *Kogyo Kagaku Zasshi*,**74**, 1811 (1971).

8) R. J. Andrulis, M. J. S. Dewar, D. R. Dietz, and R. L. Hunt, *J. Amer. Chem. Soc.*, **88**, 5473 (1966).

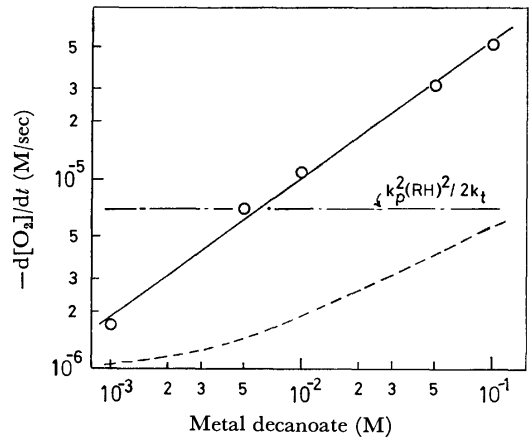

Fig. 1. The rate of oxidation of cyclohexanone as a function of manganese decanoate concentration at 60 °C. A broken line represents the rate of oxidation with cobalt decanoate

oxidation $k_p^2(RH)^2/2k_t$ 7×10^{-6} M/sec calculated from azobisisobutyronitrile initiated autoxidation of cyclohexanone. This shows that manganese decanoate is more effective than cobalt decanoate as an oxidation catalyst of neat cyclohexanone.

When manganese acetate was used as a catalyst in acetic acid solution, the rate of oxidation of cyclohexanone became extremely high. For example, it was 4×10^{-4} M/sec at manganese concentration of 0.02 M and 60 °C, and almost independent of catalyst concentration in contrast to the half order relation of cobalt acetate[7] (Fig. 2). A sudden decrease in the rate at manganese concentrations below 5×10^{-4} M suggests a change of the rate determining step and also a slow regeneration of manganic ion by the oxidation of manganous ion due to the peroxidic intermediates as peracids.

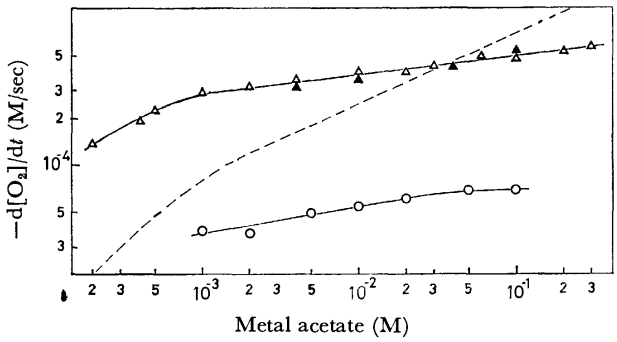

Fig. 2. The rate of oxidation of a 1: 1 mixture by volume of cyclohexanone and acetic acid as a function of metal acetate concentration.
△: manganous acetate at 60 °C, ▲: manganic acetate at 60 °C, ○: manganous acetate at 40 °C.
A broken line represents the rate of oxidation with cobalt acetate.

The rate of oxidation reached a steady state within a few minutes, the solution turning dark brown due to manganic ion. A portion of the solution in the steady state of oxidation was taken out and titrated potentiometrically to determine the concentration of manganic ion. Approximately 90% of the manganese ions was found to be manganic in the manganese concentration range 0.01—0.05 M.

The rate of oxidation catalyzed by pure manganic acetate is also shown in Fig. 2. There seems to be no difference between the catalysis by manganous and manganic acetates. This indicates that manganese ions rapidly reach a steady concentration in course of oxidation at manganese concentrations above 0.005 M.

The decomposition rate of hydroperoxide by manganese salt[6c] in acetic acid is usually slow as compared with that by cobalt. This corresponds to the fact that the rate of oxidation of tetralin,[5c] ethylbenzene,[9] and cumene[10] catalyzed by manganese acetate in acetic acid is much smaller than that catalyzed by cobalt acetate. In contrast, the decomposition of hydroperoxide by manganese salt does not seem to affect the rate of oxidation of cyclohexanone, since the actual rate of oxidation by manganese salt represents a similar value to that by cobalt salt, far exceeding the limiting rate.

The fact that the rate of oxidation exceeds the limiting rate of oxidation $k_p^2(RH)^2/2k_t$ by a factor of 100 indicates that the ordinary hydrogen abstraction step by peroxy radical plays only a minor role as explained by Walling,[11] since the chain length is nearly unity under the limiting rate conditions. If the rate of autoxidation $k_p(RH)(RO_2\cdot)$ increases one hundred times as fast as the limiting rate, the termination reaction should increase by a factor of ten thousands, and the oxidation should stop undoubtedly.

The important step of manganese-catalyzed autoxidation of cyclohexanone should be the oxidation of cyclohexanone due to manganic ion as in the case of cobalt acetate. However, the reaction mechanism by manganese catalyst seems to differ greatly from that by cobalt salt, since the rate of oxidation is almost independent of manganese concentration in a wide range of concentration above 0.001 M.

The rate of oxidation of cyclohexanone with manganese acetate was enhanced from 4.1×10^{-4} M/sec to 1.15×10^{-3}, 9.9×10^{-4}, and 8.2×10^{-4} M/sec in the presence of 0.5 M of lithium acetate, sodium acetate and potassium acetate, respectively. This effect seems to result from the enhancement of enolization rate of cyclohexanone. Lienhard and Wang[12] reported that sodium acetate and sodium pivalate increased the rate of enolization of cyclohexanone as acid and base. The effect of alkali acetate strongly supports the view that enol intermediate is involved in the rate-determining step of the oxidation of cyclohexanone catalyzed by manganese.

Oxidation of Cyclohexanone by Manganic Acetate in Nitrogen Atmosphere. Since the manganese ion in acetic acid solution during the course of oxidation is mostly manganic and radical formation by the manganese-catalyzed decomposition of hydroperoxide is not considered to be of significance, the oxidation of cyclohexanone by manganic ion seems to play an important role. The rate of Mn(III) reduction with Mn(III) of

9) Y. Kamiya, *Kogyo Kagaku Zasshi*, **69**, 897 (1966).
10) Y. Kamiya, This Bulletin, **43**, 830 (1970).
11) C. Walling, *J. Am. Chem. Soc.*, **91**, 7590 (1969).
12) G. E. Lienhard and T. C. Wang, *ibid.*, **91**, 1146 (1969).

9×10^{-3} M and cyclohexanone of 4.83 M in acetic acid at 40 °C in the absence of oxygen was 5.2×10^{-5} M/sec, which agrees with the value of 5.4×10^{-5} M/sec, the rate of oxygen absorption of cyclohexanone with manganese acetate 0.01 M at 40 °C. Agreement of the two rates strongly support the view that the rate-determining step is the oxidation of cyclohexanone by Mn(III), since the molar ratio of oxygen molecule absorbed by oxidized cyclohexanone should be 1.0—1.5 according to oxidation products.

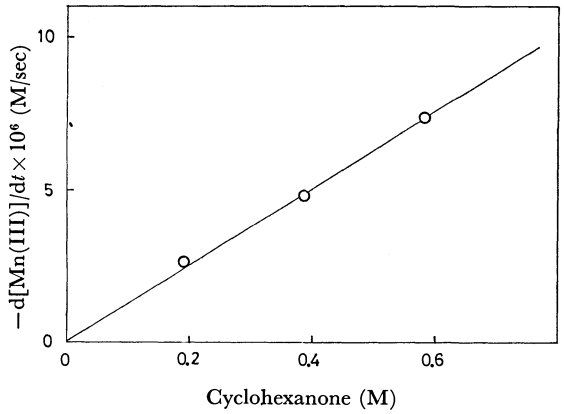

Fig. 3. The rate of reduction of manganic acetate with cyclohexanone as a function of cyclohexanone concentration in acetic acid at 40 °C. Initial manganic acetate 0.0285 M.

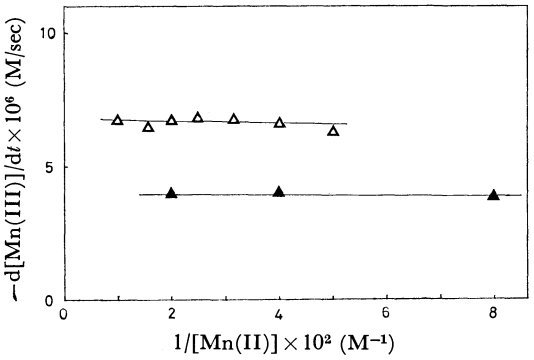

Fig. 4. The rate of reduction of manganic acetate with cyclohexanone as a function of manganous acetate in acetic acid at 40 °C.
Cyclohexanone 0.545 M, △: Mn(III) 0.02 M, ▲: Mn(III) 0.005 M.

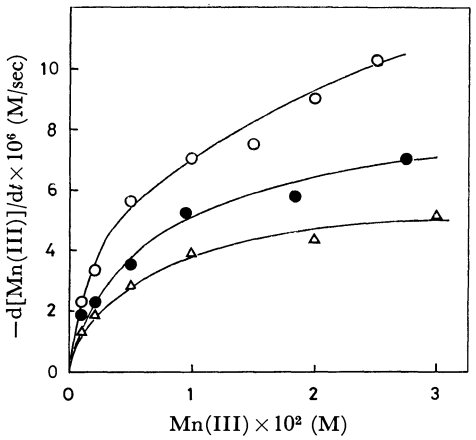

Fig. 5. The rate of reduction of manganic acetate with cyclohexanone as a function of manganic acetate concentration in acetic acid at 40 °C.
Cyclohexanone: ○ : 0.771 M, ● : 0.545 M, △ : 0.370 M.

Oxidation of cyclohexanone with manganic acetate under nitrogen atmosphere was studied under various conditions (Figs. 3, 4, and 5). The rate of reduction of Mn(III) was of first order with respect to cyclohexanone (Fig. 3) and independent of manganous ion (Fig. 4) in contrast to the case of cobalt salt.[7] The reduction of Mn(III) increased slowly with the increase of its concentration (Fig. 5).

There are several reasons for the rate determining step in the manganese-catalyzed autoxidation of cyclohexanone being the enolization of cyclohexanone and not the electron transfer step.

Den Hartog and Kooyman[13] confirmed that the enolization step of acetophenone was rate determining in the manganese-catalyzed autoxidation of acetophenone. There was no significant difference between the rates of oxidation of cyclohexanone by cobaltic and manganic acetates at 0.01 M, although the rate of oxidation of toluene by cobaltic acetate[14] was much higher than the rate by manganic acetate.[8] The rate of oxidation of cyclohexanone by manganic acetate was independent of manganous ion concentration and increased in the presence of alkali acetates.

When the oxidation of cyclohexanone by Mn(III) proceeds through enol intermediates, the reaction scheme and the rate of equation can be expressed as follows.

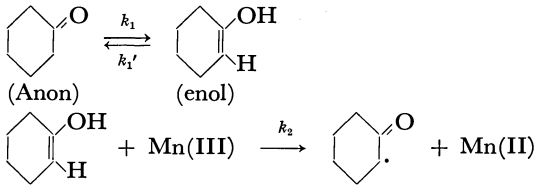

$$-d[Mn(III)]/dt = k_1k_2[Mn(III)][Anon]/(k_1' + k_2[Mn(III)]) \quad (5)$$

$$[Anon]/(-d[Mn(III)]/dt) = (1/k_1) + k_1'/k_1k_2[Mn(III)] \quad (6)$$

A plot of $[Anon]/(-d[Mn(III)]/dt)$ against $1/[Mn(III)]$ should give a straight line with an intercept equal to $1/k_1$ and a slope of k_1'/k_1k_2. The results

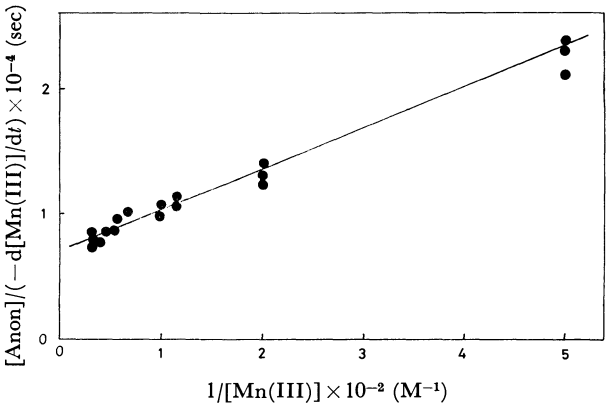

Fig. 6. [Anon]/(−d[Mn(III)]/dt) versus 1/[Mn(III)].

13) H. J. Den Hartog, E. C. Kooyman, *J. Catal.* **6**, 347 (1966).
14) K.Sakota, Y. Kamiya, and N. Ohta, *Can. J. Chem.*, **47**, 387 (1969).

obtained in several cyclohexanone-acetic acid mixtures are plotted in this manner in Fig. 6. A straight line through the experimental points is consistent with an intercept of 7×10^4 sec as required for the value of $1/k_1$. Scattering of points might be mainly due to experimental error, with possible effects of other reactions.

The satisfactory linear correlation in Fig. 6 supports the enolization mechanism.

Comparison of the Rate of Oxygen Absorption and the Rate of Reduction of Mn(III). From the value of k_1 (1.43×10^{-5} sec^{-1}), the limiting rate of Mn(III) reduction at 4.83 M cyclohexanone and 40 °C was calculated to be 6.9×10^{-5} M/sec.

The measured rate of oxygen absorption at 40 °C did not exceed the value of 6.8×10^{-5} M/sec (Fig. 2). Thus, the maximum rate of oxygen absorption can be predicted by Eq. (5). There is no significant difference between the rate of reduction of Mn(III) and that of oxygen absorption at manganese concentrations above 5×10^{-3} M, provided that the ratio of manganic to total manganese ions is kept 0.9 and the molar ratio of absorbed oxygen to reacted cyclohexanone 1—1.5.

The ratio of the rate of oxygen absorption to the rate of reduction of Mn(III) increases with decreasing manganese concentration and reaches 1.8 at 10^{-3} M manganese. This may be partly due to the participation of acylperoxy radical in the propagation step and also to a trace of oxygen remaining in the solution, since the regeneration of Mn(III) from the reaction of Mn(II) and peroxidic compounds would be affected even in the presence of 10^{-4} M of oxygen at manganese concentrations as low as 10^{-3} M.

Synergistic Effect of Metal Acetates. For the case in which one component is manganese acetate and the other a transition metal such as cobalt, the rate of oxidation was studied as a function of composition. A remarkable synergistic effect was observed in the mixture of manganese and cobalt as shown in Fig. 7. When the metal concentration is as low as 10^{-5} M, the synergistic effect was found to be more remarkable, since the rate of autoxidation by single component falls to values less than 10^{-5} M/sec.

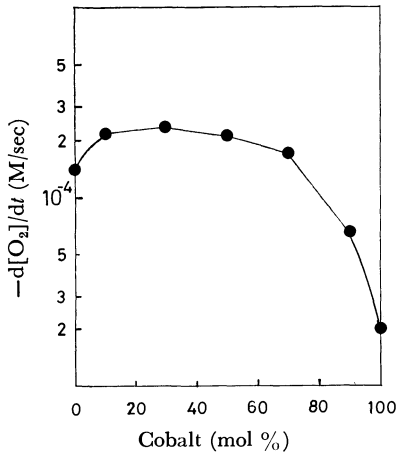

Fig. 7. The mixing effect of manganese with cobalt acetate at total concentration of 2×10^{-4}M on the oxidation of a 1:1 mixture by volume of cyclohexanone and acetic acid at 60 °C.

In the case of cobalt acetate, the rate of oxidation of cyclohexanone can be expressed as k[Co(III)]^2[Anon]/[Co(II)] and the rate of oxygen absorption catalyzed by cobalt acetate in acetic acid is of about half order in total cobalt concentration. On the other hand, the manganese-catalyzed autoxidation showed a small dependence on catalyst concentration. The marked decrease in the rate of oxidation at low manganese concentration can be attributed mostly to the slow regeneration of Mn(III) by the oxidation of Mn(II) with peracids, since the rate of decomposition of peracids with manganese acetate in acetic acid is much smaller than that with cobalt acetate.

Thus, if cobalt is mixed with manganese at low catalyst concentrations, cobalt would take over the role of peroxide decomposition and the resulting cobaltic ion would oxidize manganous ion to manganic. As a result, the rate of oxidation catalyzed by a mixture of cobalt and manganese would assume the theoretical value represented by Eq. (5).

A similar synergistic effect was observed in the mixture of nickel and manganese acetates. This can also be explained in the same manner.

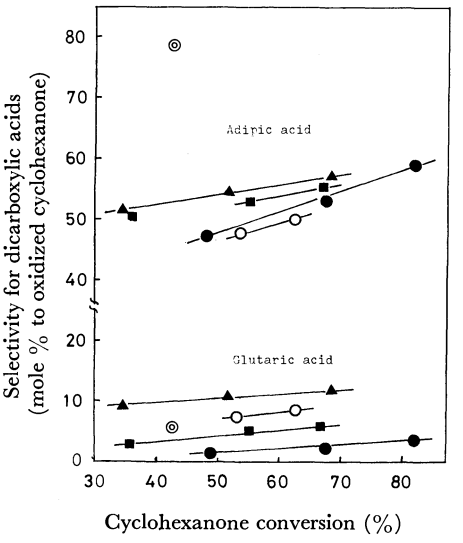

Fig. 8. The selectivities for adipic and glutaric acids in the oxidation of a 1:1 mixture by volume of cyclohexanone and acetic acid as a function of cyclohexanone conversion with 10^{-3}M metal acetates.
▲: Cobalt, ●: Manganese, ○: Cobalt/Manganese=1/1, ■: Manganese/Nickel 1/1, ◎: Manganese/Copper=1/1.

Oxidation Products. Selectivity to adipic and glutaric acids *versus* the conversion of cyclohexanone is given in Fig. 8. The selectivity for adipic acid increased gradually as the conversion increased and the highest value of 79% was obtained for all catalysts tested in the 1:1 mixture of manganese and copper. The reason why the yield of adipic acid by Mn–Cu catalyst is considerably high can be attributed to the retardation effect of Cu(II) on the coupling reaction of alkyl radicals, since Cu(II) is known to oxidize alkyl radicals[15] and the rate of oxidation of cyclo-

15) J. K. Kochi, A. Bemis, and C. L. Jenkins, *J. Amer. Chem. Soc.*, **90**, 4616 (1968).

hexanone catalyzed by 6.4×10^{-4} M Mn decreased from 9.2×10^{-5} to 5.2×10^{-5} M/sec after 50% of Mn was replaced by Cu.

Cobalt showed a higher yield of glutaric acid than the other catalysts. This may be due to its activity[16] in the decarboxylation reaction of adipic acid. The ratio of carbon dioxide to glutaric acid was 1—1.5, and almost independent of cyclohexanone conversion at conversion 40—70%. The selectivity for adipaldehyde was 6—8% in the case of manganese catalyst but only 1—2% in the presence of cobalt acetate. It seems reasonable that cobalt is more effective in the oxidation of intermediate aldehydes than manganese.

The oxidation products described above can not explain the carbon distribution satisfactorily except for the products obtained by Mn–Cu. The balance may be mostly polymerized products such as 2-cyclohexan-1-yl cyclohexanone[2] and other intermediate products[1d,2] such as dione and oxycyclohexanone.

16) a) W. A. Waters, *Discuss. Faraday Soc.*, **46**, 158 (1969). b) H. B. Tinker, *J. Catal.* **19**, 237 (1970).

BULLETIN OF THE CHEMICAL SOCIETY OF JAPAN, VOL. 46, 2784—2787 (1973)

Photochemical Reactions of Uranyl Ions with Organic Compounds. V. Effects of Temperature and Solvent on the Photooxidation of Alcohols

Shukichi SAKURABA, Soichi MIMURA, and Ryoka MATSUSHIMA*

Department of Industrial Chemistry, Faculty of Engineering, Shizuoka University, Hamamatsu 432

(Received July 19, 1972)

A comparative study of the photokinetic behaviors of aliphatic alcohols and related substrates was made for the photooxidation with uranyl ions. Ethylene glycol, glucose, sucrose and some other substrates showed abnormal results compared to a series of simple aliphatic alcohols: the photoredox quantum yields ϕ for the former substrates decreased with substrate concentration (at their higher concentrations) and temperature rise, in contrast to simple aliphatic alcohols. In aqueous acetone solution ϕ increased with the increase in acetone content, the reaction constant ρ^* being more negative than in aqueous solution. In 40% aqueous acetone solution the ϕ values for simple aliphatic alcohols varied in a complicated way with temperature. The abnormal results were interpreted in terms of the relative importance of physical quenching competing with the primary chemical process.

As regards the mechanism of the photooxidation of some aliphatic alcohols by uranyl ions, the initial stage was assumed to be the α-hydrogen abstraction (one-equivalent redox) *via* bimolecular collision of the excited uranyl ion with the substrates, followed by the two disproportionation reactions of the primary intermediates.[1,2]

However, in the course of the photokinetic investigations, we observed that some alcohols, such as glucose and benzyl alcohol, exhibited abnormal behaviors.

In the present paper the effects of temperature, substrate concentration and solvent on the photokinetics are discussed.

Experimental

Guaranteed reagents were used without purification. 0.02 M uranyl nitrate solution was prepared from a 0.1 M stock solution. The solutions (pH=1) were deaerated by the passage of oxygen-free nitrogen for 20—30 min per 5—15 ml, kept air-tight with liquid paraffin and then exposed to irradiation (mostly 405 and 436 nm) using a suitable combination of glass filters or an interference filter from a 100 or 500 W high pressure mercury lamp. The temperature was controlled with a thermostat.

Methods for actinometry and determination of the photoproducts were the same as those previously described.[1] Since the molar ratio of the products, aldehyde or ketone/uranium(IV), was unity regardless of the conditions,[1] only the formation of the uranium(IV) species was followed for the estimation of the photoredox quantum yield ϕ.

Results and Discussion

Effects of Temperature and Substrate Concentration. The plot of the reciprocal of the photoredox quantum yield $1/\phi$ as a function of the reciprocal of alcohol concentration gave a straight line for the photooxidation of simple aliphatic alcohols by uranyl ions in aqueous acidic media, in agreement with the empirical equation: $1/\phi=\alpha+\beta/[\text{alcohol}]$, where $\alpha=2$ at pH$\geqq$1[1] (Fig. 1). The relation seems to hold under some different conditions (temperature and solvent) for *n*-propyl alcohol (Fig. 1). The photoredox reaction of ethyl and three butyl alcohols with uranyl ions has been explained by a mechanism which involves one-equivalent redox reaction between the excited uranyl ions and the substrates *via* bimolecular collision, followed by thermal disproportionation reactions of the primary redox intermediates.[1] The fact that the photoredox quantum

1) S. Sakuraba and R. Matsushima, This Bulletin, **43**, 2359 (1970).

2) R. Matsushima and S. Sakuraba, *J. Amer. Chem. Soc.*, **93**, 5421 (1971).

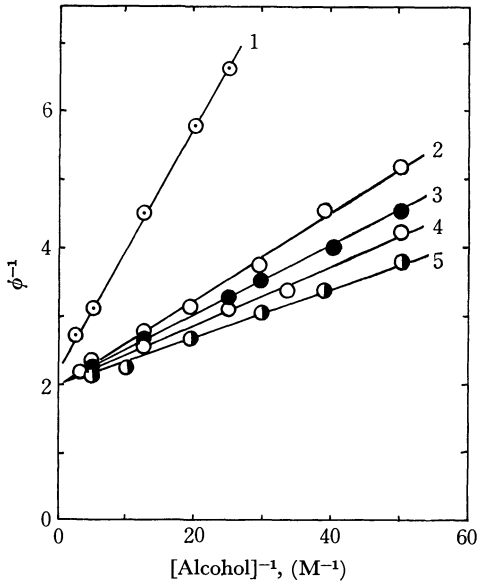

Fig. 1. Plot of ϕ^{-1} *vs.* [alcohol]$^{-1}$ in aqueous acidic solutions (pH=1). 1: methyl, 2: ethyl, 3: *n*-propyl, 4: *n*-butyl, 5: *sec*-butyl alcohol.

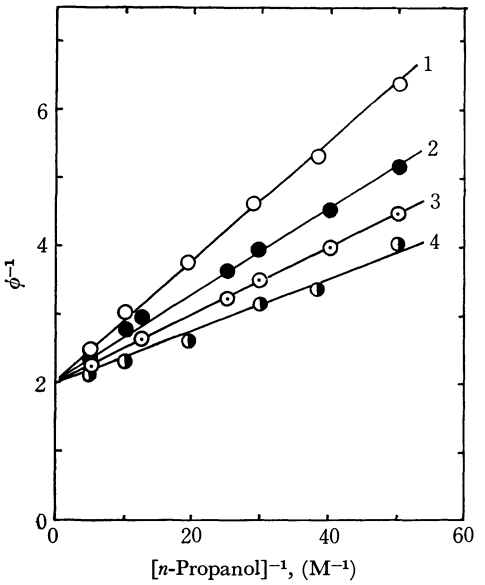

Fig. 2. Plot of ϕ^{-1} *vs.* [*n*-propyl alcohol]$^{-1}$ at different temperatures at pH 1. 1: 3 °C, 2: 10 °C, 3: 20 °C, 4: 20 °C in 40% aqueous acetone.

yield increases with temperature (Fig. 2) might support the bimolecular collision mechanism.

In contrast, the plot $1/\phi$ *vs.* 1/[substrate] for ethylene glycol, glucose, and sucrose gave no straight line (Fig. 3). This implies that some depression of the photoredox reaction becomes significant with the increase in substrate concentration at higher concentrations (>0.1 M). The photoredox quantum yield decreases with temperature rise for thse substrates, whereas the reverse is the case for simple aliphatic alcohols (Fig. 2). Plots of log ϕ *vs.* $1/T$ for simple aliphatic alcohols are given in Fig. 4. Ethyl, isopropyl, *n*-butyl and isobutyl alcohols gave similar results. Plots for glucose and benzyl alcohol are given in Fig. 5. Qualitatively, the positive apparent activation energies for simple aliphatic

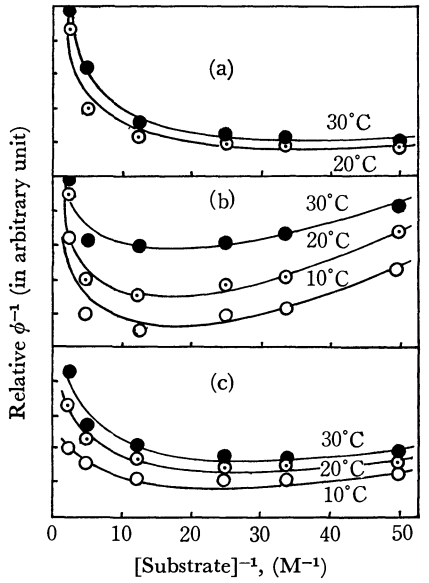

Fig. 3. Plot of relative ϕ^{-1} *vs.* [substrate]$^{-1}$ at different temperatures in aqueous acidic solutions (pH=1) (a): ethylene glycol, (b): glucose, (c): sucrose.

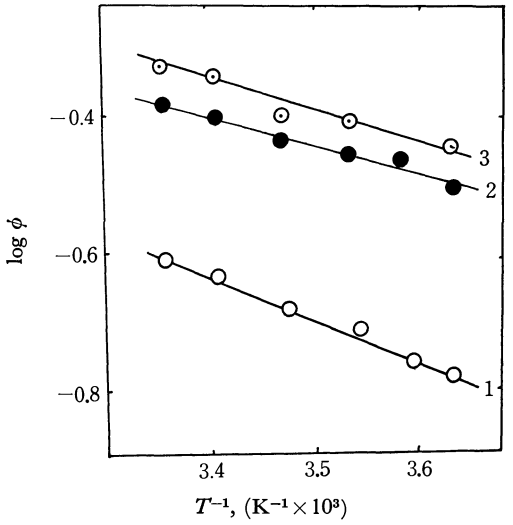

Fig. 4. Plot of log ϕ *vs.* $1/T$. 1: methyl, 2: *n*-propyl, 3: *sec*-butyl alcohol, in 0.1 M. Aqueous acidic medium (pH=1).

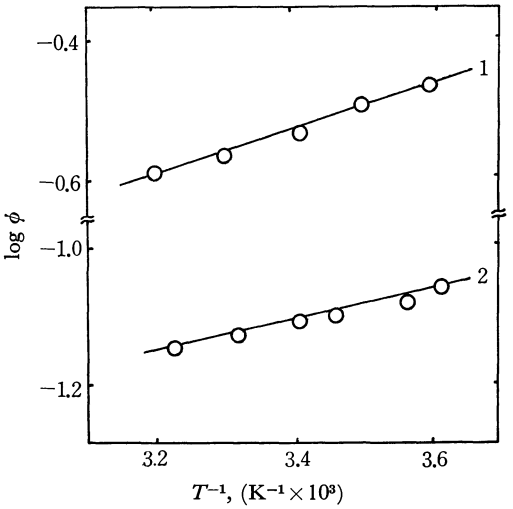

Fig. 5. Plot of log ϕ *vs.* $1/T$ for glucose (1) and benzyl alcohol (2) in aqueous acidic medium (pH=1).

Table 1. Variation in the photoredox quantum yield with acetone content[a)]

Acetone/vol%	ϕ
0	0.38
5	0.43
20	0.44
40	0.45
60	0.46

a) Ethyl alcohol 0.1 M, uranyl ion 0.02 M, pH=1, 20 °C.

alcohols, 2—5 kcal/mol, might support a bimolecular collision mechanism, but not negative apparent activation energies for glucose and benzyl alcohol, −1.5 kcal/mol.

Solvent Effects. Change in the photoredox quantum yield with acetone content is given in Table 1. The increase in ϕ with the acetone content is partly attributable to the increase in the mean lifetime of uranyl fluorescence. The Stern-Volmer plots gave straight lines for most aliphatic alcohols in 40% aqueous acetone as well as in aqueous medium.

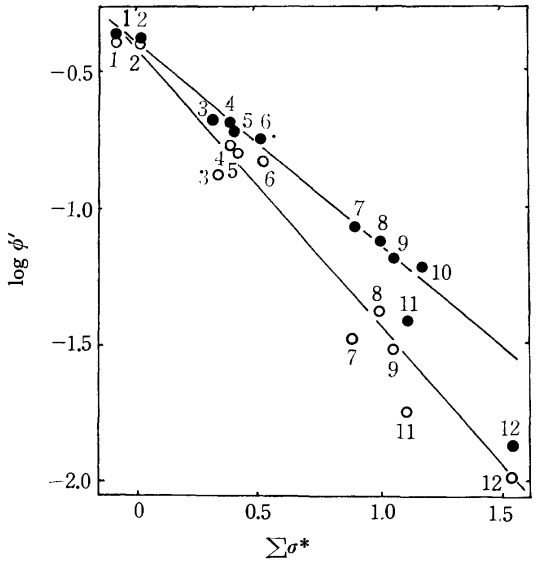

Fig. 6. Plot of log ϕ' *vs.* $\sum\sigma^*$ at pH 1, 20 °C. $\sum\sigma^*=\sigma(R_1)+\sigma^*(R_2)$; $\sigma^*(R_1)$ and $\sigma^*(R_2)$ are Taft σ^*-values of the substituents R_1 and R_2 in R_1R_2CHOH. ϕ' is the photoredox quantum yield divided by the number of the α-hydrogen atoms of each alcohol. 1: *sec*-butyl, 2: isopropyl, 3: isobutyl, 4: *n*-butyl, 5: *n*-propyl, 6: ethyl, 7: 3-chloro-*n*-propyl, 8: methyl, 9: 2-hydroxyethyl, 10: 2-propenyl, 11: benzyl, 12: 2-chloroethyl alcohols; 0.1 M in each alcohol.
○: 40% aqueous acetone, ●: aqueous medium.

Figure 6 shows the polar substituent effect of alcohols on the photoredox quantum yield in 40% aqueous acetone as compared with that in aqueous medium. The ρ*-values under some different conditions are in the range $-1.4<\rho^*<-0.6$, an indication of a free radical reaction.[3)] The ρ*-value remains unchanged with the changes in temperature and alcohol concentration, but it changes with the change in the medium

Table 2. Effects of temperature, solvent and alcohol concentration on the ρ*-value

Temperature/°C	Solvent	[Alcohol]/M[a)]	−ρ*
4	water	0.04	0.80
20	water	0.10	0.80
35	water	0.04	0.80
20	40 % acetone	0.06	0.95

a) Alcohols are the same as in Fig. 6.

(Table 2). This might be attributed to the effect of solvent polarity.

The Stern-Volmer formula, the linearity of the plot of log ϕ' *vs.* $\sum\sigma^*$, and the range of the ρ*-value, indicate that the primary process in 40% aqueous acetone is similar to that in aqueous medium, *i.e.*, α-hydrogen abstraction.[1,2)]

On the other hand, plot 4 in Fig. 2 shows a straight line with the intercept of 2 in 40% aqueous acetone medium. The intercept of 2 suggests that the secondary process in this medium is similar to that in aqueous medium, *i.e.*, disproportionation reactions of the primary redox intermediates.[1)]

Thus, it is very likely that the photoredox reaction in aqueous acetone proceeds through a similar mechanism to that in aqueous medium with different efficiency.

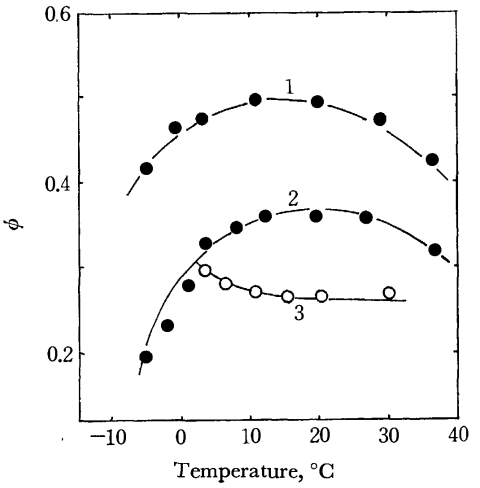

Fig. 7. Temperature dependence of ϕ in 40% aqueous acetone at pH 1. 1: *n*-butyl alcohol, 2: ethyl alcohol, 3: glucose, 0.1 M in each.

The temperature dependence of the photoredox quantum yield in 40% aqueous acetone is shown in Fig. 7. Ethyl and butyl alcohols show abnormal temperature effect in this medium compared to aqueous medium (Fig. 4). Glucose shows a different dependence.

Discussion on the Abnormal Results. Some authors[4,5)] have postulated a ground state complex as the photosensitive species for the photooxidation of sugars and alcohols by uranyl ions. Multidentate alcohols (ethylene glycol, glucose, and sucrose) would have stronger coor-

3) a) R. E. Pearson and J. C. Martin, *ibid.*, **85**, 3142 (1963); b) C. A. Russell and R. C. Williamson, Jr., *ibid.*, **86**, 2357 (1964); c) R. L. Huany and K. H. Lee, *J. Chem. Soc., C*, **1966**, 935. d) P. M. Nave and W. S. Trahanovsky, *J. Amer. Chem. Soc.*, **90**, 4755 (1968); **92**, 1120 (1970).

4) a) L. J. Heidt and K. A. Moon, *ibid.*, **75**, 5803 (1953); b) L. J. Heidt, *ibid.*, **76**, 5962 (1954).

5) a) K. Venkatarao and M. Santappa, *Z. Phys. Chem.* (Frankfurt), **54**, 101 (1967); b) K. Venkatarao and M. Santappa, *Indian J. Chem.*, **5**, 304 (1967).

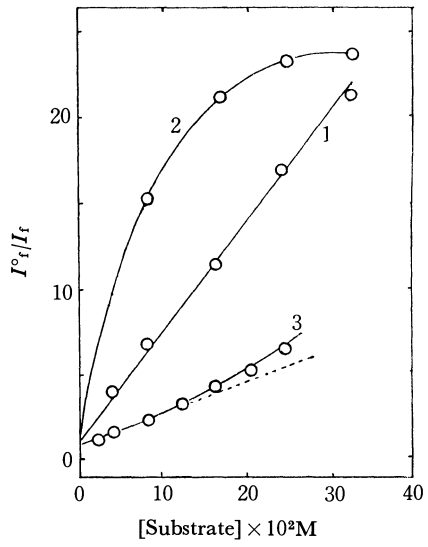

Fig. 8. Typical Stern-Volmer plots for the uranyl fluorescence by alcohols and the related substrates. Uranyl ion: 0.02 F, pH=1 (aqueous medium), 25 °C, λ_{ex}=405 nm, λ_{an}=510 nm.
1: *n*-propyl alcohol, 2: glucose, 3: lactic acid

dination power than unidentate alcohols.[6] The negative apparent activation energies for the multidentate alcohols (Figs. 3 and 5) might be interpreted in terms of the formation of a ground state complex as the photosensitive species in contrast to the positive ones for the unidentate alcohols (Figs. 2 and 4).

If complex formation takes place between the substrates and the uranyl ions, changes in the absorption and/or the fluorescence spectra of the solutions might be expected. The Stern-Volmer plots for the quenching of the uranyl fluorescence by these substrates should give lines concave upward (as is the case for lactic acid, Fig. 8), since the quenching efficiency should increase because of the additional static (intracomplex) quenching process, which is more efficient than a bimolecular collision process.[7] However, the absorption spectra (visible region) and shapes of the fluorescence spectra of uranyl ions in aqueous solution at pH 1 were entirely unchanged by the addition of these substrates in the range of uranyl concentration 0.001—0.1 M. This is in contrast to the fact that even weak complexes with many carboxylic acids show significant spectral changes,[8] though the lack of spectral changes does not always exclude complex formation. The Stern-Volmer plot for glucose gave a line concave downward (the reverse of expectation) as shown in Fig. 8. It seems difficult to explain the decrease in ϕ at higher substrate concentrations (Fig. 3) in terms of complex formation, since increase in substrate concentration should accelerate the formation. Thus, the formation of a ground state complex as the photosensitive species is unlikely and negligible at most.

The relative importance of physical quenching which competes with the primary chemical process might be a possible interpretation of our results. It should be noted that the quenching constants for the multidentate alcohols and phenyl-substituted alcohols are large compared to their photoredox quantum yields.[9] This implies the important role of physical quenching for these substrates, while for simple aliphatic alcohols (physical quenching is small), temperature rise is qualitatively equivalent to the increase in substrate concentration in the sense that the number of effective collisions for the primary chemical act is roughly proportional to substrate concentration and absolute temperature. However, this is not the case for substrates with significant physical quenching efficiencies or for even simple aliphatic alcohols at higher temperature in more complicated media where solute-solvent interaction becomes more sensitive to temperature change. The abnormal temperature dependence of ethyl and butyl alcohols in 40% aqueous acetone (Fig. 7) may be assumed to be the latter case.

For complicated substrates or those for which physical quenching is dominant, effective collision for the chemical process will be restricted, hence the greater part of the primary interaction is apt to fall into physical quenching, giving rise to large quenching constants compared to their photoredox quantum yields. For these substrates the increase in temperature will decrease the viscosity of solutions so as to increase the number of collisions between the reactants, but it will depress the efficient abstraction of α-hydrogen because of the increased steric hindrance (thermal rotations of the bulky groups) of the substrate molecules. It is probable that the increment of the primary chemical act (α-hydrogen abstraction) due to the decreased viscosity (or increased number of collisions) is small compared to its decrement due to the increased physical quenching (steric hindrance). The observed negative activation energies for these substrates may be interpreted as the superposition of these effects.

The decrease in ϕ and the deviation of the Stern-Volmer plot at higher concentrations of the multidentate alcohols (Figs. 3 and 8) may be partly due to the increase in the viscosity which depresses the bimolecular collision between the reactants. However, some other significant effects must be operative, since the decrease in ϕ and the deviation of the Stern-Volmer plot at higher concentrations of the multidentate alcohols are far beyond the effect of increased viscosity.

The stronger affinities of the multidentate alcohols to uranyl ions will accelerate the reverse recombination reactions of the primary redox intermediates, and the higher viscosity of these solutions will depress the secondary bimolecular process (the disproportionation processes of the primary intermediates): both lead to additional increase in the physical quenching constants.

The authors wish to thank Miss S. Yamamura for her assistance.

6) C. K. Jørgensen, "Inorganic Complexes," Academic Press, London, (1963), p. 101.

7) a) A. Heller and E. Wasserman, *J. Chem. Phys.*, **42**, 949 (1965); b) G. A. Crosby, *Molecular Crystals*, **1**, 37 (1966); c) N. Filipescu and G. W. Mushrush, *J. Phys. Chem.*, **72**, 3516 (1968).

8) a) E. Rabinowitch and R. L. Belford, "Spectroscopy and Photochemistry of Uranyl Compounds," Pergamon Press, London, (1964), pp. 91—183; b) S. Sakuraba and R. Matsushima, This Bulletin, **43**, 1950 (1970).

9) R. Matsushima, *J. Amer. Chem. Soc.*, **94**, 6010 (1972).

Kinetics of the Oxidation of Ascorbic Acid by the Copper(II) Ion in an Acetate Buffer Solution

Katumitu HAYAKAWA, Shoko MINAMI, and Sumio NAKAMURA

Department of Chemistry, Faculty of Science, Kagoshima University, Kamoike-cho, Kagoshima 890

(Received October 7, 1972)

The kinetics of the oxidation of ascorbic acid by the copper(II) ion has been studied spectrophotometrically by a stopped-flow technique. At pH 4—6, the initial rate of the decrease in the monohydroascorbate anion is of the second-order with respect to the total concentration of the copper(II) ion and of the first-order with respect to the concentrations of the monovalent and divalent ions of ascorbic acid:

$$-(\mathrm{d}[HA^-]/\mathrm{d}t)_{t=0} = k_1[Cu(II)]_T^2[HA^-] + k_2[Cu(II)]_T^2[A^{2-}]$$

where HA^- and A^{2-} are the monovalent and divalent ions of ascorbic acid respectively. k_1, k_2, and the activation parameters are obtained as follows: $k_1 = 3.1 \times 10^4$, $k_2 = 6.1 \times 10^{10}$ M^{-2} s^{-1}, $\Delta H^{\neq} = 17$ kcal/mol, $\Delta S^{\neq} = 8.3$ cal/deg mol, and $\Delta G^{\neq} = 15$ kcal/mol. The EPR signal from the ascorbate radical is not observed in the kinetic run by either a flow technique or a quenching technique. Some discussions of the mechanism of the reaction are given.

It is known that the oxidation of ascorbic acid, H_2A, to dehydroascorbic acid, DA, by molecular oxygen is catalyzed with a remarkable activity by the copper(II) ion. Many kinetic studies of the reaction have been made.[1-7] However, the rate of the reaction depends complicatedly on the pH, the catalyst, the oxygen pressure, the buffer, *etc.* and so the rate equation has not been determined.

The present study was undertaken to obtain some information on the kinetics of the reaction between ascorbic acid and the copper(II) ion in the absence of oxygen as a fundamental study of the copper(II) ion-catalyzed autoxidation of ascorbic acid. The electron paramagnetic resonance (EPR) spectra were measured in order to obtain some information on the mechanism of the reaction. The rates were measured in an acetate buffer solution. The stoichiometry of the reaction is as follows:

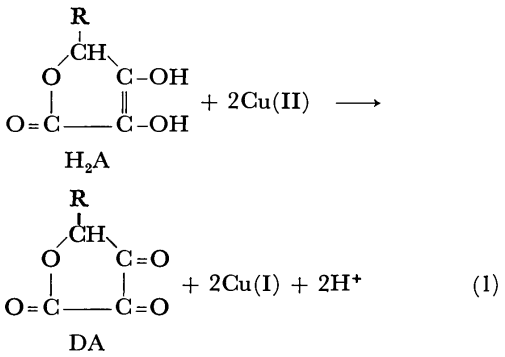

(1)

Experimental

Reagents. The ascorbic acid, copper(II) sulfate, copper(II) acetate, acetic acid, and sodium acetate were obtained commercially (all GR). The copper(II) sulfate and copper(II) acetate were purified by recrystallization. The other materials were used without further purification. The water used was distilled and bubbled by nitrogen gas for 30 min before the preparation of the reactant solutions. The acetate buffer solution, which had been prepared from 0.1 M acetic acid and 0.1 M sodium acetate, was used between pH 4—6. The ascorbic acid solution was freshly prepared for every kinetic run.

Kinetic Measurements. The absorbance maximum of ascorbic acid is 265 nm in a neutral solution and 245 nm in an acidic solution for the monohydroascorbate anion, HA^-, and ascorbic acid, H_2A, respectively. At pH 4—6, the monohydroascorbate anion is the predominant species present in solution. In the rate study, the decrease in the absorbance was followed at 265 nm by a stopped-flow apparatus constructed in our laboratory, using a Shimadzu SV 50 spectrophotometer and a 5 mm quartz cell. The acetate buffer and the 1 mM $CuSO_4$ solution do not interfere with the absorbance at 265 nm. The initial rate method was used for the analysis of the rate in order to neglect the complexity resulting from the decrease in the reactants and the increase of products during a kinetic run. Nitrogen gas was bubbled through the reactant solutions for 30 min before each kinetic run and during each kinetic run in order to exclude the oxygen. The pH was measured using a Hitachi-Horiba F-5 pH meter. The formation of precipitates by the hydrolysis of the copper(II) ion and copper(I) oxide produced interfered with the kinetic measurements above pH 6.

EPR Measurements. To obtain the EPR signal from the kinetic run, the continuous-flow technique was used with various flow rates.[8] Also, to obtain the EPR signals from the solid phase solutions containing 0.05 M $CuSO_4$ and 0.13 M ascorbic acid in 0.1 M NaOH aqueous solutions (pH *ca.* 5) were rapidly injected into liquid nitrogen and the mixing solutions were quickly quenched after the mixing.[9] The EPR spectra were measured for the solid sample at the temperature of liquid nitrogen. The EPR spectra were recorded using an X-band spectrometer with a 455 kHz field modulation constructed by the Professor Kuwata's Laboratory in Osaka University.

1) Y. Ogata, Y. Kosugi and T. Morimoto, *Tetrahedron*, **24**, 4054 (1968).
2) A. Weissberger and J. E. LuVall, *J. Amer. Chem. Soc.*, **66**, 700 (1944).
3) E. Silverblatt, A. L. Robinson and C. G. King, *ibid*, **65**, 137 (1943).
4) L. W. Mapson, *Biochem. J.*, **39**, 228 (1945).
5) I. Ohnishi and T. Hara, This Bulletin, **37**, 1317 (1960).
6) V. S. Butt and M. Hallaway, *Arch. Biochem. Biophys.*, **92**, 24 (1961).
7) A. O. Dekker and R. G. Dickinson, *J. Amer. Chem. Soc.*, **62**, 2165 (1940).
8) I. Yamazaki, H. S. Mason, and L. Piette, *J. Biol. Chem.*, **235**, 2444 (1960).
9) Y. Shimizu, T. Shiga and K. Kuwata, *J. Phys. Chem.*, **74**, 2929 (1970).

Results and Discussion

The plot of the absorbance at 265 nm, D_{265}, *versus* the concentration of HA^-, which was calculated using the equilibrium constant ($pK_1=4.12$) for $H_2A \rightleftarrows HA^- + H^+$, is given in Fig. 1 in the absence of copper(II). As a straight line passing through the original point is obtained, it may be concluded that the absorbance at 265 nm is based on HA^- under the present experimental conditions; this is consistent with the report by Ogata *et al.*[10] The molar extinction coefficient of HA^- obtained at 265 nm, ε_{HA}, is $(1.62\pm0.02)\times10^4$ $M^{-1}cm^{-1}$ at 20 °C. The spectra of 0.2 mM $CuSO_4$ and the buffer solution and a kinetic run at pH *ca.* 5 are given in Fig. 2. It is found that the absorbance of $CuSO_4$ and the buffer solution do not interfere with the absorbances of HA^- at 265 nm. The absorption bands of the copper(I) compound and dehydroascorbic acid produced by the reaction are absent between 240 to 350 nm. At pH 6.5, the formation of the precipitate of copper (I) oxide[11] interfere with the measurement of the spectra. The copper(II) ion is present as the acetatocopper(II) complex ion in this buffer solution.

In the presence of the copper(II) ion, the formation

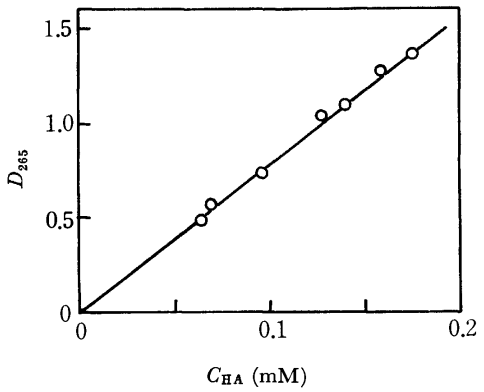

Fig. 1. The plot of the absorbance at 265 nm *versus* the concentration of monohydroascorbate ion; the total concentration of ascorbic acid: 0.08—0.2 mM.

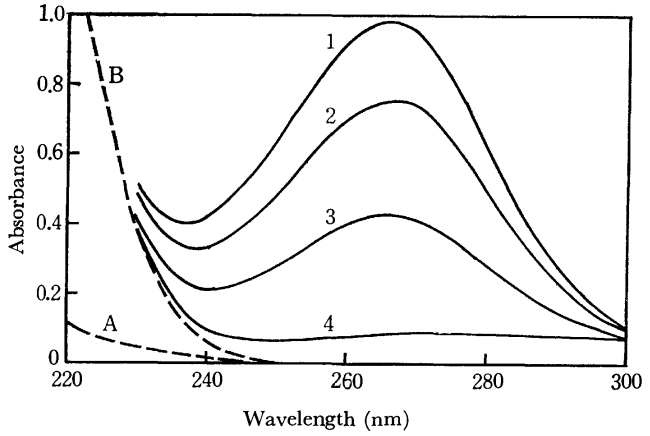

Fig. 2. The absorption spectra of 0.2 mM $CuSO_4$ aqueous solution (broken line A), 0.1 M acetate buffer (broken line B) and kinetic run at pH *ca.* 5 (solid lines; time 1<2<3<4)

of the monohydroascorbatocopper(II) complex ion, M(II)HA, has been reported by studies of the copper-(II) ion-catalyzed autoxidation of ascorbic acid[1,12] and by spectroscopic studies.[10]

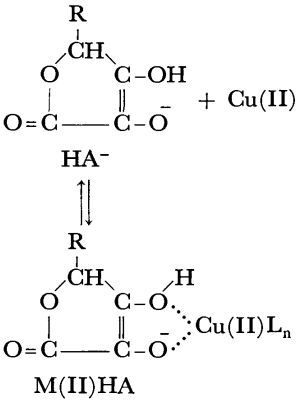

(2)

where L is the other ligand. The λ_{max} of the complex is reported to shift to a shorter wavelength than that of HA^-,[10] but the molar extinction coefficient of the complex at 265 nm is not given. The fact that the absorbance, D_{265}, after a mixing of the reactants is equal to a half of the absorbance before mixing suggests that the concentration of the complex, C_{MHA}, is small compared with that of HA^- and/or that the molar extinction coeffieient of M(II)HA is nearly equal to that of HA^-. From Equilibrium (2), $C_{MHA}=K_{MHA}C_MC_{HA}$, where K_{MHA} is the formation constant of the complex. As C_M is *ca.* 0.1 mM and K_{MHA} is *ca.* 40 M^{-1},[12] it is found that C_{MHA} is very small compared with C_{HA} under the present experimental conditions. Therefore, the decrease in D_{265} corresponds to that of HA^-.

Table 1. Apparent first-order rate constant k'
Temperature 30 °C, $[H_2A]_0$ $(0.73-2.53)\times10^{-4}$ M

$CuSO_4$ ($\times10^4$M)	k' (sec^{-1}) pH=4.80	pH=4.96	pH=5.25	pH=5.50
4.81	170±2	204±2	345±4	457±5
4.01	128±2	161±5	262±3	335±5
3.21	95±1	102±1	185±3	241±2
2.40	59±3	65±4	147±1	168±3
1.60	47±2	46±2	96±7	113±4

The initial rate, $V_0(=-(dD/dt)_{t=0})$, is directly proportional to the initial concentration of ascorbic acid, C_A^0. It is found that this reaction is a first-order reaction with respect to C_A^0. The apparent first-order rate constants, k', are given in Table 1. The apparent first-order rate constant is directly proportional to the square of the initial concentration of the copper(II) ion, C_M^0. It is found that the reaction is a second-order reaction with respect to C_M^0. Therefore, the rate equation is as follows:

$$V_0 = C_A^0(k''C_M^{0^2}+a) \quad (3)$$

where it is considered that the second term is a term resulting from the effect of a very small quantity of oxygen dissolved in the solution. k'' and a are given in Table 2.

10) Y. Ogata and Y. Kosugi, *Tetrahedron*, **26**, 4711 (1970).
11) J. Erkama, *Acta Chem. Scand.*, **3**, 844 (1949).
12) M. M. T. Khan and A. E. Martell, *J. Amer. Chem. Soc.*, **89**, 4176 (1967).

TABLE 2. RATE CONSTANT k'' AND a IN EQUATION (3) AT 30 °C

pH	k'' ($\times 10^{-8}$ $sec^{-1}M^{-2}$)	a (sec^{-1})
4.80	61±1	29±4
4.96	81±3	23±4
5.25	119±3	69±4
5.50	166±1	71±1

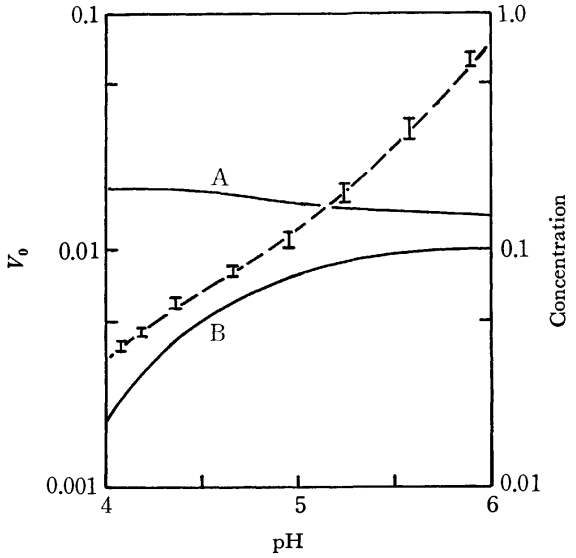

Fig. 3. Dependence of the initial rate at 0.37 mM Cu(II) ion and 0.11 mM ascorbic acid on pH (I) and the dependences of the concentrations of mono- and bis-acetatocopper(II) complex ion on pH (solid line A and B respectively). The broken line is calculated from the next equation:
$V_0=7.5\times10^{-3}/(1+1.3\times10^4C_H)+6.8\times10^{-8}/C_H(1+1.3\times10^4C_H)$.

The logarithm plot of V_0 *versus* the concentration of the hydrogen ion, C_H, is given in Fig. 3 at 0.11 mM H_2A and 0.25 mM Cu(II). It is considered that the dependence of the rate on pH is primarily due to the difference in reactivity between the undissociated form and the dissociated forms of ascorbic acid and, secondary, to the difference in reactivity between the copper(II) ion and the acetatocopper(II) complex ion. According to Weissberger *et al.*, the apparent first-order rate constants of the copper(II)-catalyzed autoxidation of ascorbic acid obtained in phosphate, acetate, and carbonate buffer solutions depend on the pH with a smooth curve.[2] This suggests that the second effect is small. Figure 3 shows that the dependence of the rate on the pH is not consistent with the dependence of the concentrations of the acetatocopper(II) complex ions (solid line), which are calculated using the formation constants of the mono- and bis-acetatocopper(II) complex ions ($K_1=251$ M^{-1} and $K_2=7.94$ M^{-1} respectively[13]). From the plot of $1/V_0$ *versus* C_H in Fig. 4, the next relations are obtained:

$$V_0 = k_1''/(1+bC_H) \quad (pH\leq5) \quad (4a)$$

$$V_0 = k_2''/C_H \quad (pH>5) \quad (4b)$$

13) L. G. Sillén and A. E. Martell, "Stability Constants of Metal-ion Complexes," Chemical Society, London (1964), p. 365.

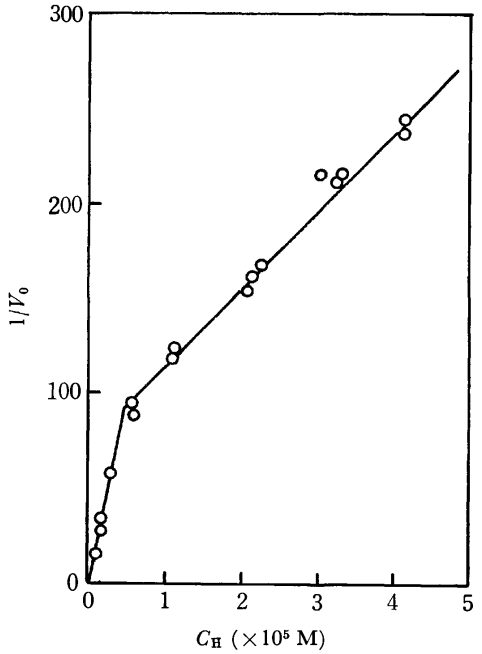

Fig. 4. Dependence of the reciprocal of the initial rate on the concentration of hydrogen ion.

In analogy with the autoxidation of ascorbic acid,[14] it is considered that both the monovalent and divalent ions of ascorbic acid are able to participate in the present reaction. From the dissociation constants of ascorbic acid ($pK_1=4.04$ for $H_2A\rightleftarrows H^+ + HA^-$ and $pK_2=11.34$ for $HA^-\rightleftarrows H^+ + A^{2-}$ at 25 °C), $C_{HA}=C_A^0/(1+K_{-1}C_H)$ and $C_A=C_A^0/K_{-2}C_H(1+K_{-1}C_H)$ at pH 4—6, where $K_{-1}=1/K_1$, $K_{-2}=1/K_2$ and C_{HA} and C_A are the concentrations of HA^- and A^{2-} respectively. Therefore,

$$V_0 = k_1'C_A^0/(1+K_{-1}C_H) + k_2'C_A^0/K_{-2}C_H(1+K_{-1}C_H) \quad (5)$$

Substituting the values of $k_1'C_A^0$, $k_2'C_A^0/K_{-2}$, and K_{-1} (7.5×10^{-3}, 6.8×10^{-8}, and 1.3×10^4 respectively, which are obtained using a curve-fitting method[15]) in Eq. (5), the broken line in Fig. 3 is obtained. The curve is very consistent with the experimental data. Therefore, the experimental rate equation is as follows:

$$V_0/\varepsilon_{HA} = k_1C_M{}^{0^2}C_A^0/(1+bC_H) + k_2C_M{}^{0^2}C_A^0/C_H(1+bC_H) \quad (6)$$

where $k_1=3.1\times10^4$ M^{-2} s^{-1}, $k_2=0.28$ M^{-1} s^{-1}, and $b=1.3\times10^4$ M^{-1}.

In the oxidation of H_2A by the peroxidase and in the autoxidation of H_2A at pH 6.6—9.6, the free radical from H_2A was detected by EPR measurements.[8,16,17] The EPR spectra of kinetic runs containing 0.05 M $CuSO_4$ and 0.13 M H_2A in a 0.1 M NaOH aqueous solution (pH *ca.* 5) were measured using a continuous-flow technique and the quenching technique. The blue solution became brown quickly after mixing. The EPR signal from the copper(II) ion is observed, but that from the ascorbate radical is not observed under

14) A. Weissberger, J. E. LuValle and D. S. Thomas, Jr., *J. Amer. Chem. Soc.*, **65**, 1934 (1943).

15) L. G. Sillén, *Acta Chem. Scand.*, **10**, 186 (1956); D. Dyrssen and L. G. Sillén, *ibid.*, **7**, 663 (1953).

16) I. Yamazaki and L. Piette, *Biochim. Biophys. Acta*, **50**, 62 (1961).

17) C. Lagercrantz, *Acta Chem. Scand.*, **18**, 562 (1964).

the condition of a varying flow rate. It is found by the stopped-flow technique that the EPR signal of the copper (II) ion from the brown solution decreases with the time because of the formation of the copper(I) compound, but the EPR signal from the ascorbate radical is not observed.

The above facts and discussions suggest the following mechanism for the oxidation of ascorbic acid by the copper(II) ion at pH 4—6, C_A^0 *ca.* 0.1 mM, C_M^0 *ca.* 0.1 mM, and 30 °C:

$$H_2A \overset{K_1}{\rightleftharpoons} H^+ + HA^- \quad (7)$$

$$HA^- \overset{K_2}{\rightleftharpoons} H^+ + A^{2-} \quad (8)$$

$$HA^- + Cu(II) \overset{K_9}{\rightleftharpoons} Cu(II)HA \quad (9)$$

$$A^{2-} + Cu(II) \overset{K_{10}}{\rightleftharpoons} Cu(II)A \quad (10)$$

$$Cu(II)HA + Cu(II) \xrightarrow{k_{11}} DA + 2Cu(I) + H^+ \quad (11)$$

$$Cu(II)A + Cu(II) \xrightarrow{k_{12}} DA + 2Cu(I) \quad (12)$$

Assuming that Reactions (11) and (12) are the rate-determining steps and applying the preliminary equilibrium treatment to Reactions (7), (8), (9) and (10), the following expression is obtained:

$$V_0/\varepsilon_{HA} = k_{11}K_9C_M{}^{0^2}C_A{}^0/(1+K_{-1}C_H) + k_{12}K_{10}C_M{}^{0^2}C_A{}^0/K_{-2}C_H(1+K_{-1}C_H) \quad (13)$$

where the next approximations are used: $C_M \gg C_{MHA}$, $C_M \gg C_{MA}$, $C_A \ll C_{HA}$, and $C_A \ll C_A{}^0$. $k_{11}K_9 = 3.1 \times 10^4$ $M^{-2}\,s^{-1}$, $k_{12}K_{10} = 6.1 \times 10^{10}\,M^{-2}\,s^{-1}$ (when $K_{-2} = 2.2 \times 10^{11}\,M^{-1}$ [12]) and $K_{-1} = 1.3 \times 10^4\,M^{-1}$ are also obtained. According to Khan *et al.*, $K_{-1} = 1.1 \times 10^4\,M^{-1}$ at 25 °C.[12] Before the rate-determining steps, the Cu(II)HA⇄Cu(I)HA· and Cu(II)A⇄Cu(I)A· equilibria are considered, but no evidence of the presence of a radical was obtained.

Table 3. Effect of temperature and activation parameters

pH 4.95, $[CuSO_4]_0$ 3.01×10^{-4} M, $[H_2A]_0$ $(0.6—2.5) \times 10^{-4}$ M

Temperature (°C)	k' (sec^{-1})
24.5	70±3
32	137±3
38	281±4
42	360±6

$\Delta H^* = 17$ kcal, $\Delta S^* = 8.3$ cal/deg, $\Delta G^* = 15$ kcal

The dependence of k' on the temperature is given in Table 3. From the Arrhenius plot based on the theory of the transition state, the activation parameters of the present reaction were obtained as follows: $\Delta H^* = 17$ kcal/mol, $\Delta S^* = 8.3$ cal deg^{-1} mol^{-1} and $\Delta G^* = 15$ kcal/mol. These values are comparable with those in the copper(II)-catalyzed autoxidation of H_2A ($\Delta H^* = 15.5$ kcal/mol, $\Delta S^* = 14$ cal deg^{-1} mol^{-1} and $\Delta G^* = 11.3$ kcal/mol[12]).

The authors wish to thank Professor Keiji Kuwata, Department of Chemistry, Osaka University, for kindly putting EPR spectrometer at his disposal and for his valuable advice.

Catalytic Function of Metal Chelates in the Hydration of 2-Pyridinecarbonitrile

Ken-ichi WATANABE, Shigeo KOMIYA, and Shinnichiro SUZUKI*

Department of Chemistry, Faculty of Science, Tokyo Metropolitan University, Setagaya-ku, Tokyo 158

(Received November 1, 1972)

The catalytic effects of various transition metal complexes on the hydration of 2-pyridinecarbonitrile have been investigated. In these homogeneous catalytic reactions, free 2-pyridinecarboxamide was obtained as the sole reaction product. The transition metal species of the complexes used were Cu(II), Ni(II), Co(II), Co(III), and Pt(IV), while the ligands were ethylenediamine, bipyridine, glycine ion, and 2-pyridinecarboxamide. The complexes of Cu(II), Ni(II), and Co(II) were all catalytically active for the hydration, but those of Co(III) and Pt(IV) were inactive. No reaction occurred with 3- and 4-pyridinecarbonitriles under the same reaction conditions. The effect of the pH was remarkable. The active complex catalysts were classified into three types.

It has been reported[1,2] that 2-pyridinecarbonitrile is hydrated to afford the metal chelate of 2-pyridinecarboxamide by the catalytic action of transition metal ions such as Ni(II) or Cu(II). No hydration occurred with 2-pyridinecarbonitrile in a neutral solution without the metal ions. In this catalytic reaction, however, when an excess of 2-pyridinecarbonitrile was employed, free 2-pyridinecarboxamide was obtained together with its metal chelate, and the yield of the free amide increased with the reaction time.

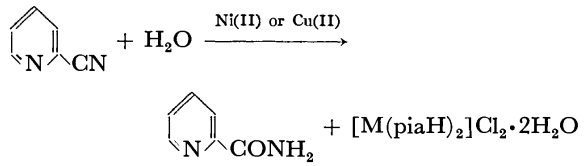

M: Metal ion
piaH: 2-pyridinecarboxamide

It has been proved[1] that the Ni(II) or Cu(II) chelate of 2-pyridinecarboxamide also shows catalytic activity for the hydration of 2-pyridinecarbonitrile.

With this view, we have taken up an idea that metal chelates other than Ni(II) and Cu(II) chelates of 2-pyridinecarboxamide may also act as catalysts for this hydration; we have found that some chelates have enough catalytic activities. A brief note has been already reported.[3]

In this paper, we will report in detail on our studies of the catalytic hydration of 2-pyridinecarbonitrile with various kinds of metal chelates. The relation between the nature and the catalytic activity of the complex catalysts will be discussed.

The meal species of the complexes used were Cu(II), Ni(II), Co(II), Co(III), and Pt(IV), and the ligands were ethylenediamine(en), 2,2′-bipyridine(bipy), glycine ion(gly), and 2-pyridinecarboxamide(piaH). These metal complex catalysts are summarized in Table 1. To make a comparison, aquo metal ions were also used as catalysts. It is characteristic that no hydrolysis occurred; that is, no ammonia was generated in these chelate-catalyzed reactions. The only product was 2-pyridinecarboxamide, and the complex catalysts were recovered without any change in all except a few cases.

TABLE 1. HYDRATION OF 2-PYRIDINECARBONITRILE WITH METAL CHELATES

2-pyridinecarbonitrile 0.0475 M, Reaction temp. 60 °C, Metal chelate 0.0058 M, Reaction time 5 hr

Exp. No.	Metal chelate	pH[a] S	pH[a] E	Yield of amide (%)
1	$[Cu(en)_2]Cl_2\cdot 2H_2O$	7.6	8.0	20
2	$Cu(gly)_2\cdot H_2O$	6.7	7.2	46
3	$[Cu(bipy)(NO_3)_2]3H_2O$	6.1	5.6	32
4	$[Ni(en)(H_2O)_4]SO_4\cdot H_2O$	6.3	6.7	20
		7.0	7.5	39
5	$[Ni(en)_3]Cl_2\cdot 2H_2O$	8.0	8.0	14
6	$[Ni(bipy)(H_2O)_4]SO_4\cdot 2H_2O$	6.3	6.2	16
7	$[Cu(piaH)_2]Cl_2\cdot 2H_2O$	6.3	6.3	48
8	$[Ni(piaH)_2]Cl_2\cdot 2H_2O$	6.5	6.6	29
9	$[Co(piaH)_2]Cl_2\cdot 2H_2O$	6.9	6.8	22
10	*cis*-$[CoCl_2(en)_2]Cl$	6.4	7.9	16
11	$[Co(en)_3]Cl_3$	6.7	6.8	0
12	$[Pt(en)_3]Cl_4$	7.3	6.9	0
13	$CuCl_2\cdot 2H_2O$	4.8	4.3	29
14	$NiCl_2\cdot 6H_2O$	6.9	6.1	30

a) pH: S, starting point; E, end point (after 5 hr reaction).

Results and Discussion

Generally, an aqueous solution of 2-pyridinecarbonitrile containing a complex catalyst was kept at 60 °C, and a definite quantity of the reaction mixture was sampled every hour. The samples were submitted to an ion-exchange column (Dowex 50×2, H-form) and developed with water. The eluate was a solution of unreacted pure 2-pyridinecarbonitrile, which was separated completely from the reaction mixture. The decrease in the amount of the starting material was followed spectrophotometrically at 272 nm, and the yield of the reaction product, 2-pyridinecarboxamide, was calculated.

In other experiments, aqueous reaction mixture con-

* Present address: Institute of Chemistry, College of General Education, Osaka University, Toyonaka, Osaka.

1) K. Sakai, T. Ito, and K. Watanabe, This Bulletin, **40**, 1660 (1967).

2) P. F. B. Barnard, *J. Chem. Soc., A*, **1969**, 2140.

3) S. Komiya, S. Suzuki, and K. Watanabe, This Bulletin, **44**, 1140 (1971).

taining 2-pyridinecarbonitrile and catalyst were refluxed and then concentrated to small amounts in order to be extracted with ether. From the ethereal solution, only 2-pyridinecarboxamide was obtained in a high yield. The metal complex catalyst was recovered from the water layer.

The labile complexes of Cu(II), Ni(II), and Co(II) were catalytically active. On the other hand, the inert Co(III) and Pt(IV) complexes were inactive.

The Effect of pH on the Hydration of 2-Pyridinecarbonitrile. The effect of hydroxide ions on the hydration was preliminarily examined without catalysts. The reactions were caused to proceed at 60 °C for 5 hr in the pH range of 2—11, and the reactivity of 2-pyridinecarbonitrile was examined spectrophotometrically as has been described above. No reaction occurred in the 2.5—9 pH range, but it proceeded rapidly above pH 10.

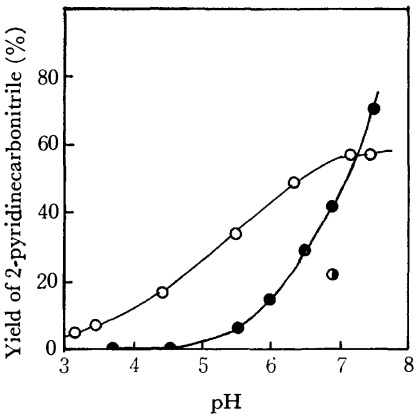

Fig. 1. Effect of pH on the hydration of 2-pyridinecarbonitrile with catalysts.
2-pyridinecarbonitrile: 0.0475 M, metal chelate: 0.00578 M, temp. 60 °C, time 5 hr.
○ $[Cu(piaH)_2]Cl_2 \cdot 2H_2O$, ● $[Ni(piaH)_2]Cl_2 \cdot 2H_2O$,
◑ $[Co(piaH)_2]Cl_2 \cdot 2H_2O$.
In our previous paper,[3] pH 6.0 of $[Ni(piaH)_2]Cl_2 \cdot 2H_2O$ (Fig. 1.) should be corrected to pH 6.5.

All the reactions with the complex catalysts proceeded in the 6—8 pH range. The pH dependence of these chelate-catalyzed reactions are remarkable; *e.g.*, the reactivity of 2-pyridinecarbonitrile was very low in the 9—10 pH range without catalysts, but the reaction with $[Ni(en)_3]Cl_2 \cdot 2H_2O$ was extremely fast in this pH range and the yield of 2-pyridinecarboxamide was about 75% after a 5 hr reaction. On the other hand, the yield decreased to 14% at pH 8 in the same reaction (Table 1). In order to investigate the effect of the pH in detail, solutions of 2-pyridinecarbonitrile and $[Ni(piaH)_2]Cl_2 \cdot 2H_2O$ or $[Cu(piaH)_2]Cl_2 \cdot 2H_2O$ were kept at 60 °C for 5 hr in the 3—7.5 pH range and the reactivities were examined. As is shown in Fig. 1, the reactivity becomes higher with a rise in the pH. Especially, for the nickel(II) complex, no reaction occurred below pH 4.5. The nickel(II) ion showed no catalytic activity at pH 3.9. 2-Pyridinecarbonitrile may not coordinate to the Ni(II) ion below pH 4.5. A solution of 2-pyridinecarbonitrile and nickel(II) chloride (1 : 1 mol) gave the same absorption spectrum as that of nickel(II) chloride at pH 3.8 and at room temperature.

Coordination of 2-Pyridinecarbonitrile. It is conceivable that the labile complexes exchange their ligands with the 2-pyridinecarbonitrile, and that, therefore, the hydration of the nitrile group occurs. The coordination of 2-pyridinecarbonitrile may be due to that of the nitrogen atom of the pyridine ring rather than that of the nitrile group. It is expected that 3- or 4-pyridinecarbonitrile also coordinates with the nitrogen atom of the pyridine ring. The catalytic hydration of the three kinds of pyridinecarbonitrile isomers was examined with $[Ni(en)(H_2O)_4]SO_4 \cdot H_2O$ and $Cu(gly)_2 \cdot H_2O$, but no reaction occurred with the 3- and 4-isomers. Thus, the effect of the coordination of 2-pyridinecarbonitrile is specific. It has been pointed out by Breslow[4] that the nitrile group of 1,10-phenanthroline-2-carbonitrile, although poorly placed for coordination, still has an interaction with the metal ion–Cu(II) or Ni(II)– and undergoes hydration.

Hydration of 2-Pyridinecarbonitrile. The results of the hydration of 2-pyridinecarbonitrile with various metal chelates are given in Table 1. The features of the reactions are not simple. In general, these homogeneous catalytic reactions proceed more rapidly at elevated temperatures. For example, the yield of amide was 22% in Exp. No. 9 (at 60 °C), but it became almost 100% when the reaction mixture was refluxed for three hours. However, no reaction occurred with the inert complex —Exp. Nos. 11—12— even when it was refluxed.

In the case of a metal ion-catalyzed reaction, 2-pyridinecarbonitrile first formed a complex with the metal ion, and then gradually underwent hydration along with a change in the color of the reaction mixture. However, when the initial pH value was about 7 or higher, metal ions afforded precipitates of thier hydroxides in the reaction systems. For this reason, the pH value of the reaction mixture was maintained in the acid region in Exp. No. 13. On the other hand, no hydroxides formed in the reaction with metal complexes, even in a basic solution. Further, metal complexes show different catalytic activities according to the kinds of thier ligands, as is shown in Table 1.

Function of Complex Catalysts. The catalytic functions of the complexes were classified into three types (Type I—III). Free 2-pyridinecarboxamide was obtained with the Type I and Type II complexes. The Type III complex afforded only the mixed complex.

Type I Complexes: The complexes used in Exp. Nos. 1, 2, 5, 7, 8, and 9 (Table 1) belong to Type I. They are recovered without any change after the reactions. Therefore, the complexes of Type I work as ideal catalysts.

Type II Complexes: The complexes used in Exp. Nos. 3, 4, and 6 belong to Type II. A part of their ligands is unidentate, NO_3 or H_2O. With these complexes, the hydration of 2-pyridinecarbonitrile proceeded, but the complexes were changed in composition after the reaction. For example, in the reaction with

4) R. Breslow, R. Fairwether, and J. Keana, *J. Amer. Chem. Soc.*, **89**, 2135 (1967).

$[Ni(en)(H_2O)_4]SO_4 \cdot H_2O$, the color of the reaction mixture changed from light blue to violet blue. The complex recovered was a mixture of tris(ethylenediamine)nickel(II) and bis(2-pyridinecarboxamide)nickel-(II).

Type III Complex: In Exp. No. 10 (Table 1), the catalytic behavior of *cis*-$[CoCl_2(en)_2]Cl$ was different from that of the labile complexes. The amount of reacted 2-pyridinecarbonitrile was 16% after 5 hr, but it was 18% even after a 15 hr reaction. After the reaction, an orange complex was obtained as the main product, and it had almost no catalytic activity.

Experimental

Materials. The 2- and 4-pyridinecarbonitriles (Tokyo Kasei Co., Ltd, Tokyo) were recrystallized from ether (mp 28.5—29.5 °C and 78—79 °C respectively). The 3-pyridinecarbonitrile (Aldrich Chemical Co., Inc.) was used without further purification (mp 49—50 °C). The $CuCl_2 \cdot 2H_2O$ and $NiCl_2 \cdot 6H_2O$ were extra-pure chemicals (Wako Junyaku, Tokyo). $[Cu(piaH)_2]Cl_2 \cdot 2H_2O$,[5] $[Ni(piaH)_2]Cl_2 \cdot 2H_2O$,[5] $[Co(piaH)_2]Cl_2 \cdot 2H_2O$,[5] $Cu(gly)_2 \cdot H_2O$, $[Cu(en)_2]Cl_2 \cdot 2H_2O$, $[Ni(en)(H_2O)_4]SO_4 \cdot H_2O$, $[Ni(en)_3]Cl_2 \cdot 2H_2O$, $[Co(en)_3]Cl_3$, *cis*-$[CoCl_2(en)_2]Cl$, $[Pt(en)_3]Cl_4$, $[Cu(NO_3)_2(bipy)]3H_2O$, and $[Ni(bipy)(H_2O)_4]SO_4 \cdot 2H_2O$ were all prepared and recrystallized several times (piaH: 2-pyridinecarboxamide, en: ethylenediamine, bipy: 2,2′-bipyridine, gly: glycine ion).

Blank Test. In a 25 ml volumetric flask, were placed 10 ml of a 2-pyridinecarbonitrile solution (0.119 M) and 10 ml of a buffer (pH 1—4: 0.1 M gly—0.1 M NaCl—0.1 M HCl, pH 4—7: 0.2 N CH_3COOH—0.2 N CH_3COONa, pH 7—12: 0.1 M gly—0.1 M NaCl—0.1 M NaOH): the content was then made up to 25 ml with distilled water. Ten ml of the solution was placed in a sealed glass tube and kept at 60 °C for 5 hr. The content was charged on a column of ion-exchange resin (Dowex 50×2, H-form) and developed with water. By this elution, only the unreacted 2-pyridinecarbonitrile was obtained. This solution was then diluted to a definite quantity and analyzed spectrophotometrically (λ_{max}=272 nm).

The VIS-UV absorption spectra were obtained with a Hitachi Recording Spectrophotometer EPS-3T.

Hydration of 2-Pyridinecarbonitrile with Metal Chelates or Ions. In a sealed glass tube, were placed 10 ml of a solution containing 2-pyridinecarbonitrile (0.0475 M) and the metal chelate or ion (0.0058 M). The mixture was adjusted to the pH range of 6.0—8.0 with small amounts of 0.1 N HCl or 0.1 N KOH solution, and was then kept at 60 °C for 5hr. After the reaction, an aliquot quantity of the reaction mixture was charged on a column of the cation exchange resin (column: diameter 1 cm, length 3 cm) and developed with water. Thus, unreacted 2-pyridinecarbonitrile was separated completely from the reaction mixture. The decrease in the amount of the starting material was followed spectrophotometrically at 272 nm, and the yield of the reaction product, 2-pyridinecarboxamide, was calculated. The only reaction product was 2-pyridinecarboxamide. Yield (%)=100−unreacted 2-pyridinecarbonitrile (%).

Hydration of 2-Pyridinecarbonitrile with Chelates under Reflux. Thirty ml of a solution containing 2-pyridinecarbonitrile (0.160 M) and chelate (0.02 M) was refluxed for 5 hr. Then, the reaction mixture was concentrated and extracted with ether several times. From the ethereal solution, the reaction product, pure 2-pyridinecarboxamide (white crystals) were obtained in the free form (about a 100% yield; mp 105 °C). No other reaction products were found. From the mother liquor, only the chelate was obtained.

Hydration of 3- and 4-Pyridinecarbonitriles with Metal Chelates. The reaction conditions were the same as in the case with 2-pyridinecarbonitrile. After the reaction, the content was charged on a column of ion-exchange resin (Dowex 50×2, H-form) and developed with a 5.5% ammonia solution. Then, the eluate was analyzed spectrophotometrically; no change of absorbance was observed (3-isomer, 265 nm; 4-isomer, 276 nm). Therefore, it was concluded that no reaction occurred with the two isomers.

In the other reaction, 60 ml of a solution containing 4-pyridinecarbonitrile (0.158 M) and $[Cu(en)_2]Cl \cdot 2H_2O$ (or $Cu(gly)_2 \cdot H_2O$) (0.019 M) was kept at 65 °C for 6 hr. After the reaction mixture has been extracted with ether several times, only the starting material was obtained from the ethereal solution. No 4-pyridinecarboxamide was found at all.

The authors wish to offer their hearty thanks to Professor Masayoshi Nakahara, Rikkyo University, for his valuable advice.

5) M. Sekizaki and K. Yamasaki, *Nippon Kagaku Zasshi*, **87**, 1053 (1966).

H^+ Ion Equilibria in Solutions of Copolypeptides of L-Lysine and L-Aspartic Acid and of L-Lysine and L-Glutamic Acid

M. Atreyi and R. C. Gupta
Department of Chemistry, University of Delhi, Delhi, India
(Received July 10, 1972)

pH and conductometric titration curves of copolypeptides containing L-lysine and either L-glutamic acid or L-aspartic acid residues have provided necessary evidence to believe that in the copolypeptides the zwitterion formation is complete at the isoionic point. The amounts of acid/alkali used up at the final inflexion/break in the titration curves agreed with the analytically determined quantity of basic/acid groups in the copolypeptides. Besides, the titration curves showed additional inflexions/breaks which distinguished between the various kinds of acid/basic groups present.

Polyamino acids, in particular, copolypeptides, serve as good model systems for understanding the behaviour of proteins. Investigations of the H^+ ion equilibria of copolypeptides in aqueous solutions had been shown[1-4] to be useful in studying conformational changes that occur on reaction with an acid or base. The role of vicinal charged sites on the titrations of polyacids, polybases, and polyampholytes, in general, had been worked out by Katchalsky *et al.*[5,6] but this aspect has received a rather limited attention in the study of polypeptide titrations. The abnormal behaviour of some proteins, however, had been explained[7-10] as arising out of such effects. Using non-peptidic ampholytes, the authors[11,12] had shown that a clear differentiation could be made, studying the titration behaviour of non-equimolar polyampholytes, between groups that take part and those that do not, in the formation of a zwitterion. Further, it had also been demonstrated that conductometric titrations, carried out for the first time on such systems, proved extremely useful in the identification and estimation of different kinds of prototropic groups. The present study is an application of the same kind of approach to the amphoteric polypeptides made up of L-lysine and L-aspartic acid/L-glutamic acid.

Experimental

N-Carboxy anhydrides (NCA) required for the polymerization were prepared starting from the corresponding amino acids, suitably protected, by using either directly phosgene or Leuch's method. The amino acids were modified as follows: L-glutamic acid to γ-benzyl L-glutamate,[13] L-aspartic acid to β-benzyl L-aspartate,[14] and L-lysine to α,ε,N-dicarbobenzoxy L-lysine.[15] Copolymerization was effected in dioxane (4%) with sodium methoxide (A/I=100) as initiator. After polymerization the protecting groups were removed simultaneously by treatment with HBr in acetic acid. The hydrobromide was converted to the free base by passing through a column of Amberlite IRA-400 in its hydroxy form. The isoionic form was obtained by passing through a mixed bed column of Amberlite IRA-120 and IRA-400.

Number-average molecular weights were determined following Sela and Berger.[16] Their amino acid composition was obtained following the method of Giri *et al.*[17]

The isoionic copolypeptide (10—15 mg) was dissolved in 20 ml of water in a titration vessel in which nitrogen could be swept continuously and was titrated with HCl/KOH (0.07—0.1N). pH/specific conductivity was measured after equilibration (2—5 min) after each addition of acid or alkali. A Leeds-Northrup conductivity (drum-type) bridge was used in conjunction with certified Sullivan resistances and a Muirhead Audio frequency oscillator. pH was measured with a Beckman Zeromatic pH meter. All adequate precautions such as using carbonate free alkali and maintaining an inert atmosphere were taken. Titrations were performed at room temperature (25—27°C).

Results and Discussion

Table 1 gives the amino acid composition of the copolypeptides, obtained as stated above, as also the amounts of acidic COOH groups and basic (NH_2) groups expected to be present. It can be seen that while A and C are acidic, B and D are basic. Considering these polypeptides as zwitterions, it follows that whereas the polypeptides under consideration have the acidic or the basic monomer in excess, at the isoionic point, there would be available in the molecule "free" carboxyl or amino groups which have not taken part in zwitterion. In other words, copolypeptides A and C would have the following prototropic groups available: i) COO^- anions, ii) COOH groups, and iii)

1) P. Doty, K. Imahori, and E. Klemperer, *Proc. Natl. Acad. Sci., U. S.*, **44**, 424 (1958).
2) K. Morita, E.R. Simon, and E.R. Blout, *Biopolymers*, **5**, 259 (1967).
3) A. Wada, *Mol. Phys.*, **3**, 409 (1960).
4) M. Nagasawa and A. Holtzer, *J. Amer. Chem. Soc.*, **86**, 538 (1964).
5) A. Katchalsky, J. Mazur, and P. Spitnik, *J. Polym. Sci.*, **23**, 513 (1957).
6) J. Mazur, A. Silbery, and A. Katchalsky, *ibid.*, **35**, 43 (1959).
7) L.M. Riddiford and H.A. Scheraga, *Biochemistry*, **1**, 95 (1962).
8) J. F. Foster and K. Aoki, *J. Phys. Chem.*, **61**, 1369 (1971).
9) H. B. Bull, R. L. Antrim, and K. Breese, *Arch. Biophys. Biochem.*, **110**, 163 (1965).
10) G. E. Perlmann, A. Oplatka, and A. Katchalsky, *J. Biol. Chem.*, **242**, 5163 (1967).
11) R. P. Mitra, M. Atreyi, and R. C. Gupta, *J. Electroanal. Chem.*, **15**, 399 (1967).
12) R. P. Mitra, M. Atreyi, and R. C. Gupta, *ibid.*, **17**, 227(1968).
13) H. Yuki, S. Sakakibara, and H. Tani, This Bulletin, **29**, 654 (1956).
14) A. K. Bose and R. E. Straube, *J. Pharm. Sci.*, **52**, 847 (1963).
15) H. Bergamann, L. Zervas, and W. F. Ross, *J. Biol. Chem.*, **111**, 245 (1935).
16) M. Sela and A. Berger, *J. Amer. Chem. Soc.*, **77**, 1893 (1955).
17) K. V. Giri, A. N. Radhakrishnan ,and C. S. Vaidyanathan, *J. Indian. Inst. Sci.*, **35**, 145 (1953).

Table 1. Amino acids analysis

Copolypeptide	Ratio of lys. to asp. acid residues	Ratio of lys. to glu. acid residues	mequiv. basic groups/100 g of copolypeptide	mequiv. acid groups/100 g of copolypeptide	Mol. wt.
A	1.00/1.59		322	516	21500
B	2.65/1.00		573	220	10700
C		1.00/1.27	342	436	15200
D		2.54/1.00	557	219	10700

NH_3^+ as the titratable groups. IR spectra fully support this in that B and D do not show any characteristic absorption for COOH group (1400 cm^{-1}).[18] Consequently, the copolypeptides A and C have only one kind of basic group, *viz.*, COO^-, to react with an acid, while B and D would have two kinds, COO^- and NH_2. In other words, copolypeptides having an excess of basic groups would be expected to have a two-stage reaction with acid and those with excess of acidic groups a two step reaction with alkali.

Figures 1 and 2 give the representative titration curves of the copolypeptides A and B with HCl and KOH, respectively. It can be seen that the conductometric titration curves marked (2) and (4), show fairly sharp breaks indicating the culmination of one type of reaction. The pH curves have corresponding inflexions, *i.e.*, changes in curvature, which are however less prominent. (In arriving at the position of the inflexions care was taken to scan the regions as carefully as possible with very small additions of acid or alkali and also checking with repetitive experiments. Also refer to modified plots.) Titration curves for the

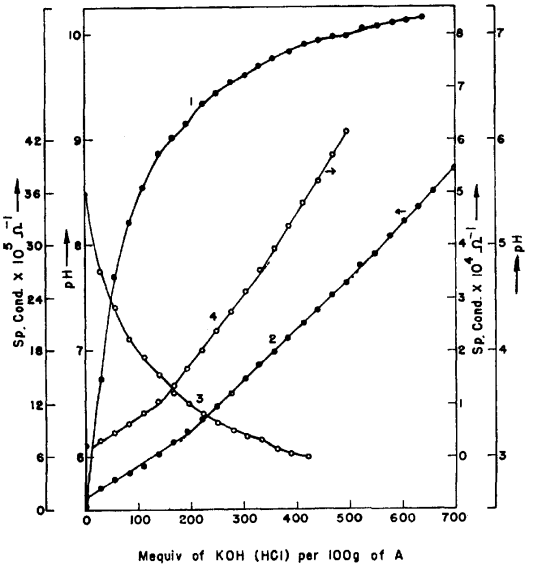

Fig. 1. Variation in pH (1,3) and sp. cond. (2,4) on addition of KOH/HCl to aq. solutions of isoionic copolypeptide A.

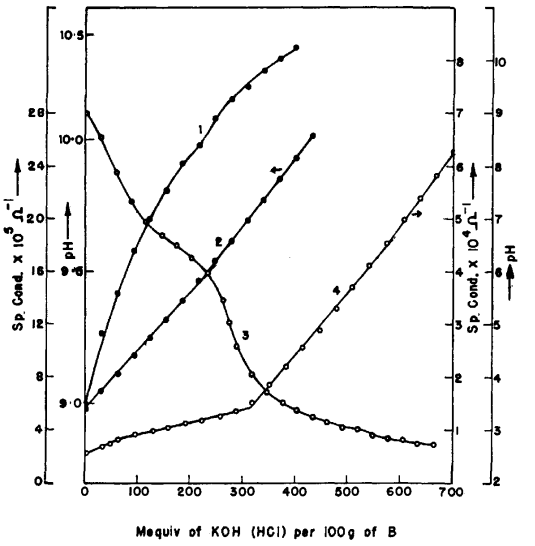

Fig. 2. Variation in pH (1,3) and sp. cond. (2,4) on addition of KOH/HCl to aq. solutions of isoionic copolypeptide B.

Table 2.

Copoly-peptide	Measurement	HCl added in mequiv./100 g at inflexion/break			KOH added in mequiv./100 g at inflexion/break		Total no. of prototropic groups	
		1st	2nd	3rd	1st	2nd	By titration	By analysis
A	pH	155	330		200	515		
	Cond.	150	330		190	520		
	Average	152	330		195	517	847	838
B	pH	55	275	550	230			
	Cond.	65	315	560	225			
	Average	60	290	555	227		782	793
C	pH	190	340		105	440		
	Cond.	195	335		110	435		
	Average	192	337		107	437	774	774
D	pH	65	315	535	235			
	Cond.	95	335	540	225			
	Average	80	325	537	230		767	776

18) E. R. Blout and M. Idelson, *J. Amer. Chem. Soc.*, **80**, 4909 (1958).

copolypeptides C and D are not given as they are very similar in nature to those of A and B. However, Table 2 summarizes the amounts of acid/base which had to be added to reach the various inflexions/breaks for all the copolypeptides.

In the first place it can be seen that the total amounts of acidic/basic groups which titrate with alkali/acid between the final inflexion/break in the titration curves are in fair agreement with the amount obtained from amino acid analysis. As to the fine features, it is interesting to note in what follows that as anticipated from the zwitterion structure the titration with alkali of A and C did show a two-stage reaction as against the one step reaction in copolypeptides B and D.

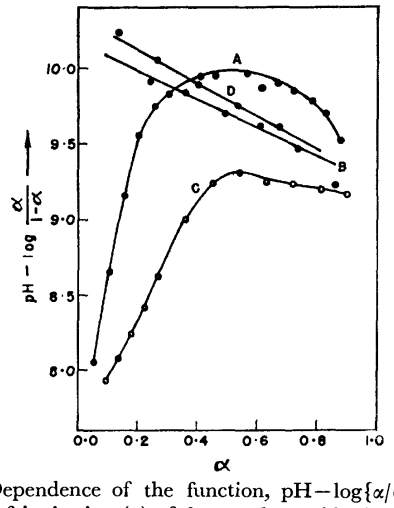

Fig. 3. Dependence of the function, pH−log{α/(1−α)} on degree of ionisation (α) of the copolypeptides in the alkaline region.

The first inflexion/break in the titration of A with KOH (Fig. 1, Curves 1, 2) corresponds to an addition of 195 milliequivalents (mequiv.)/100 g of A. The modified plot, α *versus* pH−log {α/(1−α)}, Fig. 3, shows a sharp change in curvature about the same region (α~0.35). Being an acidic polypeptide this should have two kinds of groups reacting with alkali and the first to react would be the COOH groups, not involved in zwitterion formation, followed by NH_3^+ cations. Amino acid analysis indicates (Table 1) that there would be 194 mequiv. (516—322) of COOH groups and 322 mequiv. of NH_3^+. The titration data leads to values of 195 and 322 mequiv./100 g which is in very good agreement with the expected values. In Fig. 3 can also be seen the modified plot of the acidic copolypeptide C, which is very similar to that of A and showing the expected behaviour of a two-stage neutralization phenomenon (Table 2).

Figure 1 (Curves 3, 4) gives the titration curve of copolypeptide A with HCl and the corresponding modified plots, β *versus* pH+log {β/(1−β)}, are presented in Fig. 4, which bring out the similarity between A and C more clearly. There is a two-stage neutralization against the one stage anticipated. It can be seen from Fig. 1 that it is the second inflexion/break at 322 mequiv./100 g of A that corresponds with the total anticipated COO^- anions of 330 mequiv./100 g (Table 2). The modified plots in Fig. 4 make it clear that in

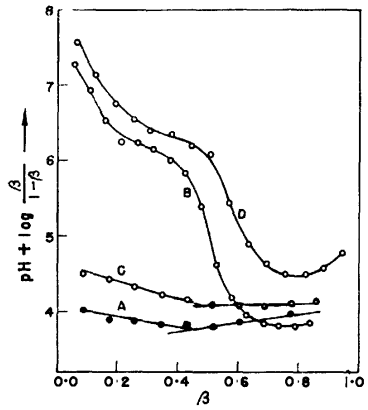

Fig. 4. Dependence of the function, pH+log {β/(1−β)} on the degree of ionisation (β) of the copolypeptides in the acidic region.

both A and C about half of the COO^- groups are stronger (the two segments in the modified plots cannot extrapolate to same pK) indicating the different energies of protonation for the carboxylate anions. This difference perhaps arises out of specific interactions such as hydrogen bond formation[19] and/or interactions between vicinally situated similar charges.[5]

Copolypeptides B and D, as suggested earlier, would be expected to have the ammonium cations as the only kind of acidic group to react with KOH. The modified plots, α *versus* pH−log {α/(1−α)} (Fig.3), show a linear behaviour and the representative titration curves of B (Fig. 2, Curves 1 and 2) show a single inflexion/break at the expected value (Table 2).

Titrations with the acid (HCl), as in the case of those with A and C, seem to deviate from the expected behaviour in having three instead of the two-stage reaction (see Table 2). Figure 3, showing the modified plots, also suggests the same and here again it appears that the protonation of NH_2 groups takes place in two stages followed by a single stage reaction of COO^- anions. This behaviour is again similar to that found in the case of polyvinylamine by Katchalsky *et al.*[5] where the vicinally situated prototropic groups were having a marked influence on their reactivity with acid.

To summarize, the amounts of COO^-, NH_2, and NH_3^+ groups found in the copolypeptides on titration are what one would expect on the basis of the assumption that zwitterion formation is complete at the isoionic point, and consistent with their chemical composition. The sequence in which the groups titrate follows the order $COO^- < NH_2 < NH_3^+$ of their pKs. The difference in the lengths of the side chains of L-aspartic acid and L-glutamic acid residues does not appear to influence the titration pattern of the copolypeptides, though this difference has been found to influence their conformation.[20]

The authors wish to thank Prof. R. P. Mitra for the fruitful discussions. Facilities provided by the Director, Shri Ram Institute for Industrial Research, Delhi (India) for the preparation of amino acid anhydrides are gratefully acknowledged.

19) H. Eisenberg, *J. Polymer Sci.*, **23**, 781 (1957).
20) J. Brahms and G. Spach, *Nature*, **200**, 72 (1963).

The Reaction of Nitriles under High Pressure. II. The Catalytic Effects of Amines and Water on the Formation of Trisubstituted 1,3,5-Triazines from Nitriles[1]

Masahiko YASUMOTO, Koshin YANAGIYA, and Masahiro KURABAYASHI

6th Division, National Chemical Laboratory for Industry[2] (Tokyo Kogyo Shikensho), Mita, Meguro-ku, Tokyo 153

(Received December 1, 1972)

When a mixture of benzonitrile and methanol is kept under a high pressure of a few thousand atoms at an elevated temperature, methyl benziminoether is produced and trimerized to triphenyl-1,3,5-triazine.[1] In the present study it was confirmed that the addition of ammonium salts or some nucleophiles with an active hydrogen atom such as water, amines, and ammonia at several per cents in the molar fraction increases the rate of the formation of this triazine by several times. It was found that the nucleophilic benzamidines produced by the reaction of benziminoether with amines attacked the second molecule of the iminoether and successively took the third iminoether molecule to form a triazine ring. The addition of water to the nitrile-methanol mixture produced amidine, methyl ester, amide, and amidinium carboxylate, of which the carboxylate exhibited the highest promotive effect. Some benzamidines were obtained in fairly good yields from amines and benzonitrile under similar high-pressure conditions. It is thought that this could be useful for synthesizing amidines.

It was found in a previous study[1] that triphenyl-1,3,5-triazine (TPT) is formed under high pressures by the cyclotrimerization of the benziminoether produced from benzonitrile and alcohol and that the triazine formation proceeds through the following reactions:

$$C_6H_5CN + ROH \longrightarrow C_6H_5C(=NH)OR \quad (1)$$

$$2\,C_6H_5C(=NH)OR \xrightarrow[\text{slow}]{-ROH} [C_6H_5C(OR)=NC(=NH)C_6H_5]$$

$$\xrightarrow{+C_6H_5C(=NH)OR} \text{TPT} + 2\,ROH \quad (2)$$

The formation was promoted by the addition of a dipolar aprotic substance such as dimethylformamide.[1] In the present investigation, the influence of protic substances other than alcohol on this reaction was examined under high pressures up to 10000 kg/cm^2.

It was revealed that the cyclotrimerization was intensely promoted by amidines or their salts, which were produced by the reaction of iminoether with substances such as water, ammonia, ammonium salts, and primary or secondary amines. These substances were added in catalytic amounts. The catalytic effects of these nucleophiles and salts were compared with the results obtained by Cairns, Larchar, and McKusick with ammonium acetate and concentrated aqueous ammonia as catalyzers[3] and with the results obtained by Kume and Moriyoshi with water.[4]

Results and Discussion

Influence of Amines. In contrast to the limited effect of tertiary amines with no active hydrogen atoms, ammonia, and primary or secondary amines showed a marked promotive effect on the production of TPT from benzonitrile in the presence of methanol, as is shown in Table 1. Methyl benziminoether (MBI),

TABLE 1. EFFECT OF VARIOUS AMINES ON THE FORMATION OF TPT IN THE MIXTURE OF BENZONITRILE AND METHANOL[a]

Exp. No.	Amines	C_6H_5CN : CH_3OH : Amine[b] (molar ratio)	Yields (%)[c]			
			C_6H_5CN	MBI[f]	TPT[f]	$C_6H_5C(=NH)NR^1R^2$[d]
1	—	1 : 3.2 : 0	56.7	41.8	1.6	
2	NH_3	1 : 3.2 : 0.05	38.0	38.6	18.3	4.6
3	n-$C_4H_9NH_2$	1 : 3.2 : 0.14	52.1	9.5	14.0	14.3
4	$(C_2H_5)_2NH$	1 : 3.2 : 0.14	46.7	8.8	28.3	6.6
5	$(C_2H_5)_3N$[e]	1 : 2.5 : 0.20	82.9	6.9	1.0	
6	Pyridine[e]	1 : 2.7 : 0.20	74.2	19.9	3.4	
7	$(C_2H_5)_2NH$	1 : 0 : 1	100			

a) Reaction conditions: 6600 kg/cm^2, 100 °C, 10 hr.
b) Molar ratio in the initial mixtures.
c) Theoretical yield based on benzonitrile.
d) R^1, R^2: H or alkyl groups corresponding to those of the added amines.
e) Results of these two runs have already been reported.[1]
f) The abbreviations of methyl benzimino ether and triphenyl-1,3,5-triazine respectively.

1) Part I of this series: M. Kurabayashi, K. Yanagiya, and M. Yasumoto, This Bulletin, **44**, 3413 (1971).
2) The name of this Institute, Government Chemical Industrial Research Institute, Tokyo, was formally changed in April, 1972.
3) T. L. Cairns, N. W. Larchar, and R. C. McKusick, US 2503979 (1950).
4) Y. Kume and T. Moriyoshi, Presented at the 6th Meeting of the High-Pressure Symposium, Tokushima, Japan, 1964.

Table 2. Effect of benzamidine on the formation of TPT in relation to that of ammonia[a)]

Exp. No.	Promoter	C_6H_5CN : CH_3OH : Promoter (molar ratio)	Yields (%)			
			C_6H_5CN	MBI	TPT	$C_6H_5C(NH)NH_2$
1	—	1 : 3.2 : 0	56.7	41.8	1.6	
2	NH_3	1 : 3.2 : 0.05	38.0	38.6	18.3	4.6
8	$C_6H_5C(NH)NH_2$	1 : 3.2 : 0.05	34.1	35.2	29.9	4.5

a) Reaction conditions were the same as those in Table 1.

which was found to be an intermediate[1)] in the above scheme of Eq. (1), was detected again in every run of the present experiment. Benzamidines were formed when benzonitrile, methanol, and one of the following substances ammonia and primary and secondary amine, were employed. These experimental results, as well as the fact that amidines are synthesized from amines and iminoethers under atmospheric pressure,[5)] indicate that the benzamidines were produced by the reaction of amines with the intermediate, MBI:

$$C_6H_5C(=NH)OCH_3 + RR'NH \quad (3)$$
MBI
$$\longrightarrow C_6H_5C(=NH)NRR' + CH_3OH$$
R, R': H or alkyl group

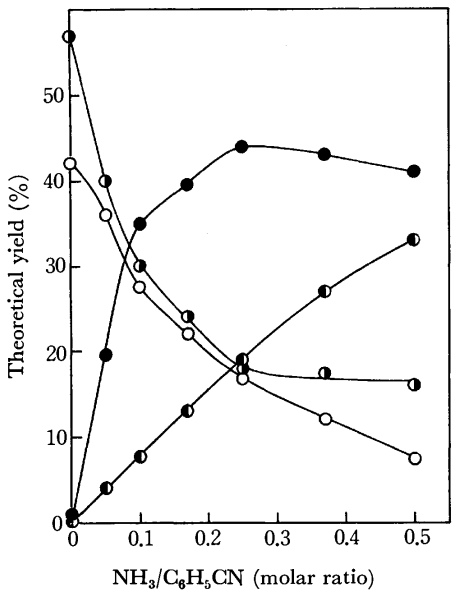

Fig. 1. Dependence of the yields of the reaction products on the amount of ammonia added to the mixture C_6H_5CN: CH_3OH = 1 : 3.2 in mol, at 6800 kg/cm² and 100 °C for 10 hr.
●: TPT, ◑: C_6H_5CN, ○: MBI, ◐: $C_6H_5C(=NH)NH_2$.

Figure 1 shows the relationship between the amount of ammonia added to the benzonitrile–methanol mixture and the amounts of the reaction products. The yield of benzamidine increased with the increase in the amount of ammonia added. The yield of TPT increased to a maximum when the amount of ammonia increased to 25 per cent in the molar fraction; above this fraction the yield decreased gradually, probably because of a decrease in [MBI] × [Benzamidine]. This may be evident from the mechanism described later. The increase in the rate of TPT formation by the addition of ammonia or amines may be assumed to be due to the catalytic effect of amidines derived from these additives. The assumption is supported by the experimental results listed in Table 2, which indicates that, in Exp. 8, the addition of benzamidine only 5 per cent of benzonitrile in the molar fraction yielded a large amount of TPT in the benzonitrile–methanol mixture in contrast to the small yield obtained without any additives in Exp. 1. On the other hand in Exp. 2 the addition of ammonia, the same molar fraction as the added benzamidine in Exp. 8, gave a fairly good yield of TPT amounting to 3/5 of that in Exp. 8 and yielded benzamidine in an amount nearly stoichiometrical to the added ammonia.[6)]

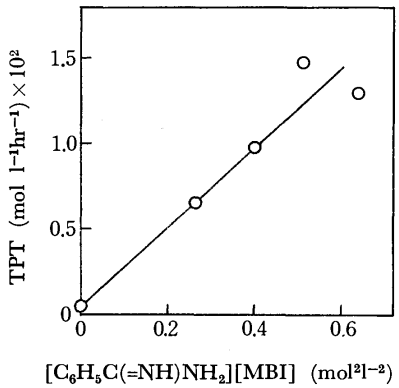

Fig. 2. Relation between the mean rate* of the formation of TPT and the concentrations of bemzamidine and MBI in the mixture C_6H_5CN: CH_3OH: NH_3 = 1 : 3.2 : 0—0.5 in mole, at 4500 kg/cm² and 100 °C for 10 hr.
* The mean rate of the formation of TPT (in mol $l^{-1}hr^{-1}$) is the value of the concentration of TPT divided by the reaction time. The volume of the reaction medium is assumed to be the sum of each volume of the initial material in the atmospheric pressure.

An approximately linear relationship was found between the rate of TPT formation and [MBI] × [Benzamidine] in Fig. 2. This suggests that TPT is produced *via* a rate-determining reaction in which an intermediate, *N*-benzimidoylbenzamidine(I), is formed by an attack of nucleophilic benzamidine on the carbon atom of MBI. This step is expected to proceed more favorably than the rate-determining reaction, Eq. (2), without a catalyzer. This is because benzamidine is a stronger nucleophile (base) than MBI. This step may be followed by the cyclic addition of another molecule

5) R. L. Schriner and F. W. Neumann, *Chem. Rev.*, **35**, 351 (1944); E. S. Hand and W. P. Tencks, *J. Amer. Chem. Soc.*, **84**, 3505 (1962); F. C. Schaefer and G. A. Peters, *J. Org. Chem.*, **26**, 412 (1961).

6) The existence of a benzamidine-rich equilibrium among methyl benziminoether, ammonia, benzamidine, and methanol under high pressures has been confirmed.

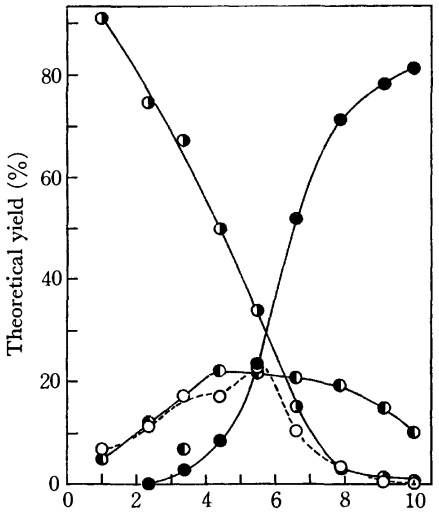

Fig. 3. Dependence of the yields of the reaction products in the mixture C_6H_5CN: CH_3OH: NH_3=1: 3.2: 0.25 in mole on the reaction pressure, at 110 °C for 10 hr.
●: TPT, ◑: C_6H_5CN, ○: MBI, ◐: $C_6H_5C(=NH)NH_2$.

of MBI to form TPT. This mechanism may be expressed as follows:

$$C_6H_5-C(=NH)-NH_2 + C_6H_5-C(=NH)-OR \xrightarrow{-ROH} \left[C_6H_5-C(NH_2)=N-C(=NH)-C_6H_5 \right] (I) \xrightarrow{+C_6H_5C(=NH)OR} TPT + NH_3 + ROH \quad (4)$$

Figure 3 shows that the effect of the pressure on the formation of TPT in the presence of ammonia is as remarkable as in the absence of ammonia.[1)]

Influence of Water. As is shown in Table 3 and Figs. 4 and 5, one of the remarkable effects of the water added to the benzonitrile–methanol mixture is the intense promotion of the TPT formation; another is the formation of benzamide, methyl benzoate, benzamidine, and benzamidinium benzoate. Some experiments were carried out in order to clarify the mechanism of the catalytic effect of water.

The same molar fractions of the by-products described above and some compounds related to the by-products were added to the benzonitrile–methanol mixture. The results of these experiments are listed in Table 4. Of these additives, benzamidinium benzoate and ammonium acetate promoted the TPT formation most. It is certain that the ammonium acetate added to the

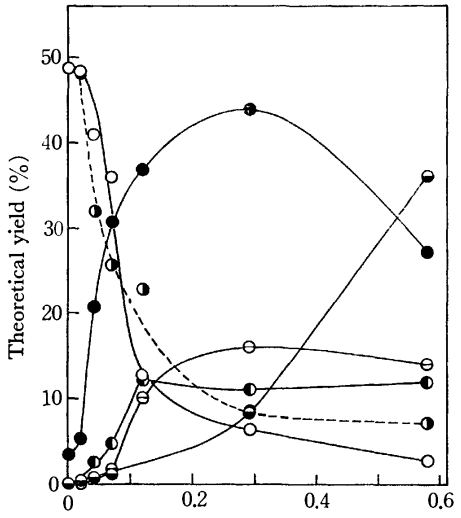

Fig. 4. Dependence of the yields of the reaction products on the amount of water added to the mixture C_6H_5CN: CH_3OH=1: 3.2 in mole, at 6800 kg/cm^2 and 100 °C for 10 hr.
●: TPT, ◑: C_6H_5CN, ○: MBI, ◒: $C_6H_5CONH_2$, ◐: $C_6H_5CO_2CH_3$, ⊖: $C_6H_5C(NH_2)_2 \cdot C_6H_5CO_2$.

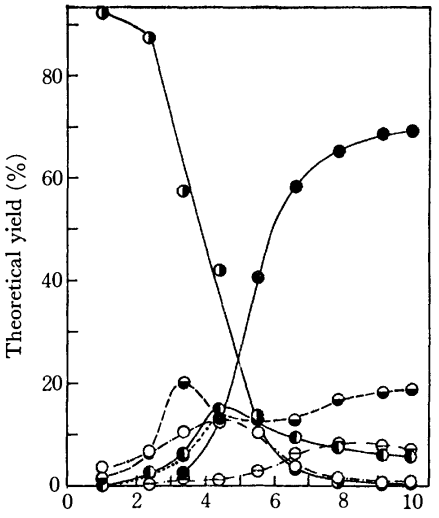

Fig. 5. Dependence of the yields of the reaction products in the mixture C_6H_5CN: CH_3OH: H_2O=1: 3.2: 0.25 in mole on the reaction pressure, at 110 °C for 10 hr.
●: TPT, ◑: C_6H_5CN, ○: MBI, ◒: $C_6H_5CONH_2$, ⊖: $C_6H_5C(NH_2)_2 \cdot C_6H_5CO_2$, ◐: $C_6H_5CO_2CH_3$, ------: $C_6H_5C(NH)NH_2$*.
* Determination of benzamidine was done only when the reaction pressure was less than 4400 kg/cm^2.

TABLE 3. EFFECT OF WATER ON THE FORMATION OF TPT IN THE MIXUTRE OF BENZONITRILE AND METHANOL[a)]

Exp. No.	C_6H_5CN: CH_3OH: H_2O (molar artio)	Yields (%)						
		C_6H_5CN	MBI	TPT	$C_6H_5C(=NH)-NH_2$	$C_6H_5C(NH_2)_2 \cdot C_6H_5CO_2$	$C_6H_5CONH_2$	$C_6H_5CO_2CH_3$
1	1 : 3.2 : 0	56.7	41.8	1.6				
9	1 : 3.2 : 0.04	32.4	41.0	20.6	+	1.5	1.1	2.6

a) Reaction conditions were the same as those in Table 1.

Table 4. Effects of both the by-products produced in the water-added mixture of benzonitrile and methanol and some reagents related to them on the formation of TPT in the benzonitrile and methanol mixture[a)]

Exp. No.	By-product and reagent	$C_6H_5CN : CH_3OH$: B&R (molar ratio)	Yields (%)						
			C_6H_5CN	MBI	TPT	$C_6H_5C(=NH)NH_2$	$C_6H_5C(NH_2)_2 \cdot C_6H_5CO_2$	$C_6H_5CONH_2$	$C_6H_5CO_2CH_3$
1	—	1 : 3.2 : 0	56.7	41.8	1.6				
8	$C_6H_5C(NH)NH_2$	1 : 3.2 : 0.05	34.1	35.2	29.9	4.5			
10	$C_6H_5C(NH_2)_2 \cdot C_6H_5CO_2$	1 : 3.2 : 0.05	12.9	6.8	74.1	+	+		
11	$C_6H_5CONH_2$	1 : 3.2 : 0.05	30.9	41.1	20.2	+	+	−2.2[b)]	4.4
12	$C_6H_5CO_2CH_3$	1 : 3.2 : 0.05	53.4	36.5	7.4				+
13	$NH_4 \cdot CH_3CO_2$	1 : 3.2 : 0.05	11.3	11.9	67.9	+	+		
14	$K \cdot CH_3CO_2$	1 : 3.2 : 0.05	18.5	15.1	1.0				

a) Reaction conditions were the same as those in Table 1.
b) Remainder of the substruction of the amount of the added benzamide from that of the observed benzamide in the reaction mixture.

benzonitrile–methanol mixture was converted to benzamidinium acetate, because several amidine salts are synthesized from iminoether salts and ammonia under atmospheric pressure. The fact that sodium acetate had no influence means that the formation of TPT is not influenced by a usual electrolyte. Therefore, the catalytic effects of those salts may be attributed merely to the benzamidinium cation. Figure 4 shows the noticeable yield of benzamidinium benzoate in the reaction with added water. Considering the strong effect of the amidinium cation as a catalyzer, it is likely that the greater part of the promotive effect of water is caused by the benzamidine benzoate derived from water. The rate-determining reaction is inferred to be the attack of the imino-nitrogen of MBI on the strongly positive carbon atom of the benzamidinium cation, which gives *N*-methoxybenzylidenebenzamidinium cation (II) as an intermediate. The whole reaction course is proposed to be as follows:

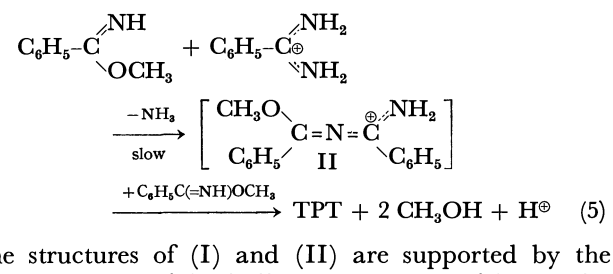

The structures of (I) and (II) are supported by the literature, in which similar compounds with a polyperhalogenomethylene group have been reported.[7)]

The route of the formation of methyl benzoate may be assumed to be Eq. (6), since the rapid hydrolysis of iminoether into the ester and ammonia under atmospheric pressure is well known:

$$C_6H_5C(=NH)OCH_3 + H_2O \longrightarrow C_6H_5COOCH_3 + NH_3 \quad (6)$$

The ammonia thus liberated will attack MBI to give benzamidine by means of Eq. (3). The nearly equimolar yields of the ester and amidine in the low pressure range shown in Fig. 5 support this reaction scheme.

The experiments shown in Table 5 were carried out to determine the route of benzamide formation in the benzonitrile–methanol mixture. The results of Exp. 15 shows that benzamide is produced more or less by the direct hydration of benzonitrile:

$$C_6H_5CN + H_2O \longrightarrow C_6H_5CONH_2 \quad (7)$$

However, when Exp. 15 is compared with Exp. 16, it appears that there is another route yielding benzamide with the aid of methanol. The hydrolysis of benzamidine is most likely, since this hydrolysis is known to take place smoothly under atmospheric conditions:

$$C_6H_5C(=NH)NH_2 + H_2O \longrightarrow C_6H_5CONH_2 + NH_3 \quad (8)$$

The hydrolysis of MBI to benzamide has not been reported. The ammonolysis of methyl benzoate is unlikely, since the reverse reaction, the methanololysis of benzamide to methyl benzoate, proceeds (see Exp. 17):

$$C_6H_5CONH_2 + CH_3OH \longrightarrow C_6H_5COOCH_3 + NH_3 \quad (9)$$

Benzamide promotes the TPT formation, as may be seen in Exp. 11 in Table 4. The promotion mechanism may be partially explained by Eq. (9).

The route of the formation of benzamidinium benzoate has not yet been clarified, although the overall reaction may be expressed as follows:

$$C_6H_5C(=NH)NH_2 + C_6H_5COOCH_3 + H_2O \longrightarrow C_6H_5C(=NH)NH_2 \cdot C_6H_5COOH + CH_3OH \quad (10)$$

Figures 4 and 5 show that the total amount of benzamide, methyl benzoate, and benzamidinium benzoate was nearly stoichiometrical to the added water. This indicates the fair stability of these by-products. Of these by-products, benzamide amounted to the largest part when much water was added. The addition of a small amount of water may be effective to obtain TPT in a good yield. The marked positive effect of pressure on the production of TPT as well as on the production of the by-products is shown in Fig. 5.

7) The polymer of perfluorogultaric acid (H. C. Brown, *J. Polymer Sci.*, **44**, 9 (1960)) and $CCl_3C(=NH)NHC(=NH)CCl_3$ (F. C. Schaefer, G. A. Peters, and V. P. Wystrach, *J. Amer. Chem. Soc.*, **81**, 1466 (1959)) correspond to (I). The hydrochloride of the dimer of perfluoroadipo(or glutaro-)iminoether (A. Ya. Yakubovcih, *et al.*, *J. General Chem. USSR*, **36**, 878 (1966)) corresponds to (II).

TABLE 5. ACTION OF WATER ON BENZONITRILE IN THE PRESENCE OR ABSENCE OF METHANOL, AND THE REACTION OF THE RESULTING BENZAMIDE WITH METHANOL[a)]

Exp. No.	C_6H_5CN:CH_3OH:H_2O:$C_6H_5CONH_2$ (molar ratio)	Yield (%)						
		C_6H_5CN	MBI	TPT	$C_6H_5C(=NH)NH_2$	$C_6H_5C(NH_2)_2 \cdot C_6H_5CO_2$	$C_6H_5CONH_2$	$C_6H_5CO_2CH_3$
15	1 : 0 : 1.15 : 0	86.1					11.2	
16	1 : 0.4 : 1 : 0	9.0		1.7			89.6	1.0
17	0 : 1 : 0 : 0.16						81.2[b)]	19.2[b)]

a) Reaction conditions were the same those as in Table 1.
b) These were calculated based on benzamide.

TABLE 6. EFFECT OF WATER ON THE TRIMERIZATION OF ACETONITRILE IN THE METHANOL SOLUTION[a)]

Exp. No.	CH_3CN:CH_3OH:H_2O (molar ratio)	Yield (%)			
		CH_3CN	TMT[c)]	CH_3CONH_3	$CH_3CO_2CH_3$
18	1 : 1.28 : 0	92.1	6.3		
19	1 : 1.22 : 0.12	48.0	38.9	5.4	3.8
20	1 : 1.15 : 0.23	28.7	39.9	13.2	5.2

a) Reaction conditions were similar to those in Table 1.
b) Theoretical yield based on acetonitrile.
c) The abbreviation of trimethyl-1,3,5-triazine.

TABLE 7. PREPARATION OF BENZAMIDINES UNDER HIGH PRESSURE[a)]

Exp. No.	Amine	C_6H_5CN:CH_3OH: Amine (molar ratio)	Yield (%)[b)]			
			C_6H_5CN	MBI	Amidine	TPT
21	NH_3	1 : 3.2 : 0.5	16.3	7.4	33.0 (65.7)	41.1
22	n-$C_4H_9NH_2$	1 : 1.5 : 0.7	16.6	3.2	69.1 (98.7)	4.8
23	$(C_2H_5)_2NH$	1 : 1.5 : 0.7	40.0	7.6	32.0 (44.6)	11.8

a) Reaction conditions were similar to those in Table 1.
b) Theoretical yield based on benzonitrile.
c) Theoretical yield based on the amine.

The reaction products in the mixtures of several combinations of acetonitrile, methanol, water, and acetamide under high pressures are listed in Table 6; the table indicates that the behavior of water in the acetonitrile–methanol mixture is similar to that in the benzonitrile–methanol mixture.

Reaction Conditions for Synthesizing Trisubstituted 1,3,5-Triazines. It is known that noticeable amounts of trisubstituted 1,3,5-triazines are produced in nitrile–alcohol mixtures without a catalyzer under pressures of more than 4000 kg/cm² and at temperatures of more than 100 °C.[1,2)] The rate of the triazine formation increases with an increase in the pressure or with an increase in the equilibrium concentration of iminoether.[1)] This concentration is altered parallel with the pressure and is dependent on the choice of nitrile and alcohol.[1)] The elevation of temperature increases the rate.[1)] However, at temperatures above 140 °C the formation of a by-product, *N*-methylbenzamidine,[8)] was remarkable in the benzonitrile–methanol mixture. The employment of the catalyzers described above may give rise to a rapid progress of the triazine formation, even in somewhat low ranges of the temperature and the pressure.

New Preparative Method of Amidines. Figure 3 shows that the yield of benzamidine increased, until it was nearly stoichiometrical to the added ammonia when the reaction pressure increased to about 5000 kg/cm², above that pressure range it gradually decreased. Those facts suggest the usefulness of this high-pressure reaction for preparing amidines by means of a good selection of reaction conditions. This usefulness is supported by the results listed in Table 7. This procedure is thought to be an excellent method for preparing amidines from nitriles because it does not need any catalyzer. The known one-step methods all require the keeping of nitriles at fairly elevated temperatures with more drastic agents than methanol, such as, ammonium halide, ammonium salts in ammonia,[9)] mixtures of amines and Lewis acids,[10)] and metal amides in benzene or ammonia.[11)]

Experimental

Reaction Apparatus and Procedure. An initial mixture for a reaction was placed in a collapsible lead capsule and was then kept in the desired conditions of pressure and tempera-

8) The route of the formation of the *N*-substituted amide is still unsolved, although one conceivable route is the Chapman rearrangement of the iminoether. The formation of *N*-methyl-2,3,3-tricyanoacrylamide from tetracyanoethylene and methanol at 5000 kg/cm² has been reported (M. Price and J. Horniak, *Chem. Commun.*, **1966**, 455).

9) E. F. Cornell, *J. Amer. Chem. Soc.*, **50**, 3311 (1928).
10) F. C. Schaefer and A. P. Krapcho, *J. Org. Chem.*, **27**, 1255 (1962).
11) P. Oxley, M. W. Partridge, and W. F. Short, *J. Chem. Soc.*, **1947**, 1110.

ture for the desired time, as has been described previously.[1]

Material Supply. The drying and distillation of EP-grade reagents, such as acetonitrile, benzonitrile, methanol, *n*-butylamine, diethylamine, and methyl benzoate, supplied this experiment with the samples of these substances. The water contents of benzonitrile and methanol were less than 0.017 per cent. Ammonia of a chemical grade was evaporated, dried on sodium hydroxide, and absorbed in methanol. The benzamide, ammonium acetate, and potassium acetate were of an EP-grade. The benzamidine was prepared from ethyl benziminoether hydrochloride[1] and ammonia[12] (mp 68.3 °C (80[13])). The melting point of the picrate was 228.5 °C. The benzamidinium benzoate was obtained by mixing an ethereal solution of benzoic acid with a stoichiometric amount of the benzamidine in a benzene solution and by recrystallizing the resulting raw product from water (mp 234.0 °C). Trimethyl-1,3,5-triazine (TMT) was prepared as follows: ethyl acetiminoether hydrochloride was prepared from acetonitrile and ethanol by Pinner's method. The iminoether was liberated by neutralization, fractionated at 87—90.5 °C, mixed with acetic acid (8 mol per cent of the iminoether), and kept at room temperature overnight.[14] The resulting TMT was extracted and distilled. The yield was 50.7 per cent (based on the iminoether) (bp 155 °C (155[14])); C, 58.38 (Calcd 58.52); H, 7.64 (7.37); N, 34.44% (34.12)).

Identification of Reaction Products. MBI and TPT: These substances were identified in a manner described previously.[1]

Amidines: A mixture of benzonitrile, ammonia, and methanol (1: 0.25: 3.2 in mole) was kept at 5500 kg/cm² and 110 °C for 10 hr. The reaction mixture was then separated from a volatile matter *in vacuo* and from TPT by extraction with toluene. A methanolic solution of picric acid was added to this mixture. Benzamidine picrate was precipitated and recrystallized from water to give yellow needles (mp 229 °C (232[15])); C, 44.73 (44.71); H, 3.01 (3.18); N, 20.51% (20.05); Infrared (IR) spectrum, 3400, 3200, 1675, and 1610 cm^{-1} for the amidinium group). The melting point was not decreased by mixing this picrate with the authentic sample described above. *N-n*-butylbenzamidine was collected at 170 °C by the fractionation of the reaction mixture of Exp. 22 by means of preparative gas-liquid phase chromatography (glc) (Reoplex-400, 9×750 mm, 70—200 °C, 4 °C/min, He 150 ml/min) (C, 74.52 (74.96); H, 9.22 (9.15); N, 15.42% (15.89); IR, 3250, 3050, 2930, 1645, 1600, 1570, 1360, 1190, 775, and 690 cm^{-1}). *N,N*-diethylbenzamidine was collected at 146 °C by the fractionation of the reaction mixture of Exp. 23 by the same procedure (C, 74.92 (74.96); H, 9.02 (9.15); N, 15.65% (15.89); IR, 3320, 3050, 2980, 1585, 1570, 1445, 1380, 1225, 1175, 775, and 700 cm^{-1}).

Benzamidinium Benzoate: A mixture of benzonitrile (2.39 g), methanol (2.29 g), and water (0.105 g) (1: 3.2: 0.25 in mol) was kept at 8000 kg/cm² and 110 °C for 10 hr. TPT was removed from the reaction mixture by filtration, and the volatile products were evaporated. The remaining crude benzoate, which amounted to 0.22 g (mp 210 °C; yield, 7.9% based on benzonitrile), was washed with toluene and recrystallized from water (mp 222.8 °C (230[16])); C, 69.53 (69.40); H. 5.91 (5.82); N, 11.65% (11.56); IR, 3200, 3000, 1710, 1610, 1570, 1520, 1490, 1390, 1035, 840, 720, and 690 cm^{-1}). The melting point was not decreased by mixing this crystal with the sample described above. The IR spectrum agreed with that of the sample as well.

Benzamide and N-Methylbenzamide: A mixture of benzonitrile (2.3 g), methanol (2.3 g), and water (0.10 g) (1: 3.2: 0.25 in mol) was kept at 4400 kg/cm² and 170 °C for 10 hr. The reaction mixture was fractionated by preparative glc (Reoplex-400, 9×750 mm, 100—205 °C, 4 °C/min, He 125 ml/min). *N*-Methylbenzamide (0.1 g) (4% based on the benzonitrile) was collected at 190—205 °C (mp 62.5 °C(75[17])); C, 71.33(71.09); H, 6.51(6.71); N, 10.27%(10.36); mol wt (from a parent peak of mass spectroscopy (MS)), 135(135.16); IR, 3350, 3050, 2950, 1640, 1550, 1490, and 1410 cm^{-1}). Benzamide was collected at 250 °C to give (0.8 g) (29% based on the benzonitrile). The melting point, 122 °C (128[13]), and the IR spectrum agreed with those of the authentic sample.

Methyl Benzoate and Acetate: Their presence in the reaction mixtures was assured by the agreement with the authentic samples on glc.

TMT: The reaction mixture of Exp. 19 was fractionated by preparative glc (DNP, 9×750 mm, 100 °C—, 2 °C/min, He 125 ml/min) to give 0.4 g at 121—127 °C (mp 58 °C (59—60[3])); C, 58.21(58.52); H, 7.48(7.37); N, 32.42%(34.12); mol wt (MS), 123 (123.15); IR, 2930, 1560, 1540, 1390, 1020, 925, and 765 cm^{-1}). The melting point, the retention time of glc, and the IR spectrum agreed with those of the authentic sample described above.

Acetamide: The reaction mixture of Exp. 20 gave 0.07 g at 150—174 °C by prepartive glc (Versamide, 9×750 mm, 60 °C—, 6 °C/min, He 125 ml/min) mp 73.5 °C(82.0[13]); C, 40.65(40.67); H, 8.59(8.53); N, 23.31%(23.71). The melting point, the retention time of glc, and the IR spectrum agreed with those of the authentic sample.

Methyl Acetate: This substance was identified from the agreement of the retention time in the glc of the reaction product of Exp. 20 with that of the authentic sample.

Analysis of Reaction Products. The yields of TPT in the reaction products were determined in a manner previously described.[1] The benazmidine was determined as the picrate. The benzamidinium benzoate was determined as a non-volatile and toluene-insoluble matter. The yields of the reaction products other than the above-mentioned substances were determined by two kinds of glc, Reoplex-400, 3×750 mm, 50—200 °C, 4 °C/min, He 25 ml/min and THEED+TEP, 3×2000 mm, 40—110 °C, 2° C/min, He 25 ml/min.

12) "Organic Synthesis," Coll. Vol. 1, (1941), p. 7.
13) "Kagaku Binran," Maruzen, Tokyo (1966), p. 335.
14) F. C. Schaefer and G. A. Peters, *J. Org. Chem.*, **26**, 2778 (1961).
15) H. H. Strain, *J. Amer. Chem. Soc.*, **49**, 1564 (1927).
16) A. Pinner, *Ber.*, **23**, 2936 (1890).
17) Beilstein, "Handbuch der Organische. Chemie," Bd. 9, H., p. 201.

The Reaction of Nitriles under High Pressure. III. The Cyclotrimerization of Aliphatic Nitriles in the Presence of Alcohols and the Rearrangement of the Resulting Trialkyl-1,3,5-triazines to 4-Aminopyrimidines[1]

Koshin YANAGIYA, Masahiko YASUMOTO, and Masahiro KURABAYASHI
6th Division, National Chemical Laboratory for Industry (Tokyo Kogyo Shikensho), Mita, Meguro-ku, Tokyo 153
(Received December 1, 1972)

The examination of the simultaneous formation of symmetrically tri-substituted 1,3,5-triazines, 4-amino-2,5,6-substituted pyrimidines and *N*-pyrimidylamidines in mixtures of lower alcohol and nitrile with more than two hydrogen atoms on the α-position under pressures of a few thousand atm afforded the following information: (1) the triazine is formed by the cyclo-trimerization of the iminoether which is derived from the nitrile and the alcohol; (2) the pyrimidine is formed by the rearrangement of the previously-formed triazine. This rearrangement is caused by an attack of the nucleophilic iminoether on a carbon atom of the triazine ring; and (3) the amidine is assumed to be formed, together with the pyrimidine, by the same attacking mechanism.

In 1952 Cairns, Larchar, and McKusic[2] found that the cyclo-trimerization of acetonitrile to 2,4,6-trimethyl-1,3,5-triazine accompanied the formation of 4-amino-2,6-dimethylpyrimidine and *N*-(2,6-dimethylpyrimidin-4-yl)-acetamidine when acetonitrile was kept under a few thousand atm in the presence of methanol or aqueous ammonia or piperidine at elevated temperatures, and that the triazine was slowly converted to the pyrimidine at 8500 kg/cm² and 150 °C in the presence of methanol. They reported that it was not evident to what extent the triazine may have been an intermediate to the pyrimidine in the trimerization of acetonitrile. This investigation was undertaken in an attempt to determine the mechanism of the conversion of nitriles with more than two hydrogen atoms on their α-carbons into the corresponding 2,4,6-tri-substituted 1,3,5-triazines (I) and the mechanism of the rearrangement of I to the isomeric 4-amino-2,5,6-tri-substituted pyrimidines (II) and to *N*-(2,5,6-substituted pyrimidin-4-yl)-amidine (III), which have the same moieties as the nitriles. Another aim was the elucidation of the above-mentioned unsolved problem proposed by Cairns *et al.*[2]

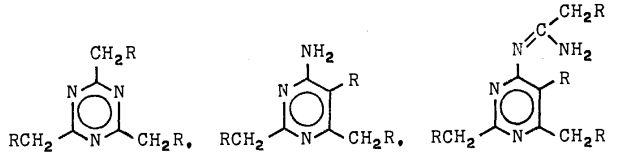

Iabc IIabc IIIabc

a: R=H, b: R=CH_3, c: R=C_2H_5

Results and Discussion

In order to get an overall view of this reaction, acetonitrile was chosen as the nitrile with more than two α-hydrogen atoms and was kept in lower alcohols or other popular solvents at 6600 kg/cm² and 120 °C for 10 hr. The results listed in Table 1 indicate that alcohol is the only promoter of the formation of Ia and that the promotive effect decreases with the increase in the molecular weight of alcohol.[3] The fact that the formation of IIa and IIIa was always accompanied by that of Ia was remarkable in connection with the mechanism of the formation of II and III, (which will be discussed below).

Table 1. Influence of solvents on the formation of Ia, IIa, and IIIa from acetonitrile

Solvent[b]	Reaction conditions			Yields (%)[a]		
	kg/cm²	°C	hr	Ia	IIa	IIIa
CH_3OH	7950	120	10	29.0	5.0	4.0
C_2H_5OH	7950	120	10	5.6	0.1	0.2
H_2O	6650	100	10			
$(C_2H_5)_2O$	6650	100	10			
$(CH_3)_2SO$	6650	100	10			

a) Theoretical yield based on nitrogen atom.
b) The weight of each solvent was the same as that of acetonitrile.

To examine the influence of the moieties of the nitriles, mixtures of ethanol and the same-weight acetonitrile or propionitrile or *n*-butyronitrile were kept under the same reaction conditions. The results are collected in Table 2. The yield of I decreased with the increase in the length of the alkyl chain in the moieties. Similar relations are found between the yield of II or III and the chain length. The fact that three

Table 2. Influence of the moieties of nitriles on the composition of reaction products[a]

R-CH_2CN	Yields (%)				
R	RCH_2CN	$RCH_2C(=NH)OC_2H_5$	I	II	III
H	83.1	1.8_7	11.2	1.5_8	1.5_5
CH_3	90.1	2.1_7	6.6_6	$(0.4)^{b}$	$(0.4)^{b}$
C_2H_5	96.7	1.4_8	1.2_5		

a) Reaction conditions: R-CH_2CN:C_2H_5OH=1:1 (by weight), 8000 kg/cm², 120 °C, and 30 hr.
b) These are assumed to be IIb and IIIb respectively.

1) Part II of this series, M. Yasumoto, K. Yanagiya, and M. Kurabayashi, This Bulletin, **46**, 2798 (1973).
2) T. L. Cairns, A. W. Larchar, and B. C. McKusic, *J. Amer. Chem. Soc.*, **74**, 5633 (1952).
3) This fact was similar to Cairns's data for benzonitrile[2].

Table 3. Influence of iminoether on the reaction products[a)]

CH_3CN (g)	$CH_3C(=NH)OC_2H_5$ (g)	(molar ratio)	C_2H_5OH (g)	Yields (%) Ia	IIa	IIIa
1.93	—	(1: 0)	2.17	16.2	7.1	5.2
1.40	1.50	(2: 1)	1.60	23.7	5.6	4.8
0.67	2.91	(1: 2)	0.68	28.4	7.5	5.5
—	5.03	(0: 1)	—	45.9	6.3	5.8

a) Reaction conditions: 7950 kg/cm², 120 °C, and 24 hr.

kinds of ethyl iminoethers were formed from the respective nitriles gives rise to the assumption that I is formed *via* an iminoether, which is known to be quickly produced from a nitrile and an alcohol under high pressures.[4)] To confirm this assumption, acetonitrile, ethyl acetiminoether, and a mixture of the two were kept in the presence of ethanol under the same pressure. As is shown in Table 3, the greater concentration of the iminoether in the initial mixture resulted the greater yield of Ia. This finding supports the above assumption, which is expressed by Eq. (1):

$$RCH_2CN + R'OH \longrightarrow RCH_2C(=NH)OR' \longrightarrow 1/3\,I + R'OH \quad (1)$$

A similar mechanism has been kinetically proven with an aromatic nitrile by the present authors.[4)]

In Fig. 1, the yields of the products in the acetonitrile–methanol mixture are plotted against the reaction time. In contrast to the gradual increases in the yields of IIa and IIIa with the lapse of the reaction time, the yield of Ia increased to a maximum when the reaction time passed about 50 hr and then decreased gradually with the gradual decrease in the acetonitrile. This fact indicates the conversion of the previously-produced Ia into IIa and IIIa. With the view of determining the mechanism of this conversion, several kinds of amines were added one by one to mixtures consisting of Ia and methanol in the same weight. These mixtures were kept under the same high-pressure conditions. The results are listed in Table 4. The formation of IIa and IIIa was seen

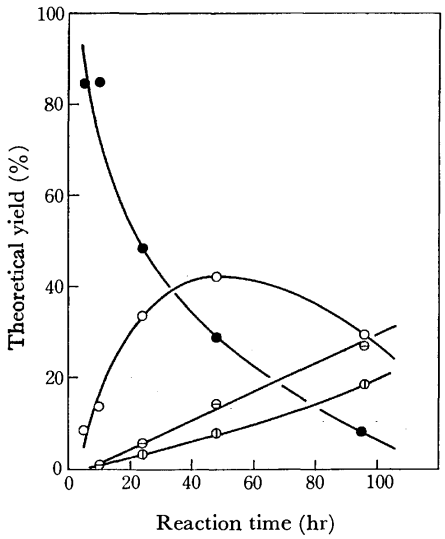

Fig. 1. Time dependence of the composition of the reaction products (theoretical yield based on nitrogen atom) at the starting ratio CH_3CN: CH_3OH=1: 1 (by weight) at 6600 kg/cm² and 100 °C.
●: CH_3CN, ○: Ia, ⊖: IIa, ⓘ: IIIa

only when an amine with less than one active hydrogen atom, such as ammonia, primary amine and secondary amine, was added.[5)] The yield of IIa increased with the increase in the number of the active hydrogen atoms of the additives. Considerable amounts of amines were recovered when ammonia or diethylamine was added, but when *n*-butylamine was added considerable

Table 4. Effect of amines on the rearrangement of I to II and III[a)]

Amines	Yields (%)[c)] CH_3CN[e)]	Ia	IIa	II'a[f)]	IIIa	Amine	Acetamidine[g)]
—[b)]		98.6		—		—	—
NH_3		41.2	38.9	—	5.6	(46.8)[d)]	[h)]
n-$C_4H_9NH_2$		27.3	11.3	42.1 (83.8)[d)]	14.8	[i)]	0.9 (5.2)[d)]
$(C_2H_5)_2NH$		94.9	0.7_5		1.0_7	(69.0)[d)]	3.6 (21.4)[d)]
$(C_2H_5)_3N$		98.8		—		—	—

a) Reaction conditions: Ia: Amine: CH_3OH=1: 0.5 (mole); 1 (weight), 8000kg/cm², 100 °C, and 30 hr.
b) In the case without amine, the mixture of same weight of Ia and ethanol was kept at 8000 kg/cm² and 120 °C for 24 hr.
c) Theoretical yield based on nitrogen in the initial Ia.
d) Figures putted in the parenteses are the theoretical yield based on the amines added.
e) Acetonitrile was never detected in the all runs listed in the table.
f) II'a means IIa with the moiety of added amine on its amino-nitrogen.
g) The yields of amidines were determined by use of glc. The details of the identification of them will be mentioned in a later report.
h) Acetamidine was expected to be produced, but its determination was prevented by the coexistence of inseparable Ia.
i) Ammonia yielded in 53% based on the added *n*-butylamine.

4) M. Kurabayashi, K. Yanagiya, and M. Yasumoto, This Bulletin, **44**, 3413 (1971).

5) The promotive effect of ammonia on the rearrangement of Ib to IIb has already been reported.[2)]

amounts of 2,6-dimethyl-4-*n*-butylaminopyrimidine (II'a) and ammonia were isolated without any recovery of *n*-butylamine. The following rearrangement mechanism is proposed for the conversion of I into II and II' on the basis of these experimental results:

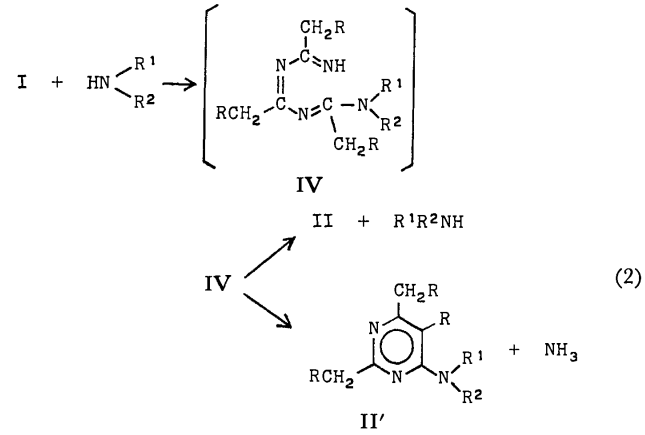

(2)

A triazine ring is attacked on its carbon atom by a neucleophilic nitrogen atom of amine. An open-chain intermediate (IV) is formed by the cleavage of the ring involving the shift of a hydrogen atom of the attacking amine. A ring closing takes place accompanied by a twist of the C–N bond and an elimination of the amine or ammonia. These eliminations both give II and II'.

It may be inferred that, when a reaction is initiated in a nitrile–alcohol mixture, the intermediate iminoether behaves as an amine with an active hydrogen atom and causes I to shift to II and III in the manner shown by Eq. (3):

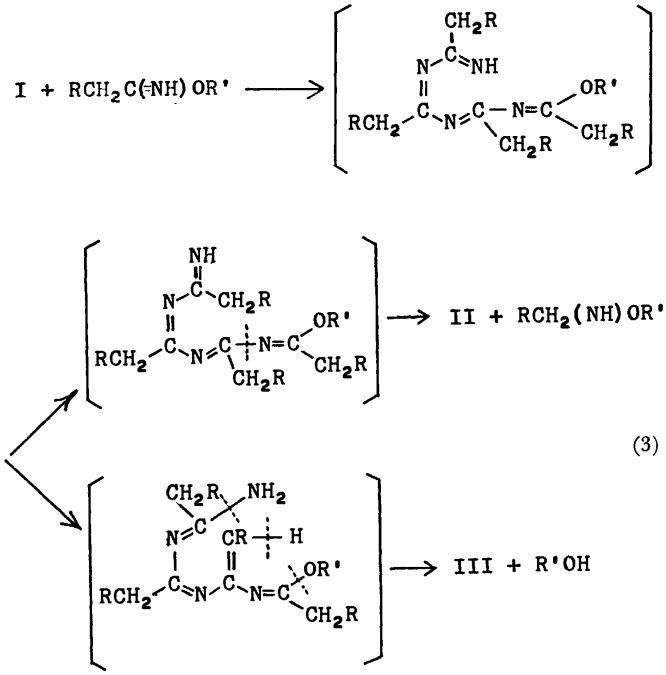

(3)

This inference is supported by the experimental results listed in Table 5, in which larger yields of IIa and IIIa are seen both in the ethanolic solution of acetonitrile and Ia and in the ethanolic solution of ethyl acetiminoether and Ia than in the ethanolic solution of acetonitrile alone, while no yield of IIa is seen in the ethanolic solution of Ia alone.

It is assumed that the small amounts of acetamidines, which were isolated in the Ia–methanol–amine mixtures (see Table 4), are formed by the partial decomposition of the IVa intermediate to an amidine and acetonitrile:

$$\text{IV} \longrightarrow \text{RCH}_2\text{C(=NH)NR}^1\text{R}^2 + 2\,\text{RCH}_2\text{CN} \qquad (4)$$

It is also assumed that methyl acetiminoether is formed from the acetonitrile thus liberated to satisfy the equilibrium of Eq. (1) and that it attacks Ia to form IIa and IIIa by means of Eq. (3). These assumptions are substantiated by the experimental results that small amounts of IIIa are formed in Ia–methanol–amine mixtures (see Table 4).

It is not speculated that III is formed by an attack of an amino-nitrogen of II on an iminoether under high pressure because of the experimental finding that IIa and ethyl acetiminoether were recovered unreacted from an ethanolic solution of them after a long reflux.

$$\text{CH}_3\text{C}(=\text{NH})\text{OC}_2\text{H}_5 + \text{IIa} \not\longrightarrow \text{IIIa} \qquad (5)$$

On the other hand, we ignored the possibility that, if I is attacked by an amino-nitrogen of II, the resulting IV will give III by means of Eq. (4); we did this in view of the experimental finding that IIIa was not detected in a methanolic or pyrimidine solution of an equimolar mixture of Ia and IIa after 30 hr's standing at 8000 kg/cm² and 120 °C.

$$\text{Ia} + \text{IIa} \not\longrightarrow \left[\text{IVa, R}^1\text{=H; R}^2\text{=}\right.\text{ 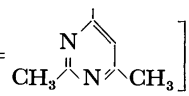 }\left.\right] \not\longrightarrow \text{IIIa} + 2\,\text{CH}_3\text{CN} \qquad (6)$$

As is shown in Figs. 2 and 3, the elevation of both the reaction pressure and the temperature caused the yields

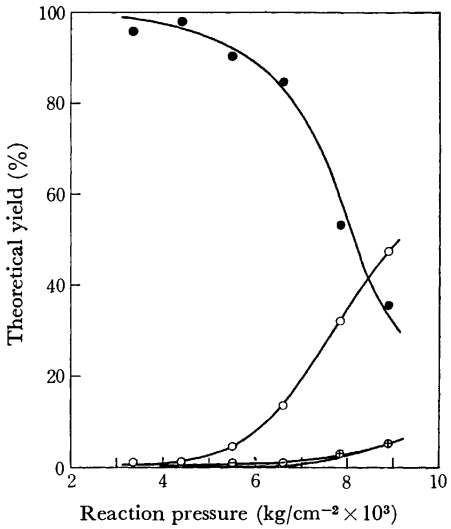

Fig. 2. Pressure dependence of the composition of the reaction products at the same starting ratio CH_3CN/CH_3OH as shown in Fig. 1 at 100 °C for 10 hr.
●: CH_3CN, ○: Ia, ⊖: IIa, ◐: IIIa.

Table 5. Effect of nitrile or iminoether on the rearrangement of Ia to IIa and IIIa in the presence of ethanol[a)]

CH_3CN (g)	$CH_3C(=NH)OC_2H_5$ (g)	Ia (g)	C_2H_5OH (g)	Yields (%)[b)]			
				CH_3CN	Ia	IIa	IIIa
1.47	—	—	1.64	85.7	6.5_9	0.4_4	0.2_9
0.74	—	0.73 (3:1)[c)]	1.65	37.1	41.5	3.8_0	7.1_2
—	1.54	0.73 (3:1)	0.82	24.7	51.5	5.6_4	7.4_2
—	—	1.46	1.64		96.5		

a) Reaction conditions: 8000 kg/cm², 120 °C, and 8 hr.
b) Theoretical yield based on nitrogen in the initial mixtures.
c) Molar ratio of CH_3CN or $CH_3C(=NH)OC_2H_5$ to Ia.

Table 6. Identification of triazines produced in the runs listed in Table 2

Triazines	Preparative glc			Elementary analysis Found (%)			mol wt		IR spectra for triazine ring
	Column conditions	Retention time (min)	Yields (g)	C	H	N	(MS)[a)]	(Calcd)	(cm^{-1})
Ia	DNP, 100°C—, 2 °C/min	13.2	0.42	58.21	7.48	32.42	123	(123.15)	1560, 1540, 1435
Ib	Carbowax-1500, 67 °C—, 4 °C/min	17.4	0.14	65.32	9.16	26.27	165	(165.24)	1540, 1460, 1420
Ic	Polyphenylether(6-ring), 150 °C	15.9	0.21	69.73	10.30	20.24	207	(207.31)	1550, 1535, 1420

a) From a parent peak of mass spectroscopy.

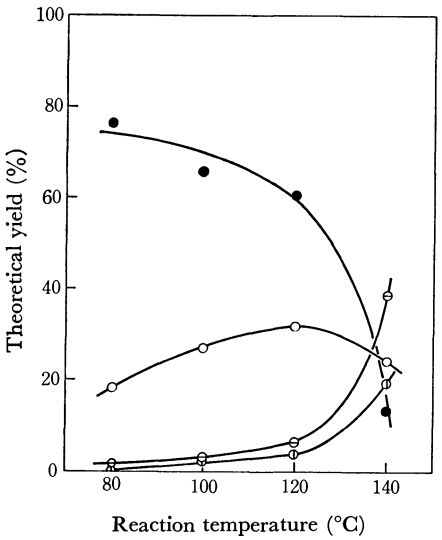

Fig. 3. Temperature dependence of the composition of the reaction products at the same starting ratio CH_3CN/CH_3OH as shown in Fig. 1 at 8900 kg/cm² for 5 hr.
●: CH_3CN, ○: Ia, ⊖: IIa, ⓘ: IIIa.

of Ia, IIa, and IIIa to increase and also caused the yield ratio of IIa to Ia and that of IIIa to Ia to increase. One of the most reasonable interpretations of this experimental fact may be that these elevations promote not only the production of Ia but also the conversion of Ia into IIa and IIIa.[6)]

It is certain that, in a mixture of nitrile and alcohol under high pressures, II and III are produced by the reaction of I with iminoether, although it can not be decided whether this route is the only possible one for the formation of II and III.

Experimental

Reaction Apparatus and Procedure. A mixture of the starting materials was placed in a collapsible lead capsule, was held in a pressure vessel, and was kept under the desired reaction conditions of pressure, temperature, and time by means of a previously-described high-pressure apparatus and procedure.[4)]

Material Supply. The nitriles, alcohols, amines, glacial acetic acid, and solvents were all EP-grade reagents and were dried and distilled. A commercial-grade ammonia was evaporated, dried on sodium hydroxide, and absorbed in methanol.

Ethyl Iminoethers: An iminoether was prepared from a nitrile and ethanol as a hydrochloride by Pinner's method and was liberated by neutralization. $CH_3C(=NH)OC_2H_5$: bp 87—90.5 °C(91[7)]); C, 55.54(55.15 Calcd); H, 10.46(10.41); N, 15.31%(16.08). $C_2H_5C(=NH)OC_2H_5$: 58—59 °C/110 mmHg(110—111[7)]); 59.62(59.37); 11.10(10.96); 13.61% (13.85). n-$C_3H_7C(=NH)OC_2H_5$: 54—55 °C/70 mmHg, 63.03 (62.57); 11.17(11.38); 11.97%(12.16). Methyl acetiminoether was obtained as a mixture containing large amounts of methanol and acetonitrile because of its instability at distillation.

Trialkyl-1,3,5-triazines: These triazines were prepared by the procedure of Schaefer and Peters,[7)] in which an iminoether was cyclotrimerized by the addition of a small amount of acetic acid. Trimethyl-1,3,5-triazine (Ia): yield, 50.7%; bp 155 °C(155[7)]); mp 58.1 °C(59—60[2)]); C, 58.38(58.52); H, 7.64(7.37); N, 34.44%(34.12). Triethyl-1,3,5-triazine (Ib): 74%; 123—125 °C/90 mmHg(128—130/90[7)]); 23 °C(25[7)]); 65.63(65.42); 9.18(9.15); 25.19(25.43). Tri-*n*-proply-1,3,5-triazine (Ic): 36%; 120 °C/13 mmHg(71—72/1[8)]); 69.83 (69.52); 10.01(10.21); 20.16%(20.27).

4-Amino-2,6-dimethylpyrimidine (IIa): The procedure of

6) It will be reported shortly by the present authors that the ring-opening of trialkyl-1,3,5-triazines, similar to that shown by Eq. (3) under high pressures is promoted by the elevation of the pressure or the temperature.

7) F. C. Schaefer and G. A. Peters, *J. Org. Chem.*, **26**, 2778 (1961).

8) A. Ya. Yakubovich, E. L. Zaitseva, G. I. Broz, and V. P. Bazov, *Chem. Abstr.*, **58**, 526 (1963).

Ronzio and Cook as modified by Cairns *et al.*[2] was employed. Acetonitrile was kept in an autoclave with a small amount of sodium methoxide at 150 °C for 12 hr; this yielded the pyrimidine in a 53.8% yield (mp 184.4 °C(182—183[2])); N, 33.63%(34.12)).

4-Chloro-2,6-dimethylpyrimidine: The aminopyrimidine (6.16 g) (0.05 mol) was dissolved in concentrated hydrochloric acid (10 ml) (0.11 mol); the solution was placed in a test tube and then cooled. A concentrated sodium nitrate solution (0.1 mol) was then gently poured into the bottom of the tube. The reaction mixture was neutralized after it had stood overnight and was extracted with ether. The extract was distilled to yield the chloropyrimidine (2.88 g, 46.8%) (bp 82 °C/15 mmHg(182[9])); mp 7.3 °C(7[9])); C, 50.42(50.54); H, 5.09(4.95); N, 18.42(19.65); Cl, 24.11%(24.86).

2,6-Dimethyl-4-n-butylaminopyrimidine (II'a, R^1: H, R^2: n-C_4H_9): A mixture of 4-chloro-2,6-dimethylaminopyrimidine (1.62 g) (0.011 mol) and *n*-butylamine (1.66 g) (0.022 mol) was heated on a water bath. The amount of pyrimidine aimed at in the reaction mixture was determined to be 1.59 g (77.6%) by means of gas-liquid phase chromatography (glc) glc-a (Reoplex-400, 3×750 mm, 50—200 °C, 4 °C/min, He 25 ml/min). When the mixture was fractionated by preparative glc (Carbowax-20 M, 9×750 mm,[10] 220 °C, He 125 ml/min) it gave essentially one fraction (0.5 g) with the retention time of 6—9 min. Found: C, 64.60; H, 9.53; N, 23.10%; infrared (IR), 2960, 2932, 2872, 2862, 1468, 1460, 1384, and 734 cm^{-1} for the *n*-butyl group, 1600, 1505, 1440, and 1360 cm^{-1} for the pyrimidine ring. Calcd for $C_{10}H_{17}N_3$: C, 67.00; H, 9.56; N, 23.44%.

Identification of Reaction Products. *Iminoethers*: Each experiment listed in Table 2 gave one peak of iminoether upon glc-b (Carbowax-1500, 3×1000 mm, 47 °C, He 25 ml/min). These peaks agreed with the corresponding peaks of the authentic samples described above (ethyl acetiminoether: 5.5 min; ethyl propio-: 7.8 min; ethyl *n*-butyro; 16.7 min). Ethyl propioiminoether (0.01 g) was isolated by glc (Carbowax-1500, 67 °C—, 4 °C/min). The IR spectrum of this fraction (3350, 3000, 1655, 1465, 1380, 1345, 1280, 1090, and 835 cm^{-1}) agreed with that of the authentic sample described above.

Trialkyl-1,3,5-triazines: The reactions listed in Table 2 each gave one fraction of triazine in a preparative glc (see Table 6). The retention times of glc-a and the IR spectra of these fractions agreed individually with those of the authentic samples described above.

IIa and IIIa: The mixture of acetonitrile (4.08 g) and methanol (4.08 g) was kept at 145 °C and 8900 kg/cm^2 for 30 hr. The reaction product was then removed from a volatile matter *in vacuo* and co-distilled with kerosene (25 ml) to yield a yellow solid (1.46 g). This solid was extracted with petroleum ether. The residue amounted to 0.79 g. The 0.79 g portion was recrystallized from toluene to yield a white powder (0.62 g) (mp 182—184 °C; C, 58.61 (58.52); H, 7.54 (7.37); N, 33.73% (34.12); λ_{max}^{MeOH} 235 mμ (234, EtOH[2])); log ε, 4.11 (4.02, EtOH[2])); IR, 1594, 1541, 1478, and 1410 cm^{-1} for the pyrimidine ring). These data and the retention time of glc-a agreed with those of the above-described authentic sample of 4-amino-2,6-dimethylpyrimidine. The extract (0.37 g) was recrystallized from petroleum ether to give yellow needles (0.28 g) (mp 148.5 °C (147—148[2])); C, 58.21 (58.52); H, 8.29 (7.37); N, 33.76% (34.12); λ_{max}^{MeOH} 340 mμ (340, EtOH[2])); log ε, 4.51 (4.49, EtOH[2])); IR, 1530 and 1420 cm^{-1} for the pyrimidine ring). This crystal is identical to *N*-(2,6-dimethylpyrimidin-4-yl)-acetamidine.

IIb and IIIb: The reaction products from propionitrile and ethanol listed in Table 2 gave two peaks of glc-a. The former peak, at the retention time of 31 min, is assumed to be that of 4-amino-2,6-diethyl-5-methylpyrimidine. The latter peak, at 35 min, is assumed to be that of *N*-(2,6-diethyl-5-methylpyrimidin-4-yl)-propioamidine.

II'a (R^1: H, R^2: n-C_4H_9): The reaction products from Ia and *n*-butylamine listed in Table 4 were removed from the volatile matter and fractionated by glc (Carbowax-20 M, 312 °C); this gave a fraction (0.2 g) at the retention time of 9 min (C, 66.81; H, 9.49; N, 23.69%; mol wt (from a parent peak of mass spectroscopy), 179 (Calcd 179.25)). These data, the results of glc-a, and the IR spectrum agreed with those of the authentic 2,6-dimethyl-4-*n*-butylaminopyrimidine described above.

Analysis of Reaction Products. The yields of the reaction products were determined mainly by the use of glc-a, but also sometimes by the use of glc (Reoplex-400, 4×2000 mm, 110 °C, He 90 ml/min).

9) J. Schmidt, *Ber.*, **35**, 1575 (1902).

10) The column size and the flow rate of helium for the preparative glcs were always the same in these experiments.

The Reaction of Nitriles under High Pressure. IV. The Replacement of the Substituents of Trialkyl-1,3,5-triazines[1]

Koshin YANAGIYA, Masahiko YASUMOTO, and Masahiro KURABAYASHI

6th Division, National Chemical Laboratory for Industry, Mita, Meguro-ku, Tokyo 153

(Received December 1, 1972)

It was found that, when some symmetrically 2,4,6-tri-substituted 1,3,5-triazines are kept with an iminoether or an amidine under high pressures and at elevated temperatures, unsymmetrically 2,4,6-tri-substituted 1,3,5-triazines are produced by way of the replacement of one or two $\diagup N \diagdown C \diagup R$ groups of the triazines with the $-N=\overset{|}{C}-R'$ group of the iminoether or that of the amidine. Several mixtures of nitriles and methanol can be used for this replacement reaction in place of iminoethers or amidines at 4000—8000 atm and 100—150 °C. In these mixtures, equilibrium amounts of methyl iminoethers are rapidly formed. Increases in the size of the substituents of the original triazine and in their electron-releasing power inhibit this replacement reaction. Nitriles with an electron-releasing moiety give tri-substituted triazines replaced selectively by one of the original substituents.

There have been reported no excellent method giving tri-substituted 1,3,5-triazines with two or three different kinds of substituents in a molecule. The stepwise method from cyanuric halide,[2] as one example, requires many synthetic steps and gives a poor yield. The co-trimerization of two kinds of nitriles[3,4] or iminoethers[5] or amidines,[6] and the co-trimerization of an iminoether and an amidine, each of which has a different moiety,[7] as a second example, gives a mixture of four kinds of tri-substituted 1,3,5-triazines, each of which has a different combination of the three substituents. The distribution among the yields of the four triazines was substantially governed by statistical laws, although some cases have been reported in which a triazine with a certain combination of substituents was selectively produced.[4,6,7] The method of substitution on the less available unsubstituted 1,3,5-triazine with iminoethers[8] or amidines,[9] as a third example, gives mono- and di-substituted 1,3,5-triazines, but no tri-substituted one.

It has been made clear[1] that some trialkyl-1,3,5-triazines are rearranged to 4-amino-2,5,6-trialkylpyrimidines by the attack of a nucleophile with an active hydrogen atom, such as primary and secondary amines and ammonia, under a pressure of a few thousand atm in the following manner:

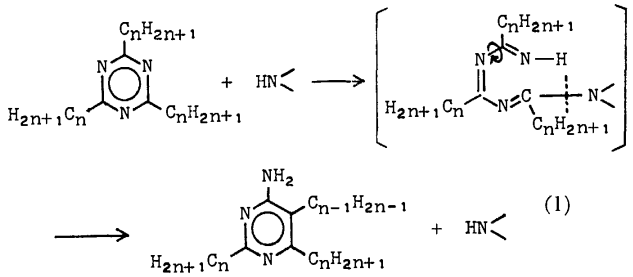

(1)

It was assumed from this rearrangement mechanism that, if a trialkyl-1,3,5-triazine (R_3) is treated with an iminoether ($R'-C\langle^{NH}_{OR''}$) or an amidine ($R'-C\langle^{NH}_{N\langle}$), each of which has a different moiety from the substituents of the triazine, at least one of the three substituents (R) of the triazine may be replaced by the moieties (R') according to the following reaction scheme;

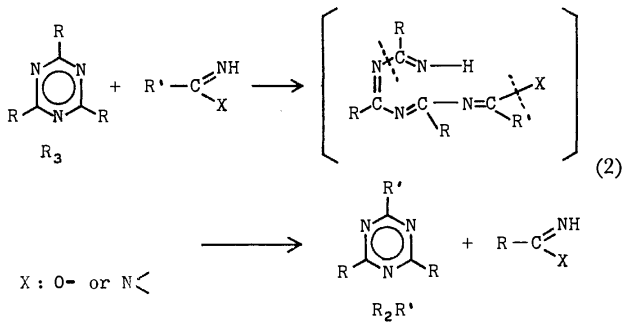

(2)

On the other hand, it is known[10] that an equilibrium amount of iminoether is quickly formed in a mixture of a nitrile and a lower alcohol by means of Eq. (3):

$$R'CN + R''OH \rightleftharpoons R'C\begin{matrix}\diagup NH \\ \diagdown OR''\end{matrix} \qquad (3)$$

Therefore, a mixture of R_3, nitrile R'CN and methanol was kept at 6000—9000 kg/cm² and 100—150 °C. As a result, a mono-replaced triazine (R_2R') was obtained in a good yield. The reaction scheme of Eq. (2) was thus proved actually to take place.

Iminoethers and amidines are known to be synthesized from nitriles under atmospheric pressure. Therefore, many mixtures of nitriles and lower alcohols are thought to be better reagents than iminoethers or amidines for this reaction. This finding may offer a

1) Part III of this series: K. Yanagiya, M. Yasumoto, and M. Kurabayashi. This Bulletin, **46**, 2804 (1973).

2) E. M. Smoline and L. Rapoport, "*s*-Triazine and Derivatives," Interscience Publishers, New York (1959), p. 154.

3) C. Grundmann, G. Weiss, and S. Seide, *Ann. Chem.*, **577**, 77 (1952).

4) K. Wakabayashi, M. Tsunoda, and Y. Suzuki, This Bulletin, **42**, 2924 (1969); *ibid.*, **44**, 148 (1971).

5) E. L. Zaitseva, G. I. Braz, A. Ya. Yakubovich, and V. F. Bazob, *Zh. Obshch. Khim.*, **33**, 199 (1963); *Chem. Abstr.*, **58**, 13957 (1963).

6) a) F. C. Schaefer, I. Hechenbleikner, G. A. Peters, and V. P. Wystrach, *J. Amer. Chem. Soc.*, **81**, 1466 (1959); b) F. C. Schaefer, U. S. 3294798 (1966).

7) Amer. Cyanamid Co., Brit. 905545 (1962).

8) F. C. Schaefer and G. A. Peters, *J. Org. Chem.*, **26**, 2784 (1961).

9) F. C. Schaefer and G. A. Peters, *J. Amer. Chem. Soc.*, **81**, 1470 (1959).

10) M. Kurabayashi, K. Yanagiya, and M. Yasumoto, This Bulletin, **44**, 3413 (1971).

TABLE 1. EFFECT OF PRESSURE ON THE REACTION OF BENZONITRILE WITH Me_3[a] IN THE PRESENCE OF METHANOL[b]

Reaction pressure (kg/cm²)	Yields (%)[c]								
	MeCN	PhCN	PhC(=NH)OMe	Me_3[a]	Me_2Ph[a]	$MePh_2$[a]	Ph_3[a]	Pyrimidine[d]	Amidine[d]
2000	11.9	65.9	3.66	81.5	18.1				
4000	40.8	24.9	4.52	41.5	65.7	1.39			
6000	40.4	1.13	0.70	15.8	94.7	2.97	0.43	3.04	1.11
7950	34.2	0.25	trace	16.8	91.6	3.85	0.44	6.30	2.68
8000[e]		72.9		87.4	6.12				

a) These symbols mean the tri-substituted 1,3,5-triazines with the substituents represented by the each symbol.
b) Reaction conditions: mixtures of Me_3, benzonitrile (the same molar amount with Me_3), and methanol (the same weight with Me_3) were kept at 100 °C for 30 hr under the various pressures.
c) Mole fraction based on Me_3.
d) Abbreviations of 4-amino-2,6-dimethylpyrimidine and *N*-2,6-dimethylpyrimidin-4-yl-acetamidine respectively.
e) Methanol was not added.

useful method for the preparation of unsymmetrically tri-substituted 1,3,5-triazines. Some electronic or steric properties of the original substituent and those of the introducing radical, and the relationship between the former and the latter, were shown to have a marked influence on this replacement reaction.

Results and Discussion

The trimethyl-1,3,5-triazine (Me_3), benzonitrile and methanol were kept at 100 °C and 2000—8000 kg/cm² as is shown in Table 1. Methanol was chosen from among the lower alcohols because of the highest equilibrium constant in Eq. (3) among those of the lower alcohols.[10] The reaction scheme proposed by Eq. (2) is supported by the fact that, in contrast to the good yield of Me_2Ph and the fair yields of acetonitrile and methyl benziminoether (MBI) in the presence of methanol at 6000—8000 kg/cm², only an inconsiderable amount of Me_2Ph was yielded without methanol at the same pressure. The progress of the reaction of Eq. (1) was negligibly slow in comparison with that of Eq. (2).

Table 1 shows the marked positive effect of the pressure on this replacement reaction. The ratio of the yield of Me_2Ph at 4000 kg/cm² to that at 2000 kg/cm² was 3.63: 1. This pressure effect is assumed to be due to two factors. One of them is an increase in the equilibrium concentration of iminoether in Eq. (3) with an increase in the pressure, and the other is an increase in the rate constant of Eq. (2) with an increase in the pressure. Here Eq. (2) is supposed to be the rate-determining step. The equilibrium concentrations at the initial point of the reactions at 4000 and 2000 kg/cm² are calculated on the bases of the experimental results reported in a previous paper.[10] These concentrations amount to 0.733 and 0.360 mol l^{-1} respectively.[11] The ratio of the former to the latter amounts to 2.04: 1.[12] This ratio is considerably smaller than the ratio in the yields of Me_2Ph, 3.67: 1 described above. It is clear from these examinations that the pressure effect depends not only upon the increase in the equilibrium constant with an increase in the pressure, but also partially upon the increase in the rate constant of Eq. (2) with that increase. The latter dependence is supported also by the experimental results listed on the first line of Table 2. On the line it is shown that hardly no substituent of Me_3 was replaced by MBI without an increase in the pressure, even at a high concentration of MBI. This high concentration was attained by starting the reaction with a mixture of benzonitrile, MBI, and methanol; it was kept over the equilibrium level throughout the reaction time. It is clear that this replacement reaction does not take place under a pressure of less than a few thousand atm; it starts either with a mixture of R_3 and iminoether or with a mixture of R_3, nitrile, and alcohol.

TABLE 2. REACTION OF METHYL BENZIMINOETHER WITH Me_3 WITHOUT INCREASING PRESSURE[a]

Additive	Yields (%)[b]					
	PhCN	PhC(=NH)OMe	Me_3	Me_2Ph	$MePh_2$	Ph_3
—	3.50	69.1	102.2	2.95		
Et_3N	24.7	47.2	101.8			
EtONa	54.8	7.23	99.1			
AcOH	36.5	6.07	97.5	5.78		13.0

a) Reaction conditions: Me_3: PhC (NH)OMe: MeOH = 1: 1 (in mole): 1 (in weight to Me_3), 100 °C, 30 hr under the saturated pressure of methanol (≈3 kg/cm² gauge.). The lead capsules were filled with the mixtures and placed in an autoclave which was filled with methanol to protect the capsules from rupture.
b) Mole percent based on Me_3.

11) It may be permissible to discuss the results at 100°C on the basis of the data calculated by means of the previously-obtained results at 110°C, because the difference between the pressure dependence of the equilibrium constant at 100°C and that at 110°C is negligible.

12) A smaller value than this can be expected when the calculation is done on the bases of the average concentration in the course of the reaction.

Table 3. Influence of the molar ratio of Me_3 to benzonitrile in the initial mixtures on the yields of the substituent-replaced triazines[a)]

Me_3 (g)	Me_3:PhCN (mol)	PhCN (g)	MeOH (g)	Yields (%)[b] MeCN	PhCN	PhC(=NH)OMe	Me_3	Me_2Ph	$MePh_2$	Ph_3	Pyrimidine	Amidine
0.512	1 : 1	0.430	0.648	24.89			10.2	84.0	7.88	0.24	19.6	4.86
0.465	1 : 1.5	0.586	0.468	26.00	7.33	1.31	3.70	103.6	18.7	1.63	9.05	0.70

a) Reaction conditions: 6000 kg/cm², 150 °C, 30 hr.
b) Mole percent based on Me_3.

Schaefer and Peters reported that, when 1,3,5-triazine was kept with some iminoethers[8] or amidines,[9] a substitution took place on the 2- or 2- and 4-position of the triazine through a scheme similar to Eq. (2). This difference in reactivity between substituted and unsubstituted 1,3,5-triazines may be caused by the difference in the electron-releasing power between the substituent and the hydrogen atom and by the difference in size between them (see below).

The mixtures of Me_3, MBI, methanol, and a small amount of acids or bases were kept at 100 °C without increasing the pressure with a view to getting a promoter for this replacement reaction. Table 2 shows that this attempt resulted in failure. Acids and bases did not noticeably influence the replacement, but did promote the dissociation of MBI to benzonitrile and methanol.

It is certain that a nitrile eliminated by Eq. (2) is partly re-cyclized to the original triazine, since it is known that nitrile is cyclotrimerized with the help of a lower alcohol under high pressures by means of Eq. (4):[1,10,13]

$$RCN + R''OH \rightleftharpoons R\text{-}C(=NH)OR'' \longrightarrow 1/3\,R_3 + R''OH \qquad (4)$$

Equation (2) is then transformed as Eq. (5) to give the stoichiometrically maximum ratio of R_2R' to R_3:

$$R_3 + 3/2\,R'CN \longrightarrow 3/2\,R_2R' \qquad (5)$$

The results collected in Table 3 indicate that the employment of more than the equimolar amount of benzonitrile to Me_3 was effective in increaseing the yield of Me_2Ph based on Me_3, although nearly quantitative yield by means of Eq. (5) was less possible because of the progress of such side reaction as Eqs. (1), (4), (6), and (7).

The influence of the property of the nitrile moiety on the replacement reaction was examined by keeping equimolar mixtures of Me_3 and various nitriles in methanol under high pressures. The results are shown in Table 4. In the cases of aromatic nitriles, nearly theoretical yields of Me_2R' were obtained. In the case of propionitrile, the only case of an aliphatic nitrile, not only the yield of Me_2R', but also the sum of the yields of Me_2R' and MeR'_2, was far less than the theoretical yields, while the ratio of the yield of MeR'_2 to that of Me_2R' was larger than those in the cases of aromatic nitriles. From these experimental results, the following considerations may be derived. Aromatic iminoether is more basic than aliphatic iminoether[14] probably because of the highly resonating structure of the iminium cation with the aromatic moiety. Therefore, aromatic iminoether may be more active in the replacement reaction, but the resulting mono-replaced triazine may be protected from the next replacement by the increasing density of the π-electron on the carbon atoms of the triazine ring. The increase in the density is caused by the strong electron-releasing power of the newly-introduced aromatic substituent. While aliphatic iminoether is less active in the replacement, the resulting mono-replaced triazine is subject to the next replacement, because the next attack of the iminoether may be less inhibited because of the less electron-releasing property of the newly introduced aliphatic substituent;

$$R_2R' + R'\text{-}C(=NH)X \longrightarrow RR'_2 + R\text{-}C(=NH)X \qquad (6)$$

Table 4. Influence of the moieties of nitriles on the substituent-replacement of Me_3[a)]

R'-CN R'	Me_3 : R'-CN (mol)	Reaction pressure (kg/cm²)	Yields (%) Me_3	Me_2R'	MeR'_2	R'_3
Et	1 : 1	6000	27.7	28.0	9.17	1.04
Ph	1 : 1	6000	15.8	94.7	2.97	0.43
p-$CH_3C_6H_4$	1 : 1	6000	10.8	95.2	1.71	
	1 : 1	8000	22.7	104.6		
p-ClC_6H_4	1 : 1	6000	12.0	92.0	2.20	0.88
β-Naphthyl	1 : 0.70	8000	34.9	70.6		
γ-Pyridyl	1 : 1	8000	39.5	75.1	4.52	4.84

a) Reaction conditions: Me_3: MeOH = 1 : 1 by weight, 100 °C, 30 hr.
b) Mole percent based on Me_3.

13) T. L. Cairns, N. W. Larchar, and B. C. McKusic, *J. Amer. Chem. Soc.*, **74**, 5633 (1952).

14) R. Roger and D. G. Neilson, *Chem. Rev.*, **61**, 179 (1961).

TABLE 5. INFLUENCE OF THE SUBSTITUENTS ON THE SUBSTITUENT-REPLACEMENT OF TRI-SUBSTITUTED 1,3,5-TRIAZINES WITH NITRILES (R'-CN)[a]

Substituents of original 1,3,5-triazine	R'-CN R'	Reaction conditions (kg/cm²)	(°C)	(hr)	Yields (%)[b] R'-CN	R'C(=NH)OMe	R_3	R_2R'	RR'_2	R'_3
Me_3	Ph	6000	100	30	0.91	0.58	15.8	94.7	2.97	0.43
Et_3	Ph	6000	100	30	49.0	21.7	75.2	29.7	1.10	0.73
n-Pr_3	Ph	6000	100	30	52.1	24.4	82—96	19.8		1.73
Me_2Ph	Ph	6000	100	30	56.6	29.4		100.4		3.56
		6000	150	30	19.9	8.3		90.1	17.4	11.2
Ph_3[c]	Me	6000	100	30	+		97.1			+

a) Reaction mixtures: triazine: R'-CN: MeOH=1: 1 (in mol): 1 (in weight to the triazine).
b) Mole per cent based on the trisubstituted triazines.
c) Ph_3 0.103 g, MeCN 0.979 g (1: 72 in mol), and MeOH 3.82 g were mixed to make into a solution.

TABLE 6. CO-TRIMERIZATION OF TWO KINDS OF NITRILES (R^1-CN AND R^2-CN) UNDER HIGH PRESSURE IN THE PRESENCE OF METHANOL, INDICATING THE DISTRIBUTION OF THE RESULTING FOUR TRISUBSTITUTED 1,3,5-TRIAZINES[a]

R^1-CN R^1	(g)	R^2-CN R^2	(g)	R'-CN: R^2-CN (mol)	MeOH (g)	Yields R^1_3 (g)	(%)[b]	$R^1_2R^2$ (g)	(%)[b]	$R^1R^2_2$ (g)	(%)[b]	R^2_3 (g)	(%)[b]
MeCN	1.050	PhCN	1.315	2 : 1	2.366	0.104	8.27	1.123	59.2	0.814	32.1	0.016	0.49
MeCN	0.372	PhCN	1.857	1 : 2	2.230	0.0062	0.60	0.209	13.5	1.323	64.3	0.556	21.6
MeCN	2.026	EtCN	2.716	1 : 1	4.744	0.161	9.51	0.665	35.2	0.835	40.1	0.345	15.2

a) Reaction conditions: 9150 kg/cm², 120 °C, 24 hr.
b) Mole per cent among the four triazines.

TABLE 7. REACTION OF BENZAMIDINE WITH Me_3 AT 6000 kg/cm AND 100 °C FOR 30 hr

Me_3 (g)	PhC(=NH)-NH_2 (g)	Me_3: $PhC(NH)NH_2$ (mol)	Dioxane (g)	Yields (%)[a] MeCN	PhCN	PhC(NH)-NH_2	Me_3	Me_2Ph	$MePh_2$	Ph_3	Pyrimidine	Amidine
1.573	1.490	1 : 1	2.369	8.54	3.56	6.50	42.6	41.9	6.52	1.18	· 4.53	10.9

a) Mole percent based on Me_3.

The influence of the chain length of the original substituents on this replacement reaction is shown in Table 5. The fact that the yields of the mono-replaced triazines decreased with an increase in the length of the original aliphatic substituents suggests that this replacement is hindered by the bulk of the original substituents. The suppressive effect resulting from the electron-releasing power of an aromatic substituent described above is indicated again in this table. The replacement of a substituent of Me_2Ph with a phenyl radical was particularly difficult in comparison with the replacement of a substituent of R_3, such as Me_3, Et_3, and n-Pr_3, by the same radical. These facts suggest that the formation of the small amounts of $MePh_2$ shown in Tables 1, 3, and 4 was due largely to the co-trimerization of the added benzonitrile and the acetonitrile liberated by Eq. (2), and less to the second replacement by Eq. (6).

$$RCN + R'CN \xrightarrow{R''OH} R_3 + R_2R' + RR'_2 + R'_3 \quad (7)$$

In order to demonstrate the excellent applicability of this replacement reaction to the synthesis of unsymmetrically tri-substituted 1,3,5-triazines, R_2R' in particular, the co-trimerization of nitriles under high pressure by means of Eq. (7) was examined as a comparative method. Table 6 indicates that this co-trimerization is not suitable for the selective preparation of a triazine with a desired combination of the three substituents.

Benzamidine, being similar in many cases, to benziminoether in its reacting manner was kept with Me_3 in dioxane at 6000 kg/cm² and 100 °C for 30 hr; this gave the expected triazine, Me_2Ph.

Experimental

Reaction Apparatus and Procedure. The reaction mixtures for these experiments were placed in a collapsible lead capsule and kept under the desired conditions of pressure and temperature for the desired time by means of a high-pressure assembly and procedure described previously.[10]

Materials. The drying and distillation of the reagents (all graded EP) supplied this experiment with benzonitrile, p-tolunitrile, methanol, triethylamine, and glacial acetic acid. The sodium ethylate was prepared in the usual manner in the form of a concentrated ethanolic solution. The β-naphthonitrile (Tokyo Chem. Ind.) and isonicotinonitrile (Koei Chem. Ltd)[10] were used without further purification. The Me_3, Et_3, and n-Pr_3 were the same as have been previously reported.[1] The Me_2Ph was prepared by the reaction of Me_3 with benzonitrile (see below).

Preparation of Authentic Samples, Identification of Reaction Products, and Analysis. Nitriles, Iminoethers, and Benzamidine: The procedures for the preparation, identification, and analysis

of these substances have been described in previous reports.[10,15]

Me_3 and Ph_3: The identification and analysis of these substances were similar in a manner to those previously reported.[15]

Me_2Et, $MeEt_2$, and Et_3: A mixture of equimolar amounts of ethyl acetiminoether and ethyl propioiminoether[1] was added to glacial acetic acid (15 per cent of the total iminoether in the molar fraction), and the resulting mixture was kept at room temperature for 24 hr. The weight ratio of the four triazines produced in the mixture was determined by means of gas-liquid phase chromatography (glc) glc-a[16] to be Me_3: Me_2Et: $MeEt_2$: Et_3=1: 0.9: 0.8: 3.1. The mixture was gradually warmed to 100 °C in 10 hr to complete the co-trimerization. This procedure was carried out with reference to the methods of Schaefer and Peters[17] and Yakubovich *et al.*[5] The reaction mixture was separated from a majority of Me_3 by filtration and was fractionated into the four triazines by glc-A.[18] On the other hand, the reaction product of the mixture of Me_3, propionitrile, and methanol listed in Table 4 was fractionated by glc-A. The first fraction, at 142—148 °C amounted to 0.03 g. Found: bp 175.6 °C; C, 61.96; H, 8.17; N, 29.71%; mol wt (from the parent peak of mass spectroscopy (MS)), 137. Calcd for $C_7H_{11}N_3$: C, 61.29; N, 8.09; N, 30.63%; mol wt, 137.18. The results of the glc-a and infrared (IR) spectrometry of this fraction agreed with those of the 2,4-dimethyl-6-ethyl-1,3,5-triazine described above. The second fraction, at 149—154 °C amounted to 0.02 g. Found: bp 190.8 °C; C, 63.53; H, 8.85; N, 27.48%. Calcd for $C_8H_{13}N_3$: C, 63.55; H, 8.67; N, 27.79%. The data of the glc-a and IR spectrometry agreed with those of the 2,4-diethyl-6-methyl-1,3,5-triazine described above. The third fraction, at 155—160 °C, was a minute amount. The retention time of the glc-a and the IR spectrum (2960, 1540, 1460, 1425, 1390, 1070, 890, 840 cm^{-1}) agreed with those of the authentic sample of triethyl-1,3,5-triazine described above.

Me_2Ph and $MePh_2$: The reaction mixture of the experiment conducted at 7950 kg/cm^2 listed in Table 1, when it was treated by means of preparative glc glc-B,[19] yielded 0.32 g at 190—200 °C (mp 38 °C (34,[7] 35—37[2])); C, 71.16 (71.33 Calcd); H, 5.84 (5.99); N, 23.26% (22.69); mol wt (MS), 185 (185.23); IR, 3070, 2970, 2940, 1540, 1435, 1375, 750, and 690 cm^{-1} for the alkyl, phenyl, and triazinyl groups). It was identified with 2,4-dimethyl-6-phenyl-1,3,5-triazine. The preparative glc gave another fraction (0.11 g) at 230—260 °C (mp 105 °C (110[2])); C, 76.36 (77.71); H, 5.34 (5.30); N, 18.09% (16.99); mol wt (MS), 247 (247.31); IR, 3050, 2950, 1535, 1525, 1425, 1380, 1365, 740, and 680 cm^{-1} for alkyl, phenyl, and triazinyl group). It was determined to be 2,4-diphenyl-6-methyl-1,3,5-triazine.

Et_2Ph and $EtPh_2$: The preparative glc-C[20] of the reaction products in the mixture of Et_3, benzonitrile, and methanol, which are shown in Table 5, gave two fractions. The first amounted to 0.02 g at 196—226 °C. Found: C, 73.48; H, 7.47; N, 19.51%; IR, 3050, 2950, 1590, 1530, 1450, 1420, 1385, 790, and 690 cm^{-1} for the alkyl, phenyl, and triazinyl groups. Calcd for $C_{13}H_{15}N_3$: C, 73.21; H, 7.09; N, 19.71%. This fraction was determined to be 2,4-diethyl-6-phenyl-1,3,5-triazine. The second amounted to 0.005 g at 226—243 °C (IR, 3050, 2950, 1520, 1440, 1380, 740, and 680 cm^{-1}). This fraction is assumed to be 2,4-diphenyl-6-ethyl-1,3,5-triazine.

n-Pr_2Ph: The fractionation by glc-C of the reaction products in the mixture of *n*-Pr_3, benzonitrile, and methanol listed in Table 5, gave a fraction of 0.04 g at 193—217 °C. Found: C, 74.84; H, 7.44; N, 17.39%; IR, 3050, 2950, 1590, 1530, 1450, 1380, 760, and 690 cm^{-1} for the alkyl, phenyl, and triazinyl groups. Calcd for $C_{15}H_{19}N_3$: C, 74.66; H, 7.94; N, 17.42%. This fraction was determined to be 2,4-di-*n*-propyl-6-phenyl-1,3,5-triazine.

Me_2 p-$CH_3C_6H_5$: The reaction products in the mixture of Me_3 and methanol (each 1.66 g) and *p*-tolunitrile (1.58 g) at 8000 kg/cm^2, listed in Table 4, were filtered. The residue was then recrystallized from ethanol to give 0.19 g. Found: mp 78.4 °C; C, 71.68; H, 6.60; N, 21.73%; mol wt (MS), 199; IR, 2920, 1610, 1530, 1430, 1405, 1370, and 790 cm^{-1} for the alkyl, phenyl, and triazinyl groups. Calcd for $C_{12}H_{13}N_3$: C, 72.33; H, 6.57; N, 21.09%; mol wt, 199.25. This crystal was determined to be 2,4-dimethyl-6-*p*-tolyl-1,3,5-triazine.

Me_2 p-ClC_6H_4 and (p-$ClC_6H_4)_3$: The reaction mixture from Me_3 and methanol (each 0.51 g) and *p*-chlorobenzonitrile (0.57 g), listed in Table 4, was separated from the precipitate by filtration, was separated from the volatile matter *in vacuo* and was then recrystallized from ethanol to give 0.55 g. Found: mp 133.1 °C; C, 60.20; H, 4.51; N, 19.24; Cl, 16.43%; mol wt (MS), 219; IR, 3030, 2900, 1570, 1530, 1430, 1400, 1380, 1370, 860, 850, and 790 cm^{-1} for the alkyl, *p*-chlorophenyl, and triazinyl groups. Calcd for $C_{11}H_{10}N_3Cl$: C, 60.14; H, 4.59; N, 19.13; Cl, 16.14%; mol wt, 219.67. It was determined to be 2,4-dimethyl-6-*p*-chlorophenyl-1,3,5-triazine. The precipitate was washed with methanol and amounted to 0.015 g. Found: mp 323 °C; C, 61.34; H, 3.06; N, 10.86; Cl, 24.73%; mol wt (MS), 412; IR, 3050, 1580, 1520, 1400, 1365, 1350, 840, and 800 cm^{-1} for the *p*-chlorophenyl and triazinyl groups. Calcd for $C_{21}H_{12}N_3Cl_3$: C, 61.12; H, 2.93; N, 10.18; Cl, 25.77%; mol wt, 412.71. It was determined to be tris(*p*-chlorophenyl)-1,3,5-triazine.

Me_2 β-Naph: The reaction products from Me_3 and methanol (each 1.55 g) and β-naphthonitrile (1.36 g), listed in Table 4, gave a fraction (0.07 g) at 210—240 °C by glc-C. Found: mp 133.4 °C; C, 75.99; H, 5.43; N, 17.85%; mlo wt (MS), 235; IR, 2950, 1600, 1530, 1470, 1390, 800, 795, and 750 cm^{-1} for the alkyl, naphthyl, and triazinyl groups. Calcd for $C_{15}H_{13}N_3$: C, 76.57; H, 5.57; N, 17.86%; mol wt, 235.27. 2,4-Dimethyl-6-naphth-2-yl-1,3,5-triazine was identical with this fraction.

Me_2 γ-Py, Me γ-Py_2, and γ-Py_3: The reaction products in the mixture of Me_3 and methanol (each 1.73 g) and isonicotinonitrile (1.46 g) listed in Table 4, were separated from the solid product and were then fractionated by glc-C. The fraction at 185—196 °C amounted to 0.48 g. Found: mp 71.8 °C; C, 64.42; H, 5.56; N, 29.93%; mol wt (MS), 186; IR, 3030, 2950, 1600, 1530, 1430, 1390, 1370, 850, 790, and 660 cm^{-1} for the alkyl and heteroaromatic groups. Calcd for $C_{10}H_{10}N_4$: C, 64.50; H, 5.41; N, 30.09%; mol wt, 186.22. This fraction was determined to be 2,4-dimethyl-6-pyrid-4-yl-1,3,5-triazine. The fraction at 228—250 °C amounted to 0.08 g. Found: mp 127.5 °C; C, 66.69; H, 4.76; N, 28.56%; mol wt (MS), 249; IR, 3030, 2950, 1600, 1525, 1430, 1380, 1370, 820, 790, and 670 cm^{-1}. Calcd for $C_{14}H_{11}N_5$: C,

15) M. Yasumoto, K. Yanagiya, and M. Kurabayashi, This Bulletin, **46**, 2798 (1973).

16) Glc-a: Reoplex 400, 3×750 mm, 50°C—, 4°C/min, He 25 ml/min.

17) S. C. Schaefer and G. A. Peters, *J. Org. Chem.*, **26**, 2778 (1961).

18) Glc-A: DNP, 9×750 mm, 120°C, 2°C/min, He 125 ml/min.

19) Glc-B Thermol-3, 9×750 mm, 100°C—, 4°C/min, He 125 ml/min.

20) Glc-C SE-30, 9×750 mm, 140°C—, 6°C/min, He 125 ml/min.

67.46; H, 4.45; N, 28.09%; mol wt, 249.28. 2,4-Bis(4-pyridyl)-6-methyl-1,3,5-triazine is identical with this fraction. The solid product amounted to 0.21 g and was recrystallized from pyridine. The melting point (362 °C) of this crystal was not reduced by mixing it with the authentic tris(4-pyridyl)-1,3,5-triazine (mp 374 °C) previouslyreported.[10] The IR spectra of the two substances agreed.

4-Amino-2,6-dimethylpyrimidine and N-2,6-Dimethylpyrimidin-4-yl-acetamidine: These were identified and analysed by the methods described in the previous report.[1]

The gas-liquid-phase chromatographies, glc-a and glc-b,[21] were employed for the determination of the yields of the products in the reaction mixtures.

21) Glc-b: SE-30, 3×750 mm, 50°C—, 6°C min, He 35 ml/min.

BULLETIN OF THE CHEMICAL SOCIETY OF JAPAN, VOL. 46, 2814—2820 (1973)

Kinetic and NMR Spectroscopic Studies of the Fusion Reactions of Chloropurines with 1,2,3,5-Tetra-*O*-acetyl-D-ribofuranoses

Akira Hosono, Kiyohisa Fujii, Toshizo Tada, Hisayuki Tanaka, Yohko Ohgo, Yoshiharu Ishido, and the late Tetsuo Sato

Department of Chemistry, Faculty of Science, Tokyo Institute of Technology, O-okayama, Meguro-ku, Tokyo 152

(Received December 4, 1972)

A kinetic study of the fusion reaction and the reaction in dimethyl sulfoxide of 2,6-dichloropurine with 1,2,3,5-tetra-*O*-acetyl-β-D-ribofuranose was undertaken, and both of them were proved to be of the second order. The activation energy and the activation entropy of the reaction in dimethyl sulfoxide were obtained: $E_a = 38.0$ kcal/mol and $\Delta S^{\neq} = +15.3$ cal/deg·mol. The reaction was thus concluded to be bimolecular involving a considerable unimolecular character. Subsequently, the fusion reactions of 2,6-dichloro- and 2,6,8-trichloropurine with 1,2,3,5-tetra-*O*-acetyl-α- and -β-D-ribofuranose were examined by NMR spectroscopy with respect to the relative content ratios of all the materials and products in each reaction mixture; the results were found to be in good agreement with those obtained by the above kinetic study. On the basis of these results, the mechanism of the fusion reaction was discussed.

In the previous paper,[1] the mechanism of the acid-catalysis and the new activating agents for the reaction of a purine with a fully-acetylated sugar were examined; it was proved that a purine is activated by the interaction with an acidic catalyst to react with an acetylated sugar. Successively, a kinetic study of the reaction of 2,6-dichloropurine (**1**) with 1,2,3,5-tetra-*O*-acetyl-β-D-ribofuranose (**2**) by means of UV absorption spectroscopy, and a study of the process of the reaction of **1** with **2** and 1,2,3,5-tetra-*O*-acetyl-α-D-ribofuranose (**3**) respectively by NMR spectroscopy, were undertaken.

Results and Discussion

*A Kinetic Study of the Reaction of 2,6-Dichloropurine with 1,2,3,5-Tetra-*O*-acetyl-β-D-ribofuranose.* No kinetic study of the synthetic reaction of glycosides by the fusion method has ever been undertaken since the discovery of the fusion reaction for the synthesis of phenyl glycosides. The reasons may be that a remarkable coloration inevitably accompanies the reaction with phenols, although it proceeds under a completely homogeneous state, and that the reaction with purines usually proceeds under a heterogeneous state in addition to a considerable coloration. Fortunately, the reaction of **1** with **2** was found to proceed autocatalytically[2a] under a completely homogeneous state, and it is accompanied by a scarce coloration which may be accepted as showing that the reaction scarcely involves decomposition of the materials or of the resultant 2,6-dichloro-9-(2′,3′,5′-tri-*O*-acetyl-β-D-ribofuranosyl)-purine (**4**). The appearance of the reaction system did not vary much even in the presence of an acidic catalyst provided that the reaction time was not extended much longer.[2b] In view of this, kinetic studies of the fusion reaction and of the reaction in dimethyl sulfoxide of **1** with **2** were undertaken by means of UV-absorption spectroscopy. It was considered possible to follow the reaction by measuring the UV spectra of the reaction mixture at different reaction times, since the spectra of **1** and **4** were found to be completely different from each other in an aqueous ethanolic sodium hydroxide solution (λ_{max} 258 nm[3] and λ_{max} 280 nm respectively). These spectra were confirmed to be unchanged under the present conditions even after 24 hr. An equimolar mixture of **1** and **2**, which were mingled as completely as possible,

1) M. Sekiya, T. Yoshino, H. Tanaka, and Y. Ishido, This Bulletin, **46**, 556 (1973).

2) a) Y. Ishido, T. Matsuba, A. Hosono, K. Fujii, T. Sato, S. Isome, A. Maruyama, and Y. Kikuchi, *ibid.*, **40**, 1007 (1967); b) Y. Ishido, A. Hosono, K. Fujii, Y. Kikuchi, and T. Sato, *Nippon Kagaku Zasshi*, **87**, 752 (1966).

3) The chloro substituent at the 6-position of **4** is known to be susceptible to hydrolysis under alkaline conditions to give 2-chloroinosine[A. Yamazaki, T. Saito, Y. Yamada, and I. Kumashiro, *Chem. Pharm. Bull.* (Tokyo), **17**, 2581 (1969); λ_{max}^{pH13} 258 nm (ε 11400)].

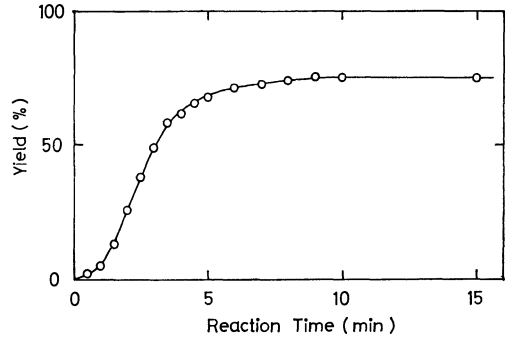

Fig. 1. A plot of the yields of the fusion reaction of **1** with 1,2,3,5-tetra-*O*-acetyl-*β*-D-ribofuranose (**2**).

in a capillary tube was heated at 152—154 °C for a scheduled reaction time in a micro melting-point apparatus. On the basis of the molar extinction coefficients of **1** ($\varepsilon_{280\text{ nm}}$ 8670 and $\varepsilon_{258\text{ nm}}$ 4150) and **4** ($\varepsilon_{280\text{ nm}}$ 2440 and $\varepsilon_{258\text{ nm}}$ 11800) in the same alkaline solvent, the yields of the reaction at each reaction time were calculated by the following simultaneous equations, where A, x, and y stand for the total molar extinctions observed at both of the wavelengths, molar concentration of **1**, and that of **4** after t hr respectively:

$$\begin{cases} A_{258\text{ nm}} = 4150 \cdot x + 11800 \cdot y \\ A_{280\text{ nm}} = 8670 \cdot x + 2440 \cdot y \end{cases}$$

A plot of the yields $[y/(x+y)]$ against the reaction times is shown in Fig. 1; it was thus proved that the equilibrium of the reaction was established at the yield of *ca.* 76%. The reaction can thus be stated to be reversible provided that the reaction is accompanied by no decomposition reaction as has been mentioned above. The reversibility of this reaction was confirmed by a tlc examination and by a UV spectral determination with respect to a mixture which had been obtained by fusing **4** with glacial acetic acid at 150 °C for 15 min. The content ratio of **1** and **4** in this mixture was determined to be 18: 82 on the basis of the total molar extinctions at 258 and 280 nm in the alkaline solvent. Supposing that a stand for the initial concentration of **1**, and that the reaction is of the second order with respect to both reactants and products, the reaction was assumed to conform to the following second-order equation, where k_1 and k_2 stand for the rate constants of the reactants and products respectively:

$$dy/dt = k_1 \cdot (a-y)^2 - k_2 \cdot y^2 \qquad (1)$$

The correlation between k_1 and k_2 can be concluded from the concentrations of **1** and **4** at the equilibrium of this reaction as below:

$$0.24^2 \cdot k_1 = 0.76^2 \cdot k_2 \qquad (2)$$

Supposing the equilibrium constants as K, moreover, Eq. (3) can be obtained:

$$k_2 = \frac{1}{K} \cdot k_1 \qquad (3)$$

When Eq. (3) was substituted into Eq. (1), the resultant equation was integrated to give Eq. (4):

$$t = \frac{2.303 \cdot \sqrt{K}}{2a \cdot k_1} \log \left| \frac{K+\sqrt{K}-(K-1)\cdot y/a}{K-\sqrt{K}-(K-1)\cdot y/a} \right| + \text{Const.} \qquad (4)$$

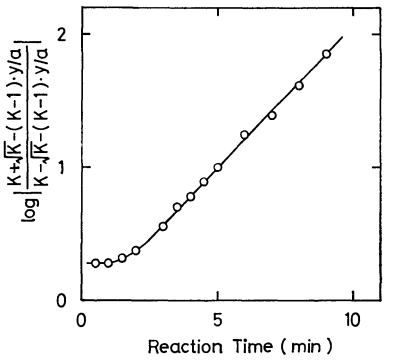

Fig. 2. A plot of $\log|\{K+\sqrt{K}-(K-1)\cdot y/a\}/\{K-\sqrt{K}-(K-1)\cdot y/a\}|$ *vs.* reaction time determined in the fusion reaction of **1** with **2**.

Moreover, y/a corresponds to the yields of the reaction, and K is $76^2/24^2$, which was obtained from Eq. (2). Thus, we can obtain the values of $\log|[K+\sqrt{K}-(K-1)\cdot y/a]/[K-\sqrt{K}-(K-1)\cdot y/a]| = \log|(475-325\cdot y/a)/(247-325\cdot y/a)|$ by measuring the yields at each reaction time. A plot of these values against the reaction time is given in Fig. 2. The deviation of the plots of the initial stage of the reaction from the linearity may be ascribed to the heterogeneity of the reaction mixture because it takes about 2.5 min until the mixture becomes almost homogeneous. According to the figure, it can be concluded that the fusion reaction of **1** with **2** is of the second order with respect to both reactants and products, and that the linear relationship implies that the reaction is reversible and that there is no catalytic effect of the acetic acid co-produced during the reaction.

Subsequently, the rate of the equimolar reaction in dimethyl sulfoxide was measured in the same way, since it was impossible to calculate the precise concentrations of **1**, **2**, and **4** in the fusion state; we thus obtained the activation energy and the activation entropy for the reaction. Supposing that the reaction in dimethyl sulfoxide also conforms to the second-order equation, the following relation can be expected to hold for the reaction:

$$k \cdot t = y/[a \cdot (a-y)] = \frac{y}{x+y} \cdot \frac{1}{a\{1-[y/(x+y)]\}}$$

The values of $y/[a\cdot(a-y)]$ can be determined from the data of UV spectroscopy, which were obtained in the same way as has previously been described; these values were then plotted against the reaction times to give the two linear relationships, which were obtained at 130 and 135 °C as demonstrated in Fig. 3. The rate constants of $k_{130°C}$ and $k_{135°C}$ were calculated as 1.46×10^{-4} l/mol·sec and 2.50×10^{-4} l/mol·sec respectively from the slopes of these linear rate plots. According to the following equations, the activation energy (E_a) and the activation entropy (ΔS^*) of this reaction were calculated as 38.0 kcal/mol and +15.3 cal/deg·mol respectively, where K, h, R, and ΔH^* stand for the Boltzmann constant, the Planck constant, the gas constant, and the activation enthalpy respectively:

$$E_a = \frac{T_1 \cdot T_2}{T_1 - T_2} \cdot R \cdot \ln \frac{k_1}{k_2}$$

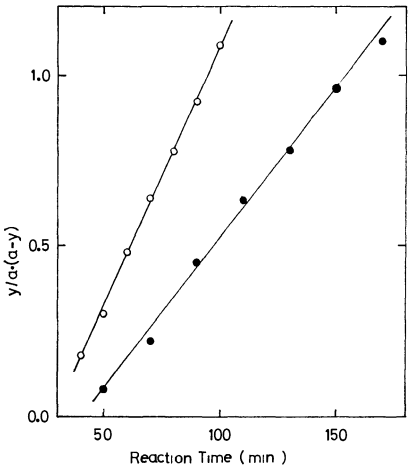

Fig. 3. A plot of $y/a(a-y)$ *vs.* reaction time in the reaction of **1** with **2** in DMSO at 130 °C (—●—) and at 135 °C (—○—).

$$E_a = \Delta H^* + R \cdot T$$

$$k = \frac{K \cdot T}{h} \cdot e^{\Delta S^*/R} \cdot e^{-\Delta H^*/R \cdot T}$$

On the basis of these results, the reaction of **1** with **2** in dimethyl sulfoxide was concluded to be second order, involving a considerable first-order character; *i.e.*, the reaction conceivably proceeds through a bimolecular mechanism involving a considerable unimolecular character. In this case, no catalytic effect of the co-produced acetic acid was also observed. Thus, this fact provides a new concept with respect to the acid-catalysis in the condensation reaction of purines with fully-acetylated sugars, although it has been generally accepted that the reaction may be induced by the interaction of the acidic catalyst with fully-acetylated sugars to give the corresponding *C*-1 carbonium ion—*i.e.*, that the rate-determining step of the reaction may be the step of the carbonium-ion formation.[4] In the autocatalytic reaction of **1** with **2**, the acidic proton of **1** must be concluded to induce the reaction in view of the lack of any catalytic effect of acetic acid. Consequently, it was deduced that the rate-determining step of the reaction must not be the step of the *C*-1 carbonium-ion formation; this was deduced from the facts that the reaction is of a second order and that the more weakly acidic compounds,

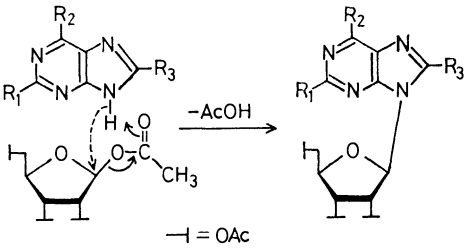

	2	6		4	7
R_1	Cl	Cl	R_1	Cl	Cl
R_2	Cl	Cl	R_2	Cl	Cl
R_3	H	Cl	R_3	H	Cl

Scheme 1.

such as 6-chloropurine (pK_a=7.68[5]) and 6-cyanopurine (pK_a=6.88[6]) *etc.*, in addition to **1** and in comparison with acetic acid, also gave the corresponding nucleosides in the reaction with **2** in the absence of such acidic catalyst as *p*-toluenesulfonic acid.[2a] Therefore, it is now necessary to postulate another reaction mechanism. On the basis of the above results, the autocatalytic reaction was postulated to proceed *via* the mechanism depicted in Scheme 1, which implies that the rate-determining step of the reaction is the step of the elimination of acetic acid from purines and fully-acetylated sugars. Thus, usual purines may be activated by interaction with acidic catalysts to react with fully-acetylated sugars, and the corresponding nucleosides may be produced accompanied by an electron transfer such as is depicted in the Scheme. The mechanism of the acid-catalysis in the fusion reaction has recently been verified by an investigation of the reaction of 1,2,3,4,6-penta-*O*-acetyl-β-D-glucopyranose with theophylline in competition with *p*-nitrophenol and in the presence of *p*-toluenesulfonic acid;[1] this reaction resulted in the selective formation of 7-(2′,3′,4′,6′-tetra-*O*-acetyl-β-D-glucopyranosyl)-theophylline.

*An Examination on the Reaction of 2,6-Dichloropurine with 1,2,3,5-Tetra-*O*-acetyl-α- and -β-*D*-ribofuranose by NMR Spectroscopy.* In order to elucidate the steric course of the fusion reaction, the reactions of **1** with **2** and with

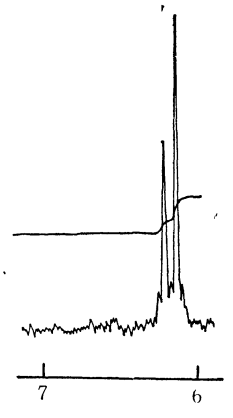

(δ-value)

Fig. 4. The anomeric region (δ 6—7 ppm) of the NMR spectrum ($CDCl_3$, TMS) of the resultant mixture from the fusion reaction of **1** with **2** at 150 °C for 10 min *in vacuo*.

4) a) The fusion reaction was suggested to proceed *via* a $C_{(1)}-C_{(2)}$ orthoester-type carbonium ion on the basis of requirement of 2-*O*-acyl groups in all sugar derivatives thus far examined[T. Shimadate, *Nippon Kagaku Zasshi*, **83**, 214(1962)]; b) The reaction was, on the other hand, considered to proceed *via* the *C*-1 carbonium ion, at least in the case of fully acylated D-ribofuranoses, because of the steric effect of the 3-*O*-acyl group, which may prevent the formation of such a carbonium ion, as has been described by Shimadate[4a] [2b]; The mechanism involving the orthoester-type carbonium ion, which had been proposed by R. U. Lemieux and W. P. Shyluk [*Can. J. Chem.*, **31**, 528 (1953)] in the acid-catalyzed condensation reaction of phenol with 1,2,3,4,6-penta-*O*-acetyl-β-D-glucopyranose, has been reinvestigated by J. I. Bose and T. R. Ingle [*Chem. Ind.*, **1967**, 1451]; they concluded that the reaction proceeded *via* the *C*-1 carbonium ion on the basis of the simultaneous formation of phenyl 2,3,4,6-tetra-*O*-acetyl-α-D-glucopyranoside and its β-anomer.

5) A. Bendich, P. J. Russel, and J. J. Fox, *J. Amer. Chem. Soc.*, **76**, 6073 (1954).

6) A. G. Sorolla, *ibid.*, **80**, 3732 (1958).

3 were examined by NMR spectroscopy. A crude mixture obtained from the fusion reaction of **1** with **2** at 150 °C for 10 min gave an NMR spectrum with the anomeric region shown in Fig. 4. The reaction was thus concluded to give **4** (*H*-1′: δ 6.24 ppm, $J_{1',2'}$= 4.7 Hz) selectively; *i.e.*, it gave a nucleoside with the same anomeric configuration as that of the fully-acetylated sugars used as the starting material. A crude mixture obtained from the same reaction after 60 min gave substantially the same spectrum, as is shown in Fig. 4. No other new anomeric proton signals could be detected, not even by an enhancement of the ratio of signal to noise. Accordingly, it can further be stated that the autocatalytic fusion reaction is not accompanied by any anomerization reaction of the nucleoside once produced in the course of the reaction.

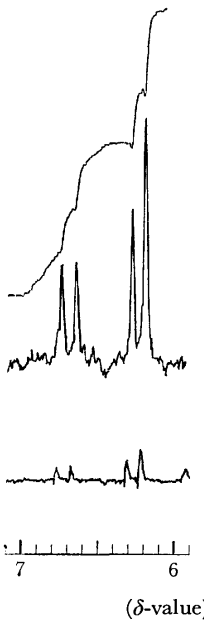

Fig. 5. The anomeric region (δ 6—7 ppm) of the NMR spectrum ($CDCl_3$, TMS) of the resultant mixture from the fusion reaction of **1** with 1,2,3,5-tetra-*O*-acetyl-α-D-ribofuranose (**3**) at 150 °C for 10 min *in vacuo*.

On the other hand, a crude mixture obtained from the reaction of **1** with **3** at 150 °C for 10 min gave a spectrum with the anomeric region shown in Fig. 5; this is in remarkable contrast with that of the reaction with **2**. A new doublet (δ 6.75 ppm, J=5.6 Hz) appeared other than that of **4** in the spectrum. The product, which gave the new doublet, was deduced to be the α-anomer of **4** (**5**) in view of the NMR data reported with respect to the α-D-ribofuranose derivatives.[7] The relative ratio of **4** to **5** in the mixture was calculated to be 59/41 from the integration curve of its spectrum.

The difference in the content ratio of the anomeric nucleosides between the above reaction mixtures were of interest in connection with the reaction mechanism, since no anomerization reaction of the nucleosides is conceivable in the autocatalytic fusion reaction. Incidentally, the fusion reactions of phenol with 2,3,4,6-tetra-*O*-acetyl-1-*O*-trichloroacetyl-β-[8] and -α-D-glucopyranose[9] have been shown to give the corresponding glycosides, with the same anomeric configuration as those of the starting material, in 70 and 20% yields respectively.[10] Thus, the reaction described here can be explained as proceeding through a bimolecular mechanism involving a considerable unimolecular character, *i.e.*, a considerably cationic character, assuming that the conclusion in the kinetic study of the reaction of **1** with **2** in dimethyl sulfoxide is the case for the fusion reaction as well. The results obtained in this section were proved to support the results of the kinetic study strongly. Accordingly, the reaction was deduced

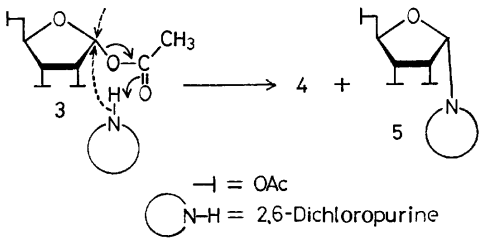

Scheme 2.

to proceed through the mechanism depicted in Schemes 1 and 2. Just after the elimination of acetic acid between **1** and **2** or **3**, accompanied by such electron transfer as is shown in the arrows with ordinary lines, the carbonium ion thus produced may be subjected to the nucleophilic attack of the anion of **1** to afford **4** or **5**. In any case, the reaction conceivably proceeds with a considerably strong interaction between the acidic proton of **1** and the 1-*O*-acetyl group of **2** or **3**. The concomitant formation of **4** and **5** in the fusion reaction with **3** can be explained as being brought about by the steric effect of the 2-*O*-acetyl group of the D-ribofuranosyl ring on the attacking of the resultant anion of **1** on the short-lived *C*-1 carbonium ion.

Subsequently, the acid-catalyzed fusion reaction of **1** with **2** was examined by the same technique in order to elucidate the effect of the acidic catalyst on the relative ratio of the anomeric nucleosides in the resultant reaction mixture. A mixture of **1**, **2**, and sulfamic acid (molar ratio=1 : 1 : 0.02) was heated at 150 °C *in vacuo* for a scheduled period in a small test tube. The resultant mixtures, obtained at the reaction times of 1, 2, 3, 4, 5, 7, and 10 min, were each dissolved in

7) J. D. Stevens and H. G. Fletcher, Jr., *J. Org. Chem.*, **33**, 1709 (1968); where the anomeric proton signals of α- and β-ribazole tri-*O*-acylates were reported to be observed in their NMR spectra ($CDCl_3$, TMS) as follows:

Ribazole	Chemical shift of anomeric protons in δ value($J_{1',2'}$, Hz)	
	Acetate	Benzoate
α-anomer	6.47 (5.0)	6.70 (5.0)
β-anomer	6.08 (5.0)	6.11 (5.0)

8) B. Helferich and B. Gootz, *Ber.*, **62**, 2788 (1929).

9) I. Karasawa and R. Onishi, *Nippon Nogei Kagaku Zasshi*, **33**, 817 (1961).

10) It was elucidated, by an examination with NMR spectroscopy, that these reactions resulted in the predominant formation of the phenyl glycosides with the same anomeric configuration as that of the fully-acylated sugars used for starting materials. The results will be published elsewhere, together with those obtained in the same way with respect to other phenyl glycoside syntheses.

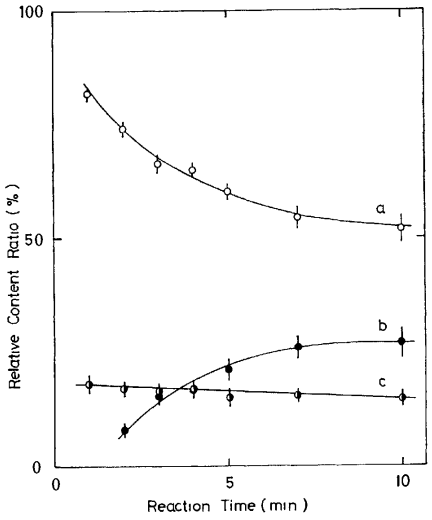

Fig. 6. The outline of the fusion reaction of **1** with **2** in the presence of sulfamic acid as a catalyst at 150 °C *in vacuo*; curves *a*, *b*, and *c* corresponds to the relative content ratio of **4**, the α-anomer of **4**(**5**), and **2** respectively.

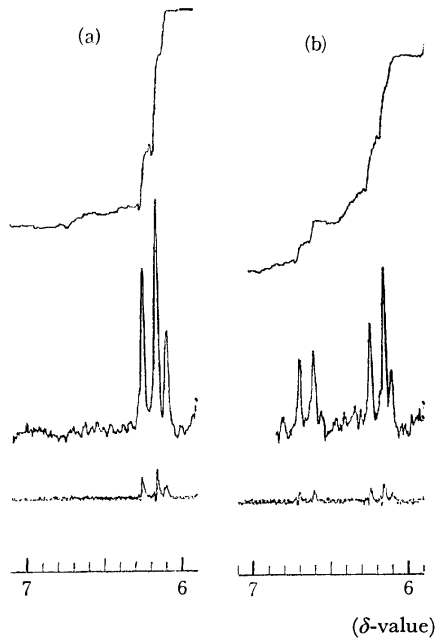

Fig. 7. The observed change in the anomeric region (δ 6—7 ppm) of the NMR spectrum ($CDCl_3$, TMS) in the acid-catalyzed fusion reaction of **1** with **2**; *a* and *b* corresponds respectively to the spectrum of the resultant mixture obtained after 1 and 10 min from the beginning of the reaction.

deuterochloroform, and their NMR spectra were taken. The relative content ratios of **2**, **4**, and **5**, which were calculated from the integration curves corresponding to the anomeric region of each NMR spectrum of the resultant mixtures, were plotted against the reaction times to give an outline of the reaction process such as is shown in Fig. 6. For reference, the spectra of the resultant mixtures obtained after 1 and 10 min are shown in Fig. 7. Judging from Fig. 6, **4** was predominantly produced in the initial stage of the reaction, and its content ratio decreased with the passage of time. Parallel with this decrease, the relative content ratio of **5** gradually increased, although a scarce anomerization of **2** into **3** was observed during the reaction. Incidentally, the anomerization of **4** into **5** was also detected by heating **4** with a catalytic amount of sulfamic acid under the same conditions; this gave the doublet at δ 6.75 ppm corresponding to the anomeric proton of **5**, in addition to that at δ 6.24 ppm corresponding to that of **4**. Consequently, the acid-catalyzed fusion reaction of **1** with **2** was deduced to proceed through this mechanism; *i.e.*, **1** might be activated by the interaction with an acidic catalyst, as was also confirmed recently in a different manner,[1] and the β-nucleoside (**4**) formed by the reaction of activated **1** with **2** might be isomerized into its α-anomer (**5**) by the effect of the acidic catalyst.

An Examination of the Fusion Reaction of 2,6,8-Trichloropurine with 1,2,3,5-Tetra-O-acetyl-D-ribofuranoses by NMR Spectroscopy. An autocatalytic fusion reaction of 2,6,8-trichloropurine (**6**) with **2** at 150 °C was found to give 2,6,8-trichloro-9-(2′,3′,5′-tri-*O*-acetyl-β-D-ribofuranosyl)-purine (**7**) selectively, much as in the reaction of **1** with **2**. The anomeric region of the NMR spectrum of the reaction mixture obtained by heating at the same temperature for 10 min is shown in Fig. 8;

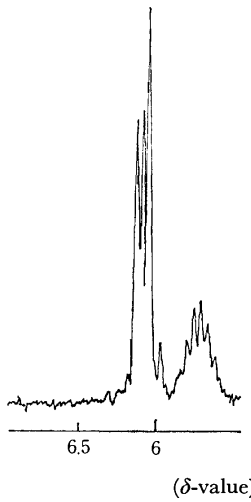

Fig. 8. The anomeric region (δ 6—7 ppm) of the NMR spectrum ($CDCl_3$, TMS) of the resultant mixture from the fusion reaction of 2,6,8-trichloropurine (**6**) with **2** at 150 °C for 10 min *in vacuo*.

the anomeric proton of **7** was observed, together with one of the other ring protons on its D-ribofuranosyl ring, at *ca.* δ 6.1 ppm. Accordingly, the steric course of this reaction can be concluded to be the same as that of the reaction of **1** with **2**. In contrast with the reaction of **1**, an autocatalytic reaction of **6** with **3** and the acid-catalyzed reactions of **6** with **2** and **3** were all found to give **7** predominantly. In the latter two cases, a new doublet (δ 6.60 ppm, J=5.0 Hz) was distinctly observed; this signal may arise from the formation of the α-anomer of **7** (**8**), in view of the data reported with respect to the α-D-ribofuranose derivatives.[7] On the basis of this assumption, the relative content ratios of **7** to **8** were calculated, from the integration curve of each NMR spectrum, as 79/21 and 81/19 respectively. In the reactions of **6**, the

relative content ratio of **8** to **7** was considerably lower than those observed in the reaction of **1** with **2** in the presence of the catalyst and in the autocatalytic and the acid-catalyzed reaction of **1** with **3**. These results can be ascribed to the steric effect of the chloro substituent at the 8-position of **6** in addition to that of the 2-*O*-acetyl group of **2** or **3**. That is, the nucleophilic attack of the anion of **6** from the α-side of the D-ribofuranosyl ring may be largely prevented by those steric effects. A bulky substituent at the 8-position of purine nucleus was also found to affect the relative content ratio of the position isomers of purine nucleosides in a condensation reaction.[11]

These facts, elucidated by the above kinetic and NMR spectroscopic investigation of the reaction of **1** or **6** with **2** or **3**, can be considered to hold for reactions involving other purine derivatives and acetylated sugars.

Experimental

The UV spectra were taken with a Hitachi EPS-3T photoelectronic spectrophotometer. The NMR spectra were taken with a JEOL JNM-C-60 spectrometer in deuterochloroform, with tetramethylsilane as the internal standard.

Rate Determination of the Reaction of 2,6-Dichloropurine with 1,2,3,5-Tetra-O-acetyl-β-D-ribofuranose. a) The Solvent for the Determination of UV Absorption Spectra (0.1 M ethanolic aqueous sodium hydroxide solution): In a measuring flask (500 ml), a 1 M (f=0.887) aqueous sodium hydroxide solution (50 ml) was mixed with ethanol (250 ml), which had then purified by distillation after having been treated with sodium hydroxide under reflux. The mixture was then diluted to the total volume of 500 ml by the addition of distilled water.

b) The UV Spectral Data of 2,6-Dichloropurine (1) and 2,6-Dichloro-9-(2',3',5'-tri-O-acetyl-β-D-ribofuranosyl)-purine (4): The UV spectra of **1** and **4** were determined in the above alkaline solution as follows:

1: $\lambda_{max}^{1M\ NaOH/EtOH\text{-}H_2O}$ 280 nm (ε 8670)

4: $\lambda_{max}^{1M\ NaOH/EtOH\text{-}H_2O}$ 258 nm (ε 11800)

Moreover, the ε_{258nm} of **1** (ε^1_{258nm}) and ε_{280nm} of **4** (ε^4_{280nm}) were determined as follows:

$\varepsilon^1_{258\,nm}$: 4150 $\varepsilon^4_{280\,nm}$: 2440

The data concerned with **4** were used as they were for the calculation of its concentration, because it was convenient to use them for the conversion of its UV spectral data in the calculations, although the data were identical with those reported with respect to 2-chloroinosine.[3]

c) Rate Determination of the Fusion Reaction: Equimolar amounts of **1**[12] (0.0187 g, 0.1 mmol) and 1,2,3,5-tetra-*O*-acetyl-β-D-ribofuranose (**2**)[13] (0.0318 g, 0.1 mmol) were mingled in an agate mortar as completely as possible, and then a suitable amount of the mixture was placed in a capillary tube. The sample in the capillary tube was heated at 152—154 °C for a scheduled period in a Micro Melting Point Apparatus (Yanagimoto Seisakusho Co., Ltd.) and then cooled immediately in an ice-bath after the reaction. The fused mixture was taken out by crushing the capillary tube, and then it was dissolved in the alkaline solvent described in a). The total coefficients of the ε_{258nm} and ε_{280nm} of the resultant solution, which had been properly diluted with the same solvent so as to enable us to determine the UV spectrum, and the yields of the reaction at each reaction time were calculated in the manner described in the text. The $y/(x+y)$[yields] thus obtained were plotted against the reaction times to give an outline such as is shown in Fig. 1.

The reversibility of this reaction was confirmed by heating **4** (300 mg) with glacial acetic acid (0.1 ml) in a small test tube at 150 °C for 15 min in an oil-bath. The tlc examination of the resultant fusion on a plate of Wakogel B5-F (0.25 mm) [the solvent system for the development: benzene–methanol (9: 1 v/v)], in comparison with the authentic **1**, **2**, and **4**, showed the formation of **1** and **2** by the reverse reaction. The spots corresponding to **1**, **2**, and **4** were easily detected by the use of a UV lamp [S. L. Light, Tokyo Machinery Co., Ltd. (2537 and 3650 Å)] or by developing with iodine or with a dilute aqueous sulfuric acid solution, followed by heating. The UV spectral determination of the resultant fusion proved it to be composed of **1** (18) and **4** (82%).

d) Rate Determination of the Reaction of 1 with 2 in Dimethyl Sulfoxide: The reaction rates were determined at 130 °C and at 135 °C. Dimethyl sulfoxide shows no absorption in the vicinity of either 258 or 280 nm under the conditions mentioned above. **1** and **4** were used for the determinations as a 40 mmol/l dimethyl sulfoxide solution. The reaction vessel used for the determinations was a three-necked, 100 ml, round-bottomed flask, fitted with a standard stopcock and an automatic stirrer. The temperature of the reaction bath (Mitamura Riken Kogyo Inc., Type 13—76) was regulated precisely with a thermostat (Jumo Co., Ltd., West Germany) within ±0.2 °C. 20 ml portions of the above freshly-prepared solution of **1** and **2** was pipetted into the reaction vessel, the mixture being constantly stirred at the reaction temperature. After each scheduled reaction time, a small amount of the reaction mixture was taken out with a pipette and diluted properly with the same alkaline solvent so as to enable us to determine the UV spectra. The data thus obtained were treated in the same way as has been described in c).

NMR Examination of the Relative Content Ratios of Anomeric Nucleosides in the Mixtures Obtained by the Fusion Reactions. a) The Sample from the Reaction of 2,6-Dichloropurine (1) with 1,2,3,5-Tetra-O-acetyl-β-D-ribofuranose (2) for NMR Determination: Equimolar amounts of **1** (1.87 g, 10 mmol) and **2** (3.18 g, 10 mmol) were sufficiently mingled in an agate mortar, and then a 200 mg portion of the mixture was put into a small glass test tube. The sample was then heated in the above-described reaction bath at 150 °C *in vacuo* for a scheduled reaction time and subsequently cooled immediately after the reaction in an ice-bath. Each of the resultant mixtures was dissolved in deuterochloroform and then subjected to an NMR determination. The deuterochloroform solution was filtered through a small cotton tampon on precipitation of some crystalline mass. In the case of the acid-catalyzed fusion reaction, a mixture of **1** (10 mmol), **2** (10 mmol), and sulfamic acid (20 mg, 0.02 mmol) was utilized after sufficient mingling in the mortar. The anomeric proton signals of 2,6-dichloro-9-(2',3',5'-tri-*O*-acetyl-β-D-ribofuranosyl)-purine (**4**)[2] and its α-anomer (**5**) were observed at 6.24 ($J_{1',2'}$=4.7 Hz) and 6.75 ($J_{1',2'}$=5.6 Hz) ppm respectively (*cf.* Figs. 4, 6, and 7).

b) The Sample from the Fusion Reaction of 1 with 1,2,3,5-

11) A similar steric effect of 8-halogeno substituents has recently been reported in the condensation reaction of 2,3,5-tri-*O*-benzoyl-D-ribofuranosyl bromide with 8-chloro(or -iodo)adenine, which brought about the preferred formation of the corresponding nucleoside glycosylated at $N_{(3)}$ in the purine nucleus[C. L. Schmidt and L. B. Townsed, *J. Org. Chem.*, **37**, 2300 (1972)].

12) G. B. Elion and G. H. Hitchings, *J. Amer. Chem. Soc.*, **78**, 3508 (1956).

13) H. Zinner, *Chem. Ber.*, **83**, 517 (1950).

Tetra-O-*acetyl*-α-D-*ribofuranose (3)*: The sirup of **3**, which had been prepared according to the method of Zinner,[14] was found to be composed of **2** and **3** in the ratio of 13/87, by a study of the integration curve of its NMR spectrum, in which a quartet (δ 6.80, *H*-1 of **3**) and a singlet (δ 6.28, *H*-1 of **2**) were observed in the anomeric region. An equimolar mixture of **1** and **3** was prepared in the way described in connection with the previous experiment, a). A 200 mg portion of this mixture was put into a small test tube and similarly subjected to a reaction. After the reaction, the resultant mixture was dissolved in deuterochloroform and used for the NMR determination (*cf.* Fig. 5).

c) The Sample from the Fusion Reaction of 2,6,8-Trichloropurine (6) with 2 or 3: The mixture of **6**[15] and **2** or **3** for the autocatalytic or acid-catalyzed fusion reaction was prepared in the way described in a) and then treated similarly. The resultant mixtures were dissolved in deuterochloroform, filtered with a small cotton tampon if needed, and used for the NMR determination. The anomeric proton signals of 2,6,8-trichloro-9-(2′,3′,5′-tri-*O*-acetyl-β-D-ribofuranosyl)-purine (**7**)[2a] and its α-anomer (**8**) were observed at *ca.* δ 6.1 ppm, together with the other one proton on the D-ribofuranosyl ring, and at 6.60 ($J_{1',2'}$=5.0 Hz) ppm respectively (*cf.* Fig. 8).

The authors wish to express their thanks to Professor Juji Yoshimura, Tokyo Institute of Technology, for his valuable discussions throughout this work, and to Mr. Keiji Eguchi, Japan Electric Optics Lab., for his help in carrying out the NMR spectral measurement of the samples. They are also grateful to the Ministry of Education, Japanese Government, for a Scientific Research Grant-in-Aid.

14) H. Zinner, *Chem. Ber.*, **86**, 817 (1953).
15) J. Davoll and B. A. Lowy, *J. Amer. Chem. Soc.*, **73**, 2936 (1951).

BULLETIN OF THE CHEMICAL SOCIETY OF JAPAN, VOL. 46, 2820—2822 (1973)

Oxidative Additions of Alkyl Halides to Palladium(0) Carbonyl Complex

Koji KUDO, Michito SATO, Masanobu HIDAI, and Yasuzo UCHIDA

Department of Industrial Chemistry, Faculty of Engineering, University of Tokyo, Hongo, Tokyo 113

(Received February 3, 1973)

Oxidative addition reactions of alkyl halides to $Pd(CO)(PPh_3)_3$ were studied. Vinyl chloride, allyl chloride, allyl bromide, methallyl chloride, benzyl bromide, methyl iodide, and iodobenzene react with $Pd(CO)(PPh_3)_3$ to afford the corresponding acyl complexes of the type *trans*-$PdX(COR)(PPh_3)_2$. The reactions proceed rapidly when the dissociation energy of carbon-halogen bond in the saturated alkyl halides is smaller than about 60 kcal/mol. In the case of the unsaturated alkyl halides the more inert carbon-halogen bond can be activated by initial formation of π complexes.

Oxidative addition reactions to lower valent metal complexes are currently drawing considerable attention in relation to transition metal catalysis. The reactions with alkyl compounds often give products possessing stable metal-carbon σ bonds.

So far the acyl complexes of palladium(II) of the type *trans*-$PdX(COR')(PR_3)_2$ reported have been limited to acetyl or benzoyl complexes such as *trans*-$PdCl(COMe)(PPh_3)_2$ prepared by oxidative addition of acetyl chloride to $Pd(PPh_3)_4$[1] and *trans*-$PdX(COR)(PEt_3)_2$ (R=Me or Ph) prepared by carbonylation of *trans*-$PdX(R)(PEt_3)_2$.[2] We found that oxidative addition of alkyl halides to $Pd(CO)(PPh_3)_3$ gives the acyl complexes of this type.[3] In this paper we wish to report the reactivity of various alkyl halides towords $Pd(CO)(PPh_3)_3$.

Results and Discussion

Reactions were carried out by addition of excess alkyl halides to toluene solutions containing $Pd(CO)(PPh_3)_3$ under carbon monoxide at 1 atm. Immediate reaction took place, the original yellow color of the solutions paled and the solutions were stirred for 1—2 hr at ambient temperature for completion of the reactions. After addition of *n*-hexane to the solutions, the acyl complexes were obtained.

Among the alkyl halides examined, allyl chloride, allyl bromide, methallyl chloride, benzyl bromide, and iodobenzene react with the carbonyl complex rapidly, giving the corresponding acyl complexes of the type *trans*-$PdX(COR)(PPh_3)_2$ in high yields.

$$Pd(CO)(PPh_3)_3 + R\text{-}X \longrightarrow PdX(COR)(PPh_3)_2$$

Methyl iodide gave two isomers of methyl complexes in addition to the expected acetyl complex. Vinyl chloride is less reactive and the oxidative addition product was obtained in a poor yield.[3] Other alkyl halides such as PhBr, $PhCH_2Cl$, MeBr, EtI, EtBr, *n*-PrCl, *n*-PrBr, *i*-PrCl, *i*-PrBr, $CCl_2{=}CCl_2$ or *cis*-CHCl=CHCl did not react, the carbonyl complex being recovered.

The reactivity of alkyl halides decreased in the order iodide>bromide>chloride, and allyl≈methallyl>benzyl>phenyl≈methyl>vinyl>propyl≈ethyl. In a series of alkyl chlorides, allyl, and methallyl chlorides give the acyl complexes in high yields but not benzyl chloride. Benzyl bromide gives the acyl com-

1) P. Fitton, M. P. Johnson, and J. E. McKeon, *Chem. Commun.*, **1968**, 6.
2) G. Booth and J. Chatt, *J. Chem. Soc., A*, **1966**, 634.
3) K. Kudo, M. Hidai, and Y. Uchida, *J. Organometal. Chem.*, **33**, 393 (1971).

Table 1. Formation of $PdX(COR)(PPh_3)_2$

R	Cl		Br		I	
	Yield %	Ed	Yield %	Ed	Yield %	Ed
CH_2=CH-	12[a]	85.5	—	73.4	—	
CH_2=$CHCH_2$-	82[a]	60	95	46	—	36
CH_2=$CMeCH_2$-	91	70	—		—	
$PhCH_2$-	X[b]		81	51	—	39
Me-	—	80	X[b]	67	26[a,c]	54
Ph-	—		X[b]	71	95	61

a) Quoted from Ref. 3.
b) No reaction occurred.
c) $PdI(Me)(PPh_3)_2$ (2 isomers) were also obtained(30%).

plex, whereas in the case of methyl and phenyl halides only iodides react with the carbonyl complex. The reaction of vinyl chloride gives the acyl complex in a poor yield. No reaction takes place in the case of propyl and ethyl halides. This is in line with the increase of the dissociation energy (Ed) of the carbon-halogen bond in alkyl halides (Table 1). The reaction of the saturated alkyl halides proceeds rapidly when Ed is smaller than about 60 kcal/mol. Unsaturated compounds which have larger Ed undergo oxidative additions. For example, methallyl chloride undergoes reaction, though Ed is 70 kcal/mol, comparable to that of methyl and phenyl bromides which do not undergo oxidative addition. Even more inert vinyl chloride (Ed=85.5 kcal/mol) gives $PdCl(COCH=CH_2)(PPh_3)_2$, though in a poor yield. This may be explained by the initial coordination of the unsaturated compounds to palladium through a π-bonding, which would cause the activation of the carbon-halogen bond, followed by isomerization to the acyl complexes.

In these oxidative addition reactions to zero-valent palladium complexes, the dissociated species are generally considered to be active species. Since $Pd(CO)(PPh_3)_3$ dissociates to a coordinatively unsaturated species $[Pd(CO)(PPh_3)_2]$ in solution,[3] the reaction probably proceeds according to the following scheme:

$$Pd(CO)(PPh_3)_3 \rightleftharpoons [Pd(CO)(PPh_3)_2] + PPh_3 \xrightarrow{R\text{-}X}$$
$$[PdX(R)(CO)(PPh_3)_2] \longrightarrow PdX(COR)(PPh_3)_2$$

The unsaturated species $[Pd(CO)(PPh_3)_2]$ is susceptible to electrophilic attack by alkyl halides, giving the unstable five-coordinate palladium(II) carbonyl complex $[PdX(R)(CO)(PPh_3)_2]$. An immediate insertion of the carbonyl ligand into the palladium-alkyl bond may occur to produce the acyl complexes $Pd(COR)X(PPh_3)_2$. The alkenyl halides initially react with the coordinatively unsaturated species $[Pd(CO)(PPh_3)_2]$ to form π complexes $[Pd(C=C)(CO)(PPh_3)_2]$, followed by isomerization to the acyl complexes. This is supported by the fact that vinyl chloride reacts with $Pd(PPh_3)_4$ affording an unstable π-complex.[4] The reaction mechanism involving the initial formation of alkyl complexes $PdX(R)(PPh_3)_2$ followed by carbonylation with atmospheric carbon monoxide is reasonably excluded for the following reasons: the acetyl complex could be obtained by a reaction of methyl iodide under nitrogen atmosphere, and Booth and Chatt reported that carbonylation of the aromatic phosphine complexes of palladium-alkyl was unsuccesful.[2]

The acyl complexes obtained here are stable in an inert atmosphere. It is reasonable that they have a *trans*-structure in analogy with $PdCl(COCH_2CH=CH_2)(PPh_3)_2$ which shows ν(Pd–Cl) at 320 cm^{-1} corresponding to a *trans*-square planar. It is known that the *trans*-isomer is more stable in these palladium(II) phosphine complexes than the *cis*, especially in the presence of excess triphenylphosphine.[1]

Table 2. IR data and decomposition points of *trans*-$PdX(COR)L_2$ (L=PPh_3)

Complex	ν(C=O)	ν(C=C) cm^{-1}	°C
$PdCl(COCH=CH_2)L_2$	1665	1620	—
$PdCl(COCH_2CH=CH_2)L_2$	1675	1636	115
$PdBr(COCH_2CH=CH_2)L_2$	1687	1640	—
$PdBr(COCH=CHCH_3)L_2$	1680	1634	—
$PdCl(COCH_2CMe=CH_2)L_2$	1695	1647	70
$PdBr(COCH_2Ph)L_2$	1696	—	105
$PdI(COMe)L_2$	1690	—	141
$PdI(COPh)L_2$	1634	—	107

IR spectra of the acyl complexes show a strong absorption at 1700—1630 cm^{-1}, assignable to C=O stretching (Table 2). The low shift of ν(C=O) for the benzoyl complex may be attributed to the conjugation between the caronyl group and phenyl ring. A slight conjugation between the carbonyl group and the carbon-carbon double bond is observed in the acryloyl complex obtained by the reaction of vinyl chloride. The product from allyl chloride exhibits absorptions at 1675 and 1636 cm^{-1} assignable to ν(C=O) and ν(C=C), respectively. Deformations of terminal vinyl group occur at 990 and 905 cm^{-1}, indicating that the complex is 3-butenoyl complex $PdCl(COCH_2CH=CH_2)(PPh_3)_2$. On the other hand, the product from allyl bromide shows ν(C=O) at 1687 and 1680 cm^{-1} and ν(C=C) at 1640 and 1634 cm^{-1}, respectively, indicating the formation of two isomers, presumably 2- and 3-butenoyl complexes. The absorption bands at 1680 and 1634 cm^{-1} are assignable to 2-butenoyl complex $PdBr(COCH=CHCH_3)(PPh_3)_2$, since the slight conjugation between C=O and C=C groups is expected to shift the bands to lower region. Separation of the two isomers was unsuccessful. The relationship between ν(C=O) and thermal stability of the acyl complexes was not observed. This may be explained by the fact that contribution of back donation from palladium to acyl group to stability is small, though the back donation is expected to strengthen the palladium-acyl bond and be reflected in ν(C=O).

Experimental

IR spectra were recorded as Nujol mulls on a JASCO DS-403 spectrophotometer. Decomposition points were measured in an argon atmosphere and are uncorrected. $Pd(CO)(PPh_3)_3$ was prepared according to Method B in literature.[3]

Reaction of Methallyl Chloride. 0.12 ml of methallyl

4) P. Fitton and J. E. McKeon, *Chem. Commun.*, **1968**, 4.

chloride was added through a syringe to a toluene solution (3 ml) containing 0.12 g of $Pd(CO)(PPh_3)_3$ at $-10°$. The solution immediately turned from orange-yellow to pale yellow. It was stirred for 2 hr at ambient temperature, during which course of time 0.085 g (91%) of *trans*-$PdCl(COCH_2CMe{=}CH_2)(PPh_3)_2$ precipitated. Decomp. 70 °C. Found: C, 65.6; H, 4.8%. Calcd for $C_{41}H_{37}OClP_2Pd$: C, 65.7; H, 5.0%.

Reaction of Allyl Bromide. A mixture of *trans*-$PdBr(COCH_2CH{=}CH_2)(PPh_3)_2$ and *trans*-$PdBr(COCH{=}CHCH_3)(PPh_3)_2$ (0.069 g; 95%) was obtained analogously from 0.086 g of $Pd(CO)(PPh_3)_3$ and 0.08 ml of allyl bromide in 3 ml of toluene. Found: C, 60.2; H, 4.7%. Calcd for $C_{40}H_{35}OBrP_2Pd$: C, 61.6; H, 4.5%.

Reaction of Benzyl Bromide. 0.10 g (81%) of *trans*-$PdBr(COCH_2Ph)(PPh_3)_2$ was obtained from 0.14 g of $Pd(CO)(PPh_3)_3$ and 0.18 ml of benzyl bromide in 3 ml of toluene. Decomp. 105 °C. Found: C, 64.1; H, 5.0%. Calcd for $C_{44}H_{37}OBrP_2Pd$: C, 63.7; H, 4.5%.

Reaction of Iodobenzene. 0.056 g (95%) of *trans*-$PdI(COPh)(PPh_3)_2$ was obtained from 0.063 g of $Pd(CO)(PPh_3)_3$ and 0.08 ml of iodobenzene in 3 ml of toluene. Decomp. 107 °C. Found: C, 59.6; H, 3.9%. Calcd for $C_{43}H_{35}OIP_2Pd$: C, 59.8; H, 4.1%.

BULLETIN OF THE CHEMICAL SOCIETY OF JAPAN, VOL. 46, 2822—2827 (1973)

Linear Conjugated Systems Bearing Aromatic Terminal Groups. XII.[1] Syntheses and Electronic Spectra of α,ω-Di-2-pyrenyl- and α,ω-Di-2-fluorenylpolyenes

Yasuhira TAKEUCHI, Akio YASUHARA, Shuzo AKIYAMA, and Masazumi NAKAGAWA

Department of Chemistry, Faculty of Science, Osaka University, Toyonaka, Osaka 560

(Received December 14, 1972)

The syntheses of α,ω-di-2-pyrenyl- and α,ω-di-2-fluorenylpolyenes I_n and I_n' ($n=1$—6) by means of the Wittig reaction are described. Aldehydes II, II′, propenals IV, IV′, pentadienals V, V′ bearing 2-pyrenyl or 2-fluorenyl terminal group and muconaldehyde VI were used as carbonyl components. Phosphoranes III, III′, VII, VII′, VIII and VIII′ were prepared from methyl-, propenyl-, and pentadienyltriphenylphosphonium bromides substituted with 2-pyrenyl or 2-fluorenyl group by the reaction with phenyllithium. I_n and I_n' were obtained by the reaction of carbonyl components with phosphoranes by proper combination. It was found that the bathochromic shift of the longest-wavelength peaks of I_n and I_n' can be expressed by the following empirical equations:

$$I_n : \lambda = 44.6n^{0.7} + 314 \text{ (nm in tetrahydrofuran)}$$

$$I_n' : \lambda = 29.5n^{0.8} + 353 \text{ (nm in tetrahyhrofuran)}$$

The bathochromic shift of the longest-wavelength absorption maxima (λ) of some α,ω-diarylpolyenes [$Ar(CH=CH)_nAr$] can be expressed by the empirical formula $\lambda = An^x + B$.[2,3] The value of x changes with terminal group and the position of linking of polyene chain. This indicates a marked influence of terminal groups on the electronic excitation of polyene chromophore. The present paper deals with the syntheses and electronic spectral regularity of α,ω-di-2-pyrenyl- and α,ω-di-2-fluorenylpolyenes (I_n and I_n', $n=1$—6) which were carried out for the purpose of getting information on the role of aromatic terminal groups on the spectral regularity of diarylpolyenes.

Syntheses. The syntheses of I_n and I_n' were carried out by the Wittig reaction. The combination of carbonyl component and phosphorane is shown in the Scheme. 2-Formylpyrene[4] (II) and 2-formylfluorene[5] (II′) were prepared by the reported methods. 3-(2-Pyrenyl)-2-propenal (IV) was prepared by the reaction of lithium ethoxyacetylide with II followed by reduction with lithium aluminum hydride and anionotropic rearrangement under acidic conditions. 3-(2-Fluorenyl)-2-propenal (IV′) could be obtained by the Meyer-Schuster rearrangement of 1-(2-fluorenyl)-2-propyn-1-ol derived from II′. The reaction of Grignard derivative of methoxybutenyne with the aldehyde (II or II′) followed by reduction and acid treatment afforded 5-aryl-2,4-pentadienal (V or V′) in a reasonable yield.

Phosphorane (III) was prepared from 2-pyrenylmethyltriphenylphosphonium bromide.[6] 2-Formyl-

1 $\underset{\text{II, II'}}{RCHO} + \underset{\text{III, III'}}{RCH=PPh_3} \longrightarrow \underset{I_1,\ I_1'}{RCH=CHR}$

2 $\underset{\text{IV, IV'}}{RCH=CHCHO} + \underset{\text{III, III'}}{RCH=PPh_3} \longrightarrow \underset{I_2,\ I_2'}{R(CH=CH)_2R}$

3 $\underset{\text{V, V'}}{R(CH=CH)_2CHO} + \underset{\text{III, III'}}{RCH=PPh_3} \longrightarrow \underset{I_3,\ I_3'}{R(CH=CH)_3R}$

4 $\underset{\text{III, III'}}{2\,RCH=PPh_3} + \underset{\text{VI}}{OCH(CH=CH)_2CHO} \longrightarrow \underset{I_4,\ I_4'}{R(CH=CH)_4R}$

1) For Part XI of this series, see Ref. 3.

2) A. Yasuhara, S. Akiyama, and M. Nakagawa, This Bulletin, **45**, 3638 (1972).

3) Y. Takeuchi, A. Yasuhara, S. Akiyama, and M. Nakagawa, *ibid.*, **46**, 909 (1973).

4) K. Nakasuji, S. Akiyama, and M. Nakagawa, *ibid.*, **45**, 875 (1972).

5) R. Rieche, H. Gross, and E. Hoft, *Chem. Ber.*, **93**, 88 (1960).

6) S. Akiyama, K. Nakasuji, and M. Nakagawa, This Bulletin, **44**, 2231 (1971).

Table 1. Physical properties of di-2-pyrenyl- and di-2-fluorenylpolyenes (I_n and I_n')

	Di-2-pyrenylpolyene (I_n)			Di-2-fluorenylpolyene (I')		
n	Color of crystals	Mp (°C)	δ (cm^{-1})	Color of crystals	Mp (°C)	δ (cm^{-1})
1	greenish yellow	>360	951	colorless	304—305	967
2	pale yellow	354—355	974	yellow	301—302	990
3	yellow	329—330	980	yellow	296—297	1000
4	yellow	320	987	yellow	289—291	1005
5	orange	303	990	yellow	277	1005
6	orange	298—299		orange	298—300	1005

5 $R(CH{=}CH)_2CHO$ (V, V′) + $R(CH{=}CH)_2CH{=}PPh_3$ (VII, VII′) ⟶ $R(CH{=}CH)_5R$ (I_5, I_5')

6 $RCH{=}CHCH{=}PPh_3$ (VIII, VIII′) + $OCH(CH{=}CH)_2CHO$ (VI) ⟶ $R(CH{=}CH)_6R$ (I_6, I_6')

fluorene (II′) was reduced to 2-hydroxymethyl derivative by sodium borohydride, which was converted into 2-bromomethylfluorene by the usual method. 2-Fluorenylmethyltriphenylphosphonium bromide prepared by the reaction of triphenylphosphine with 2-bromomethylfluorene was treated with phenyllithium to give phosphorane (III′). Reduction of propenal (IV or IV′) with sodium borohydride afforded the corresponding propenol, which was converted into propenyl bromide and treated with triphenylphosphine to give triphenylphosphonium bromide. The reaction of phenyllithium with the phosphonium bromide gave phosphorane (VIII or VIII′). Similarly, 5-aryl-2,4-pentadienal (V or V′) was converted into phosphorane (VII or VII)′ *via* pentadienol and pentadienyl bromide.

1,2-Di(2-pyrenyl)- and 1,2-di(2-fluorenyl)ethylene (I_1 and I_1') were obtained by the reaction of aldehydes (II and II′) with phosphoranes (III and III′), respectively. The combination of propenal (IV or IV′) with phosphorane (III or III′) afforded 1,4-di(2-pyrenyl)- or 1,4-di(2-fluorenyl)-1,3-butadiene (I_2 or I_2'). 1,6-Di(2-pyrenyl)- and 1,6-di(2-fluorenyl)-1,3,5-hexatrienes (I_3 and I_3') were prepared by the reaction of pentadienals (V and V′) with phosphoranes (III and III′), respectively. The reaction of muconaldehyde (VI) with III or III′ afforded 1,8-di(2-pyrenyl)- or 1,8-di(2-fluorenyl)-1,3,5,7-octatetraene (I_5 or I_5'). The reaction of propenylidenephosphorane (VIII or VIII′) with muconaldehyde (VI) gave 1,12-di(2-pyrenyl)- or 1,12-di(2-fluorenyl)-1,3,5,7,9,11-dodecahexaene (I_6 or I_6').

The color of crystals, melting points and wave number of IR absorption in the region of C–H out-of-plane deformation (δ) of *trans*-double bond are summarized in Table 1. Regular increase in melting point with the increase of n reported for α,ω-diphenylpolyenes[7] could not be observed in the series of I_n and I_n'. The solubility of both series of polyenes

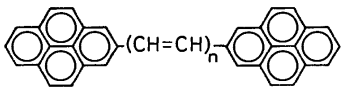

I_n

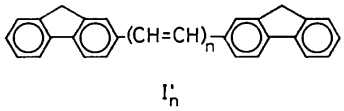

I_n'

Scheme 1. Syntheses of di-2-pyrenyl- and di-2-fluorenylpolyenes (I_n and I'_n).

Table 2. Electronic spectral data of di-2-pyrenyl- and di-2-fluorenylpolyenes (I_n and I_n')[a]

	λ_{max} (log ε) in nm in tetrahydrofuran													
n	Di-2-pyrenylpolyenes (I_n)										Di-2-fluorenylpolyenes (I_n')			
1	251 (4.77)	310 (4.87)	324 (5.03)	341.5 (4.12)	359[b]	392[c] (3.39)	415[c] (3.27)				349[b]	363 (4.93)	382 (4.71)	
2	249[b]	258 (4.54)	268[b]	314[b]	333 (5.03)	344 (5.25)	365 (4.96)	385 (4.78)	399[b]	424[c] (3.59)	364 (4.86)	380 (4.99)	404 (4.63)	
3	265 (4.48)	285 (4.20)	328 (4.79)	345 (5.07)	358 (4.96)	386 (5.05)	410 (4.51)	431[c] (4.07)			262.5[b]	379.5 (4.89)	398.5 (5.04)	424 (4.91)
4			326.5	345	351	386	401	431			275 (4.21)	394 (4.95)	432 (5.10)	461 (5.00)
5			325	342	356	402	424	452			388[b]	409 (5.00)	432 (5.16)	461 (5.09)
6	326	341	355	404	424	452	470[b]				295.5 (4.37)	423 (5.06)	446 (5.20)	476.5 (5.13)

a) Owing to poor solubility, the spectra of I_{4-6} were measured with solutions of unknown concentration employing 10 cm glass cells. b) Shoulder. c) Absorption maxima of L_b species.

7) R. Kuhn and A. Winterstein, *Helv. Chim. Acta*, **11**, 87 (1928).

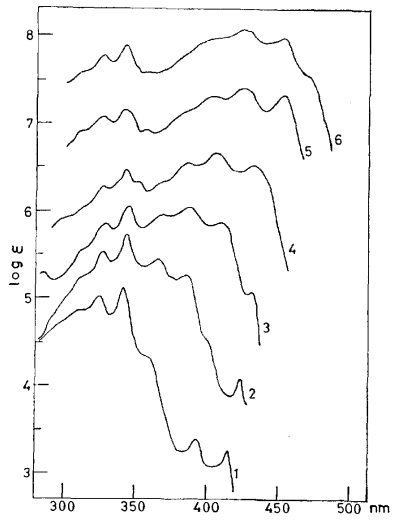

Fig. 1. Absorption curves of di-2-pyrenylpolyenes (I_n) in tetrahydrofuran. The spectra of I_{4-6} were measured with solutions of unknown concentration using 10 cm glass cells. Each curve, except for I_1, has been displaced upward by a 0.5 log ε unit increment from one immediately below it.

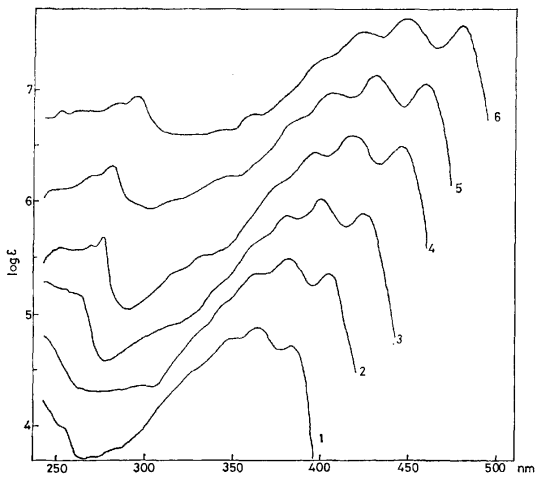

Fig. 2. Absorption curves of di-2-fluorenylpolyenes (I'_n) in tetrahydrofuran. Each curve, except for I_1', has been displaced upward by a 0.5 log ε unit increment from one immediately below it.

decreases markedly with the increase in n. Shift of δ to higher wave number along with the increase of n observed in other series of diarylpolyenes[2,3] was also found in the series of I_n and $I_{n'}$.

Electronic Spectra. Numerical data of the electronic spectra of I_n and $I_{n'}$ are summarized in Table 2. The absorption curves of both series of diarylpolyenes I_n and $I_{n'}$ exhibit well-defined vibrational fine structure (Figs. 1 and 2). The characteristic of electronic spectra of I_n and $I_{n'}$ is similar to that of other series of diarylpolyenes,[2,3] *i.e.*, the intense bands in the long-wavelength region, which seems to arise from an interaction of L_a band of the terminal group with the polyene chromophore, shift to longer wavelength with the increase in n. However, the increase in the length of polyene chain exerts a minor effect on the location of short wavelength bands. The weak absorption maxima at the longest-wavelength region observed in I_1, I_2, and I_3 can be attributed to the L_b band of pyrene nucleus. Discussion is given on the spectral regularity for the longest-wavelength sub-bands (λ) of the intense long-wavelength absorption band. It was found that the plots of λ of I_n and $I_{n'}$ *versus* $n^{0.7}$ and $n^{0.8}$, respectively, gave good straight lines (Figs. 3 and 4). The following empirical equations can well express the linear relationships:

$$\lambda = An^{\pi} + B$$

I_n : $\lambda = 44.6n^{0.7} + 314$ (nm in tetrahydrofuran)

$I_{n'}$: $\lambda = 29.5n^{0.8} + 353$ (nm in tetrahydrofuran)

The linear relationship of acetylenic analogues of I_n and $I_{n'}$, 2,2′-dipyrenylpoly-ynes[4] and 2,2′-difluorenylpoly-ynes[8] can be expressed by $\lambda=12.6\ n^{1.4}+327$ (nm in toluene) and $\lambda=9.0\ n^{1.5}+350$ (nm in tetrahydrofuran). The value of A in polyene series were found to be much larger than those in poly-yne analogues. This indicates that the electronic interaction of aromatic terminal group with polyene chromophore differs from that with poly-yne system, since the value of A can be regarded as a measure of interaction between terminal group and unsaturated function.

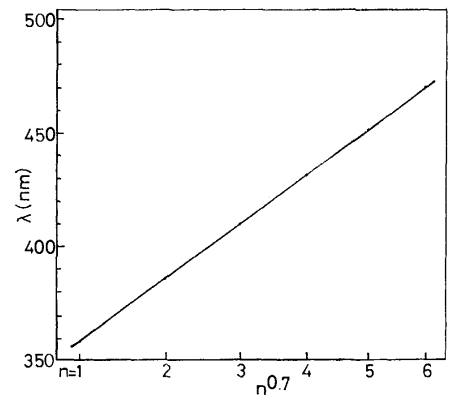

Fig. 3. Plot of λ *vs.* $n^{0.7}$ for di-2-pyrenylpolyenes (I_n).

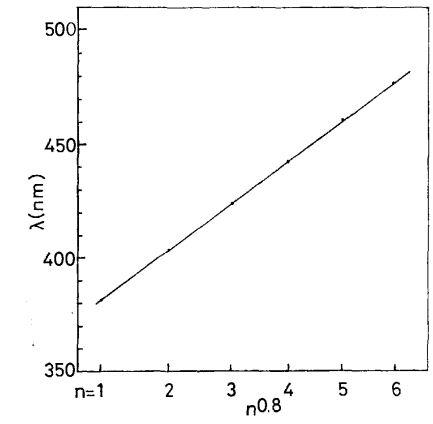

Fig. 4. Plot of λ *vs.* $n^{0.8}$ for di-2-fluorenylpolyenes (I_n').

Experimental

All melting points are not corrected. The electronic spectra were measured with a Hitachi EPS-3T spectrophotometer

8) K. Nakasuji, S. Akiyama, and M. Nakagawa, This Bulletin, **45**, 883 (1972).

using a well-matched pair of 1 cm quartz cells unless otherwise stated. IR spectra were obtained on a Hitachi EPI-2 spectrophotometer by the KBr-disk method. Preparation of phosphoranes was carried out under nitrogen atmosphere using an ethereal solution of phenyllithium as a base. The Wittig reaction was performed under shielding from light.

3-(2-Pyrenyl)-2-propenal (IV). To a solution of lithium ethoxyacetylide prepared from 2-chlorovinyl ethyl ether (7.0 g, 0.066 mol) in tetrahydrofuran (20 ml) and lithium amide (from lithium, 0.8 g, 0.12 g-atom) in liquid ammonia (130 ml) was added a solution of II[4] (3.0 g, 0.013 mol) in tetrahydrofuran (40 ml). After being stirred overnight at the boiling point of ammonia, stirring was continued overnight at 0 °C allowing the ammonia to evaporate. Ammonium chloride (10 g) and water were added to the residue. The organic layer, after washing and drying, was concentrated to give a dark brown liquid which was dissolved in tetrahydrofuran (40 ml). Lithium aluminum hydride (2.2 g, 0.058 mol) in the same solvent (50 ml) was added to the solution and the mixture was stirred for 2 hr at room temperature. Ethyl acetate (10 ml) and 2 M sulfuric acid (100 ml) were added successively, and the mixture was stirred overnight at room temperature. The aqueous layer was extracted with benzene. The combined organic layer and extract, after being washed and dried, were concentrated under reduced pressure. Crystals, 0.26 g, mp 183—194 °C obtained by trituration of the residue with a small amount of ether-tetrahydrofuran were dissolved in benzene and passed through a short column of alumina. Crystals obtained from the filtrate were recrystallized from benzene to yield pure IV, mp 205—206 °C, IR: 1693 (C=O), 973, 963 (=C-H) cm^{-1}.

Found: C, 88.57; H, 4.72%. Calcd for $C_{19}H_{12}O$: C, 89.04; H, 4.72%.

5-(2-Pyrenyl)-2,4-pentadienal (V). A solution of II[4] (4.4 g, 19 mmol) in tetrahydrofuran (50 ml) was added to a solution of Grignard derivative of methoxybutenyne prepared by the reaction of the butenyne (3.2 g, 38.9 mmol) in tetrahydrofuran (12 ml) with ethylmagnesium bromide (from ethyl bromide, 4.3 g and magnesium, 0.70 g in the same solvent, 22 ml). After being stirred overnight at room temperature, ethanol (1.3 ml) and lithium aluminum hydride (1.1 g, 29 mmol) were added and stirred for 1.5 hr. Ethyl acetate (10 ml), water (10 ml) and 2 M sulfuric acid (100 ml) were successively added to the reaction mixture and stirred for 2 hr. The aqueous layer was extracted with tetrahydrofuran, and the extract was combined with the organic layer. Light brown crude crystals, mp 212—217 °C, 3.8 g (64.2%) obtained by evaporation of the combined organic layer, after being washed and dried, were dissolved in benzene and passed through a short column of alumina. Concentration of the filtrate afforded pure V, mp 219 °C, IR: 1673 (C=O), 990 (=C-H) cm^{-1}.

Found: C, 89.17; H, 4.92%. Calcd for $C_{21}H_{14}O$: C, 88.86; H, 5.22%.

3-(2-Pyrenyl)-2-propen-1-ol. To a stirred solution of IV (0.434 g, 1.7 mmol) in a mixture of tetrahydrofuran (50 ml) and methanol (5 ml) was added a solution of sodium borohydride (0.5 g, 13 mmol) in methanol (10 ml). After being stirred for 1 hr at room temperature, dilute hydrochloric acid was added to the reaction mixture, the organic solvent being removed under reduced pressure. The residue was extracted with benzene. The extract, after being washed and dried, was concentrated to give pale yellow crystals, mp 111—118 °C, 0.30 g (quantitative), which were recrystallized from benzene to yield pure propenol, colorless plates, mp 130.5—131.1 °C, IR: 3300—3200 (O-H), 1105 (C-O), 993, 974, 965 (=C-H) cm^{-1}.

Found: C, 87.30; H, 5.99%. Calcd for $C_{19}H_{14}O$: C, 87.15; H, 6.02%.

5-(2-Pyrenyl)-2,4-pentadien-1-ol. A solution of sodium borohydride (1.0 g, 27 mmol) in methanol (40 ml) was added to a stirred solution of V (1.5 g, 5.6 mmol) in tetrahydrofuran (100 ml). After being stirred for 2 hr at room temperature, dilute hydrochloric acid and water were successively added to the reaction mixture. Yellow plates deposited, 1.05 g (69.5%), were recrystallized from benzene to give pure pentadienol, yellow plates, mp 175—176 °C, IR: 3300 (O-H), 987 (=C-H) cm^{-1}.

Found: C, 88.47; H, 5.67%. Calcd for $C_{21}H_{16}O$: C, 88.20; H, 5.92%.

3-(2-Pyrenyl)-2-propenyltriphenylphosphonium Bromide. A solution of phosphorus tribromide (0.85 g, 3.0 mmol) in chloroform (15 ml) was added, under cooling on an ice-salt bath, to a solution of 3-(2-pyrenyl)2-propen-1-ol (0.43 g, 1.66 mmol) in the same solvent containing 5 drops of pyridine. After being stirred for further 1 hr at room temperature, the reaction mixture was poured onto ice-water. The organic layer was successively washed with water, dilute hydrochloric acid, and water, and dried. Pale yellow crystals obtained by evaporating the solvent were mixed with triphenylphosphine (0.65 g, 2.4 mmol) in benzene (20 ml) and the mixture was refluxed overnight to give phosphonium bromide, colorless crystals, mp 240—252 °C, 0.338 g (34.9%).

5-(2-Pyrenyl)-2,4-pentadienyltriphenylphosphonium Bromide. Crude bromide obtained as greenish yellow crystals by the reaction of pyrenylpentadienol (0.80 g, 2.94 mmol) with phosphorus tribromide (1.8 g, 6.75 mmol) by the above procedure were mixed with triphenylphosphine (1.3 g, 5.0 mmol) in benzene (50 ml) and the mixture was refluxed for 15 hr to give phosphonium bromide, pale yellow crystals, mp 239—244 °C, 1.4 g (79.8%).

1,2-Di(2-pyrenyl)ethylene (I_1). To a suspension of 2-pyrenylmethyltriphenylphosphonium bromide[6] (0.67 g, 1.2 mmol) in benzene (20 ml) was added phenyllithium (0.88N, 1.4 ml). After being stirred for 20 min at room temperature, a solution of II[4] (0.23 g, 1.0 mmol) in benzene (20 ml) was added to the resulting orange red solution of III, and the mixture was stirred for 24 hr at room temperature. The solvent was removed under reduced pressure and the residue was extracted with hot benzene. Pale greenish yellow needles, mp>360 °C, 0.110 g (25.7%) obtained by cooling the extract were dissolved in hot benzene and passed through a short column of alumina to give pure I_1, greenish yellow plates, mp>360 °C, IR: 1598, 1440, 951, 865, 833, 807, 700 cm^{-1}.

Found: C, 95.39; H, 4.72%. Calcd for $C_{34}H_{20}$: C, 95.30; H, 4.70%.

1,4-Di(2-pyrenyl)-1,3-butadiene (I_2). A solution of 3-(2-pyrenyl)-2-propenal (0.26 g, 1.0 mmol) in benzene (45 ml) was added to a solution of III prepared from 2-pyrenylmethyltriphenylphosphonium bromide[6] (0.67 g, 1.2 mmol) in benzene (20 ml) and phenyllithium (0.73N, 1.6 ml). After the mixture had been stirred for 24 hr at room temperature, the solvent was removed under reduced pressure, and the residue was extracted with hot toluene. Yellow needles, mp 339—340 °C, 0.024 g (5.3%) obtained by concentrating the extract were dissolved in hot toluene, and the hot solution was percolated through a short column of alumina. Pure I_2, pale yellow needles, mp 354—355 °C, IR: 1600, 1440, 974, 870, 835, 818, 700 cm^{-1} was obtained from the filtrate.

Found: C, 94.62; H, 4.76%. Calcd for $C_{36}H_{22}$: C, 95.12; H, 4.88%.

1,6-Di(2-pyrenyl)-1,3,5-hexatriene (I_3). To a solution of III prepared from phosphonium bromide[6] (0.61 g, 1.1 mmol)

in benzene (20 ml) and phenyllithium (0.89N, 1.2 ml) was added a solution of 5-(2-pyrenyl)-2,4-pentadienal (0.24 g, 0.9 mmol) in benzene (70 ml) and the mixture was stirred for 26 hr at room temperature. Crystalline residue obtained by evaporating the solvent was extracted with hot benzene. Yellow fine needles, mp 308—315 °C, 0.035 g (8.1%), obtained on cooling the extract, were dissolved in hot toluene and passed through a short column of alumina to give pure I_3, yellow plates, mp 329—330 °C, IR: 1597, 1440, 980, 875, 870, 833, 804, 700 cm^{-1}.

Found: C, 95.18; H, 5.07%. Calcd for $C_{38}H_{24}$: C, 94.97; H, 5.03%.

1,8-Di(2-pyrenyl)-1,3,5,7-octatetraene (I_4). 2-Pyrenylmethyltriphenylphosphonium bromide[6] (0.67 g, 1.2 mmol) in benzene (20 ml) was treated with phenyllithium (0.88N, 1.4 ml) to give a solution of III. A solution of muconaldehyde (VI, 0.055 g, 0.5 mmol) in benzene (10 ml) was added to the solution of III and the mixture was stirred for 24 hr at room temperature. The solvent was removed under reduced pressure and the residue was digested with hot toluene. Fine orange yellow needles, mp 269—276 °C, 0.109 g (21.5%) obtained by concentrating the extract were dissolved in hot toluene. Percolation of the hot solution through a thin layer of alumina afforded pure I_4, mp 320 °C, IR: 1595, 1440, 992, 878, 853, 833, 810, 700 cm^{-1}.

Found: C, 93.89; H, 5.23%. Calcd for $C_{40}H_{26}$: C, 94.83; H, 5.17%.

1,10-Di(2-pyrenyl)-1,3,5,7,9-decapentaene (I_5). To a dark red solution of VII prepared from 5-(2-pyrenyl)-2,4-pentadienyltriphenylphosphonium bromide (0.283 g, 0.47 mmol) in benzene (25 ml) and phenyllithium (0.73N, 0.7 ml) was added a solution of 5-(2-pyrenyl)-2,4-pentadienal (0.11 g, 0.40 mmol) in the same solvent (65 ml). After being stirred for 24 hr at room temperature, the solvent was removed under reduced pressure. The residue dissolved in hot toluene was passed through a short column of alumina. Concentration of the filtrate afforded pure I_5, orange needles, mp 303 °C, IR: 1595, 1440, 990, 880, 860, 835, 700 cm^{-1}.

Found: C, 94.49; H, 5.37%. Calcd for $C_{42}H_{28}$: C, 94.70; H, 5.30%.

1,12-Di(2-pyrenyl)-1,3,5,7,9,11-dodecahexaene (I_6). A solution of muconaldehyde (VI, 0.0265 g, 0.25 mmol) in benzene (7 ml) was added to a solution of VIII prepared from 3-(2-pyrenyl)-2-propenyltriphenylphosphonium bromide (0.338 g, 0.58 mmol) in benzene (20 ml) and phenyllithium (0.84N, 0.7 ml). After the mixture had been stirred for 22 hr, the solvent was removed under reduced pressure. The residue dissolved in hot toluene was passed through a thin layer of alumina. Concentration of the filtrate yielded pure I_6, orange needles, mp 298—299 °C, 3 mg.

Found: C, 94.06; H, 5.31%. Calcd or $C_{44}H_{30}$: C, 94.59; H, 5.41%.

3-(2-Fluorenyl)-2-propenal (IV'). A mixture of concentrated sulfuric acid (2.4 ml), water (20 ml), dioxane (118 ml) and 1-(2-fluorenyl)-2-propyn-1-ol[8] (5.9 g, 26.8 mmol) was refluxed for 48 hr. Water was added to the reaction mixture and the aqueous layer was extracted with benzene. The combined organic layer, after being washed and dried, was concentrated to give a dark brown liquid. The liquid was triturated with a small amount of ethyl acetate containing a trace of ether to cause crystallization (yellow crystals, mp 97—107 °C, 3.05 g). The filtrate, after being evaporated, was dissolved in benzene and shaken with a saturated sodium hydrogen sulfite solution for 48 hr. Decomposition of sulfite adduct with a dilute sodium hydroxide afforded an additional amount of yellow crystals, mp 100—105 °C, 0.805 g. The combined crystals (3.85 g, 65.2%) were recrystallized from benzene to yield pure IV', mp 114 °C, colorless crystals, IR: 1675 (C=O), 970 (=C-H) cm^{-1}.

Found: C, 86.91; H, 5.42%. Calcd for $C_{16}H_{12}O$: C, 87.24; H, 5.49%.

5-(2-Fluorenyl)-2,4-pentadienal (V'). Methoxybutenyne (3.2 g, 38.9 mmol) in tetrahydrofuran (12 ml) was converted into the Grignard derivative by the reaction with ethylmagnesium bromide in the same solvent (22 ml) (from ethyl bromide, 4.4 g and magnesium, 0.70 g, 28 mg-atom). A solution of II'[5] (3.7 g, 19 mmol) in the same solvent (12 ml) was added to the Grignard reagent and the mixture was stirred for 15 hr at room temperature. Ethanol (1.3 ml) and lithium aluminum hydride (1.1 g, 29 mmol) were added to the reaction mixture. After being stirred for 1 hr at room temperature, water (6 ml) and 2 M sulfuric acid (100 ml) were successively added under ice-cooling, and worked up by the usual way to yield crude V', orange yellow crystals, mp 137—143 °C, 2.4 g (51.3%) which were recrystallized from ethyl acetate, yielding pure V', yellow plates, mp 158—159 °C, IR: 1665 (C=O), 995 (=C-H) cm^{-1}.

Found: C, 87.55; H, 5.76%. Calcd for $C_{18}H_{14}O$: C, 87.88; H, 5.73%.

3-(2-Fluorenyl)-2-propen-1-ol. Treatment of 3-(2-fluorenyl)-2-propenal (0.110 g, 0.5 mmol) with sodium borohydride according to a procedure similar to that for 2-pyrenyl analogue afforded fluorenylpropenol, colorless crystals, mp 133—143 °C, 1.02 g (92.5%), which were recrystallized from benzene to yield pure material, colorless plates, mp 155—156 °C, IR: 3300—3200 (O-H), 1010 (C-O), 995, 968 (=C-H) cm^{-1}.

Found: C, 86.10; H, 6.28%. Calcd for $C_{16}H_{14}O$: C, 86.45; H, 6.35%.

5-(2-Fluorenyl)-2,4-pentadien-1-ol. According to a similar procedure to that for 2-pyrenyl analogue, 5-(2-fluorenyl)-2,4-pentadienal (1.0 g) was reduced with sodium borohydride, yielding fine yellow crystals, mp 106—113 °C, 0.90 g (78.8%).

3-(2-Fluorenyl)-2-propenyltriphenylphosphonium Bromide. Fluorenylpropenol (1.40 g, 6.3 mmol) in chloroform (50 ml) containing 4 drops of pyridine was treated with phosphorus tribromide (1.2 g, 4.4 mmol) in chloroform (20 ml). The reaction of crude bromide in boiling benzene (25 ml) with triphenylphosphine (1.9 g, 7.3 mmol) afforded fine pale yellow crystals, 1.26 g which were recrystallized from ethanol-benzene to give pure phosphonium bromide, colorless crystals, mp 158—159 °C.

Found: C, 76.67; H, 5.42; Br, 12.66%. Calcd for $C_{34}H_{28}BrP \cdot C_6H_6$: C, 76.79; H, 5.48; Br, 12.77%.

5-(2-Fluorenyl)-2,4-pentadienyltriphenylphosphonium Bromide. Fluorenylpentadienol (0.75 g, 3.0 mmol) was converted into bromide by the reaction of phosphorus tribromide (0.41 g, 1.5 mmol) according to a procedure similar to that for pyrenyl analogue. Crude bromide, fine yellow crystals, was mixed with a solution of triphenylphosphine (0.95 g, 3.6 mmol) in benzene (40 ml) and the mixture was refluxed for 9.5 hr. The reaction mixture was allowed to stand overnight at room temperature to yield phosphonium bromide, fine colorless crystals, mp 243—257 °C, 0.24 g (18.0%).

1,2-Di(2-fluorenyl)ethylene (I_1'). To a suspension of 2-fluorenylmethyltriphenylphosphonium bromide[8] (0.78 g, 1.2 mmol) in benzece (25 ml) was added phenyllithium (0.73N, 1.8 ml) and the mixture was stirred for 30 min at room temperature. To the resulting solution of III' was added II'[9] (0.19 g, 1.0 mmol) in benzene (10 ml). After being stirred for 26 hr at room temperature, the solvent was removed under reduced pressure. Crude crystals, colorless plates, mp 268—300 °C, 0.102 g (29.6%) obtained by extraction of the residue with hot benzene followed by concentration were

dissolved in hot benzene and passed through a short column of alumina. Pure I_1', colorless plates, mp 304—305 °C, IR: 1454, 1428, 1395, 967, 870, 767, 732 cm^{-1} was obtained from the filtrate.

Found: C, 94.34; H, 5.66%. Calcd for $C_{28}H_{20}$: C, 94.45; H, 5.59%.

1,4-Di(2-fluorenyl)-1,3-butadiene (I_2'). To a benzene solution of III′ prepared from 2-fluorenylmethyltriphenylphosphonium bromide (0.73 g, 1.5 mmol) and phenyllithium (0.48N, 3.1 ml) was added a solution of IV′ (0.22 g, 1.0 mmol) in the same solvent (15 ml). After the mixture had been stirred for 40 hr at room temperature, the solvent was removed under reduced pressure and the residue was extracted with hot benzene. Yellow crystals, mp 297—300 °C, 0.124 g (32.4%) obtained by concentrating the extract were dissolved in benzene and percolated through a thin layer of alumina to give pure I_2', yellow plates, mp 301—302 °C, IR: 1453, 1418, 1395, 990, 878, 763, 730 cm^{-1}.

Found: C, 94.41; H, 5.75%. Calcd for $C_{30}H_{22}$: C, 94.20; H, 5.80%.

Concentration of mother liquor of the first crop of crystals afforded the second crop of I_2', yellow plates, mp 267—277 °C, 0.147 g (36%).

1,6-Di(2-fluorenyl)-1,3,5-hexatriene (I_3'). A solution of V′ (0.36 g, 1.5 mmol) in benzene (26 ml) was added to a solution of III′ prepared from phosphonium bromide (0.935 g, 1.8 mmol) and phenyllithium (0.47N, 3.8 ml) and the mixture was stirred for 46 hr. The residue obtained by removing the solvent under reduced pressure was extracted with hot benzene and toluene. The extract was concentrated to give yellow fine crystals, mp 272—286 °C, 0.519 g (84.5%) which were dissolved in hot toluene and percolated through a short column of alumina to give pure I_3', yellow plates, mp 296—297 °C, IR: 1452, 1425, 1395, 1000, 880, 764, 730 cm^{-1}.

Found: C, 93.74; H, 5.93%. Calcd for $C_{32}H_{24}$: C, 94.08; H, 5.92%.

1,8-Di(2-fluorenyl)-1,3,5,7-octatetraene (I_4'). A solution of III′ was prepared from phosphonium bromide (0.625 g, 1.2 mmol) in benzene (20 ml) and phenyllithium (0.50N, 2.4 ml). A solution of VI (0.055 g, 0.5 mmol) in the same solvent (15 ml) was added to the solution of III′. After being stirred for 26 hr at room temperature, the solvent was removed under reduced pressure. Yellow fine crystals, mp 279—287 °C, 0.205 g (94.3%) obtained by extracting the residue with hot toluene followed by concentration were dissolved in hot toluene and passed through a short column of alumina, yielding pure I_4', yellow needles, mp 289—291 °C, IR: 1450, 1395, 1005, 880, 830, 760 cm^{-1}.

Found: C, 93.72; H, 6.03%. Calcd for $C_{34}H_{26}$: C, 93.97; H, 6.03%.

1,10-Di(2-fluorenyl)-1,3,5,7,9-decapentaene (I_5'). A solution of V′ (0.0985 g, 0.40 mmol) in benzene (10 ml) was mixed with a solution of VII′ in the same solvent (15 ml) prepared from 5-(2-fluorenyl)-2,4-pentadienyltriphenylphosphonium bromide (0.240 g, 0.54 mmol) and phenyllithium (0.58N, 0.9 ml). After the mixture had been stirred for 28 hr at room temperature, the solvent was removed under reduced pressure and the residue was extracted with hot toluene. Yellow fine crystals, mp 268—276 °C, 0.0684 g (37.2%) obtained by concentrating the extract were dissolved in hot toluene. Percolation of the hot solution through a thin layer of alumina afforded pure I_5', fine yellow needles, mp 277 °C, IR: 1453, 1395, 1005, 882, 836, 817, 760 cm^{-1}.

Found: C, 93.52; H, 6.03%. Calcd for $C_{36}H_{28}$: C, 93.87; H, 6.13%.

1,12-Di(2-fluorenyl)-1,3,5,7,9,11-dodecahexaene (I_6'). To a solution of VIII′ prepared from 3-(2-fluorenyl)-2-propenyltriphenylphosphonium bromide (0.656 g, 1.2 mmol) in benzene (20 ml) and phenyllithium (1.04N, 1.1 ml) was added a solution of VI (0.055 g, 0.5 mmol) in the same solvent (7 ml) and the mixture was stirred for 20 hr at room temperature. Orange powder obtained by evaporating the solvent under reduced pressure was digested with hot toluene. Concentration of the extract afforded orange fine crystals, mp 267—279 °C, 0.104 g (21.4%) which were dissolved in hot toluene and passed through a short column of alumina. Pure I_6', fine orange crystals, mp 298—300 °C, IR: 1452, 1395, 1005, 882, 760 cm^{-1} was obtained from the filtrate.

Found: C, 93.26; H, 6.20%. Calcd for $C_{38}H_{30}$: C, 93.79; H, 6.21%.

Linear Conjugated Systems Bearing Aromatic Terminal Groups. XIII.[1] Syntheses of α-(*p*-Methoxyphenyl)-ω-(*p*-nitrophenyl)polyenes

Yasuhira TAKEUCHI, Shuzo AKIYAMA, and Masazumi NAKAGAWA

Department of Chemistry, Faculty of Science, Osaka University, Toyonaka, Osaka 560

(Received February 21, 1973)

α-*p*-Methoxyphenyl-ω-*p*-nitrophenylpolyenes (III_n, $n=1$—5) were prepared by the Wittig reaction of *p*-methoxyphenylpolyenals (I, $n=1$—5) with phosphorane derived from *p*-nitrobenzyltriphenylphosphonium bromide (II). The electronic spectra of III_n showed broad and structureless absorption curves. However, the trend of bathochromic shift of long wavelength absorption maxima with increasing length of polyene chain suggests that no alternation in the type of light-absorption of polyene chromophore is caused by the introduction of electron donating and withdrawing substituents in the terminal phenyl groups.

In view of prominent effect of terminal groups of α,ω-diarylpolyenes on the electronic spectral regularity,[2-5] it seemed to be of interest to prepare a series of polyenes bearing electron donating and withdrawing substituents in each of the terminal aromatic rings. The present paper deals with the syntheses of a series of α-*p*-methoxyphenyl-ω-*p*-nitrophenylpolyenes (III_n $n=1$—5).

Syntheses of III_n were performed by the Wittig reaction of ω-*p*-methoxyphenyl polyene aldehydes (I, $n=1$—5)[6] with phosphorane prepared from *p*-nitrobenzyltriphenylphosphonium bromide (II).[7]

The physical properties of III_n are summarized in Table 1. We see that the frequency of C–H out-of-plane deformation (δ_{C-H}) and that of C=C stretching vibration ($\nu_{C=C}$) move to higher and lower wave number, respectively, along with the increase in *n*. The absorption curves of electronic spectra of III_n in tetrahydrofuran at room temperature are illustrated in Fig. 1. Owing to the broad and structureless feature of the absorption curves, estimation of the exact wavelength of maxima of long wavelength bands was difficult and no discussion could be given on the regularity of electronic spectra. However, it was observed that the magnitude of bathochromic shift of long wavelength band between III_{n+1} and III_n ($\Delta\lambda$) decreases with the increase of n (Table 1). This indicates that the introduction of electron donating and withdrawing groups does not alter the type of light-absorption properties of α,ω-diarylpolyene system (convergent type).[8]

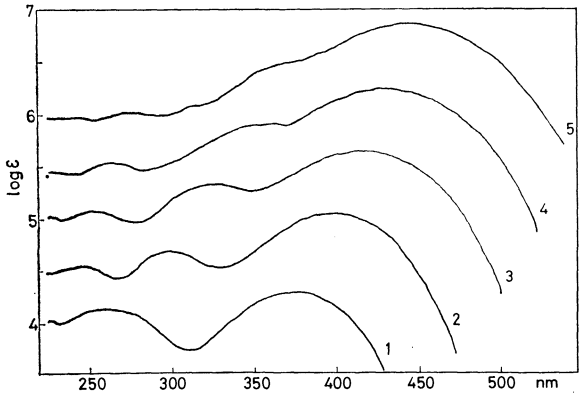

Fig. 1. Absorption curves of α-*p*-methoxyphenyl-ω-*p*-nitrophenylpolyenes (III_n) in tetrahydrofuran. Each curve, except for the lowest one, has been displaced upward by a 0.5 log ε unit increment from one immediately below it.

TABLE 1. PHYSICAL PROPERTIES OF α-*p*-METHOXYPHENYL-ω-*p*-NITROPHENYLPOLYENES (III_n)

n	Color of crystals	Mp (°C)	λ_{max} (log ε) (nm)	$\Delta\lambda$	δ_{C-H} (cm^{-1})	$\nu_{C=C}$ (cm^{-1})
1	yellow	130—131	374 (4.29)		968	1587
				26		
2	yellow	173—175	400 (5.56)		993	1585
				19		
3	orange yellow	178—179	419 (4.65)		1000	1580
				11		
4	orange	204—205	430 (4.75)		1002	1565
				12		
5	reddish brown	229—231	442 (4.85)		1002	1552

1) For Part XII of this series, see Ref. 5.

2) T. Takeuchi, S. Akiyama, and M. Nakagawa, This Bulletin, **45**, 3183 (1972).

3) A. Yasuhara, S. Akiyama, and M. Nakagawa, *ibid.*, **45**, 3638 (1972).

4) Y. Takeuchi, A. Yasuhara, S. Akiyama, and M. Nakagawa, *ibid.*, **46**, 909 (1973).

5) Y. Takeuchi, A. Yasuhara, S. Akiyama, and M. Nakagawa, *ibid.*, **46**, 2822 (1973).

6) D. Marshall and M. C. Whiting, *J. Chem. Soc.*, **1956**, 4082.

7) R. N. McDonald and T. W. Campbell, *J. Org. Chem.*, **24**, 1969 (1959).

8) $\Delta\lambda$ of diarylpoly-ynes was found to increase with the increase of n ($n=1-6$) [M. Nakagawa, S. Akiyama, K. Nakasuji, and K. Nishimoto, *Tetrahedron*, **1971**, 5401] and $\Delta\lambda$ of charge resonance system such as cyanine dyes has been found to be constant regardless of change of *n* (nonconvergent type).

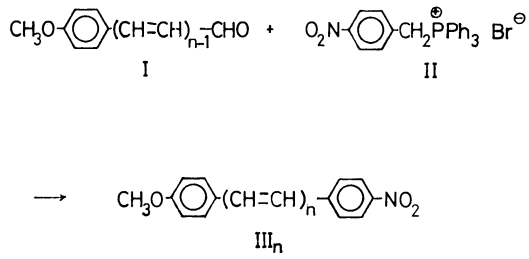

Experimental

All melting points are not corrected. The electronic spectra in tetrahydrofuran were obtained on a Hitachi EPS-3T spectrophotometer using a well-matched pair of 1 cm quartz cells, the shoulder being denoted by an asterisk. The IR spectra were measured with a Hitachi EPI-2 spectrophotometer by the KBr-disk method. Preparation of phosphorane was performed under nitrogen atmosphere using an ethereal solution of phenyllithium as a base. The Wittig reaction was carried out under shielding from light. Initially deposited crystals in the final recrystallization were used in the measurements of electronic spectra to avoid contamination with an isomer containing *cis*-linkage.

1-p-*Methoxyphenyl-2*-p-*nitrophenylethylene* (III_1). To a suspension of *p*-nitrobenzyltriphenylphosphonium bromide[7] (II, 1.44 g, 3.0 mmol) in benzene (15 ml) was added a solution of phenyllithium (0.24 N, 12.5 ml). After being stirred for 2 hr at room temperature, a solution of *p*-methoxybenzaldehyde (I, n=1, 0.27 g, 2.0 mmol) in benzene (5 ml) was added and the mixture was stirred overnight. The residue obtained by evaporation of the solvent *in vacuo* was extracted with hot benzene. Crude crystals deposited on concentration of the extract were recrystallized from ethanol to give yellow plates, mp 127—128 °C, 0.124 g (24.3%) which were recrystallized from the same solvent to give pure III_1, yellow plates, mp 130—131 °C (lit,[9] mp 131—132.5 °C), UV, λ_{max} (log ε): 258 (4.14), 270*, and 374 (4.29) nm.

1-p-*Methoxyphenyl-4*-p-*nitrophenyl-1,3-butadiene* (III_2). A solution of *p*-methoxycinnamaldehyde (I, n=2, 0.32 g, 2.0 mmol) in benzene (6 ml) was added to a solution of phosphorane prepared from II[7] (1.44 g, 3.0 mmol), benzene (15 ml) and phenyllithium (0.28N, 11.5 ml). After the mixture had been stirred for 21 hr at room temperature, the solvent was removed under reduced pressure. The residue was digested with boiling benzene and the extract was passed through a short column of alumina. Yellow needles, mp 169—178 °C, 0.292 g (42.6%) obtained on concentrating the filtrate were recrystallized from benzene to give pure III_2, yellow needles, mp 173—175 °C, UV, λ_{max} (log ε): 248 (4.06), 295 (4.21), and 400 (4.56) nm.

Found: C, 72.77; H, 5.40%. Calcd for $C_{17}H_{15}NO_3$: C, 72.58; H, 5.37%.

1-p-*Methoxyphenyl-6*-p-*nitrophenyl-1,3,5-hexatriene* (III_3). A solution of phosphorane was prepared from II[7] (1.44 g, 3.0 mmol), benzene (15 ml) and phenyllithium (0.24N, 8.4 ml). A solution of 5-*p*-methoxyphenyl-2,4-pentadienal[6] (I, n=3, 0.38 g, 2.0 mmol) in benzene (6 ml) was added to the solution and the mixture was stirred overnight at room temperature. The residue obtained by evaporating the solvent under reduced pressure was extracted with hot benzene, and the extract was percolated through a short column of alumina. Concentration of the filtrate afforded orange yellow plates, mp 175—180 °C, 0.235 g (38.2%) which were recrystallized from benzene to give pure III_3, orange yellow plates, mp 178—179 °C, UV, λ_{max} (log ε): 254 (4.14), 325 (4.32), 336 (4.32), and 419 (4.06) nm.

Found: C, 74.29; H, 5.56%. Calcd for $C_{19}H_{17}NO_3$: C, 74.25; H, 5.57%.

1-p-*Methoxyphenyl-8*-p-*nitrophenyl-1,3,5,7-octatetraene* (III_4). A solution of 7-*p*-methoxyphenyl-2,4,6-heptatrienal[6] (I, n=4, 0.43 g, 2.0 mmol) in benzene (35 ml) was added to a solution of phosphorane prepared from II[7] (1.44 g, 3.0 mmol), benzene (20 ml) and phenyllithium (0.24N, 12.5 ml), and the mixture was stirred for 21 hr at room temperature. Brown powder deposited was digested with boiling benzene. Concentration of the extract, after being filtered, afforded fine orange crystals, mp 200—202 °C, 0.222 g (33.3%). Recrystallization of this material from benzene afforded pure III_4, orange plates, mp 204—205 °C, UV, λ_{max} (log ε): 265 (4.06), 360 (4.41), 430 (4.75), and 445* nm.

Found: C, 75.81; H, 5.72%. Calcd for $C_{21}H_{19}NO_3$: C 75.65; H, 5.74%.

1-p-*Methoxyphenyl-10*-p-*nitrophenyl-1,3,5,7,9-decapentaene* (III_5). To a solution of phosphorane prepared from II[7] (0.94 g, 1.95 mmol), benzene (15 ml) and phenyllithium (0.24N, 8.2 ml) was added a solution of 9-methoxyphenyl-2,4,6,8-nonatetraenal[6] (I, n=5, 0.32 g, 1.3 mmol) in benzene (60 ml) and tetrahydrofuran (10 ml). After the mixture had been stirred for 21 hr, reddish brown solid deposited was collected by filtration. The soild was extracted with boiling benzene. The extract was filtered and concentrated. Reddish brown crystals, mp 229—230 °C, 0.123 g (26.3%) thus obtained were recrystallized from benzene to give pure III_5, reddish brown rods, mp 229—230 °C, UV, λ_{max} (log ε): 277 (4.01), 370 (4.49), 442 (4.85), and 455* nm.

Found: C, 76.86; H, 5.89%. Calcd for $C_{23}H_{21}NO_3$: C, 77.01; H, 5.83%.

9) R. Ketcham, D. Jambotkar, and L. Martinelli, *J. Org. Chem.*, **27**, 4666 (1962).

Linear Conjugated Systems Bearing Aromatic Terminal Groups. XIV.[1] On the Electronic Spectral Regularity of α,ω-Diarylpolyenes

Shuzo AKIYAMA, Yasuhira TAKEUCHI, Akio YASUHARA, Masazumi NAKAGAWA,[2] and Kichisuke NISHIMOTO*

Department of Chemistry, Faculty of Science, Osaka University, Toyonaka, Osaka 560
**Department of Chemistry, Faculty of Science, Osaka City University, Sumiyoshi-ku, Osaka 558*

(Received February 21, 1973)

The bathochromic shift of the longest wavelength absorption maxima (λ) of several series of polyenes along with the increase in number of ethylenic double bond (n) can be expressed excellently by the empirical formula $\lambda=An^x+B$. The value of x varies from 0.5 to 0.8 [$0.5\leq x\leq 0.8$] depending on the nature of terminal groups and the position of linking of polyene chain to terminal aryl nucleus, being $x=0.5$ in the case of parent polyenes (I) and $x=0.8$ for di(3-phenanthryl)- (VI) and di(2-fluorenyl)polyenes (VII). The linear relationship could be reproduced fairly well by the HMO method using the usual bond-alternation approximation ($\beta_{C=C}=1.1\,\beta$; $\beta_{C-C}=0.9\,\beta$; $\beta_{C\equiv C}=\beta$. C≡C denotes aromatic double bond). The calculation based on a modified bond-alternation approximation ($\beta_{C=C}=[1+0.5/(n+4)]\beta$; $\beta_{C-C}=[1-0.5/(n+4)]\beta$; $\beta_{C\equiv C}=\beta$) which is analogous to that successfully applied to diarylpoly-ynes did not reproduce the spectral regularity of diarylpolyenes. This seems to offer further support for the pertinence of assumption of increasing contribution of cumulenic structure in diarylpoly-ynes along with the increase in n.

The bathochromic shift of the longest wavelength absorption maxima (λ) in the electronic spectra of α,ω-diarylpoly-ynes along with the increase in number of acetylenic bond (n) can be expressed well by the empirical formula $\lambda=An^x+B$, indicating a prominent effect of aromatic terminal groups on the electronic spectral regularity.[3,4] The finding prompted the authors to synthesize various α,ω-diarylpolyenes to reveal the influence of the aromatic terminal groups on the electronic excitation of conjugated polyene chain.[5-9] Five series of α,ω-diarylpolyenes (III, IV, V, VI, and VII) exhibited electronic spectra with well-developed vibrational fine structure. The bathochromic shift could be expressed by the same type of empirical formula. The present paper gives the results of a HMO treatment to reproduce the linear relationship between λ and n^x observed in α,ω-diarylpolyenes.

The empirical formulas are summarized in Table 1 together with those for the corresponding acetylenic analogues. The plots of the reported values of the longest wavelength absorption maxima (λ) of polyenes (I)[10] and those of diphenylpolyenes (II)[11] against $n^{0.5}$ and $n^{0.6}$, respectively, gave straight lines. The empirical formulas for (I) and (II) are also included in Table 1.

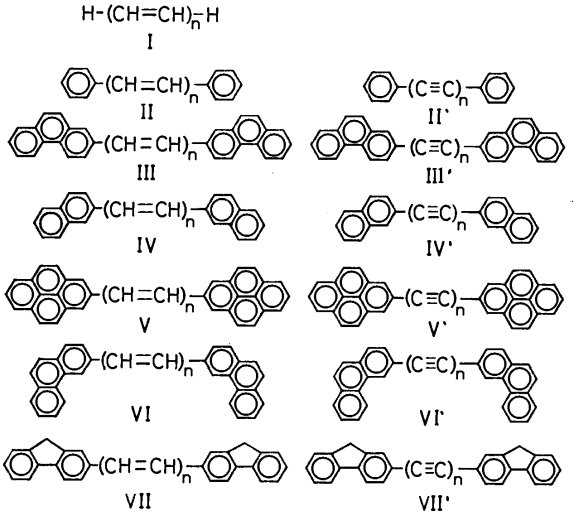

The values of A, x, and B are dependent on the nature of terminal group and the position of linking of unsaturated chain to terminal aryl system. The fact that the B-values of the polyene series and the poly-yne series are similar is understandable since they formally correspond to the absorption wavelength of hypothetical coplanar biaryls ($n=0$). The trend of variation of A, x, and B was found to be similar in both diarylpoly-ynes[4] and diarylpolyenes. The values of x and B increase with the augmentation of conjugate system in the terminal groups. On the other hand, the values of A decrease along with the increase in x and B. It is to be noted that the increase of x-value with the variation of terminal group accords to the same sequence as that found in diarylpoly-yne series. Diphenylpolyenes (II)[11] exhibit the longest wavelength absorption maxima at longer wavelength (Table 2) as compared with those of corresponding diphenylpoly-ynes (II', $n=1$, 297; $n=2$, 326; $n=3$, 358; $n=4$, 397;

1) For Part XIII, see Ref. 9.
2) To whom inquiries should be addressed.
3) K. Nakasuji, S. Akiyama, and M. Nakagawa, This Bulletin, **45**, 883 (1972) and the preceding papers.
4) M. Nakagawa, S. Akiyama, K. Nakasuji, and K. Nishimoto, *Tetrahedron*, **27**, 5401 (1971).
5) Y. Takeuchi, S. Akiyama, and M. Nakagawa, This Bulletin, **45**, 3183 (1972).
6) A. Yasuhara, S. Akiyama, and M. Nakagawa, *ibid.*, **45**, 3638 (1972).
7) Y. Takeuchi, A. Yasuhara, S. Akiyama, and M. Nakagawa, *ibid.*, **46**, 909 (1973).
8) Y. Takeuchi, A. Yasuhara, S. Akiyama, and M. Nakagawa, *ibid.*, **46**, 2822 (1973).
9) Y. Takeuchi, S. Akiyama, and M. Nakagawa, *ibid.*, **46**, 2828 (1973).
10) F. Sondheimer, D. A. Ben-Efraim, and R. Wolovsky, *J. Amer. Chem. Soc.*, **83**, 1675 (1961).
11) K. W. Hausser, R. Kuhn, and A. Smakula, *Z. Phys. Chem.*, **B29**, 384 (1935).

Table 1. Electronic spectral regularity of polyenes and poly-ynes[a)]

R		$R(CH=CH)_nR$	n		$R(C\equiv C)_nR$	n
H-	I	$\lambda=132.3\ n^{0.5}+39$	3—6			
Phenyl-	II	$\lambda=65.2\ n^{0.6}+253$	1—6	II′	$\lambda=33.0\ n^{1.0}+263$	1—6
2-Phenanthryl-	III	$\lambda=57.9\ n^{0.6}+303$	1—6	III′	$\lambda=13.9\ n^{1.3}+333$	1—6
2-Naphthyl-	IV	$\lambda=45.4\ n^{0.7}+302$	1—6	IV′	$\lambda=15.5\ n^{1.3}+319$	1—6
2-Pyrenyl-	V	$\lambda=44.6\ n^{0.7}+314$	1—6	V′	$\lambda=12.6\ n^{1.4}+327$	1—6
3-Phenanthryl-	VI	$\lambda=30.3\ n^{0.8}+348$	1—6	VI′	$\lambda=10.8\ n^{1.4}+347$	1—6
2-Fluorenyl-	VII	$\lambda=29.5\ n^{0.8}+353$	1—6	VII′	$\lambda=9.0\ n^{1.5}+350$	1—6

a) The spectral data in tetrahydrofuran were used except for I, II, and II′ to which the reported values in isooctane, benzene, and ethanol, respectively, were used.

$n=5$, 431, and $n=6$, 460 nm)[12] within a limited length of linearly conjugated system ($n=1$—4). This seems to reflect an enhanced electronic interaction of the ethylenic bond with the phenyl group as compared with the acetylenic bond. The value of A can be regarded as a measure of electronic interaction between terminal group and unsaturated function. Therefore, much larger A-values found in various kinds of polyene series indicate that the interaction of ethylenic bond with aromatic nucleus is stronger than that of the acetylenic bond, regardless of the nature of terminal aromatic system.

One of the authors (K. N.) pointed out that the Hückel molecular orbital (HMO) energy difference between the highest occupied and the lowest vacant orbitals (Δm) (in β-unit) and the absorption wavelength (λ) associated with the ^1L_a band can be correlated by the equation[13]

$$\lambda(^1L_a) = 474(\Delta m)^{-1/2} - 145\ \text{nm} \qquad (1)$$

The electronic spectral regularity of various kinds of α,ω-diarylpoly-ynes could be reproduced satisfactorily by means of the HMO method using Eq. (1). The resonance integrals were assumed as follows [modified bond-alternation approximation, Eq. (2)] considering increasing contribution of dipolar cumulenic structure (VIII) along with the increase of chain length (n):[4,14]

$$\beta_{C\equiv C} = [1+1/(n+4)]\beta;\ \beta_{C-C} = [1-1/(n+4)]\beta;$$
$$\beta_{C=C} = \beta \qquad (2)$$

Experimental support for this assumption has been obtained by comparing the wave number of spacing of vibrational sub-band of the electronic spectra with that of C≡C stretching vibration in the IR spectra.[4]

$$Ar\text{-}(C\equiv C)_n\text{-}Ar \longleftrightarrow {}^+Ar=(C=C)_n=Ar^- \longleftrightarrow {}^-Ar=(C=C)_n=Ar^+ \qquad \text{(VIII)}$$

Since the electronic spectral characteristic of linear polyene system has been explained in terms of bond-alternation,[15,16] we carried out the HMO calculation using the usual bond-alternation model in which the resonance integrals are assumed as follows:

$$\beta_{C=C} = 1.1\beta;\ \beta_{C-C} = 0.9\beta;\ \beta_{C=C} = \beta \qquad (3)$$

(C=C denotes aromatic double bond.)

In the case of di(2-fluorenyl)polyenes (VII), the resonance integral of the central C–C bond linking two benzene rings was assumed to be 0.9β. The observed and calculated values of absorption wavelength are summarized in Table 2. The present calculation reproduced the experimental relationship $\lambda=An^x+B$ except for the constant term B (Fig. 1). In the series of V and VII, calculation gave less satisfactory A-values than those of the other series. However, agreement between experimental and calculated results seems to be rather good in view of the simple treatment based on HMO.

The HMO calculation employing other parameters such as $\beta_{C=C}=1.2\beta$; $\beta_{C-C}=0.8\beta$; and $\beta_{C=C}=\beta$ gave less satisfactory results. The results based on the following modified bond-alternation approximation (Eq.

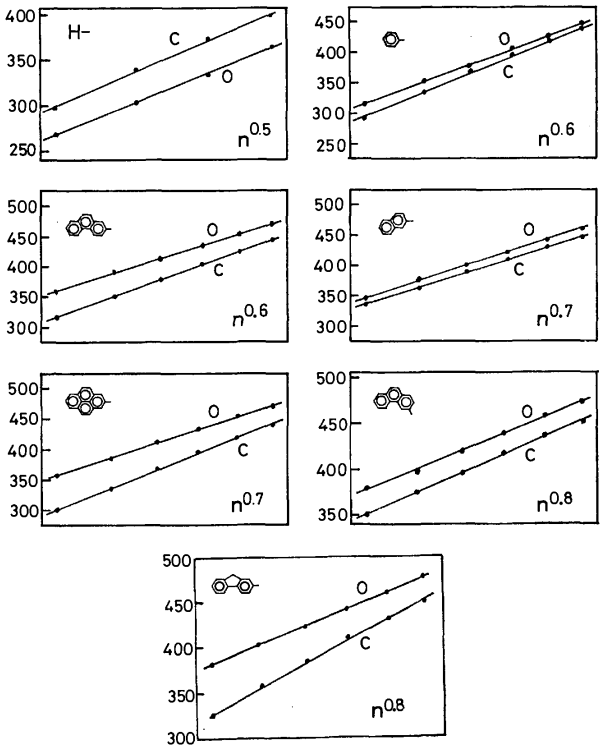

Fig. 1. Plots of λ (nm) *vs.* n^x.
C=Calculated values by bond-alternation approximation (Eq. (3)).
O=Observed values.

12) a) M. Nakagawa, A. Nakamura, and T. Inui, *Nippon Kagaku Zasshi*, **73**, 141 (1952) and the preceding papers. b) J. B. Armitage, N. Entwistle, E. R. H. Jones, and M. C. Whiting, *J. Chem. Soc.*, **1954**, 147. c) H. H. Schlubach and V. Franzene, *Ann. Chem.*, **573**, 110 (1951).
13) K. Nishimoto, This Bulletin, **39**, 645 (1966).
14) K. Nishimoto, R. Fujishiro, S. Akiyama, and M. Nakagawa, *ibid.*, **39**, 2320 (1966).
15) Y. Ooshika, *J. Phys. Soc. Jap.*, **12**, 1238, 1246 (1957).
16) H. C. Longuet-Higgins and L. Salem, *Proc. Roy. Soc., Ser. A*, **251**, 172 (1959).

Table 2. Observed and calculated longest absorption wavelength of $R(CH=CH)_nR$

R		method	n=1	2	3	4	5	6
H-	I	Obsd			268	304	334	364
		BA	175	245	298	339	372	399
Phenyl-	II	Obsd	319	352	377	404	424	445
		BA	294	334	367	395	418	438
		MBA	294	339	380	412	452	485
2-Phenanthryl-	III	Obsd	360	392	414	436	455	471.5
		BA	318	351	379	404	425	444
		MBA	318	355	392	427	460	492
2-Naphthyl-	IV	Obsd	347	377	401	423	441	462
		BA	337	362	388	411	431	448
		MBA	337	368	401	434	465	496
2-Pyrenyl-	V	Obsd	359	385	410	431	452	470
		BA	299	336	369	396	419	438
		MBA	299	357	382	418	453	485
3-Phenanthryl-	VI	Obsd	379	399	420	440	458	474
		BA	351	375	398	418	437	453
		MBA	351	379	410	441	472	501
2-Fluorenyl-	VII	Obsd	382	404	424	442	461	476.5
		BA	329	359	386	410	430	447
		MBA	329	368	409	449	487	524

Obsd = Observed values.
BA = Calculated values by bond-alternation approximation (Eq. (3)).
MBA = Calculated values by modified bond-alternation approximation (Eq. (4)).

(4)) analogous to Eq. (2) are given in Table 2.

$$\beta_{C=C} = [1+0.5/(n+4)]\beta;\ \beta_{C-C} = [1-0.5/(n+4)]\beta;\ \beta_{C=C} = \beta \quad (4)$$

(C=C denotes aromatic double bond.)

The plots of calculated wavelength against corresponding n^x yielded no straight lines. This can be regarded as a further support for the pertinence of assumption of increasing contribution of cumulenic structure (VIII) in diarylpoly-ynes along with the increase in the number of n.

It is accepted that the square of wavelength of the longest wavelength absorption maxima (λ^2) of various kinds of linear polyenes varies linearly with the number of ethylenic bond (n) [*i.e.*, $\lambda = An^{0.5} + B$]. However, the present study demonstrates that the validity of $\lambda = An^{0.5} + B$ relationship is restricted to polyenes (I) and presumably to α,ω-dialkylpolyenes, the power of $n(x)$ varying from 0.5 to 0.8 [$0.5 \leq x \leq 0.8$] depending on the nature of terminal groups and the position of linking of polyene chain to terminal aromatic system.

Stereospecific and Stereoselective Reactions. II.[1] Preparation of Esters of *N*-Phthaloyl-α-amino Acid from Esters of α-Hydroxy Acid

Makoto WADA, Takashi SANO, and Oyo MITSUNOBU*

Department of Chemistry, College of Science and Engineering, Aoyama Gakuin University, Chitosedai, Setagaya-ku, Tokyo 157

(Received March 20, 1973)

Functional selectivity and stereospecificity of the intermolecular dehydration between alcohols and phthalimide (III) by means of diethyl azodicarboxylate (I) and triphenylphosphine (II) was examined. The reaction of allyl alcohol, 2-chloroethanol or (±)-ethyl lactate with I, II, and III led to the formation of corresponding *N*-alkylphthalimide. The reaction was further applied to the synthesis of esters of *N*-phthaloyl-α-amino acid. (*S*)-(−)-ethyl 2-hydroxy-3-phenylpropionate was converted into (*R*)-(+)-*N*-phthaloylphenylalanine ethyl ester with high stereospecificity.

In previous reports, we described the efficient, stereospecific intermolecular dehydration between alcohols and acidic compounds with $pK_a<13$ by means of diethyl azodicarboxylate (I) and triphenylphosphine (II).[2] The present work was undertaken to examine functional selectivity of the reaction and stereospecific α-amino acid synthesis.

Functional Selectivity. Intermolecular dehydration by means of I and II proceeds under mild neutral conditions. Thus, when alcohols bearing another functional group such as halogen or double bond were used, the hydroxyl group would selectively undergo the reaction giving the corresponding condensation products which can be used in the subsequent displacement or addition reaction.

When allyl alcohol, 2-chloroethanol or (±)-ethyl lactate was allowed to react with I, II and phthalimide (III) at room temperature, *N*-allyl-, *N*-(2-chloroethyl)-phthalimide and (±)-*N*-phthaloylalanine ethyl ester was obtained in 73, 72, and 58% yield, respectively. No affection of functional groups other than the hydroxyl group was observed. It would be reasonable to assume the formation of an alkoxyphosphonium salt (IV) as an intermediate.

The reaction of benzyl alcohol with I and II resulted in the formation of diethyl *N*-benzylhydrazodicarboxylate and triphenylphosphine oxide in good yields.[3] Benzyl-oxygen bond in a benzyloxyphosphonium salt is readily cleaved by the attack of nucleophiles.[4] These facts led us to test the benzylation of III by the present method. When benzyl alcohol was treated with I, II, and III in a similar manner to that described above, *N*-benzylphthalimide was isolated in a 70% yield and no diethyl *N*-benzylhydrazodicarboxylate was obtained.

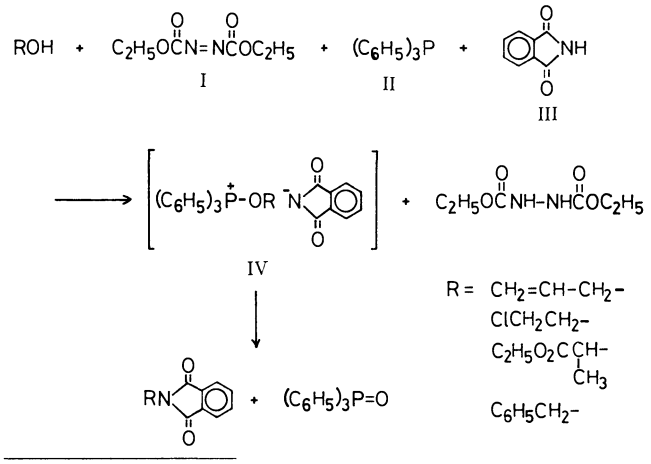

α-Hydroxy acids are easily dehydrated to afford the corresponding alkenes if carbon-carbon double bonds formed are particularly stabilized by conjugation with carbonyl and phenyl groups. In order to know limitations of the present procedure, the following reactions were attempted. (*S*)-(−)-Ethyl 2-hydroxy-3-phenylpropionate was allowed to react with equimolar amounts of I, II, and III, *N*-phthaloylphenylalanine ethyl ester (V) being isolated in a 46% yield. When the reaction was carried out by the use of 2 molar equivalents each of I and II, the yield of V increased to 66%. The reaction of methyl 2-hydroxy-2-methylpropionate, a tertiary alcohol, with I, II, and III gave only a 15% yield of methyl 2-phthalimido-2-methylpropionate. On the other hand, the reaction of diethyl malate with I, II, and III exclusively gave diethyl fumarate in a 59% yield. Diethyl fumarate was also obtained when the reaction was carried out in the absence of III.

The reaction can be explained by assuming the formation of an alkoxyphosphonium salt (VI). The

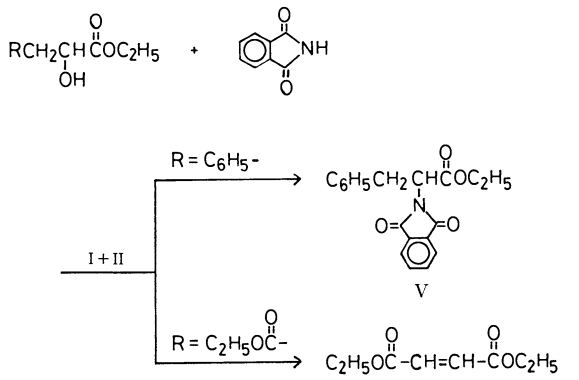

* To whom correspondence should be addressed.

1) This work has been presented in part at the 26th Meeting of the Chemical Society of Japan, April 3, 1972. For paper I. see Ref. 2a.

2) a) O. Mitsunobu, M. Wada, and T. Sano, *J. Amer. Chem. Soc.*, **94**, 679 (1972); b) M. Wada and O. Mitsunobu, *Tetrahedron Lett.*, **1972**, 1279.

3) O. Mitsunobu, M. Yamada, and T. Mukaiyama, This Bulletin, **40**, 935 (1967).

4) a) O. Mitsunobu, T. Obata, and T. Mukaiyama, *J. Org. Chem.*, **30**, 1071 (1965); b) T. Mukaiyama, O. Mitsunobu, and T. Obata, *ibid.*, **30**, 101 (1965).

TABLE 1. PREPARATION OF ESTERS OF *N*-PHTHALOYL-α-AMINO ACID

α-Hydroxy acid ROH R	*N*-Phthaloyl-α-amino acid 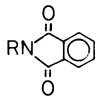 R	Yield, %
CH_3-CH-$CO_2C_2H_5$	CH_3-CH-$CO_2C_2H_5$	58
$C_6H_5CH_2$-CH-$CO_2C_2H_5$	$C_6H_5CH_2$-CH-$CO_2C_2H_5$	46 (66)[a]
$(CH_3)_2$C-CO_2CH_3	$(CH_3)_2$C-CO_2CH_3	15
$C_2H_5O_2C$-CH_2-CH-$CO_2C_2H_5$	$C_2H_5O_2C$-CH_2-CH-$CO_2C_2H_5$	0[b]

a) ( ): Two molar equivalents of I and II were used.
b) Diethyl fumarate was obtained in a 59% yield.

hydrogen atom at α'-carbon of the intermediate was abstracted by the anion of diethyl hydrazodicarboxylate giving diethyl fumarate, diethyl hydrazodicarboxylate and triphenylphosphine oxide. An alternative process in which active hydrogen atom at α'-carbon was abstracted by the anion of phthalimide is conceivable. Such a reaction has also been observed in the anhydrobond formation of uridine.[2b,5] Whether intermolecular dehydration takes place or intramolecular dehydration occurs would depend on relative acidities of active hydrogen of the alkoxyphosphonium salt, diethyl hydrazodicarboxylate and/or phthalimide.

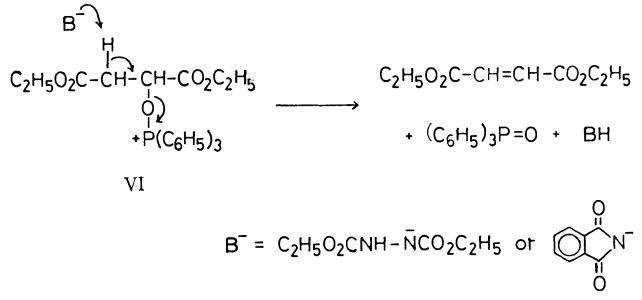

Stereospecificity. Various esters of α-hydroxy acid were converted into the corresponding esters of *N*-phthaloyl-α-amino acid. The results are summarized in Table 1. For the preparation of α-amino acids, it is necessary to determine the steric course. In view of the results so far obtained,[2a,6] the present reaction can be expected to proceed with the inversion of configuration when displacement occurs at an asymmetric carbon.

N-Phthaloylphenylalanine ethyl ester (V) prepared by the reaction of (*S*)-(−)-ethyl 2-hydroxy-3-phenylpropionate with I, II, and III had $[\alpha]_D$ +206±4°. That V possesses *R*-configuration was established by comparison with the reference compound, (*S*)-(−)-*N*-phthaloylphenylalanine ethyl ester ($[\alpha]_D$ −205±1°), prepared from (*S*)-(−)-phenylalanine by stereochemically unambiguous sequences. This result indicates that the complete or almost complete inversion occurred in the intermolecular dehydration reaction.

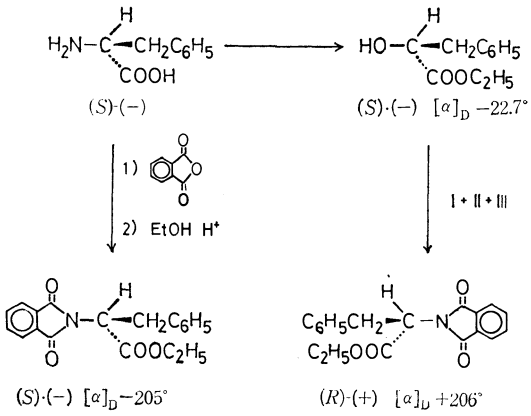

Experimental

The IR spectra were measured on a Nippon Bunko IR-G spectrophotometer. The NMR spectra were obtained on a Hitachi Perkin-Elmer R-20 high resolution spectrometer at 60 MHz. The chemical shifts (δ) are expressed in ppm from internal tetramethylsilane. The optical rotation was measured with JASCO ORD/UV-5. Thin layer chromatography (tlc) was carried out on Wakogel B-5 or Merck PF_{254}.

N-Allyl- and N-(2-Chloroethyl)-phthalimide. A solution of I (174 mg, 1 mmol) in tetrahydrofuran (THF, 2 ml) was added dropwise to a solution of II (262 mg, 1 mmol), III (147 mg, 1 mmol) and either allyl alcohol (117 mg, 2 mmol) or 2-chloroethanol (161 mg, 2 mmol) in THF (3 ml) with stirring at room temperature. After the solution was kept standing overnight, it was applied to a silica gel plate which was then developed in benzene giving the desired products.

N-Allylphthalimide: 136 mg, 73%, mp 72—73 °C (from *n*-heptane). NMR (CCl_4); 4.2 (2H, $-CH_2-$), 5—6.2 (3H, $-CH=CH_2$), 7.7 (4H, aromatic H).

N-(2-Chloroethyl)phthalimide: 151 mg, 72%, mp 82—84 °C (from *n*-heptane containing a small amount of ether). NMR (CCl_4); 3.5—4.1 (4H, $-CH_2-CH_2-$), 7.75 (4H, aromatic H).

N-Phthaloylalanine Ethyl Ester. (±)-Ethyl lactate (118 mg, 1 mmol) was treated with I (147 mg, 1 mmol), II (262 mg, 1 mmol) and III (147 mg, 1 mmol) in THF (3 ml) in the same manner as above. After 3.5 hr, the solution was concentrated and applied to a silica gel plates, developed in chloroform giving *N*-phthaloylalanine ethyl ester; 144 mg, 58%, mp 60—61 °C (from petroleum ether). Found: C, 63.14; H, 5.30%. Calcd for $C_{13}H_{13}NO_4$: C, 63.15; H, 5.30%.

5) J. P. H. Verheyden and J. G. Moffatt, *J. Org. Chem.*, **35**, 2319 (1970).

6) a) W. Gerrard and W. J. Green, *J. Chem. Soc.*, **1951**, 2550; b) J. P. Schaefer and D. S. Weinberg, *J. Org. Chem.*, **30**, 2635 (1965); c) J. B. Lee and I. M. Dowie, *Tetrahedron*, **23**, 359 (1967); d) J. Hooz and S. S. H. Gilani, *Can. J. Chem.*, **46**, 86 (1968); e) R. G. Weiss and E. I. Snyder, *J. Org. Chem.*, **35**, 1627 (1970); f) O. Mitsunobu and M. Eguchi, This Bulletin, **44**, 3427 (1971). g)R Aneja, A. P. Davies, and J. A. Knaggs, *Chem. Comm.*, **1973**, 110.

NMR (CCl_4); 1.25 and 4.2 (3H and 2H, CH_3–CH_2–O–), 1.7 (3H, >CH–C$\underline{H}_3$), 4.85 (1H, >C$\underline{H}$–CH_3), 7.75 (4H, aromatic H). IR (KBr) cm^{-1}; 1780, 1720 (C=O).

N-Benzylphthalimide and Methyl 2-Phthalimido-2-methylpropionate. In the same manner as above, *N*-benzylphthalimide was isolated in a 75% yield by preparative tlc (benzene). When the reaction was carried out in an ice bath, the yield of *N*-benzylphthalimide decreased to 70%; NMR (CCl_4): 4.75 (2H, $-CH_2-$), 7—8 (9H, aromatic H). IR (KBr) cm^{-1}: 1770, 1720 (C=O).

Similarly, methyl 2-hydroxy-2-methylpropionate was converted into methyl 2-phthalimido-2-methylpropionate in a 15% yield. NMR (CCl_4): 1.8 (6H, $(CH_3)_2C$<), 3.7 (3H, CH_3O–), 7.74 (4H, aromatic H). IR (liquid film) cm^{-1}: 1770, 1730 (C=O).

Reaction of Diethyl Malate with I and II in the Presence or Absence of III. Diethyl malate (190 mg, 1 mmol) was allowed to react with equimolar amounts of I, II, and III in THF (4 ml) at room temperature for 3 hr. The reaction mixture was separated by preparative tlc (chloroform) giving diethyl fumarate; 105 mg, 59%. NMR: 1.30 and 4.18 (6H and 4H, CH_3–CH_2–O–), 6.75 (2H, ^{H}>C=C<$_{H}$). IR (liquid film) cm^{-1}: 1715 (C=O), 1640 (>C=C<). When the reaction was carried out in the absence of III, diethyl fumarate was afforded in a 51% yield.

(R)-(+)-N-Phthaloylphenylalanine Ethyl Ester. (*S*)-(−)-Ethyl 2-hydroxy-3-phenylpropionate[7] (194 mg, 1 mmol, $[\alpha]_D$ −22.7° (*c* 4.52 in benzene); lit,[7a] $[\alpha]_D^{24}$ −22.6° (*c* 4.33 in benzene)) was allowed to react with equimolar amounts of I, II, and III at room temperature for 3 hr. The reaction mixture was separated by preparative tlc (benzene) giving (*R*)-(+)-*N*-phthaloylphenylalanine ethyl ester; 148 mg, 46%, mp 65—66 °C. NMR (CCl_4): 1.2 and 4.2 (3H and 2H, CH_3–CH_2–O–), 3.5 (2H, $C_6H_5C\underline{H}_2$–), 5.05 (1H, >C–H), 7.1 and 7.6 (5H and 4H, aromatic H). IR cm^{-1}: 1780, 1720 (C=O). $[\alpha]_D$ +210.6° (*c* 0.470 in benzene) and +201.5° (*c* 0.428 in benzene). Average $[\alpha]_D$ +206±4°.

(S)-(−)-N-Phthaloylphenylalanine Ethyl Ester. Dry hydrogen chloride was passed through a solution of (*S*)-(−)-phthaloylphenylalanine[8] (2.95 g, 10 mmol) in ethanol (9.20 g) for 1 hr and the solution was refluxed for 1 hr. After removal of the solvent, the residue was applied to a silica gel plate which was developed in benzene. The crude (*S*)-(−)-*N*-phthaloylphenylalanine ethyl ester (1.31 g) thus obtained was again purified by tlc, mp 56—57 °C. This product was further recrystallized from petroleum ether; $[\alpha]_D$ −206.2° (*c* 0.456 in benzene) and −204.1° (*c* 0.446 in benzene). Average $[\alpha]_D$ −205±1°.

7) a) S. G. Cohen and S. Y. Weinstein, *J. Amer. Chem. Soc.*, **86**, 5326 (1964); b) K. Koga, C. C. Wu, and S. Yamada, *Tetrahedron Lett.*, **1971**, 2283.

8) J. C. Shechan, D. W. Chapman, and R. Roth, *J. Amer. Chem. Soc.*, **74**, 3822 (1952).

BULLETIN OF THE CHEMICAL SOCIETY OF JAPAN, VOL. 46, 2835—2839 (1973)

Synthesis of Pyrimidines and Condensed Pyrimidines

Shigeru KOBAYASHI

Chemical Research Laboratories, Central Research Division, Takeda Chemical Industries, Ltd., Osaka 532

(Received March 31, 1973)

A new one-step synthesis of pyrimidines and condensed pyrimidines by heating carboxamides or cyclic lactams with formamide in the presence of $POCl_3$ in a sealed tube is described.

This paper provides the full version of the new one-step synthesis of pyrimidine and condensed pyrimidine compounds published in a previous communication.[1)]

4-Aminopyrimidine (**1a**) was obtained when a mixture of acetamide and formamide (FA) was heated in the presence of $POCl_3$ at 120 °C in a sealed vessel for 12 hr. The structure was established by comparing its IR spectrum with that of an authentic material.

Several workers have already reported the one-step synthesis of pyrimidines. Davies *et al.*[2a)] reported syntheses of 4-amino-5-arylpyrimidines in yields of 4—54%, by heating arylacetonitriles and FA under nitrogen flow. However, under these conditions, aliphatic nitriles and FA did not react. Tsatsaronis and Kehayoglov[2b)] also obtained 4-amino-5-arylpyrimidines in yields of 7—54% by the reaction of tris(formylamino)methane with substituted acetonitriles, acetamides, and the corresponding esters. But the yield of 4-amino-5-methylpyrimidine was only 1.8%. Bredereck *et al.*[3)] obtained purine in 19% yield by heating aminoacetonitrile and FA. Loader and Timmons[4)] obtained benzo[*f*]quinazoline by heating β-naphthylamine and FA in the presence of $POCl_3$ in a yield of 3.5%. Yamada and Okamoto[5)] also obtained purine by heating FA alone for 28 hr in 20.5% yield.

Experiments designed to maximize the yield of **1a** showed that the best yields were obtained when the reaction was carried out between 120—160 °C (Fig. 1), with the optimum reaction time being 12—20 hr (Fig.

1) K. Morita, S. Kobayashi, H. Shimadzu, and M. Ochiai, *Tetrahedron Lett.*, **1970**, 861.

2) a) W. H. Davies, and H. A. Piggott, *J. Chem. Soc.*, **1945**, 347; W. H. Davies, A. W. Johnson, and H. A. Piggott, *ibid.*, **1945**, 352. b) G. C. Tsatsaronis, and A. H. Kehayoglov, *J. Org. Chem.*, **35**, 438 (1970).

3) H. Bredereck, H. Ulmer, and H. Waldman, *Chem. Ber.*, **89**, 12 (1956).

4) C. E. Loader, and C. J. Timmons, *J. Chem. Soc., C*, **1967**, 1343.

5) H. Yamada, and T. Okamoto, *Chem. Pharm. Bull.* **20**, 632 (1972).

2). Although the yield did not change significantly as the molar ratio of FA to acetamide varied, maximum yield was obtained when this ratio was between 2: 1 and 3: 1 (Fig. 3). The final and most crucial factor varied in this study of reaction conditions was the condensing agent (Table 1). Of the several condensing agents tested, $POCl_3$ and PCl_5 proved to be effective, with $POCl_3$ giving higher yields of **1a**. The best

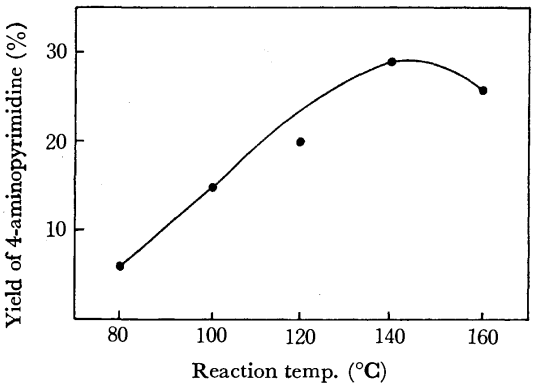

Fig. 1. Effect of reaction temperature on the yield of 4-aminopyrimidine (**1a**).
Mol. ratio: CH_3CONH_2: FA: $POCl_3$=1: 2: 3
Reaction time: 5 hr

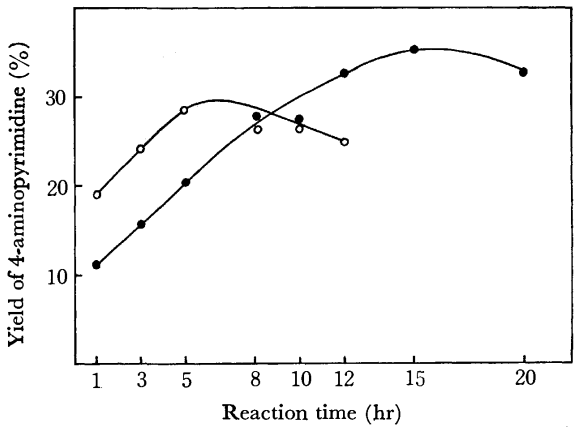

Fig. 2. Effect of reaction time on the yield of 4-aminopyrimidine (**1a**).
Mol. ratio: CH_3CONH_2: FA: $POCl_3$=1: 2: 3
Reaction temp.: ●—●: 120 °C; ○—○: 140 °C

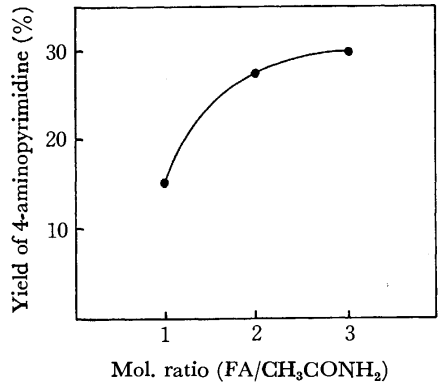

Fig. 3. Effect of mol. ratio (FA to CH_3CONH_2) on the yield of 4-aminopyrimidine (**1a**).
Reaction temp.: 140 °C Reaction time: 5 hr

Table 1. Effect of condensing agents on the yield of 4-aminopyrimidine (**1a**)

Reagent	Yield of 4-aminopyrimidine (%)
$POCl_3$	34
PCl_5	9
PCl_3	trace
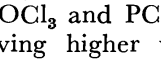	0
H_3CSO_2Cl	0
$SOCl_2$	0

Reaction temp.: 120 °.
Reaction time: 12 hr.
Mol. ratio: CH_3CONH_2: H_2NCHO: reagent (1: 2: 3).

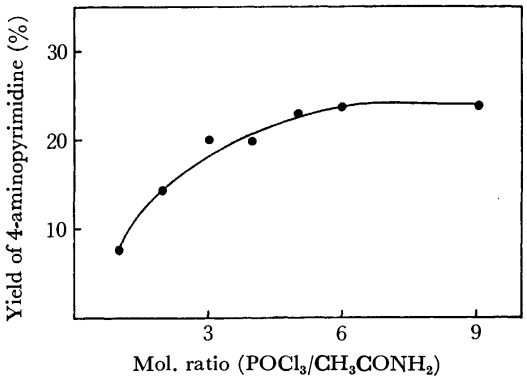

Fig. 4. Effect of mol. ratio ($POCl_3$ to CH_3CONH_2) on the yield of 4-aminopyrimidine (**1a**).
Reaction temp.: 120 °C, Reaction time: 10 hr
Mol. ratio (FA/CH_3CONH_2): 2

$POCl_3$ to acetamide ratio was between 3 and 9 (Fig. 4). The isolated yield of **1a** was 32% when a mixture of acetamide, FA and $POCl_3$ (molar ratio 1: 2: 3) was heated in a sealed tube at 120 °C for 12 hr.

When acetic acid and ethyl acetate were used instead of acetamide, **1a** was also obtained in yields of 13 and 12%, respectively. In these cases, acetamide is thought to be formed in the reaction media *via* acid-amide exchange reaction and then similarly converted to **1a**. Acetic chloride and acetic anhydride also gave **1a** although the yields diminished significantly, as shown in Table 2.

One-Step Synthesis of 4-(Substituted amino)pyrimidines. Although the reaction mechanism of this novel one-step synthesis is far from clear, it is worthwhile to note that

Table 2. Yields of 4-aminopyrimidine (**1a**) from acetic acid derivatives

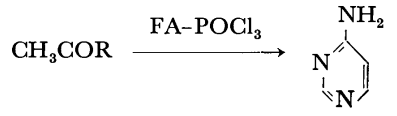

R	Yield of 4-aminopyrimidine (%)
NH_2	34
OH	13
OCH_2CH_3	12
Cl	4.7
$OCOCH_3$	3.5

Reaction temp.: 120°.
Reaction time: 12 hr.

two nitrogen atoms on a pyrimidine nucleus originate from FA, as shown in the following examples. *N,N*-Dimethylacetamide, when treated with FA–$POCl_3$, gave 4-(dimethylamino)pyrimidine (**2**). Similarly, acetanilide gave 4-anilinopyrimidine (**3**).

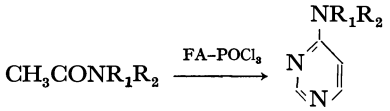

2: $R_1=R_2=CH_3$ (17%)
3: $R_1=H$, $R_2=Ph$ (9%)

One-Step Synthesis of 4-Amino-5-alkylpyrimidines. In other attempts to generalize the one-step synthesis, propionamide and stearamide were treated with FA–$POCl_3$. The product isolated from the propionamide experiment was the anticipated 4-amino-5-methylpyrimidine (**1b**). Similarly, stearamide gave 4-amino-5-hexadecylpyrimidine (**1i**). Other aliphatic carboxamides could be used and the same class of compounds was obtained, as shown in Table 3. Thus, these reactions furnish a convenient one-step synthesis of 4-amino-5-alkylpyrimidines, as illustrated by the general equation:

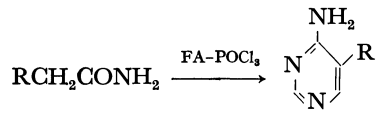

1

One-Step Synthesis of Condensed Pyrimidines. Cyclic lactams could also be the substrates of this novel one-step synthesis. Thus, α-pyrrolidone (**4**), δ-valerolactam (**5**), and ε-caprolactam (**6**) gave 5,6-dihydro-7*H*-pyrrolo-[2,3-*d*]pyrimidine (**7**), 5,6,7,8-tetrahydropyrido[2,3-*d*]-pyrimidine (**8**) and 5,6,7,8-tetrahydro-9*H*-pyrimido[4,5-*b*]azepine (**9**), respectively.

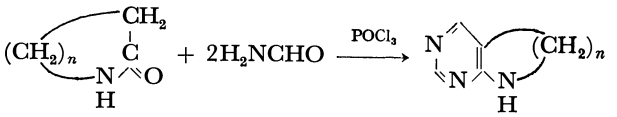

4: $n=2$
5: $n=3$
6: $n=4$

7: $n=2$ (9%)
8: $n=3$ (15%)
9: $n=4$ (7%)

When adipamide was treated with FA–$POCl_3$, the isolated product was white and crystalline, and its analysis agreed with the formula $C_7H_9N_3$. Its NMR spectrum was consistent with the structure of 4-amino-6,7-dihydro-5*H*-cyclopenta[*d*]pyrimidine (**10**).

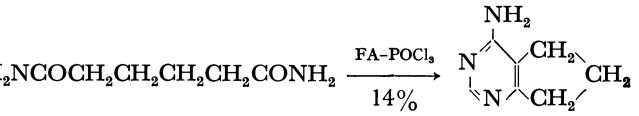

10

The UV characteristics were also in accord with the values described in literature.[9] A plausible reaction mechanism for the formation of **10** is as follows:

Table 3. Analytical and spectral data of 4-aminopyrimidines: 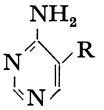

Compd.	R	Mp (°C)	Recrystn solvent	Yield (%)	Formula	Analysis (%) Calcd C	H	N	Found C	H	N
1a	H–	149—151[a]	—	32	$C_4H_5N_3$	50.51	5.30	44.19	50.53	5.30	43.79
1b	CH_3–	170—173[b]	$CHCl_3$	28	$C_5H_7N_3$	55.03	6.47	38.51	54.56	6.23	37.45
1c	CH_3CH_2–	160—162[c]	EtOH	16	$C_6H_9N_3$	58.51	7.37	34.12	58.08	7.37	34.01
1d[e]	$CH_3CH_2CH_2$–	162	EtOAc	24	$C_7H_{11}N_3$	61.28	8.08	30.63	61.37	8.17	30.23
1e[f]	$CH_3(CH_2)_2CH_2$–	103—105	EtOAc	17	$C_8H_{13}N_3$	63.54	8.67	27.79	63.54	8.71	27.54
1f[g]	$CH_3(CH_2)_4CH_2$–	119	Benzene	18	$C_{10}H_{17}N_3$	66.99	9.57	23.44	67.04	9.85	23.13
1g[h]	$CH_3(CH_2)_6CH_2$–	125—126	*n*-Hexane	16	$C_{12}H_{21}N_3$	69.52	10.21	20.27	69.22	10.43	19.07
1h[i]	$CH_3(CH_2)_{12}CH_2$–	118—119	EtOH	27	$C_{18}H_{33}N_3$	74.17	11.41	14.42	74.16	11.36	14.23
1i[j]	$CH_3(CH_2)_{14}CH_2$–	113—114	EtOH	21	$C_{20}H_{37}N_3$	75.18	11.67	13.15	75.09	11.97	13.13

a) Lit,[6] mp 151°. MS: Mol wt 95 (100%).
b) Lit,[7] mp 176°. MS: Mol wt 109 (100%).
c) Lit,[8] mp 163°. MS: Mol wt 123 (100%).
d) NMR Spectra were determined in d_6-DMSO. NMR Signals for singlet are designated as s, triplet as t, and multiplet as m.
e) NMR (δ): 0.89 (t), 1.10–1.85 (m), 2.35 (M), 6.63 (s), 7.87 (s), 8.23 (s); ratio: 3: 2: 2: 2: 1: 1.
f) NMR (δ): 0.91 (t), 1.10–1.80 (m), 2.43 (M), 5.69 (s), 7.70 (s), 8.05 (s); ratio: 3: 4: 2: 2: 1: 1.
g) NMR (δ): 0.89 (t), 1.05–1.90 (m), 2.42 (M), 5.45 (s), 8.07 (s), 8.47 (s), ratio: 3: 8: 2: 2: 1: 1.
h) NMR (δ): 0.89 (t), 1.30 (s), 2.43 (M), 5.41 (s), 8.10 (s), 8.32 (s): ratio: 3: 12: 2: 2: 2: 1.
i) NMR (δ): 0.89 (t), 1.27 (s), 2.42 (M),5.60 (s), 8.03 (s). 8.36 (s),; ratio: 3: 24: 2: 2: 1: 1.
j) NMR (δ): 0.87 (t), 1.29 (s), 2.43 (M), 5.15 (s), 8.10(s), 8.52 (s); ratio: 3: 28: 2: 2: 1: 1.

6) E. Büttner, *Ber. Deutsch. Chem. Ges.* **36**, 2227 (1903).
7) O. Gerngrass, *ibid.*, **38**, 3394 (1905).
8) A. V. Merkatz, *ibid.*, **52**, 369 (1919).
9) L. O. Ross, L. Goodman, and B. R. Baker, *J. Amer. Chem. Soc.*, **81**, 3108 (1959).

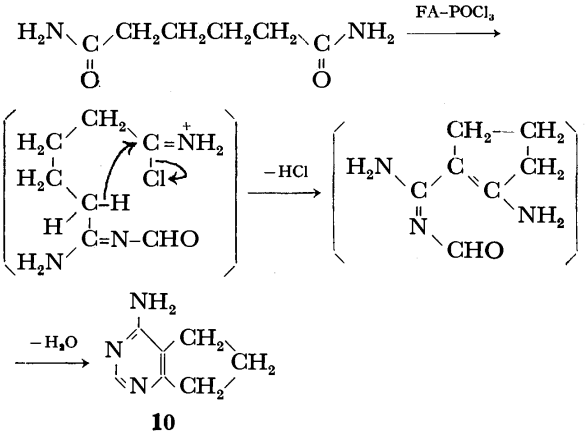

Glycinamide, when treated with FA–$POCl_3$, did not give 4,5-diaminopyrimidine (**11**); instead, purine (**12**) was obtained in 7% yield. From the above arguments it is clear that the reaction proceeded *via* intermediary formation of **11**.

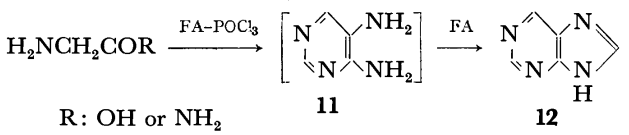

Glycine itself also yielded purine when treated under the same conditions. Here again, the conversion of glycine to glycinamide could be the first step in this reaction, as in the case of the formation of 4-aminopyrimidine from acetic acid.

Further Aspects of This One-Step Synthesis. With the hope of ultimately employing the present reaction as a practical synthetic tool, we tried to synthesize a hitherto unknown diazaisolog (**16**) of the antidepressant drug, 5-(3-dimethylaminopropyl)-10,11-dihydro-5*H*-dibenz[*b*,*f*]azepine[10] (**17**), which is clinically used extensively. The results are shown in Chart 1. Interestingly, 5,6-dihydro-11*H*-dibenz[2,3]azepino[7,6-*d*]-pyrimidine (**15a**) and 9-chloro-5,6-dihydrobenz[2,3]-azepino[7,6-*d*]pyrimidine (**15b**) were obtained from homohydrocarbostyril (**13a**) and 8-chloro-homohydrocarbostyril (**13b**) in 29 and 42% yields, respectively. Similarly, **16a** and **16b** were obtained from **14a** and **14b** as shown in Chart 1.

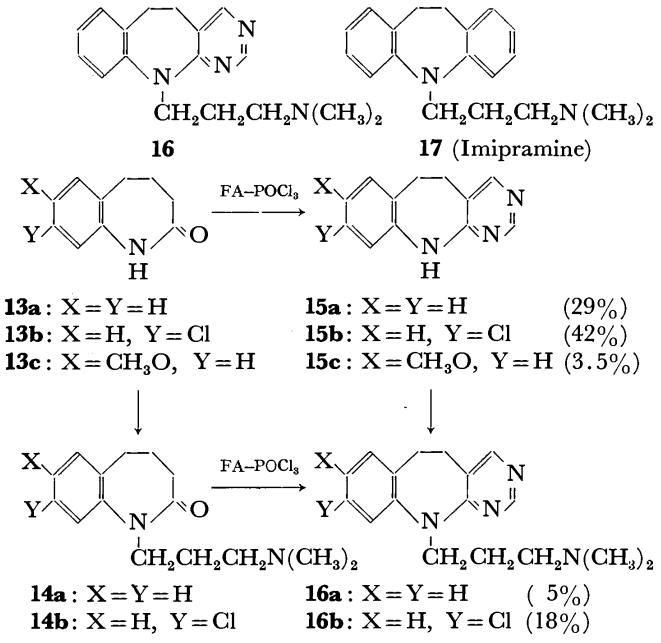

Chart 1

Both **16a** and **16b** showed weak antidepressant activities; the biological effects of these compounds will be described elsewhere.

Experimental

Mps were taken in open capillaries and are uncorrected. NMR spectra were recorded for solns in $CDCl_3$ or in d_6-DMSO (internal TMS standard), using a Varian A-60 spectrophotometer. Mass spectra (70 eV) were recorded on a Hitachi RMU-6D double focusing spectrometer and UV spectra on a Hitachi recording spectrophotometer.

Reactants. **13a**, **13b**, and **13c** were prepared by reported procedures.[11] All other reactants were obtained from commercial sources and purified by distillation or recrystallization where necessary.

General Procedure. To a mixture of carboxamides (0.01 mol) and FA (0.02 mol) in a stainless steel vessel (30 ml), $POCl_3$ (0.03 mol) was added under dry ice–acetone cooling. After being closed tightly, the vessel was heated at 120 °C for 12 hr. Then water (15 ml) was added to dissolve the reaction mixture. After neutralization with aqueous NaOH, the products were extracted with 3×5 ml EtOAc, dried over Na_2SO_4, filtered and evaporated. Column chromatography of the residue on silica gel using $CHCl_3$: acetone: EtOH (70: 30: 3) as solvent, yielded the products.

The following compounds were prepared by the general procedure unless otherwise stated.

4-Dimethylaminopyrimidine (2). *N,N*-Dimethylacetamide (0.87 g, 0.01 mol) yielded 0.21 g of **2**; mp *ca.* 40 °C (lit,[12] *ca.* 40 °C); NMR (δ) $CDCl_3$: 3.10 (s, 6H), 6.30 (broad d, 1H), 8.20 (broad s, 1H), 8.55 (broad s, 1H). Found: C, 58.35; H, 7.32; N, 34.01%.

4-Anilinopyrimidine (3). Acetanilide (1.35 g, 0.01 mol) gave 0.15 g of **3**; mp 139—142 °C (lit,[13] 142—143 °C); NMR (δ) $CDCl_3$: 6.75 (dd, J=3 and 10 Hz, 1H), 7.20—7.50 (m, 5H), 8.25 (d, J=10 Hz, 1H), 8.52 (broad s, 1H), 8.66 (s, 1H). Found: C, 70.21; H, 5.31; N, 24.29%.

5,6-Dihydro-7H-pyrrolo[2,3-d]pyrimidine (7). α-Pyrrolidone (0.85 g, 0.01 mol) yielded 0.11 g of **7**; mp 113—114 °C; NMR (δ) $CDCl_3$: 2.86—3.36 (m, 2H), 3.54—3.92 (m, 2H), 6.24 (broad s, 1H), 7.96 (s, 1H), 8.34 (s, 1H); UV (mμ) λ_{max} (ε) H_2O (pH 1): 266 (10700); H_2O (pH 11): 250 (7560), 284 (4180). Found: C, 59.32; H, 5.89; N, 34.51%. Calcd for $C_6H_7N_3$: C, 59.48; H, 5.82; N, 34.69%.

5,6,7,8-Tetrahydropyrido[2,3-d]pyrimidine (8). δ-Valerolactam (0.99 g, 0.01 mol) gave 0.19 g of **8**; mp 106—108 °C; NMR (δ) $CDCl_3$: 1.65—2.15 (m, 2H), 2.5—2.9 (m, 2H), 3.3—3.6 (m, 2H), 6.64 (broad s, 1H), 7.94 (s, 1H), 8.35 (s, 1H); UV (mμ) λ_{max} (ε) H_2O (pH 1): 262 (12100), H_2O (pH 11): 247 (9730), 286 (4750). Found: C, 62.38; H, 6.62; N, 30.92%. Calcd for $C_7H_9N_3$: C, 62.20; H, 6.71; N, 31.09%.

10) W. Schindler, and F. Häfliger, *Helv. Chim. Acta*, **37**, 472 (1954).

11) M. Tomita, S. Minami, and S. Uyeo, *J. Chem. Soc., C*, **1969**, 183.

12) D. J. Brown, and L. N. Short, *ibid.*, **1953**, 331.

13) W. Winkelmann, *J. Prakt. Chem.*, **115**, 292 (1927).

5,6,7,8-Tetrahydro-9H-pyrimido[4,5-b]azepine (9). ε-Caprolactam (1.13 g, 0.01 mol) gave 0.11 g of **9** after recrystallization from *n*-hexane; mp 99.5—101 °C; mol wt 149 (100%) (mass); NMR (δ) $CDCl_3$: 1.6—2.1 (m, 4H), 2.5—2.9 (m, 2H), 3.2—3.5 (m, 2H), 5.85 (braod s, 1H), 8.04 (s, 1H), 8.40 (s, 1H); UV (mμ) λ_{max} (ε) H_2O (pH 1): 274 (11500); H_2O (pH 11): 251 (7640), 282 (5210). Found: C, 64.16; H, 7.24; N, 28.10%. Calcd for $C_8H_{11}N_3$: C, 64.40; H, 7.43; N, 28.17%.

4-Amino-6,7-dihydro-5H-cyclopenta[d]pyrimidine (10). Adipamide (1.44 g, 0.01 mol) yielded 0.19 g of **10**; mp 231—234 °C (lit,[9] 235—238 °C); mol wt 135 (100%) (mass); NMR (δ) d_6-DMSO: 1.65—2.35 (m, 2H), 2.45—2.95 (m, 4H), 6.55 (broad s, 2H), 8.20 (s, 1H); UV (mμ) λ_{max} (ε) H_2O (pH 11): 238 (10800), 266 (5640) [lit,[9] H_2O (pH 13) 237 (8610), 266 (5370)]. Found: C, 61.94; H, 6.67; N, 30.98%.

Purine (12). Following the general procedure, 1.10 g of glycinamide hydrochloride (0.01 mol) was reacted with FA-$POCl_3$. Chromatography on Amberlite CG-120 and silica gel [MeOH: $CHCl_3$ (1: 1)] yielded 0.09 g of **12**. The IR spectra agreed well with that of an authentic sample.

5,6-Dihydro-11H-benz[2,3]azepino[7,6-d]pyrimidine (15a). 1,3,4,5-Tetrahydro-2*H*-1-benzazepin-2-one (**13a**, 1.61 g, 0.01 mol) gave 0.57 g of **15a**; mp 168—170.5 °C; NMR (δ) d_6-DMSO: 3.02 (s, 4H), 6.75—7.35 (m, 4H), 8.13 (broad s, 1H), 8.15 (s, 1H), 8.57 (s, 1H). Found: C, 72.67; H, 5.53; N, 21.15%. Calcd for $C_{12}H_{11}N_3$: C, 73.07; H, 5.62; N, 21.31%.

9-Chloro-5,6-dihydro-11H-benz[2,3]azepino[7,6-d]pyrimidine (15b). 8-Chloro-1,3,4,5-tetrahydro-2*H*-1-benzazepin-2-one (**13b**, 1.96 g, 0.01 mol) gave 0.97 g of **15b**, mp 177—178 °C; NMR (δ) $CDCl_3$: 3.00 (s, 4H), 6.8—7.2 (m, 3H), 8.15 (broad s, 1H), 8.21 (s, 1H), 8.61 (s, 1H). Found: C, 62.00; H, 4.35; N, 18.44; Cl, 15.47%. Calcd for $C_{12}H_{10}N_3Cl$: C, 62.21; H, 4.35; N, 18.14; Cl, 15.30%.

8-Methoxy-5,6-11H-benz[2,3]azepino[7,6-d]pyrimidine (15c). 7-Methoxy-1,3,4,5-tetrahydro-2*H*-1-benzazepin-2-one (**13c**, 1.91 g, 0.01 mol) yielded 0.08 g of **15c**; mp 145—146 °C; NMR (δ) $CDCl_3$: 2.99 (s, 4H), 3.79 (s, 3H), 6.6—6.9 (m, 2H), 6.85 (s, 1H), 8.05 (broad s, 1H), 8.15 (s, 1H), 8.53 (s, 1H). Found: C, 68.80; H, 5.56; N, 18.30%. Calcd for $C_{13}H_{13}ON_3$: C, 68.70; H, 5.77; N, 18.49%.

11-(3-Dimethylaminopropyl)-5,6-dihydro-11H-benz[2,3]azepino-[7,6-d]pyrimidine (16a). 1-(3-Dimethylaminopropyl)-1,3,4,5-tetrahydro-2*H*-1-benzazepin-2-one (**14a**, 2.46 g, 0.01 mol) gave a yellow powder of **16a** (0.14 g); NMR (δ) $CDCl_3$: 1.6—2.1 (m, 2H), 2.12 (s, 6H), 2.2—2.35 (m, 2H), 3.00 (s, 4H), 4.22 (t, J=11 Hz, 2H), 7.0—7.3 (m, 4H), 8.20 (s, 1H), 8.52 (s, 1H).

The dihydrochloride was prepared and recrystallized from EtOH-ether; mp 233—234 °C. Found: C, 57.49; H, 7.20; N, 16.06; Cl, 19.99%. Calcd for $C_{17}H_{22}N_4 \cdot 2HCl$: C, 57.47; H, 6.81; N, 15.77; Cl, 19.96%.

9-Chloro-11-(3-dimethylaminopropyl)-5,6-dihydro-11H-benz[2,3]-azepino[7,6-d]pyrimidine (16b). Method 1: Following the general procedure, 8-chloro-1-(3-dimethylaminopropyl)-1,3,4,5-tetrahydro-2*H*-1-benzazepin-2-one (**14b**, 2.81 g, 0.01 mol) gave 0.57 g of **16b**; mp 93—94 °C; NMR (δ) $CDCl_3$: 1.5—2.0 (m, 2H), 2.15 (s, 6H), 2.25—2.45 (m, 2H), 2.97 (s, 4H), 4.18 (t, J=12 Hz, 2H), 7.05—7.3 (m, 3H), 8.11 (s, 1H), 8.61 (s, 1H).

The dihydrochloride was prepared and recrystallized from EtOH-ether; mp 234—235 °C. Found: C, 51.92; H, 5.78; N, 14.41; Cl, 26.96%. Calcd for $C_{17}H_{21}N_4Cl \cdot 2HCl$: C, 52.39; H, 5.95; N, 14.37; Cl, 27.29%.

Method 2: To a solution of 9-chloro-5,6-dihydro-1H-benz-[2,3]azepino[7,6-*d*]pyrimidine (**15b**, 1.16 g, 0.005 mol) and 3-dimethylaminopropylchloride (1.83 g, 0.015 mol) in 4 ml of DMSO, 0.43 g of NaH (54% in mineral oil) in 6 ml of DMSO was added with stirring under nitrogen. After being stirred for 4 hr at room temperature, the reaction mixture was poured into 30 ml of water and extracted with 2×20 ml ether. The usual work up and chromatography on basic alumina using benzene: ethyl acetate (1: 1) as solvent yielded 0.62 g og **16b**.

The following compounds (**14a** and **14b**) were prepared by this method.

1-(3-Dimethylaminopropyl)-1,3,4,5-tetrahydro-2H-1-benzazepin-2-one (14a). 1,3,4,5-Tetrahydro-2*H*-1-benzazepin-2-one (**13a**, 16.1 g, 0.1 mol) gave a yellow oil of **14a** which did not crystallize (17.4 g); NMR (δ) $CDCl_3$: 1.5—2.0 (m, 2H), 2.14 (s, 6H), 2.15—2.35 (m, 4H), 2.35—2.45 (m, 2H), 2.6—2.9 (m, 2H), 3.90 (t, J=11 Hz, 2H), 7.1—7.3 (m, 4H). Found: C, 73.21; H, 9.18; N, 11.55%. Calcd for $C_{15}H_{22}ON_2$: C, 73.13; H, 9.00; N, 11.37%.

8-Chloro-1-(3-dimethylaminopropyl)-1,3,4,5-tetrahydro-2H-1-benzazepin-2-one (14b). 8-Chloro-1,3,4,5-tetrahydro-2*H*-1-benzazepin-2-one (**13b**, 45.0 g, 0.23 mol) gave a yellow oil of **14b** (44.3 g); NMR (δ) d_6-DMSO: 1.4—1.9 (m, 2H), 2.10 (s, 6H), 2.1—2.4 (m, 6H), 2.45—2.8 (m, 2H), 3.82 (t, J=12 Hz, 2H), 7.25 (d, 2H), 7.43 (broad s, 1H). Found: C, 63.73; H, 7.64; N, 9.46; Cl, 12.37%. Calcd for $C_{15}H_{21}ON_2Cl$: C, 64.16; H, 7.54; N, 9.98; Cl, 12.63%.

The hydrochloride was recrystallized from EtOH–ether; mp 160—161 °C. Found: C, 56.77; H, 7.15; N, 8.82; Cl, 22.12%. Calcd for $C_{15}H_{21}ON_2Cl \cdot HCl$: C, 56.80; H, 6.99; N, 8.83; Cl, 22.35%.

The author is grateful to Drs. S. Tatsuoka, E. Ohmura, K. Morita, and M. Ochiai of the same division for their discussion and encouragement throughout this work. Thanks are also given to Mr. H. Shimadzu for his assistance with the experimental work.

New Furanoeremophilane Derivatives from *Farfugium japonicum* Kitamura

Hajime NAGANO, Yoshiaki TANAHASHI, Yoshihiko MORIYAMA, and Takeyoshi TAKAHASHI

Department of Chemistry, Faculty of Science, The University of Tokyo, Bunkyo-ku, Tokyo 113

(Received April 2, 1973)

Five new furanoeremophilane derivatives, I, II, III, IV, and V, have been isolated from *Farfugium japonicum* Kitamura, and their structures have been determined. Conformations of some furanoeremophilane derivatives are discussed.

In addition to the previously reported farfugin A and B,[1] five new furanoeremophilane derivatives, I, II, III, IV, and V, have been isolated from *Farfugium japonicum* Kitamura (=*Ligularia tussilaginea* Makino). In this paper we wish to describe the structure determination of these compounds.

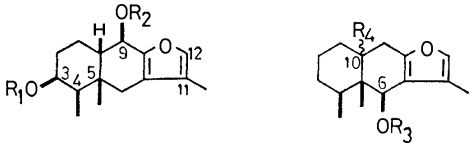

	R_1	R_2
(I)	$-CO-C(CH_3)=CH-CH_3$	$-CO-C(CH_3)=CH-CH_3$
(II)	$-CO-C(CH_3)=CH-CH_3$	H
(VI)	H	H
	R_3	R_4
(IV)	$-CO-C(CH_3)=CH-CH_3$	β-OH
(V)	$-CO-C(CH_3)=CH-CH_3$	β-H
(XIV)	H	β-OH
(XV)	H	β-H

Compound I, a viscous oil, M^+ at *m/e* 414 ($C_{25}H_{34}O_5$), $[\alpha]_D$ +17° (in MeOH), was positive to the Ehrlich test. IR, UV, PMR, and mass spectra (*cf.* Experimental and Table 1) suggest the presence of a β-methyl substituted furan ring, a secondary and a tertiary methyl and also that of partial structures: $(CH_3)_2C{=}CHCOO-$ and $CH_3CH{=}C(CH_3)COO-$. The latter moiety was determined as angeloyloxyl group by benzene induced solvent shift[2] ($\delta^{CCl_4}-\delta^{C_6D_6}=0.56$) of the olefinic proton found to be *trans* to the ester group.

Reduction of I with lithium aluminum hydride in ether gave a diol (VI), mp 187 °C (decomp.), M^+ at *m/e* 250 ($C_{15}H_{22}O_3$), $[\alpha]_D$ −24° (in EtOH), which on oxidation with active manganese dioxide[3] in benzene afforded a diketone (VIIa), mp 210 °C, M^+ at *m/e* 246 ($C_{15}H_{18}O_3$), $[\alpha]_D$ +26° (in $CHCl_3$), λ_{max} 282 nm (ε 15600), and a hydroxy-ketone (VIIIa), mp 176.5 °C, M^+ at *m/e* 248 ($C_{15}H_{20}O_3$), $[\alpha]_D$ −31° (in MeOH). Compound VIIa was found to be identical with known 3,9-dioxo-furanoeremophilane (VIIa) derived from kablicin, a furanoeremophilane derivative isolated from *Petasites kablikianus*.[4] Thus, the diol (VI) must be 3,9-dihydroxy-furanoeremophilane. Compound I would be either 3-angeloyloxy-9-senecioyloxy- or 3-senecioyloxy-9-angeloyloxy-furanoeremophilane.

Dehydration of VI with *p*-toluenesulfonyl chloride in pyridine at 110 °C gave two products, IX [M^+ at *m/e* 232 ($C_{15}H_{20}O_2$)] and X [M^+ at *m/e* 214 ($C_{15}H_{18}O$)]. The structures IX and X are compatible with their other spectral data, respectively (*cf.* Experimental).

Catalytic hydrogenation of IX over 10% palladium-charcoal in ethanol gave a pair of epimers at C-10: XIa, an oil, M^+ at *m/e* 234 ($C_{15}H_{22}O_2$), $[\alpha]_D$ −22° (in MeOH), and XIb, mp 79—80 °C, M^+ at *m/e* 234 ($C_{15}H_{22}O_2$), $[\alpha]_D$ +67° (in MeOH). The latter proved to be identical with furanoligularanol (XIb) (3β-hydroxy-10αH-furanoeremophilane),[5] derived from furanoligularenone.[5] Therefore, the stereochemistry including absolute configuration of 3-hydroxyl group of the diol (VI) should be β(*S*).

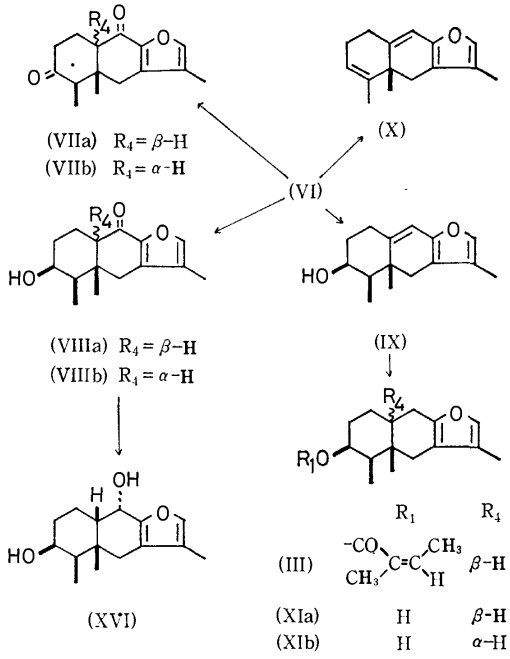

1) H. Nagano, Y. Moriyama, Y. Tanahashi, T. Takahashi, M. Fukuyama, and K. Sato, *Chemistry Lett.*, **1972**, 13.

2) J. Ronayne and D. E. Williams, *J. Chem. Soc., C*, **1967**, 2642.

3) J. Attenburrow, A. F. B. Cameron, J. H. Chapman, R. M. Evans, B. A. Hems, A. B. A. Jansen, and T. Walker, *J. Chem. Soc.*, **1952**, 1094.

4) L. Novotný, Z. Samek, V. Herout, and F. Šorm, *Tetrahedron Lett.*, **1968**, 1401.

5) F. Patil, G. Ourisson, Y. Tanahashi, M. Wada, and T. Takahashi, *Bull. Soc. Chim. Fr.*, **1968**, 1047.

Table 1. PMR spectral data (δ values)[a]

	I		II		III		IV		V
	CCl_4	C_6D_6	CCl_4	C_6D_6	CCl_4	C_6D_6	CCl_4	C_6D_6	CCl_4
$C_{(4)}$-CH_3	0.99d J=7	0.88d J=7	0.98d J=7	0.94d J=7	0.97d J=7	0.92d J=7	0.95m	0.82m	0.90m
$C_{(5)}$-CH_3	1.06s	1.12s	1.10s	1.07s	0.90s	0.73s	0.98s	1.14s	0.96s
$C_{(11)}$-CH_3	1.94d J=1.5	1.70d J=1.5	1.89	1.70d J=1	1.88	1.77d J=1	1.89	2.01	1.88
$C_{(3)}$-H	5.20m	5.27m	5.16m	5.32 quintet J=5	5.34m	5.50m			
$C_{(6)}$-H							6.07s	6.57s	6.22s
$C_{(9)}$-H	5.43s	5.82s	4.30s	4.23s			2.55 3.08 AB-type q J=19	2.87 3.07	
$C_{(12)}$-H	7.06q	6.97q	7.00m	6.98m	7.04m	7.13m	6.96m	7.09m	7.02m
CH_3(H)>C=C<CO-CH_3	1.87	1.89m	1.89	1.89m	1.88	1.92q J=1	—	—	—
$\underline{CH_3}$(H)>C=C<CO-CH_3	1.95d J=7	1.96d J=7	1.96d J=7	2.03d J=7	1.99	2.03d J=8	—	—	—
CH_3($\underline{CH_3}$)>C=C<CO-H	1.87m	1.45d J=1.5	—	—	—	—	1.89m	1.47d J=1	1.88
$\underline{CH_3}$(CH_3)>C=C<CO-H	2.16d J=1.5	2.10d J=1.5	—	—	—	—	2.17d J=1	2.14d J=1	2.17
CH_3($\underline{H}$)>C=C<CO-CH_3	5.96q J=7	5.6m	5.93q J=7	5.70q J=7	6.01q J=8	5.81q J=8	—	—	—
CH_3(CH_3)>C=C<CO-$\underline{H}$	5.54m	5.65m	—	—	—	—	5.58m	5.56m	5.67m

a) Coupling constants are expressed in Hz.
s: singlet, d: doublet, q: quartet, m: multiplet.

Compound II, an oil, M^+ at m/e 332 ($C_{20}H_{28}O_4$), $[\alpha]_D$ −11° (in MeOH), was related to I by partial hydrolysis of I with ethanolic potassium hydroxide at room temperature to give II. When I was absorped on silica gel and then eluted with solvent, II was formed.[6] Reduction of II with lithium aluminum hydride gave VI. Spectral data of II show the presence of a secondary hydroxyl and the absence of a senecioyl group. Thus, II is a desenecioyl derivative of I. In the PMR spectrum of II (Table 1), an allylic proton on hydroxy-bearing carbon resonates at δ^{CCl_4} 4.30, while the corresponding allylic proton signal of I appears at δ^{CCl_4} 5.43. These observations show that the hydroxyl group of II and the senecioyloxyl group of I are located on C-9. Therefore, I must be 3β-angeloyloxy-9-senecioyloxy-furanoeremophilane, and II should be 3β-angeloyloxy-9-hydroxy-furanoeremophilane.

Furanoeremophilane derivatives would exist in two interchangeable conformations such as **A** (steroidal) and **B** (non-steroidal conformation).[7] A number of furanoeremophilane derivatives have been isolated from the plants of Compositae. However, no description for the existence in non-steroidal conformation has yet been reported.

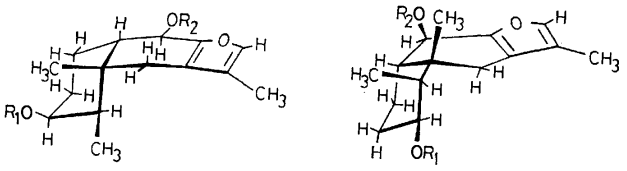

A **B**

In the PMR spectra of I, II, and VI, a broad signal (half-band width ~15 Hz) due to a proton at C-3α appears at δ^{CCl_4} 5.20, δ^{CCl_4} 5.16, and δ^{CDCl_3} 4.08, respectively, indicating an axial nature[8] for this proton. In the spectrum of II in benzene-d_6, the 3α(axial)-proton signal is observed as a quintet due to a large diaxial ($J_{2\beta.3\alpha}$=10 Hz) and two smaller axial-equatorial ($J_{2\alpha.3\alpha}=J_{3\alpha.4\alpha}$=5 Hz) vicinal couplings. An allylic proton at C-9 of I, II, and VI resonates as a singlet (half-band width ~3 Hz), suggesting a vicinal coupling ($J_{9.10}$) is small. These data can only be interpreted on the basis of the non-steroidal conformation (**B**) with the substituent at C-9 in β-configuration, in which the dihedral angle between $C_{(9\alpha)}$-H and $C_{(10\beta)}$-H is about 70—80° on Dreiding model. This dihedral angle

6) This suggests that II might be an artifact derived from I during isolation procedures involving silica gel chromatography. In the crude extract of the plant the absence of II was detected on tlc. Therefore, II is considered to be an artifact.

7) Z. Samek, J. Harmatha, L. Novotný, and F. Šorm, *Coll. Czech. Chem. Comm.*, **34**, 2792 (1969).

8) N. S. Bhacca and D. H. Williams, "Applications of NMR Spectroscopy in Organic Chemistry," Holden-Day, San Francisco (1964), pp. 77, 165.

would increase more than 80° resulting in reduction of vicinal coupling ($J_{9\alpha,10\beta}$), when a 1,3-diaxial interaction between the methyl group at C-5β and the substituent at C-9β becomes more important.

The structures including absolute configurations of I, II, and VI are thus determined as 3β-angeloyloxy-9β-senecioyloxyfuranoeremophilane (I), 3β-angeloyloxy-9β-hydroxyfuranoeremophilane (II) and 3β,9β-dihydroxy-furanoeremophilane (VI), respectively.

The hydroxy-ketone (VIIIa) exhibits an UV absorption at λ_{max} 281 nm (ε 17000), showing that the carbonyl group conjugated with furan ring is located on C-9.[9] The ORD data (*cf.* Experimental) of VIIIa is closely related to that of 9-oxo-furanoeremophilane (XIIa).[4] As VIIIa was formed by oxidation of VI, the hydroxyl group at C-3 of VIIIa must be β; this received support from the determination of absolute configuration at C-3 of VIIIa as *S* by the Horeau's method[10] (esterification 84%; optical yield (−) 25%). Therefore, the hydroxy-ketone (VIIIa) is (3*S*)-hydroxy-9-oxo-furanoeremophilane.

The same structure (VIIIa) has already been given by Rivett and Woolard for epieuryopsonol (mp 216—217 °C).[11] However, our hydroxy-ketone (VIIIa) (mp 176.5 °C) is different from epieuryopsonol. This discrepancy could be overcome when the structure of epieuryopsonol is revised from VIIIa to its 10αH-epimer, 3β-hydroxy-9-oxo-10αH-furanoeremophilane (VIIIb). This received support from an alkaline epimerization of the hydroxy-ketone (VIIIa) (mp 176.5 °C) to give its 10αH-epimer (VIIIb), mp 218—219 °C, whose PMR data are in accord with those[11] of epieuryopsonol. The structures of euryopsonol (XIIIa), dehydroeuryopsonol (VIIa), and of deoxydehydroeuryopsonol (XIIa)[11] are to be revised to XIIIb, VIIb, and XIIb, respectively. Expermiental data[11] of these euryopsonol derivatives can be best interpreted on the basis of 10αH-furanoeremophilane rather than furanoeremophilane skeleton, when compared with those of kablicin derivatives[4] (*cf.* Table 2). During isolation procedures of euryopsonol including treatment with alkali,[11] an epimerization at C-10 must have occurred to afford more stable 10αH-epimer (XIIIb).

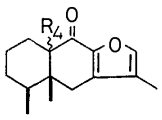

(XIIa) R_4=β-H
(XIIb) R_4=α-H

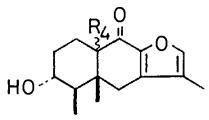

(XIIIa) R_4=β-H
(XIIIb) R_4=α-H

Compound III, an oil, M^+ at *m/e* 316 ($C_{20}H_{28}O_3$), $[\alpha]_D$ −38° (in MeOH), was positive to the Ehrlich test. The PMR spectrum (Table 1) showed the presence of an angeloyl group. Reduction of III with lithium aluminum hydride in ether gave XIa, $[\alpha]_D$ −25° (in MeOH). Therefore, III is 3β-angeloyloxy-furanoeremophilane.[12]

Spectral data of compound IV, mp 82—84 °C, M^+ at *m/e* 332 ($C_{20}H_{28}O_4$), $[\alpha]_D$ −68° (in MeOH), suggest the presence of a hydroxyl and a senecioyl groups. On reduction with lithium aluminum hydride, IV yielded a diol, mp 126 °C (decomp.), $[\alpha]_D$ +50° (in MeOH), identical with 6β,10β-dihydroxy-furanoeremophilane (XIV) isolated from *Ligularia japonica* Less.[13] Thus, the structure of IV is represented by 6β-senecioyloxy-10β-hydroxy-furanoeremophilane (IV).

The presence of a senecioyl group is suggested for compound V, an oil, M^+ at *m/e* 316 ($C_{20}H_{28}O_3$), on the basis of spectral data. Reduction of V with lithium aluminum hydride gave known petasalbin (XV),[14] $[\alpha]_D$ −14° (in MeOH). Compound V must be 6β-senecioyloxy-furanoeremophilane (V).

In the PMR spectra of III and XIa, a broad multiplet (half-band width ~15 Hz) due to a proton at C-3α appears at δ^{CCl_4} 5.34 and 4.08 respectively. This shows an axial nature for this proton, suggesting that III and XIa are in a non-steroidal rather than a steroidal conformation.

The PMR spectrum of 3β,9α-dihydroxy-furanoeremophilane[15] (XVI), prepared from VIIIa by reduction with lithium aluminum hydride, shows a broad multiplet (half-band width ~15 Hz) at δ^{CDCl_3} 4.20 due to a proton at C-3α. A proton at C-9β resonates as a doublet ($J_{9\beta,10\beta}$=6 Hz) at δ^{CDCl_3} 4.80. These data are compatible with a non-steroidal conformation for XVI.

TABLE 2[a]

Furanoeremophilanes	3α-hydroxy-9-oxo-		3β-hydroxy-9-oxo-		3,9-dioxo-		9-oxo-	
Derivaitves of kablicin[4]	XIIIa (176 °C)	XIIIb (230 °C)			VIIa (210 °C)	VIIb (225 °C)	XIIa (112 °C)	XIIb (148—149 °C)
Derivatives of euryopsonol[11]		euryopsonol (230—231 °C)		epieuryopsonol (216—217 °C)		dehydro-euryopsonol (224—225 °C)		deoxydehydro-euryopsonol (145 °C)
This report			VIIIa (176.5 °C)	VIIIb (218—219 °C)	VIIa (210 °C)			

a) Mps are indicated in parentheses.

9) L. Novotný, Ch. Tabačíkova-Wlotzká, V. Herout, and F. Šorm, *Coll. Czech. Chem. Comm.*, **29**, 1922 (1964).
10) A. Horeau and H. B. Kagan, *Tetrahedron*, **20**, 2431 (1964).
11) D. E. A. Rivett and G. R. Woolard, *ibid*, **23**, 2431 (1967).
12) Recently, we have isolated the same compound (III) from *Farfugium hiberniflorum* Kitamura.
13) M. Tada, Y. Moriyama, Y. Tanahashi, T. Takahashi, M. Fukuyama, and K. Sato, *Tetrahedron Lett.*, **1971**, 4007.
14) L. Novotný, V. Herout, and F. Šorm, *Coll. Czech. Chem. Comm.*, **29**, 2189 (1964).
15) Oxidation of XVI with active manganese dioxide led to regeneration of VIIIa.

Compounds I, II, III, VI, XIa, and XVI were thus shown to be in the non-steroidal conformation[16] such as **B**. The 3β-acyloxyl or 3β-hydroxyl group of these compounds is in an equatorial conformation, which avoids the unfavorable 1,3-diaxial interaction between 3β-substituent and 5β-methyl group; this must be the driving force to bring these compounds in a non-steroidal conformation. A predominance of this driving force over the 1,3-diaxial interaction between 9β-substituent and 5β-methyl group was shown for I, II, and VI.

Experimental

IR, UV, and Mass spectra were measured using Hitachi EPI-G2, Hitachi EPS-3 and Hitachi RMU-6 spectrometers, respectively. PMR spectra were taken on JEOL JNM-PS-100 (100 MHz) and Hitachi R-20 (60 MHz) spectrometers. Chemical shifts are expressed in δ (TMS as an internal standard). Merck Kieselgel G and Kieselgel 60 PF_{254} were used for analytical and preparative tlc, respectively. For column chromatography Wakogel C 200 was used.

Isolation. The roots of *Farfugium japonicum* Kitamura (15 kg) were extracted with ether at room temperature. The extract was then filtered, dried over anhydrous sodium sulfate and evaporated to afford a viscous oil (80 g). The oil (30 g) was again dissolved in ether, washed with 5% aqueous sodium carbonate solution, dried with anhydrous sodium sulfate and evaporated. The residue (18 g) was immediately chromatographed on silica gel (400 g) with light petroleum-ether (10: 1) as eluent (each fraction 400 ml).

Fractions 1 and 2 gave a viscous oil (1.46 g), a half of which was repeatedly chromatographed on silica gel (eluent: light petroleum-ether (100: 1)) to give an oil (124 mg). The oil was further purified by preparative tlc to afford III (77 mg) and V (16 mg).

Fraction 3 afforded I, a viscous oil (4.92 g).

Fractions 4 and 5 afforded a pale yellow oil (2.96 g), containing IV, which was isolated by preparative tlc.

The extract residue (6 g) in light petroleum was absorped on silica gel. After one day, elution with light petroleum-ether (25: 1, 3 l) and then with light petroleum-ether (10: 1. 6 l) afforded an oil (917 mg). On repeated chromatography followed by preparative tlc of the oil, II (46 mg) was obtained.

3β-Angeloyloxy-9β-senecioyloxy-furanoeremophilane (I). Compound I was a viscous oil, $[\alpha]_D^{17}$ +17° (*c* 1.45, in MeOH). Its spot on tlc plate showed yellow green color to the Ehrlich test, and developed blue color when 2% ceric sulfate reagent was sprayed and then heated. Spectral data of I are as follows; UV: λ_{max}^{MeOH} 220 nm (ε 32000); IR: ν_{max}^{liquid} 1720, 1650, and 1560 cm^{-1}; PMR (Table 1); MS *m/e* 414 (relative intensity 1.5%, M^+ ($C_{25}H_{34}O_5$)), *m/e* 83 (54%, $[CH_3CH{=}C(CH_3)CO]^+$ and $[(CH_3)_2C{=}CHCO]^+$) and *m/e* 55 (100%, $[CH_3CH{=}CCH_3]^+$ and $[(CH_3)_2C{=}CH]^+$).

3β-Angeloyloxy-9β-hydroxy-furanoeremophilane (II). Compound II, an oil, $[\alpha]_D^{14}$ −11° (*c* 0.8, in MeOH), was positive to the Ehrlich test, and displayed blue coloring with 2% ceric sulfate reagent when heated on tlc plate. Characterization of II is as follows; UV λ_{max}^{EtOH} 219 nm(ε 14500); IR: ν_{max}^{liquid} 1700, 1640, and 1560 cm^{-1}; PMR (Table 1); MS: *m/e* 332 (4%, M^+ ($C_{20}H_{28}O_4$)), *m/e* 314 (5%, $[M-H_2O]^+$), *m/e* 124 (100%, *retro*-Diels-Alder fragment), *m/e* 83 (85%, $[CH_3CH{=}C(CH_3)CO]^+$), and *m/e* 55 (70%, $[CH_3CH{=}CCH_3]^+$).

Reduction of I with Lithium Aluminum Hydride. I (996 mg) in dry ether (50 ml) was refluxed with lithium aluminum hydride (200 mg) for 1.5 hr under nitrogen atmosphere. Then, the excess of lithium aluminum hydride was decomposed with water, and extracted with ether. The usual treatment gave a crystalline product, which was recrystallized from isopropyl ether to give VI (364 mg). The residue obtained from the mother liquid was chromatographed on silica gel (30 g) with light petroleum-ether (1:1) as eluent to give further VI (40 mg). 3β,9β-Dihydroxy-furanoeremophilane (VI), mp 187 °C (decomp.), $[\alpha]_D^{19}$ −24° (*c* 0.47, in EtOH); UV: λ_{max}^{EtOH} 222.5 nm (ε 7200); IR: ν_{max}^{Nujol} 3475, 3380, and 1565 cm^{-1}; PMR ($CDCl_3$): δ 1.00 (d, *J*=7 Hz, $C_{(4)}$-CH_3), 1.14 (s, $C_{(5)}$-CH_3), 1.90 (d, *J*=1.5 Hz, $C_{(11)}$-CH_3), 1.96 (d, *J*=(−) 17 Hz, $C_{(6)}$-H), 2.66 (d, *J*=(−) 17 Hz, $C_{(6)}$-H), 4.08 (m, $C_{(3)}$-H), 4.40 (s, $C_{(9)}$-H), and 7.12 (q, *J*=1.5 Hz, $C_{(12)}$-H); MS: *m/e* 250 (6%, M^+ ($C_{15}H_{22}O_3$)) and *m/e* 124 (100%, *retro*-Diels-Alder fragment). Found: C, 72.12; H, 8.70%. Calcd for $C_{15}H_{22}O_3$: C, 71.79; H, 8.86%.

Reduction of II with Lithium Aluminum Hydride. Treatment of II with lithium aluminum hydride by the same procedures described as above gave VI, mp 187 °C (decomp.), $[\alpha]_D^{15}$ −28° (*c* 1.0, in MeOH).

Hydrolysis of I. *A*: I (1.86 g) was chromatographed on silica gel (50 g) using light petroleum-ether (50: 1) as eluent. However, only 48 mg of I was recovered and from the fractions eluted with ether a yellowish oil (640 mg) was obtained. The oil was repeatedly chromatographed on silica gel (35 g) with light petroleum-ether (10: 1) to give II (96 mg).

B: A solution of potassium hydroxide (1 g) in ethanol (25 ml) was added to I (277 mg) and the mixture was allowed to stand overnight at room temperature, added water and extracted with ether. The extract was washed with water, dried with anhydrous sodium sulfate and evaporated under reduced pressure to give an oil (191 mg) containing II and VI. VI was not detected on tlc before the evaporation of the solvent. Therefore, this compound must be formed on heating during the above procedures.

C: The residue obtained by the procedures *A* and *B* were combined, dissolved in ethanolic potassium hydroxide and refluxed for 2.5 hr under nitrogen atmosphere. After usual treatment, the resulting residue was recrystallized from isopropyl ether to give VI. The aqueous layer was acidified with dil hydrochloric acid and extracted with ether. After the solvent was distilled off, the residue was allowed to stand for several days and tiglic acid (an isomerization product of angelic acid) was obtained as crystals.

Oxidation of VI with Active Manganese Dioxide. To a solution of VI (154 mg) in benzene (50 ml) was added active manganese dioxide[3] (1.5 g) and stirred for 22 hr under nitrogen atmosphere. After filtration, the solvent was removed to afford a residue, which was chromatographed on silica gel (7 g). Fractions eluted with light petroleum-ether (1: 1) gave VIIa (64 mg), and successive elution with ether gave VIIIa (70 mg).

3,9-Dioxo-furanoeremophilane (VIIa); mp 210 °C (recrystallized from ethanol), $[\alpha]_D^{19}$ +26° (*c* 0.71, in $CHCl_3$); UV: λ_{max}^{EtOH} 282 nm (ε 15600); IR: ν_{max}^{Nujol} 1715, 1657, and 1530 cm^{-1}; PMR ($CDCl_3$): δ 0.96 (d, *J*=7 Hz, $C_{(4)}$-CH_3), 1.11

16) The PMR spectra of furanopetasine[9] (2α-angeloyloxy-9α-hydroxy-furanoeremophilane; 2β-H at δ^{CDCl_3} 5.20, half-band width ~15 Hz) and furanopetasol[9] (2α,9α-dihydroxy-furanoeremophilane; 2β-H at δ^{CDCl_3} 4.06, half-band width~15 Hz), offered through courtesy of Dr. L. Novotný, showed that these compounds also existed in a non-steroidal conformation, in which the substituents at C-2α and C-9α were equatorial.

(s, $C_{(5)}$-CH_3), 2.01 (d, J=1.5 Hz, $C_{(11)}$-CH_3), and 7.42 (q, J=1.5 Hz, $C_{(12)}$-H); MS: *m/e* 246 (39%, M^+ ($C_{15}H_{18}O_3$)), *m/e* 175 (100%), and *m/e* 122 (5%). The PMR spectrum of VIIa in the presence of Eu(dpm)$_3$ (0.45 mol equivalent) as shift reagent revealed the presence of a partial structure -CO-CH(CH_3)-$\dot{C}$-; namely, signals due to $C_{(4)}$-CH_3 and $C_{(4)}$-H appeared at δ^{CDCl_3} 3.39 (d, J=6.5 Hz) and at δ^{CDCl_3} 6.35 (q, J=6.5 Hz), respectively. Diketone (VIIa)[17] was found to be identical (mp 210 °C) with 3,9-dioxo-furanoeremophilane.

3β-Hydroxy-9-oxo-furanoeremophilane (VIIIa); mp 176.5 °C (recrystallized from isopropyl ether), $[\alpha]_D^{20}$ −31° (*c* 0.97, in MeOH); UV: λ_{max}^{EtOH} 281 nm (ε 17000); ORD (*c* 0.14, in MeOH): $[\phi]_{280}$ −6800°, $[\phi]_{260}^{trough}$ −14000°, $[\phi]_{230}^{peak}$ −10000°, $[\phi]_{208}^{trough}$ −27000° and $[\phi]_{200}$ −6800°; IR: ν_{max}^{Nujol} 3500, 1650, and 1525 cm^{-1}; PMR ($CDCl_3$): δ 0.99 (d, J=7 Hz, $C_{(4)}$-CH_3), 1.10 (s, $C_{(5)}$-CH_3), 1.98 (d, J=1.5 Hz, $C_{(11)}$-CH_3), 4.17 (m, $C_{(3)}$-H), and 7.41 (q, J=1.5 Hz, $C_{(12)}$-H); MS: *m/e* 248 (5%, M^+ ($C_{15}H_{20}O_3$)), *m/e* 91 (46%), *m/e* 77 (32%), and *m/e* 66 (100%). Found: C, 72.83; H, 7.82%. Calcd for $C_{15}H_{20}O_3$: C, 72.55; H, 8.12%.

Application of the Horeau's Method[10] to VIIIa. VIIIa (18.6 mg, 0.075 mmol) in pyridine (3 ml) was allowed to stand with α-phenylbutyric anhydride (69.6 mg, 0.224 mmol) for 18 hr at room temperature. The reaction mixture was then heated with one drop of water. After benzene was added, the mixture was titrated with 0.1 M KOH in the presence of phenolphthalein. The aqueous layer was acidified with dil sulfuric acid and then extracted with benzene. After usual treatment of the extract, the solvent was evaporated to give α-phenylbutyric acid. The optical rotation value (α_D −0.025°) was observed for the benzene solution (5 ml) of the acid using a 0.5 dm cell.

Alkaline Epimerization of VIIIa. To a solution of VIIIa (45 mg) in ethanol (20 ml), 10% aqueous sodium hydroxide (5 ml) was added and the mixture was refluxed for 1 hr under nitrogen atmosphere. After the reaction mixture was treated as usual, the residue (41 mg) was chromatographed on silica gel (3 g) using light petroleum–ether (3: 1) as eluent to give the epimerized product VIIIb (12 mg). Successive elution with ether gave VIIIa (*ca.* 30 mg). Compound VIIIb; mp 218—219 °C (recrystallized from isopropyl ether); IR: ν_{max}^{Nujol} 3480 and 1650 cm^{-1}; PMR ($CDCl_3$): δ 1.02 (s, $C_{(5)}$-CH_3), 1.16 (d, J=7 Hz, $C_{(4)}$-CH_3), 1.97 (d, J=~1 Hz, $C_{(11)}$-CH_3), 3.88 (m, $C_{(3)}$-H), and 7.32 (q, J=~1 Hz, $C_{(12)}$-H).

Dehydration of VI with p-*Toluenesulfonyl Chloride in Pyridine.* To a solution of VI (398 mg) in pyridine (10 ml), *p*-toluenesulfonyl chloride (400 mg) was added and heated at 110 °C (oil bath temperature) for 20 min under nitrogen atmosphere. Evaporation of the solvent gave a reddish residue, which was immediately chromatographed on silica gel (30 g) using light petroleum–ether (20: 1) as eluent. (each fraction *ca.* 70 ml).

Fraction 2 gave a pale yellow oil, X (20 mg); UV: λ_{max}^{MeOH} 293 nm (ε ~10000); PMR (C_6D_6): δ 1.09 (s, $C_{(5)}$-CH_3), 1.60 (m, $C_{(4)}$-CH_3), 1.78 (d, J=1.5 Hz, $C_{(11)}$-CH_3), 5.35 (m, $C_{(3)}$-H), 6.13 (d, J=~1 Hz, $C_{(9)}$-H), and 6.93 (q, J=1.5 Hz, $C_{(12)}$-H); MS: *m/e* 214 (46%, M^+ ($C_{15}H_{18}O$)), and *m/e* 199 (100%, $[M-CH_3]^+$), which was sensitive to the air. This compound (X) on tlc plate developed a bright red color with 2% ceric sulfate reagent.

Fractions 7—16 gave a pale yellow oil, IX (140 mg); UV: λ_{max}^{MeOH} 292 nm (ε ~10000); IR: ν_{max}^{liquid} 3400 cm^{-1}; PMR (CCl_4): δ 1.05 (s, $C_{(5)}$-CH_3), 1.10 (d, J=6 Hz, $C_{(4)}$-CH_3), 1.90 (d, J=1.5 Hz, $C_{(11)}$-CH_3), 3.84 (m, $C_{(3)}$-H), 5.93 (d, J=2.5 Hz, $C_{(9)}$-H), and 6.86 (m, $C_{(12)}$-H); MS: *m/e* 232 (39%, M^+($C_{15}H_{20}O_2$)), *m/e* 199 (79%, $[M-CH_3-H_2O]^+$), *m/e* 159 (100%), and *m/e* 145 (44%), which was sensitive to the air. The compound (IX) on tlc plate developed a bright red color with 2% ceric sulfate reagent.

Hydrogenation of IX over Pd–C. Hydrogenation of IX (114 mg) in ethanol was effected over Pd–C (10%) (31 mg) with stirring for 3.5 hr. Filtration of the catalyst and evaporation of the solvent under reduced pressure gave an oil (95 mg). From the oil, XIa (20 mg) and XIb (40 mg) were separated by preparative tlc. Sublimation of the latter gave colorless crystals (XIb), mp 79—80 °C (recrystallized from light petroleum), $[\alpha]_D^{25}$ +67° (*c* 0.7, in MeOH); IR: ν_{max}^{Nujol} 3350, 1640, and 1560 cm^{-1}; PMR (CCl_4): δ 0.86 (s, $C_{(5)}$-CH_3), 1.10 (d, J=7 Hz, $C_{(4)}$-CH_3), 1.86 (d, J=~1 Hz, $C_{(11)}$-CH_3), 3.84 (m, $C_{(3)}$-H), and 7.00 (m, $C_{(12)}$-H); MS: *m/e* 234 (12%, M^+ ($C_{15}H_{22}O_2$)), and *m/e* 108 (100%, *retro*-Diels-Alder fragment), which was identical with furanoligularanol (XIb),[5] mp 79—80 °C, $[\alpha]_D^{24}$ +78° (*c* 0.8, in MeOH),[18] prepared from furanoligularenone.[5] Compound XIa was an oil, $[\alpha]_D^{24}$ −22° (*c* 1.0, in MeOH); IR: ν_{max}^{liquid} 3360, 1640, and 1560 cm^{-1}; PMR (CCl_4): δ 0.94 (d, J=7 Hz, $C_{(4)}$-CH_3), 0.94 (s, $C_{(5)}$-CH_3), 1.86 (d, J=1.5 Hz, $C_{(11)}$-CH_3), 4.12 (m, $C_{(3)}$-H), and 6.91 (m, $C_{(12)}$-H); MS: *m/e* 234 (10%, M^+ ($C_{15}H_{22}O_2$)), and *m/e* 108 (100%, *retro*-Diels-Alder fragment).

3β-Angeloyloxy-furanoeremophilane (III). Compound III, an oil, $[\alpha]_D^{14}$ −38° (*c* 1.3, in MeOH), was positive to the Ehrlich test (purple). Spectral data of III are as follows; IR: ν_{max}^{liquid} 1705, 1640, and 1560 cm^{-1}; PMR (Table 1); MS: *m/e* 316 (5%, M^+ ($C_{20}H_{28}O_3$)), 108 (100%, *retro*-Diels-Alder fragment), *m/e* 83 (40%, $[CH_3CH{=}C(CH_3)CO]^+$), and *m/e* 55 (30%, $[CH_3CH{=}CCH_3]^+$).

Reduction of III with Lithium Aluminum Hydride. To a suspension of lithium aluminum hydride (48 mg) in dry ether (2 ml), III (77 mg) in dry ether (4 ml) was added and stirred at room temperature under nitrogen atmosphere. After completion of the reaction, the mixture was treated as usual and the resulting residue was chromatographed on silica gel (4 g). Fractions eluted with light petroleum–ether (10: 1) gave a compound identical with XIa, M^+ at *m/e* 234 ($C_{15}H_{22}O_2$), $[\alpha]_D^{28}$ −25° (*c* 1.3, in MeOH). Identification was effected on $[\alpha]_D$, IR, PMR, MS, and tlc.

6β-Senecioyloxy-10β-hydroxy-furanoeremophilane (IV). Compound IV, mp 82—84 °C (recrystallized from light petroleum), $[\alpha]_D^{15}$ −68° (c, 0.84, in MeOH), was positive to the Ehrlich test (purple), and displayed intense blue coloring with 2% ceric sulfate reagent when heated on tlc plate. Characterization of IV is as follows; UV: λ_{max}^{EtOH} 218 nm (ε 21000); IR: $\nu_{max}^{CCl_4}$ 3513, 1715, and 1644 cm^{-1}; PMR (Table 1); MS: *m/e* 332 (1.4%, M^+($C_{20}H_{28}O_4$)), *m/e* 83 (100%, $[(CH_3)_2C{=}CHCO]^+$), and *m/e* 55 (23%, $[(CH_3)_2C{=}CH]^+$).

Reduction of IV with Lithium Aluminum Hydride. Reduction of IV (39 mg) with lithium aluminum hydride (39 mg) in ether (5 ml) gave a crystalline product (10 mg), mp 126° (decomp.), M^+ at *m/e* 250 ($C_{15}H_{22}O_3$), $[\alpha]_D^{20}$ +50° (*c* 0.17, in EtOH), which was identified with the authentic sample of 6β,10β-dihydroxyfuranoeremophilane (XIV)[13] by mp, $[\alpha]_D$, IR, PMR, MS, and tlc.

6β-Senecioyloxy-furanoeremophilane (V). Compound V,

17) In the PMR spectra of VIIa, a remarkable benzene-induced solvent shift ($\delta^{CDCl_3}-\delta^{C_6D_6}$=0.28) was observed for the signal due to a secondary methyl adjacent to carbonyl group. This shows an axial nature[8] for the 4β-methyl group suggesting that VIIa is in a non-steroidal conformation.

18) Pure furanoligularanol (XIb) has these physical constants. Mp 63°C and $[\alpha]_D$+53° (*c* 0.5, in $CHCl_3$) were given for the same compound in the literature.[5]

a viscous oil, was positive to the Ehrlich test. Characterization of V is as follows; IR: ν_{max}^{liquid} 1710, 1645, and 1563 cm^{-1}; PMR (Table 1); MS (indirect inlet system): *m/e* 316 (1%, $M^+(C_{20}H_{28}O_3)$), *m/e* 159 (77%), *m/e* 145 (29%), *m/e* 83 (100%, $[(CH_3)_2C{=}CHCO]^+$), and *m/e* 55 (23%, $[(CH_3)_2C{=}CH]^+$).

Reduction of V with Lithium Aluminum Hydride. Treatment of V with lithium aluminum hydride by the same procedures described above gave a compound, M^+ at *m/e* 234 ($C_{15}H_{22}O_2$), $[\alpha]_D^{18}$ −14° (*c* 0.7, in MeOH), identical with petasalbin (XV)[14] (IR, PMR, MS, and tlc).

Reduction of VIIIa with Lithium Aluminum Hydride. Reduction of VIIIa (33 mg) with lithium aluminum hydride (50 mg) in ether (30 ml) with stirring for 2 hr under nitrogen atmosphere, and then usual work-up gave XVI (29 mg), mp 81—83 °C (sublimation); IR: ν_{max}^{Nujol} 3330, 1660, and 1565 cm^{-1}; PMR ($CDCl_3$): δ 0.97 (s, $C_{(5)}$-CH_3), 1.00 (d, J=7 Hz, $C_{(4)}$-CH_3), 1.90 (d, J=1.5 Hz, $C_{(11)}$-CH_3), 4.20 (m, $C_{(3)}$-H), 4.80 (d, J=6 Hz, $C_{(9)}$-H), and 7.11 (q, J=1.5 Hz, $C_{(12)}$-H); MS: *m/e* 250 (6%, M^+ ($C_{15}H_{22}O_3$)) and *m/e* 124 (100%, *retro*-Diels-Alder fragment).

Oxidation of XVI with Active Manganese Dioxide. To a solution of XVI (20 mg) in benzene (4 ml) was added active manganese dioxide[3] (100 mg) and stirred for 4 hr under nitrogen atmosphere. After filtration, the solvent was removed to afford a crystalline product, which was recrystallized from isopropyl ether to give VIIIa (12 mg).

The authors wish to express their thanks to Dr. L. Novotný, Czechoslovak Academy of Science, for a generous gift of furanopetasine and furanopetasol.

BULLETIN OF THE CHEMICAL SOCIETY OF JAPAN, VOL. 46, 2845—2849 (1973)

Transylidations of Stable Sulfonium Ylids[1)]

Haruo MATSUYAMA, Hiroshi MINATO, and Michio KOBAYASHI
Department of Chemistry, Faculty of Science, Tokyo Metropolitan University, Fukazawa, Setagaya, Tokyo 158

(Received April 3, 1973)

In the presence of a dialkoxy disulfide, sulfonium bis(methoxycarbonyl)methylids underwent transylidation with a dialkyl sulfide or pyridine at 35 °C. Thiocyanogen and benzoyl disulfide showed a similar catalytic effect. The kinetics of this reaction were investigated, and its mechanism was discussed.

A sulfur ylid containing two electron-withdrawing substituents on its negatively charged carbon atom is thermally stable, and the nucleophilicity of its negatively charged carbon atom is much less than that of an ylid containing only one electron-withdrawing substituent. While the mono-substituted ylids are used for various synthetic purposes by using their reactivity with carbonyl compounds and electron-deficient olefins,[2)] the di-substituted ylids show almost no reactivity with these electrophiles. Recently, reactions between dialkyl-sulfonium bis(methoxycarbonyl)methylids and several electrophiles have been reported on, but they require a fairly long time at high temperatures.[3)]

In the presence of a dialkoxy disulfide, dimethyl diazomalonate smoothly reacted with dialkyl sulfides at room temperature and the corresponding ylids were formed in good yields.[4)]

We have found that in the presence of a catalytic amount of dialkoxy disulfide (III), ylid (I) ($R^1R^2S^+C^-(COOMe)_2$) underwent transylidation with a dialkyl sulfide (II) very easily.

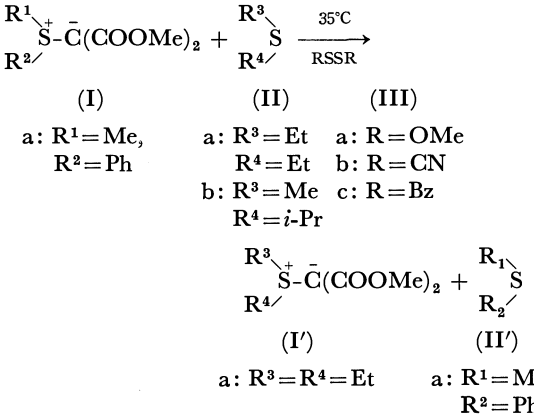

The only one example of transylidation in the literature is the case of methylarylsulfonium phenacylid in which the ylid dimerizes by dipolar attraction and then the dimer redissociates with the sulfide function scrambled.[5)]

The scope and mechanism of the transylidation between ylid I and dialkyl sulfides or pyridines are discussed in this paper.

Results and Discussion

In the absence of III, I is very stable and shows no transylidation when it is mixed with II at 35 °C.

1) Organic Sulfur Compounds. Part XLII.

2) J. Adams, L. Hoffman, and B. M. Trost, *J. Org. Chem.*, **35**, 1600 (1970); G. B. Payne, *ibid.*, **33**, 3517 (1968), *ibid.*, **32**, 3351 (1967).

3) T. Yagihara and S. Oae, *Int. J. Sulfur Chem.*, **A**, **1**, 159 (1971).

4) H. Matsuyama, H. Minato, and M. Kobayashi, This Bulletin, **46**, 1512 (1973).

5) H. Nozaki, T. Takaku, D. Tsunemoto, Y. Yamamoto, and K. Kondo, *Nippon Kagaku Zasshi*, **88**, 1 (1967).

Table 1. Transylidation of stable sulfonium ylids with sulfides[a)]

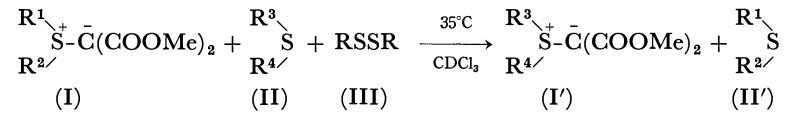

(I) (II) (III) (I′) (II′)

$R^1R^2\overset{+}{S}-$ of I	II	III	Time (min)	Products (mol%)		
				Recovered I	I′	II′
$PhMe\overset{+}{S}-$	Me_2S	$(MeOS)_2$	10	—	93	99
$PhEt\overset{+}{S}-$	Me_2S	$(MeOS)_2$	10	—	100	91
$Me_2\overset{+}{S}-\underset{\downarrow}{O}$	Me_2S	$(MeOS)_2$	150	—	91	100
$Me_2\overset{+}{S}-$	PhSMe	$(MeOS)_2$	3140	55	—	26
$Me_2\overset{+}{S}-$	Et_2S	$(MeOS)_2$	313	55	33	45
$Et_2\overset{+}{S}-$	Me_2S	$(MeOS)_2$	250	50	40	50
$EtMe\overset{+}{S}-$	Et_2S	$(MeOS)_2$	270	55	26	45
$Et_2\overset{+}{S}-$	MeSEt	$(MeOS)_2$	255	52	36	47
$PhMe\overset{+}{S}-$	Me_2S	$(BzS)_2$	900	14	78	85
$PhMe\overset{+}{S}-$	Py	$(BzS)_2$	30	—	100	100
$PhMe\overset{+}{S}-$	Me_2S	$(NCS)_2$	177	—	88	95

a) Reaction mixture consists of I (0.5—0.6 mmol), II (0.5—1.0 mmol), and III(0.2—0.4 mmol).

When Ia was heated with excess IIa (15 mol/mol Ia) in nitromethane at 86 °C for 25 hr, the mixture contained the original Ia (58%), Ia′ (34%), and IIa′ (42%). Thus, transylidation takes place upon heating, but very slowly.

However, when a catalytic amount of III is present, transylidation proceeds very easily. The results are summarized in Table 1. It is shown that dialkyl sulfides can attack all the ylids studied whereas methyl phenyl sulfide cannot carry out transylidation. It is also clear that alkyl phenyl ylids react with dialkyl sulfides rapidly but dialkyl ylids react with them rather slowly.

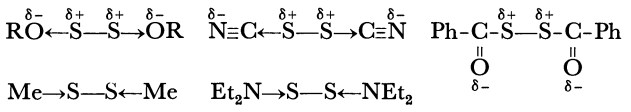

Various disulfides were examined as regards their catalytic activity in this transylidation. Neither dimethyl disulfide nor diethylamino disulfide[6)] was effective, but thiocyanogen and benzoyl disulfide possessed a catalytic activity similar to that of III (Tables 1 and 3). Thus the disulfides containing electron-withdrawing substituents catalyze the transylidation, the electron-deficiency on the –S–S–probably being responsible for the catalytic activity.

Since methylphenylsulfonium bis(methoxycarbonyl)-methylid easily reacts with dialkyl sulfides, the steric effect of alkyl groups of II on transylidation was examined by using this ylid. The results are shown in Table 2. It is evident that the sulfides with more bulky alkyl groups react more slowly; the order of reactivity is $Me_2S > (CH_2)_4S > MeSEt > Et_2S >$ MeSPr-*i*~MeSBu-*n* $\gg$ *t*-BuSBu-*t*.

Table 2. Steric effects in the transylidation of Ia with various dialkyl sulfides[a)]

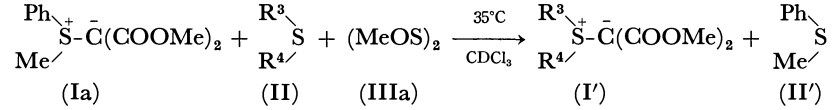

(Ia) (II) (IIIa) (I′) (II′)

II	Time (min)	Products (mol%)		
		Recovered Ia	I′	II′
MeSMe	7	—	100	98
MeSEt	35	—	94	98
MeSPr-*i*	260	23	77	77
MeSBu-*n*	28	50	50	48
EtSEt	39	25	75	75
$(CH_2)_4S$	17	9	91	91
t-BuSBu-*t*	1500	100	—	—

a) Mixture consists of Ia (0.5 mmol), II(0.6—0.8 mmol), and IIIa (0.2—0.3 mmol).

6) Q. E. Thompson, *Quart. Reports on Sulfur Chem.*, **5**, 251 (1970).

Table 3. Steric effects in the transylidation of Ia with pyridine derivatives[a)]

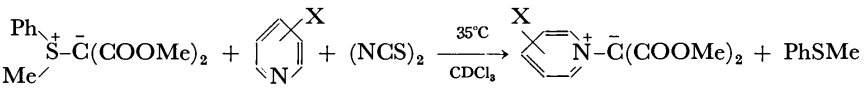

(Ia) (IV) (IIIb) (V) (II′)

IV	Time (min)	pK_a	Products (mol%)		
			Recovered (Ia)	(V)	(II′)
	2	5.2	—	100	100
 4-	4	6.0	—	96	98
3-	3	5.7	—	96	96
2-	714	6.0	72	25	28
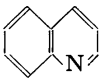	409	4.9	86	14	14
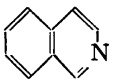	93	5.4	83	17	17
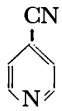	1203	1.9	89	7	7

a) Mixture consists of Ia(0.5 mmol), II (0.6—0.8 mmol), and IIIb (0.07—0.12 mmol).

It was found that S-ylids can be converted into N-ylids when pyridine derivatives are used instead of dialkyl sulfides. Table 3 shows the results of such experiments with Ia and thiocyanogen (IIIb). The methyl groups at positions 3 and 4 of pyridine show very little effect on the rate, whereas the methyl group at position 2 reduces it considerably. A similar steric retardation of rate by the 2-methyl group of 2-methylpyridine was described in its S_N2 reaction with methyl iodide.[7,8)]

The slow reaction with quinoline can be ascribed to the steric effect exerted by the hydrogen atom at position 8. The reaction with isoquinoline is a little faster than that with quinoline, and considerably slower than that of pyridine. This small reactivity of isoquinoline cannot be explained easily. The slow reaction with 4-cyanopyridine can be ascribed to its smaller nucleophilicity due to the presence of the electron-withdrawing CN group.

The reaction between isopropyl methyl sulfide (IIb) and ylid Ia was slow enough to determine its rate. The effects of concentrations of reactants and catalyst IIIa were examined. The results are summarized in Table 4. The second-order rate constants calculated by assuming $-d[Ia]/dt=k[Ia][IIb]$ increased with the initial concentration of IIb; apparently the rate depends on [IIb] to a greater extent than that expressed by means of this equation. The rates increased also with the initial concentration of IIIa.

Similarly the effects of concentrations of reactants in the reaction among Ia, 4-methylpyridine (IVa), and IIIa were examined. The results are shown in Table 5. The second-order rate constants calculated decreased with the initial concentration of IVa; apparently the rate depends on [IVa] much less. When the first-order rate constants were calculated by assuming that $-d[Ia]/dt=k[Ia]$, they were found to be almost independent of the initial concentration of IVa. As regards the initial concentration of IIIa, the rates were found to increase with [IIIa].

Table 4. Rates of transylidation between ylid Ia and methyl isopropyl sulfide in $CDCl_3$ at 35 °C

Reactants (mol/l)			Second-order rate constants
$PhMe\overset{+}{S}\overset{-}{C}(COOMe)_2$ (Ia)	*i*-Pr-S-Me (IIb)	$(MeOS)_2$ (IIIa)	calculated from $-d[Ia]/dt=k[Ia][IIb]$ $10^4\times k$ (M^{-1} sec^{-1})
0.85	0.73	0.27	4.7
0.85	1.37	0.27	7.7
0.85	2.01	0.27	13.9
0.85	1.37	0.55	21.8
0.85	1.37	1.09	34.8

7) H. C. Brown and A. Cahn, *J. Amer. Chem. Soc.*, **77**, 1715 (1955).

8) R. G. Pearson, H. Sobel, and J. Songstad, *ibid.*, **90**, 319 (1968).

Table 5. Rates of transylidation between ylid Ia and 4-methylpyridine (IVa) in $CDCl_3$ at 35 °C

Reactants (mol/l) (Ia)	Reactants (mol/l) (IVa)	Reactants (mol/l) (IIIa)	Second-order rate constants calcd from $-d[Ia]/dt=k[Ia][IVa]$ $10^4\times k$ ($M^{-1}sec^{-1}$)	First-order rate constants calcd from $-d[Ia]/dt=k[Ia]$ $10^4\times k$ (sec^{-1})
0.85	0.66	0.27	33.3	5.7
0.85	1.32	0.27	7.5	8.1
0.85	1.98	0.27	4.3	7.4
0.85	1.32	0.55	12.7	12.3
0.85	1.32	1.09	41.6	30.1

Table 6. Rates of decomposition of ylid Ia in the presence of IIIa

Reactants (mol/l) $PhMeS^+-C^-(COOMe)_2$ (Ia)	Reactants (mol/l) $(MeOS)_2$ (IIIa)	First-order rate constant calculated from $-d[Ia]/dt=k[Ia]$ $10^5\times k$ (sec^{-1})
0.85	1.36	0.8
0.85	2.27	2.7

In the absence of dialkyl sulfides, ylid Ia remained unchanged but was found to decompose slowly at 35 °C when about the same amount of IIIa was present. The products were methyl phenyl sulfide and methyl ethylenetetracarboxylate.

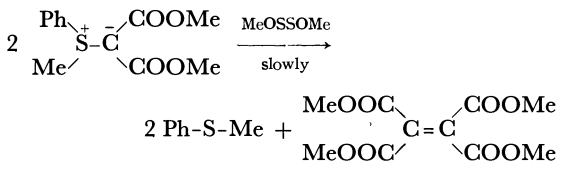

IIIa remained unchanged during the course of reaction. Table 6 shows the results of rate measurements. The first-order rate constants calculated by assuming $-d[Ia]/dt=k[Ia]$ increased with [IIIa]. The rate constants were much smaller than those obtained in the reactions among Ia, IIb, and IIIa or Ia, IVa, and IIIa. This means that almost no decomposition of Ia took place during transylidation between Ia and IIb or Ia and IVa.

The results obtained can be summarized as follows.
1) Transylidation does not take place unless an electron-deficient disulfide (MeOSSOMe, NC–SS–CN or Bz–SS–Bz) is present.
2) When I and III are mixed, I slowly decomposes. Thus, some interaction exists between I and III.
3) Substrates which can attack I possess electron-rich S or N atoms.
4) Transylidation is slower with bulky nucleophiles.
5) The rates of transylidation increase with the concentration of III.
6) During the transylidation, III does not decompose.

A plausible reaction scheme which is consistent with these results is as follows.

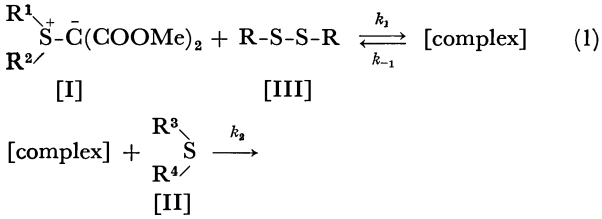

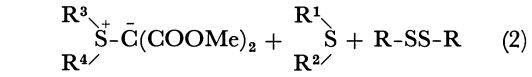

By assuming that concentration of the complex is very small and applying the steady state assumption, the rate of transylidation can be expressed as

$$-\frac{d[I]}{dt}=\frac{k_1k_2[I][II][III]}{k_{-1}+k_2[II]}$$

When 4-methylpyridine (IVa) was used in place of II, the rates appeared to be approximately of first-order in both [I] and [III], and not to depend upon [IVa]. This can be explained by assuming that in the case of 4-methylpyridine the second step proceeds very fast in comparison with the backward reaction of the first step, $k_2[IVa]\gg k_{-1}$.

Although attempts for obtaining supporting evidence by spectroscopic methods were not successful, the following structure is most plausible as the complex between I and III.

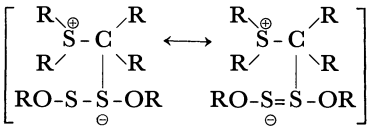

Effects of the substituents on the negatively charged carbon atom of ylid I were investigated. The results are shown in Table 7. Transylidation proceeds faster with the ylids containing COOMe and more slowly with those containing COMe. It is known that contribution of a betaine structure is greater in acetyl ylids than that in alkoxycarbonyl ylids.[9]

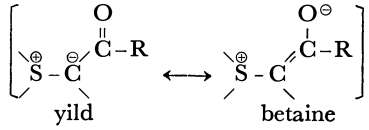

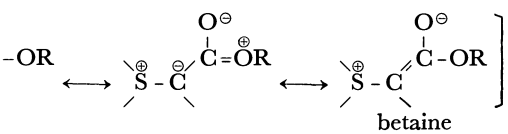

9) A. W. Johnson and R. T. Amel, *J. Org. Chem.*, **34**, 1240 (1969).

TABLE 7. TRANSYLIDATION OF YLIDS CONTAINING VARIOUS SUBSTITUENTS ON YLID CARBANION ATOMS[a)]

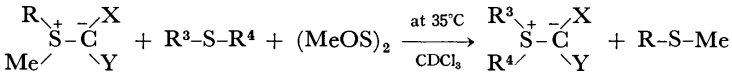

(I) (II) (IIIa) (I′) (II′)

(I)	R	X	Y	(II)	Time (min)	Products (mol%) Recovered (I)	Ylid (I′)	(II′)
(Ia)	Ph	COOMe	COOMe	Me_2S	7	—	100	98
(Ib)	Ph	COMe	COOMe	Me_2S	460	39	36	61
(Ic)	Ph	COMe	COMe	Me_2S	770[b)]	47	32	40
(Id)	Me	COOMe	COOMe	Et_2S	313	55	33	45
(Ie)	Me	CN	CN	Et_2S	174[c)]	—	—	92
(If)	Me	H	COPh	—	57[c)]	—	—	95

a) Mixture consists of I (0.5 mmol), II(0.6—0.8 mmol), and IIIa (0.2—0.3 mmol), except in the case of Ic.
b) Mixture consists of Ic (0.5 mmol), II (6.5 mmol), and IIIa (0.3 mmol).
c) Catalytic decomposition of ylid proceeded rapidly.

It is reasonable that the greater the nucleophilicity of the ylid carbanion, the easier the formation of complex with III and the faster the transylidation process.

In the presence of III, dimethylsulfonium phenacylid (I_f) was found to decompose rapidly, producing dimethyl sulfide in a quantitative yield. This suggests that the ylid carbanion with strong nucleophilicity tends to form a complex with III very rapidly.

In a study on the thermolysis of dimethylsulfonium phenacylid in cyclohexene in the presence of $CuSO_4$ or ZnI_2, Trost[10] proposed the formation of a complex between electron-deficient Cu^{2+} or Zn^{2+} and electron-rich ylid carbanion. This complex is similar to the one we proposed as regards the reaction between an electron-deficient disulfide and electron-rich ylid carbanion.

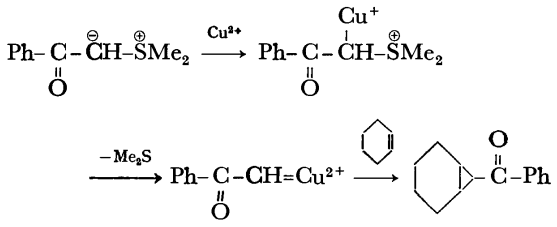

Experimental

Materials. Sulfonium bis(methoxycarbonyl)methylids were prepared by copper-catalyzed decomposition of dimethyl diazomalonate in large excess sulfides.[11]

Dimethyl sulfide, tetrahydrothiophene, di-*t*-butyl sulfide, dimethyl disulfide, pyridine, methylpyridines, 4-cyanopyridine, quinoline, and isoquinoline were of reagent grade and used without further purification. Other sulfides were prepared from the corresponding sodium mercaptides and alkyl halides.[12]

Dimethoxy disulfide was synthesized by the method of Thompson.[13] Thiocyanogen[14] and benzoyl disulfide[15] were prepared by the methods described in the literature. Diethylamino disulfide was synthesized by adding sulfur monochloride (0.1 mol) to a dichloromethane solution of diethylamine (0.4 mol) at 0 °C; bp 115 °C/6 mmHg (lit,[16] bp 137 °C/29 mmHg).

General Procedure. A $CDCl_3$ solution of I, II, and III containing nitromethane (internal standard) was placed in an NMR tube at 35 °C, and the intensity changes of the signals of the original ylid(I), new ylid(I′) and new sulfide (II′) were determined. After the original ylid(I) completely disappeared, *n*-hexane was added to the reaction mixture. The ylid crystals which precipitated were filtered and recrystallized from methanol. The melting points, IR, and NMR spectra of the ylids obtained were identical with those reported in the literature.[17]

10) B. M. Trost, *J. Amer. Chem. Soc.*, **89**, 138 (1967).

11) W. Ando, T. Yagihara, S. Tozune, S. Nakaido, and T. Migita, *Tetrahedron Lett.*, **1969**, 1979.

12) A. I. Vogel, *J. Chem. Soc.*, **1948**, 1822.

13) Q. E. Thompson, M. M. Crutchfield, M. M. Dietrich, and E. Pierron, *J. Org. Chem.*, **30**, 2692 (1965).

14) L. F. Fieser and M. Fieser, "Reagents for Organic Syntheses," Vol. 1, John Wiley, New York (1967), p. 1152.

15) "Organic Syntheses," Coll. Vol. 3, p. 116.

16) Q. E. Thompson, *Quart. Reports on Sulfur Chem.*, **5**, 258 (1970).

17) W. Ando, T. Yagihara, S. Tozune, I. Imai, J. Suzuki, T. Toyama, S. Nakaido, and T. Migita, *J. Org. Chem.*, **37**, 1721 (1972).

Synthesis and Substitution of 1,3,4,6-Tetra-substituted-3,6-dihalogeno-2,5-piperazinediones

Juji YOSHIMURA, Yuichi SUGIYAMA, and Hiroshi NAKAMURA

Laboratory of Chemistry for Natural Products, Faculty of Science, Tokyo Institute of Technology, Meguro-ku, Tokyo 152

(Received April 25, 1973)

Addition of chlorine to 3,6-dimethylene- (**3**) and 3,6-dibenzylidene-1,4-dimethyl-2,5-piperazinediones gave isomers of the corresponding tetrachloride, and substitution of 1,3,4,6-tetramethyl-2,5-piperazinedione with bromine also gave tetrabromide (**2**) of the same type *via* successive elimination and addition reactions. Treatment of **2** with water and with methanolic sodium acetate gave the corresponding 3,6-dihydroxy and dimethoxy derivatives, respectively, while treatment with sodium iodide, sodium sulfide, sodium thiocyanate, or sodium thioacetate gave only **3** and sulfur in a good yield. Similar results were obtained in the case of octahydro-5*H*,10*H*-dipyrrolo[1,2-*a*: 1′,2′-*d*]pyrazine-5,10-dione. However, bromination of 6,13-dioxo-6a,7,13a,14-tetrahydro-6*H*,13*H*-pyrazino[1,2-*a*: 4,5-*a*′]diindole gave rise only to aromatization. Configurations of the isomers obtained and the reaction processes were discussed.

3,6-Epidithio-2,5-piperazinedione skeleton is a unique partial structure of a class of antibiotics such as gliotoxin,[1] sporidesmin,[2] and others.[3,4] A few homologues were synthesized by substitution of the halogeno group of 3,6-dihalogeno-2,5-piperazinediones, having no alkyl substituents at 3- and 6-positions, with the mercapto group followed by intramolecular disulfide-ring formation.[5-7] In order to clarify the limitation of this synthetic route, synthesis and reactivity of 3,6-dihalogeno-2,5-piperazinediones were examined.

Results and Discussion

Bromination of *meso* or *racemic* 1,3,4,6-tetramethyl-2,5-piperazinedione (**1a** and **1b**) in benzene, newly obtained by condensation of two moles of *N*-methylalanine,[8] gave one isomeric 3,6-dibromo-3,6-bis(bromomethyl)-1,4-dimethyl-2,5-piperazinedione (**2**) and HBr_3 adduct of **1** which gave **1** in water with liberation of bromine. Treatment of **2** with sodium iodide gave 3,6-dimethylene-1,4-dimethyl-2,5-piperazinedione (**3**) in a good yield, which was reversely converted into **2** by addition of bromine. Bromo functions at 3- and 6-positions in **2** were selectively converted into hydroxy (**4**) or methoxy (**5**) groups in aqueous ethanol or methanolic sodium acetate, whereas attempted substitution with acetylthio, methylthio, mercapto, or cyanothio groups gave only **3** and sulfur. Similarly, substitution of octahydro-5*H*,10*H*-dipyrrolo[1,2-*a*: 1′,2′-*d*]pyrazine-5,10-dione[9] with bromine in benzene gave 1,5a,6,10a-tetrabromo-octahydro-5*H*,10*H*-dipyrrolo[1,2-*a*: 1′,2′-*d*]-pyrazine-5,10-dione (**6**) and HBr_3 adduct of the starting material. Treatment of **6** with methanol or sodium acetate in acetic acid gave 1,6-dibromo-5a,10a-dimethoxy-octahydro-5*H*,10*H*-dipyrrolo[1,2-*a*: 1′,2′-*d*]-pyrazine-5,10-dione (**7**) and 1,6-dibromo-2,3,7,8-tetrahydro-5*H*,10*H*-dipyrrolo[1,2-*a*: 1′,2′-*d*]pyrazine-5,10-dione (**8**), respectively. However, treatment of **6** with potassium iodide gave a mixture of **8** and its mono and di-debrominated compounds. Furthermore, bromination of 6,13-dioxo-6a,7,13a,14-tetrahydro-6*H*,13*H*-pyrazino[1,2-*a*: 4,5-*a*′]diindole (**9**) in methanol, obtained from two moles of ethyl 2-indoline-carboxylate,[10] deposited selectively the corresponding 2,9-dibromo derivative (**10**) in 79% yield, the position of their bromo groups being determined from the splitting of magnetically equivalent H_4 and H_{11} (δ 7.96, J=8.5 Hz) appearing in the lowest magnetic field in the NMR spectrum and characteristic absorptions (825—835 cm^{-1}) in the IR spectrum. Further bromination of **10** in chloroform gave exclusively 2,9-dibromo-6,13-dioxo-6*H*,13*H*-pyrazino[1,2-*a*: 4,5-*a*′]diindole (**11**).

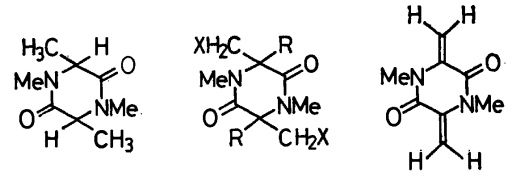

(**1**) a:
b:

(**2**) X=R=Br
(**4**) X=Br, R=OH
(**5**) X=Br, R=OMe

(**3**)

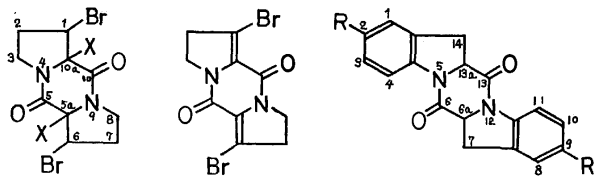

(**6**) X=Br
(**7**) X=OMe

(**8**)

(**9**) R=H
(**10**) R=Br

1) M. R. Bell, J. R. Johnson, B. S. Wildi, and R. B. Woodward, *J. Amer. Chem. Soc.*, **80**, 1001 (1958).
2) S. Safe and A. Taylor, *J. Chem. Soc., C*, **1970**, 432.
3) R. Nagarajan, L. L. Huckstep, D. H. Lively, D. C. DeLong, M. M. Marsh, and N. Neuss, *J. Amer. Chem. Soc.*, **90**, 2980 (1968).
4) D. Hauser, H. P. Weber, and H. P. Sigg, *Helv. Chim. Acta*, **53**, 1061 (1970); F. A. Anet and J. M. Muchowski, *Chem. Ind.*, **1963**, 81.
5) P. W. Trown, *Biochem. Biophys. Res. Commun.*, **33**, 402 (1968).
6) H. Poisel and U. Schmidt, *Chem. Ber.*, **104**, 1714 (1971).
7) S. G. Svokos and R. B. Angier., Ger. 2029305 (1971).
8) P. J. Fodor, V. E. Price, and J. P. Greenstein, *J. Biol. Chem.*, **180**, 193 (1949).
9) J. Kapthammer and A. Matthes, *Z. Physiol.*, **223**, 43 (1934).
10) E. J. Corey, R. J. McCaully, and H. S. Sachdey, *J. Amer. Chem. Soc.*, **92**, 2476 (1970).

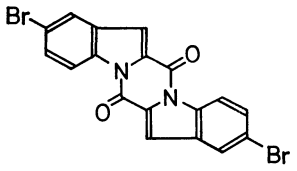

(11)

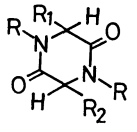

(14) $R=CH_3$, $R_1=R_2=SCH_3$
(15) $R=H$, $R_1=R_2=CH_3$
(16) $R=H$, $R_1=CH_3$, $R_2=CH_2CH(CH_3)_2$

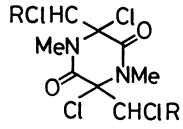

(12a—d) $R=C_6H_5$
(13) $R=H$

On the other hand, simple halogenation of 3,6-dibenzylidene-1,4-dimethyl-2,5-piperazinedione[11] or **3** with sulfur dichloride in the presence of zinc chloride or chlorine gave 3,6-bis(α-chlorobenzyl)- (**12**) and 3,6-bis(chloromethyl)-3,6-dichloro-1,4-dimethyl-2,5-piperazinedione (**13**), respectively. Although each compound from **2** to **10** consisted of only one isomer, four isomers (**12a**—**d**) among the theoretically possible four *racemic* and two *meso* forms were separated by fractional crystallization in the former case, but, not the approximate 1 to 1 mixture of *racemic* and *meso* isomers in the latter.

Table 1. Proton chemical shifts in isomeric 2,5-piperazinediones

Compounds	Chemical shift (δ) of main protons			
	N–Me or N–H	C–Me	C–H	S–Me
14 *meso*	2.06	—	4.86	3.10
racemic	2.38	—	4.60	3.09
15 *meso*	7.72	1.22	4.00	—
(D, D)	7.92	1.25	3.98	—
16 *meso*	7.83	1.21	4.13	—
(L, L)	7.93	1.27	4.07	—
1b *meso*	2.94	1.52	3.95	—
1a *racemic*	2.94	1.49	3.89	—
12a	1.53, 2.65	—	5.83, 6.47	—
b	3.29	—	5.61	—
c	2.35, 3.58	—	5.67, 5.82	—
d	3.39	—	5.74	—

Meso and *racemic* 3,6-disubstituted-2,5-piperazinediones were deduced by X-ray analysis[12] to have planar and skewed boat conformations, respectively. They do not seem to be distinguishable by NMR technique, but a comparison of NMR data of both isomers of 1,4-dimethyl-3,6-bis(methylthio)- (**14**),[6] 3,6-dimethyl- (**15**),[13] and 6-methyl-3-isobutyl-2,5-piperazinedione (**16**)[13] indicates that the chemical shift fo 3,6-hydrogens of *meso* form is usually greater (in δ) than that of the *racemic* or optically active form (Table 1). This was utilized to deduce the configuration of **1a** and **1b**, though such similarity is not observed in the C-methyl groups.

11) M. O. Forster and W. B. Saville, *J. Chem. Soc.*, **121**, 816 (1922).
12) E. Sletten, *J. Amer. Chem. Soc.*, **92**, 172 (1970).
13) A. Chemizard and S. David, *Bull. Soc. Chim. Fr.*, **1966**, 184.

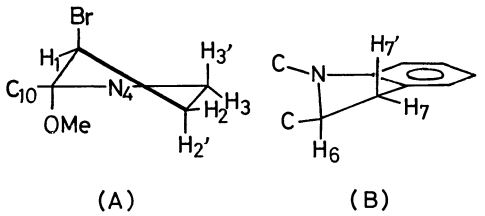

(A) (B)

Fig. 1. Conformation of the five-membered rings in **6** and **7** (A), and in **9** and **10** (B).

NMR data of **12a**—**d** indicate that they are certainly isomers to each other, although their configurations could not be determined.

On the other hand, coupling constants of protons in the five-membered ring of **7** and **9** ascertained by simulation indicated that they exist in twist and flattened envelope conformation, as shown in Fig. 1(A) and (B), respectively. Conformation (A) suggests that **7** is the *meso* isomer with planar 2,5-piperazinedione skeleton. The five-membered ring in *N*-acyl-indoline derivatives exists in a planar conformation,[14] but conformation (B) in **9** might be attributed to the condensed planar benzene ring.

The fact that tetrabromides (**2** and **6**) were obtained by simple substitution with bromine and that the former was also produced by addition reaction indicates that the substitution of 3,6-dialkyl-2,5-piperazinediones with bromine is usually followed by elimination of hydrogen bromide and re-addition of bromine, even though bromine was used in a smaller amount than stoichiometric. Exceptional formation of the elimination product **11** from **10** would be attributed to the resonance stabilization of the indole moiety. In all successful syntheses of 3,6-epidithio-2,5-piperazinediones *via* the corresponding 3,6-dibromo derivatives,[5-7] the bromides included only 3,6-substituents having no hydrogen at α-position such as the phenyl group. Easy elimination of hydrogen bromide would be due to the polarized structure of 3,6-dibromo derivatives (**17**) stabilized by mesomeric resonance of immonium and carbonium ions[6] (Fig. 2).

The fact that attempted substitution of **2** with sulfur-containing nucleophiles gave sulfur and **3** would be

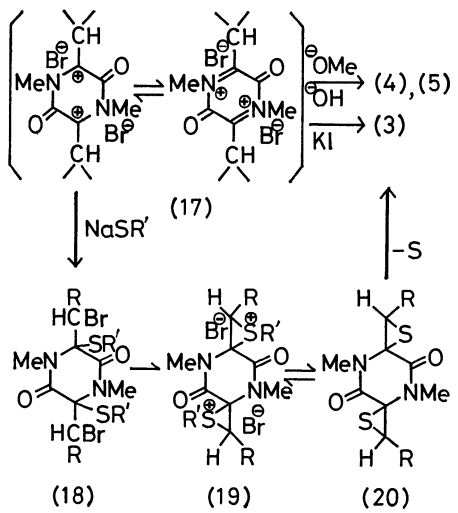

(18) (19) (20)

Fig. 2. Possible passways in substitution of **2**.

due to the character of sulfur atom and the presence of the vicinal bromine atom. Compounds (**18**) once substituted would easily shift to the spiro-type thiiranium ions (**19**). It is well-known that the sulfonium halides frequently decompose to thioether and other products depending on the conditions,[14] especially smoothly in alcohols,[15] and that ethylenesulfides having aromatic substituents such as diphenylene-dichloroethylenesulfide turned to the corresponding olefin and sulfur, even under cooling.[16] Thus, it could be concluded that **19** was smoothly transformed into **3** through the corresponding spiro-sulfide (**20**) with liberation of sulfur (Fig. 2).

Experimental

All the melting points are uncorrected. The solutions were evaporated under reduced pressure at a bath temperature not exceeding 60 °C. The infrared spectra were measured in KBr discs with a Hitachi EPI-G2 spectrometer. The NMR spectra were obtained at 100 MHz with a JNM-4H-100 spectrometer in deuteriochloroform unless otherwise stated, using TMS as an internal reference. Chemical shifts and coupling constants were recorded in δ and Hz units, and frequencies in cm^{-1}.

*1,3,4,6-Tetramethyl-2,5-piperazinedione (**1a** and **1b**).* A suspension of *N*-methylalanine (10 g, 59 mmol) in ethyleneglycol (10 g) was heated at 180—190 °C for 6 hr on an oil bath, poured into water (100 ml) and extracted with three portions of chloroform (100 ml). The combined extracts were dried over sodium sulfate and evaporated to give a sirup, which was fractionated on a silica gel column (WAKO-GEL C-200) by elution with chloroform–ligroin (3:1) to give **1a** (2.2 g, 44%) and **1b** (1.2 g, 24%) which were recrystallized from ether. Mp **1a**: 121—123 °C, **1b**: 135—136 °C. IR: **1a**: 1640 (NC=O), **1b**: 1630 (NC=O).

Found: C, 56.47; H, 8.24; N, 15.93%. Calcd for $C_8H_{14}N_2O_2$: C, 56.45; H, 8.29; N, 16.46%.

*3,6-Dibromo-3,6-bis(bromomethyl)-1,4-dimethyl-2,5-piperazinedione (**2**).* Bromine (0.7 ml, 13.3 mmol) was added to a solution of **1a** (1 g, 5.9 mmol) in dried benzene (50 ml) and kept at room temperature for 24 hr to give a yellow precipitate, which was filtered and washed with dried benzene. The precipitate was deduced to be a HBr_3 adduct of **1a** from analytical data (Found: C, 23.38; H, 3.80; N, 6.87; Br, 57.81%. Calcd for $C_8H_{15}N_2O_2Br_3$: C, 23.38; H, 3.68; N, 6.82; Br, 58.34%) and from the fact that treatment of the adduct with saturated sodium bicarbonate and sodium sulfite followed by extraction with chloroform gave **1a** in 66% recovery. Evaporation of the filtrate from the adduct gave a white precipitate of **2** (500 mg, 18%) which was washed with ethanol and recrystallized from chloroform. Mp 185—188 °C (decomp.); NMR: 3.22 ($N-CH_3$), 4.03 and 4.74 (CH_2: ABq, J=11.0). IR: 1700 (C=O).

Found: C, 19.97; H, 2.15; N, 5.80; Br, 65.62%. Calcd for $C_8H_{10}N_2O_2Br_4$: C, 19.78; H, 2.07; N, 5.77; Br, 65.77%.

*1,4-Dimethyl-3,6-dimethylene-2,5-piperazinedione (**3**).* A suspension of **2** (1 g, 2.1 mmol) and sodium iodide (2 g, 13 mmol) in ethanol (20 ml) was stirred at room temperature for 1 day and then evaporated. The residue was treated with chloroform (50 ml) and aqueous sulfite. The chloroform layer was washed with water and evaporated to give white needles which were recrystallized from ethanol. Yield, 320 mg (90%). Mp 230 °C (decomp.). NMR: 3.31 (N-Me), 4.98 and 5.87 (CH_2; ABq, J_{gem}=2.0). IR: 1600 (C=C), 1670 (NC=O).

Found: C, 58.23; H, 6.08; N, 17.09%. Calcd for $C_8H_{10}N_2O_2$: C, 57.82; H, 6.07; N, 16.86%.

*3,6-Bis(bromomethyl)-3,6-dihydroxy-1,4-dimethyl-2,5-piperazinedione (**4**).* A suspension of **2** (1 g, 2.1 mmol) in 50 ml of 50% ethanol was stirred at 70 °C for 2 days and then evaporated. The residue was triturated and recrystallized from methanol to give white crystals. Yield, 230 mg (35%); Mp 230 °C (decomp.); NMR (CF_3COOH): 3.15 (N-Me), 3.68 and 3.88 (CH_2; ABq, J_{gem}=11.5). IR: 1640 (NC=O), 3260 (OH).

Found: C, 26.61; H, 3.30; N, 7.68; Br, 43.95%. Calcd for $C_8H_{12}N_2O_4Br_2$: C, 26.68; H, 3.36; N, 7.78; Br, 44.40%.

*3,6-Bis(bromomethyl)-3,6-dimethoxy-1,4-dimethyl-2,5-piperazinedione (**5**).* A suspension of **2** (1 g, 2.1 mmol) and sodium acetate (1 g, 12 mmol) in methanol (50 ml) was stirred at room temperature for 10 hr and then evaporated. The residue was extracted with chloroform. Evaporation of the extracts gave crystals (700 mg, 86%) which were recrystallized from chloroform–ligroin. Mp 165 °C (decomp.); NMR: 3.00 (OMe), 3.20 (NMe), 3.52 and 4.10 (CH_2: ABq, J_{gem}=11.3). IR: 1670 (NC=O).

Found: C, 31.40; H, 3.91; N, 7.16%. Calcd for $C_{10}H_{16}N_2O_4Br_2$: C, 30.95; H, 4.16; N, 7.22%.

*1,5a,6,10a-Tetrabromo-octahydro-5H,10H-dipyrrolo[1,2-a: 1',2'-d]pyrazine-5,10-dione (**6**).* Bromine (0.7 ml, 13.3 mmol) was added to a dried benzene (50 ml) solution of L-proline anhydride (1 g, 5.1 mmol) and allowed to stand at room temperature for 1 day. Yellow precipitates which appeared were treated with saturated sodium bicarbonate and sodium sulfite to give insoluble white powder. A second crop was obtained from the first filtrate by evaporation and washing the residue with ethanol (5 ml). Total yield, 500 mg (19%). Unchanged starting material (700 mg) was recovered from the aqueous filtrate by extraction with chloroform (100 ml). Mp 183—185 °C (decomp.); IR: 1690 (NC=O).

Found: C, 23.18; H, 1.94; N, 5.29%. Calcd for $C_{10}H_{10}N_2O_2Br_4$: C, 23.56; H, 1.98; N, 5.49%.

*1,6-Dibromo-5a,10a-dimethoxy-octahydro-5H,10H-dipyrrolo[1,2-a: 1',2'-d]pyrazine-5,10-dione (**7**).* A solution of **6** (400 mg, 0.78 mmol) and sodium acetate (400 mg, 4.9 mmol) in methanol (50 ml) was refluxed for 8 hr, evaporated, and the residue was extracted with chloroform (50 ml). Evaporation of extracts gave a sirup which was crystallized from ethanol. Yield, 115 mg (36%); mp 267—268 °C; NMR: 2.28 (H_2 and H_7; oct), 2.71 ($H_{2'}$ and $H_{7'}$; nine peaks, $J_{2,2'}=J_{7,7'}=14.4$), 3.35 (OMe; s), 3.61 (H_3 and H_8; oct, $J_{2,3}=J_{7,8}=1.7$, $J_{2',3}=J_{7',8}=9.6$), 4.03 ($H_{3'}$ and $H_{8'}$; oct, $J_{2,3'}=J_{7,8'}=8.0$, $J_{2',3'}=J_{7',8'}=10.0$, $J_{3,3'}=J_{8,8'}=12.5$), 4.62 (H_1 and H_6; d, $J_{1,2'}=J_{6,7'}=4.6$). IR: 1660 (NC=O).

Found: C, 34.97; H, 3.79; N, 7.01; Br, 39.31%. Calcd for $C_{12}H_{16}N_2O_4Br_2$: C, 34.97; H, 3.91; N, 6.79; Br, 38.79%.

*1,6-Dibromo-2,3,7,8-tetrahydro-5H,10H-dipyrrolo[1,2-a: 1',2'-d]pyrazine-5,10-dione (**8**).* A solution of **6** (1 g, 2.1 mmol) and anhydrous sodium acetate (1 g, 12 mmol) in acetic acid (20 ml) was heated at 100 °C for 5 hr with stirring, evaporated, and the resulting residue was extracted with several portions of chloroform (50 ml). The extracts were mixed with ethanol

14) H. J. Emeleus and H. G. Heal, *J. Chem. Soc.*, **1946**, 1126; F. Krollpfeiffer and H. Hartmann, *Chem. Ber.*, **83**, 90 (1950); F. Krollpfeiffer, K. L. Schneider, and A. Wissner, *Ann. Chem.*, **566**, 139 (1950).

15) J. L. Gleave, E. D. Hughes, and C. K. Ingold, *J. Chem. Soc.*, **1935**, 236; E. D. Hughes, C. K. Ingold, and G. A. Maw, *ibid.*, **1948**, 2072; H. Böhme and P. Heller, *Chem. Ber.*, **36**, 443, 785 (1953).

16) H. Staudinger and J. Siegwart, *Helv. Chim. Acta*, **3**, 833, 840 (1920).

(10 ml), and concentrated to 5 ml, from which yellow powder was precipitated on standing in a refrigerator. It was recrystallized from ethanol. Yield, 100 mg (27%). It decomposes gradually over 150 °C. NMR: 3.03 and 3.99 (CH_2-CH_2; each t, $J=9.0$). IR: 1650 (NC=O).

Found: C, 34.00; H, 2.19; N, 8.05; Br, 46.36%. Calcd for $C_{10}H_8N_2O_2Br_2$: C, 34.51; H, 2.32; N, 8.05; Br, 45.92%.

*6,13-Dioxo-6a,7,13a,14-tetrahydro-6*H,*13*H-*pyrazino*[*1,2*-a: *4,5*-a′]*diindole* (**9**). A suspension of ethyl 2-indolinecarboxylate[10] (10 g, 52 mmol) and sodium ethoxide (900 mg, 13 mmol) in dried benzene (70 ml) was refluxed for 24 hr, washed three times with water, and evaporated to give crystals which were recrystallized from benzene–ligroin. Yield, 6.13 g (81%). Mp 263—265 °C. MNR: 3.42 ($H_{7'}$ and $H_{14'}$; q), 3.78 (H_7 and H_{14}; q, $J_{7',7}=J_{14,14'}=17.1$), 4.95 (H_{6a} and H_{13a}; q, $J_{7',6a}=J_{14,13a}=11.0$, $J_{7,6a}=J_{14',13a}=9.2$). IR: 1670 (NC=O).

Found: C, 74.19; H, 4.97; N, 9.70%. Calcd for $C_{18}H_{14}N_2O_2$: C, 74.47; H, 4.86; N, 9.65%.

*2,9-Dibromo-6,13-dioxo-6a,7,13a,14-tetrahydro-6*H,*13*H-*pyrazino*[*1,2*-a: *4,5*-a′]*diindole* (**10**). A suspension of **9** (90 mg, 0.31 mmol) and bromine (1.0 g, 19.5 mmol) in methanol (80 ml) was stirred for 1 hr to give a white powder (120 mg, 79%) which was recrystallized from chloroform–ligroin. Mp 309 °C. NMR: 7.40 (H_1; s), 7.37 (H_3; d), 8.40 (H_4; d, $J_{3,4}=8.5$). Other proton signals are almost the same as for **9**. IR: 1670, 1700 (NC=O).

Found: C, 48.07; H, 2.56; N, 6.26%. Calcd for $C_{18}H_{12}N_2O_2Br_2$: C, 48.24; H, 2.89; N, 6.25%.

*2,9-Dibromo-6,13-dioxo-6*H,*13*H-*pyrazino*[*1,2*-a: *4,5*-a′]*diindole* (**11**). Excess bromine was added to a solution of **10** (300 mg, 1.3 mmol) in chloroform (60 ml) and allowed to stand at room temperature for 1 day to give yellow precipitates (260 mg, 87%). These were recrystallized from a large amount of chloroform to give fine yellow needles. Mp 359 °C (sublime). IR: 1687 (C=O).

Found: C, 48.28; H, 1.56; N, 6.23%. Calcd for $C_{18}H_8N_2O_2Br_2$: C, 48.68; H, 1.82; N, 6.31%.

3,6-Dichloro-3,6-bis(α-chlorobenzyl)-1,4-dimethyl-2,5-piperazinedione (**12a—d**). A solution of 3,6-dibenzylidene-1,4-dimethyl-2,5-piperazinedione (12 g, 38 mmol), sulfur dichloride (40 ml) and a catalytic amount of zinc chloride in dioxane (40 ml) was allowed to stand at room temperature for 2 days, and then poured into a mixed solution of saturated sodium sulfite and chloroform. The chloroform layer was evaporated, and the residual powder was recrystallized from chloroform–ligroin to give fine crystals (**12**). **12a** (3.46 g, 20%), **12b** and **12c** (6.45 g, 37%) were separated by fractional crystallization from chloroform–ligroin. Mp **12a**; 227 °C (decomp.), **12b**; 203—205 °C (decomp.), **12c**; 186 °C. IR: **12a**; 1675, **12b**; 1670, **12c**; 1680 (NC=O).

Found: **12a**; C, 52.15; H, 3.65; N, 5.95%. **12b**; C, 52.35; H, 3.77; N, 5.77%. **12c**; C, 52.30; H, 3.93; N, 6.09%. Calcd for $C_{20}H_{18}N_2O_2Cl_4$: C, 52.20; H, 3.94; N, 6.08%.

The other isomer (**12d**) was obtained as follows. A solution of 3,6-dibenzylidene-1,4-dimethyl-2,5-piperazinedione (5.0 g, 16 mmol) in sulfur dichloride (50 ml) containing chlorine was treated as above. The white powder (2.1 g) obtained was fractionally recrystallized from chloroform–ligroin to give **12d** (0.6 g, 8%) and **12b** (1.02 g, 14%). Mp **12d**; 183 °C. IR: 1682 (NC=O).

Found: C, 51.94; H, 3.76; N, 6.09%. Calcd for $C_{20}H_{18}N_2O_2Cl_4$: C, 52.20; H, 3.94; N, 6.08%.

3,6-Dichloro-3,6-bis(chloromethyl)-2,5-piperazinedione (**13**). A solution of **3** (100 mg, 0.92 mmol) in chloroform (10 ml) saturated with chlorine was left to stand for 30 min, and then evaporated to give a crude product (175 mg), which was recrystallized from chloroform to give white crystals. Yield, 110 mg (39%). Mp 150—200 °C.

Found: C, 31.63; H, 3.43; N, 9.07%. Calcd for $C_8H_{10}N_2O_2Cl_4$: C, 31.20; H, 3.27; N, 9.10%.

NMR spectrum of this compound showed the two methylene and *N*-methyl signals with intensity ratio of nearly 1 to 1, indicating a mixture of *meso* and *racemic* isomers.

The authors are indebted to the members of the Laboratory of Organic Analysis for the microanalysis and to Mr. H. Matsumoto for NMR measurements.

Crystal and Molecular Structure of ω-Amino Acids, ω-Aminosulfonic Acids and Their Derivatives. VI. The Crystal and Molecular Structure of DL-γ-Amino-β-hydroxybutyric Acid (GABOB), A Nervous Inhibitory Chemical Transmitter

Ken-ichi TOMITA, Masahiro HARADA, and Takaji FUJIWARA

Faculty of Pharmaceutical Sciences, Osaka University, Toneyama, Toyonaka, Osaka 560

(Received May 1, 1973)

DL-γ-Amino-β-hydroxybutyric acid (GABOB), $C_4H_9O_3N$, forms monoclinic plate crystals of space group $P2_1/c$, with $a=7.43$, $b=8.29$, $c=9.34$ Å, $\beta=110.9°$, and four molecules in the unit cell. Intensity data were collected by a film method. The structure was solved by the direct method with the symbolic addition procedure, and refined by least-squares methods to $R=0.096$. GABOB molecule having the zwitterionic structure, NH_3^+-CH_2-CH(OH)-CH_2-COO^-, forms *trans-zigzag* skeletal conformation with an intramolecular OH···O hydrogen bond of 2.773 Å, and contacts with each other by three dimensional network of NH···O and OH···O hydrogen bonds.

Using chloroxypropylphthalimide as a starting material, γ-amino-β-hydroxybutyric acid (GABOB) has been originally synthesized by M. Tomita[1] in 1923, and the optical and stereo-isomers were isolated by treatment with brucin and by difference in solubility. In order to characterize these isomers, some physicochemical investigations have been carried out and the hypothetical structures, an intramolecular hydrogen bonded form and an extended one, were proposed.[2] However, the crystal structure has not yet been determined. The chemical structure of vitamin B_T, L-carnitine, which acts as a growth factor for some insects,[3] was identified as L-γ-trimethyl-β-hydroxybutyrobetaine,[4] a trimethyl-derivative of GABOB, and the crystal structure of its hydrochloride is now solved in our laboratory.[5] Moreover, it is of most interest that GABOB is also a potent inhibitory chemical transmitter[6] in central nervous system as well as γ-aminobutyric acid (GABA) of which crystal structure was recently elucidated.[7]

In a previous paper,[8] we reported briefly about some structural features of GABOB, and this paper deals with the detailed structure analysis of this compound and the comparison of its molecular structure with those of other related compounds.

Experimental

A sample of DL-γ-amino-β-hydroxybutyric acid (GABOB) was kindly supplied by Prof. A. Musashi, Kobe Women's College of Pharmacy, Kobe. GABOB crystallizes as transparent plates from *N,N*-dimethylformamide solution by slow evaporation at room temperature. Weissenberg and precession photographs indicated the crystal to be monoclinic.

Table 1. CRYSTAL DATA FOR GABOB

$C_4H_9O_3N$	F.W.=119.1
Monoclinic	Space group $P2_1/c$
$a=7.43(1)$ Å	$Z=4$
$b=8.29(1)$	$D_m=1.45$ g cm^{-3}
$c=9.34(2)$	$D_c=1.47$ g cm^{-3}
$\beta=110.9(2)°$	

Unit cell dimensions were determined from zero-layer Weissenberg photographs about the a and b axes which were calibrated with superimposed aluminum powder photographs. The systematic extinctions (*h0l*, $l=2n+1$; *0k0*, $k=2n+1$) indicated the space group to be $P2_1/c$. The density was measured by flotation in a mixture of benzene and carbon tetrachloride. The crystal data are given in Table 1. Intensity data by a crystal of approximate dimensions, $0.15\times0.03\times0.5$ mm, were obtained from multiple-film equi-inclination Weissenberg photographs taken around the a axis. Another additional data were collected on a Rigaku-Denki four-circle computer-controlled diffractometer, using Ni-filtered Cu$K\alpha$ radiation, which were only used for the scaling purpose of the former data. Altogether, 930 independent reflections were measured. Lorentz and polarization corrections were applied but absorption correction was neglected. The observed structure factors were adjusted to their absolute values by the usual procedure, then the normalized structure factors were calculated.

Structure Determination and Refinement

The structure of DL-GABOB was solved by the symbolic addition method using a computer program DPD. After three cycles of the symbolic addition procedure for 124 reflections with $|E|\geqq1.5$ and with probability greater than 97%, signs of 97 reflections were determined. Possible two E-maps were calculated, and one of which revealed clearly the correct peaks of GABOB molecule.

Refinement of the structure was carried out by a block-diagonal least-squares procedure, using a program BLLS with unit weight for non-zero reflections. Five cycles of refinement with the isotropic temperature factors for the non-hydrogen atoms reduced an *R* index ($R=\Sigma||F_o|-|F_c||/\Sigma|F_o|$) to 0.18. After the

1) M. Tomita, *Z. Physiol. Chem.*, **124**, 253 (1923).
2) M. Tomita, T. Tomita, and K. Tomita, *ibid.*, **316** 121 (1959).
3) G. Fraenkel, M. Blewett, and M. Coles, *Nature*, **161**, 981 (1948).
4) M. Tomita and Y. Sendju, *Z. Physiol. Chem.*, **169**, 263 (1927).
5) K. Tomita, K. Urabe, Y. B. Kim, and T. Fujiwara, This Bulletin, to be published.
6) T. Hayashi and K. Nagai, Proc. 20th Internatl. Physiol. Cong. p. 410 (1956).
7) K. Tomita, H. Higashi, and T. Fujiwara, This Bulletin, **46**, 2199 (1973).
8) K. Tomita, *Tetrahedron Lett.*, **1971**, 2587.

TABLE 2. FINAL POSITIONAL AND THERMAL PARAMETERS

All values $\times 10^4$ for O, N, C atoms; for H, position parameters $\times 10^3$. E.s.d.'s in parentheses are in units of least significant digit. Isotropic B's for H atoms in Å^2; for other atoms, the expression is: $\exp\{-(B_{11}h^2+B_{22}k^2+B_{33}l^2+B_{12}hk+B_{13}hl+B_{23}kl)\}$.

Atom	x	y	z	B_{11} or B	B_{22}	B_{33}	B_{12}	B_{13}	B_{23}
C1	6372(6)	1025(7)	2719(6)	23(7)	39(11)	80(7)	−9(13)	32(11)	4(13)
C2	4511(6)	1350(8)	1390(5)	40(8)	82(13)	59(6)	44(15)	27(11)	26(13)
C3	2907(6)	1866(7)	1952(5)	37(8)	64(12)	55(6)	13(14)	36(11)	17(12)
C4	1123(6)	2364(7)	620(5)	53(8)	30(11)	48(6)	44(14)	29(11)	22(11)
N	−252(5)	3159(6)	1210(5)	44(7)	47(10)	66(5)	22(12)	35(10)	20(11)
O1	7873(4)	830(6)	2391(5)	27(6)	104(9)	131(6)	64(11)	99(10)	82(12)
O2	6330(5)	868(6)	4032(4)	56(6)	152(10)	59(5)	28(12)	9(9)	25(10)
O3	2359(4)	575(5)	2717(4)	51(6)	58(8)	85(5)	24(10)	59(9)	81(10)
H1	480(9)	250(9)	80(8)	1.6					
H2	402(9)	35(9)	57(8)	1.6					
H3	341(9)	299(9)	278(8)	1.4					
H4	335(9)	4(9)	375(8)	1.7					
H5	166(9)	316(9)	11(8)	1.3					
H6	36(9)	139(9)	−9(8)	1.3					
H7	55(9)	407(9)	189(8)	1.4					
H8	−67(9)	241(9)	169(8)	1.4					
H9	−165(9)	343(9)	24(8)	1.4					

refinement with the anisotropic temperature factors for all the non-hydrogen atoms, a difference Fourier synthesis was calculated. The peaks of all nine hydrogen atoms, including three attached to the amino-nitrogen atom, were found at their proper positions. The further least-squares refinement including the hydrogen atoms with isotropic temperature factors was continued until all shifts in the atomic coordinates became less than 10% of the estimated standard deviation. The final R index was 0.096 (0.123 including $F_o=0$). The final positional and thermal parameters are listed in Table 2. A list of the observed and calculated structure factors is presented in Table 3.

All the numerical computations were done on an NEAC 2200—500 computer in the Computing Center of this University and an FACOM 230-60 in the Data Processing Center of Kyoto University, using the program written by Dr. T. Ashida and by the authors.

Results and Discussion

The bond lengths and angles of DL-GABOB are shown in Fig. 1. The bond lengths and angles of the main chain are essentially the same as the corresponding ones of γ-aminobutyric acid (GABA).[7] The C3-O3 bond length of β-hydroxyl group, 1.425 Å, corresponds

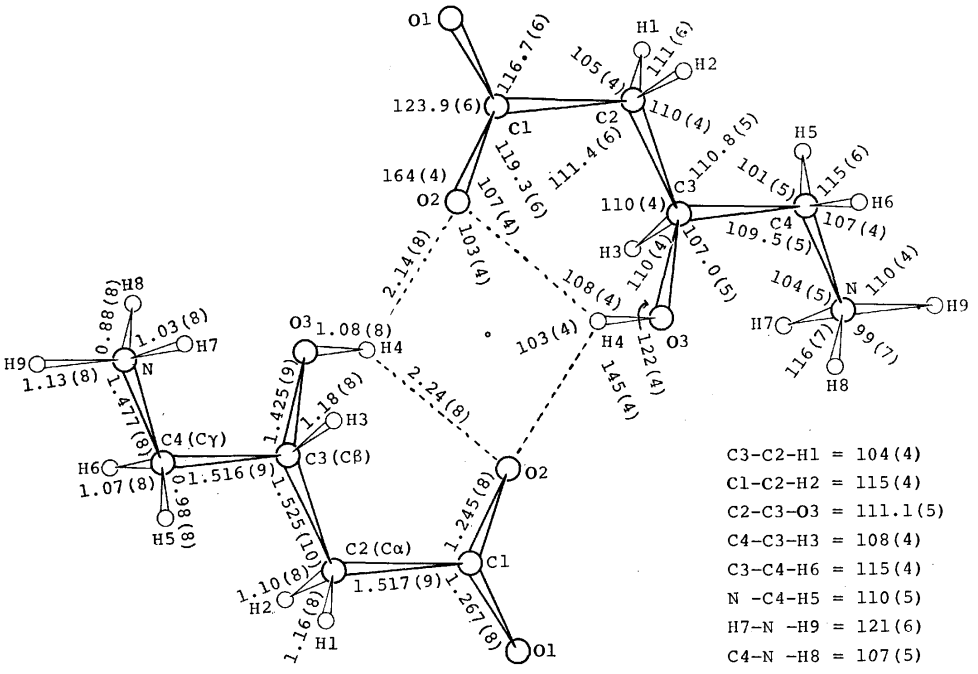

Fig. 1. Bond distances (Å) and bond angles (°). The estimated standard deviations are shown in parentheses. The broken lines indicate the hydrogen bonds.

TABLE 3. OBSERVED AND CALCULATED STRUCTURE FACTORS ($\times 10$)
Reflections marked * were omitted from the least-squares refinement.

L	FO	FC	L	FO	FC	L	FO	FC	L	FO	FC	L	FO	FC	L	FO	FC	L	FO	FC
K,K= 0	0		2	262	-251	-11	35	39	5	41	-42	-3*	0	0	-11	30	-24	1	122	-116	0	59	-57	-8	87	-73
2	566	-584	3	112	111	H,K=	5	1	6*	0	-13	-4	50	64	H,K=	4	3	2	29	23	1	301	-336	-9	93	83
4	66	61	4	157	-138	-1	152	150	7	35	-50	-5	94	98	-1	62	-44	3	76	-74	2	89	-69	H,K=	7	5
6	288	-279	5	50	42	-2*	0	8	H,K=	6	2	-6	14	-21	-2	184	174	4*	0	-14	3	124	120	-1	22	-25
8	97	88	6	131	-71	-3	93	75	0	60	-57	-7	7	-58	-3	47	48	5	36	-35	4	83	-93	-2	40	-44
10*	0	5	7	119	-156	-4	23	-26	1	38	26	H,K=	0	3	-4	75	65	6	26	21	5	50	-55	-1*	0	-5
H,K=	1	0	8*	0	148	-5	44	50	2	69	-61	1*	0	5	-5	141	-147	H,K=	6	4	6	55	46	-4	83	78
0	71	-53	9*	0	13	-6	116	-126	3	43	-39	2	296	339	-6*	0	22	0	59	-55	7	69	69	-5	32	33
2	168	-147	H,K=	2	1	-7	68	-76	4	49	-54	3	82	88	-7	47	46	1	20	-15	8*	0	-7	-6	15	-13
4	81	-73	0	117	-107	-8	40	21	5	63	61	4	87	95	-8	71	-78	2	38	24	9	59	-48	-7	19	-20
6	27	18	1	73	-57	-9*	0	-17	H,K=	7	2	5	121	-110	-9	41	37	3	59	-63	H,K=	2	5	-8	38	-33
8*	0	-3	2	338	-369	-10	41	44	0	161	-175	6	83	95	-10	29	-22	4	37	28	0	177	-161	H,K=	8	5
10	41	32	3	104	-95	-11*	0	10	1	85	82	7	25	28	-11	41	-32	H,K=	7	4	1	52	-29	-1	33	25
H,K=	2	0	4	78	-77	H,K=	6	1	2	38	30	8	135	-137	H,K=	5	3	0	72	70	2	16	-2	-2	11	22
0	316	-269	5	44	-42	-1	224	-226	3	32	23	9	53	41	-1*	0	-6	1*	0	192	3	105	101	-3	41	33
2	786	792	6	195	217	-2	81	-77	4	56	-54	10*	0	2	-2	62	58	2	28	15	4	76	71	-4	81	73
4	496	-494	7	57	65	-3	50	40	H,K=	8	2	H,K=	1	3	-3	175	-164	3	108	-126	5	19	16	-5	106	-112
6	63	54	8	38	18	-4	97	-81	0	17	36	0	339	358	-4	48	43	H,K=	8	4	6	54	-58	-6	10	-13
8	56	-53	9	34	44	-5*	0	3	1	24	-23	1	159	150	-5	114	110	0	24	23	7*	0	-23	H,K=	0	6
10	25	34	10*	0	-37	-6	91	-112	2	58	-96	2	15	8	-6	168	171	H,K=	1	4	8	67	56	1*	0	-13
H,K=	3	0	H,K=	3	1	-7	25	35	H,K=	1	2	3	83	-93	-7*	0	1	-1	109	99	H,K=	3	5	2	105	91
0	182	196	0	54	53	-8*	0	6	-1	549	-633	4	71	57	-8*	0	-9	-2	61	-64	0	40	28	3	77	90
2	200	-204	1	70	-51	-9*	0	1	2	267	-279	5	143	-147	-9*	0	-6	3	159	-151	1	30	22	4	144	-140
4	175	-181	2	98	-86	-10	24	29	-3	149	-137	6	147	-133	-10	38	-46	-4	23	-10	2*	0	-13	5	96	-100
6	79	-77	3	43	42	-11*	0	-2	-4	243	246	7	152	148	-11	23	-27	-5	101	100	3	132	-128	6	174	169
8	83	69	4	67	76	H,K=	7	1	-5	213	216	8	53	49	H,K=	6	3	-6*	0	-6	4	27	34	7	65	-55
H,K=	4	0	5	136	150	-1	62	71	-6	96	-87	9*	0	-6	-1	173	157	-7	94	-101	5	46	28	8*	0	15
0	93	75	6	36	30	-2	166	160	-7	97	88	10*	0	4	-2	135	-126	8	29	29	6	17	14	9	49	46
2	194	-202	7	24	-16	-3	36	36	-8	19	28	H,K=	2	3	-3	116	-111	-9	59	64	7	34	-34	H,K=	1	6
4	97	101	8	14	2	-4	36	-34	-9	41	-30	0	144	-133	-4	17	22	-10	79	-59	H,K=	4	5	0	68	45
6	77	-73	9	82	-88	-5	97	-86	-10*	0	-1	1	61	48	-5	35	15	H,K=	2	4	0	59	-48	1	47	-49
8	145	126	H,K=	4	1	-6	47	-43	-11	65	-64	2	58	46	-6	30	-23	-1*	0	-3	1	171	-171	2	44	37
H,K=	5	0	0	28	13	-7	59	-60	H,K=	2	2	3	108	-49	-7	64	43	-2	189	183	2	58	60	3*	0	-15
0	195	182	1	82	67	-8	59	-61	-1	263	-238	4	108	115	-8	116	107	-3	219	228	3	33	-42	4	100	78
2*	0	0	2	90	-76	-9	44	45	-2	66	54	5	59	59	-9	20	15	-4	145	155	4	46	48	5*	0	-1
4	41	57	3	29	21	-10*	0	3	-3	77	57	6*	0	7	-10*	0	-9	-5	267	-285	5	112	119	6	95	-77
6	33	-29	4	47	-50	H,K=	8	1	-4	213	-204	7	60	-57	H,K=	7	3	-6	39	-27	6	34	31	7*	0	-23
H,K=	6	0	5	70	-66	-1*	0	2	-5	171	-163	8	26	18	-1	103	-98	-7*	0	4	H,K=	5	5	8	55	61
0	41	-33	6	77	73	-2	39	43	-6	83	65	9	41	37	-2	34	-27	-8	78	-79	0*	0	1	H,K=	2	6
2	153	159	7	29	-30	-3	46	43	-7	25	6	H,K=	3	3	-3	42	33	-9*	0	1	1*	0	8	0	185	164
4	114	-115	8	101	109	-4	23	-26	-8	53	-53	0	108	119	-4	110	105	-10	27	24	2	71	78	1	115	103
6*	0	21	H,K=	5	1	-5	39	42	-9	98	92	1	150	136	-5*	0	-7	H,K=	3	4	3	36	32	2	102	-96
H,K=	7	0	0	109	-99	-6*	0	-1	-10	58	55	2	186	182	-6*	0	-8	-1	16	-17	4	32	32	3*	0	-17
0	119	-124	1	266	-270	-7*	0	3	-11	47	-37	3*	0	-1	-7	95	81	-2	108	-103	5	12	12	4*	0	38
2	127	140	2	128	126	-8	68	74	H,K=	3	2	4*	0	-5	-8	31	-27	-3	345	339	H,K=	6	5	5*	0	17
4*	0	-2	3	44	33	-9	74	-81	-1	305	-265	5	97	-98	-9	37	-37	-4	84	81	0*	0	-22	6*	0	-35
H,K=	8	0	4*	0	-7	H,K=	9	1	-2	347	323	6	125	-124	H,K=	8	3	-5	197	-210	1	113	-128	H,K=	3	6
0	104	108	5*	0	1	-2	40	41	-3	191	175	7	16	-9	-1	37	-42	-6	123	130	2	69	74	0	63	66
2	91	77	6	78	89	-3	49	-46	-4	230	-228	8	101	-93	-2	81	-90	-7	51	52	3*	0	-6	1*	0	22
H,K=	1	0	7	91	88	-4	11	17	-5	117	110	H,K=	4	3	-3	20	-27	-8	51	54	4	61	58	2	90	94
-2	465	482	H,K=	6	1	-5	32	-32	-6*	0	6	0	37	35	-4	54	-57	-9	51	-56	H,K=	7	5	3*	0	-30
-4	240	225	0	332	324	-6	40	-40	-7	77	69	1	98	80	-5*	0	-2	-10	72	-63	0	98	80	4*	0	0
-6	37	-16	1	114	114	-7	18	6	-8	135	-137	2	99	-85	-6	53	59	H,K=	4	4	1	89	-64	5	38	52
-8	29	-21	2	48	-47	H,K=	0	2	-9	184	-190	3	24	-10	-7	46	49	-1	141	139	H,K=	1	5	6	47	67
-10	97	-92	3*	0	1	1	771	-803	-10	44	47	4	117	-135	-8	32	45	-2	52	-26	-1	156	162	7*	0	0
H,K=	2	0	4	22	-26	2	327	-320	-11	96	86	5	46	-44	H,K	9	3	-3	142	-127	2	98	92	H,K=	4	6
-2	226	200	5	44	58	3	259	264	H,K=	4	2	6*	0	1	-2	36	56	-4	47	37	-3	14	17	0	132	130
-4	451	-437	6*	0	-19	4	215	203	-1	47	-31	7	44	36	-3	51	-75	-5	56	50	-4	61	-55	1	124	-145
-6	218	219	H,K=	7	1	5	199	-190	-2	41	-34	H,K=	5	3	-4	58	-78	-6	83	-80	-5	129	134	2	91	111
-8	179	165	0	50	53	6	122	-115	-3	232	-216	0	264	-267	-5	59	86	-7	29	-33	-6	72	74	3	142	195
-10	104	-106	1	53	48	7	110	102	-4	213	193	1	173	168	-6	39	-57	-8	82	86	-7	39	-31	4	30	-67
H,K=	3	0	2	75	-79	8	103	93	-5	23	-29	2	56	46	H,K=	0	4	-9	53	51	-8	18	19	5*	0	-59
-2	266	255	3	115	-119	9*	0	6	-6	116	-116	3*	0	-11	1	394	-414	-10	41	50	-9	119	-90	H,K=	5	6
-4	162	-166	4	29	31	10*	0	1	-7	180	182	4*	0	7	2	164	180	-11*	0	16	-10*	0	13	0	68	-66
-6	88	85	H,K=	8	1	11*	0	11	-8	60	-60	5	52	-48	3	88	76	H,K=	5	4	H,K=	2	5	1*	0	50
-8	92	-95	0*	0	7	H,K=	1	2	-9	45	-31	6	24	21	4	16	13	-1	385	368	-1	170	-166	2*	0	48
-10	157	167	1	107	-128	0	351	-317	-10	16	-24	H,K=	6	3	5	134	-134	-2	20	-7	-2	94	-89	3*	0	10
H,K=	4	0	2	93	101	1	140	150	-11	32	-33	0	117	102	6*	0	3	-3	197	-184	3	146	145	H,K=	6	6
-2	347	-371	H,K=	1	1	2	87	-67	H,K=	5	2	1	55	-44	7	211	217	-4	54	-35	-4	53	47	0*	0	53
-4	35	26	-1	86	-89	3	298	275	-1	112	109	2	61	-65	8	94	-98	-5	84	84	-5	31	-19	1*	0	65
-6	301	311	-2	226	240	4	20	21	-2	121	-103	3	31	24	9	70	-63	-6	117	122	-6	132	147	2*	0	60
-8*	0	0	-3	54	54	5*	0	-13	-3	138	-120	4*	0	6	10	0	-16	-7	105	-123	-7	27	25	H,K=	1	6
-10	38	-38	-4	144	127	6	217	198	-4	205	188	5	31	-29	H,K=	1	4	-8	62	-65	-8	32	-23	-1	84	45
H,K=	5	0	-5	80	-87	7	76	-73	-5	206	208	H,K=	7	3	0	222	221	-9	82	100	-9*	0	3	-2	36	-30
-2	293	-315	-6	101	-91	8	37	-30	-6	150	-165	0	61	-63	1	50	-42	-10	31	34	-10*	0	5	-3	57	-39
-4	48	33	-7*	0	-5	9	23	19	-7	259	-282	1	64	64	2	64	57	H,K=	6	4	H,K=	3	5	-4	194	-199
-6	224	-235	-8	36	36	10*	0	3	-8*	0	4	2	110	-118	3	130	-119	-1	66	-60	-1	42	32	-5	67	52
-8	318	383	-9	40	32	H,K=	2	2	-9	104	106	3	64	55	4	124	-111	-2	29	-21	-2	157	-147	-6	34	33
-10	69	-74	-10*	0	4	0	379	-365	-10	38	-42	H,K=	8	3	5	230	239	-3	135	122	-3	79	60	-7*	0	-5
H,K=	6	0	-11	34	36	1	574	582	-11	23	-30	0	82	-88	6	72	-75	-4	107	-95	-4	39	-41	-8	67	61
-2	90	-66	H,K=	2	1	2	233	235	H,K=	6	2	1	76	95	7	66	-59	-5	72	-62	-5	93	93	-9	88	72
-4	37	-5	-1	170	169	3	340	-357	-1	123	-95	H,K=	1	3	8	38	-32	-6	41	-31	-6*	0	-3	H,K=	2	6
-6*	0	-19	-2	68	77	4	105	89	-2	272	226	-1	147	161	9	21	-18	-7	55	40	-7	108	-106	-1	207	-228
-8*	0	-1	-3	128	106	5	112	106	-3	37	-38	-2	77	-64	H,K=	2	4	-8	89	72	-8	109	109	-2	119	-101
-10*	0	6	-4	29	27	6	134	141	-4	18	15	-3	269	-286	0	38	36	-9*	0	12	-9	43	36	-3	66	57
H,K=	7	0	-5	99	99	7	123	-116	-5	144	122	-4	25	-4	1	256	273	-10	28	35	H,K=	4	5	-4	22	-8
-2	82	79	-6*	0	-7	8	123	-112	-6*	0	10	-5	50	23	2	209	-196	H,K=	7	4	-1	73	-44	-5	82	60
-4	317	-305	-7	112	-103	9	39	40	-7	26	22	-6	115	-111	3	206	-219	-1	125	-130	-2	109	-100	-6	91	-80
-6	245	238	-8	51	56	H,K=	3	2	-8	80	-67	-7*	0	14	4*	0	10	-2	95	-99	-3	136	121	-7	41	43
-8	87	-81	-9	36	-19	0	44	-45	-9	79	84	-8	83	-94	5	72	84	-3	78	84	-4	75	73	-8	30	26
-10	60	56	-10	67	67	1	144	-147	-10	36	-33	-9	84	78	6	79	-65	-4	47	42	-5	47	27	-9	25	-23
H,K=	8	0	-11	23	-21	2	67	53	-11	35	-36	-10	14	15	7	93	-85	-5	163	-174	-6	51	-50	H,K=	3	6
-2	83	-77	H,K=	3	1	3	98	81	H,K=	7	2	H,K=	2	3	8*	0	3	-6	99	-83	-7	51	44	-1	62	-54
-4	76	-79	-1	291	-305	4	105	94	-1	169	-175	-1	73	65	9	85	77	-7	111	108	-8	31	-24	-2	168	-168
-6*	0	2	-2	187	-184	5*	0	-6	-2	160	158	-2	165	160	H,K=	3	4	-8	36	-30	-8	74	-79	-3	60	-34
-8	59	-43	-3	241	234	6	42	-41	-3	161	154	-3	195	-192	0	90	-80	-9	43	39	-10	24	18	-4	47	25
H,K=	9	0	-4	159	-144	7	17	2	-4*	0	-21	-4	67	-52	1	65	-39	H,K=	8	4	H,K=	5	5	-5	59	-47
-2	44	-48	-5	45	49	8	36	34	-5	180	-155	-5	54	-43	2	45	19	-1	112	129	-1	106	-102	-6	91	-89
-4	74	81	-6	38	-36	9*	0	14	-6	113	103	-6	110	99	3	98	-90	-2	47	52	-2	27	-19	-7	110	98
-6	70	-81	-7	45	41	H,K=	4	2	-7	113	103	-7*	0	-17	4	78	-81	-3	69	-64	-3	55	48	-8	91	76
H,K=	0	1	-8	25	26	0	53	36	-8	42	-41	-8	71	-73	5	51	-45	-4	44	-48	-4	126	-116	-9	25	-19
1	204	-194	-9*	0	-3	1	60	-45	-9	68	-74	-9	48	45	6*	0	13	-5	14	-20	-5	73	-63	H,K=	4	6
2	435	-458	-10	106	104	2	72	-76	-10*	0	3	-10	55	-60	7	151	153	-6	19	-22	-6	82	64	-1*	0	16
3	111	86	-11*	0	-1	3	209	195	H,K=	8	2	-11	21	16	8	26	16	-7	12	-10	-7	26	31	-2	33	14
4*	0	0	H,K=	4	1	4	144	134	-1	30	26	H,K=	3	3	H,K=	4	4	H,K=	0	5	-8	24	-20	-3	83	-73
5	76	82	-1	136	116	5	70	-50	-2	32	-24	-1*	0	9	0*	0	0	1	70	55	-9	25	19	-4	149	-127
6	32	26	-2	279	248	6*	0	-2	-3*	0	13	-2	125	-110	1	34	-36	2	123	119	-10	25	-25	-5	64	66
7	98	94	-3	132	-116	7*	0	14	-4	61	61	-3	158	-143	2	87	-99	3	52	-36	H,K=	6	5	-6	24	-16
8	63	-71	-4	285	-279	8	25	-21	-5	42	35	-4	81	77	3	47	41	4	108	-112	-1	117	104	-7	32	-28
9	102	-100	-5*	0	-13	H,K=	5	2	-6	26	-16	-5	119	-113	4*	0	24	5	92	94	-2	50	52	-8*	0	4
10*	0	8	-6	84	-88	0	240	203	-7*	0	-7	-6	75	-75	5	34	-42	6	77	-75	-3*	0	-4	-9	28	-24
11*	0	-2	-7	17	-30	1	83	77	-8	21	13	-7	125	127	6*	0	7	7	138	-156	-4*	0	-13	H,K=	5	6
H,K=	1	1	-8	44	34	2	46	-46	-9	74	-72	-8	31	28	7	34	29	8*	0	-16	-5	49	46	-1	42	-44
0	115	-120	-9	18	9	3	87	93	H,K=	9	2	-9	54	-48	H,K=	5	4	9*	0	5	-6	51	-38	-2	174	211
1	68	57	-10	36	34	4*	0	14	-2	40	-50	-10	36	-40	0	148	-140	H,K=	1	5	-7	150	-156	-3	24	-47

to the normal C–O single bond length. DL-GABOB molecule has the ziwtterionic structure, NH_3^+–CH_2–CH(OH)–CH_2–COO^-, by the protonation to the γ-amino group. D and L molecules are related by a center of symmetry as shown in Fig. 1, and the hydrogen atom attached to the O3 atom takes part in the intra- and intermolecular bifurcated hydrogen bond to form DL dimer. GABOB molecule forms the expected *trans-zigzag* conformation in crystalline state. The Cα(C2), Cβ(C3), Cγ(C4) and N atoms which compose the skeletal structure of GABOB are in a plane (plane I), and the O1, O2, and C1 atoms of the carboxyl group including the Cα(C2) atom are in another plane (plane II). Deviations of the atoms from each plane are listed in Table 4. The dihedral angle of 11.5° between these two planes indicates that all the atoms in main chain are roughly in one plane. Deviations of each atom from the best plane including all the atoms except O3 are as follows; O1: −0.19, O2: 0.06, C1: −0.03, C2: 0.17, C3: 0.10, C4: 0.14, and N: −0.20 Å. Newman projections of atoms in respect to the C1–C2, C2–C3, and C3–C4 bonds with the torsion angles are shown in Figs. 2a and 2b for GABOB and GABA, respectively. The largest conformational difference between GABOB and GABA in crystalline state is found in their torsion angles in respect to the C2–C3 bond, which are *trans* (173.7°) in GABOB and *gauche* (73.6°) in GABA, respectively. The intramolecular hydrogen

Table 4. Deviations (Å) of atoms from the least-squares planes[a)]

Plane I;	
$-0.39310X-0.91866Y-0.03919Z+2.14576=0$,	
C2	−0.065
C3	+0.064
C4	+0.078
N	−0.069
Plane II;	
$-0.13800X-0.98032Y-0.14116Z+1.67365=0$,	
C1	−0.023
C2	+0.007
O1	+0.008
O2	+0.008

a) X, Y, and Z are orthogonal coordinates in Å parallel to a, b, and c*.

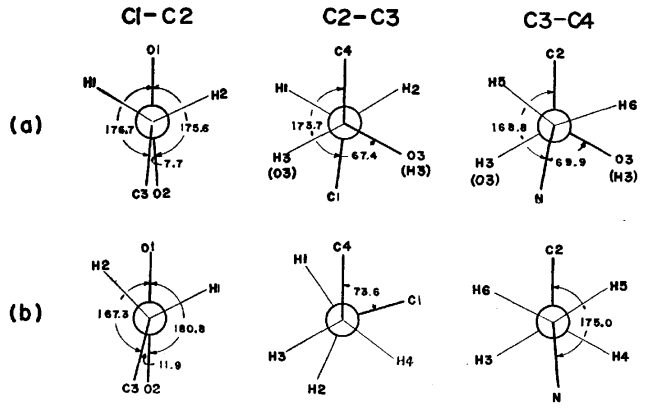

Fig. 2. Molecular conformations of DL-GABOB (a), and GABA (b).[7] Torsion angles are in degree.

bond between the O3 and the O2 atom in GABOB molecule is thought to play an important role in restricting the rotational freedom around the C2–C3 bond and keeping the extended *trans-zigzag* conformation of the molecule.

GABOB is well known as a potent inhibitory chemical transmitter in central nervous system as well as GABA, and it is of most interest that the skeletal conformation of GABOB is just the same as that of GABA hydrochloride,[9] but is different from that of GABA.[7] It is still obscure why these chemical transmitters may be released from the membrane of nerve ganglion into synapse and inhibit the transmitting of the stimulus to neighboring nerve cell, however, it may be postulated that GABA may be induced the change of its molecular conformation by binding to an ion (probably potassium or chlorine ion) due to the increase of ion concentration in presynaptic membrane by the stimulus and may be selectively released through the channel of membrane into synapse with the ion. On the other hand, the molecular conformation of GABOB is fixed as the extended *trans-zigzag* one due to the OH···O intramolecular hydrogen bond of 2.773 Å and probably released into synapse without any affection by ion concentration. GABA or GABOB in synapse may bind to the postsynaptic receptor site at neighboring nerve cell membrane in order to decrease the membrane resistance, chiefly attributable to an increase in Cl^- permeability. The nature of the interactions between the chemical transmitter and its receptor molecule is electrostatic, hydrogen bonding and van der Waals, and the resulting force between the molecules depends on the mutual orientation and conformation of the molecules. The zwitterionic form of GABA or GABOB may affect on the electrostatic interaction with the receptor and the amino group may participate in the hydrogen bonding with the receptor as a donor while the carboxyl group acts as an acceptor of hydrogen bond. In this case, the important intramolecular distances between the amino nitrogen atom and the carboxyl oxygen atoms are equal within the standard deviations; N–O1=6.052, 6.11 Å, N–O2=5.027, 5.15 Å for DL-GABOB and GABA hydrochloride, respectively. This important role of the extended *trans-zigzag* conformation for the inhibitory action may be also supported by the fact that muscimol, an isoxazole betaine isolated from *Amanita muscaria*, having a restricted similar backbone conformation, acts as a GABA-like depressant.[10] In addition, the O3 atom of GABOB is engaged in OH···O intramolecular hydrogen bond of 2.773 Å and this atom seems to interact with extra active sites of a receptor in nervous system than the GABA molecule does.

Distances and angles of the hydrogen bonds are listed in Table 5. The crystal structure of DL-GABOB is shown in Fig. 3. DL-GABOB molecules are connected by three-dimensional networks of NH···O and OH···O type hydrogen bonds, in which O3H···O2 hydrogen bond holds D-antipode of GABOB with its L-form related by a center of symmetry. There are

Table 5. Hydrogen bond distances and angles in GABOB

Distances (Å)	
donor (original) acceptor	
N ···O2 (I)	2.749 (0.007)[a)]
N ···O1 (II)	2.825 (0.007)
N ···O1 (III)	2.844 (0.007)
O3···O2 (IV)	3.080 (0.008)
O3···O2	2.773 (0.008)[b)]

Angles (degree)	
C4–N ···O2 (I)	115.7 (0.4)
C4–N ···O1 (II)	110.1 (0.4)
C4–N ···O1 (III)	96.9 (0.3)
C3–O3···O2 (IV)	137.7 (0.4)
C3–O3···O2	73.0 (0.4)[b)]

original	x	y	z
I	$-1+x$	$1/2-y$	$-1/2+z$
II	$-1+x$	y	z
III	$1-x$	$1/2+y$	$1/2-z$
IV	$1-x$	$-y$	$1-z$

a) Estimated standard deviations are in parentheses.
b) Intramolecular hydrogen bonding.

9) K. Tomita, *Jap. J. Brain Physiol.*, **61**, 1 (1965).

10) L. Brehm, H. Hjeds, and P. Krogsgaard-Larsen, *Acta Chem. Scand.*, **26**, 1298 (1972).

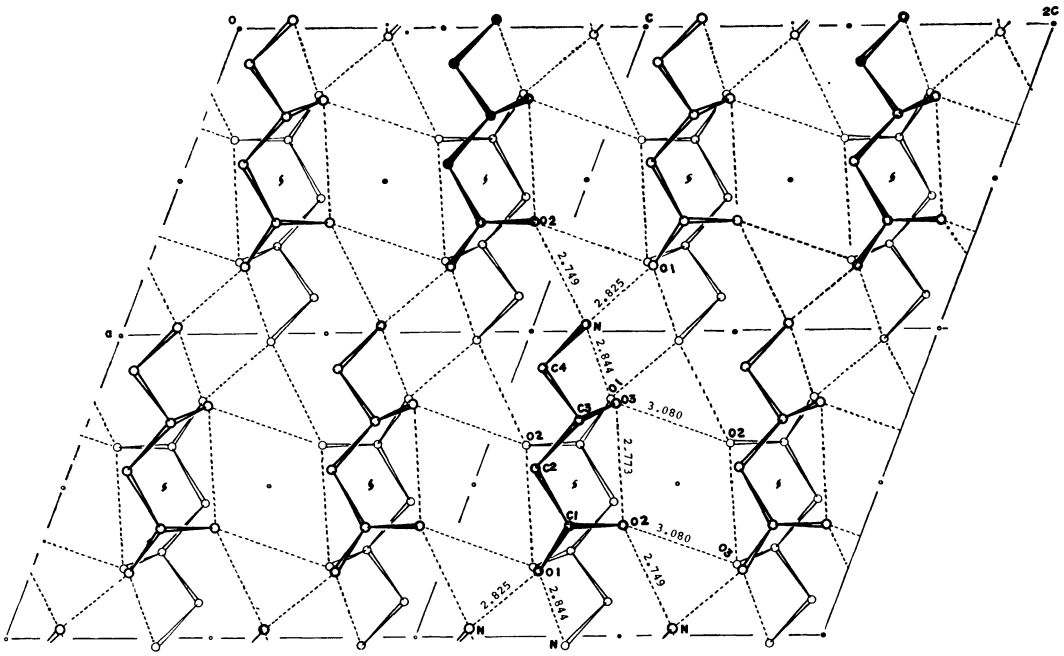

Fig. 3. The crystal structure of DL-GABOB projected along the b axis. The broken lines indicate the hydrogen bonds.

no unusual short contacts in this crystal.

The authors wish to thank the late Professor Masaji Tomita, Kobe Women's College of Pharmacy, for his valuable advice and continuous encouragement during the course of this work. This investigation was partly supported by the research grant from the Ministry of Education, Japan. We wish to express our sincere thanks for this support.

BULLETIN OF THE CHEMICAL SOCIETY OF JAPAN, VOL. 46, 2858—2861 (1973)

Restricted Rotation Involving the Tetrahedral Carbon. VII. Rotation About the Carbon-Group IV Single Bond[1]

Fumio SUZUKI, Michinori ŌKI,* and Hiroshi NAKANISHI**

Department of Chemistry, Faculty of Science, The University of Tokyo, Hongo, Tokyo 113

***National Chemical Laboratory for Industry, Shibuya, Tokyo 151*

(Received May 25, 1973)

9-*t*-Butyl-, 9-trimethylsilyl-, 9-trimethylgermyl-, and 9-trimethylstannyl-1,2,3,4-tetrachloro-9,10-dihydro-9,10-ethenoanthracenes were prepared by the addition of tetrachlorobenzyne to 1-$(CH_3)_3$M-substituted naphthalene. The carbon compound showed very high barrier to rotation, whereas the coalescence phenomenon of three methyl signals was observed for silicon, germanium, and tin compounds. The barrier ($\Delta G^{\ddagger}$) to rotation at 298 K was obtained as 19.1 ± 0.5, 17.2 ± 1.2, and 11.7 ± 0.4 kcal/mol for Si, Ge, and Sn compounds, respectively. The decrease in the barrier on increasing the atomic size was attributed to the release of repulsive interaction to a greater extent, since the longer bond length should result in the larger displacement of the methyl group even though the bond angle deformation is the same.

It was revealed, in one of the recent papers from this laboratory, that the barrier to rotation about a C–C single bond in some Diels-Alder adducts derived from 9-substituted anthracenes was extremely high.[2] These results allured the present authors to examine the outcome by the change of one of the sp^3 hybridized carbon to an atom of other fourth group elements.

One of the points of interest is to see the effect of

* To whom the correspondence should be addressed.

1) Preceding paper: M. Nakamura, M. Ōki, and H. Nakanishi, *Tetrahedron*, submitted.

2) M. Ōki and G. Yamamoto, *Chem. Lett.* **1972**, 45.

the change in bond length. As to the conformational energies of cyclohexane derivatives, it is known that chlorine, bromine, and iodine show rather similar values[3] in spite of the fact that the van der Waals radius of iodine is much greater than that of chlorine. The phenomenon has been attributed to the bond length. Namely, although the iodine atom is bulkier than chlorine, the interaction of the atom in question with the 3-hydrogen in the axial conformation is counterbalanced because the distance between hydrogen and iodine is greater.

Molecular models of 9-trimethylsilyltriptycene and its analogs indicate that the increase in bond length leads to the increased interference with the benzo bridges, because the longer C–M bond places the methyl group more closely to the substituent of the benzo group. This is just the contrary to the expectation from the analogy of the cyclohexane derivatives. This increasing interference may result in the increase in the barrier to rotation. Therefore it becomes interesting to see the effect of changing the *t*-butyl group to trimethylsilyl, trimethylgermyl, and then to trimethylstannyl.

This paper deals with the rotational barrier in 9-$(CH_3)_3$M-substituted 1,2,3,4-tetrachloro-9,10-dihydro-9,10-ethenoanthracenes, where M is C, Si, Ge, or Sn. Although the selection of the compounds was made according to the ease of syntheses, the distinct effect of the change of the central atom was observed.

Experimental

Syntheses. The syntheses of the compounds were performed by treating 1-$(CH_3)_3$M-substituted naphthalene (**1**) with tetrachlorobenzyne.[4] 1-*t*-Butylnaphthalene,[5] 1-trimethylsilylnaphthalene,[6] and 1-trimethylstannylnaphthalene[7] were known compounds and were prepared by following the procedures of literatures. The reaction of the benzyne gave both 1,4-adduct (**2**) and 5,8-adduct (**3**). The desired adduct (**2**) was separated by chromatography.

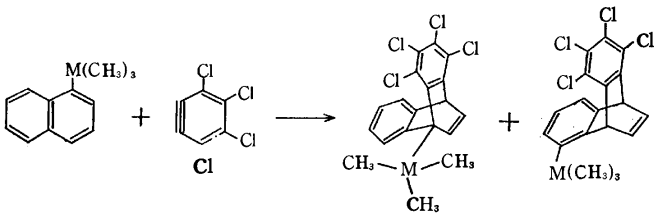

1 **2** **3**

a: M=C
b: M=Si
c: M=Ge
d: M=Sn

*1-Trimethylgermylnaphthalene (**1c**).* A solution of 1-naphthylmagnesium bromide, prepared from 10.3 g (0.05 mol) of 1-bromonaphthalene and 1.2 g (0.05 mol) of magnesium in 100 ml of ether, was added to 0.07 mol (15.0 g) of tetrachlorogermane in 50 ml of ether at −10 °C over a period of 1 hr. The mixture was set aside for 2 hr at room temperature and then heated under reflux for 0.5 hr. Methylmagnesium iodide prepared from 42.5 g (0.3 mol) of methyl iodide, 7.2 g (0.3 mol) of magnesium and 200 ml of ether was added to the above solution with vigorous stirring and the whole was refluxed for 2 hr. The mixture was cooled and treated with water. The organic layer was dried over sodium sulfate and evaporated to give a yellow oil. This crude product was directly used for the next reaction.

*1,2,3,4-Tetrachloro-9-t-butyl-9,10-dihydro-9,10-ethenoanthracene (**2a**).* A solution of butyllithium, prepared from 4.6 g (0.05 mol) of butyl bromide, 0.7 g (0.1 mol) of lithium, and 100 ml of ether, was added to a suspension of 14.2 g (0.05 mol) of hexachlorobenzene in 600 ml of ether at −30 °C over a period of 1 hr. To this mixture, a solution of 9.2 g (0.05 mol) of 1-*t*-butylnaphthalene in 50 ml of ether was added. The whole was set aside at room temperature for 1 hr, heated under reflux for 1 hr, cooled and treated with water. The organic layer was separated, washed with water, dried over sodium sulfate, and evaporated. The residue was taken up in hexane and chromatographed on alumina. Elution of the mixture with hexane gave a mixture of 1,4-adduct (**2a**) and 5,8-adduct (**3a**) in 1:2 ratio. NMR data of **3a** in $CDCl_3$ (δ from internal TMS): 1.53 (9H, s), 5.56 (1H, t, J=3.6 Hz), 6.30 (1H, t, J=3.6 Hz), 6.85—7.40 (5H, m). The NMR data for **2a** are given in Table 1.

The mixture of **2a** and **3a** was dissolved in hexane and rechromatographed on silica gel impregnated with silver nitrate. Elution with hexane gave pure **2a**, mp 162—164 °C, as a first eluate in *ca.* 5% yield based upon the starting 1-*t*-butylnaphthalene. Found: C, 60.23; H, 4.07; Cl, 35.73%. Calcd for $C_{20}H_{16}Cl_4$: C, 60.36; H, 4.06; Cl, 35.58%.

*1,2,3,4-Tetrachloro-9-trimethylsilyl-9,10-dihydro-9,10-ethenoanthracene (**2b**),* mp 157—159 °C, was similarly obtained as a mixture with the 5,8-adduct (**3b**) [NMR, $CDCl_3$, δ from TMS: 0.45 (9H, s), 5.62 (1H, q, J=4.6 and 3.0 Hz), 5.90 (1H, q, J=4.6 and 3.0 Hz), 6.95—7.43 (5H, m)] in 1:2 ratio and purified by SiO_2–$AgNO_3$ chromatography. The yield of pure **2b** was *ca.* 5%. Found: C, 55.53; H, 3.98; Cl, 34.08%. Calcd for $C_{19}H_{16}Cl_4Si$: C, 55.25; H, 3.94; Cl, 34.25%.

*1,2,3,4-Tetrachloro-9-trimethylgermyl-9,10-dihydro-9,10-ethenoanthracene (**2c**),* mp >315 °C, was similarly obtained as a mixture with **3c** (1:1.5 ratio). Pure **2c** was isolated in *ca.* 5% yield. Found: C, 49.95; H, 3.37; Cl, 31.17%. Calcd for $C_{19}H_{16}Cl_4Ge$: C, 49.74; H, 3.55; Cl, 30.89%. Only the NMR data of the 5,8-adduct (**3c**) were recorded ($CDCl_3$, δ from TMS): 0.57 (9H, s), 5.59—5.90 (2H, m), 6.97—7.41 (5H, m).

*1,2,3,4-Tetrachloro-9-trimethylstannyl-9,10-dihydro-9,10-ethenoanthracene (**2d**),* mp 165—166.5 °C, was obtained in *ca.* 5% yield. Found: C, 45.40; H, 2.98; Cl, 28.07%. Calcd for $C_{19}H_{16}Cl_4Sn$: C, 45.21; H, 2.98; Cl, 28.09%. NMR data of the 5,8-adduct (**3d**) were as follows ($CDCl_3$, δ from TMS): 0.51 (9H, s), 5.58 (2H, m), 5.70—7.50 (5H, m).

Spectral Measurement and Calculation. The NMR spectra were recorded on a Hitachi R-20B spectrometer operating at 60 MHz. The samples were dissolved in an appropriate solvent to make up *ca.* 10% solution. The temperature was read by the difference in chemical shifts of methanol protons in the lower temperature region and by that of ethylene glycol in the higher temperature region. T_2 was measured from the line-width of an appropriate additive in the sample

3) J. A. Hirsch, "Table of Conformational Energies-1967," in "Topics in Stereochemistry," N. L. Allinger and E. L. Eliel Ed., Interscience Publishers, New York (1967), vol. 1, p. 199.

4) H. Heaney and B. A. Marples, *J. Chem. Educ.*, **45**, 801 (1968).

5) H. van Bekkum, Th. J. Nieuwstad, J. van Barneveld, P. Klapwijk, and B. M. Wepster, *Rec. Trav. Chim.*, **88**, 1028 (1969).

6) H. Gilman, R. A. Benkeser, and G. E. Dunn, *J. Amer. Chem. Soc.*, **72**, 1689 (1950).

7) O. Buchman, M. Grosjean, and N. Nasielski, *Bull. Soc. Chim. Belges*, **71**, 467 (1962).

Table 1. The NMR data of compound **2** in deuteriochloroform at 34 °C (δ ppm)

2a	1.53 (3H, s)	1.77 (3H, s)	2.13 (3H, s)	5.71 (1H, q, J=6.0 and 2.0 Hz)	6.90—7.90 (6H, m)
2b	0.32 (3H, s)	0.67 (3H, s)	1.10 (3H, s)	5.67 (1H, q, J=6.0 and 1.2 Hz)	6.75—7.50 (6H, m)
2c	0.34 (3H, s)	0.67 (3H, s)	1.05 (3H, s)	5.66 (1H, q, J=6.0 and 1.6 Hz)	6.71—7.55 (6H, m)
2d		0.48 (9H, s)		5.58 (1H, q, J=6.0 and 1.2 Hz)	6.60—7.30 (6H, m)

solution: for mainly technical reasons, *t*-butylbenzene, tetrachloroethane, and dichloromethane were used for **2b**, **2c**, and **2d**, respectively.

Theoretical spectra were obtained by the use of EXNMR program.[1] The couplings of protons with ^{117}Sn and ^{119}Sn were neglected in the line-shape analysis because of the low natural abundance of the respective species. The agreement between the observed and the calculated spectra was excellent.

Results and Discussion

The NMR data of the adducts **2** in deuteriochloroform at 34 °C are summarized in Table 1. It is immediately noticed that the carbon, silicon, and germanium compounds show three kinds of methyl peaks, whereas the tin compound gives only one signal for the trimethylstannyl group. The rotation about the C_9–M bond must be slow on the NMR time scale for the compounds whose M is C, Si, or Ge, because, if the rotation in question is frozen, the three methyl groups must be in the different magnetic environment from each other (see **4**). The appearance of only one signal for the trimethylstannyl group in **2d** may be attributed to either a fortuitous coincidence of the chemical shifts of three methyl groups under the conditions or the fast exchange of the methyls on the NMR time scale. The latter was found to be the case because lowering the temperature caused the broadening of the signals and finally resulted in the appearance of three kinds of methyl signals. The chemical shifts at −58.5 °C from the internal TMS in CS_2 were 0.14, 0.51, and 0.85 ppm.

Temperature was raised to find the coalescence temperature and to observe the line shapes of compounds **2a**, **2b**, and **2c**. Spectra of **2b** and **2c** were temperature dependent and coalescence of the three signals was observed. However, the spectrum of **2a** was stout and did not show temperature dependence up to 200 °C. Even the broadening of the signal could not be observed.

From these results and the chemical shifts of the three methyl groups, the barrier to rotation about C_{Bu}–C_9 bond of **2a** is estimated to be at least 25 kcal/mol. The rate constants of rotation of other compounds were obtained by computer simulation of the curves. The activation energies were calculated by plotting the rate constants against the reciprocals of temperature. The ΔH^*, ΔS^*, and ΔG^* were obtained by putting these data to Eyring's equation. The results are shown in Table 2.

Although the use of the same solvent is desirable for the discussion, it was impossible to use a common solvent for the series of compounds. Hexachlorobutadiene is suitable for measurement at high temperatures but is too viscous to obtain a good spectra at *ca.* 50 °C. Likewise, tetrachloroethylene is good at *ca.* 50 °C but is not suitable for measurement at high and at very low temperatures. Fortunately, however, it is known that the solvent change does not affect the activation parameters of internal rotation to a great extent in the case of biphenyl derivatives.[8] This conclusion may reasonably be transferred to the present situation, since the internal rotation is the common subject in both cases. We believe the following discussion is valid, since only the nonpolar solvents are used in the present work and no strong solute-solvent interaction is anticipated.

Descending the fourth group element from carbon to the elements of the lower period gives monotonous decrease in ΔG^*'s and ΔH^*'s. This is rather unexpected from the results of examination of the molecular models, as mentioned before, and demands further consideration. Recently, Oullette and his co-workers carried out the force field calculation of various butane analogs $CH_3CH_2MH_2CH_3$ containing silicon, germanium, or tin.[9] The conclusion from that calculation is that the *gauche* conformation is strikingly stable over the *trans* conformation and the barrier to rotation is mainly controlled by the stability of the ground state where nonbonding H–H attractive interaction contributes strongly to the total energy. Thus in this series, the potential of the transition state of rotation is almost the same irrespective to the kind of element M (except carbon) and the increasing size of M decreases the

Table 2. Activation parameters for rotation (at 25 °C)

	T_c (°C)	E_a kcal/mol	ΔH^* kcal/mol	ΔS^* eu	ΔG^* kcal/mol	solvent
2a	>200				>25	hexachlorobutadiene
2b	112	20.7±0.5	20.1±0.5	0.6±1.8	19.9±0.5	hexachlorobutadiene
2c	64	15.3±0.7	14.7±0.7	−8.4±2.1	17.2±1.2	tetrachloroethylene
2d	−40	13.2±0.4	12.6±0.4	2.2±0.5	11.7±0.4	carbon disulfide

8) B. M. Grayhill and J. E. Leffler, *J. Phys. Chem.*, **63**, 1461 (1959): I. O. Sutherland and M. V. J. Ramsey, *Tetrahedron*, **21**, 3401 (1965): M. Ōki and H. Iwamura, *ibid.*, **24**, 2377 (1968): M. Ōki, H. Iwamura, and T. Nishida, This Bulletin, **41**, 656 (1968).

9) a) R. J. Oullette, *J. Amer. Chem. Soc.*, **94**, 7674 (1972): b) R. J. Oullette, D. Baron, J. Stolfo, A. Rosenblumn, and P. Weber, *Tetrahedron*, **28**, 2163 (1972).

barrier to rotation.

The phenomena in the Diels-Alder adducts dealt with here might have been explained in a similar manner, if the steric conditions of the butane analogs were applicable to the compounds in question. However, although the compound **2** is the ethane type molecule, the situations are quite different from those of $CH_3CH_2MH_2$-CH_3. In the latter compound, it is known that the distance between the two methyl groups is larger than the sum of two van der Waals radii of the methyl. The attractive term is important even at the eclipsed conformation. On the other hand, the steric situation of compound **2** is overcrowded. Inspection of the model of the ground state (**4** and **4'**) indicates that the distance between chlorine at 1-position and a closest methyl group from that atom is within the sum of the van der Waals radii of the two substituents. Therefore, although the molecule will deform to some extent to minimize the van der Waals repulsion, the steric conditions are thought to be severe at the transition state (**5**). It seems, then, natural to seek the reason for the phenomenon in repulsive forces rather than the attractive.

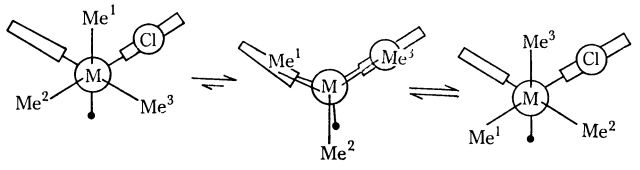

4 **5** **4'**

Since the molecular model shows severe overlap of the groups at the transition state **5**, the bond length will be stretched and the bond angle distorted to help to decrease the energy of the transition state. The energy of stretching a bond and that of deforming a bond angle may be discussed in terms of force constants obtained from the infrared study. Thus the force constants of respective moieties are collected in Table 3 from the literature.[10]

Table 3. Force constants for bond stretching and angle deformation

	C	Si	Ge	Sn
Bond Stretching constant (C–M) mdyn/A	4.50	2.97	2.70	2.12
Angle bending constant (C–M–C) mdyn/rad	0.799	0.570	0.490	0.320

Although it may seem that the smaller force constants for stretching the C–M bond should play some part in lessening the barrier to rotation when M is the large atom, the molecular model is not in conformity with this idea. When M becomes large, both the C_9–M and C_{CH_3}–M bonds become longer and, as a consequence, the overlap of the chlorine and the methyl group at the transition state becomes worse. Therefore, relief of steric strain at the transition state by stretching the bond should be small in its extent, if any.

Another way of relieving the steric interference at the transition state is to deform the bond angles concerned with the $(CH_3)_3M$ group, because the other part of the molecule is very rigid. The force constants of angle bending also decreases as M becomes large. Therefore, the ease of angle deformation increases as we descend the periodic table from carbon to tin. The important point here seems to be that even the deformation of the same degree results in the different degree of release of the steric strain. When the C–M bond is longer, the actual placement of the methyl group can become more apart from the groups which contribute mainly to the strain at the transition state, even though the angle deformation is the same. Thus we believe that the longer bond distance is the main cause for decreasing the barrier to rotation, when M is the large atom, and the smaller force constants for the C–M–C angle deformation is an additional factor which helps to decrease the barrier height.

10) Reference 9a and literatures cited therein.

An Attempt at Simultaneous Observation by Polarizing Microscopy and by Differential Thermal Analysis*

Kazuko Sasaki Kunihisa

National Chemical Laboratory for Industry, Honmachi, Shibuya-ku, Tokyo 151

(Received June 23, 1972)

An apparatus for differential thermal analysis using a polarizing microscope has been developed. With this device it is possible to observe the state of a sample under the heating or cooling conditions with a polarizing microscope and to obtain the DTA curve simultaneously. The transformations of several substances—potassium laurate, ammonium nitrate and tripalmitin— were observed. The results are in agreement with those obtained by X-ray diffraction. The relation between the appearance of Phase III of NH_4NO_3 and the water content of the sample was considered on the basis of the microscopic observations. In the case of tripalmitin, two types of transformations were observed under cooling conditions. The relation between the DTA curve of tripalmitin and the heating rate has also been studied. The apparatus may be useful for the study of liquid crystals.

Recently, various kinds of apparatus for thermal analysis have been developed. Particularly, the simultaneous measurement of two parameters, such as X-ray diffraction —differential thermal analysis or thermogravimetry— differential thermal analysis, has been established.

The apparatus has been devised to observe the state of the substance microscopically on heating or cooling and simultaneously to obtain the DTA curve. The device has been constructed by setting the furnace for DTA on the sample stage of a polarizing microscope.

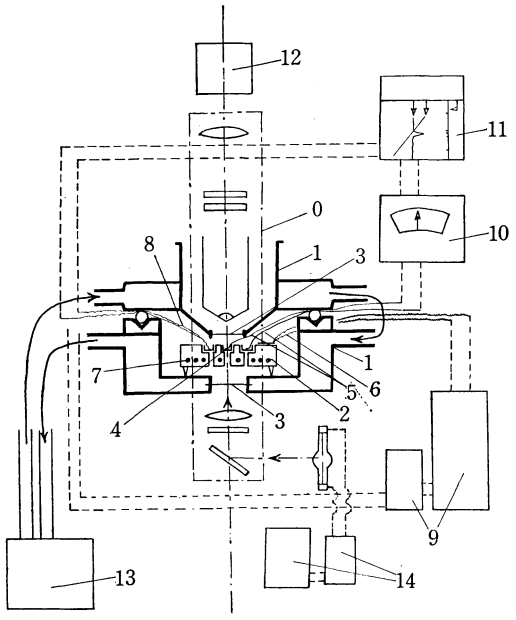

Fig. 1. The structure of DTA furnace and other parts.
0; microscope part 1; furnace body 2; copper block 3; quartz plates 4; quartz sample holders 5; differential thermocouple 6; thermocouple sheet 7; heater 8; thermocouple 9; temperature programmer 10; amplifier 11; recorder 12; photograph system 13; cooling system 14; light source system.

* Presented in part at the 4th Conf. Therm. Anal. Japan (1968) and the 23th Conf. the Chem. Soc. Japan (1970).

Apparatus

Figure 1 shows a diagram of the apparatus and illustrates the structure of the furnace. Both the lid and the base of the furnace (1) have transparent parts (3) made of quartz at their centers, water can be circurated in them from the cooling system (13). A flat cyrindrical copper block (2) was made with an embedded sheath nichrome wire heater (7) (1 mmϕ, 33 ohm) and three hollows. Each hollow has a slit at the bottom to admit light. Disc-like sample holders (4) made of quartz are inserted into the hollows of the block. The inner size is 3 mm$\phi \times$ 1 mm. The thickness of the quartz is 0.5 mm. The lid and bottom of the sample holders are polished optically. Both the differential thermocouple (5) and the temperature thermocouple (8) are Al–Cr of the sheath type (0.5 mmϕ). The input of the heater embedded in the block is controlled by a temperature programmer (9) together with a sheet-like thermocouple (6) on the block.

Microscopic observations have been made through crossed nicols and a color-sensitive plate. The multiplicity is 100. The light source (14) is usually a Tungsten lamp (30 W) or Xenon lamp (150 W).

A microswitch was set up at the tip of the release of the camera in order to interlock the camera shutter

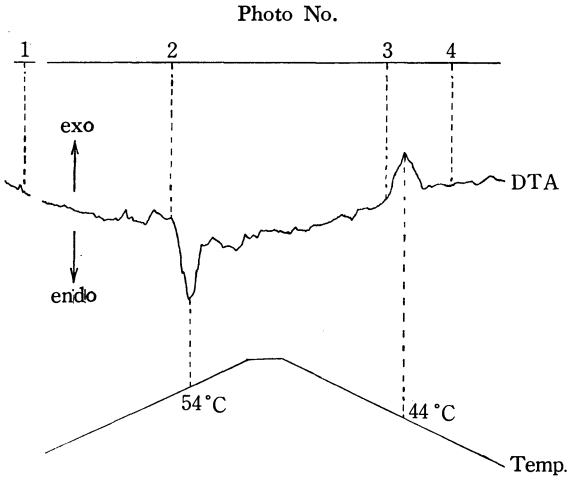

Fig. 2. DTA of potassium laurate at heating and cooling condition. Rate, 1.25 °C/min., Sensitivity, ±50 μV.

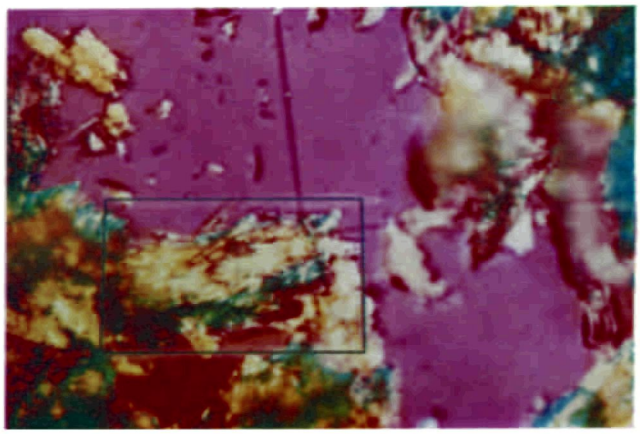

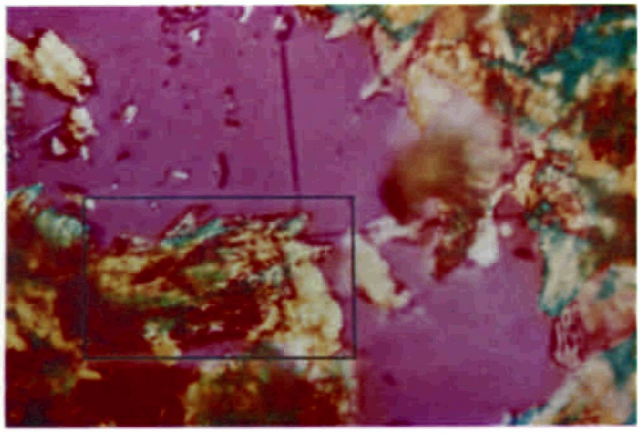

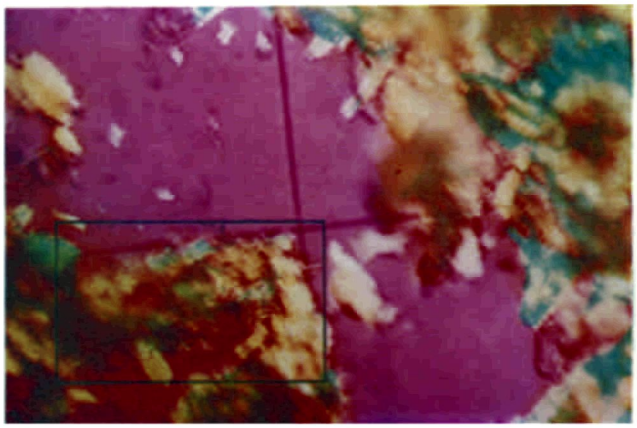

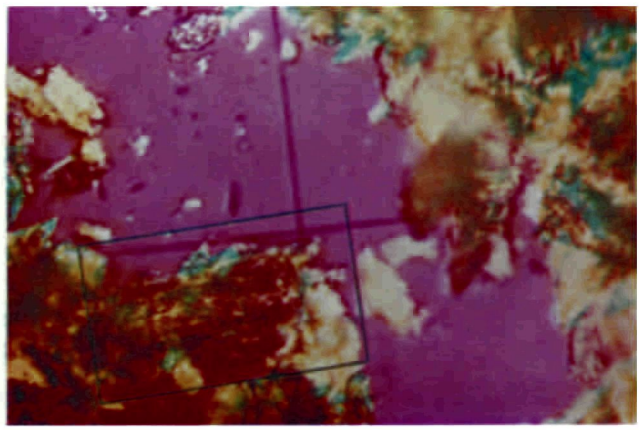

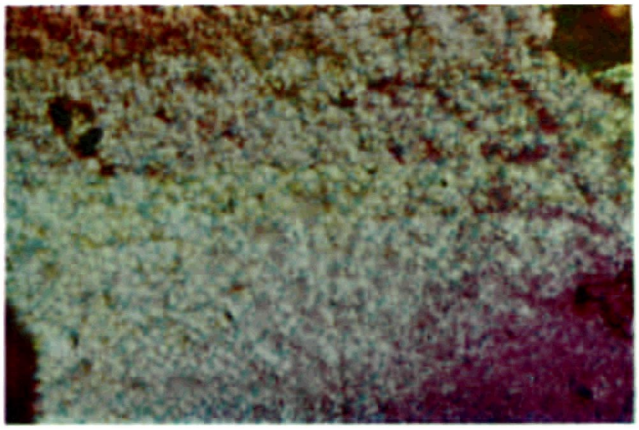

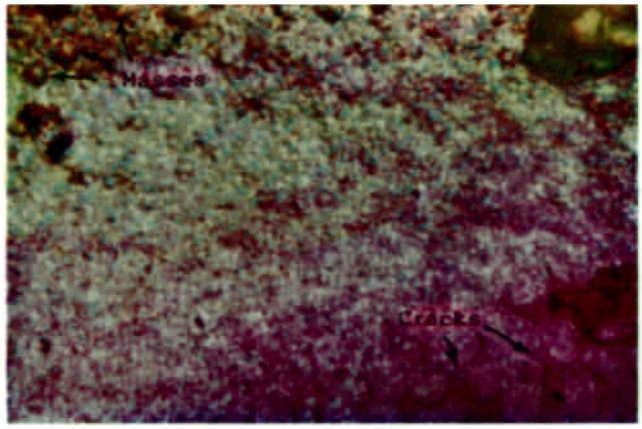
Masses
Cracks

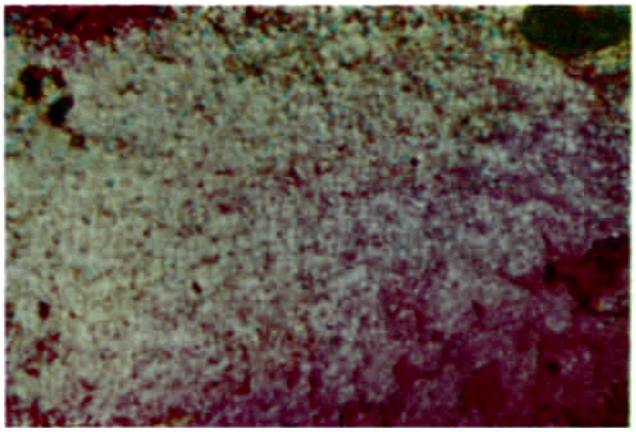

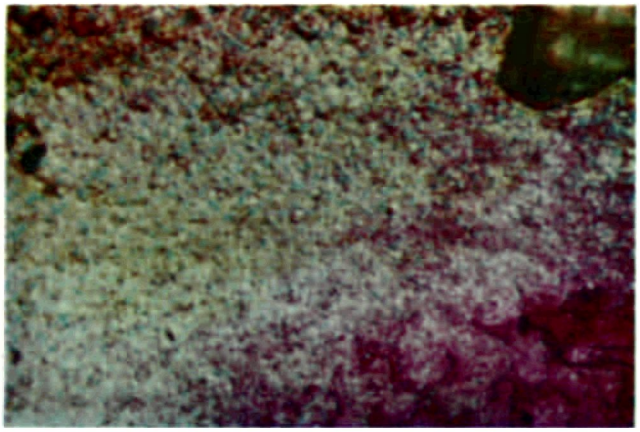

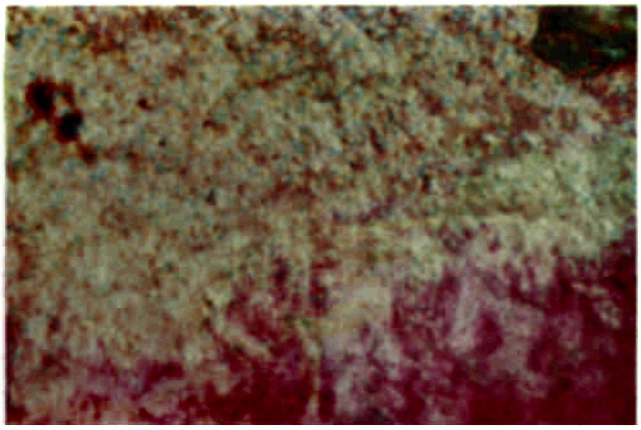

Figure 7-1 shows the thin layer of the α form made by the rapid cooling of the melt at 0 °C. Figure 7-2 shows the beginning of the transformation. The color of Fig. 7-2 is more similar to the back of the sample than that of Fig. 7-1. This means that the crystal layers are becoming transparent. At the same time, contraction occurs, as can be proved by the cracks in at the lower right in Fig. 7-2 and the several masses produced at the upper left in Fig. 7-2. Both the cracks and the masses are indicated by arrows.

At the peak of the endothermic state (Fig. 7-3), the sample becomes more transparent than at the beginning (Fig. 7-2). This means that the sample has turned more isotropic, like liquid.

Near the exothermic state, the crystalline state of the sample begins to recover. This can be deduced from the fact that Fig. 7-4 is less transparent than Fig. 7-3.

Figure 7-5 shows the sample at 58 °C. This photograph looks almost the same as Fig. 7-1 except for the cracks. Since the heating rate of this experiment is 2.5 °C/min, about 4 min elapse from Figs. 7-4 to 7-5. This means that the sample recovers a complete crystalline state after 4 min.

Figure 7-6 shows the beginning of the melting of the β form (66 °C). The photograph looks out of focus because of the movement of the crystal layer.

Upon cooling, two types of phase changes were observed. In this case, no temperature programming was carried out, as is shown in Fig. 8.

In the first case, the supercooled state was maintained from the melting point of the β form to the transition point, at which point crystallization suddenly began, accompanied by both heat absorption and evolution (Figs. 9-1 and 9-2). In the second case, crystallization took place as soon as the temperature arrived near the melting point of the β form (Figs. 11-1 and -2): afterwards, the crystal layer became transparent near the transition point (Fig. 11-3). In this case, no heat absorption was observed, but heat evolution was (Fig. 10).

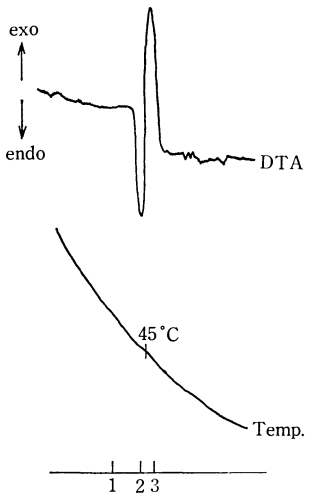

Fig. 8. DTA of tripalmitin at natural cooling. (1st case)

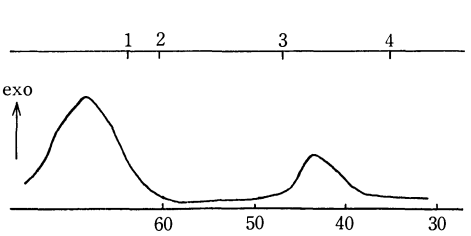

Fig. 10. DTA of tripalmitin at natural cooling. (2nd case)

Discussion

The results of the above experiments suggest that the apparatus is quite useful, even though the photographs are not very good. These results are in agreement with those obtained by X-ray diffraction.

Two transformations of ammonium nitrate made a particularly good contrast with each other. Brown and McLaren suggested that the IV—III transformation requires the presence of some moisture because of the severe structural change involved. They theorized that the transition took place by means of the dissolution and recrystallization of the solid. As proof, they cited the large increase in electrical conductance on the IV—III change. However, a large increase in electrical conductance is also observed upon the III—II change.

The transformations among IV, III, and II seem to take place with some regularities, according to the author's microscopic observations. That is, in the case of IV—III, a brightness appears longitudinally in the needle (a-axis) single crystal, but in the case of III—II, the brightness appears laterally in the crystal with expansion and contraction. If the IV—III modification takes place by means of dissolution and recrystallization, the sample should be more at random.

The III—II transition is far more drastic than that of IV—III as a phenomenon. Considering the similarities among I, II, IV, and V,[2] the presence of moisture seems to disturb the transformation of Phase IV to Phase II, on the other hand, it seems to make Phase IV turn into Phase III. Therefore, once the sample changes into Phase III, it may be forced to undergo the drastic III—II transformation (*cf.* Fig. 12).

In the case of tripalmitin, the heat absorption upon heating suggests the latent heat of melting of the α form. The successive heat evolution indicates the transformation from the α to β form, because the β form is more stable than the α form. The melting of the α form could not be observed microscopically. However, a transparency could be observed. On the other hand, at the beginning of the melting of the β form (Fig. 7-5), no transparency could be observed, even though the crystal layer started to move. Therefore, the transparency at the transformation may not indicate the melting state of the α form, but only an isotropic state during change to another form, β.

The heat absorption disappears with a decrease in the heating rate. In the case of a low heating rate it seems that the α form changes to the β form directly without actually passing through the melting state.

6) E. S. Lutton, *J. Amer. Chem. Soc.*, **67**, 524 (1945).

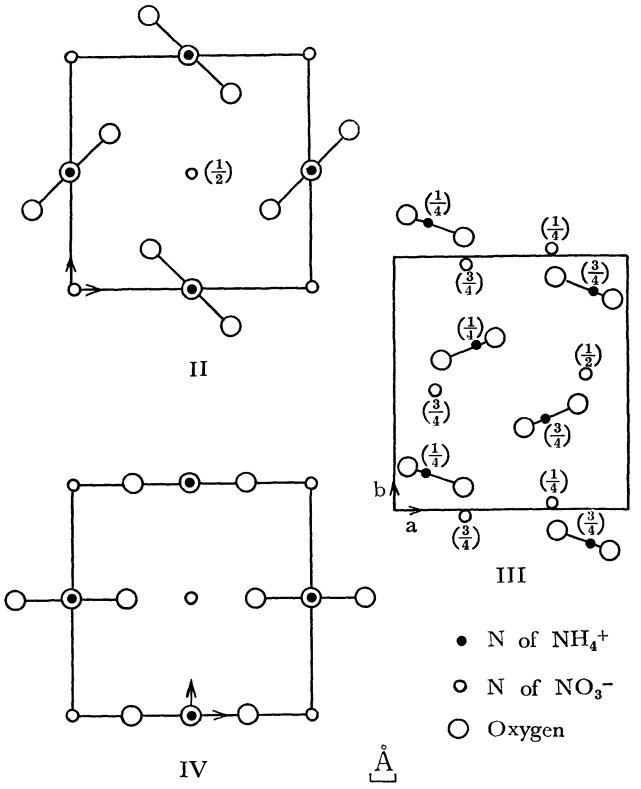

Fig. 12. Projections onto (001) of the structures of forms II, IV and III of ammonium nitrate.[2]

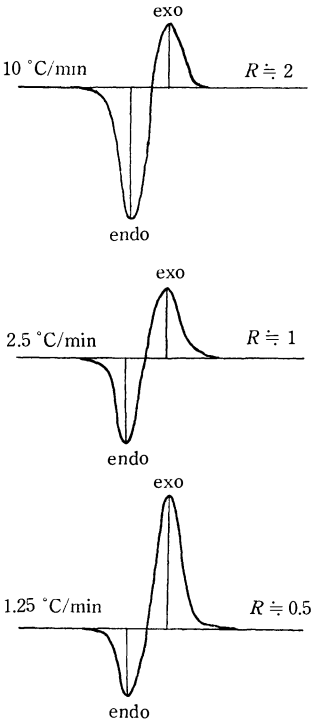

Fig. 13. The influence of heating rate on DTA curve of tripalmitin. R; ratio of endothermic peak to exothermic peak.

Figure 13 shows the relation between the heating rate and the DTA curve. The peak of the heat absorption becomes higher with increase in the heating rate, but that of the heat evolution becomes lower. These results support the theory that the α form melts directly when rapidly heated.[5] The peak of the heat absorption becomes lower with a lowering of the heating rate, but that of the heat evolution becomes higher. These results support the microscopic observation that the α form changes to the β form directly, with no melting, when slowly heated.

Upon cooling, it is reasonable to consider that the endothermic peak of the first case (Fig. 8) indicates the heat of the transformation of the β form to the α form and that the exothermic peak indicates the solidification of the α form. The second case (Fig. 10) can be interpreted as meaning that the melted sample does not cause a supercooled state; instead, the β form is deposited directly and is then transformed into the α form at the transition temperature. However, the β form does not usually change into the α form, because the β form is more stable than the α form. Considering the inhibition rule, it does not seem reasonable to assume that the first deposited phase corresponds to the β form. Since the solid state appeared over 60 °C, it did not seem to be the β′ form (mp 55.5 °C). It must be studied further in the future.

Conclusion

The above attempt at simultaneous microscopic and DTA observation has been achieved qualitatively, but not yet quantitatively. However, several useful results have been obtained by the use of this apparatus. They may contribute to the study of liquid crystals.

The present apparatus is limited to use from room temperature up to 350 °C because of the limits of the heat-resistivity of the sheet-like thermocouple and the other materials. Practically, all the experiments were done below 200 °C. Photography was restricted by the illumination of the light source.

The author wishes to thank Mrs. Midori Gotoh of this laboratory for offering the potassium laurate and tripalmitin, materials of her own study. She also kindly presented many references concerning them. The author also wishes to thank Mr. Satohiro Tanaka of this laboratory for his advice and encouragement.

NOTE

BULLETIN OF THE CHEMICAL SOCIETY OF JAPAN, VOL. 46, 2869—2870 (1973)

Evaluation of Diffusion Coefficients of Myosins from Sedimentation Boundary Curve

Masao YOKOYAMA, Atsunobu OHMOTO, and Yuji MIYAZAWA
Department of Chemistry, Science University of Tokyo, Kagurazaka, Tokyo 162
(Received November 30, 1972)

Fujita[1,2] showed that the height-area ratios of schlieren patterns obtained during a sedimentation velocity experiment can be used for the evaluation of the diffusion coefficient of the solute component in solution. This indicates that sedimentation and diffusion coefficients can be obtained under the same conditions. Considering the labile and restrictive nature of purified biological active macromolecules available for physico-chemical measurements, the evaluation of molecular weight from sedimentation and diffusion coefficients is still valuable.

The reported molecular weights of skeletal myosin are 4.2×10^5—6.2×10^5. The discrepancies were discussed in terms of the presence of aggregates in the samples.[3,4] In the present study, the diffusion coefficients for myosins prepared from smooth and skeletal muscles are evaluated from sedimentation boundary curves using Fujita's method, and the molecular weights of these myosins are calculated from the sedimentation and diffusion coefficients extrapolated to infinite dilution.

Experimental

Preparation of Sample. Smooth muscle myosin (myosin-S) was prepared from parts of the smooth muscle of horse gullet by ammonium sulfate fractionation.[5,6] Skeletal muscle myosin (myosin-A) prepared from rabbit skeletal muscle by the ammonium sulfate fractionation method[7] was supplied by Prof. T. Sekine. These myosins were dissolved in 0.5 M KCl solution containing 1/150 M phosphate buffer (pH 7.5). All sedimentation measurements were performed within three days after the final purification to minimize the formation of aggregates in the sample solutions. Concentrations of the solutions were determined from the optical densities at 279 nm. The extinction coefficients used were 600 cm^2/g[6] for myosin-S and 560 cm^2/g[8] for myosin-A.

Ultracentrifugal Experiment. A Hitachi UCA-1 ultracentrifuge equipped with schlieren optics was used. The temperature of the rotor was kept at 5.0 ± 0.1 °C. A synthetic boundary cell of double sector type and a conventional cell were used. To avoid direct contact of the sample solution with a metallic surface, which sometimes causes denaturation of proteins, either a cell made of epoxy resin or an aluminum cell coated with Teflon was used. The speed of the rotor was 10490—60000 rpm.

Results and Discussion

Sedimentation Coefficient. Sedimentation coefficients were calculated from the rates of movement of the boundary peak at several rotor speeds. The following equation[9] was used to correct the sedimentation coefficients at higher rotor speeds for pressure effect:

$$\ln(r_*/r_a)/\omega^2 t = S^0(C_0)\{1+[k_sC_0-m(1+2k_sC_0)/2(1+k_sC_0)][(r_*/r_a)^2-1]\} \quad (1)$$

where r_* and r_a are the distances from the center of rotation to the peak and the solution meniscus, respectively, ω is angular velocity, t time, $S^0(C_0)$ the sedimentation coefficient at concentration C_0, which is the initial concentration of the solution, m a parameter, and k_s a positive parameter characteristic of a given system. For the data at rotor speeds lower than 32000 rpm, at which the peak sedimented slowly and the boundary diffused quickly, the following equation was used.[10]

$$-2S\omega^2 t = \ln\left\{1-\left(\int_{r_a}^{r_p}(r^2-r_a^2)(dc/dr)dr\right)\Big/C_0r_a^2\right\} \quad (2)$$

where r_p is the distance from the center of rotation to a point arbitrarily chosen in the plateau region. The values of S obtained by Eq. (2) were equated to $S^0(C_0)$. Values of t were corrected graphically by using the conditions where $\ln(r_*/r_a)$ vanishes at $t=0$. In all experiments, the coefficient for the term $[(r_*/r_a)^2-1]$ in Eq. (1) was very small, no significant dependence of sedimentation coefficient on angular velocity being found. The sedimentation coefficients were corrected for concentration dependence by

$$1/S^0(C_0) = (1/S_0)(1+k_sC_0) \quad (3)$$

Figure 1 shows the concentration dependence of the sedimentation coefficient for myosin-S, the data being expressed by $1/S^0(C_0)=0.247(\pm0.001)+0.0230(\pm0.0003)C_0$ where C_0 is given in units of mg/ml. Figure 2 shows the results for myosin-A, the data being expressed by $1/S^0(C_0)=0.252(\pm0.004)+0.0246(\pm0.0003)C_0$.

Diffusion Coefficient. Data for the height-area ratio H/A from a series of sedimentation boundary curves could be used for the evaluation of diffusion

1) H. Fujita, *J. Phys. Chem.*, **63**, 1092 (1959).
2) H. Fujita, "Mathematical Theory of Sedimentation Analysis," Academic Press, New York, N. Y. (1962), p. 106.
3) W. W. Kielley, *Ann. Rev. Biochem.*, **34**, 403 (1964).
4) A. Stracher, P. P. Trotta, L. C. Gershman, and P. Dreizen, *J. Gen. Physiol.*, **50**, 85 (1967).
5) M. Yamaguchi, Y. Miyazawa, and T. Sekine, *Biochim. Biophys. Acta*, **216**, 411 (1970).
6) A. Kotera, M. Yokoyama, Y. Miyazawa, and M. Yamaguchi, *Biopolymers*, **7**, 99 (1969).
7) W. W. Kielley and L. B. Bradley, *J. Biol. Chem.*, **218**, 653 (1956).
8) W. W. Kielley, W. F. Harrington, and P. A. Small, *Biochim. Biophys. Acta*, **49**, 462 (1961).
9) Ref. (2), p. 137.
10) R. L. Baldwin, *Biochem. J.*, **55**, 644 (1953).

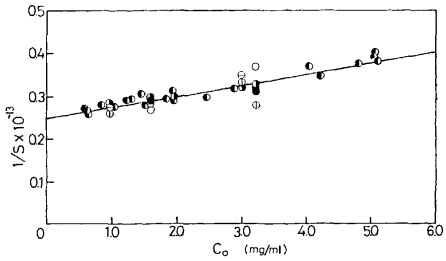

Fig. 1. Reciprocal of sedimentation coefficient for myosin-S plotted against concentration. Different symbols correspond to different rotor speeds, *i.e.*, ○: 10490 rpm; ●: 21410 rpm; ◑: 31820 rpm; ◐: 43700 rpm; ⊖: 51200 rpm; ⦶: 60000 rpm.

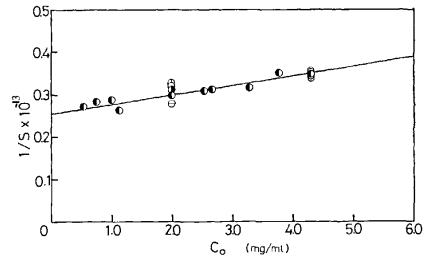

Fig. 2. Reciprocal of sedimentation coefficient for myosin-A plotted against concentration. Different symbols correspond to different rotor speeds, *i.e.*, ○: 10490 rpm; ●: 21410 rpm; ◑: 31820 rpm; ◐: 43700 rpm; ⊖: 51200 rpm; ⦶: 60000 rpm. The points at $C_0=4.34$ mg/ml read from the upper point as ◑, ●, ◐, ⦶, and ⊖.

coefficient D, when an adequate equation for H/A is available. Fujita[1,2] derived the following equation for this purpose.

$$G^{-1}(2r_a\omega^2S_0k_sC_0(H/A)t) = [r_a\omega^2k_sC_0S_0/2D^{1/2}][1-(S_0\omega^2t/2)(1-k_sC_0)]t^{1/2} \quad (4)$$

where G^{-1} is the inverse function of G. The value of D can then be determined from the slope of a plot of $[1-(1/2)(1-k_sC_0)\omega^2S_0t]t^{1/2}$ *vs.* $G^{-1}(2r_a\omega^2S_0k_sC_0(H/A)t)$. Figures 3 and 4 show the plots of $[1-(1/2)(1-k_sC_0)\omega^2S_0t]t^{1/2}$ *vs.* $G^{-1}(2r_a\omega^2S_0k_sC_0(H/A)t)$ for the smooth and skeletal muscle myosins, respectively. The zero-time corrections were made by plotting $(A/H)^2$ against time and extrapolating $(A/H)^2$ to zero. We see that the data points for each experiment lie on a straight line, most of the lines passing through the origin.

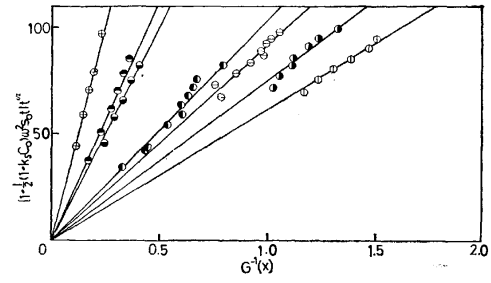

Fig. 3. Typical plots of $[1-(1/2)(1-k_sC_0)\omega^2S_0t]t^{1/2}$ against $G^{-1}(2r_a\omega^2k_sC_0S_0(H/A)t)$ for myosin-S. ⊕: $C_0=3.24$ mg/ml at 10490 rpm; ◒: 1.61 mg/ml at 21410 rpm; ◒: 0.98 mg/ml at 31820 rpm; ◐: 0.83 mg/ml; ⊖: 1.01 mg/ml; ◑: 1.25 mg/ml; ⦶: 1.95 mg/ml. The points not specified by the rotor speed were obtained at 43700 rpm.

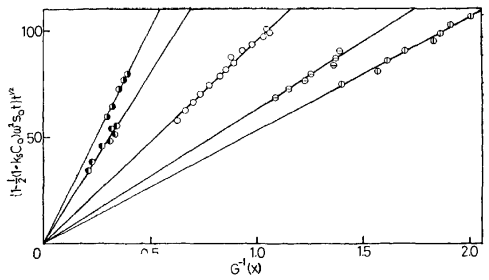

Fig. 4. Typical plots of $[1-(1/2)(1-k_sC_0)\omega^2S_0t]t^{1/2}$ against $G^{-1}(2r_a\omega^2k_sC_0S_0(H/A)t)$ for myosin-A. ◑: $C_0=2.01$ mg/ml at 21410 rpm; ◐: 0.76 mg/ml; ○: 1.13 mg/ml; ⊖: 1.85 mg/ml; ⦶: 2.46 mg/ml. The points not specified by the rotor speed were obtained at 43700 rpm.

Without zero-time corrections, however, the plots showed marked departure from the coordinate origin. According to the conditions used in deriving Eq. (4), the diffusion coefficient obtained from this equation may be taken as the one at $\bar{C}=C_0/2$.[2] The values of D for both myosins are plotted against C_0 in Fig. 5,

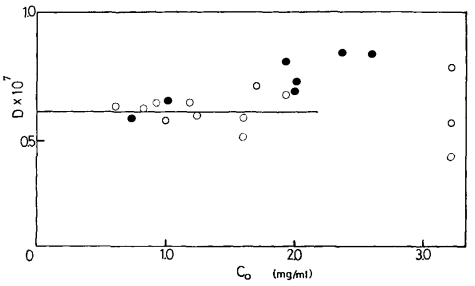

Fig. 5. Diffusion coefficients of myosins plotted against initial concentration, C_0. ○: myosin-S; ●: myosin-A.

which shows very small concentration dependence for either myosin, though the two sets of plotted points diverge considerably at higher concentrations. Considering the experimental error, the values for D at infinite dilution D_0 for both myosins may be taken as 0.64×10^{-7} cm²/sec. When this is reduced to 20 °C in water, we obtain 0.99×10^{-7} cm²/sec, which coincides with the values reported for myosin-A by other authors.[11-14] Substitution of the S_0 and D_0 values obtained into the Svedberg formula gives molecular weights of $5.2_7\times10^5$ for myosin-S and $5.1_0\times10^5$ for myosin-A. These values are slightly smaller than $5.8_7\times10^5$ for myosin-A reported by Harrington *et al.*[17] and $5.8_1\times10^5$ for myosin-S obtained from sedimantation equilibrium.[6] They are comparable with the values ranging between 5.0×10^5 and 5.5×10^5 obtained from sedimentation-diffusion measurements by others.[11-16]

11) R. G. Parrish and W. F. H. M. Mommaerts, *J. Biol. Chem.*, **209**, 901 (1954).
12) H. Mueller, J. Franzen, R. V. Rice and, R. E. Olson, *ibid.*, **239**, 1447 (1964).
13) K. Laki and W. R. Carrol, *Nature*, **175**, 389 (1955).
14) P. H. von Hippel, H. K. Schachman, P. Appel, and M. F. Morales, *Biochim. Biophys. Acta*, **28**, 504 (1958).
15) W. W. Kielley and W. F. Harrington, *ibid.*, **41**, 401 (1960).
16) P. Johson and A. J. Rowe, *Biochem. J.*, **74**, 432 (1960).
17) E. F. Woods, S. Himmelfarb, and W. F. Harrington, *J. Biol. Chem.*, **238**, 2374 (1963).

BULLETIN OF THE CHEMICAL SOCIETY OF JAPAN, VOL. 46, 2872—2873 (1973)

Solubilization of TCNQ by Anionic Surfactants

Shinya MUTO, Yoshiaki AONO,* and Kenjiro MEGURO

Faculty of Science, Science University of Tokyo, Kagurazaka, Shinjuku-ku, Tokyo 162

(Received January 30, 1973)

In a previous paper,[1] we reported on the remarkable coloration due to a charge transfer interaction between 7,7,8,8-tetracyanoquinodimethane (TCNQ) and cationic surfactants when the former was solubilized into the latter. A similar phenomenon has been reported by Deguchi *et al.*[2] for the interaction between TCNQ and nonionic surfactants.

The present paper deals with the determination of the cmc of anionic surfactants by measuring the change in shape of the absorption spectrum of TCNQ due to its solubilization.

Experimental

Lithium dodecyl sulfate (LiDS), sodium dodecyl sulfate (SDS), potassium dodecyl sulfate (KDS) and triethanol ammonium dodecyl sulfate (TDS) were used as anionic surfactants. They were synthesized by the same method as described previously.[1] All products were extracted for about 200 hr with petroleum ether and recrystallized five times from water–isopropyl alcohol mixtures. No minima were observed in the diagram of surface tension against the concentration of anionic surfactants. 7,7,8,8-tetracyanoquinodimethane (TCNQ) was synthesized by the usual method[1] and recrystallized five times from acetonitrile. Sodium chloride of extra pure grade was subjected to ignition.

Water was purified by percolation of tap water through an ion-exchanger, followed by distillation from alkaline potassium permanganate in a pyrex still. The specific conductance of water was $(1\sim1.9)\times10^{-6}$ ohm^{-1} cm^{-1} at 25 °C.

Solubilization measurement: the procedure was essentially the same as that described previously.[1] TCNQ (3 mg) was added to anionic surfactant solutions (15 ml) in L-type tubes and shaken for about three days (72 hr) in a water thermostat at 40±0.1 °C. After shaking, excess TCNQ was filtered off through glass filters. The absorption spectra of the samples were measured in 10 mm cells with a spectrophotometer (Hitachi EPS-3T) at 40±0.1 °C. The measurement was carried out on the same day as filtration, usually within 3 hr of filtration because of slow fading of color of the TCNQ-surfactant micelle complex solution.

Surface tension: measured with a Wilhelmy-type surface tensiometer (Shimazu ST-1) at 40±0.1 °C, the value obtained with 10 min of dipping being defined as surface tension.

Conductance: specific conductance was measured with a conductometer (Toa Electronics Model CM-1DS) and conductivity cell (Toa Electronics Type CG-201PL) at 40± 0.1 °C.

Results and Discussion

Remarkable coloration took place when TCNQ was solubilized in anionic surfactant solutions above cmc. The coloration was observed one day after the start of shaking in a thermostat at 40±0.1 °C. It increased gradually and reached equilibrium after about 72 hr. At equilibrium the color of TCNQ solubilized in LiDS, SDS, KDS, and TDS solutions was blue-purple, being almost the same for them all when observed with the naked eye. The absorption spectra of TCNQ solubilized in SDS and TDS solutions are shown in Figs. 1 and 2, respectively. Almost the same absorption spectra were observed for the other two surfactants. TCNQ in the solubilized state has absorption maxima

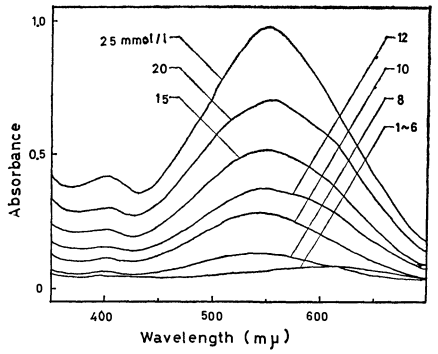

Fig. 1. Absorption spectra of TCNQ solubilized in SDS solutions. Figures show concentration of SDS solutions.

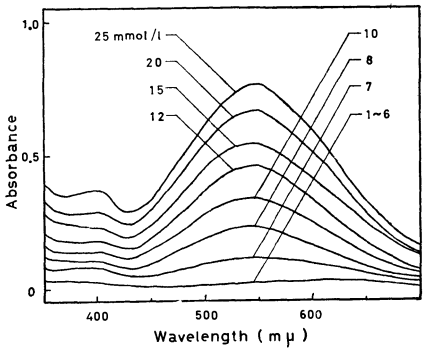

Fig. 2. Absorption spectra of TCNQ solubilized in TDS solutions. Figures show concentration of TDS solutions.

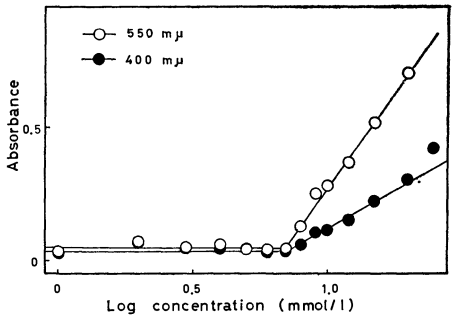

Fig. 3. Relationship between the absorbance and concentration of SDS solutions. The inflection point: 7.0 mmol/l

* Present address, Dic-Hercules Chemicals Inc., Dic Building, No. 3, Tori, 3-chome, Nihonbashi, Chuo-ku, Tokyo.

1) S. Muto, K. Deguchi, Y. Shimazaki, Y. Aono, and K. Meguro, This Bulletin, **44**, 1087 (1971).

2) K. Deguchi and K. Meguro, *J. Coll. Interface Sci.*, **38**, 596 (1972).

Table 1. Critical micelle concentration of anionic surfactants by electroconductance, surface tension and solubilization of TCNQ at 40 °C

Surfactant	Electro-conductance (mmol/l)	Surface tension (mmol/l)	Solubilization of TCNQ (mmol/l)
LiDS	8.4	7.0	7.6
SDS	8.1	6.8	7.0
KDS	7.4	6.6	5.8
TDS	6.2	5.5	6.0
Salt solution of SDS (concentration of NaCl)			
10 mmol/l	5.5	4.4	4.6
20 mmol/l	3.6	3.0	3.3

at 400 and 550 mμ above cmc but below, no remarkable absorption was observed except for some slight absorption bands at 400 and 620 mμ. Their intensities were very weak and broad. The intensities of the bands at 400 and 550 mμ increased rapidly above cmc with concentration of the surfactant.

Figure 3 shows the plot of the optical density at 400 and 550 mμ against the logarithm of surfactant concentration, in which the inflection point coincides with the cmc value. The cmc values of anionic surfactants obtained by this method are summarized in Table 1. They agree with those obtained by surface tension and electroconductance methods.

The effect of addition of sodium chloride on the spectrum of TCNQ solubilized into aqueous solution of SDS is shown in Fig. 4. The shape of the absorption spectrum is almost the same as that shown in Fig. 1. However, it was found that the addition of salt increased the intensity of the band of solubilized TCNQ and decreased the cmc of SDS. The cmc values measured in the presence of salt are given in Table 1. Increase in the intensity of the band of solubilized TCNQ by addition of salt is of particular interest (Fig. 4).

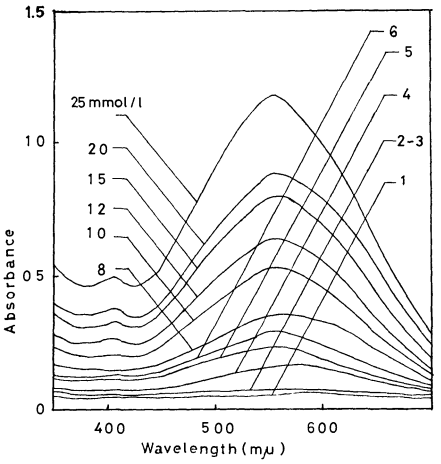

Fig. 4. The effect of addition of sodium chloride on the absorbance of spectrum of TCNQ solubilized into aqueous solution of SDS. Concentration of sodium chloride: 20 mmol/l. Figures show concentration of SDS solutions.

BULLETIN OF THE CHEMICAL SOCIETY OF JAPAN, VOL. 46, 2873—2875 (1973)

The Chlorine Nuclear Quadrupole Resonance of Several Oxygen-chlorine Bonds

Tsutomu OKUDA, Yoshihiro FURUKAWA, Koji YAMADA, and Hisao NEGITA

Department of Chemistry, Faculty of Science, Hiroshima University, Hiroshima 730

(Received February 8, 1973)

It seemed that it would be of interest to investigate the chlorine electronic structure in the O–Cl bond by means of the nuclear quadrupole resonance (NQR), since the oxygen atom is more electronegative than the chlorine atom and since various coordination states of the chlorine atom appear in the compounds with O–Cl bonds. Although many reports have been published on NQR studies of the chlorates in which the chlorine atom is bound by three oxygen atoms, there have been few reports on the other compounds with O–Cl bonds. Therefore, we have observed the ^{35}Cl NQR frequencies of the O–Cl bonds in the following compounds: *t*-butyl hypochlorite, *t*-amyl hypochlorite, sodium chlorite and its trihydrate, and silver chlorite. In these compounds, the two organic hypochlorites contain a chlorine atom bound by only one oxygen atom, whereas the chlorine atom in the chlorite is bound by two oxygen atoms. Furthermore, we have measured the NQR Zeeman effect using the single crystal of $NaClO_2 \cdot 3H_2O$.

Experimental

The sodium chlorite trihydrate was obtained by recrystallization from an aqueous solution of commercial $NaClO_2$. The single crystal was grown from its saturated aqueous solution at about 35 °C. The anhydrate salts were obtained by drying $NaClO_2 \cdot 3H_2O$ over KOH in a desiccator *in vacuo*. The silver chlorite was prepared by the reaction of $NaClO_2$ with $AgNO_3$. The alkyl hypochlorites were prepared by bubbling chlorine gas through an aqueous solution of the relevant alcohol and sodium hydroxide.

The NQR spectrometer was a self-quenching, superregenerative oscillator with frequency modulation; the ab-

1) J. S. Rigden and S. S. Butcher, *J. Chem. Phys.*, **40**, 2109 (1964).

Table 1. ^{35}Cl nuclear quadrupole resonance frequencies of several O–Cl bonds

Compound	Resonance frequency, MHz[a]	
	77 K	299 K
t-BuOCl	55.278	—
	54.941	—
t-AmOCl	55.492	—
$AgClO_2$	55.160[3]	54.052[3]
$NaClO_2$	53.342	51.802[3]
$NaClO_2 \cdot 3H_3O$	53.502	51.121

a) Experimental error is within ±0.01 MHz.

sorption lines were displayed on an oscilloscope. A Zeeman magnetic field was applied by means of a Helmholtz coil.

Results and Discussion

Table 1 shows the resonance frequencies at the temperature of liquid nitrogen and at room temperature. It is noteworthy that all the resonance frequencies in Table 1 are quite high compared with those of the usual chlorine compounds.

If the asymmetry parameter of the field gradient at the chlorine atom in R–OCl is assumed to be negligible, referred to $\eta=0.04$ for gaseous CH_3OCl,[1] the quadrupole coupling constant of 110.22 MHz (average) is obtained for *t*-BuOCl, and that of 110.98 MHz, for *t*-AmOCl, at 77 K. These values are slightly higher than that of atomic chlorine. This is an expected tendency, taking into account the electronegativity difference between oxygen and chlorine. Assuming the s character of the O–Cl bond to be 0.12, as in the case of the N–Cl bond,[2] and no $d\pi$-$p\pi$ bonding, the partial charge on the chlorine atom is $+0.16\,e$. This is in accordance with the fact that R–OCl is used as a chlorinating reagent in organic syntheses.

The resonance frequencies of $NaClO_2$ and $AgClO_2$ have been reported by Ragle;[3] they are in good agreement with our results, listed in Table 1. We have newly observed the resonance frequencies of $NaClO_2 \cdot 3H_2O$ and measured the Zeeman effect on its single crystal. Only one zero-splitting pattern was observed, as is shown in Fig. 1. This is consistent with the triclinic lattice of this compound. The asymmetry parameter of the field gradient was derived from the

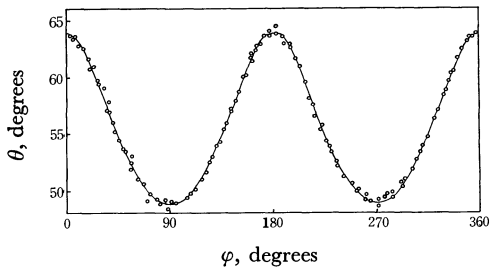

Fig. 1. Zeeman zero-splitting pattern of the chlorine atom in $NaClO_2 \cdot 3H_2O$ at room temperature.
$\sin^2\theta=2/(3-\eta\cos 2\varphi)$, $\eta=0.52$

2) R. M. Hart and M. A. Whitehead, *Trans. Faraday Soc.*, **67**, 1569 (1971).

3) J. L. Ragle, *J. Chem. Phys.*, **32**, 403 (1960).

usual equation, using the least-squares method, as 0.52 ± 0.02. From this value, the quadrupole coupling constant was calculated to be 94.348 MHz.

The bonding orbitals of the chlorine atom in the ClO_2^- ion may be presented as follows:[4]

$$\psi_1 = p_x,$$
$$\psi_2 = (\cot\theta)s - (1-\cot^2\theta)^{1/2}p_y,$$
$$\psi_3 = \sqrt{\frac{1}{2}}(1-\cot^2\theta)^{1/2}s + \sqrt{\frac{1}{2}}(\cot\theta)p_y + \sqrt{\frac{1}{2}}p_z,$$
$$\psi_4 = \sqrt{\frac{1}{2}}(1-\cot^2\theta)^{1/2}s + \sqrt{\frac{1}{2}}(\cot\theta)p_y - \sqrt{\frac{1}{2}}p_z, \quad (1)$$

where 2θ represents the $\angle$O–Cl–O bond angle. The x axis lies perpendicularly to the plane of the ClO_2^- ion and the y axis is directed along the twofold axis of the ion. We will express the electron population of the two bonding orbitals, ψ_3 and ψ_4, of the chlorine atom by A, and those of the orbitals occupied by the lone pair, ψ_1 and ψ_2, by B and 2 respectively. Using the Townes-Dailey theory, the electric-field gradients at the chlorine atom can be expressed as functions of θ, A, and B:

$$q_x/q_0(1+\varepsilon)^n = (1-\cot^2\theta)(A-2)/2 + B - A,$$
$$q_y/q_0(1+\varepsilon)^n = (1-\cot^2\theta)(2-A) + (A-B)/2,$$
$$q_z/q_0(1+\varepsilon)^n = (1-\cot^2\theta)(A-2)/2 + (A-B)/2, \quad (2)$$

where ε is 0.15 for the chlorine atom and where eq_0 is the field gradient of atomic chlorine. The symbol, n, represents the charge on the chlorine atom. The observed quadrupole coupling constant and asymmetry parameter are $|e^2Qq_i/h|$ and $(eq_k-eq_j)/eq_i$ when $|q_i|>|q_j|>|q_k|$.

The value of 2θ is in the range between 90° and 180°. If $B=2$, it can readily be found that q_x has the maximum absolute value of the field gradient when 2θ is between 90° and 109°28′. This is the case with the halogen bridge in the dimer molecule of the Group IIIb element or in the layer lattice as ScI_3, if the oxygen atom is replaced by the metal atom.[5] When 2θ is over 109°28′ and when $B=2$, the maximum field gradient becomes q_z.

The crystal structures of NH_4ClO_2 and $AgClO_2$ have been confirmed by means of X-ray diffraction.[6] The 2θ angles are found to be $110.5°\pm1.4°$ for NH_4ClO_2 and $111°\pm3°$ for $AgClO_2$. These angles are both larger than 109°28′. Also, the maximum field gradient at the chlorine atom in ClO_2 has been shown to be oriented along the axis of q_z.[7] Therefore, it seems reasonable to analyze the present data, by assuming that q_z is the maximum component of the field gradient.

As it is impossible to determine the three variables from the observed NQR parameters, we first assume the bond angle in this compound to be 111°. Substituting this value into Eq. (2), the following values

4) E. A. C. Lucken, "Nuclear Quadrupole Coupling Constants," Academic Press Inc., New York (1969).

5) See Ref. 4; P. A. Edwards and R. G. Barnes, *J. Chem. Phys.* **55**, 4664 (1971).

6) R. B. Gillespie, R. A. Sparks, and K. N. Trueblood, *Acta Crystallogr.*, **12**, 867 (1959); J. Cooper and R. E. Marsh, *ibid.*, **14**, 202 (1961).

7) R. F. Curl, *J. Chem. Phys.*, **37**, 779 (1962).

are obtained: $A=0.90$ and $B=1.73$. The decrease in B from 2 may be attributed to the presence of the $d\pi$-$p\pi$ bonding in the O–Cl bond. The value of A, 0.90, indicates that the charge of $0.60\,e$ is transferred to the oxygen atom from the chlorine atom in the σ bond of the O–Cl. The total charge on the chlorine atom is found to be $+1.47\,e$.

Taking 2θ to be larger than 111°, A becomes larger, whereas B becomes smaller. When $2\theta=123°$, $A=1.10$ and $B=2$, so the total charge on the chlorine atom is $+0.80\,e$. Actually, it may take an intermediate value between $+1.47\,e$ and $+0.80\,e$.

The temperature dependences were measured between 77 K and room temperature for $AgClO_2$, $NaClO_2$, and $NaClO_2\cdot 3H_2O$. All the frequency *vs.* temperature curves decrease steadily as the temperature is raised.

BULLETIN OF THE CHEMICAL SOCIETY OF JAPAN, VOL. 46, 2875—2876 (1973)

The ESR Spectra of Alkyl Radicals Formed in UV-irradiated Trialkyl Phosphate Glasses

Mitsuo SATO, Takashi KATSU, Yuzaburo FUJITA, and Takao KWAN
Faculty of Pharmaceutical Sciences, The University of Tokyo, Bunkyo-ku, Tokyo 113
(Received February 16, 1973)

We have recently reported the results of ESR studies of the intermediate radicals formed in UV-irradiated glasses of alkylalcohols,[1] alkanethiols,[2] and alkyl dithiophosphates.[3] As part of our continuing study of the photochemical production of intermediate radicals, we have now made a similar investigation into a series of tri-*n*-alkyl phosphates. As a result, we have found that alkyl radicals are formed rather selectively during the UV-irradiation of trialkyl phosphates at 77 K. In the present note we wish to communicate briefly the results of this investigation, since the photo-production of alkyl radicals from trialkyl phosphates has not yet been reported.

Experimental

The trialkyl phosphates employed in this work were $(CH_3O)_3PO$, $(C_2H_5O)_3PO$, $(n\text{-}C_3H_7O)_3PO$, and $(n\text{-}C_4H_9O)_3PO$. They were all commercial reagents supplied by the Tokyo Kasei Kogyo Co., and all were used without further purification. Each of the trialkyl phosphates showed a weak absorption spectrum in the region of 220—280 nm,[4] with a steep absorption edge below 220 nm. Thus, the UV light of the 253.7 nm wavelength from a low-pressure mercury lamp (Ushio Electric Co., Ltd., UL-200W) housed with a Vycor glass filter was thought to be effective. The UV-irradiation and ESR measurements were carried out at 77 K. Each sample gave a cracked-free glass upon cooling, and a few minutes' irradiation gave rise to an intense signal with a good S/N ratio. The other experimental details were similar to those of the previous report.[3]

Results and Discussion

ESR Spectra of Intermediate Radicals. Typical ESR spectra of photoproduced radicals are shown in Figs. 1 and 2.

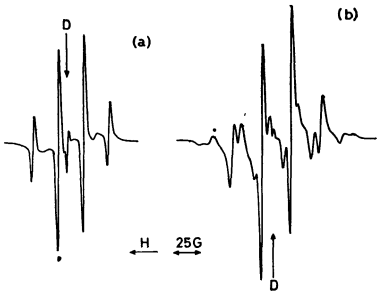

Fig. 1. ESR spectra of UV-irradiated trialkyl phosphates at 77 K.
(a) $(CH_3O)_3PO$, irradiation time 1.0 min;
(b) $(C_2H_5O)_3PO$, irradiation time 3.0 min;
D, defect signal (g=2.000) resulted from the quartz Dewar vessel.

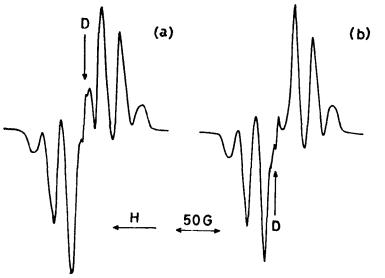

Fig. 2. ESR spectra of UV-irradiated trialkyl phosphates at 77 K.
(a) $(n\text{-}C_3H_7O)_3PO$, irradiation time 3.0 min;
(b) $(n\text{-}C_4H_9O)_3PO$, irradiation time 3.0 min.

The spectra obtained from trimethyl and triethyl phosphates were well-resolved and were assigned to methyl and ethyl radicals respectively (Fig. 1). The following hf coupling constants were in close agreement with those previously reported:[5]

1) K. Hatano, M. Yanagita, Y. Fujita, and T. Kwan, *Kogyo Kagaku Zasshi*, **72**, 123 (1969).
2) M. Yanagita, Y. Fujita, and T. Kwan, *Nippon Kagaku Zasshi*, **91**, 898 (1970).
3) M. Sato, M. Yanagita, Y. Fujita, and T. Kwan, This Bulletin, **44**, 1423 (1971).
4) This band can tentatively be assigned to a (n–π^*) transition after M. Halman and I. Platzner (*J. Chem. Soc.*, **1965**, 1440).
5) R. W. Fessenden and R. H. Schuler, *J. Chem. Phys.*, **39**, 2147 (1963).

$\dot{C}H_3$ A^H = 23.0 Gauss

$CH_3\dot{C}H_2$ A_α^H = 21.9 Gauss, A_β^H = 27.0 Gauss

It follows from Fig. 1, however, that ethyl radicals give hf lines with an unequal linewidth; moreover, the intensity distribution differs from the theoretical one, while the quartet hf lines of methyl radicals are equal in linewidth and their relative intensities are very close to the theoretical ratio of 1 : 3 : 3 : 1. Such an unequal linewidth as observed in the spectrum of the ethyl radical has already been interpreted by Cochran *et al.*[6] as arising from the effect of the anisotropic hf interaction with the α-protons. It seems, therefore, probable that the motional character of the ethyl radical differs from that of the methyl radical; such a supposition is in accordance with the decay behavior of these radicals, as will be described below.

The spectra obtained from UV-irradiated tri-*n*-propyl phosphate and tri-*n*-butyl phosphate are shown in Fig. 2. The two spectra are very similar in appearance and both consist of six broad hf lines resolved only poorly, with a splitting of 22—23 Gauss. By analogy with the spectra of radicals with the general formula of $RCH_2\dot{C}H_2$, as interpreted by Ayscough and Thomson,[7] the two spectra can be assigned to $CH_3CH_2\dot{C}H_2$ and $CH_3CH_2CH_2\dot{C}H_2$ respectively. The six hf lines may be explained on the assumption that the hf coupling constant for one of the β-protons is almost twice as great as that of the other β-proton and that of the α-protons (A_α^H=22 Gauss, $A_\beta^{H_1}$=22 Gauss, $A_\beta^{H_2}$=44 Gauss). The unequivalence of the β-protons in contrast to the ethyl radical indicates that these radicals are rather strongly constrained in the matrices, without any averaging movements of the CH_2 group. Such an interpretation is consistent with that reported by Shimada *et al.*,[8] who studied the ESR of radicals of the $CH_3\dot{C}HCH_2$-~~~ trapped in γ-irradiated polyethylene.

In general, the signal intensities of alkyl radicals were found to increase almost linearly with an increase in the irradiation time. No signal other than alkyl radicals was detected within 15 min irradiation of triethyl phosphate, tri-*n*-propyl phosphate and tri-*n*-butyl phosphate or within 2 min irradiation of trimethyl phosphate.[9] It appears from these results that alkyl radicals are formed primarily.

Since the trialkyl phosphates employed in the present work showed UV-absorption bands in the region of 220—280 nm assignable to a (n-π^*) transition, it is tempting to suppose that the electronic excitation of trialkyl phosphate molecules is associated with the rupture of the C–O bond rather than that of the C–H or P–O bond. It should be noted here that such an effect of UV-irradiation has a close resemblance, as far as the ESR information is concerned, to that of the γ-irradiation recently reported by several workers.[10,11]

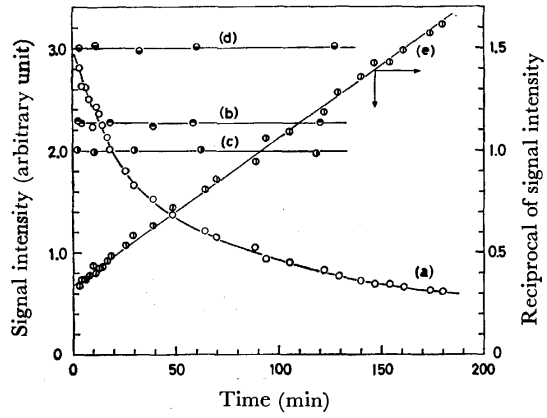

Fig. 3. Decay curves of alkyl radicals UV-produced and trapped in trialkyl phosphates at 77 K.
Signal intensity *vs.* time after UV-irradiation, (a) $\dot{C}H_3$, (b) $CH_3\dot{C}H_2$, (c) $CH_3CH_2\dot{C}H_2$, (d) $CH_3CH_2CH_2\dot{C}H_2$; Reciprocal of signal intensity *vs.* time after UV-irradiation, (e) $\dot{C}H_3$.

Stability of Alkyl Radicals. The signal intensities of the alkyl radicals trapped in the matrices were examined as a function of the time after the termination of the UV-irradiation. The results are shown in Fig. 3. It was found that ethyl, *n*-propyl, and *n*-butyl radicals did not decay at all within the period of observation, indicating that these radicals are stable in the matrices.

On the other hand, methyl radicals were found to decay, as is shown in Fig. 3, according to this equation: $-d[\dot{C}H_3]/dt = k[\dot{C}H_3]^2$. The second-order kinetics may imply that the radical recombination (1) takes place rather than the hydrogen-atom abstraction in the matrix (2).

$$\dot{C}H_3 + \dot{C}H_3 = C_2H_6 \quad (1)$$

$$\dot{C}H_3 + (CH_3O)_2P(=O)OCH_3 = CH_4 + (CH_3O)_2P(=O)O\dot{C}H_2 \quad (2)$$

However, the minor decay process due to the hydrogen-atom abstraction was proved by the appearance of a three-line spectrum (average splitting, 20 Gauss) ascribable to $(CH_3O)_2PO(O\dot{C}H_2)$ only after a considerable decay of the methyl radicals.

6) E. L. Cochran, F. J. Adrian, and V. A. Bowers, *J. Chem. Phys.*, **34**, 1161 (1961).

7) P. B. Ayscough and C. Thomson, *Trans. Faraday Soc.*, **58**, 1477 (1962).

8) S. Shimada, H. Kashiwabara, and J. Sohma, *J. Polym. Sci., A-2*, **8**, 1291 (1970).

9) In the case of trimethyl phosphate, anisotropic doublet hf lines due to the formyl radical (HCO, A^H=135 Gauss) were observed on further irradiation.

10) A. Begum, S. Subramanian, and M. C. R. Symons, *J. Chem. Soc., A*, **1970**, 1334.

11) C. M. L. Kerr, K. Webster, and F. Williams, *J. Phys. Chem.*, **76**, 2848 (1972).

BULLETIN OF THE CHEMICAL SOCIETY OF JAPAN, VOL. 46, 2877—2878 (1973)

Reactions of ^{82}Br Activated by Isomeric Transition in CH_4: A Re-Evaluation*

Richard W. HELTON, David W. OATES, and Edward P. RACK
University of Nebraska, Lincoln, Nebraska 68508 U.S.A.

(Received September 18, 1972)

In the first experiments utilizing rare-gas moderators in reactions of ^{82}Br activated by isomeric transition, Nicholas and Rack[1] found that in the $^{82}Br+CH_4$ system, the total organic product yield, extrapolated to zero mole fraction moderator, was $7.4\pm0.5\%$. The organic yield data appeared to extrapolate to $3.7\pm0.5\%$ at zero mole fraction CH_4 for the various rare-gas moderators, suggesting that 7.4% minus 3.7% was formed by excess kinetic energy processes and that 3.7% of the organic ^{82}Br was formed by thermal (kinetic energy independent) processes.

Tachikawa[2,3] studied the effect of argon moderator on the individual product yields of (I.T.)-activated ^{82}Br in CH_4. The extrapolation to zero mole fraction argon ($6.1\pm0.7\%$) agreed well with that of Nicholas and Rack, considering the larger amount of Br_2 scavenger used by Tachikawa (0.11 mol fraction Br_2), compared to a constant 15 Torr Br_2 at 700 Torr total pressure used by Nicholas and Rack. However, Tachikawa found that extrapolation to zero mole fraction CH_4 gave a total organic yield of $1.6\pm0.4\%$. Since this difference is much too large for experimental error, and the value at this extrapolation is necessary for determining the relative importances of kinetic energy dependent and thermal reactions, it was decided that a re-evaluation of the system was in order, to determine the nature of this discrepancy.

A description of our sample making techniques, irradiation procedures, and extraction techniques can be found elsewhere.[4-7] At least six samples were made for each condition, each containing 5 Torr of Br_2, and varying amounts of CH_4 and argon, for a total system pressure of 700 Torr. Neutron irradiations were for 30 sec in the Omaha, Nebraska, V. A. Hospital reactor, employing the "in-reactor technique" described by Nicholas and Rack.[1] All relative product distributions were determined by radiogas chromatography[8] employing a modified flow-through proportional counter of the type described by Wolf *et al.*[9] Only two organic products were observed in each case, $CH_3{}^{82}Br$ and $CH_2Br^{82}Br$.

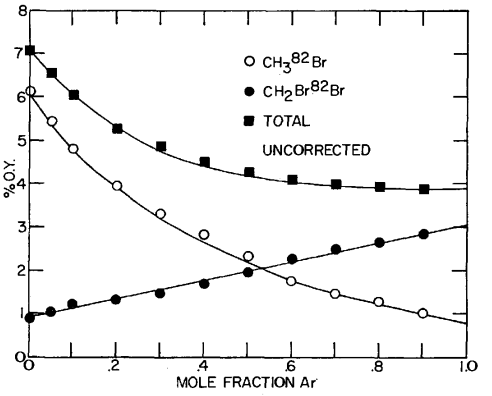

Fig. 1. Effect of Ar moderator on the product distribution in the reaction of (I.T.)-activated ^{82}Br with CH_4.

Depicted in Fig. 1 are the total organic product and individual organic product yields as a function of mole fraction argon. It can be seen that the extrapolations to zero mole fraction argon are in good agreement with both Nicholas and Rack, and Tachikawa. The $CH_3{}^{82}Br$ curve, also, strongly resembles that of Tachikawa. However, the $CH_2Br^{82}Br$ product increases linearly with increasing mole fraction argon, so that the total organic product yield resembles that of Nicholas and Rack, extrapolating to $3.8\pm0.4\%$ at zero mole fraction CH_4.

This linear dependence of organic yield upon concentration of moderator has been previously reported[10] and determined to be due to rare-gas sensitized radiation damage.

Figure 2 represents the total and individual organic product yields as a function of argon concentration, corrected for radiation damage.[10] Mixtures of CH_4

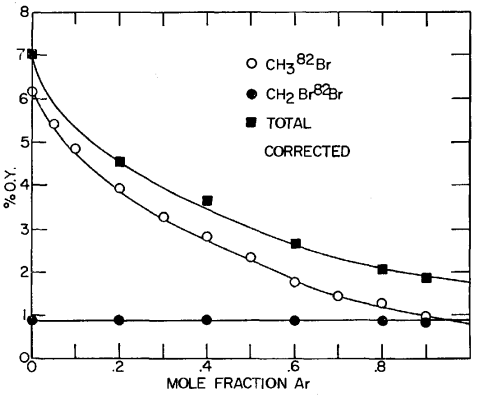

Fig. 2. Effect of Ar moderator on the reaction of (I.T.)-activated ^{82}Br with CH_4, corrected for radiation damage.

* This work was supported by the U.S. Atomic Energy Commission under Contract No. AT(11-1)-1617. This is AEC Document No. COO-1617-34.

1) J. B. Nicholas and E. P. Rack, *J. Chem. Phys.*, **48**, 9, 4085 (1968).
2) E. Tachikawa, This Bulletin, **42**, 2404 (1969).
3) E. Tachikawa, *ibid.*, **43**, 63 (1970).
4) J. A. Merrigan, W. K. Ellgren, Jr., and E. P. Rack, *J. Chem. Phys.*, **44**, 174 (1966).
5) J. A. Merrigan, J. B. Nicholas, and E. P. Rack, *Radiochim. Acta*, **6**, 94 (1966).
6) E. P. Rack and A. A. Gordus, *J. Phys. Chem.*, **65**, 944 (1961).
7) J. A. Merrigan and E. P. Rack, *ibid.*, **69**, 2795 (1965).
8) R. M. Lambrecht and E. P. Rack, *J. Chem. Phys.*, **48**, 3735 (1968).
9) M. Welch, R. Withnell, and A. P. Wolf, *Anal. Chem.*, **39**, 275 (1967).
10) E. P. Rack and A. A. Gordus, *J. Chem. Phys.*, **34**, 1855 (1961).

and argon containing 5 Torr of Br_2 and 0.1 Torr of ^{131}I labeled molecular I_2 were irradiated for 30 sec in the nuclear reactor. The percent of ^{131}I as total organic product yield was plotted as a function of argon concentration. Gas chromatographic analysis of the ^{131}I-labeled organic products was also performed. No $CH_3{}^{131}I$ product was detected at the various argon concentrations. Extrapolation of the corrected individual product yields to zero mole fraction CH_4 gives $0.9\pm0.2\%$ and $0.8\pm0.2\%$ for $CH_2Br^{82}Br$ and $CH_3{}^{82}Br$, respectively. This compares very well with the data of Tachikawa for the Br_2–CH_4–Ar system ($CH_2Br^{82}Br$, $1.1\pm0.2\%$ and $CH_3{}^{82}Br$, $0.5\pm0.2\%$), and, also, with other moderator studies.[11]

An important observation from inspection of Figs. 1 and 2 is that the only ^{82}Br labeled product affected by the argon-sensitized radiation damage is $CH_2Br^{82}Br$, which is formed exclusively by thermal (non-kinetic energy activated) ion-molecule reactions. No radiation damage is associated with the $CH_3{}^{82}Br$ product.

The apparent reason that this laboratory observes moderator-sensitized radiation damage while Tachikawa does not, is that we irradiated the premixed sample, containing all system components, and Tachikawa mixes the components after making the Br_2 radioactive.[3,11]

11) E. Tachikawa and J. Okamoto, *Radiochim. Acta*, **13**, 159 (1970).

BULLETIN OF THE CHEMICAL SOCIETY OF JAPAN, VOL. 46, 2878—2879 (1973)

Nuclear Quadrupole Resonance of Nitrogen-14 in the Naphthalene-Tetracyanoethylene Complex

Shinzaburo ONDA, Ryuichi IKEDA, Daiyu NAKAMURA, and Masaji KUBO

Department of Chemistry, Nagoya University, Chikusa, Nagoya 464

(Received May 14, 1973)

Tetracyanoethylene (TCNE) is known to be a strong electron acceptor capable of forming various stable molecular complexes,[1] of which naphthalene-TCNE is an example. The present investigation has been undertaken on the nuclear quadrupole resonance of ^{14}N in the complex in order to compare the spectra with those of TCNE previously reported[2] and to discuss the nature of intermolecular interaction between naphthalene and TCNE.

The 1:1 molecular complex of naphthalene and TCNE was prepared by a method described by Merrifield and Phillips.[3] Red-brown needle crystals deposited on mixing equimolar warm concentrated solutions of the components in ethyl acetate followed by cooling. Although the crystals gradually turned wine red on cooling to liquid nitrogen temperature, the appearance of the crystals showed no changes indicative of the first-order phase transition taking place in the temperature range investigated. The nuclear quadrupole resonance of ^{14}N was observed by means of a modified Pound-Watkins type spectrometer already described.[4] Frequency modulation was used for the determination of resonance frequencies, while Zeeman modulation was employed for the assignment of resonance signals to ν^{I} and ν^{II}. Resonance frequencies were measured by use of a Model VP-43A frequency counter from Matsushita Communication Industry Co., Ltd.

Since ^{14}N has a nuclear spin equal to unity, one can usually observe two resonance frequencies, $\nu^{I}=eQq\cdot(3+\eta)/4$ and $\nu^{II}=eQq(3-\eta)/4$, for resonant nuclei having a nonvanishing asymmetry parameter, η. Naphthalene-TCNE yielded two sets of ν^{I} and ν^{II} frequencies at liquid nitrogen temperature ($\nu^{I}=3278.2\pm0.1$ and 3246.2 ± 0.1 kHz and $\nu^{II}=3145.2\pm0.3$ and 3082.3 ± 0.1 kHz). The appearance of the two sets indicates that there are two kinds of crystallographically non-equivalent nitrogen atoms in crystals. Williams and Wallwork[5] have carried out X-ray analysis of this complex, and found that it forms monoclinic crystals belonging to the space group C2/m with two units of the complex in a unit cell. Naphthalene and TCNE molecules are stacked alternately in infinite columns aligned parallel to the c axis. Centrosymmetric TCNE molecules are located at inversion centers, and C=C bonds are directed along twofold axes. Therefore, all cyano groups are equivalent in a crystal in contradiction to the results of the present study. However, the X-ray analysis carried out at room temperature showed that the thermal vibration of a naphthalene molecule about an axis perpendicular to the molecular plane is abnormally large and that the geometry of naphthalene molecules could hardly be determined exactly. Therefore, the disagreement may be attributable to a slight change in crystal structure possibly taking place between room and liquid nitrogen temperatures. Although sharp and fairly intense signals were observed at liquid nitrogen temperature

1) D. N. Dhar, *Chem. Rev.*, **67**, 611 (1967).
2) S. Onda, R. Ikeda, D. Nakamura, and M. Kubo, This Bulletin, **42**, 2740 (1969).
3) R. E. Merrifield and W. D. Phillips, *J. Amer. Chem. Soc.*, **80**, 2778 (1958).
4) R. Ikeda, D. Nakamura, and M. Kubo, *J. Phys. Chem.*, **70**, 3626 (1966).
5) R. M. Williams and S. C. Wallwork, *Acta Crystallogr.*, **22**, 899 (1967).
6) A. Colligiani, L. Guibé, P. J. Haigh, and E. A. C. Lucken, *Mol. Phys.*, **14**, 89 (1968).

except for a very weak line of the second lowest frequency, no resonance could be detected at dry ice and room temperatures. This suggests that an order-disorder phase transition involving naphthalene molecules takes place between dry ice and liquid nitrogen temperatures.

Because two ν^{I} frequencies as well as two ν^{II} frequencies observed for naphthalene-TCNE are close to each other, one-to-one correspondence is infeasible between ν^{I} and ν^{II}. Therefore, averages were taken for the calculation of the quadurpole coupling constant and the asymmetry parameter. The results are shown in Table 1 along with those of some related compounds.

Table 1. Quadrupole coupling constants, eQq, and asymmetry parameters, η, of ^{14}N in naphthalene-TCNE and related compounds at liquid nitrogen temperature

Compound	eQq (kHz)	η (%)	Reference
Naphthalene-TCNE	4251	7.0	
TCNE	4221[a)]	4.4	2)
Acrylonitrile	3800	4.77	6)
Methacrylonitrile	3831	4.46	6)

a) eQq=4331 kHz in Table 1 of Reference 2 should read 4221 kHz.

As has been reported in a previous paper,[7] the quadrupole coupling constant and the asymmetry parameter of nitrogen in a cyano group having unequal π-electron populations, $1+i_{\pi\perp}$ and $1+i_{\pi//}$, can be expressed by

$$eQq = \left| s+i_{\sigma}-si_{\sigma}-\frac{1}{2}(i_{\pi\perp}+i_{\pi\parallel}) \right| \frac{eQq_{p}}{1+i\varepsilon} \quad (1)$$

$$\eta eQq = \frac{3}{2}\left| i_{\pi\perp}-i_{\pi\parallel} \right| \frac{eQq_{p}}{1+i\varepsilon} \quad (2)$$

Here it is assumed that the sp-hybridized σ-bond orbital and the lone pair orbital of nitrogen accommodate $1+i_{\sigma}$ and 2 electrons, respectively. The symbols, s, eQq_{p}, i, and ε denote the extent of s-character of the σ-orbital, the absolute value of the quadrupole coupling constant of an electron in a 2p-orbital of ^{14}N, the total ionicity of nitrogen, and the screening constant introduced by Townes and Schawlow,[8] respectively.

According to Eq. (2), relatively small asymmetry parameters observed for naphthalene-TCNE and TCNE indicate that the difference, $i_{\pi\perp}-i_{\pi//}$, in π-electron population is fairly small. This means that the π-electron systems of cyano groups in a TCNE molecule are not conjugated with the ethylenic double bond to a great extent. The same conclusion can be derived for acrylonitrile and methacrylonitrile. The quadrupole coupling constants of the complex and TCNE are considerably higher than those of acrylonitrile and its derivatives. This is rather difficult to interpret quantitatively because the theoretical equations involve several unknown parameters. However, Eq. (1) clearly shows that the quadrupole coupling constant decreases with increasing polarization of π-electrons in a cyano group. Accordingly, it is concluded that the π-bonds of cyano groups are less polarized in TCNE molecules than in acrylonitrile and its derivatives.

Since naphthalene-TCNE is a charge transfer complex, electron transfer is expected to take place from naphthalene to TCNE. In view of the stacking structure of the complex, such a transfer would result in an increase in the electronic population of π-orbitals directed at right angles to the molecular plane of TCNE. This leads to an increase in the asymmetry parameter and a decrease in the quadrupole coupling constant of nitrogen atoms in a TCNE molecule. In fact the observed asymmetry parameter of the complex is larger than that of TCNE. However, the difference between the observed asymmetry parameters of the two compounds is so small that it can be explained in terms of the effect of crystal field as well. Furthermore, the quadrupole coupling constant of the complex is slightly larger than that of TCNE in contradiction to the expectation. These facts suggest that the extent of charge transfer is fairly small and that the electronic state of nitrogen atoms in TCNE molecules remains essentially unaffected on forming a charge transfer complex with naphthalene.

Quite recently, Murgich and Pissanetzky[9] studied the nuclear quadrupole resonance of ^{14}N in potassium tetracyanoquinodimethanide, and found a small quadrupole coupling constant, 3.4 MHz (average), and a large asymmetry parameter, 52% (average). These results support the adequacy of the foregoing theoretical prediction.

7) R. Ikeda, S. Onda, D. Nakamura, and M. Kubo, *J. Phys. Chem.*, **72**, 2501 (1968).

8) C. H. Townes and A. L. Schawlow, "Microwave Spectroscopy," McGraw-Hill, New York, N. Y., (1955), p. 225.

9) J. Murgich and S. Pissanetzky, *Chem. Phys. Lett.*, **18**, 420 (1973).

BULLETIN OF THE CHEMICAL SOCIETY OF JAPAN, VOL. 46, 2880—2881 (1973)

Phase Transition in Organic Semiconductor. Entropy Change Due to Conduction Carriers

Yôichi IIDA

Department of Chemistry, Faculty of Science, Hokkaido University, Sapporo 060

(Received June 16, 1973)

There are a few organic semiconductors that are known to undergo phase transitions. The phase transitions of such materials are particularly interesting, because the anomalies in their electrical conductivities are associated with the phase transitions.[1-4] In a previous paper,[3] we studied the entropy for the system of conduction carriers (*i.e.*, electrons and holes) in an intrinsic semiconductor. By the use of a statistical theory, we examined to what extent this kind of entropy contributes to the total entropy change of the phase transition as determined from the heat-capacity measurements.

According to this theory, for an intrinsic semiconductor with very narrow band width, the magnitude of the entropy for the system of conduction carriers at temperature, T, is expressed by

$$S(\text{carrier}) = -4R\{f \ln f + (1-f) \ln (1-f)\}, \quad (1)$$

where $f \approx 1/\{\exp(E_g/2kT)+1\}$; E_g is the energy gap between the conduction band and the valence band. Consider the case when a first-order phase transition takes place in the intrinsic semiconductor at the T_c temperature in the solid state. The energy gaps for the low- and high-temperature phases are assumed to be E_g and E_g', respectively. At the transition temperature, the Fermi-Dirac distribution function, f, and the entropy due to the conduction carriers, S(carrier), in the low-temperature phase can be derived from the T_c and E_g values, while those in the high-temperature phase, f' and S'(carrier), from the T_c and E_g' values. Therefore, for the system of the conduction carriers, the entropy change, ΔS(carrier), associated with the phase transition is estimated to be

$$\Delta S(\text{carrier}) = S'(\text{carrier}) - S(\text{carrier}). \quad (2)$$

Let us consider two possible cases of the phase transitions. The first is of the phase transitions for intrinsic semiconductors where the E_g value in the low-temperature phase exceeds the E_g' value in the high-temperature phase. In this case, since the magnitude of S'(carrier) is larger than that of S(carrier) at $T=T_c$, a certain kind of order→disorder process with respect to the conduction carriers is involved in the phase transition, and the ΔS(carrier) value is positive in going from the low-temperature phase to the high-temperature phase. Therefore, if the phase transition of the semiconductor is endothermic, the ΔS(carrier) term plays a positive or additive contribution to the total entropy change of the phase transition, ΔS(total), as determined from heat-capacity measurements. The first-order phase transition of the semiconductive anion radical salt of $[(C_6H_5)_3PCH_3]^+ (TCNQ)_2^-$, where TCNQ is 7,7,8,8-tetracyanoquinodimethane, at $T_c=315.7$ K corresponds to one of these examples. According to the heat-capacity measurements by Kosaki *et al.*,[5] the enthalpy and the total entropy creation associated with this phase transition were experimentally determined to be 485.18 cal/mol and 1.7206 cal/K·mol, respectively. We have observed, at 315.7 K, a discontinuity in the temperature dependence of the electrical conductivity and a slight crystal volume decrease in the high-temperature phase.[1,4,6] By means of the temperature dependence of the conductivity, the E_g and E_g' values were experimentally determined to be 0.82 ± 0.04 eV and 0.60 ± 0.04 eV, respectively.[1,4] The crystal volume decrease perhaps gives rise to the fact that E_g exceeds E_g'. By the use of Eqs. (1) and (2), we have $\Delta S(\text{carrier})=1.5\times10^{-3}$ cal/K·mol for this phase transition. Therefore, we can evidently see that this positive ΔS(carrier) value contributes to the whole entropy creation of $\Delta S(\text{total})=1.7206$ cal/K·mol by 8.7×10^{-2}%.

The second case is of the phase transitions for intrinsic semiconductor where the E_g value is less than the E_g' value. This kind of phenomenon will be usually observed when a crystal volume increase is caused by the phase transition in the high-temperature phase. At this time, in going from the low-temperature phase to the high-temperature phase, a certain kind of disorder→order change with respect to the conduction carriers takes place at the phase transition, because the magnitude of S(carrier) is definitely larger than that of S'(carrier) at $T=T_c$. Therefore, for the endothermic phase transition of the semiconductor, although its over-all entropy is increased, the entropy for the system of the conduction carriers is decreased, and the ΔS(carrier) term plays a negative contribution to the total entropy change, ΔS(total), of the phase transition. We have to indicate the importance of this phenomenon. For example, the phase transition of crystalline hexamethylbenzene at $T_c=384.1$ K corresponds to this case. For this phase transtioin, the enthalpy change was experimentally determined to be 4.2×10^2 cal/mol, and the total entropy creation is estimated to be 1.1 cal/K·mol.[7,8] On the other hand, Kurematsu

1) Y. Iida, M. Kinoshita, M. Sano, and H. Akamatu, This Bulletin, **37**, 428 (1964).

2) K. Kurematsu, N. Kaneko, and S. Matsumoto, *ibid.*, **44**, 2845 (1971), and the references cited therein.

3) Y. Iida, *ibid.*, **44**, 3344 (1971).

4) Y. Iida, *J. Chem. Phys.*, in press.

5) A. Kosaki, Y. Iida, M. Sorai, H. Suga, and S. Seki, This Bulletin, **43**, 2280 (1970).

6) Y. Iida, *ibid.*, to be published.

7) M. E. Spaght, S. B. Thomas, and G. S. Parks, *J. Phys. Chem.*, **36**, 882 (1932).

8) Landort-Börnstein, "Zahlenwerte und Funktionen aus Physik, Chemie, Astronomie, Geophysik, Technik," II Band, 4 Teil, 6 Auflage, Springer-Verlag, Berlin. Göttingen. Heidelberg (1961); Nippon Kagaku-kai, "Kagaku Benran," Maruzen ,Tokyo (1966).

et al. measured the electrical conductivity and the crystal volume of this compound and found, at the transition temperature, an anomaly in the temperature dependence of the conductivity and an abrupt crystal volume increase in the high-temperature phase.[2] They assumed that the hexamethylbenzene crystal belonged to an intrinsic semiconductor, and determined experimentally the energy gaps in the low- and high-temperature phases, E_g and E_g', to be 2.5 and 4.5 eV, respectively. For this compound, the crystal volume increase perhaps gives rise to the fact that E_g is less than E_g'. By putting the E_g, E_g', and T_c values into Eqs. (1) and (2), we have $\Delta S(\text{carrier}) = -1.18 \times 10^{-14}$ cal/K·mol. Therefore, this negative ΔS(carrier) value, although its magnitude is very small, is found to make a negative contribution to the total entropy creation for this phase transition.

For such organic semiconductors as a hexamethylbenzene crystal, where the energy gap is considerably larger than kT, the magnitude of the entropy for the system of the conduction carriers is negligibly small, because the distributions of the electrons in the conduction band and of the holes in the valence band are quite limited at the temperature T. However, for semiconductors in which the energy gap is comparable to kT, the carrier population and, thus, the magnitude of the entropy due to the conduction carriers are very much increased. Consider the case when these semiconductors undergo first-order endothermic phase transitions. If the E_g value in the low-temperature phase is less than the E_g' value in the high-temperature phase, an appreciable amount of negative ΔS(carrier) value due to disorder→order process of the conduction carriers should make a significant negative contribution to the mechanism of the phase transitions. An attempt is currently under way to find such materials.

BULLETIN OF THE CHEMICAL SOCIETY OF JAPAN, VOL. 46, 2881—2883 (1973)

Carbon-13 NMR Spectra of 1-Arylpropynes and 1-Arylpropenes. Transmission of the Electronic Effects of Substituents through Carbon-Carbon Triple and Double Bonds

Kunisuke IZAWA, Tadashi OKUYAMA, and Takayuki FUENO

Department of Chemistry, Faculty of Engineering Science, Osaka University, Toyonaka, Osaka 560

(Received June 16, 1973)

It has been customary to use the Hammett $\rho\sigma$ relationship for the analysis of substituent effects on the side-chain reactions of benzene. The magnitude of reaction constant ρ usually diminishes with the increasing number of bonds intervening between the substituent and the reaction site.[1] This attenuation of the ρ value allows us to evaluate the efficiency of the intervening group in transmitting the electronic effect of substituents. A similar treatment is applicable to the ground-state properties; various spectral data have been analyzed on this basis.[2]

In the present work, we have investigated the effects of ring substituents on the ^{13}C chemical shifts of 1-phenylpropyne (**1**) and 1-phenylpropene (**2**) in order to compare the efficiencies of the C=C and C≡C bonds in transmitting the substituent effects. The C≡C bond has been found to be a less efficient transmitter.

Results

The ^{13}C NMR spectra of 1-phenylpropyne (**1**), *cis*- and *trans*-1-phenylpropenes (**2c** and **2t**) and their ring-substituted derivatives have been recorded in neat liquid. The chemical shifts were expressed in ppm *downfield* from tetramethylsilane as the standard.

The assignment of the α- and β-carbon signals of **1** was accomplished by the partial proton-decoupling technique. White and Levy[3] have recently reported the CMR spectral data of **1** and assigned the signals at 85.7 and 79.8 ppm to the α- and β-carbons, respectively, without any sound basis. On the other hand, Frei and Bernstein[4] observed the β-carbon signal at 86.8 ppm, using a ^{13}C-enriched sample. We have found that the signal at 86.4 ppm splits into quartet by partial proton-decoupling. The observed splitting must be due to the methyl protons. Although the spin coupling constants between ^{13}C and ^{1}H which are separated by more than one bond do not necessarily attenuate with an increase in the number of intervening bonds,[5] we have a good reason to say that $J_{C\text{-}C\text{-}H}$ is greater than $J_{C\text{-}C\text{-}C\text{-}H}$ in **1**. It is reported that the coupling constants between the methyl protons and the acetylenic carbons of propyne, $J_{C\text{-}C\text{-}H}$ and $J_{C\text{-}C\text{-}C\text{-}H}$, are 10.6 and 4.8 Hz, respectively.[6] Thus, the quartet signal can be assigned to the β-carbon, to which the methyl group is bonded. The assignment is compatible with the observation reported by Frei and Bernstein.[4]

1) H. H. Jaffé, *Chem. Rev.*, **53**, 191 (1953).
2) Y. Yukawa and Y. Tsuno, "Bunkokagaku 1968-B," ed. by Y. Morino, T. Shimanouchi, S. Fujiwara, and M. Oki, Nankodo, Tokyo, (1968), pp. 87—112.
3) D. M. White and G. C. Levy, *Macromolecules*, **5**, 526 (1972).
4) K. Frei and H. J. Bernstein, *J. Chem. Phys.*, **38**, 1216 (1963).
5) J. W. Emsley, J. Feeney and L. H. Sutcliffe, "High Resolution Nuclear Magnetic Resonance Spectroscopy," Vol. 2, Pergamon Press, Oxford, (1966), p. 1027.
6) J. N. Shoolery, *J. Mol. Spectrosc.*, **63**, 110 (1960).

The assignment of the α- and β-carbon signals of **2c** and **2t** was carried out with the aid of the additivity rule of Savitsky *et al.*[7] A methyl substitution of ethylene causes 12.9 ppm downfield and 7.4 ppm upfield shifts of the carbons α and β to the substitution, respectively.[7] In the same way, a phenyl substitution results in 13.0 ppm downfield and 10.5 ppm upfield shifts of the α- and β-carbons, respectively.[8] Using these shift values and the chemical shift of the ethylene carbon (122.8 ppm), we estimate the chemical shifts of the α- and β-carbons of **2** to be 128.4 and 125.2 ppm. Thus, the signals appearing at *ca.* 130 and 126 ppm of both **2c** and **2t** can be assigned to the α- and β-carbons, respectively.

Chemical shifts of sp and sp^3 carbons are substantially different from those of sp^2 carbons. Assignment of the signals of ring carbons was worked out, using both the partial proton-decoupling technique and the known additivity rule.[9]

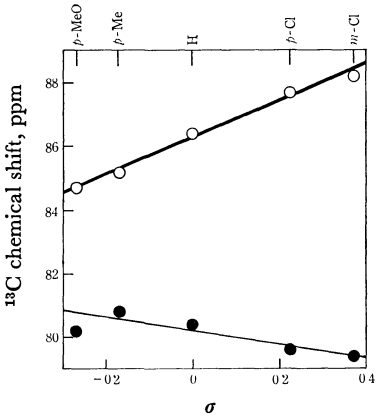

Fig. 1. Hammett plots of the ^{13}C chemical shifts of the α- (●) and β-carbons (○) of 1-phenylpropynes.

Table 1. ^{13}C chemical shifts[a] of the α- and β-carbons of ring-substituted **1**, **2c**, and **2t**

Substituent	1		2c		2t	
	α	β	α	β	α	β
p-CH_3O	80.2	84.7	130.2	125.2	131.7	123.6
p-CH_3	80.8	85.6	130.1	125.9	132.1	124.6
H	80.4	86.4	130.7	126.9	132.2	125.7
m-CH_3O					131.9	126.1
p-Cl	79.6	87.7	129.4	127.8	130.9	127.1
m-Cl	79.4	88.2				

a) In ppm downfield from TMS.

Table 2. Sensitivity constants for the ^{13}C chemical shifts of the β-carbons in **1**, **2c**, and **2t**

	1	2c	2t
ρ[a]	5.38	5.21	6.64
r[b]	0.993	0.992	0.991
s[c]	0.364	0.47	0.516

a) $\delta_X(\text{ppm})-\delta_H(\text{ppm})=\rho\sigma_X$. b) Correlation coefficient. c) Standard deviation of ρ.

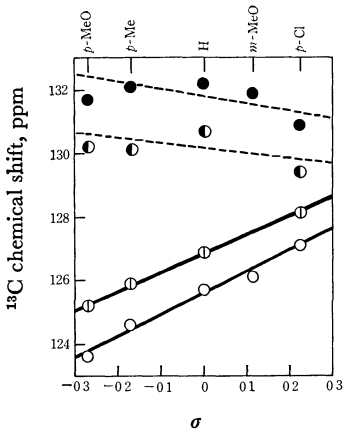

Fig. 2. Hammett plots of the ^{13}C chemical shifts of the α- and β-carbons of *cis*- and *trans*-1-phenylpropenes. **2c**; α(◐), β(◑), **2t**; α(●), β(○).

Listed in Table 1 are the ^{13}C chemical shift data obtained for the α- and β-carbons in the derivatives of **1**, **2c**, and **2t**. They are plotted against the Hammett σ constants in Figs. 1 and 2. In any case studied, the β-carbon shows a better linearity than does the α-carbon. The ρ values for the former carbon are given in Table 2, together with the related data.

Discussion

According to the present CMR data given in Table 2, the transmission efficiency of the unsaturated bond in either of **1** or **2c** is lower than that observed for **2t**. The low efficiency in **2c** may be due to the conformational effect arising from its nonplanar structure.[10] Since our specific aim here is to compare the electronic effects of the C=C and C≡C bonds in transmitting the substituent effect, the transmission efficiency of a C=C bond should be evaluated from the results for **2t**, which is coplanar and hence is free from the conformational problem. This leads to a conclusion that the efficiency of a C≡C bond is smaller than that of a C=C bond free from steric strain. The same trend is discernible in the comparison of the ρ values for the β-carbon shifts of phenylacetylene ($\rho=3.6$ ppm/σ[11]) and styrene ($\rho=4.73$ ppm/σ[8]).

It is known that ^{13}C chemical shifts well reflect the electron density (especially the π-electron density) of the carbon atom.[12] Savitsky *et al.*[7] have shown from CMR observations that the polarization of a C=C bond by an electron-donating group should effect an increase (upfield shift) in electron density at the β-carbon and a decrease (downfield shift) at the α-carbon. Most likely, the polarization effect of substituents will be the greater, the greater their electron donating or withdrawing property. The view is in line with our

7) G. B. Savitsky, P. D. Ellis, K. Namikawa, and G. E. Maciel, *J. Chem. Phys.*, **49**, 2395 (1968).
8) K. S. Dhami and J. B. Stothers, *Can. J. Chem.*, **43**, 510 (1965).
9) P. C. Lauterbur, *J. Amer. Chem. Soc.*, **83**, 1846 (1961).
10) T. Fueno, K. Yamaguchi, and Y. Naka, This Bulletin, **45**, 3294 (1972).
11) T. Higashimura and T. Masuda, private communication.
12) a) H. Spiesecke and W. G. Schneider, *Tetrahedron Lett.*, **1961**, 468; b) M. Karplus and J. A. Pople, *J. Chem. Phys.*, **38**, 2803 (1963); c) T. Tokuhiro and G. Fraenkel, *J. Amer. Chem. Soc.*, **91**, 5005 (1969); d) J. E. Bloor and D. L. Breen, *J. Pyhs. Chem.*, **72**, 716 (1968).

finding that, in both **1** and **2**, the signs of the ρ values for the α- and β-carbons are opposite to each other (Figs. 1 and 2). The small ρ-values of the β-carbon in phenylacetylenes as compared with those in styrenes may then be taken as an indication that a C≡C bond is less sensitive than a C=C bond to a perturbation in bond-polarity due to the introduction of polarizing substituents. This low sensitivity of a C≡C bond seems to be ascribable to the opposite polarization of orthogonal π-electrons in the triple bond.

The chemical shifts themselves of the α- and β-carbons seem to deserve brief comment. The polarization argument leads to the result that the side-chain unsaturated bonds of **1** and **2** are polarized in opposite directions.

$$C_6H_5-\overset{\delta-}{C}\equiv\overset{\delta+}{C}-CH_3 \qquad C_6H_5-\overset{\delta+}{C}H=\overset{\delta-}{C}H-CH_3$$

That is, for the acetylenic bond, the phenyl group appears to be less electron-donating than the methyl group, while the former is more electron-donating than the latter in the olefinic bond. However, this difference in the direction of polarization has no bearing with the lower sensitivity of the triple bond to the electronic effect of ring substituents.

Experimental

Preparation of the ring-substituted 1-phenylpropenes and 1-phenylpropynes will be described elsewhere.[13]

The ^{13}C NMR spectra of a neat liquid in an 8 mm φ sample tube were recorded at 25 °C on a JEOL C-60HL spectrometer with a 15.09 MHz RF unit. The signal to noise ratio of the spectra was enhanced by the ^{13}C–H noise decoupling. The chemical shift measurements were performed with a nuclear-resonance single-side-band technique, their accuracies being within ±0.2 ppm. CS_2 was used as an external standard. The chemical shifts are given in ppm downfield from TMS by using the chemical shift of CS_2 of 193.7 ppm.

The authors wish to thank Mr. H. Okuda for recording CMR spectra.

13) K. Izawa, T. Okuyama, and T. Fueno, to be submitted for publication.

BULLETIN OF THE CHEMICAL SOCIETY OF JAPAN, VOL. 46, 2883—2885 (1973)

The Photoconductivity of Poly(*N*-vinylcarbazole). IV.[1] The Photoconductivity of Copolymers of *N*-Vinylcarbazole with Styrene, Vinyl Acetate, and *N*-Vinylpyrrolidone[2]

Kenichi OKAMOTO,* Keishi KATO, Kenji MURAO, Shigekazu KUSABAYASHI,* and Hiroshi MIKAWA

Department of Applied Chemistry, Faculty of Engineering, Osaka University, Yamadakami, Suita, Osaka 565

(Received March 21, 1972)

In a previous paper,[1] the present authors proposed a mechanism of carrier migration in a poly-*N*-vinylcarbazole (PVCz) film based mainly on the structure of the polymer. The carriers seem to move easily along the chain from a carbazyl group to another adjacent carbazyl group through the overlap of the π-electrons of the carbazyl rings in the same polymer chain. In this note we wish to report that this manner of carrier migration is also suggested by an examination of the photoconductivity of the copolymers of *N*-vinylcarbazole (VCz) with styrene, vinyl acetate, or *N*-vinylpyrrolidone, as well as the alternate one-to-one copolymer of VCz and fumaronitrile (FN).

Copolymers rich in VCz were prepared by radical polymerization. The polymerization was carried out in a vacuum sealed tube at 60 °C for 2.5 hr. Azobisisobutyronitrile was used as the catalyst (1 mol%), and benzene as the solvent (1 mol/l). The feed ratio of monomers (VCz/comonomer) was 9/1. The copolymers thus obtained were fractionated by benzene–xylene in order to remove the PVCz homopolymer and were then purified by repeated reprecipitations (benzene–acetone). The alternate VCz–FN copolymer was prepared as has been described elsewhere.[3] The VCz content in the copolymers was determined both by elementary analysis and by UV absorption measurements. (The following absorption coefficients were used; $\varepsilon_{345}=3500$, $\varepsilon_{331}=2950$ l/mol cm.) The preparation of a sandwich-type cell and the electrical measurements were carried out in the same manner as has been described previously.[1]

The absorption spectra (both the positions of the absorption peaks and the molar extinction coefficient per carbazole unit) of the copolymers are the same as that of PVCz in the wavelength region longer than 300 mμ, where the comonomer components have no absorption. The films used in the measurement were 15 μ thick and completely absorbed the incident light shorter than 357 mμ. The fluorescence spectra of the copolymer films were almost the same as that of a PVCz film except in the case of the alternate VCz–FN

* Present address: Department of Chemical Engineering, Faculty of Engineering, Yamaguchi University, Ube, Yamaguchi.

1) Part III of this series; K. Okamoto, S. Kusabayashi, and H. Mikawa, This Bulletin, **46**, 2324 (1973).

2) Presented at the 23rd Anual Meeting of the Chemical Society of Japan (April, 1970).

3) Y. Shirota, A. Matsumoto, and H. Mikawa, *Polymer J.*, **3**, 643 (1972).

Table 1. Photocurrents of the copolymers of VCz

Polymer	Magnitude of the photocurrent, $\times 10^{-13}$A/cm^2					
	with negative electrode illumination			with positive electrode illumination		
	330mμ	360mμ	400mμ	330mμ	360mμ	400mμ
PVCz	120	900	35	300	2000	80
VCz–Vinyl acetate (8 mol%)	24 (1/5)	120 (1/7.5)	7 (1/5)	—	—	—
VCz–Vinyl acetate (17 mol%)	7.7 (1/16)	58 (1/15)	3.5 (1/10)	—	—	—
VCz–Vinylpyrrolidone (20 mol%)	4.4 (1/25)	42 (1/22)	0.6 (1/60)	12 (1/25)	60 (1/32)	1.6 (1/50)
VCz–Styrene (15 mol%)	17 (1/7)	130 (1/7)	2.3 (1/15)	23 (1/13)	290 (1/7)	8.0 (1/10)
PVCz doped with polystyrene (15 mol%)	56 (1/2)	540 (1/1.6)	20 (1/1.7)	160 (1/2)	800 (1/2.5)	35 (1/2.3)
Alternate 1:1 copolymer of VCz and FN	0	0	0	0	0	0

Values in parentheses represents the factors of decrease in the photocurrent as compared with the photocurrent of PVCz.

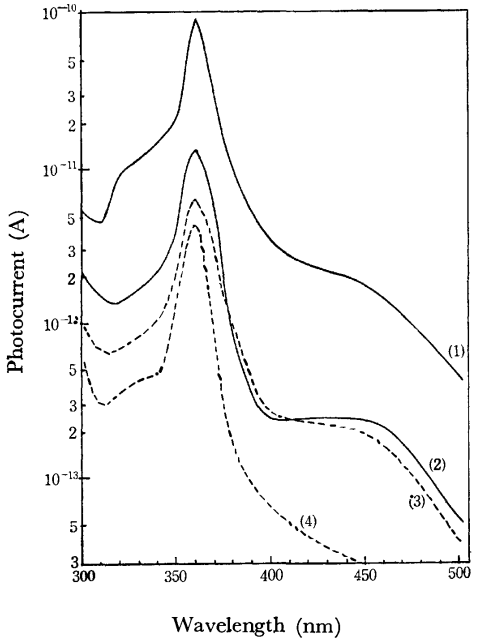

Fig. 1. Photocurrent of the copolymers of VCz with negative electrode illumination.
(1) PVCz, (2) VCz–styrene (15 mol%) copolymer, (3) VCz–vinyl acetate (17 mol%) copolymer, (4) VCz–*N*-vinylpyrrolidone (20 mol%) copolymer.

copolymer. In the film of the alternate copolymer, the excimer fluorescence was quenched almost completely and a weak emission due to the exciplex was observed.

The photocurrent was measured in a Nesa-Polymer-Gold sandwich-type cell (area of electrode: 1 cm^2) under 7000 V/cm in a high vacuum under the illumination of monochromatic light (2×10^{13} photons/cm^2 sec) at 20 °C. The copolymer films showed photoconductive properties similar to those observed in a PVCz film.[1] As is shown in Fig. 1 and Table 1, however, the photocurrent of the films of the copolymers (VCz content, 92—80 mol%), was smaller in magnitude by a factor of 5—50 than the photocurrent of the PVCz film. The photocurrent decreased in all spectral regions, irrespectively of the polarity of the illuminated electrode. The reduction of the photocurrent occurred in every copolymer, independently of the kind of comonomer. The alternate VCz–FN copolymer does not show any photoconductivity, although the FN component is thought to favor the formation of the cation of carbazole chromophore. The amount of decrease in the photocurrent depends mainly on the content of the comonomer.

On the other hand, the photocurrent in the PVCz film doped with polystyrene (dope amount, 15 mol%) decreased by only a factor of 1.5—2.5 as compared with the photocurrent in an undoped PVCz film. This decrease in the photocurrent is much smaller than that of the photocurrent in the VCz–styrene copolymer with the same content of the styrene component (15 mol%).

As has been reported in the previous paper,[1] the large photoconductivity of PVCz can be attributed both to the extrinsic carrier generation by the interaction of an exciton with some impurity and to the carrier migration through the overlap of π-electrons of the carbazyl groups in the same polymer chain. It has been found, from the study of the energy transfer,[4] that, in the films of the VCz-rich copolymers, the number of the carbazyl groups covered by an exciton during its lifetime is limited by the excimer-forming site in the copolymer chain in the same manner as in PVCz; it is evaluated to be almost the same (700) as in a PVCz film. Assuming that the conditions of the impurity (density and distribution) are almost the same in the copolymer films and in a PVCz film, the probability of an exciton interacting with any impurity will, therefore, be almost the same in both films. Consequently, the efficiency of the extrinsic carrier generation is not expected to decrease sufficiently to explain the observed results in the films of the copolymers rich in VCz. The comonomer components such as styrene may not be anticipated to act as trap centers or recombination

4) K. Okamoto, A. Yano, S. Kusabayashi, and H. Mikawa, Preprint of the 24th Anual Meeting of the Chemical Society of Japan, I-p. 142 (April, 1971). To be published in this Bulletin.

centers in view of the doping effect of some aromatic compounds on the photoconductivity of PVCz.[5] It seems, therefore, to be difficult to consider the significant decrease in the lifetime of the carrier due to trapping effect of the comonomer in the copolymer films.

Judging from the correlation between the crystallinity and the photocurrent in a PVCz film,[1] a small decrease in the crystallinity of the films does not seem to decrease the photocurrent significantly. As there was no significant difference in the crystallinity between the untreated films of the copolymers and of PVCz, the considerable decrease in the photocurrent in the films of the copolymers seems not to be due to any change in the crystallinity.

Therefore, the significant decrease in the photocurrent in the copolymers does not seem to be due to the lowering of the efficiency of the extrinsic carrier generation nor to the lowering of the crystallinity, but to the interruption effect of the comonomer components on the carrier migration. In the case of the copolymer of VCz with a comonomer such as styrene, with a small π-electron system, the sequence of the overlap of the adjacent carbazyl groups in the same polymer chain is frequently interrupted by the comonomer units introduced. As the lifetime of the carrier will be shorter than that of the exciton because of its higher energy state, it is supposed that during its lifetime a carrier covers a smaller number of the carbazyl groups than does an exciton. The excimer-forming site is hardly thought to limit the carrier migration, although it is able to act as a carrier trap. The carrier migration is, therefore, directly affected and reduced by the interruption of the overlap of the π-electrons of the carbazyl groups due to the comonomer component. This is the reason for the significant decrease in the photocurrent in the copolymers. This is also supported by the following three facts. First, as has been described previously, the decrease in the photocurrent of the copolymers does not depend on either the wavelength of the illuminated light, or the polarity of the illuminated electrode. Secondly, the decrease in the photocurrent in the PVCz film doped with polystyrene was not so large as in the film of the VCz–styrene copolymer. Thirdly, the alternate VCz–FN copolymer, where there is no sequence of carbazyl groups in the same polymer chain, has no primary photocurrent.

In conclusion, the photocurrent of the copolymers is reduced by a factor of 5—50. This might be due to the sum of the following three effects; the lowering of the efficiency of carrier generation, the reduction of the carrier life-time, and the disturbance of the carrier migration. The predominant effect seems to be the third effect, that is, the disturbance of carrier migration due to the interruption effect of the comonomer component on the overlap of the π-electrons of the carbazyl groups.

5) Part V of this series; K. Okamoto, S. Kusabayashi, and H. Mikawa, This Bulletin, **46**, 2613 (1973).

BULLETIN OF THE CHEMICAL SOCIETY OF JAPAN, VOL. 46, 2885—2887 (1973)

The Condensation of Orthophosphates with Acid Anhydrides

Makoto WATANABE, Hideaki USAMI, and Munehiro SUGASE

Department of Industrial Chemistry, Chubu Institute of Technology, Matsumoto-cho, Kasugai-shi, Aichi 487

(Received October 16, 1972)

Thilo *et al.* prepared potassium trimetaphosphate and sodium trimetaphosphate by treating monopotassium and monosodium orthophosphate respectively in a mixed solution of acetic acid and acetic anhydride.[1,2] Kasparek reported on the dehydration of various dihydrogen orthophosphates and pyrophosphates using the mixed solution mentioned above.[3,4] In a previous paper,[5] the present authors reported on the dehydration of mono-, di-, and trisodium orthophosphates in the same solution at 100 °C. In every case, the main product was the sodium trimetaphosphate. In the present work, the condensation reactions of mono- di-, and trisodium orthophosphates were carried out in mixed solutions of acetic acid and propionic, *n*-butyric, isobutyric, succinic, or maleic anhydride.

Experimental

Materials and Procedure. All the materials used were of a commercial grade. The water of the crystallization of orthophosphate was removed by heating it in an air bath at 120 °C. When propionic, *n*-butyric, or isobutyric anhydride was used as the dehydrating agent, 50 g of the anhydride was taken in a four-necked, round-bottomed, 200 ml flask; then 50 ml of acetic acid and 5 g of orthophosphate were added. The three samples of the mixture were heated, stirred, and refluxed at 100 °C for 10, 20, and 30 hr respectively. In the cases of succinic and maleic anhydrides, 25 g of the anhydride was placed in a four-necked, round-bottomed, 200 ml flask; then 100 ml of acetic acid and 5 g of orthophosphate were added, and the mixture was treated in the way described above. Each mixture was cooled after reaction periods of 10, 20, and 30 hr. The resulting precipitate was filtered off and washed with acetone. The composition of the phosphates con-

1) I. Grunze, K. Dostal, and E. Thilo, *Z. Anorg. Allgem. Chem.*, **302**, 221 (1959).
2) I. Grunze, E. Thilo, and H. Grunze, *Chem. Ber.*, **93**, 2631 (1960).
3) F. Kasparek, *Monatsh. Chem.*, **92**, 1023 (1961).
4) F. Kasparek, *ibid.*, **93**, 822 (1962).
5) M. Watanabe and T. Senda, This Bulletin, **45**, 2111 (1972).

tained in the precipitate was determined by X-ray diffractometry and paper chromatography.

X-Ray Diffractometry. The samples were ground with an agate mortar until they could pass through a 150-mesh sieve, and their X-ray diffraction pattern was taken with a Toshiba Model ADG-102 X-ray diffractometer.

Paper Chromatography. The separation and determination of condensed phosphates were performed with the method described in the present authors' previous paper.[5]

Results and Discussion

Mono-, di-, and trisodium orthophosphates were dissolved completely in a mixed solution of acid anhydride and acetic acid at 100 °C. A white product was freshly precipitated; appeared as a condensed phosphate. The quantity of the precipitate increased with increasing in the reaction time in every case. As Tables 1, 2, 3, and 4 show, except for the NaH_2PO_4–$(CHCO)_2O$–CH_3COOH system, the main product is trimetaphosphate. When propionic, *n*-butyric, or isobutyric anhydride is used as dehydrating agent, the content of trimetaphosphate in the precipitate increases with an increase in the reaction time, while the orthophosphate content decreases. In the condensation of mono- or disodium orthophosphate, a small amount of condensed phosphates, which have a longer chain than that of tripolyphosphate, exists after a reaction period of 10 hr. Tripolyphosphate also exists after reaction periods of 10, 20, and 30 hr. On the other hand, in the reaction of trisodium orthophosphate, the longer-chain phosphates and tripolyphosphate do not exist after any reaction period except in the case of the Na_3PO_4–$(CH_3CH_2CO)_2O$–CH_3COOH system. In the condensation of monosodium orthophosphate with succinic or maleic anhydride, the content of trimetaphosphate is smaller than that of di- or trisodium orthophosphate. In the reactions of di- and trisodium orthophosphates with succinic and maleic anhydrides, the content of trimetaphosphate at a reaction time of 40 hr is more than 90% in all cases.

Table 1. Distribution of phosphates in the products of the orthophosphate–propionic anhydride–acetic acid system (P%) (RT: reaction time)

RT (hr)	System	Ortho	Pyro	Tri	Tri-meta	Higher
10	Na 1	20.4	42.1	16.5	19.5	1.5
	Na 2	7.7	10.5	7.3	73.1	1.4
	Na 3	18.3	35.5	0.5	45.7	—
20	Na 1	5.9	9.5	7.3	77.3	—
	Na 2	6.6	8.9	10.4	74.1	—
	Na 3	12.3	32.6	—	55.1	—
30	Na 1	1.4	5.3	4.7	88.6	—
	Na 2	2.8	4.0	6.8	86.4	—
	Na 3	6.7	12.0	—	81.3	—

Na1: monosodium orthophosphate–propionic anhydride–acetic acid system.
Na2: disodium orthophosphate–propionic anhydride–acetic acid system.
Na3: trisodium orthophosphate–propionic anhydride–acetic acid system.

Table 2. Distribution of phosphates in the products of the orthophosphate–*n*-butyric anhydride–acetic acid system (P%) (RT: reaction time)

RT (hr)	System	Ortho	Pyro	Tri	Tri-meta	Higher
10	Na 1	19.6	39.6	15.8	23.1	1.9
	Na 2	5.9	9.5	8.8	73.5	2.3
	Na 3	19.5	33.5	—	47.0	—
20	Na 1	6.6	10.0	5.9	77.5	—
	Na 2	3.8	3.4	5.3	87.5	—
	Na 3	12.5	35.3	—	52.2	—
30	Na 1	1.8	4.2	4.3	89.7	—
	Na 2	1.2	2.3	1.0	95.5	—
	Na 3	3.0	3.4	—	93.6	—

Na1: monosodium orthophosphate–*n*-butyric anhyde–acetic acid system.
Na2: disodium orthophosphate–*n*-butyric anhydride–acetic acid system.
Na3: trisodium orthophosphate–*n*-butyric anhydride–acetic acid system.

Table 3. Distribution of phosphates in the products of the orthophosphate–isobutyric anhydride–acetic acid system (P%) (RT: reaction time)

RT (hr)	System	Ortho	Pyro	Tri	Tri-meta	Higher
10	Na 1	15.8	48.1	11.8	22.9	1.4
	Na 2	6.0	8.9	7.5	76.4	1.2
	Na 3	18.7	39.9	—	41.4	—
20	Na 1	5.1	10.3	7.6	77.0	—
	Na 2	4.9	8.5	9.3	77.3	—
	Na 3	13.9	27.6	—	58.5	—
30	Na 1	2.0	2.1	2.2	93.7	—
	Na 2	2.2	4.8	9.5	83.5	—
	Na 3	7.4	12.5	—	80.1	—

Na1: monosodium orthophosphate–isobutyric anhydride–acetic acid system.
Na2: disodium orthophosphate–isobutyric anhydride–acetic acid system.
Na3: trisodium orthophosphate–isobutyric anhydride–acetic acid system.

Table 4. Distribution of phosphates in the products of the orthophosphate–succinic anhydride–acetic acid and –maleic anhydride–acetic acid system (P%) (RT: reaction time)

RT (hr)	System	Ortho	Pyro	Tri	Tri-meta	Higher
20	SNa 1	35.2	15.2	8.5	41.1	—
	SNa 2	8.7	8.9	8.7	73.7	—
	SNa 3	7.3	5.5	8.6	78.6	—
	MNa 1	91.8	3.1	0.6	4.5	—
	MNa 2	15.9	11.3	6.7	66.1	—
	MNa 3	3.0	8.3	6.6	82.1	—
40	SNa 1	11.5	10.2	7.5	70.8	—
	SNa 2	2.5	3.0	1.2	93.3	—
	SNa 3	1.2	3.2	0.7	94.9	—
	MNa 1	57.9	22.8	1.1	18.2	—
	MNa 2	2.4	2.5	2.7	92.4	—
	MNa 3	2.0	1.8	2.1	94.1	—

(S, M, Na1, Na2, and Na3 represent succinic anhydride, maleic anhydride, mono-, di-, and trisodium orthophosphate respectively.)

Griffith and Buxton[6] reported that, when sodium polyphosphate (with a longer chain than in tetra) was hydrolyzed, trimetaphosphate was formed, while in the hydrolysis of polyphosphate with cations other than the sodium ion, scarcely no trimetaphosphate was formed. They concluded from these facts that the sodium ion is related to the formation of the trimetaphosphate ring. The fact that, in the present work, the main product is trimetaphosphate, seems related to the above conclusion. The yield of the precipitate and the theoretical value of $(NaPO_3)_3$ to be obtained per 5.00 g of each of the orthophosphates are shown in Table 5. The theoretical values are calculated assuming that the orthophosphates are completely converted into $(NaPO_3)_3$ by means of the equations described in the previous paper.[5] The formation process of sodium trimetaphosphate has already been discussed by Kasparek,[3] the same process has also been considered for these condensation reactions.

Table 5. The yields of the deposits and the theoretical amounts of $(NaPO_3)_3$ per 5 g of orthophosphates

		Acid anhydride				
	TV	PP	NBT	IBT	SC	MC
Na 1	4.25	4.20	4.15	4.10	3.45	3.04
Na 2	3.59	3.48	3.45	3.55	3.24	2.47
Na 3	3.11	2.85	2.92	3.10	2.93	2.25

Na1: monosodium orthophosphate, Na2: disodium orthophosphate, Na3: trisodium orthophosphate, TV: theoretical value, PP: propionic anhydride, NBT: *n*-butyric anhydride, IBT: isobutyric anhydride, SC: succinic anhydride, MC: maleic anhydride.

6) E. J. Griffith and R. L. Buxton, *J. Amer. Chem. Soc.*, **89**, 2884 (1967).

BULLETIN OF THE CHEMICAL SOCIETY OF JAPAN, VOL. 46, 2887—2888 (1973)

Some Palladium Complexes Containing a Benzoyl Group

Keinosuke SUZUKI and Minoru NISHIDA

Inorganic Chemistry Laboratory, Faculty of Science, Nagoya University, Chikusa-ku, Nagoya 464

(Received February 27, 1973)

The acyl complexes of transition metals are prepared by the reaction of acyl halides with low-oxidation transition metal complexes or by the insertion of CO into the metal-carbon bond of alkyl or aryl complexes. The formation of the complexes containing a benzoyl group have also been reported in several papers.[1-4] However, no palladium complex with a benzoyl group has yet been prepared. In this paper we will report on the formation and the infrared spectra of PdCl(COPh)$(PPh_3)_2$ (I) and other benzoyl complexes of palladium derived from (I) by ligand-exchange reactions.

Results and Discussion

The reaction of $Pd(PPh_3)_4$ with PhCOX gave PdX(COPh)$(PPh_3)_2$ (X=Cl, Br). The recrystallization of the chloride (I) from acetone gave (I′) containing one molecule of acetone. Two other complexes, PdCl(COPh)(P–P) (III) and PdCl(COPh)(phen) (IV) (P–P=$Ph_2PCH_2CH_2PPh_2$, phen=*o*-phenanthroline), were obtained by the ligand-exchange reaction of (I). In the solid state, all the complexes are stable enough to handle in air, but are unstable in solution. The reaction of (I) with dipyridyl did not give the expected compound, PdCl(COPh)(dipy). This failure might be due to the fact that the ligand exists in the *trans* form in the free state.

TABLE 1. IR DATA OF THE PALLADIUM COMPLEXES (cm^{-1})

	Complex	ν(C=O)	ν(Pd–Cl)
(I)	PdCl(COPh)$(PPh_3)_2$	1640	235
(I′)	PdCl(COPh)$(PPh_3)_2(CH_3)_2CO$	1702 1648	235
(II)	PdBr(COPh)$(PPh_3)_2$	1640	—
(III)	PdCl(COPh)(P–P)	1639	282
(IV)	PdCl(COPh)(phen)	1643	325

The infrared data of the complexes prepared are summarized in Table 1. As is clear from the table, all the complexes have a strong band due to ν(CO) *ca.* 1640 cm^{-1}, this is characteristic of a benzoyl group coordinated to a transition metal. The –C=O stretching frequency has been lowered *ca.* 80 cm^{-1} in comparison with the ν(CO) of the free benzoyl chloride. Green[5] suggested that the lowering may be due either to some double bonding of the metal with π-orbitals of the C=O group or to some direct interaction of the metal with the C=O group. In the ^{13}C NMR of $Fe(CO)_2(\pi\text{-}C_5H_5)(COPh)$,[6] the resonance of $^{13}COPh$ showed a large low-field shift which could be associated with the multiple bonding between the *d*-orbitals of the metal and the sp^2 carbon atom. Therefore, it was expected that the change in the donor atom *trans*

1) M. C. Baired and G. Wilkinson, *J. Chem. Soc., A*, **1967**, 865.
2) M. C. Baired, J. T. Mague, J. A. Osborn, and G. Wilkinson, *ibid.*, **1967**, 1347.
3) G. Booth and J. Chatt, *J. Chem. Soc., A*, **1966**, 1437.
4) M. Kubota and D. M. Blake, *J. Amer. Chem. Soc.*, **93**, 1368 (1971).
5) G. E. Coates, M. L. H. Green, and K. Wada, "Organometallic Compounds," Vol. 2, Methuen, London, (1968) p. 261.
6) J. A. Connor, E. M. Jones, E. W. Randall, and E. Rosenberg, *J. Chem. Soc. A*, **1972**, 2419.

to the benzoyl group has some effect on the ν(CO) of the ligand. However, the ν(CO) values of the complexes studied here remained approximately constant. Although the results may be explained by assuming either that the difference in the π-acceptor property of the donor atom is small[7] or that the direct interaction between the metal and the CO group is important, further investigations seem to be necessary to examine the effect of π-interaction on the ν(CO) of the acyl group.

In (I'), the band due to the ν(CO) of acetone was observed at 1702 cm^{-1}. The band is shifted *ca.* 30 cm^{-1} to wave numbers lower than that of free acetone. However, this shift is smaller than the lowering of ν(CO) found for the acetone which coordinates to Rh through a lone pair on the oxygen.[8] Thus, it seems to be difficult to discuss the coordination of acetone for (I') on the basis of the ν(CO) data alone.

The far infrared spectrum of (I) showed three bands, at 317, 270, and 235 cm^{-1}. The two bands at 270 and 235 cm^{-1} disappeared in the corresponding bromide. Since the ν(Pd–Cl) of (III), where P is *trans* to Cl, appeared at 281 cm^{-1}, one possible explanation of the disappearance of the band at 270 cm^{-1} is to assume the presence of the *cis*-isomer. However, its existence is rather suspected when the steric hindrance of the two bulky groups (PPh_3) in the *cis*-position is considered. Thus, the assignment of the band at 270 cm^{-1} is uncertain at present. Probably ^{31}P NMR measurements would clarify the ambiguity.

Recently Dent *et al.*[9] reported that the assignment of ν(Pt–Cl) for $PtCl(COPh)(PPh_3)_2$ made by Baired and Wilkinson[1] was incorrect and that the ν(Pt–Cl) really appeared at 261 cm^{-1}, indicating a large *trans* influence of an acyl group. This is also true in iridium complexes.[4,10] The large *trans* influence of an acyl group seems to be a general tendency, and the band at 235 cm^{-1} of (I) is probably due to the ν(Pd–Cl), where Cl is *trans* to the benzoyl group.

Experimental

Measurements. The infrared spectra were recorded with JASCO-DS-402G and HITACHI EPI-L2 spectrometers (nujol or HCB mulls).

Materials. The $Pd(PPh_3)_4$ was prepared by the method described in the literature.[11] The benzoyl chloride and benzoyl bromide were distilled before use. All the solvents used were dried over sodium and distilled under nitrogen. All the reactions were carried out under nitrogen.

Chloro(benzoyl)bis(triphenylphosphine)palladium (I): Into 0.9 g of $Pd(PPh_3)_4$ in 100 ml of benzene, we stirred 0.5 ml of C_6H_5COCl in 50 ml of benzene. After the yellow solution had then been allowed to be stirred overnight, it was concentrated to about 30 ml and filtered off to remove the small amount of precipitates formed. The filtrate was subsequently treated with 150 ml of ether. The pale yellow precipitates were filtered, washed with ether, and dried *in vacuo*. Found: C, 66.4; H, 4.9; Pd, 13.6%. Calcd for $C_{43}H_{35}ClOP_2Pd$: C, 66.9; H, 4.6; Pd, 13.8%.

The recrystallization of (I) from acetone gave $PdCl(COPh)(PPh_3)_2(CH_3)_2CO$, (I'). Found: C, 66.7; H, 4.9; Pd, 12.8%. Calcd for $C_{46}H_{41}ClO_2P_2Pd$: C, 66.6; H, 5.0; Pd, 12.8%.

Similarly, $PdBr(COPh)(PPh_3)_2$ (II) was prepared by the reaction of $Pd(PPh_3)_4$ with benzoyl bromide. Found: C, 62.5; H, 4.2; Pd, 12.9%. Calcd for $C_{43}H_{35}BrOP_2Pd$: C, 63.3; H, 4.3; Pd, 13.0%.

Chloro(benzoyl)1,2-bis(diphenylphosphino)ethanepalladium (III): To 1 g of $PdCl(COPh)(PPh_3)_2$ in 100 ml of benzene, we added 0.5 g of $Ph_2PCH_2CH_2PPh_2$ in 10 ml of benzene. About ten minutes later, yellow crystals started to precipitate. After the mixture had been stirred for 1 hr, the crystals were filtered off, washed with ether, and dried *in vacuo*. Found: C, 61.7; H, 4.6; Pd, 15.9%. Calcd for $C_{33}H_{29}ClOP_2Pd$: C, 61.4; H, 4.5; Pd, 16.5%.

Chloro(benzoyl)(*o*-phenanthroline)palladium (IV) was prepared in a similar way. Found: C, 53.1; H, 3.1; Pd, 24.5; N, 6.7%. Calcd for $C_{19}H_{13}N_2ClOPd$: C, 53.4; H, 3.1; Pd, 24.9; N, 6.7%.

7) W. D. Horrocks and R. C. Taylor, *Inorg. Chem.*, **2**, 723 (1963).
8) R. R. Schrock and J. A. Osborn, *J. Amer. Chem. Soc.*, **93**, 2397 (1971).
9) S. P. Dent, C. Eaborn, A. Pidcock, and B. Ratcliff, *J. Organometal. Chem.*, **46**, C68 (1972).
10) A. J. Deeming and B. L. Shaw, *J. Chem. Soc. A*, **1969**, 1128.
11) D. R. Coulson, "Inorganic Syntheses," Vol. 13, McGraw-Hill, New York (1972), p. 121.

BULLETIN OF THE CHEMICAL SOCIETY OF JAPAN, VOL. 46, 2889—2890 (1973)

The Hydrolysis of Y^{3+}, La^{3+}, Gd^{3+}, and Er^{3+} Ions in Heavy Water[1)]

Toshihiko AMAYA,[2)] Hidetake KAKIHANA, and Masunobu MAEDA*

Research Laboratory of Nuclear Reactors, Tokyo Institute of Technology, O-okayama, Meguro, Tokyo 152

**Department of Electrochemistry, Tokyo Institute of Technology, O-okayama, Meguro, Tokyo 152*

(Received March 2, 1973)

In the preceding papers,[3-6)] we studied the hydrolysis reactions of Be^{2+}, UO_2^{2+}, and Cu^{2+} ions in heavy water, and found that the compositions of the hydrolysis species formed in heavy water are the same as those in light water, while the stability constants of the complexes in heavy water are smaller than those in light water.

In the present work, the hydrolysis reactions of Y^{3+}, La^{3+}, Gd^{3+}, and Er^{3+} ions in heavy water have been studied and the results have been compared with those previously obtained in light water.[7)]

Symbols

The symbols used are the same as those described in Refs. 3 and 7.

Experimental

Reagents and Apparatus. The reagents used were, unless otherwise stated, prepared and analyzed as has been described in Ref. 7. A rare-earth perchlorate solution of heavy water was prepared from its solution of light water by repeated evaporation under an infrared lamp, while adding heavy water.

All the apparatuses employed were the same as those used in Ref. 7.

Procedures. All the measurements were carried out in a paraffin-oil thermostat kept at 25.00±0.01 °C and placed in a room thermostated at 25±1 °C.

The hydrolysis of the rare-earth ions was investigated by measurements of the deuterium-ion concentration with a glass electrode. A hydrolyzed test solution prepared by the procedures described in the preceding paper[7)] was electrolyzed to generate D^+ ions by means of constant-current coulometry. The same cell assembly as that described in Refs. 3 and 7 was used for the emf measurements and the constant-current coulometry.

Results and Discussion

The $Z(\log d)_B$ data for Y^{3+}, La^{3+}, Gd^{3+}, and Er^{3+} ions are graphically represented in Fig. 1.

The experimental data were analyzed by the methods

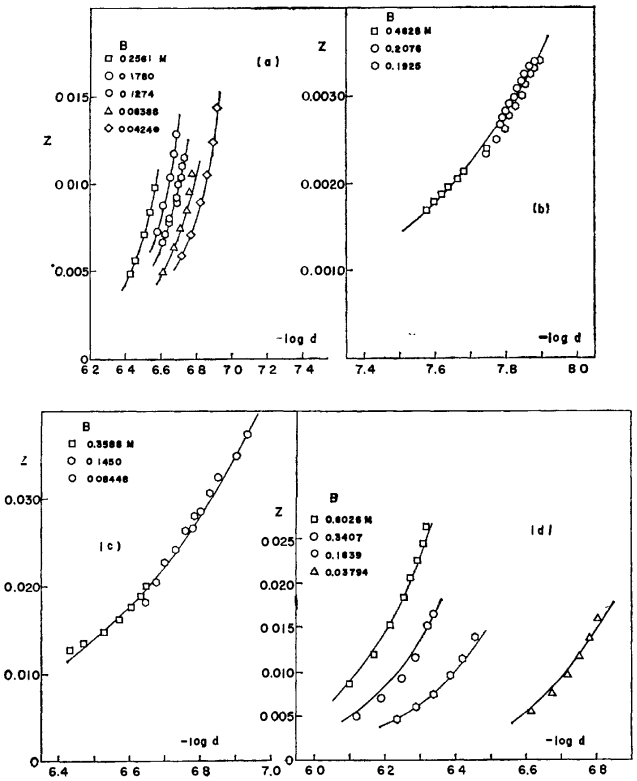

Fig. 1. Average number, Z, of OD bound per a) Y(III), b) La(III), c) Gd (III) and d) Er (III), as a function of $-\log d$. The drawn curves were calculated with the stability constants listed in Table 1.

TABLE 1. STABILITY CONSTANTS FOR THE HYDROLYSIS SPECIES OF THE RARE-EARTH IONS IN HEAVY WATER AND IN LIGHT WATER[a)]

	Y^{3+}		La^{3+}		Gd^{3+}		Er^{3+}	
	in D_2O	in H_2O	in D_2O	in H_2O	in D_2O	in H_2O	in D_2O	in H_2O
$-\log \beta_{1,1}$	—	—	10.35 ±0.01	10.04 ±0.01	8.34 ±0.02	8.20 ±0.01	—	—
$-\log \beta_{2,1}$	17.0 ±0.1	16.8 ±0.1	—	—	—	—	17.4 ±0.1	17.2 ±0.1
$-\log \beta_{2,2}$	14.75 ±0.03	14.04 ±0.01	—	—	—	—	14.29 ±0.01	13.72 ±0.01

a) The uncertainties of the constants were estimated as 3σ.

1) Ionic Equilibria in Heavy Water (Part VIII).
2) Present address: NGK Insulators Co., Mizuho, Nagoya.
3) H. Kakihana and M. Maeda, This Bulletin, **43**, 109 (1970).
4) M. Maeda and H. Kakihana, *ibid.*, **43**, 1097 (1970).
5) H. Kakihana, T. Amaya, and M. Maeda, *ibid.*, **43**, 3155 (1970).
6) H. Kakihana, T. Amaya, and M. Maeda, *Trans. Royal Inst. Tech. (Stockholm), Pure and Appl. Chem.*, **34**, 49 (1972).
7) T. Amaya, H. Kakihana, and M. Maeda, This Bulletin, **46**, 1720 (1973).

described in Ref. 7.

The most probable values for the stability constants of the hydrolysis species, calculated by means of the generalized least-squares method with the aid of an electronic computer (HITAC 5020), are listed in Table 1; the results in light water previously reported[7] are also listed for the sake of comparison.

The conclusions which we derived in the preceding works were confirmed in the present study; that is, the compositions of the species formed in heavy water are the same as those in light water, while the values of the equilibrium constants are smaller in heavy water than in light water.

We plotted the difference in the $\log \beta_{2,2}$ values in light and heavy water, $\Delta\log \beta_{2,2}=\log \beta_{2,2}(\text{in } H_2O)-\log \beta_{2,2}(\text{in } D_2O)$ against $\log \beta_{2,2}(\text{in } H_2O)$ for the (2,2) hydrolysis species of Y^{3+} and Er^{3+} ions, as well as those of the $(CH_3)_2Sn^{2+}$,[8] UO_2^{2+}, and Cu^{2+} ions.[4-6] The plot is shown in Fig. 2. The figure shows that $\Delta\log \beta_{2,2}$ is practically independent of the change in $\log \beta_{2,2}$ (in H_2O) at about 0.7.

Many workers[9] have reported that ΔpK (the difference in the pK values of an acid in light and heavy water) increased with $pK(\text{in } H_2O)$. In contrast with these conclusions, Ohtaki and Maeda[10] have pointed out that ΔpK is independent of $pK(\text{in } H_2O)$ for many organic acids with a similar structure for which a linear free-energy relationship holds. It is interesting that the same tendency has been found for the hydrolysis of the metal ions; it can be regarded as a dissociation reaction of weak acids, although no simple relation like the LFER for organic acids has been found between the acidities and other physico-chemical properties of aquated metal ions.

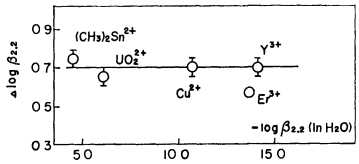

Fig. 2. $\Delta\log \beta_{2,2}=\log \beta_{2,2}$ (in H_2O) $-\log \beta_{2,2}$ (in D_2O) as a function of $-\log \beta_{2,2}$ (in H_2O).

The authors wish to thank Dr. Hitoshi Ohtaki for his valuable discussions.

8) R. S. Tobias and M. Yasuda, *J. Phys. Chem.*, **68**, 1820 (1964).

9) P. M. Laughton and R. E. Robertson, "Solute-Solvent Interactions," ed. by J. F. Coetzee and C. D. Ritchie, Marcel Dekker, New York (1969), p. 399.

10) H. Ohtaki and M. Maeda, *Z. Naturforsch.*, **B27**, 571 (1972).

BULLETIN OF THE CHEMICAL SOCIETY OF JAPAN, VOL. 46, 2890—2892 (1973)

The Anionic Polymerization of *n*-Butyraldehyde Azine

Mikiharu KAMACHI and Shunsuke MURAHASHI

Department of Polymer Science, Faculty of Science, Osaka University, Toyonaka, Osaka 560

(Received November 7, 1972)

Little is known concerning the polymerization of compounds with C=N bonds except for carbodiimides[1] and isocyanates.[2-6] We have already reported on the anionic polymerization of acetaldazine and have reported that the polymer thus obtained was a viscous oligomer.[7,8] The failure to obtain a high polymer from acetaldazine may be due to the proton transfer of the active hydrogens of the α,ω-methyl groups in the monomer. Thus, we are led to the polymerization of *n*-butyraldehyde azine, which has less active α-hydrogen than acetaldazine, and to the comparison of the molecular weight of the obtained polymer with those of formaldazine and acetaldazine under similar conditions.

The results of the polymerization of *n*-butyraldehyde azine by BuLi under various conditions are shown in Table 1. The oligomer was prepared in a good yield and was separated into a methanol-insoluble part (Oligomer 1) and a methanol-soluble part (Oligomer

Table 1. Polymerization of *n*-butyrazine by butyllithium[a]

Solvent	React. temp. (°C)	Total yield (%)	Oligomer 1 (%)	Molecular weight of Oligomer 1
Bulk[b]	−40	72.1	19.8	3130
	0	88.8	24.8	2890
	30	86.8	26.2	2870
Toluene[c]	−40	88.4	20.5	2870
	0	83.7	22.7	2670
THF[c]	−40	90.8	17.2	3030
	0	91.6	16.8	2990

a) Polymerization time 20 hr.
b) Monomer=28 mmol, BuLi=0.3 mmol.
c) Monomer=0.89 mol/l, BuLi=30 mmol/l.

1) G. C. Robinson, *J. Polymer Sci., A-1*, **2**, 3901 (1964).
2) V. E. Shashoua, *J. Amer. Chem. Soc.*, **81**, 3156 (1959).
3) V. E. Shashoua, W. Sweeny, and R. F. Tietz, *ibid.*, **82**, 866 (1960).
4) C. King, *ibid.*, **86**, 437 (1964).
5) G. Natta, J. D. Pietro, and M. Cambini, *Makromol. Chem.*, **56**, 200 (1962).
6) T. Kashiwagi, M. Hidai, Y. Uchida, and A. Misono, *J. Polymer Sci., B*, **8**, 173 (1970).
7) M. Kamachi and S. Murahashi, *Makromol. Chem.*, **119**, 232 (1968).
8) M. Kamachi and S. Murahashi, *Polymer J.*, **4**, 651 (1973).

2). In order to make it clear whether or not the addition polymerization occurs, the polymer thus obtained was characterized first.

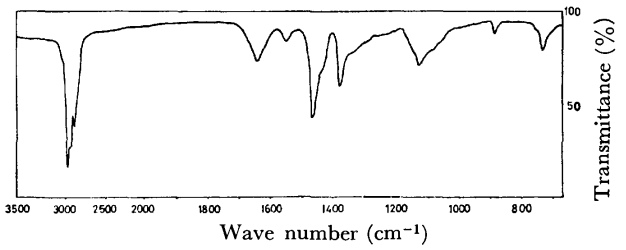

Fig. 1. The IR spectrum of oligomer 1 (KBr).

The IR spectrum of Oligomer 1 is shown in Fig. 1. It shows absorption bands at 1645 cm^{-1} ($\nu_{C=N}$) and 1555 cm^{-1} ($\nu_{N=N}$). The IR spectrum of Oligomer 2 is identical to that of Oligomer 1 except for its intensity. The UV spectrum of Oligomer 1 was measured in the range from 220 to 700 nm in a hexane solution; it showed an absorption maximum at 235 nm, a shoulder at 296 nm, and a weak absorption at 378 nm showing the -N=N- group.[12] The absorptions at 235 and 296 nm may be assigned to the n-π^* transition of the -C=N bond.[8] The NMR spectrum of Oligomer 1 is shown in Fig. 2. Each peak was assigned as is shown in Fig. 2, taking into account the conventionally available data. These assignments were consistent with the results of the IR spectra and the qualitative chemical tests. The product obtained from the treatment of the Oligomer, 1 or 2, with dilute aqueous hydrochloric acid was distilled into another ampoule containing an alcoholic solution of 2,4-dinitrophenylhydrazine by using a high-vacuum technique. An orange-yellow solid was thus formed (mp 118—122 °C). The product was identified as n-butyraldehyde hydrazone by a mixed-melting-point test with the authentic product, thus indicating the existence of pendant $-N=CH-CH_2-CH_2-CH_3$ groups.

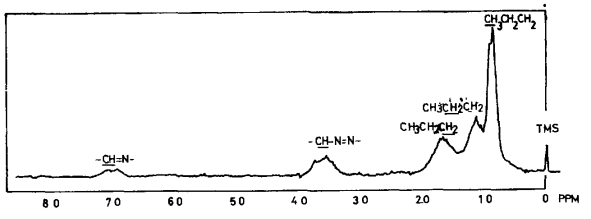

Fig. 2. The NMR spectrum of Oligomer 1 (CCl_4 5% solution).

In order to establish the existence of the $-\underset{\underset{R}{|}}{CH}-N=$ $N-\underset{\underset{R}{|}}{CH}-$ group, which is likely to cleave thermally at the C–N bonds and which evolves nitrogen molecule, the mild pyrolysis of Oligomer 1 at 200 °C was carried out under a high vacuum and the gaseous product thus obtained was collected into a vial for mass spectrometry. High-resolution mass spectrometry showed that the gas product was a nitrogen molecule (m/e 28.02).

These results suggest the following structure for the Oligomer 1:

$$C_5H_9-(\underset{\underset{N=CHC_3H_7}{|}}{CH}-N)_x-(CH-N=N-CH)_y-H$$
(C_3H_7 on each CH)

It was proved by the results of the IR spectra that Oligomer 1 is similar to Oligomer 2 except in its molecular weight.

The structure of the oligomer was consistent with that of the acetaldazine. Evidence for the hydrazone rearrangement, which was pointed out in the case of acetaldazine,[8] was found in the IR spectrum of Oligomer 2, which was allowed to stand, but not in Oligomer 1. This indicates that the rearrangement of Oligomer 1 is more difficult than that of Oligomer 2.

Table 2. Comparison of the molecular weights of the polymer obtained from various azines

Substance	State	Molecular weight (Degree of polym.)
Formaldazine[a]	Solid	$\eta_{sp/c}=0.25$[b]
Formaldazine[c,d]	Solid	Insoluble polymer
n-Butyrazine[c]		
Oligomer 1	Solid	2990 (21)
Oligomer 2	Tacky solid	1440 (10)
Acetaldazine[c]	Tacky solid	900 (10)

a) Formaldazine was polymerized by a trace of water at 0 °C.
b) H_2O Solution at 30 °C.
c) Monomer=0.89 mol/l, BuLi=30 mmol/l. Solvent, THF. Polym. temp. 0 °C.
d) Molar concentration of formaldazine was calculated by assuming that its density is the same as that of acetaldazine, because that of formaldazine was not determined.

The degree of polymerization of the oligomer of n-butyraldehyde azine was a little larger than that of the acetaldazine which was obtained under similar conditions, as is shown in Table 2, in spite of the increase in the bulkiness of the substituent group. This might be due to the decrease in the number of active hydrogens in α,ω-alkyl groups of n-butyraldehyde azine. In order to make this point clear, formaldazine, which has no active hydrogen, was polymerized to a solid polymer by a trace of water at room temperature and then explosively by butyllithium at −78 °C.[9] The intrinsic viscosity of the former was found to be 0.25 in an aqueous solution, but the latter polymer was insoluble in water as well as in common organic solvents. The degree of polymerization of the formaldazine polymer may be much larger than that of n-butyraldehyde azine. Thus, it is shown that high polymers can be anionically obtained from the C=N–N=C bond as well as from the diene bond.

These facts suggest that a cause of oligomerization in α,ω-disubstituted azine might be a proton transfer of active hydrogen.

12) H. H. Jaffe and M. Orchin, "Theory and Application of Ultraviolet Spectroscopy," John Wiley (1964), p. 186.

9) M. Kamachi and S. Murahashi, to be published.

Experimental

Reagents. The *n*-butyraldehyde azine was prepared from hydrazine hydrate and *n*-butyraldehyde according to the procedure of Curtius;[10] it was purified by reduced-pressure distillation through a Widmer column under nitrogen. The tetrahydrofuran was refluxed over metallic sodium and distilled into an ampoule on a high-vacuum system. The *n*-butyllithium was prepared in *n*-heptane by the method of Ziegler, and the concentration was determined by double titration.[11]

Polymerization. A 10 ml polymerization ampoule equipped with a nitrogen inlet with a stopcock was connected to a high-vacuum system, evacuated, and flushed with nitrogen by opening the stopcock. The ampoule was then removed under nitrogen flushing, after which a solution of butyllithium in heptane was injected by means of a hypodermic syringe into the ampoule under nitrogen. The ampoule was again connected to a high-vacuum system, the heptane was evaporated, and then the solvent and the monomer, which has previously been dried and degassed, were distilled into it. After being sealed off, the ampoule was placed in a thermostat at a given temperature. The polymerization system gradually turned orange-red in bulk polymerization, but immediately colored in a tetrahydrofuran solution.

The polymerization system became a red gel in the bulk polymerization and a red viscous solution in the solution polymerization. The reaction system was added to an excess of methanol to separate a methanol-insoluble polymer (Oligomer 1) and a methanol-soluble polymer (Oligomer 2). Oligomer 1 was filtered, washed with methanol, and dried. Oligomer 1 was a pale yellow solid, softening at 82—92 °C, which was soluble in petroleum benzine, benzene, toluene, and tetrahydrofuran.

Found: C, 69.18; H, 11.16; N, 19.83%. Calcd for $C_8H_{16}N_2$: C, 68.57; H, 11.43; N, 20.00%.

Oligomer 2 was isolated by evaporating the filtrate, and it was freed from inorganic salt by washing its ether solution with a small amount of distilled water. Oligomer 2 was a pale yellow to yellow viscous liquid (or tacky solid), soluble in aliphatic hydrocarbon, acetone, benzene, methanol, and tetrahydrofuran.

Found: C, 69.84; H, 10.99; N, 18.83%. Calcd for $C_8H_{16}N_2$: C, 68.57; H, 11.43; N, 20.00%.

The number-average molecular weights of these oligomers were determined by means of a vapour-presure osmometer (Mechro lab. 301A) in benzene.

The structure of the polymer was determined by studying its IR spectrum and NMR spectrum (Varian A 60) and by qualitative chemical tests for functional groups. The mass spectrum of the gas product obtained from the mild pyrolysis of the polymer was determined by means of a Hitachi model-10Z mass spectrometer.

The authors are grateful to Professor Shunichi Nozakura for several comments.

10) T. Curtius and E. Zinkeisen, *J. Prakt. Chem.*, **58**, 310 (1898).
11) H. Gilman, A. H. Haubein, *J. Amer. Chem. Soc.*, **66**, 1515 (1944).

BULLETIN OF THE CHEMICAL SOCIETY OF JAPAN, VOL. 46, 2892—2893 (1973)

The Synthesis of (4,5-Di(2-furyl)-2,7-octanedione) by the Electrolysis of (4-(2-Furyl)-3-buten-2-one)

Hajime SATONAKA, Zei SAITO, and Toshio SHIMURA

Industrial Research Institute of Kanagawa Prefecture, Showa-machi, Kanazawa-ku, Yokohama 236

(Received December 1, 1972)

4-(2-Furyl)-3-buten-2-one (**2**), which resembles methyl 3-(2-furyl)acrylate (**1**), was electrolyzed in methyl alcohol containing sulfuric acid as a supporting electrolyte. While **1** was oxidized to methyl 3-(2,5-dimethoxy-2,5-dihydrofuryl)acrylate[1-4] and 5,5'-bis[2-(methoxycarbonyl)vinyl]-2,2'-bifuryl,[5] **2** was reduced to 4,5-di(2-furyl)-2,7-octanedione (**3**) under similar conditions.

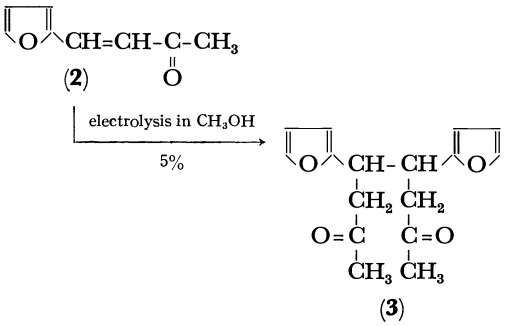

The IR spectrum of the dimer (**3**) showed a carbonyl band at 1708 cm^{-1} and bands of the furan ring at 3125, 1511, 1020, 886, and 758 cm^{-1}.[6] The UV spectrum in methyl alcohol showed a maximum peak at 220 mμ with a molar extinction coefficient of 11000. The NMR spectrum showed signals of furan-ring protons at τ 2.68 (2H, multiplet), 3.78 (2H, multiplet), and 3.91 (2H, multiplet), of methin protons at 6.40 (2H, multiplet), of methylene protons at 7.35 (4H, multiplet), and of methyl protons at 8.07 (6H, singlet). The mass spectrum exhibited its intense peaks

1) T. Shimura and Z. Saito, *Nippon Kagaku Zasshi*, **89**, 695 (1968).
2) T. Shimura, Z. Saito, M. Koizumi, and H. Satonaka, *ibid.*, **90**, 96 (1969).
3) T. Shimura, Z. Saito, and H. Satonaka, *ibid.*, **90**, 716 (1969).
4) T. Shimura, Z. Saito, and H. Satonaka, *ibid.*, **90**, 1173 (1969).
5) H. Satonaka, Z. Saito, and T. Shimura, This Bulletin, **43**, 2633 (1970).
6) M. Yamaguchi, *Bunsekikagaku*, **7**, 210 (1958).

at *m/e* 274 (M^+), 217 ($M^+-CH_2COCH_3$), 137 ($M^+/2$), and 43 ($^+COCH_3$). The elementary analysis agreed with the formula of $C_{16}H_{18}O_4$. On the basis of these results, the product was determined to be 4,5-di(2-furyl)-2,7-octanedione (**3**).

Table 1. Yields of 4,5-difuryl-2,7-octadione by the electrolyses in the various solvents (%)[a]

Solvent	Yield	Solvent	Yield
CH_3OH	5	DMF	5
C_2H_5OH	2	Pyridine	3
$(CH_3)_2CO$	7	Dioxane	Trace
THF	1		

a) Averages of the three times experiments.

Similar electrolyses were repeated for ethyl alcohol, acetone, tetrahydrofuran (THF), *N,N*-dimethylformamide (DMF), pyridine, and dioxane in the same way as was used for in methyl alcohol. The yields of the product are given in Table 1. The results when water was mixed in methyl alcohol, acetone, and DMF in various proportions, and when the reactions were carried out in these mixed solvents, are given in Table 2. It was found that the yields increased with the addition of water and came to a maximum at the point where the volume of water amounted to about 50—70%.

Table 2. Yields of 4,5-difuryl-2,7-octadione in the various water-mixed solvents (%)[a]

Solvent	H_2O (%)			
	10	25	35	50
CH_3OH	6	24	15	4
$(CH_3)_2CO$	45	52	46	34
DMF	24	30	40	15

a) Average of the three times experiments

Assuming that these reactions proceed by means of a mechanism similar to that in the hydrodimerization of acrylonitrile,[7-11] furfurylideneacetone (**2**) can be said to undergo an over-all two-electron uptake at the cathode. This probably occurs in two one-electron stages. The radical anion (**2'**) may react with water (or the proton) before the second electron is taken up. The carbanion (**2''**) may attack highly-polarized molecules of the monomer attracted to the cathode. The interaction of the dione anion (**3'**) with water (or the proton) might terminate the reactions and yield 4,5-di(2-furyl)-2,7-octanedione (**3**).

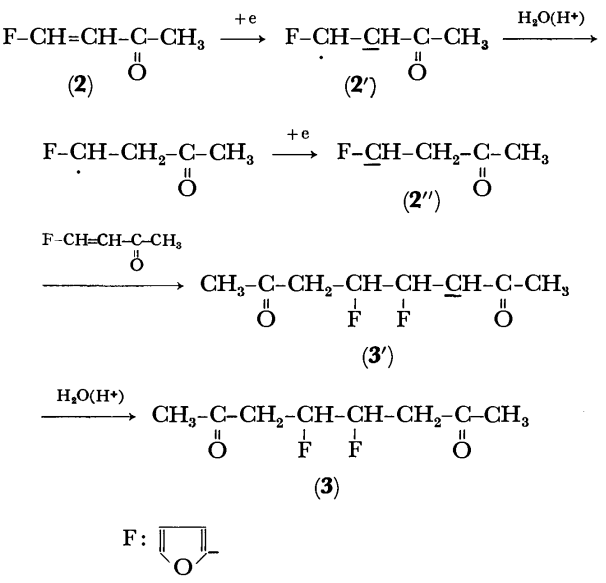

Experimental

4-(2-Furyl)-3-buten-2-one (2). This material was prepared by the condensation of furfural with acetone by the method of G. J. Leuck *et al.*[12] Yellow crystals; mp 37—39 °C.

4,5-Di(2-furyl)-2,7-octanedione (3). To a solution of 10 g of 4-(2-furyl)-3-buten-2-one in 200 ml of methyl alcohol, 1 ml of conc. sulfuric acid was added; the mixture was then electrolysed in a Clauson-Kaas electrolyser[13] for 4 hr with 15 V, 1—2 A at −40——50 °C. A product was obtained by the subsequent filtration of the electrolyzed solution. Recrystallization from methyl alcohol gave colorless needles with a melting point of 123 °C; 0.5 g (5%). The experiments using other solvents and the water-mixed solvents were carried out under similar conditions.

Found: C, 70.25; H, 6.51%. Calcd for $C_{16}H_{18}O_4$: C, 70.06; H, 6.61%.

IR (cm^{-1}, KBr): 3125 ($\nu_{=C-H}$), 1708 ($\nu_{-C=O}$), 1511, 1020, 886, 758 (furan nucleus).

UV (λ_{max} mμ(ε), in CH_3OH): 220 (11000).

NMR (τ, in CCl_4): 2.68 (2H, m), 3.78 (2H, m), 3.91 (2H, m) (furan nucleus protons), 6.40 (2H, m, methin protons), 7.35 (4H, m, methylene protons), 8.07 (6H, s, methyl protons).

Mass spectrum: *m/e* 274 (M^+), 217 ($M^+-CH_2COCH_3$), 137 ($M^+/2$), 43 ($^+COCH_3$).

The authors wish to express their thanks to Dr. Minoru Hirota, Yokohama National University, for his kind suggestions and encouragement, and Mr. Tetsuya Yokokawa and Mr. Takayoshi Ozawa for thier help in the mass-spectrum measurements and elementary analysis.

7) M. M. Baizer, *J. Electrochem. Soc.*, **111**, 215 (1964).
8) K. Sugino and T. Nakaya, *ibid.*, **112**, 1241 (1965).
9) Y. Arad, M. Levy, I. R. Miller, and D. Vofsi, *ibid.*, **114**, 899 (1967).
10) M. Figeys and H. P. Figeys, *Tetrahedron*, **24**, 1097 (1968).
11) I. Gillet, *Bull. Soc. Chim. Fr.*, **1968**, 1929.
12) G. J. Leuck and L. Cejka, "Organic Syntheses," Coll. Vol. I, p. 283 (1956).
13) N. Clauson-Kaas and F. Linborg, *Acta Chem. Scand.*, **6**, 531 (1952).

BULLETIN OF THE CHEMICAL SOCIETY OF JAPAN, VOL. 46, 2894—2895 (1973)

Formation of Trithiocarbonate by the Reaction of 2,2-Diphenylethylenesulfonamide and Carbon Disulfide

Kiyoshi HASEGAWA, Tadashi SASAKI,* and Syuzi HIROOKA

Department of Industrial Chemistry, Faculty of Engineering, Toyama University, Takaoka-shi 933

**Institute of Applied Organic Chemistry, Faculty of Engineering, Nagoya University, Furo-cho, Chikusa-ku, Nagoya 464*

(Received December 6, 1972)

We have reported[1-3] on the syntheses and intramolecular Michael cycloaddition of $RCH{=}CHSO_2N{=}CX{-}S^-M^+$ ($R{=}H$, $R^1C_6H_4$; $X{=}SR^2$, OR^2, NHR^2, $N(R^2)_2$, S^-M^+). The reaction of 2,2-diphenylethylenesulfonamide **1** with carbon disulfide and alkyl halides afforded unexpected trithiocarbonates. This paper describes the mechanism of these new reactions studied by the use of the carbon disulfide-^{35}S tracer technique.

Results and Discussion

The reaction of **1** with carbon disulfide and alkyl halides in the presence of base in DMF or DMSO gave alkyl 2,2-diphenylvinyl trithiocarbonates **2** as yellow crystals, **1** being recovered by acidifying the alkaline filtrate. The results are summarized in Table 1. The

$$\underset{\mathbf{1}}{(C_6H_5)_2C{=}CHSO_2NH_2} \xrightarrow[CS_2,\ RX]{:B} \underset{\mathbf{2}}{(C_6H_5)_2C{=}CH{-}S{-}\overset{\overset{S}{\|}}{C}{-}SR}$$

IR spectrum of **2a** displayed the strongest band at 1065 cm^{-1} due to the C=S bond,[4] but no absorption due to the SO_2 group. The NMR spectrum of **2a** exhibited a peak of the methine proton at δ 7.71. The mass spectrum showed a molecular ion peak at *m/e* 302.0270 assignable to a molecular formula $C_{16}H_{14}S_3$. Final structural elucidation of **2** was accomplished by the following degradation. Treatment of **2** with excess hydrazine afforded thiocarbohydrazid **3**, mp 167—168 °C (lit,[5] 168 °C), alkanethiol **4**, and *N,N'*-bis(2,2-diphenylvinyl)hydrazine **5** which was

$$\mathbf{2} \xrightarrow[N_2H_4]{} \underset{\mathbf{3}}{H_2NHN\overset{\overset{S}{\|}}{C}NHNH_2} + \underset{\mathbf{4}}{RSH} + ((C_6H_5)_2C{=}CHSH) \xrightarrow{N_2H_4} \underset{\mathbf{5}}{(C_6H_5)_2C{=}CHNHNHCH{=}C(C_6H_5)_2}$$

formed from 2 mol of 2,2-diphenylvinylthiol and 1 mol of hydrazine.

The yield of **2** increased with the amount of carbon disulfide and base added, but no further increase was observed when more than two equiv. of carbon disulfide and base were used. The reaction of **1** and carbon disulfide was quite rapid and a considerable yield (40%) of **2a** was obtained in a minute. The origin of three sulfur atoms in **2** were sought with carbon disulfide-^{35}S. Carbon disulfide-^{35}S was converted in to *N,N,N',N'*-tetramethylthiuram disulfide-^{35}S **6** by the usual method.[6] The specific activities of **6** and **2a** were found to be 25.84×10^5 dpm/mmol and 19.79×10^5 dpm/mmol, respectively. The fact that the relative ^{35}S atom ratio of **6** to **2a** was 4.00: 3.07 supports the mechanism that all the three sulfur atoms of **2** come from two moles of carbon disulfide. The trithiocarbonate formation was specific to the sulfonamide **1**. Neither *N,N*-dimethylsulfonamide nor 2-phenyl-2-methylethylenesulfonamide took part in it. The IR absorption peak at 2080 cm^{-1} due to the N=C=S bond was recognized in the reaction mixture of **1** and carbon disulfide. The following intramolecular rearrangement mechanism is proposed: (1) electrophilic attack of CS_2 on the N atom to form reactive **7**, (2) intramolecular S_N attack of thiolate anion on the 1-carbon atom with a loss of sulfinate anion, (3) cleavage of the C–S bond, (4) attack of CS_2 on the thiolate anion, and (5) alkylation.

The resonance stabilization of the diphenylmethylcarbanion **8** provides an important driving force which causes the thiolate anion attack on the 1-carbon atom. When DMF was removed *in vacuo* from the basic reaction mixture before alkylation, yellow hygroscopic crystals **12** ($\nu_{C=S}$ 1040, and 990 cm^{-1}) and a viscous oil ($\nu_{N=C=S}$ 2080 cm^{-1}) were obtained. This seems to be mainly composed of **11**, though it could not be

TABLE 1. $(C_6H_5)_2C{=}CH{-}S{-}C(=S){-}SR$ **2**

Compd	R	Yield (%)	Mp (°C)	Found (%)			Calcd (%)		
				C	H	S	C	H	S
2a	CH_3	57	110—111	63.78	4.62	31.45	63.53	4.67	31.80
2b	C_2H_5	57	87—88	64.37	4.98	29.93	64.55	5.10	30.35
2c	*n*-C_3H_7	44	40—41	65.50	5.39	29.14	65.44	5.49	29.06
2d	*n*-C_4H_9	44	36—37	66.09	5.74	27.51	66.27	5.85	27.88

1) K. Hasegawa and S. Hirooka, This Bulletin, **45**, 525 (1972).
2) K. Hasegawa and S. Hirooka, *ibid.*, **45**, 1567 (1972).
3) K. Nakahashi, S. Hirooka, and K. Hasegawa, *ibid.*, **45**, 3217 (1972).
4) H. C. Godt, Jr., and R. E. Wann, *J. Org. Chem.*, **26**, 4047 (1961).
5) W. Autenrieth and H. Hefner, *Ber.*, **58**, 2154 (1925).
6) E. Müller, Houben Weil, "Methoden der Organishen Chemie," Vol. IX, George Thieme Verlag, Stuttgart (1955), p. 853.

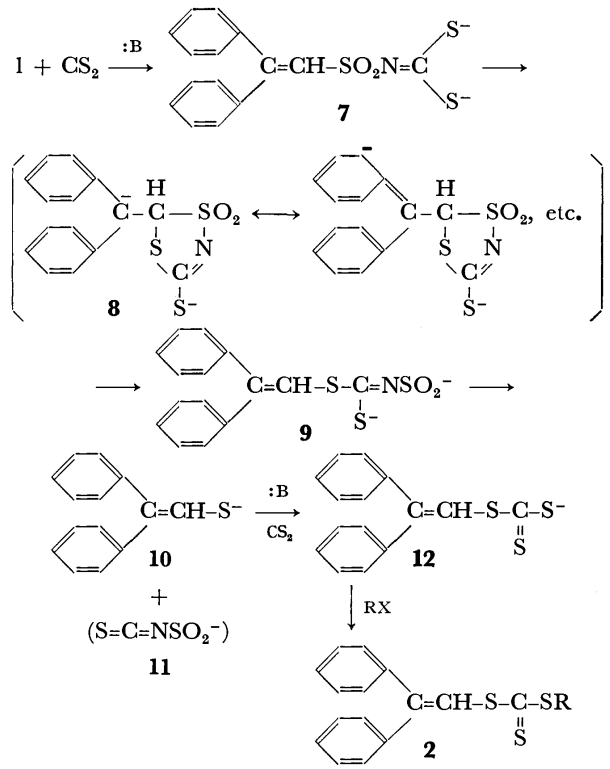

purified. Even when **1** and carbon disulfide were allowed to react for a minute followed by alkylation, **2** was the only product. This supports the view that conversion of **7** into **12** may proceed faster than the formation of **7**. The present rearrangement reaction seems to be a new case in which Smiles-type rearrangement can occur at a methine carbon atom[7] conjugated with two phenyl groups.

Experimental

All melting points are uncorrected. Specific activities of the labelled compounds were counted with a TEN-GSL-163 liquid scintillation counter using a mixture of POPOP and PPO (0.005 g and 0.4 g in 100 ml of toluene) as a scintillator.

Specific Activity of Carbon Disulfide-^{35}S Stock Solution. Radioactive carbon disulfide (2.7 mCi of ^{35}S in 15 mg) was transferred into unlabelled carbon disulfide (10 ml) by means of a vacuum line. Approximately 0.5 ml of this solution was diluted with unlabelled carbon disulfide (10 ml) to provide the stock solution used in reactions leading to labelled products. *N,N,N',N'*-Tetramethylthiuram disulfide-^{35}S was prepared from the carbon disulfide-^{35}S stock solution by the usual method[6] and its specific activity was measured.

Liquid Scintillation Counting. The radioactivity of each sample in count per minute (cpm) was measured three times with different weighing, disintegration value per minute (dpm) being obtained in reference to the quenching calibration curve.

2,2-Diphenylethylenesulfonamide ***1***. In an analogous manner to that described by B. M. Culbortson[8] for the synthesis of 2-phenylethylenesulfonamide, 1,1-diphenylethylene (48.0 g, 0.266 mol) was treated with sulfuryl chloride (60 g, 0.445 mol) in DMF (60 ml) to give 13.5 g (17%) of 2,2-diphenylethylenesulfonyl chloride. The sulfonamide was prepared in 79% yield from crude sulfonyl chloride in benzene and 28% aqueous ammonia. Recrystallization from water gave colorless crystals, mp 136—137 °C. IR (KBr): 3340 and 3240 (NH_2), 3030 (=CH), 1585 (C=C), 1310 and 1130 (SO_2) cm^{-1}. NMR (DMSO-d_6): δ 6.92 (s, 1H, =CH), 6.96 (s, 2H, NH_2), and 7.34±0.10 (m, 10H, diphenyl). Mass spectrum (75 eV) *m/e* (rel. intensity): 89 (33, $C_6H_5C^+$), 93 (8, $C^+HSO_2NH_2$), 102 (10, $C_6H_5C{=}C^+H$), 152 (20, $2C_6H_4^+$), 165 (14) and 167 (15, $(C_6H_5)_2C^+\pm H$), 178 (100, $(C_6H_5)_2C{=}C^+$), 179 (70, $(C_6H_5)_2C{=}CH^+$), 195 (23, M^+-SO_2), and 259 (53, M^+).

Found: C, 64.71; H, 4.92; N, 5.34; S, 12.38%. Calcd for $C_{14}H_{13}NO_2S$: C, 64.86; H, 5.05; N, 5.40; S, 12.35%.

Labelled Trithiocarbonate from ***1****, Carbon Disulfide-^{35}S and Methyl Iodide.* To a stirred solution of **1** (0.78 g, 3.0 mmol) in DMF (8.0 ml) were added carefully sodium hydroxide (0.24 g, 6.0 ml) in water (0.5 ml) and then a carbon disulfide-^{35}S stock solution (0.57 g, 7.5 mmol) at room temperature. The orange-yellow reaction mixture was stirred for 2 hr. Methyl iodide (0.51 g, 3.6 mmol) was then added drop by drop at 20—30 °C. The yellow reaction mixture was stirred for 2 hr at 20—30 °C, and poured into ice water (100 ml), and the resulting alkaline solution was left to stand overnight. The yellow crystals were collected and thoroughly washed twice with 20 ml portions of 1M sodium hydroxide solution to give 0.50 g (55%) of **2a**. Recrystallization from methanol gave yellow crystals. The alkaline filtrate was acidified with concentrated hydrochloric acid to recover 0.27 g (35%) of **1**. The IR, NMR, and mass spectra of unlabelled trithiocarbonate are given below. IR (KBr): 3020 (=CH), 1595 (C=C), 1065 (C=S), 815, 755 and 690 cm^{-1}. NMR ($CDCl_3$): δ 2.80 (s, 3H, CH_3), 7.34 (m, 10H, diphenyl), and 7.71 (s, 1H, =CH). Mass spectrum (75 eV) *m/e* (rel. intensity): 91 (100, C^+SSCH_3), 152 (7, $2C_6H_4^+$), 165 (15) and 167 (7, $(C_6H_5)_2C^+\pm H$), 178 (28, $(C_6H_5)_2C{=}C^+$), 179 (11, $(C_6H_5)_2C{=}CH^+$), 210 (21, $(C_6H_5)_2C{=}CS^+$), 211 (31, $(C_6H_5)_2C{=}CHS^+$), 226 (15, M^+-CS_2), 255 (4, M^+-SCH_3), and 302.0270 (43, calcd molecular weight, 302.0257).

Reaction of ***2*** *with Hydrazine.* Methanethiol was evolved when a solution of **2a** (1.46 g, 4.8 mmol) and 80% hydrazine hydrate (0.75 g, 15 mmol) in ethanol (50 ml) was refluxed for 3.5 hr. The reaction mixture was cooled overnight. Light pink precipitates (0.33 g, 65%) of **3** were obtained. Evaporation of the ethanol from the basic filtrate *in vacuo* left a yellow oily product which was acidified with sulfuric acid under cooling to afford a soft solid. It was triturated with ether to yield colorless crystals. Recrystallization from benzene-petroleum ether gave 0.64 g (69%) of **5**, mp 156—157 °C. IR (KBr): 3400 (weak, NH), 3020 (=CH), 1630 (NH), 1590 (C=C), 1490, 1450, 750, 740, and 690 cm^{-1}. NMR ($CDCl_3$): δ 5.02 (d, 2H, 2=CH), 8.25 (d, 2H, 2NH, J_{CHNH}=7.5 Hz), and 7.27 (m, 20H, phenyl). Mass spectrum (75 eV) *m/e*: 388 (M^+).

Found: C, 86.56; H, 6.06; N, 7.45%. Calcd for $C_{28}H_{24}N_2$: C, 86.56; H, 6.23; N, 7.21%.

The authors wish to thank Prof. Shigeru Oae, Osaka City University, for recommendation of the isotope experiment and encouragement throughout this work. Thanks are also due to Dr. Seizi Kozuka, Dr. Naomichi Furukawa and Mr. Yoshiyuki Tsuchida, Osaka City University, for direction in the experiment and valuable discussions, Mr. Osamu Shiokari for assistance in the preparation of some compounds, and Dr. Eizo Nakano, Nagoya University, for use of the liquid scintillation counter.

7) E. Waldan and R. Pütter, *Angew. Chem.*, **84**, 822 (1972).

8) B. M. Culbortson and S. Dietz, *J. Chem. Soc., C*, **90**, 992 (1968).

BULLETIN OF THE CHEMICAL SOCIETY OF JAPAN, VOL. 46, 2896—2897 (1973)

A Copper(II) Complex of 1,1′-Diacetylferrocene Bis(thiosemicarbazone)

Yoshimori OMOTE, Ryuichiro KOBAYASHI, and Noboru SUGIYAMA
Department of Chemistry, Tokyo Kyoiku University, Otsuka, Tokyo 112

(Received December 14, 1972)

During the course of an investigation of the intramolecular interaction between substituents in 1,1′-disubstituted ferrocenes, we examined the possibility of the intramolecular bridging in complexation of 1,1-diacetylferrocene derivatives. Among many reports on complexes of substituted ferrocenes with inorganic acceptors, there have been a few examples about complexes of 1,1′-disubstituted ferrocenes.[1-4] Hauser and Cain[1] reported a copper(II) complex of 1,1′-dibenzoylacetylferrocene in which cupric ion played a role of an electron acceptor and β-dicarbonyl group played a role of an electron donor. Pavlik and Handlir[2] reported that in the complex of 1,1′-diacetylferrocene with aluminum chloride both carbonyl groups were bound to the monomeric aluminum chloride.

These examples are characteristic to have C=O bonding in donor group. Now we want to report the synthesis and structure of copper complex of 1,1′-diacetylferrocene bis-thiosemicarbazone in which C=N bonding is expected to play a role of a donor.

Acetylferrocene thiosemicarbazone (I) and 1,1′-diacetylferrocene bis-thiosemicarbazone (II) were prepared by treatment with thiosemicarbazide. The structure of thiosemicarbazones I and II is in accordance with elemental analyses and the infrared spectra, especially absorptions by N–H stretching vibrations at 3445 to 3150 cm^{-1} and absorptions by C=N group at 1606 cm^{-1} being observed.

The copper(II) complex of acetylferrocene thiosemicarbazone (III) was prepared by treating with cupric acetate. The elemental analysis supports the structure III. In the infrared spectrum of III the intensity of the C=N band at about 1600 cm^{-1} has increased in comparison with that of the corresponding thiosemicarbazone. On the basis of this evidence, it is reasonable to suggest the structure III for the compound.

The copper(II) complex of 1,1′-diacetylferrocene bis-thiosemicarbazone (IV) was prepared in the similar manner as above. From the similarity of the infrared spectrum of this complex IV to that of III, it can be assumed that the structure around cupric ion of this compound is similar to that of III. In order to ascertain this suggestion, the changes of the absorption spectrum of I and II in ethanol by addition of cupric acetate were examined. As shown in Fig. 1, with a decrease in molar ratio of I to cupric acetate, the intensity of the band at 308 nm decreased, while that of the band at 328 nm increased. The absorption spectrum of an equimolar mixture of the thiosemicarbazone and cupric acetate gives a spectrum almost identical with that of III, indicating the formation of the complex III. There is an isosbestic point at 326 nm indicating that only two species, I and III, are present.

The absorption spectra in a series of molar ratio of II to cupric acetate are shown in Fig. 1. The change of absorption spectra with the decrease in molar ratio are very similar to the former case. The absorption spectrum of IV cannot be measured because of its slight solubility, but the absorption spectrum in molar ratio of 1 : 2, in which the formation of the complex appears to be completed, is very close to that of III. These facts also support the structure III and IV.

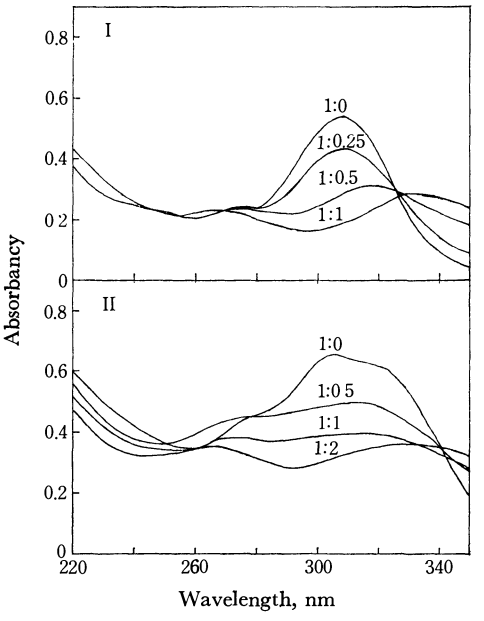

Fig. 1. The changes of the absorption spectra of acetylferrocene thiosemicarbazone(I) and 1,1′-diacetylferrocene thiosemicarbazone(II) upon the addition of cupric acetate. The figures give the molar ratio of thiosemicarbazones (2×10^{-5} mol/l) to cupric acetate.

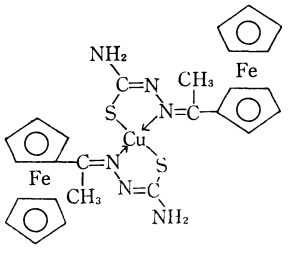

(III)

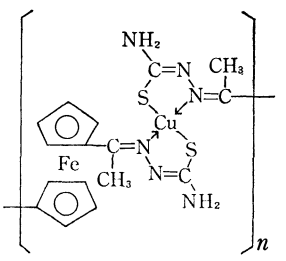

(IV)

Experimental

Acetylferrocene Thiosemicarbazone (I). The method for the preparation of copper(II) complex of formylferrocene

1) C. R. Hauser and C. E. Cain, *J. Org. Chem.*, **23**, 1142 (1958).
2) I. Pavlik and K. Handlir, *Collect. Czech. Chem. Comm.*, **31**, 1958 (1966).
3) I. Pavlik, J. Klikorka, and K. Handlir, *Z. Chem.*, **8**, 390 (1968).
4) E. B. Moynaham, F. D. Popp, and M. F. Werneke, *J. Organometal. Chem.*, **19**, 229 (1969).

thiosemicarbazone[5] was modified and used. Acetylferrocene (5 mmol) in ethanol (20 ml) was added dropwise to a solution of thiosemicarbazide (5 mmol) in water (30 ml). Glacial acetic acid (1 ml) was then added and the resulting mixture was heated in a steam bath for 1.5 hr. After the mixture was cooled the precipitate was collected, washed with aqueous ethanol, dried, and recrystallized repeatedly from ethanol, red crystals, mp 176.5—177.5 °C; yield 43%.

Found: C, 51.73; H, 4.97; N, 14.20%. Calcd for $C_{13}H_{15}FeN_3S$: C, 51.90; H, 5.00; N, 14.00%. IR (KBr) cm^{-1}: 3420, 3285, 3180, 1606, 1591. UV: λ_{max}^{EtOH} nm(ε) 239 (12600), 273 (12400), 308 (27100), 455 (960). NMR (DMSO-d_6): τ 0.10 (s, 1H), 2.00 (bs, 1H), 2.40 (bs, 1H), 5.23 (t, 2H), 5.65 (t, 2H), 5.83 (s, 5H), 7.80 (s, 3H).

1,1′-Diacetylferrocene Bis-thiosemicarbazone (II). In a similar manner as described above, the title compound was prepared and recrystallized repeatedly from ethanol, red crystals, mp 163—164.5 °C; yield 60%.

Found: C, 44.63; H, 5.26; N, 19.27%. Calcd for $C_{16}H_{20}FeN_6S_2$–H_2O: C, 44.25; H, 5.11; N, 19.35%. IR (KBr) cm^{-1}: 3445, 3250, 3150, 1606, 1593. UV: λ_{max}^{EtOH} nm(ε) 280 (22700), 305 (33000), 318 (31300), 458 (1570). NMR (DMSO)-d_6): τ 0.11 (s, 2H), 1.97 (m, 2H), 2.37 (m, 2H), 5.22 (t, 4H), 5.65 (t, 4H), 7.88 (s, 6H).

Copper(II) Complex of Acetylferrocene Thiosemicarbazone (III). Cupric acetate (2.5 mmol) in 25 ml of ethanol was added to a warm solution of acetylferrocene thiosemicarbazone (5 mmol) in 25 ml of ethanol. The resulting mixture was warmed at 70 °C for 1 hr. The precipitate, which formed after cooling, was removed by filtration, washed with aqueous hydrochloric acid solution, water, and cold ethanol, and dried, black powder, mp 160—161 °C; yield 59%.

Found: C, 46.84; H, 4.65; N, 12.05%. Calcd for $C_{26}H_{28}CuFe_2N_6S_2$: C, 47.00; H, 4.20; N, 12.60%. IR (KBr) cm^{-1}: 3465, 3425, 3325, 3200, 3095, 1611, 1598. UV: λ_{max}^{EtOH} nm(ε) 261 (10800), 328 (12000), 431 (1970).

Copper(II) Complex of 1,1′-Diacetylferrocene Bis-thiosemicarbazone (IV). In a similar manner as described above, the copper complex of 1,1′-diacetylferrocene bis-thiosemicarbazone was prepared, brown powder, mp>300 °C; yield 80%. The purification by recrystallization of this copper complex was very difficult because of its slight solubility in most solvents.

Found: C, 39.22; H, 4.02; N, 16.06%. Calcd for $(C_{16}H_{18}CuFeN_6S_2)_n$: C, 40.20; H, 3.77; N, 17.60%. IR (KBr) cm^{-1}: 3440, 3340, 3170, 1614, 1588.

UV Spectra of Copper(II) Complexes of Acetylferrocene Thiosemicarbazone and 1,1′-Diacetylferrocene Bis-thiosemicarbazone. The UV absorption spectra were measured in ethanol. The molar ratio of acetylferrocene thiosemicarbazone and cupric acetate were 1:0, 1:0.25, 1:0.5, and 1:1, while those of 1,1′-diacetylferrocene bis-thiosemicarbazone and cupric acetate were 1:0, 1:0.5, 1:1, and 1:2.

5) D. M. Wiles and T. Suprunchuk, *Can. J. Chem.*, **46**, 1865 (1968).

BULLETIN OF THE CHEMICAL SOCIETY OF JAPAN, VOL. 46, 2897—2899 (1973)

Reactions of Diazoacetophenones in the Presence of Metal Chelates. V. Reaction of *o*-Methoxy-α-diazoacetophenone

Toshikazu IBATA, Kozaburo UEDA,* and Matsuji TAKEBAYASHI**

Department of Chemistry, College of General Education, Osaka University, Toyonaka, Osaka 560

(Received December 25, 1972)

The predominant formation of carbonyl ylides takes place by the intramolecular attack of carbenoid on a carbonyl group in the copper chelate-catalyzed decomposition of *o*-alkoxycarbonyl-α-diazoacetophenones.[1] A similar facilitation might be expected in the formation of oxonium ylide by the intramolecular attack of carbenoid-carbon on ether oxygen at *ortho* position. The copper chelate-catalyzed decomposition of *o*-methoxy-α-diazoacetophenone was carried out, and formation of the oxonium ylide was confirmed.

Decomposition of *o*-methoxy-α-diazoacetophenone (I) was carried out in benzene solution containing a catalytic amount of bis(acetylacetonate)copper. Column chromatography of the reaction mixture on silica gel gave 2-methylcoumaranone (IV, 52%), bis-(*o*-methoxybenzoyl)ethylene (VIII, 7%) and a carbene-oligomer (30%).[2] Dibenzoylethylene (VIII), the formal dimer of the carbene intermediate, is considered to be obtained by the reaction of the carbene (II)

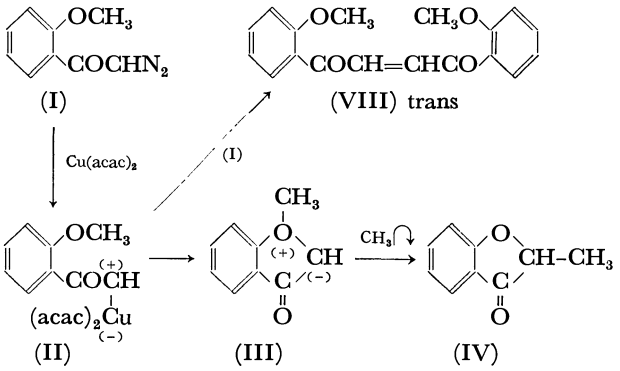

Scheme 1.

* Present address: Department of Industrial Chemistry, Faculty of Technology, Ehime University, Matsuyama, Ehime.

** Present address: Department of Chemistry, Faculty of Science and Technology, Kinki University, Higashi-osaka, Osaka.

1) K. Ueda, T. Ibata, and M. Takebayashi, This Bulletin, **45**, 2279 (1972).

2) The oligomer showed a similar IR spectrum to that described before (M. Takebayashi, T. Ibata, and K. Ueda, This Bulletin, **43**, 1500 (1970)).

with starting diazo compound (I)[3] competing with the formation of IV. Formation of IV might be explained by assuming the intermediacy of an oxonium ylide (III) produced by the intramolecular electrophilic attack of the carbenoid carbon on the ether oxygen atom, followed by methyl migration (Scheme 1).

Since the copper chelate-catalyzed decomposition of diazoketones in alcohols gives the corresponding keto-ethers,[4] facility of the oxonium ylide formation was investigated utilizing the competitive reaction between intramolecular formation of the oxonium ylide and the intermolecular reaction with alcohols. The copper-catalyzed decomposition of I was carried out in a mixed solvent of alcohol and benzene in various proportions at 80 °C for 30 min. A soluble part of the reaction mixture in *n*-heptane was analyzed by gas chromatography. Coumaranone (V), 2-methylcoumaranone (IV) and keto-ether (VI) were characterized and determined quantitatively by comparing their retention times with those of authentic samples. Molar ratios of the products are listed in Table 1.

Table 1. Decomposition of I in alcohol-benzene solution

Alcohol	wt% of Alc.	Products				
		IV	V	VI	V/IV	VI/IV+V
EtOH	50	10.8	10.9	78.3	1.01	3.61
	10	13.9	12.2	73.9	0.88	3.83
	5	14.7	12.9	72.4	0.88	2.62
	2	18.0	14.1	67.9	0.78	2.12
	1	20.8	16.9	62.3	0.81	1.65
t-BuOH	30	26.4	7.0	66.6	0.24	1.99
	10	36.4	6.9	56.7	0.19	1.31
	2	42.1	5.6	52.2	0.12	1.09
	1	49.3	2.4	48.3	0.05	0.93

With the decrease of alcohol concentration in ethyl alcohol–benzene solution, the yields of VI decreased and those of both VI and V increased. This suggests that the formation of keto-ether (VI) depends upon the concentration of alcohol and competes with the formation of IV and V. Although coumaranone (V) is produced in the acid catalysis[5] of I, a control experiment showed that I did not give V under refluxing in an alcohol–benzene solution in the absence of $Cu(acac)_2$ catalyst. Contribution of alcohol to the formation of V was supported by the fact that V was not obtained in a benzene solution in the presence of $Cu(acac)_2$ without alcohol. Decrease in the value of V/IV with the decrease in alcohol concentration is consistent with the above assumption.

Thus the formation of V might be explained in terms of the intermediacy of oxonium ylide (III) which reacts with alcohols affording coumaranone (V) *via* VII (Scheme 2).

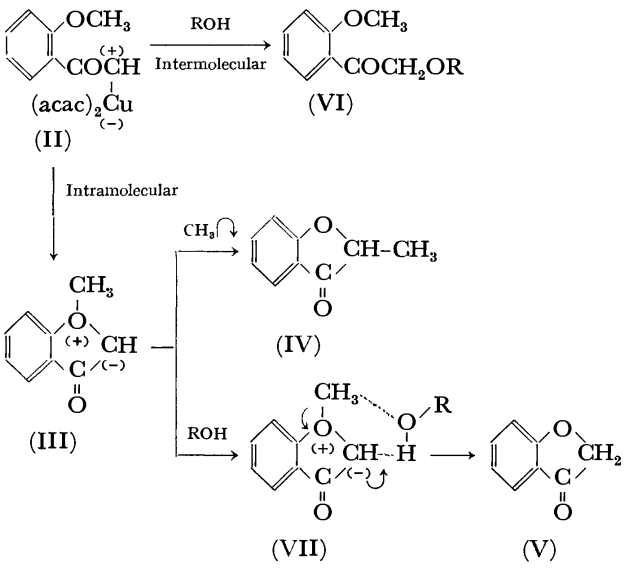

Scheme 2.

Keto-ether (VI) can be obtained by the intermolecular reaction of carbenoid (II) with alcohol competing with the intramolecular formation of the oxonium ylide (III) which gives IV and V by successive reactions. The ratio V/(IV+V) (Table 1) which decreases with decrease in alcohol concentration supports the mechanism shown in Scheme 2.

In the case of *t*-butyl alcohol, similar results were obtained except for the yields of V, which decrease with decrease in alcohol concentration. The ratio VI/IV is one third of that in ethyl alcohol reflecting the reactivity of alcohols toward copper-carbenoid (II).[4]

On the other hand, a product which could be formed through the corresponding oxonium ylide generated by the intermolecular carbenoid reaction was not recognized in a catalytic decomposition of α-diazoacetophenone in anisole in spite of careful inspection of the products.

Experimental

Material. *o*-Methoxy-α-diazoacetophenone (I) was prepared by slow addition of an ethereal solution of *o*-methoxybenzoyl chloride[6] to a large excess (about 3 molar equivalents) of cold ethereal diazomethane.[7] The oily product obtained by the evaporation of ether after drying over $MgSO_4$ was used for the reaction without further purification. IR (neat): 2200 (C=N=N), 1605 (C=O of diazoketone), 1250 (C-O-C), and 755 cm^{-1} (Ph). The elemental analysis of I was satisfactory.

Catalytic Decomposition of I in Benzene. In a flask fitted with a dropping funnel and a reflux condenser connected to a gas burette was placed 0.05 g (0.19 mmol) of $Cu(acac)_2$ dissolved in 50 ml of benzene. To the solution was added dropwise a solution of I (5.8 mmol) in 30 ml of benzene. The evolution of nitrogen was almost quantitative. When it was over, the reaction mixture was separated by silica gel

3) W. Kirmse, "Carbene Chemistry", Academic Press, New York and London, (1964) p. 131.

4) M. Takebayashi, T. Ibata, H. Kohara. and Bu. H. Kim, This Bulletin, **40**, 2392 (1967).

5) a) P. Pfeiffer and E. Ender, *Chem. Ber.*, **84**, 247 (1951). b) H. Krzikalla and B. Eistert, *J. Pract. Chem.*, **143**, 50 (1935). c) A. K. Bose and P. Yates, *J. Amer. Chem. Soc.*, **74**, 4703 (1952).

6) E. R. Marshall, J. A. Kuck, and R. C. Elderfield, *J. Org. Chem.*, **7**, 444 (1942).

7) W. E. Bachmann and W. S. Struve, "Organic Reactions", Vol. I, (1942) p. 40.

chromatography. 2-Methylcoumaranone (IV, 0.439 g, 52%) accompanied by bis(*o*-methoxybenzoyl)ethylene (VIII, 0.059 g, 7%) and an oligomer of *o*-methoxybenzoylcarbene (0.253 g, 30%)[2] was obtained. IR (neat) of IV: 1720 (C=O), 1245 (C–O–C), and 755 cm^{-1} (Ph). NMR ($CDCl_3$) of IV: 2.2—3.2 (m, 4H, aromatic proton), 5.65 (q, 1H, methine-H), and 8.61 τ (t, 3H, CH_3). Found: C, 73.12; H, 5.40%. Calcd for $C_9H_8O_2$: C, 72.96; H, 5.44%.

Competitive Reaction of I in Alcohol–Benzene Solution. A solution of I (5.7 mmol) in a mixed solvent (30 ml) of alcohol–benzene was added dropwise to 50 ml of mixed solvent of same composition containing $Cu(acac)_2$ (0.05 g, 0.19 mmol) at 80 °C. After evaporation of solvent under reduced pressure, the reaction mixture was treated with *n*-heptane, and the soluble part in *n*-heptane was analyzed quantitatively by gas chromatography. The product ratios obtained are given in Table 1. Coumaranone (V) was isolated by preparative gas chromatography (and silica gel column chromatography) of the reaction mixture. IR (KBr) of V: 1720 (C=O), 1460 (CH_2), 1190 (C–O–C), and 764 cm^{-1} (Ph). NMR ($CDCl_3$) of V: 2.2—3.1 (m, 4H, aromatic proton) and 5.40 τ (s, 2H, CH_2).

BULLETIN OF THE CHEMICAL SOCIETY OF JAPAN, VOL. 46, 2899 (1973)

Syntheses and Reactions of Metal Organics. VIII. The Formation of 2,5-Piperazinediones from Metal Alkoxides and α-Amino Acids

Norio Yoshino and Takeshi Yoshino

Department of Industrial Chemistry, Faculty of Engineering, Science University of Tokyo, Kagurazaka, Shinjuku-ku, Tokyo 162

(Received January 18, 1973)

In preliminary studies of the yellowing of wool by ultraviolet light[1] it was observed that the pretreatment of wool with an alkyl titanate, for example, tetra-*n*-butyl titanate, protects wool from yellowing. It has been proved that this protection is not due to the screening of wool from ultraviolet light by the titanate. Other observations have suggested that the titanates may react with proteins, peptides, and amino acids. Many reactions of metal (IV) alkoxides and metal (IV) chlorides with amines, amides, and carboxylic acids have been studied,[2] but few with amino acids have been studied. The present investigation is concerned with the reactions of titanium isopropoxide, *n*-butoxide, and zirconium isopropoxide with glycine and DL-α-alanine.

On heating α-amino acids, two moles of them condense to 2,5-piperazinediones, but the products are colorized by partial thermal decomposition. On the addition of metal alkoxides, they acted as dehydrating agents on α-amino acids in the presence of alcohols, but did not do so in hydrocarbon solvents.

The reactions proceeded as follows:

$$2H_2NCHRCOOH + 2M(OR')_4 \longrightarrow [RCHCONH]_2 + 2M(OR')_2O + 4R'OH$$

(R=H or Me, R'=^{i}Pr or ^{n}Bu, M=Zr or Ti)

Experimental

Reaction of Zirconium Isopropoxide with Glycine. A mixture of glycine (2.0 g, 27 mmol) and zirconium isopropoxide (13.1 g, 40 mmol) in 50 ml of ethyl alcohol was heated to boiling while being stirred. The glycine dissolved completely within 2 hr. On heating at the boiling point of the clear solution for 1.5 hr, some precipitates began to appear. Heating was continued for 20 hr in order to complete the precipitation. The white precipitates obtained were washed with cold ethyl alcohol and dried under a vacuum; yield, 1.1 g; mp 309 °C (decomp.). The product was identified with 2,5-piperazinedione by means of its melting point (lit,[3] mp 311—312 °C) and its IR spectrum.

Reaction of Zirconium Isopropoxide with DL-α-*Alanine.* The isolation of 3,6-dimethyl-2,5-piperazinedione (0.7 g) from DL-α-alanine (2.0 g, 22 mmol) and zirconium isopropoxide (11.0 g, 33 mmol) was accomplished in the same way as has been described for the preceding experiment; mp 268—269 °C (lit,[4] mp 271 °C). The IR spectrum of this product was identical with that of an authenic specimen.

Reactions of Titanium Alkoxides with Glycine. A mixture of glycine (2.0 g, 27 mmol) and titanium isopropoxide (11.3 g, 40 mmol) in 50 ml of isopropyl alcohol was heated to boiling with stirring. The glycine did not dissolve completely, but a light brown powder (1.5 g) was obtained after 20 hrs' heating; mp 307.5—308.5 °C (decomp.).

From the reaction of titanium *n*-butoxide (13.6 g, 40 mmol) and glycine (2.0 g, 27 mmol) in ethyl or isopropyl alcohol, a light brown powder (1.1—1.5 g) was also obtained. These products were identified with 2,5-piperazinedione.

Reaction of Titanium n-*Butoxide with* DL-α-*Alanine.* From the reaction of titanium *n*-butoxide (11.2 g, 33 mmol) and DL-α-alanine (2.0 g, 22 mmol) in 50 ml of methyl, ethyl, or isopropyl alcohol, colorless needles (0.7—0.8 g) were formed. All the products melted at 267 °C and were identified with 3,6-dimethyl-2,5-piperazinedione.

1) H. P. Lundgren, Proc. Intern. Wool Textile Research Conf., Melbourne, 1955C, pp. 374—395.

2) a) J. Archambault and R. Rivest, *Can. J. Chem.*, **36**, 1461 (1958); **38**, 1331 (1960); b) N. Yoshino and T. Yoshino, *Kogyo Kagaku Zasshi*, **71**, 1025 (1968); **72**, 2293 (1969); **73**, 1161 (1970); **74**, 1404, 1673 (1971); c) W. R. Trost, *Can. J. Chem.*, **29**, 877, 1075 (1951); d) H. Breederveld and H. I. Waterman, *Research*, **6**, 43S (1953).

3) R. Kempf, *J. Prakt. Chem.*, **78**, 244 (1908).

4) A. P. N. Franchimont and H. Friedmann, *Recl. Trav. Chim. Pays-Bas*, **27**, 194 (1908).

BULLETIN OF THE CHEMICAL SOCIETY OF JAPAN, VOL. 46, 2900—2901 (1973)

Syntheses and Properties of *m,m'*-Polymethylenebiphenyls

Koji YAMAMOTO, Yosihiko NAITO, Yukiyasu TANAKA, and Masao NAKAZAKI

Department of Chemistry, Faculty of Engineering Science, Osaka University, Toyonaka, Osaka 560

(Received January 26, 1973)

Reports were given on the preparation of three systems of compounds (**1**), (**2**), and (**3**), with varying lengths of polymethylene bridge spanning *o,p'*-, *m,p'*-, and *p,p'*-positions of biphenyl, respectively.[1-3]

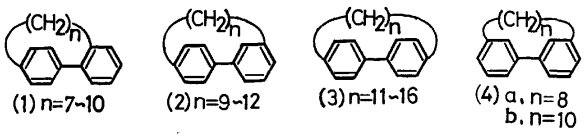

The present communication describes the syntheses and properties of biphenyls (**4**) with *m,m'*-polymethylene bridge.[4]

Preparation of (**4**) was carried out according to the sequence of reactions illustrated in Chart 1. The usual sequence involving malonic ester synthesis and LAH reduction is extended to the side chains of dibromide (**5a**), *via* (**5b**), and (**5c**), to give the homologous dibromide (**5d**). The malonic ester synthesis applied to the resulting dibromide (**5d**) afforded diester (**5g**), mp 48—49 °C, which was cyclized to acyloin (**6**) by the Prelog-Stoll acyloin condensation. The Clemmensen reduction of (**6**) gave *m,m'*-decamethylenebiphenyl (**4b**), mp 58—59 °C.

Because of severe steric strain in the lower homolog *m,m'*-octamethylenebiphenyl (**4a**), its synthesis was effected only by making a detour through the more flexible intermediates (**7**), (**8**), and (**9**) with saturated biphenyl moiety.

Hydrolysis followed by esterification of dinitrile (**5e**) secured from dibromide (**5d**), afforded diester (**5f**). Catalytic hydrogenation (1 atm, room temperature) over Adams' catalyst of ester (**5f**) in acetic acid gave saturated ester (**7**), which was cyclized by acyloin condensation to yield saturated acyloin (**8**). The Clemmensen reduction of (**8**) afforded saturated hydrocarbon (**9**).

The final step of the synthesis was dehydrogenation of (**9**) by heating with 10% Pd/C catalyst at 260—300 °C for 3 hr yielding *m,m'*-octamethylenebiphenyl (**4a**), mp 73—74 °C. Dehydrogenation under more drastic conditions (360—390 °C for 3 hr) converted (**9**) into perylene (**10**) apparently *via* biphenyl derivative (**4a**).

The electronic spectrum of *m,m'*-polymethylenebiphenyls (**4**) (**4a**: λ_{max} 253 nm, log ε 4.22; **4b**: λ_{max} 253 nm, log ε 4.21 in *n*-hexane) shifts towards longer wavelength with higher intensity compared to the reference compound (3,3'-dimethylbiphenyl: λ_{max} 250 nm, log ε 4.20 in *n*-hexane).

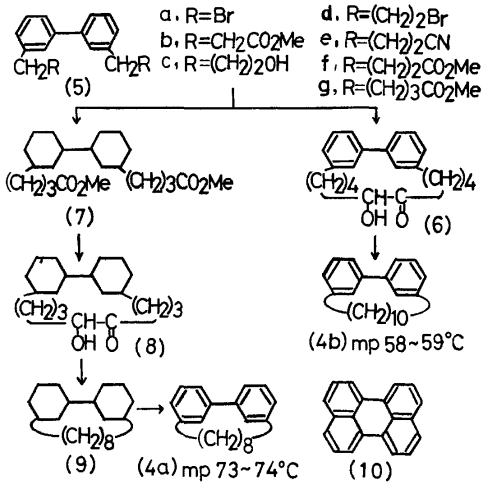

Chart 1

The NMR data of the *m,m'*-polymethylenebiphenyls are shown in Table 1. Absorptions due to the hydrogens of polymethylene bridges appear at lower field than those of the polymethylene in *o,p'*-, *m,p'*-, and *p,p'*-polymethylene bridged biphenyls. Among the *m,m'*-polymethylenebiphenyl derivatives (**4**), the methylene hydrogens of the lower homolog (**4a**) (8.45 τ) absorb at lower field than the higher homolog (**4b**) (8.67 τ).

TABLE 1. NMR SPECTRAL DATA IN CARBON TETRACHLORIDE

Compound	Aromatic protons, τ	Aliphatic protons, τ		
4a	2.62—3.15 (8H)	7.31 (4H)	8.33 (4H)	8.67 (12H)
4b	2.49—3.15 (8H)	7.26 (4H)	8.30 (4H)	8.45 (8H)

The results can be rationalized by assuming that the *m,m'*-polymethylene bridges in the biphenyl derivatives (**4**) are coplanar with the molecular planes as shown by molecular models, and that they are deshielded by the biphenyl moieties, the deshielding being apparently more effective in the shorter bridged compound (**4a**) than in (**4b**).

Experimental

m,m'-*Bis-(3-carbomethoxypropyl)-bicyclohexyl* (**7**). Six grams of diester (**5f**) was hydrogenated with 0.6 g of platinum oxide in 45 ml of acetic acid at 40 °C under 1 atmosphere. The reaction stopped after 70 hr when 90% of the theoretical amount of hydrogen had been absorbed. The catalyst was removed by filtration, the solvent was evaporated in a vacuum, and the product was distilled to yield a colorless liquid, bp 142—144 °C/0.05 mmHg, 5.4 g (87%).

1) M. Nakazaki and S. Isoe, *Chem. Ind.* (London), 224 (1965).
2) M. Nakazaki and K. Yamamoto, *ibid.*, 468 (1965).
3) M. Nakazaki, T. Horikawa, and K. Yamamoto, *Tetrahedron Lett.*, **1969**, 4551.
4) R. V. M. Campbell, L. Crombie, B. Tuck, and D. A. Whiting, *Chem. Commun.*, 1206 (1970).

4-Hydroxy-5-oxo-m,m′-*octamethylenebicyclohexyl (8)*. A solution of 2.7 g of the saturated diester (**7**) in 150 ml of xylene was added to a suspension of 1.2 g of sodium in 400 ml of xylene over 48 hr under nitrogen atmosphere. The usual work-up[5] of the reaction mixture then gave crude acyloin (**8**), 1.2 g (53%).

m,m′-*Octamethylenebicyclohexyl (9)*. Amalgamated zinc was prepared by swirling 33 g of zinc with a solution of 1 g of $HgCl_2$ and 1 ml of concd HCl in 100 ml of water. A solution of 1.2 g of acyloin (**8**) in 30 ml of toluene was added to the amalgamated zinc with 100 ml each of concd HCl and acetic acid. The mixture was heated under reflux for 48 hr, during which time four 20 ml-portions of concd HCl were added. After the usual treatment, the crude reaction product was distilled to yield a colorless liquid, bp 116—118 °C/0.1 mmHg, 0.5 g (46%).

Found: C, 86.23; H, 13.19%. Calcd for $C_{20}H_{36}$: C, 86.88; H, 13.12%.

m,m′-*Octamethylenebiphenyl (4a)*. Dehydrogenation of 0.5 g of saturated hydrocarbon (**9**) was accomplished by heating with 0.04 g of 10% palladium-on-charcoal at 260—300 °C for 3 hr. The theoretical amount of hydrogen was evolved, the reaction product was taken up in *n*-hexane, filtered free of catalyst and crystallized from ethanol to give 0.3 g (63%) of (**4a**), needles, mp 73—74 °C.

Found: C, 90.71; H, 9.32%. Calcd for $C_{20}H_{24}$: C, 90.80; H, 9.26%.

5-Hydroxy-6-oxo-m,m′-*decamethylenebiphenyl (6)*. The acyloin reaction was carried out in a manner similar to that described for (**8**). From 11 g of diester (**5g**) was obtained 4.2 g (51%) of the crude acyloin (**6**).

m,m′-*Decamethylenebiphenyl (4b)*. Four grams of acyloin (**6**) was converted into hydrocarbon with zinc and acid as described for (**9**). The product was isolated in the usual way and recrystallization from ethanol gave 0.8 g (21%) of (**4b**), needles, mp 58—59 °C.

Found: C, 90.11; H, 10.03%. Calcd for $C_{22}H_{28}$: C, 90.23; H, 9.88%.

5) D. J. Cram and H. Steinberg, *J. Amer. Chem. Soc.*, **73**, 5691 (1951).

BULLETIN OF THE CHEMICAL SOCIETY OF JAPAN, VOL. 46, 2901—2903 (1973)

Electrocatalytic Chemistry of the Transition Metal Complexes. III. Dehydrogenation of Cyclohexadienes Catalyzed by the Electro-reduced Cobalt Complex of $\alpha,\beta,\gamma,\delta$-Tetraphenylporphine

Hironori KAGEYAMA, Masanobu HIDAI, and Yasuzo UCHIDA

Department of Industrial Chemistry, Faculty of Engineering, The University of Tokyo, Hongo, Bunkyo-ku, Tokyo 113

(Received February 14, 1973)

Although there are some reports on the disproportionation of 1,3- and 1,4-cyclohexadiene (CHD) to produce benzene and cyclohexene,[1] only a few reports have appeared in which 1,3- and 1,4-CHD were dehydrogenated to produce benzene by using the homogeneous transition metal complexes such as the metal complexes of $\alpha,\beta,\gamma,\delta$-tetraphenylporphine (M(TPP)),[2] and dichloropalladium(II).[3]

In the previous papers,[4,5] the authors reported that the electro-reduced Co(TPP) had the catalytic activity of dehydrogenating cyclohexene to 1,3- and 1,4-CHD, and benzene (Bz). In this paper, the dehydrogenation reaction of 1,3- and 1,4-CHD by using the same catalyst will be described.

Experimental

Tetra-*n*-butylammonium perchlorate (TBAP),[6] Co(TPP),[7] 1,4-CHD,[8] and 1,3-CHD[9] were prepared according to the published methods. The conditions of electrolysis were: the concentration of Co(TPP), 1.0×10^{-3} mol/l; the concentration of TBAP, 2.0×10^{-1} mol/l; solvent, 10.0 ml; an anode, a platinum wire; a cathode, a platinum plate (the electrode area, 3.0 cm^2); a reference electrode, a silver wire; potential, -2.0 V; temperature, room temperature; reaction time, 24 hr; atmosphere, nitrogen; a electrolyzer, a Yanagimoto Controlled Potential Electrolyzer Model VE-3S; and an electrolytic cell, an H-type cell with a side arm to enable the insertion of an Ag wire reference electrode. The quantitative analysis of the products was performed by glc. The visible spectra of the reaction solution after electrolysis were measured using a Shimadzu Model MPS-50L Spectrophotometer.

Results and Discussion

Dehydrogenation of 1,3- and 1,4-CHD. The current efficiency for formation of benzene was defined as

1) K. Moseley, and P. M. Maitlis, *Chem. Commun.*, **1969**, 1156; J. E. Lyons, *ibid.*, **1969**, 564.
2) J. Manassen, and A. Bar-Ilan, *J. Catal.*, **17**, 86 (1970).
3) S. D. Robinson, and B. L. Shaw, *J. Chem. Soc.*, **1964**, 5002.
4) H. Kageyama, M. Hidai, and Y. Uchida, *Chem. Lett.*, **1972**, 139.
5) H. Kageyama, M. Hidai, and Y. Uchida, This Bulletin, **45**, 2898 (1972).
6) A. Misono, Y. Uchida, T. Yamagishi, and H. Kageyama, *ibid.*, **45**, 1438 (1972).
7) B. H. Ball, G. D. Dorough, and M. Calvin, *J. Amer. Chem. Soc.*, **68**, 2278 (1946); P. Rothermund, and A. R. Menotti, *ibid.*, **70**, 1808 (1948).
8) M. Amagasa, T. Yamaguchi, and M. Tanaka, Brit. 1033760 (1966).
9) T. Yamaguchi, T. Ono, K. Nagai, C. Chong Sui, and T. Shiral, *Chem. Ind.* (London), **1967**, 759.

Table 1. Dehydrogenation of 1,3- and 1,4-cyclohexadiene catalyzed by the electro-reduced Co(TPP) in various solvents

Solvent	CHD	CHD/Co molar ratio	Composition of the products (%)					η'_{Bz} (%)[c]
			cC_6[a]	cC_6'[b]	1,3-CHD	1,4-CHD	Bz	
DMF	1,3	159	0	0	100	0	0	0
	1,4	128	0	6.1	15.5	68.9	6.0	104
HMPT	1,3	154	0	0	100	0	0	0
	1,4	131	0	0	0	93.0	7.0	81.2
PhCN	1,3	147	0	0	87.0	7.0	6.0	126
	1,4	121	4.5	0	0	75.7	19.8	408

Conditions: an anode, a Pt wire; a cathode, a Pt plate; a reference electrode, an Ag wire; the concentration of Co(TPP), 1.0×10^{-2} mol/l, the concentration of TBAP, 2.0×10^{-1} mol/l, potential, -2.0 V; solvent, 10.0 ml; temperature, r.t.; reaction time, 24 hr.
a) cyclohexane b) cyclohexene c) current efficiency for formation of benzene.

follows:

$$\eta'_{Bz}\,(\%) = (\text{Amount of Bz(mole)})\times 200/\text{Current passage (Faraday)}$$

The results are shown in Table 1. In the electrolysis of 1,4-CHD with the use of dimethylformamide (DMF), hexamethylphosphoric triamide (HMPT), and benzonitrile (PhCN) as the solvent, the current efficiencies were higher than 100%, indicating that the dehydrogenation reaction is catalytic. The current efficiencies in the electrolysis of 1,3-CHD were much lower than those in the electrolysis of 1,4-CHD. Furthermore, the current efficiency in the case of PhCN used as the solvent was much higher than the current efficiencies in that of DMF and HMPT used.

In the 1,4-CHD–DMF system, 1,4-CHD was isomerized to produce 1,3-CHD. Cyclohexene and benzene were also produced in the same system, which are considered to be derived from the disproportionation of 1,4-CHD, since the amount of benzene was about equal to that of cyclohexene.[1] In the 1,4-CHD–HMPT system, 1,4-CHD was dehydrogenated to afford benzene, but 1,3-CHD was not observed in the reaction system.

In the 1,3-CHD–PhCN system, 1,3-CHD was isomerized to give 1,4-CHD, and was also dehydrogenated to produce benzene. However, in the 1,4-CHD–PhCN system, 1,4-CHD was not isomerized, but was dehydrogenated to produce benzene, and a little amount of cyclohexane was formed.

The reaction schemes in the case of the above three solvents used are summarized as follows:
in the case of DMF used as the solvent;

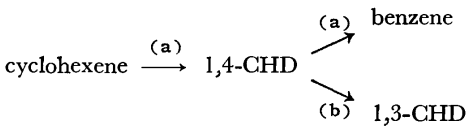

in the case of HMPT used as the solvent;

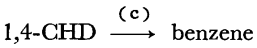

in the case of PhCN used as the solvent;

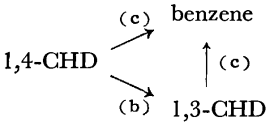

(a) disproportionation, (b) isomerization, (c) dehydrogenation

Effect of Addition of Methanol. The current efficiencies decreased with the addition of dry methanol to the reaction solution as shown in Table 2. The similar results have been reported in the dehydrogenation of cyclohexene catalyzed by the electro-reduced Co(TPP).[5] It may be reasonable to assume that added alcohol reacts with the conjugated ring of the catalytically active electro-reduced Co(TPP) to cleave or weaken the conjugated ring.

The Visible Spectra of the Reaction Solution after Electrolysis. In the visible spectrum of the HMPT solution containing 1,4-CHD after electrolysis, the new bands appeared at 620 and 417 nm, which were assigned to the Q-band and Soret-band, respectively, of the cobalt complex of $\alpha,\beta,\gamma,\delta$-tetraphenylchlorin (Co(TPC)) in which two hydrogen atoms are attached to a pyrrole

Table 2. Effect of addition of methanol

Solvent	CHD	CHD/Co molar ratio	MeOH/Co molar ratio	Composition of the products (%)					η'_{Bz} (%)
				cC_6	cC_6'	1,3-CHD	1,4-CHD	Bz	
DMF	1,3	102	138	0	0	100	0	0	0
	1,4	80	135	0	0.6	7.3	73.8	18.3	59.3
HMPT	1,3	101	131	0	0	100	0	0	0
	1,4	102	132	0	1.5	2.4	93.3	2.8	31.0
PhCN	1,3	99	137	0.1	0	56.9	0	43.0	72.6
	1,4	106	132	0	0	0	53.2	46.8	174

fragment of porphyrin skeleton.[10]

In a previous paper,[5] the authors reported that the active species for the dehydrogenation of cyclohexene could be the species electro-reduced at −2.0 V *vs.* Ag wire, *viz.*, $[Co^{I}(TPP)^{\cdot-}]^{-}$, and the formation of Co(TPC) was observed in the electrolysis of cyclohexene by using dioxane as the solvent.

From the above results, therefore, it may be reasonable to assume that the active species for the dehydrogenation of 1,3- and 1,4-CHD was analogous to that for the dehydrogenation of cyclohexene.

10) G. D. Dorough, and F. M. Huenneckens, *J. Amer. Chem. Soc.*, **74**, 3974 (1952); C. Araki, K. Yamamoto, and S. Sotomura, *Rikagaku Kenkyu-jo Hokoku*, **39**, 156 (1963).

BULLETIN OF THE CHEMICAL SOCIETY OF JAPAN, VOL. 46, 2903—2904 (1973)

Catalytic Activities of Salicylaldehyde Derivatives. III. An Improved Synthesis of 6-Nitrosalicylaldehyde

Makoto ANDO and Sakae EMOTO

The Institute of Physical and Chemical Research, Wako-shi, Saitama 351

(Received February 19, 1973)

In connection with our studies of the catalytic activities of salicylaldehyde derivatives,[1] it was necessary to synthesize 6-nitrosalicylaldehyde (**1**). Although **1** had been prepared from *m*-nitrophenol (**2**) by the Reimer-Tiemann reaction in a 3—4% yield,[2,3] our reinvestigation showed that the yield was still poor and variable. The methyl ether of **1** has been obtained in a 19% yield from 3-nitro-*o*-cresol,[4] which, in turn, is prepared from 2,6-dinitrotoluene, but this method is unsuitable for preparing a large quantity of **1**. In this paper, we wish to describe an improved synthesis of **1** *via* 5-nitro-1,3-benzodioxane (**3**); it is shown in the scheme.

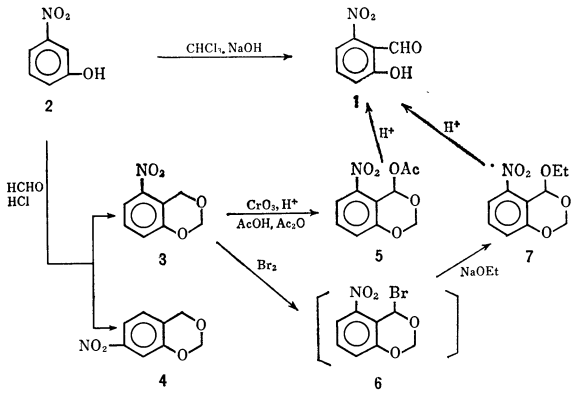

Mehta and Ayyar has previously synthesized **3** in a 13% yield,[3a] by refluxing a mixture of **2**, formaldehyde (1.5 mol equivalents), and hydrochloric acid for 2—3 hr. The yield of **3** could be increased up to 30% when we used 2 mol equivalents of formaldehyde and prolonged the reaction time to 5—6 hr (a longer reaction time decreased the yield), and after the reaction mixture had been treated according to the Mehta method, a non-crystalline residue was purified by the use of a silica gel column. A small amount of 7-nitro-1,3-benzodioxane (**4**), which had been prepared from **2**, formaldehyde, and sulfuric acid at 40 °C in a poor yield,[5] was also obtained from the non-crystalline residue. 6-Nitrosalicylic acid had previously been prepared by the oxidation of **3** with chromic anhydride and sulfuric acid in acetic acid,[3a] but when we attempted the oxidation in a mixture of acetic acid and acetic anhydride, a product (**5**), into which one acetoxy group was introduced was obtained. Because, by the acidic hydrolysis of **5**, **1** was synthesized, **5** was confirmed to be 4-acetoxy-5-nitro-1,3-benzodioxane. In carbon tetrachloride, **3** was brominated with 1 mol of bromine under the light of a tungsten lamp to give a monobrominated product (**6**); this product was very unstable and decomposed in air, so, after the bromination had been completed, a solution of **6** in carbon tetrachloride was used immediately in the next step. The solution of **6** in carbon tetrachloride was added to a solution of an excessive amount of sodium ethoxide in ethanol to convert the bromo compound into an ethoxy one (**7**), which was then hydrolyzed to **1** by acid. Consequentlyl **6** and **7** were confirmed to be 4-bromo- and 4-ethoxy-5-nitro-1,3-benzodioxanes respectively. The total yield of **1** by this route was 24% based on **2**; as compared with the synthesis by means of the Reimer-Tiemann reaction, the total yield was very much increased, and so **1** can be prepared in a large quantity.

Experimental

All the mps and bp are uncorrected.

5-Nitro-1,3-benzodioxane (3). A mixture of **2** (250 g), a 37% formaldehyde aqueous solution (375 ml), and concd hydrochloric acid (750 ml) was boiled under reflux with vigorous stirring for 5 hr. After being cooled, a clear supernatant was poured off and the residue was stirred with a

1) M. Ando and S. Emoto, This Bulletin, **42**, 2624, 2628 (1969).

2) J. N. Ashley, W. H. Perkin, Jr., and R. Robinson, *J. Chem. Soc.*, **1930**, 382.

3) a) D. R. Mehta and P. R. Ayyar, *J. Univ. Bombay*, **8**, 176 (1939); *Chem. Abstr.*, **34**, 2814 (1940). b) S. Yoshikawa, K. Kuga, Y. Ueda, M. Goto, and H. Sugiyama, *Kogyo Kagaku Zasshi*, **70**, 331 (1967).

4) G. R. Pettit, *J. Org. Chem.*, **24**, 866 (1959).

5) C. A. Buehler, G. F. Deebel, and R. Evans, *J. Org. Chem.*, **6**, 216 (1941).

hot 3 M sodium hydroxide aqueous solution (1 l). After this mixture had then been cooled, the insoluble material was separated by filtration and extraction (1 M sodium hydroxide, 1 l) was repeated twice. After the residue had been dried, it was dissolved in hot ethanol (2 l); an insoluble, oily product was filtered off with charcoal, and then the solution was allowed to stand overnight at room temperature. The resultant turbid solution was treated again with charcoal, after which the solvent was removed under diminished pressure until the solid **3** deposited, whereupon the **3** was separated by filtration. The separation of **3** was repeated until an oily product resulted. The solvent of the oily product was removed *in vacuo*; the residue was dissolved in benzene and then purified by silica gel-column chromatography (*ca.* 50 fold in weight). At first **3** was eluted by benzene; elution was then continued by the use of a mixture of benzene and ethyl acetate, and then ethyl acetate. The second fraction was collected and was confirmed to be 7-nitro-1,3-benzodioxane (**4**) by studies of the mp and by elemental analyses. Mp 91—92 °C (lit,[5] 90.5 °C); yield, 5.3 g (1.6%). The total yield of **3** was 98.5 g (30%). Mp 73—74 °C (lit,[3a] 78 °C). It was recrystallized from ethanol (mp 75 °C), but crude **3** was used in the next step.

4-Acetoxy-5-nitro-1,3-benzodioxane (5). Into a solution of **3** (65 g) in acetic acid (650 ml) and acetic anhydride (650 ml), sulfuric acid (50 ml) was stirred below 10 °C. Solid chromic anhydride (50 g) was then added to the solution in small portions at 0—5 °C; about 30 min was required for the addition. Stirring was continued for another 90 min after the chromic anhydride had been added at the same temperature; the reaction mixture was then poured into ice water and allowed to stand for several hours. A precipitate was then collected on a filter and recrystallized from methanol. Mp 98 °C; yield, 46.0 g (54%); IR (KBr) 1760 cm^{-1} (C=O).

Found: C, 50.24; H, 3.79; N, 5.94%. Calcd for $C_{10}H_9O_6N$: C, 50.21; H, 3.79; N, 5.86%.

6-Nitrosalicylaldehyde (1) from 5. A mixture of **5** (14.3 g), ethanol (75 ml), water (75 ml), and concd sulfuric acid (15 ml) was boiled for 3 hr with stirring. The cooled mixture was then diluted with water and extracted with benzene. The benzene layer was dried over anhydrous magnesium sulfate, and the solvents were removed under reduced pressure. The residue was dissolved in benzene and extracted with a dil sodium hydroxide aqueous solution. The aqueous solution was then acidified with hydrochloric acid and extracted with benzene. The solution was dried over anhydrous magnesium sulfate and concentrated under diminished pressure. Crude **1** was purified by reprecipitation with alkali-acid. Mp 51—52 °C (lit, 54—55 °C,[2] 50—51 °C[3a]); yield, 8.3 g (83%). IR of **1**, prepared from **5**, agreed with that of the authentic sample.

4-Ethoxy-5-nitro-1,3-benzodioxane (7). Under the light of a tungsten lamp, a solution of bromine (22.4 g) in carbon tetrachloride (25 ml) was added to a boiling solution of **3** (25.4 g) in carbon tetrachloride (250 ml) over a period of 1 hr, after which boiling was continued for 3 hr. After the mixture had been cooled, an insoluble product was filtered off with celite. A clear solution which contained some fuming hydrogen bromide was stirred, drop by drop, into a solution of sodium ethoxide in ethanol (prepared from 4.4 g of sodium and 90 ml of ethanol; 1.3 mol equivalents) at 10—15 °C. This required 15 min; stirring was then continued for 3 hr at room temperature. A precipitate was dissolved by the addition of water, and the carbon tetrachloride layer was separated. The aqueous solution was extracted with carbon tetrachloride, and the combined carbon tetrachloride solution was washed well with water and then dried over anhydrous magnesium sulfate. The solvent was removed under reduced pressure, and the residue was distilled in a vacuum. Bp 123—127 °C/4 mmHg; yield, 29.3 g (93%).

Found: C, 53.51; H, 4.98; N, 6.18%. Calcd for $C_{10}H_{11}O_5N$: C, 53.33; H, 4.92; N, 6.22%.

6-Nitrosalicylaldehyde (1) from 7. A mixture of **7** (10 g), ethanol (100 ml), water (100 ml), and concd sulfuric acid (20 ml) was reacted as has been described in the hydrolysis of **5**. Mp 52 °C; yield, 6.6 g (89%).

In conclusion, the authors wish to express their thanks to Dr. Haruo Homma and his staff of this Institute for elemental analyses. This work was financially supported in part by a research grant for studies of life sciences by this Institute, which help the authors acknowledge gratefully.

BULLETIN OF THE CHEMICAL SOCIETY OF JAPAN, VOL. 46, 2905—2906 (1973)

Phenolysis of *exo*- and *endo*-2-Norbornyl *p*-Toluenesulfonates. Rates and Product Distributions

Kunio OKAMOTO, Tomomi KINOSHITA, and Yuji ITO

Department of Hydrocarbon Chemistry, Faculty of Engineering, Kyoto University, Sakyo-ku, Kyoto 606

(Received February 23, 1973)

Although norbornyl arenesulfonate solvolysis has been extensively studied with regard to the non-classical nature of the norbornyl cation,[1,2] the system has never been subjected to solvolytic study with the use of a phenolic solvent, which is suitable for S_N1-solvolysis.[3]

This study was carried out in order to compare the results of 2-norbornyl tosylate (ROTs) phenolysis with those of the previous studies[1b] in common solvolytic solvents with regard to the *exo*/*endo* rate ratio and epimeric nature of the products, and to examine the distribution of the O- and C-norbornylated phenols for information on the non-classical nature of the solvolysis intermediates from *exo*- and *endo*-ROTs in the phenolic solvent.

Titrimetric first-order rate constants (k_1) for the two epimeric ROTs's in a phenol–benzene (1: 1 by wt.) solvent are given in Table 1. The *exo*/*endo* rate ratios for the phenolysis are 591 at 25 °C and 622 at 50 °C, being comparable with the acetolysis rate ratio of 185 at 50 °C,[1a] and also with the ethanolysis rate ratio of 171 at 50 °C.[2]

Phenolysis of 2-norbornyl tosylates gives the phenyl ether (ROC_6H_5), and *o*- and *p*-norbornylated phenols (*o*- and *p*-RC_6H_4OH), and a mixture of nortricyclene and norbornene. The results for representative runs are given in Table 2. Using capillary gas chromatography, we have examined the *exo*/*endo* epimer ratio of the substitution products. Control experiments showed 0.1% *endo*-epimer in ROC_6H_5 and 0.02% *endo*-epimer in both *o*- and *p*-RC_6H_4OH to be detectable. However, neither *endo*-ROC_6H_5 nor *endo*-RC_6H_4OH were observed in the phenolysis products from *exo*- and *endo*-ROTs, the *endo*-epimer content being definitely <0.1% for ROC_6H_5 and <0.02% for *o*- and *p*-RC_6H_4OH.

Table 1. Titrimetric phenolysis rates of 2-norbornyl tosylates[a]

	Tosylate M	NaOPh M	Temp. °C	k_1 sec^{-1}	*exo*/*endo*
exo	0.0998	0.1040	0.0	1.58×10^{-4}	
	0.1004	0.1040	25.0	3.78×10^{-3}	591
			50.0	5.55×10^{-2}[b]	622
endo			25.0	6.40×10^{-6}[b]	
	0.1009	0.1041	50.0	8.92×10^{-5}	
	0.1009	0.1041	75.0	8.65×10^{-4}	

a) Solvent: PhOH–Benzene (1:1 by wt.). b) Extrapolated from data at other temperatures.

Product distributions for the phenolysis of epimeric tosylates in the presence of sodium phenoxide (0.007—0.095 M) were determined in the phenoxide/substrate concentration ratios 7.6—9.5 at 50.0 °C. The distribution of products resulting from the reaction of phenol molecule with phenolysis intermediate can be estimated by the graphic extrapolation of the distribution curve to the zero phenoxide concentration, as in the case for 1-adamantyl,[3a] 2-octyl,[3b] and tetrahydrolinalyl systems;[3b] the distribution of products resulting from the reaction of phenoxide ion with phenolysis intermediate has been calculated by the method previously reported.[3] The results are given in Table 3.

The calculated product distributions for the *exo*-

Table 3. Calculated product distributions for the reactions of the phenol molecule and the phenoxide ion[a]

Substrate	Product distribution %			
	ROC_6H_5	*o*-RC_6H_4OH	*p*-RC_6H_4OH	Hydrocarbons
Reaction of the phenol molecule				
exo-ROTs	81.5	4.0	0.86	13.6
endo-ROTs	82.3	6.5	1.1	10.1
Reaction of the phenoxide ion				
exo-ROTs	51.8	42.1	6.3	0.0
endo-ROTs	50.1	44.3	5.9	0.0
Values of k_2'/k_2[b]				
exo-ROTs	223	217	78	87
endo-ROTs	268	288	79	97

a) Solvent: PhOH–Benzene (1: 1 by wt). Temperature: 50.0 °C. b) *Cf.* Ref. 2.

Table 2. Product distributions of *exo*- and *endo*-2-norbornyl tosylate phenolyses[a]

	Tosylate M	NaOPh M	Temp. °C	Time hr	ROC_6H_5[b]	*o*-RC_6H_4OH[c]	*p*-RC_6H_4OH[d]	Nortricyclene	Norbornene
exo	0.1006	0.1110	50.0	0.57	58.6	26.5	3.1	11.8	0.07
endo	0.1009	0.1061	50.0	23	54.3	23.6	2.6	23.0	0.44

a) Solvent: PhOH–Benzene (1: 1 by wt.).
b, c, d) *exo*-% >99.9% for b; >99.98% for c; >99.96% for d.

1) a) S. Winstein and D. Trifan, *J. Amer. Chem. Soc.*, **74**, 1147, 1154 (1972); S. Winstein, E. Clippinger, R. Howe, and E. Vogelfanger, *ibid.*, **87**, 376 (1965). b) P. von R. Schleyer, M. M. Donaldson, and W. E. Watts, *ibid.*, **87**, 375 (1965).

2) W. Hückel and O. Vogt, *Ann. Chem.*, **695**, 16 (1966).

3) a) K. Okamoto, K. Matsubara, and T. Kinoshita, This Bulletin, **45**, 1191 (1972). b) K. Okamoto and T. Kinoshita, *ibid.*, **45**, 2802 (1972).

and *endo*-tosylates are in line with each other within experimental error in both phenol molecule and phenoxide ion reactions. The *endo*-tosylate initially produces the classical norbornyl ion and subsequently most the classical ion becomes non-classical before it is captured by the nucleophile.[1] The distribution character for the phenolysis products probably indicates that the life of the classical ion is relatively short in the phenolysis medium, and consequently most of the products from *endo*-ROTs stem from the non-classical norbornyl cation.

Experimental[4]

Materials. *exo*-2-Norbornanol[2] and *endo*-2-norbornanol (the *exo*-epimer content 8.1% by glc)[5-8] were prepared by known methods. *exo*- and *endo*-2-Norbornyl *p*-toluenesulfonates[1a] and nortricyclene[9] were obtained in the usual manner. Sodium phenoxide was prepared by the reported method.[3a] The other organic reagents employed were of analytical reagent grade and were fractionated just prior to use.

Syntheses of exo- *and* endo-*2-Norbornyl Phenyl Ethers.* A mixture of a potassium salt of *exo*-2-norbornanol (prepared from the alcohol and potassium in benzene) and bromobenzene in hexamethylphosphoric triamide was heated at 150 °C for 32 hr. The usual work up gave *exo*-2-norbornyl phenyl ether (bp 100—103 °C/1.8 mmHg, lit,[9] bp 98 °C/1 mmHg; the *exo*-epimer content >99.9% by glc). *endo*-2-Norbornyl phenyl ether was prepared from *endo*-2-norbornanol in a similar manner; bp 102—105 °C/2 mmHg; the *endo*/*exo* ratio 35.5/64.5 by glc. Found: C, 83.13; H, 8.82%. Calcd for $C_{13}H_{16}O$: C, 83.03; H, 8.52%.

Syntheses of exo- *and* endo-*2-Norbornylphenols.* *o*- and *p*-*endo*-2-Norbornylphenols were synthesized according to the method of Kheifits and Gol'dovskii;[10] the *o*-isomer, bp 124—126 °C/1.8 mmHg (lit,[10] bp 119—123 °C/0.3 mmHg); the *p*-isomer, bp 174—177 °C/4.0 mmHg (lit,[10] bp 125—129 °C/0.3 mmHg). *o*- and *p*-*exo*-2-Norbornylphenols were obtained by *exo*-2-norbornyl tosylate phenolyses; the *o*-isomer, mp 47.3—48.5 °C (corr.) (lit,[11] mp 49—50 °C); the *p*-isomer, mp 128.6—129.4 °C (corr.) (lit,[12] mp 133—135.5 °C).

Isolation of the Phenolysis Product. A flask containing the reaction mixture was placed in a constant-temperature bath for at least ten half-lives. After the work up[3] products were separated by column chromatography or by thin-layer chromatography (silica gel).

Kinetic Measurement. This was carried out by the usual sealed-ampoule and pipetting out technique.[3] In each case, smooth first-order rate plots were obtained over 70—80% reaction.

Product Analysis by Gas Chromatography. The product distribution was analysed by glc using a 2 m × 3 mm column with Apiezon Grease on Neopak 1A at 230 °C. The epimer analysis of each product was performed by glc using a Hitachi Golay column R-45 at 83 °C for 2-norbornanol (retention time: *exo*-epimer, 51.3 min; *endo*-epimer, 56.6 min) and a Hitachi Golay column Q-45 at 230 °C for 2-norbornyl phenyl ether (retention time: *exo*-epimer, 105.1 min; *endo*-epimer, 106.9 min). Norbornylphenols were converted into norbornylanisols by the use of dimethyl sulfate[13] prior to glc analysis, carried out using the column Q-45 at 230 °C: *o*-(2-norbornyl)anisol[10] (retention time: *exo*-epimer, 116 min; *endo*-epimer, 114 min); *p*-(2-norbornyl)anisol[10] (retention time: *exo*-epimer, 79 min; *endo*-epimer, 77 min).

4) A Hitachi Model 023-6003 gas chromatographic instrument, with a flame ionization detector, a Hitachi Model 215 IR spectrophotometer, and a Hitachi Model R-24 60 MHz NMR instrument were used for the analytical work.

5) K. Alder and H. F. Rickert, *Ann. Chem.*, **543**, 15 (1940).

6) R. L. Bixler and C. Niemann, *J. Org. Chem.*, **23**, 742 (1958).

7) J. D. Roberts, C. C. Lee, and W. H. Saunders, Jr., *J. Amer. Chem. Soc.*, **76**, 4501 (1954).

8) W. D. Closson, P. Wriede, and S. Bank, *ibid.*, **88**, 1581 (1966).

9) J. D. Roberts, E. S. Trumbull, Jr., W. Bennett, and R. Armstrong, *ibid.*, **72**, 3116 (1950).

10) L. A. Kheifits and A. E. Gol'dovskii, *Zh. Org. Khim.*, **5**, 1798 (1969).

11) L. A. Kheifits, G. I. Moldovanskaya, and L. M. Shulov, *Zh. Anal. Khim.*, **18**, 267 (1963).

12) L. A. Kheifits and A. E. Gol'dovskii, *Zh. Obshch. Khim.*, **33**, 3399 (1963).

13) T. J. Curphey, E. J. Hoffman, and C. McDonald, *Chem. Ind.*, **1967**, 1138.

BULLETIN OF THE CHEMICAL SOCIETY OF JAPAN, VOL. 46, 2907—2908 (1973)

Preparation of 9-Butadiynyltriptycene and 9,9′-Ditriptycyltetraacetylene

Shuzo AKIYAMA, Fumio OGURA, and Masazumi NAKAGAWA

Department of Chemistry, Faculty of Science, Osaka University, Toyonaka, Osaka, 560

(Received March 7, 1973)

The preparation of 9-ethynyltriptycene (I_1) and 9,9′-ditriptycyldiacetylene (II_2) was given in a previous paper.[1] The present paper deals with the preparation of their higher analogues, 9-butadiynyltriptycene (I_2) and 9,9′-ditriptycyltetraacetylene (II_4), which was performed according to the following scheme.

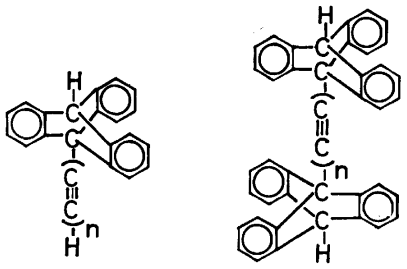

I_n II_n

n = 1, 2 n = 2, 4

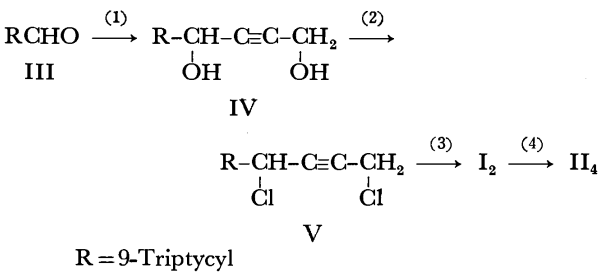

R = 9-Triptycyl

(1): $BrMgC{\equiv}C\text{-}CH_2OMgBr$; (2): $SOCl_2$-pyridine;
(3): $NaNH_2$ in liq. NH_3; (4): $Cu(OAc)_2$-pyridine

Scheme

9-Butadiynyltriptycene (I_2) was found to be highly stable in sharp contrast to the instability of other butadiynyl compounds such as phenanthryldiacetylene[2] and pyrenyldiacetylene.[3] The oxidative coupling of I_2 by Eglinton's method afforded highly stable and scarcely soluble II_4 in a quantitative yield. Theilacker and co-workers have pointed out that the introduction of an electron-attractive group at 9-position of triptycene nucleus causes an appreciable hypochromism of long wavelength absorption.[4] As shown in the Table, I_2 exhibits more enhanced hypochromism in a long wavelength region than I_1.[1]

The unusually high stability of I_1,[1] I_2, II_2,[1] and II_4, which can be attributed to the rigid and bulky cage structure of the triptycyl group, indicates the possibility of preparing much higher members of this class of polyacetylene. However, this seemed impracticable in view of the extremely poor solubility of II_4.

TABLE 1. HYPOCHROMISM OF 9-SUBSTITUTED TRIPTYCENES
(λ in nm in ethanol)

Triptycene		I_1		I_2	
λ	ε	λ	ε	λ	ε
197	62900	198	59000	198	62200
211	64200	210.5	63800	211	65200
270	3600	269.5	2800	270	2500
278	4900	277	3600	277.5	3200

Experimental

All the melting points were uncorrected. The IR and NMR spectra were measured with Hitachi EPI-2 and Varian A-60 spectrometers, respectively. The UV spectra were obtained on Hitachi EPS-3T and Zeiss PMQII,M4QIII spectrometers.

1-(9-Triptycyl)-2-butyne-1,4-diol (IV). To an ice-cooled solution of bis-Grignard derivative of propargyl alcohol [prepared from magnesium, 2.30 g; ethyl bromide, 10.5 g; propargyl alcohol, 2.69 g and tetrahydrofuran, 70 ml] was added over 20 min period a solution of 9-formyltriptycene[5] (III, 4.51 g, 0.061 mol) in the same solvent (150 ml). The cooling bath was then removed and the mixture was stirred overnight at room temperature. A saturated solution of ammonium chloride was added to the reaction mixture and the aqueous layer was extracted with benzene. The residue obtained by evaporating the combined organic layer *in vacuo* was mixed with benzene (30 ml) to give IV as colorless crystalline powder in a quantitative yield. A solution of IV thus obtained in tetrahydrofuran was passed through a thin layer of alumina. A small amount of benzene was added to the concentrated filtrate to yield pure IV, colorless tiny cubes, mp 284—285 °C, IR (KBr-disk): 3560—3050 (O-H), 1063, 1023 (C-O) cm^{-1}.

Found: C, 85.16; H, 5.56%. Calcd for $C_{24}H_{18}O_2$: C, 85.18; H, 5.36%.

9-Butadiynyltriptycene (I_2). A solution of thionyl chloride (3.57 g, 0.03 mol) in tetrahydrofuran (5 ml) was added over a 20 min period to an ice-cooled solution of IV (3.38 g, 0.01 mol) in a mixture of pyridine (2.37 g, 0.03 mol) and tetrahydrofuran (40 ml). After the mixture had been stirred for 2 hr at 55 °C, cracked ice was added and extraction was carried out with benzene (150 ml). The extract, after being washed and dried, was concentrated under reduced pressure. A solution of the residue (crude V) in tetrahydrofuran (5 ml) was added to a solution of sodium amide [prepared from sodium, 3.0 g, 0.13 g-atom] in liquid ammonia (150 ml) at

1) S. Akiyama, F. Ogura, and M. Nakagawa, This Bulletin, **44**, 3443 (1971).
2) S. Akiyama and M. Nakagawa, *ibid.*, **44**, 2237 (1971).
3) K. Nakasuji, S. Akiyama, and M. Nakagawa, *ibid.*, **45**, 875 (1972).
4) W. Theilacker, K. Albrecht, and H. Uffmann, *Chem. Ber.*, **98**, 428 (1965).
5) E. C. Kornfeld, P. Barney, J. Blankley, and W. Faul, *J. Med. Chem.*, **8**, 342 (1965).

−70 °C. After being stirred for 2 hr, the ammonia was allowed to evaporate. The residue was mixed with a saturated solution of ammonium chloride and the organic solvent was removed under reduced pressure. Insoluble material was collected by filtration, washed with water and dried. The material was crystallized from benzene–cyclohexane to give faint brown crystalline powder, 1.52 g (50%). A solution of crude I_2 in carbon tetrachloride was percolated through a thin layer of alumina. Concentration of the filtrate afforded colorless cubes which were recrystallized from benzine to give pure I_2, mp 189—191 °C, IR (KBr-disk): 3285 (≡C–H), 2245 (C≡C) cm^{-1}, NMR ($CDCl_3$): τ 2.25—3.08 (m, 12H, aromatic H), 4.65 (s, 1H, bridgehead H), 7.67 (s, 1H, –C≡C–H).

Found: C, 95.65; H, 4.59%. Calcd for $C_{24}H_{14}$: C, 95.33; H, 4.67%.

9,9′-Ditriptycyltetraacetylene (II_4). Treatment of analytically pure I_2 with cupric acetate monohydrate in pyridine afforded colorless tiny cubes in a quantitative yield, mp >300 °C, IR (KBr-disk): 2230 (C≡C) cm^{-1}. The crystals were digested with dilute hydrochloric acid and washed with water to remove a trace of inorganic material. Recrystallization of II_4 was found to be unfeasible on account of extremely poor solubility.

Found: C, 95.22; H, 4.38%. Calcd for $C_{48}H_{26}$: C, 95.65; H, 4.35%.

BULLETIN OF THE CHEMICAL SOCIETY OF JAPAN, VOL. 46, 2908—2909 (1973)

Formation and Reduction of 2-Acyl-1-tetralones

Masaaki IWATA and Sakae EMOTO

The Institute of Physical and Chemical Research, Hirosawa, Wako-shi, Saitama 351

(Received March 8, 1973)

Following the synthesis of co-enzyme model compounds, we have attempted to synthesize the substituted polycyclenes from 7-methyl-1-tetralone (I), an important intermediate in the preparation of natural products. In the present pa er we deal with the formation and reduction of 2-acyl-1-tetralone from I.

In the presence of sodium methoxide in methanol under nitrogen atmosphere, I could not be acylated with methyl acetate or phenyl acetate under any conditions and only afforded 7-methyl-1-naphthol, while sodium hydride in dimethyl sulfoxide (DMSO) gave 7-methyl-2-phenylacetyl-1-tetralone (II) in good yield besides the formation of methyl 2,4-diphenylacetoacetate (III), a self-condensation product of the ester. II and III were enolized in $CDCl_3$ and CCl_4 in 73 and 55% yield, respectively. They were determined by integral ratio of enolic hydroxyl and methine protons in the NMR spectra.

In the preparation of β-diols from β-diketones metallic sodium often gives unsatisfactory results particularly in β-diketones containing aroyl groups as the functional group.[1] Catalytic hydrogenation of aliphatic β-diketones in the presence of Raney nickel afforded β-diols in excellent yield, but this method requires high temperature and high pressure.[2] Thus it is desirable to find a mild reduction method of β-diketones to β-diols. Recent works[3] on reduction with the use of $LiAlH_4$ are valuable as regards the accomplishment of mild reduction. We attempted the reduction of II with $NaBH_4$ and found an interesting solvent effect in subsequent dehydration of β-diols (IV).

Reduction of II with $NaBH_4$ in ethanol followed by

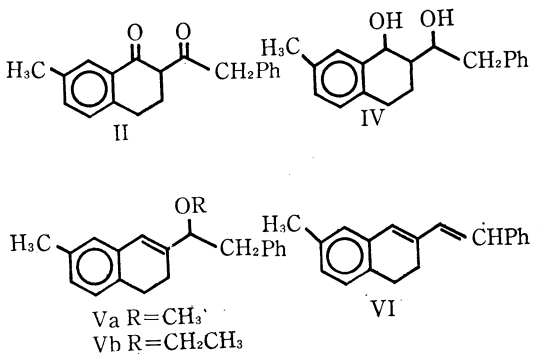

treatment with hydrochloric acid afforded 2-(1-hydroxy-2-phenylethyl)-7-methyl-1,2,3,4-tetrahydro-1-naphthol (IV) (53%), 3-(1-ethoxy-2-phenylethyl)-6-methyl-1,2-dihydronaphthalene (Vb) (6%), and 3-styryl-6-methyl-1,2-dihydronaphthalene (VI) (5%). Since Vb and VI were expected from IV in the work up, treatment of IV with acid was investigated. On being treated with 9M H_2SO_4 in benzene–methanol, IV was converted into 3-(1-methoxy-2-phenylethyl)-6-methyl-1,2-dihydronaphthalene (Va) (78%) and VI (22%). When IV was treated with the same acid in 2-propanol (more bulky alcohol), only VI was obtained quantitatively. VI gave neither Va nor Vb. These results suggest that Va and Vb were formed from IV by the S_N2 acid-catalyzed substitution of hydroxyl group on the side chain after the completion of dehydration of hydroxyl group on the ring and that both V were irreversibly dealkoxylated to VI.

Experimental

Instruments for spectral measurements were Shimadzu IR 27 (IR), Hitachi 124 spectrophotometer (UV), Japan Electron Optics Model C-60 (NMR) and JMS-OISG (MS). Merck Art. 7734 was used for separation of products on a silica gel

1) E. Bauer, *C. R. Acad. Sci., Paris*, **154**, 1092 (1912).

2) P. S. Stutzman and H. Adkins, *J. Amer. Chem. Soc.*, **61**, 3303 (1939).

3) a) L. Cazaux and P. Maroni, *Bull. Soc. Chim. Fr.*, **1972**, 773, 780; b) P. Maroni and J-P. Gorrichon, *ibid.*, **1972**, 785; c) P. Maroni and P. Tisnes, *ibid.*, **1972**, 794.

column by elution chromatography and Wakogel B-5 UA for thin layer chromatography (tlc).

Materials. 7-Methyl-1-tetralone (I) was synthesized in three steps from toluene and succinic anhydride, mp 31.5—32.5 °C (lit,[4] 33 °C).

7-Methyl-2-phenylacetyl-1-tetralone (II). I (0.04 mol) was treated with methyl phenylacetate (0.08 mol) and sodium hydride (0.08 mol) in DMSO (20 ml). After completion of the reaction, the mixture was poured into ice water (200 ml) containing 15 ml of concd. HCl and extracted with ether. The etheral extract was added dropwise to 200 ml of a hot aqueous cupric acetate solution (10%), and the mixture was stirred overnight. The precipitate was collected by filtration and washed with water, methanol and ether successively. For analytical use, a part of the precipitate was recrystallized from benzene–methanol as dark green crystals, mp 232—235 °C (decomp.). Found: Cu, 10.24%. Calcd for $C_{38}H_{34}O_4Cu$: Cu, 10.35%. UV: $\lambda_{max}(\varepsilon)$ (in methanol) 211 (40800), 253.6 (37700), 260 (35400), 334 (10200), 338.5 (3100), and 410 (2500) nm.

The copper chelate was treated with 10% sulfuric acid (60 ml) and the organic layer was extracted with benzene. After evaporation of the solvent, the residue was chromatographed on a silica gel column with benzene to give II (65%) and III (24%).

II was obtained as dark red plates, mp 56.5—58 °C. Found: C, 81.86; H, 6.71%. Calcd for $C_{19}H_{18}O_2$: C, 81.98; H, 6.52%. UV: $\lambda_{max}(\varepsilon)$ (in methanol) 236 (11000), 245s (9200), 258 (6900), 310 (10700), and 347 (18400) nm. NMR ($CDCl_3$): 2.32 (3H, singlet, $-CH_3$), 7.28 (5H, s, phenyl protons), 7.72 (1H, broad s, isolated aromatic proton in tetralone ring), 7.10 (2H, multiplet, two neighboring aromatic protons in tetralone ring), 2.66 (centered) (4H, m, two methylene protons in tetralone ring), 3.80 (2H, s, benzyl protons in the chain), 3.97 (0.2667H, s, CO–CH–CO), and 16.50 (0.7333H, s, enol proton) ppm.

III was obtained as light yellow needles, mp 60—62.5 °C. Found: C, 76.19; H, 6.07%. Calcd for $C_{17}H_{16}O_3$: C, 76.10; H, 6.01%. MS (75 eV): parent peak at *m/e* 268 and base peak at *m/e* 91 ($C_7H_7^+$). UV: $\lambda_{max}(\varepsilon)$ (in methanol) 210 (13600), 254 (3700), and 264s (3370) nm. IR (KBr disk): ν_{max} 1770 (–COOMe) and 1740 (–CO–) cm^{-1}. NMR (CCl_4): 3.59 (3H, s, $-OCH_3$), 3.61 (2H, s, $-CH_2-$), 4.62 (0.455H, s, –CH–), and 13.05 (0.545H, s, enol proton) ppm.

Reduction of II with Sodium Borohydride. In Ethanol: Sodium borohydride was added at room temperature to I (6.13 mmol) in 60 ml of ethanol at once. The color of the orange-red solution gradually vanished. The reaction was accomplished after 8 hr. The solution was acidified with 6M hydrochloric acid and the solvent was removed under reduced pressure by repeated addition of methanol. The residue was chromatographed on a silica gel column with benzene to give IV (53.2%), Vb (6%), and VI (5%).

A part of IV crystallized during the course of chromatographic separation; fine white needles, mp 164—174.5 °C. Found: C, 80.76; H, 8.12%. Calcd for $C_{19}H_{22}O_2$: C, 80.81; H, 7.85%. Exact mass measurement: For parent peak, Found: 282.16121, Calcd for $C_{19}H_{22}O_2$: 282.16198. UV: $\lambda_{max}(\varepsilon)$ (in methanol) 262s (600), 264 (650), 269 (780), and 278.5 (760) nm. NMR ($CDCl_3$): 2.30 (3H, s, $-CH_3$) and 7.23 (5H, s, phenyl protons) ppm.

Vb was obtained as colorless oily liquid showing fluorescence. Found: C, 86.17; H, 8.03%. Calcd for $C_{21}H_{24}O$: C, 86.25; H, 8.27%. Exact mass measurement: For parent peak, Found: 292.17921, Calcd for $C_{21}H_{24}O$: 292.18272. IR (NaCl plates): ν_{max} 1085 (C–O–C) and 700 (–Ph) cm^{-1}. NMR ($CDCl_3$): 1.14 (3H, triplet, $J=12.0$ Hz, $-OCH_2\underline{CH_3}$), 2.27 (3H, s, Ar–CH_3), 3.33 (2H, quartet, $J=12.0$ Hz, $-OC\underline{H_2}-CH_3$), 4.00 (1H, t, $J=11.0$ Hz, –CH–O–), 6.21 (1H, s, –C–CH–), 6.95 (2H, broad s, two adjacent aromatic protons), and 7.22 (5H, s, phenyl protons) ppm.

VI was obtained as light yellow amorphous solid, mp 118—126 °C. Found: C, 91.71; H, 6.94%. Calcd for $C_{19}H_{18}$: C, 92.36; H, 7.37%. Exact mass measurement: For parent peak, Found: 246.13723, Calcd for $C_{19}H_{18}$: 246.14085. IR (KBr disk): ν_{max} 960 (C=CH) cm^{-1}. UV: $\lambda_{max}(\varepsilon)$ (in methanol) 213 (16500), 230 (11000), 237s (9900), 245 (9800), 252s (7900), 261 (6600), 309s (18000), 325 (31000), 340 (40000), and 358 (29700) nm. NMR ($CDCl_3$): 2.29 (3H, s, Ar–CH_3) and 2.65 (centered) (4H, AA′BB′, $-CH_2CH_2-$) ppm, (aliphatic protons): (olefinic and aromatic protons) = 7: 11.

In Methanol: IV was vigorously stirred in benzene–methanol (3: 2 v/v) with sulfuric acid (9M) until no IV was detected on tlc. The mixture was extracted with benzene after neutralization with sodium bicarbonate on a silica gel column with benzene to give Va (78%) and VI (22%).

Va was obtained as colorless oily liquid showing fluorescence. Found: C, 86.28; H, 7.95%. Calcd for $C_{20}H_{22}O$: C, 86.28; H, 7.97%. IR (NaCl plates): ν_{max} 1095 (C–O–C) and 700 (–Ph) cm^{-1}. UV: $\lambda_{max}(\varepsilon)$ (in methanol) 266 (12000), 274 (11000), and 303 (1700) nm. NMR ($CDCl_3$): 2.26 (3H, s, Ar–CH_3), 3.23 (3H, s, $-OCH_3$), 3.90 (1H, t, $J=11.5$ Hz, –CH–O–), 6.23 (1H, s, C=CH), 6.81 (1H, s, isolated aromatic protons), 6.96 (2H, s, two adjacent aromatic protons), and 7.22 (5H, s, –Ph) ppm.

In Benzene: IV was vigorously stirred in benzene with 9M sulfuric acid until no IV was detected on tlc. The same work up as in methanol gave VI quantitatively.

In 2-Propanol: As the same operation as in methanol was carried out in 2-propanol. VI was quantitatively obtained after the work up. No alkoxylated product was detected.

Reaction of Va with Acid. To Va in methanol was added a small amount of concd. sulfuric acid and the mixture was allowed to stand at room temperature for 24 hr. From the solution VI crystallized quantitatively. Even when the solution containing only VI was allowed to stand further, no detectable amount of Va was found on tlc, indicating that formation of VI from Va was irreversible.

This study was supported in part by a Grant for Life Science from this Institute.

4) F. Krollpfeiffer and W. Schaefer, *Ber.*, **56**, 620 (1923).

BULLETIN OF THE CHEMICAL SOCIETY OF JAPAN, VOL. 46, 2910—2911 (1973)

Aromatic Substitution of Olefins. XX. Reactions of Triphenylamine, -phosphine, -arsine, -stibine, and -bismuth with Styrene in the Presence of Palladium(II) Salts

Ryuzo Asano, Ichiro Moritani, Yuzo Fujiwara, and Shiichiro Teranishi
Faculty of Engineering Science, Osaka University, Toyonaka, Osaka 560

(Received March 13, 1973)

We reported[1-3] that direct substitution of benzene derivatives with olefins can take place in the presence of palladium(II) salts, and that nonbenzenoid aromatic compounds such as ferrocene, furan and thiophene can also react with olefins to give alkenyl-derivatives. In continuation of these studies we wish to determine the reactivity of triphenylphosphine, which has both aromatic ring and donor P atom, toward olefins. Extensive studies on reactions of triphenylphosphine with transition metals have been carried out. It is well known that phosphine metal halide complexes form an internal metal-carbon bond.[4] However, little is known about the reaction of triphenylphosphine in the presence of transition metal compounds involving the cleavage of the phosphorus-carbon bond.[5] In this paper we report a study of the reaction of styrene with triphenylamine, -phosphine, -arsine, -stibine, or -bismuth.

Table 1. Reaction of styrene with group V triphenyl-compounds by palladium (II) acetate[a]

Triphenyl-compound	Product and yield, %[b]	
NPh_3	*trans*-*p*-Diphenylaminostilbene	41
PPh_3	*trans*-Stilbene	64
	Methyldiphenylphosphine oxide	22
$AsPh_3$	*trans*-Stilbene	99
	Biphenyl	14
$SbPh_3$	*trans*-Stilbene	67
	Biphenyl	108
$BiPh_3$	*trans*-Stilbene	7
	Biphenyl	108
	trans, *trans*-1,4-Diphenylbutadiene	11
$BiPh_3$[c]	Biphenyl	3
	Benzene	
$P(p\text{-}CH_3C_6H_4)_3$	*trans*-*p*-Methylstilbene	41
	p,*p*′-Dimethylbiphenyl	3
	Methyldi-*p*-tolylphosphine oxide	10
$PdCl_2(PPh_3)_2$[d]	*trans*-Stilbene	3

a) Equimolar amounts of the triphenyl-compound, styrene, and palladium (II) acetate were used. All the reactions were carried out under reflux for 6 hr. b) Yields are based on palladium (II) acetate. c) The reaction was carried out in the absence of palladium (II) acetate. d) Dichlorobis (triphenylphosphine) palladium (II) was used in place of triphenylphosphine and palladium (II) acetate.

Results and Discussion

A solution of styrene, triphenylphosphine (1 mol equiv.), palladium(II) acetate (1 mol equiv.) in acetic acid and dioxane was stirred under relux for 6 hr, to give *trans*-stilbene (64%) with methyldiphenylphosphine oxide and metallic palladium. Reactions with other group V triphenyl-compounds such as triphenylamine, -arsine, -stibine, and -bismuth were carried out under similar reaction conditions. The results are given in Table 1. It is evident that these triphenyl-compounds can easily react with styrene to give *trans*-stilbene involving the cleavage of the M–C bond except for the case of triphenylamine (Eq. (1)).

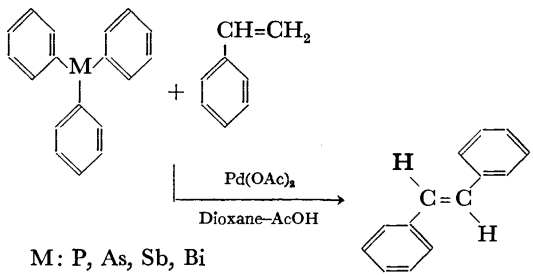

(1)

M: P, As, Sb, Bi

In the reaction of triphenylamine with styrene, the product is not *trans*-stilbene but *trans*-*p*-diphenylaminostilbene which is the normal substitution product (Eq. (2)). This may be due to the higher energy of the N–C bond.

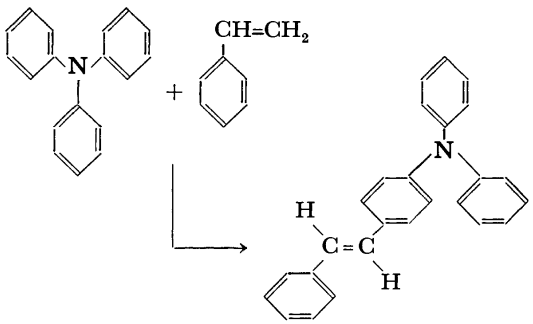

(2)

With respect to the formation of *trans*-stilbene, the reactivity is in the order triphenylarsine>triphenylstibine≃triphenylphosphine>triphenylbismuth>triphenylamine. The donor ability decreases in the order $NPh_3>PPh_3>AsPh_3>SbPh_3\gg BiPh_3$,[6] and the M–C bond energy increased in the same order M=Bi<Sb<As<P<N.[7] The yields of *trans*-stilbene for the tri-

1) Y. Fujiwara, I. Moritani, S. Danno, R. Asano, and S. Teranishi, *J. Amer. Chem. Soc.*, **91**, 7166 (1969).
2) R. Asano, I. Moritani, A. Sonoda, Y. Fujiwara, and S. Teranishi, *J. Chem. Soc., C*, **1971**, 3691.
3) R. Asano, I. Moritani, Y. Fujiwara, and S. Teranishi, This Bulletin, **46**, 663 (1973).
4) G. W. Parshall, *Accounts Chem. Res.*, **3**, 139 (1970).
5) K. Kikukawa, T. Yamane, M. Takagi, and T. Matsuda, *Chem. Commun.* **1972**, 695.
6) S. Murahashi, "Yūkikinzoku Handobukku," Asakura Shoten, Tokyo (1967), p. 706.
7) T. Saito, "Kaisetsu Yūkikinzoku Kagaku," Hirokawa Shoten, Tokyo (1970), p. 4.

BULLETIN OF THE CHEMICAL SOCIETY OF JAPAN, VOL. 46, 2912—2913 (1973)

Electrochemistry of Organic Sulfur Compounds. IV.[1] Anodic Sulfonium Formation from Alkyl Phenyl Sulfides

Sigeru TORII, Yuziro MATSUYAMA, Koji KAWASAKI, and Kenji UNEYAMA

Department of Industrial Chemistry, School of Engineering, Okayama University, Tsushima, Okayama 700

(Received March 19, 1973)

In recent years, various sulfonium salts and sulfonium ylides have been utilized as key intermediates for organic syntheses.[2] We have examined the electrochemical preparation of useful sulfonium salts which would provide sulfonium ylides. In a previous paper,[1] we described a novel anodic synthesis of a sulfonium salt from diphenyl sulfide and proposed a mechanism for the anodic process; sulfides (Ph–S–R) are oxidized in the anodic process to provide primarily a radical cation $[Ph–S–R]^{+\cdot}$, which undergoes either S–R bond cleavage to give thiyl radical and cation R^+, or electrophilic attack by water and/or sulfide to provide sulfoxide and/or sulfonium salt. The S–R cleavage is promoted by a substituent R such as benzyl and triphenylmethyl groups due to the stability of the cation R^+. Selection of the reaction pathway, either sulfoxidation or sulfonium salt formation, probably depends on the stability of the cation radical **2** and the presence of water in the reaction media.[3] This paper shows that anodic oxidation of alkyl phenyl sulfides **1** in general gives sulfonium salts **3** in anhydrous media and some chemical properties of **3**.

Alkyl phenyl sulfides **1** (2.5 mmol) dissolved in acetonitrile containing lithium perchlorate were electrolyzed at room temperature using platinum foils as electrodes without separation of the anodic compartment. Thus, 1.2 equivalent of constant current (200 mA) was applied with the terminal voltage kept at about 5.5 V. Products were separated by column chromatography on silica gel. The results are listed in Table 1.

TABLE 1. PRODUCTS OF ANODIC OXIDATION OF **1** IN ACETONITRILE

1 R	**3** (%)[a]	Sulfoxide (%)[a]	Recovered **1** (%)[b]
Methyl (**1a**)	60 (**3a**)	trace	19
3-Butenyl (**1b**)	67 (**3b**)	4	6
Cyclohexyl (**1c**)	57 (**3c**)	trace	20
Phenyl[1]	71	trace	19

a) The yield is calculated on the basis of **1**. b) *m*-Chlorothioanisole, diphenyl sulfide, and phenyl benzyl sulfide were employed for internal standards for glpc.

Alkyl phenyl sulfides **1** afforded the corresponding sulfonium perchlorates **3** in *ca.* 60—70% yields on the basis of **1**. This suggests that in the absence of water anodic oxidation of **1** takes place predominantly leading to the formation of the salts **3** in contrast to the results obtained with water–acetonitrile[3] or water–hydrogen chloride giving sulfoxides.[4]

Formation of **3b** from **1b** reveals that the divalent sulfide would be more reactive as compared with the double bond[5] of **1b**, since the phenyl group of **1** should undergo electrophilic attack by the cation radical of **2** rather than intramolecular attack of the double bond. No evidence of the S–R bond cleavage of **1** was observed during the course of electrolysis since no diphenyl disulfide was detected in glpc.[3]

Accordingly, the cation radical **2** would attack the *para*-position of the phenyl ring to give a cyclohexadienyl radical intermediate **4**, which would be readily oxidized to **5** followed by deprotonation to give **3**. Or, a dication formed incipiently from further oxidation of **2** would couple with the sulfide **1** leading to **5**.

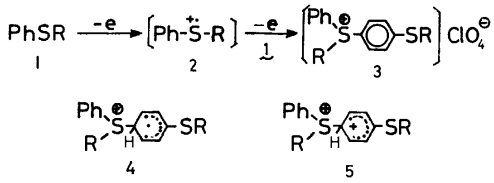

The sulfonium salt **3a**, pale brownish crystals, could be purified by recrystallization from dichloromethane–ether. Its IR spectrum had a characteristic strong band at 1095 cm^{-1} due to the sulfonium group and its NMR spectrum showed a singlet (3H) at δ 3.62 corresponding to the methyl group attached to the trivalent sulfur atom of **3a**. Treatment of **3a** with *n*-butyllithium followed by benzaldehyde in tetrahydrofuran at −78 °C gave the epoxide **6** (50%) and the sulfide **7** (50%).[6] Reduction of **3a** with lithium aluminum hydride gave **7** (60%).[7]

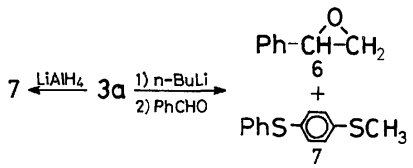

1) Part III, K. Uneyama and S. Torii, *J. Org. Chem.*, **37**, 367 (1972).

2) a) A. W. Johnson, "Ylide Chemistry," Academic Press, New York, N. Y., (1966); b) C.R. Johnson, G.F. Katekar, R.F. Huxol, and E. R. Janiga, *J. Amer. Chem. Soc.*, **93**, 3771 (1971); c) B. M. Trost and M. J. Bogdanowicz, *ibid.*, **93**, 3773 (1971).

3) K. Uneyama and S. Torii, *Tetrahedron Lett.*, **1971**, 329.

4) F. Fichter, P. Sjostedt, W. Wenk, and F. Braun, *Chem. Ber.*, **47**, 1526 (1914).

5) The halfwave potentials of the monosubstituted double bonds and phenyl sulfide group are about 2.7—2.8 V *vs.* Ag and 1.5 V *vs.* SCE, respectively. N. W. Weinberg and H. R. Weinberg, *Chem. Rev.*, **68**, 449 (1968); C. K. Mann and K. K. Barnes, "Electrochemical Reactions in Nonaqueous Systems," Marcel Dekker, Inc., New York (1970).

6) M. J. Bogdanowicz and B. M. Trost, *Tetrahedron Lett.*, **1972**, 887.

7) Electrochemical reduction of sulfonium salts: See M. Finkelstein, R. C. Petersen, and S. D. Ross, *J. Electrochem. Soc.*, **110**, 422 (1963). Phosphonium salts are also reduced to the corresponding phosphines by lithium aluminum hydride: W. J. Bailey and S. A. Buckler, *J. Amer. Chem. Soc.*, **79**, 3567 (1957); S. T. D. Gough and S. Trippett, *J. Chem. Soc.*, **1961**, 4263.

The structure of the sulfonium salt **3b**,[8] a brown oil, was characterized by its IR and NMR spectra. Treatment of **3b** with potassium hydroxide in ethylene glycol at 80 °C provided **8** and butadiene, the latter being trapped in a bromine–carbon tetrachloride solution.

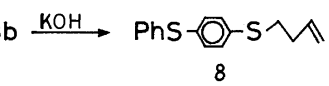

8

Structural assignment of the salt **3c**,[8] a slightly brownish amorphous solid, was carried out by comparison of its IR and NMR spectral data with those of the homologous compounds **3a** and **3b**.

Experimental

Preparation of Sulfides. Sulfides **1a** and **1c** were prepared from sodium thiophenoxide and the corresponding alkyl halides.[9] Sulfide **1b** was prepared as follows. Thiophenol (22.0 g) in 25 ml of dioxane was refluxed with 1,4-dibromobutane (50 g) and pyridine (18.0 g) with stirring for 12.5 hr. The mixture was poured onto ice and extracted with $CHCl_3$. Distillation of the extracts gave phenyl δ-bromobutyl sulfide (31%): bp 151—157 °C/8.0 mmHg. Refluxing of the sulfide with an equimolar amount of potassium *t*-butoxide in dry *t*-butanol for 1 hr provided sulfide **1b** (60%): bp 95—98 °C/6.0 mmHg; IR (Neat) 1640 (m, C=C), 1580 (m, Ph-S), 915, 740, 690 cm^{-1}; NMR ($CDCl_3$) δ 7.00—7.40 (m, 5H, Ph), 5.40—6.20 (m, 1H, -CH=C), 4.80—5.30 (m, 2H, C=CH_2), 2.80—3.10 (m, 2H, CH_2-C=C), 2.40 (t, 2H, J= 8 Hz, CH_2-S); Mass (*m/e*) 164 (M^+). Found: C, 73.00; H, 7.25%. Calcd for $C_{10}H_{12}S$: C, 73.13; H, 7.37%.

Electrolysis. Electrolysis of **1a** was carried out as follows: A solution of **1a** (310 mg) and $LiClO_4$ (500 mg) in 10 ml of dry CH_3CN in a 20 ml tall beaker was electrolyzed under N_2 at *ca.* 20 °C using two 3 cm^2 platinum foils without separation of the compartment. Constant current (200 mA, 1.2 equiv) was applied while the terminal voltage was about 5.5 V. Electrolyses of **1b** and **1c** were carried out in a similar manner to that for **1a**.

*Phenyl Methyl-*p*-methylthiophenyl-sulfonium Perchlorate (3a).* The reaction mixture combined with *m*-chlorothioanisole (79 mg, 0.5 mmol) as an internal standard for glpc was concentrated. The residue was taken up in $CHCl_3$, washed with water, dried (Na_2SO_4) and concentrated. The residue was developed on silica gel column with $CHCl_3$ and then acetone. The $CHCl_3$ eluent was subjected to glpc analysis (Diasolid L, 10% polyneopentyl glycol succinate (PNGS) coated column, 1 m long, 150 °C). The amount of recovered **1a** was calculated by comparison of the peak area with that of the internal standard. The acetone eluent was crude sulfonium salt **3a** (261 mg), which was solidified in a vacuum. Crystallization of the salt from CH_2Cl_2-ether (1:2) gave slightly brownish white crystals: mp 132.0—132.5 °C; IR (Nujol) 1580 (m), 1120—1070 (vs, sulfonium), 820, 760, 695 cm^{-1}; NMR ($CDCl_3$) δ 7.30—8.00 (m, 9H, Ph), 3.62 (s, 3H, $=S^+-CH_3$), 2.43 (s, 3H, S-CH_3). Found: C, 48.30; H, 4.28%. Calcd for $C_{14}H_{15}ClO_4S_2$: C, 48.48; H, 4.35%.

Reaction of 3a with n*-Butyllithium.* To a mixture of **3a** (347 mg) in 5 ml of dry THF under N_2 at −78 °C was added dropwise with stirring 0.9 ml of *n*-butyllithium in ether (1.64 M). The yellow solution was stirred for 45 min and to this was added 0.1 ml (*ca.* 1 mmol) of benzaldehyde in 3 ml of THF. The mixture was stirred for 1 hr at −78 °C, then the bath was removed. After tetralin (66 mg, 0.5 mmol) and phenyl benzyl sulfide (100 mg) had been added as internal standards for glpc, the reaction mixture was poured onto ice and extracted with ether. The extracts were washed, dried (Na_2SO_4), and distilled. The fraction, bp below 123 °C/13 mmHg, was analyzed by glpc (Diasolid L, 10% PNGS coated column, 2 m long, 100 °C) giving benzaldehyde (53 mg) and **6** (60 mg); their retention times in glpc were consistent with those of authentic samples, their spectral data supporting their structures. Continued distillation of the pot residue gave a fraction, bp below 120 °C/0.08 mmHg, which was analyzed by glpc (Diasolid L, 10% Silicone SE-30, 2 m long, 180—210 °C) giving **7** (147 mg) as a colorless oil: IR (neat) 1580 (m), 1480 (m), 810, 740, 690 cm^{-1}; NMR ($CDCl_3$) δ 7.10—7.40 (9H, Ph), 2.45 (s, 3H, S-CH_3); Mass (*m/e*) 232 (M^+), 217, 185, 108. Found: C, 67.21; H, 5.30%. Calcd for $C_{13}H_{12}S_2$: C, 67.19; H, 5.21%.

*Phenyl-3-butenyl-*p*-(3-butenylthio)phenyl-sulfonium Perchlorate (3b).* Crude sulfonium salt **3b** was purified by passing through a short silica gel column with $CHCl_3$-acetone (1:1), followed by tlc on silica gel with ethyl acetate to afford a brown oily **3b**:[8] IR (neat) 1650, 1580, 1120—1070 (s), 930, 820, 750, 680 cm^{-1}; NMR ($CDCl_3$) δ 7.20—8.10 (m, 9H, Ph), 5.50—6.20 (m, 2H, -CH=C), 4.90—5.30 (m, 4H, -C=CH_2), 4.22 (t, 2H, J=8 Hz, $=S^+-CH_2$), 3.03 (t, 2H, J=7 Hz, S-CH_2), 2.30—2.80 (m, 4H, CH_2-C=C).

*Phenyl Cyclohexyl-*p*-cyclohexylthiophenyl-sulfonium Perchlorate (3c).* Isolation was carried out in a similar manner to that for **3a**. The sulfonium salt **3c**, a slightly brownish amorphous solid:[8] IR (Nujol) 1580, 1070—1110 (s), 820, 750, 685 cm^{-1}; NMR ($CDCl_3$) δ 7.20—8.40 (m, 9H, Ph), 4.50—5.20 (m, 1H, $=S^+-CH$), 2.90—3.60 (m, 1H, S-CH), 1.00—2.30 (m, 20H, CH_2).

Reduction of 3a by Lithium Aluminum Hydride. To a mixture of **3a** (347 mg) in 4 ml of dry THF under N_2 was added at once 57 mg of $LiAlH_4$. This was stirred at 5 °C for 1 hr and quenched by addition of 5 ml of saturated aqueous ammonium chloride. After phenyl benzyl sulfide (100 mg) had been added as an internal standard for glpc, the mixture was extracted with ether, washed and dried (Na_2SO_4). The residue was analyzed by glpc (Diasolid L, 10% Silicone SE-30, 2 m long, 180—210 °C) giving **7** (139 mg). The retention time of **7** in glpc and its spectral data support the structure.

Reaction of 3b with Potassium Hydroxide. A mixture of **3b** (580 mg) and KOH (120 mg) in 4 ml of ethylene glycol was heated at 80 °C for 1 hr in a 10 ml tall beaker equipped with N_2 bubbler. The N_2 gas was passed through a trap containing 5 ml solution of CCl_4 with bromine. The mixture was extracted with ether, washed and dried (Na_2SO_4). Separation of the concentrated extracts by tlc on silica gel with CH_2Cl_2 gave **8** (133 mg) as a major product: IR (neat) 1650, 1580, 920, 740, 690 cm^{-1}; NMR ($CDCl_3$) δ 7.10—7.40 (broad s, 9H, Ph), 5.50—6.20 (m, 1H, -CH=C), 4.80—5.20 (m, 2H, C=CH_2), 2.70—3.10 (m, 2H, S-CH_2), 2.10—2.60 (m, 2H, -CH_2-C=C); Mass (*m/e*) 272 (M^+), 231, 218, 197. Found: C, 70.67; H, 6.03%. Calcd for $C_{16}H_{16}S_2$: C, 70.54; H, 5.96%.

From the CCl_4 solution white crystals were obtained and assigned to be 1,2,3,4-tetrabromobutane in comparison with its spectral data with that of authentic sample.

8) Difficulties were encountered in the microanalyses of **1b** and **1c** because of their hygroscopic nature.

9) A. I. Vogel, *J. Chem. Soc.*, **1948**, 1820.

BULLETIN OF THE CHEMICAL SOCIETY OF JAPAN, VOL. 46, 2914—2915 (1973)

The Catalytic Effect of Acid on the *O*→*N* Migration of the *s*-Triazinyl Group of *O*-(*s*-Triazinyl)-2-aminophenols

Takeo SHIOJIMA, Yōji HASHIDA, and Kohji MATSUI

Department of Synthetic Chemistry, Faculty of Engineering, Gunma University, Tenjincho, Kiryu, Gunma 376

(Recieved March 20, 1973)

In a previous paper[1] we have reported that *O*-(*s*-triazinyl)-2-aminophenols (I) rearrange readily in the presence of acid to give *N*-(*s*-triazinyl)-2-aminophenols. However, the details of the rearrangement in the presence of acid have not yet been given. This paper will report the quantitative results on the influence of acid on the rearrangement of *O*-(*s*-triazinyl)-2-aminophenols.

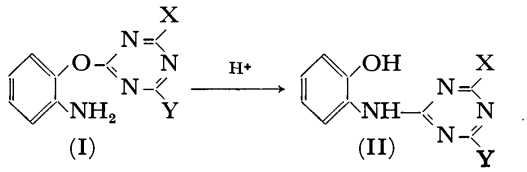

(I) (II)

a: X=OCH_3 Y=$N(CH_3)_2$
b: X=Y=$N(CH_3)_2$

Experimental

Materials. The *O*-(*s*-triazinyl)-2-aminophenols were synthesized by the method described in a previous paper.[2] The *O*-(2,4-dinitrophenyl)-2-aminophenol (III) was prepared by the method of Roberts.[3]

Kinetic Measurements. The kinetic measurements were carried out in a manner similar to that described in a previous paper[2] in buffer solutions of a constant ionic strength of 0.1 at 25 °C; the apparent first-order rate constants were calculated using Eq. (1);

$$k' = -2.303/t \log \{D_\infty - (D_t)/(D_\infty) - D_0\} \quad (1)$$

where D_0, D_∞, and D_t denote the optical densities of a solution at an appropriate wavelength observed at initial and infinite times, and at time t. The measurements were carried out in aqueous solutions in the cases of the compounds (I) and in a 50% (vol) methanolic solution in the case of compound (III).

Results and Discussion

The effect of the pH of the solution on the apparent rate constants (k') for the rearrangement of Ia, Ib, and III were investigated; compound (III) was used in order to elucidate the function of the *s*-triazine nucleus by means of a comparison of the results of I and III. The results are shown in Fig. 1.

In the case of III, the apparent rate constant decreased with an increase in the acidity of the solution; the result is considered to be due to a decrease in the concentration of III by protonation at the amino group.

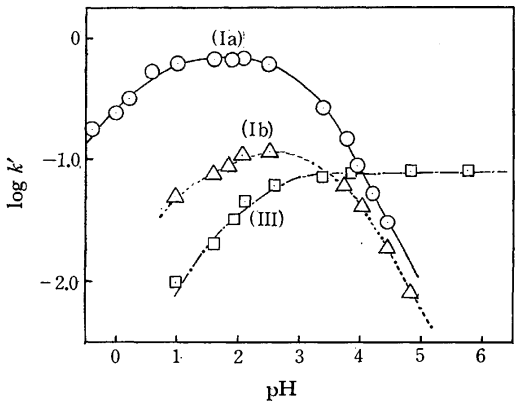

Fig. 1. pH dependence of the apparent rate constants for the rearrangement reactions of compounds (Ia, Ib, and III). (unit of k' is min^{-1})

On the contrary, in the case of Ia or Ib, no simple relation between log k' and pH value was observed. With an increase in the acidity of the solution, the apparent rate constant increased in the pH region above 3; however, it decreased in the pH region below 2. In these cases, the presence of two kinds of basic groups, *i.e.*, the amino and *s*-triazinyl groups, is considered to be the reason for the complexity. Under the present experimental conditions, the four species indicated by (A)—(D) may be assumed to be present in the solutions:

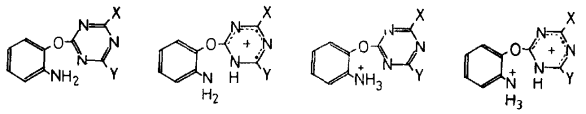

(A) (B) (C) (D)

Among these, B is expected to be the most reactive species, for in this case an intramolecular nucleophilic attack by the amino group is considered to take place most readily by lowering the electron density of the ring-carbon atoms of the *s*-triazine nucleus. In the pH region above 3, the fact that the rate constant increased with an increase in the acidity of the medium can be explained by assuming that the concentration of B increases with the increase in the acidity by a preferential protonation at the ring-nitrogen atom of the *s*-triazine nucleus.[4,5] On the other hand, in the pH region below 2, it is assumed that the apparent rate constant decreased because of a decrease in the concentration of B as a result of further protonation at the amino group to give D.

If we assume that the protonation (expressed by Eq.

1) T. Harayama, S. Sekiguchi, and K. Matsui, *J. Heterocycl. Chem.*, **7**, 981 (1970).
2) N. Maeno, T. Itagaki, S. Uno, and K. Matsui, This Bulletin, **45**, 3133 (1972).
3) K. C. Roberts, C. G. M. deWorms, and H. B. Clark, *J. Chem. Soc.*, **1935**, 196.
4) G. Morimoto, *Nippon Kagaku Zasshi*, **87**, 790 (1966).
5) T. Tashiro and M. Yasuda, *Kobunshi Kagaku*, **26**, 853 (1969).

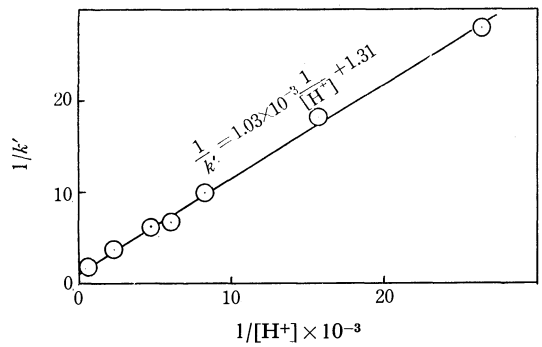

Fig. 2. Plots of $1/k'$ against $1/[H^+]$ for the rearrangement of compound (Ia) in the pH range of 4.42 to 2.50.

(2)) proceeds much faster than the rearrangement (Eq. (3)), and that B is the only reactive species, the apparent rate constant may be expressed by Eq. (4):[6]

$$(A) + H^+ \overset{K_a}{\rightleftarrows} (B) \quad (2)$$

$$(B) \overset{k}{\longrightarrow} (II) \quad (3)$$

$$1/k' = 1/k + 1/kK[H^+] \quad (4)$$

K_a: equilibrium constant

6) From Eq. (2) and (3), the rate of the rearrangement of B is expressed by Eq. (5):

$$v = k[B] = kK[A] \times [H^+] \quad (5)$$

Since the apparent rate constant was calculated in the manner described in the Experimental section, the rate of the rearrangement in the presence of acid can be written by Eq. (6):

$$v = k'([A]+[B]) = k'[A](1+K[H^+]) \quad (6)$$

From the assumption presented above, Eq. (4) is obtained by putting Eqs. (5) and (6) as equal.

Table 1. Rate constants and dissociation constants (pK_a)

Compound	$pK_a(TH^+)$[a]	pK_a (NH_3^+)	k (min^{-1})
Ia	3.11	0.33	7.63×10^{-1}
Ib	3.64	0.886	1.32×10^{-1}
III		1.99	7.50×10^{-2}

a) TH^+ denote the species (B).

From Eq. (4), the plots of $1/k'$ against $1/[H^+]$ may be expected to give a straight line. Indeed, a linear relation was observed, as is shown in Fig. 2 in the case of (Ia).

From the intercepts and slopes of the lines, the rate constants of the reactive species (B) and the equilibrium constants were calculated; they are listed in Table 1. From the data obtained in the pH region below 2, the equilibrium constants attributable to the amino group were also obtained. Using these values, the relations between $\log k'$ and pH values can be calculated; they are shown in Fig. 1 by full, dotted, and dashed lines. It can be seen that the corresponding experimental results (expressed by circles, squares, and triangles respectively) lie close to the calculated lines. This finding supports the assumptions that the basicity of the *s*-triazine nucleus is stronger than that of the amino group and that the reactive species in the presence of acid is the protonated product at the ring nitrogen of the *s*-triazine nucleus (B), which rearranges faster by a factor of 4 orders or more than the neutral molecule.[2]

BULLETIN OF THE CHEMICAL SOCIETY OF JAPAN, VOL. 46, 2915—2917 (1973)

The Reaction of 2-Chlorotropone with Methyl Methacrylate

Hitoshi TAKESHITA,* Masatoshi SHIMA, and Shô ITÔ

Department of Chemistry, Faculty of Science, Tohoku University, Sendai 980

(Received March 22, 1973)

The Diels-Alder reaction of troponoids with cyclic dienophiles including maleic anhydride is known to give only respective *endo*-adducts[1] with exception for tropolones[2-4] which yielded two stereoisomers. Our recent study[5] has disclosed even in the last case that the *endo*-adduct was initially formed but it underwent an acyloin rearrangement to the *exo*-isomer at the later stage. Contrary to the reactions with cyclic dienophiles, troponoids formed four regio- and stereoisomeric adducts in concerted fashion when an acyclic dienophile, acrylonitrile, was used.[6] We have extended our study to the reaction using 2-chlorotropone with methyl methacrylate, another acyclic dienophile for the generalization of the reaction.

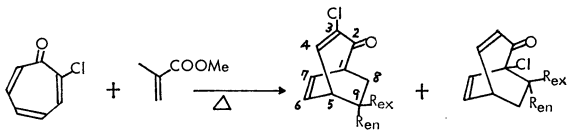

III: R_{ex}=Me, R_{en}=COOMe V: R_{ex}=COOMe, R_{en}=Me
IV: R_{ex}=COOMe, R_{en}=Me VI: R_{ex}=Me, R_{en}=COOMe

Results and Discussion

When 2-chlorotropone (I) was heated with methyl methacrylate (II) at 135—140 °C for 48 hr, four 1 : 1

* Present Address: Research Institute of Industrial Science, Kyushu University, Hakozaki, Fukuoka 812.

1) For a general reference, see T. Nozoe, *et al.*, "Comprehensive Organic Chemistry", Vol. 13, Asakura Shoten, Tokyo (1960), p. 148.

2) E. Sebe and Y. Osako, *Proc. Japan Acad.*, **28**, 282 (1952).

3) E. Sebe and Y. Itsuno, *ibid.*, **29**, 110 (1953).

4) S. Itô, H. Takeshita, Y. Shoji, Y. Toyooka, and T. Nozoe, *Tetrahedron Lett.*, **1969** 3215.

5) S. Itô, A. Mori, Y. Shoji, and H. Takeshita, *ibid.*, **1972** 2685.

6) S. Itô, H. Takeshita, and Y. Shoji, *ibid.*, **1969** 1815.

Table 1. NMR parameters of the adducts, III—VI (Solvent: CCl_4)

Compounds	III	IV	V	VI
Positions of hydrogens	Chemical shifts (in δ)			
1	3.70	3.67		
3			5.80	5.83
4	7.10	7.15	6.88	7.05
5	3.58	3.47	3.22	3.42
6	6.52	6.53	6.50	6.50
7	6.05	6.19	5.92	6.03
8 *ex*	1.62	2.67		
8 *en*	2.95	1.72		
9 *ex*			2.73	1.87
9 *en*			1.77	2.39
Me	1.35	1.29	1.47	1.27
MeO	3.62	3.69	3.60	3.63
*J*s between	Coupling constants (in Hz)			
1—7	7.5	7.0		
1—8 *ex*	0	0		
1—8 *en*	7.7	7.0		
3—4			11.0	11.0
3—5			1.0	0.5
4—5	9.5	9.3	8.7	8.5
5—6	6.8	6.8	7.7	7.5
5—7	1.0	1.0	1.0	0.5
5—9 *ex*			1.0	0.5
5—9 *en*			5.0	4.7
6—7	8.7	9.0	8.5	9.0
6—9 *ex*			1.0	1.0
7—8 *ex*	0.5	0		
8 *ex*—8 *en*	14.5	14.3		
9 *ex*—9 *en*			13.3	13.5

adducts, III (19), IV (23), V (2), and VI (2.3%), were produced. The structures of these adducts were deduced by spectroscopic analyses. Thus, all the compounds have α,β-unsaturated carbonyl chromophore in IR and UV spectra showing them to be normal ${}_{\pi}4+{}_{\pi}2$ adducts, bicyclo[3.2.2]nona-3,6-dien-2-one derivatives. The presence of the absorption maximum around 260 nm for III and IV revealed them to be 3-chloro-derivatives,[7] and the absence of this particular absorption in the other two (V and VI) is therefore discernible as 1-chloro-derivatives. The methylene proton signals, in NMR spectra of all the four (III—VI) appears as AB patterns of ABX systems. Therefore, the methyl and methoxycarbonyl groups in V and VI can be located at C-8 position (Otherwise the signal should appear primarily as AB type). In order to confirm the poistion of these groups in III and IV the corresponding deuterio-derivatives were prepared using 2-chlorotropone-3,5,7-d_3 (I-d_3) and the major products, III-d_3 and IV-d_3, were isolated. The NMR signals of the methylene protons appeared as the AB type both in III-d_3 and IV-d_3, establishing the position of the substituents at C-9. The orientation of the substituents in III and IV was again deduced from the differences in chemical shifts of the methylene protons, which should suffer the magnetic anisotropy from the adjacent carbonyl group of the substituent. The *exo*-protons, having smaller coupling constants with bridge head protons and long-range couplings with one of olefinic protons in III and VI appeared in considerably higher field than those in IV and V, revealing the formers (III and VI) to have *exo*-methyl and *endo*-methoxycarbonyl groups and the latters (IV and V) the opposite orientations.

All of the adducts are the primary products of the reaction of I and II because each adduct was quantitatively recovered after being heated in the presence of II at 140 °C for 48 hr.

Table 2. Relative yield of Diels-Alder adducts of 2-chlorotropone

Dienophiles	Sites of the reaction[a]					
	[4,7]		[5,2]		[7,4]	
	exo	*endo*	*exo*	*endo*	*exo*	*endo*
II			4.3	5.0	49.7	41.0
Acrylonitrile	8.6	11.1	39.5			40.8

a) [*m*,*n*] denotes the positions of I which formed a bond between β- and α-positions of dienophiles, respectively.

Thus, the dienophile reacted rather regiospecifically but nonstereospecifically. As summarized in Table 2, this is quite a contrast with the reaction of I and acrylonitrile[6] which afforded the adducts with stereospecificity but without regiospecificity. In the present reaction, the polar effect due to electron-releasing chlorine atom and electron-withdrawal ester group appears to be reinforced with steric repulsion between chlorine and the substituents at α-carbon atom of II to exhibit the high regiospecificity. The lack of stereospecificity may come from the stabilization of transition state by the methyl group as well as the methoxycarbonyl group.[8,9]

Experimental

Reaction of 2-Chlorotropone (I) and Methyl Methacrylate (II). I (2 g) and II (9 ml) were heated at 135—140 °C for 48 hr in a sealed glass tubing. After the removal of the excess of II, the residual oil was distilled under reduced pressure to give faintly yellow liquid (1.95 g) which was chromatographed through silica gel (40 g) with chloroform-pet. ether (4: 1). From the least polar fractions, the adduct III was separated out as colorless crystals whose recrystallization from cyclohexane yielded colorless prisms, mp 98—99 °C (320 mg).

Found: C, 60.27; H, 5.59%. Calcd for $C_{12}H_{13}O_3Cl$: C, 59.88; H, 5.44%. λ_{max}^{MeOH} 241 (ε=6020), 262 (sh), 320 nm (ε=100). ν^{KBr}: 1738, 1685 cm^{-1} (C=O), 1632, 1598 cm^{-1} (C=C, strong). Following fractions yielded the adduct IV which was distilled on a cold finger to give colorless liquid, bp 130 °C/1.5 mmHg (bath temp.) (190 mg) with a distinct single spot on thin layer chromatograms. Found: C, 60.12;

7) S. Itô, H. Takeshita, Y. Shoji, Y. Toyooka, and T. Nozoe, *Tetrahedron Lett.*, **1969**, 443.

8) Y. Kobuke, T. Fueno, and J. Furukawa, *J. Amer. Chem. Soc.*, **92**, 6548 (1970).

9) However, there is an experiment which shows a contravention to this explanation. *cf.* K. N. Houk and L. J. Luskus, *ibid.*, **93**, 4606 (1971).

H, 5.63%. λ_{max}^{MeOH} 240.5 (ε=6000), 262 (sh), 323 nm (ε=100). ν^{liq}: 1735, 1685 cm^{-1} (C=O), 1631, 1598 cm^{-1} (C=C, strong). Subsequent fractions contained the adduct V and a few mg of recovered I which was removed by brief extraction with concd hydrochloric acid. Analytical specimen of V was obtained by cold finger distillation to give 76 mg of colorless liquid, bp 130 °C/1.5 mmHg (bath temp.). Found: C, 59.79; H, 5.75%. λ_{max}^{MeOH} 225 (ε=8050), 330 nm (ε=200), ν^{liq}: 1736, 1680 cm^{-1} (C=O), 1630, 1600 cm^{-1} (C=C, weak). The most polar fraction afforded the adduct VI (80 mg) as colorless plates, mp 110.5—112 °C (fr. cyclohexane). Found: C, 60.12; H, 5.74%. λ_{max}^{MeOH} 225 (ε=8000), 330 nm (ε=180). ν^{KBr}: 1735, 1680 cm^{-1} (C=O), 1630, 1598 cm^{-1} (C=C, weak). Repeated chromatography of intermediary fractions further afforded some amounts of the adducts, III to VI, but the absence of their isomer was confirmed by NMR spectral analysis of every fraction of the chromatography. Final yields of the products were estimated by NMR analysis as 19 (III), 23 (IV), 2 (V), and 2.3% (VI), respectively.

Reaction of 2-Chlorotropone-3,5,7-d_3(I-d_3) and II. I-d_3 (200 mg) and II (1 g) were heated in a sealed glass tubing at 135—145 °C for 60 hr. A similar work up with the above afforded III-d_3, mp 98—99 °C (20 mg) and IV-d_3, colorless liquid (30 mg). The other two compounds were not isolated.

Heating of the Adducts (III, IV, V, and VI) with II. Each adduct (10—20 mg) was mixed with II (1—2 ml) in a sealed tube and heated at 140±5 °C for 48 hr. After the evaporation of II, whole residue was analyzed by NMR spectral determination. Only the starting compound was shown to be presented in each reaction.

BULLETIN OF THE CHEMICAL SOCIETY OF JAPAN, VOL. 46, 2917—2918 (1973)

The Oxidation of Alkylbenzenes and Acylcarbinols by Means of Benzopinacol Diesters

Katuzi KITATANI, Tamio SHIRAFUJI, and Hitosi NOZAKI

Department of Industrial Chemistry, Kyōto University, Yoshida, Sakyō-ku, Kyōto 606

(Received March 30, 1973)

The thermal decomposition of benzopinacol diesters (I) in benzene at 150—160 °C results in the (a) cleavage of the central carbon-carbon bond of I, followed by the acyl radical-release or hydrogen-abstraction of the resulting acyloxydiphenylmethyl radical, thus affording benzophenone (II) and benzhydryl esters (III). The trace amount of tetraphenylethylene (IV) (<5%) thus obtained was ascribed to the (b) cleavage.[1,2]

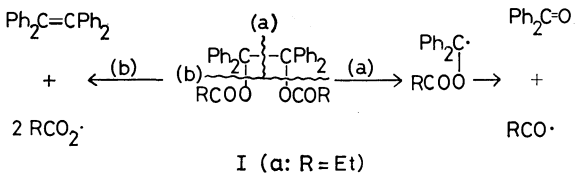

I (a: R=Et)

We have found that benzopinacol dipropionate (Ia) serves as a catalyst in the autoxidation of ethylbenzene, cumene, and tetralin. Table 1 summarizes the yields of the resulting ketones, acetophenone and α-tetralone, and of the products (II and IV) arising from Ia. No trace of III has been observed. Each mol of Ia accounted for *ca.* 20 mol of acetophenone or α-tetralone.

We found also that benzoin and an acyloin were oxidized to the corresponding α-diketones by Ia. The heating of a 0.1 M anisole solution of benzoin and Ia in a mol ratio of 2: 1 at 130 °C under a nitrogen atmosphere gave a quantitative yield of benzil, the Ia being converted to II (43) and IV (26%). The reaction of 2-hydroxycyclododecanone with Ia under the same conditions gave cyclododecane-1,2-dione in a 50% yield, besides II (34) and IV (31%). The yields are based on the amount of each component consumed, either the substrate or Ia. In order to examine the possible autoxidation, a mixture of benzoin and Ia in a mol ratio of 4: 1 was heated under an oxygen atmosphere. About 50% of benzoin was oxidized to afford the corresponding yield of benzil. 2-Hydroxycyclododecanone also behaved similarly, or it was not autoxidized at all under such conditions.

The exact nature of this stoichiometric oxidation is still not known, but the oxidation of benzylic methylene is apparently catalyzed by radicals generated from Ia. It should be added that the reaction of *N,N*-dimethylaniline as a solvent with Ia and Cu(II)Cl_2 (in a mol ratio of 1: 2) afforded an acylated product, *N*-methyl-

TABLE 1. AUTOXIDATION OF ALKYLBENZENES IN THE PRESENCE OF BENZOPINACOL DIPROPIONATE

Substrate	Reaction[a] temp °C	hr	Product (%)[b]	Ph_2CO[c]	$Ph_2C=CPh_2$[c]
Ethylbenzene	150	48	Acetophenone 47 (30)	67	33
Cumene	150	48	Acetophenone 36 (84)	60	12
Tetralin	120	17	α-Tetralone 45 (50)	32	25

a) A mixture of Ia and the alkylbenzene in a mol ratio of *ca.* 1: 200 was heated in oxygen atmosphere.
b) The yields of products are based on the consumed amount of the hydrocarbon. Data in the parentheses show the conversion (%) of hydrocarbons.
c) The yields are based on the added amount of Ia.

1) T. Shirafuji, Y. Yamamoto, and H. Nozaki, This Bulletin, **45**, 2574 (1972).

2) Copper (II) carboxylates in aqueous DMF catalyze the decomposition of diphenyldiazomethane to afford benzopinacol diesters. This reaction constitutes the only available approach to the novel class of I esters. See T. Shirafuji, Y. Yamamoto, and H. Nozaki, *Tetrahedron*, **27**, 5353 (1971).

propionanilide (V), in a 44% yield (based on both propionyl groups of Ia). In the absence of Cu(II), the formation of V was not detected. This can be explained by assuming that the intermediary propionyl radical, after having been generated *via* the cleavage (a), is oxidized by Cu(II) to the acyl cation.[3] The ion is trapped by *N,N*-dimethylaniline to afford the intermediate, $(Me_2N(Ph)–COEt)^+$, which loses its methyl cation to provide V.

The acyloxy and alkyl radicals assumed to be generated *via* the (b) cleavage have not yet been characterized, but we cannot exclude the possibility of their being due, partly at least, to the oxidations mentioned above. The reasons are that consistently higher yields of IV have been obtained in these cases and IV can not be ascribed to diphenylcarbene,[4] but instead possibly results from the acyloxydiphenylmethyl radical in the (a) cleavage.

Experimental

All the melting and boiling points are uncorrected. The glc analyses and separations were performed with columns (1 m) packed with HVSG (30%) on Celite 545 or SE 30 (5%) on Chromosorb. Unless otherwise stated, the yields were estimated by glc analyses.

The Oxidation of Ethylbenzene by Means of the Oxygen-Benzopinacol Dipropionate (Ia) System. A mixture of ethylbenzene (0.95 g, 9.0 mmol) and Ia (25 mg, 0.050 mmol) was heated under stirring and refluxing (140—150 °C) in an oxygen atmosphere for 48 hr. The reaction mixture was first heated at 60 °C for 30 min with 2 N aqueous NaOH (1 ml), neutralized with aqueous sulfuric acid, and then extracted with ether. The extract was washed with an aqueous solution (1%) of $FeSO_4$, dried (Na_2SO_4), and concentrated *in vacuo*. Glc separation (HVSG 30%, 1 m; 150 °C) gave acetophenone (0.15 g, 47%), benzophenone (15 mg, 67%), tetraphenylethylene (6.0 mg, 33%), and the recovered ethylbenzene (0.66 g, 70%).

The Oxidation of Benzoin by Ia. An anisole solution (5 ml) of a mixture of benzoin (0.21 g, 1.0 mmol) and Ia (0.24 g, 0.50 mmol) was heated at 130 °C for 24 hr under a nitrogen atmosphere. The concentration of the reaction mixture *in vacuo*, followed by glc separation (SE 30 30%, 1 m; 180 °C), gave benzil (0.20 g, 95%), benzophenone (80 mg, 43%), and tetraphenylethylene (40 mg, 26%).

The Reaction of N,N-*Dimethylaniline with Ia in the Presence of Cupric Chloride.* A mixture of *N,N*-dimethylaniline (1 ml), Ia (0.10 g, 0.20 mmol), and $CuCl_2 \cdot 2H_2O$ (70 mg, 0.40 mmol) was heated at 150—160 °C for 17 hr under stirring in a nitrogen atmosphere. Heating was continued until the solution turned blue. The reaction mixture was then washed with aqueous $NaHCO_3$ and extracted with benzene. The extract was concentrated and subjected to glc (SE 30 30%, 1 m; 150 °C) to afford *N*-methylpropionanilide (30 mg, 44%), benzophenone (40 mg, 60%), and tetraphenylethylene (15 mg, 22%). The *N*-methylpropionanilide (mp 56 °C (lit,[5] 56—58 °C)) was identical with an authentic sample[5] (IR, NMR, MS, and glc retention time).

Financial support from the Ministry of Education, Japanese Government, is acknowledged with pleasure.

3) C. L. Jenkins and J. K. Kochi, *J. Amer. Chem. Soc.*, **94**, 843, 856 (1972).

4) H. Nozaki, H. Takaya, S. Moriuti, and R. Noyori, *Tetrahedron*, **24**, 3655 (1968).

5) L. M. Norton and A. W. Allen, *Ber.*, **18**, 1998 (1885).

BULLETIN OF THE CHEMICAL SOCIETY OF JAPAN, VOL. 46, 2918—2919 (1973)

Synthesis of Dihydrofarfugin B

Hidekazu SHIRASAKI, Hideo KOMATSU, Hajime NAGANO, Yoshihiko MORIYAMA, Yoshiaki TANAHASHI, and Takeyoshi TAKAHASHI

Department of Chemistry, Faculty of Science, The University of Tokyo, Bunkyo-ku, Tokyo 113

(Received April 2, 1973)

Farfugin A (I) and farfugin B (II) have been isolated from the benzene extract of *Farfugium japonicum* Kitamura (=*Ligularia tussilaginea* Makino). Spectral data of the latter and its derivatives led to two alternative structures, II and III for farfugin B. The structure of farfugin B was finally deduced to be 3,5-dimethyl-6-(*trans-n*-3-pentenyl)benzofuran (II) on the basis of NOE (Nuclear Overhauser Effect) experiments.[1,2]

We report here the synthesis of dihydrofarfugin B (IV); this confirms the structure of II for farfugin B.

Grignard reagent prepared from 1-methyl-2-bromo-4-methoxybenzene (V)[3] was treated with *n*-pentanal to give an alcohol (VI). Dehydration of VI with iodine[4] gave the dehydrated product (VII), which was subjected to hydrogenation over Pd–C to afford VIII. Demethylation of VIII with hydrobromic acid in acetic acid gave a phenol (IX).

Finally the furan moiety was introduced as follows. Phenoxyacetone (X), prepared from the reaction of the phenol (IX) with chloroacetone, was cyclized with polyphosphoric acid on heating. This cyclization occurred toward two directions to give two isomeric benzofuran derivatives, (IV) and (XI), in the ratio of 5: 2. The PMR spectrum of the minor component showed a signal of AB type quartet (δ_A=6.91 and δ_B=7.03 ppm; J=9 Hz) due to the aromatic *ortho*-

1) H. Nagano, Y. Moriyama, Y. Tanahashi, T. Takahashi, M. Fukuyama, and K. Sato, *Chemistry Lett.*, **1972**, 13.

2) M. Tada, Y. Moriyama, Y. Tanahashi, and T. Takahashi, *Tetrahedron Lett.*, **1972**, 5251; M. Tada, Y. Tanahashi, Y. Moriyama, and T. Takahashi, *ibid.*, **1972**, 5255.

3) E. Müller, A. Rieker, and K. Scheffler, *Ann.*, **645**, 92, (1961).

4) B. A. Nagasampagi, Sukh Dev, C. Rai, and K. L. Murthy, *Tetrahedron*, **22**, 1971 (1966).

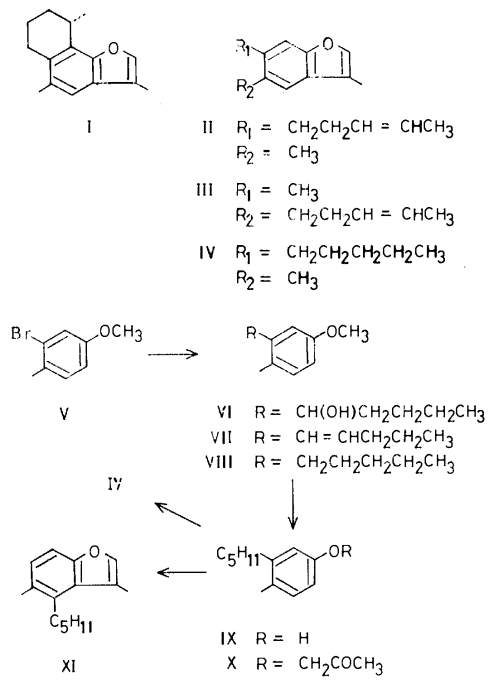

protons. This led to the structure of 3,5-dimethyl-4-*n*-pentylbenzofuran (XI) for the minor component. The major one was consequently assigned to be 3,5-dimethyl-6-*n*-pentylbenzofuran (IV), which was found to be identical with dihydrofarfugin B in all respects (IR, PMR, UV, and mass spectra). The presence of *trans*-*n*-3-pentenyl side chain was already shown for farfugin B.[1] Thus, the structure of farfugin B was confirmed to be 3,5-dimethyl-6-(*trans*-*n*-3-pentenyl) benzofuran (II).

Experimental

IR spectra were taken in neat film, and PMR spectra were measured in $CDCl_3$ containing TMS as internal standard.

*1-(1-Hydroxy-*n*-pentyl)-2-methyl-5-methoxybenzene (VI).* To the Grignard reagent prepared from 1-methyl-2-bromo-4-methoxybenzene (V)[3] (12.1 g, 58 mmol) in dry tetrahydrofuran (50 ml) and magnesium ribbon (1.75 g, 72 mmol), a solution of *n*-pentanal (6.02 g, 70 mmol) in dry tetrahydrofuran (20 ml) was added dropwise and stirred for 1 hr at room temperature. The reaction material was poured on a mixture of crashed ice (100 g) and concentrated hydrochloric acid (10 ml). This was extracted with ether three times (each 100 ml). After usual work-up, the extract gave a residue (14.0 g) containing VI, a part of which was purified by chromatography on silica gel with benzene as eluent to give pure VI, an oil, IR: ν_{max} 3380 cm^{-1} (OH); PMR: δ 0.90 (m, terminal C$\underline{H}_3$ on a side chain), 2.24 (s, aromatic C$\underline{H}_3$), 3.79 (s, OC$\underline{H}_3$), 4.88 (t, J=6 Hz, -C$\underline{H}$-OH), and 6.50—7.10 (aromatic protons); MS: *m/e* 208 (M^+; $C_{13}H_{20}O_2$). Found: C, 74.91; H, 9.72%. Calcd for $C_{13}H_{20}O_2$: C, 74.96; H, 9.68%.

*1-(*n*-1-Pentenyl)-2-methyl-5-methoxybenzene (VII).* The above residue (3.51 g) was heated with iodine (170 mg)[4] at 100 °C for 3 hr. The reaction mixture was chromatographed on silica gel (150 g) with benzene as eluent to afford VII (2.23 g; yield 78% from V), an oil, PMR: δ 0.95 (m, terminal C$\underline{H}_3$), 2.18 (m, 2H, allylic protons), 2.24 (s, aromatic C$\underline{H}_3$), 3.78 (s, OC$\underline{H}_3$), and 6.10—7.30 (aromatic and olefinic protons); MS: *m/e* 190 (M^+; $C_{13}H_{18}O$). Found: C, 81.88; H, 9.68%. Calcd for $C_{13}H_{18}O$: C, 82.06; H, 9.54%.

*1-*n*-Pentyl-2-methyl-5-methoxybenzene (VIII).* Hydrogenation of VII (1.16 g, 6.1 mmol) was effected in ethanol over 10% palladium-charcoal. After usual treatment, VIII (926 mg; yield 79%), an oil, was obtained. Characterization of VIII is as follows; PMR: δ 0.89 (m, terminal C$\underline{H}_3$), 2.21 (s, aromatic C$\underline{H}_3$), 2.54 (m, 2H, benzyl protons), 3.74 (s, OC$\underline{H}_3$), and 6.50—7.20 (aromatic protons); MS: *m/e* 192 (M^+; $C_{13}H_{20}O$). Found: C, 81.28; H, 10.68%. Calcd for $C_{13}H_{20}O$: C, 81.20; H, 10.48%.

*1-*n*-Pentyl-2-methyl-5-hydroxybenzene (IX).* To a solution of VIII (0.79 g, 4.1 mmol) in acetic acid (5 ml), 48% hydrobromic acid (5 ml) was added and the mixture was heated under reflux for 20 hr. Acetic acid was removed under reduced pressure and ether (100 ml) was added to the residue. The ether solution was washed with saturated aqueous solution of sodium bicarbonate and then treated as usual. The residue was chromatographed on silica gel (50 g) with benzene as eluent to give IX (285 mg; yield 39%), an oil, IR: ν_{max} 3380 cm^{-1} (OH); PMR: δ 0.88 (m, terminal C$\underline{H}_3$), 2.19 (s, aromatic C$\underline{H}_3$), 2.49 (m, 2H, benzyl protons), 5.57 (s, O$\underline{H}$), and 6.45—7.10 (aromatic protons); MS: *m/e* 178 (M^+; $C_{12}H_{18}O$). Found: C, 80.87; H, 10.48%. Calcd for $C_{12}H_{18}O$: C, 80.85; H, 10.18%.

*1-*n*-Pentyl-2-methyl-5-acetonyloxybenzene (X).* A solution of IX (266 mg, 1.5 mmol) in dry acetone (10 ml) was heated under reflux with chloroacetone (299 mg) and potassium iodide (130 mg) for 20 hr. The solvent was distilled off and ether (100 ml) was added to the residue, and the ether solution was treated as usual. The residue was chromatographed on silica gel (30 g) with benzene as eluent to afford X (252 mg; yield 72%), an oil, IR: ν_{max} 1720 cm^{-1} (CO); PMR: δ 0.90 (m, terminal C$\underline{H}_3$), 2.16 (s, 6H, aromatic C$\underline{H}_3$ and -COC$\underline{H}_3$), 2.51 (m, 2H, benzyl protons), 4.35 (s, -OC$\underline{H}_2$CO-) and 6.40—7.02 (aromatic protons); MS: *m/e* 234 (M^+; $C_{15}H_{22}O_2$). Found: C, 76.64; H, 9.48%. Calcd for $C_{15}H_{22}O_2$: C, 76.88; H, 9.46%.

*3,5-Dimethyl-6-*n*-pentylbenzofuran (IV) and 3,5-Dimethyl-4-*n*-pentylbenzofuran (XI).* Acetonyloxy derivative (X) (200 mg, 0.86 mmol) was heated with polyphosphoric acid (4 g) at 100 °C for 10 min under a nitrogen atmosphere. After cooling, the reaction material was poured on a mixture of crashed ice (50 g) and concentrated hydrochloric acid (5 g) to decompose the excess polyphosphoric acid. This was extracted with ether and the ethereal solution was washed with saturated aqueous solution of sodium bicarbonate (100 ml) and then treated as usual. The residue obtained was chromatographed on silica gel to give a mixture (45.4 mg; yield 25%) of IV and XI. The mixture was further chromatographed using 20% $AgNO_3$-impregnated silica gel with petroleum ether as eluent and IV (17.7 mg) and XI (7.5 mg) were obtained. Spectral data of IV, an oil, are as follows; IR: ν_{max} 1625, 1580, 800, 780 cm^{-1}; PMR: δ 0.90 (m, terminal C$\underline{H}_3$), 2.20 (d, J=2 Hz, C$\underline{H}_3$ on a furan ring), 2.38 (s, aromatic C$\underline{H}_3$), 2.66 (m, 2H, benzyl protons), and 7.05—7.20 (protons on a furan and a benzene ring); UV: λ_{max}^{EtOH} 251.5 nm (ε 11300); MS: *m/e* 216 (M^+; $C_{15}H_{20}O$). The compound IV was found to be identical with dihydrofarfugin B (IR, PMR, UV, and mass spectra).

Characterization of XI, an oil, is as follows; IR: ν_{max} 1580, 780 cm^{-1}; PMR: δ 0.93 (m, terminal C$\underline{H}_3$), 2.36 (two methyl groups on a furan and a benzene ring), 2.87 (m, 2H, benzyl protons), 6.97 (an AB quartet, δ_A=6.91, δ_B=7.03, J=9 Hz), and 7.16 (d, J=2 Hz, a proton on a furan ring); UV: λ_{max}^{EtOH} 254.3 nm (ε 12400); MS: *m/e* 216 (M^+; $C_{15}H_{20}O$). Found: C, 83.06; H, 9.55%. Calcd for $C_{15}H_{20}O$: C, 83.28; H, 9.32%.

BULLETIN OF THE CHEMICAL SOCIETY OF JAPAN, VOL. 46, 2920—2921 (1973)

Stereostructure of Zonarene

Masanobu IGUCHI, Masatake NIWA, and Shosuke YAMAMURA*

Faculty of Pharmacy, Meijo University, Showa-ku, Nagoya 468

(Received May 1, 1973)

Zonarene, a cadinane-type sesquiterpene, has been isolated from the brown seaweed (*Dictyopteris zonarioides*), and the structure of this hydrocarbon also been established by Fenical and his co-workers except for its stereostructure.[1] In the present paper, we wish to describe the stereostructure of zonarene including the absolute configuration by means of chemical transformation from preisocalamendiol, which has been synthesized from *l*-santonin,[2] to (+)-zonarene.

As described in the previous papers,[3,4] the epoxy-diol (I) was obtained from isocalamendiol, an acid-catalyzed cyclization product of preisocalamendiol, the absolute configuration of which had been already established. Further treatment of I with $POCl_3$–pyridine afforded the known dehydration product (II)[4] and a hydroxy-olefin (III)[5] in 40 and 27% yields, respectively. The structure of the latter was confirmed by its spectral data, in particular by the NMR signal at δ 3.46 ppm (2H, s) assigned to two protons attached to the carbon atom bearing the ether-oxygen atom. Catalytic hydrogenation of II on PtO_2 in AcOEt (room temp., 1.5 hr) afforded a mixture of two dihydro-compounds [IV (mp 69—70 °C) and V (mp 77—80 °C) in 82 and 6% yields, respectively]. On the basis of the comparison of the NMR spectra between IV and V, the newly formed secondary methyl group in the main product (IV) must be in an axial configuration (δ 1.05 ppm), whereas the corresponding methyl group in the latter is in an equatorial configuration (δ 0.85 or 0.87 ppm).[6] When treated with $LiAlH_4$ in ether (room temp., 2 hr), IV was converted into the corresponding diol (VI, mp 104—105 °C) in 92% yield. Finally, action of $POCl_3$–pyridine (room temp., overnight, and then 40 °C, 2 hr) on VI converted it to a mixture of two dehydration products (VII and VIII in 30 and 38% yields, respectively). The former was completely identical with an authentic sample of zonarene (glc and IR spectrum) except for the sign of the optical rotation cited in the literature.[1] The structure of the latter was characterized by its physical data [ν_{max}(film) 3550 cm^{-1}; $\delta(CCl_4)$ 1.63 (3H, br.s) and 5.48 ppm (1H, br.s)]. In conclusion, the stereostructure of zonarene including the absolute configuration should be represented by IX. Recently, the same result has also been obtained by Andersen and his co-workers.[7]

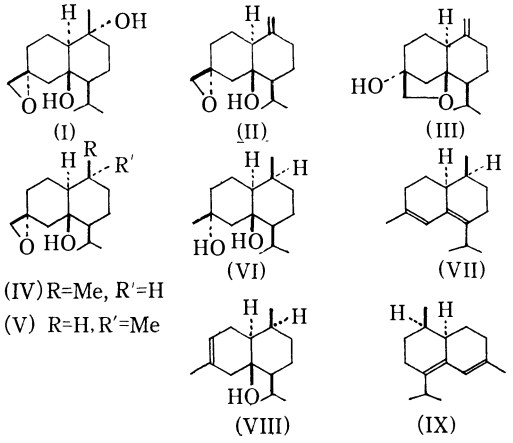

Experimental

All the melting-points are uncorrected. The IR spectra were recorded on a Hitachi-215 spectrophotometer. The NMR spectra were taken on Varian A-60 and Nihondenshi JNM-60H (60 MHz) spectrometers, using $CDCl_3$ as the solvent, unless otherwise stated. Only prominent peaks are cited. The chemical shifts are given in ppm relative to the internal TMS. The coupling constants are given in Hz (s: singlet; d: doublet; t: triplet; q: quartet; m: multiplet). The mass spectra were obtained on a Hitachi RMU-6D mass spectrometer operating with an ionization energy of 70 eV. Optical rotation was measured on a JASCO ORD/UV-5 spectrometer using MeOH as a solvent.

Dehydration of the Epoxy-diol (I). According to essentially the same condition as previously reported,[4] dehydration of the epoxy-diol (560 mg) in pyridine (10 ml) with $POCl_3$ (2 ml) in pyridine (4 ml) was carried out to give a pale brown oil (500 mg), which was chromatographed on alumina (Katayama Co. Ltd., 150—250 mesh; 10 g) and eluted with *n*-hexane–ether (1 : 1) to give the known colorless liquid (208 mg) of II[4] as the first fraction. After elution of II, a colorless liquid (140 mg) of III was isolated; ν_{max}^{film} 3460 br., 3080, 1645, 900, and 885 cm^{-1}; δ 0.91 (3H, d, J=7.0 Hz), 0.94 (3H, d, J=7.0 Hz), 3.46 (2H, s), 4.80 (1H, br.s), and 4.98 ppm (1H, br.s). Found: *m/e* 236.1785. Calcd for $C_{15}H_{24}O_2$: *m/e* 236.1776.

Catalytic Hydrogenation of the Epoxy-olefin (II). Catalytic hydrogenation of the epoxy-olefin (220 mg) in AcOEt (5 ml) over PtO_2 (5 mg) was carried out at room temp. for 1.5 hr, and then filtered to remove the catalyst. The filtrate was concentrated under reduced pressure to give a colorless liquid (220 mg), from which two reduction products were separated by preparative tlc (neutral alumina (E. Merck,

* To whom inquires should be addressed.

1) W. Fenical, J. J. Sims, R. M. Wing and P. C. Radlick, *Phytochemistry*, **11**, 1161 (1972).

2) K. Kato, Y. Hirata, and S. Yamamura, *Tetrahedron*, **27**, 5987 (1971).

3) S. Yamamura, M. Iguchi, A. Nishiyama, M. Niwa, H. Koyama, and Y. Hirata, *ibid.*, **27**, 5419 (1971); M. Iguchi, M. Niwa, and S. Yamamura, *Chem. Commun.*, **1971**, 974.

4) S. Yamamura, M. Iguchi, M. Niwa and Y. Hirata, This Bulletin, **45**, 266 (1972).

5) This compound had not been detected in the previous experiment (see Ref.4).

6) Y. Kawazoe, Y. Sato, M. Natsume, H. Hasegawa, T. Okamoto, and K. Tsuda, *Chem. Pharm. Bull.* (Tokyo), **10**, 338 (1962); R. F. Zurcher, *Helv. Chim. Acta*, **46**, 2054 (1963).

7) N. H. Andersen, D. D. Syrdal, B. M. Lawernce, S. J. Terhune and J. W. Hogg, *Phytochemistry*, **12**, 827 (1973).

A. G., Germany)) using *n*-hexane–benzene (1: 1). The upper fraction gave white crystals (181 mg) of IV; mp 69—70 °C (from *n*-hexane); ν_{max}^{KBr} 3570 cm^{-1}; δ (CCl_4) 0.87 (3H, d, J=6.9 Hz), 0.90 (3H, d, J=6.9 Hz), 1.05 (3H, d, J=7.0 Hz), and 2.46 ppm (2H, s). Found: *m/e* 238.1940. Calcd for $C_{15}H_{26}O_2$: *m/e* 238.1933. From the lower fraction, a colorless liquid (31 mg) was obtained, which was further purified by preparative tlc (Kieselgel GF_{254}) using *n*-hexane–ether (2: 1) to give white crystals (14 mg) of V; mp 77—80 °C (from *n*-hexane); ν_{max}^{film} 3570 cm^{-1}; δ (CCl_4) 0.85 and 0.87 (9H, each br.d, $J\simeq$6.3 Hz), and 2.48 ppm (2H, s). Found: *m/e* 238.1901. Calcd for $C_{15}H_{26}O_2$: *m/e* 238.1933.

Reduction of Dihydro-epoxide (IV) with $LiAlH_4$. $LiAlH_4$ (10 mg) was added to a solution of IV (130 mg) in anhyd. ether (10 ml), and then the mixture was stirred at room temp. for 2 hr. After the decomposition of the excess reagent with three drops of water, the reaction solution was filtered. The filtrate was concentrated under reduced pressure to give white crystals, which was purified by preparative tlc (Wakogel B5-F) using *n*-hexane–ether (2: 1) to give white crystals (120 mg) of the diol (VI); mp 104—105 °C; ν_{max}^{KBr} 3340 br. cm^{-1}; δ 0.93 (6H, d, J=7.0 Hz), 1.05 (3H, d, J=7.0 Hz), 1.20 (3H, s), and 2.85 ppm (2H, s, OH); *m/e* 240 (M^+). Found: C, 74.70; H, 12.01%. Calcd for $C_{15}H_{28}O_2$: C, 74.95; H, 11.74%.

Dehydration of the Diol (VI). Into a solution of the diol (110 mg) in anhyd. pyridine (10 ml) was slowly stirred a solution of $POCl_3$ (2 ml) in anhyd. pyridine (2 ml) at −15 °C. The reaction solution was further stirred at room temp. overnight, and then at 40 °C for 2 hr. The reaction solution was then poured into large amounts of ice and extracted with ether. The ether extract was washed successively with 5% hydrochloric acid and with water, and then dried over anhydrous Na_2SO_4. The subsequent removal of the solvent gave a pale yellow oil (100 mg), from which two dehydration products were obtained by preparative tlc (Wakogel B5-F) using *n*-hexane–benzene (2: 1). The upper fraction afforded a colorless oil (33 mg), which was further purified by preparative tlc (10% $AgNO_3$-Wakogel B5-F) using *n*-hexane–benzene (2: 1) to give a colorless liquid (28 mg) of (+)-zonarene (VII, $[\alpha]_D^{25}$ +322°) (glc, tlc, and IR spectrum). On the other hand, the lower fraction afforded a colorless oil (42 mg), which was also purified by preparative tlc (Wakogel B5-F) using *n*-hexane–benzene (1: 1) to give a colorless liquid (39 mg) of VIII; ν_{max}^{film} 3550 cm^{-1}; δ (CCl_4) 0.94 (6H, d, J=6.4 Hz), 1.04 (3H, d, J=6.0 Hz), 1.63 (3H, br.s), and 5.48 ppm (1H, br.s). Found: *m/e* 222.1975. Calcd for $C_{15}H_{26}O$: *m/e* 222.1984).

The authors wish to thank Dr. W. Fenical (University of California, U.S.A.) for an authentic sample of zonarene. They are also indebted to Professor Akira Tatematsu and Mr. Hiroshi Sakurai (Meijo University) for measurements of high resolution mass spectra.

BULLETIN OF THE CHEMICAL SOCIETY OF JAPAN, VOL. 46, 2921—2922 (1973)

Reaction of Sydnones with Phosphorus Pentasulfide

Kosaku SUGIMOTO and Masaki OHTA

Department of Chemistry, Faculty of Science, Tokyo Institute of Technology, Ookayama, Meguro-ku, Tokyo 152

(Received June 11, 1973)

The reaction of 3-phenylsydnone(Ia) with phosphorus pentasulfide has been reported by Baker[1] in which the reactants were heated in toluene under reflux for six hours and 1,4-diphenyl-1,2,4,5-tetrazine (II) was obtained. Other example of the reaction of sydnone with phosphorus pentasulfide has not been reported in the literature.

In this note, reactions of 3,4-diphenylsydnone (Ib), 3-benzylsydnone (Ic), and 3-isopropyl-4-phenylsydnone (Id) with phosphorus pentasulfide are described.

We now found that the reaction of Ia with phosphorus pentasulfide in methylene chloride proceeded even at room temperature yielding II. When this reaction was carried out in the presence of dimethyl acetylenedicarboxylate or acrylonitrile, II was obtained suggesting that the formation of 1,3-dipolar intermediate from sydnone could be excluded. Reaction of Ib with phosphorus pentasulfide in a mixture of methylene chloride and carbon disulfide at room temperature afforded *N*-phenyl-*N*-thiobenzoylhydrazine (IIIa). When this reaction was carried out in benzene under reflux, IIIa was obtained and tetrazine derivative was not formed.

Reaction of Ic with phosphorus pentasulfide in a mixture of methylene chloride and carbon disulfide at room temperature afforded *N*-benzyl-*N*-thioformylhydrazine (IIIb). The reaction of Id with phosphorus pentasulfide under the same condition resulted in the recovery of the starting material, while in benzene under reflux afforded *N*-isopropyl-*N*-thiobenzoylhydrazine (IIIc) was obtained.

It seems probable that the present reaction proceeds through 1,3-addition of P=S double bond to sydnone under elimination of carbon dioxide, but the formation of *N*-substituted-*N*-thioacylhydrazine instead of tetrazine derivative cannot be explained satisfactorily.

II

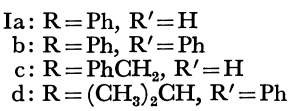

Ia: R=Ph, R′=H
b: R=Ph, R′=Ph
c: R=$PhCH_2$, R′=H
d: R=$(CH_3)_2CH$, R′=Ph

IIIa: R=R′=Ph
b: R=$PhCH_2$, R′=H
c: R=$(CH_3)_2CH$, R′=Ph

1) W. Baker, W. D. Ollis, and V. D. Poole, *J. Chem. Soc.*, **1950**, 3389.

Experimental

Reaction of Ia with P_4S_{10}. To a solution of Ia (2.5 g) in 50 ml of methylene chloride was added 2.0 g of P_4S_{10} and the mixture was stirred for 5 days at room temperature and filtered. The filtrate was evaporated *in vacuo* and the residue was crystallized from methylene chloride to give 0.5 g of II, mp 196—197 °C (lit,[1] mp 193 °C).

Found: C, 71.01; H, 5.29; N, 23.50%. Calcd for $C_{14}H_{12}N_4$: C, 71.19; H, 5.08; N, 23.73%.

Reaction of Ib with P_4S_{10}. To a solution of Ib (2.0 g) in 30 ml of methylene chloride was added a suspension of P_4S_{10} (1.1 g) in 40 ml of carbon disulfide and the mixture was stirred at room temperature for 7 days under nitrogen atmosphere. The solvent was removed *in vacuo* and the residue was subjected to column chromatography using silica gel and 0.6 g of IIIa was obtained. Recrystallization from methylene chloride–hexane afforded crystals of IIIa, mp 116—117 °C.

Found: C, 68.45; H, 5.32; N, 12.45; S, 13.91%. Calcd for $C_{13}H_{12}N_2S$: C, 68.42; H, 5.22; N, 12.28; S, 14.08%. IR (KBr): 3230, 3170 cm^{-1}. NMR ($CDCl_3$): 2.8 (s, 10H), 3.9 (s, 2H) (exchangeable by D_2O).

Reaction of Ic with P_4S_{10}. Three grams of Ic and 0.8 g of P_4S_{10} were reacted in a similar manner as described above and the product was isolated by column chromatography (0.4 g) and recrystallized from benzene–hexane, mp 111—112 °C.

Found: C, 58.11; H, 6.12; N, 16.81; S, 19.07%. Calcd for $C_8H_{10}N_2S$: C, 57.82; H, 6.06; N, 16.85; S, 19.29%. IR (KBr): 3240, 3170 cm^{-1}. NMR ($CDCl_3$): 0.7 (s, 1H), 2.5 (s, 5H), 5.1 (s, 2H) (exchangeable by D_2O).

Reaction of Id with P_4S_{10}. A mixture of Id (3.0 g), P_4S_{10} (0.8 g) and 40 ml of benzene was refluxed for 3 hr. After removal of the solvent, the residue was subjected to column chromatography and 0.9 g of IIIc was obtained which was recrystallized from benzene–cyclohexane, mp 68—69 °C.

Found: C, 62.02; H, 7.14; N, 14.24; S, 16.26%. Calcd for $C_{10}H_{14}N_2S$: C, 61.86; H, 7.22; N, 14.43; S, 16.49%. IR (KBr): 3240, 3130 cm^{-1}.

BULLETIN OF THE CHEMICAL SOCIETY OF JAPAN, VOL. 46, 2922—2924 (1973)

Diels-Alder Reaction of "Anhydrochloral-urethane" with 1,3-Dienes[1]

Takeshi IMAGAWA, Keiiti SISIDO, and Mituyosi KAWANISI
Department of Industrial Chemistry, Kyoto University, Kyoto 606

(Received January 24, 1973)

"Anhydrochloral-urethane" *N*-(2,2,2-trichloroethylidene)alkoxycarbonylamine (I), known since 1891,[2] was not actually synthesized until 1968 by Ulrich and his coworkers.[3] They gave good evidences of the reactivity of the C=N double bond in imine I toward the addition of nucleophiles.

The strongly electrophilic C=N double bond in some imines is successfully applied to the Diels-Alder reaction.[4] The enhanced electrophilicity and the simplicity of substituents prompted us to subject imine I ($R=C_2H_5$) to the Diels-Alder reaction as a dienophile affording the 2-ethoxycarbonyl-3-trichloromethyl-2-azabicyclo[2.2.1]heptenes (IIa, b) or 1-ethoxycarbonyl-2-tri-chloromethyl-1,2,3,6-tetrahydropyridines (III).

Reaction of I with cyclopentadiene in refluxing benzene for 3 hr gave two isomeric adducts in the ratio 2:1 (90% combined yield). The 1:1 nature of these adducts was evidenced by elemental analyses and MS spectroscopy which gave a peak corresponding to the $M^+ - CCl_3$ fragment ion as the base peak originated from the fragmentation β to the nitrogen atom, accompanied by a very weak molecular ion peak. The predominant crystalline adduct (IIa) was shown to possess an *exo* trichloromethyl group and the minor oily product (IIb) an *endo* trichloromethyl function, by NMR and IR spectroscopy. Especially noteworthy was the coupling constant between the proton α to the trichloromethyl group and the bridgehead proton. The value for IIa was 3.0 Hz, whereas that for IIb was nearly 0 Hz (Table 1). This difference is recognized in the elucidation of the sterochemistry of bicyclo[2.2.1]heptane ring systems.[5] It is further endorsed by the chemical shifts of the bridge methylene protons. Although both the methylene protons of IIb were degenerated at δ 1.66, the signals of those of IIa appeared at δ 1.45 and 2.74, indicating the anisotropic effect of the *exo* trichloromethyl on the nearer *syn* proton. The assignment of the configuration is also supported by IR spectra in CCl_4 solution, showing the carbonyl frequency of the urethane moiety of IIa at a higher wave number than that of IIb resulting from the decrease of overlap between the electrons of the carbonyl group and the lone-pair electrons of the nitrogen atom of IIa by a steric hindrance.

Kresze and Albrecht reported on the reaction of *N*-trichloroethylidene-*p*-toluenesulfonamide (IV) with

1) Partly presented at the 24th Annual Meeting of the Chemical Society of Japan, Osaka, April 1, 1971.

2) R. Moscheles, *Ber.*, **24**, 1803 (1891); for the revised structure, see F. Feist, *ibid.*, **45**, 945 (1912).

3) H. Ulrich, B. Tucker, and A. A. R. Sayigh, *J. Org. Chem.*, **33**, 2887 (1968).

4) a) J.-P. Anselme, "The Chemistry of the Carbon-Nitrogen Bond", S. Patai, Ed., Interscience, New York, 1970, p. 299. b) A. B. Evnin, A. Lam, and J. Blyskal, *J. Org. Chem.*, **35**, 3097 (1970). c) D. Ben-Ishai and A. Warshawsky, *J. Heterocycl. Chem.*, **8**, 865 (1971) and their earlier works. d) D. vor der Brück, R. Bühler, and H. Plieninger, *Tetrahedron*, **28**, 791 (1972).

5) For pertinent reference see M. Z. Haq, *J. Org. Chem.*, **37**, 3015 (1972).

Table 1. NMR chemical shifts,[a] multiplicities,[b] and coupling constants for II and III

	H-3	H-4	H-5,6	H-1	H-7	*N*-Substituent
IIa	3.79(s)	3.54(bm)	6.52(cm)	4.81(m)	1.45(bd) 2.74(bd) (9.5 Hz)	1.30(t) 4.12(q) (7.0 Hz)
IIb	4.85(d)	3.80(bm)	6.47(m)	5.09(m)	1.66(t)	1.31(t) 4.18(q) (7.0 Hz)
IIc	4.04(s)	3.66(bm)	6.60(cm)	4.85(bm)	1.48(bd) 2.68(bd) (10.5 Hz)	2.38(s)(Me) 7.44(m)(ArH)
	H-3	H-6	H-2	=CH	$=CCH_3$	*N*-Substituent
IIIa	2.70(bs)	−4.2(AB)	5.22(m)	5.78(bs)	—	1.33(t) 4.22(q) (6.9 Hz)
IIIb	2.56(bs)	−4.0(AB)	5.25(m)	5.46(bs)	1.78(bs)	1.32(t) 4.21(q) (6.9 Hz)
IIIc	2.52(bs)	−3.8(AB)	5.14(m)	—	1.69(bs)	1.30(t) 4.18(q) (7.1 Hz)

a) δ values in CCl_4 (60 MHz). b) s, singlet, b, broad; d, doublet; m, multiplet; cm, complex multiplet; t, triplet; q, quartet; AB, AB quartet composed of broad lines (Only the central position is shown in δ values).

cyclopentadiene to give an adduct of mp 134 °C in 93% yield,[6] but no mention seems to have been made about its stereochemistry. On reexamining the reaction we confirmed that the configuration of the adduct IIc is in the same situation as that of our predominant adduct IIa by comparison of their NMR spectra. Both showed similar patterns of the protons in the azabicyclo[2.2.1]heptene rings.

$CCl_3CH{=}NCOOR$

I

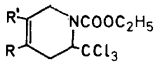

IIa: $R=CCl_3$, $R'=H$, $R''=COOC_2H_5$
b: $R=H$, $R'=CCl_3$, $R''=COOC_2H_5$
c: $R=CCl_3$, $R'=H$, $R''=SO_2C_6H_4CH_3$-*p*

IIIa: $R=R'=H$
b: $R=CH_3$, $R=H'$
c: $R=R'=CH_3$

Formula.

At first glance, the *exo* orientation of the trichloromethyl group in the exclusive or major adduct seems inconsistent with the so-called *endo* addition rule.[7] However, the results are well explained on the basis of the rule of maximum accumulation of double bonds as follows (Scheme 1). When dienophiles I and IV are assumed to have *anti* configuration[8] at the transition state of the reaction, course A is more favorable than B, since not the trichloromethyl group but the conjugated ethoxycarbonyl or *p*-toluenesulfonyl group should play a dominant role in the maximum overlapping of unsaturation. Consequently, the major or exclusive product has the trichloromethyl group in the *exo* arrangement. The reason for IV exclusively giving the *exo* adduct but I the *exo*- as well as *endo*-adduct may be ascribed to the stronger directive effect of the sulfonyl group, since the Diels-Alder reaction of *trans*-1-benzoyl-2-benzenesulfonylethylene and cyclopentadiene has been reported[9] to give the *endo* benzenesulfonyl adduct and the *endo* benzoyl adduct in the ratio 3: 1.

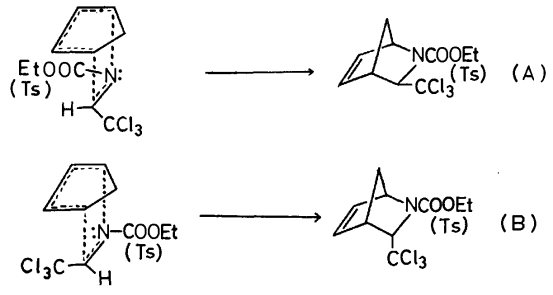

Scheme 1.

Heating benzene solutions of I and butadiene, isoprene, and 2,3-dimethylbutadiene in a pressure bottle at 100—120 °C gave 1-ethoxycarbonyl-2-trichloromethyl-1,2,3,6-tetrahydropyridines (IIIa—c) in 55, 75, and 78% yield, respectively. The adduct of isoprene was a single compound and tentatively assigned to IIIb, because the chemical shift of the protons of C_3 was nearer that of IIIc than IIIa; this assignment and the regiospecificity are consistent with the result in an analogous reaction.[10]

Experimental[11]

Reaction of I with Cyclopentadiene. Refluxing a benzene (25 ml) solution of freshly prepared I (5.00 g) and cyclopentadiene (2.5 g) for 3 hr gave an oily mixture after evaporation. This was chromatographed over 80 g of alumina with benzene as an eluent.

The faster moving zone gave, after removal of the solvent, 3.85 g (59%) of oily IIa; bp 136—138 °C/4 mmHg, $n_D^{23.5°}$

6) G. Kresze and R. Albrecht, *Chem. Ber.*, **97**, 490 (1964).
7) K. Alder and G. Stein, *Angew. Chem.*, **50**, 510 (1937); R. B. Woodward and R. Hoffmann, "The Conservation of Orbital Symmetry", Academic Press, New York, 1970. p. 145.
8) Although *syn-anti* isomerism in I and IV has not been established, the distribution of products may be safely discussed on the *anti* configuration which is stable in the transition state; for *syn-anti* isomerism in imines, see a) M. Raban and E. Carlson, *J. Amer. Chem. Soc.*, **93**, 685 (1971); b) R. M. Moriarty, C.-L. Yeh, K. C. Ramey, and P. W. Whitehurst, *ibid.*, **92**, 6350 (1970); and the references cited therein.
9) J. Sauer, H. Wiest, and A. Mielert, *Chem. Ber.*, **97**, 3183 (1964).
10) R. Albrecht and G. Kresze, *Chem. Ber.*, **98**, 1431 (1965).
11) MS spectra were obtained with an ionization potential of 70 eV. We are grateful to Dr. Simpei Kojima for permission to use the NMR spectrometer. I and IIc, prepared by the reported procedures, had spectral properties in agreement with those in literature.

1.5159. IR (CCl_4): 1730, 1270 cm^{-1}. MS: *m/e* 283 (small, M^+), 166 (100%, M^+-CCl_3), 138 (16), 94 (46), 67 (30), 66 (30), 56 (45%), M: M+2: M+4: M+6=100: 98: 32: 4. Found: C, 42.15; H, 4.24; N, 4.65%. Calcd for $C_{10}H_{12}Cl_3NO_2$: C, 42.20; H, 4.25; N, 4.92%.

From the slower moving zone, 2.01 g (30%) of IIb was obtained as colorless crystals, mp 47.5—48.0 °C. IR (CCl_4): 1708, 1270 cm^{-1}. MS: *m/e* 283 (small, M^+), 166 (M^+-CCl_3, 110%), 138 (18), 94 (36), 67 (33), 66 (40), 56 (51%), M: M+2: M+4: M+6=100: 100: 32: 4. Found: C, 42.31; H, 4.21; N, 4.71%. Calcd for $C_{10}H_{12}Cl_3NO_2$: C, 42.20; H, 4.25; N, 4.92%.

Reactions of I with Other 1,3-Dienes. A solution of 4 g of I and a large excess of 1,3-dienes in 10 ml of benzene was heated in a pressure bottle. Removal of the solvent and vacuum distillation gave oily products. Analytically pure samples were obtained by column chromatography (alumina, benzene).

IIIa was obtained from I and butadiene (100 hr at 115 °C, 55%); bp 126—127 °C/3 mmHg, $n_D^{24.0°}$ 1.5114. IR (neat): 1720 cm^{-1}. MS: *m/e* 271 (M^+, small), 154 (M^+-CCl_3, 100%), 126 (16), 108 (14), 82 (33), 80 (26), 54 (9%), M: M+2: M+4: M+6=100: 100: 31: 4. Found: C, 39.74; H, 4.51; N, 4.90%. Calcd for $C_9H_{12}Cl_3NO_2$: C, 39.66; H, 4.44; N, 5.14%.

IIIb was obtained from I and isoprene (80 hr at 100 °C, 75%); bp 125—127 °C/3 mmHg, $n_D^{25.0°}$ 1.5062. IR (neat): 1718 cm^{-1}. MS: *m/e* 285 (M^+, small), 168 (100%, M^+-CCl_3), 140 (15), 122 (10), 96 (25), 94 (19), 79 (10), 68 (10), 56 (19%), M: M+2: M+4: M+6=100: 100: 32: 4. Found: C, 42.10; H, 4.96; N, 4.80%. Calcd for $C_{10}H_{14}Cl_3NO_2$: C, 41.91; H, 4.92; N, 4.89%.

IIIc was obtained from I and 2,3-dimethylbutadiene (48 hr at 100 °C, 78%); bp 126—130 °C/3 mmHg, $n_D^{20.8°}$ 1.5074. IR (neat): 1720 cm^{-1}. MS: *m/e* 299 (M^+, 7%), 264 (13), 182 (M^+-CCl_3, 100), 154 (27), 136 (14), 110 (31), 108 (36), 93 (38), 67 (15), 56 (18%), M: M+2: M+4: M+6=100: 98: 31: 4.

The authors wish to thank Professors Hitosi Nozaki and Tyuzo Isida for help and encouragement.

BULLETIN OF THE CHEMICAL SOCIETY OF JAPAN, VOL. 46, 2924—2926 (1973)

The Novel Synthesis of Two Diastereomers of γ-Hydroxyproline[1)]

Yong Kyun LEE* and Takeo KANEKO**

Department of Chemistry, Faculty of Science, Osaka University, Toyonaka, Osaka 560

(Received May 1, 1973)

L-γ-Hydroxyproline is known as a component amino acid of limited proteins such as gelatine or collagen. Although several synthetic routes had been studied by many researchers, no satisfactory methods have been developed yet in view of the yield of the product and of the separation of two diastereomers formed. As far as literatures were concerned, γ-hydroxyproline had been synthesized through either 2-amino-5-halogeno-4-valerolactone[2-8)] or 2-halogeno-5-amino-4-valerolactone[9)] starting from epichlorohydrin. Alternatively, it had been also synthesized through 2,5-dichloro-4-valerolactone from either epichlorohydrin or alkyl halide.[10,11)] In every case, comparable amounts of racemic diastereomers, *i.e.*, DL- and DL-*allo*-γ-hydroxyproline have been formed. When these mixtures were attempted to be separated each other through their copper complexes, the purification of the more soluble DL-*allo* complex met often difficulty, though the less soluble DL-complex has been obtained in relatively pure state.

The authors found now a new synthetic method to lead to γ-hydroxyproline from 2-amino-5-bromo-4-valerolactone hydrobromide which was obtained as a diastereomeric mixture in good yield by heating 2,3-dibromopropylacetamidomalonate with hydrobromic acid. This mixture was readily separable from aqueous solution due to the difference in solubilities. This improvement in the synthetic route established a new way through which DL- and DL-*allo*-γ-hydroxyproline are available both in pure states.

Thus, diethyl acetamidomalonate (I) was condensed with equimolar allyl bromide (II) using sodium

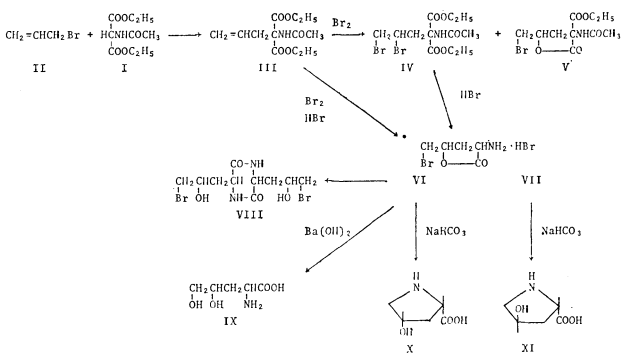

Fig. 1. Synthetic route for γ-hydroxyproline.

* Present address: Department of Polymer Engineering, Hanyang University, Seoul, Korea.

** Present address: Shiseido Laboratories, Nippa-cho, Kohoku-ku, Yokohama.

1) This work was presented at the 10th Annual Meeting of the Chemical Society of Japan, Tokyo, April, 1957.
2) H. Leuchs, *Ber.*, **38**, 1937 (1905).
3) E. Hammarsten, *C. R. Trav. Iab. Carlsberg*, **11**, 223 (1916).
4) V. V. Feofilaktov, A. S. Onishchenko, *Co. R. Acad. Sci. U. R. S. S.*, **20**, 133 (1938).
5) F. McIlwain, G. M. Richardson, *Biochem. J.*, **33**, 44 (1939).
6) J. Capkova-Jirků, J. V. Kostir, M. Vondracek, *Chem. Listy*, **44**, 19 (1950).
7) R. Gaudry, L. Berlinguet, A. Langis, G. Paris, *Can. J. Chem.*, **34**, 502 (1956).
8) T. Wieland, U. Wintermeyer, *Chem. Ber.*, **90**, 1721 (1957).
9) W. Traube, R. Johow, W. Tepohl, *Ber.*, **56**, 1861 (1923).
10) H. Leuchs, M. Giua, J. F. Brewster, *ibid.*, **45**, 1960 (1912).
11) R. Gaudry, C. Godin, *J. Amer. Chem. Soc.*, **76**, 139 (1954).

alkoxide in absolute ethanol according to the method of Albertson.[12] To the resulting allylacetamidomalonate (III), bromine was added in absolute ether to afford crystals of dibromo compound (IV). When the mother liquor thus obtained was kept for long time, 5-bromo-4-valerolactone derivative (V) was crystallized out slowly. The bromination in chloroform or carbon tetrachloride resulted in an improved yield of V but not that of IV. When the dibromo compound IV was hydrolyzed with hydrobromic acid, a mixture of two racemic diastereomers of 2-amino-5-bromo-4-valerolactone hydrobromide was obtained in good yield. This mixture was separated successfully into a less soluble isomer (VI) and a more soluble isomer (VII) from aqueous solution. The mixture of VI and VII could be also obtained in satisfactory yield even when the bromination product was hydrolyzed directly without separation of IV. The amount ratio of VI and VII in any mixtures thus obtained was always close to 1:1.

The treatment of the less soluble salt VI with pyridine gave the dioxopiperazine (VIII) composing of two molecules of 5-bromo-4-hydroxy-2-aminovaleric acid, the structure of which was confirmed by elemental analyses and IR spectrum: ν_{max}, 3210 and 3050 cm^{-1} (NH), 1637 cm^{-1} (NHCO).

Table 1. Formation of DL-allohydroxyproline and DL-γ-hydroxyproline from 2-amino-5-bromo-4-valerolactone (VI, VII)

Basic reagent	Reaction		Yield (%)	
	Temp. (°C)	Time (hr)	DL-*allo* (from VI)	DL (from VII)
28% Aqueous ammonia	100	5	30	20
Ammonia (Saturated in abs. CH_3OH)	40	5	72	42
$NaHCO_3$(10% aq. sol.)	90	1	80	46
$Ba(OH)_2$ (0.2N sol)	100	2	54	30—35

For conversion of the aminobromolactone hydrobromide (VI or VII) into γ-hydroxyproline, various basic reagents, were examined as shown in Table 1. Among these reagents, sodium hydrogen carbonate gave best result giving 55% overall yield of hydroxyproline from I. When barium hydroxide was used in the above reaction, a compound giving deep purple color with ninhydrin and a positive test with periodic acid, was obtained. The structure of this compound was deduced to 2-amino-4,5-dihydroxyvaleric acid (IX) from its elemental analysis in addition to the properties mentioned above. From the less soluble salt (VI), very pure DL-*allo*-hydroxyproline was obtained solely, while the more soluble salt (VII) gave DL-hydroxyproline after purification of its crude material through copper complex.

According to the conventional method for separation of the final synthetic product, γ-hydroxyproline, through copper complex, it was difficult to secure the pure *allo* compound. The present method has advantage of ease of separation of DL-*allo*-γ-hydroxyproline in very pure form and also of DL-γ-hydroxyproline due to the less solubility of its copper complex. The stereochemistries of the lactone VI and VII were unambiguously deduced from those of hydroxyproline that was derived from each compound. Thus orientation of amino and bromomethyl groups must be *cis* in VI and *trans* in VII.

12) N. F. Albertson, *ibid.*, **68**, 450 (1946).

Experimental

All melting points are uncorrected.

Ethyl 2-Acetamido-4,5-dibromo-2-ethoxycarbonylvalerate (IV). To a solution of 5 g of diethyl allylacetamidomalonate[12] (III) in 40 ml of absolute ether, 3.5 g of bromine was added dropwise at −10—−15 °C for 1 hr. The reaction mixture was stirred at −10 °C for another 2 hr and then at 0 °C for 2 hr. Ether was removed under reduced pressure. The residue was triturated with a small amount of water to give crystals of IV. These were filtered and recrystallized from 90% aqueous ethanol, yield 5.4 g (67%), mp 83—84 °C.

Found: C, 34.63; H, 4.42; N, 3.32; Br, 38.44%. Calcd for $C_{12}H_{19}O_5NBr_2$: C, 34.55; H, 4.59; N, 3.36; Br, 38.32%.

2-Acetamido-5-bromo-2-ethoxycarbonyl-4-valerolactone (V). When the mother liquor from IV was kept for two weeks, crystals of V appeared. The crystals were filtered and recrystallized twice from 50% aqueous ethanol, mp 141—142 °C.

Found: C, 39.29; H, 4.48; N, 4.41; Br, 27.53%. Calcd for $C_{10}H_{14}O_5NBr$: C, 38.98; H, 4.58; N, 4.55; Br, 25.94%.

2-Amino-5-bromo-4-valerolactone Hydrobromide (VI and VII). *Method A*: The compound IV (30 g) was refluxed with 48% hydrobromic acid for 4 hr. Hydrobromic acid was removed by evaporation under reduced pressure. After the residue was kept in a refrigerator overnight, a solid mixture of VI and VII was filtered, yield 19 g (95%). It was dissolved in 5 ml of hot water and kept in a refrigerator overnight. The crystals of VI were separated out. These were filtered and washed with little acetone, yield 8 g. A solution of these crystals in 60 ml of methanol was treated with charcoal, and then concentrated to about 15 ml. Crystals formed were filtered and recrystallized from methanol, mp 244 °C (decomp.).

Found: C, 21.68; H, 3.30; N, 5.04; Br, 57.98%. Calcd for $C_5H_9O_2NBr_2$: C, 21.84; H, 3.30; N, 5.09; Br, 58.13%.

The mother liquor from VI was concentrated under reduced pressure. After addition of acetone, the solution was set aside for a few days to recover further crops of VI. However, easy soluble salt VII could not be obtained in crystalline state from the filtrate by this procedure.

Method B: To a solution of 20 g of III in 40 ml of chloroform, a solution of 15 g of bromine in 15 ml of chloroform was added at 20 °C with stirring for 1 hr. The stirring was continued for another 2 hr. Chloroform was removed under reduced pressure. To the syrupy residue obtained, 150 g of 48% hydrobromic acid was added. After refluxing for 3 hr, the solution was evaporated under reduced pressure and then cooled. The resulting crystals were filtered off to afford 19.6 g (92%) of a mixture of VI and VII hydrobromides. Through the treatment of the mixture as in the method A, 9.4 g of the less soluble salt VI in crystalline state, mp 222 °C (decomp.) and 9 g of the more soluble salt VII as syrup were obtained.

2,4-Bis(3-bromo-2-hydroxypropyl)-3,6-dioxopiperazine (VIII). Into a solution of 500 mg of VI in a small amount of water, 0.2 g of pyridine was added and the reaction mixture was allowed to stand at room temperature overnight. A crys-

talline product was separated out, mp 183 °C (decomp.). After recrystallization from water, the melting point raised up to 186 °C (decomp.).

Found: C, 31.06; H, 4.20; N, 7.02; Br, 40.45%. Calcd for $C_{10}H_{16}O_4N_2Br_2$: C, 30.95; H, 4.16; N, 7.22; Br, 41.19%.

Hydrolysis of VI and VII. *a) By Aqueous Ammonia*: A mixture of 5 g of the less soluble salt VI and 110 ml of 28% aqueous ammonia was heated at 90—100 °C in a pressure bottle for 5 hr and then kept at room temperature for 24 hr. The ammonia and water were removed under reduced pressure and 30 ml of concentrated hydrochloric acid was added into the residue. The solution was heated at 80—90 °C for 1.5 hr and then evaporated under reduced pressure to obtain a syrupy residue. A solution of the residue in a small amount of water was made alkaline to phenolphthalein with 1M sodium hydroxide and then heated for about 10 min. After cooling, the solution was acidified with 1M hydrochloric acid and evaporated under reduced pressure. The inorganic materials were removed by treating several times with ethanol and finally with silver carbonate. The syrupy residue was crystallized from water and ethanol to give DL-*allo*-γ-hydroxyproline (X), yield 0.7 g, mp 238 °C (decomp.). Found: C, 45.99: H, 6.65; N, 10.44%. Calcd for $C_5H_9O_3N$: C, 45.79; H, 6.92; N, 10.68%.

The more soluble salt VII (5 g) was treated like as mentioned above. The resulting syrupy residue was dissolved in 50 ml of water and heated with cupric carbonate for 1 hr giving sky-blue copper complex, yield 1.5 g. A suspension of the copper complex in water was treated with hydrogen sulfide. The filtrate from copper sulfide was evaporated to the residue which was crystallized from water and ethanol giving pure DL-γ-hydroxyproline (XI), yield 0.5 g (20%), mp 246 °C (decomp.). Found: C, 45.80; H, 6.87; N, 10.69%

2-Amino-4,5-dihydroxyvaleric Acid (IX) A solution of 5 g of VI in 200 ml of 0.2N barium hydroxide was heated in a boiling water bath for 2 hr. From the hydrolyzate X was separated by usual way. The mother liquor from X was treated with cupric carbonate and the precipitate was recrystallized from water and ethanol to give a sky-blue copper complex. This copper compound was treated with hydrogen sulfide and filtered. The filtrate was evaporated and the residue was crystallized from water and ethanol giving IX, yield 0.7 g. This was recrystallized from 50% aqueous ethanol twice, mp 105 °C (decomp. at 175 °C).

Found: C, 36.10; H, 7.53; N, 8.19; H_2O, 9.15%. Calcd for $C_5H_{11}O_4N \cdot H_2O$: C, 35.92; H, 7.84; N, 8.38; H_2O, 10.78%.

BULLETIN OF THE CHEMICAL SOCIETY OF JAPAN, VOL. 46, 2926—2928 (1973)

Thiocyanoacetate. V. Reaction of Thiocyanoacetic Esters with Aromatic Aldehydes in the Presence of Potassium Acetate[1]

Satoshi KAMBE*

The Institute of Physical and Chemical Research, Wako-shi, Saitama 351

(Received October 21, 1972)

In the course of studies on the reaction of thiocyanoacetic ester (**1**) with aldehydes, it was found that the base as a catalyst might have some distinct effect on the nature of the reaction.[1,2] For the confirmation the author has investigated the effects of potassium acetate–acetic acid system on the reaction course.

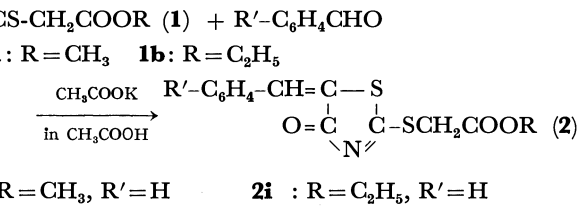

Scheme 1.

The reaction of **1** with aromatic aldehydes was carried out in an acetic acid containing potassium acetate, direct synthesis of 1,3-oxathiolan-2-one derivatives being expected.

However, an unexpected acid-unstable crystalline product was obtained upon the treatment of **1b** with benzaldehyde in acetic acid containing potassium acetate. The structure of 5-benzylidene-2-ethoxycarbonylmethylthio-1,3-thiazolin-4-one (**2i**) was indicated by elemental analysis, IR, NMR, and mass spectra. **2i** was identical with an authentic sample prepared from 5-benzylidene-1,3-thiazolidine-2-thione-4-one (**3**) and ethyl chloroacetate with sodium ethoxide in ethanol.

On the other hand, **2i** is readily hydrolyzed with hydrochloric acid to yield 5-benzylidene-1,3-thiazolidine-2,4-dione (**4**).[3] Furthermore, **1b** reacted easily with ethyl thioglycollate (**5**) in acetic acid containing potassium acetate to give 2-ethoxycarbonylmethylthio-1,3-thiazolin-4-one (**6**), which gave **2i** in the reaction

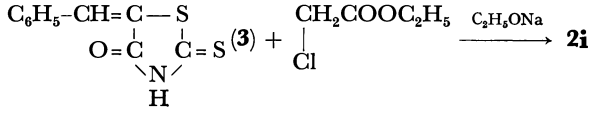

Scheme 2.

* Present address: Oyama Technical College, Oyama-shi, Tochigi.

1) Part IV of this series: S. Kambe and T. Hayashi, This Bulletin, **45**, 3192 (1972).

2) S. Kambe, T. Hayashi, H. Yasuda, and H. Midorikawa, *ibid.*, **44**, 1357 (1971).

3) S. Kambe, T. Hayashi, H. Yasuda, and A. Sakurai, *Nippon Kagaku Zasshi*, **92**, 867 (1971).

Table 1. Properties and analyses of product **2**

Product 2	Reac. time (hr)	Yield (%)	Mp °C	Formula	Analysis (%) Found (Calcd) C	H	N	S	IR spectrum (cm^{-1}) ester C=O	ring C=O	C=N	C=C
a	5	54	139—140	$C_{13}H_{11}O_3NS_2$	53.24 (53.24)	3.77 (3.78)	4.45 (4.78)	21.69 (21.82)	1750 s	1710 s	1610 m	1600 w
b	7	41	147—149	$C_{14}H_{13}O_4NS_2$	52.31 (52.02)	4.42 (4.05)	4.38 (4.33)	19.82 (19.79)	1740 s	1690 s	1590 s	1550 w
c	6	38	162—163	$C_{14}H_{13}O_4NS_2$	52.21 (52.02)	4.19 (4.05)	4.35 (4.33)	19.82 (19.79)	1740 s	1700 s	1590 s	1560 w
d	5	31	151—152	$C_{13}H_{10}O_3NS_2Cl$	47.91 (47.60)	3.10 (3.05)	4.30 (4.27)	19.62 (19.53)	1740 s	1700 s	1600 m	1580 w
e	4	28	156—157	$C_{13}H_{10}O_3NS_2Cl$	47.71 (47.60)	3.09 (3.05)	4.31 (4.27)	19.82 (19.53)	1740 s	1700 s	1610 m	1590 w
f	7	33	152—153	$C_{13}H_{10}O_5N_2S_2$	46.24 (46.12)	2.80 (2.95)	8.31 (8.27)	19.18 (18.90)	1740 s	1710 s	1600 m	1570 w
g	6	22	199—201	$C_{13}H_{11}O_4NS_2$	50.50 (50.49)	3.62 (3.59)	4.60 (4.53)	20.72 (20.69)	1740 s	1700 s	1600 m	1580 w
h	7	43	164—166	$C_{14}H_{13}O_3NS_2$	54.87 (54.72)	4.32 (4.26)	4.61 (4.56)	20.78 (20.82)	1740 s	1700 s	1600 m	1570 sh
i	6	52	138—139	$C_{14}H_{13}O_3NS_2$	54.68 (54.72)	4.25 (4.26)	4.62 (4.56)	21.20 (20.82)	1730 s	1700 sh	1600 m	1570 w
j	5	43	127—128	$C_{15}H_{15}O_4NS_2$	53.51 (53.41)	4.50 (4.48)	4.20 (4.15)	19.01 (18.97)	1740 s	1690 s	1590 m	1570 sh
k	6	50	130—131	$C_{15}H_{15}O_4NS_2$	53.52 (53.41)	4.49 (4.48)	3.99 (4.15)	18.69 (18.97)	1730 s	1700 s	1600 s	1570 w
l	6	45	158—159	$C_{14}H_{12}O_3NS_2Cl$	49.09 (49.15)	3.56 (3.51)	4.07 (4.09)	21.62 (21.82)	1740 s	1700 s	1600 s	1580 w
m	6	42	153—154	$C_{14}H_{12}O_3NS_2Cl$	49.13 (49.15)	3.51 (3.51)	4.17 (4.09)	21.99 (21.82)	1730 s	1710 s	1600 m	1590 m
n	5	40	138—139	$C_{14}H_{12}O_5N_2S_2$	47.75 (47.73)	3.49 (3.43)	8.00 (7.95)	18.24 (18.16)	1730 s	1710 s	1610 m	1570 sh
o	5	30	203—204	$C_{14}H_{13}O_4NS_2$	52.45 (52.02)	4.36 (4.05)	4.41 (4.33)	19.81 (19.79)	1740 s	1710 s	1610 m	1570 w
p	5	45	163—164	$C_{15}H_{15}O_3NS_2$	56.05 (56.07)	4.72 (4.71)	4.36 (4.36)	19.52 (19.92)	1740 s	1700 s	1600 s	1570 sh

with benzaldehyde in acetic acid containing potassium acetate.

1,3-Thiazolin-4-one derivatives (**2**) could be obtained by the reaction of **1** with other aldehydes. The results are summarized in Table 1. **1** might be led to mercaptoacetate (**5**) in the presence of potassium acetate, since thiocyanates are converted into mercaptanes when treated with basic reagents.[4] The reaction of **1b** with benzaldehyde in acetic acid without using potassium acetate gave only product **4** in poor yield. Heintz[5] and Klason[6] reported that 1,3-thiazolidine-2,4-dione was obtained when **1** was treated with acid.

$$HSCH_2COOC_2H_5\ (\mathbf{5}) + \mathbf{1b} \xrightarrow[\text{in } CH_3COOH]{CH_3COOK} \underset{\mathbf{(6)}}{O{=}C(N)C{-}S{-}CH_2COOC_2H_5}$$

$$\mathbf{6} + C_6H_5CHO \xrightarrow[\text{in } CH_3COOH]{CH_3COOK} \mathbf{2i}$$

Scheme 3.

Accordingly, it seems that **1b** was hydrolyzed with acetic acid, yielding the 1,3-thiazolidine-2,4-dione which is then condensed with benzaldehyde to give **4**.

A reaction pathway is postulated in Scheme 4.

$$\mathbf{1} \xrightarrow{CH_3COOK} \mathbf{5} \xrightarrow{(1)} \mathbf{6} \xrightarrow{R'\text{-}C_6H_4CHO} \mathbf{2}$$

Scheme 4.

Experimental

All the melting points are uncorrected. IR spectra were measured with a Shimadzu IR-27G spectrophotometer in KBr pellets. NMR spectra were determined in DMSO-d_6 with a JEOLCO JNM-C-60 high-resolution NMR spectrometer (60 MHz), using tetramethylsilane as an internal standard. Mass spectra were measured with a JMS-O1S instrument operating at 75 eV.

*Reaction of Thiocyanoacetate Ester (**1**) with Aromatic Aldehyde. Procedure.* A mixture of **1** (0.04 mol), aromatic aldehyde (0.02 mol) and potassium acetate (2 g) in acetic acid (15 ml) was stirred at 90—100 °C,[7] and then poured into crushed ice with vigorous stirring. The resulting precipitates were collected, washed with ether and recrystallized from ethanol. The yield and properties are summarized in Table 1. NMR (δ): **2a**; 4.00 (OCH_3), 4.50 (SCH_2), 7.55 (C_6H_5), and 8.30

4) J. W. Dienske, *Rec. Trav. Chim. Pays-Bas*, **50**, 21 (1931).
5) W. Heintz, *Ann.*, **136**, 232 (1865).
6) P. Klason, *Ber.*, **10**, 1350 (1877).
7) Reaction times in each case are indicated in Table 1.

(=CH). **2i**; 1.40 (CH_3), 4.50 (OCH_2), 4.60 (SCH_2), 6.50 (C_6H_5), and 8.45 (=CH). MS spectrum: **2i** (relative abundance); *m/e* 307 (87), 262 (24), 234 (11), 188 (8), 161 (39), 133 (100), and 101 (30). NMR and MS data of other compounds are deleted.

Reaction of 5-Benzylidene-1,3-thiazolidine-2-thione-4-one (3) with Ethyl Chloroacetate. To a solution of **3** (0.01 mol) in absolute ethanol (30 ml) containing metallic sodium (0.3 g) was added ethyl chloroacetate (0.01 mol), and the solution was stirred for 15 hr under gentle reflux. The sodium chloride thus precipitated was then filtered out. After the filtrate had been left to stand overnight, crystalline matter was separated which was collected and washed with water. Recrystallization from ethanol gave **2i**; yield 23%, mp 138—139 °C. Unreacted **3** was recovered from the filtrate of **2i**.

Reaction of Ethyl Thiocyanoacetate (1b) with Ethyl Thioglycollate (5). To a mixture of **1b** (0.02 mol) and potassium acetate (0.02 mol) in acetic acid (15 ml) was added dropwise **5** (0.02 mol) with stirring. The raection temperature was maintained at 25—30 °C. After completion of addition, stirring was continued for 10 hr. The reaction mixture was poured into water with vigorous stirring. The resulting precipitate was filtered and washed with ether. Recrystallization from CCl_4 gave **6**; yield 60%; mp 78—79 °C. IR (cm^{-1}): 1750 (O–C=O) and 1700 (C=O). NMR (δ): 1.35 (CH_3), 4.40 (OCH_2), 4.45 (ring CH_2), and 4.60 (SCH_2). Found: C, 38.11; H, 4.06; N, 6.39; S, 29.20%. Calcd for $C_7H_9O_3S_2N$: C, 38.36; H, 4.14; N, 6.39; S, 29.20%.

Reaction of 2-Ethoxycarbonylmethylthio-1,3-thiazolin-4-one (6) with Benzaldehyde. A solution of **6** (5 mmol) and benzaldehyde (5 mmol) in acetic acid (10 ml) containing potassium acetate (5 mmol) was refluxed for 2 hr. After cooling, the solution was poured into water and allowed to stand for several hours. The solid product (**2i**) precipitated was recrystallized from ethanol; yield 48%, mp 138—139 °C.

Hydrolysis of **2i**. To ethanol (5 ml) containing concd. hydrochloric acid (15 ml) was added **2i** (5 mmol). The mixture was refluxed for 2 hr and then cooled to room temperature. Deposited solid product (**4**) was recrystallized from ethanol; yield 32%; mp 239—240 °C (lit,[3] 239—240 °C).

Reaction of Ethyl Thiocyanoacetate (1b) with Benzaldehyde in Acetic Acid. A solution of **1b** and benzaldehyde in acetic acid (10 ml) was refluxed for 15 hr. The reaction mixture, on cooling, was poured onto cracked ice. The crystalline matter thus formed was collected and washed with ether. Recrystallization from ethanol gave **4**; yield 0.5%; mp 239—240 °C.

The author wishes to express his thanks to Dr. Hiroshi Midorikawa, Dr. Heinosuke Yasuda, and Mr. Toshio Hayashi for their helpful discussions and encouragement. Thanks are also due to Dr. Haruo Homma and his staff for the microanalyses.

The ESR Study of the Interaction of O_2 with Ag Dispersed on Silica Gel

Natsuko SHIMIZU, Kazuo SHIMOKOSHI, and Iwao YASUMORI

Department of Chemistry, Tokyo Institute of Technology, O-okayama, Meguro-ku, Tokyo 152

(Received January 31, 1973)

The state of adsorbed oxygen on metallic silver dispersed on silica gel has been studied by ESR. The spectra observed by the interaction of oxygen and the surface were found to be composed of spectra due to two different species. One of the species, which was formed separately by the contact with oxygen at −110 °C, was identified with O_2^- chemisorbed on metallic silver by a comparison of the observed g values and the other features with those previously reported. The other species has a doublet at $g=2.036$. This spectrum was reproduced by the interaction of N_2O with the silver surface. Further, the γ-irradiation of the silver samples in the presence of O_2 and N_2O markedly enhanced the intensity of this spectrum, showing a low-field hump. On the basis of the g values and the splitting of the high-field doublet, assuming that the doublet is due to the hyperfine interaction of an unpaired electron with the silver nucleus, the species was assigned to Ag^{2+} in the present system. It is postulated that this species is possibly formed by the dissociative and/or charge-transfer chemisorption of O_2 and N_2O, suggesting the presence of non-paramagnetic oxygen species, such as O^{2-}, as a counter ion of Ag^{2+}.

It is of importance to investigate the nature of adsorbed oxygen on silver because of its interesting behavior in the catalytic oxidation of ethylene. Recently Clarkson and Cilliro[1] have reported the ESR observation of O_2^- chemisorbed on a metallic silver surface supported by Vycor glass, together with the reactivity of the O_2^- with CO. However, the nature of the adsorbed states of oxygen has not yet been satisfactorily elucidated, since various forms of adsorbed oxygen have been suggested to be present on the silver surface.[2-5] The work of the present paper was initiated to investigate the catalytic activity of metallic silver in the oxidation of olefins by means of electron spin resonance spectroscopy (ESR).

In the present study we found ESR evidence for the presence of two kinds of oxygen species adsorbed on metallic silver dispersed on silica gel; we then incorporated our results with those of experiments with the γ-irradiation of the silica gel samples.

On the other hand, the ESR spectra of γ-irradiated silica gel and the effects of some additives have been reported previously.[6-9] However, no ESR study of the effects of metallic adsorbates on the irradiation has yet been reported despite the relevance to radiation chemistry.[10,11] In the present paper we will also report on the effects of γ-irradiation on the ESR spectra.

Experimental

Silica gel was prepared by the hydrolysis of ethyl orthosilicate, followed by drying at 110 °C and heating at 450 °C in air. Ethyl orthosilicate was distilled several times before the hydrolysis. Silver was impregnated on silica gel from the solution of silver nitrate, followed by drying and heating as above. The concentrations of silver were in the range of 0.5—6.0 wt%. The samples were reduced with hydrogen of 40 Torr at 100 °C and then at 300 °C for 2 hours in each case. High-purity gases of H_2, O_2 and N_2O from the Takachiho Chemical Co. were used without further purification.

γ-Irradiation was carried out by exposure to ^{60}Co at room temperature. The dose was 1—2 Mrads. The ESR measurements were made by means of a JEOL JES-3BS-X spectrometer with 100 kHz modulation. All the spectra were recorded at −110 °C.

Results and Discussion

Figure 1 (a) shows the spectrum (A) ($g=1.98$, $\Delta H=175\pm5$G) observed in the sample of the dispersed silver (2 wt%) on the silica gel after reduction. The intensity of this signal increased with the amount of silver. As has been suggested by Nicolau *et al.*,[12] who observed the spectra in the systems of Pt and Pd supported on charcoal, this signal (A) may be attributed to the unpaired electron produced by the strong interaction of the silver with the silica gel surface.

When the silver samples were exposed to oxygen of 5 Torr at 26 °C, new spectra were observed, as is shown in Fig. 1 (b). By heating the samples to 200 °C, the spectra were changed; particularly, the lower-field shoulder increased and became distinct (Fig. 1 (c)). Therefore, the signal is possibly composed of spectra due to two different species. This was further confirmed by the following experiments. When oxygen came into contact with the silver samples at −110 °C and the spectra were recorded at the same temperature, only the B signal was observed as a new signal (Fig. 2 (a)). The lower-field pattern in Fig. 1 (c) was reproduced when the silver samples were exposed to N_2O (110 Torr) at room temperature for about 60 hours, as is shown in Fig. 2 (b).

From these results, it was concluded that the spectra in Figs. 1 (b) and (c) consist of three signals, A, B, and

1) R. B. Clarkson and A. C. Cilliro, Jr., *J. Vac. Sci. Techn.*, **9**, 1073 (1972).
2) A. I. Kurilenko, N. U. Kul'kova, N. A. Rybakova, and M. I. Temkin, *Zhur. Fiz. Khim.*, **32**, 797; 1043 (1958).
3) L. Ya. Margolis, *Advan. Catal.*, **14**, 429 (1963).
4) P. D. Klugherz and P. Harriott, *A. I. Ch. E. J.*, **17**, 856 (1971).
5) R. E. Kenson and M. Lapkin, *J. Phys. Chem.*, **74**, 1493 (1970).
6) H. W. Kohn, *J. Chem. Phys.*, **33**, 1588 (1960).
7) V. B. Kazanskii, G. B. Pariiskii, and V. V. Voevodsky, *Discuss Faraday Soc.*, **31**, 203 (1961).
8) R. Haul, J. Karra, and J. Turkevich, *J. Amer. Chem. Soc.* **87**, 2092 (1965).
9) P. K. Wong and J. E. Willard, *J. Phys. Chem.*, **73**, 2226 (1969).
10) J. M. Caffrey, Jr., and A. O. Allen, *ibid.*, **62**, 33 (1958).
11) J. W. Sutherland and A. O. Allen, *J. Amer. Chem. Soc.*, **83**, 1040 (1961).
12) C. S. Nicolau, H. G. Thom, and E. Pobitschka, *Trans. Faraday Soc.*, **55**, 1430 (1959).

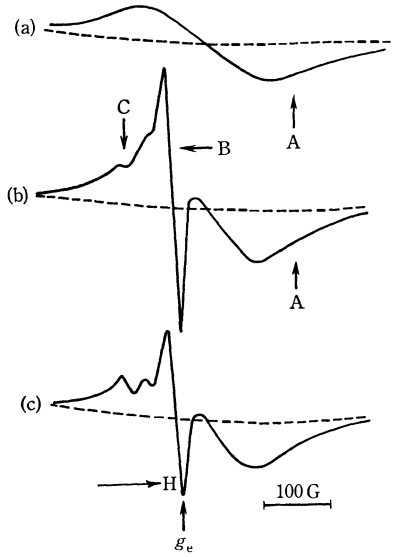

Fig. 1. Electron spin resonance spectra obtained after a) reduction of Ag dispersed silica gel, b) exposure of the Ag–SiO_2 to oxygen (5 Torr) at 26 °C, and c) heating at 200 °C in the presence of oxygen. All spectra were recorded at −110 °C. The broken line shows the signal from silica gel treated under the same conditions as the Ag–SiO_2 samples. g_e indicates the resonance field of free electron.

C. By evacuation at room temperature, the B signal decreased in its intensity, but after heating at 200 °C in the presence of oxygen the B signal became independent of the evacuation. The contact of O_2 and N_2O with the silica gel did not give any spectra of the surface species under the same conditions as those described for the silver samples.

The g tensors for oxygen species adsorbed on various surfaces have been reported.[13-14] According to the recent report by Clarkson and Cilliro,[1] the spectrum observed in the system of O_2–Ag supported on Vycor glass has been identified with that of O_2^-. The g values estimated from the B spectrum, which was obtained by subtracting the A and C signals from the observed spectra, were $g_{xx}=2.002\pm0.001$, $g_{yy}=2.010\pm0.001$, and $g_{zz}=2.040\pm0.005$. These g values, though they have some experimental error, are only reasonable for O_2^- as the oxygen species, and they are comparable to those reported by Setaka and Kwan.[14] Therefore, the B spectrum can be identified with that of O_2^-.

In order to obtain a definite assignment of these spectra, the γ-irradiations of silica gel and the silver samples were carried out. In the irradiations of the silver samples, the signals due to the paramagnetic centers formed by the irradiation, as is shown in Fig. 3, were observed in addition to the broad signal, A. The spectra were composed of a sharp and intense single line near $g=2.001$ and a number of lines due to other centers.

These spectra were essentially the same as those reported by Kazanskii *et al.*,[7] though the resolution and the relative intensity of each component were different. As may clearly be seen in Fig. 3, the spectra obtained by reducing the field modulation showed a number of lines which could not simply be identified, as has been done by Kazanskii *et al.*, with the center that couples with four equivalent protons on the surface. In the irradiation of silica gel itself, unlike the case with silver samples, the lines due to the surface centers were relatively intense compared to the sharp line. It has been suggested[7] that the sharp line can be assigned to the spectrum of the trapped electron in the bulk. Therefore, the fact that the relative intensity of the sharp line to the surface centers was larger in the irradiated silver samples than in the irradiated silica gel may suggest that the formation of the surface centers by the irradiation is hindered by the surface silver metal.

When the silver samples were irradiated in the presence of O_2 (5 Torr), in addition to the signals in Fig. 3 the B and C signals were observed with an increased intensity compared with those observed before the

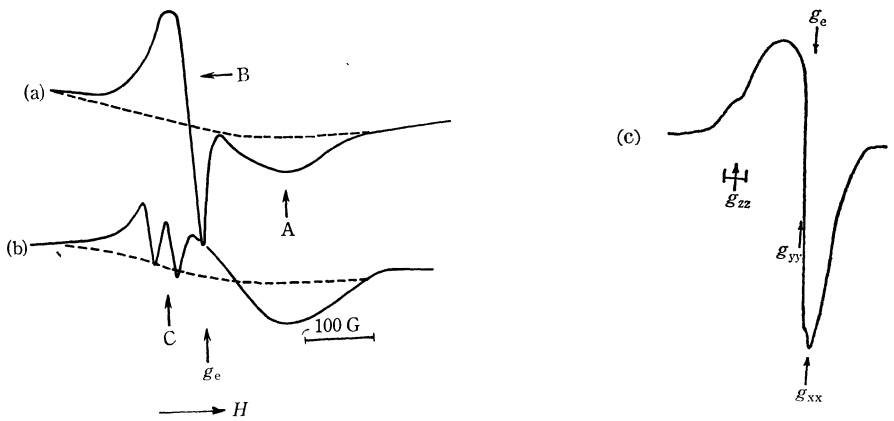

Fig. 2. Electron spin resonance spectra obtained after exposure of the Ag–SiO_2 samples to a) oxygen (5 Torr) at −110 °C, and b) nitrous oxide (110 Torr) at 26 °C for 60 hours. The spectra were recorded at −110 °C.
c) The spectrum obtained by subtracting the spectrum A from (a) in order to estimate the g- values of the spectrum B.

13) J. H. Lunsford and J. P. Jayne, *J. Chem. Phys.*, **44**, 1487 (1966).

14) M. Setaka and T. Kwan, This Bulletin, **43**, 2727 (1970).

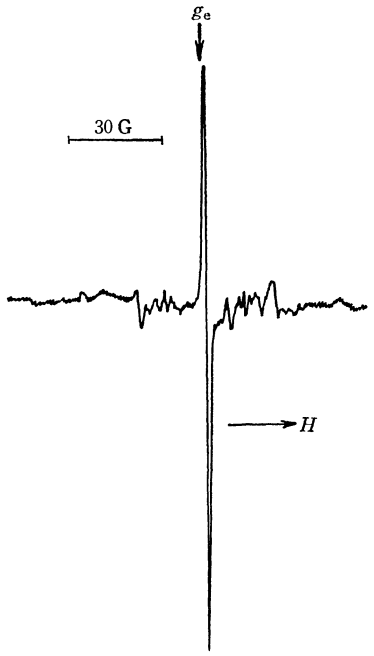

Fig. 3. Electron spin resonance spectrum obtained after γ-irradiation of the Ag–SiO_2 samples at 26 °C, and recorded at −110 °C.

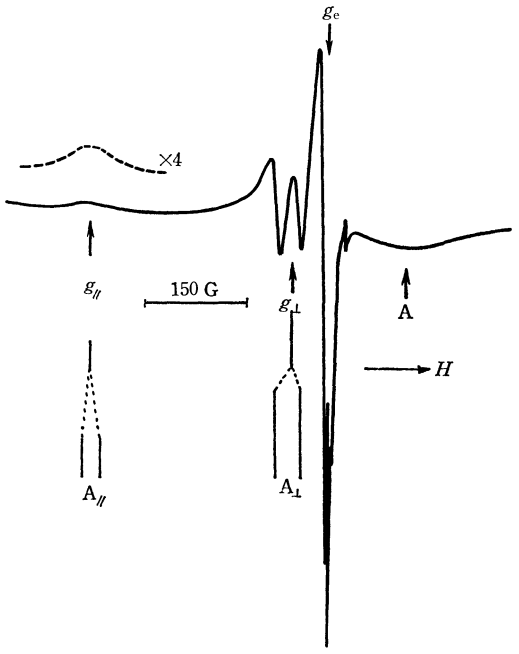

Fig. 4. Electron spin resonance spectrum obtained after γ-irradiation of the Ag–SiO_2 sample at 26 °C in the presence of O_2. The stick diagram indicates our assignment for the g and A of Ag^{2+}. The broken line at extremity corresponds to a signal amplification of 4.0. $g_\perp$ and $g_{//}$ corresponds to the resonance fields of the perpendicular and parallel components. $A_\perp$ and $A_{//}$ are the hfs of silver nucleus in perpendicular and parallel components. The value from reference (16) is used for $A_{//}$.

irradiation. The intensity of the sharp signal decreased in the presence of O_2. This is, possibly, a result of the interaction between the electron trapped in the center and oxygen, this interaction forming O_2^-.[7] The spectra are given in Fig. 4. The γ-irradiation of

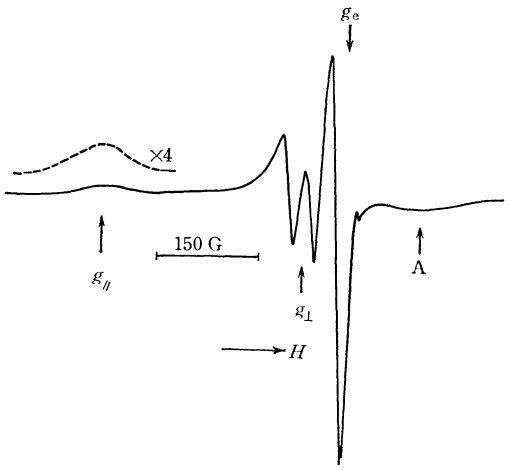

Fig. 5. Electron spin resonance spectrum obtained after γ-irradiation of the Ag–SiO_2 in the presence of nitrous oxide at 26 °C, and recorded at −110 °C.

the silver samples in the presence of N_2O (300 Torr) provided spectra almost identical with those obtained in the presence of O_2, as is shown in Fig. 5, though the intensity of B relative to C was slightly different.

The irradiation of the silica gel in the presence of O_2 and N_2O was also examined. A signal with a broad linewidth was observed upon the irradiation in the presence of O_2. The signal was similar to the B signal and has been assigned to the surface peroxide on silica gel[7] by Kazanskii. The irradiation of the silica gel with N_2O did not give the broad line, unlike the results of the irradiation of the silver samples. Further, it was found that the intensity of the surface peroxide was decreased to about 55% by warming the samples from −110 °C to 25 °C, while that of the B signal was decreased to about 35%. Therefore, the spectra obtained in the irradiation of the silver samples with O_2 and N_2O are not likely to be the surface peroxide on the silica gel, though the simultaneous formation of the surface peroxide can not be excluded in the irradiation of the silver sample with O_2. Consequently, the formation of O_2^- on the surface of the silver samples is the result of the interaction of O_2 not with silica gel, but with the metallic silver dispersed on silica gel.

In the identification of the C signal, assuming that the low-field hump, which becomes distinct by γ-irradiation, shows the parallel component of C, and that the doublet at g=2.036 is due to the hyperfine splitting, the magnetic parameters of this signal were

Table 1. ESR parameters for Ag^{2+}

$\mathbf{A}_\perp$ (G)	32±1	—	31.6
$\mathbf{A}_{//}$ (G)	—	25±3	48.0
$g_\perp$	2.036	—	2.065
$g_{//}$	2.249	2.233	2.265
Reference	This work	16)	15)[a]

a) The values were obtained from the spectra of Ag^{2+} formed in frozen acid solution at 77 K.

estimated to be as listed in Table 1. This was further confirmed by the fact that the intensity ratios of the high-field doublet to the low-field hump were constant in different experimental run with a variety of dosages. Since these values are almost equivalent with those of Ag^{2+} which have been reported by McMillan and Smaller,[15] the C signal can be identified with that of Ag^{2+} in the present system, though the poor resolution of the spectrum made it difficult to measure the splitting in the parallel component. More recently, Starkie and Symons[16] have reported their observation of Ag^{2+} trapped on silica gel formed by the γ-irradiation of the silica gel samples, which were integrated with an alcoholic solution of silver nitrate. The spectra of Ag^{2+} were only obtained in samples which had been dried for a long time *in vacuo*, while the irradiation of the wet samples provided the spectra of atomic silver. The magnetic parameters reported are also listed in Table 1.

The observation of Ag^{2+} in the present system suggests that there is a particular state of adsorbed oxygen which stabilizes Ag^{2+} by abstracting electrons from Ag. In the case of N_2O adsorption without the irradiation, though Ag^{2+} was obtained, the spectrum of O_2^- was not observed. Therefore, Ag^{2+} may be formed by the interaction with the electron-accepting species such as O_2 and N_2O, forming non-paramagnetic oxygen species such as O^{2-} as a counter ion of Ag^{2+}.

The observation of the O_2^- spectrum in the irradiation of the N_2O-silver sample can be explained if one takes into consideration the possibility that the molecular oxygen is produced by the catalytic[17] or radiolytic decomposition of N_2O by the irradiation on the silver surface.

In addition, the reactivity with ethylene of these oxygen species adsorbed on the silver surface was examined. The results obtained preliminarily showed that, when ethylene (5 Torr) was added to the silver samples, showing the B and C spectra, at 200 °C for 4 hours, the C spectrum was gradually decreased and the B spectrum disappeared. From the present results, it is not sufficient to conclude the participation of those oxygen species in the epoxidation reaction of ethylene. However, it is evident that the species identified with O_2^-, and Ag^{2+}, which was possibly formed accompanied by non-paramagnetic oxygen species, can react with ethylene.

In the present experiments we have for the first time observed Ag^{2+}, which may be formed by the interaction of metallic silver with such electron-accepting species as O_2 and N_2O. As a counter ion of Ag^{2+}, we postulated the presence of non-paramagnetic species such as O^{2-} [2] which may be formed by the dissociative adsorption of O_2 and N_2O. The presence of O_2^- on the surface of metallic silver was confirmed.

15) J. A. McMillan and B. Smaller, *J. Chem. Phys.*, **35**, 1698 (1961).
16) H. C. Starkie and M. C. R. Symons, *J. Phys. Chem.*, **75**, 2705 (1971).
17) W. Herzog, *Ber. Bunsenges. Physik. Chem.*, **74**, 216 (1970).

BULLETIN OF THE CHEMICAL SOCIETY OF JAPAN, VOL. 46, 2932—2936 (1973)

ESR Studies of the Cation Radicals Produced by $SbCl_5$ Oxidation of Some Biphenyls with *ortho-* and *para*-Dialkyl Substituents

Kazuhiko Ishizu, Muneki Ohuchi, Fujito Nemoto, and Masao Suga

**Department of Chemistry, Faculty of Science, Ehime University, Bunkyo-cho, Matsuyama 790*

(Received February 8, 1973)

The cation radicals of some alkylbiphenyls such as 4,4′-bitolyl, 4,4′-di-*t*-butylbiphenyl, and 2,2′, 4,4′, 6,6′-bimesityl, were generated by $SbCl_5$ oxidation in CH_2Cl_2. The ESR observation was carried out, and the Q values of the methyl and *t*-butyl were estimated based on either the theoretical spin density or the experimentally-determined spin density from the ^{13}C-hyperfine splitting. The Q value of the methyl in the cation radical was found to be 1.5 times that for the anion radical. The *t*-butyl groups of the cation radical also showed a much larger Q value than that for the anion radical. The perturbation of the spin density due to the steric hindrance was investigated with reference to the prediction of the McLachlan's MO calculations carried out for the hindered biphenyl. The experimentally-determined spin density derived from the Q value established for the *para*-derivative can be adequately interpreted on the assumption that the planar character of the biphenyl would be much reduced, contrary to the tendency found for the anion radicals. This effect suggests that a different delocalization of the unpaired electron may be expected between the cation and the anion radical: that is, the unpaired electron brings about a fair bonding on the central 1–1′ bond in the anion radical, but an antibonding for the cation radical, because the odd π-orbital of the cation has its node between the central 1–1′ bond.

The oxidation of aromatic hydrocarbons with $SbCl_5$ in CH_2Cl_2 is now one of the standard methods for preparation of the cation radicals in solution.[1] There have been numerous ESR studies of the aromatic cation radicals, which have often provided a useful test of molecular orbital theories. In the previous papers, we have reported several studies of the alkyl biphenyl anion radicals;[2-5] we hoped to compare the alkyl proton splitting with that of the cation radicals in order

1) I. C. Lewis and L. S. Singer, *J. Chem. Phys.*, **43**, 2712 (1965).
2) K. Ishizu, This Bulletin, **36**, 938 (1963).
3) K. Ishizu, *ibid.*, **37**, 1093 (1964).
4) K. Ishizu, H. Hasegawa, H. Chikaki, H. Nishiguchi, and Y. Deguchi, *Kogyo Kagaku Zasshi*, **68**, 1522 (1965).
5) K. Ishizu, K. Mukai, H. Hasegawa, K. Kubo, H. Nishiguchi, and Y. Deguchi, This Bulletin, **42**, 2808 (1969).

to demonstrate the importance of the hyperconjugation mechanism in these derivatives. The ESR studies of the *ortho*-derivatives would be attractive, because the conformational change in the biphenyl ring can be elucidated by an investigation of the steric hindrance observed for the cation radical and the anion radical.

In the present paper, we wish to report the results of ESR studies of the cation radicals generated by the usual $SbCl_5$ oxidation of some alkyl biphenyls, such as 4,4′-bitolyl, 4,4′-di-*t*-butylbiphenyl, and 2,2′, 4,4′,6,6′-bimesityl. The alkyl proton splitting was determined and the splitting parameters, Q^R, of the methyl and *t*-butyl groups were calculated on the basis of McLachlan's spin density for the ring carbon atoms. The twisting angle between the two phenyls was estimated with reference to the theoretical spin density of the hindered biphenyl. The experimentally-determined spin density for the cation radical was compared with that for the anion radical, and we will present new experimental evidence that the presence of the unpaired electron in the frontier orbital actually plays an important role in causing a large modification of the conformation of biphenyl.

Experimental

Materials and ESR Samples. 4,4′-bitolyl, (mp 121—122 °C), 4,4′-di-*t*-butylbiphenyl, (mp 198—199 °C), and 2,2′, 4,4′, 6,6′-bimesityl (mp 102—103 °C) were synthesized by Ullman reactions in the manner described bofore.[4] Commercial-grade dichloromethane was dried over P_2O_5 and fractionally distilled. Antimony pentachloride purchased from Nakarai Chemicals Ltd was used without further purification. About a 10% solution of $SbCl_5$ was prepared using CH_2Cl_2 as the solvent and it was stocked in a refrigerator. The materials (*ca.* 2 mg) were placed in a reaction tube (I) and 1 ml of the 10% $SbCl_5$ solution was mixed with 5 ml of CH_2Cl_2 in the side arm tube (II), shown in Fig. 1. The inside of the reaction tube was evacuated, and the reaction tube (I) was placed in liquid N_2; then $SbCl_5$ and CH_2Cl_2 were distilled into the reaction tube (I), which was placed in an aceton-dry ice bath after the removal of the oxidizing agent. As the frozen reaction mixture was melted in an aceton-dry ice bath, the oxidation of the materials proceeded smoothly and the reaction mixture began change in color from deep-blue to blue-green for the *para*-derivatives and to yellow for the *ortho*-derivatives.

The radical solution thus prepared was inserted in a pre-cooled ESR cell, and the ESR spectra were recarded at −40—70 °C. The ESR apparatus employed here was JEOL ME-3X spectrometer operating with a 100 kHz magnetic-field modulation. The magnetic field was calibrated by means of the ring proton hyperfine coupling constant of the perylene cation radical prepared in concentrated sulfuric acid.

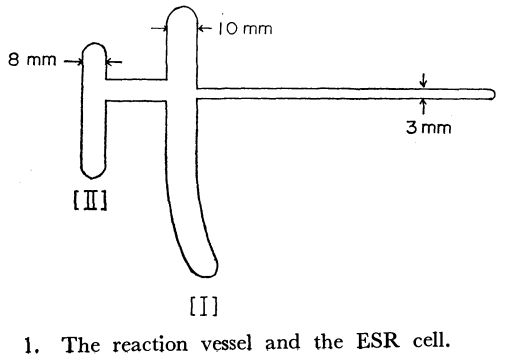

Fig. 1. The reaction vessel and the ESR cell.

Results and Discussion

4,4′-Bitolyl. The spectrum of the 4,4′-bitolyl cation radical observed at −50 °C is shown in Fig. 2. The ESR signal intensity was rapidly depressed when the observing temperature was brought to −30 °C. The largest septet splitting (8.79 Gauss) was easily assigned to those of methyl protons (a_4^H), and the quintet splitting (2.64 Gauss) was ascribed to the *ortho*-ring protons (a_2^H) taking into account McLachlan's MO calculation of the spin density. The *meta*-proton splitting could not be detected in the observed spectrum. The hyperfine coupling constants of each proton thus determined are; $a_4^{CH_3}=8.79$, $a_2^H=2.64$, and $a_3^H<0.03$ Gauss.[6] These values are nearly comparable with those of the cation radical generated by the XeF_2 oxidation of toluene.[7] Besides the proton hyperfine structure, three kinds of ^{13}C-hyperfine splitting were recorded, as is shown in Fig. 3. We found that the absolute values of these hyperfine coupling constants are much like those of the *ortho* (a_2^C)-, the *meta* (a_3^C)-, and the *para* (a_4^C)-ring carbon atoms of the 3,3′,5,5′-tetra-*t*-butylbiphenyl anion radical, as has already been reported,[8] but the splitting of a_1^C, was not resolved in the present case. The ^{13}C hyperfine splittings were assumed to be as follows; $a_2^C=1.83$, $a_3^C=-3.59$, and $a_4^C=8.47$ Gauss.

4,4′-Di-t-butyl Biphenyl. The ESR spectrum of 4,4′-di-t-butylbiphenyl, shown in Fig. 4, was observed in the temperature range of −70 °C to −60 °C. Besides the *ortho*-proton splitting of 2.67 Gauss, one may see the t-butyl proton splitting (0.38 Gauss), which is three times larger than that of the anion radical.[9] The proton hyperfine coupling constants thus estimated are $a_2^H=2.67$ and $a_4^{t\text{-}But}=0.38$ Gauss.

Bimesityl. The ESR spectrum of the cation radical, given in Fig. 5-a, was recorded at −55 °C.

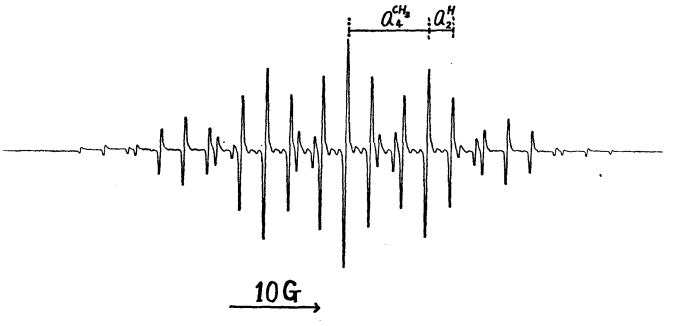

Fig. 2. The ESR spectrum of 4,4′-bitolyl cation radical observed at −50 °C.

6) The maximum resolution of the ESR spectrometer.
7) M. J. Shaw, J. A. Weil, H. H. Hyman, and R. Filler, *J. Amer. Chem. Soc.*, **72**, 5096 (1970).
8) K. Ishizu, Y. Inui, K. Mukai, H. Shikata, and H. Hasegawa This Bulletin, **43**, 3956 (1970).
9) M. D. Curtis and A. L. Allred, *J. Amer. Chem, Soc.*, **87**, 2554 (1965).

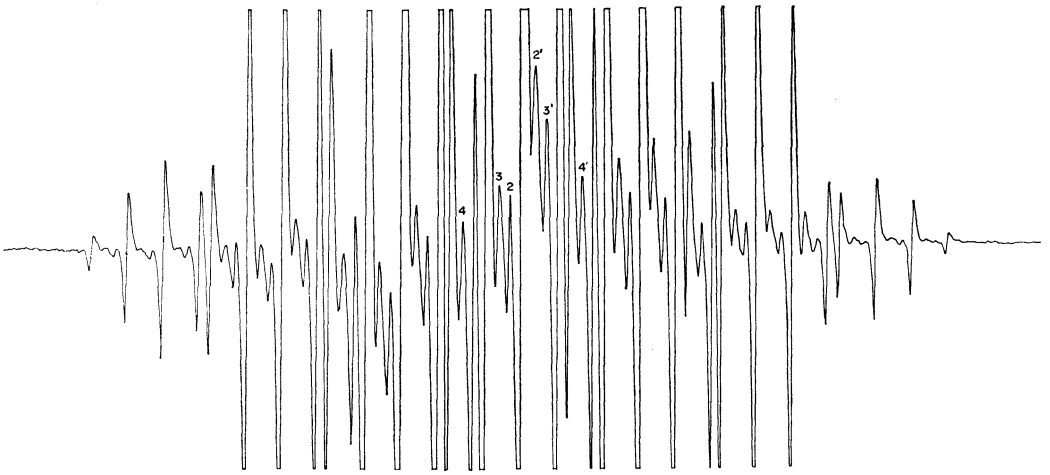

Fig. 3. The ^{13}C-splitting of the ring carbon atoms of 4,4'-bitolyl cation radical. The figures denote the ring position.

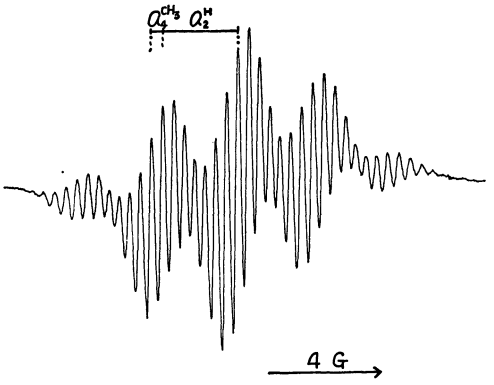

Fig. 4. The ESR spectrum of 4,4'-di-*t*-butylbiphenyl cation radical observed at −70 °C.

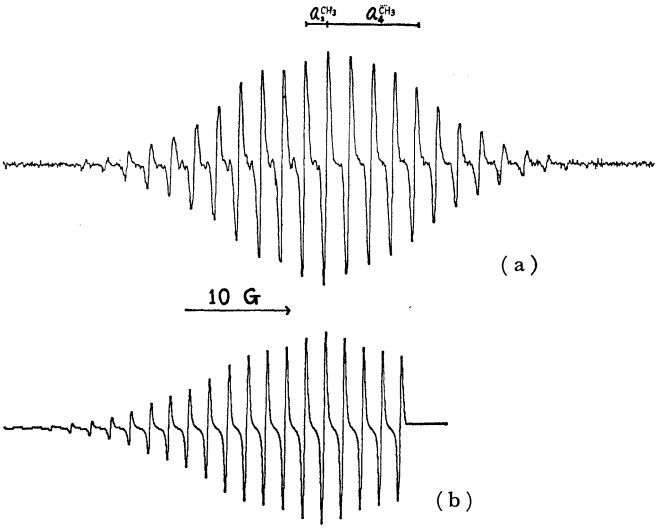

Fig. 5. a) The ESR spectrum of 2,2',4,4',6,6'-bimesityl cation radical observed at −60 °C.
b) The computer simulated spectrum.

Table 1. The observed hyperfine coupling constants of the alkyl biphenyl anion and cation radicals (Gauss)

		$a_2^H, a_2^{CH_3}$	a_3^H	a_4^R
4,4'-Bitolyl	Anion	2.66	0.51	5.63
	Cation	2.64		8.79
4,4'-Di-*t*-butyl Biphenyl	Anion	2.64	0.60	0.10[9]
	Cation	2.67		0.38
2,2', 4,4', 6,6'-Bimesityl	Cation	2.19	0.13	8.79

The bimesityl cation radical is fairly stable for a continuous observation of the ESR spectrum for about 4 hr, but the cation radicals of the other *ortho*-methyl biphenyls, such as 2,2'-bitolyl and 2,2',6,6'-bixylyl, were not successfully generated. The hyperfine structures of the observed spectrum can be well analyzed in terms of the septet splitting of the *para*-methyl protons (8.79 Gauss) and of the *ortho*-methyl proton splitting (2.19 Gauss). The computer-calculated spectrum, shown in Fig. 5-b, is in good agreement with the observed spectrum. Under the higher resolving conditions, the ring proton splitting of the *meta*-position, a_3^H was measured to be 0.13 Gauss. The hyperfine coupling constants thus determined are $a_2^{CH_3}=2.19$, $a_3^H=0.13$ and $a_4^{CH_3}=8.79$ Gauss.

Biphenyl and the Other Alkylbiphenyl. Biphenyl was dissolved in CH_2Cl_2 and treated with $SbCl_5$ in the same manner. The resulting blue solution showed a strong ESR absorption split into eleven equally-spaced hyperfine lines (2.12 Gauss). The hyperfine structure of the spectrum was, however, identical with that for the 4,4'-dichlorobiphenyl cation radical previously reported.[7] The 4-chlorobiphenyl also gave the same ESR spectrum of dichlorobiphenyl. The 3,3',5,5'-tetra-methylbiphenyl and the 3,3',5,5'-tetra-*t*-butylbiphenyl afforded poorly-resolved ESR spectrum, but we failed to detect the ESR absorptions of the alkylbiphenyls, such as 4,4'-diethylbiphenyl and 4,4'-di-isopropylbiphenyl.

Hyperconjugation of the Alkyl Group. McLachlan's MO calculations of the spin density were carried out for 4,4'-bitolyl using two different models, the inductive and the hyperconjugative models. In the inductive model, the Coulomb integral of the ring-carbon atoms

TABLE 2. THEORETICAL AND EXPERIMENTAL SPIN DENSITY FOR THE 4,4′-BITOLYL ANION AND CATION

Position	1	2	3	4	CH_3
Anion					
Inductive	0.1272	0.1189	−0.0316	0.1982	
Hyperconjugative	0.1259	0.1046	−0.0170	0.1885	0.0141
Experimental		0.1033	−0.0187	0.2011[a]	
Cation					
Inductive	0.1297	0.0931	−0.0090	0.2021	
Hyperconjngative	0.1242	0.0946	−0.014	0.1955	0.0192
Experimental		0.0939	0.0172	0.1945[b]	

a) $Q^{CH_3}=-27$ Gauss was used. b) Estimated from the a_3^C and a_4^C values, based on the Karplus and Fraenkels formula.

neighboring the methyl group, α_{CH_3}, was estimated to be $\alpha_{CH_3}=\alpha-0.2\beta$. The Coulson-Crawford parameters were used for the hyperconjugation model of the methyl groups ($>C_1-C_2\equiv H_3$) as follows; $\alpha_2=\alpha-0.1\beta$, $\alpha_{H_3}=\alpha-0.5\beta$, $\beta_{C-C}=0.7\beta$, $\beta_{C-H_3}=2.5\beta$.[10] McLachlan's parameter was taken as $\lambda=1.1$ everywhere. Based on the observed values of the ring-proton splitting (a_i^H), the experimental values of the spin density (ρ_i^π) were calculated based on the Colpa-Bolton's formula, expressed as follows;

$$a_i^H = Q_{CH}^H\rho_i^\pi \pm K_{CH}^H[\rho_i^\pi]^2$$

where the negative sign is applicable to the cation, and the positive sign, to the anion radicals, and where the parameters were taken as $Q_{CH}^H=-27$ Gauss and $K_{CH}^H=-12$ Gauss. Both the experimental and theoretical values of the spin density (ρ_i^π) are summarized in Table 2,

It has been well known that the methyl protons of the cation radical usually give a much larger splitting than those of the anion radical, and this effect has been accepted as being straightfoward evidence supporting the importance of the hyperconjugation mechanism in the methyl group.[12] The methyl proton splitting of the 4,4′-bitolyl cation radical is indeed 1.5 times larger than that for the anion radical, as may be seen in Table 1.

In the case of the cation radical, however, the ρ_4^π can not be derived from the methyl proton splitting, because the Q^{CH_3} value has not been widely established. In the present works, the experimental values of ρ_3^π and ρ_4^π were estimated from the ^{13}C-hyperfine splitting constant, a_3^C, a_4^C using the Karplus-Fraenkel formula:[13]

$$a_i^C = (S^C-\sum_{i=1}^{3}Q_{C_iX_i}^C)\rho_i^\pi - \sum_{i=1}^{3}Q_{X_kC_i}^C\rho_k^\pi$$

where $S^C=-12.7$ Gauss, the contribution from the 1s electron of C_i; where $Q_{C_iX_k}^C$ ($Q_{C_iH}^C=19.5$, $Q_{C_iC_k}^C=14.4$ Gauss), the $\sigma-\pi$ interaction parameter produced by the ρ_i^π on the C_i atom bonded to sp^2-hybridized ring carbon atoms, and where $Q_{C_kC_i}^C=-13.9$ Gauss represents a polarization from the neighboring sp^2-carbon atom. The parameters ($Q_{CC'}^C=30.0$, $Q_{C'C}^C=-20.9$ Gauss) for a sp^2-hybridized carbon bonded to the sp^3-carbon of the methyl group (C′) are referred to the value calculated by Strauss and Fraenkel.[14]

By substituting these parameters into the equation, the following equations were derived, neglecting the spin density on the methyl carbon at the *para*-position:

$$a_3^C = 35.5\rho_3^\pi - 14.4(\rho_2^\pi+\rho_3^\pi)$$

$$a_4^C = 46.1\rho_4^\pi - 28.8\rho_3^\pi$$

Using the experimental value of ρ_2^π obtained from the ring-proton splitting, ρ_3^π and ρ_4^π were thus calculated to be $\rho_3^\pi=0.0172$ and $\rho_4^\pi=0.1945$, which showed an excellent agreement with the theoretically-calculated values shown in Table 2.

The methyl-proton splitting parameter, Q^{CH_3}, was calculated to be 43.5 Gauss on the basis of the calculated value, assuming an inductive model of hyperconjugation. It can also be estimated to be 45.2 Gauss on basis of the experimental spin density, ρ_4^π, as determined from the ^{13}C-hyperfine splitting.

Of interest is the comparison of the *t*-butyl proton splitting, $Q^{t\text{-But}}$, which is tentatively estimated using the theoretical spin density calculated by the inductive model for the methyl group.

The $Q^{t\text{-But}}$ value for the cation radical (1.88) is about four times that for the anion radical (0.50).

Steric Hindrance of the Biphenyl Cation Radical. Molecular orbital calculations of the spin density were carried out for hindered models of the 2,2′,4,4′, 6,6′-bimesityl cation radical, assuming that the value of the resonance integral between the central 1-1′ bond varies with the function of the twisting angle, θ, of the two phenyls; that is, $\beta_{11'}=\beta\cos\theta$.

In Fig. 6, we show the dependence of the twisting angle, θ, on the theoretical spin density at the ring carbon atoms. The calculation results of both the inductive and hyperconjugative models suggested that the steric hindrance may cause a large depression in the spin density at the *ortho*-position (ρ_2^π), but may have scarcely any effect on the *para*-position (ρ_4^π). Therefore, either the degree of the depression in ρ_2^π or the increment in ρ_4^π/ρ_2^π would also be a good measure for estimating the degree of the steric hindrance, as has been described before.[3,4] According to the MO calculation, there is a possibility that the negative

10) C. A. Coulson and V. A. Crawford, *J. Chem. Soc.*, **1953**, 2052.
11) J. P. Colpa and J. R. Bolton, *Mol. Phys.*, **6**, 273 (1963).
12) J. R. Bolton, A. Carrington, and A. D. Mclachlan., *Mol. Phys.*, **5**, 31 (1962).
13) M. Karplus and G. K. Fraenkel, *J. Chem. Phys.*, **35**, 1312 (1961).
14) H. L. Strauss and G. K. Frenkel, *ibid.*, **35**, 1738 (1961).

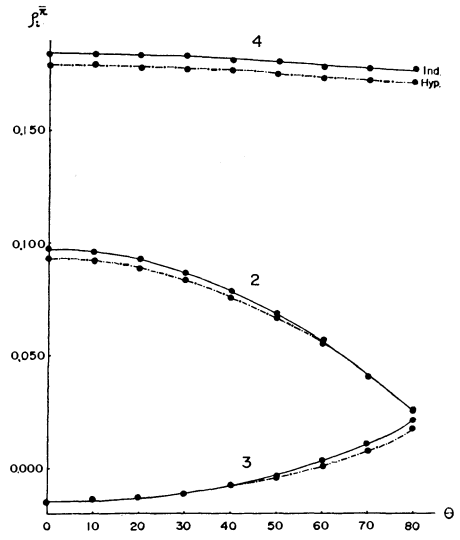

Fig. 6. Dependence of theoretical spin density of ring carbon atoms on twisting angle θ between the phenyl rings in 2,2′,4,4′,6,6′-bimesityl cation radical.
—●—●— calculation using the Inductive model (Ind)
—-●-—● calculation using the hyperconjugation model (Hyp).
The numbers represent the positions on the biphenyl ring.

spin densities at the *meta*-position, ρ_3^π, change to positive sign with an increase in the steric effect.

We have, however, disregarded the effect on the *meta*-position, because the observed *meta*-proton splitting is too small for us to qualify the steric effect on the basis of the present ESR observations. The experimental spin densities of the ρ_2^π and ρ_4^π/ρ_2^π values were calculated using the Q^{CH_3} value estimated for the p,p'-bitolyl cation radical; that is, $\rho_2^\pi=0.050$, $\rho_4^\pi=0.2021$, and $\rho_4^\pi/\rho_2^\pi=4.40$. Unfortunately, the ESR observation of the 2,2′,4,4′,6,6′-bimesityl anion radical has never been successfully achieved. However, for the 2,2′,6,6′-bixylyl anion radical, these values were already known to be $\rho_2^\pi=0.082$ and $\rho_4^\pi/\rho_2^\pi=2.30$.[4] Furthermore, the ρ_2^π of the anion radicals of the *ortho*-alkyl derivatives hitherto studied have been coincidently close to this value, and the ratios of ρ_4^π/ρ_2^π lay together in the range from 2.30 to 2.50.[2,4,5]

A large discrepancy in the ρ_2^π and ρ_4^π/ρ_2^π values can be seen between the cation and the anion radical. This suggests that the more stronger steric hindrance may work on the cation radical rather than on the anion radical.

According to the MO calculation, the twisting angle of the two phenyls would be around 70° in this cation radical, rather close to the values for the neutral molecules,[15], while it is assumed to be 45°∼50° for the anion radicals of hindered alkylbiphenyls. In order to explain the different planar characters of the biphenyl observed for the cation and the anion radical, the bonding character between the central 1–1′ bond may be considered in terms of the partial bond order in the frontier molecular orbital of each ion radical.

In the case of the anion radical, the conjugation between the two phenyl rings may be enhanced by the presence of the unpaired electron, which has a positive bond order between the central 1–1′ bond in the π_{n+1} molecular orbital. The similar enhanced planar character of biphenyl reported for the excited triplet state of *ortho*-methyl derivatives[16,17] has also been interpreted in terms of the delocalization of the unpaired electron across the two phenyl rings.

On the contrary, the unpaired electron occupies the molecular orbital in the case of cation radicals, and the conjugation of the two phenyls may be strongly reduced, just as in the neutral molecules, because the wave function has the node and there is a negative bond order between the 1–1′ bonds in these molecules.

The numerical calculations were carried out on the FACOM 230—60 at the Data Processing Center, Kyoto University.

15) H. Suzuki, This Bulletin, **32**, 1350, 1357 (1959); **33**, 109 (1960).
16) P. J. Wagner, *J. Amer. Chem. Soc.*, **89**, 2820 (1967).
17) A. Imamura, and R. Hoffman, *ibid.*, **87**, 5379 (1967).

The Kinetics of Oxygen Exchange between Arsenate Ions and Solvent Water

Akiko OKUMURA and Nobukazu OKAZAKI

Department of Chemistry, Nara Women's University, Nara 630

(Received February 12, 1973)

The rates of oxygen exchange between arsenate ions and water have been measured at 14.5 °C and 30 °C over the pH range of 6.5—12.5. The rate, R, may be expressed by the rate law:

$$R = k_1[H_2AsO_4^-] + k_2[HAsO_4^{2-}] + k_3[AsO_4^{3-}] + k_4[H_2AsO_4^-]^2 + k_5[H_2AsO_4^-][HAsO_4^{2-}] + k_6[HAsO_4^{2-}]^2.$$

The exchange rates at 30 °C and $I=0.55$ have been analyzed in terms of this rate law to obtain the values of the rate constants, k_1—k_6. The activation energy of the over-all exchange reaction is 13.2±0.2 kcal/mol at pH 7.51 and 22.14±0.02 kcal/mol at pH 9.79. The reaction shows a negative salt effect in the region of pH 7.5, and a positive salt effect at pH 9.3.

The oxygen exchange of arsenate ions in an aqueous solution has been studied, except for the earlier qualitative studies,[1] mainly from the biochemical point of view.[2] In order to explore the possibility of the use of ^{18}O-labelled arsenate in biochemical tracer work, Kouba and Varner[3] have measured the exchange half-times at several pH's between 2 and 10 at 32 °C; they estimated a very low activation energy of 3.7 kcal/mol for the exchange reaction at pH 8.0. We have studied the kinetics of this reaction in more detail in order to elucidate its mechanisms.

Experimental

Materials. Disodium hydrogen arsenate heptahydrate (Special grade, JIS) was recrystallized from water. Water enriched in oxygen-18 (*ca.* 2 atom%) and guanidine hydrochloride were treated as has been described in a previous paper.[4] Lithium perchlorate was obtained by neutralizing lithium carbonate (Special grade, JIS) with perchloric acid (Special grade, JIS), and was repeatedly recrystallized. The other chemicals were of an analytical reagent grade, and were used without further purification.

Procedure. The procedures were almost the same as those used in the previous work.[4] The exchange reaction was started by diluting an isotopically-equilibrated solution of disodium hydrogen arsenate in oxygen-18 water with a relatively large amount of isotopically normal water. The pH value of the solution was controlled by adding a small amount of hydrochloric acid or of a sodium hydroxide solution. The ionic strength was adjusted by the addition of sodium chloride. The reactions were carried out in an ice-water bath or in a constant temperature bath. At appropriate intervals a portion of the solution was removed, and the arsenate ions were precipitated by adding a barium chloride solution. The compositions of the precipitates from the solutions at pH 5.6 and 8.9 were shown by chemical analysis to be $BaHAsO_4 \cdot H_2O$. The precipitate was separated by means of a centrifuge, washed three times with absolute ethanol, dried in an oven at 110 °C, and converted into carbon dioxide by the guanidine hydrochloride method.[5] The isotopic analysis of the carbon dioxide was made on a Hitachi RMS-I-type mass spectrometer.

The rate of oxygen exchange in g atom per 1 in unit of time was calculated by means of the formulas:

$$R = \frac{4[\mathrm{As(V)}][H_2O]}{4[\mathrm{As(V)}]+[H_2O]} \cdot k_{ex},$$

and

$$k_{ex} = -\frac{1}{t} \cdot \ln\left\{1 - \frac{O_0 - O_t}{O_0 - O_\infty}\right\}, \quad \text{(I)}$$

where O_0, O_t, and O_∞ are the oxygen-18 contents of the arsenate oxygen at the times 0, t, and infinity respectively, and where [As(V)] and $[H_2O]$ are the molar concentrations of the arsenate and water respectively. The McKay plots were satisfactorily linear over two half-lives except for the runs at pH>11.

Induced Exchange. It has been found in the preliminary work that oxygen exchange between arsenate ions and water is induced on the precipitation of arsenates by metallic ions. The extent of the induced exchange varies with the nature of the metallic ions; it is found to be larger for the ions of transition metals and for the cations with higher charges. With the barium ion as precipitant, which induces the oxygen exchange least of all the metal ions tried, the induced exchange amounts to *ca.* 20% of the total exchange at pH 9.0 and 30 °C. The extent increases with an increase in the acidity. Prestwood and Wahl[6] have discussed the effect of induced exchange on the kinetics of Tl(I)–Tl(III) exchange reaction. They have shown that, when the separation-induced exchange and the incomplete separation effects are reproducible, the equation of the form of (I), with the values of specific activities measured after separation, gives the real rate that occurs in solution. Their argument, with necessary changes, applies to the present case. The presence of the crystal water in the precipitate of barium arsenate may be treated as a case of incomplete separation in the sense of these authors. Since the precipitate has a definite composition, and since the oxygen-18 content of the crystal water is approximately equal to that of the normal water, we may make use of Eq. (I) in calculating the exchange rate in solution.

To check the above arguments experimentally, we have carried out the following two experiments. 1) In a kinetic run (pH 7.40, 30 °C), the precipitate of barium hydrogen arsenate monohydrate was divided into two portions. One portion was dried at 110 °C for an hour and then analysed as has been described above. Barium hydrogen arsenate monohydrate loses its water of crystallisation above 120 °C.[7]

1) T. Titani and K. Goto, This Bulletin, **14**, 77 (1939); N. F. Hall and O. R. Alexander, *J. Amer. Chem. Soc.*, **62**, 3455 (1940).

2) D. H. Slocum and J. E. Varner, *J. Biol. Chem.*, **235**, 492 (1960); N. Itada and M. Cohn, *ibid.*, **238**, 2026 (1963).

3) R. F. Kouba and J. E. Varner, *Biochem. Biophys. Res. Communs.*, **1**, 129 (1959).

4) A. Okumura and N. Okazaki, This Bulletin, **46**, 1080 (1973).

5) P. D. Boyer, D. J. Graves, C. H. Suelter, and M. E. Dempsey, *Anal. Chem.*, **33**, 1906 (1961).

6) R. J. Prestwood and A. C. Wahl, *J. Amer. Chem. Soc.*, **71**, 3137 (1949).

7) R. H. Vallance, "A Text-book of Inorganic Chemistry," ed. by J. N. Friends, Vol. VI, Part IV, (1938), Charles Griffin Co., London, p. 194.

The other portion was dehydrated at 170 °C for two hours to the anhydrous salt and then analysed for its oxygen-18 content. The two methods gave approximately equal ^{18}O-concentrations, the difference being not more than 5 per cent. This fact shows that the scrambling of oxygen atoms occurs between arsenate ions and crystal water in the course of the dehydration of barium hydrogen arsenate monohydrate. Similar phenomena have been observed with disodium hydrogen and sodium dihydrogen arsenates at room temperature.[8] The first-order rate constants of ^{18}O-exchange, k_{ex}, obtained by the two methods are 0.233 ± 0.001 hr^{-1} and 0.234 ± 0.002 hr^{-1} for the drying temperatures of 110 °C and 170 °C respectively. 2) An oxygen-exchange reaction of arsenate ions (pH 8.89, 30 °C, [As(V)]=1.2 M) was followed by two different methods of ^{18}O-analysis, one by analysing the arsenate oxygen by the method described above, and the other by measuring the increase in the ^{18}O-content of the solvent water. The solvent water was separated by the freeze-dry method and was analysed by the guanidine hydrochloride method. The values of k_{ex} obtained are 0.0880 ± 0.0002 hr^{-1} and 0.0928 ± 0.0007 hr^{-1} for the arsenate analysis and the water analysis respectively. Taking into consideration the difference in the analytical methods, the agreement between the two values of k_{ex} may be considered to be satisfactory. These results show that the induced exchange does not affect the kinetics of the oxygen-exchange reaction of arsenate ions.

Determination of the Dissociation Constants of Arsenic Acid. For the analysis of the exchange rate, it is desirable to obtain the pK_2 and pK_3 values of arsenic acid under the conditions of the kinetic runs. These have been determined by potentiometric titrations with a glass electrode. Solutions of potassium dihydrogen arsenate containing an amount of potassium chloride necessary to maintain the desired ionic strength were titrated with a solution of carbonate-free potassium hydroxide. The concentrations of the solutions were so chosen as to give the desired ionic strength at the half-neutralisation point. The values obtained are given in the following table.

Table 1. The values of pK_2 and pK_3 of arsenic acid[a]

	Temp. °C	Ionic strength 0.13	0.30	0.55
pK_2	0	$6.83_7\pm0.00_5$	—	$6.59_6\pm0.01_5$
	14.5	$6.77_7\pm0.00_4$	—	$6.56_1\pm0.00_6$
	30.0	$6.75_0\pm0.00_3$	—	$6.53_1\pm0.01_4$
pK_3	14.5	—	$11.30_6\pm0.02_6$	$11.19_2\pm0.01_0$
	30.0	—	$11.21_5\pm0.01_3$	$11.01_5\pm0.01_0$

a) Here the dissociation constant is defined by $K=a_{H^+}\cdot[A^-]/[HA]$, where a_{H^+} is the activity of the hydrogen ion and where [HA] and [A$^-$] are the molar concentrations of an acid and its conjugate base. The values of the pK's were obtained from two series of titrations, each with ten titrations. The errors indicated are the probable errors.

Results and Discussion

pH *Dependence of the Exchange Rate.* The dependence of the exchange rate on the pH is shown in Fig. 1. In the neighbourhood of pH=pK_2, the logarithm of the rate varies linearly with the pH, and the rate is approximately first-order in the hydrogen-ion concentration. At pH≃9, the dissociation of $H_2AsO_4^-$ is almost complete and the dissociation of $HAsO_4^{2-}$ begins. In this pH region, the variation in the exchange rate with the pH slows down, and at 30 °C the rate is nearly independent of the pH. At pH>10, the rate falls off again with the increase in the dissociation of $HAsO_4^{2-}$.

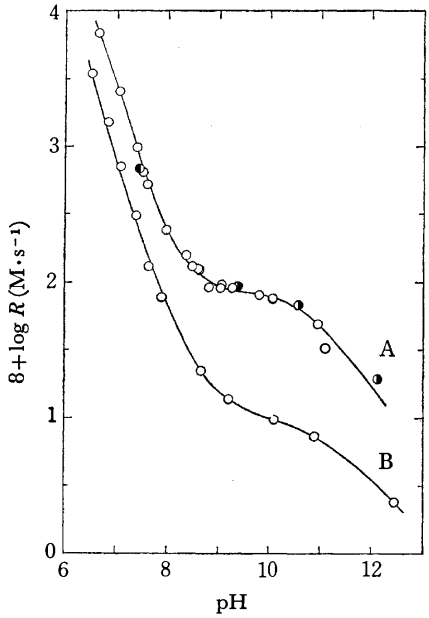

Fig. 1. pH-Rate profiles of the oxygen exchange between arsenate ions and water at 30°(A) and 14.5 °C(B). I= 0.55 M (○: NaCl, ◐: $NaClO_4$, ◑: $LiClO_4$). [As(V)] ≃6.8×10^{-2} M. The curves at 30 °C were calculated by the use of the rate constants obtained.

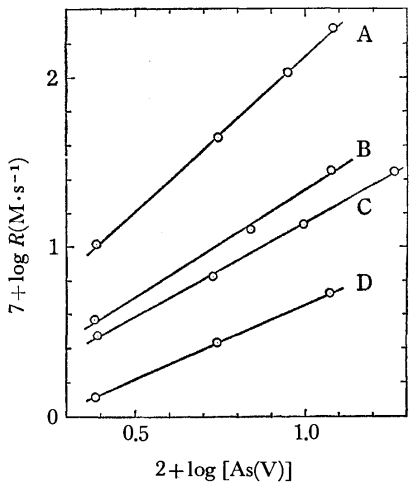

Fig. 2. Dependence of the exchange rate on [As(V)]. 30 °C. I=0.55 M. A: pH 7.51, B: pH 8.47, C: pH 9.27, D: pH 11.1.

Dependence on the Total Arsenate Concentration, [As(V)]. This was studied at four pH's, 7.51, 8.47, 9.27, and 11.1, at 30 °C and I=0.55 M (Fig. 2). Plots of log R against log [As(V)] yield straight lines with slopes of 1.83 ± 0.02, 1.26 ± 0.03, 1.11 ± 0.01, and 0.89 ± 0.01 for the pH values of 7.51, 8.47, 9.27, and 11.1 respectively.

8) A. Okumura and N. Okazaki, This Bulletin, **46**, 2981 (1973).

Mechanisms of the Oxygen Exchange. At pH≃7.5 and at 30 °C, the rate of oxygen exchange may be expressed as $R=k[H^+][As(V)]^{1.8}$. In this region, bimolecular mechanisms between arsenate ions predominate:

$$H_2AsO_4^- + H_2AsO_4^- \overset{k_4}{\rightleftharpoons} H_2As_2O_7^{2-} + H_2O, \quad (4)$$

$$H_2AsO_4^- + HAsO_4^{2-} \overset{k_5}{\rightleftharpoons} HAs_2O_7^{3-} + H_2O, \quad (5)$$

$$HAsO_4^{2-} + HAsO_4^{2-} \overset{k_6}{\rightleftharpoons} As_2O_7^{4-} + H_2O. \quad (6)$$

The role of the hydrogen ion is to shift the pre-equilibrium:

$$H_2AsO_4^- \rightleftharpoons HAsO_4^{2-} + H^+,$$

from right to left in favour of the more reactive arsenate species, $H_2AsO_4^-$. It has been believed that the diarsenate ion hydrolyzes very rapidly and therefore cannot exist in aqueous solutions.[9] However, the present result shows that, in an aqueous solution, the condensation of the arsenate ions occurs as well as the hydrolysis of the diarsenate ion. The order with respect to the [As(V)] of 1.8 suggests the occurrence of some first-order paths of the oxygen exchange. These are probably:

$$H_2AsO_3O^{*-} + H_2O \overset{k_1}{\rightleftharpoons} H_2AsO_4^- + H_2O^*, \quad (1)$$

and

$$HAsO_3O^{*2-} + H_2O \overset{k_2}{\rightleftharpoons} HAsO_4^{2-} + H_2O^*. \quad (2)$$

In the region of pH≃9 at 30 °C, where the dissociation of $H_2AsO_4^-$ is almost complete and where $HAsO_4^{2-}$ begins to dissociate, the observed rate law is $R\simeq k'[H^+]^0[As(V)]^{1.1}$. Since, in this region, $[HAsO_4^-]$ is nearly independent of pH, a zero-order dependence on $[H^+]$ may be expected. The observed [As(V)] dependence of 1.1 suggests that, above pH 9, the first-order path (2) controls the total exchange rate. At pH 11.1, the contribution of the bimolecular path (6) becomes negligible. In addition to the above five paths, a pseudo-first-order path:

$$AsO_3O^{*3-} + H_2O \overset{k_3}{\rightleftharpoons} AsO_4^{3-} + H_2O^*, \quad (3)$$

may be expected to make a contribution, if slight, to the total rate.

The rate law of oxygen exchange of arsenate ions may be written as:

$$\begin{aligned} R &= R_1 + R_2 + R_3 + R_4 + R_5 + R_6 \\ &= k_1[H_2AsO_4^-] + k_2[HAsO_4^{2-}] + k_3[AsO_4^{3-}] \\ &\quad + k_4[H_2AsO_4^-]^2 + k_5[H_2AsO_4^-][HAsO_4^{2-}] \\ &\quad + k_6[HAsO_4^{2-}]^2. \end{aligned} \quad (7)$$

Temperature Dependence of the Exchange Rate. This has been studied at pH 7.51 (0 °C, 20 °C, and 30 °C) and at pH 9.79 (30 °C, 40 °C, and 50 °C). Plots of log R against $1/T$ are shown in Fig. 3. From the slopes of the plots, the values of the activation energy are calculated to be 13.2±0.2 kcal/mol at pH 7.51 and 22.14±0.02 kcal/mol at pH 9.79. At 30 °C and pH 9.79, it can be estimated that nearly 95% of the oxygen exchange occurs through Path (2). The value of 22 kcal/mol gives the approximate value of the activation energy of this path. At 30 °C and pH 7.51, the contributions of the second-order rate terms, R_4 and R_5, to the total rate are estimated to be 44 and 38% respectively. The value of 13 kcal/mol gives an upper limit for the activation energies of these bimolecular paths between arsenate ions.

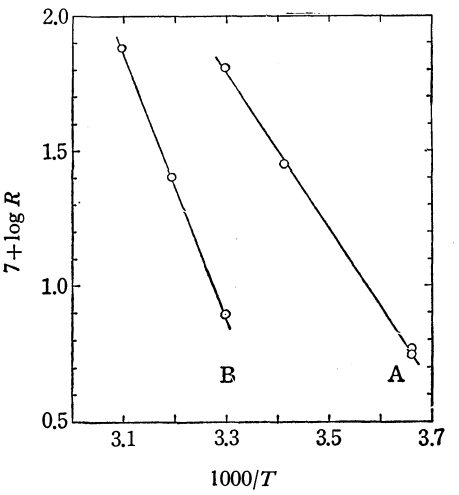

Fig. 3. Temperature dependence of the exchange rate at pH 7.51(A) and 9.79(B). [As(V)]=0.068 M, I=0.55 M.

Salt Effect. On the rate-pH profile at 30 °C (Fig. 1), the plots at pH 7.45, 9.37, 10.58, and 12.12 were obtained with solutions whose ionic strengths had been adjusted with sodium or lithium perchlorate instead of sodium chloride. These plots fall on a curve with the other plots within the range of experimental error. This fact shows the absence of any specific effects of the chloride and perchlorate ions.

The effect of the ionic strength on the exchange rate has been studied at 30 °C at pH 7.72 and 9.29. At a fixed total concentration of the arsenate, the ionic strength was varied by the addition of sodium chloride. The values of the exchange rate thus obtained are listed in the following table:

Table 2. The effect of the ionic strength on the exchange rate ($R\times10^6$) at 30°C

pH	Ionic strengths.			
	0.2	0.55	0.7	1.0
7.72	5.64	—	5.07	3.83
9.29	0.854	0.906	—	0.926

The salt effect is negative at pH 7.72 and positive at pH 9.29. The exchange paths (4), (5), and (6), which predominate in the region of pH 7.72 are expected to exhibit a positive salt effect. Thus, the negative salt effect observed must be due to an equilibrium salt effect which overcomes the kinetic salt effect. An increase in the ionic strength decreases the concentration of the more active species, $H_2AsO_4^-$, by increasing the dissociation constant of $H_2AsO_4^-$. In the region of pH 9, where the extent of the dissociation of

9) "Gmelins Handbuch der Anorganischen Chemie," 8-te Aufl. Syst. -Nr. 17, (1952), Verlag Chemie, Weinheim/Bergstrasse. S. 358.

$HAsO_4^{2-}$ is small, the change in the dissociation constant of $HAsO_4^{2-}$ is without appreciable effect on the concentration of $HAsO_4^{2-}$, and so the kinetic salt effect predominates.

Analysis of the Exchange Rate at 30 °C. The exchange rates observed can be analyzed by the use of the rate law (7). The concentrations of the ionic species were calculated by the relations:

$$[As(V)] = [H_2AsO_4^-] + [HAsO_4^{2-}] + [AsO_4^{3-}], \quad (8)$$

$$K_2 = a_{H^+} \cdot [HAsO_4^{2-}]/[H_2AsO_4^-], \quad (9)$$

$$K_3 = a_{H^+} \cdot [AsO_4^{3-}]/[HAsO_4^{2-}]. \quad (10)$$

Over the range of pH<9, the k_3-term in the rate law may be neglected, and by using the (8), (9), and (10) relations, Eq. (7) can be rewritten in the form:

$$\frac{R}{[H_2AsO_4^-]} = \left(k_1 + k_2\frac{K_2}{a_{H^+}}\right) + [As(V)] \times \left\{\frac{k_4}{1+(K_2/a_{H^+})+(K_2K_3/a_{H^+}^2)} + \frac{k_5}{1+(a_{H^+}/K_2)+(K_3/a_{H^+})} + \frac{k_6}{(a_{H^+}/K_2)\{1+(a_{H^+}/K_2)+(K_3/a_{H^+})\}}\right\}. \quad (11)$$

In Fig. 4, the data of Fig. 2 are replotted according to

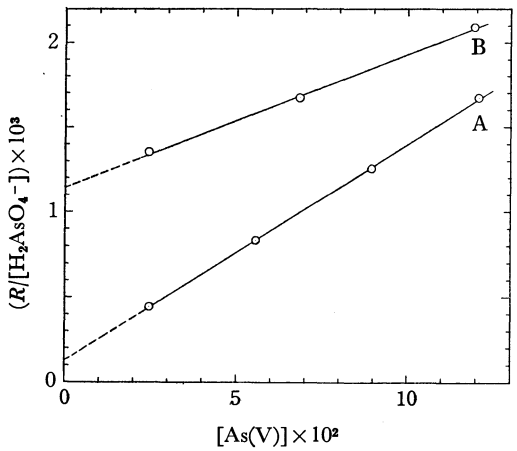

Fig. 4. $R/[H_2AsO_4^-]$ as a function of [As(V)] at pH 7.51(A) and 8.47(B) at 30 °C.

Eq. (11). The least-squares treatment of the plots yields:

$$k_1 + 9.48k_2 = (0.124 \pm 0.006) \times 10^{-3}, \quad (12)$$

$$0.954k_4 + 0.905k_5 + 8.58k_6 = (0.128\pm0.001)\times10^{-1}, \text{ at pH } 7.51, \quad (13)$$

and:

$$k_1 + 87.7k_2 = (1.15\pm0.02) \times 10^{-3}, \quad (14)$$

$$0.0112k_4 + 0.986k_5 + 86.5k_6 = (0.0784\pm0.002)\times10^{-1}, \text{ at pH } 8.48. \quad (15)$$

In the region of pH>9, by neglecting the k_1- and k_4-terms, Eq. (7) can be transformed into:

$$\frac{R}{[HAsO_4^{2-}]} = \left(k_2 + k_3\frac{K_3}{a_{H^+}}\right) + [As(V)]\left\{\frac{k_5}{1+(K_2/a_{H^+})+(K_2K_3/a_{H^+}^2)} + \frac{k_6}{1+(a_{H^+}/K_2)+(K_3/a_{H^+})}\right\}. \quad (16)$$

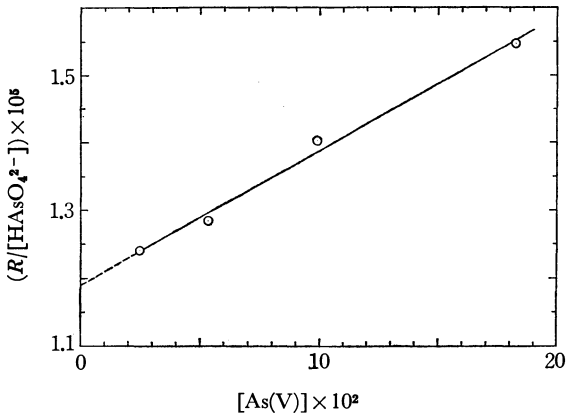

Fig. 5. $R/[HAsO_4^{2-}]$ as a function of [As(V)] at pH 9.27 and 30 °C.

Fig. 5 shows a plot of $R/[HAsO_4^{2-}]$ against [As(V)] at pH 9.27 and I=0.55 M, the data used being the same as those of Fig. 2C. From the intercept and the slope of a line passing through the plots, we obtain:

$$k_2 + 0.0179k_3 = (1.19\pm0.01) \times 10^{-5}, \quad (17)$$

and

$$0.00180k_5 + 0.981k_6 = (0.0198\pm0.0008) \times 10^{-3}. \quad (18)$$

Since k_2 may be reasonably assumed to be larger than k_3, the value of k_2 may be fixed from (17), with an uncertainty of 2% at most to be:

$$k_2 = (1.19\pm0.01) \times 10^{-5}\,s^{-1}.$$

Eqs. (13), (15), and (18) can be solved simultaneously for k_4, k_5, and k_6. The results are:

$$k_4 = 0.74 \times 10^{-1}\,M^{-1}s^{-1},$$

$$k_5 = 0.64 \times 10^{-2}\,M^{-1}s^{-1},$$

and

$$k_6 = 0.85 \times 10^{-5}\,M^{-1}s^{-1}.$$

The value of k_1 is subject to some uncertainty. By using the value of k_2 obtained above, k_1 is evaluated from (12) to be 1.1×10^{-4} and from (14) to be 1.1×10^{-5}. The former value may be better, because the k_1-path plays a more important role at pH 7.51 than at pH 8.48.

The value of k_3 is also attended with uncertainty, because the k_3-path plays an important role only in the most alkaline region of this study, where experimental troubles make the exact determination of the exchange rate difficult. At pH>9.5, where the contribution of the k_5-path to the total rate is negligible, the rate law (7) becomes:

$$R = k_2[HAsO_4^{2-}] + k_3[AsO_4^{3-}] + k_6[HAsO_4^{2-}]^2,$$

which can be transformed into:

$$R - k_6[HAsO_4^{2-}]^2 = k_2[As(V)] + (k_3-k_2)[AsO_4^{3-}].$$

In this pH region, the contribution of the k_6-term is small, being *ca.* 5% of the total rate at pH 9.79. Fig. 6 shows a plot of $R-k_6[HAsO_4^{2-}]^2$ against $[AsO_4^{3-}]$ at a constant value of [As(V)], the value of k_6 obtained above being used. The observed rates were normalized to $[As(V)]=6.8\times10^{-2}$ M by assuming $R\propto[As(V)]$. The least-squares treatment of the plots yields the value: $k_2[As(V)]=(0.080\pm0.003)\times10^{-5}$, and $k_3-k_2=-(0.010\pm0.001)\times10^{-3}$, whence we ob-

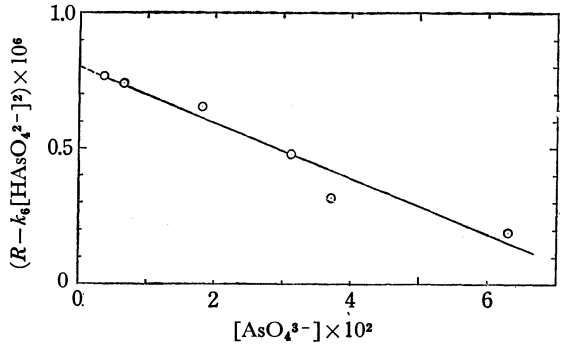

Fig. 6. A plot of $R-k_6[HAsO_4^{2-}]^2$ against $[AsO_4^{3-}]$. 30 °C. [As(V)]=0.068 M. I=0.55 M.

tain:

$$k_2 = 1.18 \times 10^{-5}\ s^{-1},$$

and

$$k_3 = 0.15 \times 10^{-5}\ s^{-1}.$$

The values of the rate constants obtained are summarized in the following table. Other methods of evaluating the rate constants yielded values which are in satisfactory agreement with those above. The rate-pH profile at 30 °C in Fig. 1 was calculated by using these rate constants; it shows a satisfactory agreement with the plots obtained by the experiments except for the most alkaline region.

The rate constant, k_1', of the oxygen exchange of dihydrogen phosphate ions:

$$H_2PO_4^- + H_2O^* \rightleftharpoons H_2PO_3O^{*-} + H_2O,$$

has been found to be $4\times10^{-6}\ s^{-1}$ at 100 °C.[10] If the activation energy of this process is assumed to be about the same as that of the hydrolysis of the monoanion of methyl dihydrogen phosphate (30 kcal/mol),[10] k_1' has a value of 4×10^{-10} at 30 °C, which is smaller by a factor of 10^6 than the corresponding rate constant, k_1, of the dihydrogen arsenate ion.

Table 3. Rate constants of the oxygen exchange between arsenate ions and water at 30 °C (I=0.55 M)

Exchange path	Rate constants
$H_2AsO_4^- + H_2O \rightleftharpoons$	k_1: $1\times10^{-4}\ s^{-1}$
$HAsO_4^{2-} + H_2O \rightleftharpoons$	k_2: $1.2\times10^{-5}\ s^{-1}$
$AsO_4^{3-} + H_2O \rightleftharpoons$	k_3: $1.5\times10^{-6}\ s^{-1}$
$H_2AsO_4^- + H_2AsO_4^- \rightleftharpoons H_2As_2O_7^{2-} + H_2O$	k_4: $7.4\times10^{-2}\ M^{-1}\ s^{-1}$
$H_2AsO_4^- + HAsO_4^{2-} \rightleftharpoons HAs_2O_7^{3-} + H_2O$	k_5: $6.4\times10^{-3}\ M^{-1}\ s^{-1}$
$HAsO_4^{2-} + HAsO_4^{2-} \rightleftharpoons As_2O_7^{4-} + H_2O$	k_6: $8.5\times10^{-6}\ M^{-1}\ s^{-1}$

A hydrogen-bonded cyclic intermediate between a dihydrogen phosphate ion and a water molecule has been postulated for the oxygen exchange of dihydrogen phosphate ions.[11] Such a special reactivity of the monoanion was not observed in the oxygen exchange of arsenate ions, the rate constant, k_1, being only an order of magnitude larger than k_2, which in turn is also an order of magnitude larger than k_3. The exchange paths, (1)—(3), involve probably the nucleophilic attack of a water molecule on the arsenic atom of arsenate ions.

From the values of the constant, k_2, and the activation energy of Path (2) (22 kcal/mol), the entropy of activation of this path is calculated to be $\Delta S^{\ddagger}_2 = -11$ cal K^{-1} mol^{-1} (30 °C). This value is consistent with a mechanism which involves a bimolecular substitution process between an arsenate ion and a water molecule as the rate-limiting step.

The authors wish to thank Professor Shinichi Kawaguchi of Osaka City University for his helpful discussions.

10) C. A. Bunton, D. R. Llewellyn, K. G. Oldham, and C. A. Vernon, *J. Chem. Soc.*, **1958**, 3574.

11) C. A. Bunton, D. R. Llewellyn, C. A. Vernon, and V. A. Welch, *ibid.*, **1961**, 1636.

An MO-simulation of Elementary Reactions in Hydrocarbon Oxidation. I. A Bimolecular Coupling Reaction of the Methyl Radical and Molecular Oxygen

Katsutoshi OHKUBO and Futoshi KITAGAWA

Department of Synthetic Chemistry, Kumamoto University, Kurokami, Kumamoto 860

(Received February 24, 1973)

An MO-simulation of the geometrical change in the bimolecular methane oxidation, $CH_3+O_2\rightarrow CH_3O_2$, was performed using the CNDO/2 approximation. The geometry of CH_3O_2 was predicted to take $r_{OO}=1.19$ Å and $\angle COO=111°$ with fixed distances of $r_{CO}=1.44$ Å and $r_{CH}=1.09$ Å. The coupling reaction proceeds smoothly, without any appreciable activation energy, with the geometric transformation of the momentarily-living CH_3--O_2, with $r_{CO}=2.36\sim1.44$ Å, $r_{OO}=1.132\sim1.19$ Å, and $\angle COO=90\sim111°$. The magnitude of the electron migration between CH_3 and O_2 throughout the reaction was estimated.

Recent shock-tube[1,2] or ignition-delay[3,4] investigations have been concerned with methane oxidation involving the elementary bimolecular reaction of CH_3 and O_2, from the kinetic point of view.[5] Clark *et al.*[2] have reported the rate constant for the CH_3 and O_2 coupling reaction to be 1.987×10^7 M^{-1} s^{-1}, while Basco *et al.*[6] have evaluated the rate constant to be 2.7×10^8 M^{-1} s^{-1}; the coupling reaction may thus proceed very rapidly and easily. In this respect, the activation energy for the reaction has been estimated to be 18.0 kcal/mol by the ignition-delay investigation of Skinner *et al.*[4]

No theoretical investigation has, however, been concerned with the process of the coupling reaction of CH_3 and O_2 from the energetic and electronic points of view. Therefore, it is necessary to perform the MO-simulation for the $CH_3+O_2\rightarrow CH_3O_2$ reaction.

The goal of the present investigation using the CNDO/2 theory[7] was to get a reliable prediction of the geometrical changes (and those of the electronic structures) of CH_3 and CH_3O_2 generated in the course of methane oxidation and to shed some light on the elementary bimolecular reaction of CH_3 and the $^3\Sigma_g^-$ state of O_2.

Method of Calculation

In this work, the following three systems were investigated: (a) the methyl radical, CH_3, (b) the methylperoxyl radical, CH_3O_2, and (c) the bimolecular coupling reaction of CH_3 and the $^3\Sigma_g^-$ O_2.

The geometric parameters are shown in the proper figures, but the interatomic distrances of C–H and C–O were fixed at 1.09 Å and 1.44 Å respectively for the sake of simplicity.

The method of calculation was CNDO/2, using the integrals and parametrization in Ref. 7.

Results and Discussion

Methyl Radical and Triplet Molecular Oxygen. The geometry of neutral CH_3 has long been known to take the "planar C_{3v}" (*viz.* D_{3h}) $^2A_2''$ state as the energetically most stable species. The vacuum UV spectroscopic study of Herzberg[8] gave the planar D_{3h} structure with the optimized bond length of C–H (r_{CH}), 1.079 Å, while some semiempirical[9] and nonempirical[10–12] treatments of CH_3 have favored a planar or nearly planar C_{3v} configuration.

The present CNDO/2 calculations on CH_3 at the angle of 70°32′∼90° between a C–H bond and a threefold axis suggest that the planar D_{3h} structure is most likely, as had been expected. Here, the predicted CH_3 geometry resulting from the semiempirical and *ab initio* calculations is summarized in Table 1 for the sake of comparison.

On the other hand, the equilibrium bond length of O–O in the $^3\Sigma_g^-$ O_2 has now been established to be 1.132 Å[7] (CNDO/2 calculation) or 1.207 Å[13] (experiment). The former value was used for the present MO-simulations.

The frontier orbitals of the singly-occupied (SO), nonbonding carbon 2p-orbital of the D_{3h} CH_3 (−13.188 eV) and of the doubly-degenerate SO $1\pi_g$-orbitals of O_2 (−14.856 eV) play a predominant role in the bimolecular coupling reaction of both species. The coupling reaction may be initially made possible by the maximum overlapping of the frontier orbitals mentioned above at the right angle of C–O–O (see below).

Methylperoxyl Radical. Neither the semiempirical nor the *ab initio* treatment has hitherto been concerned with the CH_3O_2 geometry, except in the case of an

1) T. P. J. Izod, G. B. Kistiakowsky, and S. Matsuda, *J. Chem. Phys.*, **55**, 4425 (1971).
2) T. C. Clark, T. P. J. Izod, and S. Matsuda, *ibid.*, **55**, 4644 (1971).
3) A. Lifshitz, K. Scheller, A. Burcat, and G. B. Skinner, *Combust. Flame*, **16**, 311 (1971).
4) G. B. Skinner, A. Lifshitz, K. Scheller, and A. Burcat, *J. Chem. Phys.*, **56**, 3853 (1972).
5) Other kinetic analyses of methane oxidation can be seen in the following references: R. M. R. Higgin and A. Williams, *Symp. Combust.*, 12th, Poitiers, France, **579** (1969); D. J. Seery and C. T. Bowman, *Combust. Flame*, **14**, 37 (1970); C. T. Bowman, *Combust. Sci. Technol.*, **2**, 161 (1970).
6) N. Basco, D. G. L. James, and F. C. James, *Chem. Phys. Lett.*, **8**, 265 (1971).
7) J. A. Pople and D. L. Beveridge, "Approximate Molecular Orbital Theory," McGraw-Hill, New York (1970).
8) G. Herzberg, *Proc. Roy. Soc., Ser. A*, **262**, 291 (1961).
9) D. L. Beveridge, P. A. Dobosh, and J. A. Pople, *J. Chem. Phys.*, **48**, 4802 (1968).
10) K. Morokuma, L. Pederson, and M. Karplus, *ibid.*, **48**, 4801 (1968).
11) W. A. Lathan, W. J. Hehre, and J. A. Pople, *J. Amer. Chem. Soc.*, **73**, 808 (1971).
12) P. Millie and G. Berthier, *Int. J. Quantum Chem. Symp.*, No. 2, 67 (1968).
13) G. Herzberg, "Spectra of Diatomic Molecules," Van Nostrand, Princeton, N. J. (1950).

Table 1. Prediction of CH_3 geometry

Basis set	Configuration	r_{CH} (Å)	∠HCH (deg)	Reference
Present CNDO/2	planar $^2A_2''$	1.090	120	
INDO	nearly planar $^2A_1$	1.080	119.7	9
ab initio	planar $^2A_2''$	1.080	120	10
STO-3G	pyramidal $^2A_1$	1.080	118.3	11
4-31G	planar $^2A_2''$	1.070	120	11
Exptl.	planar $^2A_2''$	1.079	120	8

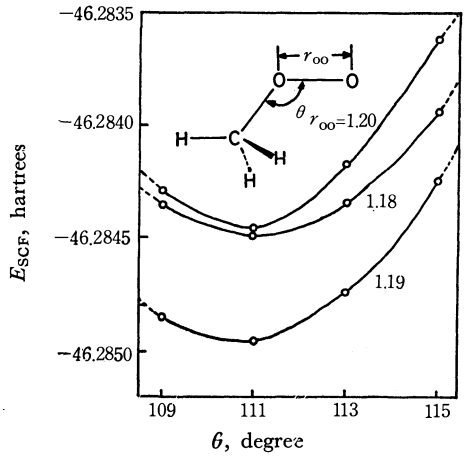

Fig. 1. SCF total energies E_{SCF} of CH_3O_2 as a function of two geometric parameters (r_{OO} and θ).

iterative extended Hückel MO treatment.[14] The CNDO/2 investigation is carried out on CH_3O_2 with the O–O bondlength (r_{OO}) of 1.15∼1.45 Å and the bond angle of C-O-O (θ) of 103∼115° under the fixed angle of HCH, 109°28′. Fig. 1 presents the SCF total energies, E_{SCF}, of CH_3O_2 as a function of two geometric parameters, r_{OO} and θ. As can be seen from Fig. 1, CH_3O_2 with r_{OO}=1.19 Å and θ=111° is shown to be the energetically most stable species. The predicted angle of 111° differs by only 3° from that of HO_2 (108°) obtained from the vibration spectrum study of Paukert and Johnston,[15] but it differs considerably from the HO_2 angle of 104.6°[16] predicted using the *ab initio* SCF–CI calculation.

On the other hand, our predicted O–O bond distance, 1.19 Å, is much closer to that of diatomic O_2 (1.207 Å[13]) than that of H_2O_2 (1.475 Å[17]) or HO_2 (1.458 Å[16]).

Some remarks will be now made concerning the electronic property of CH_3O_2 on the basis of the computed results listed in Table 2. The estimated ionization potential of 13.83 eV is slightly less than that of 14.66 eV[18] found in HO_2. This may be in harmony with the opinion that the larger the alkyl group, R, in the RO_2 radical becomes, the more the ionization potential is lowered.[14] Moreover, the g value (2.003) computed by the Stone equation[21] is somewhat less than that of the experiment (2.015).[14]

Here, it may be worthy of emphasis that the expansion of the radical spin orbital is perpendicular to the cross-section of the C–O–O (xy-plane in Table 2).

Table 2. Electronic property of CH_3O_2

Minimum energy, hartrees		−46.285
Bond length of O-O, Å		1.19
Bond length of C-O, Å		1.44
Bond angle of C-O-O, deg.		111
Dipole moment,[a] Debye		2.163
Ionization potential,[b] eV		13.83
g value		2.003
Electron density	O_α	6.032
	O_β	6.106
	C	3.899
AO electron density of O_β	p_x[c]	1.106
	p_y[c]	1.986
	p_z[c]	1.188

a) The direction of dipole moment (μ) is indicated below. b) This is derived from the MO level of the highest occupied orbital of CH_3O_2. c) As to the directions of orbital expansions, see the following figure:

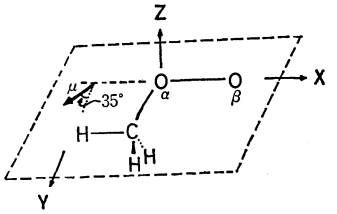

Bimolecular Coupling Reaction of CH_3 and $^3\Sigma_g^-$ O_2. The interacting system of CH_3–O_2 has four geometric parameters,[22] *i.e.*, the bond lengths of O–O and C–O and the bond angles of C–O–O and H–C–O. The SCF total energies, E_{SCF}, as a function of the above four geometric parameters have only one minimum

14) O. Yamamoto, H. Kato, and T. Yonezawa, *Nippon Kagaku Zasshi*, **91**, 907 (1970).
15) T. T. Paukert and H. S. Johnston, University of California Radiation Laboratory Report, No. UCRL-19109 (1969).
16) D. H. Liskow, H. F. Schaefer III, and C. F. Bender, *J. Amer. Chem. Soc.*, **93**, 6734 (1971).
17) R. H. Hunt, R. A. Leacock, C. W. Peters, and K. T. Hecht, *J. Chem. Phys.*, **42**, 1931 (1965).
18) The ionization potential of the energetically most stable HO_2 (r_{OO}=1.19 Å, r_{OH}=0.96 Å, and the bond angle=111°) was estimated to be 14.66 eV by the CNDO/2 treatment (K. Ohkubo *et al.*, unpublished data). Experimentally, that of the HO_2 was found to be 11.53 eV[19] and/or 12.2 eV.[20]
19) S. N. Foner and R. L. Hudson, *J. Chem. Phys.*, **36**, 2681 (1962).
20) A. J. B. Robertson, *Trans. Faraday Soc.*, **48**, 228 (1952).
21) A. J. Stone, *Mol. Phys.*, **6**, 509 (1963).
22) One unknown geometric parameter of the C–H interatomic distance can be settled uniformly to be 1.09 Å on the basis of usual C–H bond length (1.09 Å).[23]
23) L. E. Sutton, Editor, "Interatomic Distances," The Chemical Society, London (1958).

Table 3. Electron densities of momentarily-living intermediate CH_3-O_2.[a)]

Atom	AO	Electron densities as a function of C-O distance				
		∞	2.0 Å	1.8 Å	1.6 Å	1.44 Å
C	p_y' [b)]	1.000		0.838		0.858
	p_z	0.978	1.005	1.006	1.003	0.998
	net charge	4.097	3.984	3.961	3.932	3.899
H	s	0.968	0.966	0.971	0.978	0.989
O_α	s	1.802	1.780	1.746	1.698	1.644
	p_x	1.198	1.209	1.205	1.201	1.191
	p_y	1.500	1.273	1.292	1.339	1.402
	p_z	1.500	1.772	1.791	1.797	1.795
	net charge	6.000	6.034	6.034	6.035	6.032
O_β	s	1.802	1.818	1.821	1.822	1.822
	p_x	1.198	1.140	1.127	1.117	1.106
	p_y	1.500	1.910	1.949	1.976	1.986
	p_z	1.500	1.228	1.207	1.195	1.188
	net charge	6.000	6.096	6.104	6.110	6.106

a) The geometry of CH_3-O_2 is the same to that in Table 2.
b) The nonbonding carbon p-orbital of CH_3.

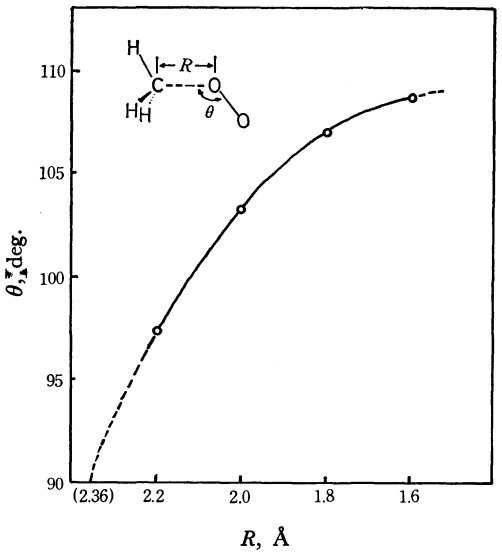

Fig. 2. Bond angle of C-O-O (θ) as a function of C-O distance (R) along the minimum potential barrier.

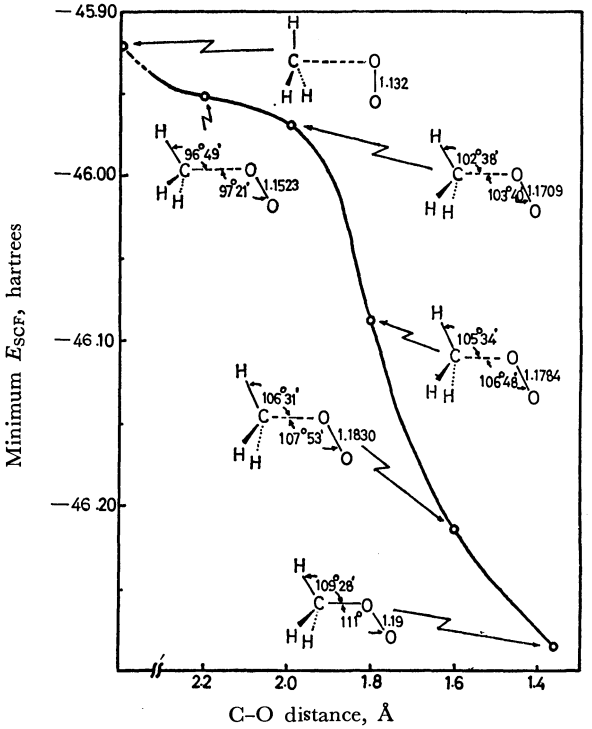

Fig. 3. Changes in minimum SCF total energies and configurations of CH_3--O_2 along the reaction path, $CH_3+O_2 \rightarrow CH_3$--$O_2$.

E_{SCF} value: this is an inevitable consequence from the basic quantum principle. The process of the coupling reaction of CH_3 and O_2 will, then, be estimated by gradually curtailing the C–O distance, giving attention to the minimum energy surface and the geometric transformation of the momentarily-living CH_3–O_2. The curve of the minimum E_{SCF} value as a function of the C–O distance is shown in Fig. 2, together with the configuration of CH_3–O_2. As Fig. 2 indicates, the coupling reaction proceeds smoothly, without any appreciable peak of the electronic energy path.

It is of interest to predict the C–O distance at the start of the reaction between CH_3 and O_2 before discussing the geometric transformation of CH_3–O_2. Bearing in mind the initial mode of the interaction between CH_3 and O_2 (*viz.*, $\angle COO=90°$), the abovementioned C–O distance surely corresponds to the R value (C–O distance) at $\angle COO=90°$ under a minimum energy surface. Judging from the correlation between R and θ (angle of C–O–O) under such a minimum energy surface (see Fig. 2), the coupling reaction of CH_3 and O_2 should start at $R=2.36$ Å ($\theta=90°$).

With regard to the geometric transformation of CH_3—O_2 through the reaction progress, the following aspects are noticeable: slack expandings of $\angle HCO$ and $\angle COO$ with a gradual stretching of the O–O follows the hasty widening of both the angles with the lengthening of the O–O under $R<2.0$ Å (see Fig. 2).

Mention should also be made here of the electron migration between CH_3 and O_2 through the reaction. Taking into consideration the electron densities of

the s and p orbitals on the carbon or oxygen atom (see Table 3), the predominant electron-migration can be depicted by the following representations.

The electron once transferred from the nonbonding half-occupied carbon p_y'-orbital to the O_α p_y-orbital through a $p\sigma$-type overlapping migrates further to the O_β p_y-orbital through $p\pi$-delocalization:

$$p_y'^{(C)} \xrightarrow{\text{through } p\sigma \text{ of C-O}\alpha} p_y^{(O\alpha)} \xrightarrow{\text{through } p_y\pi \text{ of } O_2} p_y^{(O\beta)}$$

There exists a back-donation from the O_β p_z-orbital to the O_α p_z-orbital through the $p\pi$-conjugation:

$$p_z^{(O\beta)} \xrightarrow{\text{through } p_z\pi \text{ of } O_2} p_z^{(O\alpha)}$$

However, further back-donation from the O_β p_z-orbital to the C p_z-orbital through the pseudo π orbital of the C–O_α bond cannot be expected, as may be seen from Table 3.

The calculations were carried out on a FACOM 230—60 computer at the Data Processing Center of Kyushu University.

BULLETIN OF THE CHEMICAL SOCIETY OF JAPAN, VOL. 46, 2945—2949 (1973)

The Crystal Structure of an *N*-Methylphenothiazine–7,7,8,8-Tetracyanoquinodimethane Complex, *N*-MePZT–TCNQ

Hayao KOBAYASHI

Department of Chemistry, Faculty of Science, Toho University, Narashino, Chiba 275

(Received March 2, 1973)

Crystals of the 1 : 1 charge-transfer complex of *N*-MePZT-TCNQ are monoclinic with those lattice constants: $a=10.904$, $b=13.321$, $c=7.086$ Å, and $\beta=91.06°$, and with the space group C2/m. X-ray structure analysis showed that the mixed-stacks of *N*-MePZT and TCNQ exist along the c axis. *N*-MePZT is disordered, and its apparent molecular symmetry is C_{2h}, taking four possible conformations. The molecular geometry of TCNQ indicates that the amount of the charge transferred from *N*-MePZT is very small ($<0.2e$).

7,7,8,8-tetracyano-*p*-quinodimethane (TCNQ) is a powerful electron acceptor and forms a number of charge-transfer complexes. *N*-methylphenothiazine (*N*-MePZT) is an electron donor. A neutral *N*-MePZT molecule has a folded structure,[1] while the PZT skeleton is planar in crystals of trinitrobenzene-PZT.[2] As was pointed out by Fritchie,[2] the van der Waals packing requirement of an alternating donor-acceptor stack might suggest that PZT is essentially planar in a 1 : 1 complex. Crystals of *N*-MePZT-TCNQ were subjected to X-ray structure analysis in order to examine the molecular structure of the component molecules.

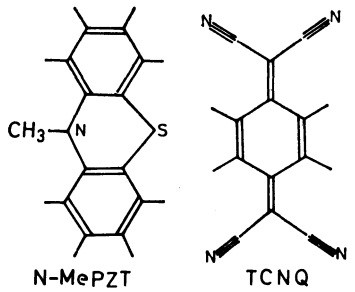

Fig. 1. The molecular structures of *N*-MePZT and TCNQ.

Experimental

Black crystals of *N*-MePZT-TCNQ were obtained by the slow evaporation of an equimolar acetone solution of the components. Oscillation and Weissenberg photographs showed the crystal to be monoclinic. The systematic absence for *hkl* with $h+k=2n+1$ indicated that the space group is C2/m, Cm, or C2. The unit-cell dimensions, as determined by means of a diffractometer with Mo$K\alpha$ radiation, are $a=10.904\pm0.002$, $b=13.321\pm0.002$, $c=7.086\pm0.001$ Å, and $\beta=91.06\pm0.04°$. The density measured by the flotation method was 1.32 g/cm^3, whereas the calculated density on the assumption of $Z=2$ is 1.347 g/cm^3. The intensity data were collected on a Rigaku automated four-circle diffractometer by employing a ω–2θ scan technique. A crystal with dimensions of $0.25\times0.13\times0.18$ mm was used. Of the 1274 accessible reflections with $2\theta\leqq55°$, significant counts were recorded for 576 reflections. Measurements of two reference reflections, (2,0,0) and (0,0,2), were repeated every fifty reflections.

Structure and Determination

The trial structure was easily deduced from packing considerations. The space group C2/m was assumed; this was verified at a latter stage. Refinements were performed by means of Fourier synthesis, followed by the block-diagonal least-squares method. Three hydrogen atoms (H1, H2, and H3 in Table 1) were found on the three-dimensional-difference Fourier maps and were refined isotropically. No hydrogen atoms of the methyl group came out. Because of the requirements of the space group, the orientation of *N*-MePZT must be disordered and the apparent molecular symmetry is C_{2h}, which seems to be consistent with the fact that diffuse scattering appears around strong Bragg reflections. Possible models of the disordered structure of *N*-MePZT were easily deduced. The model shown in Fig. 2 is the most plausible one because the difference Fourier synthesis shows nitrogen and sulfur atoms

1) N. Wakayama, This Bulletin, **44**, 2847 (1971).
2) C. J. Fritchie, *J. Chem. Soc.*, *A*, **1969**, 1328.

TABLE 1. FINAL ATOMIC PARAMETERS (ALL $\times 10^4$) AND THEIR ESTIMATED STANDARD DEVIATIONS

Temperature factor $= \exp[-(B_{11}h^2+B_{22}k^2+B_{33}l^3+2B_{12}hk+2B_{13}kl+2B_{23}kl)]$

	x	y	z	B_{11}	B_{22}	B_{33}	B_{12}	B_{13}	B_{23}
				N-MePZT					
S	−290	1482	487	135	112	331	2	−59	7
	8	5	12	13	5	29	5	10	9
N1	0	963	0	276	181	422	0	−185	0
		6		10	4	21		9	
C1	1152	524	502	190	95	167	17	−53	10
	5	3	6	6	4	10	4	6	6
C2	2225	1026	983	199	96	212	−22	3	34
	5	4	6	7	4	12	5	7	7
C3	3289	521	1435	147	142	327	−31	81	22
	4	4	7	7	6	14	5	8	7
C4	−171	1808	449	109	154	183	−10	−74	157
	37	15	32	36	18	90	25	45	33
H1	2115	1658	921	9.1[a]					
	43	40	66	1.5					
H2	3964	865	1264	8.2					
	40	36	62	1.5					
				TCNQ					
N2	3686	1645	6407	138	75	398	−13	−12	−4
	3	3	5	5	3	12	3	6	6
C5	604	941	5220	93	43	281	2	22	−2
	3	3	6	4	2	11	3	6	5
C6	1252	0	5449	68	49	210	0	24	0
	5		8	6	4	15		7	
C7	2483	0	5933	115	32	236	0	21	0
	5		8	8	4	17		9	
C8	3166	900	6207	108	52	254	12	0	4
	4	3	6	5	3	11	3	6	5
H3	1033	1603	5335	5.1					
	33	33	54	1.1					

a) Isotropic temperature factor *B*.

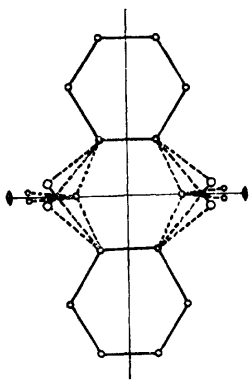

Fig. 2. The model of the disordered structure of *N*-MePZT.

separately. The nitrogen atom lies on the twofold axis, while the sulfur atom is in general position. Anisotropic refinement gave an *R*-value of 0.096. Other models were also considered, but they did not give good *R*-values. The final positional and thermal parameters are given in Table 1. The observed and calculated structure factors are compared in Table 2.

Results and Discussion

The structure is shown in Fig. 3. It consists of mixed stacking columns of alternating donor (*N*-MePZT) and acceptor (TCNQ) molecules. The mode of overlapping is shown in Fig. 4. The average intermolecular distance is 3.44 Å; the least-squares planes of both the molecules are given in Table 3.

The crystal structure analyses of neutral phenothiazine (PZT) and *N*-MePZT have revealed that these molecules have a non-planar structure folded along the N–S direction. A PZT molecule in a crystal of a PZT-3,5-dinitrobenzene complex has a folded structure with a dihedral angle of 156°,[3] and it is planar in a PZT-TNB (trinitrobenzene) complex.[2] Fritchie suggested that a PZT molecule in PZT-TNB is actively folding at room temperature, taking two possible conformations with dihedral angles of about 165—172°.

3) C. J. Fritchie and B. L. Trus, *Chem. Commun.*, **1968**, 833.

TABLE 2. COMPARISON OF OBSERVED AND CALCULATED STRUCTURE FACTORS (×10)

H	K	FO	FC
	L=0		
11	1	40	44
11	3	18	18
11	5	29	28
11	9	24	20
10	0	27	25
9	1	39	48
9	3	41	40
8	4	64	67
8	6	126	126
8	8	23	24
8	10	26	23
7	1	48	50
7	3	66	66
7	5	45	45
7	11	19	19
7	15	27	26
6	0	48	54
6	2	28	30
6	4	35	38
6	8	45	43
6	10	28	34
5	1	116	111
5	3	208	201
5	5	28	35
5	7	87	91
5	11	27	24
4	0	128	127
4	2	59	58
4	4	69	69
4	6	65	59
4	8	66	69
4	10	42	53
3	1	321	315
3	3	255	248
3	5	111	103
3	7	45	34
3	9	59	60
3	11	35	36
3	13	32	22
2	0	143	150
2	2	223	216
2	4	93	91
2	10	55	55
0	2	559	585
0	4	373	375
0	6	52	41
0	8	30	22
	L=1		
-14	2	27	3
-11	5	20	10
-10	0	41	44
-10	2	28	12
-10	8	20	5
-9	3	21	3
-9	5	63	69
-9	7	50	54
-8	2	19	19
-8	4	67	73
-8	6	97	96
-8	8	42	31
-7	1	29	33
-7	3	29	41
-7	5	26	24
-7	9	37	30
-6	0	47	38
-6	2	73	74
-6	4	25	29
-6	6	16	17
-6	8	47	43
-6	10	38	40
-5	1	82	79
-5	3	180	172
-5	5	98	91
-5	7	21	24
-5	9	55	65
-5	11	62	71
-5	13	23	16
-4	0	73	74
-4	2	101	95
-4	4	45	43
-4	6	117	113
-4	10	35	27
-3	1	103	101
-3	3	241	233
-3	5	169	166
-3	7	66	66
-3	11	45	43
-3	15	45	42
-2	0	196	192
-2	2	156	144
-2	4	61	69
-2	6	173	178
-2	10	39	29
-2	12	28	41
-2	14	24	20
-1	1	115	106
-1	3	127	120
-1	5	38	45
-1	7	42	31
-1	9	107	107
-1	11	106	107
0	0	83	65
0	4	37	55
0	6	82	70
0	8	83	77
0	10	141	137
0	12	99	109
1	1	110	98
1	3	335	321
1	5	112	108
1	7	102	107
1	9	82	86
1	13	41	34
2	0	84	94
2	2	70	74
2	4	211	198
2	6	125	122
2	8	49	45
2	10	33	25
2	14	55	39
3	3	95	94
3	5	112	110
3	7	118	117
3	9	25	17
3	11	38	38
3	13	36	0
3	15	29	14
4	0	291	284
4	2	176	170
4	4	278	266
4	6	45	51
4	8	37	49
4	10	42	53
4	12	56	53
4	14	22	11
5	1	104	104
5	3	26	18
5	5	61	54
5	9	61	72
5	11	30	34
6	0	111	112
6	4	15	11
6	6	78	83
6	10	33	28
7	1	37	33
7	3	84	93
7	5	76	79
7	7	59	66
7	9	27	13
8	0	61	64
8	2	24	25
8	4	72	72
8	6	101	106
8	8	23	32
9	1	60	57
9	3	29	32
9	9	28	18
10	2	20	15
10	8	17	14
11	1	22	19
11	9	22	11
12	6	26	17
	L=2		
-12	0	36	38
-12	4	19	8
-11	1	36	31
-10	2	26	35
-10	6	20	15
-9	3	32	31
-9	5	83	83
-9	7	55	54
-8	2	78	76
-8	4	69	72
-8	6	43	41
-8	8	23	13
-7	1	14	1
-7	3	25	27
-7	7	34	36
-7	9	29	23
-6	0	58	56
-6	2	114	110
-6	4	49	47
-6	6	52	60
-6	10	25	24
-6	14	19	13
-5	1	136	131
-5	3	21	6
-5	5	30	38
-5	7	16	10
-5	9	53	56
-4	0	187	185
-4	2	32	34
-4	4	92	88
-4	6	73	67
-4	8	43	47
-4	14	20	6
-4	16	21	21
-3	1	69	65
-3	3	135	140
-3	5	27	7
-3	9	60	55
-3	11	19	18
-2	0	30	25
-2	2	50	44
-2	6	60	52
-2	8	30	38
-2	16	21	1
-1	1	983	1000
-1	3	76	77
-1	5	157	150
-1	7	20	19
-1	11	89	101
-1	13	64	47
0	0	577	588
0	2	220	217
0	4	92	96
0	6	49	37
0	8	22	26
0	10	40	50
0	12	51	40
0	14	27	7
1	1	195	201
1	3	63	63
1	7	18	24
1	9	19	18
1	11	43	43
2	0	417	412
2	2	82	79
2	4	232	229
2	8	61	60
2	10	41	30
2	12	33	36
2	16	36	33
3	3	103	101
3	5	112	111
3	9	65	71
3	11	18	31
3	15	21	1
4	0	82	74
4	2	186	182
4	4	110	103
4	6	78	91
4	8	57	59
4	10	22	14
5	1	42	46
5	3	137	146
5	7	15	16
5	9	67	63
6	0	28	31
6	2	15	10
6	4	25	30
6	8	16	6
7	1	24	30
7	5	104	112
7	7	96	88
7	13	25	15
8	0	98	106
8	2	31	35
8	6	40	43
9	1	21	13
9	5	21	14
9	7	22	12
10	0	22	26
10	2	49	46
10	4	20	2
10	6	39	41
10	10	36	30
11	5	21	6
	L=3		
-10	0	18	18
-9	1	27	20
-9	5	63	73
-9	7	57	54
-8	6	16	10
-8	8	24	20
-7	1	20	23
-7	3	50	52
-7	5	17	11
-7	9	20	23
-6	0	34	22
-6	4	51	53
-6	6	41	37
-6	8	32	39
-6	10	64	66
-6	12	36	30
-5	1	20	13
-5	3	55	61
-5	5	23	8
-5	13	21	3
-4	0	135	137
-4	2	53	54
-4	4	156	155
-4	6	59	60
-4	10	34	26
-3	1	26	14
-3	5	76	74
-3	7	55	57
-3	13	22	23
-3	15	23	14
-2	0	104	108
-2	2	21	20
-2	4	69	65
-2	8	46	45
-2	10	71	66
-2	12	27	30
-1	1	29	23
-1	3	47	48
-1	5	53	52
-1	7	65	68
-1	9	84	78
-1	11	114	115
-1	13	51	57
-1	15	24	7
0	0	73	76
0	2	109	109
0	4	74	69
0	6	88	88
0	8	26	37
0	10	68	55
1	3	53	52
1	5	101	100
1	7	66	61
1	11	18	6
1	13	27	25
1	15	23	26
2	0	59	53
2	2	28	24
2	4	55	51
2	6	105	103
2	8	50	50
2	10	37	30
3	1	71	71
3	3	270	268
3	5	42	38
3	7	81	85
3	9	22	20
3	11	34	42
3	13	33	14
4	0	131	130
4	2	22	24
4	4	80	79
4	6	36	31
4	8	36	45
4	10	46	57
4	12	33	30
4	14	25	10
5	1	67	60
5	3	19	29
5	5	40	49
5	7	50	52
5	13	23	16
5	15	26	11
6	0	103	107
6	2	42	46
6	4	85	89
6	8	36	25
7	1	74	76
7	3	43	44
7	5	112	111
7	7	68	68
8	0	104	107
8	4	45	48
9	1	35	35
9	5	23	7
10	0	35	32
10	2	17	13
11	3	28	15
	L=4		
-12	0	34	27
-10	4	35	37
-10	6	31	38
-9	3	24	31
-9	5	51	49
-9	7	35	30
-8	0	24	15
-8	4	26	22
-7	1	44	40
-7	3	30	33
-6	0	110	108
-6	2	44	41
-6	4	20	4
-6	6	20	25
-5	1	21	29
-5	3	22	21
-5	5	33	46
-5	7	47	47
-5	11	26	19
-4	0	16	13
-4	2	42	39
-4	4	37	33
-4	8	32	32
-3	1	69	66
-3	3	22	23
-3	5	24	24
-3	7	16	6
-3	11	21	16
-2	0	410	397
-2	2	187	183
-2	4	58	60
-2	6	59	57
-2	10	45	48
-2	12	43	44
-2	14	27	0
-1	1	291	280
-1	3	33	24
-1	5	52	51
-1	9	24	28
-1	11	51	54
-1	13	24	26
0	0	143	141
0	2	25	26
0	4	25	31
0	8	17	9
0	14	30	1
1	1	53	55
1	3	113	114
1	5	34	29
1	9	45	47
2	0	75	69
2	2	28	22
2	4	108	105
2	6	38	37
2	8	25	31
2	10	35	42
3	1	82	83
3	3	91	88
3	7	61	60
3	9	31	33
3	13	25	3
4	0	52	56
4	2	80	75
4	4	69	73
4	6	43	49
4	8	17	20
4	10	45	39
5	3	15	6
5	9	24	21
6	0	50	47
6	4	22	25
6	6	79	83
6	10	34	31
7	1	84	87
7	5	44	43
7	7	40	41
8	0	51	53
8	4	20	16
8	6	22	7
8	10	19	7
9	3	47	39
11	1	26	7
	L=5		
-10	4	36	27
-10	6	42	39
-9	3	19	15
-9	9	19	7
-8	2	27	21
-8	8	24	8
-7	9	40	40
-6	2	16	6
-6	4	27	21
-6	12	27	15
-5	1	40	31
-5	3	63	66
-5	5	57	54
-4	0	48	50
-4	4	53	49
-4	6	38	38
-3	1	20	25
-3	3	20	19
-3	9	24	24
-2	0	46	45
-2	6	43	47
-2	8	41	40
-2	10	58	61
-2	12	54	57
-1	1	37	36
-1	3	22	21
-1	9	33	43
-1	11	23	24
0	4	35	36
0	6	44	45
0	12	20	17
1	1	36	44
1	3	47	44
1	5	49	51
1	7	49	49
1	11	24	21
2	2	72	67
2	4	78	79
2	6	39	42
2	8	40	37
2	12	21	16
3	1	44	44
3	3	47	44
3	5	40	51
3	9	33	36
3	11	31	40
4	0	35	29
4	2	24	16
4	4	17	10
4	6	32	32
4	8	21	12
5	1	32	33
5	3	55	56
5	9	31	28
6	0	89	88
6	4	69	73
6	6	67	65
7	1	61	62
7	3	28	33
7	5	32	31
8	0	48	52
8	2	25	2
9	1	33	25
	L=6		
-9	5	18	5
-8	0	26	14
-7	1	32	44
-6	6	20	29
-4	0	58	58
-4	6	19	11
-4	10	18	7
-3	1	98	100
-3	5	33	37
-2	0	148	149
-2	2	84	89
-2	12	28	35
-1	1	30	34
-1	3	37	37
0	2	21	19
1	3	37	37
1	5	43	48
2	0	55	58
2	2	29	33
2	4	23	29
2	8	26	37
3	1	21	25
3	3	44	44
3	11	23	7
4	4	18	11
5	1	19	15
5	5	20	23
6	0	76	71
6	2	28	24
6	6	40	41
10	0	25	10
	L=7		
-7	3	23	5
-6	4	32	26
-6	6	18	13
-4	0	19	10
-3	7	28	21
-2	8	20	16
-1	5	19	15
0	0	36	42
0	4	35	32
0	8	20	21
2	4	29	33
3	3	18	19
5	1	29	35
5	5	27	44
5	7	28	22
6	0	38	45
7	1	25	20
	L=8		
-4	0	29	28
-3	1	49	58
-2	2	26	13
-1	1	19	22
-1	3	17	4
0	0	20	2
1	1	20	23
2	0	30	32
2	2	25	16
5	1	32	27
6	0	28	27
	L=9		
-2	0	21	13

TABLE 3. LEAST-SQUARES PLANES

	Direction cosines with respect to		
	a	*b*	*c**
N-MePZT	−0.2727	−0.0074	0.9621
TCNQ	−0.2386	−0.0046	0.9711

Deviation (Å)								
N-MePZT	C1	−0.004	C2	0.002	C3	0.001	C4[a]	0.341
	S[a]	0.405	N1[a]	−0.010				
TCNQ	C5	−0.011	C6	−0.016	C7	−0.001	C8	0.005
	N2	0.004						

a) The atoms C4, S, and N1 were not used for the the calculation of least-squares plane.

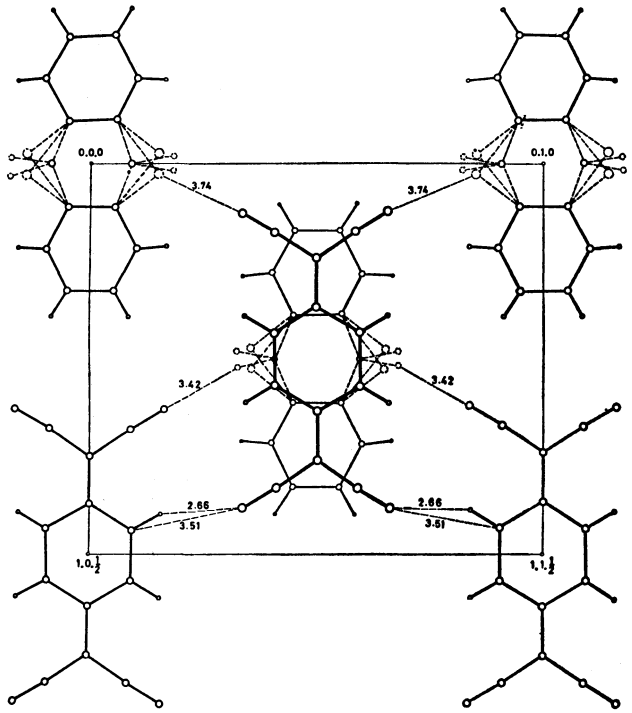

Fig. 3. The molecular arrangement and the short contacts in the plane (102), viewed along the *c* axis.

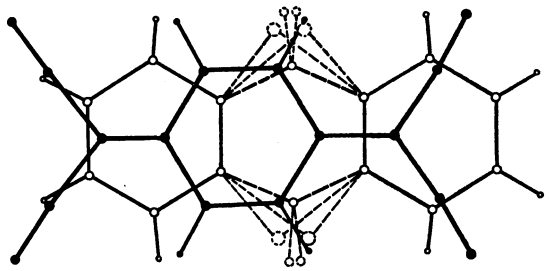

Fig. 4. The molecular overlap as viewed in the direction perpendicular to the mean molecular planes.

In view of the fact that the molecular symmetry of *N*-MePZT is C_{2h} and that the sulfur atom deviates about 0.4 Å from the molecular plane (Table 3), it may be reasonable to conclude that *N*-MePZT is disordered, taking four conformations with dihedral angles of about 160—170 °C with equal probability as is shown in Fig. 5. In addition, the nitrogen atom is

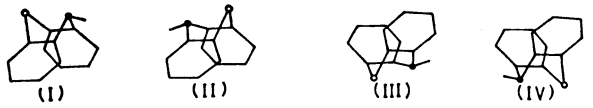

Fig. 5. The accessible structures and orientations of *N*-MePZT.

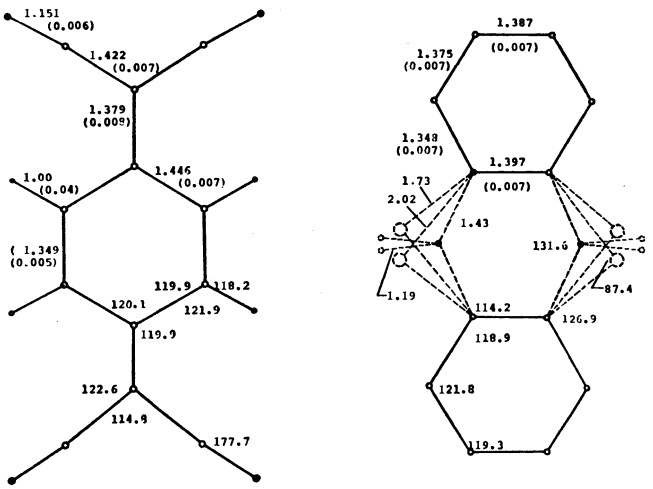

Fig. 6. Bond lengths(Å) and angles(°).
The estimated standard deviations of bond lengths are shown in parentheses. Those of bond angles are about 0.50° for all the angles spanned by non-hydrogen atoms except carbon atom of methyl group and about 4.0° for the angles involving the hydrogen atoms and carbon atom of methyl group.

on the twofold axis, that is, on the molecular plane; this is consistent with the small deviation of the nitrogen atom from the molecular plane in neutral *N*-MePZT and PZT[1,4] (0.07, 0.03 Å).

The bond lengths and angles are shown in Fig. 6. The two C–S bonds are 1.73 and 2.02 Å, giving a mean value of 1.87 Å (Fig. 6), and N–C is 1.43 Å. These values are consistent with those of neutral *N*-MePZT, (1.82, 1.43 Å). The C–C bonds parallel to the twofold axis of the molecule are longer than the others, and the N–C (methyl) bond is very short. These facts are undoubtedly due to the disorder of *N*-MePZT.

The molecular structure of TCNQ is normal. The

4) J. D. Bell, J. F. Blount, O. V. Briscoe, and H. C. Freeman, *Chem. Commun.* **1968**, 1656.

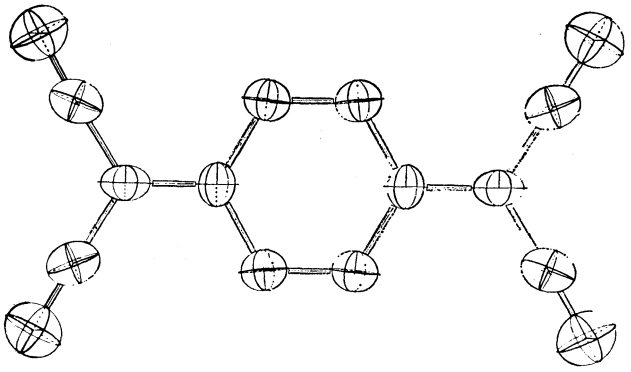

Fig. 7. *ORTEP* plot of the thermal motion ellipsoid of TCNQ.

TABLE 4. RIGID-BODY THERMAL PARAMETRES OF TCNQ

Principal axes in the form: **La+Mb+Nc**

axis	**L**	**M**	**N**
1	0.0894	0.0	0.0340
2	0.0	−0.0751	0.0
3	−0.0204	0.0	0.1370

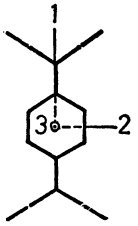

Molecular vibrational tensors

$$\mathbf{T}\times 10^4 = \begin{pmatrix} 624 & 0 & 48 \\ & 352 & 0 \\ & & 508 \end{pmatrix} \text{Å}^2 \qquad \boldsymbol{\omega}\times 10 = \begin{pmatrix} 323 & 0 & 9 \\ & 9 & 0 \\ & & 41 \end{pmatrix} \text{deg}^2$$

Principal axes of the **T** and $\boldsymbol{\omega}$ tensors relative to the molecular axes.

R.m.s. amplitude	Direction cosines		
0.19 Å	0.0	1.0	0.0
0.22	0.335	0.0	−0.942
0.25	0.942	0.0	0.336
0.9°	0.0	1.0	0.0
2.0	0.030	0.0	0.999
5.7	0.999	0.0	0.030

bond lengths shown in Fig. 6 are uncorrected for thermal libration. Some rigid-body parameters for TCNQ are given in Table 4 and Fig. 7. The translational motion nearly isotropic while the libration is quite anisotropic. The r.m.s. amplitude of 5.7° about the long axis is the largest.

Recent studies of TCNQ anion radical salts have revealed a dependence of the molecular geometry on its formal charge ($TCNQ^0$, $TCNQ^{-1/2}$, $TCNQ^-$).[5,6] In a charge-transfer complex, TCNQ may be charged to some extent according to the magnitude of the charge-transfer interaction. If the bond lengths obtained are sufficiently accurate, they will show values intermediate between those of $TCNQ^0$ and $TCNQ^-$. The bond lengths of TCNQ in the charge-transfer complexes so far reported are summarized in Fig. 8. The standard bond lengths of $TCNQ^0$, $TCNQ^{-1/2}$, and $TCNQ^-$ are taken mainly from Refs. 5 and 6. This

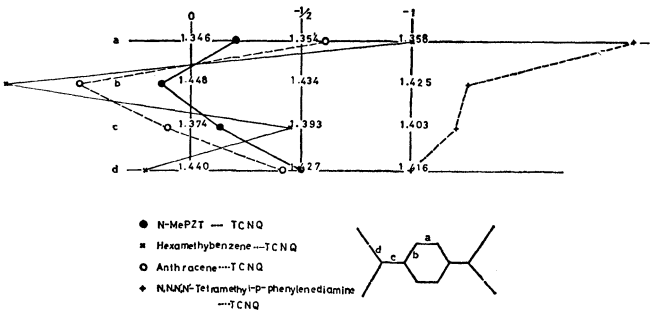

Fig. 8. The bond lengths of TCNQ.
The values are corrected for thermal vibration.

figure can be regarded as a diagram which relates bond length to the amount of transferred charge, δ ($TCNQ^{-\delta}$). The "a" bond lengths of $TCNQ^0$ (neutral molecule), $TCNQ^{-1/2}$, and $TCNQ^-$ are 1.346, 1.354, and 1.358 Å respectively. The "a" bond elongates with an increase in the charge transferred from a donor to TCNQ. Thus, the bond lengths seem to be a rough measure of the amount of charge-transfer. For example, the "a" bond seems to show the formal charge, δ, of TCNQ ($TCNQ^{-\delta}$) of about 0.25 in an *N*-MePZT-TCNQ complex. The dots corresponding to the observed bond length are scattered, probably because of the inaccuracy of the experiments. Despite the inaccuracy, the diagram seems to indicate that the average bond lengths of TCNQ in *N*-MePZT, anthracene-TCNQ,[7] and hexamethylbenzene-TCNQ[8] correspond to those of molecules with a small formal charge ($\delta<0.2$). In the case of *N*-MePZT-TCNQ, the amount of transferred electrons seems to be about 0.15e. The ESR, IR, and electronic spectra indicate that an *N*-MePZT-TCNQ complex is not an ionic type but almost neutral,[9] and they support the above conclusion. In tetramethyl-*p*-phenylenediamine (TMPD)-TCNQ,[10] the distribution of the bond lengths differs from the distributions of those of the other non-ionic complexes. The electron transferred from TMPD to TCNQ seems to be more than one, which is a rather unexpected situation.

The crystal structure of *N*-MePZT-TCNQ is similar to that of the average structure of PZT-TCNQ.[11] The main difference between the two complexes is that the former has the orientational disorder of *N*-MePZT, while the latter is a sinusoidally modulated structure. In the crystal of PZT-TCNQ, PZT are held by hydrogen bonds of N–H=N type. On the other hand, in *N*-MePZT-TCNQ, *N*-MePZT are packed loosely by van der Waals forces. Thus, the orientation of *N*-MePZT is likely to be easily disordered.

The author would like to express his thanks to Professor Yoshihiko Saito for his keen interest. He also wishes to thank Professor Minoru Kinoshita and Dr. N. S. Bhat for valuable discussions and information.

5) T. Sundaresan and S. C. Wallwork, *Acta Crystallogr.*, *B***28**, 1163 (1972).
6) P. Goldstein, K. Seff, and K. N. Trueblood, *ibid.*, *B***24**, 778 (1968).
7) R. M. Williams and S. C. Wallwork, *ibid.*, *B***24**, 168 (1968).
8) R. H. Colton and D. E. Henn, *J. Chem. Soc.*, *B*, **1970**, 1532.
9) N. S. Bhat and M. Kinoshita, private communication.
10) A. W. Hanson, *Acta Crystallogr.*, **19**, 610 (1965).
11) H. Kobayashi and Y. Saito, to be published.

The Effects of Doubly-excited Configurations in the P-P-P-CI Calculation

Hiroyuki SHINODA, Hidenobu TATEMATSU, and Tomoo MIYAZAKI

Department of Applied Chemistry, Faculty of Science and Engineering, Waseda University, Nishi-Ohkubo, Shinjuku-ku, Tokyo 160

(Received March 7, 1973)

The effects of doubly-excited configurations, especially of the χ_{kl}^{mn} type, on the results of P-P-P-CI calculations of unsaturated compounds have been discussed by comparing the results obtained by three different types of CI treatment. The calculations of the pi-electronic total energies of ground states, the electronic transition energies, the oscillator strengths, and the pi-electronic densities of sixteen molecules were performed. The core resonance integrals and electronic repulsion integrals were readjusted so that the transition energies, obtained by CI calculations considering all the singly- and doubly-excited configurations, might coincided with the experimental results. From the results of these calculations, it is found that χ_{kl}^{mn}-type configurations play an important role in CI calculation.

Although the configuration interaction (CI) treatment considering singly-excited configurations has been investigated in detail in connection with molecular orbital (MO) calculations, few studies of the CI treatment considering doubly-excited configurations have been done.[1-6] Evleth[1] calculated transition energies by means of the P-P-P method,[7-9] the LCAO-SCF-MO method in the Pariser-Parr-Pople scheme, followed by CI treatment considering doubly-excited configurations (DEC's) under the restriction of considering only the highest two occupied levels of MO. He concluded that the DEC's are important to the calculation for transition energies which are also affected by the parameters used in the SCF-MO calculation. Allinger and Stuart[2] investigated the contribution of higher excited configurations in the CI calculations of transition energies for several unsaturated hydrocarbons. They concluded that it is not necessary to include all of the doubly-excited configurations, but it is necessary to include some triply-excited configurations, and that the higher excited configurations may be cut off at 20 eV over the ground configuration. Kashiwagi[3] calculated several electronic properties of non-alternant hydrocarbons by the P-P-P-CI method, taking account of a cut-off treatment such as has been described above. He found that the oscillator strengths and pi-electronic densities of excited states are sensitive to the introduction of DEC to the CI calculation, while transition energy to low excited states are rather insensitive, and that the introduction of DEC gives satisfactory results in the calculation of oscillator strengths. The appropriate condition of the cut-off treatment determined in his work was 13 eV. Hirota and Nagakura[4] discussed the effects of parameters and DEC's on several electronic properties calculated by the P-P-P-CI method for the molecules containing hetero-atoms. They found that the CI treatment including DEC's reduced the effect of one-center core integrals upon the calculated energy levels, and that the oscillator strengths for electronic transitions and the separations between the lowest and the second-lowest excited states were improved by this CI treatment.

The present investigation was undertaken in order to clarify the effects of DEC, especially of the χ_{kl}^{mn} type, which includes four orbitals k, l, m, and n, each containing a single electron, on the pi-electronic properties as calculated by the P-P-P-CI method for the ground and excited singlet states of unsaturated molecules. In the P-P-P-CI calculation the values of parameters, which were included in the core resonance integrals and electronic repulsion integrals, were determined so that the transition energies to some excited states might coincide with the experimental results.

Methods of Calculation

In the molecular orbital calculation of the P–P–P scheme used in this work, the core resonance integral, $\beta_{\mu\nu}$, and the two-center electronic repulsion integral, $\gamma_{\mu\nu}$, were approximated as follows:

$$\beta_{\mu\nu} = \frac{1}{2}\kappa(\beta_\mu^\circ + \beta_\nu^\circ)S_{\mu\nu} \quad (1)$$

$$\gamma_{\mu\nu} = b_{AB}/(R_{\mu\nu} + a_{AB}) \quad (2)$$

Equation (1) is the formula used in the modified CNDO method proposed by Bene and Jaffé.[10,11] Equation (2) is similar to the Mataga-Nishimoto's formula.[12] For one-center core integrals and one-center electronic repulsion integrals, the values of Table 1 in Ref. 13 were used. The parameters in these equations for carbon were readjusted so that the three transition energies of benzene (B_{2u}, B_{1u}, and E_{1u}) might coincide with the experimental values, the CI treatment in this calculation including all singly- and doubly-excited configurations. The appropriate values of these parameters were 0.645, 3.32 Å, and 35.10 Å eV for κ, a_{AB}, and b_{AB} respectively, provided that the unit of $R_{\mu\nu}$ in Eq. (2) is Å. Then, these parameter values were adopted for the calculations of all the molecules treated in this work. This value of the parameter, κ, was larger than that adjusted by the calculation including the CI treatment with singly-

1) E. M. Evleth, *J. Chem. Phys.*, **46**, 4151 (1967).
2) N. L. Allinger and T. W. Stuart, *ibid.*, **47**, 4611 (1967).
3) H. Kashiwagi, This Bulletin, **44**, 624 (1971).
4) F. Hirota and S. Nagakura, *ibid.*, **43**, 1010 (1970).
5) T. Anno and A. Sado, *J. Chem. Phys.*, **39**, 2293 (1963).
6) J. N. Murrell and K. L. McEwen, *ibid.*, **25**, 1143 (1956).
7) R. Pariser and R. G. Parr, *ibid.*, **21**, 446 (1953).
8) R. Pariser and R. G. Parr, *ibid.*, **21**, 767 (1953).
9) J. A. Pople, *Trans. Faraday Soc.*, **49**, 1375 (1953).
10) J. D. Bene and H. H. Jaffé, *J. Chem. Phys.*, **48**, 1807 (1968).
11) J. D. Bene and H. H. Jaffé, *ibid.*, **48**, 4050 (1968).
12) K. Nishimoto and N. Mataga, *Z. Physik. Chem.* (Frankfurt), **12**, 335 (1957).

Table 1. Values of parameters in two-center electronic repulsion integrals

Pair of atoms	a_{AB}[a] (Å)	b_{AB}[a] (Å·eV)	Molecules as reference
Carbon - Carbon	3.20	35.10	Benzene
Carbon - Nitrogen	3.17	36.10	Pyridine
Nitrogen - Nitrogen	3.09	37.97	Pyrazine, Pyrimidine, and Pyridazine
Carbon - Oxygen	3.08	38.17	Phenol
Nitrogen - Oxygen	2.89	39.76	Pyridine *N*-oxide
Oxygen - Oxygen	2.87	43.68	1,4-Dioxin

a) See text.

excited configurations alone; this fact has been pointed out by other investigators as well.[5] The values of a_{AB} and b_{AB} for other pairs of atoms (C, N, and O) were determined so that the calculated values might agree very well with the observed transition energies of reference molecules. These parameter values are listed in Table 1. Before the calculation according to the parameters determined in this work were applied to several molecules, the variations in the transition energies of benzene with the change in the value of κ were discussed, the $\gamma_{\mu\nu}$ in this calculation being estimated by the Pariser-Parr approximation. Also, these transition energies obtained by calculations using the $\gamma_{\mu\nu}$ from Eq. (2) were compared with those calculated by the use of the parameters estimated by Bene and Jaffé.[10]

The configurations in CI treatments may be classified into seven basic types: χ_0, χ_k^m, χ_{kk}^{mm}, χ_{kk}^{mn}, χ_{kl}^{mm}, χ_{kl}^{mn} (1), and χ_{kl}^{mn} (2), in accordance with the Murrell and McEwen's notation.[6] χ_{kl}^{mn} (1) and χ_{kl}^{mn} (2) indicate the doubly-excited configurations which include four orbitals, k, l, m, and n, each containing a single electron; the number in parentheses is the symbol classifying the two wave functions which are eigenfunctions of the spin operator, $\mathbf{S}^2$. In order to investigate the effect of DEC on the calculated pi-electronic properties, three types of calculations were performed. They are different from each other in the point of the number of configurations included in the CI calculation. Method I includes all singly-excited configurations, while Method II includes singly- and doubly-excited configurations except for the χ_{kl}^{mn} type, and Method III, all singly- and doubly-excited configurations.

The ground-state energies, transition energies, oscillator strengths, and pi-electronic densities obtained by these three type of calculations were compared with each other for sixteen compounds. The geometries of molecules followed the data listed in Ref. 14.

Results and Discussion

Figure 1 shows the variation in the transition energies

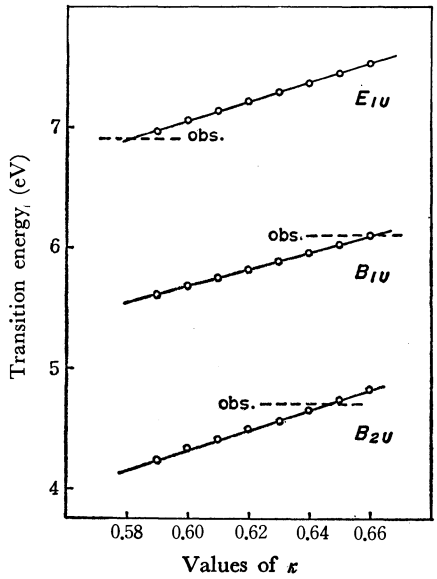

Fig. 1. The variation of transition energies of benzene with κ.

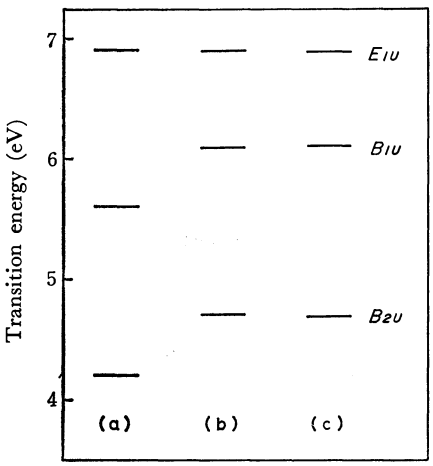

Fig. 2. Transition energies of benzene calculated by the use of different parameters.
a) Parameters are equivalent to Bene and Jaffés'.
b) Parameters were estimated by the approximation of this work.
c) observed values.

of benzene with the change in the value of κ. The transition energies increase linearly with the increased value of κ. However, the energy difference between excited states is not affected by the value of κ. In Fig. 2, the transition energies of benzene calculated by the use of the parameters estimated by Bene and Jaffé[10] are compared with the results obtained from the parameters estimated in this work. It may be seen that the energy difference between excited states of molecule is remarkably affected by the value of $\gamma_{\mu\nu}$.

In Method I, it is a matter of course that the energy of the ground state is not affected by the CI treatment considering singly-excited configurations alone. However, the ground states are stabilized by CI treatments considering singly- and doubly-excited configurations in Methods II and III, because the CI matrix elements between the ground configuration and DEC are not equal to zero. The magnitude of this stabilization

13) D. L. Beveridge and J. Hinze, *J. Amer. Chem. Soc.*, **93**, 3107 (1971).
14) "Tables of Interatomic Distances and Configuration in Molecules and Ions," The Chemical Society, London (1958), and its Supplement (1965).

TABLE 2. THE STABILIZATIONS OF GROUND STATE ENERGY AND THE WEIGHTS OF GROUND CONFIGURATION

Molecule	Method II		Method III	
	ΔE_0(eV)[a]	Weight	ΔE_0(eV)[a]	Weight
Benzene	0.269	0.980	0.545	0.957
trans-Butadiene	0.219	0.983	0.455	0.961
cis-Butadiene	0.206	0.985	0.451	0.962
Fulvene	0.387	0.966	0.674	0.941
Pyridine	0.252	0.982	0.519	0.961
Aniline	0.260	0.981	0.547	0.957
Pyrrole	0.295	0.978	0.465	0.962
Pyrazine	0.256	0.982	0.518	0.963
Pyrimidine	0.235	0.984	0.480	0.966
Pyridazine	0.262	0.982	0.533	0.962
s-Triazine	0.220	0.986	0.421	0.972
Phenol	0.263	0.981	0.544	0.957
Furan	0.263	0.982	0.436	0.966
1,4-Dioxin	0.211	0.986	0.515	0.957
Pyridine *N*-oxide	0.466	0.981	0.776	0.937
Pyrazine *N*-oxide	0.472	0.965	0.758	0.942

a) ΔE_0 is schematically shown in Fig. 3-a.

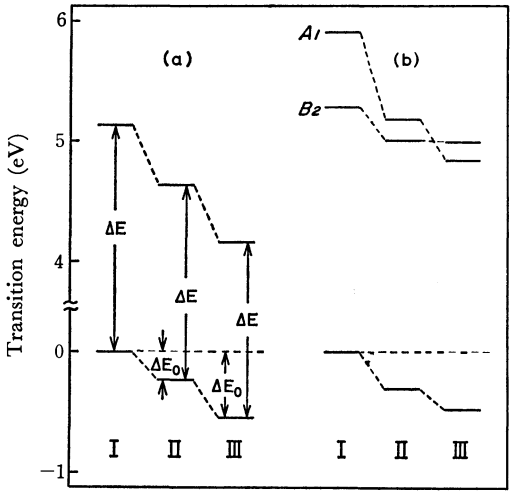

Fig. 3. Relation between energy levels calculated by different methods. (I: Method I, II: Method II, III: Method III) a) B_{2u} state of benzene b) A_1 and B_2 states of pyrrole.

energy and the contribution of the ground configuration for the ground state are listed in Table 2. From the table, it may be seen that the ground states are stabilized by from 0.20 to 0.47 eV in Method II, and by from 0.42 to 0.78 eV in Method III, and that the contributions of the ground configuration for the ground state are about 98% and 96% in Methods II and III respectively. These results show that the degree of effects of χ_{kl}^{mn}-type configurations on the results of CI calculation for the ground state is the same as that of other DEC's. The calculated transition energies and oscillator strengths are listed in Table 3, in which the experimental values are also included. In the results of Methods II and III, the transition energies are seen to depend upon the stabilization of the ground states; the energy scheme is given in Fig. 3. From Table 3 it may be found that the transition energies to low excited states calculated by Method III are in good agreement with the experimental results, and that the differences between the results from Methods I and II and between those from Methods II and III are generally less than 0.2 eV, though there are some exceptions. From these results, it is found that the degree of the effect of χ_{kl}^{mn}-type configurations on the calculated transition energies is the same as that of other DEC's. Furthermore, it is noteworthy that the energy differences between the lowest and the second-lowest excited states are improved by Method III, considering χ_{kl}^{mn}-type configurations, and that there are inversions in the order of excited levels for some molecules, as is indicated in Fig. 3-b.

The oscillator strengths calculated by Method I for the electronic transition are larger than the experimental results, but they are very much improved by Methods II and III, which consider the DEC's. From the fact that the differences between the results from Methods I and II are almost the same as those from Methods II and III, it is found that the effect of χ_{kl}^{mn}-type configurations on the oscillator strength is comparable with that of the other DEC's.

When the transition energies of molecules involving degenerate levels, such as benzene and *s*-triazine, are calculated, it should be noted that there is a defect in Method II, which considers DEC's without χ_{kl}^{mn}-type configurations, for the levels of excited states, which must be degenerate, are obtained as split levels, although the degree of splitting is very small (about 0.01 eV).

The pi-electronic densities of atomic sites in molecules varies slightly with each method of calculation. Generally, these variations in electronic densities for excited states are larger than those for the ground states of molecules. Table 4 indicates the electronic densities of fulvene and pyridazine as calculated by Methods I, II, and III. The variations between the electronic densities of these molecules calculated by the different methods are larger than those of the other molecules considered in this work. For ground states, the electron distributions in molecules were averaged by Method III as compared with other methods; the order of the magnitudes of electronic densities of the atomic sites in a molecule, except in the case of fulvene, was not affected by the method of calculation. For excited states, the calculated electron distribution did not always show the tendencies described above (see Table 4). The electronic densities of atomic sites in molecules calculated by Method III may be inferred to be reliable from the fact that the oscillator strengths are improved by this method.

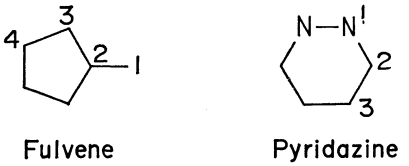

Fulvene Pyridazine

Fig. 4. Numbering of atomic sites in molecules.

TABLE 3. THE TRANSITION ENERGIES AND THE OSCILLATOR STRENGTHS

	Method I		Method II		Method III		Obsd.	
	ΔE(eV)	f	ΔE(eV)	f	ΔE(eV)	f	ΔE(eV)	f
Benzene								
B_{2u}	5.129	0.0	4.906	0.0	4.713	0.001	4.7	0.001[a]
B_{1u}	5.737	0.0	5.897	0.001	6.089	0.0	6.1	0.1[a]
E_{1u}	6.834	1.172	6.787	1.067	6.906	0.937	6.9	0.7[a]
trans-Butadiene								
B_u	5.816	1.032	5.919	0.871	6.155	0.765	5.9[b]	
A_g	7.065	0.0	6.404	0.0	6.275	0.0		
A_g	8.508	0.0	8.196	0.0	8.326	0.0		
cis-Butadiene								
B_2	5.322	0.400	5.448	0.360	5.693	0.316		
A_1	7.053	0.193	6.306	0.043	6.241	0.024		
A_1	8.670	0.688	8.361	0.634	8.428	0.404		
Fulvene								
B_2	3.368	0.043	3.356	0.022	3.401	0.015	3.3	0.012[c]
A_1	5.182	0.575	5.217	0.248	5.248	0.194	5.2	0.32[c]
B_2	6.659	0.202						
A_1	6.672	1.053	6.113	0.483	6.148	0.305		
B_2			6.403	0.154	6.365	0.112		
Pyridine								
B_2	5.134	0.135	4.908	0.124	4.783	0.080	4.9	0.04[d]
A_1	5.936	0.056	6.006	0.074	6.192	0.044	6.2	0.10[d]
B_2			7.012	0.289	7.070	0.337		
A_1	7.229	1.160	7.184	0.943	7.230	0.838	6.9	1.3[d]
B_2	7.280	0.928						
Aniline								
B_2	4.693	0.066	4.470	0.056	4.323	0.033	4.40	0.028[e]
A_1	5.182	0.575	5.217	0.248	5.248	0.194	5.39	0.144[e]
A_1	6.515	1.034	6.384	0.700				
B_2	6.517	0.797	6.392	0.600	6.418	0.418	6.40	0.510[e]
A_1					6.528	0.298		
Pyrrole								
A_1					5.305	0.000		
B_2	5.287	0.257	5.306	0.219	5.446	0.185	5.9[f,g]	
A_1	5.916	0.003	5.469	0.003				
A_1	7.232	0.978	7.014	0.761	7.002	0.603	6.8[f,g]	
Pyrazine								
B_{2u}	4.809	0.274	4.609	0.249	4.552	0.183	4.8	0.10[a]
B_{1u}	6.050	0.126	6.103	0.146	6.323	0.134	6.3	0.145[a]
B_{1u}	7.699	1.135	7.664	0.983	7.729	0.897	7.5	1.0[a]
Pyrimidine								
B_2	5.393	0.152	5.130	0.148	5.032	0.096	5.0	0.052[a]
A_1	6.219	0.123	6.282	0.110	6.340	0.106	6.5	0.16[a]
A_1	7.427	0.861	7.224	0.633	7.275	0.467	7.4	1.0[a]
B_2	7.731	1.053	7.608	0.890	7.614	0.736		
Pyridazine								
A_1	5.374	0.102	5.150	0.079	5.021	0.050	4.9	0.02[a]
B_2	6.084	0.002	6.138	0.017	6.321	0.007	6.2	0.10[a]
B_2	7.127	1.084	7.055	0.952	7.140	0.855	7.1	1.0[a]
A_1	7.577	1.131	7.451	0.932	7.510	0.763		
s-Triazine								
A_2'	6.065	0.0	5.866	0.004	5.650	0.0	5.6[h]	
A_1'	6.970	0.0	6.921	0.000	6.928	0.0	6.9[i]	
E'	7.665	1.025	7.465	0.828	7.476	0.725		
Phenol								
B_2	4.833	0.063	4.604	0.060	4.452	0.037	4.6	0.02[e]

TABLE 3. (Continued)

	Method I		Method II		Method III		Obsd.	
	ΔE(eV)	f	ΔE(eV)	f	ΔE(eV)	f	ΔE(eV)	f
A_1	5.445	0.084	5.569	0.086	5.699	0.112	5.8	0.132[e]
B_2					6.655	0.607		
A_1	6.647	1.177	6.535	0.908	6.691	0.694	6.7	0.636[e]
B_2	6.686	0.980	6.597	0.801				
Furan								
A_1					5.586	0.013		
B_2	5.375	0.252	5.449	0.226	5.625	0.200	5.8[g]	
A_1	6.169	0.066	5.706	0.036				
A_1	7.835	0.991	7.753	0.873	7.763	0.700	7.4[g]	
B_2	8.201	0.205	8.205	0.207	8.242	0.175		
1,4-Dioxin								
B_{3g}	4.244	0.0	4.453	0.0	4.555	0.0	4.7[j]	
B_{1u}	5.830	0.284	5.850	0.247	6.094	0.207	6.2[j]	
B_{3g}			7.203	0.0	6.645	0.0		
B_{1u}	7.371	1.047	7.529	0.905	7.831	0.713		
B_{3g}	7.620	0.0						
Pyridine *N*-oxide								
B_2	4.229	0.026	3.816	0.017	3.723	0.002	3.8	0.016[k]
A_1	4.401	0.401	4.321	0.364	4.360	0.365	4.4	0.205[k]
B_2	5.748	0.568	5.634	0.418	5.651	0.299	5.7	0.196[k]
A_1	6.314	0.628						
A_1			5.809	0.002	5.709	0.005		
Pyrazine *N*-oxide								
B_2			4.127	0.041	4.004	0.025		
A_1	4.484	0.444	4.315	0.400	4.322	0.399	4.52	0.186[l]
B_2	4.526	0.042						
B_2	5.656	0.504	5.389	0.385	5.443	0.272		

a) J. E. Perkin and K. K. Innes, *J. Mol. Spectrosc.*, **15**, 407 (1965). b) R. S. Mulliken, *Rev. Mod. Phys.*, **14**, 265 (1942). c) J. Thiec and J. Wiemann, *Bull. Soc. Chim. Fr.*, 177 (1956). d) R. L. Flurry, E. W. Stout, and J. J. Bell, *Theoret. Chim. Acta* (Berl.), **8**, 203 (1967). e) K. Kimura and S. Nagakura, *Mol. Phys.*, **9**, 117 (1965). f) L. W. Pickett, N. E. Corning, G. W. Wieder, D. A. Semenow, and J. M. Buckley, *J. Amer. Chem. Soc.*, **75**, 1618 (1953). g) J. C. Tai and N. L. Allinger, *Theoret. Chim. Acta*, **15**, 133 (1969). h) R. C. Hirt, F. Halverson, and R. G. Schmitt, *J. Chem. Phys.*, **22**, 1148 (1954). i) J. C. Brinen, R. C. Hirt, and R. G. Schmitt, *Spectrochim. Acta*, **18**, 863 (1962). j) L. W. Pickett and E. Sheffield, *J. Amer. Chem. Soc.*, **68**, 216 (1946). k) M. Yamakawa, T. Kubota, and H. Akazawa, *Theoret. Chim. Acta*, **15**, 244 (1969). l) T. Kubota, This Bulletin, **35**, 946 (1962).

TABLE 4. THE PI-ELECTRONIC DENSITIES[a]

Atomic sites[b]	Ground State			1st Excited State			2nd Excited State			3rd Excited State		
	I[c]	II[c]	III[c]	I[c]	II[c]	III[c]	I[c]	II[c]	III[c]	I[c]	II[c]	III[c]
Fulvene				(ΔE=3.401 eV)			(ΔE=5.248 eV)			(ΔE=6.148 eV)		
1	0.949	0.956	0.965	1.347	1.119	1.153	0.885	0.938	0.875	0.957	1.081	1.106
2	0.955	0.950	0.952	1.078	1.180	1.154	0.798	0.876	0.893	0.942	0.760	0.765
3	1.047	1.047	1.042	0.828	0.838	0.825	1.164	1.104	1.116	0.907	1.082	1.068
4	1.001	1.000	0.999	0.959	1.013	1.022	0.994	0.990	1.000	1.143	0.998	0.996
Pyridazine				(ΔE=5.021 eV)			(ΔE=6.321 eV)			(ΔE=7.140 eV)		
1	1.134	1.135	1.130	1.194	1.154	1.135	1.135	1.185	1.184	1.140	1.151	1.158
2	0.908	0.907	0.911	0.760	0.814	0.846	0.931	0.912	0.921	0.932	0.910	0.898
3	0.957	0.958	0.959	1.046	1.032	1.019	0.934	0.907	0.895	0.927	0.938	0.944

a) ΔE is the transition energy obtained by Method III. b) Numbering of atomic sites is shown in Fig. 4. c) I, II, and III indicate Methods I, II, and III, respectively.

Conclusion

In the P-P-P-CI calculation considering the doubly-excited configurations, the effects of the κ parameter, referring to the resonance integral, β, and of the two-center electronic repulsion integral, $\gamma_{\mu\nu}$, on the transition energies of benzene were discussed. Also these parameters were readjusted so that the transition energies might coincide with the experimental results. The energy difference between the excited states of a molecule was affected remarkably by the value of $\gamma_{\mu\nu}$. By comparing the results from the three different types of calculations, which are different from each other in the point of the number of configuration included in the CI calculation, it is found that the introduction of the doubly-excited configurations to the CI treatment is effective in calculating the pi-electronic properties and that the effects of χ_{kl}^{mn}-type configurations on the results are the same as those of other doubly-excited configurations.

In these calculations, we were helped by "The University Contribution" of UNIVAC Japan, Ltd.

BULLETIN OF THE CHEMICAL SOCIETY OF JAPAN, VOL. 46, 2955—2959 (1973)

The Electronic States of *p*-Bromanil and Its Anion Radical as Studied by Means of Their Infrared Spectra

Yôichi IIDA

Department of Chemistry, Faculty of Science, Hokkaido University, Sapporo 060

(Received March 14, 1973)

The infrared spectra (400—4000 cm^{-1}) were measured with neutral *p*-bromanil and its anion radical. Appreciable frequency differences between their corresponding bands were observed. The fundamental frequencies were assigned, and the simple Urey-Bradley force fields were determined for both the neutral *p*-bromanil and its anion radical. The differences in the molecular and electronic structures between these two molecules were discussed on the basis of these results. The half-occupied molecular orbital of the *p*-bromanil anion radical was found to belong to the b_{3g} irreducible representation.

The infrared spectrum of an ion radical is known to be appreciably different from that of its neutral molecule.[1-12] The spectrum difference may be attributed to the difference in their intramolecular force fields. Up to now, however, attempts have scarcely been made to study such differences quantitatively.[8,12] In a previous paper,[8] we examined the infrared spectra (650—4000 cm^{-1}) of *p*-chloranil and its anion radical (see Fig. 1). In order to explain the appreciable frequency differences between their corresponding bands, the fundamental frequencies were assigned, and the simple Urey-Bradley force fields (UBFF's) were determined for both the neutral and anion radical molecules. It was found that the difference in the infrared spectra between these two molecules could be understood in terms of the difference in their electronic structures caused by the extra electron on the *p*-chloranil anion radical.[8,9]

In the present paper, the infrared spectra (400—4000 cm^{-1}) were measured with *p*-bromanil and its anion radical (see Fig. 1). In order to make vibrational assignments and to determine the force constants for these molecules, the normal coordinate treatments were carried out for the in-plane vibrations by using the simple UBFF's. The electronic states of the neutral *p*-bromanil and its anion radical were discussed on the basis of these experimental and theoretical investigations. We shall examine how the extra electron on the anion radical causes the difference in the molecular and electronic structures between the neutral *p*-bromanil and its anion radical. On the other hand, the substituent effects upon the molecular and electronic structures of the halogen-substituted *p*-benzoquinones and their anion radicals are interesting in comparison with the results previously reported for *p*-chloranil and its anion radical.[8]

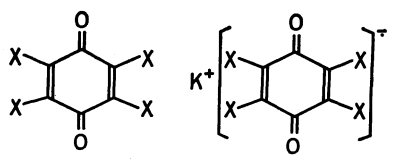

(a) ; X = Cl
(b) ; X = Br

Fig. 1. (a) *p*-Chloranil and its anion radical salt with potassium cation, and (b) *p*-bromanil and its anion radical salt with potassium cation.

1) Y. Matsunaga, *Can. J. Chem.*, **38**, 1172 (1960).
2) Y. Matsunaga, *Helv. Phys. Acta*, **36**, 800 (1963).
3) Y. Matsunaga, *J. Chem. Phys.*, **41**, 1609 (1963).
4) M. Kinoshita and H. Akamatu, *Nature*, **207**, 291 (1965).
5) J. Stanley, D. Smith, B. Latimer, and J. P. Devlin, *J. Phys. Chem.*, **70**, 2011 (1966).
6) Y. Matsunaga, *Nippon Kagaku Zasshi*, **89**, 905 (1968).
7) Y. Iida, *J. Phys. Soc. Japan*, **27**, 1371 (1969).
8) Y. Iida, This Bulletin, **43**, 345 (1970).
9) Y. Iida, *ibid.*, **44**, 1271 (1971).
10) J. C. Moore, D. Smith, Y. Youhne, and J. P. Devlin, *J. Phys. Chem.*, **75**, 325 (1971).
11) I. N. Juchnovski and I. G. Binev, *Chem. Phys. Lett.*, **12**, 40 (1971).
12) Y. Iida, This Bulletin, **46**, 423 (1973).

Experimental

Materials. Commercially-available *p*-bromanil (Tokyo Kasei Kogyo Co., Ltd., GR grade) was used without further purification. Its anion radical salt with the potassium cation (K^+ *p*-Bromanil$^-$) was synthesized according to the method of Torrey and Hunter.[13]

Measurements. The infrared spectra of these solid compounds were measured as Nujol mulls in the range from 400 to 4000 cm^{-1} using a Japan Spectroscopic Co., Ltd. IR-G infrared spectrometer. The infrared spectra in the regions where the absorption due to Nujol appears were measured using hexachlorobutadiene mulls. The spectra obtained for these compounds are reproduced in Fig. 2.

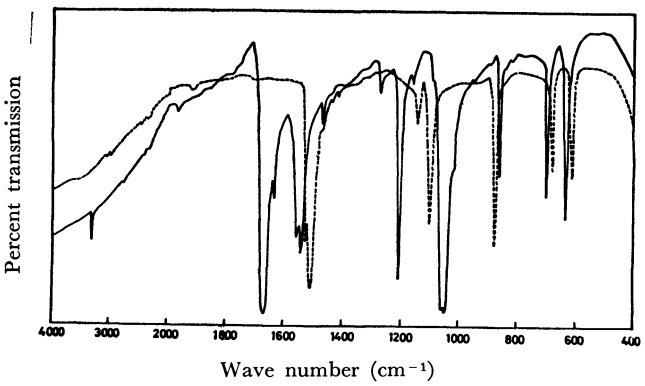

Fig. 2. The infrared spectra of *p*-bromanil and its anion radical salt with potassium cation.
———: *p*-Bromanil, ·····: K^+ *p*-Bromanil$^-$

Since the counter cation of the salt is a simple alkali metal cation, the observed spectrum of K^+ *p*-Bromanil$^-$ in the region under investigation should be due to that of the *p*-bromanil anion radical itself. The values of the absorption peaks observed for the neutral *p*-bromanil and its anion radical are listed in Table 1.

TABLE 1. THE OBSERVED AND CALCULATED FREQUENCIES (cm^{-1}) FOR IN-PLANE FUNDAMENTAL VIBRATIONS OF THE INFRARED SPECTRA OF THE NEUTRAL *p*-BROMANIL AND ITS ANION RADICAL[a]

The neutral *p*-bromanil		Its anion radical		Assign.
Obsd	Calcd	Obsd	Calcd	
1672 (s)	1672	1515 (s)	1507	B_{2u}, ν(C=O)
1565 (s)	1557	1531 (s)	1528	B_{3u}, ν(C=C)
1549 (s)				
1212 (s)	1212	1150 (w)	1256 (?)	B_{3u}, ν(C–C)
1066 (s)	1060	1105 (s)	1098	B_{2u}, ν(C–C)
1054 (s)				
869 (m)	869	879 (s)	870	B_{2u}, ν(C–C), ν(C–Br)
705 (m)		684 (m)		
650 (m)	650	618 (m)	618	B_{3u}, ν(C–Br)

a) s: strong, m: medium, w: weak.

13) H. A. Torrey and W. H. Hunter, *J. Amer. Chem. Soc.*, **34**, 702 (1912).

Normal Coordinate Treatment for In-plane Vibrations

In the infrared spectra of neutral *p*-bromanil and its anion radical, we observed appreciable frequency differences between their corresponding bands. For example, the C=O stretching mode of 1672 cm^{-1} in the neutral *p*-bromanil was found to be considerably red-shifted to 1515 cm^{-1} in the anion radical. Since only the intramolecular vibrations are expected to appear in the region from 400 to 4000 cm^{-1}, we attributed the spectrum difference between the neutral *p*-bromanil and its anion radical to the difference in their intramolecular force fields. The effect of crystal fields upon the vibrational frequencies is small in comparison with that of the intramolecular force fields. Therefore, to a first approximation, the contribution of the crystal fields to the spectra of *p*-bromanil and its anion radical was ignored in the present investigation.

The vibrational spectra of *p*-bromanil and its anion radical were then treated under the molecular point group, D_{2h}, and were analyzed by using a normal coordinate treatment. The molecular and crystal structures of the neutral *p*-bromanil have not yet been ascertained, although those of *p*-chloranil were determined by Chu, Jeffrey, and Sakurai.[14] It was assumed that the *p*-bromanil molecule was planar. By referring to the molecular structure of *p*-chloranil, the equilibrium bond lengths of *p*-bromanil were taken as l(C=O)=1.195 Å, l(C=C)=1.342, l(C–C)=1.477, and l(C–Br)=1.89, while the bond angles were taken as $\angle$(O=C–C)=121°22′, $\angle$(C–C–Br)=116°15′, and $\angle$(C=C–Br)=122°23′ (see Fig. 1). Since the structure of K^+ *p*-Bromanil$^-$ has not yet been determined, it was assumed that the molecular structure of the anion radical was almost identical with that of the neutral *p*-bromanil. This assumption means that the ***G*** matrix calculated for *p*-bromanil was also used for its anion radical (see below). Hence, thirty normal modes of vibrations for *p*-bromanil or its anion radical were reduced to the symmetry species:

$$\Gamma = 6A_g(R) + 5B_{1g}(R) + 5B_{2u}(IR) + 5B_{3u}(IR) + 1B_{2g}(R) + 3B_{3g}(R) + 2A_u(\text{inactive}) + 3B_{1u}(IR), \quad (1)$$

where the first four are the in-plane vibrations, and the rest, the out-of-plane vibrations. The signs of (R) and (IR) indicate the Raman and infrared active modes respectively. We calculated only the in-plane vibrations, because no out-of-plane vibration is expected to appear in the region now under consideration.

Wilson's ***GF*** matrix method was used in this work.[15] A representative example of each type of internal coordinate for the in-plane vibrations is given in Fig. 3. A simple UBFF was employed as the potential function. Then, four bond-stretching (K(C=O), K(C=C), K(C–C) and K(C–Br)), five angle-bending (H(O=C–C), H(C–C–Br), H(C=C–Br), H(C–C–C) and H(C=

14) S. Chu, G. A. Jeffrey, and T. Sakurai, *Acta Crystallogr.*, **15**, 661 (1962).

15) E. B. Wilson, Jr., *J. Chem. Phys.*, **7**, 1047 (1939); **9**, 76 (1941).

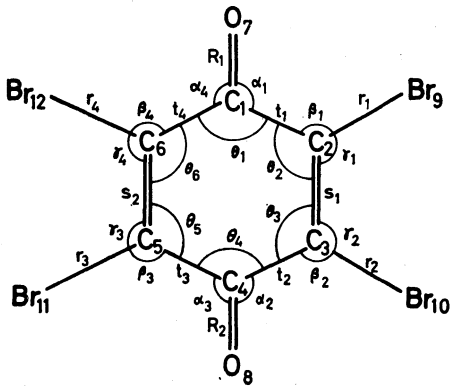

Fig. 3. The internal coordinates for the in-plane fundamental vibrations of *p*-bromanil or its anion radical.

C–C)), and five non-bonded repulsion force constants (F(O=C–C), F(C–C–Br), F(C=C–Br), F(C–C–C), F(C=C–C)) were necessary. At this time, it was assumed that the stretching force constants of *p*-bromanil were different from those of its anion radical, while the other force constants remained almost constant. Within the framework of this approximation, we could well explain the difference in the observed fundamental frequencies between *p*-bromanil and its anion radical. The trial force constants for *p*-bromanil were taken by referring to the values for benzene, halogen-substituted benzenes, *p*-benzoquinone, and *p*-chloranil,[8,16–18] while those for the *p*-bromanil anion radical were taken by modifying the force constants for the neutral *p*-bromanil. Refinements of the force constants were then carried out by the trial-and-error method, making use of the Jacobian matrix. The final sets of force constants thus obtained for the neutral *p*-bromanil and its anion radical are given in Table 2, while the frequencies calculated with these constants are compared in Table 1 with the observed values. In both of these molecules, the calculated values of the fundamental vibrations were found to agree well with the observed values, except for the following two points, which remain to be elucidated:

(1) Two absorption peaks were observed, at 705 cm^{-1} and 650 for the neutral *p*-bromanil or at 684 cm^{-1} and 618 for its anion radical, while only one fundamental vibration was expected to appear around this region.[19] It seems improbable to assign one of them to an out-of-plane vibration, because such a vibration would not appear around this region.

(2) The calculated 1256 cm^{-1} band in the anion radical cannot be assigned to any of the observed bands, presumably because of its weak intensity.

Table 2. The force constants estimated for the neutral *p*-bromanil and its anion radical (md/Å)[a]

Force constant	The neutral *p*-bromanil	Its anion radical
K(C=O)	9.62	7.10
K(C=C)	6.67	6.26
K(C–C)	2.96	3.33
K(C–Br)	2.63	2.17
H(O=C–C)	0.32	0.32
H(C–C–Br)	0.050	0.050
H(C=C–Br)	0.042	0.045
H(C–C–C)	0.210	0.237
H(C–C=C)	0.205	0.284
F(O=C–C)	0.801	0.793
F(C–C–Br)	0.710	0.710
F(C=C–Br)	0.710	0.710
F(C–C–C)	0.300	0.300
F(C–C=C)	0.370	0.500

a) $F' = -0.1F$.

16) Y. Kakiuchi, *Nippon Kagaku Zasshi*, **75**, 143 (1954).
17) T. Anno and A. Sado, This Bulletin, **31**, 734 (1958).
18) J. R. Scherer, *Spectrochim. Acta*, **20**, 345 (1964).

Discussion

The Electronic States of p-*Bromanil and Its Anion Radical.* Since a total of 14 force constants of *p*-bromanil or its anion radical were evaluated from an experimental assignment of 6 frequencies, we suspect that these values of the force constants are not the best ones for these compounds. However, the stretching force constants are still meaningful, because the observed fundamental frequencies are almost all due to the bond-stretching modes. Therefore, below, we will discuss only the difference in the stretching force constants between the neutral *p*-bromanil and its anion radical. As is shown in Table 2, K(C=O)=9.62 md/Å, K(C=C)=6.67, K(C–C)=2.96, and K(C–Br)=2.63 for the neutral *p*-bromanil, while K(C=O)=7.10 md/Å, K(C=C)=6.26, K(C–C)=3.33, and K(C–Br)=2.17 for its anion radical. We can see that an extra electron on the *p*-bromanil anion radical markedly causes a decrease in the K(C=O), K(C=C) and K(C–Br) values and an increase in the K(C–C) value.

It is well known that the stretching force constant, $K(12)$, of a bond (12) in a conjugated system is greatly affected by its bond order, $p(12)$. According to Coulson and Longuet-Higgins,[20] $K(12)$ can be expressed by

$$K(12) = \{(1-p(12))K_s + p(12)K_d\} + \left\{\frac{K_sK_d(s-d)}{K_s(1-p(12))+K_dp(12)}\right\}^2 \frac{\pi(1212)}{2}, \quad (2)$$

where K_s and K_d are the force constants associated with pure single and double bonds respectively; $\pi(1212)$ is the self-polarizability of the bond (12); s and d are the bond lengths of pure single and double bonds respectively.

In a homopolar carbon-carbon bond, the second

19) In *p*-chloranil, the corresponding bands were observed at 752 cm^{-1} and 715, and in its anion radical, at 725 cm^{-1} and 694. It appears that the bands at 752 cm^{-1} and 725 in *p*-chloranil and its anion radical shift to 650 cm^{-1} and 618 in *p*-bromanil and its anion radical, respectively, but it is not adequate to consider such band shifts in the cases of the other bands. Therefore, the bands at 650 cm^{-1} and 618 in *p*-bromanil and its anion radical were assigned to the fundamental vibrations of the C–Br stretching mode. See Ref. 8.

20) C. A. Coulson and H. C. Longuet-Higgins, *Proc. Roy. Soc. Ser. A*, **193**, 456 (1948).

term involving the self-polarizability may be small.[21] In this case, the stretching force constant, $K(12)$, is predominantly determined by the bond order, $p(12)$. By the use of the empirical relationship between $K(12)$ and $p(12)$ given in a previous paper,[8] we can evaluate the bond orders of the C=C and C–C bonds in *p*-bromanil and its anion radical. From the values of K(C=C) and K(C–C) in the infrared spectra, the p(C=C) and p(C–C) values for the neutral *p*-bromanil were estimated to be 0.88 and 0.27 respectively, while those for its anion radical were estimated to be 0.82 and 0.36 respectively. Therefore, we can see that the extra electron on the *p*-bromanil anion radical causes a decrease in p(C=C) by 0.06 and an increase in p(C–C) by 0.09. On the other hand, in order to confirm these results, we further calculated the p(C=C) and p(C–C) values of the neutral *p*-bromanil and its anion radical by the use of the molecular orbitals. For the sake of simplicity, the SCF molecular orbitals of the neutral *p*-benzoquinone calculated by Kunii and Kuroda (see Fig. 4) were used,[22] because the electronic state of the π-conjugated system in *p*-bromanil can be regarded as very similar to that in *p*-benzoquinone. It was also assumed that the extra electron of the anion radical enters into the lowest vacant molecular orbital of the neutral *p*-benzoquinone. As is shown in Fig. 4, this orbital has the irreducible representation of the symmetry, b_{3g}, where the coefficients of the C_1, C_2, and O_7 atomic orbitals were given by +0.35887, +0.31428, and −0.41674 respectively.[22] From the molecular orbital method, the p(C=C) and p(C–C) values for the neutral *p*-bromanil were estimated to be 0.91 and 0.30 respectively, while those for its anion radical were estimated to be 0.81 and 0.41 respectively. Therefore, the extra electron causes a decrease in p(C=C) by 0.10 and an increase in p(C–C) by 0.11 compared to the values of the neutral *p*-bromanil. These molecular orbital results are found to agree well with those evaluated from the infrared spectra.

Next, let us examine the heteropolar C=O bond. If we take, in Eq. (2), the values of K_s=5.0 md/Å and K_d=10.7 proposed by Bratoz and Besnainou,[23] and

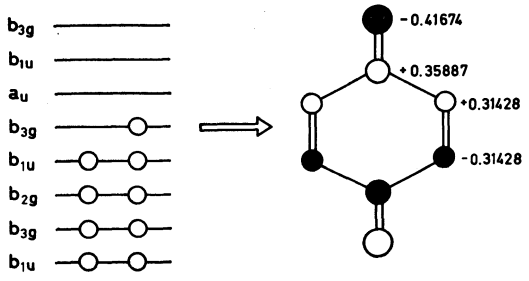

Fig. 4. Schematic representation of the molecular orbitals of the *p*-benzoquinone anion radical molecule. For the half-occupied molecular orbital with the b_{3g} irreducible representation, the open and closed circles indicate that the coefficients of the atomic orbitals are positive and negative, respectively. See text.

if we neglect the contribution of the self-polarizability to K(C=O), those C=O stretching force constants for *p*-bromanil and its anion radical give the values of p(C=O) of 0.81 and 0.37 respectively. These values should be compared with those of 0.85 and 0.70 respectively calculated from their molecular orbitals. In the neutral *p*-bromanil, the agreement is rather satisfactory. Although the extra electron definitely decreases the C=O bond order, no quantitative agreement is obtained in the anion radical. One reason for this might be the neglect of the self-polarizability.

As for the C–Br bond, although the description of K(C–Br) *versus* p(C–Br) for the neutral *p*-bromanil and its anion radical is not simple, the extra electron on the *p*-bromanil anion radical causes a decrease in K(C–Br); this decrease will definitely lead to a decrease in p(C–Br). However, the estimation of p(C–Br) by the molecular-orbital method is rather complicated, because we have some difficulties in finding appropriate parameters for the Br atomic orbitals.

Some Information on the Molecular Structures of p-*Bromanil and Its Anion Radical.* There is a well-known relation between the bond order, $p(12)$, and the bond length, $l(12)$, of a carbon-carbon bond (12); this was first derived by Coulson.[21,24] By using this relationship, the p(C=C) and p(C–C) values estimated from the infrared spectra give l(C=C) and l(C–C) respectively. The l(C=C) and l(C–C) values for the neutral *p*-bromanil were thus estimated to be 1.35_6 Å and 1.47_5 respectively, while those for its anion radical were estimated to be 1.36_8 Å and 1.45_6 respectively. The values of the neutral *p*-bromanil are in good agreement with those of l(C=C)=1.342 Å and l(C–C)=1.477 respectively, which were employed in the previous calculation. We can further see that the extra electron on the anion radical may cause an increase of 0.01 Å in l(C=C) and a decrease of 0.02 Å in l(C–C) compared to the values of *p*-bromanil. However, no observation of the molecular structure has yet been made for the anion radical.

As for the relation between the stretching force constant and the bond length of a C=O bond, Badger proposed the following equation:[25]

$$K(\text{C=O}) = 1.86/\{l(\text{C=O}) - 0.68\}^3, \qquad (3)$$

where K and l are in md/Å and Å units respectively. For *p*-bromanil and its anion radical, the values of l(C=O) derived from their force constants by Eq. (3) are 1.26 Å and 1.32 respectively. The former value is rather larger than the observed value of 1.195 Å. We may expect that the C=O bond length of the *p*-bromanil anion radical is longer than that of its neutral molecule by 0.06 Å; however, no experimental result is available at present.

Although we have no information on the relation between the stretching force constant and the bond length of the C–Br bond, the extra electron on the *p*-bromanil anion radical probably causes the difference in l(C–Br)

21) A. Streitwieser, Jr., "Molecular Orbital Theory," John Wiley & Sons, New York and London (1961).
22) T. L. Kunii and H. Kuroda, *Rep. Compt. Center, Univ. Tokyo*, **1**, 119 (1968).
23) S. Bratoz and M. S. Besnainou, *J. Chem. Phys.*, **34**, 1142 (1961).
24) C. A. Coulson, *Proc. Roy. Soc. Ser. A*, **169**, 413 (1939).
25) R. M. Badger, *J. Chem. Phys.*, **3**, 710 (1935); see also J. A. Ladd, W. J. Orville-Thomas and B. C. Cox, *Spectrochim. Acta*, **20**, 1771 (1964).

between *p*-bromanil and its anion radical.

Comparison with the Results of p-*Chloranil and Its Anion Radical.* In a previous paper,[8] the values of the stretching force constants for the neutral *p*-chloranil were reported to be $K(C{=}O)=9.7$ md/Å, $K(C{=}C)=6.6$, $K(C{-}C)=3.0$, and $K(C{-}Cl)=2.67$, while those for its anion radical were reported to be $K(C{=}O)=7.3$ md/Å, $K(C{=}C)=6.1$, $K(C{-}C)=3.5$, and $K(C{-}Cl)=2.67$. In comparison with those of the neutral *p*-bromanil and its anion radical, we can see that, in either the neutral molecule or its anion radical, the stretching force constants of the benzoquinone system are scarcely affected by replacing the chlorine substituents by the bromine substituents. This means that the molecular and electronic structures of the benzoquinone systems of *p*-bromanil and its anion radical are very similar to those of *p*-chloranil and its anion radical respectively. Although the previous paper described that the extra electron on the *p*-chloranil anion radical did not decrease the $K(C{-}Cl)$ value,[8] this description is no longer adequate. More accurate assignments of the fundamental frequencies of *p*-chloranil and its anion radical will show the decrease in the $K(C{-}Cl)$ value in the anion radical; this situation seems to be analogous to that of *p*-bromanil and its anion radical.

Concluding Remarks

The present investigation clearly shows that the predominant factor in the difference in the vibrational spectra between the neutral *p*-bromanil and its anion radical can be understood in terms of the differences in their electronic structures. By using these differences, the half-occupied molecular orbital of the *p*-bromanil anion radical was found to belong to the b_{3g} irreducible representation. However, we noticed some disagreements between the C=O bond orders obtained from the infrared spectra and those obtained from the molecular orbitals. We consider that these disagreements may be caused not only by the neglect of the self-polarizability, but also by the frequency shifts due to the crystal-field effect. Although the crystal-field effect may be more important for the anion radical salt than for the neutral molecular crystal, this contribution to the frequency shifts of *p*-bromanil and its anion radical may be small in comparison with the difference in their intramolecular force fields.

Rigorously speaking, the $\boldsymbol{G}$ matrix for the anion radical is no longer identical with that for the neutral *p*-bromanil, since the molecular structure of the anion radical was found to be slightly different from that of the neutral *p*-bromanil. Although the difference in their $\boldsymbol{G}$ matrices may make some contribution to the frequency differences, this contribution can be disregarded for the bands due to the bond-stretching modes.

The set of force constants presented in Table 2 cannot be regarded as a unique solution, since the observations of the fundamental frequencies are limited to the infrared spectra. In this sense, it is quite desirable to measure the Raman spectra of *p*-bromanil and its anion radical. We consider, however, that the set of force constants presented here is reliable enough for studying the difference in the stretching force constants between the neutral *p*-bromanil and its anion radical.

In conclusion, the application of the infrared spectra of a neutral molecule and its ion radical can provide valuable knowledge on their electronic structures as well as on their molecular structures. It is interesting to see that their frequency differences give some information concerning the nature of the half-occupied orbital in the ion-radical molecular orbitals.

The Crystal Structure of Trimellitic Acid for the Pseudo-cell

Fusao TAKUSAGAWA, Ken HIROTSU, and Akira SHIMADA

Department of Chemistry, Faculty of Science, Osaka City University, Sugimoto-cho, Sumiyoshi-ku, Osaka 558

(Received March 19, 1973)

The crystal structure of trimellitic acid(benzene-1,2,4-tricarboxylic acid) for the pseudo-cell was determined by the method of X-ray diffraction. The crystal is monoclinic, with the space group of I2/c and with a=15.91, b=61.35, c=8.99 Å, and β=95.4°. The appearence of diffraction patterns strongly indicated the existence of the pseudo-cell with $b/5$ and with the space group of I2/c. The structure of the pseudo-cell was determined by the symbolic addition method. The final R value is 13.6%. There is no intramolecular hydrogen bond between the adjacent carboxyl groups, and one of these carboxyl groups twists greatly out of the plane of a benzene ring so that the repulsion between the oxygen atoms is reduced. Each molecule is joined, through three kinds of hydrogen bonds, with three neighboring molecules. These hydrogen bonds are formed between the carboxyl groups related by the center of symmetry and the two-fold axis. The molecular dimensions and packing obtained by the refinement for the pseudo-cell do not seem to contain unacceptable results.

In a series of benzene derivatives which are substituted with one to six carboxyl groups, the crystal structures of several members have already been studied by means of X-ray studies to obtain valuable information in the field of crystal chemistry: benzoic acid,[1] phthalic acid,[2,3] isophthalic acid,[4] terephthalic acid,[5] trimesic acid,[6] hemimellitic acid,[7] pyromellitic acid,[8,9] and mellitic acid.[10] Since the trimellitic acid has a pair of adjacent carboxyl groups, just like phthalic acid, hemimellitic acid, pyromellitic acid, and mellitic acid, it is of interest to elucidate the steric hindrance of these carboxyl groups. There has been no intramolecular hydrogen bond between the adjacent carboxyl groups in these crystals. Hence, it is also of interest to examine the hydrogen bond formation in this crystal and also to compare the molecular dimensions of this compound with those of other similar carboxylic acids.

Experimental

The crystal was obtained in the form of a colorless plate by recrystallization from an aqueous solution. The cell dimensions were measured from zero-layer Weissenberg photographs, which were calibrated with superimposed Al powder lines. They are given with other crystal data in Table 1. The density was determined by the flotation method in a mixture of tetrachloromethane and benzene.

The diffraction patterns strongly suggest the existence of a pseudo-cell with the parameters shown in Table 1. The intensity data were collected for the 0—8 layers around the a and b(pseudo-cell) axes by the use of the multiple-film equi-inclination Weissenberg technique with Cu$K\alpha$ radiation. The intensities of the diffraction spots were estimated visually by comparison with a calibrated intensity standard. The characteristics of the intensity data were as follows:

$k=5n$, Strong reflections

$k=5n\pm2$, Weak reflections

$k=5n\pm1$, Absent

The intensity distribution in $0kl$ is shown in Fig. 1. There were 1424 independent reflections for the pseudo-cell ($k=5n$), while about 3500 reflections were measured for the real cell. The data were corrected for spot shape and for Lorentz and polarization factors. No absorption correction was

TABLE 1. CRYSTAL DATA FOR TRIMELLITIC ACID

Molecular formula		$C_6H_3(COOH)_3$	
Molecular weight		210.15	
		Real-cell	Pseudo-cell
Crystal system		Monoclinic	Monoclinic
Space group		I2/c	I2/c
Cell dimensions;	a	15.91±0.02 Å	15.91±0.02 Å
	b	61.35±0.06	12.27±0.01
	c	8.99±0.01	8.99±0.01
	β	95.4 ±0.1°	95.4 ±0.1°
	V	8733 ±5 Å^3	1746 ±1 Å^3
Z		40	8
Density(calc.)		1.60 g/cm^3	
Density(obs.)		1.58	

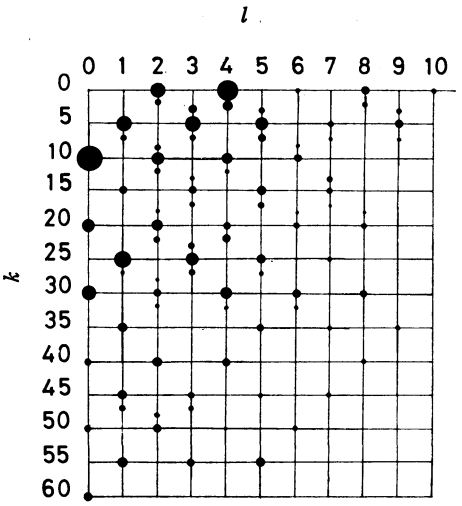

Fig. 1. Intensity distribution of $0kl$ reflections.

1) G. A. Sim, J. M. Robertson and T. H. Goodin, *Acta Crystallogr.*, **8**, 157 (1955).
2) H. Jaggi, *Z. Kristallogr.*, **109**, 3 (1957).
3) W. Nowacki and H. Jaggi, *ibid.*, **109**, 272 (1957).
4) R. Alcala and S. M. Carrera, *Acta Crystallogr.*, **B28**, 1671 (1972).
5) M. Bailery and C. J. Brown, *ibid.*, **22**, 387 (1966).
6) D. J. Duchamp and R. E. Marsh, *ibid.*, **B25**, 5 (1969).
7) F. Takusagawa and A. Shimada, This Bulletin, **46**, 2998 (1973).
8) F. Takusagawa, K. Hirotsu, and A. Shimada, *ibid.*, **44**, 1274 (1971).
9) F. Takusagawa, K. Hirotsu, and A. Shimada, *ibid.*, **42**, 3368 (1969).
10) S. F. Darlow, *Acta Crystallogr.*, **14**, 159 (1961).

TABLE 2. THE OBSERVED AND CALCULATED STRUCTURE FACTORS

F_o, F_c and DF have been multiplied by 5. The unobserved reflection is indicated by an asterisk. The reflection with the $|F_o-F_c|/|F_o|$ larger than 0.3 is indicated by a plus sign.

H	FO	FC	DF	H	FO	FC	DF	H	FO	FC	DF	H	FO	FC	DF	H	FO	FC	DF	H	FO	FC	DF	H	FO	FC	DF
K,L=	0	0		4	124	-128	4	-10	29	26	3	-9	37	47	-9	-8*	0	0	0	-4	43	39	4	15*	0	4	-4
2	87	102	-14	6	52	59	-6	-8	42	-31	-10	-7+	37	-12	-25	-6*	0	-11	11	-2	86	63	22	17*	0	-2	2
4	54	-46	-8	8	47	50	-3	-6	30	-22	-8	-5	71	-53	-18	-4*	0	2	-2	0	44	35	8	K,L=	4	2	
6	71	-62	-9	10	57	66	-8	-4*	0	-7	7	-3+	21	-35	13	-2*	0	9	-9	2	98	102	-4	-18*	0	-6	6
8+	9	-2	-7	12*	0	-8	8	-2	93	100	-7	-1	68	-79	10	0*	0	-8	8	4+	15	-8	-7	-16	14	-12	-2
10+	24	40	-16	14*	0	4	-4	0+	28	8	19	1	116	-116	0	K,L=	2	11		6	100	97	2	-14*	0	-4	4
12*	0	5	-5	16	23	23	0	2	48	38	9	3	245	-263	17	-3*	0	10	-10	8*	0	-17	17	-12+	15	10	5
14*	0	-10	10	18*	0	5	-5	4	12	9	3	5	90	75	14	K,L=	3	0		10	93	-89	-3	-10+	13	9	4
16*	0	-3	3	K,L=	1	2		6	14	11	3	7	43	44	-1	1	227	228	0	12+	29	20	9	-8	76	-67	-8
18*	0	1	-1	-17*	0	-4	4	8	23	-25	1	9*	0	-2	2	3+	7	14	-7	14*	0	-8	8	-6+	31	-15	-16
K,L=	0	2		-15*	0	-10	10	10*	0	-9	9	11	28	-25	-2	5	137	-118	-18	K,L=	3	6		-4	73	-57	-15
-16*	0	19	-19	-13*	0	-10	10	K,L=	1	8		13*	0	0	0	7	67	-47	-20	-17*	0	1	-1	-2	177	-175	-1
-14*	0	9	-9	-11*	0	0	0	-15*	0	0	0	15	41	-36	-5	9*	0	10	-10	-15+	6	12	-5	0	140	-145	4
-12*	0	-8	8	-9	112	-111	-1	-13*	0	5	-5	17	18	-14	-3	11+	52	29	22	-13*	0	-5	5	2	266	-285	19
-10	81	66	14	-7	61	59	2	-11*	0	1	-1	K,L=	2	4		13*	0	-1	1	-11	18	20	-1	4	151	-157	6
-8	157	-152	-5	-5	28	28	0	-9*	0	-1	1	-18*	0	4	-4	15	39	-33	-5	-9+	19	-12	-6	6+	38	20	17
-6	163	119	44	-3	97	98	-1	-7	12	-14	1	-16*	0	-13	13	17*	0	9	-9	-7*	0	0	0	8	37	43	-6
-4	384	432	-48	-1	93	96	-2	-5	19	17	2	-14*	0	-14	14	K,L=	3	1		-5	69	-49	-19	10	42	32	10
-2	286	299	-13	1	33	-42	9	-3	24	18	6	-12	18	19	+1	-18*	0	-1	1	-3	67	-49	-18	12	35	-27	-7
0	163	178	-15	3	228	-229	1	-1	33	39	-5	-10*	0	-1	1	-16*	0	1	-1	-1*	0	-2	2	14	11	9	1
2+	22	14	8	5*	0	8	-8	1+	17	24	-6	-8+	22	15	7	-14	32	-33	1	1	29	-34	4	16	9	6	2
4	216	233	-16	7	28	-20	-8	3	29	-22	-7	-6+	23	-8	-14	-12	17	-21	3	3	55	-48	-7	K,L=	4	3	
6	75	-96	21	9	136	131	5	5+	28	6	22	-4+	12	19	-7	-10*	0	4	-4	5	64	45	18	-17*	0	3	-3
8	80	84	-3	11	23	25	-2	7	57	43	14	-2	133	-146	12	-8	71	63	8	7	121	-129	7	-15*	0	-8	8
10	39	-37	-1	13*	0	15	-15	K,L=	1	9		0	97	105	-8	-6	56	62	-6	9	20	-19	0	-13	11	11	0
12	30	-26	-4	15	21	19	1	-12*	0	-3	3	2+	40	26	13	-4	17	-12	-5	11	52	-39	-13	-11	46	-43	-2
14*	0	0	0	17+	18	10	7	-10*	0	3	-3	4	58	-52	-6	-2	179	175	3	K,L=	3	7		-9*	14	21	-7
16	21	-22	0	K,L=	1	3		-8*	0	5	-5	6	18	21	-3	0	41	-33	-8	-16*	0	0	0	-7*	0	4	-4
K,L=	0	4		-18*	0	1	-1	-6+	14	-4	-9	8+	27	-18	-8	2	102	-111	9	-14*	0	3	-3	-5+	24	-1	-22
-14	31	28	3	-16*	0	2	-2	-4+	32	-21	-10	10	61	70	-8	4	54	42	11	-12*	0	2	-2	-3	109	88	21
-12*	0	-2	2	-14*	0	4	-4	-2	46	-40	-5	12*	0	0	0	6	112	-101	-10	-10*	0	6	-6	-1	123	-114	-9
-10*	0	-5	5	-12	68	-57	-10	0	47	38	8	14	45	-32	-12	8	59	64	-5	-8	28	21	7	1+	7	3	4
-8	32	-29	-3	-10+	14	-20	6	2	50	45	4	K,L=	2	5		10	21	19	2	-6+	34	-17	-17	3	173	186	-12
-6	130	124	6	-8	124	133	-8	4	22	-18	-4	-7+	34	18	15	12	41	46	-4	-4+	6	2	4	5+	8	-13	4
-4	21	-19	-1	-6	124	115	9	K,L=	1	10		-5	111	-94	-17	14*	0	1	-1	-2	50	47	3	7+	8	4	3
-2	202	204	-1	-4	85	85	0	-9*	0	4	-4	-3+	15	-8	-7	16	16	-11	-4	0	31	-26	-5	9	39	-40	1
0	377	-396	19	-2	120	-134	13	-7*	0	0	0	-1	35	-33	-2	18*	0	1	-1	2	100	88	11	11	16	-17	1
2+	17	7	10	0	262	278	-16	-5*	0	-7	7	1	36	32	4	K,L=	3	2		4*	0	2	-2	13*	0	-4	4
4+	153	200	-47	2*	0	8	-8	-3*	0	0	0	3	22	20	2	-17*	0	5	-5	6	24	-25	0	15+	24	16	7
6	91	93	-1	4	348	368	-19	-1*	0	-1	1	5	44	-43	-1	-15+	26	16	9	8+	15	-10	-5	K,L=	4	4	
8	46	59	-12	6	43	-51	8	1	20	14	5	7	46	-40	-5	-13	19	17	1	10*	0	4	-4	-18*	0	-6	6
10	50	-55	5	8	94	-80	-14	K,L=	1	11		9	148	144	4	-11	30	-35	4	K,L=	3	8		-16*	0	6	-6
12	66	-71	5	10	25	22	2	-8*	0	-7	7	11	22	-24	2	-9	106	105	1	-15*	0	0	0	-14*	0	-8	8
14*	0	16	-16	12*	0	-4	4	-6+	5	-11	5	13*	0	-7	7	-7	64	-59	-5	-13*	0	-7	7	-12	39	-28	-10
16+	20	-26	6	14	43	32	11	-4	11	12	-1	K,L=	2	6		-5	86	72	14	-11*	0	-1	1	-10*	0	6	-6
K,L=	0	6		16+	13	-2	-11	K,L=	2	0		-18*	0	0	0	-3	58	-61	3	-9*	0	-4	4	-8	30	28	2
-16*	0	-4	4	K,L=	1	4		0	458	-495	36	-16*	0	4	-4	-1+	15	-22	7	-7	46	47	0	-6	50	-40	-9
-14*	0	4	-4	-15*	0	-10	10	2	184	195	-10	-14*	0	-1	1	1	21	26	-5	-5+	30	-21	-9	-4	9	-10	0
-12*	0	12	-12	-13	34	-31	-2	4	37	35	2	-12*	0	-8	8	3	22	19	3	-3	75	-69	-10	-2	169	-147	-21
-10*	0	4	-4	-11	24	-21	-3	6+	10	5	5	-10*	0	2	-2	5	133	-123	-9	-1	21	-19	-2	0	31	34	-2
-8	39	36	3	-9	20	18	2	8+	17	-9	-7	-8+	23	-15	-8	7	87	90	-2	1+	13	-8	-5	2	51	-43	-8
-6	14	-13	-1	-7	50	53	-3	10	75	-65	-9	-6*	0	4	-4	9	118	-125	6	3+	16	8	7	4	79	80	-1
-4	176	-164	-12	-5	29	-29	0	12*	0	11	-11	-4	44	53	-8	11+	20	-13	-7	5	46	-41	-4	6	43	-50	6
-2	44	-43	0	-3+	32	-19	-13	14*	0	8	-8	-2+	19	-26	7	13	24	-19	-4	7	64	-56	-7	8	16	13	3
0*	0	4	-4	-1	11	-13	1	16*	0	11	-11	0	51	45	5	15	33	-23	-9	K,L=	3	9		10	57	-56	-1
2	69	70	-1	1	44	50	-5	18+	9	-3	-6	2	17	-13	-3	17+	24	-14	-9	-12	8	9	0	12	38	41	-2
4	86	-88	1	3	28	37	-8	K,L=	2	1		4	27	22	4	K,L=	3	3		-10*	0	-10	10	14	34	24	10
6	20	15	4	5	93	89	3	-17*	0	8	-8	6	44	47	-3	-18*	0	-3	3	-8*	0	-2	2	K,L=	4	5	
8	50	41	8	7	87	83	4	-15*	0	7	-7	8	50	-57	6	-16*	0	-7	7	-6*	0	1	-1	-17*	0	4	-4
10*	0	3	-3	9	29	29	0	-13	32	27	4	10	33	-26	-6	-14	17	-17	0	-4+	2	-3	1	-15*	0	3	-3
12*	0	-12	12	11	40	49	-9	-11*	0	3	-3	12*	0	9	-9	-12	39	41	-2	-2	10	9	0	-13*	0	5	-5
K,L=	0	8		13	70	60	9	-9	38	41	-2	K,L=	2	7		-10+	26	-13	-13	0	10	8	1	-11	36	-36	0
-14*	0	-6	6	15*	0	-10	10	-7	124	108	16	-17*	0	0	0	-8+	18	-9	-8	2+	15	0	-14	-9	14	12	1
-12*	0	4	-4	K,L=	1	5		-5	306	311	-5	-15*	0	-1	1	-6	108	103	5	4+	16	10	6	-7*	0	-12	12
-10*	0	7	-7	-16*	0	-4	4	-3	264	-253	-11	-13*	0	3	-3	-4	44	40	3	K,L=	3	10		-5	52	46	5
-8*	0	7	-7	-14	12	8	3	-1	93	-74	-19	-11*	0	-16	16	-2+	37	23	14	-11*	0	5	-5	-3+	34	19	15
-6	38	-33	-5	-12*	0	9	-9	1	181	-190	8	-9*	0	-18	18	0	62	54	8	-9*	0	-2	2	-1	29	-24	-5
-4+	38	-14	-24	-10*	0	6	-6	3	110	-110	0	-7	29	21	8	2	78	76	1	-7*	0	-3	3	1+	15	-6	-8
-2	68	-78	10	-8+	28	-19	-9	5	39	-37	-1	-5*	0	17	-17	4	61	53	7	-5*	0	6	-6	3	81	66	15
0	85	-61	-24	-6	120	108	12	7+	71	-43	-28	-3*	0	13	-13	6+	14	6	7	-3*	0	9	-9	5	86	78	8
2+	55	-29	-25	-4	30	-24	-5	9	135	-121	-14	-1*	0	-5	5	8	97	99	-2	-1*	0	-3	3	7	77	-78	1
4	49	59	-10	-2	58	67	-9	11	30	35	-4	1+	32	-21	-11	10+	23	-1	-22	1	37	-32	-4	9	101	-101	0
6	10	-7	-2	0	165	160	5	13	50	-47	-2	3	84	72	11	12*	0	-5	5	K,L=	4	0		11	29	23	5
8*	0	-5	5	2	53	46	7	15*	0	-7	7	5	57	52	4	14	47	-42	-4	0	335	-380	45	13	15	-12	-3
K,L=	0	10		4	118	114	3	17*	0	-14	14	7	64	60	3	16	14	12	1	2	143	-157	14	K,L=	4	6	
-4+	22	-12	-9	6	14	15	-1	K,L=	2	2		9*	0	-14	14	K,L=	3	4		4	175	-182	7	-16*	0	-1	1
-2	42	-38	-3	8	23	-24	0	-18*	0	3	-3	K,L=	2	8		-17*	0	-6	6	6	39	-33	-6	-14*	0	-1	1
0*	0	1	-1	10+	12	-16	4	-16*	0	-2	2	-14*	0	3	-3	-15	29	21	8	8	56	-49	-6	-12*	0	-1	1
2	33	-28	-4	12	57	-58	0	-14*	0	-4	4	-12*	0	-5	5	-13	38	34	4	10	50	45	4	-10+	16	-9	-7
K,L=	1	0		14*	0	0	0	-12*	0	-13	13	-10*	0	0	0	-11	26	21	4	12	17	-15	-1	-8+	16	-9	-7
3	137	153	-16	K,L=	1	6		-10	41	-40	-1	-8*	0	2	-2	-9*	0	-12	12	14	9	11	-2	-6+	5	8	-3
5	21	-27	5	-17*	0	-1	1	-8	136	123	13	-6*	0	-9	9	-7	103	-94	-8	16	19	-15	-3	-4+	6	13	-7
7	74	-92	18	-15*	0	-9	9	-6	80	-64	-16	-4*	0	12	-12	-5	79	70	9	18*	0	1	-1	-2	59	74	-14
9	21	-24	2	-13*	0	1	-1	-4+	15	-22	6	-2	24	24	0	-3+	13	-4	-8	K,L=	4	1		0	50	41	8
11*	0	-6	6	-11*	0	-10	10	-2	142	124	17	0*	0	6	-6	-1	112	-101	-11	-17*	0	-5	5	2+	53	35	17
13*	0	4	-4	-9*	0	8	-8	0	111	-107	-4	2*	0	7	-7	1	127	-141	14	-15+	11	-2	-8	4	81	73	7
15	20	19	0	-7*	0	-9	9	2+	58	-39	-19	4	47	-36	-10	3	53	-44	-8	-13+	11	-4	-6	6	138	-127	-11
17*	0	-2	2	-5	28	25	3	4	179	-178	-1	6	21	-20	-1	5	60	47	12	-11+	22	-15	-7	8+	17	-8	-8
K,L=	1	1		-3+	28	37	-9	6	50	49	0	8	24	19	5	7	27	23	4	-9	28	-27	-1	10+	15	-10	-4
-18*	0	-4	4	-1*	0	8	-8	8	31	-36	4	K,L=	2	9		9	36	-32	-4	-7	73	80	-6	K,L=	4	7	
-16+	22	-15	-7	1	35	36	0	10	24	27	-2	-9*	0	4	-4	11	114	-99	-14	-5	75	-63	-11	-15*	0	1	-1
-14*	0	-9	9	3	133	141	-8	12	41	46	-5	-7*	0	0	0	13	118	-83	-35	-3	95	92	3	-13+	16	-1	-15
-12	19	-24	5	5*	0	2	-2	14*	0	-5	5	-5*	0	13	-13	15	20	15	4	-1	147	128	19	-11*	0	11	-11
-10*	0	2	-2	7	39	38	1	16*	0	1	-1	-3	36	41	-4	K,L=	3	5		1	27	26	0	-9+	15	5	10
-8+	26	-12	-13	9	12	15	-3	18	14	-14	0	-1	32	31	1	-16*	0	8	-8	3	202	-218	15	-7	15	-15	0
-6	229	-218	-10	11+	46	31	14	K,L=	2	3		1*	0	9	-9	-14*	0	1	-1	5	130	-118	-11	-5+	6	-1	-4
-4	715	709	6	K,L=	1	7		-17*	0	-4	4	3	65	50	14	-12*	0	-3	3	7	81	76	5	-3	81	-84	3
-2	48	53	-5	-16+	9	2	7	-15*	0	11	-11	5	15	18	-2	-10+	26	16	9	9	90	81	8	-1	64	57	6
0	77	-86	9	-14*	0	2	-2	-13*	0	-21	21	K,L=	2	10		-8	21	20	1	11	40	-42	1	1	122	102	19
2	111	-112	1	-12	15	13	2	-11	71	67	4	-10*	0	0	0	-6+	15	10	4	13	25	24	1	3	113	-114	0

TABLE 2. (Continued)

H	FO	FC	DF	H	FO	FC	DF	H	FO	FC	DF	H	FO	FC	DF	H	FO	FC	DF	H	FO	FC	DF	H	FO	FC	DF
5	32	-22	-9	-11*	0	7	-7	-7	53	-43	-9	-11*	0	-2	2	-15*	0	-6	6	-3+	17	-6	-11	-1*	0	-36	36
7*	0	-13	13	-9*	0	5	-5	-5+	21	-14	-6	-9*	0	0	0	-13	13	-10	-3	-1	67	-56	-11	1	43	30	12
9	23	21	1	-7	107	86	21	-3+	31	43	-12	-7+	3	12	-9	-11*	0	0	0	1*	0	1	-1	3+	12	-8	-4
K,L=	4	8		-5	64	-65	0	-1	97	-96	-1	-5+	15	-20	5	-9*	0	0	0	3	25	-27	2	K,L=	9	7	
-14*	0	-1	1	-3	78	-59	-18	1	47	-41	-6	-3	95	85	10	-7*	0	-8	8	5	72	69	3	-8*	0	-3	3
-12+	12	6	5	-1+	30	-17	-13	3	57	43	14	-1	46	-51	4	-5	64	47	16	7+	21	-14	-6	-6	26	20	6
-10+	26	-4	-21	1	33	-36	3	5	143	131	11	1	93	-108	14	-3	31	23	7	K,L=	8	4		-4+	24	-15	-8
-8+	36	-20	-16	3	72	67	5	7*	0	2	-2	3*	0	0	0	-1*	0	-3	3	-8*	0	-1	1	-2	12	15	-2
-6	50	38	12	5+	9	-16	7	9	56	50	5	5	46	-42	-4	1	32	31	0	-6+	57	38	19	0	25	29	-4
-4+	4	7	-2	7	78	-79	1	11*	0	9	-9	7*	0	-1	1	3	32	36	-4	-4+	16	0	16	K,L=	9	8	
-2	84	92	-8	9	79	-72	-7	13+	8	5	3	K,L=	6	8		K,L=	7	5		-2*	0	1	-1	-7*	0	0	0
0	34	33	0	11	21	19	1	15*	0	1	-1	-12*	0	-4	4	-16	5	4	1	0	46	48	-2	-5*	0	0	0
2+	9	-14	4	13*	0	-3	3	17	23	23	0	-10*	0	0	0	-14*	0	-3	3	2*	0	17	-17	K,L=	9	9	
4	46	-47	1	K,L=	5	5		K,L=	6	2		-8	19	16	2	-12*	0	2	-2	4*	0	-16	16	-6*	0	2	-2
6*	0	0	0	-16	8	-7	-1	-16*	0	2	-2	-6*	0	-3	3	-10	37	-29	-8	6*	0	0	0	K,L=	10	0	
K,L=	4	9		-14*	0	-3	3	-14*	0	2	-2	-4*	0	1	-1	-8	22	-22	0	8+	23	-15	-7	0+	43	29	13
-11	19	16	2	-12*	0	-4	4	-12+	15	22	-6	-2	74	-76	2	-6+	37	24	12	K,L=	8	5		2	32	-34	1
-9*	0	2	-2	-10*	0	0	0	-10	20	-21	1	0	37	34	3	-4	42	-41	-1	-7	18	13	4	4	106	-104	-2
-7	35	-28	-7	-8	14	10	4	-8	22	-21	-1	2*	0	5	-5	-2	41	28	12	-5	20	-18	-2	6	59	53	5
-5*	0	-10	10	-6	76	-74	-1	-6	76	76	0	4*	0	2	-2	0	34	-33	0	-3*	0	-18	18	8	16	-15	-1
-3*	0	-5	5	-4	23	-23	0	-4	51	-41	-10	6*	0	-7	7	2	39	30	8	-1+	39	23	15	K,L=	10	1	
-1*	0	0	0	-2	74	-60	-14	-2+	46	20	26	K,L=	6	9		4	46	33	13	1+	83	32	50	-7	54	44	10
1*	0	-6	6	0	51	50	1	0	71	61	9	-11*	0	-7	7	6	87	-96	8	3+	36	-66	30	-5	88	68	19
3*	0	0	0	2	96	-95	0	2+	26	16	10	-9*	0	-1	1	8	28	-22	-5	K,L=	8	6		-3	64	54	9
K,L=	4	10		4	84	-91	6	4	66	65	0	-7	30	34	-3	10	8	6	2	-8	18	-16	-2	-1	69	63	6
-10*	0	0	0	6	57	-60	2	6	31	-29	-1	-5+	15	-20	4	12*	0	0	0	-6*	0	12	-12	1	165	-167	2
-8*	0	7	-7	8*	0	1	-1	8	26	18	7	-3	24	-24	0	K,L=	7	6		-4	21	-14	-6	3	46	-32	-13
-6	19	14	4	10	61	55	5	10*	9	0	-9	-1	41	-46	4	-15*	0	2	-2	-2*	0	-13	13	5	25	-27	2
-4*	0	3	-3	12	19	16	3	12+	15	-22	7	1	7	-7	0	-13*	0	-2	2	0+	46	-11	-34	7+	12	16	-3
-2+	18	12	5	K,L=	5	6		14	17	-14	-3	3	32	-28	-3	-11	14	-13	0	2*	0	-31	31	K,L=	10	2	
0*	0	-7	7	-17*	0	1	-1	16*	0	6	-6	K,L=	6	10		-9*	0	0	0	4+	27	11	15	-8	40	-38	-1
K,L=	5	0		-15*	0	-3	3	K,L=	6	3		-6*	0	-3	3	-7*	0	8	-8	6*	0	27	-27	-6	43	-40	-2
1+	27	37	-9	-13*	0	7	-7	-17+	12	7	4	-4	10	10	0	-5	32	33	-1	K,L=	8	7		-4	46	43	3
3	153	-157	4	-11*	0	-1	1	-15*	0	4	-4	-2+	9	-3	-6	-3+	15	-3	-12	-7*	0	2	-2	-2*	0	3	-3
5+	6	11	-5	-9*	0	1	-1	-13	21	-17	-4	K,L=	7	0		-1	75	60	14	-5	34	34	0	0	68	-48	-20
7	79	73	6	-7+	14	0	-13	-11+	17	-6	-11	1+	23	-14	-8	1	100	-81	-19	-3*	0	-10	10	2*	0	-2	2
9+	0	13	-12	-5	15	-15	0	-9	24	-19	-5	3	27	-19	-7	3	84	88	-4	-1+	19	7	11	4	27	-19	-7
11	22	-17	-5	-3	19	-18	-1	-7+	9	1	8	5	80	69	10	5	46	42	3	1*	0	-15	15	6*	0	-1	1
13*	0	-1	1	-1*	0	-15	15	-5+	11	-3	-7	7	16	-13	-2	7	25	25	0	K,L=	8	8		8	17	19	-2
15*	0	11	-11	1	139	139	0	-3	149	-142	-6	9	26	-23	-2	9*	0	-7	7	-8*	0	-1	1	K,L=	10	3	
17	14	-11	-3	3	97	-98	1	-1	120	110	10	11+	19	9	10	K,L=	7	7		-6	14	-10	-3	-7	67	61	5
K,L=	5	1		2	55	61	-6	1+	67	45	22	13*	0	5	-5	-12*	0	7	-7	-4+	14	-19	5	-5	9	6	2
-16+	14	7	6	4	183	-173	-9	3	73	85	-11	15*	0	7	-7	-10*	0	-5	5	-2*	0	1	-1	-3+	8	-17	9
-14+	35	24	10	6+	7	0	-6	5	67	60	7	17*	0	3	-3	-8+	10	0	-10	0	16	-19	3	-1	64	-73	8
-12*	0	6	-6	8	25	-31	5	7*	0	5	-5	K,L=	7	1		-6*	0	-11	11	K,L=	9	0		1+	12	5	7
-10	18	13	5	10	32	-40	8	9+	28	-37	8	-18*	0	-3	3	-4+	35	-22	-13	1	71	63	8	3	70	76	-6
-8+	26	-18	-8	K,L=	5	7		11	22	22	0	-16*	0	-3	3	-2	24	20	3	3	98	85	12	5	23	-19	-3
-6	47	42	5	-14*	0	-2	2	13	24	26	-2	-14*	0	7	-7	0+	16	-5	-11	5	135	-132	-3	7+	15	23	-8
-4	90	-83	-6	-12	12	-9	-2	15*	0	-3	3	-12	17	15	2	2	18	-15	-2	7+	15	-3	-12	K,L=	10	4	
-2	65	-72	7	-10*	0	-7	7	K,L=	6	4		-10*	0	-1	1	4	75	-72	-2	K,L=	9	1		-8	23	26	-3
0	258	-263	5	-8+	11	-7	-4	-16*	0	5	-5	-8	51	-49	-2	6*	0	1	-1	-8	64	65	-1	-6	9	-7	-1
2	49	36	12	-6	27	24	3	-14	16	12	4	-6*	0	-3	3	K,L=	7	8		-6	54	58	-4	-4	29	30	0
4	28	28	0	-4	62	48	13	-12	16	12	3	-4	63	55	7	-11*	0	5	-5	-4+	28	-17	-11	-2*	0	4	-4
6	79	59	20	-2	81	-73	-8	-10*	0	-4	4	-2	54	-46	-7	-9*	0	-4	4	-2*	0	3	-3	0+	16	-1	-14
8	42	-44	2	0	13	-13	0	-8	22	-17	-5	0+	60	40	20	-7+	23	12	11	0	71	69	1	2	28	-31	3
10+	33	-16	-17	2	137	-123	-14	-6+	18	-4	-13	2	103	-105	2	-5*	0	-5	5	2	62	-73	10	4+	28	45	-17
12	21	-22	0	4	25	27	-1	-4	14	-18	3	4	64	-53	-11	-3*	32	-22	-10	4	23	-25	1	6	49	-58	9
14*	0	-1	1	6*	0	-9	9	-2	94	90	4	6	63	57	5	-1	54	53	0	6*	0	-13	13	8+	9	1	7
16*	0	-12	12	8	18	19	-1	0	118	-127	8	8	8	7	1	1*	0	9	-9	8	35	43	-7	K,L=	10	5	
K,L=	5	2		K,L=	5	9		2+	12	-3	-8	10*	0	10	-10	3	41	31	9	K,L=	9	2		-7*	0	3	-3
-17*	0	0	0	-13*	0	2	-2	4	19	-13	-5	12+	20	-14	-6	5	14	-10	-4	-7+	26	-14	-12	-5	37	-35	-1
-15*	0	-6	6	-11*	0	-4	4	6	106	130	-24	14+	17	-11	-5	K,L=	7	9		-5	18	-16	-1	1	56	58	-2
-13	8	9	-1	-9	10	7	3	8*	0	2	-2	16	21	15	5	-10*	0	2	-2	-3	56	50	6	3	30	27	2
-11	38	36	2	-7	56	-52	-3	10	56	-54	-1	K,L=	7	2		-8	14	14	0	-1	48	40	7	5	14	-15	1
-9*	0	-2	2	-5+	18	8	10	12	27	-24	-3	-17*	0	-4	4	-6	22	-25	2	1+	30	15	15	7+	6	8	-2
-7+	11	1	10	-3	94	93	1	14*	0	0	0	-15*	0	4	-4	-4*	0	2	-2	3+	35	25	10	K,L=	10	6	
-5+	34	17	16	-1	27	-31	4	K,L=	6	5		-13	30	-38	7	-2	14	-13	0	5*	0	6	-6	-8	11	9	2
-3	106	98	7	1	28	-27	0	-17*	0	0	0	-11*	0	3	-3	0	18	-15	-2	7	32	34	-1	-6	15	19	-4
-1+	61	-42	-18	3	54	-45	-9	-15*	0	-1	1	-9+	9	12	-2	2+	18	11	6	K,L=	9	3		0+	22	33	-10
1	247	-245	-2	5	21	-17	-4	-13*	0	0	0	-7*	0	1	-1	K,L=	7	10		-8	15	17	-1	2*	0	-9	9
3	46	39	7	K,L=	5	9		-11	13	15	-1	-5	28	-27	-1	-5*	0	-7	7	-6+	23	-13	-10	4	18	-19	0
5*	0	-6	6	-10*	0	4	-4	-9+	12	-18	5	-3	46	49	-3	-3	8	8	0	-4	52	52	0	6*	0	-8	8
7	23	-20	-2	-8+	19	-7	-11	-7	27	-29	2	-1*	0	5	-5	K,L=	8	0		-2	14	-15	1	K,L=	10	7	
9	35	26	9	-6	26	24	1	-5+	12	21	-8	1	102	86	16	0	29	25	4	0	30	36	-5	-7	18	-14	-3
11+	12	-8	-3	-4*	0	4	-4	-3*	0	10	-10	3	116	-113	-3	2	74	74	0	2	41	34	6	1	18	24	-5
13	34	-28	-5	-2*	0	-2	2	-1	82	78	3	5	62	59	2	4	88	111	-23	4	46	45	1	3+	4	1	3
15*	0	-1	1	0	18	-14	-4	1	42	32	9	7*	0	-2	2	6+	16	9	7	6*	0	10	-10	K,L=	10	8	
17*	0	2	-2	2+	26	-17	-8	3*	0	6	-6	9	57	49	8	8+	13	4	8	8+	27	41	-14	-8	8	-9	1
K,L=	5	3		K,L=	5	10		5	145	-156	10	11*	0	2	-2	K,L=	8	1		K,L=	9	4		-6+	7	-3	-4
-16*	0	-7	7	-9*	0	0	0	7	43	45	-1	13	64	57	7	-7	43	-34	-9	-7*	0	-9	9	K,L=	11	0	
-14	19	16	3	-7*	0	7	-7	9	11	-14	2	15*	0	-6	6	-5+	33	7	25	-5	22	29	-6	3	44	-40	-4
-12*	0	6	-6	-5*	0	9	-9	11*	0	-4	4	K,L=	7	3		-3	9	-8	0	-3	20	20	0	5	80	68	12
-10	9	10	0	-3	14	-15	0	K,L=	6	6		-16	18	16	1	-1	91	-102	11	-1	37	-37	0	7	32	-24	-7
-8+	14	-22	8	-1*	0	2	-2	-16*	0	-1	1	-14*	0	1	-1	1	24	-20	-3	1	35	25	10	K,L=	11	1	
-6	93	-82	-10	K,L=	6	0		-14*	0	5	-5	-12	31	-27	-4	3	46	36	10	3	44	-41	-3	-8+	16	-8	-8
-4	120	-111	-8	0	219	226	-7	-12*	0	6	-6	-10+	10	3	7	5	15	-19	3	5	91	71	19	-6	17	13	4
-2	57	-51	-5	2	37	36	1	-10*	0	-1	1	-8+	24	-12	-11	7	37	33	3	7	52	47	5	-4	70	71	-1
0	167	-177	9	4	55	42	12	-8	19	15	4	-6+	20	-10	-9	K,L=	8	2		K,L=	9	5		-2*	0	13	-13
2	46	33	13	6	90	-104	14	-6	37	-38	0	-4+	30	-42	11	-8	37	41	-4	-8*	0	-10	10	0	111	-112	1
4	102	-110	7	8+	13	19	-6	-4+	4	-5	1	-2	58	-72	14	-6*	0	1	-1	-6*	0	-14	14	2+	17	8	9
6	66	56	10	10	22	25	-2	-2+	17	-26	8	0*	0	7	-7	-4	68	65	2	-4	45	38	6	4*	0	-5	5
8	26	-22	-3	12+	8	5	3	0	61	-53	-7	2+	12	4	7	-2	61	58	2	-2+	27	42	-15	6*	0	6	-6
10	28	23	4	14	16	-16	0	2	81	64	17	4	84	90	-5	0	67	77	-9	0+	54	14	39	8	26	18	7
12	30	-31	0	16*	0	2	-2	4	15	-12	-3	6*	0	8	-8	2	74	73	1	2+	17	59	-42	K,L=	11	2	
14	8	9	0	K,L=	6	1		6+	13	8	5	8	46	-52	6	4*	0	-4	4	4	27	22	4	-7*	0	-8	8
16*	0	-6	6	-17*	0	-3	3	8	18	-17	0	10	60	-48	-12	6+	11	25	-13	6+	25	16	8	-5	31	34	0
K,L=	5	4		-15*	0	-3	3	10	17	15	2	12	19	14	5	8*	0	2	-2	K,L=	9	6		-3	95	-116	20
-17+	16	10	6	-13	13	-14	1	K,L=	6	7		14+	38	26	11	K,L=	8	3		-7*	0	-1	1	-1+	24	35	-10
-15+	14	-8	-5	-11+	13	6	6	-15*	0	1	-1	K,L=	7	4		-7	16	-20	3	-5	19	-13	-3	1*	0	-23	23
-13*	0	6	-6	-9	58	-47	-10	-13*	0	1	-1	-17	11	-10	-1	-5	37	-31	-6	-3+	37	-13	-24	3	46	48	-2

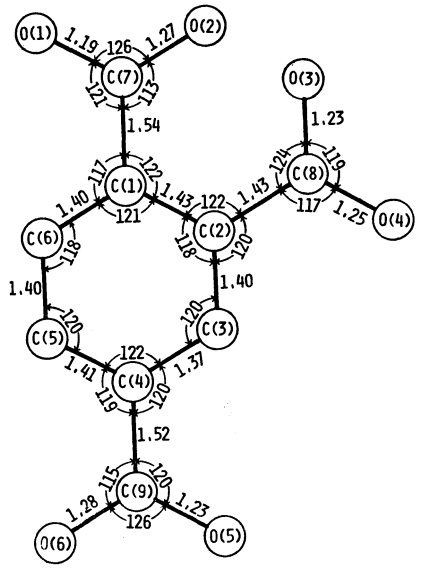

Fig. 2. Molecular dimensions of trimellitic acid. The estimated standard deviations are as follows:
C–C=0.02 Å, C–O=0.01~0.02 Å, C–C–C=0.8~1.0°, C–C–O=0.6~0.9°, O–C–O=0.5~1.0°

applied. They were then corrected and reduced to the structure factors by means of the procedure described by Hamilton, Rollet, and Sparks.[11]

Both cells, real and pseudo, were found to be monoclinic, with a space group of I2/c or Ic. The former was tentatively assumed on the basis of the statistical averages and distributions of normalized structure amplitudes in the pseudo-cell.

Phase Determination

Since the phase determination procedure for this crystal was applied only to the pseudo-cell, the indices were transformed to refer to this cell; *i.e.*, only those data with $k=5n$ were used, and the k index was divided by five. The absolute scale and approximate temperature factors were determined by means of Wilson's statistics.[12] The normalized structure amplitudes, $|E|$, were computed from these values. The symbolic addition procedure was used to determine the phases.[13] The origin was specified by assigning the signs to two linearly independent reflections.[14] Three additional E's were assigned arbitrary symbols.

Table 3. Assignment of the two origin specifying reflections and three other reflections as a starting set

h	k	l	$\|E\|$	Sign	N.I.P.[a]
4	1	3	3.34	+	88
1	10	1	3.06	−	72
9	2	5	3.40	A	50
−4	1	1	3.18	B	161
7	3	6	3.01	C	43

a) N. I. P.=Number of interaction pairs.

The starting set of phases is listed in Table 3. 114 signs for $|E|>1.5$ were determined by the application of the Σ_2 relations. From the accumulated information about the signs of the 114 reflections, it was obvious that the sign of A was +, while that of B was + and that of C was −. An E-map computed on the basis of these 114 terms revealed most of atomic positions. The peak values for all the atoms were higher than 127, the average value was 244. The maximum value of the ghost peaks was 197. A Fourier map was calculated on the basis of the structure amplitudes phased on the contributions of eight peaks(higher than 200) in order to rule out wrong peaks in the E-map.

The refinement of the positional parameters, the thermal parameters, and one scale factor was carried out by means of the block-diagonal least-squares method, with a modified version of the HBLS-IV program.[15] Four cycles of refinement with isotropic thermal parameters lowered the R value to 23.3%. At this stage of refinement, anisotropic thermal parameters were introduced; four subsequent cycles of

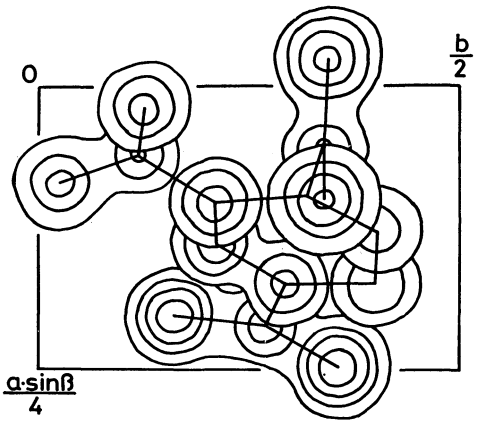

Fig. 3. Electron density map along the c axis.

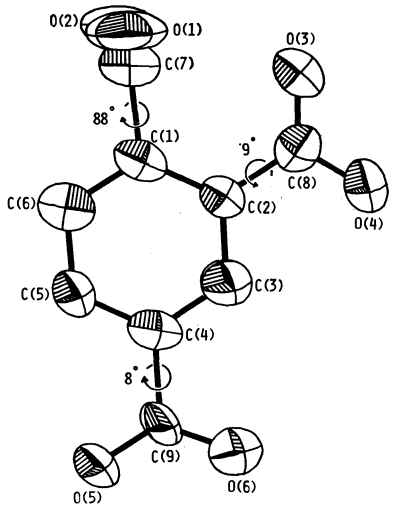

Fig. 4. Thermal ellipsoids of non-hydrogen atoms, which are scaled to include 20% probability.

11) W. C. Hamilton, J. S. Rollet and A. Sparks, *Acta Crystallogr.*, **18**, 129 (1965).
12) A. J. C. Wilson, *Nature* (London), **150**, 151 (1942).
13) J. Karle and I. L. Karle, *Acta Crystallogr.*, **21**, 849 (1966).
14) H. Hauptman and J. Karle, *ibid.*, **12**, 93 (1959).
15) Y. Okaya and T. Ashida, HBLS-IV. The Universal Crystallographic Computing System (I), p. 65. The Crystallographic Society of Japan (1967).

Table 4. The final parameters and their estimated standard deviations (in parentheses)

The coordinates have been multiplied by 10^4. The anisotropic thermal parameters are of the exp $[-(B_{11}h^2+B_{22}k^2+B_{33}l^2+B_{12}hk+B_{13}hl+B_{23}kl)]$, and have been multiplied by 10^4.

Atom	x	y	z	B_{11}	B_{22}	B_{33}	B_{12}	B_{13}	B_{23}
C(1)	994(7)	3199(9)	997(12)	61(5)	60(10)	103(11)	−15(10)	−61(11)	−15(16)
C(2)	1016(6)	2133(8)	1643(12)	63(5)	42(9)	88(10)	−14(9)	−47(11)	−5(13)
C(3)	1415(6)	2008(9)	3089(12)	53(5)	51(9)	116(11)	7(9)	−54(11)	2(14)
C(4)	1738(7)	2895(9)	3869(12)	60(4)	61(9)	85(10)	−4(10)	−53(11)	−8(14)
C(5)	1756(8)	3932(9)	3209(15)	88(6)	37(9)	124(13)	−13(12)	−91(15)	−7(16)
C(6)	1403(8)	4084(9)	1743(15)	77(6)	71(11)	118(12)	−27(12)	−65(14)	13(18)
C(7)	539(7)	3424(9)	−558(13)	56(4)	78(10)	97(11)	−6(10)	−43(11)	11(15)
C(8)	637(8)	1213(9)	864(13)	60(5)	48(9)	127(12)	−20(10)	−51(12)	47(16)
C(9)	2120(7)	2752(8)	5468(12)	60(4)	28(8)	97(10)	7(9)	−48(10)	−45(13)
O(1)	−195(5)	3651(8)	−716(9)	61(4)	140(9)	102(9)	−3(9)	−76(9)	50(14)
O(2)	1022(5)	3353(8)	−1595(9)	80(4)	135(9)	92(8)	38(10)	−57(9)	−38(13)
O(3)	197(7)	1283(7)	−328(12)	132(7)	60(7)	136(10)	−56(11)	−127(14)	−5(13)
O(4)	736(8)	304(7)	1478(15)	168(9)	44(8)	209(14)	−63(12)	−215(19)	31(15)
O(5)	2454(5)	3535(6)	6145(9)	77(4)	38(6)	111(8)	−8(7)	−76(9)	−29(10)
O(6)	2011(5)	1809(6)	6025(9)	74(4)	55(6)	107(8)	5(8)	−43(9)	4(11)

Table 5. Least-squares plane of benzene ring

Equation of the plane defined by six carbon atoms of benzene ring:

$$-0.915X+0.194Y+0.355Z=-0.339$$

X, Y, and Z are coordinates in Å referred to an orthogonal set of axes and parallel to the a, b, and c* axes. Deviations of atoms:

Atom	From the plane	Atom	From the plane
C(1)	0.04 Å	C(9)	0.07 Å
C(2)	0.01	O(1)	1.20
C(3)	−0.02	O(2)	−0.98
C(4)	0.03	O(3)	0.22
C(5)	−0.01	O(4)	−0.08
C(6)	−0.04	O(5)	0.04
C(7)	0.14	O(6)	0.22
C(8)	0.04		

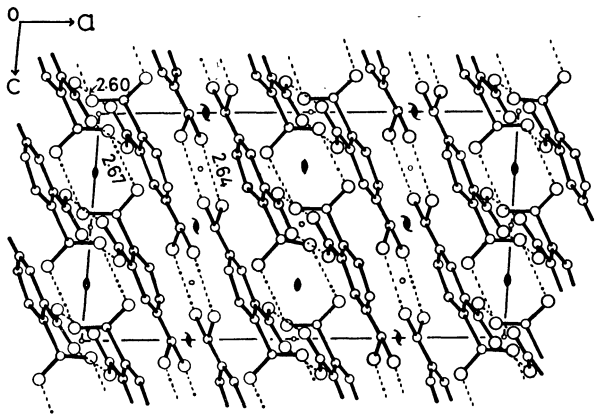

Fig. 5. A view of the crystal structure down the b axis. Hydrogen bonds are shown by broken lines.

refinement dropped the R value to 13.6%, excluding unobserved reflections. The observed and calculated structure factors are listed in Table 2.

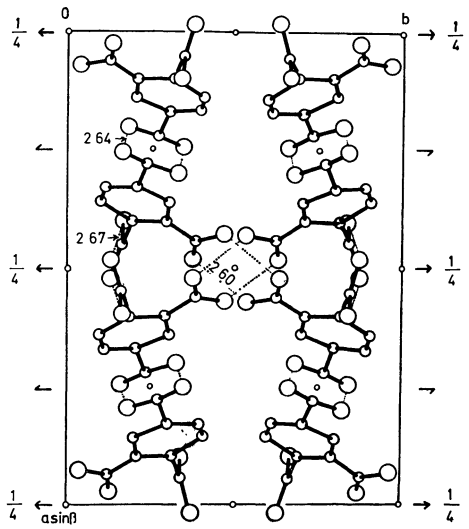

Fig. 6. A view of the crystal structure down the c axis. Hydrogen bonds are shown by broken lines.

Results and Discussion

The final positional and anisotropic thermal parameters are listed, along with their estimated standard deviations, in Table 4. Figures 3 and 4 show the electron density map along the c axis, calculated at the end of the refinement, and the thermal ellipsoids, which are scaled to include a 20% probability, respectively. The bond lengths and angles are given in Fig. 2. The equation of the least-squares plane of a benzene ring is given, along with the deviations of all the atoms from this plane, in Table 5.

A benzene ring is planar with the maximum deviation of 0.04 Å. The average values of the C(ring)–C(ring) and C(ring)–C(carboxyl) bond lengths are

1.40 and 1.49 Å, respectively. All the C–C–C bond angles lie within the range of 120±3°. In the carboxyl groups at the 1- and 4-positions, the C–O(H) and C–O bond lengths differ significantly from each other, while those of the carboxyl group at the 2-position are approximately equal. There is no intramolecular hydrogen bond between the adjacent carboxyl groups, and these groups twist by 88° (C(7)-O(1)O(2)) and 9°(C(8)O(3)O(4)) out of the plane of a benzene ring, so that the repulsion between the oxygen atoms is reduced, as is shown in Fig. 4.

The crystal structure is shown in Figs. 5 and 6. Each molecule is joined, through three kinds of hydrogen bonds (2.60, 2.64 and 2.67 Å), with three neighboring molecules. These hydrogen bonds are formed between the carboxyl groups related by the center of symmetry and the two-fold axis, as is usual in carboxylic acids.

The molecular dimensions and packing obtained by the refinement for the pseudo-cell do not seem to contain unacceptable results in comparison with other carboxylic acids[1-10] with a benzene ring. A crystal structure analysis based on the real cell is now in progress.

BULLETIN OF THE CHEMICAL SOCIETY OF JAPAN, VOL. 46, 2965—2968 (1973)

Hydrates of Organic Compounds. I. Solid-Liquid Phase Equilibria in the Water+1,4-Dioxane System and Some Properties of 1,4-Dioxane Hydrate

Haruo NAKAYAMA and Masao TAHARA

Department of Applied Chemistry, Faculty of Engineering, Yokohama National University, Ooka-machi, Minami-ku, Yokohama 233

(Received March 22, 1973)

The solid-liquid phase diagram for the water +1,4-dioxane system has been determined by the ordinary cooling curve method and with the aid of a differential scanning calorimeter (DSC). The diagram shows the existence of a hydrate which is stable in rather narrow ranges of temperature (−15.8∼−13.5 °C) and of composition (37.0∼46.5 wt% dioxane). From the phase relations and an analysis of the calorimetric data, the composition and the heat of formation (from the liquid states of both components) of the hydrate have been estimated to be $C_4H_8O_2 \cdot mH_2O$ with $m=36\sim39$ and $\Delta H_1=-51.3$ (for $m=36$)∼−55.6 (for $m=39$) kcal/mol respectively. This hydrate seems to be the same as that recently reported by Rosso *et al.*, though the compositions and the temperature ranges are very different.

In our previous papers,[1-3] from the thermodynamic measurements (heat of mixing, vapour pressure, volume change on mixing, and so forth) for aqueous solutions of various ethers, the dissolution states of ether molecules in water have been discussed. The main conclusion from these results is that the most important factor which characterizes the properties of these solutions is the structural modifications of water around the solute. In the present paper, an attempt will be made to examine some properties of the crystalline hydrates of cyclic ethers. It is conceivable that, in an aqueous solution, the local order of the water molecule induced around the solute is very similar to the state of a hydrogen-bonded water which surrounds a guest molecule in a clathrate. The propriety of such an analogy has been pointed out by a number of investigators.[4]

By various experimental techniques (such as X-ray diffraction,[5-7] phase diagram,[8,9] and dielectric absorption,[10,11]) it is now apparent that the crystalline hydrates of several cyclic ethers (such as propylene oxide, trimethylene oxide, and tetrahydrofuran) are clathrate hydrates. However, the phase diagrams[9,12,13] for the binary system of water and 1,4-dioxane, a typical cyclic ether, show no indication of a hydrate; furthermore, it has been pointed out that this rather abnormal behavior is closely associated with the unusual behavior of dilute aqueous solutions of 1,4-dioxane.[9] Very recently, nevertheless, from the phase diagram studies as well, Rosso and others[14] have reported a hitherto unknown 1,4-dioxane hydrate which contains

1) H. Nakayama and K. Shinoda, *J. Chem. Thermodynamics*, **3**, 401 (1971).
2) H. Nakayama, This Bulletin, **45**, 1371 (1972).
3) H. Nakayama, *ibid.*, **43**, 1683 (1970).
4) J. L. Kavanau, "Water and Solute-Water Interactions," Holden-Day, Inc., San Francisco (1964).
5) M. von Stackelberg and B. Meuthen, *Z. Elektrochem.*, **62**, 130 (1958).
6) R. K. McMullan and G. A. Jeffrey, *J. Chem. Phys.*, **42**, 2725 (1965).
7) D. F. Sargent and L. D. Calvert, *J. Phys. Chem.*, **70**, 2689 (1966).
8) J. Erva, *Suomen Kemistilehti*, **29B**, 183 (1956).
9) K. W. Morcom and R. W. Smith, *J. Chem. Thermodynamics*, **3**, 507 (1971).
10) D. W. Davidson, M. M. Davies, and K. Williams, *J. Chem. Phys.*, **40**, 3449 (1964).
11) R. E. Hawkins and D. W. Davidson, *J. Phys. Chem.*, **70**, 1889 (1966).
12) F. Hovorka, R. A. Schaefer, and D. Dreisbach, *J. Amer. Chem. Soc.*, **58**, 2264 (1936).
13) J. R. Goates and R. J. Sullivan, *J. Phys. Chem.*, **62**, 188 (1958).
14) J. C. Rosso and L. Carbonnel, *C. R. Acad Sci. Paris, Ser. C*, **272**, 136 (1971).

34 moles of water to one mole of dioxane. The temperature and composition ranges in which it can exist are −12.3 °C(peritectic)∼−14.2 °C(eutectic) and 31.5∼33.5 wt% dioxane. However, there are two notable features in their results. First, their phase diagram is appreciably different from those hitherto reported[6,12,13] over almost the entire range of composition. Secondly, as has been mentioned above, the estimated composition of the hydrate is expressed as $C_4H_8O_2 \cdot 34H_2O$; this is very different from the characteristic composition of the cubic Structure II hydrate (Structure II clathrate has 17 moles of water to one mole of the guest species). All the experimental data at present available show that the hydrates of low molecular-weight cyclic ethers, except ethylene oxide, are normal Type II hydrates.

In order to clarify these ambiguous points, the present work has first been undertaken in order to re-examine the solid-liquid phase equilibria in this binary system. Furthermore, from the phase diagram obtained and from the heat changes observed at peritectic and eutectic temperatures, the composition of a hydrate and the heat reaction accompanying its formation from liquid water and liquid dioxane have been estimated.

Experimental

Reagent-grade 1,4-dioxane was further purified by both crystallization and fractional distillation from sodium. The freezing points were always determined from the cooling curves. The apparatus to measure the freezing points was, for the most part, conventional. It consisted of a Pyrex tube (2.5×15 cm) sealed inside an outer jacket connected to a vacuum. The thermocouple, coated with Teflon, was inserted directly into the freezing tube, and its out-put was connected to a 1 mV recorder. Stirring was established with either a motor-driven glass stirrer or a Teflon disk-vibrator that moved vertically at high periods. A flexible Teflon sleeve was used to seal the opening between the cap and the stirring mechanism. A dry ice+acetone mixture was used as a coolant.

In order to measure the amount of heat absorbed when a hydrate melted and/or was decomposed, a differential scanning calorimeter (DSC) was employed (Shimadzu Seisakusho, SC-20). A small amount (10—20 mg) of the 1,4-dioxane+water mixture of a known composition, sealed in an aluminium pan, was cooled to about −40 °C. After being annealed at this temperature for about two hours, the sample was slowly heated at the rate of 0.5 °C/min. Pure water was used as the reference sample. The correction for the temperature and for the amount of heat was established by comparing, under the same experimental conditions, the melting point and the heat of fusion of pure water (1.436 kcal/mol[15] at 0 °C). The determination of a peritectic temperature was carried out from temperature reading on a DSC chart since, in the cooling-curve method, the change in the curve at such a temperature is somewhat ambiguous.

Results and Discussion

The Existence of a 1,4-Dioxane Hydrate. The solid-liquid phase diagram for the 1,4-dioxane+water system is shown in Fig. 1, in which most of the peritectic temperatures are obtained from DSC measurements. This phase diagram obviously shows the existence of a 1,4-dioxane hydrate in the temperature range of −13.5°C (peritectic temperature)——15.8 °C (eutectic temperature) and in the composition range of 37.0—46.5 wt% dioxane. This phase diagram is in fair agreement with the other data[6,12,13] over the major part of the composition, yet all the data except ours overlook the existence of a hydrate in a rather narrow composition range. As has been mentioned above, the measurements of Rosso and Carbonnel[14] deviate appreciably from all the data, including ours, though their report was the first to point out the existence of a hydrate. The compositions and temperatures of characteristic points in the phase diagram for this binary system are summarized in Table 1, together with the values available in the literature.

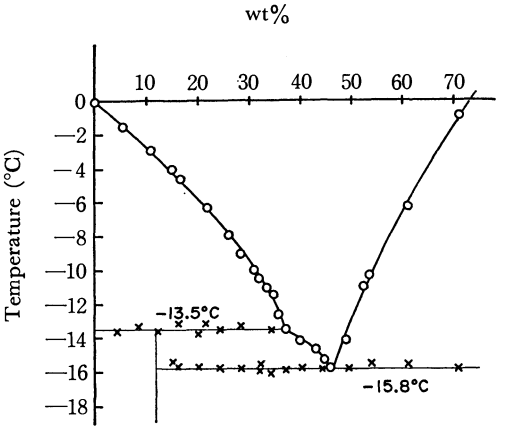

Fig. 1. The solid-liquid phase diagram for the 1,4-dioxane+water system.

Table 1. Characteristic points in the phase diagram of 1,4-dioxane+water system

Points	This work	Other work
Peritectic point		
composition(X_p)[a]	0.107	0.086[14]
temperature(T_p)[b]	−13.5	−12.3[14]
Eutectic point		
composition(X_e)	0.151	0.146,[12] 0.148,[13] 0.093[14]
temperature(T_e)	−15.8	−15.1,[9] −14.9,[12] −15.6,[13] −14.2[14]

a) X is the mole fraction of dioxane. b) in °C.

The composition of the hydrate cannot be clearly determined solely from the phase diagram since it exhibits a peritectic decomposition at −13.5 °C and since, unfortunately, the concentration dependence of the peritectic-halt length in cooling curves is quite uncertain. Thus, the composition of the hydrate was estimated by analyzing the heat change observed in the DSC measurements (Section (2)).

Typical results of the DSC measurements are illustrated in Fig. 2 as a function of the dioxane content. As may be seen from this figure, two characteristic peaks are observed around −13 °C and −16 °C.

15) D. Eisenberg and W. Kauzmann, "The Structure and Properties of Water", Oxford University Press, London, (1969).

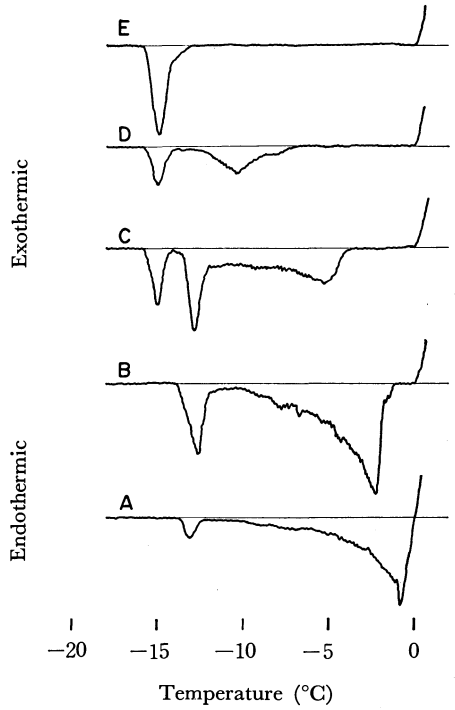

Fig. 2. Representative DSC charts for the 1,4-dioxane+water system as a function of weight per cent of 1,4-dioxane. A: X=0.009 (4%), B: X=0.027 (12%), C: X=0.061 (24%), D: X=0.088 (32%), E: X=0.143 (45%).

It is reasonable to ascribe the endothermic peak near −13 °C to the peritectic decomposition of a hydrate, thus presenting further support for the existence of a 1,4-dioxane hydrate. The other peak, near −16 °C, is unquestionably due to the melting of solids (hydrate and/or solid dioxane) at the eutectic temperature. The remarkably exothermic peak near 0 °C is due to the melting of pure water sealed in a reference pan.

Estimation of the Composition and of the Heat of Formation of the 1,4-*Dioxane Hydrate.* It is obvious that the hydrate has a hydration number greater than 17, which is the typical composition of the Type II clathrate hydrate, since, in the above phase-diagram experiments (Figs 1 and 2), the eutectic halt (at −15.8 °C) has been clearly observed at mole fractions lower than 1/18. In order to determine the probable composition of the hydrate and, at the same time, the heat of reaction, ΔH_1, accompanying its formation from liquid water and liquid dioxane, *i.e.*,

$$\text{1,4-dioxane}(l) + m\text{H}_2\text{O}(l) \rightarrow \text{1,4-dioxane}\cdot m\text{H}_2\text{O}(s), \quad (1)$$

the heat changes observed in the DSC measurements were analyzed as follows.

We assume that the composition of the hydrate can always be expressed as a stoichiometric compound, $C_4H_8O_2\cdot m H_2O$, in which m is a constant. The observed heat changes can be classified into the following four groups. The notations X_p, X_e, T_p, and T_e have the same meanings as in Table 1.

(a) The Heat Change, ΔH_p, at T_p and in the Composition Range between 0 and X_i. X_i denotes the mole fraction of dioxane in the solid hydrate, *i.e.*, $X_i=1/(m+1)$. The ΔH_p corresponds to the enthalpy change when, on heating, all the hydrate decomposes into a mixture of ordinary ice and a solution whose concentration is X_p. Thus, ΔH_p can be given by the following relation:

$$\frac{\Delta H_p}{n_2} = -\Delta H_i + \left(\frac{1}{X_p} - m - 1\right)\cdot\Delta H_{f,w} + \frac{\Delta H_M}{X_p} \quad (2)$$

where n_2 is the total number of moles of dioxane contained in the sample, $\Delta H_{f,w}$ is the heat of fusion of ordinary ice at T_p, and ΔH_M is the hypothetical heat of mixing (per mole of mixture) of liquid dioxane with water at T_p and X_p. If m is a constant, as is supposed above, the right-hand side of Eq. (2) should be constant. In Fig. 3 the observed values of $\Delta H_p/n_2$ are plotted against the mole fraction of dioxane (X). At first, it increases with an increase in X; then it reaches an almost constant value of 10.1 kcal/mol near X=0.02, after which it decreases drastically above $X>0.027$. The concentration dependence at a low mole fraction ($X<0.02$) reflects the situation that there is a minimum concentration necessary to make the hydrate stable. The marked decrease above $X>0.027$ presumably shows that Eq. (2) can not hold over X=0.027; *i.e.*, X_i is close to 0.027.

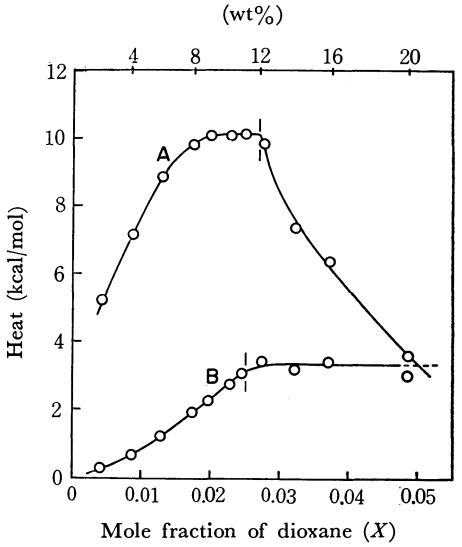

Fig. 3. The concentration dependence of the value of the left-hand side of Eq. (2) (curve A), and of Eq. (3) (curve B).

(b) The Heat Change, $\Delta H_p'$, at T_p and in the Composition Range between X_i and X_p. The $\Delta H_p'$ corresponds to the enthalpy change when the hydrate, after having been in equilibrium with an aqueous solution of dioxane, decomposes into a mixture of ordinary ice and an X_p solution. Simple calculation leads to the following equation:

$$\frac{\Delta H_p'}{(n_1+n_2)X_p - n_2} = -\frac{\Delta H_i}{mX_p-(1-X_p)} - \frac{1}{X_p}\cdot\Delta H_{f,w} + \left\{\frac{m+1}{mX_p-(1-X_p)} - \frac{1}{X_p}\right\}\cdot\Delta H_M \quad (3)$$

where n_1 is the number of moles of water in the sample. From the DSC measurements, unfortunately, only approximate values of $\Delta H_p'$ can be obtained (especially in the concentration range above X=0.05 (about 20 wt%)), because great difficulty is experienced in separating the peak corresponding to $\Delta H_p'$ from that due to the heat change at T_e and also from those of

subsequent reactions occurring in the temperature range between T_e and T_p. In Fig. 3, the observed values of $\Delta H_p'/\{(n_1+n_2)X_p-n_2\}$ are also plotted against X. At first it increases with an increase in X and reaches an almost constant value (about 3 kcal/mol) above $X=0.025$. It seems reasonable to consider that the inconstancy of the values of $\Delta H_p'/\{(n_1+n_2)X_p-n_2\}$ at low mole fractions ($X<0.025$) is due to the fact that Eq. (3) cannot hold in this region; *i.e.*, X_i is approximately equal to 0.025.

Therefore, from the concentration dependences of Eqs. (2) and (3), we arrive at the conclusion that $X_I=0.025-0.027$; that is, $m=36$—39. The change in m from 36 to 39 corresponds to a variation in dioxane content of less than one per cent (11.1∼12.0 wt%).

(c) The Heat Change, ΔH_e, at T_e and in the Composition Range between X_i and X_e. This enthalpy change corresponds to the melting of solid dioxane and of a part of the hydrate, and to the establishment of an equilibrium between the rest of the hydrate and an X_e solution. The ΔH_e must satisfy the following equation:

$$\frac{\Delta H_e}{n_2-n_1/m} = -\frac{1-X_e}{(m+1)X_e-1}\cdot\Delta H_I + \Delta H_{f,d} + \frac{m}{X_e(m+1)-1}\cdot\Delta H_M' \qquad (4)$$

is which $\Delta H_{f,d}$ is the heat of fusion of pure dioxane at T_e and $\Delta H_M'$ is the hypothetical heat of mixing (per mole of mixture) of dioxane with water at T_e and X_e. The temperature dependence of the ΔH_I is neglected. The average value of the left-hand side of Eq. (4) over six solutions of different compositions is found to be 11.6 kcal/mol.

(d) The Heat Change, $\Delta H_e'$, at T_e and in the Composition Range between X_e and $X=1$. This $\Delta H_e'$ is an enthalpy change when all of the hydrate and a part of a solid dioxane melt and when the rest of the solid dioxane comes to be in equilibrium with an aqueous solution of X_e. Thus, $\Delta H_e'$ is expressed as:

$$\frac{\Delta H_e'}{n_1} = -\frac{\Delta H_I}{m} + \left(\frac{X_e}{1-X_e}-\frac{1}{m}\right)\cdot\Delta H_{f,d} + \frac{\Delta H_M'}{1-X_e} \qquad (5)$$

in which all the notations are the same as above. The average value of the experimental data for $\Delta H_e'/n_1$ is 1.74 kcal/mol.

In order to calculate the most probable pair of values of m (as has been concluded above, $m=36$—39) and ΔH_I from these experimental results, the following numerical values are employed: $X_p=0.107$ (Table 1), $X_e=0.151$ (Table 1), $\Delta H_{f,w}=1.436$ kcal/mol,[16] $\Delta H_{f,d}=3.632$ kcal/mol,[17] $\Delta H_M=-0.150$ kcal/mol,[18] and $\Delta H_M'=-0.165$ kcal/mol.[18] As a result of calculation, it has been found that the most plausible pairs of m and ΔH_I, which meet above four equations simultaneously, are $m=36$ and $\Delta H_I=-51.3$ kcal/mol, $m=37$ and $\Delta H_I=-52.7$ kcal/mol, $m=38$ and $\Delta H_I=-54.1$ kcal/mol, and $m=39$ and $\Delta H_I=-55.6$ kcal/mol. Tentatively, if we insert $m=37$ and $\Delta H_I=-52.7$ kcal/mol into Eqs. (2)—(5), the following values are obtained: Eq. (2)=10.1 kcal/mol, Eq. (3)=3.3 kcal/mol, Eq. (4)=11.8 kcal/mol, and Eq. (5)=1.78 kcal/mol. These values are in good agreement with the experimental results presented above.

From these results, the following two features are worth noting: (a) The determined composition of the 1,4-dioxane hydrate ($C_4H_8O_2\cdot(36$—$39)H_2O$) differs greatly from that characteristic of the Structure II hydrate. This suggests, therefore, that the 1,4-dioxane hydrate has a structure either new or one of those described by Jeffrey and his co-workers.[19] (b) The estimated values of ΔH_I happen to be very close to $-\Delta H_{f,w}\cdot m$, irrespective of the choice of m (the differences between the two are 0.4—0.5 kcal/mol). The reason for this can be considered to be as follows. The reaction of Eq. (1) can be divided into the following three hypothetical processes: $m_2HO(l)\rightarrow mH_2O(s,\alpha)\rightarrow mH_2O(s,\beta)$ and a dissolution of liquid dioxane into the vacant $H_2O(s,\beta)$ lattice. The $H_2O(s,\alpha)$ means an ordinary ice I, and $H_2O(s,\beta)$ means the metastable clathrate lattice (the β-modification of water). The heat change in the first process is simply equal to $-\Delta H_{f,w}\cdot m$, *i.e.*, $-1.436\cdot m$ kcal/mol, if the temperature dependence of the heat of fusion of ice is neglected. The heat change in the second process can be approximately taken as zero (Eucken's assumption), as has been verified for several gas hydrates.[20,21] Finally, if, in the hydrate, there is no specific interaction, such as hydrogen bonding, between the dioxane molecule and the water host lattice, the heat change in the third process may also be slight, because this heat change[22] can be approximately expressed as $\Delta H_{vap}-\sqrt{\Delta H_{vap}\cdot\Delta H_{ice}}$, in which ΔH_{vap} is the heat of vaporization of liquid dioxane and ΔH_{ice} is the heat of sublimation of ice, and because the numerical value of ΔH_{ice} (8.0 kcal/mol[20]) is very close to the ΔH_{vap}. Thus, we may expect that the heat change in Eq. (1), that is, ΔH_I, will be close to $-1.436\cdot m$ kcal/mol provided the above assumptions are appropriate. In conclusion, we may expect that there are no specific interactions, such as hydrogen bonding, between dioxane (guest molecule) and water (host lattice).

16) This value is the heat of fusion of water at 0 °C (Ref. 15). Temperature correction is not made because of the experimental accuracy in DSC measurements.

17) C. J. Jacobs and G. S. Parks, *J. Amer. Chem. Soc.*, **56**, 1513 (1934). The value 3.632 kcal/mol is the sum of the heat of fusion at its melting point (3.070 kcal/mol) and the heat of transition at −0.3 °C (0.562 kcal/mol). In this case also temperature correction is not made.

18) These values are obtained from a long extrapolation of the experimental data (K. W. Morcom and R. W. Smith, *Trans. Faraday Soc.*, **66**, 1073 (1970)) for the temperature dependence of the heat of mixing of the 1,4-dioxane+water system.

19) P. T. Beurskens and G. A. Jeffrey, *J. Chem. Phys.*, **40**, 906 (1964), and earlier papers.

20) R. M. Barrer and W. I. Stuart, *Proc. Roy. Soc. Ser. A*, **243**, 172 (1957).

21) J. C. Platteeuw and J. H. van der Waals, *Mol. Phys.*, **1**, 91 (1958).

22) This heat change is a sum of two types of heat; heat of vaporization of liquid dioxane (ΔH_{vap}) and cohesive energy between gaseous dioxane and vacant $H_2O(s,\beta)$ lattice. The latter heat (exothermic) can be expressed, as a first approximation, as a geometrical mean of cohesive energies of both components, *i.e.*, $-\sqrt{\Delta H_{vap}\cdot\Delta H_{ice}}$, provided that there are no specific interactions between dioxane and H_2O lattice.

The Microwave Spectrum of Methyl Iodide in Excited Vibrational States. Fermi and Coriolis Interactions among v_3+v_6, v_5, and v_2 Vibrations

Yoshiyuki KAWASHIMA and Chiaki HIROSE

Laboratory of Molecular Spectroscopy, Tokyo Institute of Technology, O-okayama, Meguro-ku, Tokyo 152

(Received April 4, 1973)

The J=2←1 transitions of methyl iodide in the v_3, v_6, $2v_3$, v_2, v_3+v_6, and v_5 vibrationally-excited states are observed. In v_3+v_6, the central component, ν_{36}^0, of the J=2←1, K=1←1 transition is observed at 14.6 MHz, higher than the ν_{36}^+ of the *l*-type doubling. This is interpreted by the fact that the E state with $K=-l=\pm1$ is affected more strongly by the Fermi resonance through k_{356} than is the A state with $K=l=\pm1$. The Fermi resonance through k_{356} causes the Coriolis coupling between v_2 and v_5 through $\zeta_{25}^{(y)}$ to be transferred to v_3+v_6. As a result, the *l*-type doubling constant, q_6, is determined to be −5.8 MHz. The Stark effect in the presence of the *l*-type doubling and nuclear quadrupole splitting is formulated and used in the analysis.

The vibration-rotation bands of CH_3I were studied by Jones and Thompson, who determined the vibration-rotation constants, α_v^B, for several vibrational modes.[1] Further studies by Morino *et al.* by infrared[2] and microwave spectroscopy[3] made clear that the Fermi resonance was present through k_{356} between the v_3+v_6 and v_5 states. According to a recent study of the vibration-rotation spectra by Matsuura *et al.*,[4] the Coriolis interactions through $\zeta_{25}^{(y)}$ and a higher-order term $\xi_{356}^{(y)}$ should also be taken into account to make the infrared and microwave spectra consistent with each other. With their results at hand, the J=2←1 microwave transitions have been observed in the present study, and the effect of the Fermi resonance on the *l*-type doubling has been analyzed.

Buckingham and Stephens analyzed the Stark effect of CH_3I by taking into account cross-product terms between the molecular Stark effect, H_E, and the electric quadrupole coupling, H_Q, of the iodine atom as H_EH_Q and $H_E{}^2H_Q$ in order to get a more accurate dipole moment.[5] Their formulation has been extended in the present study to include the effect of the *l*-type doubling used in the assignment of the spectra.

Experimental

The sample of CH_3I was distilled before use. The microwave spectrometer used was of a conventional 100-kHz Stark-modulation type. The absorption cell was made of an X-band waveguide 3 m long. In order to increase the intensities for higher vibrational levels, the absorption cell was heated to about 60—80 °C. The J=2←1 transitions were observed with an Oki 30V10 klystron.

Assignment of the Spectra

The Stark effect of the J=2←1 and K=1←1 transitions is of the first order, whereas that of the J=2←1 and K=0←0 transitions is of the second order. The K=1←1 transitions were observed at the relatively low Stark field of about 15 V/cm.

The observed transition frequencies of the lines for v_3, v_6, $2v_3$, and v_2 coincided with those predicted from the constants obtained from the measurement of the J=1←0 transitions.[3] The satellite lines which appeared equally spaced at the upper- and lower-frequency sides of the v_6 spectra, ν_6^0, were identified as the ν_6^+ and ν_6^- components of the *l*-type doubling. The ν_v^+ and ν_v^- notations refer, respectively, to the transitions between the upper and lower levels of the *l*-type doubling, *i.e.*, the transitions between the levels with $K=l=\pm1$, the A symmetry, and ν_v^0 corresponds to the transition between the levels with $K=-l=\pm1$, the E symmetry.

The spectra for v_5 and v_3+v_6 were assigned by the use of their Stark effects. The Stark effects of the ν_v^+ and ν_v^- lines are different from that of the ν_v^0 line because a nonvanishing matrix element of the Stark effect is present between the *l*-type doublets. The Stark effect in the presence of both nuclear quadrupole coupling and *l*-type doubling has been formulated; it will be described in the Appendix. The calculated Stark effects for the F=7/2←5/2, J=2←1, and K=1←1 transitions are shown in Figs. 1a and 2a. The observed Stark effects of the candidate lines, which were not resolved into M_F components, are shown in Figs. 3 and 4. To make a better comparison between the observed and calculated Stark patterns, the line shape of the merged spectrum was calculated on the assumption of the Lorentzian line shapes, with the half-width at the half-height of $\Delta\nu$=0.5 MHz. The peak frequencies of the resultant curves at various strengths of the Stark field are plotted in Figs. 1b and 2b for the transitions in v_6 and v_3+v_6 respectively. The value of 0.5 MHz for $\Delta\nu$ was estimated from the zero-field line width of the square-wave modulated spectra. From Figs. 1b and 3, ν_6^-, ν_6^0, and ν_6^+ were assigned to the lines appearing from the lower to higher frequencies. A similar comparison of Figs. 2b and 4 established that ν_{36}^0 was observed at a frequency higher than ν_{36}^+. The ν_5^0 was not observed for some unknown reason, but ν_5^+ and ν_5^- were assigned on similar grounds.

The observed frequencies for v_3, $2v_3$, and v_2 are summarized in Table 1. The deviations were calculated by means of the rotational constant and eQq, which were derived from the least-squares fitting of the ob-

1) E. W. Jones and H. W. Thompson, *Proc. Roy. Soc. Ser. A*, **288**, 50 (1965).
2) Y. Morino, J. Nakamura, and S. Yamamoto, *J. Mol. Spectrosc.*, **22**, 34 (1967).
3) Y. Morino and C. Hirose, *ibid.*, **22**, 99 (1967).
4) H. Matsuura, T. Nakagawa, and J. Overend, *J. Chem. Phys.*, **59**, 1449 (1973).
5) A. D. Buckingham and P. J. Stephens, *Mol. Phys.*, **7**, 481 (1964).

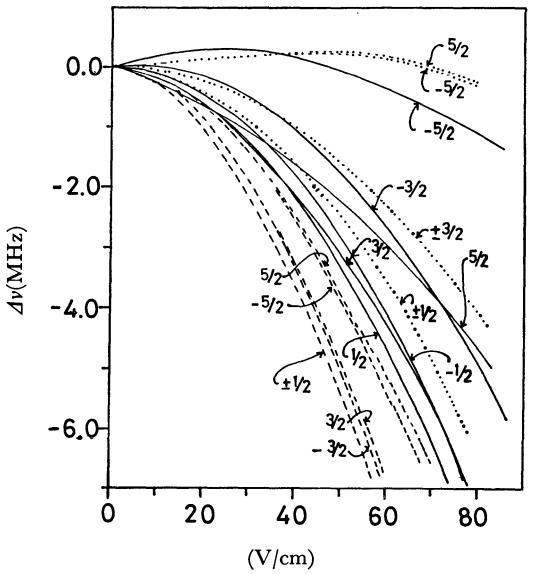

Fig. 1a. Calculated Stark shifts of ν_6^+, ν_6^0, and ν_6^- lines; J=2←1, F=7/2←5/2, K=1←1. M_F values are shown in the figure. Relative intensities of M_F components are 3 : 5 : 6 for M_F=5/2 : 3/2 : 1/2. Broken, solid, and dotted lines indicate the M_F components of ν_6^+, ν_6^0, and ν_6^-.

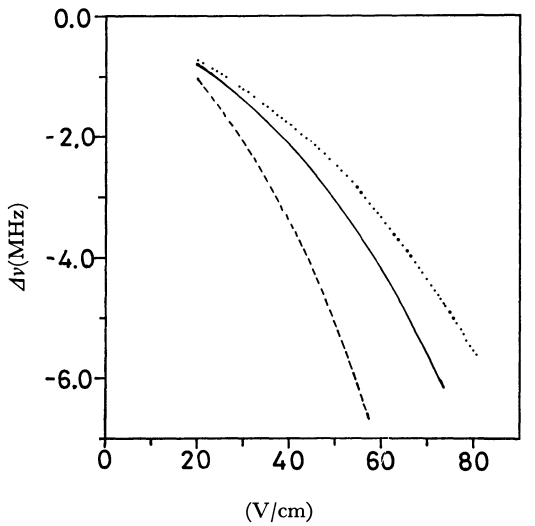

Fig. 1b. Calculated peak frequency *vs.* the Stark field.

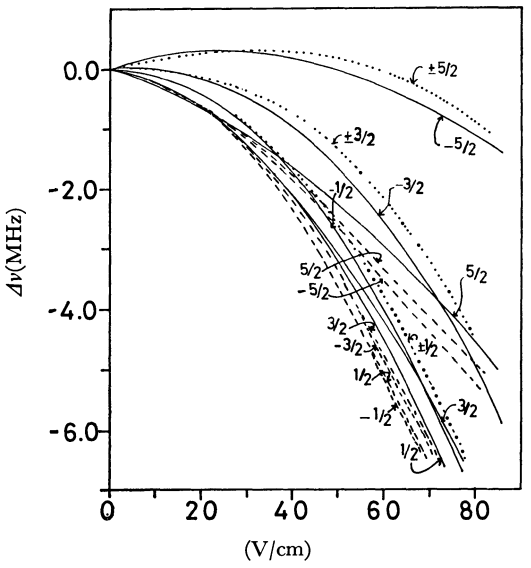

Fig. 2a. Calculated Stark shifts of ν_{36}^+, ν_{36}^0, and ν_{36}^- lines; J=2←1, F=7/2←5/2, K=1←1. The relative intensities of M_F structures are 3 : 5 : 6 for M_F=5/2 : 3/2 : 1/2. Broken, solid, and dotted lines indicate the M_F components of ν_{36}^+, ν_{36}^0, and ν_{36}^-.

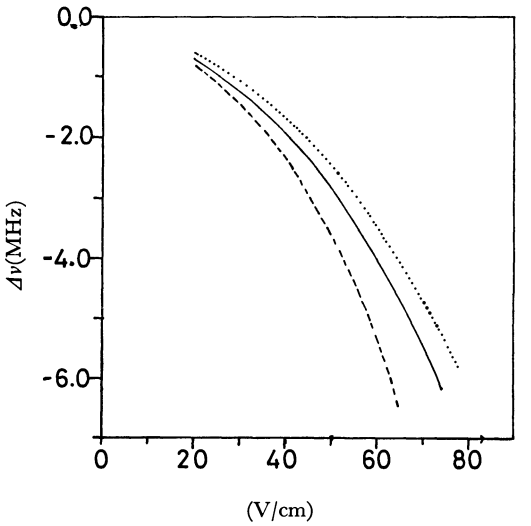

Fig. 2b. Calculated peak frequency *vs.* Stark field.

served frequencies of the J=2←1 and K=±1,0 transitions for v_3, $2v_3$, and v_2. The second-order correction on eQq was made by the procedure Gordy *et al.*[6] used in their analysis of the rotational spectra of the ground vibrational state of CH_3I. Table 2 lists the vibration-rotation constants, defined as $\alpha_v = B_0 - B_v$, and eQq.

The transitions, ν_v^+, ν_v^-, or ν_v^0, listed in Table 3 were analyzed in terms of the effective rotational constants, B_v^+, B_v^-, and B_v^0, and in terms of eQq separately from the other set; the differences in the effective rotational constants, $B_v^+ - B_v^-$, were taken as $|q_v|$. They are listed in Table 4.

Kuczkowski showed that, for CD_3I[7], the effects of asymmetry in eQq, which is induced by the degenerate vibrations on transition frequencies, were not more than 0.7 MHz. Therefore, these effects were neglected in the present study.

Discussion

Table II shows that the values of α_v^B are in good agreement with those obtained from the J=1←0 transitions[3] and infrared spectroscopy.[1,4,8] From this it is clear that there is no significant perturbation working on these vibrational states. However, v_2 is perturbed by the $\zeta_{25}^{(y)}$ Coriolis coupling, as will be discussed below.

6) W. Gordy, J. W. Simmons, and A. G. Smith, *Phys. Rev.*, **74**, 243 (1948).

7) R. L. Kuczkowski, *J. Mol. Spectrosc.*, **45**, 261 (1973).

8) H. Matsuura and J. Overend, *J. Chem. Phys.*, **56**, 5725 (1972).

Table 1. Observed frequencies and their deviations from the calculated values of the J=2←1 transitions (in MHz)

v_3 state	K	F′←F	$\nu^{a)}_{obsd}$	$\Delta\nu^{b)}$
	0	3/2 3/2	29654.75*	−0.09
	0	5/2 3/2	29380.85*	−0.25
	0	3/2 5/2	30235.71*	−0.19
	0	5/2 5/2	29962.05*	−0.11
	0	7/2 5/2	29862.07*	0.02
	0	5/2 7/2	29556.76*	0.39
	0	7/2 7/2	29456.49*	0.23
	1	3/2 3/2	29999.23*	0.44
	1	5/2 3/2	29858.0	0.21
	1	3/2 5/2	29705.90*	−0.44
	1	5/2 5/2	29564.90*	−0.44
	1	7/2 5/2	29518.45*	0.15
	1	5/2 7/2	29769.72*	0.02
	1	7/2 7/2	29723.0	0.34
	1	9/2 7/2	29905.98*	−0.27
$2v_3$ statc	K	F′←F	$\nu^{a)}_{obsd}$	$\Delta\nu^{b)}$
	0	3/2 3/2	29437.2	0.30
	0	5/2 3/2	29163.7	0.55
	0	7/2 5/2	29644.48*	0.34
	0	7/2 7/2	29238.3	0.00
	0	9/2 7/2	29611.97*	0.58
	1	3/2 5/2	29488.3	−0.14
	1	5/2 5/2	29347.0	−0.40
	1	7/2 5/2	29300.0	−0.37
	1	5/2 7/2	29551.0	−0.80
	1	7/2 7/2	29504.7	−0.06
v_2 state	K	F′←F	$\nu^{a)}_{obsd}$	$\Delta\nu^{b)}$
	0	5/2 3/2	29433.6	0.24
	0	3/2 5/2	30290.2	0.08
	0	5/2 5/2	30016.31*	0.56
	0	7/2 7/2	29509.0	0.31
	1	1/2 3/2	30173.6	−0.20
	1	3/2 3/2	30052.2	−0.26
	1	3/2 5/2	29759.4	0.06
	1	5/2 5/2	29617.8	−0.22
	1	7/2 5/2	29570.42*	−0.45
	1	7/2 7/2	29775.5	−0.20
	1	9/2 7/2	29959.8	0.08

a) Estimated error limits are ±0.2 MHz and, for transitions with asterisk, ±0.1 MHz.
b) $\Delta\nu=\nu_{obsd}-\nu_{calcd}$.

Table 2. Vibration-rotation constants and eQq in the vibrationally-excited states of CH_3I (in MHz)

	Present study		M. W. value[c)]	I. R. value[d)]
	α^B_v [a)]	eQq	α^B_v	α^B_v
v_3	54.42±0.04[b)]	−1934.3±0.7[b)]	54.2_8±0.1	54.8_6
$2v_3$	108.90±0.12	−1934.5±1.9	108.8_3±0.05	109.7_2
v_2	41.13±0.04	−1938.7±0.7	40.9_7±0.1	40.1_7

a) Vibration-rotation constants α^B_v is defined here as $\alpha^B_v=B_0-B_v$, where $B_0=7501.25$ MHz.
b) 2.5 times variance. c) Reference 3. d) Reference 1.

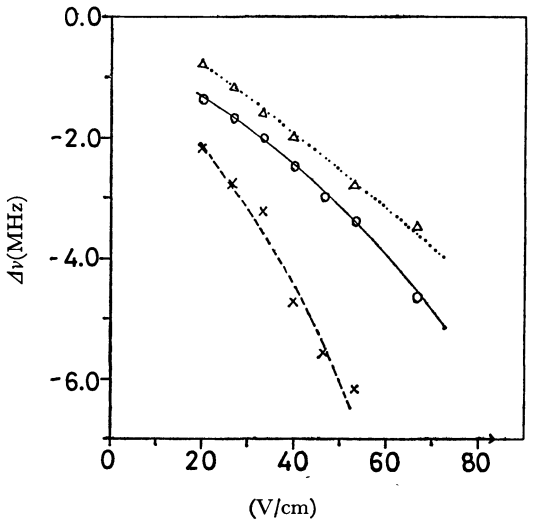

Fig. 3. Observed Stark shifts in v_6 state; J=2←1, F=7/2←5/2, K=1←1. Points denoted as ×, ○, and △ indicate the observations for ν_6^+, ν_6^0, and ν_6^-, respectively.

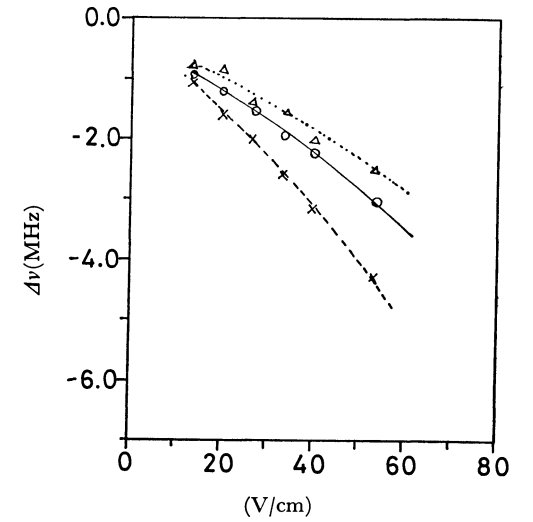

Fig. 4. Observed Stark shifts in the v_3+v_6 state; J=2←1, F=7/2←5/2, K=1←1. Points denoted as ×, ○, and △ indicate the observations for ν_{36}^+, ν_{36}^0, and ν_{36}^-, respectively.

l-Type Doubling Affected by Coriolis Coupling. As has been pointed out by Morino and Hirose, who studied CH_3Br and CD_3Br,[9] the rotational levels in v_5 are remarkably affected by the Coriolis coupling with v_2, while the effective rotational constants for v_2 are essentially unchanged.

The application of their formula to CH_3I indicates that the Coriolis coupling between v_2 and v_5 should be taken into account, but the higher-order interaction through $\xi^{(y)}_{356}$, which was reported by Matsuura *et al.*, was found to be negligible in the present case. Thus, the present problem is to solve the Fermi resonance through k_{356} and the Coriolis coupling through $\zeta^{(y)}_{25}$ as principal perturbers of the rotational levels in v_3+v_6, v_5, and v_2.

l-Type Doubling Affected by Fermi Resonance. The degenerate Coriolis coupling constant, $\zeta^{(z)}_5$, has a negative value, whereas $\zeta^{(z)}_6$, which should apply to

9) Y. Morino and C. Hirose, *J. Mol. Spectrosc.*, **24**, 204 (1967).

TABLE 3. OBSERVED FREQUENCIES OF THE J=2←1 K=1←1 TRANSITIONS IN THE DEGENERATE VIBRATIONAL STATES (in MHz)

v_6 state F′←F	ν^+ a)	$\Delta\nu$ b)	ν^0 a)	$\Delta\nu$ b)	ν^- a)	$\Delta\nu$ b)
1/2 3/2	30256.0	−0.16	30242.9	−0.11	30233.3	0.48
3/2 3/2	3.135.13*	0.47	—		30110.89*	−0.49
5/2 3/2	29993.22*	0.06	29980.3	0.24	29969.8	−0.15
3/2 5/2	29840.2	−0.96	29827.8	−0.30	29818.89*	0.87
5/2 5/2	29699.69*	0.02	—		29676.8	0.21
7/2 5/2	29652.95*	0.49	29639.49*	0.06	29629.47*	0.07
5/2 7/2	—		29891.8	0.12	29881.1	−0.48
7/2 7/2	—		29844.40*	−0.08	29833.6	−0.80
9/2 7/2	30041.88*	0.08	30028.76*	0.07	30018.85*	0.29

v_3+v_6 state F′←F	ν^+ a)	$\Delta\nu$ b)	ν^0 a)	$\Delta\nu$ b)	ν^- a)	$\Delta\nu$ b)
1/2 3/2	—		—		30056.0	0.22
5/2 5/2	29512.0	0.10	29527.5	0.19	29500.4	0.03
7/2 5/2	29464.5	−0.08	29480.0	−0.17	29453.9	0.64
7/2 7/2	29670.2	−0.02	—		29656.8	−1.15
9/2 7/2	—		29869.0	−0.02	29842.1	0.27

v_5 state F′←F	ν^+ a)	$\Delta\nu$ b)	ν^0 a)	$\Delta\nu$ b)	ν^- a)	$\Delta\nu$ b)
3/2 3/2	30233.3	0.48	—		30181.7	−0.91
5/2 5/2	29799.4	0.09	—		29749.0	−0.26
7/2 5/2	29752.3	0.05	—		—	
9/2 7/2	30139.7	−0.61	—		30091.3	1.17

a, b) See a, b) in Table 1.

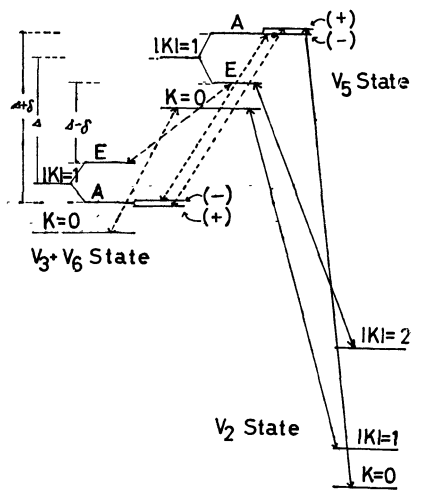

Fig. 5. Schematic interaction diagram of the Fermi resonance and Coriolis coupling among the rotational levels of v_2, v_3+v_6, and v_5. Broken lines indicate the levels interacting with each other by the Fermi resonance, and dotted lines indicate the levels coupled by the Coriolis interaction.

v_3+v_6, is positive.[1,4,10] The energy levels with $K\neq 0$ are split by the degenerate Coriolis coupling into doublets with A and E symmetries by the separation of

TABLE 4. EFFECTIVE ROTATIONAL CONSTANTS, eQq, AND l-TYPE DOUBLING CONSTANTS IN THE DEGENERATE VIBRATIONAL STATES OF CH_3I (in MHz)

		B_v(obsd)	eQq(obsd)	$\lvert q_v\rvert$(obsd)
v_6 state	ν^+	7480.61±0.12 a)	−1941.2±1.9 a)	
	ν^0	7477.34±0.05	−1940.8±0.8	5.80±0.20 a)
	ν^-	7474.81±0.12	−1940.3±2.0	
v_3+v_6 state	ν^+	7433.81±0.10	−1946.3±1.6	
	ν^0	7437.45±0.12	−1938.8±1.6	
	ν^-	7430.67±0.20	−1937.4±3.1	
v_5 state	ν^+	7505.34±0.15	−1934.7±2.6	12.5±0.6
	ν^-	7492.80±0.45	−1934.0±9.0	

a) 2.5 times variance.

$-4A_v K l_v \zeta_v^{(z)}$; one of the levels with $K=l_v=\pm 1$, which has the A symmetry, is further split by the l-type doubling. A schematic diagram is shown in Fig. 5. If we take Δ as the vibrational separation of the unperturbed levels, v_3+v_6 and v_5, the separation between the E levels ($K=\pm 1$) is smaller than Δ by $-2\times(A_5^0\zeta_5^{(z)}-A_{36}^0\zeta_6^{(z)})+(A_5^0-A_{36}^0)$, while that between the A levels ($K=\pm 1$) is larger by the same amount. Substituting the values of $A_5^0=5.127$ cm^{-1}, $A_{36}^0=5.2116$ cm^{-1},

10) Y. Morino and J. Nakamura, This Bulletin **38**, 443 (1965).

$\zeta_5^{(z)}=-0.2444$, and $\zeta_6^{(z)}=0.2019$,[4] we get 4.611 cm^{-1} for $-2({}^0_5A\zeta_5^{(z)}-A_{36}^0\zeta_6^{(z)})+(A_5^0-A_{36}^0)$, which is as much as 20% of the vibrational difference, Δ, of about 24.0 cm^{-1}.

The basic formulas to be applied to the Fermi resonance in the present case were given in a preceding paper.[3] When the corrections for the above-mentioned term are included, we get the following equations for the effective (perturbed) rotational constants:

$$B_5(K=0) = \{(1+\Delta/[\Delta^2+4W^2]^{1/2})B_5^0 + (1-\Delta/[\Delta^2+4W^2]^{1/2})B_{36}^0\}/2, \quad (1)$$

$$B_{36}(K=0) = \{(1-\Delta/[\Delta^2+4W^2]^{1/2})B_5^0 + (1+\Delta/[\Delta^2+4W^2]^{1/2})B_{36}^0\}/2, \quad (2)$$

$$B_5(K=1, E) = [\{1+(\Delta-\delta)/[(\Delta-\delta)^2+4W^2]^{1/2}\}B_5^0 + \{1-(\Delta-\delta)/[(\Delta-\delta)^2+4W^2]^{1/2}\}B_{36}^0]/2, \quad (3)$$

$$B_{36}(K=1, E) = [\{1-(\Delta-\delta)/[(\Delta-\delta)^2+4W^2]^{1/2}\}B_5^0 + \{1+(\Delta-\delta)/[(\Delta-\delta)^2+4W^2]^{1/2}\}B_{36}^0]/2, \quad (4)$$

$$B_5^{\pm}(K=1, A) = [\{1+(\Delta+\delta)/[(\Delta+\delta)^2+4W^2]^{1/2}\}(B_5^0\pm q_5/2) + \{1-(\Delta+\delta)/[(\Delta+\delta)^2+4W^2]^{1/2}\} \times (B_{36}^0\pm q_6/2)]/2, \quad (5)$$

and

$$B_{36}^{\pm}(K=1, A) = [\{1-(\Delta+\delta)/[(\Delta+\delta)^2+4W^2]^{1/2}\} + (B_5^0\pm q_5/2) + \{1+(\Delta+\delta)/[(\Delta+\delta)^2+4W^2]^{1/2}\} \times (B_{36}^0\pm q_6/2)]/2, \quad (6)$$

where:

$$\Delta = v_5^0 - v_{36}^0 + A_5^0(\zeta_5^{(z)})^2 - A_{36}^0(\zeta_6^{(z)})^2, \quad (7)$$

$$W = k_{356}/2\sqrt{2}, \quad (8)$$

$$\delta = -2(A_5^0\zeta_5^{(z)}-A_{36}^0\zeta_6^{(z)}) + (A_5^0-A_{36}^0), \quad (9)$$

where A_5^0, A_3^0, B_5^0, and B_{36}^0 denote the rotational constants for the unperturbed v_5 and v_3+v_6 states respectively, and where q_5 and q_6 are the l-type doubling constants. The constants, $\zeta_{36}^{(z)}$ and q_{36}, are set equal to $\zeta_6^{(z)}$ and q_6 respectively in the above equations. Equations (1) and (2) are identical with Eqs. (2) and (3) of Ref. 3. Thus, the J=2←1 and K=0←0 transitions can be predicted from the results given in Ref. 3.

Using the results reported in Refs. 3 and 4, we get the values listed in Table 5. The results show that the central line, $\nu_{36}{}^0$, which gives B_{36}(K=1,E), is shifted up by 12.6 MHz from the K=0 line, in agreement with the predicted value. The $\nu_{36}{}^0$ frequency can exceed that of the $\nu_{36}{}^+$ line; the assignment we have given indicates that this is the case for CH_3I.

The analysis of the spectra in v_6 has given $|q_6|=5.8$ MHz (Table 4),[11] and q_5 can not be very different from the calculated value of 13.4 MHz.[12] Furthermore, the substitution of the above-mentioned values of q_6 and q_5 into Eq. (6) gives $B^+{}_{36}-B^-{}_{36}=3.9\pm0.2$ MHz, significantly different from the observed value, 3.1 ± 0.2 MHz. This difference can be accounted for by taking account of both the Fermi resonance and the Coriolis coupling, as will be discussed below.

Table 5. Effective rotational constants and energy differences[a]

B_5(K=0)[a]	7498.10 MHz	B_5(K=1, E)[a]	7495.01 MHz
B_{36}(K=0)[a]	7433.88 MHz	B_{36}(K=1, E)[a]	7436.96 MHz
$B_5^{\pm}$(K=1, A)[a]	$7500.34\pm\|0.4515q_5+0.0485q_6\|$ MHz		
$B_{36}^{\pm}$(K=1, A)[a]	$7431.64\pm\|0.0485q_5+0.4515q_6\|$ MHz		
Δ[b]	23.997 cm^{-1}	B_5^0[d]	7508.61 MHz
W[b]	10.470 cm^{-1}	B_{36}^0[d]	7423.37 MHz
δ[c]	4.522 cm^{-1}		

a) Rotational constants perturbed by the Fermi resonance through k_{356}. b) Ref. 4. c) $\delta=-2(A_5^0\zeta_5^{(z)}-A_{36}^0\zeta_6^{(z)})+(A_5^0-A_{36}^0)$. d) Ref. 3.

l-Types Doubling Affected by Both Fermi and Coriolis Interactions. The Fermi resonance causes the rotational levels in v_5 and v_3+v_6 to be mixed up considerably. Since the Coriolis coupling through $\zeta_{25}^{(y)}$ is expected to be significant, the two perturbations should be solved simultaneously in order to make a more complete analysis of the spectra.

One of the two levels of the (K=1,A) state, designated as (−) in Ref. 9, is not coupled by the Coriolis interaction to any rotational level of v_2, while the (+) state is coupled to the (J,K=0) level of v_2 through $\zeta_{25}^{(y)}$ (see case I(a) of Ref. 9). The present case can be reduced to two problems. One is for the (−) state, where only the Fermi resonance is present, and the secular equation is expressed by:

$$\begin{vmatrix} E_1-\lambda & W \\ W & E_2-\lambda \end{vmatrix} = 0 \quad (10)$$

where

$$E_1 = v_3^0 + v_6^0 + B_{36}^0J(J+1) + A_{36}^0 - B_{36}^0 - 2A_{36}^0\zeta_6^{(z)} - q_6J(J+1)/2 + A_{36}^0(\zeta_6^{(z)})^2,$$

$$E_2 = v_5^0 + B_5^0J(J+1) + A_5^0 - B_5^0 - 2A_5^0\zeta_5^{(z)} - q_5{}^*J(J+1)/2 + A_5^0(\zeta_5^{(z)})^2,$$

$$W = k_{356}/2\sqrt{2}$$

and $q_5{}^*$ is the unperturbed l-type doubling constant for the v_5 state, −0.66 MHz.[4] The other is for the (+) state, (K=1,E), and K=0, where the Fermi resonance between v_5 and v_3+v_6 and the Coriolis coupling between v_5 and v_2 have to be taken into account simultaneously; the secular equation to be solved is expressed by Eq. (11)[13]:

$$\begin{vmatrix} E_1-\lambda & W & 0 \\ W & E_2-\lambda & C \\ 0 & C & E_3-\lambda \end{vmatrix} = 0. \quad (11)$$

The expressions for the E_i and C elements are for the K=0 level:

11) Evidence for a negative sign of q_6 is given in the Discussion part.

12) The harmonic term of the l-type doubling constant q_5 for CD_3I, CH_3Br, and CD_3Br are calculated to be 15.5, 26.0 and 32.0 MHz, respectively, while the corresponding observed values are 15.2, 26.3 and 32.2 MHz.

13) Equations (10) and (11) do not apply to the K=±1 levels of v_2, since they are further connected to the K=±2 levels of v_5 through $\zeta_{25}^{(y)}$. Thus the solution of Eq. (11) obtained from Eq. (12) is not exact for λ_3.

$$E_1 = v_3^0 + v_6^0 + B_{36}^0 J(J+1) + A_{36}^0(\zeta_6^{(z)})^2,$$
$$E_2 = v_5^0 + B_5^0 J(J+1) + A_5^0(\zeta_5^{(z)})^2,$$
$$E_3 = v_2^0 + B_2^0 J(J+1) + A_2^0 - B_2^0, \quad (12)$$
$$C = \{(v_2^0/v_5^0)^{1/2} + (v_5^0/v_2^0)^{1/2}\}[J(J+1)/2]^{1/2} B_e \zeta_{25}^{(y)},$$

for the (K=1,E) level:

$$E_1 = v_3^0 + v_6^0 + B_{36}^0 J(J+1) + A_{36}^0 - B_{36}^0 + 2A_{36}^0\zeta_6^{(z)} + A_{36}^0(\zeta_6^{(z)})^2,$$
$$E_2 = v_5^0 + B_5^0 J(J+1) + A_5^0 - B_5^0 + 2A_5^0\zeta_5^{(z)} + A_5^0(\zeta_5^{(3)})^2,$$
$$E_3 = v_2^0 + B_2^0 J(J+1) + 4(A_2^0 - B_2^0), \quad (13)$$
$$C = \{(v_2^0/v_5^0)^{1/2} + (v_5^0/v_2^0)^{1/2}\}[(J-1)(J+2)/2]^{1/2} B_e \zeta_{25}^{(y)},$$

and for the (+) level:

$$E_1 = v_3^0 + v_6^0 + B_{36}^0 J(J+1) + A_{36}^0 - B_{36}^0 - 2A_{36}^0\zeta_6^{(z)} + q_6 J(J+1)/2 + A_{36}^0(\zeta_6^{(z)})^2,$$
$$E_2 = v_5^0 + B_5^0 J(J+1) + A_5^0 - B_5^0 - 2A_5^0\zeta_5^{(z)} + q_5^* J(J+1)/2 + A_5^0(\zeta_6^{(z)})^2,$$
$$E_3 = v_2^0 + B_2^0 J(J+1), \quad (14)$$
$$C = \{(v_2^0/v_5^0)^{1/2} + (v_5^0/v_2^0)^{1/2}\}[J(J+1)]^{1/2} B_e \zeta_{25}^{(y)},$$

where the equilibrium rotational constant, B_e, is set equal to the ground-state rotational constant, B_0, 7501.25 MHz.[3]

A computer calculation was performed by using the values reported in Refs. 3 and 4; the results are listed in Table VI. The Coriolis interaction through $\zeta_{25}^{(y)}$ was corrected for the B_5^0 listed in Table V; 7500.16 MHz was used in the calculation. The agreement with the observed values confirms the reported values.

TABLE 6. EFFECTIVE ROTATIONAL CONSTANTS FOR v_3+v_6 AND v_5 (in MHz)

		B_v(obsd)[a]	B_v(calcd)
v_3+v_6 state	v^+	7433.81±0.10	7433.49
	v^0	7437.45±0.12	7437.44
	v^-	7430.67±0.20	7429.97
v_5 state	v^+	7505.34±0.15	7505.91
	v^-	7492.80±0.45	7493.54

a) 2.5 times variance.

Determination of the Sign of q_6. The combined effect of the Fermi and Coriolis interactions enables us to determine the sign of the l-type doubling constant, q_6, by microwave spectroscopy. The effect on B_{36}^+ is different from that on B_{36}^-; the difference between B_{36}^+ and B_{36}^- is 1.7 MHz, even when we assume q_6=0.0 MHz. This difference can be interpreted as indications that the $\zeta_{25}^{(y)}$ term, which is dominant in the l-type doubling of v_5, is transferred to v_3+v_6 through the Fermi resonance. We have to add the normal l-type doubling in v_3+v_6, which is supposedly the same as in v_6, to make the resultant B_{36}^+ and B_{36}^- values agree with the observed values. The dotted lines and broken lines in Fig. 6 show the predicted rotational constants *vs.* the absolute value of q_6 for the cases of $q_6>0$ and $q_6<0$, respectively, while the solid lines are the observed rotational constants. For the $|q_6|$=5.8 MHz value, the broken lines are closer to the observed values than the dotted lines, the latter

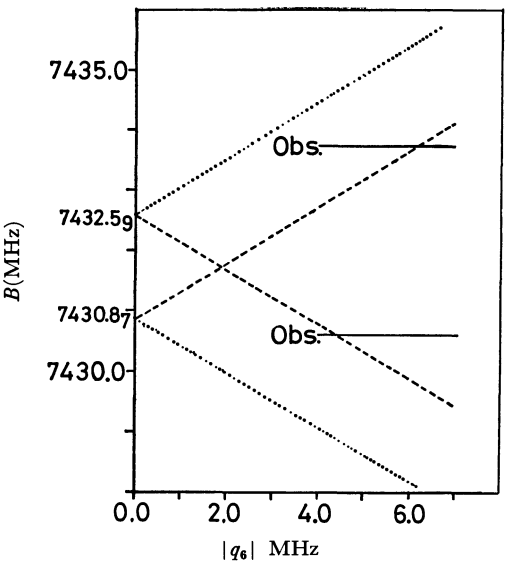

Fig. 6. Predicted rotational constants of the l-type doubling in v_3+v_6, v_{36}^+ and v_{36}^-, *vs.* $|q_6|$. Dotted and broken lines correspond to the prediction for $q_6>0$ and for $q_6<0$, respectively, and the solid lines indicate the observed rotational constants.

difference being too large to be accounted for the higher-order terms ignored in the present analysis. Therefore, the negative sign of q_6, that is, q_6=−5.8 MHz, is preferred. This is in agreement with the conclusion of Matsuura *et al.*[4]

Appendix

Stark effect in the degenerate vibrational states of CH_3I.

The effective Hamiltonian which has to be solved is expressed as:

$$H = H_{rot} + H_Q + H_l + H_E, \quad (A1)$$

where H_{rot}, H_Q, H_l, and H_E are the Hamiltonian operators for the rotation, the nuclear quadrupole coupling caused by the iodine nucleus, the l-type doubling, and the Stark effect respectively.

Since the differences in energy for different J values (more than 15 GHz) are much larger than those among the splittings caused by H_Q or H_l, only the terms which are diagonal in J need to be considered for the present purpose; the off-diagonal terms can be treated as second-order perturbations. Furthermore, an appropriate representation for the present case of a weak-field case is $|v_t,l_t\rangle|F,M_F,J,K,M_J\rangle$. We set another restriction: The degenerate vibration is singly excited, *i.e.* v_t=1, $l_t=\pm1$. However, combination tones of the v_3+v_6 type are not excluded from the present considerations, since the degenerate vibration is still singly-excited.

The nonvanishing matrix elements of H_Q and H_E for the $|F,M_F,J,K,M_J\rangle$ wave function have been given in textbooks[14,15] or papers.[16,17] We still have to consider H_l. Since H_l is of no significance when K=0, $|K|\geqq2$, or K=

14) C. H. Townes and A. L. Shawlow, "Microwave Spectroscopy", Chap. 10. McGraw-Hill, New York, 1955.
15) W. Gordy and R. L. Cook, "Microwave Molecular Spectra", Chap. 10. Interscience Publishers, New York, 1970.
16) W. Low and C. H. Townes, *Phys. Rev.*, **76**, 1295 (1949).
17) F. Coester, *ibid.*, **77**, 454 (1950).

$-l_t=\pm1$,[18] the Stark effect is essentially equal to that in the ground-vibrational state. The effect of H_l is significant only when $K=l_t=\pm1$, where the proper representations are expressed as:

$$|v_t, l, F, M_F, J, l, M_J; + \rangle = \{|v_t, l, F, M_F, J, l, M_J\rangle + |v_t, -1, F, M_F, J, -1, M_J\rangle\}/\sqrt{2} \quad \text{(A2)}$$

and:

$$|v_t, l, F, M_F, J, l, M_J; - \rangle = \{|v_t, l, F, M_F, J, l, M_J\rangle - |v_t, -1, F, M_F, J, -1, M_J\rangle\}/\sqrt{2}. \quad \text{(A3)}$$

The functions expressed in Eqs. (A2) and (A3) diagonalize both H_{rot} and H_l. The nonvanishing matrix elements of H_Q and H_E in the above representations are:

$$\langle v_t, l, F, M_F, J, l, M_J; + |H_Q| v_t, l, F, M_F, J, l, M_J; + \rangle = \langle v_t, l, F, M_F, J, l, M_J; - |H_Q| v_t, l, F, M_F, J, l, M_J; - \rangle = \langle F, M_F, J, K=1, M_J|H_Q|F, M_F, J, K=1, M_J\rangle = (eQq/2)\{3K^2-J(J+1)\}\{3C(C+1)/4-I(I+1)J(J+1)\}/\{I(2I-1)J(2J-1)(J+1)(2J+3)\}, \quad \text{(A4)}$$

where:

$$C = F(F+1) - I(I+1) - J(J+1),$$

$$\langle v_t, l, F, M_F, J, l, M_J; + |H_E|v_t, l, F, M_F, J, l, M_J; - \rangle = \langle F, M_F, I, K=1, M_J|H_E|F, M_F, J, K=1, M_J\rangle = -\mu E\, M_F\{J(J+1)+F(F+1)-I(I+1)\}/\{2J(J+1)F(F+1)\}, \quad \text{(A5)}$$

and where:

$$\langle v_t, l, F, M_F, J, l, M_J; + |H_E|v_t, l, F+1, M_F, J, l, M_J; - \rangle = \langle v_t, l, F+1, M_F, J, l, M_J; + |H_E|v_t, l, F, M_F, J, l, M_J; - \rangle = \langle F, M_F, J, K=1, M_J|H_E|F+1, M_F, J, K=1, M_J\rangle = \langle F+1, M_F, J, K=1, M_J|H_E|F, M_F, J, K=1, M_J\rangle = -\mu E[\{(F+1)^2-M_F^2\}\{(F+1)^2-(I-J)^2\} \times \{(I+J+1)^2-(F+1)^2\}]^{1/2}/[2J(J+1)(F+1)\{(2F+1)(2F+3)\}^{1/2}], \quad \text{(A6)}$$

where eQq is the electric quadrupole coupling constant of the iodine atom, μ is the electric dipole moment, and E is the applied electric field.

Since H_E is nonvanishing only between the (+) and (−) levels which are split by the l-type doubling, the secular equation to be solved is twice as large as that in the case of $K=-l_t=\pm1$. These off-diagonal elements, in combination with the relatively small splitting caused by H_l (about a few tens of MHz in contrast to about a hundred MHz of splittings among different F levels), can complicate the Stark effect. Especially, the F levels lying in between the other F levels can be severely perturbed.

In the actual analysis, a computer was used in both cases, and the shifts in transition frequencies due to the Stark field were derived for the $J=2\leftarrow1$, $F=7/2\leftarrow5/2$, and $K=1\leftarrow1$ transitions of the v_6 and v_3+v_6 vibrational states in order to compare them with the observations.

The authors are very grateful to Professor Kunio Kozima for his encouragement during the course of this work. We are much indebted to Professor Kozo Kuchitsu for his assistance in preparing the manuscript. Thanks are also due to Professor Emeritus Yonezo Morino for his critical reading of this paper and Dr. Hiroatsu Matsuura for his helpful discussion.

18) The energy levels for $K\geqq2$, which consists of four levels, are not in strict degeneracy; for $|K-l_t|=3n\pm1$ ($n=0,1,2,\cdots$), they are split into two doubly degenerate levels, and for $|K-l_t|=3n$ ($n=0,1,2,\cdots$), there are three levels with A_1, A_2, and E symmetries. Since the splittings among the levels interrelated by H_E are negligible for CH_3I, we can treat them as though the levels were degenerate. It should be noted, however, that H_E has an off-diagonal element between A_1 and A_2 levels in contrast to the diagonal element for the E levels.

The Electronic Structure of Nickelocene by Means of the Configurational Interaction Method

Shunsuke KOBINATA

Research Laboratory of Resources Utilization, Tokyo Institute of Technology, Meguro-ku, Tokyo 152

(Received Auguest 1, 1972)

The electronic structures of nickelocene have been investigated by means of the configurational interaction method. The locally-excited configurations of the central metal ion and the charge-transfer configurations corresponding to an electron transfer from the ligand system to the central metal ion have been taken into account. A correspondence with the crystal-field treatment has been obtained using the partitioning technique of solving the secular equation. The energies of the charge-transfer configurations, the resonance integrals, and the Racah parameters were determined so as to obtain the best fit with the observed d-d transition energies.

The nature of the bonding in the sandwich complexes has been the subject of extensive experimental and theoretical investigations. Many calculations based on the MO theory or the crystal-field (CF) theory have been made, but they had led to rather scattered results.[1-7] With regard to the spectral assignment of the low-lying absorption bands (d-d transitions), the CF treatment seems more reliable than the MO treatment for the present.

Recently, a detailed study of the electronic state of nickelocene has been successfully made by I. Pavlik *et al.* using the CF treatment.[8] This method is based on an electrostatic model. On the other hand, many experiments, for example, NMR[9,10] and ESR,[11,12] clearly show the presence of a considerable covalency between nickel and cyclopentadienyl rings.

In this respect it is interesting to inquire into the origin of the validity of the CF treatment and the physical contents of the CF parameters (D_s and D_t) of nickelocene. Previously we have dealt with Cu(II) complexes by means of the configurational interaction (CI) method and have shown that the CF and CI methods give approximately equivalent results with regard to the d-d transition energies. The comparison of the CF parameters with the CI parameters gives useful information about the nature of bonding of Cu(II) complexes.[13]

In this study the electronic structures of nickelocene were treated by means of the CI method, and the physical content of the CF parameters and the nature of bonding in nickelocene were investigated.

Method

In the treatment of the CI method[14,15] nickelocene is considered to be a composite of two component groups: nickel ion and a ligand system composed of two cyclopentadienyl (cp) rings. The total electronic state is described as a superposition of various configurational wave functions: the ionic configurations (locally-excited configurations of the central metal ion or the ligand system) and the charge-transfer (CT) configurations, which correspond to an electron transfer from the ligand system, and *vice versa* if necessary. The ionic configurations are defined as those configurations in which the nickel ion has eight valence electrons (Ni^{2+}).

With regard to the ionic configurations, we took into account only the locally-excited configurations of the central metal ion, which arise from the rearrangement of d electrons within the d-shells, because we are interested primarily in the d-d transitions. In the ionic configurations the fivefold degenerate d AO's of the central metal ion are split into three levels:[16]

$$\left.\begin{aligned} \langle d_0|V_c|d_0\rangle &= 2D_s^{ion} - 6D_t^{ion} \\ \langle d_{\pm1}|V_c|d_{\pm1}\rangle &= D_s^{ion} + 4D_t^{ion} \\ \langle d_{\pm2}|V_c|d_{\pm2}\rangle &= -2D_s^{ion} - D_t^{ion} \end{aligned}\right\} \quad (1)$$

as a result of the electrostatic potential (V_c) from the ligands, where D_s^{ion} and D_t^{ion} are the CF parameters. They are usually determined so as to obtain the best coincidence between the calculated and the observed d-d transition energies. Here, they are considered to be the quantities which contain only the contribution of the electrostatic potential from the ligands. The energies of various terms of Ni^{2+} (d^8 configuration; ^3F, ^3P, ^1D, ^1G, ^1S) under the influence of V_c are shown in Ref. 8. The basic wave functions used in the CF method, $\Phi_M^{ion}(S, M_S, L, M_L)$, should be replaced by:

$$\Phi_M^{ion}(S,M_S,L,M_L) = A\Phi_L^0\Phi_M^{ion}(S,M_S,L,M_L) \quad (2)$$

in the CI treatment, where Φ_L^0 is the wave function of two cp anions in their ground state. A is the antisymmetrizer for the exchange of the electrons between

1) W. Moffitt, *J. Amer. Chem. Soc.*, **76**, 3386 (1954).
2) A. T. Armstrong, D. G. Carroll, and S. P. McGlynn, *J. Chem. Phys.*, **47**, 1104 (1967).
3) R. D. Fisher, *Theoret. Chim. Acta*, **1**, 418 (1963).
4) Y. S. Sohn, D. N. Hendrickson, and H. B. Gray, *J. Amer. Chem. Soc.*, **93**, 3603 (1971).
5) A. D. Liehr and C. J. Ballhausen, *Acta Chem. Scand.*, **11**, 207 (1957).
6) D. R. Scott and F. A. Matsen, *J. Phys. Chem.*, **72**, 16 (1968).
7) R. Prins and J. D. W. Voost, *J. Chem. Phys.*, **49**, 4665 (1968).
8) I. Pavlik, V. Cerny, and E. Maxova, *Collect. Czech. Chem. Commun.*, **35**, 3063 (1970).
9) D. A. Levy and L. E. Orgel, *Mol. Phys.*, **3**, 583 (1960).
10) H. M. Mcconell and C. H. Holm, *J. Chem. Phys.*, **28**, 749 (1958); **27**, 314 (1957).
11) R. Prins, *ibid.*, **50**, 4804 (1969).
12) R. E. Robertson and H. M. Mcconnell, *J. Phys. Chem.*, **64**, 70 (1960).
13) S. Kobinata, to be published.
14) J. Hubbard, D. E. Rimmer, and F. R. A. Hopgood, *Proc. Phys. Soc.*, **88**, 13 (1966).
15) I. Hanazaki, F. Hanazaki, and S. Nagakura, *J. Chem. Phys.*, **50**, 265 (1969).
16) D. R. Scott and R. S. Becker, *J. Organometal. Chem.*, **4**, 409 (1965). See also Ref. 2—8.

the nickel ion and the ligand system. S, M_S and L, M_L are the quantum numbers of the spin and the orbital angular momentum.

As to the CT configurations, those which are formed by an electron transfer to 3d AO of the central metal ion from the filled ligand π MO were considered first (3d-CT). The filled π MO's which belong to the same irreducible representation as the d AO under the D_{5d} molecular symmetry group are given as:[17]

$$\left.\begin{array}{ll}(d_0); & \phi(a_{1g}) = 1/\sqrt{2}\,(\phi_a(a_2) + \phi_b(a_2)) \\ (d_{\pm1}); & \phi(e_{1g}\pm) = 1/\sqrt{2}\,(\phi_a(e_1\pm) + \phi_b(e_1\pm))\end{array}\right\} \quad (3)$$

where the suffixes a and b indicate the two cp rings. $\phi(a_2)$ and $\phi(e_1)$ are the π MO's of a cp ring, corresponding to the lowest and highest occupied π MO of the cp anion respectively.

$$\left.\begin{array}{l}\phi(a_2) = 1/\sqrt{5}\,(x_1+x_2+x_3+x_4+x_5) \\ \phi(e_1\pm) = 1/\sqrt{5}\,(x_1+\sigma^{\pm1}x_2+\sigma^{\pm2}x_3+\sigma^{\pm3}x_4+\sigma^{\pm4}x_5)\end{array}\right\} \quad (4)$$

where x_t is the $2p\pi$ AO of the carbon atom. $\sigma=\exp(2\pi i/5)$.

The energies of 3d-CT configurations were represented as $E_0^{CT}(a_{1g})$ or $E_1^{CT}(e_{1g})$, depending on whether an electron was transferred from $\varphi(a_{1g})$ or $\varphi(e_{1g})$. The wave functions of the CT configurations are written as:

$$\Phi_\alpha^{CT}(S,M_S,L,M_L) = \sum A\Phi_L^{CT}(S',M_S'',M_L')\Phi_M^{CT}(S'',M_S'',L'',M_L'') \\ <S',M_S',S'',M_S''|S,M_S><M_L',M_L''|M_L> \quad (5)$$

where summation is taken over S',M_S',S'',M_S'',M'_L and M_L''. $<S,'M_S',S,''M_S''|S,M_S>$ and $<M_L',M_L''|M_L>$ are the vector coupling coefficients for the spin angular momentum and the irreducible representation of the molecular symmetry group, D_{5d}.[18] $\Phi_M^{CT}(S, M_S, L, M_L)$, and $\Phi_L^{CT}(S, M_S, M_L)$ are the wave functions of the central metal ion (d^9 configuration) and the ligand system in a 3d-CT configuration (11π electrons). α is used to distinguish the independent Φ^{CT}'s belonging to the same irreducible representation. They are tabulated in Table 1. For the triplet state (S=1), we considered exclusively the state with the spin magnetic quantum number $M_S=1$.

The resonance interactions between the ionic configurations and CT configurations are calculated by the method of Longuett-Higgins and Murrell,[19] which lead to the group resonance integrals (β_0 and β_1) between the 3d AO of the central metal ion and the $2p\pi$ MO of cp rings,

$$\left.\begin{array}{l}\beta_0 = <d_0|\mathcal{H}|\phi(a_{1g})> \\ \beta_1 = <d_{\pm1}|\mathcal{H}|\phi(e_{1g}\pm)>\end{array}\right\} \quad (6)$$

The diagonal and off-diagonal matrix elements of the secular equations are tabulated in Table 2, in which the Φ^{ion} (S=1, L=3) state, corresponding to the lowest state of the Ni^{2+} ion, *i.e.*, ^3F, is chosen as the standard of energy. B and C are the Racah parameters.

The CT configurations, formed by an electron transfer from a filled π-MO of the ligand system to the 4s or 4p AO of the central metal ion (4s-CT or 4p-CT), can easily be constructed using the vector coupling coefficients, in a manner similar to that used to construct the 3d-CT configurations. It is apparent that the effect of the 4s and 4p-CT configurations on the low-lying d^8 configurations is a uniform stabilization of these energies. Hence, these configurations do not affect the d AO splittings in a higher approximation.[14] The CT configurations corresponding to an electron transfer from the ligand σ orbital to the central metal ion can also be neglected in a higher approximation, because ESR[11] and NMR[20] experiments have shown that, in nickelocene, the electron delocalization between the cp rings and the nickel ion takes place mainly through the π orbitals of the cp rings.

To see the relation between the cf and CI treatments, it is necessary first to transform the basis of the CI method (ionic and CT configurations) to the ionic configurations which appear in the CF treatment.

By means of the partitioning technique,[21,22] the secular equation in the CI treatment (Table 2) is transformed to:

$$\sum_{j=1}^{N_1}\left\{<\Phi_i^{ion}|\mathcal{H}|\Phi_j^{ion}> - \sum_{p=N_1+1}^{N_1+N_{CT}}\frac{<\Phi_i^{ion}|\mathcal{H}|\Phi_p^{CT}><\Phi_p^{CT}|\mathcal{H}|\Phi_i^{ion}>}{<\Phi_p^{CT}|\mathcal{H}|\Phi_p^{CT}>-E}\right\}c_i^{ion} = Ec_i^{ion} \quad (7)$$

Table 1. The wave functions of CT configurations

$$\begin{aligned}
\Phi^{CT}(^3A_{2g}) &= (1/\sqrt{2})(L(1/2,E_1^+)M(1/2,E_1^-) \\
&\quad -L(1/2,E_1^-)M(1/2,E_1^+)) \\
\Phi_1^{CT}(^3E_{1g}) &= L(1/2,E_1^-)M(1/2,E_2^+) \\
\Phi_2^{CT}(^3E_{1g}) &= L(1/2,E_1^+)M(1/2,A_1) \\
\Phi_3^{CT}(^3E_{1g}) &= L(1/2,A_1)M(1/2,E_1^+) \\
\Phi_1^{CT}(^3E_{2g}) &= L(1/2,E_1^+)M(1/2,E_1^+) \\
\Phi_2^{CT}(^3E_{2g}) &= L(1/2,E_1^-)M(1/2,E_2^-) \\
\Phi_3^{CT}(^3E_{2g}) &= L(1/2,A_1)M(1/2,E_2^+) \\
\Phi_1^{CT}(^1A_{1g}) &= (1/2)(L(1/2,E_1^+)M(-1/2,E_1^-) \\
&\quad -L(-1/2,E_1^+)M(1/2,E_1^-) \\
&\quad +L(1/2,E_1^-)M(-1/2,E_1^+) \\
&\quad -L(-1/2,E_1^-)M(1/2,E_1^+)) \\
\Phi_2^{CT}(^1A_{1g}) &= 1/\sqrt{2})(L(1/2,A_1)M(-1/2,A_1) \\
&\quad -L(-1/2,A_1)M(1/2,A_1)) \\
\Phi_1^{CT}(^1E_{1g}) &= (1/\sqrt{2})(L(1/2,E_1^+)M(-1/2,A_1) \\
&\quad -L(-1/2,E_1^+)M(1/2,A_1)) \\
\Phi_2^{CT}(^1E_{1g}) &= (1/\sqrt{2})(L(1/2,E_1^-)M(-1/2,E_2^+) \\
&\quad -L(-1/2,E_1^-)M(1/2,E_2)) \\
\Phi_3^{CT}(^1E_{1g}) &= (1/\sqrt{2})(L(1/2,A_1)M(-1/2,E_1^+) \\
&\quad -L(-1/2,A_1)M(1/2,E_1^+)) \\
\Phi_1^{CT}(^1E_{2g}) &= (1/\sqrt{2})(L(1/2,E_1^+)M(-1/2,E_1^+) \\
&\quad -L(-1/2,E_1^+)M(1/2,E_1^+)) \\
\Phi_2^{CT}(^1E_{2g}) &= (1/\sqrt{2})(L(1/2,E_1^-)M(-1/2,E_2^-) \\
&\quad -L(-1/2,E_1^-)M(1/2;E_2^-)) \\
\Phi_3^{CT}(^1E_{2g}) &= (1/\sqrt{2})(L(1/2,A_1)M(-1/2,E_2^+) \\
&\quad -L(-1/2,A_1)M(1/2,E_2^+))
\end{aligned}$$

$L(1/2,E_1^+)$ and $M(-1/2,E_1^-)$ indicate $\Phi_L^{CT}(S=1/2,M_S=1/2, M_L=1)$ and $\Phi_M^{CT}(S=1/2,M_S=-1/2,M_L=-1)$, respectively. (Eq. (5)).

17) W. Moffitt, *J. Amer. Chem. Soc.*, **76**, 3386 (1954).
18) J. S. Grifith, "The Theory of Transition-Metal Ions", Cambridge University Press, London (1961).
19) H. C. Longuett-Higgins and Murrell, *Proc. Phys. Soc., Ser. A*, **68**, 601 (1955).
20) M. F. Retting and R. S. Drago, *J. Amer. Chem. Soc.*, **91**, 1361 (1969).
21) P. O. Löwdin, *J. Mol. Spectrosc.*, **10**, 12 (1963).
22) P. O. Löwdin, *J. Math. Phys.*, **3**, 969 (1962).

TABLE 2a. THE MATRIX ELEMENTS BETWEEN Φ^{ion} AND Φ^{CT} FOR TRIPLET STATES

	Diagonal		Off-diagonal	
$^3A_{2g}$	$^3F(0)$	$-0.8D_s^{ion}-6D_t^{ion}$	$^3F(0)\sim{}^3P(0)$	$2.4D_s^{ion}+4D_t^{ion}$
	$^3P(0)$	$15B+2.8D_s^{ion}$	$^3F(0)\sim\Phi^{CT}(^3A_{2g})$	$-\sqrt{8/5}\,\beta_1$
	$\Phi^{CT}(^3A_{2g})$	E_1^{CT}	$^3P(0)\sim\Phi^{CT}(^3A_{2g})$	$\sqrt{2/5}\,\beta_1$
$^3E_{1g}$	$^3F(1)$	$-0.6D_s^{ion}-D_t^{ion}$	$^3F(1)\sim{}^3P(1)$	$(\sqrt{6}/5)(4D_s^{ion}-5D_t^{ion})$
	$^3P(1)$	$15B-1.4D_s^{ion}$	$^3F(1)\sim\Phi_1^{CT}(^3E_{1g})$	$\sqrt{3/5}\,\beta_1$
	$\Phi_1^{CT}(^3E_{1g})$	E_1^{CT}	$^3F(1)\sim\Phi_2^{CT}(^3E_{1g})$	$-\sqrt{2/5}\,\beta_1$
	$\Phi_2^{CT}(^3E_{1g})$	E_1^{CT}	$^3F(1)\sim\Phi_3^{CT}(^3E_{1g})$	$-\sqrt{2/5}\,\beta_0$
	$\Phi_3^{CT}(^3E_{1g})$	E_0^{CT}	$^3P(1)\sim\Phi_1^{CT}(^3E_{1g})$	$\sqrt{2/5}\,\beta_1$
			$^3P(1)\sim\Phi_2^{CT}(^3E_{1g})$	$\sqrt{3/5}\,\beta_1$
			$^3P(1)\sim\Phi_3^{CT}(^3E_{1g})$	$\sqrt{3/5}\,\beta_0$
$^3E_{2g}$	$^3F(-3)$	$D_s^{ion}-3D_t^{ion}$	$^3F(-3)\sim\Phi_2^{CT}(^3E_{2g})$	$-\beta_1$
	$\Phi_2^{CT}(^3E_{2g})$	E_1^{CT}		
$^3E_{2g}$	$^3F(2)$	$7D_t^{ion}$	$^3F(2)\sim\Phi_3^{CT}(^3E_{2g})$	$-\beta_0$
	$\Phi_3^{CT}(^3E_{2g})$	E_0^{CT}		

$^3F(0)$ indicates $\Phi^{ion}(S=1,M=1,L=3,M_L=0)$ of Eq. (2).

TABLE 2b. THE MATRIX ELEMENTS BETWEEN Φ^{ion} AND Φ^{CT} FOR SINGLET STATES

	Diagonal		Off-diagonal	
$^1A_{1g}$	$^1D(0)$	$5B+2C$	$^1G(0)\sim{}^1D(0)$	$(24\sqrt{5}/35)D_s^{ion}-(20\sqrt{5}/7)D_t^{ion}$
		$+(6/7)D_s^{ion}+(24/7)D_t^{ion}$	$^1G(0)\sim{}^1S(0)$	$2\sqrt{14}\,D_t^{ion}$
	$^1G(0)$	$12B+2C$	$^1D(0)\sim{}^1S(0)$	$2\sqrt{14}/5D_t^{ion}$
		$-(20/7)D_t^{ion}+(18/7)D_t^{ion}$	$^1D(0)\sim\Phi_1^{CT}$	$-\sqrt{2/7}\,\beta_1$
	Φ_1^{CT}	E_1^{CT}	$^1D(0)\sim\Phi_2^{CT}$	$\sqrt{4/7}\,\beta_0$
	Φ_2^{CT}	E_0^{CT}	$^1G(0)\sim\Phi_1^{CT}$	$-\sqrt{32/35}\,\beta_1$
			$^1G(0)\sim\Phi_2^{CT}$	$-\sqrt{36/35}\,\beta_0$
			$^1S(0)\sim\Phi_1^{CT}$	$\sqrt{4/5}\,\beta_1$
			$^1S(0)\sim\Phi_2^{CT}$	$-\sqrt{2/5}\,\beta_0$
$^1E_{1g}$	$^1D(0)$	$5B+2C$	$^1D(1)\sim{}^1G(1)$	$(4\sqrt{6}/7)D_s^{ion}-(5\sqrt{6}/7)D_t^{ion}$
		$+(3/7)D_s^{ion}-(16/7)D_t^{ion}$	$^1D(1)\sim\Phi_1^{CT}$	$-\sqrt{1/7}\,\beta_1$
	$^1G(1)$	$12B+2C$	$^1D(1)\sim\Phi_2^{CT}$	$\sqrt{6/7}\,\beta_1$
		$-(17/7)D_s^{ion}+(9/7)D_t^{ion}$	$^1D(1)\sim\Phi_3^{CT}$	$\sqrt{1/7}\,\beta_0$
	Φ_1^{CT}	E_1^{CT}	$^1G(1)\sim\Phi_1^{CT}$	$\sqrt{6/7}\,\beta_1$
	Φ_2^{CT}	E_1^{CT}	$^1G(1)\sim\Phi_2^{CT}$	$\sqrt{1/7}\,\beta_1$
	Φ_3^{CT}	E_0^{CT}	$^1G(1)\sim\Phi_\alpha^{CT}$	$-\sqrt{6/7}\,\beta_0$
$^1E_{1g}$	$^1G(-4)$	$12B+2C+4D_s^{ion}+2D_t^{ion}$		
$^1E_{2g}$	$^1D(2)$	$5B+2C$	$^1D(2)\sim{}^1G(2)$	$(4\sqrt{3}/7)D_s^{ion}+(30\sqrt{3}/7)D_t^{ion}$
		$-(6/7)D_s^{ion}+(4/7)D_t^{ion}$	$^1D(2)\sim\Phi_1^{CT}$	$-\sqrt{6/7}\,\beta_1$
	$^1G(2)$	$12B+2C$	$^1D(2)\sim\Phi_2^{CT}$	$-\sqrt{4/7}\,\beta_0$
		$-(8/7)D_s^{ion}-(11/7)D_t^{ion}$	$^1G(2)\sim\Phi_1^{CT}$	$\sqrt{8/7}\,\beta_1$
	Φ_1^{CT}	E_1^{CT}	$^1G(2)\sim\Phi_2^{CT}$	$-\sqrt{3/7}\,\beta_0$
	Φ_2^{CT}	E_0^{CT}		
$^1E_{2g}$	$^1G(-3)$	$12B+2C+D_s^{ion}-3D_t^{ion}$	$^1G(-3)\Phi_2^{CT}$	$-\beta_1$

$^1D(0)$ indicates $\Phi^{ion}(S=0,M_S=0,L=2,M_L=0)$ of Eq. 2.

where N_I and N_{CT} are the numbers of bases of the ionic and CT configurations respectively. c_i^{ion} and c_p^{CT} are the CI coefficients acting on Φ_i^{ion} and Φ_p^{CT} respectively. E is the eigenvalue. The secular equation obtained above is different from those ordinarily obtained, because E is present in the denominator. An eigenvalue, E, is composed of the uniform stabilization energies produced by the 4s-CT and 4p-CT configurations, ΔE(4s-CT) and ΔE(4p-CT), and of the stabilization energy produced by 3d-CT (Fig. 1). Writing the average stabilization energy by 3d-CT as ΔE(3d-CT), a constant

$$\Delta E = \Delta E(3d-CT) + \Delta E(4s-CT) + \Delta E(4p-CT) \quad (7)$$

may be added to E without any influence on the splitting of 3d levels. If the E in the denominator is replaced by an average energy, $\bar{E}$, after the above procedure, the secular equation (7) is reduced to an ordinary one, the basis of which is the same as that of the CF treatment. Each matrix element depends only on 3d-CT, not on 4s-CT and 4p-CT. The above replacement would be a good approximation for

low-lying d-d transition energies if $E_1^{CT}-\bar{E}$ is much larger than the breadth of the eigenvalues corresponding to the locally-excited configurations of the central metal ion, *i.e.*, the d-d transition energies. As will be shown in the next section, the quite large value of $E_1^{CT}-\bar{E}$ estimated by means of the CI treatment confirms that this is the case. Furthermore, the success of the CF treatment itself implies that this replacement is a good approximation. Therefore, using these definitions:

$$\left.\begin{aligned}\sigma_1 &= \beta_1^2/(E_1^{CT}-\bar{E})\\ \sigma_0 &= \beta_0^2/(E_0^{CT}-\bar{E})\end{aligned}\right\} \quad (8)$$

the average stabilization energy by 3d-CT can be represented, so as to satisfy the center of gravity rule, as:

$$\Delta E(3d-CT) = (4/5)\sigma_1 + (2/5)\sigma_0 \quad (9)$$

We obtain exactly the same form of the secular equations as those obtained by means of the CF treatment by defining as follows:

$$D_s = D_s^{ion} + D_s^{cov}$$
$$D_t = D_t^{ion} + D_t^{cov}$$

where:

$$\left.\begin{aligned}D_s^{cov} &= (5/35)\sigma_1 + (5/35)\sigma_0\\ D_t^{cov} &= (4/35)\sigma_1 - (3/35)\sigma_0\end{aligned}\right\} \quad (10)$$

The only differences are the replacement of the D_s^{ion} and D_t^{ion} of the CF treatment by the D_s and D_t in Eq. 10. These differences lose all meaning when the D_s^{ion} and D_t^{ion} are considered as parameters which should be determined so as to obtain the best fit with the observed d-d transition energies, as is usually done in the CF calculations. This implies that the CF parameter treatment is approximately equivalent to the CI treatment with respect to the d-d transition energies. Hence, the CF treatment is valid even in the presence of considerable covalency.

Results and Discussion

CI Parameters. In order to calculate the d-d transition energies theoretically by means of the CI method, it is necessary to estimate the eight quantities, D_s^{ion}, D_t^{ion}, E_1^{CT}, E_0^{CT}, B, C, β_1 and β_0, shown in Table 2. At present, it is difficult to estimate these quantities theoretically with sufficient confidence. Therefore, it seems justifiable to use an alternative method of estimating these quantities empirically, considering them as CI parameters which should be determined so as to obtain the best fit with the observed d-d transition energies.

In order to reduce the number of unknown parameters, the following approximations were made. In the first place, the D_s^{ion}, and D_t^{ion} in Table 2 were assumed to be negligible, because it is known that the effect of the electrostatic terms on the d-orbital splitting is generally rather small.[24] The validity of this approximation was confirmed by the consistency of the results obtained under this approximation. E_0^{CT} was estimated to be equal to E_1^{CT} plus the difference between the second and the first ionization potentials of the cp anion. This difference was calculated by the method of Pariser-Parr-Pople,[25,26] and using Koopmans' theorem, as 5.145 eV. Hence, we obtained:

$$E_0^{CT} = E_1^{CT} + 5.145\ \text{eV}$$

We carried out two types of calculation, Calcn. 1 and Calcn. 2. In Calcn. 1, $C/B=4.0$ was assumed, as is usually done in a CF treatment.[23] In Calcn. 2, B and C were considered to be independent parameters. With these assumptions, the number of independent CI parameters to be determined is reduced to four in Calcn. 1 (β_1, β_0, E_1^{CT} and B) and to five in Calcn. 2 (β_1, β_0, E_1^{CT}, B and C). Because five d-d bands have been observed for nickelocene, we can determine these CI parameters uniquely so as to obtain the best coincidence with the observed d-d transition energies. The results are shown in Table 3. The average deviation is about 1 kK for Calcn. 1 and 0.2 kK for Calcn. 2. This small deviation must result from the neglect of the two-electron charge-transfer configurations and the locally-excited configurations of the ligand system. Calcn. 2 gives the $B/C=6.85$ ratio, which is rather large compared with the value of the free ion. It is very near to that of $C/B=6.87$ obtained in the CF treatment of nickelocene by Pavlik *et al.*[8] The ratio of B to the free ion value B_{ion}, the nephelauxetic ratio, was obtained as $\beta=0.80$ by means of Calcn. 2, using $B_{ion}=1030\ \text{cm}^{-1}$. In the CF treatment, $\beta=0.56$ has been obtained.[8] Calc. 1 gives the unreasonable value of $\beta=1.0$. This probably results from the unreasonable

Table 3. The calculated d-d transition energies and the CI parameters

	Calcn. 1	Calcn. 2	Obsd.[8]
$^3E_{1g}\leftarrow{}^3A_{2g}$	13.12 kK	14.12 kK	14.4 kK
$^3E_{2g}\leftarrow{}^3A_{2g}$	15.78	16.68	16.9
$^3E_{1g}\leftarrow{}^3A_{2g}$	24.46	23.99	23.45
$^3E_{2g}\leftarrow{}^3A_{2g}$	32.64	35.46	
$^3A_{2g}\leftarrow{}^3A_{2g}$	52.82	52.77	
$^1E_{2g}\leftarrow{}^3A_{2g}$	10.83	11.68	11.72
$^1A_{1g}\leftarrow{}^3A_{2g}$	17.93	18.96	19.15
$^1E_{1g}\leftarrow{}^3A_{2g}$	24.54	26.51	
$^1E_{1g}\leftarrow{}^3A_{2g}$	28.70	30.10	
$^1E_{2g}\leftarrow{}^3A_{2g}$	32.14	32.98	
$^1A_{1g}\leftarrow{}^3A_{2g}$	43.42	47.78	
$^1E_{2g}\leftarrow{}^3A_{2g}$	48.37	52.35	
β_0	−3.901 eV	−3.712 eV	
β_1	−6.40	−6.40	
E_1^{CT}	10.64	9.53	
E_0^{CT}	15.785	14.675	
B	1030 cm^{-1}	824 cm^{-1}	
C	$4B$	5650 cm^{-1}	
$E_G(3d-CT)$	−4.959 eV	−5.282 eV	

23) H. L. Schläfer and G. Gliemann, "Basic Principles of Ligand Field Theory," Wiley-Interscience (1969).
24) C. K. Jørgensen, "Modern Aspects of Ligand Field Theory," North-Holland Publishing Company, Amsterdam-London (1971).
25) R. Pariser and R. G. Parr, *J. Chem. Phys.*, **21**, 466, 767 (1953).
26) J. A. Pople, *Trans. Faraday Soc.*, **49**, 1375 (1953).

assumption that the C/B ratio is independent of the complex formation, that is, $C/B=4.0$.[27] It is known that the nephelauxetic ratio consists of two factors, the central-field covalency and the symmetry-restricted covalency.[24] Because, in the CI treatment, the latter effect is taken into account to some extent, it seems reasonable that the nephelauxetic ratio in the CI treatment is larger than in the CF method.

As to the resonance integral the value of $\beta_1=-6.40$ eV and $\beta_0=-3.712$ eV were obtained. At first sight these values seem too large compared with the corresponding values of ferrocene, which is known to be more covalent than nickelocene, for which $\beta_1=-3.3468$ eV and $\beta_0=0$ have been used in the MO calculation.[28] In the Wolfsberg-Helmholz approximation, the resonance integral, β_{ij}, is estimated to be:

$$\beta_{ij} = -F(I_i+I_j)G_{ij}/2 \qquad (11)$$

where G_{ij} is the group overlap integral and where F is a constant, for which a value of about 2 has usually been used. I_i and I_j are the valence-state ionization potentials of the relevant AO's. I_i and I_j depend strongly on the electronic charge and the electronic configuration of the relevant atom. The β_{ij} in the MO calculation is related to the value for the self-consistent charge distribution and electron configuration, whereas the β_{ij} in the CI treatment would be more closely related to the value for the "zeroth-order" charge distribution and the electron configuration. In nickelocene the β_1 and β_0 of the CI treatment may be estimated as:

$$\left.\begin{aligned}\beta_1 &= -(1/2)F(I(\mathrm{Ni^{2+}}) + I(\mathrm{C^{-1/5}}))\langle \mathrm{d}_1|\psi(\mathrm{e_{1g}}^+)\rangle \\ \beta_0 &= -(1/2)F(I(\mathrm{Ni^{2+}}) + I(\mathrm{C^{-1/5}}))\langle \mathrm{d}_0|\psi(\mathrm{a_{1g}})\rangle\end{aligned}\right\} \qquad (12)$$

where $I(\mathrm{Ni^{2+}})$ and $I(\mathrm{C^{-1/5}})$ are the ionization potentials of $\mathrm{Ni^{2+}}$ and $I(\mathrm{C^{-1/5}})$, which were estimated to be 35.17 eV and 9.10 eV respectively.[30] The group overlap integrals, $\langle \mathrm{d}_1/\psi(\mathrm{e_{1g}}^+)\rangle$ and $\langle \mathrm{d}_0/\psi(\mathrm{a_{1g}})\rangle$, were calculated, on the basis of the radial 3d functions tabulated by Richardson *et al.*, to be 0.139 and 0.059 respectively.[31] This calculation made use of the geometry reported by Ronova and Alekseev.[32] With these values and taking $F=2$, the values of $\beta_1=-6.16$ eV and $\beta_0=-2.64$ eV are obtained from Eq. (12). These values coincide fairly well with the values obtained empirically by the CI method (Table 3). Hence, the values of the resonance integrals obtained from the CI treatment seem not to be unreasonable.

As to the energy of CT configuration, the value of $E_1^{CT}=9.53$ eV was obtained. The electronic absorption band at about 32700 $\mathrm{cm^{-1}}$ of nickelocene has been assigned to an intramolecular CT band by Scott and Becker.[33] Therefore, the above value of E_1^{CT}

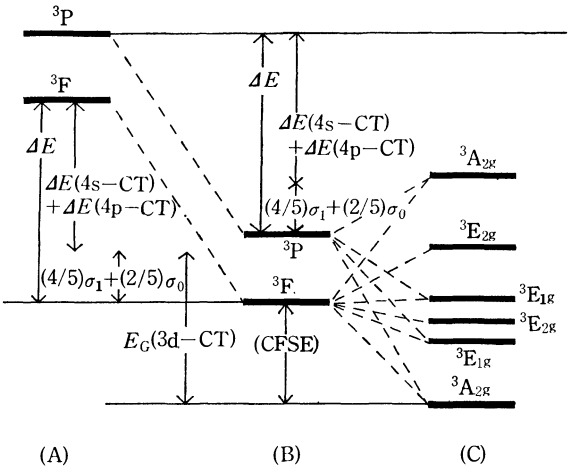

Fig. 1. Schematic illustration of the relation between the quantities ΔE, ΔE(4s-CT)+ΔE(4p-CT), $(4/5)\sigma_1+(2/5)\sigma_0$, E_G(3d-CT) and CFSE.
(A) represents the position of energy level of the ionic configurations. (B) represents the energy level after the uniform shift of Eq. 7. (C) is the final energy level.

implies that the CT state is the state of the strong mixing of the CT and the appropriate locally-excited configurations. A more detailed study of the resonance integrals in the CI and MO treatments and an analysis of the CT states will be undertaken in the future.

The E_G (3d-CT) value of −5.28 eV was obtained for the ground-state stabilization energy due to the 3d-CT, which is considerably larger than the value of Cu(en)$_2$(NCS)$_2$, E_G(3d-CT)$=-2.35$ eV. As can be seen from Fig. 1, E_G(3d-CT) is equal to the sum of the ground-state stabilization energy measured from the center of gravity of the ^{3}F term and the average stabilization energy due to 3d-CT, ΔE(3d-CT) of Eq. (9). The former should be equal to the crystal-field stabilization energy (CFSE) of the CF treatment, CFSE$=-2.89$ eV. From the values of $D_s=3290$ $\mathrm{cm^{-1}}$ and $D_t=1696$ $\mathrm{cm^{-1}}$ obtained in the CF treatment, we can estimate

$$\sigma_1 = 18.38\,\mathrm{kK}: \qquad \sigma_0 = 4.66\,\mathrm{kK}$$

following to Eqs. (8) and (10), neglecting D_s^{ion} and D_t^{ion}. Thus, we obtain:

$$E_G(3d-CT) = \mathrm{CFSE} - (4/5)\sigma_1 - (2/5)\sigma_0 = -4.94\,\mathrm{eV}$$

which agrees reasonably well with the value obtained from the CI calculation, E_G(3d-CT)$=-5.28$ eV. Hence, the large value of E_G(3d-CT) of nickelocene seems reasonable.

Although, the physical meaning of the average energy of Eq. (8) is complicated, it is expected, for the theory to be self-consistent as a whole, that the $\bar{E}$ derived from σ_1 and σ_0 are equal. Substituting the values of β_1, β_0, E_1^{CT}, and E_1^{CT} tabulated in Table 3 into the right-hand side of Eq. 8, the average energy, $\bar{E}$, is determined to be:

Calcn. 1 $\bar{E}=-7.32$ eV from σ_1
$\bar{E}=-9.35$ eV from σ_0
average $\bar{E}=-8.34\pm1.0$ eV

27) H. Witzke, *Theoret. Chim. Acta*, **20**, 171 (1971).
28) E. M. Shustorovish and M. E. Dyatkina, *J. Struct. Chem. USSR*, **1**, 98 (1960).
29) M. Wolfsberg and L. Helmholz, *J. Chem. Phys.*, **20**, 837 (1952).
30) C. E. Moore, *Natl. Bur. Std., Circ.* No. 467 (1949).
31) J. W. Richardson, W. C. Nieuwpoort, and W. F. Edgell, *J. Chem. Phys.*, **36**, 1057 (1962).
32) I. A. Ronova and N. V. Alekseev, *Zh. Struk. Khim.*, **7**, 886 (1966).
33) D. R. Scott and R. S. Becker, *J. Chem. Phys.*, **35**, 516 (1961).

Calcn. 2 $\left.\begin{array}{l}\overline{E} = -8.43\,\text{eV from } \sigma_1 \\ \overline{E} = -9.03\,\text{eV from } \sigma_0\end{array}\right\}$

average $\overline{E} = -8.76 \pm 0.3\,\text{eV}$

In Calcn. 2 a much smaller deviation of $\overline{E}$ was obtained, similarly to the case of the d-d transition energies. The good agreement between the $\overline{E}$'s obtained above implies that the values of β_1, β_0, E_1^{CT} and E_0^{CT} obtained in the CI treatment are "self-consistent."

The author would like to thank Professor Ichiro Hanazaki of Osaka University for his helpful discussions and advice.

BULLETIN OF THE CHEMICAL SOCIETY OF JAPAN, VOL. 46, 2981—2984 (1973)

Oxygen Exchange between Arsenate Ions and Water of Crystallization in the Course of Hydration and Dehydration of Disodium Hydrogen Arsenate and Sodium Dihydrogen Arsenate

Akiko Okumura and Nobukazu Okazaki

Department of Chemistry, Nara Women's University, Nara 630

(Received October 23, 1972)

Oxygen exchange between arsenate ions and crystal water in the course of hydration of anhydrous salt with water vapor and subsequent dehydration of the resulting hydrate has been studied with disodium hydrogen arsenate and with sodium dihydrogen arsenate. There is a remarkable difference in the exchange behavior between the anhydrous salt prepared by dehydration *in vacuo* at room temperature and that prepared at higher temperatures. In the former, the degree of exchange increases with increasing molar ratio of the reactants(arsenate to water), while in the latter, it is independent of the molar ratio. In the exchange reactions of the anhydrous salt prepared at higher temperatures, the number of exchangeable oxygen atoms of an arsenate ion is found to be 0.5 (that is, one atom for two arsenate ions) for disodium hydrogen arsenate, and 4 for sodium dihydrogen arsenate.

In previous publications,[1-3] we reported on the studies of deuterium and oxygen-18 exchange reactions between crystal water and anhydrous salt(or lower hydrate) in the course of hydration of anhydrous salt with water vapor and subsequent dehydration of the resulting hydrate. The characteristics of these reactions are: 1) With crystalline anhydrous salt prepared by dehydration at higher temperatures(*ca.* 100 °C), the amount of anhydrous salt which takes part in the exchange reaction is always equivalent to the amount of water used for hydration. On the other hand, with highly dispersed anhydrous salt prepared by dehydration *in vacuo* at room temperature, the amount of anhydrous salt which takes part in the exchange reaction increases, for a given amount of water, with increasing amount of anhydrous salt used. 2) In the exchange reactions of oxalic acid,[1] copper sulfate monohydrate,[2] sodium dihydrogen phosphate and racemic acid,[3] all the hydrogen atoms which are easily replaced by the hydrogen atoms of water in aqueous solutions are exchangeable for those of crystal water. The oxygen-18 exchange of copper sulfate monohydrate has shown that scrambling of the "fifth" water molecule of copper sulfate pentahydrate with the remaining four molecules of crystal water occurs in the process of hydration and dehydration.[2] In these exchange reactions, exchange equilibrium is reached during the process of hydration and dehydration. Thus, with regard to the exchangeability of hydrogen or oxygen atom, the exchange reactions of anhydrous salt with crystal water seem to be analogous to the exchange reactions in solution. The present paper describes the oxygen exchange reactions of arsenate ions with crystal water in the course of hydration and dehydration, in one of which the exchangeability of arsenate oxygen has been found to differ greatly from that of arsenate oxygen in aqueous solutions.

1) N. Okazaki and E. Takemura, This Bulletin, **34**, 977 (1961).
2) N. Okazaki, A. Okumura and K. Nakagawa, *ibid.*, **34**, 983 (1961).
3) N. Okazaki and A. Okumura, *ibid.*, **34**, 985 (1961).

Experimental

Materials. Disodium hydrogen arsenate heptahydrate(Special grade, JIS) was used without further purification. Sodium dihydrogen arsenate monohydrate was prepared as follows. Arsenic acid(60%, chemically pure) was neutralized to its first neutralization point with a sodium hydroxide solution(Special grade, JIS). The salt obtained on concentrating the solution was recrystallized twice from water. Oxygen-18 water(excess density *ca.* 800γ) was obtained by the fractionation of water. Its deuterium content was normalized by repeated exchange with ammonium chloride. It was refluxed with alkaline permanganate and distilled twice.

Preparation of Anhydrous Salts. Two kinds of anhydrous salts were studied both for disodium hydrogen arsenate and for sodium dihydrogen arsenate. One, probably in a highly dispersed state, was prepared by dehydration *in vacuo* at 30 °C. The other, crystalline, was prepared by dehydration to a constant weight at higher temperatures under the atmospheric pressure. In practice, the hydrates were partially dehydrated *in vacuo* at room temperature and then dehydrated and annealed at higher temperatures(95 °C for disodium hydrogen arsenate, 70 °C for sodium dihydrogen arsenate). To check the composition of the arsenates obtained, a portion of the anhydrous salt was heated to yield

pyro- or meta-arsenate, and the water released was collected and weighed. The amount of the water was in satisfactory agreement with the stoichiometric amount.

Procedure. The procedure was the same as that used earlier.[1] A weighed amount of anhydrous salt was hydrated in a vacuum system at a constant temperature with heavy water vapor. After the completion of hydration, which took about 10 hours, the hydrate was dehydrated by condensing the water vapor in a trap cooled with a dry ice-ethanol bath. The water obtained was purified thoroughly, and its excess density was measured by the flotation method. The excess density of oxygen-18 water is, to a good approximation, proportional to its oxygen-18 atom fraction in excess of the natural.

Results and Discussion

The reaction can be formulated as follows:

$$(Na,\ H)_3AsO_4 + H_2{}^{18}O \rightleftarrows \text{Hydrate} + \text{Anhydrous salt} \rightleftarrows (Na,\ H)_3AsO_3{}^{18}O + H_2O.$$

The balance of oxygen-18 atoms in this reaction is,

$$M_wD_i = M_wD_f + n_OM_s'k_OD_f, \quad (1)$$

where D_i and D_f: the excess oxygen-18 atom fractions of water before hydration and after dehydration respectively,

M_w: the number of moles of water used for the hydration,

M_s': the number of moles of the arsenate taking part in the exchange reaction,

n_O: the number of exchangeable oxygen atoms in an arsenate ion,

k_O: the oxygen-18 partition coefficient between the arsenate and the hydrate water ($k_O \simeq 1$).

Eq. (1) can be rewritten as:

$$(D_i - D_f)/D_fk_O = \Delta D/D_fk_O = n_O(M_s'/M_w). \quad (2)$$

As the anhydrous salt was always used in excess, a part of it is left unhydrated even after the completion of hydration. If, of the M_s moles of the anhydrous salt used, M_s' moles take part in the exchange reaction, Eq. (2) can be written as:

$$\Delta D/D_fk_O = n_O(M_s'/M_s)(M_s/M_w). \quad (3)$$

Accordingly, if we plot the result of the exchange reaction, taking $\Delta D/D_fk_O$ as ordinate and M_s/M_w as abscissa, the slope of a line drawn through the plotted point and the origin gives the value of $n_O(M_s'/M_s)$, and hence of (M_s'/M_s).

As a special case, when the anhydrous salt and the hydrate water take part in the exchange reaction in the equivalent proportion corresponding to the formula $(Na,H)_3AsO_4 \cdot mH_2O$, $mM_s' = M_w$. Eq. (2) then becomes:

$$\Delta D/D_fk_O = n_O/m. \quad (4)$$

In this case the value of $\Delta D/D_fk_O$ becomes independent of M_s/M_w. This situation is realized when the exchange reaction occurs exclusively in the reaction zone and the hydrate lattice.[1]

Disodium Hydrogen Arsenate. The results obtained with disodium hydrogen arsenate are shown in Fig. 1. Hydration was carried out at 20 °C with water vapor of *ca* 10 mmHg, and dehydration at 30 °C *in vacuo*. It will be seen that there is a qualitative difference in exchange behavior between the anhydrous salt prepared *in vacuo* at room temperature and that prepared at 95 °C. In the former case, the degree of oxygen exchange, $\Delta D/D_fk_O$, increases with increasing excess of the anhydrous salt. The line passing through the plotted points and the origin gives a slope $(=n_O(M_s'/M_s))$ of 1.71. If the value of n_O is taken to be 4, which is the case with the oxygen exchange of arsenate ions in aqueous solution, $M_s'/M_s = 0.43$. That is, 43% of the anhydrous salt used takes part in the exchange reaction irrespective of the value of the molar ratio M_s/M_w. This fact suggests that the enhanced exchangeability of the anhydrous salt prepared at room temperature is the property of the anhydrous salt itself. In this case, the exchange reaction probably occurs mainly on the surface of the highly dispersed solid, M_s'/M_s being a measure of surface-to-bulk ratio of the anhydrous salt.

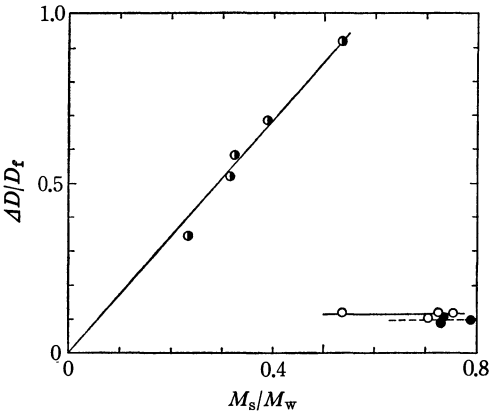

Fig. 1. Degree of exchange $\Delta D/D_f$ as a function of the ratio of moles of anhydrous disodium hydrogen arsenate to moles of water, M_s/M_w. ◑, Oxygen exchange of the anhydrous salt prepared by dehydration *in vacuo* at 30 °C. ○: Oxygen exchange of the anhydrous salt prepared at 95 °C, ●: Deuterium exchange of the anhydrous salt prepared at 95 °C.

On the other hand, with the anhydrous salt prepared at 95 °C, the value of the degree of oxygen exchange, $\Delta D/D_fk_O$, is 0.1, independent of the values of M_s/M_w. The anhydrous salt and the hydrate water react with each other in a fixed proportion. From (4) we get:

$$n_O/m = 0.1, \quad (5)$$

where m is the number of crystal water of the hydrate formed on hydration of the anhydrous salt.

By using the deuterium exchange reaction in the process of hydration and dehydration, we can estimate the value of m.[3] For the deuterium exchange, an appropriate equation corresponding to (2) is

$$\Delta D/D_fk_D = M_s'/2M_w, \quad (6)$$

where k_D is the deuterium partition coefficient between the arsenate and crystal water in the hydrate. The deuterium exchange of the anhydrous salt prepared at 95 °C was studied under the same conditions as those of the oxygen-18 exchange (Fig. 1). It will be seen that the values of $\Delta D/D_f$ are independent of M_s/M_w. The anhydrous salt and the hydrate water take part in the exchange reaction in the stoichiometric

proportion determined by the formula, $Na_2HAsO_4 \cdot mH_2O$. By using the relation, $mM_s' = M_w$, and the mean value of $\Delta D/D_f = 0.095$, Eq. (6) can be written as:

$$m = k_D/0.19. \quad (7)$$

The value of k_D was determined as follows. Disodium hydrogen arsenate labelled with deuterium was prepared by crystallization from HDO solution. The salt was dehydrated *in vacuo* at 25 °C to remove the crystal water. The anhydrous salt obtained was then heated to 200 °C to yield pyroarsenate. The excess density of the water obtained in each step was measured by the flotation method. The value of k_D is given by the ratio of the excess density of water obtained in the second step to that in the first step. Four determinations yielded a value $k_D = 0.78 \pm 0.01$.

The value of m is calculated to be 4.1 from Eq. (7). Tetrahydrate of disodium hydrogen arsenate has not been reported. Pentahydrate is the nearest to it in composition among the known hydrates of disodium hydrogen arsenate.[4] Thus, the deuterium and the oxygen-18 exchange reactions under the given conditions proceed by way of the formation of penta- or tetra-hydrate. From Eq. (5) we obtain $n_O = 0.5$ or 0.4, that is, in the oxygen-18 exchange reaction in question, the number of exchangeable oxygen atoms is 0.5 per arsenate ion, or an atom for two arsenate ions.

It may be suspected that the exchange reaction does not attain the exchange equilibrium during the process of hydration and dehydration. To check this point, the anhydrous arsenate, after being hydrated partially with heavy water vapor, was kept at a constant temperature for a definite time before dehydration. The conditions for the hydration and dehydration were the same as those shown in Fig. 1. Deuterium exchange as well as oxygen exchange was studied, the results being shown in Fig. 2. The exchange reaction does not proceed appreciably in the partially hydrated arsenate at 20 °C, but does so at 30 °C and 40 °C. The data at 30 °C were obtained by using the doubly labelled water $HD^{18}O$. In this case, both the deuterium and oxygen-18 exchange reactions can be studied in a single process of hydration and dehydration. After the dehydration, the deuterium and the oxygen-18 contents of the water were measured separately.

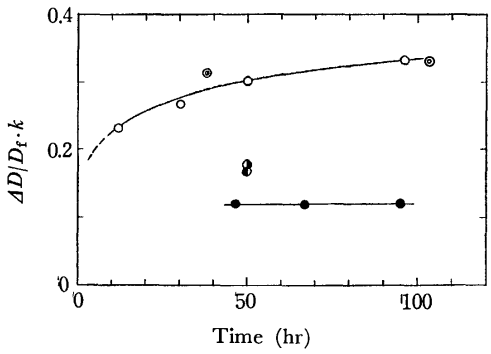

Fig. 2. Oxygen and deuterium exchange reactions in the partially hydrated disodium hydrogen arsenate. ●: Oxygen exchange; 20 °C, ◑: Oxygen exchange; 30 °C, ◐: Deuterium exchange; 30 °C, ○: Oxygen exchange; 40 °C, ◎: Deuterium exchange; 40 °C.

For the deuterium exchange it has been shown[1-3] that, during the process of hydration and dehydration, exchange equilibrium is established between the hydrate water and that part of the anhydrous salt which has taken part in the exchange reaction, and that the progress of the exchange reaction in the partially hydrated arsenate is due to the participation of fresh anhydrous arsenate which has not taken part in the exchange reaction. Fig. 2 shows that the progress of the oxygen-18 exchange keeps pace with that of the deuterium exchange. This suggests that also for the oxygen-18 exchange reaction exchange equilibrium is established during the process of hydration and dehydration, and that the progress of the exchange in partially hydrated arsenate is due to the participation of the fresh part of the anhydrous arsenate.

The number of exchangeable oxygen atoms in an arsenate ion, n_O, can also be calculated without the knowledge of the value of m. By dividing Eq. (2) by Eq. (6), we obtain:

$$k_D(\Delta D/D_f)_O/k_O(\Delta D/D_f)_D = 2n_O, \quad (8)$$

where the suffixes O and D refer to the oxygen and the deuterium exchange reactions, respectively. Here it has been assumed that $(M_s'/M_w)_D = (M_s'/M_w)_O$. The parallel progress of the oxygen and deuterium exchange reactions (Fig. 2) suggests the assumption to be probable. It is valid with doubly labelled water, since the oxygen and the deuterium exchange reactions are studied in a single process of hydration and dehydration. Fig. 2 shows that $(\Delta D/D_f)_O/k_O \simeq (\Delta D/D_f)_D/k_D$ for the experiments at 40 °C and 30 °C with doubly labelled water. Hence, $2n_O \simeq 1$, or $n_O \simeq 0.5$, in agreement with the result obtained above.

In the exchange reactions of the anhydrous salt prepared at room temperature, it has been shown that, assuming all four oxygen atoms of arsenate ion to be exchangeable, 43% of the anhydrous arsenate used takes part in the exchange reaction. If two of the four oxygen atoms are assumed to be exchangeable, 86% of the anhydrous arsenate should participate. However, the number of exchangeable oxygen atoms should not be smaller than 2, for then more than 100% of the anhydrous arsenate used should have taken part in the exchange reaction. Thus there is a remarkable difference in the number of exchangeable oxygen atoms between the crystalline and the highly dispersed anhydrous arsenate. In the latter, the ions would be rather loosely bound with each other, and the exchange reaction with adsorbed water or with hydrate water may be considered to be more or less analogous to the exchange reaction in solution. On the other hand, with the crystalline anhydrous arsenate, the exchange reaction would be controlled by the geometry of the crystal lattice of the anhydrous arsenate, and it is possible that the number of exchangeable oxygen atoms is also limited by the crystal structure of the anhydrous arsenate. In the absence of information on the crystal structures of the anhydrous and the

4) H. Menzel and W. Hagen, *Z. Anorg. Allgem. Chem.*, **233**, 209 (1937).

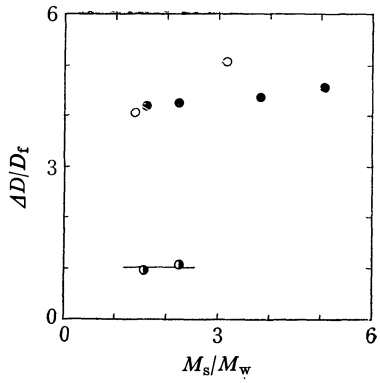

Fig. 3. Degree of exchange $\Delta D/D_f$ as a function of the ratio of moles of anhydrous sodium dihydrogen arsenate to moles of water, M_s/M_w. ○: Oxygen exchange of the anhydrous salt prepared *in vacuo* at 22 °C, ●: Oxygen exchange of the anhydrous salt prepared at 70 °C, ◑: Deuterium exchange of the anhydrous salt prepared at 70 °C.

hydrated forms of the arsenate, we cannot give a picture of hydration and dehydration, or an explanation of the number of exchangeable oxygen atoms.

Sodium Dihydrogen Arsenate. The results obtained with sodium dihydrogen arsenate are given in Fig. 3. For the anhydrous salt prepared *in vacuo* at 30 °C, hydration was carried out at 30 °C with water vapor of *ca* 16 mm, and dehydration at 30 °C *in vacuo*. For the anhydrous salt prepared at 70 °C, hydration was carried out at 22 °C with water vapor of *ca* 13 mm, and dehydration at 22 °C *in vacuo*. The characteristics of the exchange reaction of the crystal water may be seen, but the difference in behavior between the two kinds of anhydrous arsenate is not so well marked as in the case of disodium hydrogen arsenate. The values of $\Delta D/D_f$ for the anhydrous arsenate prepared at 70 °C increase with increasing M_s/M_w. From the results of deuterium exchange of the anhydrous arsenate prepared at 70 °C, the number of crystal water of the hydrate formed on hydration of the anhydrous salt, m, can be calculated by the relation:

$$m = k_D/(\Delta D/D_f)_D. \quad (9)$$

where k_D is the deuterium partition coefficient between the dihydrogen arsenate ion and crystal water in the hydrate of sodium dihydrogen arsenate. This was determined as follows. $NaHDAsO_4 \cdot HDO$ was prepared by crystallization from HDO solution. The salt obtained was dehydrated *in vacuo* at 30 °C to separate the crystal water, and then the resulting anhydrous salt was heated at 350 °C to yield metaarsenate. k_D is given by the ratio of the deuterium atom fraction of the arsenate hydrogen, that is, that of the water obtained in the second step, to that of the crystal water. Three determinations yielded a value $k_D = 0.845 \pm 0.002$. By using this value and that of $\Delta D/D_f$ for the deuterium exchange (Fig. 3), m is calculated to be 0.85 from Eq. (9). The exchange reaction between the crystal water and the arsenate ion in sodium dihydrogen arsenate proceeds through the formation of monohydrate under the condition of the experiments.

By substituting the value of m obtained and the value of $\Delta D/D_f$ of the oxygen exchange (Fig. 3) in Eq. (4), the number of exchangeable oxygen atoms of sodium dihydrogen arsenate, n_O, is calculated to be 4.3 ± 0.1. In the exchange reaction of sodium dihydrogen arsenate, all four atoms of the arsenate oxygen are exchangeable. This is in strong contrast to the exchange reaction of disodium hydrogen arsenate, where one atom for two arsenate ions is found to be exchangeable.

The authors wish to thank Professor Shinichi Kawaguchi of Osaka City University for his helpful discussions and Mrs. Kazuko Ando for her assistance.

Acidic properties of Binary Metal Oxides

Katsue SHIBATA, Tadamitsu KIYOURA, Jun KITAGAWA, Takashi SUMIYOSHI,* and Kozo TANABE*

Central Research Laboratory, Mitsui Toatsu Chemicals, Inc., Totsukaku, Yokohama 247

**Department of Chemistry, Faculty of Science, Hokkaido University, Sapporo 060*

(Received February 3, 1973)

Eighteen binary metal oxides consisting of TiO_2–M_mO_n, ZnO–M_mO_n and Al_2O_3–M_mO_n (M_mO_n: metal oxide) were prepared by the usual co-precipitation method, their acid amounts and strengths being determined by *n*-butylamine titration using various acid-base indicators. The acid strengths of fourteen of the tested binary oxides of molar ratio 1 : 1 were found to be remarkably higher than those of the component single oxides. High acid strengths were as follows: $H_0 \leqq -8.2$ for TiO_2–SiO_2, $H_0 \leqq -5.6$ for TiO_2–Al_2O_3 and Al_2O_3–ZrO_2 and $H_0 \leqq -3$ for TiO_2–CdO, TiO_2–SnO_2 and ZnO–SiO_2. The acid amounts of sixteen binary oxides were larger than those of the component oxides. The effect of the composition of binary oxides on acidity was examined for TiO_2–Al_2O_3, ZnO–Al_2O_3 and Al_2O_3–ZrO_2. The acidity maxima appearing for TiO_2–Al_2O_3 and ZnO–Al_2O_3 were found to be of molar ratio $\simeq 9 : 1$ and for Al_2O_3–$ZrO_2 \simeq 3 : 2$. A fairly good correlation has been demonstrated between the observed highest acid strengths and the average electronegativities of metal ions of binary oxides.

Some binary metal oxides such as SiO_2–Al_2O_3, SiO_2–ZrO_2, SiO_2–MgO and Al_2O_3–Bi_2O_3 are known to show acidic property and have long been used as solid acid catalysts.[1] These combinations of oxides contain either SiO_2 or Al_2O_3, both essential constituents of clay minerals. However, combinations such as TiO_2–ZnO, TiO_2–ZrO_2 and ZnO–Bi_2O_3 containing no clay mineral component were recently found to exhibit remarkable acidic property[2-6] and catalytic activity.[2,4] Since many other combinations are also expected to exhibit acidic property and it is considered important for theoretical development and practical use of mixed oxides to find combinations of oxides giving acidic property and to correlate it with the physico-chemical properties of metal oxides, we prepared various binary oxides and examined their acid amounts and sterngths. The binary oxides are restricted to colorless materials to which an acidity measurement by the amine titration method using indicators can be applied. The observed acid strengths are correlated with the electronegativities of metal ions of binary oxides. The effect of the composition of some binary oxides on acidic property was also examined.

Experimental

Preparation of Metal Oxides. Binary metal oxides were prepared by the thermal decomposition of their hydroxides at 500 °C for 3 hr. in air. The hydroxides were co-precipitated by adding 28% of ammonia water to the mixed aqueous solution of water soluble metal salts (Table 1). The precipitates were washed thoroughly to remove adhering anions such as chloride ion. Each single oxide was prepared similarly as above. Binary oxides containing silica were prepared by kneading the wetted hydroxides of silicon and other metal and calcining at 500 °C for 3 hr after drying at 70—80 °C. The silicon hydroxide was prepared from aqueous sodium silicate by adding aqueous hydrochloric acid and drying at 70—80 °C for 3 hr. The amount of oxide in the binary oxides containing silica was determined by gravimetric analysis of the oxide obtained by calcining the hydroxide.

TABLE 1. STARTING MATERIALS OF OXIDES

Oxides	Starting materials	Oxides	Starting materials
TiO_2	$TiCl_4$	Bi_2O_3	$BiCl_3$
ZnO	$ZnCl_2$	SiO_2	Na_2SiO_3
Sb_2O_5	$SbCl_5$	PbO	$Pb(NO_3)_2$
ZrO_2	$ZrOCl_2$	CdO	$CdCl_2$
Al_2O_3	$AlCl_3$	SnO_2	$SnCl_2$
MgO	$MgCl_2$		

Measurement of Specific Surface Area and Acidity. Specific surface area was obtained by applying the BET method to the adsorption isotherm of nitrogen at −196 °C. Surface acidity was measured by *n*-butylamine titration using the following indicators: methyl red ($pK_a = +4.8$), phenylazonaphthylamine (+4.0), *p*-dimethylaminoazobenzene (+3.3), benzeneazodiphenylamine (+1.5), dicinnamalacetone (−3.0), benzalacetophenone (−5.6) and anthraquinone (−8.2).

X-Ray Diffraction. X-Ray powder diffraction diagrams were recorded with an X-ray diffractometer (Rigakudenki, Geigerflex SG-7). Nickel filtered CuK_α was used as X-ray radiation source.

Results and Discussion

Single Oxides and Binary Oxides Containing Titanium Oxide. The acidity distribution of single oxides which are component oxides of binary oxides are shown in Table 2, together with the surface areas. SiO_2 gave no X-ray diffraction lines indicating its amorphous form. Al_2O_3 gave only weak diffraction lines indicating its partial crystal and TiO_2, ZrO_2, CdO, SnO_2, ZnO, Sb_2O_5 and PbO gave strong diffraction lines indicating each crystal. We see that the acid strengths of the single oxides are generally weak ($H_0 > +1.5$), TiO_2 and ZnO weaker than those observed previously.[2] This is considered to be due to the difference in the mode of preparation.

1) K. Tanabe, "Solid Acids and Bases," Kodansha, Tokyo, Academic Press, New York, London (1971).
2) K. Tanabe, C. Ishiya, I. Matsuzaki, I. Ichikawa, and H. Hattori, This Bulletin, **45**, 47 (1972).
3) K. Shibata and T. Kiyoura, *J. Res. Inst. Catalysis, Hokkaido Univ.*, **19**, 35 (1971).
4) K. Tanabe, I. Ichikawa, H. Ikeda and H. Hattori, *ibid.*, **19**, 185 (1971).
5) K. Shibata, T. Kiyoura and K. Tanabe, *ibid.*, **18**, 189 (1970).
6) "Cracking activity and acidity of hydrous oxide composites," Honors Thesis of Mariel Meents (1961) with Professor J. D. Danforth, Grinnell College, Grinnell, Iowa.

Table 2. Acidity distribution of single oxides

Oxides	Surface area m^2/g	Acid amount (mmol/g) at different pK_a's						
		+4.8	+4.0	+3.3	+1.5	−3.0	−5.6	−8.2
TiO_2	38.5	0.057	0.057	0				
ZnO	7.4	0.006	0					
Al_2O_3	190	—	0.285	0.075	0			
SiO_2	289	0.264	0.109	0.066	0			
ZrO_2	72.0	—	0.280	0.060	0.060	0		
MgO	49.1	0						
Bi_2O_3	6.5	0.250	0.250	0				
Sb_2O_5	77.0	—	0.055	0.055	0			
PbO	0.7	0.065						
CdO	2.2	0.289						
SnO_2	27.7	0.133						

Table 3. Acidity distribution of binary oxides

Binary oxides	Surface area m^2/g	Acid amount (mmol/g) at different pK_a's						
		+4.8	+4.0	+3.3	+1.5	−3.0	−5.6	−8.2
TiO_2-Al_2O_3	204	0.422	0.422	0.337	0.252	0.220	0.060	0
TiO_2-SiO_2	222	0.565	0.565	0.565	0.565	0.565	0.248	0.053
TiO_2-ZrO_2	230	—	0.475	0.380	0.350	0.375	0.125	0.050
TiO_2-MgO	13.6	0.089	0.089	0.022	0			
TiO_2-Bi_2O_3	35.6	0.099	0.049	0.025	0.025	0		
TiO_2-CdO	35.0	0.193	0.136	0.136	0.090	0.064	0	
TiO_2-SnO_2	12.1	0.154	0.108	0.046	0.031	0.018	0	
ZnO-Al_2O_3	117	0.332	0.332	0.270	0.166	0		
ZnO-SiO_2	77.0	0.216	0.175	0.175	0.175	0.042	0	
ZnO-ZrO_2	29.4	0.144	0.144	0.144	0.144	0		
ZnO-MgO	6.0	0.025	0					
ZnO-Sb_2O_5	68.3	0.011	0.011	0				
ZnO-Bi_2O_3	11.0	0.175	0.015	0.015	0			
ZnO-PbO[a)]	5.5	0						
Al_2O_3-ZrO_2	320	—	0.590	0.205	0.205	0.045	0.045	0
Al_2O_3-Sb_2O_5	38.1	0.079	0.079	0.079	0			
Al_2O_3-Bi_2O_3	21.2	0.087	0.083	0.088	0.070	0		
ZrO_2-CdO	102	—	0.399	0.391	0.343	0.106	0	

a) Color of the indicator (pK_a = +6.8) changed.

The acid amounts and strengths of the binary oxides containing TiO_2 (molar ratio=1) are shown in Table 3. The X-ray diffraction diagrams of TiO_2–SiO_2 and TiO_2–ZrO_2 showed only diffused or weak diffraction lines and were assumed to be amorphous. TiO_2–Al_2O_3 gave only the diffraction lines of TiO_2. Thediffraction lines of TiO_2–MgO, TiO_2–Bi_2O_3, TiO_2–CdO and TiO_2–SnO_2 were those of the component oxides. The results indicate the binary oxides are not mechanically mixed oxides. The acid strengths of TiO_2–SiO_2 and TiO_2–ZrO_2, found to be surprisingly high, were $H_0 \leqq -8.2$ and those of TiO_2–Al_2O_3 and TiO_2–CdO, also high, −5.6 and −3, respectively. Since SiO_2–ZrO_2 is known to have very high acid strength ($H_0 \leqq -8.2$),[7] it can be said that the combinations of oxides of metals (Si, Ti and Zr) which belong to the same fourth group in the periodic table show the highest acid strength. All the binary oxides containing TiO_2 showed higher acid strength than each component oxide. The acid amount at a certain acid strength per unit surface area of any binary oxide was larger than the sum of the acid amounts divided by the sum of the surface areas of the component oxides. The results indicate that the new acidic sites which differ from those of single oxides are created on the surface of binary oxides.

The acidity change with variation of composition was examined in the case of TiO_2–Al_2O_3. As shown in Fig. 1, the acidity maximum was observed when the molar ratio of TiO_2–Al_2O_3 is about 1 : 9. It is interesting to note that the acidity maximum of SiO_2–Al_2O_3 appears when the molar ratio is about 8 : 2,[8] despite the fact that both TiO_2 and SiO_2 are oxides

7) V. A. Dzisko, Proc. Intern. Congr. Catalysis, 3rd, Amsterdam, I, No. 19 (1964).

8) see ref. 1), p. 126.

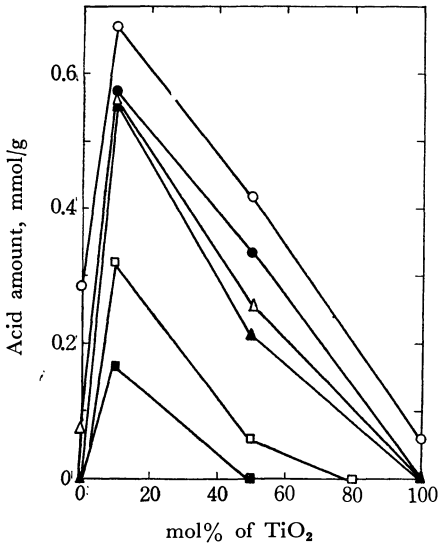

Fig. 1. Acid amounts at various acid strengths of TiO_2–Al_2O_3 *vs.* mol% of TiO_2.
(-○-): $H_0 \leqq 4.8$, (-●-): $H_0 \leqq 3.3$, (-△-): $H_0 \leqq 1.5$, (-▲-): $H_0 \leqq -3.0$, (-□-): $H_0 \leqq -5.6$, (-■-): $H_0 \leqq -8.2$

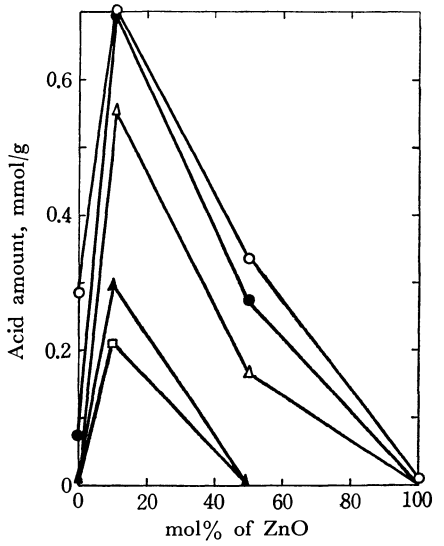

Fig. 2. Acid amounts at various acid strengths of ZnO–Al_2O_3 *vs.* mol% of ZnO.
(-○-): $H_0 \leqq 4.8$, (-●-): $H_0 \leqq 3.3$, (-△-): $H_0 \leqq 1.5$, (-▲-): $H_0 \leqq -3.0$, (-□-): $H_0 \leqq -5.6$

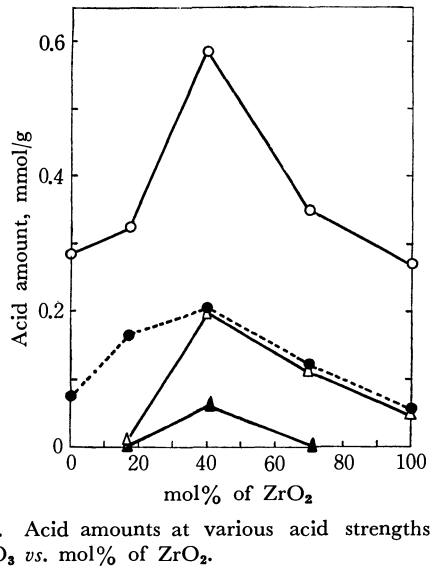

Fig. 3. Acid amounts at various acid strengths of ZrO_2–Al_2O_3 *vs.* mol% of ZrO_2.
(-○-): $H_0 \leqq 4.0$, (-●-): $H_0 \leqq 3.3$, (-△-): $H_0 \leqq 1.5$, (-▲-): $H_0 \leqq -3.0$

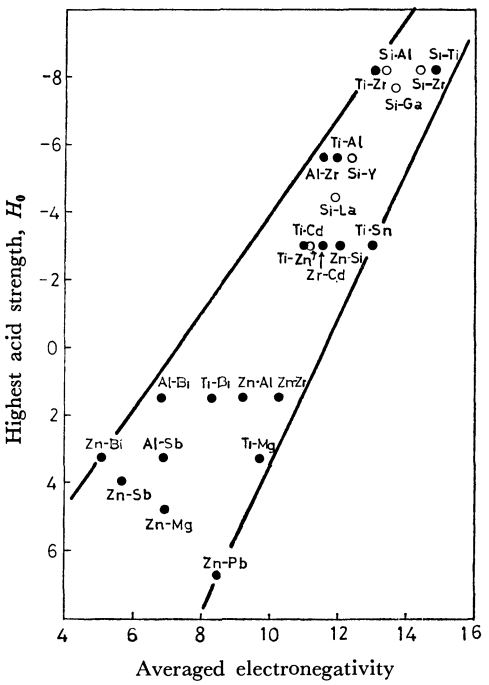

Fig. 4. Highest acid stength *vs.* averaged electronegativity of metal ions of binary oxides (molar ratio=1).

of metals of the same fourth group in the periodic table and that the acidity maximum of TiO_2–ZnO[2] appears when the molar ratio is 1 : 9 as in the case of TiO_2–Al_2O_3. Recently, TiO_2–Al_2O_3 was reported to show high catalytic activity for the synthesis of aniline from phenol and ammonia.[9] The high activity can be now understood to be due to its high acid strength. SiO_2–TiO_2 shows higher activity than SiO_2–Al_2O_3 for the aniline synthesis.[10]

Binary Oxides Containing Zinc Oxide or Alumina and Other Binary Oxides. The acidity distribution of the binary oxides containing ZnO or Al_2O_3 and other binary oxides (molar ratio=1) is shown in Table 3. According to X-ray diffraction, ZnO–SiO_2 and Al_2O_3–ZrO_2 were amorphous and ZnO–MgO gave only the diffraction lines of ZnO. ZnO–Al_2O_3, ZnO–ZrO_2, ZnO–Sb_2O_5 and ZnO–PbO gave diffraction lines differing from those of the component oxides. The results indicate that these binary oxides are not mechanically mixed oxides. The binary oxides which showed high acid strength were ZnO–SiO_2, Al_2O_3–ZrO_2 and ZrO_2–CdO. The acid strengths of binary oxides containing ZnO are relatively weak. The acidity changes of ZnO–Al_2O_3 and Al_2O_3–ZrO_2 with composition are shown in Figs. 2 and 3, where the acidity maxima are found when the molar ratios are

9) R. S. Parker, Japanese Pat. Sho 42-23571.
10) K. Tanabe, M. Ito, and M. Sato, *Chem. Commun.*, in press.

approximately 1 : 9 and 3 : 2, respectively. Many binary oxides show higher acid amount and strength than each component oxide (Table 3). The acid strengths of ZnO–MgO and Al_2O_3–Sb_2O_5 were the same as those of one of the component oxides, whereas their acid amounts per unit surface area were smaller. In the case of ZnO–Sb_2O_5 and ZnO–PbO, both acid strength and amount were lower than those of the component oxides. It was reported that both SiO_2 and ZnO are almost inactive for the isomerization of butenes, although the combination of both oxides is active.[11] The activity is considered to be due to the action of strong acid sites generated on the surface of SiO_2–ZnO.

Correlation between Acid Strengths of Binary Oxides and Electronegativities of Metal Ions of Metal Oxides. The observed highest acid strengths of binary oxides (molar ratio=1) are plotted against the algebraically averaged electronegativities of metal ions in Fig. 4, where the data indicated by open circles were cited from the literature (Ref. 2 for TiO_2–ZnO; Ref. 7 for SiO_2–ZrO_2; Ref. 12 for SiO_2–Al_2O_3, SiO_2–Y_2O_3, SiO_2–La_2O_3). The electronegativity values of various metal ions were cited from the work of Tanaka and Ozaki.[13] The highest acid strengths were found to increase with the increase of the algebraically averaged electronegativities. The correlation between the acid strengths and the geometrically averaged values of electronegativities was slightly worse than but almost the same as that shown in Fig. 4. Since the electronegativity of metal ion (Me^{+n}) is related to its acid strength (pK_a) as shown in $Me^{+n}+H_2O \rightleftarrows [Me(OH)]^{+(n-1)}+H^+$, the relation given in Fig. 4 seems to be reasonable. However, the reason why the algebraically or geometrically *averaged* values of electronegativities are correlated with the acid strengths is not yet clear. Nevertheless, the correlation in Fig. 4 is useful for predicting the acid strengths of unknown binary oxides.

11) K. Tanabe, T. Sumiyoshi, and H. Hattori, *Chem. Lett.*, **1972**, 723.

12) N. S. Kotsarenko, L. G. Karakchiev, and V. A. Dzisko, *Kinet. Katal.*, **9**, 158 (1968).

13) K. Tanaka and A. Ozaki, *J. Catal.*, **8**, 1 (1967); K. Tanaka, "Shokubai Kogaku Koza," Vol. 10, ed. by A. Ozaki, K. Tamaru, K. Tanabe, and S. Nishimura, Chijinshokan & Co. Ltd., Tokyo, (1967), p. 752.

BULLETIN OF THE CHEMICAL SOCIETY OF JAPAN, VOL. 46, 2988—2992 (1973)

Solvent Effect under High Pressure. Participation of Solvent in the Activated Complex in the Menschutkin Reaction

Katsuhiro TAMURA, Yoshiaki OGO, and Tatsuya IMOTO

Department of Applied Chemistry, Faculty of Engineering, Osaka City University, Sumiyoshi-ku, Osaka 558

(Received February 8, 1973)

Rates of the reaction between 3,5-lutidine with ethyl iodide have been measured at 50 °C over the pressure range 1—1,940 kg/cm² in benzene-nitrobenzene mixtures. The solvation number and average pressure within the solvation-shell of activated complex have been estimated from the rates and the compression of solvent. The solvation number was almost independent of solvent composition, but not the average pressure within the solvation-shell. Estimation of the structural term of the activation volume $\Delta_1 V^{\neq}$ in the reaction has been discussed. The logarithms of the rate constants showed a linear relation with the E_T-values under atmospheric pressure.

The fundamental equation for the effect of pressure on the rate constant of a chemical reaction is

$$\left(\frac{\partial \ln k}{\partial P}\right)_T = -\frac{\Delta V^{\neq}}{RT} \quad (1)$$

where $\Delta V^{\neq}$ is the activation volume of the reaction, *i.e.* the difference of the partial molar volumes of the reactants in the transition state and the initial state. The activation volume gives important information on the structure and properties of the transition state. The activation volume is of use for the mechanistic interpretation of chemical reactions since there is no method for investigating the detailed shape of activated complexes.

The reaction of alkylhalides with tertiary amines, known as the Menschutkin reaction, is a well-known heterolytic reaction under high pressure. The importance associated with the "ionic-solvation" component of $\Delta V^{\neq}$ implies that the magnitude of activation volume should depend on the nature o solvent. There are experimental evidences that $\Delta V^{\neq}$ is solvent-dependent. An extensive study of the influence of the solvent on the Menschutkin reaction under high pressure was made by Gonikberg and his collaborators.[1] The solvation number and the average pressure within the solvation-shell in the transition state for the Menschutkin reaction was estimated by Kondo *et al.*[2] Their investigation deals with the average values of various solvents. Actually, the values would change because of the variation of the influence of solvent on the activated complex if the nature of solvent

1) M. G. Gonikberg, "Khimicheskoe ravnovesie i skorost' reaktsii pri vysokikh davleniyakh," 3rd ed., Khimiya, Moscow (1969), p. 206, 278; Y. Ogo "Koatsu Kagaku" (Japanese Translation of Gonikberg's Book), Nikkan Kogyo Shinbunsha, Tokyo (1972), p. 180, 245.

2) Y. Kondo, M. Uchida, and N. Tokura, This Bulletin, **41**, 992 (1968).

(solvent polarity) is altered.

Some attempts have been made to correlate the rate constants for the Menschutkin reactions with the polarity parameters of solvents representing various aspects of solvation. A solvent dielectric constant has been widely used as a measure of solvent polarity. However, it represents only a single macroscopic characteristic of solvent and cannot express adequately all the interactions between solute and solvent molecules. Thus empirical parameters of solvent polarity have been proposed for understanding the complexities of molecular interactions in solution. E_T-values are known as a solvent polarity scale which covers a greater range of solvents. The scale was obtained by determining the molar transition energy E_T for the solvatochromic band in the spectrum of a pyridinium *N*-phenolbetaine in various solvents.

This work deals with the scale as regards the reaction of 3,5-lutidine with ethyl iodide. The solvation number and average pressure within the solvation-shell in transition state for benzene-nitrobenzene mixtures were obtained by means of the compression of solvents. The relationships between the polarity of the solvent and the reaction rate were studied by the use of the E_T-value as an empirical parameter of solvent polarity.

Experimental

Materials. Commerical 3,5-lutidine was dried overnight with sodium hydroxide and distilled twice at reduced pressure; bp 59 °C/14 mmHg, n_D^{25} 1.5030. Commerical ethyl iodide of special grade was washed with dilute potassium hydroxide solution and water, dried with calcium chloride and filtered. After addition of sodium metal to the filtered substance, the solution was distilled at atmospheric pressure; bp 71.3 °C, n_D^{20} 1.5131.

Commercial benzene and nitrobenzene of special grade were purified according to method given in literature;[3] n_D^{20} (benzene) 1.5013, n_D^{20} (nitrobenzene) 1.5526.

N-(4-Hydroxy-3,5-diphenyl-phenyl)-2,4,6-triphenylpyridinium betaine, a color change indicator used for the measurement of the E_T-value, was synthesized as follows. 2,6-Diphenyl-4-aminophenol was prepared from dibenzyl ketone and sodium nitromalonaldehyde monohydrate synthesized from mucobromic acid. Betaine was obtained from the reaction between this substance and 2,4,6-triphenylpyrylium perchlorate synthesized from acetophenone and benzaldehyde.[4] The betaine was recrystallized in a methanol-water mixture (1 : 1); mp 207—280 °C. Found; C, 83.58; H, 5.26; N, 2.61%. Calcd for $C_{41}H_{33}O_3N$: C, 83.79; H, 5.66; N, 2.38%.

The E_T-values were determined for the solvatochromic band in the spectrum of a pyridinium betaine by using the following equation.

$$E_T = h\nu = 2.859 \times 10^5/\lambda_{max} \text{ (in Å)} \qquad \text{(kcal/mol)}$$

Procedures. Solutions of equimolar concentration (0.25 M) of 3,5-lutidine and ethyl iodide were introduced into a 5-ml reaction cell, and placed in a high pressure apparatus held at 50±0.12 °C during the reaction and quickly pressurized. After decompression the reaction cell was emptied into a flask containing 15-ml water. The reaction product was extracted by vigorous shaking with water. A portion of the aqueous layer was analyzed by titration with a silver nitrate solution.

E_T-values were measured with a Hitachi 139-type UV-VIS spectrophotometer.

Measurement of Compression. The compression, $K = (V_0 - V_p)/V_0$, was determined by the measurement of the solvent volumes at atmospheric pressure V_0 and at P atom pressure V_p. The experiments for the benzene-nitrobenzene mixtures were carried out at 50 °C by means of Adams' method using a piezometer of about 11-ml capacity.[5] The pressure was measured by a Heise Bourdon-type gauge, the accuracy being checked with a pressure balance (free-piston pressure gauge). The rates of compression were in the order of 100 atm/min. The volume changes of Pyrex glass and mercury at high pressure was corrected with the values in literature.[6]

Results and Discussion

The rate constants of the reaction of 3,5-lutidine with ethyl iodide in benzene–nitrobenzene mixtures at 50 °C over the pressure range 1—1940 kg/cm² are summarized in Table 1. All the reaction rates followed second-order equation. The rate constants increased with an increase in pressure and concentration of nitrobenzene. The unexpected large rate constant at 0.8 mole fraction nitrobenzene and 1940 kg/cm² pressure suggests an unusual high concentration of reactants resulting from the freezing of solvent. The freezing temperatures of benzene and nitrobenzene under 2000 kg/cm² have been reported to be 58.0 and 49.5 °C, respectively.[7]

Estimation of Activation Volume. In order to evaluate ΔV^* it is necessary to confirm the functional dependence of rate constant upon pressure. Derivation of an analytical expression for the dependence has been discussed by various workers. Golinkin *et al.*[8] concluded that the quadratic function (3) provided the best representation of the dependence of logarithm of rate constant on pressure for some organic reactions. We checked the following three functions by the least-mean-squares method. It was concluded that a second-order polynomial (3) gives the best description of this system.

$$\ln k = A + BP \tag{2}$$

$$\ln k = A + BP + CP^2 \tag{3}$$

$$\ln (k/k_o)/P = A + BP^{0.523} \tag{4}$$

It is assumed in Eq. (2) that the dependence of the logaithm of the rate constant on pressure is linear. Eq. (4) is the Benson-Berson equation modified by means of the Tait equation.

3) J. A. Riddick and W. B. Bunger, "Organic Solvents," John Wiley & Sons, Inc., New York, N. Y. (1970), p. 796.

4) K. Dimroth, C. Reichardt, T. Siepmann, and F. Bohlmann, *Ann. Chem.*, **661**, 1 (1963).

5) L. H. Adams, *J. Amer. Chem. Soc.*, **53**, 3769 (1931).

6) K. E. Bett, K. E. Weale, and D. M. Newitt, *Brit. J. Appl. Phys.*, **5**, 243 (1954); D. S. Tsiklis, "Handbook of Techniques in High Pressure Reaction and Engineering," Plenum Press, New York (1968), p. 24.

7) "The International Critical Tables," Vol. 4, McGraw-Hill, New York (1933), p. 9.

8) H. S. Golinkin, W. G. Laidlaw, and J. B. Hyne, *Can. J. Chem.*, **44**, 2193 (1966).

Table 1. Rate constants at 50°C, $k \times 10^4$(l mol^{-1} s^{-1})

Pressure (kg/cm^2)	Mole fraction of nitrobenzene					
	0	0.2	0.4	0.6	0.8	1.0
0	0.197	1.13	2.28	3.33	3.89	4.58
410	(0.460)	2.12	4.05	5.51	6.07	6.63
920	0.613	3.20	5.82	7.88	8.24	9.03
1430	0.963	4.47	8.42	10.5	11.8	10.9
1940	—	5.48	10.3	12.2	15.2	13.8

Table 2. Functional constants of Eq. (3) and standard deviation

	Mole fraction of nitrobenzene					
	0	0.2	0.4	0.6	0.8	1.0
A	−10.84	−9.059	−8.7977	−7.977	−7.870	−7.648
$B \times 10^3$ (cm^3/kg)	1.464	1.416	1.301	1.171	0.9452	0.8058
$C \times 10^7$ (cm^4/kg^2)	−2.435	−3.239	−2.755	−2.688	−1.191	−1.378
$SD \times 10^2$	3.00	8.55	3.47	4.65	5.20	6.26

Table 3. Activation volumes, molar volume of solvent, compression and average pressure within solvation-shell[a)]

	Mole fraction of nitrobenzene					
	0	0.2	0.4	0.6	0.8	1.0
$\Delta V^{\ddagger}$ (cm^3/mol)	−40.1	−38.8	−35.6	−32.0	−25.9	−22.1
$\Delta_2 V^{\ddagger}$ (cm^3/mol)	−22.1	−20.8	−17.6	−14.0	−7.9	−4.1
V_0 (cm^3/mol)	92.231	94.470	96.873	99.469	102.18	104.87
K	0.120	0.110	0.0908	0.0704	0.0387	0.0195
$\Delta P \times 10^{-3}$ (atm)	(2.0)	2.0	1.7	1.3	0.70	0.37

a) $n=2$, $\Delta_1 V^{\ddagger} = -18$ cm^3/mol

The functional constants of Eq. (3) and the standard deviation are given in Table 2.

Substituting Eq. (3) into Eq. (1) we obtain the following equation for the evaluation of $\Delta V^{\ddagger}$.

$$\Delta V^{\ddagger} = -RT(B+2CP) \quad (5)$$

The activation volumes at atmospheric pressure calculated by this equation are listed in Table 3.

$\Delta V^{\ddagger}$ denotes the change of partial molar volumes which occurs when the transition state is formed from the initial species as given by Eq. (6). $\Delta V^{\ddagger}$ may be also expressed by Eq. (7) by considering the solvation term of the activated complex with partial electric charge. Eq. (8) is given in terms of compression.

$$\Delta V^{\ddagger} = \overline{V}^{\ddagger} - (\overline{V}_L + \overline{V}_E) \quad (6)$$

$$= [V^{\ddagger} - (\overline{V}_L + \overline{V}_E)] - n(V_0 - V) \quad (7)$$

$$= [V^{\ddagger} - (\overline{V}_L + \overline{V}_E)] - nKV_0 \quad (8)$$

The bar represents a partial molar volume, L and E refer to 3,5-lutidine and ethyl iodide, respectively, n the number of solvent molecules incorporated into transition state (solvation number), V_0 molar volume of solvent, V molar volume of compressed solvent due to solvation, and K compression of the solvent.

By measurement of the partial molar volume of 3,5-lutidine and ethyl iodide, the partial molar volumes of both reagents were almost independent of solvent composition and were obtained as 116 and 84.3 cm^3 at 50 °C, respectively. Thus the partial molar volumes of the reactants seem to be equal to their molar volumes.

The $\Delta V^{\ddagger}$ value is the sum of $\Delta_1 V^{\ddagger}$ and $\Delta_2 V^{\ddagger}$, the former being the volume change of reacting particles themselves when they form the activated complex (structural effect), and the latter the corresponding volume change in the solvent (solvation effect). The value $\Delta_1 V^{\ddagger}$ corresponds to the first term and $\Delta_2 V^{\ddagger}$ to the second term on the right-hand side of Eqs. (7) and (8). Thus, the magnitude of K in Eq. (8) denotes the volume change due to the interaction of the surrounding solvent molecules with the activated complex, *i.e.* the compression of the solvent due to solvation. If Gonikberg's value[9] −18 cm^3/mol obtained from the reaction of pyridine with ethyl iodide can be used as the value $[V^{\ddagger} - (\overline{V}_L + \overline{V}_E)]$ in Eq. (8), the product of the solvation number and the compression, (nK), can be estimated from the observed values $\Delta V^{\ddagger}$ and V_0. Since the solvation number n can be evaluated we can estimate the average pressure within the solvation-shell of activated complex ΔP from the corresponding compression-pressure curve.

Estimation of Solvation Number and Average Pressure within Solvation-shell of Activated Complex. Eq. (9) is given by differentiation of Eq. (7) with respect to V_0 assuming that n and V are independent of external

9) M. G. Gonikberg and B. S. El'yanov, *Izv. Akad. Nauk SSSR, Otd. Khim. Nauk*, **1960**, 629.

pressure over the pressure range studied.

$$\frac{\partial \Delta V^{\neq}}{\partial V_0} = \frac{\partial}{\partial P}[V^{\neq}-(V_L+V_E)]\frac{\partial P}{\partial V_0} - n \qquad (9)$$

$$= -(\beta+n)$$

$$\beta = -\frac{\partial}{\partial P}[V^{\neq}-(V_L+V_E)]\frac{\partial P}{\partial V_0}$$

A similar equation was introduced by Gonikberg and El'yanov.[9]

If we assume that $\beta=0$, then we obtain the following expression for solvation number.

$$n = -\frac{\partial \Delta V^{\neq}}{\partial V_0} \qquad (10)$$

There is no evidence that β is zero. However, the partial molar volumes of 3,5-lutidine and ethyl iodide are nearly equal to their molar volumes. Therefore $[V^{\neq}-(V_L+V_E)]$ gives the structural effect of the activation volume $\Delta_1 V^{\neq}$. In a free-radical chain reaction without the participation of solvent, the activation volume is independent of the pressure over small pressure range. This suggests that the influence of β is negligible.

Figure 1 shows a plot of $\Delta V^{\neq}$ against V_0 under various pressures in nitrobenzene. We see that good linearity holds. The solvation number is evaluated to be 2 from the slope. Similar values have been estimated by the same plot for the other mixtures and benzene. The value K in Eq. (8) can be calculated by the use of these values. The results are listed in Table 3. Figure 2 shows the experimental results on the compression of the solvent at various pressures. The average pressures within the solvation-shell of activated complex ΔP were estimated from this graph (Table 3). The values of ΔP are not independent of solvent composition and show higher values for the solvents rich in benzene.

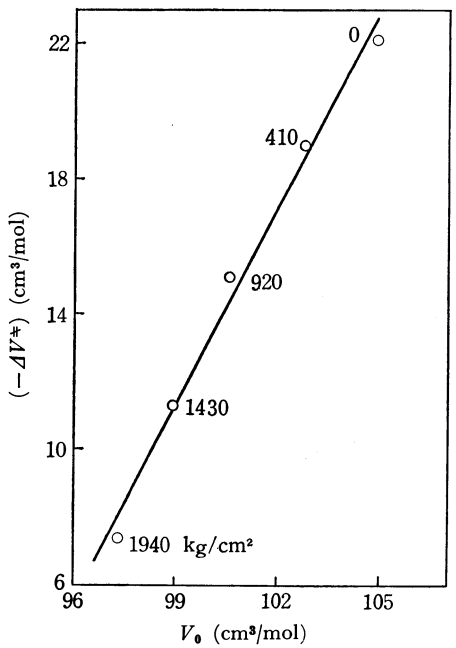

Fig. 1. Plots of activation volumes *vs.* molar volumes of solvent for the reaction of 3,5-lutidine with ethyl iodide at 50 °C in nitrobenzene.

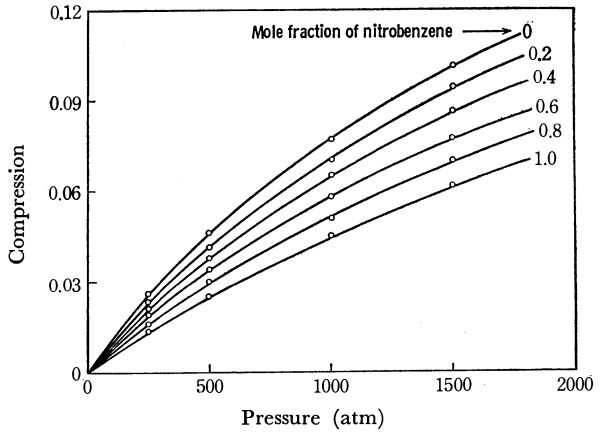

Fig. 2. Variation of the compression of solvent with pressure.

Gonikberg and El'yanov[9] tried to calculate $\Delta_1 V^{\neq}$ in the reaction of pyridine with ethyl iodide. They proposed three values of activation volume, −14, −18, and −22.5 cm³/mol, which were obtained by different analytical procedures. It seems reasonable to assume that −22.5 cm³/mol is too small since the over-all activation volume in nitrobenzene was observed to be −22.1 cm³/mol. The value −14 cm³/mol is also unfavorable since ΔP in benzene was calculated to be 2800 kg/cm², being extremely higher than the freezing pressure of benzene at 50 °C. It was concluded that the value −18 cm³/mol is reasonable. The data in Table 3 were calculated from $\Delta_1 V^{\neq}=-18$ cm³/mol. The ΔP of benzene was slightly higher than the value of freezing pressure. This was estimated by extrapolating the compression-pressure curve to freezing pressure. The unfavorable result might be due to the fact that inaccuracy of the starting data on the estimation of $\Delta V^{\neq}$ is large since the reaction in benzene takes place very slowly as compared with that in other solvents. Consequently, the value of ΔP of benzene is of low reliability.

The value ΔP can be evaluated also as follows. Isothermal compressibility is defined by $\kappa=-1/V(\partial V/$

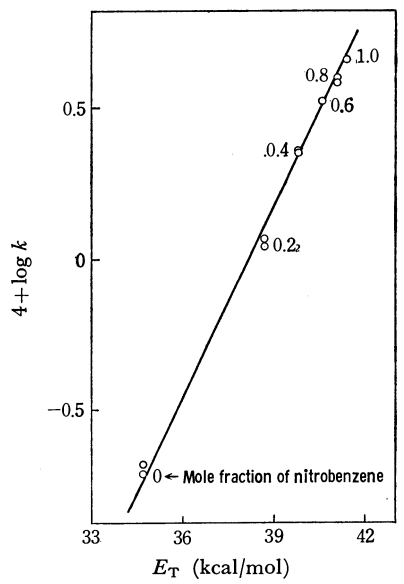

Fig. 3. Relation of $\log k$ *vs.* E_T-values.

$\partial P)_T$. We can write $\kappa'=(V_0-V_p)/V_0\cdot 1/\Delta P=K/\Delta P$ at certain pressure interval ΔP, and obtain an equation analogous to (8).

$$\Delta V^{\neq} = [V^{\neq}-(V_L+V_E)] - n\kappa' V_o \Delta P \qquad (11)$$

However, κ' at pressure interval of ΔP cnanot be obtained experimentally, and κ at atmospheric pressure is generally used as κ' for the estimation of the ΔP in Eq. (11). Thus the procedure by means of the direct measurement of K is more accurate than that with the use of Eq. (11).

E_T-value. The E_T-values and the λ_{max} of benzene–nitrobenzene mixtures at 25 °C are shown in Table 4. Figure 3 gives a plot of the E_T-values against logarithms of the rate constants under atmospheric pressure. It seems that the E_T-value is an available empirical parameter of the solvent polarity for the present reaction because of the linearity. Gonikberg and El'yanov[10] reported that the volume contraction due to solvation in the transition state is 1/6—1/14 of that in the final state in the Menschutkin reaction. It is suggested that the E_T-values are useful parameters in this type of reaction. The activation volumes and E_T-values at atmospheric pressure became greater with an increase in the quantity of nitrobenzene, but no particular correlation has yet been established between them. In order to correlate the E_T-values to the activation volumes, it is necessary to observe the pressure dependence of the E_T-values, since the pressure dependence of the rate constant is required for the calculation of activation volume.

TABLE 4. λ_{max} AND E_T-VALUES FOR BENZENE–NITROBENZENE MIXTURES AT 25°C

	Mole fraction of nitrobenzene					
	0	0.2	0.4	0.6	0.8	1.0
λ_{max} (nm)	824	739	718	704	695	690
E_T (kcal/mol)	34.7	38.7	39.8	40.6	41.1	41.4

The authors are indebted to Dr. Takashi Moriyoshi for the measurement of the compression.

10) M. G. Gonikberg and B. S. El'yanov, *Dokl. Akad. Nauk SSSR*, **130**, 545 (1960).

BULLETIN OF THE CHEMICAL SOCIETY OF JAPAN, VOL. 46, 2992—2997 (1973)

Kinetic Studies of Fast Reactions in Aqueous Solutions of Amylamine by Means of Ultrasonic Absorption

Sadakatsu NISHIKAWA, Tatsuya YASUNAGA, and Kojiro TAKAHASHI

Department of Chemistry, Faculty of Science, Hiroshima University, Higashisenda-machi, Hiroshima 730

(Received March 22, 1973)

The ultrasonic absorptions in aqueous solutions of amylamine were measured in the frequency range of 3.5—220 MHz and in the concentration range of 0.01—3.06 M. Two kinds of relaxations were observed. One was attributed to the 5A—A_5 reaction of non-ionized molecules of amylamine, and the rate constants were determined from the concentration dependence of the relaxation time at various temperatures. The thermodynamic parameters were determined from the temperature dependence of the rate and equilibrium constants. The other was attributed to hydrolysis, which is a diffusion-controlled reaction. In order to clarify the relation between the stability of the aggregate and the length of the hydrophobic group, the ultrasonic absorptions in aqueous solutions of propylamine were also measured. The excess absorption due to the association-dissociation reaction was not observed; only that due to hydrolysis was observed. It was deduced from this investigation that the aggregate formed by the hydrophobic bonding exists in the aqueous solutions of normal amines, the carbon numbers of which are more than 4.

The method of ultrasonic absorption has been successfully applied to the investigation of reaction kinetics which occur rapidly, since the relaxation time and excess absorption determined from the absorption data are related to the kinetic parameters. It is well known that a number of binary mixtures exhibit a maximum in their excess absorptions at an intermediate concentration.[1] It has been previously reported by the present authors[2,3] that there are two kinds of relaxation processes in aqueous solutions of butylamine. One, associated with the maximum excess absorption phenomena, was attributed to the association-dissociation reaction of the non-ionized molecules, and the other, to hydrolysis. Accordingly, the same phenomena may be expected to be observed in aqueous solutions of other amines.

Andreae and his co-workers[1] have explained the excess absorption of ultrasonic waves in aqueous solutions of amylamine as a solute-solvent interaction. However, this analysis employs a rather unusually defined equilibrium constant, and some of the stoichiometries reported appear to be implausible. Moreover, the data reported are insufficient for a reasonable analysis of the excess absorption mechanism.

The purpose of the present investigation is to clarify in detail the excess absorption mechanism of ultrasonic

1) J. H. Andreae, P. D. Edmonds, and J. F. McKellar, *Acustica*, **15**, 74 (1965).

2) S. Nishikawa and T. Yasunaga, This Bulletin, **46**, 1098 (1973).

3) S. Nishikawa, T. Nakamoto, and T. Yasunaga, *ibid.*, **46**, 324 (1973).

waves in aqueous solutions of amylamine on the basis of that in the aqueous solution of butylamine[2] and to reveal the characteristic properties of the aqueous solutions of amines. This type of information is particularly desirable for an understanding of the more complex biochemical reactions.

Experimental

The amylamine and propylamine were of a guaranteed reagent grade, and KOH was added to them to remove the water because the relatively concentrated solutions were made at the required concentrations by weight. They were distilled after the filtration of KOH. The purities were verified by gas chromatography to be higher than 99.9%. Deionized and distilled water was used as the solvent. The relatively dilute solutions (less than 0.5 M) were prepared by the dilution of the stock solution. The other chemicals used were all of a guaranteed reagent grade. The measurements of the ultrasonic absorption were carried out at the odd harmonic frequencies of 0.5, 5, and 20 MHz X-cut quartz transducers by means of the pulse technique.[4] The frequency range of the measurement was 3.5—220 MHz. Since the aqueous solutions of amines are highly basic, the cell was designed to be air-tight and dry nitrogen gas was passed over the solutions to prevent the contamination of the specimens by oxidation with air. The sing-around method was employed at 1.92 MHz to measure the sound velocity. The densities were measured by means of a standard pycnometer. The pH values of the solutions were measured by means of a Hitachi Horiba type F-5 pH meter. All the measurements for the aqueous solutions of amylamine were made at 15, 20, 25, and 30 °C, and for those of propylamine, at 20 °C.

Results

In Fig. 1 the plots of α/f^2 *vs.* the concentration for the aqueous solutions of amylamine at 20 °C are shown, where α is the sound absorption coefficient, and f, the frequency. As may be seen in this figure, the absorption and the peak sound absorption concentration (P.S.A.C) depend on the frequency. This behavior leads us to predict the existence of the relaxation phenomena. In general, the sound absorption caused by the several relaxation processes can be described by the following equation:

$$\alpha/f^2 = \sum_i \frac{A_i}{1+(f/f_{ri})^2} + B \qquad (1)$$

where f_{ri} is the relaxation frequency for the i-th process and where A_i and B are constants. Figure 2 shows the representative ultrasonic absorption spectra of the aqueous solutions of amylamine at 20 °C. The spectra in the concentration range of more than 1 M and less than 0.4 M show the characteristic behavior due to the single relaxation process, which is expressed by the case of $i=1$ in Eq. (1). On the other hand, the spectra in the concentration range between 1.0 and 0.4 M can be represented by the double relaxation process, which correspond to the case of $i=2$ in Eq. (1). These facts indicate that there are two kinds of relaxation processes in the aqueous solution of amylamine. The relaxation parameters, A_i, B, and f_{ri}, were determined so as to obtain the best fit of the

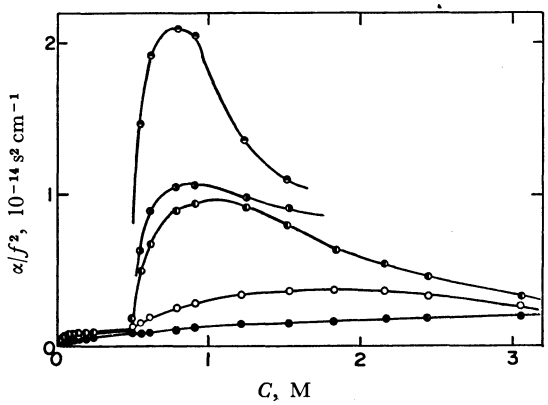

Fig. 1. The plots of α/f^2 *vs.* concentration for aqueous solutions of amylamine at 20°C. ◓: f=6.5 MHz, ◑: f=11.5 MHz, ◐: f=15 MHz, ○: f=45 MHz, ●: f=100 MHz.

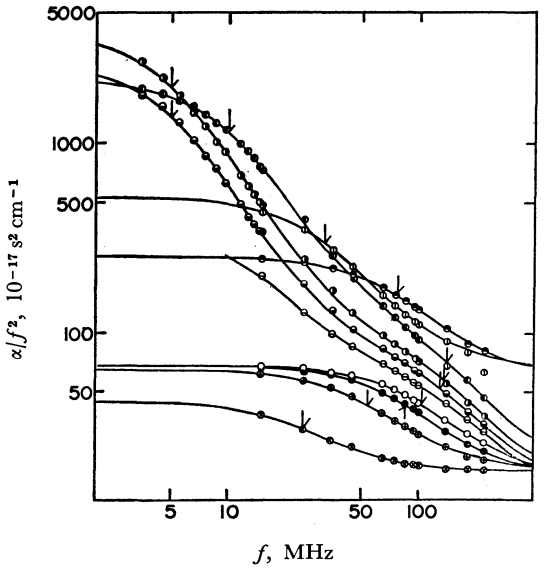

Fig. 2. Ultrasonic absorption spectra in aqueous solutions of amylamine at 20°C. ⊗: 0.00918 M, ⊕: 0.0685 M, ●: 0.147 M, ○: 0.245 M, ⊖: 0.490 M, ◒: 0.551 M, ◑: 0.612 M, ◐: 0.918 M, ⓘ: 1.84 M, ◓: 3.06 M.

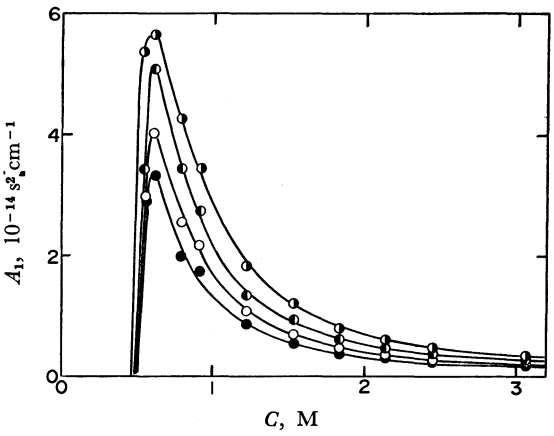

Fig. 3. Concentration dependence of the excess absorption A_1 in aqueous solutions of amylamine. ◐: 15 °C, ◐: 20 °C, ○: 25°C, ●: 30 °C.

4) N. Tatsumoto, *J. Chem. Phys.*, **47**, 4561 (1967).

TABLE 1. RELAXATION PARAMETERS, SOUND VELOCITY AND DENSITY IN THE AQUEOUS SOLUTIONS OF AMYLAMINE AND PROPYLAMINE AT 20°C

C (M)	pH	γ	ρ (g·cc^{-1})	c (m·s^{-1})	f_{r1} (MHz)	f_{r2}	A_1 (10^{-17} s^2 cm^{-1})	A_2	B
				(amylamine)					
3.06	12.54	0.8276	0.9300	1470.8	77	—	257	—	80.7
2.45	12.53	0.8295	0.9446	1479.1	54	—	386	—	69.2
2.14	12.52	0.8302	0.9535	1483.7	48	—	490	—	86.5
1.84	12.51	0.8315	0.9597	1488.8	32	—	604	—	92.1
1.53	12.50	0.8328	0.9685	1494.0	25	—	992	—	107
1.22	12.48	0.8353	0.9753	1498.9	18	—	1338	—	138
0.918	12.46	0.8379	0.9824	1505.0	10	140	2763	115	23.0
0.796	12.44	0.8404	0.9845	1506.6	8.5	120	3454	109	23.0
0.612	12.42	0.8429	0.9887	1511.5	5.0	133	5066	98.0	21.3
0.551	12.41	0.8442	0.9904	1514.8	5.0	130	3454	86.0	19.5
0.245	12.31	0.8565	0.9943	1506.5	—	105	—	64.9	23.0
0.196	12.24	0.8650	0.9950	1501.9	—	95	—	63.0	24.3
0.147	12.15	0.8749	0.9954	1497.4	—	85	—	64.2	23.9
0.107	12.06	0.8908	0.9961	1493.2	—	70	—	60.3	23.9
0.0685	11.93	0.8977	0.9971	1490.0	—	55	—	59.4	25.2
0.0300	11.64	0.9228	0.9978	1487.0	—	35	—	48.4	25.8
0.00918	11.20	0.9509	0.9989	1485.3	—	25	—	32.7	25.0
				(propylamine)					
0.201	12.37	0.8492	0.9949	1497.0	—	100	—	61.0	23.0
0.161	12.30	0.8577	0.9955	1494.6	—	85	—	61.0	23.6
0.121	12.23	0.8659	0.9961	1491.7	—	73	—	63.6	24.0
0.0805	12.11	0.8793	0.9964	1490.2	—	60	—	59.3	24.8
0.0604	12.03	0.8879	0.9969	1488.2	—	53	—	58.7	24.8
0.0403	11.82	0.9079	0.9969	1485.6	—	35	—	43.3	22.3
0.0121	11.47	0.9350	0.9975	1485.7	—	25	—	29.1	25.0

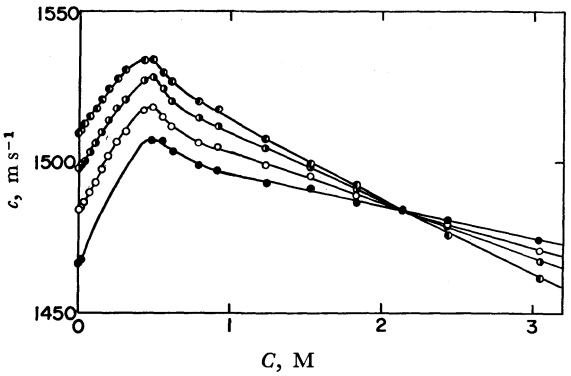

Fig. 4. Concentration dependence of the sound velocity in aqueous solutions of amylamine, ●: 15 °C, ○: 20 °C, ◑: 25 °C, ◐: 30 °C.

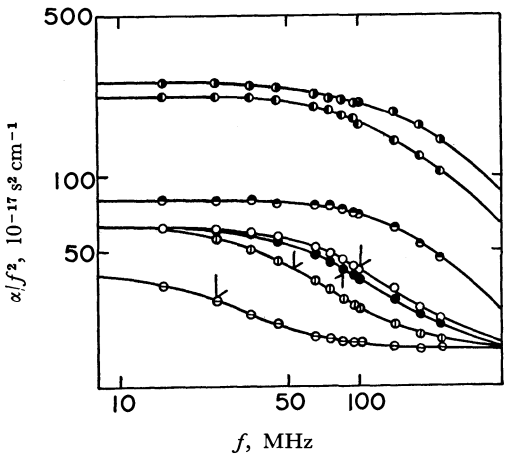

Fig. 5. Ultrasonic absorption spectra in aqueous solutions of propylamine at 20 °C. ⊖: 0.0121 M, ◫: 0.0604 M, ●: 0.161 M, ○: 0.201 M, ◓: 2.07 M, ◐: 3.05 M, ◑: 4.04 M.

data to Eq. (1). However, the spectrum at 0.490 M could not be analyzed because the absorption coefficients at low frequencies could not be observed. The excess absorptions, A_1, which were observed in the concentration range of more than 0.5 M in the lower frequency range are shown in Fig. 3. As may be seen in this figure, the positions of the P.S.A.C are independent of the temperature. The sound velocity also shows the peak at an intermediate concentration, as may be seen in Fig. 4. The concentration at which the sound velocity shows its maximum is lower than that of the excess absorption.

The ultrasonic absorptions in aqueous solutions of propylamine were also measured; same representative spectra are shown in Fig. 5. As may be seen in this figure, no double relaxation processes were observed, but only a single one was observed; no characteristic excess absorption such as is observed in the relatively concentrated solutions of butylamine and amylamine was found. In Table 1, the ultrasonic parameters and sound velocity obtained for the aqueous solutions of

amylamine and propylamine are listed, together with the density, the pH, and the activity coefficient of the ions, the last of which was calculated by means of Davies equation:[5] $-\log\gamma=0.5[\{\sqrt{I}/(1+\sqrt{I})\}-0.3I]$, where γ is the activity coefficient, and I, the ionic strength.

Interpretation of Results

First, for the excess absorption observed in the lower frequency range in the aqueous solution of amylamine, the following reaction is considered.

$$nA \underset{k_b}{\overset{k_f}{\rightleftharpoons}} A_n \qquad (2)$$

where A is the monomer, A_n, the aggregate, n, the aggregation number, and k_f and k_b, the forward and backward rate constants respectively. If one denotes the molar concentrations of the A and A_n components by C_1 and C_2, the relaxation time, τ_1, and the maximum excess absorption per wavelength, μ_{max_1}, can be written as follows:

$$2\pi f_{r_1} = \tau_1^{-1} = \overline{k_f} n^2 (\overline{C_1})^{n-1} + \overline{k_b} \qquad (3)$$

$$\mu_{max_1} = \frac{1}{2} A_1 f_{r_1} c = \frac{\pi\rho c^2}{2} \cdot \frac{(\Delta V_1^\circ)^2}{RT} \overline{k_f} \cdot (\overline{C_1})^n \cdot \tau_1 \qquad (4)$$

where ρ is the density, c, the velocity of sound, ΔV_1°, the standard volume change, R, the gas constant, and T, the absolute temperature. The equilibrium values of the rate constants and the concentrations are indicated by a bar over each symbol. The detailed derivatives of Eqs. (3) and (4) were reported in a previous paper.[2] In aqueous solutions of amines, there also exists the following equilibrium:

$$R\text{-}NH_3^+ + OH^- \underset{k_2}{\overset{k_1}{\rightleftharpoons}} R\text{-}NH_2 + H_2O \qquad (5)$$

where k_1 and k_2 are the forward and backward rate constants respectively. The dissociation constant, K_b, is defined by:

$$K_b = \frac{\overline{k_2}}{\overline{k_1}} = \frac{\gamma^2[OH^-]^2}{[R-NH_2]} \qquad (6)$$

where γ is the mean activity coefficient of the ion. If the non-ionized molecules are associated with the aggregation, Eqs. (3) and (4) can be expressed in terms of K_b and $\gamma[OH^-]$ as follows:

$$2\pi f_{r_1} = \tau_1^{-1} = \overline{k_f} n^2 \left(\frac{\gamma^2[OH^-]^2}{K_b}\right)^{n-1} + \overline{k_b} \qquad (7)$$

$$\mu_{max_1} = \frac{\pi\rho c^2}{2} \cdot \frac{(\Delta V_1^\circ)^2}{RT} \cdot \overline{k_f} \left(\frac{\gamma^2[OH^-]^2}{K_b}\right)^n \cdot \tau_1 \qquad (8)$$

The aggregation number was determined from the slope of the plots of $\log(\mu_{max_1}/\rho c^2\tau_1)$ *vs.* $\log(\gamma^2[OH^-]^2)$; the result was $n=5$. Figure 6 shows the plots of f_{r_1} *vs.* $(\gamma^2[OH^-]^2)^4$ for the aqueous solution of amylamine at 20 °C. If the dissociation constant, K_b, is known, the rate constants, $\overline{k_f}$ and $\overline{k_b}$, may be determined from the slope and intercept respectively. However, no dissociation constant has been reported except

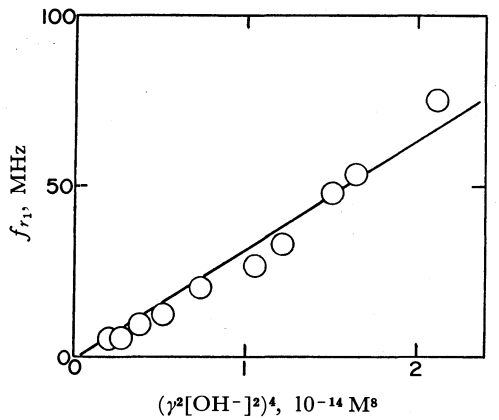

Fig. 6. The plots of f_{r_1} *vs.* $(\gamma^2[OH^-]^2)^4$ for aqueous solutions of amylamine at 20 °C.

for one at 25 °C,[6] and the intercept of these plots in Fig. 6 is close to zero. Therefore, the rate constants were determined in the following manner. Equation (7) can be rewritten as:

$$2\pi f_{r_1} = \tau_1^{-1} = n\overline{k_b} K_b \cdot \frac{C_0}{\gamma^2[OH^-]^2} - (n-1)\overline{k_b} \qquad (9)$$

where $C_0=[R-NH_2]+n[(R-NH_2)_n]$. Then, one can determine the values of $\overline{k_b}$ and $\overline{K_b}$ from the intercept and the slope of the plots of f_{r_1} *vs.* $C_0/\gamma^2[OH^-]^2$, which are shown in Fig. 7. The value of $\overline{k_f}$ was obtained using the slope of the plots of f_{r_1} *vs.* $(\gamma^2[OH^-]^2)^4$ in Fig. 6. The standard volume change was calculated by means of Eq. (4). In Table 2, the rate constants, the dissociation constant, and the standard volume change obtained are listed, together with the free energy, ΔF, which was calculated by means of: $K=\overline{k_b}/\overline{k_f}=\exp(-\Delta F/RT)$. The dissociation constant, K_b, was also determined from the $K_b=\gamma^2[OH^-]^2/(C_0'-[OH^-])$ relation in the concentration range of less than 0.25 M, in which it is expected that only the equilibrium expressed by Eq. (5) exists, where $C_0'=[R-NH_2]+[R-NH_3^+]$. These dissociation constants are indicated by K_b' in Table 2.

Secondly, for the sake of explaining the excess absorption observed in the aqueous solution of propylamine and the other one observed in the aqueous solution of amylamine, let us consider the hydrolysis which is expressed by Eq. (5). The relation between the relaxation time, τ_2, and the concentration can be

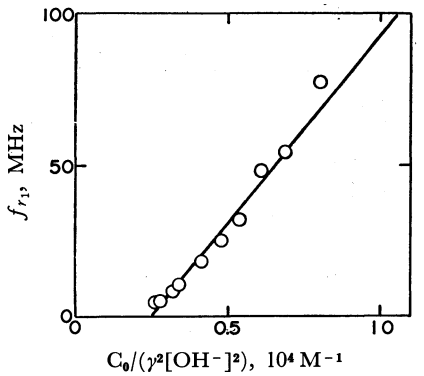

Fig. 7. The plots of f_{r_1} *vs.* $C_0/(\gamma^2[OH^-]^2)$ for aqueous solutions of amylamine at 20 °C.

5) C. W. Davies, "Ion Association," Butterworths, London (1962).

6) C. W. Hoerr, M. R. McCorkle, and A. W. Ralston, *J. Amer. Chem. Soc.*, **65**, 328 (1943).

Table 2. The rate and thermodynamic constants obtained for the association-dissociation reaction of amylamine

T (°C)	$\bar{k}_f$ (10^7 M^4 s^{-1})	$\bar{k}_b$ (10^7 s^{-1})	ΔV_1° (ml mol^{-1})	ΔF (kcal mol^{-1})	K_b	K_b' (10^{-4} M)	K_b [a]
15	0.64	5.5	17	−1.2	6.6	6.2	—
20	0.88	4.9	16	−1.0	3.2	4.8	—
25	1.2	5.0	17	−0.87	4.2	5.5	4.3
30	1.5	5.5	15	−0.80	3.0	3.6	—

a) Ref. 6).

Table 3. Rate constants and standard volume changes of hydrolysis at 20°C

System	$\bar{k}_1$ (M^{-1} s^{-1})	$\bar{k}_2$ (s^{-1})	ΔV_2° (ml mol^{-1})	Reference
$NH_4^+ + OH^- \rightleftharpoons NH_3 + H_2O$	3.6×10^{10}	6.0×10^5	26.8	(11)
$CH_3NH_3^+ + OH^- \rightleftharpoons CH_3NH_2 + H_2O$	3.7×10^{10}	1.6×10^7	26.1	(11)
$C_2H_5NH_3^+ + OH^- \rightleftharpoons C_2H_5NH_2 + H_2O$	3.2×10^{10}	1.4×10^7	24.3	(11)
$C_3H_7NH_3^+ + OH^- \rightleftharpoons C_3H_7NH_2 + H_2O$	3.0×10^{10}	1.2×10^7	24.0	(14)
	2.5×10^{10}	3.7×10^7	21	this work
$C_4H_9NH_3^+ + OH^- \rightleftharpoons C_4H_9NH_2 + H_2O$	4.1×10^{10}	1.2×10^7	32	(3)
$C_5H_{11}NH_3^+ + OH^- \rightleftharpoons C_5H_{11}NH_2 + H_2O$	3.0×10^{10}	7.5×10^7	25	this work
$C_8H_{17}NH_3^+ + OH^- \rightleftharpoons C_8H_{17}NH_2 + H_2O$	1.0×10^{10}	7.6×10^7	32	(13)

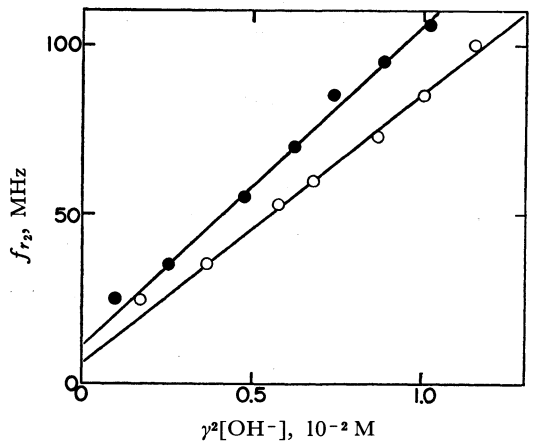

Fig. 8. The plots of f_{r_2} *vs.* γ^2[OH$^-$] at 20°C. ●: aqueous solutions of amylamine, ○: aqueous solutions of propylamine.

expressed as follows:

$$2\pi f_{r_2} = \tau_2^{-1} = 2\bar{k}_1\gamma^2[OH^-] + \bar{k}_2 \quad (10)$$

The excess absorption per wavelength can be written as:

$$\mu_{max_2} = \frac{1}{2}A_2 f_{r_2} c = \frac{1}{2}\pi\rho c^2 \frac{(\Delta V_2^\circ)^2}{RT}\Gamma_c \quad (11)$$

where $\Gamma_c = (1/[OH^-] + 1/[R{-}NH_3^+] + 1/[R{-}NH_2])^{-1}$. Figure 8 shows the plots of f_{r_2} *vs.* γ^2[OH$^-$] for the aqueous solutions of amylamine and propylamine. The forward and backward rate constants were determined from the slope and intercept respectively. The standard volume change associated with the hydrolysis was calculated by means of Eq. (11). In Table 3, the rate constants and standard volume change obtained in the present investigation are listed, together with the results for other monoamines.

Discussion

First, the excess absorption mechanism observed in an aqueous solution of amylamine in the lower frequency range will be discussed. For the mechanism associated with the peak sound absorption, several models have been proposed, such as AA+BB→2AB[7] and A+nB→AB$_n$,[1] where A is the solute, and B, the solvent molecules. All these models are due to the solute-solvent interaction. However, they are not acceptable in the case of the aqueous solutions of amines, as has been discussed in a previous paper.[2] In addition, if the cause of this excess absorption is associated with this solute-solvent interaction, the same absorption should be observed in any aqueous solution of amines. The fact that no excess absorption due to this mechanism was observed in the aqueous solution of propylamine also rules out these models. As is shown in Figs. 6 and 7, the linearities of the plots of f_{r_1} *vs.* $(\gamma^2[OH^-]^2)^4$ and f_{r_1} *vs.* $C_0/\gamma^2[OH^-]^2$ and the reasonable values of the dissociation constants, K_b, lead to the conclusion that the cause of the excess absorption is the association-dissociation reaction of amine. The theoretical maximum excess absorption per wavelength, which was calculated by Eq. (4) using the obtained values of $\bar{k}_f$ and ΔV_1°, are shown in Fig. 9, together with the experimental results. The agreement between the observed and calculated values also confirms the present model. In order to ascertain the natures of the aggregate, the ultrasonic absorptions were measured in aqueous solutions of butylamine hydrochloride and amylamine hydrochloride and in cyclohexane solutions of butylamine and amylamine. However, no excess absorptions were observed, as may be seen in Fig. 10. These facts lead us to the conclusions that the aggregate considered here consists of non-ionized amine molecules and that the water molecules participate in the aggregation of amines. In general, the molecules which consist of hydrophilic and hydrophobic groups have a tendency to aggregate in an aqueous solution. This aggregate is formed

7) R. N. Barfield and W. G. Schneider, *J. Chem. Phys.*, **31**, 488 (1959).

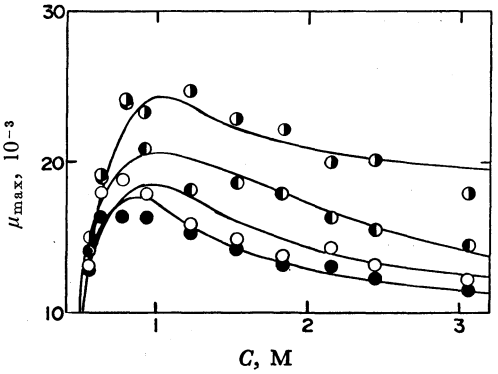

Fig. 9. Comparison of the experimental values of μ_{max} with the theoretical ones for aqueous solutions of amylamine. ◑: 15 °C, ◐: 20 °C, ○: 25 °C, ●: 30°C.

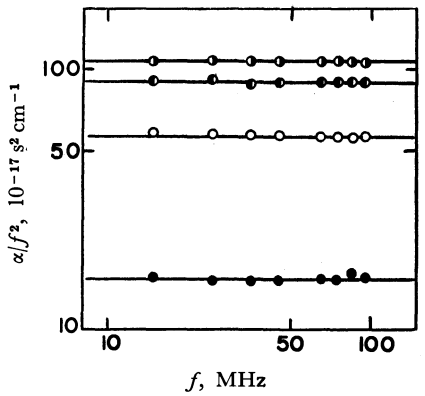

Fig. 10. Ultrasonic absorption spectra at 25 °C.
◑: cyclohexane solution of amylamine, 1.0 M.
◐: cyclohexane solution of butylamine, 2.3 M.
○: aqeous solution of butylamine hydrochloride, 2.0 M
●: aqeous solution of amylamine hydrochloride, 1.0 M.

by hydrophobic bonding, by which the ice berg structures of water which are formed around the nonpolar group of the molecule are broken and change to the normal structures of water. Since the standard volume change associated with the association-dissociation reaction of amines is comparatively large, this may be due to the change in the structure of the solvent water. The relaxation time[8] associated with this structural change in water is so small that the contribution of this relaxation to the association-dissociation reaction of amines may be neglected.

The thermodynamic parameters can be determined from the temperature dependence of the rate constants and the equilibrium constant obtained for the association-dissociation reaction of amylamine. According to the rate theory of reaction, the rate constant, k_i, is expressed by:

$$k_i = PT\exp\left(-\frac{\Delta F_i^{\neq}}{RT}\right) = PT\exp\left(-\frac{\Delta H_i^{\neq} - T\Delta S_i^{\neq}}{RT}\right) \quad (12)$$

where $\Delta H_i^{\neq}$ is the activation enthaply, $\Delta S_i^{\neq}$, the activation entropy, and P, the constant. The activation enthalpy is determined from the slope of the plots of $\ln(k_i/T)$ *vs.* $1/T$; the results are $\Delta H_f^{\neq}=8.7$ kcal/mol and $\Delta H_b^{\neq}=0$ kcal/mol. The enthalpy change was found to be -9.0 kcal/mol from the plots of $\ln K$ *vs.* $1/T$. Furthermore, through $\Delta F=\Delta H-T\Delta S$ the entropy change was calculated to be $\Delta S=-14$ e.u. It is well known that surface-active agents form a micelle by hydrophobic bonding in an aqueous solution with more than critical micelle concentration.[9] The thermodynamic parameters for micelle formation show the same temperature dependence as those of the association of amylamine, though the enthalpy change that in the latter is comparatively large. This confirms the aggregate of amylamine is formed by hydrophobic bonding. Compared with the case of the aqueous solution of butylamine,[2] the aggregation number increases with an increase in the chain length of the hydrophobic group and the dissociation rate constant of the aggregate for amylamine is smaller than that of butylamine. These facts mean that the aggregate is stabilized with an increase in the chain length of the hydrophobic group. It is also noteworthy that the aqueous solution of octylamine forms a mesomorphic phase, which consists of highly associated molecules. The ultrasonic investigation for this phase has previously been done by the present authors.[10]

Next, let us discuss the excess absorption mechanism in the aqueous solution of propylamine and the other one in the aqueous solution of amylamine. It has been reported by many authors[11-14] that there exists an excess absorption associated with hydrolysis in aqueous solutions of amines. As may be seen in Fig. 8, the linearities of the plots of f_{r_2} *vs.* $\gamma^2[OH^-]$ show that the cause of the excess absorption mechanism is attributed to the perturbation of the equilibrium expressed by Eq. (5). The obtained values of the rate constant, k_1, are pertinent for the proton transfer reaction. As may be seen in Table 3, the rate constants for the proton transfer reaction for normal amines are not appreciably dependent on the hydrophobic chain length, though the long chain length may affect the rate of the reaction.[13]

Finally, since there exist two types of equilibria in the solution of amylamine, it may be necessary to consider precisely the following two step mechanism, that is, the reaction which is coupled by Eqs. (2) and (5):

$$A^+ + B^- \rightleftharpoons A \rightleftharpoons \frac{1}{n}A_n \quad (13)$$

However, as has been described in the previous paper,[2] it has been verified that the contribution of the faster process, which is associated with hydrolysis, to the slower one, which is associated with the association-dissociation reaction, is so small that two different relaxation processes can be interpreted independently.

8) L. Hall, *Phys. Rev.*, **73**, 775 (1948).

9) K. Shinoda and T. Nakagawa, "Colloidal Surfactants," Academic Press (1963).

10) S. Nishikawa, *J. Colloid Interface Sci.*, in press.

11) M. Eigen, G. Maass, and G. Schwarz, *Z. Phys. Chem.*, **74**, 319 (1971).

12) M. M. Emara, G. Atkinson, and E. Baumgartner, *J. Phys. Chem.*, **74**, 334 (1972).

13) S. Nishikawa, T. Yasunaga, and N. Tatsumoto, This Bulletin, **46** 1657 (1973).

14) G. Maass, Ph. D. Thesis, Univ. of Göttingen (1962).

The Crystal Structure of Hemimellitic Acid Dihydrate

Fusao TAKUSAGAWA and Akira SHIMADA

Department of Chemistry, Faculty of Science, Osaka City University, Sugimoto-cho, Sumiyoshi-ku, Osaka 558

(Received March 27, 1973)

The crystal structure of hemimellitic acid dihydrate (benzene-1,2,3-tricarboxylic acid dihydrate) has been determined by the X-ray diffraction method. The crystals are triclinic, with a space group of $P\bar{1}$ and with cell dimensions of $a=11.02$, $b=9.12$, $c=8.72$ Å, $\alpha=106.2°$, $\beta=140.2°$, and $\gamma=84.2°$. The structure was determined by an inspection of a sharpened Patterson map. The final R value was 9.25% for 1532 observed reflections. The hemimellitic acid molecule has the approximate C_s symmetry. Three carboxyl groups twist by 4.5°, 86.8°, and 10.3° out of the plane of a benzene ring. The hemimellitic acid and water molecules are joined by seven independent O-H···O hydrogen bonds to form a three-dimensional network. The water molecules are hydrogen-bonded to each other around a center of symmetry to form a unique four-membered ring. The hydrogen bonds observed are classified by means of the combination of donor and acceptor groups in five types. These types of hydrogen bonds are discussed in the comparison with several carboxylic acid hydrates.

This work is a part of series of hydrogen-bonding studies by means of X-ray crystal structure analyses of several compounds which have the adjacent carboxyl groups substituted on a benzene ring. These kinds of compounds, which have already been analyzed by the X-ray diffraction method, are phthalic acid,[1] trimellitic acid,[2] pyromellitic acid,[3] and mellitic acid.[4] No intramolecular hydrogen bond has been found between the adjacent carboxyl groups in these crystal structures, but the vicinal carboxyl groups are twisted out of the plane of a benzene ring so that the repulsions were reduced between the oxygen atoms in these groups. Since the present compound has three adjacent carboxyl groups, it seemed that it would be of interest to elucidate the mutual relations of the steric hindrance by adjacent carboxyl groups. Moreover, all the hydrogen bonds in the crystal structures of benzene-carboxylic acids,[1-8] except for pyromellitic acid dihydrate are found to exist between the carboxyl groups related by a center of symmetry or a two-fold axis. On the other hand, there is no such type of hydrogen bond in the crystal of pyromellitic acid dihydrate; however, the observed types were similar to those of oxalic acid dihydrate. In view of the fact that the present compound contains water molecules, it seemed that it would also be of interest to examine the way of hydrogen bonding system in the crystal.

Experimental

The crystals were obtained in the form of colorless plates by recrystallization from a H_3PO_4 aqueous solution. Weissenberg photographs showed the crystal to be triclinic, with a space group of $P1$ or $P\bar{1}$. The unit-cell dimensions were measured from zero-layer Weissenberg photographs which had been calibrated with superimposed Al powder lines. The crystal data are given in Table 1. The crystals were shaped to cylinders with an average diameter of 0.4 mm for the a and c axes specimens. The intensity data were collected for the 0—10 layers around the a axis and for the 0—1 layers around the c axis by the use of the multiple-film equi-inclination Weissenberg technique with CuKα radiation. The intensities were estimated visually by comparison with an intensity scale. Of the possible 2425 reflections within the CuKα sphere, 1975 independent reflections were measured; 443 were too weak to be observed.

TABLE 1. CRYSTAL DATA FOR HEMIMELLITIC ACID DIHYDRATE

Molecular formula	$C_9H_6O_6\cdot 2H_2O$
Molecular weight	228.17
Crystal system	Triclinic
Space group	$P\bar{1}$
Cell dimensions;	
a	11.02±0.01 Å
b	9.12±0.01
c	8.72±0.01
α	106.2±0.1°
β	140.2±0.1
γ	84.2±0.1
V	529.2±1.0 Å^3
Z	2
Density (calculated)	1.544 g/cm^3
Density (observed)	1.52
Radiation	CuKα ($\lambda=1.5418$ Å)
Linear absorption coefficient	13.9 cm^{-1}
Atom numbering	

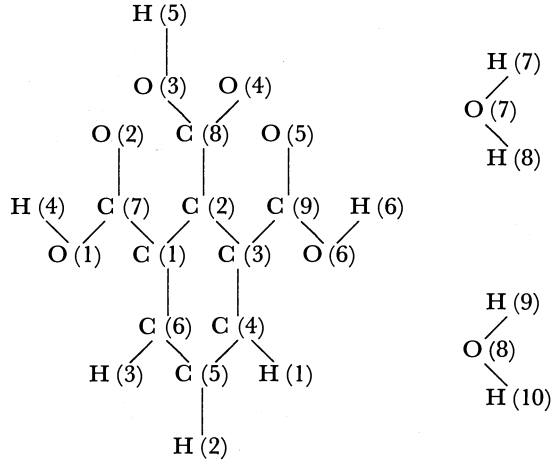

1) H. Jaggi, *Z. Kristallogr.*, **109**, 3 (1957).
2) F. Takusagawa, K. Hirotsu, and A. Shimada, This Bulletin, **46**, 2960 (1973).
3) F. Takusagawa, K. Hirotsu, and A. Shimada, *ibid.*, **44**, 1274 (1971).
4) S. F. Darlow, *Acta Crystallogr.*, **14**, 159 (1961).
5) G. A. Sim, J. M. Robertson, and T. H. Goodin, *ibid.*, **8**, 157 (1955).
6) R. Alcala and S. M. Carrera, *ibid.*, **B28**, 1671 (1972).
7) M. Bailery and C. J. Brown, *ibid.*, **22**, 387 (1966).
8) D. J. Duchamp and R. E. Marsh, *ibid.*, **B25**, 5 (1969).

No absorption and extinction corrections were applied. The space group was identified as $P\bar{1}$ on the basis of the statistical average for normalized structure factors.

Structure Determination and Refinement

The crystal structure was solved by an inspection of a sharpened Patterson map which had been resolved sufficiently enough to give the orientation and location of a hemimellitic acid molecule in the unit cell. The first postulated structure gave an R value of 59%; this decreased to 49% in three cycles of least-squares refinements with individual isotropic thermal parameters. A difference Fourier map showed the positions of the water oxygen atoms.

Anisotropic thermal parameters were introduced and the block-diagonal least-squares refinement was continued in order to reduce the R value to 11.5%. At this stage of refinement, a difference Fourier synthesis was computed, and from this the positions of ten hydrogen atoms were located (Fig. 1). There are

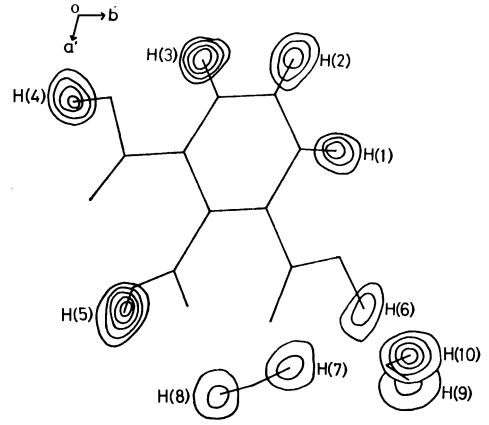

Fig. 1. A composite drawing of the electron density associated with the hydrogen atoms. The contours at intervals of 0.1 e·Å^{-3}, beginning with 0.2 e·Å^{-3} contour.

several spurious peaks on this map besides those due to hydrogen atoms. With anisotropic thermal parameters for non-hydrogen atoms and with isotropic thermal parameters for hydrogen atoms, the final R value was 9.25%, excluding unobserved reflections. The $\Sigma w(F_o-F_c)^2$ function was minimized, where:

$$w = 0.5 \text{ for } |F_o| \leqq 0.5,$$
$$w = 1.0 \text{ for } 0.5 < |F_o| < 5.0 \text{ and}$$
$$w = 5.0/|F_o| \text{ for } 5.0 \leqq |F_o|.$$

The atomic scattering factors used were those listed in the International Table for X-ray Crystallography for C, N, and O atoms and the spherical scattering factors proposed by Stewart, Davidson, and Simpson[9] for the H atom. The observed and calculated structure factors are listed in Table 2.[10] The fractional coordinates and thermal parameters are listed in Table 3.

9) R. F. Stewart, E. R. Davidson and W. T. Simpson, *J. Chem. Phys.*, **42**, 3175 (1965).

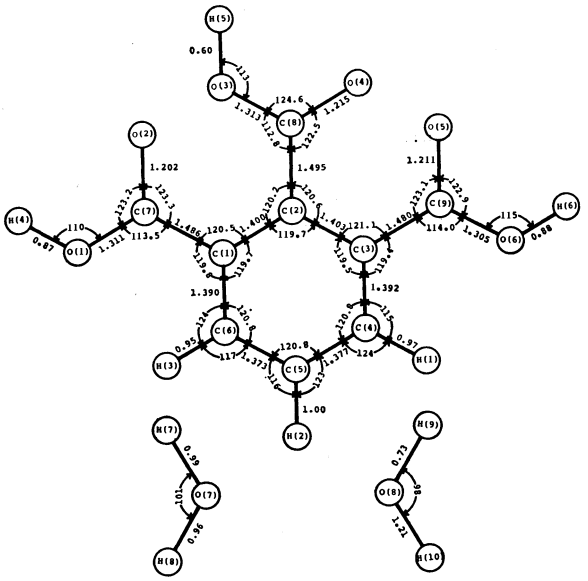

Fig. 2. Dimensions of hemimellitic acid dihydrate. The estimated standard deviations are as follows: C–C=0.007~0.008 Å, C–O=0.007 Å, C–H=0.06~0.07 Å, O–H=0.07~0.09 Å, C–C–C=0.5~0.6°, C–C–O=0.5°, C–C–O=0.5°, C–C–H=3~4°, C–O–H=3~7°.

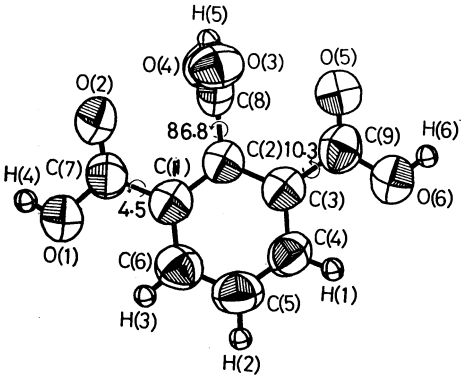

Fig. 3. The anisotropic thermal ellipsoids of non-hydrogen atoms. Ellipsoids are scaled to include the 74% probability. The hydrogen atoms are presented as artificially small spheres. The numbers indicate the dihedral angle between the planes of benzene ring and carboxyl group.

Results and Discussion

Molecular Structure of Hemimellitic Acid. The bond lengths and angles, along with their estimated standard deviations, are shown in Fig. 2. Figure 3 shows the anisotropic thermal ellipsoids of non-hydrogen atoms. Ellipsoids are scaled to include the 74% probability. Figure 4 presents the π-bond orders and net charges calculated by the use of the CNDO/2 method.[11]

The equations of the least-squares planes through six carbon atoms of a benzene ring and through all

10) Table 2 has been submitted to, and is kept by the office of the Chemical Society of Japan, 1–5, Kanda, Surugadai, Chiyoda-ku, Tokyo. (Document No. 7315).

11) J. A. Pople and D. L. Beverige, "Approximate Molecular Orbital Theory," McGraw-Hill Book Co., New York (1970).

Table 3. The final parameters and their estimated standard deviations (in parentheses)

The coordinates of the non-hydrogen atoms have been multiplied by 10^4; those of the hydrogen atoms, by 10^3. The anisotropic thermal parameters of non-hydrogen atoms are of the form of $\exp[-(B_{11}h^2+B_{22}k^2+B_{33}l^2+B_{12}hk+B_{13}hl++B_{23}kl)]$, and have been multiplied by 10^3. For the hydrogen atoms, the values are isotropic thermal parameters B(Å^2).

Atom	x	y	z	B(Å^2)	B_{11}	B_{22}	B_{33}	B_{12}	B_{13}	B_{23}
C (1)	4018 (5)	4919 (4)	1009 (6)	—	200 (7)	160 (5)	369 (12)	94 (10)	445 (17)	181 (13)
C (2)	5074 (5)	6276 (4)	3077 (6)	—	184 (7)	150 (5)	341 (11)	80 (9)	408 (16)	161 (12)
C (3)	6693 (5)	6180 (4)	5524 (6)	—	203 (7)	161 (5)	378 (13)	108 (10)	460 (18)	195 (13)
C (4)	7236 (5)	4746 (4)	5850 (7)	—	228 (8)	173 (6)	376 (13)	175 (11)	452 (18)	251 (14)
C (5)	6193 (6)	3420 (5)	3802 (8)	—	312 (9)	156 (6)	525 (17)	192 (13)	650 (24)	262 (17)
C (6)	4610 (6)	3508 (4)	1404 (7)	—	270 (9)	155 (5)	436 (15)	115 (11)	563 (21)	171 (15)
C (7)	2251 (5)	4972 (4)	−1602 (6)	—	202 (7)	157 (5)	330 (12)	65 (10)	388 (17)	128 (13)
C (8)	4516 (5)	7813 (4)	2672 (6)	—	188 (7)	153 (5)	261 (11)	51 (9)	305 (15)	109 (12)
C (9)	7846 (5)	7583 (4)	7767 (6)	—	185 (7)	182 (6)	360 (13)	97 (13)	404 (17)	195 (14)
O (1)	1482 (4)	3630 (4)	−3345 (5)	—	309 (8)	170 (5)	351 (11)	132 (10)	371 (16)	126 (12)
O (2)	1592 (4)	6132 (3)	−2073 (5)	—	259 (6)	177 (5)	324 (10)	137 (9)	336 (14)	159 (11)
O (3)	3370 (4)	8211 (3)	2731 (5)	—	294 (7)	177 (4)	591 (13)	195 (9)	711 (18)	287 (12)
O (4)	5077 (4)	8589 (3)	2321 (5)	—	258 (6)	191 (5)	504 (12)	114 (9)	571 (16)	293 (12)
O (5)	7622 (4)	8888 (3)	7632 (5)	—	316 (7)	155 (4)	423 (11)	110 (9)	486 (16)	172 (11)
O (6)	9115 (4)	7288 (3)	9905 (5)	—	277 (6)	183 (5)	358 (10)	108 (9)	426 (14)	176 (11)
O (7)	2377 (5)	9588 (4)	−2039 (7)	—	391 (9)	285 (7)	619 (16)	291 (14)	789 (23)	442 (18)
O (8)	11011 (4)	9736 (4)	13819 (5)	—	277 (7)	208 (5)	479 (12)	41 (10)	572 (17)	140 (13)
H (1)	837 (6)	477 (5)	759 (8)	6.1 (10)						
H (2)	640 (6)	235 (5)	396 (9)	6.9 (11)						
H (3)	390 (5)	254 (4)	9 (7)	4.4 (8)						
H (4)	43 (7)	371 (6)	−482 (9)	7.3 (12)						
H (5)	304 (5)	875 (5)	240 (7)	4.6 (9)						
H (6)	974 (8)	810 (7)	1125 (9)	7.7 (13)						
H (7)	155 (7)	991 (6)	−193 (9)	8.5 (15)						
H (8)	336 (7)	924 (6)	−59 (9)	7.7 (13)						
H (9)	1187 (7)	1014 (6)	1438 (9)	7.0 (11)						
H (10)	1174 (7)	960 (6)	1572 (9)	5.0 (10)						

Table 4. Deviations(Å) from the least-squares planes

The deviation(I) is the distance from the least-squares plane defined by six carbon atoms of benzene ring, and the deviation(II) is the distance from the least-squares plane defined by nine carbon atoms of a molecule.

Atom	(I)	(II)	Atom	(I)	(II)
C (1)	0.007	−0.001	O (6)	0.213	0.244
C (2)	−0.005	0.003	O (7)	−1.533	−1.512
C (3)	0.002	0.014	O (8)	0.333	0.392
C (4)	−0.001	0.001	H (1)	−0.00	0.01
C (5)	0.003	−0.010	H (2)	0.16	0.13
C (6)	−0.006	−0.023	H (3)	0.07	0.04
C (7)	0.055	0.043	H (4)	0.06	0.03
C (8)	−0.067	−0.048	H (5)	1.11	1.14
C (9)	−0.005	0.023	H (6)	0.29	0.33
O (1)	−0.018	−0.044	H (7)	−0.64	−0.61
O (2)	0.144	0.144	H (8)	−1.48	−1.46
O (3)	1.119	1.143	H (9)	−0.30	−0.24
O (4)	−1.117	−1.093	H (10)	0.93	0.99
O (5)	−0.177	−0.140			

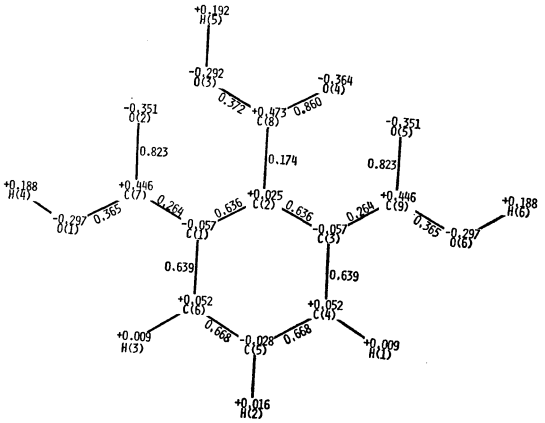

Fig. 4. The π-bond orders and net charges calculated by the CNDO/2 method. The hemimellitic acid molecule is assumed to have the C_s symmetry.

nine carbon atoms are:

$$-0.9843X - 0.1725Y + 0.0382Z = -4.8629 \text{ and}$$

$$-0.9854X - 0.9854Y + 0.0452Z = -4.8202,$$

where X, Y, and Z are coordinates in Å referred to an orthogonal set, where the X and Z axes are parallel to the a and b* axes and where Y lies on the ab plane. This coordinate system is used throughout this paper. The maximum deviation of ring atoms from the least-squares plane of a benzene ring is 0.007 Å. The benzene ring is essentially planar. The displacements of all the atoms from two planes are listed in Table 4. A molecule is approximately planar except for the O(3), O(4), and H(5) atoms of one carboxyl group.

The maximum differences among the C–C bond lengths and among the C–C–C bond angles in the benzene ring, 0.030(7) Å and 1.6(5)°, are significant from their estimated standard deviations (the values in parentheses denote the e.s.d.'s in the last digits). In two halves of the benzene ring divided through the line from C(2) to C(5) atoms, the differences between the corresponding bond lengths and angles are 0.003(7) Å (C(2)—C(3) and C(2)—C(1)), 0.002(7) Å (C(3)—C(4) and C(1)—C(6)), 0.004(7) Å (C(4)—C(5) and C(6)—C(5)), 0.2(5)° (C(2)—C(3)–C(4) and C(2)–C(1)–C(6)) and 0.0(5)° (C(3)–C(4)–C(5) and C(1)–C(6)–C(5)). These values show that the benzene ring in this molecule has the approximate C_{2v} symmetry. The significant differences in the C–C bond lengths and C–C–C bond angles in the benzene ring are due to the substitution of the carboxyl groups. This fact is supported by the π-bond orders calculated by the use of the CNDO/2 method, as is shown in Fig. 4. In this calculation, the molecule is assumed to have the C_s symmetry. The bond orders of the C(4)–C(5) and C(5)–C(6) bonds are the largest, those of the C(3)–C(4) and C(1)–C(6) bonds are second, and those of the C(1)–C(2) and C(2)–C(3) bonds are the smallest.

In these C–C bonds joining the carboxyl groups to a benzene ring, the slight differences between the C(2)–C(8) and C(1)–C(7) bond lengths, and between the C(2)–C(8) and C(3)–C(9) bond lengths, 0.009(7) and 0.015(7) Å, lie within the limits of their estimated standard deviations. However, the significance in these differences may be supported by the fact that the observed bond lengths are correlated well with their calculated bond orders, as is shown in Fig. 4. The differences between the C(7)–C(1)–C(6) and C(7)–C(1)–C(2) bond angles, between the C(8)–C(2)–C(1) and C(8)–C(2)–C(3) bond angles, and between the C(9)–C(3)–C(2) and C(9)–C(3)–C(4) bond angles are 0.7(5)°, 0.4(5),° and 1.5(5)°. These values have no significance and show that the repulsions between the carboxyl groups are reduced not by the changes in the C–C–C bond angles, but by the twists of the C–C bonds, as will be seen below.

The dimensions of three carboxyl groups agree with each other within the limits of experimental error. Two C–O bond lengths in each carboxyl group are clearly different from each other. The bonds between the carbon and carbonyl oxygen atoms, C(7)–O(2), C(8)–O(4), and C(9)–O(5), are shorter than those between the carbon and hydroxyl oxygen atoms, C(7)–O(1), C(8)–O(3), and C(9)–O(6) by an average value of 0.100(7) Å. This supports the fact that the carboxyl hydrogen atoms of hemimellitic acid are definitely associated with hydroxyl oxygen atoms. The carboxyl groups at the 1- and 3-positions twist slightly

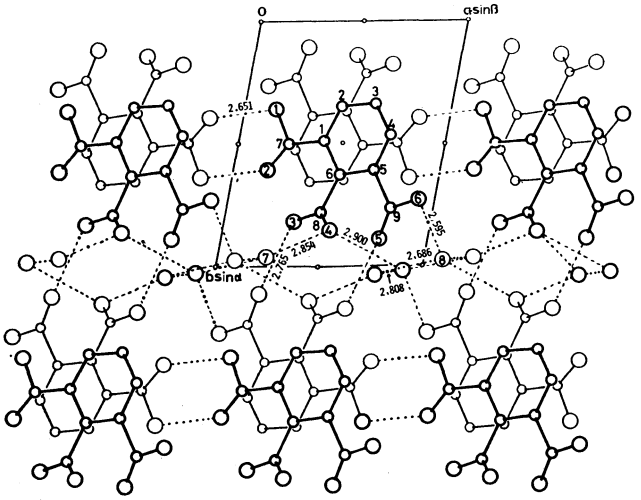

Fig. 5. A view of the crystal structure down the c axis. The hydrogen bonds are shown by broken lines.

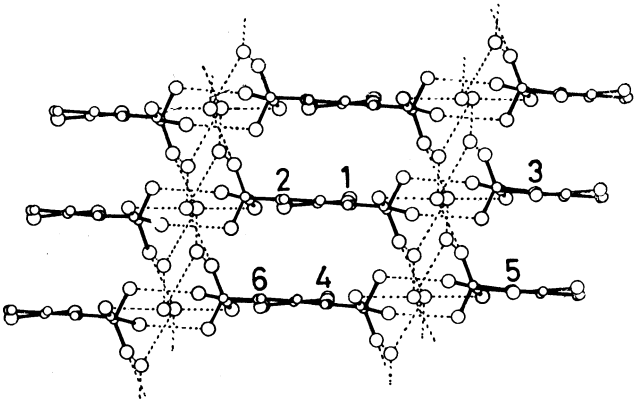

Fig. 6. A view of the crystal structure parallel to the (3 1 $\bar{2}$) plane. The hydrogen bonds are shown by broken lines.

Table 5. Hydrogen bond distances(Å) and angles(degree)

O—H···O	Symmetry	O···O	e. s. d.	O—H	e. s. d.	O···H	e. s. d.	Angle	e. s. d.
O (1)-H (4) ···O (2)	(1, 1, 2)	2.651	0.006	0.87	0.08	1.79	0.08	173	8
O (3)-H (5) ···O (5)	(1, 1, 3)	2.765	0.006	0.60	0.07	2.20	0.07	163	8
O (6)-H (6) ···O (8)	(1, 1, 1)	2.595	0.006	0.88	0.09	1.72	0.09	176	9
O (7)-H (7) ···O (8)	(1, 1, 3)	2.808	0.007	0.99	0.08	1.94	0.08	145	7
O (7)-H (8) ···O (4)	(1, 1, 1)	2.854	0.007	0.96	0.08	1.90	0.08	172	7
O (8)-H (9) ···O (4)	(1, 1, 5)	2.900	0.006	0.73	0.08	2.23	0.08	153	8
O (8)-H (10)···O (7)	(1, 1, 8)	2.686	0.007	1.21	0.08	1.49	0.08	170	7

C=O···H	Symmetry	Angle	e. s. d.	C=O···O	Symmetry	Angle	e. s. d.
C (7)=O (2)···H (4)	(1, 1, 2)	125	3	C (7)=O (2)···O (1)	(1, 1, 2)	125.7	0.4
C (8)=O (4)···H (8)	(1, 1, 1)	123	2	C (8)=O (4)···O (7)	(1, 1, 1)	120.3	0.4
C (8)=O (4)···H (9)	(1, 1, 5)	118	2	C (8)=O (4)···O (8)	(1, 1, 5)	124.5	0.4
C (9)=O (5)···H (5)	(1, 1, 3)	169	2	C (9)=O (5)···O (3)	(1, 1, 3)	169.7	0.4

H···O···O	Symmetry	Angle	e. s. d.	O···O···O	Symmetry	Angle	e. s. d.
H (9)···O (4)···H (8)	(5, 1, 1)	117	3	O (8)···O (4)···O (7)	(5, 1, 1)	113.1	0.2
H (6)···O (8)···H (7)	(1, 1, 3)	83	4	O (6)···O (8)···O (7)	(1, 1, 3)	91.8	0.2

H—O···H	Symmetry	Angle	e. s. d.	O···O···O	Symmetry	Angle	e. s. d.
H (7)-O (7)···H (10)	(1, 1, 9)	119	5	O (8)···O (7)···O (8)	(3, 1, 9)	92.4	0.2
H (8)-O (7)···H (10)	(1, 1, 9)	139	6	O (4)···O (7)···O (8)	(1, 1, 9)	149.0	0.3
H (9)-O (8)···H (6)	(1, 1, 1)	118	7	O (4)···O (8)···O (6)	(5, 1, 1)	131.1	0.2
H (9)-O (8)···H (7)	(1, 1, 3)	138	7	O (4)···O (8)···O (7)	(5, 1, 3)	135.4	0.2
H (10)-O (8)···H (6)	(1, 1, 1)	118	5	O (7)···O (8)···O (6)	(8, 1, 1)	121.3	0.2
H (10)-O (8)···H (7)	(1, 1, 3)	104	4	O (7)···O (8)···O (7)	(8, 1, 3)	87.6	0.2
H (7)-O (7)-H (8)	(1, 1, 1)	101	7	O (8)···O (7)···O (4)	(3, 1, 1)	117.0	0.2
H (9)-O (8)-H (10)	(1, 1, 1)	98	7	O (4)···O (8)···O (7)	(5, 1, 8)	80.0	0.2

[Symmetry code]

1=(x, y, z) 4=(1+x, y, z) 7=(−x, 2−y, −z)
2=(−x, 1−y, −1−z) 5=(1−x, 2−y, 2−z) 8=(1−x, 1−y, 1−z)
3=(1−x, 2−y, 1−z) 6=(1−x, 1−y, −z) 9=(−1+x, −1+y, −1+z)

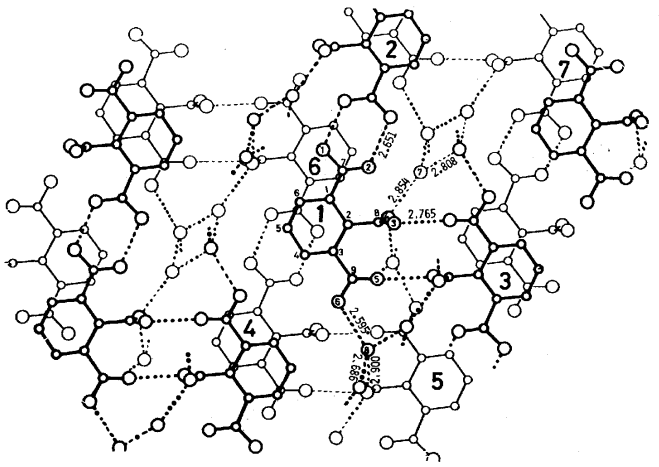

Fig. 7. A view of the erystal structure perpendicular to the (3 1 $\bar{2}$) plane, showing the relative orientation of the plane.

by 4.5° and 10.3° out of the plane of a benzene ring, while the carboxyl group at the 2-position twists greatly, by 86.8° so that the repulsions are reduced among the O(2), O(3), O(4), and O(5) atoms. Hence, the hemimellitic acid molecule has the approximate C_s symmetry in solids.

Molecular Arrangement and Hydrogen-bond System. The crystal structure is shown in Figs. 5, 6, and 7. The distances and angles of the hydrogen bonds are listed in Table 5. The hemimellitic acid molecule and one water molecule are arranged in layers closely parallel to the (3 1 $\bar{2}$) plane, with a spacing of 3.514 Å, except for the O(3), O(4), and H(5) atoms of one carboxyl group, and the O(7), H(7), H(8), H(9), and H(10) atoms of water molecules. The least-squares plane through the non-hydrogen atoms of a hemimellitic acid molecule and a water oxygen atom O(8), except for the O(3) and O(4) atoms, is:

$$-0.9836X-0.1792Y+0.0206Z=-4.8973.$$

The dihedral angle which this plane makes with the (3 1 $\bar{2}$) plane is 6.5°. Figures 6 and 7 show the views parallel to and perpendicular to the (3 1 $\bar{2}$) plane respectively; they illustrate the relative orientation of the molecules in two neighboring layers. In Figs. 5, 6 and 7, the same numerals designate the same molecules. The symmetry codes corresponding to these numbers are shown in Table 5.

Each hemimellitic acid molecule on the same plane is joined through two kinds of hydrogen bonds, with distances of 2.651(6) and 2.765(6) Å, around the center of symmetry with two neighboring molecules and forms a zig-zag chain along the [1 1 2] direction. In the O(3)-H(5)···O(5) hydrogen bond, the C(9)-O(5)···

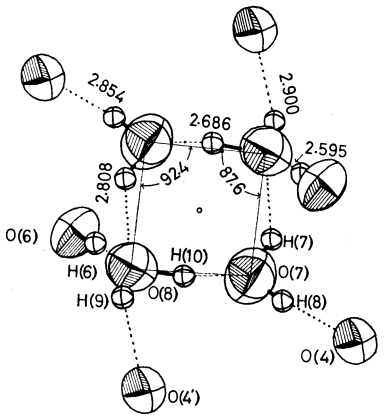

Fig. 8. Perspective view showing the environment of four-membered ring of water molecules. The hydrogen bonds are shown by broken lines.

H(5) and C(9)–O(5)···O(3) hydrogen bonding angles are 169(2)° and 169.7(4)° respectively. These values indicate that the bisector of lone pairs in the carbonyl oxygen atom O(5) is directed toward a hydrogen-bond donor group. Although the hydrogen atom in most of the O–H···O hydrogen bonds interacts with one lone pair of the acceptor oxygen atom, the H(5) atom in this hydrogen bond does so with two lone pairs of the O(5) atom.

The water molecules which lie among these chains are hydrogen-bonded around the center of symmetry to form the four-membered ring. This is a unique example of the four-membered ring being formed only by the use of water oxygen atoms, as is shown in Fig. 8. In this ring, the angles of O···O···O are 87.4° and 92.3°, and the O···O distances are 2.686(7) and 2.808(7) Å. These values show that this ring conformation is an approximate square.

The zig-zag chains of hemimellitic acid molecules are linked to each other by three kinds of hydrogen bonds with the distances of 2.595(6), 2.854(7), and 2.900(6) Å, through the medium of the four-membered ring of water molecules, thus forming the three-dimensional network.

It may be noted that the structure of hemimellitic acid dihydrate contains all the types of O–H···O hydrogen bonds among the water molecules and carboxyl groups. The observed seven hydrogen bonds can be classified by means of the combination of the donor and acceptor groups in five types, as is shown in Fig. 9. The (a) type is the most popular hydrogen bond in carboxylic acids. However, this type was not found in hydrate compounds, such as pyromellitic acid dihydrate and oxalic acid dihydrate. The observed distance, 2.651 (6) Å, is quite normal and is shorter than that of the (b) type, 2.765 Å. Types (b), (c) and (d) are found in pyromellitic acid dihydrate, which is the only hydrate compound in the crystal structures of benzene-carboxylic acids determined hitherto. The agreements between the hydrogen bonding distances, and between the hydrogen bonding angles of hemimellitic acid dihydrate and those of pyromellitic acid dihydrate, are quite good; these values are listed

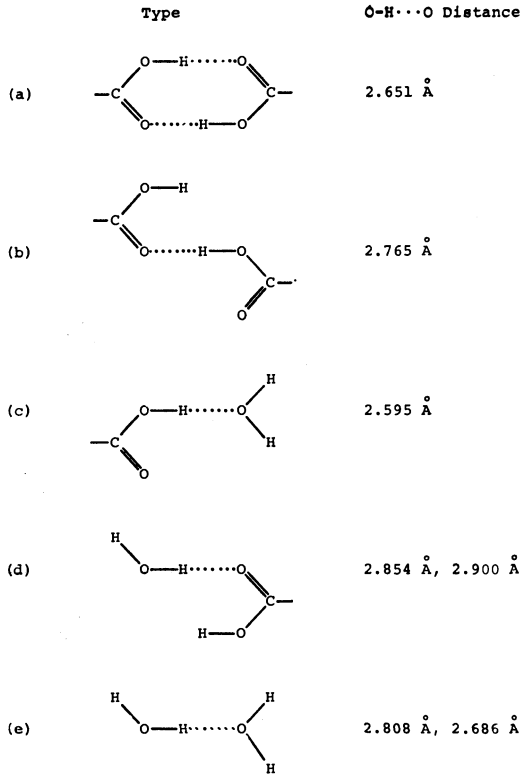

Fig. 9. The types of hydrogen bonds among the carboxyl groups and water molecules.

Table 6. Comparison of hydrogen bond distances and angles

Distance	HMA	PMA	OXA
O (5) ··· O (3)	2.765 Å	2.687 Å	— Å
O (4) ··· O (7)	2.854	2.807	2.864
O (4) ··· O (8)	2.900	2.876	2.883
O (6) ··· O (8)	2.595	2.549	2.512
Angle			
C (9) = O (5) ··· O (3)	169.7°	152.2°	— °
C (8) = O (4) ··· O (7)	120.3	120.2	127.0
C (8) = O (4) ··· O (8)	124.5	146.2	136.3
O (7) ··· O (4) ··· O (8)	113.1	93.7	96.7
O (6) ··· O (8) ··· O (7)	121.3	130.3	134.7
O (6) ··· O (8) ··· O (7′)	91.8	107.1	119.4
O (7) ··· O (8) ··· O (7′)	87.6	86.3	83.3

HMA = Hemimellitic acid dihydrate (This study)
PMA = Pyromellitic acid dihydrate (Ref. 3)
OXA = α-Oxalic acid dihydrate (Ref. 11)

with those of α-oxalic acid dihydrate[12] in Table 6. In the (b) type, the hydrogen bonding angle, C=O···O, is significantly larger than 120°. Those angles in hemimellitic acid dihydrate, pyromellitic acid dihydrate, and dipicolinic acid monohydrate[13] are 169.7°, 152.2°, and 170.6°. Both (c) and (d) types are often found in carboxylic-acid hydrates. The hydrogen-bond distances of these two types are distinctly

12) R. G. Delaplane and J. A. Ibers, *Acta Crystallogr.*, **B25**, 2423 (1969).

13) F. Takusagawa, K. Hirotsu and A. Shimada, This Bulletin, **46**, 2020 (1973).

different from each other. Most of the water oxygen atoms in the (c) type act as one acceptor of a short hydrogen bond. However, in the present compound, the water oxygen atom acts as an acceptor from two donors. This fact may cause the differences in the hydrogen bonding distances and angles in comparison with pyromellitic acid dihydrate. The carboxyl oxygen atom in the (d) type participates in two long hydrogen bonds with waters as donor groups; these bonds have the approximately equal distances. Types (c) and (d) reveal the remarkable feature of a hydrogen bond between the water molecule and carboxyl group.

Computer Programs. All the calculations were performed on a FACOM 270-30 computer at the Computer Center of Osaka City University by the use of the following programs: RSLC-3 (cell constant),[14] RSSFR-3 (Fourier synthesis),[15] HBLS-IV (block-diagonal least-squares refinement),[16] DAPH (bond length, bond angle, and least-squares plane),[17] SCALE (film factor, Lp and layer scaling),[18] TE-I (thermal ellipsoid),[19] and CNINDO (CNDO and INDO calculations).[10]

The authors wish to express their thanks to Dr. Kichisuke Nishimoto of this faculty for his useful advice on the CNDO calculation. The authors are also indebted to Mr. Ken Hirotsu for his useful advice.

14) T. Sakurai, The Universal Crystallographic Computing System (I) edited by T. Sakurai, p. 18, The Crystallographic Society of Japan, 1967.
15) T. Sakurai, *ibid.*, p. 45.
16) T. Ashida, *ibid.*, p. 65.
17) T. Ashida, *ibid.*, p. 76.
18) H. Yoshioka, K. Hirotsu, and F. Takusagawa, Unpublished work.
19) F. Takusagawa, Unpublished work.

BULLETIN OF THE CHEMICAL SOCIETY OF JAPAN, VOL. 46, 3004—3007 (1973)

The Ultrasonic Velocity and the Absorption of Aqueous *t*-Butyl Alcohol Solutions in Relation to the Structures of Water and Solutions

Harumi ENDO and Otohiko NOMOTO

Department of Applied Physics, Defense Academy, Yokosuka 239

(Received March 30, 1973)

The adiabatic compressibility *vs.* concentration curves in aqueous solutions of *t*-butyl alcohol (*t*-Bu) over a certain temperature range have a common intersection at a fixed concentration (μ_c^β). The sound absorptions of solutions are nearly constant and are independent of the concentration up to a concentration (μ_1^α) nearly the same as the μ_c^β. On the basis of the value of $\mu_c^\beta(\cong\mu_1^\alpha)$, the properties and the dissolved state of *t*-Bu in liquid water discussed in terms of the liquid clathrate hydrate model. At this concentration, the liquid clathrate hydrate of *t*-Bu consists of 18-hedron, containing 32 water molecules for each *t*-Bu molecule. For higher concentrations than μ_c^β, the breakdown of the liquid clathrate hydrate by the addition of excess *t*-Bu occurs, accompanied by an increase in the number of clusters.

In previous papers,[1,2] the sound velocity (V), the density (ρ), and the adiabatic compressibility (β) in aqueous solutions of nonelectrolytes have been investigated as functions of the concentration (μ: mole fraction). For each aqueous solution, it has been found that the V-μ curves and β-μ curves have common intersections at the fixed concentrations of μ_c and μ_c^β respectively, the sound velocity (V_c) and the compressibility (β_c) at these concentrations being independent of the temperature over a certain range (ΔT_c^V and ΔT_c^β) respectively.

From the temperature dependency of the β-μ curves in these systems, it can be concluded that the structural unit termed "liquid clathrate hydrate" with a composition of μ_c^β or r_c^β=(water/solute) does exist for various aqueous systems.

A number of papers have been published on the ultrasonic absorption (α) in aqueous solutions of nonelectrolytes—alcohol homologs,[3-6] substituted alcohols,[7,8] urea and its derivatives,[9] acetone,[3] dioxane,[3,10,11] dioxolane,[12] amines,[13,14] *etc.*; the main interest is, however, the behavior of an absorption peak in the α-μ curve. Blandamer *et al.* have pointed out that the sound absorption for some aqueous systems—alcohols,[4,5] substituted alcohols,[7] dioxolane,[12] amine[13]—in a lower concentration range is

1) H. Endo, This Bulletin, **46**, 1106 (1973).
2) H. Endo, *ibid.*, **46**, 1586 (1973).
3) C. J. Burton, *J. Acoust. Soc. Amer.* **20**, 186 (1948).
4) M. J. Blandamer, N. J. Hiden, M. C. R. Symons, and N. C. Treloar, *Trans. Faraday Soc.*, **64**, 3242 (1968).
5) M. J. Blandamer, D. E. Clarke, N. J. Hidden, and M. C. R. Symons, *ibid.*, **64**, 2691 (1968).
6) L. R. O. Storey, *Proc. Phys. Soc.*, **65B**, 943 (1952).
7) M. J. Blandamer, N. J. Hidden, M. C. R. Symons, and N. C. Treloar, *Trans. Faraday Soc.*, **64**, 1805 (1968).
8) J. Thamsen, *Acustica*, **16** 14 (1965/66).
9) K. Sasaki and K. Arakawa, This Bulletin, **42**, 2485 (1969).
10) K. Arakawa and N. Takenaka, *ibid.*, **42** 5 (1969).
11) G. G. Hammes and W. Knoche, *J. Chem. Phys.*, **45**, 4041 (1966).
12) M. J. Blandamer, N. J. Hidden, K. W. Morcom, R. W. Smith, N. C. Treloar, and M. J. Wooten, *Trans. Faraday Soc.*, **42**, 2633 (1969).
13) M. J. Blandamer, N. J. Hidden, and M. C. R. Symons, *ibid.*, **66**, 316 (1970).
14) R. N. Barfield and W. G. Schenider, *J. Chem. Phys.*, **31**, 488 (1959).

relatively insensitive to the compositions of the solutions (see also Thamsen[8]). Above this concentration, the value of α increases rapidly, reaches a maximum, and then gradually decreases to a lower value of α. According to Blandamer *et al.*,[4,5,7,12,13] this behavior of the α-μ curve in the lower concentration range is attributable to the formation of a clathrate in a solution. In one group of theories, the absorption peaks are explained in terms of a chemical relaxation process (*cf.* Andrea *et al.*[15]) involving the formation and decomposition of associated complexes, but the behavior of the α-μ curve in the lower concentration range can not be interpreted in terms of this mechanism.

In the present work, the acoustical properties of an aqueous solution of *t*-Bu have been studied both for the sound velocity and the absorption. It was found that the concentration (μ_1^{α}) at the sudden increase of the α-μ curve corresponds to μ_c^{β}. On the basis of this result, we will report that the low-concentration absorption-behavior of a *t*-Bu solution can also be explained on the basis of the liquid clathrate hydrate model used for the explanation of the behavior of β.

Experimental

Materials. Water was purified by two distillations. In order to purify the *t*-Bu, the reagent-grade product was refluxed with calcium oxide and then distilled.

Ultrasonic Apparatus. The ultrasonic pulse method was used for the absorption measurement. The absorption coefficients were determined at 60 MHz, and the mean value of 5~9 measurements was used. A crystal-controlled ultrasonic interferometer operating at a frequency of 5 MHz was used for the velocity measurements. The experimental error for the absorption data was about ±2%, and the overall accuracy of the sound velocity data was within ±0.2 m/s.

Measurements of Viscosity and Density. The viscosity coefficient (η) was measured for aqueous solutions by means of a modified Ostwald capillary viscometer. The density measurement was made by means of an Ostwald-type pycnometer. All the measurements were carried out between 20° and 50 °C at 5.0±0.1 °C intervals.

Classical Absorption Coefficient (α_η). The α_η at frequency (f) was calculated by the relation:

$$\alpha_\eta/f^2 = \frac{8\pi^2\eta}{3\rho V^3}$$

Results

Ultrasonic Velocity. In Fig. 1, the sound velocity is plotted against the mole fraction for aqueous solutions of *t*-Bu. The intersection point of V-μ curves for various temperatures converges to one point (μ_c^V= 0.032), at which V_c is constant (=1601 m/s) in this temperature range (20—35 °C). The parameters, V_c, μ_c^V, v_c^V, r_c^V, and ΔT_c^V, were obtained from Fig. 1; they are summarized in the left-hand half of Table 1. Here the notations used were the same as those used in Refs. 1 and 2.

15) J. H. Andreae, P. D. Edmonds and J. F. McKellar, *Acustica*, **15**, 74 (1965).

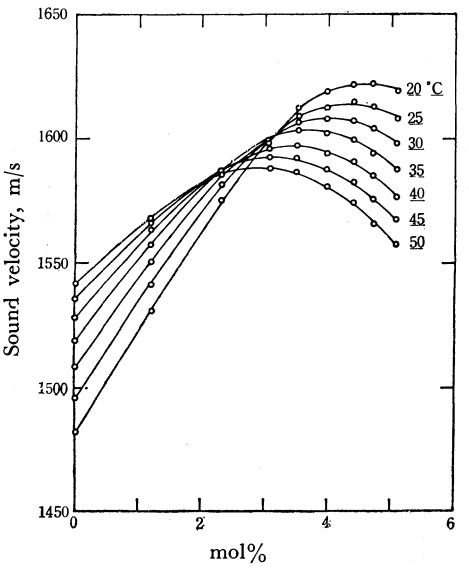

Fig. 1. Concentration dependence of sound velocity.

Table 1. Data concerning V-μ curve and β-μ curve of aqueous *t*-Bu solutions

	Sound velocity		Adiabatic compressibility
V_c	1601 m/s	β_c	40.0×10^{-12} cm²/dyn
μ_c^V	3.2 mol%	μ_c^β	3.0 mol%
v_c^V	14.7 vol.%	v_c^β	13.9 vol.%
r_c^V	30	r_c^β	32
ΔT_c^V	20—35 °C	ΔT_c^β	20—35 °C

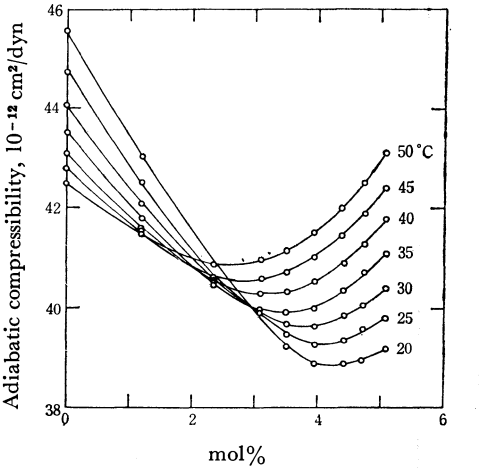

Fig. 2. Concentration dependence of adiabatic compressibility.

Adiabatic Compressibility. In Fig. 2, the adiabatic compressibility is plotted against the mole fraction for aqueous solutions of *t*-Bu. It is found that the β-μ curves at various temperatures intersect at one common point (μ_c^β=0.030), at which β_c is constant ($=40.0\times10^{-12}$ cm²/dyn). The values of β_c, μ_c^β, r_c^β, v_c^β, and ΔT_c^β are shown in the right-hand half of Table 1. The behavior of the V-μ and β-μ curves for various temperatures is similar to that of other nonelectrolytes.[1,2]

Viscosity and Classical Absorption Coefficients. The

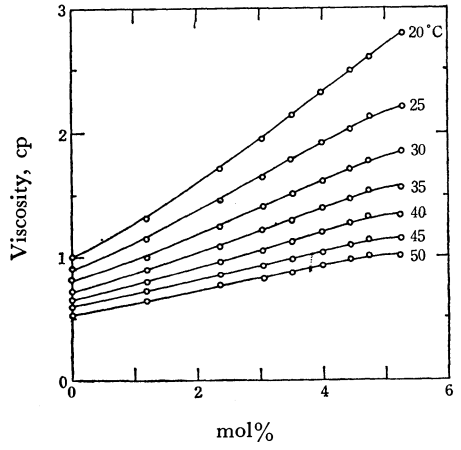

Fig. 3. Concentration dependence of viscosity.

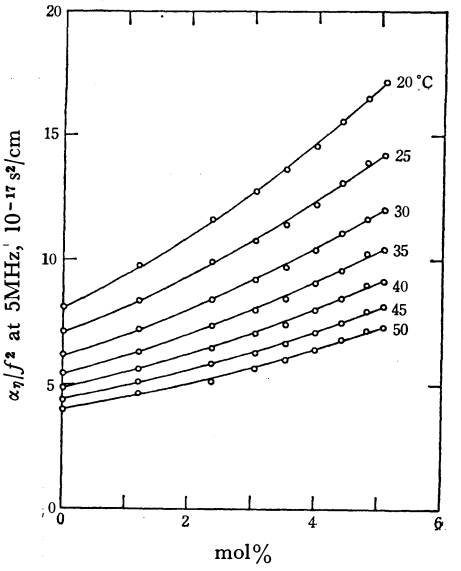

Fig. 4. Concentration dependence of classical absorption.

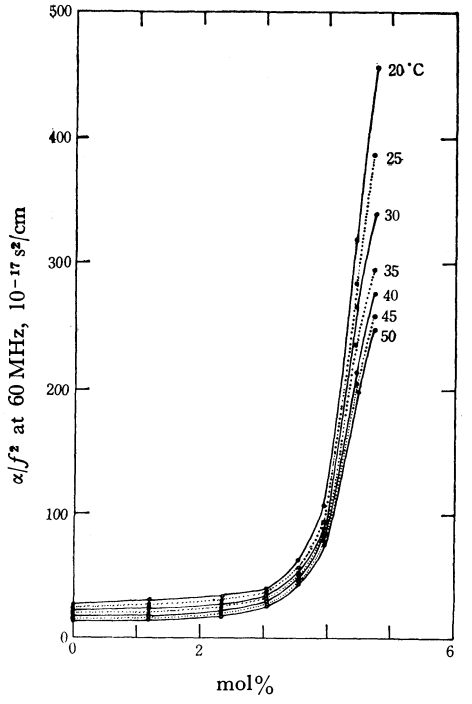

Fig. 5. Concentration dependence of sound absorption.

η-μ curves are shown in Fig. 3. The values of η at various temperatures increased monotonously with an increase in the concentration. The classical absorption coefficients (α_η/f^2) are shown in Fig. 4. The behavior of the α_η/f^2-μ curves at various temperatures is almost like that of the η-μ curves.

Ultrasonic Absorption Coefficients. The α/f^2-μ curves are given in Fig. 5. It is seen that α/f^2 was relatively insensitive to the change in μ in a low concentration range, and that it increased suddenly at a definite concentration. This limiting concentration is denoted by μ_1^a. It is seen that $\mu_1^a \cong 0.03$ mole fraction for the 20—35 °C temperature range, and that it decreases slightly in the higher temperature range ($\mu \cong 0.02$ for 40—50 °C). In the 20—35 °C temperature range, the value of μ_1^a for the α/f^2-μ curves coincides with that of μ_c^β for the β-μ curves. The behavior of the excess absorption ($\Delta\alpha/f^2=\alpha/f^2-\alpha_\eta/f^2$) is not significantly different from that of α/f^2 alone.

Discussion

The experimental results shown above can be interpreted in terms of the same model of aqueous non-electrolyte solutions as was employed in previous papers.[1,2] In our model, μ_c^β corresponds to the concentration where $d\beta_{st}/dT$ (β_{st}=structural compressibility) becomes zero. Solute molecules are accommodated in water clusters without changing their size and ice-1 structure up to this concentration. Therefore, the β_{st} of the solution decreases with an increase in the concentration up to this point, thus keeping the water-cluster structure intact. On the other hand, the β_∞(instantaneous compressibility) is constant and $d\beta_\infty/dT=0$ up to this concentration in order to keep the number of water cluster constant. We have seen[1,2] that the ratio r_c^β(=water/solute) at this concentration, μ_c^β, corresponds to the specific molecular ratios for some clathrate-making substances, and we assumed that the "liquid clathrate hydrate" exists at this composition. Here, the β_{st} of the "water-solute-cluster" at the composition of r_c^β is small, but this value is not zero since the size of this "water-solute-cluster" is significantly larger than that of this structure unit. Beyond this concentration, the number of clusters increases, resulting in a decrease in their mean size. This increase in the number of clusters takes place slowly, accompanying a decrease in β_{st} up to the concentration of $d\beta/d\mu=0$, at which the "water-solute-cluster" is destroyed separately. This is also accompanied by an increase in the β_∞($d\beta_\infty/dT>0$).

Now that the r_c^β for *t*-Bu—water system becomes 32, as was observed for tetra-ethyl ammonium chloride, the shape of the clathrate was assumed to be 18-hedron. (The solid clathrate hydrate of this composition of the *t*-Bu—water system is not known, but a "double hydrate" with help gas (H_2S) of the $16X8Y136H_2O$ (X=H_2S and Y=*t*-Bu) composition is known).

The above finding, that the ultrasonic absorption remains nearly constant, that it is not very different from that of water in the lower concentration range, and that it increases rather rapidly from a certain

concentration $\mu_1^{\alpha}(\cong\mu_c^{\beta})$, is of prime importance in elucidating the mechanism of the ultrasonic absorption in aqueous nonelectrolyte systems. This behavior is not explicable on the basis of the reaction-type theory[14,15] between a solute and solvent molecules. It can, however, be explained easily, at least qualitatively, on the basis of the "entropy of mixing"-type diffusion-theory[16,17] of sound absorption in aqueous systems if we employ the same model of the aqueous systems as was employed previously[1,2] in explaining the behavior of the sound velocity and the adiabatic compressibility. According to this theory,[16,17] the excess sound absorption in aqueous nonelectrolytes arises from the irreversible entropy production caused by the diffusion of solutes into the groups of water molecules produced by the collapse of water-clusters under sound pressure. If we assume that the solute molecules are all incorporated in water-clusters up to the concentration of μ_c^{β} as has been assumed previously,[1,2] almost no diffusion can be expected when some of the clusters are collapsed under the sound pressure, because the collapse of clusters does not accompany a local concentration change. This explains the initial concentration-independent part of the absorption curves. The increase in ultrasonic absorption beyond $\mu_c^{\beta}(\cong\mu_1^{\alpha})$ is to be expected, because free solute molecules or smaller clusters of different compositions are present at higher concentrations, as has been assumed previously.[1,2]

16) O. Nomoto, *J. Phys. Soc. Japan*, **11**, 827 (1956).
17) O. Nomoto, *ibid.*, **12**, 300 (1957).

We[1,2] ourselves have also previously pointed out that when V_c and β_c are plotted as functions of v_c^V and v_c^{β} respectively, the various solutes can be classified into three groups according to the shapes of the curves. Here, v_c^V and v_c^{β} indicate the volume fractions corresponding to μ_c^V and μ_c^{β} at 20 °C respectively.

The first group (I) consists of the urea-homolog series, hexamethylenetetramine, and glycerine. The molecules of the solutes belonging to this group collaborate in making the framework of water constituent part of liquid water. The sound velocity, V_c, and v_c^V and the adiabatic compressibility, β_c, at v_c^{β} for this series of solutes are represented by:

$$V_c = 403\,v_c^V + 1547 \text{ (m/s)}$$

$$\beta_c = (45.6-42.7\,v_c^{\beta})\times 10^{-12} \text{ (cm}^2\text{/dyn)}$$

respectively.

The second group (II) consists of formamide, acetamide, and the alcohol homolog series except for the lowest-molecular-weight substances in each homolog. These solutes only fill up the cavity of the liquid water structure. The V_c *vs.* v_c^V and β_c *vs.* v_c^{β} relations for this group are represented, respectively, by:

$$V_c = 1143\,v_c^V + 1390 \text{ (m/s)}$$

$$\beta_c = (77.5-236.7\,v_c^{\beta})\times 10^{-12} \text{ (cm}^2\text{/dyn)}$$

The third group (III) consists of the lowest-molecular-weight substances in each homolog series. This group will presumably have intermediate properties between Groups (I) and (II).

Notice that *t*-Bu, although of the alcohol homolog series, belongs to Group (I).

BULLETIN OF THE CHEMICAL SOCIETY OF JAPAN, VOL. 46, 3007—3011 (1973)

ESR Evidence for the Destruction of the Four-membered Chelate Structure of Bis(*O,O'*-diethyldithiophosphato)oxovanadium(IV) by Pyridine Bases

Mitsuo SATO, Yuzaburo FUJITA, and Takao KWAN

Faculty of Pharmaceutical Sciences, The University of Tokyo, Bunkyo-ku, Tokyo 113

(Received March 31, 1973)

The interaction of bis(*O,O'*-diethyldithiophosphato)oxovanadium(IV), $VOdtp_2$, with pyridine bases has been studied in toluene by ESR. It has been found that the four-membered chelate structure of $VOdtp_2$ is disrupted by pyridine bases to form the complex species identified as $VOdtp_2 \cdot Py$ and $VOdtp_2 \cdot Py_2$ by their characteristic ESR spectra. The coordination structures of the newly-formed complexes are discussed in association with the substitution equilibria involved.

It is well known that square pyramidal oxovanadium(IV) complexes coordinated with bidentate ligands form 1 : 1 adducts in solutions with a variety of bases according to this expression:[1]

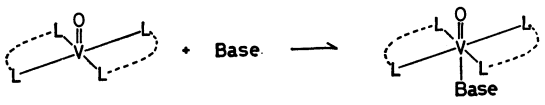

For example, the base adducts of bisacetylacetonato oxovanadium(IV) have been worked out[2] and the effects of adduct formation on the optical absorption and ESR spectra have also been reported.[3]

We have made an ESR investigation of the reaction of bis(*O,O'*-diethyldithiophosphato)oxovanadium(IV),

1) J. Selbin, *Chem. Rev.*, **65**, 153 (1965).

2) A. Rosenheim and H. Yu Mong, *Z. Anorg. Chem.*, **148**, 34 (1925); M. M. Jones, *J. Amer. Chem. Soc.*, **76**, 5995 (1964); R. T. Claunch, T. W. Martin, and M. M. Jones, *ibid.*, **83**, 1073 (1961); K. Nakamoto, Y. Morimoto, and A. E. Martell, *ibid.*, **83**, 4533 (1961); J. Selbin, H. R. Manning, and G. Cessac, *J. Inorg. Nucl. Chem.*, **25**, 1253 (1963).

3) I. Bernal and P. H. Rieger, *Inorg. Chem.*, **2**, 256 (1963); J. Selbin and T. R. Ortolano, *J. Inorg. Nucl. Chem.*, **26**, 37 (1964); R. L. Carlin and F. A. Walker, *J. Amer. Chem. Soc.*, **87**, 2128 (1965); F. A. Walker, R. L. Carlin, and P. H. Rieger, *J. Chem. Phys.*, **45**, 4181 (1966).

$VOdtp_2$, with pyridine bases. As a result, we found that pyridine bases displace equatorial sulfur ligands, leading to the partial destruction of the four-membered chelate rings, as is indicated below:

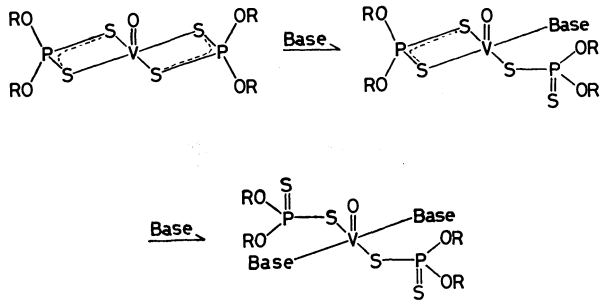

In the present report, we wish to describe the evidence for the destruction of the chelate structure, together with the characteristics of this reaction, since no such type of reaction has yet been reported for oxovanadium complexes.

Experimental

Materials. *O,O'*-Diethyldithiophosphoric acid (dtpH) was prepared as has been described previously.[4] Vanadyl sulfate hydrate ($VOSO_4 \cdot nH_2O$) was obtained from the Kishida Kagaku Co. Toluene and pyridine (G.R. Grade, Wako Junyaku Kogyo Co.) were purified by distillation from calcium hydride and potassium hydroxide respectively. All the other reagents used were of a G.R. grade and were also obtained commercially.

Preparation of Bis(O,O'-diethyldithiophosphato)oxovanadium(IV), $VOdtp_2$. Vanadyl sulfate hydrate was treated with sodium carbonate, and the precipitate was filtered and washed with distilled water until free of sodium sulfate. The precipitate was immediately added to an isopentane solution of dtpH under a flow of dry nitrogen. The suspended mixture was then stirred at room temperature until the precipitate almost dissolved. The resulting purple solution was filtered; the filtrate was then cooled by the rapid evaporation of isopentane with a vigorous flow of nitrogen to separate out a crystalline solid. The repeated recrystallization of the solid from isopentane under an atmosphere of nitrogen gave blue-purple, needle-like crystal. (Anal. Calcd. for $VO[S_2P(OC_2H_5)_2]_2$: C, 21.97; H, 4.61; V, 11.64%. Found: C, 22.12; H, 4.69; V, 11.90%.).

Measurements of the ESR Spectra. Since toluene and pyridine solutions of $VOdtp_2$ were unstable to air, all the measurements were carried out on sample solution carefully prepared in an atmosphere of nitrogen or *in vacuo*. The ESR spectra were recorded both at room temperature and at 77 K with JEOL spectrometers, Model P-10 and ME-1X (X-band), using 100 KHz field modulation. The magnetic field was calibrated with an ESR marker, MgO : Mn^{2+} powder, supplied by JEOL. Powdered DPPH was used as the reference in the determination of the *g*-values.

Results and Discussion

Interpretation of ESR Spectra and Structures of Oxovanadium Complexes in Solutions. Toluene solutions containing $VOdtp_2$ and pyridine bases in various mole ratios, as well as toluene and pyridine solutions of $VOdtp_2$, were subjected to ESR measurements both at room temperature and at 77 K. Typical ESR spectra thus obtained are illustrated in Figs. 1 and 2, while the ESR parameters calculated by the method of Kivelson and Lee[5] are presented in Table 1.

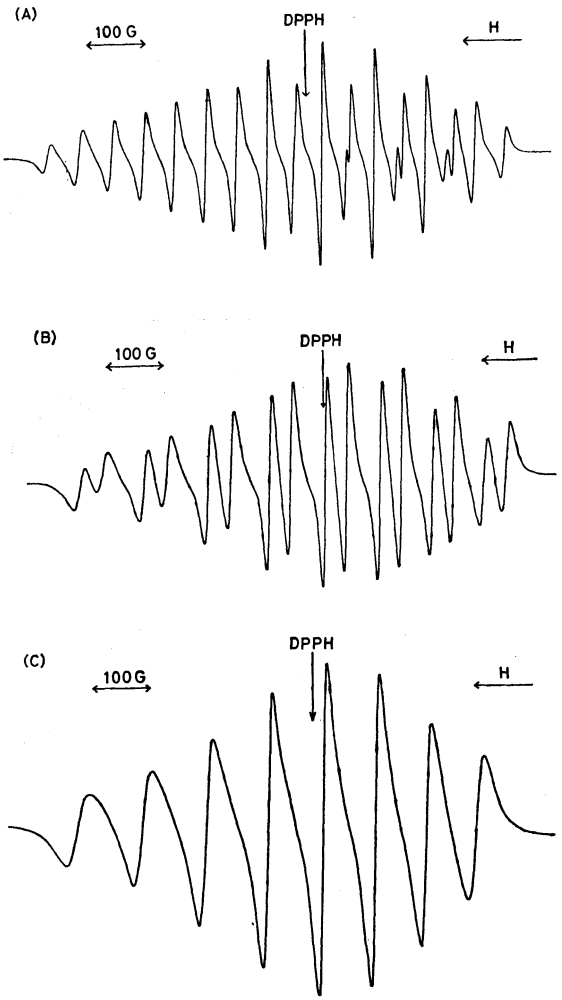

Fig. 1. ESR spectra of toluene-pyridine solutions of $VOdtp_2$ at room temperature.
(A) $VOdtp_2$ in toluene, $[VOdtp_2]=0.012$ M;
(B) $VOdtp_2$-pyridine in toluene, $[VOdtp_2]=0.018$ M, [pyridine] = 0.36 M;
(C) $VOdtp_2$ in pyridine, $[VOdtp_2]=0.024$ M.

$VOdtp_2$ in Toluene Solution: As is illustrated in Figs. 1–A and 2–A, a toluene solution of $VOdtp_2$ gave spectra quite similar to those previously reported[6,7] for $VOdtp_2$ in non-coordinating solvents. It can be seen from Figs. 1–A and 2–A that eight hf lines characteristic of the

4) M. Sato, M. Yanagita, Y. Fujita, and T. Kwan, This Bulletin, **44**, 1423 (1971).

5) D. Kivelson and S. K. Lee, *J. Chem. Phys.*, **41**, 1896 (1964).

6) N. S. Garif'yanov and B. M. Kozyrev, *Teor. Eksp. Khim.*, **1**, 525 (1965); N. S. Garif'yanov, B. M. Kozyrev, and I. F. Gainnulin, *Zh. Strukt. Khim.*, **9**, 529 (1968); I. V. Obchinnikov, I. F. Gainnulin, N. S. Garif'yanov, and B. M. Kozyrev, *Dokl. Akad. Nauk SSSR*, **191**, 395 (1970); R. G. Cavell, E. D. Day, W. Byers, and P. M. Watkins, *Inorg. Chem.*, **11**, 1591 (1972).

7) J. R. Wasson, *ibid.*, **10**, 1531 (1971); M. Sato, M. Yanagita, Y. Fujita, and T. Kwan, Preprints of 10th Electron Spin Resonance Symp. Japan, Osaka (1971), p. 59.

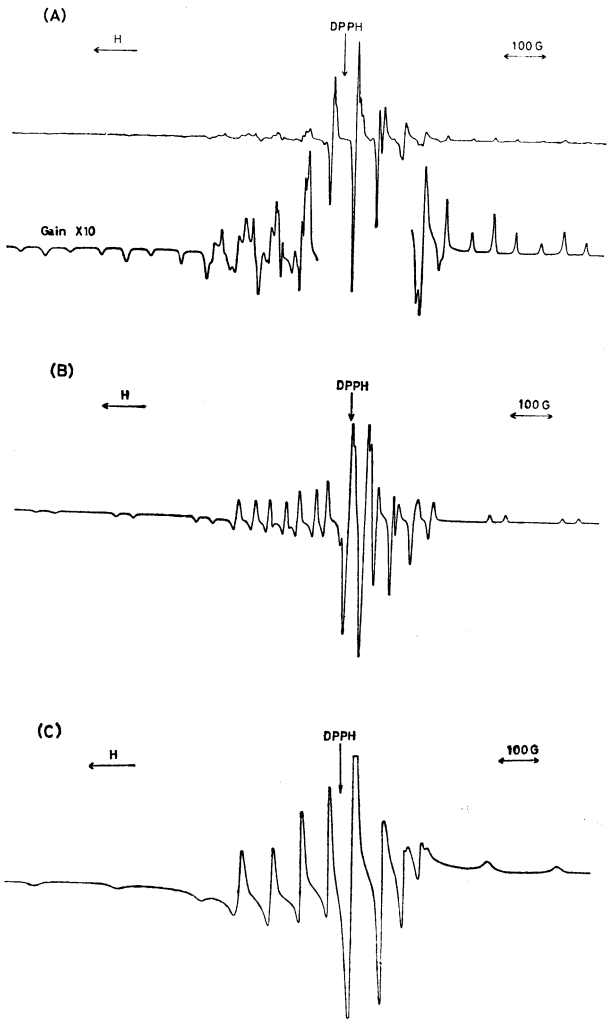

Fig. 2. ESR spectra of toluene-pyridine solutions of $VOdtp_2$ at 77 K.
(A) $VOdtp_2$ in toluene, $[VOdtp_2]=0.012$ M;
(B) $VOdtp_2$-pyridine in toluene, $[VOdtp_2]=0.012$ M, [pyridine]$=0.062$ M;
(C) $VOdtp_2$ in pyridine, $[VOdtp_2]=0.024$ M.

vanadium nucleus ($I=7/2$) are further split into three components with the intensity ratio of 1 : 2 : 1, probably by means of the shf interaction with the two equivalent phosphorus nuclei ($I=1/2$). The ESR parameters (Table 1) are in good agreement with those obtained by previous workers.[6,7]

On the other hand, it has already been suggested[6,7] that $VOdtp_2$ has a tetragonal pyramidal structure which can be depicted as:

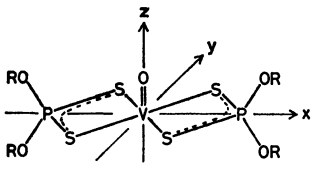

[I] $VOdtp_2$

Such a structural model seems to be quite reasonable, since this is the basic type of coordination known for many oxovanadium(IV) complexes[8] and since dithiophosphate ligands have, in general, a great tendency to form a four-membered chelate structure with metal ions.

Furthermore, the suggested structure [I], which possesses a local symmetry of C_{2v},[9] can well satisfy the ESR parameters shown in Table 1. The g-values and vanadium hf constants are in good agreement with the theory that assumes a single unpaired electron located in an A_1 orbital mainly consisting of the vanadium $3d_{x^2-y^2}$ orbital.[5,10] The isotropic phosphorus constant ($a^P=51$ Gauss) can also be interpreted in terms of a direct vanadium($3d_{x^2-y^2}$)– phosphorus(3S) interaction.[7] It is important for us to note that the vanadium $3d_{x^2-y^2}$ orbital possesses the correct symmetry so as to interact directly with the two equivalent phosphorus 3s orbitals.

Our interpretation of the ESR spectra of $VOdtp_2$ in toluene is, in fact, in good agreement with those given by the previous workers and can be taken to furnish further support for the proposed structure [I]. We have, however, noted that such a structure is valid only when $VOdtp_2$ is present in non-coordinating solvents.[11]

$VOdtp_2$-Pyridine Bases in Toluene Solutions: When a certain amount of pyridine bases, such as pyridine, 4-methylpyridine, and 4-cyanopyridine, was added to a toluene solution of $VOdtp_2$, the spectra shown in Figs. 1–A and 2–A were replaced by the spectra characterized by 16 resonance lines. Typical examples are illustrated in Figs. 1–B and 2–B. It seems to us that such spectra are quite a new type of spectra. However, these spectra can easily be explained if the shf interaction due to one phosphorus nucleus split each of the eight vanadium hf lines into two components equal in intensity. In accordance with this assumption, the liquid solution spectrum (Fig. 1–B) consists of 16 resonance lines, while the frozen solution spectrum (Fig. 2–B) consists of two sets of 16 resonance lines, corresponding to the parallel and perpendicular directions ($g_\parallel$ and $g_\perp$).

The intensity of the 16-line spectrum was examined at room temperature as a function of the concentrations of the pyridine bases. The intensities of the 16-line spectrum relative to the 24-line spectrum[12] were found to be strongly dependent upon the mole ratios of the pyridine bases to $VOdtp_2$ in solutions. For example, the gradual addition of pyridine to a toluene solution of $VOdtp_2$ brought about a progressive decrease in the intensity of the 24-line spectrum, accompanied by a simultaneous appearance of the 16-line spectrum; the superimposed spectra of the 16- and 24-line spectra with comparable intensities were observ-

8) R. J. Clark, "The Chemistry of Titanium and Vanadium," Elsevier Publishing Co., New York (1968), p. 202.

9) The ligand field can be considered as a strong C_{4v} component with a perturbation lowering the symmetry to C_{2v}.

10) B. R. McGarvey, *Transition Metal Chemistry*, **3**, 89 (1966).

11) We have been unable to observe such spectra as are shown in Figs. 1-A and 2-A for $VOdtp_2$ dissolved in coordinating solvents, such as methyl alcohol, ethyl alcohol, diethylether, and tetrahydrofuran. This indicates that $VOdtp_2$ is highly reactive toward the coordinating solvents to be converted into another complex species. Further study along this line is now in progress.

12) The spectrum shown in Fig. 1–A is conveniently denoted as the "24-line spectrum," although fewer than the 24 expected lines are resolved because of line overlappings.

ed when the mole ratio of [pyridine]/[$VOdtp_2$] was around 2; the 24-line spectrum completely disappeared to give such a typical 16-line spectrum as is shown in Fig. 1–B when the [pyridine]/[$VOdtp_2$] ratio reached more than 10. A further increase in the [pyridine]/[$VOdtp_2$] ratio beyond 100, however, caused a decrease in the intensity of the 16-line spectrum, with an appearance of the 8-line spectrum, as will be described below.

On the other hand, Job's method of continuous variations, as applied to the $VOdtp_2$–pyridine base system at room temperature, showed that the intensity of the 16-line spectrum reached a maximum at about 50 mol% of the pyridine base. It is thus evident that one mole of $VOdtp_2$ reacts with one mole of the pyridine base to form a complex species, which then gives rise to the 16-line spectrum. It seems, therefore, probable that the complex species may result either from the addition of the pyridine base to the open coordination position of $VOdtp_2$ or from the displacement of the sulfur ligand by the pyridine base, and that the complex species may have a stoichiometry of $VOdtp_2$·Py, where Py denotes the pyridine base.

On the basis of the above considerations, we can now discuss the following structural models:

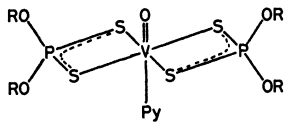

[II] $VOdtp_2$·Py

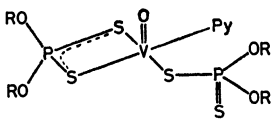

[III] $VOdtp_2$·Py

where it is assumed that the pyridine base in [II] is weakly coordinated as the sixth ligand, while the pyridine base in [III] is rather strongly coordinated as an equatorial ligand and the sulfur ligand displaced by the pyridine base is free or weakly coordinated to the axial site *trans* to the oxygen atom.

Both of the presumed models are compatible with the *g*-values and vanadium hf constants obtained (Table 1), if these structures are taken to have an approximate symmetry of C_{2v} with the electronic ground state of $^2A_1$, having an unpaired electron mainly in the vanadium $3d_{x^2-y^2}$ orbital, as in the case of $VOdtp_2$[I].

However, the observed shf splitting due to one phosphorus nucleus is in accord with the [III] structure rather than the [II] structure, because it can be expected from [II] that the two phosphorus nuclei take part in the shf interaction equivalently. On the other hand, one can reasonably expect from [III] that only the phosphorus nucleus located in the direction of the lobes of the vanadium $3d_{x^2-y^2}$ orbital contributes to the shf splitting, while the other phosphorus nucleus does not give rise to the resolved shf splitting because of its situation removed from interaction with the vanadium $3d_{x^2-y^2}$ orbital.

It is interesting to note that the isotropic shf constant (a^P=37 Gauss) for $VOdtp_2$·Py[III] is decreased considerably as compared with that (a^P=51 Gauss) found for $VOdtp_2$ [I]. This implies that the extent of the delocalization of the unpaired electron over the phosphorus 3s orbital is reduced from 1.4% for $VOdtp_2$ to 1.0% for $VOdtp_2$·Py.[13] Such a reduction may be explained on the assumption that either the lowering of the structural symmetry or the weakening of the four-membered chelate structure caused by the introduction of the pyridine base in the square plane results in the reduction of a direct vanadium($3d_{x^2-y^2}$)-phosphorus(3s) interaction.

TABLE 1. ESR PARAMETERS FOR $VOdtp_2$ DISSOLVED IN TOLUENE–PYRIDINE SOLUTIONS[a]

Solvents	Toluene	Toluene–Pyridine[b]	Pyridine
Typical spectra assignment	Figs. 1-A, 2-A	Figs. 1-B, 2-B	Figs. 1-C, 2-C
	$VOdtp_2$[I]	$VOdtp_2$·Py[III]	$VOdtp_2$·Py_2[IV]
Isotropic values			
g_0	1.981	1.976	1.974
$\|a^V\|$ Gauss	95.5	95.5	96.0
$\|a^P\|$ Gauss	51.0(2P)[c]	37.0(1P)[c]	—[d]
Anisotropic values			
$g_\parallel$	1.967	1.958	1.955
$g_\perp$	1.987	1.982	1.980
$\|A_\parallel^V\|$ Gauss	168	170	171
$\|A_\perp^V\|$ Gauss	59	59	59
$\|A_\parallel^P\|$ Gauss	52(2P)	37(1P)	—
$\|A_\perp^P\|$ Gauss	50(2P)	38(1P)	—

a) Isotropic and anisotropic values, obtained from the liquid solution spectra (Fig. 1) and the frozen solution spectra (Fig. 2) respectively, are presented. It is noted that all the experimental values thus obtained fit closely to the relations of $g_0=(g_\parallel+2g_\perp)/3$, $a^V=(A_\parallel^V+2A_\perp^V)/3$, and $a^P=(A_\parallel^P+2A_\perp^P)/3$. Uncertainty in the values is as follows: $g_0(\pm0.003)$; $g_\perp(\pm0.004)$; $g_\parallel(\pm0.008)$; a^V,a^P (±1.0); $A_\perp^V$, $A_\parallel^P$, $A_\perp^P(\pm2.0)$; $A_\parallel^V(\pm4.0)$.

b) No significant difference was found in ESR parameters between the spectra derived from the addition of pyridine, 4-methylpyridine, and 4-cyanopyridine.

c) Shf coupling constants due to the two equivalent phosphorus nuclei (2P) and due to one phosphorus nucleus (1P).

d) Shf splitting was not observed.

VOdtp$_2$ in Pyridine Solution: The spectra observed in a pyridine solution of $VOdtp_2$ are shown in Figs. 1–C and 2–C. It can be seen that the spectra consist of eight vanadium hf lines, without any phosphorus shf splitting. Quite similar spectra were also observed in toluene solutions of $VOdtp_2$ containing a large excess of pyridine bases.

The absence of phosphorus shf splitting is taken to indicate clearly that the complex species in pyridine does not carry the coordination unit consisting of the four-membered chelate structure with the phosphorus atom located diagonally to the vanadium atom. It seems likely that pyridine causes the complete destruc-

13) The spin densities of the phosphorus 3s orbital were calculated by using a hf interaction for unit occupancy of a phosphorus 3s orbital as 3640 Gauss (P. W. Atkins and M. C. R. Symons, "The Structure of Inorganic Radicals," Elsevier, Amsterdam (1967)).

tion of the chelate structure as a result of the displacement of equatorial sulfur ligands. Thus, one can tentatively presume that the complex species in pyridine has a stoichiometry of $VOdtp_2 \cdot Py_2$ and such a coordination model:

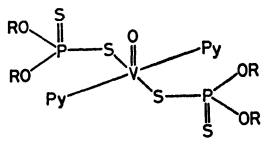

[IV] $VOdtp_2 \cdot Py_2$

The *g*-values and vanadium hf constants (Table 1) are also interpretable on the basis of this structural model which places the unpaired electron in the vanadium $3d_{x^2-y^2}$ orbital in the first approximation, as in the cases of $VOdtp_2$[I] and $VOdtp_2 \cdot Py$[III]. On the other hand, one might expect from the [IV] structure that the nitrogen instead of the phosphorus shf splitting is resolved. However, one may recall that oxovanadium complexes coordinated with nitrogen ligands seldom exhibit a resolved shf splitting.[5,14]

Reaction Scheme between $VOdtp_2$ and Pyridine Bases. The most important ESR information presented above is that the four-membered chelate structure of $VOdtp_2$[I] is destroyed by pyridine bases to form $VOdtp_2 \cdot Py_2$[III] or $VOdtp_2 \cdot Py_2$[IV], depending upon the concentrations of the pyridine bases in solutions. Accordingly, we can summarize the reactions of $VOdtp_2$ with pyridine bases as follows:

$$\underset{[I]}{VOdtp_2} + Py = \underset{[III]}{VOdtp_2 \cdot Py} \quad (1)$$

$$\underset{[III]}{VOdtp_2 \cdot Py} + Py = \underset{[IV]}{VOdtp_2 \cdot Py_2} \quad (2)$$

When pyridine concentrations are lower, $VOdtp_2$ reacts with the pyridine bases according to Reaction (1) to form the 1 : 1 complex, $VOdtp_2 \cdot Py$. It should be noted that Reaction (1) is not a simple process in which pyridine bases add to the open coordination position *trans* to the oxygen atom to form six-coordinate adducts. However, it seems quite possible that $VOdtp_2 \cdot Py$[III] is formed *via* an associative pathway[15] in which pyridine bases add first to the open coordination site, producing intermediate six-coordinate adducts with the [II] structure. The fact that the presence of the intermediate adduct [II] was not evidenced by ESR and optical absorption spectra probably implies that such a coordination structure is unstable and is rapidly converted into the [III] structure.

On the contrary, Reaction (2) takes place when $VOdtp_2 \cdot Py$ interacts with a large excess of pyridine bases. Thus, on the dissolution of $VOdtp_2$ in pyridine, both of the four-membered chelate rings are disrupted as a result of Reactions (1) and (2) to give $VOdtp_2 \cdot Py_2$ with the [IV] structure. The pyridine solution of $VOdtp_2 \cdot Py_2$ was found to be rather unstable and to liberate slowly a blue precipitate on standing *in vacuo*.

The reaction schemes, (1) and (2), disclosed here is of particular interest because the Reaction (1) affords a marked contrast to the well-established scheme of the formation of 1 : 1 adducts of $VO(acac)_2$ with a variety of bases,[2,3] where the addition of bases occurs to the sixth position of the otherwise unaltered complex. Such a difference in the scheme of base addition arises partly from the different nature of equatorial ligands in oxovanadium complexes.

This work was supported in part by a grant of the Ministry of Education, to which the authors' grateful acknowledgements are made.

14) J. M. Assour, J. Goldmacher, and S. E. Harrison, *J. Chem. Phys.*, **43**, 159 (1965); M. Sato and T. Kwan, *ibid.*, **50**, 558 (1969); M. A. Hitchman, B. W. Moores, and R. L. Belford, *Inorg. Chem.*, **8**, 1817 (1969).

15) C. H. Langford and H. B. Gray, "Ligand Substitution Process," W. A. Benjamin, New York (1965).

Photolysis of Ethylene at 1634 Å and 1849 Å

Hiroshi HARA and Ikuzo TANAKA

Department of Chemistry, Tokyo Institute of Technology, Ohokayama, Meguro-ku, Tokyo 152

(Received April 2, 1973)

The photolysis of ethylene was carried out at room temperature at 1634 Å and 1849 Å. Products at both wavelengths were hydrogen, acetylene, ethane, *n*-butane and 1-butene. Product analysis and the radical scavenger technique indicate the primary processes to be as follows.

$$C_2H_4 + h\nu \longrightarrow \begin{cases} C_2H_2 + H_2 \\ C_2H_2 + 2H \\ C_2H_3 + H \end{cases}$$

The molecular elimination process in the primary processes varied with wavelengths, and was determined to be 47% and 53% at 1634 Å and 1849 Å, respectively. With reference to the percentage reported at other wavelengths, it is pointed out that molecular elimination is suppressed with the increase in excitation energy.

The photochemistry of ethylene has long been studied[1-6] and the reaction mechanism is proposed from the results of investigations at 1236 Å and 1470 Å,[1-3]

$$C_2H_4 + h\nu \longrightarrow \begin{cases} C_2H_2 + H_2 & \Phi_1 \\ C_2H_2 + 2H & \Phi_2 \end{cases}$$

where Φ_1 and Φ_2 stand for the quantum yields of the respective reactions. These are followed by the secondary processes,

$$H + C_2H_4 \longrightarrow C_2H_5$$

$$C_2H_5 + C_2H_5 \longrightarrow \begin{cases} C_2H_4 + C_2H_6 \\ n\text{-}C_4H_{10} \end{cases}$$

The quantum yield Φ_1 relative to Φ_2 decreases as the excitation energy increases. Since some molecules such as ethane show a wavelength dependence of the quantum yield of molecular elimination, it seems interesting to study the wavelength dependence of Φ_1 relative to Φ_2 over a wider range.

Ethylene was studied at longer wavelengths. For quantitative treatment, the percentage of the molecular mechanism is expressed by $\Phi_1/(\Phi_1+\Phi_2+\Phi_3)$, where Φ_3 is the quantum yield of the vinyl radical formation process

$$C_2H_4 + h\nu \longrightarrow C_2H_3 + H$$

which was recently found in the photolysis of ethylene at 1470—1931 Å by Potzinger *et al.*[7] In the present study, the primary process of the vinyl radical formation is discussed in detail.

Ethyl radicals were formed in the secondary process of the photolysis of ethylene, and underwent disproportionation reaction or recombination reaction. A number of investigators have determined the ratio of the constants of these two reactions, generating ethyl radicals from different source. The reported ratios show a spread but most values lie in the range 0.10—0.17. The ratio in the photolysis of ethylene is discussed in the present study.

The V–N system beginning near 2650 Å consists of a long progression of broad diffuse bands, starting at 2150 Å and rising rapidly in intensity with decreasing wavelength. At 1744 Å, the V–N bands disappear under the intense bands of the first Rydberg transition, but the V–N system obviously continues, and finally reaches a broad flat maximum at about 1620 Å. At still shorter wavelengths the absorption decreases fairly steadily, down to the next strong Rydberg transition which begins at 1393 Å.[11]

Thus the absorption at 1236 Å corresponds to the second R–N transition, and that at 1470 Å to the mixture of the R–N and V–N transitions. On the other hand, the absorptions at both 1634 Å and 1849 Å in this study correspond to V–N transition.

Experimental

The light source of 1634 Å was an electrodeless discharge bromine lamp, construction of which was reported elsewhere,[12,13] and that of 1849 Å was a conventional low-pressure mercury lamp. The reaction system was a quartz cylinder with quartz windows and a glass-made circulator.

Nitrogen gas was allowed to flow between the lamp and the cell during the photolysis to avoid the absorption of oxygen at 1634 Å.

Ethylene was obtained from Takachiho Chem. Ind. Co. Gas chromatographic analysis showed the presence of impurity, 0.1% ethane. After purification by gas chromatography using an active carbon column, the impurity level was below 0.01%. Nitric oxide was also obtained from

1) J. R. McNesby and H. Okabe, *Advan. Photochem.*, **3**, 157 (1964).
2) M. C. Sauer, Jr., and L. M. Dorfman, *J. Chem. Phys.*, **35**, 497 (1961).
3) H. Okabe and J. R. McNesby, *ibid.*, **36**, 601 (1962).
4) E. Tschuikow-Roux, J. R. McNesby, W. M. Jackson, and J. L. Faris, *J. Phys. Chem.*, **71**, 1531 (1967).
5) R. A. Back and D. W. L. Griffiths, *J. Chem. Phys.*, **46**, 4839 (1967).
6) Y. Inel, A. Siddiqi, and G. G. Meisels, *J. Phys. Chem.*, **75**, 1317 (1971).
7) P. Potzinger, L. C. Glasgow, and G. von Bunau, *Z. Naturforsch.*, **27a**, 628 (1972).
8) J. A. Kerr and A. F. Trotman-Dickenson, *Prog. Reaction Kinetics*, **1**, 105 (1961).
9) A. F. Trotman-Dickenson and G. S. Milene, "Tables of Bimolecular Gas Reactions," NSRDS-NBS9, National Bureau of Standards, Washington, D. C., 1967 and literatures cited therein.
10) L. E. Reid and D. J. LeRoy, *Can. J. Chem.*, **46**, 3275 (1968).
11) A. J. Merer and R. S. Mulliken, *Chem. Rev.*, **69**, 639 (1969).
12) B. A. Thompson, R. R. Reeves, and P. Harteck, *J. Phys. Chem.*, **69**, 3964 (1965).
13) K. Obi, Ph. D. Thesis, Tokyo Institute of Technology (1966).

Takachiho Chem. Ind. Co. and was used without further purification. The reaction was followed by freezing out the unreacted ethylene and any condensable products with liquid nitrogen to a sample collection tube. The condensables were analyzed with a Hitachi Model KGL-2A gas chromatograph equipped with a flame ionization detector using a 2 m long column of silica gel-squalane, and with a Hitachi Model 063 gas chromatograph, equipped with a flame ionization detector for hydrocarbon products using a 9 m long column of squalane on Chromosorb P support. For hydrogen, a 1 m long column of active carbon and a thermal conductivity detector were used, a copper oxide furnace being provided between the column and the detector to convert hydrogen into water for higher sensitivity. In order to determine the ratio of hydrogen to ethylene, the reaction system was attached to the Toepler pump system to collect the entire amount of products and the unreacted into the sample collection tube. All experiments were carried out at room temperature.

Results

Photolysis at 1634 Å. The products of photolysis with radiation at 1634 Å were hydrogen, acetylene, ethane, *n*-butane and 1-butene. They are the same as in the photolysis at 1236 Å and 1470 Å except that only traces of 1-butene and hexane were detected and no C-4 compounds other than *n*-butane were observed.[2,3]

In order to see the effect of the secondary photolysis which should be negligibly small, the yields of acetylene, ethane and *n*-butane, were determined for different irradiation times. The relative yields are plotted as a function of irradiation time in Fig. 1. This result provided a linear function of time so that complications due to the secondary photolysis was not significant within one percent of conversion. The following photolysis was conducted within this limit.

Photolysis in the presence of nitric oxide was performed with a constant pressure of ethylene and a fixed time of irradiation. No appreciable decrease in the yield of acetylene was observed in these experiments.

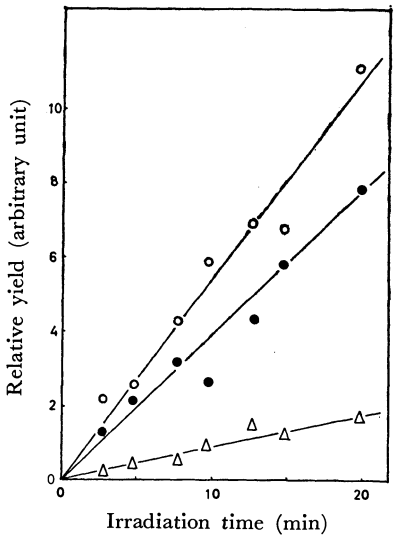

Fig. 1. Relative yields of products *vs.* irradiation time. C_2H_2 (○), *n*-C_4H_{10} (●), and C_2H_6 (△).

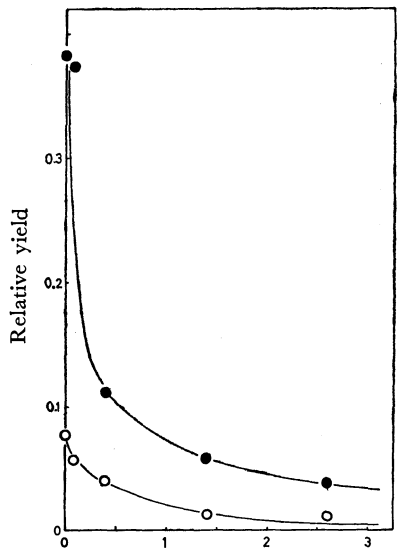

Fig. 2. Relative yields of *n*-C_4H_{10} and C_2H_6 to C_2H_2 *vs.* added NO pressure (C_2H_4; 20 Torr). *n*-C_4H_{10} (●) and C_2H_6 (○).

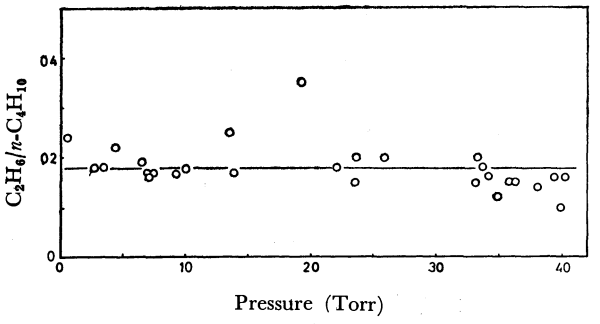

Fig. 3. C_2H_6 to *n*-C_4H_{10} ratio *vs.* C_2H_4 pressure at 1634 Å.

As shown in Fig. 2, ethane and *n*-butane decreased remarkably with increasing concentration of nitric oxide which was an effective free-radical scavenger. These results support the view that acetylene, at least the majority of it, was formed in the primary processes, and that ethane and *n*-butane were formed in the radical reaction.

The ratio of ethane to *n*-butane is plotted as a function of ethylene pressure in the range 0.6—40 Torr in Fig. 3. The ratio calculated to be 0.18±0.04 is independent of ethylene pressure.

The ratio of 1-butene to *n*-butane as products is almost constant, 0.045±0.008 in the pressure range 5—40 Torr.

Photolysis at 1849 Å. The products of the photolysis with light of 1849 Å were hydrogen, acetylene, ethane, *n*-butane and 1-butene as in the case of the photolysis at 1634 Å.

The ratio of ethane to *n*-butane was measured at various pressures of ethylene as shown in Fig. 4. It is independent of ethylene pressure and gives the average value of 0.30±0.06.

The ratio of 1-butene to *n*-butane was determined to be 0.19±0.04, pressure independent in the range 5—35 Torr.

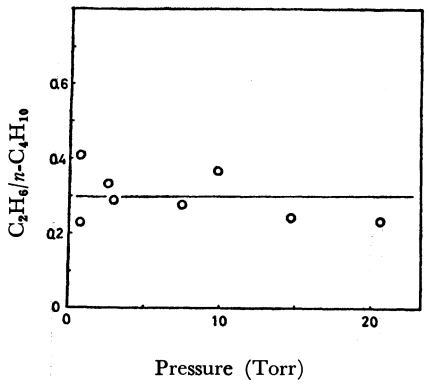

Fig. 4. C_2H_6 to n-C_4H_{10} ratio *vs.* C_2H_4 pressure at 1849 Å.

Discussion

Reaction Mechanism. The formation of a considerable amount of 1-butene at 1634 Å and 1849 Å affords the following processes which account for the products of the present work as well as those of the previous work using shorter wavelengths.

$$C_2H_4 + h\nu \xrightarrow{\Phi_1} C_2H_2 + H_2 \quad (1)$$

$$\xrightarrow{\Phi_2} C_2H_2 + 2H \quad (2)$$

$$\xrightarrow{\Phi_3} C_2H_3 + H \quad (3)$$

$$H + C_2H_4 \xrightarrow{k_4} C_2H_5 \quad (4)$$

$$C_2H_5 + C_2H_5 \xrightarrow{k_5} C_2H_4 + C_2H_6 \quad (5)$$

$$\xrightarrow{k_6} n\text{-}C_4H_{10} \quad (6)$$

$$C_2H_3 + C_2H_5 \xrightarrow{k_7} 2C_2H_4 \quad (7)$$

$$\xrightarrow{k_8} C_2H_2 + C_2H_6 \quad (8)$$

$$\xrightarrow{k_9} 1\text{-}C_4H_8 \quad (9)$$

Steady state treatment led to the relationship

$$\frac{R(C_2H_6) + R(n\text{-}C_4H_{10})}{R(C_2H_2)} = \frac{\Phi_2 + \Phi_3 \cdot \dfrac{k_8}{k_7+k_8+k_9}}{\Phi_1 + \Phi_2 + \Phi_3 \cdot \dfrac{k_8}{k_7+k_8+k_9}} \equiv \alpha \quad (10)$$

$$1 - \frac{R(H_2)}{R(C_2H_2)} = \frac{\Phi_2 + \Phi_3 \cdot \dfrac{k_8}{k_7+k_8+k_9}}{\Phi_1 + \Phi_2 + \Phi_3 \cdot \dfrac{k_8}{k_7+k_8+k_9}} \equiv \beta \quad (11)$$

$$\frac{R(C_2H_6)}{R(n\text{-}C_4H_{10})} = \frac{k_5}{k_6} + \frac{\Phi_3}{\Phi_2} \cdot \frac{k_5+k_6}{k_6} \cdot \frac{k_8}{k_7+k_8+k_9} \equiv \gamma \quad (12)$$

$$\frac{R(1\text{-}C_4H_8)}{R(n\text{-}C_4H_{10})} = \frac{\Phi_3}{\Phi_2} \cdot \frac{k_5+k_6}{k_6} \cdot \frac{k_9}{k_7+k_8+k_9} \equiv \delta \quad (13)$$

where α, β, γ, and δ are the experimentally available values of the product ratios, and R(M) is the formation rate of M.

Reaction (8) is an important process which explains the difference in the ratio of ethane to n-butane at 1634 Å and at 1849 Å. According to a recent work. k_8 is not negligibly small compared with k_7 and k_9, namely $k_7 : k_8 : k_9 = 1.00 : 0.43 : 0.89$.[14] Potzinger *et al.* did not include Reaction (8) on the basis that the addition of oxygen to ethylene had no effect on the quantum yield for acetylene.[7] It might be because the contribution of Reaction (8) at the formation of acetylene was not important. In the present study, however, the Reaction (8) must not be ruled out.

TABLE 1. k_5/k_6 IN THE PHOTOLYSES OF ETHYLENE AT DIFFERENT WAVELENGTHS

Excitation wavelength	k_5/k_6	Ref.
1236 Å[a)]	0.18	(3)
1470 Å	0.15	(2)
	0.19	(14)
1634 Å	0.16±0.04	this work
1849 Å	0.21±0.06	this work

a) CH_2CD_2

Disproportionation and Recombination of Ethyl Radicals. Ethyl radical is formed in the photolysis of ethylene. If ethane and n-butane are formed only through ethyl radical reactions, the ratio of the formed amount of ethane to that of n-butane directly leads to k_5/k_6. The photolyses at 1236 Å and 1470 Å are such cases. In the present study, the ratios of ethane to n-butane are 0.18 at 1634 Å and 0.30 at 1849 Å, suggesting the additional amount of ethane from Reaction (8). Thus from Eqs. (12) and (13), we obtain the relation.

$$\frac{k_5}{k_6} = \gamma - \frac{k_8}{k_9} \cdot \delta$$

From our experimental values of γ, δ and reported value of k_8/k_9, 0.48,[14] the value of k_5/k_6 should be obtained.

At 1634 Å, γ is 0.18±0.04 and δ is 0.045±0.008, then k_5/k_6 is 0.16±0.04. At 1849 Å, γ and δ are 0.30±0.06 and 0.19±0.04, respectively, so k_5/k_6 is 0.21±0.06. Comparison of this ratio at different wavelengths is made in Table 1. In consideration of this ratio 0.13+0.02,[8-10] obtained previously from different sources of ethyl radicals, these values in the photolysis of ethylene agree well within the error limit.

Molecular Mechanism of the Primary Processes at 1634 Å *and* 1849 Å. Substitution of our values of k_5/k_6 and the reported relative values, $k_7 : k_8 : k_9 = 1.00 : 0.43 : 0.89$,[14] into Eqs. (12) and (13) gives the following.

$$\frac{R(C_2H_6) + R(n\text{-}C_4H_{10})}{R(C_2H_2)} = \frac{\Phi_2 + 0.19\Phi_3}{\Phi_1 + \Phi_2 + 0.19\Phi_3} \equiv \alpha \quad (15)$$

$$1 - \frac{R(H_2)}{R(C_2H_2)} = \frac{\Phi_2 + 0.19\Phi_3}{\Phi_1 + \Phi_2 + 0.19\Phi_3} \equiv \beta \quad (16)$$

$$\frac{R(C_2H_6)}{R(n\text{-}C_4H_{10})} = 0.16 + 0.22\frac{\Phi_3}{\Phi_2} \equiv \gamma \text{ (for 1634 Å)} \quad (17\text{-}8)$$

$$= 0.21 + 0.22\frac{\Phi_3}{\Phi_2} \equiv \gamma \text{ (for 1849 Å)} \quad (17\text{-}2)$$

$$\frac{R(1\text{-}C_4H_8)}{R(n\text{-}C_4H_{10})} = 0.44\frac{\Phi_3}{\Phi_2} \equiv \delta \text{ (for 1634 Å)} \quad (18\text{-}1)$$

$$= 0.46\frac{\Phi_3}{\Phi_2} \equiv \delta \text{ (for 1849 Å)} \quad (18\text{-}2)$$

Relative quantum yields of the primary processes can

14) T. Ibuki and Y. Takezaki, private communication.

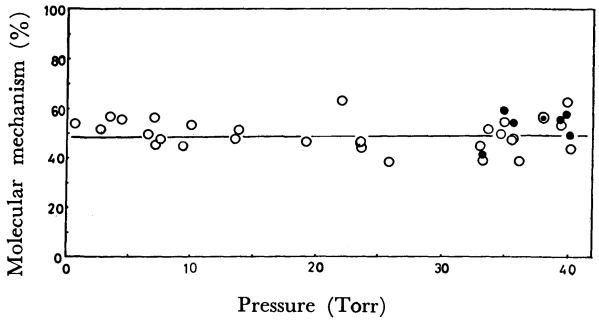

Fig. 5. Molecular mechanism (%) *vs.* C_2H_4 pressure at 1634 Å.
(○) from Eqs. (15) and (17—1); (●) from Eqs. (16) and (17—1).

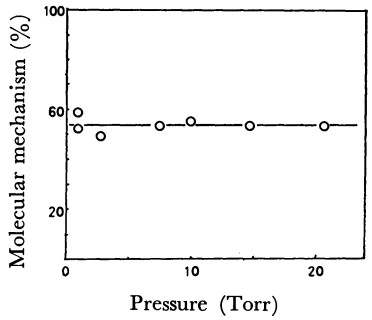

Fig. 6. Molecular mechanism (%) *vs.* C_2H_4 pressure at 1849 Å.

be obtained using Eqs. (15)—(18) with the values of α, β, γ, and δ.

In most experiments, α and γ values were used to obtain the percentage of the molecular elimination process, which is shown in Fig. 5 as a function of ethylene pressure at 1634 Å and in Fig. 6 at 1849 Å. It is pressure independent at both wavelengths. The average values of molecular mechanism, Φ_1, are 47% at 1634 Å and 53% at 1849 Å.

Φ_1 at 1634 Å calculated from β and γ values is also shown in Fig. 5, giving the average value 51%.

The value of δ from the ratio of 1-butene and *n*-butane is 0.045 at 1634 Å and 0.19 at 1849 Å. The relative quantum yields of the primary processes also can be calculated at 1634 Å and 1849 Å using δ values instead

Table 2. Relative quantum yield at 1634 Å and 1849 Å

		Relative quantum yield from			
		(15) and (17)	(16) and (17)	(15) and (18)	(16) and (18)
1634 Å	Φ_1	47 (±6) %	51 (±6) %	47 (±5) %	51 (±4) %
	Φ_2	48 (±6)	45 (±4)	48 (±5)	45 (±4)
	Φ_3	5 (±4)	4 (±4)	5 (±1)	4 (±2)
1849 Å	Φ_1	53 (±3) %	—	53 (±6) %	—
	Φ_2	33 (±5)	—	33 (±4)	—
	Φ_3	14 (±2)	—	14 (±4)	—

15) Y. Ogata, unpublished data.
16) In an unpublished experiment at 1470 Å, we found the relative quantum yield of the primary process (3) to be 1~2%.
17) K. Obi, Y. Ogata, and I. Tanaka, This Bulletin, **44**, 3190 (1971).

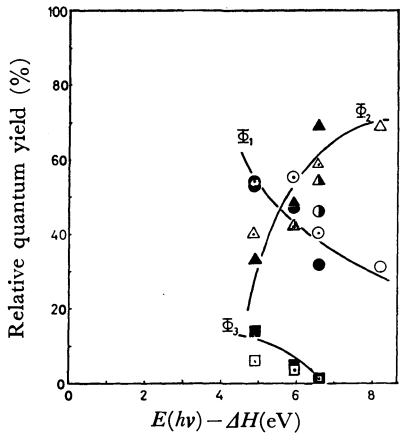

Fig. 7. Relative quantum yield *vs.* $E(h\nu)-\Delta H$.
circle, Φ_1; triangle, Φ_2; square, Φ_3.
(●, ▲, ■) this work, and Ref. 15, (◑, ◭) Ref. 2, (○, △) Ref. 3, (⊙, ◬, ⊡) Ref. 7.

of γ values. They are summarized in Table II, and are in good agreement within experimental error.

Formation of vinyl radical in the primary process, proposed in the flash photolysis study of ethylene[5] and 1470—1931 Å photolysis of ethylene,[7] explains the presence of 1-butene as a product which should be formed by the recombination reaction of vinyl and ethyl radicals.

Another fact supporting the formation of vinyl radical is the good agreement between the ratio of Φ_3 to Φ_2 from γ and that from δ. At 1634 Å, the ratio of Φ_3 to Φ_2 is 0.091 from γ and 0.10 from δ. At 1849 Å it is 0.41 from γ and 0.41 from δ. Agreement of the ratios indicates the formation of vinyl radical in the primary process.

The precursors proposed by Potzinger *et al.*, leading to the three different primary processes, are of great interest. In this study, however, the quantum yields determined are relative and cannot support or deny their proposed mechanism. Our data can be compared with their data extrapolated to zero pressure in their mechanism.

The relative quantum yields obtained in this investigation are shown in Fig. 7 as a function of the excess energy together with the reported results[2,3,7,15,16]. The excess energy is defined by

$$E(\text{excess energy}) = E(h\nu) - \Delta H \quad (18)$$

where $E(h\nu)$ is the photon energy of the excitation light, and ΔH is heat of reaction:

$$C_2H_4 = C_2H_2 + H_2 \quad \Delta H = 41.7\,\text{kcal/mol} = 1.8\,\text{eV} \quad (19)$$

Figure 7 would permit the interpretation that the internal energy of an excited ethylene molecule increases as the irradiation photon energy increases, so that molecular mechanism of the primary process could take place less easily than atomic mechanism at shorter wavelengths.

It is concluded that ethylene shows a similar wavelength dependence of the primary processes to that of ethane, where the experimental data of some simple molecules, such as ethylene, ethane ammonia and water, have been qualitatively interpreted by a simple theoretical treatment of the RRKM theory.[17]

Molecular Interactions of *p*-(*N*,*N*-Dimethylamino)-Benzonitrile. Electrostatic Self-Complex and Hetero-Complex Formation in the Ground and Excited States

Nobuaki NAKASHIMA and Noboru MATAGA[1)]

Department of Chemistry, Faculty of Engineering Science, Osaka University, Toyonaka, Osaka 560

(Received May 24, 1973)

Electrostatic self-complex formation of *p*-(*N*,*N*-dimethylamino)-benzonitrile and its hetero-complex formation with benzonitrile in cyclohexane matrix were studied in detail. The possibilities of ground state complex and excimer formation in various liquid solvents were examined thoroughly.

p-(*N*,*N*-Dimethylamino)-benzonitrile(DMABN) exhibits dual fluorescence bands in polar solvents, F_a at longer wavelength side (*ca.* 400—500 nm) and F_b at shorter wavelength side (*ca.* 360 nm). In nonpolar solvents and rigid matrix at low temperatures only the F_b band can be observed. Lippert *et al.*[2)] ascribed this phenomenon to two emitting electronic states, a strongly polar one (^1L_a) and a less polar one (^1L_b).

On the other hand, Rotkiewicz *et al.* assigned the emissions to the existence of two isomers α and β differing in polarity and in the orientation of the dimethylamino group.[3)] In the case of α form which is strongly polar and emits the F_a fluorescence, the lone pair of amino nitrogen is assumed parallel to the plane of benzene ring. In the case of less polar β form emitting the F_b fluorescence, the lone pair is considered to be perpendicular to the benzene ring.

Recently, we have measured time-resolved fluorescence spectra and fluorescence rise and decay curves of DMABN in MTHF (methyltetrahydrofuran) and have demonstrated clearly the relaxation process due to the interaction between the solvent and the strongly polar state of the solute, leading to the dual fluorescence.[4)] Either of the above two interpretations by Lippert *et al.* and Rotkiewicz *et al.* may be consistent with our result of time-resolved fluorescence studies if we assume that α isomer is formed from the β isomer in the excited state. In the course of this study, we have found that the ground state DMABN forms self-complexes and also complexes with benzonitrile in cyclohexane matrix.[4)] We have made more detailed investigations on these aggregation phenomena in cyclohexane matrix and, moreover, examined the possibilities of the ground state aggregates as well as excimer formations in various liquid solvents. We have found no definite ground state complex formation in the liquid solution.

On the other hand, McGlynn and co-workers have recently reported absorption and luminescence spectra which they ascribed to the dimer of DMABN.[5)] Moreover, they claimed that the F_a band is an excimer emission. According to our present study, their dimer band is due to some unknown impurity and their claim of excimer fluorescence is erroneous.

Experimental

DMABN (K and K) was recrystallized several times from *n*-hexane (Wako, spectrograde). Diethyl ether (Merck, spectrograde), toluene (Merck, spectrograde), acetonitrile (Merck, spectrograde), tetrahydrofuran (THF) (Wako, spectrograde) and methylcyclohexane (Wako, spectrograde) were used without purification. Methanol, propylene glycol, benzonitrile and ethanol were all Wako analytical grade reagents and used without further purification.

The absorption spectra were measured by a Cary 15 and a Shimadzu MPS-50L spectrometer. Cells with optical paths of 1 mm, 400 μ, 25 μ and 2 μ were made by inserting thin packings between quartz plates. Fluorescence spectra were measured by an Aminco-Bowman spectrophotofluorometer. The detector for luminescence was photomultiplier of type RCA 1P28. The temperature of a solution for the measurement was controlled by a constant flow of cold nitrogen gas in a metal Dewar vessel with quartz windows or a cuvette was immersed in ethanol in a quartz Dewar vessel and the temperature of ethanol was controlled by drop ping liquid nitrogen. Solutions for the measurement were not deaerated but some of them were flushed with nitrogen.

Results and Discussion

The extinction coefficient of the absorption band at 330—360 nm in propylene glycol solution decreased to about one-third or one-half of the initial value, respectively, when DMABN was recrystallized once from *n*-hexane or water. We observed that the extinction coefficient around 250 nm also decreased by recrystallization. After being recrystallized five times from *n*-hexane, DMABN did not show practically any absorption band at 330—360 nm region. Thus, it seems to be clear that the absorption band at 330—360 nm ascribed by McGlynn *et al.* to the dimer of DMABN is due to some unknown impurity. This impurity appears to show absorption band not only at 330—360 nm but also at about 250 nm. The impurity absorption band seems to become strong in such hydroxylic solvents as water and alcohols. However, it is quite weak in various non-hydroxylic solvents such as aliphatic as well as aromatic hydrocarbons, ethers and nitriles, even when a crude sample is used. Therefore, the intensity of the impurity band does not depend on the solvent polarity but seems to be affected by hydrogen bonding interaction.

1) To whom the correspondence should be adressed.

2) E. Lippert, W. Luder, and H. Boos, "Advances in Molecular Spectroscopy," Pergamon Press, London (1962), p. 443.

3) K. Rotkiewicz, K. H. Grellmann and Z. R. Grabowski, *Chem. Phys. Lett.*, **19**, 315 (1973).

4) N. Nakashima, H. Inoue, N. Mataga, and C. Yamanaka This Bulletin, **46**, 2288 (1973).

5) O. S. Khalil, R. H. Hofeldt, and S. P. McGlynn, *Chem. Phys. Lett.*, **17**, 479 (1972).

If there occurs the ground state dimerization of DMABN, its absorption spectra should show a concentration dependence. We have examined the concentration effect upon the absorption and fluorescence spectra of DMABN in propylene glycol by changing its concentration within the range 1×10^{-5} up to 5×10^{-3} M. We found no change in the spectra. This result is contrary to that of McGlynn *et al.*, and the fluorescence band assigned by them to the ground state dimer is clearly due to the unknown impurity.

We can observe true spectral change due to the ground state aggregation of DMABN in cyclohexane matrix at low temperatures as described in detail in section B. In the case of highly concentrated solutions (0.1—2 M), we can recognize a little change in the fluorescence spectra. We have confirmed, however, that this spectral change is not due to the excimer formation claimed by McGlynn *et al.*

A. On the Possibility of Excimer Formation in Highly Concentrated Solutions of DMABN. If F_a and F_b bands are an excimer and monomer emission of DMABN, respectively, as claimed by McGlynn *et al.*, the intensity ratio $I(F_a)/I(F_b)$ should increase as the concentration is increased. However, the ratio does not show any concentration dependence within the range 1×10^{-5} M up to 1×10^{-2} M in all solvents we have examined. Therefore, the excimer formation cannot be responsible for the F_a fluorescence. In toluene and ether solutions, the ratio increases and F_a band shows a red shift at very high concentration as indicated in Fig. 1 and Table 1. However, in such polar solvents as methanol and acetonitrile, the intensity ratio decreases and F_a band shows a little blue shift at a very high concentration as one can see from Fig. 2 and Table 1.

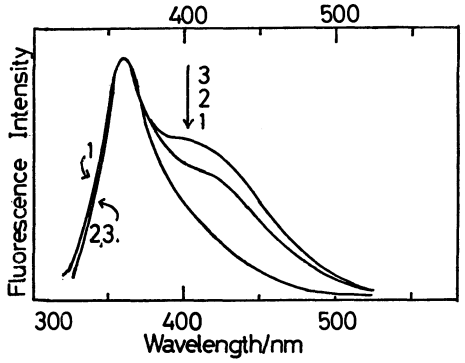

Fig. 1. Concentration effect of the fluorescence spectra of of DMABN in diethylether. [DMABN], 1: 5×10^{-5} M, 2: 1×10^{-1} M, 3: 2.5×10^{-1} M. The spectra were corrected for the response of the entire analyzing system.

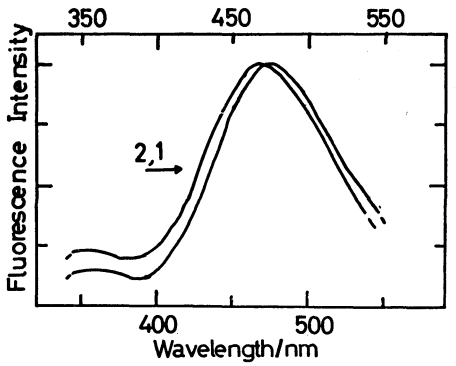

Fig. 2. Concentration effect on the fluorescence spectra of DMABN in acetonitrile. [DMABN], 1: 4×10^{-5} M, 2: 2M.

Table 1. Concentration effect on the fluorescence spectra of DMABN in various solvents (at 20±2 °C)

Solvent	ε [a] (°C)	[DMABN] (M)	$\lambda_{max}(F_b)$ (nm)	$\lambda_{max}(F_a)$ (nm)
Toluene	2.379	5×10^{-5}	360±2	c)
	(25)	1	360±5	428±2
Diethyl ether	4.335	5×10^{-5}	360±2	c)
	(20)	2.5×10^{-1}	360±2	427±2
Tetrahydrofuran	7.58	2×10^{-5}	360±2	435±2
	(25)	2	b)	460±2
Methanol	32.70	5×10^{-5}	b)	480±2
	(25)	1	b)	475±2
Acetonitrile	37.5	4×10^{-5}	b)	475±2
	(20)	2	b)	465±2

a) Dielectric constant of the solvent. Taken from J. A. Riddick and W. B. Bunger, "Techniques of Chemistry," 2. Organic Solvents., Third ed., John Wiley and Sons, New York (1970), p. 563. b) The intensity was too weak to determine the wavelength of the band maximum. c) Because of the overlapping of the F_b band which is much stronger than F_a band, the determination of the peak wavelength was not possible.

In highly concentrated solutions, DMABN seems to play not only the role of the solute but also that of the polar solvent molecule. Presumably, DMABN molecule may be more polar than toluene and ethers. Therefore, in the case of the highly concentrated solutions in these solvents, the electrostatic dipolar interactions between the strongly polar excited state and ground state DMABN molecules may facilitate the appearance and red shift of the F_a band. Contrary to this, dielectric constant of "DMABN solvent" may be smaller than those of methanol and acetonitrile, leading to the decrease of the intensity ratio and the blue shift of the F_a band at a very high concentration in these solvents.

The above electrostatic interactions, however, appear to involve not only the long range one determined by the bulk dielectric constant but also short range interactions which may be deemed 1 : 1 or 1 : *n* electrostatic loose "self-complex" formation. For the increase of the F_a band intensity in toluene and ethers starts already at 5×10^{-2} M where the increase of the bulk dielectric constant due to the added DMABN may certainly be neglected. The self-complex in the present case does not mean the formation of such a definite stoichiometric complex by a specific short range interaction as the typical exciplex, but loose association of excited DMABN with ground state DMABN molecules by means of dipole-dipole interactions.

The electrostatic self-complex formation may be rather difficult in strongly polar solvents such as methanol and acetonitrile, since the interaction between the polar solvent molecules and the excited DMABN may be quite strong. Therefore, the bulk electrostatic effect may be rather important in this case.

We have confirmed in the case of highly concen-

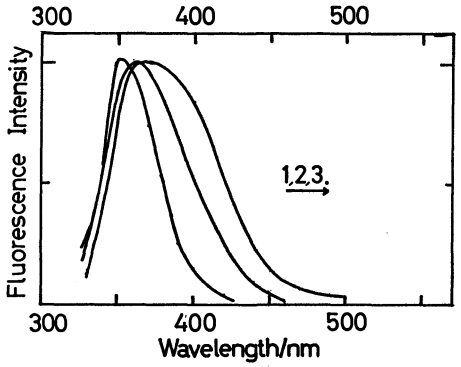

Fig. 3. Effect of the addition of benzonitrile upon the fluorescence spectra of DMABN in methylcyclohexane.
[DMABN] $=2\times10^{-5}$ M.
1. [benzonitrile] $=0$ M 21 °C.
2. [benzonitrile] $=4.9\times10^{-2}$ M, 21 °C.
3. [benzonitrile] $=4.9\times10^{-2}$ M, -17 °C.
The spectra were corrected.

trated solutions that the fluorescence excitation spectra measured at F_a band coincides with those measured at F_b band. Accordingly, the increase of the F_a band intensity at high concentration does not seem to be ascribed to the ground state complex formation. Moreover, it has been confirmed that the absorption spectra of highly concentrated solutions in methanol and ethanol are the same as those of 2×10^{-5} M solutions. Therefore, the electrostatic interactions leading to the fluorescence spectral changes are occurring in the excited state.

The excited DMABN molecule will make the electrostatic complex not only with the same kind of molecules but also with different kind of polar molecules. We have examined its interaction with benzonitrile in methylcyclohexane. As shown in Fig. 3, one can recognize a considerable change of the fluorescence spectra at 5×10^{-2} M of added benzonitrile. The spectra show an apparent red shift and intensity increase at the long wavelength side of the band by temperature lowering, which may be ascribed to the appearance of the F_a band caused by electrostatic "hetero-complexes" formation with benzonitrile molecules. In this case too, we have confirmed that the absorption spectra of DMABN do not show any change by the addition of 5×10^{-2} M benzonitrile. Therefore, the interaction with benzonitrile molecules leading to the appearance of F_a band is occurring in the excited state. The present hetero-complex also is not a definite complex but loose aggregation of excited DMABN with benzonitrile by means of dipole-dipole interactions, since one cannot recognize a definite isoemissive point in the emission spectra. Electrostatic loose complex formation of an excited polar solute molecule with polar solvent molecules has been assumed, for example, in the case of indole or tryptophan in alcohol or aqueous solution[6,7] as well as DMABN-propionitrile-methylcyclohexane system.[8]

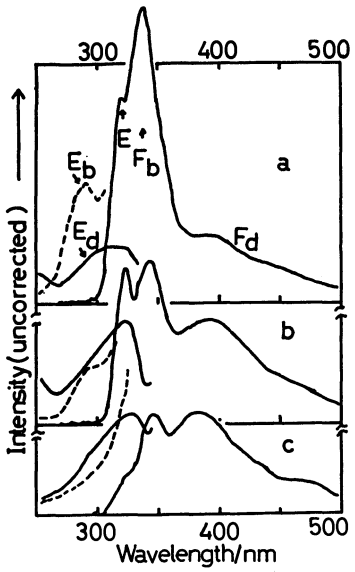

Fig. 4. Concentration effect on the fluorescence and excitation spectra of DMABN in cyclohexane matrix at -45 ± 3 °C.
[DMABN]: a. 5×10^{-5} M, b. 5×10^{-4} M, c. 5×10^{-3} M.
E: exciting light. E_b: excitation spectra of F_b band.
E_d: excitation spectra of F_d band.

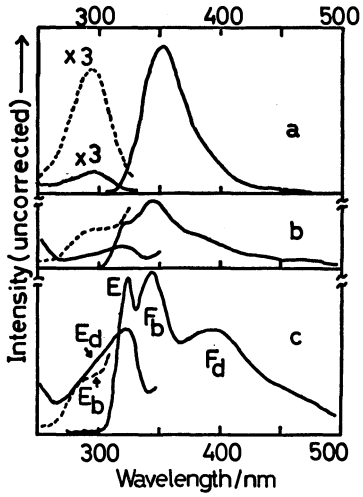

Fig. 5. Temperature effect on the fluorescence and excitation spectra of DMABN in cyclohexane matrix.
[DMABN] $=5\times10^{-4}$ M.
a. 20 ± 3 °C, b. -24 ± 3 °C, c. -45 ± 3 °C.
The meanings of E, E_b and E_d are the same as those in Fig. 4.

At any rate, the above results in nonpolar and slightly polar solvents may be well understood as due to the loose 1 : 1 or 1 : n electrostatic self-complex or hetero-complex formation and the results in strongly polar solvents may be ascribed mainly to an electrostatic bulk effect. Change of the fluorescence spectra due to the complex formation of DMABN occurs also in cyclohexane matrix at low temperatures as we have briefly reported previously. In the case of cyclohexane matrix, however, the complex is formed already in the ground state. The studies in cyclohexane matrix may be quite useful for the elucidation of the aggregation phenomena of DMABN. We have made a de-

6) N. Mataga, Y. Torihashi, and K. Ezumi, *Theor. Chim. Acta*, **2**, 158 (1964).
7) J. Eisinger and G. Navon, *J. Chem. Phys.*, **50**, 2069 (1969).
8) E. A. Chandross and H. T. Thomas, *Chem. Phys. Lett.*, **9**, 397 (1971).

tailed investigation along this line.

B. Aggregation in Cyclohexane Matrix. The effects of DMABN concentration as well as temperature upon the luminescence and excitation spectra have been investigated as shown in Figs. 4 and 5. When temperature is kept constant at -45 ± 3 °C and concentration is increased, the intensity of the band at 390 nm (F_d band) increases and its peak wavelength does not depend on the concentration as one can see from Fig. 4. When the temperature is lowered keeping the concentration at 5×10^{-4} M, the F_d band intensity increases as indicated in Fig. 5. In both of Figs. 4 and 5, we can observe the F_b band at *ca.* 340 nm together with the F_d band. The excitation spectrum of F_b band is observed at *ca.* 290 nm, the wavelength of the absorption band of DMABN. However, that of the F_d band is observed at about 320 nm which is different from the absorption peak of DMABN monomer. Since the excitation spectra at shorter wavelengths than 250 nm were not accurate, they are not shown here.

In view of its concentration and temperature dependences and its excitation spectra different from those of the monomer, the F_d band may be ascribed to an aggregated state of DMABN. In order to confirm the change of absorption spectra in cyclohexane matrix, we have measured directly the absorption spectra at several temperatures as shown in Fig. 6. Temperature lowering causes the intensity increase of the bands at 320 ± 10 nm and at 240 ± 5 nm. The absorption peak at 320 nm is in good agreement with the peak of the excitation spectra of F_d band. One can see also in Fig. 6 that the temperature lowering causes the intensity decrease of the 285 nm band. Presumably, the absorption bands at 320 and 240 nm may be assigned to the dimer of DMABN and the F_d band to its fluorescence. The F_d band may be mainly due to the F_a band appeared as a result of the electrostatic interaction between the halves in the dimer. However, the wavelength of the F_d band is a little shorter than that of the F_a band in highly concentrated toluene solution or diethyl ether solution. This result may be ascribed to the fact that the ground state of the aggregate is stabilized considerably and there is no reorientation stabilization due to the surrounding solvent dipoles in the case of the cyclohexane matrix. Moreover higher aggregate may be formed in the excited state of highly concentrated liquid solution, leading to the larger red shift of the F_a band.

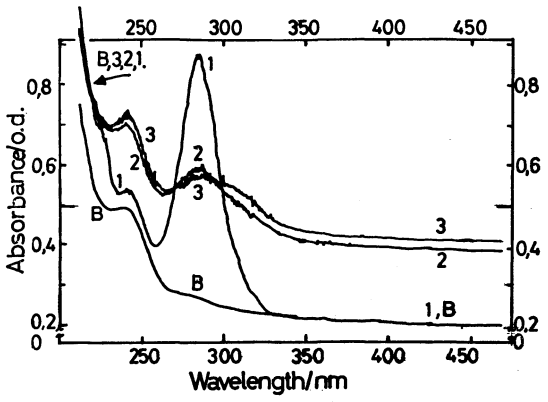

Fig. 6. Absorption spectra of DMABN in cyclohexane matrix.
Optical path ~400 μ. B. Base line (absorbance of the Dewar vessel and cell containing cyclohexane only).
[DMABN] = 5×10^{-4} M.
1. −20 °C, 2. -30 ± 2 °C, 3. -46 ± 1°C,
Because of the increase of scattering of light by the crystallization of cyclohexane, the base line is elevated at lower temperatures. However, it is elevated almost uniformly at all observed wavelengths.

Since the absorption bands of the aggregate as well as the F_d band do not show any shift caused by the temperature lowering and the concentration increase, higher aggregates do not appear to be formed in the ground state as well as in the excited state. In the case of the most concentrated solution in Fig. 4(c), we can recognize a fluorescence band at 460 nm in addition to the 390 nm band. In the previous report we also assigned this band to the dimer. However, we have confirmed that the excitation spectra of 460 nm band appears at longer wavelength (~360 nm) than 320 nm and there occurs a considerable decrease in the intensity of 460 nm band after repeated recrystallization of DMABN from *n*-hexane. Moreover, this band was not detectable in a concentrated liquid solution. Therefore, we conclude here that this fluorescence band is due to an aggregate of unknown impurity in DMABN.

If the dimer takes the sandwich configuration where the dimethylamino group lies over the cyano group, the simplified exciton resonance model predicts that the transition between the higher energy exciton state and the ground state is allowed. However, we cannot observe the intensification of the absorption at shorter wavelength side of the monomer band, but we can see only the appearance of the 320 nm band in Fig. 6. The 240 nm band is too much blue shifted from the 285 nm band to be assigned to the higher energy excited state, if we assume the 320 nm band is the lower energy one. The appearance of the 320 and 240 nm bands can be well understood as due to the electrostatic interaction between the excited and non-excited halves in the dimer causing the red shift of the monomer bands at 285 nm and at shorter wavelength than 235 nm, respectively. Of course, we cannot reject entirely the exciton type interaction mechanism

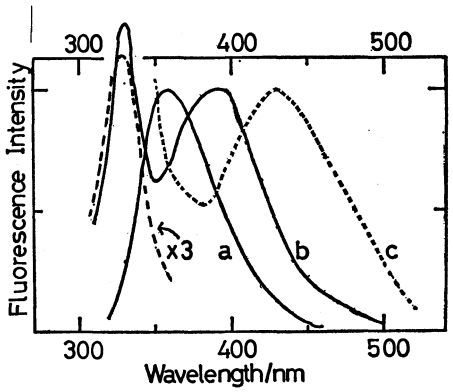

Fig. 7. Fluorescence spectra of DMABN-benzonitrile system in cyclohexane matrix.
[DMABN] = 2×10^{-5} M, [benzonitrile] = 4.9×10^{-2} M.
a. 20 °C, b. 0 ± 1 °C, -17 ± 2 °C.
The spectra were corrected.

on the basis of the above experimental results. There might be more or less contribution of the exciton type interaction to the excited state of the dimer, leading to a little longer fluorescence lifetime of the dimer than that of the monomer.[4] However, it may not be important for the shift of the spectra.

We have examined also the interaction of DMABN with benzonitrile in cyclohexane matrix as shown in Fig. 7. We reported similar spectra in the previous report,[4] where the concentration of DMABN was 5×10^{-4} M. At this concentration, self-complex formation in addition to the formation of hetero-complexes with benzonitrile might be possible. Therefore, we have studied the interaction with benzonitrile, keeping the concentration of DMABN at 2×10^{-5} M, where the self-complex formation can be neglected.

One can see from Fig. 7 that the fluorescence spectra show a remarkable red shift by temperature lowering. As shown in Table 2, not only the fluorescence band but also the excitation spectra show a considerable red shift by the temperature lowering. Whether this hetero-complex is 1 : 1 or 1 : n ($n\geqq2$) aggregate is not very clear at the present stage of the investigation.

We should note here that, we can see only one fluorescence band at 20 °C in Fig. 7. However, we observe two bands at 0 °C as well as at −17 °C, of which the longer wavelength band may be assigned to the complex as discussed above. In the previous report, we have assigned tentatively the short wavelength band to the uncomplexed DMABN. However, this assignment is not well-founded. We cannot make final conclusion at present about the nature of this band.

TABLE 2. TEMPERATURE EFFECT ON THE FLUORESCENCE AND EXCITATION SPECTRA OF DMABN-BENZONITRILE-CYCLOHEXANE SYSTEM

[Benzonitrile] (M)	Temperature (°C)	λ^{f}_{max} (nm)	λ^{e}_{max} (nm)
0	20±1	350±3	284±2
5×10^{-2}	20±1	360±3	288±2
5×10^{-2}	0±1	390±3	292±2
5×10^{-2}	−17±1	430±3	297±2

λ^{f}_{max}: fluorescence band maximum (corrected).
λ^{e}_{max}: maximum of excitation spectra (uncorrected).

At any rate, we have proved that DMABN forms (classical) electrostatic complexes with polar molecules, including the self-complex formation and that the complexation is facilitated in cyclohexane matrix.

BULLETIN OF THE CHEMICAL SOCIETY OF JAPAN, VOL. 46, 3020—3031 (1973)

Calorimetric Study of the Glassy State. VIII. Heat Capacity and Relaxational Phenomena of Isopropylbenzene

Koji KISHIMOTO, Hiroshi SUGA, and Syûzô SEKI

Department of Chemistry, Faculty of Science, Osaka University, Toyonaka, Osaka 560

(Received June 25, 1973)

The heat capacities of isopropylbenzene were measured with an adiabatic calorimeter for the crystal from 14 to 177.13 K (T_m), for the glassy state from 14 to around 126 K (glass transition temperature: T_g) and for the liquid from T_g to 313 K, with a sample of 99.93% purity. The heat and entropy of fusion were found to be 7326 J mol^{-1} and 41.36 J K^{-1} mol^{-1}, respectively. Based on these data, a set of thermodynamic functions are tabulated at rounded temperatures. In addition to the primary glass transition phenomenon, a secondary enthalpy relaxation as well as a step-like heat capacity anomaly was observed at around 70 K. These facts were discussed in correlation with the β-relaxation already observed by dielectric measurement. Configurational entropies of the supercooled liquid and of the glassy state were calculated to investigate a relation with relaxational properties. The agreement is found between the temperatures where catastrophe occurs in viscosity (T_0), and where the configurational entropy vanishes (T_2). Finally, a kind of heat capacity break observed in the liquid state is discussed against the view that this behavior is compatible with a third-order thermodynamic transition.

Recently a considerable number of papers on the glassy state have been accumulated and the concept of "*glassy state*" as a kind of state of matter is getting familiar to the wider circle of investigators. Nevertheless, rather scanty are quantitative treatments to describe this state from the thermodynamic point of view and further to clarify a relationship between dynamical and static properties. One of the purposes of this study is to elucidate a correlation between such dynamical properties as viscosity and relaxation time, and the static ones such as heat capacity, *etc.* In answer to this subject, Adam and Gibbs[1] proposed a description of the relaxation time, τ, in terms of the configurational entropy, S_c. The relation proposed by them is as follows:

$$\tau = A \exp(C/TS_c), \quad (1)$$

where A and C are constants. It was reported that this equation conformed well to the experimental results.[2,3]

As is well known, relaxations found below the glass transition temperature, T_g, are usually designated as

1) G. Adam and J. H. Gibbs, *J. Chem. Phys.*, **43**, 139 (1965).

2) S. S. Chang and A. B. Bestul, *ibid.*, **56**, 503 (1972).

3) J. Greet and D. Turnbull, *ibid.*, **47**, 2185 (1967).

β-relaxation, γ-relaxation, *etc.* in their order of appearance with decreasing temperature. β-relaxation phenomena are frequently observed by mechanical,[4] dielectric and/or nuclear magnetic resonance[5] methods not only for polymers but also for low molecular weight compounds. It is widely believed that heat capacity is not seriously affected by the molecular motions giving rise to these mechanical or dielectric relaxations. We have examined the possible observation by precise calorimetry in the present investigation. On the other hand, several workers have suggested a possible existence of a phase change in a liquid state. In 1953 Moore *et al.*[6] found the discontinuities in the several physical properties such as heat capacity, vapor pressure, density, compressibility, and viscosity in the liquid alkanes. Davies *et al.*[7] pointed out that the discontinuities in viscosity in the liquid states should correspond to thermodynamic transitions of the third order in the sense of Ehrenfest. The verification of the validity of their discussions on the nature of the transition is another principal object of the present investigation.

Experimental

Material. About 40 cm^3 of isopropylbenzene (Tokyo Kagaku Seiki Co. Ltd., claimed purity better than 99.9%) was first purified by molecular sieve (Linde 4A) under vacuum to remove low molecular weight impurities, and subjected to vacuum distillation. The purified sample of 24.997 g of the middle fraction of the distillate was introduced into a container for the heat capacity measurements by vacuum distillation. Helium exchange gas to aid heat transfer in the container was not used. But, no difficulty in establishments of thermal equilibrium was encountered except for the glass transition and the melting temperature ranges. The analysis of the fractional melting process of the sample, as will be described later, indicated the impurity content of 0.07 mol%.

Apparatus. The measurement of heat capacity of isopropylbenzene was carried out by using an adiabatic calorimeter which had been constructed already in this laboratory.[8] A capsule-type platinum resistance thermometer used for the measurement was already calibrated in our laboratory by comparison with the laboratory standard thermometer which had been calibrated at the US National Bureau of Standards according to the International Practical Temperature Scale (1948) above 90 K and the provisional NBS scale below 90 K.

Results

DTA. As a preliminary study of the thermal properties of this material, the differential thermal analysis (DTA) was performed. The results are shown in Fig. 1. Run-1 is for a cooling with a rate of about −0.7 K/min. In Run-1 a sharp exothermic peak was observed at 102 K following after a slight and gradual shift in the base line around 130 K. This

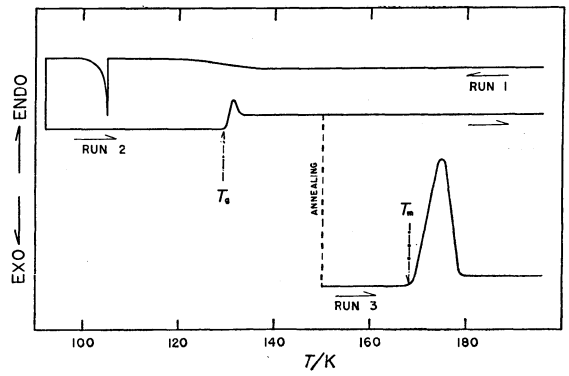

Fig. 1. DTA curves of isopropylbenzene.

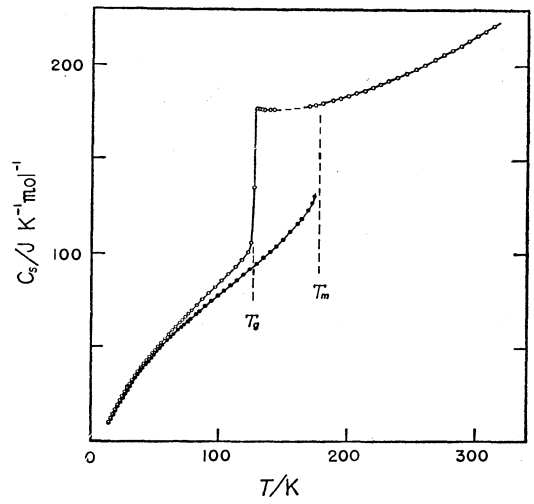

Fig. 2. Heat capacities of isopropylbenzene.
●: Crystalline phase,
○: Glassy, supercooled liquid and liquid phases.

sharp exothermic peak is attributed to the formation of cracks in the sample when the sample vitrifies. The evolution of heat is accompanied with sounding and flashing of visible light. The details of this phenomenon will be published elsewhere.[9] Run-2 is the subsequent heating (heating rate: 1.8 K/min). Only a peak due to the glass transition was observed at 130 K. Run-3 shows the heating curve of the sample which is subjected to annealing at 150 K for over two hours. The endothermic peak at 176 K was attributed to the fusion of the crystalline phase.

Heat Capacity Measurements. The heat capacity data for isopropylbenzene are listed in Table 1 and are depicted in Fig. 2. These series are numbered chronologically so that the thermal history may be followed. Estimation of the vaporization correction was performed by use of the equation given by Hoge.[10] With the aid of the data on the vapor pressure[11] and the specific volume,[12] the correction on the heat capacities

4) Y. Ishida, *J. Polymer Sci.*, **A-27**, 1835 (1969).
5) W. P. Slichter, *J. Chem. Educ.*, **47**, 193 (1970).
6) R. J. Moore, P. Gibbs, and H. Eyring, *J. Phys. Chem.*, **57**, 172 (1953).
7) D. B. Davies and A. J. Matheson, *J. Chem. Phys.*, **45**, 1000 (1966).
8) H. Suga and S. Seki, This Bulletin, **38**, 1000 (1965).
9) To be published in *J. Non-Cryst. Solids.*
10) H. J. Hoge, "Precision Measurement and Calibration, selected NBS Papers on Heat," ed. by D. C. Ginnings (1970).
11) R. C. Wilhoit and B. J. Zwolinski, "Handbook of Vapor Pressures and Heats of Vaporization of Hydrocarbons and Related Compounds," Thermodynamic Research Center Department of Chemistry, Texas A & M University, College Station, Texas 77843 (1971).
12) A. J. Barlow, J. Lamb and A. J. Matheson, *Proc. Roy. Soc., Ser. A*, **292**, 322 (1966).

Table 1. The molar heat capacities of isopropylbenzene
Mol. wt.=120.20 0 °C=273.15 K

T_{av}/K	$\Delta H/\Delta T$/J K^{-1} mol^{-1}	ΔT/K
	(crystalline state)	
	Series 10	
14.54	9.718	1.356
16.16	11.618	1.868
18.06	13.931	1.926
19.99	16.277	1.918
21.80	18.552	1.704
23.53	20.658	1.736
25.37	22.836	1.934
27.21	25.014	1.742
28.97	27.005	1.780
30.83	29.034	1.952
32.92	31.285	2.213
35.04	33.569	2.029
37.00	35.363	1.895
38.87	37.084	1.839
40.91	38.892	2.228
43.07	40.777	2.094
	Series 20	
47.06	43.838	2.288
50.53	46.552	2.386
52.85	48.279	2.259
55.14	49.899	2.346
57.43	51.626	2.235
59.73	53.231	2.387
62.07	54.914	2.302
64.44	56.622	2.435
66.83	58.138	2.364
69.16	59.630	2.297
	Series 11	
72.68	61.921	2.379
75.17	63.464	2.599
77.73	65.003	2.524
	Series 9	
79.36	66.066	2.654
81.90	67.763	2.430
84.31	69.239	2.388
86.67	70.692	2.334
101.09	78.847	2.499
103.57	80.121	2.465
106.01	81.545	2.417
108.50	83.016	2.569
111.05	84.449	2.530
	Series 8	
88.85	71.985	2.336
91.17	73.303	2.290
93.61	74.740	2.602
96.19	75.957	2.552
98.73	77.496	2.519
	Series 12	
113.36	85.767	2.511
115.85	87.147	2.473
118.41	88.700	2.641
121.03	90.089	2.604
123.61	91.676	2.563
126.16	93.239	2.525
128.66	94.672	2.491
131.25	96.134	2.684
133.92	97.851	2.644
136.54	99.567	2.607
139.13	101.159	2.573
141.69	102.602	2.541
	Series 13	
144.00	104.145	2.617
146.60	105.968	2.586
149.17	107.655	2.550
151.82	109.492	2.759
154.56	111.723	2.716
157.40	113.777	2.956
160.32	116.003	2.901
163.36	118.393	3.168
168.56	122.928	3.068
171.60	126.722	2.999
	(supercooled liquid and glassy states)	
	Series 5	
14.53	10.363	1.334
16.00	12.286	1.592
17.69	14.551	1.760
19.44	16.821	1.749
21.29	19.321	1.938
23.09	21.711	1.664
24.86	23.942	1.861
26.73	26.241	1.887
28.54	28.356	1.722
30.35	30.376	1.899
32.38	32.675	2.170
34.47	34.930	1.998
36.70	37.065	2.463
39.07	39.253	2.283
41.28	41.224	2.138
43.36	42.979	2.022
45.55	44.831	2.362
	Series 18	
45.35	44.579	2.312
47.60	46.400	2.187
49.85	48.201	2.307
52.09	49.899	2.185
54.35	51.518	2.337
56.65	53.270	2.255
58.86	54.895	2.186
61.08	56.666	2.253
63.29	58.413	2.162
65.56	60.229	2.375
67.88	61.961	2.268
70.14	63.370	2.253
72.31	64.876	2.089
74.49	66.452	2.284
76.86	68.209	2.444
	Series 6	
69.31	62.796	1.857
71.44	64.277	2.413
73.82	65.950	2.347
76.14	67.609	2.279
78.65	69.658	2.761
81.37	71.615	2.680
84.01	73.543	2.594
	Series 4	
80.23	70.773	2.252
82.45	72.456	2.198
84.62	74.053	2.149
86.79	75.601	2.184
89.13	77.183	2.497
91.61	78.756	2.458
94.14	80.347	2.613
96.73	82.025	2.559
99.26	83.742	2.508
101.75	85.372	2.461
104.30	87.036	2.634
106.91	88.897	2.581
	Series 7	
105.12	87.627	2.398
107.50	89.325	2.359
109.93	91.056	2.500
112.41	92.946	2.463
114.87	94.773	2.428
117.30	96.663	2.382
119.70	98.803	2.339
122.09	100.87	2.299
124.45	105.79	2.222

TABLE 1. (Continued)

T_{av}/K	$\Delta H/\Delta T$/J K^{-1} mol^{-1}	ΔT/K	T_{av}/K	$\Delta H/\Delta T$/J K^{-1} mol^{-1}	ΔT/K	T_{av}/K	$\Delta H/\Delta T$/J K^{-1} mol^{-1}	ΔT/K
126.60	135.17	1.865	182.77	180.41	2.892	241.41	194.75	3.553
128.30	176.86	1.534	185.65	180.87	2.871	244.96	195.95	3.534
130.03	176.61	1.926				248.63	197.01	3.807
131.96	176.34	1.927		Series 1		252.28	198.21	3.496
134.08	176.31	2.309				255.76	199.54	3.479
136.38	176.61	2.306	187.49	181.35	2.919	259.23	200.59	3.453
138.22	176.27	2.620	190.40	181.63	2.912	260.35	200.99	3.452
140.84	176.12	2.614	193.30	182.34	2.896	263.79	202.27	3.435
			196.19	182.99	2.882	267.22	203.38	3.418
	Series 16		199.25	183.52	3.227	270.62	204.76	3.398
			202.47	184.31	3.224	274.02	206.04	3.386
129.82	177.49	2.077	205.70	185.10	3.240	277.39	207.12	3.364
131.90	176.36	2.083	208.93	185.70	3.211	280.79	208.55	3.427
135.33	176.33	2.597	212.18	186.62	3.298	284.30	209.88	3.599
138.97	176.34	4.771	215.47	187.52	3.285			
141.48	176.15	2.511	218.75	188.14	3.268		Series 3	
			222.03	189.21	3.298			
	(supercooled liquid and					287.41	211.07	3.268
	liquid states)			Series 2		290.67	212.43	3.252
						293.92	213.61	3.234
	Series 14		217.81	187.98	3.544	297.14	214.84	3.218
			221.21	189.01	3.252	300.35	216.26	3.196
169.16	178.27	2.250	224.45	189.94	3.229	303.54	217.62	3.178
171.60	178.56	2.626	227.67	190.81	3.218	306.71	218.62	3.166
174.22	179.11	2.613	230.88	191.70	3.197	309.86	220.11	3.145
176.98	179.36	2.909	234.27	192.77	3.587	313.14	221.61	3.410
179.88	179.80	2.894	237.85	193.52	3.575			

was assessed to be less than 0.004% at the highest temperature of the measurements. This figure is within an experimental error of our apparatus. As a consequence, the measured heat capacities are regarded as ones under saturated pressure, C_s. The curvature correction is not taken into consideration.

The glassy state of the specimen was established by cooling the supercooled liquid sample to the liquid nitrogen temperature with a rate of −0.7 K/min in the glass transition region. In order to measure the heat capacities of the supercooled liquid just below the melting point and also just above T_g, we have prepared the sample by two different ways. The supercooled liquid obtained by raising temperature just above T_g was observed to crystallize around 145 K. The measurement on the supercooled liquid in the range from T_g to 141 K was performed in this manner. The measurement from 169 K to the melting point was made for the liquid cooled down to the temperatures not below 165 K to avoid the crystallization during measurements.

The crystalline phase was obtained from the supercooled liquid which had been prepared by heating the glassy state above T_g. The crystal was usually annealed at around 165 K to ensure the completion of the crystallization. No evidence for the existence of a metastable crystalline phase was found from the pursuit of spontaneous temperature rise of the sample during the crystallization process.

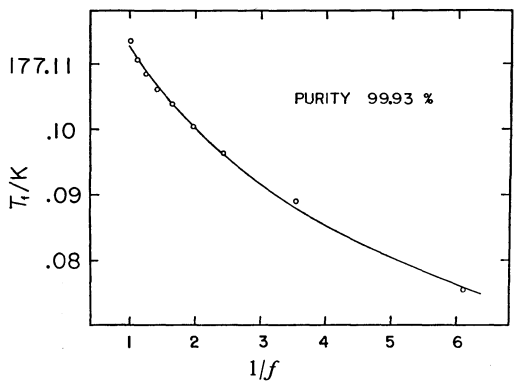

Fig. 3. Melting curve for isopropylbenzene
Open circle: experimental values,
Solid line: theoretical curve.

Determination of the Purity. To determine the melting point and the purity of the present material, a fractional melting experiment was carried out. In Fig. 3 the reciprocal of the fraction of the sample melted, $1/f$, is plotted against the equilibrium final temperature, T_f, of each energy input. As ample time was required for the establishment of thermal equilibrium during the melting process, the extrapolated value of the temperature to the time being infinite at each input was used as T_f. These values are given in Table 2. It is apparent that T_f *versus* $1/f$ plot does not yield a straight line. Therefore, White-

Table 2. The equilibrium temperatures during fusion process

Fraction melted (f)	$1/f$	T_f/K
0.1639	6.103	177.0755
0.2827	3.537	177.0890
0.4127	2.423	177.0964
0.5102	1.960	177.1004
0.6079	1.645	177.1028
0.7052	1.418	177.1061
0.8026	1.246	177.1084
0.8985	1.113	177.1106
0.9933	1.007	177.1135

The melting point of pure isopropylbenzene=177.13 K
Mol% of impurity=0.07%

Taylor-Rossini's method[13,14] which treats impurities as solid-insoluble and liquid-soluble is not applicable. Then, we adopted Mastrangelo-Dornte's method[15] in which they derive a solid solutions treatment for calorimetric melting point data. The equation derived by them is as follows:

$$T_f = T^* - \frac{R(T^*)^2}{\Delta H_F} \frac{X_2}{\frac{K}{1-K}+f}, \qquad (2)$$

where T^* is the triple point of a hypothetical 100% pure material whose heat of fusion is ΔH_F, R the gas constant and X_2 a mole fraction of the impurity whose distribution between the solid and liquid phases is expressed by K. For the determination of K, T^* and X_2 the method of least squares was applied. From this treatment X_2 and T^* are determined to be 0.7×10^{-3} and 177.13 K, respectively. The solid curve in Fig. 3 is the theoretical curve of Eq. (2) with the value of 0.2128 for K. As is seen, data fit this theoretical curve fairly well.

The heat of fusion was measured twice and the values of the molar heat of fusion are given in Table 3.

Table 3. The molar heat of fusion

	ΔH / kJ mol^{-1}
Experiment 1	7.325
Experiment 2	7.326
Mean value	7.326

Estimation of the Heat Capacity for the Supercooled Liquid. Since the heat capacity of the supercooled liquid between 142 and 169 K could not be measured as a result of interference from the crystallization, it was estimated by graphical interpolation of the measured heat capacity data of the supercooled liquid below T_m and just above T_g. A dashed curve in Fig. 2 represents the interpolated heat capacity. The errors arising from arbitrariness in this interpolation are at most 0.2% of C_s of the supercooled liquid. Adequacy of the interpolation as well as the absence of crystal or crystallite in the actual specimen in the glassy state obtained was confirmed by comparing the enthalpy of the supercooled liquid at 142.74 K obtained from the direct measurement with that calculated by use of the interpolated heat capacity. The former is 13.33 kJ mol^{-1} and the latter is 13.34 kJ mol^{-1}. Reference 16 illustrates the procedure of the direct measurement.

Table 4. The third law entropy of liquid at 177.13 K

via crystal

Temperature	Contribution	ΔS/J K^{-1} mol^{-1}
0 —14.0	Effective frequency spectra	4.00±0.05
14.0—177.13	$\int C_s$(cry.)d ln T	131.56±0.13
177.13	Transition $\left(\frac{7326}{177.13}\right)$	41.36±0.04
		176.92±0.22

via glassy state

Temperature	Contribution	ΔS/J K^{-1} mol^{-1}
0 —14.0	Effective frequency spectra	4.17±0.06
14.0—126	$\int C_s$(glass)d ln T	107.79±0.11
126—177.13	$\int C_s$(supercooled liq.)d ln T	52.95±0.05
		164.90±0.22

Residual Entropy of Glassy State. The entropy of the crystal at 0 K was concluded to obey the third law of thermodynamics by comparison of the gaseous entropy determined from thermal data with that computed from the calculated data, as described later. Based on this result the residual entropy of the glassy phase was calculated by a well-defined method which is given in Table 4. Contributions from entropy below 14 K for the crystalline and the glassy phases were determined by adopting the method of effective frequency distribution[17] with some modification. The necessary preset-parameters in this modified method include the two Debye and the Einstein cut-off frequencies. After the conversion of the measured heat capacity C_p into C_v with the aid of the Nernst-Lindemann[18] equation, the effective frequency distributions were determined for several sets of these preset-parameters by using about 20 values for C_v between 14 and 50 K. Fig. 4(A) shows the frequency distributions which reproduce best the heat capacity for the crystalline state of isopropylbenzene and Fig. 4 (B) for the glassy state. The values of entropy below 14 K used in order to assess the residual entropy and to derive the thermodynamic functions of the glassy, crystalline and

13) W. P. White, *J. Phys. Chem.*, **24**, 393 (1920).
14) W. J. Taylor and F. D. Rossini, *J. Res. Nat. Bur. Stand.*, **32**, 197 (1944).
15) S. V. R. Mastrangelo and R. W. Dornte, *J. Amer. Chem. Soc.*, **77**, 6200 (1955).
16) K. Adachi, H. Suga, and S. Seki, This Bulletin, **44**, 78 (1971).
17) M. Sorai and S. Seki, *J. Phys. Soc. Japan*, **32**, 382 (1972).
18) "Handbuch der Experimentalphysik, Band 8, 1. Teil, Energie und Wärmeinhalt" ed. by A. Eucken, Akademische Verlargsgesellschaft M. B. H., Leipzig (1929).

TABLE 5. THERMODYNAMIC FUNCTIONS OF ISOPROPYLBENZENE

T / K	C_s° / J K$^-$ mol^{-1}	S_s° / J K^{-1} mol^{-1}	$(H^\circ-H_0^\circ)/T$ / J K^{-1} mol^{-1}	$-(G^\circ-H_0^\circ)/T$ / J K^{-1} mol^{-1}
		(crystalline phase)		
10	(4.60)	(1.76)	(1.28)	(0.48)
20	16.26	8.39	5.77	2.63
30	28.12	17.28	11.29	6.00
40	38.09	26.79	16.79	10.00
50	46.12	36.17	21.87	14.30
60	53.46	45.24	26.53	18.71
70	60.18	53.99	30.87	23.13
80	66.49	62.44	34.92	27.52
90	72.62	70.63	38.78	31.86
100	78.20	78.58	42.44	36.13
110	83.86	86.29	45.95	40.34
120	89.62	93.84	49.35	44.49
130	95.48	101.24	52.67	48.57
140	101.64	108.54	55.95	52.59
150	108.31	115.77	59.21	56.56
160	115.75	123.00	62.51	60.49
170	124.54	130.26	65.88	64.38
		(glassy state)		
10	(4.83)	(13.81)	(349.89)	(−336.08)
20	17.60	20.94	180.46	−159.52
30	30.01	30.51	128.31	−97.80
40	40.08	40.59	105.06	−64.46
50	48.30	50.44	92.90	−42.46
60	55.92	59.92	86.10	−26.18
70	63.27	69.09	82.32	−13.23
80	70.66	78.01	80.39	−2.38
90	77.76	86.75	79.71	7.04
100	84.21	95.28	79.84	15.44
110	91.16	103.62	80.54	23.08
120	99.03	111.88	81.74	30.14
		(liquid state)		
130	176.62	122.11	85.34	36.77
140	176.23	135.18	91.84	43.34
150	(176.47)	147.34	97.47	49.87
160	(177.21)	158.75	102.43	56.32
170	177.38	169.53	106.86	62.67
180	179.90	179.77	110.87	68.89
190	181.74	189.54	114.55	74.99
200	183.78	198.91	117.96	80.95
210	186.10	207.93	121.15	86.78
220	188.69	216.65	124.16	92.49
230	191.48	225.10	127.03	98.07
240	194.37	233.31	129.77	103.54
250	197.47	241.31	132.42	108.89
260	200.88	249.12	134.98	114.13
270	204.49	256.77	137.49	119.27
280	208.22	264.27	139.95	124.32
290	212.14	271.64	142.37	129.27
300	216.15	278.90	144.76	134.14
310	220.16	286.06	147.13	138.92
298.15	215.40	277.57	144.21	133.36

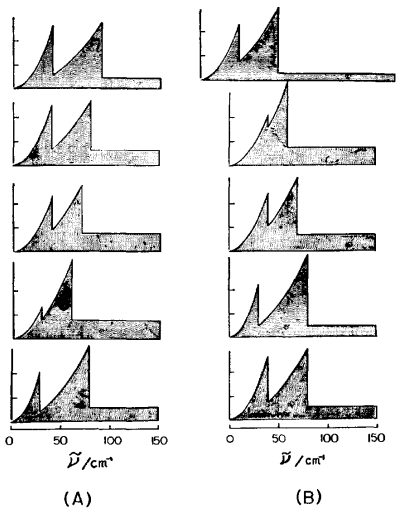

Fig. 4. Frequency distribution spectra determined from the heat capacities below 50 K,
(A) for the crystalline state,
(B) for the glassy state.

liquid phases were obtained by averaging the values of entropy which were calculated based on each lattice frequency spectrum shown in Fig. 4. The residual entropy of the glassy state turns out to be 12.0± 0.5 J K^{-1} mol^{-1}.

Thermodynamic Functions. Thermodynamic functions for the crystalline, glassy and liquid states were derived from the smoothed heat capacity data based on the values listed in Tables 3 and 4, and were all tabulated in Table 5. In the derivation of these values, the crystalline phase at 0 K was taken as a reference state.

Verification of the Third Law for the Crystalline Phase. The calorimetric entropy of isopropylbenzene as an ideal gas at 298.15 K was determined and given in Table 6, together with the values for the heat of vaporization,[19] the critical temperature and pressure.[20] The values of the spectroscopic entropy calculated by Taylor *et al.*[21] for isopropylbenzene, *n*-propylbenzene and *n*-butylbenzene in their ideal gas states

TABLE 6. THE THIRD LAW ENTROPY AT 298.15 K OF ISOPROPYLBENZENE IN IDEAL GAS STATE

Contribution	S/J K^{-1} mol^{-1}
Effective frequency distribution (0—14 K)	4.00
Heat capacity measurement (14—298.15 K)	273.62
Vaporization at 298.15 K	151.40
Gas imperfection correction	0.013
Compression to 1 atm	−42.50
	386.53

19) F. D. Rossini, K. S. Pitzer, R. L. Arnett, R. M. Braun, and G. C. Pimentel, "Selected Values of Physical and Thermodynamic Properties of Hydrocarbons and Related Compounds," Carnegie Press, Pittsburgh, Pa. (1953).
20) K. A. Kobe and R. E. Lynn, Jr., *Chem. Rev.*, **52**, 117 (1953).
21) W. P. Taylor, D. D. Wagman, M. G. Williams, K. S. Pitzer, and F. D. Rossini, *J. Res. Nat. Bur. Stand.*, **37**, 95 (1946).

TABLE 7. MOLAR ENTROPY OF IDEAL GAS AT 298.15 K

	Third law entropy (S/J K^{-1} mol^{-1})	Calculated entropy (S/J K^{-1} mol^{-1})	δ
Isopropylbenzene	386.53	388.57	−0.528
n-Propylbenzene	397.86[a]	400.66	−0.704
n-Butylbenzene	437.86[a]	439.49	−0.372

a) J. F. Messerly, S. S. Todd, and H. L. Finke, *J. Phys. Chem.*, **69**, 4304 (1965).

are compared with the calorimetric ones in Table where δ means $[S(\text{calorimetric})-S(\text{calculated})]/S(\text{calorimetric})\times 100$. The calculated values for these benzene derivatives show systematically positive deviations from the calorimetric ones. These discrepancies seem to exceed the estimated inaccuracies of respective experiments. In view of the approximate method adopted in calculating the spectroscopic entropies, however, it seems plausible to conclude that the third law of thermodynamics is applicable to the crystalline phase of isopropylbenzene rather than to assume a possible existence of randomness at zero Kelvin.

β-Relaxational Phenomenon. In the preceding series[22] of papers we concerned ourselves exclusively with the relaxational effect of primary glass transition phenomena. Glassy state or glassy-crystalline state is a non-equilibrium state and tends to be stabilized by releasing its excess enthalpy toward an equilibrium state. The practical observation of the enthalpy relaxation phenomena is usually limited within a temperature interval of 10—30 K below T_g, owing to the elongation of relaxation time.

During the course of heat capacity measurement in the glassy state, we encountered unusual temperature drifts and a step-like heat capacity increment at around 70 K, far below the primary glass transition temperature. Figure 5 shows the change of the temperature drifts in series 6. Slight exothermic drifts revealed themselves at around 50 K and gradually increased up to about 70 K. On the contrary, above 70 K endothermic drifts were observed and disappeared gradually at higher temperatures. This variation of the temperature drifts is quite similar to that observed in the usual glass transition region. The magnitude of the drifts

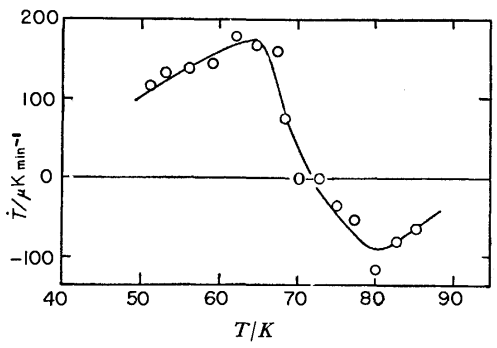

Fig. 5. Temperature-drift change around T_β.

22) K. Adachi, H. Suga, and S. Seki, This Bulletin, **45**, 1960 (1972); *Idem, ibid.*, **43**, 1916 (1970); M. Sugisaki, K. Adachi, H. Suga, and S. Seki, *ibid.*, **41**, 593 (1968).

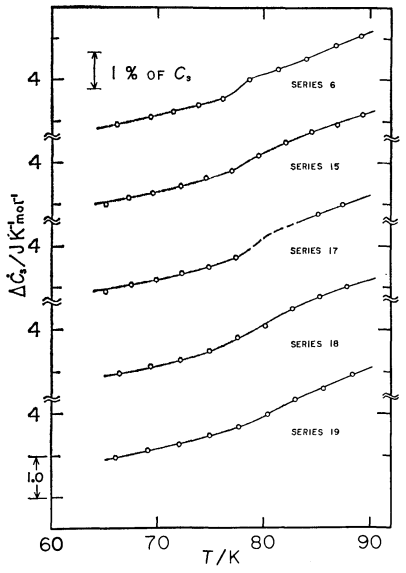

Fig. 6. Excess heat capacity of the glassy phase over the crystalline phase around T_β.

Table 8. Excess heat capacity of the glassy over the crystalline phase

T/K	ΔC_s/J K^{-1} mol^{-1}	T/K	ΔC_s/J K^{-1} mol^{-1}
Series 6		Series 18	
66.22	2.92	66.39	2.95
69.31	3.10	69.33	3.12
71.44	3.22	72.16	3.26
73.82	3.39	74.89	3.48
76.14	3.54	77.52	3.81
78.65	4.00	80.12	4.07
81.37	4.25	82.69	4.48
84.01	4.51	85.29	4.77
86.79	4.84	87.81	5.00
89.13	5.06		
Series 15		Series 19	
65.10	2.99	66.04	2.95
67.25	3.14	69.12	3.11
69.52	3.24	72.09	3.24
72.17	3.42	74.94	3.47
74.55	3.62	77.69	3.67
76.99	3.78	80.36	3.96
79.49	4.16	82.95	4.31
82.04	4.48	85.62	4.56
84.52	4.75	88.37	4.92
86.93	4.91		
89.30	5.17		
Series 17			
65.08	2.88		
67.49	3.06		
69.86	3.17		
72.30	3.34		
74.83	3.48		
77.39	3.71		
85.09	4.75		
87.43	4.98		

Table 9. Thermal history of each run

Series number	Cooling rate around T_g (K/min)	Cooling rate around 70 K (K/min)
6	0.7	2
15	4	0.3
17	3	0.9
18	1	0.5
19	2	3

in this case is far smaller than that around T_g, but larger than that due to a heat leak to or from the calorimetric cell arising from the incompleteness of adiabatic conditions.

Heat capacity measurements for the glassy state in this region were performed several times under different conditions. The C_s values of the glassy state subtracted by those of the crystalline phase were depicted in Fig. 6 for each run and tabulated in Table 8. One can find the abrupt increase in the heat capacity at around 80 K which has a resemblance to that at an ordinary glass transition point. For each series, the specimen was cooled from temperatures far above the melting point down to the liquid nitrogen temperature and then cooled further to around 50 K except for series 6 by use of liquid hydrogen or solid nitrogen as a refrigerant. The thermal history for each series is listed in Table 9. In series 6, the specimen in the glassy state was allowed to stand at the liquid nitrogen temperature for one night prior to being cooled down to 14 K. The thermal drifts were already mentioned for this series (Fig. 5). In the case of series 15, exothermic drifts change into endothermic ones at around 72 K. In series 17, the changeover of the drifts occurs at 78 K. In series 18 the specimen was annealed for 15 days at the liquid nitrogen temperature. In this case only endothermic drifts appeared in the temperature range from 55 to 80 K. The temperature drifts in series 19 were almost the same as in series 18. As is shown in this figure, the hystereses in the heat capacity due to the different thermal histories were perceptible, which reminds us of glass transition phenomena.

The temperature drifts similar to those in the primary glass transition region and the abrupt increase in C_s seem to support the view that a β-transition exists around 70—80 K.

Discussion

β-Relaxation. Johari *et al.*[23] found the β-relaxation for isopropylbenzene by means of dielectric measurements and showed that the Arrhenius plot of the frequency of maximum loss f_{max} against $1/T$ gives a straight line with an activation energy of 8 kcal/mol. Using their data, we extrapolated this Arrhenius plot and determined the temperature at which f_{max} becomes equal to 10^{-3} Hz to be 76 K.

The calorimetric β-transition temperature, T_β, of

23) G. P. Johari and M. Goldstein, *J. Chem. Phys.*, **53**, 2372 (1970).

about 80 K, is in agreement with that inferred from the dielectric measurement. However, the behavior of the thermal drifts in the β-transition region was not interpreted in terms of cooling rates around T_g, and T_β, respectively.

This failure in explanation may be attributed to the small magnitude of the observable temperature drifts which are apt to be significantly influenced by the incomplete adiabatic conditions. The other explanation may be that we could not quench the specimen instantly from the temperature above T_g to far below T_β because at least a few hours were compelled to be consumed under our experimental conditions. As a result the cooling rate could not be varied definitely from run to run. This makes a possible correlation between the cooling rates around both T_g and T_β and the behavior of the temperature drifts difficult to be clarified.

Goldstein[24] proposed that β-relaxation is intrinsic to the glassy state and arising from such degrees of freedom whose freezing out is responsible for the main glass transition. To explain β-relaxation on the basis of the earlier description given by Orowan[25] for viscous flow as an activated process, he put an additional hypothesis to Orowan's picture. The hypothesis is that the packing of molecules in an amorphous state is always such as to give rise to a distribution of barrier height against molecular motions responsible for viscous flow. The existence of lower barriers makes some molecular motions possible to be excited even at temperatures where viscous flow can no longer occur at a detectable rate. When these modes of motion become frozen-in, the β-relaxation would be observed.

However, this hypothesis alone can not account for a question why a maximum of dielectric loss or an abrupt change in heat capacity does appear. The existence of β-relaxation will lead to a hump or a shoulder in relaxation spectra in a shorter time-region than that responsible for the main glass transition, though the broadening out of relaxation spectra can be interpreted by cooperative molecular motions as well as by the distribution of potential barrier heights. If a hump or a shoulder does not exist in the spectra, a maximum of dielectric loss or an abrupt increase in heat capacity below T_g will not be expected and only a continuous loss will appear. In Goldstein's picture there is no reason for the existence of a hump (*i.e.*, the existence of many barriers with the same heights in a particular range). However, by taking into account molecular rearrangements involving defects or holes as a hypothesis in addition to Goldstein's description, the above question can be explained. Around holes less cooperative molecular motions should occur in a shorter time than those in other normal parts. Such molecular motions are expected to be responsible for a hump in the spectra and consequently related to β-relaxation.

Relation between Relaxation Time and Configurational Entropy. The validity of the Adam-Gibbs equation (Eq. (1)) was examined along the following line. Viscosity, η, in a supercooled liquid region is given by the Fulcher-Tammann-Hesse equation

$$\ln \eta = A' + B'/(T - T_0), \tag{2}$$

where A', B' and T_0 are constants. η is also related to τ by the equation

$$\eta = G_\infty \tau, \tag{3}$$

where G_∞ is the limiting high frequency shear modulus. If Eq. (1) holds, combination of Eqs. (1) and (3) yields

$$\ln \eta = \ln G_\infty + \ln A + \frac{C}{TS_c}. \tag{4}$$

The temperature dependence of G_∞ is given by the following equation[26]

$$G_\infty = G_0 + \frac{B''}{T - T_0'},$$

where G_0 is the rigidity modulus at the temperature T_0', and B'' a constant. On the other hand, τ and η usually vary exponentially with temperature. Therefore, the temperature dependence of G_∞ may be neglected compared with those of τ and η, and comparing Eq. (2) with Eq. (4), one is led to a conclusion that the quantity TS_c is proportional to $T - T_0$ and S_c must vanish at T_0 as far as the approximation adopted above is correct. The temperature at which the configurational entropy vanishes is designated as T_2. Experimentally, T_2 temperature is determined from the intersection of the extrapolated entropy curve of a supercooled liquid (curve *c–d* in Fig. 7) and the entropy curve (*a–g*) which is obtained by subtracting the residual entropy (segment *e–a* of the ordinate) from the entropy curve for the glassy state (*e–f*). Curve *a–g* is corresponding to the entropy curve of a hypothetical phonon system in the glassy state. However, estimation of the entropy of the hypothetical phonon system of this ideal glass by the method described above is not accurate. If the temperature of supercooled liquid is lowered along the equilibrium curve *d–c*, volume contraction takes place mainly by virtue of the change in the configura-

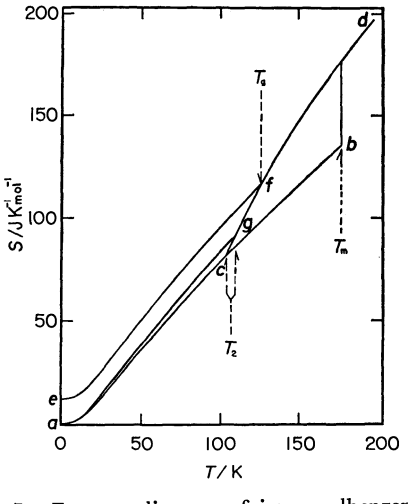

Fig. 7. Entropy diagram of isopropylbenzene.

24) M. Goldstein, *J. Chem. Phys.*, **51**, 3728 (1969).
25) E. Orowan, "Creep in Metallic and Non-Metallic Materials," Proceedings of the First U. S. National Congress of Applied Mechanics, A. S. M. E., (1952) p. 453.
26) A. J. Barlow, J. Lamb, A. J. Matheson, P. R. K. L. Padmini, and J. Richter, *Proc. Roy. Soc. A*, **298**, 467 (1967).

tion. This volume contraction will change the frequency distribution spectra and in turn affects the entropy of the phonon system[27] in a decreasing direction. Accordingly, T_2 thus obtained is an upper limit of the temperature at which the configurational entropy vanishes. On the other hand, the temperature at which the entropy curve of crystal (a–b) intersects curve c–d is considered as a lower limit.

For comparison, T_2 temperature along with the values of T_0 obtained from the viscosity data based on the Fulcher-Tammann-Hesse equation (Eq. (2).) are listed in Table 10 for two compounds. The second

Table 10. Comparison between T_2 and T_0

	Calorimetric T_2	Viscosity T_0
Isopropylbenzene	109.5—103.5K	93.8K
o-Terphenyl	207 —204K	200K

column shows the upper and the lower limits for T_2. Consistency between the values of T_2 obtained by the static method of calorimetry and T_0 by the dynamical method of viscosity measurements is fairly good. This agreement supports the Adam-Gibbs equation. Figure 8 depicts TS_c plotted against temperature for isopropylbenzene. Although estimation of S_c includes an unavoidable ambiguity due to the extrapolation of curve a–g (Fig. 7) up to about 160 K, a fairly well linear relationship was observed between them. For propan-1-ol[28] small deviation is seen in the plot of TS_c *vs.* T. For the supercooled liquid phases of o-terphenyl[2] and 2-methylpentane[38] as well as for the supercooled plastic crystalline phase of 2,3-dimethylbutane,[16] this relationship was found to hold also fairly well. In such a way, we can propose a rough method to interpret the relaxation time in terms of the configurational entropy by using the Adam-Gibbs equation for an equilibrium supercooled liquid phase and/or for a supercooled plastic crystalline phase.

It may be added that the relation $TS_c \propto T-T_2$ has to lead the following thermodynamic functions:

$$C_{conf} \propto \frac{1}{T}\theta(T-T_0)$$

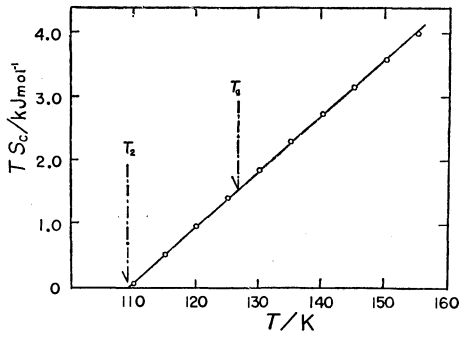

Fig. 8. Temperature dependence of the configurational entropy multiplied by temperature for isopropylbenzene.

and

$$H_c \propto \ln\frac{T}{T_2}\theta(T-T_0) ,$$

where C_{conf} is configurational heat capacity and θ the step function.

Anomalous Behavior of the Heat Capacity in the Liquid State. Recently there have been suggested the possible existence of a phase change in a liquid state by several workers. In 1953 Moore *et al.*[6] found the discontinuities in the several physical properties such as heat capacity, vapor pressure, density, compressibility, and viscosity of liquid alkanes. For example, they found that the change of the heat capacity of *n*-heptane with temperature can be well represented by two straight lines with a more or less gradual transition from one to the other over a rather narrow temperature range. They attributed these discontinuities to the onset of specific molecular motions (*i.e.*, translation↔libration↔free rotation). Davies *et al.*[7] pointed out that the discontinuity in viscositity of liquid should correspond to a thermodynamic transition which is due to the restriction of the rotation of molecules (translation↔one axis rotation↔two axes rotation equivalent to free rotation). They referred to the analysis of the heat capacity data by Moore *et al.*, mentioned above, and they concluded that the transition should correspond to the third order in the sense of Ehrenfest.

As is well known, the viscosity, η, of liquids at temperatures fairly above their melting points is well described by the Arrhenius equation

$$\ln\eta = A+E/RT, \qquad (5)$$

where A is a constant, R the gas constant, and E the activation energy for viscous flow. However, this equation is not usually applicable to liquids of high viscosity or to supercooled liquids. Fulcher[29] and Tammann & Hesse[30] found an empirical equation for these liquids

$$\ln\eta = A'+B'/(T-T_0) , \qquad (2)$$

where A', B' and T_0 are constants. For some liquids it became apparent[31] that the viscosity could not be

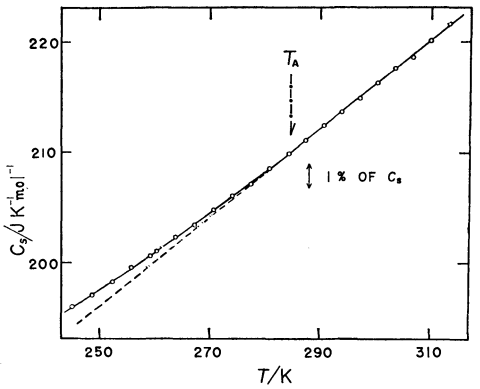

Fig. 9. Heat capacity of isopropylbenzene in the liquid state.

27) C. M. Guttman, *J. Chem. Phys.*, **56**, 627 (1972).
28) J. F. Counsell, E. B. Lees, and J. F. Martin, *J. Chem. Soc., Sec. A*, No. 8, 1819 (1968).
29) G. S. Fulcher, *J. Amer. Ceram. Soc.*, **8**, 339 (1925).
30) G. Tammann and W. Hesse, *Z. Anorg. Allgem. Chem.*, **156**, 245 (1926).
31) A. J. Barlow, J. Lamb, and A. J. Matheson, *Proc. Roy. Soc., Ser. A*, **292**, 322 (1966).

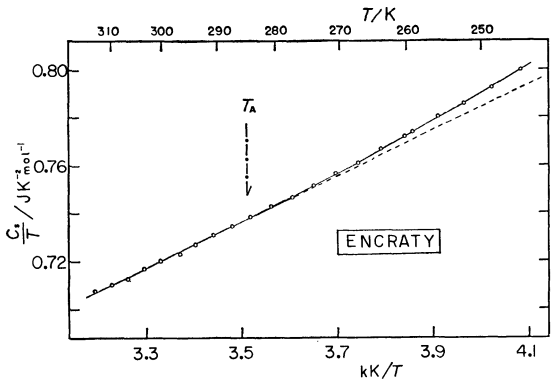

Fig. 10. Encraty *vs.* $1/T$ plot for isopropylbenzene in the liquid state.

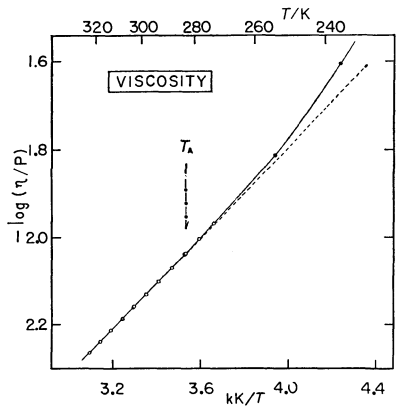

Fig. 11. Arrhenius plot of viscosity which can be compared with Fig. 10,
●: from Ref. 12. ○: from Ref. 19.

described by a single equation (Eq. (2)) over the whole temperature range except for the high temperature Arrhenius region. Thus, two sets of constants in Eq. (2) are required in two separate temperature regions. The temperature at which Arrhenius type temperature dependence changes into non-Arrhenius one is designated as Arrhenius temperature T_A. The temperature at which transformation of one type of non-Arrhenius behavior occurs into another type of non-Arrhenius behavior is designated as intersection temperature T_K. It is interesting to know how heat capacity behaves at T_A and T_K, and also to investigate the order of transitions if they exist.

The heat capacity data of isopropylbenzene over the temperature range in question are reproduced in Fig. 9 in an enlarged scale. Above *ca.* 285 K the heat capacity is well represented by a straight line, while below that it fails. The change of the heat capacity with temperature below T_A is not described by a straight line as was suggested by Moore *et al.* in the case of *n*-heptane. This is true of many compounds described later we examined for which the heat capacity data are available in the literature. The lowest temperature below which the heat capacity deviates from the straight line can not be determined within the temperature range of some 5 K because of the restriction of the precision in our heat capacity measurement. But it agrees with the Arrhenius temperature, T_A, of

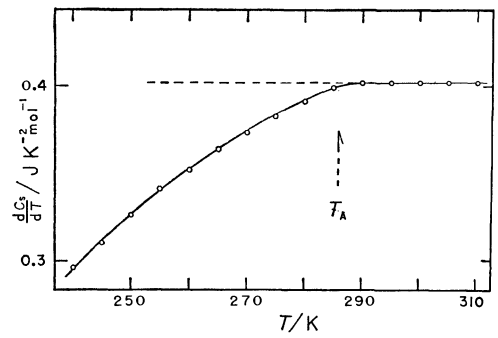

Fig. 12. Temperature derivative of heat capacity for isopropylbenzene in the liquid state.

283 K.[7] The encraty, C_s/T, of isopropylbenzene is plotted against $1/T$ in Fig. 10, which will be compared with the plots of $\ln\eta$ *vs.* $1/T$ of the same substance given in Fig. 11. These figures show that above *ca.* 285 K both C_s/T and $\ln\eta$ vary linearly with $1/T$.

At the third-order transition point the third derivative of the Gibbs free energy with respect to temperature $(\partial^3 G/\partial T^3)_p = -\partial(C_p/T)/\partial T$ is discontinuous, which should lead to a jump in dC_p/dT. dC_s/dT of isopropylbenzene determined from the smoothed curve of C_s is plotted in Fig. 12. By the way, in the case of isopropylbenzene $(C_p - C_s)/C_p$ at 313 K amounts to 0.63×10^{-4} which is within an experimental error, so we can regard C_s as C_p over the whole temperature range of our observation. No jump in dC_p/dT or d^2C_p/dT^2 is found, as is seen in Fig. 12. If dC_p/dT *vs.* T curve is concave upward up to T_A and then horizontal, the anomalous behavior of the heat capacity at T_A is compatible with the fourth-order transition because a jump appears in d^2C_p/dT^2 *vs.* T curve in this case. Actually, however, the dC_p/dT *vs.* T curve is convex upward, so this anomalous behavior is a transition, if any, of higher order than fourth. This fact is quite the same for *n*-butylbenzene,[32] *n*-propylbenzene[32] and ethylbenzene[33], *etc.* In order to discuss the nature of the anomalous behavior of this kind, more detailed heat capacity measurements with higher precision and resolution would be required.

Liquids composed of spherical molecules such as neopentane[19,34] and carbon tetrachloride[35-37] show Arrhenius behavior of the viscosity and the linear temperature dependence of the heat capacity, C_s, over the whole temperature range investigated. These are just the behavior of isopropylbenzene and analogous compounds in the limiting higher temperature region above T_A. These facts suggest a similarity of

32) J. F. Messerly, S. S. Todd, and H. L. Finke, *J. Phys. Chem.*, **69**, 4304 (1965).
33) G. B. Guthrie, Jr., R. W. Spitzer, and H. M. Huffmann, *J. Amer. Chem. Soc.*, **66**, 2120 (1944); R. B. Scott and F. G. Brickwedde, *J. Res. Nat. Bur. Stand.*, **35**, 501 (1945).
34) J. G. Aston and G. H. Messerly, *J. Amer. Chem. Soc.*, **58**, 2354 (1936).
35) J. Timmermanns, "Physico-Chemical Constants of Pure Organic Compounds," Elsevier Publ. Co. New York (1950).
36) D. Horrison and E. A. Moelwyn-Hughes, *Proc. Roy. Soc., Ser. A*, **230**, 230 (1957).
37) W. T. Richards and J. H. Wallance, Jr., *J. Amer. Chem. Soc.*, **54**, 2705 (1932).
38) D. R. Douslin and H. M. Huffman, *ibid.*, **68**, 1704 (1946).

rotational modes in a period of successive translational jump for non-spherical molecules above T_A to those modes for spherical molecules.

In passing, we should call attention to the way of compilation of heat capacity data of liquids. Usually the temperature dependence of the heat capacity of liquid is expressed as a following equation over a whole temperature range.

$$C_p = a + bT + cT^2 + dT^3,$$

where a,b,c and d are constants. However, based on our results we propose to divide the temperature range of liquid at least into two parts for more appropriate method of the compilation, *i.e.*, above and below T_A.

Summary

(1) The heat capacities of isopropylbenzene were measured for the crystal from 14 to T_m (177.13 K), for the glassy state from 14 to T_g (around 126 K) and for the liquid from T_g to 313 K, on a sample with purity of 99.93%. The heat and entropy of fusion were found to be 7326 J mol^{-1} and 41.36 J K^{-1} mol^{-1}, respectively. Gibbs energy function, enthalpy function and entropy in the solid and liquid states were calculated at selected temperatures from 15 to 310 K.

(2) The calorimetric entropy in the ideal gas state at 298.15 K, 386.53 J K^{-1} mol^{-1}, was compared with the calculated one given by Taylor *et al.* It was concluded that the crystal follows the third law of thermodynamics. Based on this result, the residual entropy for the glassy state was determined to be 12.0$\pm$0.5 J K^{-1} mol^{-1}.

(3) Aside from the primary glass transition phenomenon, a secondary relaxation was found in temperature drifts of the calorimetric cell in the temperature region centered at around 70 K and a step-like heat capacity anomaly was observed at around 75 K. This phenomenon was discussed with relation to the β-relaxation already observed by dielectric measurement.

(4) Temperature dependence of the configurational entropy of the supercooled liquid was investigated to see whether the Adam-Gibbs equation holds or not. And also, the agreement was found between the temperature at which catastrophe occurs in viscosity and the temperature at which the configurational entropy vanishes.

(5) A kind of heat capacity break was observed in the liquid state, which was discussed against the view that this behavior was compatible with the third-order thermodynamic transition. The temperature *ca.* 285 K at which anomalous behavior of heat capacity occurred was in agreement with that where a discontinuity in the temperature dependence of the viscosity was found.

BULLETIN OF THE CHEMICAL SOCIETY OF JAPAN, VOL. 46, 3031—3035 (1973)

Brillouin Scattering and Elastic Constants of Potassium Bromide

Hiroatsu MATSUURA and Tatsuo MIYAZAWA

Institute for Protein Research, Osaka University, Yamada-kami, Suita, Osaka 565

(Received July 12, 1973)

The Brillouin scattering of KBr crystals was measured by using a helium-neon laser and a pressure-scanned Fabry-Perot interferometer. The Brillouin shifts were measured for various crystal orientations with the scattering vector in the [110] plane. In addition to the strong Brillouin peaks due to the longitudinal acoustic mode, relatively weak Brillouin peaks due to the transverse mode with admixture of the longitudinal mode were clearly resolved for a certain range of crystal orientations. From these Brillouin shifts, the frequencies and velocities of thermally excited sound waves of the wavelength 286.9 nm were obtained, and the three independent elastic constants of the KBr crystal for sound waves of microwave frequencies 6—12 GHz were determined as $C_{11}=3.37\times10^{11}$, $C_{12}=0.61\times10^{11}$ and $C_{44}=0.51\times10^{11}$ dyn/cm^2. The elastic constants determined in the present study were close to the ultrasonic values, indicating little dispersion of the sound velocities for the regions between 10 MHz and 10 GHz.

Brillouin spectroscopy has become a valuable technique for studying thermal and transport properties of matter, with the introduction of lasers as intense monochromatic sources, combined with high-resolution interferometers. One of the important applications is the measurement of velocities of thermal sound-waves in crystals in the microwave region. The sound-wave velocity obtained from Brillouin scattering is used to determine the elastic constants, without any external acoustic excitation. The Brillouin scattering technique has been employed for determining the elastic constants of some alkali halide crystals. The elastic constants determined accurately for KCl, RbCl and KI crystals[1] agreed very well with the results of ultrasonic measurements, indicating that there was no dispersion of sound-wave velocities for the regions between 10 MHz and 10 GHz.

In the present study, the Brillouin scattering of KBr crystals was measured by using a helium-neon laser and a pressure-scanned Fabry-Perot interferometer. The elastic constants determined are compared with ultrasonic values and the sound velocity dispersion is discussed. The present results are also compared with previous results of a Brillouin scattering study on KBr.[2]

1) G. B. Benedek and K. Fritsch, *Phys. Rev.*, **149**, 647 (1966).
2) H. Kaplan, J. Shaham, and W. Low, *Phys. Lett.*, **31A**, 201 (1970).

TABLE 1. FREQUENCIES AND VELOCITIES OF SOUND WAVES OF 286.9 nm WAVELENGTH AS A FUNCTION OF PROPAGATION DIRECTION IN THE [110] PLANE IN KBr

Angle ϕ (deg)	Longitudinal mode (L)		Mixed mode (M)	
	Frequency[a] (GHz)	Velocity[a] (m/sec)	Frequency[a] (GHz)	Velocity[a] (m/sec)
24	11.52	3306		
25	11.44	3284		
26	11.39	3270		
29	11.18	3207		
30	11.08	3181	6.19	1776
31	11.00	3157	6.27	1800
34	10.79	3097	6.46	1855
36	10.68	3063	6.61	1896
39	10.46	3002	6.83	1960
40	10.39	2981	6.89	1976
41	10.36	2973	6.97	1999
44	10.16	2916	7.07	2030
46	10.08	2891		
49	9.97	2861		
51	9.93	2851		
55	9.91	2843		
60	9.99	2866		
65	10.12	2903		
70	10.24	2938		
75	10.38	2980		
80	10.44	2997		
85	10.53	3021		
90	10.54	3025		

a) Averaged experimental errors for the frequency and the velocity are ± 0.07 GHz and ± 20 m/sec, respectively.

Experimental

The experimental arrangement for the observation of Brillouin scattering spectra used in the present study is shown schematically in Fig. 1. The light source was a helium-neon gas laser (Nippon Electric Co., Model GLG 108), which was operated in the fundamental transverse mode at 632.8 nm with an output of about 50 mW. The laser beam passed through the sample which was rotated in such a way that any direction in a [110] plane could be set parallel to the scattering vector. The light scattered at 90° away from the direction of the incident beam was led to a pressure-scanned Fabry-Perot interferometer of Mizojiri Kogaku Kogyo Co. The ring pattern was centered on an aperture of a 1 mm diameter and the intensity of the emerging light was detected by an S20 photomultiplier (Hamamatsu Corp., R374), whose output was measured by an electronic picoammeter and recorded on an X–Y recorder. The electric vector of the incident laser light was set perpendicular to the scattering plane. The spacer between the interferometer etalons had a thickness of 6 mm, giving a free spectral range of 25 GHz. The exact thickness was measured by a micrometer to within 4 μm. The interferometer was scanned by evacuating the optical chamber and then allowing air leakage slowly.

In the measurements of the Brillouin scattering, the crystal

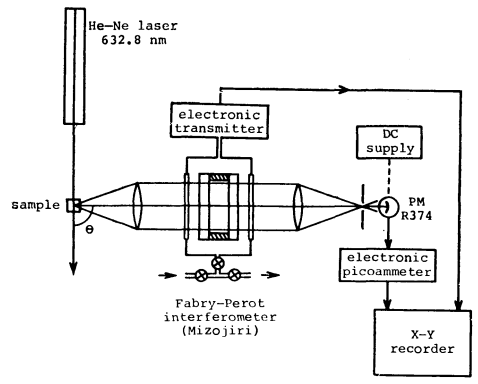

Fig. 1. Experimental arrangement for Brillouin scattering measurements.

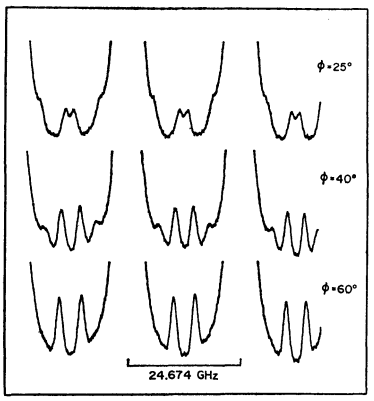

Fig. 2. Brillouin spectra of KBr for $\phi = 25°$, 40° and 60°.

sample of KBr, a cube with 5 mm on an edge, was immersed in anethole ($CH_3CH{=}CHC_6H_4OCH_3$). This liquid had nearly the same index of refraction as KBr, and surface scattering from KBr crystal was largely eliminated. The sample was supported by a rotatable holder so that the scattering vector was kept in the [110] plane of the crystal. The Brillouin spectra were measured as a function of the angle ϕ (24°—90°) between the scattering vector and the [001] direction. For $\phi<25°$, the Stokes Brillouin line overlapped the anti-Stokes line (and *vice versa*) of the adjacent spectral order. The spectra were scanned as slowly as about ten minutes over one free spectral range of 25 GHz, so as to resolve relatively weak Brillouin lines due to the transverse mode with admixture of the longitudinal mode. The scattering measurements were made at 20±1 °C at least six times for each orientation of the crystal.

Typical examples of the observed spectra for $\phi=25°$, 40° and 60° are shown in Fig. 2, and the observed frequency shifts and sound velocities are listed in Table 1.

Brillouin Scattering and Elastic Constants

Brillouin scattering shifts are proportional to the velocity of thermally excited sound waves whose wavelengths are of the same order as the wavelength of light. The sound velocity, V, in the medium is related to the frequency shift, Ω, due to the Doppler effect on the light from reflection by the sound wave:[1,3]

$$\Omega/\omega = \pm 2(V/c)n\sin(\theta/2), \tag{1}$$

where ω is the frequency of the incident light wave, c is the velocity of light in vacuum, n is index of refraction of the medium and θ is the angle of scattering. The frequency shift, Ω, is equal to the frequency of the sound wave responsible for the light scattering.

In a crystal, there are in general three modes of elastic waves, one longitudinal and two transverse modes, propagating with different velocities. Thus, V in Eq. (1) can take three values and accordingly one should observe generally three pairs of Brillouin components with different frequency shifts in the scattering by any crystal.[4] Also, in the crystal, one may obtain from the Brillouin spectra the frequencies and velocities of sound waves as a function of crystal orientation. This observation can be made by bringing different crystal directions parallel to the scattering vector. For a cubic crystal, each of the three acoustic waves which propagate in the direction of principal symmetry, namely the [001], [111] or [110] direction, is a pure longitudinal or transverse wave, and the two transverse modes are degenerate for the [001] and [111] directions. In general for the cubic crystal, the sound waves which propagate in the [110] plane have the following polarizations; the first acoustic wave (T) is purely transverse for any crystal direction, the second wave (M) is largely transverse with admixture of the longitudinal mode, and the third wave (L) is almost entirely longitudinal.

The elastic constants are closely related to the sound velocities of the three waves in the acoustic branches. The sound velocities, V, are given as roots of the following equation[5]

$$\begin{vmatrix} \lambda_{11}-\rho V^2 & \lambda_{12} & \lambda_{13} \\ \lambda_{12} & \lambda_{22}-\rho V^2 & \lambda_{23} \\ \lambda_{13} & \lambda_{23} & \lambda_{33}-\rho V^2 \end{vmatrix} = 0, \tag{2}$$

where ρ is the mass density, and λ_{ab} is given by

$$\lambda_{ab} = l^2C_{1a1b} + m^2C_{2a2b} + n^2C_{3a3b} + mn(C_{2a3b}+C_{3a2b}) + nl(C_{3a1b}+C_{1a3b}) + lm(C_{1a2b}+C_{2a1b}), \tag{3}$$

where l, m and n are the direction cosines of the propagation direction of the sound wave and the suffixes to the elastic constants are written in full. However, the elastic constants C_{iajb} in Eq. (3) may be converted into C_{pq} in the more usual notation by changing the suffixes ia and jb to p and q, respectively, in manner that 11→1, 22→2, 33→3, 23→4, 31→5 and 12→6. The general expression in Eq. (2) is specialized for the case of a cubic crystal as a function of the propagation direction, ϕ, in the [110] plane, where ϕ is the angle between the [001] direction and the propagation direction of the sound wave,

$$\begin{vmatrix} \frac{1}{2}[(C_{44}+C_{11}) + (C_{44}-C_{11})\cos^2\phi] - \rho V^2 & -\frac{1}{2}(C_{44}+C_{12})\sin^2\phi & -\frac{1}{\sqrt{2}}(C_{44}+C_{12})\sin\phi\cos\phi \\ -\frac{1}{2}(C_{44}+C_{12})\sin^2\phi & \frac{1}{2}[(C_{44}+C_{11}) + (C_{44}-C_{11})\cos^2\phi] - \rho V^2 & \frac{1}{\sqrt{2}}(C_{44}+C_{12})\sin\phi\cos\phi \\ -\frac{1}{\sqrt{2}}(C_{44}+C_{12})\sin\phi\cos\phi & \frac{1}{\sqrt{2}}(C_{44}+C_{12})\sin\phi\cos\phi & C_{44}-(C_{44}-C_{11})\cos^2\phi - \rho V^2 \end{vmatrix} = 0. \tag{4}$$

Equation (4) may be rewritten into a more convenient form by transforming the coordinates a, b and c into $(1/\sqrt{2})(a+b)$, $(1/\sqrt{2})(a-b)$ and c. Of these new coordinates, the first one is perpendicular to the [110] plane and corresponds to the pure transverse mode (T), and the hybridization of the second and third, both in the [110] plane, gives the longitudinal mode (L) and mixed mode (M). The transformed equation is given by

$$\begin{vmatrix} \frac{1}{2}[(C_{11}-C_{12}) + (2C_{44}+C_{12}-C_{11})\cos^2\phi] - \rho V^2 & 0 & 0 \\ 0 & \frac{1}{2}[(2C_{44}+C_{11}+C_{12}) - (C_{11}+C_{12})\cos^2\phi] - \rho V^2 & -(C_{44}+C_{12})\sin\phi\cos\phi \\ 0 & -(C_{44}+C_{12})\sin\phi\cos\phi & C_{44} - (C_{44}-C_{11})\cos^2\phi - \rho V^2 \end{vmatrix} = 0. \tag{5}$$

3) R. S. Krishnan, "The Raman Effect," ed. by A. Anderson, Marcel Dekker, New York (1971), p. 343.

4) If the birefringence is taken into consideration, there should in general be twelve pairs of Brillouin components.[3]

5) M. J. P. Musgrave, *Proc. Roy. Soc. London*, **A226**, 339 (1954).

Accordingly, the velocities of the three sound waves, V_T, V_L and V_M, are obtained as

$$\rho[V_T(\phi)]^2 = \frac{1}{2}[(C_{11}-C_{12}) + (2C_{44}+C_{12}-C_{11})\cos^2\phi], \tag{6}$$

$$\rho[V_L(\phi)]^2 = \frac{1}{4}[(4C_{44}+C_{11}+C_{12}) - (2C_{44}+C_{12}-C_{11})\cos^2\phi + \{(C_{11}+C_{12})^2 + (2C_{44}+C_{12}-C_{11}) \times [(8C_{44}+14C_{12}+6C_{11})\cos^2\phi - (6C_{44}+15C_{12}+9C_{11})\cos^4\phi]\}^{1/2}], \tag{7}$$

and

$$\rho[V_M(\phi)]^2 = \frac{1}{4}[(4C_{44}+C_{11}+C_{12}) - (2C_{44}+C_{12}-C_{11})\cos^2\phi - \{(C_{11}+C_{12})^2 + (2C_{44}+C_{12}-C_{11}) \times [(8C_{44}+14C_{12}+6C_{11})\cos^2\phi - (6C_{44}+15C_{12}+9C_{11})\cos^4\phi]\}^{1/2}]. \tag{8}$$

For the directions of principal symmetry [001], [111] and [110], corresponding to $\phi=0°$, 54.7° and 90°, respectively, Eqs. (6), (7) and (8) are reduced to the following simplified forms; for the [001] direction, $\rho V_L^2=C_{11}$ and $\rho V_M^2=\rho V_T^2=C_{44}$; for the [111] direction, $\rho V_L^2=[2(2C_{44}+C_{12})+C_{11}]/3$ and $\rho V_M^2=\rho V_T^2=(C_{44}+C_{11}-C_{12})/3$; and for the [110] direction, $\rho V_L^2=(2C_{44}+C_{12}+C_{11})/2$, $\rho V_M^2=C_{44}$ and $\rho V_T^2=(C_{11}-C_{12})/2$.

The intensity of the Brillouin scattering in a crystal is determined by the polarization directions of the incident and scattered light waves and of the sound wave, the propagation direction of the sound wave, and the magnitude of the elasto-optical constants.[6] The formulas for the Brillouin intensity have been derived for a cubic crystal as a function of the angle ϕ.[1] The formulas indicate that the Brillouin intensity of the longitudinal mode (L) in the entire ϕ region and of the mixed mode (M) in a certain ϕ region is strong enough, but the intensity of the purely transverse mode (T) is much weaker than the former two modes. Therefore, the Brillouin component due to the transverse mode is not expected to be observable in the spectra.

Results

In the present study, the Brillouin scattering measurements were made for the scattering angle $\theta=90°$, and the wavelength of the scattering sound wave λ_s is given from Eq. (1) by

$$\lambda_s = \lambda_0/(\sqrt{2}n), \tag{9}$$

where λ_0 is the wavelength of the incident light in vacuum. By substituting $\lambda_0=632.8$ nm for a helium–neon laser and $n=1.5594$ for KBr,[7] $\lambda_s=286.9$ nm is obtained, which is common to all orientations of the crystal.

The observed spectra in Fig. 2 exhibit two kinds of Brillouin components, a stronger one with a larger frequency shift and a weaker one with a smaller frequency shift. The former is assigned to the longitudinal mode (L) and the latter to the mixed mode (M) (a largely transverse mode with admixture of the longitudinal mode), as suggested from the theoretical relative intensities. The Brillouin component due to the mixed mode was resolved clearly for $\phi=30°$—44°. The intensity of this mode was previously expected to be strong enough only for this ϕ region.[1,2] Also, if ϕ is smaller than 30°, the velocity of the mixed mode is so low that the mixed-mode peak apparently merges into the strong central peak. Variation of the relative intensity of the longitudinal mode with the angle ϕ is also noted in Fig. 2. The intensity increases progressively as ϕ is increased up to 60°, and reaches maximum and finally decreases slightly as ϕ is further increased to 90°. This pattern is in agreement with the intensity variation previously calculated for KBr by Kaplan *et al.*[2]

The sound velocities listed in Table 1 were obtained from the observed frequency shifts by Eq. (1). In Fig. 3, the observed sound velocities V_L and V_M for the longitudinal and mixed modes are plotted against the angle ϕ. From the observed sound velocities, the three independent elastic constants C_{11}, C_{12} and C_{44} were determined from Eqs. (7) and (8) by the method of least squares. The mass density[8] of $\rho=2.744$ g/cm^3 was used for the calculation. The values of the elastic constants are listed in Table 2, and the sound velocities V_L, V_M and V_T calculated from these

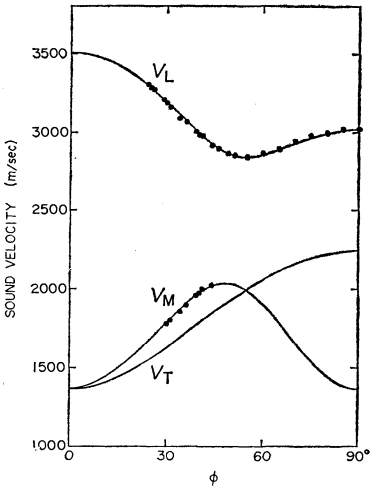

Fig. 3. Velocity of sound waves in KBr as a function of propagation direction in the [110] plane; ϕ is the angle between the propagation direction and the [001] axis.
●: observed value; ——: calculated value.

6) I. L. Fabelinskii, "Molecular Scattering of Light," Plenum Press, New York (1968), p. 139.

7) "Kagaku Benran," ed. by the Chemical Society of Japan, Maruzen, Tokyo (1966).

8) O. D. Slagle and H. A. McKinstry, *J. Appl. Phys.*, **38**, 437 (1967).

Table 2. Elastic constants of KBr at room temperature, in units of 10^{11} dyn/cm^2

	C_{11}	C_{12}	C_{44}
Brillouin scattering			
Present study (20 °C)	3.37±0.03	0.61±0.03	0.51±0.02
Kaplan *et al.*[a] (22.5 °C)	3.34±0.08	0.35±0.04	0.47±0.04
Ultrasonic technique			
Huntington[b]	3.45±0.07	0.54±0.03	0.508±0.005
Galt[c]	3.46	0.58	0.505
Merkulov[d]	3.50	0.62	0.506
Slagle and Mckinstry[e] (25 °C)	3.468	0.580	0.507
Thermal diffuse scattering of X-rays			
Ramachandran and Wooster[f]	3.8	0.60	0.64

a) Ref. 2. b) H. B. Huntington, *Phys. Rev.*, **72**, 321 (1947). c) J. K. Galt, *Phys. Rev.*, **73**, 1460 (1948). d) L. G. Merkulov, *Soviet Phys.-Acoustics*, **5**, 444 (1960). e) Ref. 8. f) Ref. 9.

elastic constants are shown in Fig. 3.

Discussion

In the present study, the elastic constants C_{11}, C_{12} and C_{44} of KBr were determined for sound waves of microwave frequencies 6—12 GHz by the Brillouin scattering technique. The elastic constants thus determined may be compared with the values for the ultrasonic region (10 MHz region) as measured by externally generated sound waves. In Table 2, previous results of ultrasonic measurements are also listed for comparison with the Brillouin results. Although there are some discrepancies among the ultrasonic results by different workers, the present hypersonic values by Brillouin scattering and the ultrasonic values are close to each other, indicating little dispersion of the sound-wave velocity for the regions between 10 MHz and 10 GHz corresponding to the frequency change of three orders of magnitude. Kaplan *et al.*[2] have also measured Brillouin scattering spectra of KBr and have obtained the elastic constants. However, their C_{12} value is appreciably smaller than ours (see Table 2). Comparison of Fig. 3 in this paper and Fig. 1b in Ref. 2 indicates that the sound velocity measured by Kaplan *et al.* is slightly smaller than the present result for the longitudinal mode but larger for the mixed mode; these differences make their C_{12} value smaller. The previous Brillouin study[1] on other alkali halides of KCl, RbCl and KI indicated the absence of dispersion of the sound-wave velocity for the hypersonic and ultrasonic regions. Accordingly, the little dispersion found for KBr in the present study seems to be reasonable.

The elastic constants of KBr have also been obtained by the technique of thermal diffuse scattering of X-rays,[9] in which measurements were made of the intensity of weak diffuse X-rays reflected from crystals. The elastic constants determined by this method are also listed in Table 2. However, the accuracy of this method is not high enough for discussing the dispersion of the sound velocity for the visible and X-ray regions.

In the present measurements of Brillouin scattering of KBr, the Brillouin component due to the mixed mode was observed for $\phi=25°$—$50°$, but the frequency-shift data for $\phi=30°$—$44°$ were used for the calculation of the elastic constants. The observation of the mixed mode is necessary for determining C_{12} and C_{44} separately; the velocity of the longitudinal mode depends largely on $(2C_{44}+C_{12})$ and C_{11}, as seen from Eq. (7), but the velocity of the mixed mode is sensitive to C_{44}. Our observation of the mixed mode for $\phi=30°$—$44°$ and the longitudinal mode for $\phi=24°$—$90°$ was good enough for the determination of the three elastic constants.

Numerical calculations in the present study were carried out with a NEAC 2200—700 computer at the Computer Center of Osaka University.

9) G. N. Ramachandran and W. A. Wooster, *Acta Crystallogr.*, **4**, 431 (1951).

The Photoelectron Spectra of Alcohols, Mercaptans and Amines

Hitoshi OGATA, Hatsuki ONIZUKA, Yoshimasa NIHEI, and Hitoshi KAMADA

Department of Industrial Chemistry, Faculty of Engineering, The University of Tokyo, Bunkyo-ku, Tokyo 113

(Received December 19, 1972)

The HeI photoelectron spectra of aliphatic amines, alcohols and mercaptans were measured. These spectra, especially those of methylsubstituted compounds, were interpreted in terms of the orbital energies and corresponding eigenvectors calculated by the CNDO/2 and the INDO type self-consistent field molecular orbital techniques. Modification of CNDO/2 was also performed and the results are briefly discussed.

Photoelectron spectroscopy (pes) has become a powerful tool for the interpretation of the electronic structure of molecules and the corresponding ions, and widely used for studies of various molecular systems. The present paper is meant to make a contribution to the interpretation of the photoelectron (pe) spectra of some aliphatic alcohols, ROH, mercaptans, RSH, and amines, RNH_2. The CNDO/2[1] and the INDO[2] calculations have been performed on these molecules in order to interpret the pe spectra. We assume throughout the validity of Koopmans' theorem.[3] Since the calculations have been performed in the ground state geometries, the calculated ionization potentials will be compared with the experimental vertical values throughout.

Experimental

A Jasco Model PE-1 Photoelectron Spectrometer was used for measurements. The resonance line of He(584 Å) was emitted by means of DC glow discharge. A hemispherical electrostatic condenser with 100 mm diameter was used for electron energy analysis, a channel electron multiplier for detection and a pulse counting method for signal processing system. As low energy electrons are largely affected by terrestrial magnetic field and fluctuating magnetic field around the apparatus, they were eliminated by μ-metal shielding. In order to obtain ionization potentials from spectra, xenon gas is mixed into the sample gas as internal standards of ionization potential. We have measured the spectra of aliphatic amines, RNH_2, alcohols, ROH and mercaptans, RSH, where R=CH_3, C_2H_5, *n*-C_3H_7, *iso*-C_3H_7, *n*-C_4H_9, *iso*-C_4H_9, *sec*-C_4H_9 and *tert*-C_4H_9. The spectra were obtained in gas phase at room temperature. The compounds were obtained commercially, and further purification was not performed. Theoretical calculations were based on the CNDO/2 and the INDO method.

Results and Discussion

Alcohols. Figure 1 shows the pe spectra of eight aliphatic alcohols.[4] Each spectrum contains a relatively sharp and symmetrical peak in the lowest ionization potential (i.p.) region (termed as the first band) and a series of broad peaks in the higher i.p. region.

The first band of methanol shows fine structure ascribable to the vibration of the ion in the ground electronic state. It consists of at least three peaks, and the spacing is about 960 cm^{-1}. The intense band in the infrared absorption spectra of methanol located in 990 to 1050 cm^{-1} is complicated and may be related to CO stretching, OH bending and CH bending (CH rocking) modes. Fine structure observed in the pe spectra of methanol may be due to these vibrational modes of methanol ion.

Refaey and Chupka measured the photoionization total cross section of methanol and found six sharp peaks in the region of photon energy from 10.5 to 12.0 eV.[5] They concluded that these peaks might be due to vibration of methanol ion in the electronic ground state. They also stated that to ascertain this assignment it would be necessary to measure the pe spectra of CH_3OH.

Brehm *et al.* measured the pe spectra of methanol using Lyα line (12.08 eV) and He resonance line as light sources.[6] Their results show that both first

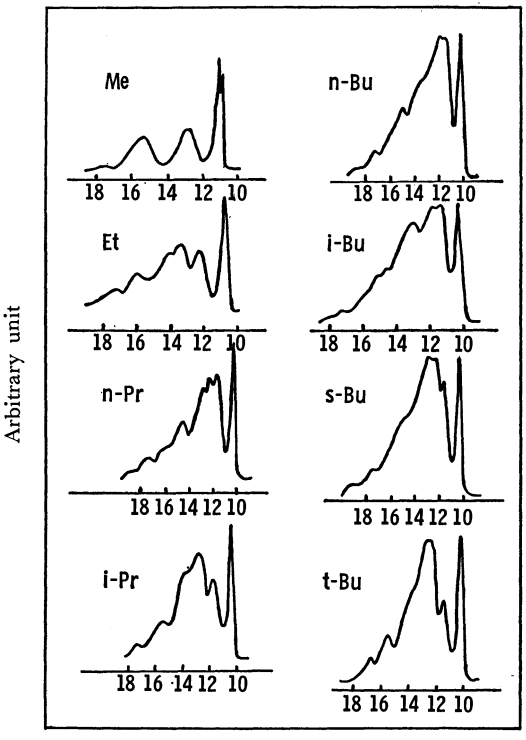

Fig. 1. The photoelectron spectra of alcohols.

1) J. A. Pople and G. A. Segal, *J. Chem. Phys.*, **44**, 3298 (1966).
2) J. A. Pople, D. L. Beveridge, and P. A. Dobosh, *ibid.*, **47**, 2026 (1967).
3) T. Koopmans, *Physica*, **1**, 104 (1934).
4) Some of the spectra shown here have already been published. A. D. Baker, *Anal. Chem.*, **43**, 375 (1971).
5) K. M. A. Refaey and W. A. Chupka, *J. Chem. Phys.*, **48**, 5205 (1968).
6) B. Brehm, V. Fucks, and P. Kebarle, *Int. J. Mass Spectrom. Ion Phys.*, **6**, 279 (1971).

bands of methanol obtained by Lyα and He resonance line give similar fine structure, *i.e.*, there are only three peaks due to vibration of CH_3OH^+. Of the six peaks in the derivative curve of the total ionization cross section presented by Chupka, the envelope of three peaks located in the region from 10.8 to 11.2 eV bears a striking resemblance to that of the first band of the pe spectra. On the other hand, the remaining three peaks in the derivative curve which are in 11.3 to 11.6 eV cannot be found in the pe spectra. Accordingly, three of six peaks located in higher energy region reported by Chupka may be due to some other process than the direct ionization, presumably due to auto-ionization process.

It is interesting while the 0–0 peak is the most intense in the first pe band of water,[7] the 0–1 peak is the most intense in the case of methanol. This fact, perhaps, indicates that the character of the highest occupied molecular orbital (HOMO) of methanol is considerably different from that of water. In fact, this is ascertained by the calculated HOMO's: the HOMO of water is wholly composed of an oxygen 2p atomic orbital, but, as for methanol, only 62% of the HOMO is composed of an oxygen 2p atomic orbital.

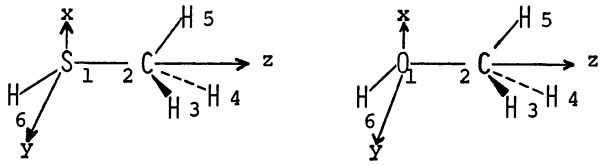

Fig. 2. Models employed for calculations.

Table 1. Calculated ionization potentials and eigenvectors[a] of methanol

Ionization potentials (eV)					
CNDO/2	22.87	21.93	19.25	16.16	15.28
MCNDO/2[b]	21.63	20.23	18.13	14.84	13.00
INDO	22.32	21.97	18.67	15.16	14.24
Obsd	17.53	15.69	15.09	12.66	10.95
1OS	0.170		0.116	−0.197	
1OZ	0.118		−0.722	0.183	
1OX	0.582			−0.564	
1OY		0.606			−0.788
2CS					
2CZ	−0.144		0.545	−0.110	
2CX	0.519		0.199	0.426	
2CY		0.598			0.362
3HS	−0.223	0.370		0.244	0.352
4HS	−0.223	−0.370		0.244	−0.352
5HS	0.313		0.295	0.409	
6HS	−0.366		0.180	0.360	
MO Sym.	3a′	1a″	4a′	5a′	2a″

a) Eigenvectors are those calculated by CNDO/2.
b) Modified CNDO/2. See text for explanation.

7) D. W. Turner, C. Baker, A. D. Baker, and C. R. Brundle, "Molecular Photoelectron Spectroscopy," Wiley-Interscience, London, New York, Sydney and Toronto (1970).

Fig. 2 shows the models of methanol and methyl mercaptan used in theoretical calculations. Results for methanol obtained by the CNDO/2 and the INDO method are summarized in Table 1. In Table 1 1OZ, for example, indicates the $2p_z$ atomic orbital of an oxygen atom. Wave functions are approximated as a linear combination of atomic orbitals and the coefficients, C_{ht}, are given in Table 1. The calculated orbital energies are compared with observed vertical i.p.'s. The first band of the pe spectrum of methanol is thought to be due to the ionization from a "lone pair" orbital localized on an oxygen atom. This is ascertained by the fact that the first band of the pe spectrum is considerably sharp. But this "lone pair" orbital is not completely atomic: only 62% of this orbital is composed of an oxygen $2p_y$ atomic orbital. Relationship between band shapes of the photoelectron spectra which can be assigned to "lone pair" orbitals and the wave functions obtained from theoretical calculations has been considered in detail elsewhere.[8]

As for methanol, ethanol, 2-propanol, *sec*-butanol and *tert*-butanol, the well-defined second i.p.'s can be determined. But as for alcohols with straight chain alkyl group, the second band overlaps with higher ionization potential bands and the second i.p.'s cannot be determined. Figure 1 shows that the more the alkyl group is branched, the second ionization band is the more clearly isolated.

Table 1 shows that the nature of the 5a′ orbital of methanol is rather indistinct. This orbital consists of contribution of CH and OH bonding character. It is interesting that the second occupied orbitals of alcohols that have strongly electron-releasing branched alkyl groups, *i.e.*, *iso*-propanol, *tert*-butanol, have con-

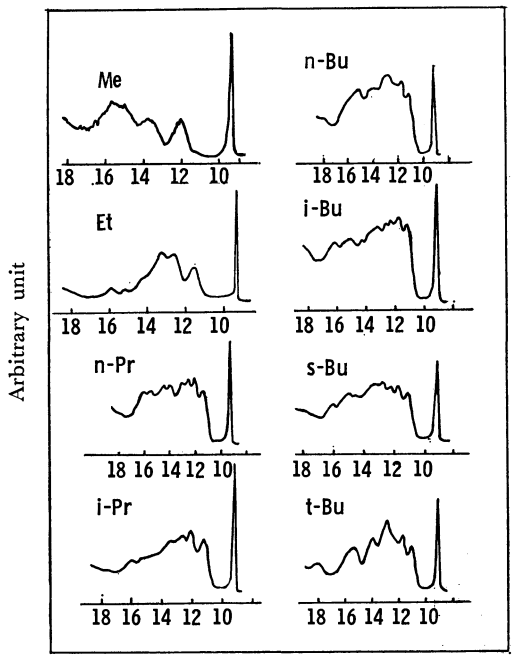

Fig. 3. The photoelectron spectra of mercaptans.

8) H. Ogata, H. Onizuka, Y. Nihei, and H. Kamada, *Chem. Lett.*, **1972**, 895.

siderable CO bonding character. Though third i.p.'s cannot be given from pe spectra except for methanol and ethanol, calculations show that the third occupied orbitals consist of mainly CO bonding orbitals. In the case of methanol the fourth pe band is thought to be the ionization from CH_3 group.

Mercaptans. The pe spectra of eight aliphatic mercaptans are shown in Fig. 3. Calculated ionization potentials and the corresponding eigenvectors are given in Table 2. The first to the third vertical i.p.'s can be readily obtained from spectra and they are summarized in Table 3. Since an oxygen and a sulfur atoms belong to the same column of the periodic table, pe spectra of mercaptans might be expected to contain some of the characteristic features of the spectra of alcohols, *i.e.*, they would contain a sharp intense peak ascribable to a 3p "lone pair" electrons localized on the sulfur atom in the lowest i.p. region, and a series of broader bands in higher i.p. region. The i.p.'s of the "lone pair" electrons may be expected to be lower in mercaptans than in alcohols because a sulfur atom has 3p "lone pair" electrons. Comparison of Fig. 3 with Fig. 1 shows the validity of these predictions.

Table 2. Calculated ionization potentials and eigenvectors[a] of methyl mercaptan

	Ionization potentials (eV)				
CNDO/2	21.04	20.41	17.09	14.81	12.07
MCNDO/2[b]	19.14	19.03	15.01	12.16	9.97
INDO	20.03	19.84	16.20	13.37	11.30
Obsd		15.63	13.67	12.08	9.44
1SS	0.249			−0.369	
1SZ			−0.605	0.378	
1SX	0.426		−0.187	−0.578	
1SY		0.372			0.923
2CS					
2CZ	−0.190		0.544	−0.212	
2CX	0.591		0.251	0.267	
2CY		0.673			−0.236
3HS	−0.289	0.452		−0.186	−0.236
4HS	−0.289	−0.452		−0.186	0.192
5HS	0.381		0.359	0.243	
6HS	−0.229		0.319	0.376	
MO Sym.	3a′	1a″	4a′	5a′	2a″

a) Eigenvectors are those calculated by CNDO/2.
b) Modified CNDO/2. See text for explanation.

Table 3. The first to the third ionization potentials of mercaptans

	1st	2nd	3rd
CH_3SH	9.44	12.08	13.67
C_2H_5SH	9.29	11.59	12.61
n-C_3H_7SH	9.19	11.38	12.08
i-C_3H_7SH	9.14	11.19	12.15
n-C_4H_9SH	9.15	11.15	11.80
i-C_4H_9SH	9.12	11.14	11.69
s-C_4H_9SH	9.10	11.07	11.64
t-C_4H_9SH	9.03	11.01	11.67

Mercaptans give pe spectra composed of a sharp intense peak at the lowest i.p. region and a series of broader but well-resolved bands in higher i.p. region.

Table 2 shows that the largest contribution to the HOMO is given by 1SY, and amounts to more than 80%. The first band of each mercaptan is assigned to the ionization from the "lone pair" orbital localized on a sulfur atom on the ground that this band is composed of single sharp peak and that calculations show the HOMO is non-bonding. That the first bands of mercaptans are sharp compared with those of alcohols and that though the first band of methanol contains vibrational fine structure, mercaptan shows no vibrational structure, are consistent with the difference between the degree of contribution of 1OY and 1SY to the HOMO.

When the comparison is made between methyl- and *tert*-butyl-substituted compounds, the contribution of 1NX and 1OY to the highest occupied orbital reduces from 51% to 32% for amines and from 62% to 36% for alcohols. On the contrary, the contribution of 1SY to it only reduces from 85% to 82%. This property is the marked characteristic of the "lone pair" orbital of aliphatic mercaptan. Of the eight alkyl-substituted amines, alcohols and mercaptans, methyl-substituted compounds have the highest i.p.'s and *tert*-butyl-substituted compounds have the lowest i.p.'s. Difference of ionization potentials of methyl and *tert*-butyl-substituted compounds is 0.40 eV for amine, 0.77 eV for alcohol and 0.41 eV for mercaptan. The first i.p.'s of amines, alcohols and mercaptans are given graphically in Fig. 4.

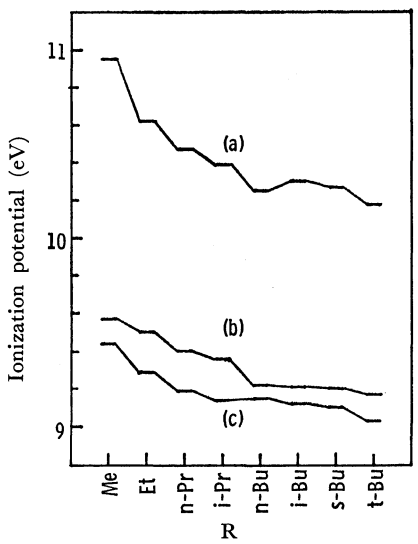

Fig. 4. The first adiabatic i.p.'s of (a) alcohols, (b) amines and (c) mercaptans.

Unlike alcohols, the second bands of mercaptans are all separated from the higher i.p. bands. The second occupied molecular orbital of methyl mercaptan is indistinct in character but has the feature that the electronic population is relatively high on the SH functional group of this molecule. The third vertical ionization potentials can be determined from spectra and calculations indicate that the third occupied molecular orbital of methyl mercaptan is rich in SC bonding

character. As in the case of methanol, the fourth ionization band of methyl mercaptan is largely contributed to by CH_3 group.

Amines. The first i.p.'s of the aliphaticamines have been measured by photoionization[9] and by low resolution pes.[10] Recently, the i.p.'s of methylamine determined by the high resolution pe spectra and those predicted by the INDO type MO calculations have been reported by McDowell *et al.*[11]

The pe spectra of aliphatic amines are shown in Fig. 5. Since the lowest i.p. bands of amines are very broad and show no vibrational fine structure, it is difficult to determine the first adiabatic i.p.'s. But if the onsets of these bands are taken for the adiabatic i.p.'s, our values are in good agreement with those reported by Watanabe *et al.*[9] The first pe bands of amines can be assigned to the ionization from the so-called "lone pair" orbitals. That these bands are very broad compared with those of the first i.p. bands of alcohols and mercaptans is the characteristic feature of amines.[8] As in the case of alcohols, the second i.p.'s can be determined only for amines which have the strong electron-releasing alkyl group, *i.e.* *iso*-C_3H_7 and *tert*-C_4H_9. Calculated results for ethylamine are summarized in Table 4.

Although one center exchange integrals are neglected in CNDO/2, they are taken into account in the INDO method. It is supposed that the inclusion of one center exchange integrals most affects the energy level of an orbital which is localized. Tables

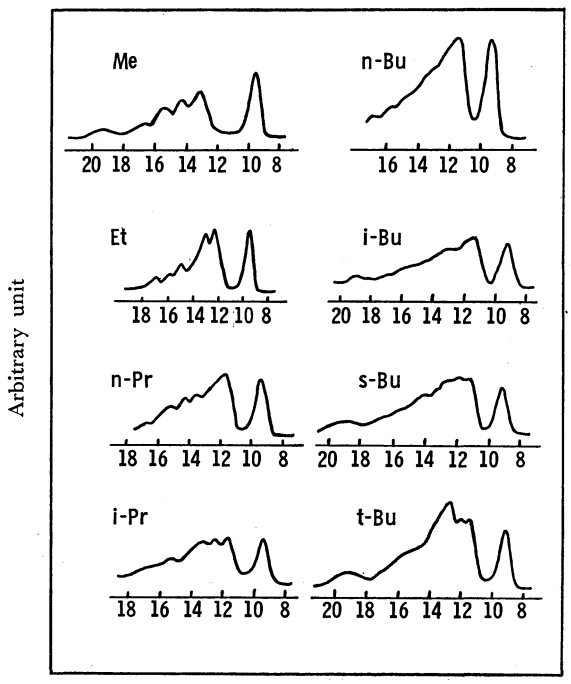

Fig. 5. The photoelectron spectra of amines.

Table 4. Calculated and observed i.p.'s of ethylamine (eV)

CNDO/2	13.69	14.95	16.08	18.70
MCNDO/2	11.87	14.19	15.22	17.80
INDO	12.20	14.83	15.88	18.49
Obsd	9.50	12.27	13.01	14.80
MO Sym.	a′	a″	a′	a′

1, 2 and 4 show that the first i.p.'s calculated by INDO are, in all cases, lower than those calculated by CNDO/2 and the remaining i.p.'s obtained by INDO are somewhat lower but the two methods give essentially the same results.

Modification of the CNDO/2 method. Making a comparison between the observed i.p.'s and the calculated orbital energies by the use of Koopmans' theorem, the calculated values are too large as can be seen from Tables 1 and 2. In order to improve calculated orbital energies, some changes of approximations were introduced to the CNDO/2 method.

From the preliminary calculations, it became clear that the change in the coulombic repulsion integrals causes the parallel translation of the orbital energies and that the bonding parameters have relationship to the intervals of the orbital energies. Taking these facts into consideration, it is necessary first to investigate the parametrization of the electron repulsion integrals, γ_{AB}. These integrals calculated by using the Slater orbitals in the original CNDO/2 method are much larger compared with those semiempirically evaluated.[12] In the present modification, therefore, these integrals are calculated by Klopman's equation.[12] The next modification relates to bonding parameters. In the CNDO/2 approximation, β_A^0 is treated as a parameter characteristic of atom A. In our modification, the following approximations were introduced:

$$\beta^0_{AB} = (1/2)K(z_A' + z_B')$$

where z_A' is the effective nuclear charge of atom A, and K is a constant determined for each row.

Figure 6 shows the variation of orbital energies of

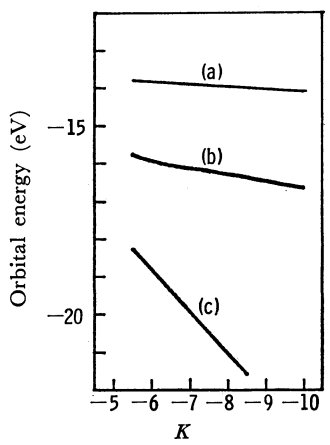

Fig. 6. Orbital energies of water *vs.* parameter *K*. (a) $1b_1$, (b) $3a_1$ and (c) $1b_2$ orbitals.

9) K. Watanabe and J. R. Mottl, *J. Chem. Phys.*, **26**, 1773 (1957).

10) M. I. Al-Joboury and D. W. Turner, *J. Chem. Soc.*, **1964**, 4434.

11) A. B. Cornford, D. C. Frost, F. G. Herring, and C. A. McDowell, *Can. J. Chem.*, **49**, 1135 (1971).

12) G. Klopman, *J. Amer. Chem. Soc.*, **87**, 3300 (1965).

H_2O. The observed difference between the first and the second i.p.'s is 2.1 eV and that between the second and the third ionization potential is 3.7 eV. The value of -6.5 was adopted for K so as to fill these conditions. The same procedure has been performed for the determination of K of the third-row atoms and the value of -2.3 was obtained citing H_2S as instance.

Results for methanol, methyl mercaptan and ethylamine are given in Tables 1, 2 and 4, respectively. Ionization potentials obtained by these modifications are still larger compared with the observed values but considerable improvement was obtained. It should be noted that the CNDO/2, INDO and the modified CNDO/2 calculations lead to the same ordering of the molecular orbital energy levels.

The authors wish to thank Mr. H. Matsumoto for his continuous help in the measurements of the photoelectron spectra.

BULLETIN OF THE CHEMICAL SOCIETY OF JAPAN, VOL. 46, 3040—3043 (1973)

The Electrification of Iron Oxide in Water

Tetsuo MORIMOTO and Shigeharu KITTAKA*

Department of Chemistry, Faculty of Science, Okayama University, Tsushima, Okayama 700

** Department of Chemistry, Faculty of Science, Okayama College of Science, Ridaicho, Okayama 700*

(Received April 20, 1973)

The electrification of iron oxides pretreated at various temperatures from 600 to 1200 °C has been investigated in water by measuring the ζ-potential as a function of the pH. From the surface-chemical point of view, iron oxides pretreated at temperatures lower than 800 °C behave differently from those pretreated at higher temperatures; the isoelectric point of the former samples reaches an equilibrium value in a few hours, while that of the latter samples increases slowly to an equilibrium value with an increase in the surface hydration. On the other hand, the equilibrium isoelectric point of iron oxide decreases sharply upon heat treatment at 800—1000 °C, corresponding to the change in the chemical composition of iron oxide from Fe_2O_3 to Fe_3O_4.

Metal oxide surfaces are usually hydrated in water to produce surface hydroxyl groups, which should have extensive effects on the surface properties of metal oxides.[1-4] The electrification of metal oxide surfaces has also been explained in terms of the dissociation of surface hydroxyl groups and the adsorption of H^+ on them:[5,6]

$$MO^-(s) + 2H^+ \rightleftharpoons MOH_2^+(s) \quad (1)$$

The sign of the charge, positive or negative, carried on the surface may be considered to depend on the nature of the metal oxides and the surface properties. With regard to the former effect, Parks[6] has found the empirical rule that the larger the ionic valency, and the smaller the ionic radius of the metal ion, the smaller the isoelectric point of metal oxide. On the other hand, the effects of the crystal structure and of the surface state (especially the surface hydration) on the surface charge have not been investigated in detail. Here, on iron oxide carefully prepared, the effect of the surface hydration on the surface charge is examined, and the dependence of the electrification on the pretreatment temperature is discussed.

Experimental

Materials. Three kinds of iron oxides were prepared in this work. The addition of an excess amount of 3 mol/l ammonia water to a 1 mol/l $Fe(NO_3)_3$ solution yielded a precipitate of iron hydroxide gel. The precipitate was washed fully with distilled water through a glass filter and then dried at 100 °C for 24 hr. Dried iron hydroxide was decomposed in air at 600 °C into iron oxide and washed with distilled water. Furthermore, iron oxide was heated in air at various temperatures between 600 °C and 1400 °C for 3 hr. Finally, the samples were thoroughly washed with distilled water until the conductivity of the filtrate became nearly that of pure water (FI). Since soluble impurities were detected in the filtrate after the recalicination of the FI samples, calcination and washing were repeated more than ten times in order to purify the samples further. This procedure improved the purity of samples so much that we were not able to detect soluble impurities in the final filtrate (FII). Pure iron (99.99%) was oxidized in air at 1400 °C for 3 hr to produce Fe_3O_4. This sample was then crushed in an agate mortar and heated in air at various temperatures between 200 °C and 1400 °C (FIII).

The nitrogen adsorption was measured at the temperature of liquid nitrogen on the FII samples, and the specific surface areas obtained were 6.57 and 1.50 m^2/g for samples treated at 600 and 800 °C (FII-600 and FII-800) respectively. For the samples treated at temperatures higher than 1000 °C, the specific surface area was found to be less than 0.1 m^2/g.

X-Ray diffraction analysis proved that iron oxides calcined below 1200 °C exhibit the rhombohedral α-Fe_2O_3 structure, while in the sample calcined at 1400 °C two types of structures coexist: a large part of Fe_3O_4 and a very small part of α-Fe_2O_3.

1) M. M. Egorov and V. F. Kiselev, *J. Phys. Chem.* (USSR). **36**, 318 (1962).

2) W. H. Wade and N. Hackerman, *J. Phys. Chem.*, **64**, 1196 (1960).

3) J. P. Peri and R. B. Hannan, *ibid.*, **64**, 1526 (1960).

4) R. Mars, J. J. F. Scholten, and P. Zwietering, "Advances in Catalysis," Vol. 14, ed. by D. D. Eley, H. Pines, and P. B. Weisz, Academic Press, New York (1963), p. 101.

5) T. Morimoto and M. Sakamoto, This Bulletin, **37**, 719 (1964).

6) G. A. Parks, *Chem. Rev.*, **65**, 177 (1965).

Determination of the Isoelectric Point. The isoelectric points of iron oxide were determined by the measurement of the ζ-potential in solutions with various pH values at 25 °C by means of the streaming potential method.[7] The potential values were calculated by using the Helmholtz-Smoluchowski equation. The pH value of the solutions was controlled with HCl and NaOH, and NaCl was used to adjust the ionic strength of the solutions (10^{-3} mol/l). The solid reagents used were recrystallized once from guaranteed-grade reagents. The water which was used for preparing the iron hydroxide and electrolyte solutions and for washing the samples was redistilled one. The second distillation was performed from an alkaline permanganate solution. Before preparing the electrolyte solution, purified water was bubbled with N_2 in order to exclude any dissolved CO_2.

Measurements of Hydration.[8] FII samples calcined at 600 and 1200 °C were immersed into water for various time intervals in order to obtain differently-hydrated samples. After degassing the hydrated samples in a vacuum of 10^{-5} Torr at 25 °C for 10 hr, by which almost all the physisorbed water molecules were removed. The samples were calcined at 1000 °C and the water vapor released was condensed into a dry-ice trap. The condensed water was vaporized and determined volumetrically at 25.0 °C.

Results and Discussion

Immediately after the calcination of the FII samples at various temperatures, they were mounted in the cell of the streaming potential apparatus; then the potential was measured at intervals. During the time between successive measurements, the solution was forced to stream through the diaphragm by applying pressure with N_2 (100 mmHg); the streaming velocity was 4.1 and 110 ml/hr in the cases of FII-600 and FII-1200 respectively. In Fig. 1, the ζ-potential values of FII samples in solutions of different pH values are plotted against the time elapsed after the contact of the solid surface with a solution. Figure 1 shows that the ζ-potential value increases steeply in the

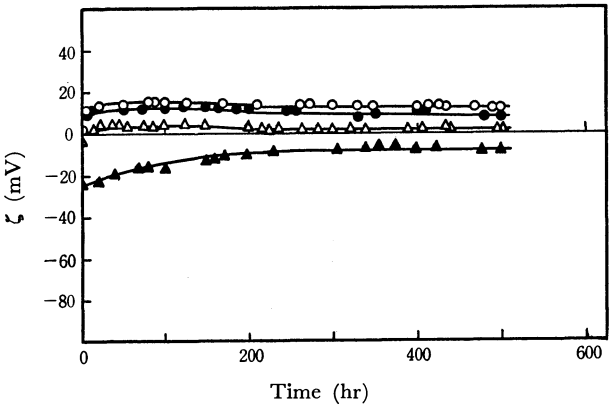

Fig. 1a. ζ-potential of FII pretreated at 600 °C against hydration time. ○: pH 7, ●: pH 8, △: pH 9, ▲: pH 10.

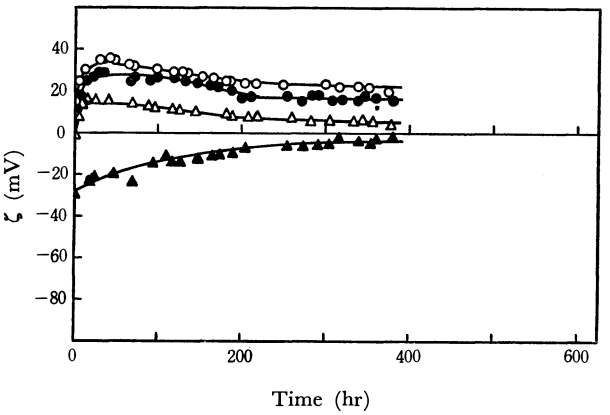

Fig. 1b. ζ-potential of FII pretreated at 800 °C against hydration time. ○: pH 7, ●: pH 8, △: pH 9, ▲: pH 10.

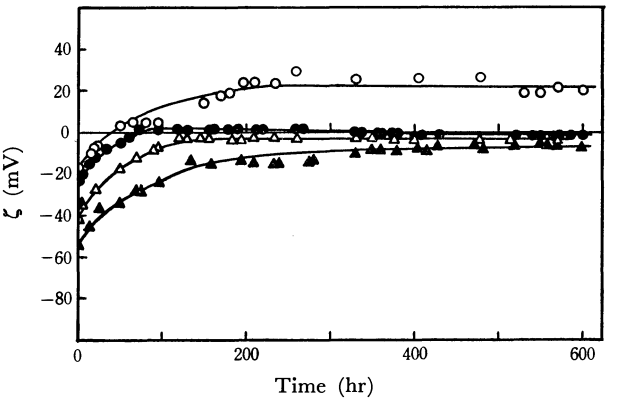

Fig. 1c. ζ-potential of FII pretreated at 1000 °C against hydration time. ○: pH 3, ●: pH 4, △: pH 5, ▲: pH 6.

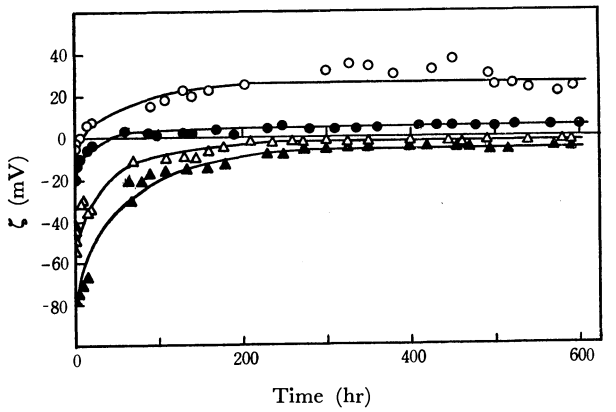

Fig. 1d. ζ-potential of FII pretreated at 1200 °C against hydration time. ○: pH 3, ●: pH 4, △: pH 5, ▲: pH 6.

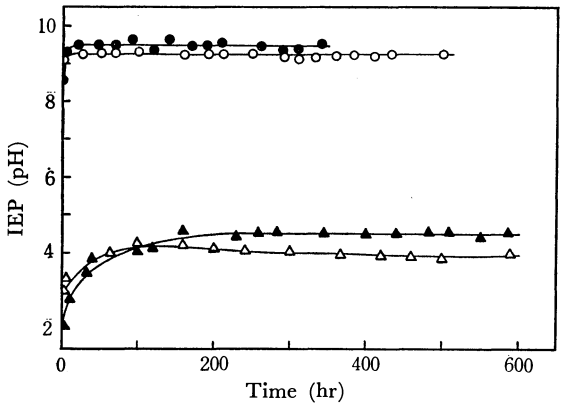

Fig. 2. Isoelectric point (IEP) of FII against hydration time. Pretreatment temperature, ○: 600 °C, ●: 800 °C, △: 1000 °C, ▲: 1200 °C.

7) T. Morimoto, This Bulletin, **37**, 386 (1964).
8) T. Morimoto, M. Nagao, and F. Tokuda, *J. Phys. Chem.*, **73**, 243 (1969).

first stage and then slowly; in some cases, the sign of the surface charge changes from negative to positive. The ζ-potential value of FII–600 and FII–800 could attain an equilibrium in a few hours, but it took a long time in the cases of FII–1000 and FII–1200 (about 200 hr). From the data given in Fig. 1 the isoelectric point can be determined to be changed with the immersion time (Fig. 2). It may be understood from Fig. 2 that the isoelectric point of iron oxides calcined at lower temperatures rapidly approaches higher equilibrium values, while those calcined at higher temperatures attain lower equilibrium values very slowly.

In Fig. 3, the water content of the FII–600 and FII–1200 surfaces is plotted as a function of the immersion time. This is expressed as the number of OH groups per 1 g of the sample left on the surface after long outgassing at 25 °C. It has been made clear that the water content thus obtained is mostly composed of chemisorbed water.[9] It can be seen from Fig. 3 that the surface of FII–600 can hydrate very rapidly in water to attain a saturated water content, while the hydration of FII–1200 proceeds very slowly. Taking into account the specific surface area, the water content of FII–600 can be expressed as about 13 OH's per 100 Å^2, irrespective of the hydration time. On the other hand, the specific surface area of FII–1200 is so small that it could not be determined exactly and that it was impossible to estimate the density of the surface water content, but it is evident that the density increases with the hydration time. The difference in hydration properties between the FII–600 and FII–1200 surfaces may be considered to correspond to the difference in the surface structure. Figure 4 shows the isoelectric point and the water content of FII–600 and FII-1200 as a function of the hydration time, where a good parallelism can be seen between the two quantities in each iron oxide.

It has been proposed that surface hydration may affect the surface charge of metal oxide.[6,10–12] However, no experimental evidence for this proposition has been reported. Therefore, the present results of direct measurements of the isoelectric point and of the surface hydration give the first verification of the proposition (Fig. 4). An increase in the water content of the FII surface must be due to the increase in chemisorbed water, as has been described above.

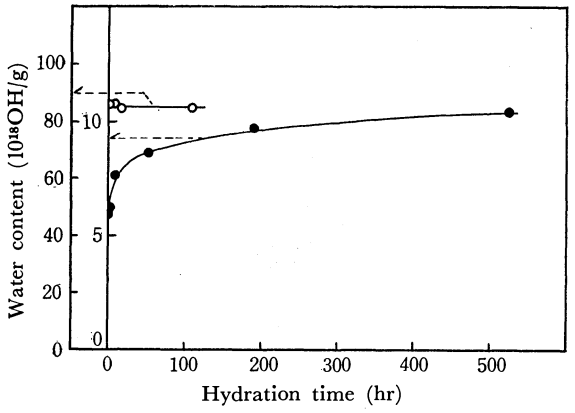

Fig. 3. Water content of FII against hydration time. Pretreatment temperature, ○: 600 °C, ●: 1200 °C.

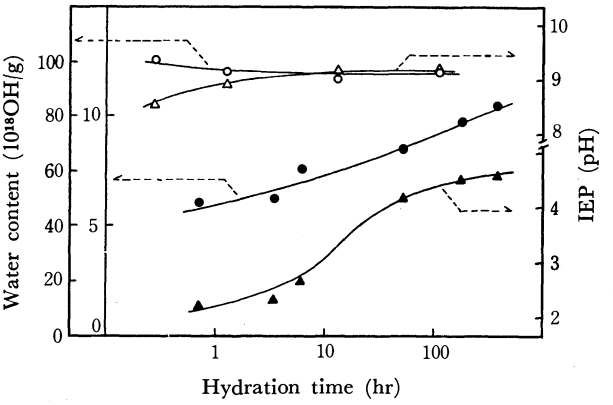

Fig. 4. Water content and IEP of FII against hydration time. ○: Water content, △: IEP. Open symbol, 600 °C; filled symbol, 1200 °C.

As is shown in Fig. 4, the progress of hydration gives rise to an enhanced density of the surface water content of iron oxide, which may itself possibly result in the mutual interaction of neighboring hydroxyl groups through hydrogen bonding:

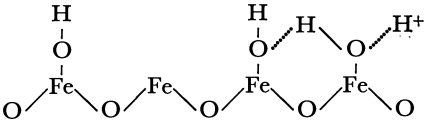

The hydrogen-bond formation will make the oxygen atom less free and, at the same time, slightly richer in electron density compared with that in an isolated hydroxyl group, facilitating the attraction of another proton to it from the solution. Thus, it is reasonable that the isoelectric point of iron oxide is raised by the progress of hydration.

In Fig. 5, the equilibrium value of the isoelectric points of iron oxides is plotted against the calcination temperature. Generally, it can be seen from Fig. 5

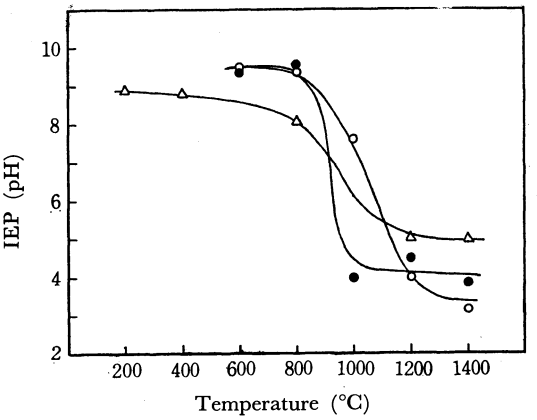

Fig. 5. Equilibrium IEP value of FI, FII and FIII against pretreatment temperature. ○: FI, ●: FII, △: FIII.

9) T. Morimoto and H. Naono, This Bulletin, **46**, 2000 (1973).
10) M. D. Robinson, J. A. Pask and D. W. Fuerstenau, *J. Amer. Ceram. Soc.*, **47**, 516 (1964).
11) Y. G. Berube and P. L. de Bruyn, *J. Colloid Interface Sci.*, **27**, 305 (1968).
12) D. J. O'Connor, P. G. Johansen and N. S. Buchanan, *Trans. Faraday Soc.*, **52**, 229 (1956).

that the isoelectric point of iron oxides (FI, FII) calcined below 800 °C shows an almost constant value (9.3—9.5), irrespective of the pretreatment temperature, while it falls sharply when pretreated at temperatures higher than 800 °C. The isoelectric point of FI falls sharply upon treatment at a temperature higher than in the case of FII, but an additional test showed that prolonged heating for more than 6 hr made the isoelectric point of FI similar to that of FII. The FIII samples which were prepared by the crushing and subsequent calcination of iron oxide in air at various temperatures represent the isoelectric points approximate to those of FI and FII; the variation in the isoelectric point between 800 and 1000 °C is similar to that of FI and FII.

Isoelectric points of the samples treated at lower temperatures (FI, FII, and FIII) are 8.1—9.5, approximate to the values of 8.2—9.1[13,14] reported for Fe_2O_3 samples, while the values (4.0—5.7) obtained with the samples treated at higher temperatures are close to that for Fe_3O_4 (6.5).[15] X-Ray diffraction analysis demonstrated that the crystal structure of FI and FII changes from Fe_2O_3 to Fe_3O_4 upon treatment at 1400 °C. Furthermore, the crystal structure of FIII calcined below 1200 °C was found to be α-Fe_2O_3, like those of the other two samples, though the FIII sample exhibits the Fe_3O_4 structure just after preparation by oxidizing pure iron. These facts suggest that iron oxides calcined below 800 °C have the higher isoelectric points characteristic of the Fe_2O_3 crystal structure, whereas those calcined above 1000 °C have the lower isoelectric points characteristic of the Fe_3O_4 structure, which might be produced on the surface even at temperatures (1000—1200 °C) lower than the decomposition temperature (1390 °C)[16] of Fe_2O_3 to Fe_3O_4.

13) G. Y. Onoda, Jr and P. L. de Bruyn, *Surface Sci.*, **4**, 48 (1966).

14) G. K. Korpi, "Measurement of Streaming Potentials," M. S. Thesis, Department of Metallurgy, MIT, 1960.

15) P. H. Tewari and A. W. Mc Lean, *J. Colloid Interface Sci.*, **40**, 267 (1972).

16) A. Muan, "Phase Diagrams," Vol. 2, ed. by A. Alper, Academic Press, New York (1963), p. 5.

BULLETIN OF THE CHEMICAL SOCIETY OF JAPAN, VOL. 46, 3043—3048 (1973)

The Effect of the Temperature on the Mass Spectra of Aliphatic Primary Alcohols and 1-Alkenes. I.

Hiroko HOSHINO, Susumu TAJIMA, and Toshikazu TSUCHIYA
National Chemical Laboratory for Industry, Honmachi, Shibuya-ku, Tokyo 151

(Received April 23, 1973)

The decomposition of the $(M-18)^+$ ion of aliphatic alcohols and that of the M^+ ion of 1-alkenes are studied. The temperature effect of the ion source of a mass spectrometer on the ratios of the intensities of these ions, those of the ions produced from them by C_2H_4 elimination, and those of the metastable ions for the corresponding fragmentation was measured and was compared with the results to be expected from a simple QET consideration. A discrepancy between the result expected and the experimental result was found for 1-alkenes. In order to clarify the cause of the discrepancy, the photoelectron spectrum was measured for 1-hexanol and for 1-hexene and was assumed to represent the internal energy distribution function, $P(E)$, for each of these substances. Taking the shape of the $P(E)$ into account, the result for 1-alkenes was explained.

It is well known that there is so striking a similarity between the mass spectra of aliphatic primary alcohols and those of 1-alkenes that a group of peaks in the mass spectra of alcohols is called as "olefin peaks," this has prompted studies of the fragmentation mechanism of these alcohols. By study of the appearance potentials of the ion corresponding to the "olefin molecule" or by study of the time variation in the intensity of the "olefin peaks" in the mass spectra of alcohols, it has been shown that no olefin molecule is actually formed by, for instance, any surface reaction, in the ionization chamber before ionization takes place.[1] The mass spectra of primary alcohols, particularly the intensities of the $(M-18)^+$ ion peak and the peaks related to the ion, are known to be strongly dependent on the conditions of measurement, such as the temperature or the materials of the sample manifold of the instrument used.[2] However, the details of these phenomena have not yet been clarified.

It is of primary importance to obtain reproducible mass spectra in the various applications of mass spectrometry to organic chemistry. As a first step to finding the conditions under which we can obtain reproducible results, it is desirable that the mechanism of fragmentation resulting in the poorly reproducible peaks be clarified. In the present work, the effect of the temperature of the ion source of a mass spectrometer on a few peaks, mentioned above, in the mass spectra of primary alcohols and those of 1-alkenes was investigated.

1) J. H. Beynon, "Mass Spectrometry and Its Applications to Organic Chemistry," Elsevier Publ. Co., Amsterdam (1960),

2) R. A. Brown, W. S. Young, and N. Nicolaides, *Anal. Chem.*, **26**, 1653 (1954),

Experimental

A CEC21-103C mass spectrometer was used to obtain the mass spectra of aliphatic primary alcohols and the corresponding 1-alkenes. The number of carbon atoms of the alcohols and the 1-alkenes investigated ranged from 5 to 12 and from 6 to 10, respectively. For alcohols, ions in the following decompositions were investigated, because the $(\text{alcohol}-H_2O)^+$ ion is known to be sensitive to the temperature of the ion source:

$$\begin{aligned} C_nH_{2n+1}OH &\rightarrow (C_nH_{2n+1}OH)^+ \\ &\rightarrow (C_nH_{2n})^+ + H_2O \\ &\quad {}^{*'}\big\downarrow \\ &\quad\longrightarrow (C_nH_{2n}-28)^+ + C_2H_4 \end{aligned} \tag{1}$$

In the decomposition, the intensities of the $(C_nH_{2n})^+$ and $(C_nH_{2n}-28)^+$ ions and that of the metastable ion, $*'$, are denoted as M', F', and m' respectively. For 1-alkenes, the following decomposition was studied:

$$C_nH_{2n} \rightarrow C_nH_{2n}^+ \xrightarrow{*} (C_nH_{2n}-28)^+ + C_2H_4 \tag{2}$$

In the decomposition, the intensities of the $(C_nH_{2n})^+$, and $(C_nH_{2n}-28)^+$ ions and that of the metastable ion, $*$, are denoted as M, F and m respectively. The height of the metastable peak was taken as the m or m′ intensity. When the metastable peak was partly masked by an adjacent peak, the height of the metastable peak was determined after it had been resolved with a Du Pont 310 Curve Resolver.

F'/M', m'/M', and m'/F' for alcohols, and F/M, m/M, and m/F for 1-alkenes were measured under various temperatures, and the relation between the values of these intensity ratios and the temperature of the ion source was investigated from the standpoint of QET. The temperature range covered was between 120 and 250 °C.

The appearance potentials, A, of the $C_nH_{2n}^+$ ions from hexanol and 1-hexene, $A(M')$ and $A(M)$ respectively, and that of the $(C_nH_{2n}-28)^+$ ion from the hexene, $A(F)$, were measured at the ion-source temperature of 250 °C using the EDD technique.[3] The constant, b, in the EDD calculation was taken as 0.67. In the measurement, the influence of the filament-shielding voltage of the ion source on the appearance potential obtained was taken into account.[4] Xenon was used for the correction of the energy axis. The results obtained were $A(M)=9.33$ eV and $A(M)-A(F)=0.12$ eV. The photoelectron spectra of hexanol and 1-hexene were measured with a photoelectron spectrometer, PE-1, made by the Japan Spectroscopic Co., Ltd., using He I. The temperature of the sample in the measurement was less than 100 °C. Xenon was used for calibrating the energy axis again.

The alcohols were obtained from the Tokyo Kasei Co., Ltd., and were used after distillation. The olefins were API Standard Samples, the purity of which was guaranteed to be more than 99.7%. All the reagents were mass-spectroscopically confirmed to be pure.

Results and Discussion

The relations between the temperature of the ion source and the m'/M', m'/F', F'/M', m/M, m/F, and F/M ratios are shown in Figs. 1—6 respectively. As may be seen from the figures, the tangents of the curves for the m/M, m'/M', F/M, F'/M' and m/F ratios *versus* the temperature are positive, whereas the tangent of the curve for the m'/F' ratio is negative. Though Figs. 1—6 were obtained with an electron-accelerating voltage, V_e, of 70 eV, the tangent for each curve was found to keep the same sign when V_e was lowered until $V_e=10.0$ eV.

According to QET in its simplest form,[5] the rate constant, k, for the unimolecular fragmentation with a metastable ion, m:

$$A^+ \longrightarrow B^+ \tag{3}$$

is written as:

$$k = \nu\left(1 - \frac{\varepsilon}{E}\right)^{n-1} \tag{4}$$

where ν is the frequency factor, ε is the activation energy, E is the internal energy of the A^+ ion, and n is the effective number of harmonic oscillators of which the A^+ molecule is assumed to be composed. In Reaction (3), it is assumed that B^+ does not decompose further.

Before applying QET to the results shown in Figs. 1—6, the effect of the potential successive decompositions from F'^+ or F^+ and that of the potential competitive decompositions from M'^+ or M^+ on the results shown in Figs. 1—6 have to be investigated in order to examine whether the rate constant in the form of Eq. (4) can be used for Reactions (1) and (2).

When bombarded by electrons of $V_e=70$ eV, the $(M'-28)^+$ ions from alcohols and the $(M-28)^+$ ions from 1-alkenes are shown to decompose further into the $(M'-43)^+$, and $(M'-45)^+$ ions, and into the $(M-43)^+$, $(M-45)^+$ ions, respectively, by the appearance of the corresponding metastable peaks. However, in the spectra obtained at electron-acceleration voltages lower than $V_e=12$ eV, the intensities of the ions produced by the successive fragmentations were found to be nearly zero. Because the signs of the tangent of the curves shown in Figs. 1—6 remain the same down to $V_e=10.0$ eV, it is reasonable to assume that the rate constant in the form of Eq. (4) can be used to discuss qualitatively the temperature effect on the intensity of the ions in Reactions(1) and (2) without taking the influence of the successive fragmentations into account.

At low electron-acceleration voltages, two reactions, (5) and (6), competing with Reactions (1) and (2) respectively, were observed:

$$M'^+ \longrightarrow (M'-29)^+ \tag{5}$$

$$M^+ \longrightarrow (M-29)^+ \tag{6}$$

The appearance potentials for these ions, A, were measured for 1-alkenes, such as 1-hexene and 1-octene, and were found to be $A(M-28)<A(M-29)$, as was to be expected for the reasons to be given below. As for the appearance potentials of the corresponding ions for alcohols, $A(M'-28)^+$ is inferred to be smaller than $A(M'-29)^+$, because the $(M'-28)^+$ ion is considered to be produced by rearrangement, and the $(M'-29)^+$

3) R. E. Winters, J. H. Collins, and W. L. Courchene, *J. Chem. Phys.*, **45**, 1931 (1966).

4) S. Tajima, Y. Shimizu, and T. Tsuchiya, This Bulletin, **45**, 931 (1972).

5) H. M. Rosenstock and M. Krauss, *Adv. Mass Spectrometry*, **2**, 251 (1962).

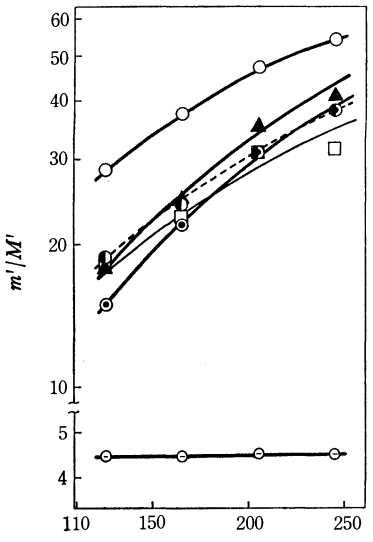

Fig. 1.

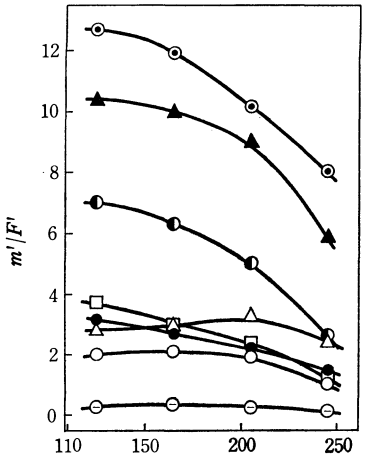

Fig. 2.

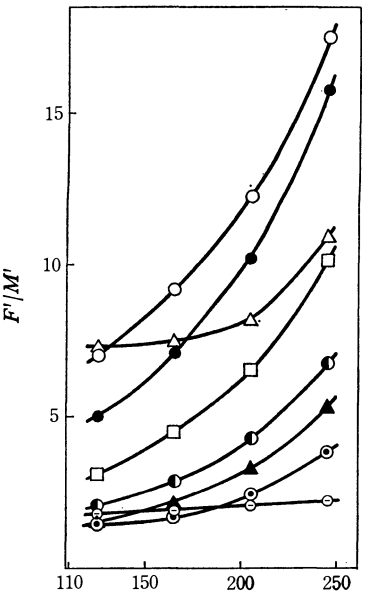

Fig. 3.

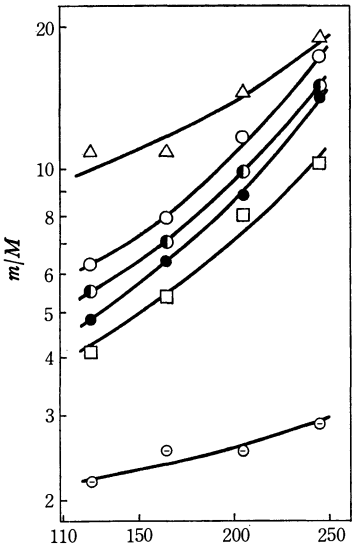

Fig. 4.

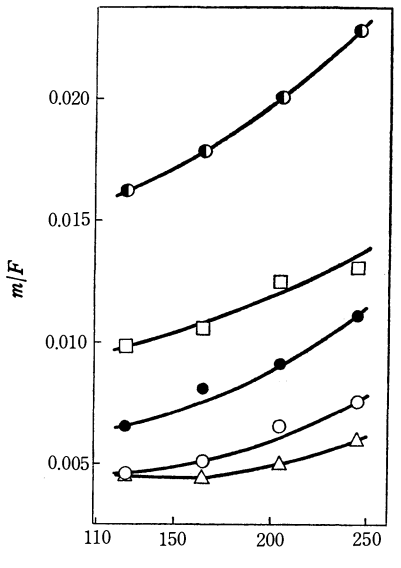

Fig. 5.

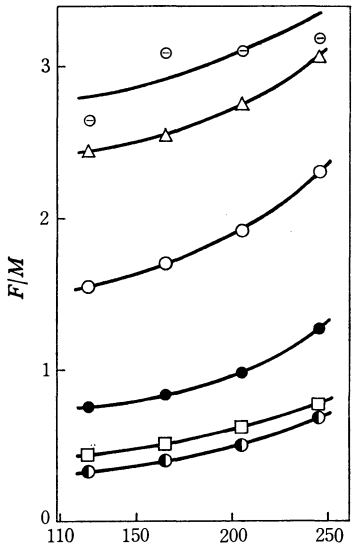

Fig. 6.

Figs. 1—6 show the relation of intensity ratios of ions in Reaction (1) or (2) *versus* the temperature of the ion source. The mark for each curve stands for the carbon number of the compound as indicated below.
⊖ 5; △ 6; ○ 7; ● 8; □ 9; ◐ 10; ▲ 11; ⊙ 12.

ion, to be a simple cleavage of a bond from the $M^{\cdot+}$ ion[6,7]. Actually, the values of the $(M'-29)^+/(M'-28)^{\cdot+}$ and $(M-29)^+/(M-28)^{\cdot+}$ intensity ratios, which were 1—0.5 at $V_e=70$ eV, were found to decrease as the electron energy was lowered. The implication of these results is that the competitive reactions, (5) and (6), have no serious effect upon the general behavior of the curves shown in Figs. 1—6, at least not in the low-electron energy range, the sign of the tangent of the curves can, therefore, be investigated without taking the influences of these reactions into account as long as the qualitative considerations are concerned, although the influences of Reactions (5) and (6) on the intensities of $M'^{\cdot+}$ or $M^{\cdot+}$ respectively can not be neglected in any quantitative consideration. Such being the circumstances, the results of Figs. 1—6 were investigated as follows. In the investigation, the $M'^{\cdot+}$ ion, produced by water elimination from alcohol, is considered to be the parent ion for Reaction (2), since the $F'^{\cdot+}$ ion is shown to be produced from the $M'^{\cdot+}$ ion by the presence of the metastable ion.

Using the expression given by Eq. (4) for the rate constant, McLafferty *et al.*,[8] Cooks *et al.*,[9] Jennings

6) D. H. Williams and R. G. Cooks, *Chem. Comm.*, **1968**, 663.
7) A. N. H. Yeo and D. H. Williams, *J. Amer. Chem. Soc.*, **92**, 3984 (1970).
8) F. W. McLafferty and W. T. Pike, *ibid.*, **89**, 5951 (1967).
9) R. G. Cooks and D. H. Williams, *Chem. Comm.*, **1968**, 627.

et al.[10] and Williams *et al.*[6,11] have investigated quantitatively the effects of n[8,9], ε[10], E[11] and ν[6] in Eq. (4) on the fragmentation patterns of an appropriate series of compounds or of appropriate combinations of compounds.

In the present investigation, the A^+ ion in the unimolecular decomposition reaction, (3), is assumed to have an internal energy distribution function of $P(E)$. The times spent by an ion in various parts of the mass spectrometer were assumed to be as follows. The mean time spent by a newly-formed ion in the ionization chamber is t_1. After being accelerated, the ions dissociated between the times t_2 and t_3 are observed as a metastable peak, and the A^+ ions which do not dissociate until t_4, are observed as the parent ion, A^+. Then, of the total ions produced, the fractions of the ions, A, B, and m, are given by:[12]

$$[A] = \int_0^{\varepsilon} P(E)dE + \int_{\varepsilon}^{\infty} P(E)\exp\{-k(E)t_4\}dE \quad (7)$$

$$[B] = \int_{\varepsilon}^{\infty} P(E)[1-\exp\{-k(E)t_1\}]dE \quad (8)$$

$$[m] = \int_{\varepsilon}^{\infty} P(E)[\exp\{-k(E)t_2\}-\exp\{-k(E)t_3\}]dE \quad (9)$$

Ehrhardt *et al.*[13] have given an expression for $P(E)$, based on statistical mechanics, as follows:

$$P(E) = F(E)G(T)\exp(-E/kT)$$

For the sake of simlicity, the following expression for $P(E)$ was assumed in the present investigation:

$$P(\mathrm{E}) = \frac{E}{(kT)^2}\exp(-E/kT) \quad (10)$$

where k is the Boltzmann constant and where T is the temperature of the molecule. Figure 7 shows schematically the behavior of $P(E)$ for two different temperatures. As the temperature rises, the maximum value of $P(E)$ decreases and the mean value of E increases. This tendency is in accordance with the results previously reported.[13-15]

Assuming Eq. (10) for $P(E)$, the $R\equiv$[B]/[A], $R'\equiv$[m]/[B], and $R^*\equiv$[m]/[A] ratios were calculated using Eqs. (7)—(9). In the calculation, it was assumed that the $m/e=100$ ion is focused at the ion-acceleration voltage of 1000 V and that $t_1=t_2=3$ μs, $t_3=4$ μs, and $t_4=12$ μs. The results are shown in Fig. 8. From the figure, it may be seen that, under these assumptions, as the temperature of the molecules increases and as, consequently, the mean internal energy and the rate constant increase, both R and R^* increase and R′ decreases in the range of $kT < 1.5$ eV.

The results shown in Fig. 8 can be applied to Reactions (1) and (2), and the ratios, F/M, m/M, *etc*, given in Figs. 1—6 can be expected to behave qualitatively,

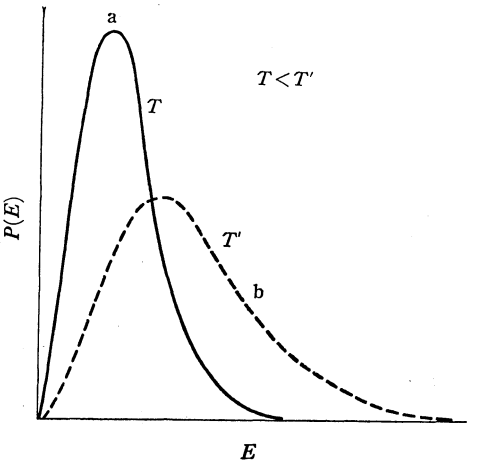

Fig. 7. Illustration of typical behavior expected for a simple internal energy distribution function.
a : lower temperature.
b : higher temperature.

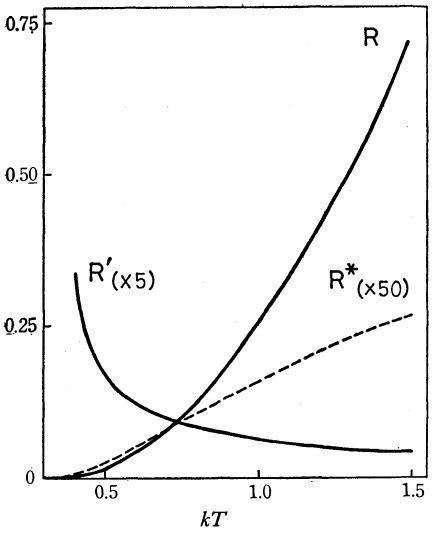

Fig. 8. Intensity ratios of ions calculated from Eqs. (7)—(9) *versus* internal energy E.

in accord with the curves shown in Fig. 8 under the assumption cited.

A comparison of Figs. 1—6 with each of the corresponding curves in Fig. 8 reveals that the expectation is met in all with the exception of Fig. 5; *i.e.*, the signs of the tangents of the curves in Figs. 1—4 and Fig. 6 are in accord with those of the corresponding curves in Fig. 8. On the contrary, the sign of the tangent for the curve in Fig. 5 is positive, whereas that for the curve, R', in Fig. 8 is negative.

In order to explain this discrepancy, the shape of the internal energy distribution function, $P(E)$, was investigated as follows. McLafferty *et al.*,[14] in their study of substituent effects in unimolecular decompositions of diphenylethane derivatives, have taken the effect of the shape of $P(E)$ curves into account in explaining the temperature dependence of the ratio of the intensity of the metastable ion to the parent ion, R^* in the present study, for their sample substances. They synthesized the photoelectron spectrum for a substance from the known spectrum for each moiety

10) K. R. Jennings and J. H. Futrell, *J. Chem. Phys.*, **44**, 4315 (1966).
11) D. H. Williams, R. G. Cooks, and I. Howe, *J. Amer. Chem. Soc.*, **90**, 6759 (1968).
12) I. Howe and D. H. Williams, *ibid.*, **91**, 7137 (1969).
13) H. Ehrhardt and O. Osberghaus, *Z. Naturforschg.*, **15a**, 575 (1960).
14) F. W. McLafferty, T. Wachs, C. Lifshitz, G. Innorta, and P. Irving, *J. Amer. Chem. Soc.*, **92**, 6867 (1970).
15) W. A. Chupka, *J. Chem. Phys.*, **54**, 1936 (1971).

compound of which the substance was composed, and used the synthesized photoelectron spectrum as $P(E)$ for the substance. Using the structure of the synthesized $P(E)$ curve and the value of internal energy corresponding to the range of the abscissa called the "metastable window," which is considered to mainly contribute to the production of the metastable ion observed, they explained the temperature effect on metastable ions.

There have been various investigations[16-19] of possible methods for the evaluation of the internal energy distribution functions resulting in ions from the impact of energetic electrons; their shortcomings have been analysed by Meisels *et al.*[20] According to them, the photoelectron spectrum gives a resonable representation of the actual functions for molecules where multiple ionization and autoionization occur to only a relatively minor extent. On the other hand, another report notes[21] that it is too crude an approximation to use photoelectron spectra as a representation of the internal energy distribution function for some compounds in interpreting their mass spectra. It seems difficult to reach a decisive conclusion concerning the problem for the time being.

Under these circumstances, the photoelectron spectra were used as an approximate representation of the internal energy distribution function in the present study, and the temperature effects shown in Figs. 1—6, especially the effect shown in Fig. 5, were investigated following McLafferty *et al.*[14]

In the present report, *n*-hexanol and 1-hexene were taken as examples, and the photoelectron spectrum of each of these compounds was measured. Figures 9 and 10 show the spectra for *n*-hexanol and 1-hexene respectively. The ionization potentials of $^2P_{1/2}$ and $^2P_{3/2}$

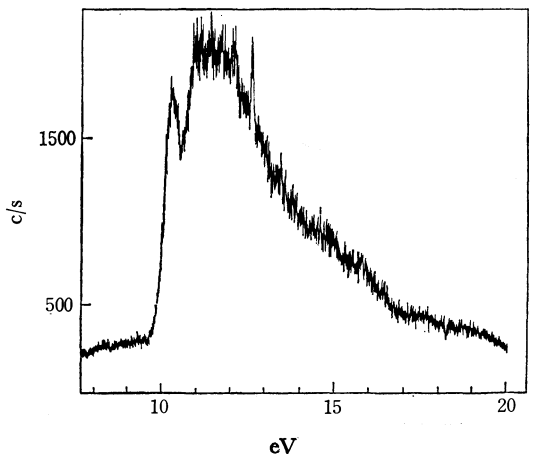

Fig. 9. Photoelectron spectrum of 1-hexanol.

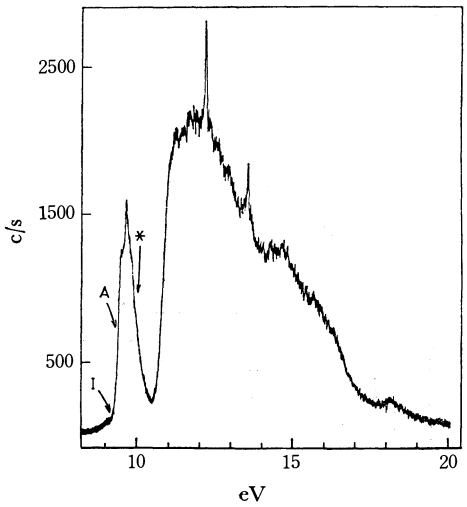

Fig. 10. Photoelectron spectrum of 1-hexene.
1, Ionization potential.
A, Appearance potential of $C_4H_8^+$.
*, "Metastable Window."

for xenon, 13.44 eV and 12.14 eV respectively, were used for energy calibration. The vertical ionization potential and the adiabatic ionization potential[22] for 1-hexene were found to be 9.61 eV and 9.31 eV respectively. The ionization potential of 1-hexene, measured by the photoionization method, has been reported to be 9.45±0.02 eV[17] and 9.46±0.02 eV.[23] The appearance potentials of M^+ and F^+ for 1-hexene, $A(M)$ and $A(F)$, respectively, as measured by electron impact in the present study, are shown by arrows in Fig. 10. The $A(M)$ value thus obtained, 9.33 eV, coincides with the result obtained from the photoelectron spectrum mentioned above, but it is lower than the literature value. Though the reason for the disagreement is not clear, it is noticeable that the mean value, 9.46 eV, of the vertical and the adiabatic ionization potentials obtained from the photoelectron spectrum is consistent with the literature value.

In order to obtain the internal energy value corresponding to the "metastable window," as is shown in the report of McLafferty *et al.*,[14] $\log k(E)$ was calculated for 1-hexene by Eq. (4) as a function of E. In the calculation, ε was taken as 0.12 eV and n was assumed to be $n=(3N-6)/3$, where N is the number of atoms in the molecule. Figure 11 shows the results. Generally, the ν value for a fragmentation with a rearrangement, such as the McLafferty rearrangement, is smaller than that for a simple cleavage of a bond[5,6]. Yeo *et al.*[7] used $\nu=3\times10^6$ for fragmentations with the rearrangement of a hydrogen atom or an oxygen atom and thus obtained results which are close to those obtained in their experiments. Both the log $k(E)$ *versus* E curves for $\nu=10^7$ and $\nu=10^6$ were calculated; they are shown in Fig. 11. The real value for ν was assumed to be in the range between these two values. It may be seen from the figure that the

16) H. Ehrhardt, F. Linder, and T. Tekaat, *Adv. Mass Spectrometry*, **4**, 705 (1968).
17) B. Steiner, C. F. Giese, and M. G. Inghram, *J. Chem. Phys.*, **34**, 189 (1961).
18) J. D. Morrison, *ibid.*, **21**, 1767 (1953).
19) H. von Koch, *Arkiv Fysik*, **28**, 559 (1965).
20) G. G. Meisels, C. T. Chen, B. G. Giessner, and R. H. Emmel, *J. Chem. Phys.*, **56**, 793 (1972).
21) G. Innorta, S. Torroni, and S. Pignataro, *Org. Mass Spectrom.*, **6**, 113 (1972).
22) A. D. Baker, D. P. May, and D. W. Turner, *J. Chem. Soc., Ser. B*, **1968**, 22.
23) K. Watanabe, T. Nakayama, and J. Mottl, *J. Quant. Spectrosc. Radiat. Transfer*, **2**, 369 (1962).

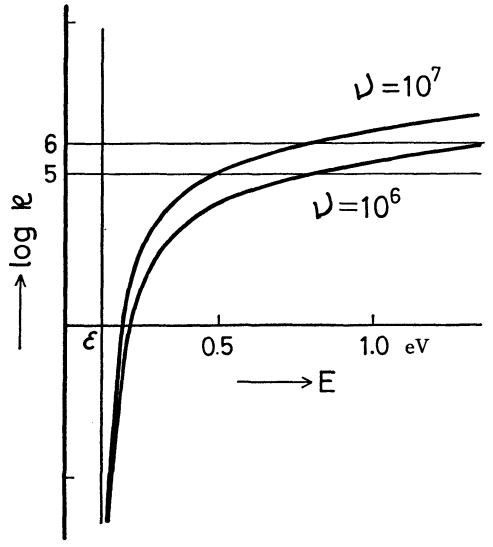

Fig. 11. log k *versus* internal energy E calculated by Eq. (4) for 1-hexene.

internal energy corresponding to the "metastable window" in this case is in a small range centered about $E=1$ eV, as is shown by an asterisk in Fig. 10. As the temperature is increased, the curve in Fig. 10 takes a flatter form as a whole, like the broken curve in Fig. 7, and the fraction of the area under the curve, which covers the energy region marked by an asterisk in Fig. 10, gets larger, resulting in an increase in the metastable-ion intensity. On the other hand, because the fractional change in the area under the curve corresponding to the fragment ion F^+, as the temperature is increased, is relatively small, as may be seen from Fig. 3 cited above,[14] the behavior of the curves shown in Fig. 5 is explained. The results given in Figs. 4 and 6 can be understood as has been discussed before.

The signs of the tangents of all the curves, shown in Figs. 1—3, for 1-hexanol, are as would be expected from the simple consideration, in which no particular structure is assumed for the internal energy distribution function for the precursor ion, M'^+, which itself, in this case, is produced from the molecular ion. This suggests that the internal energy distribution function for M'^+ is of a simple form, as is the curve given in Fig. 7, which has no structure, in contrast to the photoelectron spectrum of 1-hexene (Fig. 10). This implies that no 1-hexene molecule is actually produced in the ion source of the mass spectrometer; this is consistent with an observation cited before.[1]

Danby *et al.*[24] report that the sum of the coincident electron spectra corresponding to the parent ion and the fragment ion from methylene chloride agrees with the photoelectron spectra for all the electrons. If this result is also valid for 1-hexanol, it follows from the inference described above that the internal energy distribution function for the fraction of the molecular ion, which is observed as the parent ion in the mass spectrum of 1-hexanol, may be of a simple form without any marked structure, at least in the vicinity of the "metastable window," because the photoelectron spectrum of 1-hexanol is of a simple form without any marked structure, as may be seen in Fig. 10.

The authors are indebted to Mr. Hiroshi Matsumoto and Mr. Tadashi Miyazaki for carrying out the photoelectron spectrometry experiments, to Mr. Mikitake Nakayama for purifying the alcohols, and to Miss Fusako Isogai for preparing the manuscript.

24) C. J. Danby and J. H. D. Eland, *Int. J. Mass Spectrom. Ion Phys.*, **8**, 153 (1972).

BULLETIN OF THE CHEMICAL SOCIETY OF JAPAN, VOL. 46, 3048—3051 (1973)

Molecular Structure of Acetamide as Studied by Gas Electron Diffraction

Mitsuo KITANO and Kozo KUCHITSU

Department of Chemistry, Faculty of Science, The University of Tokyo, Hongo, Bunkyo-ku, Tokyo 113

(Received May 4, 1973)

The bond distances (r_g) and angles (r_a) in acetamide CH_3CONH_2 have been determined by gas electron diffraction as follows: C–C=1.519±0.006 Å, C–N=1.380±0.004 Å, C=O=1.220±0.003 Å, C–H (average)=1.124±0.010 Å, N–H (average)=1.022±0.011 Å, ∠N–C=O=122.0±0.6°, ∠C–C–H (average)=109.8±2°, and ∠C–C–N=115.1±1.6° (or 112.2±1.6°). In comparison with the molecular structure in the crystal, the C–N bond is about 0.05 Å longer, whereas the C=O bond is about 0.04 Å shorter. The C–N and C=O bonds appear to be slightly shorter than the corresponding bonds in *N*-methylacetamide.

The present paper is a part of the systematic analyses of simple amide structures by gas electron diffraction, following the study of *N*-methylacetamide reported in a previous paper.[1] The gas-phase structure of acetamide was first determined by Kimura and Aoki[2] by the visual method of electron diffraction, and the molecular structures in the trigonal and orthorhombic crystals were studied by Senti and Harker[3] and by Hamilton,[4] respectively. The purpose of the present study is to improve the accuracy by an order of magnitude by the sector-microphotometer method of elec-

1) M. Kitano, T. Fukuyama, and K. Kuchitsu, This Bulletin, **46**, 384 (1973).

2) M. Kimura and M. Aoki, *ibid.*, **26**, 429 (1953).

3) F. Senti and D. Harker, *J. Amer. Chem. Soc.*, **62**, 2008 (1940).

4) W. C. Hamilton, *Acta Crystallogr.*, **18**, 866 (1965).

tron diffraction.

Experimental

A commercial sample was heated to about 160 °C by a high-temperature nozzle,[5] and diffraction photographs were taken with 40 kV electrons at camera distances of 112.30 mm (short) and 246.86 mm (long). The scale factors of the diffraction patterns were calibrated to within 0.10% with reference to the r_a(C=O) distance of carbon dioxide (1.1646 Å).[6] The densities of four plates taken at each camera distance were measured by a digital microphotometer.[7] Other experimental conditions are described elsewhere.[6,8]

Molecular intensities in the ranges $s=2.2$—15.7 and 9.4—37.7 Å^{-1} were obtained from the long and short distance data, respectively.[9] Since they agreed with each other in the overlapping region within experimental error (about 0.03 in the absolute $sM(s)$ scale), they were joined at $s=11.6$ Å^{-1} (Fig. 1). Most of the calculations were carried out on a HITAC-5020E in the Computer Centre of the University of Tokyo.

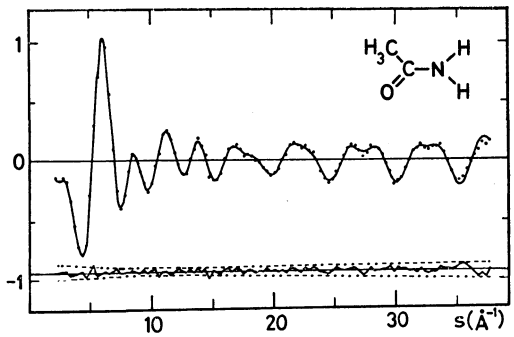

Fig. 1. Experimental and theoretical molecular intensities for acetamide. Typical observed $sM(s)$ values are shown in dots, and the best-fit theoretical is shown in the solid curve. The indices of resolution for long and short camera distances are 0.935 and 0.985, respectively. The lower solid and broken curves represent the residuals and the error limits in the $sM(s)$ to a fractional error of 1×10^{-3} of the original photocurrent,[7] respectively.

Analysis

The molecular intensity was analyzed under the following assumptions:

1) All the atoms except for the two hydrogen atoms of the methyl group are coplanar.

2) One of the hydrogen atoms of the methyl group eclipses the C=O bond.[10] The threefold potential barrier of the methyl torsion is 1 kcal/mol.[10]

3) The methyl group has local C_{3v} symmetry with the tilt angle equal to zero.

4) Two N–H distances (r_g) are equal to each other.

5) The C–N–H_1 and C–N–H_2 angles (r_α), which are *trans* and *cis* to the C=O bond, are equal to the corresponding r_s angles in formamide,[11] 120.0° and 118.5°, respectively.

The mean amplitudes of vibration and the vibrational corrections for the shrinkage effect (r_a-r_α)[12,13] were calculated from a set of modified Urey-Bradley force constants reported by Suzuki[1] and a number of force constants for out-of-plane displacements reported by Itoh[15] for *N*-methylacetamide, both determined from frequencies observed in the liquid phase. The results are given in Table 1. The contributions to the vibrational corrections from the methyl and C–N torsions were estimated in the way described in a previous paper.[1] The asymmetry parameters κ for the bonded C–H and N–H distances were assumed to be 1.8×10^{-5} Å^3, and the rest of the κ parameters were ignored.[16]

The r_g distances and r_α angles derived from least-squares analyses[17] are listed in Table 2 with limits of error estimated from the internal consistency and reproducibility of the parameters, with additional account for systematic errors.[17–19] The mean amplitudes for the C=O, C–N, and C–C bonds were varied and were

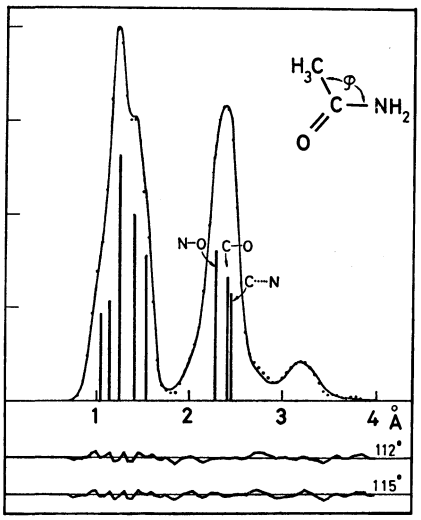

Fig. 2. Experimental (dots) and theoretical radial distribution curves. The lower curves represent residuals based on the models with the C-C-N angle (φ) assumed to be 112° and 115°. Vertical bars represent principal atom pairs based on the 115° model. A damping factor, exp $(-0.0016s^2)$, is used.

5) A. Yokozeki and K. Kuchitsu, This Bulletin, **44**, 72 (1971).
6) Y. Murata, K. Kuchitsu, and M. Kimura, *Japan. J. Appl. Phys.*, **7**, 591 (1970).
7) Y. Morino, K. Kuchitsu, and T. Fukuyama, This Bulletin, **40**, 423 (1967).
8) M. Tanimoto, K. Kuchitsu, and Y. Morino, *ibid.*, **43**, 2776 (1970).
9) Numerical experimental data of the leveled total intensity and the background have been deposited with the Chemical Society of Japan (Document No. 7316).
10) J. P. Lowe, *Progr. Phys. Org. Chem.*, **6**, 1 (1968).
11) E. Hirota, R. Sugisaki, C. J. Nielsen and G. O. Sørensen, *J. Mol. Spectrosc.*, in press.
12) K. Kuchitsu and S. Konaka, *J. Chem. Phys.*, **45**, 4342 (1966).
13) K. Kuchitsu and S. J. Cyvin, "Molecular Structures and Vibrations," ed. by S. J. Cyvin, Chapter 12, Elsevier, Amsterdam (1972).
14) I. Suzuki, This Bulletin, **35**, 1279 (1962).
15) K. Itoh, Ph. D. Thesis, The University of Tokyo (1969).
16) K. Kuchitsu, This Bulletin, **40**, 505 (1967).
17) Y. Morino, K. Kuchitsu, and Y. Murata, *Acta Crystallogr.*, **18**, 549 (1965).
18) K. Kuchitsu, T. Fukuyama, and Y. Morino, *J. Mol. Struct.*, **1**, 463 (1968).
19) K. Kuchitsu, "Molecular Structures and Vibrations," ed. by S. J. Cyvin, Chapter 10, Elsevier, Amsterdam (1972).

TABLE 1. MEAN AMPLITUDES AND VIBRATIONAL CORRECTIONS FOR ACETAMIDE[a] (in 10^{-4} Å)

	l	$r_a - r_\alpha$		l	$r_a - r_\alpha$
C′=O	399	18	N···H_3	1016	−369
C′-N	431	13	N···H_4	1792	88
C-C′	522	5	O···H_1	904	41
N-H	736	57	O···H_2	1266	11
C-H	787	68	O···H_3	1410	−232
N···O	533	−1	O···H_4	1376	−190
C···O	628	−9	H_1···H_2	1172	21
C···N	676	−12	H_3···H_4	1283	30
C′···H_1	947	41	H_1···H_3	1539	82
C′···H_3	1068	13	H_1···H_4	2804	−130
C···H_1	1408	−9	H_2···H_3	1314	92
C···H_2	960	31	H_2···H_4	1856	71

a) Calculated at 160 °C. The carbonyl carbon atom is denoted as C′. The amide hydrogen atoms which are *trans* and *cis* to the C=O bond are denoted as H_1 and H_2, respectively, and H_3 and H_4 are the inplane and out-of-plane hydrogen atoms, respectively, in the methyl group.

TABLE 2. STRUCTURAL PARAMETERS FOR ACETAMIDE AND *N*-METHYLACETAMIDE[a]
(Distances in Å and angles in degrees)

	Gas AA[b]	Gas AA[c]	Cryst. AA[d]	Cryst. AA[e]	Gas NMAA[f]
C-C	1.519(6)	1.53(3)	1.51	1.505(13)	1.520(5)
C-N	1.380(4)	1.36(2)	1.38	1.334(17)	1.386(4)
C=O	1.220(3)	1.21(2)	1.28	1.260(11)	1.225(3)
C-H (av)	1.124(10)	1.09 (as)[g]	—	—	—
N-H (av)	1.022(11)	1.02 (as)[g]	—	—	—
∠C-C-N	115.1(16)	113	109	117.2(15)	114.1(15)
	or 112.2(16)				
∠O=C-N	122.0(6)	125(3)	122	123.1(5)	121.8(4)
∠C-C=O	123.0	122(4)	129	119.7	124.1
	or 125.9				
∠C-C-H (av)	109.8(20)	109.5 (as)[g]	—	—	—

a) Numbers in parentheses represent uncertainties attached to the last significant figures. b) Present study for acetamide (AA): the parameters determined in the least-squares analyses (r_g distances and r_α angles) with estimated limits of error. c) Ref. 2. d) Ref. 3. e) Ref. 4. f) The r_g distances and r_α angles for *N*-methylacetamide (NMAA) with estimated limits of error.[1] g) Assumed.

TABLE 3. ERROR MATRIX FOR ACETAMIDE

	X_1	X_2	X_3	X_4	X_5	X_6	X_7	X_8	l_1	l_2	l_3	k_1	k_2
X_1	14	7	−6	−4	5	8	12	−5	3	5	3	17	−6
X_2		13	−6	4	13	−13	−7	13	3	−4	−6	11	−36
X_3			44	12	−13	12	4	11	−4	−12	−6	−40	58
X_4				9	5	16	−8	10	6	−7	3	−9	38
X_5					41	−21	−8	−19	11	1	−4	−31	−43
X_6						139	−27	−65	35	25	36	68	192
X_7							23	−22	−10	−2	−8	−15	−47
X_8								153	−23	−22	−26	−56	−114
l_1									18	14	18	20	82
l_2										19	19	21	57
l_3											26	22	84
k_1												100	95
k_2													446

X_1=C-C′, X_2=C′-N, X_3=N-H (average), X_4=C′=O, X_5=C-H (average), X_6=∠C-C′-N, X_7=∠N-C′=O, X_8=∠C′-C-H (average), $l_1=l$(C′=O), $l_2=l$(C-N), $l_3=l$(C-C′), k_1=index for long and k_2=index for short. Units ($\times 10^{-4}$) for the distances and mean amplitudes are Å, those for the angles are rad, and those for the indices are dimensionless.

found to be 0.043±0.005, 0.049±0.005, and 0.055± 0.007 Å, respectively. In comparison with the corresponding calculated values in Table 1 (0.040, 0.043, and 0.052 Å), a slight discrepancy is observed in the C–N amplitude. This difference is possibly due to that in the C–N stretching force constants in the gas and liquid phases (See Discussion for the C-N bond lengths in the gas and condensed phases). The rest of the mean amplitudes were fixed to the calculated values listed in Table 2. The error matrix is given in Table 3. The theoretical molecular intensity and radial distribution curves based on this structure are compared in Figs. 1 and 2, respectively, with the corresponding observed curves.

The least-squares analyses resulted in two alternative choices for the C–C–N and C–C=O angles. The C–C–N angle converged to about 115° and 112° when its initial estimates were larger and smaller, respectively, than 114°. The double minimum character of the weighted sum of squared residuals arises from the alternative assignments of the nonbonded C–O and C–N distances to 2.40 and 2.44 Å. All the rest of the parameters, including the O=C–N angle, are not essentially influenced by this ambiguity. As illustrated in Fig. 2, the radial distribution curves based on these alternative sets are almost equally acceptable, and therefore, no definite conclusion can be reached by electron diffraction alone. Since the 115° model is closer to the structure of *N*-methylacetamide,[1] it seems to be more plausible than the 112° model.

As for the torsional motion of the methyl group, the present experimental data are insensitive to the minimum position and the barrier of the potential. A least-squares analysis based on the model that the methyl group is staggered with the C=O bond gave a set of structural parameters essentially equal to those given in Table 3.

Discussion

The structure of acetamide determined in the present study is compared in Table 2 with those in the gas and crystal phases reported in the past and with the structure of *N*-methylacetamide. The most remarkable differences in the gas and crystal structures are found in the C–N and C=O bond distances, which are about 0.05 Å longer and 0.04 Å shorter, respectively, in the gas phase than in the crystal phase. This trend, which is also observed in *N*-methylacetamide, may be interpreted as due to the effect of intermolecular hydrogen bonds in the crystal.[1] Acetamide and *N*-methylacetamide have nearly equal C–C bond distance and O=C–N angles, whereas the former molecule has slightly shorter C–N and C=O bonds than the latter.

BULLETIN OF THE CHEMICAL SOCIETY OF JAPAN, VOL. 46, 3051—3055 (1973)

Intermediates and Mechanism of Photo-Oxygenation Reaction of Triethylamine

Hiroshi TSUBOMURA, Teruo YAGISHITA*, and Hiroo TOI

Department of Chemistry, Faculty of Engineering Science, Osaka University, Toyonaka, Osaka 560

(Received June 4, 1973)

The electronic absorption spectrum caused by the charge transfer interaction between oxygen and triethylamine was studied quantitatively. It is concluded that there is no particular stabilization between them due to the charge transfer interactions. The intermediate radicals produced by the excitation of triethylamine-O_2 in the region of the charge transfer band were studied by the ESR method at various temperatures from 77 to 300 K. The chemical analysis of the irradiation products of the same system was also carried out. The radicals observed are methyl, ethyl, and possibly, $(C_2H_5)_2\dot{N}CHCH_3$, $\dot{O}OH$ and $(C_2H_5)_2NO\cdot$. The products identified are acetaldehyde and diethylamine. Based on these results, the various reactions taking place in the overall photochemical process were speculated.

It is well known that oxygen gives rise to charge transfer(CT) absorption spectra with various organic substances.[1] The upper states for the absorption processes are theoretically predicted to be almost pure ionic pairs, $D^+\cdots O_2^-$, where D is an electron donor. In the case of aniline derivatives, we have found that an ion-pair formation occurs from this excited CT state followed by electron recombination leading mostly to the ground state of aniline.[2] In the case of aliphatic compounds, on the other hand, oxidation reactions seem to ensue generally.

Systematic studies of the photo-chemical reactions of such oxygen CT complexes seem to be very important, because, by doing so, we might be able to get a general information on the chemical driving forces for the CT complexes which are related with such biological processes as photosynthesis. The photo-oxygenation process is also very important as one taking part in the auto-oxidation. In spite of these importances, there seems to have been rather scanty work on direct photo-oxygenation reactions so far, aside from numerous works concerning photo-sensitized oxygenation reactions.[3] In the case of ethyl ether, Stenberg *et al.*[4]

* Present address: Fujitsu Laboratory Ltd., Kamiodanaka, Nakahara-ku, Kawasaki.

1) H. Tsubomura and R. S. Mulliken, *J. Amer. Chem. Soc.*, **82**, 5966 (1960), and earlier papers cited there.

2) M. Hori, H. Itoi, and H. Tsubomura, This Bulletin, **43**, 3765 (1970).

3) For instance, C. S. Foote, *Science*, **162**, 963 (1968).

4) V. I. Stenberg, R. D. Olson, C. T. Wang, and N. Kulevsky, *J. Org. Chem.*, **32**, 3227 (1967).

found that the excitation of the O_2-ether system in the region of its CT absorption leads mainly to the formation of ethyl acetate. For aliphatic amines, Stratford[5] studied the direct photo-oxidation of trialkylamines in detail. He found that, in the case of tri-*n*-butylamine, dibutylamine, butyric acid and tributylamine *N*-oxide are among the products.

Experimental

Materials. Reagent grade triethylamine was dried overnight with potassium hydroxide, and fractionally distilled with a Widmer column. *n*-Heptane and most other hydrocarbons were treated with concentrated sulfuric acid, washed, dried with calcium chloride and then with sodium wire, and fractionally distilled. Acetonitrile was dried with calcium chloride and refluxed with phosphorus pentoxide and fractionally distilled. Commercially available pure oxygen was dried by liquefaction with liquid nitrogen.

Measurements of the CT Absorption Spectra. Pure triethylamine (TEA) or the *n*-heptane solution of TEA was placed in an ampoule with a magnetic rotor inside and a side arm connected to a quartz cell for the spectral measurements. The ampoule was connected through a ground glass joint to a vacuum line, and the TEA or the solution was degassed by means of the freeze-pump-thaw technique. After the absorption spectrum was measured at room temperature, oxygen was introduced into the line at *ca.* 1 atm pressure, the line being closed and the pressure being read quickly with a mercury manometer. Then, the liquid was vigorously stirred by the magnetic stirrer for a few minutes and the pressure drop was read. By this procedure, the concentration of the oxygen in the solution could be determined. The solution was transferred to the quartz cell and its ultraviolet absorption spectrum was measured by use of a Cary 15 spectrophotometer.

ESR Measurements. The ESR measurements were made using a JES-3BX or a JES-ME-2X spectrometer of Japan Electron-Optics Laboratory Co. at the X band. The magnetic field was measured by use of the proton magnetic resonance signal. The *g*-values of short-life species were determined by inclusion of a Mn^{2+} reference sample.

The solution containing TEA was put into a pyrex ampoule connected to a quartz ESR capillary cell. After dried oxygen gas was bubbled in, the solution was transferred into the ESR cell, which was then placed into a Dewar vessel and cooled with liquid nitrogen. The cell was irradiated with a Ushio 500 W high pressure mercury lamp through a Toshiba UV-D2 glass filter which transmits the light in the region of the CT band (300—400 nm).

The Analysis of the Photo-Oxygenation Products. TEA in a reaction vessel (a cylinder, 24 mm in diameter) made of sodium glass, transparent beyond 310 nm, was irradiated with the 500 W high pressure mercury lamp 25 cm apart from the reaction vessel with oxygen bubbling in through a glass capillary tube. The reaction products were analyzed by the gas chromatographic, chemical and IR techniques.

Results

UV Absorption Spectra. In Fig. 1, the absorption spectra of *n*-heptane solutions of TEA dissolving oxygen are shown, the absorption of the deoxygenated solution being subtracted for each curve. From the absorbances and the amount of dissolved oxygen determined by the manometric method, the Benesi-Hildebrand plot[6] was made, which leads to molar extinction coefficients of 640 at 310 nm, 970 at 300 nm, and 1550 at 290 nm. The equilibrium constants obtained ranged from 0.05 to 0.08, showing that the binding between oxygen and TEA is very weak or practically nil. In Fig. 2, the Benesi-Hildebrand plot for λ=290 nm is shown as an example.

ESR Studies. The excitations of TEA in *n*-heptane in the range of the CT band at 77 K for about 10 min gave an ESR spectrum as shown by curve A in Fig. 3. The spectrum is symmetric with respect to the magnetic field, the *g* value being 2.0025. The intensity increased with irradiation till about 2 hr, after which it began to be saturated. At 77 K, the

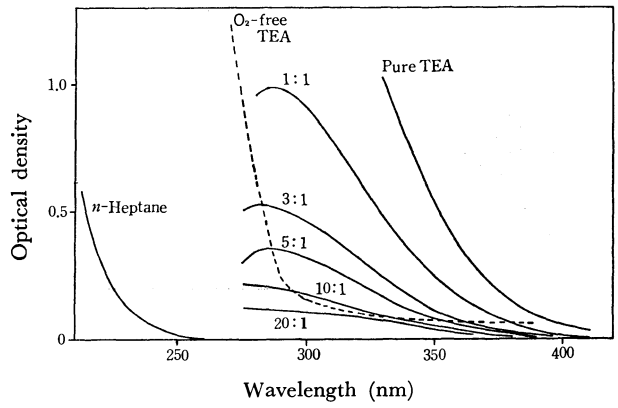

Fig. 1. The ultraviolet absorption spectra caused by oxygen dissolved in *n*-heptane, triethylamine, and their *n* : 1 mixtures (The absorption of the degassed solution is subtracted for each curve.).

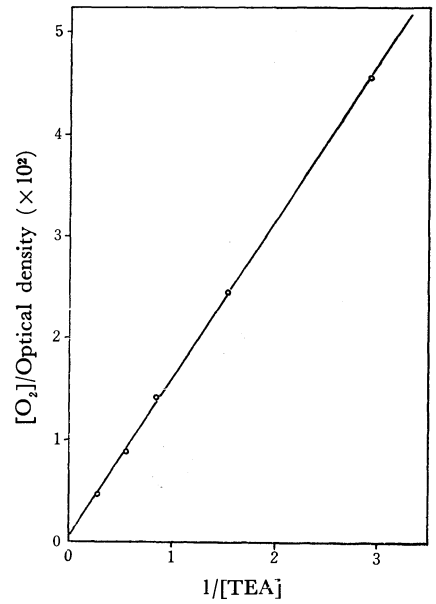

Fig. 2. The Benesi-Hildebrand plot of the absorption caused by oxygen dissolved in *n*-heptane solutions of triethylamine at 290 nm.

5) M. J. W. Stratford, U. S. Dept. Com., Office Tech. Serv., P. B. Report, 144250, p. 46 (1959).

6) For instance, L. E. Orgel and R. S. Mulliken, *J. Amer. Chem. Soc.*, **79**, 4839 (1957).

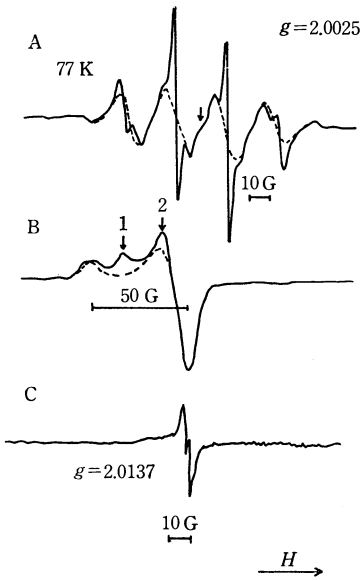

Fig. 3. The ESR spectra of the species produced by the UV-irradiation of triethylamine(1) : *n*-heptane(5)–O_2 at 77 K (A), followed by warming in the dark (B and C).

spectrum stayed unchanged after the light was turned off. The intensity was proportional to the concentration of oxygen. It was confirmed that *n*-heptane and methylcyclohexane dissolving oxygen did not show any ESR signal when irradiated.

The spectrum has a prominent quartet, with an intensity ratio of approximately 1 : 3 : 3 : 1 and a hyperfine coupling constant of 26 G. These features show that methyl radical is present in the solution. It has been confirmed that similar spectra were obtained when TEA in acetonitrile or a 1 : 1 mixture of *n*-propyl and isopropyl alcohols was UV-irradiated at 77 K.

When the component of the spectrum due to the methyl radical is subtracted from the spectrum of Fig. 3A, the curve shown by the broken line is obtained. This appears to be a symmetric quartet, but might more probably be a sextet which is due to a five proton system (see later sections). From the present situation, the species most relevant to this spectrum is the ethyl radical.

In the case of the decalin solution, an ESR spectrum was obtained as shown in Fig. 4. A similar spectrum was obtained for the methylcyclohexane solution. Here, the structure due to the methyl radical is much weaker, and the sextet is prominent. This result can be understood by assuming that the methyl radical is more mobile in these solvents at 77 K than in the other solvents and is unable to survive at 77 K, while the larger radical relevant to the sextet is less mobile

Table 1. The *g*-factors of peroxy radicals

	g_1	g_2	g_3
In isopentane matrix at 77 K	2.0034	2.0034	2.0369
In *n*-heptane matrix at elevated temp	2.0029	2.0029	2.0353
OOH[7]	2.0044	2.0044	2.0393

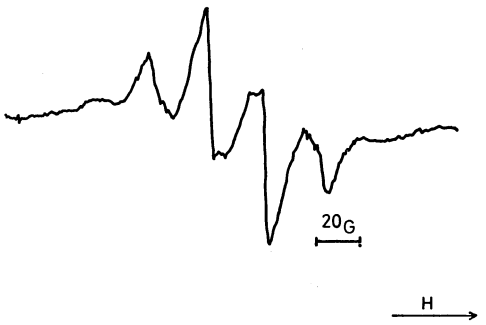

Fig. 4. The ESR spectrum of UV-irradiated triethylamine(1): decalin(1)-O_2 at 77 K.

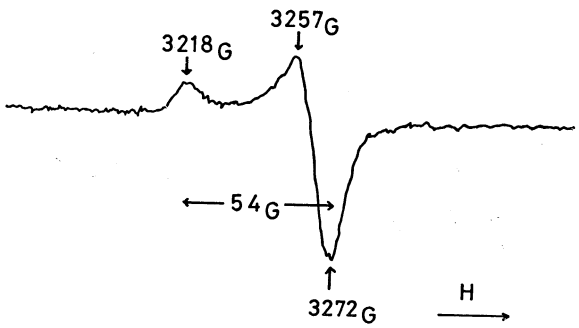

Fig. 5. The ESR spectrm of UV-irradiated triethylamine(1): isopentane(5)–O_2 at 77 K.

and more stable at the same temperature.

For the case of the isopentane solution, a spectrum was obtained showing large anisotropic *g*-factors (Fig. 5 and Table 1). The *g*-factors are a little different from those of OOH and the species for the spectrum may be assigned to an organic peroxy radical. It is often recognized that the isopentane matrix at 77 K is softer than other matrices, so that oxygen can move through the matrix at 77 K, making encounter with a radical and reacting with it even at that temperature.

When the liquid nitrogen in the Dewar vessel was removed and the irradiated solution of TEA was allowed to warm up, the ESR spectrum changed as shown in Fig. 3 for the case of *n*-heptane solution. The analysis of curve B as assigned to a peroxy radical reveals that the peak indicated by an arrow (1) is no doubt due to a different species and the peak indicated by an arrow (2) shows that a small amount of methyl radical still survives in that spectrum. What remains is very much similar to the spectrum of the isopentane solution (Fig. 5 and Table 1) and undoubtedly represents that the same species are present in the two cases. At intermediate temperatures between those for curve A and B, the methyl quartet gets weaker while at the same time the peroxy signal gets stronger. These results indicate that as the matrix begins to soften, the methyl and ethyl radicals transform into diamagnetic species and the oxygen molecules begin to move through the matrix and react with a carbon radical to form the peroxide.

7) F. J. Adrian, E. L. Cochran, and V. A. Bowers, *J. Chem. Phys.*, **47**, 5441 (1967).

At the still higher temperature, the ESR signal almost disappears once, and then reappears taking the form shown by curve C in Fig. 3. This is a slightly split singlet with the g-value of 2.016, which is not accurate because of the fast scanning. The spectrum fades out quickly at higher temperature. The average g-value for the peroxy spectrum of curve B is 2.0137, fairly close to the above-mentioned value and therefore the spectrum C is attributable to the same peroxy radical as that for curve B rapidly rotating in the warm matrix. The disappearance of the signal at the intermediate temperature then indicates a dimerization reaction as shown below,

$$\mathrm{ROO\cdot} + \mathrm{ROO\cdot} \longrightarrow \mathrm{ROOOOR},$$

taking place when the radicals gets fairly mobile. The dimer then dissociates into the monomer radicals at higher temperature, giving spectrum C. Such a dimerization-redissociation phenomenon was observed before.[8]

By irradiating continuously a n-heptane solution of TEA at room temperature, an ESR spectrum was obtained as shown in Fig. 6. The spectrum was very weak and the intensity was proportional to the oxygen pressure. It disappeared immediately when the light is extinguished. The spectrum shows the characteristics of the nitrogen hyperfine structure, with $g=2.0036$ and the nitrogen coupling constant $a_N=15$ G. From the stability of this species, it is most probably an N-oxyl radical. The a_N value of diethylamine-N-oxyl radical observed is 16.7 G.[9] Also, g and a_N of di-t-butylamine-N-oxyl are 2.00595 and 15.36 G, respectively.[10] These values nearly agree with those obtained for the observed spectrum, and from the present situation, it seems most probable that the species obtained is diethylamine-N-oxyl (Et_2NO).

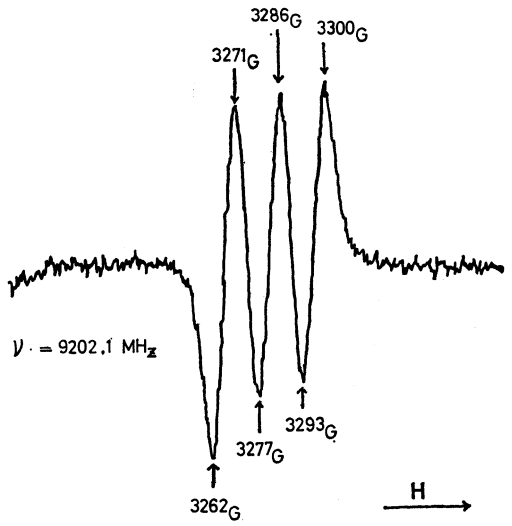

Fig. 6. The ESR spectrum of a species formed by continuous UV-irradiation of triethylamine (1): n-heptane(5)-O_2 at room temperature.

8) N. Yamamoto, H. Tsubomura, and F. Sakiyama, An unpublished result.
9) A. Hudson and A. Hussain, *J. Chem. Soc., Ser. B*, **1967**, 1299.
10) R. J. Faber, F. W. Markley, and J. A. Weil, *J. Chem. Phys.*, **46**, 1652 (1967).

The Analyses of the Photo-Oxygenation Reaction Products. When TEA bubbled with oxygen was irradiated at room temperature in the region of the CT band for a few minutes as described in Experimental section, the amine became turbid, and then began to color yellow. By further irradiation, the yellow color deepened and brown viscous liquid gradually accumulated at the bottom. These processes took about one hour. In the case where the oxygen gas, together with some volatile reaction products, was passed into a cold trap, containing a dilute sulfuric acid solution of 2,4-dinitrophenylhydrazine, a yellow precipitate was immediately formed. The precipitate was purified by recrystallization and identified as the phenylhydrazone of acetaldehyde by elementary analysis and by comparison of its IR spectrum with that of the authentic sample. The yellow-colored sample was also found to contain diethylamine, by treating the sample with p-toluenesulfonyl chloride under Hinsberg's method.

The gas-chromatographic analyses of the amine solutions were carried out also at various stages of the irradiation. At the stage where the amine became first turbid, a peak whose retention time agreed with that of acetaldehyde appeared, together with an unidentified one and the large peak of TEA. By further irradiation, another peak was found. Then, from a sample taken at the stage of yellow coloration, a peak was obtained which is assigned to diethylamine by its retention time, together with at least two small peaks at the longer retention time. The last one agreed in the retention time with that of a product obtained from a reaction mixture of acetaldehyde and diethylamine. The amounts of acetaldehyde and diethylamine obtained are estimated to be about 1 mol% of TEA. The gas-chromatogram of the brown, viscous, bottom layer was very broad and no component was clearly identified.

The infrared spectra of the irradiated sample at various stages were measured as shown in Fig. 7. By the irradiation, absorptions appear at the regions

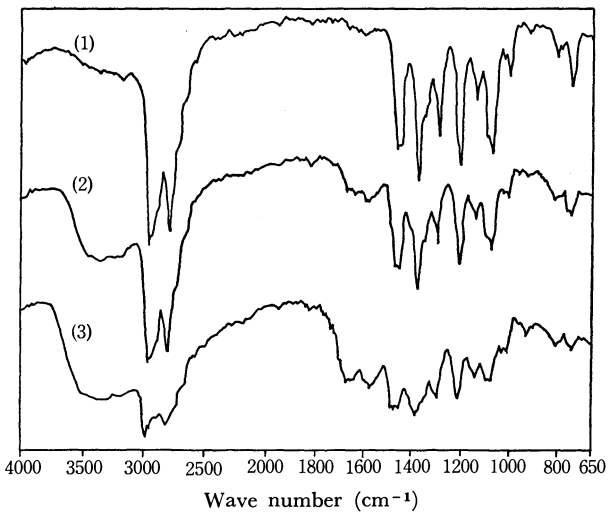

Fig. 7. The infrared absorption spectra of the UV-irradiated triethylamine.
(1) Before irradiation.
(2) The upper layer of the yellow-colored sample.
(3) The lower layer of the same sample.

of 3300 and 1600 cm^{-1}, which suggest the appearance of an amino group or a hydrogen-bonded OH species and carbonyl groups, respectively.

Discussion

Under the present experimental conditions, it is obvious that the first step of the photo-oxygenation reaction of TEA is the formation of the charge transfer state.

$$Et_3N\cdots O_2 \xrightarrow{h\nu} Et_3N^+\cdots O_2^- \qquad (1)$$

At 77 K, the following two processes can be considered.

1. The proton transfer process from the charge transfer state.

$$Et_2N^+\text{-}CH(H)\text{-}CH_3 \longrightarrow Et_2N\text{-}\dot{C}H\text{-}CH_3 \qquad (2)$$
$$O\text{-}O^- \qquad\qquad \cdot O\text{-}OH$$

(named R· hereafter)

The calculation of the enthalpy change for this process by use of known thermochemical data leads to the conclusion that the above process is almost isothermal or slightly endothermic.

2. Re-excitation from the charge transfer singlet state. Though there is no data for the lifetime of the CT state, it might be possible that the CT triplet state which is first attained by photo-excitation degrades to a more stable CT singlet state having a spin different from that of the ground state or to the amine's triplet state, then reabsorbs another photon, and is excited to a higher state. From such higher states, the dissociation of the C–H, C–C, or C–N bond might be probable.

$$^3[Et_3N^+\cdots O_2^-] \longrightarrow \underbrace{^1[Et_3N^+\cdots O_2^-] \text{ or } ^3[Et_3N]\cdots O_2}_{\downarrow h\nu'} \qquad (3)$$
$$\dot{C}H_3,\ \dot{C}_2H_5,\ \dot{E}t_2N,\ R\cdot,\ etc.$$

This second process probably accounts for the methyl and ethyl signals of our ESR measurements at 77 K. It might be possible also that the radical produced by the first process(designated by R·) and the HOO· radical form a pair with $S=0$, or 1. This might be the reason why the signals for R· and HOO· were too weak to be observed in our experiments.

By warming up the matrix, our results tell that the signals for the methyl and ethyl radicals become weaker, and simultaneously, the signal for the peroxy radical increases. These changes can easily be attributed to the softening of the matrix, making the alkyl radicals unstable and the oxygen molecules to diffuse through the matrix till they encounter and react with the larger radicals, for instance, R·, to form the peroxy radical ROO·.

$$R\cdot + O_2 \longrightarrow ROO\cdot$$

The peroxy signal observed, with a slight splitting by a proton, seems to support its assignment to the above-mentioned species, ROO·. The presence of *N*-oxyl radical found from the ESR measurements by continued irradiation at room temperature and that of acetaldehyde from chemical analysis suggest the following process from this ROO·.

$$Et_2N\text{-}CH\text{-}CH_3 \longrightarrow Et_2NO\cdot + CH_3CHO$$
$$\cdot O\text{-}O$$

(ROO·)

The origin of the diethylamine isolated from the photolysis product is not clear, but at least part of the material might have been formed from diethylamino radical obtained in process 2.

The overall processes leading to the yellow viscous material seem to be extremely complex. One possible route is the condensation reaction between acetaldehyde and diethylamine *via* the formation of an enamine.

$$CH_3CHO + Et_2NH \longrightarrow CH_2{=}CH\text{-}NEt_2 + H_2O$$
$$\downarrow$$
$$\lesssim$$
$$\downarrow$$

More condensation reactions

The *N*-oxyl radical, some peroxides and other radicals formed photo-chemically may take part in the further reactions.

The authors gratefully acknowledge the aid given by Professor K. Kuwata, Professor K. Itoh(Osaka University) and Professor T. Matsuura(Kyoto University) for the interpretations of the ESR spectra.

Molecular Association and Electronic Spectra of Naphthoic Acids: Formation of an Excimer-like Complex in 1-Naphthoic Acid in Rigid-Glass Matrix

Michio KITAMURA and Hiroaki BABA

Division of Chemistry, Research Institute of Applied Electricity, Hokkaido University, Sapporo 060

(Received June 16, 1973)

Absorption and fluorescence spectra of 1- and 2-naphthoic acid (1- and 2-NA) have been studied in a hydrocarbon rigid-glass matrix at 77 K and in the crystal. Each of these acids is associated to form a hydrogen-bonded dimer. On increasing the concentration of 1- or 2-NA, the dimer is further associated to give a higher-order complex that may be assumed to be a tetramer. The fluorescence spectra of the monomer and dimer are in mirror-image relation to their respective absorption spectra in both 1- and 2-NA. When the tetramer of 1-NA is photo-excited, a broad structureless fluorescence emission appears, with the maximum at *ca.* 7000 cm^{-1} to the red from the 0–0 band of the dimer fluorescence. The structureless fluorescence spectrum, which has no mirror-image relation to the absorption spectrum of the tetramer, is supposed to originate from an "excimer-like tetramer" of 1-NA. Photo-excitation of the 2-NA tetramer results in a structured fluorescence emission which is considered to come from the simple excited state of the tetramer. The fluorescence lifetimes, quantum yields, and fluorescence-polarization spectra were measured for various molecular species of 1- and 2-NA. The natural fluorescence lifetime of the excimer-like tetramer of 1-NA is evaluated to be 320 nsec, which is 51 times as long as that of the dimer, and the fluorescence from the excimer-like tetramer is polarized mainly along the short molecular axis of the naphthalene nucleus. It is concluded from these observations that the excimer-like tetramer has a symmetrical configuration, with the planes of the constituent dimer molecules parallel to each other, and its fluorescence process is essentially symmetry forbidden.

In a previous paper,[1] we reported the emission spectra of benzoic acid in a hydrocarbon matrix at 77 K with particular regard to effects of dimer formation. As in the case of benzoic acid, 1-naphthoic acid (1-NA) and 2-naphthoic acid (2-NA) are each associated easily to form a dimer containing two O–H··· O hydrogen bonds. The monomer of benzoic acid gives no fluorescence and only its dimer fluoresces, whereas both the monomer and dimer of the naphthoic acids are known to fluoresce.[2]

In the present study, absorption and fluorescence spectra of 1- and 2-NA have been examined in detail from the viewpoint of molecular association. It was found that, as the concentration of 1- or 2-NA in a hydrocarbon rigid-glass matrix is increased, the hydrogen-bonded dimer is associated further to form a tetramer. In 1-NA, the fluorescence was found to originate from an "excimer-like tetramer." The fluorescence spectra of crystal samples of the naphthoic acids were also obtained for the sake of comparison.

Experimental

1-Naphthoic acid (1-NA), G. R. grade, obtained from Wako Pure Chemical Industries, and 2-naphthoic acid (2-NA), G. R. grade, from Tokyo Kasei Industries were recrystallized from 95% ethyl alcohol and sublimed *in vacuo*. Isopentane, methylcyclohexane, and ethyl ether were purified by the same methods as described in the previous paper.[1] A mixture of isopentane and methylcyclohexane (6 : 1 by volume) was used as solvent, which is referred to as PM in this paper.

Absorption spectra were obtained at 77 K or at room temperature with a Hitachi EPS-3 spectrophotometer, and emission and excitation spectra with a Hitachi MPF-2A spectrophotometer or with an apparatus constructed in our laboratory.[3] Absorption measurements at 77 K were carried out on rigid-glass samples in a quartz cell of 10 mm or 1 mm path length placed in a glass Dewar vessel with quartz windows. Emission measurements at 77 K were made using a 10 mm square quartz cell and a quartz tube cell, 4 mm in diameter. The correction of emission and excitation spectra was made by the relative methods.[1]

Fluorescence decays were observed using 8-nsec exciting light pulses generated by electric discharges through the atmosphere, and the fluorescence lifetimes were obtained by the deconvolution method. Fluorescence quantum yields were determined according to the same procedure as described in Ref. 1.

The measurements of fluorescence polarization were made by the photoselection method.[3,4] The degree of polarization, P is defined as $P=(I_{\parallel}-I_{\perp})/(I_{\parallel}+I_{\perp})$, where $I_{\parallel}$ and $I_{\perp}$ are the intensities of the emitted light polarized, respectively, parallel and perpendicular to the exciting light, which is polarized with the electric vector perpendicular to the plane formed by the excitation and emission beams. The P values were corrected in the usual manner for instrumental and other factors.[3]

Absorption spectra of crystals were measured at room temperature and 77 K using crystal films prepared by evaporation. The crystal fluorescence and excitation spectra were obtained by the front-surface viewing method using crystal powder and crystal films.

The fluorescence spectrum of 1-NA in PM at 4.2 K was observed by immersing the sample cell (a 4-mm quartz tube) directly in liquid helium in a quartz Dewar vessel.

Results and Discussion

The naphthoic acids have large association constants in a hydrocarbon solvent. The monomer–dimer equilibrium constants, K, in PM at room temperature were determined through the procedure of Hosoya *et al.*[5] Since the solubilities of the acids

1) H. Baba and M. Kitamura, *J. Mol. Spectry.*, **41**, 302 (1972).
2) R. M. Hochstrasser, *Can. J. Chem.*, **39**, 1776 (1961).
3) T. Takemura and H. Baba, This Bulletin, **42**, 2756 (1969).
4) F. Dörr, "Creation and Detection of the Excited State," Part A, ed. by A. A. Lamola, Marcel Dekker, New York (1971), pp. 53—122.
5) H. Hosoya, J. Tanaka, and S. Nagakura, *J. Mol. Spectry.*, **8**, 257 (1962).

are very poor in PM, the concentrations of the acids were of the order of 10^{-4} to 10^{-7} mol/l. The results are as follows:

1-naphthoic acid, $K=7.6\times10^4$ l/mol

2-naphthoic acid, $K=3.4\times10^4$ l/mol

Absorption Spectra. The absorption spectra at 77 K of 1- and 2-NA in PM are shown in Figs. 1(a) and 2. The K values obtained at room temperature, together with the large binding energies (~10 kcal/mol)[6] estimated for the formation of the dimer, indicate that virtually no monomeric species exists in PM at 77 K with the concentrations adopted in this study. As was reported,[1] the benzoic acid monomer exists in PM even at 77 K. It was confirmed that the naphthoic acids do not show such an unusual phenomenon. In Figs. 1(a) and 2, the absorption spectra in PM containing 5% ethyl ether by volume are regarded as representing approximately the spectra of the monomers.

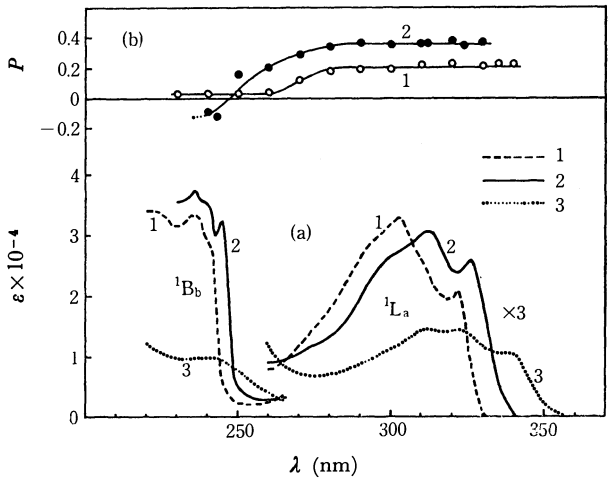

Fig. 1. (a) Absorption spectra of 1-naphthoic acid in PM at 77 K. (1) monomer (see text); (2) dimer (solute concentration, 1.0×10^{-5} mol/l); (3) a mixture of dimer and tetramer (1.0×10^{-4} mol/l).
(b) Excitation-polarization spectra of 1-naphthoic acid at 4.0×10^{-5} mol/l, obtained by monitoring the fluorescence at two wavelengths: (1) 440 nm (excimer-like tetramer fluorescence region); (2) 353 nm (dimer fluorescence region).

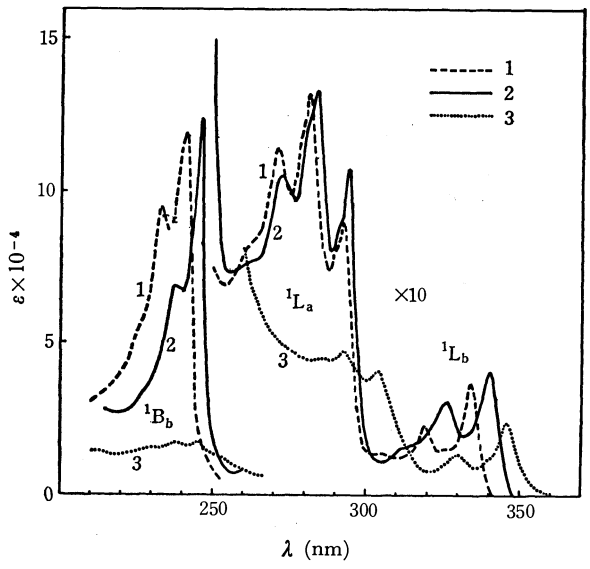

Fig. 2. Absorption spectra of 2-naphthoic acid in PM at 77 K. (1) monomer (see text); (2) dimer (solute concentration, 1.0×10^{-5} mol/l); (3) tetramer (1.0×10^{-4} mol/l).

When the concentration of 1- or 2-NA is 10^{-5} mol/l, only the spectrum of the dimer is obtained at 77 K. As the concentration is increased from 10^{-5} mol/l to 10^{-4} mol/l, new absorption grows up at somewhat longer wavelengths. The absorption spectra corresponding to different concentrations of the acid give an isosbestic point, indicating the existence of an equilibrium between the dimer and a new molecular complex. The new complex is assumed here to be a tetramer of 1- or 2-NA. In Fig. 1(a) or 2, the absorption spectrum represented by the dotted line is considered to be due to the tetramer, but in Fig. 1(a) the spectrum is attributed in part to the dimer. It is further assumed that the tetramer consists of two dimer molecules with their molecular planes parallel to each other; here the hydrogen-bonded dimer is regarded as planar. From the absorption-spectral data, the dimer–tetramer equilibrium constant was estimated to be *ca.* 2.5×10^4 l/mol for 1-NA. This value involves some uncertainty, because the amount of the tetramer produced varies according to the rate of cooling the solution.

In Figs. 1(a) and 2, the values for the molar extinction coefficients, ε, for the dimer and tetramer are defined as the values per monomer. It is evident that the ε values for the dimer defined in this way are comparable to those for the monomer, which fact shows that the π-electronic interaction between the unit monomer molecules is relatively weak in the dimer. This is consistent with the fact that the dimer is formed through the hydrogen bonds and is essentially planar as a whole.[7,8]

The ε values for the tetramer are considerably different from those for the monomer and dimer. This shows a strong π-electronic interaction to occur between the unit dimer molecules in the tetramer, and supports the preceding assumption concerning the configuration of the tetramer. However, inspection of the absorption spectra in Figs. 1(a) and 2 will lead to the following broad assignments of the electronic absorption bands, irrespective of the form of absorbing species (*i.e.*, monomer, dimer or tetramer). In 1-NA, the first absorption band is assigned to the $^1A\rightarrow{}^1L_a$ transition in the Platt notation, with the weak $^1A\rightarrow{}^1L_b$ transition being assumed to be hidden under the $^1A\rightarrow{}^1L_a$ (*vide infra*), and the second band is assigned to the $^1A\rightarrow{}^1B_b$ transition. In 2-NA, the first, second, and third absorption bands are assigned respectively to the $^1A\rightarrow{}^1L_b$, $\rightarrow{}^1L_a$, and $\rightarrow{}^1B_b$ transitions.

In Fig. 3 are shown the absorption spectra of crystal films of the naphthoic acids. These spectra are very broad and clearly different from the absorption spectra

6) G. C. Pimentel and A. L. McClellan, "The Hydrogen Bond," W. H. Freemann and Company, San Francisco (1960), pp. 351—353.

7) J. Trotter, *Acta Crystallogr.*, **13**, 732 (1960).

8) J. Trotter, *ibid.*, **14**, 101 (1961).

of the tetramers in solution (Figs. 1(a) and 2).

Fluorescence and Excitation Spectra. Figures 4(a) and 5(a) show the fluorescence spectra of 1- and 2-NA in PM solution and in the crystal at 77 K. The fluorescence spectra in PM containing 5% ethyl ether are attributed to the monomer as in the case of the absorption spectra.

The fluorescence spectrum at the solute concentration of 10^{-5} mol/l is due to the dimer. The fluorescence spectra of the monomer and dimer are in mirror-image relation to their respective absorption spectra. For 1-NA, on increasing the concentration, the intensity of the structured dimer fluorescence decreases and, at the same time, a new broad structureless fluorescence emission appears, its maximum being shifted to the red by about 7000 cm^{-1} from the 0-0 band of the dimer fluorescence. The new fluorescence spectrum has no mirror-image relation to the absorption spectrum of the tetramer. Only the broad spectrum with its maximum at 440 nm is observed upon excitation

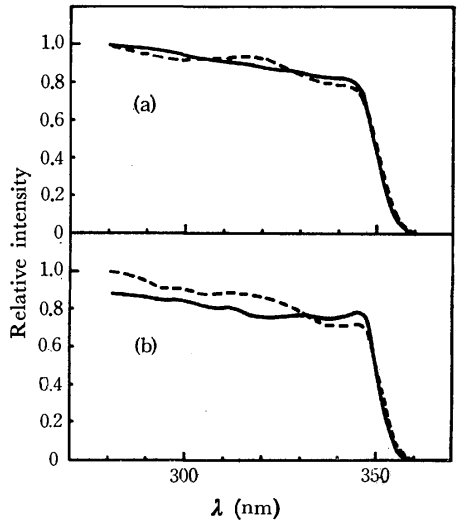

Fig. 3. Absorption spectra (——) and excitation spectra (----) in the crystal of 1-naphthoic acid (a) and 2-naphthoic acid (b) at 77 K.

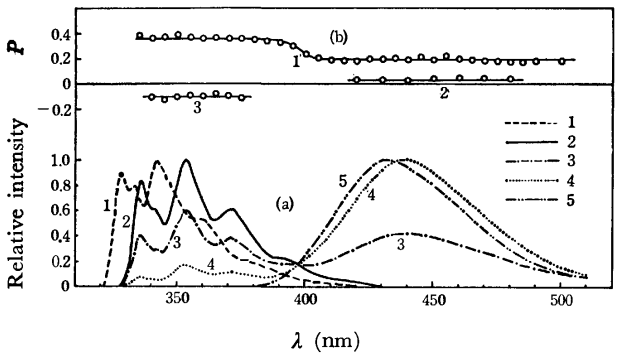

Fig. 4. (a) Fluorescence spectra of 1-naphthoic acid in PM and in crystal at 77 K. (1) monomer (see text); (2) dimer (solute concentration, 1.0×10^{-5} mol/l); (3) a mixture of dimer and excimer-like tetramer (4.0×10^{-5} mol/l); (4) a mixture of dimer and excimer-like tetramer (1.0×10^{-4} mol/l); (5) crystal.

(b) Fluorescence-polarization spectra of 1-naphthoic acid in PM at 4.0×10^{-5} mol/l, obtained by excitation at two wavelengths: (1) 310 nm, (2) and (3) 240 nm.

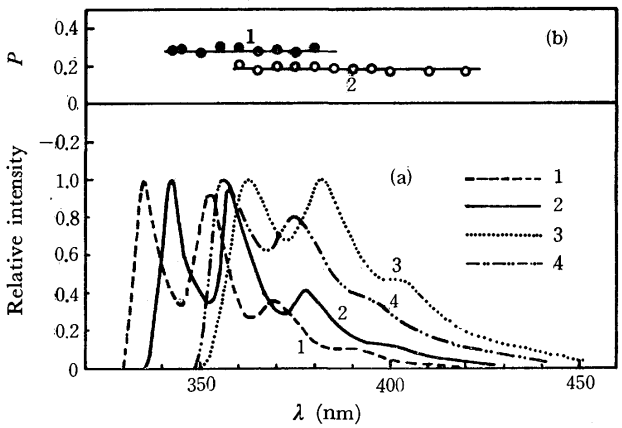

Fig. 5. (a) Fluorescence spectra of 2-naphthoic acid in PM and in crystal at 77 K. (1) monomer (see text); (2) dimer (solute concentration, 1.0×10^{-5} mol/l); (3) tetramer (1.0×10^{-4} mol/l); (4) crystal.

(b) Fluorescence-polarization spectra of 2-naphthoic acid dimer (1) and tetramer (2) in PM at 77 K, obtained by excitation in the region of the longest wavelength absorption (the ^1L_b band).

at 340 nm, where the tetramer alone is considered to be excited (*cf.* Fig. 1(a)). For 2-NA, the increase of the concentration results in a structured fluorescence which is red shifted by only 1700 cm^{-1} from the 0-0 band of the dimer fluorescence.

The new broad structureless fluorescence of 1-NA is considered to originate from an "excimer-like tetramer" in which the interplanar distance between the dimer molecules constituting the tetramer is definitely shortened as a result of the excitation of the tetramer. It should be noted that 1-NA dimer is here regarded as corresponding to the monomer in the ordinary excimer.[9-12] On the other hand, the new structured fluorescence of 2-NA is assigned to the simple tetramer.

In each of the monomer, dimer, and tetramer of the naphthoic acids, the corrected excitation spectrum related to the fluorescence was found to be in good agreement with the corresponding absorption spectrum.

The corrected excitation spectrum of the excimer-like tetramer of 1-NA is shown in Fig. 6 by a broken line. The excitation spectrum is similar to but somewhat different from the absorption spectrum for the 10^{-4} mol/l solution of 1-NA. Since in this solution the tetramer is considered to be largely responsible for the latter spectrum, it must be reasonable to assume that, actually, the excitation spectrum fully agrees with the absorption spectrum of the tetramer alone. The discrepancy between the excitation and absorption spectra for the 10^{-4} mol/l solution can then be at-

9) B. Stevens, "Advances in Photochemistry," Vol. 8, ed. by J. N. Pitts, Jr., G. S. Hammond, and W. A. Noyes, Jr., Interscience Publishers, New York (1971), pp. 161—226.

10) J. B. Birks, "Photophysics of Aromatic Molecules," Wiley-Interscience, London (1970), pp. 301—371.

11) N. Mataga and T. Kubota, "Molecular Interactions and Electronic Spectra," Marcel Dekker, New York (1970). pp. 411—436.

12) S. P. McGlynn, A. T. Armstrong, and T. Azumi, "Modern Quantum Chemistry," Part III, ed. by O. Sinanoğlu, Academic Press, New York (1965), pp. 203—228.

Table 1. Fluorescence lifetimes and quantum yields for 1- and 2-naphthoic acids at 77 K

Compound		τ_f(nsec)	Φ_f	τ_f^0(nsec)	k_f(sec^{-1})
1-Naphthoic acid	Dimer	1.9	0.30	6.3	1.6×10^8
	Excimer-like tetramer	83.7	0.26	320	3.1×10^6
	Crystal	69.7			
2-Naphthoic acid	Dimer	23	0.54	43	2.3×10^7
	Tetramer	25	0.53	47	2.1×10^7
	Crystal	18			

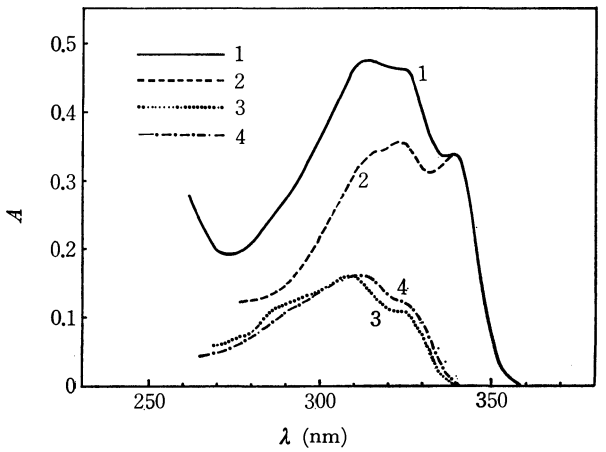

Fig. 6. Excitation spectrum related to the fluorescence from excimer-like tetramer and absorption spectra of 1-naphthoic acid. (1) absorption spectrum of a mixture of dimer and tetramer (solute concentration, 1.0×10^{-4} mol/l); (2) excitation spectrum of excimer-like tetramer; (3) subtracted spectrum (see text for the derivation of this spectral curve); (4) absorption spectrum of dimer (1.0×10^{-5} mol/l).

tributed to the fact that the absorption spectrum involves to some extent the contribution of the dimer. On the basis of the finding that the absorption band at 340 nm (Fig. 1(a)) is due to the tetramer alone, the excitation and absorption spectra are so drawn in Fig. 6 that the both spectra may have the same intensity at that wavelength. Under these conditions, subtraction of the excitation spectrum from the absorption spectrum for the 10^{-4} mol/l solution will yield the absorption spectrum for the dimer. This proves to be true, as is seen in Fig. 6. These considerations clearly indicate that the excimer-like tetramer of 1-NA is formed when the tetramer which exists already in the ground state is photo-excited.

The fluorescence spectra for the crystals of 1-NA and 2-NA are similar to those for the excimer-like tetramer of 1-NA and the simple tetramer of 2-NA, respectively, but the crystal spectra are slightly shifted to the blue (see Figs. 4(a) and 5(a)). The corrected excitation spectra associated with the crystal fluorescence emissions agree well with the crystal absorption spectra in both 1- and 2-NA (see Figs. 3(a) and 3(b)). It may be noted that the structureless excimeric fluorescence spectra of 1-NA in the crystal as well as in the rigid-glass matrix disappeared when a phosphoroscope (50 rps) was used.

Formation of the Excimer-like Tetramer. We are now in a position to examine in detail the excimer-like tetramer of 1-NA in comparison with the simple tetramer of 2-NA. To inquire into the mechanism of the formation of the excimer-like tetramer, it is desirable to know the nature of the excited states of the dimer. For this purpose we shall first consider the fluorescence lifetimes.

Table 1 shows observed fluorescence lifetimes, τ_f, and quantum yields, Φ_f, for 1- and 2-NA at 77 K. The τ_f value for the 1-NA dimer is 1.9 nsec, while that for the 2-NA dimer is 23 nsec. The natural lifetimes, τ_f^0, obtained by the use of the quantum yields are also shown in the table. The τ_f^0 values for the dimers of 1- and 2-NA are 6.3 and 43 nsec, respectively. This suggests that the lowest excited singlet state (fluorescent state), S_1, of the 1-NA dimer is the ^1L_a state and S_1 of the 2-NA dimer is the ^1L_b state. In fact, these values of τ_f^0 agree well with the ones calculated from the Strickler-Berg equation[13] on the basis of the above state assignments; the calculated values are 6.2 and 29.2 nsec, respectively, for the 1- and 2-NA dimers. In the 1-NA dimer the ^1L_a and ^1L_b absorption bands cannot be separated from each other, so that it is tentatively assumed here that the intensity of the ^1L_a absorption band is 80% of the whole absorption intensity in the region from 270 nm to 340 nm (see Fig. 1(a)). This assumption is based on the expectation that the ratio between the intensities of the ^1L_a and ^1L_b bands in the 1-NA dimer is not appreciably different from the corresponding ratios in other simpler naphthalene derivatives.[14-16]

In the 2-NA dimer, it follows from the absorption spectrum given in Fig. 2 that the ^1L_a state, which is the second excited singlet state, is located at an energy about 4600 cm^{-1} above the ^1L_b (S_1) state. It is generally known that the ^1L_a state is responsible for the formation of an excimer,[17,18] and that if the ^1L_a level is much higher than the ^1L_b, the excimer formation is hardly possible.[19] Thus, the difference in the tendency to form an excimer-like tetramer between 1- and 2-NA dimers seems to come from the difference in their electronic structure.

The potential curves illustrating the interaction of the two dimer molecules are shown schematically in Fig. 7. In 1-NA, the attractive force leading to the excimer-like tetramer may result from the inter-

13) S. J. Strickler and R. A. Berg, *J. Chem. Phys.*, **37**, 814 (1962).
14) L. S. Forster and K. Nishimoto, *J. Amer. Chem. Soc.*, **87**, 1459 (1965).
15) K. Nishimoto, *J. Phys. Chem.*, **67**, 1443 (1963).
16) H. Baba and S. Suzuki, This Bulletin, **34**, 82 (1961).
17) T. Azumi and S. P. McGlynn, *J. Chem. Phys.*, **41**, 3131 (1964).
18) A. K. Chandra and E. C. Lim, *ibid.*, **48**, 2589 (1968).
19) E. A. Chandross and H. T. Thomas, *J. Amer. Chem. Soc.*, **94**, 2421 (1972).

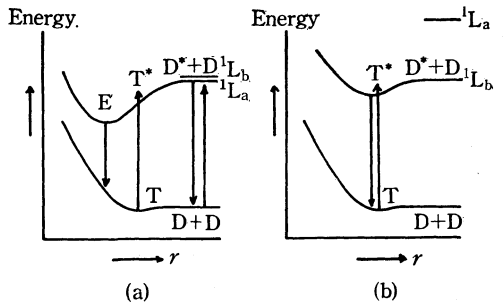

Fig. 7. Schematic potential energy curves showing the formation of excimer-like tetramer of 1-naphthoic acid (a) and tetramer of 2-naphthoic acid (b). r represents the interplanar distance.

action of the ^1L_a state and charge resonance states.[17] The excimer-like tetramer is thus formed along the potential curve for the excited state in Fig. 7(a).

As may be inferred from Fig. 7(b), the situation is different in the case of 2-NA, where the fluorescence is emitted from the simple excited state of the tetramer.

A broad structureless fluorescence emission to be assigned to the excimer-like tetramer was also observed at 4.2 K for 1-NA in PM. In this case, the fluorescence band maximum shows a slight blue shift of *ca.* 140 cm^{-1} compared with the fluorescence at 77 K. The probable increase of the matrix rigidity accompanying the temperature decrease will prevent the excimer-like tetramer from reaching its equilibrium state during its lifetime. This may result in the blue shift mentioned above.

Crystals of 1- and 2-NA are known to consist of nearly planar centrosymmetrical dimer molecules that are formed by the two O–H···O hydrogen bonds,[7,8] and the adjacent dimer molecules have their molecular planes parallel to each other. The difference in spectral behavior between the fluorescence emissions of the 1- and 2-NA crystals (Figs. 4(a) and 5(a)) may be interpreted, as before, in terms of the difference in the relative positions of the ^1L_a and ^1L_b levels. Furthermore, in 1-NA the crystal structure is more favorable for the strong π-electronic interaction to occur.[7,8]

Geometrical Configuration and Electronic Structure of the Excimer-like Tetramer. The geometrical configuration of excimers has been studied by means of intramolecular excimer fluorescence and excimer fluorescence in the crystal.[20,21] The results seem to indicate that a symmetrically overlapping configuration is favorable for the excimer formation. For such a configuration, theoretical considerations predict that the electronic transition associated with the excimer fluorescence should be symmetry forbidden.[11] However, the fact that most of the observed lifetimes of excimers in solution are relatively short is inconsistent with the above prediction.[9]

The lifetimes and quantum yields of the naphthoic acids are given in Table 1. It is seen that in 1-NA the excimer-like tetramer has a much longer natural lifetime τ_f^0 than does the dimer. The radiative rate constants $k_f(=1/\tau_f^0)$ for the dimer, excimer-like tetramer, and tetramer will be denoted by k_f^D, k_f^E, and k_f^T, respectively. Then, from the data in Table 1 the following are obtained:

$$\text{1-naphthoic acid,}\quad k_f^D/k_f^E = 51$$

$$\text{2-naphthoic acid,}\quad k_f^D/k_f^T = 1.1$$

The results suggest that the fluorescence transition in the excimer-like tetramer is electronically forbidden.

The electronic structure of the excimer of naphthalene has attracted much attention.[12,18,22] McGlynn *et al.* showed that in a naphthalene excimer of relatively high symmetry, the transition between its fluorescent and ground states is forbidden.[12] In a similar manner it may be concluded that the excimer-like tetramer of 1-NA has a symmetrical configuration, with the planes of the constituent dimer molecules parallel to each other, and that its fluorescence process is essentially symmetry forbidden. Mataga *et al.* measured the fluorescence lifetimes of excimers of anthracene, perylene, and other aromatic hydrocarbons in cyclohexane matrix at 77 K,[23] and found that the lifetimes are of the order of 10^2 nsec and are longer than the fluorescence lifetimes of the corresponding monomers. Thus, with respect to the configuration and fluorescent state of the excimers, they reached a conclusion similar to the one we have just derived.

The question may then be raised why the "forbidden" fluorescence transition from the excimer-like tetramer of 1-NA has a relatively small but non-zero value of radiative rate constant ($k_f^E = 3.1 \times 10^6$ sec^{-1}). In general, an electronically-forbidden transition in a molecule may become allowed through vibronic interaction. Thus, for instance, in aromatic hydrocarbons like naphthalene, $k_f(^1L_a)/k_f(^1L_b)$ is of the order of 10 to 10^2,[11] where $k_f(^1L_a)$ and $k_f(^1L_b)$ are the radiative rate constants for the $^1L_a \rightarrow {}^1A$ and $^1L_b \rightarrow {}^1A$ transitions, respectively; the former transition is allowed, while the latter is essentially forbidden. As has been shown, $k_f^D/k_f^E = 51$, so that it would be reasonable to consider that the "forbidden" fluorescence transition in the excimer-like tetramer steals a transition probability from other allowed transitions. Alternatively, we may suppose that the excimer-like tetramer deviates slightly from the symmetrical configuration, resulting in the non-zero value of the rate constant k_f^E.

Only a few studies have hitherto been made on the polarization of the excimer fluorescence because of experimental difficulties.[24–26] The excimer fluorescence has been observed not only in fluid solutions, but also in rigid matrices.[27,28] However, most of these matrices are opaque ones, *e.g.*, frozen cyclohexane and *n*-hexane, and are not suitable for the polarization measurement.

20) E. A. Chandross and C. J. Dempster, *J. Amer. Chem. Soc.*, **92**, 3586 (1970).
21) J. Ferguson, *J. Chem. Phys.*, **28**, 765 (1958).
22) A. K. Chandra and E. C. Lim, *ibid.*, **49**, 5066 (1968).
23) N. Mataga, Y. Torihashi, and Y. Ota, *Chem. Phys. Lett.*, **1**, 385 (1967).
24) R. M. Hochstrasser and A. Malliaris, *J. Chem. Phys.*, **42**, 2243 (1965).
25) S. K. Chakrabarti, *Mol. Phys.*, **18**, 275 (1970).
26) E. Sackmann and D. Rehm, *Chem. Phys. Lett.*, **4**, 537 (1970).
27) J. Ferguson, *J. Chem. Phys.*, **43**, 306 (1965).
28) E. Loewenthal, Y. Tomkiewicz, and A. Weinreb, *Spectrochim. Acta*, **25A**, 1501 (1969).

We observed the fluorescence- and excitation-polarization spectra for the dimer and excimer-like tetramer of 1-NA in the transparent rigid-glass PM solution, together with the fluorescence-polarization spectra of the dimer and tetramer of 2-NA in the same solution. Figures 1(b) and 4(b) show respectively the excitation- and fluorescence-polarization spectra of 1-NA. Figure 4(b) is concerned with the fluorescence-polarization spectrum of 1–NA at the concentration of 4×10^{-5} mol/l, where both dimer and tetramer exist in the ground state. In the region of the excimer-like tetramer fluorescence (between 410 and 500 nm), the P values are 0.20 with respect to excitation at 310 nm (line 1), and 0.04 with respect to excitation at 240 nm (line 2). It may be noted that excitation at 340 nm, where only the tetramer is excited, leads to the same P values as excitation at 310 nm. In the region of the dimer fluorescence (between 335 and 380 nm), the P values are 0.36 for excitation at 310 nm (line 1) and -0.10 for excitation at 240 nm (line 3). The same results were also obtained at the 1-NA concentration of 10^{-5} mol/l, where only the dimer exists.

The fluorescence-polarization spectra of 2-NA are shown in Fig. 5(b). The polarization spectrum of the dimer was obtained at the 2-NA concentration of 1.0×10^{-5} mol/l, and that of the tetramer at 1.0×10^{-4} mol/l. The P values are 0.28 for the dimer (line 1) and 0.18 for the tetramer (line 2) with respect to the excitation in the region of the longest-wavelength absorption band.

In 1-NA, the $^1A\rightarrow{}^1L_a$ and $^1A\rightarrow{}^1B_b$ transitions are considered to be polarized largely along the short and long axes of the naphthalene nucleus, respectively.[29] Then, the polarization data for the 1-NA dimer (Figs. 1(b) and 4(b)) are reasonably explained by assuming that the dimer fluorescence has a transition moment parallel to the short axis. The fluorescence spectra of the dimer and tetramer of 2-NA are positively polarized with respect to the excitation into the ^1L_b state (Fig. 5(b)), so that the fluorescent state is regarded as the ^1L_b in either case. However, the P value is somewhat smaller for the tetramer, showing that the increase in the degree of molecular association is accompanied by a factor which leads to depolarization.

A comparison of the polarization data for the excimer-like tetramer of 1-NA with the corresponding data for the dimer (Figs. 1(b) and 4(b)) shows that depolarization occurs obviously in the fluorescence emission in passing from the dimer to the excimer-like tetramer. However, referring to the situation in 2-NA, one may say that the fluorescence emitted from the excimer-like tetramer is polarized essentially along the short axis, as in the case of the dimer fluorescence.

As has been mentioned, the "forbidden" transition associated with the fluorescence of the excimer-like tetramer may become partially allowed either by vibronic interaction or by deviation from the symmetrical configuration. Among the lower excited states of the excimer-like tetramer, there should exist an electronic state from which the transition to the ground state is symmetry allowed. The energy of this allowed transition must be higher than that of the forbidden transition, since the latter transition is related to the lowest excited state. According to the proposed mechanism of the formation of the excimer-like tetramer (*cf.* Fig. 7), the transition moment of the allowed transition in question should be parallel to the moment of the $^1A\rightarrow{}^1L_a$ transition in the dimer or simple tetramer of 1-NA. As regards the vibronic interaction, the forbidden transition will steal the transition probability efficiently from the allowed transition, because the energy difference between the two transitions concerned would not be large. On the other hand, the deviation from the symmetrical configuration, if it occurs at all, will result in a mixing of the allowed transition metioned above with the forbidden transition. These considerations account for the observed polarization of the fluorescence from the excimer-like tetramer.

We wish to express our thanks to Professor S. P. McGlynn for his criticism and discussion, and to Mr. Masahisa Fujita for his help in carrying out the lifetime measurement.

29) S. Suzuki, T. Fujii, and H. Baba, *J. Mol. Spectry.*, in press.

Electron-donating Strengths of Some Ketimines Intermolecular Charge Transfer Studies

R. ABU-EITTAH and M. M. HAMED

Department of Chemistry, Faculty of Science, University of Cairo, Giza, Egypt

(Received March 6, 1972)

The electron-donating strengths of some ketimines have been investigated *via* the formation of charge transfer complexes with iodine as electron-acceptor. Two types of ketimines were chosen as electron-donors, namely, the =N– unsubstituted as well as the =N– substituted ketimines. With the first type of donors the "n" charge transfer complex was obtained whereas with the second type the "π" charge transfer complexes were obtained. The equilibrium constants were computed for the different types of complexes. An attempt is made to estimate the ionization potentials of the donors from the position of the charge transfer band characteristic of the specific complex.

The electron-donating properties of a Lewis-base can very well be investigated through its ability of forming an intermolecular charge transfer complex with a Lewis-acid. The more stable the complex formed, the stronger is the Lewis base. A wide variety of such complexes has been studied. Different types of electron donors are known, organic as well as inorganic molecules.[1] The donors are usually classified as either "n" or "π" donors depending on the type of their molecular orbital that overlaps with the empty molecular orbital of the acceptor.[2–6] Also, a number of electron acceptors have been used but mainly iodine, chloranil, tetracyanoethylene and maleic anhydride are well known.[7] It has been confirmed that the "n" complexes are much more stronger than the "π" ones. Literature is very rich with intermolecular charge transfer studies and many reviews are available.[8,9] Also, Drago[10–13] and his co-workers, Tamres[14–16] and his co-workers have extensively investigated a wide variety of the charge transfer complexes.

The donor properties of many, nitrogen containing, organic molecules have been investigated.[4,6,13,17] However the electron-donating properties of "Ketimines" have not yet been studied. The "Ketimine" molecule contains a C=N– group which may be called an electron sink. Hence it will be interesting to investigate the donating properties of such a group of compounds. The donating properties will essentially depend on some steric factors as well as on the planarity of the molecule.

Experimental

Materials. *1,1-Diphenylmethylenimine*:

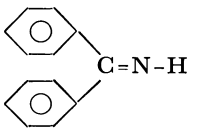

It was prepared from Grignard reaction between freshly distilled bromobenzene and phenyl cyanide. Decomposition of the complex was carried out by absolute methanol.[18] The product was purified by vaccum distillation. Refractive index of the prepared sample is the same as that reported in the literature (n_D^{19} 1.6191).[18]

N-*(Diphenylmethylene)aniline*:

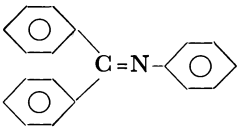

It was prepared by condensation of benzophenone and aniline till the calculated volume of water is collected.[19] The sample was purified by several recrystallization. Melting point is 112—113 °C as compared with 113—114 °C found in literature.[19]

N-*(Diphenylmethylene)*m-*toluidine*.

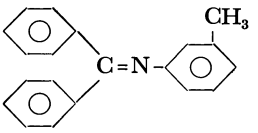

It was prepared by the same procedure used for the *N*-phenyl derivative. Melting point is 81—82 °C as compared with 82.5 found in the literature.[20]

Solvent. Cyclohexane (Apolda Laboratory product)

1) D. Meyerstein and A. Treinin, *Trans. Faraday Soc.*, **59**, 1114 (1963).
2) G. Briegleb, J. Czekalla, and G. Reuss, *Z. Phys. Chem.* (Frankfurt am Main), **30**, 333 (1961).
3) R. P. Lange, *J. Amer. Chem. Soc.*, **84**, 4438 (1962).
4) V. G. Krishna and M. Chowdhury, *J. Phys. Chem.*, 1067 (1963).
5) M. Ashraf El-Bayoumi and O. S. Khalil, *J. Chem. Phys.*, **47**, 4863 (1967).
6) S. Nagakura, *J. Amer. Chem. Soc.*, **80**, 520 (1958).
7) Z. Yoshida and T. Kobayashi, *Tetrahedron*, **26**, 267 (1970).
8) O. Hassel and Chr. Rømming, *Quart. Rev.*, **16**, 1 (1962).
9) G. Briegleb, "Elektronen Donator-Acceptor-Komplexe," Springer Verlag. Berlin (1963).
10) R. S. Drago and D. A. Wenz, *J. Amer. Chem. Soc.*, **84**, 526 (1962).
11) R. S. Drago, B. Wayland, and R. L. Carlson, *ibid.*, **85**, 3125 (1963).
12) R. L. Middaugh, R. S. Drago, and R. J. Niedzielski, *ibid.*, **86**, 388 (1964).
13) R. S. Drago, D. W. Meek, R. Longhi, and M. Joesten, *Inorg. Chem.*, **2**, 1056 (1963).
14) M. Tamres and S. Searles, Jr., *J. Phys. Chem.*, **66**, 1099 (1962).
15) A. F. Grand and M. Tamres, *ibid.*, **74**, 208 (1970).
16) A. F. Grand and M. Tamres, *Inorg. Chem.*, **8**, 2495 (1968).
17) H. Yada, J. Tanaka and, S. Nagakura, This Bulletin, **33**, 1660 (1960).
18) P. L. Pickard and T. L. Tolbert, *J. Org. Chem.*, **26**, 4886 (1961).
19) A. W. Weston and R. J. Michaels, Jr., *J. Amer. Chem. Soc.*, **73**, 1381 (1951).
20) G. Reddelien, *Ber.*, **42**, 4761 (1909).

was purified by vigorously stirring with fuming sulphuric acid for eight hours. It was washed with water, saturated sodium carbonate and finally with water. The solvent was dried by keeping over anhydrous magnesium sulphate for 24 hr. The solvent was distilled and then used for scanning the spectra.

Apparatus. Beckman DK spectrophotometer was used. The cells were fused silica of 1.0 cm thickness.

Results and Discussion

1,1-Diphenylmethylenimine-Iodine System. Equilibrium Studies: When solutions of the ketimine (D), and iodine, in cyclohexane, are mixed the following equilibrium exists assuming that only a 1 : 1 complex is formed.

$$D + I_2 \rightleftharpoons D \cdot I_2 \quad (1)$$

The equilibrium constant K is given by:

$$K = [C_c]/[C_D - C_c][C_{I_2} - C_c] \quad (2)$$

where, C_C is the molar concentration of the charge transfer complex, C_D is the initial concentration of the ketimine and C_{I_2} is the initial concentration of iodine. If the absorbance "A" is due to complexed as well as noncomplexed iodine and A_0 corresponds to the absorbance of the initial iodine solution then, assuming Beer's law is obeyed, Eq. (2) will read, after rearrangement:[21]

$$K^{-1} = \frac{A - A_0}{\varepsilon_c - \varepsilon_{I_2}} - C_{I_2} - C_D + \frac{C_D C_{I_2}(\varepsilon_c - \varepsilon_{I_2})}{A - A_0} \quad (3)$$

This equation will be used to calculate the equilibrium constant for some "Ketimine-iodine" system from the variation of the absorbance of the iodine 520 nm band on mixing with the donor.

If at a given wavelength, the absorbance is only due to the charge transfer complex, then A_0 and ε_{I_2} are zero and Eq. (3) becomes:

$$K^{-1} = \frac{A}{\varepsilon_c} - C_{I_2} - C_D + \frac{C_D C_{I_2}}{A}\varepsilon_c \quad (4)$$

When both C_D and C_{I_2} are both small and each is much more than C_C, then Eq. (4) can be rearranged to read:

$$\frac{C_{I_2} C_D}{A} = \frac{1}{K\varepsilon_c} + \frac{C_{I_2} + C_D}{\varepsilon_c} - \frac{K C_{I_2} C_D}{\varepsilon_c} \quad (5)$$

If C_D is equal to or of the order of C_{I_2} (and both are small), the last term of (5) can be neglected and a plot of $C_{I_2} \cdot C_D/A$ *versus* $(C_{I_2} + C_D)$ will give a straight line. According to Scott,[22] the best straight line is drawn through the experimental points. From the slope and intercept ε_C and K are computed.

Figure 1 show the absorption spectra of mixtures of the ketimine and iodine solutions in the 465—330 nm region. Cyclohexane is used as the solvent and as the blank. The best experimental conditions for studying this CT system were found to use equal concentrations of both the donor and the acceptor. In the 465—330 nm region neither iodine nor the ketimine has an absorption band and their absorbance in this region is quite negligible. However, the spectra of the "iodine-ketimine" mixtures show a discrete and well defined band with λ_{max} at 398 nm. This band is assigned to a charge transfer transition characteristic of the charge transfer complex $(C_6H_5)_2C{=}NH \cdot I_2$ obtained on mixing the ketimine with iodine. The spectra of a number of "donor-acceptor" mixtures were scanned. Equation (5) is used to compute ε_C and K. Figure 2 shows a

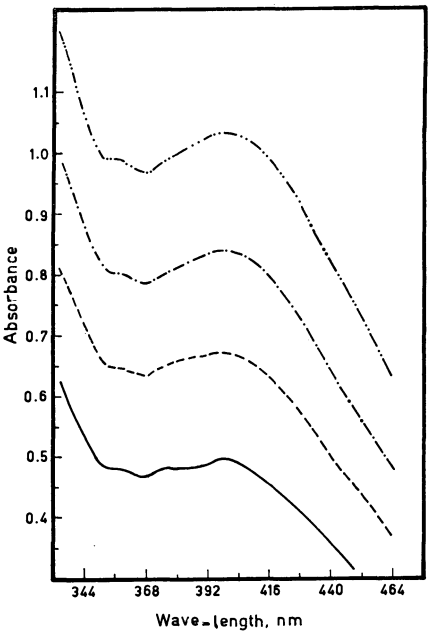

Fig. 1. Absorbance spectra of ketimine-iodine mixtures in cyclohexane.
——— $[I_2]=[\text{Ketimine}]=1.7728\times10^{-3}$ M
----- $[I_2]=[\text{Ketimine}]=2.0682\times10^{-3}$ M
— · — $[I_2]=[\text{Ketimine}]=2.3637\times10^{-3}$ M
— ·· — $[I_2]=[\text{Ketimine}]=2.6592\times10^{-3}$ M

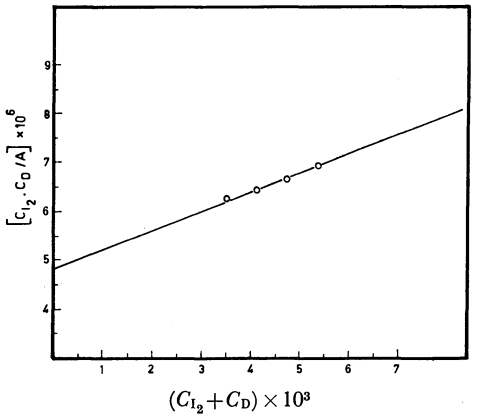

Fig. 2. Variation of $C_{I_2} \cdot C_D/A$ with $C_{I_2}+C_D$ at 398 nm.

Table 1. Variation of absorbance, at $\lambda=398$ nm, with concentration of 1,1-diphenylmethylenimine and iodine

$C_{I_2}=C_D$	Absorbance A	$C_{I_2} \cdot C_D/A$	$C_{I_2}+C_D$
1.7728×10^{-3}	0.50	6.28×10^{-6}	3.5456×10^{-3}
2.0682×10^{-3}	0.67	6.38×10^{-6}	4.1364×10^{-3}
2.3637×10^{-3}	0.84	6.65×10^{-6}	4.7274×10^{-3}
2.6592×10^{-3}	1.03	6.86×10^{-6}	5.3184×10^{-3}

21) N. J. Rose and R. S. Drago, *J. Amer. Chem. Soc.*, **81**, 6138 (1959).
22) R. L. Scott, *Rec. Trav. Chim.*, **75**, 787 (1956).

plot of $C_{I_2} \cdot C_D/A$ (at λ=398 nm) *versus* $(C_{I_2}+C_D)$. A quite satisfactory straight line relationship is obtained. Data needed to plot Fig. 2 are given in Table 1 and are obtained from Fig. 1. Several plots, as shown in Fig. 2, were drawn at different wavelengths. Results are highly reproducible as shown in Table 2. Variation of K with wavelength has been attributed to the formation of I_3^-.[23]

Table 2. Numerical values of K and ε for the 1,1-diphenylmethylenimine-iodine charge transfer complex at room temperature (18 °C)

λ, nm	K	$1/\varepsilon K$	ε
410	83.49	4.90×10^{-6}	2445
404	83.50	4.85×10^{-6}	2469
398	83.33	4.80×10^{-6}	2500
392	85.37	4.80×10^{-6}	2440
386	84.08	4.90×10^{-6}	2427

The numerical value of the equilibrium constant K of the charge transfer complex of the 1,1-diphenylmethylenimineiodine system is of the order of 84. Reproducibility of the results is quite satisfactory. The relatively high value of "K" suggests strongly that one is dealing with an "n" charge transfer complex. The π charge transfer complexes are much weaker than the n ones. The equilibrium constants for π charge transfer complexes vary between 0.15 and 1.35 for benzene or alkyl benzenes-iodine systems.[25,26]

Position of the Charge Transfer Band and Ionization Potential of 1,1-Diphenylmethylenimine. Figure 3

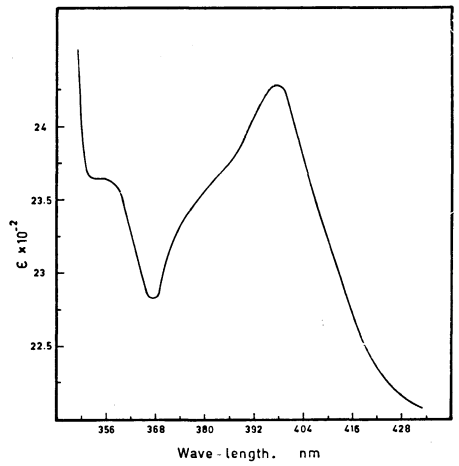

Fig. 3. Charge transfer band of "iodine-1,1-diphenylmethylenimine" System.

shows the charge transfer band of 1,1-diphenylmethylenimine-iodine complex. There are some semiempirical relations which predict the position of the charge transfer band if the ionization potential of the donor is known and others which predict the ionization potential of the donor knownig the position of the charge transfer band. Ionization potentials are determined by a number of methods but most of them cannot differentiate between n and π ionization potentials. On the other hand, ionization potentials obtained from charge transfer studies can be identified as either n or π ionization potentials.

Briegleb[9] *Equation.*

$$E_{CT} = I_D - 5.2 + 1.5/(I_D - 5.2)$$

gives the relation between the energy of the charge transfer band (E_{CT}) and the ionization potential of the donor (I_D) when iodine is the acceptor. Using 3.115 eV for E_{CT} for the 1,1-diphenylmethylenimine-iodine system the n ionization potential of 1,1-diphenylmethylenimine is found to be 7.72 eV.

N-*(Diphenylmethylene)aniline-iodine System. Equilibrium Studies*: Figures 4a and b show the absorption spectra of the pure ketimine, pure iodine and mixtures of both in the 650—350 nm region. Cyclohexane is the solvent and the blank and spectra were scanned at room temperature. Iodine concentration (in the free solution and in the mixtures) was kept constant at 8.5038×10^{-4} M whereas that of the ketimine varied between 1.8153×10^{-2} and 4.8410×10^{-2}. The spectra in Fig. 4 show only the perturbed visible iodine band. That is, no new characteristic band was obtained for the charge transfer transition. On mixing iodine solution with that of the ketimine, the 520 nm band of iodine was blue shifted and the absorbance decreased as the concentration of the ketimine increased. Figure 4a shows one clear and definite isosbestic point. These experimental observations are characteristics of a charge transfer complex. However, since the perturbation of the iodine band is slight and no characteristic charge transfer band was obtained (Fig. 4a) we conclude that we are dealing with a weak charge transfer complex,

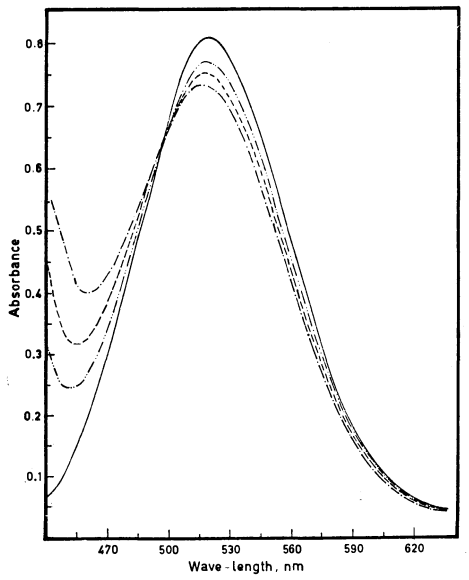

Fig. 4a. Electronic absorption spectra in cyclohexane.
—— Free iodine (8.5038×10^{-4} M)
— · — I_2+Ketimine (Ketimine=4.8410×10^{-2} M)
----- I_2+Ketimine (Ketimine=3.0256×10^{-2} M)
—··— I_2+Ketimine (Ketimine=1.8153×10^{-2} M)
Concn. of I_2 in all mixtures=8.5038×10^{-4} M

23) A. D. Autery and R. E. Connick, *J. Amer. Chem. Soc.*, **73**, 1842 (1951).
24) N. Ebara, This Bulletin, **34**, 1151 (1961).
25) N. W. Blake, H. Winston, and J. A. Patterson, *J. Amer. Chem. Soc.*, **73**, 4437 (1951).
26) L. S. Andrews and R. M. Keefer, *ibid.*, **74**, 4500 (1952).

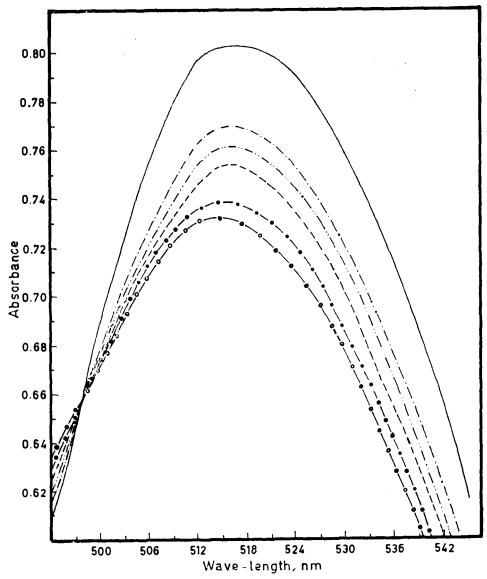

Fig. 4b. Enlarged part of the spectra of *N*-(diphenylmethylene), aniline–iodine system.
——— Free iodine (8.5038×10^{-4} M)
-o-o- I_2+Ketimine (Ketimine=4.8410×10^{-2} M)
-•-•- I_2+Ketimine (Ketimine=4.2359×10^{-2} M)
----- I_2+Ketimine (Ketimine=3.0256×10^{-2} M)
—··— I_2+Ketimine (Ketimine=2.4205×10^{-2} M)
— · — I_2+Ketimine (Ketimine=1.8153×10^{-2} M)
Concn of I_2 in all mixtures=8.5038×10^{-4} M

TABLE 3. NUMERICAL VALUES OF K AND ε FOR THE *N*-(DIPHENYLMETHYLENE) ANILINE-IODINE CHARGE TRANSFER COMPLEX (at 20°C)

Mixtures	K	ε_c
1,2	7.2191	610
1,3	6.3734[a)]	578[a)]
1,4	7.3980	616
1,5	7.8308	629
2,4	7.4510	618
2,5	7.9617	634
3,6	6.9783	605
Average (calculated for the 95% probability limite)	7.4731 ± 0.3875	619

a) Excluded values

most probably a "π" one. The explicit Eq. (3) was used to calculate "K", results are given in Table 3.

Results given in Table 3 are quite reproducible. Figure 4a led to the conclusion that we are dealing with a weak complex. Table 3 confirms this conclusion. Most probably we are dealing with a π complex since K is of the order of 7 whereas that for the 1,1-diphenylmethylenimine-iodine complex K is of the order of 84. It is known that the π complexes are much weaker than those of the n ones. It is worthy to rationalize why, when 1,1-diphenylmethylenimine (a) was the donor an n charge transfer complex is obtained whereas

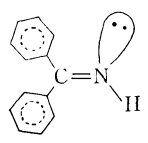

(a)

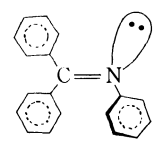

(b)

when *N*-(diphenylmethylene)aniline (b) was the donor a π complex was obtained. Assuming sp^2 hybridization for nitrogen atom, the lone pair of electrons occupies one of the sp^2 hybrid orbitals which is perpendicular to the π atomic orbitals of the rest of the molecule. Hence, overlap of this n orbital with the σ^* molecular orbital of iodine is not sterically hindered and a quite stable n charge transfer complex is obtained. On the other hand, in case of the *N*-(diphenylmethylene)aniline, the phenyl group attached to the -*N* atom is not coplanar with the rest of the molecule. As a result the n orbital is conjugated with the π system of the phenyl group attached to the –N atom. Hence, we have no free n orbital to overlap with the σ^* molecular orbital of iodine and only a π charge transfer complex is botained. The π charge transfer complexes are much weaker than the n ones and usually, donot show an absorption band of their own.[25,26] Overlap of transitions is commonly encountered with π complexes.

The above discussion is confirmed when we consider the electronic absorption spectra of the two donors: 1,1-diphenylmethylenimine (a) and *N*-(diphenylmethylene)aniline (b) as shown in Fig. 5. The spectra of

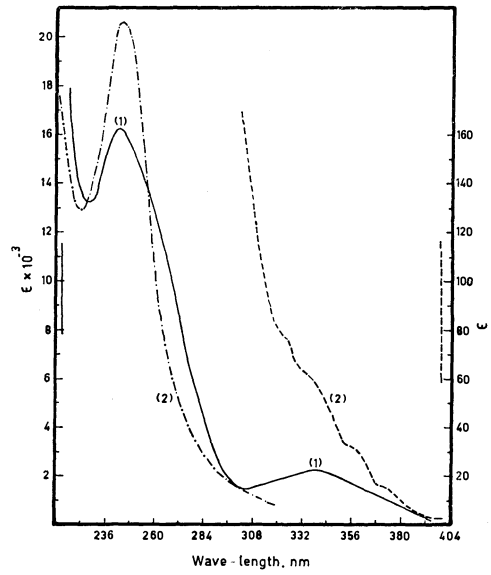

Fig. 5. Electronic absorption spectra of 1,1-(diphenylmethylenimine) (2) and *N*-(diphenylmethylene) aniline (1) in cyclohexane.

the two compounds are very much similar and each show two $\pi\rightarrow\pi^*$ electronic transitions in the ultraviolet region (discussion of the spectra of some ketimines will be subjected in a separate comunication). If conjugation extended over the whole molecule in (b) (molecule is completely planar), then its spectrum would have been significantly different from that of (a). This means that in (b), the benzene ring attached to the nitrogen atom does not lie in the plane of the molecule but may be perpendicular to it. Consequently the n orbital of the nitrogen atom is conjugated with its π cloud and is not free to form an n charge transfer complex when mixed with iodine. This is also confirmed by the fact that the spectrum of 1,1-diphenylmethylenimine shows a separate band for the $n\rightarrow\pi^*$

transition whereas the spectrum of *N*-(diphenylmethylene)aniline does not show this band (Fig. 5). Deviation from coplanarity was also indicated when the spectra of benzylidine aniline were investigated.[24] However, numerical values of the equilibrium constant of "*N*-(diphenylmethylene)aniline-iodine" charge transfer complex indicate that the lone pair of electrons on the nitrogen atom contributes substantially to the relative stability of such a complex. On the other hand, steric factors (in addition to conjugation of n electrons with the π system) inhibit strong interaction with iodine.

Position of the Charge Transfer Band and Ionization Potential of the Donor. When the spectra of pure iodine (3.4270×10^{-5} M), pure *N*-(diphenylmethylene)-aniline (2.4018×10^{-4} M) and their mixtures were scanned in the visible-near ultraviolet region 400—300 nm

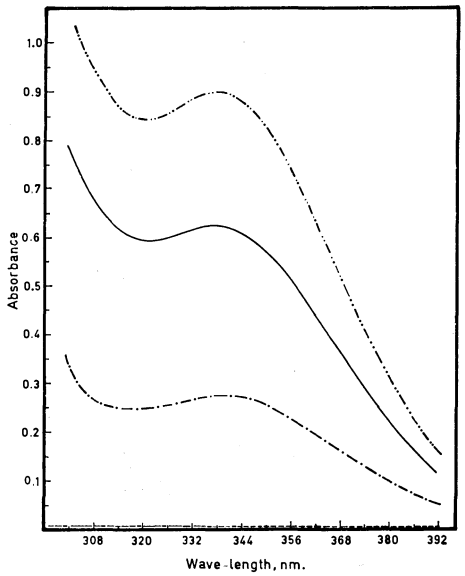

Fig. 6. Electronic absorption spectra of iodine, *N*-(diphenylmethylene) aniline and their charge transfer complex in cyclohexane.
----- Iodine [3.4270×10^{-5} M]
— · — Charg transfer complex
—— Ketimine [2.4018×10^{-4} M]
—··— Mixture of I_2 and ketimine

the absorbance of the mixture is significantly greater than the sum of the absorbances of the free ketimine (Fig. 6) and free iodine. The difference is the absorbance of the charge transfer complex. Thus, in this system, the charge transfer transition and the first $\pi\rightarrow\pi^*$ transition of the donor are overlapping. The energy of the charge transfer band, E_{CT}, is 3.67 eV ($\lambda_{max}=338$ nm) is substituted in Briegleb's equation to yield 8.40 eV as the first ionization potential of *N*-(diphenylmethylene)aniline. Results of Fig. 6 indicate clearly that the electronic transition of the donor with λ_{max} at 338 is $\pi\rightarrow\pi^*$ one ($\varepsilon=2160$). However this transition may be overlapping on the $n\rightarrow\pi^*$ one.

N-*(Diphenylmethylene)*-m-*Toluidine-iodine Systems.* To confirm the above results we used *N*-(diphenylmethylene)-*m*-toluidine as the donor and iodine as the acceptor. The same procedure used with *N*-(diphenylmethylene)aniline was followed. The results obtained with the two donors were very much similar. On mixing iodine solution with that of *N*-(diphenylmethylene) *m*-toluidine the 520 nm iodine band was slightly perturbed, a clear isosbestic point is obtained and no new charge transfer band was obtained. Equation (3) was used to calculate the equilibrium constant. Results are given in Table 4.

Table 4. Numerical values of the equilibrium constant *K* and the molar extinction coefficient ε of the *N*-(diphenylmethylene)-*m*-toluidine-iodine charge transfer complex at room temperature (25 °C)

Mixtures	*K*	ε_c
1,2	5.6895	656
1,3	5.6401	654
1,4	6.2227	676
2,3	5.5481	650
2,4	6.3645	683
3,4	6.7114	695
Average (calculated for the 95% probability limit)	6.0294 ± 0.4949	669

Results of Table 4 are quite reproducible. Also the values of *K* agree fairly well with these obtained for the *N*-(diphenylmethylene)aniline-iodine charge transfer complex. This what one expects when the two donors forms the same type of complex with iodine. The relatively small values of "*K*" as well as the slight perturbation of the iodine band on complexation suggest that we have a weak charge transfer complex.

ESR Line Width and Exchange Narrowing in Powder Samples

B. N. MISRA and S. K. GUPTA
Department of Physics, Allahabad University, Allahabad, India
(Received November 4, 1972)

Electron Spin Resonance Spectra of 1-1 Diphenyl-2-Picryl Hydrazyl (DPPH) recrystallized from some aliphatic and aromatic solvents have been studied at room temperature in the X-band region. Measurements of lineshape, linewidth and *g* value were carried out, all the samples being subjected to microchemical analyses with determination of density and melting point. A theoretical study of ESR linewidths has been carried out by means of the Kubo-Tomita theory of ESR linewidth. A quantitative estimation of dipolar width, exchange frequency, exchange integral and asymptotic Curie temperature for each sample was made. A reduction of exchange narrowing has been suggested to be the main cause of broadening.

Earlier ESR studies[1-7] showed that broader ESR lines with a notable change in shape and *g* value are obtained when free radicals are recrystallized from different solvents. In order to make a detailed theoretical study of various interactions, we used powder samples of 1-1 Diphenyl-2-Picryl-Hydrazyl recrystallized from various organic solvents. The changes obtained in ESR parameters have been quantitatively interpreted with the help of the Kubo-Tomita theory of ESR linewidth. The decrease in exchange coupling has been suggested as the main cause of broadening in the lines. The resulting broadening of the lines has been interpreted in terms of the nature and structure of the solvent used for recrystallization.

Experimental Technique and Method of Measurement

A Bruker X-Band BER 402 Reflection type ESR Spectrometer was used. An Alpha NMR Gaussmeter was used for field measurement, and a Hewlett-Packard frequency counter (hp-525-A) and converter (hp-524-B) for frequency measurement.

The powder free radical DPPH (Purum grade, M/s Fluka, Switzerland) was used. This was prepared from the corresponding hydrazine by oxidation in chloroform solution with lead dioxide. The recrystallized samples were prepared by using analytical grade solvents by slow evaporation technique. The density and melting point of each sample was measured. The linewidth, lineshape and *g*-values were determined by the usual method.[3]

Microchemical analysis of the samples was carried out by direct titration of their solutions in pyridine against chlorauric acid (solution of gold chloride in water) using gallocyanine (in glacial acetic acid) solution as an indicator. The colour changes sharply from bluish green to brownish pink at end point. It was observed that the reaction between chlorauric acid and DPPH takes place in the ratio of 1: 1, confirmed by potentiometric titration.

Results and Discussion

The results of microchemical analysis, density, melting point and ESR parameters such as linewidth and *g* value are given in Table 1.

Line Shape. The shape of ESR lines depends on crystal structure, magnetic dilution and on exchange coupling. The Lorentzian lineshape of the recrystallized samples suggests that the samples are a case of large exchange effect.[9,10] Samples obtained by recrystallization from other solvents have also been reported to show Lorentzian shape of the ESR lines over a wide range of magnetic dilution, frequency and temperature.[11-14]

Line Width. The data in Table 1 indicate that the linewidth of recrystallized powder samples have increased as compared to that of the parent free radical DPPH. This simply suggests that the factors responsible for narrowing the ESR lines have sufficiently reduced after recrystallization of the free radical. It is known that the linewidth from the single crystal of DPPH are highly anisotropic[15,16] changing by as much as a factor of 2. In the polycrystalline sample, a linewidth is averaged out over all orientations of the crystallites with the result that a broader line should be observed. The linewidth of 1.9 Gauss (K-band) for a single crystal of DPPH changes to 3.7 Gauss in powder.[3]

In free radicals, apart from the anisotropy effect, the main causes of linewidth are dipole-dipole and exchange interactions, the latter playing the main role in narrowing the lines. Hence, it can be assumed that the broadening of the lines of the recrystallized sample excluding the anisotropy effect may be due to the change in exchange coupling. A quantitative estimation of the parameters, dipolar broadening and exchange frequency have been made.

1) F. Bruin and M. Bruin, *Physica*, **22**, 129 (1958).
2) G. E. Pake and T. R. Tuttle Jr., *Phys. Rev. Lett.*, **3**, 423 (1969).
3) G. A. Hutchison, R. C. Pastor, and A. Kowalsky, *J. Chem. Phys.*, **20**, 534 (1952).
4) J. J. Lothe and G. Eia, *Acta. Chem. Scand.*, **12**, 1535 (1958).
5) J. P. Goldsborough, M. Mandel, and G. E. Pake, *Phys. Rev. Lett.*, **4**, 13 (1960).
6) J. R. Singer, Paramagnetic Resonance Vol. II, Proceedings of first International Conference, Jerusalem, 16—20 July (Academic Press Inc. New York), 577 (1963).
7) A. Ye. Arbuzov. F. G. Valitova, N. S. Garifyanov, and B. M. Kozyrev, *Doklady Akad. Nauk SSSR*, **126**, 774 (1959).
8) B. N. Misra, S. K. Gupta, and S. D. Sharma, II, *Nuovo Cimento*, **5B**, 145 (1971).
9) J. H. van Vleck, *Phys. Rev.*, **74**, 1168 (1948).
10) P. W. Anderson and M. T. Weiss, *Rev. Mod. Phys.*, **25**, 269 (1953).
11) J. W. Meyer, Ph. D. Thesis, University of Wisconsin, 1955.
12) P. Swarup, *Canad. J. Phys.*, **37**, 848 (1959).
13) Krishnaji and B. N. Misra, *Phys. Rev.*, **135**, A1068 (1964).
14) B. N. Misra, *Ind. J. Pure Appl. Phys.*, **3**, 54 (1965).
15) M. G. Berthet, *C. R. Acad. Sci., Paris*, **240**, 57 (1955).
16) R. Livingston and H. Zelder, *J. Chem. Phys.*, **24**, 170 (1956).

Table 1.

S. No.	Sample	Density gm/ml	Microchemical analysis ratio of DPPH to solvent by wt.	Mp °C	ΔH_{pp} Oersteds	g values	Mean spin distance dÅ
1.	DPPH Powder	1.29	—	137	1.689	2.0036	7.89
	Its sample recrystallized form						
2.	Benzylamine	1.24	1:19.8	70	6.962	2.0036	22.23
3.	Isobutylamine	1.44	1: 6.0	81	6.069	2.0028	14.69
4.	Dibenzylamine	1.33	1:10.0	90	8.071	2.0034	17.56
5.	Benzaldehyde	1.25	1: 5.9	116	5.526	2.0031	15.35
6.	Benzyl chloride	1.36	1: 5.5	110	7.152	2.0036	14.62
7.	2,4-Dinitrofluorobenzene	1.55	1: 4.5	175	7.176	2.0034	13.23
8.	Dimethyl formamide	1.35	1: 3.2	110	6.857	2.0033	12.69
9.	Chlorobenzene	1.53	1: 1.2	116	7.967	2.0033	9.80
10.	Carbon tetrachloride	1.29	1: 1.2	110	2.027	2.0035	10.38
11.	Benzyl alcohol	1.42	1: 1.1	175	7.596	2.0033	9.89
12.	Chloroform	1.47	1: 1.0	105	1.952	2.0036	9.62
13.	Methylene chloride	1.54	1: 1.0	85	2.019	2.0035	9.47
14.	Benzene	1.03	1: 0.7	120	1.864	2.0036	10.26
15.	*n*-Propyl cyanide	—	1: 0.25	—	5.168	2.0035	—
16.	Di-*n*-amylamine	1.05	—	145	5.296	2.0037	—
17.	Diallyl amine	1.51	—	230	8.119	2.0037	—

The theory of linewidth has been developed on the basis of these interactions by van Vleck,[9] Anderson and Weiss[10] and Kubo and Tomita.[17] The expressions given by Chirkov and Kokin[18] from the Kubo-Tomita theory have been used for computation:

The half width between half power points

$$\Delta\omega = 4.18\omega_{10}^2/\omega_{20} \text{ radian s}^{-1} \quad (1)$$

ω_{10}^2, the dipolar width $= 3.79\, g^4\beta^4\hbar^{-2}d^{-6}$ radian^2 s^{-2} (2)

ω_{20}, the exchange frequency $= 3.65|J|/\hbar$ radian s^{-1} (3)

and the exchange integral $J = k\theta/12$

where k is the Boltzmann constant, θ is the asymptotic Curie temperature and all other symbols have their usual meanings. Since the crystal structure and hence d^{-6} is not known for all the samples, we assumed as a very rough approximation that the system has a simple cubic structure. Thus

$$\sum_k r_{jk}^{-6} = 8.4d^{-6}$$

where d is the lattice constant for the crystal, and

$$r_{jk}^{-3} = N\rho/M$$

where N is Avogadro's number, ρ is density and M the molecular weight. This gives an average distance of 7.98 Å between the spins in DPPH powder which is comparable with the value obtained from crystal structure data. Data of microchemical analysis and density (Table 1) have been used to evaluate the value of mean spin distance.

The values of dipolar width ω_{10}^2, exchange frequency ω_{20} and half width between half powder points for DPPH have been computed by taking Curie temperature[1,18] $\theta = -10$ K:

$$\omega_{10}^2 = 15.76\times10^{17} \text{ radian}^2 \text{ s}^{-2}$$
$$\omega_{20} = 3.89\times10^{11} \text{ radian s}^{-1}$$
$$\Delta\omega = 16.54\times10^{6} \text{ radian s}^{-1}$$

The full width $\Delta H_{1/2} = 2\Delta\omega/r = 1.88$ Oersteds

The dipolar broadening ω_{10}^2 was computed by means of (2). The values of ω_{20} was obtained by means of (1) by utilizing the computed values of ω_{10}^2 and measured values of $\Delta\omega$. With these values, exchange integral J and asymptotic Curie temperature θ were calculated for all samples including DPPH. The results are given in Table 2. The lower values of ω_{20} of DPPH powder indicate that the linewidth has been averaged out due

Table 2. Variation of half width between half power points $\Delta\omega$, dipolar frequency ω_{10}^2 exchange frequency ω_{20}, exchange integral J and Curie temperature θ at room temperature

Sample	$\Delta\omega$ $\times10^{-7}$ a) s^{-1}	ω_{10}^2 $\times10^{-17}$ s^{-2}	ω_{20} $\times10^{-9}$ s^{-1}	$J\times10^{25}$ Joules	$\lvert\theta\rvert$ K
DPPH powder	2.57	11.2	181.9	52.6	4.6
Its samples recrystallized form					
Benzylamine	10.60	<0.1	0.1	<0.1	<0.1
Isobutylamine	9.24	0.3	1.3	0.4	<0.1
Dibenzylamine	12.29	<0.1	0.3	<0.1	<0.1
Benzaldehyde	8.41	0.2	1.1	0.3	<0.1
Benzyl chloride	10.88	0.3	1.1	0.3	<0.1
2,4-Dinitrofluoro benzene	10.93	0.5	2.1	0.6	<0.1
Dimethyl formamide	10.44	0.7	2.8	0.8	<0.1
Chlorobenzene	12.13	3.3	11.3	3.3	0.3
Carbon tetrachloride	3.10	2.3	31.4	9.1	0.8
Benzyl alcohol	11.56	3.0	10.8	3.0	0.3
Chloroform	3.00	3.7	51.6	15.0	1.3
Methylene chloride	3.07	4.0	61.7	18.0	1.6
Benzene	2.84	2.5	36.6	10.6	0.9

a) $\Delta\omega = \gamma\sqrt{3}\,\Delta H_{pp}/2$ (For Lorentzian line shape) and $\gamma = 1.758\times10^{7}$.

17) R. Kubo and K. Tomita, *J. Phys. Soc. Jap.*, **9**, 888 (1954).

18) A. K. Chirkov and A. A. Kokin, *J. Expt. Theoret. Phys. USSR*, **30**, 50 (1958).

to the polycrystalline nature of the free radical. The computed values of dipolar width decrease in all the recrystallized samples. The simultaneous decrease in exchange narrowing ω_{20} is sufficiently large. This is also the case in exchange integral J. Thus it can be said that the exchange is more effective in controlling the linewidth. The difference in decrease of exchange coupling for the same magnetic dilution of two different samples is probably controlled by the nature of solvent. The dilution may be due to the permanent inclusion of solvent molecules in the free radical unit cell[19] or a solvent molecule may have associated with the free radical molecule and a molecular addition complex may have formed.[4-6] It can be concluded from the data of microchemical analysis that a greater affinity of complex formation or association was found for the compounds having benzene ring attached with the amino group and chlorine (solvents 2—4). The samples recrystallized from these solvents show a maximum decrease in the exchange coupling. The amino group was found to be more effective in lowering the value of exchange coupling even without benzene ring *viz.* isobutylamine. These form the first category of solvents used here. The second category of solvents include benzyl alcohol and chlorobenzene. The results of their microanalysis do not indicate much dilution but the change in linewidth is comparable with the samples of the first category of solvents. The unexpected broadening present in their ESR lines may be due to the presence of lone pair of electrons on their oxygen and chlorine atoms. The other solvents (Table 1) form the third catagory where the changes in linewidth and exchange coupling parameters are not abnormal and are in agreement with the data on microchemical analysis.

g *Value.* A different value of g has been obtained for different samples. In general, the g value of a substance depends upon many factors such as nuclear and molecular magnetic fields, crystal orientation and applied magnetic field. Crystal orientation has been found to be very effective in DPPH, with the result that a quite measurable anisotropy in the g value of a single crystal of DPPH[3,20] is observed. In polycrystalline sample one gets g factor averaged out over all possible orientations of the polycrystallites present. Hence the changes in g value contain an unknown contribution of g anisotropy and no definite conclusion can be drawn from the change in g value. The change in structure of the free radical responsible for the change in g values does occur[19] after recrystallization of free radical.

Conclusion. The broadening in ESR lines and resulting decrease in exchange coupling depends upon the nature and affinity of the solvents to form complex with the free radical molecule. The changes thus produced in exchange coupling and structure of the free radical due to addition complex formation have not been effective in changing the shape of ESR lines.

Thanks are due to the Council of Scientific and Industrial Research, India, for financial assistance.

19) H. W. Dewijn and J. C. M. Hennig, *Physica*, **28**, 592 (1962).

20) C. Kikuchi and V. W. Cohen, *Phys. Rev.*, **93**, 394 (1954).

Intramolecular Rotations in 1,2-Dialkoxyethanes in the Liquid State

Arati DAS, Alpana GHATAK, Abul HASAN, and S. B. ROY
Department of Optics, Indian Association for the Cultivation of Science, Calcutta-32, India
(Received April 2, 1973)

Dielectric measurements have been made in 1,2-dimethoxy- and 1,2-diethoxyethane in the liquid state in 1.62, 3.17, and 3.49 cm microwave region. Both the molecules are found to relax mostly by methoxy/ethoxy group rotations.

The methoxy group rotation has been reported in anisole both in pure liquid[1,2] and in dilute solutions[3,4] in non polar solvents. It was observed that while the weight factor C_2 for methoxy group rotation in anisole in dilute solution is about 0.8,[3,4] it is only about 0.2[2] in the pure liquid state. The decrease in the value of C_2 from dilute solution to the pure liquid was explained by Garg and Smyth[2] to be due to some restraint in the C–O bond resulting the methoxy group rotation not completely free but hindered.

Similar rotation of the methoxy group has not been reported in aliphatic molecules. In order to study how the methoxy or ethoxy group behave to dipolar relaxation in aliphatic molecules, dielectric studies have been made in the case of 1,2-dimethoxy- and 1,2-diethoxyethane in pure liquid state in 1.62, 3.17, and 3.49 cm microwave region. The results are presented and discussed in the paper.

Experimental

Pure samples of 1,2-dimethoxy- and 1,2-diethoxyethane procured from Schuchardt (Germany) were first dried and fractionated. The proper fraction was distilled under reduced pressure before use in the investigations. The experimental arrangements for measuring the complex dielectric permittivity (ε' and ε''), static dielectric constant ε_0 refractive index n_D and viscosity η were the same as described earlier.[5] The temperature of the experiment was kept constant within ± 1 °C by means of a thermostat. The accuracy in the measurements of ε' and ε'' are about 3 and 5% respectively.

Results

The experimental values of ε', ε'', ε_0, n_D^2 and η are given in Table 1. Cole-Cole arc plots (Fig. 1) were

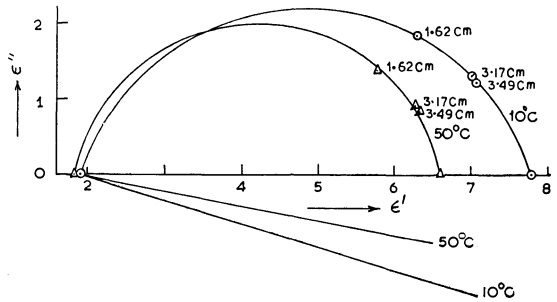

Fig. 1a.

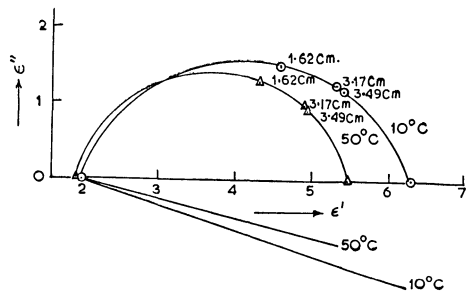

Fig. 1b.

Fig. 1. Cole arc plots of (a) 1,2-dimethoxyethane, (b) 1,2-diethoxyethane.

TABLE 1. VALUES OF n_D^2, ε', ε'', ε_0 AND η

T°C	n^2_D	λ=1.62		λ=3.17		λ=3.49		ε_0	η (cp)
		ε'	ε''	ε'	ε''	ε'	ε''		
				1,2-Dimethoxyethane					
10	1.92	6.29	1.83	7.01	1.30	7.07	1.20	7.80	0.4483
30	1.88	6.10	1.54	6.63	1.03	6.69	0.09	7.14	0.3806
50	1.85	5.78	1.37	6.26	0.91	6.32	0.08	6.61	0.3293
70	1.83	5.60	1.12	5.93	0.70	5.97	0.63	6.14	0.2925
				1,2-Diethoxyethane					
10	2.00	4.57	1.51	5.30	1.26	5.39	1.18	6.30	0.6424
30	1.96	4.44	1.40	5.11	1.09	5.18	1.04	5.86	0.4878
50	1.92	4.30	1.30	4.88	0.96	4.94	0.92	5.47	0.3937
70	1.88	4.20	1.18	4.67	0.84	4.74	0.77	5.12	0.3332

1) W. E. Vaughan and C. P. Smyth, *J. Phys. Chem.*, **65**, 98 (1961).
2) S. K. Garg and C. P. Smyth, *J. Chem. Phys.*, **46**, 375 (1967).
3) D. B. Farmer and S. Walker, *Can. J. Chem.*, **46**, 4645 (1969).
4) G. Klages and G. Krauss, *Z. Naturforsch*, **26a**, 1272 (1971).
5) A. Hasan, A. Das, and A. Ghatak, This Bulletin, **44**, 322 (1971).

drawn with the dielectric data at each temperature. The values of the distribution parameter α were obtained from the arc plots and the most probable relaxation times were calculated by the usual method. The activation energy for dielectric relaxation $\Delta H\tau$ was obtained from the straight line plots of $\log \tau T$ *vs.* $1/T$ (Fig. 2) and the activation energy for viscous flow $\Delta H\eta$ was obtained from the plots of $\log \eta$ *vs.* $1/T$. The values of α, τ, $\Delta H\tau$, and $\Delta H\eta$ are given in Table 2.

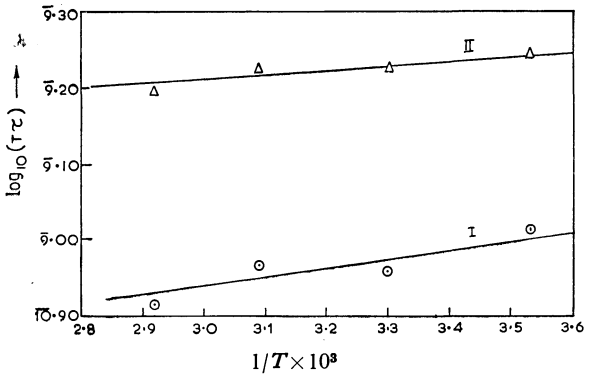

Fig. 2. Plots of $\log \tau T$ *vs.* $1/T$. (I) 1,2-dimethoxyethane (II) 1,2-diethoxyethane

Table 2. Values of α, τ, $\Delta H\tau$ and $\Delta H\eta$

T°C	α	$\tau \times 10^{12}$ s	$\Delta H\tau$ kcal/mol	$\Delta H\eta$ kcal/mol
		1,2-Dimethoxyethane		
10	0.19	3.64		
30	0.16	3.00	0.520	1.30
50	0.13	2.86		
70	0.10	2.39		
		1,2-Diethoxyethane		
10	0.20	6.23		
30	0.17	5.54	0.254	2.30
50	0.14	5.20		
70	0.12	4.59		

Discussion

It can be seen from Table 2 that the distribution parameter in both the liquids are appreciable. So attempts were made to analyse the data in terms of two relaxation processes but were not successful. In order to understand whether the τ-values in the Table 2 belong to orientation of molecules or the groups, the following consideration will help us to clarify the mechanism of the relaxation processes involved in the present case.

The molecule of 1,2-dibromoethane is smaller in size than the molecule of 1,2-dimethoxyethane (since CH_3 group is of the same size as the Br-atom). But the τ-value in the former is 8.6 ps[5] at 30 °C which is much larger than the value of 3.0 ps at 30 °C obtained for the latter molecule. Evidently, the τ-value of 3.0 ps can not correspond to the relaxation time due to molecular orientation in 1,2-dimethoxyethane. Moreover, this τ-value of 3.0 ps at 30 °C in this molecule compares very well with the τ-value of 3.2 ps at 20 °C for the methoxy group rotation in anisole[2] in the liquid state. So it is reasonably concluded that the τ-value of 3.0 ps is due to the methoxy group rotation in 1,2-dimethoxyethane. That the dielectric data could not be resolved into group and molecular relaxation may be due to the fact that the relaxation in this molecule is mostly from methoxy group rotation. In this respect the behaviour of molecules of 1,2-dimethoxyethane differs markedly from that of anisole in the liquid state where contribution from methoxy group rotation is only 0.2.[2] The difference in the weight factor for group rotation in anisole and in 1,2-dimethoxyethane can be understood from consideration of the respective values of dipolar activation energy $\Delta H\tau$. The activation energy for group rotation ($\Delta H\tau_2$) in the former molecule is 1.5 kcal[2] while in the latter it is only 0.53 kcal/mol. This shows that the methoxy group is more flexible in 1,2-dimethoxyethane than in anisole in the liquid state. The high flexibility of the methoxy group makes it possible for 1,2-dimethoxyethane molecule to have four rotational isomers as is reported from spectroscopic studies.[6]

From similar considerations, it is seen that the value of 5.5 ps at 30 °C for τ-value in 1,2-diethoxyethane compares fairly well with the value of about 4 ps at 20 °C in the ethoxy group rotation in phenetole[7] in the liquid state. So in the case of 1,2-diethoxyethane also the relaxation is mainly due to orientation of the ethoxy group. The activation energy of dielectric relaxation in this molecule as can be seen from Table 2 is about 0.25 kcal/mol, which is even smaller than that in 1,2-dimethoxyethane. This means that the ethoxy group in 1,2-dimethoxyethane is more flexible than the methoxy group in 1,2-dimethoxyethane. A larger number of rotamers reported to be present in 1,2-diethoxyethane[6] lends support to this. It is to be noted here that the τ-value of methoxy group rotation at any temperature is less than that of the τ-value of the ethoxy group rotation at the same temperature, which is consistent with the sizes of the groups.

The authors are thankful to Professor G. S. Kastha for his interest in the work.

6) R. Iwamoto, *Spectrochim. Acta*, **27a**, 2385 (1971).
7) J. Bhattacharyya, A. Hasan, S. B. Roy, and G. S. Kastha, *J. Phys. Soc. Jap.*, **28**, 204 (1970).

Polarographic Study of the Substitution Reactions between Nickel(II) Ions and Copper(II) Chelates of Triethylenetetraminehexaacetic Acid

Md. Shamsul HAQUE and Miloslav KOPANICA*

Department of Chemistry, Bangladesh Agricultural University, Mymensingh, Bangladesh

**J. Heyrovsky Polarographic Institute, Czechoslovak Academy of Sciences, Prague, Czechoslovakia*

(Received September, 30, 1972)

The mechanism of substitution reaction between nickel ion and Cu-TTHA chelate was studied by polarographic technique. During the study of the substitution reaction the existence of mixed binuclear chelate $CuXNi^{2-}$ was verified and the value of the stability constant was calculated on the basis of polarographic data. Formation of the mixed binuclear chelate was further verified by the amperometric titration of the equimolar mixture of both metal ions with TTHA. Finally the existence of mixed binuclear chelate $CuXNi^{2-}$ was verified by potentiometric titration method. When nickel is present in large excess the replacement of Cu^{2+} ions from Cu_2X^{2-} occurred directly without formation of intermediate mixed binuclear chelate. The stability constant of Cu_2X^{2-} was calculated from equilibrium study.

The practical utility of EDTA as a titrant for metal ions and in some other fields has encouraged the researchers for ligands with a greater affinity and selectivity for metal ions. One fruitful approach has been the study of higher homologs of EDTA, such as DTPA and TTHA. Their acid dissociation constants were determined by Frost[1] while Grimes *et al.*[2] reported the formation constants of alkaline earth metal chelates with TTHA. The analytical application of TTHA has been studied by Pribil and Vesely[3] mainly in complexometric titration. The interaction between TTHA and various metal ions in aqueous solution was studied by many authors who used mostly potentiometric method[4-8] and in some cases they employed polarographic measurement[9-11] and the stability constants of the metal chelates of TTHA are reported.

During last decade a great interest has been given to study the nature and the mechanism of the electrophilic substitution reaction involving metal ion 'M' and metal chelate M–EDTA by polarographic method[12-15] and by spectrophotometric method.[16-17] It has been found that during the substitution reaction between the metal ion M' and M–EDTA chelate a mixed binuclear intermediate chelate of the type M–EDTA–M' was formed.[17-18] Kopanica[19] has suggested that the substitution reaction between calcium ion and Zn–TTHA chelate proceed through a mixed binuclear chelate which is comparitively stable.

From the review of the literature it appeared that the nature and the mechanism of the substitution reaction of metal chelates of TTHA was not studied intensively. The present work was undertaken with a view to study the mechanism and kinetics of the substitutions reactions of metal chelate of TTHA. In course of the study special attention has been given to verify the existence of the reaction intermediates and also to determine their stability constants. It has been found that under given conditions the attack of the metal ion M' on the chelate molecule M–TTHA results in the formation of relatively stable mixed binuclear chelate M–TTHA–M'.

Experimental

Reagents. Triethylenetetraminehexaacetic acid (TTHA) is sparingly soluble in water. A 0.01 M stock solution was prepared by dissolving 2.484 g of TTHA in 13 ml of 1 M NaOH and by diluting to 500 ml with redistilled water.[10] The solution was standardized against standard zinc solution amperometrically and also by complexometric titration using Eriochrome Black T as an indicator. Solutions of 0.01 M Cu(II) and 0.01 M Ni(II) were prepared from the respective sulphate salt and were standardised against standard Na_2-EDTA solution by amperometric titration[20-21] and also by complexometric titration against standard Na_2EDTA solution using murexide indicator.[22] A 0.2 M acetate buffer (pH 3.55—5.76) and 0.2 M $NaClO_4$ solution (pH 5.0—5.55) were prepared according to the known method.[23-24]

1) A. E. Frost, *Nature*, **178**, 322 (1956).
2) J. H. Grimes, A. J. Huggard, and S. P. Wilford, *J. Inorg. Nucl. Chem.*, **25**, 1225 (1963).
3) R. Pribil and V. Vesely, *Talanta*, **9**, 939 (1962),; **10**, 899 (1963); **11**, 1319 (1964); **12**, 475, 925 (1965).
4) T. A. Bohigian, Jr., and A. E. Martell, *J. Amer. Chem. Soc.*, **89**, 832 (1967).
5) T. A. Bohigian, Jr., and A. E. Martell, *Inorg. Chem.*, **4**, 1264 (1965).
6) L. Harju, *Anal. Chim. Acta.*, **50**, 475 (1970).
7) V. Linden and A. Georgio, *Helv. Chim. Acta*, **53**, 569 (1970).
8) K. H. Schroder, *Acta. Chem. Scand.*, **20**, 881 (1966).
9) K. S. Klausen, G. O. Kalland and E. Jacobsen,, *Anal. Chim. Acta*, **33**, 76 (1965).
10) G. Gonradi, M. Kopanica, and J. Koryta, *Collect. Czech. Chem. Commun.*, **30**, 2029 (1965).
11) D. N. Purohit, *J. Polarog. Soc.*, **12**, 109 (1966).
12) N. Tanaka, K. Kato, and R. Tamamushi, This Bulletin, **31**, 283 (1958).
13) N. Tanaka and K. Kato, *ibid.*, **32**, 1376 (1959); **33**, 1236 (1960).
14) K. Kato, *ibid.*, **33**, 600 (1960).
15) N. Tanaka and M. Kodama, *ibid.*, **35**, 1596 (1962).
16) T. J. Bydalek and D. W. Margerum, *J. Amer. Chem. Soc.*, **83**, 4326 (1961).
17) D. W. Margerum, D. L. Janes, and H. M. Rosen, *ibid.*, **87**, 4463 (1965).
18) T. J. Bydalek, *Inorg. Chem.*, **4**, 232 (1965).
19) M. Kopanica, *Talanta*, **15**, 1457 (1968).
20) N. Tanaka and Y. Sakuma, This Bulletin, **32**, 578 (1959).
21) N. Tanaka, M. Kodama, M. Sakaki, and M. Sugino, *Bunseki Kagaku*, **6**, 86 (1957).
22) F. J. Welcher, "The Analytical Uses of Ethylenediaminetetraacetate Acid," D. Van Nostrand Co., Inc., (1957), pp. 241, 234, 149.
23) A. I. Vogel, "A Text Book of Qualitative Inorganic Analysis,." Longmans Green and Co., New York.
24) J. Heyrovsky, "Practical Polarography," Academic Press, London and New York, p. 101.

Apparatus. *Polarographic Arrangement*: The current–voltage curves were measured with a pen-recording polarograph model LP-60. This polarograph was designed and produced by the Czechoslovak National Enterprise Laboratorni Pristroje (Laboratory Instrument) in Prague and exported through the foreign trade company KOVO of Czechoslovakia. A saturated calomel electrode of large surface area was prepared in one compartment of the Kalousek cell and used as reference electrode. The other compartment was used for electrolysis of the solution under investigation. Dropping mercury electrode (DME) was used as indicating electrode. The capillary characteristics, measured in 0.2 M KNO_3 solution at a mercury height of 60.0 cm at temperature 20 °C and at a potential −0.60 V, were $m=2.34$ mg/s and $t=3.675$ s.

Procedure. The polarographic current–voltage curves were recorded with a pen-recording polarograph as described before. Polarographic measurements were carried out in 0.2 M acetate buffer of pH 4.7 and in 0.2 M $NaClO_4$ solution of pH 5.15 at 20 °C unless it is mentioned otherwise. Gelatin was added as a maximum suppressor by 0.003% in concentration. The corrected height of the mercury reservior was kept constant at 60.0 cm. The dissolved oxygen from the sample solutions was removed by bubbling pure nitrogen gas through the solutions prior measurement.

Copper(II) and nickel(II) form Cu_2X^{2-} and Ni_2X^{2-} with TTHA (H_6X=TTHA) when copper(II) ions and nickel(II) ions react separately with TTHA. Amperometric titration of equimolar mixture of copper(II) ions and nickel(II) ions with TTHA was carried out in 0.2 M acetate buffer and 0.2 M $NaClO_4$ solution to ascertain the joint behaviour and it was observed that both copper wave and nickel wave diminished simulatneously and became zero when the molar ratio Cu: Ni: TTHA=1: 1: 1.

Exactly equimolar amounts of copper and TTHA solutions were mixed in a number of flasks containing 0.2 M $NaClO_4$ solution and then exactly equimolar amount of nickel solution was added. The ionic strength was adjusted to $\mu=0.2$ with requisite amount of concentrated $NaClO_4$ solution and the volumes of all the samples were made equal by the supporting electrolyte. Polarograms were recorded after 20 min, 24 and 72 hr and it was found that all the nickel ions added have entered into the Cu–TTHA chelate and no copper was released from the chelate. Both the above experiments indicate the formation of a stable mixed binulcear $CuXNi^{2-}$ chelate.

The effect of excess of Ni^{2+} ions on $CuXNi^{2-}$ chelate was investigated in acetate buffer and in $NaClO_4$ solution as follows. Solutions $CuXNi^{2-}$ were prepared in 12 measuring flasks and varying amount of nickel solution was added. The ionic strength was adjusted by adding concentrated $NaClO_4$ solution and the volumes of all the samples were made equal by the supporting electrolyte. The samples were kept in a thermostat at 20 °C for 72 hr and polarograms were recorded. The concentrations of released copper and unreacted nickel were measured directly from the polarograms with the help of calibration curves for copper and nickel. The effect of excess of Ni^{2+} ions on Cu_2X^{2-} was studied as above. In all cases limiting currents of free metal ions were corrected for residual current.

Potentiometric Measurement. The interaction of hexabasic TTHA acid with metal ions was studied potentiometrically. A Radiometer pH meter model PHM 4 with pH scale 0 to 14 and reproducibility of ±0.001 pH unit was calibrated so as to determine the hydrogen ion concentration directly and this was done by direct titration of standard dil. HCl with standard NaOH solution in a medium of constant ionic strength ($\mu=0.2$) maintained by KNO_3 solution. A stream of pure nitrogen gas was passed through the titration vessel and the solution was stirred with a magnetic stirrer before each measurement. The hexabasic TTHA acid was first titrated with standard NaOH solution. Since TTHA is a decadentate ligand, both 1: 1 and 2: 1 metal chelates were expected to be formed and therefore mixtures of metal and ligand of the above ratios were investigated. To ascertain the formation of mixed binuclear metal chelates Cu–X–Ni type, mixtures of Cu^{2+} ions, Ni^{2+} ions and TTHA of ratios 1: 1: 1 were titrated against standard NaOH solution.

Results

Polarographic Investigation of the Reaction between Copper(II), Nickel(II) and TTHA. Amperometric titration of Cu(II) ions and Ni(II) ions with TTHA separately showed that Cu_2X^{2-} chelate and Ni_2X^{2-} chelate were formed. An equimolar mixture of Cu(II) ions and Ni(II) ions was titrated amperometrically with TTHA in 0.2 M acetate buffer and also in 0.2 M $NaClO_4$ solution. The titration polarograms, recorded 20 hr after addition of TTHA, consist of three waves; first one due to the reduction of free copper ions, second one due to the reduction of copper from the chelate and third one due to the reduction of free nickel ions. No wave for the reduction of nickel chelate is appeared. The limiting currents of Cu(II) ions, chelate and Ni(II) ions were measured at −0.20, −0.80, and −1.25 V *vs.* SCE respectively. The height of the limiting currents of Cu(II) ions and Ni(II) ions decreased simultaneously with the addition of TTHA and the height of the chelate wave increased. The height of the waves of Cu(II) ions and Ni(II) ions became zero at the molar ratio 1: 1: 1 of Cu^{2+}, Ni^{2+}, and TTHA and only the wave of the chelate appeared (Fig. 1). The titration curves indicate that most probably a mixed binuclear $CuXNi^{2-}$ chelate is formed which is quite stable and polarographically active. An increase of concentration of TTHA beyond the above ratio shifted the half-wave potential of the chelate wave towards negative potential.

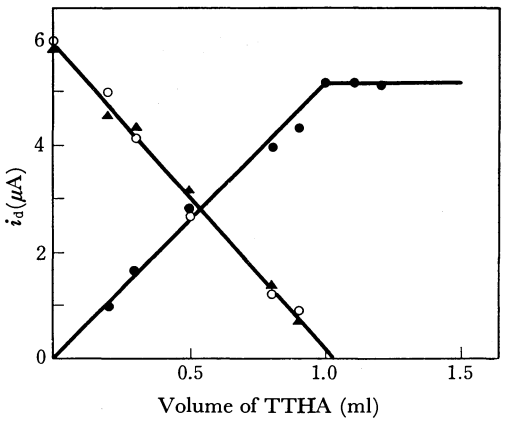

Fig. 1. Amperometric titration of a mixture of Cu(II) ions and Ni(II) ions (1: 1) with TTHA in acetate buffer of pH 4.7. Recorded 20 hr after addition. ○: wave of free copper ions, ●: wave of chelate, ▲: wave of free nickel ions.

Polarographic Behaviour of $CuXNi^{2-}$ Chelate. Polarogram recorded from solution containing Cu^{2+}, TTHA and Ni^{2+} in the molar ratio 1:1:1 in 0.2 M acetate buffer shows that only a single well-defined wave appears due to the reduction of copper from the chelate $CuXNi^{2-}$. The half-wave potential of the wave is −0.248 V *vs.* SCE. The polarographic behaviour such as the effect of (a) pressure, (b) excess TTHA, (c) temperature and (d) gelatin on the reduction wave of $CuXNi^{2-}$ chelate is similar to the corresponding behaviour of Cu_2X^{2-} chelate wave. The effect of pH on the reduction wave of $CuXNi^{2-}$ is different from its effect on the reduction wave of Cu_2X^{2-} when all other conditions are maintained constant. In case of $CuXNi^{2-}$, the second wave does not appear at higher pH as it appears in case of Cu_2X^{2-} chelate. The height of the limiting current of $CuXNi^{2-}$ remains unchanged with pH of the buffer but the half-wave potential of $CuXNi^{2-}$ wave shifted towards negative with the increase of pH. The above observations supported the proposal of the formation of a mixed binuclear $CuXNi^{2-}$ chelate.

Potentiometric Titration Studies. Potentiometric titration curves of TTHA acid in absence of metal ions and in presence of one and two moles of metal ions per mole of TTHA are presented in Fig. 2. The

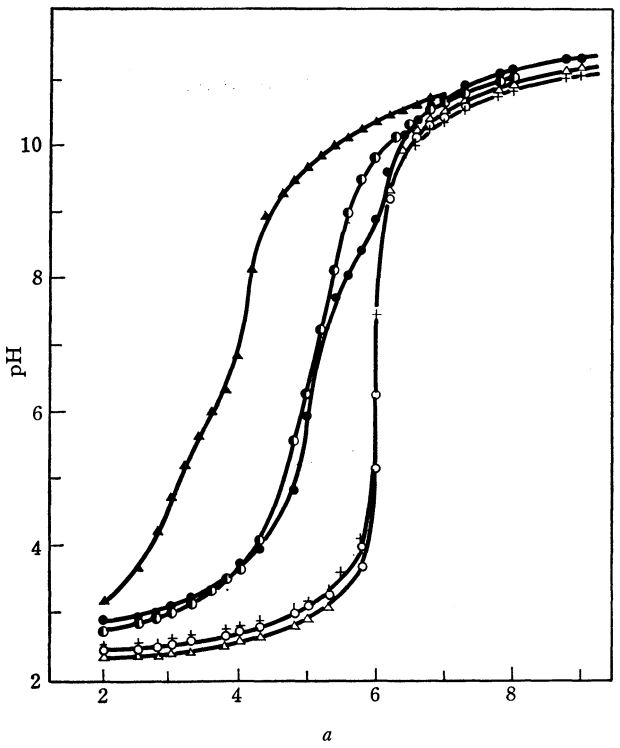

Fig. 2. Potentiometric titration of Cu(II) & Ni(II) chelates of TTHA at 20 °C in 0.20 M KNO_3 with the following molar ratios of metal ions to TTHA.
1) TTHA alone, 2) Cu: TTHA (1:1), 3) Ni: TTHA (1:1), 4) Cu: TTHA (2:1), 5) Cu: Ni: TTHA (1:1:1), 6) Ni: TTHA (2:1). '*a*'=mol of base added per mol of ligand. $C_{TTHA}=8.3\times10^{-4}$ M.

pH is plotted against '*a*', the number of moles of hydroxide ion added per mole of TTHA. The neutralization of the free TTHA occurs in three steps, which has a weak inflection at $a=3$ and a strong inflection at $a=4$. The first step is the reaction of the neutral form of the ligand to form a trinegative anion. The next step occurs at an '*a*' value 4 and results in the formation of tetranegative anion. The neutralization of 5th and 6th protons occurs between an '*a*' value 4 and 6 in overlapping dissociation steps.

The titration curve of 1:1 Cu: TTHA consists of two inflections at an '*a*' value of 5 and 6 indicating the formation of a protonated metal chelate which dissociates at relatively higher pH value to form a normal chelate (Fig. 2). In case of 1:1 Ni: TTHA system the subsequent dissociation step is not as sharp as in the case of Cu: TTHA system. The reaction in case of Cu(II): TTHA system can be represented as follows:

$$H_6X + Cu^{2+} + 5OH^- \longrightarrow CuHX^{3-} + 5H_2O,\ 5OH^-/TTHA \quad (1)$$

where H_6X represents TTHA. Since $CuHX^{3-}$ is a relatively weak acid, the second reaction step involves the neutralization of the remaining proton to form a normal chelate CuX^{4-}.

$$CuX^{3-} + OH^- \longrightarrow CuX^{4-} + H_2O,\ OH^-/TTHA \quad (2)$$

The reactions of Ni(II) occur similarly.

The titration curve of 2:1 Cu: TTHA indicates that the 6 protons of the ligand are neutralized in a single step at an '*a*' value of 6 and a binuclear Cu_2X^{2-} chelate is formed.

$$H_6X + 2Cu^{2+} + 6OH^- \longrightarrow Cu_2X^{2-} + 6H_2O,\ 6OH^-/TTHA \quad (3)$$

Similar titration curve is obtained when 2:1 Ni: TTHA is titrated. No indication of the formation of hydroxo chelate is observed at higher pH.

The titration curve of a mixture of Cu^{2+} ions, Ni^{2+} ions and TTHA of molar ratio 1:1:1 has a single inflection at an '*a*' value of 6 indicating the formation of stable mixed binuclear chelate $CuXNi^{2-}$. The reaction is represented as follows:

$$Cu^{2+} + Ni^{2+} + H_6X + 6OH^- \longrightarrow CuXNi^{2-} + 6H_2O,\ 6OH^-/TTHA \quad (4)$$

There is no subsequent hydrolysis step at higher pH and this indicates that the mixed binuclear chelate $CuXNi^{2-}$ is quite stable.

Polarographic Investigation of the Reaction between $CuXNi^{2-}$ Chelate and Nickel(II) Ions. Amperometric titration of an equimolar mixture of Cu(II) ions and Ni(II) ions with TTHA, and potentiometric titration of 1:1:1 molar ratio of Cu(II) ions, Ni(II) ions and TTHA bear the evidence of formation of a mixed binuclear $CuXNi^{2-}$ chelate over the pH range 4.7—5.15. Polarogram of $CuXNi^{2-}$ chelate is a well-defined wave ($E_{1/2}=-0.248$ V *vs.* SCE) due to the reduction of copper from the chelate. Addition of further amount of Ni(II) ions to the solution of $CuXNi^{2-}$ shows that copper is replaced by nickel from $CuXNi^{2-}$ to form binuclear Ni_2X^{2-} chelate. The exchange reaction is represented as follows:

$$CuXNi^{2-} + Ni^{2+} \rightleftharpoons Ni_2X^{2-} + Cu^{2+} \quad (5)$$

TABLE 1. STABILITY CONSTANT OF $CuXNi^{2-}$ CHELATE AT 20 °C AND IONIC STRENGTH $\mu=0.20$

Cu:X:Ni	C_{Cu} $\times10^4$M	C_X $\times10^4$M	C_{CuXNi} $\times10^4$M	C_{Ni} $\times10^4$M	Equilibrium concentration $[Cu^{2+}]$ $\times10^4$M	$[CuXNi^{2-}]$ $\times10^4$M	$[Ni_2X^{2-}]$ $\times10^4$M	$[Ni^{2+}]$ $\times10^4$M	K_{eq}	log K_{eq}	log K^{Cu}_{CuXNi}
1 : 1 : 2	8.0	8.0	8.0	16.0	1.09	6.91	1.09	4.97	3.46×10^{-2}	−1.46	15.76
1 : 1 : 3	8.0	8.0	8.0	24.0	1.78	6.22	1.78	13.02	3.91×10^{-2}	−1.41	15.71
1 : 1 : 4	8.0	8.0	8.0	32.0	1.87	6.13	1.87	20.70	2.76×10^{-2}	−1.56	15.86
1 : 1 : 5	8.0	8.0	8.0	40.0	2.34	5.66	2.34	27.60	3.51×10^{-2}	−1.46	15.76
											Av. 15.77
1 : 1 : 2	8.0	8.0	8.0	16.0	1.592	6.408	1.592	5.52	7.14×10^{-2}	−1.15	15.45
1 : 1 : 3	8.0	8.0	8.0	24.0	2.682	5.318	2.682	13.27	10.18×10^{-2}	−0.99	15.29
1 : 1 : 4	8.0	8.0	8.0	32.0	3.160	4.840	3.160	19.81	10.42×10^{-2}	−0.98	15.28
1 : 1 : 5	8.0	8.0	8.0	40.0	3.740	4.260	3.740	27.90	11.76×10^{-2}	−0.93	15.23
1 : 1 : 2	4.0	4.0	4.0	8.0	1.01	2.99	1.01	3.20	10.30×10^{-2}	−0.99	15.29
1 : 1 : 3	4.0	4.0	4.0	12.0	1.63	2.37	1.36	7.33	15.30×10^{-2}	−0.82	15.12
1 : 1 : 2	12.0	12.0	12.0	24.0	2.59	9.41	2.59	9.08	7.86×10^{-2}	−1.11	15.41
1 : 1 : 3	12.0	12.0	12.0	36.0	3.90	8.10	3.90	19.60	9.60×10^{-2}	−1.004	15.30
											Av. 15.30

First set: in 0.2M acetate buffer of pH 4.70
Second set: in 0.2M $NaClO_4$ solution of pH 5.15
X=TTHA

The kinetic study of the Eq. (5) showed that the equilibrium reached within 48 hr, still to ensure completion of the reaction, the equilibrium concentrations were studied after 72 hr. The equilibrium constant K_{eq} of the reaction (5) can be defined as

$$K_{eq} = \frac{[Ni_2X^{2-}]\times[Cu^{2+}]}{[CuXNi^{2-}]\times[Ni^{2+}]} \quad (6)$$

$$= \frac{[Ni_2X^{2-}]}{[NiX^{4-}]\times[Ni^{2+}]} \times \frac{[Cu^{2+}]\times[NiX^{4-}]}{[CuXNi^{2-}]}$$

$$= K^{Ni}_{Ni_2X}\cdot K^{Cu}_{CuXNi} \quad (6a)$$

where

$$NiX^{4-} + Ni^{2+} = Ni_2X^{2-},$$

$$K^{Ni}_{Ni_2X} = \frac{[Ni_2X^{2-}]}{[NiX^{4-}]\times[Ni^{2+}]} \quad (7)$$

and

$$CuXNi^{2-} = Cu^{2+} + NiX^{4-},$$

$$K^{Cu}_{CuXNi} = \frac{[Cu^{2+}]\times[NiX^{4-}]}{[CuXNi^{2-}]} \quad (8)$$

The determination of the equilibrium constant K_{eq} leads directly to the determination of the stability (formation) constant of $CuXNi^{2-}$ which is related to K_{eq} by Eq. (6a). The Eq. (7) represents formation constant of Ni_2X^{2-} and Eq. (8) represents the dissociation constant of $CuXNi^{2-}$ and its reciprocal is the stability (formation) constant K^{Cu}_{CuXNi} of $CuXNi^{2-}$chelate.

In equilibrium state, the concentrations of released copper ions and unreacted nickel ions are measured from the polarograms by means of calibration curves. As the metal ions and the metal chelates are not hydrolysed at the pH used, the concentrations of other species in the equilibrium state were calculated according to the method of M. Kopanica[19] and can be given by

$$[CuXNi^{2-}] = C_{Cu} - [Cu^{2+}] \quad (9)$$

$$[Ni_2X^{2-}] = C_X - [CuXNi^{2-}] = C_X - C_{Cu} + [Cu^{2+}] \quad (10)$$

where C_{Cu}, C_X represent the total concentration of copper and the ligand respectively. Substituting the value of $[Cu^{2+}]$, $[Ni^{2+}]$, $[CuXNi^{2-}]$, and $[Ni_2X^{2-}]$ into Eq. (6) gives the Eq. (11)

$$K_{eq} = \frac{[Cu^{2+}]^2}{\{C_{Cu}-[Cu^{2+}]\}[Ni^{2+}]} \quad (11)$$

The equilibrium constant K_{eq} is calculated with the help of Eq. (11). When K_{eq} is substituted into Eq. (6a) and the reciprocal of dissociation constant is taken as stability constant of $CuXNi^{2-}$, then the Eq. (6a) is reduced to Eq. (12).

$$K^{Cu}_{CuXNi} = \frac{K^{Ni}_{Ni_2X}}{K_{eq}} \quad (12)$$

The formation constant $K^{Ni}_{Ni_2X}$ is known[25] and hence K^{Cu}_{CuXNi} is calculated from Eq. (12) and the values of log K^{Cu}_{CuXNi} are presented in Table 1.

Reaction between Cu_2X^{2-} Chelate and Ni(II) Ions. Amperometric titration and potentiometric titration results showed that Cu_2X^{2-} chelate is formed in acetate buffer and $NaClO_4$ solution when copper ions and TTHA are present in the molar ratio 2: 1. When excess of Ni(II) ions are added to the solution of Cu_2X^{2-}, copper is released from the chelate and Ni_2X^{2-} is formed. At higher concentration of Ni^{2+}, the exchange reaction takes place directly without the formation of mixed intermediate binuclear chelate. The exchange reaction is expressed as follows:

$$Cu_2X^{2-} + 2Ni^{2+} \rightleftharpoons Ni_2X^{2-} + 2Cu^{2+} \quad (13)$$

The equilibrium constant K_{eq} of the reaction (13) is represented by

$$K_{eq} = \frac{[Ni_2X^{2-}]\times[Cu^{2+}]^2}{[Ni^{2+}]^2\times[Cu_2X^{2-}]} \quad (14)$$

$$= \frac{[Ni_2X^{2-}]}{[Ni^{2+}]^2\times[X^{6-}]} \times \frac{[Cu^{2+}]^2\times[X^{6-}]}{[Cu_2X^{2-}]} = \frac{K_{Ni_2X}}{K_{Cu_2X}} \quad (14a)$$

where K_{Ni_2X} and K_{Cu_2X} are the formation constants of Ni_2X^{2-} and Cu_2X^{2-} respectively. The Eq. (13) is studied in 0.2 M $NaClO_4$ of pH 5.15 and the equi-

25) L. Harju and A. Ringbom, *Anal. Chim. Acta*, **49**, 221 (1970).

Table 2. Stability constant of Cu_2X^{2-} chelate at 20 °C and ionic strength $\mu=0.2$. 0.2M $NaClO_4$ solution of pH 5.15 is used as supporting electrolyte. X=TTHA

Cu:X:Ni	C_{Cu} $\times 10^4$M	C_X $\times 10^4$M	C_{Ni} $\times 10^4$M	Equilibrium concentration				K_{eq}	$\log K_{eq}$	$\log K_{Cu_2X}$
				$[Cu^{2+}]$ $\times 10^4$M	$[Cu_2X^2]$ $\times 10^4$M	$[Ni^{2+}]$ $\times 10^4$M	$[Ni_2X^{2-}]$ $\times 10^4$M			
2 : 1 : 4	4.0	2.0	8.0	2.36	0.82	6.38	0.81	1.37×10^{-1}	−0.863	33.26
2 : 1 : 8	4.0	2.0	16.0	2.87	0.565	14.85	0.575	0.38×10^{-1}	−1.42	33.82
2 : 1 : 4	8.0	4.0	16.0	4.59	1.71	12.37	1.82	1.47×10^{-1}	−0.83	33.23
2 : 1 : 8	8.0	4.0	32.0	5.88	1.06	28.50	1.75	0.703×10^{-1}	−1.15	33.55
2 : 1 : 4	12.0	6.0	24.0	6.80	2.60	18.30	2.85	1.54×10^{-1}	−0.813	33.21
2 : 1 : 8	12.0	6.0	48.0	8.64	1.68	43.30	2.35	0.557×10^{-1}	−1.25	33.65
										Av. 33.45

librium concentrations of released copper ions and unreacted nickel ions are measured polarographically 72 hr after mixing. The total concentrations of Cu^{2+}, Ni^{2+} and TTHA are known, the concentrations of Cu_2X^{2-} and Ni_2X^{2-} are calculated and hence the value of K_{eq} is calculated from Eq. (14). The formation constant K_{Ni_2X} is known[25] and hence the formation (stability) constant K_{Cu_2X} of Cu_2X^{2-} is calculated from Eq. (14a) and the values of $\log K_{Cu_2X}$ are presented in Table 2.

Discussion

During the study of the substitution reactions between Cu–TTHA chelate and nickel ions, the existence of the mixed binuclear chelate $CuXNi^{2-}$ is established. This has been done by amperometric titration of equimolar mixture of Cu^{2+} ions and Ni^{2+} ions with TTHA. Figure 1 shows the simultaneous decrease of free Cu^{2+} ions and free Ni^{2+} ions waves during the addition of TTHA while new wave appeared which is not the wave of Cu_2X^{2-} chelate ($E_{1/2Cu_XNi}=-0.248$ V, $E_{1/2Cu_2X}=-0.240$ V *vs.* SCE). Section of polarographic behaviour of $CuXNi^{2-}$ chelate is a summary of proofs that the new wave observed does not correspond to the wave of Cu_2X^{2-} chelate. Further evidence of the existence of the mixed binuclear chelate $CuXNi^{2-}$ is the quantitative treatment of the system containing Cu^{2+} ions, Ni^{2+} ions and TTHA ligand. The polarographic measurement enables to collect the data of the concentrations of free Cu^{2+} ions and Ni^{2+} ions which are used for the calculation of the formation constant K^{Cu}_{CuXNi}, the log value of which is 15.30. This constant value calculated under different concentration conditions (Table 1) verifies the proposal of mixed binuclear chelate formation. Further verification of the system of calculation and the accuracy of the experimental data is done by the determination of the stability constant of Cu_2X^{2-} chelate based on the substitution reaction between Cu_2X^{2-} chelate and Ni^{2+} ions (Table 2). The agreement of the obtained value of the stability constant K_{Cu_2X} with the literature value[25] is satisfactory.

Finally the existence of the mixed binuclear chelate $CuXNi^{2-}$ is verified by potentiometric study of neutralization of the mixture of Cu^{2+} ions, Ni^{2+} ions and TTHA ligand (Fig. 2).

Comparison of the results obtained by the polarographic study of the substitution reaction of Cu-chelate with Ni^{2+} ions led to the following conclusion. In the reaction between CuY^{2-} (H_4Y=EDTA) and Ni^{2+} ions the mixed binuclear chelate CuYNi exists only as an intermediate state. During the polarographic examination of the substitution reaction $CuY^{2-}+Ni^{2+}$ (1 : 1) it has been found that in equilibrium state, which comes after 24 hr of mixing, the concentration of free Ni^{2+} ions is equal to the concentration of CuY^{2-} chelate. At the beginning of the reaction the concentration of CuY^{2-} chelate is higher than that of free Ni^{2+} ions. This indicates that at the beginning of the reaction Ni^{2+} ions enter into the CuY^{2-} chelate to form the intermediate CuYNi chelate of sufficient concentration which gradually dissociates to Cu^{2+} and NiY^{2-} chelate. When the substitution reaction of DTPA chelate is studied the formation of mixed binuclear chelate $CuZNi^{-}$ (H_5Z=DTPA) is established and the stability constant of this chelate is determined.[26] In the case of substitution reaction of TTHA chelate the formation of the mixed binuclear chelate is again established. From the above results it is evident that the stability of the mixed binuclear chelate increases with the increase of the number of the donor groups in the ligand molecule.

26) M. S. Haque and M. Kopanica, "Polarographic Study of the Substitution Reactions between Metal Ions and Copper Chelates of Diethylenetriaminepentaacetic Acid," Indian Journal of Applied Chemistry. (Submitted for publication).

A UV Study of the Magnesium Haematoporphyrin Complex

V. D. ANAND* and W. R. CARPER

Garvey Research Center, Department of Chemistry, Wichita State University, Wichita, Kansas, 67208 USA

(Received April 10, 1973)

The interaction between magnesium and haematoporphyrin has been studied spectrophotometricaly as a function of concentration, pH and temperature and the existence of a strong 1 : 1 complex has been established. The Benesi-Hildebrand equation was used to determine K_c's at various wavelengths and temperatures, at pH's of 7.4, 8.2, and 9.0. The enthalpy of complex formation is seen to change from +9.78 kcal/mol to −9.50 kcal/mol as the pH changes from 8.2 to 9.0. This change may be a reflection of the change in the various ligands which coordinate to the magnesium ion in addition to the porphyrin ring.

The porphyrins are a group of compounds that play an extremely important role in the metabolism of plants and animals. A large number of porphyrin derivatives have been isolated, all of which contain the basic prophyrin nucleus.[1-6] One of the first porphyrins to be isolated was haematoporphyrin, about which this report is concerned.

In the present study, addition of magnesium acetate to haematoporphyrin produced marked changes in the difference spectra and these changes were analyzed as a function of pH, concentration and temperature. Equilibrium constants and ΔH's for a 1 : 1 complex have been determined at the pH's of 7.4, 8.2, and 9.0 for the following equilibrium:

$$PH_2 + Mg^{2+} \rightleftharpoons \{MgPH_2\}^{2+} \quad (1)$$

As is indicated in the text, the above equilibrium is far stronger than a displacement equilibrium of the type studied by Brisbin and Balahura.[7] They have measured the equilibrium constants for copper(II) and zinc(II) complexes with haematoporphyrin which result in the following proton displacements:

$$Zn^{2+} + PH_2 \rightleftharpoons ZnP + 2H^+ \quad (2)$$

$$Cu^{2+} + PH_4^{2+} \rightleftharpoons CuP + 4H^+ \quad (3)$$

In their analysis, the 500—600 mμ region was used, and K_C for Eq. (2) was 1.3×10^{-7} at a pH of 7.0.

Experimental

Reagent grade chemicals were used throughout the investigation. Haematoporphyrin dihydrochloride was obtained initially from Calbiochem and finally in recrystallized form from Mann Laboratories. Tris buffer solutions at 0.05 M were used at all pH's.

It should be emphasized that unless the commercial haematoporphyrin is recrystallized, it will be found to contain numerous impurities. However, it can be easily separated from its impurities by the use of Sephadex G-25 in a borate buffer of pH 8.6. This separation has been extensively studied by Momenteau, Ropars and Rougee[8] and Rimington and Belcher.[9]

Survey spectra were recorded with a Beckman DK-2 and a Beckman DU was used to record the actual absorbances. Each spectrophotometer was thermostatted to within 0.1 °C of the desired temperature. The wavelengths used for the analysis were 425, 430, 435, 440, and 445 mμ. The solutions were made up such that the metal concentration was at least 100 times greater than the heamatoporphyrin concentration over a ten-fold range. At least ten points were used at each of the five wavelengths, and the resulting formation constants are an average of the results at each of these wavelengths. As is required in the analysis, Beer's law was obeyed by al of the data used.

Results and Discussion

Some typical difference spectra are given in Fig. 1. Here magnesium acetate was added to haematoporphyrin in a tris buffer of pH 9.0. The haematoporphyrin absorbance was subtracted out and yielded

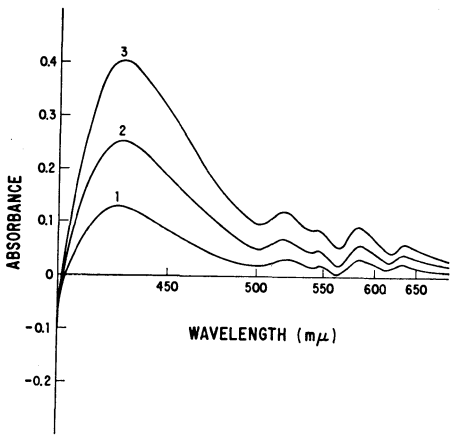

Fig. 1. Recorded difference spectra of the complex as a function of concentration at 25 °C in a tris buffer, pH 9.0. In all cases the haematoporphyrin concentration is 10^{-4} M. The concentrations of magnesium acetate are 10^{-2} M in 1, 4×10^{-2} M in 2 and 0.1 M in 3.

* Present address: NRC Senior Resident, Research Associate, Biochemical Assessment Branch, USAF School of Aerospace Medicine, Brooks Air Force Base, Texas 78235. The view expressed herein are those of the author and do not necessarily reflect the view of the U.S. Air Force or the Department of Defense.

1) S. Aronoff, *Chem. Revs.*, **47**, 175 (1950).
2) R. J. P. Williams, *Biol. Revs.*, **56**, 299 (1956).
3) R. Lemberg and J. W. Legge, "Hematin Compounds and Bile Pigments," Interscience, New York (1949).
4) R. J. P. Williams, "Haematin Enzymes," ed. by J. E. Falk, R. Lemberg, and R. K. Morton, Pergammon, London (1961).
5) J. N. Phillips, "Comprehensive Biochemistry.," Vol. 9, ed. by M. Florkin and E. H. Stotz, Elsevier, New York (1963), Chapter II.
6) J. E. Falk, "Porphyrins and Metalloporphyrins," Vol. 2, Elsevier, New York (1964).
7) D. A. Brisban and R. J. Balahura, *Can. J. Chem.*, **44**, 2157 (1966).
8) M. Momenteau, C. Ropars, and M. Rougee, *J. Chem. Phys.*, **65**, 1635 (1968).
9) C. Rimington and R. V. Belcher, *J. Chromatog.*, **28**, 112 (1967).

the resulting curves. It was routinely possible to vary the absorbance reversibly with respect to temperature.

A Job's plot made at 430 mμ of a pH 9.0 solution is given in Fig. 2 and establishes the presence of a 1 : 1

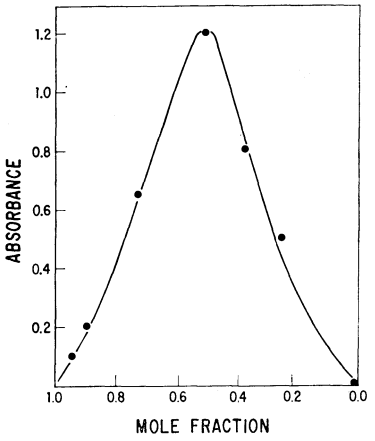

Fig. 2. Job's plot of magnesium-haematoporphyrin complex in a pH 9.0 buffer at 430 mμ at 28 °C.

magnesium-haematoporphyrin complex. Having defined the stoichiometry of the complex, it was possible to analyze the difference spectra of the complex, using the Benesi-Hildebrand (BH) method.[10] In this approach, the relationship

$$1/\log [I_0/I] = 1/K_c\varepsilon_c[M][H] + 1/\varepsilon_c[H] \quad (4)$$

is valid, providing that [M] ⋙ [H], where ε_C is the absorbance coefficient of the complex and [M] and [H] are the molar concentrations of the magnesium ion and haematoporphyrin, respectively.

A plot of $[H]/\log [I_0/I]$ *vs.* 1/[M] gives a slope of $1/K_C\varepsilon_C$, a y intercept of $1/\varepsilon_C$ and a x intercept of $-K_C$. It should be pointed out that if K_C is small, or if Beer's law is not obeyed, then the BH method can no longer be used.

Tables 1 and 2 contain the results of the UV analysis at the pH 's 7.4, 8.2 and 9.0. It should be emphasized that at a pH of 7.4, one is approaching the limits of solubility with respect to haematoporphyrin. As can be readily seen, the formation constants roughly decrease with increasing pH in the vicinity of 37 °C and the enthalpy of complex formation goes from endothermic to exothermic between a pH of 8.2 and 9.0.

In order to explain the drastic change in enthalpy with pH, one may invoke either of the following models or a combination thereof. The initial model (I) is concerned with the changing species that are coordinated to the magnesium ion in addition to the porphyrin nucleus. This effect may be due solely to

10) H. A. Benesi and J. H. Hildebrand, *J. Amer. Chem. Soc.*, **71**, 2703 (1949).

TABLE 1. COMPLEX FORMATION CONSTANTS AND EXTINCTION COEFFICIENTS

T(°C)	K^c pH=7.4	ε_c
40	26.0±0.0	12000
35	25.0±1.2	12500
30	25.1±0.5	13200
25	22.2±1.8	12200
	pH=8.2	
40	32.5±1.2	13300
35	27.5±0.9	14000
30	18.6±0.3	15400
25	14.7±0.7	16000
	pH=9.0	
40	5.6±0.9	34500
35	7.5±0.3	29400
30	10.9±1.6	18200
25	12.5±1.1	17800

TABLE 2. ENTHALPIES OF COMPLEX FORMATION

pH	ΔH(kcal/mol)
7.4	+1.14
8.2	+9.78
9.0	−9.50

a more exothermic bond between the metal and hydroxyl ion than that between the metal ion and a water molecule or a tris anion. However, there is also the possibility of a polymerization effect where the ionized propionic sidechains from one porphyrin complex coordinate to the magnesium of another complex. This was suggested by Loach and Calvin for the manganese haematoporphyrin complex.[11] As porphyrins and metalloporphyrins are known to dimerize, this is not an unreasonable idea, particularly at high pH's.

Model (II) would concern itself with the effect of pH upon the pyrrole hydrogen atoms and the subsequent or simultaneous complex formation between the dianion and the magnesium ion. Unfortunately, the neutral species is stable even in concentrated sodium hydroxide[6] and it would appear that this event is unlikely.

In conclusion, it seems that the environmental changes around the magnesium ion drasticly affect its thermodynamic properties with respect to the complex. As a result, the function of the complex as an efficient electron acceptor may be considerably altered by a pH variation of less than one unit.

V. D. A. acknowledges the award of a University Postdoctoral Fellowship and W. R. C. wishes to thank the University Research Fund for support.

11) P. A. Loach and M. Calvin, *Biochem. J.*, **2**, 361 (1963).

Some Reversible and Irreversible Electrode Processes at DME. A Study on Uranyl and Zinc Complexes of L-Hydroxyproline in Aqueous and Aqueous-Methanolic Solutions

P. C. RAWAT and C. M. GUPTA*

Department of Chemistry, M.R. Engineering College, Jaipur, India

**Chemical Laboratories, University of Rajasthan, Jaipur, India*

(Received October 23, 1972)

Complexes of zinc and uranyl ions with L-hydroxyproline (LHP) have been investigated by polarographic method of analysis at 25±1 and 35±1 °C. At pH 4.5, formation of uranyl-LHP complex was observed with metal to ligand ratio of 1: 1 in aqueous and aqueous-methanolic solutions. The stability constant for the complex species is log K_c=1.50, 1.30, 1.61, 1.87 in aqueous (25 °C), aqueous (35 °C), aqueous-methanolic (10% v/v) and aqueous-methanolic (50% v/v) media respectively. Between pH 3.0—12.0, zinc–LHP complex has been observed to be reduced irreversibly at DME. Detailed investigations have been reported on the system at 25±1 °C and 35±1 °C at pH 10.0 in varying concentrations of the ligand. Kinetic parameters—the formal rate constant $K^\circ_{f,h}$ and transfer coefficient α have been calculated.

Owing to their numerous advantages and interesting properties, amino-acids are finding an increasingly wider applications in chemical technology, biochemistry and various fields of analytical chemistry. Moreover, this class of compounds is characterstically provided with two or more functional groups, the donor atoms from which are capable of combining with a metal atom and, so situated in the molecule, that they permit the formation of a chelate ring with the metal atom as the closing member. L-hydroxyproline (LHP) is one such compound and there are scanty references[1-4] as to the chelate forming capabilities of this acid. The paper is a continuation of our earlier insestigations on the complex forming abilities of L-hydroxyproline with different metal ions. The properties of Cd(II) and Pb(II) complexes have been previously investigated in aqueous and aquo-nonaqueous media.[5] There is however, no reference in literature to the study of uranyl–LHP and zinc–LHP system, and hence the present work has been initiated. The present communication describes the nature of the complexes formed between uranyl ion or zinc ion with LHP by polarographic technique of analysis.

Experimental

L-Hydroxyproline (W. Germany) and AnalaR(BDH) potassium nitrate, potassium chloride, zinc sulphate and uranyl nitrate were used. All solutions were prepared in air free conductivity water. Gelatin at a concentration of 0.004% in final solutions was found satisfactory as maxima suppresor in uranyl–LHP system. No maxima supressor was used in zinc–LHP Studies.

Polarographic waves were recorded with a manual polarograph using a H-cell in conjunction with saturated calomel electrode as reference electrode. The DME had the characterstics: −2.768 mg/s and t=2.8 s (in μ=0.5 M KNO_3 or KCl at −1.15 V *vs.* SCE).

The experiments were performed with 0.5 mM uranyl or zinc in varying concentrations of LHP (0.0 to 0.035 M). Ionic strength was kept constant at μ=0.5 M by adding requisite amounts of KNO_3 (Zinc–LHP system) and KCl (Uranyl–LHP system). Dilute solutions of HCl or NaOH (0.01 M) were used for adjusting pH of the solutions on a Cambridge bench pattern (null-deflection type) pH meter.

Studies on the systems were performed at two temperatures 25±1 °C and 35±1 °C in order to calculate thermodynamic parameters.

Our earlier investigations[5-9] on the behaviours of complexation processes in aqueous-aquo-nonaqueous mixtures furnished significant polarographic data pertaining to stability and composition of the complex species. In sequence to these studies, uranyl–LHP system was further investigated under identical conditions in aqueous-methanolic solutions (10—50% v/v).

Uranyl–LHP system has been throughout studied in weakly acid media (pH=4.5) at μ=0.5 M KCl, in order to obtain diffusion controlled, reversible and one electron reduction of U(VI) to U(V) at DME.[10]

Results and Discussion

Uranyl–LHP System. Reduction: Uranyl ion in LHP gives a one electron reduction at DME which is diffusion controlled and reversible, as revealed by constant values of $i_d/h^{1/2}_{eff}$, the temperature coefficient (1.1—1.5%) and slope of the conventional log i/i_d–i plots (60±3) mV. The wave nature remained the same in all the experimental conditions studied.

Effect of Ligand Concentration: A cathodic shift in $E_{1/2}$, coupled with decrease in diffusion current with increasing concentration of the ligand (0.0—0.035 M) indicates complexation. The plot of $E_{1/2}$ *vs.* $-\log C_X$ results in a straight line (Fig. 1). It is therefore reasonable to conclude the complex being reduced is composed of only one species. The number of ligand/uranyl ion as estimated by expression[11]

1) J. Schubert, *J. Amer. Chem. Soc.*, **76**, 3442 (1954).
2) N. C. Li, N. Doddy, and J. H. White, *ibid.*, **80**, 5001 (1956).
3) D. D. Perrins, *J. Chem. Soc.*, **1956**, 3125.
4) D. D. Perrins, *ibid.*, **1959**, 290.
5) P. C. Rawat and C. M. Gupta, *Talanta*, (1972), Communicated.
6) P. C. Rawat and C. M. Gupta, *J. Inorg. Nucl. Chem.*, **34**, 951 (1972).
7) P. C. Rawat and C M. Gupta, *ibid.*, **34**, 1621 (1972).
8) P. C. Rawat and C. M. Gupta, *Talanta*, **19**, 706 (1972).
9) P. C. Rawat and C. M. Gupta, *Ind. J. Chem.*, **11**, 186 (1973).
10) G. W. C. Milner, "The Principles and Applications of Polagography," Longmans Publication (1962).
11) J. J. Lingane, *Chem. Rev.*, **29**, 1 (1941).

TABLE 1. POLAROGRAPHIC DATA FOR UO_2^{2+} -LHP SYSTEM IN AQUEOUS 25±1 °C(a), 35±1°C(b), 10% METHANOLIC(c), AND 50% METHANOLIC (d) MEDIA (UO_2^{2+}=0.5 mM, KCl=0.5 M, pH=4.5)

Concn of Ligand M	(a)		(b)		(c)		(d)	
	$-E_{1/2}$ (*vs.* SCE) V	i_d μA	$-E_{1/2}$ (*vs.* SCE) V	i_d μA	$-E_{1/2}$ (*vs.* SCE) V	i_d μA	$-E_{1/2}$ (*vs.* SCE) V	i_d μA
0.0	0.204	1.976	0.195	2.280	0.205	1.596	0.260	1.406
0.02	0.205	1.862	0.196	2.204	0.211	1.406	0.272	1.216
0.03	0.215	1.900	0.202	2.223	0.216	1.406	0.283	1.102
0.04	0.220	1.824	0.209	2.166	0.223	1.368	0.289	1.102
0.05	0.225	1.710	0.212	2.143	0.228	1.482	0.293	1.121
0.06	0.230	1.634	0.215	2.014	0.233	1.464	0.300	1.102
0.07	0.234	1.634	0.219	2.014	0.237	1.482	0.306	1.102
0.08	0.240	1.596	0.225	1.976	0.243	1.464	0.311	1.120

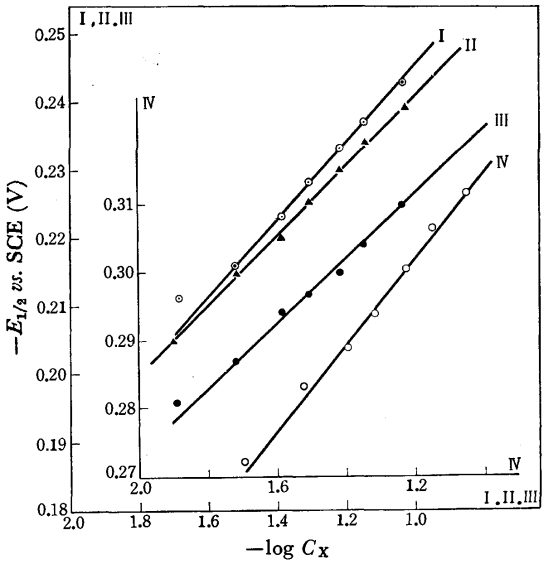

Fig. 1. Plots of $E_{1/2}$ *vs.* $-\log C_x$ for UO_2^{2+}-LHP system at 25 °C (▲), 35 °C (●), 10% methanolic (⊙), and 50% methanolic (○) media.

$$p = -\frac{d(E_{1/2})_c}{d\log C_x} \Big/ \frac{RT}{0.4343nF}$$

is found to be unity. The overall formation constant $\log K_C$ as derived from expression.[11]

$$\Delta E_{1/2} = (E_{1/2})_c - (E_{1/2})_s = \frac{RT}{0.4343nF}\log \beta_p + \mathrm{P}\cdot\frac{RT}{0.4343nF}\log C_x$$

and other polarographic data for different temperature and media are summarised in Table 1.

Effect of Non-aqueous Media: The stability constant $\log K_C$ is found to increase with increasing non-aqueous concentration (methanol) in the media. This suggests stronger metal to ligand binding in the media. This is quite significant and in conformity with our earlier studies on different systems[5-9] and also with similar studies by other workers.[12-14]

Effect of Temperature: Stability constants $\log K_C$ value shows a decrease at increased temperature. This establishes exothermic nature of the interaction between U(VI) and LHP. The thermodynamic constants ΔG, ΔH, and ΔS as calculated from standard equations[15] are summarized in Table 2.

TABLE 2. THERMODYNAMIC CONSTANTS FOR UO_2^{2+}-LHP SYSTEM

Temp. (°C)	$\log K_c$	ΔG kcal	ΔH (kcal)	ΔS (cal/deg/mol)
25±1	1.50	−2.04	—	—
35±1	1.30	−1.83	−8.4	−21.3

L-Hydroxyproline is an amino-acid with pK_1=9.58 and pK_{12}=1.93.[16] Therefore at pH (4.5) on which the system has been investigated, the predominant ligand species must be a dipole molecule rather than the L-hydroxyprolinate ion. In the light of this discussion the complex species and electrode reaction can be possibly formul ated as under.

$$UO_2^{2+} + HL \text{ (dipole molecule)} \rightleftharpoons [UO_2(HL)]^{2+}$$

UO_2^{2+} and $[UO_2(HL)]^{2+}$ co-exist and undergo electrode reaction

$$UO_2^{2+} + [UO_2(HL)]^{2+} + H^+ + 2e \rightleftharpoons 2UO_2^+ + (HL\text{-}H)^+$$

Zinc-LHP System. Reduction: Zinc in LHP (Zn=0.5 mM, μ=0.5 M KNO_3, LHP=0.125 M) was initially investigated in a wide range of pH of the solutions (3.0 to 12.0) at 25±1 °C. The metal ion was observed to give a well defined, diffusion controlled wave in all the solutions. The conventional log plots were linear, but the resulting slopes were not found to be in agreement with the theoretical values, thus indicating the irreversible nature of the electrode reaction. However, the H.W.E.T. shifted towards more negative values with increase in pH suggesting formation of a stable, soluble Zn-LHP complex. Further, studies on the system were preferred at pH=10.0.

12) H. Kodama and K. Hayashi, *J. Electroanal Chem.*, **14**, 209 (1967).
13) P. K. Migal, G. F. Sarova, *Zh. Neorg. Khim.*, **10**, 2513 (1965).
14) P. K. Migal, *Zh. Neorg. Khim.*, **7**, 675 (1962).
15) K. B. Yatsimirskii and Y. P. Vasil'ev, "Instability Constanst of Complex Compounds." Pergamon Press, Oxford (1960).
16) L. G. Sillén and A. E. Martell, "Stability Constants of Metal Ion Complexes." Special Publication No. 17, The Chemical Society, London (1964).

Table 3. Polarographic data for Zn–LHP system at 25±1 °C (a) and 35±1 °C (b)
(Zn=0.5 mM, KNO_3 μ=0.5 M, pH=10.0)

Concn of ligand M		$-E_{1/2}^{o}$ (*vs.* SCE) V	Slope of log plots. mV	i_d μA	αn	$D_0^{1/2}$ 10^{-3}	$K^{o}_{f,n}$
0.005	(a)	1.238	43	3.002	1.26	2.11	9.22×10^{-25}
	(b)	—	—	—	—	—	—
0.015	(a)	1.288	45	2.850	1.20	2.00	9.59×10^{-25}
	(b)	1.266	41	3.306	1.32	2.32	9.70×10^{-26}
0.020	(a)	1.295	46	2.964	1.18	2.08	1.77×10^{-24}
	(b)	1.273	42	3.306	1.29	2.32	2.93×10^{-25}
0.025	(a)	1.303	47	2.85	1.15	2.00	3.32×10^{-24}
	(b)	1.280	43	3.306	1.26	2.32	7.03×10^{-25}
0.030	(a)	1.309	50	2.774	1.08	1.95	4.47×10^{-23}
	(b)	1.285	45	3.154	1.20	2.22	4.23×10^{-24}
0.035	(a)	1.315	52	2.736	1.04	1.92	1.92×10^{-22}
	(b)	1.290	49	3.040	1.11	2.14	1.55×10^{-22}

Effect of Concentration of the Ligand: The zinc–LHP reduction wave, however remained irreversible and diffusion controlled in all the concentrations of the ligand (0.0 to 0.035 M) corresponding to 0.5 mM zinc at μ=0.5 M (KNO_3) and pH=10.0. The wave nature did not change at higher temperature 35±1 °C as well.

Kinetic Parameters: From Koutecky's[17] treatment of irreversible waves as modified by Meites and Israel[18] it follows that for a cathodic wave (at 25 °C) with $E_{1/2}$ more then −1.0 V *vs.* SCE

$$E_{DME} + 0.2412 = \frac{0.05915}{\alpha n}\log\frac{1.349K^{\circ}_{f,h}}{D_0^{1/2}} - \frac{0.0542}{\alpha n}(\log i/(i_d-i) - 0.546\log t) \quad (1)$$

and

$$E^{\circ}_{1/2} = -0.2412 + \frac{0.05915}{\alpha n}\log\frac{1.349K^{\circ}_{f,h}}{D_0^{1/2}} \quad (2)$$

17) J. Koutecky, *Coll. Czech. Chem. Commun.*, **18**, 597 (1953).
18) L. Meites and Y. Israel, *J. Amer. Chem. Soc.*, **83**, 4903 (1961).

The kinetic parameters have thus been calculated by employing Eqs. (1) and (2). The αn was obtained by equating the slope of the straight line plot E_{DME} *vs.* $(\log i/(i_d-i) - 0.546\log t)$ with $0.0542/\alpha n$. The same plot gives the intercept where the quantity being plotted along the abscissa is zero, which is equal to the parameter $E_{1/2}$ defined by the Eq. (2), which was then used to calculate $K^{o}_{f,h}$. The values of $K^{o}_{f,h}$ and αn at 25±1 °C and 35±1 °C (using analogous equations valid at this temperature) in various concentrations of the ligand are summarized in Table 3. From the perusal of the results, it is obvious that the electrode reaction is highly irreversible and increased concentration of the ligand further adds to the irreversibility of the reaction. There is no significant change in this character even at higher temperature.

The authors feel grateful to Prof. R. M. Advani, Principal M. R. E. College, Jaipur and Prof. Dr. R. C. Mehrotra of University of Rajasthan, Jaipur for their interest and provision of research facilities.

Liquid-Liquid Extraction of Zinc with Thiothenoyltrifluoroacetone Direct Photometric Determination in the Organic Phase

K. R. SOLANKE and S. M. KHOPKAR

Department of Chemistry, Indian Institute of Technology, Bombay, 400076 India

(Received January 5, 1973)

The thioderivative of 2-thenoyltrifluoroacetone [1,1,1-trifluoro-4-(2-thienyl)-4-mercaptobut-3-en-2-one (STTA)] is used for the simultaneous extraction and direct photometric determination of zinc. About 68 μg of zinc was quantitatively extracted at pH 7—7.5 with 10 ml of 0.001 M STTA in carbon tetrachloride as yellow green colored complex. It was measured spectrophotometrically at 450 nm. The system conformed to Beer's law over the concentration range of 0.4 to 30 μg of zinc per ml. The color of the complex was stable for more than 96 hr. Zinc was extracted quantitatively and was determined in the presence of large excess of (1: 300) ions which are associated with it. The method was made selective by using sequestering agents like ascorbic, oxalic, citric acids or alkali cyanide to form unextractable negatively charged complexes. The selective extraction with mesityl oxide was used to eliminate the interferences due to iron and chromium. The procedure was found to be applicable for the analysis of zinc in gun metal and brass. The proposed method is comparable with the standard methods for the extraction of zinc.

Thiothenoyltrifluoroacetone (1,1,1-Trifluoro-4-(2-thienyl)-4-mercaptobut-3-en-2-one (STTA) has been used as the extracting and colorimetric reagent for the number of transition elements.[1] It was observed that zinc can be quantitatively extracted at pH 7.0—7.5 with 0.001 M STTA in carbon tetrachloride. The yellow green complex can be measured spectrophotometrically at 450 nm.

The method proposed in this paper with thiothenoyltrifluoroacetone as the extracting and colorimetric reagent is simple, rapid and selective. It is possible to accomplish clean cut separation of zinc at micro gram concentrations. It was found to be applicable to analysis of zinc in alloys such as gun metal and brass.

Experimental

Apparatus and Reagents. Type SF-4 quartz spectrophotometer with 10 mm matched cells. Type FEK-57 photoelectric filter photometer with 10 mm Corex glass cells. Cambridge pH meter with glass electrode; wrist action flask shaker.

Thiothenoyltrifluoroacetone (1,1,1-trifluoro-4-(2-thienyl)-4-mercaptobut-3-en-2-one (STTA) was synthesised from 2-thenoyltrifluoroacetone (Koch-light England) as per the method indicated in earlier paper[2] with all the necessary precautions to get the best yield as described by Kiba.[3] About 0.001 M reagent in carbon tetrachloride was used. The reagent was always preserved in the refrigerator.

A stock solution of zinc was prepared by dissolving about 1.2 gm of zinc sulphate hexahydrate in 100 ml of distilled water containing 0.001% of sulphuric acid. The solution was standardized complexometrically[4] with EDTA, and was found to contain 2.7 mg of zinc per ml. The dilute solution containing 67.5 μg per ml of zinc was prepared by appropriate dilution.

General Procedure. An aliquot of solution containing about 67.5 μg of zinc was taken. After addition of 10 ml of water, the pH of the solution was adjusted to 7—7.5 with 0.01 M sulphuric acid or ammonium hydroxide. The solution was diluted to 25 ml with water. It was then transferred into a 250 ml separating funnel. Then 10 ml of 0.001 M STTA in carbon tetrachloride was added. The solution was then extracted on the wrist action flask shaker for about ten minutes. The solution was allowed to settle and separate. The yellow green colored organic phase was withdrawn in a ten ml volumetric flask. It was then measured spectrophotometrically at 450 nm against the reagent blank prepared similarly. The amount of zinc was then calculated from the calibration curve.

For interference studies the solution containing desired ion was added before the pH adjustment.

Results and Discussion

Absorption Spectra. The absorption spectra of Zn–STTA complex (Zn=9.333×10^{-3} M) extracted at pH 7 against the reagent blank (A) and that of complex against carbon tetrachloride (B) is shown in Fig. 1. The spectrum of reagent blank against carbon tetrachloride (C) is also shown. The yellow green Zn–STTA chelate solution showed the maximum absorption at 450 nm. The cruve steadily fell until absorbance became negligible beyond 500 nm. The reagent blank had strong absorbance at 410 nm. This became insignificant compared to chelate solution from 450 nm onwards. Therefore, all the absorbance measurements were taken at 450 nm. The molar absorptivity was 6.697×10^{3} calculated on the basis of zinc contents (9.3×10^{-3} M) with the absorbance of 0.300 at 450 nm when 1 cm cells were used. The sensitivity (as per Sandell's definition) is 0.0022 μg/cm^2.

Extraction as the Function of pH. The solvent extraction behaviour of Zn–STTA system was studied over the pH region of 0.5—10.0 (Fig. 2). It was observed that there is no extraction in the pH region of 0—3.5. The extraction commenced at pH 4.0 and half of the zinc was extracted at pH 6. The extraction was quantitative at pH 7.0—7.5. Beyond this pH region the extraction had decreased. It became insignificant at pH 9.0. Therefore the optimum pH of extraction is 7.0—7.5.

1) V. M. Shinde and S. M. Khopkar, *Chem. Ind.* (London), 1785 (1967).

2) A. K. De, S. M. Khopkar, and R. A. Chalmers, "Solvent Extraction of Metals" Von Nostrand Reinhold Co., London (1970).

3) S. B. Akki and S. M. Khopkar, This Bulletin, **45**, 167 (1972).

4) T. Honjyo and T. Kiba, *ibid.*, **45**, 185 (1972).

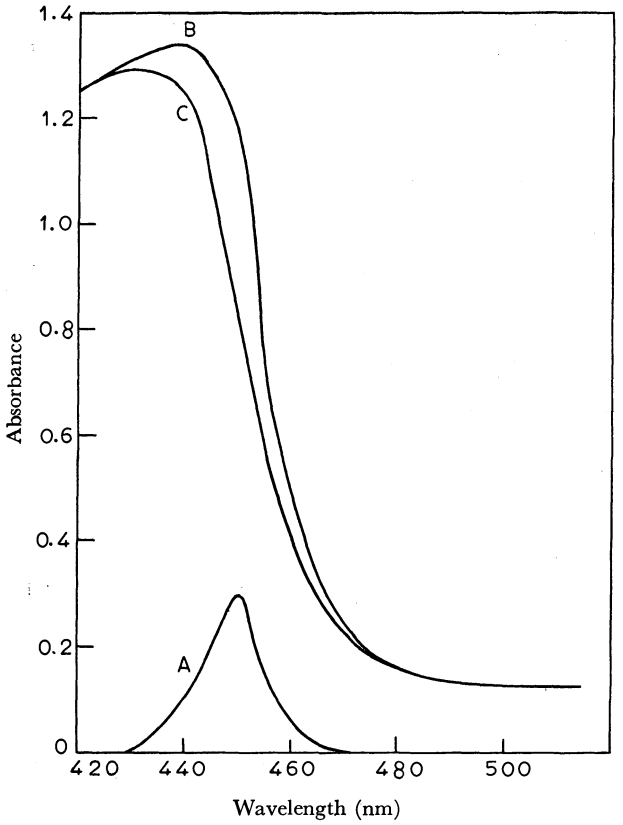

Fig. 1. Absorption spectra of Zn–STTA complex.
$Zn=9.33\times10^{-3}$ mM pH=7.0 1×10^{-3} M STTA–CCl_4
A) Zinc–thiothenoyltrifluoroacetone in carbon tetrachloride *vs.* reagent blank.
B) Reagent blank *vs.* carbon tetrachloride.
C) Complex *vs.* carbon tetarchloride.

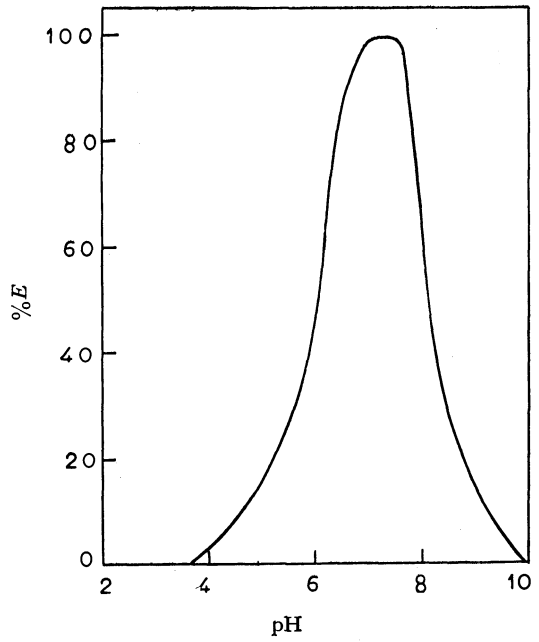

Fig. 2. Extraction as the function of pH.
$Zn=9.333\times10^{-3}$ M STTA=1×10^{-3} M in CCl_4

Adherence to Beer's Law. The varying amounts of zinc ranging from 4.25 to 303.75 μg per ml were taken. They were extracted at pH 7.0 with 0.001 M STTA in carbon tetrachloride as described earlier. To observe the adherence of the system to Beer's law, their absorbances were measured at three different wave lengths namely 440, 450, 460 nm (Table 1). The yellow green zinc–STTA system conformed to Beer's law at 450 nm over the concentration range of 0.4 to 30.3 μg/ml of zinc.

Table 1. Applicability of Beer's law
pH=7, 0.001 M STTA in carbon tetrachloride

Zinc taken μg	Absorbance		
	440 nm	450 nm	460 nm
4.25	0.015	0.030	0.020
8.5	0.025	0.060	0.035
17.0	0.040	0.100	0.070
33.75	0.080	0.180	0.160
67.5	0.120	0.300	0.250
84.5	0.125	0.390	0.270
118.25	0.130	0.410	0.290
168.75	0.170	0.640	0.470
236.25	0.200	0.860	0.610
303.75	0.290	1.100	0.890

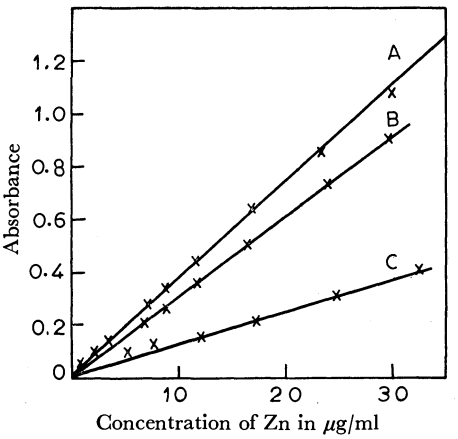

Fig. 3. Beer's law.
A) 450 nm B) 460 nm C) 440 nm

Stability of Colour of the Complex. The absorbance of the colored complex was measured at elapsed interval of 0.5, 8, 16, 24, 48, 96, and 120 hr. The value of the absorbance was found to be constant *viz.* 0.300 until 96 hr. The absorbance after 120 hr was about 0.280. This showed that the complex was stable for at least 96 hr.

Period of Equilibration. With all other factors constant the period of shaking was varied from 3—30 min, on wrist action flask shaker. It was seen that the extraction was quantitative if period of equilibration was 7.5 min. Hence in all measurements, extraction was carried out for at least 10 min.

Effect of Reagent Concentration. The concentration of the reagent was varied from 1×10^{-4} M to 2×10^{-3} M. Similarly the volume of 1.0×10^{-3} M reagent was varied from 2.5 to 20 ml. It was seen (Table 2) that the extraction was quantitative with the reagent concentration of 1×10^{-3} M. It was incomplete with low concentration of the reagent. The extractions did not improve substantially at the higher reagent concen-

Table 2. Effect of reagent concentration
Zn=67.5 μg pH=7.00

STTA concetration (M) × 10^{-3}	STTA added	Absorbance at 450 nm
0.10	10	0.240
0.25	10	0.290
0.50	10	0.300
0.75	10	0.300
1.00	10	0.300
1.5	10	0.300
2.0	10	0.290
1.0	2.5	0.170
1.0	5	0.230
1.0	7.5	0.300
1.0	10	0.300
1.0	15	0.210
1.0	20	0.150

tration. The variation in volume of the reagent showed that the extraction was quantitative with 10 ml of 1.0×10^{-3} M of the reagent in carbon tetrachloride.

Effect of the Salting-out Agents. Various salting-out agents such as sulfates of sodium, lithium, potassium, ammonium, magnesium and calcium were tried as the salting-out agents. The extraction of zinc was carried out in the presence of the salting-out agents, with 0.001 M STTA in carbon tetrachloride. It was observed from values of absorbance that the extraction remained constant with the use of 0.2—2 M of lithium, sodium, potassium and ammonium sulfates (Table 3). There was insignificant decrease in the extractability of zinc with 2 M calcium or magnesium sulfate. There was some enhancement in extraction if 1—3 M ammonium sulfate was used as the salting-out agent. On the whole the results revealed that the salting-out agents did not materially enhance the extraction.

Table 3. Effect of salting-out agent
Zn=67.5 μg pH=7.0 0.001 M STTA-CCl_4

Salting-out agent	Molarity (M)	Absorbance at 460 nm
Li_2SO_4	0.5—3.0	0.300
Na_2SO_4	0.5—2.0	0.300
K_2SO_4	0.5—2.0	0.300
$(NH_4)_2SO_4$	1.0—3.0	0.320
$MgSO_4$	0.5—1.0	0.300
	2.0	0.280
$CaSO_4$	0.5—1.0	0.300
	2.0	0.270

Effect of Diverse Ions. The effect of presence of several ions on the extraction behaviour of zinc was studied (Table 4). The tolerance limit was set as the amount required to cause ±2% error in zinc recovery.

It was observed that complexing anions like oxalate, citrate, tartrate are tolerated in the ratio 1 : 300. While thalium, alkali and alkaline earths and anions such as molybdate, selenite, phosphate, thiosulfate *etc.* are tolerated in the ratio of 1 : 150. Other ions were

Table 4. Effect of diverse ions
Zn=67.5 μg pH=7.5 STTA=0.001 M

Foreign ions	Added as	Tolerance limit, μg	Foreign ions	Added as	Tolerance limit, μg
Tl^+	$TlNO_3$	10000	Ba^{2+}	$BaCl_2 \cdot 2H_2O$	10000
In^{3+}	$InCl_3 \cdot 3H_2O$	100[a]	Sr^{2+}	$SrCl_2 \cdot 6H_2O$	10000
Ag^+	$AgNO_3$	None	Ge^{4+}	$GeCl_4$	20000
Pb^{2+}	$Pb(NO_3)_2 \cdot 2H_2O$	None	Rb^+	RbCl	10000
Hg^{2+}	$Hg(NO_3)_2$	200[b]	Cs^+	CsCl	10000
Cu^{2+}	$CuSO_4 \cdot 5H_2O$	1000[b]	ReO^{4-}	$KReO_4$	1000
Cd^{2+}	$CdCl_2$	None	VO_3^-	NH_4VO_3	5000
Sn^{2+}	$SnCl_2 \cdot 2H_2O$	None	$Mo_7O_{24}^{6-}$	$(NH_4)_6 \cdot Mo_7O_{24}$	10000
Sb^{3+}	$SbCl_3 \cdot 3H_2O$	1000[c]	WO_4^{2-}	Na_2WO_4	5000
As^{3+}	$AsCl_3$	20000	SeO_3^{2-}	Na_2SeO_3	10000
Au^{3+}	$HAuCl_4 \cdot XH_2O$	1000[b]	TeO_3^{2-}	Na_2TeO_3	500
Pt^{4+}	$H_2PtCl_6 \cdot XH_2O$	1000	NO_2^-	$NaNO_2$	10000
Os^{8+}	OsO_4	500	F^-	NaF	5000
Ti^{4+}	$TiCl_4 \cdot 4H_2O$	1000[a]	Br^-	NaBr	1000
Fe^{3+}	$Fe(NO_3)_3 \cdot 6H_2O$	100[e]	I^-	NaI	1000
Cr^{3+}	$Cr(NO_3)_3$	100[e]	CN^-	KCN	2500
Al^{3+}	$Al(NO_3)_3 \cdot 9H_2O$	1000[d]	SCN^-	KSCN	1000
Mn^{2+}	$MnCl_2 \cdot 4H_2O$	1000[b]	$S_2O_3^{2-}$	$Na_2S_2O_3 \cdot 5H_2O$	10000
UO_2^{2+}	$UO_2(NO_3)_2 \cdot 6H_2O$	5000	PO_4^{3-}	Na_3PO_4	5000
Th^{4+}	$Th(NO_3)_4 \cdot 4H_2O$	1000	$C_2O_4^{2-}$	$H_2C_2O_4 \cdot 2H_2O$	20000
Ce^{4+}	$Ce(SO_4)_2 \cdot 4H_2O$	500[d]	CH_3COO^-	CH_3COOH	20000
Be^{2+}	$BeSO_4 \cdot 4H_2O$	100	$Malonate^{2-}$	$(COOH)_2CH_2$	20000
Zr^{4+}	$Zr(SO_4)_2$	500	$Ascorb^-$	Ascorbic acid	20000
			Cit^{3-}	Citric acid	20000
			$Tart^{3-}$	Tartaric acid	20000
			$EDTA^{4-}$	EDTA(disodium salt)	None

Masked with a) ascorbic, b) alkali cyanide, c)oxalic, d) citric acid, e) selective extraction with pure mesityl oxide for Fe at 3.5M HCl, Cr from 1M HCl+2.5M KCl (2)

tolerated in the ratios exceeding 1 : 15. Some ions such as lead, silver, cadmium, tin formed characteristic colored complex with reagent and showed strong interference. The interference of some of the ions could be removed by complexing with sequestering agents. As a matter of fact sequestering agents are tolerated in larger amounts (*viz.* 20000 μg) and hence can be used for masking number of metals. Further some of the ions which might hydrolyse at very high concentrations can be successfully complexed with sequestering agents to prevent hydrolytic precipitation. Thus sequestering agents play two fold role to eliminate interference and mitigate hydrolysis of certain ions. Hence antimony was complexed with oxalic acid; aluminium, cerium and zirconium with citric acid and silver, copper and gold were complexed with alkali cyanide. The process of selective extraction (2) with mesityl oxide (4-methyl-3-pentane-2-one) was also used to eliminate the interferences due to iron(III) and chromium(III).

Separation of Zinc from Gun Metal. About one gm of gun metal was dissolved in concentrated nitric acid. Tin was removed as metastannic acid and was determined gravimetrically. The filtrate was evaporated to dryness. The residue was dissolved in water, and made up to 1 litre. One ml of the diluted solution was taken. It was adjusted to pH 2.5 to extract copper with 0.1 M acetylacetone in benzene as described in earlier[2] paper. The aqueous solution was taken. To this solution 3 M hydrochloric acid and 2 M lithium chloride was added. It was extracted with a 10 ml of tributyl phosphate in MIBK to quantitatively remove lead.[6] The aqueous phase containing zinc was taken. Its pH was adjusted to 7.0. Then zinc was extracted with 10 ml of 0.001 M STTA in carbon tetrachloride. The yellow green colored complex was measured spectrophotometrically at 450 nm. Another aliquot of solution containing zinc after removal of copper and lead as described earlier was taken. The acidity was adjusted to 3 M with hydrochloric acid. Then it was extracted twice with 10 ml of 8% tribenzoylamine.[7] Zinc from the combined organic phase was stripped with 10 ml of 0.1 M hydrochloric acid and was determined as usual.[8] It was found that the percentage of zinc found by STTA method was 4.6, 4.9, 4.8 while percentage of zinc by TBA method was 4.5, 4.4, 4.3 as against 4.5% actually present.

Separation of Zinc from Brass. About 0.885 gm of brass sample was dissolved in concentrated nitric acid. Tin was which was present in traces was removed as insoluble residue of metastannic acid. The filtrate was evaporated to dryness and extracted with water. The solution was made up to 1 litre. Then 2 ml of diluted solution was taken and copper from it was removed by extraction as described earlier.[2] The aqueous phase was then taken. The pH was adjusted to 7.0. Then it was extracted with 10 ml of 0.001 M STTA in carbon tetrachloride. The yellow green colored complex was measured at 450 nm. The percentage of zinc was found to be 35.9, 35.4, 36.2 as against 36%. Another aliquot of solution containing zinc after removing tin and copper was taken. It was then extracted with 8% tribenzylamine[7] from 3 M hydrochloric acid. It was stripped to the aqueous phase with 0.1 M hydrochloric acid and was determined as usual.[8] The percentage of zinc was found to be 35.8, 35.2, 36.0 as against 36%. This shows the method proposed by us for the extractive separation and colorimetric determination of zinc compares favourably well with standard method.[7]

Comparison with Other Methods. Four sets of five samples containing varying amounts of zinc were taken. Then zinc from each sample was determined by extraction with thiothenoyltrifluoroacetone (STTA); tribenzoylamine (TBA);[7] triisooctylamine (TIOA)[9] and dithizone[10] methods (Table 5). It was interesting to

Table 5. Comparison with other methods

Zinc taken μg	Zinc found (%) by			
	STTA method	TBA method (7)	TIOA method (9)	Dithizone method (10)
6.35	6.30	6.0	6.4	6.4
12.75	12.5	12.2	12.70	12.5
48.0	48.0	47.9	48.4	48.2
101.25	102.0	100.00	101.3	103.0
202.5	200.5	198.7	202.6	204.0

observe that the amount of zinc found by STTA method compares favourably well with other methods for the extraction of zinc. This further shows that the proposed method is rapid, simple, selective as well as sensitive. Total operation of each run requires only 30 min. It is possible to accomplish clean-cut separation of zinc from cadmium, mercury, copper, silver, gold, aluminium and iron with which it is usually associated.

Thanks are due to Council of Scientific and Industrial Research (India) for sponsoring this project and awarding research fellowship to one of the authors (K.R.S.).

5) A. I. Vogel, "A Textbook of Quantitative Inorganic Analysis," 3rd Ed. Longmans and Green (1961).
6) A. A. Yadav and S. M. Khopkar, *Talanta*, **18**, 833 (1971).
7) H. A. Mahlman, G. W. Leddicotte, and F. Moore, *Anal. Chem*, **26**, 1939 (1954).
8) E. B. Sandell, "Colorimetric Determination of Traces of Metals," Interscience, 3rd Ed. (1959), p. 965.
9) L. E. Scroggie and J. A. Dean, *Anal. Chim. Acta*, **21**, 282 (1959).
10) D. W. Margerum and F. Santacana, *Anal. Chem.*, **32**, 1157 (1960).

Thermometric Titration in the Investigation of the Formation of Polyanions of Molybdenum(VI), Tungsten(VI), Vanadium(V), and Chromium(VI). III. Titration of Molybdic Acid with Sodium Hydroxide Solution

Nobutoshi KIBA and Tsugio TAKEUCHI

Department of Synthetic Chemistry, Faculty of Engineering, Nagoya University, Chikusa-ku, Nagoya 464

(Received December 21, 1972)

To define the properties of molybdenum-containing species which appear in the acidification of neutral molybdate solution with mineral acid, the reverse process, *i.e.* the titration of molybdic acid of acidified molybdate solution with sodium hydroxide, was examined and the titration curves were obtained thermometrically as well as potentiometrically. In the thermometric titration curves there are inflections not found on the pH-titration curves of the same systems. Titration curves of both methods change with molybdenum concentration, the reaction process being found to be responsible for the change. Polymolybdate anions were identified with the aid of the ultraviolet spectrophotometry of Punger *et al.* A neutral salt such as sodium perchlorate or lithium perchlorate was found to affect the shape of the thermometric titration curve, since in the presence of such salt octamolybdate ion was readily converted into heptamolybdate ion.

In a previous paper we reported on the formation of molybdenum-containing polyanions in the process of acidification of neutral molybdate solution,[1] the investigation being carried out by means of thermometric titration. The inflections on the titration curves gave useful information. The reverse reaction, *i.e.* neutralization of molybdic acid or acidified molybdate solution with alkali hydroxide, seems to be of interest in connection with the above process. We carried out the thermometric titration with a titrator of a new type.[2]

The reaction between molybdic acid and alkali hydroxide has been investigated mainly by pH-titration and conductometric titration. Cannon[3] reported two inflections at P-values 0.5 and 2.0 the alkali/Mo equivalent ratio, on the pH-titration curve of 0.310 M molybdic acid solution prepared by Auger's method.[4] He also reported that in the presence of 3 M sodium chloride the first inflection shifted to a larger P-value while the second remained unchanged. The shift was accounted for by the variation of the activity coefficient of hydrogen ion in the solution containing sodium chloride. Richardson[5] tried pH- and conductometric titrations with 2.2×10^{-1}—3.4×10^{-4} M molybdic acid prepared by an ion-exchange technique, and reported two inflections on the titration curves at P-values 0.5 and 2.0. The form of titration curve changes with the concentration of molybdic acid solution. Jain and Jain[6] carried out pH-titration with 0.018 M molybdic acid prepared by ion-exchange and also found two inflections on the titration curve at 0.5 and 2.0; in the presence of 4 M sodium chloride, the first shifted to 0.85 while the second remained constant. From the results they concluded that octamolybdate ($Mo_8O_{26}^{4-}$) exists in the initial molybdic acid solution and can be transformed into heptamolybdate($Mo_7O_{24}^{6-}$) in a medium with high ionic strength.

We observed four distinct inflections on the thermometric titration curve when acidified molybdate solution in the concentration range of molybdenum 2.29×10^{-1}—1.07×10^{-1} M was titrated with sodium hydroxide solution. The heat of the reaction of the four steps was estimated from each titration curve.[1] Richardson[5] and Heitner-Wirguin and Cohen[7] concluded that a similar equilibrium could be applied to an acidifed molybdate solution and a molybdic acid solution as a result of pH- and conductometric titrations[5] and ion-exchange technique.[7] We have examined the ionic equilibria by means of thermometric titration of acidified molybdate solution and molybdic acid solution in wide concentration ranges. The titration curves were compared with each other and also with the curve obtained by potentiometric titration. The effect of a neutral salt such as sodium perchlorate or lithium perchlorate on shape of the titration curve was also examined.

Experimental

Reagents. *Molybdic acid solution*[8]: Twenty grams of sodium molybdate dihydrate of reagent grade was dissolved in 200 ml of distilled water, and the solution was passed through a column of polystyrene cation-exchange resin(Amberlite IR-120, mesh 32—100). In order to remove sodium ion completely, the effluent was poured on the other column of the same cation-exchanger. The process was repeated till no sodium ion could be found in the effluent. 0.2 M molybdic acid solution was prepared by adjusting the volume of the solution to a definite volume. Standardization of the molybdenum content was made gravimetrically after precipitating molybdenum as 8-hydroxyquinolinate.[11]

1) N. Kiba and T. Takeuchi, *J. Inorg. Nucl. Chem.*, in press.
2) N. Kiba and T. Takeuchi, *Talanta*, **20**, 875 (1973).
3) P. Cannon, *J. Inorg. Nucl. Chem.*, **9**, 252 (1959).
4) V. Auger, *C. R. Acad. Sci., Paris*, **206**, 913 (1938).
5) E. Richardson, *J. Inorg. Nucl. Chem.*, **9**, 267 (1959).
6) D. V. S. Jain and C. M. Jain, *Indian J. Chem.*, **7**, 821 (1969).
7) C. Heitner-Wirguin and R. Cohen, *J. Inorg. Nucl. Chem.*, **26**, 161 (1964).
8) Sasaki and Sillén[9] prepared 1 M molybdic acid solution by the use of cation exchanger (Dowex 50 X-8). The solution was found to show a strong Tyndall effect. After being left to stand for a few days a white precipitate appeared. However, the 0.2 M molybdic acid solution we prepared was very stable, the Tyndall effect being observed eventually after ten days and no precipitate appearing after one month. We prepared a fresh solution of molybdic acid every three days and the octamer was defined as the predominant species in the solution by the differential spectrophotometric method of Pungor and Halasz.[10]
9) Y. Sasaki and L. G. Sillén, *Arkiv Kemi*, **29**, 253 (1967).
10) E. Pungor and A. Halasz, *J. Inorg. Nucl. Chem.*, **32**, 1187 (1970).
11) I. M. Kolthoff and E. B. Sandell, "Textbook of Quantitative Inorganic Analysis," 3rd Ed., Macmillan, New York, p. 89.

Preparation of Ion-exchanger Column: The cation exchanger should be free from reducing substance. 100 ml of powdered resin was suspended in acetone for about three hours to remove acetone-soluble substance. The resin was then poured into distilled water to let the resin particles settle, followed by repeated washing with water and decantation. The resin particles were put into 0.2% potassium dichromate solution and allowed to stand for a day. A slurry of the resin was poured into a glass tube 1.5×60 cm for chromatographic use, fitted with a sintered glass filter at one end. 500 ml of 3 M hydrochloric acid and 200 ml of 2 M sodium chloride solution were passed successively through the column. 200 ml of 3 M hydrochloric acid was then passed to make the hydrogen form of resin. Finally the column was washed with distilled water to remove chloride ion.

Acidified Molybdate Solution: A sodium molybdate solution was made acidic by adding perchloric acid of 2.00 times the molarity of the molybdate. The concentration of molybdenum was determined gravimetrically in a similar manner to that described above.[11]

All the other reagents were of guaranteed reagent grade (Wako Chemicals Co.) unless otherwise stated, and used without further purification.

Apparatus. *Thermometric titrator*: A thermometric titrator (TOA Electric Co.) was used. Construction has been described in detail.[2]

All pH measurements were made using a Metrohm potentiograph E 336 with a glass-calomel electrode system calibrated with buffer solutions complying with accepted standards.

All spectrophotometric measurements were carried out with an automatic Shimadzu ultraviolet spectrophotometer. Silica microcuvettes of path lengths 1.0—0.02 mm were used.

Procedure. The procedure was just the same as before.[1,2] Titration was carried out for molybdic acid in the concentration range 0.2—0.004 M. Following Richardson's prescription, the molybdic acid solution was left to stand for about twelve hours after preparation to attain homogeneity.[5] Titration with sodium hydroxide was performed under conditions where the volume of the titrant to be required was not to exceed 10% of the total volume of the final solution in the titration cell.

The spectra of the solutions examined were measured against distilled water and neutral monomeric molybdate solution according to the method by Pungor and Halasz.[10] All experiments were conducted at 25 °C.

Results and Discussion

Thermometric Titration Curves of Molybdic Acid and Acidified Molybdate Solution with Sodium Hydroxide. The titration curves of molybdic acid in 2.29×10^{-1} M and 4.58×10^{-3} M are shown in Figs. 1 and 2, respectively. We see four inflections in the former and two in the latter. The P-values are listed in Table 1. In consequence of the titration of acidified molybdate solution in 2.14×10^{-1} to 5.35×10^{-3} M with sodium hydroxide solution, similar titration curves to those as in the case of molybdic acid were obtained. The P-values of each titration curve are listed in Table 2. It is evident that the shape of the titration curve depends upon the initial concentration of molybdenum. A variation of the P-value could be observed in a wide range of concentration of molybdic acid rather than in that of acidified molybdate. This may be

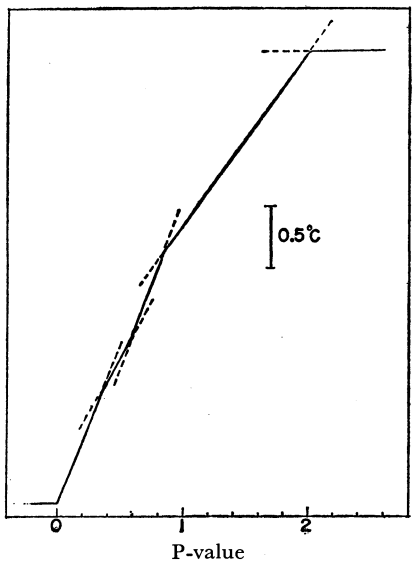

Fig. 1. Thermometric titration of 2.29×10^{-1} M molybdic acid with sodium hydroxide.
P-value=number of moles of base added per mole of molybdenum and the ordinate is relative heat change during the titration.

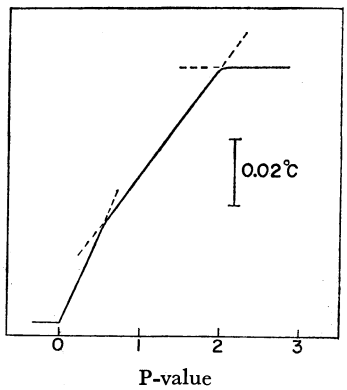

Fig. 2. Thermometric titration of 4.58×10^{-3} M molybdic acid with sodium hydroxide.

Table 1. Results of thermometric titration of molybdic acid in various concentrations with sodium hydroxide

Molybdic acid taken (mol/l)	P-value[a] inflections 1st	2nd	3rd	4th
2.29×10^{-1}	0.375	0.571	0.857	2.00
1.14×10^{-1}	0.315	0.519	0.722	2.00
9.16×10^{-2}	0.264	0.400	0.687	2.00
6.87×10^{-2}	—	0.312	0.664	2.00
4.58×10^{-2}	—	0.304	0.658	2.00
2.29×10^{-2}	—	—	0.558	2.00
1.14×10^{-2}	—	—	0.511	2.00
9.16×10^{-3}	—	—	0.509	2.00
6.87×10^{-3}	—	—	0.503	2.00
4.58×10^{-3}	—	—	0.501	2.00

a) P-value=number of moles of base added per mole of molybenum.

TABLE 2. RESULTS OF THERMOMETRIC TITRATION OF ACIDIFIED MOLYBDATE SOLUTION[a] IN VARIOUS CONCENTRATIONS WITH SODIUM HYDROXIDE

Molybdate taken (mol/l)	P-value			
	inflections			
	1st	2nd	3rd	4th
2.14×10^{-1}	0.375	0.571	0.857	2.00
1.50×10^{-1}	0.375	0.570	0.857	2.00
1.07×10^{-1}	0.373	0.570	0.857	2.00
8.56×10^{-2}	0.366	0·549	0.850	2.00
6.56×10^{-2}	0.305	0.500	0.827	2.00
4.28×10^{-2}	—	0.463	0.689	2.00
1.07×10^{-2}	—	0.311	0.543	2.00
8.56×10^{-3}	—	—	0.527	2.00
5.35×10^{-3}	—	—	0.508	2.00

a) The ratio of acid added to molybdate in an acidified molybdate solution is 2.00.

attributed to the variation of ionic strength during the titration of molybdic acid solution, since in the latter case sodium ion is initially present in the solution and the change of ionic strength is relatively small. Thus, the shape of the titration curve seems to be determined not only by the concentration of molybdic acid taken initially but by the variation of the ionic strength in the solution during titration.

pH-Titration Curves of Molybdic Acid and Acidified Molybdate Solution with Sodium Hydroxide. The pH-titration curves of molybdic acid in the range 2.10×10^{-1}—4.20×10^{-3} M are shown in Fig. 3. Two inflections can be seen in all of them. The P-values of the inflections estimated by secondary differentiation

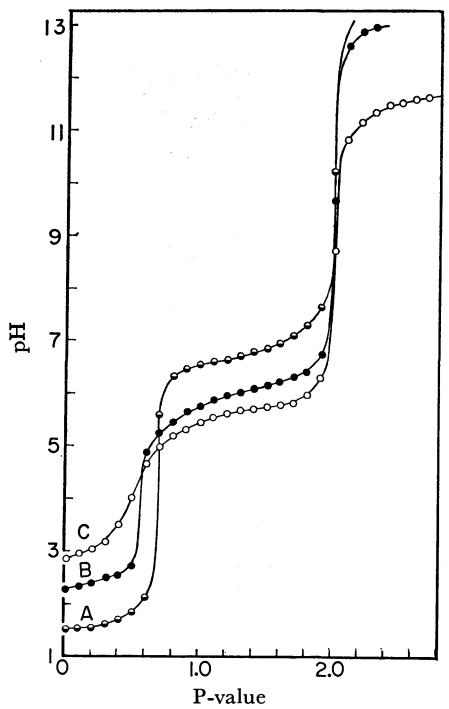

Fig. 3. pH-titration of
A: 100 ml 0.210 M molybdic acid with 2.14 M NaOH
B: 100 ml 0.0420 M molybdic acid with 0.42 M NaOH
C: 100 ml 0.00420 M molybdic acid with 0.042 M NaOH

TABLE 3. RESULTS OF pH-TITRATION OF MOLYBDIC ACID IN VARIOUS CONCENTRATIONS WITH SODIUM HYDROXIDE

Molybdic acid taken (mol/l)	P-value	
	1st inflection	2nd inflection
2.10×10^{-1}	0.66	2.0
1.05×10^{-1}	0.63	2.0
9.03×10^{-2}	0.63	2.0
6.45×10^{-2}	0.61	2.0
4.20×10^{-2}	0.59	2.0
2.10×10^{-2}	0.54	2.0
1.05×10^{-2}	0.52	2.0
6.45×10^{-3}	0.51	2.0
4.20×10^{-3}	0.50	2.0

TABLE 4. RESULTS OF pH-TITRATION OF ACIDIFIED MOLYBDATE SOLUTION IN VARIOUS CONCENTRATIONS WITH SODIUM HYDROXIDE

Molybdate taken (mol/l)	P-value	
	1st inflection	2nd inflection
2.14×10^{-1}	0.64	2.0
1.50×10^{-1}	0.63	2.0
1.07×10^{-1}	0.63	2.0
8.56×10^{-2}	0.61	2.0
6.56×10^{-2}	0.60	2.0
4.28×10^{-2}	0.57	2.0
1.07×10^{-2}	0.52	2.0
8.56×10^{-3}	0.52	2.0
5.35×10^{-3}	0.51	2.0

of the curve are shown in Table 3. In the pH-titration of acidified molybdate solution in the range 2.14×10^{-1}—5.35×10^{-3} M with sodium hydroxide, similar titration curves were obtained. The P-values of the inflections are listed in Table 4.

We see that the P-value of the second inflection was held constant at about 2.0, while that of the first inflection was 0.6 in higher and 0.5 in lower concentration of molybdic acid. Previous investigations[3] showed that the first inflection does not depend on the concentration of molybdic acid, its P-value being held constant at 0.5, potentiometrically and conductometrically. However, Heitner-Wirguin and Cohen reported variations of the P-values of both the first and second inflections with the concentration of molybdic acid from their results on the pH-titration of molybdic acid with sodium hydroxide solution.[7] This discrepancy is difficult to interpret because of the lack of understanding of the chemical species existing in the solution or appearing during the course of titration.

Richardson[5] pointed out that the variety of titration curves might result to some extent from the hydrolysis of the salt formed in a dilute solution. He assumed the hydrolysis from the results of his conductometric titration of molybdic acid with sodium hydroxide solution, in which a variation of titration curves was found in every case. We proposed a different assumption from his, since the variation of titration

curves, either potentiometric and thermometric, depends upon the initial concentration of molybdic acid or acidified molybdate. The variation should show a difference in the reaction process in each case. The chemical species existing in the solution before titration was identified by spectrophotometry as octamolybdate ion and that after titration monomeric molybate ion.[9]

From Tables 1—4 and spectrophotometric measurements, we conclude that the titration of about 2×10^{-1} M molybdic acid or acidified molybdate solution with sodium hydroxide solution might proceed through the following four reaction process:

$$H_4Mo_8O_{26} + 3OH^- = HMo_8O_{26}^{3-} + 3H_2O \quad (P=0-0.375) \quad (1)$$

$$7HMo_8O_{26}^{3-} + 11OH^- = 8H_2Mo_7O_{24}^{4-} + H_2O \quad (P=0.375-0.571) \quad (2)$$

$$H_2Mo_7O_{24}^{4-} + 2OH^- = Mo_7O_{24}^{6-} + 2H_2O \quad (P=0.571-0.857) \quad (3)$$

$$Mo_7O_{24}^{6-} + 8OH^- = 7MoO_4^{2-} + 4H_2O \quad (P=0.857-2.00) \quad (4)$$

On the other hand, in the titration of *ca.* 5×10^{-3} M molybdic acid or acidified molybdate solution, P-values of the inflections seem to prove the existence of two reaction processes:

$$H_4Mo_8O_{26} + 4OH^- = Mo_8O_{26}^{4-} + 4H_2O \quad (P=0-0.500) \quad (5)$$

$$Mo_8O_{26}^{4-} + 12OH^- = 8MoO_4^{2-} + 6H_2O \quad (P=0.500-2.00) \quad (6)$$

It is supposed that in the range above 4×10^{-2} M reactions (1)—(4) are predominant and (5) and (6) subdominant, while below that concentration reactions (5) and (6) become predominant and (1)—(4) subdominant.

Titration of Molybdic Acid with Sodium Hydroxide Solution in the Presence of Sodium Perchlorate or Lithium Perchlorate. Molybdic acid of concentrations 2.00×10^{-1}—2.00×10^{-2} M in 4 M sodium perchlorate solution was titrated with sodium hydroxide solution and thermometric titration curves were obtained; the curve of 2.00×10^{-1} molybdic acid is shown in Fig. 4 and that of 2.00×10^{-2} M molybdic acid in Fig. 5. P-values of the inflections of titration curves for molybdic acid in various concentrations are given in Table 5. Three inflections were observed in the case of 2.00×10^{-1} M molybdic acid. In the case of 2.00×10^{-2} M, the P-value of the first inflection was 0.856, but 0.542 in absence of sodium perchlorate. The pH-titration curves were also obtained under the same conditions for 2.00×10^{-1}—2.00×10^{-2} M molybdic acid in 4 M sodium perchlorate solution. Each titration curve was similar to the corresponding one of the pH-titration curves (Fig. 3). The P-values of the inflections of the curves are given in Table 6. The influence of sodium perchlorate on the P-values of the first inflections seems to be important in various concentrations of molybdic acid.

We examined exclusively the first inflections of the thermometric titration curves for 2.00×10^{-2} M molybdic acid in the presence of the perchlorate in varying concentrations. The results are shown in Table 7. The second inflection remained constant at the P-value of 2.00 in all runs. We see that the amount of neutral salt necessary to change the P-value of the first inflection from 0.542 to 0.856 differs for sodium and lithium salts, *i.e.*, above 3.0 M of sodium

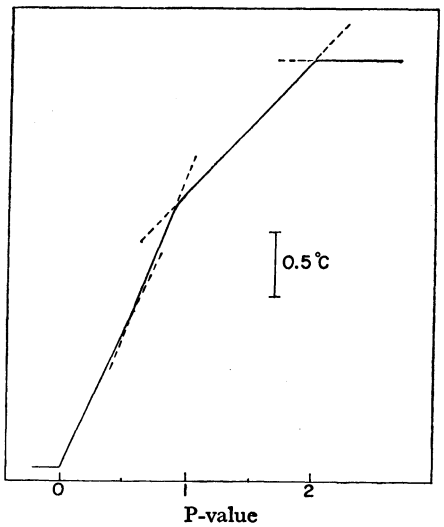

Fig. 4. Thermometric titration of 2.00×10^{-1} M molybdic acid with sodium hydroxide in the presence of 4.0 M sodium perchlorate.

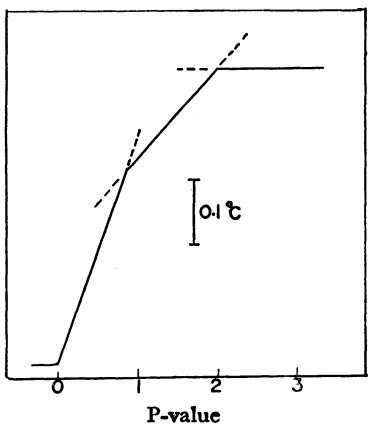

Fig. 5. Thermometric titration of 2.00×10^{-2} M molybdic acid with sodium hydroxide in the presence of 4.0 M sodium perchlorate.

Table 5. Results of thermometric titration of molybdic acid in various concentrations with sodium hydroxide in the presence of 4.0 M sodium perchlorate

Molybdic acid taken (mol/l)	P-value		
	1st inflection	2nd inflection	3rd inflection
2.00×10^{-1}	0.602	0.857	2.00
1.00×10^{-1}	0.670	0.857	2.00
3.00×10^{-2}	0.735	0.857	2.00
6.00×10^{-2}	0.814	0.858	2.00
4.00 ± 10^{-2}	0.835	0.857	2.00
2.00 ± 10^{-2}	—	0.856	2.00

TABLE 6. RESULTS OF pH-TITRATION OF MOLYBDIC ACID IN VARIOUS CONCENTRATIONS WITH SODIUM HYDROXIDE IN THE PRESENCE OF 4.0 M SODIUM PERCHLORATE

Molybdic acid taken (mol/l)	*P*-value	
	1st inflection	2nd inflection
2.00×10^{-1}	0.81	2.0
1.00×10^{-1}	0.82	2.0
8.00×10^{-2}	0.82	2.0
6.00×10^{-2}	0.82	2.0
4.00×10^{-2}	0.84	2.0
2.00×10^{-2}	0.84	2.0

perchlorate and above 4.4 M of lithium perchlorate. The difference of salt concentration between sodium perchlorate and lithium perchlorate required to display the salt effect sufficiently seems therefore to be in conflict with Cannon's interpretation of the salt effect, for which discussion was given only from the data in the presence of sodium chloride. The difference might be caused by the extent of protonation of molybdate owing to the difference in hydration of cations and anions of the salt added.[7] We have obtained the spectrum with only a well defined maximum at 258 mμ in the absorption of 2.00×10^{-2} M molybdic acid in 4 M sodium perchlorate solution against sodium monomeric molybdate in the region 210—330 mμ.[11] The molybdenum-containing species in this solution was revealed as being heptamolybdate ion and not octamolybdate ion. This shows the validity of the assumption on salt effect described by Jain and Jain.[6] Thus, we concluded that the reactions proceeding in the titration of 2.00×10^{-2} M molybdic acid in 3 M sodium perchlorate or in 4.4 M lithium perchlorate with

TABLE 7. SALT-EFFECT OF SODIUM PERCHLORATE AND LITHIUM PERCHLORATE ON P-VALUE OF THE FIRST INFLECTION OF THE THERMOMETRIC TITRATION CURVE
Molybdic acid: 2.00×10^{-2} M

Perchlorate taken (mol/l)	P-value of the first inflection
none	0.542
Sodium perchlorate	
0.5	0.747
1.0	0.765
1.5	0.783
2.0	0.843
2.5	0.850
3.0	0.858
3.5	0.857
4.0	0.858
4.5	0.858
Lithium perchlorate	
1.1	0.702
1.7	0.730
2.2	0.768
2.8	0.779
3.3	0.788
3.9	0.831
4.4	0.857
5.0	0.857

sodium hydroxide solution might consist of the following two steps:

$$H_6Mo_7O_{24} + 6OH^- = Mo_7O_{24}^{6-} + 6H_2O \quad (P=0-0.857)$$

$$Mo_7O_{24}^{6-} + 8OH^- = 7MoO_4^{2-} + 4H_2O \quad (P=0.857-2.00)$$

The Thermal Properties of Gallium-bearing Allophane

Mitsuhiro KASAI, Yoshiyuki KUDO, and Shuichi HAMADA

Department of Chemistry, Faculty of Science, Science University of Tokyo, Kagurazaka, Shinjuku-ku, Tokyo 162

(Received February 8, 1973)

The DTA patterns of synthesized coprecipitated gels, SiO_2–Al_2O_3–Ga_2O_3–H_2O system, resembled that of allophane, and the exothermic peak temperature in the DTA was lowered continuously from 980 to 810 °C with an increase in the gallium content, while that on mixed gels scarcely lowered. The apparent activation energy for this exothermic reaction on the coprecipitated gels decreased with an increase in the gallium content, while that on the mixed gels hardly changed. The crystallization process during the heat treatment of the gels depended on the content and on the coexistence state of the gallium. A unit cell volume of a mullite crystallized at 1200 °C in the coprecipitated gels was enlarged by forming a solid solution with the gallium ion, in contrast to the small change in that formed in the mixed gels. Further, the exothermic peak in the DTA was considered to originate not only from the formation of the mullite, but also from that of the silico-alumina spinel in the gallium-bearing gels; the exothermic reaction products seem to depend on the composition or the coexistence state of gallium in the gels.

The lower crystalline minerals of the SiO_2–Al_2O_3–H_2O system, found in nature as allophane, frequently contain iron. In a previous paper,[1] a synthesized iron-coprecipitated gel was recognized to be an iron-bearing allophane. Gallium occurs widely, but in trace amounts, and it is considered to coexist as a solid solution in aluminum minerals, as in nature. Mixed systems of aluminum and gallium have been studied in connection with those of the Al_2O_3–Ga_2O_3–H_2O system,[2] (Al, Ga)$_2O_3$,[3,4] $2SiO_2 \cdot 3$(Al, Ga)$_2O_3$,[5] and gallium-bearing feldspar.[6]

In this work, the properties of the synthesized gallium-coprecipitated gels of the SiO_2–Al_2O_3–Ga_2O_3–H_2O system were studied in order to examine the coexistence state of gallium in them.

Experimental

Materials. The gallium-coprecipitated samples were prepared in the following manner:[1,7] coprecipitated gels were obtained by boiling mixed solutions of aluminum sulfate, sodium silicate, and gallium sulfate at pH 5.9—6.4, a pH value obtained by adding hexamethylenetetramine. The $Ga_2O_3/(Al_2O_3+Ga_2O_3)$ molar ratio in the mixed solutions was varied from zero to 1.0 at a constant molar ratio of 2.0 as $SiO_2/(Al_2O_3+Ga_2O_3)$. The gels thus coprecipitated were washed by decantation and then air-dried for three weeks. The gallium-mixed samples were prepared by mixing a synthesized allophane, free from gallium, and a hydrated gallium(III) oxide in order to compare the properties of the coprecipitated samples. The amorphous hydrated gallium(III) oxide was prepared by precipitation with ammonia water at pH 4.0 and by subsequent air-drying, like the coprecipitated samples, as one of the components in the mixed samples. The air-dried hydrated gallium(III) oxide gel obtained at pH 4.0 was identified as amorphous from its X-ray powder diffraction pattern, and its chemical composition was estimated to be $Ga_2O_3 \cdot 4.1H_2O$ (corresponding to $Ga(OH)_3 \cdot 0.5H_2O$) from the ignition loss, though the air-dried gels obtained at pH 5.3 and 7.7 were found to contain a crystalline GaOOH[8] and their chemical compositions were $Ga_2O_3 \cdot 2.0H_2O$ and $Ga_2O_3 \cdot 1.2H_2O$ (corresponding to $Ga(OH)_3 \cdot$GaOOH and $Ga(OH)_3 \cdot 9$GaOOH) respectively.

Procedure. The chemical compositions of the samples were estimated gravimetrically for SiO_2, Al_2O_3, and H_2O (±),[9] and colorimetrically for Ga_2O_3.[10]

The differential thermal analysis was carried out in the temperature range from room temperature to 1000 °C and at the heating rate of 10 °C/min with a Rigaku Denki Thermoflex model 8002 differential thermal analyzer.

The X-ray powder diffractogram of the sample was taken with an X-ray diffractometer, model JDX-5P, of the Japan Electron Optics Laboratory Co. The diffraction angles were calibrated by using those of silicon. The sample, in a quartz tube, was heated at 800, 900, 1000, 1100, and 1200 °C for 5 hr in an electric furnace. The firing products were identified and their relative amounts were estimated by using the diffraction peaks at (120) and (210) of the mullite, that at (101) of the cristobalite, those at (200) and (004) of the β-gallia, and those at (220) and (311) of the silico-alumina spinel. The unit-cell dimensions of the mullite, one of the firing products at 1200 °C, were calculated by using the diffraction peaks at (400), (041), (331), and (002) of the mullite.

Results

The chemical compositions of the gallium-bearing samples are shown in Table 1. The $SiO_2/(Al_2O_3+Ga_2O_3)$ and the $H_2O(\pm)/(Al_2O_3+Ga_2O_3)$ molar ratios in the coprecipitated samples decreased with an increase in the gallium content, while the $H_2O(\pm)/(Al_2O_3+Ga_2O_3)$ ratio in the mixed samples did not vary in spite of the change in the gallium content.

The Differential Thermal Analysis of the Samples. All the samples were amorphous or lower crystalline materials, for there were few sharp X-ray powder diffraction peaks. The Ga-0 sample, free from gallium, showed a broad endothermic peak and a sharp exothermic peak at 100 and 980 °C respectively in the

1) J. Ossaka, S. Iwai, M. Kasai, T. Shirai, and S. Hamada, This Bulletin, **44**, 716 (1971).
2) V. G. Hill, R. Roy, and E. F. Osborn, *J. Amer. Ceram. Soc.*, **35**, 135 (1952).
3) J. McDonald, J. A. Gard, and F. P. Glasser, *J. Inorg. Nucl. Chem.*, **29**, 661 (1967).
4) J. A. Gard, *Bull. Groupe France Argiles*, **17**, 19 (1966).
5) G. Gelsdorf, H. Hüller-hesse, and H. E. Schwiete, *Arch. Eisenhüttenw.*, **29**, 513 (1958).
6) J. R. Goldsmith, *J. Geol.*, **58**, 518 (1950).
7) J. Ossaka, S. Iwai, M. Kasai, T. Shirai, and S. Hamada, *Nippon Kagaku Zasshi*, **90**, 1288 (1969).
8) R. Roy, V. G. Hill, and E. F. Osborn, *J. Amer. Chem. Soc.*, **74**, 719 (1952).
9) The values were estimated from the ignition loss.
10) T. Moeller, *Anal. Chem.*, **22**, 686 (1950).

TABLE 1. CHEMICAL COMPOSITIONS OF GALLIUM-BEARING SAMPLES

Sample	Chemical composition, wt%					Molar ratio	
	SiO_2	Al_2O_3	Ga_2O_3	$H_2O(\pm)$	Total	SiO_2/R_2O_3[a]	$H_2O(\pm)/R_2O_3$[a]
Ga-0[b]	36.34	29.66	0	33.86	99.86	2.07	6.46
Ga-1C[c]	37.16	31.04	1.13	30.98	100.31	1.99	5.54
Ga-2C	37.32	27.59	2.82	31.76	99.39	2.13	6.00
Ga-3C	35.62	28.03	4.64	32.43	100.72	1.98	6.00
Ga-4C	36.56	27.18	5.67	30.93	100.34	2.05	5.79
Ga-5C	36.47	27.22	6.39	29.74	99.82	2.02	5.49
Ga-6C	36.45	25.76	7.84	29.51	99.61	2.06	5.57
Ga-7C	36.18	24.57	10.52	28.98	100.25	2.02	5.42
Ga-8C	35.36	22.65	15.25	27.36	100.62	1.94	5.01
Ga-9C	33.66	20.64	17.72	28.44	100.46	1.89	5.32
Ga-10C	33.07	19.61	19.64	27.72	100.04	1.85	5.18
Ga-11C	32.76	17.34	23.53	26.74	100.37	1.84	5.03
Ga-12C	32.29	16.71	25.83	25.68	100.52	1.78	4.73
Ga-13C	30.50	11.70	34.57	23.53	100.30	1.70	4.37
Ga-14C	26.48	0	53.01	20.65	100.14	1.56	4.06
Ga-15M[c]	34.68	28.30	2.82	34.07	99.87	1.97	6.46
Ga-16M	32.47	26.50	6.57	34.46	100.00[d]	1.83	6.49
Ga-17M	30.25	24.69	10.32	34.74	100.00[d]	1.69	6.49
Ga-18M	27.40	22.36	15.16	34.98	99.90	1.52	6.47
Ga-19M	22.45	18.33	23.54	35.60	99.92	1.22	6.48

a) $Al_2O_3+Ga_2O_3$. b) Allophane, free from gallium. c) The postscripts "C" and "M" denote the coprecipitated and mixed samples, respectively. d) Calculated.

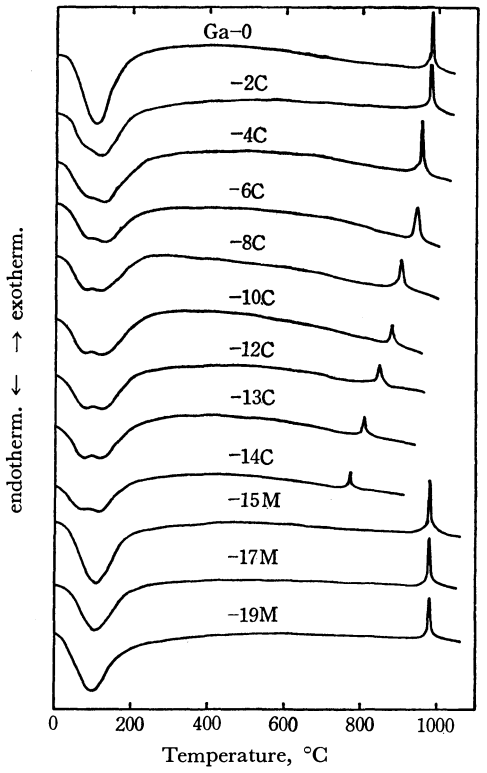

Fig. 1. DTA curves of gallium-bearing samples.

DTA which were assigned to the allophane. The patterns of the DTA of the samples were also similar to that of the allophane, though the endothermic peak split into two peaks with an increase in the gallium content, as is shown in Fig. 1. The exothermic peak temperature in the DTA on the coprecipitated samples

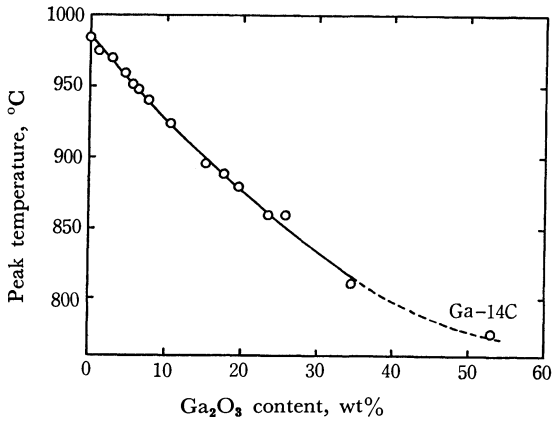

Fig. 2. Plot of exothermic-peak temperature in DTA of coprecipitated samples against gallium content.

was lowered from 980 to 810 °C with an increase in the gallium content, in contrast to the small shift of the exothermic peak temperature of the mixed samples, as is shown in Fig. 2. The peak temperature of the Ga-14C sample, free from aluminum, was 775 °C.

The Variation in the Firing Products in the Samples during Heat Treatment. The crystalline phases formed in the heat-treated samples at 800, 900, 1000, 1100, and 1200 °C for 5 hr were identified as the mullite, the silico-alumina spinel,[11] the β-gallia, and the cristobalite by means of X-ray powder diffractometry. The firing products at each temperature are shown in Table 2. The crystallization process of the coprecipitated samples was found to vary, depending on the con-

11) G. W. Brindley and M. Nakahira, *J. Amer. Ceram. Soc.*, **42**, 314 (1959).

Table 2. Firing products in gallium-bearing samples

Sample	Temperature, °C				
	800	900	1000	1100	1200
Ga-0	A	M	M	M	M, C
Ga-1C	A	M	M	M	M, C
Ga-2C	A	M	M	M	M, C
Ga-3C	A	M	M	M	M, C
Ga-4C	A	M	M	M	M, C
Ga-5C	A	M	M	M	M, C
Ga-6C	A	Sp	M, Sp	M	M, C
Ga-7C	A	Sp	Sp	M, Sp	M, C
Ga-8C	A	Sp	Sp	M, Sp	M, C
Ga-9C	Sp	Sp	Sp	Sp	M, C
Ga-10C	Sp	Sp	Sp	Sp, G	M, G, C
Ga-11C	Sp	Sp	Sp	Sp, G	M, G, C
Ga-12C	Sp	Sp	Sp	G	G, C
Ga-13C	Sp	Sp	Sp	G	G, C
Ga-14C	Sp	Sp	G	G	G, C
Ga-15M	A	M, G	M, G	M, G, C	M, G, C
Ga-16M	G	M, G	M, G	M, G, C	M, G, C
Ga-17M	G	M, G	M, G	M, G, C	M, G, C
Ga-18M	G	M, G	M, G	M, G, C	M, G, C
Ga-19M	G	M, G	M, G	M, G, C	M, G, C

A: amorphous, M: mullite, Sp: silico-alumina spinel, G: β-gallia, C: cristobalite.

dition of the original samples, as is shown in Table 2. The crystallization of the mullite tended to become difficult with an increase in the gallium content of the samples; thus, the mullite was not observed as a firing product in the samples with more than 25.83 wt% of Ga_2O_3.

On the contrary, the crystallization process of the mixed samples was analogous with each other in spite of the variation in the gallium content without forming the silico-alumina spinel. Therefore, the coexistence state of gallium in the coprecipitated samples were considered to be different from that of the mixed samples, judging from the dissimilarity between the crystallization processes of the coprecipitated and of the mixed samples.

In order to examine the cause of the exothermic peak around 900 °C in the DTA, the Ga-1C, -3C, -8C, -11C, -13C, -14C, and -16M samples were preheated up to temperatures just below and above their peak temperatures at the rate of 10 °C/min in the DTA equipment. The phases of these preheated samples were identified by X-ray diffractometry to be as is shown in Table 3. When these samples were again examined by the DTA, the sharp exothermic peak was observed only in the samples which retained the amorphous state after preheating just below the peak temperatures, except for the Ga-16M sample. As is shown in Table 3, the exothermic change in the coprecipitated samples was found to lead to the formation of the mullite or the silico-alumina spinel from the amorphous state.

The apparent activation energy, E_a, for the exothermic change was estimated by the following Kissinger equation:[12]

$$d(\ln \theta/T_m^2)/d(1/T_m) = -E_a/R$$

where θ is the heating rate (3, 5, 10, 15, and 20 °C/min); T_m, the peak temperature in the DTA, and R, the gas constant.

Table 3. Phases of preheated samples

Sample	Peak temp. of original state, °C	Phase after heat treatment	
		below peak temp.	above peak temp.
Ga-1C	975	A (960 °C)	M (990 °C)
Ga-3C	959	A (930 °C)	M (985 °C)
Ga-8C	895	A (872 °C)	Sp (910 °C)
Ga-11C	859	A (848 °C)	Sp (875 °C)
Ga-13C	810	A (798 °C)	Sp (834 °C)
Ga-14C	775	A (762 °C)	Sp (787 °C)
Ga-16M	980	G (970 °C)	M, G (995 °C)

A: amorphous, M: mullite, Sp: silico-alumina spinel, G: β-gallia.

The E_a values of the exothermic change in the coprecipitated samples decreased with an increase in the gallium content, while those in the mixed samples were nearly equal to that of the Ga-0 sample and scarcely changed at all in spite of the variation in the gallium content, as is shown in Table 4.

Table 4. Apparent activation energy for exothermic change around 900 °C

Sample	E_a, kcal/mol
Ga-0	243
Ga-7C	215
Ga-11C	209
Ga-14C	196
Ga-17M	227
Ga-19M	239

The Unit Cell Dimensions of the Mullite Formed in the Heat-treated Samples. The relationship between the unit cell volume, V, of the mullite heat-treated at 1200 °C for 5 hr and the gallium content in the original samples is shown in Fig. 3. The V of the mullite formed in the coprecipitated samples increased with an increase in the gallium content up to 15.25 wt% as Ga_2O_3, and then decreased above 17.72wt%, while those in the mixed samples scarcely changed at all in spite of variation in the gallium content in all except the Ga-18M sample.

The relationship between the unit cell length along the c axis, c_0, and the V of the mullite formed in the coprecipitated samples was approximately linear, as is shown in Fig. 4, in contrast to the case in the heat-treated mixed samples. Although the c_0 and V values of gallium-free mullite varied with the silica/alumina ratio,[13] the variation in the c_0 and the V of

12) H. E. Kissinger, *Anal. Chem.*, **29**, 1702 (1957).
13) S. O. Agrell and J. V. Smith, *J. Amer. Ceram. Soc.*, **43**, 69 (1960).

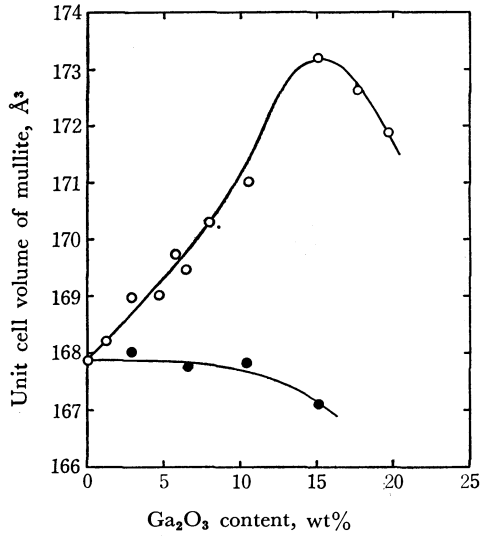

Fig. 3. Plot of unit cell volume of mullite formed at 1200 °C against gallium content.
○; coprecipitated samples, ●; mixed samples

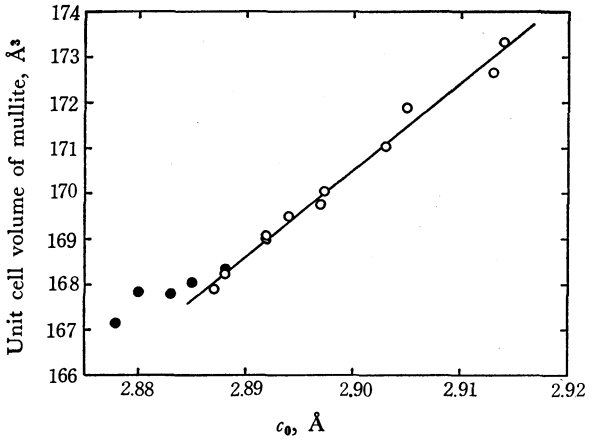

Fig. 4. Plot of unit cell volume against c_0 of mullite formed at 1200°C.
○; coprecipitated samples, ●; mixed samples

the mullite formed in the coprecipitated samples remarkably exceeded those caused by a change in the silica/alumina ratio.

Therefore, much of the gallium in the coprecipitated samples was considered to be included in the mullite by forming a solid solution, although a limit of the amount of gallium included in the mullite was obscure.

The maximum value of the V (173.3 Å^3, the Ga–8C sample) was larger than the reported value of the gallium-bearing mullite (170.1 Å^3).[5] However, it is difficult to compare them directly, since the substantial amount of gallium in the mullite formed in the Ga–8C sample can not be estimated.

Discussion

Because the exothermic peak around 900 °C in the DTA on the coprecipitated gels shifted continuously toward lower temperatures as the gallium content increased, the causes of all the exothermic peak must have the same pattern. The exothermic peak around 900 °C on the silica-alumina gel has been explanied as originating from the formation of mullite[14,15] or γ-alumina.[16] In the case of the coprecipitated gels with less gallium (*e.g.*, the Ga–1C and –3C samples), the results shown in Table 3 favor the conclusion that the formation of the mullite was responsible for this peak. On the contrary, the exothermic reaction product from the coprecipitated gels with more gallium (*e.g.*, the Ga–8C, –11C, and –13C samples) was found to be the silico-alumina spinel, similar to that of the Ga–14C sample, free from aluminum.

If the exothermic peak originates from the formation of the mullite, the inconsistency between a reduction in the apparent activation energy for the exothermic reaction and a rising trend of the crystallization temperature of the mullite with an increase in the gallium content can not be explained. A direct examination of the preheated samples indicated that the exothermic peak in the DTA resulted not only from the formation of the specified mineral, *i.e.*, mullite, but also from that of the silico-alumina spinel, which was a metastable phase. Furthermore, this exothermic peak is considered to originate in a structural change in the silica-alumina based gels, a change which arises from the formation of the mullite or the silico-alumina spinel, although its details are obscure; the kind of exothermic reaction products will depend on the composition, the coexistence state of gallium in the gels, and the crystallographic geometry.

The β-gallia formed was found to include aluminum ions as a solid solution, since the spacings of the β-gallia, one of the firing products in the gallium-rich coprecipitated samples and the aluminum-free one, decreased with the decrease in the gallium content. For example, the spacing for the (311) of the β-gallia[17] crystallized at 1200 °C in the Ga–11C, –12C, and –14C samples were 1.518, 1.529, and 1.545 Å respectively, while those in the two mixed samples, Ga–17M and –19M, were 1.542 and 1.545 Å respectively.

Judging from the chemical compositions and the results of the DTA and of the X-ray powder diffractometry of the heat-treated samples, the coprecipitated samples, the SiO_2–Al_2O_3–Ga_2O_3–H_2O system, prepared in this work are considered to be an allophane-like material, *i.e.*, a gallium-bearing allophane.

14) T. Demediuk and W. F. Cole, *Nature*, **181**, 1400 (1953).
15) J. Ossaka, "Nendokagaku no Shinpo," Vol. 4, ed. by S. Iwao, Gihodo, Tokyo (1962), p. 33.
16) Y. Tsuzuki and K. Nagasawa, Ref. 15, p. 1.
17) The reported value for the (311) of the β-gallia is 1.542 Å; J. A. Kohn, G. Katz, and J. B. Broder, *Amer. Mineral.*, **42**, 398 (1957).

An MO-theoretical Interpretation of the Reductive Cleavage of Organic Halides by Pentacyanocobaltate(II)

Katsutoshi OHKUBO, Hirokazu KANAEDA, and Kohji TSUCHIHASHI

Department of Synthetic Chemistry, Faculty of Engineering, Kumamoto University, Kurokami, Kumamoto 860

(Received February 14, 1973)

The mechanism of the reductive cleavage of organic halides (RX) by pentacyanocobaltate(II) $Co(CN)_5^{3-}$ was investigated by means of the extended Hückel MO theory. First, the molecular structure of $Co(CN)_5^{3-}$ was considered to be the square-pyramidal C_{4v} configuration, without H_2O as its sixth ligand. Secondly, the order of the observed rate constants for the $Co(CN)_5^{3-}+RX \rightarrow Co(CN)_5X^{3-}+R\cdot$ reaction was found to be in satisfactory accordance with that of the calculated binding energies of the R–X bond. Thirdly, the reductive cleavage of RX by $Co(CN)_5^{3-}$ proceeds by the aid of the predominant electron-migration from the highest-occupied, lone-pair halogen-orbital to the singly-occupied d_{z^2} Co-orbital and from the highest-occupied d_{xz} (or d_{yz}) Co-orbital to the lowest-unoccupied, antibonding $p\sigma^*$ orbital of the R–X bond. Finally, the mode of the interaction between $Co(CN)_5^{3-}$ and RX was precisely discussed in terms of the homolytic cleavage of the R–X bond.

It has been well established that organocobalt compounds can be easily formed by the reductive cleavage of organic halides with pentacyanocobaltate(II)[1-6]:

$$2Co(CN)_5^{3-} + RX \rightarrow Co(CN)_5R^{3-} + Co(CN)_5X^{3-} \quad (1)$$

The mechanism of such a reaction has been interpreted mainly, by the kinetic and other studies of Halpern *et al.*,[2,3,6] in terms of the free-radical reaction according to:

$$Co(CN)_5^{3-} + RX \rightarrow Co(CN)_5X^{3-} + R\cdot \quad \text{(rate-determining)} \quad (2)$$

$$Co(CN)_5^{3-} + R\cdot \rightarrow Co(CN)_5R^{3-} \quad (3)$$

Since any precise discussion referred to the above reactions, however, depends in the early stages on a molecular level, molecular orbital study seems significant.

The present study was undertaken in order to elucidate the mechanism of the reductive cleavage of RX by $Co(CN)_5^{3-}$, using throughout the extended Hückel MO method, with particular reference to the plausible model of the interaction between the two compounds.

Method of Calculation

An extended Hückel MO (EHMO) method[7] involving metal d-orbitals was used for the calculations on the following three systems:

(a) pentacyanocobaltate(II) : square-pyramidal C_{4v} and trigonal-bipyramidal D_{3h} $Co(CN)_5^{3-}$, (b) organic halides: RI (R=CH_3, C_2H_5, *i*-C_3H_7, and *t*-C_4H_9), $XCH_2CO_2CH_3$ and XCH_2CONH_2 (X=Cl, Br, and I), and (c) an interacting system of $Co(CN)_5^{3-}$ and RX (CH_3I was tentatively taken).

The orbital exponents and ionization energies for the s and p orbitals of the C, N, O, and halogen atoms were supplied by Clementi[8] and by Jaffé[9] respectively. The ionization energies for the s, p, and d orbitals of the Co atom were, respectively, taken to be 10.0 eV,[10] 8.0 eV,[10] and 11.0 eV.[10]

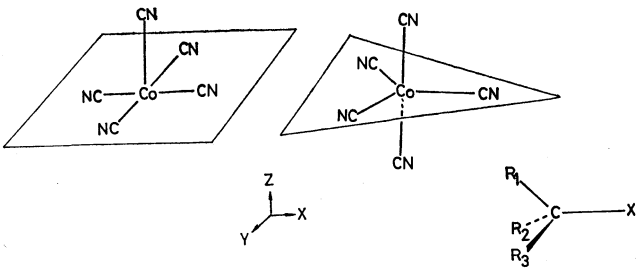

Co-C=2.30−1.50 Å
C-N=1.30 Å
C-Cl=1.767 Å
C-Br=1.939 Å
C-I=2.139 Å

Fig. 1. Geometries of pentacyanocobaltate(II) and organic halides used for the calculation.

The geometries used for the calculations are illustrated in Fig. 1; the interatomic distance and the valence angles for $XCH_2CO_2CH_3$ and XCH_2CONH_2 were determined uniformly from those[12] of $CH_3CO_2CH_3$ and CH_3CONH_2, with the fixed angle of C–C–X (109°28′), for the sake of simplicity.

Results and Discussion

Molecular Structure of $Co(CN)_5^{3-}$. The molecular structure of $Co(CN)_5^{3-}$ in solution has not yet been strictly established; the square-pyramidal C_{4v} $Co(CN)_5^{3-}$ has been predominantly discussed as compared with the trigonal-bipyramidal D_{3h} one.

1) J. Halpern and J. P. Maher, *J. Amer. Chem. Soc.*, **86**, 2311 (1964).
2) J. Halpern and J. P. Maher, *ibid.*, **87**, 5361 (1965).
3) J. Kwaitek and J. K. Seyler, *J. Organometal. Chem.*, **3**, 421 (1965).
4) J. Kwiatek and J. K. Seyler, *Advance in Chemistry Series*, No. 70, American Chemical Society, Washington, D. C. (1968), p. 207.
5) J. Kwiatek, *Catalysis Rev.*, **1**, 37 (1967).
6) P. B. Chock and J. Halpern, *J. Amer. Chem. Soc.*, **91**, 582 (1969).
7) K. Ohkubo and H. Kanaeda, *J. Chem. Soc. Faraday Trans. II*, **68**, 1164 (1972); For the basic principles, see R. Hoffmann, *J. Chem. Phys.*, **39**, 1397 (1963); *ibid.*, **40**, 2474 (1964).
8) E. Clementi and D. L. Raimondi, *J. Chem. Phys.*, **38**, 2686 (1963).
9) J. Hinze and H. H. Jaffé, *J. Amer. Chem. Soc.*, **84**, 540 (1962).
10) L. L. Lohr, Jr., and W. W. Lipscomb, *Inorg. Chem.*, **3**, 22 (1964). Another values of the ionization energies, for the s, p, and d Co-orbitals, such as 5.66 eV,[11] and 7.84 eV[11] respectively, were found to be unsuitable for the present calculations on $Co(CN)_5^{3-}$, because in the calculations with the above parameters, Co was much positively charged and the bond population of Co–C was negatively calculated.
11) F. A. Cotton and T. E. Haas, *ibid.*, **3**, 1004 (1964).
12) L. E. Sutton, Editor, "Interatomic Distances," The Chemical Society, London (1958).

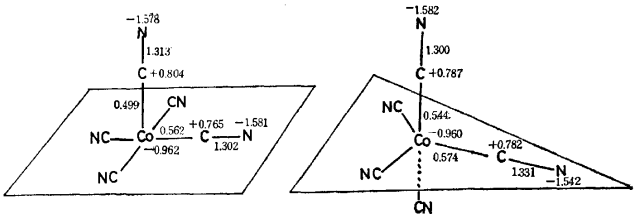

C_{4v} $E_{EH} = -1009.116$ eV

D_{3h} $E_{EH} = -1009.770$ eV

Fig. 2. Electronic structures of C_{4v} and D_{3h} $Co(CN)_5^{3-}$.

We will first discuss which structure, the C_{4v} or the D_{3h}, is more likely for $Co(CN)_5^{3-}$. Fig. 2 shows the formal charges (Q_A), the bond populations (M_{A-B}), and the total electronic energies (E_{EH}) of C_{4v} and D_{3h} $Co(CN)_5^{3-}$ at a fixed Co–C distance of 1.81 Å.[13] As Fig. 2 indicates, the electronic structures of the C_{4v} and the D_{3h} $Co(CN)_5^{3-}$ resemble each other, since they have almost the same values of Q_A, M_{A-B}, and E_{EH}.

According to the E_{EH} values of the C_{4v} and D_{3h} $Co(CN)_5^{3-}$ at the Co–C distances of 1.5~2.3 Å (Table 1), the latter cobaltate seems to be slightly more stable than the former. The energy difference between the two cobaltates is, however, quite small; that is, it is difficult to conclude the stability of the trigonal-pyramidal D_{3h} structure for $Co(CN)_5^{3-}$ from the total energy, neglecting the electron-electron and nuclear-nuclear repulsions.

On the other hand, the 10 Dq value estimated from the energy difference between the lowest-unoccupied (LU) and the singly-occupied (SO) orbitals[14] of the Co atom offers some information about the molecular structure of $Co(CN)_5^{3-}$. The 10 Dq value for the C_{4v} $Co(CN)_5^{3-}$, 32.09 kK, at the Co–C distance of 1.81 Å was found to be in good agreement with that of 33 kK obtained experimentally by Caulton.[15]

Since the C_{4v} structure was demonstrated by Alexander and Gray[16] in their ESR and UV spectroscopic investigations of $Co(CN)_5^{3-}$, and since the theoretical values of 10 Dq agree with those in the experiments, the square-pyramidal C_{4v} $Co(CN)_5^{3-}$ seems to be more likely than the trigonal-pyramidal D_{3h} one, and the Co–C distance seems to be about 1.81 Å.

Table 1. Total electronic energies of C_{4v} and D_{3h} $Co(CN)_5^{3-}$

	$Co(CN)_5^{3-}$ geometry	1.50 Å	1.81 Å	2.30 Å
E_{EH}(eV)	D_{3h}	−1013.015	−1009.770	−1006·616
	C_{4v}	−1012.333	−1009.116	−1006.217
Nuclear-nuclear repulsion (eV)	D_{3h}	7516.707	6821.210	5938.764
	C_{4v}	7606.707	6821.210	5938.764
10Dq (kK)	D_{3h}	29.77	18.88	3.47
	C_{4v}	126.3	33.04	3.19

Table 2. Bond populations of Co-C and C-N[a]

Bond	σ Overlap	σ N_{Co-C}	π Overlap	π N_{Co-C}
Co-C	s-s	0.0476	p_y-p_y	0.0178
	s-p_x	0.0430	p_z-p_z	0.0462
	p_x-p_x	0.0899	d_{xz}-p_z	0.0381
	p_x-s	0.1442	d_{xy}-p_y	0.0376
	$d_{x^2-y^2}$-s	0.0317	d_{z^2}-p_z	0.0067
	total	0.4225	total	0.1464

Bond	σ Overlap	σ N_{C-N}	π Overlap	π N_{C-N}
C-N	s-s	0.1701	p_y-p_y	0.2471
	s-p_x	0.2432	p_z-p_z	0.2443
	p_x-p_x	0.1744		
	p_x-s	0.2226		
	total	0.8103	total	0.4914

a) Co-CN bond on x-axis.

On the other hand, there have been some discussions[17] referred to $Co(CN)_5^{3-}$ coordinated by H_2O as its sixth ligand in aqueous solutions. According to the calculated results of the C_{4v} $Co(CN)^{3-}$, H_2O, and octahedral $Co(CN)_5OH_2^{3-}$ (Co–O was taken to be 1.93 Å,[18] the isolated systems of $Co(CN)_5^{3-}$ and H_2O (the sum of their E_{EH} values = −1169.72 eV) can be said to be energetically more stable than $Co(CN)_5OH_2^{3-}$ ($E_{EH} = -1167.96$ eV). It may be deduced, therefore, that H_2O does not coordinate directly to $Co(CN)_5^{3-}$.

Here, the bond nature of the C_{4v} $Co(CN)_5^{3-}$ will be discussed briefly. Table 2 lists the AO bond populations (N_{A-B}) of the Co–C and C–N bonds. The d Co-orbitals contribute mainly to the dp-π-type bond

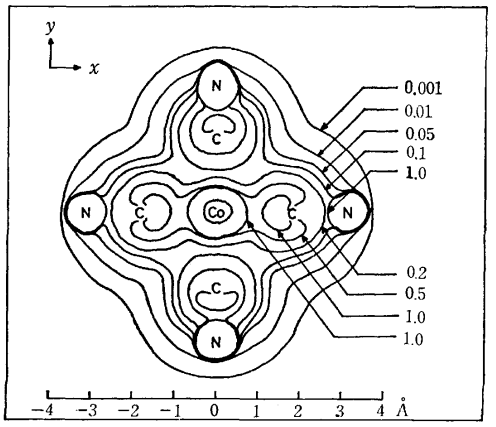

Fig. 3. Charge density contour of C_{4v} $Co(CN)_5^{3-}$. (The representation is in xy cross section.)

13) Lipscomb *et al.*[10] emphasized the Co–CN distance of 1.81 Å by their study on $Co(CN)_5H^{3-}$.

14) The LUMO and the SOMO are, respectively, $d_{x^2-y^2}$ and d_{z^2} orbitals for the C_{4v} $Co(CN)_5^{3-}$ and are, respectively, d_{z^2} and d_{xy} orbitals for the D_{3h} $Co(CN)_5^{3-}$.

15) K. G. Caulton, *Inorg. Chem.*, **7**, 392 (1968).

16) J. J. Alexander and H. B. Gray, *J. Amer. Chem. Soc.*, **89**, 3356 (1967).

17) For instance, see J. M. Pratt, and R. J. P. Williams, *J. Chem. Soc., Ser.* A, **1967**, 1291.

18) The purely covalent bond-distance was used because the usual bond-distances of metal-oxygen in aquo-complexes are purely covalent (see Ref. 12).

Table 3. Correlation between the electronic properties and reactivities of RX and the k_{obs} values for the reaction, $RX + Co(CN)_5^{3-} \rightarrow R\cdot + Co(CN)_5X^{3-}$

RX	k_{obs}[a] ($M^{-1}s^{-1}$)	D_{298}[b] (kcal/mol)	Binding[c] energy (kcal/mol)	M_{C-x}	N_{p_σ}	$N_{lone-pair}$
CH_3I	9.5×10^{-3}	56.0	60.88	0.5107	0.3435	1.9995
C_2H_5I	5.9×10^{-2}	53.0	58.40	0.580	0.3384	1.9990
i-C_3H_7I	1.2	50.0	54.11	0.5153	0.3319	1.9987
t-C_4H_9I	9.1	50.0	53.24	0.5197	0.3285	1.9983
$ClCH_2CO_2CH_3$	$\sim10^{-3}$		28.05	0.6030	0.3648	1.9965
$ClCH_2CONH_2$	$\sim6\times10^{-4}$		32.28	0.6266	0.3638	1.9934
$BrCH_2CO_2CH_3$	~34		37.68	0.5980	0.3862	1.9977
$BrCH_2CONH_2$	16.4		40.61	0.6218	0.3845	1.9948
$ICH_2CO_2CH_3$	8.8×10^{4}		55.71	0.5037	0.3417	1.9988
ICH_2CONH_2	2.95×10^{4}		62.43	0.5190	0.3419	1.9975

a) 1:1 methanol-water by volume at 25°C for $XCH_2CO_2CH_3$ and XCH_2CONH_2, and 2:8 water-methanol at 25°C for RI. Cited from Refs. 2 and 6. b) Quoted from J. A. Kerr, *Chem. Rev.*, **66**, 465 (1966). c) Binding energy $=|E_{EH}(RX) - (E_{EH}(R\cdot) + E_{EH}(X\cdot))|$.

Table 4. Bond populations of C-I in various modes of interaction between CH_3I and $Co(CN)_5^{3-}$

Type of interaction	θ, (deg.)	Bond population of C-I		
		Initial	Transition	Final[a]
A	0	0.5065	0.1237	−0.0057
	30	0.5.73	0.1251	−0.0001
	45	0.5082	0.1281	0.3104
	60	0.5089	0.1413	0.0045
	90	0.5090	0.1455	0.0082
B	12	0.5065	0.1215	−0.0053
	22.5		0.1160	−0.0050
	33	0.5051	0.1081	−0.0046
	45	0.5011	0.1005	−0.0031

a) Co-I=3.60 Å, C-I=2.139 Å, and ∠HCI=109°28′ for the initial system, Co-I=2.90 Å, C-I=2.82 Å, and ∠HCI=99°44′ for the transition system, and Co-I=2.52 Å, C-I=3.50 Å, and ∠HCI=90° for the final system.

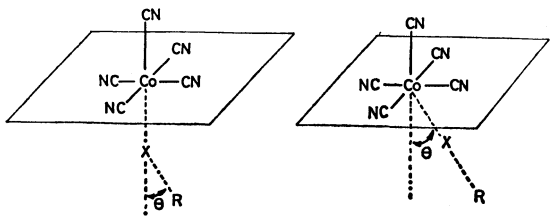

Type A Type B

Table 5. Electron densities of I in CH_3I and Co in $Co(CN)_5^{3-}$ in their various states

Atom	Orbital	Electron densities					
		CH_3I[a]	CH_3I[b]	$Co(CN)_5^{3-}$[c]	Initial[d]	Transition[d]	Final[d]
I	s	1.8207	1.9731		1.8046	1.7657	1.6344
	p_x	1.3582	1.5690		1.3025	1.2714	1.4452
	p_y	1.9995	1.9999		1.9967	1.9496	1.8324
	p_z	1.9995	1.9999		1.9948	1.6552	1.2559
Co	d_{xz}			1.5844	1.6068	1.4552	1.2878
	d_{yz}			1.5844	1.5848	1.5909	1.6063
	d_{xy}			1.3491	1.3507	1.3827	1.4657
	$d_{x^2-y^2}$			1.1621	1.1696	1.1523	1.1262
	d_{z^2}			0.9511	0.9805	1.2595	1.0930

a) In the geometry of the initial state (see Fig. 1).
b) In the geometry of the transition state (see Table 4).
c) In the geometry of the initial state (see Fig. 1).
d) Interacting system between CH_3I and $Co(CN)_5^{3-}$, and the geometries were shown in Table 4.

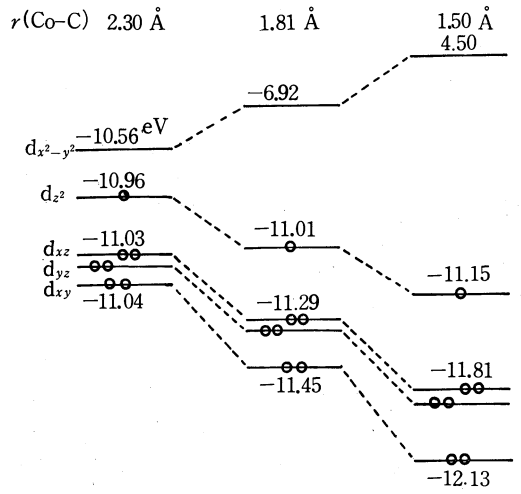

Fig. 4. d-Orbital separation of C_{4v} $Co(CN)_5^{3-}$ as a function of Co–C distance.

formation of the Co–C bond, and the $d_{x^2-y^2}$ Co-orbital takes part in the ds-σ-type bond formation of the Co–C in some measure. The net charge-density contour for the C_{4v} $Co(CN)_5^{3-}$ is illustrated in Fig. 3 to facilitate an understanding of the bond nature discussed above and the electron distribution of the compound.

Frontier Orbitals of $Co(CN)_5^{3-}$ and RX. The d-orbital separation on the Co atom of the C_{4v} $Co(CN)_5^{3-}$ is shown in Fig. 4; the cobaltate is characterized by the SO d_{z^2} and the doubly-degenerate, highest occupied (HO) d_{xz} and d_{yz} Co-orbitals. On the other hand, the frontier orbitals of RX are the doubly-degenerate, HO lone-pair p_z and p_y orbitals on X and the antibonding, LU $p\sigma^*$ orbital on the C–X axis. It seems certain that the above-mentioned orbitals corresponding to the frontier MOs play an important role in the reductive cleavage of RX by $Co(CN)_5^{3-}$: The SOMO (and/or the HOMO) of $Co(CN)_5^{3-}$ interacts predominantly with the LUMO, the HOMO, or both the MOs of RX respectively in the nucleophilic, electrophilic, or radical attack of the former on the latter.

Correlation between the Electronic States of RX and the Reaction Rates for $Co(CN)_5^{3-}+RX \rightarrow Co(CN)_5X^{3-}+R\cdot$. In this section, we will discuss the correlation between the bond nature of RX and the observed rate constants, k_{obsd}, for Eq. (2) (see Introduction). As can be seen from Table 3, the order of k_{obsd} values is satisfactorily reflected in that of the dissociation energies, D_{298} (in other words, binding energies or M_{C-X} values). On the other hand, no parallelism between the order of the AO-bond population of the $p\sigma$-orbitals on the C–X axis (N_{p_σ}) or of the lone-pair p_z-orbital on X ($N_{lone-pair}$) and that of the k_{obsd} values can be consistently realized between the two series of RI and $XCH_2CO_2CH_3$ and/or XCH_2CONH_2; that is, the order of the k_{obsd} values cannot be explained by only that of the N_{p_σ} or $N_{lone-pair}$ values. It can be deduced, therefore, that both the $p\sigma^*$ C–X orbital and the lone-pair X-orbital take part directly in the interaction with $Co(CN)_5^{3-}$.

Interacting System of $Co(CN)_5^{3-}$ and RX. We will here determine the most plausible mode of the interaction between $Co(CN)_5^{3-}$ and RX in terms of the homolytic cleavage of the R–X bond. The EH-MO calculations were performed on the two modes of interaction between $Co(CN)_5^{3-}$ and RX (CH_3I was tentatively used), *i.e.*, Type-A and Type-B, both illustrated in Table 4.

It may be found from Table 4 that the C–I bond of CH_3I is most weakened by the Type-B interaction at $\theta=45°$ in view of the fact that the M_{C-I} values of such interaction are the smallest throught the reaction progress. The Type-B interaction at $\theta=45°$ seems to be the most appropriate interacting form in which plausible overlappings between the frontier orbitals of both compounds can be established (see Fig. 5).

With regard to the electron migrations between $Co(CN)_5^{3-}$ and RX, the migrations depicted by Eqs. (4)~(7) can be considered on the basis of the changes in the electron densities of the s and p X-orbitals and the d Co-orbitals, as is indicated in Table 5:

$$p_z^{(X)}\ \text{(lone-pair)} \xrightarrow{\text{through } d_{z^2}{}^{(Co)}-p_z{}^{(X)}} d_{z^2}{}^{(Co)}\ \text{(predominant)} \quad (4)$$

$$p_y{}^{(X)}\ \text{(lone-pair)} \xrightarrow{\text{through } d_{yz}{}^{(Co)}-p_y{}^{(X)}} d_{yz}{}^{(Co)} \quad (5)$$

$$\xrightarrow{\text{through } d_{xy}{}^{(Co)}-p_y{}^{(X)}} d_{xy}{}^{(Co)} \quad (6)$$

$$d_{xz}{}^{(Co)} \xrightarrow{\text{through } d_{xz}{}^{(Co)}-p_x{}^{(X)}} p_x{}^{(X)}\ \text{(predominant)} \quad (7)$$

The predominant electron-migrations depicted by Eqs. (4) and (7) bring about, respectively, the decrease in the bonding character of the R–X and the increase in the antibonding character of the same bond, as may be seen from the energy-change in the frontier orbital levels of RX (*viz.* CH_3I) in Fig. 5.

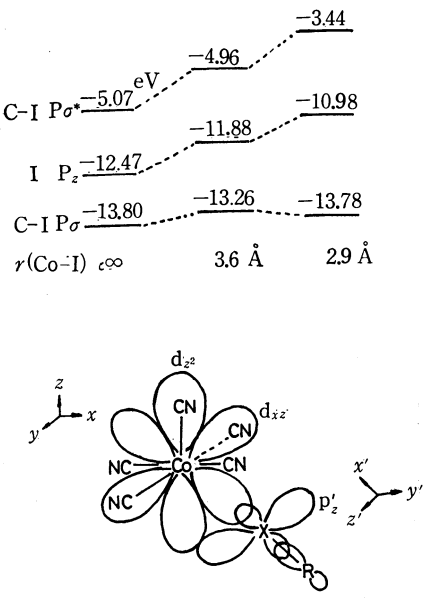

Fig. 5. MO-energy changes in frontier orbitals of RX by optimized interaction of $Co(CN)_5^{3-}$.

The present calculations were carried out on a FACOM 230-60 computer at the Data Processing Center of Kyushu University.

The Solubility of Sulfur in Na_2O-SiO_2 Melts under Various Oxygen Partial Pressures at 1100 °C, 1250 °C, and 1300 °C

Shigeru NAGASHIMA and Takashi KATSURA

Department of Chemistry, Faculty of Science, Tokyo Institute of Technology, Ookayama, Meguro-ku, Tokyo 152

(Received February 17, 1973)

The solubility of sulfur in Na_2O–SiO_2 melts with the Na_2O/SiO_2 molar ratios of 1/3, 1/2, and 1/1 was investigated by varying the oxygen partial pressure at 1100, 1250, and 1300 °C. The results at 1100 °C are complicated, for the equilibrium state within the gas phase is not established. From the experiments at 1250 and 1300 °C, the following conclusions are reached: (1) When the temperature and the Na_2O/SiO_2 ratio in the melt are constant, the solubility of sulfur increases with an increase of the total amount of sulfur in the gas phase. (2) When the temperature, the Na_2O/SiO_2 ratio, and the total amount of sulfur in the gas phase are constant, the solubility of sulfur shows its minimum at a specific oxygen partial pressure; at higher oxygen partial pressures, the sulfur dissolves in the melts mostly as sulfate, while at lower oxygen partial pressures, the sulfur dissolves mostly as sulfide. (3) When the temperature and the total amount of sulfur in the gas phase are constant, the solubility rises greatly with an increase in the Na_2O/SiO_2 ratio in the melt. (4) When the Na_2O/SiO_2 ratio in the melt and the total amount of sulfur in the gas phase are constant, the minimum point of the solubility shifts in the direction of higher oxygen partial pressures as the temperature increases. This corresponds to the shifts of the equilibrated gas composition as the temperature increases.

The solubility of sulfur in melts at high temperatures is important not only for geochemistry but also for metallurgy and ceramics. Fincham and Richardson[1] investigated the effect of the oxygen partial pressure on the solubility of sulfur in silicate and alumino silicate melts by equilibrating the melts with gas mixtures (SO_2–CO_2–H_2) at 1350—1650 °C. On the basis of thermodynamic calculations at 1425—1650 °C, they concluded that sulfur dissolves in the CaO–Al_2O_3–SiO_2 melts as sulfate at oxygen partial pressures higher than about 10^{-3} atm, and that sulfur dissolves as sulfide at oxygen partial pressures lower than about 10^{-5} atm. Similar results were obtained later by other investigators[2-3] using different kinds of melts. However, no study has been published on the alkali silicate systems.

The present objectives are to: (1) obtain fundamental thermodynamic information about the solubility of sulfur in the Na_2O–SiO_2 melts and (2) actually prove the dissolving state of sulfur in silicate melts by chemical analysis. The solubility of sulfur was studied at very high oxygen partial pressures by Holmquist,[4] but no study has ever been made over wider range of oxygen partial pressures.

Experimental

Furnace, Temperature Control, and Procedure. These were almost the same as those adopted by Iwasaki and Katsura.[5]

Gas Mixture. Commercial gases (SO_2, CO_2, and H_2) were purified with phosphorus pentoxide and were mixed in the required ratio by a capillary technique. The rate of gas flow was fixed at 0.66 cm/s throughout the present experiments. Preliminary experiments at about 0.3 cm/s proved that the gas-flow rate does not have any significant effect on the results.

Materials. Sodium silicate glasses with the required compositions (the Na_2O/SiO_2 molar ratios of 1/1, 1/2, and 1/3) were prepared by melting mixtures of sodium carbonate and silica of an analytical grade in platinum crucibles. The sodium contents of these glasses were chemically analyzed in the form of Na_2SO_4 after dissolving the glasses with HF and H_2SO_4; the results agreed well with the calculated values within an error of 0.5%. The sulfur content of these glasses was less than 0.001%. Samples with a known amount of sulfur were also prepared by melting mixtures of sodium carbonate, sodium sulfate, and silica.

Chemical Analysis of Total Sulfur. The total sulfur in the quenched samples was determined by the following two methods, according to the sulfur content: (1) for high concentrations of sulfur (>0.5%), the sulfur was determined by the method of Kiba *et al.*[6] with some modifications; (2) for low concentrations of sulfur (0.001—0.5%), the sulfur was determined as in a previous paper.[7] In order to check the reliability of the methods, the sample with a known amount of sulfur mentioned above was analyzed by the methods, (1) and (2). Some results for the samples with the Na_2O/SiO_2 ratio of 1/2 were as follows: (Added: 4.0% S, Found: 3.9, 4.0, 3.7% S; Added: 0.34% S, Found: 0.32, 0.34, 0.33% S).

Chemical Analysis of Sulfide- and Sulfate-Sulfur. The sulfide- and sulfate-sulfur in the samples was determined with tin(II)-strong phosphoric acid and strong phosphoric acid in the same way as has been reported previously.[7]

Results and Discussion

Establishment of Equilibration. (1) Equilibrium Composition of the Gas Phases: The equilibrium composition of the gas phase at 1100, 1250, and 1300 °C was obtained by means of a digital computer using the linear programing method of White *et al.*[8] and using the thermodynamic data on the chemaical species (H_2, CO_2, CO, H_2O, O_2, SO_3, SO_2, SO, S_2, HS, H_2S,

1) C. J. B. Fincham and F. D. Richardson, *Proc. Roy. Soc. Ser. A*, **223**, 40 (1954).
2) G. R. St. Pierre and J. Chipman, *Trans. AIME*, **206**, 1474 (1956).
3) E. T. Turkdogan and L. S. Darken, *ibid.*, **221**, 464 (1961).
4) S. Holmquist, *J. Amer. Ceram. Soc.*, **47**, 467 (1966).
5) B. Iwasaki and T. Katsura, This Bulletin, **40**, 554 (1967).
6) T. Kiba, T. Takagi, Y. Yoshida, and I. Kishi, *ibid.*, **28**, 641 (1955).
7) S. Nagashima, M. Yoshida, and T. Ozawa, *ibid.*, **45**, 3446 (1972).
8) W. B. White, S. M. Johnson, and G. B. Dantzig, *J. Chem. Phys.*, **28**, 751 (1958).

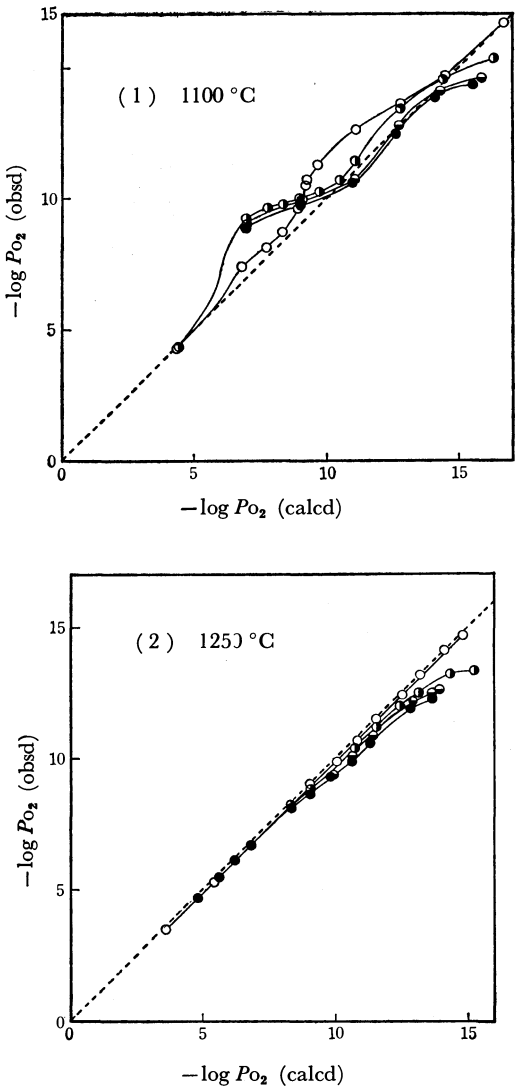

Fig. 1. Relationship between measured oxygen partial pressure and calculated oxygen partial pressure.
○ $(SO_2)_i$ 0 (0 cc/sec)
◑ 0.5% (0.03 cc/sec)
◐ 1.3% (0.08 cc/sec)
● 2.1% (0.13 cc/sec)

COS, CS, CS_2); the values of the standard free energy of the formation of each gas species were taken from "JANAF" Thermochemical Tables.[9] A HITAC-8500 was used for the computations.

Since it is not feasible to confirm whether the actually-established partial pressure of each gaseous species coincides with the thermodynamically-calculated value, the actual oxygen partial pressure was measured for each gas mixture by using a solid electrolyte composed of $(ZrO_2)_{0.85}(CaO)_{0.15}$,[10,11] and the establishment of equilibration was judged through a comparison of the measured value with the calculated one.

A comparison of the measured oxygen partial pressure, P_{O_2}(obsd), with the calculated one, P_{O_2}(calcd) is given in Fig. 1(1) and -(2). As Fig. 1(1) shows, at 1100 °C the measured oxygen partial pressures deviate greatly from the values calculated by the thermodynamic data; this suggests a significant deviation from the equilibrium state within the gas phase. On the other hand, as is shown in Fig. 1(2), at 1250 °C the measured values are in fairly good agreement with the calculated ones, although they deviate slightly with a decrease in the oxygen partial pressure and with an increase in the $(SO_2)_i$ concentration. The results at 1300 °C were almost the same as those at 1250 °C. Therefore, at 1250 and 1300 °C the gas phase is considered to be approximately in equilibrium. The present study was mainly carried out at relatively high oxygen partial pressures above 10^{-12} atm P_{O_2} at 1250 and 1300 °C. The calculated P_{O_2} was adopted except for that at 1100 °C.

(2) Equilibration between Melts and the Gas Phase: The equilibrium amount of total sulfur in the melt was determined by varying the reaction time and by using various starting samples with the same Na_2O/SiO_2 ratio but containing different amounts of sulfur. Examples of the results are given in Fig. 2. The Na content of each sample after heating was analyzed to prove it to be unchanged in the bulk composition throughout the reaction.

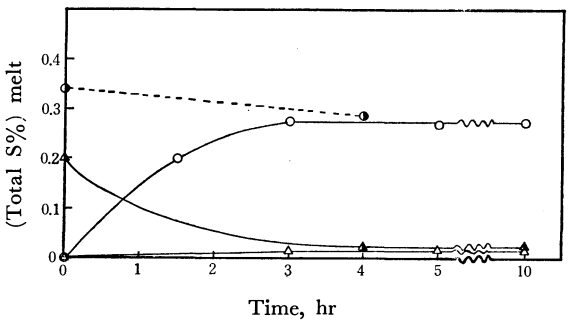

Fig. 2. Saturation time and sulfur content of Na_2O–SiO_2(1:2) melts at 1250 °C.
○, ◑ $(CO_2)_i$: 6 cc/s
△, ◭ $(CO_2)_i$: 6 cc/s, $(H_2)_i$: 0.1 cc/s
in all cases, $(SO_2)_i$ is fixed to 0.03 cc/s.

Experiments at 1100 °C. Preliminary experiments were performed at 1100 °C, although, as was mentioned above, the gas phase was not equilibrated at this temperature. The solubility of gaseous species in silicate and phosphate melts has been studied by several investigators.[4,12-13] Of these, Pearce[12] studied the solubility of CO_2 in Na_2O–SiO_2 melts and observed that the solubility of CO_2 increases with an increase in the Na_2O/SiO_2 ratio. He explained that the solubility of CO_2 depends on the oxygen-ion activity ($a_{O^{2-}}$) in the melts.

In the present study, the solubility of sulfur decreases rapidly with a decrease in the oxygen partial pressures, ranging from 10^{-5} to 10^{-10} atm P_{O_2}, when the Na_2O/SiO_2 ratio is constant, while the solubility

9) "JANAF" Thermochemical Tables. U. S. Department of Commerce/National Bureau of Standards, (1965—1966).
10) T. Katsura and M. Hasegawa, This Bulletin, **40**, 561 (1967).
11) K. Shibata, *ibid.*, **40**, 830 (1967).
12) M. L. Pearce, *J. Amer. Ceram. Soc.*, **47**, 342 (1964).
13) A. Kato, R. Nishibashi, M. Nagano, and I. Mochida, *ibid.*, **55**, 183 (1972).

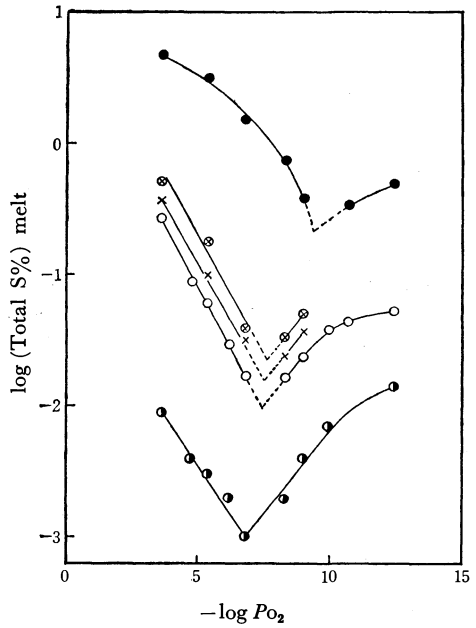

Fig. 3. Variation of sulfur content of Na_2O–SiO_2 melts with oxygen partial pressure at 1250 °C.
Na_2O–SiO_2 (1:1) melts
● $(SO_2)_I$: 0.5%
Na_2O–SiO_2 (1:2) melts
⊗ $(SO_2)_I$: 2.1%
× 1.3%
○ 0.5%
Na_2O–SiO_2 (1:3) melts
◑ $(SO_2)_I$: 0.5%
These symbols are also used in Figs. 3—8.

remains substantially constant though the P_{O_2} value decreases from 10^{-10} to 10^{-15} atm except for the case of $Na_2O/SiO_2=1$. These results are very different from those by Fincham and Richardson.[1] The difference can not be well explained, since the gas phase deviated far from the equilibrium state.

Experiments at 1250 °C. (1) The Solubility of Sulfur Affected by the Oxygen Partial Pressure: Fig. 3 shows the relationship between the solubility of sulfur in sodium silicate melts and the oxygen partial pressure at 1250 °C. The solubility increases greatly with an increase in the Na_2O/SiO_2 ratio, in the same way as was seen at 1100 °C, when the $(SO_2)_I$ concentration is constant. The solubility increases with an increase in the $(SO_2)_I$, as shown in Fig. 3, when the Na_2O/SiO_2 value is 1/2. When both the Na_2O/SiO_2 ratio in the melts and the $(SO_2)_I$ concentration are constant, the solubility shows its minimum at a specific oxygen partial pressure. Fincham and Richardson[1] also obtained the minimum solubility of sulfur in the CaO–Al_2O_3–SiO_2 systems and presumed the following two equilibria:

$$\frac{1}{2}S_2 + \frac{3}{2}O_2 + (O^{2-})_{melt} = (SO_4^{2-})_{melt} \quad (1)$$

$$K_1 = \frac{a_{SO_4^{2-}}}{P_{S_2}^{1/2} P_{O_2}^{3/2} a_{O^{2-}}}$$

$$\frac{1}{2}S_2 + (O^{2-})_{melt} = (S^{2-})_{melt} + \frac{1}{2}O_2 \quad (2)$$

$$K_2 = \frac{P_{O_2}^{1/2} a_{S^{2-}}}{P_{S_2}^{1/2} a_{O^{2-}}}$$

If the oxygen ion activity of the melts, $(a_{O^{2-}})$, is constant in the constant melt composition and at a given temperature, and if, in addition, the activities of SO_4^{2-} and S^{2-} in the melt are proportional to the total sulfur concentrations, $(\%\ S)_{melt}$, the equilibrium constants, K_1 and K_2, may be written as K_1' and K_2' respectively:

$$K_1' = \frac{(\%S)_{melt}}{P_{S_2}^{1/2} P_{O_2}^{3/2}} \quad (1)'$$

$$K_2' = \frac{P_{O_2}^{1/2} (\%S)_{melt}}{P_{S_2}^{1/2}} \quad (2)'$$

Figure 4 illustrates the relationship between the apparent equilibrium constants, K_1' and K_2', and the oxygen partial pressure on the basis of the present experiments. The results show that $\log K_1'$ is almost constant at high oxygen partial pressures, and that $\log K_2'$ is almost constant at low oxygen partial pressures, although the constant, K_1', varies somewhat in the case of melts with the Na_2O/SiO_2 ratio of 1/1 at high oxygen partial pressures. This suggests that the sulfur dissolves as sulfate at high oxygen partial pressures and as sulfide at low oxygen partial pressures.

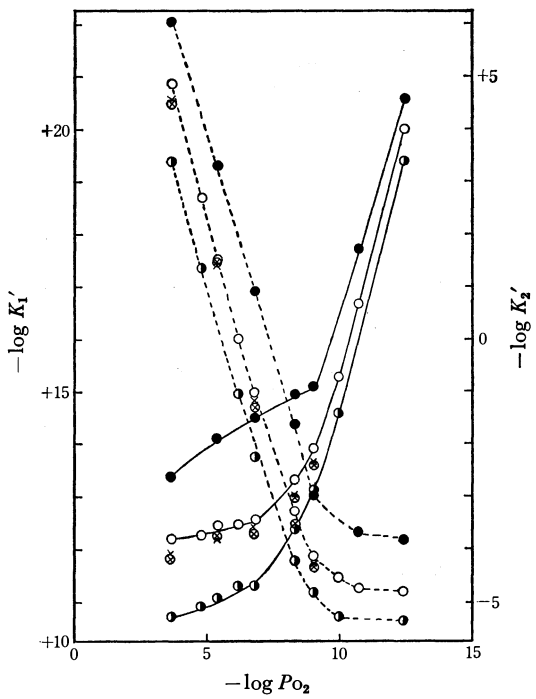

Fig. 4. Sulfate (K_1')(——) and sulfide (K_2')(——) equilibrium constants as a function of oxygen partial pressure for Na_2O–SiO_2 melts at 1250 °C.

(2) Relationship between the Solubility of Total Sulfur and the Partial Pressures of the Sulfur Compounds: The relationship between the solubility of sulfur in the melts and the calculated partial pressures of various sulfur compounds in the gas phase was examined. Figs. 5-(1) and -(2) show the relationship between the total sulfur content of the melts, and P_{SO_3} and P_{H_2S}, respectively. The number in parentheses placed close to each individual point indicates the value of $-\log P_{O_2}$. However, in order to avoid illegibility, the values are omitted at some points in the figures.

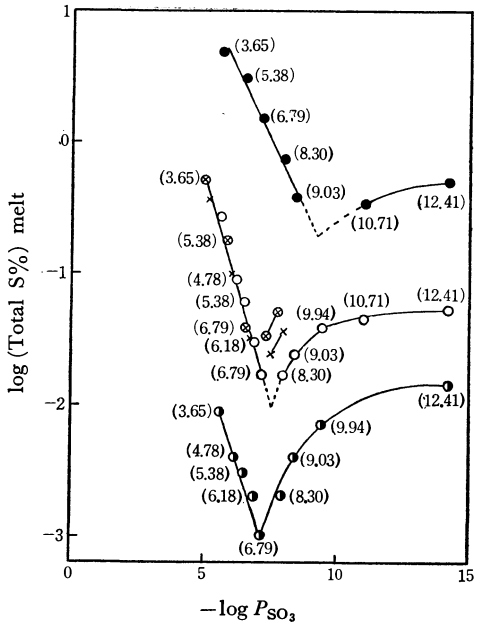

Fig. 5(1). Variation of sulfur content of Na_2O–SiO_2 melts with P_{SO_3} at 1250 °C.

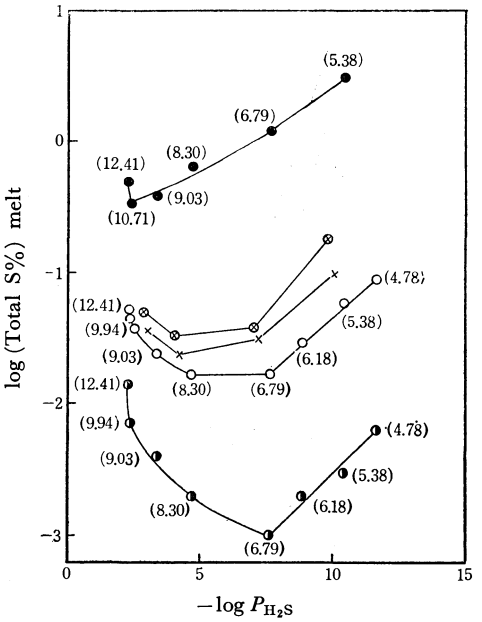

Fig. 5(2). Variation of sulfur content of Na_2O–SiO_2 melts with P_{H_2S} at 1250 °C.

As may be seen in Fig. 5-(1), the total sulfur content of a melt increases with an increase in P_{SO_3} at relatively high oxygen partial pressures; this relation may be expressed as a linear equation as follows:

$$\log (\%\ S)_{melt} = k_1 + (0.7 \sim 0.75) \times \log P_{SO_3} \qquad (3),$$

where k_1 is constant and where Equation (3) is applicable in the range above 10^{-9} atm P_{O_2} when the Na_2O/SiO_2 ratio is 1/1 and in the range above $10^{-6.8}$ atm P_{O_2} when the Na_2O/SiO_2 ratios are 1/2 and 1/3. These results support the idea that the sulfur dissolves mainly as sulfate at high oxygen partial pressures. On the other hand, as is shown in Fig. 5-(2), the total sulfur content of a melt increases with an increase in P_{H_2S} at relatively low oxygen partial pressures, though we can not obtain a simple equation such as has just been obtained at relatively high oxygen partial pressures. However, this trend may also support the idea that the total sulfur may dissolve mainly as sulfide at low oxygen partial pressures.

The relationships between the solubility of sulfur and the sulfur compounds in the gas phase other than SO_3 and H_2S were also examined, but the relationships showed significant discrepancies in all cases from the general rules expected thermodynamically.

(3) Determination of Sulfide- and Sulfate-Sulfur in Melts: One of the most direct and definite methods to distinguish the state of dissolved sulfur in a melt is to chemically analyze the sulfide- and sulfate-sulfur separately. The method of determining sulfide and sulfate has been established, as has been mentioned before.[7] Here, in Table 1 we show some analytical results in the case of the $Na_2O/SiO_2=1/2$.

As may clearly be seen in Table 1, the total sulfur is mostly in the form of sulfate at higher oxygen partial pressures (above $10^{-6.8}$ atm P_{O_2}). On the other hand, at lower oxygen partial pressures (below 10^{-9} atm P_{O_2}), the total sulfur is mostly in the form of sulfide.

TABLE 1. SULFIDE- AND SULFATE-SULFUR CONTENT OF Na_2O–SiO_2 (1:2) MELTS AT 1250°C

$(SO_2)_I$: 0.5% (0.03 cc/sec)					
$(CO_2)_I$ (cc/s)	$(H_2)_I$	$-\log P_{O_2}$ (calcd.)	Total-S	Sulfide-S	Sulfate-S
6	0	3.65	0.27	<0.001	0.27
	0.02	5.38	0.060	<0.001	0.060
	0.1	6.79	0.017	0.001	0.016
5.5	0.5	8.30	0.017	0.008	0.009
5	1	9.03	0.024	0.021	0.003
3	3	10.71	0.044	0.042	0.002
1	5	12.41	0.053	0.052	0.001

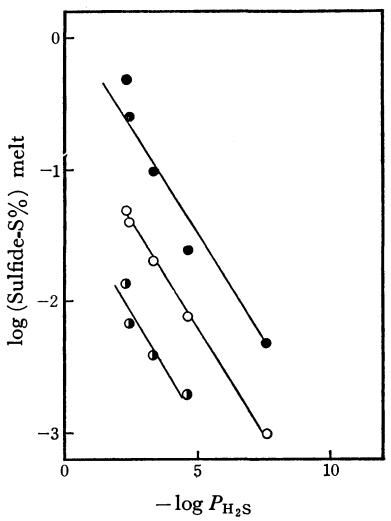

Fig. 6. Variation of sulfide-sulfur content of Na_2O-SiO_2 melts with P_{H_2S} at 1250 °C.

Fig. 6 shows the relationship between the analyzed sulfide-sulfur content in the melts and P_{H_2S}. As may be seen in Fig. 6, the sulfide-sulfur content increases almost linearly with an increase in P_{H_2S}, leading to the

following equation:

$$\log (\%\ S)_{melt} = k_2 + 0.3 \times \log P_{H_2S},$$

where k_2 is constant.

This fact proves the thermodynamic prediction that sulfur should dissolve in the form of sulfide when the melt was at relatively low oxygen partial pressures.

Effect of the Temperature on the Solubility of Sulfur. Figure 7 shows the relationship between the sulfur content of the sodium silicate melts and the oxygen partial pressure at 0.5% of $(SO_2)_I$ and at 1250 and 1300 °C. As may be seen in Fig. 7, the minimum point of the solubility moves in the direction of higher oxygen partial pressures as the temperature increases. Fig. 7 indicates that the increase in the solubility of the total sulfur does not necessarily correspond to the temperature change. This is because the partial pressure of each sulfur compound varies according to the temperature change. The experimental results at 1100 °C were complicated, since the gas phase was not in the chemical equilibrium state. However, in some experiments at 1100 °C, *i.e.*, under the conditions of $(CO_2)_I$: 6 cc/s and $(SO_2)_I$: 0.03 cc/s, the measured oxygen partial pressure showed a good agreement with the calculated value [P_{O_2}(obsd) $= 10^{-4.33}$ atm, P_{O_2}(calcd) $= 10^{-4.35}$ atm], and the results corresponded reasonably to the experiments at 1250 and 1300 °C, *i.e.*, under the conditions of $(CO_2)_I$: 6 cc/s and (SO_2): 0.03 cc/s. At these three temperatures, P_{SO_2} and P_{SO_3} were nearly the same and were calculated to be $10^{-2.3}$ atm and $10^{-5.6}$ atm respectively. In Fig. 8, the sulfate content in each melt is plotted against $1/T$, where T is the absolute temperature. This shows that the solubility of the sulfate decreases with an increase in the temperature. Moreover, from Fig. 8, the following empirical equations were obtained:

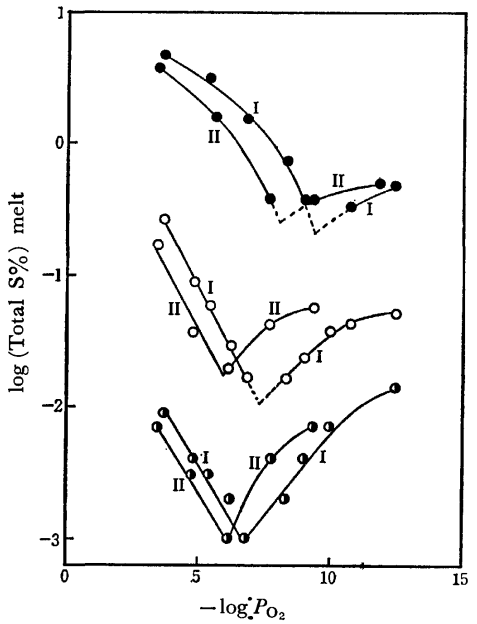

Fig. 7. Variation of sulfur content of Na_2O-SiO_2 melts with partial pressure of oxygen at 1250 °C and 1300 °C and at 0.5% of $(SO_2)_I$. I at 1250 °C, II at 1300 °C.

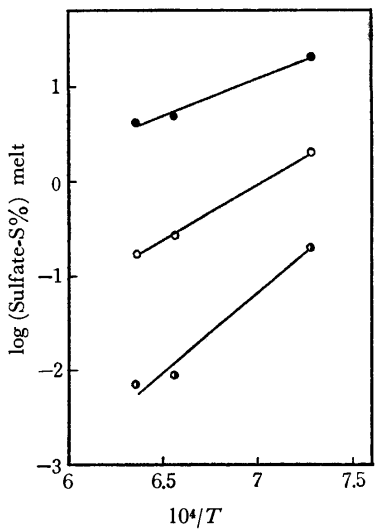

Fig. 8. Change of sulfate-solubility with temperature. [$(CO_2)_I$: 6 cc/sec, $(SO_2)_I$: 0.03 cc/s]

$$\log (\%S)_{melt} = 0.76 \times \frac{10^4}{T} - 4.2$$

for Na_2O-SiO_2 (1:1) melt

$$\log (\%S)_{melt} = 1.16 \times \frac{10^4}{T} - 8.1$$

for Na_2O-SiO_2 (1:2) melt

$$\log (\%S)_{melt} = 1.74 \times \frac{10^4}{T} - 13.4$$

for Na_2O-SiO_2 (1:3) melt

The change in solubility with the temperature can be written as in following equation[14]: $R \ln a = \bar{L}/T +$ constant, where R is the gas constant, a is the activity of solute, and $\bar{L}$ is the relative partial molal enthalpy of a solution. When this equation is compared with the above three ones, it is found that the relative partial molal enthalpies have positive values. However, the change in the solubility of sulfur in the form of sulfide with the temperature is complicated, and it was impossible to obtain a simple relation similar to that obtained above for the sulfate solubility.

The authors wish to thank Dr. Hisajiro Osada of the Tokyo Institute of Technology for his help in calculating the partial pressures of gaseous species. The authors also wish to thank Dr. Takejiro Ozawa and Mr. Kenzo Kitayama of the Tokyo Institute of Technology for their encouragement and many discussions during this study.

14) G. N. Lewis and M. Randall, "Thermodynamics," revised by K. S. Pitzer and L. Brewer, McGraw-Hill, New York (1961), p. 393.

Stereoselectivity in Mixed Tris-type Complexes of Cobalt(III) with L-Proline and L- or D-Aspartic Acid[1]

Toshitsugu MATSUDA and Muraji SHIBATA

Department of Chemistry, Faculty of Science, Kanazawa University, Kanazawa 920

(Received March 22, 1973)

Mixed complexes with L-proline and L- or D-aspartic acid, $[Co(L\text{-pro})_{3-n}(L\text{-(or D-)asp})_n]^{n-}$ (n=1,2), have been prepared and separated into a number of stereoisomers by means of ion-exchange chromatography. The structures of the isomers have been characterized by various spectral data. As to the $[Co(L\text{-pro})(D\text{-asp})_2]^{2-}$ and $[Co(L\text{-pro})_2(D\text{-asp})]^{-}$ complexes, all of three possible *mer*-isomers have been isolated in their Δ-forms. The formation ratios among the isomeric species in the reaction system have been estimated spectrophotometrically. Marked differences in stereoselectivity have been found between the L-aspartato complexes and the corresponding D-aspartato complexes. These selectivities have been qualitatively explained in terms of the interaction between the dangling β-carboxylate group in a chelated aspartate ion and the adjacent ligand.

Through several experiments on the stereoselectivity in mixed-ligand complexes of cobalt(III) containing L-aspartic acid as a bidentate ligand, we have isolated a number of complexes and ascertained their stereoselective formations in various degrees.[2-5] In comparison with these aspartato complexes, the mixed complexes containing L-glutamic acid have also been investigated.[6] On the other hand, Denning and Piper[7] have obtained three of the four possible isomers of tris(L-prolinato)cobalt(III) in different yields; they have said that the absence of one isomer (*i.e.*, *mer*-Λ) is predictable on steric grounds. Yasui *et al.*[8] have obtained only one isomer (*i. e.*, *fac*-Λ), consistent with the consideration of the molecular models.

Thus, in the present work L- or D-aspartic acid and L-proline were chosen as the ligands. That is, two series of complexes, $[Co(L\text{-pro})_{3-n}(L\text{-asp})_n]^{n-}$ and $[Co(L\text{-pro})_{3-n}(D\text{-asp})_n]^{n-}$ (n=1,2), have been prepared, and their diastereoisomers have been isolated. These isomers have been characterized on the basis of the spectral data; the degree of the stereoselectivity has also been evaluated spectrometrically.

Experimental

Preparations. Freshly prepared (7.2 g, 0.02 mol) sodium tricarbonatocobaltate(III) trihydrate[9] and 4.6 g (0.04 mol) of L-proline were dissolved in 50 ml of water; the mixture was then stirred at 60 °C for 2 hr, whereupon the solution became blue-violet in color. Then, 4.0 g (0.03 mol) of L-aspartic acid was added to the above solution. After activated charcoal (1.0 g) had then been added, the reaction mixture was stirred for an additional 3 hr at 60 °C; the solution turned red-violet, and a small amount of a water-insoluble material was precipitated. After the removal of the precipitates and charcoal by filtration, the filtrate was passed through a column containing a cation-exchange resin in hydrogen form (Dowex 50W-X8, 100—200 mesh). By this treatment, the coexisting $[CoCO_3(L\text{-pro})_2]^{-}$ species was converted to a cationic species, which was adsorbed on the column. The effluent was adjusted to pH ~8.5 with an aqueous solution of sodium hydroxide. The resulting solution was charged on an anion-exchange resin column containing 100—200 mesh Dowex 1-X8 in chloride form (column diameter, 7.0 cm; resin height, 45 cm). The same experiment was then carried out using D-aspartic acid instead of L-aspartic acid.

When water was passed through the column, a non-charged tris(L-prolinato)cobalt(III) complex flowed out. Then, chromatographic separation was carried out with a $CaCl_2$ solution (prepared initially in 0.03 M and finally in 0.05 M) at the rate of *ca.* 0.5 ml/min. Through the prolonged elutions, five bands for the L-aspartato-L-prolinato series complexes and ten bands for the D-aspartato-L-prolinato series complexes were separated. These eluted bands were collected in fractions and labeled from L-1 to L-5 for the L-aspartato complexes and from D-1 to D-10 for the D-aspartato complexes, according to the elution order. The four fractions of L-1, L-3, D-5 and D-10 were colored red, and the other fractions, violet. Except the L-2, L-5 and D-4 fractions, each of the other fraction was concentrated to a small volume under reduced pressure at a temperature below 35 °C. Ethanol was added to the concentrate to precipitate calcium salt of the desired isomer. This crude salt was dissolved in a small amount of water, and then the solution was passed through a column containing Dowex 50W-X8 resin in hydrogen form. By this chromatographic procedure, each salt obtained from the L-3 and D-3 fractions was separated into two bands, alternately colored violet and red. These were again labeled as L-3′ and L-3″, and as D-3′ and D-3″. All the effluents thus obtained were evaporated to dryness at 35 °C, and the following procedures were employed. Each residue of the D-2, D-3′, D-5, D-7, and D-8 fractions was dissolved in a minimum amount of water, and acetone was added. After that, the solution was kept in an ice-box for several days to crystallize a hydrogen compound of each isomer. On the other hand, each residue of the L-1, L-3″, D-1, D-3″, D-6, D-9, and D-10 fractions was dissolved in an aqueous solution slightly alkalined with a Na_2CO_3 solution; the solution was then acidified with aqueous hydrochloric acid to precipitate the desired isomer as the hydrogen compound. Each residue obtained from the L-3′ and L-4 fractions was dissolved in a minimum amount of water, after which the solution was passed again through a Dowex 50W-X8 column in hydrogen form. The effluent was evaporated

1) Presented at the 22nd Symposium on Coordination Chemistry, Osaka, November, 1972.
2) K. Kawasaki, J. Yoshii, and M. Shibata, This Bulletin, **43**, 3819 (1970).
3) T. Matsuda, T. Okumoto, and M. Shibata, *ibid.*, **45**, 802 (1972).
4) Y. Kojima and M. Shibata, *Inorg. Chem.*, **10**, 2382 (1971).
5) Y. Kojima and M. Shibata, *ibid.*, in press.
6) K. Kawasaki and M. Shibata, This Bulletin, **45**, 3100 (1972).
7) R. G. Denning and T. S. Piper, *Inorg. Chem.*, **5**, 1056 (1966).
8) T. Yasui, J. Hidaka, and Y. Shimura, This Bulletin, **38**, 2025 (1965).
9) H. F. Bauer and W. G. Drinkard, *J. Amer. Chem. Soc.*, **82**, 5031 (1960).

Table 1. Elemental analyses, absorption[a] and CD[a] spectral data

Label	Complex	Elemental anal., %[b] C	H	N	Band I $10^{-3}\nu_{max}$ cm^{-1}	ε_{max}	Band II $10^{-3}\nu_{max}$ cm^{-1}	ε_{max}	CD $10^{-3}\nu_{max}$ cm^{-1}	$\Delta\varepsilon_{max}$
L-1	*fac*-*Δ*-[Co(L-pro)$_2$ (L-aspH)]·2H$_2$O	37.03 (36.93)	6.09 (5.76)	8.88 (9.23)	19.19	118	26.52	126	18.08	−1.63
L-2	*mer*-*Δ*-Ca$_{1/2}$[Co(L-pro)$_2$ (L-asp)]·0.5 H$_2$O	37.60 (37.59)	5.46 (4.96)	9.36 (9.39)	*ca.* 19.0	92	26.65	139	17.86	−2.25
L-3′	*mer*-1-*Δ*-[Co(L-pro) (L-aspH)$_2$]·1.5H$_2$O	33.85 (33.63)	4.98 (4.99)	9.25 (9.05)	*ca.* 18.8	105	26.74	157	18.52	−1.89
L-3″	*fac*-*Δ*-[Co(L-pro) (L-aspH)$_2$]·2H$_2$O	33.50 (32.99)	5.33 (5.11)	8.71 (8.88)	19.31	141	26.67	122	18.42	−1.71
L-4	*mer*-2-*Δ*-[Co(L-pro) (L-aspH)$_2$]·H$_2$O	34.42 (34.30)	4.95 (4.87)	9.23 (9.23)	*ca.* 18.9	126	26.80	183	18.28	−2.28
L-5	*mer*-*Δ*-[Co(L-pro) (L-aspH)$_2$]·0.5H$_2$O	35.00 (34.99)	5.16 (4.74)	9.34 (9.42)	*ca.* 18.7	128	26.93	186	19.12	+3.91
D-1	*mer*-*Δ*-[Co(L-pro)$_2$ (D-aspH)]·*n*H$_2$O[c]	—	—	—	*ca.* 18.9	—	26.67	—	19.27	+
D-2	*mer*-1-*Δ*-[Co(L-pro)$_2$ (D-aspH)]·0.5H$_2$O	39.22 (39.26)	5.98 (5.41)	9.92 (9.81)	*ca.* 18.7	115	26.60	175	18.21	−2.73
D-3′	*mer*-2-*Δ*-[Co(L-pro)$_2$ (D-aspH)]·H$_2$O	38.47 (38.45)	5.97 (5.53)	9.52 (9.61)	*ca.* 19.1	109	26.58	171	18.21	−2.97
D-3″	*fac*-*Δ*-[Co(L-pro)$_2$ (D-aspH)]·2H$_2$O	37.29 (36.93)	6.08 (5.76)	9.23 (9.23)	19.16	125	16.53	141	18.18	−1.57
D-4	*mer*-3-*Δ*-Ca$_{1/2}$[Co(L-pro)$_2$ (D-aspH)]·4H$_2$O	33.00 (32.94)	6.18 (5.73)	8.28 (8.23)	*ca.* 18.6	110	26.52	169	17.86	−1.93
D-5	*fac*-*Δ*-[Co(L-pro)$_2$ (D-aspH)]·*n*H$_2$O[c]	—	—	—	18.87	—	26.39	—	18.38	+
D-6	*mer*-1-*Δ*-[Co(L-pro) (D-aspH)$_2$]·0.5H$_2$O	35.51 (34.99)	4.96 (4.74)	9.07 (9.42)	*ca.* 18.5	104	26.81	155	18.98	−2.42
D-7	*mer*-*Δ*-[Co(L-pro) (D-aspH)$_2$]·2H$_2$O	32.95 (32.99)	5.20 (5.11)	9.24 (8.88)	*ca.* 18.9	120	26.88	205	18.98	+4.01
D-8	*mer*-2-*Δ*-[Co(L-pro) (D-aspH)$_2$]·2H$_2$O	33.38 (32.99)	5.54 (5.11)	8.58 (8.88)	*ca.* 18.8	110	26.88	160	18.80	−2.30
D-9	*mer*-3-*Δ*-[Co(L-pro) (D-aspH)$_2$]·1.5H$_2$O	33.54 (33.63)	5.34 (4.99)	8.84 (9.05)	*ca.* 18.8	112	26.67	169	18.48	−3.57
D-10	*fac*-*Δ*-[Co(L-pro) (D-aspH)$_2$]·H$_2$O	34.73 (34.30)	5.14 (4.87)	9.26 (9.23)	19.01	188	26.46	157	18.59	+2.24

a) Measured in 60% perchloric acid. b) ( ): calcd. c) Because of the poor yield, no elemental analyses were carried out.

to dryness at 30 °C. A violet, glassy material was thus obtained.

To the L–2 and D–4 fractions, acetone was added to precipitate calcium salts of the complexes. Attempts to isolate these isomers as hydrogen compounds were unsuccessful. The remaining fraction, L–5, was once concentrated to precipitate crude calcium salt, and the crude material was dissolved in 60% perchloric acid. When an aqueous NaOH solution was added to the solution drop by drop, the hydrogen compound of the complex began to precipitate.

The recrystallizations were repeated with all the compounds except those obtained from the L-3′ and L–4 fractions until their main CD peaks showed constant intensities. The results of the elemental analyses are summarized in Table 1.

Formation Ratios. From the spectral data of the fractions, the formation ratios among the bands separated chromatographically were evaluated. For some isomers not isolated as crystals, we assumed their ε values from the known ε values of the corresponding isomers (that is, 100 for the D–1 and 120 for the D–5).

Measurements. The absorption spectra were measured with a Hitachi Perkin-Elmer Model 139 UV-VIS spectrophotometer. The circular dichroism spectra were recorded on a JASCO Model ORD/UV-5 spectropolarimeter. The proton magnetic resonance spectra were recorded on a JEOL Model C–60H spectrometer at about 25 °C, using deuterium oxide containing an equivalent mole of Na_2CO_3 as the solvent. The values of the chemical shifts were referred to internal sodium 2,2-dimethyl-2-silapentane-5-sulfonate (DSS).

Results and Discussion

Characterization of the Isomers. From the results of the elemental analyses and the elution order, it was apparent that the compounds obtained from the L–1 and L–2 fractions were the isomers of the bis(L-prolinato)L-aspartatocobaltate(III) complex, while the compounds obtained from the L–3′, L–3″, L–4, and L–5 fractions were the isomers of the L-prolinatobis(L-aspartato)cobaltate(III) complex. Likewise, for the D-aspartato complexes, it was apparent that the compounds obtained from the D–1∼D–5 fractions were the isomers of the bis(L-prolinato)D-aspartatocobaltate(III) complex, and that the compounds from the D–6∼D–10 fractions were the isomers of L-prolinatobis(D-aspartato)cobaltate(III), although for the compounds from the D–1 and D–5 fractions we have no results of elemental analyses because of their extremely poor yields. The geometrical form (*mer* or *fac*) of each compound could easily be identified on the basis

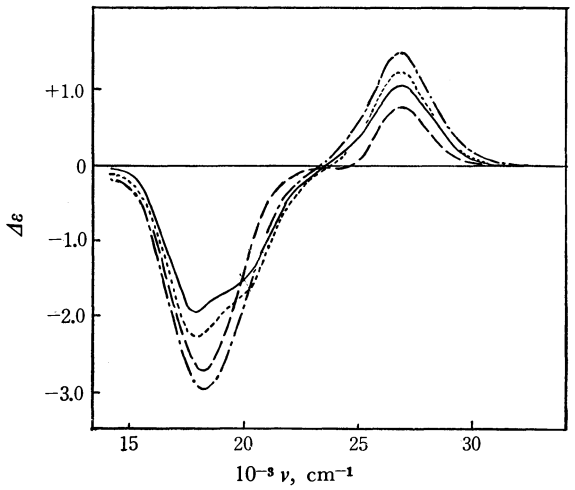

Fig. 1. CD spectra of *mer*-[Co(L-pro)$_2$(aspH)] in 60% $HClO_4$
····· *mer*-*Δ*-$Ca_{1/2}$[Co(L-pro)]$_2$(L-asp)]
– – *mer*-1-*Δ*-[Co(L-pro)$_2$(D-aspH)]
—·— *mer*-2-*Δ*-[Co(L-pro)$_2$(D-aspH)]
—— *mer*-3-*Δ*-$Ca_{1/2}$[Co(L-pro)$_2$(D-asp)]

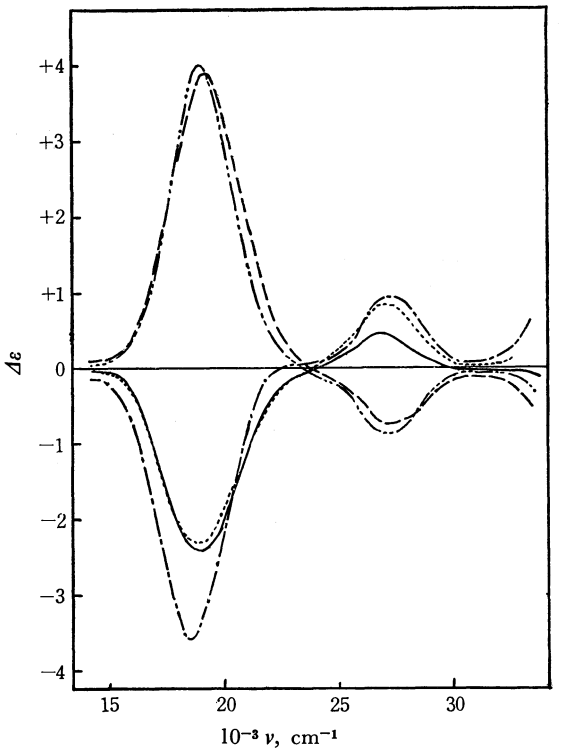

Fig. 2. CD spectra of *mer*-[Co(L-pro)(aspH)$_2$] in 60% $HClO_4$
– – – *mer*-*Δ*-[Co(L-pro)(L-aspH)$_2$]
—·— *mer*-*Δ*-[Co(L-pro)(D-aspH)$_2$]
—— *mer*-1-*Δ*-[Co(L-pro)(D-aspH)$_2$]
····· *mer*-2-*Δ*-[Co(L-pro)(D-aspH)$_2$]
—·— *mer*-3-*Δ*-[Co(L-pro)(D-aspH)$_2$]

of its absorption spectrum; the violet compounds could be identified as *mer* forms, and the red ones, as *fac* forms. The absorption spectral data in 60% perchloric acid are given in Table 1. The absolute configurations of the isomers were determined from the signs of the main CD peaks in the first absorption band region. The CD spectra of the isolated compounds

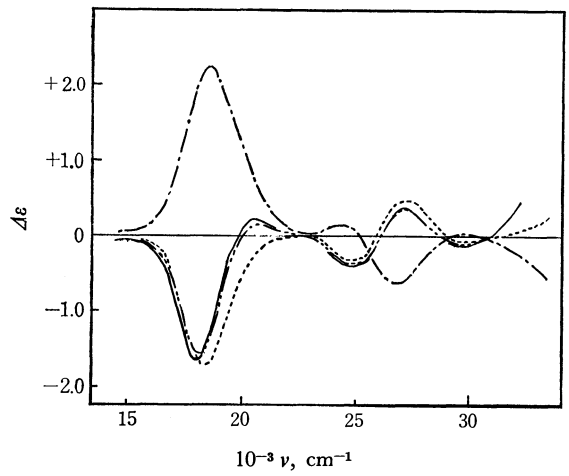

Fig. 3. CD spectra of *fac* isomers in 60% $HClO_4$
—— *fac*-*Δ*-[Co(L-pro)$_2$(L-aspH)]
—·— *fac*-*Δ*-[Co(L-pro)$_2$(D-aspH)]
····· *fac*-*Δ*-[Co(L-pro)(L-aspH)$_2$]
—·— *fac*-*Δ*-[Co(L-pro)(D-aspH)$_2$]

are shown in Figs. 1—3.

Through the experiments, an interesting fact has been found with regard to the elution order; for the D-aspartato complexes, the *mer* isomers were eluted earlier than the corresponding *fac* ones. This was a general trend in geometrical isomers of a complex. However, for the L-aspartato complexes, the *fac* isomers were eluted earlier than the corresponding *mer* ones.

Structure of mer *Isomers.* In a tris-chelated complex with two kinds of α-aminoacidato ligands, three geometrical isomers are possible for the *mer* form (Fig. 4). In our previous works,[3,6] at least two isomers among the three have been found. In the present work, three isomers were separated for the *mer*-*Δ*-[Co(L-pro)(D-asp)$_2$]$^{2-}$ species. For the sake of convenience, these will be labeled *mer*-1-*Δ*, *mer*-2-*Δ*, and *mer*-3-*Δ*, according to the elution order. The absorption spectra of these isomers are shown in Fig. 5. These spectra, as well as the CD spectra (Fig. 2), exhibit different shapes among the three isomers.

With the *mer*-[Co(L-pro)(L-asp)$_2$]$^{2-}$ complex, only one isomer of the *Δ* form was isolated (see Table 2), and no other two isomers of the same form were detected. The molecular models for the three possible isomers of this *Δ* form indicate that a certain steric interaction exists between a pyrrolidine ring of the chelated L-prolinate ion and a side-chain of a chelated L-aspartate in the geometry of each *cis*(N)*cis*(O) and *trans*(N)*cis*(O), while no such interaction exists in the geometry of *cis*(N)*trans*(O). From these facts, it may

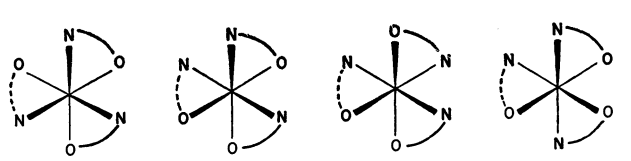

fac *cis*(N)*cis*(O) *cis*(N)*trans*(O) *trans*(N)*cis*(O)
mer

Fig. 4. Possible geometrical isomers.

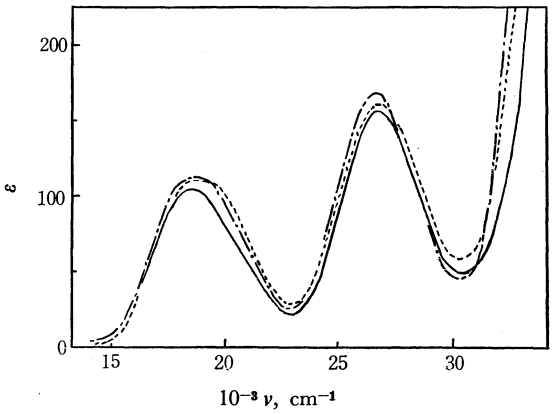

Fig. 5. Absorption spectra of three isomers of *mer*-*Δ*-[Co(L-pro)(D-aspH)$_2$] in 60% $HClO_4$
—— *mer*-1-*Δ* isomer
····· *mer*-2-*Δ* isomer
—·— *mer*-3-*Δ* isomer

be considered that formations of the isomers of both *cis*(N)*cis*(O) and *trans*(N)*cis*(O) will be less favored than that of the isomer of *cis*(N)*trans*(O). This consideration leads to the conclusion that the *mer*-*Λ*-[Co(L-pro)-(L-aspH)$_2$] complex, in which only one *Λ*-isomer is isolated, has the *cis*(N)*trans*(O) structure.

The PMR spectra concerning the methylene proton signals due to the coordinated aspartate ions in the bis(aspartato) complexes are shown in Fig. 6. Each spectrum is characteristic of each isomer. For the CH_2 signal of an aspartate ion, the AB portion of a ABX pattern is expected, and the separation width of the appeared doublet is represented by the expression of $(J_{AX}+J_{BX})/2$.[10] Moreover, since the vicinal coupling constant depends on the dihedral angle,[11] it is considered that the width of the doublet reflects the orientation of the side-chain of the coordinated aspartate. From this point of view, it is considered that two side-chains of the aspartate ions in the *mer*-1-*Δ* isomer are oriented differently, for considerably different widths are observed (Fig. 6(a)). Separately, measurements with the *fac*-[Co(L-asp)$_3$]$^{3-}$ complexes gave different spectra between the *Δ* and *Λ* isomers

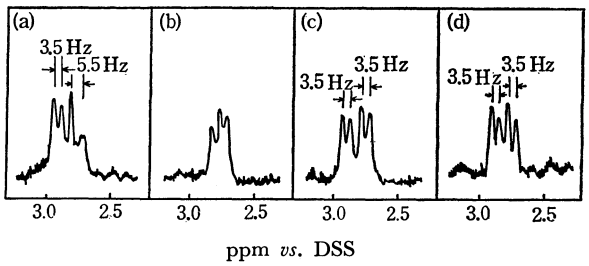

Fig. 6. PMR spectra of [Co(L-pro)(asp)$_2$]$^{2-}$ in D_2O (pD ~7), (methylene proton resonance of aspartate ion)
(a) *mer*-1-*Δ*-[Co(L-pro)(D-asp)$_2$]$^{2-}$
(b) *mer*-2-*Δ*-[Co(L-pro)(D-asp)$_2$]$^{2-}$
(c) *mer*-3-*Δ*-[Co(L-pro)(D-asp)$_2$]$^{2-}$
(d) *mer*-*Λ*-[Co(L-pro)(L-asp)$_2$]$^{2-}$

10) J. W. Emsley, J. Feeney, and L. H. Sutcliffe, "High Resolution Nuclear Magnetic Resonance Spectroscopy," Pergamon Press, London (1965), p. 357.
11) M. Karplus, *J. Amer. Chem. Soc.*, **85**, 2870 (1963).

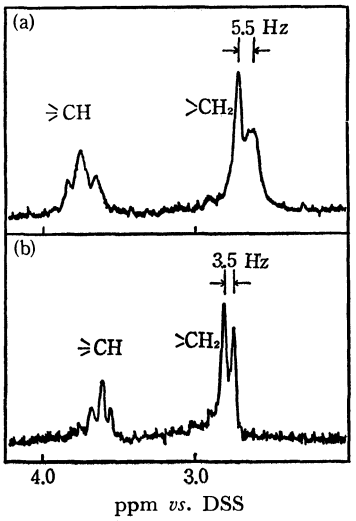

Fig. 7. PMR spectra of *fac*-[Co(L-asp)$_3$]$^{3-}$ in D_2O (pD ~8)
(a) *fac*-*Λ* isomer (b) *fac*-*Δ* isomer

(Fig. 7); the *Λ* isomer exhibits a more separated doublet than the *Δ* isomer. This fact means that the orientations of the aspartate side-chain will be affected by the interactions of the *β*-carboxylate groups with adjacent ligands. Thus, it is considered on the basis of a comparison of the spectra (c) and (d) in Fig. 6 that the *mer*-3-*Δ* isomer of the bis(D-aspartato) complex and the *mer*-*Λ* isomer of the bis(L-aspartato) complex have the same geometry, *cis*(N)*trans*(O). In this geometry, both *β*-carboxylate groups in an isomer are able to interact equally with the adjacent NH_2 groups, while in the other geometries one *β*-carboxylate interacts with the NH_2 group and the other *β*-carboxylate, with adjacent carboxylate group. The structural assignments of the other *mer*-1-*Δ* and *mer*-2-*Δ* complexes are difficult at present. For the [Co(L-pro)$_2$(D-asp)]$^-$ complex, three *mer*-*Δ* isomers have been isolated, but their geometrical assignments are also difficult.

Absorption and CD Spectra. Figure 8 shows the absorption spectra of the *fac*-*Δ*-[Co(L-pro)$_{3-n}$(L-aspH)$_n$]

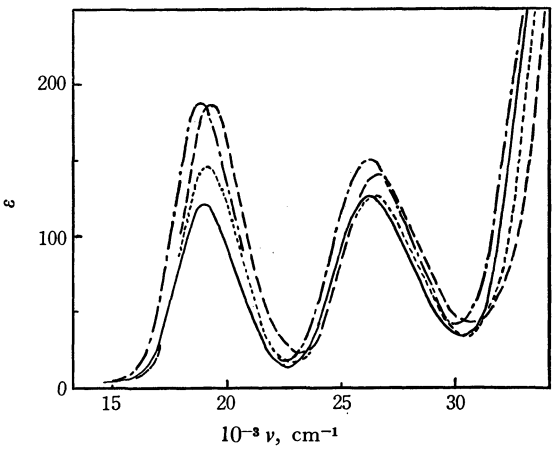

Fig. 8. Absorption spectra of *fac*-[Co(L-pro)$_{3-n}$(aspH)$_n$] in 60% $HClO_4$
—— *fac*-*Δ*-[Co(L-aspH)$_3$]
····· *fac*-*Δ*-[Co(L-pro)(L-aspH)$_2$]
—— *fac*-*Δ*-[Co(L-pro)$_2$(L-aspH)]
=:=: *fac*-*Λ*-[Co(L-pro)(D-aspH)$_2$]

TABLE 2. FORMATION RATIOS

n	Label	Isomer	Ratio
a) $[Co(L\text{-pro})_{3-n}(L\text{-asp})_n]^{n-}$			
1	L-1	*fac*-Δ	4
	L-2	*mer*-Δ	14
2	L-3'	*mer*-1-Δ	1
	L-3''	*fac*-Δ	5
	L-4	*mer*-2-Δ	1
	L-5	*mer*-Λ	8
b) $[Co(L\text{-pro})_{3-n}(D\text{-asp})_n]^{n-}$			
1	D-1	(*mer*-Λ)[a]	1
	D-2	*mer*-1-Δ	8
	D-3'	*mer*-2-Δ	52
	D-3''	*fac*-Δ	1
	D-4	*mer*-3-Δ	8
	D-5	(*fac*-Λ)[a]	1
2	D-6	*mer*-1-Δ	3
	D-7	*mer*-Λ	2
	D-8	*mer*-2-Δ	4
	D-9	*mer*-3-Δ	28
	D-10	*fac*-Λ	8

a) No analyses.

(n=1,2,3) and *fac*-Λ-$[Co(L\text{-pro})(D\text{-aspH})_2]$ complexes. In the L-aspartato complex species, both the first and second absorption bands show bathochromic shifts with an increase in the number of the chelated proline, as is to be expected from a weaker ligand field of a secondary amine group than that of primary amine. Moreover, the differences in the absorption and CD spectral data (Table 1) among the three *mer*-Δ isomers of the $[Co(L\text{-pro})(D\text{-aspH})_2]$ complex seem to be attributable mainly to a weaker ligand field of secondary amine group of proline. It is interesting that the absorption maxima of the *fac*-Λ-$[Co(L\text{-pro})(D\text{-aspH})_2]$ (D–10) complex are observed at a lower energy than the maxima of the *fac*-Δ-$[Co(L\text{-pro})(L\text{-aspH})_2]$ (L–3'') complex. The former complex differs from the latter merely in the orientation of the pyrrolidine ring of the chelated proline, since the mirror image of the *fac*-Λ-$[Co(L\text{-pro})(D\text{-asp})_2]^{2-}$ is the *fac*-Δ-$[Co(D\text{-pro})(L\text{-asp})_2]^{2-}$.

Stereoselectivity. Each fraction separated chromatographically showed distinctly a plus or a minus CD sign in the first absorption-band region. With each fraction, the ratio of the observed intensity of the main CD peak to the absorbance at the Band I maximum was estimated. On the other hand, the ratio of the $\Delta\varepsilon_{max}$ to the ε_{max} of Band I was estimated with each complex isolated. When the former ratio was divided by the latter, the quotient was within 0.8~1 in all the fractions. Since this fact indicated that only one isomer predominated in each fraction, the minor species were ignored in evaluating the formation ratios. The results are given in Table 2.

In the bis(L-aspartato) complex species, the selective formation of the Δ isomer is found for the *fac* form, while the selective formation of the Λ isomer is found for the *mer* form. In the bis(D-aspartato) complex species, the Λ isomer for the *fac* form and the Δ isomer for the *mer* are found preferentially. The *fac*/*mer* ratios have been estimated as *ca.* 1/2 and 1/4.6 for the bis(L-aspartato) and the bis(D-aspartato) complex species respectively.

In the bis(L-prolinato) species, remarkable differences in selectivity occur depending upon the optical form of the chelated aspartate ion (*i.e.*, L or D). The L-aspartato complex species exhibit preferential formations of Δ isomers for both the *fac* and *mer* forms. The *fac*/*mer* ratio is estimated as 1/3.5. On the other hand, the D-aspartato complex species exhibit a preferential formation of the Δ isomer for the *mer* form, while no preferential formation is observed in the *fac* form, and the formation amounts themselves are very poor; the *fac*/*mer* ratio is estimated to be *ca.* 1/35, indicating serious inter-ligand interactions.

Until now, the selectivity in the mixed L-aspartato complexes with other amino acids[2,3] or diamines[4,5] has been interpreted in terms of hydrogen-bonding between the β-carboxylate group of the chelated L-aspartate ion and the amino group in the adjacent ligand. The stereoselectivity observed in this study can also be interpreted in this way. The interactions between the side-chain of an aspartate ion and the adjacent ligand can now be classified into the following four types from the stereo models: (A) a favorable interaction through a hydrogen bond, in which the apical position (a) in Fig. 9 is occupied by an amino group; (B) an electrostatic repulsive interaction between the β-carboxylate group and the chelated oxygen atom occupying the apical position (a); (C) some interactions of the side-chain with the pyrrolidine ring of the chelated proline, in which hydrogen-bonding is not favorable because of the existence of the pyrrolidine ring; (D) a marked steric crowding

TABLE 3. INTERACTION OF THE SIDE-CHAIN OF COORDINATED ASPARTATE

Complex \ Isomer	Config.	*fac*	*mer*		
			cis(N)*cis*(O)	*cis*(N)*trans*(O)	*trans*(N)*cis*(O)
$Co(L\text{-pro})_2(L\text{-asp})^-$	Δ	A	B	B	A
	Λ	B	D	B(X)	D
$Co(L\text{-pro})(L\text{-asp})_2^{2-}$	Δ	A A	A B	A B	B B
	Λ	B B	B D	A A	B D
$Co(L\text{-pro})_2(D\text{-asp})^-$	Δ	B	A	B	A
	Λ	C	B	B(X)	C
$Co(L\text{-pro})(D\text{-asp})_2^{2-}$	Δ	B B	A B	A A	A B
	Λ	A C	A B	B C	B B

A: polar interaction with the amino group in the adjacent ligand. B: polar interaction with the carboxylate group in the adjacent ligand. C: some interaction with the pyrrolidine ring. D: steric interaction with the pyrrolidine ring. X: steric interaction between two pyrrolidine rings.

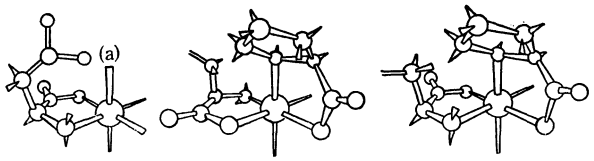

Fig. 9. Interactions of coordinated aspartate.

between the pyrrolidine ring and the side-chain of the chelated aspartate ion. These four types are drawn in Fig. 9. The relation between the types and the geometrical arrangements are given in Table 3. In this table, the symbol X expresses the existence of a steric hindrance between the two pyrrolidine rings.

Thus, the preferential formations of the Δ isomer in the *fac*-[Co(L-pro)(L-asp)$_2$]$^{2-}$ and of the Λ isomer in the *fac*-[Co(L-pro)(D-asp)$_2$]$^{2-}$ can be explained by the favorable interaction of Type A. The preference of the Δ isomers in the *mer*-[Co(L-pro)$_2$(D-asp)]$^-$ can also be explained in this way. The preferential formation of the Λ isomers in the *mer*-[Co(L-pro)$_2$(L-asp)]$^-$ can be explained by considering there to be less stability in the opposed Λ isomers containing the interactions of Types D and X. Moreover, the poorer formation of the *fac* isomers of the [Co(L-pro)$_2$(D-asp)]$^-$ complex than of the *mer* ones can be interpreted in terms of the lack of a favorable interaction of Type A.

This work was partially supported by a grant from the Ministry of Education.

BULLETIN OF THE CHEMICAL SOCIETY OF JAPAN, VOL. 46, 3109—3116 (1973)

Molecular Complexes of Arenetricarbonylchromium

Hiroshi KOBAYASHI, Mitaka KOBAYASHI, and Youkoh KAIZU

Department of Chemistry, Tokyo Institute of Technology, Ookayama, Meguro-ku, Tokyo 152

(Received April 11, 1973)

Arenetricarbonylchromium forms a charge-transfer molecular complex with electron acceptors such as 1,3,5-trinitrobenzene and tetracyanoethylene but not with electron donors such as *N,N,N′,N′*-tetramethyl-*p*-phenylenediamine. The ionization potentials of arenetricarbonylchromium complexes were determined from the charge-transfer transition energies in the molecular complexes. The molecular complexes are formed by a charge-transfer interaction of electron acceptor toward the π-coordinating benzene ring of arenetricarbonylchromium in the case of 1,3,5-trinitrobenzene, and by a charge-transfer toward the central chromium in the case of tetracyanoethylene.

Effects of the tricarbonylchromium group on the chemical properties of the π-coordinating benzene ring in arenetricarbonylchromium are more likely those of an electron-withdrawing group such as a para-nitro substituent. In fact, pK_a of phenylacetic acid coordinating to tricarbonylchromium is as high as that of *p*-nitrophenylacetic acid. Benzoic acid-tricarbonylchromium is an acid stronger than benzoic acid and anilinetricarbonylchromium is a base weaker than aniline.[1,2] Furthermore arenetricarbonylchromium complexes show a higher susceptibility to nucleophilic substitutions such as[1,3]

$$C_6H_5ClCr(CO)_3 \xrightarrow{NaOCH_3} C_6H_5OCH_3Cr(CO)_3$$

whereas the complexes are less susceptible to electrophilic substitutions such as Friedel-Crafts acylation.[4] This indicates an electron-withdrawing effect of tricarbonylchromium group. Larger dipole moments of arenetricarbonylchromium complexes might indicate a large charge-migration toward tricarbonylchromium.[5-7]

In the present work, arenetricarbonylchromium complexes were found to behave as electron donor rather than electron acceptor in charge-transfer molecular complex formation. Arenetricarbonylchromium forms molecular complexes with 1,3,5-trinitrobenzene (1,3,5-TNB) and tetracyanoethylene (TCNE) but not with *N,N,N′,N′*-tetramethyl-*p*-phenylenediamine (TMPD). Bis-π-benzenechromium, however, forms a 1 : 1 salt-like molecular complex with TCNE described as $[\pi\text{-}(C_6H_6)_2Cr]^+TCNE^-$.[8] Arenetricarbonylchromium is not so readily oxidized as bis-π-benzenechromium but a charge-transfer molecular complex formation of arenetricarbonylchromium with 1,3,5-TNB has been reported.[9-10] An X-ray crystallography study has revealed a geometry of "face to face" contact of the counterpart benzene rings in a molecular complex of anisoletricarbonylchromium and 1,3,5-TNB.[11] We have obtained the ionization potentials of arenetricarbonylchromium complexes from the charge-transfer transition energies in the molecular complexes of

1) B. Nicholls and M. C. Whiting, *J. Chem. Soc.*, **1959**, 551.
2) E. O. Fischer, K. Öfele, H. Essler, W. Fröhlich, J. P. Mortensen, and W. Semmlinger, *Chem. Ber.*, **91**, 2763 (1958).
3) D. A. Brown and J. R. Raju, *J. Chem. Soc. A*, **1966**, 40.
4) R. Riemschneider, O. Becker, and K. Franz, *Monatsh. Chem.*, **90**, 571 (1959).
5) E. W. Randall and L. E. Sutton, *Proc. Chem. Soc.*, **1959**, 93.
6) E. O. Fischer and S. Schreiner, *Chem. Ber.*, **92**, 938 (1959).
7) W. Strohmeier and H. Hellmann, *Ber. Bunsenges. Physik. Chem.*, **68**, 481 (1964).
8) J. W. Fitch, III and J. J. Lagowski, *Inorg. Chem.*, **4**, 864 (1965).
9) G. Huttner, E. O. Fischer, R. D. Fischer, O. L. Carter, A. T. McPhail, and G. A. Sim, *J. Organometal. Chem.*, **6**, 288 (1966).
10) J. W. Fitch, III and J. J. Lagowski, *ibid.*, **5**, 480 (1966).
11) O. L. Carter, A. T. McPhail, and G. A. Sim, *J. Chem. Soc., A*, **1966**, 822.

TABLE 1. ANALYSES OF ARENETRICARBONYLCHROMIUM COMPLEXES

Complexes	Found (%)				Calcd (%)			
	C	H	N	Cr	C	H	N	Cr
$C_6H_5COOHCr(CO)_3$	46.3	2.2		20.1	46.5	2.3		20.1
$C_6H_5COCH_3Cr(CO)_3$	51.2	3.0		20.4	51.5	3.1		20.3
$C_6H_5FCr(CO)_3$	—	—		22.0	46.6	2.2		22.4
$C_6H_5ClCr(CO)_3$	43.8	2.2		20.9	43.5	2.0		20.9
$C_6H_6Cr(CO)_3$	51.0	2.9		24.2	50.5	2.8		24.3
$C_6H_5CH_3Cr(CO)_3$	52.2	3.3		22.5	52.6	3.5		22.8
$C_6H_5OCH_3Cr(CO)_3$	49.0	3.3		21.2	49.2	3.3		21.3
o-$C_6H_4(CH_3)_2Cr(CO)_3$	55.3	4.6		21.2	54.5	4.2		21.5
m-$C_6H_4(CH_3)_2Cr(CO)_3$	55.5	4.3		21.5	54.5	4.2		21.5
p-$C_6H_4(CH_3)_2Cr(CO)_3$	54.8	4.2		21.5	54.5	4.2		21.5
1,3,5-$C_6H_3(CH_3)_3Cr(CO)_3$	55.9	4.7		20.4	56.2	4.7		20.3
$C_6H_5N(CH_3)_2Cr(CO)_3$	51.0	4.3	5.5	20.3	51.4	4.3	5.5	20.2

arenetricarbonylchromium with TCNE or 1,3,5-TNB.

Experimental

Materials. Arenetricarbonylchromium complexes were prepared according to the methods in the literature[1] by refluxing hexacarbonylchromium (High Pressure Chem. Co. Penn. U.S.A.) with the corresponding benzene derivatives under dry nitrogen atmosphere. For the arenes of low boiling point such as fluorobenzene, chlorobenzene, benzene, toluene, and acetophenone, diglyme was used as solvent. Solid benzoic acid was also dissolved in diglyme. The refluxed mixture was filtered, the filtrate being then condensed by vacuum distillation. The residue thus obtained was recrystallized from petroleum ether. The complexes were identified by elemental analysis (Table 1). Diglyme, petroleum ether and benzene derivatives used for the preparation of arenetricarbonylchromium complexes were dried and distilled by the usual methods.[12]

N,N,N',N'-Tetramethyl-*p*-phenylenediamine (TMPD) dihydrochloride (Tokyo Kasei Co.) was neutralized with NaOH and the free amine thus obtained was purified by vacuum distillation. 1,3,5-Trinitrobenzene (1,3,5-TNB, Tokyo Kasei Co.) was recrystallized from dil HNO_3 and then from ethanol. Tetracyanoethylene (TCNE, Tokyo Kasei Co.) was recrystallized from chlorobenzene.

Preparation of Molecular Complexes with 1,3,5-*Trinitrobenzene.* 150 mg of toluenetricarbonylchromium (tolueneCr$(CO)_3$) in 5 ml *n*-heptane and 70 mg of 1,3,5-TNB in 5 ml *n*-heptane were separately heated up to 80 °C and then mixed. When the solution was cooled, red crystals of a 1 : 1 molecular complex of tolueneCr$(CO)_3$ and 1,3,5-TNB were precipitated. The complex was repeatedly recrystallized from *n*-heptane. mp 85.5—86.0 °C (mp of tolueneCr$(CO)_3$: 80.0—81.0 °C; mp of 1,3,5-TNB: 123.0—123.5 °C).

Found: C, 43.0; H, 2.3; N, 10.1; Cr, 11.8%. Calcd for $C_{16}H_{11}N_3O_9Cr$: C, 43.5; H, 2.5; N, 9.5; Cr, 11.8%. Chromium was determined by colorimetry after carbonate fusion.

The 1 : 1 1,3,5-TNB molecular complexes of *o*-xyleneCr$(CO)_3$, *N,N*-dimethylanilineCr$(CO)_3$ and anisoleCr$(CO)_3$ were prepared by similar methods: *o*-xyleneCr$(CO)_3$–1,3,5-TNB mp 86.0—87.0 °C (mp of *o*-xyleneCr$(CO)_3$: 90.0—90.5 °C).

Found: C, 44.9; H, 2.8; N, 9.3; Cr, 11.7%. Calcd for $C_{17}H_{13}N_3O_9Cr$: C, 44.9; H, 2.9; N, 9.2; Cr, 11.4%. *N,N*-dimethylanilineCr$(CO)_3$·1,3,5-TNB mp 102.0—102.5 °C (mp of *N,N*-dimethylanilineCr$(CO)_3$: 143.5—144.0 °C).

Found: C, 43.5; H, 2.8; N, 12.3; Cr, 11.2%. Calcd for $C_{17}H_{14}N_4O_9Cr$: C, 43.4; H, 3.0; N, 11.9; Cr, 11.1%. AnisoleCr$(CO)_3$·1,3,5-TNB mp 93.0—93.5 °C (mp of anisoleCr$(CO)_3$: 84.5—85.0 °C).

Found: C, 42.1; H, 2.2; N, 9.4; Cr, 11.3%. Calcd for $C_{16}H_{11}N_3O_{10}Cr$: C, 42.0; H, 2.4; N, 9.2; Cr, 11.4%.

Measurements of Absorption Spectra and Determination of the Complex Formation Constants. Absorption spectra were recorded on a Shimadzu automatic recording spectrophotometer Model MPS-50. The cell compartment was thermostatted at a constant temperature (25 °C).

The solvent 1,2-dichloroethane (Wako Pure Chem. Co.) was dried and purified by the usual procedure.[12]

The equilibrium constant K of a 1 : 1 molecular complex formation between electron donor D and electron acceptor A is given by

$$K = \frac{[D\cdot A]}{([D]_0-[D\cdot A])([A]_0-[D\cdot A])},$$

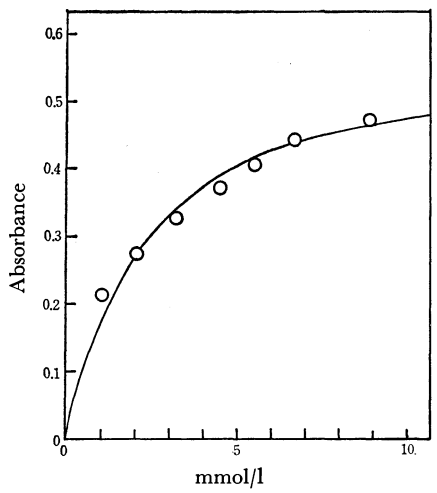

Fig. 1. Change of the absorbance at 13800 cm^{-1} in the charge-transfer band of 1:1 molecular complex of tolueneCr$(CO)_3$ and TCNE as a function of the initial concentration of tolueneCr$(CO)_3$ at 25°C.
$[TCNE]_0 = 1.06\times10^{-3}$ $mol\cdot l^{-1}$.

12) D. D. Perrin, W. L. F. Armarego, and D. R. Perrin, "Purification of Laboratory Chemicals," Pergamon Press, Oxford (1966).

where $[\ ]_0$ denotes the initial concentrations, and [D·A], the concentration of molecular complex D·A. Measurements were carried out at a wave number in the charge-transfer band of the molecular complex where molar absorption coefficients ε_D and ε_A are negligibly small. Assuming Beer's law, [D·A] is rewritten in terms of the observed absorbance $E=\varepsilon_C\cdot[D\cdot A]\cdot l$, where ε_C is the molar absorption coefficient of molecular complex formed in solution, and l, the optical path length. Thus it follows that

$$[D]_0[A]_0\, l/E = \{[D]_0+[A]_0-E/\varepsilon_C\cdot l\}\cdot 1/\varepsilon_C+1/K\varepsilon_C\,.$$

Measurements were carried out at 25 °C for various initial concentrations of D and A. K and ε_C were then evaluated according to the methods described by Rose and Drago,[13] and Lang.[14] In Fig. 1, the absorbance measured at 13800 cm^{-1} is shown as a function of the initial concentration o toluene$Cr(CO)_3$ in the presence of constant initial concentration of TCNE (1.06×10^{-3} mol·l^{-1}). Plots of $[D]_0[A]_0l/E$ *versus* $\{[D]_0+[A]_0-E/\varepsilon_C\cdot l\}$ give a straight line (Fig. 2) for a self-consistent value of ε_C obtained by iterative calculations.

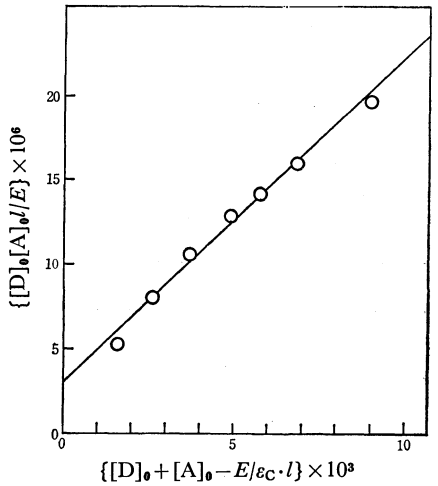

Fig. 2. Plots of $[D]_0[A]_0\cdot l/E$ *versus* $\{[D]_0+[A]_0-E/\varepsilon_C\cdot l\}$ for a self-consistent of ε_C at 25 °C. $[D]_0\equiv$[toluene-$Cr(CO)_3$]$_0$; $[A]_0\equiv[TCNE]_0=1.06\times10^{-3}$ mol·l^{-1}; $\varepsilon_C=520$.

Infrared Absorption Spectra. Infrared absorption spectra of arenetricarbonylchromium complexes and their molecular complexes with 1,3,5-TNB were taken on a Hitachi spectrophotometer Model EPI-G3.

NMR and ESR Spectra. NMR spectra in 1,2-dichloroethane were recorded on a 60 MHz Varian spectrometer Model T-60. Tetramethylsilane was used as an internal standard. ESR spectra in 1,2-dichloroethane were measured with a Japan Electron Optics Laboratory Co. spectrometer Model JES-3BX.

Results and Discussion

No molecular complex formation of arenetricarbonylchromium with electron-donating TMPD was detected in the absorption measurements. We have not succeeded so far in the isolation of a molecular complex of arenetricarbonylchromium with TMPD, but some 1 : 1 molecular complexes with 1,3,5-TNB could be isolated in a pure state. A charge-transfer band at 20200 cm^{-1} (Fig. 3) implies a molecular complex formation between toluene$Cr(CO)_3$ and 1,3,5-TNB in 1,2-dichloroethane. Molar absorption coefficient of the molecular complex and the equilibrium constant of complex formation were determined to be $\varepsilon_C=55$ l·mol^{-1}·cm^{-1} and $K=70$ l·mol^{-1} at 25 °C from the measurements for various initial concentrations of toluene$Cr(CO)_3$ and 1,3,5-TNB. Since TCNE is a stronger acceptor than 1,3,5-TNB and thus the charge-transfer band in the molecular complex with TCNE shows a remarkable shift toward lower wave number, a good resolution of the charge-transfer band is ob-

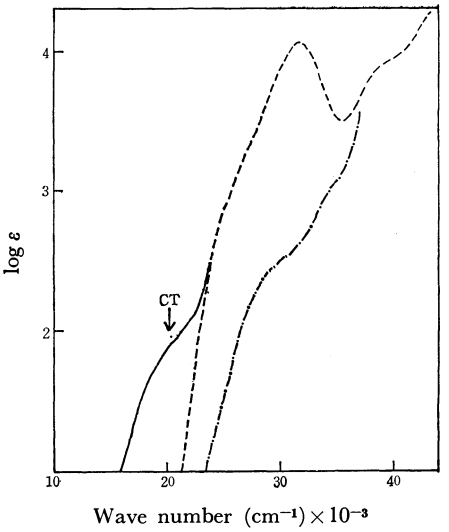

Fig. 3. The charge-transfer band (CT) of toluene$Cr(CO)_3$-1,3,5-TNB system in 1,2-dichloroethane at 25 °C.
[toluene$Cr(CO)_3$]$_0$=0.442 mol·l^{-1};
[1,3,5-TNB]$_0$=0.462 mol·l^{-1}
——: toluene$Cr(CO)_3$-1,3,5-TNB
– – –: toluene$Cr(CO)_3$
—·—: 1,3,5-TNB

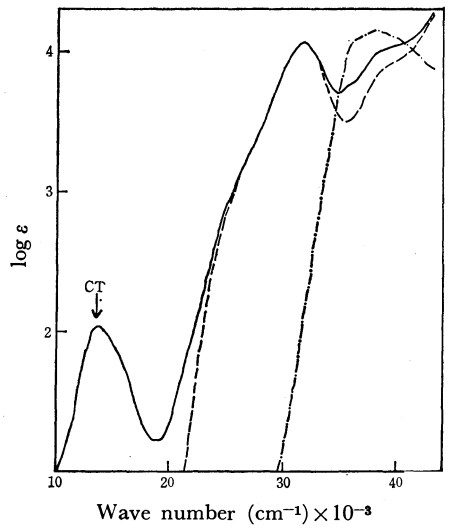

Fig. 4. The charge-transfer band (CT) of toluene$Cr(CO)_3$-TCNE system in 1,2-dichloroethane at 25 °C.
[toluene$Cr(CO)_3$]$_0=4.51\times10^{-3}$ mol·l^{-1};
$[TCNE]_0=1.06\times10^{-3}$ mol·l^{-1}.
——: toluene$Cr(CO)_3$-TCNE
– – –: toluene$Cr(CO)_3$
—·—: TCNE

13) N. J. Rose and R. S. Drago, *J. Amer. Chem. Soc.*, **81**, 6138 (1959).
14) R. P. Lang, *ibid.*, **84**, 1185 (1962).

Table 2. Molar absorption coefficients and complex formation constants of 1 : 1 molecular complexes of arenetricarbonylchromium with 1,3,5-TNB and TCNE

Donors	Acceptors	K at 25 °C ($l \cdot mol^{-1}$)	ε_c (max) ($l \cdot mol^{-1} \cdot cm^{-1}$)
$C_6H_6Cr(CO)_3$	1,3,5-TNB	67	50
$C_6H_5CH_3Cr(CO)_3$	1,3,5-TNB	70	55
$C_6H_5OCH_3Cr(CO)_3$	1,3,5-TNB	76	56
o-$C_6H_4(CH_3)_2Cr(CO)_3$	1,3,5-TNB	56	44
1,3,5-$C_6H_3(CH_3)_3Cr(CO)_3$	1,3,5-TNB	60	47
$C_6H_5N(CH_3)_2Cr(CO)_3$	1,3,5-TNB	79	60
$C_6H_5COOHCr(CO)_3$	TCNE	4400	410
$C_6H_5COCH_3Cr(CO)_3$	TCNE	3960	444
$C_6H_5FCr(CO)_3$	TCNE	2000	528
$C_6H_5ClCr(CO)_3$	TCNE	1030	800
$C_6H_6Cr(CO)_3$	TCNE	1070	553
$C_6H_5CH_3Cr(CO)_3$	TCNE	661	520
$C_6H_5OCH_3Cr(CO)_3$	TCNE	265	538
o-$C_6H_4(CH_3)_2Cr(CO)_3$	TCNE	952	667
m-$C_6H_4(CH_3)_2Cr(CO)_3$	TCNE	504	482
p-$C_6H_4(CH_3)_2Cr(CO)_3$	TCNE	240	616
1,3,5-$C_6H_3(CH_3)_3Cr(CO)_3$	TCNE	686	703
$C_6H_5N(CH_3)_2Cr(CO)_3$	TCNE	139	2510

Table 3. Ionization potentials (I_p) of arenes and arenetricarbonylchromium complexes evaluated from the charge-transfer excitation energies ($h\nu_{CT}$) in the 1 : 1 molecular complexes with 1,3,5-TNB and TCNE

Donors	Acceptors: 1,3,5-TNB			Acceptors: TCNE			Photoionization potentials[4] (eV)
	$h\nu_{CT}$ (kK)	solvent	I_p (eV)	$h\nu_{CT}$ (kK)	solvent	I_p (eV)	
C_6H_6	35.2[1]	$CHCl_3$	9.20	25.9	1,2-$C_2H_4Cl_2$	9.13	9.245
$C_6H_6Cr(CO)_3$	20.5	1,2-$C_2H_4Cl_2$	7.23	13.4	1,2-$C_2H_4Cl_2$	7.33	
$C_6H_5CH_3$	33.0[2]	CCl_4	8.91	24.2[3]	$CHCl_3$	8.90	8.82
$C_6H_5CH_3Cr(CO)_3$	20.2	1,2-$C_2H_4Cl_2$	7.18	13.9	1,2-$C_2H_4Cl_2$	7.40	
$C_6H_5OCH_3$	29.1[1]	CH_2Cl_2	8.40	19.9	1,2-$C_2H_4Cl_2$	8.33	8.20
$C_6H_5OCH_3Cr(CO)_3$	20.1	1,2-$C_2H_4Cl_2$	7.17	14.2	1,2-$C_2H_4Cl_2$	7.47	
o-$C_6H_4(CH_3)_2$	31.4[1]	CH_2Cl_2	8.70	22.8[3]	$CHCl_3$	8.70	8.56
o-$C_6H_4(CH_3)_2Cr(CO)_3$	20.0	1,2-$C_2H_4Cl_2$	7.16	13.9	1,2-$C_2H_4Cl_2$	7.42	
1,3,5-$C_6H_3(CH_3)_3$	29.1[1]	CH_2Cl_2	8.40	21.3[3]	$CHCl_3$	8.52	8.39
1,3,5-$C_6H_3(CH_3)_3Cr(CO)_3$	19.8	1,2-$C_2H_4Cl_2$	7.14	14.0	1,2-$C_2H_4Cl_2$	7.43	
$C_6H_5N(CH_3)_2$	20.7	1,2-$C_2H_4Cl_2$	7.26	14.9[3]	$CHCl_3$	7.57	
$C_6H_5N(CH_3)_2Cr(CO)_3$	18.9	1,2-$C_2H_4Cl_2$	6.99	16.1	1,2-$C_2H_4Cl_2$	7.77	

1) R. Foster, "Organic Charge-transfer Complexes," Academic Press, London and New York, (1969) p. 40. 2) Ref. 17. 3) Ref. 18. 4) K. Watanabe, *J. Chem. Phys.*, **26**, 542 (1957).

tained as shown in Fig. 4. Molar absorption coefficients and complex formation constants of 1 : 1 molecular complexes of arenetricarbonylchromium with 1,3,5-TNB or TCNE are given in Table 2.

Although an ESR signal has been reported for bis-π-benzenechromium with TCNE,[8] no signal was found for the molecular complexes of arenetricarbonylchromium with 1,3,5-TNB or TCNE formed in 1,2-dichloroethane. Thus their ground state should be a singlet. In fact, proton NMR spectra were observed in the usual region even when most part of the arenetricarbonylchromium complex present in solution forms a molecular complex with acceptor. Since no appreciable shift was observed in molecular complex formation, no further information has been obtained from the NMR spectra.

The charge-transfer transition energies of the molecular complexes with a common acceptor are given by a linear function of the ionization potential I_p of the donor

$$h\nu_{CT} = \{I_p - C_1\} + C_2/\{I_p - C_1\},$$

where C_1 and C_2 are constants determined only by the acceptor. The values given for 1,3,5-TNB are $C_1 = 5.00$ and $C_2 = 0.70$,[15] and for TCNE, $C_1 = 6.10$ and $C_2 = 0.54$.[16] The ionization potential of toluene$Cr(CO)_3$ was estimated to be 7.18 eV from the charge-transfer excitation energy in a molecular complex with 1,3,5-TNB, and 7.40 eV from the one with TCNE.

15) G. Briegleb and J. Czekalla, *Z. Elektrochem.*, **63**, 6 (1959).
16) G. Briegleb, J. Czekalla, and G. Reuss, *Z. Physik. Chem., N. F.*, **30**, 333 (1961).

Table 4. Ionization potentials (I_p) of arenetricarbonylchromium complexes evaluated from the charge-transfer excitation energies ($h\nu_{CT}$) in the molecular complexes with TCNE

AreneCr(CO)$_3$	$h\nu_{CT}$ (kK)	I_p (eV)	$\tilde{\nu}_{CO}$ in areneCr(CO)$_3$ (cm^{-1}) in 1,2-$C_2H_4Cl_2$	in C_6H_{12}	I_p of corresponding arenes[3] (eV)
$C_6H_5COOHCr(CO)_3$	12.3	7.06	1983	—	9.59[4]
$C_6H_5COCH_3Cr(CO)_3$	12.1	7.00	1979	—	(9.42)[5]
$C_6H_5FCr(CO)_3$	12.9	7.22	1977	1996[1]	9.36[4]
$C_6H_5ClCr(CO)_3$	12.7	7.16	1975	1992[2]	9.14
$C_6H_6Cr(CO)_3$	13.4	7.33	1970	1987[1]	9.13[4]
$C_6H_5CH_3Cr(CO)_3$	13.9	7.40	1965	1982[1]	8.90
$C_6H_5OCH_3Cr(CO)_3$	14.2	7.47	1964	1982[1]	8.27, 8.33[4]
o-$C_6H_4(CH_3)_2Cr(CO)_3$	13.9	7.42	1962	—	8.70
m-$C_6H_4(CH_3)_2Cr(CO)_3$	14.0	7.43	1962	—	8.69
p-$C_6H_4(CH_3)_2Cr(CO)_3$	14.2	7.46	1960	1979[1]	8.52
1,3,5-$C_6H_3(CH_3)_3Cr(CO)_3$	14.0	7.43	1958	1975[1]	8.52
$C_6H_5N(CH_3)_2Cr(CO)_3$	16.1	7.77	1951	1969[1]	7.57

1) Ref. 19. 2) Ref. 20. 3) Ref. 18; evaluated from the charge-transfer excitation energies in the molecular complexes with TCNE. 4) determined in the present work. 5) Plots shown in Fig. 5 predict I_p=9.42 eV from the observed carbonyl stretching frequency in $C_6H_5COCH_3Cr(CO)_3$ 1979 cm^{-1}. The charge-transfer band in the molecular complex with TCNE is not well resolved from the (n, π^*) transition of $C_6H_5COCH_3$ and thus the ionization potential is not determined directly by method 3).

The ionization potential of toluene in the molecular complex with 1,3,5-TNB is 8.91 eV,[17] while that in the complex with TCNE is 8.90 eV.[18] The ionization potential of toluene$Cr(CO)_3$ is lower than that of free toluene by 1.73 eV in the complex with 1,3,5-TNB and 1.5 eV in that with TCNE. The ionization potentials of some arenes and their coresponding arenetricarbonylchromium complexes, evaluated from the charge-transfer excitation energies in the molecular complexes with 1,3,5-TNB and TCNE, are given in Table 3. The empirical linear functions used to estimate the ionization potentials of arenetricarbonylchromium complexes originally fitted naphthalene.[15,16] The functions, however, can well reproduce the ionization potentials of various aromatic hydrocarbons and show a difference of less than 0.1 eV of the ionization potentials obtained for molecular complexes with 1,3,5-TNB and TCNE. It should be noted that the ionization potentials of arenes evaluated from the charge-transfer excitation energies agree in the 1,3,5-TNB and TCNE systems, whereas those of arenetricarbonylchromium complexes differ in the two systems beyond experimental error. The ionization potentials of arenetricarbonylchromium complexes in the TCNE system obtained are given in Table 4, together with the carbonyl stretching frequencies of arenetricarbonylchromium in 1,2-dichloroethane measured in the present work and those in cyclohexane taken from literature.[19,20] A shift of the infrared peak toward higher frequency was observed in the order

$$C_6H_5COOH > C_6H_5COCH_3 > C_6H_5F > C_6H_5Cl > C_6H_6 > C_6H_5CH_3 > C_6H_5OCH_3 > o\text{-}C_6H_4(CH_3)_2 \geqq m\text{-}C_6H_4(CH_3)_2 > p\text{-}C_6H_4(CH_3)_2 > 1,3,5\text{-}C_6H_3(CH_3)_3 > C_6H_5N(CH_3)_2 .$$

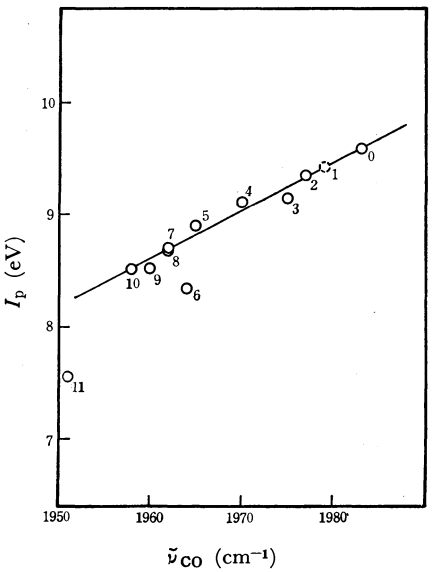

Fig. 5. Plots of the ionization potentials of arenes *versus* the carbonyl stretching frequencies in arenetricarbonylchromium complexes.
Arenes: 0, C_6H_5COOH; 1, $C_6H_5COCH_3$; 2, C_6H_5F; 3, C_6H_5Cl; 4, C_6H_6; 5, $C_6H_5CH_3$; 6, $C_6H_5OCH_3$; 7, *o*-$C_6H_4(CH_3)_2$; 8, *m*-$C_6H_4(CH_3)_2$; 9, *p*-$C_6H_4(CH_3)_2$; 10, 1,3,5-$C_6H_3(CH_3)_3$; 11, $C_6H_5N(CH_3)_2$.

When the antibonding orbital of carbonyl is given a certain charge by chromium-carbonyl back-donation, the carbonyl stretching frequency is shifted toward lower frequency. The above order was in good agreement with that observed in the ionization potentials of arenes (Fig. 5). The stronger donating arene gives rise to more back-donation from chromium to carbonyl groups in arenetricarbonylchromium complex. Plots of the ionization potentials of arenetricarbonylchromium in the molecular complexes with 1,3,5-TNB against the carbonyl frequencies give a straight line except the point of dimethylanilineCr(CO)$_3$, where the ionization potential is much reduced (Fig. 6).

17) G. Briegleb and J. Czekalla, *ibid.*, **24**, 37 (1960).
18) P. G. Farrell and J. Newton, *J. Phys. Chem.*, **69**, 3506 (1965).
19) R. D. Fischer, *Chem. Ber.*, **93**, 165 (1960).
20) D. A. Brown and H. Sloan, *J. Chem. Soc.*, **1962**, 3849.

TABLE 5. INFRARED FREQUENCIES OBSERVED IN ARENETRICARBONYLCHROMIUM AND THEIR TNB COMPLEXES

Complex	Medium[1]	Absorption peak (cm^{-1})[2]					
		I	II	III	IV	V[3]	VI[3]
$C_6H_5CH_3Cr(CO)_3$	KBr	1959 s		814w			665m
	$C_2H_4Cl_2$	1965 s		811w			—
$C_6H_5CH_3Cr(CO)_3TNB$	KBr	1960 s	1343 s	820w	729m	713m	667m
	$C_2H_4Cl_2$	1965 s	1345 s	814w	731m	—	—
$C_6H_5OCH_3Cr(CO)_3$	KBr	1960 s		812w			662m
	$C_2H_4Cl_2$	1964 s		808w			—
$C_6H_5OCH_3Cr(CO)_3TNB$	KBr	1960 s	1345 s	820w	731m	717m	663m
	$C_2H_4Cl_2$	1962 s	1344 s	811w	730m	—	—
$C_6H_5N(CH_3)_2Cr(CO)_3$	KBr	1935 s		800w			673m
	$C_2H_4Cl_2$	1951 s		797w			—
$C_6H_5N(CH_3)_2Cr(CO)_3TNB$	KBr	1957 s	1343 s	813w	731m	717m	681m
	$C_2H_4Cl_2$	1951 s	1345 s	802w	731m	—	—

1) KBr: disk, $C_2H_4Cl_2$: 1,2-dichloroethane solution. 2) I: symmetrical CO valence stretching frequency, III: symmetrical carbon-hydrogen bending vibration of the π-coordinating benzene ring, VI: metal-CO bending vibration, II, IV and V: 1,3,5-trinitrobenzene peaks. 3) The peaks V and VI could not be well resolved in 1,2-dichloroethane from the bands of the solvent.

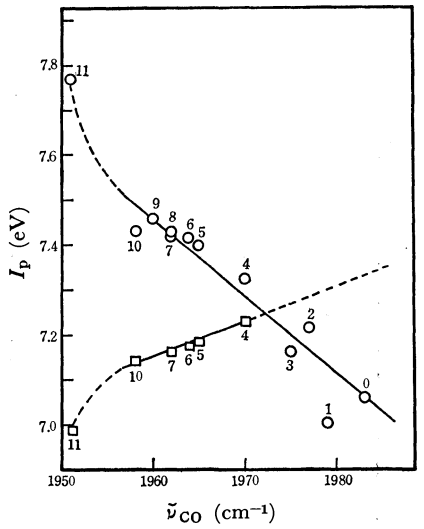

Fig. 6. Plots of the ionization potentials of arenetricarbonylchromium complexes in the molecular complex *versus* the carbonyl stretching frequencies in arenetricarbonylchromium complexes.
○: TCNE molecular complexes
□: 1,3,5-TNB molecular complexes
Arenes: 0, C_6H_5COOH; 1, $C_6H_5COCH_3$; 2, C_6H_5F; 3, C_6H_5Cl; 4, C_6H_6; 5, $C_6H_5CH_3$; 6, $C_6H_5OCH_3$; 7, *o*-$C_6H_4(CH_3)_2$; 8, *m*-$C_6H_4(CH_3)_2$; 9, *p*-$C_6H_4(CH_3)_2$; 10, 1,3,5-$C_6H_3(CH_3)_3$; 11, $C_6H_5N(CH_3)_2$.

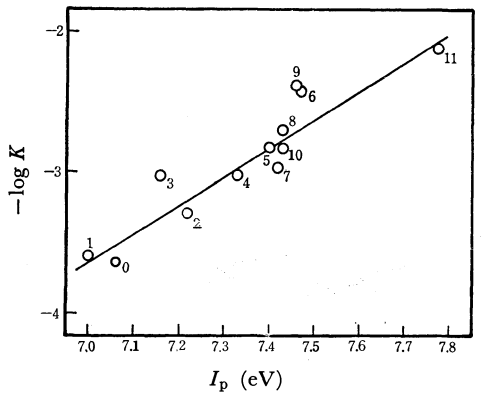

Fig. 7. Plots of the free energy changes of 1:1 molecular complex formation of arenetricarbonylchromium with TCNE against the ionization potentials of arenetricarbonylchromium in the molecular complex with TCNE.
Arenes: 0, C_6H_5COOH; 1, $C_6H_5COCH_3$; 2, C_6H_5F; 3, C_6H_5Cl; 4, C_6H_6; 5, $C_6H_5CH_3$; 6, $C_6H_5OCH_3$; 7, *o*-$C_6H_4(CH_3)_2$; 8, *m*-$C_6H_4(CH_3)_2$; 9, *p*-$C_6H_4(CH_3)_2$; 10, 1,3,5-$C_6H_3(CH_3)_3$; 11, $C_6H_5N(CH_3)_2$.

However, it is evident that the ionization potential of arenetricarbonylchromium in the 1,3,5-TNB molecular complex decreases with a decrease in the ionization potential of coordinating arene. Since the coordinating arene enhances the charge density on carbonyl groups, the acceptor 1,3,5-TNB might exert a charge-transfer interaction toward the carbonyl groups other than the coordinating arene. Apparently no shift was observed in the carbonyl stretching frequencies upon molecular complex formation in solution. The molecular complexes even in the solid state showed no appreciable shift of the IR peaks except dimethylanilineCr$(CO)_3$ (Table 5). DimethylanilineCr$(CO)_3$ shows an appreciable shift of the carbonyl frequency in KBr disk, arising from an intermolecular interaction between dimethylanilineCr$(CO)_3$ in the solid state. Thus the remarkable difference of carbonyl stretching frequencies in the KBr disk of dimethylanilineCr$(CO)_3$ and its 1,3,5-TNB complex does not necessarily imply a reduction in the bond order of the carbonyl groups by a direct charge-transfer interaction of 1,3,5-TNB toward the carbonyl groups. In fact, the carbonyl stretching frequency makes no sizable shift in 1,2-dichloroethane solution, even when the concentrations of dimethylanilineCr$(CO)_3$ and 1,3,5-TNB were so chosen as to obtain an almost complete complex formation. An X-ray crystallography study of a molecular complex anisoleCr$(CO)_3$·1,3,5-TNB has revealed that the acceptor 1,3,5-TNB makes a charge-transfer interaction with coordinating arene rather than carbonyl groups.[11] The absorption spectra of the KBr disk of anisoleCr$(CO)_3$·1,3,5-TNB and dimethylanilineCr-

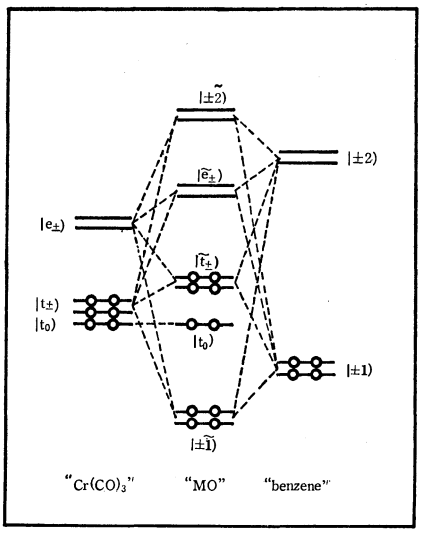

Fig. 8. Molecular orbital levels in arenetricarbonylchromium (schematic). "$Cr(CO)_3$" implies molecular orbitals mainly localized on zero-valent chromium d orbitals which are split by σ ligand field and π back-donation in tricarbonyl chromium, and "benzene" implies the highest occupied and the lowest vacant orbitals of benzene. Chromium d orbitals are given by

$$|e_+) = \sqrt{\frac{2}{3}}|+1) - \sqrt{\frac{1}{3}}|-2)$$

$$|e_-) = \sqrt{\frac{2}{3}}|-1) + \sqrt{\frac{1}{3}}|+2)$$

$$|t_+) = \sqrt{\frac{1}{3}}|+1) + \sqrt{\frac{2}{3}}|-2)$$

$$|t_-) = \sqrt{\frac{1}{3}}|-1) - \sqrt{\frac{2}{3}}|+2)$$

$$|t_0) = |0)$$

The MO's formed are denoted by ~with the name of a component orbital in the highest contribution.

$(CO)_3 \cdot$1,3,5-TNB were measured. The solid state spectra thus obtained were in good agreement with the solution spectra. This implies that the molecular complex formed in solution should have a similar geometry to the structure formed in the solid state. In the case of the TCNE complexes, however, the ionization potential increases with a decrease in the ionization potential of coordinating arene (Fig. 6). As Fig. 7 shows, the stability of molecular complexes with TCNE increases with a decrease in the ionization potential of arenetricarbonylchromium in the TCNE molecular complex and also a decrease in the charge-density of the carbonyl groups. No shift was observed in the carbonyl stretching frequencies upon molecular complex formation with TCNE. Thus it should be concluded that the acceptor TCNE makes a direct interaction with the central chromium.

Schematic molecular orbital levels of the outer electrons in arenetricarbonylchromium are shown in Fig. 8. An interaction of the highest filled benzene orbitals $|\pm1)$ and vacant chromium $d\sigma$ orbitals $|e_\pm)$ gives rise to a charge-migration from π-coordinating benzene to chromium. In the contrast, an interaction of the filled chromium orbitals $|t_\pm)$, participating in the back-donation in Cr–CO, and the lowest vacant benzene orbitals $|\pm2)$ gives a charge-migration from chromium $d\pi$ orbitals to coordinating benzene. A semi-empirical molecular orbital calculation predicted that the resulting charge-migration occurs from π-coordinating benzene to carbonyl groups.[21] Regardless of the charge-migration, the highest filled orbitals $|\pm1)$ are stabilized by interaction with the chromium $d\sigma$ orbitals $|e_\pm)$, leading to increase of the ionization potentials of coordinating arene. The ionization potential of arenetricarbonylchromium is a work to be done for detachment of an electron in the molecular orbital $|\tilde{t}_\pm)$ or $|t_0)$. The orbital $|t_0)$ is delocalized over the chromium and the carbonyls but has no population on the π-coordinating arene, whereas the orbitals $|\tilde{t}_\pm)$ have populations not only on the carbonyls but also on the π-coordinating arene.

When a molecular complex is formed by a charge-transfer interaction involving the orbital $|t_0)$, the acceptor accepts electronic charge from the carbonyl groups in an outer-sphere mechanism or directly from the central chromium in an inner-sphere mechanism. In fact, a protonation of arenetricarbonylchromium results in the formation of a hydrido complex,[22,23] in which a proton forms a direct binding with the central chromium. However, a bulky acceptor such as 1,3,5-TNB can not make an appreciable interaction with the chromium-localized $|t_0)$ orbital for steric hindrance, the molecular complex being formed by a charge-transfer interaction involving the molecular orbital $|\tilde{t}_\pm)$ delocalized over the π-coordinating benzene and carbonyl groups. Direct interaction between 1,3,5-TNB and carbonyl groups could be eliminated because of the small overlapping between the acceptor and carbonyl orbitals despite the high population of chromium $d\pi$ electron on the carbonyl groups.

In the case of TCNE, an enhancement in the charge-populations in π-coordinating arene and carbonyl groups of the donor reduces the stability of the molecular complex. Thus the acceptor TCNE makes direct interaction with the orbital $|t_0)$ localized on the central chromium by an inner-sphere mechanism, although TCNE is not so small. The stability of the molecular complex increases with a decrease in the ionization potential of the orbital $|t_0)$. With the decrease of ionization potential of arene the back-donation in Cr–CO is enhanced. By a charge-migration from the top filled orbitals $|\pm1)$ of arene, orbital $|t_0)$ is stabilized by an enhancement of the back-donation in Cr–CO, whereas orbital $|\tilde{t}_\pm)$ is rather destabilized. As is shown in Fig. 6, the ionization potential of arenetricarbonylchromium in the molecular complex with TCNE is the ionization potential of $|t_0)$, which increases with a decrease in the ionization potential of arene, while the ionization potential of arenetricarbonylchromium in the molecular complex with 1,3,5-TNB is the ionization potential of $|\tilde{t}_\pm)$, which decreases with a decrease in the ionization potential of arene.

Since orbital $|\pm1)$ of the π-coordinating arene is stabilized by interaction with orbital $|t_\pm)$, which makes

21) D. G. Carroll and S. P. McGlynn, *Inorg. Chem.*, **7**, 1285 (1968).
22) A. Davison, W. McFarlane, L. Pratt, and G. Wilkinson, *J. Chem. Soc.*, **1962**, 3653.
23) C. P. Lillya and R. A. Sahatjian, *Inorg. Chem.*, **11**, 889 (1972).

a charge-transfer from arene to chromium-carbonyl orbitals, the substitution reactions in the π-coordinating benzene ring are more likely those of the benzene ring with electron-withdrawing substituents. However, the chromium-localized orbitals $|t_0)$ and $|\tilde{t}_\pm)$ play important roles in the charge-transfer molecular complex formation, and thus arenetricarbonylchromium acts as an electron donor rather than an electron acceptor as shown in the nucleophilic substitutions in π-coordinating benzene ring of arenetricarbonylchromium. The acceptor TCNE can accept electronic charge by an inner-sphere interaction with orbital $|t_0)$ on the π-coordinating arene.

The authors wish to express their thanks to Professor Seinosuke Otsuka, Osaka University, for valuable discussions on the interaction of TCNE.

BULLETIN OF THE CHEMICAL SOCIETY OF JAPAN, VOL. 46, 3116—3118 (1973)

Circular Dichroism of Copper(II) Complexes with Optically Active Tetradentate Ligands in Aqueous Solutions

Tasuku MURAKAMI and Masahiro HATANO

Chemical Research Institute of Non-aqueous Solutions, Tohoku University, Sendai 980

(Received April 17, 1973)

The circular dichroism(CD) spectra of copper(II) complexes containing the asymmetric tetradentate ligands, such as ethylenediamine-*N,N'*-di-L-α-propionate, ethylenediamine-*N,N'*-di-L-α-isovalerate, and ethylenediamine-*N,N'*-di-L-α-hydrocinnamate, were measured in an aqueous solution. Each of the CD curves can be resolved into four components in the d–d region by Gaussian analysis; these components are related to the four possible d–d transitions of the copper(II) ion. The visible CD spectrum profile of the complexes varies with the variation in ligands; this implies that the conformation of the complexes is affected appreciably by the bulkiness of the side chain in the ligand.

In the analyses of the absolute configurations of many metal complexes by means of CD measurements, the empirical rule, that the conformations of complexes containing similar ligands may be identical with each other when the CD spectra observed for these complexes resemble each other in shape and sign, has been very often employed. It has been reported that the copper(II) complexes containing a series of L-α-amino acids exhibit similar CD curves in an aqueous solution. Therefore, the conformations of these complexes seem to be identical with each other in an aqueous solution.[1-3]

In this study, we wish to report that the observed CD spectra of three copper(II) complexes containing optically active tetradentate ligands, prepared by joining the amino groups of identical amino acid with one ethylene group, are very different from each other, and that these complexes may adopt different conformations in an aqueous solution.

Experimental

The asymmetric tetradentate ligands used in this study are ethylenediamine-*N,N'*-di-L-α-propionic acid(abbreviated to $EDDPH_2$), ethylenediamine-*N,N'*-di-L-α-isovaleric acid ($EDDVH_2$), and ethylenediamine-*N,N'*-di-L-α-hydrocinnamic acid($EDDCH_2$), prepared from L-alanine, L-valine, and L-phenylalanine respectively by a method similar to that described in the literature.[4]

Each of the complex solutions for the spectral observation was prepared by mixing equimolar aliquots of an aqueous stock solution of copper(II) nitrate with the tetradentate acids. An equivalent quantity of a base (sodium hydroxide) was always added to assure the virtually complete formation of the complexes. The copper(II) solution was standardized by EDTA titration, using murexide as the metal-ion indicator.[5] The CD curves were obtained by means of a JASCO J-20A spectropolarimeter in the region from 200 to 1000 nm. The absorption measurements were made by means of a Hitachi EPS-3T spectrophotometer at room temperature.

Results and Discussion

The CD spectra of [Cu(EDDP)], [Cu(EDDV)], and [Cu(EDDC)] in an aqueous solution are shown in Fig. 1. The visible CD spectra are very different from each other. Especially, the main CD components of the two complexes, [Cu(EDDP)] and [Cu(EDDV)], are opposite in sign. Applying the "empirical rule" described above to the present case, it seems reasonable to expect that these complexes include different extents of some types of conformers in an aqueous solution.

By an examination of the molecular models, two conformations can be constructed for these complexes, as is illustrated in Fig. 2. In the (I) conformation the orientation of the ring substituent groups is equatorial,

1) T. Yasui, This Bulletin, **38**, 1746 (1965).
2) C. J. Hawkins and C. L. Wong, *Aust. J. Chem.*, **23**, 2237 (1970).
3) R. D. Gillard and S. H. Laurie, *J. Chem. Soc., A*, **1970**, 59 (1970).
4) L. N. Schoenberg, D. W. Cooke, and C. F. Liu, *Inorg. Chem.*, **7**, 2386 (1968).
5) G. Schwarzenbach, "Complexometric Titrations," Methuen, London, p. 82 (1957).

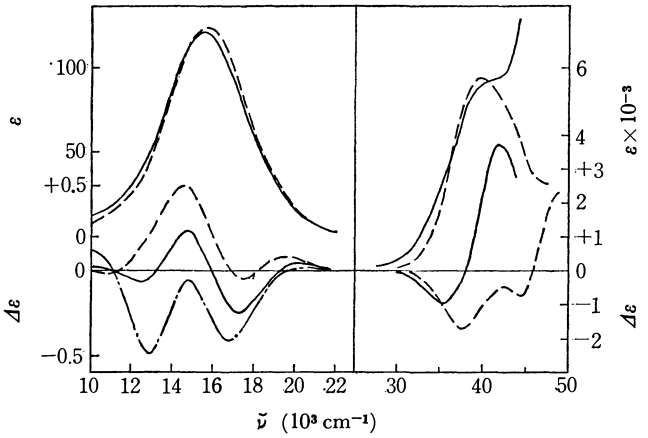

Fig. 1. Absorption and CD spectra of [Cu(EDDP)](— —), [Cu(EDDV)](—·—), and [Cu(EDDC)](——) in aqueous solution.

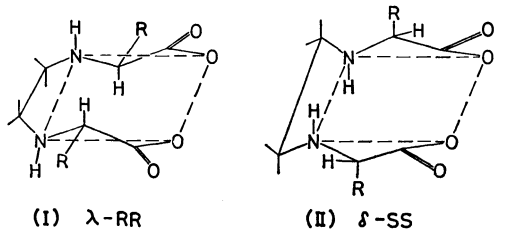

Fig. 2. The two possible conformers. The symbols δ and λ represent the conformations of the central en-type chelate ring, and R and S the configurations of the asymmetric donor nitrogen.

whereas in the (II) conformation the orientation is axial. In general, it is accepted that the equatorial orientation is more stable than the axial orientation in most chelate complexes. However, the energy difference between the two types of orientations of the substituent groups in the amino acid chelate portions of the present tetradentate ligands is much smaller than that in the en-type chelate ring, since, in the en-type chelate ring, the *gauche* structure discriminates greatly between the two orientations, whereas in the amino acid chelate ring this is not the case because of its planarity.[6] Furthermore, the energy difference between the two orientations in square-planar complexes can be expected to be much smaller than that in octahedral complexes. In square-planar complexes, the interaction of the axially-oriented substituent group with the molecules occupying the apical positions may be small.[7] Therefore, the energy difference between the two conformers, (I) and (II), in Fig. 2 seems to be not so large that an equilibrium may exist between the two conformers in an aqueous solution. The equilibrium distribution between the two conformers should vary with the bulkiness of the substituents; hence, these three complexes are speculated to have different equilibrium constants in (I)⇌(II). Thus, we seem to be able to account convincingly for the spectral results observed here in terms of the equilibrium.

If there is such an equilibrium in the complexes, an appreciable change in the CD curves of these complexes would be expected with a variation in the temperature because of the temperature dependence of the equilibrium. In practice, the CD curves observed for these complexes change considerably with a variation in the temperature, despite the limited temperature range. For example, the temperature dependence of the CD curve in the EDDV complex is shown in Fig. 3.

As the origins of the temperature dependence of the CD spectra, vibronic effects or an equilibrium between some conformers may be expected. Since it has been suggested that the magnitudes of the CD bands of metal complexes are only weakly influenced by the vibronic effects,[8] the temperature dependence may be mainly due to the existence of an equilibrium. Furthermore, the presence of an isosbestic point in Fig. 3 indicates the binary equilibrium. Thus, the temperature dependence observed here may be attributed to the equilibrium between the two conformers, (I) and (II), in Fig. 2.

It is clear that the visible CD spectra in Fig. 1 are composed of some d-d transition components. The observed shapes of the CD curves depend essentially on the relative magnitudes of these components, which should subsequently change with the variation in the equilibrium distribution described above. Therefore, it seemed that it would be worthwhile to resolve each of the CD spectra into their transition components.

Each of the visible CD spectra in Fig. 1 can be apparently resolved into four CD bands, although these four bands may not correspond exactly to the four com-

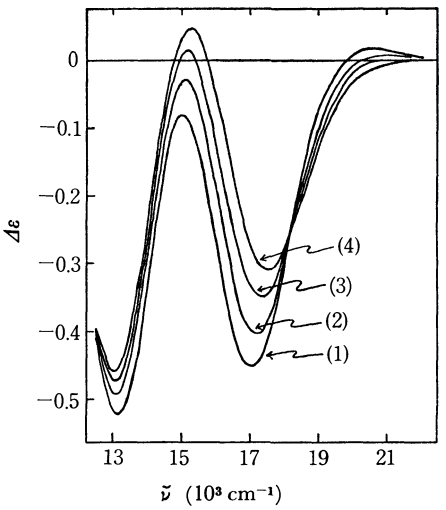

Fig. 3. CD variation with the temperature in the EDDV complex; (1) 3°±1 °C, (2) 27.5°±0.2 °C, (3) 51.2°±0.2 °C, (4) 72.0°±0.3 °C

6) Equatorial and axial orientations in these tetradentate ligands are somewhat different from the so-called 'quasi'-equatorial and 'quasi'-axial orientations in amino acid chelates. By the examination of the molecular models, the *gauche* structure of the N-C-C-N skeleton may be responsible for the orientation of the substituents, and the energy difference between the two orientations seems to be larger than that in the amino acid chelates.

7) C. J. Hawkins, "Absolute Configuration of Metal Complexes," Wiley-Interscience, New York, p. 203 (1971).

8) F. S. Richardson, *J. Phys. Chem.*, **75**, 692 (1971), and references therein.

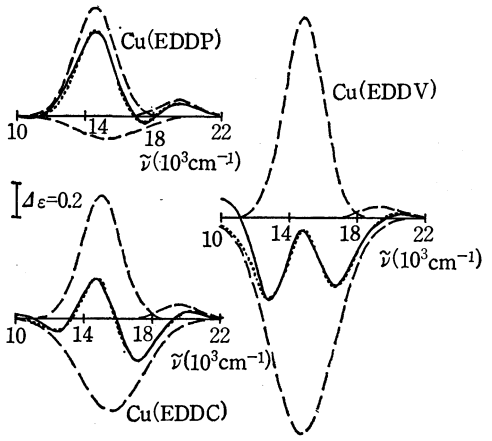

Fig. 4. Gaussian analyses of the CD spectra observed at room temperature: The solid curves are measured spectra; the dashed curves are the Gaussian components; the dotted curves represent the Gaussian summations.

ponents of the d-d transitions. From a comparison of the CD shapes in the 12000—18000 cm^{-1} region, it can be anticipated that each of the CD curves in this region is composed of two components, each of which has one peak near 15000 cm^{-1} with an opposite sign. In the CD spectrum of the EDDV complex at room temperature, the positive one of the two components is not observed in any appreciable amount (Fig. 1). However, the positive component emerges at the higher temperature, as is shown in Fig. 3. Moreover, small positive CD bands appear at about 10000 and 20000 cm^{-1}, and finally these CD curves could be composed of four components.

In order to support the view that these CD curves are composed of four components, we attempted to resolve the CD spectra by Gaussian analysis.[9] A set of Gaussian analyses is presented in Fig. 4. The analyses led to only the three bands at the higher wavenumber side, for we failed to observe the whole of the CD band at the lowest wave number. The slight discrepancies between the summed curves and the measured curves are within the limits of experimental error. Thus, it is almost certain that the curves in the visible region are composed of four components, which are related to the four possible d-d transitions.[10] The corresponding resolved components in the three spectra are situated at almost the same wave numbers, but with different magnitudes. Since the relative magnitudes of the respective components change with the variation in the equilibrium distribution between the two conformers, different CD spectra might be observed for the present three complexes. On the basis of the curve resolutions for the obtained CD curves, the assignments of the four components in the visible region of these complexes will be reported in the next paper.

9) The analyses of the band envelopes were accomplished by trial and error, assuming a symmetrical and purely Gaussian shape for every component band, and assuming that the corresponding resolved components in the respective curves may be the same d-d origin and hence have the same band widths.

10) Wilson and Martin reported that four ligand field bands are identified in the solution circular dichroism of the bis type complex of *N*-methyl-L-alanine with copper(II). E. W. Wilson, Jr., and R. B. Martin, *Inorg. Chem.*, **10**, 1197 (1971).

Derivatographic Studies on Transition Metal Complexes. XI.[1] Thermal Ligand-exchange Reaction of *cis*- and *trans*-[CoXY(N$_4$)]SCN·*n*H$_2$O Type Complexes[2]

Ryokichi Tsuchiya, Tatsuo Murakami,* and Eishin Kyuno

Department of Chemistry, Faculty of Science, Kanazawa University, Kanazawa 920

(Received April 20, 1973)

The thermal ligand-exchange reaction was investigated by derivatographic and isothermal methods for the following complex thiocyanates: *cis*-[CoCl$_2$en$_2$]SCN, *cis*-[CoClBren$_2$]SCN·H$_2$O, *cis*-[CoBr$_2$en$_2$]SCN·H$_2$O and the corresponding *trans*-complexes, and several corresponding triethylenetetramine complexes *cis*-α-[CoXYtrien]-SCN·H$_2$O, where X and Y represent Cl$^-$ and Br$^-$ ion, respectively. *cis*-Complexes, except for *cis*-[CoCl$_2$en$_2$]SCN were found to exhibit obviously the ligand-exchange reaction in which Cl$^-$ or Br$^-$ is substituted by SCN$^-$ just after the liberation of lattice water takes place. On the other hand, *cis*-[CoCl$_2$en$_2$]SCN showed only partial ligand-exchange reaction accompanied by immediate thermal decomposition even at higher temperature than in the other monohydrates. In contrast, all the anhydrated *trans*-complexes *trans*-[CoCl$_2$en$_2$]SCN, *trans*-[CoClBren$_2$]-SCN and *trans*-[CoBr$_2$en$_2$]SCN did not give such a reaction upon heating. The activation energies of *cis*-[CoClBren$_2$]SCN·H$_2$O were found to be $E_a=26\pm2$ kcal/mol for dehydration and $E_a=54\pm2$ kcal/mol for ligand-exchange. The thermal ligand-exchange reaction proceeded in *cis*-type complexes without change in the geometrical configuration of the original complexes. No racemization or inversion could be observed in the optically active complex.

Of several types of thermal reactions on transition metal complexes in a solid phase, the isomerization reactions for *trans*-[CoCl$_2$(NH$_3$)$_4$]IO$_3$·2H$_2$O,[3] *cis,trans*-[CoCl$_2$(NH$_3$)$_2$en]ClO$_4$[4] and *trans*-[CoCl$_2$pn$_2$](H$_5$O$_2$)·Cl$_2$,[5,6] and the racemization reactions for *d-cis*-[CrCl$_2$en$_2$]Cl,[7] *d*-[Coen$_3$]I$_3$·H$_2$O,[7] and *l*-K$_3$[Co(C$_2$O$_4$)$_3$]·*n*H$_2$O[8,9] have been reported. In most cases, solid phase reactions occurred without exchange of the ligand by counter ions. However, few studies have been carried out on the ligand-exchange reaction between anionic ligand coordinated and the counter ion in outer coordination sphere.

Radioactive chloride exchange reaction takes place when *trans*-[Co*Cl$_2$pn$_2$](H$_5$O$_2$)·Cl$_2$ or *trans*-[CoCl$_2$pn$_2$](H$_5$O$_2$)·*Cl is heated.[6] In this reaction, the complete chloride scrambling might occur during the course of dehydration or dehydrochlorination. This suggests that the aquation-anation mechanism is acceptable.

Another type of thermal exchange reaction was found[10] in *cis,trans*-[CoCl$_2$(NH$_3$)$_2$en]SCN·H$_2$O. It contains not only stereochemical change in the coordination sphere but also ligand-exchange with the counter ion: *i.e.*, the reaction of this complex proceeds in two steps as follows.

(1) *cis, trans*-[CoCl$_2$(NH$_3$)$_2$en]SCN·H$_2$O → *cis, trans*-[CoCl$_2$(NH$_3$)$_2$en]SCN + H$_2$O

(2) *cis, trans*-[CoCl$_2$(NH$_3$)$_2$en]SCN → *cis, cis*-[CoCl(NCS)(NH$_3$)$_2$en]Cl

In (2) the stereochemical change and ligand-exchange occur simultaneously, water of crystallization playing no important role. For thermal reaction in this complex, an associative mechanism with seven coordinated reaction intermediates was proposed.[10]

Thermal reaction in a solid phase is affected by several factors, one of which is the steric effect of a chelate ring. Thus, it is of interest to investigate the effect of chelation of neutral ligands in *cis*- and *trans*-[CoXY(N$_4$)]SCN·*n*H$_2$O, as compared with *cis,trans*-[CoCl$_2$(NH$_3$)$_2$en]SCN·H$_2$O. Coordinated halogen ions will also affect the thermal reaction.

We have also attempted to survey the role of lattice water on the ligand-exchange reaction and examine the influence of isomeric configurations of starting complexes; *viz.*, the effect brought about by the difference in coordination site of two halogen ions.

We have prepared *cis*- and *trans*-[CoXY(N$_4$)]SCN·*n*H$_2$O type complexes and investigated their thermal ligand-exchange reactions in detail.

Experimental

Preparation of Complex Thiocyanates. Complexes *cis*-[CoCl$_2$en$_2$]Cl, *cis*-[CoClBren$_2$]Br and *cis*-[CoBr$_2$en$_2$]Br and the corresponding trans complexes were prepared by the methods in literature.[11,12] Their thiocyanates were obtained by adding an excess amount of potassium thiocyanate to the cold saturated solution of the corresponding chloride or bromide. Recrystallization was carried out from a dilute solution of potassium thiocyanate. The crystals were filtered and washed with small amounts of water, ethanol and ether

* Present address: Fuji Kagaku Kogyo Co., Ltd., Kami-ichi, Toyama.

1) Part X of this series; R. Tsuchiya, S. Joba, A. Uehara, and E. Kyuno, This Bulletin, **46**, 1454 (1973).

2) Presented in part at the 20th Annual Meeting of the Chemical Society of Japan, Hiratsuka, 4, April, 1972.

3) H. E. LeMay, Jr. and J. C. Bailar, Jr., *J. Amer. Chem. Soc.*, **89**, 5577 (1967).

4) R. Tsuchiya, A. Nakata, and E. Kyuno, This Bulletin, **44**, 705 (1971).

5) R. Tsuchiya, K. Murai, and E. Kyuno, *ibid.*, **43**, 1383 (1970).

6) H. E. LeMay, Jr., *Inorg. Chem.*, **10**, 1990 (1971).

7) H. E. LeMay, Jr. and J. C. Bailar, Jr., *J. Amer. Chem. Soc.*, **90**, 1729 (1968).

8) J. Brady, F. Dachille, and C. D. Schmulbach, *Inorg. Chem.*, **2**, 803 (1963).

9) J. Brady, F. Dachille, and C. D. Schmulbach, *ibid.*, **7**, 287 (1968).

10) R. Tsuchiya, M. Suzuki, and E. Kyuno, This Bulletin, **44**, 709 (1971).

11) W. C. Fernelius, "Inorganic Synthesis," Vol. 2, p. 223 (1946); *ibid.*, Vol. 9, p. 163 (1967).

12) A. Werner, L. J. Lorie, and J. Rapiport. *Ann*, **386**, 112 (1912).

Table 1. Elemental analysis

Complex	C%		H%		N%	
	Found	Calcd	Found	Calcd	Found	Calcd
trans-[$CoCl_2en_2$]SCN	19.60	19.49	5.74	5.24	22.07	22.73
trans-[$CoClBren_2$]SCN	17.32	17.03	4.77	4.58	19.87	19.87
trans-[$CoBr_2en_2$]SCN	15.42	15.12	4.34	4.07	17.40	17.64
cis-[$CoCl_2en_2$]SCN	19.56	19.49	5.53	5.24	22.42	22.73
cis-[$CoClBren_2$]SCN·H_2O	16.78	16.20	4.66	4.91	18.77	18.90
cis-[$CoBr_2en_2$]SCN·H_2O	15.04	14.47	4.52	4.38	17.07	16.88
cis-α-[$CoCl_2$trien]SCN·H_2O	23.92	23.87	5.89	5.74	19.83	19.89
cis-α-[CoClBrtrien]SCN·H_2O	21.28	21.19	5.25	5.01	17.90	17.66
cis-α-[$CoBr_2$trien]SCN·H_2O	19.31	19.06	4.77	4.58	16.33	15.88
$(-)_D$-*cis*-α-[$CoBr_2$trien]SCN·H_2O	19.36	19.06	4.70	4.58	16.36	15.88

and then air-dried.

The triethylenetetramine complexes *cis*-α-[$CoCl_2$trien]Cl,[13] *cis*-α-[CoClBrtrien]Br[14] and *cis*-α-[$CoBr_2$trien]Br[15] were obtained by the known methods. The thiocyanates were obtained by a similar method to that for the corresponding ethylenediamine complexes. The optically active complex $(-)_D$-*cis*-[$CoBr_2$trien]SCN·H_2O was obtained by the reaction of $(-)_D$-*cis*-α-[$CoBr_2$trien]Br with potassium thiocyanate in an aqueous solution.

The complexes obtained were identified by elemental analysis and spectral measurement. The results are given in Table 1.

Derivatographic Measurement. The apparatus and technique for derivatography were the same as described previously.[5]

Isothermal Measurement. A Shimadzu TM-1A Thermanobalance and an Abderhalden apparatus were used for isothermal measurement. The procedures of measurement and analysis were also the same as given previously.[16]

Spectral Measurement. The electronic, infrared and circular dichroism spectra were measured with a Hitachi ERS spectrophotometer, JASCO Model IR-E, IR-F spectrophotometer, and JASCO Model ORD/UV-5 spectrophotometer, respectively.

Results and Discussion

Structure of Reaction Products. When freshly prepared *cis*-type complexes except for *cis*-[$CoCl_2en_2$]SCN were heated, the original violet color turned brick-red, showing that the counter ion may coordinate in place of halogen ligand after dehydration. The IR spectra of *cis*-[$CoClBren_2$]SCN·H_2O and the reaction product are shown in Fig. 1.

We see that C≡N stretching band is shifted from 2040 cm^{-1} to 2100 cm^{-1} upon heating. It is well-known[17] that there is a characteristic difference between the infrared spectra of the complexes containing SCN^- of different

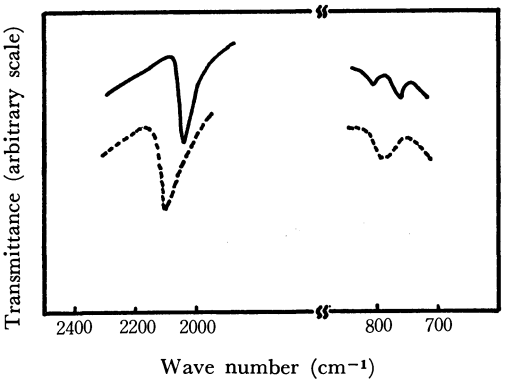

Fig. 1. IR spectra of *cis*-[$CoClBren_2$]SCN·H_2O (——) and its reaction product (----).

coordination modes and those of the complexes having SCN^- as counter ion, *viz.*, the infrared absorption band assigned to C≡N stretching vibration in the thiocyanate ion attached to a metal ion appears in the higher wavenumber region than that in the inorganic thiocyanate anion. The shift from 2040 cm^{-1} to 2100 cm^{-1} may be attributed to a cobalt(III)-thiocyanate bonding formation, and the thiocyanate ion in outer sphere probably coordinates to the central metal after dehydration.

The linkage isomerism of N-bonded or S-bonded thiocyanate ion in the coordination is distinct from the presence of a C–S stretching vibration band in the frequency region 690—860 cm^{-1} and NCS bending in the region 400—490 cm^{-1}. It is known[17] that the C–S stretching band appears in 780—860 cm^{-1} for M–NCS and 690—720 cm^{-1} for M–SCN and NCS bending band, in 450—490 cm^{-1} for M–NCS and 400—440 cm^{-1} for M–SCN.

After the exchange reaction is over, the C–S stretching band shifts towards the higher wave number region from 760 cm^{-1} which is given by SCN^- counter ion, partly overlapping the NH_2 deformation band. Although there is no obvious evidence for the change of frequency in NCS bending, it may be concluded that the thiocyanate ion participates in bonding through nitrogen atom to central cobalt(III) ion.

The IR spectra of *cis*-[$CoBr_2en_2$]SCN·H_2O and its reaction product are very similar to those of *cis*-[$CoClBren_2$]SCN·H_2O.

13) E. Kyuno, L. J. Boucher, and J. C. Bailar, Jr., *J. Amer. Chem. Soc.*, **87**, 4458 (1965).
14) E. Kyuno, and J. C. Bailar, Jr., *ibid.*, in press.
15) E. Kyuno and J. C. Bailar, Jr., *ibid.*, **88**, 1125 (1966).
16) R. Tsuchiya, Y. Kaji, and E. Kyuno, This Bulletin, **42**, 1881 (1969).
17) P. C. Mitchell and R. J. P. Williams, *J. Chem. Soc.*, **1960**, 1912; K. Nakamoto, "Infrared Spectra of Inorganic and Coordination Compounds," 2nd Ed., John Wiley & Sons, Inc., New York (1970), p. 187.

TABLE 2. ABSORPTION MAXIMA OF STARTING COMPLEXES AND REACTION PRODUCTS

	Starting complex	Reaction product
cis-$[CoCl_2en_2]SCN$	540 (2.11)	a)
cis-$[CoClBren_2]SCN \cdot H_2O$	549 (2.03)	505 (2.21)
cis-$[CoBr_2en_2]SCN \cdot H_2O$	554 (2.05)	510 (2.25)
cis-α-$[CoCl_2trien]SCN \cdot H_2O$	539 (2.08)	506 (2.32)
cis-α-$[CoClBrtrien]SCN \cdot H_2O$	546 (2.11)	506 (2.34)
cis-α-$[CoBr_2trien]SCN \cdot H_2O$	552 (2.10)	508 (2.40)

Values in parentheses are absorption coefficients.

a) *cis*-$[CoCl_2en_2]SCN$ could not be completely converted into *cis*-$[CoCl(NCS)en_2]Cl$.

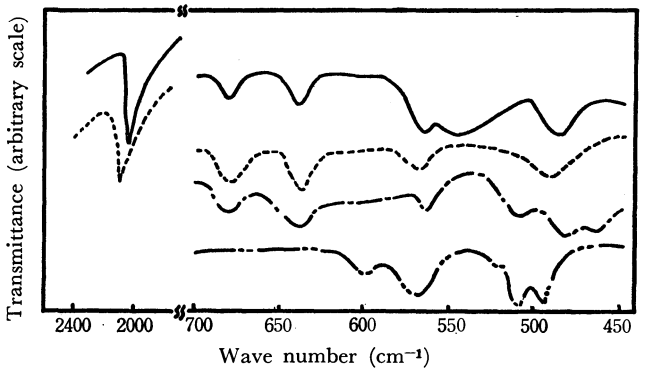

Fig. 2. IR spectra of *cis*-α-$[CoCl_2trien]SCN \cdot H_2O$ (——), its reaction product (·····), *cis*-α-$[CoCl_2trien]Cl$ (– – –) and *cis*-β-$[CoCl_2trien]Cl$ (— — —).

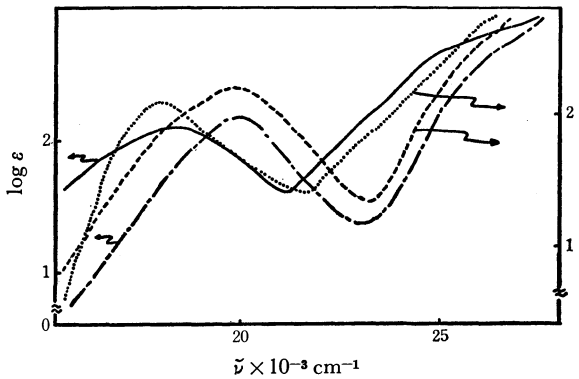

Fig. 3. Absorption spectra of *cis*-$[CoClBren_2]SCN \cdot H_2O$ (——), its reaction product (– – –), *cis*-$[CoCl(NCS)en_2]Cl$ (– – –) and *trans*-$[CoCl(NCS)en_2]Br$ (·····).

The corresponding trien complexes give a similar pattern to the bis-en complexes in IR spectra before and after the thermal reaction. The IR spectra of *cis*-α-$[CoCl_2trien]SCN \cdot H_2O$, the reaction product, and the related complexes are shown in Fig. 2.

In the far-infrared region, the pattern of the absorption bands originating from the skeletal vibration in each complex does not change much after thermal reaction. There are three geometrical isomers, *cis*-α, cis-β and trans ones, in the octahedral complex involving the trien chelate. The skeletal vibration is more useful in distinguishing these isomers. The configuration of the reaction product of *cis*-α-$[CoCl_2trien]SCN \cdot H_2O$ is considered to be the same as that of the starting complex (Fig. 2). Thus, the ligand-exchange reaction does not involve the stereochemical change, the isomerization from *cis*-α to *cis*-β or *trans*-form.

When two halogen ions in the preheating complex are the same, the chromophore of the reaction product is easily seen. For example, when *cis*-$[CoBr_2en_2]SCN \cdot H_2O$ is heated the product obtained is obviously $[CoBr(NCS)en_2]Br$, but it can not be deduced from only IR data whether Cl^- or Br^- ion is substituted by SCN^- ion upon heating the *cis*-chloro-bromo complex. UV spectra can be used to assign the geometrical isomers and the chromophore of cobalt(III) complexes.[18,19] Numerical values of the absorption maxima of the complexes and their reaction products are shown in Table 2. All the reaction products have absorption maxima at *ca.* 505 nm, and no shoulders at *ca.* 550 nm.

In the chromophore of $[CoX(NCS)(N_4)]$, the first absorption band of *cis*-compound, in general, appears in rather higher frequency than that of *trans*-one. *cis*-$[CoCl(NCS)en_2]Cl$ and *trans*-$[CoCl(NCS)en_2]Br$ were found to exhibit the first absorption maxima at 505 nm and 555 nm, respectively.[20] The absorption spectra of *cis*-$[CoClBren_2]SCN \cdot H_2O$, its reaction product, and the related complexes are given in Fig. 3.

The spectral feature of the reaction product of *cis*-$[CoClBren_2]SCN \cdot H_2O$ is in good agreement with that of *cis*-$[CoCl(NCS)en_2]Cl$. It is therefore concluded that the reaction product from *cis*-$[CoClBren_2]SCN \cdot H_2O$ is *cis*-$[CoCl(NCS)en_2]Br$. Thus, the thiocyanate ion in outer sphere is considered to substitute the coordinated bromide ion but not chloride ion, the *cis*-structure in thermal ligand-exchange reaction being retained. The reaction product from *cis*-$[CoBr_2en_2]SCN \cdot H_2O$, the chromophore of which is $[CoBr(NCS)en_2]$, has a first absorption maxima at 510 nm, and is considered to be *cis*-$[CoBr(NCS)en_2]Br$. This is due to the fact that the ligand field of Cl^- ion is stronger than that of Br^- ion.

Three trien complexes give a similar spectral behavior to that in the bis-en complexes (Table 2). It is concluded that the ligand-exchange reaction proceeds retaining *cis*-form.

Optically active $(-)_D$-*cis*-α-$[CoBr_2trien]SCN \cdot H_2O$ was also used. Apparent difference in activity of the complex was observed before and after the reaction. Their CD and UV spectra are given in Fig. 4.

18) H. Yamatera, This Bulletin, **31**, 95 (1958).

19) R. A. O. Wentworth and T. S. Piper, *Inorg. Chem.*, **4**, 709 (1965).

20) H. Kuroya and R. Tsuchida, This Bulletin, **15**, 427 (1940).

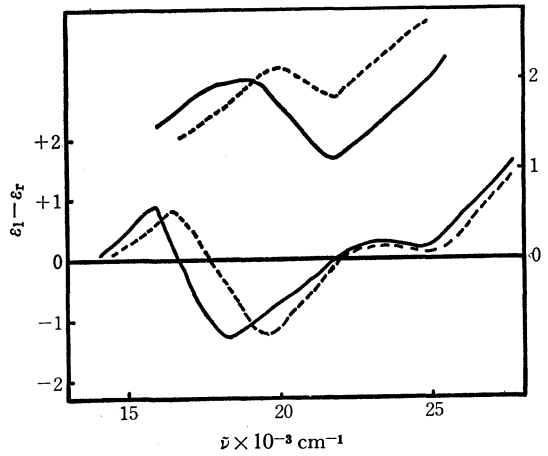

Fig. 4. CD and absorption spectra of $(-)_D$-*cis*-α-[$CoBr_2$trien]-SCN·H_2O (----) and its reaction product (----).

Although the CD spectrum of the reaction product shifts slightly towards the higher frequency side due to the substitution of Br^- by SCN^-, its pattern remains almost unchanged with the same sign even after the reaction. $(+)_D$-*cis*-$[CoCl_2en_2]^+$ and $(+)_{5461}$-*cis*-[Co(NCS)en_2]$^+$ have similar CD curves with the same sign, and their absolute configurations are found to be the same, namely, *Λ*.[21] Complex $(-)_D$-*cis*-α-[$CoBr_2$trien]SCN·H_2O and its reaction product $(-)_D$-*cis*-α-[CoBr(NCS)trien]Br were found to have the same absolute configuration, since the ring chirality of the trien complex is almost equal to that of bis-en complex. The thermal reaction in the optically active complex is found to accompany neither racemization nor inversion reactions.

It is thus concluded that the thermal ligand-exchange reaction for *cis*-[CoXY(N_4)]SCN·H_2O type complexes proceeds retaining both geometrical and optical configurations giving the formula *cis*-[CoX(NCS)-(N_4)]Y.

Derivatographic Studies. The derivatograms for the complexes examined are given in Figs. 5, 6 and 7. *cis*-[$CoClBren_2$]SCN·H_2O and *cis*-[$CoBr_2en_2$]SCN·H_2O each exhibit a small exothermic peak at *ca.* 125 °C after the appearance of the endothermic peak due to the dehydration in DTA curve (Fig. 5). The exothermic peak corresponds to the ligand-exchange reaction between Br^- ion in the coordination and SCN^- ion in outer sphere as for *cis,trans*-[$CoCl_2(NH_3)_2$en]SCN·H_2O[10] in which the exchange between the chloride ion and the thiocyanate ion takes place with an exothermic peak.

cis-[$CoCl_2en_2$]SCN with no lattice water shows no peak in this temperature range, but an exothermic peak overlapping with complicated decomposition peaks at higher temperature. Even upon isothermal heating, it decomposes as soon as the color change begins to appear. At this stage, the C≡N stretching band splits into two peaks at 2040 cm^{-1} and 2100 cm^{-1}. The ligand-exchange reaction does not proceed stoichiometrically for *cis*-[$CoCl_2en_2$]SCN unlike that for *cis*-[$CoClBren_2$]SCN·H_2O.

21) T. E. MacDermott, A. M. Sargeson, *Austr. J. Chem.*, **16**, 334 (1963).

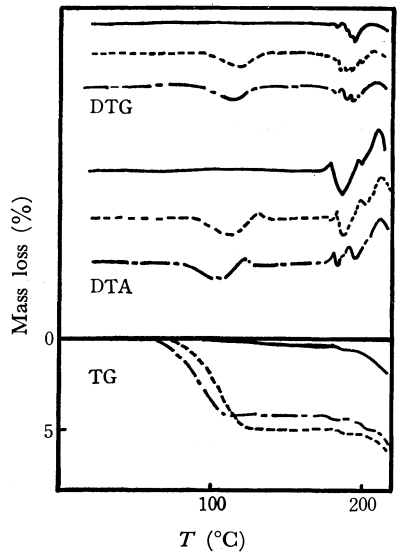

Fig. 5. Derivatograms of *cis*-[$CoCl_2en_2$]SCN (——), *cis*-[$CoClBren_2$]SCN·H_2O (----) and *cis*-[$CoBr_2en_2$]SCN·H_2O (——).

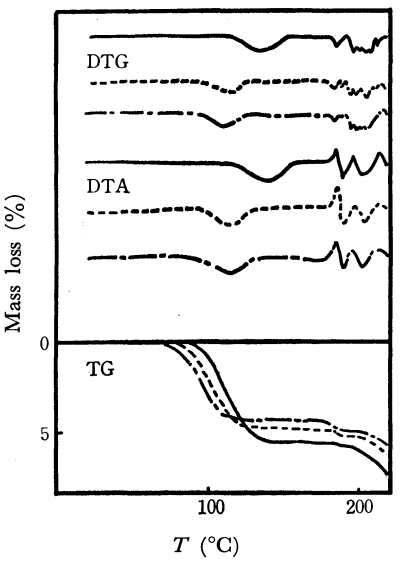

Fig. 6. Derivatograms of *cis*-α-[$CoCl_2$trien]SCN·H_2O (——), *cis*-α-[CoClBrtrien]SCN·H_2O (----) and *cis*-α-[$CoBr_2$trien]-SCN·H_2O (——).

Each derivatogram of the three trien complexes exhibits only one peak attributable to the liberation of lattice water (Fog. 6). The color of the sample changed from violet to brick red after appearance of the endothermic peak, the C≡N stretching band being shifted to 2100 cm^{-1}. The ligand-exchange reaction for the trien complexes might take place in the temperature range of thermal dehydration, since the peak is considered to overlap that of dehydration.

cis-α-[$CoBr_2$trien]SCN·H_2O readily loses a certain amount of lattice water with no color change on being kept in a vacuum desiccator at room temperature. The derivatogram of this complex exhibits a small exothermic peak at 100 °C due to the lack of a large endothermic peak. This peak appearing with color change could be attributed to the ligand-exchange reaction occurring on heating.

Table 3. Thermochemical functions

Complex	ΔH_d kcal/mol[a)]	E_a^d kcal/mol[b)]	ΔH_e kcal/mol[c)]	E_a^e kcal/mol[d)]
cis-$[CoClBren_2]SCN \cdot H_2O$	10.8±2.0	26±3	−1.2±1.0	50±5
cis-α-$[CoCl_2trien]SCN \cdot H_2O$	8.6±2.0	33±3		
cis-α-$[CoClBrtrien]SCN \cdot H_2O$	7.8±2.0	31±3		
cis-α-$[CoBr_2trien]SCN \cdot H_2O$	7.2±2.0	30±3		

a) and c) are enthalpy changes of dehydration and ligand-exchange reaction, respectively. b) and d) are activation energies of dehydration and ligand-exchange reaction, respectively.

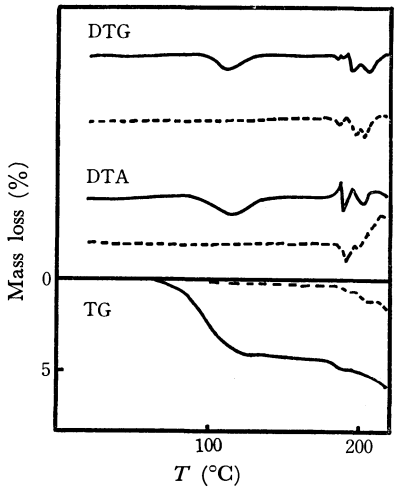

Fig. 7. Derivatograms of $(-)_D$-*cis*-α-$[CoBr_2trien]SCN \cdot H_2O$ (——) and *trans*-$[CoClBren_2]SCN$ (——).

The deviatogram of optically active $(-)_D$-*cis*-α-$[CoBr_2trien]SCN \cdot H_2O$ given in Fig. 7 is similar to that of the corresponding racemic complex. Since all the reaction products indicate the same spectral behavior, it can be concluded that the thermal ligand-exchange reaction occurs just after thermal dehydration.

The following reaction sequence for the *cis*-type complexes is proposed.

(1) *cis*-$[CoXY(N_4)]SCN \cdot H_2O$
$\rightarrow$ *cis*-$[CoXY(N_4)]SCN + H_2O$

(2) *cis*-$[CoXY(N_4)]SCN$
$\rightarrow$ *cis*-$[CoX(NCS)(N_4)]Y$.

In the case of coexistence of Cl^- and Br^- ions in the coordination sphere, the ligand-exchange of Br^- by SCN^- will be more predominant than Cl^-.

On the other hand, the green *trans*-complexes *trans*-$[CoCl_2en_2]SCN$, *trans*-$[CoClBren_2]SCN$ and *trans*-$[CoBr_2en_2]SCN$ have no lattice water, and exhibit no color change on heating. The derivatogram of *trans*-$[CoClBren_2]SCN$ is given in Fig. 7 as an example. In the DTA, DTG and TG curves of this derivatogram, neither the peak for dehydration nor that for the ligand-exchange reaction appears below 185 °C when the complicated thermal decomposition is initiated.

It is understood that the ligand-exchange reaction does not take place in the three dehydrated *trans*-complexes, whereas in the anhydrated *cis*-$[CoCl_2en_2]SCN$ the partial ligand-exchange reaction occurs just before thermal decomposition takes place. This indicates that the configuration of trans isomers should prevent the occurrence of the thermal ligand-exchange reaction.

The thermochemical functions calculated from DTA and DTG curves of the derivatograms are given in Table 3. Because of the incomplete separation of the peaks in DTA curves, no genuine enthalpy changes corresponding to each process of dehydration and ligand-exchange reaction could be calculated separately for *cis*-$[CoClBren_2]SCN \cdot H_2O$, and no DTG and DTA curves of the derivatogram of *cis*-$[CoBr_2en_2]SCN \cdot H_2O$ could be analyzed.

Isothermal Studies. In the isothermal study of *cis*-$[CoClBren_2]SCN \cdot H_2O$, the rate constants of dehydration and ligand-exchange reaction were determined at various temperatures.

Since *cis*-$[CoClBren_2]SCN \cdot H_2O$ and its reaction product *cis*-$[CoCl(NCS)en_2]Br$ have the absorption coefficients 64.9 and 161.8 at 505 nm and 108.5 and 132 at 549 nm in DMSO, respectively, with a 1.0 cm cell, the ratios of the concentration of chloro-bromo/chloro-isothiocyanato complex in the reaction products at a given heating time can be determined spectrophotometrically by means of the equations

$$64.9X + 161.8Y = D_{505}$$
$$108.5X + 132Y = D_{549},$$

where X and Y are the concentrations (in mol^{-1}) of the chloro-bromo and chloro-isothiocyanato complexes, respectively, and D_{505} and D_{549} the absorbances at 505 nm and 549 nm, respectively. The rate constants of the ligand-exchange reaction were calculated from the conversion ratios of the two isomers in each product X/Y. The rate of dehydration was estimated from the weight change of sample with a thermobalance.

The rate constants k_d for dehydration and the rate constants k_e for the ligand-exchange reaction are given in Table 4. The Arrhenius plots of the rate constants are shown in Fig. 8.

The activation energies are (26±1) kcal/mol and (54±2) kcal/mol for dehydration and ligand-exchange reaction, respectively. The values agree with those obtained by analysis of the derivatogram.

Table 4. Rate constants of dehydrvtion and ligand-exchange reaction for *cis*-$[CoClBren_2]SCN \cdot H_2O$

T °C	k_d, s^{-1}	T °C	k_e, s^{-1}
95	$7.8\pm0.5\times10^{-6}$	100	$4.0\pm0.3\times10^{-6}$
100.0	$1.1\pm0.3\times10^{-5}$	110.8	$8.9\pm0.5\times10^{-5}$
105	$1.7\pm0.3\times10^{-5}$	121.8	$4.7\pm0.4\times10^{-5}$
108.5	$2.6\pm0.3\times10^{-5}$	131.7	$1.2\pm0.4\times10^{-4}$
111	$3.0\pm0.4\times10^{-5}$		
	$E_a=26\pm2$ kcal/mol		$E_a=54\pm2$ kcal/mol

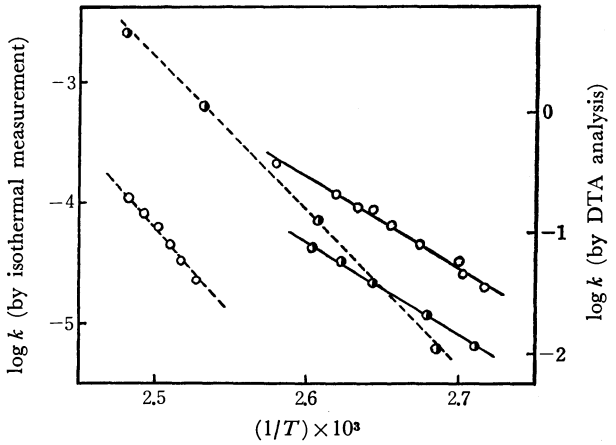

Fig. 8. Arrhenius plots for *cis*-[CoClBren$_2$]SCN·H_2O in the dehydration (——) and ligand-exchange reaction (----) by DTA analysis (○) and isothermal measurement (◑).

If the thermal reaction in a solid phase proceeds through the aquation-anation pathway, the activation energy of the thermal reaction will be nearly equal to that of dehydration, and if the reaction proceeds by intramolecular mechanism, the activation energy would be comparatively higher than that by aquation-anation mechanism.

In the study of *cis*-[CoClBren$_2$]SCN·H_2O, the two Arrhenius plots for dehydration and the ligand-exchange reaction were not parallel with each other (Fig. 8), and the activation energy of the ligand-exchange reaction was considerably higher than that of dehydration. It is assumed that the lattice water plays no important role in the ligand-exchange reaction.

The ligand-exchange reaction occurs after dehydration and thus proceeds *via* the intramolecular mechanism. All the reaction products of *cis*-[CoXY(N$_4$)]-SCN·H_2O type complexes were of *cis*-structure with respect to a halogen ion originally coordinated and an isothiocyanate ion entering the coordination sphere.

When *cis*-[CoClBren$_2$]SCN·H_2O and $CuSO_4 \cdot 5H_2O$ separately placed in a sealed tube were heated, the reaction product of the former differed from that obtained in an open system, *viz.*, it was a mixture of *cis*- and *trans*-[CoCl(NCS)en$_2$]Br. In such a closed system, the gaseous water molecule evolving from the sample and $CuSO_4 \cdot 5H_2O$ can not escape from the reaction system, and may aquate the complex catalytically at the solid surface. The thermal reaction might proceed through the aquation-anation pathway accompanied by the stereochemical change, isomerization from *cis* to *trans*-form.

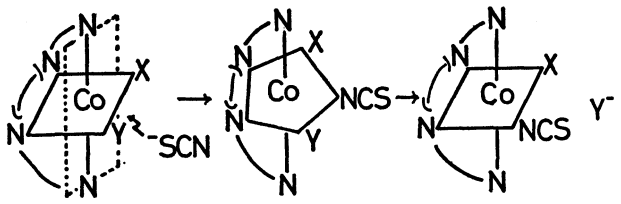

Fig. 9. Probable reaction mechanism.

The following reaction mechanism for the ligand-exchange reaction of *cis*-[CoXY(N$_4$)]SCN·H_2O type complex in the solid phase is postulated (Fig. 9).

The thiocyanate ion would attack at a position *cis* to the two halogen ions coordinated to form the seven coordinated reaction intermediates and then one of the halogen ions would be removed to outer coordination sphere. In the case of the coexistence of Cl^- and Br^- ions in the coordination, the Co–Br bond breaking takes place after making the seven coordinated intermediate, since the Co–Br bond energy is considered to be smaller than the Co–Cl one.

The thermal reaction products through this pathway should be of *cis*-structure without any stereochemical change such as racemization or an inversion in the optically active complex. The exchange reaction and isomerization from *cis,trans*-[CoCl$_2$(NH$_3$)$_2$en]SCN·H_2O to *cis,cis*-[CoCl(NCS)(NH$_3$)$_2$en]Cl occurred simultaneously, where the thiocyanate ion in outer sphere attacked at a position trans to the two halogen ions. In the case of *cis*-[CoXY(N$_4$)]SCN·H_2O, however, the chelate ring of ethylenediamine or triethylenetetramine might prevent the thiocyanate ion from attacking the trans site and make the *cis*-attack more easily. After the liberation of water molecule from the crystal lattice upon heating, packing may somewhat loosen as in an amorphous substance.

The looseness would affect the acceleration of the mobility of the thiocyanate ion in the solid phase. The assumption seems plausible, since the monohydrated *cis*-complexes exhibit a perfect ligand-exchange after dehydration, while the other anhydrous *cis*-[CoCl$_2$en$_2$]SCN showed only partial ligand-exchange just before thermal decomposition.

Kinetic Studies of the Nickel Lactate Complex Formation in Solution by the Pressure-jump Method

Shoji HARADA, Hideyuki TANABE, and Tatsuya YASUNAGA

Department of Chemistry, Faculty of Science, Hiroshima University, Higashi-sendamachi, Hiroshima 730

(Received April 23, 1973)

The nickel lactate complex formation reaction in an aqueous solution was studied by the pressure-jump method and the overall rate constants, the stability constants, and the activation parameters were determined. The results were interpreted by the use of the step-by-step complex formation mechanism, and it was revealed that the rate-determining step is the chelate-ring formation process. The ligand effect on the rate of the complex formation was also considered.

With the help of the relaxation techniques,[1,2] fast metal complex formation reactions in solution have been studied. In many cases, the relaxation effects have been interpreted by the step-by-step mechanism,[3] and it has been revealed that the rate-determining step is the dissociation of a water molecule from the inner-coordination sphere of the metal ion. For the complex formation with the bidentate ligand, one more step of chelation should be added to the unidentate-complex-formation mechanism. Kinetic studies of some of the nickel dicarboxylate-complex-formation reactions have been performed[4–7] by the use of the above mechanism. For the assignment of the relaxation effect, however, two different theories have been proposed. In one theory,[4,5] the rate-determining step was considered to be the first-bond formation between the nickel ion and the ligand. In the other,[6,7] it was ascribed to the chelation process. The present authors have studied the nickel dicarboxylate-complex-formation reactions[8–10] and discussed if one of the two theories can be properly applied. In the present studies, the same attempts have also been made in the case of the univalent-bidentate-ligand complex of the nickel ion. The results obtained will be compared to the kinetic data of other bidentate-ligand complexes.

Experimental

All of the chemicals used were of a reagent grade. A stock solution of the nickel lactate was prepared by mixing a stoichiometric amount of $NiSO_4$ and lactic acid where the sulfate ion was precipitated out as $BaSO_4$ by $Ba(OH)_2$ titration. The concentration of the nickel lactate was determined by dimethylglyoxime titration. The solutions studied were prepared by the dilution of the stock solution to the desired concentration. The pH's of the solutions were 5.5—5.8, where most of the ligand was in the dissociated form.

The pressure-jump apparatus used has been described in considerable detail elsewhere.[8] To ensure that the observed relaxation is due to the complex formation reaction of the nickel lactate, blank experiments were carried out with solutions containing only nickel nitrate or sodium lactate under the same conditions. In no case was a relaxation effect observed. The measurements were carried out at 10, 15, 20, 25 and 30 °C in the concentration range from 1.01×10^{-3} to 5.04×10^{-2} M of nickel lactate. The relaxation times quoted are the mean values of at least four runs.

Results and Discussion

The experimental conditions and the reciprocal relaxation times observed at 25 °C are shown in Table 1. The concentration dependence of the relaxation time can be interpreted in terms of the following simple mechanism:

$$M^{2+} + L^- \underset{k_d}{\overset{k_f}{\rightleftharpoons}} ML^+ \qquad (1)$$

where M^{2+} is the metal ion, L^- is the ligand ion, ML^+ is the complex, and k_f and k_d are the formation and the dissociation rate constants respectively. Taking into account the small stability constant and the experimental conditions of the low concentration of the nickel lactate, the concentrations of ML_2 or higher-order complexes are assumed to be negligible. For the mechanism (1), the relaxation time, τ, is related to the rate constants as follows:

$$1/\tau = k_f\gamma_M\gamma_L(C_M+C_L) + k_d\gamma_{ML} \qquad (2)$$

where γ is the activity coefficient, C is the equilibrium concentration, and the subscript indicates the corresponding ionic species. Assuming that $\gamma_{ML}=\gamma_L$, Eq. (2) is rearranged to:

$$1/(\tau\cdot\gamma_{ML}) = k_f\gamma_M(C_M+C_L) + k_d. \qquad (3)$$

When the stability constant is given, the concentrations of each ionic species can be calculated. The activity coefficients are calculated by the following Davies[11] equation.

$$\log\gamma_i = -\left(\frac{1}{2}\right)\cdot Z_i^2\left(\frac{\mu^{1/2}}{1+\mu^{1/2}} - 0.3\,\mu\right) \qquad (4)$$

where Z_i is the charge of the i-th ion and where μ is the ionic strength of the solution. If the suggested

1) M. Eigen and L. DeMaeyer, "Technique of Organic Chemistry," Vol. VIII, 2nd Ed., S. L. Friess, Interscience Publishers Inc., New York, N. Y. (1963), Part 2, p. 895.
2) G. H. Czerlinski, "Chemical Relaxation," M. Dekker Inc., New York, N. Y. (1966).
3) M. Eigen and K. Tamm, *Z. Elektrochem.*, **66**, 93, 107 (1962).
4) G. H. Nancollas and N. Sutin, *Inorg. Chem.*, **3**, 360 (1964).
5) F. P. Cavasino, *J. Phys. Chem.*, **69**, 4380 (1965).
6) U. Nickel, H. Hoffmann, and W. Jaenicke, *Ber. Bunsenges. Physik. Chem.*, **72**, 526 (1968).
7) H. Hoffmann and U. Nickel, *ibid.*, **72**, 1096 (1968).
8) S. Harada, K. Amidaiji, and T. Yasunaga, This Bulletin, **45**, 1752 (1972).
9) S. Harada and T. Yasunaga, *ibid.*, **46**, 502 (1973).
10) S. Harada, H. Tanabe, and T. Yasunaga, *ibid.*, **46**, 2450 (1973).
11) C. W. Davies, "Ion Association," Butterworths, London (1962).

TABLE 1. RELAXATION TIMES AND EXPERIMENTAL CONDITIONS FOR THE NICKEL LACTATE SYSTEM AT 25 °C

C_0[a] (10^{-4} M)	C_{Ni} (10^{-4} M)	C_L (10^{-4} M)	C_{NiL} (10^{-4} M)	μ (10^{-4})	γ_{Ni}	$\gamma_L = \gamma_{NiL}$	$1/\tau$ (10^2 s^{-1})
10.1	7.9	18.0	2.1	26	0.80	0.95	2.1
20.2	13.4	33.6	6.8	47	0.75	0.93	2.4
40.3	21.0	61.3	19.3	82	0.69	0.91	3.1
60.5	26.3	86.7	34.2	113	0.65	0.90	3.4
100.8	33.6	134.4	67.3	168	0.60	0.88	4.1
201.6	43.2	244.8	158.5	288	0.53	0.85	5.0
302.4	48.3	350.7	254.1	399	0.49	0.84	5.4
403.2	51.6	454.8	351.7	506	0.46	0.82	6.7
504.0	53.8	557.8	450.2	612	0.44	0.81	7.1

a) C_0 refers to the total stoichiometric concentrations of the nickel lactate.

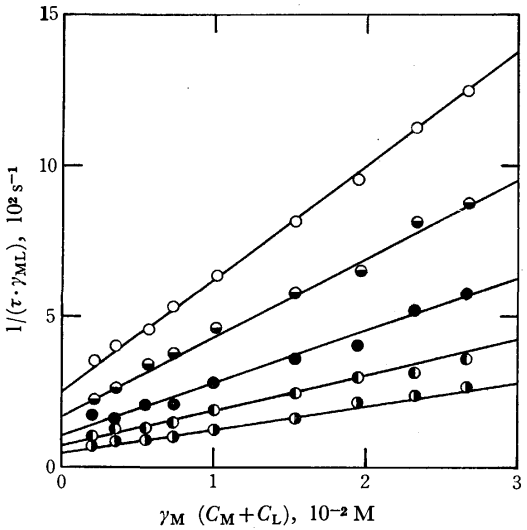

Fig. 1. $1/(\tau\cdot\gamma_{ML})$ *vs.* $\gamma_M(C_M+C_L)$ plot at 10 °C (◑), 15 °C (◐), 20 °C (●), 25 °C (◒), and 30 °C (○).

mechanism is correct, the plot of $1/(\tau\cdot\gamma_{ML})$ *vs.* $\gamma_M(C_M+C_L)$ should be linear; then, k_f and k_d are obtained from the slope and the intercept of the straight line respectively. The stability constant $K(=k_f/k_d)$, which should coincide with the first assumed value, was obtained from the ratio between k_f and k_d. Successive approximations were performed until a constant K was obtained. The final plots at various temperatures are shown in Fig. 1. The lines are the best fit ones based on a least-squares treatment. The rate and the stability constants are summarized in Table 2.

The Arrhenius energies of activation, $\Delta E_f^{\neq}$ and $\Delta E_d^{\neq}$, were obtained from the plot of $\log k_f$ and $\log k_d$ against $1/T$ respectively. Other thermodynamic parameters of the complex formation, *i.e.*, the entropy of activation, $\Delta S_f^{\neq}$; the enthalpy of activation, $\Delta H_f^{\neq}$, and the free energy of activation, $\Delta G_f^{\neq}$, were calculated from the following equations; they are listed in Table 3:

$$\log A = \log\frac{eRT}{Nh} + \frac{\Delta S_f^{\neq}}{2.3R} \quad (5)$$

$$\Delta H_f^{\neq} = \Delta E_f^{\neq} - RT \quad (6)$$

$$\Delta G_f^{\neq} = \Delta H_f^{\neq} - T\Delta S_f^{\neq} \quad (7)$$

where A is the frequency factor.

TABLE 2. THE FORMATION AND THE DISSOCIATION RATE CONSTANTS AND THE STABILITY CONSTANTS OF THE NICKEL LACTATE ($\mu\rightarrow 0$)

t, °C	k_f (10^3 M^{-1} s^{-1})	k_d (s^{-1})	K (10^2 M^{-1})
10	7.7±1.0	48±8	1.6±0.4
15	11.5±1.2	72±10	1.6±0.4
20	17.3±1.3	108±22	1.6±0.4
25	26.0±3.1	170±38	1.5±0.4
30	37.5±4.9	250±44	1.5±0.4

TABLE 3. KINETIC DATA OF THE NICKEL LACTATE COMPLEX FORMATION AT 25°C ($\mu\rightarrow 0$)

K, M^{-1}	$1.5(\pm 0.4)\times 10^2$
k_f, M^{-1} s^{-1}	$2.60(\pm 0.31)\times 10^4$
k_d, s^{-1}	$1.70(\pm 0.38)\times 10^2$
$\Delta E_f^{\neq}$, kcal·mol^{-1}	13.5±2.3
$\Delta E_d^{\neq}$, kcal·mol^{-1}	14.1±3.0
$\Delta G_f^{\neq}$, kcal·mol^{-1}	11.4±2.3
$\Delta H_f^{\neq}$, kcal·mol^{-1}	12.9±2.3
$\Delta S_f^{\neq}$, cal·K^{-1}·mol^{-1}	5±8

The kinetic data obtained for the nickel lactate are compared with the other literature values. The stability constant is very close to the value obtained by Evans *et al.*[12] by the use of conductivity method. The value is also close to the stability constant of the nickel glycollate.[13] At the same time, k_f and k_d are also very close to those of the nickel glycollate.[14] Considering the structural resembrance of the two ligands, the above coincidences of the data can be easily understood. The activation parameters are very close to those of the oxalate[4] and the malonate complexes[5]: *i.e.*, $\Delta E_f^{\neq}$=14—16 kcal·mol^{-1}, $\Delta H_f^{\neq}$=13—15 kcal·mol^{-1}, $\Delta S_f^{\neq}$=5—16 cal·mol^{-1}·K^{-1}, and $\Delta G_f^{\neq}$=10—11 kcal·mol^{-1}. These coincidences imply that the relaxations observed result from similar reactions.

The lactate ligand makes a chelate complex where the carboxyl group and the hydroxyl group are coordinated to the nickel ion. Therefore, the complex

12) W. P. Evans and C. B. Monk, *Trans. Faraday Soc.*, **50**, 132 (1954).
13) W. P. Evans and C. B. Monk, *J. Chem. Soc.*, 550 (1954).
14) H. Hoffmann, *Ber. Bunsenges. Physik. Chem.*, **73**, 432 (1969).

TABLE 4. THE RATE AND THE STABILITY CONSTANTS FOR THE NICKEL CARBOXYLATE COMPLEXES AT 25°C

Ligard	K (M^{-1})	k_f ($M^{-1}s^{-1}$)	k_d (s^{-1})	K_0k_1 ($M^{-1}s^{-1}$)	k_{-1} (s^{-1})	k_2 (s^{-1})	k_{-2} (s^{-1})	Ref.
Oxalate	2.1×10^4	7.4×10^4	3.6	8.5×10^5	7×10^3	6.7×10^2	4	4a)
Glycollate	1.65×10^2	3.3×10^4	2×10^2	1.5×10^5	9×10^3	2.5×10^3	2.6×10^2	14
Lactate	1.5×10^2	2.6×10^4	1.7×10^2	1.5×10^5	9×10^3	1.9×10^3	2.1×10^2	This work

a) The rate constant of the individual steps were calculated from the original data in the same way as that carried out in the nickel lactate system.

formation reaction (1) must be composed of the following step-by-step mechanism:

$$Ni^{2+}+L^- \overset{K_0}{\rightleftharpoons} Ni^{2+}O\overset{H}{\underset{H}{\diagup\diagdown}}L^- \underset{k_{-1}}{\overset{k_1}{\rightleftharpoons}} Ni^+-L \underset{k_{-2}}{\overset{k_2}{\rightleftharpoons}} Ni^+ = L \quad (8)$$

(I) (II) (III) (IV)

where (I) is the free ions, (II) is the outer-sphere complex, (III) is the unidentated complex (probably coordinated by the carboxyl group), (IV) is the chelate complex, and K_0 is the outer-sphere stability constant. The observed relaxation phenomena can be characterized by a single relaxation time; therefore, it may be ascribed to one of the steps in the above mechanism. On the assumption that the intermediate species, (II) and (III), are in the steady state, the rate constants in Eq. (8) are related to the overall formation and the dissociation rate constants, k_f and k_d, in Eq. (1) by the following equations:

$$k_f = K_0k_1\left(\frac{k_2}{k_2+k_{-1}}\right) \quad (9)$$

$$k_d = k_{-1}\left(\frac{k_{-2}}{k_2+k_{-1}}\right). \quad (10)$$

It has usually been admitted[1,3] that k_1 is equal to the water-substitution rate constant of the nickel ion,[15] $2.7\times10^4\ s^{-1}$. Moreover, K_0 can be calculated to be $5.4\ M^{-1}$ for the 2—1 electrolyte by means of this equation:[16,17]

$$K_0 = (4\pi Na^3/3000)\cdot e^{-U(a)/kT} \quad (11)$$

where N is Avogadro's number, $U(a)$ is the Coulomb energy, and a is the distance of the closest approach of ion-pair partners, which was assumed to be 5 Å. Therefore, $K_0k_1=1.5\times10^5\ M^{-1}s^{-1}$. The same value of K_0k_1 is also obtained from the kinetic studies of the nickel acetate. The fact that k_f in Table 2 is about an order of magnitude smaller than K_0k_1 means that the value in the parentheses in Eq. (9) is much smaller than unity, *i.e.*, $k_2 \ll k_{-1}$, and that the rate-determining step of the complex formation is not the first-bond formation, but the chelate-ring formation step. If the value of k_{-1} is given, k_2 and k_{-2} can be calculated from Eqs. (9) and (10) by the use of k_f and k_d. Hoffmann *et al.*[7,14] have reported that log k_{-1} bears a linear relationship to the basicity of the ligand. Applying this relationship to the lactate complex, k_{-1} was estimated to be $9\times10^3\ s^{-1}$. By the use of these values, k_2 and k_{-2} were calculated; they are listed in Table 4. The data in Table 4 show that the rate-determining step of the complex formation is the chelation step of the OH group and that of the complex dissociation process is the chelate-ring rupture.

The rate constants of all the steps of the lactate complex formation are very close to those of the glycollate. This means that the rate constants and the stability constants are not affected by the small difference in structure between the two ligands. In comparison with the six-membered dicarboxylate complex, *i.e.*, the oxalate, the lactate is two orders less stable; this may be ascribed not only to the stabilities of the ion-pair formation, but also, and mainly, to the stabilities of the chelate or the rate of the chelate-ring rupture.

15) T. J. Swift and R. E. Connick, *J. Chem. Phys.*, **37**, 307 (1962).
16) R. Fuoss, *J. Amer. Chem. Soc.*, **80**, 5059 (1958).
17) G. Hammes and J. I. Steinferd, *ibid.*, **84**, 4639 (1962).

Application of the Zone Melting Technique to Metal Chelate Systems. VII. Computer-assisted Consideration on the Solute Distribution Profiles in Zone Melting Process

Shigeru MAEDA, Hiroshi KOBAYASHI, and Keihei UENO

Department of Organic Synthesis, Faculty of Engineering, Kyushu University, Fukuoka 812

(Received Feburary 1, 1973)

A new equation is derived which gives the solute distribution along a column after a zone melting chromatography (ZMC) process, where the initial charge of a sample mixture of $k<1$ is placed on the upper end of the column, one zone length high. The solute distribution differs significantly from that obtained by Pfann's equation on an infinite ingot, in the neighborhood of the upper end as expected from the difference in the initial conditions. The solute distribution is calculated numerically for the case in which the initial charge is placed by several zone lengths on the column top. The present multiple zone charge method shows little difference in solute distribution from the conventional single zone charge method, having the advantage of increasing the sample amount to be fractionated. Numerical calculation is performed to find the zone length with which the greatest amount of the solute of $k<1$ is concentrated into the bottom fraction of a certain length of a given column after each zone pass. A series of resulting zone lengths, showing a stepwise shortening, pass after pass, provides the optimum mode of decrease in the zone length.

We successfully applied the zone melting method to systems containing metal chelates.[1-6] The basic theory of zone melting was thoroughly covered by Pfann.[7] We have extended the theory by presenting mathematical expressions which give the solute distribution profile in specific methods of zone melting operation for a higher separation efficiency. Discussion is given on the theoretical basis for the experimental work. Since the equations are not given in simple analytical forms, the solute distribution profiles were computed numerically by use of FACOM 230—60 of the Computer Center of Kyushu University.

Solute Distribution on a Semi-infinite Column in Zone Melting Chromatography (ZMC)

The basic equation determining the solute distribution along the solid column after n-th zone pass was described in the form of difference differential equation on the basis of mass balance as follows.[8]

$$dC_n(x)/dx = k\{C_{n-1}(x+l) - C_n(x)\}/l \qquad (1)$$

where l is the length of a molten zone, x denotes the position of the freezing interface of the zone which travels in the positive x direction, $C_n(x)$ is the solute concentration at x after the n-th zone pass, and k, the distribution coefficient, is defined as a ratio of solute concentration (weight/volume) in the frozen solid to that in the molten liquid.

Analytical solutions of Eq. (1) were derived by Reiss and Helfand[8] for various types of ZMC methods on the following assumptions for simplification:

1) a constant distribution coefficient k, regardless of the concentration of the solute or freezing conditions,
2) no diffusion in the solid,
3) infinitely rapid mixing in the melt,
4) a negligibly small change in density upon freezing,
5) a constant zone length, l,
6) flat solid-melt interfaces perpendicular to the column axis,
7) a uniform cross section of the column.

When the initial charge of a sample is placed at midpoint on an infinitely long column of a uniform unit cross section (Fig. 1), distribution of the solute is given by an analytical expression,[8] which is further simplified by Pfann[9] as

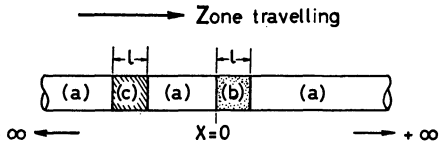

Fig. 1. ZMC on an infinitely long column
(a): Pure solid solvent
(b): Initial charge of sample mixture
(c): Molten zone

$$C_n(x) = C_i k[k\{(x/l)+m\}]^m \exp[-k\{(x/l)+m\}]/m! \qquad (2)$$

where $m=n-1$, $-\infty<x<+\infty$, and C_i is the concentration of a solute in the initial charge.[10]

Practically it is much easier to place the initial charge of a solute mixture on either end than at the midpoint of a pure solid solvent column.

* Contribution No. 287 from the Department of Organic Synthesis, Kyushu University. Presented in part before the International Congress on Analytical Chemistry, April 7, 1972 in Kyoto. Part VI by the same authors, Ref. 6.

1) K. Ueno, H. Kaneko, and Y. Watanabe, *Microchem. J.*, **10**, 244 (1966).
2) H. Kaneko and K. Ueno, *Talanta*, **13**, 1525 (1966).
3) H. Kaneko, H. Kobayashi, and K. Ueno, *ibid.*, **14**; 1403 (1967).
4) H. Kaneko, H. Kanagawa, H. Kobayashi, and K. Ueno, *ibid.*, **14**, 1411 (1967).
5) N. Fukuda, H. Kobayashi, and K. Ueno, *ibid.*, **18**, 807 (1971).
6) S. Maeda, H. Kobayashi, and K. Ueno, *ibid.*, **20**, 653 (1973).
7) W. G. Pfann, "Zone Melting," 2nd ed., John Wiley and Sons, Inc., New York, N. Y. (1966).
8) H. Reiss and E. Helfand, *J. Appl. Phys.*, **32**, 228 (1961).
9) W. G. Pfann, *Anal. Chem.*, **36**, p. 2231 (1964).

10) According to Pfann. [Ref. 7, pp. 10, 30 and 59 and *J. Appl. Phys.*, **35**, 258 (1964)], Eq. (2) is valid without the third and fourth assumptions, if concentration is expressed in weight fraction or mole fraction, l defined as the length of solid that is melted to form the zone and k is an effective value consistent with the freezing conditions.

Solutes with k less than unity move in the direction of zone travelling, and no ZMC column is required which extends in the opposite direction to that of the zone travelling from the position of the initial charge.

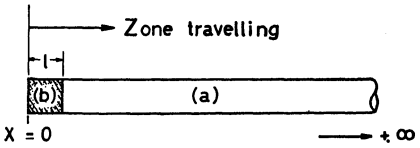

Fig. 2. ZMC on a semi-infintely long column
(a): Pure solid solvent
(b): Initial charge of sample mixture and molten zone.

Assuming that the initial charge is placed one zone length high on the upper end of a semi-infinite column extending from $x=0$ to $x=+\infty$, and that the zone travels downwards, Eq. (1) can be solved using iterative methods for each succeeding pass. After the first zone pass, it can be rewritten as

$$(l/k)\{dC_1(x)/dx\} + C_1(x) = C_0(x+l) \quad (3)$$

where $C_0(x+l)=0$ regardless of x in the region $x>0$. Thus

$$dC_1(x)/C_1(x) = (-k/l)dx \quad (4)$$

A solution of this equation is

$$C_1(x) = C_1(0)\exp(-kx/l) \quad (5)$$

where $C_1(0)=kC_i$

After the second zone pass, the basic differential equation is written as

$$(l/k)\{dC_2(x)/dx\} + C_2(x) = C_1(x+l) \quad (6)$$

The right hand side of this equation is given by Eq. (5), and we have

$$dC_2(x)/dx + (k/l)C_2(x) = (k/l)C_1(0)\exp\{-k(x+l)/l\} \quad (7)$$

A solution of this equation is analytically derived as

$$C_2(x) = \exp(-k/l)\{C_2(0) + (kx/l)C_1(0)\exp(-k)\} \quad (8)$$

where

$$C_2(0) = (k/l)\int_0^l C_1(x)dx \quad (9)$$

Repeating similar treatments, after the n-th zone pass we have the following solution.

$$C_n(x) = \exp(-kx/l)\{\sum_{r=0}^{n-1}(k/l)^r C_{n-r}(0) \times \exp(-rk)x(x+rl)^{r-1}/r!\} \quad (10)$$

where

$$C_n(0) = (k/l)\int_0^l C_{n-1}(x)dx$$
$$= \{1-\exp(-k)\}C_{n-1}(0) + \sum_{r=1}^{n-2} C_{n-1-r}(0)\exp(-rk) \times \left[\{1-\exp(-k)\} + (k/l)^r \sum_{p=0}^{r-1} \frac{lp(rl)^{r-p-1} - l(p+1)\exp(-k)\{(r+1)l\}^{r-p-1}}{(k/l)^p(r-p)!}\right] \quad (11)$$

Equation (10) can be readily proved to be one of the analytical solutions of Eq. (1) by the method of mathematical induction (Appendix).

Equations (10) and (11) are highly iterative and can be calculated only by a digital computer for relatively large n-values, the results being illustrated in Fig. 3 along with those of Eq. (2) for comparison. Solute distribution by Eq. (10) differs from that by Eq. (2) with respect to the fact that the solute does not distribute in the region of negative x, namely

$$\int_0^{+\infty} C_n(x)dx = 1$$

for Eq. (10) in contrast to

$$\int_{-\infty}^{+\infty} C_n(x)dx = 1$$

for Eq. (2).

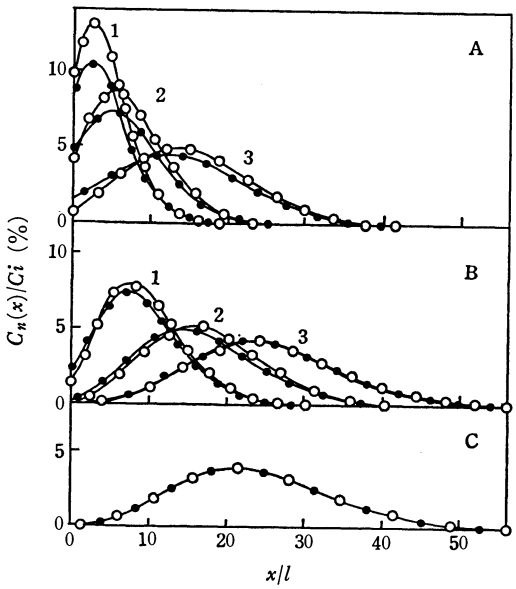

Fig. 3. Comparisons of the distribution profiles between Reiss-Helfand's and the present equations.
○—○ the present equation (10)
●—● Reiss-Helfand's equation (2)
A: $k=0.80$, 1; $n=10$, 2; $n=20$, 3, $n=50$
B: $k=0.56$, 1; $n=10$, 2; $n=20$, 3; $n=30$
C: $k=0.30$, $n=10$.

A comparison of curves from both equations indicates that the distribution curves of Eq. (10) shift to the direction of positive x slightly greater than those of Eq. (2), obviously owing to the effect of a semi-infinite column as mentioned above. This tendency is especially marked when the solute distribution peak is in the neighborhood of the column top. Otherwise, the distribution curves from Eq. (10) are almost superimposable on those from Eq. (2).

If we refer to Eq. (2), the peak position x_{max} increases linearly with n, as is given by

$$x_{max}/l = (n-1)(1-k)/k \quad (12)$$

On the other hand, if we refer to Eq. (10), it is difficult to obtain such a relationship mathematically. Numerical calculation affords the relationship between x_{max}/l and n, which is slightly deviated from linearity in the range of small n-values (Fig. 4), x_{max}/l being generalized dimensionless expression of the peak position.

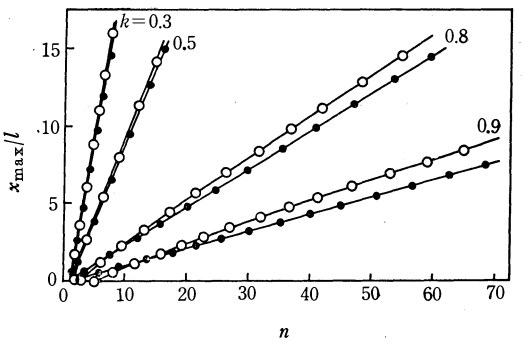

Fig. 4. The peak position *versus* number of zone passes.
○—○ The present equation (10)
●—● Reiss-Helfand's equation (2)

ZMC Distribution Curve on a Multiple Zone Charge Method

The theory of ZMC fractionation tells us that the separation between two components having different k-values becomes more effective with increasing number of zone passes n, as shown by Eq. (12),[9] the shorter zone length being required for attaining the more efficient separation on the column of a limited length, L. However, such shortened zone length would decrease the amount of the sample to be fractionated, as long as the sample mixture was placed initially one zone length high. Thus the question arises of how the separation is affected when the initial charge of a sample mixture is placed by more than single zone length on the column top.

Assuming that the sample mixture of k less than unity is charged by T-folds of a unit zone length l on the upper end of a column from which a zone starts to travel downwards (Fig. 5), the solute distribution after a ZMC process can be calculated as follows.

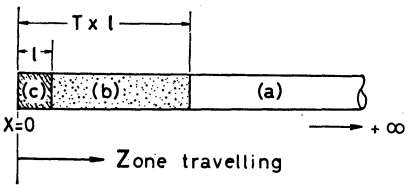

Fig. 5. Multiple zone charge method.
(a): Pure solid solvent
(b): Initial charge of sample mixture
(c): Molten zone

At the first zone pass, in so far as the freezing interface of a molten zone moves in the region $0<x<(T-1)l$, the solute is distributed by an ordinary zone melting process according to the equation,[7]

$$C_1(x)/C_i = 1 - (1-k)\exp(-kx/l) \quad (13)$$

where $0<x<(T-1)l$.

When the freezing interface arrives at $x=(T-1)l$, the solute concentration in the solid just frozen at this point is given by

$$C_1(x)/C_i = 1 - (1-k)\exp\{-k(T-1)\} \quad (14)$$

The solute concentration in the molten zone is therefore given by

$$C_i' = C_i[1-(1-k)\exp\{-k(T-1)\}]/k \quad (15)$$

From this point, ZMC process begins with C_i' as the initial concentration according to an equation analogous to Eq. (5):

$$C_1\{x-(T-1)l\} = kC_i'\exp[-k\{x-(T-1)l\}/l] \quad (16)$$

After the second zone pass, the solute is redistributed according to Eq. (1) from the solute distribution profile developed on the preceding zone pass. The analytical method for determining the solute distribution profile is generally too complicated, and a numerical computation provides much easier solution.

Computation was carried out by the Runge-Kutta-Gill method for Eq. (1), taking the zone length l and the initial concentration C_i both as unity, the grid spacing being one twentieth of the zone length.[11] The solute concentration at the upper end of the column on each pass $C_n(0)$ is given by

$$C_n(0) = k\int_0^1 C_{n-1}(x)\mathrm{d}x \quad (17)$$

which was also computed by use of Simpson's numerical integration method with an integration step equal to the grid spacing.

Numerically computed concentration profile after each pass was counter-checked by Simpson's integration of a solute amount over the whole range of solute distribution in a similar procedure to that described above. The integrated magnitude of the solute amount remained constant from pass to pass, being equal to that in the initial charge TlC_i.

A few examples of solute distribution profiles after 20 zone passes are shown in Fig. 6. Each curve is normalized for comparison, which suggests that are very little differences between the distribution curves where T-values are less than 5, especially in the case of small k-values. The situation is further clarified by Figs. 7 and 8 showing the peak position and the half peak width plotted against n for a certain range of T-values, respectively, which were also numerically computed. If one compares the peak position of the multiple zone charge method with that of the ordinary single zone charge method ($T=1$) in the case of $k=0.3$ after 40 zone passes, the peak position by the former method shifts towards positive x only 1.3% of that by the latter method. Even in the case of $k=0.8$, the relative distance of the shift is within 8%. Fig. 8 indicates that the difference in the half peak widths between the two methods is also insignificant; the relative differences are within only 0.4 and 3.5% for

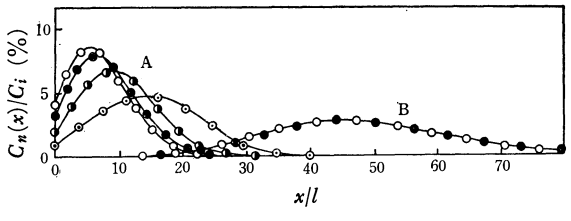

Fig. 6. Solute distribution curves by multiple zone charge method after 20th zone pass, where T means multiplicity of multiple zone charge.
○ $T=1$, ● $T=5$, ◐ $T=10$, ⊙ $T=20$
A: $k=0.8$, B: $k=0.3$

11) L. Lapidus, "Digital Computation for Chemical Engineers," McGraw-Hill, Inc., New York, N. Y. (1962), p. 89.

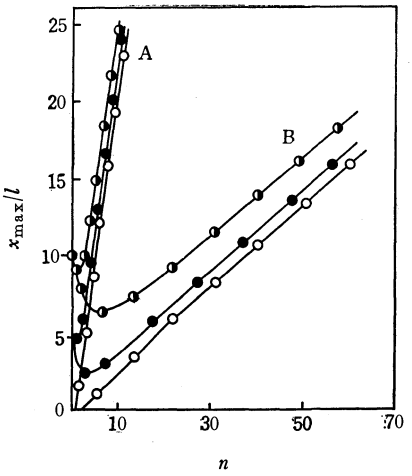

Fig. 7. Peak position of multiple zone charge sample.
○ $T=1$, ● $T=5$, ◑ $T=10$
A: $k=0.3$, B: $k=0.8$

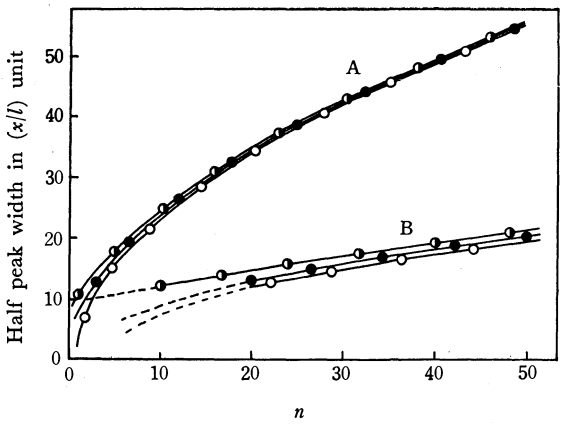

Fig. 8. Half peak width of distribution profiles *versus* number of zone passes.
○ $T=1$, ● $T=5$, ◑ $T=10$
A: $k=0.3$, B: $k=0.8$

$k=0.3$ and 0.8 after 40 zone passes, respectively, the difference decreasing considerably with increase in number of zone passes. As far as the efficacy as a separating method is concerned, we could find no disadvantages in the present multiple zone charge method as compared with the ordinary single zone charge method.

This method should be useful working with a large quantity of sample or solutes, solubilities of which in a solid solvent are relatively small. With use of the single zone charge method, even if the length of the initial charge is not rigorously equal to a unit zone length, no significant difference would result as regards the solute distribution profile.

An Optimum Mode of Stepwise Decreasing Zone Length for Improving the Concentrating Efficiency by Zone Melting Method

Regarding the efficiency of the zone melting method as a separating technique, normal freezing was the most effective at the first zone pass and the shorter zone length was the more effective after an indefinitely large number of zone passes,[12] and the solute concentration profile is expected to approach very rapidly the ultimate distribution by adjusting the zone length in the following manner; at the first zone pass, $l=L$, namely normal freezing process, and after the second pass, zone length decreases stepwise pass after pass. Such a method would be useful from the viewpoint of saving time.

Eckschlager and co-workers calculated the efficiency as a refining method for the cases where zone length decreased in seemingly arbitrary manner with increase in zone passes.[13] We have also investigated the technique, and calculated the optimum mode of stepwise decrease of zone length, which gave the maximum concentration in the bottom portion of a given length S after each zone pass.

Optimization of zone length is carried out in the following procedure for a set of specified k- and S values:
1) At the first zone pass ($n=1$), zone length is equal to the total column length L, the solute distribution being therefore determined by the normal freezing process, which has been given analytically[14] as

$$C_1(x) = kC_0(1-x/L)^{k-1} \tag{18}$$

where x denotes the position of the freezing interface as $x=0$ at the column top, and C_0 the initial concentration of a solute of k less than unity in the ingot.
2) At the second pass ($n=2$), based upon the distribution profile developed by the normal freezing process, distribution profiles are numerically calculated for 200 different zone lengths l_j with an increment of $0.005L$ unit from $0.005L$ to $1.0L$.

$$l_j = 0.005\,Lj \qquad j = 1, \cdots\cdots, 200 \tag{19}$$

Computation for the region of the zone melting process was programmed by the Runge-Kutta-Gill method for Eq. (1)[11], where $n=2$ and $l=l_j$ ($j=1, \cdots\cdots, 200$), taking $L=100$ and $C_0=1$, and grid spacing defined as $L/2000$. Normal freezing on the last zone length of the column is calculated numerically for the points in the region in $L-l_j<x<L$ with an increment of $L/2000$, which is equal in magnitude to the grid spacing, according to the analytical equation

$$C_{nj}(x) = kC'_j\{(L-x)/l_j\}^{k-1} \tag{20}$$

where

$$C'_j = C_{nj}(L-l_j)/k \tag{21}$$

$n=2$ and $L-l_j<x<L$.

Solute concentration at the column top, $C_{2j}(0)$, is given by

$$C_{2j}(0) = k\int_0^{l_j} C_1(x)\mathrm{d}x \tag{22}$$

This was computed by Simpson's numerical method with an integration step equal to the grid spacing defined in the Runge-Kutta-Gill calculation.

Solute amount in the bottom portion of a specified length S is given by

12) a) L. Burris, Jr., C. H. Stockman, and I. G. Dillon, *Trans. AIME*, **203**, 1017 (1955). b) W. G. Pfann, Ref. 7, pp. 31 and 42—45.
13) K. Eckschlager, V. Ettel, P. Stopka, and Z. Kodejs, *Coll. Czech. Chem. Commun.*, **36**, 3900 (1971).
14) W. G. Pfann, Ref. 7, p 11.

$$M_{nSj} = C_0L - \int_0^{L-S} C_{nj}(x)\mathrm{d}x \qquad (23)$$

where $n=2$, assuming a unit cross section of the column. The second term for each distribution profile was computed also by Simpson's method in a similar manner to that described above.

The distribution profile giving the highest value of M_{2Sj} with different j is then stored into the memory for calculation of zone lengths in the 3rd pass, and the zone length bringing the highest M_{2Sj}-value is defined as the optimum zone length in the 2nd pass.

3) At the n-th pass after the third pass, the optimum zone length is determined in a similar manner to that described above, from the distribution profile which is brought by the optimized $(n-1)$-th zone pass. The distribution profile which is formed by the zone length optimized for the n-th pass, is then stored for computation of the zone lengths in the $(n+1)$-th pass.

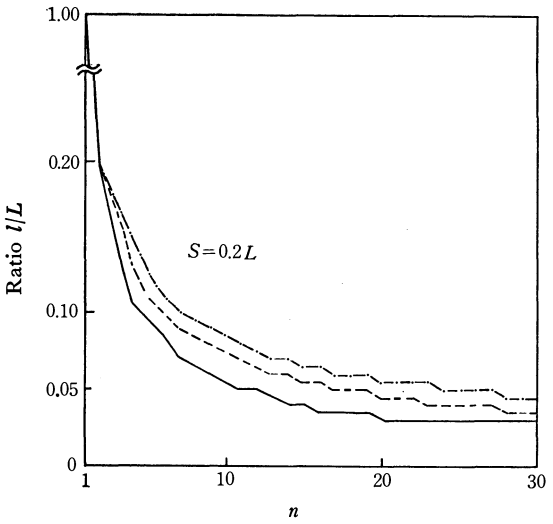

Fig. 9—1. Optimum zone length in ratio to L on each zone pass.
—·—· $k=0.8$, ——— $k=0.5$, —— $k=0.2$

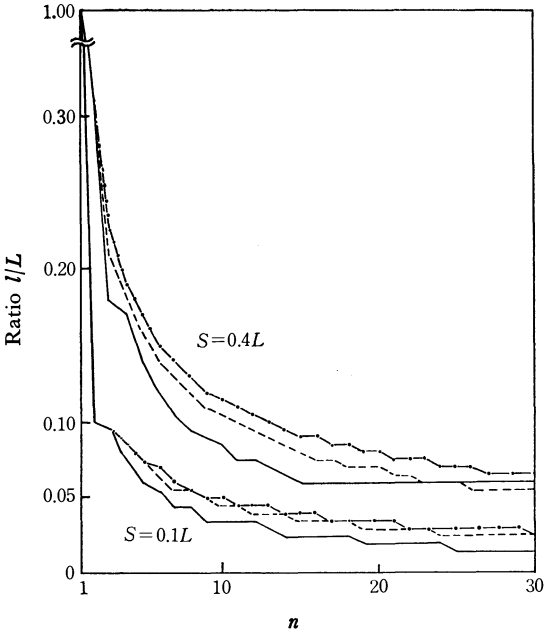

Fig. 9—2. Optimum zone length in ratio to L on each zone pass.
—·—· $k=0.8$, ——— $k=0.5$, —— $k=0.2$

Fig. 9 shows a few examples of the optimized mode of stepwise decrease of zone length for various k and S-values.

The superior efficacy of the present decreasing zone length (DZ) method is shown in Fig. 10 and Tables 1 and 2, in comparison with the conventional constant zone length (CZ) method.

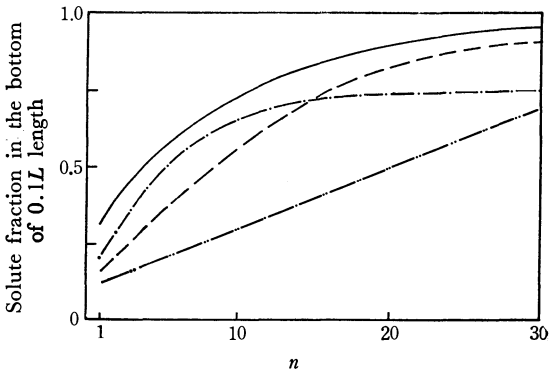

Fig. 10. Solute fraction concentrated into the bottom portion of $0.1L$ length after n-th zone pass, $k=0.5$.
—— DZ method, ——— CZ method, $l=0.05L$, —·—· CZ method, $l=0.10L$, —··— CZ method, $l=0.02L$

In Fig. 10 the solute fraction, which is concentrated in the bottom portion of $S=0.1\ L$, is plotted against number of zone passes upon applying the DZ- and CZ methods to a system of $k=0.5$. It is apparent that, though the solute is concentrated in various ways to the bottom portion, efficiency in concentrating a solute by the DZ method is always superior to the CZ method, when compared at the same number of zone passes.

Table 1. Fraction concentrated into a portion of $0.1\ L$ at the bottom after the 30 th zone pass

k	DZ method	CZ method		
		$l=0.1L$	$l=0.05L$	$l=0.02L$
0.1	1.0000	0.9899	0.9997	1.0000
0.2	1.0000	0.9599	0.9970	1.0000
0.3	0.9997	0.9099	0.9883	0.9906
0.4	0.9955	0.8399	0.9663	0.8915
0.5	0.9600	0.7491	0.9077	0.6883
0.6	0.8435	0.6337	0.7716	0.4977
0.7	0.6388	0.4911	0.5661	0.3535
0.8	0.4081	0.3355	0.3584	0.2445
0.9	0.2195	0.1976	0.2000	0.1614

Table 1 gives a comparison of the two methods as regards concentrating techniques. Values indicate the fraction of the solute concentrated into the bottom portion of 0.1 L after 30 zone passes.

Table 2 gives a comparison from a viewpoint of refining efficiency. Values indicate the length (% to L) of the portion which is purified to the average concentration level indicated on each heading. After 30 zone passes of the DZ method, for example, within 79.7% of the column length from the top, averaged

TABLE 2. LENGTH OF PURIFIED PORTION IN % OF A WHOLE LENGTH FROM THE COLUMN TOP AFTER THE 30 TH ZONE PASS

	DZ method		CZ method					
			$l=0.1L$		$l=0.05L$		$l=0.02L$	
C_{av}/C_0	1/100	1/1000	1/100	1/1000	1/100	1/1000	1/100	1/1000
$k=0.1$	97.9	96.5	89.7	82.3	94.9	91.2	97.9	96.5
0.2	96.8	95.1	83.6	74.6	91.9	87.6	96.8	95.0
0.3	95.7	93.1	77.9	65.9	89.3	83.5	89.4	62.7
0.4	91.8	81.7	70.5	54.6	85.3	72.3	49.5	29.9
0.5	79.7	48.7	59.3	32.3	62.7	24.2	25.1	9.6
0.6	43.4	2.2	31.2	0	20.2	0	8.1	0
0.7	0	0	0	0	0	0	0	0
0.8	0	0	0	0	0	0	0	0
0.9	0	0	0	0	0	0	0	0

concentration C_{av} of an impurity of $k=0.5$ is less than 1/100 of the initial concentration C_0, and within 48.7 % of the column length, the impurity level is less than 1/1000, while by the CZ method of $l=0.02\,L$, the corresponding length is 25.1 and 9.6% for the respective impurity levels.

It should be mentioned that, since a series of the optimum zone lengths is determined by a specified set of k- and S values of a system under consideration, and since the mode of stepwise decrease of zone length differs considerably with k- and S values, difficulties remain in the instrumentation of the present DZ method.

Appendix

Proof that Eq. (10) is a solution of Eq. (1).

If $K_n(x)$ is defined by

$$K_n(x) = \exp(\beta x)C_n(x) \tag{24}$$

where $\beta=k/l$, then Eqs. (1) and (10) can be rewritten respecitively as

$$dK_n(x)/dx = \beta\exp(-k)K_{n-1}(x+l) \tag{25}$$

$$K_n(x) = \sum_{r=0}^{n-1}\beta^r C_{n-r}(0)\exp(-rk)x(x+rl)^{r-1}/r! \tag{26}$$

Equation (10) can be verified to be a solution of Eq. (1) by showing that Eq. (26) is a solution of Eq. (25).

First, we verify that Eq. (26) is a solution of Eq. (25) when $n=1$.

From Eq. (26), $K_1(x)$ is given by

$$K_1(x) = C_1(0) \tag{27}$$

By substituting Eq. (5) into Eq. (24) where $n=1$, Eq. (27) can be found to hold under the present initial conditions.

Assuming that Eq. (26) is the right solution at $n=N$, we verify that it also holds for $n=N+1$.

Equation (25) is written for $n=N+1$ as

$$dK_{N+1}(x)/dx = \beta\exp(-k)K_N(x+l) \tag{28}$$

By integrating the equation over the region from 0 to x, we have

$$\int_0^x dK_{N+1}(x) = \beta\exp(-k)\int_0^x K_N(x+l)dx \tag{29}$$

or

$$K_{N+1}(x) - K_{N+1}(0) = \beta\exp(-k)\int_0^x K_N(x+l)dx \tag{30}$$

By substituting Eq. (26) into Eq. (30), the right-hand side is written as

$$\beta\exp(-k)\int_0^x K_N(x+l)dx = \beta\exp(-k)\sum_{r=0}^{N-1}[\{\beta^r C_{N-r}(0)\exp(-rk)/r!\} \times \int_0^x (x+l)\{x+(r+1)l\}^{r-1}dx] \tag{31}$$

The last integration can be readily performed to give

$$\int_0^x (x+l)(x+(r+1)l\}^{r-1}dx = x\{x+(r+1)l\}^r/(r+1)$$

Substituting this relation into Eq. (31), we obtain

$$\beta\exp(-k)\int_0^x K_N(x+l)dx = \beta\exp(-k)\sum_{r=0}^{N-1}\beta^r C_{N-r}(0) \times \exp(-rk)x\{x+(r+1)l\}^r/r!(r+1) = \sum_{r=0}^{N-1}\beta^{(r+1)}C_{N-r}(0) \times \exp\{-(r+1)k\}x\{x+(r+1)l\}^r/(r+1)! \tag{32}$$

Substituting this relation into Eq. (30), and considering the identity

$$K_{N+1}(0) = C_{N+1}(0) \tag{33}$$

which is readily derived from Eq. (24), we have

$$K_{N+1}(x) = C_{N+1}(0) + \sum_{r=0}^{N-1}\beta^{(r+1)}C_{N-r}(0) \times \exp\{-(r+1)k\}x\{x+(r+1)l\}^r/(r+1)! = \sum_{s=0}^{N}\beta^s C_{N+1-s}(0)\exp(-sk)x(x+sl)^{s-1}/s! \tag{34}$$

where $s=r+1$.

This can readily be seen to be equivalent to Eq. (26), where $n=N+1$. Equation (26) is proved by mathematical induction to be a solution of Eq. (25) for all n, n being any positive integer. Thus by introducing Eq. (26) into Eq. (24), we obtain Eq. (10).

The authors are grateful to Dr. S. Gondo, Department of Chemical Engineering, and Mr. T. Tsuneyuki, Department of Organic Synthesis, Kyushu University, for their helpful advice in FORTRAN programming.

Circular Dichroism and Absolute Configuration of Triammine(sarcosinate-*N*-monopropionato)cobalt(III) Chloride and Several Analogues

Ken-ichi OKAMOTO, Jinsai HIDAKA, and Yoichi SHIMURA

Department of Chemistry, Faculty of Science, Osaka University, Toyonaka, Osaka 560

(Received June 13, 1973)

cis(O)- and *trans(O)*-Triammine(sarcosinate-*N*-monopropionato)cobalt(III) salts, which have an asymmetrically coordinated nitrogen atom, were prepared and the *cis(O)* isomer was optically resolved through its diastereomeric salt with $(+)_{546}$-(ethylenediaminetetraacetato)cobaltate(III) anion. The less soluble diastereomeric salt produced $(+)_{546}$-*cis(O)* isomer of the triammine cation, and its absolute configuration (*R*) was established from circular dichroism spectrum, referring to the stereochemistry of the several analogous triammine complexes stereospecifically formed, which contain L-alaninate- and L-prolinate-*N*-monocarboxylate ligands, where the carboxylate stands for acetate or propionate. Two diastereomeric isomers, *R*(N)-L(C) and *S*(N)-L(C), were synthesized for the *cis(O)*-(L-alaninate-*N*-monopropionato)triamminecobalt(III) perchlorate salt.

In previous papers,[1,2] the stereochemistry was studied for cobalt(III) complexes with several *O,N,O*-tridentate ligands such as L-alaninate-*N*-monoacetate (L-alama^{2-})[1] and L-prolinate-*N*-monopropionate (L-promp^{2-}).[2] Most of these *O,N,O*-tridentate ligands contain an asymmetric carbon atom, and the cobalt(III) complexes formed have two or more kinds of chiral centers, namely each one of asymmetric carbon (L) and nitrogen (*R* or *S*) atoms per one ligand, and in some cases a configurational chirality (*Δ* or *Λ*). The additivity of the two or more kinds of circular dichroism (CD) contributions was discussed, but the lack of an appropriate model complex which contains only one asymmetric nitrogen atoms prevented us from thorough elucidation. The present paper deals with such a model complex newly synthesized, triammine(sarcosinate-*N*-monopropionato)cobalt(III) cation. The ligand sarcosinate-*N*-monopropionate (sarmp^{2-}) forms a five- and a six-membered chelate rings by coordination of an α-aminocarboxylate foot and an *N*-propionate one, respectively. This allowed the existence of two geometrical isomers, *cis(O)* and *trans(O)*, of the triammine complex.

The optical resolution of the *cis(O)* isomer was made successfully and the absolute configuration was established from the consideration of the CD spectrum, referring to the stereochemistry and CD spectra of analogous triammine complexes with L-alama^{2-}, L-alamp^{2-} (L-alaninate-*N*-monopropionate), L-proma^{2-} (L-prolinate-*N*-monoacetate), and L-promp^{2-}. The conclusion coincides with that obtained by an X-ray crystal structure study of the diastereomer, $(+)_{546}$-*cis(O)*-[Co(sarmp)$(NH_3)_3$]·$(+)_{546}$-[Co(edta)]·H_2O, of which a preliminary report has been presented recently.[3]

Experimental

Preparation of Ligands. (1). L-alanine-*N*-monoacetic, L-proline-*N*-monoacetic and L-proline-*N*-monopropionic acids were described in the previous papers.[1,2]

(2) L-Alanine-N-monopropionic Acid. A solution of 41 g (0.46 mol) of L-alanine in 92 ml of 5 M potassium hydroxide was mixed with the solution of 50 g (0.46 mol) of 3-chloropropionic acid in 92 ml of 2.5 M potassium hydroxide, and 92 ml of 7.5 M potassium hydroxide was added drop by drop to the mixture with vigorous stirring at 80—85 °C on an oil bath. The mixture was maintained in the pH range 8—9 during the reaction. The reaction mixture was further stirred for about 15 min, cooled to 40 °C, and 119 ml (1.44 mol) of 70% perchloric acid was added to it. The potassium perchlorate resulted was filtered off. The filtrate was concentrated in a vacuum evaporator at 40 °C. The solution concentrated was neutralized with 18 g (0.45 mol) of sodium hydroxide in 20 ml of water. The white deposit was filtered, and recrystallized from warm water. The crystals were washed with ethanol and ether, and then dried in a vacuum desiccator. Yield 33 g. $[\alpha]_D^{20}=+3.2°$ (*c.* 2.47, water). Found: C, 43.93; H, 6.89; N, 8.54%. Calcd for L-alampH$_2$=$C_6H_{11}NO_4$: C, 44.72; H, 6.88; N, 8.69%.

(3). Sarcosine-*N*-monopropionic acid was prepared by the procedure similar to that in (2), and more soluble in water than the other acids. Found: C, 43.49; H, 6.82; N, 8.43%. Calcd for sarmpH$_2$·1/4H_2O=$C_6H_{11}NO_4$·1/4-H_2O: C, 43.50; H, 7.00; N, 8.46%.

Preparation and Separation of Complexes. A solution of 8.9 g (0.17 mol) of ammonium chloride and 9.9 ml (0.15 mol) of 28% aqueous ammonia in 40 ml of water was mixed with a solution of the *O,N,O*-tridentate acid (0.042 mol) neutralized by sodium hydroxide in 20 ml of water. To this was added a solution of 10 g (0.042 mol) of cobalt(II) chloride hexahydrate in 10 ml of water. The molar ratio among Co^{2+}, *O,N,O*-tridentate ligand, NH_3, and NH_4^+ takes 1 : 1 : 3.5 : 4. Ten grams of lead dioxide was added to the mixture, and this was stirred at about 40—50 °C for an hr. The color of the solution turned from dark red to reddish violet. After having been allowed to stand at room temperature for 30 min, the reaction mixture was filtered to remove an excess of lead dioxide, and the filtrate was kept in a refrigerator. A small amount of yellow deposit, [Co$(NH_3)_6$]Cl_3, was filtered off. The filtrate was poured into a column (35 mm × 500 mm) containing strong-acid cation exchange resin (Dowex 50WX8 200—400 mesh, sodium form). After the column had been swept with water, the adsorbed band was eluted with 0.1 M aqueous solution of sodium perchlorate at a rate of 2.5 ml per min.

(4) trans(O)- *and* cis(O)-[*Co*(L-*promp*)$(NH_3)_3$]ClO_4. The complexes were already reported.[2] A great portion of the complex obtained consisted of the *cis(O)* isomer, and the *trans(O)* one occurred in a trace amount.

(5) trans(O)-[*Co(sarmp)*$(NH_3)_3$]ClO_4 *and* cis(O)-[*Co-(sarmp)*-$(NH_3)_3$]*Cl*. Two colored bands, violet one (i)

1) K. Okamoto, J. Hidaka, and Y. Shimura, This Bulletin, **44**, 1601 (1971).

2) K. Okamoto, J. Hidaka, and Y. Shimura, *ibid.*, **46**, 475 (1973).

3) K. Okamoto, T. Tsukihara, J. Hidaka, and Y. Shimura, *Chem. Lett.*, **1973**, 145.

in a small amount and red one (ii) in a large amount, were eluted in this order. These eluates were separately concentrated in a vacuum evaporator and a large amount of ethanol was added to the concentrated solution. The desired complex was collected by filtration and recrystallized from a small amount of water by adding ethanol. It was confirmed by absorption measurements that the eluate (i) contained *trans(O)*-[Co(sarmp)$(NH_3)_3]^+$ and the eluate (ii) *cis(O)* one. The pure complexes were obtained as perchlorate salts. The *cis(O)* perchlorate was dissolved in a small amount of water and the solution was poured into a column containing strong-base anion exchange resin (Dowex 1-X8, 200—400 mesh, chloride form). The column was eluted with water and an appropriate amount of acetone was added to the eluate. In this procedure, the *cis(O)* perchlorate was converted into the chloride salt and washed with acetone and then dried in a vacuum desiccator.

(6) cis(O)-[*Co(ida)*$(NH_3)_3]ClO_4$. Two colored bands, a reddish violet one (i) in a small amount and a red one (ii) in a large amount, were eluted in this order. It was identified by absorption measurements and analytical results that the eluate (i) was a by-product containing two iminodiacetate ligands and the eluate (ii) was *cis(O)*-[Co(ida)$(NH_3)_3]^+$. The eluate (ii) was treated as in (5) and the desired complex was obtained as perchlorate salt.

(7) cis(O)-[*Co(*L-*proma)*$(NH_3)_3]ClO_4$. Two colored bands, violet one (i) in a small amount and red one (ii) in a large amount, were eluted in this order. From the absorption measurements, the eluate (i) was confirmed to be a by-product as in (6) and the eluate (ii) *cis(O)*-[Co(L-proma)$(NH_3)_3]^+$. The eluate (ii) was treated as in (5).

(8) cis(O)-[*Co(*L-*alama)*$(NH_3)_3]ClO_4$. Only one red band was eluted and the desired complex was obtained by adding a large amount of ethanol to the concentrated eluate and recrystallized from a small amount of water by adding ethanol. Two kinds of crystals were obtained and it was confirmed that one was *cis(O)*-[Co(L-alama)$(NH_3)_3]ClO_4 \cdot 1/2H_2O \cdot 1/4C_2H_5OH$ and the other *cis(O)*-[Co(L-alama)$(NH_3)_3]ClO_4 \cdot 3/4H_2O$, from their absorption and NMR spectra and by elemental analysis (see Table 1).

(9) trans(O)-[*Co(*L-*alamp)*$(NH_3)_3]ClO_4$, R- *and* S-cis(O)-[*Co(*L-*alamp)*$(NH_3)_3]ClO_4$. By elution, a reddish purple band (i) in a large amount and two adjacent red bands (ii) and (iii) in small amounts were obtained. By absorption measurements, it was confirmed that the eluate (i) contained *trans(O)*-[Co(L-alamp)$(NH_3)_3]^+$ and the eluates (ii) and (iii) *cis(O)*-[Co(L-alamp)$(NH_3)_3]^+$. These eluates were separately concentrated in a vacuum evaporator. The perchlorate of *trans(O)* isomer was precipitated by concentrating the eluate (i) and recrystallized from a small amount of water by adding ethanol. The perchlorates of *cis(O)* isomers ii (*R*) and iii (*S*) were obtained by adding a large amount of ethanol to the concentrated eluates (ii) and (iii), respectively. The isomer iii was recrystallized from ethanol and obtained as hygroscopic crystals. These pure complexes were washed with ethanol and dried in a vacuum desiccator.

Optical Resolution of Complex.

(10) $(+)_{546}$-cis(O)-[*Co(sarmp)*$(NH_3)_3]Cl$. Silver acetate (0.30 g) was added to a solution of 0.54 g of racemic *cis(O)*-[Co(sarmp)$(NH_3)_3]$Cl in a minimum amount of water and the silver chloride resulted was filtered off. A solution of 0.375 g of $(+)_{546}$-K[Co(edta)]$\cdot 2H_2O$[4] in a minimum amount of water was added to the filtrate. The mixture was concentrated by stream of air at room temperature and then kept in a refrigerator overnight. The violet crystals deposited as the less soluble diastereomer were collected by filtration (yield: 95 mg) and recrystallized from a small amount of water by adding ethanol. The pure diastereomer was washed with ethanol and dried in a vacuum desiccator. An aqueous solution of the diastereomer was poured into a column containing strong-base anion exchange resin (Dowex 1-X8, 200—400 mesh, chloride form) and the column was washed with water. An appropriate amount of acetone was added to the eluate to obtain the desired complex. The optically active $(+)_{546}$-*cis(O)*-[Co(sarmp)-$(NH_3)_3]$Cl was washed with acetone and dried in a vacuum desiccator. $\Delta\varepsilon_{546} = +0.35$.

The analytical results for the cobalt(III) complexes obtained are shown in Table 1.

Measurements. The electronic absorption spectra were measured by a Beckman DU spectrophotometer and Shimadzu spectrophotometer UV-200. The CD spectra were recorded with a JASCO Model J-10 or J-20 spectropolarimeter with a CD attachment or by Roussel-Jouan Dichrograph. A Yanagimoto spectropolarimeter, Model 185, was used to examine the eluates from the chromatographic column. All the measurements were made in aqueous solution at room temperature.

The infrared spectra were measured with a JASCO DS-402G spectrophotometer with NaCl prism using KBr disk samples. The proton nuclear magnetic resonance spectra of the complexes were recorded with a Japan Electron Optics JNM-4H 100 spectrometer operating at 100 MHz, in D_2O solutions. Measurements were carried out using *t*-butanol as an internal standard. All the signals lie at a lower field than that of the standard. The chemical shifts are referred to NaTMS (sodium trimethylsilylpropanesulfonate) as zero; *t*-butanol resonate at 1.234 ppm down field of NaTMS.

Results and Discussion

Visible Absorption Spectra. The present triammine complexes which belong to a $[Co^{III}(O)_2(N)_4]$ type are divided into two groups on the characteristics of splitting of their first d–d absorption bands. The first group has a shoulder at higher energy side of the major peak which is located at $18.3—19.0 \times 10^3$ cm^{-1}, and the second group a vague shoulder at lower energy side of the major peak, $19.3—19.9 \times 10^3$ cm^{-1} (Fig. 1 and Table 2). By referring to a general theory of the splitting pattern of first absorption bands of cobalt(III) complexes,[5,6] it is concluded that the first group (including L-alamp, L-promp, and sarmp complexes) has *trans(O)* structure with a meridionally coordinated *O,N,O*-tridentate ligand and the second (including ida, L-alama, and L-proma complexes and another set of L-alamp, L-promp, and sarmp ones) has *cis(O)* structure with a facially coordinated *O,N,O*-tridentate ligand. The ligands ida, L-alama, and L-proma form two five-membered chelate rings by coordination and the ligands L-alamp, L-promp, and sarmp form each one of five- and six-membered chelate ring with an α-aminocarboxylate part and an *N*-propionate foot, respectively. Thus the inclusion of the six-membered

4) F. P. Dwyer and F. L. Garvan, "Inorg. Syntheses," Vol. 6, p. 192 (1960).

5) H. Yamatera, This Bulletin, **31**, 95 (1958); C. E. Schäffer and C. K. Jørgensen, *Mat. Fys. Medd. Dan. Vid. Selsk.*, **34**, No. 13 (1965).

6) N. Matsuoka, J. Hidaka, and Y. Shimura, This Bulletin, **40**, 1868 (1967).

TABLE 1. ANALYTICAL DATA

Complex	C (%)		H (%)		N (%)	
	Calcd	Found	Calcd	Found	Calcd	Found
trans(*O*)-[Co(L-alamp)$(NH_3)_3$]$ClO_4 \cdot 1/2H_2O$	19.08	18.63	5.07	5.08	14.84	14.72
trans(*O*)-[Co(sarmp)$(NH_3)_3$]$ClO_4 \cdot 1/2H_2O \cdot 1/4NaClO_4$	17.65	17.96	4.69	4.74	13.72	13.92
cis(*O*)-[Co(ida)$(NH_3)_3$]$ClO_4 \cdot 1/4H_2O$	13.92	13.97	4.24	4.33	16.24	16.23
cis(*O*)-[Co(L-alama)$(NH_3)_3$]$ClO_4 \cdot 3/4H_2O$	16.31	16.35	4.79	4.82	15.22	15.27
cis(*O*)-[Co(L-alama)$(NH_3)_3$]$ClO_4 \cdot 1/2H_2O \cdot 1/4C_2H_5OH$	17.60	17.22	4.97	4.93	14.94	15.26
cis(*O*)-[Co(L-proma)$(NH_3)_3$]$ClO_4 \cdot 1/4H_2O$	21.83	22.17	4.84	4.82	14.55	14.43
cis(*O*)-[Co(L-alamp)$(NH_3)_3$]$ClO_4 \cdot H_2O$ (isomer ii)	18.63	18.47	5.21	5.20	14.49	14.27
cis(*O*)-[Co(L-alamp)$(NH_3)_3$]$ClO_4 \cdot H_2O$ (isomer iii)	18.63	18.35	5.21	5.01	14.49	14.51
cis(*O*)-Co(sarmp)$(NH_3)_3$]Cl	23.66	23.34	5.96	5.97	18.39	18.19
$(+)_{546}$-*cis*(*O*)-[Co(sarmp)$(NH_3)_3$]$Cl \cdot H_2O$	22.36	22.29	6.25	6.28	17.37	17.24

TABLE 2. ABSORPTION MAXIMA OF [Co(*O*,*N*,*O*-tridentato)$(NH_3)_3$]$^+$ IONS

Complex ion	I band		II band	
	$\tilde{\nu}_{max}$	($\log \varepsilon_{max}$)	$\tilde{\nu}_{max}$	($\log \varepsilon_{max}$)
trans(*O*)-[Co(L-alamp)$(NH_3)_3$]$^+$	19.0	(2.24)	27.7	(2.14)
trans(*O*)-[Co(L-promp)$(NH_3)_3$]$^+$	18.5	(2.23)	27.1	(2.24)
trans(*O*)-[Co(sarmp)$(NH_3)_3$]$^+$	18.3	(2.17)	27.0	(2.20)
cis(*O*)-[Co(ida)$(NH_3)_3$]$^+$	19.9	(2.00)	28.3	(2.13)
cis(*O*)-[Co(L-alama)$(NH_3)_3$]$^+$	19.8	(1.96)	28.2	(2.09)
cis(*O*)-[Co(L-proma)$(NH_3)_3$]$^+$	19.4	(1.99)	28.5	(2.06)
cis(*O*)-*R*-[Co(L-alamp)$(NH_3)_3$]$^+$	19.8	(2.07)	27.7	(2.07)
cis(*O*)-*S*-[Co(L-alamp)$(NH_3)_3$]$^+$	19.9	(2.02)	27.6	(2.02)
cis(*O*)-[Co(L-promp)$(NH_3)_3$]$^+$	19.3	(1.94)	27.5	(2.00)
cis(*O*)-[Co(sarmp)$(NH_3)_3$]$^+$	19.3	(1.97)	27.3	(2.02)

The wave numbers are given in 10^3 cm^{-1}.

TABLE 3. CD DATA OF [Co(*O*,*N*,*O*-tridentato)$(NH_3)_3$]$^+$ IONS

Complex ion	I band		II band	
	$\tilde{\nu}_{ext}$	($\Delta\varepsilon_{ext}$)	$\tilde{\nu}_{ext}$	($\Delta\varepsilon_{ext}$)
trans(*O*)-*R*-[Co(L-alamp)$(NH_3)_3$]$^+$	17.2	(−0.06)	27.8	(+0.08)
	19.0	(+0.28)		
	21.4	(−0.81)		
trans(*O*)-*R*-[Co(L-promp)$(NH_3)_3$]$^+$	17.2	(−0.64)	27.2	(−0.09)
	19.0	(+0.92)		
	21.3	(−0.10)		
cis(*O*)-*R*-[Co(L-alama)$(NH_3)_3$]$^+$	18.1	(−0.17)	28.4	(−0.22)
	19.8	(+0.12)		
	21.9	(−0.17)		
cis(*O*)-*R*-[Co(L-proma)$(NH_3)_3$]$^+$	17.9	(−0.30)	28.1	(−0.46)
	19.9	(+1.04)		
cis(*O*)-*R*-[Co(L-alamp)$(NH_3)_3$]$^+$ (isomer ii)	18.4	(+0.38)	27.4	(−0.18)
	21.2	(−0.39)		
cis(*O*)-*S*-[Co(L-alamp)$(NH_3)_3$]$^+$ (isomer iii)	17.3	(+0.08)	27.8	(+0.34)
	19.5	(−0.22)		
cis(*O*)-*R*-[Co(L-promp)$(NH_3)_3$]$^+$	18.7	(+0.66)	27.4	(−0.18)
$(+)_{546}$-*cis*(*O*)-*R*-[Co(sarmp)$(NH_3)_3$]$^+$	19.2	(+0.52)	27.8	(−0.14)

The wave numbers are given in 10^3 cm^{-1}.

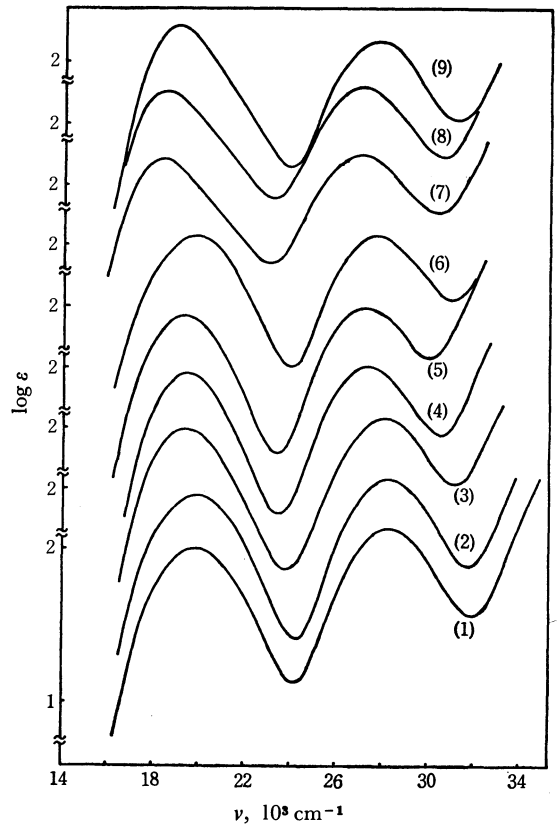

Fig. 1. Absorption curves of $[Co(O,N,O\text{-tridentato})(NH_3)_3]^+$ complexes: (1) ida *cis(O)*, (2) L-alama *cis(O)*, (3) L-proma *cis(O)*, (4) sarmp *cis(O)*, (5) L-promp *cis(O)*, (6) L-alamp *cis(O)-R*, (7) sarmp *trans(O)*, (8) L-promp *trans(O)*, and (9) L-alamp *trans(O)*.

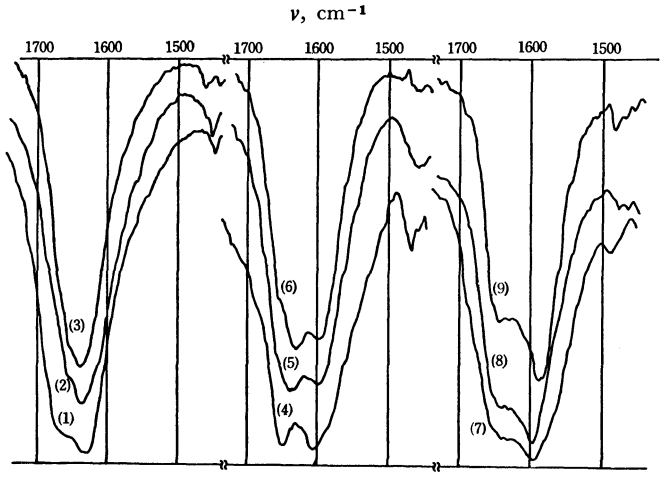

Fig. 2. Infrared curves in antisymmetric C=O stretching band region: (1) ida *cis(O)*, (2) L-alama *cis(O)*, (3) L-proma *cis(O)*, (4) sarmp *cis(O)*, (5) L-alamp *cis(O)-R*, (6) L-promp *cis(O)*, (7) sarmp *trans(O)*, (8) L-alamp *trans(O)*, and (9) L-promp *trans(O)*.

chelate ring is probably a reason for the stable existence of the meridionally coordinated form of the L-alamp, L-promp, and sarmp ligands. It may be worthwhile to note that the maximum intensities of the longer wavelength components of the first absorption bands for the *trans(O)* isomers are unusually large, and this fact is a reason for the apparently weak splitting of the first absorption bands of the *trans(O)* complexes.

Infrared Spectra. The IR spectra in the 1500—1800 cm^{-1} region are illustrated in Fig. 2. The *cis(O)* complexes with ida, L-alama, and L-proma show a strong band at 1630—1640 cm^{-1} and the *cis(O)* complexes with L-alamp, L-promp, and sarmp two strong bands at 1590—1610 cm^{-1} and 1630—1650 cm^{-1}, while the *trans(O)* complexes with L-alamp, L-promp, and sarmp show a strong band at 1585—1600 cm^{-1} with a shoulder at about 1635 cm^{-1}. The bands at 1620—1650 cm^{-1} region are assigned to the antisymmetric C=O stretching of the five-membered chelate ring.[7] The bands at 1585—1610 cm^{-1} region can be assigned to the corresponding carboxylate stretching of the six-membered chelate ring as in the case of $[Co(aspartato)_2]^-$[8] and [Co(ethylenediaminedisuccinato)]$^-$[9].

Stereospecific Formation of Isomers. Since the coordinated nitrogen atom of the *O,N,O*-tridentate complexes is asymmetric except for the ida complex, two isomers *R* and *S* with respect to the nitrogen atom are possible for each of the complexes. Experimentally, only one *cis(O)* isomer was obtained for $[Co(L\text{-proma})(NH_3)_3]^+$, while each one of *cis(O)* and *trans(O)*

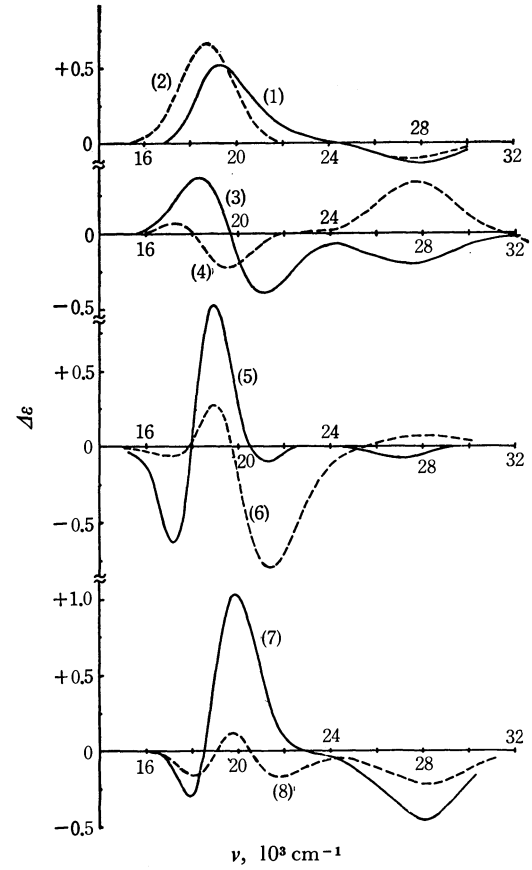

Fig. 3. CD curves of $[Co(O,N,O\text{-tridentato})(NH_3)_3]^+$ complexes: (1) sarmp *cis(O)-R*, (2) L-promp *cis(O)-R*, (3) L-alamp *cis(O)-R*, (4) L-alamp *cis(O)-S*, (5) L-promp *trans(O)-R*, (6) L-alamp *trans(O)-R*, (7) L-proma *cis(O)-R*, and (8) L-alama *cis(O)-R*.

7) K. Nakamoto, "Infrared Spectra of Inorganic and Coordination Compounds", Wiley-Interscience, 1970, p. 232.

8) S. Yamada, J. Hidaka, and B. E. Douglas, *Inorg. Chem.*, **10**, 2187 (1971).

9) J. A. Neal and N. J. Rose, *ibid.*, **7**, 2405 (1968).

isomer for [Co(L-promp)$(NH_3)_3$]$^+$. It has been well established that the configuration of the nitrogen atom of L-prolinate-*N*-monocarboxylate is restricted to *R* by coordination.[1,2] Accordingly, the three complexes are resonably assigned to *R* configuration. As shown in Fig. 3 and Table 3, CD behavior of *cis(O)*-R-[Co(L-promp)$(NH_3)_3$]$^+$ is similar to that of *cis(O)*-R-[Co(sarmp)$(NH_3)_3$]$^+$, of which the absolute configuration has been determined by an X-ray study.[3]

One *trans(O)* and two *cis(O)* isomers were isolated for the [Co(L-alamp)$(NH_3)_3$]$^+$ complex. Of the two *cis(O)* isomers the latter eluent (isomer iii) was obtained in an extremely low yield. Molecular model constructions indicate that a repulsion between the methyl group of *N*-alaninate chelate ring and the ethylenic portion of the *N*-propionate ring exists so far as the nitrogen atom takes *S* configuration, while no repulsion arises for *R* configuration. This suggests that the isomer ii takes *R* configuration and the isomer iii *S* one, and the NMR data of the two *cis(O)* isomers lead us to the same conclusion. One methyl doublet appears at 1.57 and 1.56 ppm for the isomer ii and iii, respectively. According to a theory of C–O interchelate ring magnetic anisotropic deshielding,[11] the methyl protons in the *S* configuration should resonate up field from that of the *R* one. Accordingly, the isomer ii is assigned to *R* and the isomer iii to *S*. The stereospecific dominancy for *R* configuration of L-alamp is also substantiated for the *trans(O)* isomer, because the CD pattern of this isomer (−, +, and − longer wavelength side) isomer similar to that of *trans*-*(O)*-*R*-[Co(L-promp)$(NH_3)_3$]$^+$ in the first absorption band region (Fig. 3).

Contrary to the L-alamp complex, only one *cis(O)* isomer is obtained for the L-alama one. The NMR spectrum points out that the isomer obtained is not a mixture of *R* and *S* isomers. In a former work,[1] two isomers (*RR* and *RS*) of three possible ones (*RR*, *RS*, and *SS*) were obtained for *trans(N)*-[Co(L-alama)$_2$]$^-$ and the non-existence of *SS* isomer and the lower yield of *RS* isomer were explained from the repulsion between the *N*-alaninate methyl group and the protons of acetate of an *S* ligand. The same situation can be supposed for the present triammine complex, *cis(O)*-[Co(L-alama)$(NH_3)_3$]$^+$. It is thus concluded that the *cis(O)* L-alama isomer obtained takes *R* configuration.

CD and Absolute Configuration. The CD spectra are shown in Fig. 3 and Table 3. The diastereomeric pair of isomers of L-alamp *cis(O)* complex, *R*(N)–L(C) and *S*(N)–L(C), provides a tool to evaluate three vicinal CD contributions *R*(N), *S*(N), and L(C) by adoption of additivity rule[1,11,12]; *i.e.*, the curves (9) *R*(N), (10) *S*(N), and (11) L(C) in Fig. 4 were obtained.

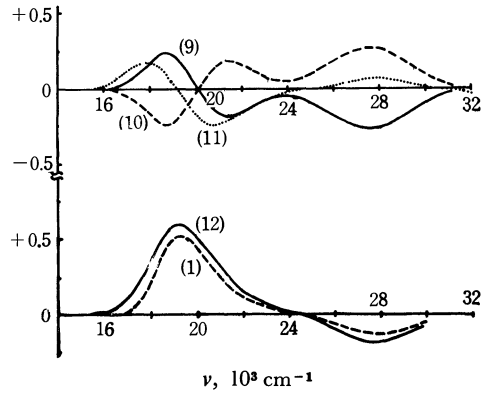

Fig. 4. Curve analyses of *cis(O)*-[Co(*O*,*N*,*O*-tridentato)-$(NH_3)_3$]$^+$ complexes: (9) *R* vicinal curve in L-alamp complex, $1/2\times\{(3)-(4)\}$, (10) *S* vicinal curve in L-alamp complex, $1/2\times\{(4)-(3)\}$, (11) L vicinal curve in L-alamp complex, $1/2\times\{(3)+(4)\}$, (12) *R* vicinal curve in L-promp complex, (2)—(11), compared with the observed R vicinal curve (1) of sarmp *cis(O)*-*R* complex.

Substraction of the curve (11) from the curve (2) in Fig. 3 produces a vicinal curve (12) for the *R*(N) contribution of L-promp *cis(O)* complex, and this coincides well with the observed CD curve (1) for the $(+)_{546}$-*cis(O)*-[Co(sarmp)$(NH_3)_3$]$^+$ complex, which has only one vicinal contribution of the asymmetric nitrogen center. This fact establishes the absolute configuration *R* of the sarmp $(+)_{546}$-*cis(O)* complex in accordance with the result from the X-ray study employing the Bijvoet method.[3] It is noteworthy that the *R*(N) vicinal curve (12) or (1) disagrees with the curve (9), but this may be acceptable since the former is for a tertiary amine nitrogen atom, while the latter for secondary amine nitrogen. Maricondi, Jordan, and Douglas[13,14] showed that a drastic change of the CD intensity of vicinal contribution occurred between the two kinds of coordinated nitrogen centers in some cobalt(III) complexes of edta and its derivatives.

In the first absorption band region, three CD components (−, +, and − from longer wavelength side) are observed for the L-promp *trans(O)*-*R* complex and this pattern corresponds well with that of the L-alamp *trans(O)*-*R* one, though there are some differences in intensities (Fig. 3 and Table 3). A similar correlation in CD components is also observed for the L-proma *cis(O)*-*R* and L-alama *cis(O)*-*R* complexes. In the last two pairs of complexes, it is not possible to evaluate the individual vicinal contributions of *R*(N) and L(C), because the sarmp *trans(O)* complex was not resolved (due to its lower yield) and the diastereomeric pair of *R*(N)–L(C) and *S*(N)–L(C) of L-alama complex was also not obtained.

10) E. A. Berends and J. G. Brushmiller, *Inorg. Nucl. Chem. Lett.*, **6**, 531, 847 (1970).
11) N. Matsuoka, J. Hidaka, and Y. Shimura, *Inorg. Chem.*, **9**, 719 (1970); This Bulletin, **45**, 2491 (1972).
12) N. Koine, N. Sakota, J. Hidaka, and Y. Shimura, *Chem. Lett.*, **1972**, 543.
13) C. W. Maricondi and B. E. Douglas, *Inorg. Chem.*, **11**, 688 (1972).
14) W. T. Jordan and B. E. Douglas, *ibid.*, **12**, 403 (1973).

The Tautomeric Equilibria of 4-(Dialkylamino)azobenzene Derivatives. II.[1] 2- and/or 2′-Methyl-4-(dimethylamino)azobenzene Derivatives

Shunzo YAMAMOTO

Department of Chemistry, Faculty of Science, Okayama University, Tsushima, Okayama 700

(Received November 16, 1972)

The tautomeric equilibrium constants, K_t=[ammonium ion]/[azonium ion], of the first conjugate acids of 2- and/or 2′-methyl-4-dimethylaminoazobenzene derivatives were estimated by the spectrophotometric method. The effects of the 2- and 2′-methyl groups on the basicity of the amino and the azo nitrogens were examined in order to explain the effects on the tautomeric equilibrium. The effects of the 2- and 2′-methyl groups on the basicity of the amino nitrogen is an inductive one only, while the effects on the basicity of the azo nitrogens are both electronic and steric. The latter effect of the 2′-methyl group is very large, but that of the 2-methyl group is not significant. The order of K_t in a series of compounds is almost the same as that of the basicity of the azo nitrogens. That is to say, the magnitude of K_t is mainly governed by the basicity of the azo nitrogens.

The tautomeric equilibrium constants between the ammonium and the azonium ions of 4-dimethylaminoazobenzene derivatives have been reported by several workers.[2-6] Jaffé *et al.*[4] reported that the constants for 4′-substituted-4-dimethylaminoazobenzenes follow the Hammett equation.

In a previous paper,[7] we studied the effects of *N*-alkyl groups on the tautomeric equilibria for 4-dialkylaminoazobenzene derivatives and found that the base strength of the azo and the amino nitrogens is mainly governed by the degree of resonance interaction between the amino group and the rest of the molecule.

Recently, Haselbach[8] measured the pK_a values of a number of *p*- and *o*-substituted azobenzenes and showed that the *o*-methyl group exhibits both electronic and steric effects. For 2- and/or 2′-methyl-4-dimethylaminoazobenzene derivatives, the basicity of the azo nitrogens may be similarly influenced by the 2- and 2′-methyl groups, but the basicity of the amino nitrogen may be not so much influenced. Therefore, it can be expected that the tautomeric equilibrium is greatly affected by the 2- and 2′-methyl groups. As far as we know, there has been no systematic study of the effects of 2- and/or 2′-methyl groups on the tautomeric equilibrium. The purpose of the present paper is to examine to what extent the tautomeric equilibrium of the first conjugate acids of 4-dimethylaminoazobenzene derivatives is influenced by the introduction of the methyl groups into the *ortho* positions.

Experimental

Compounds. The 4-dimethylaminoazobenzene derivatives were prepared and purified by procedures described in previous papers.[7,9]

2-Methyl-4-dimethylaminoazobenzene: mp 67—67.5 °C (lit, 68—68.5 °C)

2′-Methyl-4-dimethylaminoazobenzene: mp 73.5 °C (lit, 73.5—74 °C)

2,4′-Dimethyl-4-dimethylaminoazobenzene: mp 126 °C (lit, 121 °C)

2′,4′-Dimethyl-4-dimethylaminoazobenzene: mp 137 °C (Found: C, 75.48; H, 7.70; N, 16.32%. Calcd: C, 75.85; H, 7.56; N, 16.59%).

2-Methyl-4′-chloro-4-dimethylaminoazobenzene: mp 96 °C (Found: C, 65.61; H, 6.31; N, 15.67%. Calcd: C, 65.81; H, 5.89; N, 15.35%).

2′-Methyl-4′-chloro-4-dimethylaminoazobenzene: mp 117 °C (Found: C, 65.41; H, 6.13; N, 15.09%. Calcd: C, 65.81; H, 5.89; N, 15.35%).

Measurements. The absorption spectra of the azo compounds and their conjugate acids, and the pH values of the solutions, were measured in *ca.* 50% aqueous ethanol at 25±0.5 °C by the methods described in a previous paper.[7] The dissociation constants, pK_a, were calculated by a standard method.[10] The average deviations for all the compounds were within ±0.05 pH units.

Results and Discussion

Table 1 shows the absorption bands of 4-dimethylaminoazobenzene derivatives and their conjugate acids (the B band is the conjugation band of the base, and the A and C bands are the conjugation bands of the ammonium and the azonium ions respectively). The $\varepsilon_a/\varepsilon_c$ ratio gives a measure of the tautomeric equilibrium, where ε_a is the apparent molar extinction coefficient at the peak of the A band, and where ε_c is that at the peak of the C band. As is shown in Table 1, the tautomeric equilibrium is sensitive to 2- and 2′-methyl groups. Especially for 2-methyl derivatives, the equilibrium greatly shifts to the azonium form, while for 2′-methyl derivatives the equilibrium shifts to the ammonium form.

According to Eq. (2) in Ref. (7), the tautomeric equilibrium constant, K_t, may be expressed as:

$$K_t = \frac{[\text{ammonium ion}]}{[\text{azonium ion}]} = \frac{\varepsilon_c^{III}}{\varepsilon_a^{II}} \cdot \frac{\varepsilon_a}{\varepsilon_c} - \frac{\varepsilon_a^{III}}{\varepsilon_a^{II}} \qquad (1)$$

where ε_a^{II} and ε_a^{III} are the molar extinction coefficients of the ammonium and azonium ion at the wavelength

1) Part I of this series: Ref. 7.

2) G. M. Badger, R. G. Buttery, and G. E. Lewis, *J. Chem. Soc.*, **1954**, 1888.

3) E. Sawicky, *J. Org. Chem.*, **21**, 605 (1956); **22**, 365, 621, 743 (1957).

4) Si-Jung Yeh and H. H. Jaffé, *J. Amer. Chem. Soc.*, **81**, 3283 (1959); M. Isaks and H. H. Jaffé, *ibid.*, **86**, 2209 (1964).

5) F. Gerson and E. Heilbronner, *Helv. Chim. Acta*, **45**, 42 (1962).

6) A. J. Ryan, *Tetrahedron*, **20**, 1547 (1964).

7) S. Yamamoto, N. Nishimura, and S. Hasegawa, This Bulletin, **46**, 194 (1973).

8) E. Haselbach, *Helv. Chim. Acta*, **53**, 1526 (1970).

9) S. Yamamoto, N. Nishimura, and S. Hasegawa, This Bulletin, **44**, 2018 (1971).

10) L. A. Flexser, L. P. Hammett, and A. Dingwall, *J. Amer. Chem. Soc.*, **57**, 2103 (1935).

TABLE 1. ABSORPTION SPECTRA OF 4-DIMETHYLAMINOAZOBENZENE DERIVATIAES AND THEIR CONJUGATE ACIDS

No.	Substituent	λ_{max} ($\varepsilon \times 10^{-3}$)			$\varepsilon_a/\varepsilon_c$
		A band	B band[a)]	C band	
1	Unsubstituted	320 (10.1)	400 (30.4)	516 (33.6)	0.30
2	2-Methyl	327 (6.3)	405 (30.2)	516 (47.1)	0.13
3	2′-Methyl	327 (19.7)	394 (29.9)	515 (5.8)	3.40
4	2, 2′-Dimethyl	330 (14.8)	400 (28.8)	514 (17.0)	0.87
5	4′-Methyl	331 (13.2)	400 (31.8)	528 (30.1)	0.44
6	2, 4′-Dimethyl	336 (6.5)	405 (30.5)	528 (45.2)	0.14
7	2′, 4′-Dimethyl	340 (20.9)	393 (31.0)	522 (4.1)	5.10
8	2, 2′, 4′-Trimethyl	342 (17.8)	399 (29.9)	525 (12.7)	1.40
9	4′-Chloro	325 (12.9)	410 (34.1)	520 (33.0)	0.39
10	2-Methyl-4′-chloro	332 (7.4)	415 (32.8)	517 (47.4)	0.16
11	2′-Methyl-4′-chloro	334 (22.7)	413 (32.6)	511 (3.5)	6.49
12	2,2′-Dimethyl-4′-chloro	335 (20.1)	411 (31.0)	513 (12.4)	1.62

a) Conjugation band of the base in cyclohexane.

TABLE 2. VARIOUS EQUILIBRIUM CONSTANTS OF 4-DIMETHYLAMINOAZOBENZENE DERIVATIVES

Group	No.[a)]	$\varepsilon_a/\varepsilon_c$	$\varepsilon_c^{III}/\varepsilon_a^{II}$	K_t	pK_a	pK_1	pK_2
1	1	0.30	2.64	0.78	2.00	1.64	1.75
	2	0.13	2.65	0.24	2.81	2.10	2.72
	3	3.40	2.32	7.89	2.00	1.95	1.05
	4	0.87	2.75	2.39	2.42	2.27	1.89
2	5	0.44	2.54	1.12	2.17	1.89	1.85
	6	0.14	2.40	0.24	2.84	2.13	2.75
	7	5.10	2.50	12.75	2.08	2.05	0.95
	8	1.40	2.67	3.74	2.53	2.43	1.85
3	9	0.39	2.53	0.99	1.88	1.58	1.58
	10	0.16	2.34	0.27	2.63	1.96	2.53
	11	6.49	2.50	16.23	1.90	1.87	0.69
	12	1.62	2.75	4.46	2.20	2.11	1.46

a) Key is shown in Table 1.

maximum of the A band, and where ε_c^{III} is that of the azonium ion at the wavelength maximum of the C band. As has been described in the previous paper, when ε_a is sufficiently large ($\varepsilon_a > 10000$), as in the cases of dimethylaminoazobenzene and the like, the contribution of the second term on the right-hand side of Eq. (1) can be neglected. For 2-methyl derivatives, however, the second term can not be neglected. This can be estimated in the following way. According to Jaffé and Yeh,[4] the molar extinction coefficient (ε_a^{III}) of the azonium ion at about 320 nm is about 2000. On the other hand, ε_a^{II} is more than 20000.[7] Therefore, the $\varepsilon_a^{III}/\varepsilon_a^{II}$ value is about 0.1. The $\varepsilon_c^{III}/\varepsilon_a^{II}$ values were estimated in the manner described in a previous paper;[7] they are listed in Table 2. The K_t values calculated are listed in Table 2.

The tautomeric equilibrium constant is a measure of the difference between the basicity of the amino nitrogen (pK_1) and that of the azo nitrogen (pK_2). Hence, an examination of the effects of 2- and 2′-methyl groups on both pK_1 and pK_2 is necessary in order to interpret the effects on K_t. The pK_1 and pK_2 values were calculated according to the method described in a previous paper;[7] they are given in Table 2.

For all three groups in Table 2, the pK_1 increases in this order: unsubstituted < 2′-methyl < 2-methyl < 2,2′-dimethyl derivatives. The resonance effects of the 2-methyl group might not be significant, since this group is in the *meta* position to the amino group. As for the 2′-methyl group, this effect also does not seem to be important. Further, the steric effect of these groups on the pK_1 is not significant, since these groups are apart from the amino group. Therefore, of the effects of the 2- and 2′-methyl groups the inductive effect may be predominant.

The ΔpK_1 and ΔpK_2 values, which show the differences in pK_1 and pK_2 between 2- and/or 2′-methylated and the corresponding unmethylated compounds, are shown in Table 3 (a) and (b). An inspection of the ΔpK_1 values in Table 3 (a) shows that the introduction of an extra methyl group on the 2-position always results in a definite increase in pK_1. The same thing holds for the 2′-methyl group as well (see Table 3 (b)). This can easily be understood by remembering that the effects of the 2- and 2′-methyl groups on the pK_1 are only inductive.

As is shown in Table 2, the introduction of a methyl group into the 2-position increases the pK_2, while that into the 2′-position decreases the pK_2. These findings

TABLE 3. THE EFFECTS OF 2- AND 2′-METHYL GROUPS ON pK_1 AND pK_2

a) 2-methyl group

No.[a)]	2′- and/or 4′-substituents	2-substituent	pK_1	ΔpK_1	pK_2	ΔpK_2
1	H	H	1.64		1.75	
2	H	CH_3	2.08	0.44	2.73	0.98
5	4′-CH_3	H	1.89		1.85	
6	4′-CH_3	CH_3	2.10	0.21	2.76	0.91
9	4′-Cl	H	1.58		1.58	
10	4′-Cl	CH_3	1.93	0.38	2.53	0.95
3	2′-CH_3	H	1.95		1.03	
4	2′-CH_3	CH_3	2.27	0.32	1.89	0.86
7	2′,4′-diCH_3	H	2.05		0.95	
8	2′, 4′-diCH_3	CH_3	2.43	0.38	1.82	0.87
11	2′-CH_3-4′-Cl	H	1.87		0.73	
12	2′-CH_3-4′-Cl	CH_3	2.11	0.24	1.46	0.73
	average			0.33±0.02		0.88±0.02

a) Key is shown in Table 1.

b) 2′-methyl group

No.[a)]	2- and/or 4′-substituents	2′-substituent	pK_1	ΔpK_1	pK_2	ΔpK_2
1	H	H	1.64		1.75	
3	H	CH_3	1.95	0.31	1.03	−0.72
5	4′-CH_3	H	1.89		1.85	
7	4′-CH_3	CH_3	2.05	0.16	0.95	−0.90
9	4′-Cl	H	1.58		1.58	
11	4′-Cl	CH_3	1.87	0.29	0.73	−0.85
2	2-CH_3	H	2.08		2.72	
4	2-CH_3	CH_3	2.27	0.19	1.89	−0.83
6	2, 4′-diCH_3	H	2.10		2.76	
8	2, 4′-diCH_3	CH_3	2.43	0.33	1.82	−0.94
10	2-CH_3-4′-Cl	H	1.93		2.53	
12	2-CH_3-4′-Cl	CH_3	2.11	0.18	1.46	−1.07
	average			0.24±0.02		−0.89±0.03

a) Key is shown in Table 1.

show that the 2′-methyl group sterically hinders the addition of a proton and decreases the pK_2, while the 2-methyl group does not hinder the addition, but, rather, increases the pK_2 through its electronic effect.[9] This supports the idea that the azonium ion of 4-dimethylaminoazobenzene derivatives is of the following resonance-stabilized type:[11]

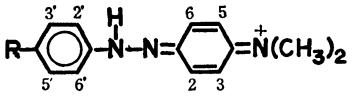

As is shown in Table 3 (a) and (b), the constancy of the ΔpK_2 values shows the additivity of the effects of 2- and 2′-methyl groups on the basicity of the azo nitrogens. The values of 0.88 and −0.89 for the ΔpK_2 values of the 2- and 2′-methyl groups roughly agree with the corresponding values obtained by Haselbach[8] for 4-methoxyazobenzene derivatives.

The effects of the 2- and 2′-methyl groups on pK_1 are only inductive; therefore, the order of pK_1 is simple (unsubstituted < 2′-methyl < 2-methyl < 2,2′-dimethyl derivatives). On the other hand, the effects on pK_2 may be both electronic and steric, and the order of pK_2 is more complicated (2′-methyl < 2,2′-dimethyl ≈ unsubstituted < 2-methyl derivatives). The order of K_t is almost the same as that of pK_2. This shows that the magnitude of K_t is mainly governed by the basicity of the azo nitrogens.

The author would like to thank Professor Shigeo Hasegawa and Dr. Norio Nishimura for their kind guidance.

11) G. E. Lewis, *Tetrahedron*, **10**, 129 (1960).

Liquid Crystalline Properties of Substituted Azo- and Azoxy-benzenes. I[1]

Kei MURASE and Haruaki WATANABE

Ibaraki Electrical Communication Laboratory, Nippon Telegraph and Telephone Public Corporation, Tokai, Ibaraki 319—11

(Received November 27, 1972)

In order to obtain low-temperature mesomorphic materials, thirty-two *p*-alkyl-*p'*-alkoxy-azo- and -azoxy-benzenes have been synthesized. The former have been made by the condensation of *p*-*n*-alkylnitrosobenzenes and *p*-*n*-alkoxyanilines, and the latter, by the oxidation of the former. Twenty-nine of the compounds show nematic behavior. In the majority of cases, the nematic temperature range of the azoxy compounds, which have been considered to consist of two isomers synthesized simultaneously, is appreciably wide.

In order to use a new electro-optic effect of nematic liquid crystals[2] to display elements, the present authors are studying the preparation of new mesomorphic materials[3,4] which, it is hoped, will exhibit nematic behavior at a low and wide temperature range, and will respond at high speeds and with high contrast ratios to an applied electric field.

Many compounds of *p,p'*-di-*n*-alkoxy-benzylideneanilines, -azobenzenes, and -azoxybenzenes are well known to show mesomorphism.[5] Recently, almost all the compounds of *p*-*n*-alkoxybenzylidene-*p'*-*n*-alkylanilines have been found to be mesomorphic.[3,6,7] Because their less polar alkyl substituents make the molecular interactions weak, they show mesomorphic transitions at much lower temperatures than the corresponding *p,p'*-dialkoxybenzylideneanilines.

For the same reason, it was presumed that *p*-*n*-alkyl-*p'*-*n*-alkoxy-azo- or -azoxy-benzenes would be mesomorphic in a low temperature range. This work was carried out to ascertain the validity of this assumption. Thirty-two new compounds have been synthesized in this work; some of them have recently been studied by a method different from ours, and the same results have been shown.[8,9,10]

Experimental

The transition temperatures were determined with a Mitamura Riken micro hot stage. The NMR spectra were measured on a JEOL C-60 HL apparatus, using CCl_4 as the solvent.

Raw Materials. *p*-Nitrotoluene and *p*-ethylnitrobenzene were purchased from commercial sources and were not distilled further. *p*-*n*-Propylnitrobenzene (bp 96—100 °C/2 mmHg) and *p*-*n*-butylnitrobenzene were prepared by the nitration of the corresponding *n*-alkylbenzenes. *p*-Anisidine and *p*-phenetidine were purchased from commercial sources and were not refined. *p*-*n*-Propoxyaniline (bp 74—75 °C/1.5 mmHg), *p*-*n*-butoxyaniline (bp 103—104 °C/1.5 mmHg), and *p*-*n*-hexyloxyaniline (bp 155—158 °C/5 mmHg) were prepared by the reduction of corresponding *p*-*n*-alkoxynitrobenzenes.[11]

Preparation of p-*Alkylnitrosobenzenes. General Procedure*: A solution of *p*-*n*-alkylnitrobenzene (14—18 g) in 60 ml of ethanol and an aqueous solution of ammonium chloride (5.4 g) were mixed and then kept at 60—65 °C. Zinc dust (15 g) was added to the mixture under vigorous stirring for two or three minutes. Then the zinc oxide was removed and the filtrate was cooled at dry ice-methanol temperature. The resulting solid was filtered and washed with benzene. After vacuum drying white *p*-alkylphenylhydroxylamine was obtained in a 10—20% yield.

Then, a solution of the hydroxylamine (3 g) in 100 ml of ethanol was poured into an ice-cooled aqueous solution of $FeCl_3 \cdot 6H_2O$ (10.8 g). By extraction with ether, the green *p*-*n*-alkylnitrosobenzene was separated. The yield was about 90%.

Preparation of p-*Alkyl*-p'-*alkoxyazobenzenes. General Procedure*: A solution of *p*-*n*-alkylnitrosobenzene (3 g) in 25 ml of ethanol and a solution of an equimolar quantity of the appropriate *p*-*n*-alkoxyaniline in 10 ml of acetic acid were cooled with ice-water and then mixed. After the cooling had been continued for about an hour, an orange-red crystalline product was given by filtration in a 70—90% yield. The product was recrystallized twice from a methanol solution. IR(KBr): 1580 (N=N), 1255 (C-O-C) and 835 (*p*-subst. benzene-ring) cm^{-1}. NMR(CCl_4): τ 2.20 and 2.28 (double d, J=9 Hz, inner aromatic 4H), 2.87 and 3.20 (double d, J=8 Hz, outer aromatic 4H).

Preparation of p-*Alkyl*-p'-*alkoxyazoxybenzenes. General Procedure*: The azobenzene (6 g) was dissolved in acetic acid (90 ml) and then warmed to 60—70 °C. While the solution was being stirred continuously, a 90-ml portion of aqueous hydrogen peroxide (30%) was added. After the color of the solution became yellow, cold water (100 ml) was added. Then the product was extracted with *n*-hexane (300 ml). The yield was 55—85%. The additional recrystallization of the product was done twice. IR (Nujol): 1565—70 and 1280 (N=N→O), 1255 (C-O-C) and 835 (*p*-subst. benzene-ring) cm^{-1}. NMR (CCL_4): τ 1.80 (m, inner aromatic 4H), 2.81 and 3.20 (double d, J=8 Hz, outer aromatic 4H).

Results and Discussion

Sixteen compounds of *p*-*n*-alkyl-*p'*-*n*-alkoxyazoxybenzenes were synthesized, and all were converted into the corresponding azoxybenzenes (strictly speaking, each of the compounds seems to be a mixture of Compounds I and II[10]) by oxidation.

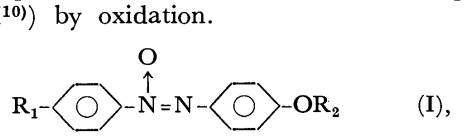

(I),

1) Presented in part at the 25th Annual Meeting of the Chemical Society of Japan, Oct., 1971 (Osaka).
2) G. H. Heilmeier, L. A. Zanoni, and L. A. Barton, *Proc. IEEE.*, **56**, 1162 (1968).
3) K. Murase, This Bulletin, **45**, 1772 (1972).
4) K. Murase, *Chem. Lett.*, **1972**, 471.
5) Cf., for example, W. Kast, "Landort-Börnsteins Tabellen," 6th ed., Bd II (2a), 288 (1960).
6) H. Kelker and B. Scheurle, *Angew. Chem.*, **81**, 903 (1969).
7) J. B. Flannery and W. Haas, *J. Phys. Chem.*, **74**, 3611 (1970).
8) H. Kelker and B. Scheurle, *Angew. Chem.*, **82**, 984 (1970).
9) R. Steinsträsser, *Z. Naturforsch.*, **B26**, 577 (1971).
10) R. Steinsträsser and L. Phol, *Tetrahedron Lett.*, **1971**, 1921.
11) G. O. Gutekunst and H. L. Gray, *J. Amer. Chem. Soc.*, **44**, 1741 (1922).

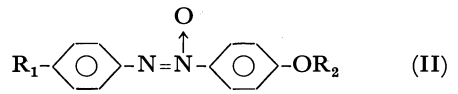

(II)

The structures of the obtained compounds were confirmed by means of their IR and NMR spectra. Although *p,p'*-dialkyl and *p,p'*-dialkoxy compounds were expected to have also been produced by exchange reaction,[12] it can be concluded from the characterization of the NMR spectra of the aliphatic protons that the obtained compounds do not contain those mentioned above.

Contrary to Steinsträsser's result,[10] the difference in NMR spectra between Compounds I and II was not apparent in ours. Therefore, the isomer compositions of the azoxybenzenes are ambiguous.

The elemental compositions of the obtained compounds were also confirmed. The analyzed C, H, and N contents are in fair agreement with the calculated values.

The transition temperatures of the obtained compounds are shown in Tables 1 and 2. It is apparent from these results that the majority of the compounds show nematic behavior in the relatively low temperature range, which is appreciably wide, especially in the azoxybenzenes. The wide nematic range of the azoxy compounds gives evidence that each of them consists of two isomers synthesized simultaneously.

The deviations in the transition temperatures of some of the obtained compounds from those of the

Table 1. Transition temperatures of synthsized azo compounds, 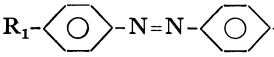

Substituents		Transition temperatures (°C)		
R_1	R_2	mp	CNpt.	NLpt.
CH_3	CH_3	110 (111) [a]		(64) [a]
CH_3	C_2H_5	120 (118) [a]		90 (87) [a]
CH_3	n-C_3H_7	91		
C_2H_5	CH_3	80 (80) [a]		41 (37) [a]
C_2H_5	C_2H_5	102 (97)		80 (60)
C_2H_5	n-C_3H_7	91		
C_2H_5	n-C_4H_9	69 (68) [a]		68 (67) [a]
C_2H_5	n-C_6H_{13}		67	69
n-C_3H_7	CH_3		58 (60) [a]	69 (69) [a]
n-C_3H_7	C_2H_5		88 (88) [a]	100 (100) [a]
n-C_3H_7	n-C_3H_7	86		74
n-C_3H_7	n-C_4H_9		74	85
n-C_3H_7	n-C_6H_{13}		65	81
n-C_4H_9	CH_3		31 (32) [a,b]	46 (42 [b], 47 [a])
n-C_4H_9	C_2H_5		47 (48) [a,b]	84 (81 [b], 83 [a])
n-C_4H_9	n-C_3H_7	62 [c]	(67) [a]	54 [c] (68) [b]

a) Ref. 9, b) Ref. 8, c) Recrystallized only once.

12) Y. Ogata, M. Tsuchida, and Y. Takagi, *J. Amer. Chem. Soc.*, **79**, 3397 (1957).

Table 2. Transition temperatures of synthesized azoxy compounds, 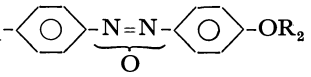

Substituents		Transition temperatures (°C)		
R_1	R_2	mp	CNpt.	NLpt.
CH_3	CH_3	98		
CH_3	C_2H_5		105	114
CH_3	n-C_3H_7	88		62
C_2H_5	CH_3		38 (37 [a])	71 (71 [a])
C_2H_5	C_2H_5		54	100
C_2H_5	n-C_3H_7	72		68
C_2H_5	n-C_4H_9		47	85
C_2H_5	n-C_6H_{13}		51	81
n-C_3H_7	CH_3		41	94
n-C_3H_7	C_2H_5		55	119
n-C_3H_7	n-C_3H_7		52	90
n-C_3H_7	n-C_4H_9		44	102
n-C_3H_7	n-C_6H_{13}		58	98
n-C_4H_9	CH_3		18 (19 [b], 16 [b])	73 (75—76 [b], 76 [a])
n-C_4H_9	C_2H_5		45	98
n-C_4H_9	n-C_3H_7		49 (39 [a])	73 (78 [a])

a) Ref. 10, b) Ref. 8.

Table 3. Deviations in the transition temperatures of $C_nH_{2n+1}O$- 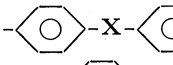 -C_nH_{2n+1} from those of $C_nH_{2n+1}O$- 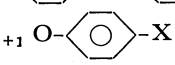 -OC_nH_{2n+1} [13]

n	Deviations in transition temperature (°C)			
	X: -N=N-		X: -N(→O)=N-	
	CNpt or mp	NLpt	CNpt or mp	NLpt
1	−45		−18	
2	−57	−70	−80	−68
3	−60		−64	−32

analogous compounds which have two *n*-alkoxy groups as the *para* substituents[13] are shown in Table 3. As expected, all the transition temperatures of the obtained compounds are much lower than those of the comparable analogues.

Consequently, the materials obtained in this study may be used in the practical display so far as the transition temperature is concerned. Further study of the electro-optic effect of these materials is now in progress; the results will be presented in a subsequent paper.

The authors wish to thank Mr. Toshikuni Kaino and Mr. Tetsuo Wachi for their helpful cooperation in the measurements.

13) C. Weygand and R. Gabler, *Ber.*, B **71**, 2399 (1938).

The Reaction of Nucleophilic Reagents at the β-Position of 3-Bromo-4-nitropyridine *N*-Oxide

Eizo MATSUMURA and Masahiro ARIGA

Department of Chemistry, Osaka Kyoiku University, Tennoji-ku, Osaka 543

(Received January 9, 1973)

Some nucleophilic substitutions on the β-position of the pyridine nucleus were carried out. The reactions of 3-bromo-4-nitropyridine *N*-oxide(**1**) with diethyl sodiomalonate, ethyl sodiocyanoacetate, and ethyl sodioacetoacetate in diethyl carbonate or pyridine afforded 3-bis-(ethoxycarbonyl)methyl-4-nitropyridine *N*-oxide (**2**), 3-cyano(ethoxycarbonyl)methyl-4-nitropyridine *N*-oxide (**3**), and 3-acetyl(ethoxycarbonyl)methyl-4-nitropyridine *N*-oxide (**4**) respectively, and ethyl sodioacetoacetate, when treated at a higher temperature, gave 3-ethoxycarbonyl-2-methyl-furo(3,2-*c*)pyridine *N*-oxide (**5**). A probable mechanism of the reaction was presented.

The nucleophilic substitution reaction of pyridine homologues and their *N*-oxides have been widely investigated for a long time, and there are several reviews on the subject.[1-3] Most of such substitutions of the pyridine ring take place at the α or γ-position, especially with the carbanions. In this connection, several carbanion sources, such as active methylenes, enamines, Grignard reagents, alkyl metals, and metal cyanides, have been developed,[4] but only a few examples of the introduction of carbanions to the β-position of the pyridine ring have been reported, among which are the followings.[5,6]

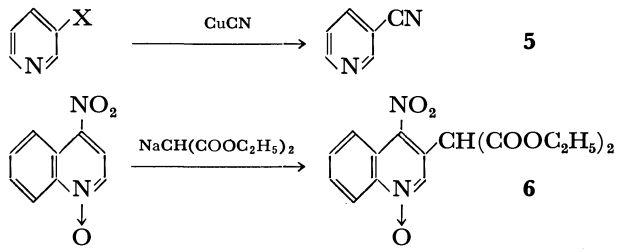

In the present investigation, since the authors' interests focussed on the carbanion introduction to the β-position of the pyridine ring, the reactions of 3-bromo-4-nitropyridine *N*-oxide with several active methylene compounds were worked out. The choice of the substrate was based on the following considerations; in the case of a nucleophilic attack, a bromide anion is a better leaving group than a hydride anion, and the β-carbon occupied by the bromine is activated by the inductive and tautomeric effects of the neighbouring nitro group.[7]

Results and Discussion

Diethyl malonate, ethyl cyanoacetate, and ethyl acetoacetate were employed as nucleophilic reagents.

The Reaction of 3-Bromo-4-nitropyridine N-*Oxide (1) with Diethyl Sodiomalonate.* On the treatment of **1** with diethyl sodiomalonate in diethyl carbonate at 50 °C, pale yellow needles (**2**) were obtained in a satisfactory yield after purification through a silica gel column. The NMR spectrum of Compound **2** showed four different kinds of hydrogens; a triplet at δ 1.28 and a quartet at 4.27 (CH_3CH_2OCO), a singlet at 5.31($CHPy(COOEt)_2$), and several peaks between 7.93—8.25 (aromatic hydrogens) in an area ratio of 6 : 4 : 1 : 3. The infrared spectrum of **2** indicated the presence of ester carbonyl, nitro, and *N*-oxide groups. The treatment of **2** with 20% sulfuric acid at 130 °C for 3 hours gave 3-(1-oxido-4-nitro)pyridylacetic acid. On the basis of these data, **2** was proved to be 3-bis(ethoxycarbonyl)methyl-4-nitropyridine *N*-oxide (**2**), showing that the malonate anion was introduced into the β-position of the pyridine nucleus.

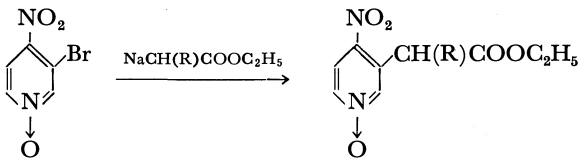

(**1**)

(**2**, **3**, and **4**)
2: R=$COOC_2H_5$
3: R=CN
4: R=$COCH_3$

The Reaction of 1 with Ethyl Sodiocyanoacetate. When **1** was treated with ethyl sodiocyanoacetate, the reaction proceeded similarly, and 3-cyano(ethoxycarbonyl)methyl-4-nitropyridine *N*-oxide (**3**) was obtained. The NMR spectrum of **3** was analogous to that of **2** with the exception of the fact that the methine proton at δ 5.58 was exchangeable with deuterium. The acidity of **3** was also shown by the capacity to form a deeply-coloured quaternary ammonium salt, even with aqueous ammonia.

The Reaction of 1 with Ethyl Sodioacetoacetate. The treatment of **1** with ethyl sodioacetoacetate had results different from those of the two preceding reactions.

At a lower temperature (30—35 °C), the reaction proceeded much as in the above two reactions to give 3-acetyl(ethoxycarbonyl)methyl-4-nitropyridine *N*-oxide

1) H. S. Mosher, "Heterocyclic Compounds," Vol. 1, Chap. 8, ed. by R. C. Elderfield, John Wiley & Sons, New York, 1950.
2) E. Ochiai, "Aromatic Amine Oxides," Elsevier Publishing Co., Amsterdam (1967).
3) A. R. Katritzky and J. M. Lagowski, "Chemistry of the Heterocyclic N-oxides," Academic Press, London (1970).
4) For example, M. Hamana, "The Chemistry of the Heterocycles," Vol. 3, ed. by Y. Kitahara, T. Kametani, and T. Kato, Nankodo & Co., Tokyo (1971).
5) S. M. McElvain and M. A. Goese, *J. Amer. Chem. Soc.*, **63**, 2283 (1941); W. T. Caldwell, F. T. Tyson, and L. Lauer, *ibid.*, **66**, 1479 (1944).
6) H. J. Richter and N. E. Rustad, *J. Org. Chem.*, **29**, 3381 (1964).
7) *Cf.* Th. J. de Boer and I. P. Dirdx, "The Chemistry of the Nitro and Nitroso Groups," Chap. 8, ed by H. Feuer, Interscience Publishers, New York (1969).

(**4**). However, the NMR spectrum of **4** showed a different aspect from the two preceding products (**2** and **3**). The singlet due to the methine proton was weakened to a negligible intensity, and a new D_2O-exchageable singlet corresponding to one proton appeared at δ 13.07, indicating that **4** exists as an enol, but the O–H absorption band was not observed in the IR spectrum. The fact that the methylene signal, which should originally be a quartet, splits into twelve peaks suggests that **4** exists in more than two enol forms. It seems also that the reactivity of the methine proton might act as a driving force to further the reaction.

When the reaction was followed by further treatment at a higher temperature (80—90 °C), colourless crystals (**5**) were obtained which had the empirical formulas of $C_{11}H_{12}NO_{4.5}$ and $C_{11}H_{11}NO_4$ after drying over phosphorus pentoxide. The IR spectrum of **5** indicated the subsistence of the carbonyl group and the *N*-oxide group and the lack of a nitro group. The NMR spectrum of **5** showed 6 different kinds of hydrogens. From the above data, **5** was assumed to be either **5a**, or **5b**.

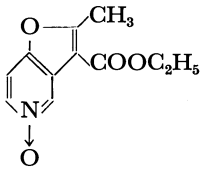

(**5a**)

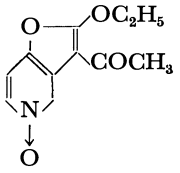

(**5b**)

The reaction of **1** with diethyl sodiomalonate and ethyl sodiocyanoacetate did not produce a compound corresponding to **5**, even at a higher temperature. This fact suggests that the acetyl carbonyl group rather than the ester carbonyl group takes part in the reaction and that **5** might be **5a** rather than **5b**. This inference was supported by the fact that the treatment of **5** with 10% hydrochloric acid gave a colourless carboxylic acid (**6**), $C_9H_7NO_4$. Thus, **5** was proved to be **5a**, 3-ethoxycarbonyl-2-methylfuro(3,2-*c*)pyridine *N*-oxide, and **6** was proved to be 2-methyl-5-oxidofuro-(3,2-*c*)pyridine-3-carboxylic acid.

The above results prove that ethyl sodioacetoacetate behaved, at a higher temperature, differently from the other reagents and gave a fused heterocyclic compound; this was because of the outstanding activity of the methine proton and the acetyl carbonyl group of **4** as has been mentioned above. The judgment that **5** was formed *via* **4** was supported by the facts that **4** was obtained at a lower temperature, that **5** was a preferential product at a higher temperature, and the fact that a deep red-purple in colour of the reaction mixture as was common to all the reactions yielding **2**, **3**, and **4**, faded in the case of **5** with a rise in the temperature. A probable course of the formation of **5** was proporsed as in the following scheme.

A methine proton of the preliminary product, **4**, is extracted by the excess base to give an anion, **7**, which is shown as a resonance of two canonical formula. The *O*-anion internally attacks the 4–*C*, which is activated by the nitro and *N*-oxide group; this is followed by the departure of the nitrate anion to give **5**.

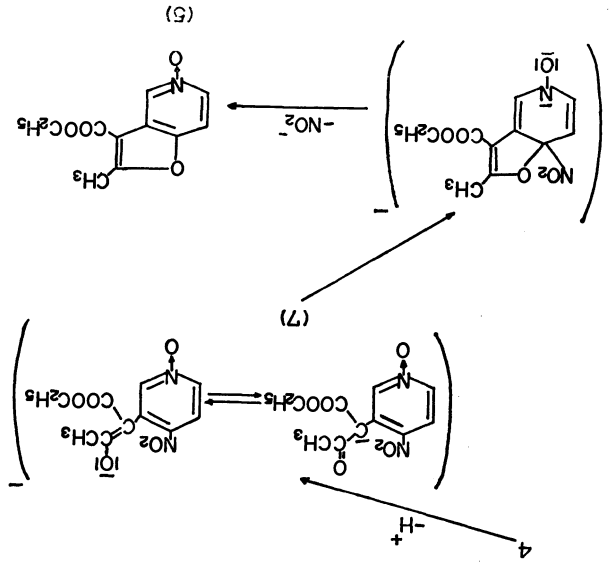

Scheme

Consequently, the introduction of carbanion to the β-position of the pyridine ring was successfully achieved by the displacement of the bromide anion activated by the *ortho*-nitro group. The results were of great value not only in the point of the accomplishment of the introduction of the *C*-anion into the β-position of the pyridine nucleus with ease, but also in the point of the use of the product (**2**, **3**, and **4**) as synthetic intermediates, because the 4-nitro group of the products was still active in response to the nucleophilic attack. Further work is in progress on this point.

Experimental

All the melting points are uncorrected. The IR spectra were obtained on a Hitachi Infrared Spectrophotometer, EPI-S2, as Nujol mulls. The NMR spectra were recorded on a Hitachi High Resolution NMR Spectrometer, 20B, with TMS as the internal standard.

3-Bromo-4-nitropyridine N-*oxide* (**1**). 3-bromopyridine[8] was treated with 5 equivalent amounts of 30% hydrogen peroxide and 100 equivalent amounts of glacial acetic acid at 70—80 °C for 20 hr to give 3-bromopyridine *N*-oxide in a 92.3% yield as hydrochloride. 3-Bromo-4-nitropyridine *N*-oxide (**1**) (mp 152—152.5 °C) was obtained in a 57.5% yield from 3-bromopyridine *N*-oxide by the method of Jujo.[9]

The Reaction of **1**. *(a) With Diethyl Sodiomalonate*: Into a solution of 1.0 g of 3-bromo-4-nitropyridine *N*-oxide (**1**) in 50 ml of diethyl carbonate, a solution of diethyl sodiomalonate, which had been formed from 0.3 g of sodium and 2.2 g of diethyl malonate in 50 ml of diethyl carbonate, was stirred from a dropping funnel at 15—20 °C over a period of an hour; then the mixture was heated at 50—60 °C for 5 hr. The resulting mixture was neutralized with dil hydrochloric acid to pH 3. The organic layer was separated, and the water layer was extracted with chloroform. After drying over anhydrous sodium sulfate, the combined organic layers were evaporated; the residue was dissolved in 10 ml of chloroform and refined through a silica gel (Wakogel C-300) column. After the elution of diethyl malonate with chloro-

8) S. M. McElvain and M. A. Goese, *J. Amer. Chem. Soc.*, **65**, 2227 (1943).

9) R. Jujo, *Yakugaku Zasshi*, **66**(**B**), 49(1946).

form, the evaporation of the ethereal elute gave 1.25 g (91.9%) of 3-bis(ethoxycarbonyl)methyl-4-nitropyridine *N*-oxide (**2**) as pale yellow needles; mp 97—98 °C (recrystallized from acetone-isopropyl ether). Found: C, 48.08; H, 4.51; N, 9.19%; Calcd for $C_{12}H_{14}N_2O_7$: C, 48.33; H, 4.73; N, 9.39%. IR: 1750 cm^{-1} (C=O), 1520 and 1350 (NO_2), and 1245 (N→O). NMR($CDCl_3$): δ 1.28 (6H, t), 4.27 (4H, q), 5.31 (1H, s), and 7.93—8.25 (3H, m).

(b) With Ethyl Sodiocyanoacetate: A similar treatment of **1** with ethyl sodiocyanoacetate formed from 0.3 g of sodium and 2.0 g of ethyl cyanoacetate in pyridine at 0 °C, but with the solvent being evaporated before the neutralization, gave 0.92 g (80.3%) of 3-cyano(ethoxycarbonyl)-methyl-4-nitropyridine *N*-oxide (**3**) as pale yellow needles; mp 147 °C (recrystallized from methyl alcohol). Found: C, 47.75; H, 3.65; N, 16.57%; Calcd for $C_{10}H_9N_3O_5$: C, 47.81; H, 3.59; N, 16.73%. IR: 2225 cm^{-1} (CN), 1745 (C=O), 1520 and 1340 (NO_2), and 1240 (N→O). NMR($CDCl_3$): δ 1.34 (3H, t), 4.34 (2H, q), 5.58 (1H, s), and 8.06—8.45 (3H, m).

(c) With Ethyl Sodioacetoacetate at a Lower Temperature: A solution of 1.0 g of **1** and ethyl sodioacetoacetate from 0.3 g of sodium and 2.1 g of ethyl acetoacetate in 100 ml of diethyl carbonate was kept at 30—35 °C for 12 hr; then the reaction mixture was treated as above to give 0.8 g (65.4%) of 3-acetyl(ethoxycarbonyl)methyl-4-nitropyridine *N*-oxide (**4**) as yellow leaflets; mp 95—96 °C (recrystallized from ethyl ether). Found: C, 49.46; H, 4.48; N, 10.26%; Calcd for $C_{11}H_{12}N_2O_6$: C, 49.25; H, 4.48; N, 10.26%. IR: 1645 cm^{-1} (C=O), 1620 (C=C), 1510 and 1350 (NO_2), and 1260 (N→O). NMR($CDCl_3$): δ 1.13 (3H, t), 1.96 (3H, s), 4.24 (2H, m), 7.90—8.27 (3H, m), and 13.07 (1H, s).

(d) With Ethyl Sodioacetoacetate at a Higher Temperature: The reaction mixture of the above reaction was further heated at 80—90 °C for an additional 5 hr. The resulting mixture was treated by the same procedure, and from the alcoholic elute, 0.82 g (78.2%) of 3-ethoxycarbonyl-2-methylfuro(3,2-*c*)pyridine *N*-oxide (**5**) semihydrate was obtained as colourless prisms; mp 150 °C (recrystallized from acetone). Found: C, 57.31; H, 5.23; N, 5.92%; Calcd for $C_{11}H_{11}NO_4 \cdot 1/2\ H_2O$: C, 57.39; H, 5.22; N, 6.09%, after drying over phosphorus pentoxide, Found: C, 59.64; H, 4.88; N, 6.08%; Calcd for $C_{11}H_{11}NO_4$: C, 59.28; H, 4.96; N, 6.33%. IR: 1695 cm^{-1}(C=O) and 1245 (N→O). NMR($CDCl_3$): δ 1.42 (3H, t), 2.78 (3H, s), 4.40 (2H, q), 7.31 (1H, d), 8.10 (1H, dd), and 8.82 (1H, d).

Hydrolysis of ***5***. A mixture of **5** and 10 ml of 10% hydrochloric acid was refluxed for 5 hr, and then cooled. The crystalline precipitates were collected and recrystallized from 0.1% hydrochloric acid to give 0.15 g (89.4%) of 2-methyl-5-oxidofuro(3,2-*c*)pyridine-3-carboxylic acid (**6**) as colourless needles; mp 254 °C (decomp.). Found: C, 55.69; H, 3.46; N, 7.06%; Calcd for $C_9H_9NO_4$: C, 55.96; H, 3.65; N, 7.25%. IR: 1690 cm^{-1}(broad)(COOH), 1245 (N→O). NMR(CD_3COOD): δ 2.83(3H, s), 7.71 (1H, d), 8.55 (1H, dd), and 9.10 (1H, d).

Hydrolysis of ***2***. A mixture of 1.0 g of **2** and 10 g of 30% sulfuric acid was heated at 130 °C for 3 hr; the reaction mixture was then neutralized with sodium carbonate to pH 2. The precipitates were collected by filtration and recrystallized from methyl alcohol to give 0.5 g (81.0%) of 3-(1-oxide-4-nitro)pyridylacetic acid as colourless needles; mp 161—162 °C. Found: C, 42.65; H, 2.56; N, 14.21%; Calcd for $C_7H_4N_2O_5$: C, 42.68; H, 2.58; N, 14.08%. IR: 1530 and 1350 cm^{-1}(NO_2), 1710 (C=O), and 1260 (N→O).

Ammonium Salt of ***3***. A tenth gram of **3** was dissolved in 10 ml of concd. ammonium hydroxide; then the mixture was evapolated to dryness, and recrystallized from acetone-isopropyl ether to give 0.09 g of ammonium salt of **3** as dark violet needles; mp 160—161 °C. Found: C, 44.75; H, 4.42; N, 20.57%. Calcd for $C_{10}H_{12}N_4O_5$: C, 44.77; H, 4.48; N, 20.89%.

The Catalytic Effect of Bases on the O→N Migration of the s-Triazinyl Group in *O*-(*s*-Triazinyl)-2-aminophenols

Takeo SHIOJIMA, Yōji HASHIDA, and Kohji MATSUI

Department of Chemistry, Faculty of Engineering, Gunma University, Tenjincho, Kiryu, Gunma 376

(Received March 20, 1973)

The catalytic effect of bases on the O→N migration of the *s*-triazinyl group in *O*-(*s*-triazinyl)-2-aminophenols has been studied kinetically. In the rearrangement of *N*-(acyl)-*O*-(*s*-triazinyl)-2-aminophenols (II) in alkaline aqueous methanol, the reactive species was found to be an ion formed by the ionization of the acylamino group. In the case of *O*-(*s*-triazinyl)-2-aminophenols (I), the rearrangement was subjected to a general base catalysis, although the extent was small.

Many examples of Smiles rearrangement have been known to be catalysed by an acid or a base.[1] In the course of our studies of the Smiles rearrangement of *s*-triazine derivatives, we reported[2-4] that *O*-(*s*-triazinyl)-2-aminophenols and N^1,N^1-bis(*s*-triazinyl)-*o*-phenylenediamines rearrange readily in protic solvents, especially in the presence of an acid or a base, to give *N*-(*s*-triazinyl)-2-aminophenols and N^1,N^2-bis(*s*-triazinyl)-*o*-phenylenediamines respectively. A similar O→N migration of the *s*-triazinyl group was also observed in the reaction of *N*-(acyl)- or *N*-(*s*-triazinyl)-*O*-(s-triazinyl)-2-aminophenol in the presence of a base.[2] However, these studies have been limited to qualitative discussions, and details of the effects of acids and bases on the rearrangement have not been sufficiently elucidated. This paper will report quantitative results on the influences of bases on the rearrangement.

Results and Discussion

O-(*s*-Triazinyl)-2-aminophenol (I) was prepared by a known method,[5] while *N*-acyl-*O*-(*s*-triazinyl)-2-aminophenols (IIa—b) were synthesized by acylating *O*-(4-dimethylamino-6-methoxy-*s*-triazin-2-yl)-2-aminophenol with acetic anhydride or 4-substituted benzoyl chlorides.[2] The new compounds thus obtained are listed in Table 1.

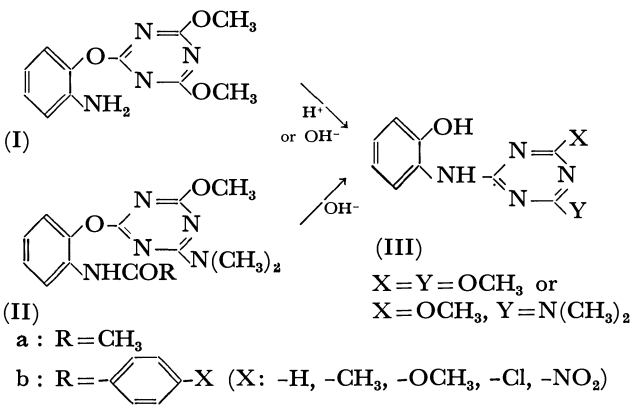

Effect of a Base on the Rearrangement of N-*(Acyl)*-O-*(s-triazinyl)-2-aminophenols (II).* The compounds (II) are stable in neutral and acidic solutions, but give rearranged products (III)[5] under the hydrolytic cleavage conditions of the acyl group when dissolved in an alkaline solution. Since the molar extinction coefficients of the original compounds at the absorption maxima (280—310 nm) are much smaller than those of the rearranged products, the apparent rate constants of the rearrangement were obtained spectrophotometrically from Eq. (1):

$$k' = -\frac{2.303}{t}\log\frac{D_\infty - D_t}{D_\infty - D_0} \quad (1)$$

where D_0, D_∞, and D_t denote the optical densities of a solution observed at initial and infinite times and at time t respectively. In every case, a plot of $\log D_\infty - D_t / D_\infty - D_0$ against the reaction time (t) gave a straight line.

The apparent rate constants (k') for the rearrangement of *N*-acetyl (IIa) and *N*-benzoyl (IIb) derivatives measured at various pH values are listed in Table 2. Fig. 1 shows the pH —rate profile in the case of (IIa).

As is shown in Fig. 1, the dependence of $\log k'$ on pH was linear with a unit slope. A similar relation was observed in the cases of *N*-benzoyl derivatives (IIb); however, no increase in the rate constant was

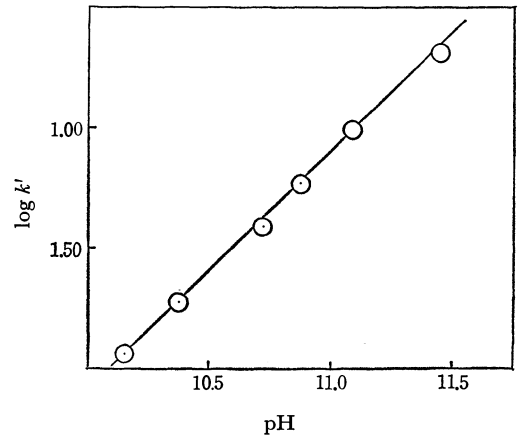

Fig. 1. pH Dependence of the apparent rate constants for the rearrangement of *N*-acetyl-*O*-(4-dimethylamino-6-methoxy-*s*-triazin-2-yl)-2-aminophenol (IIa).

1) For example, W. E. Truce, E. M. Kreider, and W. W. Brand, "The Smiles and Related Rearrangements of Aromatic Systems," in "Organic Reactions," Vol. 18, John Wiley & Sons, New York (1970), p. 99.

2) T. Shiojima, T. Kuroda, S. Ohkawa, Y. Hasegawa, and K. Matsui, This Bulletin, **46**, 2549 (1973).

3) T. Harayama, K. Okada, S. Sekiguchi, and K. Matsui, *J. Heterocycl. Chem.*, **7**, 981 (1970).

4) K. Nakamura, N. Nohara, and K. Matsui, This Bulletin, **45**, 3140 (1972).

5) N. Maeno, T. Itagaki, S. Uno, and K. Matsui, *ibid.*, **45**, 3133 (1972).

Table 1. *N*-(4-Substituted benzoyl)-*O*-(4-dimethylamino-6-methoxy-*s*-triazin-2-yl)aminophenols (IIb)

Substituent (X) in IIb	Yield (%)	Mp (°C)	Solvent for recrystallization	Elemental analysis (%) Found C	Found H	Calcd C	Calcd H
OCH_3	98	159—160	Benzene	60.99	5.23	60.75	5.35
CH_3	95	124—125	Benzene	63.63	5.21	63.31	5.58
Cl	95	138—139	Benzene-Ligroin	57.14	4.61	57.07	4.54
NO_2	96	161—162	Benzene	55.93	4.54	55.60	4.42

Table 2. Rate constant for the rearrangement of *N*-acetyl(IIa) and *N*-benzoyl-*O*-(4-dimethylamino-6-methoxy-*s*-triazin-2-yl)-2-aminophenol (IIb, X=H) in 10% (vol) methanolic buffer solutions at 20°C (μ=0.20)

(IIa)	pH	10.16	10.38	10.78	10.87	11.10	11.43
	$k'(min^{-1})\times 10$	0.116	0.195	0.382	0.572	0.974	1.99
(IIb, X=H)	pH	10.75	10.92	11.14	11.43		11.69
	$k'(min^{-1})\times 10$	0.442	0.686	1.09	1.99		3.47

observed in the presence of a base such as pyridine at a constant pH value, suggesting that the rate-determining step of the reaction does not involve an abstraction of a proton from the NH– acyl group. Therefore, two reaction sequences can be considered:

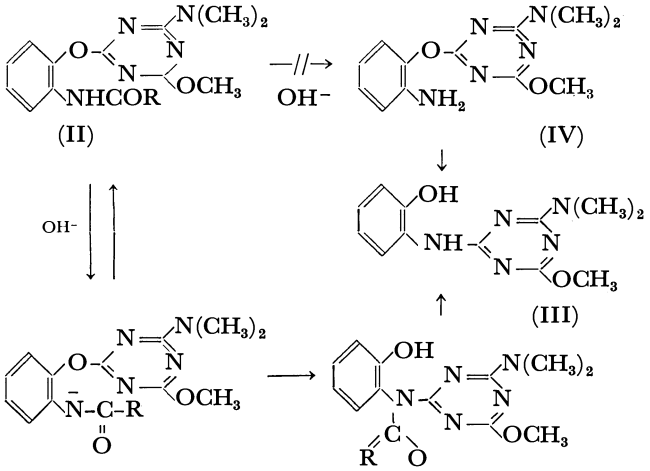

One is a process involving a preferential hydrolytic cleavage of the acyl group to give (IV), followed by the O→N migration of the *s*-triazinyl group. However, under similar reaction conditions, no hydrolytic fission of an acyl group was observed in *N*-acyl arylamines. In addition, the rearrangement of (II) proceeded much more rapidly than that of (I) in the presence of alkali. Therefore, another path, one involving the rate-determining formation of the *N*-acyl-*N*-*s*-triazinyl derivative by the O→N rearrangement, followed by a hydrolytic cleavage of the acyl group, is considered to be reasonable. Although an intermediary *N*-acyl-*N*-triazinyl derivative was not obtained in every case, this reaction sequence may be supported by the consideration that generally, since the nucleophilic reactivity of a Ar–NH–acyl group is known to be lower than that of the parent amino group, the rearrangement of *N*-(acyl)-*O*-(2,4-dinitrophenyl)-2-aminophenols is slower than that of the parent aminoether.[6] Therefore, it seems unreasonable to consider that the reaction of (II) in the presence of alkali proceeds by a direct nucleophilic attack of the NH–acyl group; the reactive species may be assumed to be an anion formed by the dissociation of the NH–acyl group and the rate may be expressed by Eq. (2):

$$v = k\ (\text{Anion}) \qquad (2)$$

This assumption is verified by the fact that the dependence of $\log k'$ on pH was linear with a unit slope; the result may be understood by assuming that the concentration of the anion increases by a factor of ten per pH unit under a given set of reaction conditions. Since these compounds rearrange readily in alkaline solutions, the measurement of their pK_a values is impossible experimentally; the concentration of the anion remains unknown, and the real value of the rate constant could not be determined.

Recently, it has been suggested[7] that the rearrangement of *O*-*s*-triazinyl-*N*-acyl derivatives of 1-amino-8-hydroxynaphthalene-3,6-disulfonic acid to *N*-*s*-triazinyl-*N*-acyl derivatives proceeds by means of a direct nucleophilic attack on the acylamino group. However, further examinations will be necessary before this postulation can be accepted.

The effect of a substituent in the benzoyl group of *N*-(benzoyl)-*O*-(*s*-triazinyl)-2-aminophenol (IIb) was also studied at a constant pH value. The results are

Table 3. Rate constants for the rearrangement of *N*-(4-substituted benzoyl)-*O*-(4-dimethylamino-6-methoxy-*s*-triazin-2-yl)-2-aminophenols (IIb) in 50% (vol) methanolic buffer solutions at 20°C (pH=10.91, μ=0.20)

Substituent (X)	$k'(min^{-1})$
p-OCH_3	1.08×10^{-2}
p-CH_3	1.97×10^{-2}
H	3.80×10^{-2}
p-Cl	1.29×10^{-1}
p-NO_2	3.88×10^{-1}

6) K. C. Roberts and C. G. M. deWorms, *J. Chem. Soc.*, **1934**, 727; **1935**, 1309.

7) R. Budziarrek, *J. Chem. Soc., C*, **1971**, 74.

Table 4. Rate constants for the rearrangement of *O*-(4,6-dimethoxy-*s*-triazin-2-yl)-2-aminophenol (I) in aqueous buffer solutions at 25°C (μ=0.10)

pH	8.75	9.50	10.15	10.61	11.36	12.66
$k'(\text{min}^{-1})\times10^2$	1.02	1.12	1.14	1.14	1.24	2.29

Table 5. Base catalysis of pyridine derivatives for the rearrangement of *O*-(4,6-dimethoxy-*s*-triazin-2-yl)-2-aminophenol (I) in methanol at 25°C.

Pyridine	c[a] (mol/l)×10	0.785	1.57	2.36	3.14	4.71
$k_c=4.43\times10^{-3}$	k[b] $(\text{min}^{-1})\times10^3$	2.53	2.98	3.31	3.58	4.32
γ-Picoline	$c\times10$	0.774	1.55	2.32	3.10	4.64
$k_c=6.53\times10^{-3}$	$k\times10^3$	2.78	3.35	3.81	4.34	5.31
β-Picoline	$c\times10$	0.750	1.50	2.25	3.00	4.50
$k_c=5.59\times10^{-3}$	$k\times10^3$	2.68	3.04	3.41	3.95	4.74
α-Picoline	$c\times10$	0.615	1.23	1.85	2.40	3.69
$k_c=4.24\times10^{-3}$	$k\times10^3$	2.54	2.78	3.09	3.36	3.82
2,6-Lutidine	$c\times10$	0.555	1.31	1.97	2.62	3.93
$k_c=3.15\times10^{-3}$	$k\times10^3$	2.66	2.74	2.98	3.18	3.66
2,4-Lutidine	$c\times10$	0.611	1.32	1.98	2.64	3.97
$k_c=5.27\times10^{-3}$	$k\times10^3$	2.60	3.04	3.39	3.84	4.40
3,5-Lutidine	$c\times10$	0.658	1.32	1.98	2.63	3.95
$k_c=6.46\times10^{-3}$	$k\times10^3$	2.71	3.15	3.50	4.05	4.82
s-Colidine	$c\times10$	0.614	1.23	1.84	2.45	3.68
$k_c=4.96\times10^{-3}$	$k\times10^3$	2.53	2.69	3.00	3.47	3.97

a) Figures in the upper column indicate the concentrations of pyridine derivatives. b) Figures in the lower column indicate the rate constants.

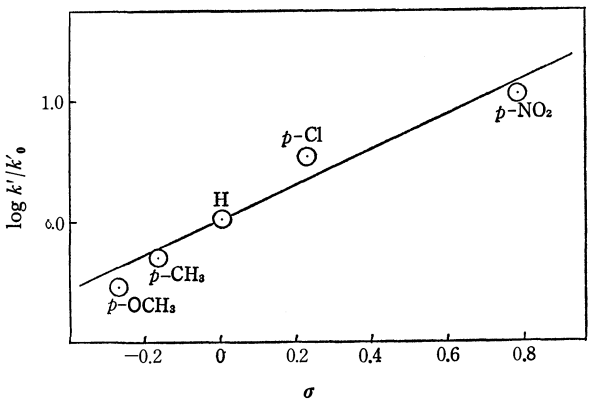

Fig. 2. Plot of the rate constants for the rearrangement of *N*-(4-substituted benzoyl)-*O*-(4-dimethylamino-6-methoxy-*s*-triazin-2-yl)-2-aminophenols (IIb) against the substituent constants.

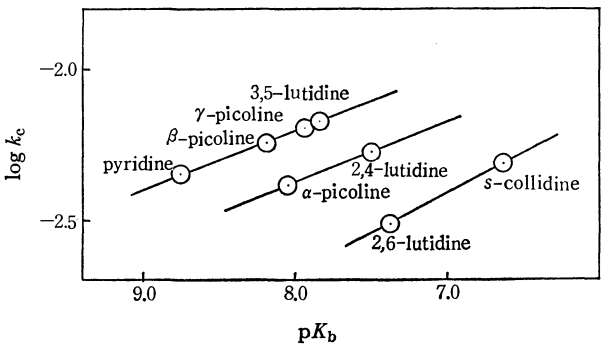

Fig. 3. Brönsted plot for the base-catalytic rearrangement of *O*-(4,6-dimethoxy-*s*-triazin-2-yl)-2-aminophenol (I).

given in Table 3, while a plot of log k'/k'_0 (where k' and k'_0 denote the apparent rate constants of substituted and unsubstituted benzoyl derivatives respectively) against the σ-value of the substituent is shown in Fig. 2. The substituent effect may be considered from two points of view. One is the effect upon the pK_a value of the benzamido group, namely, the effect on the concentration of the reactive anion, and the other is the effect upon the nucleophilic reactivity of the attacking anion. In the former, an electron-attracting substituent favors the rearrangement by increasing the concentration of the anion, while an electron-releasing substituent favors the latter.

As is shown in Fig. 2, it can be seen that the effect on the concentration of the anion dominates the rate change.

Effects of Bases on the Rearrangement of O-*(s-Triazinyl)-2-aminophenols (I).* In Table 4 are listed the rate constants for the rearrangement of (I) at various pH values. It is obvious from Table 4, that the rate constant (k) increases slightly with an increase in pH value in the pH range above 11.5. In this case, however, it is unlikely that an abstraction of the proton from the amino group occurs prior to the rearrangement, because an increase in the rate constant was not proportional to an increase in the pH value.

As is shown in Table 5, the rearrangement was also accelerated by such organic bases as pyridine and its methyl derivatives. Under the present reaction conditions, the rates were proportional to the concentration of bases. Therefore, the rate constant in the presence of a base can be expressed by Eq. (3):

$$k = k_0 + k_c\ (\text{Base}) \qquad (3)$$

where k, k_0, and k_c represent the rate constant observed, the rate constant in pure methanol, and the catalytic

constant by the base respectively. The catalytic constants obtained are summarized in Table 5, while Fig. 3 shows the relations between the log k_c and pK_b values of pyridine derivatives, which are given in three parallel lines.

Pyridine derivatives containing no methyl group in the α-position belong to Type 1, while those containing one methyl group in the α-position belong to Type 2 and those containing two methyl groups in the α,α'-positions belong to Type 3; among the pyridine derivatives of the same series, the Brönsted rule was found to hold. These facts indicate that the steric hindrance plays an important role in the catalytic efficiency of pyridine derivatives.

An acceleration of rearrangement was also observed in triethylamine; the catalytic constant in this case was found to be $k_c=6.58\times10^{-3}$.

Furthermore, a similar catalytic effect by triethylamine was observed in the rearrangement of *O*-(2,4-dinitrophenyl)-2-aminophenol in methanol at 25 °C ($k=2.88\times10^{-2}$), indicating that the base catalysis is not limited to the case of the *s*-triazine derivative.

Ordinary nucleophilic substitution reactions of activated aromatic halogen or aryloxy compounds with nucleophiles are considered to proceed by means of an addition-elimination process involving the intermediary formation of the σ-complex.[8,9] When an amine is used as a nucleophile, the catalytic effect by a base has been observed.[9,10] In the reaction of 2,4-dinitrophenyl phenyl ether with piperidine, the catalytic functions of bases have been interpreted in terms of the reaction mechanism involving the reversible transformation of the intermediate complex into its conjugate base, followed by the general acid-catalyzed detachment of the leaving group.[11,12]

Generally, Smiles rearrangements including the reaction of compound (I) can be considered to proceed in a manner similar to that of the ordinary nucleophilic aromatic substitution involving the formation of an intermediate complex;[13] this assumption may be supported by the facts observed in the rearrangement of 4- and 2-nitro-2'-hydroxydiphenyl sulfones,[14] in which the reactions are accompanied by a striking color change from deep-red to pale yellow, suggesting the formation of a Meisenheimer-type intermediate.

From these facts and considerations, it may be reasonable to consider that, in the rearrangement of *O*-(*s*-triazinyl)-2-aminophenol (I), a base participates in the proton transfer and detachment of the leaving group in the intermediate complex, as is shown below:

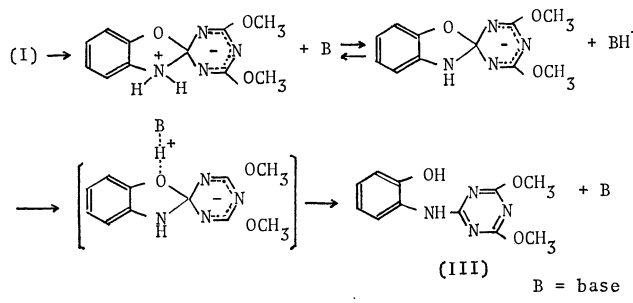

Experimental

All the melting points are uncorrected. The ultraviolet spectra were recorded on a Hitachi-124 UV-VIS spectrophotometer. The elemental analyses were performed at the Microanalytical Center of Gunma University.

Materials. N-*(4-Substituted benzoyl)*-O-*(s-triazinyl)-2-aminophenols*: A typical preparation is shown below in the case of *N*-(4-chlorobenzoyl)-*O*-(4-dimethylamino-6-methoxy-*s*-triazin-2-yl)-2-aminophenol. Into a mixture of 2.6 g (0.01 mol) of *O*-(4-dimethylamino-6-methoxy-*s*-triazin-2-yl)-2-aminophenol and 0.8 g (0.01 mol) of sodium bicarbonate in 10 ml of water in 50 ml of acetone, was added 1.7 g (0.01 mol) of *p*-chlorobenzoyl chloride in 30 ml of acetone dropwise with stirring at room temperature. After having been stirred for 6 hr at room temperature, the reaction mixture was poured into 500 ml of ice-water; the precipitate thus obtained was filtered and dried.

Kinetic Measurements. The kinetic measurements were carried out in buffered solutions at a constant ionic strength.

8) P. Rys, A. Schmitz, and H. Zollinger, *Helv. Chim. Acta*, **54**, 163 (1971).

9) J. Miller, "Aromatic Nucleophilic Substitution," Elsevier Publishing Company, Amsterdam (1968), pp. 139, 164, *etc.*

10) S. D. Ross, "Nucleophilic Aromatic Substitution Reactions," in "Progress in Physical Organic Chemistry," Vol. 1, Interscience Publishers, New York (1963), p. 31.

11) J. F. Bunnett and R. H. Garst, *J. Amer. Chem. Soc.*, **87**, 3879 (1965).

12) F. Pietra, *Tetrahedron Lett.*, **1965**, 2405.

13) Th. J. de Boer and I. P. Dirkx, "Activating Effects of the Nitro Group in Aromatic Substitutions," in "The Chemistry of the Nitro and Nitroso Groups," Part I, ed. by H. Feuer, Interscience Publishers, New York (1969), p. 588.

14) B. A. Kent and S. Smiles, *J. Chem. Soc.*, **1934**, 422.

Kinetics of Multidentate Ligand Substitution Reactions. XV. Substitution Reactions of 1,2-Cyclohexanediamine-*N*,*N*,*N*′,*N*′-tetraacetic Acid (CyDTA) with Zinc(II) Iminodiacetate (IDA), *N*-(2-Hydroxyethyl)iminodiacetate (HIDA), and Nitrilotriacetate (NTA) Complexes and Those with Cobalt(II)-IDA, -HIDA, NTA, -*N*-(2-Hydroxyethyl)ethylenediamine (EtEN), and Diethylenetriamine (Dien) Complexes

Mutsuo KODAMA[1] and Kaoru HAGIYA*

Department of Chemistry, College of General Education, Hirosaki University, Bunkyo, Hirosaki, Aomori 036

**Department of Chemistry, Faculty of Science, Ibaraki University, Bunkyo, Mito, Ibaraki 310*

(Received March 22, 1973)

The kinetics of the substitution reactions of CyDTA with zinc(II)-IDA, -HIDA, and -NTA complexes and those with cobalt(II)-IDA, -HIDA, -NTA, -EtEN, and Dien complexes were studied by using the polarographic technique. All the substitution reactions studied in this paper were found to have a common reaction mechanism. They were first-order with respect to the CyDTA anion, and they were also first-order with respect to the metal(II) complex with a 1 : 1 composition; their reaction mechanism could be formulated as:

$$MX_2^{(2-2m)+} \rightleftharpoons MX^{(2-m)+} + X^{m-} \quad \text{in a rapid equilibrium}$$

$$MX^{(2-m)+} + \begin{cases} HY^{3-} \rightleftharpoons MY^{2-} + HX^{(1-m)+} \\ Y^{4-} \rightleftharpoons MY^{2-} + X^{m-} \end{cases} \quad \text{rate determining steps}$$

From a comparison of the observed rate constants with those estimated on the basis of the proposed reaction intermediate, the detailed reaction mechanism and structures of the reaction intermediates were discussed. The steric effect of the cyclohexane ring on the rate of the substitution reaction was also discussed.

We have studied a series of substitution reactions involving metal(II) aminopolycarboxylate complexes and have determined their detailed reaction mechanism.[2] Usually, the nucleophilic substitution reactions involving zinc(II) complexes proceed so rapidly that one can not determine their reaction rates accurately by employing a conventional technique. However, the substitution reaction of CyDTA with the zinc(II) aminopolycarboxylate complex proceeds at a measurable rate under the usual experimental conditions. In this paper, we will deal with the kinetics of the substitution reactions of CyDTA with zinc(II)-IDA, -HIDA, and -NTA complexes, and will discuss the detailed reaction mechanism and the steric effect of the cyclohexane ring on their reaction rates. To describe more precisely the reaction mechanism and the above steric effect, the substitution reactions of CyDTA with the cobalt(II) complexes of IDA, HIDA, NTA, EtEN, and Dien will also be studied.

Experimental

Reagents. The preparation and the standardization of zinc(II) and cobalt(II) solutions were described previously.[3,2a] Reagent-grade IDA, HIDA, NTA, and CyDTA were recrystallized from their aqueous solutions by adding pure hydrochloric acid and ethanol. The Dien and EtEN used in this study were purified by distilling them under reduced pressure. The other chemicals used were of an analytical reagent grade and were used without further purification.

Apparatus and Experimental Procedures. The apparatus and the experimental procedures were the same as those described previously.[2c] In this study, all the measurements were conducted in solutions of an ionic strength of 0.30 ($NaClO_4$ for the IDA, HIDA, and NTA systems; KNO_3 for the EtEN and Dien systems). No buffer reagent was used in this study, because free IDA, HIDA, NTA, EtEN, and Dien have enough buffer capacity to maintain the pH values of sample solutions constant over the entire pH range covered. The sample solutions used in the kinetic study of the substitution reactions of CyDTA with the cobalt(II)-IDA, -HIDA, and -NTA complexes always contained large excesses of complexed and uncomplexed IDA, HIDA, and NTA over CyDTA, while those in the reactions of CyDTA with zinc(II)-IDA, -HIDA, and -NTA complexes and with the cobalt(II)-EtEN and -Dien complexes contained large excesses of CyDTA and uncomplexed IDA, HIDA, NTA, EtEN, and Dien over the metal(II) complex. Therefore, all the substitution reactions studied in this paper could be treated as pseudo first-order reactions. The rates of the substitution reactions of CyDTA with the zinc(II) complexes and those of the reactions with the cobalt(II)-polyamine complexes were followed by measuring the change in the reduction wave-height of the zinc(II) complex and the oxidation wave-height of the cobalt(II) complex respectively. On the other hand, the rates of the substitution reactions with the cobalt(II)-IDA, -HIDA, and -NTA complexes were followed by determining the change in the dissolution wave-height due to the uncomplexed CyDTA.

Results and Discussion

Although not all the results will be shown here, the following facts were found in preliminary experiments. Provided that the other experimental conditions are kept constant, the forward pseudo first-order rate constant, k^+_{ap}, obtained from the slope of the linear relation between $\log(i_0/i_t)$ and t, was (1) inversely proportional to the concentration of the uncomplexed

1) To whom correspondence should be addressed.

2) a) M. Kodama, This Bulletin, **40**, 2575 (1967). b) M. Kodama, C. Sasaki, and M. Murata, *ibid.*, **41**, 1333 (1968). c) M. Kodama, *ibid.*, **42**, 2532 (1969). d) M. Kodama, *ibid.*, **42**, 3330 (1969). e) M. Kodama and T. Ueda, *ibid.*, **43**, 419 (1970).

3) M. Kodama and N. Oyama, *ibid.*, **45**, 2169 (1972).

IDA, HIDA, NTA, EtEN, and Dien, $[X]_f$, (2) exactly proportional to the concentration of the metal(II) complex (the cobalt(II)-IDA, -HIDA, and -NTA systems), [Me(II)], or the CyDTA concentration (the cobalt(II)-EtEN and -Dien systems and the zinc(II)-IDA, -HIDA, and -NTA systems), $[Y]_f$, and (3) independent of the initial concentration of CyDTA (the cobalt(II)-IDA, -HIDA, and -NTA systems) or that of the metal(II) complex (the cobalt(II)-EtEN and -Dien systems and the zinc(II)-IDA, -HIDA, and -NTA systems). Furthermore, as is shown by the results obtained in the reactions with zinc(II)-HIDA, cobalt-(II)-Dien and cobalt(II)-HIDA complexes (Figs. 1, 2, and 3), the k^+_{ap} multiplied by $K_2\cdot[X]_f\cdot(\alpha_H)_Y/(\alpha_H)_X[Ex]$

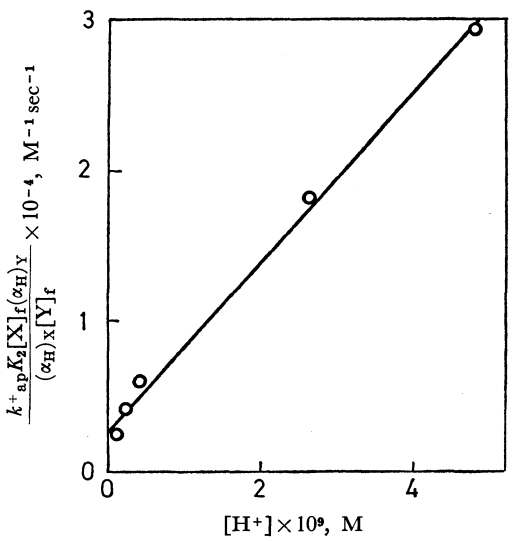

Fig. 1. The plot of $k^+_{ap}\cdot K_2\cdot[X]_f\cdot(\alpha_H)_Y/(\alpha_H)_X\cdot[Y]_f$ against $[H^+]$ 0 °C, μ=0.30.
The concentration of zinc(II) ion=1.0 mM
The concentration of CyDTA=12.5 mM
The concentration of uncomplexed HIDA=17.8 mM
pH ranged from 8.30 to 9.80

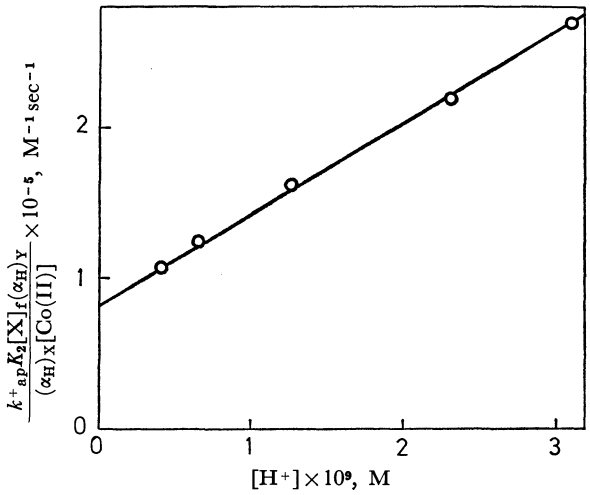

Fig. 2. The plot of $k^+_{ap}\cdot K_2\cdot[X]_f\cdot(\alpha_H)_Y/(\alpha_H)_X\cdot[Co(II)]$ against $[H^+]$ 25.0 °C, μ=0.30.
The concentration of cobalt(II) ion=7.27 mM
The concentration of CyDTA=0.545 mM
The concentration of uncomplexed HIDA=10.9 mM
pH ranged from 8.50 to 9.50

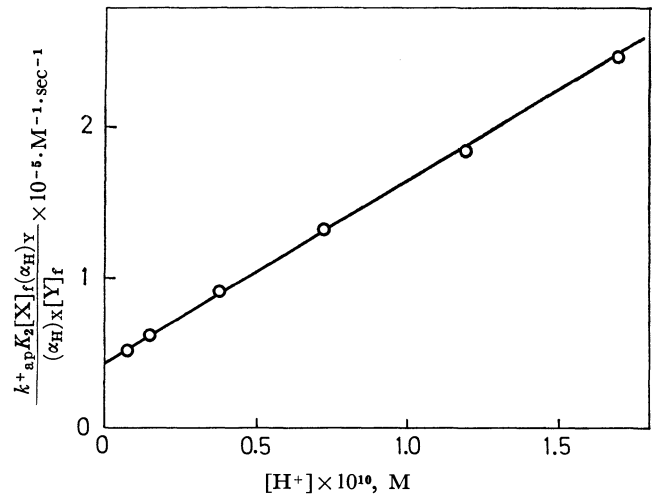

Fig. 3. The plot of $k^+_{ap}\cdot K_2\cdot[X]_f\cdot(\alpha_H)_Y/(\alpha_H)_X\cdot[Y]_f$ against $[H^+]$ 0 °C, μ=0.30.
The concentration of cobalt(II) ion=1.16 mM
The concentration of CyDTA=11.6 mM
The concentration of uncomplexed Dien=131 mM

is a linear function of the concentration of the hydrogen ion, $[H^+]$, and is given by:

$$\frac{k^+_{ap}K_2[X]_f\cdot(\alpha_H)_Y}{(\alpha_H)_X[Ex]} = k_\alpha + k_\beta\cdot[H^+] \qquad (1_a)$$

where [Ex] denotes $[Y]_f$ or [Me(II)], and where $(\alpha_H)_Y$ and $(\alpha_H)_X$ are the (α_H) values of CyDTA and IDA, HIDA, NTA, EtEN, or Dien respectively, and where the other symbols used in the equation (1) have their usual meanings.[4,5,6] Considering that, under the present experimental conditions (8.90<pH<9.80 in the IDA system, 8.30<pH<9.80 in the HIDA system, 9.00<pH<9.60 in the NTA system, 9.70<pH<10.70 in the EtEN system, and 9.50<pH<11.0 in the Dien system), all the metal ions are considered to exist in the form of $MX_2^{(2-2m)+}$, the above experimental facts suggest that all the substitution reactions have the following common reaction mechanism:

$$MX_2^{(2-2m)+} \rightleftharpoons MX^{(2-m)+} + X^{m-} \quad \text{in a rapid equilibrium}$$

$$MX^{(2-m)+} + \begin{cases} HY^{3-} \overset{k_H}{\rightleftharpoons} MY^{2-} + HX^{(1-m)+} \\ Y^{4-} \overset{k_o}{\rightleftharpoons} MY^{2-} + X^{m-} \end{cases} \quad \text{rds}$$

For the above reaction mechanism, Eq. (1_a) can be rewritten as:

$$\frac{k^+_{ap}\cdot K_2\cdot[X]_f\cdot(\alpha_H)_Y}{(\alpha_H)_X[Ex]} = k_o + k_H\cdot\frac{[H^+]}{|K_4} \qquad (1_b)$$

where $|K_4$ is the fourth dissociation constant of CyDTA. From the slopes and the intercepts of the linear relations between $k^+_{ap}\cdot K_2\cdot[X]_f\cdot(\alpha_H)_Y/(\alpha_H)_X\cdot[Ex]$ and $[H^+]$, the k_H and k_0 values were determined; they are listed in Tables 1, 2, and 3. As is clear from the data in Table 1, the rates of the substitution reactions of CyDTA with zinc(II) complexes are much larger than

4) M. Kodama, S. Karasawa, and T. Watanabe, *ibid.*, **44**, 1815 (1971).
5) M. Kodama, T. Sato, and S. Karasawa, *ibid.*, **45**, 2757 (1972).
6) M. Kodama and N. Oyama, *ibid.*, **44**, 2849 (1971).

Table 1. Rate constants for the substitution reactions of CyDTA with the zinc(II) complexes
0 °C, $\mu = 0.30$

System		IDA	HIDA	NTA
k_o, $M^{-1}sec^{-1}$		$2.7_7\times10^{4a)}$	$2.6_5\times10^3$	7.5
k_H, $M^{-1}sec^{-1}$		5.90×10^2	2.08×10^1	5.4×10^{-2}
log K_{MX}		6.72	8.02	10.0
log K_{st}		0.30	0.30	0.48
log K_{elec}		−0.50	−0.50	−1.0
Δ log k	calcd	1.30	0	−2.30
	obsd k_o	1.02[a)]	0	−2.55
	obsd k_H	1.45	0	−2.59

a) Less accurate.

Table 2. Rate constants for the substitution reactions of CyDTA with the cobalt(II) aminopolycarboxylate complexes
25.0 °C, $\mu = 0.30$

System		IDA	HIDA	NTA
k_o, $M^{-1}sec^{-1}$		—	8.2×10^4	8.5×10^1
k_H, $M^{-1}sec^{-1}$		3.17×10^3	$2.3_0\times10^2$	0.58
log K_{MX}		6.64	7.66	10.15
log K_{st}		0.30	0.30	0.48
log K_{elec}		−0.50	−0.50	−1.0
Δ log k	calcd	1.02	0	−2.81
	obsd k_o	—	0	−2.98
	obsd k_H	1.19	0	−2.61

Table 3. Rate constants for the substitution reactions of CyDTA with the cobalt(II)-polyamine complexes
0 °C, $\mu = 0.30$

System		EtEN	Dien
k_o, $M^{-1}sec^{-1}$		8.7×10^5	4.3×10^4
k_H, $M^{-1}sec^{-1}$		4.49×10^4	4.53×10^3
log K_{MX}		6.58	8.00
log K_{st}		0	0.30
Δ log k	calcd	1.12	0
	obsd k_o	1.30	0
	obsd k_H	1.00	0

their corresponding dissociation rates.[7] This can be explained in terms of the formation of the mixed-ligand-complex reaction intermediates involving the CyDTA anion. As was attempted in the substitution reaction of EDTA or EDTAOH with the nickel(II) ethylenediaminemonoacetate (EDMA) complex,[8] we tried to estimate the structure of the reaction intermediate in the substitution reaction by comparing the relative rate constant observed with that calculated on the basis of the proposed reaction intermediate. The substitution reactions of CyDTA with the zinc(II)-HIDA and -NTA complexes proceed at measurable rates, but the corresponding EDTA reactions proceed so rapidly that one can not determine their rates by employing a conventional method. Usually, this can be ascribed to the steric effect of the cyclohexane ring on the substitution reaction. Generally speaking, it is reasonable to believe that the steric hindrance which will be encountered in the substitution reaction of CyDTA with the zinc(II)-HIDA complex is quite similar to that in the reaction with the zinc(II)-NTA complex. If the above assumption is correct, one can determine the structure of the reaction intermediate by comparing the relative rate constants for the zinc(II)-HIDA and -NTA complexes with those estimated on the basis of the proposed reaction intermediates. In the polarographic study of zinc(II)-HIDA and -NTA complexes in an acetate buffer solution, we found that these complexes dissociate through the glycinate reaction intermediate, where the leaving group is bonded to the zinc(II) ion through the glycinate chelate ring.[7] Therefore, it is natural to consider that the HIDA and NTA anions in the reaction intermediates in the substitution reactions of CyDTA are also bonded to the zinc(II) ion through the glycinate chelate ring. As is shown by the data in Table 1, the relative rate constants calculated with the aid of this well-known relation: $k=k_{rds}\cdot K_L\cdot K_A\cdot K_{st}\cdot K_{elec}/K_{MX}$,[5] on the basis of reaction intermediates given in Fig. 4 agree well with those observed. The relative

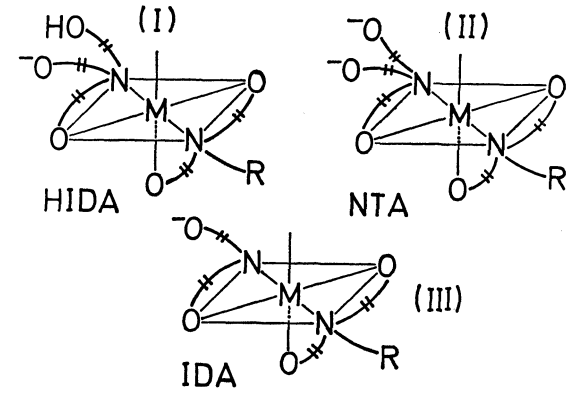

Fig. 4. Reaction intermediates.

rate constants calculated on the basis of the reaction intermediates other than those shown in Fig. 4 showed no satisfactory agreement with the observed ones. Since it is reasonable to consider that the steric effect brought about by the cyclohexane ring in the CyDTA reaction of the zinc(II)-NTA complex is not different from that of the zinc(II)-HIDA complex, the above agreement can be said to be an indication that the CyDTA anion in the reaction intermediate coordinates to the zinc(II) ion through the iminodiacetate group. In the calculation of the relative rate constants, the formation constants determined at 20 °C were used. Previously,[4] we ascribed the sluggishness of the substitution reaction of CyDTA with the nickel(II)-HIDA complex to the steric interaction of the cyclohexane ring with the hydroxyethyl group of the HIDA anion. However, the Fisher-Hirschfelder-Taylor molecular model shows that the steric interaction of the

7) M. Kodama, K. Namekawa, and T. Horiuchi, This Bulletin, to be published.

8) M. Kodama, M. Hashimoto, and T. Watanabe, *ibid.*, **45**, 2761 (1972).

cyclohexane ring with the hydroxyethyl group of the HIDA anion in the reaction intermediate is negligibly small. Furthermore, the fact that the rates of the reactions with zinc(II)- and cobalt(II)-IDA complexes can also be understood by assuming the reaction intermediates III (Tables 1 and 2) shows that the sluggishness of the CyDTA reaction with the metal(II)-HIDA complex can not be ascribed solely to the above steric interaction. For the successful formation of I and II in Fig. 4, the approach of the CyDTA anion to the coordination sphere and the formation of the zinc(II)-CyDTA bond should not be hindered by the steric interaction between the glycinate chelate ring, through which the leaving group is bonded to the zinc(II) ion, and the free iminodiacetate group of the CyDTA anion. The above steric requirement will be satisfied completely only when the rotation of the uncoordinated IDA group of CyDTA around the C–N bond is not hindered. However, as is shown by the molecular model, the cyclohexane ring in the CyDTA anion provides a greater barrier to the rotation of its uncoordinated IDA group. Therefore, the I and II structures can be formed, but only with some difficulty. Thus, the slow substitution reaction of CyDTA can be ascribed mainly to the above difficulty encountered in the reaction-intermediate formation. Undoubtedly, if the above steric effect of the cyclohexane ring on the rate of the substitution reaction can be neglected, the rate constant ratio between the dissociation of the zinc(II)-HIDA complex and its substitution reaction with CyDTA should be $10^{7.58}$. The observed ratio was $10^{3.42}$. Although the dissociation and substitution rates were determined at different temperatures (25 and 0 °C respectively), the above discrepancy can be accounted for by the steric effect of the CyDTA anion on the substitution reaction. Previously,[5] we mentioned in our kinetic study of the substitution reactions of Calmagite with the cobalt(II) and nickel(II) aminopolycarboxylate complexes that the reaction of the cobalt(II) complex proceeds through a reaction intermediate with the same structure as that in the reaction of the nickel(II) complex. Therefore, the finding that the reaction intermediate in the substitution reaction involving the zinc(II) aminopolycarboxylate complex has the same structure as that of the reaction involving thenickel(II) complex[4] suggests that the substitution reactions of CyDTA with the cobalt(II)-aminopolycarboxylate complexes proceed through the same reaction intermediate as that of the zinc(II) complex. In Table 2, the relative rate constant calculated on the basis of the reaction intermediates in Fig. 4, using the numerical data listed there also are compared with those observed. The calculated values agreed well with the observed ones. As in the case of the substitution reaction of CyDTA with the nickel(II) aminopolycarboxylate complex, the k_H value is much smaller than the k_0 value. Since the protonation of the CyDTA anion bonded to the metal(II) ion will reduce the electrostatic repulsion between the uncoordinated carboxylate groups and will stabilize the reaction intermediate, the fact that the k_H value is smaller than the k_0 value suggests the importance of the deprotonation of the attacking group in the formation of the reaction intermediate. The molecular model also shows that the protonation of the nitrogen atom in the uncoordinated IDA group in the CyDTA anion will provide a greater barrier to the formation of the reaction intermediate. Thus, the small k_H value can be understood in terms of the above barrier to the formation of the reaction intermediate. In this investigation, we also dealt with the substitution reactions of CyDTA with the cobalt(II)-EtEN and -Dien complexes. The rate constants for the two elementary reaction pathways are listed in Table 3. Previously,[8] we reported that the substitution reaction of EDTA with the nickel(II)-Dien complex proceeds through the outer-sphere complex, where the leaving Dien is bonded to the nickel(II) ion through the ethylenediamine chelate ring. The rates of the substitution reactions of CyDTA with the cobalt(II)-EtEN and -Dien complexes can also be understood by assuming an outer-sphere complex formation between the cobalt(II) complex ion and CyDTA anion. The rate constant ratio between the Dien and EtEN systems, calculated on the basis of the outer-sphere complex in which the leaving group is bonded to the cobalt(II) ion through the ethylenediamine chelate ring, agrees fairly well with the observed one. The k_H values for the cobalt(II)-polyamine systems are about ten times smaller than the k_0 values. This factor is clearly consistent with the relative electrostatic attraction of the ions concerned. Although the substitution reaction involving the cobalt(II)-EtEN complex was studied at 0 °C, the k_0 value is nearly identical to the characteristic rate constant for the water-loss from the cobalt(II) aquo ion at 25 °C. In considering the fact that the rate constant for the water loss at 0 °C must be smaller than that at 25 °C, and the fact that the equilibrium constant for the outer-sphere association between the cobalt(II) complex and the CyDTA anion is larger than unity,[9] the above agreement can also be taken as evidence for the water-loss mechanism proposed for the reactions of CyDTA with the cobalt(II)-polyamine complexes.

9) R. M. Fuoss, *J. Amer. Chem. Soc.*, **80**, 5059 (1958).

A-Substituted 5β-Steroids. V.[1] Syntheses and Some Reactions of 1-Oxygenated 5β-Cholestanes

J. Yasuo SATOH, Katsumi MISAWA, T. Tomoyoshi TAKAHASHI, Masakatsu HIROSE, C. Akira HORIUCHI, Shin-ichiro TSUJII*, and Akira HAGITANI

Department of Chemistry, St. Paul's (Rikkyo) University, Nishi-Ikebukuro, Toshima-ku, Tokyo 171
** Rock Paint Co., Ltd., Himejima, Nishi-Yodogawa-ku, Osaka 555*

(Received March 22, 1973)

1-Oxygenated 5β-cholestanes were synthesized in good yield from 3-oxygenated 5β-cholestane through 5β-cholest-1-en-3-one. The reaction of 1β,2β-epoxy-5β-cholestan-3-one with hydrogen halide occurs with a normal ring cleavage resulting in the formation of 2-halo-5β-cholest-1-en-3-one. The reaction of 1β-hydroxy-5β-cholest-2-ene with chromium trioxide gave the allylic rearrangement product, 5β-cholest-1-en-3-one. The oxidative acetylation and bromination of 5β-cholestan-1-one is described.

Although studies have been made on the syntheses of 1-oxygenated 5α-steroids,[2] only very little information can be found on 5β-steroids concerning the reactions of introducing oxygenated groups at the C_1 position.[3]

In a previous paper, we reported on the synthesis of 5β-cholest-1-en-3-one as a key intermediate for the synthetic pathway of 1-oxygenated 5β-cholestanes.[4] In the present paper, the synthesis of 1-oxygenated 5β-cholestanes is given in detail together with reactions of some of them.

Djerassi *et al.*[5] reported that 1-oxygenated 5α-cholestanes were synthesized from 5α-cholest-1-en-3-one derived from 3-oxygenated 5α-cholestane. Since the bromination of 3-oxo-5α-steroid gives a 2-brominated product, the 1-en-3-oxo derivative could easily be derived from the product by dehydrobromination. However, this procedure can be applied to 5β-steroid because the bromination of the 3-oxo derivative does not occur at C_2. Williamson and Johnson reported the synthesis of 4α-bromo-5α-cholestan-3-one, a compound that can be produced only with difficulty by the direct bromination of 5α-cholestan-3-one, or by the reductive monodebromination of the 2α,4α-dibromo-3-oxo derivative with chromous acetate.[6] We attempted the preparation of 2-bromo-5β-cholestan-3-one by the application of this method to 2β,4β-dibromo-5β-cholestan-3-one (**1**),[7] and achieved good results. The syntheses of 1-oxygenated 5β-cholestanes from 5β-cholest-1-en-3-one (**3**) were then carried out following the procedure of Djerassi *et al.*[5] for the synthesis of 1-oxygenated 5α-cholestanes. Some reactions have been examined for the 1-oxygenated derivatives thus obtained.

Results and Discussion

The α-bromoketone derived from 2β,4β-dibromo-5β-cholestan-3-one (**1**) by reductive monodebromination with chromous acetate was determined as 2β-bromo-5β-cholestan-3-one (**2**) from its NMR spectrum. The bromine susceptible to reductive elimination was found to be at C_4 rather than that at C_2 in the 5β-series, but at C_2 in the 5α-series.[6] By treating the product with calcium carbonate/dimethylformamide, 5β-cholest-1-en-3-one (**3**) was formed in good yield. Thus it seems that this pathway improves the insertion of the 1-en-3-oxo function in 5β-steroid.

The epoxy ketone derived from the 1-en-3-oxo derivative (**3**) with alkaline hydrogen peroxide was identified as 1β,2β-epoxy-5β-cholestan-3-one (**4**) from the fact that it shows a negative Cotton curve in its ORD spectrum.[8] The structure is also supported by the ring opening reaction of the epoxy ketone with hydrogen halide. If the epoxy ring has a β-orientation, it will be transformed into 2-halo-5β-cholest-1-en-3-one (**5**) in this reaction. In the present instance, the chemical shift of the C_1-vinyl proton in the presumed structure was calculated from the equation proposed by Matter *et al.*,[9] and the values (**5a**, τ 2.74; **5b**, 3.01) agreed very closely with the ones observed (τ 2.75 and 3.01, respectively) for the compound obtained. These results show that in the epoxydation of derivative (**3**) the attack of the reagent took place at the β-side of the molecule. The attack is the reverse of that in the epoxydation of 5α-cholest-1-en-3-one.[5] This is attritable to the environmental complexity of the α-side of 5β-steroids.

Reductive elimination of the 1β,2β-epoxy-3-oxo derivative (**4**) with 100% hydrazine hydrate gave an allylic alcohol (**6**). Catalytic hydrogenation of (**6**) followed by its acetylation gave 1β-acetoxy-5β-cholestane (**7b**). This shows that the hydrazine reduction product has a β-oriented hydroxy group at C_1. Oxidation of the catalytic hydrogenation product (**7a**) gave 5β-cholestan-1-one (**8**), which shows a negative Cotton curve having a shoulder near 310 nm similar to 5β-cholestan-2-one[10] in the ORD spectrum.

1) Part IV: J. Y. Satoh, T. T. Takahashi, H. Toda, and A. Hagitani, *Nippon Kagaku Zasshi*, **90**, 1267 (1969).

2) L. F. Fieser and M. Fiesser, "Steroids," Reinhold publishing, Inc., New York (1959), p. 254; C. W. Shoppee, S. K. Roy, and R. S. Goodrich, *J. Chem. Soc.*, **1961**, 1583.

3) a) W. Schlegel and Ch. Tamm, *Helv. Chim. Acta*, **40**, 160 (1957); b) K. Morita, *Chem. Pharm. Bull.* (Tokyo), **5**, 494 (1957); This Bulletin, **32**, 791 (1959); c) E. Glotter, M. Weissenberg, and D. Labie, *Tetrahedron*, **26**, 3857 (1970).

4) J. Y. Satoh, T. T. Takahashi, T. Aoki, and A. Hagitani, This Bulletin, **42**, 1465 (1969).

5) C. Djerassi, D. H. Williams, and B. Berkoz, *J. Org. Chem.*, **27**, 2205 (1962).

6) K. L. Williamson and W. S. Johnson, *ibid.*, **26**, 4563 (1961).

7) C. Djerassi and G. Rosenkranz, *Experientia*, **7**, 93 (1951).

8) C. Djerassi and W. Klyne, *Tetrahedron*, **21**, 163 (1965).

9) U. E. Matter, C. Pascual, E. Pretsch, A. Pross, W. Simon, and S. Sternhell, *ibid.*, **25**, 691 (1969).

10) M. Tomoeda and T. Koga, *Tetrahedron Lett.*, **1965**, 3231; J. Y. Satoh, C. A. Horiuchi, and A. Hagitani, This Bulletin, **43**, 491 (1970).

In the synthetic pathway of 5β-cholestan-1-one from 5β-cholest-1-en-3-one (**3**), the synthesis from **3** to **7a** without purification of each product, followed by chromatographic separation of the oxidation product of **7a** in the last step, gave the 1-oxo derivative (**8**) in 55% yield based on the 1-en-3-oxo derivative.

Catalytic reduction of derivative (**8**) proceeds stereospecifically to give an equatorial hydroxy group. The configuration of the product (**9a**) was determined from the NMR spectrum of its acetate (**9b**). C_1-H of the acetate appeared in a higher field than that of the 1β-acetoxy epimer (**7b**), showing a triplet. This stereospecificity is attributable to preferential attack from the β-side rather than the α-side, which has a stereochemical complexity similar to the epoxy ketone (**4**). This catalytic reduction of the 1-oxo derivative is identical with that of Schlegel and Tamm on the catalytic reduction of methyl 1-oxo-etianate.[3a]

Oxidation of 2-en-1β-ol (**6**) with chromium trioxide gave predominantly 5β-cholest-1-en-3-one (**3**) along with a minor component, 5β-cholest-2-en-1-one (**10**). This may be attributed to the small interaction involved with respect to the 19-methyl group in the case of the reaction pathway through a six-membered transition state (A) between the 1β-chromic ester formed and the allylic position, as compared with that in the case of the pathway through a cyclic transition state (B) between the 1β-chromic ester and $C_{1\alpha}$-H (Fig. 1). We see that the properties of 1β-hydroxy-5β-cholest-2-ene (**6**) are similar to those of 1β-halo-5β-cholestan-2-one, which gave a 3-substituted product through various reactions.[11]

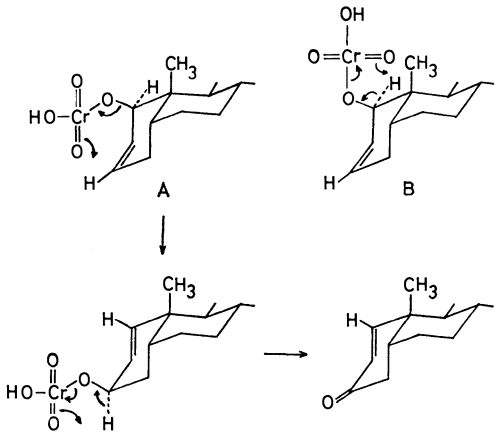

Fig. 1.

The reaction of 5β-cholestan-1-one (**8**) with bromine in acetic acid gave mainly a compound melting at 118—119 °C with two minor products: "A", mp 69—70.5 °C and "B", mp 141.5—143.5 °C. The main product was determined to be 2β-bromo-5β-cholestan-1-one (**11a**) from the fact that the ORD curve showed a negative Cotton effect and its λ_1 had a blue shift of 5 nm from that of the parent ketone (**8**), and from the coupling constant in the NMR spectrum. Dehydrobromination of bromoketone (**11a**) with Ca-

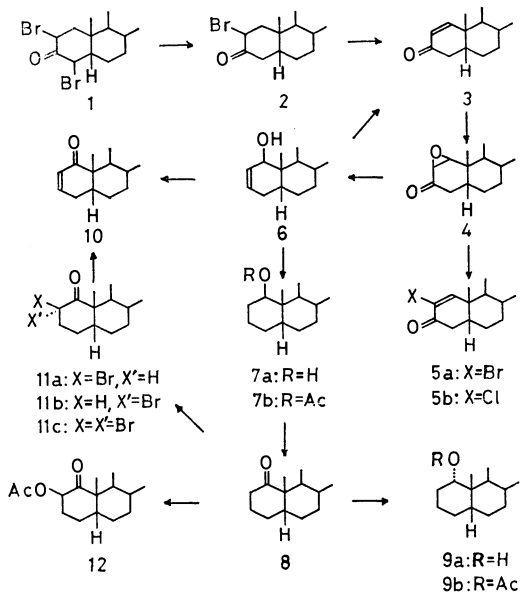

CO_3/DMF gave an α,β-unsaturated ketone, identical with 5β-cholest-2-en-1-one (**10**) obtained from 1β-hydroxy-5β-cholest-2-ene (**6**) with chromium trioxide. The minor product "A" was determined to be the 2α-bromo epimer (**11b**) from the small half-height width of the peak at τ 5.69 in its NMR spectrum, as compared with that of the 2β-epimer (**11a**), and from the ORD curve showing a red shift of 28 nm from that of the parent ketone (**8**). The product could easily be converted into the 2β-epimer (**11a**) with HBr/AcOH. The NMR spectrum of the other product "B" did not reveal any peaks due to –CH(Br)–. Hence the product was concluded to be a 2,2-dibromo-1-oxo derivative (**11c**).

Oxidative acetylation of 5β-cholestan-1-one (**8**) with lead tetraacetate gave 2β-acetoxy-5β-cholestan-1-one (**12**). It was found from the NMR spectrum that the acetate was not deformed, as was the case with the other α-acyloxy-keto-5β-steroids having an equatorial acyloxy group in ring A.[12]

Experimental

All melting points are uncorrected. The IR spectra were measured on a Shimadzu model IR-27B infrared spectrometer, ORD spectra on a JASCO model ORD/UV-5 spectrometer, and NMR spectra on Hitachi-Perkin Elmer R-20A and JEOL model JNM-4H-100 instruments using TMS as an internal standard.

2β-Bromo-5β-cholestan-3-one (2). To a solution of **1** (31.7 g) in acetic acid (600 ml) and chloroform (240 ml) was added chromous acetate prepared from chromic chloride according to the method of Williamson and Johnson.[6] The end point of the reaction was confirmed by tlc. Ether extracts from the reaction mixture were neutralized, washed and evaporated. Crystallization of the residue from ethanol gave needles (22.2 g), mp 138—140 °C, IR (KBr): 1727 cm^{-1}; ORD (*c* 0.216, dioxane) at 16 °C: $[\alpha]_{311}$ −296° (trough) and $[\alpha]_{267}$ +494°; NMR (CCl_4) τ: 5.42 (dd, $J_{1\alpha,2}$=5 and

11) J. Y. Satoh, C. A. Horiuchi, and A. Hagitani, *Chem. Lett.*, **1972**, 995.

12) T. T. Takahashi, J. Y. Satoh, and A. Hagitani, *Nippon Kagaku Zasshi*, **89**, 974 (1968); J. Y. Satoh, C. T. Kimura, M. Y. Tajima, T. T. Takahashi, and A. Hagitani, *ibid.*, **90**, 500 (1969).

$J_{1\beta,2}=14$ Hz, 1H).

Found: C, 69.45; H, 9.79%. Calcd for $C_{27}H_{45}OBr$: C, 69.66; H, 9.74%.

*5β-Cholest-1-en-3-one (**3**).* A mixture of **2** (19.4 g), calcium carbonate (20 g), and DMF (300 ml) was refluxed for 2 hr. After the usual work-up, the resultant residue, on crystallization from ethanol, gave needles (12.8 g), mp 108—109 °C (lit,[3c] 105—106 °C).

*Synthesis of 5β-Cholestan-1-one (**8**) from 5β-Cholest-1-en-3-one (**3**).* The synthesis was carried out following the procedure of Djerassi *et al.*[5] for the synthesis of 5α-cholestan-1-one from 5α-cholest-1-en-3-one. Details are therefore omitted. Reaction of **3** (10 g) with 1 M sodium hydroxide solution (100 ml), dioxane (510 ml), and 30% hydrogen peroxide (35 ml) at room temperature for 15 hr gave **4** (7.4 g), mp 107—108.5 °C (lit,[3c] 107—109 °C), from ethanol. When the temperature was raised to 34—40 °C, the reaction was completed in 5 hr. By refluxing **4** (2.42 g) with 100% hydrazine hydrate (14.7 ml) for 15 min, **6** was obtained as a colorless amorphous substance (1.26 g), mp 95—96 °C (lit,[3c] 98—99 °C), from acetone. Hydrogenation of **6** (9.8 g) was carried out with 10% Pd-C (7 g) in cyclohexane (35 ml). Since crystallization of **7a** could not be accomplished from the residue (9.8 g, IR: 3330 cm^{-1}), the following procedure was used. A solution of **7a** (10 g) in acetic acid (605 ml) was treated with chromium trioxide (2.6 g) in acetic acid (242 ml) and water (12 ml) at room temperature. After being stirred for 5 hr, the reaction mixture was treated in the usual manner. The residue was chromatographed on silica gel. Elution with benzene–petroleum ether (1 : 1) gave needles of **8** (4.9 g), mp 101—102 °C (lit,[3c] 101—102 °C), from ethanol (Found: C, 83.79; H, 12.02%).

*Epoxy Ring Opening Reaction of 1β,2β-Epoxy-5β-cholestan-3-one (**4**).* A solution of **4** (200 mg) in chloroform (20 ml) was treated with 48% hydrobromic acid (2 ml) at room temperature for 24 hr. The reaction mixture was poured into water and the chloroform layer was worked up in the usual manner. Crystallization of the resulting oil from ethanol gave **5a** (156 mg), mp 137—139 °C; λ_{max}^{EtOH} 257 nm (ε 12500); IR (KBr): 1696 and 1600 cm^{-1}; ORD (*c* 0.611, dioxane) at 18.5 °C: $[\alpha]_{375.5}$ +200° (sh), $[\alpha]_{360}$ +237° (peak), $[\alpha]_{350}$ +193° (trough), $[\alpha]_{345.5}$ +198° (peak), $[\alpha]_{334}$ +148° (trough), $[\alpha]_{331}$ +149° (peak), $[\alpha]_{323}$ +136° (trough), and $[\alpha]_{300}$ +265°; NMR (CCl_4) τ: 2.75 (s, 1H) and 8.77 (s, 3H).

Found: C, 69.76; H, 9.43%. Calcd for $C_{27}H_{43}OBr$: C, 69.96; H, 9.36%.

When the epoxide was treated with 35% hydrochloric acid under the same conditions, **5b** (137 mg) mp 130—132.5 °C, was obtained from ethanol. λ_{max}^{EtOH} 249 nm (ε 10500); IR (KBr): 1703 and 1606 cm^{-1}; ORD (*c* 0.434, dioxane) at 18.5 °C: $[\alpha]_{373}$ +761° (sh), $[\alpha]_{359.5}$ +885° (peak), $[\alpha]_{350}$ +747° (trough), $[\alpha]_{344}$ +789° (peak), $[\alpha]_{334}$ +630° (trough), $[\alpha]_{328}$ +685° (peak), $[\alpha]_{323}$ +643° (trough), and $[\alpha]_{300}$ +1266°; NMR (CCl_4) τ: 3.01 (s, 1H), and 8.79 (s, 3H).

Found: C, 77.17; H, 10.27%. Calcd for $C_{27}H_{43}OCl$: C, 77.38; H, 10.34%.

*1β-Acetoxy-5β-cholestane (**7b**).* **7a** (2.3 g) was treated with acetic anhydride (55 ml) and pyridine (55 ml) for 10 hr at room temperature. After the usual work-up, the residue was chromatographed on silica gel. Benzene elution, on crystallization from ethanol, gave needles (1.48 g), mp 104—105.5 °C (lit,[3c] 100—101 °C).

*1α-Acetoxy-5β-cholestane(**9b**).* Sodium borohydride (500 mg) was gradually added to a solution consisting of **8** (1 g), ether (75 ml) and methanol (25 ml). After the usual work-up, an oily product (1.1 g; IR; 3400 cm^{-1}) was obtained. Attempts to crystallize it with several solvents were unsuccessful, and it was acetylated in the usual manner. **9b** was obtained as needles (783 mg) from ethanol. Mp 40—42 °C, IR (KBr): 1735 and 1242 cm^{-1}; NMR (CCl_4) τ: 5.57 (t, $J_{1.2}=7.5$ Hz, 1H) and 8.06 (s, 3H).

Found: C, 80.59; H, 11.72%. Calcd for $C_{29}H_{50}O_2$: C, 80.87; H, 11.71%.

*Oxidation of 5β-Cholest-2-en-1β-ol (**6**).* A solution of **6** (900 mg) in acetone (7 ml) was treated with chromium trioxide (560 mg) and 40% H_2SO_4 solution (0.8 ml) at 10—15 °C. After 30 min, a small amount of methanol was added to the reaction mixture. The ether extracts from the solution were washed with sodium hydrogen carbonate solution and water, dried and evaporated. The residue was chromatographed on silica gel. From the first elution with benzene–petroleum ether (1 : 1), **10** (36 mg) was obtained from ethanol as needles, mp 100—101.5 °C (lit,[3c] 99—100 °C); IR (KBr): 1672 and 1631 cm^{-1}; λ_{max}^{EtOH} 223 nm (ε 7000); ORD (*c* 0.196, dioxane) at 23.5 °C: $[\alpha]_{400}$ −143°, $[\alpha]_{384}$ −250° (trough), $[\alpha]_{373}$ −89° (peak), $[\alpha]_{366}$ −189° (trough), $[\alpha]_{356}$ +92° (peak), $[\alpha]_{349}$ −59° (trough), $[\alpha]_{342}$ +120° (peak), $[\alpha]_{334}$ +20° (trough), $[\alpha]_{327}$ +112° (peak), $[\alpha]_{322}$ +94° (trough), and $[\alpha]_{280}$ +339°; NMR (CCl_4) τ: 3.40 (dq, $J_{3.4\alpha}=2.1$, $J_{3.4\beta}=5.0$ and $J_{2,3}=10.2$ Hz, 1H) and 4.32 (dd, $J_{2.4\beta}=1.7$ and $J_{2.3}=10.2$ Hz, 1H).

Found: C, 84.02; H, 11.46%. Calcd for $C_{27}H_{44}O$: C, 84.31; H, 11.53%.

The next fraction eluted with the same solvent, on crystallization from ethanol, gave needles of **3** (640 mg), mp 108—109 °C.

*Bromination of 5β-Cholestan-1-one (**8**).* To a solution of **8** (2.89 g) in acetic acid (200 ml) was added bromine (1.2 g) in acetic acid (50 ml). After being stirred for 30 min at room temperature, the reaction mixture was treated in the usual manner. The resulting oil (3.7 g) was chromatographed on silica gel. From the first elution with benzene–petroleum ether (1 : 9), **11c** was obtained as needles (184 mg), mp 141.5—143°C, IR (KBr): 1714 cm^{-1}; ORD (*c* 0.22, dioxane) at 21 °C: $[\alpha]_{350}$ +854° (peak) and $[\alpha]_{294}$ −1240° (trough); NMR ($CDCl_3$) τ: 8.70 (s, 3H).

Found: C, 59.65; H, 8.19%. Calcd for $C_{27}H_{44}OBr_2$: C, 59.56; H, 8.15%.

The second fraction, eluted with benzene–petroleum ether (2 : 8), on crystallization from ethanol gave plates of **11b** (494 mg), mp 69—70.5 °C, IR (KBr): 1699 cm^{-1}; ORD (*c* 0.66, dioxane) at 20 °C: $[\alpha]_{350}$ +555° (peak), $[\alpha]_{324}$ +350° (sh), and $[\alpha]_{304}$ −400° (trough); NMR ($CDCl_3$) τ: 5.67 m, $W_{h/2}=6.5$ Hz, 1H) and 8.85 (s, 3H).

Found: C, 69.76; H, 9.84%. Calcd for $C_{27}H_{45}OBr$: C, 69.66; H, 9.74%.

The third fraction, eluted with the same solvent, on crystallization from ethanol, gave needles (1.22 g) of **11a**, mp 118—119 °C, IR (KBr): 1711 cm^{-1}; ORD (*c* 0.46, dioxane) at 30 °C: $[\alpha]_{317}$ −1150° (trough), $[\alpha]_{308}$ −1020° (sh), and $[\alpha]_{272}$ +1080° (peak); NMR ($CDCl_3$) τ: 5.04 (dd, $J_{2,3\alpha}=6$ and $J_{2,3\beta}=12.5$ Hz, 1H) and 8.76 (s, 3H).

Found: C, 69.58; H, 9.96%. Calcd for $C_{27}H_{45}OBr$: C, 69.66; H, 9.74%.

Epimerization of **11b** with hydrogen bromide in acetic acid gave **11a**.

A solution of the 2β-bromo derivative (**11b**) (1.5 g) in DMF (25 ml) was refluxed with calcium carbonate (1.5 g). After 3 hr, the reaction mixture was treated in the usual manner. Crystallization of the product from ethanol gave needles (1.1 g), mp 99—101 °C. The compound was identical with 5β-cholest-2-en-1-one (**10**) in the IR and NMR spectra.

*2β-Acetoxy-5β-cholestan-1-one (**12**).* A mixture consisting of **8** (1 g), lead tetraacetate (1.2 g), boron trifluoride etherate (1.9 ml), and benzene (30 ml) was stirred at 30 °C in a nitrogen atmosphere. After 20 hr, the reaction mixture was poured into water and the benzene layer was taken up in ether. The ethereal solution was washed with water, dried and evaporated. Crystallization of the residue from ethanol gave needles (320 mg), mp 88—90 °C, IR (KBr): 1747 and 1711 cm^{-1}; ORD (*c* 0.23, dioxane) at 20 °C: $[\alpha]_{312}$ −1662° (trough), $[\alpha]_{304}$ −1386° (sh), and $[\alpha]_{264}$ +1586° (peak); NMR ($CDCl_3$) τ: 4.60 (dd, $J_{2,3\alpha}=5.8$ and $J_{2,3\beta}=12.7$ Hz, 1H) and 7.88 (s, 3H).

Found: C, 78.11; H, 11.02%. Calcd for $C_{29}H_{48}O_3$: C, 78.33; H, 10.88%.

The authors are indebted to Japan Electron Optics Laboratory Co., Ltd., for measurement of 100 MHz NMR spectra.

BULLETIN OF THE CHEMICAL SOCIETY OF JAPAN, VOL. 46, 3158—3160 (1973)

Catalytic Decomposition of Stable Sulfur Ylids[1]

Haruo MATSUYAMA, Hiroshi MINATO, and Michio KOBAYASHI

Department of Chemistry, Faculty of Science, Tokyo Metropolitan University, Fukazawa, Setagaya, Tokyo 158

(Received April 26, 1973)

In the presence of dimethoxy disulfide, such stable sulfur ylids as Me_2S^+–$C^-(COOMe)_2$, Me_2S^+–$C^-(CN)_2$, and Me_2S^+–C^-HCOPh were found to decompose at 35 °C, forming methyl sulfide and an olefin or a cyclopropane. Thiocyanogen and trifluoromethyl disulfide were found to possess similar catalytic activity. The scope and mechanism of these reactions are discussed.

Sulfur ylids possessing two electron-withdrawing substituents on the negatively-charged carbon atom are thermally stable, and their nucleophilicity is much less than that of mono-substituted sulfur ylids. Recently, we have reported that methylphenylsulfonium bis(methoxycarbonyl)methylid (Id) undergoes transylidation with alkyl sulfides and pyridines at 35 °C when dimethoxy disulfide (II) is present.[2]

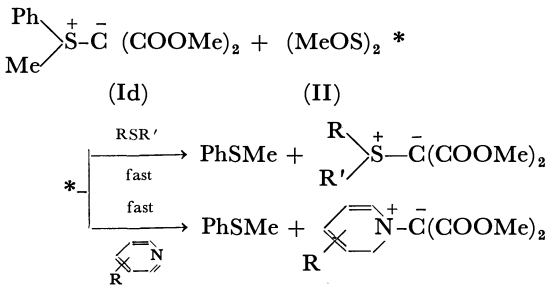

It has been found that, when an alkyl sulfide or a pyridine is absent and II is present, Id slowly decomposes, yielding methyl phenyl sulfide and methyl ethylenetetracarboxylate almost quantitatively.

$$[Id] + [II] \xrightarrow{slow} PhSMe + (MeOOC)_2C{=}C(COOMe)_2$$

The decompositions of ylids under acidic conditions[3] or at higher temperatures[4] have been reported, but the decomposition of thermally stable ylids under such mild conditions have never been reported yet. In order to clarify the mechanism of this reaction, the effects of catalysts and ylid substituents on the decomposition have now been studied; the results will be described in this paper.

Results and Discussion

In the absence of dimethoxy disulfide [II], the ylids [I] listed in Table 1 are stable for a long time at 35 °C and show no change. However, when equimolar amounts of I and II are mixed in, the decomposition of I takes place slowly.

Ic is a mono-substituted ylid; it decomposes much faster than di-substituted ylides, producing methyl sulfide and *trans*-1,2,3-tribenzoylcyclopropane. Di-substituted ylids (Ia, Ib, and Id) decompose slowly and give the corresponding sulfide and olefin. Two ylids containing acetyl groups (Ie: Me_2S^+—C^-(COOMe)(COMe), If: Me_2S^+—$C^-(COMe)_2$) do not decompose under the same conditions.

Thiocyanogen $(SC{\equiv}N)_2$ and bistrifluoromethyl disulfide showed catalytic activity similar to that of II. The common feature in these sulfides is that the electron density on the –S–S– group is much lowered by the electron-withdrawing substituents:

$$\overset{\delta-}{MeO}\leftarrow\overset{\delta+}{S}—\overset{\delta+}{S}\rightarrow\overset{\delta-}{OMe} \qquad \overset{\delta-}{N}{\equiv}C\leftarrow\overset{\delta+}{S}—\overset{\delta+}{S}\rightarrow C{\equiv}\overset{\delta-}{N}$$

$$\overset{\delta-}{F_3C}\leftarrow\overset{\delta+}{S}—\overset{\delta+}{S}\rightarrow\overset{\delta-}{CF_3}$$

Trost reported that, when an ylid was heated with copper(II) sulfate, it quantitatively decomposed.[5] In order to explain this reaction, he proposed that the copper(II)-ylid complex is formed.

In order to compare the disulfide-catalyzed decomposition with the Cu(II)-catalyzed decomposition, Ia and Ib were heated under the conditions used by Trost. In the presence of Cu(II), Ia decomposed and formed the corresponding sulfide and olefin, but Ib did not decompose appreciably. Id slowly decomposed

1) Organic Sulfur Compounds. Part XLIII.

2) H. Matsuyama, H. Minato, and M. Kobayashi, This Bulletin, **46**, 2845 (1973).

3) T. Yagihara and S. Oae, *Int. J. Sulfur Chem.*, **A**, **1**, 159 (1971).

4) W. Ando, T. Yagihara, S. Tozune, I. Imai, J. Suzuki, T. Toyama, S. Nakaido, and T. Migita, *J. Org. Chem.*, **37**, 1721 (1972).

5) B. M. Trost, *J. Amer. Chem. Soc.*, **89**, 138 (1967).

Table 1. Decomposition of stable sulfur ylids in the presence of a catalytic disulfide in $CDCl_3$ at 35°C

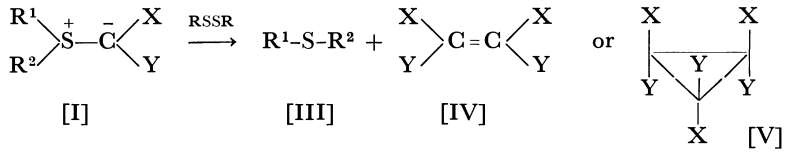

[I] [III] [IV] [V]

	I				Catalyst	Time (hr)	Products (mol%)			
	R^1	R^2	X	Y			Recovered I	III	IV	V
Ia	Me	Me	COOMe	COOMe	$(MeOS)_2$	21	—	93	88	—
Ib	Me	Me	CN	CN	$(MeOS)_2$	4	36	64	46	—
					$(N{\equiv}CS)_2$	27	8	83	57	—
					$(F_3CS)_2$	67	36	60	50	—
Ic	Me	Me	H	COPh	$(MeOS)_2$	1	—	95	—	90
Id	Ph	Me	COOMe	COOMe	$(MeOS)_2$	24	—	98	92	—

Table 2. Thermal and Cu(II)-catalyzed decomposition of sulfur ylids[a]

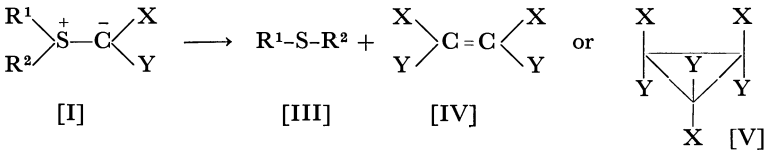

[I] [III] [IV] [V]

Ylid	Solvent	Catalyst[b]	Temp. (°C)	Time (hr)	Products (mol%)			
					Recovered I	III	IV	V
Ia	$CHCl_3$	$CuSO_4$	62	48	30	60	60	—
Ib	$CHCl_3$	$CuSO_4$	62	48	92	—	—	—
Ic	$CHCl_3$	—[c]	62	144	100	No Reaction		
		$CuSO_4$[c]	83	24	—	90	—	90
Id	CH_3NO_2	—	86	48	80	18	18	—
	—	—[d]	155	>20	Rearrangement			

a) When a solvent was used, [I] was about 0.5 M. b) Molar ratio, $CuSO_4$: I, was about 2. c) Ref. 5; benzoylnorcarane was found in 4.9% yield. d) Ref. 4; the Stevens-type product, $PhSC(CH_3)(COOCH_3)_2$, was found in 10% yield.

Table 3. Rates of decomposition of Ia in the presence of II in $CDCl_3$ at 35°C

$$Me_2S^+—C^-(COOMe)_2 + (MeOS)_2 \rightarrow Me_2S + (MeOOC)_2C{=}C(COOMe)_2$$

[Ia] [II]

Concentration (mol/l)		[II]/[Ia]	First-order Rate Constant[a] 10^5k_1 (s^{-1})
[Ia]	[II]		
0.46	0.45	1.0	0.7
0.46	0.91	2.0	1.8
0.46	1.82	4.0	8.3
0.46	2.73	6.0	19.0

a) Calculated from $-d[Ia]/dt = k[Ia]$.

even in the absence of $CuSO_4$. The results are shown in Table 2.

When Tables 1 and 2 are compared, it is clear that the disulfide-catalyzed decomposition proceeds much faster under milder conditions than the Cu(II)-catalyzed decomposition.

Then, the effect of the concentration of IIa on the rate of the decomposition of Ia was examined; the results are shown in Table 3. The first-order rate constants for the decomposition of Ia were greater when the concentration of IIa was greater.

The results of the investigations of the disulfide-catalyzed transylidation and decomposition of ylids can be summarized as follows:

1) Disulfides containing electron-withdrawing substituents catalyze both the transylidation and decomposition.

2) The rates of both reactions increase with the concentration of catalytic disulfide.

3) The catalytic disulfide does not decompose during the reaction.

4) The order of reactivity for transylidation[2] is:

$$R_2S^+—C^-(COOMe)_2 > R_2S^+—C^-(COOMe)(COMe) \gg R_2S^+—C^-(COMe)_2$$

and that for decomposition is:

$$R_2S^+—C^-HCOPh > R_2S^+—C^-(COOMe)_2 \approx R_2S^+—C^-(CN)_2 \gg R_2S^+—C^-(COOMe)(COMe)$$

and $R_2S^+—C^-(COMe)_2$

These orders are similar to the order of the nucleophilicity of the negatively-charged carbon atom of ylids.

The transylidation and ylid decomposition may be

expressed by the following scheme, involving a disulfide-ylid adduct:

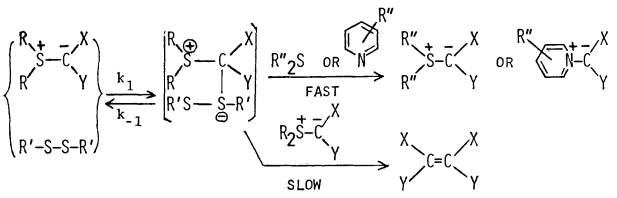

When an alkyl sulfide or pyridine is present, their nucleophilic attack on the adduct takes place rapidly, and the corresponding new ylid is formed. When such a powerful nucleophile is absent, the ylid itself functions as a nucleophile, the nucleophilic attack of the negatively-charged carbon atom of the ylid on the adduct results in the C–C bond formation, and the corresponding olefin is obtained. This process may be represented as follows:

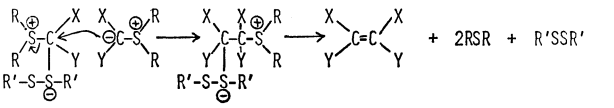

As Table 1 shows, Ic decomposed very rapidly. This is reasonable, because the mono-substituted ylid with great nucleophilicity must form the adduct readily; furthermore, the nucleophilic attack of Ic on the adduct must be faster than that of di-substituted ylids. Since Ic is known to undergo a Michael addition with dibenzoylethylene,[5] the olefin formed by the decomposition-dimerization of Ic reacts with another molecule of Ic faster than the adduct, and *trans*-1,2,3-tribenzoylcyclopropane is the final product.

The nucleophilicity of Ia and Ib is much smaller, and the olefins formed do not receive any further nucleophiclic attack of ylids. Two ylids, Ie and If, which did not decompose under the reaction conditions, underwent transylidation extremely slowly. The nucleophilicity of these ylids is very small, the adduct is formed to a very small extent, and both the transylidation and ylid decomposition take place very slowly.

Experimental

Materials. The ylids (Ia, Ib,[6] Ic,[5] Id,[4] Ie, and If[7]), dimethoxy disulfide,[8] and thiocyanogen[9] were synthesized according to the procedures described in the literature. Bistrifluoromethyl disulfide was synthesized by the reaction between trichloromethanesulfenyl chloride and sodium fluoride in sulfolane.[10]

Decomposition of Ib in the presence of Thiocyanogen. A chloroform solution (50 ml) of Ib (1.15 g, 9.14 mmol) was mixed with thiocyanogen (3.0 g, 0.66 mmol; dissolved in CCl_4) in a 50-ml, egg-shaped flask at 35 °C. The disappearance of Ib (Me_2S^+—, δ, 2.80 ppm) and the formation of Me_2S (δ, 2.10 ppm) were followed by use of NMR spectroscopy. When the Me_2S^+— signal completely disappeared, the reaction mixture was concentrated with a rotatory evaporator. The residue was chromatographed (Wakogel Q-22, 200 mesh), and with a benzene–ether (1 : 1) mixture 0.66 g of tetracyanoethylene (5.2 mmol, 57%) was obtained. Sublimation gave 0.49 g (3.8 mmol, 42%), melting at 197—199 °C (lit,[11] 200 °C) and possessing the same infrared spectrum as that of an authentic sample.[12]

The Decomposition of Id in the Presence of II. A mixture of Id (0.85 g, 3.33 mmol), nitromethane (20 ml), and II (0.54 g, 4.32 mmol) in a 50-ml, egg-shaped flask was placed in a constant-temperature bath at 35 °C. The decrease in Id (PhMeS$^+$–, δ, 3.26 ppm) and the increase in PhSMe (δ, 2.50 ppm) were followed by NMR spectroscopy, using 1,1,2,2-tetrachloroethane as the internal standard. The chromatographic separation of the residue gave 0.40 g (3.08 mmol, 92%) of methyl ethylenetetracarboxylate. Its identity was established by a comparison of its infrared absorptions ($\nu_{C=O}$, 1740 cm^{-1}), mp (121—122 °C) and gas-chromatographic retention time (Carbowax 20 M, 10%, 2 m, 200 °C) with those of an authentic sample synthesized by the copper-catalyzed decomposition of methyl diazomalonate.

The Decomposition of Ic in the Presence of II. The reaction in a mixture of Ic (0.54 g, 3.0 mmol), nitromethane (20 ml), and II (0.63 g, 5.0 mmol) at 35 °C was followed by NMR spectroscopy, with 1,1,2,2-tetrachloroethane as the internal standard. After evaporation and chromatography, *trans*-1,2,3-tribenzoylcyclopropane was obtained; Yield, 0.32 g (0.27 mmol, 90%); mp 214—216 °C (lit,[13] 215 °C); IR ($\nu_{C=O}$ 1670 cm^{-1}); NMR, identical with that reported in the literature.[14]

The $CuSO_4$-Catalyzed Decomposition of Ia. A mixture of Ia (1.74 g, 9.04 mmol), chloroform (20 ml), and anhydrous $CuSO_4$ (3.42 g, 21.4 mmol) was refluxed for 48 hr. When the $CuSO_4$ was filtered and the solvent was evaporated, white solids remained. Their IR absorptions indicated the presence of methyl ethylenetetracarboxylate ($\nu_{C=O}$, 1740 cm^{-1}) and Ia ($\nu_{C=O}$, 1620—1660 cm^{-1}). The amount of Ia was determined by NMR, using nitromethane as the internal standard. Methyl ethylenetetracarboxylate was separated by column chromatography and determined by gas chromatography (5.42 mmol, 60%).

The Thermal Decomposition of Id in the Absence of a Catalyst. A mixture of Id (0.20 g, 0.77 mmol) and nitromethane (10 ml) in a 50-ml flask was heated at 86 °C for 48 hr. After the mixture had been concentrated, the amounts of methyl phenyl sulfide (0.14 mmol, 18%) and the remaining Id (0.62 mmol, 80%) were determined by NMR spectroscopy, using 1,1,2,2-tetrachloroethane as the internal standard.

The Determination of the Rate of Decomposition of Ia. A $CDCl_3$ solution of Ia (0.320 mmol) and a suitable amount of dimethoxy disulfide were mixed in an NMR tube. After nitromethane (0.79 mmol; δ, 4.33 ppm) had been added as the internal standard, more $CDCl_3$ was added with a microsyringe so that the total volume became 700 μl. The disappearance of Ia was followed by observing the decrease in Me_2S^+– (δ, 2.89 ppm).

6) W. J. Middleton, E. L. Buhle, J. G. McNally, Jr., and M. Zanger, *J. Org. Chem.*, **30**, 2384 (1965).
7) H. Nozaki, D. Tsunemoto, Z. Morita, K. Nakamura, K. Watanabe, M. Takaku, and K. Kondo, *Tetrahedron*, **23**, 4279 (1967).
8) Q. E. Thompson, M. M. Crutchfield, M. W. Dietrich, and E. Pierron, *J. Org. Chem.*, **30**, 2692 (1965).
9) L. F. Fieser and M. Fieser, "Reagents for Organic Syntheses," John Wiley & Sons, New York (1967), Vol. 1, 1152.
10) C. W. Tullock and D. D. Coffman, *J. Org. Chem.*, **25**, 2016 (1960).
11) T. L. Cairns, R. A. Carboni, D. D. Coffman, V. A. Engelhardt, R. E. Heckert, E. L. Little, E. G. McGeer, B. C. McKusick, W. J. Middleton, R. M. Scribner, C .W. Theobald, and H. E. Winberg, *J. Amer. Chem. Soc.*, **80**, 2775 (1958).
12) C. E. Looney and J. R. Downing, *ibid.*, **80**, 2840 (1958).
13) G. Mair, *Chem. Ber.*, **95**, 611 (1962).
14) J. D. Graham and M. T. Rogers, *J. Amer. Chem. Soc.*, **84**, 2249 (1962).

The Synthesis of Azulene Derivatives Condensed with Several Heterocycles[1)]

Tetsuo NOZOE,* Toyonobu ASAO,** and Masao KOBAYASHI***

Department of Chemistry, Faculty of Science, Tohoku University, Aramaki, Aoba, Sendai 980

(Received May 28, 1973)

The reactions of ethyl 1,2-diaminoazulene-3-carboxylate with formic acid, nitrous acid, glyoxal sodium bisulfite, diacetyl, and benzil afforded the corresponding azulene derivatives condensed at the 1,2-position with nitrogen-containing heterocycles, namely, imidazole, triazole, and pyrazine rings. 2-Amino-1-formylazulene reacted with guanidine or thiourea to give 2-aminoazuleno[2,1-*d*]pyrimidine. The ultraviolet and visible absorption spectra of these azulenes are presented.

Azulene derivatives condensed with furans,[2,3)] pyrroles,[4)] thiophenes,[5)] pyridines,[6,7)] pyrazines,[8)] thiapyran,[9)] and azepine[9)] have already been synthesized.

During the course of an investigation of the reactions of 1,2-diaminoazulene derivatives and 2-amino-1-formylazulene, the present authors have synthesized azuleno[1,2-*d*]imidazole, azuleno[1,2-*d*]triazole, azuleno[2,1-*b*]pyrazine and azuleno[2,1-*d*]pyrimidine derivatives; the results will be reported in this paper.

The heating of 1,2-diacetamidoazulene (I)[10)] in acetic anhydride or acetic acid in anticipation of the formation of an azulenoimidazole derivative led to the complete recovery of the starting material, and the treatment of I in hydrochloric acid at the boiling point resulted in the formation of a resinous product besides the starting compound.

The reaction of the hydrochloride of ethyl 1,2-diaminoazulene-3-carboxylate (II)[10)] and 40% aqueous formic acid yielded yellow crystals (III) in a good yield. The results of the elemental analyses ($C_{14}H_{14}O_3N_2$) and the infrared spectrum (3420 and 3300 cm^{-1} (NH_2)) indicate that Compound (III) is not the expected azulenoimidazole, but ethyl 2-amino-1-formamidoazulene-3-carboxylate. An alternative structure for III, ethyl 1-amino-2-formamidoazulene-3-carboxylate, may be excluded because an amino group at the 1-position is less sterically hindered and must be more basic than one at the 2-position.[10)]

The acetylation of III afforded the 2-acetamido derivative (IV), whose ultraviolet spectrum shows a curve very similar to that of ethyl 1,2-diacetamidoazulene-3-carboxylate.[10)]

The reaction of II with anhydrous formic acid yielded light purple crystals, the elemental analyses ($C_{14}H_{12}O_2N_2$) and the infrared spectrum of which show one sharp carbonyl band at 1680 cm^{-1}; the compound may, therefore, be assumed to be ethyl azuleno[1,2-*d*]-imidazole-9-carboxylate (V).

The treatment of the solution of II in hydrochloric acid with sodium nitrite afforded orange crystals (VI) in a fairly good yield. From the analyses ($C_{13}H_{11}O_2N_3$) and the similarity of the ultraviolet spectrum (Fig. 1) to that of Compound (V), Compound (VI) is considered to be ethyl azuleno[1,2-*d*]triazole-9-carboxylate.

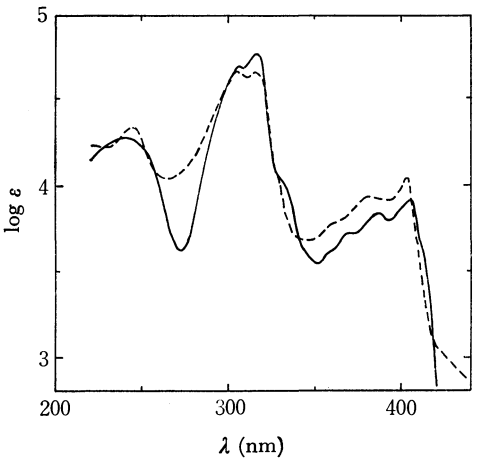

Fig. 1. UV absorption spectra of V (——) and VI (------) in methanol.

The attempted derivation of V and VI to azuleno-[1,2-*d*]imidazole and azuleno[1,2-*d*]triazole respectively by alkaline hydrolysis, followed by thermal decarboxylation, resulted in the formation of a resinous substance; no objective compounds could be obtained.

The reactions of II and an aqueous solution of glyoxal or glyoxal sodium bisulfite under various conditions yielded resinous products; no pure products could be isolated. However, when unstable ethyl 1,2-diaminoazulene-3-carboxylate (IIa), obtained by passing a methanolic solution of II through an ion-exchange resin (Amberlite IRA-410), was reacted with glyoxal sodium bisulfite, ethyl azuleno[2,1-*b*]pyrazine-10-car-

* Present address: No. 811, 2-5-1, Kamiyoga, Setagaya-ku, Tokyo 158.

** Present address: Department of Chemistry, College of General Education, Tohoku University, Kawauchi, Sendai 980.

*** Present address: Mitsubishi Rayon Co., Ltd., Otake, Hiroshima 739-06.

1) Presented at the Tohoku Local Meeting of the Chemical Society of Japan, Yamagata, October, 1961; M. Kobayashi, Master Thesis, Tohoku University, Sendai, March, 1962.

2) K. Takeda and W. Nagata, *Chem. Pharm. Bull.* (Tokyo), **1**, 164 (1953).

3) T. Nozoe, S. Seto, and S. Matsumura, *Chem. Ind.*, **1961**, 1715.

4) K. Matsui and T. Nozoe, *Chem. Ind.*, (London), **1960**, 1302; K. Matsui, *Nippon Kagaku Zasshi*, **82**, 1517, 1520, 1522, 1665, 1667 (1961); L. L. Replogle, K. Katsumoto, and H. L. Ammon, *J. Amer. Chem. Soc.*, **90**, 1086 (1968); H. L. Ammon, L. L. Replogle, D. H. Watts, Jr., K. Katsumoto, and J. M. Stewart, *ibid.*, **93**, 2196 (1971).

5) T. Nozoe, K. Takase, and T. Tada, This Bulletin, **36**, 1016 (1964).

6) T. Nozoe and K. Kikuchi, *Chem. Ind.* (London), **1962**, 358; This Bulletin, **36**, 633 (1963).

7) L. L. Replogle, *J. Amer. Chem. Soc.*, **86**, 3137 (1964).

8) T. Nozoe, P. W. Yang, H. Ogawa, and T. Toda, This Bulletin, **41**, 2095 (1968).

9) L. L. Replogle, K. Katsumoto, T. C. Morrill, and C. A. Minor, *Tetrahedron Lett.*, **1965**, 1877; *J. Org. Chem.*, **33**, 823 (1968).

10) T. Nozoe, T. Asao, and M. Kobayashi, This Bulletin, **46**, 3266 (1973).

boxylate (VII) was obtained as greenish brown crystals in a low yield.

The reaction of II with diacetyl and benzil proceeded smoothly to give the corresponding products, 2,3-dimethyl and 2,3-diphenyl derivatives (VIII and IX respectively).

The hydrochloride of ethyl 1,2-diamino-5-isopropylazulene-3-carboxylate (X)[10] afforded the 8-isopropyl derivative (XI) by means of a reaction with benzil.

The hydrolysis of Compounds VIII, IX, and XI with ethanolic alkali gave the corresponding carboxylic acids, and the thermal decarboxylation yielded 2,3-dimethyl-, 2,3-diphenyl-, and 2,3-diphenyl-8-isopropylazuleno[2,1-*b*]pyrazine (XII, XIII, and XIV respectively).

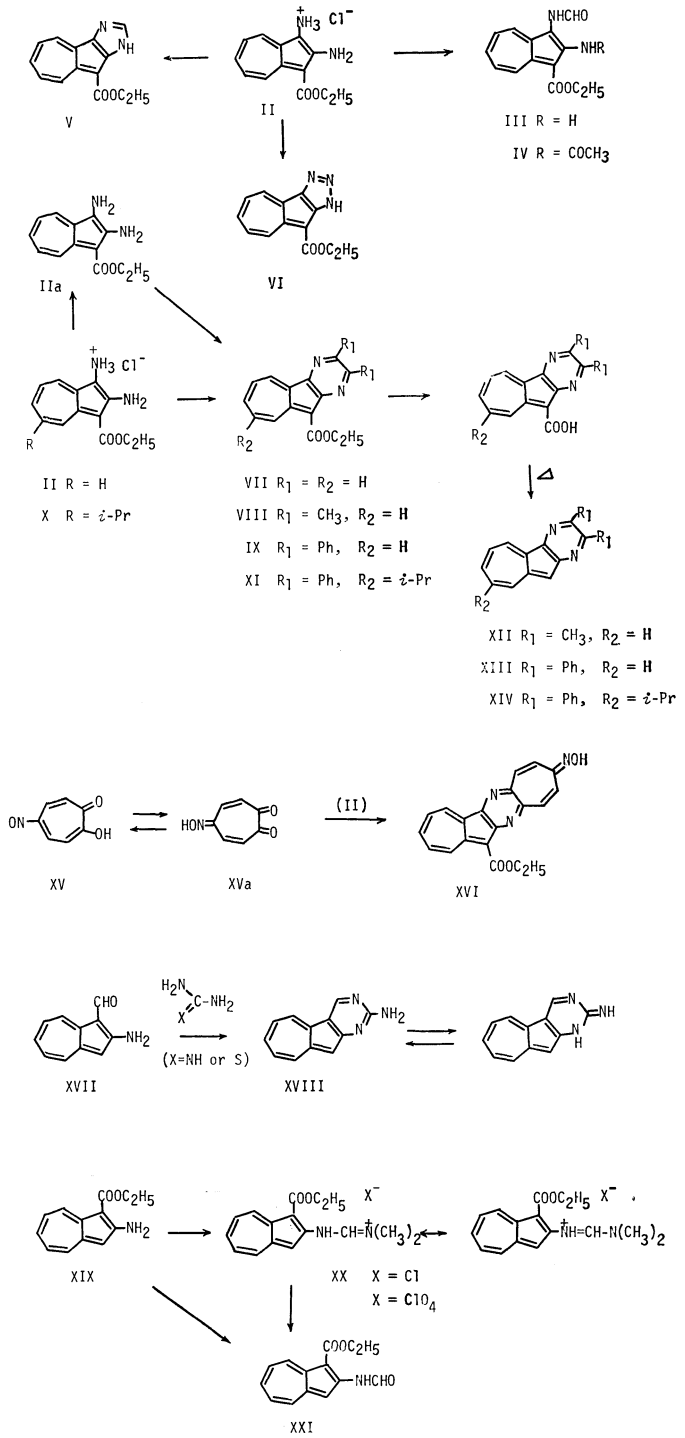

It has been shown that 5-nitrosotropolone (XV) reacted with *o*-diamine derivatives *via* its tautometic *o*-diketone form (XVa) to give troponoids fused with pyrazine or quinoxaline rings.[11,12]

The reaction of II with XV gave yellowish-green crystals (XVI) as an insoluble precipitate. The infrared spectrum of XVI shows an OH band at 3400 cm^{-1}, and the permanganate oxidation of XVI, followed by methylation with diazomethane, afforded tetramethyl pyrazinetetracarboxylate;[12] therefore, Compound XVI must has the structure shown in the scheme.

2-Amino-1-formylazulene (XVII)[6] reacted with guanidine, and orange needles (XVIII) were obtained. The analyses of the compound accord with the $C_{12}H_9N_3$ formula, and the infrared spectrum displays bands at 3300 and 3100 cm^{-1} similar to those of 2-aminopyrimidine;[13] thus, the compound may be considered to be 2-aminoazuleno[2,1-*d*]pyrimidine.

A similar reaction of XVII with thiourea gave the same compound (XVIII); this fact shows that the aza-nitrogen at the 1-position of XVIII came from an amino group at the 2-position of XVII in the reaction with thiourea.

The reactions of XVII with formamide and of 2-chloro-1-formylazulene with guanidine resulted in the recovery of the starting compounds in both cases.

The attempted formylation of ethyl 2-acetamidoazulene-1-carboxylate by the Vilsmeier method resulted in the complete recovery of the starting azulene. However, the similar formylation of ethyl 2-aminoazulene-1-carboxylate (XIX) afforded crystalline chloride (XX: X=Cl), which was easily converted to perchlorate (XX: X=ClO_4). The mild treatment of the chloride with sodium hydrogen carbonate yielded ethyl 2-formamidoazulene-1-carboxylate (XXI), which was also obtained by the direct formylation of XIX with formic acid. Therefore, Compound (XX) may be considered to have the structure shown in the scheme.

The unreactivity of the azulene attached by the ethoxycarbonyl group at the 1-position to the Vilsmeier reaction must be attributable to the electron-withdrawing effect of the ethoxycarbonyl group, as is observed in the diazo-coupling reaction of the same compound.[10]

Experimental[14]

Ethyl 2-Amino-1-formamidoazulene-3-carboxylate (III). A solution of II (134 mg) in 40% formic acid (2 ml) was heated on a water bath for 30 min. After cooling, the crystals which separated out were filtered to yield 135 mg of yellowish-brown crystals; mp 200 °C. The crystals were chromatographed on alumina, using acetone as the solvent, and then recrystallized from ethyl acetate to give III as orange-yellow

11) T. Nozoe, M. Sato, and T. Matsuda, *Sci. Repts. Tohoku Univ.*, **I, 37**, 407 (1953); S. Ito, *ibid.*, **42**, 236 (1958); T. Nozoe, S. Ito, S. Suzuki, and K. Hiraga, *Proc. Japan Acad.*, **32**, 344 (1956).
12) T. Asao, This Bulletin, **34**, 151 (1961).
13) L. N. Short and H. W. Thompson, *J. Chem. Soc.*, **1952**, 168.
14) All melting points are uncorrected.

micro needles; mp 203—204 °C.

Found: C, 64.82; H, 5.45; N, 11.04%. Calcd for $C_{14}H_{14}O_3N_2$: C, 65.10; H, 5.46; N, 10.85%.

λ_{max}^{MeOH} nm (log ε); 242 (3.94), 315.5 (4.46), and 355 (3.62).

Ethyl 2-Acetamido-1-formamidoazulene-3-carboxylate (IV). A solution of III (100 mg) in acetic anhydride (0.5 ml) was heated on a water bath for 50 min. The solvent was then removed to leave a violet residue, which was dissolved in chloroform, and passed through an alumina column; 70 mg of violet needles were thus obtained. Recrystallization from ethanol afforded IV as violet micro needles; mp 220—222 °C.

Found: C, 63.88; H, 5.64; N, 9.28%. Calcd for $C_{16}H_{16}O_4N_2$: C, 63.99; H, 5.37; N, 9.33%.

λ_{max}^{MeOH} nm (log ε); 225^{sh} (4.32), 248 (4.35), 314 (4.73), 360 (3.84) 375^{sh} (3.70) and 535 (2.67).

Ethyl Azuleno[1,2-d]imidazole-9-carboxylate (V). A solution of II (196 mg) in anhydrous formic acid (1.5 ml) was heated on a water bath for 1 hr. To the solution we then added water (10 ml), after which the solution was neutralized with sodium hydrogen carbonate and extracted with chloroform. When the extract was dried and passed through an alumina column, violet crystals were obtained, recrystallization from benzene afforded light brownish-purple crystals (V); mp 202 °C.

Found: C, 70.13; H, 5.30; N, 10.93%. Calcd for $C_{14}H_{12}O_2N_2$: C, 69.99; H, 5.03; N, 11.66%.

λ_{max}^{MeOH} nm (log ε): 243.5 (4.28), 305 (4.70), 317 (4.72), 332^{sh} (4. 1), 370 (3.73), 386 (3.84), 405 (3.92), 475^{sh} (2.27), 515 (2.36) and 550^{sh} (2.32).

Ethyl Azuleno[1,2-d]triazole-9-carboxylate (VI). To a solution of II (134 mg) in acetic acid (60 mg), water (7 ml), and dioxane (2 ml), a solution of sodium nitrite (38 mg) in water (2 ml) was added under cooling. After the addition, the solution was stirred for 15 min at 60 °C and then for 2 hr at room temperature. After cooling with ice, an 80 mg portion of a brown product was obtained; it was recrystallized from benzene to give orange needles (VI); mp 178 °C (decomp.).

Found: C, 64.46; H, 4.72; N, 17.30%. Calcd for $C_{13}H_{11}O_2N_3$: C, 64.72; H, 4.60; N, 17.42%.

λ_{max}^{MeOH} nm (log ε); 244 (4.35), 302 (4.68), 316 (4.71), 360^{sh} (3.78), 380 (3.95), 402 (4.06), and 480 (2.50).

Ethyl Azuleno[2,1-b]pyrazine-10-carboxylate (VII). To a stirred solution of 200 mg of II in methanol (30 ml), ion-exchange resin (Amberlite IRA-410) was added in small portions to almost the neutral point, after which the resin was filtered off. To the solution, a solution of glyoxal sodium bisulfite (260 mg) in water (40 ml) was added drop by drop, after which the solution was kept at room temperature overnight. The methanol was removed under reduced pressure, and the residue was extracted with chloroform and dried. The evaporation of the solvent gave a greenish brown residue; when this residue was dissolved in benzene and passed through an alumina column, yellowish green crystals were obtained. Recrystallization from ethanol–petroleum ether gave VII as pale greenish crystals; mp 112—115 °C.

Found: C, 71.43; H, 4.46; N, 10.73%. Calcd for $C_{15}H_{12}O_2N_2$: C, 71.41; H, 4.80; N, 11.11%.

λ_{max}^{MeOH} nm (log ε): 224 (4.32), 251 (4.36); 318 (4.63), 330 (4.64), 369 (3.79), 391 (3.96), 417 (4.03), 468 (2.39), 505 (2.46) 540 (2.47), and 585 (2.33).

Ethyl 2,3-Dimethylazuleno[2,1-b]pyrazine-10-carboxylate (VIII). A solution of II (300 mg) and diacetyl (200 mg) in ethanol (40 ml) was stirred for 3 hr at room temperature. Water (500 ml) was then added, and the solution was extracted with chloroform. After drying, the extract was passed through an alumina column; yellowish green crystals were thus obtained. Recrystallization from benzene–cyclohexane yielded 210 mg of VIII as greenish needles; mp 138—139 °C.

Found: C, 72.72; H, 5.46; N, 9.76%. Calcd for $C_{17}H_{16}O_2N_2$: C, 72.84; H, 5.75; N, 9.99%.

λ_{max}^{MeOH} nm (log ε): 227 (4.34), 255 (4.39), 325 (4.68), 338 (4.74), 373 (3.85), 395 (3.89), 416 (3.89), 520 (2.38), 554 (2.41), 600^{sh} (2.29), and 660^{sh} (1.75).

2,3-Dimethylazuleno[2,1-b]pyrazine (XII). A solution of VIII (120 mg) in ethanol (6 ml) and a 1M sodium hydroxide solution (4 ml) was refluxed for 6 hr. The ethanol was removed, water was added, the solution was acidified with hydrochloric acid, and then the solution was extracted with chloroform. The dark brown product obtained by removing the solvent was heated under reduced pressure to afford a dark greenish product. Recrystallization from cyclohexane gave XII as violet prisms; mp 143 °C.

Found: C, 80.94; H, 5.70; N, 13.15%. Calcd for $C_{14}H_{12}N_2$: C, 80.74; H, 5.81; N, 13.45%.

λ_{max}^{MeOH} nm (log ε): 470 (2.00), 505 (2.11), 550 (2.24), 595 (2.28), and 650 (2.16).

Ethyl 2,3-Diphenylazuleno[2,1-b]pyrazine-10-carboxylate (IX). When a solution of II (60 mg) and benzil (50 mg) in ethanol (7 ml) was heated on a water bath for 10 min, greenish needles were precipitated out. After cooling, 70 mg of crystals were obtained; recrystallization from ethanol then gave IX as yellowish green silky needles; mp 209—210 °C.

Found: C, 80.10; H, 5.00; N, 6.93%. Calcd for $C_{27}H_{20}O_2N_2$: C, 80.18; H, 4.98; N, 6.92%.

λ_{max}^{MeOH} nm (log ε): 235 (4.41), 287 (4.50), 361 (4.71), 410^{sh} (5.07), 520^{sh} (2.51), 560 (2.58), and 604 (2.50).

2,3-Diphenylazuleno[2,1-b]pyrazine (XIII). A solution of IX (304 mg) in ethanol (50 ml) and a 1M sodium hydroxide solution (8 ml) was refluxed for 5 hr. The ethanol was then removed, water (30 ml) was added, the solution was acidified with hydrochloric acid, and the dark greenish crystals thus precipitated out were filtered and dried. The crystals were submitted to decarboxylation by heating under reduced pressure to afford greenish crystals, which were dissolved in chloroform, passed through an alumina column, and recrystallized from benzene–cyclohexane to give XIII as greenish crystals (75 mg); mp 180—181 °C.

Found: C, 86.90; H, 4.85; N, 8.33%. Calcd for $C_{24}H_{16}N_2$: C, 86.72; H, 4.85; N, 8.43%.

λ_{max}^{MeOH} nm (log ε): 290.5 (4.37), 354 (4.63), 410^{sh} (3.95), 510 (2.29), 555 (2.36), 605 (2.38), 660 (2.24), and 738 (1.88).

Ethyl 2,3-Diphenyl-8-isopropylazuleno[2,1-b]pyrazine-10-carboxylate (XI). A solution of ethyl 2-amino-5-isopropyl-1-(*p*-tolylazo)azulene-3-carboxylate in ethyl acetate was submitted to catalytic hydrogenation in the presence of 5% Pd-C. After two molar equivalents of hydrogen had been absorbed, the catalyst was removed, to the filtrate was added a solution of benzil (250 mg) in ethanol (5 ml), and the resulted solution was kept at room temperature overnight. The solvent was then removed, and the residue was dissolved in chloroform and passed through an alumina column. The product obtained from greenish effluents was recrystallized from cyclohexane and then from ethanol to give XI (100 mg) as yellowish green needles; mp 211 °C.

Found: C, 80.98; H, 5.73; N, 6.21%. Calcd for $C_{30}H_{26}O_2N_2$: C, 80.69; H, 5.87; N, 6.27%.

λ_{max}^{MeOH} nm (log ε): 237 (4.41), 291 (4.51), 364 (4.72), 410^{sh} (4.15), 430^{sh} (3.91), 565 (2.63), and 620 (2.55).

2,3-Diphenyl-8-isopropylazuleno[2,1-b]pyrazine (XIV). A solution of XI (140 mg) in ethanol (16 ml) and a 1M sodium hydroxide solution (4 ml) was refluxed for 5 hr. The ethanol was then removed, water was added, and the solution was acidified to give a dark brown solid. The solid was dried

and decarboxylated by heating under reduced pressure, thus yielding a yellowish solid, which was subsequently purified by chromatography and repeated sublimation to afford yellowish green crystals, mp 61 °C.

Found: N, 7.64%. Calcd for $C_{27}H_{22}N_2$: N, 7.48%.

λ_{max}^{MeOH} nm (log ε): 281 (4.30), 355 (4.51), 410^{sh} (3.80), 440^{sh} (3.39), 510^{sh} (1.96), 560 (2.07), 605 (2.09), 660 (1.98), and 740^{sh} (1.54).

The Reaction of II and 5-Nitrosotropolone (XV). To a solution of 150 mg of II in methanol (20 ml), a solution of XV (100 mg) in methanol (10 ml) was added, and the resulting solution was stirred at room temperature from 2 hr. After cooling, the precipitate (90 mg) was filtered and then recrystallized from diluted pyridine to give yellowish green micro crystals (XVI): the mp blackens from around 290 °C.

Found: C, 68.49; H, 4.02; N, 11.44%. Calcd for $C_{20}H_{15}O_3N_3$: C, 69.55; H, 4.38; N, 12.17%.

λ_{max}^{MeOH} nm (log ε): 229 (3.41), 245 (4.35), 314 (4.55), 397 (4.58), 590 (2.80), 630 (2.79), and 690^{sh} (2.56).

Oxidation of XVI. Into a solution of XVI (300 mg) in a 10% potassium hydroxide solution (40 ml), a solution of potassium permanganate (3.6 g) in water (110 ml) was added drop by drop at 70—80 °C. After 2 hr, a small amount of methanol was added, manganese dioxide was filtered out and washed with a dilute pottassium hydroxide solution, and the combined filtrate and washing were concentrated to about 20 ml. The solution was then acidified with hydrochloric acid and extracted with ether; 30 mg of pale yellow crystals (mp 191 °C) were thus obtained. The crystals were methylated with diazomethane, and the product was purified by chromatography to give colorless crystals (mp 181 °C), whose infrared absorption spectrum was superimposable upon that of authentic tetramethyl pyrazinetetracarboxylate.

2-Aminoazuleno[2,1-d]pyrimidine (XVIII). a) To a solution of guanidine hydrochloride (168 mg) in ethanol (3 ml) containing sodium ethoxide prepared from 42.8 mg of sodium, 2-amino-1-formylazulene (XVII) (250 mg) was added, and the resulting solution was refluxed for 15 hr. After cooling, the precipitate was filtered and washed with water to give 90 mg of crystals. Recrystallization from ethanol gave XVIII as brown needles; mp 283 °C (decomp.).

Found: C, 73.59; H, 4.36; N, 21.22%. Calcd for $C_{12}H_9N_3$: C, 73.83; H, 4.65; N, 21.53%.

λ_{max}^{MeOH} nm (log ε): 250 (4.09), 324 (4.82), 336 (4.78), 391 (3.50), 418 (3.16), 514 (3.62), 550 (2.43), and 610 (2.06).

b) A solution of 2-amino-1-formylazulene (300 mg) and thiourea (160 mg) in ethanol (10 ml) containing sodium ethoxide prepared from 50 mg of sodium was refluxed for 12 hr. The solvent was then removed, and the residue was washed with water. Crystallization from ethanol gave 80 mg of brown crystals, and the starting azulene (150 mg) was recovered from the filtrate. The recrystallization of the former crystals from ethanol gave brown needles (mp 282 °C (decomp.)), whose infrared spectrum was superimposable upon that of the XVIII obtained by means of Method a).

Vilsmeier Reaction of Ethyl 2-Aminoazulene-1-carboxylate (XIX). Into a solution of XIX (1 g) in dimethylformamide (20 ml), a solution of phosphorus oxychloride (2 g) in dimethylformamide (6 ml) was stirred under cooling with ice. After standing at room temperature overnight, the precipitate was filtered and washed with chloroform to give 1.19 g of crystals. Recrystallization from ethanol afforded orange crystals (XX: X=Cl); mp 205—206 °C (decomp.). Perchlorate (XX: X=ClO_4); pink crystals (from ethanol); mp over 280 °C.

Found: C, 51.98; H, 4.78; N, 7.11%. Calcd for $C_{16}H_{19}O_6N_2Cl$: C, 51.83; H, 5.17; N, 7.56%.

Ethyl 2-Formamidoazulene-1-carboxylate (XXI). a) A solution of chloride (XX) (100 mg) in water was made slightly alkaline by adding sodium carbonate solution, and then it was extracted with chloroform. The extract was dried, passed through an alumina column, and recrystallized from benzene to afford 50 mg of XXI as orange needles; mp 81—83 °C.

Found: C, 67.28; H, 5.31; N, 5.63%. Calcd for $C_{14}H_{13}O_3N \cdot 1/2H_2O$: C, 66.65; H, 5.59; N, 5.56%.

b) A solution of ethyl 2-aminoazulene-1-carboxylate (XIX) (100 mg) in formic acid (1 ml) and pyridine (0.5 ml) was allowed to stand at room temperature for 2 days. The precipitate which separated out was filtered; 108 mg of reddish brown crystals (mp 83 °C) were thus obtained. The infrared spectrum of the crystals was superimposable upon that of XXI obtained by means of Method a).

This work was financially supported by grants from the Ministry of Education of Japan and the Sankyo Co., Ltd., to which the authors' thanks are due.

Synthesis of "Reversed" Nucleosides of Some Purine and Pyrimidine Bases

Shunzo FUKATSU,* Yoshiro TAKEDA,** and Sumio UMEZAWA

Department of Applied Chemistry, Faculty of Engineering, Keio University, Hiyoshi, Yokohama 222

(Received Feburary 3, 1973)

The title compounds have been synthesized by condensation of terminal iodo-sugars with purine bases and pyrimidine bases in dimethylformamide in the presence of sodium hydride or lithiu ı hydride.

As part of investigations of the synthesis of new nucleosides and analogues,[1-3] the synthesis of "reversed" nucleosides[4] (ribose derivatives of adenine bonded at C-5 of the sugar moiety) and their analogues seemed to be of interest, the compounds being useful as synthetic intermediates as in the synthesis[5] of eritadenine (lentynasine). Some reversed nucleosides were synthesized by Leonard *et al.*[4] and Hildesheim *et al.*[6] as compounds related to kinetin, a cell division factor.

The reversed nucleosides were synthesized by use of C-5 sulfonate derivatives of 2-deoxy-D-ribose and D-ribose.[4,5] Martinez and Lee[7] prepared 1-(2',2'-diethoxyethyl)uracil by the reaction of uracil with 2-bromo-1,1-diethoxyethane in dimethylformamide in the presence of sodium hydride. This was the first direct *N*-monoalkylation of uracil. We have extended the reaction to the preparation of reversed nucleosides by an alternative method using terminal iodo derivatives of sugars.

In the conventional synthesis of nucleosides using glycosyl halides, the mercuri-method[8] and fusion method[9] are known to be convenient, but attempts to apply these condensation methods to the present synthesis were unsuccessful.

Methyl 5-deoxy-5-iodo-2,3-*O*-isopropylidene-D-ribofuranoside (**1**) was synthesized from the corresponding 5-*O*-methyl derivative by the procedure of Kissman and Baker.[10] The iodo compound (**1**) reacted smoothly with 6-benzamidopurine (**2**) in dimethylformamide in the presence of lithium hydride to afford, after removal of the protecting groups, methyl 5-(6-aminopurin-9-yl)-5-deoxy-α- and β-D-ribofuranoside (**3** and **4**) in a total yield of 24% (Scheme 1). The methyl riboside of this

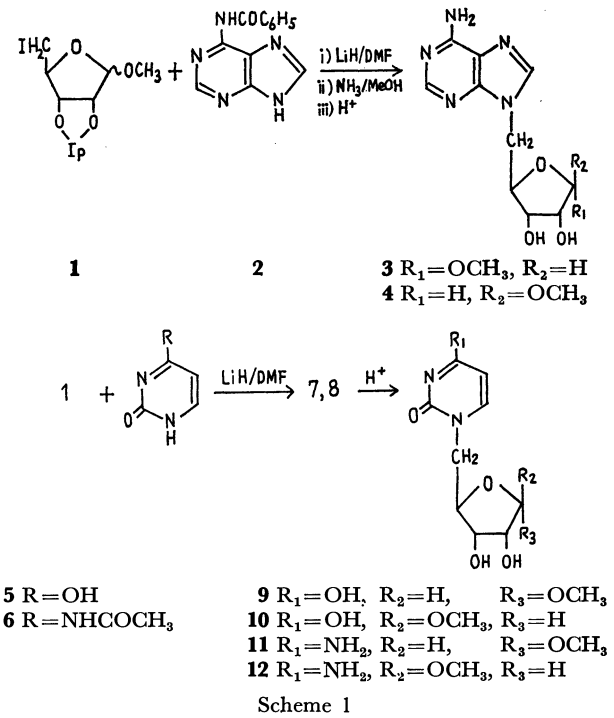

1 **2** **3** R_1=OCH_3, R_2=H; **4** R_1=H, R_2=OCH_3

5 R=OH; **6** R=NHCOCH$_3$

9 R_1=OH, R_2=H, R_3=OCH_3; **10** R_1=OH, R_2=OCH_3, R_3=H; **11** R_1=NH_2, R_2=H, R_3=OCH_3; **12** R_1=NH_2, R_2=OCH_3, R_3=H

Scheme 1

β-compound was previously synthesized by Kawazu *et al.*[5] by an alternative procedure. An analogous reaction of **1** with uracil (**5**) or 4-*N*-acetylcytosine (**6**) gave a masked condensation product (**7** or **8**), which afforded, after removal of the protecting groups, methyl 5-deoxy-5-(uracil-1-yl)-α- and β-D-ribofuranoside (**9** and **10**) or methyl 5-(cytosin-1-yl)-5-deoxy-α- and β-D-ribofuranoside (**11** and **12**) (Table 1).

On the other hand, methyl 2,3,4-tri-*O*-acetyl-6-deoxy-6-iodo-α-D-glucoside (**13**) was prepared by treatment of methyl 2,3,4-tri-*O*-acetyl-6-tosyloxy-α-D-glucoside[11] with sodium iodide in acetic anhydride in a good yield. Condensation of **13** with **2** in dimethylformamide in the presence of sodium hydride afforded the masked condensation product (**15**), in a 35% yield, which gave, after removal of the protecting groups, methyl 6-(6-aminopurin-9-yl)-6-deoxy-α-D-glucoside (**17**) in a 60% yield. A similar condensation of 2,6-benzamidopurine (**14**), uracil (**5**) or 4-*N*-acetylcytosine (**6**) with **13** afforded the masked condensation products (**16**, **19**, or **20**), which gave, after removal of protecting groups, methyl 6-(2,6-diaminopurin-9-yl)-6-deoxy-α-D-glucoside (**18**), methyl 6-deoxy-6-(uracil-1-yl)-α-D-glucoside (**21**), and methyl 6-(cytosin-1-yl)-6-deoxy-α-D-glucoside (**22**) (Scheme 2).

9-Substitution on the purine bases and 1-substitution

* Present address: Development Laboratories, Meiji Seika Kaisha, Ltd. 580 Horikawa-cho, Saiwaiku, Kawasaki 210.

** Present address: Osaka Factories, Sumitomo Kagaku Kogyo Co., Ltd. 278-3 Kasugade-cho, Konohanaku, Osaka 554.

1) S. Fukatsu and S. Umezawa, This Bulletin, **38**, 1443 (1965).

2) H. Yanagisawa, M. Kinoshita, S. Nakada, and S. Umezawa, *ibid.*, **43**, 246 (1970).

3) O. Makabe, S. Fukatsu, and S. Umezawa, *ibid.*, **45**, 2577 (1972).

4) N. J. Leonard, F. C. Sciavolino, and V. Nair, *J. Org. Chem.*, **33**, 3169 (1968).

5) M. Kawazu, T. Kanno, N. Takamura, T. Mizoguchi, S. Saito, and K. Okumura, *Chem. Commun.*, **1970**, 1047.

6) J. Hildesheim, J. Cleophax, S. D. Gero, and R. D. Guthrie, *Tetrahedron Lett.*, **1967**, 5013.

7) A. P. Martinez and W. W. Lee, *J. Org. Chem.*, **30**, 317 (1965).

8) J. A. Montgomery and H. J. Thomas, *Advan. Carbohyd. Chem.*, **17**, 301 (1962).

9) K. Onodera, S. Hirano, H. Fukumi, and F. Matsuda, *Carbohyd. Res.*, **1**, 254 (1965).

10) H. M. Kissman and B. B. Baker, *J. Amer. Chem. Soc.*, **79**, 5534 (1957).

11) B. Helferich and E. Himmen, *Ber.*, **61**, 1825 (1928).

Table 1. Properties and elemental analyses

Compound	Mp, °C	Formula	Calcd, %			Found, %			Yield, %	$[\alpha]_D^{16}$(in water)
			C	H	N	C	H	N		
3	170 (dec)	$C_{11}H_{15}N_5O_4$	46.97	5.38	24.90	46.63	5.68	24.58	4	+34 (*c* 0.4)
4	197—198	$C_{11}H_{15}N_5O_4$	46.97	5.38	24.90	47.59	5.61	24.62	20	−12 (*c* 0.5)
9	81—85	$C_{10}H_{14}N_2O_6$	46.51	5.47	10.85	46.07	5.84	11.01	10	+62.8 (*c* 0.5)
10	84.5—85.5	$C_{10}H_{14}N_2O_6 \cdot H_2O$	43.48	5.84	10.14	43.98	6.00	10.55	20	+13.3 (*c* 0.5)
11	68—74	$C_{10}H_{15}N_3O_5$	47.62	5.84	16.34	47.48	6.26	15.91	4	+93 (*c* 0.5)
12	235—236.5	$C_{10}H_{15}N_3O_5$	47.62	5.84	16.34	47.90	6.02	16.73	11	+19.0 (*c* 0.5)
17	199—200(dec)	$C_{12}H_{17}N_5O_5$	46.30	5.50	22.51	45.98	5.58	22.13	20.7	+85 (*c* 0.5)
18	258—261(dec)	$C_{12}H_{18}N_6O_5$	44.17	5.52	24.54	44.60	5.98	24.83	16.7	+84.8 (*c* 0.35)
21	129—133	$C_{11}H_{16}N_2O_7 \cdot C_2H_5OH$	46.70	6.63	8.38	46.77	6.83	8.45	5.6	+122.4 (*c* 0.5)
22	170	$C_{11}H_{17}N_3O_6 \cdot C_2H_5OH$	46.85	6.91	12.61	46.57	6.93	12.51	27	+136 (*c* 1.0)

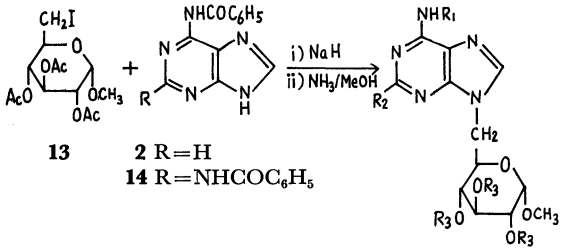

13 **2** R=H
14 R=NHCOC$_6$H$_5$

15 R_1=COC$_6$H$_5$, R_2=H, R_3=OAc
16 R_1=COC$_6$H$_5$, R_2=NHCOC$_6$H$_5$, R_3=OAc
17 R_1=R_2=R_3=H
18 R_1=R_3=H, R_2=NH$_2$

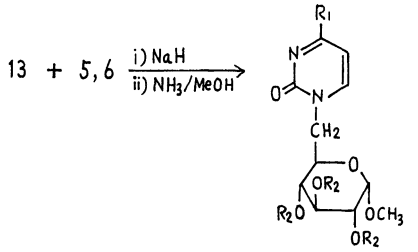

19 R_1=OH, R_2=COCH$_3$
20 R_1=NHCOCH$_3$, R_3=COCH$_3$
21 R_1=OH, R_2=H
22 R_1=NH$_2$, R_2=H

Scheme 2

on the pyrimidine bases have been established by determination of ultraviolet spectra (Table 2). The structures and stereochemistry of the above products have been confirmed by analyses of their NMR and IR spectra.

Table 2. Ultraviolet spectral data

Compound	λ_{max} mμ (ε × 10^3)		
	0.01N HCl	Water	0.01N NaOH
3	260(12.7)	262(12.4)	261(12.8)
4	260(15.4)	261(15.3)	261(15.1)
9	264(10.3)	265(11.2)	266(7.4)
10	266(13.1)	265(11.2)	265(9.8)
11	283(8.0)	273(5.0)	275(5.2)
12	285(11.4)	275(8.0)	275(8.6)
17	260(13.8)	260(13.9)	260(14.1)
18	253(10.0)	255(8.4)	256(8.8)
	291(10.0)	280(10.2)	281(10.4)
21	266(12.1)	266(12.1)	265(9.0)
22	282(12.0)	274(9.0)	277(6.6)

Since the aminopurines alkylated on the nitrogen atoms **7** or **9** have rarely been obtained by direct alkylation of the aminopurines,[12] the above-mentioned results are interesting.

Experimental

*Methyl 5-(6-Aminopurin-9-yl)-5-deoxy-α- and β-D-Ribofuranoside (**3** and **4**).* To a solution of 6-benzamidopurine (1.42 g, 6.0 mmol) in 60 ml of anhydrous dimethylformamide was added lithium hydride (48 mg, 6.0 mmol) with stirring. To this was added a solution of methyl 5-iodo-5-deoxy-2,3-*O*-isopropylidene-D-riboside (1.85 g, 6.0 mmol) in 10 ml of anhydrous dimethylformamide. The mixture was heated at 130—135 °C for 12 hr. After cooling to room temperature, the dimethylformamide solution was evaporated to dryness *in vacuo*. The residue was extracted with two 45 ml portions of chloroform, filtered and washed with two 30 ml portions of water. The chloroform solution was dried over anhydrous sodium sulfate, filtered and evaporated to dryness *in vacuo*. The residue (3.13 g) was dissolved in 30 ml of methanol and filtered. Alumina (8 g, Merck) was added, and the resulting suspension was evaporated to dryness. The residue was placed on the top of a column of 60 g (2×29 cm) of alumina packed with benzene and eluted successively with benzene, benzene–ethyl acetate (1: 1), ethyl acetate, and ethyl acetate–methanol (3: 1). Evaporation of the last eluate afforded 0.84 g of colorless solid, which was dissolved in 28 ml of anhydrous methanol. The solution was saturated with ammonia at 0 °C, sealed, and allowed to stand at 10 °C for 18 hr. The solution was evaporated to dryness *in vacuo*. The residue was dissolved in 11 ml of methanol and the mixture was refluxed for 4 hr after addition of 5 ml of 0.4N sulfuric acid. The solution was cooled and barium carbonate was added until the pH was neutral. The precipitate was removed by filtration and washed with warm 50% methanol solution. The combined filtrate and washings were evaporated *in vacuo* to give a sirup. The residue was dissolved in water (10 ml) and chromatographed on a Dowex 1×2 (OH form) column (1×38 cm) and eluted with water. Fractions monitored by their ultraviolet absorption were separated into two portions. The first portion was evaporated to dryness to yield **3**, 0.07 g (0.25 mmol, 4%), α-anomer.

12) See, for example, G. A. Howard, "Purines and Related Ring Systems," Chapt. XX in "Chemistry of Carbon Compounds," Vol. IV, E. H. Rodd, Ed., Elsevier Publishing Co. (1960), p. 1691; J. H. Lister, "Physicochemical Aspects of Purines" in "Advances in Heterocyclic Chemistry," Vol. 6, A. R. Katritzky, Ed., Academic Press (1966), p. 40.

The solid was found homogenous by tlc, but could not be crystallized. The second portion was evaporated to dryness to yield **4**, 0.33 g (1.2 mmol, 20%) as colorless needles, β-anomer.

Methyl 5-(Uracil-1-yl)-5-deoxy-α- and β-D-Ribofuranoside (9 and 10). To a mixture of uracil (0.57 g, 5.2 mmol) and lithium hydride (41.5 mg, 5.2 mmol) in 10 ml of anhydrous dimethylformamide was added a solution of **1** (1.7 g, 5.2 mmol) in anhydrous dimethylformamide with stirring. The solution was heated at 130—132 °C for 12 hr. It was then evaporated *in vacuo* to give a sirup, which was dissolved in 16 ml of chloroform. The resulting solution was washed two 28 ml portions of water, dried over sodium sulfate and filtered. The filtrate was evaporated to dryness *in vacuo*. The residue (1.6 g) was recrystallized from ethanol to yield 0.54 g (1.6 mmol, 31%) of methyl 5-deoxy-2,3-*O*-isopropylidene-5-(uracil-1-yl)-D-riboside (**7**) as needles, mp 189—190 °C, $[\alpha]_D^{17}$ +78.7° (*c* 0.5, chloroform), λ_{max}^{MeOH} 266 mμ (ε 9940), ν_{max}^{KBr} (cm^{-1}), 3000 (NH, OH), 1715, 1680 (uracil), 1098 (C–O–C). Found: C, 52.63; H, 6.03; N, 9.01%. Calcd for $C_{13}H_{18}N_2O_6$: C, 52.34; H, 6.08; N, 9.39%; mol wt, 298.

A sample of **7** (0.54 g, 1.6 mmol) was dissolved in a solution of methanol, the solution being refluxed for 2 hr after addition of 0.8N sulfuric acid (3 ml). It was then neutralized with barium carbonate and filtered. The filtrate was passed through a column of 20 ml (0.8×2.6 cm) of CG-400 (OH form), and eluted with 0.1% ammonia solution. Fractions monitored by their ultraviolet absorption were separated into two portions. The first portion was evaporated to dryness to yield **9**, α-anomer, 0.13 g (0.51 mmol), and the second to yield **10**, β-anomer, 0.26 g (1.02 mmol). The total yield including α- and β-anomers was 30%.

NMR (DMSO-d_6), α-anomer: δ 11.05 (1H, s, pyrimidine C_4–OH), 7.49 and 5.53 (1H, each d, J=8.0 Hz, pyrimidine H_5 and H_6), 4.64 (1H, s, $H_{1'}$), 3.25 (3H, s, CH_3O–); β-anomer: δ 4.82 (1H, d, J=3 Hz, $H_{1'}$).

Methyl 5-(Cytosin-1-yl)-5-deoxy-α- and β-D-Ribofuranoside (11 and 12). *N*-Acetylcytosine (1.54 g, 1.0 mmol) was made to react with lithium hydride (90 mg, 1.1 mmol) and **1** (3.4 g, 1.04 mmol) in 55 ml of anhydrous dimethylformamide. The solution was evaporated to give a sirup, which was dissolved in 120 ml of chloroform. The solution was washed with two 50 ml portions of water, dried over sodium sulfate, and filtered. The filtrate was evaporated *in vacuo* to give a gum, which was chromatographed on a column (2×36 cm) of alumina (100 g, acid washed, Merck), and eluted successively with benzene, benzene–ethyl acetate (1:1), ethyl acetate and ethyl acetate–methanol (1:1). Fractions as determined by their ultraviolet absorption were combined and evaporated to dryness *in vacuo*. The residue was recrystallized from ethanol to give methyl 5-(*N*-acetylcytosin-1-yl)-5-deoxy-2,3-*O*-isopropylidene-D-riboside (**8**) (1.37 g, 41%) as needles, mp 209—211 °C, $[\alpha]_D^{13}$ +75.4° (*c* 0.5, chloroform), λ_{max}^{MeOH} 248 mμ (ε 13200), 301 mμ (ε 6650), ν_{max}^{KBr} (cm^{-1}), 3290 (NH, OH), 1700 (*N*-acetyl), 1670, 1625 (pyrimidine), 1098 (C–O–C).

A 1.0 g portion of **8** was dissolved in 30 ml of methanolic ammonia (saturated at 0 °C) and kept at 0 °C for 16 hr. The solution was evaporated *in vacuo* to dryness. The residue was dissolved in a solution of 0.8N sulfuric acid (6.5 ml) and methanol (15 ml) and the solution was heated under reflux for 1 hr. The solution was neutralized to about pH 7 (test paper) with barium carbonate powder and filtered. The filtrate was passed through a column (1.5×30 cm) of CG-400 (OH form, 40 ml) and eluted with water. Fractions monitored by their ultraviolet absorption were separated into two portions, the first being evaporated to dryness to yield 0.1 g (4%) of **11**, α-anomer, and the second to yield 0.26 g (11%) of **12**, β-anomer.

Methyl 2,3,4-Tri-O-acetyl-6-deoxy-6-iodo-α-D-glucopyranoside (13). A solution of methyl 2,3,4-tri-*O*-acetyl-6-*O*-*p*-tolylsulfonyl-α-D-glucopyranoside[10] (41.9 g, 0.088 mol) in 450 ml of acetic anhydride was refluxed with dry sodium iodide (25 g, 0.17 mol) for 1 hr. The mixture was cooled and poured with stirring into 1.2 l of ice water. The suspension was allowed to stand at about 10 °C in the refrigerator for 18 hr. The solid acetate was then filtered, washed with water, and dried *in vacuo* to yield 16.9 g (45%) of **13**, wihch was recrystallized from ethanol, mp 149—150 °C (lit,[10] mp 150—151 °C).

Methyl 6-(6-Aminopurin-9-yl)-6-deoxy-α-D-glucoside (17). 6-Benzamidopurine (**2**) (2.10 g, 8.8 mmol) was made to react with sodium hydride (250 mg, 10.4 mmol) and methyl 2,3,4-tri-*O*-acetyl-6-deoxy-6-iodo-α-D-glucoside (**13**) (3.50 g, 8.2 mmol) in 80 ml of dimethylformamide. The solution was evaporated *in vacuo* to give a sirup, which was extracted with two 75 ml portions of chloroform. The filtered chloroform extract was washed with two 75 ml portions of water, dried with sodium sulfate, filtered, and evaporated to dryness. The residue (4.96 g) was dissolved in 40 ml of methanol, the insoluble matter being removed by filtration. To the filtrate, was added alumina (10 g, acid washed, Merck) and the mixture was evaporated to dryness. The residue was placed on a column of alumina (80 g) and eluted with ethyl acetate–chloroform (6:4), ethyl acetate–methanol (1:1) and methanol, successively. Fractions monitored by their ultraviolet absorption (λ_{max}^{MeOH} 280 mμ) were combined and evaporated to dryness *in vacuo* to give a crude solid of **15**, 2.71 g, λ_{max}^{MeOH} 280 mμ.

A 1.7 g portion of the crude solid of **15** was dissolved in 600 ml of anhydrous methanol at room temperature, and the solution was saturated with dry ammonia at 0 °C. After storage in a refrigerator for 18 hr, the solution was evaporated to dryness *in vacuo*. The residue was dissolved in 30 ml of water, the solution was placed on a column of 120 ml of Dowex 1×2 (OH form, 200—400 Mesh) and the column was eluted with water. The fractions having ultraviolet absorption at 260 mμ were combined and evaporated to dryness *in vacuo*. The residue was crystallized from hot water to yield 0.57 g of **17**, colorless needles (20.7%, based on the iodo sugar), ν_{max}^{KBr} (cm^{-1}), 3380, 3340, 3210 (NH, OH), 1646, 1613, 1583 (purinyl), 1053, 1006 (C–O–C); NMR (DMSO-d_6), δ 8.12 and 8.22 (1H, each s, purine H_2 and H_8), 7.23 (2H, s, $-NH_2$), 4.55 (1H, d, J=3 Hz, $H_{1'}$), 3.90 (3H, s, CH_3O–).

Methyl 6-(2,6-Diaminopurin-9-yl)-6-deoxy-α-D-glucoside (18). 2,6-Benzamidopurine (**14**) was made to react with sodium hydride (50 mg, 2.0 mmol) and **13** (0.5 g, 1.2 mmol) in 16 ml of dimethylformamide and treated under the same conditions as for **15**. Chromatography of the residue (0.59 g) on a column of alumina (20 g) gave **16** as a colorless glass, 0.169 g (28.6%); λ_{max}^{MeOH} 248 mμ (ε 19150), 304 mμ (ε 8700), 345 mμ (ε 11600), ν_{max}^{KBr} (cm^{-1}), 1757 (ester), 1640, 1600, 1570 (purinyl). Found: N, 12.57%. Calcd for $C_{32}H_{32}N_6O_{10}$: N, 12.72%.

A 0.169 g portion of **16** was treated with methanolic ammonia followed by chromatography as the hydrolysis of **15** to **17** to give needles of **18**, 66 mg (16.7%).

Methyl 6-Deoxy-6-(uracil-1-yl)-α-D-glucoside (21). Uracil (6.0 g, 53.5 mmol) was made to react with sodium hydride (1.28 g, 53.5 mmol) and **13** (21.3 g, 49.5 mmol) to give a gum (25.1 g), which was chromatographed on a column of alumina (500 g, acid washed, Merck), being eluted succes-

sively with benzene, benzene–ethyl acetate (1: 1), ethyl acetate, ethyl acetate–methanol (5: 1) and methanol. Fractions containing the product of ultraviolet absorption (λ_{max}^{MeOH} 260 mμ) were combined and evaporated to dryness *in vacuo*. The residue was crystallized from ethanol to give needles of **19**, 2.46 g (12%), mp 195 °C $[\alpha]_D^{13}$ +133.6° (*c* 0.5, chloroform), λ_{max}^{MeOH} 260 mμ (ε 10300) NMR (DMSO-d_6) δ 5.53 and 7.52 (1H, each d, J=8 Hz, pyrimidine H_5 and H_6), 11.25 (1H, s, pyrimidine C_4–OH), 4.89 (2H, s, $-CH_2-$), 3.19 (3H, s, CH_3O-), 1.99 (6H, s, CH_3CO-), 1.93 (3H, s, CH_3CO-). Found: C, 49.46; H, 5.46; N, 6.65%. Calcd for $C_{17}H_{22}N_2O_{10}$: C, 49.28; H, 5.35; N, 6.76%; mol wt, 414.

A 0.53 g (1.3 mmol) portion of **19** was treated with methanolic ammonia as in the hydrolysis of **15** to **17** and then chromatographed on a column of Dowex 1×2 (OH form). Elution was effected with water and 0.3N ammonia, elution with 0.1N hydrochloric acid (40 ml). Fractions as determined by their ultraviolet absorption (266 mμ) were combined, and evaporated to dryness *in vacuo*. The residue was crystallized from ethanol–water to give needles of **21**, 0.2 g (46.5%). NMR (DMSO-d_6): δ 5.60 and 7.62 (1H, each d, pyrimidine H_5 and H_6), 4.60 (1H, d, J=3 Hz, $H_{1'}$), 3.16 (3H, s, CH_3O-).

*Methyl 6-(Cytosin-1-yl)-6-deoxy-α-D-glucoside (**22**).* *N*-Acetylcytosine (**6**) (2.8 g, 18.5 mmol) was made to react with sodium hydride (450 mg, 18.5 mmol) and **13** (7.4 g, 17.2 mmol) in 170 ml of anhydrous dimethylformamide to give a residue, which was dissolved in 253 ml of chloroform, washed with two 105 ml portions of water, dried with sodium sulfate, filtered, and evaporated to dryness. The residue was crystallized from ethanol to give needles, 2.73 g (35%) of methyl 6-(*N*-acetylcytosin-1-yl)-2,3,4,6-tetradeoxy-2,3,4-tri-*O*-acetyl-α-D-glucoside (**20**), mp 242—243 °C, $[\alpha]_D^{16}$ +260° (*c* 0.5, chloroform), λ_{max}^{EtOH} 243 mμ (ε 15600), 301 mμ (ε 7240), ν_{max}^{KBr} (cm^{-1}), 1760 (ester), NMR ($CDCl_3$), δ 7.68 and 7.37 (1H, each d, J=7.5 Hz, pyrimidine H_5 and H_6), 4.91 (2H, s, $-CH_2-$), 3.16 (3H, s, CH_3O-), 2.28 (3H, s, $-N-COCH_3$), 2.08, 2.04 and 1.99 (3H, each s, $-O-COCH_3$). Found: C, 49.73; H, 5.59; N, 8.96%. Calcd for $C_{19}H_{25}N_3O_{10}$: C, 50.22; H, 5.32; N, 9.25%; mol wt, 455.

A 2.0 g (4.4 mmol) portion of **20** was treated with methanolic ammonia followed by chromatography as in the hydrolysis of **15** to **17**. The fractions containing ultraviolet absorbing material were combined and evaporated to dryness. The residue was crystallized from ethanol–water (10: 1) to give 1.13 g (27%) of needles of **22**.

BULLETIN OF THE CHEMICAL SOCIETY OF JAPAN, VOL. 46, 3168—3173 (1973)

Formation and Reaction of Cyclohexanone Oxime Hydrogen Sulfate[1)]

Kiyoshi FUKUI, Masaru UCHIDA, and Mitsuo MASAKI

Polymer Research Laboratory, Ube Industries, Ltd., Goi, Minamikaigan, Ichihara, Chiba 290

(Received May 11, 1973)

Cyclohexanone oxime hydrogen sulfate, prepared by the reaction of cyclohexanone oxime with sulfur trioxide–1,4-dioxane complex under mild conditions, was isolated as stable salts with various Lewis bases. It was found that a Beckmann rearrangement of the oxime hydrogen sulfate to 3,4,5,6-tetrahydro-2*H*-azepin-7-ol hydrogen sulfate was retarded by the weak Lewis base 1,4-dioxane and prevented by a stronger Lewis base aniline. The rearrangement of the oxime hydrogen sulfate was also found to be promoted by Lewis acids such as sulfur trioxide, tin tetrachloride or zinc chloride. Hydrogen chloride retarded the rearrangement. Alcoholysis of the oxime hydrogen sulfate gave cyclohexanone oxime and monoalkyl sulfate quantitatively, while hydrolysis of the oxime hydrogen sulfate gave cyclohexanone, cyclohexanone oxime and ε-caprolactam.

It has been suggested that the Beckmann rearrangement of cyclohexanone oxime (**1**) by sulfuric acid and/or sulfur trioxide involves cyclohexanone oxime hydrogen sulfate (**2**) and 3,4,5,6-tetrahydro-2*H*-azepin-7-ol hydrogen sulfate (**3**) as intermediates.[2,3)] Ogata *et al.*[3)] obtained **2** as an unstable solid in the reaction of **1** with chlorosulfonic acid. Csuros *et al.*[4)] reported that the reaction of cyclohexanone with hydroxylamine-*O*-sulfonic acid in the presence of potassium bicarbonate led to the formation of potassium salt of **2** (**5a**), which was hydrolyzed to ε-caprolactam (**4**) in aqueous acidic or basic solution. **3** was isolated in the reaction of **1** with the sulfur trioxide–1,4-dioxane complex by Turbak,[5)] who postulated that **2** was an intermediate in the reaction. However, very little is known about the reactivity of these intermediates. This paper deals with the formation and reactions of **2**.

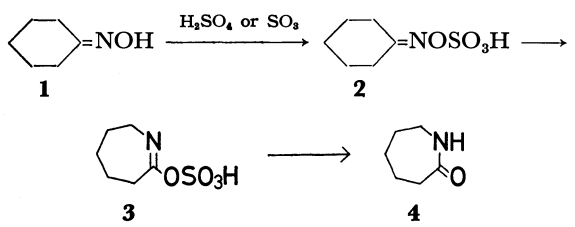

Formation of **2** by the reaction of **1** with sulfur trioxide has not been reported, presumably because the reactivity of free sulfur trioxide is too great to permit

1) A Japanese patent has been applied for a part of this work: M. Masaki and M. Uchida (to Ube Ind., Ltd.), Japanese Patent Application, S. 44-67955 (1969).

2) D. E. Pearson and F. Ball, *J. Org. Chem.*, **14**, 118 (1949).

3) Y. Ogata, M. Okano, and K. Matsumoto, *J. Amer. Chem. Soc.*, **77**, 4643 (1955).

4) Z. Csuros, K. Zech, S. Zech, and G. Binder, *Acta Chim. Hung.*, **1**, 83 (1951).

5) A. F. Turbak, *Ind. Eng. Chem., Prod. Res. Develop.*, **7**, 189 (1968).

Table 1. Salt of cyclohexanone oxime hydrogen sulfate (**2**) with Lewis bases

Lewis Base	Yield %	Mp °C	Formula	Anal, %	
				Calcd	Found
Diethylamine	91	136—138[a]	$C_{10}H_{22}N_2O_4S$	C, 45.09	45.20
				H, 8.33	8.05
				N, 10.52	10.79
				S, 12.04	12.03
Triethylamine	87	—[b]	$C_{12}H_{26}N_2O_4S$	N, 9.51	9.13
				S, 10.89	11.52
n-Propylamine	96	125—128	$C_9H_{20}N_2O_4S$	C, 42.84	42.87
				H, 7.99	7.84
				N, 11.10	10.45
				S, 12.71	12.90
Isopropylamine	94	107—110	$C_9H_{20}N_2O_4S$	N, 11.10	11.26
				S, 12.71	12.98
t-Butylamine	99	160—163[a]	$C_{10}H_{22}N_2O_4S$	N, 10.52	10.14
				S, 12.04	11.91
Cyclohexylamine	95	156—158[a]	$C_{12}H_{24}N_2O_4S$	N, 9.58	9.29
				S, 10.96	10.78
Aniline	92	170—175[c]	$C_{12}H_{18}N_2O_4S$	C, 50.33	50.19
				H, 6.34	6.53
				N, 9.78	10.01
Imidazole	100	114—116[d]	$C_9H_{15}N_3O_4S$	C, 41.37	41.54
				H, 5.79	5.78
				N, 16.08	16.18

a) Recrystallized from methanol–ether.
b) Attempts to determine the melting point of the salt were unsuccessful as the salt was extremely hygroscopic.
c) Recrystallized from ethanol.
d) Recrystallized from methanol–acetone.

a controlled reaction. Recently, Kelly and Matthews[6] reported the reaction of **1** with the complexes of sulfur trioxide with various Lewis bases, which resulted in the formation of **2**. Independently of this, we found that the reaction of **1** with the sulfur trioxide–1,4-dioxane complex afforded **2** under mild conditions.[1]

When the complex was treated with **1** in ethylene dichloride below 20 °C, **2** was formed as a crystalline precipitate. Since it is extremely hygroscopic and decomposes explosively, **2** was confirmed by treatment of the reaction mixture with ammonia or aniline under cooling, giving the corresponding ammonium (**5b**) or anilinium salt (**5c**). In a similar way salts with various organic bases such as diethylamine, triethylamine, *n*-propylamine, isopropylamine, *t*-butylamine, cyclohexylamine or imidazole were obtained.

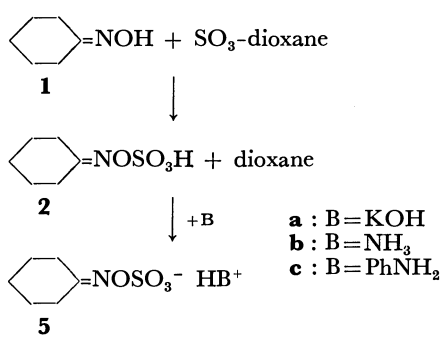

Attempts to rearrange **5c** were unsuccessful. When **5c** suspended in ethylene dichloride was heated at refluxing temperature for 20 min, the statring material was recovered in a high yield. Treatment of **5b** with potassium hydroxide and **5c** with potassium bicarbonate in aqueous solution led to the formation of **5a**, which was identical with the specimen prepared according to the method described by Csuros.[4] When **5c** was treated with 2,4-dinitrophenylhydrazine under acidic conditions, 2,4-dinitrophenylhydrazone of cyclohexanone was formed.

When **2** was heated at 50 °C for about 15 min in the presence of 1/2 equiv. of 1,4-dioxane in ethylene dichloride, it was exothermically transformed into **3**, which was confirmed by treatment of the reaction mixture with aniline, giving anilinium phenylsulfamate and **4**.[7] In the presence of 1 equiv. of 1,4-dioxane, however, the exothermic rearrangement of **2** to **3** occurred after heating for 20—30 min at the same temperature. Apparently 1,4-dioxane retarded the rearrangement of **2** to **3**, which is probably due to the formation of the salt-like compound between 1,4-dioxane and **2**. The retarding effect by 1,4-dioxane as a Lewis base is also supported by the fact that the rearrangement of the salt of **2** with a stronger base,

6) K. K. Kelly and J. S. Matthews, *J. Org. Chem.*, **36**, 2159 (1971).

7) It was found that the reaction of 3,4,5,6-tetrahydro-2*H*-azepin-7-ol hydrogen sulfate with 2 equiv. of aniline in refluxing ethylene dichloride led to exclusive formation of anilinium phenylsulfamate and ε-caprolactam: M. Masaki, M. Uchida and K. Fukui, This Bulletin, **46**, 3174 (1973).

5c, did not occur even when it was heated at 82 °C for 20 min under anhydrous conditions. The retarding effect of bases for the rearrangement suggests that **2** would be formed if sulfur trioxide was gradually added to **1** under mild conditions, since **2** formed initially would be stabilized by the unreacted oxime, a Lewis base.

As expected, cyclohexanone oxime hydrogen sulfate (**2**) was obtained as a colorless crystalline precipitate by the gradual addition of sulfur trioxide to **1** in ethylene dichloride below −6 °C. The suspension of **2** in ethylene dichloride was then heated in order to examine the rearrangement of **2** in the absence of the Lewis base. As soon as the temperature of the suspension reached 44 °C, a vigorous exothermic reaction occurred, **2** being transformed into **3**. The conditions under which **2** began to rearrange were apparently milder than those needed in the presence of 1,4-dioxane. However, when the addition of sulfur trioxide was attempted at room temperature, the reaction accompanied decomposition.[8]

On the other hand, an inverse addition method did not lead to the formation of **2**. When **1** was added to sulfur trioxide in ethylene dichloride below −2 °C, a vigorous exothermic reaction occurred, no formation of **2** being observed. However, after hydrolysis of the reaction product **4** was obtained in 85% yield. This indicates that sulfur trioxide promotes the rearrangement of **2**. The rearrangement of **2** took place even below −3 °C, when sulfur trioxide was added to a suspension of **2** in ethylene dichloride. Kuhara and Todo[9] demonstrated that the rates of rearrangement of a series of ester of benzophenone oxime were proportional to the acid strength of the esterifying acid. The rate-determining step in a Beckmann rearrangement is known to be the partial ionization of the nitrogen-oxygen bond of the oxime.[10] The promoting effect by sulfur trioxide might be explained by a formation of cyclohexanone oxime hydrogen pyrosulfate (**6**), or by a simple coordination (**7**) of sulfur trioxide to the oxygen atom of **2**.

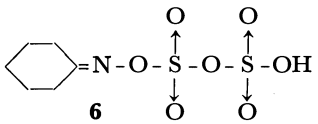

6

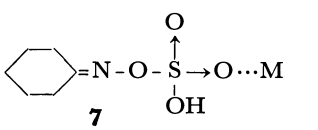

7

M: SO_3, $SnCl_4$, $ZnCl_2$

Thus, we examined whether other Lewis acids promote the rearrangement of **2**. When tin tetrachloride was added to the suspension of **2** in ethylene dichloride, the exothermic rearrangement began to occur below 15 °C, as expected. An analogous effect was observed by using zinc chloride.

The effect of hydrogen chloride on rearrangement of **2** was also studied, a retarding effect being observed. Treatment of cyclohexanone oxime monohydrochloride with sulfur trioxide below −2 °C, and heating of the reaction mixture at 50 °C for 30 min followed by hydrolysis of the product yielded only 52% of **4**. This might be rationalized by the fact that hydrogen chloride protonated on the nitrogen atom[11] of **2** to give **8**, contrary to the case of a Lewis acid, and the nitrogen-oxygen bond became difficult to be cleaved.

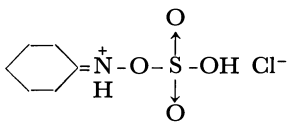

8

Hydrolysis of **2** under refluxing conditions gave **4** in 64% yield and a mixture of cyclohexanone and **1** in 17% yield. In a similar way, the hydrolysis of **2** in the presence of Lewis bases such as 1,4-dioxane, **4** and aniline yielded three products. These results are in contrast to those of Kelly and Matthews,[6] who reported the hydrolysis of **2** in the presence of 1,4-dioxane or **4** resulting exclusively in the formation of **4**.

In contrast, methanolysis of **2** gave rise to the formation of **1** and monomethyl sulfate, which was confirmed by treatment of the reaction mixture with aniline, giving the corresponding anilinium salt in 96% yield. Analogous alcoholysis of **2** with *n*-butanol gave **1** in 81% and mono-*n*-butyl sulfate in 76% yield.

Experimental

Concentration and evaporation were carried out under reduced pressure with a rotary evaporator. All melting points were determined in a liquid bath and are uncorrected.

Reaction of Cyclohexanone Oxime (1) with Sulfur Trioxide–1,4-Dioxane Complex. A solution of 1,4-dioxane (2.3 g, 26 mmol) in ethylene dichloride (10 ml) was added dropwise below 10 °C, with stirring, to a solution of sulfur trioxide (2 ml, 48 mmol) in ethylene dichloride (40 ml). To the resulting suspension of sulfur trioxide–1,4-dioxane complex was added dropwise a solution of **1** (5.43 g, 48 mmol) in ethylene dichloride (30 ml) with stirring below 20 °C. The complex dissolved and then colorless crystals separated gradually. The crystals was confirmed to be cyclohexanone oxime hydrogen sulfate (**2**).

Oxime hydrogen sulfate (**2**) is hygroscopic and becomes like honey when allowed to stand in an atmosphere after filtration. When dried over phosphorus pentoxide in a vacuum desiccator it decomposed within a few hour.

Aniline Salt of Cyclohexanone Oxime Hydrogen Sulfate (5c). To a suspension of **2** prepared from sulfur trioxide (5 ml, 120 mmol), 1,4-dioxane (10.5 g, 120 mmol) and **1** (13.6 g, 120 mmol) in ethylene dichloride (150 ml) was added dropwise aniline (33.5 g, 360 mmol) with stirring below 10 °C. The resulting mixture was stirred at room temperature for 1 hr. A crystalline substance, aniline salt of cyclohexanone

8) It has been shown that when cyclohexanone oxime hydrogen sulfate was heated in the presence of cyclohexanone oxime or ε-caprolactam, the oxime hydrogen sulfate decomposed to give an intractable substance: M. Masaki, K. Fukui, M. Uchida, K. Yamamoto, and I. Uchida, This Bulletin, **46**, 3179 (1973).

9) M. Kuhara and Y. Todo, *Memoirs Coll. Sci., Kyoto*, **2**, 387 (1910).

10) G. Donaruma and W. Z. Heldt, "Organic Reactions," Vol. 11, ed. by A. C. Cope et al., Wiley, New York, N. Y., (1960) p. 1.

11) a) H. Saito, K. Nukada, and M. Ohno, *Tetrahedron Lett.*, **1964**, 2124; b) H. Saito, *Nippon Kagaku Zasshi*, **85**, 724 (1964).

oxime hydrogen sulfate (**5c**), was collected by filtration (35.2 g). Recrystallization from ethanol gave colorless needles. Yield 31.5 g. Mp and analytical results are shown in Table 1.

A solution of **5c** (0.5 g, 0.17 mmol) in water (40 ml) and methanol (40 ml) was treated with a solution of 2,4-dinitrophenylhydrazine[12] to give 2,4-dinitrophenylhydrazone of cyclohexanone (0.48 g, 99%). Recrystallization from ethanol gave orange leaves, mp 159 °C (lit,[13] 160 °C).

A suspension of **5c** (13.13 g, 46 mmol) in ethylene dichloride (100 ml) was heated under reflux for 20 min and then stirred at room temperature for 41 hr. The crystalline substance collected by filtration was identified as the starting material. Yield 10.6 g (81%).

*Ammonia Salt of Cyclohexanone Oxime Hydrogen Sulfate (**5b**).* To a suspension of **2** prepared from sulfur trioxide (5 ml, 120 mmol), 1,4-dioxane (10.5 g, 120 mmol) and **1** (13.6 g, 120 mmol) in ethylene dichloride (150 ml) was added gaseous ammonia below 0 °C. The resulting mixture was stirred at room temperature for 1 hr and allowed to stand overnight. A crystalline substance, ammonia salt of cyclohexanone oxime hydrogen sulfate (**5b**), was collected by filtration. Yield 22.8 g (91%). Mp 140—145 °C decomp.

*Diethylamine Salt of Cyclohexanone Oxime Hydrogen Sulfate (**5d**).* A suspension of **2** (48 mmol) in ethylene dichloride prepared in a similar way to that for **5b** was treated with a solution of diethylamine (3.5 g, 49 mmol) in ethylene dichloride (10 ml) with stirring below 0 °C. The resulting mixture was stirred at room temperature for 1 hr and concentrated, the residue being treated with ether. A crystalline substance, diethylamine salt of cyclohexanone oxime hydrogen sulfate (**5d**) was collected by filtration. Yield 11.7 g. Mp and analytical results are given in Table 1.

*Triethylamine, n-Propylamine, Isopropylamine, and t-Butylamine Salts of Cyclohexanone Oxime Hydrogen Sulfate (**5e**, **5f**, **5g**, and **5h**).* These ammonium salts were prepared by treating **2** with the corresponding amines in a similar way to that for **5d**. The results are given in Table 1.

*Cyclohexylamine and Imidazole Salts of Cyclohexanone Oxime Hydrogen Sulfate (**5i** and **5j**).* These salts were prepared by treating **2** with cyclohexylamine and imidazole, respectively, in a similar way to that for **5c**. The results are shown in Table 1.

*Potassium Salt of Cyclohexanone Oxime Hydrogen Sulfate (**5a**).* *a) From Aniline Salt of Cyclohexanone Oxime Hydrogen Sulfate (**5c**):* A saturated aqueous solution of potassium bicarbonate was added to an aqueous solution of **5c** (2.86 g, 10 mmol) until gas evolution ceased. The resulting mixture was washed with benzene and concentrated. The residue was treated with an aqueous ethanol. The crystalline precipitate was collected by filtration and identified with authentic potassium salt of cyclohexanone oxime hydrogen sulfate (**5a**)[4] by infrared spectrum. Yield 1.6 g (69%). Extraction with ethanol by means of Soxhlet extractor gave colorless needles as an extract, mp 172—180 °C (lit,[4] 155—180 °C decomp.).

*b) From Ammonia Salt of Cyclohexanone Oxime Hydrogen Sulfate (**5b**):* An aqueous solution of potassium hydroxide (0.56 g, 10 mmol) was added under ice cooling to an aqueous solution of **5b** (2.1 g, 10 mmol). The resulting solution was concentrated. Treatment of the residue with an aqueous ethanol afforded the potassium salt of cyclohexanone oxime hydrogen sulfate (**5a**), the infrared spectrum of which was superimposable on that of the authentic sample.[4] Yield 1.3 g (56%).

*Addition of Sulfur Trioxide to Cyclohexanone Oxime (**1**).* *a) Addition under Ice-Salt Cooling:* A solution of sulfur trioxide (2 ml, 48 mmol) in ethylene dichloride (40 ml) was added dropwise with stirring below −6.5 °C to a solution of **1** (5.4 g, 48 mmol) in ethylene dichloride (40 ml). The resulting solution was stirred under ice-salt cooling for 1 hr and then treated with a solution of aniline (4.46 g, 48 mmol) in ethylene dichloride (20 ml) below −5 °C. The mixture was stirred at room temperature for 3 hr and filtered to give aniline salt of cyclohexanone oxime hydrogen sulfate (**5c**) as a crystalline substance. Yield 11.23 g (82%).

b) Addition at Room Temperature: A solution of sulfur trioxide (5 ml, 120 mmol) in ethylene dichloride (40 ml) was added dropwise at room temperature to a solution of **1** (13.5 g, 120 mmol) in ethylene dichloride (60 ml). The temperature of the mixture rose to a refluxing temperature. The reaction mixture was treated under ice-salt cooling with water (20 ml) and aqueous ammonium hydroxide (20 ml of a 28% solution) and concentrated. The residue was dissolved in water (40 ml) and extracted with chloroform (40 ml×4). Evaporation of chloroform from the combined extracts afforded a brown crystalline residue, the solution of which in benzene (50 ml) was extracted with water (50 ml×4). The combined aqueous layers were concentrated to about 40 ml and extracted with chloroform (40 ml×4). The combined extracts were dried over anhydrous sodium sulfate and evaporated to give **4**. Yield 6.4 g (47%).

*Addition of Cyclohexanone Oxime (**1**) to Sulfur Trioxide.* A solution of **1** (5.4 g, 48 mmol) in ethylene dichloride (60 ml) was gradually added dropwise below −2 °C, with stirring, to a solution of sulfur trioxide (2 ml, 48 mmol) in ethylene dichloride (40 ml). The mixture was stirred under cooling for 1 hr and at room temperature for 3 hr, treated under ice-salt cooling with water (20 ml) and aqueous ammonium hydroxide (20 ml of a 28% solution) and concentrated. The residue was dissolved in water (40 ml) and extracted with chloroform (40 ml×4). The combined extracts were dried over anhydrous sodium sulfate and evaporated to give **4**. Yield 4.6 g (85%).

Reaction of Cyclohexanone Oxime Monohydrochloride with Sulfur Trioxide. A solution of sulfur trioxide (2 ml, 48 mmol) in ethylene dichloride (40 ml) was added dropwise, with stirring, below −2.5 °C to a solution of cyclohexanone oxime monohydrochloride (7.2 g, 48 mmol), prepared according to the method of Saito,[11b] in ethylene dichloride (60 ml). The resulting mixture was heated at 50 °C for 30 min, stirred at room temperature for 1.5 hr, treated with water (20 ml) and aqueous ammonium hydroxide (20 ml of a 28% solution) under ice-salt cooling, and concentrated. The residue was dissolved in water (40 ml) and extracted with chloroform (40 ml×4). The combined extracts were dried over anhydrous sodium sulfate and evaporated to give a mixture of **1** and **4** (4 g), which was confirmed by vapor-phase chromatographic analysis. The mixture (0.5 g) was treated with a solution of 2,4-dinitrophenylhydrazine[12] to afford 2,4-dinitrophenylhydrazone of cyclohexanone (0.38 g), the amount of **1** being 1.2 g and that of **4** 2.8 g (52%).

*Rearrangement of Cyclohexanone Oxime Hydrogen Sulfate (**2**).* *a)* A solution of sulfur trioxide (2 ml, 48 mmol) in ethylene dichloride (40 ml) was added dropwise, with stirring, below −1.5 °C to a solution of **1** (5.4 g, 48 mmol) in ethylene dichloride (60 ml). When the resulting suspension of **2** was heated to 44 °C, the suspended **2** disappeared and the temperature of the mixture rose to 49.5 °C. The resulting solu-

12) The solution of 2,4-dinitrophenylhydrazine used was prepared from 2,4-dinitrophenylhydrazine (3 g), conc. sulfuric acid (15 ml), methanol (70 ml), and water (20 ml): R. L. Shriner, R. C. Fuson, and D. Y. Curtin, "The Systematic Identification of Organic Compound," Wiley, New York (1956), p. 111.

13) C. F. H. Allen, *J. Amer. Chem. Soc.*, **52**, 2955 (1930).

tion was stirred at room temperature, treated with water (20 ml) and aqueous ammonium hydroxide (20 ml of a 28% solution) under ice-salt cooling, and then concentrated. The residue was dissolved in water (40 ml) and extracted with chloroform (40 ml×5). The combined extracts were dried over anhydrous sodium sulfate and evaporated to give **4**. Yield 4.3 g (80%).

b) In the Presence of 1/2 Equiv. of 1,4-Dioxane: To a suspension of sulfur trioxide–1,4-dioxane complex, prepared from sulfur trioxide (2 ml, 48 mmol) and 1,4-dioxane (2.3 g, 26 mmol) in ethylene dichloride (50 ml) was added dropwise a solution of **1** (5.42 g, 48 mmol) in ethylene dichloride (30 ml) below −5 °C with stirring. When the resulting suspension was heated at 50 °C for 15 min, the suspended **2** disappeared and the temperature of the mixture rose rapidly to 58 °C. The resulting solution was stirred at room temperature for 3 hr and then treated with a solution of aniline (8.93 g, 96 mmol) in ethylene dichloride (20 ml) under ice-salt cooling. The mixture was stirred at room temperature for 20 min, heated at refluxing temperature for 1 hr, and then allowed to stand at room temperature overnight. The crystalline substance, anilinium phenylsulfamate, was collected by filtration. Yield 11.15 g (87%). Mp 185—195 °C. Found: C, 54.01; H, 5.26; N, 10.85; S, 12.24%. Calcd for $C_{12}H_{14}N_2O_3S$: C, 54.12; H, 5.30; N, 10.52; S, 12.04%.

The filtrate was concentrated. The residue was dissolved in water (30 ml) and aqueous hydrochloric acid (10 ml of 1 N solution) and extracted with chloroform (40 ml×4). The combined extracts were dried over anhydrous sodium sulfate and evaporated to give **4**. Yield 4.59 g (85%).

c) In the Presence of 1 Equiv. of 1,4-Dioxane: When a suspension of **2** in the presence of 1 equiv. of 1,4-dioxane, prepared from sulfur trioxide (2 ml, 48 mmol), 1,4-dioxane (4.4 g, 50 mmol) and **1** (5.4 g, 48 mmol) in ethylene dichloride (100 ml) was heated at 50 °C for 26 min, the suspended **2** disappeared and the temperature of the mixture rose rapidly to 60 °C. The mixture was treated with water (20 ml) and aqueous ammonium hydroxide (20 ml of a 28% solution) under ice-salt cooling and concentrated. The residue was dissolved in water (40 ml) and extracted with chloroform (40 ml×4). The combined extracts were evaporated to give **4**. Yield 4.7 g (87%).

d) In the Presence of Sulfur Trioxide: To a suspension of **2** prepared by the addition of sulfur trioxide (2 ml, 48 mmol) in ethylene dichloride (40 ml) to **1** (5.4 g, 48 mmol) in ethylene dichloride (60 ml) was added a solution of sulfur trioxide (12 mmol) in ethylene dichloride (10 ml) dropwise below −5 °C with stirring. The suspension turned solution, the temperature of the mixture rising to 10 °C. The mixture was stirred at room temperature for 1.5 hr and heated at 50 °C for 30 min, no exothermic phenomenon being observed. The mixture was then treated with water (20 ml) and aqueous ammonium hydroxide (20 ml of a 28% solution) under ice-salt cooling and concentrated. The residue was dissolved in water (40 ml) and extracted with chloroform (40 ml×4). The combined extracts were dried over anhydrous sodium sulfate and evaporated to give **4**. Yield 4.7 g (87%).

e) In the Presence of Tin Tetrachloride: To a suspension of **2**, prepared from sulfur trioxide (2 ml, 48 mmol) and **1** (5.4 g, 48 mmol) in ethylene dichloride (80 ml) was added a solution of tin tetrachloride (6.25 g, 24 mmol) in ethylene dichloride (20 ml) dropwise below −4 °C. The resulting solution was gradually warmed with stirring. After reaching 15 °C, the temperature of the mixture rose exothermically to 36.5 °C and colorless crystals separated. The suspension was stirred at room temperature for 2.5 hr, treated with water (20 ml) and aqueous ammonium hydroxide (20 ml of a 28% solution) under ice-salt cooling, and concentrated. The residue was treated with water (40 ml) and the precipitate was removed by filtration. The filtrate was extracted with chloroform (40 ml×4). The combined extracts were dried over anhydrous sodium sulfate and evaporated to give **4**. Yield 4.7 g (87%).

f) In the Presence of Zinc Chloride: A solution of sulfur trioxide (2 ml, 48 mmol) in ethylene dichloride (40 ml) was added dropwise, with stirring, below −8 °C to a solution of cyclohexanone oxime–zinc chloride complex (8.7 g, 24 mmol) in ethylene dichloride (60 ml). The resulting mixture of **2** and zinc chloride was stirred at room temperature for 2 hr. The temperature of the mixture rose exothermically to 32 °C. The mixture was then treated with water (20 ml) and aqueous ammonium hydroxide (20 ml of a 28% solution) under ice-salt cooling and concentrated. The residue was dissolved in water (40 ml) and extracted with chloroform (40 ml×5). The combined extracts were dried over anhydrous sodium sulfate and evaporated to give **4**. Yield 4.73 g (87%).

Cyclohexanone Oxime–Zinc Chloride Complex. A solution of zinc chloride (21 g, 150 mmol) in acetone (50 ml) was added dropwise with stirring at room temperature to a solution of **1** (34 g, 300 mmol) in ethyl acetate (50 ml). The mixture was stirred at room temperature for 3 hr and concentrated. The residue was treated with isopropyl ether and the crystalline cyclohexanone oxime–zinc chloride complex was collected by filtration. Yield 31 g (57%). Recrystallization from isopropyl ether gave colorless crystals, mp 90—91 °C. Found: C, 39.87; H, 6.40; Cl, 19.38%. Calcd for $C_{12}H_{22}Cl_2N_2O_2Zn$: C, 39.75; H, 6.12; Cl, 19.55%.

Hydrolysis of Cyclohexanone Oxime Hydrogen Sulfate (2). To a suspension of **2**, prepared from sulfur trioxide (2 ml, 48 mmol) and **1** (5.42 g, 48 mmol) in ethylene dichloride (80 ml), was added water (20 ml) under ice-salt cooling. The mixture was then heated under refluxing for 1 hr, and neutralized with aqueous potassium hydroxide under ice-salt cooling. The precipitate, potassium sulfate (2.95 g), was removed by filtration, and the filtrate was divided into an organic layer and an aqueous layer.

The organic layer was dried over anhydrous sodium sulfate, and evaporated to give a mixture (3.34 g) of cyclohexanone, **1** and **4**, which were identified by vapor-phase chromatographic analysis. One gram of the mixture was dissolved in aqueous methanol (100 ml of a 50% solution) and treated with 2,4-dinitrophenylhydrazine to give 2,4-dinitrophenylhydrazone of cyclohexanone (0.64 g). Thus, the amount of cyclohexanone and **1** in the mixture was 7.69 mmol (16%) and that of **4** was calculated to be 2.47 g (46%).

The aqueous layer was extracted with chloroform (60 ml×3). The combined extracts were evaporated to give a mixture (1.03 g) of cyclohexanone and **1** (0.467 mmol, 1%), and **4** (0.98 g, 18%), the amounts of which were determined by a treatment of the mixture with 2,4-dinitrophenylhydrazine.

Hydrolysis of Cyclohexanone Oxime Hydrogen Sulfate (2) in the Presence of Lewis Base. a) In the Presence of 1,4-Dioxane: A suspension of **2**, prepared from sulfur trioxide (2 ml, 48 mmol), 1,4-dioxane (4.4 g, 50 mmol) and **1** (5.42 g, 48 mmol) in ethylene dichloride (100 ml), was treated with water (20 ml) under ice-salt cooling. The mixture was heated under refluxing for 1 hr, and neutralized with aqueous potassium hydroxide under ice-salt cooling. A precipitate, potassium sulfate (4.01 g), was removed by filtration, and the filtrate was treated in a similar way to that described above.

The organic layer was confirmed to involve cyclohexanone

and **1** (11.38 mmol, 24%) and **4** (2.15 g, 40%).

The aqueous layer included cyclohexanone and **1** (0.647 mmol, 1.3%) and **4** (0.75 g, 14%).

b) In the Presence of ε-Caprolactam (4): To a suspension of **2**, prepared from sulfur trioxide (2 ml, 48 mmol) and **1** (5.42 g, 48 mmol) in ethylene dichloride (70 ml), was added a solution of **4** (5.42 g, 48 mmol) in ethylene dichloride (30 ml) under ice-salt cooling. The resulting solution was treated with water (20 ml) under ice-salt cooling, heated under refluxing for 1 hr, and neutralized with aqueous potassium hydroxide under ice-salt cooling. A precipitate, potassium sulfate (3.88 g), was removed by filtration, and the filtrate was treated as above.

The organic layer was confirmed to involve cyclohexanone and **1** (14.8 mmol, 31%) and **4** (60 mmol).

The aqueous layer included cyclohexanone and **1** (0.647 mmol, 1.3%) and **4** (18.5 mmol).

Hydrolysis of Aniline Salt of Cyclohexanone Oxime Hydrogen Sulfate (5c). A solution of **5c** (4.43 g, 15 mmol) in water (50 ml) was heated under reflux for 1 hr and extracted with chloroform (50 ml×4). The combined extracts were dried over anhydrous sodium sulfate and evaporated to give a mixture of cyclohexanone, **1** and **4**. Yield 1.42 g. The mixture was dissolved in aqueous methanol (100 ml of a 50% solution) and treated with a solution of 2,4-dinitrophenylhydrazine to give 2,4-dinitrophenylhydrazone of cyclohexanone (0.33 g, 1.19 mmol, 8%). Thus, the amount of **4** in the mixture was calculated to be 1.29 g (75%).

Methanolysis of Cyclohexanone Oxime Hydrogen Sulfate (2). To a suspension of **2**, prepared from sulfur trioxide (2 ml, 48 mmol), 1,4-dioxane (4.4 g, 50 mmol) and **1** (5.42 g, 48 mmol) in ethylene dichloride (90 ml), was added a solution of methanol (2 g, 63 mmol) in ethylene dichloride (10 ml) dropwise with stirring below −11.5 °C. The mixture was stirred at room temperature for 18.5 hr and treated with a solution of aniline (4.47 g, 48 mmol) in ethylene dichloride (20 ml) with stirring below −3 °C. The mixture was stirred at room temperature for 3 hr and aniline salt of monomethyl sulfate precipitated was collected by filtration. Yield 9.17 g (93%). Recrystallization from acetonitrile gave colorless needles, mp 160 °C. Found: C, 40.98; H, 5.20; N, 7.06; S, 15.45%. Calcd for $C_7H_{11}NO_4S$: C, 40.98; H, 5.37; N, 6.83; S, 15.61%.

The filtrate was concentrated and the residue was treated with benzene (100 ml) to give 0.29 g of crystals, whose infrared spectrum was identical with that of the crystals obtained above. Total yield 96%.

The filtrate was washed with water (50 ml×3), dried over anhydrous sodium sulfate and evaporated to give **1** (4.62 g, 85%). The combined washings were concentrated to about 50 ml and extracted with chloroform (50 ml×4). The combined extracts were dried over anhydrous sodium sulfate and evaporated to give further **1** (0.22 g, 4%).

n-Butanolysis of Cyclohexanone Oxime Hydrogen Sulfate (2). To a suspension of **2**, prepared from sulfur trioxide (2 ml, 48 mmol), 1,4-dioxane (4.2 g, 48 mmol), and **1** (5.4 g, 48 mmol) in ethylene dichloride (70 ml) was added a solution of *n*-butanol (3.6 g, 49 mmol) in ethylene dichloride (15 ml) dropwise with stirring at −5—0 °C. The mixture was stirred for 1 hr and then treated with a solution of aniline (4.47 g, 48 mmol) in ethylene dichloride (15 ml) under ice-salt cooling. The resulting suspension was stirred at room temperature for 2 hr and then concentrated. The residue was treated with cyclohexane (60 ml), and aniline salt of mono-*n*-butyl sulfate precipitated was collected by filtration. Yield 10 g (84%). Recrystallization from ethyl acetate gave colorless needles, mp 110—115 °C. The infrared spectrum was superimposable on that of an authentic sample (mp 111.5—112 °C).[14]

The filtrate was washed with water, dried over anhydrous sodium sulfate, and evaporated to give **1** (4.1 g, 76%).

14) F. Popelier, *Bull. Soc. Chim. Belg.*, **35**, 264 (1926).

Reaction of 3,4,5,6-Tetrahydro-2*H*-azepin-7-ol Hydrogen Sulfate with Nucleophilic Reagents

Mitsuo MASAKI, Masaru UCHIDA, and Kiyoshi FUKUI

Polymer Research Laboratory, Ube Industries, Ltd., Goi, Minamikaigan, Ichihara, Chiba 290

(Received May 11, 1973)

The reaction of 3,4,5,6-tetrahydro-2*H*-azepin-7-ol hydrogen sulfate with nucleophilic reagents was studied. The tetrahydroazepin-7-ol hydrogen sulfate reacted with alcohols and oximes to give respectively ε-caprolactam and the corresponding hydrogen sulfate of the reagents in good yields. Treatment with cyclohexylamine or benzylamine afforded ε-caprolactam, the amine salt of the corresponding sulfamic acid, and the corresponding amine salt of the tetrahydroazepin-7-ol hydrogen sulfate, while anilinium phenylsulfamate was formed exclusively in the reaction with aniline. From these results, the tetrahydroazepin-7-ol hydrogen sulfate was confirmed to undergo exclusively a cleavage of the oxygen-sulfur bond by an attack of nucleophiles on the sulfur atom.

3,4,5,6-Tetrahydro-2*H*-azepin-7-ol hydrogen sulfate (**1**) is known as an isolatable intermediate in a Beckmann rearrangement of cyclohexanone oxime to ε-caprolactam (**2**), when sulfuric acid and/or sulfur trioxide is used as the rearranging agent.[1,2] However, the reactivity of **1** has not been studied except for hydrolysis,[2] which gave ε-caprolactam (**2**) and sulfuric acid. The hydrolytic reaction can be envisaged to take place through two pathways (Scheme 1); A which involves a nucleophilic attack by water (**3a**) on the sulfur atom of **1**, resulting in the tetrahydroazepinyl substituted oxygen-sulfur bond fission, and B which involves a nucleophilic attack by water (**3a**) on the carbon atom, resulting in the carbon-oxygen bond fission. No report has referred to the mechanism of the hydrolysis, presumably because both pathways give rise to identical products.

When nucleophilic reagents other than water such as alcohol or amine are used with **1**, a reaction along path A would give ε-caprolactam (**2**) and the corresponding sulfonated derivatives of reagent (**4**), while path B would give rise to the formation of sulfuric acid and 7-substituted 3,4,5,6-tetrahydro-2*H*-azepine derivatives (**5**), such as 7-alkoxy (**5b**) or 7-amino compound (**5c**). Reactions of 2-aza-1-cycloalkenyl benzenesulfonates with amine[3,4] or enamine[5] have been reported to yield α-substituted cyclic imino compounds resulting from the cleavage of the carbon-oxygen bond (Scheme 2). Thermal rearrangement of cycloalkanone oxime benzenesulfonates in the presence of alcohols or amines is also known to give α-substituted cyclic imino compounds.[6] The reaction of the oxime benzenesulfonates with acetic acid or methanol afforded lactam as a main product.[7]

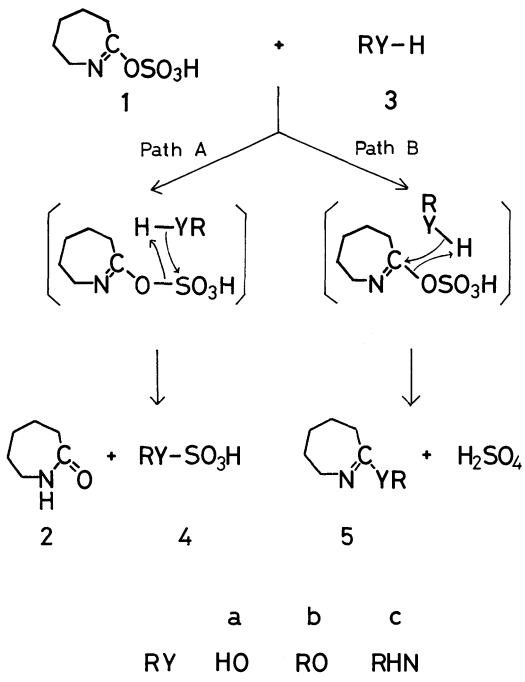

Scheme 1.

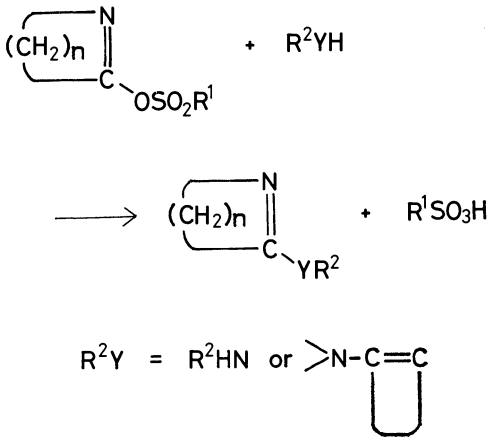

Scheme 2.

We have found that nucleophilic reagents caused an exclusive cleavage of the oxygen-sulfur bond of tetrahydroazepin-7-ol hydrogen sulfate (**1**, path A). This paper describes the reaction of **1** with alcohols, amines, and oximes.

1) L. Giuffre, G. Sioli, and E. Losio, *Chim. Ind.* (*Milan.*), **50**, 983 (1968).
2) A. F. Turbak, *Ind. Eng. Chem., Prod. Res. Develop.*, **7**, 190 (1968).
3) P. Oxley, D. A. Peak, and W. F. Short, *J. Chem. Soc.*, **1948**, 1618.
4) R. Huisgen, D. Vossius, and M. Appl, *Chem. Ber.*, **91**, 1 (1958).
5) S. Hünig, W. Lücke, V. Meuer, and W. Grässmann, *Angew. Chem.*, **75**, 295 (1963).
6) P. Oxley and W. F. Short, *J. Chem. Soc.*, **1948**, 1514.
7) W. Z. Heldt, *J. Amer. Chem. Soc.*, **80**, 5880 (1958).

Results and Discussion

Reaction of 3,4,5,6-Tetrahydro-2H-azepin-7-ol Hydrogen Sulfate (1) with Alcohols. When **1** was treated with methanol (**6a**) in ethylene dichloride at 50 °C, ε-caprolactam (**2**) and monomethyl sulfate (**7a**) were obtained in 99 and 85% yields, respectively. The latter was isolated as a sodium salt. A similar treatment of **1**

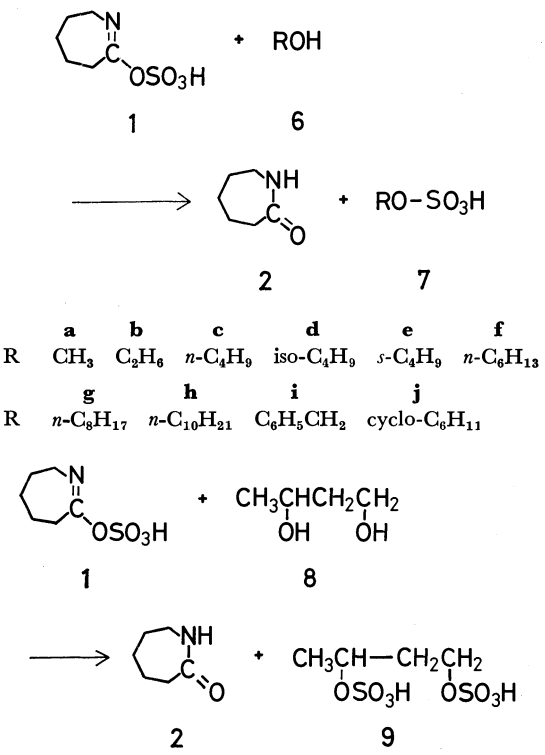

with a half equiv. of 1,3-butanediol (**8**) yielded ε-caprolactam and 1,3-butanediol bis(hydrogen sulfate) (**9**) in 96 and 90% yields, respectively. **9** was isolated as a barium salt. Similarly, reactions of **1** with various alcohols (**6**) gave ε-caprolactam and the corresponding monoalkyl sulfates (**7**) in good yields. Monoalkyl sulfates (**7**) were isolated as stable salts with *S*-benzylthioformamidine. The results are summarized in Tables 1 and 2.

Table 1. Reaction of 3,4,5,6-tetrahydro-2*H*-azepin-7-ol hydrogen sulfate (**1**) with alcohols

	Alcohol	Products, yields %	
		Lactam	Monoalkyl sulfate
6a	Methanol	99	85[a]
6b	Ethyl alcohol	90	51[b]
6c	Butyl alcohol	98	95[b]
6d	Isobutyl alcohol	97	89[b]
6e	*sec*-Butyl alcohol	94	86[b]
6f	Hexyl alcohol	77	78[b]
6g	Octyl alcohol	83	80[b]
6h	Decyl alcohol	72	86[b]
6i	Benzyl alcohol	65	89[b]
6j	Cyclohexanol	98	83[b]
8	1,3-Butanediol	96	90[c]

a) Based on conversion into the sodium salt.
b) Based on conversion into the *S*-Benzylthioformamidinium salt.
c) Based on conversion into the barium salt.

Table 2. *S*-Benzylthioformamidinium monoalkyl sulfates

$R\text{-}OSO_3^-\ \ H_2N^+=C(NH_2)\text{—}S\text{—}CH_2C_6H_5$

R	Mp, °C	Formula		Anal % Calcd	Anal % Found
C_2H_5	112—114	$C_{10}H_{16}N_2O_4S_2$	C	41.10	41.11
			H	5.52	5.38
			N	9.59	9.61
			S	21.90	21.56
C_4H_9	99—100	$C_{12}H_{20}N_2O_4S_2$	N	8.74	8.66
			S	20.01	19.82
iso-C_4H_9	134—137	$C_{12}H_{20}N_2O_4S_2$	N	8.74	8.85
			S	20.01	20.31
sec-C_4H_9	124—126	$C_{12}H_{20}N_2O_4S_2$	N	8.74	8.92
			S	20.01	20.10
C_6H_{13}	83—84.5	$C_{14}H_{24}N_2O_4S_2$	C	42.27	42.49
			H	6.94	6.78
			N	8.04	8.16
			S	18.37	18.57
C_8H_{17}	69—70.5	$C_{16}H_{28}N_2O_4S_2$	C	51.05	50.96
			H	7.50	7.27
			N	7.44	7.80
			S	17.00	17.22
$C_{10}H_{21}$	63—66	$C_{18}H_{33}N_2O_4S_2$	C	53.45	53.83
			H	7.98	7.95
			N	6.92	6.53
			S	15.85	15.65
$C_6H_5CH_2$	145—147	$C_{15}H_{18}N_2O_4S_2$	C	50.83	50.69
			H	5.12	5.09
			N	7.90	7.79
			S	18.09	18.41
cyclo-C_6H_{11}	170—173	$C_{14}H_{22}N_2O_4S_2$	C	48.53	48.67
			H	6.40	6.17
			N	8.09	8.31

In these reactions, formation of 7-alkoxy-3,4,5,6-tetrahydro-2*H*-azepine (**5b**, path B) was not detected. In a reaction of **1** with *tert*-butyl alcohol, ε-caprolactam (**2**) and sulfuric acid were isolated. Formation of sulfuric acid could be explained by the decomposition[8] of mono-*tert*-butyl sulfate formed initially, along path A.

Reaction of 3,4,5,6-Tetrahydro-2H-azepin-7-ol Hydrogen Sulfate (1) with Amines. Treatment of **1** with 2 equiv. of aniline (**10a**) in ethylene dichloride at refluxing temperature afforded **2** and anilinium phenylsulfamate (**13a**) in 93 and 87% yields, respectively. However, reaction of **1** with 2 equiv. of benzylamine (**10b**) afforded not only **2** and benzylammonium benzylsulfamate (**13b**), but also benzylamine salt of **1** (**11b**). A considerable amount of the latter was obtained even when the reaction was carried out at 80 °C for 7 hr. Similarly, reaction of **1** with 2 equiv. of cyclohexylamine (**10c**) afforded **2**, cyclohexylammonium cyclohexanesulfamate (**13c**), and cyclohexylamine salt of **1**

8) C. M. Suter and J. D. Malkemus, *ibid.*, **63**, 978 (1941).

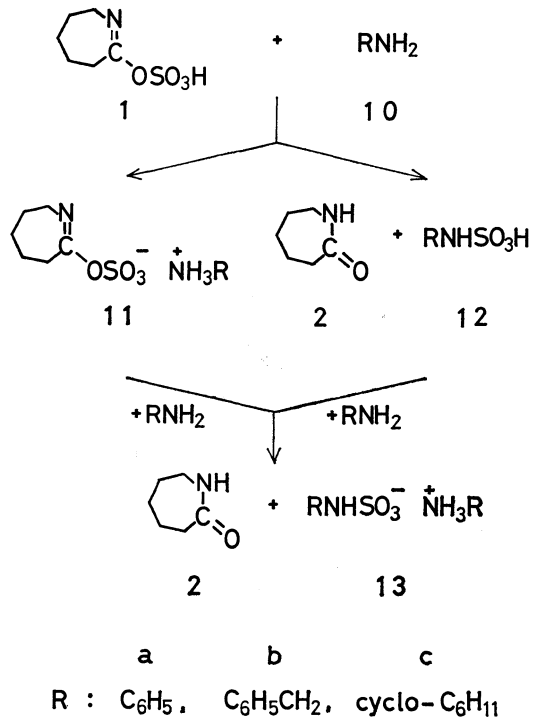

(**11c**) in 22, 27, and 69% yields, respectively.

Thus, the reaction of **1** with an amine could be explained to consist of two competitive reactions, a simple salt formation between **1** and the amine, and a nucleophilic attack of the amine on sulfur atom of **1** to give **2** and the corresponding sulfamic acid (**12**) which afforded the corresponding ammonium salt (**13**). Exclusive formation of **13a** in the reaction with aniline was rationalized by the fact that **11a** could undergo a further nucleophilic attack by another molecule of aniline to give **2** and **13a**.

When **1** was treated with 1 equiv. of aniline below −8 °C, aniline salt of **1** (**11a**) was produced in 75% yield. A reaction of **11a** with aniline at 80 °C resulted in the formation of **13a** in 67% yield. The cyclohexylamine salt (**11c**) was obtained by a treatment of **1** with 1 equiv. of cyclohexylamine (**10c**) in 76% yield. Reaction of **11c** with aniline was carried out at 80 °C for 1 hr, the starting materials being recovered.

The difference in reactivity of **11a** and **11c** could be ascribed to the basicity of the parent amines (**10**). The anionic character of sulfate moiety of the salt (**11**) would increase with increasing basicity of **10**. The electron density on the sulfur atom of sulfate (**11c**) would be larger than that of sulfate (**11a**), and it would become difficult for the former to undergo a nucleophilic attack by an amine on the sulfur atom as compared with the case of aniline salt (**11a**). Analogous phenomena have been observed in the Beckmann rearrangement of cyclohexanone oxime hydrogen sulfate (**15a**), its rearrangement being retarded by the Lewis base.[9] Salt formation with the base would increase the electron density on the sulfur atom of **15a** and make the heterolytic fission of nitrogen-oxygen bond more difficult, which is a rate-determining step in the rearrangement.[10]

Table 3. Reaction of 3,4,5,6-tetrahydro-2*H*-azepin-7-ol hydrogen sulfate (**1**) with oximes

	Oxime	Products, yield %	
		Lactam	Oxime hydrogen sulfate
14a	Cyclohexanone oxime	82	90[a]
14b	Acetoxime	100	85[b]
14c	Acetophenone oxime	66	50[b]
14d	Cyclopentanone oxime	96	63[b]
14e	Cyclododecanone oxime	100	68[b]

a) Based on conversion into the anilinium salt.
b) Based on conversion into the imidazolium salt.

Table 4. Imidazolium salts of oxime hydrogen sulfates (**15**)

$R_3 \atop R_4$>CNOSO$_3$H·Imidazole

R^3	R^4	Mp, °C	Formula	Anal %	Calcd	Found
CH_3	CH_3	102—105[a]	$C_6H_{11}N_3O_4S$	N	18.99	18.84
				S	14.49	14.37
CH_3	C_6H_5	92—95[b]	$C_{11}H_{13}N_3O_4S$	N	14.87	14.86
				S	11.32	11.08
$-(CH_2)_4-$		79—84[b]	$C_8H_{13}N_3O_4S$	N	16.99	16.90
				S	12.97	12.13
$-(CH_2)_{11}-$		157—159[c]	$C_{15}H_{27}N_3O_4S$	N	12.16	12.56
				S	9.28	9.67

a) Recrystallized from methanol–acetone.
b) Recrystallized from methanol–ether.
c) Recrystallized from methanol.

In every reaction of **1** with amines, no formation of 7-amino derivatives of 3,4,5,6-tetrahydro-2*H*-azepine (**5c**) could be observed which might be formed according to path B.

*Reaction of 3,4,5,6-Tetrahydro-2*H*-azepin-7-ol Hydrogen Sulfate (1) with Oximes.* **1** was treated with cyclohexanone oxime (**14a**) in ethylene dichloride to give cyclohexanone oxime hydrogen sulfate (**15a**) and **2** in

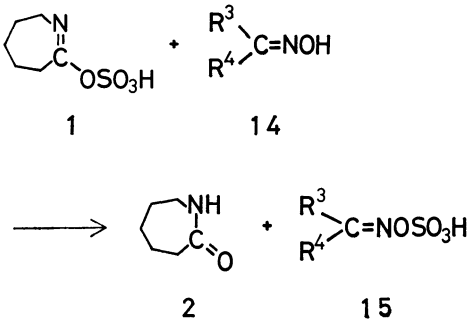

a $-(CH_2)_5-$
b CH_3 CH_3
c CH_3 C_6Ht
d $-(CH_2)_4-$
e $-(CH_2)_{11}-$

9) K. Fukui, M. Uchida, and M. Masaki, This Bulletin, **46**, 3168 (1973).

10) L. G. Donaruma and W. Z. Heldt, "Organic Reactions," Vol. 11, ed. by A. C. Cope, Wiley, New York, N. Y. (1960), p. 1.

good yields. Formation of **15a** was confirmed by treatment of the reaction mixture with aniline, giving aniline salt of cyclohexanone oxime hydrogen sulfate in 90% yield. Similar reactions of **1** with acetoxime (**14b**), acetophenone oxime (**14c**), cyclopentanone oxime (**14d**), and cyclododecanone oxime (**14e**) resulted in the formation of the corresponding oxime hydrogen sulfate (**15**) and **2** in good yields. Most of the oxime hydrogen sulfate (**15**) were isolated as stable salts with imidazole. The results are summarized in Tables 3 and 4.

Experimental

Concentration and evaporation were performed with a rotary evaporator under reduced pressure. Melting points were determined in a liquid bath and are uncorrected. Reagents and organic solvents for reactions were used as anhydrous states.

3,4,5,6-Tetrahydro-2H-azepin-7-ol Hydrogen Sulfate (1). A solution of **1** in ethylene dichloride was prepared by two methods. *a*) A modification of the method of Giuffre *et al*:[1] A solution of sulfur trioxide (2 ml, 48 mmol) in ethylene dichloride (40 ml) was added dropwise to a solution of ε-caprolactam (5.42 g, 48 mmol) in an appropriate amount of ethylene dichloride with stirring under ice cooling; *b*) A modification of the method of Turbak:[2] A suspension of cyclohexanone oxime hydrogen sulfate was heated to 40—50 °C until exothermic rearrangement took place.

Reaction of 1 with Methanol. Methanol (3.8 g, 120 mmol) was added dropwise with stirring at room temperature to a solution of **1** (120 mmol) in ethylene dichloride (250 ml). The mixture was then stirred at room temperature for 30 min, heated to 50 °C and further stirred for 30 min. The reaction mixture was concentrated. The syrup-like residue was dissolved in ice water (50 ml) and treated with a solution of sodium hydroxide (4.8 g, 120 mmol) under cooling. The solution was then extracted with chloroform (50 ml×4). The combined extracts were dried over anhydrous sodium sulfate and evaporated to give **2.** Yield 13.5 g (99%).

The aqueous solution remaining after chloroform extraction was concentrated to 10 ml, and ethyl alcohol (50 ml) was added to the concentrate. The crystalline precipitate was collected by filtration and found to be identical with authentic sodium monomethyl sulfate monohydrate by infrared spectrum. Yield 15.5 g (85%).

Reaction of 1 with 1,3-Butanediol. A solution of 1,3-butanediol (5.4 g, 60 mmol) in ethylene dichloride (20 ml) was added dropwise to a solution of **1** (120 mmol) in ethylene dichloride (250 ml) with stirring at room temperature. The mixture was thereafter stirred for 30 min at room temperature, heated to 50 °C and stirred for 30 min. The reaction mixture was concentrated. The syrup-like residue was dissolved in ice water (50 ml) and neutralized with an aqueous barium hydroxide. The aqueous solution was extracted with chloroform (50 ml×4). The combined extracts were dried over anhydrous sodium sulfate and evaporated to give **2.** Yield 13 g (96%).

The aqueous solution remaining after chloroform extraction was treated with activated carbon and concentrated to 20 ml. Ethyl alcohol was added to the concentrate to cause precipitation of barium 1,3-butanediol bis(hydrogen sulfate) dihydrate, which was collected by filtration and confirmed by an infrared spectroscopic comparison with that of an authentic sample. Yield 19.2 g (90%).

Reaction of 1 with Ethyl Alcohol. To a solution of **1** (48 mmol) in ethylene dichloride (85 ml) was added dropwise at room temperature a solution of ethyl alcohol (2.2 g, 48 mmol) in ethylene dichloride (15 ml). The mixture was stirred for 1 hr at room temperature, heated to 50 °C, and further stirred for 30 min. The reaction mixture was concentrated. The syrup-like residue was dissolved in water (25 ml) and neutralized with sodium bicarbonate. The aqueous solution was then extracted with chloroform (30 ml× 5). The combined extracts were dried over anhydrous sodium sulfate and evaporated to give **2.** Yield 4.85 g (89%).

The aqueous solution remaining after chloroform extraction was treated with activated carbon. A solution of *S*-benzylthioformamidine hydrochloride (9.72 g, 48 mmol) in water (15 ml) was then added to the aqueous solution. The resulting solution was concentrated and ethyl alcohol was added to the residue. An insoluble matter was removed by filtration and the filtrate was treated with water (30 ml) to give *S*-benzylthioformamidinium monoethyl sulfate as pale yellow needles. Yield 1.05 g (7%). The mp and analytical results are shown in Table 2.

The filtrate was concentrated and the residue was treated with methanol (90 ml) to afford more *S*-benzylthioformamidinium monoethyl sulfate. Yield 5.8 g (41%).

Reaction of 1 with Butyl Alcohol, Isobutyl Alcohol, sec-*Butyl Alcohol, Hexyl Alcohol, Octyl Alcohol, Decyl Alcohol, Benzyl Alcohol, or Cyclohexanol.* In a similar way to that for the reaction of **1** with ethyl alcohol, a solution of **1** (48 mmol) in ethylene dichloride (85 ml) was treated with a solution of the alcohol (48 mmol) in ethylene dichloride (15 ml). The results are summarized in Tables 1 and 2.

Reaction of 1 with tert-*Butyl Alcohol.* To a solution of **1** (48 mmol) in ethylene dichloride (70 ml) was added dropwise with stirring below 0 °C a solution of *tert*-butyl alcohol (3.6 g, 48 mmol) in ethylene dichloride (10 ml). The mixture was stirred at room temperature for 2 hr and at 40 °C for 1 hr, and then treated with aniline (4.5 g, 48 mmol) under 0 °C. The resulting mixture was allowed to stand overnight. The crystalline substance collected by filtration was confirmed as anilinium sulfate by comparison of its infrared spectrum with that of the authentic sample. Yield 6.76 g (48% based upon **1**). The filtrate was concentrated to half, and treated with aniline (4.5 g, 48 mmol) under ice cooling to afford more anilinium sulfate. Yield 5.56 g (39%).

The ethylene dichloride solution separated from the above crystalline substance by filtration was concentrated. The residue was dissolved in water (40 ml) and hydrochloric aicd (1N, 10 ml) and extracted with chloroform (50 ml×4). The combined extracts were dried over anhydrous sodium sulfate and evaporated to give **2.** Yield 4.93 g (91%).

Reaction of 1 with Two Equiv. of Aniline. To a solution of **1** (48 mmol) in ethylene dichloride (80 ml) was added dropwise below −5 °C with stirring a solution of aniline (8.93 g, 96 mmol) in ethylene dichloride (20 ml). Stirring was continued for 30 min. The mixture was heated under reflux for 1 hr, and then allowed to stand at room temperature to cool down. The precipitated crystals were collected by filtration and identified as anilinium phenylsulfamate (**13a**) by comparison of its infrared spectrum with that of the authentic sample.[9]

The mother liquor separated from the crystals was concentrated. Water (50 ml) was added to the residue, and the aqueous solution was washed with ether (50 ml) and extracted with chloroform (50 ml×5). The combined extracts were dried over anhydrous sodium sulfate and evaporated to give **2.** Yield 5 g (93%).

Reaction of 1 with One Equiv. of Aniline. A solution of aniline (4.47 g, 48 mmol) in ethylene dichloride (30 ml) was added dropwise to a solution of **1** (48 mmol) in ethylene dichloride (100 ml) with stirring below −8 °C, taking about 15 min. Stirring was continued for 2 hr below −5 °C and overnight at room temperature. The mixture was filtered to give 11.94 g of colorless powder, which was identified by elemental analysis and infrared spectrum as a homogeneous mixture of aniline salt of 3,4,5,6-tetrahydro-2*H*-azepin-7-ol hydrogen sulfate and anilinium hydrogen sulfate (4:1 in molar ratio). Mp 124—146 °C. Found: C, 48.43; H, 6.06; N, 9.43; S, 12.24%. Calcd for $(C_{12}H_{18}N_2O_4S)_4 \cdot C_6H_9NO_4S$: C, 48.53; H, 6.07; N, 9.44; S, 11.99%. The infrared spectrum exhibited characteristic absorption bands at 1650 cm^{-1} (C=N), and 1270 and 1200 cm^{-1} (SO_2). The yield of **11a** was 10.23 g (75%).

The filtrate was concentrated, and the residue was dissolved in water (12 ml) and extracted with chloroform (20 ml×5). The combined extracts were dried over anhydrous sodium sulfate and concentrated to dryness, yielding 1.13 g (21%) of **2**.

Reaction of Aniline Salt of 1 (11a) with Aniline. A solution of aniline (2.81 g, 30 mmol) in ethylene dichloride (20 ml) was added with stirring below 0 °C to a suspension of a mixture of **11a** (6.5 g, 22.8 mmol) and anilinium hydrogen sulfate (1.1 g, 5.7 mmol) in ethylene dichloride (40 ml). The mixture was stirred at room temperature for 1 hr and then at the refluxing temperature for 1 hr. Filtration afforded 7 g of colorless powder which was identified by infrared spectrum as a mixture consisting of anilinium phenylsulfamate (**13a**) and a small amount of anilinium sulfate.

Reaction of 1 with Two Equiv. of Benzylamine. To a solution of **1** (48 mmol) in ethylene dichloride (80 ml) was added dropwise at room temperature with stirring a solution of benzylamine (10.27 g, 96 mmol) in ethylene dichloride (20 ml) over 17 min period. When the reaction temperature reached 40 °C at the highest, crystals were precipitated. It was then heated under reflux for 7 hr and cooled. The crystalline precipitate was collected by filtration. 7.09 g of benzylammonium benzylsulfamate (**13b**) was obtained, which was identified by comparison of its infrared spectrum with that of the sample synthesized by a reaction of sulfur trioxide–1,4-dioxane complex with 2 equiv. of benzylamine. Yield 50%.

The filtrate separated from **13b** was concentrated and the residue was treated with benzene (50 ml). The crystalline substance collected by filtration was identified by infrared spectrum as a mixture (4.33 g) of **13b** and benzylamine salt of **1** (**11b**), which exhibited characteristic absorption bands at 1630 cm^{-1} (C=N), and 1260 and 1210 cm^{-1} (SO_2). The mixture was dissolved in water (50 ml), and the resulting solution was heated under reflux for 1 hr and extracted with chloroform (50 ml×4). The combined extracts were dried over anhydrous sodium sulfate and evaporated to give **2**. Yield 1.39 g (26%). The yield of **11b** was 3.74 g (26%) and that of **13b** 0.59 g (4%).

The filtrate was concentrated, and the residue was dissolved in aqueous sulfuric acid (0.5N, 40 ml) and extracted with chloroform (40 ml×5). Concentration of the combined extracts afforded a yellow oily substance (7.16 g), which was extracted with hot hexane (50 ml×4). Evaporation of hexane from the combined extracts afforded **2** as colorless crystals. Yield 2.99 g (55%).

Reaction of 1 with Two Equiv. of Cyclohexylamine. To a solution of **1** (48 mmol) in ethylene dichloride (80 ml) was added dropwise with stirring below −2 °C a solution of cyclohexylamine (9.5 g, 96 mmol) in ethylene dichloride (20 ml). The mixture was stirred at room temperature for 1.5 hr, heated under reflux for 1 hr, and allowed to stand at room temperature to cool down. The crystalline substance collected by filtration was identified by infrared spectrum as cyclohexylammonium cyclohexanesulfamate (**13c**). Yield 4.06 g (27%).

The filtrate separated from **13c** was concentrated and the residue was treated with benzene (100 ml). The crystalline precipitate was collected by filtration and identified by infrared spectrum as cyclohexylamine salt of **1** (**11c**), which exhibited characteristic absorption bands at 1630 cm^{-1} (C=N), and 1260 and 1210 cm^{-1} (SO_2). Yield 9.72 g (69%).

The filtrate was concentrated, and the residue was dissolved in water (35 ml) and extracted with chloroform (40 ml×4). Concentration of the combined extracts afforded an oily substance (2.77 g), which was extracted with hot hexane (60 ml×4). Evaporation of hexane from the combined extracts afforded **2** as colorless crystals. Yield 1.22 g (22%).

Reaction of 1 with One Equiv. of Cyclohexylamine. A solution of cyclohexylamine (4.75 g, 48 mmol) in ethylene dichloride (20 ml) was added dropwise to a solution of **1** (48 mmol) in ethylene dichloride (80 ml) with stirring below −7 °C. Stirring was continued for 30 min below −9 °C and overnight at room temperature. The mixture was filtered to give 7.42 g of colorless powder, which was identified by infrared spectrum as cyclohexylamine salt of **1** (**11c**). Yield 53%.

The filtrate separated from **11c** was evaporated and the residue was treated with benzene (100 ml) to give more **11c** as an insoluble matter. Yield 3.19 g (23%).

Reaction of Cyclohexylamine Salt of 1 (11c) with Aniline. A solution of aniline (2.79 g, 30 mmol) in ethylene dichloride (10 ml) was added with stirring at room temperature to a suspension of **11c** (8.76 g, 30 mmol) in ethylene dichloride (50 ml). The mixture was heated under reflux for 1 hr and stirred at room temperature for 2 hr. The mixture was concentrated and the residue was treated with benzene (50 ml). The crystalline substance collected by filtration was identified as the starting material, amine salt (**11c**). Yield 7.36 g (84%).

Benzylammonium Benzylsulfamate (13b). A solution of 1,4-dioxane (4.4 g, 50 mmol) in ethylene dichloride (20 ml) was added dropwise to a solution of sulfur trioxide (2 ml, 48 mmol) in ethylene dichloride (40 ml) with stirring below 4 °C. To the resulting suspension of sulfur trioxide–1,4-dioxane complex was added dropwise with stirring below −1 °C a solution of benzylamine (10.3 g, 96 mmol) in ethylene dichloride (30 ml). The mixture was stirred at room temperature for 4 hr, and the crystalline substance, benzylammonium benzylsulfamate (**13b**), was collected by filtration. Yield 11.45 g (81%). Recrystallization from methanol gave colorless needles, mp 174—176 °C. Found: C, 57.04; H, 6.40; N, 9.71%. Calcd for $C_{14}H_{18}N_2O_3S$: C, 57.14; H, 6.12; N, 9.52%.

Cyclohexylammonium Cyclohexanesulfamate (13c). A suspension of sulfur trioxide–1,4-dioxane complex (1:1 in molar ratio, 48 mmol) in ethylene dichloride (60 ml) was treated with a solution of cyclohexylamine (9.5 g, 96 mmol) in ethylene dichloride (30 ml) in a similar way to that for **13b**. The mixture was stirred at room temperature and filtered to give 9.48 g of cyclohexylammonium cyclohexanesulfamate (**13c**). Yield 71%. Recrystallization from methanol–ether gave colorless crystals, mp 191 °C (lit,[11] 198—200 °C). Found: N, 10.18; S, 11.37%. Calcd for $C_{12}H_{26}$-

11) L. F. Audrieth and M. Sveda, *J. Org. Chem.*, **9**, 89 (1944).

N_2O_3S: N, 10.07; S, 11.51%.

Reaction of ***1*** *with Cyclohexanone Oxime.* A solution of cyclohexanone oxime (13.6 g, 120 mmol) in ethylene dichloride (50 ml) was added dropwise to a solution of **1** (120 mmol) in ethylene dichloride (170 ml) with stirring below 3 °C. Stirring was continued further for 30 min under cooling and for 1 hr at room temperature. The mixture was then treated with a solution of aniline (11.2 g, 120 mmol) in ethylene dichloride (30 ml) below 0 °C and stirred at room temperature for 1 hr. The crystalline precipitate was collected by filtration and identified by comparison of its infrared spectrum with that of authentic aniline salt of cyclohexanone oxime hydrogen sulfate.[9] Yield 31.3 g (90%).

Concentration of the filtrate afforded an oily substance which was dissolved in water (50 ml), washed with benzene (10 ml) and extracted with chloroform (50 ml×4). The combined extracts were dried over anhydrous sodium sulfate and evaporated to give **2**. Yield 11.2 g (82%).

Reaction of ***1*** *with Acetoxime.* To a solution of **1** (48 mmol) in ethylene dichloride (90 ml) was added dropwise with stirring below −2 °C a solution of acetoxime (3.5 g, 48 mmol) in ethylene dichloride (20 ml). The mixture was stirred for 1 hr at room temperature, and then cooled down to −5 °C or below. A solution of imidazole (3.3 g, 48 mmol) in ethylene dichloride (50 ml) was then added dropwise to the mixture. A colorless precipitate was formed at once. Stirring was continued for further 30 min under cooling. The precipitated imidazole salt of acetoxime hydrogen sulfate was collected by filtration. Yield 8.9 g (84%). Recrystallization from methanol–acetone gave colorless prisms, mp 102—105 °C. Found: N, 18.84; S, 14.37%. Calcd for $C_6H_{11}N_3O_4S$: N, 18.99; S, 14.49%.

Concentration of the filtrate afforded a syrup-like residue which was extracted with benzene (30 ml), the extract being evaporated to give **2**. Yield 5.3 g (98%).

Reaction of ***1*** *with Acetophenone Oxime, Cyclopentanone Oxime, and Cyclododecanone Oxime.* In a similar way to that for the reaction of **1** with acetoxime, a solution of **1** (48 mmol) in ethylene dichloride (80 ml) was treated with a solution of acetophenone oxime (6.5 g, 48 mmol), cyclopentanone oxime (4.7 g, 48 mmol), or cyclododecanone oxime (9.5 g, 48 mmol) in an appropriate amount of ethylene dichloride. The reaction mixture was then treated with a solution of imidazole (3.8 g, 48 mmol) in chloroform (30 ml). The results are summarized in Tables 3 and 4.

BULLETIN OF THE CHEMICAL SOCIETY OF JAPAN, VOL. 46, 3179—3183 (1973)

Reaction of 3,4,5,6,-Tetrahydro-2*H*-azepin-7-ol Hydrogen Sulfate with Cyclohexanone Oxime–Tin Tetrachloride Complex

Mitsuo MASAKI, Kiyoshi FUKUI, Masaru UCHIDA, Koichi YAMAMOTO, and Izuhiko UCHIDA

Polymer Research Laboratory, Ube Industries, Ltd., Goi, Minamikaigan, Ichihara, Chiba 290

(Received May 11, 1973)

Cyclohexanone oxime hydrogen sulfate was found to undergo facile rearrangement to 3,4,5,6-tetrahydro-2*H*-azepin-7-ol hydrogen sulfate in the presence of ε-caprolactam–tin tetrachloride complex, while the oxime hydrogen sulfate decomposed in the presence of ε-caprolactam. Other metal halides were studied to see if the oxime hydrogen sulfate undergoes rearrangement in the presence of the lactam. Cyclohexanone oxime–tin tetrachloride complex was synthesized. Its reaction with the tetrahydroazepin-7-ol hydrogen sulfate was found to give the lactam–tin tetrachloride complex and the oxime hydrogen sulfate which regenerated the tetrahydroazepin-7-ol hydrogen sulfate in the reaction system. Tin tetrachloride complex was prepared with several oximes.

Tetrahydroazepin-7-ol hydrogen sulfate undergoes an oxygen-sulfur bond fission exclusively on treatment with nucleophilic reagents.[1] The reaction of 3,4,5,6-tetrahydro-2*H*-azepin-7-ol hydrogen sulfate (**1**) with cyclohexanone oxime (**2**) afforded ε-caprolactam (**3**) and cyclohexanone oxime hydrogen sulfate (**4**) in good yields. The reaction indicates a possible regeneration of **1** in the reaction system, since the compound has been known to be produced by a thermal rearrangement of **4**.[2] It is of interest to examine the possibility, because a Beckmann rearrangement using sulfuric acid and/or sulfur trioxide as a rearranging agent has been known to require at least one equiv. of the agent.[3] Preliminary experiments revealed, however, that **4** decomposed in the presence of **3** and did not undergo rearrangement. Though the decomposition products

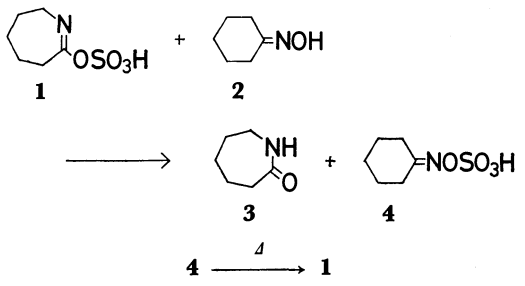

1) M. Masaki, M. Uchida, and K. Fukui, This Bulletin, **46**, 3174 (1973).

2) K. Fukui, M. Uchida, and M. Masaki, *ibid.*, **46**, 3168 (1973).

3) a) L. G. Donaruma and W. Z. Heldt, "Organic Reactions," Vol. 11, ed. by A. C. Cope *et al.*, John Wiley & Sons, Inc., New York, N. Y., (1960) p. 57; b) N. Tokura, R. Asami, and R. Tada, *Sci. Repts. Research Inst., Tohoku Univ., Ser.* **A8**, 151 (1956).

and mechanism are not clear,[4] the decomposition seems to be ascribable to an interaction between the oxime hydrogen sulfate (strong acid) and the lactam function (weak base). Thus **4** might be expected to undergo rearrangement normally, when the lactam function is protected by converting the lactam into a complex with Lewis acid.

This paper describes a Beckmann rearrangement of oxime hydrogen sulfate (**4**) in the presence of lactam–Lewis acid complex and a conversion of cyclohexanone oxime–tin tetrachloride complex into ε-caprolactam-tin tetrachloride complex by means of a circulatory use of sulfur trioxide moiety in **4** or tetrahydroazepin-7-ol hydrogen sulfate (**1**).

Results and Discussion

When a mixture of cyclohexanone oxime hydrogen sulfate (**4**) and 1 equiv. of ε-caprolactam–zinc chloride complex (2: 1 in molar ratio, **5a**) in ethylene dichloride was heated to 64 °C, no exothermic phenomenon nor any remarkable coloration of the reaction mixture was observed, in contrast to the fact that **4** decomposes with a remarkable coloration of the mixture in the presence of ε-caprolactam (**3**) under similar conditions, and when alone, undergoes rearrangement exothermally under milder conditions.[2] After hydrolysis and neutralization of the reaction product, **3** was obtained in 152% yield based upon the lactam complex (**5a**). The results showed that more than 52% of **4** underwent rearrangement to **1** and less than 48% decomposed, competitively. The partial decomposition might be due to a partial dissociation of **5a** into **3** and zinc chloride.

When a mixture of **4** and 1 equiv. of ε-caprolactam–tin tetrachloride complex (2: 1 in molar ratio, **5b**) in ethylene dichloride was gradually heated to 48 °C, exothermic rearrangement of **4** occurred to afford **3** in 190% yield, after hydrolysis and neutralization. It is apparent that at least 90% of **4** rearranged in the presence of **5b**.

Various metal halides were similarly examined to see whether **4** underwent rearrangement in their presence with ε-caprolactam (**5**). The results are summarized in Table 1. Tin tetrachloride was found to be most effective among the metal halides examined.

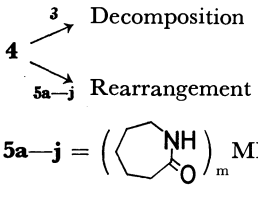

	a	b	c	d	e
MX_n	$ZnCl_2$	$SnCl_4$	BF_3	$CdCl_2$	$HgCl_2$
m	2	2	1	1	1
	f	**g**	**h**	**i**	**j**
MX_n	$FeCl_3$	$ZrCl_4$	$SbCl_5$	$SbCl_5$	$SnBr_4$
m	2	2	1	2	2

Table 1. Rearrangement of cyclohexanone oxime hydrogen sulfate (**4**) in the presence of ε-caprolactam–metal halide complex (**5**)

Metal halide	Reaction temp °C	Risen temp °C	Color of reaction mixture	ε-Caprolactam yield Based on **5**, %	Based on **4**, %
$ZnCl_2$	64	0	colorless	152	52
$SnCl_4$	48	17	colorless	190	90
BF_3	55	10.5	colorless	188	88
$CdCl_2$	55	0	pale yellow	122	22
$HgCl_2$	55	0	pale yellow	124	24
$FeCl_3$	25	few	yellowish brown	148	48
$ZrCl_4$	25	16	colorless	180	80
$SbCl_5$	55	0	yellowish brown	178	78
$SnBr_4$	50	0	orange	157	57

It might be concluded that a regeneration of **1** in the reaction system is possible, when tin tetrachloride is added subsequently to the formation of **4** and **3** in the reaction of **1** with **2**. It might be expected that a reaction of **1** with cyclohexanone oxime–tin tetrachloride complex (**6**) affords **5b** and **1**.

Treatment of **2** with 1/2 equiv. of tin tetrachloride in ethylene dichloride gave cyclohexanone oxime–tin tetrachloride complex (2: 1 in molar ratio, **6**), which was confirmed by elemental analysis and infrared spectrum. Since this was the first example of complexes of oximes with tin tetrachloride, several other oximes were treated in a similar way with tin tetrachloride. The results are summarized in Table 2. All complexes (**7**—**11**) synthesized consist of two oximes and one tin tetrachloride in molar ratio.

When **6** was treated with 1 equiv. of 3,4,5,6-tetrahydro-2*H*-azepin-7-ol hydrogen sulfate (**1**) in ethylene dichloride at room temperature, a slight exothermic reaction occurred, **5b** being obtained as a crystalline

Table 2. Oxime–tin tetrachloride complexes

Complex	Yield %	Mp °C	Formula	Anal %	Calcd	Found
6	97	170(dec.)	$(C_6H_{11}NO)_2SnCl_4$	C	29.57	29.60
				H	4.52	4.47
				N	5.75	5.93
7	89	169—170	$(C_5H_9NO)_2SnCl_4$	C	26.16	26.23
				H	3.92	3.97
				N	6.10	6.02
8	96	217—219	$(C_3H_7NO)_2SnCl_4$	C	17.70	17.83
				H	3.44	3.40
				N	6.88	6.76
9	96	139.5—140	$(C_8H_9NO)_2SnCl_4$	C	36.16	35.08
				H	3.39	3.38
				N	5.27	5.21
10	85	161—163	$(C_7H_{13}NO)_2SnCl_4$	C	32.68	32.81
				H	5.06	4.93
				N	5.45	5.46
11	72	144.5—145.5	$(C_{12}H_{23}NO)_2SnCl_4$	C	43.71	44.00
				H	7.03	6.99
				N	4.28	4.29

4) The oxime hydrogen sulfate decomposed when heated in the presence of 1 equiv. of ε-caprolactam, giving an intractable mixture consisting of more than at least three components. A similar decomposition also took place when substances having amide function were used in place of ε-caprolactam.

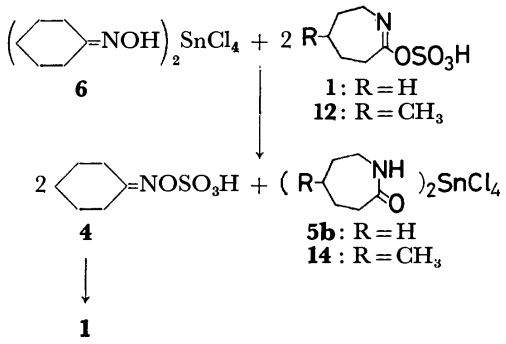

Scheme 1

precipitate in 65% yield. Hydrolysis and neutralization of products in the solution afforded **3** in 113% yield based on **1**, showing the presence of more than 13% yield of **5b** in the solution. The reaction can be summarized as in Scheme 1.

Although oximes are known to be transformed into amides or lactams by means of Lewis acid,[5] such a rearrangement requires more drastic conditions. Control experiments showed that the starting material was recovered when the oxime complex was heated under reflux in ethylene dichloride alone or in the presence of excess tin tetrachloride. We were able to isolate a reaction intermediate, the oxime hydrogen sulfate derived from the oxime complex.

When a reaction of 4-methyl-3,4,5,6-tetrahydro-2*H*-azepin-7-ol hydrogen sulfate (**12**) with cyclohexanone oxime-tin tetrachloride complex (**6**) in ethylene dichloride below 5 °C was followed by treatment with imidazole, 4-methyl-ε-caprolactam (**13**) and imidazole salt of cyclohexanone oxime hydrogen sulfate were obtained in 87 and 62% yields, respectively.

When the reaction mixture resulting from the reaction of **1** and 1 equiv. of **6** (Scheme 1) was further treated with 1 equiv. of **6**, a slight exothermic reaction occurred and **5a** was obtained as a crystalline precipitate in 85% yield based upon **6**. The regeneration of **1** in the reaction mixture was thus confirmed.

Experimental

Concentration and evaporation were carried out with a rotary evaporator under reduced pressure. All melting points were determined in a liquid bath, and are uncorrected unless otherwise stated. Solvents were used after drying and distillation.

Materials. Complexes of ε-caprolactam with zinc chloride (**5a**),[6] tin tetrachloride (**5b**),[6] boron trifluoride (**5c**),[7] cadmium chloride (**5d**),[8] mercuric chloride (**5e**),[8] ferric chloride (**5f**),[8] and zirconium tetrachloride (**5g**)[8] were prepared by known methods. The suspension of cyclohexanone oxime hydrogen sulfate (**4**) in ethylene dichloride was prepared by a reaction of cyclohexanone oxime with sulfur trioxide–1,4-dioxane complex.[2] The solution of 3,4,5,6-tetrahydro-2*H*-azepin-7-ol hydrogen sulfate (**1**) in ethylene dichloride was prepared by two methods.[1]

ε-Caprolactam–Antimony Pentachloride Complex. The reaction of **3** with antimony pentachloride in methylene chloride has been reported by Rothe *et al.*[7a] to give ε-caprolactam–antimony pentachloride complex (3:2 in molar ratio). However, we obtained two complexes (2:1 and 1:1).

Complex (1: 1, 5h): A solution of **3** (2.71 g, 24 mmol) in ethylene dichloride (30 ml) was added dropwise to a solution of antimony pentachloride (7.18 g, 24 mmol) in ethylene dichloride (20 ml) with stirring below 0 °C. Crystals formed were collected by filtration. Yield 2.81 g (28%). Mp 135—145 °C (on a hot plate). Found: Cl, 42.72%. Calcd for $C_6H_{11}NO \cdot SbCl_5$: Cl, 43.01%.

The filtrate was concentrated and the residue was treated with benzene to give 4.2 g of crystals, whose infrared spectrum was identical with that of crystals obtained above. Total yield 70%.

Complex (2: 1, 5i): A solution of antimony pentachloride (7.17 g, 24 mmol) in ethylene dichloride (20 ml) was added to a solution of **3** (5.42 g, 48 mmol) in ethylene dichloride with stirring below −5 °C. The mixture was stirred at room temperature for 1 hr and filtered to give crystals. Yield 5.69 g (45%). Found: C, 27.33; H, 4.25; N, 5.21; Cl, 33.96%. Calcd for $C_{12}H_{22}N_2O_2 \cdot SbCl_5$: C, 27.43; H, 4.23; N, 5.33; Cl, 33.74%.

The filtrate was concentrated and the residue was treated with ethyl acetate to give 5.43 g of crystals, whose infrared spectrum was identical with that of crystals obtained above. Total yield 87%.

ε-Caprolactam–Tin Tetrabromide Complex (5j). A solution of tin tetrabromide (65.7 g, 0.15 mol) in ethylene dichloride (70 ml) was added dropwise to a solution of **3** (34 g, 0.3 mol) in ethylene dichloride with stirring under ice cooling. The mixture was stirred for 2 hr at room temperature and filtered to afford crystals. Yield 80.8 g (81%). Mp 145—146.5 °C. Found: C, 21.51; H, 3.16; N, 4.09; Br, 48.07%. Calcd for $C_{12}H_{22}N_2O_2 \cdot SnBr_4$: C, 21.67; H, 3.31; N, 4.21; Br, 48.11%.

Rearrangement of Cyclohexanone Oxime Hydrogen Sulfate (4).

a) In the Presence of ε-Caprolactam–Zinc Chloride Complex (5a): A solution of **5a** (8.7 g, 24 mmol) in ethylene dichloride (20 ml) was added dropwise to a suspension of **4** (48 mmol) in ethylene dichloride (70 ml) with stirring below −5.5 °C. The mixture was stirred at room temperature until dissolution, and then heated gradually to 64 °C. Stirring was continued for 1 hr, during which the temperature fell gradually to room temperature. The mixture was treated with water (20 ml) and then with aqueous ammonia (28%, 20 ml) under ice cooling, and concentrated. The residue was dissolved in water (50 ml) and extracted with chloroform (50 ml × 5). The combined extracts were dried over anhydrous sodium sulfate and concentrated to dryness, giving 8.24 g of **3**. The yield was 152% based upon the lactam complex.

b) In the Presence of ε-Caprolactam–Tin Tetrachloride Complex (5b): The complex (**5b**, 11.7 g, 24 mmol) was added to a suspension of **4** (48 mmol) in ethylene dichloride (80 ml) at room temperature. When the mixture was gradually heated to 48 °C, the temperature of the mixture rose to 65 °C. The resulting mixture was stirred at room temperature overnight, and then filtered to give colorless crystals which were identified by infrared spectrum as **5b**. Yield 7.15 g (61%). The filtrate was concentrated and the residue

5) C. R. Hanser and D. S. Hoffenberg, *J. Org. Chem.*, **20**, 1482 (1955).

6) Inventa AG, Swiss 326165 (1958).

7) a) M. Rothe, G. Reinisch, W. Jaeger, and I. Schopov, *Makromol. Chem.*, **54**, 183 (1962); *b*) J. Duynstee, W. van Raayen, J. Smidt, and Th. A. Veerkamp, *Rec. Trav. Chim. Pays-Bas.*, **80**, 1323 (1961).

8) K. Sturzer, *Z. Naturforsch.*, **17b**, 197 (1962).

9) L. Giuffre, G. Sioli, and E. Losio, *Chim. Ind.* (Milan), **50**, 983 (1968).

10) A.F. Turbak, *Ind. Eng., Chem. Prod. Res. Develop.*, **7**, 190 (1968).

was treated with water (50 ml), neutralized with aqueous ammonia under ice cooling, and evaporated to about half in volume. Tetrahydrofuran (50 ml) was added to the residual mixture and the gelatinous precipitate was removed by filtration and washed with tetrahydrofuran. The combined filtrate and washing were concentrated and the residue was dissolved in water (40 ml) and extracted with chloroform (40 ml×5). The combined extracts were dried over anhydrous sodium sulfate and concentrated to dryness, giving 7 g of **3**. Yield 129%. Total yield of **3** was 190% based upon **5b**.

c) In the Presence of Complexes of ε-Caprolactam with Boron Trifluoride, Cadmium Chloride, Mercuric Chloride, Ferric Chloride, Zirconium Tetrachloride, Antimony Pentachloride, or Tin Tetrabromide (5c—h, or 5j): Twenty four mmol of **5c**, **5d**, **5e**, **5f**, **5g** or **5j**, or 48 mmol of **5h** as crystals or a solution in ethylene dichloride was added with stirring to a suspension of **4** (48 mmol) in ethylene dichloride (80 ml) below −10 °C. The mixture was stirred for 20—60 min, during which time the temperature returned gradually to room temperature. The mixture was then slowly heated to the temperature given in Table 1, when an exothermic phenomenon was observed, the temperature of the reaction mixture being raised by degrees. After stirring for 2 hr at room temperature, the mixture was concentrated and the residue was treated with water (50 ml), neutralized with aqueous ammonia and treated with methanol (50 ml). The gelatinous precipitate was filtered and washed with methanol. The combined filtrate and washing were concentrated and the residue was dissolved in water (40 ml) and extracted with chloroform (50 ml×5). The combined extracts were dried over anhydrous sodium sulfate and concentrated to give **3**. A ratio of conversion of **4** into **1** was calculated by subtraction of the theoretical yield 5.42 g of **3** based on **5c—h**, or **5j** from the yield of **3** obtained from the extraction. The results are summarized in Table 1.

Cyclohexanone Oxime–Tin Tetrachloride Complex (6). To a solution of cyclohexanone oxime (**2**) (11.3 g, 100 mmol) in ethylene dichloride (50 ml) was added dropwise a solution of tin tetrachloride (13.0 g, 50 mmol) in ethylene dichloride (20 ml) with stirring below 10 °C. A colorless precipitate was soon formed. After being left to stand overnight, the mixture was filtered to give 23.7 g of colorless crystals. The results are given in Table 2.

Cyclopentanone Oxime–Tin Tetrachloride Complex (7). To a solution of cyclopentanone oxime (9.9 g, 100 mmol) in ethylene dichloride (50 ml) was added dropwise a solution of tin tetrachloride (13.0 g, 50 mmol) in ethylene dichloride (20 ml) with stirring below 10 °C. The mixture was stirred for 2 hr at room temperature and concentrated. Ethyl acetate (50 ml) was added to the sirupy residue and the resulting solution was allowed to stand at room temperature to give 20.1 g of colorless crystals. The results are given in Table 2.

Tin Tetrachloride Complex with Acetoxime (8), Acetophenone Oxime (9), and 4-Methylcyclohexanone Oxime (10). The complexes were synthesized as in the case of **6** (Table 2).

Cyclododecanone Oxime–Tin Tetrachloride Complex (11). This was synthesized as in the case of **7** (Table 2).

Reaction of 3,4,5,6-Tetrahydro-2H-azepin-7-ol Hydrogen Sulfate (1) with 1 Equiv. of Cyclohexanone Oxime–Tin Tetrachloride Complex (6). **6** (11.7 g, 24 mmol) was added to a solution of **1** (48 mmol) in ethylene dichloride (80 ml) with stirring at room temperature. The temperature of the mixture rose above *ca.* 2—3 °C, a homogeneous solution being formed within 20 min. Stirring was continued for approximately 90 min after the addition of the complex, when the temperature began to fall, the solution becoming turbid, and a precipitate formed gradually. After being allowed to stand at room temperature overnight, the mixture was filtered to give 7.6 g of colorless crystals, which were identified by infrared spectrum as ε-caprolactam–tin tetrachloride complex (**5b**). The yield based on the used oxime complex (**6**) was 65%. The filtrate was concentrated and the residue was dissolved in water, neutralized with ammonia, and extracted with chloroform to afford 6.5 g of **3**.

Reaction of 3,4,5,6-Tetrahydro-2H-azepin-7-ol Hydrogen Sulfate (1) with 2 Equiv. of Cyclohexanone Oxime–Tin Tetrachloride Complex (6). **6** (11.7 g, 24 mmol) was added to a solution of **1** (48 mmol) in ethylene dichloride (100 ml) with stirring at room temperature. The mixture rose by 2—3 °C, and became homogeneous within *ca.* 20 min. 90 min after addition of the complex, the temperature began to fall. **6** (11.7 g, 24 mmol) was again added to the mixture and stirring was continued. The reaction mixture rose 2—3 °C above room temperature. It was stirred overnight at room temperature, and then filtered to give 20.0 g of colorless crystals, which were identified by infrared spectrum as lactam complex (**5b**). The yield based upon the added oxime complex was 85%. The filtrate was treated as in the case of the reaction described above, 5.8 g of **3** being obtained.

Reaction of 4-Methyl-3,4,5,6-tetrahydro-2H-azepin-7-ol Hydrogen Sulfate (12) with Cyclohexanone Oxime–Tin Tetrachloride Complex (6): **6** (11.7 g, 24 mmol) was added with stirring at −10 °C to a solution of **12** (48 mmol) in ethylene dichloride (80 ml), prepared by the reaction of 4-methyl-ε-caprolactam (6.10 g, 48 mmol) and sulfur trioxide (2 ml, 48 mmol). The temperature of the mixture rose to −3 °C. The resulting suspension was stirred at 5 °C for approximately 1.5 hr, when it became a clear solution. This was cooled to −10 °C, and a solution of imidazole (6.5 g, 96 mmol) in chloroform (50 ml) was added dropwise. Stirring was continued, and the mixture was allowed to gradually return to room temperature. The colorless solid formed after the imidazole addition turned into an oily matter with temperature rise. After stirring at room temperature for 30 min the mixture was concentrated to remove ethylene dichloride and chloroform. To the oily residue was added tetrahydrofuran (100 ml) and the precipitated colorless solid was collected by filtration. The precipitate was hygroscopic. It was confirmed by infrared spectrum to be a mixture of imidazole salt of **1** and imidazole–tin tetrachloride complex. The mixture was added to acetonitrile (60 ml) and stirred at room temperature, in order to dissolve the imidazole salt of **1**. The insoluble imidazole–tin tetrachloride complex was separated by filtration. The filtrated cake weighed 5.8 g. The acetonitrile filtrate was concentrated to afford 7.8 g of imidazole salt of **1**, whose infrared spectrum was identical with that of the authentic specimen.[2] The yield based upon the added oxime complex (**6**) was 62%.

The tetrahydrofuran filtrate separated from the above colorless solid was concentrated, and the residue was treated with water (50 ml) and neutralized with aqueous ammonia under ice cooling. After a gelatinous precipitate was removed by filtration and washed with tetrahydrofuran, the combined filtrate and washing were concentrated. The residue was dissolved in 50 ml of water and extracted with chloroform (50 ml×5). The combined extracts were dried and concentrated to give 5.3 g of 4-methyl-ε-caprolactam. The yield based upon the employed 4-methyl-3,4,5,6-tetrahydro-2*H*-azepin-7-ol hydrogen sulfate (**12**) was 87%.

Attempted Thermal Rearrangement of Cyclohexanone Oxime–Tin Tetrachloride Complex (6). *a)* A suspension of **6** (2 g, 4.1 mmol) in ethylene dichloride (40 ml) was heated at

reflux temperature for 1.5 hr. The starting material **6** (1.9 g) was recovered in 95% yield.

b) To a suspension of **6** (10 g, 20.5 mmol) in ethylene dichloride (100 ml) was added tin tetrachloride (5.35 g, 20.5 mmol) and the mixture was heated at reflux temperature for 7.5 hr. After the mixture returned to room temperature the precipitate was collected by filtration. 8.6 g of **6** was recovered.

BULLETIN OF THE CHEMICAL SOCIETY OF JAPAN, VOL. 46, 3183—3187 (1973)

The Synthesis and the Absolute Configurations of Lilac Alcohols, New Naturally Occurring Odorous Ingredients of Lilac Flower

Seiji WAKAYAMA, Satoshi NAMBA, Kazuo HOSOI,* and Masaji OHNO*

Chemical Laboratory, Hokkaido University of Education, Sapporo 060

**Basic Research Laboratories, Toray Industries, Inc., Kamakura 248*

(Received July 18, 1972)

The conversion of racemic linalyl acetate to racemic lilac alcohols has been completed in 5 steps and four diastereoisomers of β,5-dimethyl-5-vinyl-2-tetrahydrofuranethanol were obtained. *d*-Lilac alcohols were also synthesized from *d*-linalyl acetate and confirmed to be identical with natural ones. The absolute configurations of lilac alcohol-a, -b, -c, and -d were respectively shown to be (β*S*, 2*S*, 5*S*), (β*R*, 2*S*, 5*S*), (β*R*, 2*R*, 5*S*), and (β*S*, 2*R*, 5*S*) by the chemical and physical evidences.

In previous papers,[1,2] it has been reported that four new terpene alcohols with exquisite floral fragrance have been isolated from the flower of lilac, *Syringa vulgaris* L. They have been named lilac alcohol-a, -b, -c, and -d according to decreasing order of the relative abundance and the diastereomers of β,5-dimethyl-5-vinyl-2-tetrahydrofuranethanol (I) were assigned as the structures of lilac alcohol-a and -b. It was soon confirmed by spectroscopic evidence that lilac alcohol-c and -d are also diastereomers of (I). (*cf.* Table 1).

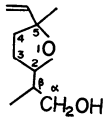

I

TABLE 1. CHARACTERIZATION OF LILAC ALCOHOLS

Lilac alcohol	a	b	c	d
Relative abundance	9.7	3.5	2.5	1
R_t[a] (min)	17.8	13.4	20.8	14.8
$[\alpha]_D^{21}$(natural)	+12.2	−6.6	−1.4	+4.3
$[\alpha]_D^{25}$(from *d*-II)	+ 6.7	−1.4	−0.5	+1.4
$[\alpha]_D^{25}$(from *l*-II)	−11.6	+3.0	+2.5	−2.9

a) Gas chromatographic analyses were carried out at 120 °C with a 3mm×3m column packed with 20% DEGS on Chromosorb W using JEOL GC-750.

Therefore, the lilac flower oil contains interestingly all diastereomers expected from the structure (I), but their extremely low yield from natural flower oil (-c and -d) made it difficult to investigate their stereochemical relationships. In this paper we wish to report the synthesis of lilac alcohols from linalyl acetate and their absolute configurations.[3]

Synthesis of Lilac Alcohols and the Absolute Configurations at C-2 and C-5. Four diastereomers of β,5-dimethyl-5-vinyl-2-tetrahydrofuranethanol (I) were obtained from racemic linalyl acetate in the following manner (Chart 1).

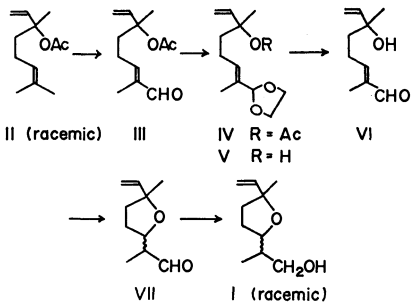

Chart 1.

Racemic linalyl acetate (II) was treated with selenium dioxide to afford α,β-unsaturated aldehyde (III) in 40% yield. Treatment of (III) with ethylene glycol in the presence of *p*-toluenesulfonic acid in benzene gave ethylene acetal (IV) which was hydrolysed with a 5% solution of sodium hydroxide to afford V. When the elution chromatography of V was carried out through a silica gel column, the ethylene acetal group underwent easy hydrolysis to afford VI (77% overall yield from III).[4] The direct hydrolysis of III afforded VI in only 6% yield along with VII. The intramolecular Michael addition of the tertiary alcohol to the α,β-

1) S. Wakayama, S. Namba, and M. Ohno, *Nippon Kagaku Zasshi*, **92**, 256 (1971).

2) S. Wakayama, S. Namba, and M. Ohno, This Bulletin, **43**, 3319 (1970).

3) S. Wakayama, S. Namba, K. Hosoi, and M. Ohno, *ibid.*, **44**, 875 (1971).

4) During the course of our synthetic work on lilac alcohols from linalyl acetate, Naegeli and Weber published the use of the aldehyde III as an intermediate to davanone synthesis. P. Naegeli and G. Weber, *Tetrahedron Lett.*, **1970**, 959.

unsaturated aldehyde was effected with triethylamine to give a tetrahydrofuran derivative VII in 43% yield. Reduction of VII with $LiAlH_4$ afforded a mixture of four diastereomers of racemic lilac alcohol in 75% yield. From the mixture, each diastereomer was cleanly separated and purified by vapor phase chromatography. The relative concentration of the synthetic lilac alcohol-a, -b, -c, and -d was 2.0, 3.0, 2.5, and 1.0, respectively. The identity of the synthetic lilac alcohols with natural ones was confirmed by IR, NMR, and R_t (vpc) except for the optical activity.

In order to establish the absolute configuration of natural lilac alcohols, *d*-linalyl acetate[5] (*d*-II, $[\alpha]_D^{25}$ +2.9) and *l*-linalyl acetate (*l*-II, $[\alpha]_D^{25}$ −5.0) were separately converted into the corresponding lilac alcohols in the manner described above for the racemic case. Although these starting materials were not optically pure, they proved to be pure enough for the diagnostic purpose of the absolute configuration.

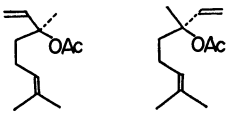

d-II l-II

Thus, the physical properties of *d*-lilac alcohol-a, -b, -c, and -d derived from *d*-II were found to be consistent with the data obtained from the natural alcohols, as shown in Table 1.

Stereochemistry of the Tetrahydrofuran Ring. In a previous paper[2] lilac alcohol-a and -b and racemic *trans*-linalool oxide[6-8] (VIII) were converted into the same derivative (X).

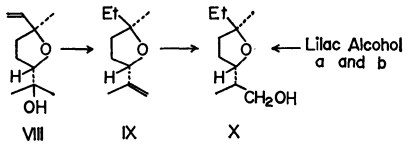

VIII IX X

Therefore, the stereochemitry of lilac alcohol-a and -b was clearly shown to be *trans* as for the tetrahydrofuran ring, and also concluding that the stereochemistry of lilac alcohol-c and -d must be *cis* as for the tetrahydrofuran ring.

Furthermore, since the absolute configuration of *d*-linalool[9] is known, it follows from the above results that the absolute configurations at C-2 and C-5 of lilac alcohol-a, -b, -c, and -d are (2*S*, 5*S*), (2*S*, 5*S*), (2*R*, 5*S*), and (2*R*, 5*S*), respectively.

Configurations at C-2 and C-β. The NMR spectra

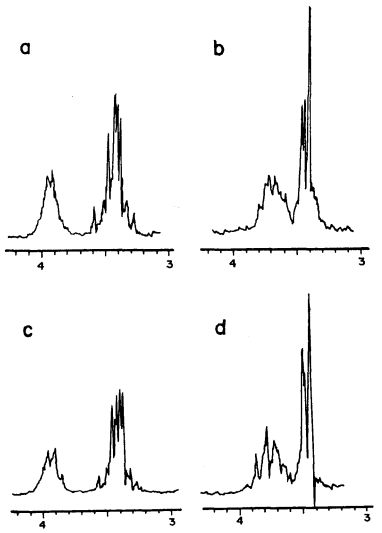

Fig. 1. The signal patterns of $-CH_2OH$ group.

of lilac alcohols are very similar to one another except for the signal of the carbinol methylene shown in Fig. 1.

Lilac alcohol-a and -c show common patterns (ABX type) regarding the methylene signal of the CH_2OH group, while lilac alcohol-b and -d show another common signal for the same group. This fact suggests that the former pair and the latter pair have respectively the same configurations at C-2 and C-β, and it was considered that such configurational problem might be solved by the study of intramolecular hydrogen bonding between the hydroxyl group and the ether oxygen, as seen in the formula of *threo* isomer, for example.

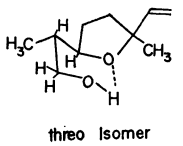

threo Isomer

Therefore, we determined the relative extent of hydrogen bonding[10,12,13] in the diastereomeric lilac alcohol-a, -b, -c, and -d by (1) measuring the hydroxyl absorption of their IR spectra in high dilution and (2) observing the dilution shift of the hydroxyl proton in the NMR spectrum of each isomer. In addition, we examined in detail the coupling constants (half-height width), $J_{2,\beta}$, since the magnitude of the vicinal proton coupling constant $J_{2,\beta}$ is a measure of the relative population of the various conformations.[10] Consideration of non-bonded interactions and intramolecular hydrogen bonding between the hydroxyl group and the ether oxygen in the rotational isomers of *threo* lilac alcohols[11] suggests that conformer A would be more stable than B or C (Chart 2). Similar consideration suggests that conformer E and F of the *erythro* isomer would be more stable than D.

5) *d*-Linalyl acetate was synthesized from *d*-linalool (coriabder oil). The oil and *l*-linalyl acetate were supplied by Takasago Perfumery Co., Ltd., Japan.

6) This compound is a mixture of equal amount of (2*R*, 5*R*)- and (2*S*, 5*S*)-configuration.

7) D. Felix, A. Melera, J. Seibe, and E. Sz. Kovatz, *Helv. Chim. Acta*, **46**, 1513 (1963); *ibid.*, **47**, 918 (1964).

8) E. Klein, H. Farnow, and W. Rojahn, *Ann. Chem.*, **675**, 73 (1964).

9) R. H. Cornforth, J. W. Cornforth, and V. Prelog, *ibid.*, **634**, 197 (1960).

10) K. D. Carlson, D. Weisleder, and M. E. Daxenbichler, *J. Amer. Chem. Soc.*, **92**, 6232 (1970), and references contained therein.

11) In the case of lilac alcohol, the ether oxygen and the hydroxy methylene group, and the ring methylene and methyl group are taken as the like groups, respectively.

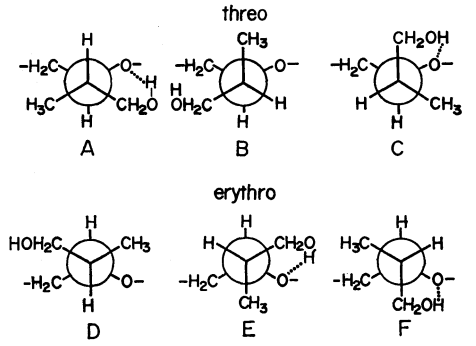

Chart 2. Staggered rotational isomers of the diastereoisomeric lilac alcohols*
(*Only one enantiomer is shown in each case.)

Infrared Study: Hydroxyl bands in the 3600 cm^{-1} region in the IR spectra of lilac alcohols were examined in carbon tetrachloride (0.005—0.025 M). At concentrations lower than 0.025 M, each alcohol shows two OH bands independent of concentration, which are assigned to free (3634—3640 cm^{-1}) and intramolecularly bonded (3520—3525 cm^{-1}) hydroxyl groups, showing that intermolecular hydrogen bonding is negligible in these concentrations. Table 2 shows

Table 2. Infrared data for lilac alcohols

Lilac alcohol	ν OH (free, cm^{-1})	ν OH (bonded, cm^{-1})	$\Delta\nu$ (cm^{-1})	Ratio of integrated band intensity (bonded/free)
a	3638	3525	113	5
b	3640	3520	120	12
c	3634	3522	112	4
d	3640	3520	120	14

that lilac alcohol-b and -d exhibit a longer frequency shift, $\Delta\nu$, than lilac alcohol-a and -c, and the former isomers have most significantly a clearly larger ratio of the integrated band intensity of bonded and free hydroxyl bands than that of the latter isomers. Therefore, lilac alcohol-b and -d should have a much more populous hydrogen bonded conformation than lilac alcohol-a and -c. From this evidence, it was assumed that lilac alcohol-b and -d have the *threo* configuration and -a and -c have the *erythro* configuration. In the latter case, conformers E and F may be composed to the similar order as acyclic analog, 3-methoxypropanol[12] $CH_3OCH_2CH_2CH_2OH$, and in the former case conformer A may be most stable owing to not only the nonbonded interaction but also the intramolecular hydrogen bonding.

NMR Studies: NMR spectra (100 MHz) of the alcohols were obtained in carbon tetrachloride. In Fig. 2, the chemical shift of each hydroxyl proton (tetramethylsilane as an internal standard) is plotted as a function of concentration of lilac alcohols. The smaller limiting slope of the lilac alcohol-b and -d compared with lilac alcohol-a and -c is consistent with stronger bonding[13,14] as confirmed by our IR studies.

12) A. B. Foster, A. H. Haines, and N. Stacey, *Tetrahedron*, **16**, 177 (1961).

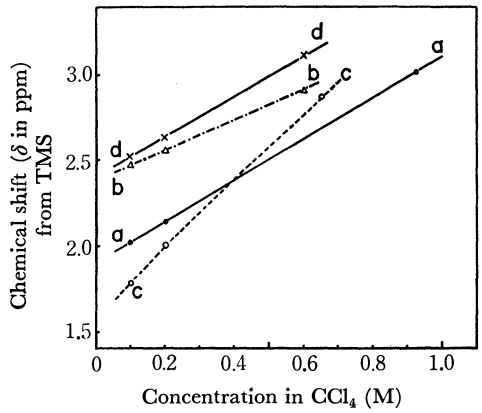

Fig. 2. Hydroxy proton chemical shift dependence on concentration of Lilac alcohols in CCl_4.

The -b and -d isomers have the larger limiting chemical shift for the hydroxyl proton. Thus, it was tentatively proposed to assign the *erythro* configuration to lilac alcohol-a and -c, and the *threo* configuration to lilac alcohol-b and -d.

If this conclusion is reasonable, *threo* isomers should have a larger vicinal coupling constant ($J_{2,\beta}$) than *erythro* isomers, because the coupling of the hydrogen at C-2 of *threo* and *erythro* isomers to the neighboring methylene group in the ring is considered to be the same order, but the coupling to the hydrogen at C-β should be stronger in *threo* configuration (anti conformation). In the *erythro* configuration, the contribution of conformer E and F seems to be larger than D to decrease the proton dihedral angle ($\phi_{2,\beta}$) of the averaged conformers (*gauche* conformation) or causing a smaller coupling constant than that of conformer A. The magnitudes of the vicinal coupling constants, $J_{2,\beta}$, are obtained as half-height width (Table 3), clearly showing as expected that lilac alcohol-b and -d have the larger coupling constants than those of lilac alcohol-a and -c.

Table 3. Half-height width of the vicinal coupling constants ($J_{2,\beta}$)

Lilac alcohol	Half-height width of >CH–O– (Hz)
a	13
b	22
c	15
d	22

All of the spectroscopic evidences obtained above consistently support the view that lilac alcohol-a and -c have *erythro* configuration and lilac alcohol-b and -d have *threo* configuration.

Both chemical and physical evidences indicate that the absolute configurations of lilac alcohol-a, -b, -c, and -d are (βS, 2*S*, 5*S*), (βR, 2*S*, 5*S*), (βR, 2*R*, 5*S*), and (βS, 2*R*, 5*S*), respectively.

13) R. J. Ouellette, K. Liptak, and G. E. Booth, *J. Org. Chem.*, **32**, 2394 (1967).

14) C. J. Cheer and C. R. Johnson, *J. Amer. Chem. Soc.*, **90**, 178 (1968).

Experimental

General Methods. The IR spectra were measured with a Hitachi EPI S-2 IR spectrophotometer and hydroxyl absorption bands in the 3600 cm^{-1} region in the IR spectra of lilac alcohols were examined in carbon tetrachloride (0.005—0.025 M), using Perkin-Elmer Model 125 infrared grating spectrophotometer. A 5.0 cm sodium chloride cell was used for the carbon tetrachloride solutions and the temperature of the measurements was about 25 °C. Spectrograde carbon tetrachloride was used directly after passing a molecular sieve column.

The NMR spectra were recorded on a Varian Associates HA-100 instrument and chemical shifts (δ) are given relative to internal tetramethylsilane standard.

The optical rotations were mersured on a Carl Zeiss photoelectric polarimeter in chloroform.

2,6-Dimethyl-6-acetoxy-2,7-octadienal (III): Linalyl acetate (II, 39.2 g, 0.2 mol) and selenium dioxide (22.2 g, 0.2 mol) were dissolved in 100 ml of 90% dioxane and the solution was heated at 80 °C for 5 hr. After removal of selenium deposited by filtration, the solvent was removed under a reduced pressure. The residue was treated with 100 ml of a mixed solvent of ether and petroleum ether (1: 1). The organic layer was separated by decantation. The solvent was removed and the residue was subjected to vacuum distillation (bp 113—115 °C/1.3 mmHg), affording 16 g (38% yield) of 2,6-dimethyl-6-acetoxy-2,7-octadienal (III).

Vpc: R_t 15.5 min (PEG 20 M, 180 °C, 3 mm×2 m, He 30 ml/min)

IR: ν_{max} 2720, 1735, 1685, 1640, 1365, 1245, 1170, 1105, 1020, 930 cm^{-1}.

NMR: 1.57 (*t*-Me, s), 1.73 (CH_3-C=C, d J=0.7 Hz), 1.98 (CH_3COO, s), 5.12, 5.16, 5.96 (-HC=CH_2), 6.49 (-HC=C-), 9.38 δ (CHO).

Found: C, 68.53; H, 8.58%. Calcd for $C_{12}H_{18}O_3$: C, 68.54; H, 8.63%.

6-Hydroxy-2,6-dimethyl-2,7-octadienal (VI): 2,6-Dimethyl-6-acetoxy-2,7-octadienal (III, 6.3 g, 0.03 mol), ethylene glycol (2.1 g, 0.033 mol), and *p*-toluenesulfonic acid (0.05 g) were dissolved in 100 ml of dry benzene, and the solution was refluxed for about 3 hr until 0.9 ml of water was removed, using a moisture collector. The solvent was removed under a reduced pressure and the residue was treated with 40 ml of 5% sodium hydroxide solution in aqueous methanol (75%) for 1 hr at room temperature. After removal of methanol, the residue was extracted with ether, and the ethereal solution was dried over anhydrous sodium sulfate. The solvent was removed and the residue was subjected to silica gel chromatography, using chloroform as an eluent. 6-Hydroxy-2,6-dimethyl-2,7-octadienal (VI) (3.9 g, 77% yield) was obtained, showing that the ethylene acetal group was hydrolysed during the chromatography.

Vpc: R_t, 12.1 min (PEG 20 M, 180 °C, 3 mm×2 m, He 30 ml/min)

IR: ν_{max} 3420 (OH), 2720 (CHO), 1680 (CHO), 1640 (C=C)cm^{-1}.

NMR: ($CDCl_3$) 1.32 (*t*-Me, s); 1.73 (CH_3-C=C); 5.01, 5.25, 5.93 (-CH=CH_2); 6.50 (-C=C-H), 9.31 δ (CHO).

Found: C, 71.21; H, 9.63%. Calcd for $C_{10}H_{16}O_2$: C, 71.39; H, 9.59%.

2-(1-Formylethyl)-5-methyl-5-vinyltetrahydrofuran (VII): The hydroxyaldehyde (VI, 1.0 g) dissolved in 10 ml of methanol was treated with a catalytic amount of triethylamine under nitrogen atmosphere at 50 °C for 5 hr.

After removal of the solvent, the residue was subjected to silica gel chromatography. The fractions eluted with a mixed eluent of petroleum ether and ether (20: 1) afforded 0.23 g of VII and 0.7 g of the starting hydroxyaldehyde (VI) was recovered from the fractions eluted with methylene chloride–ether (10: 1). The recovered material was subjected to the same procedure for the intramolecular Michael reaction, giving 0.20 g of VII. The total yield was 43%.

Vpc: R_t 2.65 and 2.90 min (2: 1).

IR: ν_{max} 2720, 1720 (CHO), 1640 (C=C), 1040 (-O-) cm^{-1}.

NMR: ($CDCl_3$) 1.26 (*t*-Me, s); 4.07, 5.00, 5.76 (-CH=CH_2); 9.70 δ (CHO).

The analytical sample was purified by vacuum distillation, bp 99—101 °C/23 mmHg.

Found: C, 71.53; H, 9.48%. Calcd for $C_{10}H_{16}O_2$: C, 71.53; H, 9.59%.

Lilac Alcohols (I): The cyclic aldehyde (VII, 1.17 g) was dissolved in 20 ml of dry ether and 0.4 g of lithium aluminum hydride was added in small portions. After stirring at room temperature for 30 min followed by decomposition of the excess lithium aluminum hydride with water, the reaction mixture was acidified with 1M sulfuric acid and extracted with a mixed solvent of methylene chloride and ether. The organic layer was dried over sodium sulfate. After removal of the solvent, the residue was subjected to chromatography on alumina. Elution with ether gave 0.88 g (75%) of lilac alcohols, which were shown to be a mixture of four diastereomers and separated by vapor phase chromatography to afford each alcohol in pure state. The relative concentration of the synthetic lilac alcohol-a, -b, -c, and -d was 2.0, 3.0, 2.5, and 1.0, respectively. The identity of the synthetic lilac alcohols with natural ones was confirmed by IR, NMR and R_t (vpc).

Vpc: R_t; 12.3 (b), 13.75 (d), 15.8 (a), 19.1 (c) min. (PEG 20 M, 120 °C, 3 mm×2 m, He 30 ml/min)

IR: ν_{max} 3420 (OH), 1640 (C=C), 1100, 1025 (-O-) cm^{-1}.

NMR: see Fig. 1 and Table 4.

TABLE 4. NMR SPECTRAL DATA (δ in ppm in $CDCl_3$)[a)]

Lilac alcohol		a	b	c	d
s-CH_3		0.94 d	0.80 d	0.93 d	0.78 d
		J=6.0	J=6.0	J=6.0	J=6.0
t-CH_3		1.31 s	1.30 s	1.27 s	1.28 s
-CH_2-CH_2- -C- H CH_3		1.82 m	1.80 m	1.80 m	1.80 m
>C-CH_2OH H		3.66	3.62	3.59	3.60
>C(O-)H		4.12 m	3.80 m	4.10 m	3.78 m
H_3>C=C(H_1)(H_2)	H_1[a)]	4.99	5.01	5.01	5.01
	H_2	5.17	5.19	5.19	5.19
	H_3	5.87	5.89	5.89	5.89

a) The signals of alcohols appear at 2.96—2.60 δ, depending on the concentration, and typical signals of vinyl group are observed with $J_{1,2}$=1.6Hz, $J_{1,3}$=8.0Hz and $J_{2,3}$=18 Hz.

The analytical sample was prepared by vacuum distillation, bp 110—112 °C/18 mmHg.

Found: C, 70.50; H, 10.69%. Calcd for $C_{10}H_{18}O_2$: C, 70.54; H, 10.66%.

d-Lilac alcohols were synthesized from *d*-linalyl acetate with $[\alpha]_D^{25}$ +2.9 (*c* 3.2) according to the same manner as described above and cleanly separated by vpc. The optical rotation was measured in chloroform, showing +6.7 (*c* 2.7), −1.4 (*c* 2.9), −0.5 (*c* 1.6), and +1.4 (*c* 2.8) for *d*-lilac alcohol-a, -b, -c, and -d, respectively.

l-Lilac alcohols were synthesized from *l*-linalyl acetate with $[\alpha]_D^{25}$ −5.0 (*c* 0.8) according to the same manner as described above, and cleanly separated by vpc. The optical rotations were measured in chloroform, showing −11.6 (*c* 1.1), +3.0 (*c* 1.0), +2.5 (*c* 0.8), and −2.9 (*c* 1.0) for *l*-lilac alcohol-a, -b, -c, and -d, respectively. The optical rotations of natural lilac alcohols listed in Table 1 were measured in chloroform, showing +12.2 (*c* 4.1), −6.6 (*c* 3.6), −1.4 (*c* 1.8), and +4.3 (*c* 1.7) for the alcohol-a, -b, -c, and -d, respectively.

BULLETIN OF THE CHEMICAL SOCIETY OF JAPAN, VOL. 46, 3187—3193 (1973)

Synthetic Studies of Bacitracin. VIII.[1] Synthesis of Cyclohexapeptide Moiety[2]

Eisuke MUNEKATA,* Yoshihiro MASUI,* Tetsuo SHIBA, and Takeo KANEKO**
Department of Chemistry, Faculty of Science, Osaka University, Toyonaka, Osaka 560

(Received May 1, 1973)

For the purpose of synthesis of antibiotic bacitracin of six amino acids-membered ring formula, the following intermediate peptides, *i.e.*, cyclo-(N^{α}-benzyloxycarbonyl-L-lysyl-N^{δ}-cyclopentyloxycarbonyl-D-ornithyl-L-isoleucyl-D-phenylalanyl-L-histidyl-α-methyl-L-aspartyl) (III) and N^{α}-benzyloxycarbonyl-N^{ε}-*t*-butyloxycarbonyl-L-lysyl-N^{δ}-cyclopentyloxycarbonyl-D-ornithyl-L-isoleucyl-D-phenylalanyl-N^{im}-benzyl-L-histidyl-L-aspartyl-D-isoasparagine benzyl ester (IV) were prepared. In this synthesis, cyclopentyloxycarbonyl group was introduced to protect δ-amino group of ornithine residue and cleavability of this protecting group for hydrogen fluoride was investigated.

Bacitracin A is an antibiotic peptide produced by *Bacillus licheniformis*.[3] The investigations on the chemical structure of bacitracins were performed by several groups since twenty five years ago.[4,5] Craig and his collaborators had suggested a chemical structure I of six amino acids-membered ring for bacitracin A as the most probable one in 1961.[5] However, Ressler *et al.* later proposed another formula II of seven amino acids-membered ring for the antibiotic.[6] A decisive judgment for a correct structure must be awaited after completion of the total synthesis of this antibiotic peptide unless it is conclusively determined by unobjectionable method like X-ray analysis. In connection with the situation, we attempted to synthesize both of the proposed structures in order to identify with the natural antibiotic.

In our previous papers,[7,8] we prepared a peptide

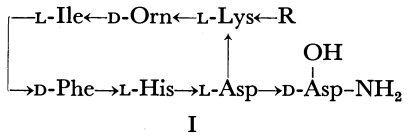

I

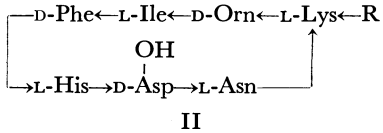

II

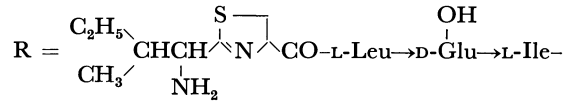

analogue possessing a cysteinyl residue in the place of a thiazoline ring in bacitracin A of Craig's formula I, and demonstrated that it was unable to lead to the compound I through thiazoline ring cyclization from the cysteinyl peptide by the treatment with strong acid such as concentrated hydrochloric acid.[9] Therefore, the ring closure of the cysteine peptide in the final step of a synthetic program must be avoided. On the contrary, it seems most promising to accomplish the synthesis by the condensation of thiazoline moiety corresponding to *N*-terminal peptide with a remaining peptide fragment containing a macrocyclic structure at an appropriate synthetic stage followed by an exhaustive deprotection. We already developed the synthetic method of thiazoline peptides through the coupling of iminoether derivative of *N*-protected amino acids with cysteine ester or cysteinyl peptide.[1,10] This synthetic

* Present address: Peptide Institute, Protein Research Foundation, Minoh, Osaka.
** Present address: Shiseido Laboratory, Nippa-cho, Kohoku-ku, Yokohama.

1) Part VII: Y. Hirotsu, T. Shiba, and T. Kaneko, This Bulletin, **43**, 1870 (1970).
2) This work was presented at the 5th Symposium on Peptide Chemistry, Kyoto, November, 1967 and at the 8th same Symposium, Osaka, November, 1970.
3) B. A. Johnson, H. Anker, and F. L. Meleney, *Science*, **102**, 376 (1945).
4) D. W. Swallow and E. P. Abraham, *Biochem. J.*, **72**, 326 (1959).
5) W. Stoffel and L. C. Craig, *J. Amer. Chem. Soc.*, **83**, 145 (1961).
6) C. Ressler and D. V. Kashelikar, *ibid.*, **88**, 2025 (1966).
7) Y. Ariyoshi, T. Shiba, and T. Kaneko, This Bulletin, **40**, 1709 (1967).
8) Y. Ariyoshi, T. Shiba, and T. Kaneko, *ibid.*, **40**, 2648 (1967).
9) Y. Hirotsu, T. Shiba, and T. Kaneko, *ibid.*, **40**, 2950 (1967).
10) Y. Hirotsu, T. Shiba, and T. Kaneko, *ibid.*, **40**, 2945 (1967).

strategy may also be applied to a synthesis of bacitracin F which is known to be a peptide transformed from bacitracin A *via* oxidative deamination under mild alkaline or neutral condition and possess a keto-thiazole moiety instead of amino-thiazoline in *N*-terminal part of the molecule of bacitracin A.

In this paper, we synthesized hexa- and heptapeptide derivatives corresponding to the ring peptide moiety of the structure I proposed by Craig *et al.*[5] in order to investigate a possibility to elongate these intermediate peptides to the whole structure of bacitracins. However, prior to this synthesis, we must overcome the difficult problem concerned with the selection of protective groups in building up these peptide chains. Particularly, the protection of δ-amino group of D-ornithine residue is in problem, since this protective group must remain throughout the whole synthetic pathway including cyclization of macro-ring as far as the final condensation step on the one hand, and, for the removal of this protection, reaction conditions such as in catalytic hydrogenation, reduction with sodium in liquid ammonia, and saponification, cannot be applied in view of instability of thiazoline or thiazole ring on the other hand. Furthermore, this protective group is also required to be resistant enough for catalytic hydrogenation, hydrazinolysis as well as mild acidolysis, those conditions being needed on a way of making up the cyclic peptide containing ornithine residue. The fact that both thiazoline and thiazole ring are stable under acidic condition, suggests a possible use of anhydrous hydrogen fluoride as reagent for removal of the all protective groups at the final step of the synthesis. These considerations lead us to utilize *s*-alkyloxycarbonyl group for protection of δ-amino group of ornithine residue, since this special protection may resist to the reaction condition mentioned above with the exception of facile cleavability with hydrogen fluoride.

In preliminary tests, *s*-alkyloxycarbonyl groups such as isopropyloxycarbonyl, *s*-butyloxycarbonyl, 1-ethylpropyloxycarbonyl, cyclopentyloxycarbonyl, and cyclohexyloxycarbonyl were introduced into δ-amino group of L-ornithine. The derivatives thus prepared were treated with anhydrous hydrogen fluoride respectively. From the results obtained in the experiments as shown in Table 1, it was demonstrated that cyclopentyloxycarbonyl group was the most suitable for our purpose. Although this protective group had been introduced by McKay and Albertson who used hydrogen bromide in glacial acetic acid as removing agent,[11] its behavior for hydrogen fluoride has not been reported yet.

Table 1. Cleavability of N^{δ}-*s*-alkyloxycarbonyl group of L-ornithine in treatment with hydrogen fluoride

	0 °C 30 min	0 °C 60 min	20 °C 60 min
Isopropyloxycarbonyl		−	−
s-Butyloxycarbonyl		−	−
1-Ethylpropyloxycarbonyl	−	±	+
Cyclopentyloxycarbonyl	±	+	
Cyclohexyloxycarbonyl	−	±	+

+: cleavable −: stable

Using such a special protective group, the hexa- and heptapeptides, *i.e.*, cyclo-(N^{α}-Z-L-lysyl-L-N^{δ}-Poc-D-ornithyl-L-isoleucyl-D-phenylalanyl-L-histidyl-α-methyl-L-aspartyl) (III)[12] and N^{α}-Z-N^{ε}-Boc-L-lysyl-N^{δ}-Poc-D-ornithyl-L-isoleucyl-D-phenylalanyl-N^{im}-benzyl-L-histidyl-L-aspartyl-D-isoasparagine benzyl ester (IV)[12] were prepared.

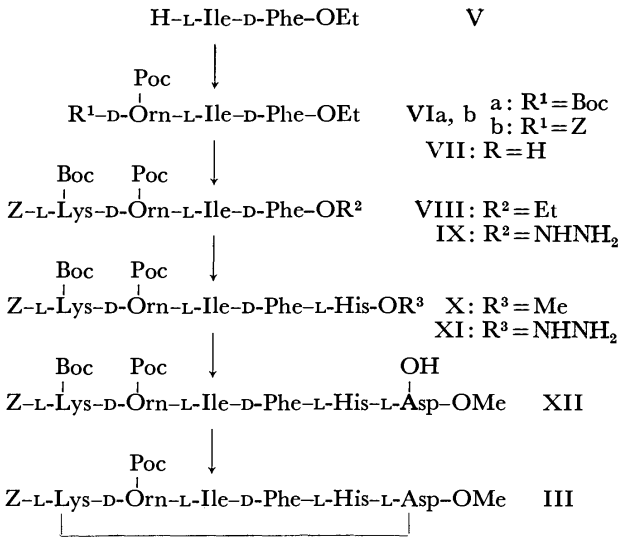

Poc: cyclopentyloxycarbonyl, Boc: *t*-butyloxycarbonyl, Z: benzyloxycarbonyl

Scheme 1.

Thus the synthesis of these peptides was started with the coupling reaction of Z-L-isoleucine with ethyl D-phenylalaninate through the active ester method as shown in Scheme 1. The resulting acyl dipeptide ester was treated with hydrogen bromide in glacial acetic acid to afford V hydrobromide.[7] This compound was coupled with N^{α}-Boc-N^{δ}-Poc-D-ornithine or N^{α}-Z-N^{δ}-Poc-D-ornithine either by the active ester method or by the mixed anhydride method to give two corresponding acyl tripeptide derivatives VIa and VIb respectively. The Boc group was removed from VIa by exposing to hydrogen chloride in ethyl acetate and the Z group of VIb was removed by catalytic hydrogenation in the presence of hydrogen chloride.

The same tripeptide ester VII hydrochloride thus obtained was coupled with N^{α}-Z-N^{ε}-Boc-L-lysine *via* the active ester method to give VIII. This acyl tetrapeptide ester VIII was converted to a corresponding hydrazide IX. The protected tetrapeptide azide prepared from IX was coupled with methyl L-histidinate dihydrochloride to afford acyl pentapeptide ester X. The ester X was converted to the hydrazide XI which was then used for azide coupling reaction with aspartic acid moiety. Thus, removal of Z group from α-methyl Z-L-aspartate was carried out by heating with trifluoroacetic acid applying Weygand's technique[13]

11) F. C. McKay and N. F. Albertson, *J. Amer. Chem. Soc.*, **79**, 4686 (1957).

12) Abbreviations: Z, benzyloxycarbonyl; Poc, cyclopentyloxycarbonyl; Boc, *t*-butyloxycarbonyl.

13) F. Weygand and W. Steglich, *Z. Naturforsch.*, **14b**, 472 (1959).

to give α-methyl L-aspartate trifluoroacetate. This compound was condensed with the azide prepared from the protected pentapeptide hydrazide XI mentioned above in the presence of triethylamine to afford a linear hexapeptide derivative XII. Attempts to obtain the same peptide by stepwise elongation method starting from *C*-terminal side failed, because of difficulty in purification of intermediate tri- or tetrapeptides due to their hygroscopic natures or troublesome tendencies to form gelatinous solid.

After removal of N^{ε}-Boc group of lysine residue in hexapeptide derivative XII obtained above, cyclization between ε-amino group of lysine residue and β-carboxyl group of aspartic acid residue was attempted in high dilution by *p*-nitrophenyl ester method, 1-succinimidyl ester method or carbodiimide method. However no satisfactory results were obtained in all cases. Only when cyanomethyl ester of the hexapeptide XII was tried to be cyclized, expected cyclohexapeptide III was obtained but in an extremely low yield. This cyclic peptide corresponds to macrocyclic part of Craig's formula. However, this cyclohexapeptide methyl ester III was resistant to conversion into a hydrazide which is a necessary intermediate to be coupled with *C*-terminal isoasparagine residue by the azide method. Therefore, we could not extend this synthetic route to reach to the heptapeptide (6—12) of the Craig's formula, and turned our efforts to an alternative way through coupling of the tetrapeptide fragment IX with *C*-terminal tripeptide derivative as shown in Scheme 2.

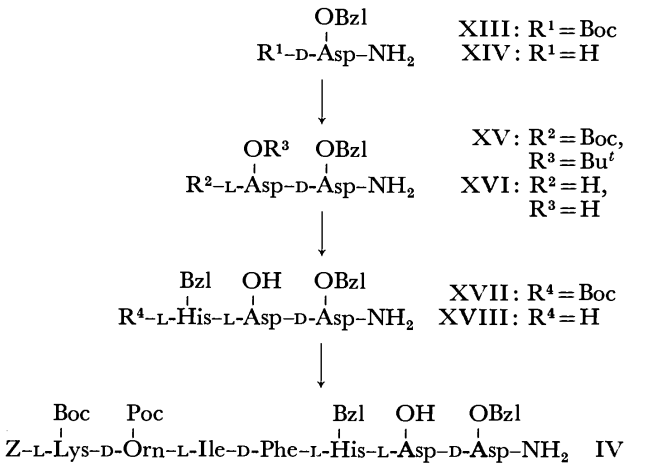

Bzl: benzyl, Z: benzyloxycarbonyl, Boc: *t*-butyloxycarbonyl, Poc: cyclopentyloxycarbonyl, Bu^t: *t*-butyl

Scheme 2.

Thus, β-benzyl Boc-D-aspartate was converted to benzyl Boc-D-isoasparaginate (XIII) by the active ester method. Boc group in XIII was removed by trifluoroacetic acid and the resulting deblocked product XIV was coupled with β-*t*-butyl Boc-L-aspartate by the 1-succinimidyl ester method to give acyl dipeptide ester XV. This compound XV thus obtained was treated with trifluoroacetic acid to afford L-aspartyl-D-isoasparagine benzyl ester (XVI) which was then acylated with N^{α}-Boc-N^{im}-benzyl-L-histidine-2,4,5-trichlorophenyl ester. In this case, we used benzyl group for protection of imidazole nitrogen in histidine residue in order to prevent the side reaction at cyclization reaction by the cyanomethyl ester method and to facilitate a purification of the product by silica gel column chromatography. The resulting tripeptide derivative XVII was exposed to trifluoroacetic acid to give deblocked ester XVIII. This compound XVIII was coupled with the tetrapeptide azide derived from the hydrazide IX prepared before to afford a linear heptapeptide derivative IV. All attempts to cyclize this compound, after removal of N^{ε}-Boc group on lysine residue, either by dicyclohexylcarbodiimide method, 1-succinimidyl ester method or cyanomethyl ester method did not give satisfactory results at the stage of this investigation.

Therefore, the presented results indicate that synthetic approaches from the intermediate hexa- and heptapeptides mentioned above to the whole structure of bacitracins of six amino acids-membered ring formula must be reinvestigated.

Experimental

All melting points are uncorrected. Silica gel G according to Stahl, Merck was used for thin-layer chromatography. Paper electrophoresis was carried out using Toyo filter paper No. 51 in a Toyo paper electrophoresis C apparatus at a potential gradient of 13 V/cm for 1—2 hr. The buffer used was pyridine–acetic acid–water (30: 4: 966, v/v/v, pH 6.4) unless otherwise stated. For silica gel column chromatography, Kieselgel 0.05—0.2 mm, Merck 70—325 mesh ASTM, was used.

N$^{\delta}$-s-*Alkyloxycarbonylornithines*. These compounds were prepared by the reaction of copper complex of ornithine with corresponding *s*-alkyloxycarbonyl chlorides through usual Schotten-Baumann type acylation. The complexes of the N^{δ}-acylornithines thus obtained were operated with hydrogen sulfide and the products were recrystallized from water. Reaction yields, melting points, elemental analyses, and optical properties of those compounds are shown in Table 2.

Treatment of N$^{\delta}$-*Alkyloxycarbonyl-L-ornithine with Hydrogen Fluoride*. N^{δ}-*s*-Alkyloxycarbonyl-L-ornithines were treated with hydrogen fluoride under the following three reaction conditions, *i.e.*, i) at 0 °C, for 30 min, ii) at 0 °C, for 60 min, iii) at 20 °C, for 60 min, respectively. After the given reaction period, excess hydrogen fluoride was removed *in vacuo* and the reaction vessel was dried over sodium hydroxide under reduced pressure. The residue was dissolved in water and the solution was extracted with ether. An aqueous layer was concentrated by lyophilization. The degree of deprotection was checked by thin-layer chromatography and paper electrophoresis. The quantitative results are shown in Table 1.

N$^{\delta}$-*Cyclopentyloxycarbonyl-D-ornithine*. This compound was prepared using cyclopentyloxycarbonyl chloride[11] by the same procedure described above for N^{δ}-*s*-alkyloxycarbonylornithines; yield, 64%; mp 251—253 °C; $[\alpha]_D^{20}$ −17.6° (*c* 1, 3 M HCl).

Found: C, 54.05; H, 8.29; N, 11.51%. Calcd for $C_{11}H_{20}O_4N_2$: C, 54.08; H, 8.25; N, 11.47%.

N$^{\alpha}$-t-*Butyloxycarbonyl*-N$^{\delta}$-*cyclopentyloxycarbonyl-D-ornithine*. This compound was prepared by acylation of N^{δ}-Poc-D-ornithine (22.3 g, 0.09 mol) with *t*-butyl azidoformate (15 g, 0.1 mol) and sodium carbonate (12 g) in dioxane–water (1: 1, v/v 800 ml). The reaction mixture was operated in the usual manner and the product was recrystallized from

TABLE 2. RESULTS OF PREPARATIONS OF N^{δ}-*s*-ALKYLOXYCARBONYL-L-ORNITHINE

s-Alkyloxycarbonyl group	Formula of derivatives	Yield (%)	Mp (°C) (Decomp.)	Elemental analysis Found (Calcd) C	H	N	$[\alpha]_D$ (Temperature, Concentration)
Isopropyloxycarbonyl	$C_9H_{18}O_4N_2$	52.0	237—240	49.43 (49.53)	8.34 (8.31)	12.82 (12.84)	+18.6° (18°, *c* 1, M HCl)
s-Butyloxycarbonyl	$C_{10}H_{20}O_4N_2$	44.0	227—230	51.38 (51.70)	8.60 (8.68)	11.92 (12.06)	+20.6° (19°, *c* 1, M HCl)
1-Ethylpropyloxycarbonyl	$C_{11}H_{22}O_4N_2$	59.2	225—228	53.43 (53.64)	9.06 (9.00)	11.31 (11.37)	+22.1° (19°, *c* 1, M HCl)
Cyclopentyloxycarbonyl	$C_{11}H_{20}O_4N_2$	64.0	250—253	54.13 (54.08)	8.39 (8.25)	11.25 (11.47)	+17.7° (20°, *c* 1, 3M HCl)
Cyclohexyloxycarbonyl	$C_{12}H_{22}O_4N_2$	56.0	229—232	54.99 (54.84)	8.70 (8.63)	10.48 (10.66) [a]	+16.3° (19°, *c* 1, M HCl)

a) Calculated values are based on formula of $C_{12}H_{22}O_4N_2 \cdot 1/4\ H_2O$.

ethyl acetate–petroleum ether; yield, 28.5 g (91%); mp 144—146 °C; $[\alpha]_D^{18}$ +7.9° (*c* 1, dimethylformamide).

Found: C, 55.63; H, 8.11; N, 7.83%. Calcd for $C_{16}H_{28}O_6N_2$: C, 55.80; H, 8.20; N, 8.13%.

Dicyclohexylammonium salt: (recrystallized from ethanol); mp 170—172 °C; $[\alpha]_D^{19}$ −9.3° (*c* 1, ethanol).

Found: C, 64.08; H, 9.83; N, 8.06%. Calcd for $C_{16}H_{28}O_6N_2 \cdot C_{12}H_{23}N$: C, 63.97; H, 9.78; N, 7.99%.

N^{α}-t-*Butyloxycarbonyl*-N^{δ}-*cyclopentyloxycarbonyl*-D-*ornithine* p-*Nitrophenyl Ester*. *N,N'*-Dicyclohexylcarbodiimide (6.6 g, 32 mmol) was added to an ice-cold solution of N^{α}-Boc-N^{δ}-Poc-D-ornithine (10.3 g, 30 mmol) and *p*-nitrophenol (4.2 g, 30 mmol) in ethyl acetate (200 ml) with stirring. The mixture was stirred at 0—3 °C for 1 hr and then at room temperature for 4 hr. Dicyclohexylurea formed was filtered off, washed with ethyl acetate and the combined filtrate was concentrated under reduced pressure. The residue was recrystallized from ethanol; yield, 8.0 g (57%); mp 146—147 °C; $[\alpha]_D^{19}$ +27.9° (*c* 1, dimethylformamide).

Found: C, 56.77; H, 6.77; N, 8.93%. Calcd for $C_{22}H_{31}O_8N_3$: C, 56.76; H, 6.71; N, 9.03%.

N^{α}-t-*Butyloxycarbonyl*-N^{δ}-*cyclopentyloxycarbonyl*-D-*ornithine 1-Succinimidyl Ester*. *N,N'*-Dicyclohexylcarbodiimide (3.1 g, 15 mmol) was added to an ice-cold solution of N^{α}-Boc-N^{δ}-Poc-D-ornithine (5.2 g, 15 mmol) and *N*-hydroxysuccinimide (1.8 g, 16 mmol) in tetrahydrofuran (150 ml) with stirring. The stirring was continued at 0—3 °C for 30 min and then at room temperature for 5 hr. Dicyclohexylurea formed was filtered off and washed with tetrahydrofuran. The combined filtrate was concentrated *in vacuo*. The residual syrup was crystallized from 2-propanol–isopropyl ether; yield, 5.2 g, (79%); mp 152—155 °C; $[\alpha]_D^{18}$ +21.1° (*c* 1, dimethylformamide).

Found: C, 54.48; H, 7.04; N, 9.42%. Calcd for $C_{20}H_{31}O_8N_3$: C, 54.41; H, 7.08; N, 9.52%.

N^{α}-t-*Butyloxycarbonyl*-N^{δ}-*cyclopentyloxycarbonyl*-D-*ornithyl*-L-*isoleucyl*-D-*phenylalanine Ethyl Ester (VIa)*. *(i) By 1-Succinimidyl Ester Procedure*: A solution of N^{α}-Boc-N^{δ}-Poc-D-ornithine 1-succinimidyl ester (5.7 g, 13 mmol) in dimethylformamide (60 ml) was added to an ice-cold solution of V hydrobromide[7] (5.0 g, 13 mmol) in dimethylformamide (150 ml) containing triethylamine (1.9 ml). The mixture was stirred in an ice bath for 1 hr and then at room temperature for 30 hr. The solution was concentrated under reduced pressure. Precipitate formed upon addition of water to the residue was filtered, washed with water and recrystallized from methanol; yield, 6.6 g, (80%); mp 188—190 °C; $[\alpha]_D^{19}$ +18.7° (*c* 1, dimethylformamide).

Found: C, 62.59; H, 8.30; N, 8.91%. Calcd for $C_{33}H_{52}O_8N_4$: C, 62.63; H, 8.28; N, 8.85%.

(ii) By p-*Nitrophenyl Ester Procedure*: The same compound VIa was prepared by coupling of N^{α}-*t*-Boc-N^{δ}-Poc-D-ornithine *p*-nitrophenyl ester (5.1 g, 11 mmol) and V hydrobromide[7] (4.3 g, 11 mmol) according to the usual procedure; yield, 5.3 g, (76%); mp 188—190 °C; $[\alpha]_D^{20}$ +18.9° (*c* 1, dimethylformamide).

Found: C, 62.60; H, 8.25; N, 8.86%.

(iii) By Mixed Anhydride Procedure: The same compound VIa was also prepared from a mixed anhydride of N^{α}-Boc-N^{δ}-D-ornithine (26.5 g, 77 mmol) with ethyl chloroformate (8.4 g, 77 mmol), and V hydrobromide[7] (29.8 g, 77 mmol) by the usual procedure; yield, 42 g, (86%); mp 187—190 °C; $[\alpha]_D^{20}$ +18.9° (*c* 1, dimethylformamide).

Found: C, 62.43; H, 8.41; N, 8.69%.

N^{α}-*Benzyloxycarbonyl*-N^{δ}-*cyclopentyloxycarbonyl*-D-*ornithine*. This compound was prepared by acylation of N^{δ}-Poc-D-ornithine (10 g, 40 mmol) with benzyloxycarbonyl chloride (8.5 g, 50 mmol) and aqueous 1M sodium hydroxide by the usual procedure. The oily product (14.3 g, 95%) thus obtained was used directly to the following esterification.

N^{α}-*Benzyloxycarbonyl*-N^{δ}-*cyclopentyloxycarbonyl*-D-*ornithine* p-*Nitrophenyl Ester*. *N,N'*-Dicyclohexylcarbodiimide (6.8 g, 33 mmol) was added to the chilled solution of N^{α}-Z-N^{δ}-Poc-D-ornithine (12.5 g, 33 mmol) and *p*-nitrophenol (4.6 g, 33 mmol) in ethyl acetate (50 ml). The mixture was stirred in an ice-bath for 1 hr and at room temperature for 3 hr. Dicyclohexylurea precipitated was filtered off and the residue was washed with ethyl acetate. The combined filtrate was concentrated and residual oil was kept under petroleum ether. The solidified material was collected by filtration and recrystallized from ethanol; yield, 12.9 g (78%); mp 118—120 °C; $[\alpha]_D^{21}$ +22.4° (*c* 1, dimethylformamide).

Found: C, 60.28; H, 5.85; N, 8.42%. Calcd for $C_{25}H_{29}O_8N_3$: C, 60.11; H, 5.85; N, 8.41%.

N^{α}-*Benzyloxycarbonyl*-N^{δ}-*cyclopentyloxycarbonyl*-D-*ornithyl*-L-*isoleucyl*-D-*phenylalanine Ethyl Ester (VIb)*. N^{α}-Z-N^{δ}-Poc-D-ornithine *p*-nitrophenyl ester (5.0 g, 10 mmol) in dimethylformamide (30 ml) was added to a solution of V hydrobromide[7] (4.0 g, 10 mmol) in dimethylformamide (100 ml) containing triethylamine (1.4 ml) with stirring in an ice-bath. The stirring was continued on ice cooling for 30 min and at room temperature for 20 hr. The solvent was removed *in vacuo* and residue was triturated with water. The precipitate was collected, washed with 5% sodium carbonate, water, 1M hydrochloric acid and water successively. The product was reprecipitated from ethanol; yield, 5.7 g (85%); mp 231—233 °C, $[\alpha]_D^{20}$ +9.6° (*c* 1, dimethylformamide).

Found: C, 64.94; H, 7.57; N, 8.40%. Calcd for $C_{36}H_{50}$-

O_8N_4: C, 64.84; H, 7.56; N, 8.40%.

N^{δ}-*Cyclopentyloxycarbonyl*-D-*ornithyl*-L-*isoleucyl*-D-*phenylalanine Ethyl Ester (VII) Hydrochloride.* *(i) From VIa*: The tripeptide derivative VIa (6.6 g, 10.4 mmol) was suspended in ethyl acetate (300 ml) and treated with hydrogen chloride in ethyl acetate (about 6.4 M, 150 ml). As vigorous stirring was continued, a clear solution was obtained and then the deposition of crystals was observed. The reaction mixture was kept at room temperature for 40 min. Upon addition of petroleum ether (800 ml), crystalline hydrochloride was deposited. It was filtered, washed with petroleum ether and dried over potassium hydroxide *in vacuo*. The crude product was combined with a second crop secured from the mother liquor, and recrystallized from methanol-ethyl ether; yield, 5.4 g, (92%); mp 197—200 °C (decomp.); $[\alpha]_D^{19}$ +1.4° (*c* 1.5, dimethylformamide).

Found: C, 58.93; H, 8.05; N, 9.78; Cl, 6.32%. Calcd for $C_{28}H_{44}O_6N_4 \cdot HCl$: C, 59.09; H, 7.97; N, 9.85; Cl, 6.23%.

(ii) From VIb: The tripeptide derivative VIb (10 g, 15 mmol) was dissolved in ethanol (200 ml) containing concentrated hydrochloric acid (2 ml). Palladium black was added to the solution and hydrogen gas was bubbled through the solution at room temperature for 10 hr. The catalyst was filtered off with the aid of celite and the filtrate was concentrated *in vacuo*. The precipitated solid was collected and recrystallized from methanol-ether; yield, 7.7 g, (91%); mp 198—199 °C (decomp.); $[\alpha]_D^{20}$ +1.2° (*c* 1.5, dimethylformamide).

Found: C, 59.17; H, 8.25; N, 9.61; Cl, 6.27%.

N^{α}-*Benzyloxycarbonyl*-N^{ε}-t-*butyloxycarbonyl*-L-*lysyl*-N^{δ}-*cyclopentyloxycarbonyl*-D-*ornithyl*-L-*isoleucyl*-D-*phenylalanine Ethyl Ester (VIII).* *(i) By 1-Succinimidyl Ester Procedure*: N^{α}-Z-N^{ε}-Boc-L-lysine 1-succinimidyl ester[14] (13.5 g, 28 mmol) in dimethylformamide (100 ml) was added to an ice-cold solution of the tripeptide ester VII hydrochloride (16 g, 28 mmol) and triethylamine (4 ml) in dimethylformamide (400 ml). The mixture was stirred at 0—3 °C for 30 min and then at room temperature for 30 hr. After most of the solvent had been removed under reduced pressure, the residue was diluted with water to yield a precipitate. It was collected by filtration, washed with 5% aqueous sodium carbonate, water, 5% aqueous citric acid and water successively. The product was reprecipitated from dimethylformamide-water and then dried *in vacuo* at 30 °C over phosphorus pentoxide; yield, 23.7 g, (94%); mp 218—221 °C (decomp.); $[\alpha]_D^{19}$ −10.8° (*c* 1, dimethylformamide).

Found: C, 63.09; H, 8.01; N, 9.35%. Calcd for $C_{47}H_{70}O_{11}N_6$: C, 63.06; H, 7.88; N, 9.39%.

Amino acid analysis: Lys+Orn, 2.10; Ile, 1.00; Phe, 0.97.

(ii) By p-*Nitrophenyl Ester Procedure*: The same tetrapeptide derivative VIII was obtained from N^{α}-Z-N^{ε}-Boc-L-lysine *p*-nitrophenyl ester[15] (3.2 g, 6.4 mmol) and the tripeptide ester VII hydrochloride (3.6 g, 6.3 mmol) by the usual method; yield, 4.4 g, (79%); mp 216—219 °C (decomp.); $[\alpha]_D^{19}$ −11.1° (*c* 1, dimethylformamide).

Found: C, 62.75; H, 7.96; N, 9.33%.

N^{α}-*Benzyloxycarbonyl*-N^{ε}-t-*butyloxycarbonyl*-L-*lysyl*-N^{δ}-*cyclopentyloxycarbonyl*-D-*ornithyl*-L-*isoleucyl*-D-*phenylalanine Hydrazide (IX) Hemihydrate.* Hydrazine hydrate (15 ml) was added to a solution of the tetrapeptide derivative VIII (7.3 g, 8.2 mmol) in dimethylformamide (150 ml) and the mixture was kept at room temperature for 48 hr. The solvent was removed *in vacuo* and the residue was solidified by addition of water. The resulting gelatinous mass was collected, washed with water, and dried *in vacuo*; yield, 6.8 g (93%); mp 187—190 °C (decomp.); $[\alpha]_D^{20}$ +8.9° (*c* 1, dimethylformamide).

Found: C, 60.56; H, 7.80; N, 12.46%. Calcd for $C_{45}H_{68}O_{10}N_8 \cdot 1/2\,H_2O$: C, 60.72; H, 7.81; N, 12.59%.

N^{α}-*Benzyloxycarbonyl*-N^{ε}-t-*butyloxycarbonyl*-L-*lysyl*-N^{δ}-*cyclopentyloxycarbonyl*-D-*ornithyl*-L-*isoleucyl*-D-*phenylalanyl*-L-*histidine Methyl Ester (X) Dihydrate.* A solution of sodium nitrite (1 g) in water (5 ml) was added to an ice-cold solution of the tetrapeptide hydrazide IX hemihydrate (8.9 g, 10 mmol) in a mixture of 60% acetic acid (200 ml) and 1M hydrochloric acid (20 ml) at −3—0 °C with vigorous stirring. After 10 min, excess cold water was added to the mixture. The resulting precipitate was filtered and washed thoroughly with water. The acyl tetrapeptide azide thus obtained was dissolved in dimethylformamide (200 ml) and cooled to 2—3 °C. This solution was added to an ice-cold solution of methyl L-histidinate dihydrochloride (5 g, 21 mmol) in dimethylformamide (100 ml) containing triethylamine (4 ml) with stirring. The mixture was stirred at 0—2 °C for 18 hr and then at room temperature for 24 hr. The mixture was concentrated *in vacuo* and the residue was triturated with water. The amorphous solid precipitated was collected and washed thoroughly with water. The product was reprecipitated from dimethylformamide-water, and dried over phosphorus pentoxide at 30—35 °C; yield, 8.4 g, (80%); mp 186—190 °C; $[\alpha]_D^{19}$ +6.0° (*c* 1, dimethylformamide).

Found: C, 59.53; H, 7.58; N, 11.90%. Calcd for $C_{52}H_{75}O_{12}N_9 \cdot 2H_2O$: C, 59.24; H, 7.55; N, 11.96%.

Amino acid analysis: Lys+Orn, 1.95; Ile, 1.00; Phe, 1.05; His, 0.96.

N^{α}-*Benzyloxycarbonyl*-N^{ε}-t-*butyloxycarbonyl*-L-*lysyl*-N^{δ}-*cyclopentyloxycarbonyl*-D-*ornithyl*-L-*isoleucyl*-D-*phenylalanyl*-L-*histidine Hydrazide (XI) Hydrate.* Hydrazine hydrate (10 ml) was added to a solution of the pentapeptide ester X dihydrate (5.5 g, 5.2 mmol) in dimethylformamide (150 ml). After the mixture had been kept at room temperature for 48 hr, the solvent was evaporated *in vacuo* and the residue obtained was diluted with water. The amorphous solid precipitated was filtered and washed with water. The product was reprecipitated from dimethylformamide-water and dried *in vacuo* over phosphorus pentoxide at 35 °C; yield, 5.1 g, (94%); mp 206—208 °C (decomp.); $[\alpha]_D^{17}$ +6.3° (*c* 1, dimethylformamide).

Found: C, 59.07; H, 7.46; N, 14.74%. Calcd for $C_{51}H_{75}O_{11}N_{11} \cdot H_2O$: C, 59.11; H, 7.49; N, 14.87%.

α-*Methyl* L-*Aspartate Trifluoroacetate.* α-Methyl Z-L-aspartate[16] (11.3 g, 40 mmol) prepared from the corresponding dicyclohexylammonium salt was dissolved in trifluoroacetic acid (40 ml) and the solution was heated under refluxing for 30 min. Excess acid was removed *in vacuo* and the residue was triturated with ethyl ether. The precipitate formed was collected by filtration and recrystallized from methanol-ethyl ether; yield, 9.4 g, (90%); mp 117—119 °C; $[\alpha]_D^{15}$ +13.0° (*c* 1, methanol).

Found: C, 32.31; H, 3.95; N, 5.36%. Calcd for $C_5H_9O_4N \cdot CF_3COOH$: C, 32.19; H, 3.86; N, 5.36%.

N^{α}-*Benzyloxycarbonyl*-N^{ε}-t-*butyloxycarbonyl*-L-*lysyl*-N^{δ}-*cyclopentyloxycarbonyl*-D-*ornithyl*-L-*isoleucyl*-D-*phenylalanyl*-L-*histidyl*-L-*aspartic Acid* α-*Methyl Ester (XII).* The pentapeptide hydrazide XI hydrate (4.0 g, 3.9 mmol) was dissolved in aqueous acetic acid (CH_3COOH 40 ml, H_2O 16 ml). Sodium nitrite (400 mg) in water (1 ml) was added to the soltuion at 0 °C and the reaction mixture was vigorously stirred at the

14) H. Otsuka, K. Inouye, M. Kanayama, and F. Shinozaki, This Bulletin, **39**, 882 (1966).

15) R. Schwyzer and W. Rittel, *Helv. Chim. Acta*, **44**, 159 (1961).

16) E. Wünsch and A. Zwick, *Z. Physiol. Chem.*, **333**, 108 (1963).

same temperature for 10 min. Saturated sodium chloride solution (250 ml) was added to the solution on ice cooling and the precipitated material was collected and washed thoroughly with ice-cold water. The solid thus obtained was dissolved in cold dimethylformamide (200 ml). This preparation was added to the cooled solution of α-methyl L-aspartate trifluoroacetate (1.6 g, 6.1 mmol) in dimethylformamide (100 ml) containing triethylamine (2 ml). The mixture was stirred at 0 °C for 12 hr and at room temperature for 24 hr. The solvent was removed *in vacuo* and excess water was added to the residue. The precipitate formed was collected, washed with water and reprecipitated from dimethylformamide–water; yield, 4.1 g, (93%); mp 167—175 °C; $[\alpha]_D^{19}$ +9.1° (*c* 1, dimethylformamide).

Found: C, 59.77; H, 7.60; N, 11.49%. Calcd for $C_{56}H_{80}O_{15}N_{10}$: C, 59.35; H, 7.12; N, 12.36%.

Cyclo-(N$^{\alpha}$-benzyloxycarbonyl-L-lysyl-N$^{\delta}$-cyclopentyloxycarbonyl-D-ornithyl-L-isoleucyl-D-phenylalanyl-L-histidyl-α-methyl-L-aspartyl) (III) Hydrate. To a solution of the hexapeptide derivative XII (6.0 g, 5.3 mmol) in dimethylformamide (50 ml), there were added chloroacetonitrile (3 ml) and triethylamine (6 ml). The reaction mixture was stirred at room temperature for 48 hr. The solvent was evaporated *in vacuo* and water was added to the residue. Solid formed was filtered and dried over phosphorus pentoxide *in vacuo*. The product (5.8 g) was treated with trifluoroacetic acid (60 ml) at room temperature for 30 min with stirring. Excess trifluoroacetic acid was removed *in vacuo*, and the residue was triturated with ethyl ether. The deblocked product thus obtained was dissolved in a mixture of dimethylformamide (20 ml) and acetic acid (5 ml). The solution was dropped into large excess pyridine (5 l) for 6 hr and the reaction mixture was stirred at 40—45 °C for 48 hr. The reaction mixture gave a spot showing positive Pauly and negative ninhydrin reaction at R_f 0.71, besides the original spot of deblocked linear peptide at R_f 0.1—0.2, and a minor spot of positive iodine test but negative both to Pauly[17] and ninhydrin reaction at R_f 0.91 on thin-layer chromatography using methanol–chloroform (2 : 8, v/v) as developing solvent. The solvent was evaporated *in vacuo* and the residue was purified by silica gel column chromatography (elution solvent: chloroform–methanol, 1:19—1:9 v/v) to obtain the cyclization product of R_f 0.71 on thin-layer chromatogram; yield, 53 mg (0.97%); mp 160—165 °C (decomp.); $[\alpha]_D^{18}$ +11.4° (*c* 1, dimethylformamide).

Found: C, 59.04; H, 7.03; N, 13.78%. Calcd for $C_{51}H_{70}O_{12}N_{10}\cdot H_2O$: C, 59.29; H, 7.03; N, 13.56%.

Amino acid analysis: Lys+Orn, 1.98; Ile, 1.11; Phe, 1.00; His, 0.95; Asp, 0.89.

Benzyl t-Butyloxycarbonyl-D-isoasparaginate (XIII). Concentrated aqueous ammonia (5 ml) in tetrahydrofuran (50 ml) was added to a cooled solution of Boc-D-aspartic acid β-benzyl α-1-succinimidyl ester (21.0 g, 50 mmol) in tetrahydrofuran (200 ml). The mixture was stirred at room temperature for 3 hr. The solution was concentrated and the residual solid was recrystallized from methanol–ethyl ether; yield, 12.3 g, (76%); mp 159—160.5 °C (decomp.); $[\alpha]_D^{15}$ −1.3° (*c* 1, methanol).

Found: C, 59.54; H, 6.89; N, 8.69%. Calcd for $C_{16}H_{22}O_5N_2$: C, 59.61; H, 6.83; N, 8.69%.

Benzyl D-Isoasparaginate (XIV) Trifluoroacetate. The compound XIII (4.8 g, 15 mmol) was dissolved in trifluoroacetic acid (30 ml). The solution was stirred at room temperature for 20 min. Excess trifluoroacetic acid was evaporated and the residue obtained was triturated with anhydrous ethyl ether. The precipitate was recrystallized from methanol–ethyl ether; yield, 4.5 g, (90%); mp 185—186.5 °C (decomp.); $[\alpha]_D^{15}$ −1.1° (*c* 1, methanol).

Found: C, 46.32; H, 4.52; N, 8.33%. Calcd for $C_{11}H_{14}O_3N_2\cdot CF_3COOH$: C, 46.43; H, 4.50; N, 8.33%.

t-Butyloxycarbonyl-L-aspartic Acid β-t-Butyl α-1-Succinimidyl Ester. *N*-Hydroxysuccinimide (11.5 g, 0.1 mol) and β-*t*-butyl Boc-L-aspartate obtained from its dicyclohexylammonium salt (47.1 g, 0.1 mol) by desalting with citric acid were dissolved in tetrahydrofuran (300 ml) and cooled on an ice-bath. *N,N'*-Dicyclohexylcarbodiimide (20.6 g, 0.1 mol) was added to the solution and the reaction mixture was stirred on ice cooling for 2 hr and then at room temperature for 3 hr. The precipitate was filtered off and the combined filtrate was concentrated *in vacuo*. The residual solid was collected by filtration with the aid of petroleum ether and recrystallized from ethyl acetate–petroleum ether; yield, 27.5 g, (71%); mp 105—105.5 °C; $[\alpha]_D^{15}$ −15.2° (*c* 1, ethyl acetate).

Found: C, 52.97; H, 6.82; N, 7.21%. Calcd for $C_{17}H_{26}O_8N_2$: C, 52.84; H, 6.78; N, 7.25%.

t-Butyloxycarbonyl-β-t-butyl-L-aspartyl-D-isoasparagine Benzyl Ester (XV). A solution of Boc-L-aspartic acid β-*t*-butyl α-1-succinimidyl ester (9.7 g, 25 mmol) in chloroform (100 ml) was added to an ice-cold solution of benzyl D-isoasparaginate (XIV) trifluoroacetate (8.4 g, 25 mmol) in chloroform (200 ml) containing triethylamine (4 ml). The mixture was stirred on an ice-bath for 1 hr and at room temperature for 12 hr. The solvent was removed *in vacuo* and the residue was dissolved in ethyl acetate (200 ml). The ethyl acetate solution was washed with water and dried over anhydrous sodium sulfate. The solvent was removed *in vacuo* and the residue was kept under petroleum ether. The precipitate was collected and recrystallized from methanol–petroleum ether; yield, 11.0 g (89%); mp 120—121 °C; $[\alpha]_D^{14}$ −3.2° (*c* 1, methanol).

Found: C, 58.35; H, 7.12; N, 8.52%. Calcd for $C_{24}H_{35}O_8N_3$: C, 58.40; H, 7.15; N, 8.51%.

L-Aspartyl-D-isoasparagine Benzyl Ester (XVI) Hemihydrate. The dipeptide diester XV (4.0 g, 8.1 mmol) was dissolved in trifluoroacetic acid (15 ml). The mixture was stirred at room temperature for 30 min. Excess trifluoroacetic acid was evaporated *in vacuo*. The residue was kept under ethyl ether and the resulting solid was recrystallized from methanol–ethyl ether. During recrystallization, trifluoroacetic acid in salt form of the product was eliminated from the deblocked peptide derivative; yield, 2.6 g, (93%); mp 160—165 °C; $[\alpha]_D^{15}$ +6.7° (*c* 1, acetic acid).

Found: C, 52.26; H, 5.53; N, 12.05%. Calcd for $C_{15}H_{19}O_6N_3\cdot 1/2H_2O$: C, 52.02; H, 5.82; N, 12.13%.

t-Butyloxycarbonyl-N^{im}-benzyl-L-histidyl-L-aspartyl-D-isoasparagine Benzyl Ester (XVII) Hydrate. Boc-N^{im}-benzyl-L-histidine 2,4,5-trichlorophenyl ester[18] (7.9 g, 15 mmol) in dimethylformamide (30 ml) was added to a chilled solution of the compound XVI hemihydrate (5.2 g, 15 mmol) in dimethylformamide (70 ml) containing triethylamine (4.2 ml). The mixture was stirred at 0 °C for 1 hr and at room temperature for 12 hr. The solvent was removed *in vacuo* and the residual oil was diluted with water. The precipitate formed was collected by filtration. The product was purified by silica gel column chromatography (elution solvent: chloroform–methanol 9 : 1—7 : 3 v/v); yield, 3.2 g, (31%); mp 125—128 °C; $[\alpha]_D^{15}$ +6.5° (*c* 1, methanol).

Found: C, 58.48; H, 6.22; N, 12.20%. Calcd for $C_{33}H_{40}$-

17) Faint yellow: This spot is assumed to be N^{im}-cyanomethylated cyclohexapeptide.

18) B. O. Handford, T. A. Hylton, K.-T. Wang, and B. Weinstein, *J. Org. Chem.*, **33**, 4251 (1968).

$O_9N_6 \cdot H_2O$: C, 58.05; H, 6.20; N, 12.31%.

Amino acid analysis: N^{im}-Bzl-His, 1.08; Asp, 2.00; N^{im}-benzylhistidine was eluted with citrate buffer of pH 6.80 from the short column of amino acid analyzer.

N^{im}-Benzyl-L-histidyl-L-aspartyl-D-isoasparagine Benzyl Ester (XVIII) Bistrifluoroacetate. The compound XVII hydrate obtained above (683 mg, 1 mmol) was dissolved in trifluoroacetic acid (5 ml). The solution was stirred at room temperature for 30 min and excess acid was evaporated *in vacuo*. The residue was triturated with ethyl ether. The precipitate formed was collected by filtration. This product was homogeneous on paper electrophoresis at pH 4.8; yield, 713 mg (90%); mp 104—118 °C (decomp.); $[\alpha]_D^{15}$ +4.4° (*c* 1, methanol).

Found: C, 48.51; H, 4.42; N, 10.50%. Calcd for $C_{28}H_{32}O_7N_6 \cdot 2CF_3COOH$: C, 48.49; H, 4.32; N, 10.60%.

N^{α}-Benzyloxycarbonyl-N^{ε}-t-butyloxycarbonyl-L-lysyl-N^{δ}-cyclopentyloxycarbonyl-D-ornithyl-L-isoleucyl-D-phenylalanyl-N^{im}-benzyl-L-histidyl-L-aspartyl-D-isoasparagine Benzyl Ester (IV) Hydrate. The tetrapeptide hydrazide IX hemihydrate (291 mg, 0.33 mmol) was dissolved in a mixture of acetic acid (4 ml) and 1M hydrochloric acid (1.7 ml). A solution of sodium nitrite (40 mg) in water (0.5 ml) was added to the cooled solution mentioned above and the mixture was stirred at 0 °C for 30 min. Ice-cold saturated aqueous sodium chloride (50 ml) was added to the above solution. The deposit was collected by filtration and washed with cold water thoroughly. The product was dissolved in dimethylformamide (30 ml) and added to a solution of the tripeptide derivative XVIII bistrifluoroacetate (270 mg, 0.34 mmol) in dimethylformamide (20 ml) containing triethylamine (0.1 ml) at 0 °C. The solution was stirred at 5 °C for 48 hr and then at room temperature for 24 hr. The solvent was removed *in vacuo* and the residual oil was triturated with water. The precipitate was collected by filtration. The crude product was purified by silica gel column chromatography (elution solvent: chloroform–methanol 9:1—8:2; v/v); yield, 330 mg (70%); mp 185—195 °C; $[\alpha]_D^{15}$ +15.0° (*c* 1, dimethylformamide).

Found: C, 60.80; H, 7.04; N, 11.74%. Calcd for $C_{73}H_{96}O_{17}N_{12} \cdot H_2O$: C, 61.24; H, 6.90; N, 11.74%.

Amino acid analysis: Lys+Orn, 1.92; Ile, 1.00; Phe, 0.95; N^{im}-Bzl-His, 1.05; Asp, 1.85.

The authors are grateful to Peptide Center, Institute for Protein Research of Osaka University for carrying out the amino acid analyses and also deeply indebted to Ajinomoto Co., Ltd. and Commercial Solvent Corporation, U.S.A. for their kind offers of amino acids.

BULLETIN OF THE CHEMICAL SOCIETY OF JAPAN, VOL. 46, 3193—3197 (1973)

Telomerization of Ethylene with Carbon Tetrachloride Initiated by *N*-Chloroalkylamines

Teruzo ASAHARA, Manabu SENŌ, and Noritaka OHTANI

Institute of Industrial Science, The University of Tokyo, Roppongi, Minato-ku, Tokyo 106

(Received May 18, 1973)

By using various *N*-chloroalkylamines, the telomerization of ethylene with carbon tetrachloride was carried out in a stainless steel autoclave at 130 °C. It was found that the yields and the compositions of telomers varied widely according to the kinds and the structures of *N*-chloroalkylamines. When *N*-chloromonoalkylamines or *N*-chlorodialkylamines were used, the total yield of telomers was high compared with the case using *N,N*-dichloroalkylamines. In the presence of both *N*-chloromonoalkylamines and *N*-chlorodialkylamines, the total yield of telomers became higher and the greater part of the telomers was 1:1 adduct ($n=1$ telomer $CCl_3CH_2CH_2Cl$) of ethylene with carbon tetrachloride.

The telomerization of ethylene with carbon tetrachloride by using various initiators, has been examined by many investigators. *N*-Chloroamine, which is known to have a small value of bond energy and a large value of chain transfer constant, adds easily to olefins by a free radical mechanism.[1] As an initiator of polymerization or telomerization, however, *N*-chloroalkylamine was not noticed except for some studies.[2-3] The previous report from our laboratory illustrated that telomerization of ethylene with carbon tetrachloride occurred by use of systems of *N,N*-dichloro-*n*-butylamine and amines to give the $n=1$ telomer, $CCl_3CH_2CH_2Cl$, as a main product.[4]

On the other hand, we found that *N,N*-dichloroalkylamines reacted with primary or secondary amines to produce *N*-chloromonoalkylamines and *N*-chlorodialkylamines as shown by the following equation.[5]

$$RNCl_2 + R'R''NH \longrightarrow RNHCl + R'R''NCl$$

R, R′=alkyl, R″=alkyl or H

These findings lead us to the attempt of telomerizations initiated by various *N*-chloroalkylamines. Furthermore, the systems of *N,N*-dichloroalkylamines and

1) R. S. Neale and N. L. Marcus, *J. Org. Chem.*, **33**, 3457 (1968); R. S. Neale and N. L. Marcus, *ibid.*, **32**, 3273 (1967) and references cited therein; F. Minisci, R. Galli, and M. Cecere, *Tetrahedron Lett.*, **1966**, 3163; F. Minisci and R. Galli, *ibid.*, **1964**, 167.

2) T. Otsu, S. Aoki, and K. Itakura, *J. Polym. Sci., Part A-1*, **8**, 445 (1970).

3) T. Otsu, S. Aoki, M. Nishimura, M. Yamagucni, and Y. Kusuki, *Polym. Lett.*, **5**, 835 (1967).

4) T. Asahara and T. Sato, *Kogyo Kagaku Zasshi*, **74**, 1845 (1971).

5) This result was presented at the 26th Annual Meeting of Chemical Society of Japan, Tokyo (1972).

amines were studied in detail and the result was compared with that for the cases of *N*-chloromonoalkylamines and *N*-chlorodialkylamines.

Experimental

Materials. Ethylene (purity 99.8%), carbon tetrachloride, and amines of commercial special grade were used without purification. *N,N*-Dichloroalkylamines[6] and *N*-chlorodialkylamines were prepared by bubbling chlorine gas into the aqueous solution of amines and sodium bicarbonate and were purified by distillation. *N,N*-Dichloro-*n*-butylamine, bp 55°C/28 mmHg, *N,N*-dichloro-*t*-butylamine, bp 42 °C/19.5 mmHg, *N,N*-dichloro-*s*-butylamine, bp 45.5 °C/20 mmHg, *N,N*-dichloroisobutylamine, bp 39 °C/25 mmHg, *N*-chlorodi-*n*-butylamine, bp 33 °C/2.5 mmHg, *N*-chloropiperidine, bp 29 °C/10 mmHg.

N-Chloromonoalkylamines[7] were prepared by mixing slowly the solution of corresponding amine hydrochloride with the aqueous solution of sodium hypochlorite in the presence of carbon tetrachloride. The resulting carbon tetrachloride solution was dried over sodium sulfate and the concentration was determined by the iodometric analysis.

Apparatus and Method. Telomerization was carried out in a 200 ml stainless steel (SUS 7) autoclave with a magnetic stirrer. In the autoclave, 1 mol of carbon tetrachloride and prescribed amounts of *N*-chloroamines were placed. After the autoclave was sealed, the air inside was replaced several times by ethylene. Ethylene was then charged to show a definite pressure. The autoclave was heated up to 130 °C and kept for a desired time. After the reaction, the autoclave was chilled to room temperature and the reaction mixture was washed by an aqueous potassium iodide solution and then an aqueous sodium thiosulfate solution. The product was fractionated by distillation into $n=1$ and $n=2$ telomers, which were identified by boiling point and NMR spectra.

Results and Discussion

Reactions of N,N-*Dichloroalkylamines with Primary or Secondary Amines.* It was made clear from the observations described later that primary and secondary amines react with *N,N*-dichloroalkylamines to form *N*-chloromonoalkylamine and *N*-chlorodialkylamine, respectively.

The reaction of *N,N*-dichloro-*n*-butylamine with *n*-butylamine in isooctane at 40 °C was examined by means of UV spectrometer. The absorption at 309 nm by *N,N*-dichloro-*n*-butylamine diminished in strength instead of the increase in strength of the absorption at 264 nm, which was identified to be owing to *N*-chloromono-*n*-butylamine. The ^{1}H NMR measurement of this reaction in carbon tetrachloride showed that the triplet absorption at δ 3.60 diminished and at the same time the triplet at δ 3.03 appeared and became greater. The former is owing to α-methylene protons of *N,N*-dichloro-*n*-butylamine and the latter was ascribed to that of *N*-chloromono-*n*-butylamine.

The reaction of *N,N*-dichloro-*n*-butylamine with di-*n*-butylamine was examined in the same way. The absorption at about 270 nm in the UV spectra and the triplets at δ 2.84 and δ 2.99 in the NMR spectra appeared and increased in strength as the reaction proceeded. The absorption around 270 nm can be explained as a combined peak of two absorptions, *i.e.*, that of *N*-chlorodi-*n*-butylamine at 274 nm and that of *N*-chloromono-*n*-butylamine at 264 nm, which have the similar molar absorption coefficient of about 400 $l \cdot cm^{-1} \cdot mol^{-1}$. The peak at δ 2.84 in the NMR spectra is owing to the α-methylene protons of *N*-chlorodi-*n*-butylamine and the peak at δ 2.99 to that of *N*-chloromono-*n*-butylamine. In these reactions, the concentration of the positive chlorine of *N*-chloroamines decreased by only 5—10%, when the conversion of *N,N*-dichloroamine was 50%. The similar results were obtained in the other systems of *N,N*-dichloroalkylamines and amines. The rate of reaction was low for amines with the bulky alkyl groups. In the case of dicyclohexylamine, the replacement reaction did not take place and dicyclohexylamine hydrochloride was obtained. The details will be reported in a separate paper.

Telomerization of Ethylene with Carbon Tetrachloride using N-*Chloroalkylamines.* The results of telomerizations using *N,N*-dichloroalkylamines, *N*-chloromonoalkylamines, and *N*-chlorodialkylamines are shown in Tables 1, 2, and 3, respectively.[8] When *N,N*-dichloroalkylamines were used, the yield of telomers was generally low. In the case of *N,N*-dichloro-*t*-butylamine, the yield of telomers is particularly low. The composition ratio of $n=1$ telomer was, however, very high compared with that of other cases using di-*t*-butyl peroxide (DTBP) and di-*n*-butylamine.

N-Chloromonoalkylamines were more reactive for initiation of telomerization than *N,N*-dichloroalkylamines and the following order with higher yields of telomers was observed: *t*-Bu<*s*-Bu and *n*-Bu<*i*-Bu. The same order was observed in the case of *N,N*-dichlorobutylamines. In addition, it was noticed that the yield of telomers increased and the composition ratio of $n=1$ telomer decreased when the alkyl group of *N*-chloromonoalkylamine was more bulky. The similar result was obtained in the case of *N*-chlorodialkylamines.

Table 1. Telomerization of ethylene with carbon tetrachloride using *N,N*-dichloroalkylamines[a]

Dichloroamine	Total yield of telomers g	Composition of telomers mol%		
		$n=1$	$n=2$	$n\geqq3$
n-$BuNCl_2$	20	77	17	6
i-$BuNCl_2$	31	78	19	3
s-$BuNCl_2$	16	80	15	5
t-$BuNCl_2$	2	—	—	—

a) Telomerization conditions: *N,N*-dichloroalkylamine, 0.02 mol; initial ethylene pressure, 20 kg/cm^2; carbon tetrachloride, 1 mol; reaction temperature, 130 °C; reaction time, 2 hr.

6) L. K. Jackson, G. N. R. Smart, and G. F. Wright, *J. Amer. Chem. Soc.*, **69**, 1539 (1947).

7) V. L. Heasley, P. Kovacic, and R. M. Lange, *J. Org. Chem.*, **31**, 3050 (1966).

8) The telomerization using *N,N*-dichloroalkylamines has an induction period, which is about 30 min or longer and is dependent upon the concentration of dichloroamine and other reaction conditions.

Table 2. Telomerization of ethylene with carbon tetrachloride using *N*-chloromonoalkylamines[a)]

Chloroamine	Total yield of telomers g	Composition of telomers mol%		
		$n=1$	$n=2$	$n\geqq3$
n-BuNHCl	36	61	34	5
i-BuNHCl	57	75	22	3
s-BuNHCl	32	67	30	3
t-BuNHCl[b)]	11	42	48	10
n-PrNHCl[c)]	21	76	20	4
i-PrNHCl[c)]	9	78	22	0
EtNHCl[c)]	6	—	—	—

a) Telomerization conditions: *N*-chloromonoalkylamine, 0.01 mol; initial ethylene pressure, 20 kg/cm²; carbon tetrachloride, 1 mol; reaction temperature, 130 °C; reaction time, 1.5 hr.
b) Reaction time; 2.0 hr.
c) *N*-Chloromonoalkylamine: 0.02 mol.

Table 3. Telomerization of ethylene with carbon tetrachloride using *N*-chlorodialkylamines[a)]

Chloroamine	Total yield of telomers g	Composition of telomers mol%		
		$n=1$	$n=2$	$n\geqq3$
$(n\text{-Bu})_2$NCl	63	73	20	7
$(n\text{-Pr})_2$NCl	30	75	22	3
Et_2NCl	18	79	18	3
N-Chloro-piperidine	5[b)]	—	—	—

a) Telomerization conditions: *N*-chlorodialkylamine, 0.02 mol; initial ethylene pressure, 20 kg/cm²; carbon tetrachloride, 1 mol; reaction temperature, 130 °C; reaction time, 1.5 hr.
b) Reaction time; 2.0 hr.

Telomerization of Ethylene with Carbon Tetrachloride using N,N-*Dichloroalkylamine–Amine Systems.* The effect of the composition ratio of *N,N*-dichloro-*n*-butylamine to *n*-butylamine is listed in Table 4. The yield of telomers decreases, but the composition ratio of $n=1$ telomer increases with the increase of the ratio of *N,N*-dichloroamine. The decrease in the yield of total telomers can be explained from the fact that the replacement reaction above-mentioned takes place as the amine interacts stronger with *N,N*-dichloroamine than carbon tetrachloride.

Table 4. Telomerization of ethylene with carbon tetrachloride using the system of *N,N*-dichloro-*n*-butylamine and *n*-butylamine[a)]

n-BuNCl$_2$ $\times10^{-2}$ mol	n-BuNH$_2$ $\times10^{-2}$ mol	Total yield of telomers g	Composition of telomers mol%		
			$n=1$	$n=2$	$n\geqq3$
0	2.0	46	57	35	8
0.5	1.5	37	57	33	10
1.0	1.0	17	73	17	10
1.5	0.5	11	72	19	9
2.0	0	4	—	—	—

a) Telomerization conditions: initial ethylene pressure, 20 kg/cm²; carbon tetrachloride, 1 mol; reaction temperature, 130 °C; reaction time, 1.5 hr.

As is shown in Table 5, both the yield of telomers and the composition ratio of $n=1$ telomer increase by adding di-*n*-butylamine to *N,N*-dichloroalkylamine. This binary system is more reactive than the single system of *N,N*-dichloroalkylamine, *N*-chloromonoalkylamine, or *N*-chlorodialkylamine. The reactivity of this system was dependent upon the alkyl group of *N,N*-dichlorobutylamines and the order of reactivity was the same to that of *N*-chloromonobutylamines and *N,N*-dichlorobutylamines.

Table 5. Telomerization of ethylene with carbon tetrachloride using the system of *N,N*-dichloroalkylamine and di-*n*-butylamine[a)]

Dichloroamine	Total yield of telomers g	Composition of telomers mol%		
		$n=1$	$n=2$	$n\geqq3$
n-BuNCl$_2$	60	86	12	3
i-BuNCl$_2$	91	87	12	1
s-BuNCl$_2$	70	88	9	3
t-BuNCl$_2$	23	77	18	5

a) Telomerization conditions: *N,N*-dichloroalkylamine, di-*n*-butylamine, 0.02 mol; initial ethylene pressure, 20 kg/cm²; carbon tetrachloride, 1 mol; reaction temperature, 130 °C; reaction time, 1.5 hr.

Table 6. Comparison of the system of *N*-chloromono-*n*-butylamine and *N*-chlorodi-*n*-butylamine with the system of *N,N*-dichloro-*n*-butyl amine and di-*n*-butylamine[a)]

Initiator system	Total yield of telomers g	Composition of telomers mol%		
		$n=1$	$n=2$	$n\geqq3$
n-BuNCl$_2$/$(n\text{-Bu})_2$NH	51	85	11	4
n-BuNHCl/$(n\text{-Bu})_2$NCl	52	82	14	4

a) Telomerization conditions: *N*-chloroamine, amine, 0.01 mol; initial ethylene pressure, 20 kg/cm²; carbon tetrachloride, 1 mol; reaction temperature, 130 °C; reaction time, 1.5 hr.

Table 6 shows the comparison of the result for the system of *N,N*-dichloro-*n*-butylamine and di-*n*-butylamine with that for the system of *N*-chloromono-*n*-butylamine and *N*-chlorodi-*n*-butylamine. The latter system is to be formed from the reaction in the former one. For the both systems, essentially the same results were obtained as expected. It was supposed that the reaction of *N,N*-dichloro-*n*-butylamine with di-*n*-butylamine at room temperature takes place rapidly to be almost completed within 30 min which is necessary to heat up the autoclave to the reaction temperature of 130 °C. The result for the 1 : 1 system of *N,N*-dichloro-*n*-butylamine–*n*-butylamine in Table 4 does not coincide with that for the *N*-chloromono-*n*-butylamine system in Table 2. This would show that the rate of the reaction of primary amines is slower than secondary amines.

Effects of Metal or Its Salts on the Telomerization Using N-*Chloroalkylamines.* The effect of iron, copper and their chlorides on the telomerization of ethylene with carbon tetrachloride using *N*-chloroalkylamines is

shown in Table 7. Remarkable decreases of the yield of telomers were observed when copper, its salts, and ferric chloride are added except the case of *N,N*-dichloro-*n*-butylamine. The addition of iron did not affect the reactivity of *N*-chloroalkylamines. The effect of ferrous chloride varied with the kind of *N*-chloroalkylamines. Particularly, the system of ferrous chloride and *N*-chlorodi-*n*-butylamine showed a marked increase in the yield of telomers and the ethylene

Table 7. Telomerization of ethylene with carbon tetrachloride using the system of *N*-chloroalkylamines and metal or its salts[a)]

Chloroamine	Metal or its salt	Total yield of telomers g	Composition of telomers mol% $n=1$	$n=2$	$n\geqq3$
n-$BuNCl_2$	—	4	—	—	—
	Fe	18	83	14	3
	$FeCl_2$	22	70	27	3
	$FeCl_3$	4	—	—	—
	Cu	8	58	40	2
	CuCl	1	—	—	—
	$CuCl_2$	3	—	—	—
n-BuNHCl	—	36[c)]	61	34	5
	Fe	40	85	13	2
	$FeCl_2$	38	73	23	4
	$FeCl_3$	4	—	—	—
	Cu	27	81	16	3
	CuCl	11	76	24	0
	$CuCl_2$	7	90	10	0
$(n\text{-Bu})_2NCl$	—	63	73	20	7
	Fe	63	87	9	4
	$FeCl_2$	80[b)]	87	11	2
	$FeCl_3$	35	87	9	4
	Cu	20	86	14	0
	CuCl	13	83	17	0
	$CuCl_2$	14	87	13	0

a) Telomerization conditions: chloroamine, metal, and salt, 0.02 mol; initial ethylene pressure, 20 kg/cm²; carbon tetrachloride, 1 mol; reaction temperature, 130 °C; reaction time, 1.5 hr.
b) Reaction time, 22 min.
c) Chloroamine, 0.01 mol.

Table 8. Telomerization of ethylene with carbon tetrachloride using the system of di-*n*-butylamine and metal or its salts[a)]

Metal or salt	Total yield of telomers g	Composition of telomers mol% $n=1$	$n=2$	$n\geqq3$
—	63	64	18	18
Fe	84	81	16	3
$FeCl_2$	73	71	24	5
$FeCl_3$	63	88	10	2
Cu	27	85	10	5
CuCl	54	90	7	3
$CuCl_2$	52	90	8	2

a) Telomerization conditions: metal or salt, 0.02 mol; di-*n*-butylamine, 0.02 mol; initial ethylene pressure, 20 kg/cm²; carbon tetrachloride, 1 mol; reaction temperature, 130 °C; reaction time, 1.5 hr.

charged into the autoclave was completely consumed within 25 min.

These results are to be compared with those for the systems of di-*n*-butylamine and metal or its salts. As is shown in Table 8, the high yields of telomers were obtained for all systems and the inhibition effect of copper salts or ferric chloride was not found.

Mechanism of Initiation. It is supposed that the telomerization would be initiated by *N*-chloroalkylamine through following reactions (1—3).

$$\mathrm{R\text{-}N(X)(Cl)} \xrightarrow{\Delta} \mathrm{R\text{-}N\cdot(X)} + \mathrm{Cl\cdot} \quad (1)$$

(I)

$$\mathrm{R\text{-}N(X)(Cl)} + \mathrm{HCl} \longrightarrow \mathrm{R\text{-}\overset{+}{N}(X)(Cl)(H)\ Cl^-}$$

(II)

$$\xrightarrow{\Delta} \mathrm{R\text{-}\overset{+}{N}(X)(Cl)\ Cl^-} + \mathrm{Cl\cdot} \quad (2)$$

(III)

$$\mathrm{R\text{-}N(X)(Cl)} + \mathrm{CCl_4} \longrightarrow \mathrm{R\text{-}\overset{+}{N}(X)(H)\ Cl^-} + \mathrm{\cdot CCl_3} \quad (3)$$

(III′)

X=R, H, or Cl

In Reaction 1, amino radical (I) is formed through a thermal scission of nitrogen-chlorine bond. *N,N*-dichloro-*n*-butylamine was utilized for the chlorination of polybutadiene by Kagiya *et al.*[9] This decomposition is probably the main process of radical formation in the case of *N*-chloro-*t*-alkylamines having no hydrogen bonded to α-carbon and *N,N*-dichloroalkylamines.

N-Chlorodialkylamine and *N*-chloromonoalkylamine having α-hydrogen easily undergo thermal decomposition at high temperatures to release hydrogen chloride. In the same manner as Hofmann-Loeffler reaction of *N*-chloroalkylamine in sulfuric acid,[10] hydrogen chloride maybe forms a salt (II) with *N*-chloroalkylamine and II decomposes to form aminium radical (III) and chlorine atom. Practically, II was formed stably at −60 °C and decomposed at room temperature in methanol. The decomposition products from II were amine hydrochloride and chlorine gas.

One-electron transfer from *N*-chloroalkylamine to carbon tetrachloride results in the formation of aminium radical (III′) and trichloromethyl radical (Reaction 3). It was reported that amines, such as triethylamine, and carbon tetrachloride form an *n*-σ complex which shows a charge-transfer spectrum.[11] But the basicity of *N*-chloroalkylamines is weaker than that of amines and, therefore, an electron donation is not feasible. Then, the radical formation by Reaction 3 might be excluded.

The telomerization of octene-1 instead of ethylene with carbon tetrachloride was carried out in a 20 ml glass ampule and the result was compared with that of

9) H. Okamoto, S. Hagiwara, and T. Kagiya, *Kogyo Kagaku Zasshi*, **74**, 1466 (1971).
10) M. E. Wolff, *Chem. Rev.*, **63**, 55 (1963).
11) D. P. Stevenson and G. M. Coppinger, *J. Amer. Chem. Soc.*, **84**, 149 (1962).

the same reaction in the 200 ml stainless steel autoclave under the same reaction conditions. The yield of telomers in the ampule was less than one fifth of that in the autoclave. This suggests that the metal surface or the trace amount of metal resolved has a large effect on the initiation of *N*-chloroalkylamine as does the case for the system of triethanolamine–carbon tetrachloride[12] or the system of cellulose–water–carbon tetrachloride.[13] The telomers in the ampule was probably produced *via* the initiations indicated by Eqs. (1)—(2). On the other hand, most part of the telomers in the autoclave was likely formed *via* the following reactions.

$$2\,R\text{–}\underset{Cl}{\overset{X}{N}} + Fe \longrightarrow 2\,R\text{–}\overset{X}{N}\cdot + Fe^{2+} + 2\,Cl^- \quad (4)$$

$$n\,R\text{–}\underset{Cl}{\overset{X}{N}} + Fe^{2+} \longrightarrow \underset{(IV)}{[(RNXCl)_nFe^{2+}]} \quad (5)$$

$$R\text{–}\underset{Cl}{\overset{X}{N}} + Fe^{2+} \longrightarrow R\text{–}\overset{X}{N}\cdot + Fe^{3+} + Cl^- \quad (6)$$

$$IV + CCl_4 \longrightarrow \left[\begin{matrix}(RNXCl)_nFeCl^{2+}\\ \cdot CCl_3\end{matrix}\right]_{(V)} \quad (7)$$

Amino radical and ferrous ion are formed by the action of iron to *N*-chloroalkylamine, as suggested from studies by Otsu *et al.*[3] Although a part of ferrous ions is oxidized by *N*-chloroalkylamine to form ferric ion (Eq. (6)), most part of ferrous ions forms a complex (IV) with *N*-chloroalkylamine (Eq. (5)). This complex reacts with carbon tetrachloride to form trichloromethyl radical (Eq. (7)). The trichloromethyl radical thus formed seems to coordinate to iron–*N*-chloroalkylamine complex or to be trapped within the cage of this complex and carbon tetrachloride as in the system of triethyl phosphite–iron salts–carbon tetrachloride.[14]

Parts of amino radicals, aminium radicals, and chlorine atoms formed through Reactions 1, 2, 4, and 6 act as free radical initiators and give the telomers with the composition similar to that by usual radical initiators such as DTBP (Eqs. (8)—(9)).

$$I\cdot + n\,C_2H_4 \longrightarrow I(C_2H_4)_n\cdot \xrightarrow{CCl_4} I(C_2H_4)_nCl + \cdot CCl_3 \quad (8)$$

$$\cdot CCl_3 + n\,C_2H_4 \longrightarrow CCl_3(C_2H_4)_n\cdot \xrightarrow{CCl_4} CCl_3(C_2H_4)_nCl + \cdot CCl_3 \quad (9)$$

On the other hand, coordinated radicals (V) react with ethylene to produce $n=1$ telomer almost selectively.[14]

$$V + C_2H_4 \longrightarrow IV + CCl_3C_2H_4Cl \quad (10)$$

The telomerization of ethylene with chloroform using the system of *N*-chlorodi-*n*-butylamine and *N*-chloromono-*n*-butylamine afforded the product, a greater part of which was of chlorine abstracted type, *i.e.*, $CHCl_2(C_2H_4)_nCl$. To a contrary, the product of telomerization by DTBP or di-*n*-butylamine was of hydrogen abstracted type, $CCl_3(C_2H_4)_nH$. This result seems to support the above suggestion.

The authors would like to express their thanks to Mr. T. Suzuki for the assistance in the experiments.

12) T. Asahara and J. Hirano, *Kogyo Kagaku Zasshi*, **69**, 1512 (1966).
13) Y. Igi, N. Kinoshita, and M. Imoto, *ibid.*, **74**, 295 (1971).
14) T. Asahara, M. Senō, and T. Sato, *ibid.*, **74**, 2288 (1971).

Photoinduced Reactions. LXXIII. Solvent Dependence in the Photochemical Reaction of α-Nitroepoxides[1]

Isao SAITO, Masaaki TAKAMI, Toshiro KONOIKE, and Teruo MATSUURA
Department of Synthetic Chemistry, Faculty of Engineering, Kyoto University, Sakyo-ku, Kyoto 606
(Received June 21, 1973)

The photochemical reaction of α-nitroepoxides showed marked solvent dependence. The photolysis of (1,2-epoxy-2-nitropropyl)benzene (I) in 2-propanol led to the formation of three products 1-phenyl-1-isopropoxy-2-propanone (IIb), 1-phenyl-1,2-propanedione oxime (III) and 1-hydroxy-1-phenyl-2-propanone oxime (IV), whereas on irradiation in ether I gave exclusively IV. However, in *t*-butyl alcohol, benzene, acetone, acetonitrile or *n*-hexane, I was not susceptible to photolysis. The photolysis of α,α'-epoxy-α-nitrobibenzyl (V) in ether gave benzoin oxime (VII) in addition to benzaldehyde and benzoic acid, whereas in methanol it gave benzoin methyl ether (VI) in the dark. These reactions are interpreted in terms of effects of the acidity and hydrogen-donating property of solvents on the excited α-nitroepoxides. The pyrolysis of I and V were also examined.

The photochemical reaction of carbonyl compounds attached to a small ring has been extensively investigated.[2,3] Among these compounds, α,β-epoxyketones are known to give β-diketones and α-hydroxyketones[4-6] *via* mechanisms involving the initial n-π^* excitation followed by opening the epoxy ring.[5,6] In view of the similarity between photochemical behaviors of isoelectronic carbonyl and nitro groups,[7] such as photoreduction and α-cleavage, the photochemical behavior of α-nitroepoxides drew our attention. It also encouraged us that the solution photochemistry of aliphatic nitro compound has yet been little investigated.[8] The present paper deals with results obtained with certain α-nitro epoxides which undergo solvent-depending photochemical reactions.

Results and Discussion

Photolysis of (E)-(1,2-Epoxy-2-nitropropyl)benzene (I). In methanol, I[9] was found to be slowly converted into a methoxyketone IIa[10] with the participation of the solvent even in the dark, whereas I was stable to 2-propanol and ether in the absence of light. Irradiation of I in 2-propanol, ether and mixutres of them was carried out with light through Pyrex under bubbling nitrogen at room temperature. The ratio of photoproducts IIb,[10] III,[11] and IV[9] was solvent-dependent (Table 1). The photochemical conversions appear to occur in protic or hydrogen-donating solvents or ones having both properties since I was unsusceptible to photolysis in benzene, acetone, acetonitrile, and *n*-hexane, but was converted very slowly into III in *t*-butyl alcohol.

TABLE 1. PHOTOLYSIS OF I IN VARIOUS SOLVENTS

Solvent	Yields of products(%)[a]			
	II	III	IV	I
MeOH	85	—	—	12
i-PrOH	31	41	11	17
i-PrOH–Et_2O 9:1	20	25	15	39
i-PrOH–Et_2O 1:1	8	—	31	57
i-PrOH–Et_2O 1:9	—	—	30	67
Et_2O	—	—	20	80

a) The yields were determined by NMR analyses.

The conversion of I in methanol into IIa was accelerated by irradiation. The protic nature of solvents could be responsible for the formation of II. The decrease of the yield of II in the order, methanol > 2-propanol ≫ *t*-butyl alcohol, is probably due to steric hindrance of the solvents. The hydrogen-donating ability of solvents could be responsible for the formation of IV, since irradiation of I in ether gave exclusively IV. On the other hand, the formation of III should be ascribed to both protic and hydrogen-donating properties of solvents.

TABLE 2. QUENCHING EXPERIMENTS OF I WITH 1,3-PENTADIENE

Quencher concentration (mol/mol of I)	Yields of products (%)[a]					
	In 2-propanol				In ether	
	II	III	IV	I	IV	I
0	24	40	14	22	45	0
1.0	13	7	27	53	—	—
1.5	14	6	11	69	—	—
2.0	6	2	6	86	22	57
3.0	5	1	5	89	—	—
5.0	—	—	—	—	5	93

a) The yields were determined by NMR analyses.

1) Part LXXII: T. Matsuura, A. Horinaka, and R. Nakashima, *Chem. Lett.*, **1973**, 887. Part of this work was reported as a short communication; I. Saito, M. Takami, T. Konoike, and T. Matsuura, *Tetrahedron Lett.*, **1972**, 2689.

2) A. Padwa, "Organic Photochemistry," ed. by O.L. Chapman, Vol. 1, Marcel Dekker Inc., New York (1967), p. 91.

3) A. Padwa, *Accounts Chem. Res.*, **4**, 48 (1971).

4) S. Bodforss, *Chem. Ber.*, **51**, 214 (1918).

5) C. Lehmann, K. Schaffner, and O. Jeger, *Helv. Chim. Acta*, **45**, 1031 (1962).

6) H. Wehrli, C. Lehmann, K. Schaffner, and O. Jeger, *ibid.*, **47**, 1336 (1964).

7) H.A. Morrison, "The Chemistry of the Nitro and Nitroso Groups", part 1, ed. by H. Feuer, Interscience, New York, N. Y., (1969), p. 165.

8) a) S. T. Reid and J. N. Tucker, *Chem. Commun.*, **1970**, 1286. b) S. T. Reid and E. J. Wilcox, *Tetrahedron Lett.*, **1972**, 1759. c) C. Chachaty and A. Forchioni, *ibid.*, **1968**, 1079.

9) H. Newmann and R. B. Angier, *Tetrahedron*, **26**, 825 (1970).

10) V. Auwers and L. Muller, *Ann. Chem.*, **524**, 155, 162, 170 (1936).

11) O. L. Chapman, *Pure Appl. Chem.*, **9**, 585 (1964).

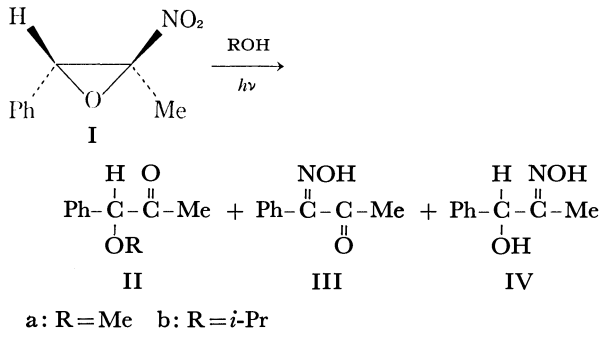

a: R=Me b: R=*i*-Pr

Photolysis of (E)-α,α'-Epoxy-α-nitrobibenzyl (V). Analogously to the dark reaction of I in methanol, V[9] reacted readily with methanol in the absence of light resulting in the formation of benzoin methyl ether (VI).[12] Irradiation of V in ether under similar conditions gave a complex mixture of products, from which benzoin oxime (35%) corresponding to IV, benzaldehyde (15%) and benzoic acid (11%) were isolated. The photolysis of V in 2-propanol was more complex and the isolation of pure products was unsuccessful, whereas V did not undergo photochemical change in *t*-butyl alcohol, benzene, and *n*-hexane under similar conditions.

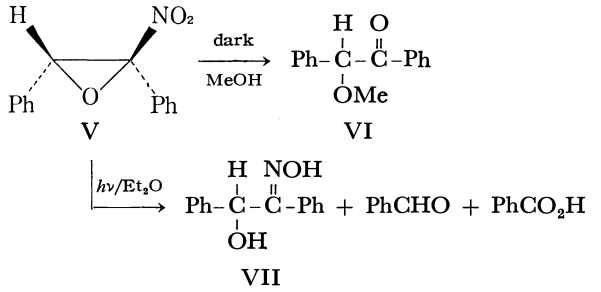

Mechanistic Consideration. As already pointed out, the presence of an aprotic solvent is requisite for the formation of II and III during the photolysis of I. This may be interpreted by considering on 1,3-dipolar intermediate VIII which is derived from the excited state of I, probably with the assistance of a solvent proton. The intermediate VIII may undergo two competitive processes, path a and path b shown in Scheme 1. In path a, VIII reacts with an alcohol to form II with the elimination of nitrous acid. Nitrogen oxides resulted from nitrous acid were experimentally detected. The photochemical addition of alcohols to simple epoxides has been reported,[13-15] although the reaction suffers auto-catalysis by a trace amount of acidic matter formed during the photolysis.[13,14] In methanol, which is more nucleophilic and has a more acidic proton than 2-propanol, the solvent can attack even in the ground state of I to the β-C–O bond having a considerably polar character attributable to the nitro group.

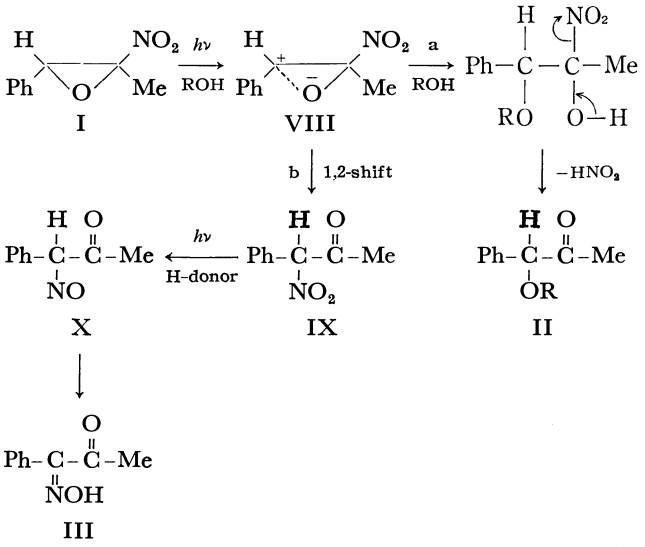

Scheme 1.

In path b, the 1,3-dipolar intermediate VIII undergoes a 1,2-shift of the nitro group to form an α-nitro ketone IX in competition with the attack of an alcohol to the cationic β-carbon. An analogous rearrangement of I to IX is known to occur by acid catalysis with boron trifluoride.[9] The α-nitroketone IX may be photochemically reduced in a hydrogen-donating solvent to III possibly *via* an α-nitrosoketone X. Supporting this scheme, IX was found to be rapidly reduced upon irradiation in 2-propanol to give III in good yield. To the best of our knowledge, the photoreduction of an aliphatic nitro compound to an oxime is the first example. The photoreduction of IX to III may be rationalized by a mechanism involving the intermediary formation of a coupling product XI between IX and 2-propanol (Scheme 2). Similar intermediates have been proposed by Reid and co-workers.[8]

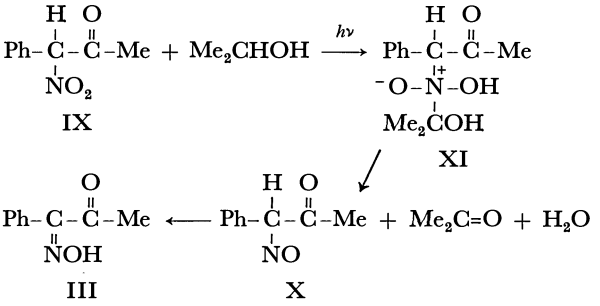

Scheme 2.

For the formation of III, an alternative pathway should be considered, which involves photochemical deoxygenation of the epoxy ring of I followed by rearrangement of a nitroolefin XII to form III (Scheme 3). In fact, the photochemical rearrangement of XII into III has been reported by Chapman and co-workers.[16] We found that *cis*-α-nitrostilbene (XIII) underwent the same rearrangement to benzil oxime (XIV) in addition to the known isomerization to

12) J. Wier, *J. Chem. Soc.*, **91**, 1391 (1905).
13) K. Tokumaru, This Bulletin, **40**, 242 (1967).
14) M. Hisaoka and K. Tokumaru, *Chem. Lett.*, **1973**, 351.
15) R. C. Petterson, C. S. Irving, A. M. Khan, G. W. Griffin, and I. M. Sarkar, 18th. National Meeting of the American Chemical Society, September, 1969, New York, ORGN-10.
16) O. L. Chapman, P. G. Cleveland, and E. D. Hogauson, *Chem. Commun.*, **1966**, 101.

trans-α-nitrostilbene (XV).[17] Considering the fact that neither XIV nor XV was obtained by the photolysis of V, which is expected to form XIII according to Scheme 3, the pathway involving the initial deoxygenation is less probable than Scheme 1.

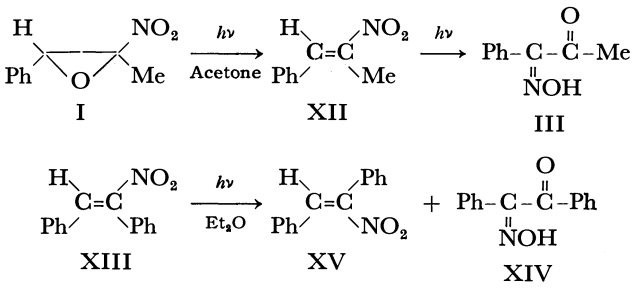

Scheme 3.

Four possible pathways were considered for the formation of α-hydroxyimino alcohols IV and VII by the photolysis in a hydrogen-donating solvent of I and V respectively (Scheme 4). Path a involves rearrangement to an α-nitroketone XVI analogous to the photorearrangement of α,β-epoxyketones to β-diketones,[4] followed by photoreduction leading to IV or VII. This pathway was eliminated by the finding that XVIb was unsusceptible to photolysis in ether. Path b involves reduction to an α-nitro alcohol XVII followed by further photoreduction leading to IV or VII. Path b was also excluded by the finding that neither XVIIa[9] or XVIIb[18] was susceptible to photolysis in ether.

Path c and path d involve photoreduction of the nitro group leading to a hydroxylamine XVIII and a nitrosoepoxide XIX respectively. The former will be tautomerized and the latter photoreduced to IV or VII. Attempts to synthesize these possible intermediates were unsuccessful. Available evidences at present cannot distinguish between path c and path d.

In order to obtain informations on the nature of the excited state of α-nitroepoxides, quenching experiments were carried out with I in 2-propanol and ether. Piperylene was found to quench both the disappearance of I and the formation of II, III, and IV in 2-propanol and of IV in ether. A triplet state of I may be responsible for the first step of the over-all reactions.

In conclusion, the photochemistry of α-nitroepoxides distinctly differs from that of α,β-epoxyketones, an isoelectronic analog. It may be reasonable to assume that the difference is due to a more polar character of nitro group which alters the electronic situation of the epoxy ring as already seen from the reactivity to methanol in the ground state.

Pyrolysis of α-Nitroepoxides I and V. When I was heated at 120—130 °C at atmospheric pressure, three products, IX (33%), XXIa[9] (21%) and benzaldehyde (6%) were obtained. Pyrolysis of I at 150 °C at 20 mmHg gave exclusively XXIa. A similar temperature dependence was observed in the pyrolysis of V. Thus XVIb was exclusively obtained on pyrolysis at 100 °C, while benzil (XXIb) (80%), benzaldehyde (15%) and benzoic acid (5%) were obtained at 150 °C.

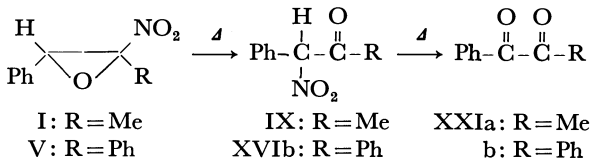

It is evident that α-nitroketones IX and XVIb are an intermediate in the formation of XXI, since pyrolysis of IX at 150 °C and XVIb at 200 °C was found to give XXIa and XXIb respectively. The initial step

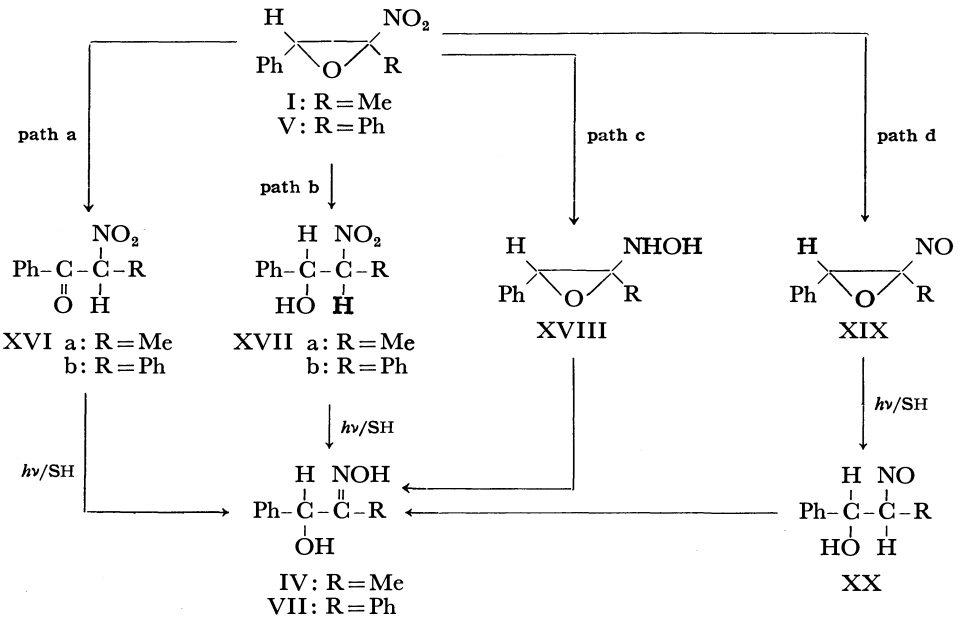

Scheme 4.

17) J. A. Sousa, J. Weinstein, and A. L. Bluhm, *J. Org. Chem.*, **34**, 3320 (1969).

18) F. G. Bordwell and E. W. Garbisch, Jr., *ibid.*, **27**, 2322 (1962).

of these pyrolysis reactions may be a homolytic cleavage of the C–NO_2 bond as seen in the pyrolysis of nitromethane.[19]

Experimental

All mps are uncorrected. IR spectra were obtained by a Japan Spectroscopic Co., Model IRS spectrometer. NMR spectra were obtained on a Varian T-60 NMR spectrometer with TMS as an internal standard. Elemental analyses were performed at Elemental Analysis Center of Kyoto University.

Dark Reaction of (E)-(1,2-Epoxy-2-nitropropyl)benzene (I) with Methanol. A solution of I[9] (20 mg) in 20 ml of anhydrous methanol in a Pyrex tube was let to stand for 21 hr at room temperature under nitrogen atmosphere. After evaporating under reduced pressure, the residue showed two spots on tlc. Analysis of the residue by NMR indicated that it consisted of unreacted I (59%) and IIa (41%). After purifying by glpc (DC-550 Silicone on Celite column at 160 °C), IIa was obtained as a colorless oil, which was identified by a comparison of its IR spectrum with that of an authentic sample.[10] ν_{max} (neat) 1720 cm^{-1}; NMR ($CDCl_3$): δ 2.13 (s, 1H), 3.60 (s, 3H), 6.67 (s, 1H), and 7.40 (s, 5H).

Irradiation of (E)-(1,2-Epoxy-2-nitropropyl)benzene (I).

A) In Methanol: A solution of I [λ_{max}^{EtOH}: 290 nm (ε 450) and 230 nm (ε 4500)] (0.23 g) in 100 ml of purified methanol was irradiated with a 100 W high-pressure mercury lamp (Pyrex filter) under bubbling nitrogen for 5 hr. The gas outlet tube was connected to a trap containing a solution of sulfanilic acid (5 g) and *N,N*-dimethylnaphthylamine (5 g) in 200 ml of acetic acid. The trap solution was turned to red, indicating the liberation of nitrogen oxides.[20] The reaction mixture was evaporated to give a residue, the NMR spectrum of which showed the same spectral pattern as that of the dark reaction products. After purifying by glpc (DC-550 Silicone on Celite column at 160 °C), IIa was obtained as a colorless oil, which was identical with an authentic sample (IR).[10] The yields were determined by NMR analysis; IIa in 69% and I in 31%.

B) In 2-Propanol: A solution of I (0.50 g) in 5 ml of 2-propanol in a Pyrex tube was externally irradiated for 40 hr under nitrogen atmosphere with a 100 W high-pressure mercury lamp at room temperature. The reaction mixture was evaporated and the residue was chromatographed on neutralized alumina (15 g). Elution with benzene afforded 0.1 g of recovered I. Further elution with benzene yielded 0.15 g of IIb as a slightly yellow oil, which was identical with an authentic sample (IR).[10] Elution with chloroform gave a brown mass. After recrystallization from ethyl acetate colorless crystals were obtained (0.2 g), mp 160—161 °C, which were identified to be III by a comparison of its IR spectrum with that of an authentic sample.[11] ν_{max} (nujol) 3300 and 1670 cm^{-1}; NMR ($(CD_3)_2CO$): δ 2.47 (s, 3H), 7.36 (s, 5H), and 11.50 (s, 1H). Further elution with chloroform gave a brown mass. After recrystallization from ethyl acetate IV was obtained as colorless crystals (0.05 g), mp 111—112 °C, which were identical with an authentic sample (IR),[9] NMR ($(CD_3)_2CO$): δ 1.68 (s, 3H), 4.72 (s, 1H), 5.31 (s, 1H), 7.39 (s, 5H), and 11.40 (s, 1H).

C) In Ether: A solution of I (0.5 g) in 5 ml of anhydrous ether in a Pyrex tube was irradiated for 40 hr as above. The reaction mixture was evaporated and the resulting brown oil was chromatographed on neutralized alumina (15 g). Elution with chloroform gave colorless crystals. Recrystallization from ethyl acetate gave IV (0.15 g), mp 111—112 °C, which was identical with an authentic sample (IR).[9]

D) In Mixtures of 2-Propanol and Ether of Different Ratios: Solutions of I (50 mg) in each 20 ml of three solvent systems (2-propanol and ether; 9:1, 1:1, and 1:9) in Pyrex tubes under nitrogen atmosphere were irradiated for 40 hr with a 100 W high-pressure mercury lamp using a merry-go-round apparatus at room temperature. After evaporating, the yields of II, III, and IV were determined by NMR analysis. These results are shown in Table 1.

E) In Other Solvents (t-Butyl Alcohol, Benzene, Acetone, Acetonitrile, and n-Hexane): Solutions of I (50 mg) in each 20 ml of the solvents were externally irradiated under the same conditions as described in D). The reaction mixtures were monitored by tlc. After evaporating, the residues were analyzed by NMR indicating that I was recovered completely in benzene, acetone, acetonitrile, and *n*-hexane. Analyses of the product mixture obtained in *t*-butyl alcohol by tlc and NMR showed the existence of a small amount of III.

Dark Reaction of (E)-α,α'-Epoxy-α-nitrobibenzyl (V) in Methanol. A solution of V[9] (0.35 g) in 4 ml of anhydrous methanol in a Pyrex tube was let stand for 1 day at room temperature under nitrogen atmosphere. After evaporating, the residue showed a single spot on tlc and a single peak on glpc (DC-550 Silicone on Celite column at 160 °C). After purifying by glpc, the product VI was obtained as an oil, which was identical with an authentic sample (IR).[12] ν_{max} (neat) 1670 cm^{-1}; NMR ($CDCl_3$): δ 3.45 (s, 3H), 5.53 (s, 1H), and 8.20—7.20 (m, 10H).

Irradiation of (E)-α,α'-Epoxy-α-nitrobibenzyl (V). *A) In Methanol*: A solution of V [λ_{max}^{EtOH}: 290 (ε 800) and 232 nm (ε 6000)] (0.35 g) in 4 ml of anhydrous methanol was externally irradiated with a 100 W high-pressure mercury lamp for 40 hr under nitrogen atmosphere. After evaporating, glpc, tlc, and NMR analyses of the residue showed that it consisted of only IV.

B) In Ether: A solution of V (1.8 g) in 50 ml of dry ether was irradiated with a 100 W high-pressure mercury lamp under bubbling nitrogen at room temperature. After 11 hr V was completely consumed, which was monitored by tlc. The reaction mixture was evaporated and the residue was chromatographed on silica gel column (50 g). Elution with 90 ml of benzene afforded an oil (0.09 g), identified as benzaldehyde (IR). Elution with 800 ml of a mixture of benzene and chloroform (*ca.* 1:1) gave colorless crystals (0.28 g), identified as benzoic acid (IR). Elution with 100 ml of chloroform gave VII (0.63 g) as colorless crystals, mp 150—153 °C, which were identical with an authentic commercial sample (IR). NMR (DMSO-d_6): δ 5.60 (s, 1H), 7.27 (s, 10H), and 10.87 (s, 1H).

C) In 2-Propanol: A solution of V (0.1 g) in 20 ml of 2-propanol was externally irradiated with a 400 W high-pressure mercury lamp for 20 hr under nitrogen atmosphere at room temperature. After evaporating, the residue showed nine spots on tlc (silica gel with chloroform). The isolation of pure products was unsuccessful.

Irradiation of 2-Nitro-1-phenyl-1-propanol (XVIIa). A solution of XVIIa[9] (0.18 g) in 20 ml of ether in a Pyrex tube was externally irradiated with a 400 W high-pressure mercury lamp under nitrogen atmosphere for 50 hr at room temperature. After evaporating, the residue was analyzed by tlc and NMR showing that it consisted of only recovered XVIIa.

Irradiation of 1,2-Diphenyl-2-nitroethanol (XVIIb). A

19) a) C. G. Crawforth and D. J. Waddington, *Trans. Faraday Soc.*, **65**, 1334 (1969). b) K. Glänzer and J. Troe, *Helv. Chim. Acta*, **55**, 2884 (1972).

20) F. G. Germuth, *Ind. Eng. Chem., Anal. Ed.*, **1**, 28 (1929).

solution of XVIIb[18] (0.464 g) in 70 ml of ether was irradiated with a 100 W high-pressure mercury lamp (Pyrex filter) under bubbling nitrogen at room temperature for 20 hr. Analyses of the photolyzate by tlc, glpc, and NMR indicated no consumption of XVIIb.

Irradiation of 1-Nitro-1-phenyl-2-propanone (IX). A solution of IX[9] (50 mg) in 20 ml of 2-propanol in a Pyrex tube was externally irradiated for 22 hr with a 400 W high-pressure mercury lamp under nitrogen atmosphere at room temperature. After removal of 2-propanol under reduced pressure, a crystalline mass was obtained. Recrystallization from ethyl acetate gave III as colorless crystals (13 mg), mp 160—161 °C, which were identical with an authentic sample (IR and NMR).[11]

Preparation of 2-Nitro-2-phenylacetophenone (XVIb). To a solution of 1,2-diphenyl-2-nitroethanol (XVIIb;[18] 5 g) in 50 ml of acetone was added dropwise (30 min) under stirring a solution of chromium trioxide (13 g) in a mixture of 40 ml of water and 10 ml of conc. sulfuric acid at room temperature. After the addition of chromium trioxide, the reaction mixture was stirring for about 3 hr. The mixture was diluted with 150 ml of acetone and 150 ml of water, then extracted with ether. The ethereal layer was washed with water and dried over anhydrous sodium sulfate. After the removal of ether, a crystalline mass was obtained, which was recrystallized from a mixture of benzene and *n*-hexane gave 2 g of XVIb, mp 75 °C; ν_{max} (nujol) 1680, 1560, and 1350 cm^{-1}; NMR ($CDCl_3$): δ 7.3—8.0 (m).

Found: C, 69.51; H, 4.52; N, 5.83%. Calcd for $C_{14}H_{11}NO_2$: C, 69.70; H, 4.59; N, 5.80%.

Irradiation of 2-Nitro-2-phenylacetophenone (XVIb). A solution of XVIb (0.5 g) in 40 ml of ether in a Pyrex tube was externally irradiated with a 400 W high-pressure mercury lamp for 20 hr under nitrogen atmosphere at room temperature. After the removal of ether, analysis of the residue by tlc and NMR indicated no consumption of XVIb.

Quenching Experiments. *A) I with 1,3-Pentadiene in 2-Propanol*: 1,3-Pentadiene was distilled prior to use. Five solutions of I[9] (50 mg; 0.28×10^{-3} mol) in 20 ml of 2-propanol were prepared in Pyrex tubes. To each solution given amounts of 1,3-pentadiene, 0 μl, 30 μl (0.28×10^{-3} mol), 45 μl (0.42×10^{-3} mol), 60 μl (0.56×10^{-3} mol), and 90 μl (0.84×10^{-3} mol) were added. These five tubes were irradiated with a 400 W high-pressure mercury lamp using a merry-go-round apparatus for 13 hr under nitrogen atmosphere at room temperature. After evaporating, the residues were analyzed by NMR. The yields of recovered I and products were determined by NMR analysis. The results were summarized in Table 2.

B) I with 1,3-Pentadiene in Ether: Three solutions containing I (50 mg; 0.28×10^{-3} mol) and a given amount of 1,3-pentadiene (0 μl, 60 μl (0.56×10^{-3} mol) and 150 μl (1.40×10^{-3} mol), in 20 ml of ether were prepared in Pyrex tubes. These three tubes were irradiated for 18.5 hr as above. After evaporating each solution, the yields of recovered I and product IV were determined by NMR analysis. The results were summarized in Table 2.

Pyrolysis of (E)-(1,2-Epoxy-2-nitropropyl)benzene (I). *A) At 150 °C*: The pyrolysis of 20 mg of I[9] was done at 150 °C for 5 min under 20 mmHg. Analysis of the resulting yellow oil by NMR showed complete consumption of I and the yellow oil showed two peaks on glpc (DC-550 Silicone on Celite column at 150 °C). Glpc separation (DC-550 Silicone at 150 °C) gave XXIa as a yellow oil (13 mg), which was identical with an authentic sample.[9] ν_{max} (neat) 1710 and 1680 cm^{-1}; NMR (CCl_4): δ 2.13 (s, 3H) and 7.25—8.20 (m, 5H).

B) At 120—130 °C: A glass tube containing I[9] (25 mg) was heated at 120—130 °C for 10 min. Analysis of the resulting yellow oil by NMR showed that it consisted of recovered I (8%), XXIa (21%), benzaldehyde (6%), IX (33%), and an unknown product (30%). Among XXIa,[9] benzaldehyde, and the unknown product separated by glpc, the former two were identified by a comparison of the NMR and IR spectra with those of authentic samples. The methine proton peak of IX in the NMR spectrum of the product mixture was in accord with that of an authentic sample.[9] When an authentic sample of IX was heated at 150 °C for 5 min, XXIa was obtained quantitatively, which was monitored by NMR.

Pyrolysis of (E)-α,α'-Epoxy-α-nitrobibenzyl (V). *A) At 160 °C*: The pyrolysis of V[9] (24 mg) was done at 160 °C for 1 hr. Analysis of the resulting yellow oil by NMR showed complete consumption of V. Three products were isolated by glpc separation (DC-550 Silicone on Celite column at 160 °C), benzaldehyde (15%), benzoic acid (5%) and benzil (XXIb) (80%), which were identical with authentic samples (IR). The yields were determined by NMR analysis.

B) At 100 °C: The pyrolysis of V[9] (50 mg) was done at 100 °C for 2 hr under 20 mmHg. The reaction mixture solidified to give slightly yellow crystals, which were recrystallized from a mixture of benzene and *n*-hexane to give 25 mg of XVIb as colorless crystals, mp 75 °C, which were identical with an authentic sample (IR and NMR). Pyrolysis of XVIb at 200 °C in a glpc column gave a peak of XXIb.

Branched-chain Sugars. III. Addition of Vinylmagnesium Bromide to 5,6-Dideoxy-1,2-*O*-isopropylidene-6-*C*-nitro-3-*O*-substituted-α-D-*xylo*-hex-5-enofuranoses[1]

Takao IIDA, Masuo FUNABASHI, and Juji YOSHIMURA

Laboratory of Chemistry for Natural Products, Faculty of Science, Tokyo Institute of Technology, Ookayama, Meguro-ku, Tokyo 152

(Received April 20, 1973)

Addition of vinylmagnesium bromide to 3-*O*-acetyl (**1**) and 3-*O*-benzyl (**3**) derivatives of 5,6-dideoxy-1,2-*O*-isopropylidene-6-*C*-nitro-α-D-*xylo*-hex-5-enofuranose gave the corresponding 5-deoxy-5-*C*-vinyl derivatives of L-*ido*-type, of which the configurations were proved by intramolecular cyclization into the corresponding nitrocyclitols. Conformations of **1** and **3** and that of the transition state in the addition reaction were discussed on the basis of their NMR parameters.

In order to find out a synthetic passway of 5,6-dideoxy-5-*C*-formyl-6-*C*-nitro-D-glucose as a key intermediate for synthesis of tetrodotoxin from D-glucose,[2] addition of vinylmagnesium bromide to 5,6-dideoxy-1,2-*O*-isopropylidene-6-*C*-nitro-3-*O*-substituted-α-D-*xylo*-hex-5-enofuranoses was examined and the configuration of products were determined to be of L-*ido*-type by intramolecular cyclization into the corresponding branched-chain nitrocyclitols.

Results and Discussion

A few papers on addition of the Grignard reagents to nitroolefins have been published,[3-6] however, no report on the similar reaction of sugar derivatives has been appeared in literatures. Baer and Rank synthesized 3-*O*-acetyl-6-deoxy-1,2-*O*-isopropylidene-6-*C*-nitro-α-D-*xylo*-hex-5-enofuranose (**1**) from 1,2-*O*-isopropylidene-α-D-glucofuranose by periodate oxidation, nitromethane condensation, 3,5-di-*O*-acetylation and elimination.[7] By the similar way, the corresponding 3-*O*-benzyl derivative (**3**) was obtained from 3-*O*-benzyl-1,2-*O*-isopropylidene-α-D-glucofuranose,[8] in which 5-*O*-acetyl-3-*O*-benzyl-1,2-*O*-isopropylidene-β-L-idofuranose (**2**) was obtained as crystals. The configuration of **2** was determined by comparison of its optical rotation ($[\alpha]_D$ −58.2°) with that of the corresponding 3-*O*-acetyl derivatives (D-*gluco* type, $[\alpha]_D$ +18.8°; L-*ido* type, $[\alpha]_D$ −30.1°).[9]

Reaction of **1** and **3** with four equivalents of vinylmagnesium bromide in tetrahydrofuran at 0 °C gave 3-*O*-acetyl (**4**) and 3-*O*-benzyl (**5**) derivatives of 5,6-dideoxy-1,2-*O*-isopropylidene-6-*C*-nitro-5-*C*-vinyl-β-L-idofuranose in 28 and 41% yield, respectively. The epimeric D-*gluco*-type isomer could not be detected by NMR spectra. Reaction of **1** with other Grignard reagents such as methyl, allyl, β-styryl, and phenylmagnesium bromide gave only intractable sirups, and the original nitro group could not be detected in IR spectra of the products, when large excess amount of reagents were used. Vinyllithium reaction of **3** gave **5** in much lower yield than that of the Grignard reaction. Hydrogenation of **5** in the presence of palladium-charcoal gave quantitatively the corresponding 5-*C*-ethyl derivative (**6**).

In order to prove the configuration at *C*-5, both **4** and **5** were respectively de-*O*-isopropylidenated in 70% acetic acid at 80—85 °C for 7—8 hr under monitoring with tlc, and then the hydrolyzed products were intramolecularly cyclized into the corresponding nitro cyclitols, without separation in a pure state. In the case of **5**, cyclization in ethanol at pH 8—9 for 2 days and successive acid-catalyzed acetylation gave 2,4-di-*O*-acetyl-3-*O*-benzyl-1-*O*-ethyl-(1,3,5/2,4,6)-6-nitro-5-vinylcyclohexanetetrol (**7**)[10] in 83% yield. When the cyclization was performed in methanol–water in the presence of equimolar amount of sodium bicarbonate, 3-*O*-benzyl-(3,5/1,2,4,6)-6-nitro-5-vinylcyclohexanetetrol (**8**)[10] was obtained in 52% yield, which was then converted into the corresponding 1,2,4-tri-*O*-acetate (**9**). Acetylation of the sirup obtained from the mother liquor of **8** gave the *C*-1 epimer of **9** (**10**). The ratio of **10** to **9** was 1 : 1.54. In the case of **4**, a similar cyclization and *O*-acetylation gave 1,2,3,4-tetra-*O*-acetyl-(1,3,5/2,4,6)-6-nitro-5-vinylcyclohexanetetrol (**11**)[10] as crystals in 11.4% yield. Hydrogenation of **8** in ethanol–acetic acid in the presence of platinum-charcoal gave 3-*O*-benzyl-(3,5/1,2,4,6)-6-amino-5-ethylcyclohexanetetrol (**12**)[10] as an acetate.

First-order analysis of NMR spectra of nitrocyclitols (**7**—**11**) by double resonance technique clarified their configurations (Table 1). The hydrogen signals at the branched point were distinguished by its multi-splittings and higher resonating magnetic field than others. Other ring-protons appeared in a lower field in the order of alkoxy, nitro, and acetoxy position. They have com-

1) Part II. This Bulletin, **46**, 1515 (1973).
2) J. Yoshimura, K. Kobayashi, K. Sato, and M. Funabashi, *ibid.*, **45**, 1806 (1972).
3) E. P. Kohler and J. F. Stone, *J. Amer. Chem. Soc.*, **52**, 761 (1930).
4) G. D. Buckley and E. Ellery, *J. Chem. Soc.*, **1947**, 1497.
5) A. Lambert, J. D. Rose, and B. C. L. Weedon, *ibid.*, **1949**, 42.
6) J. Colonge and G. Lartigan, *Bull. Soc. Chim. Fr.*, **1965**, 738.
7) H. H. Baer and W. Rank, *Can. J. Chem.*, **43**, 3330 (1965).
8) M. L. Wolfrom and S. Hanessian, *J. Org. Chem.*, **27**, 1800 (1962).
9) J. M. Grosheints and H. O. L. Fischer, *J. Amer. Chem. Soc.*, **70**, 1476 (1948).
10) For easier understanding, the numbering and figures of nitrocyclitols for nomenclature were cited from that of original compounds. Other points were followed by "Tentative Rules for Cyclitol Nomenclature" of IUPAC (1967 rule).

TABLE 1. NMR PARAMETERS OF *O*-ACETYLATED NITROCYCLITOLS

Compound	H_1	H_2	H_3	H_4	H_5	H_6	Other protons
7	3.95(t) $J_{1.2}=10.0$	5.27(t) $J_{2.3}=10.0$	3.64(t) $J_{3.4}=10.0$	5.04(t) $J_{4.5}=10.0$	2.72 $J_{5.6}=12.5$	4.47(dd) $J_{1.6}=10.0$	7.30 (Ph; m), 5.60 (H; m, $J_{5.7}=7.5$), 5.20—5.00 (H_{8a}, H_{8b}; m), 4.62 ($PhCH_2O$; s), 3.54 (OCH_2; q, $J_{CH_3.CH_2}=6.5$), 1.07 (CH_3; q), 2.00 and 1.93 (OAc; s).
9	5.95(t) $J_{1.2}=2.5$	5.00(dd) $J_{2.3}=10.0$	3.92(t) $J_{3.4}=10.0$	5.07(dd) $J_{4.5}=10.5$	3.25 $J_{5.6}=12.5$	4.65(dd) $J_{1.6}=2.5$	7.30 (Ph; m), 5.80—5.10 (H_7, H_{8a} and H_{8b}; m), 4.67 ($PhCH_2O$; s), 2.18, 2.00 and 1.98 (OAc).
10	5.60(t) $J_{1.2}=10.0$	5.20(t) $J_{2.3}=10.0$	3.75(t) $J_{3.4}=10.0$	5.08(dd) $J_{4.5}=12.5$	2.80 $J_{5.6}=12.5$	4.62(dd) $J_{1.6}=10.0$	7.29 (Ph; m), 5.60 (H_7; m), 5.2—5.0 (H_{8a}, H_{8b}; m), 4.62 ($PhCH_2O$; s), 2.08, 1.98 and 1.93 (OAc).
11	4.9—5.9 (H_1-H_4)				2.92 $J_{5.6}=10.5$	4.12 $J_{1.6}=12.5$	4.9—5.9 (H_7, H_{8a} and H_{8b}; $J_{5.7}=8.5$), 1.98 (4×OAc).

monly large *trans*-diaxial coupling constants except H_1 of **9**. Thus, the configuration of **4** and **5** was proved to be of L-*ido* type.

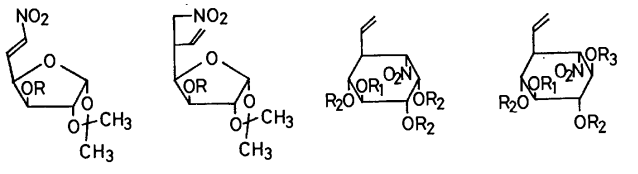

(**1**) R=Ac (**4**) R=Ac (**8**) R_1=Bzl, R_2=H (**7**) R_1=Bzl, R_2=Ac, R_3=Et
(**3**) R=Bzl (**5**) R=Bzl (**9**) R_1=Bzl, R_2=Ac (**10**) R_1=Bzl, R_2=R_3=Ac
(**11**) R_1=R_2=R_3=Ac

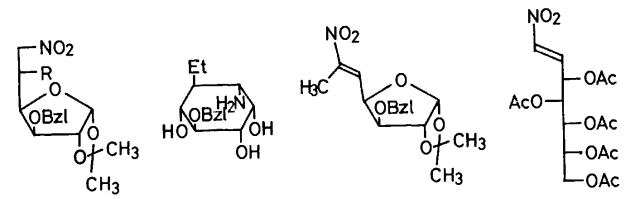

(**2**) R=OAc (**12**) (**13**) (**14**)
(**6**) R=Et

In order to deduce the conformation of nitroolefin function of **1** and **3**, 6-*C*-methyl derivative of **3** (**13**) was synthesized by a similar method to that of **3**, and also D-*gluco*-3,4,5,6,7-pentaacetoxy-1-nitro-1-heptene (**14**) from the corresponding 1-*C*-nitro-1-deoxyalditol[11] by the usual procedure.

NMR parameters of nitroolefin function of these compounds and 1-nitro-1-pentene (**15**)[12] (Table 2) showed that α-proton signals of **1** and **3** appear in the lower magnetic field than that of **14** and **15**, and $J_{\beta,\gamma}$ values in **1** and **3** are smaller than that of others. These facts indicate that the dihedral angle between H_4 and H_5 in **1** and **3** equals nearly 72° [13] in a conformation with a hydrogen-bonding between H_6 and the lactol oxygen, as shown in Fig. 1(A). While that of **13** means the angle should be larger than 140°, indicating the both protons are oriented to an almost true-*trans* as shown in (B).

TABLE 2. NMR PARAMETERS IN NITRO OLEFIN FUNCTIONS

Compound	(H_γ) (H_4)	(H_β) (H_5)	(H_α) (H_6)
1	5.05(t) $J_{4.5}=2.5$	7.10(dd) $J_{5.6}=13.0$	7.29(d)
3	4.91(t) $J_{4.5}=2.5$	7.13(dd) $J_{5.6}=15.5$	7.30(d)
13	4.82(dd) $J_{4.5}=7.5$	7.18(d)	
	(H_3)	(H_2)	(H_1)
14	5.62(m) $J_{2.3}=4.5$	7.22(dd) $J_{2.1}=14.0$	6.97(d)
15	2.30(q) $J_{2.3}=6.5$	7.30(td) $J_{2.1}=14.0$	7.06(d)

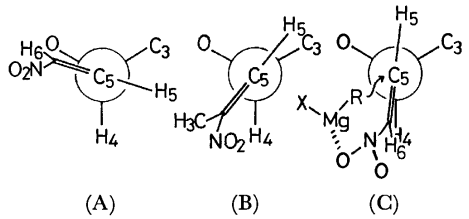

(A) (B) (C)

Fig. 1. Conformation of nitro olefin functions.

If conformation (A) is maintained in the transition state of the Grignard reaction, vinyl group will approach to C_5 from the less-hindered down-side to give D-*gluco* type product, however, the configuration of products were L-*ido* type. Therefore, it will be concluded that the conformation in the transition state

11) J. Yoshimura and H. Ando, *Nippon Kagaku Zasshi*, **85**, 138 (1964).
12) A. I. Meyers and J. C. Sircar, *J. Org. Chem.*, **32**, 4134 (1967).
13) E. W. Garbish, *J. Amer. Chem. Soc.*, **86**, 5561 (1964).

was changed from (A) to (B) by coordination of the Grignard reagent to the nitro-oxygen, and the vinyl group attacked from less-hindered lactol-oxygen site, as shown in (C).

Experimental

All melting points are uncorrected. The solutions were evaporated under diminished pressure at a bath temperature not exceeding 45 °C. Specific rotations were measured in a 0.5-dm tube, with a Carl Zeiss photoelectric polarimeter. The IR spectra were recorded with a Hitachi Model EPI-GS spectrophotometer. The NMR spectra were taken in deuteriochloroform with a JMN-4H-100 MHz Spectrometer using tetramethylsilane as an internal standard. Chemical shifts and coupling constants were recorded in δ and Hz units, and frequencies in cm^{-1}.

5-O-Acetyl-3-O-benzyl-6-deoxy-1,2-O-isopropylidene-6-C-nitro-β-L-idofuranose (2). To a solution of 3-*O*-benzyl-1,2-*O*-isopropylidene-α-D-glucofuranose (60 g, 0.193 mol)[8] in benzene (500 ml) was added lead tetraacetate (80 g, 0.20 mol) portionwise under refluxing, filtered after cooling, and evaporated. The residual sirup was extracted with chloroform, and the extract was washed with water, dried, and evaporated to give the corresponding 5-aldehyde derivative (56 g) as a sirup. A solution of the sirup and nitromethane (40 ml, 0.65 mol) in ethanol (100 ml) was adjusted to pH 7.8—8.0 with 2M-sodium hydroxide, stood at room temperature for 5 hr, neutralized with acetic acid, and evaporated. The residual sirup was extracted with chloroform, and the extract was washed twice with water, dried, and evaporated to give sirupy mixture of 6-deoxy-6-*C*-nitro derivatives (52 g). A solution of this sirup and *p*-toluenesulfonic acid (0.5 g) in acetic anhydride (50 ml) was kept at room temperature for 3.5 hr, poured into ice-water to give semi-crystalline product in 75.1% (55 g) total yield.

Recrystallization from ethanol gave a pure isomer in 47.2% (33.2 g) yield. Mp 96—97 °C, $[\alpha]_D^{23}$ −58.2° (*c* 0.97, chloroform); IR: 1740 (ester), 1550 and 1368 (NO_2); NMR: 7.36 (Ph; s), 5.92 (H_1; d, $J_{1.2}$=3.5), 5.73 (H_5; m), 4.92 and 4.68 (H_{6a} and H_{6b}; ABq, J_{ab}=14.0, $J_{5.6a}$=3.5, $J_{5.6b}$=7.5), 4.69 and 4.51 (-CH_2-; ABq, J_{ab}=11.5), 4.62 (H_2; d), 4.40 (H_4; dd, $J_{3.4}$=3.0, $J_{4.5}$=5.0), 4.07 (H_3; d), 2.03 (OAc), 1.51 and 1.36 (2×C-CH_3).

Found: C, 56.78; H, 5.98; N, 3.48%. Calcd for $C_{18}H_{23}NO_8$: C, 56.68; H, 6.08; N, 3.67%.

3-O-Benzyl-5,6-dideoxy-1,2-O-isopropylidene-6-C-nitro-α-D-xylo-hex-5-enofuranose (3). A solution of **2** (2.0 g, 5.25 mmol) in benzene (70 ml) was refluxed in the presence of potassium carbonate (4.0 g, 28.6 mmol), filtered, and evaporated to give a sirup (1.8 g). Fractionation of the sirup on a Kieselgel column with benzene as an effluent gave the pure product as a sirup (1.14 g, 71.3%). $[\alpha]_D^{23}$ −29.1° (*c* 0.96, chloroform); IR: 1650 (C=C), 1510 and 1340 (conjugated NO_2), 735 and 691 (Ph); NMR: 7.35 (Ph; m), 7.30 (H_6; d, $J_{5.6}$=15.5), 7.13 (H_5; dd, $J_{4.5}$=2.5), 6.01 (H_1; d, $J_{1.2}$=3.5), 4.91 (H_4; t, $J_{3.4}$=2.5), 4.68 (H_2; d), 4.68 and 4.46 (CH_2; ABq, $J_{a.b}$=11.5), 4.06 (H_3; d), 1.52 and 1.37 (2×C-CH_3).

Found: C, 60.07; H, 6.08; N, 4.58%. Calcd for $C_{16}H_{19}NO_6$: C, 59.80; H, 5.96; N, 4.36%.

3-O-Benzyl-5,6-dideoxy-1,2-O-isopropylidene-6-C-nitro-5-C-vinyl-β-L-idofuranose (5). To a solution of a sirupy **3** [3.5 g, obtained from 5 g (13.1 mmol) of **2**] in THF (30 ml) was added dropwise a solution of vinyl magnesium bromide[14] in THF (30 ml) prepared from magnesium (1.25 g, 52.4 mmol) and excess amount of vinyl bromide under ice-cooling. After stirring for 1 hr at room temperature, the reaction mixture was neutralized with acetic acid (6 ml) under cooling, and extracted with chloroform. Evaporation of the extract gave a sirup (3.5 g) which was crystallized from ethanol. Yield, 41% (1.86 g); mp 103 °C; $[\alpha]_D^{23}$ −71.4° (*c* 1.23, chloroform); IR: 1640 (C=C), 1540 and 1373 (NO_2). NMR: 7.34 (Ph; s), 5.88 (H_1; d, $J_{1.2}$=3.8), 5.65 (H_7; octet, $J_{5.7}$=8.5, $J_{7.8a}$=17.5, $J_{7.8b}$=10.0), 5.18 and 5.14 ($J_{8a.8b}$=2.5), 4.66 and 4.39 (CH_2; ABq, $J_{a.b}$=10.3), 4.58 (H_2; d), 4.39 (H_6; d, $J_{5.6}$=6.0), 4.14 (H_4; dd, $J_{4.5}$=6.8), 3.84 (H_3; d, $J_{3.4}$=3.0), 3.45 (H_5; m), 1.29 and 1.46 (2×C-CH_3).

Found: C, 62.08; H, 6.79; N, 3.98%. Calcd for $C_{18}H_{23}NO_6$: C, 61.88; H, 6.64; N, 4.01%.

3-O-Acetyl-5,6-dideoxy-1,2-O-isopropylidene-6-C-nitro-5-C-vinyl-β-L-idofuranose (4). In the same manner as **5**, **1** (2.68 g, 9.85 mmol) was treated with 4 equimolar amount of vinylmagnesium bromide in THF. Fractionation of the product on a Kiesel Gel 60 column gave 0.87 g (28%) of **4** as a sirup. $[\alpha]_D^{23}$ −35.6° (*c* 0.96, chloroform); IR: 1745 (ester), 1635 (C=C), 1544 and 1381 (NO_2).

Found: C, 52.25; H, 6.49; N, 4.64%. Calcd for $C_{13}H_{19}NO_7$: C, 51.82; H, 6.36; N, 4.65%.

3-O-Benzyl-5,6-dideoxy-5-C-ethyl-1,2-O-isopropylidene-6-C-nitro-β-L-idofuranose (6). Hydrogenation of **5** (150 mg) in ethanol in the presence of palladium-charcoal (5%, 70 mg) at a room temperature showed the absorption of calculated amount of hydrogen (10.2 ml) within 6 min. Evaporation of the filtrate of the reaction mixture gave a sirup which was crystallized from petroleum ether. Mp 78—79 °C; $[\alpha]_D^{23}$ −50.5° (*c* 0.78, chloroform); IR: 1540 and 1374 (NO_2); NMR: 7.36 (Ph; s), 5.93 (H_1; d, $J_{1.2}$=4.0), 4.70 and 4.44 (CH_2; ABq, $J_{a.b}$=11.5), 4.66 (H_2; d), 4.47 and 4.23 (H_{6a} and H_{6b}; each q, $J_{6a.6b}$=12.5, $J_{5.6a}$=3.0, $J_{5.6b}$=6.0), 4.18 (H_4; q, $J_{3.4}$=3.0, $J_{4.5}$=8.0), 3.93 (H_3; d), 2.67 (H_5; m), 1.70—1.20 (H_7; m), 1.51 and 1.34 (2×C-CH_3), 0.97 (H_8; t, $J_{7.8}$=6.5).

Found: C, 61.57; H, 7.30; N, 3.79%. Calcd for $C_{18}H_{25}NO_6$: C, 61.52; H, 7.17; N, 3.99%.

2,4-Di-O-acetyl-3-O-benzyl-1-O-ethyl-(1,3,5/2,4,6)-6-nitro-5-vinylcyclohexanetetrol (7). A solution of **5** (0.35 g, 1 mmol) in 70% acetic acid (10 ml) was heated at 80—85 °C for 7.5 hr, evaporated to give a sirup. A solution of the sirup in ethanol (20 ml) adjusted to pH 8—9 with 2M potassium hydroxide was kept at room temperature for 2 days, neutralized with Amberlite IR-120, evaporated to give sirupy nitrocyclitol (0.28 g, 83%). Acid-catalyzed acetylation of the sirup gave the corresponding di-*O*-acetate in a quantitative yield, which was recrystallized from ethanol. Mp 146—147 °C; $[\alpha]_D^{23}$ −14.0° (*c* 0.96, chloroform). IR: 1743 and 1732 (ester), 1540 and 1368 (NO_2).

Found: C, 59.66; H, 6.40; N, 3.18%. Calcd for $C_{21}H_{27}NO_8$: C, 59.85; H, 6.46; N, 3.32%.

Intramolecular Cyclization of 3-O-Benzyl-5,6-dideoxy-6-C-nitro-5-C-vinyl-β-L-idofuranose in the Presence of Sodium Bicarbonate. A solution of a sirup obtained by de-isopropylidenation of **5** (1.91 g, 5.47 mmol), and sodium bicarbonate (60 mg) in methanol-water (each 30 ml) was kept at a room temperature for 11 hr, neutralized with Amberlite IR-120, and concentrated to give a semi-crystalline sirup which gave 3-*O*-benzyl-(3,5/1,2,4,6)-6-nitro-5-vinylcyclohexanetetrol (**8**) as crystals from ethanol. Yield, 0.88 g (52%); mp 168—169 °C; $[\alpha]_D^{23}$ −46.5° (*c* 0.99, methanol); IR: 3430, 3330, and 3190 (OH), 1548 and 1362 (NO_2), 734 and 700 (Ph).

Found: C, 58.27; H, 6.33; N, 4.38%. Calcd for $C_{15}H_{19}$-

14) D. Seyferth, "Organic Syntheses", Coll. Vol. IV, p. 258, (1963).

NO_6: C, 58.24; H, 6.19; N, 4.53%.

Acid-catalyzed acetylation of **8** (110 mg) gave quantitatively the corresponding tri-*O*-acetate (**9**) (160 mg) as a sirup which crystallized by standing for 1 month. Mp 95—96 °C; $[\alpha]_D^{23}$ −33.1° (*c* 1.01, chloroform); IR: 1740 (ester), 1550 and 1360 (NO_2).

Found: C, 58.35; H, 5.97; N, 3.09%. Calcd for $C_{21}H_{25}NO_9$: C, 57.92; H, 5.79; N, 3.22%.

On the other hand, evaporation of the mother liquor from **8** gave a sirup (0.52 g) which on acid-catalyzed acetylation gave 1,2,4-tri-*O*-acetyl-3-*O*-benzyl-(1,3,5/2,4,6)-6-nitro-5-vinylcyclohexanetetrol (**10**) as crystals which was recrystallized from ethanol. Yield, 0.7 g (34.2%); mp 165.5—166.5 °C; $[\alpha]_D^{23}$ −14.5° (*c* 1.83, chloroform); IR: 1740 (ester), 1545 and 1360 (NO_2).

Found: C, 57.66; H, 6.05; N, 3.10%. Calcd for $C_{21}H_{25}NO_9$: C, 57.92; H, 5.79; N, 3.22%.

1,2,3,4-Tetra-O-*acetyl-(1,3,5/2,4,6)-6-nitro-5-vinylcyclohexanetetrol (**11**).* De-isopropylidenation of **4** (0.34 g, 11.6 mmol) with 70% acetic acid gave a sirup (0.29 g). A solution of the sirup, and sodium bicarbonate (300 mg) in 50% methanol (20 ml) was kept at a room temperature for 1 day, neutralized with Amberlite IR-120, decolorized with charcoal, and evaporated to give a sirup (0.19 g). Acetylation of the sirup by the usual manner gave sirupy **11** (250 mg) which was crystallized from ether, and recrystallized from ethanol. Yield, 50 mg (11.4%); mp 169—170 °C; $[\alpha]_D^{23}$ −14.9° (*c* 0.74, chloroform).

Found: C, 49.57; H, 5.47; N, 3.69%. Calcd for $C_{16}H_{21}NO_{10}$: C, 49.26; H, 5.47; N, 3.62%.

*3-O-Benzyl-(3,5/1,2,4,6)-6-amino-5-ethylcyclohexanetetrol (**12**).* Hydrogenation of **8** (0.21 g) in ethanol in the presence of palladium-charcoal (110 mg, 5%) and a small amount of acetic acid for 1 day, and evaporation of the filtrate of the reaction mixture gave **12** as an acetate. Mp 203—204 °C; $[\alpha]_D^{32}$ −29.3° (*c* 1.27, methanol); IR: 3400 (OH), 3200 (NH_2) and 1680 (COOH).

Found: C, 59.80; H, 7.92; N, 4.02%. Calcd for $C_{17}H_{27}NO_6$: C, 59.81; H, 7.97; N, 4.10%.

*3-O-Benzyl-5,6,7-trideoxy-1,2-O-isopropylidene-6-C-nitro-α-D-xylo-hept-5-enofuranose (**13**).* A solution of 3-*O*-benzyl-1,2-*O*-isopropylidene-α-D-*xylo*-pentodialdose-(1,4), prepared from 3-*O*-benzyl-1,2-*O*-isopropylidene-α-D-glucofuranose (5.0 g, 16.1 mmol) by lead tetraacetate (8 g) oxidation, and nitroethane (10 ml) in ethanol (10 ml) was adjusted to pH 9.0 with 2M potassium hydroxide, kept at a room temperature for 17 hr, neutralized with acetic acid, and then evaporated. The residual sirup was extracted with chloroform, and the extract was washed twice with water, and evaporated to give sirupy nitro alcohol (3.7 g). Acetylation of the sirup by the usual manner gave the corresponding nitro acetate (4.5 g) as a sirup. A solution of the nitro acetate (2.1 g) in benzene was refluxed for 2.5 hr in the presence of anhydrous potassium carbonate (2.8 g), and evaporation of the filtrate of the reaction mixture gave a sirup (2.0 g). Fractionation of the sirup (1.07 g) on a Kiesel Gel 60 column (20 g) with benzene–ethyl acetate (100: 3) as an effluent gave **13** (0.69 g) as a sirup. $[\alpha]_D^{23}$ −49.4° (*c* 0.93, chloroform); IR: 1520 and 1340 (conjugated NO_2). NMR: 7.31 (Ph; s), 7.18 (H_5; d, $J_{4,5}$=7.5), 6.01 (H_1; d, $J_{1,2}$=4.0), 4.82 (H_4; dd, $J_{3,4}$=3.5), 4.67 (H_2; d), 4.68 and 4.42 (CH_2; ABq, $J_{a,b}$=12.5), 3.46 (H_3; d), 2.07 (H_7; s), 1.50 and 1.33 (2× C–CH_3).

Found: C, 60.51; H, 6.31; N, 4.46%. Calcd for $C_{17}H_{21}NO_6$: C, 60.88; H, 6.31; N, 4.18%.

D-gluco-*3,4,5,6,7-Pentaacetoxy-1-nitro-1-heptene (**14**).* Acetylation of 1-*C*-nitro-1-deoxy-D-*glycero*-D-*gulo*-heptitol[11] (0.92 g, 3.8 mmol) by the usual manner gave the corresponding hexaacetate (1.88 g) as a sirup. The benzene solution of the sirup was refluxed in the presence of anhydrous potassium carbonate for 1.5 hr, filtered, and the filtrate was evaporated to give a sirup which was crystallized from ethanol. Yield, 1.10 g (77%), mp 105—106 °C; $[\alpha]_D^{23}$ +20.1° (*c* 1.16, chloroform); IR: 3090 (olefinic C–H), 1740 (ester), 1650 (C=C), 1520 and 1357 (conjugated NO_2); NMR: 7.22 (H_2; dd, $J_{1,2}$=13.0, $J_{2,3}$=5.0), 6.97 (H_1; d), 5.62 (H_3; m), 5.45—5.20 (H_4 and H_5; m), 5.03 (H_6; m), 4.23 and 4.04 (H_{7a} and H_{7b}; $J_{a,b}$=12.5, $J_{6,7a}$=3.0, $J_{6,7b}$=5.0), 2.125, 2.08, 2.05, and 2.025 (5×OAc).

Found: C, 47.26; H, 5.33; N, 3.39%. Calcd for $C_{17}H_{23}NO_{12}$: C, 47.11; H, 5.35; N, 3.23%.

The authors are indebted to Mr. H. Matsumoto for NMR measurements, and members of Laboratory of Organic Analysis for microanalysis.

Branched-chain Sugars. IV. Synthesis of 5,6-Dideoxy-5-*C*-hydroxymethyl-1,2-*O*-isopropylidene-6-*C*-nitro-3-*O*-substituted-α-D-glucose Derivatives[1]

Juji YOSHIMURA, Takao IIDA, Hiroo WAKAI, and Masuo FUNABASHI

Laboratory of Chemistry for Natural Products, Faculty of Science, Tokyo Institute of Technology
Ookayama, Meguro-ku, Tokyo 152

(Received June 22, 1973)

Addition of nitryl iodide to 5-deoxy-1,2,*O*-isopropylidene-3-*O*-methyl-5-*C*-methylene-6-*O*-substituted-α-D-*xylo*-hexofuranoses (**3** and **4**), and subsequent hydrogenation with sodium borohydride gave a mixture of the corresponding 5,6-dideoxy-5-*C*-hydroxymethyl-6-*C*-nitro derivatives of D-*gluco* and L-*ido* forms. The configuration of both isomers were determined by intramolecular cyclization into the corresponding nitrocyclohexanetetrols. The ratios of D-*gluco* to L-*ido* product were 1:2 in the case of 6-*O*-trityl derivative (**3**) and 4:5 in the case of 6-*O*-benzyl derivative (**4**), respectively.

In the previous paper,[1] addition of vinylmagnesium bromide to 5,6-dideoxy-1,2-*O*-isopropylidene-6-*C*-nitro-3-*O*-substituted-α-D-*xylo*-hex-5-enofuranoses gave exclusively the corresponding L-*ido*-type product. In order to synthesize a 5,6-dideoxy-6-*C*-nitro-5-*C*-hydroxymethyl derivative of D-*gluco* configuration, another pathway including addition of nitryl iodide[2] to 5-deoxy-1,2-*O*-isopropylidene-3-*O*-methyl-5-*C*-methylene-6-*O*-substituted-α-D-*xylo*-hexofuranoses (**3** and **4**) and hydrogenation with sodium borohydride was examined, and the configuration of the product was determined to be a mixture of D-*gluco* and L-*ido* forms by intramolecular cyclization into the corresponding nitrocyclitol.

Results and Discussion

As the starting materials, 6-*O*-trityl (**1**) and 6-*O*-benzyl derivatives (**2**) of 1,2-*O*-isopropylidene-3-*O*-methyl-α-D-*xylo*-hexofuranos-5-ulose were synthesized by dimethyl sulfoxide oxidation of the corresponding 5-hydroxy derivatives,[3,4] respectively. Treatment of **1** and **2** with triphenylphosphonium methylide gave the corresponding 5-*C*-methylene derivatives (**3** and **4**) in 50 and 85% yield, respectively. Addition of nitryl iodide, prepared from silver nitrite and iodine, to **3** and **4** in ether in the dark place gave the corresponding addition product as crystals (**5**) and a sirup (**6**) in good yields, respectively. The homogeneity of **5** was deduced from the presence of the single methoxy signal in the NMR spectrum, however, the configuration at C_5-position could not be determined because of its instability. **6** was deduced to be a mixture of C_5-epimers and a small amount of unchanged **4**, and was used without further purification. Attempted elimination of **5** and **6** into the corresponding nitro olefin by use of potassium carbonate or 1,5-diazabicyclo-[5.4.0]undec-5-ene were unsuccessful. Hydrogenation of **5** and **6** in ethanol–tetrahydrofuran with sodium borohydride at 0 °C gave the corresponding 5,6-dideoxy-5-*C*-hydroxymethyl-6-*C*-nitro derivatives (**7** and **8**) in 55 and 79% yield, respectively. Both the compounds showed two kinds of methoxy proton signals in NMR spectra, indicating they are a mixture of C_5-epimers in the ratios of 1 to 2 and of 2 to 3, respectively. For resolution and assignment of both the epimers, **7** and **8** were de-*O*-isopropylidenated by treatment with 70% acetic acid at 90 °C for 10 hr under monitering with tlc, and cyclized intramolecularly without further purification. In the case of **8**, cyclization in ethanol at pH 9 for 40 hr at 30 °C, neutralization with Amberlite IR-120, and purification of the product on silica-gel column with benzene–ethyl acetate (2:3) gave the corresponding nitrocyclitols in 30% yield, which on acetylation gave 1-*O*-ethyl-3-*O*-methyl-(3,6/1,2,4,5)-5-benzyloxymethyl-6-nitrocyclohexanetetrol (**9**)[5] as crystals. When the cyclization was accomplished in 50% aqueous methanol in the presence of sodium bicarbonate at 30 °C for 3 days and the reaction mixture was then treated as above, two kinds of sirupy nitrocyclohexanetetrol were obtained in 31 and 21% yield, which upon acetylation gave 1,2,4-tri-*O*-acetyl-3-*O*-methyl-(3,6/1,2,4,5)-5-benzyloxymethyl-6-nitrocyclohexanetetrol (**10**)[5] and its (1,3,5/2,4,6)-diastereoisomer (**11**) as crystals. The ratio of the both

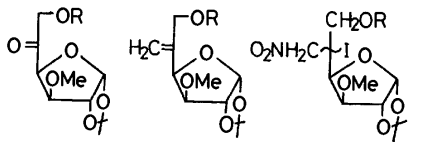

(**1**) R=Trityl (**3**) R=Trityl (**5**) R=Trityl
(**2**) R=Benzyl (**4**) R=Benzyl (**6**) R=Benzyl

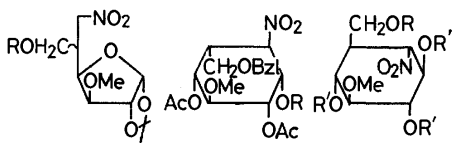

(**7**) R=Trityl (**9**) R=Et (**11**) R=Benzyl, R′=Ac
(**8**) R=Benzyl (**10**) R=Ac (**12**) R=R′=H
(**13**) R=R′=Ac

1) Part III. This Bulletin, **46**, 3203 (1973).
2) W. A. Szareck, J. S. Jewell, J. Szazerek, and J. K. N. Jones, *Can. J. Chem.*, **47**, 4473 (1969).
3) G. W. Huffman, B. A. Lewis, F. Smith, and D. R. Spriestersbach, *J. Amer. Chem. Soc.*, **77**, 4346 (1955).
4) J. Kenner and G. N. Richards, *J. Chem. Soc.*, **1954**, 3277.
5) For easier understanding, the numbering and figures of nitrocyclitols for nomenclature were cited from that of original compounds. Other points were followed by "Tentative Rules for Cyclitol Nomenclature" of IUPAC (1967 rule).

Table 1. NMR parameters of *O*-acetylated nitrocyclitols

Compound	H_1	H_2	H_3	H_4	H_5	H_6	Other protons
9	4.C8(dd) $J_{1,2}=3.7$	5.47(td) $J_{2,3}=3.7$	3.8—3.2 $J_{3,4}=3.0$	5.28(td) $J_{4,5}=2.5$	2.85(m) $J_{5,6}=12.0$	4.80(t) $J_{1,6}=10.0$	7.29 (Ph), 4.48 and 4.27 ($PhCH_2O$; ABq, $J=12.0$), 3.48 (OMe), 3.8—3.2 ($C-CH_2O$, OCH_2Me), 1.05 (C-Me; t, $J=7.0$), 2.01 and 1.88 (OAc)
10	5.59(dd) $J_{1,2}=3.5$	5.50 $J_{2,3}=3.5$	3.7—3.3 $J_{3,4}=3.0$	5.27(m) $J_{4,5}=3.0$	2.92(m) $J_{5,6}=11.5$	4.45(t) $J_{1,6}=11.5$	7.27 (Ph), 4.47 and 4.27 ($PhCH_2O$; ABq, $J=12.0$), 3.48 (OMe), 3.7—3.3 ($C-CH_2O$; m), 2.02, 1.93 and 1.88 (OAc)
11	5.54(dd) $J_{1,2}=10.0$	5.05(dd) $J_{2,3}=9.5$	3.55 $J_{3,4}=9.0$	5.19(dd) $J_{4,5}=11.0$	2.39(tm) $J_{5,6}=10.5$	4.89(t) $J_{1,6}=10.5$	7.28 (Ph), 4.38 ($PhCH_2O$; s), 3.40 (OMe), 3.55—3.07 ($C-CH_2O$; m), 2.02 and 1.95 (OAc)
13	5.55(t) $J_{1,2}=10.0$	5.06(dd) $J_{2,3}=9.0$	3.46(t) $J_{3,4}=9.0$	5.09(t) $J_{4,5}=9.0$	2.55(tm) $J_{5,6}=11.5$	4.28(dd) $J_{1,6}=10.0$	4.22 and 3.72 ($C-CH_2O$; each q, $J_{5'a,5'b}=12.5$, $J_{5'a,5}=3.5$, $J_{5'b,5}=2.5$), 3.43(OMe), 2.10, 2.05 and 1.98(OAc)

epimers in the original crude nitrocyclitol was again estimated to be 4: 5 from the intensities of H_5 proton signals (δ 2.92 and 2.39) of the corresponding acetate. The main product **11** indicates that the L-*ido* form was predominant in **8**. In the case of **7**, a similar cyclization gave 3-*O*-methyl-(1,3,5/2,4,6)-5-hydroxymethyl-6-nitrocyclohexanetetrol (**12**)[5] as crystals in 37% yield, which on acetylation gave the corresponding tetra-*O*-acetate (**13**). The ratio of the expectable isomers in the crude nitrocyclitol estimated by the similar way as above (δ 2.92 and 2.55) was 1: 2, indicating again L-*ido* form was predominant in **7**, but the minor isomer could not be isolated in a pure state.

Configurations of **9**, **10**, **11**, and **13** predicted above were determined from the NMR parameters shown in Table 1, which were analyzed by double resonance technique. The proton signals at the branched point were distinguished by its multi-splittings and higher resonating magnetic field than others. Other ring protons appeared in a lower field in the order of alkoxy, nitro and acetoxy positions. The large *trans*-diaxial coupling constants in **11** and **13** indicate that the all substituents are in equatorial conformation, while small *gauche* coupling in H_2–H_4 of **9** and **10** indicate that substituents at these position are in axial conformation. As shown in Fig. 1, this conformation would be caused by the preferential adoption of the nitro group[6] and benzyloxymethyl group into an equatorial orientation.

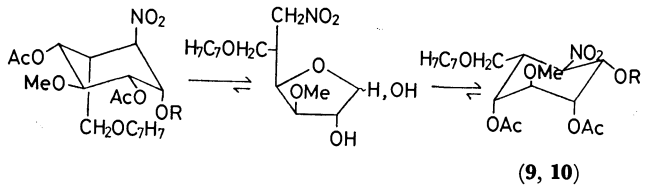

(**9**, **10**)

Fig. 1. Conformation of (3,6/1,2,4,5)-type isomers

Experimental

All melting points are uncorrected. The solutions were evaporated under diminished pressure at a bath temperature not exceeding 45 °C. Specific rotations were measured in a 0.5-dm tube, with a Carl Zeiss photoelectric polarimeter. The IR spectra were recorded with a Hitachi Model EPI-GS spectrophotometer. The NMR spectra were taken in deuteriochloroform with a JMN-4H-100 MHz Spectrometer using tetramethylsilane as an internal standard. Chemical shifts and coupling constants were recorded in δ and Hz units, and frequencies in cm^{-1}.

1,2-O-Isopropylidene-3-O-methyl-6-O-trityl-α-D-xylo-hexofuranos-5-ulose (1). A solution of 1,2-*O*-isopropylidene-3-*O*-methyl-6-*O*-trityl-α-D-glucofuranose (41.5 g) in dimethyl sulfoxide (200 ml) and acetic anhydride (70 ml) was stood at room temperature for 21 hr, poured into ice-water (5 l) with stirring. The gummy precipitate was separated from the water layer by decantation, and dissolved in benzene. The benzene solution was washed with saturated sodium bicarbonate solution and water, and evaporated to give crystals which were recrystallized from ligroin. Yield, 17.5 g (45%), mp 146—147 °C, $[\alpha]_D^{23}$ −41° (*c* 0.5, $CHCl_3$). IR: 1740 (C=O), NMR: 7.5—7.1 (Ph_3C-; m), 5.87 (H_1; d, $J_{1,2}=3.5$), 4.85 (H_4; d, $J_{3,4}=3.5$), 4.47 (H_2; d), 4.09 (H_3; d), 4.01 (H_6; s), 3.18 (OCH_3), 1.46 and 1.28 ($2\times C-CH_3$).

Found: C, 73.00; H, 6.22%. Calcd for $C_{29}H_{30}O_6$: C, 73.40; H, 6.37%.

6-O-Benzyl-1,2-O-isopropylidene-3-O-methyl-α-D-xylo-hexofuranos-5-ulose (2). A solution of 6-*O*-benzyl-1,2-*O*-isopropylidene-3-*O*-methyl-α-D-glucofuranose (3.0 g, 9.35 mmol) in dimethyl sulfoxide (50 ml) and acetic anhydride (10 ml) was kept at room temperature for 1 day, poured into ice-water (500 ml), and extracted with chloroform. The extract was washed with saturated sodium bicarbonate solution and water, evaporated, and the sirup obtained was fractionated on a silicagel (Wakogel C-200) column with benzene–methanol (50: 1) to give a pure sirup (1.5 g, 50%). $[\alpha]_D^{23}$ −73° (*c* 0.5, $CHCl_3$). IR: 1728 (C=O); NMR: 7.32 (Ph; m), 5.96 (H_1; d, $J_{1,2}=3.0$), 4.71 (H_4; d, $J_{3,4}=3.5$), 4.55 (H_6; s), 4.51 (H_2; d), 4.35 ($-CH_2-$; s), 4.06 (H_3; d), 3.28 (OCH_3), 1.42 and 1.28 ($2\times C-CH_3$).

Found: C, 62.53; H, 6.72%. Calcd for $C_{17}H_{22}O_6$: C, 63.34; H, 6.88%.

5-Deoxy-1,2-O-isopropylidene-3-O-methyl-5-C-methylene-6-O-trityl-α-D-xylo-hexofuranose (3). To a suspended solution of triphenylmethylphosphonium bromide (28.2 g, 77.6 mmol) in tetrahydrofuran (400 ml) was added dropwise *n*-butyllithium in *n*-hexane (41.4 ml of 15% solution, 97 mmol) with stirring at 0 °C, and after 10 min was further added a solution of **1** (18.4 g, 38.8 mmol) in tetrahydrofuran (60 ml). The resulted solution was stirred for 1 hr, filtered, and evaporated. The resulted sirup was extracted with *n*-hexane, and

6) F. W. Lichtentnaler, "Fortschritte der Chemischen Forschung; Topics in Current Chemistry," Vol. 14, No. 4, p. 556 (1970).

the extract was washed with water, dried, and evaporated to give a sirup which was crystallized and recrystallized from ethanol–*n*-hexane. Yield, 9 g (50%), mp 97—98.5 °C, $[\alpha]_D^{23}$ −44° (*c* 0.5, $CHCl_3$). IR: 1650 (C=C); NMR: 7.58—7.17 (Ph_3C), 5.92 (H_1; d, $J_{1,2}$=3.5), 5.37 (H_5'; m, $J_{4,5'} \simeq J_{5',6a} \simeq J_{5',6b} \simeq 2$), 4.82 ($H_4$; m), 4.49 ($H_2$; d), 3.75 and 3.50 ($H_{6a}$ and H_{6b}; ABq, $J_{a,b}$=12.0), 3.49 (H_3; d, $J_{3,4}$=3.0), 3.07 (OCH_3), 1.50 and 1.30 (2×C-CH_3).

Found: C, 76.16; H, 7.04%. Calcd for $C_{30}H_{32}O_5$: C, 76.24; H, 6.83%.

*6-O-Benzyl-5-deoxy-1,2-O-isopropylidene-3-O-methyl-5-C-methylene-α-*D-xylo-*hexofuranose (4).* Compound **3** (3.45 g, 10.7 mmol) was treated with triphenylmethylphosphonium bromide (7.6 g, 21.4 mmol) and *n*-butyllithium (26.7 mmol) as above to give a sirupy product in 85% (3 g) yield. $[\alpha]_D^{23}$ −57° (*c* 0.5, $CHCl_3$). IR: 1640 (C=C).

Found: C, 67.05; H, 7.95%. Calcd for $C_{18}H_{24}O_5$: C, 67.48; H, 7.55%.

*5,6-Dideoxy-5-iodo-1,2-O-isopropylidene-3-O-methyl-6-C-nitro-5-C-trityloxymethyl-α-*D-xylo-*hexofuranose (5).* To a suspended solution of iodine (5.30 g, 21.0 mmol) and silver nitrite (2.66 g, 17.2 mmol) in ether (500 ml) under stirring at 0 °C in the dark state, was added a solution of **3** (0.7 g, 14.8 mmol) in ether, and after stirring 1 day at room temperature the reaction mixture was filtered and evaporated. The resulted sirup was extracted with chloroform, and the extract was washed with sodium thiosulfate solution and water, dried, and evaporated to give a sirup (6.7 g, 70%) which was crystallized from benzene–*n*-hexane. Mp 171—172 °C, $[\alpha]_D^{23}$ −8° (*c* 0.5, $CHCl_3$). IR: 1540 and 1370 (NO_2); NMR: 7.63—7.20 (Ph_3C), 5.83 (H_1; d, $J_{1,2}$=3.5), 4.95 and 4.81 (H_{6a} and H_{6b}; ABq, $J_{a,b}$=13.0), 4.88 (H_4; d, $J_{3,4}$=3.0), 4.37 (H_2; d), 3.97 and 3.27 ($H_{5'a}$ and $H_{5'b}$; ABq, $J_{a,b}$=10.0), 3.47 (H_3; d), 2.81 (OCH_3), 1.55 and 1.30 (2×C-CH_3).

Found: C, 55.90; H, 5.02; N, 2.26%. Calcd for $C_{30}H_{32}NO_7I$: C, 55.82; H, 5.00; N, 2.17%.

*5,6-Dideoxy-1,2-O-isopropylidene-3-O-methyl-6-C-nitro-5-C-trityloxymethyl-α-*D-gluco- *and β-*L-ido-*furanose (7).* To a solution of **5** (6.0 g, 9.1 mmol) in tetrahydrofuran (90 ml) and ethanol (800 ml) was added portionwise sodium borohydride (2.46 g) at 0 °C, and after stirring for 1 day a small amount of water was added to decompose the hydride. The reaction mixture was then evaporated, the resulted residue was extracted with chloroform, and the extract was washed with water, dried, and evaporated to give a sirup which was crystallized from benzene–ethanol. Yield, 2.4 g (55%), mp 152—153 °C, $[\alpha]_D^{23}$ −46° (*c* 0.5, $CHCl_3$). IR: 1540 and 1365 (NO_2).

Found: C, 69.53; H, 6.46; N, 2.76%. Calcd for $C_{30}H_{33}NO_7$: C, 69.35; H, 6.39; N, 2.70%.

NMR spectrum of this crystal showed still two methyl proton signals (δ 3.17 and 2.99) in the intensity ratio 1:2.

*5-C-Benzyloxymethyl-5,6-dideoxy-1,2-O-isopropylidene-3-O-methyl-6-C-nitro-α-*D-gluco- *and β-*L-ido-*furanose (8).* Compound **4** (2.67 g, 0.34 mmol) was treated with nitryl iodide prepared from iodine (2.93 g, 11.5 mmol) and silver nitrite (1.49 g, 9.6 mmol) by a similar manner as in the case of **5**. NMR spectrum of the sirupy product (3.36 g, 85%) showed three kinds of methoxy proton signals (δ 3.14, 3.23, and 3.43), indicating the presence of C_5-epimers and a small amount of **4**. This sirup (3.3 g, 6.8 mmol) was hydrogenated with sodium borohydride (7 equimolar amount) to give a sirupy product which was purified with silica-gel column. Yield, 2.0 g, (79%), $[\alpha]_D^{23}$ −50° (*c* 0.5, $CHCl_3$). IR: 1540 and 1370 (NO_2).

Found: C, 59.86; H, 7.27; N, 3.50%. Calcd for $C_{18}H_{25}NO_7$: C, 58.84; H, 6.86; N, 3.81%.

NMR spectrum of this product showed two kinds of methoxy proton signals (δ 3.25 and 3.28) in the intensity ratio of 2:3, indicating the presence of C_5-epimers.

2,4-Di-O-acetyl-1-O-ethyl-3-O-methyl-(3,6/1,2,4,5)-5-benzyloxymethyl-6-nitrocyclohexanetetrol (9). A solution of **8** (300 mg, 0.82 mmol) in acetic acid (70%, 20 ml) was heated at 90 °C for 10 hr, and evaporated to give the de-*O*-isopropylidenated product as a sirup (260 mg). The pH of a solution of this sirup in ethanol (20 ml) was adjusted to 8.5—9 with 2M potassium hydroxide, stood for 40 hr at 30 °C, neutralized with Amberlite IR-120, evaporated to give a sirup which was fractionated on a silica-gel column (Wakogel C-200), using benzene–ethyl acetate as effluent. The purified sirupy nitrocyclitol (90 mg, 35%) was acetylated with acetic anhydride in the presence of *p*-toluenesulfonic acid as a catalyst to give **9** (70 mg, 70%). Mp 123—124 °C, $[\alpha]_D^{23}$ +45° (*c* 0.5, $CHCl_3$). IR: 1740 and 1720 (ester), 1540 and 1370 (NO_2).

Found: C, 57.67; H, 6.82; N, 3.15%. Calcd for $C_{21}H_{29}NO_9$: C, 57.39; H, 6.65; N, 3.19%.

1,2,4-Tri-O-acetyl-3-O-methyl-(3,6/1,2,4,5)-5-benzyloxymethyl-6-nitrocyclohexanetetrol (10) and Its (1,3,5/2,4,6)-Diastereomer (11). A solution of de-isopropylidenated **8** (520 mg), prepared from **8** (613 mg, 1.67 mmol) as above, and sodium bicarbonate (135 mg, 1.6 mmol) in aqueous methanol (50%, 40 ml) was stood at 30 °C for 3 days with stirring, neutralized with Amberlite IR-120, and evaporated to give a sirup which was fractionated into two nitrocyclitols [the first fraction, 160 mg (31%) and the second one, 110 mg (21%)], on a silica-gel column (Wakogel C-200) with benzene–ethyl acetate (1:1) as the effluent. Acid-catalyzed acetylation of the both nitrocyclitols gave the corresponding tri-*O*-acetate **10** (60 mg) and **11** (70 mg), respectively. **10**; mp 123—124 °C, $[\alpha]_D^{23}$ +44° (*c* 0.5, $CHCl_3$). IR: 1750 and 1730 (ester), 1545 and 1360 (NO_2).

Found: C, 55.71; H, 6.12; N, 3.05%. Calcd for $C_{21}H_{27}NO_{10}$: C, 55.62; H, 6.00; N, 3.09%.

11; mp 155—156 °C, $[\alpha]_D^{23}$ +29° (*c* 0.5, $CHCl_3$). IR: 1730 (ester), 1550 and 1360 (NO_2).

Found: C, 55.82; H, 5.98; N, 3.19%. Calcd for $C_{21}H_{27}NO_{10}$: C, 55.62; H, 6.00; N, 3.09%.

3-O-Methyl-(1,3,5/2,4,6)-5-hydroxymethyl-6-nitrocyclohexanetriol (12) and Its Tetra-O-acetate (13). A solution of *7* (1.0 g, 1.92 mmol) in 70% acetic acid (40 ml) was heated at 90 °C for 10 hr, evaporated, and the sirup obtained was redissolved in water and extracted three times with benzene. Evaporation of the water layer gave the hydrolyzed product (450 mg) as a sirup. A solution of this sirup (300 mg, 1.27 mmol) and sodium bicarbonate (106 mg, 1.26 mmol) in aqueous methanol (50%, 12 ml) was kept at 30 °C for 3 days, neutralized with Amberlite IR-120, and evaporated to give a sirup. Fractionation of this sirup on a silica-gel column with benzene–ethyl acetate gave crystalline **12**, which was recrystallized from ethanol. Yield, 110 mg (37%), mp 119—120 °C, $[\alpha]_D^{23}$ −17° (*c* 0.2, water). IR: 3540 and 3350 (OH), 1530 and 1365 (NO_2).

Found: C, 38.35; H, 6.42; N, 5.57%. Calcd for $C_8H_{15}NO_7 \cdot 1/2\ H_2O$: C, 39.02; H, 6.55; N, 5.69%.

Acid-catalyzed acetylation of **12** gave the corresponding tetra-*O*-acetate in 40% yield. Mp 166—167 °C, $[\alpha]_D^{23}$ −4° (*c* 0.5, $CHCl_3$). IR: 1730 (ester), 1544 and 1360 (NO_2).

Found: C, 47.54; H, 5.84; N, 3.36%. Calcd for $C_{16}H_{23}NO_{11}$: C, 47.41; H, 5.72; N, 3.46%.

The authors arei ndebted to Mr. H. Matsumoto for NMR measurements, and members of Laboratory of Organic Analysis for microanalyses.

Studies on Aminosugars. XXXVI. Syntheses of 3′,4′-Dideoxy- and 3′,4′,5″-Trideoxyribostamycin[1]

Daishiro IKEDA,* Toshihisa SUZUKI,* Tsutomu TSUCHIYA,* Sumio UMEZAWA,* and Hamao UMEZAWA**

*Department of Applied Chemistry, Faculty of Engineering, Keio University, Hiyoshi, Yokohama 223
**Institute of Microbial Chemistry, Kamiosaki, Shinagawa-ku, Tokyo 141

(Received July 9, 1973)

3′,4′-Dideoxyribostamycin and 3′,4′,5″-trideoxyribostamycin have been prepared from ribostamycin *via* 3′,4′-unsaturation and 5″-iodo-3′,4′-unsaturation intermediates, respectively.

As described in previous papers, the 3′-deoxy[2,3] and 3′,4′-dideoxy[4,5] derivatives of kanamycins and neamine have been found to exhibit strong antibiotic activity against resistant bacteria carrying R factor and *Pseudomonas aeruginsoa*. The syntheses of these deoxy compounds were designed on the basis of mechanism of resistance[6] in resistant bacteria and as an extension of these works, we have now synthesized deoxyderivatives of another aminoglycoside antibiotic, ribostamycin,[7] which undergoes 3′-phosphorylation by the same enzymes,[8] kanamycin phosphotransferases I and II of resistant bacteria.

In order to protect the four amino groups, ribostamycin were treated with benzyl chloroformate in aqueous methanol in the presence of sodium carbonate to give tetra-*N*-benzyloxycarbonylribostamycin (**1**). The compound **1** was allowed to react with 1,1-dimethoxycyclohexane in dimethyl formamide (DMF) in the presence of catalytic amount of *p*-toluenesulfonic acid at 50 °C under diminished pressure. As described by Bissett, Evans, and Parrish,[9] the reaction under diminished pressure effectively removed the methanol which was liberated and the reaction was completed within 2 hr to give a tricyclohexylidene derivative (**2**), in a yield of 60%, in which one of the cyclohexylidene groups presented in a 1-methoxycyclohexyl form. The presence of the hemiketal group was confirmed by the observation of methoxyl group at τ 6.83 in the NMR spectrum. Acetylation of **2** gave the 6-*O*-acetyl derivative (**3**). Selective removal of the 5″-*O*-protecting group was achieved by treatment with acetone–40% acetic acid (4: 1) at room temperature to give a di-*O*-cyclohexylidene derivative (**4**) in a yield of 82%. Further acetylation gave the 5″,6-di-*O*-acetyl derivative (**5**). The cyclohexylidene group attached to the *trans* hydroxyl groups at 3′ and 4′ was selectively removed

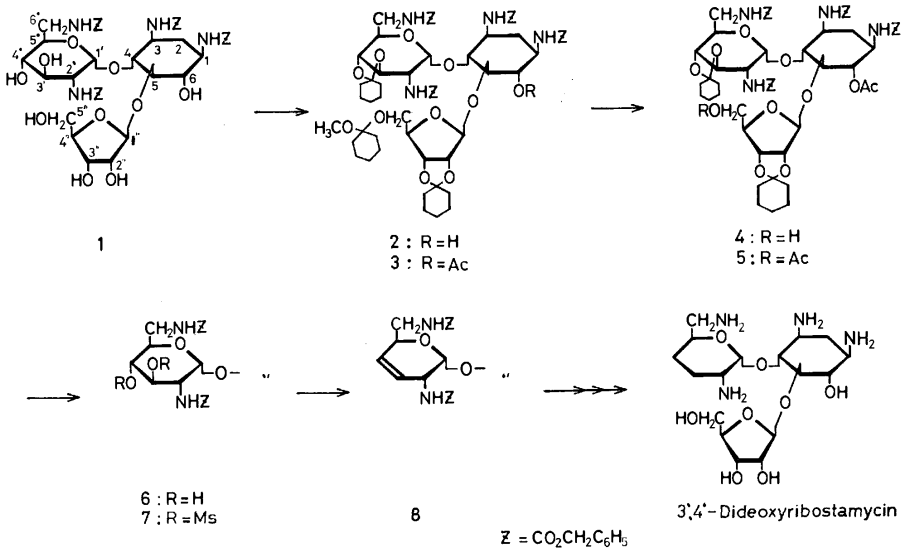

1) A part of this paper was read by S. Umezawa at Symposium of New Natural Product Syntheses, XXIIIrd International Congress of Pure and Applied Chemistry at Boston, U.S.A., July 28, 1971; XXIIIrd ICPAC, Vol. 2, 173, Butterworths, London. Short communication: S, Umezawa. T. Tsuchiya, D. Ikeda, and H. Umezawa, *J. Antibiot.* (Tokyo), **25**, 613 (1972).

2) S. Umezawa, T. Tsuchiya, R. Muto, Y. Nishimura, and H. Umezawa, *ibid.*, **24**, 274 (1971); S. Umezawa, Y. Nishimura, H. Hineno, K. Watanabe, S. Koike, T. Tsuchiya, and H. Umezawa, This Bulletin, **45**, 2847 (1972).

3) Y. Takagi, T. Miyake, T. Tsuchiya, S. Umezawa, and H. Umezawa, *J. Antibiot.* (Tokyo), **26**, in press.

4) H. Umezawa, S. Umezawa, T. Tsuchiya, and Y. Okazaki, *ibid.*, **24**, 485 (1971); S. Umezawa, H. Umezawa, Y. Okazaki, and T. Tsuchiya, This Bulletin, **45**, 3624 (1972).

5) S. Umezawa, T. Tsuchiya, T. Jikihara, and H. Umezawa, *J. Antibiot.* (Tokyo), **24**, 711 (1971); This Bulletin, in press.

6) H. Umezawa, Progress in Antimicrobial and Anticancer Chemotherapy, **2**, 567, University of Tokyo Press, 1970.

7) E. Akita, T. Tsuruoka, N. Ezaki, and T. Niida, *J. Antibiot.* (Tokyo), **23**, 173 (1970).

8) M. Yagisawa, H. Yamamoto, H. Naganawa, S. Kondo, T. Takeuchi, and H. Umezawa, *ibid.*, **25**, 748 (1972).

9) F. H. Bissett, M. E. Evans, and F. W. Parrish, *Carbohyd. Res.*, **5**, 184 (1967).

by treatment with hot acetone–60% acetic acid (1:1) to give the di-*O*-acetyl-mono-*O*-cyclohexylidene derivative (**6**) in a yield of 94%. Mesylation of **6** gave the 3′,4′-di-*O*-mesyl derivative (**7**). Subsequent 3′,4′-unsaturation was carried out by sodium iodide-zinc dust method reported by Tipson and Cohen[10] and Horton *et al.*[11] to give the 3′-eno derivative (**8**), which was obtained in a fairly good yield as expected from our works[12] on 3,4-unsaturated sugars. Treatment of **8** with methanolic ammonia gave the deacetylated derivative (**9**), which was then catalytically hydrogenated and decyclohexylidenated to give 3′,4′-dideoxyribostamycin in a yield of 54% from **8**.

On the other hand, the above-mentioned compound **3** was led to 3′,4′,5″-trideoxyribostamycin. Treatment of **3** with hot acetone–aqueous acetic acid gave the mono-*O*-cyclohexylidene derivative (**10**), which was then mesylated to give 3′,4′,5″-tri-*O*-mesyl derivative (**11**). Treatment of **11** with sodium iodide and zinc dust in DMF afforded the unsaturated iodo derivative **12**, namely, 6-*O*-acetyl-tetra-*N*-benzyloxycarbonyl-2″, 3″-*O*-cyclohexylidene-3′,4′-dideoxy-3′-eno-5″-iodoribostamycin (**12**) in a yield of 73%. Reduction of the iodo compound with Raney nickel and hydrogen in the presence of triethylamine gave the unsaturated 5″-deoxy derivative (**13**). Removal of the acetyl group by treatment with methanolic ammonia gave **14**, which was then catalytically hydrogenated with palladium black and hydrolyzed with acid to give the final product, 3′,4′,5″-trideoxyribostamycin.

The semisynthetic 3′,4′-dideoxyribostamycin showed[1] antibacterial activity similar to the parent ribostamycin against most of bacteria and, moreover, activity against *E. coli* carrying R factor of kanamycin phosphotransferase II and *Pseudomonas aeruginosa* resistant to ribostamycin. On the other hand, 3′,4′,5″-trideoxyribostamycin was found[1] to be less active than the parent antibiotic, indicating the involvement of the 5″-hydroxyl in antibacterial activity.

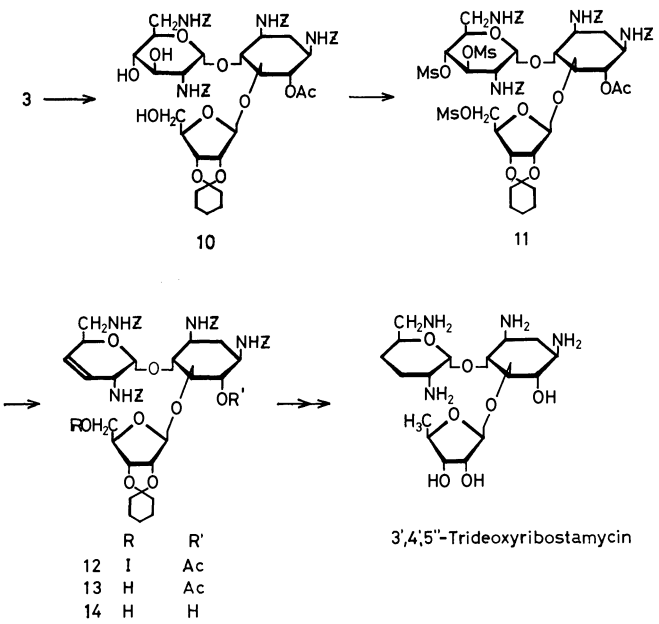

Experimental

Thin layer chromatography (tlc) was carried out on silica gel and the spots were visualized with sulfuric acid. Paper chromatography was performed on Toyo-Roshi paper No. 50 and the spots were detected with 0.5% ninhydrin in pyridine.

1,2′,3,6′-Tetra-N-*benzyloxycarbonylribostamycin (1).* To a mixture of ribostamycin sulfate (10 g, as ribostamycin·1.3 H_2SO_4) and anhydrous sodium carbonate (9 g) in 75% aqueous methanol (300 ml), benzyl chloroformate (15 g) was added under stirring at 5 °C and stirring was continued for 1 hr at that temperature. On tlc with benzene–methanol (4: 1), a spot (R_f 0.48) appeared. The reaction mixture was evaporated to dryness. The residue was extracted with hot acetone (100 ml × 3). Evaporation of the solution gave a solid, 15.3 g.

Found: C, 58.29; H, 5.80; N, 5.37%. Calcd for $C_{44}H_{58}N_4O_{18}\cdot H_2O$: C, 58.33; H, 5.99; N, 5.55%.

1,2′,3,6′-Tetra-N-*benzyloxycarbonyl-3′,4′;2″,3″-di*-O-*cyclohexylidene-5″*-O-*(1-methoxycyclohexyl)ribostamycin (2).* To a solution of **1** (2.76 g) and anhydrous *p*-toluenesulfonic acid (100 mg) in dry DMF (40 ml), 1,1-dimethoxycyclohexane (5.5 ml) was added and the solution was heated at 50 °C for 2 hr under reduced pressure (30—35 Torr). On tlc with benzene–diisopropyl ether (5: 1) a spot (**2**, R_f 0.49) accompanied by spots of R_f 0.90 and 0.59, appeared, but the spot for the starting material (R_f 0) was still strong. Therefore another 1,1-dimethoxycyclohexane (6 ml) and anhydrous *p*-toluenesulfonic acid (15 mg) were added and the solution was again heated at 50 °C under the reduced pressure for 2 hr. After addition of sodium hydrogen carbonate solution, the mixture was evaporated to dryness and the residue was extracted with acetone. Evaporation of the acetone solution gave a solid, which was chromatographed on a column of silica gel (240 g) with benzene–ethyl acetate (7: 2) containing triethylamine (0.5%). The portion containing **2** was evaporated to give a residue, which was reprecipitated from benzene–*n*-hexane yielding 1.93 g (60%), mp 92—94 °C, $[\alpha]_D^{17}$ +16.2° (*c* 2, $CHCl_3$).

Found: C, 64.39; H, 6.80; N, 4.58%. Calcd for $C_{68}H_{86}N_4O_{19}$: C, 64.65; H, 6.86; N, 4.43%.

NMR (in $CDCl_3$): τ 8.8—8.1 (30H broadened signals, cyclohexylidene protons), 6.83 (3H, s, $OC\underline{H}_3$), 2.65 (20H, $CO_2CH_2C_6\underline{H}_5$).

6-O-Acetyl-1,2′,3,6′-tetra-N-*benzyloxycarbonyl-3′,4′;2″,3″-di*-O-*cyclohexylidene-5″*-O-*(1-methoxycyclohexyl)ribostamycin (3).* To a solution of **2** (1.65 g) in dry pyridine (33 ml), acetic anhydride (1.96 g) was added and the solution was allowed to stand overnight at 37 °C. On tlc with benzene–ethyl acetate (7: 2) a spot (R_f 0.42) appeared. After addition of a small amount of methanol followed by standing for 1 hr, the solution was evaporated and the residue was dissolved in chloroform. The solution was washed with saturated sodium hydrogen carbonate solution and water, dried over sodium sulfate and evaporated to give a colorless solid. Reprecipitation from benzene–*n*-hexane yielded 1.60 g (95%), mp 95—97 °C, $[\alpha]_D^{17}$ +8.3° (*c* 1, $CHCl_3$).

Found: C, 64.39; H, 6.86; N, 4.43%. Calcd for $C_{70}H_{88}N_4O_{20}$: C, 64.40; H, 6.80; N, 4.29%.

NMR (in $CDCl_3$): τ 8.8—8.2 (30H broadened signals), 7.94 (3H, s, OAc), 6.85 (3H, s, $OC\underline{H}_3$), 2.65 and 2.63 (20H in total, $CO_2CH_2C_6\underline{H}_5$).

10) R. S. Tipson and A. Cohen, *ibid.*, **1**, 338 (1965).
11) E. Albano, D. Horton, and T. Tsuchiya, *ibid.*, **2**, 349 (1966).
12) S. Umezawa, Y. Okazaki, and T. Tsuchiya, This Bulletin, **45**, 3619 (1972).

6-O-Acetyl-1,2',3,6'-tetra-N-benzyloxycarbonyl-3',4';2'',3''-di-O-cyclohexylideneribostamycin (4). A solution of **3** (450 mg) in acetone–40% acetic acid (4:1, 5 ml) was allowed to stand at room temperature for 3 hr. On tlc with benzene–ethyl acetate (5:2) a spot (**4**, R_f 0.22) accompanied by a minor spot (**10**, R_f 0) appeared. The solution was poured into a mixture of chloroform and saturated sodium hydrogen carbonate solution under stirring. The chloroform solution separated was washed with water, dried over sodium sulfate and evaporated. The syrup (430 mg) was chromatographed on a column of silica gel (22 g) with the same solvent system. The portion containing **4** was evaporated to give a solid (330 mg, 82%), mp 109—111 °C, $[\alpha]_D^{17}$ +18° (*c* 2, $CHCl_3$).

Found: C, 63.62; H, 6.32; N, 4.88%. Calcd for $C_{63}H_{76}N_4O_{18}$: C, 63.41; H, 6.42; N, 4.70%.

NMR (in $CDCl_3$): τ 8.8—8.2 (20H broadened signals, cyclohexylidene protons), 7.97 (3H, s, OAc), 2.72 and 2.68 (5H and 15H, s, respectively, $CO_2CH_2C_6\underline{H}_5$).

5'',6-Di-O-acetyl-1,2',3,6'-tetra-N-benzyloxycarbonyl-3',4';2'',3''-di-O-cyclohexylideneribostamycin (5). To a solution of **4** (200 mg) in pyridine (4 ml), acetic anhydride (27.4 mg) was added and the solution was allowed to stand at room temperature overnight. On tlc with benzene–ethyl acetate (5:2) a spot (R_f 0.37) appeared. The solution was poured into ice water with stirring. The resulting precipitate was filtered, washed with water and dried to give a solid, 200 mg (97%), which was reprecipitated from benzene–*n*-hexane, mp 95—98 °C, $[\alpha]_D^{17}$ +22° (*c* 0.67, $CHCl_3$).

Found: C, 63.06; H, 6.16; N, 4.64%. Calcd for $C_{65}H_{78}N_4O_{20}$: C, 63.19; H, 6.37; N, 4.54%.

NMR (in $CDCl_3$): τ 8.8—8.2 (20H broadened signals) 7.99 and 7.97 (both 3H, s, OAc), 2.69 and 2.66 (5H and 15H, s, respectively, $CO_2CH_2C_6\underline{H}_5$).

5'',6-Di-O-acetyl-1,2',3,6'-tetra-N-benzyloxycarbonyl-2'',3''-O-cyclohexylideneribostamycin (6). A solution of **5** (200 mg) in acetone–60% acetic acid (1:1, 7 ml) was heated at 50 °C for 1 hr. A single product (R_f 0.14 on tlc with benzene–ethyl acetate (3:2)) appeared. The solution was evaporated with toluene to give a solid, which was dissolved in chloroform. The solution was washed with saturated sodium hydrogen carbonate solution and water, dried over sodium sulfate and evaporated to give a solid. Reprecipitation from benzene–*n*-hexane yielded 175 mg (94%), mp 102—105 °C, $[\alpha]_D^{17}$ +7.7° (*c* 1.8, $CHCl_3$).

Found: C, 61.22; H, 5.95; N, 4.89%. Calcd for $C_{59}H_{70}N_4O_{20}$: C, 61.34; H, 6.11; N, 4.85%.

NMR (in $CDCl_3$): τ 8.9—8.2 (10H broadened signals, cyclohexylidene protons), 8.00 (6H, s, OAc), 2.73 and 2.70 (5H and 15H, s, respectively, $CO_2CH_2C_6\underline{H}_5$).

5'',6-Di-O-acetyl-1,2',3,6'-tetra-N-benzyloxycarbonyl-2'',3''-O-cyclohexylidene-3',4'-di-O-mesylribostamycin (7). To a solution of **6** (280 mg) in pyridine (5 ml), methanesulfonyl chloride (110 mg) was added and the solution was allowed to stand at room temperature overnight. After addition of a small amount of water, the solution was evaporated and the residue was dissolved in chloroform. The solution was washed successively with saturated potassium hydrogen sulfate solution, saturated sodium hydrogen carbonate solution and water, dried over sodium sulfate and evaporated to give a glassy solid, which was reprecipitated from benzene–*n*-hexane to give a solid, 279 mg (88%), mp 109—114 °C, $[\alpha]_D^{17}$ −4.7° (*c* 1.1, $CHCl_3$).

Found: C, 56.16; H, 5.61; N, 4.35; S, 4.58%. Calcd for $C_{61}H_{74}N_4O_{24}S_2$: C, 55.86; H, 5.69; N, 4.27; S, 4.89%.

NMR (in $CDCl_3$): τ 8.8—8.2 (10H), 7.93 (6H, s, OAc), 7.18 and 6.92 (both 3H, s, SO_2CH_3), 2.65, 2.62 and 2.59 (5H, 5H and 10H, s, respectively, $CO_2CH_2C_6\underline{H}_5$).

5'',6-Di-O-acetyl-1,2',3,6'-tetra-N-benzyloxycarbonyl-2'',3''-O-cyclohexylidene-3',4'-dideoxy-3'-eno-ribostamycin (8). To a solution of **7** (270 mg) in dry DMF (6 ml), anhydrous sodium iodide (3.0 g) and zinc dust (1.5 g) were added and the mixture was heated in an oil bath (91 °C) for 1 hr under vigorous stirring. Chloroform (30 ml) was added and the reaction mixture was filtered to remove the insoluble matters, which were washed with chloroform. The filtrate and the washings combined were washed successively with saturated sodium chloride solution, sodium thiosulfate solution and with water, dried over sodium sulfate and evaporated to give a yellow syrup (214 mg). On tlc with benzene–ethyl acetate (5:2), the syrup showed two spots of R_f 0.34 (**8**) and 0 (minor). The syrup was chromatographed on a column of silica gel (6 g) with benzene–ethyl acetate (5:2). The eulate containing **8** was evaporated to give a colorless solid, 156 mg (70%), mp 82—85 °C, $[\alpha]_D^{20}$ −30° (*c* 2, $CHCl_3$).

Found: C, 63.44; H, 6.02; N, 4.83%. Calcd for $C_{59}H_{68}N_4O_{18}$: C, 63.20; H, 6.11; N, 5.00%.

NMR (in $CDCl_3$): τ 8.8—8.2 (10H), 8.00 (6H, s, OAc), 4.42 (2H slightly broadened singlet, H-3',4'), 2.75, 2.71, 2.69, and 2.67 (each 5H, s, $CO_2CH_2C_6\underline{H}_5$).

1,2',3,6'-Tetra-N-benzyloxycarbonyl-2'',3''-O-cyclohexylidene-3',4'-dideoxy-3'-eno-ribostamycin (9). A solution of **8** (130 mg) in 10% ammonia in methanol (3 ml) was allowed to stand at room temperature overnight. The solution was evaporated and the residue was dissolved in benzene-ethyl acetate (1:1). The solution was passed through a short column of silica gel and the eluate containing **8** was evaporated to give a solid, 118 mg (98%), mp 89—93 °C, $[\alpha]_D^{21}$ −10° (*c* 2, $CHCl_3$).

Found: C, 64.05; H, 6.31; N, 5.24%. Calcd for $C_{55}H_{64}N_4O_{16}$: C, 63.69; H, 6.22; N, 5.40%.

NMR (in $CDCl_3$): τ 8.8—8.2 (10H), 4.45 (2H, slightly broadened singlet, H-3',4'), 2.75 and 2.72 (5H and 15H, s, respectively, $CO_2CH_2C_6\underline{H}_5$).

3',4'-Dideoxyribostamycin. A solution of **9** (50 mg) in aqueous dioxane (1:1, 2 ml) was hydrogenated with palladium black and hydrogen (50 psi) at 40 °C for 18 hr. The reaction mixture was filtered and the filtrate was evaporated to dryness. The residue was dissolved in 1M hydrochloric acid (0.5 ml) and the solution was heated at 60 °C for 1 hr. Addition of acetone gave a solid. The solid was charged on a column of CM Sephadex C-25 (NH_4^+) and, after washing the column with water (80 ml), it was developed with 0.01—0.4M ammonia with gradual increase in concentration. The product was eluted at the concentration of 0.3M ammonia. The portion was evaporated to give a solid, 11 mg (52%), mp 155—156 °C (decomp.), $[\alpha]_D^{20}$ +35° (*c* 1, H_2O). On paper chromatography with *n*-butanol–pyridine–water–acetic acid (6:4:3:1), it gave $R_{f\ \text{ribostamycin}}$ 1.50.

Found: C, 46.10; H, 8.38; N, 12.53%. Calcd for $C_{17}H_{34}N_4O_8\cdot H_2O$: C, 46.35; H, 8.24; N, 12.72%.

NMR (in D_2O): τ 9.0—7.7 (6H, m, H-2,3',4'), 4.65 (1H slightly broadened doublet, $J\sim1$ Hz, H-1''), 4.52 (1H, m, H-1').

On hydrolysis with 1M hydrochloric acid at 60 °C overnight, the product (R_f 0.40) gave 3',4'-dideoxyneamine[5] (R_f 0.56 on tlc with chloroform–methanol–17% ammonia (1:4:3)).

6-O-Acetyl-1,2',3,6'-tetra-N-benzyloxycarbonyl-2'',3''-O-cyclohexylideneribostamycin (10). Compound **3** (966 mg) was treated in a similar manner as described in the preparation of **6** from **5**. The solid obtained was reprecipitated from benzene–*n*-hexane yielding 808 mg (98%), mp 104—107 °C, $[\alpha]_D^{14}$ +1.3° (*c* 0.78, $CHCl_3$).

Found: C, 61.34; H, 5.80; N, 5.18%. Calcd for $C_{57}H_{68}N_4O_{19}$: C, 61.50; H, 6.16; N, 5.03%.

NMR (in $CDCl_3$): τ 8.9—8.2 (10H), 8.00 (3H, s, OAc), 2.73, 2.70 and 2.69 (5H, 10H and 5H, s, respectively, $CO_2CH_2C_6\underline{H}_5$).

6-O-Acetyl-1,2′,3,6′-tetra-N-benzyloxycarbonyl-2″,3″-O-cyclohexylidene-3′,4′,5″-tri-O-methanesulfonylribostamycin (11). Compound **10** (737 mg) was treated with methanesulfonyl chloride (465 mg) in pyridine (15 ml) in a similar manner as described in the preparation of **7** from **6**. The solid obtained was chromatographed on a short column of silica gel with benzene–ethyl acetate (2: 1). The eluate containing **11** was evaporated to give a solid, 840 mg (95%), mp 112—114 °C, $[\alpha]_D^{17}$ −8.8° (*c* 2.6, $CHCl_3$).

Found: C, 53.74; H, 5.60; N, 4.29; S, 7.31%. Calcd for $C_{60}H_{74}N_4O_{25}S_3$: C, 53.48; H, 5.54; N, 4.16; S, 7.14%.

NMR (in $CDCl_3$): τ 8.8—8.2 (10H), 7.97 (3H, s, OAc), 7.18, 6.98 and 6.96 (3H, s, each, $SO_2C\underline{H}_3$), 2.71, 2.70, 2.67 and 2.66 (5H, s, each, $CO_2CH_2C_6\underline{H}_5$).

6-O-Acetyl-1,2′,3,6′-tetra-N-benzyloxycarbonyl-2″,3″-O-cyclohexylidene-3′,4′,5″-trideoxy-3′-eno-5″-iodoribostamycin (12). To a solution of **11** (544 mg) in dry DMF (11 ml), anhydrous sodium iodide (5.45 g) and zinc dust (2.73 g) were added and the mixture was heated in an oil bath (90 °C) for 1 hr under vigorous stirring. Chloroform (50 ml) was added and the reaction mixture was filtered from the precipitates, which were washed with chloroform. The filtrate and washings combined were washed successively with saturated sodium chloride solution, sodium thiosulfate solution and with water, dried over sodium sulfate and evaporated. On tlc with benzene–ethyl acetate (5: 2), the slightly yellowish syrup showed two spots of R_f 0.61 (**12**) and 0.47 (**11**, minor). The syrup (500 mg) was chromatographed on a column of silica gel (25 g) with benzene–ethyl acetate (3: 1). The eluate containing **12** was evaporated to give a colorless solid, 350 mg (73%), mp 88—90 °C, $[\alpha]_D^{16}$ −30° (*c* 2, $CHCl_3$).

Found: C, 57.47; H, 5.38; N, 4.73; I, 11.08%. Calcd for $C_{57}H_{65}N_4O_{16}I$: C, 57.57; H, 5.51; N, 4.71; I, 10.68%.

NMR (in $CDCl_3$): τ 8.8—8.2 (10H), 8.00 (3H, s, OAc), 4.35 (2H slightly broadened singlet, H-3′,4′), 2.71, 2.68, 2.67 and 2.63 (each 5H, s, $CO_2CH_2C_6\underline{H}_5$).

6-O-Acetyl-1,2′,3,6′-tetra-N-benzyloxycarbonyl-2″,3″-O-cyclohexylidene-3′,4′,5″-trideoxy-3′-eno-ribostamycin (13). A solution of **12** (240 mg) in dioxane (3 ml) was hydrogenated with Raney nickel and hydrogen (50 psi) in the presence of triethylamine (0.1 ml) for 15 hr at 40 °C. On tlc with benzene–ethyl acetate (5: 2), the reaction mixture showed three spots of R_f 0.44 (**13**), 0.25 (de-OAc derivative) and 0.61 (**12**). After filtration, the solution was treated again with a fresh Raney nickel and hydrogen in the presence of triethylamine for 15 hr at 40 °C. The reaction mixture was filtered and the filtrate was evaporated to give a brown solid (171 mg). The solid was chromatographed on a column of silica gel (10 g) with benzene–ethyl acetate (3: 1). From the earlier eluate, **13** was obtained as a colorless solid, which was reprecipitated from benzene–*n*-hexane, yielding 91 mg (43%), mp 90—93 °C, $[\alpha]_D^{14}$ −29.8° (*c* 1.3, $CHCl_3$).

Found: C, 64.67; H, 6.17; N, 5.22%. Calcd for $C_{57}H_{66}N_4O_{16}$: C, 64.39; H, 6.26; N, 5.27%.

NMR (in $CDCl_3$): τ 8.82 (3H, d, J=6.5 Hz, $C\underline{H}_3$–CH(4″)), 8.8—8.2 (10H), 7.98 (3H, s, OAc), 4.38 (2H, s, H-3′,4′), 2.70, 2.66, 2.64 and 2.61 (each 5H, s, $CO_2CH_2C_6\underline{H}_5$).

From the late eluate, the de-*O*-acetylated product (**14**) was obtained in a yield of 57 mg (28%).

1,2′,3,6′-Tetra-N-benzyloxycarbonyl-2″,3″-O-cyclohexylidene-3′,4′,5″-trideoxy-3′-eno-ribostamycin (14). Compound **13** was treated similarly as described in the preparation of **9** from **8**. Yield 89%, mp 87—90 °C, $[\alpha]_D^{14}$ −26.6° (*c* 1.2, $CHCl_3$).

Found: C, 64.79; H, 6.14; N, 5.57%. Calcd for $C_{55}H_{64}N_4O_{15}$: C, 64.69; H, 6.32; N, 5.49%.

NMR (in $CDCl_3$): τ 8.78 (3H, d, J=6.5 Hz, CH_3–C(4″)), 8.8—8.2 (10H), 4.41 (2H, s, H-3′,4′), 2.71 and 2.67 (5H and 15H, s, respectively, $CO_2CH_2C_6\underline{H}_5$).

3′,4′,5″-Trideoxyribostamycin. A solution of **14** (120 mg) in aqueous dioxane (1: 1, 4 ml) was hydrogenated with palladium black and hydrogen (50 psi) at 35—40 °C for 15 hr. When water was added, the reaction mixture became turbid indicating that the hydrogenation was incomplete. The reaction mixture was filtered and the filtrate was evaporated to dryness. The residue was again treated as above with a fresh palladium black and hydrogen for 20 hr. The reaction mixture was filtered and the filtrate was evaporated to give a solid, which was dissolved in 1M hydrochloric acid (1 ml) and the solution was heated at 50 °C for 1 hr. After cooling, acetone was added to give a solid. The solid was charged on a column of Amberlite CG-50 (NH_4^+) and, after washing the column with water, it was developed with 0.1—0.4M ammonia with gradual increase in concentration. The product was emerged at the concentration of 0.3M ammonia. The eluate was evaporated to give a solid, 20 mg (40%), $[\alpha]_D^{14}$ +56° (*c* 0.7, H_2O). On paper chromatography with *n*-butanol–pyridine–water acetic acid (6:4:3:1), it gave $R_{f\ \text{ribostamycin}}$ 1.6.

Found: C, 48.32; H, 8.48; N, 13.11%. Calcd for $C_{17}H_{34}N_4O_7 \cdot H_2O$: C, 48.10; H, 8.55; N, 13.21%.

NMR (in D_2O): τ 9.0—7.7 (6H, m), 8.65 (3H, d, J= 6.5 Hz, $CH_3C\underline{H}$), 4.75 (1H slightly broadened singlet, H-1″), 4.62 (1H, m, H-1′).

The authors wish to thank Mr. Saburo Nakada for the elemental analysis and to Mr. Hiroshi Miyamoto for the technical assistance.

Kinetic Studies on the Cationic Ring-Opening Polymerization of Tetrahydrofuran Initiated by Superacid Esters[1)]

Shiro KOBAYASHI, Hidenori DANDA, and Takeo SAEGUSA

Department of Synthetic Chemistry, Faculty of Engineering, Kyoto University, Kyoto 606

(Received July 13, 1973)

The present paper descibes kinetic studies on the cationic ring-opening polymerization of tetrahydrofuran (THF) initiated by superacid esters such as ethyl fluorosulfate ($EtOSO_2F$), chlorosulfate ($EtOSO_2Cl$), and trifluoromethanesulfonate ($EtOSO_2CF_3$). The phenoxyl end-capping method was found to de applicable to kinetic analyses of the THF polymerization initiated by superacid esters. Also, the rate constants of propagation (k_p) and of initiation (k_i) were determined directly by NMR spectroscopic method. Rate constants determined by these two methods were in good agreement within experimental error. As a polymerization mechanism it was established that the propagation proceeds *via* cyclic oxonium species. The k_p values of superacid esters varied depending upon the nature of the counter anion, OSO_2X^-, *e.g.*, k_p at 0 °C in CH_2Cl_2: 0.66×10^{-3} (X=F), 1.4×10^{-3} (X=Cl), and 1.7×10^{-3} ($X=CF_3$) l/mol·sec, respectively. These magnitudes, however, were at least lower than one half of those of typical Lewis acid initiators. Initiation by superacid ester is a dipole-diple reaction, and k_i values were about 1/10—1/20 of the corresponding value of triethyloxonium tetrafluoroborate ($Et_3O^+BF_4^-$). Activation parameters were calculated for both the propagation and initiation reactions. In order to compare the present systems with those of superacid initiators, model reactions were examined by NMR spectroscopy.

In the last decade chemistry of superacid systems has widely been developed especially in the field of cationic reactions.[2)] Thus, it has become possible to observe directly a variety of cationic species in such superacid media.[2a,b)] Superacids are, according to Gillespie[2c)] more acidic than 100% sulfuric acid, the most frequently used strong acid solvent. With this respect fluorosulfuric, chlorosulfuric and trifluoromethanesulfonic acids are the well-known among superacids.

It has been reported preliminarily in our recent presentation[3)] that ester derivatives of fluorosulfuric and chlorosulfuric acids are very effective initiators for the cationic ring-opening polymerization of tetrahydrofuran (THF), oxetane, β-propiolactone, 2-oxazoline, epichlorohydrin, and propylene oxide. At almost the same time with our presentation,[3)] Simith and Hubin[4)] have reported semi-quantitative studies of the THF polymerization initiated by superacid derivatives including methyl trifluoromethanesulfonate. In the present paper we wish to report kinetic studies on the ring-opening polymerization of THF initiated with superacid esters. The superacid esters employed were ethyl fluorosulfate ($EtOSO_2F$), chlorosulfate ($EtOSO_2Cl$), and trifluoromethanesulfonate ($EtOSO_2CF_3$). The kinetic analyses were made on the basis of our "phenoxyl end-capping" method[5,6)] which enabled the determination of the concentration of the propagating species [P*]. Furthermore, the kinetic analyses were also performed by NMR spectroscopy. Thus, rate constants were determined, for the first time, directly by NMR spectroscopic method.

Results and Discussion

Determination of [P*]. In the ring-opening polymerization of THF by superacid ester initiators the phenoxyl end-capping procedure is shown in Scheme 1. For the determination of [P*], the modification of the original procedure was made; *i.e.*, phenetole produced directly from the initiator was successfully separated from the polymer phenyl ether by vacuum distillation with the aid of Decalin as the distillation entrainer.[7)]

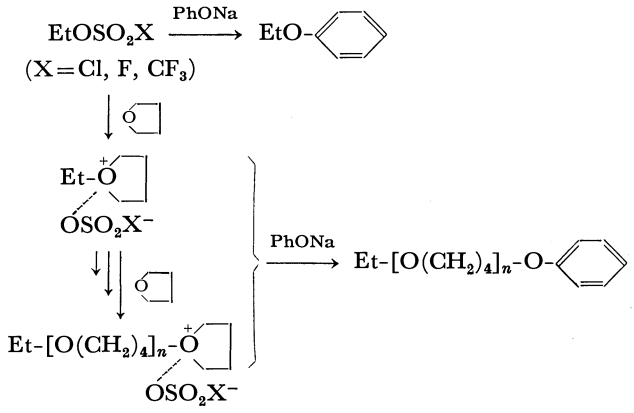

Scheme 1.

In Scheme 1, the reaction of sodium phenoxide with the propagating species and with the unreacted initiator should be quantitative in producing the polymer phenyl ether and phenetole, respectively. It has already been established that the propagating cyclic oxonium could be quantitatively converted into the polymer phenyl ether.[5)] In the present study, the reactions of sodium phenoxide with superacid esters were examined. $EtOSO_2F$ and $EtOSO_2Cl$

1) "Superacids and Their Derivatives," Part I.

2) For review see a) G. A. Olah and C. U. Pittman, Jr., *Adv. Phys. Org. Chem.*, **4**, 305 (1966); b) G. A. Olah, *Angew. Chem.*, **85**, 183 (1973); c) R. J. Gillespie, *Accounts Chem. Res.*, **1**, 202 (1968); d) R. J. Gillespie and T. E. Peel, *Adv. Phys. Org. Chem.*, **9**, 1 (1971).

3) T. Saegusa and S. Kobayashi, presented at the 21st Annual Meeting of the Society of Polymer Science, Japan, May, 1972.

4) S. Smith and A. J. Hubin, "Polymer Preprints," Vol. 13, p. 66 (1972).

5) T. Saegusa and S. Matsumoto, *J. Polym. Sci., Part A-1*, **6**, 1559 (1968).

6) T. Saegusa and S. Matsumoto, *Macromolecules*, **1**, 442 (1968).

7) T. Saegusa and S. Matsumoto, *J. Macromol. Sci. Chem.*, **A4**, 873 (1970).

$$EtOSO_2X + NaO\text{-}\langle\bigcirc\rangle \xrightarrow{\text{in THF}} EtO\text{-}\langle\bigcirc\rangle + NaOSO_2X \quad (1)$$

X=F, Cl

were allowed to react with sodium phenoxide in THF at room temperature, and the reaction mixture was treated in a similar manner as that for the polymerization system. The amount of phenetole produced was determined by UV spectroscopy. Reaction (1) has been regarded as quantitative (in Table 1). Thus, the phenoxyl end-capping method has been shown valid for the kinetic analysis of the THF polymerization initiated by superacid esters as in the case of the $Et_3O^+BF_4^-$ initiator system.[7]

Table 1. Reactions of $EtOSO_2F$ and $EtOSO_2Cl$ with sodium phenoxide at room temperature

$EtOSO_2X$[a] $\times 10^{-3}$, mol	X	NaO-⟨⟩[b] $\times 10^{-3}$, mol	Reaction time (min)	Yield[c] (%)
0.99	F	4.0	10	96
0.59	F	2.9	30	95
1.15	Cl	3.5	5	93

a) Solution in 3 ml of THF.
b) Solution in 6 ml of THF.
c) Based on $EtOSO_2X$. Determined by UV analysis.

Polymerization by Superacid Esters. Figure 1 shows the [P*]-time (Curve A) and conversion-time (Curve B) relationships in the THF polymerization initiated by $EtOSO_2F$. Throughout the polymerization, [P*] continued to increase. After 20 hr, [P*] reached to 63% of the initial concentration of the initiator. The induction period was observed in the conversion-time relationship and then, monomer was consumed monotonously. These observations indicate a slow initiation followed by a fast propagation.

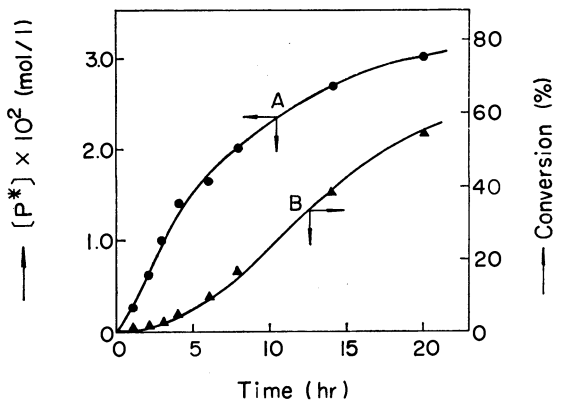

Fig. 1. Polymerization of THF by $EtOSO_2F$ at 0 °C. [P*]-time (Curve A) and monomer conversion-time (Curve B) relationships: $[I]=4.8\times10^{-2}$ mol/l, $[M]_0=9.80$ mol/l in CH_2Cl_2 solution.

It has been already established that in the cationic polymerization of THF the propagation reaction can be expressed by

$$\sim\sim\overset{+}{O}\langle\rangle + O\langle\rangle \overset{k_p}{\rightleftharpoons} \sim\sim O(CH_2)_4\text{-}\overset{+}{O}\langle\rangle \quad (2)$$

(A⁻ counterion)

On the basis of S_N2 mechanism the rate equation of propagation is given by

$$-\frac{d[M]}{dt} = k_p[P^*]\{[M]-[M]_e\} \quad (3)$$

where [M] and $[M]_e$ represent the instantaneous and equilibrium monomer concentrations, respectively, and k_p is the rate constant of propagation. Integration of Eq. (3) with respect to time gives

$$\ln\frac{[M]_{t_1}-[M]_e}{[M]_{t_2}-[M]_e} = k_p\int_{t_1}^{t_2}[P^*]dt \quad (4)$$

where $[M]_{t_1}$ and $[M]_{t_2}$ represent the monomer concentrations at time t_1 and t_2, respectively.

Based on the data in Fig. 1, the plot of Eq. (4) was made (Fig. 2). The slope of the straight line gave a k_p value of 0.66×10^{-3} l/mol·sec at 0 °C.

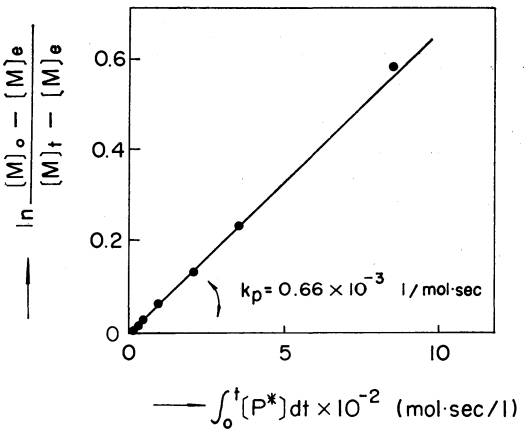

Fig. 2. Polymerization of THF by $EtOSO_2F$ at 0 °C: $[I]_0=4.8\times10^{-2}$ mol/l, $[M]_0=9.80$ mol/l in CH_2Cl_2 solution. $[M]_e=1.7$ mol/l.[8]

The initiation reaction can be formulated as

$$EtOSO_2X + O\langle\rangle \overset{k_i}{\rightleftharpoons} Et\text{-}\overset{+}{O}\langle\rangle \quad (5)$$

(OSO_2X^- counterion)

According to a bimolecular mechanism the rate equation of initiation is given by

$$-\frac{d[I]}{dt} = k_i[I][M] \quad (6)$$

Integration of Eq. (6) gave

$$\ln\frac{[I]_{t_1}}{[I]_{t_2}} = k_i\int_{t_2}^{t_1}[M]dt \quad (7)$$

where k_i is the rate constant of initiation and $[I]_{t_1}$ and $[I]_{t_2}$ are the instantaneous concentrations of the unreacted initiator at time t_1 and t_2, respectively.

Figure 3 shows the plot of Eq. (7) on the reasonable assumption that the amount of the reacted initiator corresponds to [P*] of Curve A in Fig. 1. The slope of the straight line of Fig. 3 gave the initiation rate constant, 0.33×10^{-5} l/mol·sec at 0 °C.

8) E. A. Ofstead, "Polymer Preprints," Vol. 6, p. 674 (1965).

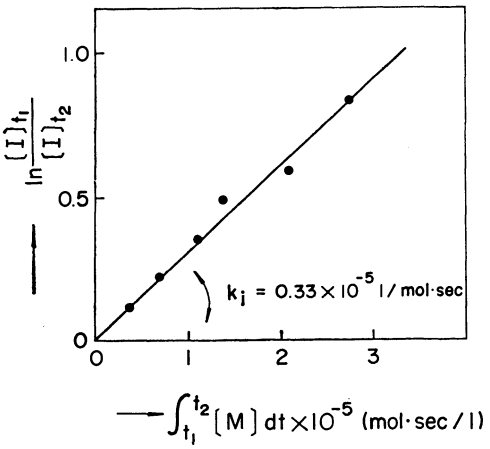

Fig. 3. Plots of Eq. (7) in the THF polymerization by $EtOSO_2F$ in CH_2Cl_2 at 0 °C. t_1=1.0 hr.

In a similar manner k_p and k_i values were determined at other temperatures. Furthermore, kinetic analyses were carried out on the THF polymerizations initiated by $EtOSO_2Cl$ and $EtOSO_2CF_3$. These results are summarized in Table 2.

TABLE 2. RATE CONSTANTS OF PROPAGATION (k_p) AND INITIATION (k_i) OF THE THF POLYMERIZATION[a]

Initiator	Temp (°C)	$10^3\cdot k_p$ (l/mol·sec)	$10^5\cdot k_i$ (l/mol·sec)
$EtOSO_2F$	8.4	1.4	0.67
	0	0.66	0.33
	−8.0	0.32	0.13
$EtOSO_2Cl$	6.5	2.2	0.50
	0	1.4	0.38
	−4.5	0.89	0.19
	−11.9	0.45	0.09
$EtOSO_2CF_3$	9.5	3.0	1.6
	0	1.7	0.80
	−7.8	0.76	0.45

a) Solution polymerization in CH_2Cl_2. $[M]_0$=9.80 mol/l, $[I]_0$=0.048 mol/l.

In all cases Arrhenius plots were linear, and the activation parameters were calculated (Table 3). For the purpose of comparison the k_p and k_i values at 0 °C are listed again, and the data with triethyloxonium tetrafluoroborate ($Et_3O^+BF_4^-$) initiator are also given in Table 3. The k_p value of $EtOSO_2F$ initiator is extremely small, *e.g.*, about 1/6 of that of $Et_3O^+BF_4^-$ initiator. The k_p values of $EtOSO_2Cl$ and $EtOSO_2CF_3$ initiators are between those of $EtOSO_2F$ and $Et_3O^+BF_4^-$. In the THF polymerization initiated by various Lewis acids such as BF_3, $SnCl_4$, $EtAlCl_2$, and Et_3Al–H_2O systems, the k_p values were determined by us using the phenoxyl end-capping methods.[11] The k_p values are in a narrow range between 3.7 and 9.9×10^{-3} l/mol·sec at 0 °C in CH_2Cl_2. Therefore, the k_p values by superacid esters of the present study are 1/15—1/2.2 for those of Lewis acid initiators. Since the activation parameters ($\Delta H_p^{\ddagger}$ and $\Delta S_p^{\ddagger}$) of $EtOSO_2X$ are very close to those of $Et_3O^+BF_4^-$, it is evident that the propagation of the polymerizations by superacid esters proceeds *via* an oxonium mechanism as shown in Eq. (2). Significant difference in k_p values between superacid esters and Lewis acids initiators may reasonably be attributed to the difference in the nature of the counter anions, A^- of Eq. (2). A recent report has revealed that the THF polymerization by $Et_3O^+BF_4^-$ proceeds *via* two species, *e.g.*, the free-ion and the ion-pair.[12] It may be likely that the effect of the counter anion on k_p is attributed partly to the different contribution of above two species toward k_p. Elucidation of this point must await further studies.

The initiation is a dipole-dipole reaction producing an oxonium ion (Eq. (5)). With this respect the initiation is similar to Menschutkin reaction in which an ammonium ion is formed from amine and alkyl halide (Eq. (8)). The initiation rate constant, k_i is at

$$R_3N + R'Y \longrightarrow R_3\overset{+}{R'}N\,Y^- \qquad (8)$$

least 2×10^2 times smaller than k_p in superacid ester systems. The k_i values of superacid esters are 1/20—1/10 of k_i of $Et_3O^+BF_4^-$. The activation parameters of the initiation exhibited relatively low $\Delta H_i^{\ddagger}$ and

TABLE 3. ACTIVATION PARAMETERS OF PROPAGATION AND INITIATION IN THE THF POLYMERIZATION BY SUPERACID ESTERS AND OXONIUM SALT IN CH_2Cl_2

Initiator	$EtOSO_2F$[a]	$EtOSO_2Cl$[a]	$EtOSO_2CF_3$[a]	$Et_3O^+BF_4^-$[b]
Propagation				
$10^3\cdot k_p$ at 0 °C (l/mol·sec)	0.66	1.4	1.7	3.7
$\Delta H_p^{\ddagger}$ (kcal/mol)	13.0	11.8	11.6	12
$\Delta S_p^{\ddagger}$ (e.u.)	−26	−28	−29	−26
Initiation				
$10^5\cdot k_i$ at 0 °C (l/mol·sec)	0.33	0.38	0.80	6.1[c]
$\Delta H_i^{\ddagger}$ (kcal/mol)	13.5	12.8	10.5	16.4
$\Delta S_i^{\ddagger}$ (e.u.)	−34	−37	−44	−16

a) Present work.
b) Taken from Refs. 7, 9, and 10.
c) Data at 2.5 °C; see Ref. 10.

9) T. Saegusa, S. Matsumoto, M. Motoi, and H. Fujii, *Macromolecules*, **5**, 236 (1972).
10) T. Saegusa, Y. Kimura, H. Fujii, and S. Kobayashi, *ibid.*, in press.
11) a) T. Saegusa, *J. Macromol. Sci. Chem.*, **A6**, 997 (1972); b) T. Saegusa and S. Kobayashi, "Progress in Polymer Science, Japan," Vol. 6, Kodansha Scientific, Tokyo, 1973.
12) J. M. Sangster and D. J. Worsfold, *Macromolecules*, **5**, 229 (1972).

also, low (unfavorable) $\Delta S_i^{\neq}$ values. This is in accordance with a dipole-dipole S_N2 mechanism (Eq. (5)) as seen in Menschutkin reaction.[13] Similar results have been obtained also in the molar reactions between superacid esters and tetrahydropyran (Eq. (9)).[14]

$$EtOSO_2X + O \rightleftharpoons Et\text{-}O^{+} \quad OSO_2X^{-} \qquad (9)$$

X=F, Cl, CF_3

NMR Studies. It has already been presented that the kinetics of the THF polymerization by superacid esters could be studied by means of NMR spectroscopy as well as the phenoxyl end-capping method.[15] In order to compare the kinetic data obtained by two different methods, the THF polymerization by superacid esters was examined also by NMR spectroscopy. A mixture of THF–$EtOSO_2CF_3$ (5: 1 molar ratio) in CH_2Cl_2 solution was introduced into an NMR sample tube at −78 °C. The tube was sealed and then the course of the reaction was followed by the change of NMR spectrum of the system. Figure 4 shows an

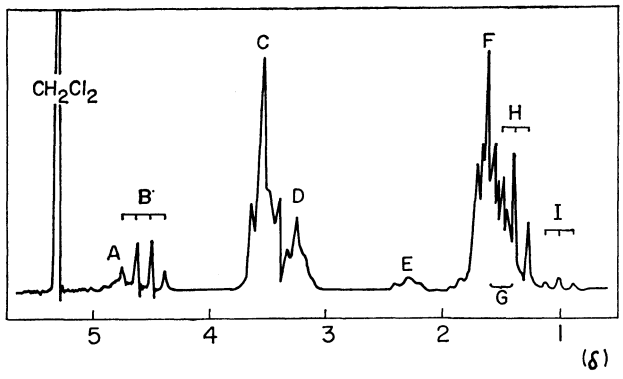

Fig. 4. NMR spectrum of the THF polymerization mixture by $EtOSO_2CF_3$ in CH_2Cl_2 after 20 min at 0 °C.

example NMR spectrum of the reaction system which was taken after 20 min at 0 °C. Signals C and D are due to α-methylene protons of THF monomer and of linear polymer, respectively. Peak F is due to β-methylene protons of THF monomer, while signal G due to β-methylene protons of polymer is overlapping with peaks F and H. A sharp quartet (B) and triplet (H) are due to methylene and methyl protons, respectively, of the initiator. Signals A (δ 4.72) and E (δ 2.32) are reasonably assigned to α- (six protons) and β- (four protons) methylene protons of cyclic oxonium of the propagating species. This assignment coinsides with that of our previous work[10] in which the formation of cyclic oxonium ions was clearly shown by NMR in the reaction of $Et_3O^+BF_4^-$ with cyclic ethers. Finally, a triplet (peak I) can be assigned to methyl protons of ethoxy group at polymer end. A

13) K. Wiberg, "Physical Organic Chemistry," John-Wiley & Sons, Inc., New York (1966), p. 379.

14) S. Kobayashi, T. Ashida, and T. Saegusa, presented at the 22nd Annual Meeting of the Society of Polymer Science, Japan, May, 1973.

15) T. Saegusa, S. Kobayashi, and H. Danda, presented at the 21st Symposium of the Society of Polymer Science, Japan, November 1972.

Table 4. Signal assignments in the polymerization mixture of THF by $EtOSO_2CF_3$

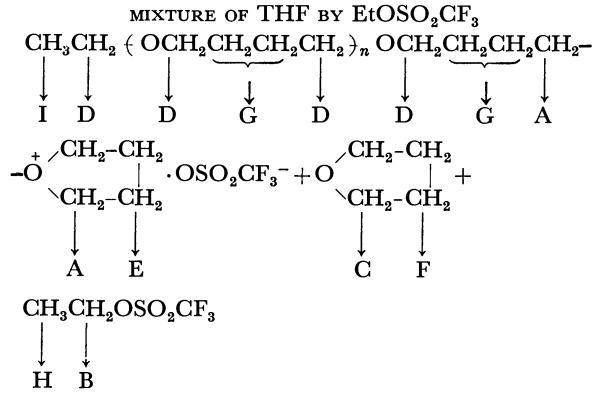

Signal	Chemical shift in ppm (from Me_4Si)[a]
A	4.72(m)
B	4.55(q)
C	3.52(m)
D	3.28(m)
E	2.32(t)
F	1.67(m)
G	1.50(m)
H	1.40(t)
I	1.02(t)

a) Multiplicity: m=multiplet, q=quartet, and t=triplet.

quartet due to methylene protons of the ethoxy group is overlapping with peak D. Table 4 summarizes the chemical shift assignments.

The concentrations of monomer, the initiator consumed and P* were determined by integration of signals C, I, and E, respectively. Thus, the kinetic analysis could be made in a similar way to that of the phenoxyl end-capping method. Figure 5 shows the variations of [P*]-time (Curve A) and of monomer conversion-time (Curve B), respectively. The molar concentration of cyclic oxonium species (obtained from the signal E) was equal to that of ethoxy group at the polymer end (obtained from the signal I) throughout the polymerization, *i.e.*, the system was of living character without termination. Therefore, the concentration of P* could be determined by either the

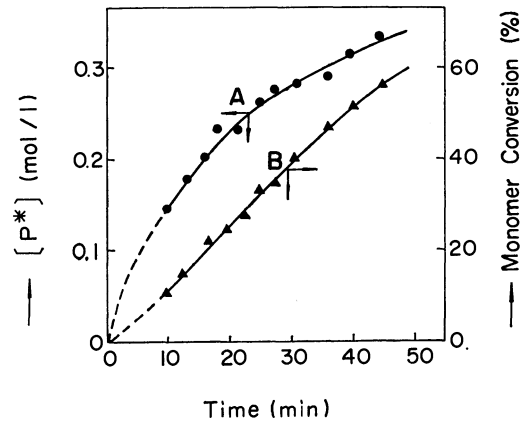

Fig. 5. Polymerization of THF with $EtOSO_2CF_3$ monitored by NMR spectroscopy. Solution polymerization at 0 °C. [P*]-time (Curve A) and monomer conversion-time (Curve B) relationships: $[I]_0$=1.27 mol/l, $[M]_0$=7.70 mol/l.

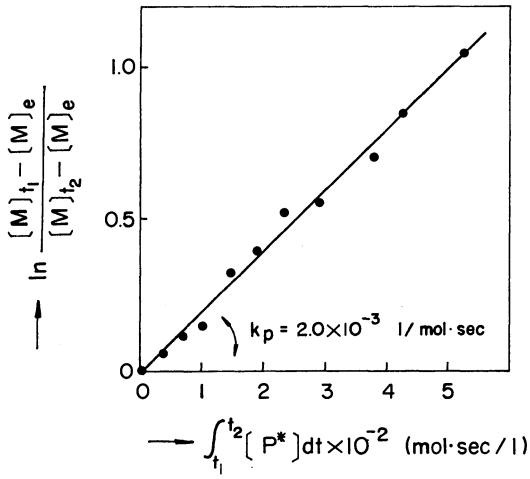

Fig. 6. Polymerization of THF by $EtOSO_2CF_3$ in CH_2Cl_2 at 0 °C: $[I]_0=1.27$ mol/l, $[M]_0=7.70$ mol/l, $[M]_e=1.7$ mol/l[18], $t_1=10$ min.

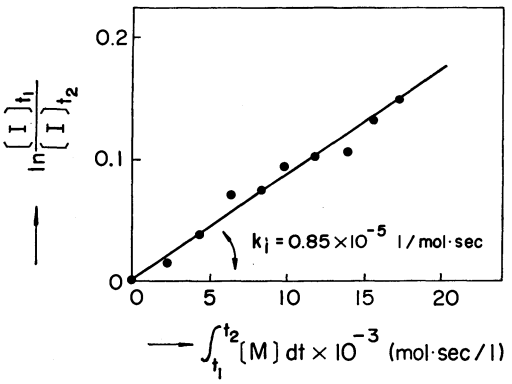

Fig. 7. Plots of Eq. (7) in the THF polymerization by $EtOSO_2CF_3$ in CH_2Cl_2 at 0 °C. $t_1=13$ min

signal E or I.

Based on the data in Fig. 5 the plots of Eq. (4) gave a straight line. From the slope a k_p value was obtained as 2.0×10^{-3} l/mol·sec at 0 °C (Fig. 6). On the basis of the relationship that the concentration of the propagating species is equal to that of the initiator consumed, the [P*]-time relationship in Fig. 5 was plotted according to Eq. (7) as shown in Fig. 7. Then, a k_i value was obtained as 0.85×10^{-5} l/mol·sec at 0 °C from the slope of the straight line.

In an analogous manner k_p and k_i values were determined by NMR spectroscopy for the systems of $EtOSO_2F$ and $EtOSO_2Cl$ initiators (in Table 5). It can be seen that the rate constant values by NMR spectroscopy and by phenoxyl end-capping method

Table 5. Rate constants of propagation (k_p) and initiation (k_i) of the THF polymerization determined by NMR spectroscopy in CH_2Cl_2 solution at 0 °C[a]

Initiator	$10^3\cdot k_p$ (l/mol·sec)	$10_5\cdot k_i$ (l/mol·sec)
$EtOSO_2F$	0.8	0.5
$EtOSO_2Cl$	1.5	0.6
$EtOSO_2CF_3$	2.0	0.85

a) $[M]_0=7.70$mol/l, $[I]_0=1.27$ mol/l.

(Tables 5 and 2) are in good agreement within experimental error.

In all systems of three initiators, the polymerization proceeded *via* oxonium propagating species in accordance with the mechanism of Scheme 1. An equilibrium of oxonium-ester species (Eq. (10)) may come into play during the polymerization.

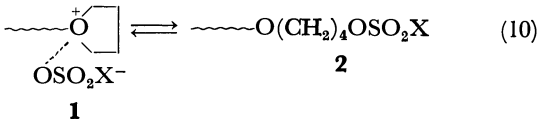

(10)

If the ester type species **2** were involved in the system, a peak should have appeared which is a characteristic signal of the α-methylene protons of an ester type ~~~~CH_2OSO_2X. However, any peak was not detected in the region of τ 4.25 throughout the THF polymerization initiated by a series of superacid esters under NMR measurement conditions. This indicates that the contribution of **2** to the propagation is, if any, very small during the THF polymerization where monomer is present in large excess, although the molar reaction of superacid ester and tetrahydropyran (Eq. (9)) has been proved to be an equilibrium system.[14]

Very recently, Pruckmayr and Wu have reported NMR studies on the THF polymerization initiated by superacids such as FSO_3H.[16] However, they did not determine the rate constants of such polymerization systems, in which "acidic" proton was present in a significant amount. Consequently, such proton made the polymerization systems complicated, bringing about termination, chain-transfer, the breaking of the polyether chain, the proton-proton exchange and so forth. Unlike these systems, the present reaction of superacid ester initiator is quite clean, since no "acidic" proton is involved. Therefore, NMR spectra were simple in all cases as shown in Fig. 4. So far as we know the present study is the first case that the initiation and propagation rate constants in the THF ploymerization were determined directly by means of high resolution NMR spectroscopy.

As to NMR spectral assignments Pruckmayr and Wu[16] ascribed a peak at δ 4.25 to α-methylene protons of cyclic trialkyloxonium in benzene. For a peak at δ 4.65 they assigned it to α-methylene protons of cyclic dialkyloxonium ion. Their assignment of cyclic trialkyloxonium ion, however, is not compatible with that of the present work. It is unlikely that cyclic dialkyloxonium ion (the protonated THF, **3**) was observed as a long-lived species at their NMR measurement conditions, since proton exchange reaction (Eq. (11)) is very fast. We attempted to observe **3** directly by NMR spectroscopy.

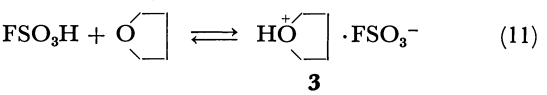

(11)

However, the direct observation of **3** as a long-lived species was unsuccessful in FSO_3H–benzene at 0 °C or in FSO_3H–CH_2Cl_2 solution even at lower temperature of −50 °C. Rapid proton exchange still took place at

16) G. Pruckmayr and T. K. Wu, *Macromolecules*, **6**, 33 (1973).

−50 °C. This rapid proton exchange is suggested from their observations[16] that the signal of α-methylene protons of monomer THF was shifted downfield to δ 3.75 in the presence of "acidic" protons[16] from δ 3.52 of free THF in the absence of such protons (Table 4) whereas the peak of α-methylene protons of polymer chain were less affected.

On the basis of above findings we think that a peak at δ 4.65 is due to α-methylene protons of cyclic trialkyloxonium ion (propagating species) and that a peak at δ 4.25 must be due to another species. For such species we propose here a polymer alkyl ester species of superacid as given by **2**. To support this,

$$\sim\!\sim\!\sim CH_2OSO_2X$$

2 (X=F)

a model compound (**4**) was prepared from 4-ethoxy-1-butanol and sulfuryl chloride according to Eq. (12). **4** is recognized as a 1:1 adduct of $EtOSO_2Cl$ and

$$CH_3CH_2O(CH_2)_4OH + SO_2Cl_2 \xrightarrow{\text{in } CH_2Cl_2} CH_3CH_2O(CH_2)_4OSO_2Cl + HCl \quad (12)$$

4

THF. The reaction of alcohol and sulfuryl chloride is probably the best one to prepare alkyl chlorosulfate.[17] Figure 8 shows NMR spectra of the reaction mixture of Eq. (12). At 30 min after the addition of sulfuryl chloride to the above ether alcohol a peak (A) due to α-methylene protons of OSO_2Cl group appeared at δ 4.25 (spectrum I in Fig. 8). After the reaction mixture was concentrated under reduced pressure with bubbling of dry nitrogen at 0 °C a spectrum of II (Fig. 8) was obtained. Additionally two peaks appeared at δ 4.70 (B) and δ 2.35 (C). They are assigned to α-(B) and β-(C) methylene protons of cyclic trialkyloxonium ion (**5**). This indicate that 30% of **4** (from integration) underwent an intramolecular cyclization to produce **5**. It should be added here that the chemical shifts are not changed by the nature of X (X= F, Cl, or CF_3) of OSO_2X in **4** or **5**.[18]

$$CH_3CH_2\ddot{O}(CH_2-CH_2)_2\,\delta^-OSO_2Cl \rightleftharpoons CH_3CH_2-\overset{+}{O}\!\left(\begin{matrix}CH_2-CH_2\\ \diagdown\ \diagup\\ O\end{matrix}\right)\,OSO_2Cl^- \quad (13)$$

4 **5**

All of these findings are taken to substantiate our assignments, *i.e.*, peaks at δ 4.65 and δ 4.25 are respectively due to α-methylene protons of cyclic trialkyloxonium ion (propagating species, **1**) and to α-methylene protons of superacid ester (**2**, X=F) of polymer chain. By the same reason, β-methylene protons of **1** corresponds to a peak at δ 2.40, which was assigned to β-methylene protons of **3**.[16] As to our assignment, the production of **2** is explained reasonably. For example, the initiator reacts with hydroxyl group at the polymer end to produce a polymer alkyl ester of fluorosulfuric acid as shown by Eq. (14). This kind of reaction, *i.e.*, a reaction of alcohol and superacid, provides a

$$FSO_3H + \sim\!\sim\!\sim CH_2OH \longrightarrow \sim\!\sim\!\sim CH_2OSO_2F + H_2O \quad (14)$$

2

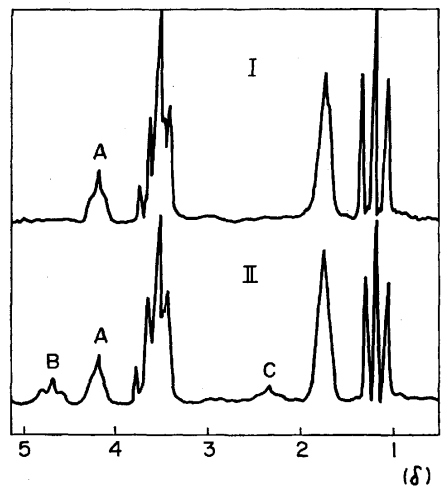

Fig. 8. NMR spectra of the reaction mixture of 4-ethoxy-1-butanol and sulfuryl chloride in CH_2Cl_2: (I) At 30 min after the addition of sulfuryl chloride at **0** °C; (II) After concentration at reduced pressure with bubbling of dry nitrogen at **0** °C.

good synthetic method of superacid ester.[19] Another possibility of the production of **2** is a reaction of the propagating species given by Eq. (10), in which the counter anion, OSO_2X^-, attacks nucleophilically the α-carbon atom of cyclic oxonium ion **1**. This type of reaction (Eq. (10)) may be facilitated in the presence of "acidic" protons. Thus, propagating cyclic trialkyloxonium ion **1** will eventually convert into species **2** according to Eq. (10). This agrees with the observation that peaks at δ 4.65 and 2.40 disappeared and instead a peak at δ 4.25 appeared at a long reaction time.[16]

Experimental

Materials. THF and solvents were purified as previously reported.[5,6] The THF solution of sodium phenoxide was prepared in a similar manner as reported.[5] Fluorosulfuric acid was prepared from hydrogen fluoride and fuming sulfuric acid, bp 69 °C/50 mmHg (lit,[20] 163 °C). $EtOSO_2F$ and $EtOSO_2CF_3$ were prepared by the reaction of diethyl sulfate with FSO_3H and with CF_3SO_3H, bp the former 88 °C/390 mmHg (lit,[19] 113 °C/752 mmHg) and the latter 55—58 °C/100 mmHg (lit,[20] 115 °C). $EtOSO_2Cl$ was prepared by the usual procedure[17] from sulfuryl chloride and ethanol, bp 58 °C/25 mmHg (lit,[17] 43 °C/10 mmHg). 4-Ethoxy-1-butanol was prepared from 1,4-butanediol, ethyl iodide and sodium, bp 70—72 °C/9 mmHg (lit,[21] 72 °C (8 mmHg)).

Polymerization Procedure. Polymerization was carried out under nitrogen. At a polymerization temperature 1.0 ml CH_2Cl_2 solution of the initiator (0.24 mmol) was added to 50 mmol of THF monomer, which resulted in the initial

17) E. Buncel and J. P. Millington, *Can. J. Chem.*, **43**, 556 (1964).
18) S. Kobayashi and T. Saegusa, unpublished results.
19) J. Meyer and G. Schramm, *Z. Anorg. Allg. Chem.*, **206**, 24 (1932).
20) T. Gramstad and R. N. Haszeldine, *J. Chem. Soc.*, 173 (1956).
21) M. Lj. Mihailović and M. Miloradivić, *Tetrahedron*, **22**, 723 (1966).

monomer and catalyst concentrations of 9.80 mol/l and 0.048 mol/l, respectively. After a desired reaction time 1.5 ml THF solution of sodium phenoxide (0.5 mol/l) was added to stop the polymerization. The reaction mixture was stirred further for 30 min at room temperature. Then, it was treated with a large excess of 1M aqueous sodium hydroxide solution. The reaction mixture was extracted three times with 5 ml of CH_2Cl_2. The extracts were combined and dried over K_2CO_3 and centrifuged. The CH_2Cl_2 solution was diluted to 25 ml and the total amount of phenyl ether was determined by UV spectroscopy. A 1.0 ml portion of this CH_2Cl_2 solution was mixed with 4 ml of Decalin and the mixture was subjected to distillation at room temperature under reduced pressure (below 0.3 mmHg). The residue was dissolved in CH_2Cl_2 to the total volume of 20 ml. Then, the amount of phenyl ether at the polymer end was determined by UV analysis. Conversion percent was determined from the amount of the product polymer.

UV Measurements. All UV spectra were taken on Shimadzu UV-200 spectrometer in CH_2Cl_2 solution at room temperature.

NMR Measurements. Into 14.6 mmol of THF 2.4 mmol of $EtOSO_2CF_3$ in 0.40 ml CH_2Cl_2 was added slowly at −78 °C. After mixing a portion of the reaction mixture was transfered into an NMR sample tube, and then the tube was sealed at the same temperature. The extent of the reaction was negligible at −78 °C. The tube was then placed in the NMR probe insert which was kept constant at 0 °C. The time of the insertion was assumed to be the start of the reaction. Then, the reaction was followed. The instrument used was a Hitachi R-20B NMR spectrometer. The reaction temperature was kept constant within ±1 °C and the experimental error of the integration was within ±2%.

The authors are indebted to Minnesota Mining and Manufacturing Co. (Minnesota) for a gift of CF_3SO_3H. They also express appreciation to Daikin Kogyo Co. Ltd., (Osaka, Japan) for providing anhydrous hydrogen fluoride.

BULLETIN OF THE CHEMICAL SOCIETY OF JAPAN, VOL. 46, 3220—3224 (1973)

Kinetic Study on the Ring-Opening Polymerization of Tetrahydrofuran by Pyrosulfuryl Chloride Initiator[1]

Shiro KOBAYASHI, Takeo SAEGUSA, and Yoshiaki TANAKA[2]

Department of Synthetic Chemistry, Faculty of Engineering, Kyoto University, Kyoto 606

(Received July 13, 1973)

This paper deals with a kinetic study of the ring-opening polymerization of tetrahydrofuran (THF) initiated by pyrosulfuryl chloride (PSC). The kinetic analysis was based on the determination of the concentration of propagating species, [P*], by the phenoxyl end-capping method. The rate constants of the three elementary processes, propagation (k_p), initiation (k_i), and termination (k_t), were determined. Activation parameters for the propagation were; $\Delta E_p^{\neq}=12$ kcal/mol, and $A_p=7.6\times10^6$ l/mol·sec. From the k_p values and the NMR study of the THF–PSC reaction, it is concluded that the propagation proceeds *via* the bis-oxonium species **5b**. The ester type species **5a** may be involved at a very early stage of polymerization. However, its contribution was quite small throughout the polymerization. The THF polymerization initiated by PSC was characterized by the fast initiation. The mechanism of termination was also examined. The THF polymerization by trifluoromethanesulfonic anhydride was also studied kinetically, which was characterized by a living propagation by bis-oxonium species.

Relatively few studies have been reported on the reaction of pyrosulfuryl halides in the organic chemistry. Very recently, however, attention has been paid on the reactions of pyrosulfuryl fluoride.[3] We have recently reported a kinetic study of the polymerization of tetrahydrofuran (THF) by using superacid esters such as ethyl chlorosulfate, fluorosulfate, and trifluoromethanesulfonate.[4] As an extension of our previous study we report in the present study the kinetics of the THF polymerization initiated by pyrosulfuryl chloride, $Cl\text{-}SO_2\text{-}O\text{-}SO_2Cl$, (PSC). PSC is a derivative of superacid, *i.e.*, an anhydride of chlorosulfuric acid. Furthermore, it could be a bifunctional initiator for the cyclic ether polymerization.

Results and Discussion

Determination of [P] by the Phenoxyl End-Capping Method.* The phenoxyl end-capping method has originally been developed by Saegusa and Matsumoto[5] for the determination of [P*] in THF polymerization. Since then, this method has successfully been employed in kinetic analyses of polymerizations of various cyclic ethers including mono and bicyclic monomers.[6] This

1) "Superacids and Their Derivatives," Part II. For Part I, See Ref. 4.

2) Present Address: Industrial Research Laboratories, Kao Soap Co. Ltd., Wakayama-shi, Japan.

3) M. M. Boudakian, G. A. Hyde, and S. Kongpricha, *J. Org. Chem.*, **36**, 940 (1971).

4) S. Kobayashi, H. Danda, and T. Saegusa, This Bulletin, **46**, 3214 (1973).

5) T. Saegusa and S. Matsumoto, *Macromolecules*, **1**, 442 (1968).

6) For review, see a) T. Saegusa, *J. Macromol. Sci.*, **A-6**, 997 (1972); b) T. Saegusa and S. Kobayashi, in "Progress in Polymer Science, Japan," Vol. 6, Kodansha Scientific, Tokyo, 1973.

method was used also in the present study. It has been established in the polymerization of THF that the conversion of the propagating species into the phenyl ether group is quantitative under the phenoxyl end-capping reaction conditions regardless of the nature of the propagating species, *e.g.*, oxonium type (**1**) or ester type (**2**).[7] The concentration of the phenyl ether

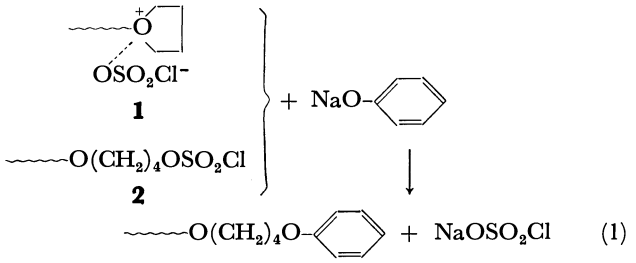

(1)

group formed by the reaction of **1** or **2** with sodium phenoxide (Eq. (1)) was analyzed by its UV absorption at 272 mμ. The molar extinction coefficient value of the phenyl ether was obtained to be 1.93×10^3 l/mol·cm in the THF polymerization.[5,8]

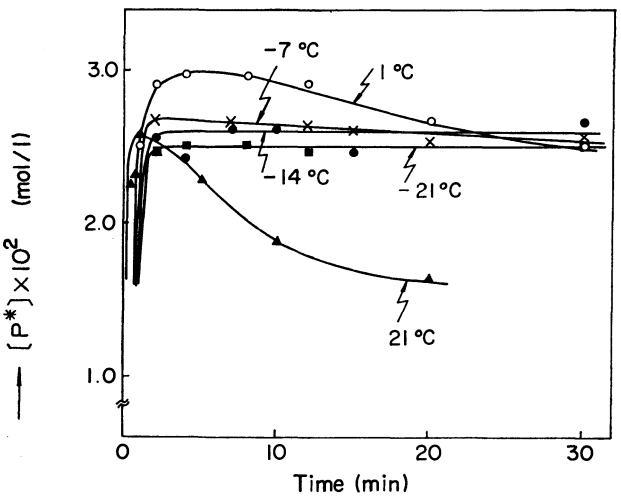

Fig. 1. [P*]-time plots in the polymerization of THF by PSC initiator in CH_2Cl_2: $[M]_0$, 9.9 mol/l; $[PSC]_0$, 0.0203 mol/l.

Polymerization of THF. The THF polymerization was carried out at five temperatures between −21 and 21 °C. The [P*] change during the THF polymerization was examined by means of the phenoxyl end-capping method. The time-[P*] relationships of the PSC-initiated polymerization are shown in Fig. 1. At −21 and −14 °C, P* was produced at an early stage of the polymerization, *i.e.*, within 3 min, and it remained constant thereafter. This indicates a rapid initiation and no occurrence of a termination at these temperatures. At higher temperatures [P*] reached to the maximum within few minutes, and then diminished slowly at 1 °C and fairly rapidly at 21 °C. The maximum concentration of P* during the polymerization is about 75% of the charged initiator concentration,

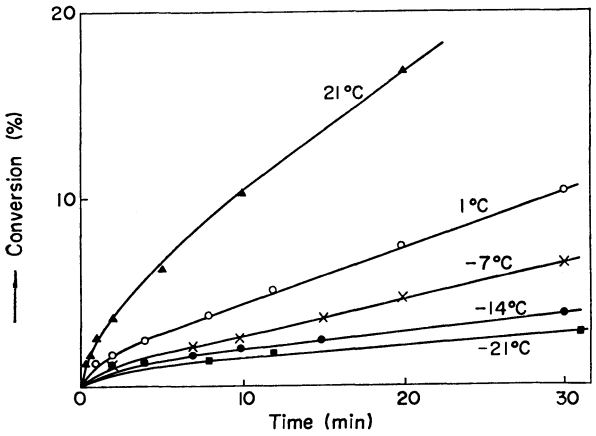

Fig. 2. Time-conversion curves in the THF polymerization by PSC initiator in CH_2Cl_2 at various temperatures: $[M]_0$, 9.9 mol/l; $[PSC]_0$, 0.0203 mol/l.

based on the assumption that PSC is a bifunctional initiator.

The time-conversion curves at five temperatures are shown in Fig. 2. From the time-[P*] and time-conversion relationships the propagation rate constant, k_p, was determined on the basis of the following procedure.

The initiation of THF by PSC must be expressed as Eq. (2)

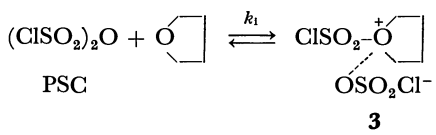

(2)

producing the oxonium species **3**. Then, the first propagation step takes place by the nucleophilic attack of THF monomer on **3**, by which the oxonium-ester type intermediate (**4**) may probably be produced

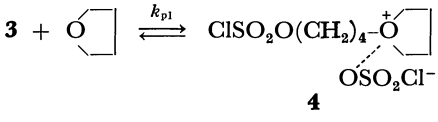

(3)

where k_{p1} represents the first propagation rate constant. In the later propagation stage, therefore, the growing chain end can be formulated as a bifunctional oxonium-ester (**5a**) and/or a bifunctional oxonium-oxonium type (**5b**) as shown in Eq. (4). As a matter of fact the formation of **5b** involves the conversion of ester into oxonium species.

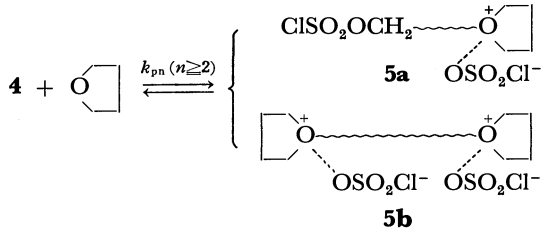

(4)

It has been already established that the propagation of the THF polymerization proceeds *via* a bimolecular reaction between the propagating species and monomer, and hence obeys a following kinetic equation

7) T. Saegusa and S. Kobayashi, presented at the 21st Annual Meeting of the Society of Polymer Science, Japan, May, 1972.

8) T. Saegusa and S. Matsumoto, *J. Polym. Sci., Part A-1*, **6**, 1559 (1968).

$$-\frac{d[M]}{dt} = k_p[P^*]\{[M]-[M]_e\} \quad (5)$$

where [M] and $[M]_e$ denote the instantaneous and equilibrium monomer concentrations, respectively.[5] Integration of Eq. (5) with respect to time gives

$$\ln\frac{[M]_{t_1}-[M]_e}{[M]_{t_2}-[M]_e} = k_p\int_{t_1}^{t_2}[P^*]dt \quad (6)$$

where $[M]_{t1}$ and $[M]_{t2}$ are the monomer concentrations at time t_1 and t_2, respectively.

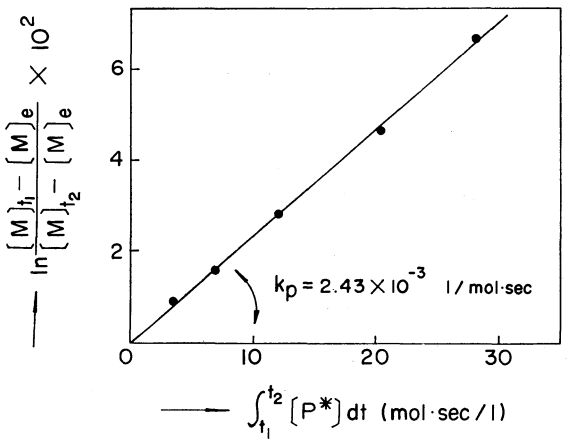

Fig. 3. Plots of Eq. (6) in the THF polymerization by PSC initiator at 1 °C: $[M]_0$, 1.7 mol/l; t_1, 8 min.

A linear plot of Eq. (6) gave a straight line passing through the origin as shown in Fig. 3, from which k_p at 1 °C was calculated. Similarly, k_p values at other temperatures were obtained and are summarized in Table 1.

Table 1. Rate constants and activation parameters of the THF polymerization by PSC[a]

°C	$10^3\times k_p$ (l/mol·sec)	$10^3\times k_i$ (l/mol·sec)	$10^4\times k_t$ (sec^{-1})
−21	0.42	—	—
−14	0.81	—	—
− 7	1.55	—	—
1	2.43	2.4	1.3
21	10.9(6.5)[b]	10(∼15)[b]	5.3
ΔE_p^* (kcal/mol)	12		
A_p (l/mol·sec)	7.6×10^6		

a) Polymerization conditions: $[M]_0$, 9.9 mol/l in CH_2Cl_2; $[PSC]_0$, 0.0203 mol/l.
b) Trifluoromethanesulfonic anhydride initiator at 21°C. Polymerization conditions were the same as those of PSC initiator.

The rate of initiation was estimated from the rate of the P* production. The rate equation is given by Eq. (7) according to the initiation reaction Eq. (2)

$$-\frac{d[PSC]}{dt} = k_i[PSC][M] \quad (7)$$

Thus, the initiation rate constant k_i was obtained from the slope of the linear plot of the integrated equation.

$$\ln\frac{[PSC]_0}{[PSC]_t} = k_i\int_0^t[M]dt \quad (8)$$

where $[PSC]_t$ was obtained on the assumption that $[PSC]_t=[PSC]_0-[P^*]$. From the [P*]-time relationship in Fig. 1 k_i was roughly calculated and given in Table 1.

A kinetic analysis of termination was also made on the basis of the [P*]-time curve. The termination of the THF polymerization has been assumed to be a unimolecular reaction.[9] Therefore, the following equation is derived

$$-\frac{d[P^*]}{dt} = k_t[P^*] - R_i \quad (9)$$

where R_i is the production rate of P* and k_t is the rate constant of termination. After the [P*] reaches to the maximum in few minitutes the production of P* ceases, *i.e.*, $R_i=0$. Hence, Eq. (9) becomes Eq. (10)

$$-\frac{d[P^*]}{dt} = k_t[P^*]$$
$$\therefore\quad -d(\ln[P^*])/dt = k_t \quad (10)$$

The plot of ln[P*] *vs.* time became a straight line after the [P*] maximum at 1 and 21 °C. These slopes gave k_t values, which are listed also in Table 1.

The k_p value initiated by PSC can reasonably be taken to represent the propagation *via* bis-oxonium species **5b** of Eq. (4) according to the following observations. Recently we have found that ethyl chlorosulfate (**6**) causes the THF polymerization *via* an oxonium ion (**7**) of Eq. (12).[4]

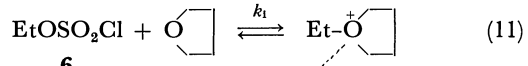

(11)

6

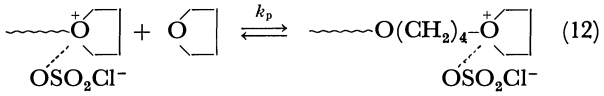

(12)

7

The k_p value obtained in the above system was 1.4×10^{-3} l/mol·sec at 0 °C in CH_2Cl_2.[4] In the PSC-initiated polymerization the conversion of ester (**5a**) into oxonium (**5b**) is not impossible because the ester **6** is able to induce the THF polymerization. However, the rate of oxonium formation, k_i of Eq. (11), 3.8×10^{-6} l/mol·sec at 0 °C, is very slow compared with k_p of Eq. (12), 1.4×10^{-3} l/mol·sec at 0 °C, *i.e.*, k_i is about 3.7×10^2 times smaller than k_p. Since ester species of **5a** has longer alkyl chain group than ethyl group of **6**, it may be less reactive than **6** as usually seen in the similar type S_N2 reactions.[10] Therefore, ester species in **5a** is at least 3.7×10^2 times less reactive than oxonium species in **5a** or **5b**. In this respect **5a** behaves like a monofunctional species of the oxonium type although ester species of **5a** is inherently not a dead species. The [P*] obtained by the phenoxyl end-capping methods represents both the oxonium (**1**) and ester (**2**) type propagating species. If the propagation proceeds *via* **5a** the fraction of the oxonium

9) H. Meerwein, D. Delfs, and H. Morshel, *Angew. Chem.*, **72**, 927 (1960).
10) C. K. Ingold, "Structure and Mechanism in Organic Chemistry," 2nd ed., Cornell University Press, (1969), Chapter VII.

concentration is one half of the observed [P*]. Then, the k_p values should be twice as large as those in Table 1 since the propagation rate of the ester type is negligible small. The k_p value, for example, at 1 °C results in 4.86×10^{-3} l/mol·sec which is too large compared with the observed k_p value of 1.4×10^{-3} l/mol·sec at 0 °C initiated by ethyl chlorosulfate **6** (Eq. (12)). The k_p values should be equal in principle when the same counter anion is involved in the propagation. Both PSC and ethyl chlorosulfate **6** initiators provide a same counter anion, OSO_2Cl^-. Even so, the k_p value of 2.43×10^{-3} l/mol·sec is still fairly larger than that of Eq. (12). All these findings indicate most likely that the PSC-initiated polymerization proceeds *via* bis-oxonium type **5b**. The contribution of **5a** is, if any, very small throughout the propagation of THF polymerization.

The k_p values obtained in the present study are interestingly compared with those initiated by typical Lewis acids.[6] For example, the k_p value at 0 °C by BF_3-epichlorohydrin initiator is reported to be 4.5×10^{-3} l/mol·sec,[5] the magnitude of which is about twice as large as that of the PSC-initiated polymerization.

Activation parameters of the propagation were also calculated. Arrhenius plot of k_p values gave a well-correlated straight line whose slope gave an activation energy ΔE_p^* of 12 kcal/mol. The same magnitude of ΔE_p^* was obtained in the BF_3-epichlorohydrin initiated polymerization.[11] This is again taken to support the bis-oxonium process **5b**.

For comparison, kinetics of the THF polymerization was carried out also by trifluoromethanesulfonic anhydride (**8**) initiator. The results are shown in Fig. 4. [P*] reached to the maximum within 2 min and kept constant thereafter. The maximum of [P*] was 85% of the charged initiator on the assumption that **8** is a bifunctional initiator. It should be noted that in the polymerization by **8** no termination took place even at a higher temperature, *e.g.*, **21** °C. From the relationships in Fig. 4 k_p values were calculated (Table 1).

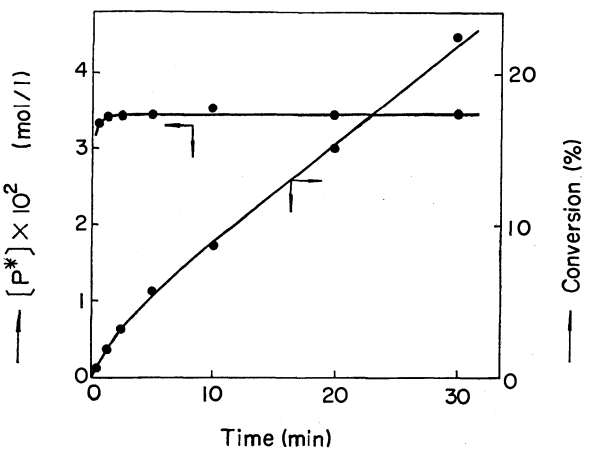

Fig. 4. Time-[P*], and time-conversion relationships in the THF polymerization initiated by trifluoromethanesulfonic anhydride at 21 °C in CH_2Cl_2: $[M]_0$, 9.9 mol/l; $[(CF_3SO_2)_2O]_0$, 0.0203 mol/l.

11) T. Saegusa, S. Matsumoto, M. Motoi, and H. Fujii, *Macromolecules*, **5**, 236 (1972).

The k_p of **8** is smaller than that of PSC initiator. It is likely that the polymerization initiated by **8** proceeds *via* bis-oxonium type **9** as suggested previously by Smith and Hubin.[12]

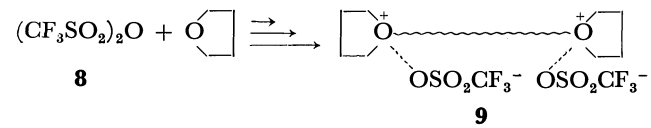

8 **9**

The PSC-initiated polymerization is characterized by a rapid initiation reaction as given in Table 1. The rate of the initiation is as fast as that of the propagation. Comparing k_i values between PSC and **6** of Eq. (11) PSC reacts with THF about 5.8×10^2 times faster than **6** at 1 °C. In addition the k_i value of PSC is also more than 10 times larger than that of triethyloxonium tetrafluoroborate in the THF polymerization.[13] The initiation rate of **8** is even faster than PSC. Therefore, the system initiated by **8** is recognized as that of a fast initiation but a slow propagation. This may account that polymer of very narrow molecular weight distribution ($M_W/M_N=1.08$) was obtained by **8** initiator.[12]

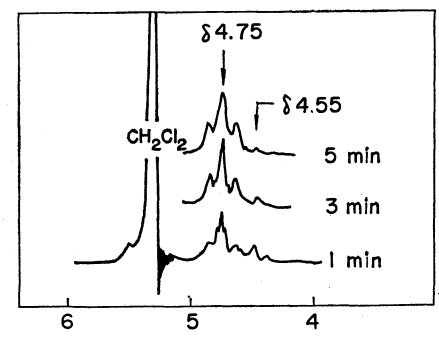

Fig. 5. NMR spectra of the reaction mixture of PSC with THF at 0 °C in CH_2Cl_2.
The molar ratio of PSC to THF was 1/5.

NMR Spectroscopy. To elucidate whether the ester type is involved or not, the reaction of THF with PSC in CH_2Cl_2 was examined by means of NMR spectroscopy. The THF to PSC molar ratio was 5/1. The reaction was carried out at 0 °C in an NMR sample tube under nitrogen. NMR spectra of the reaction system are shown in Fig. 5. After 1 min at 0 °C complex peaks appeared. Among them a triplet-like signal centered at δ 4.55 is reasonably assigned to α-methylene proton signal of the ester type **10** since that of an authentic tetramethylene bischlorosulfonate

~~~~CH_2OSO_2Cl $ClSO_2OCH_2CH_2CH_2CH_2OSO_2Cl$

10 **11**

11 appears at δ 4.60 in CH_2Cl_2 at 35 °C. Peaks centered at δ 4.75 is due to the α-methylene signal of oxonium type **12** whose assignment has already been established.[4,7,14] After 3 min at 0 °C, however, the

12) S. Smith and A. J. Hubin, "Polymer Preprints," Vol. 13, p. 66 (1972).

13) T. Saegusa and S. Matsumoto, *J. Macromol. Sci. Chem.*, **A-4**, 873 (1970).

14) T. Saegusa, Y. Kimura, H. Fujii, and S. Kobayashi, *Macromolecules*, in press.
~~~~

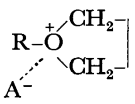

12

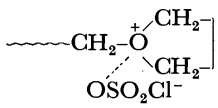

13

signal at δ 4.55 almost disappeared whereas the signal at δ 4.75 increased very much. It should be noted that the pattern of the signal at δ 4.75 changed from that of the reaction time of 1 min into a typical triplet-like one. The same triplet-like signal has been observed for the oxonium **13** at the same chemical shift.[4,14] After 5 min at 0 °C the ester signal has completely disappeared and only the oxonium signal was observed.

These findings indicate that the ester type species **10** converted into the oxonium species **13** at a very early stage to produce bis-oxonium species **5b**. This means that the contribution of ester type species **5a** is very small throughout the propagation stage which is in accordance with the kinetic results. It is interesting to note that in the PSC-initiated polymerization the reactivity of the ester involved at a very early stage is much enhanced probably due to the neighboring oxonium group.

Termination Mechanism. As seen in Fig. 1 considerable termination takes place at 21 °C in the PSC-initiated polymerization. Therefore, a reference reaction was carried out to examine the termination mechanism. At −78 °C THF was added to PSC in CH_2Cl_2 at a molar ratio of THF to PSC of 3: 1. The reaction system was allowed to warm up gradually to 25 °C and kept for 20 hr at this temperature. Then, the reaction mixture was treated with sodium phenoxide under the phenoxyl end-capping reaction conditions. White waxy polymer was obtained after work-up. The polymer was analyzed by elemental analysis, molecular weight measurement, iodometry, IR and NMR spectroscopy.

The results of elemental analysis was as follows: C, 66.56; H, 8.82 and Cl, 10.6%, respectively. The iodine value was null, *i.e.*, the polymer has no olefinic group. The molecular weight measurement by vapor pressure osmometry gave 309. From these data the polymer composition was proposed as $(C_6H_5)_{1.07}(OC_4H_8)_{2.68}Cl_{0.95}$ for the polymer. In addition, the NMR measurement of the polymer gave a polymer composition of $(C_6H_5)_{1.01}(OC_4H_8)_{2.6}$ from an integral ratio of phenyl protons *vs.* aliphatic protons. The IR spectrum of the polymer showed an absorption band at 650 cm^{-1} due to C–Cl stretching indicative of the presence of alkyl chloride.

Based on the above findings the termination mechanism is reasonably formulated as Eq. (13) which involves the nucleophilic attack of chloride anion of the counterion on the α-carbon of oxonium **13** with the liberation of SO_3. In this process it is not clear if the ester type intermediate **10** is involved or not. The termination of the PSC-initiated polymerization is in

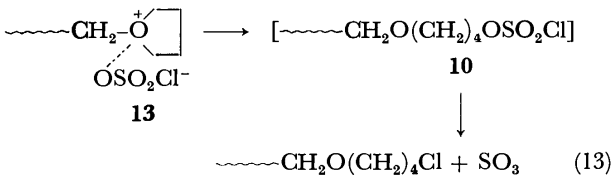

13 10

$$\sim\sim\sim\sim CH_2O(CH_2)_4Cl + SO_3 \qquad (13)$$

sharp constrast to that of the trifluoromethanesulfonic anhydride **8** initiated one where no termination was observed even at a higher temperature of 21 °C. This is obviously due to the stability difference between the counter anions, OSO_2Cl^- and $OSO_2CF_3^-$.

Experimental

Materials. The THF monomer and methylene dichloride solvent were commercial reagents and were purified in the same manner as described previously.[5,8] PSC was prepared by the reaction of sulfur trioxide with carbon tetrachloride according to the literature procedure,[15] bp 147 °C (lit,[15] 147—148 °C). Trifluoromethanesulfonic anhydride **8** was prepared by the dehydration of trifluoromethanesulfonic acid with excess phosphorus pentoxide,[16] bp 84 °C (lit,[12] 84 °C).

Tetramethylene bischlorosulfate **11** was prepared by the following procedure. To 0.1 mol of 1,4-butanediol in 10 ml of CH_2Cl_2 0.26 mol of sulfuryl chloride in 30 ml of CH_2Cl_2 was added dropwise at −20 °C. During the addition nitrogen gas was bubbled into the reaction mixture to remove sulfur dioxide and hydrogen chloride in the system. The addition took 20 min. Then, the reaction mixture was gradually warmed up to 0 °C, and kept for 4 hr at 0 °C and for 12 hr at −78 °C. A white solid precipitated. The solid was isolated and recrystallized from CH_2Cl_2, mp 49—50 °C. The NMR spectrum in CH_2Cl_2 showed two triplet-like signals centered at δ 4.60 (4H) and at δ 2.06 (4H).

Polymerization Procedure and Determination of [P].* Polymerization was carried out in CH_2Cl_2 solution under nitrogen. The reaction was initiated with the addition, at polymerization temperature, of a CH_2Cl_2 solution of PSC to a monomer solution. After a desired time of reaction, the polymerization system was short stopped by the addition of a 0.5 mol/l THF solution of sodium phenoxide. The procedure for the determination of [P*] was the same as that of the reported previously.[4,7]

The analogous procedures were taken in the polymerization of trifluoromethanesulfonic anhydride initiator.

NMR Measurement. To 0.03 mol of THF monomer in 2 ml of CH_2Cl_2 0.006 mol of PSC in 1 ml of CH_2Cl_2 was added with vigorous stirring at −78 °C under nitrogen. A portion of the reaction mixture was transferred into an NMR sample tube by using a hypodermic syringe at −78 °C. Then, the NMR spectrum was recorded at 0 °C on Hitachi R-20B NMR spectrometer.

Molecular Weight Determination. The molecular weight of the polymer was measured by a vapor pressure osmometer (Hitachi Perkin-Elmer model 115) in benzene at 35 °C.

15) M. Sveda, "Inorganic Syntheses," Vol. 3, p. 124 (1950).
16) T. Gramstad and R. N. Haszeldine, *J. Chem. Soc.*, **1957**, 4069.

Polycondensation of Malononitrile and Methylenedimalononitrile with Bis(chloromethyl)Aromatic Compounds Using Triethylamine as Acid Acceptor

Nariyoshi KAWABATA,* Kenichi MATSUBARA, and Shinzo YAMASHITA
Department of Chemistry, Kyoto Institute of Technology, Matsugasaki, Sakyo-ku, Kyoto 606
(Received November 16, 1972)

Malononitrile was found to undergo condensation reaction with benzyl chloride to give dibenzylmalononitrile in a quantitative yield under mild conditions when an organic base such as triethylamine was used as acid acceptor in dimethyl sulfoxide. The reaction was applied to the polycondensation of malononitrile and methylenedimalononitrile with *p*-xylylene dichloride and *p,p'*-bis(chloromethyl)diphenyl ether, polymers with intrinsic viscosity 0.14—0.22 dl/g being obtained in quantitative yields.

A number of research works have been carried out on the polycondensation of monomers which contain active hydrogen attached to oxygen, nitrogen or sulfur, *e.g.*, glycols, dibasic acids, diamines and dithiols. However, few works are found in the literature on the polycondensation of CH-acidic monomers.

It is well-known that active methylene compounds undergo condensation with alkyl halide to give mono- and/or dialkyl derivatives with the use of sodium hydride, sodium alkoxide, potassium alkoxide or other inorganic bases as acid acceptor. As example, the condensation of malononitrile with benzyl chloride using potassium hydroxide as base gives a mixture of mono- and dibenzylmalononitrile in 17.3 and 29.3% yields, respectively.[1] The same reaction with a combination of sodium hydride as base and dimethyl sulfoxide as solvent gives dibenzylmalononitrile in 75% yield.[2] The reaction was applied to polycondensation.[3] These reactions proceed *via* the formation of sodium or potassium salt of the active methylene compound as an intermediate, and eliminate alkali metal halides. They are thus condensations of salt of active methylene compound with organic halide. We have investigated the possibility of polycondensation of active methylene and methine compounds with bis(halomethyl)aromatic compounds without the use of an inorganic base as acid acceptor.

Results and Discussion

Model Reactions. Before carrying out the investigation, we first studied the condensation of malononitrile with benzyl chloride and related condensations as model reactions, and found that it proceeds smoothly at room temperature to give dibenzylmalononitrile (I) in a quantitative yield when an organic base such as triethylamine was used as acid acceptor in dimethyl sulfoxide under nitrogen atmosphere.

$$CH_2(CN)_2 + 2C_6H_5CH_2Cl \xrightarrow{Et_3N} C_6H_5CH_2C(CN)_2CH_2C_6H_5 \quad (1)$$

I

The reaction needs equimolar amount of triethylamine and eliminates triethylamine hydrochloride, while classical condensation with the use of an inorganic base as acid acceptor eliminates alkali metal halide. The infrared spectrum of the product was identical to that of the authentic sample. Dimethyl sulfoxide seems to be necessary for the condensation reaction. The yield of I was much lower in other solvents, *e.g.*, tetrahydrofuran.

Under similar reaction conditions, *p*-xylylene dichloride was found to undergo condensation reaction with monomethylmalononitrile to give *p*-xylylenebis(methylmalononitrile) (II) in 92% yield.

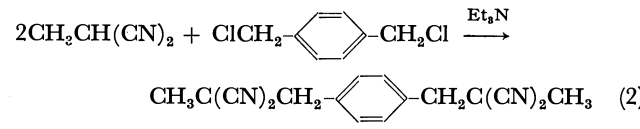

$$2CH_3CH(CN)_2 + ClCH_2\text{-}C_6H_4\text{-}CH_2Cl \xrightarrow{Et_3N} CH_3C(CN)_2CH_2\text{-}C_6H_4\text{-}CH_2C(CN)_2CH_3 \quad (2)$$

II

The structure of II was determined by elemental and spectral analyses.

Condensation of methylenedimalononitrile with benzyl chloride under similar conditions was found to afford methylenebis(benzylmalononitrile) (III) in 88% yield.

$$CH(CN)_2CH_2CH(CN)_2 + 2C_6H_5CH_2Cl \xrightarrow{Et_3N} C_6H_5CH_2C(CN)_2CH_2C(CN)_2CH_2C_6H_5 \quad (3)$$

III

The structure of III was also determined by elemental and spectral analyses.

Polycondensation Reactions. Polycondensation of malononitrile with *p,p'*-bis(chloromethyl)diphenyl ether using triethylamine as an acid acceptor in dimethyl sulfoxide was carried out at room temperature in a similar manner to that for model reactions.

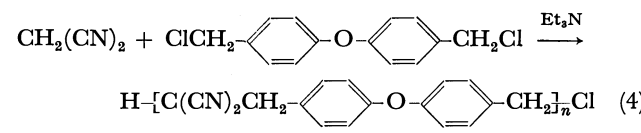

$$CH_2(CN)_2 + ClCH_2\text{-}C_6H_4\text{-}O\text{-}C_6H_4\text{-}CH_2Cl \xrightarrow{Et_3N} H\text{-}[C(CN)_2CH_2\text{-}C_6H_4\text{-}O\text{-}C_6H_4\text{-}CH_2]_n\text{-}Cl \quad (4)$$

IV

Polymer IV was obtained as a white powder in a quantitative yield and soluble in dimethylformamide, dimethyl sulfoxide and chloroform. Its structure was determined by elemental and spectral analyses, intrinsic viscosity in dimethyl sulfoxide at 30 °C being 0.15 dl/g.

* To whom inquiries should be directed.

1) H. Normant and T. Cuvigny, *Bull. Soc. Chim. Fr.*, **1965**, 1881.

2) J. J. Bloomfield, *J. Org. Chem.*, **26**, 4112 (1961).

3) a) D. Brown, M. E. B. Jones, and W. R. Maltman, *J. Polym. Sci., Part B*, **6**, 635 (1968); b) Imperial Chemical Industries Ltd., Fr. 1 547 098 (1968); *Chem. Abstr.*, **71**, 40389f (1969).

The number average molecular weight of the polymer determined by vapor pressure osmometry in chloroform was 3200, *i.e.*, the number average degree of polymerization was about 12. Polycondensation of malononitrile with *p,p'*-bis(chloromethyl)diphenyl ether using sodium hydride as acid acceptor gave IV with a molecular weight of 5100.[3]

Polycondensation of malononitrile with *p*-xylylene dichloride under similar conditions gave polymer V in a quantitative yield.

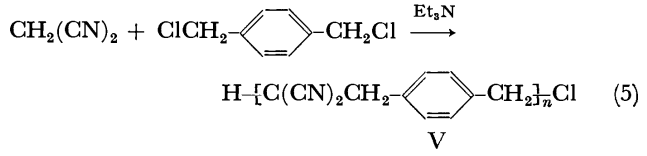

V

The polymer was soluble in sulfuric acid, but insoluble in most organic solvents. Its structure was determined by elemental and spectral analyses, intrinsic viscosity in sulfuric acid at 25 °C being 0.22 dl/g. Chemical analysis showed the presence of 0.96% of chlorine in the polymer. The result suggests that the number average degree of polymerization is about 22. Thermogravimetric analysis showed that the polymer was stable up to 330 °C under nitrogen atmosphere.

Efforts were made to increase the molecular weight of polymer V. Polycondensation (5) proceeded best in dimethyl sulfoxide. Polymer was obtained in neither diethyl ether nor chloroform. In tetrahydrofuran, low molecular weight oligomer was obtained only in 10% yield. In dimethylformamide, polymer was obtained in 60% yield, but its molecular weight was lower than that of the polymer obtained in dimethyl sulfoxide. The strong basicity of dimethyl sulfoxide seems to be essentially necessary for the polycondensation.

Polycondensation of malononitrile with *o*- and *p*-xylylene dibromides in a similar manner gave no polymeric material.

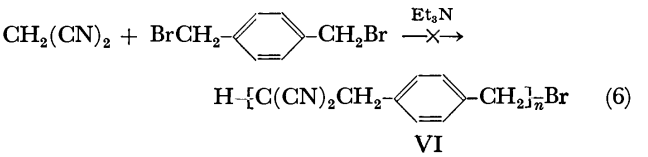

VI

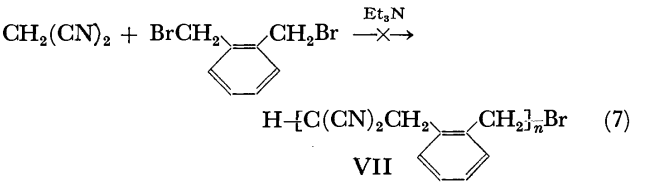

VII

Polycondensation of methylenedimalononitrile with *p,p'*-bis(chloromethyl)diphenyl ether under similar conditions was also found to proceed smoothly to give polymer VIII in a quantitative yield.

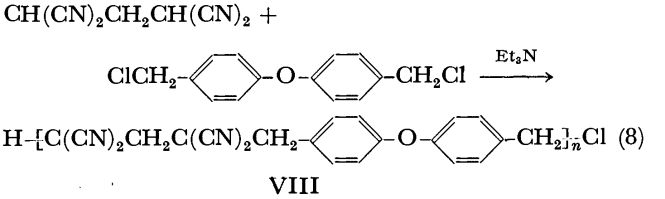

VIII

The polymer was soluble in dimethyl sulfoxide but not in most organic solvents, its intrinsic viscosity in dimethyl sulfoxide at 30 °C being 0.14 dl/g and number average degree of polymerization estimated from the chlorine content about 9.

A similar polycondensation of methylenedimalononitrile with *p*-xylylene dichloride gave polymer IX in a quantitative yield.

IX

The polymer was insoluble in most organic solvents, the number average degree of polymerization estimated from the chlorine content being about 8.

Reactions of bis(chloromethyl)aromatic compounds with diethyl malonate, methyl cyanoacetate, acetylacetone and fluorene under similar reaction conditions gave no polymeric products.

Experimental

Materials. Malononitrile was purified by distillation. Methylenedimalononitrile (1,1,3,3-tetracyanopropane) was prepared from malononitrile and formaldehyde in the presence of piperidine,[4] mp 134—135 °C (lit,[4] 136—137 °C). NMR (in a 2:1 (volume ratio) mixture of CD_3CN and CCl_4, τ): 5.63 (2H, t, J=7.3 Hz), 7.23 (2H, t, J=7.3 Hz). Monomethylmalononitrile was prepared by the dehydration of monomethylmalonamide[5] with phosphorus pentoxide. Commercial *p*-xylylene dichloride and *o*- and *p*-xylylene dibromide were used without further purification. Benzyl chloride was purified by distillation. *p,p'*-Bis(chloromethyl)-diphenyl ether was prepared by the conventional method.[6] Triethylamine was purified by distillation in the presence of phenyl isocyanate. Dimethyl sulfoxide was refluxed over calcium hydride and distilled under reduced pressure. Tetrahydrofuran and diethyl ether were refluxed in the presence of benzophenone sodium ketyl and distilled. Chloroform was dried over calcium chloride and distilled. Dimethylformamide and dimethylacetamide were purified by distillation under reduced pressure. Nitrogen was purified by passing through a tube containing copper turnings in a furnace at 170 °C followed by drying with silica gel and molecular sieves.

General Procedure. Model reactions and polycondensations were carried out under a nitrogen atmosphere in Pyrex test tubes with magnetic stirring at room temperature. Organic halide and malononitrile or methylenedimalononitrile were dissolved in dimethyl sulfoxide. Triethylamine was added dropwise to the solution. Products were recovered by pouring into a large excess of water or methanol. Products of model reactions were purified by recrystallization from ethanol. Polymers IV and VIII were purified by reprecipitation from dimethyl sulfoxide with methanol followed by drying *in vacuo* over phosphorus pentoxide for prolonged periods at 120 and 90 °C, respectively. Polymers

4) O. Diels, H. Gärtner, and R. Kaack, *Chem. Ber.*, **55**, 3439 (1922).

5) a) R. Meyer and P. Bock, *Ann. Chem.*, **347**, 98 (1906); b) N. Weiner, "Organic Syntheses," Coll. Vol. II, p. 279 (1943).

6) H. Plieninger, L. Horn, and A. Lutz, *Arch. Pharm.* (Weinheim), **286**, 285 (1953).

V and IX were purified by drying *in vacuo* over phosphorus pentoxide at 190 and 150 °C, respectively, for prolonged periods of time.

Elemental analyses were performed at the Elemental Analyses Center of Kyoto University. Infrared spectra were recorded on a Japan Spectroscopic Co. Model 402G spectrometer. Proton magnetic resonance spectra were obtained with a Japan Electron Optics Lab. Model 4H-100 spectrometer using tetramethylsilane as an external standard. Viscosity measurements of polymer solutions were carried out in dimethyl sulfoxide at 30 °C or in sulfuric acid at 25 °C with an Ubbelohde-type dilution viscometer. The number average molecular weight of polymer was determined by vapor pressure osmometry in chloroform using a Hitachi-Perkin-Elmer Model 115 Molecular Weight Apparatus. Thermogravimetric analysis was performed with a thermobalance (wire-torsion balance) under nitrogen atmosphere.

Dibenzylmalononitrile (I). Condensation of malononitrile (20 mmol, 1.3 ml) with benzyl chloride (40 mmol, 4.6 ml) using triethylamine (42 mmol, 5.9 ml) as an acid acceptor in 5.0 ml of dimethyl sulfoxide for 18 hr gave I in a quantitative yield, mp 131.5 °C (lit,[2] 131.8—132.5 °C). The IR and NMR spectra were identical to those of an authentic sample.[2]

p-*Xylylenebis(methylmalononitrile) (II).* Reaction of monomethylmalononitrile (20 mmol, 1.60 g), *p*-xylylene dichloride (10 mmol, 1.75 g) and triethylamine (20 mmol, 2.8 ml) in dimethyl sulfoxide (10.0 ml) for 24 hr afforded II in 92% yield, mp 206 °C. Found: C, 73.53; H, 5.27; N, 21.51%. Calcd for $C_{16}H_{14}N_4$: C, 73.26; H, 5.38; N, 21.36%. NMR (CD_3COCD_3, τ): 3.18 (4H, s), 7.30 (4H, s), 8.80 (6H, s). IR (KBr disk): $\nu_{C\equiv N}$, 2250 cm^{-1}.

Methylenebis(benzylmalononitrile) (III). Reaction of methylenedimalononitrile (10 mmol, 1.44 g), benzyl chloride (20 mmol, 2.3 ml) and triethylamine (20 mmol, 2.8 ml) in 4.9 ml of dimethyl sulfoxide for 18 hr afforded III in 88% yield, mp 207 °C. Found: C, 77.85; H, 4.94; N, 17.23%. Calcd for $C_{21}H_{16}N_4$: C, 77.76; H, 4.97; N, 17.27%. NMR (CD_3COCD_3, τ): 3.10 (10H, s), 7.03 (4H, s), 7.59 (2H, s). IR (KBr disk): $\nu_{C\equiv N}$, 2250 cm^{-1}.

Polymer IV. Reaction of malononitrile (10 mmol, 0.66 g), *p,p'*-bis(chloromethyl)diphenyl ether (10 mmol, 2.67 g) and triethylamine (20 mmol, 2.8 ml) in 5.0 ml of dimethyl sulfoxide for 18 hr afforded polymer IV as a white powder in a quantitative yield. Found: C, 77.42, 77.43; H, 4.70, 4.75; N, 10.40; Cl, 0.73%. Calcd for $H(C_{17}H_{12}N_2O)_{12}Cl$: C, 77.54; H, 4.63; N, 10.64; Cl, 1.12%. NMR ($CDCl_3$, τ): 2.78 (8H, A_2B_2), 6.78 (4H, s). IR (KBr disk): $\nu_{C\equiv N}$, 2250 cm^{-1}.

Polymer V. Reaction of malononitrile (20 mmol, 1.32 g), *p*-xylylene dichloride (20 mmol, 3.50 g) and triethylamine (40 mmol, 5.6 ml) in 20.0 ml of dimethyl sulfoxide for 18 hr afforded polymer V in a quantitative yield. Found: C, 77.69; H, 4.49; N, 16.16; Cl, 0.96%. Calcd for $H(C_{11}H_8N_2)_{22}Cl$: C, 77.78; H, 4.77; N, 16.49; Cl, 0.95%. IR (KBr disk): $\nu_{C\equiv N}$, 2250 cm^{-1}. The IR spectrum showed a characteristic absorption of *p*-disubstituted benzene in the region 5—6 μ.

Polymer VIII. Reaction of methylenedimalononitrile (5 mmol, 0.72 g), *p,p'*-bis(chloromethyl)diphenyl ether (5 mmol, 1.34 g) and triethylamine (10 mmol, 1.4 ml) in 10.0 ml of dimethyl sulfoxide for 18 hr afforded polymer VIII in a quantitative yield. Found: C, 73.86; H, 4.22; N, 16.54; Cl, 1.21%. Calcd for $H(C_{21}H_{14}N_4O)_9Cl$: C, 73.66; H, 4.15; N, 16.36; Cl, 1.15%. NMR (CD_3SOCD_3, τ): 2.86 (8H, A_2B_2), 6.55 (4H, s), 7.06 (2H, s). IR (KBr disk): $\nu_{C\equiv N}$, 2250 cm^{-1}.

Polymer IX. Reaction of methylenedimalononitrile (10 mmol, 1.44 g) *p*-xylylene dichloride (10 mmol, 1.75 g) and triethylamine (20 mmol, 2.8 ml) in 20.0 ml of dimethyl sulfoxide for 24 hr afforded polymer IX in a quantitative yield. Found: C, 71.68, 71.73; H, 4.17, 4.33; N, 20.70, 21.09; Cl, 1.77, 1.80%. Calcd for $H(C_{15}H_{10}N_4)_8Cl$: C, 71.83; H, 4.07; N, 22.34; Cl, 1.77%. IR (KBr disk): $\nu_{C\equiv N}$, 2250 cm^{-1}. The IR spectrum showed a characteristic absorption of *p*-disubstituted benzene in the region 5—6 μ.

Compounds Relating to Dibenzoyladenine Riboside. The Choice between the N^6,1-Dibenzoyl and N^6,N^6-Dibenzoyl Structures

Kentaro ANZAI and Masanao MATSUI

The Institute of Physical and Chemical Research, Wako-shi, Saitama 351

(Received January 29, 1973)

It was clarified, by NMR analysis and on the grounds of synthetic work, that dibenzoyladenine riboside and its analogues have the N^6,N^6-dibenzoyl structure rather than the N^6,1-dibenzoyl structure, which has customarily been used to describe the benzoyl derivatives of adenosine.

5′-*O*-Trityl-tetrabenzoyladenosine and its detritylated product were tentatively identified by Khorana and his colleagues[1] as N^6,1,2′-*O*,3′-*O*-tetrabenzoates (I and II), but without strictly excluding another possible assignment, N^6,N^6,2′-*O*-3′-*O*-tetrabenzoates (III and IV). Polybenzoylated adenosine residues in protected oligonucleotides have also been described in the N^6,1-dibenzoyl structure.[2] The perbenzoylated product of 2′,3′-*O*-ethoxymethylideneadenosine was registered by Sŏrm and his colleagues[3] as N^6,1,5′-*O*-tribenzoyl-2′,3′-*O*-ethoxymethylideneadenosine (V). The reaction product with benzoyl chloride of 6-benzamido-9-(5-deoxy-2, 3-*O*-isopropylidene-β-D-*erythro*-pent-4-enofuranosyl)purine was described by Moffatt and his colleagues[4] as the N^6,1-dibenzoate (VI).

We also met a similar situation when we synthesized derivatives of tubercidin[5] (7-deazaadenosine),[6] where two benzoyl groups were introduced into the pyrrolo-[2,3-*d*]pyrimidine moiety.[7–10] The perbenzoylated product of 2′,3′-*O*-isopropylidenetubercidin has been ambiguously described as *N*,*N*,5′-*O*-benzoyl-2′,3′-*O*-isopropylidenetubercidin.[11]

Thus, compounds relating to dibenzoyladenine riboside have been described as having the N^6,1-dibenzoyl structure, but without any reliable grounds. It is the purpose of this paper to present proof that they are actually N^6,N^6-dibenzoyl compounds.

The tetrabenzoyl derivatives of adenosine (III[1] and IV[1]) and the tribenzoyl derivatives of tubercidin (VII and VIII) show complex NMR patterns in the aromatic region; these patterns do not give any good information about the position of benzoylation. In the case of a dibenzoylated derivative (IX)[8] of adenosine and those of tubercidin (X,[8] XI,[7] and XII[7]) signals of four *ortho* protons of benzoyl groups have been observed to separate well from the signals of the other aromatic protons, and these four protons have been shown to be equivalent; IX δ 7.84 J_{ortho}=7 Hz, X δ 7.82 J_{ortho}=7 Hz, XI δ 7.84 J_{ortho}=8 Hz, XII δ 7.83 J_{ortho}=7 Hz.

To obtain more certain information about the position of benzoylation, we prepared several toluyl derivatives of adenosine and observed the signals of the methyl protons. The results are shown in Table 1. In every case the signals corresponding to two methyls of toluyl groups, which are introduced in the adenine moiety, are found never to split, exhibiting a sharp singlet. Moreover, the NMR spectrum of the ditoluyl compound (XVI) (Fig. 1) exhibits a pair of doublets (δ 7.13 and 7.74, J_{ortho}=8 Hz) assignable to aromatic protons of toluyl groups; this also supports the N^6,N^6-ditoluyl structure. In the case of a tubercidin derivative the NMR spectrum of the tritoluyl compound (XVIII) exhibited a sharp singlet at δ 2.34 corresponding to two methyls of toluyl groups introduced in the pyrrolo-[2,3-*d*]pyrimidine moiety. The spectrum of XIII was taken at lower temperatures (Fig. 2), for we expected that a signal at δ 2.28 corresponding to two methyls might split by the restricted rotation of the bond between N^6 and C-6. However, only a broadening of the signal was observed, so we devised another proof for the N^6,N^6-diacyl structure.

9-Methyladenine (XIX) was converted to its benzoyl *p*-toluyl derivative *via* two routes; thus, the benzoylated product of 9-methyl-N^6-*p*-toluyladenine and the toluylated product of N^6-benzoyl-9-methyladenine were prepared, and these two products were compared exhaustively. If they are the same compound, both acyl groups should be bound at N^6.

The reaction of 9-methyladenine (XIX) with excess *p*-toluyl chloride afforded N^6,N^6-di-*p*-toluyl-9-methyl-

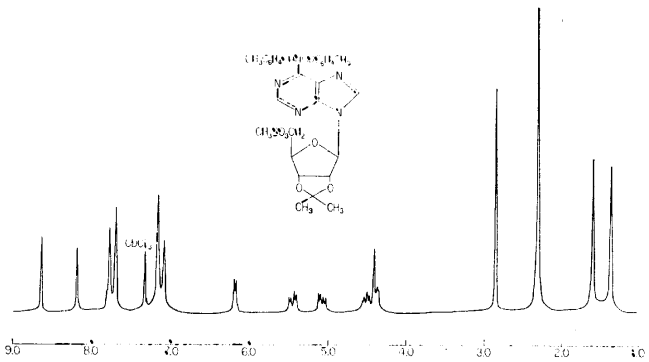

Fig. 1. NMR spectrum of N^6,N^6-di-*p*-toluyl-2′,3′-*O*-isopropylidene-5′-*O*-mesyladenosine (XVI). (100 MHz, $CDCl_3$).

1) M. Smith, D. H. Rammler, I. H. Goldberg, and H. G. Khorana, *J. Amer. Chem. Soc.*, **84**, 430 (1962).

2) K. Lohrman, D. Soell, H. Hayatsu, E. Otsuka, and H. G. Khorana, *ibid.*, **88**, 819 (1966).

3) S. Chládek, J. Zemlika, and F. Sŏrm, *Coll. Czech. Chem. Commun.*, **31**, 1785 (1966).

4) I. D. Jenkins, J. P. H. Verheyden, and J. G. Moffatt, *J. Amer. Chem. Soc.*, **93**, 4323 (1972).

5) K. Anzai, G. Nakamura, and S. Suzuki, *J. Antibiot.* (Tokyo), *Ser A*, **10**, 201 (1957).

6) S. Suzuki and S. Marumo, *ibid.*, **13**, 360 (1960); **14**, 34 (1961); Y. Mizuno, M. Ikehara, K. A. Watanabe, S. Suzaki, and T. Itoh, *J. Org. Chem.*, **28**, 3329 (1963).

7) K. Anzai and M. Matsui, This Bulletin, **46**, 618 (1973).

8) K. Anzai and M. Matsui, *Agr. Biol. Chem.* (Tokyo), **37**, 301 (1973).

9) K. Anzai and M. Matsui, *ibid.*, **37**, 345 (1973).

10) K. Anzai and M. Matsui, *ibid.*, **37**, 921 (1973).

11) Upjohn Co., Netn. 6606669 (1966); *Chem. Abstr.*, **67**, P 82375w (1967).

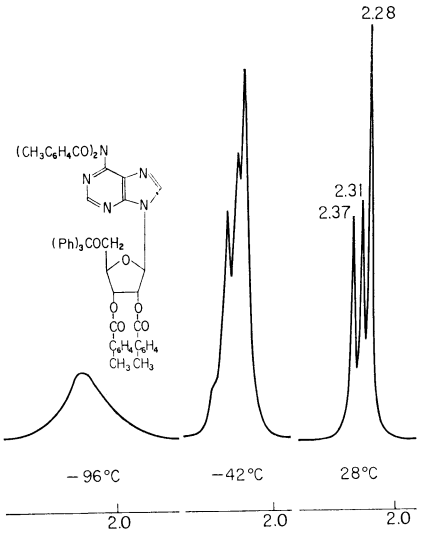

Fig. 2. NMR spectrum of N^6,N^6,2′-*O*, 3′-*O*-tetra-*p*-toluyl-5′-*O*-trityladenosine (XIII) at 28, −42, and −96 °C. (100 MHz, CS_2).

adenine (XX). The NMR spectrum of XX shows a sharp singlet at δ 2.31 corresponding to two methyls of *p*-toluyl groups. Similarly, N^6,N^6-di-*o*-toluyl-9-methyladenine (XXI) was prepared. The spectrum of XXI exhibits a six-proton singlet at δ 2.53. Attempts to prepare the monotoluyl compound (XXII), on the hydrolysis of XX, failed. In aqueous acetic acid, in a solution of sodium bicarbonate, or even in ethanol the only product obtained was XIX under the conditions where XX was partially hydrolysed. When XIX was treated with an equimolar amount of *p*-toluyl chloride, half of the starting material was converted to XX.

Compound XX was treated with lithium aluminum hydride in refluxing tetrahydrofuran to give 9-methyl-N^6-*p*-methylbenzyladenine (XXIII). However, when this reaction was carried out at room temperature, 9-methyl-N^6-*p*-toluyladenine (XXII) was obtained in a moderate yield. The benzoylation of XXII afforded N^6-benzoyl-9-methyl-N^6-*p*-toluyladenine (XXIV). Similarly, N^6,N^6-dibenzoyl-9-methyladenine (XXV) was treated with lithium aluminum hydride, and the product, N^6-benzoyl-9-methyladenine (XXVI), was treated with *p*-toluyl chloride. Thus, two samples of the benzoyl *p*-toluyl compound were prepared, and their NMR, IR (Fig. 3), UV, and Mass spectra were compared. It was shown that all of the spectral data were identical, strongly supporting the idea that dibenzoyladenine riboside and its derivatives should be described as having the N^6,N^6-dibenzoyl structure.

Preparation. The benzylidene benzoate (VIII) was prepared by the treatment of 2′,3′-*O*-benzylidenetubercidin (XXVII) with excess benzoyl chloride. The tetra-*p*-toluyl trityl ether (XIII) was prepared by the treatment of 5′-*O*-trityladenosine with excess *p*-toluyl chloride. The treatment of XIII in hot aqueous acetic acid for a short period afforded the detritylated compound (XIV). On the prolonged heating of XIII, the glycosidic bond was cloven and the isolated products were N^6,N^6-di-*p*-toluyladenine (XXVIII), N^6-*p*-toluyladenine (XXIX), and 2′,3′-*O*-di-*p*-toluylribose (XXX). The isopropylidene tri-*p*-toluyl compound (XV) was

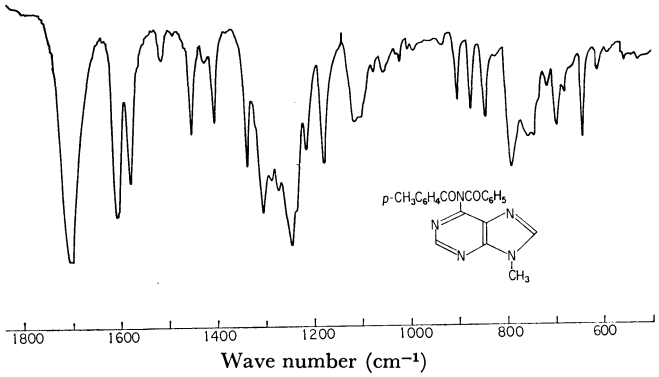

Fig. 3. IR spectrum of N^6-benzoyl-9-methyl-N^6-*p*-toluyladenine (XXIV). (KBr).

prepared by the treatment of 2′,3′-*O*-isopropylideneadenosine (XXXI) with excess *p*-toluyl chloride. Similarly, XVIII was prepared from 2′,3′-*O*-isopropylidenetubercidin (XXXII).[11] Compound XXXI was treated with ethyl vinyl ether in the presence of trifluoroacetic acid to give the acetal (XXXIII), which was then converted to the di-*p*-toluyl compound (XVII).

The treatment of XXXII with acetyl chloride afforded N^6,5′-*O*-diacetyl-2′,3′-*O*-isopropylidenetubercidin (XXXIV), and a triacetate corresponding to VII and XVIII was not obtained.

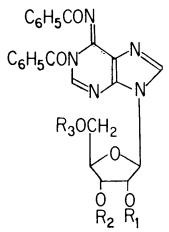

I R_1,R_2=C_6H_5CO, R_3=$(C_6H_5)_3C$
II R_1,R_2=C_6H_5CO, R_3=H
V R_1R_2=C_2H_5OCH<, R_3=C_6H_5CO

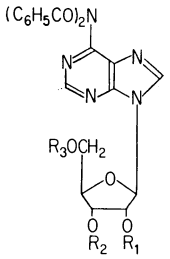

III R_1,R_2=C_6H_5CO, R_3=$(C_6H_5)_3C$
IV R_1,R_2=C_6H_5CO, R_3=H
IX R_1R_2=$(CH_3)_2C$<, R_3=CH_3SO_2

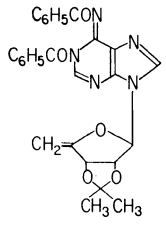

VI

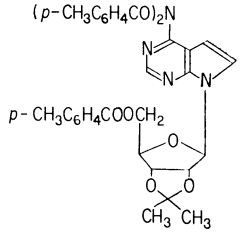

XVIII

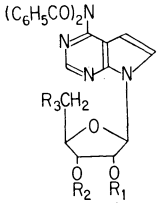

VII $R_1R_2=(CH_3)_2C<$, $R_3=C_6H_5COO$
VIII $R_1R_2=C_6H_5CH<$, $R_3=C_6H_5COO$
X $R_1R_2=(CH_3)_2C<$, $R_3=CH_3SO_3$
XI $R_1R_2=(CH_3)_2C<$, $R_3=I$
XII $R_1R_2=(CH_3)_2C<$, $R_3=H$

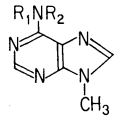

XIX $R_1,R_2=H$
XX $R_1,R_2=p\text{-}CH_3C_6H_4CO$
XXI $R_1,R_2=o\text{-}CH_3C_6H_4CO$
XXII $R_1=H$, $R_2=p\text{-}CH_3C_6H_4CO$
XXIII $R_1=H$, $R_2=p\text{-}CH_3C_6H_4CH_2$
XXIV $R_1=p\text{-}CH_3C_6H_4CO$, $R_2=C_6H_5CO$
XXV R_1, $R_2=C_6H_5CO$
XXVI $R_1=H$, $R_2=C_6H_5CO$

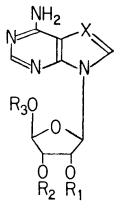

XXVII $R_1R_2=C_6H_5CH<$, $R_3=H$, X=CH
XXXI $R_1R_2=(CH_3)_2C<$, $R_3=H$, X=N
XXXII $R_1R_2=(CH_3)_2C<$, $R_3=H$, X=CH
XXXIII $R_1R_2=(CH_3)_2C<$, $R_3=CH_3CH(OC_2H_5)$, X=N

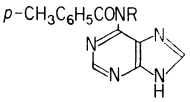

XXVIII $R=p\text{-}CH_3C_6H_5CO$
XXIX R=H

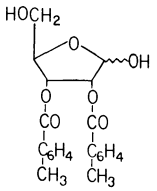

XXX

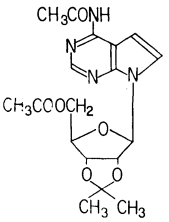

XXXIV

Experimental

2′,3′-O-Isopropylidenetubercidin (XXXII). The reported method[11] was improved to result in an increase in the yield. Tubercidin (5 g) was treated with tosyl chloride (37.5 g) in a mixture of acetone (250 ml) and acetone dimethyl acetal (25 ml) with stirring at room temperature. Within 2 hr the tubercidin was dissolved completely. The reaction mixture was poured into a cold solution of sodium bicarbonate (0.5 M, 1 liter), and the acetone was evaporated under reduced pressure. After the product had been extracted with chloroform, the organic layer was repeatedly washed with water and concentrated to dryness to afford a syrup (5.24 g, 92%), which was used without furthur purification for the succeeding processes. When acetone dimethyl acetal was excluded from this system, as has been reported previously,[11] the yield was 80%.

2′,3′-O-Benzylidenetubercidin (XXVII). A mixture of tubercidin (500 mg), zinc chloride (500 mg), and benzaldehyde (10 ml) was stirred at room temperature overnight and then poured into ice water. The product was extracted with chloroform, and the organic layer was washed with a cold solution of sodium bicarbonate and then with water. The chloroform was then evaporated, and petroleum ether was added to the residue. A syrupy sample of XXVII was separated by decantation and repeated precipitation from chloroform and petroleum ether; yield, 600 mg. An analytical sample was obtained by chromatography on silica gel (Kieselgel 0.05—0.2 mm, Merck), the developing being done with a mixture of ethyl acetate and methanol (9: 1); λ_{max}^{MeOH} mμ(ε) 270 (12000).

Found: C, 61.21; H, 5.27; N, 15.74%. Calcd for $C_{18}H_{18}O_4N_4$: C, 61.01; H, 5.12; N, 15.81%.

N⁶,N⁶,5′-O-Tribenzoyl-2′,3′-O-benzylidenetubercidin (VIII). Into a stirred solution of XXVII (5.1 g) in pyridine (50 ml), benzoyl chloride (10 g) was added dropwise keeping the temperature at −10 °C. The solution was then left at 0 °C for additional 4 hr and was then poured into an ice-cooled solution of sodium bicarbonate. The product was extracted with chloroform, and the solvent was evaporated to dryness. The residue was crystallized from ethyl acetate; yield, 6.9 g; mp 203 °C; $[\alpha]_D^{23}$ −87.5° (*c* 2.69, DMSO); λ_{max}^{MeOH} mμ(ε) 280 (sh, 12000), 224 (47000).

Found: C, 70.20; H, 4.55; N, 8.40%. Calcd for $C_{39}H_{30}O_7N_4$: C, 70.26; H, 4.54; N, 8.40%.

N⁶,N⁶,2′-O,3′-O-Tetra-p-toluyl-5′-O-trityladenosine (XIII). 5′-*O*-Trityladenosine[1] (2.6 g) was suspended in pyridine (20 ml), and then *p*-toluyl chloride (5 ml) was added at once. After stirring at room temperature for 18 hr, a clear solution was obtained. The reaction mixture was poured into an ice-cooled solution of sodium bicarbonate, and the product was extracted with chloroform. The solution was concentrated to dryness, and the residue was chromatographed on silica gel; development with a mixture of benzene and ethyl acetate (9: 1) resulted in the separation of XIII from triphenyl carbinol, the latter being eluted earlier. A crystalline mass melting at 132—138 °C was obtained from benzene and ligroin; yield, 5.1 g; $[\alpha]_D^{25}$ −71.7° (*c* 1.51, $CHCl_3$).

Found: C, 75.00; H, 5.43; N, 7.13%. Calcd for $C_{61}H_{51}O_8N_5$: C, 74.60; H, 5.24; N, 7.13%.

N⁶,N⁶,2′-O,3′-O-Tetra-p-toluyladenosine (XIV). A solution of XIII (1 g) in 70% aqueous acetic acid (50 ml) was heated on a water bath for 10 min. Several products were detected on tlc; among them one was found to be predominant; $R_{f\ major\ product}$: 1.3, 1.0, 0.3, 0 (benzene and ethyl acetate 4: 1). The major product was separated by chromatography on silica gel, developing with a mixture of benzene and ethyl acetate (4: 1) and increasing the content of the latter gradually; yield, 270 mg (36%). An analytical sample was obtained as crystals from benzene and ligroin; mp 173—174 °C; $[\alpha]_D^{25}$ −236° (*c* 1.73, $CHCl_3$).

Found: C, 68.23; H, 5.16; N, 9.35%. Calcd for $C_{42}H_{37}O_8N_5$: C, 68.19; H, 5.04; N, 9.47%.

Glycosidic Bond Cleavage of XIII. A solution of XIII (1 g) in 70% aqueous acetic acid (50 ml) was heated on a water bath for 2 hr. The formation of three products was shown on tlc (benzene and ethyl acetate 1: 1), and they

Table 1. NMR and UV data of ditoluyladenine ribosides

	Chemical shift (δ)[a]				λ_{max}^{MeOH} mμ(ε)
	$(C\underline{H}_3C_6H_4CO)_2N$-	H-2	H-8	Other signals of methyl protons	
XIII	2.31	8.54	8.28	2.35, 2.40 ($2CH_3C_6H_4CO\cdot O$-)	270 (sh,[b] 28800), 242 (44200)
XIV	2.30	8.16	8.17	2.32, 2.36 ($2CH_3C_6H_4CO\cdot O$-)	270 (sh, 35400), 244 (51700)
XV	2.34	8.60	8.16	1.42, 1.65 ($(CH_3)_2C<$)	270 (sh, 32000), 247 (36400)
XVI[9]	2.32	8.64	8.20	1.38, 1.60 ($(CH_3)_2C<$)	270 (sh, 26800), 260 (28000)
XVII	2.34	8.62	8.16	1.38, 1.64 ($(CH_3)_2C<$) 2.17 (J=3Hz) ($C\underline{H}_3CH(OC_2H_5)$-)	270 (sh, 27400), 262 (28000)

a) NMR spectra were taken in $CDCl_3$ at 100 MHz with TMS standard.
b) shoulder

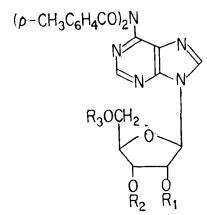

XIII R_1, R_2=p-$CH_3C_6H_4CO$, R_3=$(C_6H_5)_3C$
XIV R_1, R_2=p-$CH_3C_6H_4CO$, R_3=H
XV R_1R_2=$(CH_3)_2<$, R_3=p-$CH_3C_6H_4CO$
XVI R_1R_2=$(CH_3)_2<$, R_3=CH_3SO_2
XVII R_1R_2=$(CH_3)_2<$, R_3=$CH_3CH(OC_2H_5)$

were separated by chromatography on silica gel. The least polar one was eluted with a mixture of benzene and ethyl acetate (1: 1) and was obtained as a syrup from benzene and petroleum ether; yield, 340 mg. It was identified as 2′,3′-*O*-di-*p*-toluylribose (XXX), $[\alpha]_D^{25}$ +14.8° (*c* 1.03, $CHCl_3$); λ_{max}^{MeOH} mμ(ε) 236 (21300); NMR (100 MHz, $CDCl_3$): δ 2.34 and 2.39 (6H, two singlets, $2C\underline{H}_3C_6H_4CO$); M^+ 386.

Found: C, 65.50; H, 5.70%. Calcd for $C_{21}H_{22}O_7$: C, 65.27; H, 5.74%.

After the column had been washed with ethyl acetate, a mixture of ethyl acetate and methanol (9: 1) was used for elution. Two products were obtained. The less polar one, which was identified as N^6,N^6-ditoluyladenine (XXVIII), was crystallized from chloroform and benzene; yield, 83 mg; mp 231 °C; λ_{max}^{MeOH} mμ(ε) 290 (sh, 6500), 240 (33400); NMR (100 MHz, DMSO-*d*): δ 2.32 (6H, s, $2C\underline{H}_3C_6H_4CO$), 7.24 and 7.84 (8H, two doublets, J=8 Hz, $2CH_3C_6\underline{H}_4CO$).

Found: C, 64.70; H, 5.23; N, 18.11%. Calcd for $C_{21}H_{17}N_5O_2\cdot H_2O$: C, 64.77; H, 4.92; N, 17.99%.

The most polar compound, N^6-toluyladenine (XXIX), was crystallized from chloroform and benzene; yield, 110 mg; mp 224—225 °C; λ_{max}^{MeOH} mμ(ε) 287 (23400), 252 (16200); NMR (100 MHz, DMSO-*d*): δ 2.40 (3H, s, $C\underline{H}_3C_6H_4CO$), 7.35 and 8.04 (4H, two doublets, J=8 Hz, $CH_3C_6\underline{H}_4CO$); M^+ 253.

Found: C, 61.45; H, 4.31; N, 27.95%. Calcd for $C_{13}H_{11}ON_5$: C, 61.65; H, 4.38; N, 27.66%.

N^6,N^6,*5′*-O-p-*Toluyl-2′,3′*-O-*isopropylideneadenosine (XV)*. To a solution of XXXI (614 mg) in pyridine (50 ml), *p*-toluyl chloride (1.6 g) was added, drop by drop, at −10 °C. The solution was then kept in a refrigerator overnight and subsequently poured into an ice-cooled solution of sodium bicarbonate. The product was extracted with chloroform, and the chloroform layer was concentrated to dryness. Tlc showed the presence of two UV-positive compounds, which were separated by silica gel chromatography, developing with a mixture of benzene and ethyl acetate (8: 1), the content of the latter being gradually increased. The less polar one was identified as *p*-toluic anhydride. The more polar compound, identified as XV, was crystallized from benzene and ligroin; yield, 550 mg; mp 170 °C, $[\alpha]_D^{25}$ −11.0° (*c* 1.69, $CHCl_3$).

Found: C, 67.15; H, 5.32; N, 10.55%. Calcd for $C_{37}H_{35}O_7N_5$: C, 67.16; H, 5.33; N, 10.59%.

5′-O-*(1-Ethoxyethyl)-2′,3′*-O-*isopropylideneadenosine (XXXIII)*. To a solution of XXXI (1 g) and ethyl vinyl ether (3 ml) in dimethylformamide (50 ml) cooled at −15——20 °C, trifluoroacetic acid (3 ml) was added. After 3 hr the reaction mixture was poured into a cold solution of sodium bicarbonate (0.5 M, 500 ml). The desired product was extracted with chloroform and was separated by silica gel chromatography, being eluted with a mixture of ethyl acetate and methanol (95: 5), the content of the latter being gradually increased. The eluate was concentrated to dryness, affording a syrup; yield, 785 mg; $[\alpha]_D^{25}$ −35.7° (*c* 0.32, $CHCl_3$); λ_{max}^{MeOH} mμ(ε) 260 (13000); Mass *m/e*: 379 (M^+), 364 (M^+-CH_3), 350 ($M^+-C_2H_5$), 334 ($M^+-C_2H_5O$).

Found: C, 54.32; H, 6.77; N, 18.07%. Calcd for $C_{17}H_{25}O_5N_5$: C, 53.81; H, 6.64; N, 18.46%.

N^6,N^6-*Di*-p-*toluyl-5′*-O-*(1-ethoxyethyl)-2′,3′*-O-*isopropylideneadenosine (XVII)*. To an ice-cooled and stirred solution of XXXIII (758 mg) in pyridine (5 ml), *p*-toluyl chloride (1 g) was added; it was then kept standing in a refrigerator overnight. The reaction mixture was poured onto a cold solution of sodium bicarbonate, and the product was extracted with chloroform. Silica gel chromatography, on developing with a mixture of benzene and ethyl acetate (4: 1), afforded 580 mg of a syrup; this was repeatedly precipitated from carbon tetrachloride and *n*-hexane; $[\alpha]_D^{25}$ −52.6° (*c* 0.79, $CHCl_3$).

Found: C, 64.11; H, 5.92; N, 10.91%. Calcd for $C_{33}H_{37}O_7N_5$: C, 64.37; H, 6.06; N, 11.38%.

N^6, N^6, *5′* - O - *Tri* - p - *toluyl* - *2′*, *3′* - O - *isopropylidenetubercidin (XVIII)*. To an ice-cooled and stirred soltion of XXXII (306 mg) in pyridine (30 ml), *p*-toluyl chloride (800 mg) was added drop by drop. After it had then been

kept standing in a refrigerator overnight, the reaction mixture was poured into a cold solution of sodium bicarbonate and the product was extracted with chloroform. The solution was concentrated to dryness, and the residue was crystallized from ethyl acetate and ligroin; yield, 460 mg (70%); mp 204—207 °C; $[\alpha]_D^{25}$ −47.5° (*c* 2.51, $CHCl_3$); λ_{max}^{MeOH} mμ(ε) 240 (47500); NMR (100 MHz, $CDCl_3$): δ 1.39 and 1.64 (6H, two singlets, isopropylidene methyls), 2.34 (6H, s, $(C\underline{H}_3C_6H_4CO)_2N$), 2.39 (3H, s, $C\underline{H}_3C_6H_4COO$).

Found: C, 68.55; H, 5.54; N, 8.34%. Calcd for $C_{38}H_{36}O_7N_4$: C, 69.08; H, 5.49; N, 8.48%.

N⁶,N⁶-*Di*-p-*toluyl-9-methyladenine (XX).* 9-Methyladenine (826 mg) was suspended in pyridine (50 ml), and then *p*-toluyl chloride (3 ml) was added at once. After the solution had been stirred at room temperature overnight, it was poured into a cold solution of sodium bicarbonate and the product was extracted with chloroform. *p*-Toluic anhydride formed was separated by silica gel chromatography, developing with a mixture of benzene and ethyl acetate (2: 1); thus, 1.37 g of XX were isolated. It was crystallized from benzene and *n*-hexane; mp 216—218 °C; λ_{max}^{MeOH} mμ(ε) 262 (30000); NMR (100 MHz, $CDCl_3$): δ 2.31 (6H, s, $(C\underline{H}_3C_6H_4CO)_2N$), 3.82 (3H, s, $CH_3N\langle$), 7.12 and 7.76 (8H, two doublets, J=8 Hz, $(CH_3C_6\underline{H}_4CO)_2N$), 8.20 (1H, s, H-8), 8.64 (1H, s, H-3).

Found: C, 68.49; H, 4.99; N, 18.17%. Calcd for $C_{22}H_{19}O_2N_5$: C, 68.56; H, 4.97; N, 18.17%.

N⁶,N⁶-*Di*-o-*toluyl-9-methyladenine (XXI).* 9-Methyladenine (92 mg) was treated with *o*-toluyl chloride (300 mg), as has been described in the preceeding section. The isolated product, XXI, was crystallized from carbon tetrachloride; yield, 160 mg; mp 184—185 °C; λ_{max}^{MeOH} mμ(ε) 270 (18400), 252 (20000); NMR (60 MHz, $CDCl_3$): δ 2.53 (6H, s, $2C\underline{H}_3C_6H_4CO$), 3.97 (3H, s, $CH_3N\langle$).

Found: C, 67.26; H, 4.90; N, 17.87%. Calcd for $C_{22}H_{19}O_2N_5\cdot 1/2H_2O$: C, 67.00; H, 5.11; N, 17.76%.

N⁶,N⁶-*Dibenzoyl-9-methyladenine (XXV).* 9-Methyladenine (1 g) was treated with benzoyl chloride (3 ml), as has been described in the preceeding section. Crystals of XXV were obtained from ethyl acetate and carbon tetrachloride; yield, 1.07 g; mp 182—184 °C; λ_{max}^{MeOH} mμ(ε) 270 (sh, 20000); 249 (26000).

Found: C, 65.96; H, 4.18; N, 19.42%. Calcd for $C_{20}H_{15}O_2N_5\cdot 1/2H_2O$: C, 65.56; H, 4.40; N, 19.12%.

9-Methyl-N⁶-p-*methylbenzyladenine (XXIII).* Compound XX (165 mg) was treated with lithium aluminum hydride (95 mg) in refluxing tetrahydrofuran (70 mg) for 17 hr. After the excess lithium aluminum hydride had been destroyed with water, the product, which was shown to be homogeneous on tlc, was extracted with chloroform. The solvent was evaporated, and the residue was crystallized from carbon tetrachloride; yield, 120 mg; mp 154 °C; λ_{max}^{MeOH} mμ(ε) 270 (18200); NMR (100 MHz, $CDCl_3$): δ 2.34 (3H, s, $C\underline{H}_3C_6H_4CH_2$), 3.82 (3H, s, $CH_3N\langle$), 3.90 (2H, broad d, J=4 Hz, $CH_3C_6H_4C\underline{H}_2$).

Found: C, 65.74; H, 5.94; N, 27.86%. Calcd for $C_{14}H_{15}N_5$: C, 65.38; H, 5.97; N, 27.65%.

9-Methyl-N⁶-p-*toluyladenine (XXII).* Compound XX (180 mg) was treated with lithium aluminum hydride (68 mg) in tetrahydrofuran (100 ml) at room temperature for 4 days. After the excess reagent had been destroyed with water, the products were extracted with chloroform. Tlc exhibited several UV-positive spots; among them, two major products were isolated by silica gel chromatography, developing with a mixture of ethyl acetate and methanol (9: 1), the content of the latter being gradually increased. The less polar one was identified as XXIII; yield, 15 mg. The more polar one, identified as XXII, was crystallized from ethyl acetate; yield 75 mg; mp 176—177 °C; λ_{max}^{MeOH} mμ(ε) 282 (15400); NMR (100 MHz, $CDCl_3$): δ 2.42 (3H, s, $C\underline{H}_3C_6H_4CO$), 3.90 (3H, s, $CH_3N\langle$).

Found: C, 60.82; H, 5.02; N, 25.73%. Calcd for $C_{14}H_{13}ON_5\cdot 1/2H_2O$: C, 60.85; H, 5.11; N, 25.35%.

N⁶-*Benzoyl-9-methyladenine (XXVI).* Compound XXV (730 mg) was treated with lithium aluminum hydride (250 mg) in tetrahydrofuran (100 ml) at room temperature for 6 days. After the excess reagent had then been destroyed with water, the products were extracted with chloroform and chromatographed on silica gel, developing with a mixture of ethyl acetate and methanol (9: 1), the content of the latter being gradually increased. The less polar one (yield, 107 mg) was found to be N^6-benzyl-9-methyladenine, as had already been reported by some workers.[12] The more polar one, which was identified as XXVI, was crystallized from ethyl acetate; yield, 133 mg; mp 189—191 °C; λ_{max}^{MeOH} mμ(ε) 280 (18300), 230 (sh, 14500).

Found: C, 61.65; H, 4.38; N, 27.96%. Calcd for $C_{13}H_{11}ON_5$: C, 61.47; H, 4.37; N, 28.38%.

N⁶-*Benzoyl-9-methyl*-N⁶-p-*toluyladenine (XXIV).* Compound XXII (125 mg) was treated with benzoyl chloride (108 mg) in pyridine (5 ml) at 0 °C for 1 hr; then the reaction mixture was poured into a cold solution of sodium bicarbonate. The product was extracted with chloroform and chromatographed on silica gel developing with ethyl acetate. From carbon tetrachloride, 34 mg of a glassy substance, which was shown to be homogeneous on tlc, were obtained. The analytical data showed that the solvent was difficult to exclude even on prolonged heating *in vacuo*; *e.g.*, after heating at 56 °C for 4 hr, a 2/3 equivalent of carbon tetrachloride was found to remain, and a 1/3 equivalent still remained after it had been treated at 80 °C for 8 hr. The same compound was prepared from XXVI (85 mg) and *p*-toluyl chloride (150 mg); yield, 40 mg; λ_{max}^{MeOH} mμ(ε) 270 (sh, 18700), 255 (20000); NMR (60 MHz, $CDCl_3$): δ 2.20 (3H, s, $C\underline{H}_3C_6H_4CO$), 4.00 (3H, s, $CH_3N\langle$); Mass *m/e*: 370 (M^+), 342 (M^+-CO), 266 ($M^+-C_6H_5CO+H$), 252 ($M^+-CH_3C_6H_4CO+H$).

N⁶,*5'*-O-*Diacetyl-2',3'*-O-*isopropylidenetubercidin (XXXIV).* To an ice-cooled solution of XXXII (306 mg, 1 mml) in pyridine, acetyl chloride (800 mg, 10 mml) was added drop by drop. After 2 hr, the reaction mixture was poured into a cold solution of sodium bicarbonate. The product was extracted with chloroform and chromatographed on silica gel, developing with a mixture of benzene and ethyl acetate (2: 1), the content of the latter being gradually increased. Precipitation from ethyl acetate and ligroin afforded 183 mg of a syrup; $[\alpha]_D^{25}$ −20.0° (*c* 2.04, $CHCl_3$); λ_{max}^{MeOH} mμ(ε) 287 (7800).

Found: C, 55.69; H, 5.57; N, 14.04%. Calcd for $C_{18}H_{22}O_6N_4$: C, 55.55; H, 5.59; N, 14.35%.

12) Shell Internationale Research Maatschappij N. V., Brit. 953897 (1964); *Chem. Abstr.*, **62**, P 6494a (1965). Shell Internationale Research Matschappij, Ger. 1132784, (1962); *Chem. Abstr.*, **57**, P 13776g (1962). Johannes von Overbeek, U. S. 3013885, (1960); *Chem. Abstr.* **56**, P 14306e (1962).

The Metalation of Fluorene by Means of the Diethylmagnesium-Hexamethylphosphoramide System

Masao TOMOI and Hiroshi KAKIUCHI

Department of Applied Chemistry, Faculty of Engineering, Yokohama National University, Yokohama 233

(Received January 31, 1973)

The metalation of fluorene by means of the Et_2Mg–HMPA system was investigated. The reaction scarcely occurred at all when the mole ratio of HMPA: Et_2Mg fell below 1: 1, but it proceeded easily when the ratio was over 1: 1, and a solvent-separated ion pair of magnesium fluorenide was formed. When the ratio was 2: 1, the order of reaction was unity in both fluorene and Et_2Mg. It was demonstrated by the kinetic and NMR studies that the active species of metalation in such a case was not Et_2Mg but the Et_2Mg–HMPA complex, in which two molecules of HMPA are coordinated to Et_2Mg.

In recent years dipolar solvents, especially dipolar aprotic solvents, have frequently been used as media or reactants for organic reactions. Previously we[1] ourselves reported that Grignard's reagent (RMgX) could not polymerize styrene in toluene, but that high-molecular polystyrene could be obtained when hexamethylphosphoramide (HMPA) existed in over twice the molar quantity of RMgX. It was demonstrated that RMgX was changed to an ionic form, *i.e.*, carbanion, by the coordination of HMPA, and that the initiation reaction proceeded by means of the addition of the carbanion to the styrene monomer. In this paper, the metalation of fluorene by means of the diethylmagnesium–HMPA system will be investigated in order to make clear the role of HMPA in organomagnesium compound–HMPA systems. Normant[2] has already reported the metalation of fluorene by isopropylmagnesium chloride in HMPA, but the mechanism of the reaction has not yet been studied.

Experimental

Reagents. Fluorene (FL) was purified by recrystallization from ethanol. A solution of diethylmagnesium (Et_2Mg) was prepared by adding dioxane to an ether solution of ethylmagnesium bromide. The concentration of the solution of Et_2Mg was determined by acid-base titration.[3] HMPA was refluxed and distilled over calcium hydride *in vacuo*.

Metalation Reaction. The reaction of FL with Et_2Mg was done in 0.2 cm optical cells under an atmosphere of nitrogen. Et_2Mg in ether was added to a toluene solution of FL, and at last HMPA in toluene was introduced into the reaction system. Within two min of the mixing of the reagents, the cell was placed in a Hitachi EPS-3T recording spectrophotometer and the optical density at 373 nm was monitored as a function of the time. The absorption at this wavelength is due to the product, fluorenyl carbanion.

Measurement of the NMR Spectrum. The NMR spectrum of the Et_2Mg–HMPA system in ether was taken with a JNM C-60H spectrometer at room temperature, using teramethylsilane as the internal standard.

Results and Discussion

Electronic Spectrum of the Reaction Product. In the absence of HMPA, scarecely no reaction of FL and Et_2Mg in toluene or tetrahydrofuran (THF) occurred. However, the reaction easily proceeded in the presence of HMPA, and fluorenyl carbanion (FL^-) was formed. Figure 1 shows the spectra of the reaction product and fluorenyllithium in THF. The absorption spectrum of magnesium fluorenide has a peak at 373 nm. This peak has been assigned by Hogen-Esch and Smid[4] to the solvent-separated ion pair of alkali fluorenides in ethereal solvents. The spectrum of magnesium fluorenide in the visible region was similar to that of the solvent-separated ion pair of fluorenyllithium. These results indicate that the magnesium fluorenide produced in the presence of HMPA exists as a solvent-separated ion pair.

The NMR spectrum[5] of magnesium fluorenide produced by the reaction of FL with equimolar quantities of Et_2Mg at $[HMPA]/[Et_2Mg]=3$ indicated that the

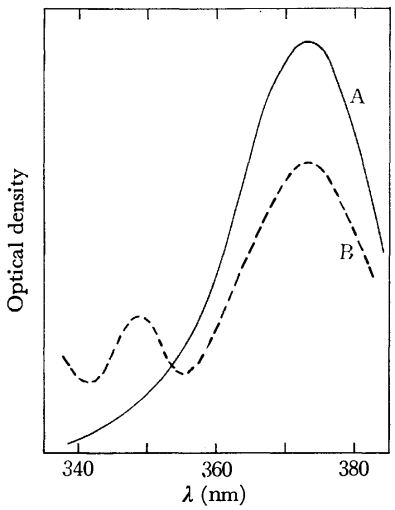

Fig. 1. Absorption spectra of lithium and magnesium fluorenides.
A: Magnesium fluorenide produced by the reaction of FL with Et_2Mg at $[Et_2Mg]/[HMPA]=2$,
B: Fluorenyllithium in THF, Temp.: 15.0 °C.

1) M. Tomoi and H. Kakiuchi, *Kogyo Kagaku Zasshi*, **73**, 2367 (1970).
2) T. Cuvigny and H. Normant, *Bull. Soc. Chim. Fr.*, **1964**, 2003.
3) H. Gilman, E. A. Zoellner, and J. B. Dickey, *J. Amer. Chem. Soc.*, **51**, 1576 (1929).
4) T. E. Hogen-Esch and J. Smid, *ibid.*, **88**, 307 (1966).
5) M. Tomoi, T. Yoneyama, and H. Kakiuchi, Abstracts, SPSJ 21th Annual Meeting, Tokyo, May 25, 1972, p. 310.

product consisted of equimolar amounts of fluorenyl and ethyl groups. The fluorenyl part of the NMR spectrum of the product was similar to that of fluorenyllithium in THF.[6] Moreover, the chemical shift of methylene protons, δ_{CH_2}, in the product was −1.1, while the value of δ_{CH_2} in Et_2Mg was −0.88 at [HMPA]/[Et_2Mg]=3 (see below). This fact indicates that the diamagnetic anisotropy induced by the aromatic ring strongly shields the ethyl protons. Consequently, the metalation seems to proceed as is shown in Reaction (1), and ethylfluorenylmagnesium (FL^-Mg^+Et) is formed:

$$FL + Et_2Mg \longrightarrow FL^-Mg^+Et + EtH \quad (1)$$

$$2FL^-Mg^+Et \rightleftarrows (FL^-)_2Mg^{2+} + Et_2Mg \quad (2)$$

The mixed reagent (FL^-Mg^+Et) may coexist at equilibrium, as is shown in Reaction (2). The NMR data, however, indicate that the structure of the magnesium fluorenide produced is a mixed reagent rather than a mixture of difluorenylmagnesium ($(FL^-)_2Mg^{2+}$) and Et_2Mg. It has been reported by House *et al.*[7] that a similar mixed reagent was formed when dicyclopentadienylmagnesium and diethylmagnesium were mixed in ether. Since a large excess of Et_2Mg over FL was used in the kinetic experiment, the equilibrium could be considered to lie far to the left.

We allowed a reaction system to come to the steady state and then diluted it with various quantities of toluene, measuring the optical density of the solution at each stage. This showed that Beer's law was accurately obeyed; the extinction coefficient of magnesium fluorenide was $\varepsilon_{373}=9900$.

Kinetic Studies. In a previous paper,[1] we reported that the molar ratio of HMPA to a organomagnesium compound was a significant factor in the polymerization of styrene by the RMgX–HMPA. In this paper, the molar ratio, α, is defined as follows:

$$\alpha = \frac{[\text{HMPA}]}{[\text{Organomagnesium compound}]} \quad (3)$$

Figure 2 shows the variation in the optical density of the reaction system with the time at $\alpha=2$. The optical density increased with the time and became a constant value after about 20 hr. In the absence of HMPA ($\alpha=0$), the optical density remained zero, even after about 22 hr. Since a large excess of Et_2Mg over FL was used in this experiment, the order of the reaction in the latter reagent could be obtained from an analysis of the optical density-time curve.[8] In this manner, we found the order of the reaction in FL to be 1.0. Thus, we may write:

$$\text{Rate of production of } FL^- = dFL^-/dt = k[FL] \quad (4)$$

where k is the first-order rate constant.

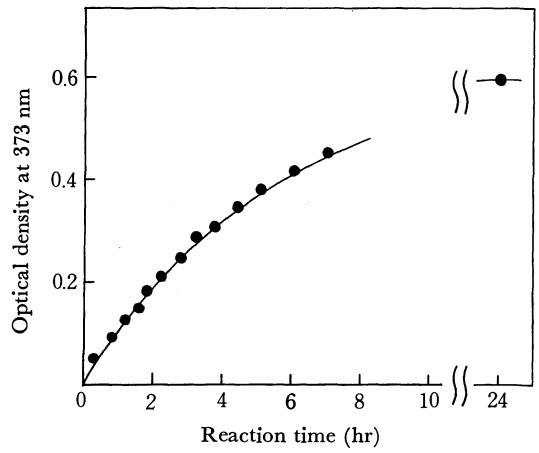

Fig. 2. A typical reaction rate plot.
$[FL]_0=3.04\times10^{-4}$ M, $[Et_2Mg]_0=2.37\times10^{-2}$ M, $[HMPA]_0=4.75\times10^{-2}$ M, Temp.: 19.0 °C.

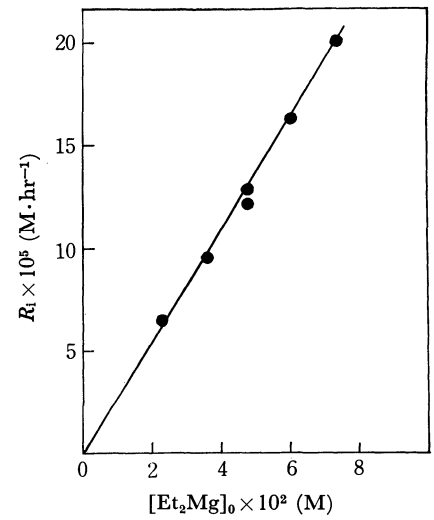

Fig. 3. Dependence of initial rate on initial diethylmagnesium concentration.
$[FL]_0=3.40\times10^{-4}$ M, $[HMPA]_0/[Et_2Mg]_0=2.0$, Temp.: 19.0 °C.

Figure 3 shows the dependence of the initial rate (R_i) on the initial diethylmagnesium concentration $[Et_2Mg]_0$ at $\alpha=2$. This finding indicates the order of the reaction in Et_2Mg to be 1.0. Consequently, the rate of the production of FL^- at $\alpha=2$ may be written as follows:

$$dFL^-/dt = k'[Et_2Mg][FL] \quad (5)$$

where k' is the second-order rate constant.

Effect of the Molar Ratio of HMPA to Et_2Mg (α). Figure 4 shows the dependence of the initial rate (R_i) on the molar ratio of HMPA to Et_2Mg (α) at a constant Et_2Mg concentration. When α is less than about unity, the rate of metalation is zero, while the reaction is significantly promoted when α is more than about unity. The relationship between R_i and α is indicated by the two straight lines, the slopes of which are dependent on the range of α. One is the range in α from about unity to about two, while the other is in the α range over about two. The increment of the rate was larger in the former range than in the latter.

The dependence of R_i on $[Et_2Mg]_0$ at a constant concentration of HMPA is shown in Fig. 5. When α was less than about two, the rate decreased greatly in spite of the increase in the concentration of Et_2Mg.

6) R. H. Cox, *J. Phsy. Chem.*, **73**, 2649 (1969).
7) H. O. House, R. A. Latham, and G. M. Whitesides, *J. Org. Chem.*, **32**, 2481 (1967).
8) See *e.g.*, A. G. Evans, and N. H. Rees, *J. Chem. Soc.*, **1963**, 6039.

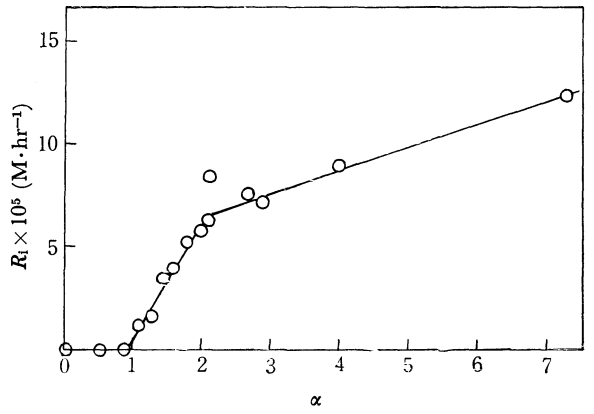

Fig. 4. Dependence of initial rate on α at a constant diethylmagnesium concentration.
$[FL]_0=2.80\times10^{-4}$ M, $[Et_2Mg]_0=3.95\times10^{-2}$ M, Temp.: 15.0 °C.

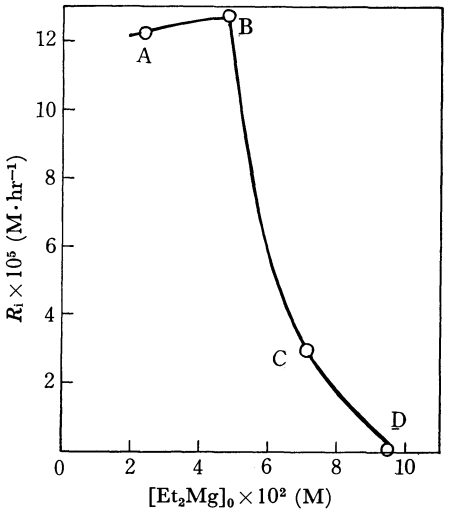

Fig. 5. Dependence of initial rate on initial diethylmagnesium concentration at a constant HMPA concentration.
$[FL]_0=3.40\times10^{-4}$ M, $[HMPA]_0=9.50\times10^{-2}$ M, Temp.: 19.0 °C.
The values of α are as follows;
A: 4.0, B: 2.0, C: 1.33, D: 1.0.

This fact indicates that, in the course of the reaction the important factor is not the Et_2Mg concentration, but the molar ratio of HMPA to Et_2Mg, this is, α.

NMR Spectrum of the Et_2Mg–HMPA System. The chemical shift of the methyl protons in Et_2Mg, δ_{CH_3}, was 1.17 in ether, while that of the methylene protons, δ_{CH_2}, was −0.65. The value of δ_{CH_2} was dependent on α. However, δ_{CH_3} scarcely changed in the presence of HMPA. Figure 6 shows the dependence of δ_{CH_2} on α. The change in δ_{CH_2} was small when α was less than about unity. The δ_{CH_2}, however, shifted upfield with an increase in α when α was between about unity and about two. When α was over about two, the magnitude of the decrease in δ_{CH_2} was small.

It is known that an approximately linear relationship exists between the internal chemical shift in ethyl compounds and the electronegativity of the substituent or the metal atom.[9] We could study the change in the

9) B. P. Dailey and J. N. Shoolery, *J. Amer. Chem. Soc.*, **77**, 3977 (1955).

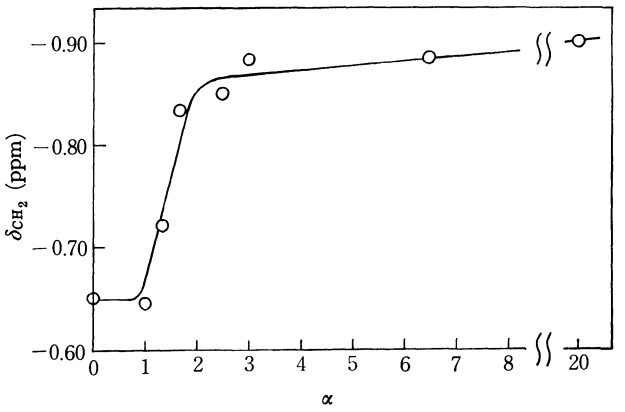

Fig. 6. Variation of δ_{CH_2} in Et_2Mg with α.
Solvent: ether, $[Et_2Mg]=0.50$—0.88 M.

electronegativity of magnesium metal in diethylmagnesium upon coordination with HMPA by using the relationship proposed by Narasimhan and Rogers:[10]

$$\text{Electronegativity} = 0.62(\delta_{CH_2}-\delta_{CH_3}) + 2.07 \quad (6)$$

where $\delta_{CH_2}-\delta_{CH_3}$ is the internal chemical shift in ethyl compounds. The electronegativity of magnesium in Et_2Mg was 0.94 (δ_{CH_2}, −0.65; δ_{CH_3} 1.17) in the absence of HMPA in ether. When α was equal to 3, the electronegativity of magnesium changed to 0.79 (δ_{CH_2}, −0.88; δ_{CH_3}, 1.17). In the presence of THF ([THF]/[Et_2Mg]=3), it was 0.89 (δ_{CH_2}, −0.74; δ_{CH_3}, 1.17).[5] This result indicates that the electronegativity of magnesium in Et_2Mg decreases upon coordination with HMPA or THF, and that HMPA coordinates to magnesium more strongly than THF, as is to be expected from the donicities of these solvents.[11] Our result is in agreement with that recently reported by Ducom,[12] who investigated the same system in benzene. Similar conclusions have been obtained in triethylalminium–donor[13,14] and diethylzinc–donor[14] systems.

Interaction of HMPA with Et_2Mg, and the Mechanism of the Metalation Reaction. It has been reported by Walker and Ashby[15] that Et_2Mg is predominantly monomeric in ether (degree of association=∼1.3 at [Et_2Mg]=∼1M). The dietherate species (I), therefore, must have changed to Species (II)—(IV) on the addition of HMPA to this system:

$$\underset{\text{(I)}}{Et_2Mg(Et_2O)_2} + HMPA \overset{K_1}{\rightleftharpoons} \underset{\text{(II)}}{Et_2Mg(Et_2O)(HMPA)} + Et_2O \quad (8)$$

$$\text{(II)} + HMPA \overset{K_2}{\rightleftharpoons} \underset{\text{(III)}}{Et_2Mg(HMPA)_2} + Et_2O \quad (9)$$

$$\text{(III)} + m\text{HMPA} \overset{K_3}{\rightleftharpoons} \underset{\text{(IV)}}{Et^-Mg^+Et(2+m)\text{HMPA}} \quad (10)$$

10) P. T. Narasimhan and M. T. Rogers, *ibid.*, **82**, 5983 (1960).
11) V. Gutmann, *Angew. Chem.*, **82**, 858 (1970).
12) J. Ducom, *Bull. Soc. Chim. Fr.*, **1971**, 3523.
13) K. Hatada and H. Yuki, *Tetrahedron Lett.*, **1968**, 213.
14) M. Ikeda, T. Hirano, and T. Tsuruta, *Makromol. Chem.*, **150**, 127 (1971).
15) F. Walker and E. C. Ashby, *J. Amer. Chem. Soc.*, **91**, 3845 (1969).

where K_1, K_2, and K_3 are the equilibrium constants in the three reactions.

The fact that the chemical shift, δ_{CH_2}, changed continuously suggests that the exchanges of these species are rapid at room temperature. If $K_1 > K_2 \gg 1$ and $K_3 \ll 1$ in these equilibria, Species (I) and Species (II), which is coordinated by one HMPA and one ether, coexist at equilibrium when α is less than unity. When α is between about unity and about two, Species (III), which is coordinated by two HMPA molecules, coexists with Species (II). The monomeric species (III) seems to change to an ionic form (IV) with the additional coordination of HMPA when $\alpha > 2$. As the δ_{CH_2} is considered to shift more upfield with an increase in the number of HMPA molecules coordinated to Mg, it is reasonable that the δ_{CH_2} of these species decreases in this order:

$$\delta_{CH_2}(I) > \delta_{CH_2}(II) > \delta_{CH_2}(III) > \delta_{CH_2}(IV).$$

A similar order has been suggested by Parris and Ashby in the case of dimethylmagnesium in THF.[16] The fact that the δ_{CH_2} shifted upfield with the increase in α at $1 < \alpha < 2$ is considered to be due to the increase in the concentration of Species (III). It can be explained that, because of the low concentration of Species (IV) formed in Reaction (10), the δ_{CH_2} decreased gradually at $\alpha > 2$.

The metalation reaction was done in a mixture of solvents of toluene and a small amount of ether. It could be assumed that Et_2Mg is present as aggregated forms (V) in a toluene–ether mixture rather than as a monomeric form. These aggregates must have been dissociated into less aggregated or monomeric forms on the addition of HMPA:

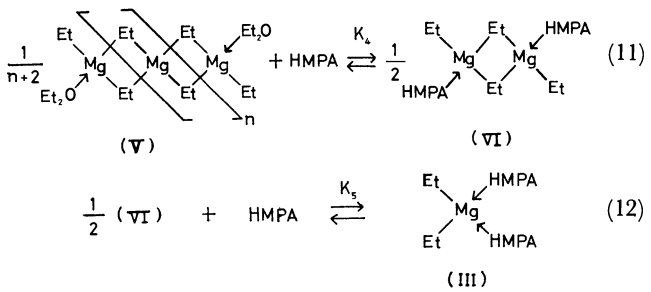

where K_4 and K_5 are the equilibrium constants in Reactions (11) and (12). The dimeric species (VI), which is coordinated by one HMPA molecule per Mg atom, seems to be present in this system. However, the monomeric form (II) shown in Reaction (8) may also coexist with Species (VI). The species which are coordinated by one HMPA per Mg must, in any event, have been changed to Species (III) coordinated with two HMPA molecules (Reactions (9) and (12)). Furthermore, Species (III) seems to change to the ionic species (IV), as is shown in Reaction (10).

If $K_4 > K_2 \approx K_5 \gg 1$ and $K_3 \ll 1$ in these reactions, the concentration of the monomeric species (III) at $\alpha \leq 2$ can be given as follows:

$$[Et_2Mg \cdot 2HMPA] \simeq 0 \text{ when } \alpha \leq 1$$
$$[Et_2Mg \cdot 2HMPA] = [HMPA] - [Et_2Mg] = [Et_2Mg](\alpha - 1) \text{ when } 1 < \alpha < 2 \quad (13)$$

where [HMPA] and $[Et_2Mg]$ are the total concentrations of HMPA and Et_2Mg respectively in the reaction system. The rate of the production of FL^- at $\alpha \leq 2$ can be given as in Eq. (14) by assuming that only Species (III) can react with FL:

$$FL + Et_2Mg \cdot 2HMPA \longrightarrow FL^-Mg^+Et \cdot 2HMPA + EtH$$
$$dFL^-/dt = k_1[Et_2Mg \cdot 2HMPA][FL] \quad (14)$$

where k_1 is the second-order rate constant. From Eqs. (13) and (14), we obtain Eqs. (15):

$$dFL^-/dt \simeq 0 \text{ when } \alpha \leq 1 \quad (15\text{-A})$$
$$dFL^-/dt = k_1(\alpha - 1)[Et_2Mg][FL] \text{ when } 1 < \alpha < 2 \quad (15\text{-B})$$
$$dFL^-/dt = k_1[Et_2Mg][FL] \text{ when } \alpha = 2 \quad (15\text{-C})$$

The dependence of the rate on α at $\alpha < 2$ (Fig. 4) could be explained in terms of Eqs. (15-A) and (15-B). The order of reaction at $\alpha = 2$ is in agreement with the experimental results shown in Eq. (5). These facts support the idea that the reactive species in the metalation reaction is the monomeric species (III) when $\alpha < 2$.

When α is more than two, the ionic species (IV) seems also to react with FL. The concentration of Species (IV) is given as follows:

$$[IV] = K_3[III][HMPA_f]^m \quad (16)$$

where $HMPA_f$ is the concentration of free HMPA and is given by the following equation:

$$[HMPA_f] = [HMPA] - 2[Et_2Mg] = (\alpha - 2)[Et_2Mg] \quad (17)$$

As the concentration of Species (IV) is considered to be low, the concentration of Species (III) is given as follows:

$$[III] = [Et_2Mg] - [IV] \simeq [Et_2Mg]. \quad (18)$$

From Eqs. (16), (17), and (18), we can obtain Eq. (19):

$$[IV] = K_3[Et_2Mg]\{(\alpha - 2)[Et_2Mg]\}^m = K_3(\alpha - 2)^m[Et_2Mg]^{1+m}. \quad (19)$$

Consequently, the rate at $\alpha < 2$ is given as follows:

$$dFL^-/dt = k_1[Et_2Mg][FL] + K_3 \cdot k_2(\alpha - 2)^m[Et_2Mg]^{1+m}[FL] \quad (20)$$

where k_2 is the rate constant in the reaction of Species (IV) with FL. The fact that a linear relationship exists between R_i and α when $\alpha \geq 2$ can be explained by assuming that m in Eq. (20) is equal to unity. That is to say, Et_2Mg probably changes to the ionic species with the coordination of three HMPA molecules. However, the formation of the ionic species from the organomagnesium compound (R_2Mg, RMgX) is considered to be dependent on the structure of the organic moiety in the compound. The relationship between the ease of carbanion formation from RMgX and the structure of the organic group, R, is now under investigation.

16) G. E. Parris and E. C. Ashby, *J. Amer. Chem. Soc.* **93**, 1206 (1971).

The Carbonylation of Alcohols Catalyzed by Cu(I) Carbonyl

Yoshie SOUMA and Hiroshi SANO

Government Industrial Research Institute, Osaka, Midorigaoka, Ikeda, Osaka 563

(Received March 1, 1973)

In conc. H_2SO_4 containing the Cu(I) compound, alcohols react with carbon monoxide at room temperature and atmospheric pressure to produce *tert*-carboxylic acids in high yields. Primary carboxylic acid is not formed. It is assumed that the unstable Cu(I) tricarbonyl ion, $Cu(CO)_3^+$, is transiently formed in conc. H_2SO_4. An amount of the Cu(I) compound as small as 0.2 mol/l is sufficient. The catalyst is effective at H_2SO_4 concentrations above 80%. The reaction rate decreases with a decrease in the H_2SO_4 concentration. At H_2SO_4 concentrations of less than 80%, no carboxylic acids are obtained.

Many attempts to obtain carboxylic acid from alcohol and carbon monoxide have been made. Reppe *et al.*[1] reported the carbonylation of alcohols with the nickel carbonyl catalyst to give mixtures of straight-chain carboxylic acids and branched carboxylic acids. Adkins and Rosenthal[2] suggested that a possible course of the reaction was the dehydration of the alcohol to an olefin. These reactions proceed at high temperatures and under high pressures. Eidus *et al.*[3] reported the carbonylation of alcohols using an acid catalyst such as H_2SO_4 or H_3PO_4. Even in this reaction, however, an elevated pressure of carbon monoxide is necessary. Koch and Haff[4] reported the synthesis of branched carboxylic acids from alcohols using formic acid in conc. H_2SO_4.

To carry out the carbonylation reaction under mild conditions, the present authors previously attempted the use of the Cu(I) carbonyl catalyst, prepared from Cu(I) compounds and carbon monoxide in conc. H_2SO_4.[5] The unstable Cu(I) tricarbonyl ion, $Cu(CO)_3^+$, acts as a catalyst for this carbonylation reaction. The carbonylation of olefin using the Cu(I) catalyst was reported; *tert*-carboxylic acids were thus obtained in high yields.[6]

In this report, the carbonylation of alcohol using the Cu(I) carbonyl catalyst was studied at room temperature and atmospheric pressure. Reactions using the Cu(I) carbonyl catalyst will prove of wide-ranging synthetic utility for carbonylation reactions.

Results and Discussion

The results of the carbonylation of alcohols using the Cu(I) carbonyl catalyst are shown in Table 1. Various alcohols (normal, secondary, and tertiary alcohols) are converted to *tert*-carboxylic acids in high yields. Alcohol is protonated and dehydrated to the carbonium ion, which rearranges to the stable tertiary carbonium ion prior to the carbonylation. Hence, no primary carboxylic acid is obtained.

The structures of the products were determined by

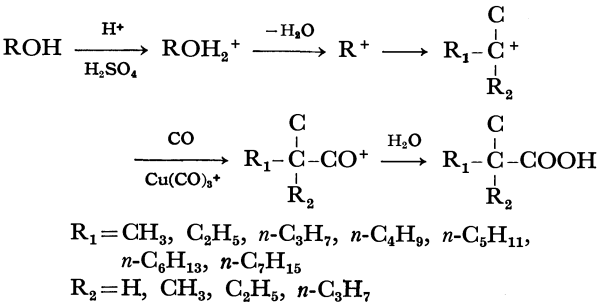

R_1=CH_3, C_2H_5, n-C_3H_7, n-C_4H_9, n-C_5H_{11}, n-C_6H_{13}, n-C_7H_{15}

R_2=H, CH_3, C_2H_5, n-C_3H_7

a study of their NMR, IR, and mass spectra as well as by elemental analysis. In most cases, the products were mixtures of the isomers. When the mixtures were easily separable by glpc, each isomer was isolated by preparative glpc and was subjected to structure analysis. When the separation was not easy by glpc, the mixture was analyzed by means of ^{13}C NMR.

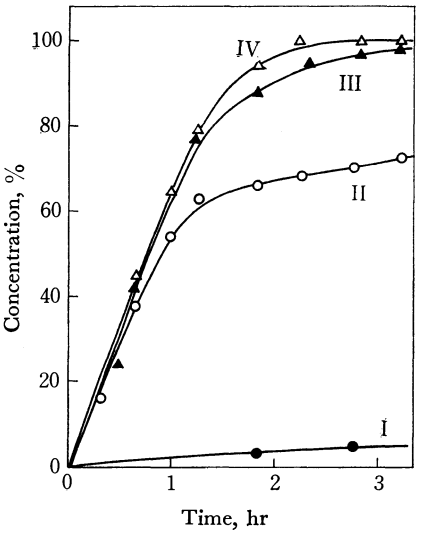

Fig. 1. Catalytic effect of Cu_2O.
98% H_2SO_4 10.5 ml and 1-hexanol 1.24 ml (10 mmol) at 30°
I: Cu_2O 0 mmol, II: Cu_2O 0.1 mmol, III: Cu_2O 1 mmol
IV: Cu_2O 4 mmol

Cuprous oxide was used as the Cu(I) compound. The effect of the amount of cuprous oxide is illustrated in Fig. 1. Without cuprous oxide, the rate of the reaction was very slow, and the yield of carboxylic acid was less than 10% after 3 hr. When cuprous oxide was added in conc. H_2SO_4, the rate of the reaction increased rapidly, and *tert*-carboxylic acid was obtained in a high yield.

1) W. Peppe, H. Kroper, N. Kutepow, and H. J. Pistor, *Ann. Chem.*, **582**, 72 (1953).
2) H. Adkins and R. W. Rosenthal, *J. Amer. Chem. Soc.*, **72**, 4550 (1950).
3) Ya. T. Eidus, K. V. Puzitskii, and S. D. Pirozhkov, *Neftekhimiya*, **8**, 343 (1968).
4) H. Koch and W. Haff, *Ann. Chem.*, **618**, 251 (1958).
5) Y. Souma and H. Sano, *Nippon Kagaku Zasshi*, **91**, 625 (1970).
6) Y. Souma and H. Sano, *J. Org. Chem.*, **38**, 2016 (1973).

Table 1. *tert*-Carboxylic acids derived from alcohols and carbon monoxide[a)]

Alcohol	R_1	R_2	Yield (%)
1-Propanol[b)]	CH_3	H	15
2-Propanol[b)]	CH_3	H	18
1-Butanol[b)]	CH_3	CH_3	22
	C_2H_5	H	23
2-Methylpropanol[b)]	CH_3	CH_3	56
2-Methyl-2-propanol[b)]	CH_3	CH_3	52
2-Butanol[b)]	CH_3	CH_3	28
	C_2H_5	H	19
1-Pentanol	C_2H_5	CH_3	62
1,1-Dimethylpropanol	C_2H_5	CH_3	30
	CH_3	CH_3	24
	C_3H_5	CH_3	7
	Other acids		8
1-Hexanol	C_3H_5	CH_3	60
	C_2H_5	C_2H_5	25
	C_2H_5	CH_3	4
	CH_3	CH_3	2
2-Hexanol	C_3H_5	CH_3	55
	C_2H_5	C_2H_5	38
	C_2H_5	CH_3	3
	CH_3	CH_3	1
4-Methyl-2-pentanol	C_3H_5	CH_3	56
	C_2H_5	C_2H_5	28
	Other acids		9
3-Methyl-3-pentanol	C_3H_5	CH_3	26
	C_2H_5	C_2H_5	30
	C_2H_5	CH_3	20
	CH_3	CH_3	10
Cyclohexanol	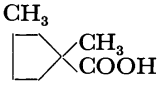		80
1-Octanol	n-C_5H_{11}	CH_3	72
	n-C_4H_9	C_2H_5	15
	n-C_3H_7	n-C_3H_7	5
2-Octanol	n-C_5H_{11}	CH_3	55
	n-C_4H_9	C_2H_5	30
	n-C_3H_7	n-C_3H_7	10
1-Decanol	n-C_7H_{15}	CH_3	75
	n-C_6H_{13}	C_2H_5	15
	n-C_5H_{11}	n-C_3H_7	5
2,5-Dimethylcyclohexanol			78

a) In most cases, 20 mmol of alcohol, 4 mmol of Cu(I) oxide, and 21 ml of 98% H_2SO_4 were used, and the reaction temperature was approximately 30°, while the reaction time varied from 1 to 2 hr. The pressure of carbon monoxide was 1 atm.
b) 10 mmol of alcohol was used.

Cuprous oxide absorbs carbon monoxide in conc. H_2SO_4 and forms an equilibrium mixture of Cu(I) carbonyl ions, $Cu(CO)^+$ and $Cu(CO)_3^+$:[5)]

$$Cu_2O + CO \overset{H^+}{\rightleftharpoons} Cu(CO)^+ + Cu(CO)_3^+$$

Only $Cu(CO)_3^+$ acts as a catalyst in the carbonylation reaction. With the absorption of carbon monoxide, the reddish color of cuprous oxide gradually changes to white. Every Cu^+ ion changes to a $Cu(CO)_3^+$ ion in conc. H_2SO_4 at -10 °C, under 7 atm of carbon monoxide. However, $Cu(CO)_3^+$ is unstable, and it exists as an equilibrium mixture with $Cu(CO)^+$ at the atmospheric pressure of carbon monoxide and at room temperature:

$$Cu(CO)_3^+ \rightleftharpoons Cu(CO)^+ + 2CO$$

In the presence of CO acceptors such as carbonium ions, CO is liberated from $Cu(CO)_3^+$ and reacts with the carbonium ion immediately. Carbon monoxide is continuously absorbed by the $Cu(CO)^+$ in the solution from the gas phase, and a constant amount of $Cu(CO)_3^+$, which acts as a catalyst, exists in conc. H_2SO_4. In the reaction system, Cu^+ acts as a "CO carrier" from the gas phase to the reaction species in the solution.

Table 2. The effect of the H_2SO_4 concentration upon the carbonylation[a)]

H_2SO_4 concn		Conversion of alcohol (%)		
Wt.%	Mole ratio H_2O/H_2SO_4	1-Hexanol	2-Hexanol	3-Methyl-3-pentanol
100.0	0.0	91	90	90
98.2	0.10	50	90	90
95.6	0.25	28	90	90
91.5	0.50	8	74	89
88.0	0.75		31	47
84.4	1.00		10	21
73.0	2.00		0	0

a) In most cases, 10.5 ml of H_2SO_4, 0.286 g of Cu_2O, and 1.25 ml of alcohol were used. The reaction temperature was 30°C, and the reaction time was 3 hr.

The influence of the H_2SO_4 concentration upon the carbonylation was also examined. The results are shown in Table 2. With the increase in the concentration above 80%, the reaction rate and the yield increased. No carboxylic acid was obtained at concentrations below 80%.

As to Cu(I) carbonyl, only $Cu(CO)^+$ exists in H_2SO_4 concentrations below 80%. It is known that $Cu(CO)_3^+/Cu(CO)^+$ gradually increases with an increase in the H_2SO_4 concentration above 80%.[5)] The effect of the H_2SO_4 concentration upon the carbonylation is parallel with the effect upon the formation of the unstable $Cu(CO)_3^+$ in the system.

Alcohol was added slowly to the Cu(I) carbonyl suspension. The absorption of carbon monoxide by the alcohol was then measured. The results are shown in Fig. 2. Among normal, secondary, and tertiary alcohols, the rates of CO absorption are different at every H_2SO_4 concentration (100, 91.5, and 84.4%). The rate increases in the following order; normal$<$secondary$<$tertiary. In normal alcohol, dehydration is difficult compared with that in secondary or tertiary alcohols. In 91.5% H_2SO_4 and 84.4% H_2SO_4, the rate of CO absorption became slower. This shows that dehydration and isomerization become more difficult with the decrease in the H_2SO_4 concentration. Roebuck and Evering studied the relation between the isomerization of the alkyl cation and the H_2SO_4 concentration,

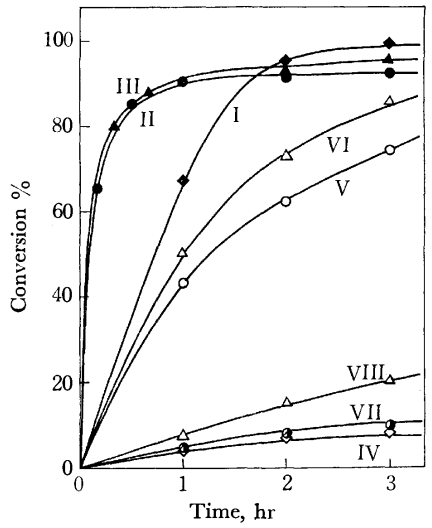

Fig. 2. The rate of CO absorption by alcohols (*n*, *sec*, *tert*). Alcohols (10 mmol) and H_2SO_4 (10 ml) were used at 30°. I: 1-hexanol in 100% H_2SO_4, II: 2-hexanol in 100% H_2SO_4, III: 3-methyl-3-pentanol in 100% H_2SO_4, IV: 1-hexanol in 91.5% H_2SO_4, V: 2-hexanol in 91.5% H_2SO_4, VI: 3-methyl-3-pentanol in 91.5% H_2SO_4, VII: 2-hexanol in 84.4% H_2SO_4, VIII: 3-methyl-3-pentanol in 84.4% H_2SO_4.

and reported that increasing the initial acid concentration from 95.5 to 99.8% increased the rate of isomerization as much as 64 fold.[7]

In the carbonylation of 3-methyl-3-pentanol, considerable amounts of 2,2-dimethylbutanoic acid and 2,2-dimethylpropionic acid are obtained as by-products. Möller[8] and Yoneda *et al.*[9] reported the same type of reactions. They explained the reaction as the disproportionation of the dimerized alkyl group in strong acid. On the other hand, Olah and Lukas[10] reported the formation of a very stable *tert*-butyl cation from C_5—C_{16} alkanes in a very strong acid medium at room temperature.

The effect of the amount of alcohol on the yield of *tert*-carboxylic acid was studied in the presence of constant amounts of 98% H_2SO_4 and Cu_2O. The results are shown in Table 3. When the amount of alcohol increases, the rate of reaction becomes very slow, and the yield of carboxylic acid decreases.

Table 3. The effect of the amount of alcohol on the yield of *tert*-carboxylic acid[a]

1-Hexanol	98% H_2SO_4	Mole ratio 1-hexanol/H_2SO_4	Yield of *tert*-C_7 acid
1.24 ml(10 mmol)	10.5 ml(200 mmol)	0.05	85%
2.24 (18 mmol)		0.09	79
5.24 (42 mmol)		0.21	53
7.24 (58 mmol)		0.29	41

a) The reaction temperature was 30°C, and 0.286 g of Cu_2O was used.

Experimental

The infrared spectra were taken as neat samples on a Hitachi EPI-S2 apparatus. The ^1H NMR spectra were taken on a JEOL PS-100 apparatus at 100 MHz in the CCl_4 solvent. The chemical shifts are given in δ units (ppm) downfield from the internal TMS. The mass spectra were measured on the Shimadzu-LKB-9000 gaschromatograph-mass spectrometer with a 70 eV ionizing current. The glpc analyses were performed using a 3 m FFAP column (10% on Chromosorb WAW). The elemental analyses were done on a Yanagimoto CHN MT-2 apparatus.

All the alcohols used in the experiment were commercial reagents and were purified by distillation. The Cu_2O, H_2SO_4, and carbon monoxide were all commercial reagents and were used without further purification.

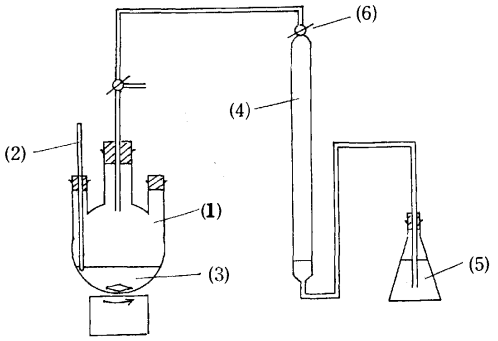

Fig. 3. The reaction apparatus of carbonylation. (1): 300 ml three-necked flask, (2): Thermometer, (3): Cu_2O +98% H_2SO_4, (4): Gas buret, (5): Leveling bottle, (6): Gas cock.

Preparation of Cu(I) Carbonyl. The apparatus is shown in Fig. 3. In a 300 ml, three-necked flask equipped with a thermometer and carbon monoxide gas buret, we placed 572 mg of Cu_2O and 21.0 ml of 98% H_2SO_4. The apparatus was evacuated by means of a diffusion pump to remove the air; then carbon monoxide was introduced from the gas buret. The mixture of Cu_2O and H_2SO_4 was then stirred vigorously. The carbon monoxide was absorbed by the Cu^+ in about 40 min. The CO/Cu^+ ratio reached 1.35 at 30°, CO 1 atm.

Carbonylation of Alcohol. By a syringe, 20 mmol of alcohol was added, drop by drop, to a Cu(I)-carbonyl suspension over a 20 min. The CO absorption by alcohol finished in from 1 to 3hr. The amount of CO absorption was measured using a CO gas buret. The amount of the conversion of alcohol to acid is equal to that of the CO absorption. The reaction mixture was then poured over ice-water. The products were extracted by benzene, and excess alkali was added to the benzene extract. The aqueous phase was acidified by H_2SO_4. The carboxylic acid was then again extracted by the use of benzene. In order to determine the yield of *tert*-carboxylic acid, a 1/10 volume of the benzene extract was titrated with a 1/10M NaOH ethanol solution. The yield of the carboxylic acid was also determined by gas chromatography by adding a known amount of the internal standard.

1,4-Dimethylcyclohexanecarboxylic Acid. This was obtained by the carbonylation of 2,5-dimethylcyclohexanol. The *cis* and *trans* isomers were separated by preparative glpc, the *trans* isomer as a white solid and the *cis* isomer as a liquid component. (lit,[4,11]) Bp 135—137°C/16—20 mmHg;

7) A. K. Roebuck and B. L. Evering, *J. Amer. Chem. Soc.*, **75**, 1631 (1953). H. Pines and N. E. Hoffmann, "Friedel-Crafts and Related Reactions," Vol. II, part 2, G. A. Olah, Ed., Interscience Publishers, Inc., New York, N. Y., (1964) Chapter 28.

8) K. E. Möller, *Brennst. Chem.*, **45**, 129 (1964).

9) T. Yoneda, Y. Matsushima, M. Matsubara, and H. Otsuka, *Nippon Kagaku Kaishi*, **1972**, 1475.

10) G. A. Olah and J. Lukas, *J. Amer. Chem. Soc.*, **89**, 2227, 4739 (1967).

$n_D^{25}=1.4576$.

trans-Isomer. Mp 69°; IR (cm^{-1}) 2950, 1703 (C=O), 1458, 1235, 1178; NMR δ 0.90 (d, 3, $J=6$ Hz, $C\underline{H}_3$-$\dot{C}H$), 1.22 (s, 3, $C\underline{H}_3$-$\dot{C}$-COOH) 1.64 (m, 4, $-CH_2-$), 0.70—1.26 (m, 3, $-\underline{H}\dot{C}H$, $-\dot{C}\underline{H}$), 2.0—2.40 (m, 2, $-HC\underline{H}$), 11.66 (br. s, 1, $COO\underline{H}$); mass spectrum (70 eV) *m/e* (rel. intensity) 156 (25, M^+), 111 (45), 87 (72), 70 (100), 69 (70). Found: C, 69.02; H, 10.09%. Calcd for $C_9H_{16}O_2$: C, 69.19; H, 10.32%.

cis-Isomer. IR (cm^{-1}) 2950, 1703 (C=O), 1470, 1295, 1130; NMR δ 0.98 (d, 3, $J=7$ Hz, $C\underline{H}_3$-$\dot{C}H$), 1.26 (s, 3, $C\underline{H}_3$-$\dot{C}$-COOH), 0.75—1.50 (m, 3, $-\underline{H}\dot{C}H$, $-C\underline{H}-$), 1.73 (m, 6, $-C\underline{H}_2-$), 11.58 (br. s, 1, $COO\underline{H}$); mass spectrum (70 eV) *m/e* 156 (10, M^+), 111 (100), 110 (73), 69 (94), 55 (53). Found: C, 69.25; H, 10.42%. Calcd for $C_9H_{16}O_2$: C, 69.19; H, 10.32%.

The 2-methylpropionic acid, 2,2-dimethylpropionic acid, 2-methylbutanoic acid, 2,2-dimethylbutanoic acid, 2,2-dimethylpentanoic acid, 2-methyl-2-ethylbutanoic acid, and 1-methylcyclopentanecarboxylic acid were identified by comparing their retention time and "spiking" with those of authentic samples. The authentic samples were obtained by the carbonylation of olefins.[6] The ratios of all the isomers of the *tert*-C_9 and *tert*-C_{11} carboxylic acids were determined by ^{13}C NMR according to the method described in a previous paper.[6]

11) W. G. Schindel and R. E. Pincock, *J. Org. Chem.*, **35**, 1789 (1970).

BULLETIN OF THE CHEMICAL SOCIETY OF JAPAN, VOL. 46, 3240—3247 (1973)

Solid Phase Peptide Synthesis by Oxidation-Reduction Condensation. Synthesis of LH-RH by Fragment Condensation on Solid Support

Rei MATSUEDA, Hiroshi MARUYAMA, Eiichi KITAZAWA, Hidekuni TAKAHAGI, and Teruaki MUKAIYAMA*

Product Development Laboratories, Sankyo Co. Ltd., Hiromachi, Shinagawa-ku, Tokyo 140
**Laboratory of Organic Chemistry, Tokyo Institute of Technology, Ookayama, Meguro-ku, Tokyo 152*

(Received March 22, 1973)

Solid phase peptide synthesis by oxidation-reduction condensation was investigated. The fragment condensation on solid support was examined by employing two types of chain elongation, that from *C*-terminal amino acid to *N*-terminal amino acid (A type elongation) and that from *N*-terminal amino acid to *C*-terminal amino acid (B type elongation). The feasibility of these two approaches A and B was demonstrated in two syntheses of LH-RH (luteinizing hormone-releasing hormone). The LH-RH prepared from the two different chain elongations showed identical mobilities on tlc, exhibiting full activities of natural LH-RH (AVS 77-33 # 215-269).

Solid phase peptide synthesis has provided a rapid method for preparation of many biologically active peptides[1] in which peptide chains have been lengthened from *C*-terminal amino acid to *N*-terminal amino acid (A type elongation). However, only a few investigations[2] have been reported on the preparation of oligopeptides by solid phase synthesis in which the peptide chain elongation was carried out from *N*-terminal amino acid to *C*-terminal amino acid (B type elongation). As regards type A, many modifications[3] have been attempted by fragment condensation to minimize the contaminants which bear similar properties to those of the desired product. On the other hand, no development was attained as regards type B because of the danger of racemization both in the deprotection and in the coupling steps. Recently, a modification[4] of this method was attempted by the use of azide coupling, but it was found not to be a general procedure because of low yields and of restrictions on reaction solvents. In the present experiment, application of the oxidation-reduction process with triphenylphosphine (Ph_3P) and 2,2′-dipyridyl disulfide ($(PyS)_2$) to solid phase peptide synthesis was investigated, taking into consideration the fact that development of both types of chain elongations would be achieved by fragment condensation with oxidation-reduction process possessing the advantages of minimizing side reactions and the racemization of a carboxyl component.[5] This paper describes successful syntheses of porcine luteinizing hormone-releasing hormone (LH-RH)[6] with a sequence of <Glu–His–Trp–Ser–Tyr–Gly–Leu–Arg–Pro–Gly–NH_2 by em-

1) R. B. Merrifield, *Biochemistry*, **3**, 1385 (1964). G. R. Marshall and R. B. Merrifield, *ibid.*, **4**, 2394 (1965). A. Marglin and R. B. Merrifield, *J. Amer. Chem. Soc.*, **88**, 5051 (1966). H. Takashima, V. du Vigneaud, and R. B. Merrifield, *ibid.*, **90**, 1323 (1968). M. Manning, *ibid.*, **90**, 1348 (1968). J. Meienhofer and Y. Sano, *ibid.*, **90**, 2996 (1968). B. Gutte and R. B. Merrifield, *ibid.*, **91**, 501 (1969).

2) R. L. Letsinger and M. J. Kornet, *ibid.*, **85**, 3045 (1963).

3) F. Weygand and U. Rahnarsson, *Z. Naturforsch.*, **216**, 1141 (1966). G. S. Omenn and C. B. Anfinsen, *J. Amer. Chem. Soc.*, **90**, 6571 (1968). H. Yajima, H. Kawatani, and H. Watanabe, *Chem. Pharm. Bull.* (Tokyo), **18**, 1333 (1970).

4) A. M. Felix and R. B. Merrifield, *J. Amer. Chem. Soc.*, **92**, 1385 (1970).

5) T. Mukaiyama, R. Matsueda, and N. Suzuki, *Tetrahedron Lett.*, **1970**, 1901. T. Mukaiyama, K. Goto, R. Matsueda, and M. Ueki, *ibid.*, **1970**, 5293.

6) H. Matsuo, Y. Baba, R. M. G. Nair, A. Arimura, and A. V. Schally, *Biochem. Biophys. Res. Commun.*, **43**, 1334 (1971). Y. Baba, H. Matsuo, and A. V. Schally, *ibid.*, **44**, 459 (1971).

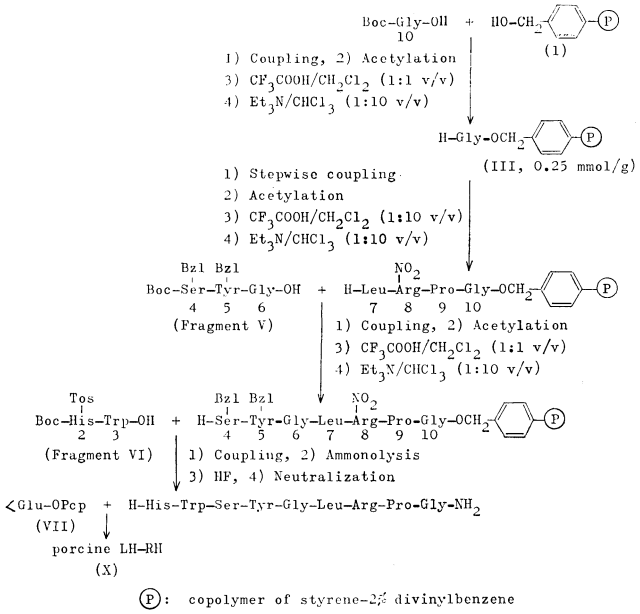

Fig. 1. Scheme for the synthesis of LH-RH by A type elongation.

ploying both A and B types of chain elongation.[7]

I. Chain Elongation from C-Terminal Amino Acid to N-Terminal Amino Acid (Type A). Attachment of the first amino acids or peptide fragments to the hydroxymethyl resin and the peptide chain elongation by fragment condensation have recently been achieved[8] by oxidation-reduction condensation. Synthesis of nonapeptide (2—10 sequence) of LH-RH was attempted by solid phase method as shown in Fig. 1. The chain elongation on solid support was designed to prepare nonapeptide since the tosyl group of the side chain of histidine was found to be partially cleaved by treatment with trifluoroacetic acid used for the removal of Boc-group. The syntheses of peptide fragments achieved by oxidation-reduction condensation in solution are outlined in Fig. 2 and physical properties of these intermediates are listed in Table 1. In the

Table 1. Physical properties of peptide fragments

Peptide fragment	Mp	$[\alpha]_D^t$° (*c*,solvent)
Fragment V	134°C	$[\alpha]_D^{20}$—6.2° (*c* 1, MeOH)
Fragment VI	148—150°C	$[\alpha]_D^{20}$ 15.2° (*c* 1, DMF)
XV	172—175°C	$[\alpha]_D^{20}$—9.6° (*c* 1, DMF)
XIX	168—171°C(decomp.)	$[\alpha]_D^{20}$—43.2° (*c* 2, DMF)

first step, esterification of a 2% crosslinked hydroxymethyl resin which was synthesized from usual chloromethyl resin (Schwarz-Mann, New York, Cl content: 2.0 mmol/g) with the first Boc-glycine was undertaken by using 3 fold excess each of Boc-glycine, Ph_3P and $(PyS)_2$ in CH_2Cl_2. The remaining free hydroxyl groups were covered by acetylation[9] in DMF.[10] The Boc-

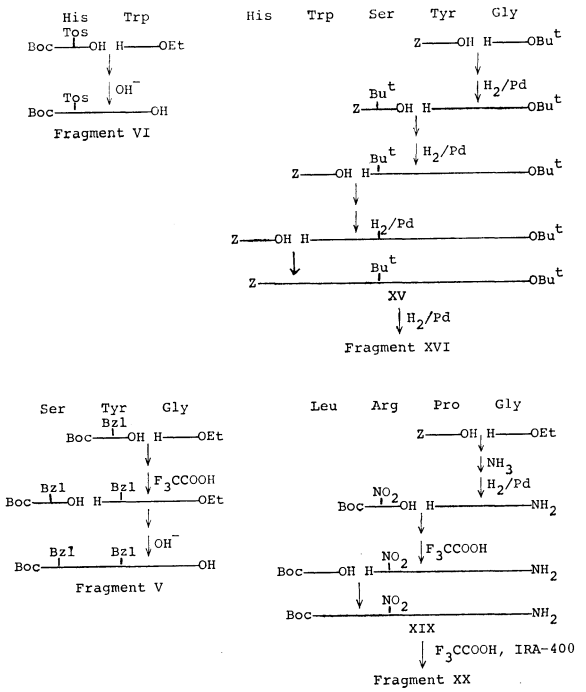

Fig. 2. Syntheses of peptide fragments.

glycine resin (III, 0.25 mmol/g) thus obtained was chain-lengthened to a tetrapeptide stage by stepwise elongation by oxidation-reduction condensation according to a similar procedure to that of the attachment of glycine to the resin. Removal of the Boc-group was performed by treatment with trifluoroacetic acid in CH_2Cl_2 (1:1 v/v) for 30 min, neutralization being carried out with triethylamine in $CHCl_3$ (1:10 v/v) for 10 min. The first coupling of tetrapeptide-resin with fragment V was achieved by treating the deprotected tetrapeptide-resin with a 1.5 fold excess of fragment V and 3 fold excess each of Ph_3P and $(PyS)_2$ in CH_2Cl_2 for 24 hr. The second coupling of heptapeptide-resin with fragment VI was also achieved by treating the deprotected heptapeptide-resin with 3 fold excess each of fragment VI, Ph_3P and $(PyS)_2$ in CH_2Cl_2 for 24 hr. A portion of this resulting resin was hydrolyzed in 3 M *p*-toluenesulfonic acid in the presence of 3-(2-aminoethyl)indole[11] after being treated with HF,[12] the amino acid analysis giving: His, 0.95; Trp, 0.84; Ser, 0.96; Tyr, 0.95; Gly, 2.12; Leu, 1; Arg, 0.93; Pro, 0.97.

Since triphenylphosphine oxide and 2-mercaptopyridine, coproducts produced in the above condensation, are very soluble in various organic solvents, they are washed away thoroughly in the washing steps. It is an important advantage over *N,N'*-dicyclohexylcarbodiimide-mediated coupling in which insoluble dicyclohexylurea are formed.

Removal of the completely protected peptide chain from the resin was undertaken by ammonolysis in absolute ethanol. The protected nonapeptide amide was purified by Avicel column in BuOH: AcOH: H_2O

7) The results were reported at the 10th Japanese Peptide Symposium held at Sapporo, 26, 27 September, 1972.

8) R. Matsueda, E. Kitazawa, H. Maruyama, H. Takahagi, and T. Mukaiyama, *Chem. Lett.*, **1972**, 379.

9) J. M. Stewart and J. D. Young, "Solid Phase Peptide Synthesis," W. H. Freeman, San Francisco, Calif. (1969), p. 33.

10) *N,N*-dimethylformamide.

11) T. Y. Liu and Y. H. Chang, *J. Biol. Chem.*, **246**, 2842 (1971).

12) S. Sakakibara, Y. Shimonishi, Y. Kishida, M. Okada, and H. Sugihara, This Bulletin, **40**, 2164 (1967).

(4: 1: 1 v/v) and Sephadex LH-20 in DMF. The pure protected nonapeptide amide Boc-His(Tos)-Trp-Ser(Bzl)-Tyr(Bzl)-Gly-Leu-Arg(NO_2)-Pro-Gly-NH_2·H_2O (IX) was obtained as a white amorphous powder, weight 373 mg (48% yield based on the amount of glycine originally esterified to the resin), mp 197—201 °C (decomp.), $[\alpha]_D^{25}$ −27.6° (*c* 1, DMF). In order to check the racemization during fragment condensation, the nonapeptide amide was digested at 37 °C for 48 hr with aminopeptidase M after HF treatment and amino acid analysis of the digest gave: His, 1.06; Trp, 1.03; Ser, 1.02; Tyr, 1.02; Leu, 1; Gly, 1.04; Arg, and Pro were not observed. This shows that the fragment condensation by oxidation-reduction condensation was achieved with L-configuration being kept.

The nonapeptide amide was deprotected with HF in the presence of anisole and 2-mercaptopyridine[13] to avoid the decomposition of tryptophan residue. Conversion into LH-RH was attempted by coupling with <Glu-OPcp according to the procedure in the synthesis of thyrotropin-releasing hormone.[14] Since excess molar ratio of pyroglutamyl residue was observed to be incorporated to nonapeptide amide when 1.5 eq of <Glu-OPcp was used, the coupling was carried out in DMF by using 0.85 eq of <Glu-OPcp to nonapeptide amide after neutralization with Amberlite IRA-400 in MeOH. The product was applied to IRP-64 column in MeOH and eluted with 1% AcOH in MeOH. The peptide was purified on CM-Sephadex C-25[15c] column after gel filtration on Sephadex G-25 in 1 M AcOH. The decapeptide amide eluted with 0.15 M ammonium acetate was desalted by lyophilization three times and gel filtration on Sephadex G-25 in 1 M AcOH. Forty nine milligrams of pure LH-RH was obtained from 161 mg of the protected nonapeptide amide (IX) after precipitation from MeOH-Et_2O and drying at 40 °C *in vacuo* over P_2O_5. $[\alpha]_D^{20}$ −54.2° (*c* 1, 1% AcOH) lit, $[\alpha]_D^{28}$ −50.5±2° (*c* 1, 1% AcOH),[15a] $[\alpha]_D^{20}$ −52.9° (*c* 0.3, 1% AcOH),[15b] and $[\alpha]_D^{25}$ −48.2° (*c* 0.5, H_2O).[15c] This decapeptide amide was characterized as diacetate and trihydrate after further drying at 80 °C for 5 hr *in vacuo* over P_2O_5. The peptide was homogeneous on various tlc detected by Pauly, Ehrlich, Sakaguchi and Cl-tolidine reactions and gave the same R_f values as those reported.[15a] LH-RH activity of the purified decapeptide amide (amino acid content: 76%) was compared at 2 dose levels with that of natural LH-RH (AVS 77-33 # 215-269, amino acid content 67.5%) in ovariectomized, estrogen-progesterone treated rats. Serum LH levels were estimated by radioimmunoassay according to Niswender *et al.*[16] The synthetic LH-RH exhibited full activity[17] of the natural LH-RH.

II. Chain Elongation from N-*Terminal Amino Acid to* C-*Terminal Amino Acid (Type B).* Since Letsinger and Kornet[2] proposed the B type elongation of peptide chain, no successful developments have been reported in this type of chain elongation. Recently, a modification[4] of this method was attempted by the use of azide coupling. However, it was shown that this was not a general procedure because of low yields and restrictions on reaction solvents. Since the direction of B type chain elongation is similar to that in biosynthesis, it seemed attractive as an approach to biosynthesis by chemical means.

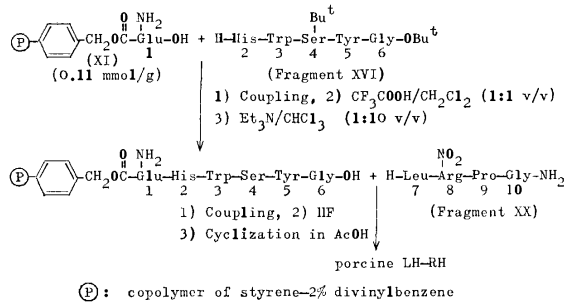

Fig. 3. Scheme for the synthesis of LH-RH by B type elongation.

The synthetic scheme for the B type elongation is shown in Fig. 3. In this approach, carboxyl protection was performed as *t*-butyl ester which is easily deprotected by trifluoroacetic acid. The building of decapeptide was designed to couple 3 fragments of 1,2—6 and 7—10 sequence in order to eliminate the trouble of preparing *t*-butyl ester of an acid-sensitive tryptophan and of racemization in fragment condensation with the use of glycine as a carboxyl component.

In the first step, an attachment of amino group of *t*-butyl glutaminate to a methylchloroformylated copolymer of styrene-2% divinylbenzene (Cl content: 1.4 mmol/g) was carried out in chloroform in the presence of triethylamine. The remaining chloroformyl group was covered by the reaction with diethylamine.[4] A resin-glutamine *t*-butyl ester containing 0.11 mmol/g was obtained. The first coupling of 2 g of resin-glutamine with fragment XVI was achieved by treating the deportected resin-glutamine with 3 fold excess each of fragment XVI, Ph_3P and $(PyS)_2$ in DMF and CH_2Cl_2 at room temperature for 10 hr and for an additional 24 hr after addition of 3 fold excess each of Ph_3P and $(PyS)_2$. The second coupling with fragment

13) Unpublished data.

14) G. Flouret, *J. Med. Chem.*, **13**, 843 (1970).

15) a) R. Geiger, W. König, H. Wissmann, K. Geisen, and F. Enzmann, *Biochem. Biophys. Res. Commun.*, **45**, 767 (1971). b) S. Sakakibara, *et al.*, "The 9th Japanese Symposium on Peptide Chemistry," Protein Research Foundation, Osaka, 1971, p. 90. c) N. Yanaihara, *et al.*, *ibid.*, p. 96.

16) G. D. Niswender, A. R. Midgley, Jr., S. Z. Monroe, and L. E. Reichert, Jr., *Proc. Soc. Exp. Biol. Med.*, **128**, 807 (1968).

17) Serum LH levels 15 min after jugular vein injection of 0.5 and 2.5 ng LH-RH in six rats in each dose level were estimated. The dose response regression lines for natural and synthetic LH-RH prepared by two procedures were parallel. Using four point factorial assay,[18] the LH-RH activity of synthetic LH-RH was calculated as follows: synthetic LH-RH of A type elongation (amino acid content 76%), 121% of the potency of natural LH-RH (AVS 77-33 # 215-269, amino acid content 67.5%); synthetic LH-RH of B type elongation (amino acid content 78%), 125% of the potency of natural LH-RH. These values show that synthetic LH-RH prepared by the two types of chain elongation have full activity of natural LH-RH taking into consideration the ratio of amino acid content of synthetic products to that of natural one.

18) C. I. Bliss, "The Statistics of Bioassay," Academic Press, Inc., (1952).

XX was carried out by the same procedure as that for the first coupling except that the deprotection of *t*-butyl group was carried out with CF_3COOH/CH_2Cl_2 (1 : 1 v/v) containing 5% of 2-mercaptopyridine[13] to avoid decomposition of the acid-sensitive tryptophan residue. The amino acid ratios of the resulting resin–decapeptide amide after hydrolysis with 3 M *p*-toluenesulfonic acid[11] were as follows: Glu, 1.10; His, 1.01; Trp, 0.80; Ser, 0.95; Tyr, 1.03; Gly, 2.05; Leu, 1; Arg, 0.95;[19] Pro, 0.94; NH_3, 2.87. This shows that fragment condensation proceeds efficiently without protection of side chains of amino acids by this new method. The recovered amino components of fragments XVI and XX in the washing solvents, DMF and CH_2Cl_2, showed the same spots on tlc as with the starting fragments: the former was detected with ninhydrin, Pauly and Ehrlich reactions and the latter by ninhydrin and Cl-tolidine reactions. It was established that couplings of 1 g of new resin–glutamine with the recovered fragments XVI and XX gave a resin peptide with nearly the same amino acid ratios as those obtained in the above chain elongation.

The resin–decapeptide amide was treated with HF at room temperature for 30 min in the presence of anisole and 2-mercaptopyridine and the decapeptide amide was extracted with DMF. Cyclization of glutaminyl residue of the decapeptide amide to pyroglutamyl derivative (LH–RH) was achieved in acetic acid[20] at 80—100 °C for 30 min in the presence of aniosle and 2-mercaptopyridine. This decapeptide amide was purified on CM-Sephadex C-25[15c] as mentioned in A type elongation after separation of 2-mercaptopyridine by gel filtration on Sephadex G-25 in 1 M AcOH. The pure LH–RH (133 mg, 51% yield from the initial resin–glutamine) was obtained after desalting, lyophilization and precipitation from MeOH–Et_2O and drying at 40 °C *in vacuo* over P_2O_5. $[\alpha]_D^{20}$ −53.1° (*c* 1, 1% AcOH). The peptide was also characterized as diacetate and trihydrate after further drying at 80 °C for 5 hr *in vacuo* over P_2O_5. LH–RH activity of the purified decapeptide amide (amino acid content: 78%) which gave the same R_f values on various tlc as with the one prepared by A type elongation was compared at two dose levels with that of natural LH–RH (AVS 77-33 # 215-269), it exhibited full activity[17] of the natural LH–RH.

These new approaches demonstrate the advantages of preparing oligopeptides in good yields by a simple purification procedure since the contamination of similar peptides with small difference in sequence is eliminated. The introduction of tryptophan residue is more feasible than the usual solid phase synthesis since the number of acidolysis required for deblocking of protecting groups can be reduced.

Superiority of the oxidation-reduction process lies in the advantage it possesses of minimizing side reactions in carboxyl components. Thus, the side reaction, formation of acyl urea derivatives in dicyclohexylcarbodiimide method, and intensive restrictions on reaction solvent and temperature in azide method are eliminated.

Special practical merits of A and B types of elongation are as follows: type A, (1) it allows an attachment of the first amino acid in a rather homogeneous environment on the resin under milder conditions and in shorter reaction time than those carried out by ordinary methods and (2) the reaction conditions and operations are the same as for the subsequent chain-lengthening acylation and consequently incorporation of the esterification step in the automated process is possible. Type B, (1) chain elongation can be carried out in most cases with readily available Z-amino acids which can be used mostly without protection of side chains except carboxyl and amino groups, (2) excess amino components can be recovered unchanged and the formation of diacyl amide[21] can be avoided since the excess amino components are used in solution.

It is to be noted that solid phase peptide synthesis by oxidation-reduction condensation provides a versatile method which combines the advantages of the usual solid phase synthesis and the classical synthesis in solution.

Experimental

All melting points are uncorrected. Optical rotations were determined with a Perkin-Elmer Model 141 polarimeter. Amino acid analyses were performed on a Hitachi Amino Acid Analyzer, Model KLB-3B. Solid phase peptide synthesis was carried out by shaking with a manual apparatus. Thin layer chromatography was performed on precoated plates of silica gel G and cellulose F (E. Merck) at 5°.

Hydroxymethyl Resin (I) and Methylchloroformylated Resin (II). Chloromethylated copolystyrene-2% divinylbenzene (Schwarz-Mann, New York, Cl: 2.0 mmol/g, 50 g) was treated with potassium acetate, subsequently hydrolyzed and was converted into hydroxymethyl resin (I, Cl: 0%).[4] Similarly the hydroxymethyl resin (20 g) was allowed to react with phosgene and was further converted into methylchloroformylated resin (II). The resin of Cl content of 1.39 mmol/g was obtained.

I. A Type Elongation. Attachment of t*-Butyloxycarbonylglycine to the Hydroxymethyl Resin.* Hydroxymethyl resin (I) (4 g, OH: 8 mmol) was suspended in 40 ml of CH_2Cl_2 and shaken for 30 min in a vessel for solid phase synthesis and the resin was washed with CH_2Cl_2 (40 ml). After addition of 3 eq (24 mmol) each of *t*-butyloxycarbonyl glycine, 2,2′-dipyridyl disulfide in CH_2Cl_2 (20 ml) and shaking for a few min, 3 eq (24 mmol) of triphenylphosphine in CH_2Cl_2 (10 ml) was added at room temperature. The mixture was shaken for 24 hr at room temperature and washed successively with CH_2Cl_2 (30 ml × 3), EtOH (30 ml × 3) and DMF (30 ml × 3). The remaining free hydroxyl groups on the resin were covered by acetylation[10] with 10 eq (80 mmol) each of acetic anhydride and triethylamine in 30 ml of DMF for 2 hr and washed successively with DMF (30 ml × 3), EtOH (30 ml × 3) and CH_2Cl_2 (30 ml × 3). An aliquot of the resin (III) was hydrolyzed and glycine content was determined by amino acid analyzer to be 0.25 mmol/g of the resin.

Boc-Tyr(Bzl)-Gly-OEt (IV). To a stirred mixture of

19) The value was calculated from the amounts of Arg, Orn and $Arg(NO)_2$.

20) H. Matsuo, A. Arimura, R. M. G. Nair, and A. V. Schally, *Biochem. Biophys. Res. Commun.*, **45**, 822 (1971).

21) M. Brenner, "Peptides, Proc. 8th Europ. Peptide Sympos.," North Holland Publ., Amsterdam, 1966, p. 1. E. Wünsch, *Angew. Chem.*, **83**, 773 (1971).

N-t-butyloxycarbonyl-*O*-benzyl-L-tyrosine (18.50 g, 50 mmol), ethyl glycinate (5.15 g, 50 mmol) and 2,2′-dipyridyl disulfide (11.00 g, 50 mmol) in 150 ml of dry CH_2Cl_2 was added triphenylphosphine (13.10 g, 50 mmol) in 50 ml of CH_2Cl_2 with ice-cooling. This was stirred for 6 hr at room temperature. After being left to stand overnight, the solvent was removed *in vacuo*, dissolved in 200 ml of ethyl acetate and washed successively with 10% citric-acid, water, 5% sodium bicarbonate and water. The solvent was evaporated after addition of silica gel (100 g) and the coated residue was applied to a dry column chromatography[22] on silica gel and the peptide was eluted with ether and crystallized from ethylacetate and petroleum ether; yield 20.0 g (87%); mp 123—126 °C; $[\alpha]_D^{20}$ 1.2° (*c* 2, MeOH).

Found: C, 65.91; H, 7.00; N, 6.25. Calcd for $C_{25}H_{32}O_6N_2$: C, 65.95; H, 7.02; N, 6.00.

Boc–Ser(Bzl)–Tyr(Bzl)–Gly–OEt (V). Compound IV (20 g, 40 mmol) was dissolved in 20 ml of CH_2Cl_2 and 50 ml of trifluoroacetic acid and stirred at room temperature for 1 hr. To the evaporated residue, 100 ml of ethyl acetate was added and washed first with saturated sodium bicarbonate, then water and dried over sodium sulfate. After evaporation of the solvent, the oily residue was used as ethyl *O*-benzyl-L-tyrosylglycinate. Dicyclohexylamine salt of *N-t*-butyloxycarbonyl-*O*-benzyl-L-serine (16.60 g, 43 mmol) was suspended in 10% citric acid (200 ml) and the mixture was extracted with ethyl acetate. The ethyl acetate layer was washed with water and dried over magnesium sulfate. The solvent was removed *in vacuo* and the residue was used as *N-t*-butyloxycarbonyl-*O*-benzyl-L-serine. To the stirred mixture of ethyl *O*-benzyl-L-tyrosylglycinate, *N-t*-butyloxycarbonyl-*O*-benzyl-L-serine and 2,2′-dipyridyl disulfide (11 g, 50 mmol) in 100 ml of CH_2Cl_2 was added triphenylphosphine (13.1 g, 50 mmol) in 50 ml of CH_2Cl_2 with ice-cooling and stirred at room temperature for 6 hr. After evaporation of solvent, the residue was dissolved in ethyl acetate and was washed successively with 10% citric acid, water, 5% sodium bicarbonate and water. Worked up as mentioned above, the tripeptide was obtained by dry column chromatography in ether and crystallization from ethyl acetate and petroleum ether; yield 19.00 g (71%); mp 63°C; $[\alpha]_D^{20}$ −9.0° (*c* 1, MeOH).

Found: C, 66.33; H, 6.87; N, 6.61. Calcd for $C_{35}H_{43}O_8N_3$: C, 66.33; H, 6.84; N, 6.63.

Boc–Ser(Bzl)–Tyr(Bzl)–Gly–OH (Fragment V). To a stirred mixture of 14.0 g (22 mmol) of IV in 100 ml of methanol was added 100 ml of water containing 1.0 g of sodium hydroxide. This was stirred at room temperature for 1 hr. The mixture was adjusted to pH 7 with acetic acid and evaporated *in vacuo*. The residue was dissolved in 100 ml of ethyl acetate and washed with 10% citric acid and water and dried over magnesium sulfate. The free acid peptide was obtained by crystallization from ethyl acetate–petroleum ether; yield 8.80 g (65%); mp 129—134°C; $[\alpha]_D^{20}$ −6.2° (*c* 1, MeOH).

Found: C, 65.51; H, 6.51; N, 7.10. Calcd for $C_{33}H_{39}O_8N_3$: C, 65.44; H, 6.49; N, 6.94. R_f 0.78 on silica gel G in *n*-BuOH: AcOH: H_2O (4: 1: 1) and R_f 0.72 on silica gel G in *n*-BuOH: AcOH: H_2O: Pyridine (30: 6: 24 :20). A portion of the peptide was deprotected with HF[12] for 2 hr at room temperature and hydrolysate in 6 M HCl gave the following amino acid ratios: Ser, 0.96; Tyr, 0.98; Gly, 1.

Boc–His(Tos)–Trp–OH (Fragment VI). Dicyclohexylamine salt of N^{α}-*t*-butyloxycarbonyl-N^{im}-tosyl-L-histidine(5.90 g, 10 mmol) and L-tryptophan ethyl ester hydrochloride (2.69 g, 10 mmol) were converted into free forms with citric acid and sodium bicarbonate respectively as in the preparation of IV. To a stirred mixture of N^{α}-*t*-butyloxycarbonyl-N^{im}-tosyl-L-histidine, L-tryptophan ethyl ester and 2,2′-dipyridyl disulfide (2.20 g, 10 mmol) in 30 ml of CH_2Cl_2 was added triphenylphosphine (2.62 g, 10 mmol) in 20 ml of CH_2Cl_2 with ice-cooling and the mixture was stirred at room temperature for 8 hr. The residue, after evaporation of solvent, was dissolved in ethyl acetate and washed successively with 10% citric acid, water, 5% sodium bicarbonate and water and dried over sodium sulfate. The solvent was evaporated and the residue was hydrolyzed with sodium hydroxide in methanol and water as in the preparation of V. After evaporation of methanol, the water layer was adjusted to pH 3 with acetic acid and extracted with *n*-buthanol saturated with water. The *n*-buthanol layer was washed with water saturated with *n*-buthanol and evaporated to dryness *in vacuo*. The dipeptide acid (4.05 g; 68%) was obtained from the residue by adding ether: mp 148—150 °C; $[\alpha]_D^{20}$ 15.2° (*c* 1, DMF).

Found: C, 58.54; H, 5.81; N, 11.80; S, 5.42%. Calcd for $C_{29}H_{33}O_7N_5S$: C, 58.47; H, 5.58; N, 11.75; S, 5.38%. R_f 0.80 on silica gel G in *n*-BuOH: AcOH: H_2O (4: 1: 1) and R_f 0.73 on silica gel G in *n*-BuOH: AcOH: H_2O: Pyridine (30: 6: 24: 20). Amino acid ratios (3M *p*-toluenesulfonic acid in the presence of 3-(2-aminoethyl)indole[11]): His, 1; Trp, 0.85.

〈Glu–OPcp (VII). To a stirred mixture of L-pyroglutamic acid (1.29 g, 10 mmol), pentachlorophenol 2.66 g (10 mmol) and 2,2′-dipyridyl disulfide (2.20 g, 10 mmol) in 40 ml of DMF was added triphenylphosphine (2.62 g, 10 mmol) in 20 ml of DMF with ice-cooling. The resulting mixture was stirred at room temperature for 5 hr and kept standing overnignt. After evaporation of solvent, the residue was crystallized from ethanol–ether and 2.32 g (62%) of the active ester was obtained: mp 196—198 °C, $[\alpha]_D^{28}$ +20.8° (*c* 2, DMF) lit,[14] mp 196—199 °C, $[\alpha]_D^{26}$ +21° (*c* 2, DMF).

Found: C, 35.26; H, 1.67; N, 3.96; Cl, 47.06%. Calcd for $C_{11}H_6Cl_5O_3N$: C, 35.00; H, 1.60; N, 3.71; Cl, 46.97%.

Boc–His(Tos)–Trp–Ser(Bzl)–Tyr(Bzl)–Gly–Leu–Arg(NO$_2$)–Pro–Gly–resin (VIII). Two grams of *t*-butyloxycarbonylglycine–resin (III, 0.25 mmol/g) were added to the vessel for solid phase peptide synthesis and the following steps were used to couple each new amino acid or peptide fragment: (1) washing with CH_2Cl_2 (15 ml×3); (2) prewash with trifluoroacetic acid/CH_2Cl_2 (1: 1 v/v); (3) removal of *t*-butyloxycarbonyl group with 15 ml of trifluoroacetic acid/CH_2Cl_2 (1: 1 v/v) for 30 min; (4) washing with CH_2Cl_2 (15 ml×3); (5) washing with $CHCl_3$ (15 ml×3); (6) neutralization with 15 ml of $Et_3N/CHCl_3$ (1: 10 v/v) for 10 min; (7) washing with $CHCl_3$ (15 ml×3); (8) addition of 3 fold excess (1.5 mmol) each of protected new amino acid or peptide fragment and 2,2′-dipyridyl disulfide in 10 ml of reaction solvent (CH_2Cl_2 or DMF); (9) addition of 3 eq (1.5 mmol) of triphenylphosphine in 5 ml of reaction solvent followed by a reaction period; (10) washing with reaction solvent (CH_2Cl_2 or DMF, 15 ml×3); (11) washing with ethanol (15 ml×3). The following *t*-butyloxycarbonyl amino acids were successively coupled at room temperature for 6 hr; Boc–Pro in CH_2Cl_2 Boc–Arg(NO$_2$)–OH in DMF[10] and Boc–Leu–OH·H_2O in CH_2Cl_2. In the case of Boc–Leu–OH·H_2O, 6 fold excess each of triphenylphosphine and 2,2′-dipyridyl disulfide was used. After the coupling of leucine, the peptide resin was treated with 10 fold excess (5 mmol) each of acetic anhydride and triethylamine in 15 ml of DMF for 2 hr[9] and was washed successively with DMF (15 ml×3) and ethanol (15 ml×3). The coupling of tetrapeptide–resin with Boc–Ser(Bzl)–Tyr(Bzl)–OH (fragment V) was carried out with a 1.5 fold excess of fragment V and 3 fold excess each of triphenylphosphine and 2,2′-dipyridyl disulfide in CH_2Cl_2 for 24 hr, followed by

22) B. Loev and K. M. Snader, *Chem. Ind.*, **1965**, 15. B. Loev and M. M. Goodman, *ibid.*, **1967**, 2026.

acetylation[9] with 10 fold excess each of acetic anhydride and triethylamine in DMF for 2 hr. The coupling of the resulting heptapeptide–resin with Boc-His(Tos)-Trp-OH (tragment VI) was achieved with 3 fold excess each of fragment VI, 2,2′-dipyridyl disulfide and triphenylphosphine in CH_2Cl_2 for 24 hr. A portion of this resin was treated with HF[12] at room temperature for 2 hr in the presence of 2-mercaptopyridine[13] and anisole and hydrolyzed in 3M *p*-toluenesulfonic acid[11] containing 0.2% of 3-(2-aminoethyl)indole for 24 hr and the hydrolysate gave the following amino acid ratios: His, 0.95; Trp, 0.84; Ser, 0.96; Tyr, 0.95; Gly, 2.12; Leu, 1; Arg, 0.93; Pro, 0.97.

Boc-His(Tos)-Trp-Ser(Bzl)-Tyr(Bzl)-Gly-Leu-Arg(NO_2)-Pro-Gly-NH_2 (IX). The nonapeptide–resin (VIII) was suspended in abs. ethanol and the stirred suspension was bubbled with a stream of ammonia from a refluxing solution of ammonia, which contained sodium as a drying agent, at −15—−30 °C for 8 hr with exclusion of moisture. The mixture was stirred overnight at −15—0 °C and subsequently at room temperature for 8 hr. After the evaporation of solvent, the residue was dried *in vacuo* over P_2O_5 and KOH. The cleaved material was extracted with DMF and methanol and the resin was removed by filtration. The combined filtrate was concentrated and applied to Sephadex LH-20 (2×130 cm) in DMF. The main peak was followed by two very small peaks detected by the absorption at 280 nm. The main peak was further purified with Avicel (Funakoshi Pharmaceutical Co., Tokyo) column (2.5×115 cm) in *n*-BuOH: AcOH: water (4: 1: 1) and followed by the filtration on Sephadex LH-20 in DMF. The fractions were condensed and the protected nonapeptide amide monohydrate was precipitated by adding ethyl acetate and ether. The precipitate was filtered, thoroughly washed with ethyl acetate and ether and dried *in vacuo* (P_2O_5 and KOH) to give an amorphous powder (373 mg, 48% based on Boc–glycine attached to the resin), mp 197—201 °C (decomp.), $[\alpha]_D^{25}$ −27.6° (*c* 1, DMF).

Found: C, 57.91; H, 6.35; N, 15.29; S, 1.81%. Calcd for $C_{76}H_{95}O_{17}N_{17}S \cdot H_2O$: C, 58.18; H, 6.23; N, 15.18; S, 2.04%. R_f 0.66 on silica gel G in *n*-BuOH: AcOH: H_2O (4: 1: 1) and R_f 0.75 on silica gel G in *n*-BuOH: AcOH: H_2O: Pyridine (30: 6: 24: 20). Amino acid analysis (3 M *p*-toluenesulfonic acid after HF treatment): His, 1.01; Trp, 0.82; Ser, 0.94; Tyr, 0.96; Gly, 2.04; Leu, 1; Arg, 0.88; Pro, 0.94; NH_3, 1.38. Amino acid analysis of an aminopeptidase M (Rohm and Hass Darmstadt) digest of the nonapeptide amide which was completely deprotected with HF in the presence of anisole and 2-mercaptopyridine gave: His, 1.06; Trp, 1.03; Ser, 1.02; Tyr, 1.02; Gly, 1.04; Leu, 1. No detection of Arg and Pro by the above amino acid analysis is due to the well-known resistance to enzymatic digestion of peptide bond involving proline.

⟨Glu-His-Trp-Ser-Tyr-Gly-Leu-Arg-Pro-Gly-NH_2 (LH-RH, X). In the coupling of completely deprotected nonapeptide with pentachlorophenyl L-pyroglutamate, 1.39 molar ratio of pyroglutamyl residue was found to be incorporated into nonapeptide when 1.5 eq of pentachlorophenyl pyroglutamate was used. The reaction conditions were so determined as not to use excess pentachlorophenyl glutamate. The protected nonapeptide (IX) 161 mg (0.123 mmol) was deprotected with 30 ml of dry HF for 1.5 hr at room temperature in the presence of 20 mg of 2-mercaptopyridine an i 1 ml of anisole. After the removal of HF and anisole *in vacuo*, the residue was washed with ether and dissolved in 100 ml of methanol and neutralized to pH 7 with Amberlite IRA-400 in methanol. The solvent was removed *in vacuo* and the residue was dissolved in 20 ml of DMF. To this mixture was added 0.85 eq of pentachlorophenyl L-pyroglutamate (VII) (35.5 mg, 0.942 mmol) and the mixture was stirred at room temperature for 2 hr and allowed to stand overnight. The solvent was evaporated and the peptide was precipitated by adding ethyl acetate and ether. The precipitate was dissolved in methanol and charged on the column of Amberlite IRP-64 (H^+) (1.5×8 cm) which was eluted first with methanol (200 ml) and then with 1% AcOH in methanol (700 ml). The elute of 1% AcOH in methanol was evaporated *in vacuo* and applied to Sephadex G-25 column (2.0×133 cm) in 1 M AcOH. After the evaporation of Ehlrich and Pauly positive fractions of the main peak, the decapeptide was precipitated from methanol–ethyl acetate–ether. The precipitate was dissolved in 150 ml of water and was further purified on CM-Sephadex C-25 (2.5×11 cm) as reported by N. Yanaihara *et al.*:[15] eluted successively with H_2O (150 ml), 0.1 M $AcONH_4$ (500 ml), 0.15 M $AcONH_4$ (500 ml) and 0.2 M $AcONH_4$ (500 ml). The main peak in 0.15 M $AcONH_4$ which was negative to ninhydrin was followed by a small peak in 0.2 M $AcONH_4$ positive to ninhydrin. The fractions containing a single component evaluated by Ehlrich, Pauly and Cl-tolidine reactions on tlc were pooled and evaporated *in vacuo* to 100 ml after acidification with AcOH. Desalting was achieved by lyophilization 3 times and further gel filtration on Sephadex G-25 in 1 M AcOH. The pure decapeptide amide was obtained by precipitation from methanol–ethyl acetate–ether after evaporation of solvent and dried *in vacuo* over P_2O_5 at 40°C for 12 hr: yield 46 mg (38% yield based on nonapeptide (IX)) $[\alpha]_D^{20}$ −54.2° (*c* 1, 1% AcOH) lit, $[\alpha]_D^{20}$ −50.5 ±2° (*c* 1, 1% AcOH)[15a], $[\alpha]_D^{20}$ −52.9° (*c* 1, 1% AcOH)[15b], $[\alpha]_D^{25}$ −48.2° (*c*0.5, H_2O)[15b]. Amino acid ratios (3 M *p*-toluenesulfonic acid[12]): Glu, 1.02; His, 0.98; Trp, 0.84; Ser, 1.01; Tyr, 0.99; Gly, 2.06; Leu, 1; Arg, 0.92; Pro, 0.96; NH_3, 1.35 and amino acid content was calculated to be 76% from the recovery value of leucine. The peptide was characterized as diacetate and trihydrate after further drying *in vacuo* at 80° over P_2O_5 for 5 hr.

Found: C, 52.32; H, 6.37; N, 17.56%. Calcd for $C_{55}H_{75}N_{17}O_{13} \cdot 2CH_3COOH \cdot 3H_2O$: C, 52.24; H, 6.61; N, 17.56%.

The product showed a single spot on various systems of tlc to Pauly, Ehlrich, Sakaguchi and Cl-tolidine reagents, the R_f values being identical with those reported in the literature[15a]: R_f 0.19 (lit, 0.16) on silica gel G and R_f 0.43 (lit, 0.44) on cellulose F in *n*-BuOH: AcOH: H_2O (4: 1: 5); R_f 0.51 (lit, 0.54) on silica gel G and R_f 0.61 (lit, 0.64) on cellulose F in $CHCl_3$: MeOH: 32%AcOH (12: 9: 4); R_f 0.44 (lit, 0.41) on silica gel G in *n*-BuOH: AcOH: Pyridine: H_2O (4: 1: 1: 2); R_f 0.79 (lit, 0.80) on cellulose F in $CHCl_3$: MeOH: 28%-NH_4OH (12: 9: 4).

II. B Type Elongation. Attachment of t-*Butyl* L-*Glutaminate to the Methylchloroformylated Resin.* The methylchloroformylated resin (II) 4 g (Cl: 1.39 mmol/g) was treated with 0.5 eq (2.78 mmol) each of *t*-butyl L-glutaminate and triethyl amine in 40 ml of $CHCl_3$ for 4 hr and successively with 10 eq (55.6 mmol) of diethylamine for 4 hr.[4] The content of glutamine of the resin (XI) was determined by amino acid analyzer to be 0.11 mmol/g.

Z-Tyr-Gly-OBu^t (XII). To a stirred mixture of 0.1 mol each of benzyloxycarbonyl-L-tyrosine (31.50 g), *t*-butyl glycinate (13.1 g) and 2,2′-dipyridyl disulfide (22 g) in 300 ml of DMF was added triphenylphosphine (26.2 g, 0.1 M) in 100 ml of CH_2Cl_2 and the mixture was stirred at room temperature for 9 hr. After working up as in the preparation of IV, crystallization from ethyl acetate–petroleum ether gave the dipeptide: 35.6 g (83%); mp 113—114°; $[\alpha]_D^{28}$ −22.4° (*c* 2, DMF).

Found: C, 64.25; H, 6.63; N, 6.70%. Calcd for $C_{23}H_{28}O_6N_2$: C, 64.47; H, 6.59; N, 6.54%.

Z-Ser(Bu^t)-Tyr-Gly-OBu^t (XIII). Compound XII 34.8 g (72 mmol) in 300 ml of methanol was hydrogenated over 10% Pd/C as a catalyst. The solvent was removed after filtration of the catalyst and dried *in vacuo* over P_2O_5. The residue, benzyloxycarbonyl-*O*-*t*-butyl-L-serine (17.7 g, 60 mmol) and 2,2'-dipyridyl disulfide 13.2 g (60 mmol), were dissolved in 200 ml of CH_2Cl_2. To this stirred mixture was added triphenylphosphine (15.70 g, 60 mmol) in 100 ml of CH_2Cl_2 with ice-cooling and the mixture was stirred at room temperature for 8 hr. After working up as in the preparation of IV, evaporation of solvent gave an amorphous powder: 27.5 g (80%); mp 105—115 °C; $[\alpha]_D^{20}$ −20.5° (*c* 1, MeOH).

Found: C, 60.92; H, 7.15; N, 7.30%. Calcd for $C_{30}H_{41}O_8N_3 \cdot H_2O$: C, 61.10; H, 7.35; N, 7.13%.

Z-Trp-Ser(Bu^t)-Tyr-Gly-OBu^t (XIV). Compound XIII (25.1 g, 44 mmol) was hydrogenated in methanol over 10% Pd/C as in the preparation of XIII. To a stirred mixture of the above *t*-butyl *O*-*t*-butyl-L-seryl-L-tyrosylglycinate, benzyloxycarbonyl-L-tryptophan (13.5 g, 40 mmol) and 2,2'-dipyridyl disulfide (8.80 g, 40 mmol) in 200 ml of DMF was added triphenylphosphine (10.5 g, 40 mmol) in 100 ml of CH_2Cl_2 with ice-cooling and the mixture was stirred at room temperature for 6 hr and kept standing overnight. The solvent was removed *in vacuo* and the residue was dissolved in 200 ml of ethyl acetate. The mixture was washed with 10% citric acid, water, 5% sodium bicarbonate and water and dried over sodium sulfate. The solvent was removed *in vacuo* after the addition of 100 g of silica gel. The coated residue was subjected to dry column chromatography and developed with ether. The coated layer was separated and the peptide was eluted with MeOH/$CHCl_3$ (1: 2 v/v). After the solvent was removed, the residue was dissolved in ethyl acetate, and washed with water. After being dried over sodium sulfate, the solution was condensed and the tetrapeptide was obtained by precipitation with the addition of petroleum ether: 23.5 g (78%); mp 138—140°; $[\alpha]_D^{20}$ −14.8° (*c* 1, DMF).

Found: C, 65.13; H, 6.89; N, 9.15%. Calcd for $C_{41}H_{51}O_9N_5$: C, 64.97; H, 6.78; N, 9.24%.

Z-His-Trp-Ser(Bu^t)-Tyr-Gly-OBu^t (XV). Compound XIV (16.65 g, 22 mmol) was hydrogenated over 10% Pd/C as in the preparation of XIII. To a stirred mixture of the above tetrapeptide, benzyloxycarbonyl-L-histidine (5.78 g, 20 mmol) and 2,2'-dipyridyl disulfide (4.40 g, 20 mmol) in 150 ml of DMF was added triphenylphosphine (5.24 g, 20 mmol) in 100 ml of CH_2Cl_2 with ice-cooling and the mixture stirred at room temperature for 8 hr. After being left to stand overnight, the solvent was evaporated *in vacuo* and the residue was dissolved in *n*-buthanol. The mixture was washed successively with 10% citric acid, water and 5% sodium bicarbonate and evaporated *in vacuo*. From the residue, pentapeptide was precipitated from methanol-ethyl acetate-ether and was further filtered with Sephadex LH-20 in DMF. It was crystallized from methanol-ethyl acetate-ether and dried *in vacuo* over P_2O_5: yield 13.90 g (78%); mp 172—175 °C; $[\alpha]_D^{20}$ −9.6° (*c* 1, DMF).

Found: C, 61.57; H, 6.58; N, 12.10%. Calcd for $C_{47}H_{58}O_{10}N_8 \cdot H_2O$: C, 61.83; H, 6.62; N, 12.27%. R_f 0.72 on silica gel G in *n*-BuOH: AcOH: H_2O (4: 1: 1) and R_f 0.74 on silica gel G in *n*-BuOH: AcOH: H_2O: Pyridine (30: 6: 24: 20). Amino acid ratios (3M *p*-toluenesulfonic acid hydrolysis): His, 1.01; Trp, 0.84; Ser, 0.98; Tyr, 0.97; Gly, 1.

H-His-Trp-Ser(Bu^t)-Tyr-Gly-OBu^t (Fragment XVI). Compound XV (679 ml, 0.66 mmol) was hydrogenated over Pd/C in methanol and the solvent was removed after filtration of the catalyst. The residue was dried *in vacuo* over P_2O_5 and was used as fragment XVI: R_f 0.47 on silica gel G in *n*-BuOH: AcOH: H_2O (4: 1: 1) and R_f 0.66 on silica gel G in *n*-BuOH: AcOH: H_2O: Pyridine (30: 6: 24: 20).

Z-Pro-Gly-NH$_2$ (XVII). To a stirred mixture of 50 mmol each of benzyloxycarbonyl-L-proline (12.50 g), ethyl glycinate 5.15 g and 2,2'-dipyridyl disulfide (11.00 g) in 150 ml of CH_2Cl_2 was added triphenylphosphine (13.10 g, 50 mmol) in 50 ml of CH_2Cl_2 with ice-cooling and the mixture was stirred at room temperature for 8 hr. After being left to stand overnight and worked up as in the preparation of XII, ethyl benzyloxycarbonyl-L-prolylglycinate was obtained as an oily substance. This product was dissolved in 1000 ml of abs. ethanol to which was added 500 ml of dry ammonia at −30 °C. After stirring was continued at room temperature for 58 hr, the solvent was removed and the dipeptide amide was obtained by crystallization from ethyl acetate: yield 13.80 g (89%); mp 120 °C; $[\alpha]_D^{20}$ −37.1° (*c* 1, MeOH).

Found: C, 58.88; H, 6.23; N, 13.92%. Calcd for $C_{15}H_{19}N_3O_4$: C, 59.02; H, 6.29; N, 13.77%.

Boc-Arg(NO$_2$)-Pro-Gly-NH$_2$ (XVIII). Compound XVII (10.10 g, 33 mmol) was hydrogenated as in the preparation of XIII. To a stirred mixture of L-prolylglycine amide, *t*-butyloxycarbonyl-N^G-nitro-L-arginine (9.60 g, 30 mmol) in 150 ml of DMF was added triphenylphosphine (7.86 g, 30 mmol) in 50 ml of DMF with ice-cooling and the mixture stirred at room temperature for 8 hr. After being left to stand overnight, the solvent was removed and dry column chromatography was developed with ethyl acetate. The coated layer was separated and the tripeptide was eluted with MeOH/$CHCl_3$ (1: 2). The solvent was removed and crystallization of the residue from ethyl acetate gave tripeptide: 11.00 g (78%); mp 157 °C; $[\alpha]_D^{20}$ −33.8° (*c* 1, MeOH).

Found: C, 45.62; H, 6.73; N, 23.45%. Calcd for $C_{18}H_{32}O_7N_8$: C, 45.66; H, 6.78; N, 23.68%.

Boc-Leu-Arg(NO$_2$)-Pro-Gly-NH$_2$ (XIX). Compound XVIII (10.40 g, 22 mmol) was dissolved in 30 ml each of trifluoroacetic acid and CH_2Cl_2 and stirred at room temperature for 1 hr. To the evaporated residue was added 500 ml of ether and the precipitate was filtered. it was dried over potassium hydroxide *in vacuo*. To a stirred mixture of the above trifluoroacetic acid salt of tripeptide, triethylamine (2.50 g, 25 mmol), 2,2'-dipyridyl disulfide (8.80 g, 40 mmol) and *t*-butyloxycarbonyl-L-leucine monohydrate (5.00 g, 20 mmol) in 100 ml of DMF was added triphenylphosphine (10.48 g, 40 mmol) in 50 ml of DMF. The mixture was stirred at room temperature for 6 hr and left to stand overnight. After evaporation of the solvent, the residue was dissolved in *n*-buthanol and washed successively with 10% citric acid, water, 5% sodium bicarbonate and water. The solvent was removed and the residue was subjected to dry column chromatography developed with ethyl acetate. From the coated layer the peptide was eluted with MeOH/$CHCl_3$ (1: 3) and crystallization from methanol-ethyl acetate-petroleum ether, after evaporation of the solvent, gave the tetrapeptide amide: 11.00 g (94%); mp 168—171 °C (decomp.); $[\alpha]_D^{20}$ −43.2° (*c* 2, DMF).

Found: C, 48.82; H, 7.42; N, 21.18%. Calcd for $C_{24}H_{43}O_8N_9$: C, 49.15; H, 7.34; N, 21.50%. R_f 0.56 on silica gel G in *n*-BuOH: AcOH: H_2O (4: 1: 1) and R_f 0.70 on silica gel G in *n*-BuOH: AcOH: H_2O: Pyridine (30: 6: 24: 20). Amino acid ratios: Leu, 1; Arg, 0.96[19]; Pro, 0.99; Gly, 1.03; NH_3, 1.39.

H-Leu-Arg(NO$_2$)-Pro-Gly-NH$_2$ (Fragment XX). Compound XIX (387 mg, 0.66 mmol) was dissolved in 20 ml of trifluoroacetic acid with ice-cooling and stirred at room temperature for 1 hr. Ether was added and the precipitate was collected by filtration. The precipitate was dissolved in methanol and neutralized with IRA-400 in methanol. The evaporated residue was dried over KOH *in vacuo* and used as

fragment XX: R_f 0.23 on silica gel G in *n*-BuOH: AcOH:H_2O (4: 1: 1) and R_f 0.61 on silica gel G in *n*-BuOH: AcOH: H_2O: Pyridine (30: 6: 24: 20).

Resin–Glu(NH_2)–His–Trp–Ser–Tyr–Gly–Leu–Arg(NO_2)–Pro–Gly–NH_2 (XXI). Two grams of resin–L-glutamine *t*-butyl ester (XI, 0.11 mmol/g) was added to the vessel for solid phase peptide synthesis and chain elongation was carried out according to the procedure for the preparation of VIII. The first coupling of the initial resin–glutamine with H–His–Trp–Ser(Bu^t)–Tyr–Gly–OBu^t (fragment XVI) was carried out by adding 3 eq (0.66 mmol) of triphenylphosphine in 5 ml of CH_2Cl_2 to a mixture of the resin and 3 eq (0.66 mmol) each of fragment XVI and 2,2′-dipyridyl disulfide in 10 ml of DMF. The mixture was shaken at room temperature for 10 hr followed by shaking for 24 hr after the further addition of 3 eq (0.66 mmol) each of triphenylphosphine and 2,2′-dipyridyl disulfide. A portion of the resulting resin was hydrolyzed in 3 M *p*-toluenesulfonic acid and the amino acid analysis gave the following ratios: Glu, 1.09; His, 0.98; Trp, 0.84; Ser, 0.96; Tyr, 0.95; Gly, 1; NH_3, 1.42. The recovered fragment XVI in the washing solvent of DMF and CH_2Cl_2 showed the same spot on tlc as the starting fragment XVI detected with ninhydrin, Pauly and Ehrlich reaction. Fragment XVI was isolated by gel filtration on Sephadex LH-20 in DMF: 160 mg (0.35 mmol). The second coupling of the resulting resin–hexapeptide with 3 eq (0.66 mmol) of H–Leu–Arg(NO_2)–Pro–Gly–NH_2 (fragment XX) was carried out by the same procedure as described in the first coupling except that the deprotection of *t*-butyl group (steps (2) and (3) in the preparation of VIII) was carried out with trifluoroacetic acid/CH_2Cl_2 (1: 1 v/v) containing 5% of 2-mercaptopyridine. The amino acid analysis (3 M *p*-toluenesulfonic acid) of an aliquot of the resin–decapeptide gave the following results: Glu, 1.10; His, 1.01; Trp, 0.80; Ser, 0.95; Tyr, 1.03; Gly, 2.05; Leu, 1; Arg, 0.95;[19] Pro, 0.94; NH_3, 2.87. The recovered fragment XX in the washing solvent was also identical on tlc with the starting material. It was established by the following experiment that the recovered fragments were used successfully in the next coupling. The coupling of 1g of a new resin–glutamine *t*-butyl ester (XI, 0.11 mmol/g) with the recovered fragment XVI (0.35 mmol) isolated as above and the recovered fragment XX in washing solvent after the evaporation of solvent gave similar results. The amino acid analysis gave: Glu, 1.07; His, 0.97; Trp, 0.80; Ser, 0.99; Tyr, 0.96; Gly, 2.06; Leu, 1; Arg, 0.94;[19] Pro, 0.98; NH_3, 2.93.

⟨Glu–His–Trp–Ser–Tyr–Gly–Leu–Arg–Pro–Gly–NH_2 (LH–RH, X). The resin–decapeptide (XXI) 2 g was treated with 30 ml of dry HF[13] for 30 ml at room temperature in the presence of 1 ml of anisole and 300 mg of 2-mercaptopyridine. After the removal of HF and anisole *in vacuo*, 150 ml of DMF was added and the resin was filtered off. The solution was condensed and the peptide was precipitated by adding ethyl acetate and ether. The glutaminyl residue of this decapeptide was cyclized[20] in 40 ml of acetic acid containing 200 mg of 2-mercaptopyridine and 20 ml of anisole at 80—100 °C for 30 min. After evaporation of solvent, the peptide was precipitated from methanol–ether. The peptide was dissolved in 200 ml of water and passed through a Dowex 1×2 (OAc) column to be converted into acetate form. The peptide was also purified on CM-Sephadex as in the preparation of X by A type elongation after the separation of 2-mercaptopyridine by gel filtration on Sephadex G-25; the main peak in 0.15 M $AcONH_4$ was proceeded by a small peak in 0.1 M $AcONH_4$. The fraction containing a single component was pooled and the pure decapeptide amide was obtained after desalting, precipitation and drying *in vacuo* over P_2O_5 at 40°: yield 133 mg (51% based on the glutamine attached to the resin); $[\alpha]_D^{20}$ −53.1° (*c* 1, 1% AcOH). Amino acid analysis (3 M *p*-toluenesulfonic acid hydrolysate: Glu, 1.02; His, 0.99; Trp, 0.81; Ser, 0.96; Tyr, 0.97; Gly, 2.02; Leu, 1; Arg, 0.96; Pro, 0.97; NH_3, 1.32 and amino acid content was calculated to be 78% from the recovery value of leucine. The peptide was homogeneous on various tlc described in the preparation of X by detection with Pauly, Ehrlich, Sakaguchi and Cl-tolidine reagents, the R_f values being identical with those of natural LH–RH and the synthetic LH–RH by A type elongation. The peptide was also characterized as diacetate and trihydrate after further drying *in vacuo* at 80°C over P_2O_5.

Found: C, 52.26; H, 6.64; N, 17.14%. Calcd for $C_{55}H_{75}N_{17}O_{13}\cdot 2CH_3COOH\cdot 3H_2O$: C, 52.24; H, 6.61; N, 17.56%.

Bioassay. LH–RH activities of the decapeptides were compared at 2 dose levels with that of natural LH–RH (AVS 77-33 #215-269, amino acid content 67.5%) in ovariectomized, estrogen-progesterone treated rats. Serum LH levels 15 min after the jugular vein injection of 0.5 and 2.5 ng LH–RH in six rats in each dose level were estimated by radioimmunoassay according to Niswender *et al.*[16] and expressed in terms of NIH-LH-S17. The dose response regression lines for natural and synthetic two decapeptides were parallel. Using four point factorial assay,[18] the LH–RH activities of synthetic LH–RH were calculated as follows: synthetic LH–RH of A type elongation (amino acid content 76%), 121% of the potency of natural LH–RH with 95% fiducial limits of 87—182%; synthetic LH–RH of B type elongation (amino acid content 78%), 125% of the potency of natural LH–RH with 95% fiducial limits of 91—173%. The values were in good agreement with the ratios of the amino acid contents of synthetic LH–RH to that of the natural one.

Appreciation is due to Drs. Y. Baba and K. Kitamura for participating in the biological assay and to Mr. T. Wada for statistical treatment. We would like to thank Drs. A. V. Schally and A. Arimura, Tulane University, for providing us with the natural LH–RH.

Studies of Reaction Mechanisms by All-valence Electron Semi-Empirical SCF MO Theories. VIII.[1] Electronic Structure and Valence Isomerization of *syn*- and *anti*-Tricyclo[4.2.0.0^{2,5}]octa-3,7-dienes

Hiizu IWAMURA, Hiroshi KIHARA, Kazuhiko MORIO, and Tosiyasu L. KUNII*

*Department of Chemistry, Faculty of Science, *Information Science Laboratory, Faculty of Science, and The Computer Centre, The University of Tokyo, Hongo, Bunkyo-ku, Tokyo 113*

(Received April 5, 1973)

The theoretical structures and heats of formation of *syn*- and *anti*-tricyclo[4.2.0.0^{2,5}]octa-3,7-dienes (**1** and **2**) have been investigated by the MINDO methods. An examination of their MO's reveals that there is an extensive mixing between the highlying σ-orbitals of the four-membered rings and the ethylenic π-orbitals, which makes the highest occupied MO's devoid of any ethylenic π-character. A degenerate valence isomerization (Eq. (7)) rather than the [2+2] cycloaddition is suggested as an excited-state reaction. An intermediately facile ($\Delta H^{\ddagger}$=23.1 kcal/mol) degenerate Cope rearrangement (Eq. (1)) is predicted for **1** under thermal conditions. The transition-state structure (**1′**) and the partitioned activation energy values obtained by the MINDO/2 methods are compared with those for the Cope rearrangement of semibullvalene (**3**) and 1,5-hexadiene. The deviation from planarity of the allyl groups in **1′** is the reason for the activation energy calculated for **1** being higher than that for **3**. The hypothetical paths from **1** to cubane in the electronic ground state are characteristic of the reaction with an anti-aromatic transition state.

Although the development of the chemistry of *syn*- and *anti*-tricyclo[4.2.0.0^{2,5}]octa-3,7-dienes (**1** and **2**) has been rather tardy since their first preparation as cyclobutadiene dimers by Nenitzescu and his co-workers in 1964,[2] their electronic structures are of great theoretical interest in that extensive through-space and/or through-bond interaction[3] between π- and high-lying σ-orbitals is expected. We will present here some possible chemical consequences of the orbital overlap as revealed by an examination of their molecular orbitals obtained by the MINDO approximations which are reputed to reproduce the ground-state properties of hydrocarbons reasonably well.[4] Two kinds of the valence isomerization of the *syn*-isomer **1**, one involving a degenerate Cope rearrangement and the other leading to cubane (Chart 1), are considered.

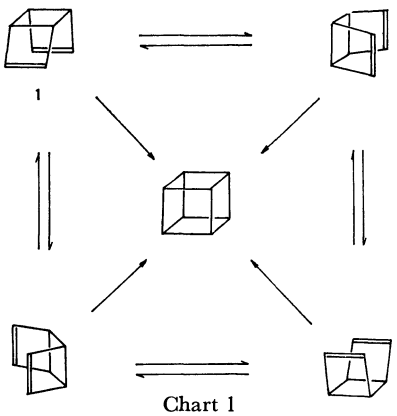

Chart 1

Method of Calculations

Since no structural data are available for **1** and **2**, their equilibrium geometries are sought by minimizing the total energies with respect to the changes in all the independent bond lengths and angles in the molecules. The geometry of the transition state **1′** for the Cope rearrangement was assumed *a priori* to have the C_{2v} symmetry, with the axis passing through the centers of the C_1–C_2 and C_4–C_7 bonds when the C_5–C_6 and C_3–C_8 bonds participate in the rearrangement (Eq. (1)); it was optimized much as in ground-state geometry.

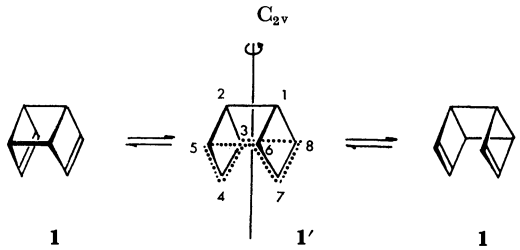

(1)

In order to help verbalize the results of the molecular orbital studies, the partitioning of the total energy into one-center and two-center terms was carried out as presented by Gordon[5] and by Fischer and Kollmar[6] for the CNDO methods. In the framework of the MINDO/2 methods, both terms are defined by standard integrals as follows, with the second term consisting of the resonance (E_{AB}^{R}), exchange (E_{AB}^{X}), and electrostatic (E_{AB}^{S}) terms, respectively:

$$E_{\text{total}} = \sum_{A} E_A + \sum_{A<B}\sum E_{AB} \tag{2}$$

$$E_A = \sum_{\mu(A)} P_{\mu\mu}U_{\mu\mu} + \frac{1}{2}\sum_{\mu(A)} P_{\mu\mu}^2\langle\mu\mu|\nu\nu\rangle + \sum_{\mu\neq\nu}^{A}\sum^{A}\left\{P_{\mu\mu}P_{\nu\nu}\left[\langle\mu\mu|\nu\nu\rangle - \frac{1}{2}\langle\mu\nu|\mu\nu\rangle\right] + P_{\mu\nu}^2\left[\frac{3}{2}\langle\mu\nu|\mu\nu\rangle - \frac{1}{2}\langle\mu\mu|\nu\nu\rangle\right]\right\} \tag{3}$$

1) Part VII: H. Iwamura, K. Morio, and H. Kihara, *Chem. Lett.*, **1973**, 457.

2) M. Avram, I. G. Dinulescu, E. Marica, G. Mateescu, E. Sliam, and C. D. Nenitzescu, *Chem. Ber.*, **97**, 382 (1964).

3) R. Hoffmann, *Accounts Chem. Res.*, **4**, 1 (1971).

4) a) N. C. Baird and M. J. S. Dewar, *J. Chem. Phys.*, **50**, 1262 (1969); N. C. Baird, M. J. S. Dewar, and R. Sustman, *ibid.*, **50**, 1275 (1969); b) M. J. S. Dewar and E. Haselbach, *J. Amer. Chem. Soc.*, **92**, 590 (1970); N. Bodor, M. J. S. Dewar, A. Harget, and E. Haselbach, *ibid.*, **92**, 3854 (1970).

5) M. S. Gordon, *ibid.*, **91**, 3122 (1969).

6) H. Fischer and H. Kollmar, *Theor. Chim. Acta*, **16**, 163 (1970).

$$E_{AB} = E_{AB}^{R} + E_{AB}^{X} + E_{AB}^{S} \quad (4)$$
$$E_{AB}^{R} = 2\sum_{\mu(A)}\sum_{\nu(B)} P_{\mu\nu}\beta_{AB}(I_\mu + I_\nu)S_{\mu\nu}$$
$$E_{AB}^{X} = -\frac{1}{2}\gamma_{AB}\sum_{\mu(A)}\sum_{\nu(B)} P_{\mu\nu}^2$$
$$E_{AB}^{S} = P_A P_B \gamma_{AB} + (-P_A Z_B - P_B Z_A)\gamma_{AB} + Z_A Z_B[\gamma_{AB} + (1/R - \gamma_{AB}) \exp(-\alpha_{AB} R_{AB})]$$

In short, the total energy of molecules is considered to be determined by the nature of the constituent atoms and the chemical bonding energy, E_{AB} corresponding to the strength of the A–B bond. By taking a partial summation, the one-center energy is further divided into one due to hydrogen and another due to carbon atoms:

$$\sum_A E_A = \sum E_A^{H} + \sum E_A^{C} \quad (5)$$

The two-center terms are further subdivided to neighboring (E_{AB}^{N}) and non-neighboring (E_{AB}^{NN}) terms, where the A and B atoms in E_{AB}^{N} are, by definition, a pair connected by the chemical bond, while the pair of A and B in E_{AB}^{NN} are not directly bonded in a molecule.

The calculations were performed on a HITAC 5020E computer, with the use of a modified MINDO program originally written by Baird and distributed by the QCPE organization.[7]

Results and Discussion

(A) Results on Ground-state Geometry and Energy. The equilibrium geometries, neighboring two-center energies, and bond indices of Wiberg, as defined as Eq. (6),[8] are summarized for **1** and **2** in Table 1.

$$W_{AB} = \sum_{\mu}^{A}\sum_{\nu}^{B} P_{\mu\nu}^2 \quad (6)$$

The calculated bond lengths and angles are generally in good agreement with those observed for many cyclobutane and cyclobutene derivatives,[9] especially when the slight underestimation of the sp^2 to sp^3 single-bond length is taken as a natural consequence of one of the disadvantages of the MINDO/2 approximations.

The heats of formation and the ionization potentials obtained by the use of Koopmans' theorem are listed in Table 2. The MINDO/1 energy values are for the geometries of **1** and **2**, which are obtained by replacing the optimized bond lengths by the MINDO/2 with the standard bond lengths tabulated in Ref. 4(a). It is generally accepted that the strain energy of cyclobutane and cyclobutene rings is underestimated by the MINDO/2 by as much as 25 kcal/mol.[4] The values of the heat of formation calculated for **1** and **2** by this method are lower than those of the MINDO/1 by *ca.* 75 kcal/mol. The value when divided by three, the number of the four-membered rings present in **1** and **2**, gives 25 kcal/mol, in good agreement with the amount of the underestimation of the strain energy per four-membered ring. Thus, the MINDO/1 values are considered to represent more realistic theoretical values for the heat of formation. The value of 108 kcal/mol is obtained for **1** and **2** by Franklin's group-equivalent method for the heat of formation.[10]

The ionization potentials calculated by the MINDO/2 are in good agreement with the experimental ones.[11] The larger value found for **2** is well reproduced by the calculation; the origin of the difference in **1** and **2** will be discussed in Section (B).

We note that the **1** isomer is always predicted to be slightly less stable than the **2** isomer irrespective of the approximation of the MO methods employed. The **1**

Table 1. Ground state geometries, two-center energy terms, and Wiberg's bond indices of tricyclo[4.2.0.0^{2,5}]octa-3,7-dienes **1** and **2**

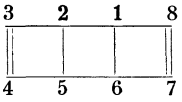

		C_1C_2	C_2C_3	C_3C_4	C_1C_6	C_3C_8	Cyclobutane-cyclobutene dihedral angle
	Bond length (Å)	1.50	1.48	1.33	1.55	2.93	
1	E_{AB}^{N} (eV)	−13.577	−14.435	−22.748	−12.468	0.060	119°
	Wiberg's bond index	0.934	0.979	1.903	0.965	0.0024	
	Bond length (Å)	1.505	1.48	1.33	1.55	3.85	
2	E_{AB}^{N} (eV)	−13.731	−14.467	−22.738	−12.432	−0.034	116°
	Wiberg's bond index	0.945	0.977	1.903	0.959	0.0084	

Table 2. Dissected total energies, heats of formation and ionziation potentials of tricyclo[4.2.0.0^{2,5}]octa-3,7-dienes **1** and **2**

	E(eV)		ΔH_f (kcal/mol)		Ionization potential (eV)		
	$\sum E_A$	$\sum\sum E_{AB}$	MINDO/1	MINDO/2	MINDO/1	MINDO/2	Observed[11]
1	−906.064	−245.275	120.8	46.3	9.38	8.86	8.20
2	−906.064	−245.424	120.2	42.9	9.25	9.07	8.27

7) Quantum Chemistry Program Exchange No. 137, Chemistry Department, Indiana University, Bloomington, Indiana 47401.

8) K. B. Wiberg, *Tetrahedron*, **24**, 1083 (1968).

9) S. L. Hsu, A. H. Andrist, T. D. Gierke, R. C. Benson, W. H. Flygare, and J. E. Baldwin, *J. Amer. Chem. Soc.*, **92**, 5250 (1970), and the papers cited therein.

10) J. L. Franklin, *Ind. Eng. Chem.*, **41**, 1070 (1949).

11) J. L. Franklin and S. R. Carroll, *J. Amer. Chem. Soc.*, **91**, 5940 (1969).

Table 3. Non-neighboring two center energies E_{AB}^{NN} (eV) for **1** and **2**

	AB	E_{AB}^{R}	E_{AB}^{X}	E_{AB}^{S}	E_{AB}^{NN}
1	C_3C_8	0.024	−0.006	0.042	0.060
	C_3H_9	−0.033	−0.010	0.009	−0.034
	H_9H_{10}	0.001	−0.000	0.074	0.074
2	C_3C_8	−0.023	−0.015	0.004	−0.034
	C_3H_9	0.025	−0.003	0.047	0.070
	H_9H_{10}	−0.054	−0.007	0.032	−0.030

isomer is calculated by the CNDO/2 method as well to be less stable by 2.4 kcal/mol. It is intuitively expected that the repulsive interaction between the 2pπ orbitals of the two facing ethylene groups in **1** might contribute to the destabilization, since the distance between the ethylene groups is only 2.93 Å. The energy partitioning study supports this expectation. The non-neighboring two-center energy value for C_3 and C_8 (=C_4 and C_7) is *ca.* 1.5 kcal/mol; the positive sign indicates destabilization, and the mechanism is found to be mostly electrostatic (see Table 3).[12] The slight widening of the angles between the cyclobutane and cyclobutene ring planes calculated for **1** compared to **2** could be due to this repulsive interaction. A further inspection of the dissected energy values reveals that, although the eclipsed hydrogen atoms, H_9 and H_{10}, in **1** also have non-neighboring repulsion, the effect is counterbalanced by the analogous interaction between pairs of eclipsed hydrogen and carbon atoms on the cyclobutane ring in **2**. The bonding interaction between the far-apart C_3 and C_8 (and C_4 and C_7 as well), together with the strengthening of the C_1–C_2 bond (and C_5–C_6) in **2**, as is shown in Table 2, suggest the role of a through-bond resonance interaction, *i.e.*, π-σ-π conjugation, between the two ethylenic moieties as another factor favoring **2** energetically.

(B) Molecular Orbital Construction. Turning now to the construction of the higher occupied molecular orbitals of **1** and **2**, we may note that the π-orbital approximations are a far from satisfactory description. The highest occcupied molecular orbitals are, first of all, not π-charactered, but are composed of σ-orbitals. The mixing of the ethylenic π-orbitals with σ-orbitals is extensive as a result of the presence of the high-lying σ-orbitals of cyclobutane and cyclobutene rings.[13] The unique topology of the carbon atoms in **1** and **2** also provides the necessary symmetry for the interaction. Ideally, three types of interaction, a, b, and c, are possible between the 2p-orbitals, as is shown in Chart 2. In connection with the relative stability of **1** and **2** discussed in the previous section, the a type interaction

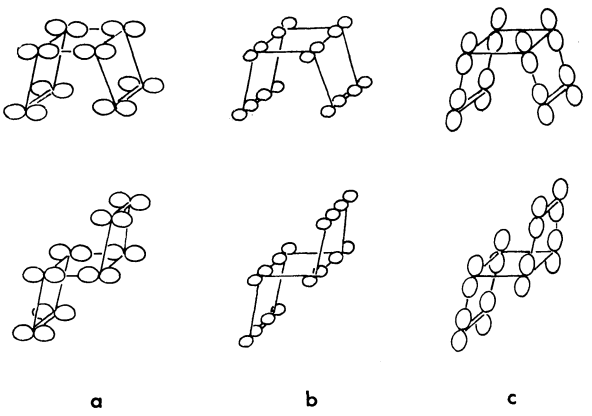

Chart 2

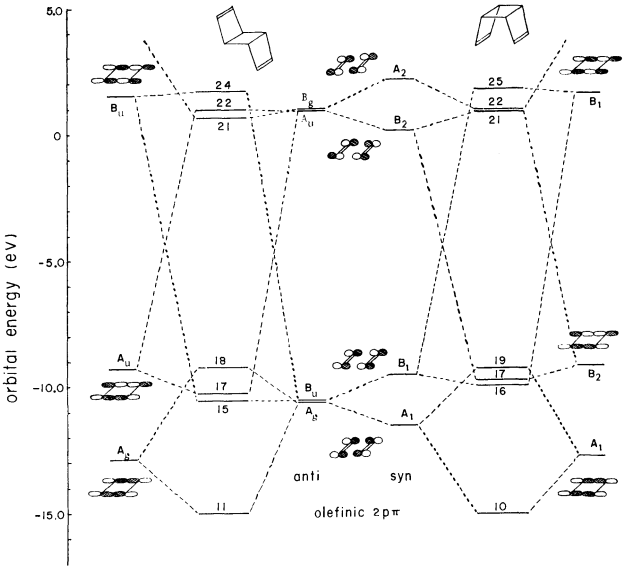

Fig. 1a. Type a interaction diagram for the mixing of two olefinic 2pπ orbitals and the σ orbitals of a cyclobutane ring. Symmetry classification uses the σ and i operations for **1** and **2**, respectively.

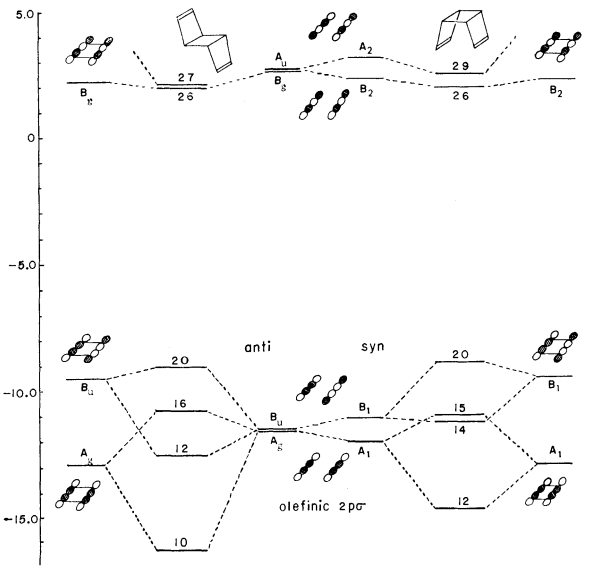

Fig. 1b. Type b interaction diagram for the mixing of two olefinic 2pπ orbitals and the σ orbitals of a cyclobutane ring. The directions of the atomic orbitals are idealized.

12) The sum of the Hückel molecular orbital energy values should not change theoretically by the interaction of the two facing ethylene groups, because the amount of the stabilization of the in-phase combination of the ethylenic π-orbitals and the destabilization of the out-of-phase combination cancel each other out. The terms other than electrostatic are, therefore, expected not to differ much between **1** and **2**.

13) L. Salem and J. S. Wright, *J. Amer. Chem. Soc.*, **91**, 5947 (1969); R. Hoffmann and R. B. Davidson, *ibid.*, **93**, 5699 (1971); J. S. Wright and L. Salem, *ibid.*, **94**, 322 (1972); P. Bischof, E. Haselbach, and E. Heilbronner, *Angew. Chem.*, **82**, 952 (1970).

is of prime importance in that many of the calculated higher occupied molecular orbitals are interpreted in terms of this type of interaction. The calculated coefficients of the atomic orbitals in the 10th, 16th, 17th, and 19th molecular orbitals of **1**, for example, are described by interaction diagram of Fig. 1a. To this is added the b type interaction, which results in the production of the highest occupied 20th molecular orbital of a σ-character. It is interesting to note that the lower ionization potential calculated for **1** compared to **2**, *i.e.*, the energy value of the highest occupied molecular orbital of **1** relative to **2** higher by 0.21 eV, is due to a larger splitting by this interaction in **1**, probably because of the through-space destabilization of the ethylenic σ-bonds. The failure to obtain cubane by the irradiation of **1** under direct and sensitized conditions[14] is possibly related to the fact that the highest occupied molecular orbital is not connected with the ethylenic π-orbitals. To make matters worse, the C_1–C_6 and C_2–C_5 bonds of the cyclobutane ring are now *anti*-bonding in the unoccupied molecular orbitals, *e.g.*, 21st and 26th, where the transannular π-orbital interaction between C_3 and C_8, and between C_4 and C_7, is effectively bonding. Thus, the cleavage of the ring would concomitantly result and a degenerate valence isomerization as depicted by Eq. (7) can be predicted as a possibility of an excited-state reaction.[1]

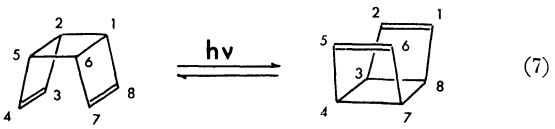

(7)

(C) Results on the Transition State for the Cope Rearrangement. Figure 2 shows the optimized geometry and (in parentheses) the Wiberg bond indices for the transition-state structure **1′**. The four-membered rings are folded so as to make a dihedral angle between the $C_2C_3C_5$ and $C_3C_4C_5$ planes of 25.8°. Notice also that each allyl group is not planar, but that the end carbon atoms, C_3, C_5, C_6, and C_8 are pyramidal, with the hydrogen atoms attached to them deviating outwards from the trigonal planes, *e.g.*, the $C_2C_3C_4$ plane, by 32.0°. The geometry is considered to be attained by an attempt to relieve the non-bonded interaction between the facing hydrogens on both sides of the allyl moieties on the one hand and to increase the overlap between the two allyl groups at their ends. In contrast, the hydrogen atoms attached to C_4 and C_7 are displaced by 14.5° from the $C_3C_4C_5$ and $C_6C_7C_8$ planes, respectively, in the direction of their approach. The deformation is favored by the smaller overlap between C_4 and C_7. When the overlap is appreciable, the intermediate will be somewhat like the geometry on the reaction coordinate leading to cubane and should be energetically unfavorable, as will be seen in Section (E). The distance between the two allyl groups in **1′** is 1.71 Å at the end carbons and 2.70 Å at the center. These values are quite similar to the corresponding values (1.75 and 2.81 Å respectively)[15] in the transition-state structure for the Cope rearrangement of semibullvalene **3**. In other words, the delocalization of electrons over the six carbon atoms (C_3 through C_8) in **1′** is expected to be as extensive as in the transition state of **3**. The heat of formation of **1′** obtained by the MINDO/2 method is 69.5 kcal/mol.

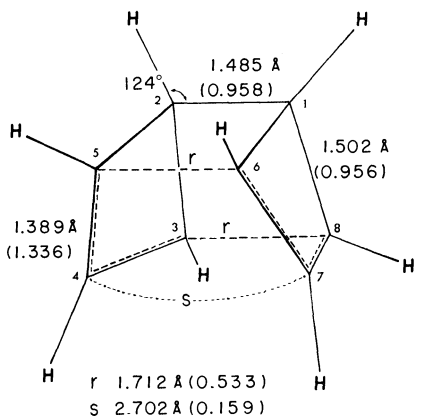

Fig. 2. The optimized bond lengths and the Wiberg's bond indices (in parentheses) for **1′**.

(D) On the Activation Energy for the Cope Rearrangement. The activation energy for the Cope rearrangement of **1** *via* **1′** is calculated as 23.1 kcal/mol on the basis of the difference between the MINDO/2 heats of formation for the ground state, **1**, and the transition state, **1′**.[16] Although the Cope rearrangement in **1** can be expected, from the similarity of the transition-state structure, to be as facile as in the case of **3** (see Section (C)), the value indicates that the reaction is not as easy as in bridged homotropilidenes, in which the activation energy is no more than 12 kcal/mol.[15] The reported thermal isomerizations of 1,3,4,6-tetrabromo-2,5,7,8-tetramethyltricyclo[4.2.0.$0^{2,5}$]octa-3,7-diene to the 1,4,5,8-tetrabromo-2,3,6,7-tetramethyl isomer (Eq. (8)) and of the hexachloro-derivative (Eq. (9)) support the result of the theoretical calculations.

14) R. Criegee, *ibid.*, **74**, 703 (1962); H. Iwamura, to be published elesewhere.

15) A. Brown, M. J. S. Dewar, and W. W. Schoeller, *J. Amer. Chem. Soc.*, **92**, 5516 (1970); M. J. S. Dewar and D. H. Lo, *ibid.*, **93**, 7201 (1971); H. Iwamura, K. Morio, and T. L. Kunii, This Bulletin, **45**, 841 (1972).

16) A more reasonable energy value which includes the correct strain energy in **1′** may be obtained by the MINDO/1 calculation. There is, however, a fatal ambiguity in the latter method as regards the choice of the correct standard bond lengths for the allyl groups in **1′**. There are no *a priori* standard bond lengths tabulated for the bonds of an intermediate bond order or hybridization, and yet the calculated energy values are rather sensitive to these bond lengths. Although there is certainly strain energy in **1′** due to the presence of two four-membered rings, and although the release of the strain energy of one cyclobutane ring can be expected on going from **1** to **1′**, the effect is considered to be partly counterbalanced by the formation of two less strained cyclobutane-like rings approaching bicyclo[2.2.0]hexane in **1′**. Thus, as long as the difference in heats of formation is concerned, the MINDO/2 value is taken to represent a more reliable estimate of the activation energy for the degenerate Cope rearrangement of Eq. 1. Since the strain energy in **1** is still underestimated relative to that in **1′**, the activation energy obtained as heats of formation of the latter minus that of the former is likely to be overestimated. The value of 23.1 kcal/mol, may, therefore, be proposed as the upper limit of the activation energy.

Table 4. One-center and two-center terms in the activation energies for the Cope rearrangements of **1**, **3** and **4**

	ΔE_A(eV)		ΔE_{AB}(eV)		ΔE_{AB}(eV) and (in parentheses) bond length (Å) in the transition state for bonds						
	H	C	N	NN	a	b	c	d	e	f	g
1	−0.010	−1.051	1.967	0.097	5.968 (1.712)	−3.527 (1.389)	4.786	−7.669	−0.025 (2.702)	−0.934	1.033
3	0.126	−0.102	−1.771	1.904	4.626 (1.752)	−2.604 (1.404)	2.841	−3.712	−0.076 (2.806)	−0.358	0.308
4	−0.104	−2.033	3.534	−0.127	4.549 (1.630)	−2.479 (1.428)	6.145	−10.013	−0.170 (2.630)	—	—

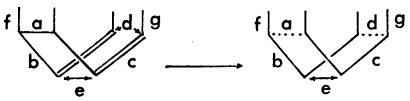

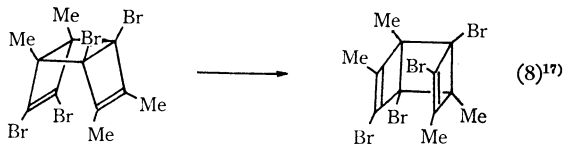

(8)[17]

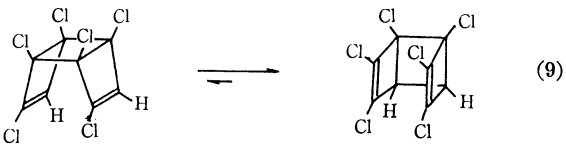

(9)

Table 4 shows the total contributions to the activation energy of the one-center term (ΔE_A) for the carbon and hydrogen atoms, and of the two-center terms (ΔE_{AB}) for the neighboring (N) and non-neighboring (NN) pairs of the AB atom. These values are compared with those of the Cope rearrangements of 1,5-hexadiene **4** *via* the boat-type transition state and of semibullvalene **3**. These examples represent two extreme cases with respect to the facility of the reaction; the activation energies are *ca.* 40 kcal/mol[18] for the former and less than a few kcal/mol for the latter.[19]

The one-center terms, ΔE_A, for **1** to **1'** are characterized by an intermediately large negative value for carbon atoms. The effect is pronounced for the carbon atoms, $C_5(C_6)$ (−0.343 eV) and $C_4(C_7)$ (−0.354), in the allyl groups. The negative values of ΔE_A^C are parallel with the change (Δq_A) in the electron population of carbon atoms in passing from the reactant to the transition state; the Δq_A's are 0.008, 0.019, and −0.034 for $C_5(C_6)$, $C_4(C_7)$, and $C_3(C_8)$ respectively. The correlation can be understood quite easily by taking into account the change in the electronegativity of the carbon atoms which undergo rehybridization. On passing to the transition state, the s character of the orbitals directed from carbon atoms C_5 and C_6 to the adjoining atoms is increased, while it is decreased at C_3 and C_8. The decrease in the electronegativity of the latter carbons should tend to force the electrons on these atoms on to the neighboring C_4 and C_7. The increase in the electron population leads to the increase in the total one-center core attraction energy, ΔE_A^U. In the ground state of **3**, two allyl carbon atoms are members of a cyclopropane ring rich in p character. The change in the hybridization of these atoms on going from the ground to the transition state is, consequently, small. At the other end of the allyl moiety, the shortening of the distance, d, on passing to the transition state is smallest; the decrease in the s character of the hybridized orbitals on these carbon atoms is also small. These effects are found in the least change in ΔE_A^C value for the rearrangement of **3**. Thus, as far as the one-center terms are concerned, the ease of rearrangement is predicted to be in the order **4**>**1**>**3**, which is just the opposite of that determined by the total contributions to the activation energy.

It will, therefore, be seen that the greater facility of reaction in **3** compared with that of **1** and, more especially, with that of **4** is due to a large decrease in the ΔE_{AB}^N terms. There are three factors which are conceivable as the origin of the large negative ΔE_{AB}^N value in **3**: i) the strength of the interaction linking two allyl groups, ii) the strength of the bonds in each allyl moiety, and iii) the relief of the ring strain. The first factor is expressed by the ΔE_{AB}^N value due to the a+d interaction at the two ends of the allyl groups; it amounts to +0.914, −1.701, and −5.450 for the rearrangement of **3**, **1**, and **4**, respectively. The stabilizing order is in harmony with the decreasing atomic distances linking the two ends of the allyl moieties in the transition state, but is, again, opposite to the net order of the relative stability of the transition state. Secondly, the ΔE_{AB}^N between the atoms pertaining to the b and c bonds within the allyl group in **1'** and **1** (+1.258 eV) is much more than that in **3** (−1.763) and much less than that in **4** (+3.666). The destabilizing effect in the rearrangement of **4** can be interpreted in terms of the relatively long b (c) distance in the transition state. The corresponding b(c) distances in the transition state of **1** and **3** are, however, nearly the same at *ca.* 1.39 Å, which is the average C–C bond length of the order of 1.5; they are typified by those of benzene. A simple atomic distance *vs.* ΔE_{AB}^N argument does not hold in this case. As has been pointed out in Section (C), the allyl groups in **1'** are not planar any longer. A more careful examination of the **1'** structure reveals that

17) R. Criegee and R. Huber, *Chem. Ber.*, **103**, 1855 (1970).
18) W. von E. Doering and W. R. Roth, *Tetrahedron*, **18**, 67 (1962).
19) H. E. Zimmerman, R. W. Binkley, R. S. Givens, G. L. Grunewald, and M. A. Sherwin, *J. Amer. Chem. Soc.*, **91**, 3316 (1969).

the formally unpaired fourth valences of C_3 (C_5, C_6, and C_8 also) are not 2p orbitals but are $sp^{4.4}$ hybridized.[20] Moreover, they are directed to the opposite side of the $C_3C_4C_5$ ($C_6C_7C_8$) plane, inwards at the C_3 (C_5, C_6, and C_3) end and outwards at the C_4 and C_7 centers. The π-type overlap between the adjacent carbon atoms is necessarily inefficient, and the destabilization of **1'** relative to the transition state of **3** results in spite of a similar bond length b(c) (see Fig. 3).

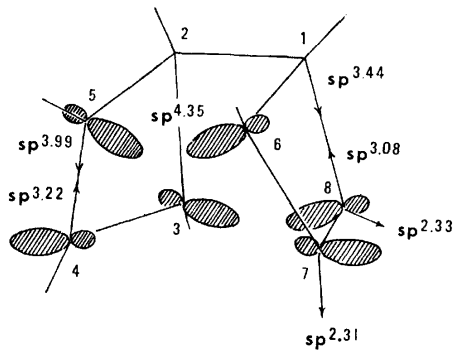

Fig. 3. Hybridization of the carbon atomic orbitals in **1'**.

Although it is not simple to define the strain energy by the E_{AB} of a specific bond, the E_{AB}^{N} (a, b, c) values in the ground state can be taken, in a sense, as a good measure of the intrinsic strain energy of these bonds, while ΔE_{AB}^{N} (f+g) may reflect the relief of the ring strain. We may note that the a bond in the cyclopropane ring of **3** is clearly weak when compared with those of **1** and **4**. The ΔE_{AB}^{N} due to bonds f and g is +0.099 and −0.050 for **1** and **3** respectively, and the stabilization of the transition state relative to the ground state is indicated. Thus, the relief of the ring strain seems to be another factor in the ease of rearrangement in **3**. The effect is not obvious in **1**.

(E) Intramolecular [2+2] Cycloaddition of 1 to Give Cubane. Several reaction paths from **1** leading to cubane were investigated in which the decrease in the cyclobutane/cyclobutene dihedral angle ($\Delta\theta$) from 119° to 90° was followed by changes in C–C bond lengths (Δr) and C–C–H bond angles ($\Delta\varphi$) according to a suitable function of $\Delta\theta$ (Eq. (10)). The general trend

$$\Delta r,\ \Delta\varphi \propto f(\Delta\theta) \qquad (10)$$

in the total energy *vs.* $\Delta\theta$ curve does not depend greatly on the type of $f(\Delta\theta)$ as long as the latter is reasonably chosen by model considerations. Figure 4 shows a typical example in which $f(\Delta\theta)=\Delta\theta$. Strictly speaking, however, the lengthening of the ethylenic double bonds and the displacement of the vinylic hydrogen atoms out of the trigonal planes appear to lag befind $\Delta\theta$ as the reaction proceeds in the energy minimum cross-section

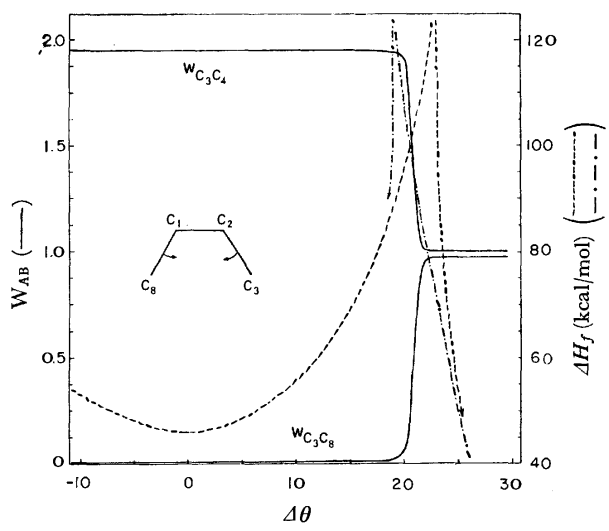

Fig. 4. The energy and the Wiberg's bond indices *vs.* $\Delta\theta$ plots for the ring closure of **1** ($\Delta\theta$=0) to give cubane ($\Delta\theta$=29.0°).

of the potential energy hypersurface interrelating **1** and cubane. The energy value rises steadily during the course of the reaction untill just before the end of change in the dihedral angle (at *ca.* 98°), when it starts to fall to the value corresponding to the heat of formation of cubane. At the same time the bond lengths r's, and the bond angles, φ's, change suddenly to values more or less close to those of cubane. The Wiberg's bond indices between atoms pertaining to bond formation and bond cleavage also change abruptly at this point of the reaction coordinate. We obtain a separate energy *vs.* $\Delta\theta$ plot when the reaction starts from cubane to **1**. All these trends indicate that the reactions refuse to occur when an attempt is made to force them, and provide a typical example of *anti*-aromatic reactions in the electronic ground state.[21-23]

The authors wish to acknowledge stimulating discussions with Professor M. Ōki. They are also indebted to the Ministry of Education for financial support of this work.

20) For the definition of the p character in individual hybrids in terms of the bond index of Wiberg, see C. Trindle and O. Sinanoglu, *ibid.*, **91**, 853 (1967).

21) M. J. S. Dewar and S. Kirschner, *ibid.*, **93**, 4291 (1971).

22) A rectangular disposition of the C_3, C_4, C_7, and C_8 and the C_{2v} symmetry as a whole, are assumed for the species throughout the reaction paths. The distortion from this geometry to a rhombic arrangement of the ethylenic carbon atoms with the total symmetry of C_2 results in the stabilization of the [2+2] interaction by means of the Jahn-Teller effect (see, *e.g.*, H. E. Zimmerman, *Accounts Chem. Res.*, **5**, 393 (1972)). However, the effect is expected to be counteracted by energy loss due to bond bending in the σ framework of the four-membered rings and, therefore, is not taken into present consideration.

23) Note added in proof. R. Gleiter, E. Heilbronner, M. Hekman, and H.-D. Martin, (*Chem. Ber.*, **106**, 28 (1973)) have reported the photoelectron spectral data and the molecular orbital analyses of **1** and **2**. Their results are in good agreement with ours.

The Reaction of Arylthallium(III) Compounds with Copper(II) and (I) Thiocyanates[1]

Sakae UEMURA, Satoru UCHIDA, Masaya OKANO, and Katsuhiko ICHIKAWA*

Institute for Chemical Research, Kyoto University, Uji, Kyoto 611

**Department of Hydrocarbon Chemistry, Faculty of Engineering, Kyoto University, Yoshida, Kyoto 606*

(Received May 10, 1973)

Arylthallium(III) acetate perchlorates reacted with copper(II) thiocyanate to afford aryl thiocyanates in various solvents. The Cu(I) salt was found to be less effective for the thiocyanation. The choice of solvent and the addition of potassium thiocyanate had a significant effect on the yield of aryl thiocyanates. The reaction with the mixture of copper(II) and potassium thiocyanates (1: 1) in dioxane showed the best result. Electron-releasing groups in the aromatic ring accelerated hydrodethallation, yielding aromatic hydrocarbons with a depression of the thiocyanate formation.

In previous papers we showed that the thallium in arylthallium(III) compounds can be replaced by the cyano group[2] or halogen[3] by a reaction with copper-(II) and (I) cyanides or with halides respectively. As another example of such replacement reactions, we will describe here how arylthallium(III) acetate perchlorate monohydrates (**1**), $ArTl(OAc)ClO_4 \cdot H_2O$, react with $Cu(SCN)_2$ in the presence of KSCN, mainly in a dioxane solvent, to afford aryl thiocyanates, sometimes along with aromatic hydrocarbons. In this connection, Taylor and McKillop have recently reported that the thiocyanation of arylthallium(III) bis(trifluoroacetates) with KSCN proceeds under UV irradiation.[4]

Results and Discussion

Phenylthallium(III) acetate perchlorate monohydrate (**1a**) and $Cu(SCN)_2$ were added to an appropriate solvent, such as water, alcohols, cyclic ethers, pyridine, or acetonitrile, and the stirred mixture was then heated under reflux to afford phenyl thiocyanate. Isomeric phenyl isothiocyanate could not be found in the products. The formation of $TlClO_4$ and a Cu (II) salt containing an acetoxy group, probably Cu(OAc)(SCN), was supposed on the basis of a study of the IR spectra. The reaction mixtures were generally heterogeneous, except in the cases of pyridine and acetonitrile solvents, because of the poor solubilities of $Cu(SCN)_2$ in water and the organic solvents used. Among the various solvents, dioxane was found to be the best solvent for preparing phenyl thiocyanate; with it the reaction proceeded even at 70 °C and was almost complete within 1 hr under reflux. However, most reactions including other solvents were carried out under reflux for 5 hr for convenience of comparison. Various results are shown in Table 1.

$$PhTl(OAc)ClO_4 \cdot H_2O + Cu(SCN)_2 \longrightarrow PhSCN + TlClO_4 + Cu(OAc)SCN + H_2O \quad (1)$$

In dioxane, the yield of phenyl thiocyanate was improved by the addition of KSCN; this addition probably caused an increased solubility of $Cu(SCN)_2$ in the solvent, even if to only a slight degree. When an equimolar mixture of $Cu(SCN)_2$ and KSCN was used in dioxane, the yield was more than 80%. A similar additive effect was observed in a homogeneous reaction using a pyridine or acetonitrile solvent, but unexpectedly, whether KSCN was present or absent, the yields of the thiocyanate were less than those in dioxane. On the contrary, when hydroxylic solvents (water, methanol, and ethanol) and tetrahydrofuran were used as solvents (in them KSCN is more soluble than in dioxane),[5] the addition of KSCN resulted in the formation of diphenylthallium(III) thiocyanate (**2**) and a depression in the yield of phenyl thiocyanate. In addition, separate experiments showed that, in hydroxylic solvents, **1a** readily reacted with KSCN at room temperature to give phenylthallium(III) dithiocyanate (**3**), which was then slowly converted into **2** on heating, while in dioxane no **3** was isolated at room temperature and considerable amounts of **2** were obtained on heating. Such a difference may arise from both the poor solubility of KSCN in dioxane and the high-boiling nature of the solvent, the latter of which is favorable for the transformation of **3** into **2**. A similar disproportionation has already been reported for phenylthallium(III) chloride and cyanide.[6] All the results are included in Table 1.

Here, let us consider the possibility of thiocyanate formation from **2** or **3**. When **2** was heated in dioxane, in either the presence or the absence of $Cu(SCN)_2$, no appreciable amounts of phenyl thiocyanate were formed. As to **3**, though its decomposition to give phenyl thiocyanate at above 120 °C had been reported,[6] such transformation was not observed, at least under reflux (65—101 °C) in the usual solvents. However, in the presence of $Cu(SCN)_2$, **3** afforded considerable amounts of phenyl thiocyanate, along with **2** (in dioxane). On the other hand, the reaction of **1a** with $Cu(SCN)_2$ under the same conditions gave only the thiocyanate in a higher yield. Thus, it may be deduced that, in

1) Presented at the 27th Annual Meeting of the Chemical Society of Japan, Nagoya, October, 1972.

2) S. Uemura, Y. Ikeda, and K. Ichikawa, *Tetrahedron*, **28**, 3025 (1972).

3) S. Uemura, Y. Ikeda, and K. Ichikawa, *ibid.*, **28**, 5499 (1972).

4) E. C. Taylor, F. Kienzle, and A. McKillop, *Synthesis*, **1972**, 38.

5) Though the solubility of KSCN in tetrahydrofuran was not so large as that in alcohols, a clear difference in its solubility between tetrahydrofuran and dioxane solvents was observed.

6) F. Challenger and O. V. Richards, *J. Chem. Soc.*, **1934**, 405.

Table 1. Results of the reaction of PhTlYZ with $Cu(SCN)_2$

PhTlYZ mmol		$Cu(SCN)_2$ mmol	KSCN mmol	Solvent 50ml	Temp. °C	Time hr	Products, yield(%)[a] PhSCN	3	2
1a	10	10	0	H_2O	100	5	40	0	0
	10	10	10	H_2O	100	5	30	0	15
	10	0	20	H_2O	20	0.05	0	57	0
	10	0	20	H_2O	100	5	0	0	36
	10	10	0	MeOH	65	5	44	0	0
	10	10	20	MeOH	65	5	7	0	25
	10	0	20	MeOH	20	0.05	0	49	0
	10	0	20	MeOH	65	5	0	0	29
	10	10	0	EtOH	78	5	46	0	0
	10	10	20	EtOH	78	5	18	0	22
	10	10	0	THF	65	5	42	0	0
	10	10	20	THF	65	5	13	0	13
	10	10	0	Dioxane	101	5	58	0	0
	10	10	10	Dioxane	101	5	82	0	0
	10	10	20	Dioxane	101	5	75	0	0
	10	10	40	Dioxane	101	5	56	0	11
	10	0	20	Dioxane	101	5	0	0	50
	10	10	20	Dioxane	101	1	75	0	0
	10	10	20	Dioxane	70	5	62	0	0
	10	10	20	Dioxane-H_2O[b]	89	5	33	0	11
	10	10	0	MeCN	82	5	8	0	0
	10	10	20	MeCN	82	5	27	0	0
	10	10	0	Pyridine	115	5	38	0	0
	10	10	10	Pyridine	115	5	45	0	0
3	5	0	5	MeOH[c]	65	5	0	0	48
	5	5	10	Dioxane[c]	101	5	27	0	27
4a	5	5	10	Dioxane[c]	101	5	trace	0	0
5	5	5	0	Dioxane[c]	101	5	trace	0	0
	5	5	10	Dioxane[c]	101	5	trace	0	0

1a: $PhTl(OAc)ClO_4 \cdot H_2O$, **2**: $Ph_2Tl(SCN)$, **3**: $PhTl(SCN)_2$, **4a**: $PhTl(OCOCF_3)_2$, **5**: $PhTlCl_2$.
a) Based on Tl compound charged (Glc determination).
b) Dioxane: H_2O=7: 3.
c) Solvent 25 ml.

dioxane, thiocyanation using a mixture of $Cu(SCN)_2$ and KSCN occurs directly by Path (a) mainly and *via* **3** by Path (b) partly, while in hydroxylic solvents it is accompanied by a significant formation of **3**, which may be responsible for the facile disproportionation. In connection with the reactivity of **3**, it is worthwhile

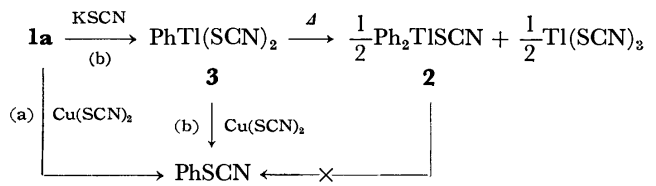

to note that phenylthallium(III) dichloride and bis(trifluoroacetate) were almost unreactive toward $Cu(SCN)_2$, even in the presence of KSCN in dioxane (see Table 1).

Although $Cu_2(CN)_2$ and CuCl could be used as reagents for cyano- and chlorodethallation respectively,[2,3] CuSCN was found to be not so effective for thiocyanodethallation. For example, the reaction of **1a** (10 mmol) with CuSCN (20 mmol) in dioxane gave a 12% yield of phenyl thiocyanate under reflux for 5 hr; the addition of KSCN (40 mmol) improved the yield to 22%. In the cases of tetrahydrofuran and pyridine solvents, only trace amounts of the thiocyanate were formed.

When certain arylthallium(III) acetate perchlorate monohydrates (**1b—e**) were treated with $Cu(SCN)_2$ in dioxane in the presence of KSCN, the corresponding arylthiocyanates and aromatic hydrocarbons were obtained, showing that both thiocyanation and protonation occurred at the position where the thallium was attached to the aromatic ring. As can be seen in Table 2, hydrodethallation is accelerated by the presence of electron-releasing groups as aromatic substituents and also with an increase in the water content in the reaction mixture. This is the same tendency as was previously observed in the reaction between **1** and $CuCl_2$.[3] Here, the proton clearly comes from water, and **1** may serve as a source of water when no external water was added to the reaction system. In thiocyanation, the reverse substituent effect was observed, indicating a nucleophilic character of the reaction; *e.g.*, the yields of aryl thiocyanates from **1d**

$$\underset{\textbf{1b—e}}{ArTl(OAc)ClO_4 \cdot H_2O} \xrightarrow[KSCN]{Cu(SCN)_2} ArSCN + ArH \quad (2)$$

b: 4-CH_3, **c**: 3,4-$(CH_3)_2$, **d**: 2,4-$(CH_3)_2$, **e**: 4-OCH_3

TABLE 2. RESULTS OF THE REACTION OF ArTlYZ WITH $Cu(SCN)_2$ IN DIOXANE

ArTlYZ mmol		$Cu(SCN)_2$ mmol	KSCN mmol	Solvent ml	Temp. °C	Time hr	Products, yield (%)[a] ArSCN	ArH
1b	10	10	0	50	101	5	42	0
	10	10	10	50	101	5	49	trace
	10	10	20	50[b]	89	5	18	19
1c	5	5	5	25	101	5	36	16
1d	5	5	5	25	101	5	13	46
1e	10	10	20	50	101	5	21	55
4b	10	10	20	50	101	5	trace	0

1b: 4-$CH_3C_6H_4Tl(OAc)ClO_4\cdot H_2O$, **1c**: 3,4-$(CH_3)_2C_6H_3Tl(OAc)ClO_4\cdot H_2O$, **1d**: 2,4-$(CH_3)_2C_6H_3Tl(OAc)ClO_4\cdot H_2O$, **1e**: 4-$CH_3OC_6H_4Tl(OAc)ClO_4\cdot H_2O$, **4b**: 4-$ClC_6H_4Tl(OCOCF_3)_2$.

a) Based on Tl compound charged (Glc determination).

b) Dioxane: H_2O=7: 3.

and **1e** were very low (below *ca.* 20%).

The following observations will also serve to make it possible to presume a probable reaction mechanism. In the reactions between equimolar amounts of **1a** and $Cu(SCN)_2$, the yields of phenyl thiocyanate sometimes exceeded 50%. Moreover, the pale green color of a dioxane solution of $Cu(SCN)_2$, though its solubility is very limited, did not change on 5 hrs' refluxing. These facts appear to exclude the possibility of thiocyanogen formation (by Eq. (3)) and its participation as reactive

$$Cu(SCN)_2 \longrightarrow CuSCN + \frac{1}{2}(SCN)_2 \qquad (3)$$

species, at least in dioxane, which has been the subject of several experiments.[7,8] A route *via* phenyl isothiocyanate was also eliminated by an experiment examining its isomerization. Further, the reaction between **1a** and a mixture of $Cu(OAc)_2$ and KSCN in dioxane afforded no phenyl thiocyanate, indicating that no ligand exchange to form $Cu(SCN)_2$ occurred. Thus, it is clear that the thiocyano group comes from $Cu(SCN)_2$ itself. Since no biphenyl was found in the reaction products from **1a**, the possibility *via* an organocopper compound can also be excluded. In addition, the reaction does not appear to involve a radical path, because when **1a** was treated with a mixture of $Cu(SCN)_2$ and KSCN in dioxane in the presence of acrylonitrile, neither an acrylonitrile polymer nor arylated acrylonitrile was formed and no effect on the yield of phenyl thiocyanate was observed.

After a consideration of all the above results, the most plausible mechanism involving a concerted nucleophilic substitution after coordination is proposed to be as follows:

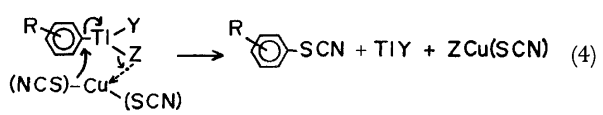

(4)

In cases where KSCN is added to the reaction system, one might expect the participation of $Cu(SCN)_4^{2-}$ as the attacking species which would be a more powerful nucleophile than $Cu(SCN)_2$, since the formation of the complex anion from $Cu(SCN)_2$ and KSCN in acetonitrile has been established.[8] However, this seems to be very unlikely; the coordination number of Cu(II) is generally known to be 4, and hence the above anion is thought to be ineffective for such a reaction involving initial coordination.

Experimental

The IR spectra were taken with Hitachi EPI-2 and EPS-3T spectrometers. The NMR spectra were recorded by a Varian A-60 spectrometer in $CDCl_3$, using TMS as the internal standard. The glc analyses were carried out on a Shimadzu 5APTF apparatus, using PEG 6000(25%)-Chromosorb W (3 m) and Apiezon L (30%)-Celite (3 m) columns (He as the carrier gas).

Materials. All the organic materials except the arylthallium(III) compounds were purified immediately before use by distillation, while commercially-available CuSCN and KSCN were used without further purification. $Cu(SCN)_2$ was preqared by the reported method from $CuSO_4\cdot 5H_2O$ and KSCN.[8] The prepatation of various arylthallium(III) compounds, except for phenylthallium(III) dithiocyanate, and diphenylthallium(III) thiocyanate, was described in previous papers.[2,3]

Formation of Phenylthallium(III) Dithiocyanate (3) and Diphenylthallium(III) Thiocyanate (2). Reactions of Phenylthallium(III) Acetate Perchlorate Monohydrate (1a) with KSCN in Hydroxylic Solvents. By the addition of a solution of 1.9 g (20 mmol) of KSCN dissolved in water (25 ml) to an aqueous solution (25 ml) of 4.6 g (10 mmol) of **1a** at room temperature, **3** was readily obtained as a white amorphous precipitate in a 57% yield; mp 130—140 °C (d) [lit,[6] mp 100—120 °C (d)]. Found: C, 24.07; H, 1.22; N, 7.15%. Calcd for $C_8H_5N_2S_2Tl$: C, 24.16; H, 1.27; N, 7.05%. A similar reaction at the refluxing temperature in water for 5 hr gave a white precipitate, **2** (which is soluble in alcohols and insoluble in water), in a 36% yield; mp 285—287 °C. Found: C, 37.40; H, 2.39; N, 3.28%. Calcd for $C_{13}H_{10}NSTl$: C, 37.41; H, 2.59; N, 3.36%. The preparations of **3** and **2** could be carried out similarly in a methanol solvent. Further, when 2.0 g (5 mmol) of **3** was heated for 5 hr in refluxing methanol (25 ml) containing 0.5 g (5 mmol) of KSCN, 0.5 g (1.2 mmol) of **2** was formed.

Reactions of Arylthallium (III) Acetate Perchlorate Monohydrates (1) with Cu(SCN)$_2$ in Dioxane. The following example shows a typical experimental procedure. A mixture of 4.6 g (10 mmol) of **1a**, 1.8 g (10 mmol) of $Cu(SCN)_2$, and 1.9 g (20 mmol) of KSCN in 50 ml of dioxane was stirred at 101°C for 5 hr, during which period the color of the heterogeneous

7) H. P. Kaufmann and K. Küchler, *Ber.*, **67**, 944 (1934).

8) C. L. Jenkins and J. K. Kochi, *J. Org. Chem.*, **36**, 3095 (1971).

solution changed from pale black to deep yellow. After the filtration of the yellow precipitate (6.2 g), the yellow filtrate was diluted with aqueous NaCl (sometimes white **2** was precipitated) and extracted with benzene. The benzene extract contained 8.2 mmol (82% yield) of phenyl thiocyanate and no phenyl isothiocyanate (determined by glc; benzyl acetate was used as the internal standard). Phenyl thiocyanate was isolated in a pure form by distillation at 101—102 °C/18 mmHg. IR ν_{SCN} 2150 cm^{-1} (s). The washing of the yellow precipitate with hot water left a greyish-yellow solid (4.3 g), which was shown by IR spectroscopy to contain thiocyano and acetate and no perchlorate groups; it was probably a mixture of CuSCN, $Cu(SCN)_2$, and Cu(SCN)(OAc). The treatment of the water-washing containing perchlorate ion with dil. HCl gave a precipitate (1.5 g) of TlCl.

In similar reactions using other arylthallium(III) salts, the formation of the corresponding aryl thiocyanates and aromatic hydrocarbons was observed. The yields of both compounds were determined by glc (benzyl acetate and ethylbenzene were used respectively as the internal standards). Aromatic thiocyanates were isolated by distillation and identified by means of their IR and NMR spectra. *p*-Tolyl thiocyanate, bp 117—118 °C/20 mmHg; 3,4-dimethylphenyl thiocyanate, bp 140—141 °C/28 mmHg; *p*-Anisyl thiocyanate, bp 159—160 °C/27 mmHg.

BULLETIN OF THE CHEMICAL SOCIETY OF JAPAN, VOL. 46, 3257—3260 (1973)

Reactions of the Iodocarbenoid of Zinc. I. The Synthesis of Alkyl-substituted 7-Ethylcyclohepta-1,3,5-trienes *via* the Ring-expansion of Alkylbenzenes with Diethylzinc and Iodoform

Sotaro MIYANO and Harukichi HASHIMOTO

Department of Applied Chemistry, Faculty of Engineering, Tohoku University, Aramaki, Sendai 980

(Received May 15, 1973)

By treatment with diethylzinc and iodoform, benzene gave 7-ethylcyclohepta-1,3,5-triene in a yield of 58%, along with a quantitative formation of ethyl iodide. Alkylbenzenes, including methyl-, ethyl-, isopropyl-, *tert*-butyl-, and *o*-dimethylbenzene, gave the corresponding alkyl-substituted 7-ethylcyclohepta-1,3,5-trienes in yields of 60, 45, 41, 35, and 52% respectively. The tropylium iodide resulting from the adduct of the iodocarbenoid of zinc to benzene (7-iodonorcaradiene) is suggested as an intermediate in the formation of the 7-ethylcycloheptatriene.

Recently Furukawa and Nishimura reported that the halocarbenoid of zinc obtained from diethylzinc and haloforms transfer the halomethylene groups to cyclohexene to give 7-halonorcaranes.[1] When iodoform was used as the halomethylene source, 7-iodonorcarane was obtained in only a trace amount.

In the course of our investigation of the zinc-carbenoid reaction, we found that alkyl-substituted 7-ethylcyclohepta-1,3,5-trienes are obtained by the treatment of diethylzinc and iodoform in alkylbenzenes.[2] In this report, we will describe the details of the reaction, and will present evidence for the tropylium iodide intermediate in the formation of 7-ethylcyclohepta-1,3,5-triene from benzene.

Results and Discussion

Reactions of Diethylzinc and Iodoform with Benzene. Table 1 shows the results of the reactions of diethylzinc and iodoform with benzene. To a stirred diethylzinc solution in benzene, iodoform was added over a 1 hr period under a nitrogen atmosphere, after which the reaction was continued for another 5 hr. Besides 7-ethylcyclohepta-1,3,5-triene and ethyl iodide, propylene and cyclohepta-1,3,5-triene were obtained as side reaction products in yields of 28 and 3% respectively (No. 4). The amount of ethyl iodide depended on the limiting component (iodoform or diethylzinc), and the total iodides recovered were almost equal to the iodoform consumed. These facts suggest the following stoichiometry for the formation of 7-ethylcycloheptatriene and propylene (Eqs. (1) and (2) respec-

TABLE 1. REACTIONS OF THE IODOCARBENOID OF ZINC FROM IODOFORM AND DIETHYLZINC WITH BENZENE[a)]

Run	CHI_3 10^{-2} mol	7-Ethylcyclohepta-1,3,5-triene 10^{-2} mol	EtI 10^{-2} mol	Iodide ion 10^{-2} eq.
1	0.53	0.22	0.55	0.98
2	1.01	0.49	1.00	1.93
3	2.03	1.12	2.04	3.88
4	2.97	1.73	3.03	5.66
5	3.51	1.74	3.06	5.70
6[b)]	3.03	1.54	3.28	5.72
7[c)]	3.02	0.28	3.11	5.44

a) To a stirred solution of Et_2Zn (0.030 mol) in benzene (50 ml), CHI_3 was added portionwise during 1 hr period at 50°C under a nitrogen atmosphere, and the reaction was continued for another 5 hr.
b) Et_2Zn was added to a CHI_3 suspension in benzene.
c) Benzene; 10 ml, *n*-hexane; 40 ml.

1) J. Nishimura and J. Furukawa, *Chem. Commun.*, **1971**, 1375.
2) S. Miyano and H. Hashimoto, *ibid.*, **1973**, 216.

Table 2. Reactions of alkylbenzenes

R	R′	Yield (%)[b]	Isomer distribution (%)[c]		
H	H	48			
CH_3	H	60	57	22	21
CH_2CH_3	H	45	44	27	29
$CH(CH_3)_2$	H	41	26	39	35
$C(CH_3)_3$	H	35	3.4	37	60
CH_3	CH_3	52	66	10	24

a) Alkylbenzene; 100 ml, Et_2Zn; 0.10 mol, CHI_3; 0.10 mol, 50 °C, 6 hr.
b) Determined by glc, and based on the CHI_3.
c) Determined by glc and NMR spectra.

tively):

$$C_6H_6 + CHI_3 + Et_2Zn \longrightarrow \text{(H, Et)} + EtI + ZnI_2 \quad (1)$$

$$CHI_3 + Et_2Zn \longrightarrow CH_3CH{=}CH_2 + EtI + ZnI_2 \quad (2)$$

Reactions of Alkylbenzenes. Table 2 shows that alkylbenzenes also gave the corresponding alkyl-substituted 7-ethylcyclohepta-1,3,5-trienes in fairly good yields on treatment with diethylzinc and iodoform. All the cycloheptatrienes were separated by distillation as mixtures of positional isomers and were confirmed by elemental analysis and by a study of their NMR and IR spectra. Though the ring-expansion of aromatic compounds by carbene or carbenoid reagents is well-known,[3] this iodocarbenoid reaction gives a convenient route for the synthesis of alkyl-substituted 7-ethylcycloheptatrienes from alkylbenzenes.

In a preliminary experiment, ethylzinc iodide[4] obtained from zinc-copper couple[5] and ethyl iodide also gave the 7-ethylcycloheptatriene when allowed to react with iodoform in benzene.

A competition study was carried out by allowing an equimolar mixture of benzene and isopropylbenzene to compete for a deficient amount of diethylzinc and iodoform. The latter gave 1.5 times more of the corresponding cycloheptatrienes than the former. This seems to show that the addition of the iodocarbenoid of zinc to the benzene nuclei is electrophilic in nature (*vide infra*).

Anisole and chlorobenzene gave complex mixtures of unidentified products which contained cycloheptatriene derivatives, judging from the NMR spectra.

Addition of the Iodomethylene Group from the Iodocarbenoid of Zinc to the Benzene Ring, and the Tropylium Iodide Intermediate in the Formation of 7-Ethylcyclohepta-1,3,5-triene. The following two reaction paths are possible for the formation of 7-ethylcyclohepta-1,3,5-triene through the ring-expansion of benzene with diethylzinc and iodoform (Path (a) and Path (b))[6] (R=Et or I):

(a) $EtZnR + CHI_3 \longrightarrow EtI + CHI_2ZnR$ (I)

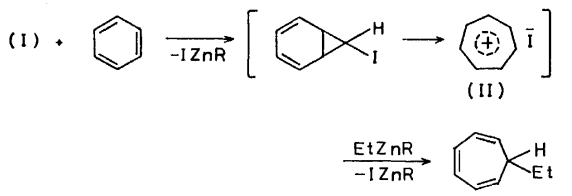

(b) $(I) + EtZnR \longrightarrow EtCHIZnR + IZnR$ (III)

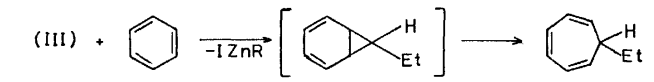

Furukawa *et al.* reported the ring-expansion of aromatic compounds by means of the methylcarbenoid of zinc formed from diethylzinc and ethylidene iodide.[7] This might suggest the addition of propylidene from the ethylcarbenoid of zinc (III) to the benzene ring (Path (b)), but the following result shows that, in the present case, Path (a) is the reasonable one. After benzene-d_6 had been allowed to react with diethylzinc and iodoform, the 7-ethylcycloheptatriene-d_6 thus formed was analyzed by studying its NMR spectra. It was found that, in the 7-ethylcycloheptatriene-d_6, the hydrogen atom derived from iodoform was statistically distributed throughout the cycloheptatriene ring:

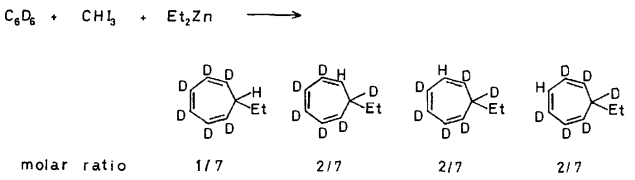

This fact can most reasonably be explained by the tropylium iodide intermediate (II) and the nucleophilic replacement of iodine by the ethyl group, thus forming 7-ethylcycloheptatriene.[8]

The isomer distribution of the cycloheptatrienes from toluene by this iodocarbenoid reaction is somewhat different from those obtained by the CH_3CHI_2–Et_2Zn[7a] and CH_2N_2-CuBr[10] systems, but it is consistent with that obtained by the chlorocarbenoid of lithium formed from methyllithium and methylene chloride.[11] For the latter reaction, tropylium chloride was detected as the intermediate in the formation of 7-methylcycloheptatriene from benzene.[12] There seems to be few reports dealing with the orientation of alkyltropylium

3) W. Kirmse, "Carbene Chemistry," 2nd ed., Academic Press, New York, London, (1971), p. 381.
4) M. H. Abraham and P. H. Rolfe, *J. Organometal. Chem.*, **7**, 35 (1967).
5) E. LeGoff, *J. Org. Chem.*, **29**, 2048 (1964).
6) D. B. Miller, *Tetrahedron Lett.*, **1964**, 989.
7) a) J. Nishimura, J. Furukawa, N. Kawabata, and T. Fujita, *Tetrahedron*, **26**, 2229 (1970). b) J. Nishimura, J. Furukawa, and N. Kawabata, This Bulletin, **43**, 2195 (1970).
8) The reaction of tropylium ions with carbanions is a synthetic route for the 7-alkylcycloheptatrienes.[9]
9) For example, a) C. Jutz, *Chem. Ber.*, **97**, 2050 (1964). b) G. A. Gladkovskii, S. S. Skorokhodov, S. G. Slyvina, and A. S. Khachaturov, *Izv. Akad. Nauk SSSR, Ser. Khim.*, **1963**, 1273.
10) E. Müller, H. Kessler, H. Fricke, and W. Kiedaisch, *Ann. Chem.*, **675**, 63 (1964).
11) O. M. Nefedov, N. N. Novitskaya, and A. D. Petrov, *Dokl. Akad. Nauk SSSR*, **158**, 411 (1964).
12) G. L. Closs and L. E. Closs, *Tetrahedron Lett.*, **1960**, 38.

Table 3. Separated cycloheptatrienes

R	R′	Yield of separated cycloheptatrienes (%)[a]	Bp[b] (°C/mmHg)	Elemental analysis C(%) (Calcd)		H(%) (Calcd)	
H	H	27	73—73.5/43	89.79	(89.94)	10.29	(10.06)
CH_3	H	39	64/11	89.39	(89.49)	10.63	(10.51)
CH_2CH_3	H	36	63—64/6.5	89.29	(89.12)	10.96	(10.88)
$CH(CH_3)_2$	H	30	62.5—63/3	88.69	(88.82)	11.02	(11.18)
$C(CH_3)_3$	H	25	72—78/3.5	88.36	(88.56)	11.63	(11.44)
CH_3	CH_3	32	70.5—71/7	89.07	(89.12)	10.80	(10.88)

a) Based on the CHI_3.
b) For the mixture of the isomers.

ions for the nucleophilic reaction,[13] and the preferential formation of 2-methyl-7-ethylcycloheptatriene from toluene is not yet explained.[14]

Propylene seems to be formed by the facile 1,2-hydride shift of the ethylcarbenoid of zinc (III).[12] Similar olefin-forming reactions have been reported for the reaction of Grignard reagents and bromoform.[16]

Experimental

Materials. Commercial diethylzinc was distilled under reduced pressure. The iodoform was recrystallized from ethanol-acetone. The alkylbenzenes and other materials were of commercial origin and were purified as usual. Distillation or recrystallization was carried out under a nitrogen atmosphere. Materials were stored under nitrogen.

The glc analysis was carried out on a Shimadzu GC 3AF apparatus equipped with hydrogen flame detectors; four different stainless steel columns (3 m×3 mm) were used, packed with Diasolid M coated with Silicone DC 550, Silicone DC 410, Apiezon Grease L, and PEG 2000 respectively.

Reaction of Benzene with Diethylzinc and Iodoform. The general procedure used for the reaction of diethylzinc, iodoform, and benzene was as follows. The reaction was carried out in a round-bottomed flask equipped with a magnetic stirrer, a thermometer, a reflux condenser topped with a nitrogen inlet, and a dropping funnel for a solid material[17] which had been charged with iodoform. The flask was flushed with prepurified nitrogen. In the flask we placed benzene and diethylzinc, and the stirred solution was heated to 40—45 °C. The iodoform was added, portion by portion, over a 1 hr period at 50 °C, and then the reaction was continued for another 5 hr. On the addition of the iodoform, an exothermic reaction was observed and the iodoform reacted smoothly. During the addition of the iodoform, white precipitates were formed in the reaction flask. At the end of the reaction, a small amount of water and then dilute nitric acid were added cautiously to the cooled mixture. The organic layer was washed successively with dilute nitric acid and water. The aqueous layer and combined aqueous washings were extracted with a small amount of benzene, and the content of the iodide ion was determined by Vorhard titration. The organic layer was washed with a dilute sodium carbonate solution and water, and then diluted with additional benzene to a 250 ml volume, from which a 10 ml portion was used for the quantitative determination of the ethyl iodide, cyclohepta-1,3,5-triene, and 7-ethylcyclohepta-1,3,5-triene formed. The remaining solution was dried over magnesium sulfate. After the removal of benzene and ethyl iodide by distillation, the residue was fractionated through a Vigreux column. Besides 7-ethylcyclohepta-1,3,5-triene, a high-boiling portion was obtained which was positive to the Beilstein test and which seemed to consist of the iodocyclopropanes derived from cyclo-

Table 4. NMR data for the 7-ethylcycloheptа-1,3,5-triene-d_6

Proton[a]	H_a	H_b	H_c	H_d	H_e	H_f
Chemical shift (ppm)[b]	6.5 (b)[c]	6.05 (b)	5.07 (b)	1.69 (q,m)[d]		1.0 (t,m)[e]
Proton distribution						
Obsd	0.25H	0.27H	0.28H	2.12H		3H
Calcd for statistical distribution	0.286H[f]	0.286H	0.286H	0.143H[g]	2H	3H

a) 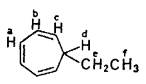
b) Downfield from internal TMS.
c) Broad.
d) Complex quintette.
e) Complex triplet.
f) 2/7 H.
g) 1/7 H.

13) D. Lloyd, "Carbocyclic Non-benzenoid Aromatic Compounds," Elsevier Publ. Co., Amsterdam-London-New York, (1966), p. 98.

14) Prof. M. Hida suggested that from the HMO calculations the frontier electron density of a methyltropylium ion for a nucleophilic reaction (f_r^N) is in the order of $f_1 > f_3 > f_2$.[15]

15) M. Hida, Private communication.

16) J. Villieras, *Bull. Soc. Chim. Fr.*, **1967**, 1511.

17) T. Suehiro, K. Tokumaru, and M. Yoshida, "Gendai no Yukikagaku Zikken," Gihodo, Tokyo, (1971), p. 139.

heptatrienes by the addition of the iodocarbenoid of zinc to the double bonds. Cyclohepta-1,3,5-triene was confirmed only by the retention time on glc because of its scarcity.

The isomer distributions of 7-ethylcycloheptatrienes from alkylbenzenes were determined by studying the glc[7a] and NMR[18] spectra (Table 2). The results of the separation of cycloheptatrienes are shown in Table 3.

Competition between Benzene and Isopropylbenzene. Benzene (0.30 mol) and isopropylbenzene (0.30 mol) competed for the iodocarbenoid reagent generated *in situ* from diethylzinc (0.050 mol) and iodoform (0.050 mol). Both gave the corresponding 7-ethylcycloheptatrienes, in yields of 0.00853 mol and 0.0126 mol respectively.

18) K. W. Egger and W. R. Moser, *J. Phys. Chem.*, **71**, 3699 (1967).

7-Ethylcyclohepta-1,3,5-triene-d_6. Under a nitrogen atmosphere, an 11 ml portion of commercial benzene-d_6 (Merck Co., deuterium content, 99%) was distilled over sodium into a reaction flask directly. The reaction was carried out as stated above using 1 ml (0.010 mol) of diethylzinc and 4.0 g (0.010 mol) of iodoform. A portion boiling at 70—72°C/45 mmHg, contaminated with a trace amount of ethyl iodide, was distilled into an NMR sample tube. The NMR analysis of the sample (*ca.* 5% solution in CCl_4, TMS) showed the statistical distribution of the hydrogen atom derived from iodoform throughout the cycloheptatriene ring within the limits of experimental error (Table 4).

The authors wish to acknowledge with pleasure their helpful discussions with Professor Mitsuhiko Hida.

BULLETIN OF THE CHEMICAL SOCIETY OF JAPAN, VOL. 46, 3260—3263 (1973)

The Preparation and Reactions of *N*-Substituted Hexafluoroisopropylideneimines

Nobuo ISHIKAWA and Tomoya KITAZUME

Department of Chemical Engineering, Tokyo Institute of Technology, Ookayama, Meguro-ku, Tokyo 152

(Received May 16, 1973)

N-Aryl- and *N*-alkylhexafluoroisopropylideneimines (**2**) were prepared from the hexafluorothioacetone dimer (**1**) by treatment with either aryl- or alkylamines. These imines reacted with alcohols and thiols to give three addition products, **7**, **8**, and **9**. Phenylhydrazone (**3**), semicarbazone (**4**), hydrazone (**5**), and azine (**6**) of hexafluoroacetone were also obtained directly from **1** and the corresponding carbonyl reagents.

Hexafluoroisopropylideneimine (**2**, R=H) and its-*N*-substituted derivatives appear to be useful intermediates for the syntheses of hexafluoroisopropyl compounds. Although Middleton *et al.*[1,2] have prepared the imine and its *N*-methyl derivative by the reaction of hexafluoroacetone with either ammonia or methylamine, followed by the dehydration of the resulting adducts, the present knowledge of the experimental conditions for the preferential elimination of water from adducts of hexafluoroacetone with other amines is far from satisfactory.

On the other hand, Zeifman *et al.*[3] prepared *N*-phenylhexafluoroisopropylideneimine (**2**, R=Ph) by a Wittig-like reaction, which involved the reaction of hexafluoroacetone with phenylisocyanate in the presence of triphenylphosphine oxide as the catalyst. Furthermore, they prepared the oxime and semicarbazone of hexafluoroacetone by the elimination of aniline from the corresponding adducts obtained from the condensation of *N*-phenylhexafluoroisopropylideneimine with hydroxylamine[4] and semicarbazide[5] respectively.

In the course of our investigation of the organic fluorine sulfur compounds, it was necessary to study the reactivity of fluoroalkylthiocarbonyl compounds. Hexafluorothioacetone is known as an unstable gas which dimerizes very readily into a stable liquid, 2,2,4,4-tetrakis(trifluoromethyl)-1,3-dithiethane (**1**).[6] Our studies of the nucleophilic reactions of this dimer have revealed that aryl- and alkylamines gave *N*-substituted hexafluoroisopropylideneimines easily, and that it is a convenient general method for the preparation of the imines of this type. Carbonyl reagents also gave the phenylhydrazone and semicarbazone of hexafluoroacetone directly.

We also carried out several nucleophilic addition reactions across the C=N– double bonds of these imines; we could thus obtain 2-alkoxy- and 2-alkylthio-2-arylaminohexafluoropropanes.

Results and Discussion

The Preparation of N-*Substituted Hexafluoroisopropylideneimines.* The dimer of hexafluorothioacetone (**1**) (bp 110 °C) can be prepared directly from hexafluoropropene and sulfur in sulfolan in the presence of potassium fluoride.[7] This compound is reported to be very

1) W. J. Middleton and C. G. Krespan, *J. Org. Chem.*, **30**, 1398 (1965).
2) W. J. Middleton, U. S. 3226439 (1965).
3) Yu. V. Zeifman, N. P. Gambaryan, and I. L. Knunyants, *Dokl. Akad. Nauk SSSR*, **153**, 1334 (1964).
4) Yu. V. Zeifman, N. P. Gambaryan, and I. L. Knunyants, *Izv. Akad. Nauk SSSR, Ser. Khim.*, **1965**, (3), 450.
5) Yu. V. Zeifman, N. P. Gambaryan, and I. L. Knunyants, *Zh. Vses Khim. Obshch. im D. I. Mendeleeva*, **10**(2), 235 (1965).
6) W. J. Middleton, E. G. Howard, and W. H. Sharkey, *J. Org. Chem.*, **30**, 1375 (1965).
7) I. L. Knunyants, *Dokl. Akad. Nauk*, **183**, 598 (1968).

Table 1. Preparation of **2**, **4**, and **5**

CF_3
CF_3 > C = N–R

	Compound R	Yield %	Bp (°C/mmHg) [mp (°C)]	IR (cm^{-1}) (C=N)	^{19}F NMR[a] *syn*	^{19}F NMR[a] *anti*	F Anal (%) Found	F Anal (%) Calcd
2	Ph	67	75/91	1680	−8.6	−16.2	47.9	47.3
	o-MeC_6H_4	78	72—73/53	1698	−8.4	−15.0	44.7	44.7
	m-MeC_6H_4	70	83—84/71	1604	−8.4	−16.4	45.3	44.7
	p-MeC_6H_4	69	85—86/53	1660	−8.4	−16.1	45.2	44.7
	2,4-$Me_2C_6H_3$	45	70—71/34	1612	−8.7	−15.7	42.0	42.3
	m-FC_6H_4	71	75—78/97	1618	−8.2	−16.2	51.6	51.3
	p-FC_6H_4	65	118—120/108	1640	−8.1	−14.7	50.9	51.3
	m-$CF_3C_6H_4$	59	80—83/48	1620	−8.0	−16.0	55.0	55.3
	m-*i*-$C_3F_7C_6H_4$	73	90—92/58	1605	−8.1	−16.0	60.9	60.4
	p-*i*-$C_3F_7C_6H_4$	76	78—81/38	1603	−6.4	−16.8	61.2	60.4
	o-ClC_6H_4	49	75/25	1594	−9.1	−15.1	40.9	41.4
	m-ClC_6H_4	78	71—72/21	1595	−8.4	−16.2	41.7	41.4
	p-ClC_6H_4	39	65—66/21	1592	−8.7	−16.1	41.1	41.4
	o-$MeOC_6H_4$	50	95—96/43	1604	−9.2	−12.7	42.7	42.0
	p-$MeOC_6H_4$	13	76—77/15	1664	−9.1	−15.4	42.5	42.0
	n-C_3H_7	18	52—53	1691	−7.4	−13.6	55.5	55.0
	n-C_5H_9	20	63—64	1634	−7.2	−14.7	51.1	51.5
3	NHPh	66	91—92/23	1664	−8.7	−15.8	44.8	44.5
4	$NHCONH_2$	90	[131—132]	1640	−11.3	−12.9	50.7	50.9
5	NH_2	43	93—96	1600	−12.0[b]	−13.4[b]	62.7	63.3

a) δ ppm from ext. CF_3CO_2H in CCl_4.
b) lit,[1] −11.5, −12.8.

susceptible to bases and reacts with sodium methoxide in methanol rapidly to give a fluorine-free compound, dimethyl α-methylthio-α-methoxymalonate, in a poor yield.[6] However, no other nucleophilic reaction of this dimer has appeared in the literature. We carried out several reactions of the dimer with amines under more moderate conditions, and found that both aryl- and alkylamines reacted with the dimer at room temperature, with a liberation of sulfur.

For example, when the dimer was allowed to react with 2 mol of *p*-toluidine in dimethylformamide, an oily material was obtained. Among the various solvents examined, such as alcohol, acetonitrile, dioxane, and other polar solvents, dimethylformamide was the most effective in promoting the reaction.

The product was sulfur-free, but it still contained trifluoromethyl groups. The structure of this compound was elucidated by a study of the IR, ^1H and ^{19}F NMR, and mass spectra to be *N*-*p*-tolylhexafluoroisopropylideneimine (**2** R=$C_6H_4CH_3$). In the IR spectrum, the presence of the C=N group was shown by the band at 1660 cm^{-1}, and in the ^{19}F NMR spectrum, two singlet peaks, −8.4 and −16.1 ppm from ext. CF_3COOH in CCl_4, appeared, corresponding to *syn*- and *anti*-CF_3 respectively.[8-10] In the mass spectrum, the parent peak, M^+ 255, and other fragment peaks, such as *m/e* 186 ($C_9H_7NF_3$), 91 (C_7H_7), and 69 (CF_3), appeared appropriately.

The other *N*-aryl hexafluoroisopropylideneimines were prepared similarly by using aniline and its substituted derivatives. Such alkylamines as *n*-propyl- and *n*-butylamine gave *N*-alkylimines, but in poorer yields. (Table 1).

Considering the yields of the products and the amount of sulfur liberated during the reaction, the reaction seemed to proceed according to the following scheme:

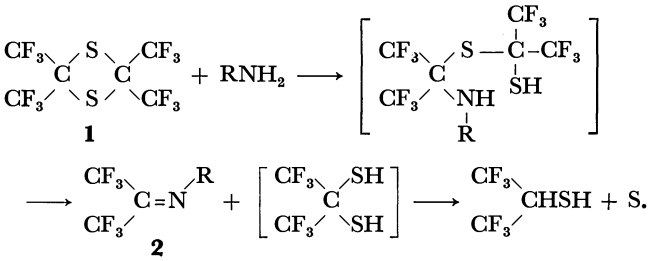

Many attempts to capture bis(trifluoromethyl)methanethiol in the reaction mixtures were unsuccessful, probably because of the extreme instability of this compound.

In addition to aryl- and alkylamines, phenylhydrazine and semicarbazide also attacked the dimer in dimethylformamide at room temperature; phenylhydrazone and semicarbazone of hexafluoroacetone were thus obtained.

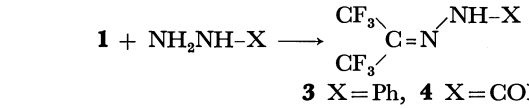

3 X=Ph, **4** X=$CONH_2$

When unsubstituted hydrazine was used as nucleophile, the reaction in dimethylformamide was too vigorous and gave only a tarry material. In a milder solvent, such as acetonitrile, the reaction proceeded smoothly and hexafluoroacetone hydrazone (**5**) and

8) J. K. Ruff, *J. Org. Chem.*, **32**, 1675 (1967).
9) G. E. Hall, W. J. Middleton, and J. D. Roberts, *J. Amer. Chem. Soc.*, **93**, 4778 (1971).
10) F. J. Weigert, *J. Org. Chem.*, **37**, 1314 (1972).

Table 2. Preparation of **7** and **8**

$$X\text{–}C(CF_3)_2\text{–}NH\text{–}Ar$$

Compound X	Compound Ar	Yield %	Bp °C/mmHg	IR (cm^{-1}) N–H	^{19}F NMR (ppm)	F Anal (%) Found	F Anal (%) Calcd
MeO	Ph	34	85/25	3306	−3.8	41.6	41.7
	o-MeC_6H_4	35	88—89/18	3360	−4.9	39.8	39.7
	m-MeC_6H_4	28	99—100/26	3332	−3.5	39.1	39.7
	p-MeC_6H_4	33	96—97/26	3358	−3.6	40.1	39.7
	2,4-$Me_2C_6H_3$	28	105/21	3343	2.0	38.0	37.8
	o-ClC_6H_4	38	98/27	3386	−4.8	37.5	37.1
	m-ClC_6H_4	51	118/28	3360	−3.5	37.6	37.1
	p-ClC_6H_4	20	106/19	3410	−3.8	37.3	37.1
	o-$MeOC_6H_4$	35	107/21	3398	1.9	38.0	37.6
EtO	Ph	28	84/24	3342	−5.2	40.0	39.8
	o-MeC_6H_4	31	93/24	3358	−3.5	37.5	37.8
	m-MeC_6H_4	42	98/26	3359	−5.2	37.5	37.8
	p-MeC_6H_4	29	96—98/24	3343	−5.1	38.6	37.8
	2,4-$Me_2C_6H_3$	26	100/24	3305	−2.8	36.9	36.2
	o-ClC_6H_4	23	96/24	3391	−2.1	35.6	35.4
	m-ClC_6H_4	33	105—106/24	3353	2.0	35.1	35.4
EtS	Ph	27	84/31	3286	−4.3	37.9	37.6
	o-MeC_6H_4	30	88/22	3303	−4.3	35.6	35.9
	m-MeC_6H_4	61	133/25	3401	−7.3	36.1	35.9
	p-MeC_6H_4	35	101—104/24	3328	−7.3	36.2	35.9
	2,4-$Me_2C_6H_3$	30	83/20	3316	−4.0	34.6	34.4
	o-ClC_6H_4	54	88/25	3321	−4.3	34.1	33.9
	m-ClC_6H_4	21	106/27	3318	−4.1	33.5	33.9

a) δ ppm from ext. CF_3CO_2H in CCl_4.

azine (**6**) were obtained in yields of 43 and 11% respectively.

$$\mathbf{1} + NH_2NH_2 \longrightarrow \underset{\mathbf{5}}{(CF_3)_2C{=}N{-}NH_2} + \underset{\mathbf{6}}{(CF_3)_2C{=}N{-}N{=}C(CF_3)_2}$$

Thus, the hydrazones of hexafluoroacetone were prepared directly from the hexafluorothioacetone dimer and the corresponding carbonyl agents; this seemed to be a convenient preparative route because several steps had previously been required for the preparation of these compounds.[5]

Hexafluoroisopropylideneimines are also susceptible to nucleophiles. Zeifman *et al.*[3,4] reported several reactions of the imines, especially reactions with amines, by which an exchange of imino groups occurred. We examined the addition of alcohols and thiols across the C=N– double bond of *N*-arylhexafluoroisopropylideneimines and prepared a number of 2-alkoxy- and 2-alkylthio-2-arylaminohexafluoropropanes, **7** and **8**, for pharmacological purposes.

Methyl and ethyl alcohols reacted with the imines by means of refluxing in the presence of a small amount of alkali, while ethanethiol reacted under a nitrogen atmosphere at room temperature. The structures of the products were evident from the IR and the ^1H and ^{19}F NMR spectra, as well as, from fluorine analysis. In each compound, only one singlet signal appeared in the ^{19}F NMR, and the presence of N–H was shown in the IR spectrum (Table 2).

$$(CF_3)_2C{=}N{-}Ar + R\text{–}ZH \longrightarrow R\text{–}Z\text{–}C(CF_3)_2\text{–}NH\text{–}Ar$$

7 Z=O, **8** Z=S

It is known that the reaction between the Schiff bases and thioglycolic acid gives 4-thiazolidinones, and that their derivatives are sometimes useful as drugs.[11,12]

Table 3. Preparation of **9**

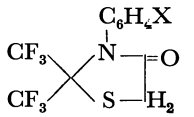

Compound X	Yield %	Mp °C	IR (cm^{-1}) C=O	F Anal (%) Found	F Anal (%) Calcd
H	85	97—98	1702	36.1	36.2
p-Me	81	119.5—120	1704	34.8	34.7
m-F	50	105—106	1710	39.3	39.9
p-F	56	108—109	1710	39.4	39.9
m-CF_3	60	101—102	1709	44.8	44.6
m-*i*-C_3F_7	46	97—98.5	1710	50.8	51.1
p-*i*-C_3F_7	52	101—102	1710	51.3	51.1
m-Cl	60	91.5—92	1705	33.0	32.6
p-Cl	58	102—102.5	1708	32.8	32.6

11) A. R. Surrey, *J. Amer. Chem. Soc.*, **69**, 2911 (1947).
12) H. D. Troutman and L. M. Long, *ibid.*, **70**, 3436 (1948).

We have also prepared 3-aryl-4-thiazolidinones (**9**), which carry geminal trifluoromethyl groups at the 2-position, by the reaction of *N*-arylhexafluoroisopropylideneimines with thioglycolic acid (Table 3).

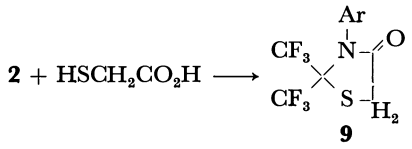

9

Experimental

Hexafluorothioacetone Dimer (1). This compound was prepared according to the method of Knunyants.[7] Bp 109—110 °C; yield, 74% (lit, bp 110—111 °C, yield, 72%).

N-*Arylhexafluoroisopropylideneimines (2).* These compounds were prepared in a similar manner; one example will be described below.

To a stirred mixture of *p*-toluidine (4.3 g, 0.04 mol) and dimethylformamide (40 ml), **1** (7.3 g, 0.02 mol) was added, drop by drop, at room temperature; stirring was then continued for 4 hr at that temperature. The liberated sulfur (0.43 g, 0.013 mol) was removed by filtration, and the filtrate was poured into water. The separated oily material was extracted with diethyl ether, and the extract was dried over magnesium sulfate. After removing the solvent, the residual oil was subjected to vacuum distillation. *N-p*-Tolylhexafluoroisopropylideneimine (**2**, R=*p*-$CH_3C_6H_4$) (3.5 g) (bp 85—86 °C/53 mmHg) was thus obtained in a yield of 35%. IR: 1660 (C=N), 1300, 1218 (C–F) cm^{-1}. NMR (in CCl_4): τ 7.69 (CH_3, s), 2.86—3.38 (arom-H).

Hexafluoroacetone Phenylhydrazone (3). Phenylhydrazine (2.5 g, 0.044 mol), **1** (8.0 g, 0.022 mol), and dimethylformamide (40 ml) were used as in the preceding reaction, and worked up similarly. A fraction with a bp of 91—92 °C/23 mmHg was collected to give **3** (3.7 g, 66%).

Hexafluoroacetone semicarbazone (**4**) was prepared in a similar manner.

Hexafluoroacetone Hydrazone (5) and Azine (6). Anhydrous hydrazine (9.6 g, 0.3 mol) was added, drop by drop, to a solution of **1** (36.4 g, 0.1 mol) in acetonitrile (80 ml), after which the mixture was stirred for 1.5 hr at room temperature. After removing the liberated sulfur by filtration, the filtrate was poured into water and worked up as usual. Two products were obtained by fractional distillation: azine, **6** (3.6 g, 11%) (bp 67—70 °C (lit,[1] bp 67—67.5 °C)) and hydrazone, **5** (15.4 g, 43%) (bp 93—96 °C (lit,[1] bp 95.5—96 °C)).

2-Alkoxy-2-arylaminohexafluoropropanes (7). An example will be given below.

A mixture of *N*-phenylhexafluoroisopropylideneimine (**2**, R=Ph) (3.7 g, 0.015 mol), methanol (6.4 g, 0.19 mol), and potassium hydroxide (1.0 g, 0.015 mol) was refluxed for 5 hr. The usual work-up process gave a product (**7**, R=Me, Ar=Ph), 1.4 g (34%) (bp 85 °C/25 mmHg). IR (KBr): 3306 (N=H), 1258, 1211, 1178 (C–F) cm^{-1}. NMR (in CCl_4): τ 5.50 (OMe), 2.55—3.27 (arom. and NH).

2-Ethylthio-2-arylaminohexafluoropropanes (8). Under a nitrogen atmosphere, a mixture of **2**, R=Ph (2.6 g, 0.011 mol), ethanthiol (0.8 g, 0.013 mol), and potassium hydroxide (0.8 g, 0.012 mol) was stirred for 5 hr at room temperature. The usual work-up process gave **8**, R=Et, Ar=Ph (0.9 g, 27%); bp 84 °C/31 mmHg. IR (KBr): 3286 (N–H), 1257, 1217 (C–F) cm^{-1}. NMR (in CCl_4): τ 7.30 (CH_2, q), 8.80 (CH_3, t), 2.12 (NH, broad), 2.79—3.32 (arom.).

2,2-Bis(trifluoromethyl)-3-aryl-4-thiazolidinones (9). A mixture of *N*-phenylhexafluoroisopropylideneimine (5.68 g), thioglycolic acid (6.0 g), triethylamine (0.5 g), and dried benzene (30 ml) was refluxed under a nitrogen atmosphere for 48 hr, and then the benzene was removed by distillation. The residue solidified on cooling; it was recrystallized from *n*-hexane to give **9**, Ar=Ph (6.3 g, 85%) (mp 97—99 °C). Other *N*-aryl compounds were prepared in a similar manner.

BULLETIN OF THE CHEMICAL SOCIETY OF JAPAN, VOL. 46, 3263—3266 (1973)

The Effect of Acylamino Groups in Diazo-coupling Reactions

Yōji HASHIDA, Kazuo MITSUMURA, Shizen SEKIGUCHI, and Kohji MATSUI
Department of Chemistry, Faculty of Engineering, Gunma University, Tenjincho, Kiryu, Gunma 376

(Received May 23, 1973)

A kinetic study has been made of the coupling reactions of diazonium salts with *N,N*-dialkyl-*N'*-acyl-*m*-phenylenediamines, including *N'*-acetyl- (I, II), *N'*-benzoyl- (III), *N'*-carboethoxy- (IV), and *N'*-*p*-toluenesulfonyl derivatives (V, VI). It was found from the pH dependence of the apparent rate constant that the reactive species of a substrate varies with the pH of the medium, from an undissociated molecule to an anion formed by the ionization of an acylamino group. In the case of I, the activating effect of the dissociated acylamino group seems to be higher than that of the undissociated acylamino group by some 8 powers of ten.

Ordinary diazo-coupling reactions between diazonium ions and aromatic compounds activated by such an electron-releasing substituent as an amino- or phenoxide group are well-known electrophilic aromatic substitutions.[1] In a previous paper,[2] we have shown that a diazonium ion couples not only with the undissociated pyrrole, but also with the pyrrole anion, and that the coupling with the pyrrole anion takes place much more rapidly than that with the undissociated pyrrole, showing that the conjugate base of the pyrrole

1) H. Zollinger, "Azo and Diazo Chemistry," Interscience Publishers, New York, N.Y. (1961), p. 221.

2) K. Mitsumura, Y. Hashida, S. Sekiguchi, and K. Matsui, This Bulletin, **46**, 1770 (1973).

is a powerfully reactive species for this reaction. Although, in the pyrrole, the N–H group participates in ring formation, a similar activation of an aromatic molecule by the ionization of a substituent can be seen in the cases of phenols.[1] However, there has been no study of the acceleration of an aromatic electrophilic reaction by the ionization of a substituent in an aromatic molecule other than those of phenolic substances. From the same point of view, it may be expected that an aromatic compound bearing an acylamino group will provide a reactive substrate for the electrophilic substitution by means of the ionization of the acylamino N–H bond. This assumption has not, however, been proved.

This paper will report on the activation caused by the ionization of an acylamino group in the coupling reaction with *m*-acylamino anilines.

Experimental

Materials. Commercial *N,N*-bis(2-hydroxyethyl)-*N'*-acetyl-*m*-phenylenediamine (I) was recrystallized from methanol. The *N,N*-dimethyl-*N'*-acetyl-*m*-phenylenediamine (II) and *N,N*-dimethyl-*N'*-benzoyl-*m*-phenylenediamine (III) were prepared from *N,N*-dimethyl-*m*-phenylenediamine by acetylation and benzoylation respectively. The *N,N*-dimethyl *N'*-carboethoxy-*m*-phenylenediamine (IV) was prepared from *N,N*-dimethyl-*m*-phenylenediamine and ethyl chloroformate by the method of Schmidt.[3] Recrystallization from petroleum ether gave an analytical sample; mp 59—60 °C. Found: C, 63.73; H, 7.85; N, 13.14%. Calcd for $C_{11}H_{16}N_2O_2$: C, 63.44; H, 7.74; N, 13.44%. The *N,N*-dimethyl-*N'*-(*p*-toluenesulfonyl)-*m*-phenylenediamine (V) was prepared by the reaction of *N,N*-dimethyl-*m*-phenylenediamine with tosyl chloride. Recrystallization from aqueous methanol gave an analytical sample; mp 138—138.5 °C. Found: C, 62.43; H, 6.57; N, 8.17%. Calcd for $C_{15}H_{18}N_2O_2S$: C, 62.07; H, 6.21; N, 8.27%. The *N,N,N'*-trimethyl-*N'*-(*p*-toluenesulfonyl)-*m*-phenylenediamine (VI) was prepared by methylating V with dimethyl sulfate in water in the presence of sodium hydroxide. Recrystallization from methanol gave an analytical sample; mp 154—156 °C. Found: C, 63.30; H, 6.49; N, 9.17%. Calcd for $C_{16}H_{20}N_2O_2S$: C, 63.13; H, 6.62; N, 9.20%. The aromatic amines employed as diazo-components were purified by fractional distillation under reduced pressure before use.

pK_a *Measurements.* The pK_a values of the *N,N*-dimethylamino and *N,N*-(2-hydroxyethyl)amino derivatives (I—VI) were measured spectrophotometrically in the same solvent as that used in the kinetic experiment at 20 °C.

Kinetic Measurements. The rate of the coupling reaction was obtained by measuring the concentration of an azo-compound formed at an appropriate wavelength using a Hitachi 124 type spectrophotometer.[4,5] All the kinetic experiments were carried out in an approproate buffer solution at 20 °C under a constant ionic strength (μ; 0.04). The components of the buffer solution have been described elsewhere.[5] In the presence of a large excess of a substrate, the reaction followed a pseudo-first-order relationship (1):

$$k't = \ln \frac{E_\infty}{E_\infty - E_t} \quad (1)$$

where E_∞ and E_t denote the optical densities at an infinite time and at time t. In every case, the k' value thus obtained was reasonably constant up to at least 80—90% of the reaction. At the end of the kinetic measurements, the acidity of a reaction mixture was measured using a Toa HM-5A-type pH meter, thus confirming the constancy of the acidity of the medium during the reaction.

Results and Discussion

It is well known that *N,N*-dialkyl-*N'*-acyl-*m*-phenylenediamines couple with diazonium salts:[6,7]

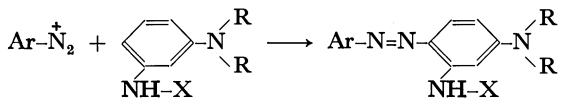

R: H, CH_3, CH_2CH_3, CH_2CH_2OH, etc.
X: $COCH_3$, SO_2CH_3, $CONH_2$, etc.

In this investigation, *N,N*-bis(2-hydroxyethyl)-*N'*-acetyl-*m*-phenylenediamine (I), *N,N*-dimethyl-*N'*-acetyl-*m*-phenylenediamine (II), *N,N*-dimethyl-*N'*-benzoyl-*m*-phenylenediamine (III), *N,N*-dimethyl-*N'*-carboethoxy-*m*-phenylenediamine (IV), *N,N*-dimethyl-*N'*-(*p*-toluenesulfonyl)-*m*-phenylenediamine (V), and *N,N,N'*-trimethyl-*N'*-(*p*-toluenesulfonyl)-*m*-phenylenediamine (VI) were used as coupling components.

Although there was the possibility that more than one azo campound would be formed, thin-layer chromatograms of the reaction products obtained under the conditions employed in the kinetic measurements showed the presence of only one azo compound in every case.

The first-order dependence of the reaction rate on the concentration of a diazonium salt is apparent from the applicability of Eq. (1) to these reactions; the reaction rate (k') also showed a first-order dependence on the substrate concentration at a constant pH. Thus, at any given acidity, the reaction rate can be expressed by Eq. (2):

$$\text{Rate} = k(\text{Ar–}\overset{+}{\text{N}}_2)(\text{Substrate}) \quad (2)$$

To establish the kinetic form of the substrate, the dependence of the apparent rate constant (k') on the acidity of a medium was examined. The results are shown in Fig. 1 by plotting log k' against the pH values in the cases of Compounds I and II. From Fig. 1, it is obvious that there are three distinct regions in the pH-rate profile. For instance, in the case of Compound I, in the pH region below 5.0 log k' decreases with an increase in the acidity of a solution, while in the pH range between 5.0 and 7.0 k' is practically independent of the acidity of the solution. However, in the pH region above 7.0, log k' increases with a decrease in the acidity, and the slope of the line is close to unity in the pH range above 8.0. A similar pH-rate relation-

3) O. Schmidt, *Z. Phys. Chem.*, **58**, 516 (1907).
4) Y. Hashida, K. Nakajima, S. Sekiguchi, and K. Matsui, *Kogyo Kagaku Zasshi*, **72**, 1132 (1969).
5) Y. Hashida, M. Kobayashi, and K. Matsui, This Bulletin, **44**, 2506 (1971).
6) K. H. Schünderhütte, "Methoden der Organischen Chemie (Houben-Weyl)," Band X/3, ed. by E. Müller, George Thieme Verlag, Stuttgart (1965), p. 245.
7) J. Dickery and E. Towne, U.S. 265719 (1953); *Chem. Abstr.*, **49**, 1335f (1955).

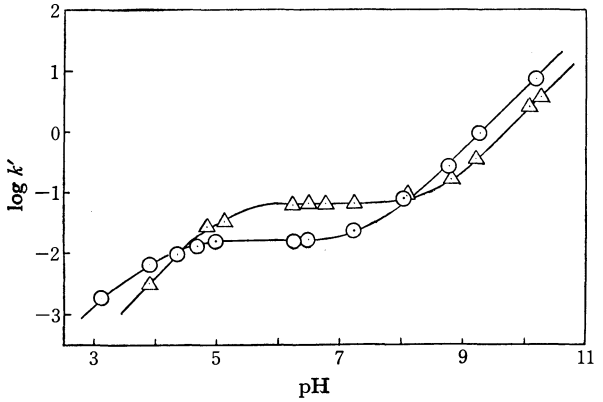

Fig. 1. pH-Rate profile for the reaction of *p*-methylbenzenediazonium salt with *N,N*-bis(2-hydroxyethyl)-*N'*-acetyl-*m*-phenylenediamine (I) (circles, ○), and with *N,N*-dimethyl-*N'*-acetyl-*m*-phenylenediamine (II) (triangles, △) in aqueous solution. (Initial concentration of substrate: 4×10^{-3} M. Initial concentration of diazonium salt: 4×10^{-5} M. k' in min^{-1})

Table 1. Ionization constants of *N,N*-bis(2-hydroxyethyl)amino- or *N,N*-dimethylamino groups of compounds (I—IV)

Compound	Solvent	pK_a
I	Water	3.55
II	Water	4.70
III	50% Methylcellosolve	3.80
IV	50% Methanol	4.36
V	50% Methylcellosolve	3.27
VI	50% Methylcellosolve	3.35

ship was also found to hold in the case of Compound II.

The pK_a value of I is 3.55, as is shown in Table 1. Therefore, the finding that the k' value decreased with an increase in the acidity of the medium in the pH region below 5 can be explained from the fact that the concentration of the free amine decreases with an increase in the acidity by means of the protonation at the *N,N*-bis(2-hydroxyethyl)amino group. The observed constancy of k' in the pH range between 5.0 and 7.0 may be due to the constancy of the concentration of the free amine in this region. Consequently, in the pH region below 7.0 the kinetic expression is given by Eq. (3), which is entirely consistent with that of the coupling reaction of ordinary aromatic amine:[1]

$$\text{Rate} = k_2(\text{Ar}\text{-}\overset{+}{\text{N}}_2)\left(\text{C}_6\text{H}_4(\text{NH-X})\text{-N}(\text{R})_2\right) \quad (3)$$

However, the finding in the pH region above 8.0 indicates the presence of a reactive species other than a free amine; the reactive species may be an anion formed by the ionization of the acylamino group, judging from the fact that the slope of the line in the pH-rate profile is close to unity, which may be understood by assuming that the concentration of the reactive anion increases by a factor of ten per pH unit in the given pH range. Accordingly, the kinetic equation in this pH region is expressed by Eq. (4):

$$\text{Rate} = k_2(\text{Ar}\text{-}\overset{+}{\text{N}}_2)\left(\text{C}_6\text{H}_4(\overset{\ominus}{\text{N}}\text{-X})\text{-N}(\text{R})_2\right) \quad (4)$$

It is well known that, in the coupling reaction of phenol, it is the phenoxide ion that reacts with a diazonium ion in a neutral or weak acidic solution. Although *N,N*-dialkyl-*N'*-acyl-*m*-phenylenediamine may be a weaker acidic substance than phenol, it is reasonable to assume that their conjugate bases also couple with a diazonium ion in a manner similar to that described above, even in a neutral solution.

The difference between the activating effects of an acetylamino and its conjugate base can be obtained by comparing their reactivities. The second-order rate constant (k_2) can be calculated according to Eq. (3) or Eq. (4) by dividing the first-order rate constant (k') by the stoichiometric concentration of the undissociated substrate or by the anion concentration respectively. However, the calculation of the anion concentration requires the pK_a value of an acetylamino compound. Unfortunately, in water, the measurements of the pK_a value of an acetylamino compound is impossible because of its high reactivity to hydrolytic cleavage in a strong alkaline solution. Therefore, the exact concentration of an anion under kinetic conditions can not be accurately determined. However, in isopropyl alcohol the acidity of acetanilide is known to be close to that of methanol.[8] On the other hand, the pK_a value of methanol was measured to be 15.5 in water.[9] Therefore, the pK_a value of acetanilide in water may also be close to this value. On the basis of the presence of an electron-releasing *N,N*-dialkylamino group in the *meta* position, I is assumed to be a weaker acid than acetanilide; therefore, we assume that the pK_a value of I is 16.0. By using this value, we obtained the rate constants (k_2) of 4.1 ($l\cdot mol^{-1}\cdot min^{-1}$) for the reaction of the undissociated molecule and 1.1×10^9 ($l\cdot mol^{-1}\cdot min^{-1}$) for the reaction of the anion; this implies that the activating effect of the conjugate base of an acetylamino group is higher than that of

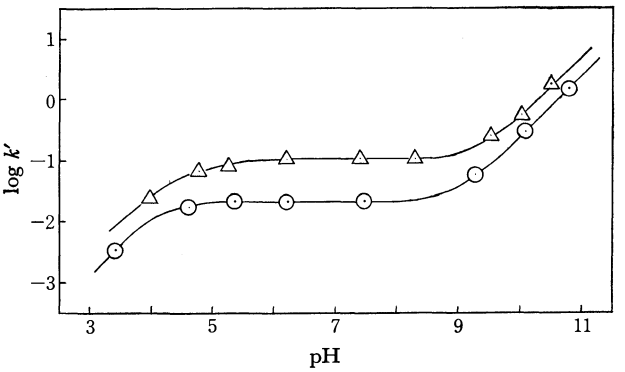

Fig. 2. pH-Rate profile for the reaction of *p*-methoxybenzenediazonium salt with *N,N*-dimethyl-*N'*-benzoyl-*m*-phenylenediamine (III) (circles, medium: 50 vol% methylcellosolve-water), and with *N,N*-dimethyl-*N'*-carboethoxy-*m*-phenylenediamine (IV) (triangles, medium: 50 vol% methanol-water). Concentration of reactants was identical to those described in Fig. 1. k' in min^{-1})

8) J. Hine and M. Hine, *J. Amer. Chem. Soc.*, **74**, 5266 (1952).
9) P. Ballinger and F. A. Long, *ibid.*, **82**, 795 (1960).

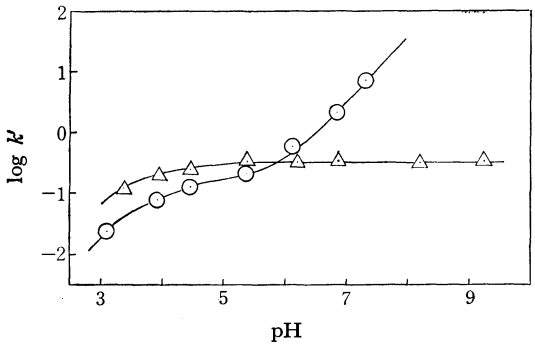

Fig. 3. pH-Rate profile for the reaction of *m*-methylbenzenediazonium salt with *N,N*-dimethyl-*N'*-(*p*-toluenesulfonyl)-*m*-phenylenediamine (V) (circles), and with *N,N,N'*-trimethyl-*N'*-(*p*-toluenesulfonyl)-*m*-pnenylenediamine (VI) (triangles) in 50 vol% methylcellosolve–water. (Concentration of reactions was identical to those described in Fig. 1. k' in min^{-1})

the parent group by some 8 powers of ten.

From a similar point of view, the coupling reactions with *N'*-benzoyl- (III), *N'*-carboethoxy- (IV), and *N'*-(*p*-toluenesulfonyl) (V) derivatives were also investigated. The pH dependences of the rate constant (k') in these cases are given in Figs. 2 and 4.

From these figures, it is obvious that the pattern of the pH-rate profile of these reactions is esesntially the same as that in the case of Compound I, although the pH region in which an anion enters the reaction varies considerably.

Additional evidence for the pariticpation of an anion was obtained from the reaction of *N,N,N'*-trimethyl-*N'*-(*p*-toluenesulfonyl)-*m*-phenylenediamine (VI), containing no acidic hydrogen atom in the acylamino group. In this case, the reaction rate was found to be independent of the pH value, even in an alkaline region, as can be seen in Fig. 3; this finding supports the validity of the view presented above.

BULLETIN OF THE CHEMICAL SOCIETY OF JAPAN, VOL. 46, 3266—3269 (1973)

The Synthesis of 1,2-Diamino- and 1,2,3-Triaminoazulene Derivatives[1)]

Tetsuo Nozoe,* Toyonobu Asao,** and Masao Kobayashi***

Department of Chemistry, Faculty of Science, Tohoku University, Aramaki, Aoba, Sendai 980

(Received May 28, 1973)

The diazo coupling reaction of 2-amino- (I), 2-acetamido-, and 2-amino-1-ethoxycarbonyl-azulene with *p*-toluene diazonium salt gave the corresponding 1-(*p*-tolylazo)azulene derivatives, II, V, and VIII respectively, in good yield; 2-amino-1,3-di(*p*-tolylazo)azulene (III) was also obtained by the reaction of I and two molar equivalents of *p*-toluene diazonium salt. The catalytic reduction of V and VIII afforded 2-acetamido-1-aminoazulene and ethyl 1,2-diaminoazulene-3-carboxylate as hydrochloride. The similar reduction of II and III yielded only a resinous product, and 1,2-diamino- or 1,2,3-triaminoazulene could not be isolated, not even as their salts. However, the reductive acetylation of II and III afforded the corresponding polyacetamidoazulenes. The ultraviolet and visible absorption spectra of these azulenes are indicated.

1-, 2-, 4-, and 6-aminoazulenes have been synthesized[2)] by several groups all as unstable compounds except for 2-aminoazulene,[2c)] and detailed investigation of 1-aminoazulene concerning to its basicity and spectroscopic properties have been reported.[2b)] Syntheses of polyaminoazulenes have also been attempted, but none of the polyaminoazulene have been reported except for their derivatives, 1,3-diacetamidozaulene[3)] and diethyl 2,5- and 2,6-diaminoazulene-1,3-dicarboxylate.[2e)]

In the present investigation, the syntheses of 1,2-diamino- and 1,2,3-triaminoazulene were attempted in order to compare their stabilities, basicities, and spectroscopic properties with those of aromatic amines and other aminoazulenes; our results will be reported herein.

Among the synthetic courses of these polyaminoazulenes, the reduction of 2-amino-1(or 1,3-di)-arylazoazulene derivatives was chosen.

The reaction of 2-aminoazulene (I)[2c)] and one molar equivalent of *p*-toluene diazonium salt in ethanol easily afforded 2-amino-1-(*p*-tolylazo)azulene (II) in a good yield, besides a small amount of 2-amino-1,3-di-(*p*-tolylazo)azulene (III). Compound (III) was also obtained by the reaction of I and two molar equivalents of the diazonium salt. The structure of the products

* Present address: No. 811, 2-5-1, Kamiyoga, Setagaya-ku, Tokyo 158.

** Present address: Department of Chemistry, College of General Education, Tohoku University, Kawauchi, Sendai 980.

*** Present address: Mitsubishi Rayon Co., Ltd., Otaka, Hiroshima 739-06.

1) Presented at the Tohoku Local Meeting of the Chemical Society of Japan, Yamagata, October, 1961; M. Kobayashi, Master Thesis, Tohoku University, Sendai, March, 1962.

2) a) A. J. Anderson, Jr., J. A. Nelson, and J. J. Tazuma, *J. Amer. Chem. Soc.*, **75**, 4980 (1953). b) J. Schulze and E. Heilbronner, *Helv. Chim. Acta*, **41**, 1492 (1958). c) T. Nozoe, S. Matsumura, Y. Murase, and S. Seto, *Chem. & Ind.*, **1955**, 1257; T. Nozoe, S. Sato, S. Matsumura, and T. Asano, *Proc. Japan Acad.*, **32**, 339 (1956). d) D. H. Reid, W. H. Stafford, and J. P. Ward, *J. Chem. Soc.*, **1958**, 1100. e) T. Nozoe, K. Takase, and M. Tada, This Bulletin, **36**, 1006 (1963).

3) A. G. Anderson, Jr., R. Scotoni, Jr., E. J. Cowles, and C. G. Fritz, *J. Org. Chem.*, **22**, 1193 (1957); A. G. Anderson, Jr., C. G. Fritz, and R. Scotoni, Jr., *J. Amer. Chem. Soc.*, **79**, 6511 (1957).

4) T. Nozoe, S. Seto, T. Asano, and T. Asao, to be published.

are assumed from the general reactivity of azulenes.[2a] By a similar method, 2-acetamidoazulene (IV)[2c] gave 2-acetamido-1-(*p*-tolylazo)azulene (V), and ethyl 2-aminoazulene-1-carboxylate (VI)[2c] and its 7-isopropyl derivative (VII)[4] afforded the corresponding 3-*p*-tolylazo derivatives (VIII and IX respectively). 2-Amino-5-isopropyl-1,3-di(*p*-tolylazo)azulene (X) was also obtained from 2-amino-5-isopropylazulene.[2c]

In contrast with the cases of Compounds IV, VI, and VII, the azo-coupling reactions of ethyl 2-acetamidoazulene-1-carboxylate[2c] and its 7-isopropyl derivative[4] were unsuccessful, and the starting materials were recovered.

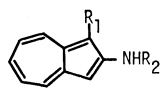

I $R_1 = R_2 = H$

II $R_1 = N{=}NC_6H_4CH_3(p)$, $R_2 = H$

IV $R_1 = H$, $R_2 = COCH_3$

V $R_1 = N{=}NC_6H_4CH_3(p)$, $R_2 = COCH_3$

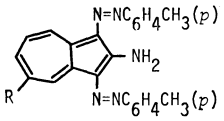

III R = H

X R = *i*-Pr

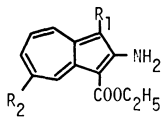

VI $R_1 = R_2 = H$

VII $R_1 = H$, $R_2 = i$-Pr

VIII $R_1 = N{=}NC_6H_4CH_3(p)$, $R_2 = H$

IX $R_1 = N{=}NC_6H_4CH_3(p)$, $R_2 = i$-Pr

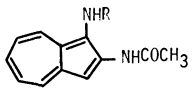

XI R = $COCH_3$

XIII R = H

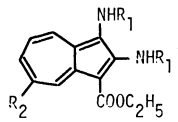

XIV $R_1 = R_2 = H$

XV $R_1 = H$, $R_2 = i$-Pr

XVI $R_1 = COCH_3$, $R_2 = H$

XVII $R_1 = COCH_3$, $R_2 = i$-Pr

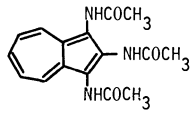

XII

It is considered that such an unreactivity of the 2-acetamidoazulene derivatives for the electrophilic attack may be attributable to a contribution of the resonance form shown below caused by the electron-attractive effect of the ethoxycarbonyl group. This assumption is supported by the following spectroscopic data: ethyl 2-acetamidoazulene-1-carboxylate shows ν_{CO} at the low frequency of 1650 cm^{-1}, and NMR signals at a lower field (δ 7.3—7.6 (m, H_5—H_7), 8.06 (s, H_3), 8.27 (d, J=9 Hz, H_4), 9.03 (d, J=9 Hz, H_8), 11.45 (bs, NH), and 2.33 (NCH_3)) than the corresponding signals of 2-acetamidoazulene (δ 7.0—7.6 (m, H_1, H_3, H_5—H_7), 7.90 (NH), 8.15 (d, J=9 Hz, H_4, H_8) and 2.28 (NCH_3)).

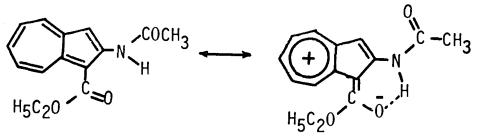

In the reduction of II in ethyl acetate using 5% Pd-C as the catalyst, two molar equivalents of hydrogen were consumed, but the product was very unstable and was rapidly decomposed to a black resinous compound and could not be isolated even as hydrochloride or picrate. Therefore, the reductive acetylation of II was attempted in acetic anhydride; 1,2-diacetamidoazulene (XI) was thus obtained in a good yield as stable violet crystals. 1,2,3-Triaminoazulene also could not be isolated in the free state by the reduction of III; however, the reductive acetylation of III afforded 1,2,3-triacetamidoazulene (XII) as yellowish-green crystals. The 2-acetamido-1-aminoazulene (XIII) obtained by the reduction of V was also so unstable that it was isolated only as hydrochloride. Various attempts to isolate the free amino compound (XIII) from the hydrochloride failed. The acetylation of the hydrochloride or the reductive acetylation of V yielded the previously-obtained 1,2-diacetamidoazulene (XI).

From the reduction mixture of ethyl 2-amino-3-(*p*-tolylazo)azulene-1-carboxylate (VIII), ethyl 2,3-diaminoazulene-1-carboxylate (XIV) could not be isolated; however, monohydrochloride of XIV was obtained in a good yield as golden yellow crystals. In a similar manner, monohydrochloride of ethyl 1,2-diamino-5-isopropylazulene-3-carboxylate (XV) was obtained from the azo compound (IX). These hydrochlorides are considerably stable, but are gradually changed to black resin, and the attempted isolations of the free amines, XIV and XV, from the hydrochlorides resulted in resinification. The acetylation of these hydrochlorides or the reductive acetylations of VIII and IX afforded the corresponding diacetates (XVI[5] and XVII respectively).

In view of the facts that the 2-amino group may form a stable hydrogen bonding with the ethoxycarbonyl group and that the 1- and 3-positions of the azulene nucleus have the highest electron densities, the 1-amino group in XIV must have a higher basicity than the 2-amino group; therefore, it is considered that hydrogen chloride may form a salt with the 1-amino group, as is shown below.

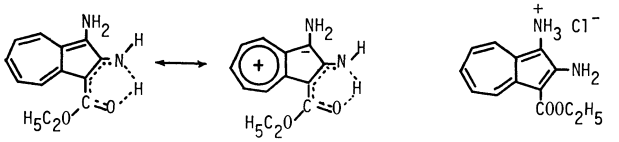

The ultraviolet and visible absorption maxima of the aminoazulene and *p*-tolylazoazulene derivatives obtained above are shown in Table 1.

The visible absorption maxima shown in Table 1, together with that of 2-acetamidoazulene [λ_{max}^{MeOH} nm

5) 1,2-Diacetamidoazulene (XVI) has also been obtained by the reduction of ethyl 2-amino-3-nitrosoazulene-1-carboxylate; T. Nozoe, P.W. Yang, H. Ogawa, and T. Toda, This Bulletin, **41**, 2095 (1968).

Table 1. Ultraviolet and visible absorption maxima

Compounds	λ_{max}^{MeOH} nm (log ε)		
II	238 (4.27),	285 (4.29),	316 (4.28),
	375^{sh} (4.64),	388 (4.66),	535^{sh} (3.69)
III	254 (4.19),	355^{sh} (4.43),	414 (4.72),
	548 (3.85)		
VIII	254 (4.23),	295^{sh} (4.42),	328 (4.51),
	345^{sh} (4.35),	385 (4.54),	510 (4.04)
IX	259 (4.16),	328 (4.56),	345^{sh} (4.40),
	390 (4.54),	500 (4.05)	
X	235^{sh} (4.20),	256 (4.24),	345^{sh} (4.33),
	355^{sh} (4.42),	418 (4.75),	542 (3.86)
XI	242 (4.25),	297 (4.81),	345^{sh} (3.63),
	360 (3.79),	380 (3.81),	395^{sh} (3.32),
	560 (2.50)		
XII	246 (4.34),	307 (4.72),	320^{sh} (4.36),
	365 (3.69),	375 (3.55),	600 (2.54)
XVI	235^{sh} (4.31),	248 (4.33),	314 (4.72),
	360 (3.82),	370^{sh} (3.77),	395^{sh} (3.21),
	535 (2.68)		
XVII	255 (4.33),	318 (4.72),	357 (3.85),
	540 (2.80)		

(log ε); 540 (2.44) and 580^{sh} (2.38)] indicate that the acetamido groups at the 1- and 3-positions cause the absorption maxima to shift to longer wavelengths, according to the expanded Plattner rule.[3,6]

Experimental[7]

Coupling Reaction of 2-Aminoazulene with p-*Toluene Diazonium Chloride.* To a stirred solution of 2 g of 2-aminoazulene in a mixture of 30 ml of ethanol and 10 ml of dioxane, a solution of *p*-toluenediazonium chloride prepared from 1.79 g of *p*-toluidine was added at once under cooling with ice. After stirring for 2 hr, the solution was allowed to stand at room temperature overnight. A deep brown solid (3.4 g) was then filtered out; to the filtrate water (150 ml) was added, and it was extracted with chloroform. The extract was washed with water, dried over sodium sulfate and evaporated, leaving a deep reddish semi-solid. A benzene solution of the combined solids was chromatographed on an alumina column and eluted with benzene. The first effluent gave brown crystals (mp 180—195 °C), which were recrystallized from ethyl acetate to give 2-amino-1-3-di(*p*-tolylazo)azulene (III) (400 mg) as deep brown needles (mp 199—200 °C).

Found: C, 75.80; H, 5.66; N, 18.19%. Calcd for $C_{24}H_{21}N_5$: C, 75.96; H, 5.58; N, 18.46%.

The second effluent gave brown crystals (mp 150—160 °C), which were recrystallized from ethyl acetate to afford 2-amino-1-(*p*-tolylazo)azulene (II) (3.1 g) as brown crystals (mp 162—163 °C).

Found: C, 78.00; H, 5.78; N, 15.74%. Calcd for $C_{17}H_{15}N_3$: C, 78.13; H, 5.79; N, 16.08%.

*2-Acetamido-1-(*p-*tolylazo)azulene (V).* a) To a stirred solution of 185 mg of 2-acetamidoazulene in 4 ml of ethanol, a solution of *p*-toluene diazonium chloride prepared from 120 mg of *p*-toluidine was added at once under cooling with ice. After stirring for 2 hr, the solution was made slight alkaline by the addition of sodium hydrogen carbonate. Brown precipitate was then filtered out, dried, and dissolved in benzene, and the solution was chromatographed on an alumina column. The recrystallization of the crystals obtained from the effluent from ethanol gave 136 mg of V as reddish violet needles (mp 185—186 °C).

Found: C, 74.79; H, 6.01; N, 13.85%. Calcd for $C_{19}H_{17}ON_3$: C, 75.22; H, 5.65; N, 13.85%.

b) The acetylation of 50 mg of 2-amino-1-(*p*-tolylazo)-azulene with acetic anhydride gave 40 mg of V (mp 185—186 °C, undepressed on admixture with a sample prepared by Method a)).

Hydrochloride of 2-Acetamido-1-aminoazulene (XIII). A solution of 210 mg of V in 15 ml of ethyl acetate was submitted to catalytic hydrogenation in the presence of 50 mg of 5% Pd-C. After two molar equivalents of hydrogen had been uptaken, the catalyst was filtered off; the filtrate was shaken with 5 ml of concentrated hydrochloric acid, thus affording 110 mg of precipitate. Recrystallization from water gave 95 mg of black-violet needles (mp over 280 °C).

Found: C, 60.80; H, 5.22; N, 11.57%. Calcd for $C_{12}H_{12}ON_2 \cdot HCl$: C, 60.89; H, 5.11; N, 11.84%.

1,2-Diacetamidoazulene (XI). A solution of 1.22 g of 2-amino-1-(*p*-tolylazo)azulene in 190 ml of acetic anhydride was submitted to catalytic hydrogenation in the presence of 500 mg of 5% Pd-C. After two molar equivalents of hydrogen had been uptaken, the catalyst was filtered and the filtrate was evaporated, leaving a dark yellow residue, from which 55 mg of acetotoluidide were obtained. After the catalyst had been washed thoroughly with acetic acid, the washings were evaporated to give 540 mg of violet crystals. Recrystallization from acetic acid gave 1,2-diacetamidoazulene as violet crystals (mp 278 °C (decomp.)).

Found: C, 69.25; H, 5.61; N, 11.46%. Calcd for $C_{14}H_{14}O_2N_2$: C, 69.40; H, 5.83; N, 11.56%.

The same compound was also obtained in a good yield by the acetylation of the hydrochloride of 2-acetamido-1-aminoazulene with acetic anhydride.

1,2,3-Triacetamidoazulene (XII). A solution of 500 mg of 2-amino-1,3-di(*p*-tolylazo)azulene (III) in 100 ml of acetic anhydride was submitted to catalytic hydrogenation in the presence of 250 mg of 5% Pd-C. After four equivalents of hydrogen had been uptaken, the catalyst was filtered and washed with acetic acid. The combined filtrate and washing was concentrated to a small volume, thus affording yellowish-orange crystals; these crystals were recrystallized from ethanol to gave 276 mg of 1,2,3-triacetamidoazulene as yellowish-green crystals (mp 271—272 °C).

Found: C, 64.11; H, 5.63; N, 13.97%. Calcd for $C_{16}H_{17}O_3N_3$: C, 64.20; H, 5.72; N, 14.04%.

*Ethyl 2-Amino-3-(*p-*tolylazo)azulene-1-carboxylate (VIII).* To a solution of 215 mg of ethyl 2-aminoazulene-1-carboxylate in 4 ml of ethanol, a solution of *p*-toluenediazonium chloride prepared from 118 mg of *p*-toluidine was added under cooling with ice. After having been allowed to stand overnight, the solution was made slight alkaline; the precipitate was filtered and washed with water. A solution of the solid in benzene was chromatographed on an alumina column; subsequent recrystallization from ethanol gave 240 mg of ethyl 2-amino-3-(*p*-tolylazo)azulene-1-carboxylate as deep reddish crystals (mp 120—121 °C).

Found: C, 71.98; H, 5.34; N, 12.76%. Calcd for $C_{20}H_{19}O_2N_3$: C, 72.05; H, 5.74; N, 12.61%.

Hydrochloride of Ethyl 2,3-Diaminoazulene-1-carboxylate (XIV). A solution of 200 mg of ethyl 2-amino-3-(*p*-tolylazo)azulene-

6) *Cf.* E. Heilbronner, "Non-Benzenoid Aromatic Compounds," ed. by D. Ginsbrug, Interscience Publ., New York (1959), pp. 218—254; T. Nozoe, and T. Asao, "Dai-Yuki Kagaku (Comprehensive Organic Chemistry)," **13**, Asakura Shoten, Tokyo (1960), pp. 450—456.

7) All melting points are uncorrected.

1-carboxylate in 15 ml of ethyl acetate was submitted to catalytic hydrogenation in the presence of 50 mg of 5% Pd-C. After two molar equivalents of hydrogen had been uptaken, the catalyst was filtered and washed with ethyl acetate; the combined filtrate and washing was shaken with concentrated hydrochloric acid to give yellowish-orange crystals. Recrystallization from dilute hydrochloric acid gave 170 mg of XIV as golden yellow needles (mp over 260 °C).

Found: C, 58.33; H, 5.33; N, 10.91%. Calcd for $C_{13}H_{14}O_2N_2 \cdot HCl$: C, 58.45; H, 5.67; N, 10.51%.

Picrate of ethyl 2,3-diaminoazulene-1-carboxylate. Mp changed to black from around 215 °C.

Found: C, 49.67; H, 3.67; N, 15.28%. Calcd for $C_{19}H_{17}O_9N_5$: C, 49.67; H, 3.73; N, 15.25%.

Ethyl 2,3-Diacetamidoazulene-1-carboxylate (XVI). A solution of 150 mg of hydrochloride of XIV in acetic anhydride (1 ml) was heated on a water bath for 30 min. The excess acetic anhydride was then removed to leave a violet residue, which was dissolved in benzene; the solution was then chromatographed on an alumina column. Recrystallization from benzene gave 160 mg of XVI as light purple needles (mp 216—218 °C).

Found: C, 65.20; H, 5.57; N, 8.66%. Calcd for $C_{17}H_{18}O_4N_2$: C, 64.95; H, 5.77; N, 8.91%.

Ethyl 2-Amino-5-isopropyl-1-(p-tolylazo) azulene-3-carboxylate (IX). To a stirred solution of 210 mg of ethyl 2-amino-5-isopropylazulene-3-carboxylate in 3 ml of ethanol, a solution of *p*-toluene diazonium chloride prepared from 150 mg of *p*-toluidine was added under cooling with ice. After stirring for 2 hr, the solution was allowed to stand at room temperature overnight. The precipitate was filtered, and dissolved in benzene, and the solution was chromatographed on an alumina column. The effluent afforded reddish crystals, which were recrystallized from ethanol to give ethyl 2-amino-5-isopropyl-1-(*p*-tolylazo)azulene-3-carboxylate (220 mg) as reddish-brown crystals (mp 118—120 °C).

Found: C, 73.35; H, 6.51; N, 11.04%. Calcd for $C_{23}H_{25}O_2N_3$: C, 73.57; H, 6.71; N, 11.19%.

2-Amino-1,3-di(p-tolylazo)-5-isopropylazulene (X). To a stirred solution of 92 mg of 2-amino-5-isopropylazulene in 2 ml of ethanol, a solution of *p*-toluene diazonium chloride prepared from 120 mg of *p*-toluidine was added. After standing for a day, water was added and then extracted with benzene; the solution was subsequently chromatographed on an alumina column, 110 mg of 2-amino-1,3-di(*p*-tolylazo)-5-isopropylazulene as yellow-brown crystals (mp 170—171 °C (from ethyl acetate)) being thus obtained.

Found: C, 76.86; H, 6.15; N, 16.43%. Calcd for $C_{27}H_{27}N_5$: C, 76.93; H, 6.46; N, 16.62%.

Hydrochloride of Ethyl 1,2-Diamino-5-isopropylazulene-3-carboxylate (XV). A solution of 1 g of IX in 80 ml of ethyl acetate was submitted to catalytic hydrogenation in the presence of 300 mg of 5% Pd-C. After two molar equivalents of hydrogen had been uptaken, the catalyst was filtered; the filtrate was shaken with 10 ml of concentrated hydrochloric acid to give 380 mg of hydrochloride of XV as yellow crystals; the mp changed to black from around 250 °C, after washing with ethyl acetate.

Found: C, 62.03; H, 6.48; N, 8.71%. Calcd for $C_{16}H_{20}O_2N_2 \cdot HCl$: C, 62.23; H, 6.85; N, 9.07%.

Ethyl 1,2-Diacetamido-5-isopropylazulene-3-carboxylate (XVII). A solution of 50 mg of hydrochloride of XV in 0.3 ml of acetic anhydride was heated on a water bath for 30 min. The solvent was then removed; the residue was purified by chromatography (alumina, benzene) and then recrystallized from cyclohexane to give 30 mg of XVII as light purple needles (mp 162—164 °C).

Found: N, 7.62%. Calcd for $C_{20}H_{24}O_4N_2$: N, 7.86%.

This work was financially supported by grants from the Ministry of Education of Japan and the Sankyo Co., Ltd., to which the authors' thanks are due.

Hydrolyses of *p*-Nitrophenyl(Oligodeoxyribonucleotide Succinate)s by Oligodeoxyribonucleotide *N*-Acetylhistidates on Polycytidylic Acid

Takeo SHIMIDZU* and Robert L. LETSINGER**

* *Department of Hydrocarbon Chemistry, Faculty of Engineering, Kyoto University, Kyoto 606*

** *Department of Chemistry, Northwestern University, Evanston, Illinois, U.S.A.*

(Received February 5, 1973)

The hydrolyses of *p*-nitrophenyl(oligonucleotide succinate)s, in which the oligonucleotides are *d*GpG, *d*GpT, *d*GpC, *d*GpA, and *d*GpGpG, by oligonucleotide *N*-acetylhistidates, in which the oligonucleotides are *d*GpG, *d*GpT, *d*GpC, *d*GpA, and *d*GpGpG, or by *d*GpG nicotinate were carried on polycytidylic acid (Poly C). While the hydrolysis did not occur at lower concentrations of them, it did take place at moderate concentrations, in the presence of Poly C. From the kinetics of the hydrolysis, it was concluded that the interaction between those oligonucleotide derivatives and Poly C was homogeneous at lower concentrations of them and heterogeneous at higher concentrations. The change in the viscosity of the reaction system was correlated with the kinetical results. The heterogeneity in the interaction can be explained as a contiguous stacking of the oligonucleotide derivatives on Poly C. The tendency of the contiguous stacking was great in *d*GpGpG *N*-acetylhistidate. The rate of the hydrolysis of Poly C was higher than that without Poly C. The order in magnitude of the interaction between the oligonucleotide derivatives and Poly C was *d*GpGpG-derivative>*d*GpGp-derivative>*d*GpC-derivative>*d*GpA-derivative>*d*GpT-derivative.

For the study of a chemical reaction on a macromolecule, it is very important to make clear the features of the interaction of a reactant onto the macromolecule. An interaction between polynucleotide and oligonucleotide will play an important role in the condensation of the oligonucleotide on the polynucleotide.

In continuation of an earlier study,[1] the present paper will report on the hydrolyses of *p*-nitrophenyl (oligodeoxyribonucleotide succinate)s, such as *p*-nitrophenyl (deoxyguanylyldeoxyguanosine succinate) (NPS-*d*GpG), -(deoxyguanylylthymidine succinate) (NPS-*d*GpT), -(deoxyguanylyldeoxycytidine succinate) (NPS-*d*GpC), -(deoxyguanylyldeoxyadenosine succinate) (NPS-*d*GpA), and -(deoxyguanylyldeoxyguanylyldeoxyguanosine succinate) (NPS-*d*GpGpG), by oligodeoxyribonucleotide *N*-acetylhistidates, such as deoxyguanylyldeoxyguanosine *N*-acetylhistidate (AH-*d*GpG), deoxyguanylylthymidine- (AH-*d*GpT), deoxyguanylyldeoxycytidine- (AH-*d*GpC), deoxyguanylyldeoxyadenosine- (AH-*d*GpA), and deoxyguanylyldeoxyguanylyldeoxyguanosine (AH-*d*GpGpG), and by deoxyguanylyldeoxyguanosine nicotinate (N-*d*GpG), on polycytidylic acid (Poly C). The hydrolysis of *p*-nitrophenyl(oligodeoxyribonucleotide succinate) proceeds by means of a nucleophilic reaction of an imidazolyl or nicotinyl group present in the latter derivatives. Though the substances used in the present work are not pure and homogeneous, they can still be used in substantially clarifying the features of the interaction of those reactants onto the macromolecule, Poly C.

The interaction between nucleotides is specific and selective, and its magnitude depends on the degree of polymerization of the nucleotides, the concentration of the nucleotides, the ionic strength of the solution, *etc.*[2] Even though guanosine is most liable to stack, no hypochromicity was, in general, observed in the cases of the guanosine dimer and Poly C at which concentrations were of the order of 10^{-4} M.[3] In the case of the enzymatic polymerization of oligonucleotide by DNA-dependent RNA polymerase, the effective degree of polymerization of the oligonucleotide was elucidated to be 6—7.[4] Nevertheless, a complex formation between Poly C and deoxyguanosine-5′-phosphate was suggested by the infrared spectrum under conditions of a higher concentration and a lower temperature.[5] Further, base-base interactions were observed in the dinucleotide model by means of studying the emission spectrum,[6] and in dinucleotide by means of studying the proton magnetic resonance spectrum.[7]

While the interaction between polynucleotide, Poly C, and the oligonucleotide derivatives used is complex, a characteristic mode of interaction is deduced in the present study of the hydrolysis.

Results and Discussion

From the mixing curves for Poly C and NPS-*d*GpG and for Poly C and AH-*d*GpG at the total nucleotide concentration of 7×10^{-4} M, the maximal hypochromicities which occurred at the minimal points were found to be about 1.0% and 2.5% respectively. The larger hypochromicity of the latter might be ascribed to the interaction between the histidyl moiety and the nucleotidic base.

Fig. 1 shows the hydrolysis of NPS-*d*GpG by AH-*d*GpG with Poly C and without Poly C. The rate[8] of the hydrolysis was negligible when the ratio of NPS-

1) T. Shimidzu and R. L. Letsinger, This Bulletin, **44**, 584 (1971).

2) R. Naylor and P. T. Gilham, *Biochemistry*, **5**, 2722 (1966).

3) M. N. Lipsett, *J. Biol. Chem.*, **239**, 1256 (1964).

4) N. K. Gupta, E. Ohtsuka, H. Weber, S. H. Chang, and H. C. Khorana, *Proc. Natl. Acad. Sci. U. S.*, **60**, 285 (1968).

5) F. B. Howard, J. Fraser, M. N. Lipsett, and H. T. Miles, *Biochem. Biophys. Res. Commun.*, **17**, 93 (1964).

6) D. T. Browne, J. Eisinger, and N. J. Leonard, *J. Amer. Chem. Soc.*, **90**, 7302 (1968).

7) C. C. McDonald and W. D. Phillips, *ibid.*, **91**, 1513 (1969).

8) The rate, R, was defined as the increase of *p*-nitrophenol concentration per unit time and per concentration of histidyl or nicotinyl group, at the initial stage of the hydrolysis; $R=[p\text{-nitrophenol}]/([N\text{-acetylhistidine in AH-derivative}]\times t)$ or $R=[p\text{-nitrophenol}]/([\text{nicotinic acid in } N\text{-derivative}]\times t)$.

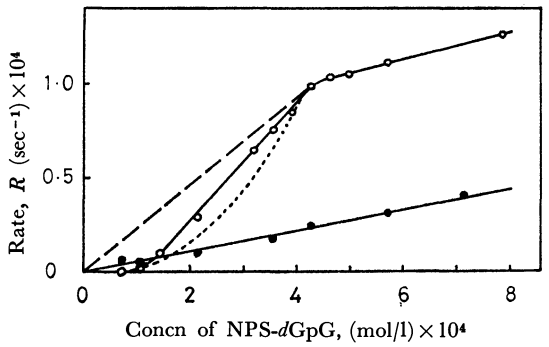

Fig. 1. The total rate of hydrolysis of NPS-*d*GpG by AH-*d*GpG *vs.* their concentration.
Solution; EtOH: H_2O=1 : 100 (0.01M $MgCl_2$, 0.0001M $Mg(OAc)_2$, buffered at a pH being 7.9 with tris(hydroxymethyl)aminomethane; Temperature; 5°C.
○, presence of Poly C (0.35×10^{-3} mol/l).
●, absence of Poly C.

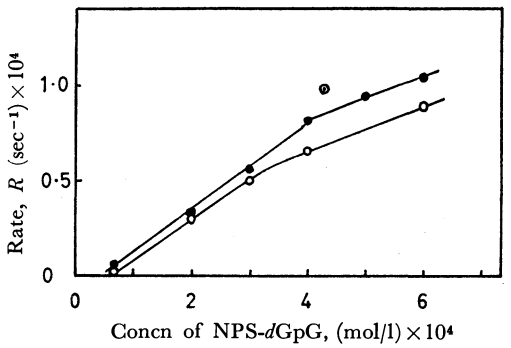

Fig. 2. The total rate of hydrolysis of NPS-*d*GpG by AH-*d*GpG at a constant concentration of AH-*d*GpG.
Conditions are the same in Fig. 1.
○; [AH-*d*GpG]=2.0×10^{-4} mol/l
●; [AH-*d*GpG]=3.0×10^{-4} mol/l
⊙; [AH-*d*GpG]=4.3×10^{-4} mol/l (taken from Fig. 1)

*d*GpG and AH-*d*GpG to Poly C was less than 0.2, but it increased linearly when the ratio exceeded 0.3. When the ratio was over 1.3 the rate of increase of the hydrolysis with Poly C was parallel to that without Poly C. On the other hand, the hydrolysis rate without Poly C was proportional to the amount of the NPS-*d*GpG and AH-*d*GpG, and the line passed through the point of origin.

From the fact that the hydrolysis of the reactants in the presence of Poly C was not observed at lower concentrations, it can be concluded that the interaction between dinucleotide derivatives and Poly C is statistically homogeneous, so that the distance between the two dinucleotide derivatives is too long to cause the hydrolysis reaction. If the two reactants are stacked on Poly C so as to be contiguous with each other, the hydrolysis reaction takes place and the hydrolysis rate can be shown by the broken line[9] in Fig. 1. From the other fact that the hydrolysis rate increased linearly with the amount of the dinucleotide derivatives in the ratio range between 0.3 and 1.3, it can be concluded that, in this range, the derivative is stacked on Poly C contiguously to the derivatives which had previously been stacked on it. If the stacking is homogeneous in this range, the hydrolysis rate can be presented as by the dotted line[10] in Fig. 1. From the other fact that the hydrolysis rate at higher concentrations of the derivatives was almost parallel to that without Poly C, it can be concluded that the stacking of the derivatives on Poly C is saturated in this range and that an excess of them reacts freely with the Poly C.

The difference between the hydrolysis rates with and without Poly C, $R_{polyC}-R_0$, indicates the hydrolysis rate on Poly C. The hydrolysis rate on Poly C increased linearly with the concentration of the reactants, the dinucleotide derivatives, in the ratio of 0.3 to 1.3.

Fig. 2 shows the hydrolysis rate when the concentration of the catalyst, AH-*d*GpG, was a constant. The profile of the increase in the rate with respect to the concentration of the substrate, NPS-*d*GpG, is almost the same as that of Fig. 1 at lower concentrations. The saturation points are different with each concentration of AH-*d*GpG used. They increase with the concentration of AH-*d*GpG. This shows that the reaction on Poly C takes place where the substrate is stacked contiguously with the catalyst. The lowest concentration at which the reaction takes place decreases with the concentrations of the catalyst and the substrate.

The observations in Figs. 1 and 2 support the above-stated conclusions. It can be considered that Poly C does not take a helical configuration under these reaction conditions. Therefore, the following plausible explanation may be offered for this finding: The reactants which were stacked remotely on Poly C at their lower concentrations might not react, while the reactants which were stacked contiguously on Poly C at a moderate concentration could react. At a higher concentration, with a ratio exceeding 1.3, the additional reactants react freely from Poly C.

To estimate the hydrolysis rate on Poly C, let us define the rate as;

$$k_{eff} = (R_{polyC}-R_o)/(C-C_i)$$

where C is the concentration of the reactant, NPS-*d*GpG, and where C_i is the concentration which is the extrapolation of the linearly-increasing part of the rate *vs.* the concentration of NPS-*d*GpG in Fig. 1 to the intercept, or the lowest concentration of which the hydrolysis takes place. The rate constants of the hydrolyses, k_{eff}'s, on Poly C were substantially constants, which were estimated to be $(2.46\pm0.10)\times10^{-1}$ mol^{-1} sec^{-1} at the [NPS-*d*GpG]/[Poly C] ratios exceeding the threshold values respectively. The constancy of the

9) When two reactants are stacked on Poly C contiguously, the hydrolysis rate should be proportional to the concentration of NPS-*d*GpG. So that, the rate is presented as a straight line which passes the origin.

10) When two reactants are stacked on Poly C at random, the average probability of contiguous stacking of those reactants is presented as;

$\bar{P}_c \cong 2n/(n_0-n)$ $(n<n_0/3)$

where n_0 denotes the total contiguous stacking site on the Poly C and n does the number of stacked reactants. The concentration of the reactant (C) is almost proportional to n and the reaction rate is also proportional to $\bar{P}_c$, so the rate is expressed as;

the rate$\cong 2\alpha C/(n_0-\alpha C)$ $(\alpha C \leqq n_0/3)$

where α denotes the stacking factor of the reactant. When $\alpha C > n_0/3$, a proportionality between the rate and the concentration of the reactant will be given.

TABLE 1. RATES OF HYDROLYSES ON AND WITHOUT POLY C

Run	Derivatives of dinucleotide		C_1	Relative rate of hydrolysis[a] ×10	
	Catalyst	Substrate		on Poly C	without Poly C
1	AH-*d*GpG (0.9)	NPS-*d*GpG (1.2)	1.05	2.06/1.05=2.34	0.54/1.05=0.52
2	N-*d*GpG (1.7)	NPS-*d*GpG (1.2)	1.05	0.40/1.45=0.28	0.20/1.45=0.14
3	AH-*d*GpT (1.1)	NPS-*d*GpT (1.4)	0		0.50/1.25=1.25
4	AH-*d*GpC (0.9)	NPS-*d*GpC (1.2)	0.7		0.64/1.05=0.60
5	AH-*d*GpA (0.9)	NPS-*d*GpA (1.1)	>0 ($\times 10^{-4}$ M)		0.48/1.00=0.48 ($1\ mol^{-1}\ sec^{-1}$)

Poly C; 0.35×10^{-3} mol/l. ( ) Shows the degree of esterification. a) The relative rate was obtained by dividing the rate by arithmetic mean values of the esterifications of the substrate and the catalyst.

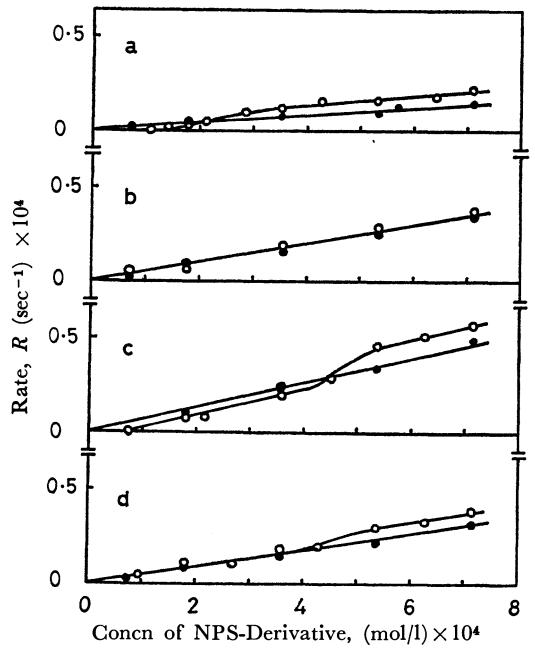

Fig. 3. Hydrolyses of dinucleotide derivatives.
a ; hydrolysis of NPS-*d*GpG by N-*d*GpG
b ; hydrolysis of NPS-*d*GpT by AH-*d*GpT
c ; hydrolysis of NPS-*d*GpC by AH-*d*GpC
d ; hydrolysis of NPS-*d*GpA by AH-*d*GpA
○, presence of Poly C (0.35×10^{-3} mol/l)
●, absence of Poly C
The other conditions are the same as in Fig. 1.

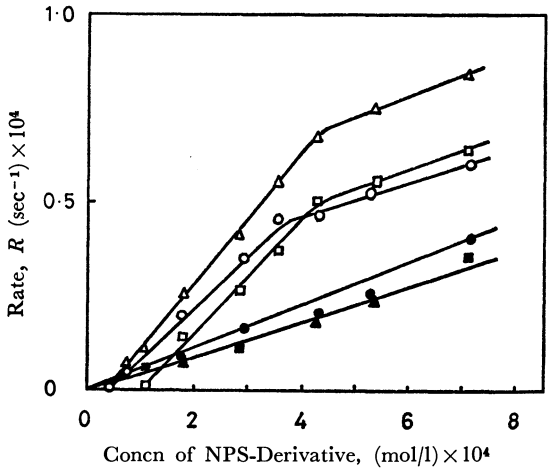

Fig. 4. Hydrolyses of NPS-deoxyguanosine oligomers by AH-deoxyguanosine oligomers.
○: NPS-*d*GpGpG, AH-*d*GpGpG
△: NPS-*d*GpG, AH-*d*GpGpG
□: NPS-*d*GpGpG, AH-*d*GpG
} in the presence of 0.35×10^{-3} mol/l of Poly C.
●: NPS-*d*GpGpG, AH-*d*GpGpG
▲: NPS-*d*GpG, AH-*d*GpGpG
■: NPS-*d*GpGpG, AH-*d*GpG
} in the absence of Poly C.
The other conditions are the same as in Fig. 1.

rate supports the above-mentioned explanation that the reactants stacked on Poly C react contiguously with each other in this range. In other words, the stacking of the reactants on Poly C takes place contiguously in the range of the [NPS-*d*GpG]/[Poly C] ratio exceeding the threshold value. From the hydrolysis rate without Poly C, which is shown in Fig. 1, the rate of the hydrolysis except on Poly C, k_0, is found to be $(0.54\pm0.1)\times10^{-1}\ l\ mol^{-1}\ sec.^{-1}$

Figure 3 shows the hydrolysis of dinucleotide derivatives with and without Poly C. In the case of the hydrolysis of NPS-*d*GpT by AH-*d*GpT, there was no evidence of the interaction with Poly C. In the cases of the hydrolyses of NPS-*d*GpC by AH-*d*GpC, of NPS-*d*GpA by AH-*d*GpA, and of NPS-*d*GpG by N-*d*GpG, similar phenomena were observed. The hydrolyses did not take place at lower concentrations of the oligonucleotide derivatives, and they were parallel to the rate without Poly C at higher concentrations. At moderate concentrations, the hydrolyses increased at a higher rate, similar to the case of the hydrolysis of NPS-*d*GpG by AH-*d*GpG.

To estimate the rate of the hydrolysis on Poly C, k_{eff}, and that without Poly C, k_0, the same calculations as have been described above have been made for each case. The results are tabulated in Table 1. Although the hydrolysis rate of NPS-*d*GpG by AH-*d*GpG on Poly C was 4 times faster than that without Poly C, the hydrolysis rate of NPS-*d*GpG by N-*d*GpG on Poly C was 2 times faster than that without Poly C. This difference might be due to different distances between the catalytic nucleophilic atoms and the stacking points of these nucleotidic materials. The fact that the concentrations at which the hydrolysis took place were substantially identical in both hydrolyses shows that the modes of the interactions of AH-*d*GpG and N-*d*GpG with Poly C are almost identical with that of AH-*d*GpG and NPS-*d*GpG with Poly C. Though it is not possible to quantify the interaction between dinucleotides and Poly C, it can be seen from the values of C_1's that its order is *d*GpG>*d*GpC>*d*GpA>*d*GpT.

Fig. 4 shows the hydrolyses of NPS-*d*GpGpG by AH-*d*GpGpG, of NPS-*d*GpG by AH-*d*GpGpG, and of NPS-

Table 2. Rates of hydrolyses of oligoguanosine derivatives on and without poly C

Run	Derivatives of oligoguanosine		C_1	Relative rates of hydrolysis[a] ×10	
	Catalyst	Substrate		on Poly C	without Poly C
1	AH-*d*GpG (0.9)	NPS-*d*GpG (1.2)	1.0(5)	2.34	0.52
2	AH-*d*GpGpG(0.9)	NPS-*d*GpGpG(1.0)	0.3(5)	0.93	0.57
3	AH-*d*GpGpG(0.9)	NPS-*d*GpG (1.0)	0.3(5)	1.34	0.46
4	AH-*d*GpG (0.9)	NPS-*d*GpGpG(1.0)	0.9	1.09	0.48
			($\times 10^{-4}$ M)	($1\ mol^{-1}\ sec^{-1}$)	

a) Notes are the sameas in Table 1.

Table 3. Reduced viscosities of several reaction systems

Reaction system	η_{sp}/c
0.35×10^{-3} M Poly C	1.15(6)
0.35×10^{-3} M Poly C $+0.20\times10^{-3}$ M NPS-*d*GpG & AH-*d*GpG	1.15(6)
0.35×10^{-3} M Poly C $+0.40\times10^{-3}$ M NPS-*d*GpG & AH-*d*GpG	1.15(6)
0.35×10^{-3} M Poly C $+0.50\times10^{-3}$ M NPS-*d*GpG & AH-*d*GpG	1.11(2)
0.35×10^{-3} M Poly C $+0.60\times10^{-3}$ M NPS-*d*GpG & AH-*d*GpG	1.11(2)
0.50×10^{-3} M NPS-*d*GpG & AH-*d*GpG	
0.35×10^{-3} M Poly G	1.31(6)
0.35×10^{-3} M Poly C+0.35×10^{-3} M Poly G	2.34(7)
	1.10(5)[a]

c: g-solute/100 ml relating to Poly C (=0.0106)
5±0.05°C; 0.01 M $MgCl_2$, 0.0001 M $Mg(OAc)_2$, EtOH–H_2O =1 : 100
a) Total concentration of Poly C and Poly G was used as*c* (=0.0225) in the calculation.

*d*GpGpG by AH-*d*GpG. Profiles of hydrolysis similar to Figs. 1 and 4 were observed.

The rates are tabulated in Table 2. From the hydrolyses of NPS-*d*GpG by AH-*d*GpG and of NPS-*d*GpGpG by AH-*d*GpGpG, it is very tempting to suppose that the distance between the substrates and the catalysts plays a role in the hydrolyses. Although the two relative rates of hydrolyses without Poly C were similar, the rates on Poly C were different. The longer distance was not preferable to the hydrolysis in spite of the tightly stacking on Poly C. The exhibition of very little increment in the hydrolysis of the latter might be due to the stacking of AH-*d*GpGpG and NPS-*d*GpGpG with each other. Furthermore, a directionality in the interaction might be considered with the difference between the rates of the hydrolyses of NPS-*d*GpG by AH-*d*GpGpG and that of NPS-*d*GpGpG by AH-*d*GpG. From the C_1's which are concentrations of the oligonucleotide derivatives when the hydrolysis took place, we learn that the mode of interaction of AH-*d*GpGpG with Poly C was rather favorable to the contiguous stacking.

The results of the reduced viscosity measurements of several reaction systems are tabulated in Table 3. While the reduced viscosity, η_{sp}/c, relating to Poly C did not change when relatively small amounts of NPS-*d*GpG and AH-*d*GpG were present in the system, the reduced viscosity decreased when amounts of NPS-*d*GpG and AH-*d*GpG of more than 0.50×10^{-3} M were present. The viscosity of the system of NPS-*d*GpG and AH-*d*GpG was negligible, of course. On the other hand, when an added Poly G existed in the Poly C solution, the reduced viscosity relating to Poly C obviously increased to 2.34(7). This increase in the viscosity was due to the added Poly G. To eliminate the effect of the viscosity of Poly G, we employed the total concentrations of those two polymeric materials, Poly C and Poly G, as the reference concentration, *c*; then, the reduced viscosity was estimated to be 1.10(5). This value was less than the arithmetic mean value of the reduced viscosities of Poly C and Poly G. This can be explained as the formation of a double strand of Poly C and Poly G by reference to the results of Fresco and Doty.[11] Using Poly A, they had obtained a lower viscosity under the condition of an interrupted helix and a higher viscosity under the condition of a random coil. Therefore, the decrease in the reduced viscosity of Poly C in the presence of a considerable amount of NPS-*d*GpG and AH-*d*GpG can be explained as a partial conformational change of Poly C at the interacting location where the stacking of those dinucleotide derivatives with Poly C took place.

Those results are compatible with the conclusions that the stacking of the dinucleotide derivatives with Poly C takes place statistically homogeneous at the initial stage and that afterwards the stacking occurs at the site contiguously to the pre-stacked one. Such a phenomenon may be caused by a conformational change in Poly C by the stacking of the oligonucleotide derivatives. This conclusion is an interesting concept compared with that of the homogeneous stacking previously believed.

Experimental

The hydrolyses reactions were carried out using a 1 : 100 ethanol-water solution containing 0.01 M of $MgCl_2$ and 0.0001 M of $Mg(OAc)_2$,[12] the pH of which was made up to 7.9 by tris-(hydroxymethyl)aminomethane.

The Poly C solution was made up to 0.7×10^{-3} M using the above buffer solution. Both solutions of dinucleotide and trinucleotide derivatives in a certain concentration were prepared fresh each time using the above buffer solution.

11) J. R. Fresco and P. Doty, *J. Amer. Chem. Soc.*, **79**, 3928 (1957).

12) Generally, existence of Mg^{2+} assists the complex formation of Poly C-Poly G, so that such magnesium salts were used in the present study. The existence of Mg^{2+} did not affect the absorbancy of Poly C in UV spectrum.

The experiments were carried out by mixing 2 ml of the Poly C solution, 1 ml of the substrate derivative of the *p*-nitrophenyl succinate solution, and 1 ml of the catalyst derivative of the *N*-acetylhistidate or nicotinates solution at 5 °C. The absolute amounts of the substrate and the catalyst were the same in all the experiments. The rates of the hydrolyses were measured by the increase in absorbance at 400 nm. In the case of the absence of Poly C, 2 ml of the above buffer solution instead a similar portion of the Poly C solution was used.

By analysing the reacted material in a paper chromatograph, it was proved that the hydrolyzed materials did not contain *p*-nitrophenylsuccinic acid. It can be said that the hydrolyses took place predominantly at the position between *p*-nitrophenyl and succinyl moieties.

The increase in absorbance can be treated as linear with the reaction time at lower conversions. The reaction followed the kinetics of the first-order with respect to the NPS-*d*GpG to the extent of 45% of the conversion. This shows that there might be no product inhibition in the reaction.

The viscosity was measured at 5±0.05 °C using a Ubbelohde-type viscometer.

Polycytidylic Acid (Poly C) and Polyguanylic Acid (Poly G). Poly C and Poly G were purchased from the Miles Chemical Co.; their sedimentation constants were 4.3 and 2.9 respectively.

p-*Nitrophenyl (deoxyguanylyldeoxyguanosine succinate) (NPS-*d*GpG).* In anhydrous pyridine, 40 mg of *N*-di-*p*-methoxytrityldeoxyguanylyl-*N*-di-*p*-methoxytrityldeoxyguanosine,[13] (DMTr)*d*G(DMTr)*d*G, and 20 mg of succinic anhydride was subjected to a reaction for 14 hr at room temperature; then we added 25 mg of *p*-nitrophenol and 40 mg of dicyclohexylcarbodiimide. After 14 hr, 10 ml of an aqueous solution of KH_2PO_4 was added. Then 90 ml of ethanol was added, and the resultant mixture was filtered. A filtrate was concentrated, and 40% acetic acid was added along with a small quantity of pyridine. After 5 hr, the solution was separated by centrifugation. The isolation of NPS-*d*GpG was achieved chromatographically in 70% ethanol using an anion-exchange resin, IR-45. The resulting NPS-*d*GpG contained 1.2 *p*-nitrophenyl groups per molecule, as indicated by the ultraviolet spectra before and after alkaline hydrolyses, which were achieved with 1 M NaOH. It is probable that the nitrophenylsuccinyl group is bonded predominantly to the 5′-O position of the nucleotide. The resulting NPS-*d*GpG did not obtain free carboxylic acid, since the present column separation showed that the resulting NPS-*d*GpG was found in one elution band, unlike the case of a free carboxylic acid.

p-*Nitrophenyl (deoxyguanylylthymidine succinate) (NPS-*d*GpT),* p-*Nitrophenyl (deoxyguanylyldeoxycytidine succinate) (NPS-*d*GpC),* p-*Nitrophenyl (deoxyguanylyldeoxyadenosine succinate) (NPS-*d*GpA),* and p-*Nitrophenyl (deoxyguanylyldeoxyguanylyldeoxyguanosine succinate) (NPS-*d*GpGpG).* The procedures to synthetize these materials were the same as that for NPS-*d*GpG, but using *N*-di-*p*-methoxytrityldeoxyguanylylthymidine, (DMTr)*d*GT, in lieu of (DMTr)*d*G(DMTr)*d*G, using *N*-di-*p*-methoxytrityldeoxyguanylyl-*N*-di-*p*-methoxytrityldeoxycytidine, (DMTr)*d*G(DMTr)*d*C, in lieu of (DMTr)*d*G(DMTr)*d*G, using *N*-di-*p*-methoxytrityldeoxyguanylyl-*N*-di-*p*-methoxytrityldeoxyadenosine, (DMTr)*d*G(DMTr)*d*A, in lieu of (DMTr)*d*G(DMTr)*d*G, and using *N*-di-*p*-methoxytrityldeoxyguanylyl-*N*-di-*p*-methoxytrityldeoxyguanylyl-*N*-di-*p*-methoxytrityldeoxyguanosine,[14] (DMTr)*d*G(DMTr)*d*G(DMTr)*d*G, in lieu of (DMTr)*d*G(DMTr)*d*G.

Deoxyguanylyldeoxygaunosine N-*acetylhistidate (AH-*d*GpG).* In anhydrous pyridine, 30 mg of *N*-di-*p*-methoxytrityldexoyguanylyl-*N*-di-*p*-methoxytrityldeoxyguanosine, (DMTr)*d*G(DMTr)*d*G, 30 mg of *N*-acetylhistidine, and 50 mg of dicyclohexylcarbodiimide were reacted for 4 days at room temperature. Then 30 ml of a KH_2PO_4 aqueous solution was added. An 50 ml of ethanol was added and filtered. Into the filtrate, the same amount of acetic acid was poured. After 5 hr the supernatant was separated by centrifugation. The isolation of AH-*d*GpG was achieved chromatographically in 70% ethanol using the anion-exchange resin. The resulting AH-*d*GpG contained 0.9 imidazolyl group per molecule, as indicated by the ultraviolet spectra in an acidic solution, in which the nucleotide had been removed by means of an ion-exchange column, before and after alkaline hydrolyses. In this case, it is probable that the histidyl group is bonded predominantly to the 5′-O position of the nucleotide.

Deoxyguanylylthymidine N-*acetylhistidate (AH-*d*GpT), Deoxyguanylyldeoxycytidine* N-*acetylhistidate (AH-*d*GpC), Deoxyguanylyldeoxyadenosine* N-*acetylhistidate (AH-*d*GpA), and Deoxyguanylyldeoxyguanylyldeoxyguanosine* N-*acetylhistidate (AH-*d*GpGpG).* The procedures to synthetize these materials were the same as that for AH-*d*GpG, but using (DMTr)*d*GT in lieu of (DMTr)*d*G(DMTr)*d*G, using (DMTr)*d*G(DMTr)*d*C in lieu of (DMTr)*d*G(DMTr)*d*G, using (DMTr)*d*G(DMTr)*d*A in lieu of (DMTr)*d*G(DMTr)*d*G, and using (DMTr)*d*G(DMTr)-*d*G(DMTr)*d*G in lieu of (DMTr)*d*G(DMTr)*d*G.

*Deoxyguanylyldeoxyguanosine nicotinate (*N-d*GpG).* Thirty mg of (DMTr)*d*G(DMTr)*d*G and 30 mg of nicotinyl chloride were reacted in anhydrous pyridine for 4 hr at room temperature. Two ml of methanol was added to esterify the excess of nicotinyl chloride; then the solution was condensed until it became cloudy, and 30 ml of acetic acid was added. After 4 hr, the isolation of N-*d*GpG was achieved chromatographically in a 50% ethanol aqueous solution, using the anion-exchange resin.

The nitrophenyl, imidazolyl, and nicotinyl contents in the above materials are tabulated in Table 4.

TABLE 4. CONTENTS OF NITRONPHENYL, IMIDAZOLYL, AND NICOTINYL GROUPS IN THE ESTERS

	Substrate	Catalyst
	p-Nitrophenyl-succinate	*N*-Acetyl-histidate
*d*GpG	1.2	0.9
*d*GpT	1.4	1.1
*d*GpC	1.2	0.9
*d*GpA	1.1	0.9
*d*GpGpG	1.0	0.9
		Nicotinate
*d*GpG		1.7

13) T. Shimidzu and R. L. Letsinger, *J. Org. Chem.*, **33**, 708 (1968).

14) T. Shimidzu and R. L. Letsinger, This Bulletin, **44**, 1673 (1971).

Studies on Pyrophosphates II. A New Method for the Synthesis of Nucleotide Coenzymes and Their Analogs

Iwao NAKAGAWA and Tsujiaki HATA

Laboratory of Chemistry for Natural Products, Faculty of Science, Tokyo Institute of Technology, Ookayama, Meguro-ku, Tokyo 152

(Received May 2, 1973)

A new method for the synthesis of unsymmetrical pyrophosphates from the reaction of alkyl phosphorothioates and disilver salt of alkyl phosphates are described. Nucleotide coenzymes such as uridine diphosphate glucose, uridine diphosphate galactose, and flavin adenine dinucleotide was synthesized.

Information on the biological significance of a large number of nucleotide derivatives has increased rapidly and the domain of biochemistry of such compounds has been extended, one of them being nucleotide conenzymes which can be defined as unsymmetrical pyrophosphates having nucleoside residues. So far no biological function has been ascribed to symmetrical dinucleoside pyrophosphates, nor has any naturally occurring symmetrical pyrophosphate has been found. Consequently, development of the method for the selective synthesis of unsymmetrical pyrophosphates is of importance. The synthesis of nucleotide coenzymes were carried out by the use of reagents such as carbodiimide and related dehydrating reagents,[1] triesters of pyrophosphates,[2] α-pyridyl ester of phosphoric acid,[3] phosphoroamidates,[4] and *S*-ethyl phosphorothioates.[5] We have found a simple method for the selective synthesis of nucleotide coenzymes *via* nucleoside phosphorothioate intermediates[6] as shown in the following.

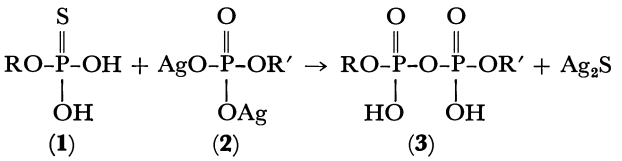

(1) (2) (3)

In this paper results of the experiments for the synthesis of nucleotide coenzymes and their analogs are described in detail.

Preparation of Phosphorothioates. The starting material, phosphorothioate derivatives (**1**), was prepared by hydrolysis of the corresponding thiophosphorodichloridate (**4**) obtained from the reactions of alcohol or nucleoside with thiophosphoryl chloride.

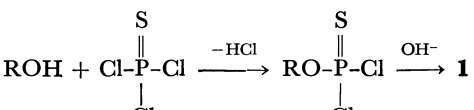

(4)

Alkyl thiophosphorodichloridates (**4**) are oily substances and purified by distillation (for their boiling points, see Experimental). Hydrolysis of **4** was performed in aqueous acetone at 0 °C in the presence of tertiary amines such as pyridine or triethylamine. Alkyl phosphorothioates (**1**) were extracted from the resulting mixture with ether and dried over sodium sulfate. After removal of ether at 5 °C, the phosphorothioates were dissolved in dry chloroform and stored in a refrigerator at 5 °C. They are stable under neutral and basic conditions at a temperature below 5 °C, but decompose in acidic medium even when kept at low temperature. Nucleoside phosphorothioates[7] were obtained by a similar procedure without isolating the intermediate **4**. Bis-triethylammonium salts of nucleoside phosphorothioates are stable solid substances. They are stable in dry pyridine at 5 °C, but unstable in acetonitrile or commercial pyridine, being converted into the corresponding P^1,P^2-bis-[nucleoside-5′-phosphoryl]disulfide (**5**).[8]

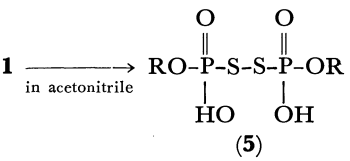

(5)

R = nucleoside residue

Preparation of Disilver Salt of Phosphates. Disilver salts (**2**) were prepared from the corresponding disodium salts and silver nitrate. In order to avoid the formation of silver oxide, a solution of the sodium salts was added slowly to a solution of excess silver nitrate with vigorous stirring. Disilver salts of *p*-nitrophenyl phosphate and adenosine 5′-phosphate precipitated from the reaction mixtures. In the cases of glucose-1-phosphate, galactose-1-phosphate, and riboflavin 5′-phosphate, the silver salts precipitated by addition of methanol.[9]

Synthesis of Unsymmetrical Pyrophosphates. Several unsymmetrical pyrophosphates (**3**) were obtained when 1 equiv. of bis-triethylammonium salt of phosphorothioate (**1**) was treated with 1.2 equiv. of disilver salt of phosphate (**2**) in dry pyridine at room temperature for five hours. The results are

1) N. A. Hughes, G. W. Kenner, and A. R. Todd, *J. Chem. Soc.*, **1957**, 3733: E. P. Kennedy, *J. Biol. Chem.*, **222**, 185 (1956); R. J. Cremlyn, G. W. Kenner, and Sir A. Todd., *J. Chem. Soc.*, **1960**, 4511.

2) F. Cramer and R. Wittmann, *Chem. Ber.*, **94**, 322, 328 (1961).

3) W. Kampe, *Chem. Ber.*, **98**, 1031, 1038 (1965); K. H. Scheit and W. Kampe, *ibid.*, **98**, 1045 (1965); W. Kampe, *ibid.*, **99**, 593 (1966).

4) J. G. Moffatt and H. G. Khorana, *J. Amer. Chem. Soc.*, **83**, 649 (1961); J. Josse and J. G. Moffartt, *Biochem.*, **4**, 2825 (1965).

5) A. L. Nussbaum and R. Tiberi, *J. Amer. Chem. Soc.*, **87**, 2513 (1965); A. F. Cook, M. J. Holman, and A. L. Nussbaum, *ibid.*, **91**, 1522 (1969).

6) T. Hata and I. Nakagawa, *ibid.*, **92**, 5516 (1970).

7) T. Hata and I. Nakagawa, This Bulletin, **43**, 3619 (1970).

8) The disulfides can be detected and distingushed from the corresponding pyrophosphates after the paper chlomatograms have been sprayed with the Grote reagent. J. G. Grote, *J. Biol. Chem.*, **93**, 25 (1931).

9) Silver nitrate does not precipitate with the addition of methanol.

TABLE 1. PREPARATION OF UNSYMMETRICAL PYROPHOSPHATES (3)

Phosphorothioate (1) R	mg (mmol)	Disilver salt of phosphate (2) R′	mg (mmol)	Pyridine (ml)	Unsymmetrical pyrophosphate (3) Yield (%)	R_f value (solv. A)	Spectral data (pH=7) $\lambda_{max}^{H_2O}$ ($\varepsilon \times 10^{-3}$)	$\lambda_{min}^{H_2O}$
C_2H_5	327 (1.0)	(*p*)O_2N-C_6H_4	508 (1.2)	20	74	0.68	290 (10.0)	242
n-C_3H_4	358 (1.0)	(*p*)O_2N-C_6H_4	508 (1.2)	20	85	0.70	290 (10.0)	242
n-C_4H_9	372 (1.0)	(*p*)O_2N-C_6H_4	508 (1.2)	20	84	0.72	290 (10·0)	242
iso-C_5H_{11}	386 (1.0)	(*p*)O_2N-C_6H_4	508 (1.2)	20	83	0.74	290 (10.0)	242
2′, 3′-*O*-Isopropylidene adenosine-(5′)	68 (0.1)	(*p*)O_2N-C_6H_4	51 (0.12)	2	54	0.65	263 (18.4)	235
2′, 3′-*O*-Isopropylidene uridine-(5′)	58 (0.1)	(*p*)O_2N-C_6H_4	64 (0.15)	1	86	0.56	267 (14.0)	237
n-C_4H_9	37 (0.1)	adenosine-(5′)	76 (0.12)	1	61	0.42	260 (15.4)	228

summarized in Table 1. The pyrophosphates were characterized by ratio of nucleoside base to phosphate and by ultraviolet absorption.

No symmetrical pyrophosphate was detected when only 1.2 equiv. of **2** was used. Satisfactory yields are maintained even when insoluble disilver salts containing crystal water were used.

Experimental

Methods. Paper chromatography was performed by the descending technique using Toyo Roshi papers No. 51 and No. 51A. The solvent system used was isopropyl alcohol-conc. aqueous ammonia-water (7 : 1 : 2 v/v) (Solvent **A**). The R_f values of different compounds are listed in Table 1. Paper electrophoresis was carried out with an apparatus similar to that described by Markham and Smith.[10] The buffer solution used was 0.05 M phosphate (pH=8.0). Estimation of the yields of unsymmetrical pyrophosphates was most frequently carried out spectrophotometrically after elution of the spot from paper chromatograms run on Solvent A.

Thiophosphoryl chloride was prepared by the procedure of Knotz.[11] It was distilled (bp 125 °C) prior to use. *p*-Nitrophenyl phosphate was prepared as described previously.[12] Commercial disodium salt of glucose-1-phosphate, galactose-1-phosphate, adenosine 5′-phosphate, and riboflavin 5′-phosphate were used.

*Alkyl Thiophosphorodichloridate (**4**).* These compounds were prepared by procedures given in literature. Boiling points of ethyl,[13] *n*-propyl,[14] and *n*-butyl[15] derivatives were 71 °C (23 mmHg), 82—82 °C (22 mmHg) and 91—93 °C (19 mmHg), respectively. Isoamyl derivative 115—116 °C (23 mmHg), was prepared by a modification of the procedure of Martin *et al.*[15].

*Alkyl Phosphorothioates (**1**). General procedure.* To 150 ml of aqueous acetone (1 : 2 v/v) was added alkyl thiophosphorodichloridate (0.1 mmol) under cooling at 0 °C in the presence of triethylamine (0.4 mmol). The mixture was concentrated to dryness under reduced pressure. Evaporation was repeated three times until triethylammonium chloride precipitated from the pyridine solution. The precipitate was then filtered off and the filtrate was concentrated. Chromatogram of the residue developed by Solvent A gave a single spot of compound **1**. The residue was dissolved in dry pyridine and a standard solution of **1** was prepared. The content of **1** was determined by phosphate measurement. The standard solution can be kept in a refrigerator for several weeks.

Disilver Salt of Adenosine 5′-Phosphate. To an aqueous solution of silver nitrate (0.2 mmol) was added disodium salt of adenosine 5′-phosphate (0.1 mmol) with vigorous stirring. The precipitate which soon appeared was collected by centrifuging. It was washed with water and then with methanol and finally with ether. The silver salt was kept in a desiccator under protection from light.

Disilver Salt of p-*Nitrophenyl Phosphate.* This was prepared in a similar way to that for adenosine 5′-phosphate.

Disilver Salts of Glucose-1-Phosphate and Galactose-1-phosphate. Experiments were carried out as for adenosine 5′-phosphate. The silver salts precipitated by addition of methanol.

Disilver Salt of Riboflavin 5′-Phosphate. The reaction was carried out under the same conditions as in the case of adenosine 5′-phosphate. The reaction mixture was filtered and the filtrate was concentrated under reduced pressure until the precipitate appeared. After addition of methanol, red colored precipitate was collected and washed with methanol. The silver salt was dried over phosphorus pentoxide in a vacuum desiccator.

P^1-*Isoamyl* P^2-p-*Nitrophenyl Pyrophosphate.* To a suspension of disilver salt of *p*-nitrophenyl phosphate (508 mg, 1.2 mmol) in dry pyridine (20 ml) was added gradually a solution of bis-triethylammonium salt of isoamyl phosphorothioate (386 mg, 1.0 mmol) in dry pyridine (5 ml) with vigorous stirring. After 5 hr, the mixture was concentrated to dryness under reduced pressure at a temperature below 40 °C. The residue was shaken with four portions of a mixture of ethanol and concd. aqueous ammonia (2 : 1 v/v). The extracts were combined and concentrated. Water was then added and insoluble material was filtered off. The aqueous solution was neutralized by Dowex 50W-X8 (pyridinium form) and cyclohexylamine was added. The solution was concentrated to dryness. The residue was washed several times with chloroform and the extracts were combined and concentrated. Dicyclohexylammonium salt of P^1-isoamyl P^2-*p*-nitrophenyl pyrophosphate, separated by addition of dry ether and purified by reprecipitation, was obtained in an 83% yield based on isoamyl phosphorothioate. Mp 180—183 °C. Found: C, 48.06; H, 7.48; N, 7.95%. Calcd for $C_{23}H_{43}N_3P_2O_9$: C, 48.60; H, 7.57; N, 7.38%.

In a similar manner, P^1-ethyl P^2-*p*-nitrophenyl pyrophos-

10) R. Markham and J. D. Smith, *Biochem. J.*, **52**, 552 (1952).
11) F. Knotz, *Österr. Chemiker Z.*, **50**, 128 (1949).
12) K. J. Chong and T. Hata, This Bulletin, **44**, 2641 (1971).
13) H. S. Booth, D. R. Martin, and F. E. Kendall. *J. Amer. Chem. Soc.*, **70**, 2523 (1948); "Inorganic Syntheses", Vol. IV, p. 75 (1953).
14) P. S. Pishchimuka, *Ber.*, **41**, 3854 (1908).
15) T. W. Martin, G. R. Norman, and E. A. Weilmuenster, *J. Amer. Chem. Soc.*, **67**, 1662 (1945).

phate, P^1-*n*-propyl P^2-*p*-nitrophenyl pyrophosphate and P^1-*n*-butyl P^2-*p*-nitrophenyl pyrophosphate were obtained. The data are given in Table 1.

Uridine Diphosphate Glucose. To a suspension of disilver salt of glucose-1-phosphate (monohydrate 59 mg, 0.12 mmol) in dry pyridine (0.5 ml) was added gradually a solution of bis-tri-*n*-butylammonium salt of 2′,3′-*O*-dibenzoyl uridine phosphorothioate (tetrahydrate 99 mg, 0.1 mmol) in dry pyridine (0.5 ml) with vigorous stirring. After 5 hr, the reaction mixture was filtered and the filtrate was passed through a column of Dowex 50W-X8 (pyridinium form). The eluate was treated with 0.2 M sodium hydroxide at room temperature for 30 min and then neutralized with Dowex 50W–X8 (pyridinium form). The solution was concentrated to a volume of 5 ml and applied to a column of Dowex 1–X8 (chloride form). Uridine 5′-phosphate was first eluted with 0.003 M hydrochloric acid in 0.01 M lithium chloride and then uridine diphosphate glucose with 0.003 M hydrochloric acid in 0.06 M lithium chloride. This was neutralized with lithium hydroxide and concentrated to a small volume. After addition of ethanol, dilithium salt of uridine diphosphate glucose was separated by addition of acetone. The precipitate was filtered and washed with acetone and then with dry ether. Uridine diphosphate glucose (dilithium salt) was obtained in 70% yield (43 mg). Found: C, 29.76; H, 4.93; N, 4.22%. Calcd for $C_{15}H_{22}N_2P_2Li_2O_{17}\cdot 2H_2O$: C, 29.31; H, 4.23; N, 4.57%. Determination of ratios of uridine, glucose, phosphorus gave 1.00 : 1.15 : 1.94; the calculated ratios 1 : 1 : 2.

Uridine Diphosphate Galactose. To a suspension of disilver salt of galactose-1-phosphate (monohydrate 59 mg, 0.12 mmol) in dry pyridine (0.5 ml) was added a solution of bis-triethylammonium salt of 2,′3,′-*O*-isopropylidene uridine 5′-phosphorothioate (48 mg, 0.10 mmol) in dry pyridine (0.5 ml) with vigorous stirring. After 5 hr, the reaction mixture was concentrated to dryness and the residue was treated with 10% sodium chloride (10 ml), hydrogen sulfide being passed into the solution. The precipitate was centrifuged and the supernatant liquid was concentrated to a small volume (*ca.* 5 ml). It was then treated with Dowex 50W-X8 (pyridinium form) and concentrated. The residue was dissolved in 80% acetic acid and heated at 100 °C for 10 min. After removal of acetic acid, the product showed the expected ultraviolet absorption characteristics ($\lambda_{max}^{H_2O}$ 262 mμ at pH=7), being homogeneous on paper electrophoresis (Mobility= 0.78 relative to uridine 5′-phosphate). The yield of uridine diphosphate galactose was 63% (630 $O.D._{262}$) based on 2′,3′-*O*-isopropylidene uridine 5′-phosphorothioate.

Flavin Adenine Dinucleotide. To a suspension of disilver salt of riboflavin 5′-phosphate (40 mg, 0.06 mmol) in dry pyridine (0.25 ml) was added slowly a solution of bis-triethylammonium salt of 2′,3′-*O*-isopropylidene adenosine phosphorothioate (tetrahydrate 25.2 mg, 0.05 mmol) in dry pyridine (0.25 ml) with vigorous stirring. After 27 hr, the mixture was concentrated under reduced pressure. The residue was treated with 10% sodium chloride (10 ml), hydrogen sulfide being then passed into the solution. The precipitate was centrifuged and the supernatant liquid was concentrated to a small volume (*ca.* 5 ml). This was treated with Dowex 50W-X8 (pyridinium form) and concentrated to dryness. The residue was dissolved in 80% acetic acid and heated at 100 °C for 10 min. This was concentrated and flavin adenine dinucleotide was obtained by electrophoretic separation. The yield was 51% based on 2′,3′-*O*-isopropylidene adenosine 5′-phosphorothioate.

$\lambda_{max}^{H_2O}$ 264, 375, 450 mμ. $\lambda_{260}/\lambda_{375}=4.00$; $\lambda_{375}/\lambda_{450}=0.95$; $\lambda_{260}/\lambda_{450}=3.80$ (at pH=7).

The authors heartily thank Professor Teruaki Mukaiyama for his encouragement and discussions throughout the investigation.

BULLETIN OF THE CHEMICAL SOCIETY OF JAPAN, VOL. 46, 3277—3280 (1973)

Reactions of *N*-Acylaminoacetamidine with 1,3-Bifunctional Compounds

Hiroaki UCHIDA, Hiroyuki IWASAWA, and Masaki OHTA

Department of Chemistry, Faculty of Science, Tokyo Institute of Technology, Ookayama, Meguro-ku, Tokyo 152

(Received May 4, 1973)

The reactions of *N*-benzoylaminoacetamidine(IIIa) and *N*-benzyloxycarbonylaminoacetamidine(IIIb) with various 1,3-bifunctional compounds were investigated. Both IIIa and IIIb were found to react with acetylacetone to produce 2-amino-3-benzoylamino-4,6-dimethylpyridine and 2-amino-3-benzyloxycarbonylamino-4,6-dimethylpyridine, respectively. On the other hand, IIIa reacted with ethyl acetoacetate or diketene to produce 2-(*N*-benzoylaminomethyl)-4-hydroxy-6-methylpyrimidine. Reaction of IIIb with malononitrile gave 1-amino-2-(*N*-benzyloxycarbonylaminoethylidene)malononitrile.

Amidines and 1,3-bifunctinal compounds react generally to form pyrimidines, and rarely to form another heterocyclic ring system. The reaction of malonamideamidine(I) with β-ethoxyacrolein diethylacetal or 1,3-dicarbonyl compounds has been reported[1,2] to produce 2-aminonicotinamide derivatives (II).

$H_2NCOCH_2C(=NH)NH_2$

I

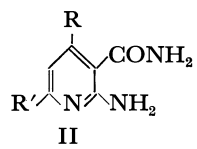

II

Goldberg and Kelly[3] reported that the reaction product between *N*-benzoylaminoacetamidine(IIIa) and acetylacetone was 2-(*N*-benzoylaminomethyl)-4,6-dimethylpyrimidine(IVa) on the basis of elemental analysis only. We have followed their procedure to prepare IVa and obtained a product having an empirical formula $C_{14}H_{15}ON_3$ and the same melting point as described. However, the IR spectrum of the product

1) A. Dornow and K. Peterlein, *Chem. Ber.*, **82**, 257 (1949).
2) A. Dornow and E. Neuse, *ibid.*, **84**, 296 (1951).
3) A. A. Goldberg and W. Kelly, *J. Chem. Soc.*, **1947**, 1372.

Table 1. Reaction of IIIa[a] with acetylacetone

Reaction	Solvent	Reaction		Alkali	Molar ratio of IIIa HCl : alkali	Yield of Va (%)
		Temp. (°C)	Time (hr)			
1[b]	C_2H_5OH	reflux	4	K_2CO_3	1 : 1	23
2	C_2H_5OH	reflux	4	K_2CO_3	1 : 2.5	17
3	C_2H_5OH	reflux	9	K_2CO_3	1 : 1	20
4	C_2H_5OH	reflux	15	K_2CO_3	1 : 1	11
5	C_2H_5OH	reflux	4	C_2H_5ONa	1 : 0.1[c]	20
6	DMF	70	4	K_2CO_3	1 : 2	21
7	DMF	90	4	K_2CO_3	1 : 2	18

a) Used in the form of hydrochloride except in Reaction 5.
b) The same conditions as given in Ref. 3.
c) Ratio of free IIIa : alkali.

showed absorptions attributed to =NH, $-NH_2$, and an amide carbonyl group. Additional information was obtained from the NMR spectrum. There were singlet peaks at τ 0.50(1H) and τ 4.37(2H) which disappeared with the addition of deuterium oxide, and two at τ 7.73(3H) and τ 7.93(3H) due to unequivalent two methyl groups.

On the basis of spectral results it is reasonable to consider that the reaction proceeded, as in the case of formation of II from I, to form 2-amino-3-benzoylamino-4,6-dimethylpyridine(Va).

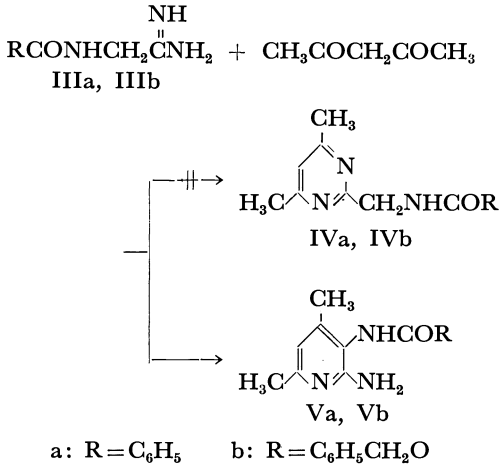

In order to collect chemical evidences on the assigned structure of Va, the following reactions were carried out. Treatment of Va with benzoyl chloride led to 2,3-dibenzoylamino-4,6-dimethylpyridine(VI). Hydrolysis of Va yielded 2,3-diamino-4,6-dimethylpyridine(VII) which condensed with benzil to produce 2,3-diphenyl-6,8-dimethylpyrido[2,3-*b*]-pyrazine(VIII). These properties can be explained satisfactorily only with Va and do not seem to occur with IVa.

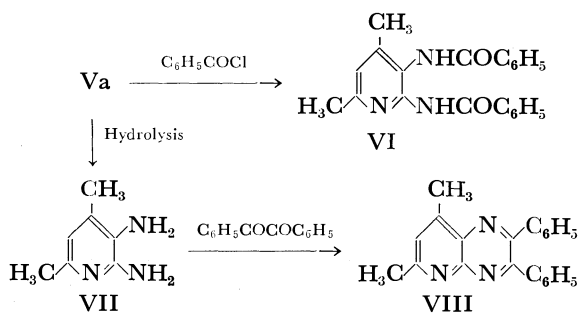

In order to learn whether the pyrimidine derivative (IVa) could be formed by the present reaction and for the purpose of improving the yield of Va, the reaction was carried out under various conditions (Table 1). All efforts to improve the yield of Va were unsuccessful. This can be attributed to the facile hydrolysis of free amidine(IIIa) in alkaline medium which competes with the formation of Va. In fact, a considerable amount of *N*-benzoylaminoacetamide was obtained as a by-product in each experiment. The reaction at room temperature, in benzene, or in acetic acid in the presence of sodium acetate gave no Va.

The reaction of *N*-benzyloxycarbonylaminoacetamidine(IIIb) with acetylacetone in ethanol in the presence of sodium ethoxide proceeded in a similar way affording 2-amino-3-benzyloxycarbonylamino-4,6-dimethylpyridine(Vb) in a poor yield. The assignment of structure Vb was based on its composition, IR and NMR spectra.

The reactivity of the methylene groups in IIIa and IIIb is considered to be much lower than that of the methylene group in I. It is notable that the methylene group in III participated in the ring formation.

Next, the reaction of IIIa with ethyl acetoacetate in the presence of sodium hydroxide was studied. The product, having an empirical formula $C_{13}H_{13}O_2N_3$, is soluble in aqueous sodium hydroxide and devoid of primary amino absorption in the IR spectrum. The doublet centered at τ 5.65 (2H, J=2.8 Hz) in the NMR spectrum assigned to methylene protons changed to a singlet, the triplet at τ 1.10(1H, J=2.8 Hz) disappearing with the addition of deuterium oxide. This indicates that the methylene protons are coupled with the =NH of the neighboring amide group. Elemental and spectrometric analyses identified the product as 2-(*N*-benzoylaminomethyl)-4-hydroxy-6-methylpyrimidine (IX).

As an alternative synthesis of IX, diketene was made to react with IIIa in ethanol at 0 °C. The product was identical with that previously prepared.

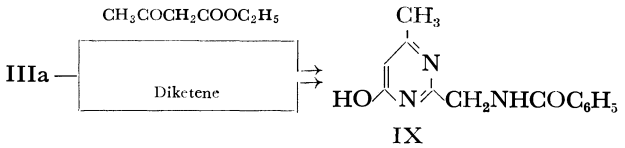

The reaction of IIIa with other 1,3-bifunctional compounds was also studied. The following reagents were used as 1,3-bifunctional compounds, *i.e.*, benzoylacetone, dibenzoylmethane, ethyl dimethylmalonate, methyl acrylate, and acetylacetaldehyde dimethylacetal. The reactions were carried out in ethanol at 45 °C for 2 days or under reflux for 4 hours in the presence of potassium carbonate or sodium ethoxide. All trials to isolate the expected product were unsuccessful.

Amidine IIIa is known to react with malononitrile and ethyl cyanoacetate to yield 1-amino-2-(*N*-benzoylaminoethylidene)malononitrile and ethyl 1-amino-2-(*N*-benzoylaminoethylidene)cyanoacetate, respectively.[3] A similar condensation of ethyl cyanoacetate with formamidine or benzamidine in the absence of alkali was reported.[4] We have now found that the reaction of IIIb with malononitrile proceeds analogously, 1-amino-2-(*N*-benzyloxycarbonylaminoethylidene)malononitrile(X) being obtained.

$$\text{IIIb} + CH_2(CN)_2 \rightarrow C_6H_5CH_2OCONHCH_2C{=}C(CN)_2 \quad (\text{X: } NH_2)$$

X

Experimental

All melting points were uncorrected. The NMR spectra were recorded at 60 MHz using tetramethylsilane as an internal standard.

2-Amino-3-benzoylamino-4,6-dimethylpyridine(Va). To a solution of 9 g (90 mmol) of acetylacetone in 75 ml of ethanol was added 15 g (70 mmol) of IIIa hydrochloride[3] and 10 g (72 mmol) of potassium carbonate, and refluxed for 4 hr with stirring. The reaction mixture was concentrated and the residue was dissolved in 70 ml of 10% hydrochloric acid. Insoluble *N*-benzoylaminoacetamide [mp 183 °C (lit,[3] 186 °C), 5 g (40%)] was removed by filtration, the filtrate being made alkaline with 10% aqueous sodium hydroxide. Precipitates were collected and recrystallized from methanol to give colorless needles of Va, mp 197—198 °C, 3.9 g (23%).

Found: C, 69.57; H, 6.51; N, 17.71%. Calcd for $C_{14}H_{15}ON_3$: C, 69.69; H, 6.27; N, 17.42%. IR(KBr) cm^{-1}: 3425, 3300, 3180, 1635, 1530. NMR ($CDCl_3$)τ: 0.50 (s, 1H), 1.80—2.67 (m, 5H), 3.55 (s, 1H), 4.37 (s, 2H), 7.73 (s, 3H), 7.93 (s, 3H).

2,3-Dibenzoylamino-4,6-dimethylpyridine(VI). To a solution of 1.2 g (5 mmol) of Va in 20 ml of 10% hydrochloric acid was added 0.7 g (5 mmol) of benzoyl chloride under ice cooling. Aqueous sodium hydroxide (10%) was added dropwise until the solution became alkaline. The precipitates were collected and recrystallized from dimethylformamide to give white powder of VI, mp 223—225 °C, 1.1 g (64%).

Found: C, 73.01; H, 5.61; N, 12.27%. Calcd for $C_{21}H_{19}O_2N_3$: C, 73.03; H, 5.54; N, 12.17%. IR(KBr) cm^{-1}: 3215, 1653, 1532. NMR (DMSO-d_6)τ: 1.77—2.63 (m, 10H), 2.90 (s, 1H), 5.87 (s, 2H) 7.54 (s, 3H), 7.71 (s, 3H).

2,3-Diamino-4,6-dimethylpyridine(VII). A solution of 2 g (8.3 mmol) of Va in 30 ml of 10% hydrochloric acid was heated under reflux for 6 hr. On cooling, benzoic acid which separated out was removed by filtration. The filtrate was treated with charcoal, concentrated to *ca.* 10 ml, and then made strongly alkaline with 10% aqueous sodium hydroxide to give crystalline substance. Recrystallization from water afforded colorless needles of VII, mp 156—158 °C, 0.9 g (79%).

Found: C, 61.59; H, 7.99; N, 30.32%. Calcd for $C_7H_{11}N_3$: C, 61.29; H, 8.08; N, 30.63%. IR(KBr) cm^{-1}: 3380, 3320. NMR (DMSO-d_6)τ: 3.81 (s, 1H), 4.74 (s, 2H), 5.86 (s, 2H), 7.88 (s, 3H), 8.00 (s, 3H).

2,3-Diphenyl-6,8-dimethylpyrido[2,3-b]pyrazine(VIII). A mixture of 0.69 g (5 mmol) of VII and 1.05 g (5 mmol) of benzil was heated for 30 min, the temperature being maintained at 120 °C. The reactants melted first and solidified again. Recrystallization from a mixture of ethanol and benzene gave colorless prisms of VIII, mp 189—190 °C, 1.4 g (89%). Found: C, 81.19; H, 5.56; N, 13.27%. Calcd for $C_{21}H_{17}N_3$: C, 81.00; H, 5.50; N, 13.50%. IR (KBr) cm^{-1}: 3030, 1590, 770, 700. NMR($CDCl_3$)τ: 2.23—2.87 (m, 10H and 1H of CH), 7.20 (s, 6H).

2-(N-Benzoylaminomethyl)-4-hydroxy-6-methylpyrimidine(IX). An ethanol solution of sodium ethoxide prepared from 0.7 g (30 mmol) of sodium and 30 ml of ethanol was added to a solution of 6.4 g (30 mmol) of IIIa hydrochloride in 20 ml of ethanol under ice cooling and the precipitated sodium chloride was removed by filtration. To the filtrate was added 3.9 g (30 mmol) of ethyl acetoacetate. This was transferred to an evaporating dish and evaporated to dryness in a desiccator over sulfuric acid. The residue was added to a mixture of 10 ml of 20% aqueous sodium hydroxide and 30 ml of ethanol, and stirring was continued at room temperature for 2 days. The reaction mixture was concentrated *in vacuo* and 20 ml of water was added. The water-insoluble substance was removed by filtration, and filtrate was neutralized with 5% hydrochloric acid to afford the precipitate. Recrystallization from dimethylformamide gave colorless needles of IX, mp 241—242 °C, 2.1 g (29%).

Found: C, 63.89; H, 5.26; N, 17.08%. Calcd for $C_{13}H_{13}O_2N_3$: C, 64.19; H, 5.38; N, 17.29%. IR(KBr) cm^{-1}: 3300, 1633. NMR (DMSO-d_6)τ: 1.10 (t, 1H), 2.1—2.5 (m, 5H), 3.93 (s, 1H), 5.65 (d, 2H), 6.67 (s, 1H), 7.87 (s, 3H).

Reaction of IIIa with diketene. A solution of IIIa (30 mmol) in ethanol was prepared by the same procedure as in the preceding experiment. To this was added dropwise 2.6 g (30 mmol) of diketene at 0 °C. Crystals began to separate out after 30 min. The reaction mixture was stirred at room temperature for 1 day. Precipitates were collected and recrystallized from dimethylformamide to give 2.2 g (32%) of IX, mp 241—242 °C. Found: C, 63.96; H, 5.30; N, 17.44%. Spectral data were identical with those obtained in the preceding experiment.

N-Benzyloxycarbonylaminoacetamidine(IIIb) hydrochloride. To a solution of ammonia in ethanol (50 ml, 15% by wt) was added 10 g (37 mmol) of ethyl imino(*N*-benzyloxycarbonylamino)acetate hydrochloride[5] and stirred for 1 hr. The resulting solution, after being allowed to stand at room temperature for 2 days, was concentrated in a desiccator over sulfuric acid. Recrystallization of the residue from acetonitrile gave colorless plates of IIIb hydrochloride, mp 112—113 °C (lit,[5] 78 °C), 5.5 g (62%). Found: C, 48.93; H, 5.52; N, 17.48%. Calcd for $C_{10}H_{14}O_2N_3Cl$: C, 49.39; H. 5.79; N, 17.24%. IR(KBr) cm^{-1}: 3500—2700, 1690, 1525. NMR(DMSO-d_6)τ: 0.87 (b.s, 4H), 2.17 (b.s, 1H), 2.63 (s, 5H), 4.90 (s, 2H), 5.92 (d, 2H).

Reaction of IIIb with acetylacetone. To an ethanol solution of sodium ethoxide prepared from 0.76 g (33 mmol) of

4) G. W. Kenner, B. Lythgoe, A. R. Todd, and A. Topham, *J. Chem. Soc.*, **1943**, 388.

5) M. Mengelberg, *Chem. Ber.*, **89**, 1185 (1956).

sodium and 30 ml of ethanol was added a solution of 6.8 g (28 mmol) of IIIb hydrochloride in 30 ml of ethanol under ice cooling. After removing sodium chloride 3.6 g (36 mmol) of acetylacetone was added and refluxed for 4 hr and then concentrated. To the residue was added 50 ml of chloroform. The crystal, insoluble in chloroform, was collected and recrystallized from ethanol to give colorless needles of *N*-benzyloxycarbonylaminoacetamide, mp 133—134 °C, 2.4 g (41%).

Found: C, 57.40; H, 6.05; N, 13.70%. Calcd for $C_{10}H_{12}O_3N_2$: C, 57.68; H, 5.81; N, 13.45%. IR(KBr) cm^{-1}: 3380, 3315, 3180, 1690, 1655, 1535.

The chloroform solution was concentrated and the residue was subjected to column chromatography on alumina and eluted with ethyl acetate to afford Vb. Recrystallization from a mixture of benzene and ligroin gave colorless needles, mp 162—163 °C, 1.0 g (13%). Found: C, 66.51; H, 6.19; N, 15.41%. Calcd for $C_{15}H_{17}O_2N_3$: C, 66.40; H, 6.31; N, 15.49%. IR(KBr) cm^{-1}: 3450, 3300, 3180, 1700, 1617, 1602. NMR($CDCl_3$)τ: 2.71 (s, 5H), 3.13 (b.s, 1H; exchanged with D_2O), 3.67 (s, 1H), 4.87 (s, 2H), 5.27 (s, 2H; exchanged with D_2O), 7.79 (s, 3H), 7.99 (s, 3H).

*1-Amino-2-(*N*-benzyloxycarbonylaminoethylidene)malononitrile(X).* A solution of IIIb (10 mmol) in 20 ml of ethanol containing sodium ethoxide (2 mmol) was prepared by a similar procedure to that in the preceding experiment. To this solution was added 0.66 g (10 mmol) of malononitrile and refluxed for 30 min. After cooling to room temperature, crystals which separated out were recrystallized from ethanol to give colorless needles of X, mp 169—170 °C, 1.5 g (62%). Found: C, 60.68; H, 4.46; N, 22.13%. Calcd for $C_{13}H_{12}O_2N_4$: C, 60.93; H, 4.72; N, 21.86%. IR(KBr) cm^{-1}: 3400, 3350, 2220, 2190, 1715, 1650, 1548. NMR (DMSO-d_6)τ: 1.33 (b.s, 1H), 1.57 (b.s, 1H), 2.61 (b.s, 1H), 2.63 (s, 5H), 4.93 (s, 2H), 5.98 (d, 2H).

BULLETIN OF THE CHEMICAL SOCIETY OF JAPAN, VOL. 46, 3280—3285 (1973)

Improved Solid-Phase Synthesis of Tryptophan-Containing Peptides. II. Use of N^{α}-*t*-Butyloxycarbonyl-N^{i}-formyltryptophan[1]

Motonori OHNO, Sadaji TSUKAMOTO, Shin-ichi SATO, and Nobuo IZUMIYA

Department of Chemistry, Faculty of Science, Kyushu University, Fukuoka 812

(Received May 14, 1973)

N^{i}-Formyltryptophan has proved to be more resistant than tryptophan against oxidation mediated by hydrogen chloride in acetic acid. N^{α}-*t*-Butyloxycarbonyl-N^{i}-formyltryptophan has been synthesized *via* nonaqueous *acylation* reaction and used for the solid-phase synthesis of tryptophan-containing peptides, in combination with hydrogen chloride in formic acid as the reagent for cleavage of the *t*-butyloxycarbonyl group. The validity of the method has been demonstrated, on the basis of several criteria, in the synthesis of the tryptophan-containing octapeptide, Lys-Gly-Val-Leu-Ala-Gly-Trp-Leu.

In solid-phase synthesis of tryptophan-containing peptide, repeated deprotection of the Boc[2] group with hydrogen chloride in acetic acid brings about more or less oxidative destruction of tryptophan even in the presence of 2-mercaptoethanol as a scavenger.[3] Because of such well-known acid lability of tryptophan, it has been of special value to develop a new reagent for cleavage of the Boc group which would not produce the undesirable oxidation and to find out an acid-stable tryptophan derivative suitable for peptide synthesis. Hydrogen chloride in formic acid has recently been introduced as a reagent for cleavage of the Boc group in the solid-phase synthesis of the tryptophan-containing heptapeptide. Its effectiveness has been demonstrated on the basis of relevant chemical and physical properties of the resulting heptapeptide and its derivatives.[3] The merit of the reagent is ascribed to its greater ability to prevent oxidation of tryptophan owing to the reductive nature of formic acid.

Tryptophan undergoes formylation at its indole nitrogen in hydrogen chloride–formic acid as described by Previero *et al.*[4] and in our previous reports.[3] This formyl group is removed easily in a weakly alkaline medium or by dissolving formylated derivatives in dimethylformamide containing hydrazine hydrate without any serious influence on other amino acids.[3] It seemed of interest to examine whether N^{i}-formyltryptophan is more resistant than tryptophan against oxidation mediated by acids, since it would satisfy the prerequisite that the group introduced for stabilization of indole nucleus should be removed under mild conditions without affecting other residues. Thus, the acid-stability of N^{i}-formyltryptophan was tested using 1 M hydrogen chloride in acetic acid and compared with tryptophan as a reference.

Changes of N^{i}-formyltryptophan[3] and tryptophan in 1 M hydrogen chloride in acetic acid were followed

1) A part of this paper was presented at the 10th Symposium on Peptide Chemistry, Sapporo, September 26 and 27, 1972.

2) All amino acids in this report are of the L-configuration. Abbreviations used are: Boc, *t*-butyloxycarbonyl; Z, benzyloxycarbonyl; Trp, trytophan; Trp(CHO), N^{i}-formyltryptophan; NCPS–Cl, 2-nitro-4-carboxyphenylsulfenyl chloride; Trp(NCPS), 2-thio-(2-nitro-4-carboxyphenyl)-tryptophan; βME, 2-mercaptoethanol; HCl, hydrogen chloride; AcOH, acetic acid; Et_3N, triethylamine; DMF, dimethylformamide; EtOH, ethanol; HF, anhydrous hydrofluoric acid.

3) M. Ohno, S. Tsukamoto, and N. Izumiya, *Chem. Commun.*, **1972**, 663; M. Ohno, S. Tsukamoto, S. Makisumi, and N. Izumiya, This Bulletin, **45**, 2852 (1972).

4) A. Previero, M. A. Coletti-Previero, and J. -C. Cavadore, *Biochim. Biophys. Acta*, **147**, 453 (1967).

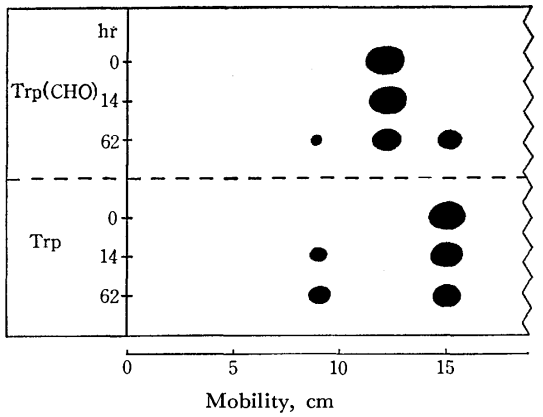

Fig. 1. Electrophoreograms of the solutions of N^{i}-formyltryptophan and tryptophan in 1 M hydrogen chloride in aceuc acid after 14 and 62 hr of standing. Fresh solutions of these amino acids in 0.1 M hydrochloric acid were used as references. The spots were developed with ninhydrin. The substance at 9 cm from the original line was Ehrlich-negative and is noted as "unidentified substance" in the text.

by paper electrophoresis and UV absorption spectra at appropriate time intervals. In Fig. 1 are shown electrophoreograms for the two solutions after 14 and 62 hr of standing. After 14 hr, an Ehrlich-negative, less mobile unidentified substance was detected for the test solution of tryptophan in an appreciable amount. On the other hand, N^{i}-formyltryptophan remained unchanged. After 62 hr of standing, however, about one-half of N^{i}-formyltryptophan had been deformylated to produce tryptophan and the unidentified substance was also present although in a very small quantity. At that time the amount of the unidentified substance in the test solution of tryptophan had increased markedly. These phenomena indicate that N^{i}-formyltryptophan in 1 M hydrogen chloride in acetic acid is first deformylated and tryptophan thus formed is successively oxidized to produce the unidentified substance. It should be noted that there was a long time lag for the conversion of N^{i}-formyltryptophan into tryptophan. It is concluded that N^{i}-formyltryptophan is more resistant than tryptophan against oxidation mediated by the acid at least within a limited period. Thus, use of N^{i}-formyltryptophan has been undertaken for the solid-phase synthesis of tryptophan peptide.

t-Butyloxycarbonylation of α-amino group of N^{i}-formyltryptophan with Boc-chloride[5] or Boc-azide[6] in an aqueous alkaline medium (pH 9.0) was unsuccessfull because of alkali lability and insolubility at a near-neutral pH of N^{i}-formyltryptophan. *Acylation,* therefore, was carried out in nonaqueous, triethylamine-buffered dimethylformamide. The method gave an yield as high as 89% for N^{α}-Boc-N^{i}-formyltryptophan. This type of nonaqueous *t*-butyloxycarbonylation might be widely applicable for hydrophobic amino acid with suitable solubility in dimethylformamide.

5) S. Sakakibara, I. Honda, K. Takada, M. Miyoshi, T. Ohnishi, and K. Okumura, This Bulletin, **42**, 809 (1969).

6) R. Schwyzer, P. Sieber, and H. Kappeler, *Helv. Chim. Acta*, **42**, 2622 (1959).

This paper describes the use of N^{α}-Boc-N^{i}-formyltryptophan and hydrogen chloride in formic acid for the Merrifield type solid-phase synthesis of tryptophan peptide. The method has been compared with two other methods: one making use of Boc-tryptophan and hydrogen chloride in formic acid, and the other Boc-tryptophan and hydrogen chloride in acetic acid containing βME. The latter method is usually applied to the solid-phase synthesis of tryptophan peptide.[7] Arbitrarily sequenced octapeptide consisting of amino acids which do not absorb near-ultraviolet light except for tryptophan, Lys–Gly–Val–Leu–Ala–Gly–Trp–Leu, was selected as a model peptide to test the methods.

The three octapeptides were built up as usual, in parallel, starting from Boc-leucyl resin and using either a 6—7 fold molar excess of hydrogen chloride (0.4 M) in formic acid or a 15-fold molar excess of hydrogen chloride (1 M) in acetic acid containing 2% βME. ε-Amino group of lysine was protected with the Z group. At every neutralization step, chlorides were determined on the combined dimethylformamide washings. As seen in Fig. 2, levels of chloride titrated for hydrogen chloride–formic acid systems were 83—84% of that for hydrogen chloride–acetic acid system. Such phenomena have always been observed in all other comparable experiments although the reason has not yet been clarified.

The larger halves of the three protected octapeptide resins [**1a** (*via* Boc–Trp(CHO)—HCl–HCOOH), **1b** (*via* Boc–Trp—HCl–HCOOH), and **1c** (*via* Boc–Trp—HCl–AcOH–βME)] were cleaved by hydrazine hydrate in dimethylformamide.[3,8] In order to remove non-peptide substances derived from the resin, the three products for Boc–Lys(Z)–Gly–Val–Leu–Ala–Gly–Trp*–Leu–$NHNH_2$[9] [**2a** (*via* Boc–Trp(CHO)—HCl–HC-

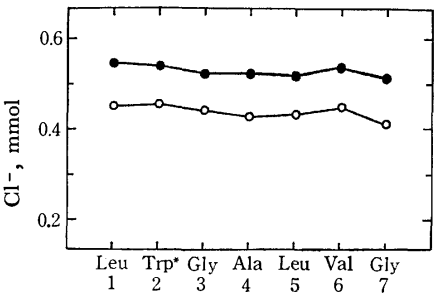

Fig. 2. Millimoles of chlorides determined at neutralization steps in the solid-phase syntheses using HCl–HCOOH (-○-) and HCl–AcOH (-●-). Values presented are those for 1.00 g each of Boc-leucyl resin used. Two runs using HCl–HCOOH gave the same titration values. Details are described in the ' Experimental" section.

7) G. R. Marshall, "Pharmacology of Hormonal Polypeptides and Proteins," ed. by N. Back, R. Paoletti, and L. Martini, Plenum Press, New York, N. Y., (1968); J. Blake and C. H. Li, *J. Amer. Chem. Soc.*, **90**, 5882 (1968); H. Matsuo, A. Arimura, R. M. G. Nair, and A. V. Schally, *Biochem. Biophys. Res. Commun.*, **45**, 822 (1971).

8) M. Ohno and C. B. Anfinsen, *J. Amer. Chem. Soc.*, **89**, 5994 (1967); M. Ohno, K. Kuromizu, H. Ogawa, and N. Izumiya, *ibid.*, **93**, 5251 (1971).

9) Asterisk signifies that Trp may or may not denote pure tryptophan. In some cases the denotation is extended to derivatives.

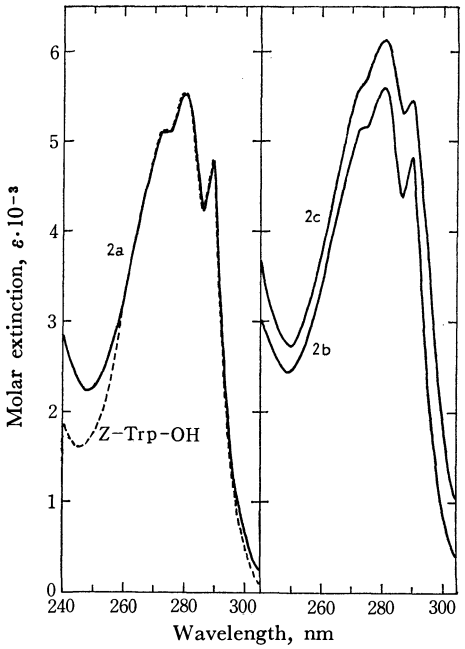

Fig. 3. Ultraviolet absorption spectra of the protected octapeptide hydrazides, **2a**, **2b**, and **2c**, and Z–Trp in methanol.

OOH), **2b** (*via* Boc–Trp—HCl–HCOOH), and **2c** (*via* Boc–Trp—HCl–AcOH–βME)] were reprecipitated (see Experimental). Yields were in parallel with levels of chloride titrated in the neutralization steps. The UV absorption spectra of **2a** and **2b** were virtually identical with that of Z-tryptophan except that a trough in the 240—250 nm region showed somewhat greater absorption and was shifted to the red by 2—3 nm (Fig. 3). Such phenomena suggest that **2a** and **2b** are contaminated to only a minor extent by oxidized species, but it seems likely that an increase of absorption in the 240—250 nm region owes to some extent to the additional peptide absorption as discussed by Beaven and Holiday.[10] On the other hand, extinction of **2c** at 280 nm, for example, was about 20% greater than those of **2a** and **2b**, reflecting oxidative destruction of indole chromophore to a considerable extent.

Small portions of **1a**, **1b**, and **1c** were cleaved with anhydrous hydrofluoric acid in the presence of anisole,[11] to produce **3a**, **3b**, and **4c**, respectively. The formyl group is still attached more or less to tryptophan residues of **3a** and **3b** since it is resistant to anhydrous hydrofluoric acid as well as anhydrous triethylamine in dimethylformamide in the neutralization step. Hydrogen chloride–acetic acid never acetylates tryptophan. **3a** and **3b** were chromatographed on a Sephadex G–25 column (Fig. 4): the peptides recovered from the major peaks are denoted by **3a**† and **3b**†, respectively. **3a**† gave a spectrum typical of N^i-formyltryptophan,[12] indicating that a N^i-formyltryptophan residue is kept intact. The spectrum of **3b**† showed that about one-half of tryptophan involved is formylated. **3a** and **3b** were then treated with 0.1 M aqueous triethylamine for removing the formyl group to produce completely deprotected peptides, **4a** and **4b**.

Figure 5 shows gel-chromatographic patterns of **4a**, **4b**, and **4c** on a Sephadex G–25 column: the peptides from the major peaks for **4a** and **4b** are denoted by **4a**† and **4b**†, respectively. In contrast to **4a** and **4b**, **4c** gave a complex profile owing to its heterogeneity. The peptide from peak II (denoted by **4c**-II) exhibited

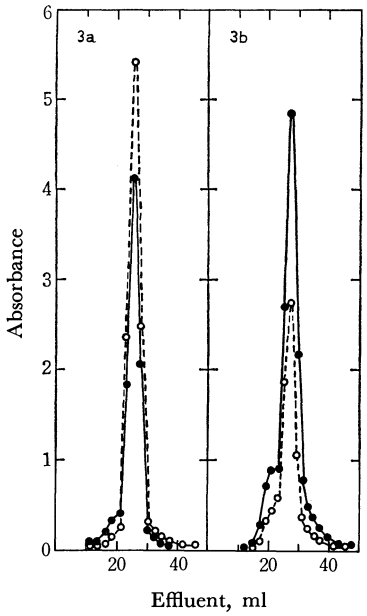

Fig. 4. Chromatographies on a Sephadex G–25 column (0.9×61 cm) of the octapeptides, **3a** and **3b** (7 mg each), which were obtained by cleavages of the peptide resins, **1a** and **1b**, with HF. Elutions were conducted with 5% AcOH and monitored by absorptions at 280 (-●-) and 300 (···○···) nm.

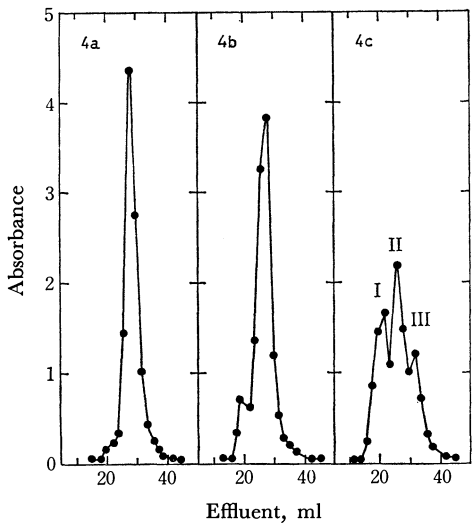

Fig. 5. Chromatographies on a Sephadex G–25 column (0.9×61 cm) of the completely deblocked peptides, **4a**, **4b**, and **4c** (5 mg each). Elutions were conducted with 5% AcOH and monitored by absorption at 280 nm.

10) G. G. Beaven and E. R. Holiday, *Advan. Protein Chem.*, **7**, 319 (1952).

11) S. Sakakibara, Y. Shimonishi, Y. Kishida, M. Okuda, and H. Sugihara, This Bulletin, **40**, 2164 (1967); J. Lenard and A. B. Robinson, *J. Amer. Chem. Soc.*, **89**, 181 (1967).

12) Spectra of N^i-formyltryptophans have been presented in a previous paper.[3]

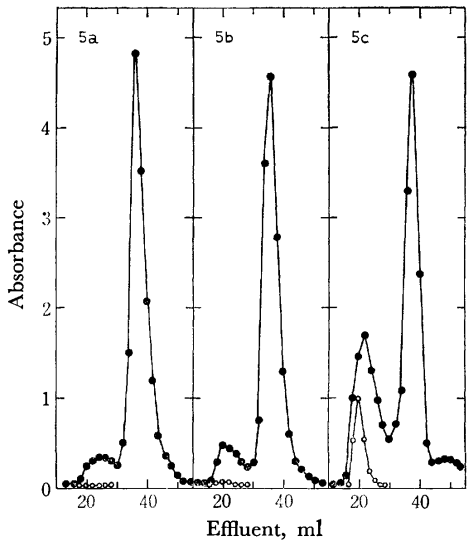

Fig. 6. Chromatographies on a Sephadex G-25 column (0.9×61 cm) of the peptides, **5a**, **5b**, and **5c**, which were obtained by reactions of **4a**, **4b**, and **4c** (7 mg each) with NCPS-Cl. Elutions were conducted with 5% AcOH and monitored by absorptions at 280 (-●-) and 585 (-○-) nm.

a similar spectrum to that given by **4a**† and **4b**† but was contaminated by a minor component of less mobility on paper electrophoresis. **4c**-I and **4c**-III consisted of peptides involving oxidized tryptophan. For further inspection of purity, **4a**, **4b**, and **4c** were treated with NCPS-Cl[13,14] as described[3] and the modified peptides (denoted by **5a**, **5b**, and **5c**, respectively) were examined chromatographically and spectrally. During the modification, the reaction mixture for **4c** became dark blue, giving an absorption maximum at 585 nm. The mixture for **4b** was yellow slightly tinged with blue but that for **4a** was yellow. If only intact tryptophan is involved, the reaction mixture should be yellow. It is extremely likely that oxidized tryptophans form blue substances upon reaction with NCPS-Cl. Chromatography of the modified peptides was carried out on the same column as for the unmodified ones, elutions being monitored by absorptions at 280 and 585 nm (Fig. 6). The peptides from the major peaks for **5a** and **5b**, denoted by **5a**† and **5b**†, were pure yellow and showed an increased adsorptivity on the gel compared with **4a**† and **4b**† (Figs. 5 and 6).[15] Such shifts suggest that **4a**† and **4b**† involve only pure tryptophan peptide. This was confirmed by the fact that **5a**† and **5b**† exhibited the same spectra as 2-thio-(2-nitro-4-carboxyphenyl)-tryptophan[14] (Table 1) and gave a single band by paper chromatography. Although **5c** gave a major peak at almost the same elution volume as for **5a**† and **5b**†, the peptide from the major peak for **5c**, denoted by **5c**†, was brownish yellow and

13) A. J. Havlik and N. Kharasch, *J. Amer. Chem. Soc.*, **77**, 1150 (1955).

14) F. M. Veronese, E. Boccú, and A. Fontana, *Ann. Chim.*, **58**, 1309 (1968).

15) The peptide containing Trp(NCPS) showed an increased adsorptivity on the gel compared with the corresponding tryptophan peptide.

Table 1. Spectral characteristics of **5a**†, **5b**†, and **5c**†

Substance	λ_{max} (nm)			$A_{282}/A_{350-\delta 56}$
Trp(NCPS)	260(s)[a]	282	355	4.80
5a†	260(s)	282	356	4.94
5b†	260(s)	282	356	4.94
5c†	257(s)	282.5	350	4.02

a) (s), shoulder.

contaminated by two additional minor impurities. The spectrum of **5c**† was rather different from that of 2-thio-(2-nitro-4-carboxyphenyl)-tryptophan.

Octapeptide samples were hydrolyzed in the presence of 3% thioglycolic acid[16] and the contents of tryptophan were analyzed on amino acid analyzer. Yields of tryptophan from the protected peptide hydrazides **2a**, **2b**, and **2c** were distinctly lower than those of the corresponding unprotected peptides, *e.g.*, **3a**, **3b**, and **4c**. The peptides **2c** and **4c** synthesized by use of HCl-AcOH-βME gave about 20—30% lower yields of tryptophan compared with the peptides prepared by use of HCl-HCOOH. Yield of tryptophan for **3b** was lower to some degree than that for **3a**, indicating that **3b** involves somewhat more oxidized peptide. As seen in the elution diagrams for **3a** and **3b** as well as **4a** and **4b** (Figs. 4 and 5), the oxidized peptides were eluted in part of shoulder prior to the major peak and shoulders for **3a** and **4a** were smaller than those for **3b** and **4b**, respectively. Considering these observations together with differences in physical properties between **2a** and **2b**, the peptides *via* Boc-Trp(CHO)—HCl-HCOOH are superior in quality to those *via* Boc-Trp—HCl-HCOOH. However, when both the crude unprotected peptides were purified on a Sephadex G-25 column, the resulting purified ones showed the same behaviors in terms of electrophoresis, chromatography, and chemical modification by NCPS-Cl and gave the same yields for tryptophan on amino acid analysis. The results demonstrate usefulness of hydrogen chloride in formic acid for the solid-phase synthesis of tryptophan peptide, and show pre-introduction of the formyl group to indole nucleus to be so effective as regards the protection of tryptophan from oxidation under solid-phase synthesis conditions. N^{α}-Boc-N^{i}-Formyltryptophan will be a useful derivative for synthesis of longer, complex tryptophan-containing peptides which may resist purification.

Experimental

General experimental and analytical procedures used were those described in the previous paper.[3] Thin-layer chromatography was performed using methanol-ethyl acetate (3 : 1 v/v) (solvent 1) and paper chromatography *n*-butanol-acetic acid-water (4 : 1 : 5 v/v, upper layer) (solvent 2). Paper electrophoresis was carried out under the following conditions: paper, Whatman 3 MM (57 cm length); solvent, 0.24 M formic acid (pH 2.08); voltage gradient, 48 V/cm; period, 90 min. All peptides in the present experiments moved towards the cathode. Amino acids and peptides were detected by a spray of ninhydrin (0.2% solution in 80%

16) H. Matsubara and R. H. Sasaki, *Biochem. Biophys. Res. Commun.*, **35**, 175 (1969).

ethanol). Modified Ehrlich reagent (0.5% solution of *p*-dimethylaminocinnamaldehyde in 0.5 M hydrochloric acid) was also used for the detection of tryptophan and its peptides. For amino acid analysis, peptides were hydrolyzed with constant boiling hydrochloric acid containing 3% thioglycolic acid in an evacuated, sealed tube at 110 °C for 24 hr. Formic acid (analytical grade, 98—100%, Merck) was used without purification. Acetic acid was refluxed over potassium permanganate, dehydrated with boron triacetate and distilled.[17] Concentration of hydrogen chloride in formic acid or acetic acid was determined by the modified Volhard method.[18]

Stability Test of N^{i}*-Formyltryptophan and Tryptophan in 1 M Hydrogen Chloride in Acetic Acid.* Trp(CHO)·HCl[3] and tryptophan (40 mg each) were respectively dissolved in 5 ml of 1 M HCl in AcOH and the solutions were allowed to stand at room temperature. After 14 and 62 hr of standing, aliquots of the solutions were subjected to paper electrophoresis, and 0.5 ml portions were taken and dried by lyophilization. The residues were dissolved in water and UV spectra were taken. After 14 hr no spectral change was observed for the test solution of tryptophan, when compared with untreated tryptophan, except for somewhat greater absorption in the 240—250 nm region, but an Ehrlich-negative, less mobile unidentified substance was detected in an appreciable amount on paper electrophoresis. On the other hand, Trp(CHO) was unchanged on paper electrophoresis although the test solution became tinged with yellow and the fine structure of the spectrum in the 280—290 nm region was only slightly disturbed. After 62 hr of standing, however, about one-half of Trp (CHO) had been deformylated to produce tryptophan and the unidentified substance was also present although in a minute quantity. Amount of the unidentified substance in the test solution for tryptophan had increased markedly but the spectrum was virtually the same as before.

N^{α}*-Boc-*N^{i}*-Formyltryptophan.* To a solution of 2.68 g (10 mmol) of Trp(CHO)·HCl in 60 ml of DMF was added 4.2 ml (30 mmol) of Et_3N followed by 3.0 ml of Boc-azide. The mixture was stirred at room temperature for 2 days. Gelatinous stuff appeared at the beginning but gradually dissolved with the progress of reaction except for Et_3N·HCl. The mixture was poured into 300 ml of 0.5 M citric acid and an oil deposited was extracted with 150 ml of ethyl acetate. The ethyl acetate layer was washed four times with water, dried over anhydrous sodium sulfate and evaporated below 40 °C nearly to dryness. The syrup was crystallized by adding petroleum ether and by scratching. Crystals were filtered and washed with petroleum ether, 2.98 g (89%); mp 102—104 °C; $[\alpha]_D^{21}$ +22.3° (*c* 1.61, EtOH); λ_{max} (EtOH) 242 (log ε 4.23), 293 (log ε 3.67), 301 nm (log ε 3.67).

Found: C, 61.24; H, 6.26; N, 8.35. Calcd for $C_{17}H_{20}O_5N_2$: C, 61.43; H, 6.07; N, 8.43%.

Boc-Leucyl Resin. Chloromethylated copolystylene-divinylbenzene (2%) resin (1.3 mmol Cl/g) obtained from the Protein Research Foundation, Osaka, was esterified with Boc-Leu.[3] Amino acid analysis indicated the leucine content to be 0.56 mmol/g.

Boc-Lys(Z)-Gly-Val-Leu-Ala-Gly-Trp-Leu-resins (**1a**, **1b**, and **1c**).* Boc-Leucyl resin (1.00 g each) was placed in three reaction vessels of the type described by Merrifield for repeated deblocking, rinsing and coupling procedures. The procedures used for the stepwise addition of the appropriate Boc-amino acids were almost the same as described[3] except that either a 6—7 fold molar excess of HCl (0.4 M) in HCOOH (8 ml) or a 15-fold molar excess of HCl (1 M) in AcOH (8 ml) was used for the cleavage of the Boc group. About 8—9 ml portions of the appropriate solvents were used for rinsing and coupling procedures. βME (2% by volume) was added to HCl-AcOH and also to the AcOH washes after deprotection. The Boc group on valine amino group was not completely cleaved by 30 min shaking in 0.4 M HCl in formic acid. The acid treatment was repeated twice for all runs. Yields: **1a**, 1.42; **1b**, 1.44; and **1c**, 1.48 g.

At every neutralization step, Et_3N-DMF for neutralization and DMF washings were pooled, chlorides being determined by the modified Volhard method (Fig. 2).

Boc-Lys(Z)-Gly-Val-Leu-Ala-Gly-Trp-Leu-*$NHNH_2$ *(**2a**, **2b**, and **2c**).* To suspensions of **1a**, **1b**, and **1c** (0.80 g each) in 3 ml of DMF was added 1.0 ml each of 100% hydrazine hydrate and the mixtures were shaken for 3 days at room temperature. The DMF solutions were separated by filtration and the resins were rinsed several times with DMF. The combined filtrates were evaporated *in vacuo* nearly to dryness. The hydrazides quickly solidified upon addition of water and were filtered and washed with water. The crystalline products were dissolved in hot methanol and insoluble materials were filtered off. The filtrates were evaporated *in vacuo* nearly to dryness and the residues were dissolved in a small volume of DMF. To these solutions were added larger volumes of water and the crystalline precipitates were filtered: **2a**, 159 mg (76% of **2c**), mp 235—236 °C, $[\alpha]_D^{21}$ −28.7° (*c* 0.223, DMF), R_f(1) 0.90; **2b**, 169 mg (81% of **2c**), mp 233—234 °C, $[\alpha]_D^{21}$ −27.7° (*c* 0.235, DMF), R_f(1) 0.89; and **2c**, 209 mg, mp 217—219 °C, $[\alpha]_D^{21}$ −25.7° (*c* 0.296. DMF), R_f(1) 0.89.[19] UV Spectra were taken in the methanolic solutions (Fig. 3), A_{281}/A_{248}[20] for **2a**, 2.42; A_{281}/A_{249} for **2b**, 2.24; and A_{282}/A_{250} for **2c**, 2.09. Amino acid analysis data are presented as 1.00 for lysine. **2a**: Lys 1.00, Trp 0.75, Gly 1.92, Ala 0.95, Val 0.97, Leu 1.92. **2b**: Lys 1.00, Trp 0.72, Gly 1.99, Ala 0.98, Val 0.94, Leu 1.91. **2c**: Lys 1.00, Trp 0.45, Gly 2.12, Ala 1.05, Val 1.08, Leu 1.95.

Found **2a**: C, 58.39; H, 7.65; N, 15.13. **2b**: C, 58.63; H, 7.76; N, 15.15. **2c**: C, 58.12; H, 7.63; N, 14.96. Calcd for $C_{54}H_{82}N_{12}O_{12}\cdot H_2O$: C, 58.46; H, 7.63; N, 15.15%.

Lys-Gly-Val-Leu-Ala-Gly-Trp(CHO)-Leu (**3a** and **3b**) and Lys-Gly-Val-Leu-Ala-Gly-Trp*-Leu (**4a**, **4b**, and **4c**).* **1a**, **1b**, and **1c** (0.140 g each) were respectively treated with 3—4 ml of HF for 1 hr at 0 °C in the presence of anisole (0.2 ml). After removal of HF *in vacuo*, the peptides released were extracted with four 3 ml portions of 20% AcOH. The aqueous solutions were shaken with ethyl ether and lyophilized. Yields: **3a**, 30 mg; **3b**, 32 mg; and **4c**, 39 mg. Amino acid analyses of the samples gave the following ratios. **3a**: Lys 1.00, Trp 0.91,[21] Gly 2.05, Ala 1.03, Val 1.00, Leu 1.95. **3b**: Lys 1.00, Trp 0.80, Gly 2.07, Ala 1.04, Val 0.97, Leu 1.97. **4c**: Lys 1.00, Trp 0.58, Gly 2.01, Ala 1.12, Val 1.07, Leu 2.12. **3a** and **3b** (7 mg each) were chromatographed on a Sephadex G-25 column (0.9×61 cm) using 5% AcOH (Fig. 4). Fractions of the major peaks were lyophilized to give **3a**† and **3b**†. Their spectra were taken in 5% AcOH and compared with those of Trp(CHO) and the mixtures of

17) L. F. Fieser, "Experiments in Organic Chemistry," 3rd Ed., D. C. Heath and Co., New York (1955), p. 281.

18) J. M. Stewart and J. D. Young, "Solid Phase Peptide Synthesis," W. H. Freeman and Co., San Francisco (1969), p. 55.

19) When 47% hydrobromic acid was sprayed to cleave the Boc group, a spot turned purple.

20) *A* signifies absorbance at the indicated wave lengths. Such ratios are presented as a sort of measure for the extent of oxidation for tryptophan.

21) The formyl group of Trp(CHO) was spontaneously removed by heating in constant boiling hydrochloric acid at 110 °C with concomitant formation of tryptophan. Thioglycolic acid produced no side reaction.

Trp(CHO) and tryptophan in varying ratios. Amino acid analyses gave the following ratios. **3a**†: Lys 1.00, Trp 0.87. **3b**†: Lys 1.00, Trp 0.86. **3a** and **3b** (15 mg each) were dissolved in 1.5 ml of 0.1 M aqueous Et_3N and the solutions were allowed to stand at 0 °C for 10 min. Lyophilization of the solutions gave **4a** and **4b** as white fluffy powders.

*Chromatographies of the Octapeptides (**4a**, **4b**, and **4c**) on a Sephadex G-25 Column.* **4a**, and **4b**, and **4c** (5 mg each) were chromatographed on a Sephadex G-25 column (0.9× 61 cm) using 5% AcOH. The elutions were monitored by absorption at 280 nm (Fig. 5). Fractions of the major peaks for **4a** and **4b** were lyophilized to give **4a**† and **4b**†. Fractions of three peaks for **4c** were lyophilized. The resulting peptides were subjected to paper electrophoresis and their spectra were taken in 5% AcOH. Mobilities on paper electrophoresis (cm): **4a**†, 13.2; **4b**†, 13.2; **4c**-I, 14.5 (broad); **4c**-II, 13.2 (major) and 24.2 (minor); and **4c**-III, 11.7 (broad). Absorbance ratios: A_{280}/A_{247} for **4a**†, 2.17; and A_{280}/A_{247} for **4b**†, 2.20; A_{282}/A_{254} for **4c**-I, 1.45; A_{280}/A_{249} for **4c**-II, 2.05; and A_{280}/A_{251} for **4c**-III, 1.98. R_f's (2): **4a**†, 0.69; **4b**†, 0.69; **4c**-I, 0.53; **4c**-II, 0.69 (major) and 0.13 (minor); and **4c**-III, 0.75. Amino acid analyses gave the following ratios. **4a**†: Lys 1.00, Trp 0.88. **4b**†: Lys 1.00, Trp 0.86.

*Reactions of the Octapeptides (**4a**, **4b**, and **4c**) with NCPS-Cl and Chromatographies of the Modified Peptides (**5a**, **5b**, and **5c**) on a Sephadex G-25 Column.* To solutions of **4a**, **4b**, and and **4c** (7.0 mg each) in 1.2 ml of 80% HCOOH were added 19.5 mg each of NCPS-Cl and the solutions were stirred for 5 hr at room temperature and lyophilized. Color changes observed during the course of reactions have been described in the text. The dried residues were scratched with five 2 ml portions of acetone containing 2% concentrated hydrochloric acid in order to remove the excess reagent. The peptides were separated by centrifugation from the acetone solutions and finally dissolved in water, and the solutions were lyophilized. The dried peptides were dissolved in 0.6 ml of 5% AcOH and chromatographed on a Sephadex G-25 column (0.9×61 cm). The elutions were monitored by absorptions at 280 and 585 nm (Fig. 6). Fractions of the major peaks for **5a**, **5b**, and **5c** were lyophilized to give **5a**†, **5b**†, and **5c**†, respectively. Their spectra were taken in 5% AcOH and compared with that of Trp(NCPS) (Table 1). **5a**† and **5b**† (both pure yellow) gave a single band on paper chromatography, R_f (2) 0.80. On paper electrophoresis they did not move from the original line owing to extreme adhesiveness to the paper. **5c**† (brownish yellow) was shown on paper electrophoresis to contain two impure peptides in addition to the yellow peptide identical with **5a**† and **5b**†. Major and minor impurities moved 0.5 and 7.7 cm, respectively.

BULLETIN OF THE CHEMICAL SOCIETY OF JAPAN, VOL. 46, 3285—3288 (1973)

The Reactions of the Hexafluorothioacetone Dimer with Nucleophiles in the Presence of the Fluoride Ion

Tomoya KITAZUME and Nobuo ISHIKAWA

Department of Chemical Engineering, Tokyo Institute of Technology, Ookayama, Meguro-ku, Tokyo 152

(Received June 11, 1973)

In the KF-DMF system, the hexafluorothioacetone dimer (**1**) reacted with alcohols, alkanethiols, and thiophenols under mild conditions. The products, **2**, **3**, **10**, and **12**, were assumed to have resulted from the hexafluorothioacetone monomer (**4**) and the nucleophiles. Cycloadducts of **4** and anthracene or styrene were also obtained readily from the dimer (**1**) and the dienes.

2,2,4,4-Tetrakis(trifluoromethyl)-1,3-dithiethane (**1**), a dimer of hexafluorothioacetone, is a stable compound derived from hexafluoropropene and sulfur.[1] In an earlier communication,[2] we reported on the reactions between the dimer and amines or carbonyl reagents, which gave *N*-substituted hexafluoroisopropylideneimines. However, attempts to have other nucleophiles, such as alcohols and thiols, react with the dimer were unsuccessful.

In our continued studies of the nucleophilic reactions of the dimer, we have found that, in the presence of potassium fluoride, **1** in dimethylformamide reacted with alcohols and thiols, thus giving the reaction products of these nucleophiles with hexafluorothioacetone itself.

Results and Discussion

Reaction of Hexafluorothioacetone Dimer with Alcohols. Although the dimer, **1**, reacted with aryl or alkyl amines in dimethylformamide at room temperature,[2] no reaction was observed with alcohols even at a higher temperature. The presence of a small amount of potassium fluoride, however, promoted the reaction very much, and it proceeded smoothly at room temperature. The products of this reaction were bis-[1-alkoxy-1-(trifluoromethyl)-2,2,2-trifluoroethyl] disulfide (**2**) and 1-alkoxy-1-(trifluoromethyl)-2,2,2-trifluoroethyl alkyl sulfide (**3**).

1) I. L. Knunyants, *Dokl. Akad. Nauk SSSR*, **183**, 598 (1968).
2) N. Ishikawa and T. Kitazume, This Bulletin, submitted for publication.

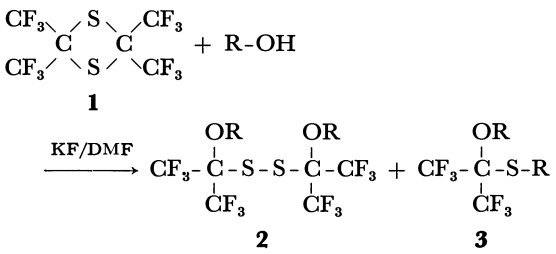

The structures of these compounds were elucidated by a study of the ^1H and ^{19}F NMR and the mass spectra. The ^{19}F NMR spectra of both **2** and **3** showed only one singlet signal each, *i.e.*, −9.2 ppm for **2** (R=Me) and −7.20 ppm for **3** (R=Me), from ext. CF_3CO_2H in CCl_4. The patterns of the ^1H NMR spectra were also simple. Only one singlet signal at τ 6.28 (OMe) for **2** (R=Me) and two singlet signals at τ 6.40 (OMe) and 7.80 (SMe) for **3** (R=Me) appeared. In the mass spectrum of **2** (R=Me), the base peak, *m/e* 181 ($C_4H_3F_6O$), and other fragment peaks, such as *m/e* 213 ($C_4H_3F_6OS$), 69 (CF_3), 64 (S_2), and 31 (OMe), appeared appropriately. The parent peak, M^+ 426, was not observed, but this is not strange because, in di-*tert*-alkyl disulfides, it is known that the parent peak appears very weakly.[3]

Among the various catalysts examined in connection with the above reaction, only alkali metal fluorides such as potassium and sodium flouride, were effective; alkalies, such as potassium and sodium hydroxide or potassium carbonate, had no catalytic activity. Further, in protonic solvents such as alcohols, no reaction occurred even in the presence of potassium fluoride. These results made it evident that the fluoride ion, especially the unsolvated active ion, catalyzed the reaction.

We presumed that the reaction proceeded according to the following scheme:

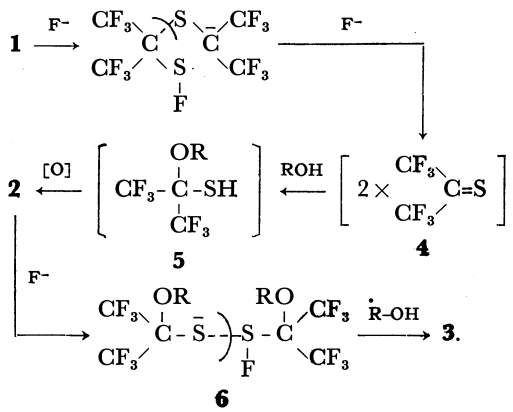

It was initiated by the active fluoride ion in the polar aprotic solvent, which attacked the sulfur atom of the dimer, **1**; it thus accelerated the formation of the reactive hexafluorothioacetone monomer, **4**. Alcohol as a nucleophile reacted with **4**, thus giving 1-alkoxy-1-(trifluoromethyl)-2,2,2-trifluoroethanethiol (**5**), which was subsequently oxidized to disulfide, **2**. The attack of the fluoride ion on sulfur occurred again, and the resulting anionic sulfur (**6**) probably reacted with alcohol to give **3**.

In order to obtain evidence for this scheme, we carried out the following reactions. To capture the intermediate thiol, **5**, the **1** and methanol in the KF–DMF system were reacted in the presence of 2,4-dinitrofluorobenzene; the 2,4-dinitrophenyl sulfide (**7**) (R=Me) was thus obtained in a good yield.

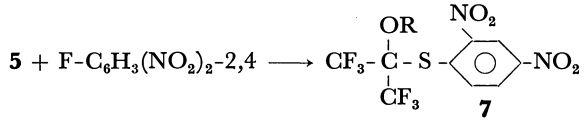

Further, the disulfide **2** (R=Me) reacted with methanol in the KF–DMF system to give **3** (R=Me), proving **2** and **3** were formed successively.

It is well known that sulfides[4] and disulfides[5] give *N*-sulfonylsulfilimines and sulfonimidosulfinsulfonylimine derivatives with Chloramine T. From disulfides, **2**, and sulfides, **3**, these derivatives were obtained as two crystalline compounds, (**8**) and (**9**) (Table 1).

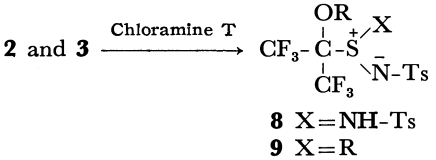

Reaction of the Dimer with Thiols. Middleton *et al.* reported that, in the reaction of the hexafluorothioacetone monomer with alkanethiols, the thiocarbonyl group behaves as would be expected if sulfur were positive; the following addition reaction was observed:

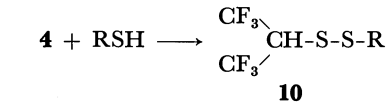

Since hexafluorothioacetone was assumed to be formed during the reaction of the dimer **1** in the KF–DMF system, we carried out the reaction using alkanethiols as the nucelophile. For example, *n*-butanethiol and **1**, together with potassium fluoride, were allowed to react in dimethylformamide at room temperature; the disulfide **10** (R=*n*-Bu) was thus obtained as the main product. Ethanethiol also gave a similar product, **10** (R=Et).

When thiophenol and thiocresol were used in the above reaction, the main products were 3:1 (C_3F_6S:ArSH) and 4:1 adducts, **12** (*n*=**2** and **3**) respectively. Adducts of this kind were also reported by Middleton *et al.*, although they did not make clear on which side the disulfide bonding was.[6]

We elucidated the structure of **12** by studying the NMR and mass spectra. For example, the ^{19}F NMR of **12** (Ar=Ph, *n*=2) revealed three signals, one doublet and two singlets of the same intensity, and the ^1H NMR contained one multiplet signal at τ 6.24 in addition to the aromatic-proton signal. The mass spectrum gave the molecular ion and other fragment ions, as is

3) D. H. Williams, J. H. Bowie, S. O. Lawesson, J. ϕ, Madsen, C. Nolde, and G. Schrole, *J. Chem. Soc. B*, **1966**, 946.

4) F. G. Mann and W. J. Pope, *J. Chem. Soc.*, **121**, 1052 (1922).

5) G. Leandri and D. Spinelli, *Ann. Chem.*, **49**, 964 (1959).

6) W. J. Middleton and W. H. Sharkey, *J. Org. Chem.*, **30**, 1384 (1965).

Table 1. Preparation of disulfide **2** and monosulfide **3**, and their chloramine T derivatives, **8** and **9**

R		Yield (%)	Bp (°C/mmHg)	^{19}F NMR (δ ppm[a])	F-Anal (%) Obsd	F-Anal (%) Calcd		Yield (%)	Mp (°C)	IR (cm^{-1}) N=S (IV)	IR (cm^{-1}) N-H	F-Anal (%) Obsd	F-Anal (%) Calcd
Me	2	68	113—115/24	−9.20	51.9	52.1	8	37	124—126	956	3452	20.4	20.7
Et		69	131—132/43	−8.40	50.8	50.2		64	125—126	978	3480	20.0	20.1
n-Pr		77	132—134/24	−8.20	47.5	47.3		58	135—135.5	958	3442	19.3	19.7
i-Pr		46	138—140/20	−8.40	47.7	47.3		60	121.5—122	945	3438	19.6	19.7
n-Bu		66	155—156/23	−8.80	45.1	44.7		65	122—123	958	3422	19.0	19.2
i-Am		51	159—160/23	−8.62	42.6	42.4		56	131.5—132	963	3418	18.7	18.8
Me	3	23	101—102/120	−7.20	50.3	50.0	9	68	109—110	945	——	28.9	28.7
Et		27	125—126/43	−8.00	44.7	44.5		66	129.5—130	956	——	27.1	26.8
n-Pr		23	118—120/24	−7.40	40.6	40.1		47	126—127	943	——	25.4	25.2
i-Pr		15	128—131/20	−7.35	40.3	40.1		44	127—129	938	——	25.6	25.2
n-Bu		21	148—149/24	−7.65	36.1	36.5		45	120—121	964	——	23.7	23.7
i-Am		33	131—134/23	−7.90	32.9	33.5							

a) Erom ext. CF_3CO_2H in CCl_4.

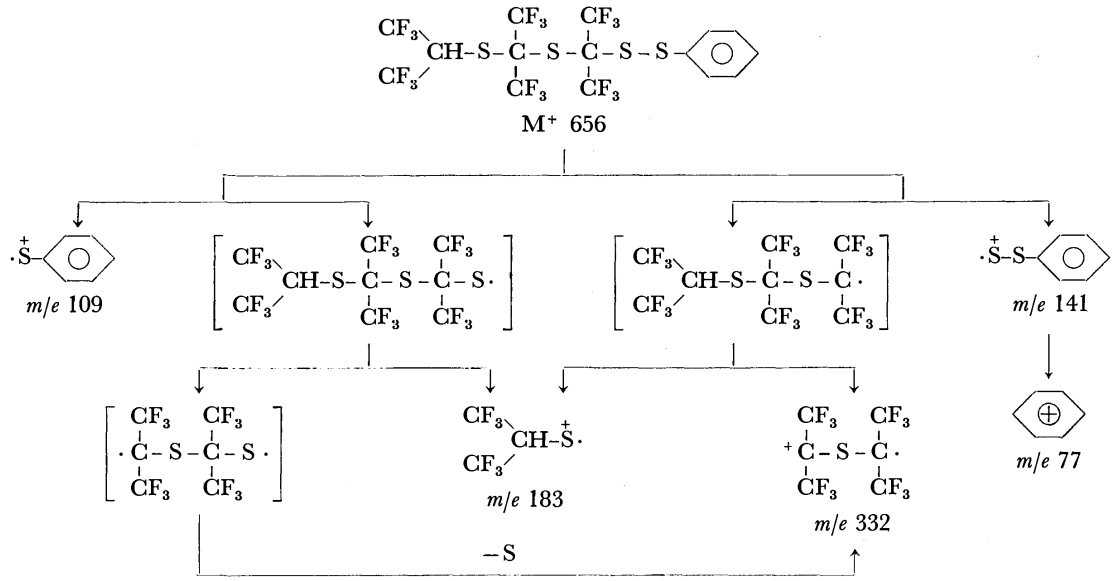

Fig. 1. Mass fragmentation of 12 (Ar = Ph).

shown in Fig. 1. On the other hand, the fragment peaks, $C_6H_5S_2^+$ and $C_3HF_6S_2^+$, which are characteristic of the disulfide bond,[3,7,8] appeared in considerable strength and no fragment corresponding to $C_3HF_6S_2^+$ was observed. This means that there is C–S_2–Ar group, but no C–S_2–CH$(CF_3)_2$ group, in the molecule.

From these results, the reaction scheme and the structures of the products were estimated to be as is shown below:

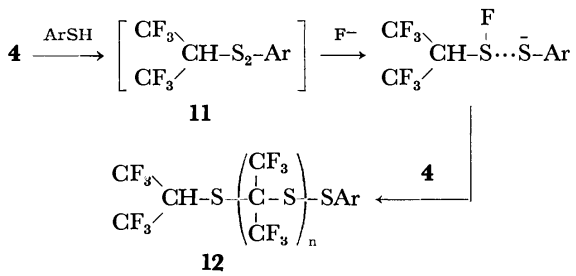

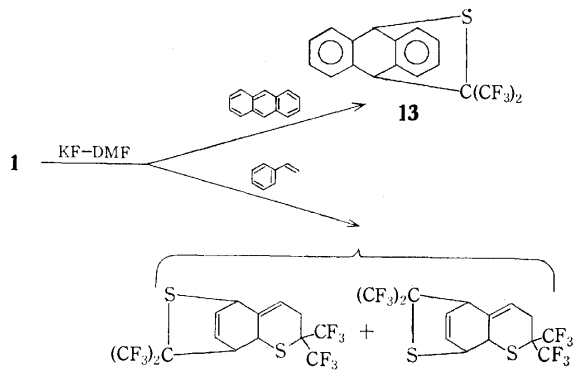

Preparation of Cycloadducts from the Hexafluorothioacetone Dimer. Further confirmation of hexafluorothioacetone as an intermediate was made by the formation of the cycloadducts with dienes.

7) S. Kozuka, H. Takahashi, and S. Oae, This Bulletin, **43**, 129 (1970).

8) I. L. Knunyants and L. S. German, *Dokl. Akad. Nauk SSSR*, **201**, 603 (1971).

Since Middleton reported that hexafluorothioacetone gives cycloadducts with dienes very easily,[9] we carried out the reaction of the dimer **1** with anthracene and with styrene in the KF–DMF system. As expected, the **13** and **14** cycloadducts were obtained respectively; they were similar to those prepared by Middleton.

Experimental

*Reaction of **1** with Methyl Alcohol.* Into a mixture of potassium fluoride (4.6 g, 0.08 mol), **1** (14.6 g, 0.04 mol), and dimethylformamide (30 ml), methyl alcohol (3.8 g, 0.12 mol) was added, drop by drop; the whole was then stirred for 24 hr at room temperature. The reaction mixture was poured into water, and the separated oily matter was extracted with ethyl ether. The extract was dried over magnesium sulfate, and the solvent was removed. The vacuum distillation of the residue gave **3** (R=Me) (bp 101—102 °C/120 mmHg (3.8 g, 23%)) and **2** (R=Me) (bp 113—115 °C/24 mmHg (5.8 g, 68%)).

The reactions with other alcohols were run similarly; two products, **2** and **3**, were obtained in each case (Table 1).

*1-Alkoxy-1-(trifluoromethyl)-2,2,2-trifluoroethyl 2',4'-dinitrophenyl Sulfide (**7**).* A mixture of **1** (7.3 g, 0.02 mol), potassium fluoride (2.4 g, 0.041 mol), methanol (1.4 g, 0.04 mol), 2,4-dinitrofluorobenzene (3.7 g, 0.02 mol), and dimethylformamide (30 ml) was stirred for 48 hr at room temperature, and then the reaction mixture was poured into water. The resulting precipitate was collected and recrystallized from cyclohexane, thus giving crystals of **7** (R=Me) (mp 76—77 °C) in a yield of 73%. Found: F, 29.5%. Calcd: F, 30.0%. IR: 1526, 1352 (NO_2) cm^{-1}. NMR: ^1H, τ 1.62 (Ph), 6.16 (OMe); ^{19}F, −8.80 ppm from ext. CF_3CO_2H in CCl_4.

The sulfide, **7** (R=Et) (mp 82—83 °C), was also prepared in a similar way. Found: F, 28.6%. Calcd: F, 28.9%.

S-[*1-Ethoxy-1-(trifluoromethyl)-2,2,2-trifluoroethyl*]-S-p-*toluenesulfonamide*-N-p-*toluenesulfonylsulfilimine (**8**).* Into a solution of **2** disulfides (R=Et, 1.0 g, 2 mmol) in ethanol (30 ml), we added Chloramine T (3.0 g, 10 mmol) at room temperature, and then the whole was stirred for 48 hr. The reaction mixture was then poured into a cold dilute sodium hydroxide solution. The precipitate was filtered and recrystallized from benzene to give **8** (R=Et, 1.6 g, 64%) (mp 125—126 °C).

9) W. J. Middleton, *J. Org. Chem.*, **30**, 1390 (1965).

S-[*1-Ethoxy-1-(trifluoromethyl)-2,2,2-trifluoroethyl*]-S-*ethyl*-N-p-*toluenesulfonylsulfilimine (**9**).* To a mixture of the **3** sulfide (R=Et, 2.05 g, 8 mmol), Chloramine T (3.0 g, 10 mmol), and methanol (30 ml), we added, drop by drop, a mixture of acetic acid (1.0 ml) and methanol (5 ml) at room temperature. The whole was then stirred for 48 hr and poured into a cold dilute sodium hydroxide solution. The precipitate was collected and washed with water. Recrystallization from benzene gave **9** (R=Et, 2.24 g, 66%) (mp 129—130 °C).

Other Chloramine T derivatives were obtained by a similar procedure (Table 1).

*Reaction of **1** with Butanethiol.* A mixture of **1** (7.3 g, 0.02 mol), butanethiol (3.6 g, 0.04 mol), potassium fluoride (2.4 g, 0.04 mol), and dimethylformamide (20 ml) was stirred for 24 hr at room temperature, and then the whole was poured into water. An oily matter was subsequently extracted with ethyl ether, and the solvent was removed. The vacuum distillation of the residue gave **10** (R=*n*-Bu) (bp 85—86 °C/21 mmHg (2.0 g, 55% on the basis of the consumed BuSH.)) and di-*n*-butyl disulfide (2.4 g, bp 118—119 °C/21 mmHg). **10** (R=*n*-Bu): Found: F, 41.4%, Calcd for $C_7H_{10}F_6S_2$: F, 41.9%. NMR: ^1H, τ 6.2 (m, $(CF_3)_2$-CH); ^{19}F, δ −12 ppm (d) (from ext. CF_3CO_2H in CCl_4).

When ethanthiol was used in the above reaction, a similar disulfide, **10** (R=Et) (bp 74—76 °C/58 mmHg), was obtained in a 47% yield. Found: F, 46.3%. Calcd: F, 46.7%. NMR: ^1H, τ 6.31 (m); ^{19}F, δ −11.6 ppm (d).

*Reaction of **1** with Thiophenol.* A mixture of thiophenol (2.2 g), **1** (3.6 g), potassium fluoride (1.2 g), and dimethylformamide (20 ml) was allowed to react as has been described above. A subsequent work-up gave an oil, **12** (Ar=Ph, *n*=2) (2.2 g, 51%, bp 94—95 °C/70 mmHg, Found: F, 51.6%, Calcd for $C_{15}H_6F_{18}S_4$: F, 52.1%).

p-Thiocresol gave a similar product, **12** (Ar=*p*-MeC_6H_4, *n*=3) (bp 87—89 °C/19 mmHg, 40%; Found: F, 53.3%. Calcd: F, 53.5%).

*Hexafluorothioacetone-anthracene Adduct (**13**).* A mixture of **1** dimer (7.3 g, 0.02 mol), anthracene (7.2 g, 0.04 mol), potassium fluoride (2.4 g), and dimethylformamide (30 ml) was stirred at room temperature for 48 hr, and then the mixture was poured into water. The precipitate was collected and recrystallized from *n*-hexane, thus, giving **13** (mp 121—122 °C (lit,[9] mp 123—124 °C)) in a yield of 82%.

Styrene reacted in a similar way, thus giving a mixture of isomers (**14**) (bp 125—127 °C/3 mmHg (lit,[9] bp 103—104 °C/1.2 mmHg)) in a 24% yield.

NOTES

BULLETIN OF THE CHEMICAL SOCIETY OF JAPAN, VOL. 46, 3289—3290 (1973)

π-Electron Structures of Aromatic Hydrocarbons in Their Low-lying Triplet States

Hiroshi KASHIWAGI,* Suehiro IWATA**, and Saburo NAGAKURA*,**

*The Institute for Solid State Physics, The University of Tokyo, Roppongi, Minato, Tokyo 106

**The Institute of Physical and Chemical Research, Wako, Saitama 351

(Received November 30, 1972)

Since Lewis *et al.*[1] found absorption bands due to transitions between the lowest and higher triplet states, many studies have been made in this field.[2] In addition to strong triplet-triplet transition bands measured at the initial stage of the study, weak low-energy bands were observed by Kellogg[3] and by other authors.[4] Polarization of these bands were investigated by El-Sayed and Pavlopoulos[5] and by others.[6] Thus, a considerable amount of T-T absorption data are now available for theoretical consideration.[7-10]

Theoretical studies of T-T transitions have been made by the composite method,[11] by the Pariser-Parr-Pople method,[12-14] and also by the open-shell SCF MO CI procedure.[15] The transition energies and oscillator strengths calculated so far agree less satisfactorily for the T-T transitions than for the singlet-singlet transitions. Furthermore, most of these theoretical studies are concerned with only a few strong absorption bands for each molecule.

In this paper, the SCF MO CI calculations based on the Pariser-Parr-Pople procedure[16] were applied to the T-T transitions of aromatic hydrocarbons by taking the stable geometrical structure of the lowest triplet state for each molecule and by considering weak T-T transition bands in addition to strong bands.

Method of Calculation

We employed the Pariser-Parr-Pople SCF MO CI procedure,[16] taking all the singly excited configurations for benzene and naphthalene and taking the lower 40 singly excited configurations for each symmetry for anthracene, pyrene, chrysene, and coronene. The penetration integrals were disregarded. The core resonance integral (β) was taken to be proportional to the overlap integral, the value at the equilibrium C-C bond distance of benzene, $\beta_0 = -2.39$ eV, being taken as the standard. Two-center Coulomb repulsion integrals were estimated by the Nishimoto-Mataga approximation.[17] One-center Coulomb integrals and orbital exponents were determined by using the method described by Iwata and Shida.[18]

The results of X-ray crystal analysis experiments[19] of naphthalene, anthracene, pyrene, chrysene, and coronene were used at the first stage of the calculation, and thereafter the geometrical configurations of the lowest triplet states were estimated by using the standdar bond order-bond length relation.[20] The bond lengths used for the final calculation are shown in Fig. 1.[2] The calculations were performed with a FACOM 270-30 computer. Weaker bands ($\varepsilon_{max} \sim 10^2$) in the longer wavelength region can be assigned to symmetry forbidden or parity forbidden transitions. The calculated transitions forbidden from both symmetry and parity are disregarded.

All the calculated transition energies were found to be larger by $\sim 2000\ cm^{-1}$ than the corresponding observed values. Therefore, we reduced all the calculated T-T transition energies by $2000\ cm^{-1}$. A similar correction was made by Orloff.[12]

1) G. N. Lewis, D. Lipkin, and T. J. Magel, *J. Amer. Chem. Soc.*, **63**, 3005 (1941).

2) D. S. McClure, *J. Chem. Phys.*, **19**, 670 (1951); D. P. Craig and I. G. Ross, *J. Chem. Soc.*, **1954**, 1589; G, Porter and M. W. Windsor, *Proc. Roy. Soc.* (London), **A 245**, 238 (1958).

3) R. E. Kellogg, *J. Chem. Phys.*, **44**, 411 (1966).

4) M. W. Windsor and J. R. Novak, "The Triplet State," ed. by A. B. Zahlan, Cambridge University Press, London (1967), p. 229; R. Astier and Y. H. Meyer, *ibid.*, p. 447; R. Astier, A. Bokobza, and Y. H. Meyer, *J. Chem. Phys.*, **51**, 5174 (1969).

5) M. A. El-Sayed and T. Pavlopoulos, *ibid.*, **39**, 834 (1963).

6) J. B. Gallivan and J. S. Brinen, *ibid.*, **50**, 1590 (1969); T. G. Pavlopoulos, *ibid.*, **52**, 3307 (1970); J. Langelaar, J. Wegdam-Van Beck, J. D. W. Van Voorst, and D. Lavalette, *Chem. Phys., Lett.*, **6**, 460 (1970).

7) J. S. Brinen, *J. Chem. Phys.*, **49**, 586 (1968).

8) W. Heinzelmann and H. Labhart, *Chem. Phys. Lett.*, **4**, 20 (1969).

9) T. M. Naumova and V. I. Glyadkovskii, *Opt. Spectrosk.*, **27**, 228 (1969).

10) T. Takemura, K. Hara, and H. Baba, This Bulletin, **44**, 977 (1971).

11) K. Kimura, *Mol. Phys.*, **15**, 109 (1968).

12) M. K. Orloff, *J. Chem. Phys.*, **47**, 235 (1967).

13) P. L. DeGroot and G. J. Hoytink, *ibdi.*, **46**, 4523 (1967).

14) J. Pancir and R. Zahradnik, *Theoret. Chim. Acta*, **14**, 426 (1969); D. Lavalette, C. Tetreau, and J. Langelaar, *Chem. Phys. Lett.*, **9**, 319 (1971).

15) L. Goodman and J. R. Hoyland, *J. Chem. Phys.*, **39**, 1068 (1963).

16) R. Pariser and R. G. Parr, *ibid.*, **21**, 466, 767 (1953); J. A. Pople, *Proc. Phys. Soc.* (London), **A68**, 81 (1955).

17) K. Nishimoto and N. Mataga, *Z. Phis. Chem.* (*N.F.*), **12**, 335 (1957).

18) S. Iwata and T. Shida, to be published. According to this method, the valence state ionization energy for the carbon $2p\pi$ orbital electron was evaluated to be 11.18 eV.

19) "Interatomic Distances," Sp. Pub. No. 11, ed. by L. E. Sutton, The Chem. Soc., London, (1958); *ibid.*, No. 18 (1965).

20) M. J. S. Dewar, H. N. Schmeising, *Tetrahedron*, **5**, 166 (1959). The spectroscopic study made by Nieman and Tinti (G. C. Nieman and D. S. Tinti, *J. Chem. Phys.*, **46**, 1432 (1967)) with benzene in a C_6D_6 host crystal at 4.2 K shows a small distortion from a hexagonal shape arised either from extrinsic or intrinsic perturbations. This small distortion is disregarded in the present study.

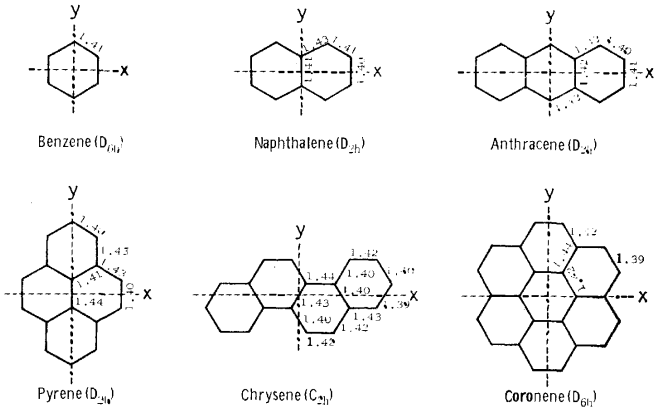

Fig. 1. The geometrical structures used for the present calculation.

Results and Discussion

The $^3E_{2g}^- \leftarrow {}^3B_{1u}^+$ transition energy, 41000 cm^{-1}, calculated for benzene agrees well with the observed band position, 40800 cm^{-1}.[9] The T-T transition energies of naphthalene were calculated to be 20600, 25200, 31100, 39100, and 47000 cm^{-1} for the transitions from the lowest triplet ($^3B_{2u}^+$) state to the $^3A_g^-$, $^3B_{1g}^-$, $^3A_g^-$, $^3B_{1g}^-$, and $^3B_{1g}^-$ states, respectively, the oscillator strengths and the directions of transition moments (in parentheses) being 0.063 (y), 0.48 (x), 0.39 (y), 0.007 (x), and 0.92 (x), respectively. Four bands were observed for naphthalene at ~20000 cm^{-1}, ~25000 cm^{-1}, 29300 cm^{-1}, and 38500 cm^{-1}.[2,4] The calculated values agree well with the observed transition energies for the four longer wavelength bands. Furthermore, the oscillator strength and the direction of the transition moment calculated for the second longest wavelength band agree well with the observed results (f=0.32, x-polarized).[5]

The four T-T absorption bands were observed for anthracene at~12000 (f=0.0017), ~20000 (f=0.038), ~24000 (f=0.68, x-polarized[5]), and 35700 cm^{-1}.[2,4] The calculated transition energies are 11900, 21000, 23600, and 35700 cm^{-1} for the transitions from the lowest triplet ($^3B_{2u}^+$) state to the $^3A_g^+$, $^3A_g^-$, $^3B_{1g}^-$, and $^3A_g^-$ states, respectively, the oscillator strengths and the directions of transition moments (in parentheses) being calculated to be 0.00, 0.061 (y), 0.80 (x), and 0.37 (y), respectively. The calculated results agree well with the observed ones obtained so far.

The transition energies and oscillator strengths observed and calculated for pyrene are shown in Table 1, together with the band assignment.

The T-T absorption bands were observed for chrysene at ~12000 (f=0.003), 17200 (f=0.40), 24900 (f=0.016), 35200 (f=0.32), and 39500 (f=0.65) cm^{-1}.[4,9] The calculated transition energies are 11900, 17400, 25600, 35400, and 37900 cm^{-1} with the calculated oscillator strengths of 0.007, 0.76, 0.021, 0.26, and 0.37, respectively. The second longest wavelength band was found experimentally to be polarized almost parallel with the L_a band,[6] in good agreement with the theoretical prediction. The five observed bands can be assigned to the $^3A_g^- \leftarrow {}^3B_u^+$ transitions.

Table 1. The observed and calculated transition energies, ΔE's (in the units of 10^3 cm^{-1}), oscillator strengths, f's, directions of polarization, and the assignments of the T-T absorption spectrum of pyrene

Observed			Calculated			
ΔE	f	Polarization[6]	ΔE	f	Polarization	Assignments
11[4]	0.0005		12.5	0		$^3B_{3u}^- \leftarrow {}^3B_{2u}^+$
13.2[4]	0.002		14.0	0		$^3B_{3u}^- \leftarrow {}^3B_{2u}^+$
16.7[4]	0.008		18.3	0		$^3B_{1g}^+ \leftarrow {}^3B_{2u}^+$
~20[4]	0.022	x	21.6	0.051	x	$^3B_{1g}^- \leftarrow {}^3B_{2u}^+$
22.2[6]			23.1	0		$^3A_g^+ \leftarrow {}^3B_{2u}^+$
			24.6	0		$^3B_{3u}^- \leftarrow {}^3B_{2u}^+$
~25[4]	0.48	y	26.7	0.84	y	$^3A_g^- \leftarrow {}^3B_{2u}^+$
27.8[8]	0.03		28.6	0		$^3B_{1g}^+ \leftarrow {}^3B_{2u}^+$
~31[8]	0.08		33.1	0.044	x	$^3B_{1g}^- \leftarrow {}^3B_{2u}^+$
34.4[8]	0.16		35.9	0.24	y	$^3A_g^- \leftarrow {}^3B_{2u}^+$
38.6[8]	0.13		40.1	0.30	x	$^3B_{1g}^- \leftarrow {}^3B_{2u}^+$

Four bands were observed for coronene at ~10000, ~16000, 20800, and ~25000 cm^{-1} with the oscillator strengths of 0.0005, 0.08, 0.16, and 0.12, respectively.[7,21] The longest wavelength band is assigned to the parity forbidden transition (ΔE=7900 cm^{-1}, $^3E_{2g}^+ \leftarrow {}^3B_{1u}^+$). The higher transition energies were calculated to be 12600, 20800, and 25900 cm^{-1} with the oscillator strengths of 0.06, 0.41, and 0.22, respectively. These three bands can be assigned to the $^3E_{2g}^- \leftarrow {}^3B_{1u}^+$ transitions.

One of the characteristics of our calculation is to adopt the stable geometrical configuration of the lowest triplet state in which the bonds are generally elongated compared with those of the structure in the ground state. This reduces the $|\beta|$ values to some extent and brings about a narrowing of the energy separation between the higher and lower transition energies for each of the aromatic hydrocarbon molecules.[22] This is a reason why the present calculation can explain quantitatively the observed peak positions over wide wavelength region. Our assignments are different from those by Orloff[12] in some points; for example, we assigned the 38500 cm^{-1} band of naphthalene to the $^3B_{1g}^- \leftarrow {}^3B_{2u}^+$ transition and the 35700 cm^{-1} band of anthracene to the $^3A_g^- \leftarrow {}^3B_{2u}^+$ transition, while Orloff assigned both bands to the $^3B_{3g}^+ \leftarrow {}^3B_{2u}^+$ transition. Our assignmens give better agreements between the observed and theoretical results concerning both transition energies and absorption intensities. Furthermore, in view of the fact that we are concerned with greater number of observed bands (including weak ones) for each molecule, our assignments are more reasonable than those by Orloff.[12]

21) Unpublished results by Windsor and Novak; private communication to one of the authors (S.N.) from Dr. Windsor, to whom the authors' thanks are due.

22) For example, the transition energies calculated for naphthalene by the use of the ground state geometry are 19400, 26200, 31900, 40700, and 50100 cm^{-1}; the corresponding value obtained by the use of the excited state geometry being 20600, 25200, 31100, 39100, and 47000 cm^{-1}.

BULLETIN OF THE CHEMICAL SOCIETY OF JAPAN, VOL. 46, 3291—3292 (1973)

Energetic Consideration of $C_5H_5^+$ Ions Produced from Various Precursors by Electron Impact

Susumu TAJIMA and Toshikazu TSUCHIYA

National Chemical Laboratory for Industry, 1-1-5, Honmachi, Shibuya-ku, Tokyo 151

(Received March 31, 1973)

It is well known[1] that the $C_7H_7^+$ ions produced from various precursors (C_7H_7Z) decompose into the $C_5H_5^+$ ions by losing C_2H_2. The structure of the $C_7H_7^+$ ions has been investigated by various methods.[1-3] To the authors' knowledge, however, the structure of the $C_5H_5^+$ ions produced by the $C_7H_7Z^+ \rightarrow C_7H_7^+ + Z \rightarrow C_5H_5^+ + C_2H_2$ reaction has not yet been examined.

Occolowitz and White have concluded[4] that the structure of the $C_5H_5^+$ ions derived from some compounds can be identified as the (a) structure rather than the (b) structure shown in Fig. 1 by measuring the heat of formation.[5] Natalis and Franklin have also reported[6] similar conclusions reached by the same method.

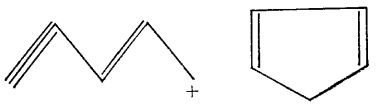

(a) ΔH_f: 277 kcal/mol (Ref. 4) (b) ΔH_f: 240 kcal/mol (Ref. 5)

Fig. 1. Schematic diagram of the structure of the $C_5H_5^+$ ion from 3-penten-1-yne (a) and cyclopentadienyl radical (b).

In order to examine the structure of the $C_5H_5^+$ ions produced from the derivatives of toluene and benzene, we have now measured the heat of formation of the $C_5H_5^+$ ions from these compounds and compared them with that of 3-penten-1-yne and the cyclopentadienyl radical.[4,5]

The apparent heat of formation of the $C_5H_5^+$ ions, $\Delta H_f(C_5H_5^+)$, is calculated from the following equation:

$$\Delta H_f(C_5H_5^+) = \Delta H_f(M) + A.P(C_5H_5^+) - \sum \Delta H_f(N) - E \quad (1)$$

where $\Delta H_f(M)$ is the heat of formation of the neutral molecule; $A.P(C_5H_5^+)$ is the appearance potential of the $C_5H_5^+$ ion, $\sum \Delta H_f(N)$ is the algebraic sum of the heat of formation of the neutral fragments, and E is the excess energy of the fragments at the threshold.

The values of $A.P(C_5H_5^+)$ from the compounds obtained in the present experiment using a CEC 21-103C mass spectrometer are given in the second column in Table 1. These A.P values were obtained by the E.D.D technique;[7] the details of the experiment have already been described.[8] Each value is the average of at least three measurements. The experimental error is within ± 0.2 eV.

Table 1. Appearance potentials (eV) and heats of formation (kcal/mol) of the $C_5H_5^+$ ion from various compounds

Compounds	$A.P(C_5H_5^+)$ This work	$A.P(C_5H_5^+)$ Ref. 4	$\Delta H_f(C_5H_5^+)$ This work	$\Delta H_f(C_5H_5^+)$ Ref. 4	Neutral products
Toluene	16.4		284.8		$H+C_2H_2$
p-Xylene	16.3		292.1		$CH_3+C_2H_2$
o-Nitrotoluene	13.5		306.8 (Eq. 2)		$OH+CO+HCN$
			259.2 (Eq. 3)		$NO_2+C_2H_2$
m-Nitrotoluene	15.2		298.4		$NO_2+C_2H_2$
p-Nitrotoluene	14.9		291.0		$NO_2+C_2H_2$
Ethylbenzene	16.2		292.6		$CH_3+C_2H_2$
n-Propylbenzene	15.5		279.9		$C_2H_5+C_2H_2$
o-Chlorotoluene	15.7		282.7		$Cl+C_2H_2$
m-Chlorotoluene	15.7		282.5		$Cl+C_2H_2$
p-Chlorotoluene	15.7		281.4		$Cl+C_2H_2$
o-Bromotoluene	15.2		285.3		$Br+C_2H_2$
m-Bromotoluene	15.2		284.5		$Br+C_2H_2$
p-Bromotoluene	15.2		285.2		$Br+C_2H_2$
o-Iodotoluene	14.3		279.9		$I+C_2H_2$
m-Iodotoluene	14.5		281.9		$I+C_2H_2$
p-Iodotoluene	14.7		286.2		$I+C_2H_2$
Aniline	15.2	15.24	290.2	288.0	$HCN+H$
Phenol	14.2	14.25	278.2	273.0	$CO+H$

The values for the heat of formation of the $C_5H_5^+$ ions calculated from Eq. (1) using the A.P values in Table 1 and the literature values[9] for $\Delta H_f(M)$ and $\Delta H_f(N)$ are given in the fourth column in Table 1. The value of E is usually determined from the width of the observed metastable peak.[4,10] The value seldom exceeds 10 kcal/mol, with a few exceptions, such as is the case of NO loss. In this experiment, we estimated

1) H. M. Grubb and S. Meyerson, "Mass Spectrometry of Organic Ions," ed. by F. W. McLafferty, Academic Press Inc., New York (1963), Chap. 10.

2) K. R. Jennings and J. H. Futrell, *J. Chem. Phys.*, **44**, 4315 (1966).

3) S. Tajima, Y. Niwa, M. Nakajima, and T. Tsuchiya, This Bulletin, **44**, 2340 (1971).

4) J. L. Occolowitz and G. L. White, *Aust. J. Chem.*, **21**, 997 (1968).

5) R. F. Pottie and F. P. Lossing, *J. Amer. Chem. Soc.*, **85**, 269 (1963).

6) P. Natalis and J. L. Franklin, *J. Phys. Chem.*, **69**, 2943 (1965).

7) R. E. Winters, J. H. Collins, and W. L. Courchene, *J. Chem. Phys.*, **45**, 1931 (1966).

8) S. Tajima, Y. Shimizu, and T. Tsuchiya, This Bulletin, **45**, 931 (1972).

9) J. L. Franklin, J. G. Dillard, H. M. Rosenstock, J. T. Herron, K. Draxl, and F. H. Field, "Ionization Potentials, Appearance Potentials and Heats of Formation of Gaseous Positive Ions," National Bureau of Standard, U.S., (1969).

10) J. H. Beynon, R. A. Saunders, and A. E. Williams, "The Mass Spectra of Organic Molecules," Elsevier Publishing Co., London (1968), Chap. 1.

the heat of formation by neglecting E. Therefore, the data will show a tendency to have a little higher value. Taking the experimental error into consideration, the overall error is considered to be less than 20 kcal/mol. It is evident from the data of the heat of formation (Table 1) that all these values coincide with the heat of formation of 3-penten-1-yne (277 kcal/mol)[4] within the limits of experimental error, except for the values from *o*-nitrotoluene (the value of *m*-nitrotoluene is slightly higher than the limit of the experimental error, but it probably belongs to the former group). The values for the former group are considerably higher than the heat of formation of the $C_5H_5^+$ ion from the cyclopentadienyl radical (240 kcal/mol).[5] According to the results of Occolowitz and White,[4] we can also regard the $C_5H_5^+$ ions from the compounds studied here as having the (a) structure in Fig. 1.

Beynon *et al.* have reported[11] that the $C_5H_5^+$ ions are produced from *o*-nitrotoluene molecular ions by the following two reactions:

$$C_7H_7NO_2^+ \xrightarrow{-OH} C_7H_6NO^+ \xrightarrow{-CO} C_6H_6N^+ \xrightarrow{-HCN} C_5H_5^+ \quad (2)$$

$$C_7H_7NO_2^+ \xrightarrow{-NO_2} C_7H_7^+ \xrightarrow{-C_2H_2} C_5H_5^+ \quad (3)$$

Therefore, the heat of formation of the $C_5H_5^+$ ion for *o*-nitrotoluene, calculated from both Eq. (2) and Eq. (3), is given in Table 1. The structure of the $C_5H_5^+$ ion produced from Reaction (2) cannot be assigned on the basis of the present experiment alone. The value calculated from Reaction (3) is considerably lower than that of *m*- and *p*-nitrotoluene. The value (259.2 kcal/mol) shown in Table 1 as having been obtained from Reaction (3) was calculated by using A.P.= 13.5 eV. However, taking the mechanism of the production of the $C_5H_5^+$ ion given in Eq. (3) into account, the structure of the $C_5H_5^+$ ion of *o*-nitrotoluene produced by Reaction (3) seems to be identical with that of the *m*- and *p*-compounds. If this assumption is valid, the $\Delta H_f(C_5H_5^+)$ obtained from Eq. (3) for *o*-nitrotoluene should be close to that obtained for *m*- and *p*-compounds. In that case, assuming the $\Delta H_f(C_5H_5^+)$ is about 290 kcal/mol, the A.P value of the $C_5H_5^+$ ions for *o*-nitrotoluene obtained from Eq. (3) must be close to 14.8 eV. Therefore, a break in the ionization efficiency curve of the $C_5H_5^+$ ion for *o*-nitrotoluene is expected to occur at about 14.8 eV. As may be seen in Fig. 2, there is a break at about 14.8 eV. Consequently, it may be inferred that, while the onset of the $C_5H_5^+$ ion from Reaction (2) is at 13.5 eV (shown by the a arrow in Fig. 2), that of the $C_5H_5^+$ ion from Reaction (3) is at about 14.8 eV (shown by the b arrow).

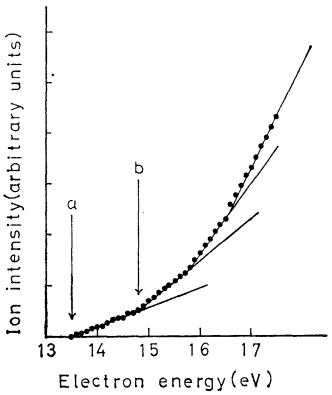

Fig. 2. Ionization efficiency curve for the $C_5H_5^+$ ion from *o*-nitrotoluene.

If the appearance potentials of the metastable ions corresponding to the $C_6H_6N^+ \rightarrow C_5H_5^+ + HCN$ and $C_7H_7^+ \rightarrow C_5H_5^+ + C_2H_2$ reactions can be measured, then the above assumption will be confirmed.

The authors wish to thank Mr. Nobuhide Wasada of this Laboratory for his valuable discussions.

11) J. H. Beynon, R. A. Saunders, and A. E. Williams, "The Mass Spectra of Organic Molecules," Elsevier Publishing Co., London (1968), Chap. 5.

BULLETIN OF THE CHEMICAL SOCIETY OF JAPAN, VOL. 46, 3293—3294 (1973)

Visual Autoclaving Studies of Hydrothermal Changes in Sugar Solutions

Tominosuke KATSURAI and Yoshihiro MAKIDE

The Institute of Physical and Chemical Research, Wako-shi, Saitama 351

(Received March 24, 1973)

Visual autoclaving studies of hydrothermal changes have so far been restricted to inorganic compounds.[1] Lately it occurred to us that an extension of the studies to organic compounds might add to our information on hydrothermal changes. Sugars were chosen because they resemble inorganic compounds as regards their behavior towards solvents; that is, they are easily soluble in water but not in organic solvents. By such a choice, we were able to find a new mode of the concentration dependence of hydrothermal changes.

Sugars. Commercial saccharose, dextrose, and levulose of the best grade were used. Solutions of various concentrations were put into 5 tubes of Pyrex glass (dia. 10 mm). They were evacuated with a water-jet pump, sealed, and subjected to visual autoclaving. Solutions with concentrations of 0.4M, 0.1M, 0.04M, 0.01M and 0.004M were autoclaved up to 230°C in 1.5 hr, and the resulting changes were observed. Coloration took place in each solution at a certain temperature, which rose with a decrease in the concentration. Reproducibility of the values of the coloration temperature was within ± 3 °C. Levulose underwent the change most easily. Above the coloration temperature, a deepening in color took place with a rise in the temperature, followed by a coagulation of the particles which separated from the solution. All the 0.4M solutions turned into two phases, a dark precipitate and a brown liquid. The sugar appeared to be charred in water.[2] The changes became less marked with a decrease in concentration, all the 0.004M solutions turning brown with hardly any precipitate. The onset of coloration of each 0.4M solution took place at a temperature slightly higher (2—8 °C) than that of the corresponding solid sugar observed when heated in an open glass tube.

The results are shown in Fig. 1. The concentration range of the solutions being great, it was necessary to reduce the scale for representation. For this, the average inter-solute distance was used instead of the logarithm of the concentration. This was found to be effective also for giving an intuitive picture of a non-dissociated solution. If we put r=inter-solute distance and c=molar concentration, their relation is given by[3]

$$r = 12/\sqrt[3]{c} \qquad (1)$$

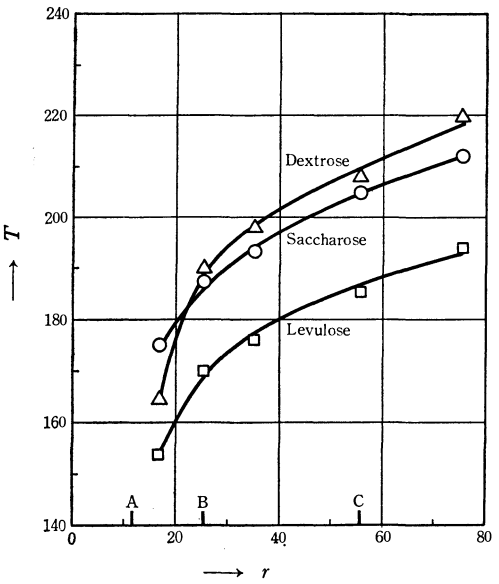

Fig. 1. Concentration dependence of coloration temperature
T=coloration temperature in °C.
r=average inter-solute distance in Å
Points A, B, and C correspond to 1M, 0.1M, and 0.01M, respectively.

The concentration dependence of the coloration temperature T is given in terms of the curve T *vs.* r. The area above the curve represents the zone in which the solution undergoes changes, while that under the curve is the zone in which the solution remains stable. The concentration dependence here is in contrast to the case of electrolytes (hydrolysis), where a high concentration makes the solution stable.

Equation (1) can be obtained as follows. We assume that solute particles are of equal size and are not dissociated. Let us take the case in which 6.02×10^{23} (Avogadro's number) particles are distributed uniformly in a space of 1 liter volume. The inter-solute distance, say l, can be taken as a unit distance corresponding to one molar solution. For its evaluation we replace the problem with one of packing. Suppose that a volume of 1 liter is closely packed with 6.02×10^{23} spheres of equal size; then the distance between the centers of the nearest neighbors, or the diameter of the

1) For the principal achievements attained by visual autoclaving, see T. Katsurai and K. Sone, This Bulletin, **41**, 519 (1968).

2) The precipitate obtained from 0.4 M levulose was subjected to electron-diffraction study. The diffraction pattern indicated that the precipitate consists of dielectric and polymerized matter differing from electro-conductive carbon. The precipitate seems to be formed by the hydrothermal polymerization of levulose. We owe this information to Dr. Shigeto Yamaguchi, National Institute for Research in Inorganic Materials.

3) This formula was found to be useful also for obtaining the empirical formula for the optimum concentration in hydrothermal precipitation; T. Katsurai, This Bulletin, **44**, 3207 (1971). The applicability of Formula (2) can be extended to a case where we have a solvent only. If we put l=10.3 Å (tetrahedral packing) and c=55.3 (number of moles of water in 1 liter), we obtain r=2.70 Å, which agrees with the distance between water molecules experimentally obtained; T. T. Wall and D. F. Hornig, *J. Chem. Phys.*, **43**, 2084 (1965).

sphere, gives the required value. It is not unique, but differs according to the mode of packing.

Mode of packing	l in Å
Closest	13.3
Cubic	11.8
Tetrahedral	10.3

Since the concentration (number of solute particles in unit volume) is inversely proportional to the third power of the inter-solute distance, we obtain the following relation for the conversion of concentration into inter-solute distance:

$$r = l/\sqrt[3]{c} \qquad (2)$$

For our present purpose, the value 12 is taken as an approximation of the average (11.8Å) of the three values of l. We thus obtain Eq. (1). This can be taken for granted when we consider the fluctuation of the positions of the solute particles.

Some modifications in the experimental procedure should be added:[4] (a) for the simultaneous observation of the changes taking place in the 5 tubes, it is advantageous to keep the circular disk supporting the sealed tubes rotating and the ring burner below the disk fixed; (b) the appropriate r.p.m. of the disk is 3, and (c) the tubes are tilted 30° from the direction of gravity. This makes the circulation of the stream in the solution caused by heating smoother, and the shock given to the test tube caused by contingent bumping smaller.

4) T. Katsurai, *Kolloid-Z.*, **170**, 57 (1960), Fig. 1.

BULLETIN OF THE CHEMICAL SOCIETY OF JAPAN, VOL. 46, 3294—3295 (1973)

On Liquefaction Caused by the Trituration of Pairs of Solid Compounds. II

Tominosuke KATSURAI and Koko MAEDA

The Institute of Physical and Chemical Research, Wako-shi, Saitama 351
Department of Chemistry, Faculty of Science, Ochanomizu University, Otsuka, Tokyo 112

(Received May 25, 1973)

In a previous paper a report was given on pairs of solid compounds which give rise to liquefaction on trituration.[1] Urea was found to cause liquefaction with most of the inorganic compounds examined. Tests, not rigorous but practical, were prescribed to find pairs for liquefaction. We have since extended our search for new pairs utilizing the tests and have been able to find some. We are still far from grasping the principle for the selection of the pairs, but a systematic representation of the data will suffice for the present (Table 1).

The experimental procedure and the mode of representation are the same as before. A pair consists of (a) an inorganic compound with water of crystallization and (b) an organic compound. The former is considered to liberate water for liquefaction as a result of interaction with the latter. For (a), sulfates were chosen because of their small hygroscopicity, while for (b) we chose salts of organic acids and bases with a fairly large solubility in water. Some inorganic and organic compounds were also chosen for the sake of

Table 1. Modes of liquefaction

(a)	(b)						
	NH_4NCS	NaNCS	KNCS	HCOONa	CH_3COONH_4	CH_3COONa	CH_3COOK
$Na_2B_4O_7\cdot 10H_2O$	++	−	++	−	++	−	−
$Na_3PO_4\cdot 12H_2O$	++	−	−	−	+	−	+
$Na_2HPO_4\cdot 12H_2O$	+++	+	++	+	+++	+	+++
$NaH_2PO_4\cdot 2H_2O$	++	−	+	++	++	+	+
$Na_2SO_4\cdot 10H_2O$	+++	+++	+++	+++	+++	+++	+++
$MgSO_4\cdot 7H_2O$	−	+	++	++	+++	+++	+++
$Al_2(SO_4)_3(NH_4)_2SO_4\cdot 24H_2O$	++	++	+	++	++	−	−
$Al_2(SO_4)_3Na_2SO_4\cdot 24H_2O$	−	+++	+++	+++	+++	+	+++
$Al_2(SO_4)_3K_2SO_4\cdot 24H_2O$	−	++	−	+++	++	−	−
$FeSO_4(NH_4)_2SO_4\cdot 6H_2O$	−	+	++	+	+	++	−
$Fe_2(SO_4)_3(NH_4)_2SO_4\cdot 24H_2O$	++	++	++	+++	+++	++	++
$CuSO_4\cdot 5H_2O$	+	+	++	+++	+++	++	+
$ZnSO_4\cdot 7H_2O$	++	−	++	+	+++	++	+
$CCl_3CH(OH)_2$	++	+	++	+++	+	++	−

1) T. Katsurai, S. Matsuo, and K. Sone, This Bulletin, **44**, 2276 (1971); this article, with the same title as the present one, is referred to as I.

(a)	(b)					
	$\begin{matrix}COONa\\ \vert\\ COONa\end{matrix}$	$NH_2(CH_2)_3$-COOH	$NH_2(CH_2)_5$-COOH	$HOOC-\overset{\overset{H}{\vert}}{\underset{\underset{NH_2}{\vert}}{C}}-(CH_2)_2COONa$	$(NH_2)_2CO$	$C_2H_5NH_2$·HCl
$Na_2B_4O_7\cdot 10H_2O$	−	−	−	−	−	+
$Na_3PO_4\cdot 12H_2O$	−	++	−	−	−	++
$Na_2HPO_4\cdot 12H_2O$	−	+++	−	−	+	+++
$NaH_2PO_4\cdot 2H_2O$	−	++	−	−	−	−
$Na_2SO_4\cdot 10H_2O$	−	+++	−	+	+++	+++
$MgSO_4\cdot 7H_2O$	−	−	−	−	+	+
$Al_2(SO_4)_3(NH_4)_2SO_4\cdot 24H_2O$	−	+	−	−	+	+
$Al_2(SO_4)_3Na_2SO_4\cdot 24H_2O$	−	++	++	+	+++	+++
$Al_2(SO_4)_3K_2SO_4\cdot 24H_2O$	−	+	−	−	+	−
$FeSO_4(NH_4)_2SO_4\cdot 6H_2O$	−	−	−	−	−	−
$Fe_2(SO_4)_3(NH_4)_2SO_4\cdot 24H_2O$	++	++	++	−	+++	+++
$CuSO_4\cdot 5H_2O$	−	−	−	+	+	++
$ZnSO_4\cdot 7H_2O$	−	++	−	−	+++	+++
$CCl_3CH(OH)_2$	−	++	++	−	+++	+++

(a)	(b)						
	NH_2OH·HCl	$(NH_2OH)_2$·H_2SO_4	$NH_2NHCONH_2$·HCl	$NH=C(NH_2)_2$·HCl	$CCl_3CH(OH)_2$	$C_6H_{12}O_6$ D-levulose	$C_{12}H_{22}O_{11}$ sucrose
$Na_2B_4O_7\cdot 10H_2O$	+++	+	+++	++	+	−	−
$Na_3PO_4\cdot 12H_2O$	++	+	+++	++	+++	−	−
$Na_2HPO_4\cdot 12H_2O$	+++	+++	+++	+++	+++	++	+
$NaH_2PO_4\cdot 2H_2O$	+++	−	−	++	−	−	−
$Na_2SO_4\cdot 10H_2O$	+++	+++	+++	+++	+++	+++	+++
$MgSO_4\cdot 7H_2O$	−	−	−	+	−	−	−
$Al_2(SO_4)_3(NH_4)_2SO_4\cdot 24H_2O$	−	−	−	−	−	−	−
$Al_2(SO_4)_3Na_2SO_4\cdot 24H_2O$	+	+	−	++	++	++	+
$Al_2(SO_4)_3K_2SO_4\cdot 24H_2O$	−	−	−	−	−	−	−
$FeSO_4(NH_4)_2SO_4\cdot 6H_2O$	−	−	−	−	−	−	−
$Fe_2(SO_4)_3(NH_4)_2SO_4\cdot 24H_2O$	+++	+++	++	+++	+	++	++
$CuSO_4\cdot 5H_2O$	++	−	++	++	−	−	−
$ZnSO_4\cdot 7H_2O$	+++	+	+++	+++	+	−	−
$CCl_3CH(OH)_2$	+	−	−	++	/	−	−

(a): Water liberating compound, (b): Compound making (a) liberate water
+++ denotes rapid, ++ moderately fast, + slow, and − no liquefaction

comparison.

We see that many of the pairs found consist of combinations of reagents with which weare familiar. They would have been found much earlier if liquefaction had attracted attention. It is expected that more pairs will be found by future attempts.

A few remarks should be added. Of (a), $Na_2SO_4\cdot 10H_2O$ and $Al_2(SO_4)_3\cdot Na_2SO_4\cdot 10H_2O$ undergo liquefaction to a great extent. Among the sodium phosphates, $Na_2HPO_4\cdot 12H_2O$ undergoes liquefaction most easily. Besides urea, several organic compounds as well as alkali thiocyanates were found to cause liquefaction with inorganic compounds.

The following combinations are suitable for the demonstration of liquefaction:

$Na_3PO_4\cdot 12H_2O + NH_2NHCONH_2\cdot HCl$

$Na_2HPO_4\cdot 12H_2O + CH_3COONH_4$

$ZnSO_4\cdot 7H_2O + C_2H_5NH_2\cdot HCl$

$ZnSO_4\cdot 7H_2O + NH=C(NH_2)_2\cdot HCl$

BULLETIN OF THE CHEMICAL SOCIETY OF JAPAN, VOL. 46, 3296—3297 (1973)

Thermal Decomposition Studies of the Ammonium Forms of the Crystalline Zirconium Phosphate Ion Exchanger

Yoshitsugu HASEGAWA

Department of Industrial Chemistry, Tokyo University of Agriculture and Technology, Nakamachi, Koganei, Tokyo 184

(Received January 16, 1973)

Ammonium-ion exchange on a crystalline zirconium phosphate (c-ZrP) had been studied, and the formation of two phases, $Zr(NH_4PO_4)_{1.33}(HPO_4)_{0.67}\cdot H_2O$ (Phase I) and $Zr(NH_4PO_4)_2\cdot H_2O$ (Phase II), has been found.[1] It is known that c-ZrP has two phosphate protons and that they exist in the ratio of 1 to 1.[2] However, the results obtained earlier for the ammonium-ion exchange showed that the phosphate protons seemed to exist in the ratio of 2 to 1. This result differs from that expected from the known properties of c-ZrP. In the present study, the thermal decomposition of the ammonium forms of c-ZrP was examined by means of thermogravimetry, and the enthalpy changes in the decomposition processes were measured by differential scanning calorimetry. Moreover, the changes in the phases of the samples during heating were analysed by means of X-ray powder diffraction. On the basis of these results, the state of the ammonium ions and the waters in the exchanger were discussed.

Experimental

Preparation of the Samples. c-ZrP and Phases I and II were prepared as has been described in the previous papers.[1,3]

Apparatus and Procedure. Thermogravimetry (TG) and Differential Scanning Calorimetry (DSC). The TG curves were obtained with a Rigaku TJG-DTA 8020 apparatus in static air, using a platinum crucible. The DSC curves were obtained with a Rigaku DSC 8000 apparatus in a dynamic nitrogen stream and at a flow rate of 300 ml/min. The measurement was made using samples of about 5—10 mg with a mesh size of 100—200 in an aluminum pan. In both thermal measurements, the heating rate was fixed at 5 °C/min. The standard substances used were KNO_3, $KClO_4$, and Zn.

X-Ray Study. The X-ray powder patterns were obtained with Ni filtered copper X-rays, using a Rigaku Geigerflex (Rigaku Denki Co., Ltd.).

Results and Discussion

Thermal Studies. The thermogravimetric data obtained are shown in Table 1. For each decomposition step, we attempted to detect ammonia by means of evolved gas analysis. Ammonia was found in the first and second steps. As is shown in the DSC curves (Fig. 1), the first decomposition reaction was complex. Thus, the detection of ammonia was carried out at the beginning and at the end of the reaction. Ammonia was not detected at the beginning. Hence, Phases I and II released one mole of water and almost simultaneously 0.33 or one mole of ammonia in the first step. One mole of ammonia was released in the second step. The last step corresponded to the polymerization of *ortho*-phosphate groups.

Table 1. Weight loss on heating phases I and II

Temperautre range (°C)	Total weight loss (%)		
	TG	DSC[a]	Theoretical
Phase I			
70—270	7.4	7.4	7.3
270—400	11.6	12.1	12.5
540—640	16.0	—	18.1
Phase II			
50—270	11.0	10.8	10.4
270—400	16.0	16.0	15.5
540—640	20.0	—	20.9

a) The samples analysed by the differential scanning calorimeter were weighed batchwise after heating.

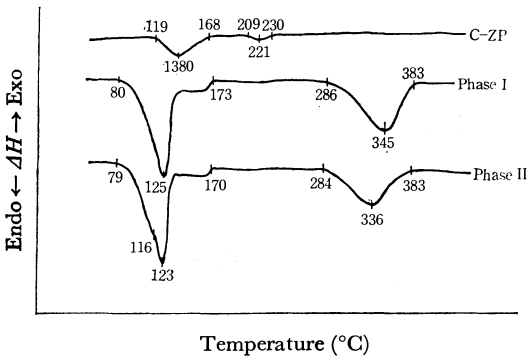

Fig. 1. The DSC curves of c-ZrP, Phases I and II.

In the DSC study, the heating rate, the gas-flow rate, and the packing manner of the samples were varied in order to isolate each reaction in the first step, but the attempt was unsuccessful. The DSC curves obtained are shown in Fig. 1. The DSC curves of Phase I agreed with that of Phase II except for the details in the first step. The DSC curves in Fig. 1 showed that the enthalpy changes in the reactions were endothermic.

When the decomposition reactions of Phases I and II were compared with those of the ammonium phosphates of some metals reported by Erdey and Gal,[4] the effect of zirconium on the release of ammonia seemed to be small and the interaction between the ammonium ions and phosphate groups appeared to be dominant. The temperature range corresponding to the first decomposition is similar to that of diammonium

1) Y. Hasegawa and H. Aoki, This Bulletin, **46**, 836 (1973).
2) A. Clearfield and J. A. Stynes, *J. Inorg. Nucl. Chem.*, **26**, 117 (1964).
3) Y. Hasegawa and I. Tomita, This Bulletin, **43**, 3011 (1970).
4) L. Erdey and S. Gal, *Talanta*, **10**, 23 (1963).

monohydrogen phosphate (max., about 170 °C). The second decomposition-temperature range is similar to the decomposition temperature of ammonium chloride (max., 345 °C) or ammonium sulfate (max., 330 °C).[5] According to Erdey *et al*,[4,5] the decomposition temperature of ammonium salts is inversely proportional to the basicity of the anion bases in the salts. Hence, the ammonia released in the first and second steps will originate from the ammonium ions exchanged with the proton on c-ZrP at higher pH values, and at lower pH values, respectively (see Fig. 1 in Ref. 1). The decomposition temperature observed in the second step is higher than that expected from the basicity of the monohydrogen phosphate group. This is mainly due to the structural change in the solid phase (*cf.* X-ray study).

From the DSC curves in Fig. 1, the characteristics of the water in the ammonium-form exchanger can be deduced to be as follows. The dehydration of c-ZrP in the first step took place at a relatively higher temperature and the enthalpy change was small. This reflects the zeolitic nature of the water in c-ZrP.[6,7] In contrast to c-ZrP, the dehydration of Phases I and II shifted to a lower temperature and the DSC curves resembled that of a hydrated water. This change in the water in the exchanger is more apparent if we compare the enthalpy change, ΔH, for c-ZrP with those for Phases I and II. The ΔH's of c-ZrP and Phases I and II for the first step were equal to 5, 15, and 25 and those for the second step, to 0.6, 13, and 14 kcal/mol, respectively. It is not apparent why the second peak for c-ZrP is present. The ΔH for the dehydration of c-ZrP is about equal to that of the hydrogen bond. The ΔH's in the second step for Phases I and II showed a good agreement. In view of the structural changes in Phases I and II by heating (see X-ray study), it is assumed that the differences in the ΔH's between Phases I and II are due to the presence of 0.67 moles of ammonium in both the forms. Therefore, the enthalpy changes can be calculated to be 10 kcal/H_2O and 15 kcal/NH_3 respectively.

As the standard heat of the formation of Phases I and II and their specific heats are not known, the heat of the reaction in each step can not be calculated. However, it is interesting to compare the ΔH's obtained in this study with the heat of reaction of the ammonium phosphates. The standard heats of the formation of mono-, di-, triammonium phosphate (crystal), and ammonia (gas) are −347, −376, −402, and −11 kcal/mol respectively.[8] The specific heat of ammonia at a constant pressure as a function of the temperature has also been established.[9] Assuming that the difference in the specific heats of solid phases is negligibly small, as is assumed in the case of aquopentaammine chromium (III) complexes,[10] the heats of the reactions of di- to mono- and of tri- to diammonium phosphate can be calculated. The resulting values are 18 kcal/mol at 500 K and 15 kcal/mol at 700 K. These values are almost equal to the ΔH's obtained for Phases I and II at the second decomposition step and to the calculated value. It may be deduced that the ammonium ions and the phosphate group in the exchanger and in the salts interact to the same extent. The deduction stated is coincident with the observation on the decomposition temperatures of Phases I and II.

Table 2. *d* Values of the compounds

Phase I		Phase II		c-ZrP 420 °C	β ZrP[a]
220 °C	420 °C	220 °C	420 °C		
7.55 vs	7.44 vs	7.50 vs	7.44 vs	7.44 vs	9.4
4.48 s	4.50 s	4.48 s	4.51 s	4.51 s	5.40
4.19 w		4.19 w			4.65
3.63 vs	3.59 s	3.63 vs	3.60 s	3.60 s	3.83
3.49 vs		3.48 vs			3.55
3.19 vw					3.30
3.08 vw		3.09 w			3.12
2.69 w	2.64 s	2.77 w	2.64 s	2.65 s	2.69
2.59 w		2.64 w			2.15
		2.58 w			

a) The values from Ref. 8.

X-Ray Study. The interplanar distances of the samples (*d* values) after heating to 220 and 420 °C in a differential scanning calorimeter are shown in Table 2. It is apparent that Phases I and II were converted to an identical phase (Phase III) by the first decomposition. After the second decomposition, both phases showed the same diffraction patterns as that of the c-ZrP heated to 420 °C. Further, the heated samples were equilibrated with vapor of ammonia and water, and then examined again. Their X-ray diffraction patterns were then identical with that of the original ones. This fact suggests that the thermal decomposition reactions are reversible. The *d* value of anhydrous zirconium bis(monohydrogen *ortho*-phosphate) obtained above did not agree with that reported by Clearfield *et al.*[11]

It is already known that c-ZrP has a layer structure and contains a cavity with a radius of about 1.3Å and that the first reflection in the X-ray diffraction patterns represents its interlayer distance.[12] The interlayer distances accompanying the thermal decomposition differ from those with the ion exchange.[1] That is, in the ion-exchange process the interlayer distance of 9.5Å changed to 8.2Å, while in the thermal decomposition it changed to 7.5Å. These facts suggest that one water molecule contributes to the structural change in the exchanger. Moreover, the shrinkage of the interlayer distance in the thermal decomposition will cause an increase in the apparent acidity of the phosphate group and the decomposition temperature in the second step will be raised.

5) L. Erdey, S. Gal, and G. Lipty, *ibid.*, **11**, 913 (1964).
6) A. Clearfield and G. D. Smith, *Inorg. Chem.*, **8**, 431 (1969).
7) N. Imai, R. Otsuka, and N. Yoshimori, *Memoirs of the School of Science & Engineering, Waseda Univ.*, **28**, 1 (1964).
8) N. A. Lange, "Handbook of Chemistry," 9th Ed., Handbook Publishers, Inc., (1956), p. 1579.
9) Din, "Thermodynamic Functions of Gases," Butterworth, London (1962), pp. 96—97.
10) R. Tsuchiya, Y. Kaji, A. Uehara, and E. Kyuno, This Bulletin, **42**, 1881 (1969).
11) A. Clearfield, R. H. Blessing, and J. A. Stynes, *J. Inorg. Nucl. Chem.*, **30**, 2249 (1968).
12) A. Clearfield, W. L. Duax, A. S. Medina, G. D. Smith, and J. R. Thomas, *J. Phys. Chem.*, **10**, 3424 (1969).

BULLETIN OF THE CHEMICAL SOCIETY OF JAPAN, VOL. 46, 3298—3299 (1973)

The Near-ultraviolet Absorption of Aqueous Solution of Copper(II) Ammine Complex with an Excess of Ammonia

Masatomi SAKAMOTO* and Sigeo KIDA

Department of Chemistry, Faculty of Science, Kyushu University, Hakozaki, Fukuoka 812

(Received June 12, 1973)

In 1941 Kubota[1] observed absorption spectra of copper(II) ammine complex in aqueous solutions with various concentration of ammonia, and found that an absorption appears in the near-ultraviolet region (~31 kK) at the presence of some excess ammonia. Kubota attributed the origin of this absorption to the formation of *trans*-$[Cu(NH_3)_4(OH)_2]$. However, his conclusion appears to be based on an old-fashioned theory, and therefore, it was attempted in this study to clarify the origin of the band in the light of the modern ligand field theory.

Recently, Kida *et al.*[2,3] studied some binuclear copper(II) complexes bridged with two alkoxo or hydroxo groups, and concluded that a band at the near-ultraviolet region (28—31 kK) is attributable to the charge transfer transition from nonbonding π-orbitals of bridged oxygen atoms to copper ions. Thus, it is expected that the origin of the near-ultraviolet band observed for copper(II)-ammonia solution should reasonably be explained by a similar basis to that of the above cases.[2,3]

Results and Discussion

Figure 1 shows the near-ultraviolet absorption spectra of copper sulfate with various concentration of ammonia. The result qualitatively agrees with that reported by Kubota. As seen in Fig. 1 the solution of Cu/NH_3= 1/10 showed the maximum absorption at 31.5 kK.

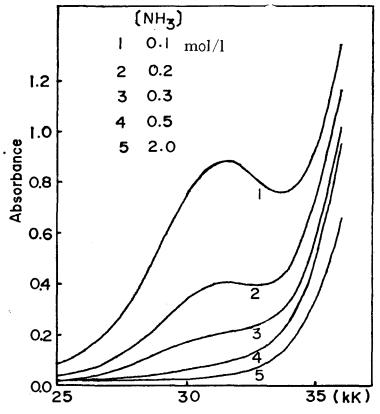

Fig. 1. UV spectra of 0.01 M $CuSO_4$ in aqueous ammonia solutions.

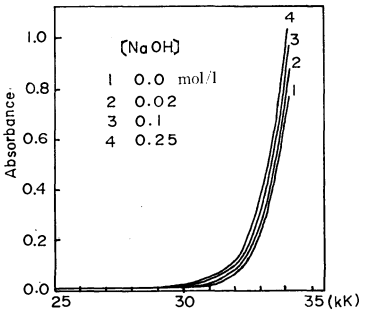

Fig. 2. UV spectra of aqueous solutions containing 0.01 M $CuSO_4$ and 0.1 M ethylenediamine at various OH^- concentrations.

However, in the copper(II)-ethylenediamine solution, as indicated in Fig. 2, no specific band was observed in the ultraviolet region (28—31 kK) even at the addition of sodium hydroxide. If the near-ultraviolet absorption were due to the formation of $[Cu(NH_3)_4(OH)_2]$ as Kubota concluded,[1] a similar absorption should have been observed for the solutions of Fig. 2 where $[Cu\ en_2(OH)_2]$ should exist in some extent. Therefore, it is obvious that the band is not due to the *trans*-coordination of two hydroxide ions.

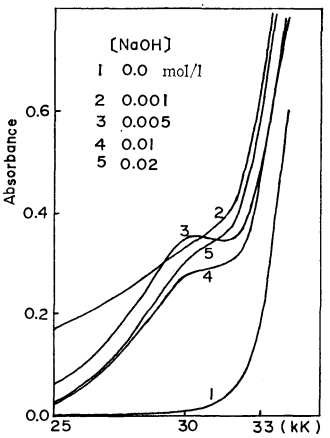

Fig. 3. UV spectra of aqueous solutions containing 0.01 M $CuSO_4$ and 0.018 M ethylenediamine at various OH^- concentrations.

As shown in Fig. 3, however, in the copper(II)-ethylenediamine solution with the mole ratio of 1: 1.8, a remarkable absorption was observed at 30.8 kK when sodium hydroxide was added. From this fact and the results of our previous studies,[2,3] we assume that the band is due to partially formed di-μ-hydroxo-bis-(ethylenediamine)dicopper(II) ion. Considering from

* Present address: Department of Industrial Chemistry, Faculty of Engineering, Ehime University, Bunkyo-cho, Matsuyama 790.

1) M. Kubota, *Nippon Kagaku Kaishi*, **62**, 509 (1941).

2) Y. Ishimura, Y. Nonaka, and S. Kida, This Bulletin, in press.

3) S. Kida, Y. Nishida, and M., Sakamoto, This Bulletin, **46**, 2428 (1973).

the stepwise stability constants[4] an appreciable amount of $[Cu\ en\ aq]^{2+}$ is present in the solution of Cu/en=1/1.8 (where aq denotes "aquated"). Accordingly, addition of sodium hydroxide to this solution will lead to formation of the dihydroxo-bridged binuclear complex. Further addition of sodium hydroxide may cause destruction of the binuclear structure, accompanying the decrease of the near-ultraviolet band, as observed in Fig. 3. Recently, the formation of the dihydroxo-bridged

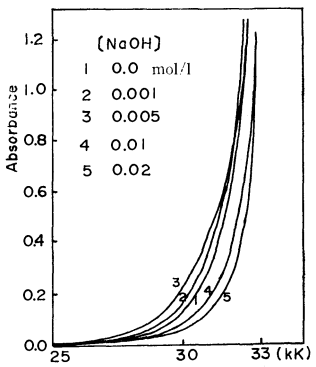

Fig. 4. UV spectra of aqueous solution containing 0.01 M $CuSO_4$ and 0.01 M diethylenetriamine at various OH^- concentrations.

binuclear complex under a similar condition was proved by the potentiometric study of Barbucci *et al.*[5]

In a solution of copper(II)-diethylenetriamine solution with the 1:1 ratio the dihydroxo-bridged binuclear complex is not liable to be formed even at a high pH region, but only mononuclear complexes, such as $[Cu\ dien\ aq]^{2+}$ and $[Cu\ OH\ dien\ aq]^{+}$, are formed. In fact, as shown in Fig. 4, no appreciable near-ultraviolet band was observed in the spectra of the copper(II)-diethylenetriamine solutions of various OH^- concentrations. This is supporting our view for the origin of the near-ultraviolet band, and eliminating the possibility that a mononuclear complex with hydroxide ion at an in-plane coordinating position, such as $[Cu(OH)_2\ en\ aq]$, $[Cu\ OH\ en\ aq]^{+}$ or $[Cu\ OH\ dien\ aq]^{+}$, is the origin of the near-ultraviolet band.

From the above discussion we may conclude that the absorption band at the near-ultraviolet region observed for the aqueous copper(II)-ammonia solution is attributable to the partially formed binuclear complex $[(NH_3)_2Cu(OH)_2Cu(NH_3)_2]^{2+}$. The decrease of intensity of the absorption at the very high concentration of ammonia can be well elucidated in terms of the conversion of the binuclear species into the mononuclear tetraammine complex.

4) "Stability Constants of Metal-ion Complexes," Sec. II, compiled by A. E. Martell, Special Publication of the Chem. Soc., London (1964), p. 371.

5) R. Barbucci, L. Fabbrizzi, and P. Paoletti, *J. Chem. Soc.*, Dalton, **1972**, 740.

BULLETIN OF THE CHEMICAL SOCIETY OF JAPAN, VOL. 46, 3299—3301 (1973)

Polarographic and ESR Studies on the Electrode Reactions of Tris(2,2′-bipyridine)iron(II) in Acetonitrile

Nobuyuki TANAKA, Tateaki OGATA, and Shigeya NIIZUMA

Department of Chemistry, Faculty of Science, Tohoku University, Sendai 980

(Received June 13, 1973)

In a previous paper[1] it was reported that in acetonitrile tris(2,2′-bipyridine)iron(II) was reduced to iron(I), iron(0) and iron(−I) complexes at the dropping mercury electrode. In that study, however, those complexes which were considered to be formed at the electrode were not isolated and their oxidation states were not confirmed by other techniques.

In this study the reduction products of tris(2,2′-bipyridine)iron(II) ($[Fe(bipy)_3]^{2+}$) were obtained by controlled potential electrolysis in acetonitrile and their ESR spectra were measured to clarify the oxidation states of those reduction products.

Experimental

Tris(2,2′-bipyridine)iron(II) perchlorate, $[Fe(bipy)_3](ClO_4)_2$, was synthesized according to the literature.[2] Acetonitrile was purified by the method presented by Coetzee.[3]

The polarographic measurement was carried out using an H-type cell and an aqueous saturated calomel electrode (SCE) at 25 °C. ESR spectra of reduction products which were obtained by controlled potential electrolysis were measured by the method of Geske and Maki[4] with an X-band JEOL P-10 ESR spectrometer and Mn^{2+} in MgO as standard.

Results and Discussion

A direct current (d.c.) polarogram of $[Fe(bipy)_3]^{2+}$ in acetonitrile with 0.05M $(C_2H_5)_4NClO_4$ as supporting electrolyte gave six reduction waves, although the sixth wave was not well-defined, as shown in Fig. 1 (Curve a). The limiting current of each of the first three waves was found to correspond to the value of one-electron reduction, while those of the fourth and fifth wave

1) N. Tanaka and Y. Sato, *Electrochim. Acta*, **13**, 335 (1968).
2) F. H. Burstall and R. S. Nyholm, *J. Chem. Soc., Ser. A*, **1952**, 3570.
3) J. F. Coetzee, *Pure Appl. Chem.*, **13**, 429 (1966).
4) D. H. Geske and A. H. Maki, *J. Amer. Chem. Soc.*, **82**, 2671 (1960).

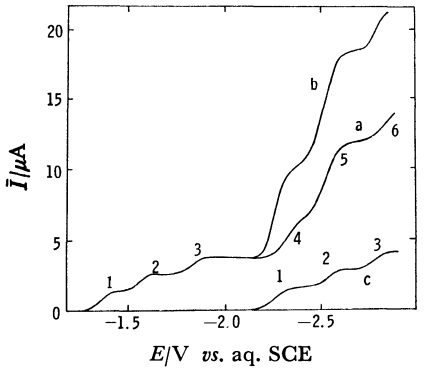

Fig. 1. D.c. polarograms of $[Fe(bipy)_3](ClO_4)_2$ and 2,2′-bipyridine in acetonitrile with 0.05 M $(C_2H_5)_4NClO_4$. (a) 0.5 mM $[Fe(bipy)_3](ClO_4)_2$, (b) a+0.6 mM 2,2′-bipyridine and (c) 0.3 mM 2,2′-bipyridine. Residual current and IR drop are corrected.

were those of two- and six-electron reduction, respectively. On the addition of free 2,2′-bipyridine the wave heights of the last three waves increased, as seen from Curve b in Fig. 1. The ligand itself undergoes reduction in acetonitrile at −2.24, −2.53, and −2.77 V *vs.* aq. SCE with the limiting current ratio of 1 : 1 : 1 (see Curve c in Fig. 1). Half-wave potentials of the reduction waves of $[Fe(bipy)_3]^{2+}$ and those of 2,2′-bipyridine in acetonitrile are given in Table 1. These

Table 1. Half-wave potentials of reduction waves of $[Fe(bipy)_3](ClO_4)_2$ and 2,2′-bipyridine

Electrolytic solution[a)]	Half-wave potential/V *vs.* aq. SCE				
	1st	2nd	3rd	4th	5th
I	−1.35	−1.55	−1.82	−2.32	−2.52
II				−2.26	−2.51
III	−2.24	−2.53	−2.77		

a) I: 0.5 mM $[Fe(bipy)_3](ClO_4)_2$+0.05 M $(C_2H_5)_4NClO_4$.
II: I+0.6 mM 2,2′-bipyridine.
III: 0.3 mM 2,2′-bipyridine+0.05 M $(C_2H_5)_4NClO_4$.

experimental results suggested that the last three waves must be attributed to the reduction of ligand coordinated in and/or dissociated from the complex. Although the first three waves are considered to be due to the reduction of tris(2,2′-bipyridine)iron complex,[1)] their electron transfer mechanisms are still in question; it has not been decided whether electrons enter to the ligand orbitals or to the metal ones.

In order to obtain the definitive information of the nature of the reduction products, ESR spectra of the reduction products which were obtained by controlled potential electrolysis at various potentials were measured at room temperature.

The parent complex $[Fe(bipy)_3]^{2+}$, which has been reported to be diamagnetic[2)], gave no ESR signal. A solution of reduction product obtained by electrolysis at −1.45 V, where a univalent complex $[Fe(bipy)_3]^+$ was considered to be formed, was purple and gave an ESR signal shown in Fig. 2. The g-value and the peak to peak width (ΔH_{msl}) were calculated to be 1.995_4 and 97 gauss, respectively. From the polarographic results and from the evidence that the intensity of this

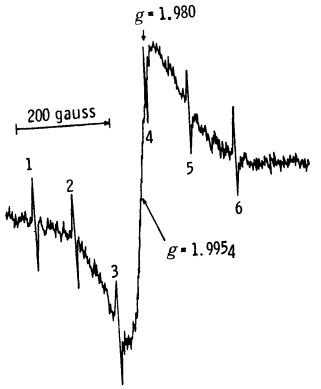

Fig. 2. ESR spectrum of the reduction product of $[Fe(bipy)_3](ClO_4)_2$ obtained by electrolysis at −1.45 V *vs.* aq. SCE. Signals of 1 to 6 are the hyperfine structures of Mn^{2+}.

signal did not change by the addition of excess free 2,2′-bipyridine, the signal of $g=1.995_4$ was considered to be due to $[Fe(bipy)_3]^+$.

It is known that most of the d^7 metal ions give g-values much greater than 2[5)]. Goodman and Raynor[6)], however, suggested that six-coordinated nominally d^7 spin-paired ion would give a low g-value if suitable π-bonded ligands were present with low-lying π^* orbitals available.

In the case of $[Fe(bipy)_3]^+$ which has a low g-value, therefore, it seems reasonable to consider that the iron exists as Fe^{2+} (d^6, spin-paired) and an unpaired electron is localized mainly on the ligand orbitals, because 2,2′-bipyridine possibly has low-lying vacant π^* orbitals.

On electrolysis at −1.70 V, where the formation of $[Fe(bipy)_3]$ was expected, black crystals grew up at the surface of the mercury electrode and the solution which was in contact with the crystals was purple. In this case, two ESR signals were observed; one had a g-value of 1.995_4 and the other, a g-value of 2.08 and ΔH_{msl} of about 800 gauss. The former signal was the same as that of $[Fe(bipy)_3]^+$, while the latter was found to coincide with that of $[Fe(bipy)_3]$ reported by Hall and Reynolds[7)]. These results seem to support that $[Fe(bipy)_3]$ was formed at the potential of the second wave and that $[Fe(bipy)_3]$ reacts with $[Fe(bipy)_3]^{2+}$ to form $[Fe(bipy)_3]^+$ in solution. The ESR signal of g-value of 2.08 suggested that $[Fe(bipy)_3]$ has the iron of d^8 configuration, although the optical spectrum of $[Fe(bipy)_3]$ obtained in 1,2-dimethoxyethane indicated that the unpaired electrons exist also in the ligand orbital.[7,8)]

The brown solution of reduction product generated by electrolysis at −2.10 V gave ESR spectrum with g-value of 1.995_4 and ΔH_{msl} of 14 gauss both in the absence and in the presence of free 2,2′-bipyridine as shown in Fig. 3.

The g-value found for this product did not coincide with the reported value of 2.0031 for the solid of $Na[Fe(bipy)_3]$,[8)] in spite of the expectation of the formation of $[Fe(bipy)_3]^-$ complex at this potential. The dif-

5) A. Abragam and B. Bleaney, "Electron Paramagnetic Resonance of Transition Ions," Clarendon Press, Oxford (1970).
6) B. A. Goodman and J. B. Raynor, *J. Chem. Soc., Ser. A*, **1970**, 2038.
7) F. S. Hall and W. L. Reynolds, *Inorg. Chem.*, **5**, 931 (1966).
8) C. Mahon and W. L. Reynolds, *ibid.*, **6**, 1927 (1967).

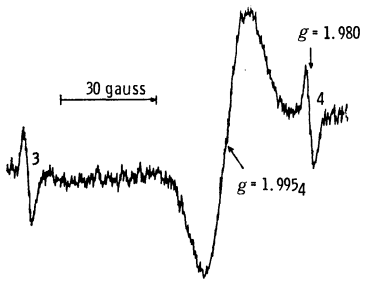

Fig. 3. ESR spectrum of the reduction product of $[Fe(bipy)_3](ClO_4)_2$ obtained by electrolysis at −2.10 V *vs.* aq. SCE. Signals of 3 and 4 are the hyperfine structures of Mn^{2+}.

ference between the observed *g*-value and the reported one is now under consideration.

The fact that, at the beginning of electrolysis at −2.10 V, ESR spectra with *g*-values of 1.995_4 and 2.08, which corresponded to those of $[Fe(bipy)_3]^+$ and $[Fe(bipy)_3]$ respectively, were also obtained seems to support proportionation reactions between the products and the parent complex taking place.

At −2.40 V, the formation of two kinds of reduction products was observed. One was the same as the product obtained by electrolysis at −2.10 V and the other was considered to be bipyridine anion radical from its *g*-value. Only the latter signal increased its intensity by continued electrolysis. This supports that bipyridine and/or its anion radical were formed by the dissociation of the reduction product such as $[Fe(bipy)_3]^{2-}$ either at the electrode surface or in the solution. Bipyridine anion radical was obtained in acetonitrile by electrolysis of 2,2′-bipyridine at −2.40 V and gave ESR spectrum with *g*-value of 2.003_6 and ΔH_{msl} of 7.5 gauss.

In conclusion, it should be emphasized that the observations mentioned above are in a sharp contrast with those in aqueous solutions, because in aqueous solutions the complexes of low oxidation states such as $[Fe(bipy)_3]^+$ and $[Fe(bipy)_3]^-$ are considered not to be formed electrochemically either at the electrode surface or in the solution.

The authors wish to thank the Ministry of Education for the financial support granted for this research.

BULLETIN OF THE CHEMICAL SOCIETY OF JAPAN, VOL. 46, 3301—3302 (1973)

Sugars Containing a Carbon-Phosphorus Bond. IV.[1] 5-(Alkylphosphonyl)-5-deoxy-*O*-methyl-D-xylopyranose[2]

Kuniaki Seo and Saburo Inokawa*, **

Department of Industrial Chemistry, Numazu Technical College, Ooka, Numazu 410
**Department of Synthetic Chemistry, Faculty of Engineering*
Shizuoka University, Johoku, Hamamatsu 432

(Received March 14, 1973)

The synthesis[1,3] of the sugar analogs, in which the ring oxygen is replaced by phosphorus, is intriguing, not only from the point of view of the chemistry, but also from that of biochemistry. In the present paper we will report on the syntheses of 5-deoxy-5-(ethylphosphonyl)-3-*O*-methyl-D-xylopyranose (IVa) and 5-(butylphosphonyl)-5-deoxy-3-*O*-methyl-D-xylopyranose (IVb).

Result and Discussion

As a starting material, we used 5-bromo-5-deoxy-1,2-*O*-isopropylidene-3-*O*-methyl-α-D-xylofuranose (I).[4] Ethyl ethyl-(5-deoxy-1,2-*O*-isopropylidene-3-*O*-methyl-α-D-xylofuranose-5)-phosphinate (IIa) and ethyl butyl-(5-deoxy-1,2-*O*-isopropylidene-3-*O*-methyl-α-D-xylofuranose-5)-phosphinate (IIb) were obtained almost quantitatively by the Michaelis-Arbuzov reaction of I with diethyl ethylphosphonite and diethyl butylphosphonite respectively. The reduction of IIa and IIb with sodium bis(methoxyethoxy) aluminum hydride (Red Al) in tetrahydrofuran (THF) gave a syrup of ethyl-(5-deoxy-1,2-*O*-isopropylidene-3-*O*-methyl-α-D-xylofuranose-5)-phosphine oxide (IIIa, 97%) and butyl-(5-deoxy-1,2-*O*-isopropylidene-3-*O*-methyl-α-D-xylofuranose-5)-phosphine oxide (IIIb, 77%) respectively. The PMR spectrum of IIIa (IIIb) in chloroform-*d* showed a characteristic J_{P-H} value[5] of 458 Hz at τ 3.08 (459 Hz at τ 3.07); it disappeared on deuteration. The IR spectrum of IIIa (IIIb) showed the absorption of a P–H group at 2320 cm^{-1} (2310 cm^{-1})[6] and that of a P=O group at 1240 cm^{-1} (1240 cm^{-1}).[7]

The hydroysis of IIIa (IIIb) with diluted hydrochloric acid (3 N) in water at 80—100 °C for 6 hr afforded a syrup of IVa (IVb) in a 61% (65%) yield. The studies of PMR (D_2O and DMSO-d_6) and the IR spectra of IVa (IVb) showed that IVa (IVb) had three OH groups and no P–H group. Moreover, the acetyla-

1) Part III: S. Inokawa, Y. Tsuchiya, K. Seo, H. Yoshida, and T. Ogata, This Bulletin, **44**, 2279 (1971).

2) We have tentatively used this name for the sugar in which O was replaced by RP(0) in the hemiacetal ring of 3-*O*-methyl-D-xylopyranose.

** To whom correspondance concerning this manuscript may be directed.

3) R. L. Whistler and C.-C. Wang, *J. Org. Chem.*, **33**, 4455 (1968).

4) S. Inokawa, H. Yoshida, C.-C. Wang, and R. L. Whistler, This Bulletin, **41**, 1472 (1968).

5) H. R. Hays *J. Org. Chem.*, **33**, 3690 (1968).

6) R. A. Chittenden and L. C. Tomas, *Spectrochim. Acta*, **20**, 861 (1964).

7) L. C. Tomas and R. A. Chittenden, *ibid.*, **20**, 467 (1964).

tion of IVa (IVb) with acetic anhydride in pyridine gave, in good yields, crystals of the tri-*O*-acetylated compound, Va (Vb), the PMR data and elemental analysis of which showed that Va (Vb) was 1,2,4-tri-*O*-acetyl-5-deoxy-(ethylphosphonyl)-3-*O*-methyl-D-xylopyranose [1,2,4-tri-*O*-acetyl-5-(butylphosphonyl)-5-deoxy-3-*O*-methyl-D-xylopyranose]. Therefore, IVa and IVb must be 5-deoxy-5-(ethylphosphonyl)-D-xylopyranose and 5-(butylphosphonyl)-5-deoxy-D-xylopyranose respectively.

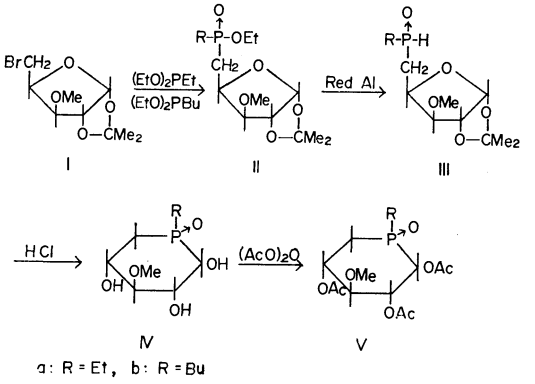

Experimental

The melting points were determinted by means of a Yanagimoto micro melting point apparatus. The infrared spectra were mesured on a Hitachi EPI-G-2 grating spectrophotometer. The nuclear magnetic resonance spectra were taken at 60 MHz on a Hitachi R-2 spectrometer, using tetramethylsilane as the internal or external standard. Thin-layer chromatography (tlc) was carried out on microscope slides coated with silica gel,[8] using ethyl acetate–petroleum ether ((1:1 v/v) (A); (3:7 v/v (B)) and methanol–chloroform ((1:7 v/v) (C)), and the spots were visualized with a sulfuric acid–ethanol solution (10%).

Ethyl Ethyl-(5-deoxy-1,2-O-isopropylidene-3-O-methyl-α-D-xylofuranose-5)-phosphinate (IIa). A mixture of 5-bromo-5-deoxy-1,2-*O*-isopropylidene-3-*O*-methyl-α-D-xylofuranose (6 g) and diethyl ethylphosphonite (15 ml) was refluxed under nitrogen for 6 hr at 130—145 °C. During the reaction, diethyl ethylphosphonite (2 ml) was added several time. The excess of the phosphonite was then distilled *in vacuo* to give colorless needles of IIa (6.9 g, an almost quantitative yield), which was sufficiently pure for the subsequent conversion; mp 67.5—70.0 °C (from ethyl acetate–*n*-hexane (1:4 v/v); R_f (Solvent B) 0.2; $[\alpha]_D^{12}$ −50° (*c* 6.2, chloroform); IR (KBr): 1240 cm^{-1} (P=O); PMR ($CDCl_3$): τ 4.20 (1H, d, $J_{1,2}$= 4 Hz, H-1), 4.45 (1H, d, overlapping with H-4, H-2), 5.97 (2H, q, $POCH_2$–), 6.35 (1H, t, H-3), 6.63 (3H, s, OCH_3).

Found: C, 50.04; H, 8.51%. Calcd for $C_{13}H_{25}O_6P$: C, 50.64; H, 8.17%.

Ethyl Butyl-(5-deoxy-1,2-O-isopropylidene-3-O-methyl-α-D-xylofuranose-5)-phosphinite (IIb). Compound I (5.5 g) was treated with diethyl butylphosphonite as has been described above to give crystals pf IIb in an almost quantitative yield: mp 45.0—46.0 °C (from ethyl acetate–*n*-hexane (1:5 v/v)); $[\alpha]_D^{19}$ −39° (*c* 1.1, chloroform); IR (KBr): 1240 cm^{-1} (P=O); PMR ($CDCl_3$): τ 4.2 (1H, d, $J_{1,2}$=4 Hz, H-1), 5.45 (1H, d, overlapping with H-4, H-2), 5.95 (2H, q, P–OCH_2–), 6.34 (1H, t, H-3), 6.60 (3H, s, OCH_3).

Found: C, 52.39; H, 9.08%. Calcd for $C_{15}H_{29}O_6P$: C, 53.56; H, 8.68%.

Ethyl-(5-deoxy-1,2-O-isopropylidene-3-O-methyl-α-D-xylofuranose-5)-phosphine Oxide (IIIa). To IIa (2.2 g) in THF (150 ml) Red Al (70% benzene solution) (2.8 g) in THF (100 ml) was added under a nitrogen atmosphere in an iced-salt bath for 30 min. After 1 hr's stirring at room temperature, the reaction mixture was neutralized with hydrochloric acid in THF and a few drops of water were added. The filtration and evaporation of the filtrate gave a syrup of IIIa (1.8 g, 97%) which was sufficiently pure for the subsequent conversion. An analytical sample was obtained by tlc separation; R_f 0.05 (Solvent A): $[\alpha]_D^{19}$ −44°[9] (*c* 2.9, chloroform); IR (KBr); 2320 cm^{-1} (P–H), 1240 cm^{-1} (P=O); PMR ($CDCl_3$): τ 3.08 (1H, *m*, disappearing on deuteration, J_{P-H}=458 Hz, P–H), 4.18 (1H, d, $J_{1,2}$=4 Hz, H-1), 5.41 (1H, d, overlapping with H-4, H-2), 6.32 (1H, t, H-3), 6.60 (3H, s, OCH_3).

Butyl-(5-deoxy-1,2-O-isopropylidene-3-O-methyl-α-D-xylofuranose-5)-phosphine Oxide (IIIb). Compound IIb (3.0 g) was treated as has been described above, and the reaction product was separated by silica gel-column chromatography (Solvent C) to give a syrup of IIIb (2.0 g, 77%): R_f 0.05 (Solvent C); $[\alpha]_D^{19}$ −43°[9] (*c* 4.3, chloroform); IR (KBr): 2310 cm^{-1} (P–H), 1240 cm^{-1} (P–O): PMR ($CDCl_3$): τ 3.07 (1H, *m*, disappearing on deuteration, J_{P-H}=459 Hz, P–H), 4.12 (1H, d, $J_{1,2}$= 4 Hz, H-1), 5.51 (1H, d, overlapping with H-4, H-2), 6.34 (1H, t, H-3), 6.65 (3H, s, OCH_3).

5-Deoxy-5-(ethylphosphonyl)-3-O-methyl-D-xylopyranose (IVa). A solution of IIIa (0.5 g) and concentrated hydrochloric acid (1.0 ml) in water (25 ml) containing small amounts of THF was heated at 80—100 °C under a nitrogen atmosphere. The THF was evaporated during the reaction. The hot solution was neutralized with silver carbonate; subsequent filtration and evaporation gave a colorless syrup of IVa (0.3 g, 71%); hydroscopic solid; R_f 0.20 (Solvent C): $[\alpha]_D^{14}$ 0.0° [9] (*c* 2.6, water); IR (KBr): 1240 cm^{-1} (P=O); PMR (D_2O): τ 6.40 (3H, s, OCH_3), 7.3—9.5 (7H, m, H-5,5′, P–C_2H_5); (DMSO-d_6): τ 6.0—7.0 (8H, m, three of them disappearing on deuteration).

5-(Butylphosphonyl)-5-deoxy-3-O-methyl-D-xylopyranose (IVb). Compound IIIb (1.0 g) was treated as has been described above to give a hydroscopic solid of IVb (0.5 g, 65%); R_f 0.20 (Solvent C); $[\alpha]_D^{17}$ 0.0° [9] (*c* 3.4, water); IR (KBr): 1240 cm^{-1} (P=O); PMR (DMSO-d_6): τ about 6.4 (4H, three of them disappearing on deuteration), 6.72 (3H, s, OCH_3), 7.8—9.8 (11H, m, H-5,5′, P–C_4H_9).

1,2,4-Tri-O-acetyl-5-deoxy-5-(ethylphosphonyl)-3-O-methyl-D-xylopyranose (Va). The treatment of IVa (0.30 g) with acetic anhydride in pyridine in the usual way gave a colorless solid (0.44 g, 94%); R_f 0.95 (Solvent C); mp 227—229 °C (from ethanol); $[\alpha]_D^{17}$ 0.0 ° (*c* 0.87, chloroform); IR (KBr): 1240 cm^{-1} (P=O); PMR ($CDCl_3$); τ 4.5—5.1 (3H, m), 6.57 (3H, s, overlapping with one proton, OCH_3(, 7.90, 7.94, 7.95 (9H, s, 1,2,4-$OCOCH_3$).

Found: C, 47.95; H, 6.85%. Calcd for $C_{14}H_{28}O_8P$: C, 48.00; H, 6.62%.

1,2,4-Tri-O-acetyl-5-(butylphosphonyl)-5-deoxy-3-O-methyl-D-xylopyranose (Vb). Compound IVb (0.50 g) was treated as has been described above to give crystals of Vb (0.70 g, 93%); R_f 0.95 (Solvent C); mp 218.5—220 °C; $[\alpha]_D^{17}$ −8.1° (*c* 4.2, chloroform); IR (KBr): 1240 cm^{-1} (P=O); PMR ($CDCl_3$): τ 4.1—5.1 (3H, m), 6.50 (3H, s, overlapping with one protone, OCH_3), 7.86, 7.92, 7.95 (9H, s, 1,2,4-$OCOCH_3$).

Found: C, 50.47; H, 7.43%. Calcd for $C_{16}H_{27}O_8P$: C, 50.79; H, 7.19%.

8) Silica-Layer G-10, Nakarai Chemicals, Ltd.

9) This sample seemed to be fairly pure from the observation of its PMR spectrum and tlc, but it was not enough pure for an elemental analysis.

BULLETIN OF THE CHEMICAL SOCIETY OF JAPAN, VOL. 46, 3303—3304 (1973)

The Formation of Carbon-Carbon and Carbon-Oxygen Bonds in the Oxidation of Enolizable Ketones with Iron(III) Chloride

Hiroo INOUE, Yoshikazu KIMURA, and Eiji IMOTO

Department of Applied Chemistry, College of Engineering, University of Osaka Prefecture, Sakai, Osaka 591

(Received April 11, 1973)

We have recently reported that the oxidation of enolizable alkyl aryl ketones with iron(III) chloride brings about carbon-carbon coupling and/or the chlorination of the α-methylene group.[1] Here we undertook the study of the heterogeneous oxidation of benzyl phenyl ketone (I) with iron(III) chloride in benzene and chlorobenzene. As a result, we found that the reaction differs from those of alkyl aryl ketones and results in the direct arylation of the α-methylene group by a two-electron oxidation. Furthermore, it was found that ring closure by carbon-oxygen coupling occurs in the oxidation of the arylation product (II) with two phenyl groups at the α-position of the carbonyl group.

$$C_6H_5COCH_2C_6H_5 + C_6H_5R \xrightarrow{FeCl_3}$$

I a: R=H b: R=Cl

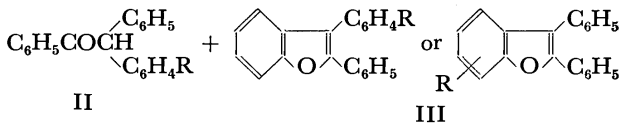

II III

When a solution of I in benzene containing dispersed iron(III) chloride was refluxed for several hours, the I was converted to 2,2-diphenylacetophenone (IIa) and 2,3-diphenylbenzofuran (IIIa) was formed. Iron(III) chloride was reduced to iron(II) chloride. The nuclear chlorination did not occur at all. The irradiation of a solution of I in benzene in the presence of iron(III) chloride also gave IIa, along with a small amount of IIIa, although I undergoes photolysis to 1,2-diphenylethane, benzaldehyde, and 1,2,3,4-tetraphenyl-1,4-butanedione in the absence of iron(III) chloride.[2] The results are shown in Table 1. The addition of a small amount of water to the reaction system did not have any significant effect on the reaction pathway.

TABLE 1. THE OXIDATION OF I WITH IRON(III) CHLORIDE IN BENZENE OR CHLOROBENZENE[a]

Solvent	Therm. or *hv*	Reaction time hr	Yield of product, % II	Yield of product, % III	Recovery %
C_6H_6	Reflux	7	83	7	7
C_6H_6[b]	Reflux	7	72	8	11
C_6H_6	*hv*	2.5	33	0.2	53
C_6H_5Cl	Reflux	7	60[c]	—	19

a) The amount of $FeCl_3$: 1.02 mmol in 5 ml of the solvent. The concentration of I: 10^{-1} mol/l. The amounts of the products were determined by glc.

b) Water was added into the reaction system (the molar ratio of $H_2O/FeCl_3$: 1.3).

c) This is the yield of the *p*-isomer.

When chlorobenzene was used as the solvent, the *p*-isomer of IIb was isolated by a treatment similar to that used in the case of benzene (Table 1). However, the *o*- and *m*-isomers and IIIb could not be isolated because their yields were considerably lower than that of the *p*-isomer. The reaction of 2-chloro-2-phenylacetophenone (IV) with chlorobenzene in the presence of aluminum chloride at room temperature also gave the *p*-isomer of IIb in a 63% yield. Furthermore, the *p*-isomer has been prepared by the Friedel-Crafts reaction of benzoin with chlorobenzene in the presence of sulfuric acid.[3] These facts suggest strongly that the reaction proceeds *via* an intermediate (V) which is formed by a two-electron oxidation, followed by the reaction with the solvent, since, in the reaction of the α-keto radical formed by a one-electron oxidation, it is predicted that the yields of the *o*- and *m*-isomers will become higher. Such a process has been considered

$$I \xrightarrow{FeCl_3} \underset{V}{C_6H_5\overset{+}{C}OCHC_6H_5} \xrightarrow{C_6H_5R} II$$

in the oxidative dimerization of phenols with a variety of oxidants.[4] In the oxidation of alkyl aryl ketones with iron (III) chloride, we have reported that the homogeneous reaction results in the coupling of the α-keto radical, while, in the heterogeneous system, α-chlorination occurs by means of a two-electron oxidation.[1] Therefore, the fact that the arylation proceeds by a two-electron oxidation may be explained as resulting from the heterogeneous oxidation by iron(III) chloride. The phenyl group at the α-position of I must be required for the reaction of V with benzene, since the oxidation of propiophenone with iron(III) chloride in benzene resulted in only chlorination, without any arylation. This result agreed with the fact that 1-bromo-1-phenyl-2-propanone undergoes Friedel-Crafts reaction, 2-bromoacetophenone showing no reaction with benzene in the presence of aluminum chloride.[5]

$$C_6H_5COCH_2CH_3 \xrightarrow[C_6H_6]{FeCl_3} C_6H_5COCHCH_3 \quad (Cl)$$

On the other hand, IIIa was produced consecutively

1) H. Inoue, M. Sakata, and E. Imoto, This Bulletin, **44**, 3490 (1971); *ibid.*, **46**, 2211 (1973).

2) J. Kenyon, A. R. A. A. Rassoul, and G. Soliman, *J. Chem. Soc.*, **1956**, 1774.

3) E. C. Dodds, L. Goldberg, E. I. Grünfeld, W. Lawson, C. M. Saffer, Jr., and R. Robinson, *Proc. Roy. Soc. Ser. B*, **132**, 83 (1944); *Chem. Abstr.*, **38**, 3637 (1944).

4) W. A. Waters, "Mechanisms of Oxidation of Organic Compounds," Wiley, New York (1964), Ch. 9; W. A. Waters, *J. Chem. Soc. B*, **1971**, 2026.

5) P. Ruggli, H. Dahn, and J. Wegmann, *Helv. Chim. Acta*, **29**, 113 (1946); *Chem. Abstr.*, **40**, 2821 (1946).

from IIa by the oxidative ring closure with iron(III) chloride; when a solution of IIa in benzene containing iron(III) chloride was refluxed for 2 hr, IIIa was obtained in a 10% yield, with an 85% recovery of IIa, although IIIa was converted to a polymeric material in a longer reaction time. The arylation and chlorination at the α-position of the carbonyl group did not occur. The formation of IIIa indicates that the stereochemical conditions of IIa strongly favor the ring closure by carbon-oxygen coupling, as is shown in the syntheses of xanthones, which can be effected by oxidizing 2,3′-dihydroxybenzophenones with alkaline ferricyanide.[6]

Experimental

Materials. The I was prepared by the method described in the literature.[7] The anhydrous iron(III) chloride was prepared by the sublimation of commercial iron(III) chloride under a reduced pressure of 1 mmHg at 300 °C.

Oxidation of I with Iron(III) Chloride. A solution of 5 mmol of Ia in 30 ml of benzene or chlorobenzene containing 10.1 mmol of the dispersed anhydrous iron(III) chloride was refluxed for 7 hr, or was irradiated under stirring with a Pyrex-covered 100-W high-pressure mercury lamp at the distance of 6 cm under a nitrogen atmosphere at room temperature for 2.5 hr. Hydrogen chloride was generated during the reaction. After the reaction period, the precipitate, which contained mainly iron(II) chloride, was filtered off. The iron(II) chloride was confirmed spectrophotometrically by the *o*-phenanthroline method.[8] The filtrate was submitted to chromatography on alumina (elution with dry benzene), leading to the separation of IIa and IIIa. After removing the benzene, the residue (IIa or IIIa) was recrystallized from ethanol. The isolation of *p*-IIb was carried out according to the method used in the case of IIa, IIa (mp 134—136 °C (lit,[9] 136 °C)) exhibited NMR (CCl_4) signals at δ 5.87 (s, 1H, CH), and 7.16—7.98 (m, 15H, aromatic protons) and an IR (KBr plate) peak at 1675 cm^{-1} (CO). Mass *m/e*, 272 (parent peak). IIIa (mp 121—122 (lit,[10] 123 °C)) exhibited NMR (CCl_4) signals of aromatic protons at δ 7.04—7.60. Mass *m/e*, 270 (parent peak). *p*-IIb (mp 102—104 °C (lit,[3] 104 °C)) exhibited NMR (CCl_4) signals at δ 5.85 (s, 1H, CH) and 7.10—7.94 (m, 14H, aromatic protons) and an IR (KBr plate) peak at 1670 cm^{-1} (CO). Mass *m/e*, 305 and 306 (parent peaks).

Reaction of IV with Chlorobenzene in the Presence of Aluminum Chloride. A solution of 1.2 mmol of IV in 3 ml of chlorobenzene containing 1.4 mmol of the dispersed aluminum chloride was refluxed for 50 min. After the solution had then cooled to room temperature, *p*-IIb was isolated by a method similar to that used in the case of IIa; the amount was determined by glc.

Oxidation of Propiophenone with Iron(III) Chloride. A solution of 1.1 mmol of propiophenone in 3 ml of benzene containing 2 mmol of the dispersed anhydrous iron(III) chloride was refluxed for 22 hr. 2-Chloropropiophenone[1] was obtained in a 40% yield, along with the recovery of propiophenone. No other products were detected by glc at all.

Oxidation of IIa with Iron(III) Chloride. A solution of 0.3 mmol of IIa in 3 ml of benzene containing 0.6 mmol of the dispersed anhydrous iron(III) chloride was refluxed for 2 hr. The reaction mixture was submitted to glc analysis. IIIa was thus obtained in a 10% yield.

Analyses. The amounts of the products in the reaction mixture were determined by means of glc using a 3 mm × 1 m column of 30% high-vacuum silicon grease on Celite 545 (80—100 mesh).

6) J. E. Atkinson and J. R. Lewis, *J. Chem. Soc., C*, **1969**, 281.

7) C. F. H. Allen and W. E. Barker, "Organic Syntheses," Coll. Vol. II, p. 156 ,(1943).

8) H. Inoue, K. Tamaki, N. Komakine, and E. Imoto, This Bulletin, **40**, 875 (1967).

9) C. F. Koelsch, *J. Amer. Chem. Soc.*, **54**, 2049 (1932).

10) B. I. Arventi, *Bull. Soc. Chim. Fr.*, [5], **3**, 598 (1936); *Chem. Abstr.*, **30**, 4495 (1936).

BULLETIN OF THE CHEMICAL SOCIETY OF JAPAN, VOL. 46, 3304—3306 (1973)

Reaction of 4-Acetylsydnones

Hsien-Ju TIEN, Kazusato KANDA, Akiko CHINONE, and Masaki OHTA

Department of Chemistry, Faculty of Science, Tokyo Institute of Technology, Ookayama, Meguro-ku, Tokyo 152

(Received June 4, 1973)

Due to their unique mesoionic character, sydnones have been the subject of continued study since their discovery in 1935.[1] Although sydnones have been extensively investigated, little is known concerning the synthesis and reaction of 4-substituted sydnones. We reported the synthesis of 4-acetylsydnones by the reaction of sydnones with acid anhydrides in the presence of perchloric acid.[2] In this paper, we describe the reaction of 4-acetylsydnones whose structures are analogous to that of acetophenone.

Reaction of 4-acetyl-3-phenylsydnone (I) with benzaldehyde in the presence of alkali afforded 4-cinnamoyl-3-phenylsydnone (III), and 4-acetyl-3-benzylsydnone (II) reacted with benzaldehyde to give α-(4-cinnamoylsydnon-3-yl)stilbene (IV). 4-(Bromoacetyl)-3-phenylsydnone (V) and 3-benzyl-4-(bromoacetyl)sydnone (VI) were obtained by the reaction of I and II with bromine, respectively, in chloroform under irradiation of visible light. Corresponding dibromoacetyl derivatives, VII and VIII, were obtained when the above reaction was carried out in the presence of two equivalents mole of bromine. However, tribromoacetyl derivatives were not obtained even in the presence of three equivalents

1) J. C. Earl and A. W. Mckney, *J. Chem. Soc.*, **1935**, 899.
2) H. Tien and M. Ohta, This Bulletin, **45**, 2944 (1972).

mole of bromine. Compound V reacted with thioures to give sydnone-substituted thiazole derivative IX, and VI afforded X. Treatment of V and VI with calcium chloride in DMSO afforded chloroacetyl derivatives, XI and XII, which reacted with thiourea to give IX and X, respectively. Haloform reaction of neither I nor II proceeded, and resulted in a recovery of the starting material. Treatment of V with sodium hydroxide and bromine yielded 3-phenylsydnone (XIII). Brief heating of an aqueous sodium hydroxide solution of VII afforded XIII, and VIII yielded 3-benzylsydnone (XIV) by the same treatment. These results show that mono- and dibromoacetylsydnones are unstable to alkali. Pyridinium salts, XV and XVI, were obtained by treatment of V and VI with pyridine, respectively. Compound XVI afforded 3-benzylsydnone-4-carboxylic acid (XVII) by treatment with alkali, while XV did not afford corresponding carboxylic acid but 3-phenylsydnone was obtained. 4-(Aminoacetyl)-3-phenylsydnone hydrochloride (XVIII) was obtained by the reaction of V with hexamethylenetetramine followed by treatment with hydrochloric acid. 3-Benzyl-4-morpholinoacetylsydnone was obtained by treating VI with morpholine. The behavior of bromo derivatives and pyridinium salts toward alkali described above suggests that the substituents at position 3 and ω-position of side chain affect, to some extent, the mode of cleavage at bond a or b of 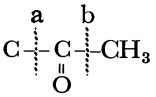 grouping.

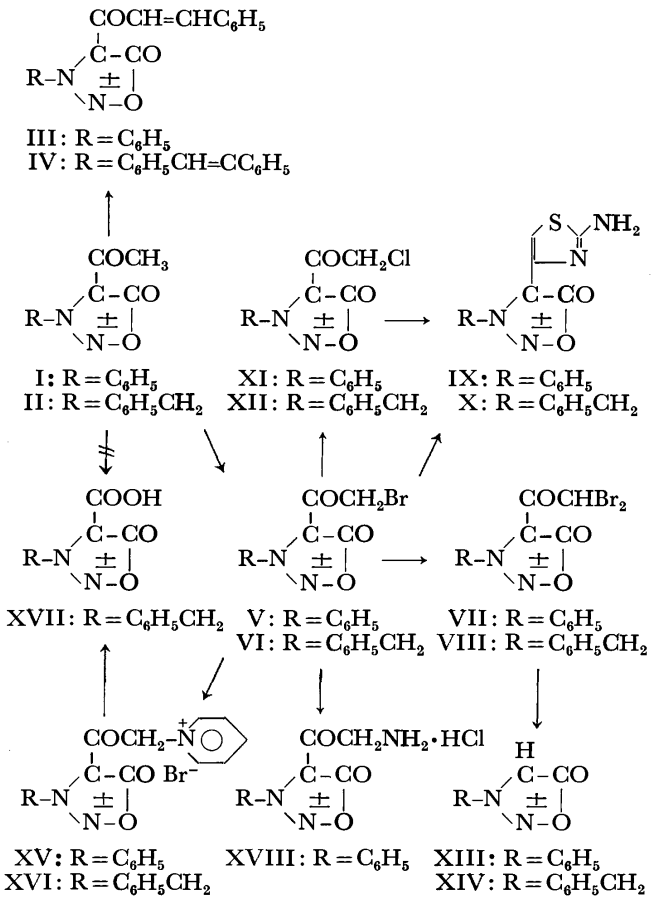

Experimental

4-Cinnamoyl-3-phenylsydnone (III). Compound I (2.0 g) was suspended in an alkaline solution (sodium hydroxide 0.5 g, water 5 ml, ethanol 3 ml) and 1.0 g of benzaldehyde was added and the reaction mixture was stirred for 10 min at room temperature. The precipitates were collected and washed well with water and then with cold ethanol. Recrystallization from ethanol afforded yellow needles with a mp of 145—147 °C (yield 52%).

Found: C, 69.86; H, 4.11; N, 9.59%. Calcd for $C_{17}H_{12}O_3N_2$: C, 70.71; H, 4.20; N, 9.78%. IR: 1785, 1655, 1590, 1420, 1040 cm^{-1}.

α-(4-Cinnamoylsydnon-3-yl)stilbene (IV). Compound IV was prepared form II and benzaldehyde by the same method as mentioned above. Recrystallization from isopropyl alcohol afforded colorless prisms with a mp of 105—106 °C (yield 30%).

Found: C, 75.73; H, 5.14; N, 7.20%. Calcd for $C_{25}H_{18}O_3N_2$: C, 76.13; H, 4.60; N, 7.10%. IR: 1780, 1650, 1470, 1050, 1038 cm^{-1}.

4-Bromoacetylsydnones, V and VI. To a solution of I (2.0 g) in 30 ml of chloroform, 1.6 g of bromine was added under irradiation of visible light. After 15 min, the color of bromine bleached. The solvent was removed *in vacuo* and the residue was recrystallized from ethanol to give pale yellow crystals with a mp of 110—111 °C (yield 70%).

Found: C, 42.69; H, 2.76; N, 10.00%. Calcd for $C_{10}H_7O_3N_2Br$: C, 42.40; H, 2.47; N, 9.89%. IR: 3050, 2975, 2925, 1790, 1680, 1420, 1010, 770, 680 cm^{-1}.

By the same method, VI was obtained from 8.8 g of II and 6.4 g of bromine in 100 ml of chloroform. Recrystallization from ethanol gave colorless needles with a mp of 64.5—65.5 °C (yield 70%).

Found: C, 44.48; H, 3.06; N, 9.63%. Calcd for $C_{11}H_9O_3N_2Br$: C, 44.44; H, 3.06; N, 9.43%. IR: 3000, 1780, 1760, 1660, 1465, 1035, 735, 705 cm^{-1}.

4-(Dibromoacetyl)sydnones, VII and VIII. To a solution of I (5.0 g) in 100 ml of chloroform, a little portion of chloroform solution of bromine (9.0 g/60 ml) was added under irradiation of visible light. After the initiation of the reaction, residual bromine solution was added dropwise and the solution was refluxed by heating with the tungsten lamp for 1 hr. During the irradiation, evolved hydrogen bromide was repelled by the stream of N_2. The solvent was removed *in vacuo* to give oily residue, to which a small amount of petroleum ether was added to crystallize. Reprecipitation of VII from a benzene solution with *n*-hexane afforded pale yellow prisms with a mp of 86—87 °C (yield 67%).

Found: C, 33.47; H, 1.86; N, 7.52%. Calcd for $C_{10}H_6O_3N_2Br_2$: C, 33.17; H, 1.66; N, 7.74%. IR: 1785, 1690, 1420, 1005, 770 cm^{-1}.

By the same method, VIII was prepared from 2.2 g of II and 3.2 g of bromine. Reprecipitation from a benzene solution with *n*-hexane afforded colorless needles with a mp of 80.5—81.5 °C (yield 80%).

Found: C, 35.11; H, 2.13; N, 7.45%. Calcd for $C_{11}H_8O_3N_2Br_2$: C, 35.25; H, 2.19; N, 7.57%. IR: 3000, 1760, 1682, 1470, 1000, 705 cm^{-1}.

Reaction of V with Thiourea. A solution of 1.4 g of V and 0.4 g of thiourea in 20 ml of ethanol was refluxed for 10 min. The precipitates were collected by filtration and dissolved in dilute ethanol (1: 1) and the solution was neutralized with sodium hydrogen carbonate. The precipitates were recrystallized from ethanol to give IX as yellow needles with a mp of 181—182 °C (yield 70%).

Found: C, 50.68; H, 3.13; N, 21.79; S, 12.10%. Calcd for $C_{11}H_8O_2N_4S$: C, 50.77; H, 3.08; N, 21.54; S, 12.31%.

IR: 3425, 3280, 3150, 1750, 1630, 1215 cm^{-1}.

Reaction of VI with Thiourea. Compound VI was treated with thiourea as mentioned above to give X. Recrystallization from ethanol gave X as yellow needles with a mp of 125—127 °C (yield 66%).

Found: C, 52.39; H, 3.73; N, 20.42; S, 11.98%. Calcd for $C_{12}H_{10}O_2N_4S$: C, 52.55; H, 3.65; N, 20.44; S, 11.68%. IR: 3375, 3295, 3200, 3120, 1745, 1730, 1620, 1520, 1325, 1180 cm^{-1}.

4-(Chloroacetyl)sydnones, XI and XII. Compound V (2.8 g) was dissolved in 20 ml of DMSO which was saturated with calcium chloride, and the solution was allowed to stand at room temperature for 48 hr. The reaction mixture was poured into ice-water and the precipitates were collected. Recrystallization from ethanol afforded colorless plates with a mp of 127—129 °C.

Found: C, 50.18; H, 2.94; N, 11.76%. Calcd for $C_{10}H_7O_3N_2Cl$: C, 50.31; H, 2.94; N, 11.74%. IR: 3060, 2990, 2945, 1790, 1775, 1693, 1280 cm^{-1}. NMR τ ($CDCl_3$) 2.15—2.60 (m, 5H), 5.33 (s, 2H).

By the same method, XII was prepared from VI and calcium chloride. Recrystallization from ethanol afforded colorless needles with a mp of 67—70 °C (yield 24%).

Found: C, 52.21; H, 3.59; N, 11.18%. Calce for $C_{11}H_9O_3N_2Cl$: C, 52.27; H, 3.56; N, 11.09%. IR: 1798, 1765, 1690, 1680, 1448, 1385, 1268, 1010 cm^{-1}.

Pyridinium Salt of VI (XVI) and 3-Benzylsydnone-4-carboxylic Acid (XVII). Compound VI was dissolved in 17 ml of pyridine and precipitates separated in a few minutes. Ether (30 ml) was added to the reaction mixture and precipitates were collected and recrystallized from ethanol, mp above 300 °C (yield 27%).

Found: C, 51.24; H, 3.87; N, 11.10%. Calcd for $C_{16}H_{14}O_3N_3Br$: C, 51.06; H, 3.72; N, 11.17%. IR 1780, 1675, 1635, 1480, 1005 cm^{-1}.

Pyridinium salt (0.75 g) thus obtained was added to a sodium hydroxide solution (sodium hydroxide 0.4 g, water 15 ml), and the solution was heated at 50 °C for 10 min. After filtering off the precipitates, filtrate was made acidic to Congo red with concentrated hydrochloric acid and kept to stand overnight at room temperature. Separated oily product was dissolved in methanol and treated with activated charcoal. Solvent was removed *in vacuo* to give XVII as colorless crystals. Recrystallization from hot water afforded colorless needles with a mp of 154—156 °C (yield 11%, calcd from pyridinium salt).

Found: C, 54.16; H, 3.81; N, 12.85%. Calcd for $C_{10}H_8O_4N_2$: C, 54.55; H, 3.64; N, 12.73%. IR: 3100—2500 (br), 1825 (sh), 1785, 1680, 1500, 1493, 1220, 1100 cm^{-1}.

Pyridinium Salt of V (XV) and its Treatment with Alkali. Compound XV was prepared from V and pyridine as mentioned above. Recrystallization from 90% ethanol afforded XV as pale yellow crystals with a mp of 226—228 °C (dec.).

Found: C, 49.49; H, 3.31; N, 11.45%. Calcd for $C_{15}H_{12}O_3N_3Br$: C, 49.72; H, 3.31; N, 11.60%. IR: 3025, 3010, 1780, 1685, 1640, 1492, 1470, 1435, 1015, 755, 685 cm^{-1}.

Pyridinium salt (1.8 g) thus obtained was heated at 50—60 °C in an alkaline solution (sodium hydroxide 1 g, water 30 ml) for 10 min. Precipitates were collected and washed with water. Recrystallization from ethanol gave 0.3 g of 3-phenylsydnone.

4-(Aminoacetyl)-3-phenylsydnone hydrochloride (XVIII). To a chloroform solution of V (5.6 g/30 ml), a chloroform solution of hexamethylenetetramine (2.8 g/30 ml) was added and the reaction mixture was stirred for 24 hr at room temperature. Precipitates were collected and washed with chloroform. The precipitates were added to ethanol–concentrated hydrochloric acid (20—8.5 ml) and the solution was stirred for 3 days at room temperature. In the course of stirring, precipitates were dissolved completely and then the reaction product separated out. Precipitates were collected and stirred for 10 min in 10 ml of water. Recrystallization from methanol gave XVIII, mp 180 °C (yield 78%).

Found: C, 46.68; H, 4.11; N, 16.11%. Calcd for $C_{10}H_{10}O_3N_3Cl$: C, 46.86; H, 3.91; N, 16.41%. IR: 3000—2850 (br), 1790, 1690 cm^{-1}.

3-Benzyl-4-morpholinoacetylsydnone. To a chloroform solution of VI (3.0 g/20 ml), a chloroform solution of morpholine (1.75 g/20 ml) was added under cooling with ice-water and the reaction mixture was kept at low temperature for 2 hr. Precipitates were filtered off and filtrate was concentrated *in vacuo*. Resulted oily product was dissolved in benzene and precipitates were filtered off. The benzene solution was concentrated and a small amount of petroleum ether was added to crystallize. Reprecipitation from acetone solution with ether afforded orange prisms with a mp of 121—123 °C (yield 97%).

Found: C, 59.62; H, 5.68; N, 13.71%. Calcd for $C_{15}H_{17}O_4N_3$: C, 59.39; H, 5.65; N, 13.86%. IR: 2955, 2875, 1840, 1770, 1755, 1673, 1432, 1110, 985, 710 cm^{-1}.

BULLETIN OF THE CHEMICAL SOCIETY OF JAPAN, VOL. 46, 3307—3308 (1973)

The Diels-Alder Reaction of 1,3,5-Cycloheptatriene with Thiobenzophenone

Yutaka OHNISHI, Yutaka AKASAKI, and Atsuyoshi OHNO

Sagami Chemical Research Center, 4-4-1 Nishiohnuma, Sagamihara-shi, Kanagawa 229

(Received June 11, 1973)

1,3,5-Cycloheptatriene (CHT) is known to undergo the Diels-Alder reaction with various dienophiles. In most cases, the structure of the adduct thus formed has tricyclo[3.2.2.$0^{2,4}$]nonane skeleton, **1**, instead of simple (2+4) cycloadduct, **2**.[1-4] There are two exceptions, one of which is the cycloadduct of CHT with nitrosobenzene and the other is that of CHT with acrolein. The structure of the former cycloadduct was initially thought to have **2**-type skeleton, but recently it was re-examined and found to have **3**-type skeleton, or a (2+6) cycloadduct.[5] The latter adduct, which was formed in minor (~10%) yield along with major (~30%) tricyclic **1**-type adduct, is believed to have a skeleton of **2**-type, but, unfortunately, the position of the formyl group in this adduct was not determined because its formation was confirmed after hydrogenation.[6]

We have found that the Diels-Alder reaction of CHT with thiobenzophenone affords **2**-type cycloadduct with regiospecificity.[7] Regiospecific formation of a bicyclic Diels-Alder adduct from unsubstituted CHT has never been reported in earlier papers.

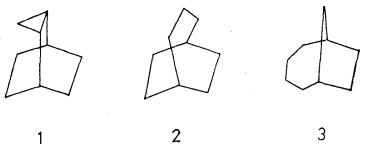

1 2 3

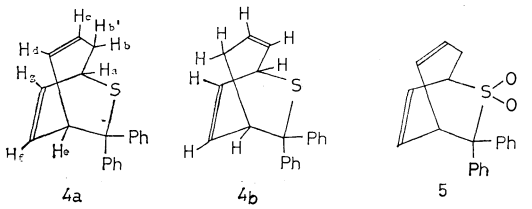

4a 4b 5

Results and Discussion

Thiobenzophenone does not react with CHT at room temperature without light.[8] However, from the reaction mixture at 90—100 °C, the Diels-Alder adduct, **4a**, was isolated in 40% yield along with some unidentified materials. The structure of **4a** was confirmed by the 100 MHz NMR spectrum (Fig. 1) with the decoupling technique and by the oxidation to the corresponding sulfone, **5**.

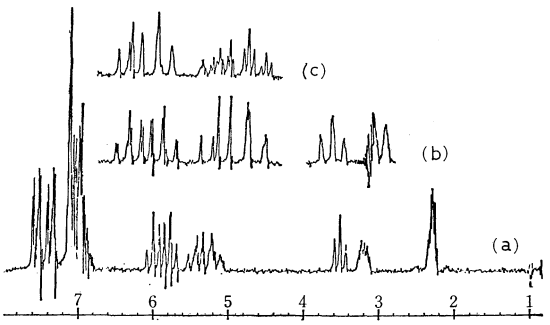

Fig. 1. The NMR spectra of (a) 6,6′-diphenyl-7-thiabicyclo-[3.2.2]nona-3,8-diene, **4a**, in benzene-d_6; (b) that with irradiation at H_b; and (c) that with irradiation at H_a. Spectra (b) and (c) are recorded with doubled scale.

The spectrum is consistent with the structure **4**, but inconsistent with any those of other cycloadducts. Although structures **4a** and **4b** are possible for the adduct, the former structure is prefered over the latter by the following reason; in **4b**, the phenyl ring at the *exo*-position should cause larger difference than that observed here in the chemical shift of signals due to H_b and H_b'. Namely, the signal at δ 2.30 in benzene-d_6 appears as an AA′XY-type multiplet. The double irradiation at the resonance positions of H_a and H_c simplifies this signal to an AA′-type quartet. Contrary the spectrum of **5** shows the large difference in chemical shifts of H_b (δ 3.13 in $CDCl_3$) and H_b' (δ 2.38 in $CDCl_3$). In addition, the signal from H_a (δ 3.94 in $CDCl_3$) in the sulfone appears at more down-field than that from H_a (δ 3.65 in $CDCl_3$) in the sulfide and the reverse is true for H_e protones in the sulfide and sulfone.

It is known that thiobenzophenone is a good dienophile.[9] The formation of the tricyclic Diels-Alder adducts from CHT is accounted for by two ways: the one proposes lower reactivity of CHT than that of norcaradiene, which is in equilibrium with the triene.[10,11] The other, based on kinetics, prefers to propose C_2–C_7 bond formation at the transition state of the cycloaddition from CHT itself.[12] Although we cannot discuss the mechanism of the cycloaddition in

1) G. H. Wahl, Jr., *J. Org. Chem.*, **33**, 2158 (1968).
2) C. J. Rostek and W. M. Jones, *Tetrahedron Lett.*, 3957 (1969).
3) M. J. Goldstein and A. H. Gevirtz, *ibid.*, 4413, 4417 (1965).
4) K. N. Houk and R. B. Woodward, *J. Amer. Chem. Soc.*, **92**, 4143 (1970).
5) a) G. Kresze and G. Schultz, *Tetrahedron*, **12**, 7 (1967); b) J. Hutton and W. A. Waters, *Chem. Commun.*, 634 (1966); c) P. Burns and W. A. Waters, *J. Chem. Soc., C*, 27 (1969).
6) E. M. Mil'vitskaya and A. F. Plate, *Zh. Obshch. Khim.*, **32**, 2566 (1962); *Chem. Abstr.*, **58**, 8927e (1963).
7) For a symmetric dienophile, see H. Ishitobi, H. Tanida, K. Tori, and T. Tsuji, This Bulletin, **44**, 2993 (1971).
8) Results on the photo-reaction of CHT with thiobenzophenone will be published elsewhere.
9) A. Ohno, Y. Ohnishi, and G. Tsuchihashi, *Tetrahedron*, **25**, 871 (1969).
10) E. Ciganek, *J. Amer. Chem. Soc.*, **89**, 1454 (1967).
11) G. Maier, *Angew. Chem. Int. Ed. Engl.*, **6**, 385 (1967).
12) T. Tsuji, S. Teratake, and H. Tanida, This Bulletin, **42**, 2033 (1969).

detail,[13] the present result suggests that the existence of reactive norcaradiene, if any, does not necessarily mean the formation of tricyclic Diels-Alder cycloadducts.

Experimental

Reaction of Thiobenzophenone with CHT. A mixture of thiobenzophenone (1.0 g) and CHT (15 ml) in an ampoule was degassed and sealed. The sample was heated at the temperature of boiling water until complete decolorization of thiobenzophenone took place (2.5 days). After excess CHT had been evaporated, the residue was chromatographed on a column of silica gel with elution by a mixture of *n*-hexane and benzene (4: 1 v/v). The first elution gave 0.26 g of unidentified material. From the second elution 0.67 g of crystals were obtained. Recrystallizations of crystals from a mixture of benzene and *n*-hexane gave **4a** in 40% yield; mp 170—172 °C.

The structure of **4a** was confirmed by the following data: NMR (δ from TMS, benzene-d_6)[14] 3.23 (H_a), 2.36 (H_b or H_b'), 2.23 (H_b' or H_b), 5.20 (H_c), 5.46 (H_d), 3.55 (H_e), 6.04 (H_f), 5.81 (H_g), and 6.8—7.7 (H_{ar}). Coupling constants (J_{xy}, Hz) 2.0 (ab), 3.2 (bc), 11.6 (cd), 8.0 (de), 7.0 (ef), 9.0 (fg), 6.0 (ag), 1.0 (eg), 1.0 (af), 18.0 (bb'). Irradiation at the resonance position of $H_b(H_b')$ made signals from H_a, H_c, and H_d to be broad doublet, doublet, and doublet of doublet, respectively, with no change for signals from H_e, H_f, and H_g. On irradiation at H_a, H_c appeared as double triplets, H_g as doublet, and H_f as doublet of doublet, but the signal from H_d did not change. Mass spectrum (*m/e*) 290 (M^+), 200, 199, 198 (Ph_2CS^+, base), 197, 121, 92, 91, and 77.

Found: C, 82.50; H, 6.34; S, 10.91%. Calcd for $C_{20}H_{18}S$: C, 82.50; H, 6.25; S, 11.40%.

Oxidation of 4a. A solution composed of **4a**, (100 mg) and two equivalents of *m*-chloroperbenzoic acid in 10 ml of dichloromethane was stirred for a day at room temperature. After working-up and recrystallizations from *n*-hexane–benzene, **5** was obtained in quantitative yield: mp 260 °C. IR: 1135 and 1305 cm^{-1}.

Found: C, 74.54; H, 5.66; S, 10.14%. Calcd for $C_{20}H_{18}O_2S$: C, 74.53; H, 5.63; S, 9.93%.

13) Note that thiobenzophenone has a heteropolar double bond and two-step mechanism is possible to this compound.

14) The spectrum in chloroform-*d* did not show well-resolved signals.

BULLETIN OF THE CHEMICAL SOCIETY OF JAPAN, VOL. 46, 3308—3310 (1973)

Nuclear Magnetic Resonance Study of the Stereoisomeric 2-Oxazolidone and 2-Phenyl-2-oxazoline Derivatives of α-Amino-β-hydroxy Acids[1)]

Shuji FUTAGAWA,* Toshishige INUI,** and Tetsuo SHIBA

Department of Chemistry, Faculty of Science, Osaka University, Toyonaka, Osaka 560

(Received June 19, 1973)

NMR studies on β-substituted α-amino acids have revealed that the coupling constant ($J_{\alpha\beta}$) between C_α–H and C_β–H is larger in *erythro* form than in *threo* form in case of β-methylleucine[2)] or isoleucine derivatives.[3)] However, it is well known that the value of the coupling constant in such >CH–CH< system is considerably effected by the environmental linkage. In fact, in our experiment for comparison of $J_{\alpha\beta}$ value of free α-amino-β-hydroxy acids, the relationship was found to be reversed, that is, *threo* form always showed the relatively larger value than *erythro* form as shown in Table 1.

Furthermore, the small differences in $J_{\alpha\beta}$ values observed in a group of α-amino-β-hydroxy acids may not allow its use for assignment of relative configurations, even if a pair of pure diastereoisomeric compounds is obtained.

Table 1. Chemical shifts and coupling constants of free α-amino-β-hydroxy acids in D_2O

$$\mathrm{R\text{-}CH(OH)\text{-}CH(NH_2)\text{-}CO_2H}$$

R	*threo*		*erythro*	
	H_α (ppm)	$J_{\alpha\beta}$ (Hz)	H_α (ppm)	$J_{\alpha\beta}$ (Hz)
CH_3	3.62	5.0	3.81	4.2
C_6H_5	3.88	4.5	4.83	4.2
CH_2CO_2H	3.70	4.1	3.92	3.8
$(CH_3)_2CH$–	a)		3.91	3.2
	4.05	5.0	4.10	4.6

a) Measurements of these values were impossible, since chemical shifts of H_α and H_β were overlapped.

Since the coupling constants in the aliphatic compounds as mentioned above are revealed as an average value contributed from relatively stable rotational isomers of each diastereomer, it is expected that a difference between J_{erythro} and J_{threo} could be enlarged if amino and hydroxy groups are fixed in an appropriate ring which prevents a free rotation of α-β carbon-carbon bond.

* Present address: Osaka Dental University, Hirakata, Osaka.

** Present address: Institute of Chemistry, College of General Education, Osaka University, Toyonaka, Osaka.

1) This study was partly presented at the 26th Annual Meeting of the Chemical Society of Japan, Kanagawa, April, 1972.

2) K. Okubo and Y. Izumi, This Bulletin, **43**, 1541 (1970).

3) J. Shoji, K. Tori, and H. Otsuka, *J. Org. Chem.*, **30**, 2772, (1965).

α-Amino-β-hydroxy acids were known to be cyclized either with phosgene or with iminoether to the corresponding 2-oxazolidone (I) or 2-phenyl-2-oxazoline (II) derivatives respectively without any configurational changes.[4] We prepared 2-oxazolidone derivative of six diastereoisomeric pairs of α-amino-β-hydroxy acids, *i.e.*, DL-threonine, β-phenyl-DL-serine, β-hydroxy-DL-glutamic acid, β-hydroxy-DL-aspartic acid, β-hydroxy-DL-leucine and β-furyl-DL-serine, the configurations of which are known definitely. We also synthesized the diastereoisomeric pairs of 2-phenyl-2-oxazoline derivative of DL-threonine, β-phenyl-DL-serine and β-hydroxy-DL-leucine.

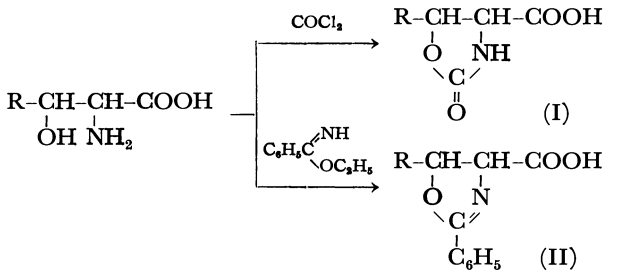

The coupling constants $J_{\alpha\beta}$ measured for those derivatives are summarized in Tables 2 and 3. The

Table 2. Chemical shifts and coupling constants of 2-oxazolidone derivatives in CD_3OD

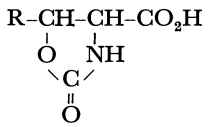

R	*cis* (*erythro*)		*trans* (*threo*)	
	H_α (ppm)	$J_{\alpha\beta}$ (Hz)	H_α (ppm)	$J_{\alpha\beta}$ (Hz)
CH_3[a]	4.39	9.0	4.04	5.0
C_6H_5[b]	4.55	9.6	4.29	5.0
CH_2CO_2H[c]	4.47	9.0	4.27	5.7
CO_2H[d]	4.70	10.2	4.37	4.0
CH_3>CH_3>CH–[e]			4.10	5.0
 [d]	5.90[f]	9.5	5.75[f]	6.0
CH_2CH_2NHZ[g,6]	4.33	9.0	4.08	5.2

a) T. Kaneko and T. Inui, This Bulletin, **35**, 1145 (1962).
b) T. Kaneko and T. Inui, *Nippon Kagaku Zasshi*, **82**, 1075 (1962); T. Inui, *ibid.*, **83**, 493 (1962).
c) R. Yoshida, Dissertation, Osaka University, 1961.
d) T. Inui, Y. Ohta, T. Ujike, H. Katsura, and T. Kaneko, This Bulletin, **41**, 2148 (1968).
e) *Cis* form was recrystallized from ethyl acetate and *n*-hexane, mp 144—146°C. Found: C, 48.62; H, 6.51; N, 7.98%. Calcd for $C_7H_{11}NO_4$: C, 48.55; H, 6.40; N, 8.09%. Assignment of H_α of this isomer was impossible, because of very close chemical shifts of H_α and H_β. *Trans* form was recrystallized from ethyl acetate and *n*-hexane, mp 118—119 °C. Found: C, 48.93; H, 6.38; N, 8.10%.
f) H_β value was mentioned, as H_α peak was masked by the solvent peak.
g) Z=$C_6H_5CH_2OCO$-

Table 3. Chemical shifts and coupling constants of 2-phenyl-2-oxazoline derivatives in $CDCl_3$

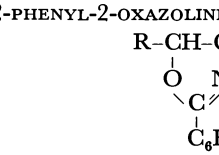

R	R′	*cis* (*erythro*)		*trans* (*threo*)	
		H_α (ppm)	$J_{\alpha\beta}$ (Hz)	H_α (ppm)	$J_{\alpha\beta}$ (Hz)
CH_3	C_2H_5	5.50	11.2	5.11	7.0
C_6H_5[a]	CH_3	5.28	11.0	4.80	7.5
CH_3>CH_3>CH–[b]	CH_3	4.95	10.0	5.01	6.0

a) S. H. Pines, M. A. Kozlowsky, and S. Karaday, *J. Org. Chem.*, **34**, 1621 (1969).
b) S. Futagawa, M. Nakahara, T. Inui, H. Katsura, and T. Kaneko, *Nippon Kagaku Zasshi*, **92**, 374 (1971).

erthro form corresponds to *cis* H_α–H_β relationship concerning with the ring plane and *threo* form to *trans* one. The $J_{\alpha\beta}$ values for both isomers of 2-oxazolidone derivatives converged within narrow range as far as tested, that is, *cis* isomers are centered to 9.6±0.6 Hz and *trans* one to 5.0±1.0 Hz. Similar separation of $J_{\alpha\beta}$ values for *cis* and *trans* compounds are observed in cases of 2-phenyl-2-oxazoline derivatives.

Although the couplings in such heterocyclic systems cannot be satisfactorily explained,[5] the observed values in this experiment indicated that the configurational relationship of *threo* and *erythro* isomers of α-amino-β-hydroxy acids can be assigned undoubtedly by the analysis of NMR spectra of their 2-oxazolidone or 2-phenyl-2-oxazoline derivatives. Furthermore, formation and purification of 2-oxazolidone derivative from a small amount of the sample of α-amino-β-hydroxy acid can be carried out very easily. Therefore, this procedure will present a convenient and practical method for determination of configurational isomerism of α-amino-β-hydroxy acid.

A criterion on an advantage of this method was tested in the case where only one form of two diastereoisomeric isomers of α-amino-β-hydroxy acid was obtained. In our another synthetic study of the new amino acid, *i.e.* β-hydroxyornithine, first we obtained only one unknown form of its derivative.[6] Thus 5-(2-benzyloxycarbonylaminoethyl)-2-oxazolidone-4-carboxylic acid prepared from synthetic DL-β-hydroxyornithine showed the coupling constant $J_{\alpha\beta}$ of 9.0 Hz. From this single value, we assigned this isomer to ***cis***, namely, *erythro* form, and this conclusion was successfully applied to further synthetic study.[6] Later we could obtain the other form of DL-β-hydroxyornithine and its 2-oxazolidone derivative gave the expected value of $J_{\alpha\beta}$ of 5.2 Hz as *trans* type, namely, *threo* isomer.[6]

Experimental

The NMR spectrum was obtained at room temperature

4) a) D. F. Elliot, *J. Chem. Soc.*, **1949**, 589; b) T. Kaneko and T. Inui, *Nippon Kagaku Zasshi*, **82**, 1075 (1961).

5) R. J. Abraham and K. Parry, *J. Chem. Soc. B*, **1971**, 446.

6) T. Wakamiya, T. Teshima, T. Shiba, and T. Kaneko, This Bulletin, to be published in detail.

with a Varian T-60 spectrometer at 60 MHz. Sodium 2,2-dimethyl-2-silapentane-5-sulfonate was used as an internal reference in deuterium oxide solution and tetramethylsilane was used for tetradeuteromethanol and deuterochloroform solutions. The chemical shifts are expressed as ppm from the reference peak.

Preparation of 2-Oxazolidone Carboxylic Acid Derivatives of α-Amino-β-hydroxy Acid. α-Amino-β-hydroxy acid (30 mg) was dissolved in 1M potassium hydroxide solution (10 ml) and was cooled to 5 °C. Then, a solution of phosgene (1.5 g) in toluene (10 ml) was added all at once. After stirring for an additional hour, the aqueous layer separated from the toluene layer was acidified with concentrated hydrochloric acid and extracted three times with 10 ml portion of ethyl acetate. The combined extract was dried and evaporated to dryness. The residue was dissolved in CD_3OD and the solution was directly analyzed by NMR.

Preparation of 2-Phenyl-2-oxazoline Ester Derivatives of α-Amino-β-hydroxy Acid. α-Amino-β-hydroxy acid methyl ester hydrochloride (50 mg) was dissolved in ethanol (10 ml) in a 30 ml flask and mixed with a solution of benziminoethyl ether (1.0 g) in ethyl ether (5 ml). The mixture was stirred vigorously at 20 °C for 1 hr. After addition of water (10 ml), the reaction mixture was extracted three times with each 10 ml portion of ethyl ether, and then evaporated to dryness. The residue was dissolved in $CDCl_3$ and the solution was directly analyzed by NMR.

BULLETIN OF THE CHEMICAL SOCIETY OF JAPAN, VOL. 46, 3310—3311 (1973)

Synthesis of Dinucleoside Analog of Uracil-Uracil

Toru SEITA, Masayoshi KINOSHITA, and Minoru IMOTO*

Department of Applied Chemistry, Osaka City University, Sumiyoshi, Osaka 558

**Department of Applied Chemistry, Kansai University, Senriyama, Suita 564*

(Received June 21, 1973)

We have been attempted to prepare nucleic acid analogs in which the ribose or deoxyribose ring is replaced with an aliphatic moiety.[1-4] In order to study base-base interaction Browne, Eisinger, and Leonard[5] have studied the synthesis of dinucleotide analogs. On the other hand, Fecher *et al.*[6] synthesized the dinucleoside such as 5'-(9-adenyl)-5'-deoxy derivatives of thymidine.

To extend this study, we have synthesized a new type dinucleoside analog of uracil-uracil.

1-(2'-Hydroxy-3'-chloropropyl)-4-ethoxy-2-pyrimidinol (**1**) was synthesized by the reaction of 4-ethoxy-2-pyrimidinol[7] with epichlorohydrin in dimethylformamide (DMF) containing potassium carbonate. The separation of product was accomplished by chromatography on silica gel using benzene–ethanol as solvent. The compound **1** was treated with 20% hydrochloric acid to give 1-(2'-hydroxy-3'-chloropropyl)uracil (**2**). Condensation of compound **1** with sodium salt of 4-ethoxy-2-pyrimidinol was carried out in DMF to give 1',3'-bis(1-4-ethoxy-2-pyrimidinol)-2'-propanol (**3**).

When compound (**3**) was treated with 20% hydrochloric acid at 85—90 °C 1',3'-bis(1-uracil)2'-propanol (**4**) was afforded in good yield.

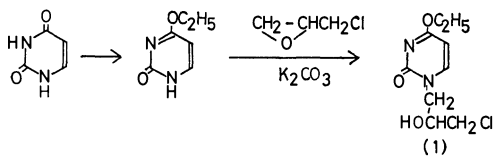

Scheme 1.

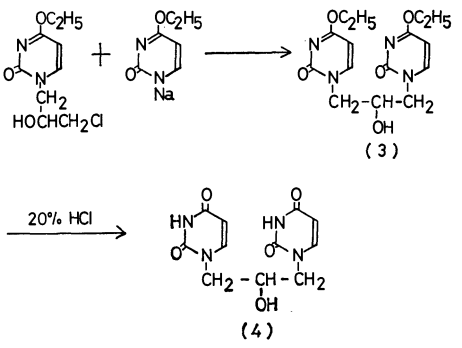

Scheme 2.

The observed extinction coefficient of **4** was approximately the same value as that of 1',3'-bis(1-uracil)-trimethylene, $Ur(CH_2)_3Ur$, shown by Browne, Eisinger, and Leonard. The compound **4** showed a small blue shift of UV when compared with the compound **2**. The compound **4** will give many derivatives through the reaction of its 2'-hydroxy group. UV data were listed in Table 1.

1) T. Seita, K. Yamauchi, M. Kinoshita, and M. Imoto, This Bulletin, **45**, 926 (1972).

2) T. Seita, K. Yamauchi, M. Kinoshita, and M. Imoto, *Makromol. Chem.*, **154**, 255 (1972).

3) T. Seita, K. Yamauchi, M. Kinoshita, and M. Imoto, This Bulletin, **46**, 1563 (1973).

4) T. Seita, M. Kinoshita, and M. Imoto, *ibid.*, **46**, 1572 (1973).

5) D. T. Browne, J. Eisinger, and N. J. Leonard, *J. Amer. Chem. Soc.*, **90**, 7302 (1968).

6) R. Fecher, K. H. Boswell, J. J. Wittick, and T. Y. Shen, *ibid.*, **92**, 1400 (1970).

7) G. E. Hibert and E. P. Jansen, *ibid.*, **57**, 552 (1935).

Table 1. UV data of uracil-uracil dimer and its related compounds

Compound	$\lambda_{max}^{H_2O}$	ε	Ref.
2	267	10300	
4	266.5	19900	
Ur–C_3	267	10130	5
Ur–C_3–Ur	266.5	19730	5

Experimental

The melting points are uncorrected. The IR and UV spectra were measured by a JASCO Model IR-G Spectrometer and Hitachi Recording Spectrometer Model ESP-3T, respectively.

1-(2'-Hydroxy-3'-chloropropyl)-4-ethoxy-2-pyrimidinol (1). A mixture of 4-ethoxy-2-pyrimidinol (5.0 g, 36 mmol), epichlorohydrin (3.3 g, 36 mmol), and a trace of anhydrous potassium carbonate in DMF (80 ml) was stirred at 70—80 °C for 10 hr. After allowing to cool to room temperature the reaction mixture was filtered off and the filtrate was evaporated under the reduced pressure. 10 ml of ethanol was poured into the residue and kept in refrigerator overnight. The resulting white precipitate was filtered off and washed with excess ethanol. The filtrate and washing were combined, then evaporated and the oil residue was chromatographed on silica gel (Mallinckrodt). Elution with benzene–ethanol (4: 1) gave the product. The product was recrystallized from benzene to give the compound (**1**) (5.1 g (62%)) as colorless needles.

Mp 121—122 °C, UV; $\lambda_{max}^{H_2O}$ 275 mμ, IR (Potassium bromide) 3200 (OH), 1620 (4-ethoxy-2-pyrimidinol ring); Found: C, 46.22; H, 5.19; N, 11.65%. Calcd for $C_9H_{13}N_2O_3Cl$: C, 46.44; H, 5.63; N, 12.05%.

1-(2'-Hydroxy-3'-chloropropyl)uracil (2). Compound (**1**) (0.46 g, 2 mmol) was treated in 20% hydrochloric acid, evaporated and the residue was recrystallized from benzene–ethanol (4: 1) to give compound (**2**) (0.32 g (80%)) as colorless needles.

Mp 153—156 °C; IR (Potassium bromide): 3350 (OH), 1660 (Uracil ring); Found: C, 41.28; H, 4.88; N, 13.88%. Calcd for $C_7H_9N_2O_3Cl$: C, 41.07; H, 4.44; N, 13.70%.

1',3'-Bis(1-4-ethoxy-2-pyrimidinol)-2'-propanol (3). Mixture of compound (**1**) (3.36 g, 20 mmol) and sodium salt of 4-ethoxy-2-pyrimidinol (4.24 g, 20 mmol) was stirred in DMF at 70 °C for 2 days. The reaction mixture was filtered off and the filtrate was evaporated under reduced pressure. The resulting white precipitate was recrystallized from ethanol to give compound (**3**) (3.9 g (58%)) as colorless pales.

Mp 229—231 °C, IR (Potassium bromide); 3250 (OH), 1630 (4-ethoxy-2-pyrimidinol ring); Found: C, 53.05; H, 6.28; N, 16.37%. Calcd for $C_{15}H_{20}N_4O_5$: C, 53.55; H, 6.00; N, 16.66%.

1',3'-Bis(1-uracil)-2'-propanol (4). Compound (**3**) (3.36 g, 10 mmol) was stirred in 20% hydrochloric acid at 90 °C for one hour, evaporating to dryness. The white precipitate was recrystallized from water to give compound (**4**) (2.68 g, (92%)) as colorless needles.

Mp 139—142 °C, IR (Potassium bromide): 3250 (OH), 1660 (Uracil ring); Found: C, 46.68; H, 4.58; N, 19.67%. Calcd for $C_{11}H_{12}N_4O_5$: C, 47.13; H, 4.32; N, 20.00%.

BULLETIN OF THE CHEMICAL SOCIETY OF JAPAN, VOL. 46, 3311—3312 (1973)

A Facile Synthesis of Mellein

Yoshitsugu ARAI, Tadao KAMIKAWA, and Takashi KUBOTA*

Faculty of Science, Osaka City University, Sugimotocho, Sumiyoshi-ku, Osaka 558

(Received June 26, 1973)

The application of the Diels-Alder reaction to the preparation of 2,3-disubstituted phenols[1] from 1-methoxycyclohexa-1,4-diene and suitable dienophiles has now been extended to the synthesis of mellein (**1a**),[2] which had been isolated from the culture broth of *Aspergillus mellus*. In this paper we report a four-step synthesis of **1a**.

4-(2-Tetrahydropyranyloxy)pent-1-yne[3] was treated with *n*-butyllithium and ethyl chloroformate to give an ethyl ester (**2**). Heating the mixture of **2** and 1-methoxycyclohexa-1,4-diene in a sealed tube at 180 °C for 22 hr gave an aromatic ester (**3**; 73%), which, on base hydrolysis and acid treatment, gave (±)-mellein methyl ether (**1b**), [mp 67—68 °C], in 87% yield. Treatment of **1b** with boron tribromide gave (±)-mellein **1a**, [mp 38—38.5 °C], in 85% yield, which was identical in all respects (IR and NMR) with the authentic sample.[2]

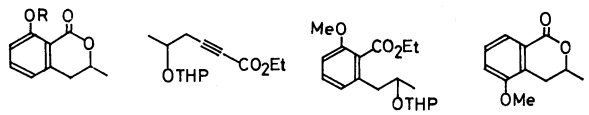

(1a) R=H (1b) R=Me (2) (3) (4)

The minor product of the Diels-Alder reaction, after hydrolysis and acid treatment, was proved to be **4** from physical data.

Birch and Dastur found that dichloromaleic anhydride catalyzes the conversion of 1-methoxycyclohexa-1,4-diene into 1-methoxycyclohexa-1,3-diene.[4]

* Present address: Kinki University, Kowakae, Higashiosaka-shi, Osaka 577.

1) Y. Arai, T. Kamikawa, and T. Kubota, *Tetrahedron Lett.*, **1972**, 1615.

2) H. Nishikawa, *J. Agr. Chem. Soc. Jap.*, **9**, 1059 (1933); T. Yabuta and Y. Sumiki, *ibid.*, **9**, 1264 (1933); M. Matsui, K. Mori, and S. Arasaki, *Agr. Biol. Chem.*, **28**, 896 (1964); N. S. Narasimhan and B. H. Bhide, *Chem. Commun.*, **1970**, 1552; *idem.*, *Tetrahedron*, **27**, 6171 (1971).

3) L. J. Haynes and E. R. H. Jones, *J. Chem. Soc.*, **1946**, 954.

4) A. J. Birch and K. P. Dastur, *Tetrahedron Lett.*, **1972**, 4195.

Hoping the improvement of the yield, we have applied this reagent to the Diels-Alder reaction. Heating the mixture of 1-methoxycyclohexa-1,4-diene, **2** and dichloromaleic anhydride gave **1b** in one step in 48% yield.

Experimental

Ethyl 5-(2-Tetrahydropyranyloxy)-2-hexynoate (2). To a solution of 4-(2-tetrahydropyranyloxy)pent-1-yne (16.8 g) in 50 ml of abs. ether was added an ethereal solution of *n*-butyllithium (prepared from 17.13 g of *n*-butyl bromide and 2.15 g of lithium in 100 ml of abs. ether) at −70 °C in 15 min under argon atmosphere and the mixture was stirred for 15 min at this temperature. The mixture was gradually allowed to warm to −10 °C during 5 hr, then poured into ice-water and extracted with ether. The solvent was removed and the residue was distilled under reduced pressure to give **2** (14.5 g, 60%), bp. 112—112.5 °C/0.15 mmHg. ν_{max} (liquid film) 2240, 1715, and 1250 cm^{-1}.

The Ester (3). (a) A mixture of 2.4 g of 1-methoxycyclohexadienes (1,3- and 1,4- 1: 3), 2.4 g of **2** and 30 mg of *N*-phenyl-2-naphthylamine was heated at 180 °C for 22 hr in a sealed tube. The crude product was distilled under reduced pressure to give 0.54 g of the recovered ester (**2**) and 2.26 g (73%) of the ester (**3**), bp 125—127 °C/0.07 mmHg. ν_{max} (liquid film) 1730, 1600, 1585, and 1470 cm^{-1}. (b) A mixture of 10 g of 1-methoxycyclohexadienes, 13.8 g of **2**, 10 mg of dichloromaleic anhydride, and 100 mg of *N*-phenyl-2-naphthylamine was heated at 180 °C for 20 hr in a sealed ube. Fractional distillation under reduced pressure gave (±)-mellein methyl ether (**1b**) bp 112—113 °C/0.03 mmHg (5.2 g, 48%), which was recrystallized from ether–light petroleum to give colorless prisms, mp 67—68 °C (lit,[2] mp 66—67 °C).

(±)-Mellein Methyl Ether (1b). The ester (**3**; 3.27 g) was dissolved in 10 ml of 0.5 M methanolic sodium hydroxide solution and the solution was allowed to stand at room temperature for 48 hr. The mixture was acidified with 40 ml of 2 M hydrochloric acid and refluxed for 30 min. After removal of the organic solvent, the aqueous phase was extracted with chloroform. Evaporation of the extract gave an oil (2.64 g) which was chromatographed on silica gel. Elution with benzene–AcOEt (9: 1) gave **4** as colorless prisms, mp 85—86 °C (from $CHCl_3$–ether), (0.27 g, 13%). ν_{max} ($CHCl_3$) 1715, 1600, and 1590 cm^{-1}, δ ($CDCl_3$) 1.50 (d, 3H, *J* 5 Hz), 2.62 (dd, 1H, *J* 11, 17 Hz), 3.14 (dd, 1H, *J* 4, 17 Hz), 3.84 (s, 3H), 5.40 (m, 1H), 7.05 (dd, 1H, *J* 2, 8 Hz), 7.32 (t, 1H, *J* 8 Hz), and 7.70 (dd, 1H, *J* 1.5, 8 Hz). Found: C, 68.69; H, 6.31%. Calcd for $C_{11}H_{12}O_3$: C, 68.73; H, 6.29%.

Further elution with the same solvent mixture gave (±)-mellein methyl ether (**1b**), mp 67—68 °C, colorless prisms (from ether–light petroleum), (1.69 g; 87%).

(±)-Mellein (1a). To a cooled soln of BBr_3 (0.4 ml) in 10 ml of dry CH_2Cl_2 was added a soln of **1b** (192 mg) in 8 ml of dry CH_2Cl_2 (−70°) under atmosphere of argon. The mixture was gradually allowed to warm up to room temperature and kept overnight. The mixture was poured into ice-water and extracted with $CHCl_3$. Removal of the solvent gave (±)-mellein (**1a**) as crystals (151 mg, 85%), which was recrystallized from *n*-hexane to give colorless prisms, mp 38—38.5 °C (lit,[2] mp 37—38 °C). The IR and NMR spectra are identical with that of the published data.[2]

BULLETIN OF THE CHEMICAL SOCIETY OF JAPAN, VOL. 46, 3312—3313 (1973)

Isolation and Characterization of a Yellow Pteridine from *Drosophila melanogaster* Mutant *sepia*

Katsura SUGIURA, Shinichiro TAKIKAWA,* Motoo TSUSUE,* and Miki GOTO

Department of Chemistry, Gakushuin University, Toshima-ku, Tokyo 171

**Biological Laboratory, Kitasato University, Sagamihara, Kanagawa 228*

(Received June 30, 1973)

It is well known that the wild type flies of *Drosophila melanogaster* have red and yellow eye-pigments and the mutant *sepia* has only yellow pigments, *i.e.* sepiapterin and isosepiapterin.[1-4] This paper describes the isolation and characterization of an additional pteridine compound from *D. melanogaster sepia*. On the basis of mass spectrum, UV spectra, NMR spectrum and chemical reactions, the structure of the third pteridine compound from the *sepia* flies was proved to be 6-acetyl-2-amino-4-hydroxy-7,8-dihydropteridine.

Experimental

Isolation of the Compound (sepiapterin C).[5-7] *D. melanogaster sepia* was reared in bottles at 25 °C with sterile yeast medium (1000 ml water, 50 g cane sugar, 9 g agar powder, 80 g dry yeast, and 5 ml propionic acid). Flies were harvested on the 1st, 5th, and 9th days after eclosion and stored at −20 °C until extraction.

The flies (50 g) were homogenized in a waring blender with 500 ml of 50% aqueous ethanol for 4 min. The homo-

1) E. Hadorn and H. K. Mitchell, *Proc. Nat. Acad. Sci. U.S.*, **37**, 650 (1951).

2) I. Ziegler and E. Hadorn, *Z. Verebungslehre*, **89**, 235 (1958).

3) H. S. Forrest, C. V. Baalen, and J. Myers, *Arch. Biochem. Biophys.*, **83**, 508 (1959).

4) S. Nawa, This Bulletin, **33**, 1555 (1960).

5) The pteridines from the *sepia* flies are named as sepiapterin A, B, and C systematically, *i.e.*, sepiapterin: sepiapterin A; isosepiapterin: sepiapterin B; actually isosepiapterin is no isomer of sepiapterin.

6) T. Fukushima and M. Akino, *Arch. Biochem. Biophys.*, **128**, 1 (1968).

7) M. Tsusue and M. Akino, *Zool. Mag.* (Tokyo), **74**, 91 (1965).

genate was heated on a boiling water bath for 20 min. It was then centrifuged at 2000 g for 10 min. The extraction procedure was repeated two more times with 50% ethanol (each 400 ml). The supernatants were combined and concentrated to a small bulk at 30 °C. The solution was put on the top of a pH 7 ECTEOLA cellulose column (5 × 30 cm), and the column washed with distilled water. A yellow, a blue and a purple fluorescent bands were eluted, successively. The eluate of the first band (main band) was evaporated to a small bulk *in vacuo*. The solution was put on the top of a P-cellulose column (4 × 30 cm), which was then eluted with distilled water. The yellow fraction was separated into three bands; each band was eluted and the eluate evaporated to dryness *in vacuo*. The yellow compounds of the first and the second bands were identified as riboflavin and sepiapterin A, respectively, by means of paper chromatography and UV absorption spectra. The eluate of the third band contained two yellow compounds, which were separated by chromatography on a cellulose column (3 × 25 cm) using the solvent, 1-butanol, ethanol, water (2 : 1 : 1), The substance of the first band was sepiapterin B and that of the second sepiapterin C. The latter fraction was concentrated to dryness and further purified on a Sephadex column (3 × 28 cm, G-25, fine) (elution: 0.005% ammonia). The eluate was concentrated to dryness and the residue was crystallized from water to give yellow needles, yield, 0.3 mg. The sepiapterin contents (mg/50 g) in sepia flies were calculated from UV absorptions (values on the 1st, 5th, and 9th days after eclosion): sepiapterin A, 19.8, 34.4, 34.4; sepiapterin B, 0.36, 1.33, 1.87; sepiapterin C, 0.27, 0.36, 0.37.

Structure of Sepiapterin C. The mass spectrum was determined with a Nihondenshi JEOL-01SG mass spectrometer (a direct inlet system). The ionizing energy was 75 eV and the temperature of the ion source 120—200 °C. The UV spectra were determined using a Hitachi ESP-3 spectrometer and the NMR spectrum using a JEOL-C60 HL spectrometer.

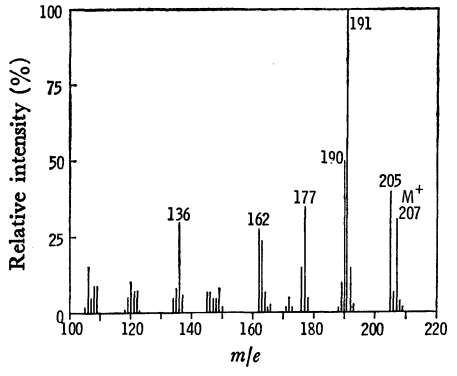

Fig. 1. Mass spectrum of sepiapterin C.

The molecular formula of sepiapterin C was determined to be $C_8H_9N_5O_2$ by mass spectrometry (M^+: 207.0774; Calcd for $C_8H_9N_5O_2$, 207.0754) (for mass spectrum, see Fig. 1). Sepiapterin C was proved to be a 6-substituted pterin, as its alkaline permanganate oxidation gives 6-carboxypterin. The formation of 2,4-dinitrophenylhydrazone showed the presence of a carbonyl group at the side chain. The UV-spectra of sepiapterin C are essentially identical with those of sepiapterin A and sepiapterin B (Fig. 2). From these evidences, the structure of 6-acetyl-2-amino-4-hydroxy-7,8-dihydropteridine was postulated for sepiapterin C.

This formulation was well supported by NMR spectrum and the fragmentation pattern of the mass spectrum (the fragmentations are summarized in Fig. 3; the fragment ion, *m/e* 191 remained to be clarified).[8] NMR (DMSO-d_6, 40 °C, TMS): 2.27 ppm (3H, singlet, $-CO-CH_3$), 4.05 (2H, singlet, $-CH_2-$), 6.62 (2H, singlet, $-NH_2$), 7.27 (1H, singlet, $-NH-$) and 9.96 (1H, singlet, $-NH-$); the signals of 6.62, 7.27, and 9.96 ppm disappeared with addition of D_2O. Finally, 6-acetyl-2-amino-4-hydroxy-7,8-dihydropteridine was prepared by the reaction of 7,8-dihydropterin and pyruvic acid.[9] The identity of the product with sepiapterin C was confirmed by means of paper chromatography, UV and mass spectral determinations. R_f-values of pteridines are summarized in Table 1.

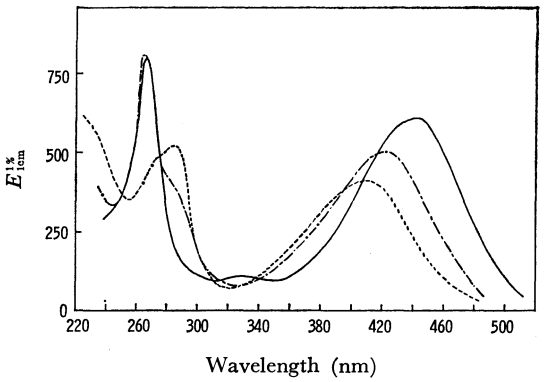

Fig. 2. Ultraviolet absorption spectra of sepiapterin C. in 0.1 M NaOH (——), in H_2O (-·-), and in 0.1 M HCl (– – –).

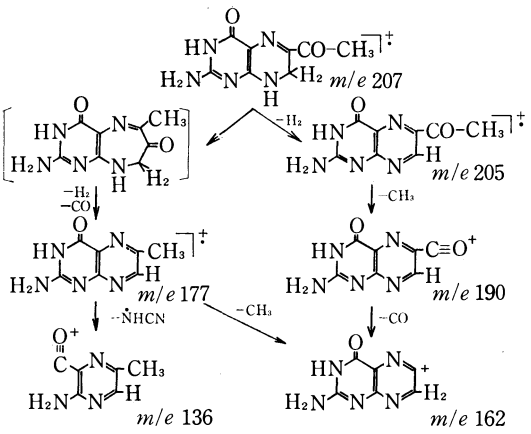

Fig. 3. Fragmentation patterns of mass spectrum of sepiapterin C. The formulae of fragment ions were determined by high resolution mass spectrometry.

Table 1. R_f values of pteridines

Pteridine	Solvents[a]				
	1	2	3	4	5
Sepiapterin A	0.29	0.34	0.47	0.27	0.36
Sepiapterin B	0.21	0.44	0.52	0.46	0.53
Sepiapterin C	0.21	0.32	0.42	0.30	0.36
6-Acetyl-7,8-dihydropterin	0.21	0.32	0.42	0.30	0.36

a) Solvents: 1; 3% ammonium chloride, 2; 2-propanol, 1% ammonia (2:1), 3; 2-propanol, 2% ammonium acetate (1:1), 4; 1-butanol, acetic acid, water (4:1:1), 5; 1-propanol, ethyl acetate, water (7:1:2).
Ascending method. Whatman filter paper, No. 1.

8) For mass spectrum of sepiapterin, see; Y. Iwanami and M. Akino, *Tetrahedron Lett.*, **31**, 3219 (1972).

9) H. S. Forrest and S. Nawa, *Nature*, **96**, 169 (1962).

BULLETIN OF THE CHEMICAL SOCIETY OF JAPAN, VOL. 46, 3314—3315 (1973)

A Note on the Kinetic Parameter Determination at the DME by Koutecký's Method

J. N. GAUR and S. K. BHARGAVA
Chemical Laboratories, University of Rajasthan, Jaipur, India

(Received May 24, 1973)

In Koutecký's[1,2] method the fundamental equation is

$$\frac{i_l}{i_d} = F(x) - \xi H_c(x) = F'(x) \tag{1}$$

where

$$x = K_f\left(\frac{12t}{7D}\right)^{1/2} \tag{2}$$

and

$$\xi = 50.4D^{1/2}m^{-1/3}t^{1/6} \tag{3}$$

i_l is the maximum instantaneous current of the single drop at the potential E, i_d is the maximum instantaneous current of the single drop in the limiting current region, $F(x)$ is a function related with the current at potential E to the current at infinity and $H_c(x)$ is a correction factor introduced because of the curvature of the drop. Koutecký has given a table of numerical values of $F(x)$ and $H_c(x)$ at particular value of x.

Meites and Israel[3] have extended this into a more mathematical form by using Koutecký's table. They found that $\log x$ varies linearly with $\log F(x)/\{1-F(x)\}$ as

$$\log\lambda = -0.1300 + 0.9163\log\frac{F(x)}{1-F(x)} \tag{4}$$

where for simplicity they have taken $\lambda=(7/12)^{1/2}x$ and they assume that diffusion at the electrode surface is linear. Then in Eq. (1) i_l/i_d is virtually equal to $F(x)$ so Eq. (4) can be written as

$$\log\lambda = -0.1300 + 0.9163\log\frac{i}{i_d-i} \tag{5}$$

Heterogeneous rate constant can be described by

$$K_{fh} = K^\circ_{fh}\exp\left(-\frac{\alpha nFE}{RT}\right) \tag{6}$$

on combining Eqs. (2), (5), and (6) yields

$$E_{d.e.} = \frac{0.05915}{\alpha n}\log\frac{1.349K^\circ_{fh}t^{1/2}}{D^{1/2}} - \frac{0.0542}{\alpha n}\log\frac{i}{i_d-i} \tag{7}$$

which may be written

$$E_{d.e.} = E_{1/2} - \frac{0.0542}{\alpha n}\log\frac{i}{i_d-i} \tag{8}$$

With

$$E_{1/2} = \frac{0.05915}{\alpha n}\log\frac{1.349K^\circ_{fh}t^{1/2}}{D^{1/2}} \tag{9}$$

In these equations both $E_{d.e.}$ and $E_{1/2}$ are referred to N.H.E.

Instead of Eq. (5) we find

$$\log\lambda = 0.0523 + 0.9619\log\frac{i}{i_d-i} \tag{10}$$

On combining Eqs. (2), (6), and (10) we obtain

$$E_{d.e.} = \frac{0.05915}{\alpha n}\log\frac{K^\circ_{fh}t^{1/2}}{1.128\times D^{1/2}} - \frac{0.05690}{\alpha n}\log\frac{i}{i_d-i} \tag{11}$$

which may be written

$$E_{d.e.} = E_{1/2} - \frac{0.05690}{\alpha n}\log\frac{i}{i_d-i} \tag{12}$$

with

$$E_{1/2} = \frac{0.05915}{\alpha n}\log\frac{K^\circ_{fh}t^{1/2}}{1.128\times D^{1/2}} \tag{13}$$

In deriving Eqs. (5) and (10) we have considered that diffusion to the electrode surface is linear, but if we consider spherical diffusion then we have to consider the second factor of Eq. (1) *i.e.* $\xi H_c(x)$. Values of $H_c(x)$ are given in the Koutecký's table and the value of ξ changes with capillary to capillary and also depends on the metal ion, solvent *etc.* In our laboratory[4,5] it has been found that the value of ξ lies between 0.05 to 0.25. Keeping this in view we have taken different values of ξ from 0.0 to 0.3 and calculated the value of $F'(x)$ for different values of ξ. We find that $\log x$ again varies linearly with $\log F'x/\{1-F'(x)\}$

TABLE 1. VALUES OF ξ, C, AND m

ξ	C	m
0.000	0.0523	0.9619
0.025	0.0606	0.9650
0.050	0.0679	0.9646
0.060	0.0711	0.9660
0.070	0.0745	0.9662
0.080	0.0778	0.9664
0.090	0.0815	0.9667
0.100	0.0845	0.9668
0.110	0.0878	0.9669
0.120	0.0912	0.9670
0.125	0.0929	0.9671
0.130	0.0945	0.9672
0.140	0.0979	0.9672
0.150	0.1012	0.9773
0.175	0.1095	0.9674
0.200	0.1179	0.9673
0.225	0.1262	0.9671
0.250	0.1345	0.9667
0.275	0.1430	0.9662
0.300	0.1512	0.9656

1) J. Koutecký, *Collect. Czech. Chem. Commun.*, **18**, 597 (1953).
2) J. Koutecký, and J. Cizek, *ibid.*, **21**, 836 (1956).
3) L. Meites and Y. Israel, *J. Amer. Chem. Soc.*, **83**, 4903 (1961).
4) D. S. Jain, Ph. D. Thesis, University of Rajasthan, Jaipur, India (1965).
5) N. K. Goswami, Ph. D. Thesis, University of Rajasthan, Jaipur, India (1967).

(For all values of ξ)

$$\log \lambda = C + m \log \frac{F'(x)}{1-F'(x)} \tag{14}$$

Different values of C and m at particular value of ξ are given in the Table 1. It is also found that the value of C increases as the value of ξ increases and a linear relation exists between ξ and C which can be represented as

$$C = 0.0523 + 0.3335\xi \tag{15}$$

Value of m also increases with the value of ξ, at lower values of ξ untill 0.1 then onwards becomes constant.

By combining Eqs. (2), (6), and (14) we obtained:

$$E_{\text{d.e.}} = \frac{0.05915}{\alpha n} \log \frac{K_{\text{fh}}^{\circ} t^{1/2}}{(\text{antilog } C) D^{1/2}} - \frac{0.05915m}{\alpha n} \log \frac{i}{i_{\text{d}}-i} \tag{16}$$

which may be written

$$E_{\text{d.e.}} = E_{1/2} - \frac{0.05915m}{\alpha n} \log \frac{i}{i_{\text{d}}-i} \tag{17}$$

With

$$E_{1/2} = \frac{0.05915}{\alpha n} \log \frac{K_{\text{fh}}^{\circ} t^{1/2}}{(\text{antilog } C) D^{1/2}} \tag{18}$$

In Eqs. (9), (13), and (18) the potentials are referred to normal hydrogen electrode. If the potentials are referred to the standard potential of that couple then the equations will correspond to the standard rate constant.

BULLETIN OF THE CHEMICAL SOCIETY OF JAPAN, VOL. 46, 3315—3316 (1973)

Synthesis of Bridged Bicycloferrocene: Participation of Anhydrous Aluminum Chloride in the Condensation Reaction

Yoshimori OMOTE, Ryuichiro KOBAYASHI, Yoshio NAKADA, and Noboru SUGIYAMA

Department of Chemistry, Faculty of Science, Tokyo Kyoiku University, Otsuka, Tokyo 112

(Received July 3, 1973)

Only a few papers[1] are known on the synthesis of bridged bicycloferrocenes. We now wish to report a new method for one-step synthesis of bridged bicycloferrocenes from 1,1′-diacetylferrocene-aluminum chloride complex (I).[2] Anhydrous aluminum chloride is known to catalyze the condensation reaction of *o*-benzoylbenzophenone with *o*-phenylenediamine.[3] Two acetyl groups of the complex (I) are expected to be accessible to two amino groups in the reaction of (I) with aromatic diamines such as *o*-phenylenediamine, because of their orientation in the same direction by aluminum chloride participation.

A mixture of (I) and *o*-phenylenediamine was heated in a molten state to give (IIa), whose structure was determined on the basis of the following evidences. The elemental analysis was in accord with (IIa). The mass spectrum of (IIa) indicated a peak at *m/e* 342 (M^+). The infrared spectrum showed a N–H absorption at 3340 cm^{-1} and a C=N absorption at 1610 cm^{-1}. The NMR spectrum is also consistent with (IIa), especially showing AB quartets at τ 6.96 (d, 1H, J= 11.4 Hz) and 7.51 (d, 1H, J=11.4 Hz) (methylene protons). In order to confirm the structure of (IIa), it was reduced with sodium borohydride in methanol to give (IIIa). In a similar manner, reaction of (I) with 4-methyl-1,2-diaminobenzene gave a product (IIb), which on reduction with sodium borohydride gave (IIIb). A nonbridged compound was obtained in the reaction of (I) and 1,8-diaminonaphthalene, which was determined to have structure (IV). The reason why no bridged ferrocene could be obtained in the reaction of (I) and 1,8-diaminonaphthalene can be considered to be that the distance between two amino groups of this diamine is too short to form a bridge with the complex (I). The formation of (II) can be explained by the condensation of carbonyl groups and aromatic amino groups, followed by intramolecular aldol type condensation.

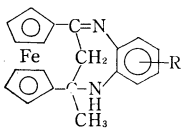

(IIa): R=H
(IIb): R=CH_3

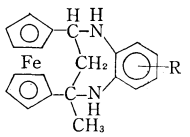

(IIIa): R=H
(IIIb): R=CH_3

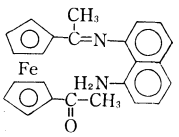

(IV)

Experimental

Bridged Bicycloferrocene (IIa). 1,1′-Diacetylferrocene-aluminum chloride complex (I) was prepared according to the literature.[2] The complex (1.44 g) was mixed with *o*-phenylenediamine (1.94 g) in a stoppered flask and the mixture was heated in a molten state at 90—100 °C in an oil bath for 5 min. The reaction mixture was extracted three times with 10 ml of benzene each. The extract was evaporated *in vacuo* and chromatographed on a silica gel column in benzene–ethyl acetate (10: 1) to give the product (6%), which was recrystallized from benzene–*n*-hexane as orange needles, mp 274—280 °C (dec.).

1) R. L. Schaaf, P. T. Kan, and C. T. Lenk, *J. Org. Chem.*, **26**, 1790 (1961); T. H. Barr and W. E. Watts, *Tetrahedron*, **25**, 3219 (1968); R. A. Schnetter, J. T. Suh, and C. I. Judd, U.S. 3417118 (1968).

2) I. Pavlik and K. Handlir, *Collect. Czech. Chem. Commun.*, **31**, 1958 (1966).

3) H. D. Perlmutter, *Chem. Commun.*, **1968**, 1202.

Found: C, 70.44; H, 5.32; N, 7.98%. Calcd for $C_{20}H_{18}FeN_2$: C, 70.19; H, 5.30; N, 8.18%. IR (KBr) cm^{-1}: 3340, 1610. UV: λ_{max}^{EtOH} nm (ε) 237 (26000), 296 (4170), 344 (5040), 443 (658). NMR ($CDCl_3$): τ 2.66—3.16 (m, 4H), 5.21 (m, 4H), 5.57 (m, 3H), 5.90 (m, 2H), 6.96 (d, 1H, J=11.4 Hz), 7.52 (d, 1H, J=11.4 Hz), 8.50 (s, 3H). Mass *m/e* 342.

Bridged Bicycloferrocene (IIb). The complex (1.44 g) was mixed with 4-methyl-1,2-diaminobenzene (2.18 g) and the mixture was heated in a molten state at 100 °C for 3 min. The reaction mixture was worked up as described above to give the product (11%), which was recrystallized from benzene–*n*-hexane as yellowish organge needles, mp 280.5—282.0 °C.

Found: C, 70.86; H, 5.70; N, 8.03%. Calcd for $C_{21}H_{20}FeN_2$: C, 70.60; H, 5.64; N, 7.86%. IR (KBr) cm^{-1}: 3345, 1615. UV: λ_{max}^{EtOH} nm (ε) 237 (26000), 266 (8700), 306 (4100), 346 (4870), 438 (673). NMR ($CDCl_3$): τ 2.78—3.41 (m, 3H), 5.21 (m, 4H), 5.57 (m, 3H), 5.91 (m, 2H), 6.97 (d, 1H, J=11.4 Hz), 7.52 (d, 1H, J=11.4 Hz), 7.68 (s, 3H), 8.50 (s, 3H).

Reduction of Bridged Bicycloferrocene (IIa). Sodium borohydride (100 mg) was added to bridged bicycloferrocene (IIa) (60 mg) in 50 ml of methanol in portions and the mixture was stirred for 30 min at room temperature. After addition of 10 ml of water, the reaction mixture was extracted with 100 ml of ethyl ether and the organic layer was washed with water, dried over anhydrous sodium sulfate, evaporated *in vacuo*, and recrystallized from benzene–*n*-hexane as yellow rods (IIIa) (78%), mp 225—227.5 °C.

Found: C, 69.71; H, 5.88; N, 7.91%. Calcd. for $C_{20}H_{20}FeN_2$: C, 69.80; H, 5.85; N, 8.15%. IR (KBr) cm^{-1}: 3360. UV λ_{max}^{EtOH} nm (ε) 222 (28400), 308 (2880), 441 (180). NMR ($CDCl_3$): τ 3.22 (s, 4H), 5.67 (m, 2H), 5.77—6.18 (m, 7H), 6.72 (bs, 2H), 7.46—8.10 (m, 2H), 8.46 (s, 3H).

Reduction of Bridged Bicycloferrocene (IIb). Sodium borohydride (140 mg) was added to bridged bicycloferrocene (IIb) (40 mg) in 60 ml of methanol in portions and the mixture was stirred for 30 min at room temperature. The reaction mixture was worked up as described above to give the product (85%), which was recrystallized from benzene–*n*-hexane as yellow prisms (IIIb), mp 195—197 °C.

Found: C, 70.38; H, 6.32; N, 7.88%. Calcd. for $C_{21}H_{22}FeN_2$: C, 70.40; H, 6.18; N, 7.81%. IR (KBr) cm^{-1}: 3365. UV: λ_{max}^{EtOH} nm (ε) 222 (30600), 312 (2960), 444 (193). NMR ($CDCl_3$): τ 3.35 (s, 3H), 5.62 (m, 2H), 5.77—6.16 (m, 7H), 6.98 (bs, 2H), 7.45—7.75 (b, 2H), 7.75 (s, 3H), 8.47 (s, 3H).

The Compound (IV). The complex (2.09 g) was mixed with 1,8-diaminonaphthalene (4.10 g) and the mixture was heated in a molten state at 90—95 °C for 1.5 hr. The reaction mixture was worked up as described above to give the product (12%), which was recrystallized from benzene–*n*-hexane as orange plates, mp 218.5—220.5 °C.

Found: C, 70.26; H, 5.38; N, 6.99%. Calcd. for $C_{24}H_{22}FeN_2O$: C, 70.26; H, 5.40; N, 6.83%. IR (KBr) cm^{-1}: 3380, 3350, 1642, 1601. UV: λ_{max}^{EtOH} nm (ε) 235 (48600), 269 (7000), 350 (13000), 463 (475). NMR ($CDCl_3$): τ 2.53—2.90 (m, 5H), 3.37—3.53 (m, 1H), 5.24 (t, 2H), 5.48 (t, 2H), 5.80 (m, 4H), 5.95 (m, 2H), 7.62 (s, 3H), 8.17 (s, 3H).

BULLETIN OF THE CHEMICAL SOCIETY OF JAPAN, VOL. 46, 3316—3317 (1973)

Photochemical Reactions of Aromatic Compounds. XVII.[1] The Photocyclization of *N*-(*o*-Chlorobenzyl)aniline

Kazuhiko MIZUNO, Chyongjin PAC, and Hiroshi SAKURAI

The Institute of Scientific and Industrial Research, Osaka University, Suita-shi, Osaka 565

(Received July 3, 1973)

The dehydrohalogenative photocyclization has been shown to be of potential use for the synthesis of some alkaloids.[2] However, the starting halides are limited to iodides and bromides, and difficulties have been generally encountered in the case of chlorides. In the previous papers,[3] we have reported the photoinduced reduction of halobenzenes with *N,N*-dimethylaniline, which affords the dehalogenative adducts in the maximum yield in the case of chlorobenzene. Therefore, *N*-(*o*-chlorobenzyl)aniline (Ia) can be expected to undergo an intramolecular dehydrohalogenative photocyclization and we did obtain the cyclized products (II) and (III) in moderate yields.

Irradiation was carried out for an acetonitrile–water (9: 1) solution of *N*-(*o*-halobenzyl)anilines (Ia—b) in the presence of sodium hydroxide through a Pyrex glass by a high pressure mercury arc. Phenanthridine (II)[4] and 5,5′,6,6′-tetrahydro-6,6′-biphenanthridyl (III)[4] were isolated from the reaction mixture by column chromatography on silica gel.

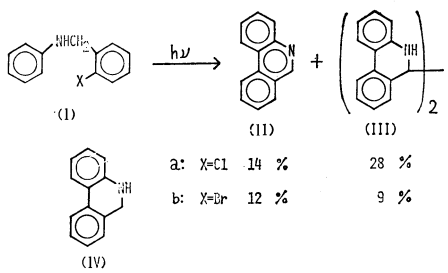

In the present photoreactions, the primary product can be expected to be 9,10-dihydrophenanthridine (IV), but it could not be isolated. However, when the photoreactions were monitored by the UV spectra, the

1) Part XVI: K. Mizuno, C. Pac, and H. Sakurai, *Chem. Commun.*, **1973**, 219.

2) T. Kametani and K. Fukumoto, *Account. Chem. Res.*, **5**, 212 (1972).

3) a) T. Tosa, C. Pac, and H. Sakurai, *Tetrahedron Lett.*, **1969**, 3635. b) C. Pac, T. Tosa, and H. Sakurai, This Bulletin, **45**, 1169 (1972).

4) J. J. Eisch and R. M. Thompson, *J. Org. Chem.*, **27**, 4171 (1962).

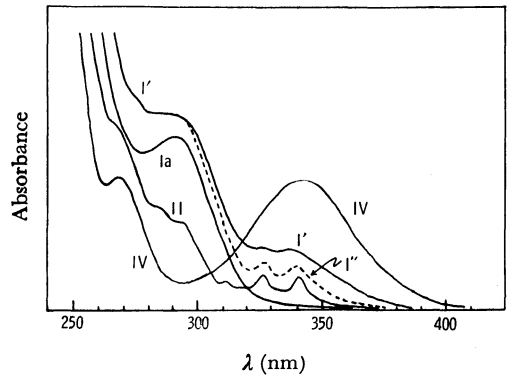

Fig. 1. The UV spectra in acetonitrile solutions: Ia (1.1×10^{-3} M of Ia); I′ (after irradiation of Ia at 313 nm in a degassed solution); I″ (after irradiation of I′ at 366 nm after I′ was air-saturated; II (phenanthridine); IV (9,10-dihydrophenanthridine). The absorption intensities are in arbitrary unit.

characteristic broad absorption maximum of IV at 342 nm appeared by the irradiation of Ia at 313 nm (Fig. 1). Further irradiation of the solution resulted in the decrease of the broad absorbtion band with the appearance of the bands similar to II at 326 and 342 nm. In fact, IV was found to be quantitatively oxidized into II by the treatment of column chromatography on silica gel and easily photolyzed into II and an unknown dimeric material (V), though III was not detected. The structure of V has not been determined, since it is insoluble in usual organic solvents. Therefore, it is suggested that the primary product IV might be oxidized into II during the work-up procedures and also photolyzed into II and the other products during the irradiation. On the other hand, the formation of III cannot be rigorously interpreted at present.

Although Ogata and Takagi have reported the photorearrangement of *N*-(*p*-chlorobenzyl)-*p*-toluidine,[5] the rearranged products, *o*-amino-*o*-chlorodiphenylmethane and *p*-amino-*o*-chlorodiphenylmethane, could not be obtained in appreciable amounts.

5) Y. Ogata and K. Takagi, This Bulletin, **44**, 2186 (1971).

Experimental

All the melting points and boiling points are uncorrected. Spectroscopic analyses of the organic products were carried out as follows; the IR spectra using a high Hitachi EPI-S2 spectrophotometer, the UV spectra using a Hitachi RMU-6E spectrometer. The acetonitrile was purified as uasul. The aniline, *o*-chlorobenzyl chloride and *o*-bromotoluene were distilled under nitrogen stream *in vacuo* before use.

The Preparation of The Starting Halides, Ia and Ib. Ia was obtained from aniline and *o*-chlorobenzylchloride according to the method described for the preparation of *N*-benzylaniline[6]: bp 160—163 °C/4 mmHg; ν_{max}^{KBr} 3380 cm^{-1} (N–H);. $\lambda_{max}^{C_2H_5OH}$ (ε) 296 (1090) and 246 nm (21010); Found: C, 71.36; H, 5.01; N, 6.37; Cl, 16.45%. Calcd for $C_{13}H_{12}NCl$: C, 71.26; H, 5.56; N, 6.43; Cl, 16.28%.

In a similar way, Ib was obtained from aniline and *o*-bromobenzyl bromide prepared by the bromination of *o*-bromotoluene with *N*-bromosuccinimide: bp 184—189 °C/7 mmHg; ν_{max}^{KBr} 3393 cm^{-1} (N–H); $\lambda_{max}^{CH_3CN}$ (ε) 293 (2470) and 244 nm (12820). Found: C, 59.63; H, 4.72; N, 5.12; Br, 30.78%. Calcd for $C_{13}H_{12}NBr$: C, 59.54; H, 4.58; N, 5.34; Br, 30.53%.

Irradiation of Ia and Ib. A solution of (Ia) (1 g) and sodium hydroxide (0.2 g) in 200 ml of acetonitrile–water (9: 1) was irradiated through a Pyrex glass under a nitrogen atmosphere at room temperature by a high-pressure mercury arc for 30 hr. After removal of the solvent *in vacuo*, the residue was dissolved in 200 ml of ether, washed by water and dried over magnesium sulfate. After removal of the ether, the residue was subjected to column chromatography on silica gel. Benzene eluted III (0.23 g) which was recrystallized from benzene–hexane: mp (dec.) 183—184 °C (lit,[4] 175—185 °C), ν_{max}^{KBr} (KBr disk) 3240 cm^{-1} (N–H); *m/e* 360 (M^+) and 180. Found: C, 87.02; H, 5.51; N, 7.69%. Calcd for $C_{26}H_{20}N_2$: C, 86.63; H, 5.59; N, 7.77%.

Benzene containing 10% of ether eluted 0.04 g of II, which was recrystallized from hexane: mp 105.5—106.5 °C (lit,[4] 105—106 °C). Found: C, 87.41; H, 4.83; N, 7.74%. Calcd. for $C_{13}H_9N$: C, 87.12; H, 5.06; N, 7.82%.

Further elution gave brownish tarry materials, the sublimation of which afforded 0.075 g of II.

In a similar way, irradiation of Ib afforded II (0.08 g) and III (0.06 g).

6) F. G. Willson and T. S. Wheeler, "Organic Syntheses," Coll. Vol. I, p. 102 (1941).

BULLETIN OF THE CHEMICAL SOCIETY OF JAPAN, VOL. 46, 3318—3319 (1973)

Chemical Effects of Osmium Neutron Capture Recoils. III. Cation Effect in Crystalline Mixtures of $K_4Os(CN)_6$-$K_4Fe(CN)_6$-$Cs_4Fe(CN)_6$

El-Hussieny M. DIEFALLAH and Jack G. KAY*

Department of Chemistry, Assiut University, Assiut, Egypt

**Department of Chemistry, Drexel University, Philadelphia, U.S.A.*

(Received July 11, 1972)

Changes in retention between crystals with different cations and the same Szilard-Chalmers component have been attributed to a cation effect. The effect is closely associated in many cases with that of changing crystal structure and thermal effects. The latter refers to the thermal response of the lattice and its effect on product distribution and is thought to differ for each crystalline modification. Studies of the effects of changing crystalline environment or cations have made us to realize the importance of certain factors involved.[1-5]

Observations with a wide variety of crystalline compounds[1] have shown that compounds with a similar crystal structure but different cations or Szilard-Chalmers elements show large variations in initial parent retention, so that cation effects may be more important than crystal structure effects. The role played by the cation in the retention reaction is not completely understood. Although the effect has been interpreted in certain cases as one of electron affinity of the cation,[5] and in others as being attributable to the state of hydration of the crystal,[2] the results do not agree. Explanations were given based on the differences due to radiation dose effects and to radiation chemical processes resulting from cation activation,[6] or to cage effects arising from differences in the masses of surrounding atoms or ions.[4]

We have studied osmium recoil effects in crystalline mixtures of the type $K_4Os(CN)_6$-$K_4Fe(CN)_6$-$Cs_4Fe(CN)_6$ in order to investigate the role of the cation in diluted systems. Crystals of the pure components were either available commercially or prepared as previously described.[7] Crystalline mixtures of $K_4Os(CN)_6$-$K_4Fe(CN)_6$-$Cs_4Fe(CN)_6$ containing a fixed Os- to Fe- mole ratio (1 : 1) and cesium to potassium mole ratios ranging from 0 : 1 to 1 : 1 were precipitated from a hot saturated solution of pure components by adding absolute alcohol. Each mixture was then filtered, washed several times with alcohol, and vacuum dried at about 100 °C. Chemical analysis of each mixture agrees well with the composition of the solution of pure components. X-Ray powder diffraction spectroscopy of the pure components and their mixtures show that the X-ray pattern for $Cs_4Fe(CN)_6$ differs from that for $K_4Fe(CN)_6$ and $K_4Os(CN)_6$; the mixture gives diffraction lines which is not properly related to the pure components.[8] This indicates that the cesium and potassium salts are not isomorphous and hence their crystalline mixtures are not true mixed crystals.

Neutron irradiations were carried out at a thermal neutron flux of 1.8×10^{12} n/cm^2/s, fast neutron flux of 1.8×10^{12} n/cm^2/s and gamma ray dose rate of about 1.4×10^7 rad/hr. The potassium-cesium salt mixtures were each irradiated for 6.0 hr and then analyzed by paper electrophoresis.[7] The duration of the electrophoretic separation was three hours and the counting of paper strips started several hours after the completion of irradiation in order to minimize the effect of any radiocesium contamination. The osmium activity appeared mainly in two peaks,[7,8] one due to OsO_2 remaining at the starting point and the other due to the parent peak migrating towards the anode. Since only the parent species should be stable in aqueous solution, it is believed that all partially reconstituted species hydrolyze or react immediately in solution to give OsO_2 and that most of the activity found in the parent peak actually comes from a cyanoosmate precursor present as such in the irradiated crystal.[7,8]

The results of cyanoosmate(II) parent retention determined as a function of $Cs_4Fe(CN)_6$ mole fraction in the cesium–potassium crystalline mixtures are given in Table 1. We see that replacement of cesium for potassium causes a large decrease in parent retention.

TABLE 1. CYANOOSMATE(II) RETENTIONS IN $K_4Os(CN)_6$-$K_4Fe(CN)_6$-$Cs_4Fe(CN)_6$ CRYSTALLINE MIXTURES WITH A FIXED 1:1 Os- to Fe- mol RATIO

$Cs_4Fe(CN)_6$ mole fraction	Cesium-to-potassium mole ratio	Percent retention
0.0	0.0	51±3
0.166	0.20	25±3
0.286	0.40	32±3
0.375	0.60	25±4
0.445	0.80	20±3
0.500	1.00	20±4

The observed decrease in cyanoosmate(II) retention due to the replacement of potassium by cesium cannot be explained on the basis of cage effects, as this would predict an increase in retention because of better caging around the recoil atom being provided by the massive Cs^+ ions. Potassium cation has a higher affinity for

1) G. Harbottle and N. Sutin, "Advances in Inorganic Chemistry and Radiochemistry," Vol. 1, ed. by H. J. Emeleus and A. G. Sharp, Academic Press, New York (1959), p. 267.
2) G. Harbottle, *J. Chem. Phys.*, **22**, 1083 (1954).
3) T. Anderson and A. G. Maddock, *Radiochim. Acta*, **2**, 93 (1963).
4) T. Anderson and A. G. Maddock, *ibid.*, **1**, 220 (1963).
5) N. Saito, F. Ambe, and H. Sano, *ibid.*, **7**, 131 (1967).
6) C. H. Collins, K. E. Collins, and C. M. Hyche, R53, 152nd, ACS Meeting, N.Y., Sept. 1966.
7) E. M. Diefallah and J. G. Kay, *Radiochim. Acta* (in press).
8) E. M. Diefallah, Ph. D. Thesis, Univ. of Illinois (Feb. 1968). Available from University Microfilms, Ann Arbor, Michigan, U.S.A.

electrons than cesium, and this could provide an explanation.[5] However, the increase in absorbed radiation dose and neutron activation with increasing cesium mole fraction in the crystalline mixtures causes excessive damage which may also account for the lowering in parent retention.

In general, the probability of parent reformation is not only determined by the density of lattice defects and radiation damage in the crystal, but also by the energy of activation for release from traps. It is believed that an increase in parent retention would correspond to an increased probability for an electron capture reaction by the parent precursor fragment taking place in the solid.[7] Changes in initial parent retention could be discussed on the basis of an electron acceptor-donor mechanism involving electron-hole traps and electron recombination centers. The energy of activation for defect release depends on the details of electronic structure of the solid which is determined by the crystal structure and types of cations, anions and ligands or the nature of the chemical bonds.[9] Thus it is expected that the more ionic cesium salt with a larger band gap would increase the trap depth and activation energy for reactions giving rise to initial retention. This interpretation is more reasonable than that based only on differences in density of lattice defects.

Partial support of this work by the U. S. Atomic Energy Commission through Contracts No. At(11-1)-891 and No. At(11-1)-1648 is gratefully acknowledged.

9) F. A. Kröger, "The Chemistry of Imperfect Crystals," North-Holland Publishing Co., Amsterdam, and Wiley, New York (1963).

BULLETIN OF THE CHEMICAL SOCIETY OF JAPAN, VOL. 46, 3319—3320 (1973)

Reactions of 3-Bromocamphor with Phenylhydrazine[1)]

Angelo G. GIUMANINI,[2)] Luciano CAGLIOTI, and Walter NARDINI
Instituto di Chimica Organicae Industriale, University of Bologna, 40136 Bologna, Italy

(Received September 25, 1972)

The interaction of 3-bromocamphor (**1**) with phenylhydrazine (**2**) at 100 °C yielded camphor phenylhydrazinophenylhydrazone,[3)] perhaps in the tautomeric formula **3**, a colorless crystalline compound, mp 136—137 °C, moderately stable in air, surprisingly[4)] stable to prolonged heating at 100 °C *in vacuo* and treatment with **2** at 150 °C. Compound **3** was identified on the basis of its molecular weight (M^+ *m/e* 348), elemental analysis and unequivocal spectral evidences.

When the reaction was carried out at 150 °C, after a few minutes a vigorous exotherm set in with the evolution of ammonia and the formation of aniline to give an excellent yield of camphor osazone **4**, a yellow crystalline compound, mp 149—152 °C, whose structure was supported by spectral characteristics. That the camphor framework was intact was ascertained by the PMR spectrum, which exibited three singlets in 1 : 1 : 1 ratio at δ 0.74, 0.87, and 1.03 ppm, an A_2B_2 quartet centered at 1.48 ppm and a deformed doublet at 2.80 ppm in addition to a complex aromatic pattern. The infrared spectrum of **4** showed two absorption bands for the γ_{NH} at *ca.* 3300 cm^{-1} due to the free and associated secondary amine[5)] and the presence of monosubstituted phenyl groups with three bands between 650 and 800 cm^{-1}. The parent peak (M^+ *m/e* 346) was also the most prominent in the mass spectrum at 70 eV. The ultraviolet spectrum was closely similar in band location and relative intensities to that of cyclohexane osazone.[6)]

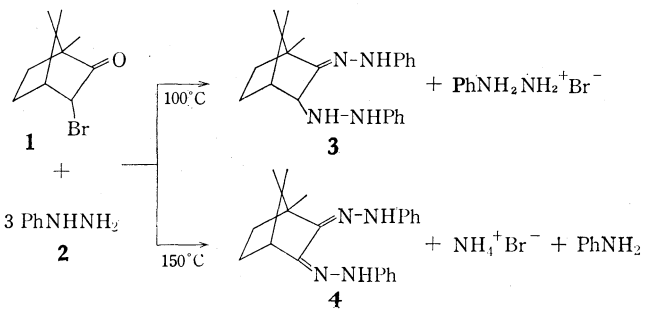

Reciprocal support for structures **3** and **4** was given by the facile conversion of the former into the latter by reflux with **2** in acetic acid.

In an experiment under the conditions and the workup procedure described by Balbiano[3)] we isolated only a compound **5** melting at 191—192 °C in a trace

1) This work was supported by Grants nos. 69.00367.115.621 (to L. C.) and 70.00143/03 (to A.G.G.) from the Italian Research Council (CNR).

2) To whom inquiries should be addressed: Center for Mass Spectrometry, University of Bologna, Via S. Giacomo, 5, 40126 Bologna.

3) A supposed camphor phenylhydrazinophenylhydrazone was described by Balbiano, *Gazz. Chim. Ital.*, **15**, 246 (1886) and **17**, 95 (1887), as a red compound, mp 55 °C.

4) Phenylhydrazinophenylhydrazones are a very rare type of compounds, only two of them having been described: L. Caglioti, G. Rosini and F. Rossi, *J. Amer. Chem. Soc.*, **88**, 3865 (1965); H. Simon, G. Heubach, and H. Wacker, *Chem. Ber.*, **100**, 3106 (1967). These compounds are believed to be the key intermediates on the way to osazones in Weygand's mechanism of osazone formation: for a recent review see: S. Kitaoka, *Kagaku-no-Ryoiki*, **18**, 475 (1964).

5) C. N. R. Rao, "Chemical Application of Infrared Spectroscopy," Academic Press, New York (1963), p. 245.

6) A. G. Giumanini, unpublished results.

amount. Its analytical data fitted the composition $C_{32}H_{41}N_5$, confirmed by the mass spectrum (M^+ *m/e* 495). Strong insolubility in common NMR solvents prevented recording of the PMR spectrum. Infrared analysis of this bright yellow product showed weak absorptions at 3320 and 3160 cm^{-1}, which can be tentatively ascribed to the ν_{NH} of hydrazone functions, strong bands between 650 and 750 cm^{-1} indicating the presence of monosubstituted phenyl groups. The characteristic bornane doublet was found at 1380 cm^{-1}, as well as intense ν_{CH} absorptions in the expected range. Mass spectral data (M^+ *m/e* 495, "aliphatic" peaks at *m/e* 15, 27, 41, 55 and the peak *m/e* 241, which can be hypothetically pictured as **6** together with the other evidences indicated a structure containing intact camphor moieties and phenyl rings, perhaps **5**.

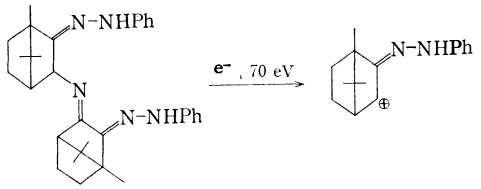

5 **6**

Our results support the theory according to which a phenylhydrazinophenylhydrazone is an intermediate in the formation of osazones under acid catalysis (HBr or AcOH), though it was not confirmed in which elementary step subsequent to **3** the acid intervened.

Experimental

Mp and bp are uncorrected. UV spectra were recorded with a spectrometer Unicam sp. 800. IR spectra were recorded with a Beckman IR 5, calibrated with polystyrene film. Spectra of solids were recorded by the KBr technique.

PMR spectra were recorded with a Varian DP 60, using TMS as internal standard and a frequency meter Hewlett Packard 241 A to establish peak locations (δ values, ppm). Mass spectra were obtained with a double focusing Perkin Elmer 270, with an ion source temperature of *ca.* 200 °C.

Camphor Phenylhydrazinophenylhydrazone (3). **1** (17 mmol) and **2** (54 mmol) were kept at 100 °C under N_2 for 1 hr. About 10 min after immersion into a warm oil bath, a homogeneous, almost colorless solution was formed from which a white precipitate appeared at once. At the end the whole mixture appeared as a red orange solid mass, from which phenylhydrazinium bromide was obtained by repeated washings with dry ether. The ether solution was extracted with chilled 15% HCl, dried over Na_2SO_4 and evaporated to yield a red oil having the smell of camphor. No osazone **4** was present (tlc). Careful sublimation gave some unreacted **1** (8%), whereas the residue solidified upon cooling, mp 55 °C. Addition of a small amount of methanol to this residue separated a compound, mp 191—192 °C after two crystallizations from methanol, in trace amount, mass spectrum (solid inlet 150 °C): M^+ 495, ten highest peaks 92 (100%), 93 (98), 77 (96), 241 (91), 91 (85), 242 (53), 94 (38), 107 (37), 108 (32) and 255 (32); Found: C, 77.00; H, 8.33; N, 14.05%; Calcd for $C_{32}H_{41}N_5$: C, 77.53; H, 8.34; N, 14.13%; IR bands at 1600, 1500, 1450, 1380, 1310, 1260, 1195, 1150, 1130, 1095, 1070, 1020, 995, 880, 775, 745, 705 and 685 cm^{-1}. This was compound **5**: the mother liquor after its precipitation gave a 47% yield of product **3**, mp 136—137 °C, after crystallization from hexane–ether, UV (95% EtOH): λ_{max} (ε): 346 (2427), 280 (32680), and 242 (24100) nm; IR: 3250, 3200, 3160, 3100, 2925, 1600, 1550, 1540, 1500, 1495, 1450, 1390, 1337, 1310, 1270, 1240, 1170, 1150, 1140, 1128, 990, 972, 917, 878, 858, 818, 798, 750, and 695 cm^{-1}; Mass spectrum (solid inlet 75 °C, 10 highest peaks): 93 (100%), 92 (99.5), 94 (25), 77 (87), 107 (37), 108 (36), 105 (29), 255 (80), 241 (20), and 159 (15) with M^+ 348; PMR ($CDCl_3$): 7.05 (m, 10H), 3.62 (s, 3H), 2.60 (s, 1H), 1.86 (s, 1H), 1.54 (d, 4H), 1.085 (s, 3H), and 0.965 (s, 3H) ppm; Found: C, 76.12; H, 8.20; N, 16.18%; Calcd for $C_{22}H_{28}N_4$: C, 75.82; H, 8.10; N, 16.08%. This compound was separated from other runs by absorption chromatography on silica gel using hexane–ether as an eluant. A quantitative transformation of **1** was achieved at 100 °C for 4 hr. Compound **3** was recovered unchanged by heating it alone at 100 °C *in vacuo*, refluxing it in methanol and heating it with phenylhydrazine at 150 °C.

Camphor Osazone (4). *A*) A mixture of 115 mmol of **1** was immersed into an oil bath at 150 °C: dissolution of **1** was promptly followed by a vigorous exothermic reaction. When the reaction subsided, the mixture was kept for 5 min at 150 °C, then cooled to 75 °C and taken up with warm water, cooled to room temperature and extracted with concentrated HCl and ether. The dried ether solution (Na_2SO_4) was evaporated to give 7.38 g of a yellow resinous mixture, which turned green at once upon exposure to air. Absorption chromatography (silica gel/ether–hexane) gave 88.5% crude **4**, mp 149.5—152 °C, after crystallization from methanol, pure yield 86%, UV (95% EtOH): λ_{max} (ε): 375 (16940), 304 (13250), and 254 (16640); IR: 3300, 2900, 1600, 1575, 1500, 1380, 1260, 1210, 1160, 1115, 1075, 1020, 995, 915, 880, 840, 785, 750, 715, and 685 cm^{-1}; PMR ($CDCl_3$): 7.21 (m, 10H), 2.80 (d, 1H, J=7 Hz), 1.48 (deformed q, 4H, J=7 and 25±2 Hz), 1.03 (s, 3H), 0.875 (s, 3H), and 0.74 (s, 3H) ppm; Mass spectrum (solid inlet 100 °C, 10 highest peaks): 346 (M^+), 254, 212, 210, 93, 92, 91, 77, 238, and 347; Found: C, 76.31; H, 7.77; N, 15.92%; Calcd for $C_{22}H_{26}N_4$: C, 76.26; H, 7.56; N, 16.17%.

B) The osazone **4** was obtained in practically quantitative yield by treating **3** with an excess of **2** and a few drops of AcOH at reflux temperature during 30 min. Direct interaction of **1** with **2** in acetic acid did not give good results.

Impurity Effect on Domain Formation in a Nematic Liquid Crystal

Jun NAKAUCHI,* Masaaki YOKOYAMA, Hiroshi SAWA,* Ken-ichi OKAMOTO,**
Hiroshi MIKAWA, and Shigekazu KUSABAYASHI**

Department of Applied Chemistry, Faculty of Engineering, Osaka University, Suita, Osaka 565

(Received February 19, 1973)

The effect of impurity on domain formation in an ethyl anisal-*p*-aminocinnamate nematic liquid crystal was investigated. With the decrease of the content of ionic impurities, the threshold voltage of the domain formation increases and the size of the domain patterns becomes larger. With blocking electrodes, the domain patterns could not be seen, although molecular orientation was still observed. When a negative electrode is coated partly with Nesa and partly with gold, the domain patterns appear first in the Nesa (*n*-type) part. When an electric field is cut and applied within one second intervals, the domains reappear at the same places. The mechanism of domain formation is discussed.

It is well-known that the optical properties of nematic liquid crystals are remarkably altered when electric fields are applied. Anomalous alignment called "domain" occurs at a low field strength. This phenomenon was first found by Williams in the nematic state of a *p*-azoxyanisole liquid crystal,[1] and has since been studied by many investigators.[2-6] Helfrich[7] proposed a quantitative theory describing the behavior of nematic liquid crystals with DC electric field near the critical field strength of domain formation. With DC electric field, ionic impurities influence the electro-optical properties of a liquid crystal.[7,8] However, there are few reports on the effect of impurities. We thought it of interest to elucidate the effect of impurities in a liquid crystal on the process of domain formation.

The present report deals with the effect of impurities on domain formation in a nematic liquid crystal. Our results for ethyl anisal-*p*-aminocinnamate (EAPAC) show that the current, probably due to ionic impurities, considerably contributes to the size and shape of the domain patterns.

Experimental

EAPAC was synthesized according to the literature.[9-11] EAPAC was purified by recrystallizations from absolute ethanol, and was dried sufficiently under reduced pressure. Three EAPAC samples (I, II, and III) each having different electrical conductivity, were obtained by recrystallization once, twice, and three times, respectively. Phase transition temperatures were determined with a differential scanning calorimeter (Rigaku Model 8001). Heating and cooling rates were controlled to within 5 °C/min.

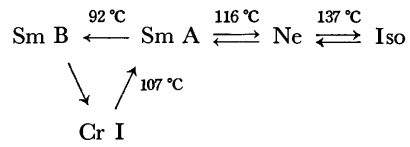

There is no conspicuous difference in phase transition temperature between samples I, II and III. Although Vorländer reported the presence of another crystal phase II with transition at 83 °C from Sm B,[11] no such phase could be observed. Other phase transition temperatures showed good agreement with those reported by Vorländer.

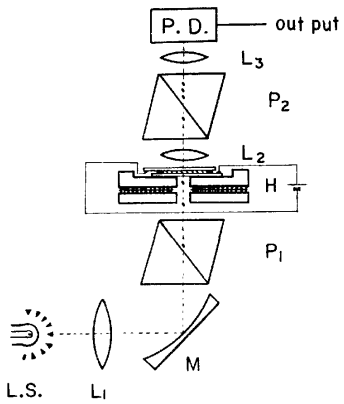

Fig. 1. Experimental alignment for observing the optical behavior of EAPAC in the nematic state. L.S: light source, M: mirror, L_1: condensing lens, L_2,L_3: objective and ocular lenses, P_1,P_2: polarizer and analyzer, P.D.: photodiode, H: heater plate.

All measurements were made in a nematic region. The domain patterns were observed under a Leitz polarizing microscope in the transmission mode with crossed nicols. The experimental alignment for observing the optical behavior is shown in Fig. 1. An EAPAC sample held between two Nesa-coated glass electrodes with a Teflon spacer (50 μ thickness), was set on a heater plate, which was then placed on the stage of a microscope. The optical response when the electric field was applied, was detected with a photodiode (NEC PD32) equipped at the top of a microscope and displayed on an oscilloscope (National VP517A). The DC current-voltage characteristics were measured by using a sandwich type cell with temperature control within 0.5 °C.

* Present address: Mitsubishi Rayon Co., Ltd., Otake, Hiroshima.

** Present address: Department of Chemical Engineering, Faculty of Engineering, Yamaguchi University, Ube, Yamaguchi.

1) R. Williams, *J. Chem. Phys.*, **39**, 384 (1963).
2) E. F. Carr, *Mol. Cryst. Liquid Cryst.*, **7**, 253 (1969).
3) H. Gruler and G. Meier, *ibid.*, **12**, 289 (1971).
4) G. H. Heilmeier, *J. Chem. Phys.*, **44**, 644 (1966).
5) H. Koelmans and A. M. von Boxtel, *Phys. Lett.*, **32A**, 32 (1970).
6) R. B. Beyer, *Phys. Rev. Lett.*, **22**, 918 (1969).
7) W. Helfrich, *J. Chem. Phys.*, **51**, 4092 (1969).
8) G. H. Heilmeier, *Proc. IEEE*, **59**, 442 (1971).
9) J. J. Broomfield and R. Fuchs, *J. Org. Chem.*, **26**, 2991 (1961).
10) E. D. Bergmann, S. Berkovic, and R. Ikan, *J. Amer. Chem. Soc.*, **78**, 6037 (1956).
11) D. Vorländer, R. Wilke, U. Haberland, K. Thinius, H. Hempel, and J. Fisher, *Ber.*, **71**, 501 (1938).

Results and Discussion

The threshold voltage of domain formation was determined from the change of the transmitted light intensity as a function of the applied voltage by a similar method to that reported by Williams.[1] The threshold field strengths of the domain formation in I, II, and III were about 560, 600, and 700 V/cm, respectively. These critical points correspond to the applied voltage for the appearance of extinction crosses which are observed by a polarizing microscope.

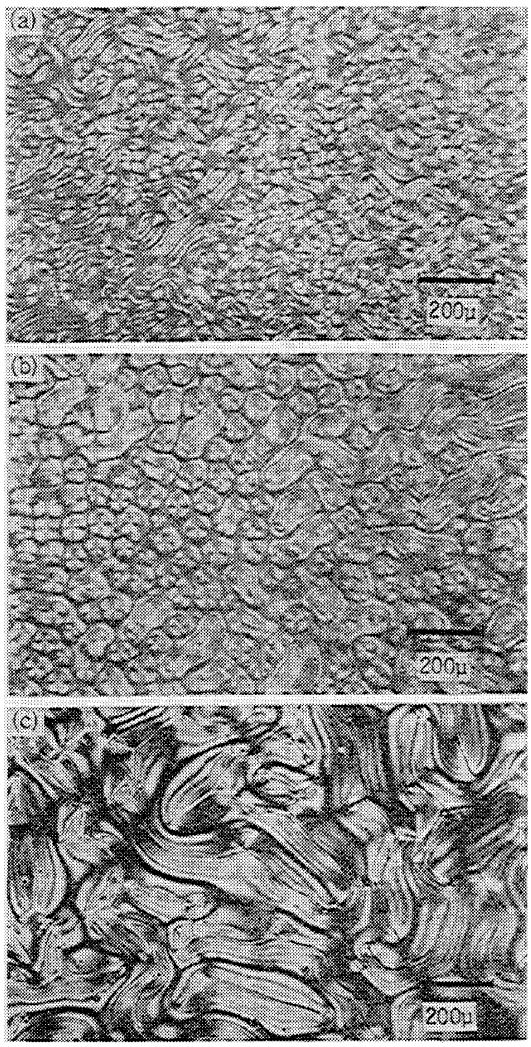

Fig. 3. The typical domain patterns of EAPAC (a) Sample I (applied voltage 4V, 50 μ thickness, 128 °C), (b) Sample II (4 V, 50 μ, 128 °C), and (c) Sample III (4.5 V, 50 μ, 128 °C).

Figure 2 shows the DC current-voltage characteristics for I, II, and III. Their conductivities are of the order 10^{-7}, 10^{-8}, and $10^{-9}\,\Omega^{-1}\,cm^{-1}$, respectively. These rather high values of conductivity at DC electric field indicate that ionic conduction is predominant. A difference in DC electrical conductivity was, however, clearly observed with the number of recrystallization times. Taking this difference in conductivity into consideration, the difference in the threshold voltage of domain formation for the samples is considered to be due to the different degree of contribution of ionic impurities. Thus, ionic impurities to some extent

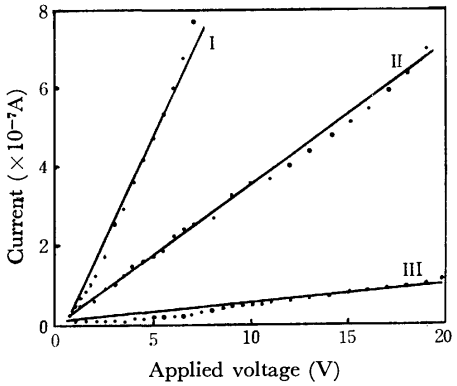

Fig. 2. Current-voltage characteristics of the EAPAC samples I, II, and III measured at 128 °C. The separation of electrodes is 50 μ.

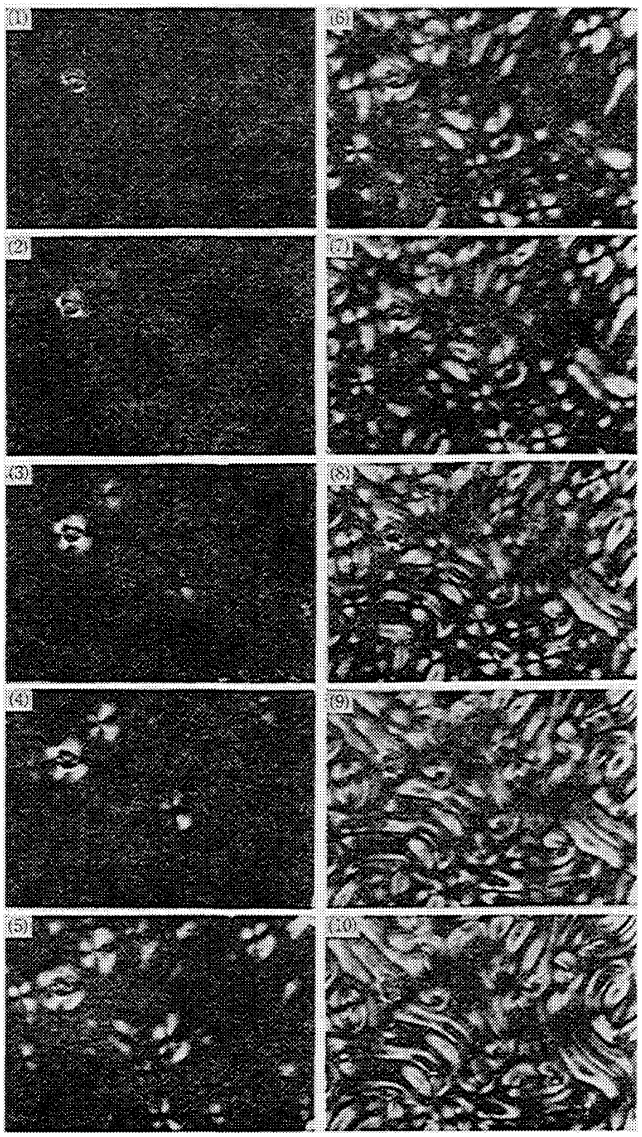

Fig. 4. The process of the domain formation of EAPAC Sample III (5 V, 50 μ, 130 °C) observed by a 16 mm moving camera. The 10 frames shown here are selected in the order of the process with appropriate intervals, 0.3 s for 1)—7) and 1 s for 7)—10).

influence the domain formation. Typical domain patterns of I, II, and III are shown in Fig. 3. The process of domain formation for III observed by a 16 mm moving camera with a crank speed of 64 frames per second is shown in Fig. 4. At the threshold voltage, Maltese cross-like extinction crosses of spherulites appear and then increase in number. As the voltage increases further, some of the crosses link with each other and gradually grow independently into long stripes everywhere, and finally form the characteristic cellular domain patterns of EAPAC. The size of the cellular domain becomes larger with the number of recrystallization times, *viz.*, with the decrease of impurities (Fig. 3). The domain patterns of III appear at slightly higher applied voltage (4.5 V) than those of the other two samples (4 V). The outer domain wall, shown in the figure as a dark obscure part with the pattern of a slightly stretched circle occurs in the neighborhood of the negative electrode. On the other hand, the inner wall which had been produced by the linking of the extinction crosses can be observed near the positive electrode by focusing a microscope in sharp focus. Penz[12] reported that even at the domain formation voltage the hydrodynamic flow of a *p*-azoxyanisole liquid crystal occurred. In the case of EAPAC it was also found that a dust particle in a domain moves in a circular motion between the two electrodes through these inner and outer domain walls. When observed carefully, a dust particle moves from the negative electrode to the positive electrode through the inner domain wall and inversely through the outer domain wall. This phenomenon may imply that the hydrodynamic flow of a liquid crystal is necessary to produce the domain pattern.

In order to examine the effect of the contact of an electrode and a liquid crystal, experiments were made with blocking electrodes, Nesa electrodes being covered with thin mica sheets (10 μ thickness). In the case of both positive and negative blocking electrodes, the domain pattern could not be observed even in the voltage region of the dynamic scattering mode. However, a transient increase of transmission was still observed under the crossed polarizers at the instant of applying an electric field, the transmission decreasing gradually to a final steady state value (Fig. 5). The transient increase of transmission may be caused by the orientation of the dipoles of EAPAC molecules to the direction of an electric field, and then the back field due to these ordered dipoles may decrease the effect of the external field, and a final arrangement of dipoles in a steady state may be attained with decreasing transmission. Thus, only the molecular orientation is observable and the domain pattern does not appear in the case of blocking electrodes. This suggests that not only the orientation of molecules but also the stationary current is necessary for the domain formation with DC electric field. Since an electron injection or electron transfer to EAPAC molecules, if any, is possible only in the case of direct contact to the electrodes and not in blocking electrodes, the electron transfer to EAPAC molecules from the negative electrode may play an important role in the domain formation.

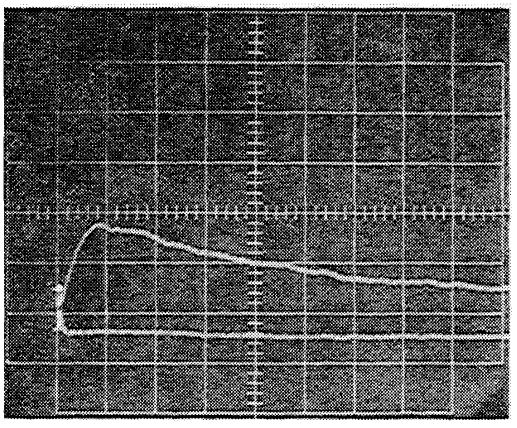

Fig. 5. Transient transmission change with blocking electrodes observed under the crossed polarizers. The upper and lower curves indicate the changes at the instant of switching on and off electric field (4×10^4 V/cm), respectively. Vertical axis: arbitrary transmittance, sweep: 100 ms/division.

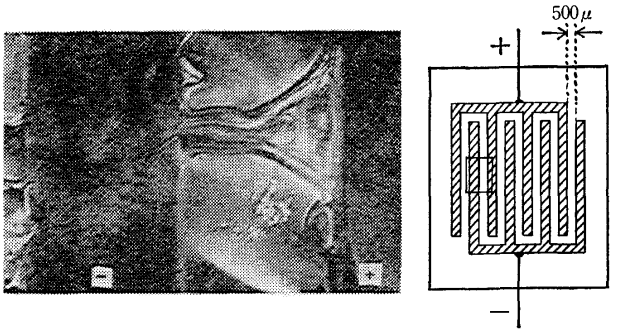

Fig. 6. The domain patterns of EAPAC observed with a gold surface cell on glass plate (10^3 V/cm, 127 °C). The place corresponding to the photograph is indicated by square in the schematic figure of the electrode.

Furthermore, in the case of the negative electrode plate coated half with Nesa and half with gold, the domain patterns appear first in the Nesa-coated part and subsequently in the gold part as the field strength increases. Provided that electron injection is required for the domain formation, this phenomenon is easily understood because an electron injection occurs more easily from the *n*-type Nesa part than from gold. The result of the optical measurement under a surface cell with the separation of 500 μ between two electrodes is shown in Fig. 6. The measurement with surface type electrodes corresponds to the case of viewing transversely the domain pattern between two sandwich type electrodes. In this case, the striped structure due to hydrodynamic flow of EAPAC molecules was observed, and the source point of the hydrodynamic flow was considered to coincide with the site of electron injection at the negative electrode.

Another experimental result suggests that the ionic impurities in a liquid crystal have an influence on the initial process of the domain formation. The extinction crosses or domain patterns reappear in the same

12) P. A. Penz, *Mol. Cryst. Liquid Cryst.*, **15**, 141 (1971).

position for the quick switching (about 1 s intervals) of the applied field, while the position as well as the shape of the domain patterns change when an electric field is applied again after an interval long enough for the ionic impurities stuck to the electrodes to diffuse. The domain patterns in the nematic state are still memorized even if the temperature once rises to the isotropic region or once falls to the crystal region keeping the applied field.

Taking all the measurements into account collectively, the process of EAPAC domain formation may be considered as follows. When an electric field is applied, ionic impurities in a liquid crystal are attracted and migrate to the negative electrode. Here, ionic impurities sticking to the electrode lower the electrode potential, and the electron transfer from the electrode to EAPAC molecules as an electron acceptor, *i.e.*, electron injection, may easily occur as Heilmeier has suggested.[8] This injection site corresponds to the place where the extinction crosses can be observed with a polarizing microscope at the threshold voltage of the domain formation. The injected electrons are captured by EAPAC molecules and cause the hydrodynamic flow of a liquid crystal and finally produce the characteristic domain pattern. Thus, (1) the domain inner wall gushes out from the negative electrode as the injection site, and (2) with a smaller amount of ionic impurities, the number of injecting sites becomes smaller and hence the size of the domain becomes larger.

BULLETIN OF THE CHEMICAL SOCIETY OF JAPAN, VOL. 46, 3324—3330 (1973)

The Self-diffusion of Chloride Ions in Divalent Metal Chloride Crystallites with $CdCl_2$-type Structure

Yoshihiro SENSUI

Institute for Atomic Energy, Rikkyo University, Yokosuka 240-01

(Received April 18, 1973)

The self-diffusion of chloride ions in $MgCl_2$- and $CoCl_2$-crystallites with the $CdCl_2$-type structure was studied, the results being compared with previous data on $MnCl_2$ and $NiCl_2$. The diffusion rate was measured through gas/solid-isotopic exchange reactions in a carefully cleaned vacuum system. The results were analyzed by the use of a model of semi-infinite crystal. The Arrhenius plots of apparent diffusion coefficient consist of two segments of line, from whose slopes the activation heat of migration E and the apparent heat of formation of vacancies H_v/n_v are determined. [H_v denotes the total heat of formation of two anion vacancies and one catoin vacancy with n_v= 2 or 3.] The values for E and H_v/n_v were 0.55 and 1.1 eV in $MgCl_2$ and 1.3 and 2.0 eV in $CoCl_2$, respectively. A linear relationship holds between the logarithms of pre-exponential factor of the diffusion coefficient and E or $(E+H_v/n_v)$; *viz.*, the theta-rule holds in this case. In the initial stage of the exchange reaction, ions or atoms in the surface region of crystals were observed to easily migrate. Sodium ions doped deliberately as impurity enhance the diffusion of chloride ions. It is concluded that the diffusion takes place through the vacancy mechanism.

Chemical processes in solids are closely related to migration of atoms or ions in crystals, which is controlled by imperfections in the crystal. The isotopic exchange reaction between crystals and gaseous molecules is one of the simplest surface reactions, and can be used as a useful means of measuring the self-diffusion of ions in crystals. Although diffusion is studied through measurements of electric conductance, it is desirable to confirm the validity of diffusion law by the tracer method.

Most studies on the self-diffusion of anions in solids have dealt with alkali halides, and a few with polyvalent metal halides.[1-3] Dearth of data on the latter crystals may be ascribed to the following. Most of such crystals are easily hydrated and volatile when dehydrated, making the manipulation of samples difficult. Chemical bonds in these crystals are partly ionic and partly covalent,[4] and theoretical interpretations of experimental data may not be as straightforward as in pure ionic crystals. As for theoretical studies, only rough ideas were applied to polyvalent metal fluoride.[5]

In the present paper, the results of studies of the self-diffusion of Cl^- ions in $MgCl_2$- and $CoCl_2$-crystallites with the $CdCl_2$-type structure are compared with the results on $MnCl_2$[2] and $NiCl_2$.[3] Some of these crystals are used as solid catalysts for chlorination of hydrocarbons in gaseous phase.[6]

1) G. M. Hood and J. A. Morrison, *J. Appl. Phys.*, **38**, 4796 (1967).
2) Y. Sensui, This Bulletin, **45**, 359 (1972).
3) Y. Sensui, *ibid.*, **45**, 2677 (1972).
4) L. Pauling, "Nature of the Chemical Bond," Third Edition, Cornell University Press, New York (1960).
5) A. D. Franklin, *J. Phys. Chem. Solids*, **26**, 933 (1965).
6) T. Shiba, (ed.), "Catalytic Engineering Vol. IX," Chijinshokan & Co., Ltd., Tokyo (1965).

Experimental

Apparatus and General Procedure. The apparatus used was made of Hario-glass, except for the two Teflon stoppers in the circulation pump (Fig. 1). The system consists of a reaction vessel, a thin-wall-type G.M. counter, a circulation pump, a Bourdon-type pressure gauge and a supplier of chlorine gas.

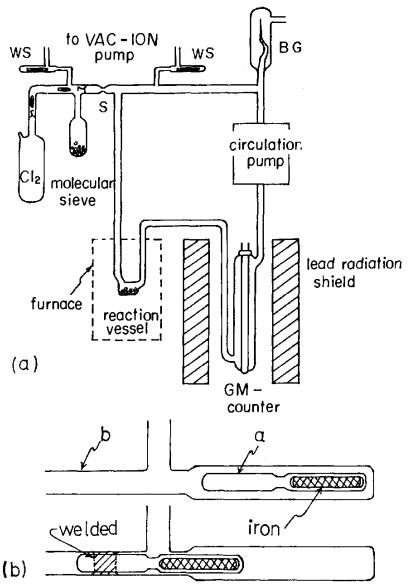

Fig. 1(a). Apparatus for the gas/solid-isotopic exchange reaction. WS, welding seal; BG, Bourdon type vaccuum gauge; S, common type seal.
(b) Detail of welding seal with a high conductance.

The samples were dehydrated by baking at 60—80 °C for 5—10 hr in a vacuum. The temperature was then gradually raised to 200 °C over 3—5 hr and kept at that temperature for 3—7 hr. After pre-baking in a vacuum, the system was sealed off from a diffusion pumping line, thus being made grease free. Further baking-out was carried out with a Vac-Ion pump. The system was isolated when the residual pressure became lower than 5×10^{-7} Torr during the course of baking of the sample at about 350 °C. The sample thus obtained was free from any external contamination of grease and water vapor, and its surface was adequately clean for the present purpose,[7] even though ultra high vacuum (below 10^{-9} Torr) could not be reached. A welding-seal was improved to be less-resistive as shown in Fig. 1 (b). To seal the system, a glass rod *a* is inserted into the outer tube *b* with the aid of magnet, the rod being welded to the outer tube.

First the temperature of the sample was raised to the reaction temperature. Purified chlorine gas was then carefully introduced into the system through a breakable seal and circulated by a circulation pump during the course of reaction. The reaction was followed by counting 0.714 MeV β-ray from ^{36}Cl in the gaseous phase, diffused from the crystallites, with the thin-wall-type GM counter. The temperature of the sample was controlled within 0.2 °C of a preset temperature by the aid of a PID-controller.

Materials Chlorine gas with a nominal purity of 99.8% (contained in a glass cylinder, Takachiho Chemical Co., Ltd.) was distilled and dehydrated with a Linde-3A molecular sieve in a vacuum system. Dehydration of chlorine gas is indispensable.[7]

Radioactive dichlorides were obtained by the isotopic dilution method. Their precipitates were prepared by a modified Marshall's method;[8] *i.e.*, by adding about 100 parts of distilled ethyl ether to one part of a nearly saturated alcoholic solution of the chlorides. Ethyl alcohol used had been dehydrated with a Linde-3A molecular sieve and distilled prior to use. After replacing the supernatant phase with ethyl ether, the precipitates were transferred into the vacuum system together with ethyl ether evaporated in situ. Conditions for preparation and properties of specimens are as follows.

$MgCl_2\cdot6H_2O$ (Merck G.R. reagent, item No. 5833) contains univalent impurities (Na^+ and K^+) nominally amounting to 20 ppm, the specific activity of the resulting radioactive dichloride being about 65 μCi/g. Special care was taken in the treatment of $MgCl_2$ specimens, since the substance is easily splashed by sudden heating in a vacuum and easily turns to magnesium hydroxychloride at 118 °C in air. The crystallites of $MgCl_2$ baked-out in a vacuum had a BET area of about 24 m^2/g.

Cobalt dichloride was prepared by the reaction between cobalt sponge (L. Light Co., Ltd., assay 99.99%) and distilled hydrochloric acid. It contained 20 ppm of sodium as determined by radio-activation analysis, the specific activity being about 5.3 μCi/g. The crystallites of $CoCl_2$ had a BET area of about 6 m^2/g.

Results and Analysis

The diffusion equation by Fick can be solved under the following boundary conditions: 1) the system is homogeneous and isotropic, 2) the initial concentration of radio-tracer is uniform over the crystals, and 3) the ratio of the amount of tracer diffused out (n) to that in the bulk is so small that the model of semi-infinite media can be used. Then n is given as a function of time t:[9]

$$n = (2AN_0)(Dt/\pi)^{1/2}, \tag{1}$$

where A denotes the surface area of specimen, N_0 the initial concentration of the tracer in the crystal, and D the diffusion coefficient. If we denote the counting rate by C, we obtain the following equation as a solution of the diffusion equation.[2,3]

$$C = C_0 + (2AN_0/\alpha\sqrt{\pi})(D_1t_1+D_2t_2+\cdots)^{1/2} \tag{2}$$

or

$$(C-C_0)^2 = (4A^2N_0^2/\alpha^2\pi)(D_1t_1+D_2t_2+\cdots) \tag{3}$$

where C_0 denotes the counting rate resulting from ^{36}C, diffused out of the surface region of the crystals, and α the conversion factor between C and n. Suffix i specifies the number of runs carried out successively for a given sample. In real crystals the properties of the surface region differ from those in the bulk, even though the bulk is homogeneous with respect to diffusion.[3,7,10] The diffusion coefficients in the surface region, in general, are much larger than those in the bulk. In the initial stage of the exchange reaction, diffusion from the surface region is observed, and then

7) T. Takaishi and Y. Sensui, *Trans. Faraday Soc.*, **63**, 1007 (1967); *Surface Science*, **19**, 339 (1970).

8) F. G. Marshall, *Phys. Rev.*, **58**, 642 (1940).

9) S. Chandrasekhar, *Rev. Modern Phys.*, **15**, 1 (1943). A. B. Lidiard and K. Thermalingam, *Discuss. Faraday Soc.*, **28**, 64 (1959).

10) G. C. Benson, P. I. Freeman, and E. Dempsey, *Adv. Chem. Ser.*, **33**, 26 (1961); *J. Chem. Phys.*, **39**, 302 (1963).

bulk diffusion takes place.[3,7] Such a surface effect is taken into consideration as a correction term C_0 in Eqs. (2) and (3).

If the single path mechanism is applicable, the plots of $(C-C_0)^2$ against time may well be fitted by a straight line, and the Arrhenius plots of D_i may become a linear line.

Magnesium Dichloride. Diffusion experiments were carried out in the temperature range 180—350 °C. The exchange reaction referred to the surface of the crystallites proceeded even at −21 °C as shown in Fig. 2, while the self-diffusion of chloride ions in the bulk did not occur appreciably at temperatures below 180 °C. This indicates that chloride ions much more easily migrate in the surface region of the crystallites than in the bulk and Eqs. (2) or (3) is applicable to the present system. Three samples of magnesium dichloride crystallites were used to check the reproducibility of the data. The total counting rate in the gaseous phase are plotted against the square root of reaction time in Fig. 3(a), which represents an initial stage of the diffusion reaction at 180 °C. Except for the initial portion, the experimental points lie on a straight line, where the bulk diffusion may control the reaction; namely, the results can be well described by Eq. (2). However, there are some ambiguities as to the start of the reaction on the time scale. Measured time t should be replaced by an effective time interval $(t+\delta)$, where the value for δ is determined by the method given previously.[2,3] The abscissa in Fig. 3 is the effective time thus corrected. On the other hand, the intersection of the asymptote with the ordinate

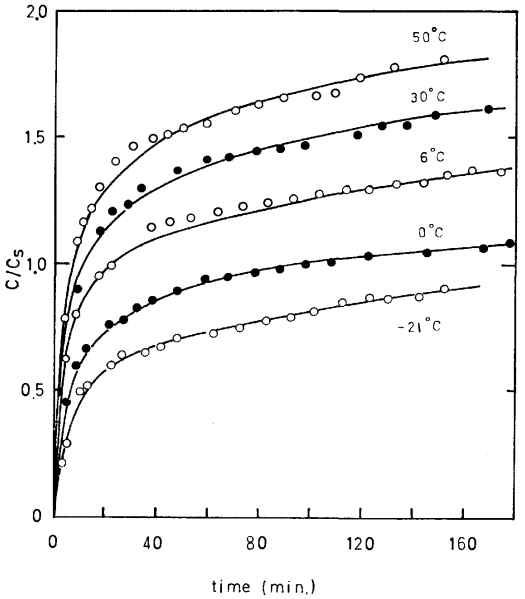

Fig. 2. Plots of counting rate against time in the exchange reaction between Cl_2 and the surface region of $MgCl_2$ crystallites. The value, $C/C_S=1$, corresponds to a monolayer exchange: Solid curves show calculated values based on Eq. (6).

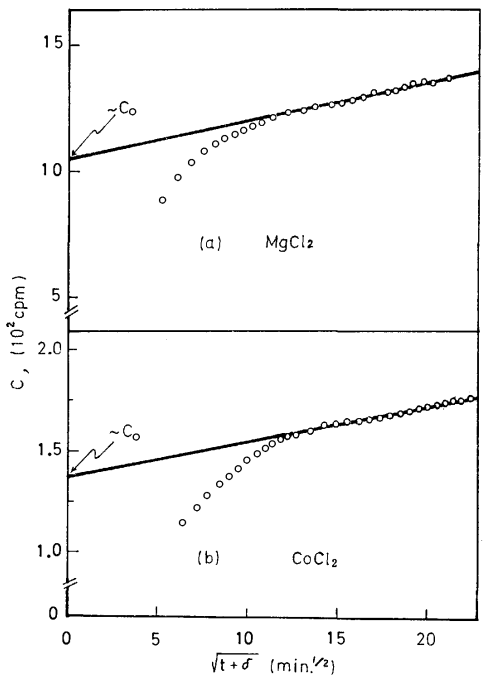

Fig. 3. Plots of C against a square root of time.
(a), $MgCl_2$; (b), $CoCl_2$.

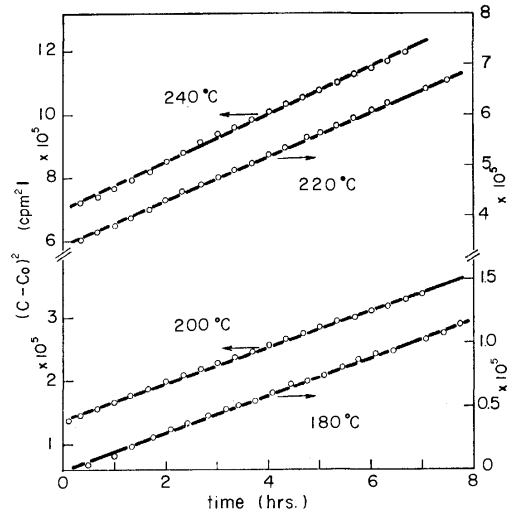

(a)

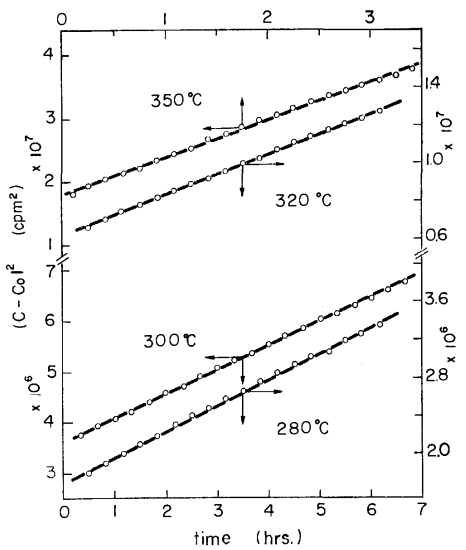

(b)

Fig. 4. Plots of $(C-C_0)^2$ against time referred to $MgCl_2$ (Sample No. I).
(a), 180—240 °C; (b), 280—350 °C.

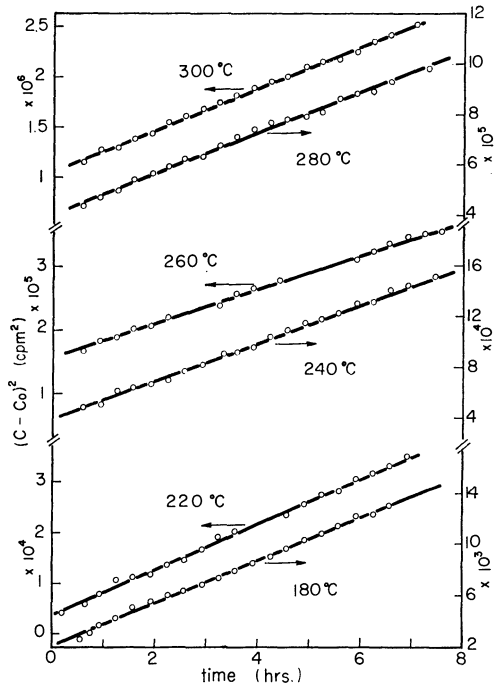

Fig. 5. Plots of $(C-C_0)^2$ against time referred to $CoCl_2$ (Sample No. I).
(a), 180—300 °C; (b), 320—360 °C.

gives a value for C_0. By using C_0-values thus determined, $(C-C_0)^2$ are plotted against time in Fig. 4, in which the points obtained lie on straight lines within experimental error. It is considered that the scattering of the data is mainly attributable to an incomplete mixing of ^{36}Cl in gaseous phase and partly to some drifts in the back-ground-counting rate. From the linear relationship the validity of the homogeneous crystal model may be envisaged. Values for $(4A^2N_0^2/\pi\alpha^2)D$ can be obtained from the slopes of the lines. Arrhenius plots of these values are shown in Fig. 6, in which all the curves consist of two segments of lines with breaks at about 270 °C ($1/T=1.85\times10^{-3}$ K^{-1}) and two kinds of slope are found.

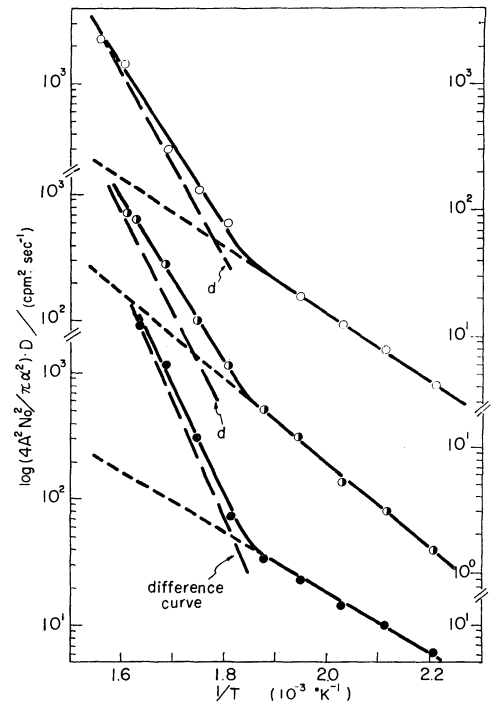

Fig. 6. Arrhenius plots of the apparent diffusion rates in $MgCl_2$.
○, Sample No. I; ◑, No. II; ●, No. III.

In the vacancy diffusion mechanism, the diffusion coefficient D may be expressed as[11]

$$D = D_0(1)\exp[-E/kT] + D_0(2)\exp[-(E+H_v/n_v)/kT] \quad (4)$$

where both $D_0(1)$ and $D_0(2)$ denote terms containing activation entropy and frequency, E is activation energy for the migration of vacancy, and H_v/n_v the apparent heat of the formation per one vacancy. The value for n_v depends on the mechanism of its formation, and we must make a choice between conceivable mechanisms.

If the vacancy mechanism of diffusion can be applied, the slopes in the lower temperature regions give the activation energy for migration of vacancy or Cl^- ions, E. When we plot the difference between the observed curve in the lower one, straight lines are obtained. The value for $(E+H_v/n_v)$ can be determined from the slope of the difference curve as given in Table 1.

Cobalt Dichloride. The temperature range studied was 180—360 °C. It may safely be assumed that chloride ions migrate more easily in the surface region than in the bulk. The total counting rate in the gaseous phase is plotted against the square root of effective time, $(t+\delta)^{1/2}$, in Fig. 3(b). In this case also experimental points lie on a straight line, except for the initial portion; namely, Eq. (2) can be applied to the $CoCl_2/Cl_2$ system. By the use of the values for C_0 obtained in Fig. 3(b), $(C-C_0)^2$ are plotted against reaction time in Fig. 5. The experimental points lie on straight lines within experimental error, the homogeneous crystal model thus being also valid in the

11) R. A. Swalin, "Thermodynamics of Solids" John Wiley & Sons, Inc., New York, N. Y. (1962).

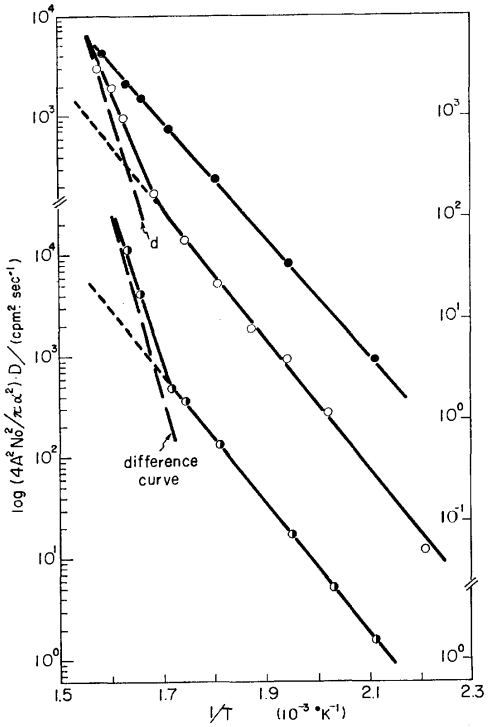

Fig. 7. Arrhenius plots of the apparent diffusion rates in $CoCl_2$.
○, undoped sample (I); ◑, undoped sample (II); ●, sample doped with Na amounting to 250 ppm.

present case. Values for $(4A^2N_0^2/\pi\alpha^2)D$ determined from the slopes of lines are plotted against $1/T$ in Fig. 7. These curves have a similar form to those in Fig. 6, having breaks at about 320 °C ($1/T=1.7\times10^{-3}$ K^{-1}). The temperature of the break point is slightly higher than that on $MgCl_2$. The values for E and $(E+H_v/n_v)$ obtained are also given in Table 1.

If monovalent metal ions are doped in crystals of divalent metal dichloride, anion vacancies may be produced to satisfy electrical neutrality conditinon in the crystal. This effect was examined for $CoCl_2$ crystallites doped with sodium, whose concentration was 250 ppm as determined by radioactivation analysis. The same diffusion law was also valid in the doped crystallites. Arrhenius plots of the apparent diffusion coefficient are shown in Fig. 7. We see that the doped crystal has no break in the line in the temperature range studied, while the undoped crystallites containing 20 ppm of sodium have a break. From the slope of the line referring to the doped crystallites, the activation heat was evaluated to be 1.2 eV which is in harmony with E of the undoped crystallites (*cf.* Table 1); namely, the activation heat observed in doped crystallites should be referred to the activation energy for migration of vacancy or Cl^- ion. Thus, the experimental results support the theoretical prediction that the position of break point depends on the content of impurity, and the assumption that the vacancy migration is a dominant mechanism.

Table 1. The values for E and $(E+H_v/n_v)$ in divalent metal dichloride crystallites with $CdCl_2$-type structure

Specimen	E (eV)	$E+H_V/n_V$ (eV)	H_V/n_V (eV)	Remarks
$MgCl_2$ I	0.53	1.4	0.87	Present work
II	0.62	1.6	0.98	
III	0.48	1.8	1.32	
Average	0.55	1.6	1.05	
$CoCl_2$ I	1.3	3.2	1.9	Present work
II	1.25	3.4	2.15	
Average	1.3	3.3	2.0	
$MnCl_2$ I	0.96	2.0	1.04	Previous work[2]
II	0.92	2.0	1.08	
III	—	2.3	1.4	
IV	—			
Average	0.9	2.1	1.2	
$NiCl_2$ I	1.0[1]	—	—	Previous work[3]
II	1.0[2]	—	—	
III	1.0[5]	—	—	
Average	1.0			

Discussion

In crystals with the $CdCl_2$-type structure, chlorine atoms are arranged in the cubic closest-packing structure and a metal atom occupies an octahedral hole made of six chlorine atoms, forming a sandwich structure with a layer arrangement ……(Cl–M–Cl)(Cl–M–Cl)……. Since the primary valence of the metal and chlorine atoms are satisfied within each sandwich, the van der Waals force operates between adjacent sandwiches.[13] However, the situation is not so simple; namely, there are two types of layer arrangements in the closest-packing structure, *i.e.*, the cubic type, ……ABC·ABC……, and the hexagonal one, ……AB-ABA……. Choice between the two structures is determined by the magnitude of the interaction between the metal layer and the chlorine layer in the adjacent sandwiches. If the interaction is very weak, the diffusion of Cl^- ions may be highly anisotropic, while, if strong, it approaches an isotropic diffusion. At the present stage of our knowledge on crystal structures, nothing can be predicted as to the magnitude of such interactions. We can only say that the experimental data are well described by a model of isotropic diffusion.

The values for $D_0(1)$ and $D_0(2)$ in Eq. (6) obtained with this model are given in Table 2. Plots of log $D_0(j)$ against the activation heat lie on a straight line as shown in Fig. 8; namely, the theta-rule[12] holds. This means that the method of analysis used is supported.

Table 2. Values for the pre-exponential factors of the apparent diffusion coefficients ($cm^2\cdot s^{-1}$)

Specimen	$D_0(1)$	$D_0(2)$	Remarks
$MgCl_2$	$(4.5\pm2)\times10^{-13}$	$(5\pm4)\times10^{-3}$	Present work
$CoCl_2$	$(2.5\pm0.5)\times10^{-5}$	2×10^{11}—2×10^{14}	Present work
$MnCl_2$	$(9\pm4)\times10^{-10}$	8 ± 5	Previous work[2,3]
$NiCl_2$	$(3.2\pm0.8)\times10^{-8}$	—	Previous work[2,3]

12) G. M. Schwab, *Advan. Catal.*, **2**, 251 (1950).
13) A. F. Wells, "Structural Inorganic Chemistry," Oxford Univ. Press, London (1962).

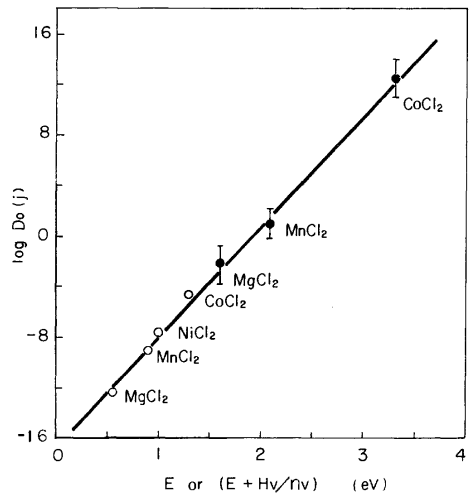

Fig. 8. Linear relationship between log $D_0(j)$ and E or $(E+H_V/n_V)$.
$D_0(j)$ is the pre-exponential factor of diffusion coefficient and given in the unit of $cm^2 \cdot s^{-1}$.
○ and ● refers to E and $(E+H_V/n_V)$, respectively.

According to Benson and his co-workers,[10] the surface of ionic crystal is deformed; namely, anions and cations in the surface region are displaced towards outer and inner directions from ideal lattice points, respectively. Such a distortion may increase the surface reactivity of the crystal. This prediction was proved quantitatively in the case of alkali chloride by Takaishi and Sensui.[7,14] Benson's theory may not be applied to divalent metal chloride crystals without further refinements, since these crystals have partly covalent nature. However, we can expect qualitatively that the surface region has different properties from the bulk, and ions in the surface region can migrate more easily than in the bulk. This prediction was semi-quantitatively proved in $NiCl_2$ crystallites.[3] Let us analyze the data on $MgCl_2$ to verify the prediction.

It may be safely assumed that there are two domains in the first layer of the crystal surface and that the distortion in the first layer influences the configuration of the second layer. The reverse reaction from the gaseous phase to the solid is ignored due to the boundary condition mentioned above, the kinetic equation being given by[3]

$$\begin{aligned}
&dn_g(i)/dt = k_1(i)n_1(i)\\
&dn_1(i)/dt = -k_1(i)n_1(i) - k_2(i)n_1(i) + k_2(i)n_2(i)\\
&dn_2(i)/dt = -k_2(i)n_2(i) + k_2(i)n_1(i) - k_3n_2(i) + k_3n_3(i)\\
&n(i) + n_1(i) + n_2(i) + n_3(i) = 3a(i), \qquad (5)
\end{aligned}$$

and

$$n_g = \sum_{i=1}^{2} n_g(i),\quad n_1 = \sum_{i=1}^{2} n_1(i),\quad n_2 = \sum_{i=1}^{2} n_2(i),\quad n_3 = \sum_{i=1}^{2} n_3(i),$$

$$a = \sum_{i=1}^{2} a(i),$$

where n_i denotes the number of ^{36}Cl in the i-th layer at time t; a, the number of ^{36}Cl contained in each layer at $t=0$; k_i, the apparent rate constant of the exchange reaction between the $(j-1)$th and the j-th layers; subscript g, the gaseous phase; and (i), the i-th kind of domain. In Eq. (5) it is assumed that $k_3(1)$ and $k_3(2)$ have the same value, k_3. If ^{36}Cl in gaseous phase amounting to a results in a counting rate C_s, it can be expressed as $C_s=\alpha \cdot a$ and $C/C_s = n_g/a$. Then, the solution of Eq. (1) is expressed[3] as

$$\begin{aligned}
\frac{C(i)}{C_s(i)} = \frac{n_g(i)}{a(i)} = {}& \frac{k_1(i)}{\rho_+(i)\rho_-(i)}\left\{\frac{k_2(i)k_3}{\lambda} - \rho_+(i) - \rho_-(i) - k_1(i)\right\}\\
&- \frac{k_1(i)k_2(i)k_3}{\lambda[\lambda+\rho_+(i)][\lambda+\rho_-(i)]}\exp(-\lambda t)\\
&- \frac{k_1(i)}{\rho_+(i)[\rho_+(i)-\rho_-(i)]}\left\{\rho_-(i) + k_1(i) - \frac{k_2(i)k_3}{\lambda+\rho_+(i)}\right\}\exp[\rho_+(i)t]\\
&- \frac{k_1(i)}{\rho_-(i)[\rho_-(i)-\rho_+(i)]}\left\{\rho_+(i) + k_1(i) - \frac{k_2(i)k_3}{\lambda+\rho_+(i)}\right\}\exp[\rho_-(i)t]
\end{aligned}$$

with

$$\begin{aligned}
2\rho_\pm = {}& -[k_1(i) + 2k_2(i) + k_3]\\
&\mp[k_1(i)^2 + 4k_2(i)^2 + k_3^2 - 2k_1(i)k_3]^{1/2} \qquad (6)
\end{aligned}$$

where λ denotes an effective rate constant for the decrease in n_3. By a comparison of Eq. (5) with the experimental curves, the best-fitting values for k_1(i), k_2(i) and k_3 are determined with the aid of an electronic computer. The results are well described by the theory, as shown in Fig. 2. The Arrhenius plots of $k_1(i)$ and $k_2(i)$ are given in Fig. 9; the activation energies for the exchange reaction are obtained to be: 3.4 kcal/mol (=0.15 eV) for the active part of the first layer, 7 kcal/mol (=0.3 eV) for the less-active one, 10 kcal/

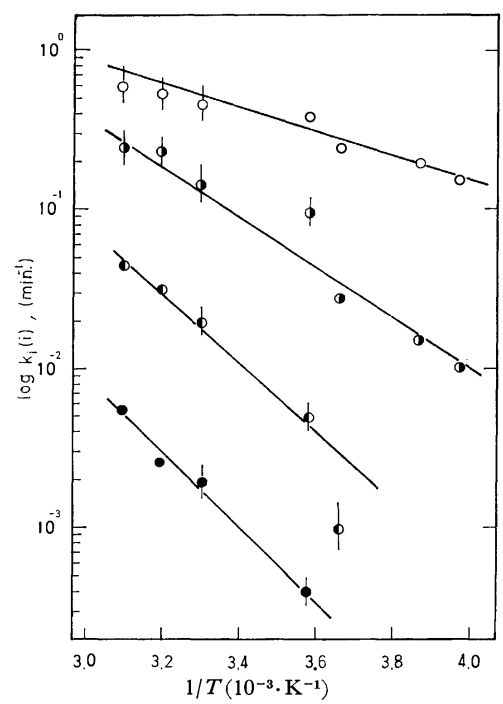

Fig. 9. Arrhenius plots of the rate constants for the exchange reaction in the surface region of $MgCl_2$ crystallites.
○, active domain in the first layer; ◑, less-active domain in the first layer; ◐, active domain in the second layer; ●, less-active domain in the second layer.

14) T. Takaishi and Y. Sensui, *Trans. Faraday Soc.*, **65**, 131 (1969).

mol (=0.43 eV) for the active part of the second layer, and 11 kcal/mol (=0.48 eV) for the less-active one. The activation energies of the exchange reaction converge to that of the self-diffusion more rapidly in $MgCl_2$ than in $NiCl_2$. This conclusion is semi-quantitative, since the present data on $MgCl_2$ are less quantitative. In $MnCl_2$ and $CoCl_2$, such a surface effect was observed only qualitatively but distinctly. Thus, we can say that high reactivity of the surface is a fairly common phenomenon which may be of value for further studies in connection with catalytic properties.

The value for n_v in Eq. (4) could not be determined. However, Simkovich[15] studied the mechanism of electrical properties and arrived at the conclusion that the associated vacancy is dominantly formed as

$$0 \rightarrow (V_{Pb}V_{Cl})' + V_{Cl}' + H_v$$

where V_x' denotes the vacancy of x atom (or ion). It may generally be considered that vacancies with effective charge, 2e, are rather unstable electrostatically and apt to form associated vacancies. If so, we may apply the above mechanism to other MeX_2 crystals; namely, $n_v=2$ may be presumed.

The author would like to express his gratitude to Prof. Tetsuo Takaishi, Rikkyo University, for valuable suggestions.

15) G. Simkovich, *J. Phys. Chem. Solids.*, **24**, 213 (1963).

BULLETIN OF THE CHEMICAL SOCIETY OF JAPAN, VOL. 46, 3330—3335 (1973)

The Reflection Spectra of Simple Salts of the Tetracyanoquinodimethane Anion Radical

Yukako Oohashi and Tadayoshi Sakata*

The Institute for Solid State Physics, The University of Tokyo, Roppongi, Minato, Tokyo 106

(Received April 20, 1973)

The reflection measurements were carried out for fourteen simple salts of the tetracyanoquinodimethane (TCNQ) anion radical over the range from 5000 to 42000 cm^{-1} by Avery's method. The solid-state spectra show three bands (CT, YI, and YII) and exhibit distinct differences depending on the cation species. According to the differences in the transition energy (σ_i) and the oscillator strength (f_i), the fourteen salts were classified into three groups (A, B, and C). The solid-state spectra of Group A resemble that of the dimer in an aqueous solution. Group B is characterized by the red shift of the CT band and the intensity increase in the YII band. The spectra of Group C exhibit a vibrational structure in the YI band which is similar to the monomer spectrum in an aqueous solution. Moreover, the large dispersion of the refractive index and the intensity increase in the bands of local excitation were observed for Group C. The electronic structures of these groups were studied by the use of the composite-system method. By taking account of the crystal structure of RbTCNQ-I, belonging to Group A, the stabilization energy (J^*) of the ground state was calculated from σ_{CT} and f_{CT}. The J^* values for ten salts in Group A correspond well to the singlet-triplet separation in the ground state observed by ESR measurements.

The electrical,[1-4] magnetic,[5-9] and optical properties,[10,11] and the crystal structures[12-20] have been extensively investigated with the anion radical salts of 7,7,8,8-tetracyanoquinodimethane (TCNQ). These results indicate that, in the crystalline state, the mode of the packing of TCNQ radicals exerts an important effect on the physical paoperties. X-ray crystal analysis studies clarified that TCNQ radicals form a one-dimensional column in a crystal and that the interplanar spacing is 3.16—3.6 Å.[12-20] The rather short interplanar spacing causes the strong charge-transfer (CT) interaction between TCNQ radicals in a column which is essential to an understanding of the electronic

* Present address: Department of Chemistry, Faculty of Engineering Science, Osaka University, Toyonaka, Osaka.

1) L. R. Melbey, R. J. Harder, W. R. Hertler, W. Mahler, R. E. Benson, and W. E. Mochel, *J. Amer. Chem. Soc.*, **84**, 3374 (1962).
2) L. R. Melbey, *Can. J. Chem.*, **43**, 1448 (1965).
3) V. Walatka, Jr. and J. H. Perlstein, *Mol. Cryst. Liquid. Cryst.*, **15**, 269 (1971).
4) T. Hibma, P. Dupuis, and J. Kommandeur, *Chem. Phys. Lett.*, **15**, 17 (1972).
5) D. S. Chesnut and W. D. Phillips, *J. Chem. Phys.*, **35**, 1002 (1961).
6) D. B. Chesnut and P. Arthur, Jr., *ibid.*, **36**, 2969 (1962).
7) R. G. Kepler, *ibid.*, **39**, 3528 (1963).
8) Z. G. Soos, *ibid.*, **43**, 1121 (1965).
9) Z. G. Soos and R. C. Hughes, *ibid.*, **46**, 253 (1967).
10) Y. Iida, This Bulletin, **42**, 71, 637 (1969).
11) N. Sakai, I. Shirotani, and S. Minomura, *ibid.*, **43**, 57 (1970).
12) C. J. Fritchie, Jr., *Acta Crystallogr.*, **20**, 892 (1966).
13) C. J. Fritchie, Jr. and P. Arthur, Jr., *ibid.*, **21**, 139 (1966).
14) A. W. Hanson, *ibid.*, **B24**, 768 (1968).
15) H. Kobayashi, Y. Ohashi, F. Marumo, and Y. Saito, *ibid.*, **B26**, 459 (1970).
16) H. Kobayashi, F. Marumo, and Y. Saito, *ibid.*, **B27**, 373 (1971).
17) T. Sundaresan and S. C. Wallwork, *ibid.*, **B28**, 491, 1163, 2474, 3065 (1972).
18) A. Hoekstra, T. Spoedler, and A. Vos, *ibid.*, **B28**, 14 (1972).
19) I. Shirotani, H. Kobayashi, and Y. Saito, to be published.
20) G. R. Anderson and C. J. Fritchie, Second National Meeting, Society for Applied Spectroscopy, San Diego, Paper 111 (1963).

properties. The absolute absorption intensity of the solid state gives quantitative knowledge about that interaction. The crystals of these radical salts, however, exhibit strong absorptions over the visible and ultraviolet regions, so that the transmission measurement is very difficult. On the other hand, the reflection measurement is useful for the determination of a strong absorption intensity, as has been described in the previous paper.[21]

In the present study, we measured the reflection intensities of the pressed pellets of fourteen simple salts of TCNQ anion radical and obtained the oscillator strength (f) for each transition. On the basis of these results and the reported crystal structures, we classify the fourteen simple salts into three groups and discuss the characteristics of each group.

Experimental

Materials. The samples used in this experiment were prepared by the method described in the literature[1] except for the Rb salts. RbTCNQ-I was prepared by the diffusion method described by Hoekstra,[18] and RbTCNQ-II was obtained by the rapid mixing of two hot acetonitrile solutions of RbI and TCNQ. The fourteen simple salts of TCNQ used are LiTCNQ, NaTCNQ, KTCNQ, RbTCNQ-I, RbTCNQ-II, CsTCNQ, NH_4TCNQ, (Ph_3PCH_3)TCNQ, MorpholiniumTCNQ (MorTCNQ), $BaTCNQ_2$, $FeTCNQ_2 \cdot 3H_2O$, $CoTCNQ_2 \cdot 3H_2O$, $NiTCNQ_2 \cdot 3H_2O$, and $MnTCNQ_2 \cdot 3H_2O$.

Measurements. The samples were ground with an agate mortar and were pressed by a KBr disc presser at about 10 kbar. The reflection intensity of the pressed pellet was measured by means of an apparatus constructed by our laboratory. The experimental details are the same as those described in the previous paper.[21] By the analysis of these reflection data, the refractive index (n) and the extinction coefficient (k) were determined, and the oscillator strength (f) for each transition was calculated by means of the equation:

$$f = \frac{m}{e^2 n_0} \int 4n(\nu)k(\nu)\nu d\nu.$$

Here, n_0 is the number of molecules in a unit volume and ν is the frequency of light. The f values were calculated in this study per TCNQ radical. In the figures of the present paper, the $4\pi n(\nu)k(\nu)/2.303\lambda C$ value (ε') will be plotted to show the wave number dependence of the absorption intensity of the solid-state spectrum (C: molar concentration of TCNQ radical, λ: wavelength).

Results and Discussion

Figure 1 shows the absorption spectra of LiTCNQ in an aqueous solution and a solid-state spectrum obtained from the reflection measurements. The TCNQ anion radical exhibits a reversible dimerization in the aqueous solution when the temperature is varied.[22] The monomer and the dimer spectra in the aqueous solution are shown in Fig. 1. From an open-shell SCF–LCAO–MO–CI calculation, t e electronic transitions at 11800 and 24800 cm^{-1} of the monomer spectrum were assigned to the locally-excited (LE) transitions in a TCNQ radical, polarized parallel to the long axis (y) of the anion radical. The present calculatoin shows that, in the region up to 50000 cm^{-1}, another band with a strong intensity (f=0.8) appears at 43000 cm^{-1}, polarized parallel to the short axis (x) of the anion radical. In the dimer state, the low-energy CT configuration exists and interacts with the LE configurations. The bands at 15800 and 36200 cm^{-1} of the dimer are shifted from the monomer positions by the interaction with the CT configuration, and the band at 11000 cm^{-1} has the CT character.

The observed solid-state spectra exhibit distinct differences depending on the species of the cation. On the basis of the transition energies (σ_i) and the oscillator strengths (f_i) of the solid-state spectra, the fourteen

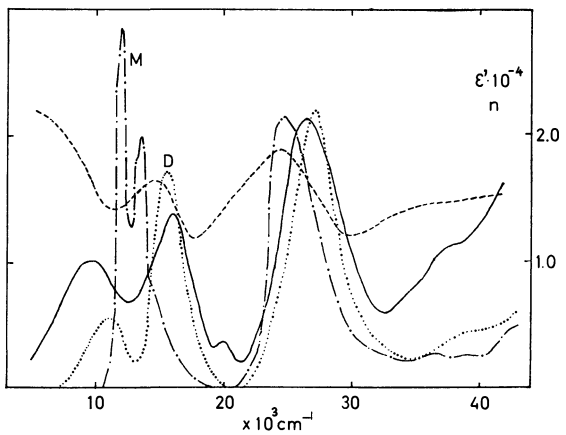

Fig. 1. The absorption spectra of LiTCNQ in the aqueous solution; monomer (M) and dimer (D). The solid-state spectra (——) and the refractive index (——) of LiTCNQ.

Table 1. Transition energy and oscillator strength of three groups of TCNQ simple salts (in cm^{-1})

	A1	A2	A3	B	Dimer in H_2O	C	Monomer in H_2O
σ_{CT}	9.7×10^3	8.8×10^3	11.0×10^3	7.4×10^3	11.0×10^3	10.2×10^3	
$\sigma_{YI}-\sigma_{CT}$	6.7	6.5	5.5	9.3	4.8	13.7[a]	11.8×10^3[a]
$\sigma_{YII}-\sigma_{YI}$	11.1	11.0	11.2	11.4	10.5	26.6[b]	23.8[b]
f_{CT}	0.24—0.41	0.26—0.28	0.25	0.39	0.09	0.1	
f_{YI}	0.25	0.36	0.41	0.33	0.22	0.51	0.27
f_{YII}	0.56	0.75	1.0	1.5	0.46	1.1	0.47
Cation	Li, K, Rb-I, NH_4, Ni	Fe, Co, Mn	Na, Ph_3PCH_3	Cs, Rb-II		Ba, Mor	

a) Transition energy of the YI band.
b) Transition energy of the YII band.

21) Y. Oohashi and T. Sakata, This Bulletin, **46**, 765 (1973).

22) R. H. Boyd and W. D. Phillips, *J. Chem. Phys.*, **43**, 2927 (1965).

simple salts of the TCNQ radical were summarized into three groups (A, B, and C), as may be seen in Table 1. Here, the absorption peaks are denoted as CT, YI, and YII. The common feature of Group A is that the f_{YI}/f_{YII} ratio (0.5) and the $\sigma_{YI}-\sigma_{CT}$ (5000—6000 cm^{-1}) and $\sigma_{YII}-\sigma_{YI}$ splittings (11000 cm^{-1}) are all almost equal to those of the dimer in the solution. However, the oscillator strengths of the YI band of Group A, with respect to that of the dimer in the solution, are equal for the TCNQ salts of the Li, K, Rb-I, NH_4, and Ni cations, 1.5 times for the salts of the Mn, Co, and Fe cations, and 2.0 times for those of the Na and (Ph_3PCH_3) cations. Therefore, Group A is further divided into three subgroups, A1, A2, and A3 (Fig. 2).

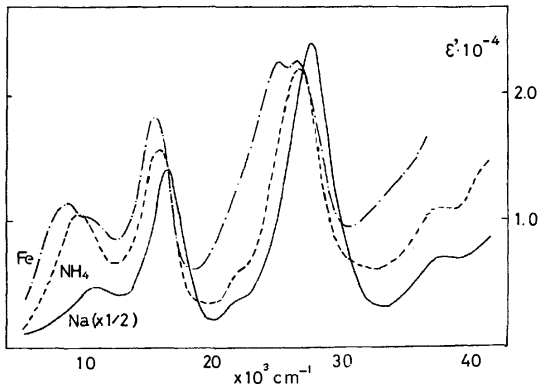

Fig. 2. The solid-state spectra of Al(NH_4TCNQ), A2(Fe-TCNQ$_2$·3H_2O) and A3(NaTCNQ). ε' in this work is the value per one TCNQ radical.

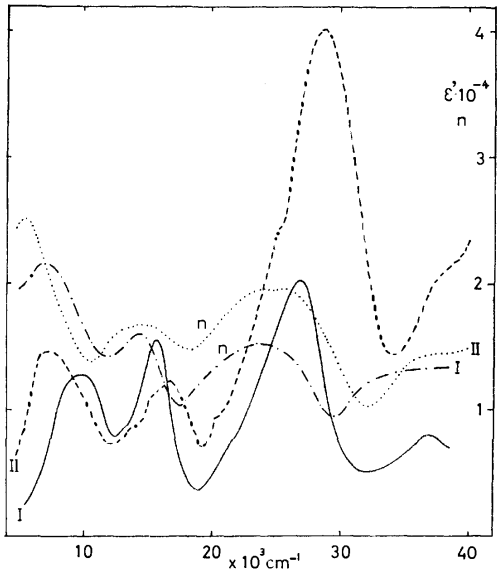

Fig. 3. The solid-state spectra and the refractive indexes of RbTCNQ-I(I) and RbTCNQ-II(II).

Figure 3 shows the solid-state spectra of RbTCNQ-I and RbTCNQ-II, together with the wave number dependence of the refractive indexes (n). The CT bands of RbTCNQ-II and CsTCNQ have an asymmetric shape and appear at 7400 and 7200 cm^{-1} respectively. These show a distinct red shift compared with the CT bands of Group A, and as a result, the

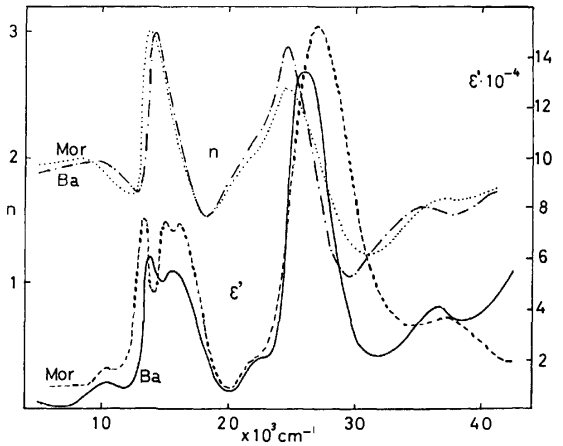

Fig. 4. The solid-state spectra and the refractive indexes of MorpholiniumTCNQ(Mor) and BaTCNQ$_2$(Ba).

$\sigma_{YI}-\sigma_{CT}$ splitting (9000 cm^{-1}) becomes large. The YII band increases remarkably in intensity. These two salts belong to Group B.

As may be seen in Fig. 4, the YI bands of the solid-state spectra of BaTCNQ$_2$ and MorTCNQ exhibit some structure, and the oscillator strengths of the YI and YII bands are larger than those of Groups A and B, especially for MorTCNQ, while the f_{YI}/f_{YII} ratios are about 0.5. The intensity of the CT band is very weak and is almost equal to that of the dimer in the solution. From the above-mentioned features, these two salts are denoted as Group C. The observed transition energies and oscillator strengths of the fourteen simple salts are tabulated in Table 2.

Group A. The solid-state spectra of Group A are shown in Figs. 1—3 and Figs. 5 and 6. Among these ten simple salts, the crystal structure has been

Table 2. Observed transition energy and oscillator strength of fourteen simple salts (σ_i: in cm^{-1})

	σ_{CT}	f_{CT}	σ_{YI}	f_{YI}	σ_{YII}	f_{YII}
Li	9.8×10^3	0.26	16.2×10^3	0.25	26.6×10^3	0.56
NH_4	9.5	0.24	16.0	0.25	26.9	0.54
Rb-I	9.8	0.31	15.7	0.23	27.1	0.56
Na	11.0	0.25	16.5	0.41	27.7	1.0
Ph_3PCH_3	10.5	0.24	15.3	0.39	26.4	0.88
K	9.5	0.36	16.0	0.27	27.7	0.62
Ni	9.0	0.44	15.7	0.49	25.3^s 26.7	1.0
Fe	8.6 10.5^s	0.58	15.4	0.63	25.5 26.9	1.3
Co	8.8 10.5^s	0.52	15.4	0.78	25.0^s 26.6	1.5
Mn	9.0^b	0.52	15.3	0.69	25.0^s 25.8	1.7
Rb-II	7.4	0.39	16.7	0.33	28.1	1.5
Cs	7.2 9.3^s	0.22	14.0^s 16.0	0.30	27.5	0.86
Ba	10.0	0.17	13.8 15.4	1.0	26.2	2.2
Mor	10.5	~0.1	13.5 15.1 16.1	0.89	27.0	2.1

s: shoulder b: broad

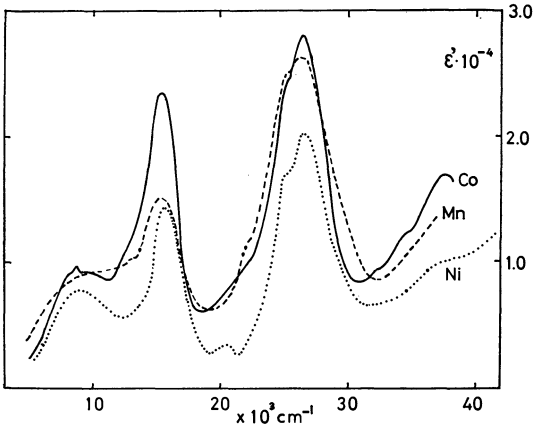

Fig. 5. The solid-state spectra of $MnTCNQ_2 \cdot 3H_2O$(Mn), $CoTCNQ_2 \cdot 3H_2O$(Co), and $NiTCNQ_2 \cdot 3H_2O$(Ni).

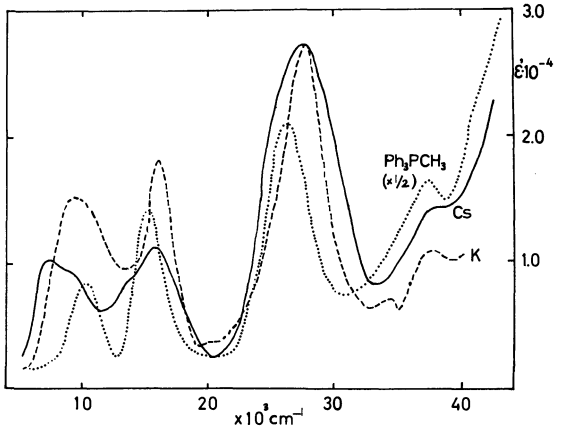

Fig. 6. The solid-state spectra of KTCNQ(K), CsTCNQ(Cs) and Ph_3PCH_3TCNQ.

reported for RbTCNQ-I,[18] and for KTCNQ[20] as the preliminary data. In the crystal of RbTCNQ-I, the dimer of TCNQ radicals (the radical spacing is 3.159 Å) form a one-dimensional column (the interval between the dimers is 3.484 Å). In the dimer unit, the radicals overlap each other, with a shift (0.84 Å) along the x axis. In the case of KTCNQ, the axis of the radical column almost coincides with the axis normal to the molecular plane.

The TCNQ radical has one odd electron in the ninth molecular orbital (φ_9). By our calculation of the open-shell SCF–CI, the lowest LE state was assigned to the $\varphi_8 \rightarrow \varphi_9$ transition, and the second lowest LE state, mainly to the $\varphi_9 \rightarrow \varphi_{10}$ transition; the higher LE state is found at 43000 cm^{-1} in the region up to 50000 cm^{-1}. Therefore, in this study of the electronic structure of the solid state, it is sufficient to take account of the interaction between the ground (G), LEI, LEII, and CT configurations. The CT configuration under consideration corresponds to the $\varphi_9 \rightarrow \varphi_{9'}$ transition (φ_9 and $\varphi_{9'}$ denote the MO's of the two radicals forming a dimer unit).

$$G = 1/\sqrt{2}\,(|8\bar{8}98'\bar{8}'\bar{9}'| - |8\bar{8}\bar{9}8'\bar{8}'9'|)$$

$$\mathrm{LEI}^{\pm} = 1/2[(|8\bar{9}98'\bar{8}'\bar{9}'| - |9\bar{8}\bar{9}8'\bar{8}'9'|) \pm (|8\bar{8}99'\bar{8}'\bar{9}'| - |8\bar{8}\bar{9}8'\bar{9}'9'|)]$$

$$\mathrm{LEII}^{\pm} = 1/2[(|8\bar{8}108'\bar{8}'\bar{9}'| - |8\bar{8}\bar{1}08'\bar{8}'9'|) \pm (|8\bar{8}98'\bar{8}'\bar{1}\bar{0}'| - |8\bar{8}\bar{9}8'\bar{8}'10'|)]$$

$$\mathrm{CT}^{\pm} = 1/\sqrt{2}\,(|8\bar{8}9'8'\bar{8}'\bar{9}'| \pm |8\bar{8}98'\bar{8}'\bar{9}|)$$

The doubly occupied MO's φ_1—φ_7 are neglected. Here, the + and — signs denote the symmetric and the antisymmetric properties with respect to the symmetric center. Since the TCNQ molecule has the symmetry of D_{2h}, LEI and LEII do not interact with CT for the above-mentioned two modes of radical packing. Therefore, the configuration interaction occurs only between G and CT^+. The oscillator strength (f_{CT}) and the transition energy (σ_{CT}) of the CT band are calculated as follows:

$$f_{CT} = 1.085 \times 10^{-5} \frac{\beta^2 \sigma_{CT} R_{CT}^2}{\sigma_{CT}^2 + \beta^2}$$

and:

$$\sigma_{CT} = 1/2(E_{CT} + \sqrt{E_{CT}^2 + 4\beta^2}) \quad (\sigma_{CT}: \text{ in } cm^{-1}).$$

Here, E_{CT} is the configuration energy of CT^+, and β is the interaction parameter between G and CT^+. R_{CT} is the distance between the radical centers in Å units. Then, from the observed values of σ_{CT}, f_{CT}, and R_{CT}, the β value can be calculated as follows:

$$|\beta| = \sigma_{CT}\left(1.085 \times 10^{-5} \frac{\sigma_{CT} R_{CT}^2}{f_{CT}} - 1\right)^{-1/2}$$

Moreover, the stabilization energy (J^*) of the ground state is obtained as β^2/σ_{CT}. Table 3 shows the values of $|\beta|$ and J^* calculated from the reflection data. The value of R_{CT} was known only for KTCNQ (3.5 Å) and RbTCNQ-I (3.42 Å); therefore, for the other eight salts, R_{CT} was assumed to be 3.42 Å. For the R_{CT} value of 3.8 Å, the change in the $|\beta|$ value is less than 10%.

Table 3. Parameters obtained from the reflection data of group A

	σ_{CT} $10^3 cm^{-1}$	f_{CT}	β eV	J^* eV	E_{CT} $10^3 cm^{-1}$	J_{ESR} eV
Li	9.8	0.26	0.62	0.32	7.2	0.23±0.2[24]
NH_4	9.5	0.24	0.58	0.32	7.2	
Rb-I	9.8	0.31	0.70	0.41	6.5	0.29±0.2[24]
Na	11.0	0.25	0.64	0.30	8.6	0.16±0.01[24]
PH_3PCH_3	10.5	0.24	0.62	0.33	8.2	
K	9.5	0.36	0.76	0.50	5.4	0.26±0.01[24]
Ni	9.0	0.22	0.54	0.26	6.9	
Fe	8.6	0.29	0.64	0.39	5.4	
Co	8.8	0.26	0.60	0.33	6.2	
Mn	9.0	0.26	0.60	0.32	6.4	
Dimer in H_2O	11.0	0.087	0.32	0.07	10.4	

On the basis of the crystal data for RbTCNQ-I, the overlap integral ($S_{99'}$) between φ_9 and $\varphi_{9'}$ was calculated by the use of the Slater-type AO's[23] as 0.037. On the other hand, β is related to $\beta_{99'}$ by this equation; $\beta = 2\beta_{99'}$. Here, $\beta_{99'} = \int \varphi_9(1)\, H^C(1)\, \varphi_{9'}(1)\, d\tau_1$ and $H^C(1)$ is the one-electron Hamiltonian of the crystal. $|\beta_{99'}|$ was found from the reflection data to be 0.35 (Table 3). The ratio of $|\beta_{99'}|$ to

23) F. Clementi and D. L. Raimondi, *J. Chem. Phys.*, **38**, 2686 (1963).

$S_{99'}$ thus obtained is 9.5; this is reasonable. Table 3 shows the signlet-triplet splitting (J_{ESR}) of the ground state as determined by the ESR studies.[4,24] The ground configuration for the dimer system splits into the singlet (^{S}G) and the triplet (^{T}G) terms due to the exchange interaction (K) between the two unpaired electrons. By means of Mulliken's approximation, K and β are expressed as follows:

$$K = -A/2(S_{99'})^2$$

and:

$$\beta = -AS_{99'}$$

$$A = -\int\varphi_9(1)\varphi_9(2)\mathscr{H}\varphi_9(1)\varphi_9(2)d\tau_{12} - \int\varphi_9(1)\varphi_{9'}(2)\mathscr{H}\varphi_9(1)\varphi_{9'}(2)d\tau_{12}$$

where $\mathscr{H}$ is the Hamiltonian for the dimer system. Then, J_{ESR} is related to K and J^* by this equation:

$$J_{ESR} = -2K + J^* = AS_{99'}(1+A/\sigma_{CT}).$$

For the case of RbTCNQ-I, the A/σ_{CT} value is evaluated to be 13 from the observed values of J_{ESR} (0.29 eV), σ_{CT} (1.2 eV), and the calculated $S_{99'}$ (0.037). Therefore, the effect of the exchange interaction is almost negligible. The correspondence of J^* and J_{ESR} is good, taking account of the experimental error and the assumptions used for the calculation. The small value of J^* (0.07 eV) for the dimer in the solution is also reasonable.

If there is interaction between the CT^- and LE^- configurations, the f_{YI}/f_{YII} ratio differs from that of the dimer in the solution, as is the case with a very weak interaction. However, the f_{YI}/f_{YII} ratio and the $\sigma_{YI}-\sigma_{CT}$ and $\sigma_{YII}-\sigma_{YI}$ splittings observed for Group A show only slight change, and they are almost equal to the corresponding values of the dimer in the solution. Therefore, it seems that the salts belonging to Group A take the same packing form of the radical pair as RbTCNQ-I. The absolute intensities of the LE bands increase from A1 to A2 and A3, while the f_{YI}/f_{YII} ratio stays constant. The reason for this increase is not clear.

Table 4. Results of open-shell SCF–CI calculation

	RbTCNQ-I		RbTCNQ-II	
	cm^{-1}	f	cm^{-1}	f
LEI	9770	0.33	11300	0.28
LEII	21900	0.68	22200	0.74
LEIII	43300	0.77	43900	0.76

Group B. The crystal structure of RbTCNQ-II was reported by Shirotani *et al.*[19] TCNQ radicals form one-dimensional columns, in which the radicals are piled with equal spacing, with a shift of 1.86 Å along the y axis.

The transition energy and the oscillator strength of the radical monomer were calculated by the use of the molecular structures of RbTCNQ-I and RbTCNQ-II (Table 4). The slight difference in the bond lengths has a considerable effect on these transitions. Although the quantitative coincidence with the experimental values is not sufficient, it may be said that the f_{LEI}/f_{LEII} ratio is smaller for RbTCNQ-II than for RbTCNQ-I. First, we will consider the dimer model in discussing the electronic states of RbTCNQ-II solid. For the type of the radical packing of RbTCNQ-II, the $CT^{\pm}$ configurations interact with all the configurations under consideration. The matrices for the configuration interaction are:

Symmetric	G	0			
	LEI^+	0	E_I^+		
	$LEII^+$	0	0	E_{II}^+	
	CT^+	$2\beta_{99'}$	$-\sqrt{2}\beta_{89'}$	$\sqrt{2}\beta_{910'}$	E_{CT}^+
Asymmetric	LEI^-	E_I^-			
	$LEII^-$	0	E_{II}^-		
	CT^-	$\sqrt{2}\beta_{89'}$	$\sqrt{2}\beta_{910'}$	E_{CT}^-	

Here, $E_{CT}^+=E_{CT}^-(=E_{CT})$ was assumed. The configuration energies were estimated in the following way. The configuration energies of the locally-excited states, E^+ and E^-, show splitting by the interradical interaction, V, of the transition dipoles. The transition moments obtained from the open-shell calculation are almost equal for LEI and LEII. Therefore, the V values calculated on the basis of the crystal structures are −0.56 and −0.23 eV for RbTCNQ-I and RbTCNQ-II respectively. By the use of the reflection results and V, $E_I=1/2\ (E_I^+ + E_I^-)=1.00$ eV and $E_{II}=1/2\ (E_{II}^+ + E_{II}^-)=2.42$ eV were obtained for RbTCNQ-I. As may be seen in Table 4, the calculated E_I and E_{II} are higher for RbTCNQ-II than for RbTCNQ-I by 1500 and 300 cm^{-1} respectively. These differences were added to the E_I and E_{II} values obtained above for the RbTCNQ-I crystal. Thus, for the RbTCNQ-II crystal, E_I and E_{II} were determined to be 1.19 and 2.46 eV, and E_I^+, E_{II}^+, E_I^-, and E_{II}^- were calculated to be 0.96, 2.23, 1.42, and 2.69 eV respectively. E_{CT} was treated as a parameter (0.50—1.50 eV), and the values of β_{ij} were varied over the range of $k=-10$——-50 ($\beta_{ij}=kS_{ij}$). The S_{ij} used was calculated by the use of the Slater-type AO's.[23] The oscillator strengths were calculated on the basis of the transition moments obtained by the open-shell calculation for LEI and LEII. By comparison with the experimental results of RbTCNQ-II, a good fit was obtained by the set of $k=-20$ and $E_{CT}=0.75$ eV (Table 5). When the radicals are piled in an infinite column, f_{CT} becomes twice as large as f_{CT} for the dimer unit. Since the

Table 5. Calculated transition energies based on the dimer model for RbTCNQ-II

	Calcd		Obsd	
	σ	f	σ	f
CT	0.92 eV	0.20	0.93 eV	0.39
YI	1.72	0.40	2.09	0.33
YII	2.95	0.56	3.52	1.48

24) R. M. Vlasova, I. A. Smirnov, L. S. Sochava, and A. I. Skerle, *Fiz. Tverd. Tela*, **10**, 2990 (1968).

25) W. Rhodes, *J. Amer. Chem. Soc.*, **83**, 3609 (1961).

Table 6. Transition energy and oscillator strength of group C

	$BaTCNQ_2$		MorTCNQ		Monomer in H_2O		Dimer in H_2O	
	cm^{-1}	f	cm^{-1}	f	cm^{-1}	f	cm^{-1}	f
CT	10000	0.09	10500	0.1			11000	0.09
YI	13800 15400	0.5	13500 15100 16100	0.9	11800 13400 14700	0.27	15800	0.22
YII	26200	1.1	27000	2.1	24800	0.47	26300	0.46

calculated CT band shows the 93% CT character, 0.20 corresponds to $0.39\times1/2$. Since this calculation does not take account of the effect of the infinite column and makes use of several assumptions, no quantitative discussion is available. The magnitudes of $k=-20$ and $E_{CT}=0.75$ eV are reasonable. In this treatment, the observed large intensity increase in the YII band could not be explained. This shows the importance of the long-range interaction. The calculations were carried out on the basis of Rhodes' [25] theory for intensity borrowing. The $\sum_{m}^{*n} G_{am\beta n}e_{am}e_{\beta n}$ factor for the YI and YII bands was four times as large for RbTCNQ-II as for RbTCNQ-I. Although a detailed discussion is impossible without the knowledge of the higher energy LE bands, it is clear that RbTCNQ-II is more sensitive to the intensity borrowing than is RbTCNQ-I.

Group C. Table 6 shows the transition energy and the oscillator strength of Group C, together with the data of the monomer and the dimer in the aqueous solution. The YI band of the monomer spectrum has a very sharp vibrational structure, the main vibrations of which are 1600 and 2900 cm^{-1} (Fig. 1). The vibrations of the YI bands, about 1600 cm^{-1} for $BaTCNQ_2$, and 1600 and 2700 cm^{-1} for MorTCNQ, are assigned to the above vibrations. The CT bands of both salts have an intensity almost equal to that of the dimer in the solution. On the other hand, the intensities of the LE bands show a remarkable increase, especially for MorTCNQ. The intense dispersion of the refractive index near the peaks of the LE bands is characteristic of Group C. This dispersion is one of the reasons for the large oscillator strength of the LE bands. Recently, it was reported that the MorTCNQ crystal contains the dimer unit of the TCNQ radicals, overlapping each other with a little shift along the x axis, and that its spacing is 3.28 Å.[26] For this mode of the radical packing, the interaction does not occur between the CT^- and the LEI^- configurations. The vibrational structure of the YI band may, therefore, be retained. Our observation of the weak CT band and the presence of the vibrational structure suggests a small contribution of the CT interaction in the solid state. However, the intensity increase in the LE bands and the outstanding dispersion of the refractive index cannot be discussed in detail at present.

The Relation of the Optical Spectrum to the Other Physical Properties. The magnitudes of the electrical resistivities of the salts of Group A are all in the order of 10^3—10^5 ohm cm, except for the case of the (Ph_3PCH_3) TCNQ (4×10^{10} ohm cm).[1,27] The salts of Group B have resistivities of 10^2 (RbTCNQ-II)[28] and 3×10^3 ohm cm (CsTCNQ).[27] By an analysis of the solid-state spectra, the CT components of the ground states are found to be a little larger for Group A (25%) than for Group B (20%). These results show that the resistivity is not sensitive to the CT character of the ground states. The TCNQ anion radical salts of Group A show the dimer formation in the solid state. On the other hand, in the salts of Group B, the radicals are piled up by equal spacings. Therefore, it may be suggested that the presence of the alternation of the radical spacing makes the resistivity large. The recent work on the MorTCNQ crystal structure also supports the above suggestion. This crystal exhibits a large alternation of the planar spacing between TCNQ anion radicals (3.28 and 3.61 Å) and shows a large electrical resistivity (10^9 ohm cm).[27]

The phase transitions of the TCNQ simple salts were observed by measurements of the absolute paramagnetic susceptbility and the electrical conductivity.[29,30] The transition temperatures are in the range of 338—391 K[29] or 348—395 K[30] for NaTCNQ, KTCNQ, and RbTCNQ-I. For RbTCNQ-II and CsTCNQ, they are 231 and 254 K[29] (210 K)[30] respectively. From our conclusion that the optically-classified groups take a different radical packing in the solid state, it is very reasonable that Group A and B behave differently in the phase transitions.

The authors would like to express their deep gratitude to Professor Saburo Nagakura of this Institute for giving them the chance to do this work and for his helpful discussions and critical reading of the manuscript. Our thanks are also due to Dr. Suehiro Iwata of the Institute of Physical and Chemical Research for his kindness in putting his computer program at our disposal.

26) T. Sandaresan and S. C. Wallwork, *Acta Crystallogr.*, **B28**, 3175 (1972).
27) W. J. Siemons, P. E. Bierstedt, and R. C. Kepler, *ibid.*, **39**, 3523 (1963).
28) N. Sakai, I. Shirotani, and S. Minomura, This Bulletin **45**, 3314 (1972).
29) *idem, ibid.*, **45**, 3321 (1972).
30) J. G. Vegter, T. Hibma, and J. Kommandeur, *Chem. Phys. Lett.*, **3**, 427 (1969).

A Note on the Intermolecular Orthogonalized Orbital

Hiroshi KATO and Shingo ISHIMARU*

Department of General Education, Nagoya University, Chikusa-ku, Nagoya 464
**Department of Hydrocarbon Chemistry, Kyoto University, Sakyo-ku, Kyoto 606*

(Received May 7, 1973)

The procedure for treating the molecular interaction is simplified by using the intermolecular orthogonalized orbital given by the method of Löwdin, and the accuracy of the approximation is examined, giving examples of the proton spin density of the solvated electron and the delocalization energy between chemically-interacting molecules. The following is then concluded: the intermolecular orthogonalized orbital is a kind of perturbed wavefunction of the molecule interacting with the other system and can most reasonably be applied when the Mulliken-type approximation for the intermolecular integrals can well be used. Its utility with regard to the three-system problem is also briefly discussed.

There have been many investigations[1-3] pointing out the important role of orbital overlapping between chemically-interacting molecules. However, the treatment considering the overlap effect is troublesome, particularly in the perturbation calculation. Consequently, in the present paper, we will try to calculate the electronic state of the composite system of molecules by the use of the intermolecular orthogonalized orbital given by the method of Löwdin[4] and will examine the accuracy of the approximation. An analogous calculation has frequently been performed in obtaining the spin density of a solvated electron on solvent molecules.[5-7] However, the wavefunction of the electron, ϕ^0, is orthogonalized only to the occupied orbitals of solvent molecules, ϕ_i, as follows:

$$\phi^0 = (\phi_e - \sum_i^{occ} S_{ei}\phi_i)/(1-\sum_i^{occ} S_{ei}^2)^{1/2}, \quad (1)$$

where ϕ_e is the non-orthogonalized orbital of the excess electron and where $S_{ei}=\langle\phi_e|\phi_i\rangle$. However, this type of orbital constructs a wavefunction which describes only the electron transfer from the occupied orbitals of solvent molecules to the excess electron orbital; in this sense, it is desirable that ϕ^0 be orthogonal also to the vacant orbitals of solvent molecules. Hence, we employ here a wavefunction satisfying this additional restriction.

Procedure

The basic notations used in this paper are summarized below:

	System A	System B
Fock operator	F_A	F_B
Occupied orbital	i, j	k, l
Vacant orbital	m, n	p, q
All orbital	a	b
Eigenvalue	ε_a	ε_b
Total energy in the ground state	W_A	W_B

Let us assume that the SCF MO's of the closed-shell systems, A and B, have already been obtained as:

$$F_A|a\rangle = \varepsilon_a|a\rangle, \quad F_B|b\rangle = \varepsilon_b|b\rangle. \quad (2)$$

The occupied orbitals orthogonalized to all of the orbitals of the other system and normalized to the second order of overlap integrals are given by:

$$\left.\begin{aligned} |i^0\rangle &= |i\rangle - \frac{1}{2}\sum_b S_{ib}|b\rangle + \frac{3}{8}\sum_b\sum_a S_{ib}S_{ba}|a\rangle \\ |k^0\rangle &= |k\rangle - \frac{1}{2}\sum_a S_{ka}|a\rangle + \frac{3}{8}\sum_a\sum_b S_{ka}S_{ab}|b\rangle \end{aligned}\right\} \quad (3)$$

which lead to $\langle i^0|j^0\rangle=O(S^3)$ and $\langle i^0|k^0\rangle=O(S^4)$, where S implies an intersystem overlap integral. We tentatively construct an antisymmetrized wavefunction using these orbitals in the following manner:

$$\Phi^0 = ||\cdots i^0\bar{i}^0\cdots j^0\bar{j}^0\cdots k^0\bar{k}^0\cdots l^0\bar{l}^0\cdots|| \quad (4)$$

where $i^0\bar{i}^0=i^0(\mu)\alpha(\mu)\ i^0(\nu)\beta(\nu)$ (μ, ν: the numbers of electrons, and α, β: spin functions). At this point of the discussion, we proceed without making definite what this wavefunction stands for. The "energy" corresponding to this wavefunction is given by:

$$W_T^0 = \langle\Phi^0|H|\Phi^0\rangle, \quad (5)$$

in which H is the hamiltonian operator of the composite system. Equation (5) is approximately written as follows:

$$\begin{aligned} W_T^0 \approx\ & W_A + W_B + Q_{AB} \\ & -2\sum_i\sum_k S_{ik}[Q_{A,ik}+Q_{B,ik}-S_{ik}(Q_{A,kk}+Q_{B,ii})] \\ & -\sum_i\sum_p S_{ip}[Q_{A,ip}+Q_{B,ip}-\frac{1}{2}S_{ip}(3Q_{B,ii}+Q_{A,pp}) \\ & +\frac{1}{2}S_{ip}(\varepsilon_p-\varepsilon_i)] \\ & -\sum_k\sum_m S_{km}[Q_{A,km}+Q_{B,km}-\frac{1}{2}S_{km}(3Q_{A,kk}+Q_{B,mm}) \\ & +\frac{1}{2}S_{km}(\varepsilon_m-\varepsilon_k)], \end{aligned} \quad (6)$$

where

$$Q_{AB} = 2\sum_i\langle i|V_B|i\rangle + 2\sum_k\langle k|V_A|k\rangle + 2\sum_i\sum_k\langle k|2J_i-K_i|k\rangle + (\text{repulsions between cores of A and B}), \quad (7)$$

$$Q_{A,ik} = \langle i|V_A+\sum_j(2J_j-K_j)|k\rangle \quad etc., \quad (8)$$

in which V is the core field and in which J and K are the Coulomb and exchange operators. In Eq. (6), the

1) H. C. Longuet-Higgins and J. N. Murrell, *Proc. Phys. Soc.*, **A68**, 601 (1955); J. N. Murrell, *ibid.*, **A68**, 969 (1955).
2) K. Fukui and H. Fujimoto, This Bulletin, **41**, 1989 (1968).
3) L. Salem, *J. Amer. Chem. Soc.*, **90**, 543, 553 (1969).
4) P. O. Löwdin, *J. Chem. Phys.*, **18**, 365 (1950).
5) W. E. Blumberg and T. P. Das, *ibid.*, **30**, 251 (1959).
6) D. E. O'Reilly, *ibid.*, **41**, 3736 (1964).
7) K. Fueki, *ibid.*, **45**, 183 (1966).

terms which are of the first and of the second order with regard to the overlap integrals are of the same order of magnitude. If the molecules considered to be non-polar, we may be permitted to put:

$$Q_{AB} \approx 0,\ Q_{A,ik} \approx Q_{B,ik} \approx \cdots \approx 0. \tag{9}$$

Hence, Eq. (6) is simplified as:

$$W_I^o \approx W_A + W_B - \frac{1}{2}\sum_i\sum_p S_{ip}^2(\varepsilon_p - \varepsilon_i) - \frac{1}{2}\sum_k\sum_m S_{km}^2(\varepsilon_m - \varepsilon_k). \tag{10}$$

On the right-hand side of this equation, the latter two terms express the stabilization brought about by the delocalization of the electronic charge between two molecules.

Other quantities are also easily obtained as follows. By the interaction with System B, the i-th orbital of A varies to:

$$\begin{aligned}\varepsilon_i^o \approx{}& \varepsilon_i + Q_{B,ii} \\ &- \frac{1}{2}\sum_b S_{ib}[Q_{A,ib} + Q_{B,ib} - \frac{1}{2}S_{ib}(\varepsilon_i - \varepsilon_b) \\ &- \frac{1}{2}S_{ib}(3Q_{B,ii} + Q_{A,bb})] \\ &- 2\sum_i\sum_j\sum_b S_{jb}\langle jb|ii\rangle - 2\sum_i\sum_a\sum_l S_{al}\langle al|ii\rangle \\ &+ \frac{1}{2}\sum_i\sum_j\sum_b S_{jb}^2(3J_{ij} + J_{ib}) + \frac{1}{2}\sum_i\sum_a\sum_l S_{al}^2(3J_{il} + J_{ia}) \\ &+ \frac{1}{2}\sum_i\sum_l\sum_b S_{ib}^2(3J_{il} + J_{lb})\end{aligned} \tag{11}$$

and the matrix elements concerning the charge transfer and the electronic excitation, which should vanish when intermolecular SCF MO's are used, are, respectively:

$$\begin{aligned}\langle\Phi_{i\to p}^o|H|\Phi^o\rangle \approx{}& \frac{1}{2}[Q_{A,ip} + Q_{B,ip} - S_{ip}(Q_{A,pp} + Q_{B,ii})] \\ &- \frac{1}{2}[\sum_{a\neq i} S_{ap}Q_{B,ia} + \sum_{b\neq p} S_{ib}Q_{A,pb}] \\ \langle\Phi_{i\to m}^o|H|\Phi^o\rangle \approx{}& Q_{B,im} - \frac{1}{2}\sum_b S_{ib}(Q_{A,mb} + Q_{B,mb}) \\ &- \frac{1}{2}\sum_b S_{bm}(Q_{A,ib} + Q_{B,ib}) \\ &+ \sum_b S_{ib}S_{mb}\Big[\frac{1}{8}(\varepsilon_i + \varepsilon_m) - \frac{1}{4}\varepsilon_b \\ &+ \frac{3}{8}(Q_{B,ii} + Q_{B,mm}) + \frac{1}{4}Q_{A,bb}\Big].\end{aligned} \tag{13}$$

Furthermore, it may be noted that the intermolecular orthogonalized orbital is convenient for treating the three-system (A, B, and C) problem; then:

$$|i^o\rangle = |i\rangle - \frac{1}{2}\sum_r S_{ir}|r\rangle + \frac{3}{8}\sum_r\sum_s S_{ir}S_{rs}|s\rangle, \tag{14}$$

where r indicates all the molecular orbitals of the two systems except A, and where s indicates all those of the two systems except the system to which r belongs. Here, $\langle i^o|i^o\rangle = 1 + O(S^3)$. The accuracy is inferior to that in the case of two systems. With the use of Eq. (14), the core integral is written as:

$$\begin{aligned}\langle i^o|H^c|i^o\rangle = {}& \langle i|H^c|i\rangle - \sum_r S_{ir}\langle i|H^c|r\rangle \\ &+ \frac{1}{4}\sum_r\sum_{r'} S_{ir}S_{ir'}\langle r|H^c|r'\rangle \\ &+ \frac{3}{4}\sum_r\sum_s S_{ir}S_{rs}\langle i|H^c|s\rangle,\end{aligned} \tag{15}$$

where $H^C = T + V_A + V_B + V_C$ (T: the one-electron kinetic operator) and where r and r' belong to the same group of molecules. It is clear in Eq. (15) that the three-center integrals emerge from the second and last terms. Thus, according to the orthogonalization procedure, the three-system problem becomes tractable.

Now, let us compare the above treatment with that of Devaquet,[9] in which the following intermolecular SCF MO for two closed-shell molecules is used:

$$|i^{int}\rangle = |i\rangle(1 - \gamma_i) - \sum_b c_{ib}|b\rangle + \cdots, \tag{16}$$

where:

$$\begin{aligned}\gamma_t &= \frac{1}{2}\sum_b c_{tb}(c_{tb} - 2S_{ib}) \\ c_{ib} &= \frac{F_{ib} - S_{ib}F_{ii}}{F_{bb} - F_{ii}} \\ &\approx \frac{\frac{1}{2}S_{ib}(\varepsilon_b - \varepsilon_t) + \left[\frac{1}{2}(Q_{A,ib} + Q_{B,ib}) - S_{ib}Q_{B,ii}\right]}{\varepsilon_b - \varepsilon_i + Q_{A,bb} - Q_{B,ii}}\end{aligned} \tag{17}$$

(F: Fock operator for the composite system of two molecules). If we set:

$$\frac{1}{2}(Q_{A,ib} + Q_{B,ib}) - S_{ib}Q_{B,ii} = 0,\ Q_{A,bb} - Q_{B,ii} = 0, \tag{18}$$

i.e.,

$$Q_{A,ib} + Q_{B,ib} = S_{ib}(Q_{A,bb} + Q_{B,ii}), \tag{19}$$

c_{ib} and γ_i become:

$$c_{ib} \approx \frac{1}{2}S_{ib} \text{ and } \gamma_i \approx -\frac{3}{8}\sum_b S_{ib}^2 \tag{20}$$

respectively. Equation (16) agrees with Eq. (3) if we take only the i term in the summation with respect to a in Eq. (3). Equation (19) is regarded as a "Mulliken-type approximation" for intermolecular integrals in the case of non-polar molecules.

The interaction energies given by Eqs. (3) and (16) are similar except for the term:

$$\left.\begin{aligned}&-2\sum_i\sum_p \frac{I_{ip}^2}{\varepsilon_p - \varepsilon_i} - 2\sum_k\sum_m \frac{I_{km}^2}{\varepsilon_m - \varepsilon_k} \\ &I_{ip} = \frac{1}{2}(Q_{A,ip} + Q_{B,ip}) \quad etc.\end{aligned}\right\} \tag{21}$$

which appears only in the expression of Devaquet. That is, the intermolecular orthogonalized orbital is a kind of approximate perturbed wavefunction of the molecule interacting with the other system, and the validity depends on the adequacy of the approximation represented by Eq. (19). Under the condition that Eq. (19) is well satisfied, the total wavefunction of the single Slater determinant composed of orthogonalized orbitals (Eq. (4)), which includes the resulting charge-transfer and polarization effects, is considered to describe the electronic state of the composite system appropriately.

8) L. Brillouin, *Actualites Sci. et Ind.*, **71**, (1933); 159 (1934).

9) A. Devaquet, *Mol. Phys.*, **18**, 233 (1970).

TABLE 1. THE CALCULATED RESULTS CONCERNING THE INSIDE PROTON SPIN DENSITY OF THE SOLVATED ELECTRON[a)]

Solvent	Previous work[b)]		The 1s AO orthogonal to all of the orbitals of solvent molecules (I)	The 1s AO orthogonal only to the occupied orbitals of solvent molecules (II)
	Total	Delocalization term		
NH_3	−0.009	+0.0008	+0.020	+0.009
H_2O	−0.012	+0.00004	+0.021	+0.007

a) The model is formed by four solvent molecules with one OH or NH bond oriented toward the cavity center. The orbital exponent of the 1s AO for the solvated electron is 0.3 a.u.$^{-1}$.
b) Ref. 10.

Examples

Table 1 shows the calculated spin densities of the solvated electron on the proton of solvent molecules. The values of I are larger than those of II; this is because in the former the delocalization, from the 1s AO of the excess electron to the vacant orbitals of solvent molecules, and from the occupied orbitals to the 1s AO, are both included, while in the latter only the delocalization from the occupied orbitals to the 1s AO is included. The discrepancy of this I from that of our previous work[10] is mainly caused by the approximation corresponding to omitting the term of (21). The result of II for the ammoniated electron differs very much from O'Reilly's.[6] This may be brought about by the differences between the wavefunctions applied and the approximation in estimating the molecular integrals. For the hydrated electron, the spin density of II is almost identical with Fueki's,[7] *ca.* 0.01, which is given in the same manner as II by the orbital exponent of the 1s AO for an excess electron, 0.312 a.u.$^{-1}$. At any rate, the spin polarization mechanism contributes dominantly in the case of a solvated electron in polar solvents; therefore, the values obtained by the orthogonalized orbital, which gives only an approximate spin delocalization term through the second order of the overlap integral, are unsatisfactory.

In Table 2, the results concerning the delocalization energies between a hydrogen molecule and carbene, between borane and borane, and between carbene and ethylene are compared with those of Fukui *et al.* For models (1) and (2), the present values are overestimated by a factor of several times.[11] For Model (3), the error is as small as *ca.* 16% and when the intermolecular distance R becomes smaller (Model (4)), the error increases. In Model (3), the perturbation expansion with the overlap is suitable because of the large intermolecular distance; besides, Eq. (19) can be expected to be satisfied successfully.

TABLE 2. THE RESULTS OF THE DELOCALIZATION ENERGY (in eV)

Model	Present value	The value given by Fukui *et al.*
(1)	0.048090	0.013575[a)]
(2)	0.603132	0.129753[b)]
(3)	0.035370	0.042354[c)]
(4)	0.105696	0.281025[c)]

a) Calculated by M. Miyagi.
b) Calculated by S. Kato.
c) Ref. 12.

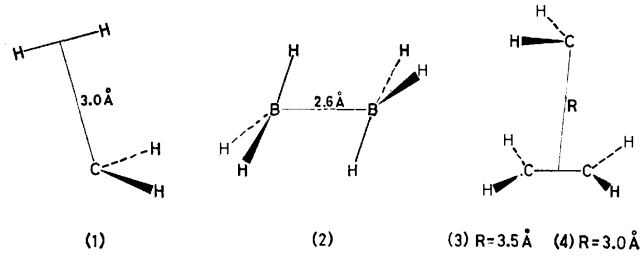

Fig. 1. The models used in the calculation of the delocalization energy.

Conclusion

The intermolecular orthogonalized orbital is a kind of perturbed wavefunction of the molecule interacting with the other system, and, with the use of the orbital, the approximate expression of the interaction energy can easily be derived. It should be noticed, however, that the wavefunction can most reasonably be applied when the Mulliken-type approximation for the intermolecular integrals can be used. This means that, for the case in which the Gaussian-type orbitals are favorably used,[13] it is appropriate to use the intermolecular orthogonalized orbital. Moreover, according to the present procedure, the three-system problem becomes tractable.

The authors wish to thank Professor Kenichi Fukui for his valuable discussions. They also wish to thank Mr. Morio Miyagi and Mr. Shigeyuki Kato for thier generous permission to cite unpublished data.

10) S. Ishimaru, H. Kato, T. Yamabe, and K. Fukui, *Chem. Phys. Lett.*, **17**, 264 (1972).
11) For model (1), the value of r.h.s. of Eq. (19) between highest occupied orbitals is −0.605 and that of l.h.s. is −0.327 in eV.
12) H. Fujimoto, S. Yamabe, and K. Fukui, This Bulletin, **45**, 2424, (1972).
13) L. Jansen, "Advances in Quantum Chemistry," Vol. 2, ed. by P. O. Löwdin, Academic Press, New York, (1965), p. 119. H. Margenau and J. Stamper, *ibid.*, Vol. 3, (1967), p. 129.

Arrangement of Acridine Orange in the Poly-α, L-glutamic Acid–Acridine Orange Complex

Yukio SATO and Masahiro HATANO

The Chemical Research Institute of Non-aqueous Solutions, Tohoku University, Sendai 980

(Received May 8, 1973)

The temperature dependencies of the absorption and circular dichroism spectra of the poly-α,L-glutamic acid-acridine orange complex were observed at the temperatures in the range of 23—95 °C. The circular dichroism spectra were resolved into several Gaussian components by means of a computer online system. Thus, the circular dichroism spectrum can be resolved to five components. The shorter-wavelength bands, consisting of one positive and one negative element, were assigned to the transitions polarized parallel to and perpendicular to the axis of the α-helix of polypeptide respectively. On the other hand, the longer-wavelength bands, having equal magnitudes but signs opposite to each other, were assigned to the transition of the acridine orange dimer bound to polymer. The fifth band, at the shortest wavelength was uncertain. On the basis of these results, the arrangement of acridine orange molecules bound to poly-α,L-glutamic acid was discussed. Thus, two kinds of arrangements of acridine orange molecules were postulated. One is a left-handed super-helix around the right-handed α-helix of the polypeptide in the acidic pH region, and the other is a right-handed super-helix around the core of the α-helix in the alkaline pH region when the molar ratio of glutamyl residues to the dye is kept around unity. In these two complexes, there are dimeric acridine orange molecules bound to the polymer; in the latter complex, the super-helix consists of dimeric acridine orange molecules. Two types of arrangements of acridine orange molecules around the polypeptide were offered for the elucidation of the circular dichroism spectra of the complex of acridine orange with poly-α,L-glutamic acid in an aqueous solution.

Stryer and Blout studied the optical rotatory properties of dyes bound to polypeptides.[1] They made the interesting observation that an extrinsic Cotton effect in the wavelength region corresponding to the absorption bands of bound dye was obtained only when the dye combined with the helical form of poly-α,L-glutamic acid (PLGA). They also explained their results in a manner consistent with the dye-aggregation concept. Thus, they postulated three types of models for the elucidation of the Cotton effects observed in the complex of acridine orange (AO) with PLGA. According to their concept, the acquired optical rotatory power of the bound dye molecule can be only one of two types, configurational or conformational. A configurationally-induced Cotton effect could arise from the interaction of the symmetric dye chromophore with the local asymmetric environment of the α-carbon atom of the polypeptide. On the other hand, a conformationally-induced Cotton effect might result from the interaction among several symmetric dye chromophores which have been oriented to one another in the axial chirality sense by binding to the asymmetric polypeptides.

A conformationally-induced Cotton effect could arise from the aggregates of the dye molecules, which superimpose on the α-helix of polypeptide to form a superhelix in a single-screw sense or which form a tangential helix to the α-helix of polypeptide. Their data favor the conformational type of induced Cotton effect.

On the other hand, Yamaoka and Resnik[2] assumed that the induced Cotton effect in the PLGA–AO complex was caused by a vicinal dissymmetry around the asymmetric carbons in PLGA, since the induced Cotton effect was observed even at very high values of the ratio of the glutamyl residue to the dye (R/D). This assumption of Yamaoka's agrees with the configurationally-induced Cotton effect proposed by Stryer and his collaborator.[1]

In a previous paper,[3] we reported that the induced Cotton effect in the PLGA–AO complex arose from an interaction between the dimerically-bound AO molecules and that the induced Cotton effect arose from a helical arrangement of the dye along the main chain of the polypeptide.

The structure of this complex has not yet been established, although the structure was discussed in another report.[4] In this paper, we wish to report on our study of the arrangement of AO molecules on PLGA by means of some analyses of the effect of the temperature on their circular dichroism and on the absorption spectra. We will consider the origin of the induced Cotton effects on the basis of curve resolution for the observed circular dichroism bands. Furthermore, we will show the possible models of the PLGA–AO complex both in the case of pH=4.5 at small R/D (the ratio of the glutamyl residues to the dye molecules) values and in the case of the alkaline pH region at a R/D value of around unity. The induced circular dichroism bands can be explained by these models.

Experimental

The materials and the procedure are the same as those described previously.[5] The temperature in the optical cell was measured by means of a Takara Thermistor, Type SPD-1D, and allowed to equilibrate for 5 min before each

1) L. Stryer and E. R. Blout, *J. Amer. Chem. Soc.*, **83**, 1411 (1961).

2) K. Yamaoka and R. A. Resnik, *J. Phys. Chem.*, **70**, 4051 (1966).

3) Y. Sato, M. Hatano, and M. Yoneyama, This Bulletin, **46**, 1980 (1973).

4) R. E. Ballard, A. J. McCaffery, and S. F. Mason, *Biopolymers*, **4**, 97 (1966).

5) Y. Sato, M. Yoneyama, and M. Hatano, This Bulletin, **45**, 1941 (1972); M. Hatano, M. Yoneyama, and Y. Sato, *Biopolymers*. **12**, 895 (1973).

reading. The computer used for the curve fitting was a JEC-6 Spectrum Computer of the Japan Electron Optics Lab. Co., Ltd.

All the data presented below are reduced to the molar basis of the total AO concentration and are expressed by the molar extinction coefficient, ε, and the molar ellipticity, $[\theta]$. The molar ellipticity of the band at 222 nm is obtained on the basis of the molar quantity of the glutamyl residue.

Results

Effect of Temperature on the PLGA–AO Complex. Although Eyring and his collaborators[6] observed the effect of the temperature on the optical rotation of the PLGA–AO complex, they did not analyze this phenomenon. Therefore, we analyzed the temperature effect on the absorption and circular dichroism spectra of the PLGA–AO system with the variation in the value of the R/D ratio and in that of the pH of the system.

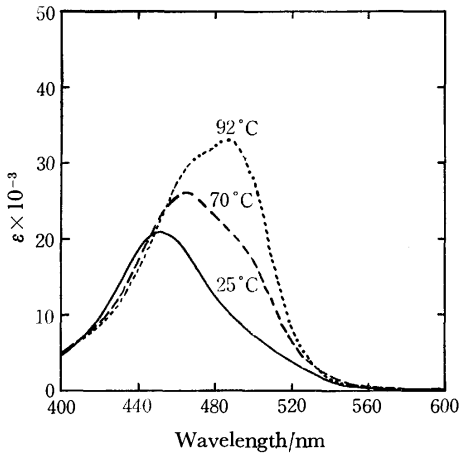

Fig. 1. Temperature dependence of absorption spectrum of PLGA–AO system. R/D=10, pH=4.5, [AO]=2×10^{-5}M.

When the PLGA–AO solution was gradually heated, the absorption spectrum changed, as is shown in Fig. 1. This variation may be due to a dissociation of AO molecules from the PLGA–AO complex or to a deaggregation of the AO molecules in the complex. This phenomenon was quite the reverse of the that anticipated. The course of the variation in the absorption spectrum was followed by measurements of the changes in the absorbance of the bands at 450 and 492 nm. The former band can be assigned to a band due to the aggregated AO, and the latter band, to the monomeric AO.[7] The temperature-dependent variations of the absorption bands at 450 and 492 nm in the R/D ratios of 10 and 1 are shown in Figs. 2 and 3 respectively. From these figures it can be seen that there are two types of shapes in these curves; this may be due to a difference between the arrangements of AO molecules bound to PLGA in the R/D ratios of 10 and 1. In order to discriminate the types of the arrangements of AO, the course of the decrease in

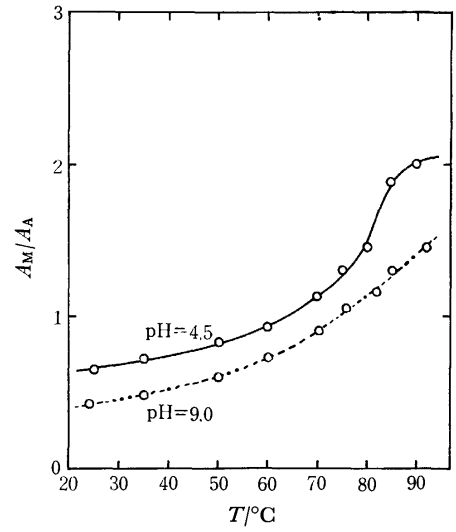

Fig. 2. Variation of ratio of absorbance at 492 nm (A_M) to absorbance at 450 nm (A_A) with changing temperature. R/D=10, [AO]=2×10^{-5} M.

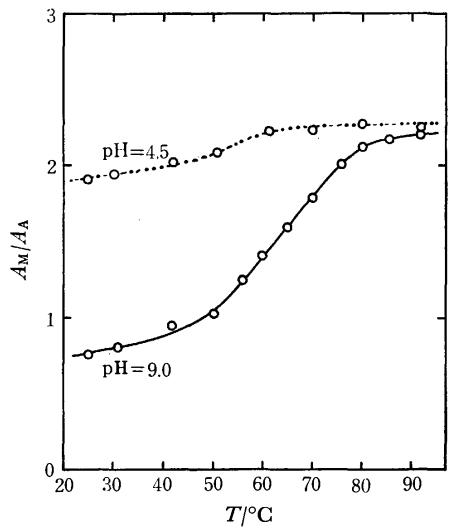

Fig. 3. Variation of ratio of absorbance at 492 nm (A_M) to absorbance at 450 nm (A_A) with changing temperature. R/D=1, [AO]=2×10^{-5} M.

the molar ellipticities at the wavelengths of 435, 465, and 520 nm were observed; the variations in the ellipticities are summarised in Fig. 4. The circular dichroism (CD) bands at 435 and 465 nm may be ascribed to the aggregated AO in a helical fashion, and that at 520 nm, to the dimerically-bound AO.[3,4] The shapes of the temperature-dependent variation curves at 435 and 465 nm are similar to each other, but the shape at 520 nm is different. This indicates that the dimeric AO molecules are not in a helical arrangement. Furthermore, the variations in the residue molar ellipticities of PLGA samples with various degrees of polymerization were measured in the presence or in the absence of AO molecules; the results are shown in Figs. 5 and 6 respectively. From Fig. 5, it may safely be said that a complete helix-coil transition of PLGA does not occur in this temperature range. This may be because the glutamyl residues acquire a somewhat negative heat of ionization with

6) E. J. Eyring, M. Kraus, and J. T. Yang, *Biopolymers*, **6**, 703 (1968).

7) V. Zanker, *Z. Phys. Chem.*, **199**, 225 (1952).

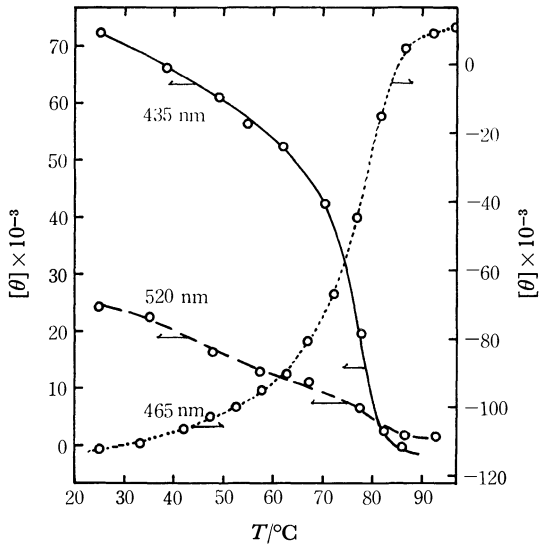

Fig. 4. Temperature dependence of the magnitudes of molar ellipticities of PLGA–AO system at each wavelength. R/D=10, pH=4.5, [AO]=2×10^{-5} M.

an increase in the temperature.[8] On the other hand, Fig. 6 shows the occurrence of the helix-coil transition for the PLGA–AO system in the observed temperature range. This may reflect the dissociation of AO molecules from the complex, or it may suggest that a raising of the temperature disturbs the formation of an array of AO molecules on PLGA anions. In other words, it is suggested that the aggregation of AO molecules on PLGA favors keeping the α-helix structure of PLGA itself.

Effect of the Degree of Polymerization of PLGA on the Dye Aggregation in the PLGA–AO Complex. As has previously been reported,[3,5] the pH, the R/D ratio, and a neutral salt addition can all affect the extent of the dye aggregation on PLGA. Figure 7 shows the

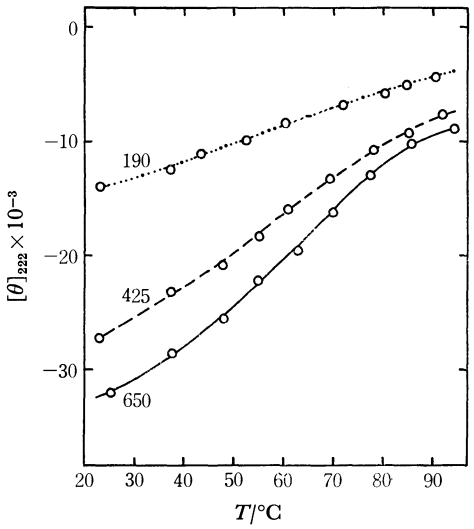

Fig. 5. Temperature dependence of the magnitudes of molar ellipticities of PLGA at 222 nm.
Numerical values in the figure shows the degree of polymerization of PLGA; pH=4.5.

8) R. Doty, A. Wada, J. T. Yang, and E. R. Blout, *J. Polymer. Sci.*, **23**, 851 (1957).

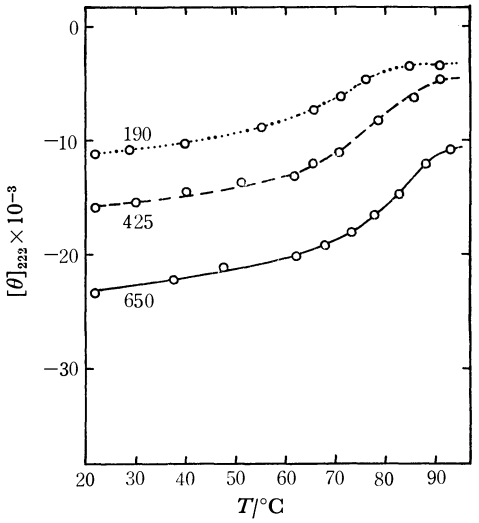

Fig. 6. Temperature dependence of magnitudes of molar ellipticities of PLGA–AO system at 222 nm. Numerical values in the figure show the degree of polymerization of PLGA; R/D=10, pH=4.5, [AO]=2×10^{-5} M.

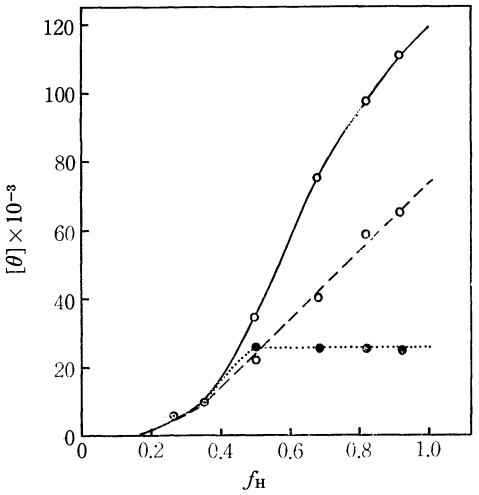

Fig 7. Plots of $[\theta]$ *vs.* helix fraction of PLGA (f_H) in the PLGA–AO systems having various R/D values.
pH=4.5. —○—: at 435 nm, —○—: at 465 nm, (−[θ]); ···●···: at 520 nm.

relation between f_H (helix fraction of PLGA in the PLGA–AO system) and the molar ellipticities of CD bands at 435, 465, and 520 nm. The values of f_H can be estimated from the residue molar ellipticities at 222 nm. The molar ellipticities at 435 and 465 nm increase with an increase in the f_H value, whereas that at 520 nm increases gradually with an increase in the f_H value up to 0.5 and then is almost constant in the case f_H values higher than 0.5. Figure 7 indicates that a higher f_H value than 0.2 is necessary to induce a Cotton effect in the visible region. The magnitudes of the molar ellipticities at 435 and 520 nm are dependent mainly on the helical aggregated and dimeric AO fractions respectively.[3,4] Figure 8 gives the relation between the degree of the polymerization of PLGA and the ratio of the molar ellipticity of the CD band at 520 nm to that at 435 nm. This indicates that none of all the AO molecules bound to PLGA

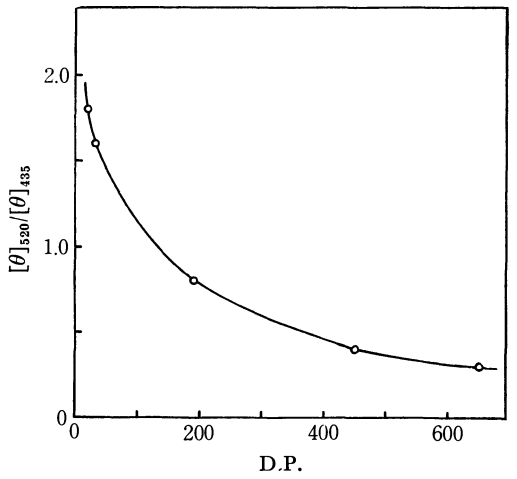

Fig. 8. Plots of ratio of magnitude of molar ellipticities at 520 nm to magnitude at 435 nm *vs.* degree of polymerization of PLGA (D.P.) in PLGA–AO system.
R/D=10, pH=4.5, [AO]=2×10^{-5} M.

are dimeric, since the relation shown in Fig. 8 is not linear. This consideration is supported by the findings on neutral salt effects on the PLGA–AO system.[3]

Curve Fitting. In order to assign the CD bands observed in the PLGA–AO system, we resolved the CD bands by a conventional Gaussian fitting method. Figure 9 shows the most favorable curve fitting for the case of R/D=10 and pH=4.5, and Fig. 10, for the case of R/D=1 and pH=9.1. In both figures, the solid lines indicate the observed curves, whereas the dotted lines indicate Gaussian curves obtained by the use of a computer.

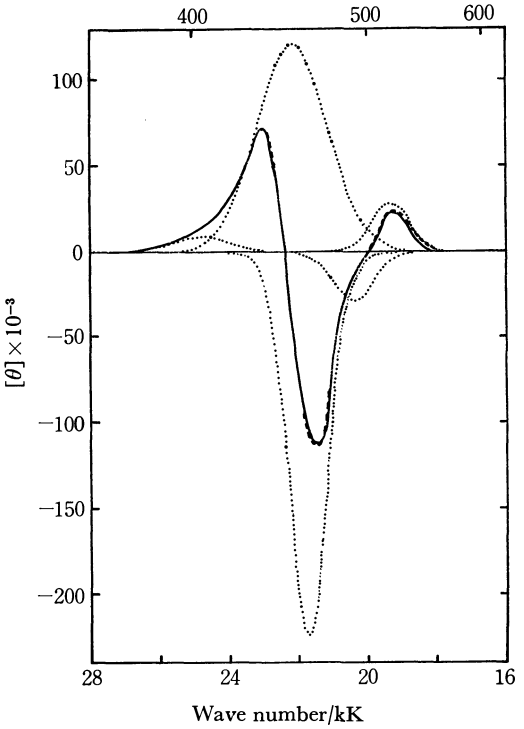

Fig. 9. CD spectrum of PLGA–AO system and its resolution into Gaussian bands; R/D=10, pH=4.5, [AO]=2×10^{-5}M.
·····: Gaussian bands, ——: Observed spectrum.

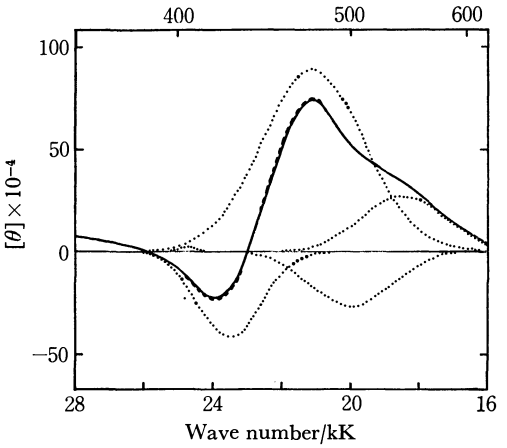

Fig. 10. CD spectrum of PLGA–AO system and its resolution into Gaussian bands; R/D=1, pH=9.1, [AO]=2×10^{-5} M.
·····: Gaussian bands, ——: Observed spectrum.

Discussion

Aggregation of AO Molecules on PLGA. Ballard *et al.*[4] reported that the aggregation of AO molecules in the PLGA–AO complex has the form of a left-handed super-helix around the core of the right-handed α-helix of PLGA in a acidic pH region. On the other hand, we found that AO molecules are arranged to form a right-handed super-helix in the alkaline pH region at a R/D of around unity.[5] In a previous paper,[3] the CD band at 520 nm was assigned to the band due to the AO dimer bound to the helical PLGA in an acidic aqueous solution. Furthermore, the magnitude of the CD band at 520 nm is nearly constant at various R/D values, from 4 to 500, (as is shown in Table 1); therefore, it may safely be said that the PLGA–AO complex consists of both dimeric AO and helical AO molecules. The dimeric AO molecules contribute almost nothing to the rotational strength at 435 and 465 nm, since the increase in dimeric AO molecules is not accompanied by an increase in the magnitude at 435 and 465 nm.[3]

TABLE 1. SUMMARY OF RESULTANT CD FOR PLGA–AO SYSTEM

	Present work			*a*		*b*
R/D	4	10	20	100	400	500
λ(nm)	520	520	520	525	522	522
$[\theta]\times10^{-3}$	26	25	23.1	26.4	23.76	29.7

a) Ballard *et al.*, Ref. 4.
b) Yamaoka and Resnik, Ref. 2.

Arrangement of AO Molecules Bound to PLGA in the Acidic pH *Region.* In the acidic pH region, it was found, by using a variation method, that one AO molecule interacts with three glutamyl residues in PLGA.[9] Since AO molecules have a strong stacking tendency, the molecules are not randomly distributed among the available sites on a helical PLGA, but occupy sites adjacent to one another on the PLGA

9) B. C. Myhr and J. G. Foss, *Biopolymers*, **10**, 425 (1971).

and stack with each other.[10] The angle, v, between the direction of the long-axis electronic-transition moment of the AO molecule and the helix axis of PLGA may have values in the range from 5° to 40°.[4] If the thickness of the AO molecule is assumed to be 3.2 Å, and if the distance between the 3-dimethyl amino group and the 6-dimethyl amino group along the long axis of the AO molecule itself is 9.6 Å, the schematic model of the PLGA–AO complex shown in Fig. 11 can be used. In this case, the geometry of the binding sites of PLGA is that of α-helix, *i.e.*, 3.6 residues/turn, a vertical distance of 1.5 Å from each other, and a radius 5.4 Å.[11]

On the basis of the geometry of AO molecules in the PLGA–AO complex, the v angle can be determined to be near 15°; this seems plausible in view of Ballard's results[4] and the geometrical positions of the binding sites on PLGA. The short axis of the AO plane may be slightly tangentially-oriented with respect to the axis of the α-helix of PLGA, since this complex gives a positive CD band near 295 nm, where a transition polarized along the short axis of AO appears.[5]

A frequency interval, $\Delta\nu$, between the two transition energies which interact each other is given by:[12]

$$\Delta\nu = 2\mu^2 G/hcd^3 \qquad (1)$$

where G is the geometric factor for the dipole-dipole interaction with the limitting values of $+2$ and -1, h is Planck's constant, c is the velocity of light, and d is the distance between the two transition moments. The dipole strength, μ^2, of the visible absorption band of monomeric AO is 47×10^{-36} c.g.s.[12]

A Gaussian analysis, as is shown in Fig. 9, for the CD curve of the PLGA–AO complex in the acidic pH region suggests the presence of one positive CD band at 520 nm and one negative CD band at 490 nm. The magnitudes of the two bands at 520 and 490 nm are nearly equal to each other, but the signs are opposite. In the pair of bands, the frequency interval is 1100 cm^{-1}. The geometric factor, G, is assumed to be $+1$ because of the antiparallel sandwich type of AO dimer, and the distance from the center of one AO molecule to that of the nearest neighbor AO molecule in the PLGA-AO complex can be estimated to be 7.6 Å, which is a reasonable value.

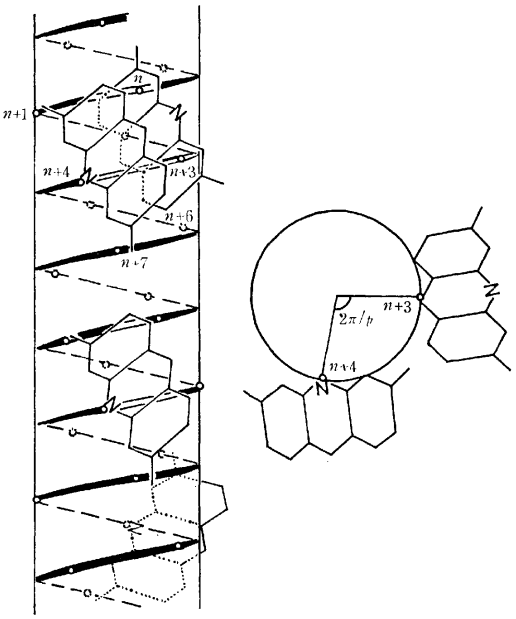

Fig. 11. Schematic model of PLGA–AO complex and the correlation between the positions of dimeric AO molecules in acidic pH.

In the PLGA–AO complex, two types of interaction between the transition dipoles of the AO molecules in the helical array bound to the helical PLGA can be expected. One is dependent on the radius of the helix, whie the other is dependent on the pitch. The radius-dependent rotational strength, R, is given by the following equation:[12]

$$R_{//} = -R_{\perp} = 2\pi a\mu_v\mu_t \sin^2(\pi/P) \qquad (2)$$

where a is the radial distance of each transition dipole from the helical axis and where $(2\pi/P)$ is the angle in radian about the axis between the two adjacent dipoles, which refer to Fig. 11. The rotational strengths, $R_{//}$ and $R_{\perp}$, arise from the resultant electronic transitions, which are polarized parallel and perpendicular to the helix axis respectively. The moments, μ_v, μ_t, and μ_r are, respectively, the vertical, tangential, and radial components of the dipole vector, μ, in the cylindrical coordinate frame of the helix. If the AO molecular planes lie at an angle of 15° to the axis of the helix, the pitch-dependent rotational strength can be neglected. Hence, the radial components of the interactions between the two excitation dipoles could be considered; the rotational strength was estimated to be 25×10^{-40} c.g.s., assuming the angle to be 15°. This value was obtained on the approximation that the dimeric AO molecules were attached to the glutamyl residues numbered (n, $n+3$, $n+6$) and ($n+1$, $n+4$, $n+7$) in the sequence along the polypeptide backbone of the α-helix of PLGA. This approximation was based on the finding that the distance between the dimeric AO molecules was nearly equal to that between the binding residues numbered $n+3$ and $n+4$. On the other hand, the experimental value of the rotational strength obtained from the CD magnitude of the bands at 520 and 490 nm was 23×10^{-40} c.g.s.; it was obtained using the following equation:

$$R = 0.696\times10^{-42}\sqrt{\pi}\,[\theta_k]\frac{\Delta_k}{\lambda_k} \qquad (3)$$

where $[\theta_k]$, Δ_k, and λ_k are the molar ellipticity, the half-band width, and the wavelength of the k-th CD band respectively. This experimental value agrees with the calculated one. Accordingly, the postulated scheme for the arrangement of AO molecules bound to PLGA may be plausible. As is shown in Fig. 11, two AO molecules attached to the glutamyl residues numbered (n, $n+3$, $n+6$) and ($n+1$, $n+4$, $n+7$) form the dimeric AO. Besides, the aggregated AO molecules have the form of a left-handed super-helix around the core of the α-helix of PLGA. These aggregated AO mole-

10) D. F. Bradley and M. K. Wolf, *Proc. Natl. Acad. Sci., U.S.*, **45**, 944 (1959).
11) I. Tinoco, Jr., R. W. Woody, and D. F. Bradley, *J. Chem. Phys.*, **38**, 1317 (1963).
12) B. J. Gardner and S. F. Mason, *Biopolymers*, **5**, 79 (1967).

cules have two CD bands, a negative CD band at 465 nm and a positive CD band at 435 nm, arising, respectively, from the transitions polarised parallel to and perpendicular to the axis of the α-helix of PLGA.[4] As is shown in Fig. 9, there are a negative component at about 460 nm and a positive component at about 450 nm in the CD curve of the PLGA–AO complex. These components can be assigned to the transitions polarized parallel and perpendicular to the axis of the α-helix of PLGA.

Arrangement of AO Molecules Bound to PLGA in the Neutral and Alkaline pH *Regions.* In the neutral and alkaline pH regions, PLGA is substantially ionized and randomly coiled in an aqueous solution. However, we have found that the PLGA–AO complex has a helical structure even in the neutral and alkaline pH regions at a R/D of unity.[5] In this case, the ring nitrogen cations of AO molecules bind to the carboxylate anions of PLGA side chains; these AO cations may be neutralized enough by the ion coupling to stack together. From the sign of the CD band near 450 nm (Fig. 10), it was considered that the arrangement of AO molecules bound to PLGA at R/D=1 and pH=9 may be such that their long axes form a right-handed super-helix around the PLGA chain. Thus, the formation of stacked dimeric AO molecules on PLGA is most plausible.

Over the same geometry of the α-helix of PLGA with that in an acidic aqueous medium, an array of aggregated AO, at R/D=1 and pH=9, may be arranged in such way as is shown in Fig. 12. In this case, one positive CD band and one negative CD band can be observed at 540 nm and at 500 nm respectively. In view of the steric hindrance between the dimethylamino groups of the AO molecules, the transition dipoles of the AO molecules may lie at an angle of about 51° to the axis of α-helix of PLGA. In this complex, AO molecules attached to the glutamyl residues numbered n, $n+3$, and $n+6$ may form two pairs of dimers. On the basis of these presumptions, the rotational strength arising from the interaction between dimeric AO molecules can be estimated to be 101×10^{-40} c.g.s. Therefore, the total rotational strength originating from dimeric AO molecules is 202×10^{-40} c.g.s. This value is very small compared with the experimental value. The rotational strength obtained from resolved CD curves using Eq. (3) amounts to 480×10^{-40} c.g.s. This extraordinarily large rotational

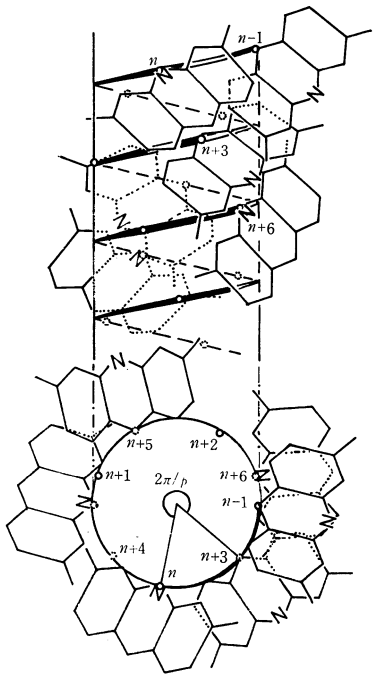

Fig. 12. Schematic model of PLGA–AO complex and the correlation between the positions of dimeric AO molecules at R/D=1, pH=9.

strength may arise from an interaction between the neighboring AO molecules on PLGA numbered $n-1$, $n+1$, $n+2$, *etc.* In the case of an R/D of unity in the alkaline pH region, the dimeric AO molecules should form an aggregate more tightly and should interact with each other. Therefore, the interaction between the dimeric AO units must be considered to be stronger in this case than in the case of a large value of R/D in the acidic pH region.

These closely-spaced AO molecules around the core of the α-helix of PLGA may also give an extraordinarily large rotational strength at 222 nm,[5] one which results from the coupling of the spin-forbidden n-π^* transition of polypeptide with some other allowed π-π^* transition of the AO molecule.

The polarization directions of the AO molecules and dimeric AO could be assigned by means of a polarization technique using a liquid crystal, one which is oriented by the application of an electric field. This experimental technique and our results will be described elsewhere in the near future.

Charge-transfer and Proton-transfer in the Formation of Molecular Complexes. VII.[1] Complex Isomerism in Several Anilinium Alkyl-substituted Picrates

Nobuaki INOUE and Yoshio MATSUNAGA

Department of Chemistry, Faculty of Science, Hokkaido University, Sapporo 060

(Received May 11, 1973)

o-Chloroanilinium and *o*-bromoanilinium methylpicrates are obtainable not only as yellow-colored salts, but also as unstable, monotropic reddish-orange forms. Spectroscopic studies have revealed that the latter are charge-transfer complexes composed of the aniline molecule acting as an electron-donor and the acid molecule acting as an acceptor. Similar monotropic forms have been found in combinations of dimethylpicric acid with *o*-iodoaniline, *o*-bromoaniline, and *N,N*-dimethylamino-*p*-benzaldehyde.

About half a century ago, Hertel found that yellow-colored *o*-bromoanilinium picrate turns reddish-orange upon heating above 95 °C.[2] On the basis of the similarity in color and melting point with the corresponding *s*-trinitrobenzene complex, he concluded that the deeply-colored high-temperature form is a molecular compound composed of the aniline and the acid. As was confirmed by our spectroscopic examinations,[3] this is a charge-transfer complex in present-day terminology. The yellow picrate and the reddish-orange picric acid complex are enantiotropically related to each other. Hertel named this phenomenon "complex isomerism". Several more combinations including *o*-iodoanilinium picrate have been reported by Hertel to behave similarly.

With the hope of finding new organic compounds which exhibit solid-state transformations accompanied by a color change, we have examined series of anilinium methylpicrates and dimethylpicrates. These alkyl-substituted picric acids have been reported by Mariella *et al.* to form salts with aniline and its *N,N*-dimethyl derivative.[4] All of them have been noted to decompose at their melting points.

Experimental

Materials. The methylpicric acid and dimethylpicric acid were prepared by the nitration of *m*-cresol and 3,5-dimethylphenol respectively.[5] All the aromatic amines used in this work were commercially obtained. The anilinium alkyl-substituted picrates were precipitated by mixing the component compounds separately dissolved in chloroform or benzene.

Measurements. The vibrational and electronic spectra were measured as has been reported in the first paper of this series.[6] The X-ray measurements were made with a Toshiba recording diffractometer, Model ADG-301, using filtered copper radiation.

Results and Discussion

The combinations of methylpicric acid with *N,N*-diethyl-*m*-toluidine (pK_a=7.12), *N,N*-dimethyl-*o*-toluidine (6.11), *N,N*-dimethyl-*m*-toluidine (5.34), *N,N*-dimethylaniline (5.15), and *N*-methylaniline (4.85) give yellow compounds in both the solid and molten states. The presence of broad vibrational bands in the region from 2250 to 2750 cm^{-1} indicates that they are true phenolates formed by means of proton-transfer from the acid to the anilines. The solid products with the following seventeen anilines (arranged in the order of decreasing pK_a values) were also found to be salts: *p*-anisidine, *p*-phenetidine, *p*-toluidine, 2,4-dimethylaniline, *m*-toluidine, aniline, *o*-anisidine, *o*-phenetidine, *o*-toluidine, *m*-anisidine, *p*-chloroaniline, *m*-chloroaniline, 3-nitro-4-methylaniline (2.96), *o*-chloroaniline (2.71), *o*-iodoaniline (2.60), *o*-bromoaniline (2.55), and *m*-nitroaniline (2.46). The first twelve salts rapidly decompose below or at the melting points; therefore, the color of the melts could not be observed at all. On the other hand, the yellow salts derived from the last five turn red or reddish-orange upon melting. As will be described in the following paragraph, this color change can be attributed to the appearance of an additional electronic absorption near 500 nm. Moreover, the melting is accompanied by the replacement of the vibrational bands assignable to the NH_3^+ group by those characteristic of the NH_2 group. Therefore, we may conclude that these phenolates isomerize into complexes of the charge-transfer type at their melting points. Such an isomerization by melting has already been observed by us in some anilinium picrates and also in 2,4-dinitrophenolates.[6,7]

The lower limit of the pK_a range of aniline, in which the phenomenon of complex isomerization by melting is observable, has been shown to be close to the pK_a value of the acid component in the cases of the 2,4-dinitrophenolates.[7] On the other hand, the limit could not be determined in the cases of the picrates because of the lack of anilines in the desired pK_a range. Nonetheless, *p*-nitroaniline, the pK_a value of which is located a little above the value of picric acid, was found to form a charge-transfer complex. In the present case, the pK_a value of the acid component has not

1) Part VI: G. Saito and Y. Matsunaga, This Bulletin, **46**, 1609 (1973).
2) E. Hertel, *Ann.*, **451**, 179 (1926).
3) R. Osawa, E. Osawa, and Y. Matsunaga, Paper presented at the Symposium on Molecular Structures, October 1971, Kyoto.
4) R. P. Mariella, M. J. Gruber, and J. Elder, *J. Org. Chem.*, **26**, 3217 (1961).
5) C. E. Moore and R. Peck, *ibid.* **20**, 673 (1955).
6) G. Saito and Y. Matsunaga, This Bulletin, **44**, 3328 (1971).
7) N. Inoue and Y. Matsunaga, *ibid.*, **45**, 3478 (1972).

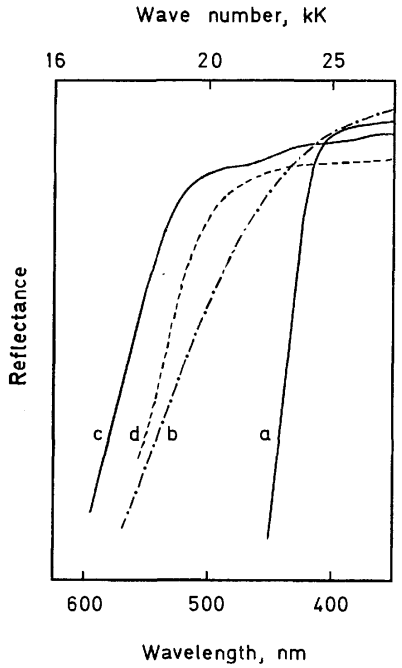

Fig. 1. Reflectance spectra, a) the stable yellow form of the *o*-chloroaniline-methylpicric acid complex, b) the same complex in the molten state, c) the unstable reddish-orange form, and d) the *o*-chloroaniline-*s*-trinitrobenzene complex.

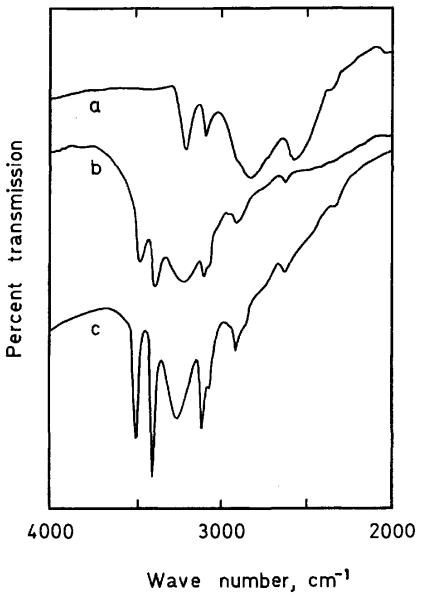

Fig. 2. Vibrational spectra, a) the stable yellow form of the *o*-chloroaniline-methylpicric acid complex, b) the same complex in the molten state, and c) the unstable reddish-orange form.

been well established. Although Moore and Peck have reported that the acidity of methylpicric acid is considerably lowered ($pK_a=2.8$) as compared to that of picric acid itself,[5] this value may be in the range from 1 to 2, according to Mariella *et al.*[4]

When the reddish-orange melts of *o*-chloroanilinium and *o*-bromoanilinium methylpicrates are solidified, the color does not return to yellow. After storage at room temperature for several days; however, a gradual change to yellow became noticeable. Contrary to the case with most of the complex isomers studied by Hertel, these reddish-orange forms are monotropically related to the yellow forms. The melting point of the yellow form of the *o*-chloroanilinium methylpicrate was found to be higher than that of the reddish-orange form (101—102 *vs.* 72—73 °C), in accordance with Hertel's observation for the only complex isomers monotropically related to each other (4-bromo-1-naphthylamine-2,6-dinitrophenol; 91—92 *vs.* 85 °C).[8] For the *o*-bromoanilinium salt, the corresponding values are 102—103 °C and 74—75 °C. As is shown in Fig. 1, the reflectance spectrum of the yellow form of the *o*-chloroaniline complex has a strong absorption below 450 nm which is assignable to the methylpicrate ion. Upon melting, a broad absorption band covering the range from 450 to 570 nm appears. The unstable form shows a strong absorption in the same region as the melt does. The similarity between the spectrum of the reddish-orange form and that of the *s*-trinitrobenzene complex (shown by Curve d) indicates that this broad absorption band arises from the charge-transfer interaction between the amine and the acid. The weakness of the charge-transfer absorption in the melt may be explained by a partial dissociation of the complex to the component molecules at high experimental temperatures.

The examination of the vibrational spectra in the region from 2000 to 4000 cm^{-1} was more rewarding, and bands characteristic of the aniline and anilinium ion were well verified. In Fig. 2, the spectrum of the yellow form is compared with that of the melt and also with that of the reddish-orange form. The broad bands located at 2550 and 2820 cm^{-1} in the yellow form constitute the pattern characteristic of the anilinium ion. The sharp bands in the unstable form appearing 3250 and 3500 cm^{-1} may be assigned to the aniline, more particularly to a NH_2 stretching vibration. The spectrum of the melt consists of rather broad bands but is undoubtedly similar to that of the reddish-orange form, in accordance with the conclusion drawn on the basis of the electronic spectra. The behavior of the *o*-bromoanilinium methylpicrate resembles that of the above-mentioned *o*-chloroanilinium salt. On the other hand, the molten charge-transfer complexes of 3-nitro-4-methylaniline, *o*-iodoaniline, and *m*-nitroaniline reversibly isomerize into yellow salts upon solidification.

N,*N*-Dimethylamino-*p*-benzaldehyde, 2,5-dichloroaniline, and *p*- and *o*-nitroanilines, the pK_a values of which are the lowest among those of the anilines examined, ranging from −0.26 to 1.62, were found to form charge-transfer complexes in both solids and melts. These observations seem to be in accordance with the view that the pK_a value of methylpicric acid is in the range from 1 to 2.

Dimethylpicric acid forms yellow salts, which rapidly decompose below or at the melting points, with the following anilines: *p*-anisidine, *p*-phenetidine, 2,4-dimethylaniline, *N*-methylaniline, *m*-toluidine, aniline, *o*-anisidine, *o*-phenetidine, *o*-toluidine, *m*-anisidine, *p*-

8) E. Hertel and J. van Cleef, *Ber.*, **61**, 1545 (1928).

chloroaniline, *m*-chloroaniline, and 3-nitro-4-methylaniline. Their pK_a values are 2.96 or higher. The dimethylpicrates derived from *o*-chloroaniline, *o*-iodoaniline, *o*-bromoaniline, *m*-nitroaniline, and *N,N*-dimethylamino-*p*-benzaldehyde turn red or reddish-orange upon melting. Their melting points are consistently higher than those of the corresponding methylpicrates, 133—134 *vs.* 101—102, 96—97 *vs.* 89—90, 124—125 *vs.* 102—103, 123—124 *vs.* 110, and 99—100 *vs.* 82 °C respectively. The isomerization to complexes of the charge-transfer type was proved by spectroscopic examinations, as has been described for the cases of the methylpicrates. Among the five, the complexes of *o*-iodoaniline, *o*-bromoaniline, and *N,N*-dimethylamino-*p*-benzaldehyde were found to solidify without any color change. However, none of them was stable enough to be heated to the melting point. Even the physical measurements at room temperature could be carried out only for the last-mentioned complex. Thus, these complex isomers are also monotropically related to the yellow salts. The acidity of dimethylpicric acid has been estimated to be lower by 0.5 pK_a unit than that of methylpicric acid.[5] Nevertheless, we found that *N,N*-dimethylamino-*p*-benzaldehyde forms a charge-transfer complex with methylpicric acid, but a true phenolate with dimethylpicric acid. Charge-transfer complexes of dimethylpicric acid were obtained with 2,5-dichloroaniline and *p*-nitroaniline.

Hertel and Schneider have found that the complex isomers of 4-bromo-1-naphthylamine-2,6-dinitrophenol have crystal structures distinctly different from each other;[9] this is also the case with ours. The X-ray diffraction patterns are schematically presented in Fig. 3 for all the pairs examined. The longest spacings in the unstable forms of the methylpicrates are shorter than those in the stable yellow forms; *e.g.*, 7.2 Å *vs.* 9.2 Å in the isomers of the *o*-chloroaniline complex.

9) E. Hertel and K. Schneider, *Z. Phys. Chem.*, **B13**, 387 (1931).

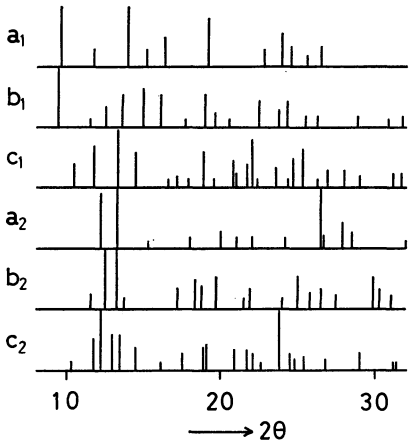

Fig. 3. X-Ray diffraction patterns, a) the *o*-chloroaniline-methylpicric acid, b) the *o*-bromoaniline-methylpicric acid, and c) the *N,N*-dimethylamino-*p*-benzaldehyde-dimethylpicric acid. The subscript 1 denotes the stable form and 2 the unstable form.

All the aromatic amines in the eight pairs of the complex isomers found by Hertel are halogenated derivatives.[2] The observations made by Hertel and also by us strongly suggest that the chance of finding complex isomers is high in the salts derived from halogenated amines, especially *o*-haloanilines. However, the amines in our five pairs of complex isomers include one free from halogen; that is, *N,N*-dimethylamino-*p*-benzaldehyde. In addition, a pair of complex isomers has been prepared by us with another amine bearing no halogen. When *o*-dianisidine is combined with tetranitrobiphenyl-4,4'-diol in a mole ratio of 1 : 1, a yellow salt and a black complex of the charge-transfer type are obtained.[1]

The authors wish to express their thanks to Professor Thosio Yokokawa for letting them use the X-ray diffractometer.

Small-angle Electron Scattering by Gases. CS_2 and CCl_4

Makoto NAGASHIMA, Shigehiro KONAKA, Takao IIJIMA, and Masao KIMURA
Department of Chemistry, Faculty of Science, Hokkaido University, Sapporo 060

(Received May 14, 1973)

The small-angle scattering intensity of 40 keV electrons by CS_2 and CCl_4 molecules has been measured by the use of a counting unit. The experimental intensities have been compared with the theoretical values for the independent-atom-model, and an analysis of the comparison has shown the consistency of the present results with Tavard's energy relation. The difference intensity, $\Delta\sigma(s)$, of CCl_4 has shown oscillatory behavior resulting from the distortion of charge distribution due to chemical-bond formation.

The study of the charge distribution of atoms and molecules by means of a small-angle scattering experiment of high-energy (~40 keV) electrons has been shown to be feasible and promising by several recent works.[1-6] In most of them, molecules consisting of light atoms were investigated and the results interpreted in terms of the effect of the chemical binding and electron correlation on the charge distribution. Since the theoretical scattering intensity calculated from the exact molecular wave function is not available except for a few very simple cases, a direct comparison of the experimental results with the theoretical intensity is generally impossible at present. The theoretical relationship between the scattering intensity and the electronic energy of the molecular system given by Tavard and co-worker[7] has been useful for a semi-quantitative discussion of the experimental results. The difficulty in intensity measurements in the small-angle region was largely decreased by the use of a new diffraction unit with the scintillation-counting system in place of the photographic plate.[4,6]

The following atom and molecules have so far been successfully investigated by the counting technique; Ne,[2] CH_4,[3] CO_2,[4,8] N_2O,[4] and N_2[5] by Bonham and co-workers, and H_2O[6] by Konaka. All of them consist of atoms in the first row of the periodic table. The present study is an extension of these previous works along the same line of interest to molecules which contain atoms in the second row of the periodic table. For these atoms, the correlation energy is fairly large. To see how far the observed scattering intensity is consistent with the correlation energy estimated by Clementi[10] was the main purpose of the present study. However, the quantitative discussion of the result has been obscured by the uncertainty in our knowledge of the relativistic effect, which can not be ignored for the second-row atoms.

Experimental

The diffraction experiment was carried out on a counting unit which was reported elsewhere.[6] The experimental conditions were as follows: accelerating voltage, 41 kV, stabilized within 0.01%; camera length, 107 cm; pressure in the diffraction chamber, 2.0×10^{-6} Torr without sample gas injection and 3.5×10^{-6} Torr during measurement. A liquid nitrogen cold trap was placed close to the nozzle. The accumulated count was in the range of 2000—600000, and the time of measurement for a single data-point was 20 s. The data covered the range of $s=0.6-9$ Å^{-1} at intervals of 0.5 Å^{-1}.

The residual gas correction was carried out by the method of Fink and Bonham.[4] However, the second nozzle for the background measurement was not placed close to the main nozzle; rather, it was in between the nozzle and the detector, about 30 cm from the main nozzle and close to the wall of the diffraction chamber. This modification was made simply because of the difficulty in doing additional machine work for the small specimen-chamber. The amount of gas-injection through the second nozzle was adjusted so that the reading of the vacuum gauge was the same as that of the first run of the scattering measurements for a gas sample from the main nozzle. The present method is effective enough to make the residual gas correction for the background scattering from the almost uniformly-distributed gas in the scattering chamber, which is the major portion of the residual gas in the present unit for condensable samples.

The measured electron counts were first corrected for the counting loss due to the finite resolving time of the scaler. Then the normalized relative intensity, I_{exp}, was obtained by;

$$I_{exp} = C\left(N_G^D\frac{N_G^{M_0}}{N_G^M} - N_B^D\frac{N_B^{M_0}}{N_B^M}\right) \quad (1)$$

where $N_{G,B}^{D,M,M_0}$ are the corrected counts of the scanning detector (D) and monitor (M) for the sample gas (G) and background (B). The superscript M_0 indicates the reference value of the monitor count, and C is the normalization constant. This equation is valid on the assumption that the variation in the scattering intensity from the sample gas is proportional to the variation due to background scattering. The incident beam current was not monitored during measurements in the unit of the present study. However, an independent observation of the scattering count from a solid specimen indicated that the stability of the beam current was within

1) D. A. Kohl and R. A. Bonham, *J. Chem. Phys.*, **47**, 1634 (1967) and references cited therein.
2) M. Fink and R. A. Bonham, *Phys. Rev.*, **187**, A114 (1969).
3) M. Fink, D. A. Kohl, and R. A. Bonham, *J. Chem. Phys.*, **52**, 5487 (1970).
4) M. Fink and R.A. Bonham, *Rev. Sci. Instrum.*, **41**, 389 (1970).
5) R. A. Bonham, M. Fink and D. A. Kohl, *Chem. Phys. Lett.*, **4**, 349 (1969).
6) S. Konaka, *Japan. J. Appl. Phys.*, **11**, 1199 (1972).
7) a) C. Tavard and M. Roux, *C. R. Acad. Sci. Paris*, **260**, 4933 (1965); b) C. Tavard, *Cahiers Phys.*, **20**, 397 (1966).
8) In Ref. 4, difficulty in the normalization of CO_2 and N_2O data to the theoretical intensity was reported. However, it was found recently that there were errors in the calculated values of the theoretical curve and the experimental data showed sufficient consistency with the Tavard's relation. Similar result for CO_2 was obtained also by the present authors.[9]
9) S. Konaka, International Symposium of the Application of Quantum Mechanics, Florida (January, 1973).
10) a) E. Clementi, *J. Chem. Phys.*, **38**, 2248 (1963); b) E. Clementi, *ibid.*, **39**, 175 (1963); c) A. Veillard and E. Clementi, *ibid.*, **49**, 2415 (1968).

TABLE 1. EXPERIMENTAL AND THEORETICAL (IAM) SCATTERED INTENSITIES FOR CS_2 AND CCl_4 AT 41 kV

CS_2				CCl_4			
s(Å^{-1})	I_{exp}[a]	σ/I_{exp}[b]	I_{IAM}	s(Å^{-1})	I_{exp}	σ/I_{exp}	I_{IAM}
0.658	1.453×10^{1}	2.2%	1.706×10^{1}	0.676	3.436×10^{1}	2.2%	3.497×10^{1}
0.955	8.122×10^{0}	1.5	9.706×10^{0}	0.973	1.683	1.5	1.784
1.350	4.235	1.0	5.133	1.468	4.796×10^{0}	1.0	5.462×10^{0}
1.744	2.698	0.9	3.176	1.962	3.074	0.9	3.492
2.139	1.956	0.9	2.210	2.457	3.184	0.8	3.540
2.534	1.377	0.8	1.531	2.951	2.295	0.7	2.484
2.929	9.246×10^{-1}	0.7	1.008	3.446	1.278	0.8	1.361
3.324	6.520	0.7	6.920×10^{-1}	3.940	9.490×10^{-1}	0.8	9.779×10^{-1}
3.719	5.314	0.8	5.549	4.435	8.807	0.8	9.081
4.114	4.660	0.8	4.827	4.930	6.807	0.8	7.060
4.509	3.941	0.8	4.009	5.424	4.188	0.9	4.256
4.904	3.031	0.8	3.069	5.915	2.576	0.9	2.595
5.299	2.212	0.9	2.257	6.413	2.216	1.0	2.223
5.693	1.685	0.9	1.710	6.908	2.069	1.0	2.098
6.088	1.347	0.9	1.367	7.402	1.683	1.1	1.683
6.483	1.082	1.0	1.108	7.897	1.240	1.2	1.227
6.878	8.836×10^{-2}	1.0	8.844×10^{-2}	8.391	9.891×10^{-2}	1.3	9.941×10^{-2}
7.273	7.240	1.0	7.136	8.886	8.813×10^{-2}	1.5	8.948×10^{-2}
7.668	6.125	1.1	6.124				
8.063	5.613	1.2	5.572				
8.458	5.054	1.3	5.076				
8.853	4.059×10^{-2}	1.5	4.436×10^{-2}				

a) Normalized to I_{IAM} at s=6.5—8

b) The symbol σ denotes the estimated standard error of I_{exp}, which include the error resulting from the uncertainty in s. The relative errors σ/I_{exp} are shown in percentage unit.

5%. Therefore, a systematic error of 5% may be included in the second term of Eq. (1); this error is, fortunately, smaller than the random error of $N_G{}^D$.

The scale factor, $L\lambda$, was calibrated by Debye-Scherrer rings of gold-foil.[11]

Results and Discussion

The experimental intensity, I_{exp}, was normalized to the theoretical intensity for the independent-atom-model,[1] I_{IAM}, in the s-range of 6.5—8. The final values of I_{exp} were obtained as the average of six sets of data from three independent measurements. Two sets of data were obtained for each measurement by scanning both sides of the main beam. The values of I_{exp} and I_{IAM} are shown in Table 1, together with the estimated uncertainties evaluated in much the same way as in Ref. 6.

The theoretical I_{IAM} value was calculated by the use of the elastic and inelastic scattering factors[12] based on the Hartree-Fock wave functions and by the use of the structure parameters[13] taken from the literature. The elastic scattering factor is the partial wave amplitude, even though Tavard's equation is valid only for the Born amplitude. The necessity and meaning of this treatment were discussed by Kohl and Bonham.[1]

The s^2I_{exp} and s^2I_{IAM} curves are compared in Figs. 1 and 2 for CS_2 and CCl_4 respectively. The difference intensities, $\Delta\sigma(s)=s^4[I_{exp}-I_{IAM}]$, are shown in Figs. 3 and 4.

Analysis of the Results by Means of Tavard's Energy Relation. In the present scheme of analysis, where I_{IAM} is calculated on the basis of the Hartree-Fock wave functions of the atoms, the energy relation given by Tavard and co-worker[7] can be reduced to the following expression;[1]

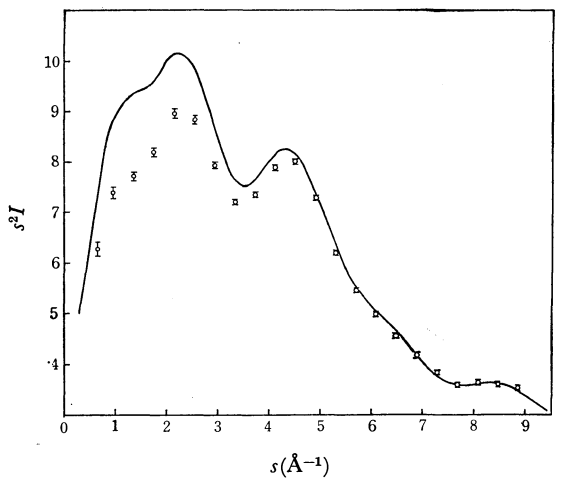

Fig. 1. Comparison between the experimental and theoretical (IAM) s^2I intensities for CS_2. ——: Theoretical intensity curve calculated using partial wave amplitude. ○: Experimental intensity. The vertical bar of experimental intensity shows the experimental standard error.

11) The lattice constant 4.078Å was used.

12) a) M. Kimura, S. Konaka, and M. Ogasawara, *J. Chem. Phys.*, **46**, 2599 (1967); b) C. Tavard, D. Nicolas, and M. Rouault, *J. Chim. Phys.*, **64**, 540 (1967).

13) a) Y. Morino and T. Iijima, This Bulletin, **35**, 1661 (1962); b) Y. Morino, Y. Nakamura, and T. Iijima, *J. Chem. Phys.*, **32**, 643 (1960).

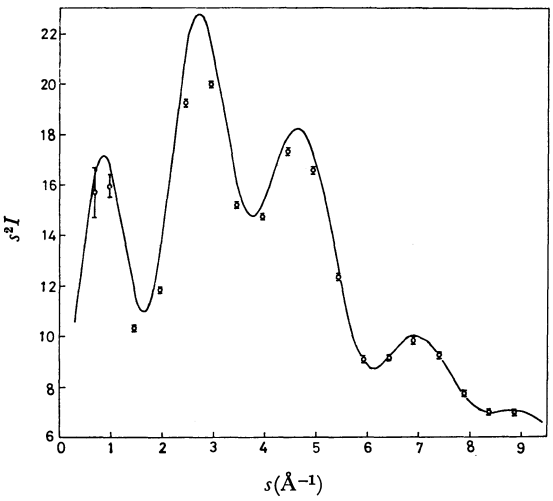

Fig. 2. Comparison between the experimental and theoretical (IAM) s^2I intensities for CCl_4. ——: Theoretical intensity curve calculated using partial wave amplitude. ○: Experimental intensity. The vertical bar of experimental intensity shows the experimental standard error.

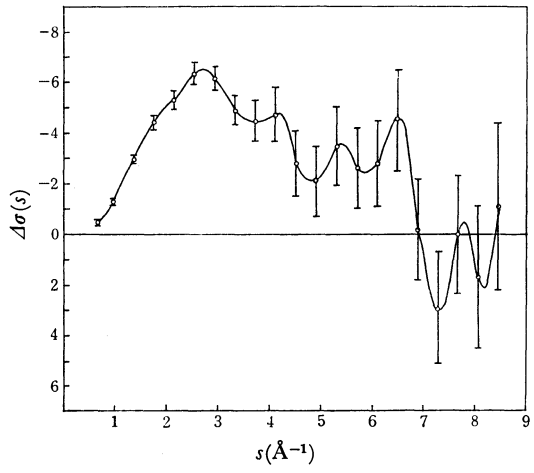

Fig. 3. Plot of $\Delta\sigma(s)$ for CS_2. The vertical bar shows the experimental standard error.

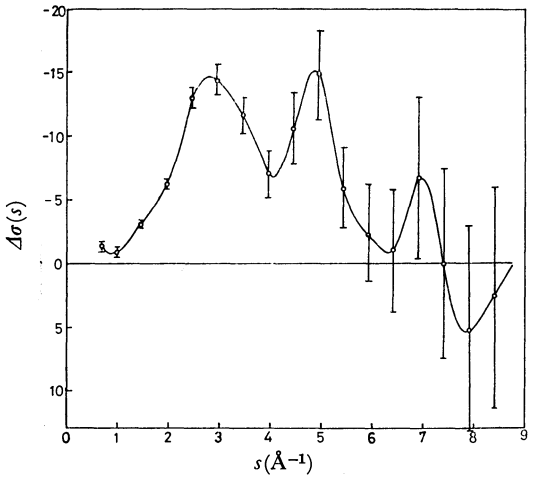

Fig. 4. Plot of $\Delta\sigma(s)$ for CCl_4. The vertical bar shows the experimental standard error.

$$E_b = \Delta E + E_1 - E_{corr} - E_{rel}, \quad (2)$$

where;

$$\Delta E = \frac{1}{2\pi}\int_0^\infty \sigma(s)ds.$$

In this equation, E_b is the binding energy of the molecule, E_1 is one-half of the lowering of the potential energy of the IAM molecule from that of the separated atoms, and E_{corr} and E_{rel} are the sum of the correlation energies for all the atoms and that of the relativistic energies respectively. All the terms in this expression have negative values.[14] The contribution to the first integral from the s-region beyond the normalization point was assumed to be zero.

According to the theoretical estimations,[10c,15] the relativistic energy, E_{rel}, is comparable to E_{corr} for the present molecules. Since the relativistic Hamiltonian contains terms other than the Coulomb interaction between charged particles, Tavard's equation in the form of Eq. (2) becomes invalid. According to Bonham and Cox,[16] a modified version of Tavard's equation can be obtained by putting a factor of 1.5—2.0 to E_{rel} for the K-shell electrons of He-like ions,[17] where the relativistic effect appears as the charge contraction due to an increase in the effective mass of electrons. However, the decrease in scattering intensity corresponding to the relativistic effect confined in the charge distribution of the inner core should show up in a wide s-range extending to large scattering angles. The integral of $\Delta\sigma(s)$, which is obtained from a rather limited s-range, could not contain the contribution from the E_{rel} term of at least K-shell electrons. By a similar argument, the K-shell correlation energy is most probably excluded from the integration of $\Delta\sigma(s)$. Although the charge contraction by the mass-effect in outer cores may be very small, the contribution of the relativistic energy of outer cores to Tavard's equation can not necessarily be assumed to be negligible. In the present stage of knowledge, it seems to be most reasonable to regard the relativistic energy of the outer cores as a theoretical uncertainty in Tavard's relation. Equation (2) was modified by this conjecture to:

$$\Delta E + E_1 = E_b + E^*_{corr} \quad \text{with} \pm E^*_{rel}, \quad (3)$$

where E^* means that the contribution from the K-shell is not included; this equation was tested by the experimental data. The results were satisfactory, as is shown in Table 2. By considering that the radius of the L-shell of S and Cl is smaller than those of the first-row atoms, it is worth comparing the experimental values with the theoretical energies, where both the K- and L-shell energy are excluded for S and Cl. This is also shown in Table 2, where the energies without the contribution of the K- and L-shells are denoted by E^{**}. The agreement is poor. The exclusion of the whole L-shell seems, therefore, to be too extreme.

14) Note that in Eq. (11) of Ref. 1 the correlation energy E_{corr} is taken as a positive quantity and the relativistic energy is neglected.

15) a) E. Clementi, *J. Mol. Spectrosc.*, **12**, 18 (1964); b) H. Hartmann and E. Clementi, *Phys. Rev.*, **133**, A1295 (1964).

16) R. A. Bonham and H. L. Cox, Jr., *J. Chem. Phys.*, **47**, 3508 (1967).

17) R. A. Bonham, *ibid.*, **43**, 1434 (1965).

TABLE 2. RESULT OF THE ANALYSIS BY TAVARD'S RELATION (Energies in a.u.)

	ΔE[a]	E_1	$\Delta E+E_1$	$E_b+E^*_{corr}$	$E_b+E^{**}_{corr}$	E_b[b]
CS_2	-1.67 ± 0.6	-0.32	-2.0 ± 0.6	-1.69	-0.92	-0.41
CCl_4	-3.58 ± 1.5	-0.41	-4.0 ± 1.5	-3.28	-1.69	-0.51
	E_{corr}[c]	E^*_{corr}[d]	E^{**}_{corr}[e]	E_{rel}[f]	E^*_{rel}[d]	E^{**}_{rel}[e]
CS_2	-1.42	-1.28	-0.51	-2.12	-0.56	-0.03
CCl_4	-3.01	-2.78	-1.19	-5.51	-1.53	-0.08

a) Experimental values obtained by the integration of $\Delta\sigma(s)$
b) Calculated from the values of enthalpy of formation in Ref. 26.
c) Ref. 10.
d) The K-shell energy is excluded.
e) The K-shell energy for C and the K- and L-shell energy for S and Cl are excluded.
f) Ref. 10c, 15.

Further correction for the vibrational effect,[18] which is of the order of the zero-point energy (a few hundredth of an a.u.), was neglected in the present analysis.

Comparison of I_{exp} and I_{IAM} in the Large s-Region by Means of Photographic Data. Since the s-range covered by the present counting experiment is rather limited, it is often uncertain whether or not the normalization at $s=6.5$—8 might have introduced a systematic error, thus leading to an underestimation of the absolute value of ΔE. In order to be sure that there is no such systematic error, the scattering intensity of CS_2 was carefully examined in the larger s-region by the use of the best photographic plate which has so far been obtained by the diffraction unit for the precise determination of the molecular structure.[19]

The s^4I_{exp} values up to $s=12$ are compared with s^4I_{IAM} in Fig. 5, where the counting data are also shown. The agreement of the counting data with the photographic intensity in the overlapping region, especially in the $7<s<9$ region is satisfactory. The agreement of the photographic data with the IAM intensity in the larger s-region up to $s=19$ is almost perfect, although the data beyound $s=12$ are not shown in the figure. The slight discrepancy between the counting and photographic data in $4.5<s<7$ seems to show an experimental imperfection still existing in the photographic data, because the increase in the intensity in this region has been experienced to be most sensitive to a slight misalignment of the slit system and/or the nozzle assembly. The photographic data in the $s<5$ region are not reliable enough because of the uncertainty in the effective sector correction and possible extraneous scattering from the main-beam stopper.

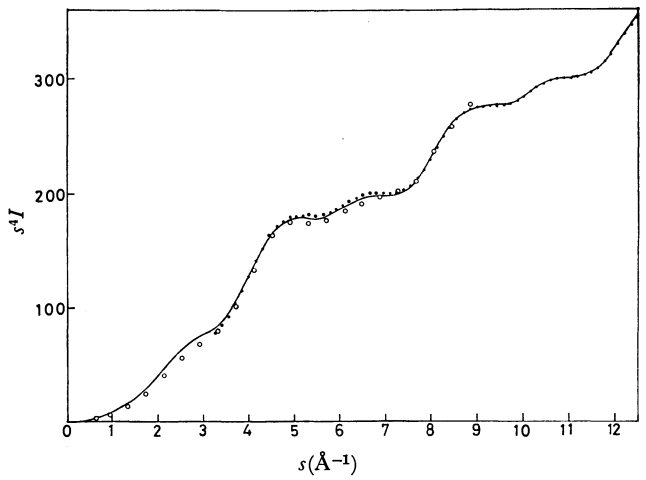

Fig. 5. Comparison of the photographic experimental, counting experimental and theoretical (IAM) s^4I intensities for CS_2. ——: Theoretical (IAM) curve calculated using partial wave amplitude.
• : The photographic experimental intensity.
o : The counting experimental intensity.

The comparison leads to the conclusion that there can be no better alternative for the normalization of the counting data in the present study, unless the precision of the intensity measurement is greatly improved.

Effect of Multiple Scattering. It has been pointed by several recent studies[20–23] that the effect of intramolecular multiple scattering appears in two ways: the double scattering, which reduces the atomic background intensity in the small s-region, and the triple scattering, which leads to a correction term containing a geometric factor. The first effect may be important in the interpretation of the experimental scattering intensity in terms of the binding and correlation energies, as in the present paper. The second one is related to the structure determination and also to the oscillatory behavior of the $\Delta\sigma(s)$ curve, as will be discussed in the next section.

The double-scattering contribution was, therefore, calculated for CCl_4 by means of Eq. (11) of Ref. 22. Also, one of the present authors (S.K) calculated the multiple effect for CCl_4 by means of the formalism of the eikonal approximation.[24] Both of these results indicated that the amount of the multiple effect for s^4I_T is less than 2 in the scale of Fig. 4, which is well within the limits of experimental uncertainty. Furthermore, the multiple effect for the atomic back-

18) R. A. Bonham, *J. Phys. Chem.*, **71**, 856 (1967).
19) M. Nagashima, H. Fujii, and M. Kimura, This Bulletin, to be published.
20) A. C. Yates and A. Tenney, *Phys. Rev.*, **5**, A2474 (1972).
21) L. S. Bartell and T. C. Wong, *J. Chem. Phys.*, **56**, 2364 (1972).
22) R. A. Bonham and E. M. A. Peixoto, *ibid.*, **56**, 2377 (1972).
23) A. C. Yates, *ibid.*, **57**, 1686 (1972).
24) a) D. P. Duncan, F. H. Tuley, Jr. and D. A. Kohl, *ibid.*, **56**, 3766 (1972); b) F. H. Tuley, Jr., Doctral Dissertation, The University of Texas at Austin, (1972); c) S. Konaka, unpublished.

ground of s^4I_T is found to be a monotonously increasing function within the s-range of 0—9; therefore, if one is to normalize the experimental intensity at s=6.5—8 to the IAM intensity which is corrected for the multiple effect, the ΔE value becomes almost equivalent to that obtained without the multiple correction, the difference being less than 0.1 a.u. Thus, the effect of multiple scattering seems to be safely ignorable in the present scheme of analysis.

Oscillatory Behavior of $\Delta\sigma(s)$. As is shown in Fig. 4, the $\Delta\sigma(s)$ curve of CCl_4 shows oscillatory behavior which is very similar to the interference pattern of diffraction pictures. In fact, the difference in s-values for the first and second maxima corresponds to that of the interference pattern for the Cl···Cl atom-pair in the CCl_4 molecule. This result can be reasonably understood in the light of the theoretical study of molecular Hartree-Fock cross sections for diatomic molecules performed by Kohl and Bartell.[25]

The oscillatory part of $\Delta\sigma(s)$ is primarily attributable to the interference of scattered electrons where the scatterers are a nucleus and the distorted part of the electron cloud around other nuclei produced by the chemical-bond formation, and it is denoted by $\Delta\sigma_{ne}$. Although the distortion of the charge density is generally not simple, it may be more or less described by an expansion around each nucleus in the Legendre polynomials, with radial function as coefficients. Then, the Fourier transform gives $\Delta\sigma_{ne}$, which consists of terms of the spherical Bessel functions, $j_n(sr_{AB})$, where r_{AB} is a nucleus-nucleus separation in the molecule. The $j_n(sr_{AB})$ can show up in a limited range of s as an oscillatory function with the characteristic distance of r_{AB}, irrespective of the order n. In general, $\Delta\sigma_{ne}$ is only a small portion of the total $\Delta\sigma$. However, the multiplicity of Cl···Cl separation due to the high symmetry of this molecule and the large scattering power of the Cl atom seem to have made the $\Delta\sigma_{ne}$ detectable, while the $\Delta\sigma_{ne}$ of CS_2 is perhaps of the order of the uncertainty of the total $\Delta\sigma$.

A similar oscillatory contribution can also be expected from the intramolecular multiple scattering. According to a preliminary calculation on the basis of the eikonal approximation,[24c] the peak-to-peak difference in the oscillatory multiple effect for CCl_4 is 1.2 or less in the scale of Fig. 4, which is only a small fraction of the observed oscillatory part of the $\Delta\sigma(s)$ curve.

The $\Delta\sigma_{ne}$ forms a part of the elastically-scattered intensity and is a one-electron property. Thus, the molecular Hartree-Fock wave function can be a satisfactorily good description for the calculation of $\Delta\sigma_{ne}$, and, conversely, the oscillatory part of the observed $\Delta\sigma$ curve can be an observable for testing a computed charge distribution of molecules. The usefulness of Tavard's equation is limited to a great extent by the uncertainties in the intensity measurement, which are amplified by the multiplication of s^4 for large s-values. A comparison of I_{exp} itself with the theoretical descriptions over all the observed region seems to be more fruitful for the future program of the small-angle scattering study, as the computation of molecular cross-sections becomes more familiar to experimentalists as well as to theoreticians.

Added Discussion. Relativistic-Hartree-Fock (RHF) calculations of atoms have been performed by several authors. The most extensive ones were obtained by Coulthard[27] and more recently by Malý and Hussonnois.[28] The first Born scattering factors were calculated by Doyle and Turner[29] on the basis of Coulthard's RHF atomic potentials; they are available for atoms from He through U. In these calculations, the Hamiltonian is expressed as:

$$\mathscr{H} = \mathscr{D} + \mathscr{B},$$

where $\mathscr{D}$ is the sum of the one-electron Dirac Hamiltonians for all the electrons plus the Coulomb interaction terms of the $1/r_{12}$ type and $\mathscr{B}$ is the sum of the relativistic two-electron terms, *viz.*, the Gaunt term and the retardation term. The wave function is made self-consistent with respect to $\mathscr{D}$, and the $\mathscr{B}$ term is neglected. The charge distribution used in the calculation of the scattering factors then corresponds to the $\mathscr{D}$ term.

By integrating $\Delta=(Z-f_x)^2_{RHF}-(Z-f_x)^2_{HF}$ for Ne up to s=60 Å^{-1}, where the integrand almost coverges to zero, it was found that the integrated value was nearly 15% larger than E_D-E_{HF}, where E_D means the eigen value of the $\mathscr{D}$ term, in absolute value. The difference, Δ, for Cl extends to more than s=60 Å^{-1}, with a small but appreciable magnitude. However, if $(Z-f_x)^2_{RHF}$ is normalized to $(Z-f_x)^2_{HF}$ at s=8 Å^{-1}, as in the present scheme of analysis, the energy obtained by integrating the differences in the $s<8$ Å^{-1} range amounts to −0.026 a.u., that is, −0.10 a.u. for four Cl atoms.

Theoretical uncertainty still remains concerning the effect of the $\mathscr{B}$ term on the charge distribution. Since the energy correction due to the $\mathscr{B}$ term is only 10% of E_D-E_{HF} for atoms heavier than Ne,[30] the uncertainty, $\pm E_{rel}$, mentioned in the text might be too pessimistic. Another uncertainty arises from the neglect of the inelastic scattering intensity in the discussion mentioned above. The inelastic part is probably important in the small-angle region investigated in the present study. The calculation of the inelastic scattering factors on the RHF basis is very much awaited.

25) a) D. A. Kohl and L. S. Bartell, *J. Chem. Phys.*, **51**, 2891 (1969); b) *idem, ibid.*, **51**, 2896 (1969).
26) The Chemical Society of Japan, "Kagaku-Binran," Maruzen Co., Ltd., Tokyo (1966), p. 819.
27) a) M. A. Coulthard, *Proc. Phys. Soc.*, **91**, 44 (1967); b) M. A. Coulthard, unpublished, cited in Ref. 29.
28) J. Malý and M. Hussonnois, *Theoret. Chim. Acta*, **28**, 363 (1973).
29) P. A. Doyle and P. S. Turner, *Acta Crystallogr*, **A24**, 390 (1968).
30) J. B. Mann and W. R. Johnson, *Phys. Rev.*, **4**, A41 (1971).

The Electronic Spectrum of *p*-Benzosemiquinone Anion in Aqueous Solution

Shun-ichi FUKUZUMI, Yoshio ONO, and Tominaga KEII

Department of Chemical Engineering, Tokyo Institute of Technology, Ookayama, Meguro-ku, Tokyo 152

(Received May 19, 1973)

The electronic spectrum of *p*-benzosemiquinone anion in aqueous solution formed through the oxidation of hydroquinone with manganese dioxide was measured at room temperature. The absorption maxima were found at 430, 404, and 316 mμ with shoulders at 371 and 310 mμ. It was confirmed that these absorption maxima are due to the same species *p*-benzosemiquinone anion, on the ground that their kinetic behaviors are the same. The molar extinction coefficients of the absorption maxima and the oscillator strengths of the absorption bands were estimated.

Semiquinones are known to be intermediates in the quinone–hydroquinone redox systems. ESR studies gave unambiguous evidence for the presence of these important radicals.[1] While the electronic spectra of the substituted *p*-benzosemiquinones such as durosemiquinone or 2,5-di-*t*-butyl-*p*-benzosemiquinone have been established,[2-5] the spectrum of non-substituted *p*-benzosemiquinone has hardly been studied at all.

Two methods of producing *p*-benzosemiquinone anions have been employed so far; the chemical oxidation of hydroquinone in alkaline solutions[4,6] and the photolysis of hydroquinone in rigid media at 77 K.[7-9]

Using a rapid flow method for the air oxidation of hydroquinone in an alkaline solution, Diebler *et al.*[6] found the absorption maxima at 430 and 404 mμ. Harada and Matsunaga[4] succeeded in the observation of fairly good electronic spectra of several substituted *p*-benzosemiquinone anions, stabilized sterically by bulky substituents, in highly viscous solutions at room temperature, but could not record a good spectrum of the simplest *p*-benzosemiquinone anion though they found the absorption maxima at 432 and 408 mμ in the visible region. A drawback in this method of preparation is that *p*-benzosemiquinone anions are too unstable in an alkaline solution.

By the ultraviolet irradiation of hydroquinone in an alkaline ethanol solution at 77 K, Kimura *et al.*[9] obtained a spectrum with three bands, each with several absorption maxima and ascribed the spectrum to *p*-benzosemiquinone anion [$\cdot OC_6H_4O^-$], on the ground that it was similar to that of 2,5-di-*t*-butyl-*p*-benzosemiquinone anion mentioned above. However, interference by the presence of other species cannot be completely eliminated with this method. It seemed of prime importance therefore to prepare semiquinone anions in a stable condition. We have found that *p*-benzosemiquinone anion is easily formed when a neutral aqueous solution of hydroquinone is passed through a column of manganese dioxide, and that the anion thus formed is quite stable at room temperature even in the atmosphere. The rate of radical decay follows the first order kinetics with the rate constant 5.7×10^{-3} (min^{-1}).

By applying this technique to the preparation of the radical we could distinctly observe the electronic spectra of *p*-benzosemiquinone anion and the molar extinction coefficients were determined.

Experimental

p-Benzosemiquinone anion was prepared by passing an aqueous solution of hydroquinone through tubing (I.D. 6 mm) packed with 0.7 g of manganese dioxide (20—30 mesh). The initial concentrations of hydroquinone were 10—30 mM. The outlet of the MnO_2 column was directly connected to the optical cell. A flat type ESR cell for aqueous solutions, supplied by Japan Electron Optics Laboratory (JEOL), was also used for the measurements of electronic spectra, enabling us to measure both electronic and ESR spectra under the same conditions. The path length of the cell is 0.38 mm.

The electronic spectra were registered with a Shimadzu spectrophotometer, Model MPS-5000. The ESR measurements were carried out with a JEOL-X band spectrometer (JES-3BS-X). The concentration of *p*-benzosemiquinone anion was determined by comparison of the area under the absorption curve of the anion and that of 1,1-diphenyl-2-picrylhydrazyl (DPPH) in benzene.

Results and Discussion

The electronic spectra were measured with various feed rates of the hydroquinone solution. Besides the bands due to hydroquinone and *p*-benzoquinone, bands appeared in the near ultraviolet and visible regions, as shown in Figs. 1 and 2, respectively. Figure 1 was obtained by subtracting the absorption of hydroquinone of the initial concentration from the observed spectra. In the visible region, there is no appreciable overlapping of the bands due to hydroquinone or *p*-benzoquinone.

1) B. Venkataraman and G. K. Fraenkel, *J. Chem. Phys.*, **23**, 588 (1955); B. Venkataraman, B. G. Segal, and G. K. Fraenkel, *ibid.*, **30**, 1006 (1959); J. E. Wertz and J. L. Vivo, *ibid.*, **23**, 2441 (1955).

2) N. K. Bridge and G. Porter, *Proc. Roy. Soc. Ser., A*, **244**, 259, 276 (1958).

3) H. R. Hardy and J. H. Baxendale, *Trans. Faraday Soc.*, **49**, 1433 (1953).

4) Y. Harada and Y. Matsunaga, This Bulletin, **74**, 585 (1961).

5) Y. Harada and H. Inokuchi, *Mol. Phys.*, **8**, 265 (1964).

6) H. Diebler, M. Eigen, and P. Matthies, *Z. Elektrochem.*, **65**, 634 (1961).

7) G. N. Lewis and J. Bigeleisen, *J. Amer. Chem. Soc.*, **65**, 2424 (1943).

8) H. Linschitz, J. Rennert, and T. M. Korn, *ibid.*, **76**, 5839 (1954).

9) K. Kimura, K. Yoshinaga, and H. Tsubomura, *J. Phys. Chem.*, **71**, 4485 (1967).

10) S. Fukuzumi, Y. Ono, and T. Keii, to be published.

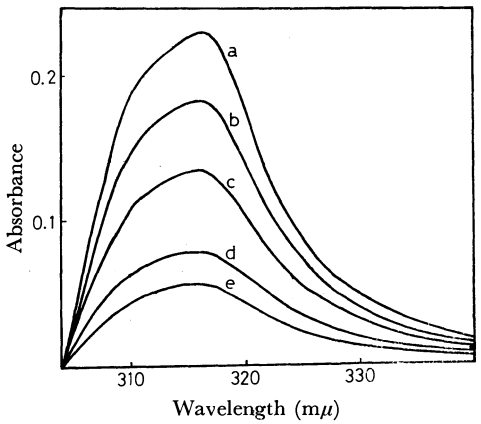

Fig. 1. Electronic spectra of *p*-benzosemiquinone anion in the ultraviolet region. The 20 mM hydroquinone solution was fed with the rates of (a) 0.15, (b) 0.38, (c) 0.81, (d) 3.9, and (e) 7.0 ml/min. (path length 0.38 mm)

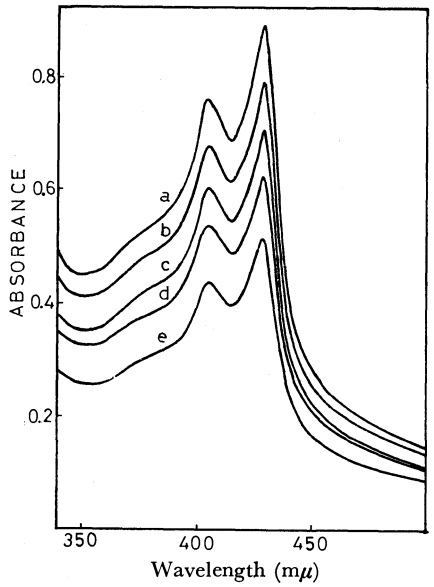

Fig. 2. Electronic spectra of *p*-benzosemiquinone anion in the visible region. The 30 mM hydroquinone solution was fed with the rates of (a): 0.68, (b): 1.0, (c): 1.3, (d): 2.2, and (e): 4.7 ml/min. (path length 1.0 cm)

The absorption maxima were observed at 430, 404, ~371, and ~310 mμ.

The kinetic behavior of the bands was studied in order to ascertain whether all the absorption maxima are due to *p*-benzosemiquinone anion. Previous ESR work showed that the concentration of the semiquinone anion was expressed as a function of the feed rate of the solution in the following way:

$$\ln \frac{[S]_\infty - [S]}{[S]_\infty} = -k\frac{V}{F} \qquad (1)$$

where [S] is the concentration of semiquinone anion at the exit of the MnO_2 column of volume V, when the feed rate of the solution is F, $[S]_\infty$ is the concentration at the infinitesimal feed rate and k the rate constant. Thus, if the absorption at the wavelength λ is caused solely by the semiquinone anion, the following relationship should hold.

$$\ln \frac{[A]^\lambda_\infty - [A]^\lambda}{[A]^\lambda_\infty} = -k\frac{V}{F} \qquad (2)$$

where $[A]^\lambda$ and $[A]^\lambda_\infty$ are the absorbance at wavelength λ when the feed rates are F and infinitesimal, respectively.

$\log([A^\lambda_\infty - [A]^\lambda)$ is plotted against $1/F$ at the wave-

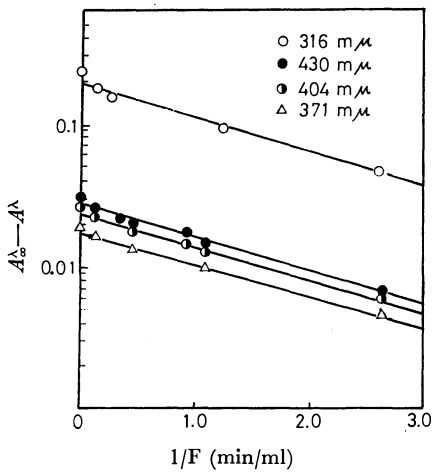

Fig. 3. Change in the absorbance with the feed rate of the 20 mM hydroquinone solution.

Table 1. Wavelengths of the absorption maxima and molar extinction coefficients of *p*-benzosemiquinone anion

Species	Method of preparation	Wavelengths (mμ) and molar extinction coefficients ($\times 10^{-3}$)	Reference
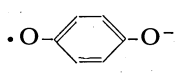	hydroquinone+MnO_2	λ 430, 404, 371*, 316, 310* ε 5.4, 4.6, 3.7, 40, 33	This work
	hydroquinone+alkaline solution	λ 430, 404, —, —, — ε 7.4, —, —, —, —	6)
	hydroquinone+alkaline solution	λ 432, 408, —, —, — ε —, —, —, —, —	5)
	photolysis of hydroquinone at 77K	λ 432, 407, 385, 316, 308, 301, 295* ε —, —, —, —, —, —, —	9)
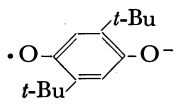	2,5-di-*t*-butylhydroquinone+alkaline solution	λ 436, 411, 373, 323.5 ε 5.3, 4.0, 4.2, 14	5)

* designates a shoulder

lengths of the absorption maxima in Fig. 3. It is evident that the changes of absorbance with feed rates are well expressed by Eq. (2) and the slope of each line gives the same value of k. In the case of other initial concentrations of hydroquinone, 20 and 30 mM, the same results were obtained. Since all the absorption maxima show the same kinetic behavior, it is concluded that all absorption maxima in Figs. 1 and 2 are due to the same species, *viz.*, *p*-benzosemiquinone anion. The ESR work confirmed that *p*-benzosemiquinone anion was the only paramagnetic species in the solution, and the neutral semiquinone ($\cdot OC_6H_4$-OH) or hydroquinone cation did not exist.

The positions of absorption maxima observed in this work are compared with those observed by other workers in Table 1. The values of the two maxima at the longer wavelengths agree with those obtained by Diebler *et al.*[6] The absorption maxima at the shorter wavelengths have not been reported for non-substituted *p*-benzosemiquinone anion at room temperature, but the corresponding maxima have been obtained for 2,5-di-*t*-butyl-*p*-benzosemiquinone anion.[4] Comparing the maxima for 2,5-di-*t*-butyl-*p*-benzosemiquinone anion with those of the non-substituted, all the bands of the former slightly red-shift. This can be understood as the effect of the electron-donating substituents [$-C(CH_3)_3$] on the benzene ring.

The molar extinction coefficients (ε_{max}) of the absorption maxima were calculated. The absolute concentration of the *p*-benzosemiquinone anion was determined from ESR intensity. The results are given in Table 1. The magnitude of the extinction coefficients suggests that all the absorption bands are caused by π-π^* transitions. The absorption maxima of 430 and 404 mμ are considered to be caused by the same π-π^* transition and their splitting is due to the C–O stretching vibration in the exited state.[4]

Table 2. Comparison between the observed and the calculated values of transition energy and the oscillator strength (f)

Observed		Calculated (11)		
Transition energy (eV)	f[a]	Transition energy (eV)	f	Symmetry type
2.88	0.06	2.960	0.03	$^2B_{3g}$–$^2B_{1u}$
3.34	0.03	3.479	0.11	$^2B_{3g}$–^2A_u
3.93	0.35	4.458	0.69	$^2B_{3g}$–$^2B_{1u}$

a) The oscillator strength f is evaluated from the well-known formula, $f=4.23\times10^{-9}\int\varepsilon(\nu)d\nu$.

Harada[11] carried out the molecular orbital calculation with the Pariser-Parr method on *p*-benzosemiquinone anion and estimated the transition energies and the oscillator strengths. The experimental values obtained in this study are compared with those calculated by Harada in Table 2. The agreement between the observed and the calculated values is fairly good for this type of calculation on molecules with hetero atoms.

11) Y. Harada, *Mol. Phys.*, **8**, 273 (1964).

BULLETIN OF THE CHEMICAL SOCIETY OF JAPAN, VOL. 46, 3355—3358 (1973)

Hydrogen Formation in the Gas-Phase Radiolysis of C_2H_4-D_2O Mixtures

Ken-ichi KUWABARA and Yoshihiko HATANO

Laboratory of Physical Chemistry, Tokyo Institute of Technology, Meguro-ku, Tokyo 152

(Received May 24, 1973)

The total hydrogen yields and their isotopic compositions have been measured in the gas-phase radiolysis of C_2H_4–D_2O mixtures at room temperature. A mixture of D_2O ($<$10 mol %) with a large amount of C_2H_4 was used to avoid the effect of the wall on the decomposition of D_2O. The contribution of thermal hydrogen atoms to the hydrogen formation may reasonably be excluded in this system. The kinetic treatment of D_2 and HD formation suggests the decomposition mechanism of D_2O. No important contribution of hot hydrogen atoms was observed. The yield of hydrogen from the D_2O formed by the unimolecular process, $G_{1D}=0.4$, was nearly equal to the molecular hydrogen yield reported previously.

In the radiolysis of pure water vapor, the hydrogen yield is very small.[1,2] The radiolysis in the presence of various organic additives, however, has shown a fairly large yield of hydrogen atoms.[3–9] The importance of excited hydrogen atoms in the physicochemical stage of the radiation effect on water vapor has been predicted by Platzman.[10] He suggested that such atoms might be electronically excited and pro-

1) R. Firestone, *J. Amer. Chem. Soc.*, **79**, 5593 (1957).
2) A. R. Anderson, B. Knight, and J. A. Winter, *Trans. Faraday Soc.*, **62**, 359 (1966).
3) J. H. Baxendale and G. P. Gilbert, *Discuss. Faraday Soc.*, **36**, 186 (1963).
4) J. H. Baxendale and G. P. Gilbert, *J. Amer. Chem. Soc.*, **86**, 516 (1964).
5) G. R. A. Johnson and M. Simic, *Nature*, **212**, 1570 (1966).
6) J.Y. Yang and I. Marcus, *J. Amer. Chem. Soc.*, **88**, 1625 (1966).
7) G. R. A. Johnson and M. Simic, *Nature*, **210**, 1356 (1966).
8) G. R. A. Johnson and M. Simic, *J. Phys. Chem.*, **71**, 1118 (1967).
9) G. R. A. Johnson and M. Simic, "The Chemistry of Ionization and Excitation," ed. by G. R. A. Johnson and G. Scholes, Taylor and Francis, London (1967), p. 211.
10) R. L. Platzman, *Radiation Res.*, **17**, 419 (1962).

duced *via* excitation from superexcitation. Actually, the measurement of the Lyman and Balmer radiation has been made in the collisions of fast electrons on water vapor, in which the possible role of superexcited water molecules as important precursors of electronically-excited hydrogen atoms has been discussed.[11] The yield of superexcited water molecules has been theoretically estimated by Santer and Bednar.[12] In the radiation chemistry of water vapor, however, few experiments have been made to examine this hydrogen atom.[13]

Recently, in the radiolysis of various hydrocarbons, evidence has been presented of the important role of hydrogen atoms with excess energy, called "hot hydrogen atoms".[14] That is, bimolecular hydrogen formation in the radiolysis of olefins or paraffins with a radical and an electron scavenger has been interpreted in terms of the hydrogen atom abstraction by hot hydrogen atoms formed by direct excitation, which must at least partially involve superexcitation.

The present investigation has been made in order to examine the nature of hydrogen atoms produced in the radiolysis of water vapor.

Experimental

Research-grade ethylene supplied by the Takachiho Shoji Co. was condensed at 77 K and degassed several times before use. Gas-chromatographic analysis using a silica gel column showed a purity of more than 99.95%, most of the impurities consisted of ethane. Deuterium oxide (>99.8 D%) stored in a nitrogen atmosphere was used without further purification except for the usual degassing at 77 K.

Cylindrical glass vessels about 300 ml in volume and fitted with break-off seals were baked in air at about 400 °C and then evacuated at less than about 10^{-5} mmHg for several hours. After this treatment, the required amounts of deuterium oxide and ethylene were introduced into the vessel. The total pressure for each sample was about 300 mmHg.

The samples were irradiated by ^{60}Co γ-rays at room temperature. The dose rate was 5.2×10^{19} eV/g·hr, and the total dose was 5.2×10^{20} eV/g of ethylene. The dose rate was based on the yield of hydrogen from ethylene, using $G(H_2)=1.31$.[15]

After irradiation the samples were attached to a vacuum line and the seals were broken. The product gases noncondensable at 77 K were collected by means of a Toepler pump. The total hydrogen yield was determined by gas chromatography using a molecular sieve-5A column. The isotopic composition of hydrogen was determined by means of a Hitachi RMU-5 mass spectrometer.

Results and Discussion

In the radiolysis of water vapor the wall has a large effect on the hydrogen formation.[2] The hydrogen yield depends considerably on the cleanliness of the vessel surface. In our case, however, the partial pressure of water vapor is less than 10% of the total, which is about 300 mmHg and which is formed mainly by ethylene. The effect of the wall mentioned above may be of lesser importance for the hydrogen formation in this experiment.

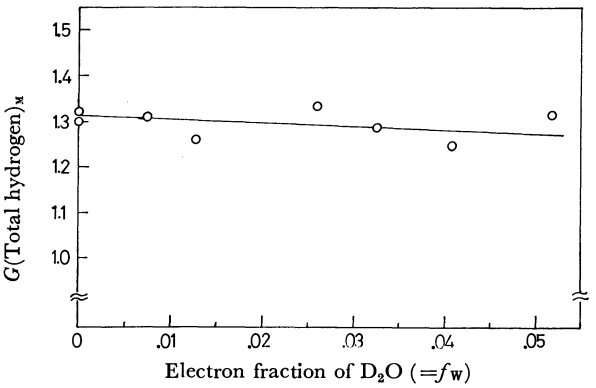

Fig. 1. Yields of hydrogen in the radiolysis of C_2H_4–D_2O mixtures.

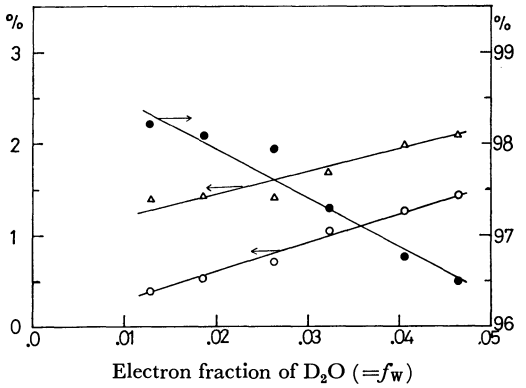

Fig. 2. The isotopic composition of hydrogen produced in the radiolysis of C_2H_4–D_2O mixtures.
●: H_2, △: HD, ○: D_2.

In Fig. 1, G(total hydrogen)$_M$, the number of hydrogen molecules formed per 100 eV of the energy absorbed by the C_2H_4–D_2O mixtures, is plotted against the electron fraction of D_2O ($=f_W$). G(total hydrogen)$_M$ decreases only a little with an increase in the D_2O concentration. Figure 2 shows the isotopic composition of the total hydrogen as a function of f_W. Both the D_2 and HD contents increase linearly with an increase in the f_W. By the extrapolation to zero concentration of D_2O, the D_2 content becomes zero, whereas the HD content has an intercept.

Now, let us consider the hydrogen formation from the C_2H_4–D_2O mixtures. In the first place, the contribution of thermal hydrogen atoms will be considered. Ethylene has a high reactivity for them[16] and the addition reaction (1) may be dominant compared with the abstraction reactions, (2) and (3):

11) D. A. Vroom and F. J. de Heer, *J. Chem. Phys.*, **50**, 1883 (1969).
12) I. Santer, "Progress and Problems in Contemporary Radiation Chemistry," Vol. 1, ed. by J. Teply (1971), p. 51 and references cited therein.
13) R. S. Dixson, *Radiation Res. Rev.*, **2**, 237 (1970).
14) Y. Hatano and S. Shida, *J. Chem. Phys.*, **46**, 4784 (1967); Y. Hatano, S. Shida, and M. Inokuti, *ibid.*, **48**, 940 (1968); Y. Hatano, S. Shida, and S. Sato, This Bulletin, **41**, 1120 (1968); Y. Hatano, *ibid.*, **41**, 1126 (1968).
15) G. G. Meisels, *J. Chem. Phys.*, **41**, 51 (1964).
16) K. R. Jennings and R. J. Cvetanovic, *ibid.*, **35**, 1233 (1961).

$$H(\text{or } D) + C_2H_4 \longrightarrow C_2H_5(\text{or } C_2H_4D) \quad (1)$$

$$H(\text{or } D) + C_2H_4 \longrightarrow H_2(\text{or } HD) + C_2H_3 \quad (2)$$

$$H(\text{or } D) + D_2O \longrightarrow HD\ (\text{or } D_2) + OD \quad (3)$$

Thus, the contribution of the abstraction reaction of thermal hydrogen atoms to hydrogen formation must be excluded. The ethyl radicals in Reaction (1) are vibrationally excited at first and possibly dissociate again. Under these experimental conditions, however, such as a total pressure of about 300 mmHg at room temperature, these excited radicals are changed predominantly to thermal ethyl radicals by collisional deactivation and are not responsible for the hydrogen formation. Thus, thermal hydrogen atoms may be unimportant for the hydrogen formation in this system.

Secondly, the possibility of hydrogen formation through various ion-molecule reactions may also be eliminated on the basis f the following discussion.[17]

Positive-charge or proton transfer from $C_2H_4^+$ to D_2O and hydrogen-atom transfer from D_2O to $C_2H_4^+$ seems to be energetically impossible.

$$C_2H_4^+ + D_2O \longrightarrow C_2H_4 + D_2O^+; \quad \Delta H = 47 \text{ kcal/mol} \quad (4)$$

$$C_2H_4^+ + D_2O \longrightarrow C_2H_3 + HD_2O^+; \quad \Delta H = 11\pm4 \text{ kcal/mol} \quad (5)$$

$$C_2H_4^+ + D_2O \longrightarrow C_2H_4D^+ + OD; \quad \Delta H = 32\pm4 \text{ kcal/mol} \quad (6)$$

However, secondary ions which are known to exist in the high-pressure mass spectrometry of ethylene[19] can possibly undergo proton transfer to D_2O to produce D_2HO^+.

The formation of D_2O^+ *via* the direct effect of ionizing radiation on D_2O will invoke the following ion-molecule reactions:

$$D_2O^+ + C_2H_4 \longrightarrow D_2O + C_2H_4^+; \quad \Delta H = -47 \text{ kcal/mol} \quad (7)$$

$$D_2O^+ + C_2H_4 \longrightarrow OD + C_2H_4D^+; \quad \Delta H = -15\pm4 \text{ kcal/mol} \quad (8)$$

$$D_2O^+ + C_2H_4 \longrightarrow D_2HO^+ + C_2H_3; \quad \Delta H = -37\pm4 \text{ kcal/mol} \quad (9)$$

$$D_2O^+ + D_2O \longrightarrow D_3O^+ + OD; \quad \Delta H = -22\pm4 \text{ kcal/mol} \quad (10)$$

Even if D_3O^+ was present in this system, it seems that, on energetic grounds, we can exclude the possibility of the hydrogen formation through ion-molecule reactions (11) and (12) between D_3O^+ and C_2H_4.

$$D_3O^+ + C_2H_4 \longrightarrow D + D_2O + C_2H_4^+; \quad \Delta H = 94\pm4 \text{ kcal/mol} \quad (11)$$

$$D_3O^+ + C_2H_4 \longrightarrow HD + D_2O + C_2H_3^+; \quad \Delta H = 68\pm6 \text{ kcal/mol} \quad (12)$$

The possibility of the hydrogen formation through ion-molecule reactions between D_2HO^+ and C_2H_4 may similarly be excluded.

The HD formation *via* the neutralization of $C_2H_4D^+$ in Reaction (8) might be considered, but such a possibility may be excluded because of the experimental finding in the radiolysis of ethylene that hydrogen formation is not affected by the addition of electron scavengers. Such a neutralization would produce thermal hydrogen atoms to be scavenged by ethylene itself.

The hydrogen observed in this experiment might be formed by the molecular detachment from C_2H_4 and D_2O, or by the hydrogen-atom-abstraction reaction of the hot hydrogen atoms, H′ and D′, produced from C_2H_4 and D_2O respectively *via* direct excitation. Hot hydrogen atoms might also be produced *via* the neutralization of D_3O^+ or D_2HO^+ with an electron.[20] In the next scheme, however, this possibility is excluded; it will be discussed later.

$$C_2H_4 \rightsquigarrow H_2(+\cdots) \quad G_{1H} \quad (13)$$

$$\searrow H'(+\cdots) \quad G_{2H} \quad (14)$$

$$D_2O \rightsquigarrow D_2(+\cdots) \quad G_{1D} \quad (15)$$

$$\searrow D'(+\cdots) \quad G_{2D} \quad (16)$$

$$H' + C_2H_4 \longrightarrow H_2 + C_2H_3 \quad k_1 \quad (17)$$

$$H' + D_2O \longrightarrow HD + OD \quad k_2 \quad (18)$$

$$D' + C_2H_4 \longrightarrow HD + C_2H_3 \quad k_3 \quad (19)$$

$$D' + D_2O \longrightarrow D_2 + OD \quad k_4 \quad (20)$$

Assuming the energy absorbed by each component in a mixture of C_2H_4 and D_2O to be proportional to the electron fraction of C_2H_4 and D_2O, one can estimate the yield of HD on the basis of the amount of energy absorbed in the mixture:

$$G(HD)_M = G_{2H}(1-f_w)\frac{1.6f_wk_2}{(1-f_w)k_1+1.6f_wk_2} + G_{2D}f_w\frac{(1-f_w)k_3}{(1-f_w)k_3+1.6f_wk_4} \quad (I)$$

Similarly, the yields of D_2 and H_2 are given, respectively, by:

$$G(D_2)_M = G_{1D}f_w + G_{2D}f_w\frac{1.6f_wk_4}{(1-f_w)k_3+1.6f_wk_4} \quad (II)$$

$$G(H_2)_M = G_{1H}(1-f_w) + G_{2H}(1-f_w)\frac{(1-f_w)k_1}{(1-f_w)k_1+1.6f_wk_2} \quad (III)$$

Now, assuming that $k_2/k_1=k_4/k_3$ $(=\alpha)$, we obtain the following equations:

17) The exothermic direction of the processes is examined assuming the following heats of formation;[18]
$\Delta H_f(C_2H_4)=12.5$ kcal/mol, $\Delta H_f(H_2O)=-57.8$ kcal,
$\Delta H_f(C_2H_4^+)=255$ kcal/mol, $\Delta H_f(H_2O^+)=232$ kcal/mol,
$\Delta H_f(C_2H_5^+)=220\pm4$ kcal/mol, $\Delta H_f(H_3O^+)=143\pm4$ kcal/mol,
$\Delta H_f(C_2H_3^+)=281\pm2$ kcal/mol,
$\Delta H_f(H)=52.1$ kcal/mol, $\Delta H_f(OH)=9.3$ kcal/mol,
$\Delta H_f(H_2)=0$, and $\Delta H_f(C_2H_3)=65$ kcal/mol.
It is also assumed that no isotope effect exists.

18) J. L. Beauchamp and S. E. Buttrell Jr., *J. Chem. Phys.* **48**, 1783 (1968).

19) P. Kebarle, R. M. Haynes, and S. Searles, "Ion-Molecule Reactions in the Gas Phase," Advances in Chemistry Series 58, American Chemical Society, Washington, D. C. (1966), p. 210.

20) It has already been suggested that D_2 or HD may not be formed directly *via* neutralization of D_3O^+ or D_2HO^+ with an electron.[7]

$$\frac{(1-f_w)f_w}{G(HD)_M} = \frac{1}{1.6G_{2H}\alpha+G_{2D}} + \frac{1.6\alpha-1}{1.6G_{2H}\alpha+G_{2D}} \times f_w \quad (I')$$

$$\frac{G(D_2)_M}{f_w} = G_{1D} + 1.6G_{2D}\alpha f_w \quad (II')$$

$$\frac{G(H_2)_M}{1-f_w} = (G_{1H}+G_{2H}) - 1.6G_{2H}\alpha f_w \quad (III')$$

whe e Eqs. (II)′ and (III)′ apply to the case of $f_W \ll 1$. The (II)/(I) ratio gives;

$$\frac{G(D_2)_M(1-f_w)}{G(HD)_M} = \frac{G_{1D}}{1.6G_{2H}\alpha+G_{2D}} + \frac{1.6\alpha(G_{1D}+G_{2D})-G_{1D}}{1.6G_{2H}\alpha+G_{2D}} \times f_w \quad (IV)$$

Plots of the left-hand side of these equations, (I)′, (II)′, (III)′, and (IV), against f_W should give straight lines. The intercepts and the slopes of these lines will give G_{1H}, G_{2H}, G_{1D}, G_{2D}, and α. They are shown in Figs. 3 and 4.

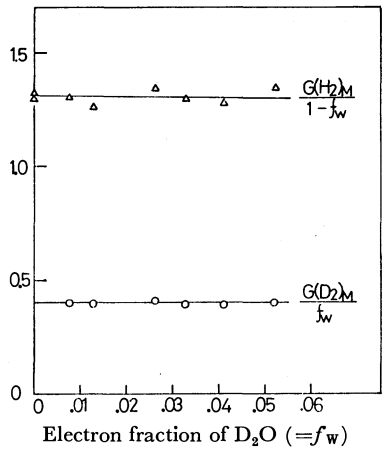

Fig. 3. $G(H_2)_M/(1-f_W)$ and $G(D_2)_M/f_W$ as a function of f_W.

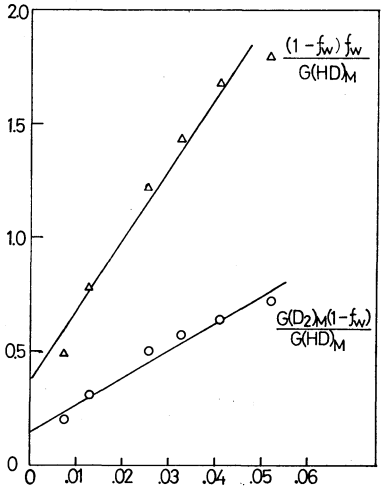

Fig. 4. $(1-f_W)f_W/G(HD)_M$ and $G(D_2)_M(1-f_W)/G(HD)_M$ as a function of f_W.

The yield of unimolecular hydrogen from C_2H_4, $G_{1H}=1.28$. The yield of the hct hydrogen atom from C_2H_4, $G_{2H}=0.03\pm0.01$. The yield of unimolecular hydrogen from D_2O, $G_{1D}=0.4$. The yield of the hot hydrogen atom from D_2O, $G_{2D}=0.0\pm0.1$. The value of α is nearly equal to 50.

These results apparently do not show that hot hydrogen atoms have an important role in this system. The conclusion does not necessarily follow, however, that they are not formed in the radiolysis of pure water vapor, where a fairly large amount of hydrogen atoms, $G(H)\cong 8$, has already been detected and divided into the following two kinds in a ratio of 3 to 5; hydrogen atoms formed *via* the neutralization process and those formed *via* direct excitation.[5,7,8] The above experimental results show that at least the latter kind of hydrogen atoms may not be hot. To describe the former, the possibility of the formation of H′ or D′ *via* the neutralization of D_3O^+ or D_2HO^+ mentioned above must be discussed here. By including this possibility in the above schemes (13)—(20) one may not easily establish the kinetic equations as (I)—(III). The yields of hot hydrogen atoms may not easily be estimated on the basis of the amount of the energy absorbed in each component. Similar experiments have been undertaken in the presence of 0.5 mol % SF_6, where the possibility of the above neutralization processes may reasonably be excluded. The same kinetic treatment as Eqs. (I)—(III) leads to exactly the same results for G_{1H}, G_{2H}, G_{1D}, G_{2D} as those obtained in the absence of SF_6.[21] On the basis of this fact, it seems that, the possibility of the formation of D′ or H′ *via* neutralization is not large. The hydrogen atoms formed *via* neutralization, however, can not be completely described; further investigations will be required.

A hot hydrogen atom here corresponds to the precursor of the bimolecular formation of hydrogen, which is non-scavengeable by ethylene. If a hot hydrogen atom reacts with ethylene such as:

$$D' + C_2H_4 \longrightarrow C_2H_3D + H$$

to form a thermal hydrogen atom which is scavenged by ethylene itself, the yield of hot hydrogen atoms estimated here will indicate the lower limit.

The value of $G_{1D}=0.4$ is nearly equal to the "molecular" hydrogen yield, which is unaffected by an electron scavenger.[2,4-6,8,22] The most reasonable process for the formation of "molecular" hydrogen is the molecular detachment of hydrogen from the excited state formed *via* direct excitation.

The authors wish to thank Professor Shoji Shida and Dr. Satoshi Takao for their valuable suggestions.

21) The value of α is nearly half of that in the absence of SF_6. The value of α itself and the decrease of α by the addition of SF_6 may not reasonably be explained here.

22) A. R. Anderson, B. Knight, and J. A. Winter, *Nature*, **201**, 1026 (1964).

Dielectric Relaxation and Molecular Structure. VII. Structure of the Molecules of Diphenylene Dioxide Type

Yoshinori KOGA, Hiroaki TAKAHASHI, and Keniti HIGASI

School of Science and Engineering, Waseda University, Shinjuku-ku, Tokyo 160

(Received May 29, 1973)

The dielectric constants and losses of diphenylene dioxide, phenoxathiin, thianthrene, xanthene and phenothiazine have been measured in dilute solution of benzene at the millimeter-wave frequency of 100 GHz at 20 °C. Diphenylene dioxide is found to have a very small dielectric relaxation time which is associated with the change in dipole orientation by the intramolecular change (butterfly motion). The dipole moment of this molecule is small but not considered to be zero. Similar to thianthrene, which has a folded structure about the S–S axis, diphenylene dioxide is also folded about the O–O axis or can easily have a folded structure. Phenoxathiin and the other two molecules have a folded structure and the dielectric relaxation times (at 100 GHz) reveal the effect of the butterfly-flapping motion associated with the barrier height for this internal motion.

Both planar and non-planar configurations of diphenylene dioxide have been concluded from measurements of the dipole moments. According to Bennett, Earp and Glasstone[1] it has a planar structure since their measurements indicated a zero moment, while Higasi[2] inferred that it would have a folded structure since its dipoe moment amounts to 0.64 D. The observed difference between ${}_{\infty}P_2$ and R_D may possibly be due to a rather large atomic polarization arising from the vibration of the molecule about the O–O axis. For this reason Smith[3] considered that diphenylene dioxide is planar.

From a recent X-ray crystal analysis[4] it was revealed that the molecule of diphenylene dioxide is not fixed at the coplanar configuration in solid. In addition Davies and Swain[5] discovered a dielectric absorption due to the butterfly-flapping motion for diphenylene dioxide in polystyrene matrix.

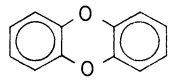

I: Diphenylene dioxide

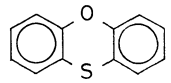

II: Phenoxathiin

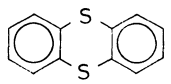

III: Thianthrene

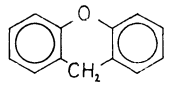

IV: Xanthene

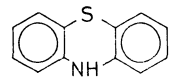

V: Phenothiazine

Diphenylene dioxide (I) and related molecules (II), (III), (IV), and (V) were studied in order to obtain further information on the molecular configuration and intramolecular configurational changes.

Experimental

The frequencies of the dielectric measurements are 96.382 GHz (*ca.* 100 GHz) and 1 MHz (for the static value). Pure samples of diphenylene dioxide (mp 119 °C) and phenoxathiin (mp 56.5 °C) were kindly provided by Professor S. Uyeo, Kyoto University. Other compounds were obtained from commercial sources, and were purified by recrystallization. Benzene employed as the solvent was prepared in the usual way. The apparatus and experimental technique for dielectric measurements were the same as those used previously.[6]

TABLE 1. REFRACTIVE INDICES, ABSORPTIONS, DIELECTRIC CONSTANTS AND LOSSES OF DIPHENYLENE DIOXIDE IN BENZENE SOLUTION AT 96.382 GHz (20 °C)

Weight fraction	n	k	ε'	ε''
0.00000	1.5110	0.0022	2.2831	0.0068
0.02126	1.5156	0.0023	2.2970	0.0069
0.05325	1.5200	0.0029	2.3104	0.0087
0.08243	1.5247	0.0030	2.3248	0.0093
0.09217	1.5258	0.0032	2.3281	0.0098

The complex refractive indices $n^*=n-ik$, n and k being the real and imaginary parts, respectively, have been measured for three or four different dilute solutions of the same sample at 20 °C. The dielectric constants ε' and the losses ε'' were obtained from n and k by $\varepsilon'=n^2-k^2$ and $\varepsilon''=2nk$ (Table 1). The slopes of a' and a'' were obtained on the assumption that the linear relationship of ε' and ε'' with the concentration (weight fraction) w_2 exists.

$$\varepsilon' = \varepsilon_1' + a'w_2$$
$$\varepsilon'' = \varepsilon_1'' + a''w_2 \quad (1)$$

In addition, a_0, a_D and b are the slopes for the static dielectric constant ε_0, the square of refractive index n_D (for the sodium D-line) and the specific volume v against the weight fraction, respectively (Table 2).

1) G. M. Bennett, D. P. Earp, and S. Glasstone, *J. Chem. Soc.*, 1179 (1934).
2) K. Higasi, *Sci. Pap. Inst. Phys. Chem. Res.*, **38**, 331 (1941).
3) J. W. Smith, "Electric Dipole Moments," Butterworths Sci. Publ., London (1955), pp. 244—245.
4) K. Osaki, Kyoto Univ. Private communication.
5) M. Davies and J. Swain, *Trans. Faraday Soc.*, **67**, 1637 (1971).
6) K. Chitoku, K. Higasi, M. Nakamura, Y. Koga, and H. Takahashi, This Bulletin, **44**, 992 (1971).

TABLE 2. SLOPES a_0, a', a'', a_G, a_D, AND b IN BENZENE SOLUTION (20 °C)

Substance	a_0	a'	a''	a_G	a_D	b
Diphenylene dioxide	0.496	0.447	0.038	0.418	0.254	−0.320
Phenoxathiin	1.035	0.521	0.135	0.486	0.380	−0.352
Thianthrene	1.470	0.511	0.111	0.498	0.434	−0.372
Xanthene	1.140	0.367	0.097	0.355	0.266	−0.281
Phenothiazine	3.227	0.676	0.311	0.638	0.480	−0.367

$$\varepsilon_0 = \varepsilon_{10} + a_0 w_2, \quad n_D^2 = n_{1D}^2 + a_D w_2$$
$$v = v_1 + b w_2, \quad \varepsilon_\infty = \varepsilon_{1\infty} + a_\infty w_2 \qquad (2)$$

The total molar polarization of the solute at infinite dilution ($w_2 \to 0$) is approximately given by Halverstadt and Kumler[7] in the following form:

$${}_\infty P_2 \simeq M_2\left\{\frac{3a_0 v_1}{(\varepsilon_{10}+2)^2} + (v_1+b)\frac{\varepsilon_{10}-1}{\varepsilon_{10}+2}\right\} \qquad (3)$$

where M_2 is the molecular weight of the solute. If a_∞ and $\varepsilon_{1\infty}$ are used instead of a_0 and ε_{10}, respectively, the distortion polarization P_A+P_E instead of ${}_\infty P_2$ will be obtained by

$$P_A + P_E \simeq M_2\left\{\frac{3a_\infty v_1}{(\varepsilon_{1\infty}+2)^2} + (v_1+b)\frac{\varepsilon_{1\infty}-1}{\varepsilon_{1\infty}+2}\right\} \qquad (4)$$

Similarly, the molecular refraction for the D-line R_D will be given by

$$R_D \simeq M_2\left\{\frac{3a_D v_1}{(n_{1D}^2+2)^2} + (v_1+b)\frac{n_{1D}^2-1}{n_{1D}^2+2}\right\} \qquad (5)$$

The atomic polarization P_A will be estimated roughly by $(P_A+P_E)-R_D$ if $R_D \approx P_E$ and $\varepsilon_{10} \approx \varepsilon_{1\infty} \approx {n_{1D}}^2$ (see Appendix 1). Thus we have an estimate for P_A by

$$P_A \simeq M_2\left\{\frac{3(a_\infty - a_D)v_1}{(\varepsilon_{10}+2)^2}\right\} \qquad (6)$$

The relaxation time of the solute τ is calculated by use of two equations:[8]

$$\tau = \frac{1}{\omega}\frac{a''}{a'-a_\infty} \equiv \tau(1) \qquad (7)$$

$$\tau = \frac{1}{\omega}\frac{a_0-a'}{a''} \equiv \tau(2) \qquad (8)$$

If one assumes a_∞ to be equal to a_D, the values τ (1) will become much smaller than τ (2); and if a_∞ is given by a_G defined in Eq. (9), τ (1) will become identical with τ (2).

$$a_\infty \simeq a_G \equiv a' - \frac{(a'')^2}{a_0-a'} \qquad (9)$$

Perhaps a_G evaluated from a' and a'' at a very high frequency (100 GHz) would be a good estimate for a_∞ and is often close to a_∞ obtained from Cole-Cole plots. Thus Eq. (4) can be rewritten by using a_G instead of a_∞:

$$P_A + P_E \simeq M_2\left\{\frac{3a_G v_1}{(\varepsilon_1'+2)^2} + (v_1+b)\frac{\varepsilon_1'-1}{\varepsilon_1'+2}\right\} \qquad (10)$$

where $\varepsilon_{1\infty}$ is also replaced with ε_1'.

The dipole moment μ is estimated by

$$\mu = \left\{\frac{9kTM_2}{4N\pi}({}_\infty P_2 - (P_A+P_E))\right\}^{1/2} \qquad (11)$$

On the assumption that $\varepsilon_{10} \approx \varepsilon_1'$ for non-polar solvents we can obtain approximately

$${}_\infty P_2 - (P_A+P_E) \simeq M_2\left\{\frac{3(a_0-a_\infty)v_1}{(\varepsilon_1'+2)^2}\right\} \qquad (12)$$

Therefore

$$\mu^2 \simeq \frac{27kTM_2 v_1}{4N\pi}\frac{a_0-a_\infty}{(\varepsilon_1'+2)^2} = B^2(a_0-a_\infty) \qquad (13)$$

where

$$B = \left\{\frac{27kTM_2}{4N\pi d_1}\right\}^{1/2}\frac{1}{(\varepsilon_1'+2)} \qquad (14)$$

and d_1 is the density of the solvent. Equations (13) and (14) are equivalent to the corresponding formulae of the previous work[8,9] (see Appendix 2). The relaxation times and polarization data are given in Tables 3 and 4, respectively.

TABLE 3. TWO RELAXATION TIMES $\tau(1)$, $\tau(2)$ AND DIPOLE MOMENTS BASED ON Eqs. (3), (10) AND (11) TOGETHER WITH LITERATURE VALUES. $\tau(1)$ IS OBTAINED ON THE ASSUMPTION OF $a_\infty = a_D$ (20 °C)

Substance	$\tau(1)$ ps	$\tau(2)$ ps	μ D	μ(lit.) D
Diphenylene dioxide	0.3	2.1	0.36	0[a], 0.64[b]
Phenoxathiin	1.6	6.3	0.99	1.09[b], 1.00[c], 0.97[d]
Thianthrene	2.4	14.3	1.37	1.41[e], 1.57[f], 1.70[g]
Xanthene	1.6	13.2	1.13	1.14[h], 1.29[i]
Phenothiazine	2.6	13.6	2.15	2.16[c]
Anthrone(25 °C)	—	21.2	—	3.63[i]
Xanthone(25 °C)	—	21.0	—	2.95[i]

a) Ref. 1.
b) Ref. 2.
c) Ref. 12.
d) Ref. 10.
e) W. S. Walls and C. P. Smyth, *J. Chem. Phys.*, **1**, 337 (1933).
f) I. G. M. Campbell, C. G. Le Fevre, R. J. W. Le Fevre and E. E. Turner, *J. Chem. Soc.*, **1938**, 404.
g) E. Bergmann and M. Tshundnowsky, *Chem. Ber.*, **B65**, 457 (1938).
h) Ref. 15.
i) A. L. McClellan, "Tables of Experimental Dipole Moments," Freeman and Co., San Francisco (1963).

TABLE 4. TOTAL MOLAR POLARIZATION ${}_\infty P_2$, DISTORTION POLARIZATION P_A+P_E OBTAINED FROM Eq. (10) AND MOLECULAR REFRACTION R_D

Substance	${}_\infty P_2$ (cm³)	P_A+P_E (cm³)	R_D (cm³)	P_A (cm³)	P_A/R_D (%)
Diphenylene dioxide	62.1	59.4	53.2	6.2	11.7
Phenoxathiin	85.7	65.2	60.7	4.5	7.4
Thianthrene	108.8	69.7	66.5	3.2	4.8
Xanthene	85.4	58.8	55.1	3.7	6.7
Phenothiazine	165.7	69.7	63.3	6.4	10.1

Discussion

The dielectric relaxation time of diphenylene dioxide (I) in benzene solution is 2.1 ps (calculated as $\tau(2)$). If $a_\infty \simeq a_D = 0.254$ is assumed, $\tau(1)$ will be only 0.3 ps. In contrast to this, anthrone (VI) and xanthone

7) I. F. Halverstadt and W. D. Kumler, *J. Amer. Chem. Soc.*, **64**, 2988 (1942).
8) K. Higasi, This Bulletin, **39**, 2157 (1966).
9) K. Higasi and O. Kiyohara, *Bull. Inst. Appl. Elect.*, **18**, 24 (1966).

(VII) have much larger relaxation times 21.2 and 21.0 ps, respectively, in benzene solution.

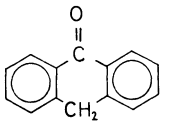

VI: Anthrone

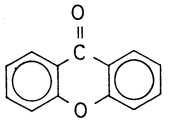

VII: Xanthone

The small values observed for τ of diphenylene dioxide are certainly not due to the change of dipole orientation by rotation of the whole molecule.

When there exist two independent paths from the same initial state to the same final state with opposite directions of the molecular dipole, a single relaxation time τ will be observed which is related to the relaxation times τ_m and τ_b for the two individual processes by

$$\frac{1}{\tau} = \frac{1}{\tau_m} + \frac{1}{\tau_b} \qquad (15)$$

Suppose that Eq. (15) is valid in this case and some internal process such as the butterfly motion (with a small τ_b value) is considered. If we assume $\tau_m=21$ ps for molecular rotation and $\tau_b=2.5$ ps for butterfly motion, we shall obtain from Eq. (15) $\tau=2.2$ ps which compares well with $\tau(2)=2.1$ ps. This would be an evidence for a slightly folded structure in the equilibrium state.

The dipole moment of diphenylene dioxide is calculated to be 0.36 D from Eqs. (3), (10), and (11). Or, we may calculate it to be 0.38 D from Eq. (A-4) on the basis of the relaxation time $\tau(2)=2.1$ ps. Both values are smaller than 0.64 D obtained from the previous measurement of the static dielectric constant.[2] However, they are not zero so that one may conclude that very likely the molecule of diphenylene dioxide would have a non-planar configuration. At the same time one may notice that the atomic polarization of this molecule is 6.2 cm^3, *i.e.*, about 12% of R_D; diphenylene dioxide has a rather large atomic polarization as Smith[3] pointed out.

The dielectric relaxation time of phenoxathiin is calculated by Eq. (8) to be $\tau(2)=6.3$ ps which compares favorably with 7.0 ps (Hufnagel *et al.*[10]), but is somewhat less than 10 ps given by Anderson and Smyth.[11] These small values of τ for phenoxathiin are related to the butterfly motion. The dipole moments of phenoxathiin in benzene at room temperature from static measurement are 1.09 D (Higasi[2]), 0.97 D (Hufnagel, Klages, and Knobloch[10]) and 1.00 D (Leonard and Sutton[12]). The present work gives the total dipole moment 0.99 D on the basis of Eqs. (3), (10) and (11).

The folded structure of thianthrene has been well established by means of both X-ray crystal analysis[13,14] and dielectric measurements in solution.[3] Anderson and Smyth[11] found the dielectric relaxation time to be 31, 24, and 19 ps at 20, 40, and 60 °C, respectively. In the present experiment, however, it is only 14.3 ps at 20 °C. This seems to indicate the imporatnce of the butterfly motion. Suppose $\tau_m=21$ ps and $\tau_b=50$ ps, τ will be given as 14.8 ps from Eq. (15). It is reasonable to assume a larger τ_b for thianthrene than τ_b of diphenylene dioxide, since thianthrene has a high barrier of inversion by the butterfly motion. The atomic polarization of thianthrene is about 5% of P_E.

From their Kerr effect studies, Aroney, Hoskins, and Le Fevre[15] concluded that the preferred solution-state conformation of xanthene is a slightly folded structure defined by a dihedral angle of 160° (±6°). The dielectric relaxation time of xanthene is somewhat smaller than that of anthrone and of xanthone. Phenothiazine obtained from thianthrene by replacing S by N–H group has also a smaller relaxation time 13.6 ps. In both cases the internal motion process seems to help decrease the relaxation time observed at 100 GHz.

The activation process of butterfly inversion of a folded molecule $C_6H_4\langle{}^{X}_{Y}\rangle C_6H_4$ may be described as a change of the valence angles of the central atoms X and Y, that is, from the valence angles, ϕ_X and ϕ_Y, of the folded configuration at an equilibrium state to the valence angles, ϕ_X and ϕ_Y,[16] at the coplanar configuration. The energy U needed to change the two valence angles from ϕ_X and ϕ_Y to ϕ_X and ϕ_Y will be approximated by

Table 5. Dihedral angles θ, valence angles ϕ, bond lengths r and angle bending force constants H

Atoms X	Atoms Y	θ (°)	ϕ_X (°)	ϕ_Y (°)	r (C–X) Å	r (C–Y) Å	H_{CXC} mdyn/Å	H_{CYC} mdyn/Å
O	O	172[a]	115[a]		1.43[b]		0.30[c]	
O	S	138[d]	118[d]	98[d]	1.40[d]	1.75[d]	0.30[c]	0.157[c]
S	S	128[e]	100[e]		1.773[e]		0.157[c]	
O	C	160[f]	118[d]	109[g]	1.43[b]	1.51[g]	0.30[c]	0.257[h]
S	N	153[i]	100[i]	122[i]	1.77[i]	1.406[i]	0.157[c]	0.20[j]

a) Ref. 4.
b) Ref. 2.
c) Ref. 17.
d) S. Hosoya, *Acta Crystallogr.*, **20**, 429 (1966).
e) Ref. 14.
f) Ref. 15.
g) L. E. Sutton, "Tables of Interatomic Distances and Configuration in Molecules and Ions," Chem. Soc. Special Publ., No. 18, (1965).
h) H. Takahashi, *Nippon Kagaku Zasshi*, **83**, 978 (1962).
i) Ref. 19.
j) T. Miyazawa, T. Shimanouchi, and S. Mizushima, *J. Chem. Phys.*, **29**, 611 (1958).

10) V. F. Hufnagel, G. Klages, and P. Knobloch, *Z. Naturforsch.*, **17a**, 96 (1962).
11) J. E. Anderson and C. P. Smyth, *J. Chem. Phys.*, **42**, 473 (1965).
12) N. J. Leonard and L. E. Sutton, *J. Amer. Chem. Soc.*, **70**, 1564 (1948).
13) H. Lynton and E. G. Cox, *J. Chem. Soc.*, **1956**, 4886.
14) I. Rowe and B. Post, *Acta Crystallogr.*, **11**, 372 (1958).
15) M. J. Aroney, G. M. Hoskins, and R. J. W. Le Fevre, *J. Chem. Soc.*, **1969**, 980.
16) ϕ can be obtained from $\cos\phi=1-2(1-\cos\phi)/(1-\cos\theta)$, where θ is the angle between the planes containing the two aromatic rings.

TABLE 6. ACTIVATION ENERGY (U) FOR INVESRION ESTIMATED FROM Eq. (16)

Atoms X	Atoms Y	$\Delta\phi_X$ (°)	$\Delta\phi_Y$ (°)	U kcal/mol	U (literature) kcal/mol
O	O	0.43		0.005	0.29,[2] 0[5]
O	S	15	10	3.9	1.20,[2] 2.63[5]
S	S	17		6.2	5.50,[2] 5.00[5]
O	C	3	2.5	0.2	
S	N	14	6	2.4	2.87[5]

$$U = (1/2)H_{CXC}r_X^2\Delta\phi_X^2 + (1/2)H_{CYC}r_Y^2\Delta\phi_Y^2 \qquad (16)$$
$$\Delta\phi_X = \phi_X - \phi_X, \quad \Delta\phi_Y = \phi_Y - \phi_Y$$

where H_{CXC} and H_{CYC} are the angle bending force constants and r_X and r_Y the bond lengths of X and Y atoms, respectively. The literature values of θ, ϕ, r, and H are given in Table 5 and the values U thus estimated in Table 6. For diphenylene dioxide, $\Delta\phi_o = 0.43°$, r(C–O)=1.43 Å[2] and H_{COC}=0.30 mdyn/Å[17] Eq. (16) gives U=0.005 kcal/mol. This is in accordance with the small value 2.5 ps assumed for τ_b. For the inversion barrier of thianthrene we can obtain 6.2 kcal/mol by using the values of $\Delta\phi_S = 17°$, r(C–S)= 1.773 Å[14] and H_{CSC}=0.157 mdyn/Å.[17] The conjugation energy at the coplanar position should decrease these barrier heights, while the viscosity of the solvent would hinder the inversion.

The observed relaxation time for phenoxathiin, 6.3 ps, is close to an average of 2.1 ps (diphenylene dioxide) and 14.3 ps (thianthrene). The inversion barrier of phenoxathiin 3.9 kcal/mol lies between those for the two molecules.

The molecular dipole of phenoxathiin has two components, $\mu_{//}$ directed along the O–S axis for the overall rotation and $\mu_\perp$ perpendicular to the same axis for the butterfly motion. Hence, two dipolar relaxations should be observed; however, the absorption due to the butterfly motion predominates overall rotation since $(\mu_\perp/\mu_{//})^2$ is estimated to be very large, *i.e.*, 12: 1.[5] One can say with certainty that the observed relaxation time at 100 GHz corresponds to that of butterfly motion.

The relaxation time of xanthene is 13.2 ps, which is smaller than that of xanthone and of anthrone by 30—40%. From the analysis of its dipole moment one would expect two dipolar relaxations, the ratio of their intensities $(\mu_\perp/\mu_{//})^2$ being about 1: 20. The observed lowering of the relaxation time might be explained in the following way. The inversion barrier of xanthene is less than 1 kcal/mol and hence the relaxation time associated with the butterfly motion would be similar to τ_b for diphenylene dioxide. If one assumes the relaxation time for the overall rotation to be 20 ps and that for the butterfly motion 2.5 ps, one can estimate $\tau(2)$ obtainable for any frequency for any value of $(\mu_\perp/\mu)^2 = C_2$ by using the method given in the preceding paper.[18] The result of calculations for 100 GHz is shown by curve A and that for 10 GHz by curve B in Fig. 1. At the frequency of this experiment, $\tau(2)$ is equal to 13.2 ps for C_2=0.1 (*cf.*, 19.4 ps for C_2=0.1 at 10 GHz). Consequently, the lowering in relaxation time might be due to the butterfly inversion, although the dipole component associated with this internal process is not significant enough.

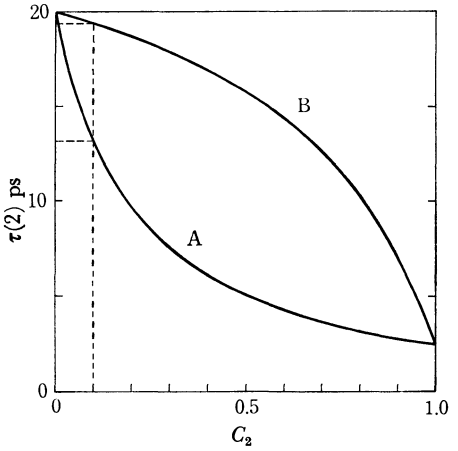

Fig. 1. Dependence of the relaxation time $\tau(2)$ upon the weight of internal process C_2.
A: 100 GHz, B: 10 GHz.

For phenothiazine we find a similar lowering in the relaxation time. Phenothiazine is assumed to have a quasi-equatorial form from X-ray evidence.[19] There are two independent relaxation processes, overall and internal. The dipole component associated with the internal motion is larger than that for xanthene, while the barrier height (see Table 6) for the inversion is found to be much larger. Increase in the above two quantities causes cancellation of the effects so that very likely the relaxation time is lowered to a similar extent to that for xanthene.

Concluding Remarks

1. Atomic polarization as well as the dipole moment of the solute can be obtained from the dilute solution method by use of extended Halverstadt-Kumler equations.

2. Atomic polarization is found to be large for diphenylene dioxide and phenothiazine.

3. Discussion is given for a small but non-zero polarity of diphenylene dioxide. As indicated by X-ray evidence[4] this molecule perhaps is folded about the O–O axis having two shallow potential minima. Or possibly it has one minimum with a very flat potential curve.

4. Thianthrene, phenoxathiin and phenothiazine are folded molecules with two potential minima. Xanthene also has a folded structure either with one potential minimum or two minima.

5. The molecules of $C_6H_4\langle\overset{X}{X}\rangle C_6H_4$ type have the single relaxation time τ which is related to the relaxation time τ_m and τ_b by Eq. (15).

6. The molecules of $C_6H_4\langle\overset{X}{Y}\rangle C_6H_4$ type have two

17) M. Hayashi, *Nippon Kagaku Zasshi*, **77**, 1804 (1956).
18) K. Higasi, Y. Koga, and M. Nakamura, This Bulletin, **44**, 988 (1971).
19) J. D. Bell, J. F. Blount, O. V. Briscoe, and H. C. Freeman, *Chem. Commun.*, **1968**, 1656.

dipolar relaxations. The average relaxation time $\tau(2)$ is a function of $(\mu_{//}/\mu)^2=C_2$ and the frequency of the measurement.[18]

Appendix

I. P_A is obtained by subtracting Eq. (5) from Eq. (4) and neglecting Δ^2.

$$P_A \simeq M_2\left\{\frac{3a_\infty v_1}{(\varepsilon_{1\infty}+2)^2}-\frac{3a_D v_1}{(n_{1D}^2+2)^2}+(v_1+b)\times\left[\frac{(\varepsilon_{1\infty}-1)}{(\varepsilon_{1\infty}+2)}-\frac{(n_{1D}^2-1)}{(n_{1D}^2+2)}\right]\right\}$$
$$\simeq M_2\left\{\frac{3[(a_\infty-a_D)(\bar{\varepsilon}_1+2)-2\Delta(a_\infty+a_D)]v_1}{(\bar{\varepsilon}_1+2)^3}+\frac{6\Delta(v_1+b)}{(\bar{\varepsilon}_1+2)^2}\right\} \quad \text{(A-1)}$$

where

$$\bar{\varepsilon}_1=\frac{1}{2}(\varepsilon_{1\infty}+n_{1D}^2) \quad \text{(A-2)}$$

and

$$\Delta=\frac{1}{2}(\varepsilon_{1\infty}-n_{1D}^2) \quad \text{(A-3)}$$

For $n_{1D}^2=\varepsilon_{1\infty}$, Eq. (6) follows immediately from (A-1).

II. For dilute solution of a polar molecule in a non-polar solvent, there is a familiar equation between the dipole moment μ and the relaxation time τ.[20]

$$\mu^2=\frac{6750kT}{NC\pi}\frac{\varepsilon''}{(\varepsilon'+2)^2}\frac{1+(\omega\tau)^2}{\omega\tau} \quad \text{(A-4)}$$

where C is the concentration in mol liter^{-1}. Introducing Eq. (8) for τ in Eq. (A-4) and assuming $\varepsilon'\approx\varepsilon_1'$, we have

$$\mu^2=\frac{6750kT}{N\pi}\frac{1}{(\varepsilon_1'+2)^2}\frac{(a_0-a')^2+(a'')^2}{a_0-a'} \quad \text{(A-5)}$$

Therefore

$$\mu^2=\frac{27000kT}{4N\pi}\frac{1}{(\varepsilon_1'+2)^2}(a_0-a_\infty)=B^2(a_0-a_\infty) \quad \text{(A-6)}$$

where

$$B=\left\{\frac{27000kT}{4N\pi}\right\}^{1/2}\frac{1}{(\varepsilon_1'+2)} \quad \text{(A-7)}$$

The value of B in (A-7) differs from that in Eq. (14) since the concentration of the solute is expressed in units of molar concentration in (A-7) and in units of weight fraction in Eq. (14).[8,9] If $a_D=a_\infty$, then

$$\mu=B(a_0-a_D)^{1/2} \quad \text{(A-8)}$$

We thank Professor S. Uyeo for the gift of valuable samples and also Toray Science Foundation for financial aids.

20) N. E. Hill, W. E. Vaughan, A. H. Price ,and M. Davies, "Dielectric Properties and Molecular Behaviour," Van Nostrand, Rheinhold, London, (1969), p. 289.

BULLETIN OF THE CHEMICAL SOCIETY OF JAPAN, VOL. 46, 3363—3366 (1973)

The Primary Photochemical Process of 4-Nitropyridine *N*-Oxide. III. Its Photochemical Behavior in an Aqueous Solution

Norisuke HATA, Isao ONO, and Kenji OSAKA

Department of Chemistry, College of Science and Engineering, Aoyama Gakuin University, Chitosedai, Setagaya-ku, Tokyo 157

(Received June 19, 1973)

4-Nitropyridine *N*-oxide does not undergo photochemical changes in an aqueous solution. When small amounts of 2-propanol or tetrahydrofuran were added to a deaerated solution, however, the 4-nitropyridine *N*-oxide was found to be reduced photochemically to afford 4-hydroxylaminopyridine *N*-oxide. From the measurements of the quantum yields and from flash-spectroscopic experiments under various conditions, such a photoinduced reduction of 4-nitropyridine *N*-oxide in deaerated water was revealed to be initiated by a hydrogen-atom abstraction from a 2-propanol or tetrahydrofuran by the triplet species. The situation was quite different from the case of an alcoholic solution, in which some intermediate species originating from the excited singlet state was responsible for the photoreduction.

As has been described in a previous paper,[1] the photochemical reaction of 4-nitropyridine *N*-oxide in alcohol (methanol, ethanol, 2-propanol, or glycerol) involves some intermediate species, A, A′, or B, originating from the excited singlet state; Process I (the photochemical formation of 4-hydroxypyridine *N*-oxide nitrate) proceeds *via* a transient complex between the intermediate A′ and the unexcited molecule, while Process II (the photochemical formation of 4-hydroxylaminopyridine *N*-oxide) is initiated by a hydrogen-atom abstraction from a solvent molecule by the intermediate B, which is produced from another intermediate, A.

However, the 4-nitropyridine *N*-oxide in water is quite stable to light.[2] Considering the fact that even Process I does not proceed in an aqueous solution, the primary process may be inferred to be quite different from that in alcohol. In order to make this point

1) N. Hata, I. Ono, and T. Tsuchiya, This Bulletin, **45**, 2386 (1972).

2) C. Kaneko, S. Yamada, I. Yokoe, N. Hata, and Y. Ubukata, *Tetrahedron Lett.*, **1966**, 4729.

clear, therefore, the present authors have carried out investigations by means of both steady-light irradiation and flash spectroscopy for the 4-nitropyridine *N*-oxide in deaerated water.

Experimental

The 4-nitropyridine *N*-oxide used in this experiment was synthesized and purified according to the method given in the literature.[3] Reagent-grade tetrahydrofuran and 2-propanol (Wako Pure Chemical Industries) were used without further purification.

The apparatus and procedures for both the steady-light and flash experiments were the same as those reported previously.[1,4]

Results and Discussion

Photochemical changes were not induced for the 4-nitropyridine *N*-oxide when it was irradiated with 313 nm light in deaerated water. The introduction of small amounts of 2-propanol or tetrahydrofuran (THF) into the solution, however, was found to result in the photochemical reduction of 4-nitropyridine *N*-oxide to the 4-hydroxylaminopyridine *N*-oxide, while no such production occurred when *tert*-butyl alcohol was added instead of 2-propanol or THF. Such a photoinduced reaction of 4-nitropyridine *N*-oxide in an aqueous solution was completely prevented by the dissolved oxygen. As an example, Fig. 1 shows the progressive spectral change of 4-nitropyridine *N*-oxide (7.0×10^{-5} M) in deaerated water containing 1.2×10^{-1} M THF on 313 nm irradiation. As can be seen from the figure, as the irradiation time increased the absorption spectrum of 4-nitropyridine *N*-oxide decreased progressively in intensity and a new absorption band with its maximum at 283 nm appeared, which coincided with that of 4-hydroxylaminopyridine *N*-oxide.

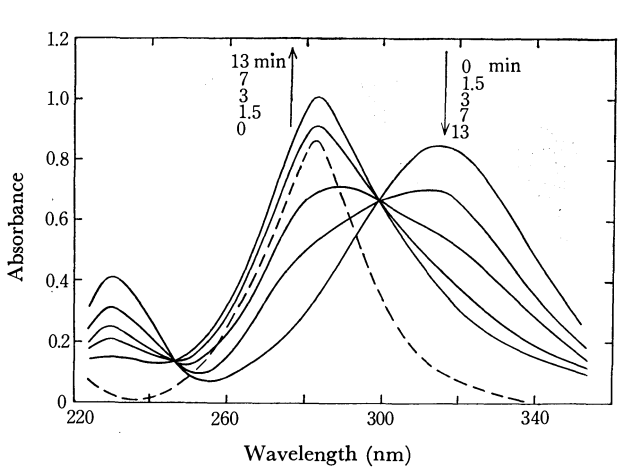

Fig. 1. The progressive spectral change of 4-nitropyridine *N*-oxide in deaerated water (7.0×10^{-5} M) containing a 1.2×10^{-1} M THF on 313 nm irradiation. Numbers refer to the irradiation time. The broken curve represents the absorption spectrum of 4-hydroxylaminopyridine *N*-oxide in water (4.7×10^{-5} M).

3) E. Ochiai, *J. Org. Chem.*, **18**, 535 (1953).

4) N. Hata, E. Okutsu, and I. Tanaka, This Bulletin, **41**, 1769 (1968).

The quantum yields (Φ) of the disappearance of 4-nitropyridine *N*-oxide were determined as a function of the concentration of 2-propanol or THF added as the reducing agent, or of the concentration of the hydrogen-donor (RH) in an aqueous solution (7.0×10^{-5} M) at room temperature. Figure 2 shows the results thus obtained; a linear relationship may be seen to exist between the reciprocals of Φ and [RH].

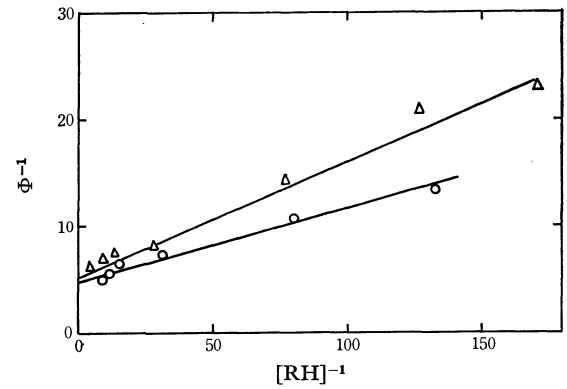

Fig. 2. Quantum yield (Φ) *vs.* concentration of hydrogen-donor (-○-: THF, -△-: 2-propanol) in deaerated aqueous solution (7.0×10^{-5} M) at room temperature, on 313 nm irradiation.

Next, in order to clarify whether or not the photochemical process of 4-nitropyridine *N*-oxide in water involves the same intermediates as in the case of an alcoholic solution, flash-spectroscopic examinations were undertaken in a deaerated aqueous solution at room temperature. Figure 3 shows the absorption spectra of the transient species produced by a flash illumination, where the spectrum was plotted after the flash and also at a specified time interval following the flash. Thus, the transient absorptions were observed around 380 and 550 nm, but they completely disappeared in the presence of oxygen. The decay analyses for these transient absorptions were carried out by applying the first-order rate law at various wavelengths; two examples, at 380 nm and at 540 nm, are presented in Fig. 4. It is clear from the figure that the decay curve for the 540 or 380 nm absorption can be resolved into

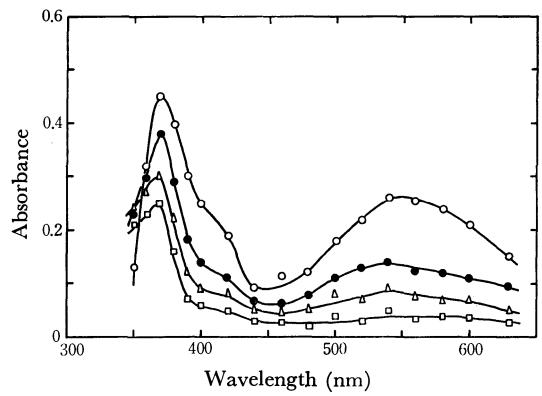

Fig. 3. Transient spectra of 4-nitropyridine *N*-oxide in deaerated water (7.0×10^{-5} M) at room temperature. (1) -○-, (2) -●-, (3) -△-, and (4) -□- indicate the spectrum taken at 20 μsec, 60 μsec, 100 μsec, and 200 μsec, respectively, after the flash.

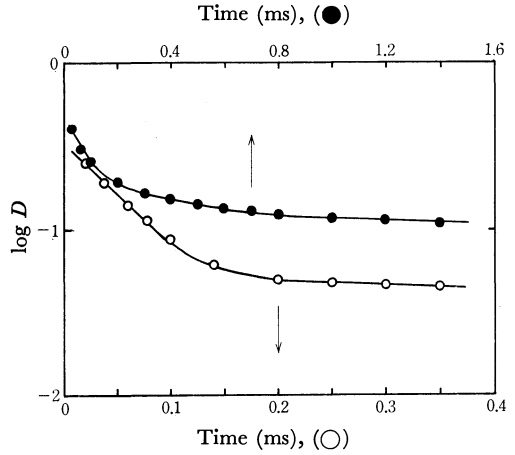

Fig. 4. Decay analysis for the transient absorption at 380 nm (●) and 540 nm (○).

a two- or three-component decay. Consequently, the transient absorptions were revealed to be due to three intermediate species, X, Y, and Z; their individual spectra are shown in Fig. 5. The intermediate X, with its absorptions around 380 and 550 nm, decayed with a rate constant (k_X) of $3.3\times10^4\ s^{-1}$, whereas the intermediates Y and Z (about 370 nm) decayed with rate constants (k_Y and k_Z) of $3.8\times10^3\ s^{-1}$ and $7.0\times10^2\ s^{-1}$ respectively.

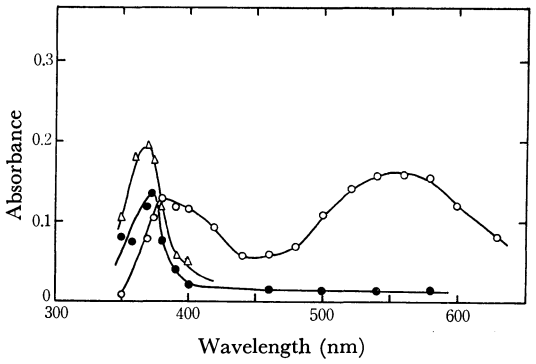

Fig. 5. Absorption spectra of the intermediate species X (-○-), Y (-●-) and Z (-△-) resolved by the decay analyses at different wavelengths.

Then, the effect of a hydrogen-donor on the decay rate was investigated in order to elucidate which intermediate is responsible for the photochemical reduction of 4-nitropyridine *N*-oxide. The decay rate (k_x) of the intermediate X, as is shown in Fig. 6, increased linearly with an increase in the concentration of THF, while that (k_Y or k_Z) of the intermediate Y or Z was independent of the concentration of THF. Quite similar results were also obtained when the 2-propanol was added as a hydrogen-donor instead of THF.[5] These results lead to the conclusion that the intermediate X is responsible for the hydrogen-atom abstraction from a THF or 2-propanol.

Although the transient spectrum in water (Fig. 3) is closely similar in appearance to that in alcohol (Figs. 1 and 2 in Ref. 1), the nature of the intermediate species involved seems to be different in each case, for a reason to be presented below. In the case of an alcoholic solution,[1] the decay of the transient absorption (~550 nm) appeared immediately after the flash had been clearly observed to be followed by the appearance of the 380 nm absorption. Moreover, these absorption spectra have been obtained even in an oxygen-saturated solution, indicating that all the intermediate involved originated from the excited singlet state of 4-nitropyridine *N*-oxide. In the case of an aqueous solution, however, apparently the two absorption systems (Fig. 3) appeared simultaneously within the time of the flash (10 μs), although they were located in the same spectral region as in the case of an alcoholic solution. In addition, they were completely quenched by the dissolved oxygen, suggesting that the intermediates involved is due to a triplet and related species. It is remarkable that, whereas the decay rate (k_Y) of the intermediate Y was independent of [RH], the absorption intensity was observed to decrease with an increase in [RH]. As an example, Fig. 7 shows the decrease in the absorption intensity of the intermediate Y with an increased concentration of 2-propanol. This can possibly be interpreted by assuming the following pathways, (i) and (ii), for the decay of the intermediate X:

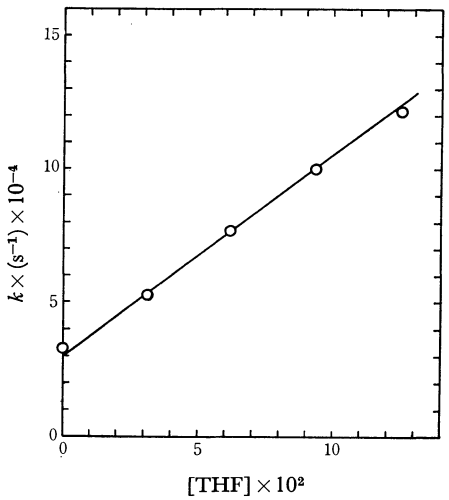

Fig. 6. The effect of THF on the decay rate of the intermediate X in deaerated water at room temperature (concentration of 4-nitropyridine *N*-oxide: 7.0×10^{-5} M).

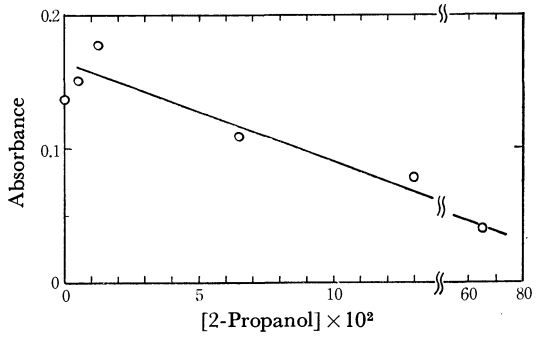

Fig. 7. The effect of the concentration of 2-propanol on the absorption intensity of the intermediate Y in deaerated water at room temperature (concentration of 4-nitropyridine *N*-oxide: 7.0×10^{-5} M).

5) In this case, the decay rate (k_Z) of the intermediate Z was observed to decrease initially with an increased concentration of 2-propanol, although the reason was quite ambiguous at present.

$$\text{Intermediate X} \xrightarrow{+RH} \begin{cases} \longrightarrow \text{Hydrogen-atom abstraction} & \text{(i)} \\ \longrightarrow \text{Intermediate Y} & \text{(ii)} \end{cases}$$

That is, as the concentration of the hydrogen-donor increases, the hydrogen-atom abstraction (i) would become much more important than the formation of the intermediate Y (ii), leading to a decrease in the absorption intensity of the intermediate Y. The fact that the absorption intensity at 350 nm was observed to increase slightly with the lapse of time (Fig. 5) seems to support the idea that the intermediate Y[6] could be produced from the intermediate X. Judging from these facts, it appears reasonable to assign the intermediate X to the lowest triplet state (T_1) of 4-nitropyridine *N*-oxide.[7] Accordingly, the following reaction scheme can be obtained.

	Rate
$S_0 + h\nu \longrightarrow S_1$	I_a
$S_1 \longrightarrow S_0$	$k_1[S_1]$
$S_1 \longrightarrow T_1$	$k_2[S_1]$
$T_1 + RH \longrightarrow$ Hydrogen-atom abstraction	$k_3[T_1][RH]$
$T_1 \longrightarrow Y$	$k_4[T_1]$
$T_1 \longrightarrow S_0$	$k_5[T_1]$

where the intermediate Z is not involved because of the ambiguous nature.

Assuming the photostationary state conditions, the quantum yield of the 4-nitropyridine *N*-oxide disappearance is given by the following equation:

$$1/\Phi = 1/\Phi_{isc} + (k_4+k_5)/\Phi_{isc}k_3[RH] \quad (1)$$

where Φ_{isc} represents the efficiency of the S_1–T_1 intersystem crossing as follows:

$$\Phi_{isc} = k_2/(k_1+k_2) \quad (2)$$

Thus, if Processes I and II, both of which proceed from the S_1 state,[1] can be neglected in an aqueous solution, a linear relationship should be expected to exist between the reciprocals of Φ and [RH]. The experimental results shown in Fig. 2 gave a straight line, in accordance with Eq. (1), and thus supporting the proposed reaction scheme. The values of Φ_{isc} and $(k_4+k_5)/\Phi_{isc}k_3$ were estimated from the slope and intercept of the straight-line respectively. Meanwhile, according to the reaction scheme presented above, the decay rate (k_X) of the intermediate X, or the triplet species, may be given by the following equation:

$$k_X = k_4 + k_5 + k_3[RH] \quad (3)$$

As has been described before, it was seen that the decay rate (k_X) of the intermediate X was directly proportional to the concentration of 2-propanol or THF; this was consistent with Eq. (3). Therefore, k_3 was evaluated from the slope of the straight line, while k_4+k_5 was estimated by extrapolating [RH] to zero. The value of Φ_{isc}, k_3 and k_4+k_5 thus obtained are listed in Table 1. The values of $(k_4+k_5)/k_3$ determined from both the steady-light and flash spectroscopic experiments are also given in Table 1; these values agree approximately with each other. This also supports the proposed reaction scheme.

TABLE 1. OBSERVED VALUES OF Φ_{isc}, k_3 AND k_4+k_5 IN AN AQUEOUS SOLUTION CONTAINING A HYDROGEN-DONOR AT ROOM TEMPERATURE

Hydrogen-donor	Φ_{isc}[a]	k_3[b] (l mol^{-1} s^{-1})	k_4+k_5[b] (s^{-1})	$(k_4+k_5)/k_3$
THF	0.20	7.5×10^5	3.0×10^4	0.016[a], 0.040[b]
2-Propanol	0.19	7.1×10^5	3.0×10^4	0.021[a], 0.042[b]

a) Represents the value determined from the steady-light experiment (Fig. 2).
b) Represents the value determined from the flash spectroscopic experiment (Figs. 6 and 7).

The following conclusions can be drawn from the experimental results described above. The photochemical reduction of 4-nitropyridine *N*-oxide in deaerated water proceeds through the lowest triplet state (probably, π,π^*),[8] whereas in an alcoholic solution the intermediate species resulting from the S_1 state is responsible for the photoreduction. Also, in an aqueous solution, approximately 20% of the 4-nitropyridine *N*-oxide in the S_1 state undergoes an intersystem crossing into the T_1 state responsible for the hydrogen-atom abstraction, but the intermediate A (and therefore B as well) and A′ are scarcely formed at all; thus, Process I does not occur. In the case of an alcoholic solution, on the other hand, the formation of the intermediate species A (and therefore, of B) and A′ from the S_1 state is considered to become much more predominant than the S_1–T_1 intersystem crossing; thus, both Processes I and II proceed. These conclusions are of particular interest in relation to the effect of the solvent on a dynamic behavior of the excited singlet state of 4-nitropyridine *N*-oxide. Further studies of these points are now in progress.

In conclusion, the authors wish to thank Professor Shiro Matsumoto for his permission to use the flash-photolysis apparatus.

6) The intermediate Y does not undergo chemical changes but it seems to be converted to the 4-nitropyridine *N*-oxide (S_0), although the structure is not clear at present.

7) Exactly, a comparison of the decay time of the transient absorption with that of the phosphorescence of 4-nitropyridine *N*-oxide in a deaerated water at 77 K must be made to identify the intermediate X to the lowest triplet state of *N*-oxide, but it was experimentally too difficult under such conditions.

8) I. Ono and N. Hata, This Bulletin, **45**, 2951 (1972).

Molar Volume of Ions

Fumio HIRATA and Kiyoshi ARAKAWA
Research Institute of Applied Electricity, Hokkaido University, Sapporo 060
(Received June 20, 1973)

A formula based on the scaled particle theory of fluids has been derived for the intrinsic volume of ions. Validity ranges of earlier semiempirical formulas are discussed in the light of the formula. Using the theoretical values of the intrinsic volumes of ions, values of volume contraction caused by ion-water interactions are estimated.

The partial molar volume of ions at infinite dilution, $\bar{V}_{\text{ion}}$, has turned out to be one of the most important quantities for elucidating the structure and properties of aqueous solutions of electrolytes. $\bar{V}_{\text{ion}}$ is given by

$$\bar{V}_{\text{ion}} = \bar{V}_{\text{int}} + \Delta\bar{V}, \tag{1}$$

where $\bar{V}_{\text{int}}$ is the inrinsic volume of ions, and $\Delta\bar{V}$ is the volume contraction caused by ion-solvent interactions. Intrinsic volume is defined as *the volume of spherical cavities in which ions are contained,*[1] *or non-hydrated partial molar volume of ions.*[2]

Studies have been carried out to estimate the magnitude of $\bar{V}_{\text{ion}}$, $\bar{V}_{\text{int}}$ and $\Delta\bar{V}$.[1-10] Hepler gave the following equation.[1]

$$\bar{V}_{\text{ion}} = Ar_{\text{X}}^3 - B/r_{\text{X}}, \tag{2}$$

where Ar_{X}^3 and $-B/r_{\text{X}}$ correspond to $\bar{V}_{\text{int}}$ and $\Delta\bar{V}$, respectively, and r_{X} is the crystal radius of an ion. From Eq. (2) and observed values of the partial molar volume, A and B were determined empirically. The values of Ar_{X}^3 given by Hepler were about twice as much as $4\pi r_{\text{X}}^3 N_{\text{A}}/3 (=2.52\, r_{\text{X}}^3)$, where N_{A} is Avogadro's number, r_{X} being given in Å.

Since the studies on $\bar{V}_{\text{ion}}$ by Stokes and Robinson[3] and by Hepler,[1] a number of studies have been carried out but with only partial success. For theoretical estimation of $\bar{V}_{\text{ion}}$, it is important to calculate the values of $\bar{V}_{\text{int}}$. Attempts were carried out to find expressions for $\bar{V}_{\text{int}}$. They are summarized as follows.[2]

$$\bar{V}_{\text{int}} = Ar_{\text{X}}^3 \tag{3}$$

$$= 2.52r_{\text{X}}^3 + A'r_{\text{X}}^2 \tag{4}$$

$$= 2.52(r_{\text{X}}+a)^3. \tag{5}$$

In Eq. (3) A is positive and larger than 2.52.[1,3-7] In Eq. (4) the contribution from a surface effect of ions in addition to the crystal volume, $2.52\, r_{\text{X}}^3$ is taken into consideration.[7,8,10] In Eq. (5), $\bar{V}_{\text{int}}$ is expressed with the assumption that the ionic radius is larger than that in crystals by an amount a. Assuming that "the dead space" in packing of hard spheres "corresponds to a hollow sphere of constant thickness", Glueckauf estimated the magnitude of an additive term to the crystal radius, a.[9] Since Eqs. (3), (4), and (5) are based on semiempirical and intuitive considerations, there remains an arbitrariness for estimating the values of $\bar{V}_{\text{int}}$. The expressions are found to be inconsistent with each other, their applicability being restricted. Thus, it is necessary to remove the uncertainty in the estimation of $\bar{V}_{\text{int}}$.

It is the purpose of this report to give a theoretical expression for the intrinsic volume of ions on the basis of the scaled particl theory of liquids[11] in order to make clear the physical meanings of the semiempirical expressions, and to investigate ion-water interactions through a discussion on $\Delta\bar{V}$.

Application of the Scaled Particle Theory

The Scaled Particle Theory.[11-13] The theory is based on the consideration of the properties of a new distribution function $G(r)$, where "$\rho G(r)$ is defined as the local concentration of molecular centers adjacent to a spherical cavity of radius r from which all molecular centers are excluded".[11] ρ is the number density of the fluid. The *key relation* of the theory is

$$G(d) = g(d), \tag{6}$$

where $g(r)$ is the radial distribution function at a separation r and d is a rigid sphere diameter. Noting that Eq. (6) is an exact relation for hard sphere fluids, Reiss *et al.* arrived at an approximate analytical expression for $G(r)$ by combining the packing of hard spheres with the thermodynamical consideration for the formation of spherical cavities. They derived an equation of state for hard sphere fluids, which is identical with the equation derived by Wertheim[14] as an analytical solution of Percus-Yevick equation for hard sphere fluids. It was proved that the equation is useful for various real fluids.[15,16] The theory is not only rigorous to the same extent as the Percus-Yevick equation, but also intuitive like a model theory.

The Partial Molar Volume of Solute. Pierotti made use of the theory to obtain the expression for solubility

1) L. G. Hepler, *J. Phys. Chem.*, **61**, 1426 (1957).
2) F. J. Millero, "Water and Aqueous Solutions," (ed,. R. A. Horne) p. 519, John Wiley & Sons, Inc., New York, N. Y. (1972).
3) R. H. Stokes and R. A. Robinson, *Trans. Faraday Soc.*, **53**, 301 (1957).
4) P. Mukerjee, *J. Phys. Chem.*, **65**, 740 (1961).
5) S. W. Benson and C. S. Copeland, *ibid.*, **67**, 1194 (1964).
6) L. Padova, *J. Chem. Phys.*, **39**, 1552 (1963).
7) R. M. Noyes, *J. Amer. Chem. Soc.*, **86**, 971 (1964).
8) B. E. Conway, R. E. Verrall, and J. E. Desnoyers, *Z. Physik. Chem.*, **230**, 157 (1965), *Trans. Faraday Soc.*, **62**, 2738 (1966).
9) E. Glueckauf, *ibid.*, **61**, 914 (1965).
10) M. H. Panckhurst, *Rev. Pure Appl. Chem.*, **45** (1969).
11) H. Reiss, *Adv. Chem. Phys.*, **9**, 1 (1964).
12) H. Reiss, H. L. Frisch, and J. L. Lebowitz, *J. Chem. Phys.*, **31**, 369 (1959).
13) H. Reiss, H. L. Frisch, E. Helfand, and J. L. Lebowitz, *ibid.*, **32**, 119 (1960).
14) M. S. Wertheim, *J. Math. Phys.*, **5**, 643 (1964).
15) H. Reiss and S. W. Mayer, *J. Chem. Phys.*, **31**, 1513 (1961).
16) S. W. Mayer, *ibid.*, **38**, 1803 (1963).

of non-polar gases in water.[17] The partial molar volume of solute at infinite dilution $\bar{V}_2$ is obtained as a partial derivative of chemical potential of the solute in a very dilute solution. The resulting equation is

$$\bar{V}_2 = (\partial\bar{G}_c/\partial p)_{N,T} + (\partial\bar{G}_i/\partial p)_{N,T} + RT\beta_T \quad (7)$$
$$= \bar{V}_c + \bar{V}_i + RT\beta_T \quad (8)$$

where β_T is the isothermal compressibility of the solvent. $\bar{V}_c$ and $\bar{V}_i$ appear since the process of introduction of a solute molecule into the solvent is considered to take place in two steps. The first step is "the creation of a cavity in the solvent of a suitable size to accomodate the solute molecule".[17] The reversible work required for the process is $\bar{G}_c$, which is given by the scaled particle theory as follows.

$$\bar{G}_c = K_0 + K_1 d_{12} + K_2 d_{12}^2 + K_3 d_{12}^3, \quad (9)$$

where d_{12} is $(d_1+d_2)/2$, and d_1 and d_2 are diameters for solvent and solute molecules, respectively. The second step is "the introduction into the cavity of a solute molecule which interacts with the solvent according to some potential law".[17] The reversible work required is $\bar{G}_c$. The K values in Eq. (9) were evaluated from the scaled particle theory[13] to be

$$K_0 = RT\{-\ln(1-y) + (9/2)[y/(1-y)]^2\} - (\pi p d_1^3)/6$$
$$K_1 = -(RT/d_1)\{[6y/(1-y)] + 18[y/(1-y)]^2\} + \pi p d_1^2$$
$$K_2 = (RT/d_1^2)\{[12y/(1-y)] + 18[y/(1-y)]^2\} - 2\pi p d_1$$
$$K_3 = (4/3)\pi p, \quad (10)$$

where $y=(\pi d_1^3\rho)/6$, ρ is the number density of solvent molecules, p pressure, R gas constant and T absolute temperature. The last term on the right-hand side of Eq. (9) is the work expended in creating a cavity of volume, $4\pi d_{12}^3/3$. The third and second terms are surface work and additive terms accounting for the curvature dependence of surface tension, respectively. The first term is a function of density and temperature.

Equations (7)—(10) are now applied to ionic solutions. By neglecting the term $RT\beta_T$, Eq. (8) is reduced to Eq. (1). $\bar{V}_{ion}$, $\bar{V}_{int}$, and $\Delta\bar{V}$ in Eq. (1) correspond to $\bar{V}_2$, $\bar{V}_c$, and $\bar{V}_i$ in Eq. (8), respectively. Thus, using the ionic radius r_X, $\bar{V}_c$ ($\equiv\bar{V}_{int}$) is expressed as follows, after sine calculations.

$$\bar{V}_c \equiv \bar{V}_{int} = 2.52r_X^3 + A'r_X^2 + A''r_X + A''' \quad (11)$$

A', A'', and A''' are expressed as

$$A' = RT\beta_T\{12y/(1-y)^2 + 36y^2/(1-y)^3\}/d_1^2$$
$$A'' = RT\beta_T\{6y/(1-y)^2\}/d_1$$
$$A''' = RT\beta_T\{y/(1-y)\}. \quad (12)$$

Validity and Interpretation of Various Semiempirical Equations

The physical meaning and validity of semiempirical Eqs. (3), (4), and (5) are interpreted on the basis of Eqs. (11) and (12). Equation (3) by Hepler, and Stokes and Robinson includes only the cubic term, the value of A being determined empirically and intuitively. Formally, Eq. (3) is seen to drop out the second, third and fourth terms in Eq. (11). Equation (4) by Conway *et al.* and other workers includes cubic and square terms, A' being determined empirically. Equation (4) is seen formally to drop out the third and fourth terms in Eq. (11). Equation (5) has a cubic polynomial form similar to Eq. (11). Concerning Eq. (5), the value a was determined by Glueckauf as follows.

$$a = (3\phi_w/4\pi N)^{1/3} - r_w = (18.02/2.52)^{1/3} - 1.38$$
$$= 0.55,$$

where ϕ_W is the molar volume of water, r_W the radius of water molecule.[18] This intuitive consideration by Glueckauf is explained theoretically by means of Eqs. (11) and (12).

The values of coefficients A', A'', and A''' calculated by means of Eq. (12) are given in Table 1. The values of a', a'', and a''' are determined by comparing Eq. (5) with Eqs. (11) and (12). Equation (5) is expanded as follows.

TABLE 1. VALUES A', A'', A''' CALCULATED BY Eq. (12) AND VALUES a', a'', a''' BY COMPARING Eq. (5′) WITH Eq. (11)[a]

Temperature (°C)	A'	A''	A'''	a'	a''	a'''
0	4.527	2.291	0.662	0.60	0.55	0.64
25	4.310	2.187	0.639	0.57	0.54	0.64
50	4.434	2.270	0.666	0.59	0.55	0.64
75	4.735	2.454	0.727	0.63	0.57	0.66

a) In calculating A and a, r_X in Eqs. (11), (12), and (5) is represented in Å.

$$\bar{V}_{int} = 2.52r_X^3 + 7.56ar_X^2 + 7.56a^2r_X + 2.52a^3. \quad (5')$$

The coefficients of the second, third and fourth term in Eq. (5′) correspond to A', A'', and A''' in Eq. (11), respectively. The values of a obtained using the values of A', A'', and A''' in Table 1 are denoted by a', a'', and a'''. From the fact that the values of a' and a'' remain nearly constant and equal to Glueckauf's value 0.55, and from the formal agreement of the formula with Eq. (11), Glueckauf's equation is found to be the most reasonable of Eqs. (3)—(5). On the other hand, disagreement of a''' indicates that a representation such as Eq. (5) is an over-simplification.

For the sake of comparison, the values of A' and a obtained by various methods are shown in Table 2,

TABLE 2. VALUES OF A' AND a OBTAINED BY VARIOUS METHODS

	A' (from Eq. (4))	a (from Eq. (5))
B. E. Conway *et al.*[8]	3.15	
R. Noyes[7]	4.09	0.45
M. Panckhurst[10]	4.03	0.436
E. Glueckauf[9]		0.55
F. J. Millero[19]	4.0	0.45

17) R. A. Pierotti, *J. Phys. Chem.*, **67**, 1840 (1963), *ibid.*, **69**, 281 (1965).

18) $\phi_w=(4/3)\pi N(r+a)^3$. The value of a was used as a constant increment over the crystal radius of ions in solutions.

19) F. J. Millero, *J. Phys. Chem.*, **73**, 2417 (1969).

A' from Eq. (4) and a from Eq. (5). It turns out that values of A' and a determined by semiempirical and intuitive methods are all underestimated when compared with those in Table 1.

Estimation of $\Delta\bar{V}$

The values of the volume contraction caused by ion-water interactions are calculated by means of Eqs. (1), (11), (12) and the experimental values of $\bar{V}_{ion}$. The assignment of $\bar{V}_{ion}$ to each ion from the observed values of $\bar{V}$ for electrolytes has attracted the interest of workers in this field, many conventional methods having been presented.[2] For the partial molar volume of H^+, the value $\bar{V}_{H^+}=0$ has been used conventionally. We adopt here the value $-5.0\,cm^3$ for $\bar{V}_{H^+}$ as the most adequate.[2] $\bar{V}_{ion}$ of other ions are obtained from the conventional values of partial molar volume of ions $\bar{V}_{conv}$ which have been estimated assuming that $\bar{V}_{H^+}=0$. The values of $\bar{V}_{conv}$ were tabulated by Millero.[2] The values $\Delta\bar{V}$ calculated from the values of $\bar{V}_{int}$ determined with the use of Eqs. (11) and (12) and those of $\bar{V}_{ion}$, are shown in Table 3 for various univalent ions. Pauling's crystal radii are used as ionic radii r_X in the calculation.

In alkali and halogen ions, the magnitudes of $|\Delta\bar{V}|$ are seen to decrease with the increase of ionic radii, except for Li^+ ion. The behavior is interpreted as an electrostatic aspect in ion-water interactions. However, it should be remarked that the obtained results depend on the choice of the value of $\bar{V}_{H^+}$ used here.[1,4]

The magnitude of $|\Delta\bar{V}|$ of the tetraalkylammonium ions increases with increasing ionic size. This behavior cannot be interpreted only in the light of electrostatic interactions between ions and water molecules but by the iceberg formation around the ions. We have shown recently by an ultrasonic study that icebergs formed around tetraalkylammonium ions have a dense and hard structure, and the trend of iceberg formation increases with the ionic size.[20] The behavior of $\Delta\bar{V}$ in tetraalkylammonium ions given in Table 3 is consistent with the conclusion of the ultrasonic study. It is interesting to compare the difference between the values of $\Delta\bar{V}$ of two subsequent ions, such as Me_4N^+ and Et_4N^+. The values of $(\Delta\bar{V}_{Et_4N^+}-\Delta\bar{V}_{Me_4N^+})$, $(\Delta\bar{V}_{Pr_4N^+}-\Delta\bar{V}_{Et_4N^+})$ and $(\Delta\bar{V}_{Bu_4N^+}-\Delta\bar{V}_{Pr_4N^+})$ at 25 °C are −14.7, −26.3, and −27.9 cm³/mol, respectively. This supports our conclusion that the trend of iceberg formation seems to be appreciable at Pr_4N^+.[20]

Table 3. The values of $\Delta\bar{V}$ $(=\bar{V}_{ion}{}^{a)}-\bar{V}_{int}{}^{b)})$ (cm³/mol)

Ion	r_X(Å)	0 °C	25 °C	50 °C	75 °C
H^+		−5.0	−5.0	−5.0	−5.0
Li^+	0.60	−9.7	−9.9	−10.4	−11.3
Na^+	0.95	−17.6	−15.0	−14.3	−13.7
K^+	1.33	−15.5	−13.1	−12.9	−13.0
Rb^+	1.48	−14.8	−12.4	−12.2	
Cs^+	1.69	−15.0	−12.5	−12.1	−12.4
F^-	1.36	−15.7	−14.1	−15.6	−17.3
Cl^-	1.81	−13.1	−10.8	−11.2	−13.2
Br^-	1.95	−13.0	−10.3	−10.2	−12.1
I^-	2.16	−13.6	−9.7	−9.1	−11.3
Me_4N^+	3.47	−84.8	−80.8	−81.0	−80.7
Et_4N^+	4.00	−101.1	−95.5	−95.4	−93.3
Pr_4N^+	4.52	−128.7	−121.8	−119.7	−118.8
Bu_4N^+	4.94	−160.1	−149.8	−143.9	−133.1
Am_4N^+	5.29		−171.7		

a) The values are obtained from the conventional values of partial molar volume of ions $\bar{V}_{conv}$ which have been estimated assuming that $\bar{V}_{H^+}=0$. That is, $\bar{V}_{ion}=\bar{V}_{conv}\pm5.0\,cm^3/mol$ (+for anions, −for cations). The values of $\bar{V}_{conv}$ are those compiled by Millero.[2]
b) The values are calculated by Eqs. (11) and (12).

20) F. Hirata and K. Arakawa, This Bulletin, **45**, 2715 (1972).

Radiotracer Studies on Adsorption of Surface Active Substance at Aqueous Surface. V. Effects of Additives on the Adsorption of Tritiated Nonionic Surfactant

Kazuo TAJIMA and Makio IWAHASHI

Department of Chemistry, Faculty of Science, Tokyo Metropolitan University, Setagaya-ku, Tokyo 158

(Received July 7, 1973)

The effects of additives on the adsorption of tritiated hexaoxyethylene dodecyl monoether ($TD(EO)_6$) at the air-solution interfaces have been determined at 30 °C. The salting-out effect has been found to follow the Hofmeister series for the sodium salts of various anions, whereas a constant amount has been found for the adsorption increase due to the addition of various chlorides varying with the type of cation. The salting-in effect is observed for denaturants such as urea, urea nitrate and guanidine nitrate, but not for di- and tri-ethylene glycols.

It was reported[1] that the adsorbed amount of tritiated hexaoxyethylene dodecyl monoether ($TD(EO)_6$) at the air-solution interface is in good agreement with the surface excess based on the Gibbs adsorption isotherm for concentration dependence of the surface tension of its solution. The molecular area at the saturated adsorption has been found to be 60.8 Å^2, the value being slightly larger than that for sodium dodecyl sulfate.[2,3]

Several papers have dealt with the effects of additives in nonionic surfactant solutions upon their surface-chemical characters such as cloud point,[4] critical micelle concentration,[5] thinning of film,[6] and surface tension lowering.[7] All these phenomena were studied basically by means of adsorption, which, however, has never been determined directly. Another problem is how to make use of the Gibbs adsorption isotherm for calculation of the adsorbed amount in a mixed solution of a nonionic surfactant and a strong electrolyte. We have made an attempt to determine the adsorbed amounts of $TD(EO)_6$ at the interfaces between humidified nitrogen and its solutions containing strong electrolytes or denaturants frequently used for studying the mechanism of salting-in and salting-out of surfactants.

Experimental

Materials. The tritiated nonionic surfactant was the same as that used in the previous experiment.[1,3] All the additives were purified by appropriate procedures; distillation for di- and triethylene glycols and recrystallization for strong electrolytes, urea, urea and guanidine nitrates. All the crystalline additives were finally degreased by Soxhlet extraction.

Procedures. The surfactant solution was prepared by dissolving $TD(EO)_6$ in an aqueous solution of an additive. The adsorbed amount was determined by the same procedures as described previously.[1-3] The radioactivity was measured by sheet scintillation counting in an atmosphere of 98%-humidified nitrogen at 30±0.1 °C. The surface tension was measured by the Wilhelmy plate method under the same conditions as in the adsorption experiments. The concentration of the nonionic surfactant solution, throughout all experiments, was kept constant at 4.00×10^{-5} mol/l, at which the adsorption reached the saturated values, 2.73×10^{-10} mol/cm^2 for the salt-free solution.

Results and Discussion

Salt Effects. Ionic specificity does not appear to influence the adsorption of $TD(EO)_6$ at its solution/nitrogen interfaces for any of Li, Na, K, and Cs chlorides (Fig. 1). The peculiar behavior of Rb^+ probably comes from some impurity contained in the sample of RbCl. On the other hand, an order of $Cl^->NO_3^->I^->SCN^-$ has been found for enhancement of the surfactant adsorption due to the addition of their sodium salt (Fig. 2). The order is in accord with the lyotropic series for hydration of various ions.[8] The same tendency has been found for the salt effects on the time required for formation of black film of polyoxyethylene nonylphenyl ether solution.[6] Malik and Jhamb[9] ob-

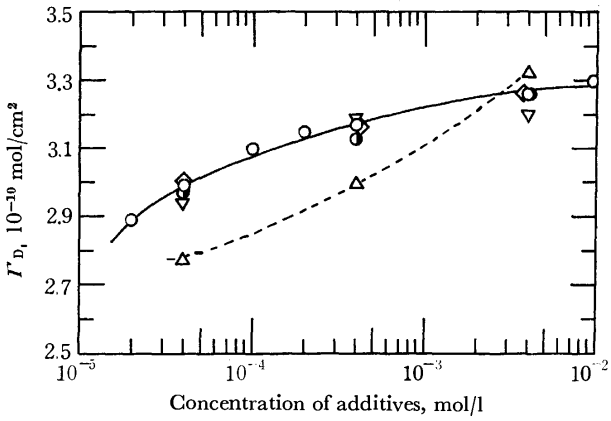

Fig. 1. Effects of various cations on the adsorbed amount of $TD(EO)_6$ at 30 °C.
The bulk concentration of $TD(EO)_6$ is 4.0×10^{-5} mol/l.
▽: LiCl, ○: NaCl, ◑: KCl, ◇: CsCl, △: RbCl.

1) K. Tajima, M. Iwahashi, and T. Sasaki, This Bulletin, **44**, 3251 (1971).
2) K. Tajima, M. Muramatsu, and T. Sasaki, *ibid.*, **43**, 1991 (1970).
3) M. Muramatsu, K. Tajima, M. Iwahashi, and K. Nukina, *J. Colloid Interf. Sci.*, **43**, 499 (1973).
4) W. N. Maclay, *J. Colloid. Sci.*, **11**, 272 (1956). M. Aoki and Y. Iwayama, *Yakugaku Zasshi*, **79**, 516 (1959).
5) K. Shinoda, T. Yamaguchi, and R. Hori, This Bulletin, **34**, 237 (1961). P. Becher, *J. Colloid Sci.*, **17**, 325 (1962). M. J. Schik and A. H. Gilbert, *ibid.*, **20**, 464 (1965). A. Ray and G. Nemethy, *J. Amer. Chem. Soc.*, **93**, 6787 (1971).
6) T. Yamanaka, This Bulletin, **43**, 633 (1970).
7) M. J. Schwuger, *Kolloid-Z. Z. Polym.*, **232**, 775 (1969).
8) A. Voet, *Chem. Rev.*, **20**, 169 (1937). R. H. Stokes and R. A. Robinson, *J. Amer. Chem. Soc.*, **70**, 1870 (1948).
9) W. U. Malik und O. P. Jhamb, *Kolloid-Z. Z. Polym.*, **242**, 1209 (1970).

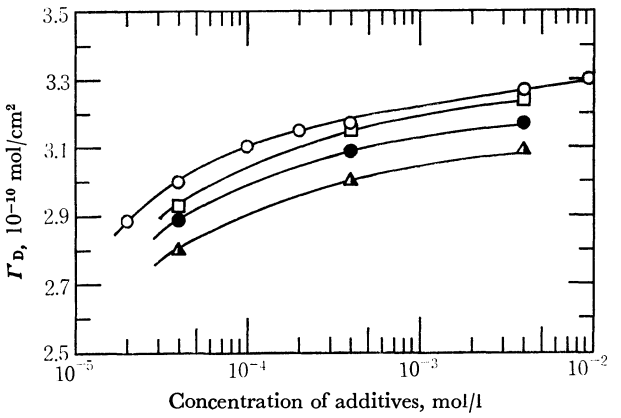

Fig. 2. Effects of various anions on the absorbed anmout of $TD(EO)_6$ at 30 °C.
The bulk concentration of $TD(EO)_6$ is 4.0×10^{-5} mol/l.
○: NaCl, □: $NaNO_3$, ●: NaI, ▲: NaSCN.

served similar effects with electrolytic additives on the lowering of cmc for Tween 20, 40, and 80 in their solutions. All these phenomena are explicable by almost the same co-ordination number, *i.e.*, 3.8 for Li^+, 3.7 for Na^+, 3.8 for K^+, and 3.5 for Cs^+, for relatively small cations surrounded by common anions (chloride) of larger size.[10] On the other hand, the result (Fig. 2) probably reflects the different charge density due to the variation of ionic radius.

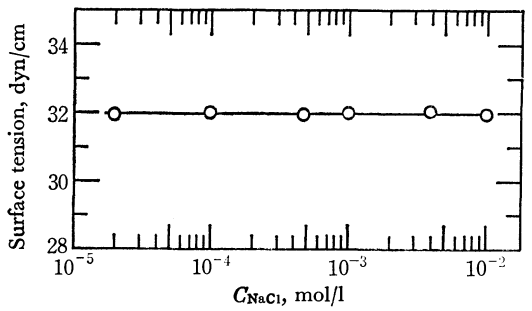

Fig. 3. Surface tension as a function of concentration of NaCl added to the solution of $TD(EO)_6$ ($C_D=4.0\times10^{-5}$ mol/l) at 30 °C.

The surface tension given as a function of NaCl added to $TD(EO)_6$ in solution is shown in Fig. 3. For such a system, the surface tension γ is expressed as

$$-d\gamma = RT\Gamma_D d\ln a_D + RT\Gamma_{Na^+} d\ln a_{Na^+} + RT\Gamma_{Cl^-} d\ln a_{Cl^-} \quad (1)$$

in terms of surface excess Γ, activity a of individual components in the solution, gas constant R, and absolute temperature T. Subscripts D, Na^+, and Cl^- denote surfactant, sodium and chloride ions, respectively. From the constancy of surfactant concentration and the electrical neutrality in surface and bulk phases, it follows that $dC_D=0$, $\Gamma_{Na^+}=\Gamma_{Cl^-}=\Gamma_{NaCl}$, and $C_{Na^+}=C_{Cl^-}=C_{NaCl}$. Thus Eq. (1) can be rewritten as follows,

$$-\frac{d\gamma}{RT\,d\ln C_{NaCl}} = \Gamma_D\frac{d\ln f_D}{d\ln C_{NaCl}} + 2\Gamma_{NaCl}\left(1+\frac{d\ln f_{\pm}^{NaCl}}{d\ln C_{NaCl}}\right) \quad (2)$$

where $f_{\pm}^{NaCl}$ is the mean activity coefficient of NaCl in the solution. Because of the small value of C_D ($=4.0\times10^{-5}$ mol/l) in comparison with C_{NaCl} ($=10^{-2}\sim10^{-5}$ mol/l), the Debye-Hückel limiting law can be applied. Thus

$$-\frac{d\ln f_{\pm}^{NaCl}}{d\ln C_{NaCl}} = \frac{A}{2}C_{NaCl}^{1/2} \quad (3)$$

where A is a constant. From the empirical relationship, $-[d\gamma/(RT\ d\ln C_{NaCl})]_D=0$ (see Fig. 3), Eq. (2) becomes

$$\Gamma_D = \frac{A\Gamma_{NaCl}}{\Delta_{NaCl}}C_{NaCl}^{1/2} - \frac{2\Gamma_{NaCl}}{\Delta_{NaCl}} \quad (4)$$

where $\Delta_{NaCl}=d\ln f_D/d\ln C_{NaCl}$. In the $\Gamma_D\sim C_{NaCl}^{1/2}$ relationship (Fig. 4), a value of 1×10^{-10} mol/cm^2/(mol/l)$^{1/2}$ is obtained for $A\Gamma_{NaCl}/\Delta_{NaCl}$ from the linear portion at $C_{NaCl}>1\times10^{-4}$ mol/l. If we assume the empirical relationship,[11]

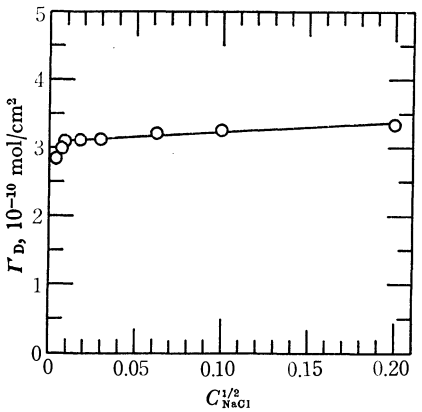

Fig. 4. Γ_D *vs.* $C_{NaCl}^{1/2}$

$$\gamma_{NaCl} = 1.92C_{NaCl} + \gamma_{H_2O} \quad (5)$$

for explaining a surface tension increase from γ_{H_2O} to γ_{NaCl} due to the addition of NaCl to water, the result $-0.762\ C_{NaCl}\times10^{-10}$ mol/cm^2 is obtained for the adsorbed amount of NaCl at its solution surface. If we furt er assume that the Γ_{NaCl} value remains unchanged by addition of $TD(EO)_6$ and A is 1.14 (l/mol)$^{1/2}$ at 30 °C, we obtain

$$-\ln f_D = 0.869C_{NaCl} \quad (6)$$

The relationship is essentially the same as the equation proposed by McDevit and Long[12] for a solution of benzene in aqueous salt solution. Mukerjee[13] derived a similar relationship for the activity coefficient for nonionic amphiphiles dissolved in aqueous salt solutions of various concentrations. It is natural to find a negative value of Δ_{NaCl} so as to give a smaller f_D value corresponding to a larger C_{NaCl} value.

10) O. Ya. Samoilov, "Structure of Aqueous Electrolyte Solutions and the Hydration of Ions," Transl. by D. J. G. Ives, Consultants Bureau Enterp., Inc., New York (1965), p. 107.

11) K. Schäfer, *Z. Elektrochem.*, **59**, 425 (1955).

12) W. F. McDevit and F. A. Long, *J. Amer. Chem. Soc.*, **74**, 1773 (1952). F. A. Long and W. F. McDevit, *Chem. Rev.*, **51**, 119 (1952).

13) P. Mukerjee, *J. Phys. Chem.*, **69**, 4038 (1965).

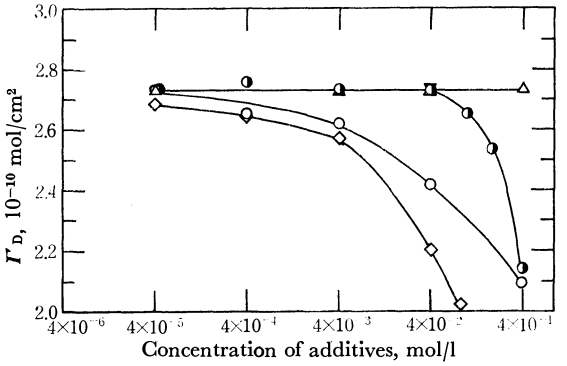

Fig. 5. Effects of various denaturants on the adsorbed amount of $TD(EO)_6$ at 30 °C.
The bulk concentration of $TD(EO)_6$ is 4.0×10^{-5} mol/l.
○: urea, ◑: urea nitrate, ▼: diethylene glycol,
△: triethylene glycol, ◇: guanidine nitrate.

Denaturant Effects. Figure 5 shows the effects of urea, urea nitrate, guanidine nitrate, di- and triethylene glycols on the adsorbed amounts of the surfactant. Addition of the denaturants causes a decrease in the adsorbed amount in the order guanidine nitrate> urea>urea nitrate>glycols, the tendency being in parallel with the effect of similar additives on the cmc elevation of Triton X-100 in its solutions[14] and on the denaturation of proteins.[15] A marked lowering of Γ_D at a concentration of urea nitrate higher than 4.0×10^{-2} mol/l might indicate a decrease in activity of ionic species. In fact, the conductivity~concentration relationship for urea nitrate (Fig. 6) gives a distinct deviation from a linear portion in log-log scale. The rather weak effect of glycols on the adsorption of $TD(EO)_6$ is understandable when we consider their weak action as denaturants.

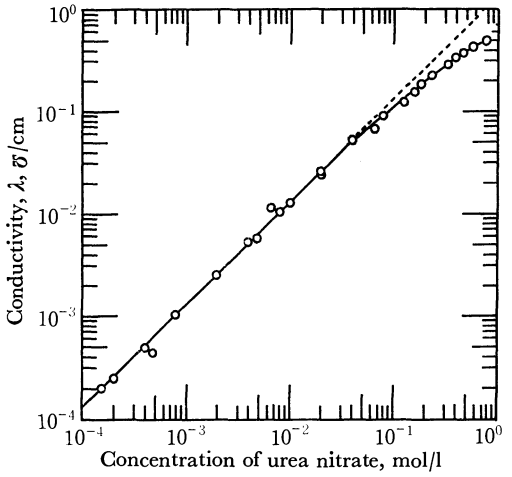

Fig. 6. Conductivity of aqueous solution of urea nitrate at 30 °C.

The surface tensions of urea solution with and without the nonionic surfactant are shown in Fig. 7. As in the derivation of Eq. (2), we obtain

$$-\left[\frac{d\gamma}{RTd\ln C_U}\right]_D = \Gamma_D\frac{d\ln f_D}{d\ln C_U} + \Gamma_U\left(1+\frac{d\ln f_U}{d\ln C_U}\right) \quad (7)$$

14) W.B. Gratzer and G.H. Beaven, *J. Phys. Chem.*, **73**, 2270 (1969).
15) P. H. von Hippel and K. Y. Wong, *J. Biol. Chem.*, **240**, 3909 (1965).

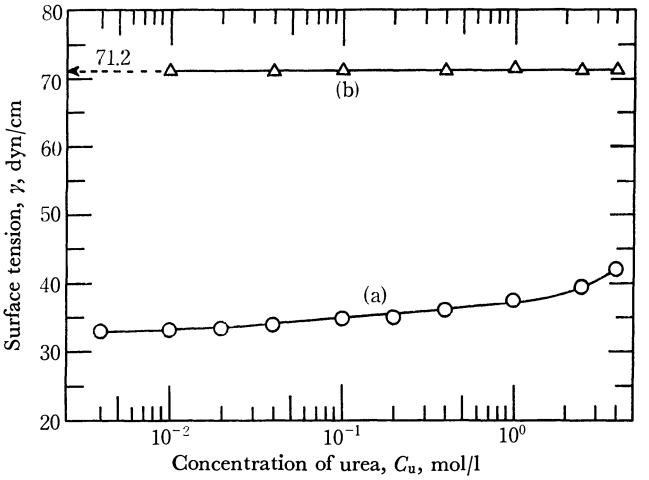

Fig. 7. Surface tension of urea solution with (a) and without (b) $TD(EO)_6$ ($C_D=4.0\times10^{-5}$ mol/l) at 30 °C.

for surface tension γ as a function of the concentration C_U and the activity coefficient f_U of urea in the solution. The left side term in Eq. (7) is given empirically by

$$\left[\frac{d\gamma}{RTd\ln C_U}\right]_D = 4.5\times10^{-11}C_U^{0.15} \quad (8)$$

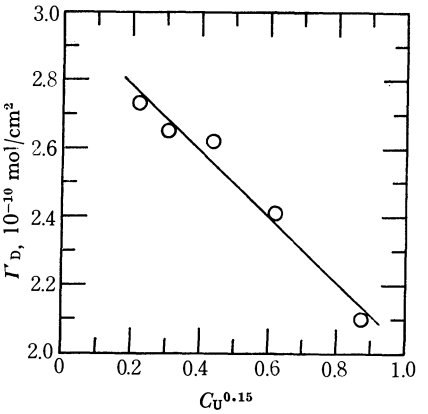

Fig. 8. Test of Eq. (9).

in the region below 0.4 mol/l of urea solution. Assuming $\Gamma_U=0$ from the inclination of curve (b) in Fig. 7, we can rewrite Eq. (7) as follows.

$$\Gamma_D = -\frac{4.5\times10^{-11}}{\Delta_U}C_U^{0.15} \quad (9)$$

where $\Delta_D=d\ln f_U/d\ln C_U$, which is obtainable as the inclination of the linear portion of $\Gamma_U\sim C^{0.15}$ relationship. It is obvious that $\Delta_U>0$ shows a salting-in effect of urea on surfactant. Sears[16] reported a marked expansion of the monolayer of stearic acid when it is spread on an aqueous urea solution, unless the surface pressure is too high. It is likely that the urea molecules are anchored on the ethoxyl groups of the surfactant.

The authors wish to express their hearty thanks to Professor M. Muramatsu for valuable discussions and for help in the preparation of the paper. Financial support from the Matsunaga Science Foundation is gratefully acknowledged.

16) D. F. Sears, *J. Colloid Interf. Sci.*, **29**, 288 (1969).

Radical Formation Initiated by the Biphotonic Excitation of Acridone

Yoshikatsu MIYASHITA, Shigeya NIIZUMA, Hiroshi KOKUBUN, and Masao KOIZUMI
Department of Chemistry, Faculty of Science, Tohoku University, Aoba, Aramaki, Sendai 980
(Received March 20, 1973)

The photochemical formation of alcohol radical has been found to occur in the rigid solvent of ethanol (77 K) and in the polyvinyl alcohol (PVA) film (77 K and at room temperature), when acridone is dissolved as a sensitizer. It has been established that by absorbing two photons stepwise acridone gives rise to radicals which abstract hydrogen atoms from alcohol molecules, this being called the radical reaction mechanism and abbreviated as R-R mechanism. The energies necessary for the radical formation were estimated by determining energy levels of acridone and examining the wavelength dependence of the reaction. They differed for ethanol (77 K), PVA (77 K) and PVA (room temp.), perhaps due to the cage effect. The feature of the R-R mechanism has been compared with that of the energy transfer type (E-T mechanism) in which the energy is transferred from the higher triplet of solute to solvent molecules. When methyl iodide with a lower dissociation energy is added to an ethanol solution of acridone (77 K) and is then irradiated by an exciting light ineffective for R-R mechanism, methyl radical is formed by E-T mechanism. When the two types of reaction were energetically possible, E-T mechanism occurred more easily than R-R mechanism.

Photochemical reactions initiated by the absorption of two photons *via* the lowest triplet state are fully established.[1-7] Studies on the biphotonic sensitized solvent decomposition so far reported have led to the conclusion that the mechanism is the energy transfer from higher triplet states of solute to solvent molecule.[2-5] Siegel *et al.*[2,3] chose the ethanol solution of naphthalene and extensively studied the formation of solvent radicals from the excited solvent molecules produced by the energy transfer from the higher excited triplet states of naphthalene. In these cases the electronic states of the solvent molecules susceptible to dissociation should be located somewhat lower than the higher triplet states of solute molecules. It was found that only the T-levels above the fourth T-level of naphthalene lying 60 kK above the ground state are effective for the solvent radical formation. In the case of ethanol the direct radical formation also occurs upon irradiating the solvent alone with a light of about 50 kK.[8] This state is possibly responsible for the sensitized reaction.

It is expected that the formation of solvent radicals occurs also *via* the biphotonic formation of solute radicals which subsequently abstract hydrogen atoms from solvent molecules. This radical reaction mechanism (R-R mechanism) is thought to be common in view of the fact that alcohols act as a H-donor to many reducible substances; for instance, the ethanol radical is formed by one photon reduction of acridine in ethanol at room temperature and also by one photon decomposition of acridan in ethanol at liquid nitrogen temperature.[9]

However, no such example has been found in literature, although the unimolecular biphotonic solute radical formation was reported for *p*-xylene.[7] We have found the occurrence of such a biphotonic solvent radical formation *via* R-R mechanism when acridone dissolved in rigid organic solvents is irradiated with the light of a lower energy than in the case of energy transfer mechanism (E-T mechanism). We have also found that radical formation by E-T mechanism also occurs when the substance with a lower dissociation energy such as CH_3I is added to the ethanol solution of acridone at 77 K.

Experimental

The decomposition of solute and solvent was examined by measuring the ESR signals and the electronic absorption spectra. A JEOL P-10 type ESR spectrometer was used. Light from a superhigh pressure mercury arc (Ushio USH-500D) was used with or without filters (Toshiba UV-39, UV-35, Hoya-crystal U-2). The intensity distribution of the radiation output from the mercury arc and transmittances of

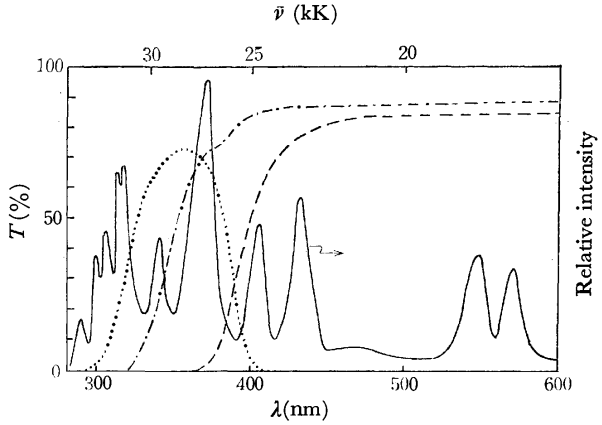

Fig. 1. Transmittances of filters and the intensity distribution of the radiation output from the mercury arc.
——: UV-39, -·-·-: UV-35, ·····U-2

1) K. D. Cadogan and A. C. Albrecht, *J. Chem. Phys.*, **43**, 2550 (1965).
2) S. Siegel and K. Eisenthal, *J. Chem. Phys.*, **42**, 2494 (1965).
3) S. Siegel and H. S. Judeikis, "The Triplet State," ed. by A. B. Zahlan, Cambridge University Press, (1967), p. 195.
4) B. Brocklehurst, W. A. Gibbons, F. T. Lang, G. Porter, and M. I. Savadatti, *Trans. Faraday Soc.*, **62**, 1793 (1966).
5) A. Terenin, V. Rylkov, and V. Kholmogorov, *Photochem. Photobiol.*, **5**, 543 (1966).
6) V. G. Vinogradova, B. N. Shelimov, N. F. Fok ,and V. V. Voevodskii, *Doklady Akad. Nauk. S. S. S. R.*, **154**, 188 (1964).
7) P. M. Johnson and S. A. Rice, *Chem. Phys. Lett*, **1**, 709 (1968).
8) P. J. Sullivan and W. S. Koski, *J. Amer. Chem. Soc.*, **85**, 384 (1963); **86**, 159 (1964). A. J. Harrison and J. S. Lake, *J. Phys. Chem.*, **63**, 1489 (1959).
9) S. Niizuma and M. Koizumi, This Bulletin, **41**, 1090 (1968).

filters are shown in Fig. 1.

Materials. Polyvinyl alcohol (PVA) (Koso-Kagaku) and ethanol (Wako-Junyaku, G.R.) were used without further purification. Methyl iodide (Wako-Junyaku, E.P.) was purified by the standard method. Acridone (Tokyo-Kasei, G.R.) was recrystallized from ethanol. The concentration of acridone was usually $10^{-3}\sim10^{-4}$ M. PVA films were about 200 μ in thickness.

Results

Triplet State of Acridone. For the present investigation it is desirable to know the triplet levels of acridone. A stepwise biphotonic process *via* the lowest triplet states requires that the triplet state concentration is appreciable and this in turn requires a long lifetime of the triplet state. These data were therefore determined.

Phosphorescence was observed near 20 kK in glassy ethanol and PVA at 77 K. The triplet lifetimes evaluated from the decay of phosphorescence are as follows.

Solvent	Temp.	τ(s)
EtOH	77 K	2.0
PVA	77 K	2.0
	R.T.	1.2

Acridone in PVA at room temperature showed phosphorescence, the lifetime of which was not much shorter than that at 77 K. T-T absorption of acridone in PVA was observed by flash technique at room temperature. The triplet lifetime was approximately the same as that of phosphorescence. T-T absorption spectrum in ethanol at room temperature is shown in Fig. 2.[10] There are two absorption bands, one near 17.5 kK and the other above *ca.* 28 kK. The energy diagram of acridone obtained from these data is given in Fig. 3.

The steady state concentration of the lowest triplet state, $\phi_{ST}I_{ab}\tau$ (ϕ_{ST}, S*-T transition probability; τ, the lifetime of the lowest triplet state) was estimated to be of the order 10^{-5} M under the present experimental conditions. It is expected that a considerable amount of the lowest triplet molecules is excited to higher triplet states. A $\Delta m=\pm2$ signal from acridone in the lowest triplet state was observed. The value of the zero-field splitting parameter D* was 0.065 cm^{-1}, which is comparable with that of acridine, 0.0688 cm^{-1}.[11]

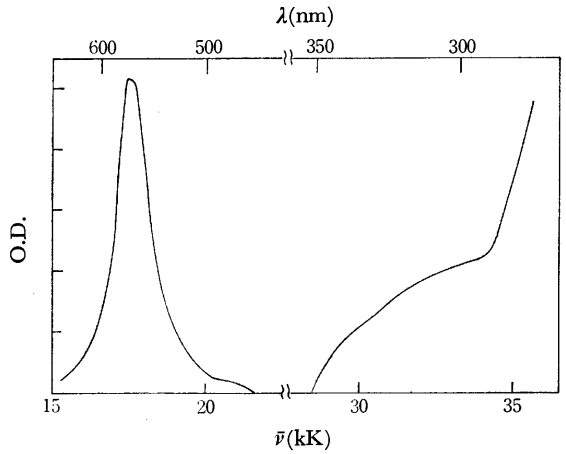

Fig. 2. T-T absorption spectrum of acridone in ethanol at room temperature.

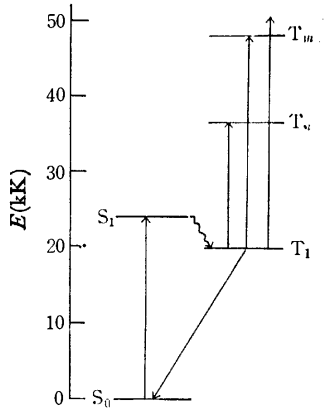

Fig. 3. Energy diagram of acridone.

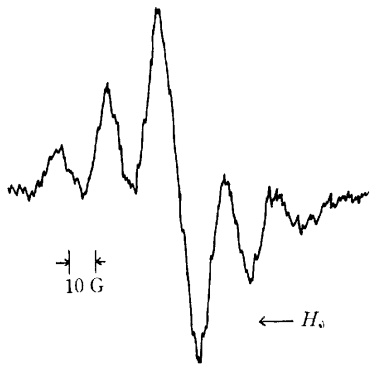

Fig. 4. ESR spectrum of photoproducts in deaerated ethanol solution irradiated with a UV-35 filter at 77 K.

Reaction in Ethanol Solution at 77 K. Deaerated ethanol solutions of acridone were irradiated with a UV-35 filter. The ESR spectrum of radicals is shown in Fig. 4. Broadly speaking, the spectrum consists of five lines, which can be safely attributed to ethanol radical ($CH_3\dot{C}HOH$), but a very high central line suggests the contamination of some other species. Irradiation with a UV-39 filter, on the other hand, did not give any signals.

The effect of light intensity on the rate of radical formation was examined by assuming the following relation between the two quantities,

$$d[R]/dt = kI_0^n \quad (1)$$

where [R] is radical concentration, I_0 light intensity, and n and k are constants characteristic for the reaction.

The value of n was found to be 1.7. Thus the rate of radical formation is nearly proportional to the square of light intensity.

Radical formation was accompanied by a purple coloration, which disappeared upon warming the ir-

10) Measured by K. Fushimi and K. Kikuchi.

11) Y. Kubota and M. Miura, This Bulletin, **42**, 2763 (1969). *Cf.* J.-Ph. Grivet, *Chem. Phys. Lett.*, **11**, 267 (1971).

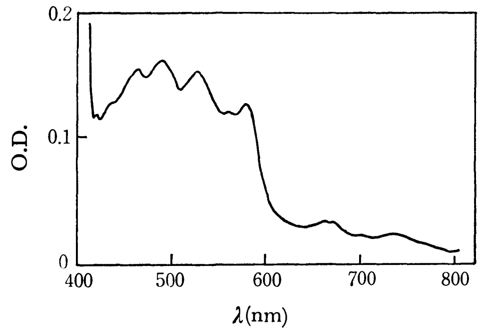

Fig. 5. Absorption spectrum of intermediates in ethanol upon irradiation with a UV-35 filter at 77 K.

radiated sample to room temperature. The absorption spectrum of the irradiated sample at 77 K is shown in Fig. 5. Since the ethanol radical does not absorb the visible light,[12] it is ovbious that some other intermediates are produced from acridone. Hence an abnormally high central line in the ESR spectrum is safely attributed to the intermediates originating from acridone.

The irradiated sample, when warmed to room temperature, showed a prominent decrease of the main absorption bands of acridone. The decrease was very slight in the case of irradiation with a UV-39 filter, the irradiated sample not being colored.

We can conclude that in ethanol at 77 K, formation of the ethanol radical is accompanied with the decomposition of acridone, as shown in Table 1.

TABLE 1. SUMMARY OF THE RESULTS

Solvent	Temp.	Filter	ESR	Abs.
EtOH	77 K	UV-39	×	×
		UV-35	○	○
PVA	77 K	UV-35	×	
		U-2	×	×
		No	○	○
	R.T.	UV-39		○
		UV-35		○
		U-2	○	○
EtOH (20% CH_3I)				
	77 K	UV-39	○	×
		UV-35	○	×

× : ESR, no signal
Abs., Acridone not decomposed
○ : ESR, signal appearance
Abs., Acridone decomposed

The effect of the dissolved oxygen on the reaction was examined. Irradiation with a UV-35 filter of the aerated solutions gave the ESR signal of an ethanol radical. But the signal was unsymmetric from the initial stage of irradiation and gradually truned into a peroxide-like signal (Fig. 6). It can be said that oxygen participates in the reaction mainly after a biphotonic process has been completed.

Reaction in Polyvinylalcohol Films. Polyvinylalcohol is a solvent which is glassy at room temperature. When PVA films containing 10^{-3} M acridone were irradiated

12) S. Fuji and J. E. Willard, *J. Phys. Chem.*, **74**, 4313 (1970).

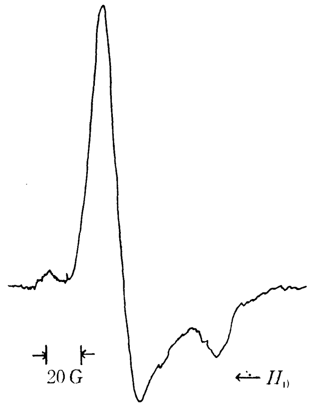

Fig. 6. ESR spectrum of photoproducts in aerated ethanol solution, 15 min. after irradiation with a UV-35 filter at 77 K.

at 77 K with a UV-35 filter and a U-2 filter whose limit of transmission is 10 nm shorter than for UV-35, they did not give any ESR signal. Irradiation with a total output from the mercury arc at 77 K gave a three line ESR spectrum (Fig. 7), no signal being detected in the case of PVA alone.

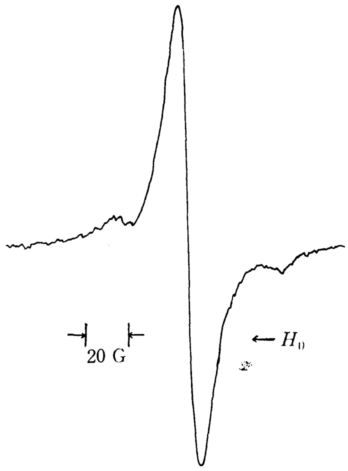

Fig. 7. ESR spectrum of photoproducts in PVA irradiated with a total output from mercury arc at 77 K.

These radical species were stable at 77 K. When irradiated samples were warmed up to room temperature, the ESR signals were still observed although the intensities were somewhat decreased and decayed slowly. When an irradiated sample was warmed to the glass transition temperature (70—80 °C), the signal disappeared completely.

Since a coupling constant of the radical is about 35 Gauss[13] there is no doubt that a polyvinylalcohol

$$(\sim CH_2\text{-}\dot{C}(OH)\text{-}CH_2\sim)$$

radical is formed. The polyvinylalcohol radical formed by γ-ray irradiation was investigated by Ogawa.[13] He reported that a crystalline region gives an ESR signal of three lines and an amorphous region, a broad line, the resulting spectrum consisting of the two com-

13) S. Ogwa, *J. Phys. Soc. Japan*, **16**, 1488 (1960).

ponents. The present result reconfirms this conclusion. The radical species not being attacked by oxygen was found to be stable in the presence of oxygen at 77 K.

The effect of light intensity on the rate of radical formation was examined by means of Eq. (1). The value of n was found to be 1.8, supporting a biphotonic nature of the main reaction. As in the ethanol solution at 77 K, irradiation with a U-2 filter which gave no ESR signal did not cause any change in the main absorption bands of acridone. Irradiation by a total output from the mercury arc caused a decrease in the main absorption bands of acridone with the appearance of a new absorption in the visible region at *ca.* 100 K.

It is remarkable that the irradiation of samples at room temperature with a U-2 fillter which caused no reaction at 77 K gave the ESR signal accompanied with a change of absorption spectrum in the visible and ultraviolet regions. The results obtained are listed in Table 1, which leads to the conclusion that the formation of a solvent radical is always accompanied by the decomposition of acridone.

Reaction in Ethanol Containing Methyl Iodide at 77 K. Since the irradiation with UV-39 (total energy $\leq$46 kK) does not decompose acridone in ethanol at 77 K, a possible mechanism for biphotonic radical formation in the wavelength region below 46 kK is only energy transfer. According to Terenin *et al.*[5] the minimum energy required for the direct photodissociation of methyl iodide is 5.0 eV (40 kK). It is therefore expected that the irradiation of acridone in ethanol containing methyl iodide gives rise to methyl radical by the biphotonic E-T mechanism.

The deaerated ethanol solutions of acridone containing methyl iodide (20%) which were glassy at 77 K were irradiated with the use of UV-39. ESR spectra due to a methyl radical (1 : 3 : 3 : 1 intensity ratio and a 24 Gauss hyperfine splitting) and an ethanol radical were detected. The height of the central line could be interpreted as originating only from the ethanol radical. The effect of light intensity on the rate of radical formation was examined by Eq. (1) and a value of 1.8 was obtained for n supporting a biphotonic process. Irradiation with UV-35 also produced the two kinds of radical. In both cases the ESR spectra in the initial stage mainly consisted of methyl radicals. The methyl radical disappeared with the life-time of 13 min, which agrees with the value in literature,[8] only the ethanol radical remaining in the later stage. Figure 8 gives an example of the variation of ESR spectra with time after irradiation. When the irradiated sample was kept in the dark, the ethanol radical increased with a decrease of the methyl radical. This implies that the methyl radical abstracts a hydrogen atom from ethanol according to $\dot{C}H_3 + C_2H_5OH \longrightarrow CH_4 + CH_3\dot{C}HOH$.

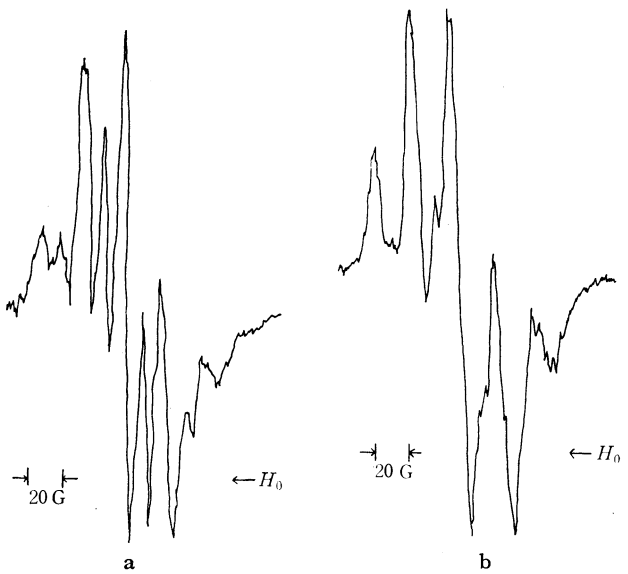

Fig. 8. ESR spectrum of photoproducts in deaerated ethanol solution containing 20% methyl iodide, a) 2 min, b) 20 min after irradiation with a UV-35 filter at 77 K.

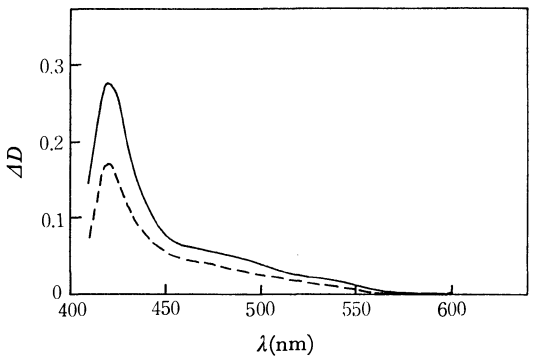

Fig. 9. The difference spectra between the irradiated (with a UV-35 filter) and non-irradiated deaerated ethanol solution containing 20% methyl iodide at 77 K.
----: 10 min irradiation, ——: 40 min irradiation.

The irradiation imparted an yellow color to the solution. The difference spectrum between the irradiated (with UV-35) and non-irradiated solution is shown in Fig. 9. The band located at 420 nm is safely assigned to iodine, the spectrum with no band near 500 nm supports an E-T mechanism, acridone not being decomposed. Irradiation with UV-35 is certainly energetically capable of bringing about R-R mechanism in addition to E-T mechanism. However, it is judged from the above results that E-T mechanism predominates, giving a larger quantity of methyl radicals in the initial stage.

It was established experimentally that the excitation in the T-T absorption band corresponding to 17.5 kK (the total excess energy, 37.5 kK) is not effective. Therefore the total energy required in the present case is 46 kK. This is consistent with the statement of Terenin *et al.*[5]

Discussion

The energy of the second photon required for the decomposition of acridone is obtained from Figs. 1 and 3. In both ethanol and PVA, irradiation with a UV-39 filter which excites the T-T absorption around 17.5 kK did not induce reaction. Thus 37.5 kK (17.5 kK plus the energy of the lowest triplet state) is not effective for the formation of an ethanol radical *via*

Table 2. Total energies required for radical formation

Sensitizer	Solvent	Temp.	Energy (kK)	Radicals
Acridone	EtOH	77 K	E≥50	$CH_3\dot{C}HOH$
	PVA	77 K	E≥53	$\sim CH_2-\dot{C}(OH)-CH_2\sim$
		R.T.	E≥46	
	EtOH (20% CH_3I)			
		77 K	E≥46	$\dot{C}H_3$, $CH_3\dot{C}HOH$
Naphthalene	EtOH	77 K	E≥60	$CH_3\dot{C}H_2$, $CH_3\dot{C}HOH$

R-R mechanism. The total energies required for the radical formation in the present systems are listed in Table 2. The results of Siegel *et al.*[2,3] on the naphthalene–ethanol system are given for the sake of comparison. Naphthalene as a sensitizer is not decomposed in ethanol at 77 K; the mechanism of radical formation is E-T. On the other hand the present mechanism is R-R.

It is interesting to compare the general features of the two mechanisms. First, the energy required for E-T mechanism is remarkably higher than that for R-R. This is natural, because ethanol does not absorb the light below *ca.* 50 kK. Sullivan and Koski,[8] using the light in this region, investigated the radicals produced by the direct photochemical decomposition of ethanol. Several radicals were detected but the main one was $C_2H_5\cdot$. The total energy of 60 kK required for radical formation which Siegel *et al.*[2,3] obtained is consistent with the result of direct photodecomposition. The energies of the four lowest triplet levels of naphthalene being about 45.6, 47, 48, and 60 kK, the lowest three are deficient in energy for exciting ethanol. On the other hand, the energy required for R-R mechanism naturally depends upon the solute employed. Once a solute radical is produced, the formation of an ethanol radical usually occurs very easily, *e.g.*, it is produced by one photon decomposition of acridan in ethanol at 77 K.[9]

Secondly, various types of radicals are produced by E-T mechanism while only the ethanol radical is produced by R-R mechanism. This is also reasonable since various types of radicals are expected to be formed with a high excitation energy followed by the secondary photochemical and thermal reactions between them and their mother substances. However, Judeikis and Siegel[14] proposed the sequence

$$^3S^* + CH_3CH_2OH \longrightarrow S + CH_3CH_2OH^* \quad (0)$$

$$CH_3CH_2OH^* \longrightarrow CH_3\dot{C}HOH + H\cdot \quad (1)$$

$$CH_3\dot{C}HOH + h\nu \longrightarrow CH_3\dot{C}HOH^* \quad (2)$$

$$CH_3\dot{C}HOH^* + CH_3CH_2OH \longrightarrow CH_3CHO + CH_3\dot{C}H_2 + H_2O \quad (3)$$

where $^3S^*$ is a highly excited triplet state solute molecule. Their finding that the $CH_3\dot{C}HOH$ radical is the only species observed during the early part of photolysis in ethanol strongly suggests that reaction (1) is the first step of dissociation. It is likely[12] that the ethanol radical has an absorption increasing from 300 to 200 nm which gives the ethyl radical according to (2) and (3).

In the case of R-R mechanism, the exciting light is so low in energy that (2) and (3) do not occur. In fact we could establish the occurrence of (2) and (3) when the deaerated solutions of acridone in ethanol were irradiated with a total output from the mercury arc. Thus the initial spectrum consisted mainly of ethanol radicals while at a later stage of continuous irradiation, the quantity of ethyl radicals gradually increased. It is not yet certain whether the decomposition of acridone is unimolecular, but this is most likely the case in view of the fact that acridone is not easily reduced by ethanol.

The cage effect is important for the formation of separate radicals. Rigidity of the medium, relative orientation of solute and solvent molecules as well as the microscopic structure around the solute molecules are important factors in addition to the excitation energy. The difference in the required energy for ethanol and PVA at 77 K may be due to the cage effect. In PVA, a rather hard medium as compared with ethanol, the diffusion of two radicals apart from each other may require a little higher energy than for ethanol. This is supported by the fact that at room temperature the required energy for PVA decreases to a smaller value than for ethanol. Another evidence is the occurrence of P-type delayed fluorescence at room temperature but not at 77 K.

It is intersting that acridone acts as a sensitizer for the biphotonic decomposition of methyl iodide. It has been established by Terenin *et al.*[5] that this compound dissociates when the energy 5.1—5.6 eV is supplied from various sensitizers raised *via* biphotonic process to higher triplet levels. Further, it is known that the absorption of light around 40 kK causes the direct dissociation of this compound. The continuous band located in this region is a n-σ* transition.[15] Therefore there is no doubt that the triplet acridone with the excess energy of ≥46 kK gives rise to dissociation of methyl iodide by E-T mechanism. The ethanol radical is formed by the secondary radical reaction which is quite reasonable in view of similar reactions already reported. It is thus strange that Terenin *et al.*, without observing the formation of ethanol radical, proposed the combination of two methyl radicals into ethane.

It is very suggestive that E-T mechanism overwhelms R-R mechanism when they are both energetically possible. Perhaps this indicates that energy transfer occurs far more quickly than the dissociation of a molecule for which rearrangement of atoms is usually required. It is not yet clear what kinds of intermediate are produced from acridone.

14) H. S. Judeikis and S. Siegel, *J. Chem. Phys.*, **43**, 3625 (1965).

15) K. Kimura and S. Nagakura, *Spectrochim. Acta*, **17**, 166 (1961).

Kinetics of the Hydrolysis of Diethyl Acetal Catalyzed by Iron(III) in Aqueous Solution

Goro WADA and Machiko SAKAMOTO

Department of Chemistry, Faculty of Science, Nara Women's University, Nara 630

(Received May 4, 1973)

The catalytic activity of iron(III) on the hydrolysis of diethyl acetal was investigated in aqueous solutions. The reaction rate was followed dilatometrically. The reaction is of the first order with respect to acetal concentration, the rate constant being expressed by

$$k_{app}=k_0+k_H[H^+]+k_{Fe}[Fe].$$

The respective rate constants are $k_0=1.30\times10^{-4}$ s^{-1}, $k_H=1.28$ M^{-1} s^{-1}, and $k_{Fe}=1.86$ M^{-1} s^{-1} at an ionic strength $\mu=0.2$ M and 25 °C. A tentative reaction scheme for iron(III) catalysis was proposed.

Diethyl acetal is known to be easily hydrolyzed on producing acetaldehyde and ethanol under the acid catalysis *via* an A-1 mechanism.

$$CH_3CH(OC_2H_5)_2 + H_2O \xrightarrow{H^+} CH_3CHO + 2C_2H_5OH \quad (1)$$

Although investigations on the solvent and substituent effects on the reaction mechanisms were carried out in detail,[1-12] the catalytic activities of various metal ions have not so far been studied. We have measured the rates of the hydrolysis of diethyl acetal in the presence of iron(III) and determined the rate constants of the individual reaction steps.

Experimental

Materials. Diethyl acetal (Schuchardt München, Germany) was used without further purification. Its density at 25 °C was 0.827 g/cm^3 which agreed with that in literature. Iron(III) perchlorate was prepared by dissolving pure iron wire in perchloric acid and oxidizing it with hydrogen peroxide. Pure water obtained by distillation of city water which had been treated with ion-exchange resin was used.

Procedure of Rate Measurement. As the hydrolysis of diethyl acetal proceeds, its aqueous solution increases in volume at constant temperature. Since the hydrolysis proceeds almost irreversibly and the increase in volume of the solution is proportional to the degree of reaction, the reaction rate can be followed by means of dilatometry. The dilatometer consists of a glass tube about 1 cm in diameter, connected with a vertical capillary of 0.03 cm in diameter and of 30 cm in height at one end of the tube. The other end is attached to a glass stop-cock, through which the reaction solution is quickly introduced from the reservoir where two reactant solutions are mixed at the initiation of hydrolysis. The content of the dilatometer is about 70 cm^3. The dilatometer and the other vessels containing the reactant solutions were set in a thermostat at 25 °C in advance. The ionic strength was always kept at $\mu=0.2$ M with sodium perchlorate.

Photometry. A Hitachi UV-VIS spectrophotometer Model 139 and a Hitachi recording spectrophotometer EPS-3T were used for the concentration determination of iron(III) and for the observation of the spectral variation during the course of reaction.

Results and Discussion

If we denote the heights of the reaction solution surface in the capillary of the dilatometer at time t and at the time of completion of the reaction by h and h_∞ respectively, the plots of $\log(h_\infty-h)$ against t always exhibit straight lines, indicating that the reaction is of the first order with respect to acetal concentration [A]. The slopes give apparent rate constants, k_{app}.

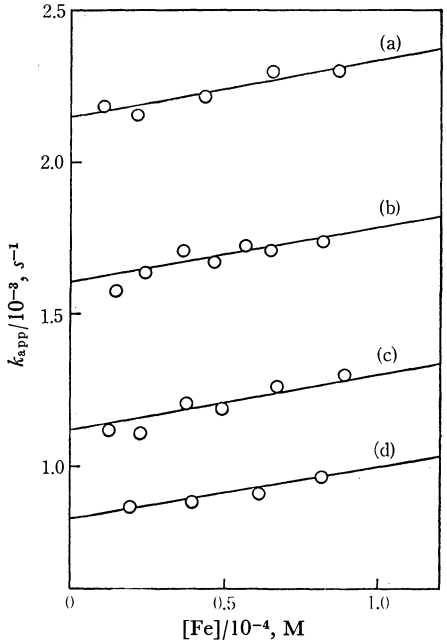

Fig. 1. Relationships between k_{app} and [Fe] at various [HClO$_4$] at [A]$=5.55\times10^{-2}$M.
[HClO$_4$]: (a): 1.44×10^{-3}M, (b); 1.00×10^{-3}M, (c): 7.50×10^{-4}M, (d): 5.00×10^{-4}M.

1) M. H. Palomaa and A. Salonen, *Ber.*, **67B**, 424 (1934).
2) L. K. J. Tong and A. R. Olson, *J. Amer. Chem. Soc.*, **65**, 1704 (1943).
3) A. R. Olson and L. K. J. Tong, *ibid.*, **66**, 1555 (1944).
4) R. K. Wolford and R. G. Bates, *J. Phys. Chem.*, **66**, 1496 (1962).
5) R. K. Wolford, *ibid.*, **67**, 632 (1963).
6) R. K. Wolford, *ibid.*, **68**, 3392 (1964).
7) J. C. Speck, Jr., D. J. Rynbrandt, and I. H. Kochevor, *J. Amer. Chem. Soc.*, **87**, 4974 (1965).
8) E. H. Cordes, *Progr. Phys. Org. Chem.*, **4**, 1 (1967).
9) B. Capon and M. C. Smith, *J. Chem. Soc. B*, **1969**, 1031.
10) A. Kankaanperä and M. Lahti, *Acta Chem. Scand.*, **23**, 1465, 1728, 2465 (1969).
11) C. A. Burton and J. D. Reinheimer, *J. Phys. Chem.*, **74**, 4457 (1970).
12) H. G. Bull, K. Koehler, T. C. Pletcher, J. J. Ortiz, and E. H. Cordes, *J. Amer. Chem. Soc.*, **93**, 3002 (1971).

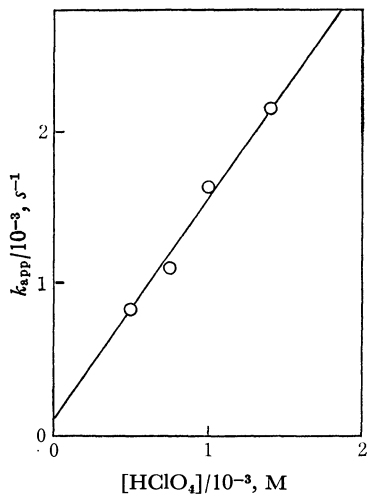

Fig. 2. Relationships between k_{app} and $[HClO_4]$ at [Fe]=0 (extrapolated) and $[A]=5.55\times10^{-2}$M.

The relationships between k_{app} and total iron concentration, [Fe], at various acid concentrations, $[HClO_4]$, are shown in Fig. 1. It is seen that k_{app} is linear with respect to [Fe] with a common slope irrespective of $[HClO_4]$. The intercepts of the straight lines also show a linear relationship with $[HClO_4]$ as is depicted in Fig. 2. The apparent rate constant can therefore be expressed by the sum of three terms, *viz.*

$$k_{app} = k_0 + k_H[H^+] + k_{Fe}[Fe] \quad (2)$$

The individual rate constants are determined from Figs. 1 and 2 as $k_0=1.30\times10^{-4}\ s^{-1}$, $k_H=1.28\ M^{-1}\ s^{-1}$, and $k_{Fe}=1.86\ M^{-1}\ s^{-1}$ at $\mu=0.2$ M and 25 °C. The value of k_H agrees fairly well with that in the literature.[4]

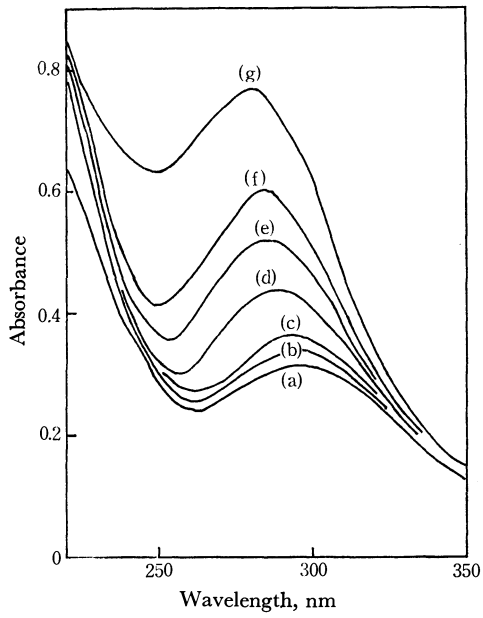

Fig. 3. Spectral changes with time of diethyl acetal hydrolysis at $[A]=5.55\times10^{-2}$M, $[Fe]=1.5\times10^{-4}$M, and $[HClO_4]=6.14\times10^{-5}$M.
(a): t=0, (b): 3 min, (c): 15 min, (d): 30 min, (e): 60 min, (f): 90 min, (g): 240 min.

The three terms in the right-hand side of Eq. (2) might correspond to the respective three reaction paths; (i) a spontaneous one without catalyst, (ii) an acid catalysis, and (iii) an iron(III) catalysis. Since k_{Fe} is independent of the acid concentration, the iron catalysis is not wholly attributed to the apparent increment of hydrogen ion concentration due to the hydrolysis of Fe^{3+}_{aq} at the given acid concentration. The expected increment of hydrogen ion concentration under the present conditions is too small to be compared with the observed catalytic effect resulting from iron(III). The chemical forms of iron(III) in the reaction system are predominantly Fe^{3+}_{aq} and $FeOH^{2+}$, and their concentration ratio should change according to the variation in the acid concentration. However, the catalytic activity of iron(III) was not seriously affected by its chemical form. A presumable reaction scheme in analogy with acid catalysis[13,14] might be as follows;

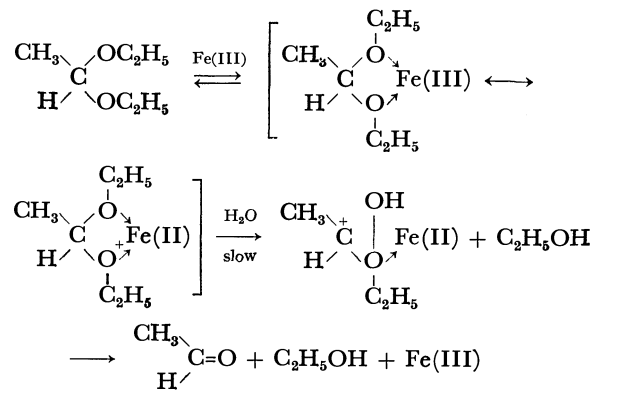

in which Fe(III) behaves as a Lewis-type acid-base catalyst.

Spectral changes during the reaction are shown in Fig. 3, where the absorption in the wavelength range 200—400 nm increases with time and finally reaches a spectrum with a peak at 280 nm. The final absorption spectrum subtracted by the initial one agrees with that in the absence of iron(III) catalyst at infinite reaction time. Thus, the reaction products are found to be the same irrespective of whether the reaction is catalyzed by acid or iron(III), although the absorption spectrum in this wavelength range is mainly due to acetaldehyde and not to acetal or ethanol. The hypothetical intermediate of a complex between iron(III) and acetal was not recognized, probably because of the fact that the formation of the complex was very minute or no distinct absorption band appeared in the wavelength range studied.

Catalytic activities of metal ions other than iron(III) were also qualitatively determined. Silver(I), copper(II), cobalt(II), and zinc(II) were found to be less catalytic than iron(III).

13) F. A. Long and M. A. Paul, *Chem. Rev.*, **57**, 925 (1957).
14) K. J. Laidler, "Chemical Kinetics," McGraw-Hill Book Company, New York (1965), p. 504.

Emission Spectra of Benzonitrile, Aniline, and Nitrobenezene by Controlled Electron Impact

Masaharu Tsuji, Teiichiro Ogawa, and Nobuhiko Ishibashi
Faculty of Engineering, Kyushu University, Hakozaki, Fukuoka 812
(Received April 24, 1973)

The emission spectra of benzonitrile, aniline, *N,N*-dimethylaniline, and nitrobenzene under controlled electron-impact excitation (60—300 eV) were investigated at a very low pressure. Bands of the parent molecules were observed in the 260—410 nm region on benzonitrile and anilines, and were assigned to the S_1–S_0 transitions. However, no emission of the parent molecule was observed on nitrobenzene and this was attributed to the spin-orbit coupling effect of the nitro group and the predissociation of the excited parent molecule. Bands of the following fragment species were observed for all four compounds: H(Balmer series), CH($A^2\Delta$–$X^2\Pi$), and CN($B^2\Sigma$–$X^2\Sigma$). In addition, NH($A^3\Pi$–$X^3\Pi$) band on aniline and NO($A^2\Sigma$–$X^2\Pi$, $B^2\Pi$–$X^2\Pi$), CO($b^3\Sigma$–$a^3\Pi$), and CO^+ ($A^2\Pi$–$X^2\Sigma$, $B^2\Sigma$–$X^2\Sigma$) bands on nitrobenzene were observed. The linear relationships between the electron beam current and the emission intensities of the parent molecules and the fragment species indicated that most of the excited species were produced by primary electron-molecule collision processes (CN of anilines, CO, and CO^+ were found to be exceptional). The mechanism of the excitation and the fragmentation of the parent molecules and the comparison of the present spectra with those by discharge and by optical excitation were discussed. It was concluded that some excited species were produced through superexcited states.

As sources for exciting the electronic levels of molecules, ultraviolet radiation, such as Hg and Xe emission (5—21 eV), and X-ray radiation (1000 eV and above) have been widely used. However, few studies have been conducted in the energy region between these two methods. The excitation by electron impact is one of the most effective methods for this region. As early as 1946 the emission spectra of various benzene derivatives under electron impact in a hollow cathode discharge were investigated by Woeldike and Schüler[1] and the effects of the substituents were discussed. However, in an electric discharge, since many secondary processes occur in many cases, it is difficult to distinguish which processes are the primary ones. In this respect, the crossed electron and molecular-beam method is of great advantage as a method for exciting molecules, for the electron beam can be controlled easily and the pressure of the collision chamber can be so low that intermolecular collisional perturbation can be almost neglected during the lifetime of the excited species.

In recent years, the emission spectra of such molecules as N_2, CO, and NO and of some simple organic molecules have been extensively investigated by this method. Among the molecules which have a nitrogen atom, nitrogen,[2] ammonia,[3,4] hydrazine,[4] and methylamine[5] have been investigated, and much interesting information has been acquired regarding the excitation, the ionization, and the fragmentation processes not only of the ionized species, which can be detected by mass spectrometry, but also of neutral unstable ones. The emission spectra of benzene have been studied by this method by Vroom[6] and Smith.[7] The former has determined absolute emission cross sections for Lyman and Balmer radiation from hydrogen atoms formed in the dissociative excitation of benzene by electron impact (0.05—6 keV). The latter has measured the lifetimes of the vibrational levels of the $^1B_{2u}$ state using an electron beam phase shift method. However, few studies have been carried out on the photoemission of other aromatic molecules.

In the previous papers, the emission spectra of aromatic hydrocarbons[8] and of aromatic halides[9] by controlled electron impact (60—300 eV) have been reported. Characteristic bands of the parent molecules have been obtained from benzene, toluene, xylenes, fluorobenzene, and anisole[10] and assigned to the S_1–S_0 electronic transitions. However, chloro- and bromobenzenes failed to show such a band; instead, they showed pronounced progression bands of HCl^+ or HBr^+ and weak lines of Cl^+ or Br^+. It has been reported that benzonitrile and aniline show a strong photoemission of the parent molecules, both by discharge[1] and by optical excitation, while nitrobenzene does not. This has been ascribed to a rapid dissipation of the electronic transition energy through the nitro group and to the dissociation of the carbon-nitrogen bond.[11] In the present study, the emission spectra of these simple benzene derivatives by controlled electron impact will be reported and compared with those obtained by discharge and by optical excitation. Moreover, the mechanism of the electron-molecule collision which gives rise to the excitation, the ionization, and the fragmentation of the parent molecules will be discussed in connection with the results of the relationships between the emission intensities and the electron beam current.

1) A. Woeldike, *Z. Naturforsch.*, **1**, 566 (1946). H. Schüler. *ibid.*, **2a**, 556 (1947).
2) For example, R. F. Holland and W. B. Maier II, *J. Chem. Phys.*, **56**, 5229 (1972).
3) N. Böse and W. Sroka, *Z. Naturforsch.*, **26a**, 1491 (1971).
4) H. Bubert and F. W. Froben, *J. Phys. Chem.*, **75**, 769 (1971).
5) K. Fukui, I. Fujita, and K. Kuwata, This Bulletin, **45**, 2278 (1972).
6) D. A. Vroom and F. J. de Heer, *J. Chem. Phys.*, **50**, 573 (1969).
7) W. H. Smith, *ibid.*, **54**, 4169 (1971).
8) T. Ogawa, M. Tsuji, M. Toyoda, and N. Ishibashi, This Bulletin, **46**, 2637 (1973).
9) T. Ogawa, M. Tsuji, M. Toyoda, and N. Ishibashi, *ibid.*, **46**, 1063 (1973).
10) T. Ogawa, M. Tsuji, M. Toyoda, and N. Ishibashi, *Chem. Lett.*, **1972**, 233.
11) G. N. Lewis and M. Calvin, *Chem. Rev.*, **25**, 273 (1939).

Experimental

The electron-impact apparatus is essentially identical to that described in the previous papers.[8,12] The electrons emitted from the hot tungsten filament were accelerated by three electrodes and were led to the collision chamber through a slit. The accelerating voltage was variable from 60 to 300 V, with an energy spread of at least 6—10 eV; the electron beam current used was 10—1000 μA. The sample gas was injected through a nozzle 0.3—1.0 mm in diameter and collided with the electron beam perpendicularly. The gas pressure was estimated to be 10^{-3}—10^{-2} mmHg in the region of collisions.

The photoemission from the excited species was observed by the use of a Jarrell-Ash JE25 monochromator, which had a reciprocal dispersion of 33 Å/mm. The slitwidth of the monochromator used was 100 μm and 300 μm.

The aniline and nitrobenzene were obtained from the Kishida Chemical Co., and the benzonitrile and *N,N*-dimethylaniline, from Wako Pure Chemical Ind. All the reagents used were of a JIS guaranteed grade. They were distilled and degassed *in vacuo* a few times just before use. The mass spectrum was taken with a Hitachi RML-6E mass spectrometer. The accelerating voltage was 100 V.

Results and Discussion

Benzonitrile. A typical emission spectrum of benzonitrile under electron-impact excitation in the 250—450 nm region is shown in Fig. 1. The impact voltage was 200 V, and the electron beam current was 700 μA in this measurement. A characteristic band of the parent molecule was observed in the 260—330 nm region. This band was assigned to the electronic transition of benzonitrile from the lowest excited singlet state to the ground state, which is related to the $^1B_{2u}$—$^1A_{1g}$ transition of benzene. Woeldike[1] observed a discrete emission spectrum in the 270—310 nm region in a hollow cathode discharge. Fluorescence spectra excited by Mn and Fe sparks at the vapor pressure of about 20 mmHg were photographed, and the vibronic bands were assigned, by Bass.[13] In the present spectrum, several discrete vibronic bands appear above the broad background (the continuous part of the band) and the vibrational structure closely resembles those of toluene[8] and fluorobenzene,[9] which are identical to benzonitrile in symmetry. The discrete band at the shortest wavelength (274 nm) was assigned to the (0,0) band of benzonitrile. Similar bands have been observed at 267 nm on toluene and at 264 nm on fluorobenzene. Other discrete bands on the longer-wavelength side of 274 nm may be interpreted as the vibrational structure with the fundamental frequencies given by Bass. On its shorter-wavelength side, weak unresolved features were observed; they were assigned to the transitions from the higher vibrational levels of the upper state to some vibrational levels of the ground state. These bands were also observed in the spectra of toluene and fluorobenzene. Since the pressure of the collision chamber was so low ($\leq 10^{-2}$ mmHg) that the intermolecular collisional perturbation was small in the lifetime of the excited state, the emission from the higher vibrational levels of the upper state was observed even from the molecule with less symmetry than benzene.

Other bands in the 355—430 nm region were assigned to the bands of fragment species. The lines at 434, 410, and 397 nm, decreasing in intensities as the wavelength becomes shorter, belong to the Balmer series of the hydrogen atom, which are denoted by H_γ, H_δ, and H_ε respectively. The band at 431 nm belongs to the (0,0) band of CH($A^2\Delta$–$X^2\Pi$). These band systems have always been observed in various benzene derivatives.[8-10] The most intense band systems in the 358—359 nm, 385—388 nm, and 415—422 nm regions were assigned to the main sequences with $\Delta v = 1, 0, -1$ of CN($B^2\Sigma$–$X^2\Sigma$), and several weak bands in the 363—403 nm region, to the tail bands of this violet system.

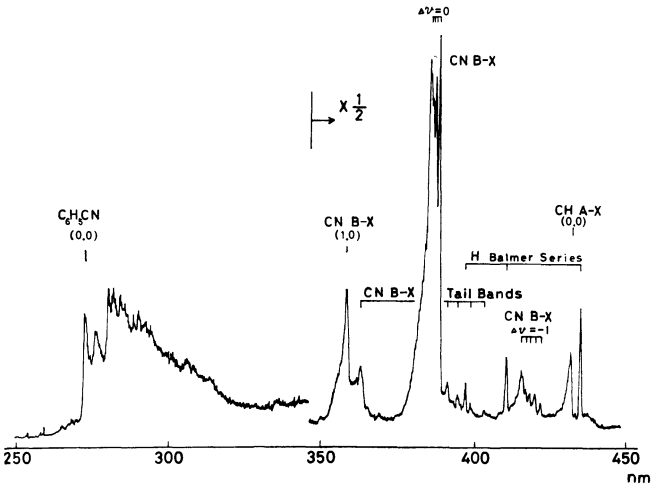

Fig. 1. Emission spectrum of benzonitrile by controlled electron impact. Impact voltage 200 V, electron beam current 700 μA.

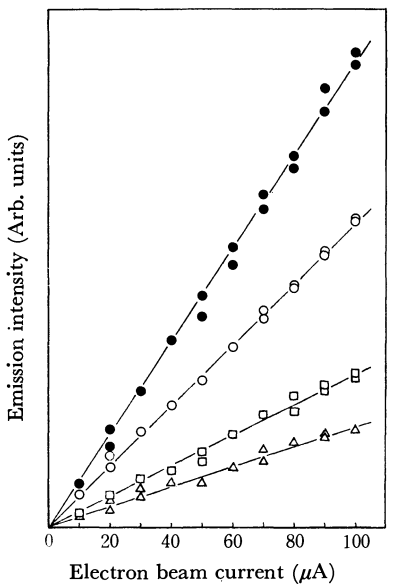

Fig. 2. Dependence of photoemission intensities of benzonitrile on the electron beam current. Impact voltage 200 V. ○: C_6H_5CN (282 nm), ●: CN (388 nm), □: $H\gamma$, △: CH (431 nm).

12) T. Ogawa, M. Toyoda, M. Tsuji, and N. Ishibashi, *Technology Repts. Kyushu Univ.*, **45**, 427 (1972).

13) A. M. Bass, *J. Chem. Phys.*, **18**, 1043 (1950).

The relationships between the emission intensities and the electron beam current are shown in Fig. 2. The emission intensities of the parent molecule and of the fragment species of H, CH, and CN are proportional to the electron beam current. This finding indicates that the excitation and the fragmentation of benzonitrile take place through primary electron-molecule collisions, just as in the cases of other benzene derivatives.[8,9] The excitation of a π electron of benzonitrile is concluded to be a one-electron process. The mechanism of the excitations and fragmentations can, then, be described as below:

$$\mathrm{PhCN} \xrightarrow{e} \mathrm{PhCN}^* \xrightarrow{h\nu} \text{ground state} \qquad (1)$$

$$\mathrm{PhCN} \xrightarrow{e} \mathrm{PhCN}^{**} \begin{cases} \xrightarrow{\text{fast}} \mathrm{PhCN}^* \\ \xrightarrow{\text{fast}} \mathrm{H}^*, \mathrm{CH}^*, \mathrm{CN}^* \end{cases} \xrightarrow{h\nu} \text{ground state} \qquad (2)$$

where superscript * signifies excited states from which the molecules radiate and where ** indicates a superexcited state, as was pointed out by Platzman,[14] which lasts for a length of time shorter than or equal to one period of vibration of the molecule. Since the excitation energy of the hydrogen Balmer series is larger than the first ionization potential of benzonitrile, it can be concluded that hydrogen atoms are produced through superexcited states. It seems that PhCN* is produced through two processes, (1) and (2), although their relative importance cannot be determined in the present study.

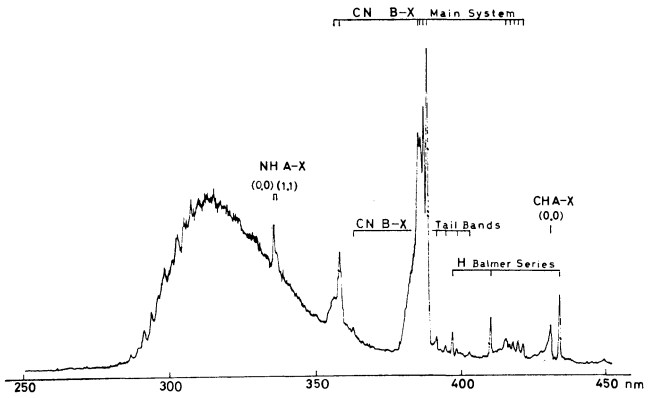

Fig. 3. Emission spectrum of aniline by controlled electron impact. Impact voltage 300 V, electron beam current 1 mA.

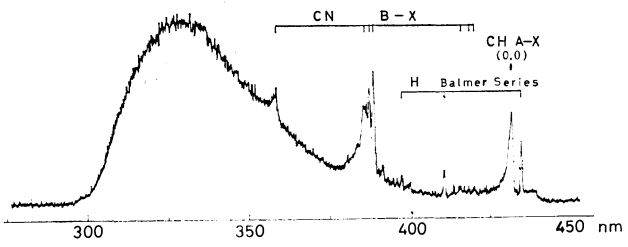

Fig. 4. Emission spectrum of *N,N*-dimethylaniline by controlled electron impact. Impact voltage 200 V, electron beam current 700 μA.

14) R. L. Platzman, *Radiation Res.*, **17**, 419 (1962).

Aniline and N,N-*Dimethylaniline.* Typical emission spectra of aniline and *N,N*-dimethylaniline under electron-impact excitation in the 250—450 nm region are shown in Figs. 3 and 4 respectively. The electron beam of 300 eV at 1 mA was used for the measurement of the former, while that of 200 eV at 700 μA was used for the latter. Bands of the parent molecules were observed in the 280—375 nm region on aniline and in the 295—410 nm region on *N,N*-dimethylaniline. These bands are shifted to longer wavelengths by about 10 nm and about 25 nm from the (0, 0) band of toluene (267 nm) respectively, and they agree well with the fluorescence bands in solution.[15] The former band was assigned to the A^1B_2–X^1A_1 electronic transition for aniline.[16] The vibrational structure of aniline is more complicated than that of benzonitrile, and the fraction of the background is larger. The emission spectrum of *N,N*-dimethylaniline is very broad, and the fine structure is no longer observed, probably because the symmetry of the aniline molecule is destroyed, as has been shown in the case of the absorption spectrum.[17] Woeldike[1] observed a continuous emission spectrum of aniline in the region from 285 to 330 nm. Blondeau, Quack, and Stockburger[18,19] investigated the resonance fluorescence spectra of various benzene derivatives, such as benzene, toluene, xylenes, and aniline, at low pressures ($\leq$0.1 mmHg) by irradiation with light of narrow bandwidth; they concluded that aromatic molecules exhibit resonance fluorescence. It was shown that the difference in the initially-irradiated levels resulted in different progression bands, and the most striking feature was the loss of structure and an increase in the fraction of the background when the molecules were excited to higher vibronic levels. It is known that, in the spectrum of aniline, pronounced progression bands due to the strongly anharmonic inversion vibration of NH_2 group exist in addition to those due to the symmetric vibration,[16,18,19] and that these progression bands complicate the vibrational structure. In addition, since the exciting energy of the present study is higher than the optical excitation, molecules are expected to be excited to the closely-spaced higher vibrational levels of the upper state, from which the fast intramolecular vibrational rearrangement occurs. Since aniline has more vibrational states which can strongly interact with the initially-excited state than do benzene, toluene, and fluorobenzene, the initial vibrational modes will be converted to other modes more easily. Thus, the complex vibrational structure and the large fraction of the background in the present spectrum are partly due to the appearance of the complicated progression bands, and partly due to the further overlapping of these progression bands because

15) I.S. Berlman, "Handbook of Fluorescence Spectra of Aromatic Molecules," Academic Press, N.Y. (1971).

16) J. C. S. Brand, D. R. Williams, and T. J. Cook, *J. Mol. Spectry.*, **20**, 359 (1966).

17) A. Mangini, A. Trombetti, and C. Zauli, *J. Chem. Soc. B*, **1967**, 153.

18) J. M. Blondeau and M. Stockburger, *Ber. Bunsenges. Physik. Chem.*, **75**, 450 (1971).

19) M. Quack and M. Stockburger, *J. Mol. Spectry.*, **43**, 87 (1972).

of the wider energy distribution of the incident electrons used and because of the higher excitation energy used in the present study.

A doublet band at 336—337 nm was assigned to the (0,0) and (1,1) bands of NH($A^3\Pi$–$X^3\Pi$). All the other bands on anilines were assigned to the H, CH, and CN bands, which appeared also on benzonitrile.

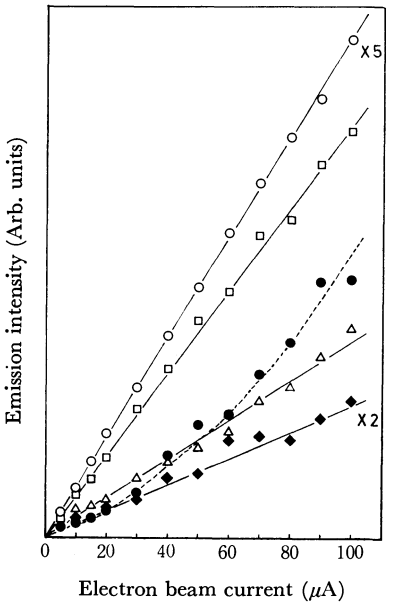

Fig. 5. Dependence of photoemission intensities of aniline on the electron beam current. Impact voltage 200 V.
○: $C_6H_5NH_2$ (314 nm), ●: CN (388 nm), □: Hγ, △: CH (431 nm), ◆: NH (336 nm).

The emission intensities of the parent molecules and the fragment species, such as H, CH, and NH of aniline and *N,N*-dimethylaniline, are found to be proportional to the electron beam current, as is shown in the case of aniline in Fig. 5. Similar results have been obtained from various benzene derivatives[8,9] and other organic molecules, such as methane,[20] methanol,[21] and amines.[5] Consequently, the excitations of the parent molecules and the fragmentations of H, CH, and NH by electron impact under the present crossed-beam method are concluded to take place generally through one-electron processes.

The emission intensities of the CN bands of aniline and *N,N*-dimethylaniline are found to be proportional to about 1.4 and about 1.2 powers of the electron beam current respectively, as is shown in Fig. 5. These results indicate that the photoemission processes of CN produced from anilines are different from those of other fragment species, such as H, CH, and NH, and that of CN produced from benzonitrile. It seems that a certain secondary process is involved in the production of the excited CN species. It is noteworthy that a similar result was obtained for the CN produced from pyridine,[22] whose emission intensity was found to be proportional to 1.5 powers of the electron beam current. Since the radiation lifetime of the CN $B^2\Sigma(v'=0)$ state was measured[23] as 39—85 ns, collisions between the excited species and the neutral molecule can be neglected at such a low pressure as 10^{-3}—10^{-2} mmHg. Furthermore, in the present experimental situation, the possibility of the second collision of one neutral species with another electron is also expected to be small. A collision process between an electron and a positive-ion may be involved in the production of CN. It should be noticed that the production of CN from benzonitrile, whose emission intensity is proportional to the electron beam current, proceeds with one C–CN bond scission, whereas the production of CN from anilines and pyridine, whose emission intensities are not linear, needs the scissions of at least two skeletal bonds. Particularly, in the case of aniline and pyridine, the cleavage of the stable ring must take place.

Nitrobenzene. A typical emission spectrum of nitrobenzene under electron-impact excitation in the 200—600 nm region is shown in Fig. 6. The impact voltage was 200 V, and the electron beam current was 1 mA in this measurement. There are pronounced bands of CO and CO^+; they were assigned as in the cases of anisole[10] and phenol,[24] as will be shown below. The emission bands at 283—331 nm were assigned to the progression, $v'=0$, of the third positive system ($b^3\Sigma$–$a^3\Pi$) of CO; those at 219—247 nm, to the progressions, $v'=0$, 1, 2, of the first negative system ($B^2\Sigma$–

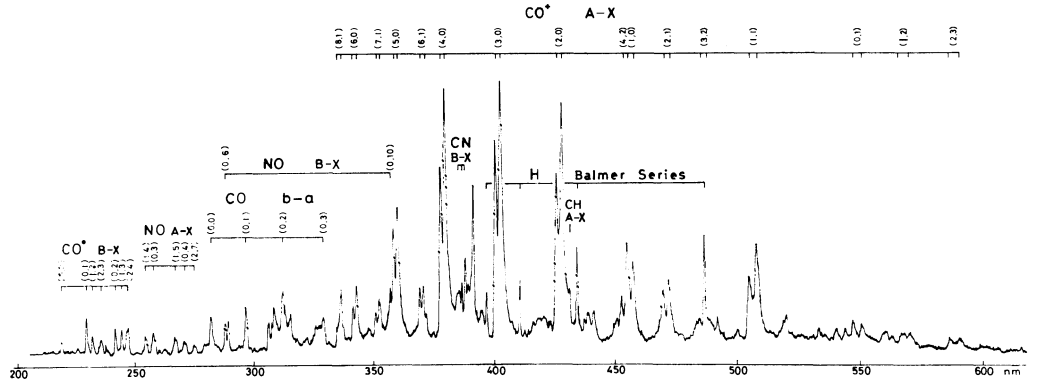

Fig. 6. Emission spectrum of nitrobenzene by controlled electron impact. Impact voltage 200 V, electron beam current 1 mA.

20) T. Ogawa, I. Fujita, M. Hatada, and K. Hirota, This Bulletin, **44**, 659 (1971).
21) I. Fujita, M. Hatada, T. Ogawa, and K. Hirota, *ibid.*, **44**, 1751 (1971).
22) M. Toyoda, T. Ogawa, and N. Ishibashi, unpublished.
23) T. J. Cook and D. H. Levy, *J. Chem. Phys.*, **57**, 5059 (1972).
24) M. Tsuji, T. Ogawa, and N. Ishibashi, unpublished.

$X^2\Sigma$) of CO^+, and the characteristic doublet bands at 335—590 nm, to the progressions, $v''=0$, 1, 2, of the comet-tail system ($A^2\Pi$–$X^2\Sigma$) of CO^+. The relative emission intensities of the main progression of this comet-tail system of nitrobenzene agree with those of CO by 200 eV impact.[25] The bands at 255—276 nm were assigned to the sequences with $\Delta v=-3$, -4 of the NO γ system ($A^2\Sigma$–$X^2\Pi$), and those at 289 and 359 nm, to the (0,6) and the (0,10) bands of the NO β system ($B^2\Pi$-$X^2\Pi$). Other bands were assigned to the H, CH, and CN bands observed on benzonitrile and anilines.

It is concluded from the linear relationships between the emission intensities and the electron beam current that H, CH, and NO species are produced by one-electron processes. Meanwhile, the emission intensities of CO and CO^+ species are found to be proportional to about 1.2 powers of the electron beam current. Thus, the production of these species is not a simple one-electron process, and it seems that positive ions of some kind are involved, as in the case of the CN produced from anilines. Since the energy of the $b^3\Sigma$ state of CO is larger than the first ionization potential of nitrobenzene, it seems that the CO species are produced through some superexcited states.

It should be noticed that there is no direct carbon-oxygen bond in the nitrobenzene molecule. The pressure of the collision chamber is so low that no recombination between carbon and oxygen atoms may occur. Meanwhile, from the analysis of the mass spectrum,[26] it was suggested that the decomposition of nitrobenzene proceeded as is shown below;

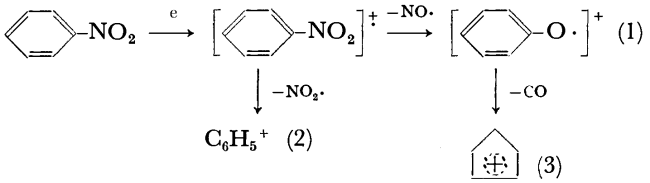

The mass spectrum was measured in order to compare the relative intensities of these peaks. The intensities of the fragment peaks, (1), (2), and (3), relative to the parent peak were found to be 0.32, 2.55, and 0.37 respectively. The fragment species of CO and CO^+ may be produced through the positive ions, as has been described above.

Nitrobenzene exhibited no emission of the parent molecule in the present study, as was found in the case of the excitations by photons and by discharge.[1] This is partly due to the fast intersystem crossing processes, since the lowest excited level is the *n* nonbonding orbital. Another reason for this is the dissociation of the carbon-nitrogen bond, as was pointed out by Lewis and Calvin.[11] The relative intensity of the phenyl cation peak to the parent one was measured as 2.55 for nitrobenzene, while those for benzonitrile[27] and chlorobenzene[9] were reported to be 0.056 and 0.68 respectively. This indicates that the cleavage of the carbon-nitrogen bond can easily take place. Thus, it is concluded that the spin-orbit interaction and the predissociation of the parent molecule prevent the appearance of the band of the parent molecule under electron-impact excitation.

Concluding Remarks. Benzonitrile, aniline, and *N,N*-dimethylaniline were found to show the emission bands of the transitions from the lowest excited singlet state to the ground state of the parent molecules. The appearances and the positions of these bands do not change appreciably when the impact energy changes between 60—300 eV. It may be concluded that the molecules receive enough excess energy even though the exciting energy is 60 eV.

A pronounced feature of the electron-impact excitation is that the optically-forbidden singlet-triplet transition may be allowed. However, such a transition could not be observed under 60—300 eV electron-beam excitation in the present study, and the observed spectra are similar to those of optical excitation because the parent molecules are excited only to the singlet states. Meanwhile, in the energy loss spectrum of benzene, optical selection rules hold for 200—300 eV electrons,[28] while three singlet-triplet transitions were observed in addition to three singlet-singlet transitions under low energy electron impact[29] (13.6 and 20.0 eV). Thus, it is expected that a singlet-triplet transition will be observed when the impact energy is lowered to the near threshold value in the present method, although several experimental difficulties have to be overcome.

The first ionization potentials of benzene, benzonitrile, aniline, *N,N*-dimethylaniline, and nitrobenzene have been reported to be 9.56,[30] 10.09,[30] 8.32,[30] 7.51,[31] and 10.18[30] or 10.26[31] eV respectively. All these values are smaller than the excitation energy of the hydrogen atom (13.32 eV for the Balmer line H_ε); the first ionization potential of nitrobenzene is also smaller than the excitation energy of the CO $b^3\Sigma(v'=0)$ state (10.38 eV).[32] It is concluded that hydrogen atoms are produced in the dissociative excitations of benzonitrile, aniline, and nitrobenzene, as has been shown before, and that these dissociative processes probably proceed through superexcited states. It seems that the superexcited states also play an important role in the production of the CO from nitrobenzene and other fragment species.

The emission intensities of the line of H_γ relative to the (0,0) band of CH and the ratios of the H atom to the CH group in these molecules are shown in Table 1. This comparison is valid because the emission intensities of H and CH are proportional to the electron beam current and also to the gas pressure of the collision

25) J. M. Ajello, *J. Chem. Phys.*, **55**, 3158 (1971).
26) H. Buzikiewicz, C. Djerassi, and D. H. Williams, "Mass Spectrometry of Organic Compounds," Holden-Day Inc., San Francisco (1967).
27) A. Cornu and R. Massot, "Compilation of Mass Spectral Data," Heyden & Son Ltd. (1967).
28) A. Skerbele and E. N. Lassettre, *J. Chem. Phys.*, **42**, 395 (1965).
29) J. P. Doering, *ibid.*, **51**, 2866 (1969).
30) G. F. Crable and G. L. Kearns, *J. Phys. Chem.*, **66**, 436 (1962).
31) A. D. Baker, D. P. May, and D. W. Turner, *J. Chem. Soc. B*, **1968**, 22.
32) G. Herzberg, "Spectra of Diatomic Molecules," D. Van. Nostrand, Princeton, N. J. (1950), p. 520.

Table 1. The ratios of H to CH in the molecules and the emission intensities of the line of H_γ relative to the (0,0) band of CH
Impact voltage: 200 V

Compounds	Estimated intensities H/CH	Emission intensities[a] H/CH
C_6H_6	1(6/6)	1.55 ± 0.08[b]
C_6H_5CN	1(5/5)	1.54
$C_6H_5NO_2$	1(5/5)	1.48
C_6H_5F	1(5/5)	1.55[c]
$C_6H_5NH_2$	1.4(7/5)	$2.09 (=1.49\times1.4)$

a) Intensities were measured in peak height and the slitwidth used was 300 μm.
b) Ref. 8.
c) Ref. 9.

chamber as has been shown in the cases of benzene[8] and fluorobenzene.[9] It should be noticed that the numbers of the second column and those of the third column correspond very well within the limits of experimental error. Therefore, the probabilities of the production of the excited H and CH species, whose fragmentation processes are competitive ones, are found to be almost equal in these simple benzene derivatives. In the case of aniline, it seems that the production of excited hydrogen atoms from the hydrogens in the NH_2 group and in the benzene ring is almost equally probable. These results may imply that similar super-excited states are involved in the collision with electrons with energy of 200 eV for the fragmentations of H and CH, whatever the substituents of the benzene ring are.

The authors wish to express their thanks to Professor Tetsuro Seiyama and Miss Shizue Saeki for the measurement of the mass spectrum, and to Mr. Minoru Toyoda and Mr. Totaro Imasaka for their discussions.

BULLETIN OF THE CHEMICAL SOCIETY OF JAPAN, VOL. 46, 3385—3391 (1973)

Dielectric Constant Measurement on Organic Crystalline Powder

Kikujiro Ishii,[1] Minoru Kinoshita,[1] and Haruo Kuroda
Department of Chemistry, Faculty of Science, The University of Tokyo, Hongo, Tokyo 113

(Received June 4, 1973)

The microwave cavity perturbation method was applied for the measurement of the dielectric constants for polycrystalline samples of ten aromatic compounds (naphthalene, anthracene, phenanthrene, pyrene, chrysene, perylene, durene, acenaphthene, biphenyl, and *p*-terphenyl.) The method is shown to give a reasonable result, if the effect of the second order perturbation term is properly included and if Böttcher's equation is carefully applied in transforming an apparent dielectric constant obtained on a powder sample into the mean dielectric constant of a crystal. The nature of the ordinarily used cavity perturbation equation and of Böttcher's transformation equation is discussed in this respect. The obtained mean dielectric constants are; naphthalene 2.87, anthracene 3.12, phenanthrene 2.96, pyrene 3.14, chrysene 3.09, perylene 3.34, durene 2.55, acenaphthene 2.94, biphenyl 2.88, and *p*-terphenyl 2.98. The molecular polarization calculated from these values agreed quite well with the values estimated from the bond polarization given by Le Fèvre *et al.*

Only few measurements have been reported on the dielectric constants of aromatic molecular crystals, although the dielectric properties are of essential significance in understanding their electric behaviors. The reason for this may be attributable to the difficulties most frequently found in the shape and the amount of a sample when the usual method of dielectric constant measurement is applied. In the usual method, we must fill up the whole space between the electrodes with a fairly good amount of sample.[2] However, it is difficult to obtain a single crystal of sufficient size and shape in the case of molecular crystal of interest. When a compressed powder specimen is used, there are a problem in fitting itself to electrode surfaces and other apprehensions[3] that the crystallites may be oriented in some direction on compression.

It is, therefore, desirable to establish a simple method to measure the dielectric constant on a small amount of crystalline material. For this purpose, we adopted the cavity perturbation method in the X-band microwave region. This method is found to be useful for polycrystalline samples if applied with proper care. In this paper we will describe the experimental procedures, and the dielectric constants of ten polycrystalline aromatic compounds determined with this method. We will discuss also some fundamental problems related to the cavity perturbation method.

Method of Measurement

Cavity Perturbation Method. In the cavity perturbation method, the change in the resonant frequency of the microwave cavity is related to the dielectric constant of the sample inserted into the cavity.

If a small sample, of which the dielectric constant and the magnetic permeability are given respectively

1) Present address: The Institute for Solid State Physics, the University of Tokyo, Roppongi, Minato-ku, Tokyo.

2) See, for example, C. P. Smyth, "Dielectric Behavior and Structure," McGraw-Hill, New York, (1955), Chapter VI.

3) C. C. Meredith and G. F. Wright, *Can. J. Chem.*, **38**, 1177, (1960).

by ε_1 and μ_1, is inserted into a resonant cavity, the change in the resonant frequency, f_1-f_0, is given[4] by,

$$-\frac{f_1-f_0}{f_1}=\frac{\int_{V_1}(\varepsilon_1-\varepsilon_0)\boldsymbol{E}_1\cdot\boldsymbol{E}_0^*\mathrm{d}v+\int_{V_1}(\mu_1-\mu_0)\boldsymbol{H}_1\cdot\boldsymbol{H}_0^*\mathrm{d}v}{\varepsilon_0\int_V\boldsymbol{E}_0\cdot\boldsymbol{E}_0^*\mathrm{d}v+\mu_0\int_V\boldsymbol{H}_0\cdot\boldsymbol{H}_0^*\mathrm{d}v} \tag{1}$$

where f_0 and f_1 are the resonant frequencies of the cavity, in the absence and presence of the sample, respectively, ε_0 and μ_0 denote the dielectric constant and magnetic permeability of vacuum, $\boldsymbol{E}_0$ and $\boldsymbol{H}_0$ the undisturbed electric and magnetic field vectors and $\boldsymbol{E}_1$ and $\boldsymbol{H}_1$ the resulting field vectors when the sample is loaded. V_1 and V indicate that the integration should be carried out within the volume of the sample and whole volume of the cavity, respectively.

The frequency, the dielectric constant and the magnetic permeability should, in general, be considered as complex quantities. However, in the case of low-dielectric-loss and diamagnetic material, we assume that all the quantities are real, and also that μ_1 is equal to μ_0. Then using the relation,

$$\varepsilon_0\int_V\boldsymbol{E}_0\cdot\boldsymbol{E}_0^*\mathrm{d}v=\mu_0\int_V\boldsymbol{H}_0\cdot\boldsymbol{H}_0^*\mathrm{d}v, \tag{2}$$

one gets Eq. (3) which concerns only the electrical field and the dielectric constant.

$$-(f_1-f_0)/f_1=(\varepsilon_s-1)\left(\int_{V_1}\boldsymbol{E}_1\cdot\boldsymbol{E}_0^*\mathrm{d}v\right)\Big/2\left(\int_V\boldsymbol{E}_0\cdot\boldsymbol{E}_0^*\mathrm{d}v\right), \tag{3}$$

where $\varepsilon_s=\varepsilon_1/\varepsilon_0$.

In the usual measurement of the dielectric constant, the equation in the first order approximation has been used[5,6] by assuming that the dielectric constant of a sample is small, and/or that its volume is also small compared with that of the cavity. In this case, putting $\boldsymbol{E}_1$ equal to $\boldsymbol{E}_0$, the dielectric constant of the sample is calculated by an equation which includes only the known electric field $\boldsymbol{E}_0$. For a rectangular cavity of the reasonance mode of TE_{k0m}, assuming that $\boldsymbol{E}_0$ is constant in the sample, this equation is written as[5]

$$-(f_1-f_0)/f_1=2(\varepsilon_s-1)\cdot V_1/V. \tag{4}$$

For a sample of relatively large volume and large dielectric constant, on the other hand, the first order equation is not promised to hold. Kaminow and Harding[7] and Hatta[8] gave equations of higher approximation which contain the quadratic term of ε_s. However, since the physical meanings of these equations are not given plainly, and since these equations lead to quite different results,[9] we tried to use another equation which was derived according to the general perturbation theory.[10]

Considering a wave equation in a cavity, and regarding the sample inserted into the cavity as a perturbation, one may derive an equation in which the square of the resulting resonant frequency is given by an expansion in ε_s-1. If one takes the first three terms of Eq. (I, 3) in Appendix I, he obtains a quadratic equation of ε_s (see Appendix I),

$$\frac{f_1^2-f_0^2}{f_1^2}=-(\varepsilon_s-1)\frac{\int_{V_1}\boldsymbol{E}_0\cdot\boldsymbol{E}_0^*\mathrm{d}v}{\int_V\boldsymbol{E}_0\cdot\boldsymbol{E}_0^*\mathrm{d}v}+(\varepsilon_s-1)^2\cdot\mathrm{A}, \tag{5}$$

where A is the factor which represents the second order perturbation effects.

Calculation of the factor A (see Appendix II) indicated that the second order term is not negligible under the experimental condition in this work. This term has a large value when ε_s is large and sometimes well exceeds five percent of the first order term in spite of our intention to get ε_s-1 with an accuracy within several percent. Therefore we explicitly took account of this term and calculated ε_s by solving the quadratic equation.

Calculation of Mean Dielectric Constant of Crystal. Many formulae have been proposed for the calculation of the dielectric constant of a crystal (which we denote by ε) from the apparent dielectric constant measured on a powder sample. We employed Böttcher's equation for the calculation of the dielectric constant of a molecular crystal, since it gives a relatively good result[11] among those equations.

Assuming that the environment of a spherical powder particle is continuous dielectric, Böttcher derived the following equation;[12]

$$\varepsilon=\frac{3\delta\varepsilon_a+2\varepsilon_a(\varepsilon_a-1)}{3\delta\varepsilon_a-(\varepsilon_a-1)}, \tag{6}$$

where ε_a is the apparent dielectric constant of the sample and δ is the ratio of the volume actually occupied by the microcrystals to the apparent volume of the powder filled in the sample cell. Polder and van Santen[13] showed that this equation also hold for non-spherical particles when the dielectric constant of the crystal is not large. Therefore we adopted it for our powder samples without correction.

We should note that ε is the mean dielectric constant of a crystal when it has anisotropic dielectric constant.

Experimental

Apparatus. The block diagram of the apparatus is shown in Fig. 1. The microwave generated by the klystron was introduced into the test cavity, of which the resonance mode is TE_{105}. The klystron was frequency-swept at a 50 Hz rate around the resonant frequency of the cavity, and the resonance was detected with a crystal detector and displayed on an oscilloscope. The output of the klystron was partly introduced into a cavity wavemeter, Hitachi M240B, through a directional coupler. Representing the resonance of it

4) F. E. Borgnis and C. H. Papas, "Encyclopedia of Physics," Vol. 16, ed. by S. Flügge, Springer, Berlin, (1958), p. 285.
5) G. Birnbaum and J. Franeau, *J. Appl. Phys.*, **20**, 817 (1949).
6) E. Nakamura and J. Furuichi, *J. Phys. Soc. Japan*, **15**, 2101 (1960).
7) I. P. Kaminow and G. O. Harding. *Phys. Rev.*, **129**, 1562 (1963).
8) I. Hatta, *J. Phys. Soc. Japan*, **24**, 1043 (1968).
9) M. Hosoya and E. Nakamura, *Japanese J. Appl. Phys.*, **9**, 552 (1970).
10) This treatment was originally proposed by Hosoya and Nakamura (Ref. 9). The authors wish to thank Dr. Hosoya for his kindness to draw our attention to their paper.
11) J. C. van Vessem and J. M. Bijvoet, *Rec. Trav. Chim.*, **67**, 191 (1948).
12) C. J. F. Böttcher, "Theory of Electric Polarization," Elsevier, Amsterdam, (1952).
13) D. Polder and J. H. van Santen, *Physica*, **12**, 257 (1946).

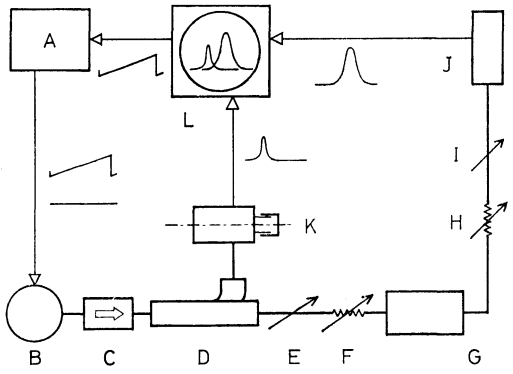

Fig. 1. Schematic diagram of the apparatus.
A: Powder supply for the klystron, B: Klystron, 2K25, C: Isolator, D: Directional coupler, E and I: Phase shifters, F and H: Attenuaters, G: Test cavity, J: Crystal detector, K: Cavity wavemeter, L: Oscilloscope. The klystron is frequency-swept by the saw-tooth wave oscillator included in the oscilloscope through the power supply. The components, from B to K, compose the wave guide circuit.

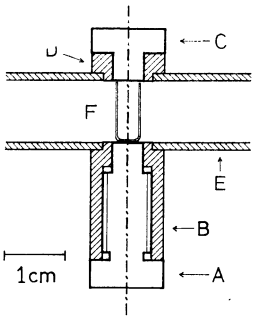

Fig. 2. The sample holder and the cell.
A and C; Brass sample holder and cap. B and D: Brass guides for the holder and the cap, bound to the copper cavity, E, with solder. F: Fused quartz sample cell.

simultaneously on the oscilloscope, the resonant frequency of the test cavity was measured.

The test cavity was made with copper waveguide and copper plates. Its volume is 25.7 cm^3. The resonant frequency and the Q-factor are about 9.36 GHz and 4500, respectively, when it contains the empty sample cell.

The sample holder and the cell are shown in Fig. 2. The sample cell made with fused quartz was bound on the brass holder with a small amount of binding agent of cyanoacrylate, and was inserted into the cavity at the point of the maximum electric field. The outer diameter of the cell is 4.0 mm, and the volume is measured to be 89.9 mm^3 by weighing cyclohexane, *n*-heptane and benzene filled in the cell.

All the measurements were carried out in atmosphere and at room temperature.

Samples. Organic liquids were used after distillation over calcium chloride. In the case of *p*-xylene, in addition to this procedure, fractional crystallization was repeated for several times. The solid samples were used after purification by sublimation *in vacuo* or recrystallization followed by drying under a reduced pressure.

The powder sample was prepared by grinding crystals in an agate mortar just before the measurement, and stuffed into the cell without pressure. The volume fraction δ was determined using the total volume of the microcrystals which was calculated from the weight and the crystal density. By changing the amount of powder and stuffing procedure, we were able to vary δ in the range around 0.4—0.5.

Table 1. Dielectric constants of organic liquids[a)]

Substance	1st Order	Corrected 1ts Order	2nd Order	Literature[b)]
n-Heptane	1.94	1.97	1.94	1.924
Cyclohexane	2.04	2.07	2.03	2.023
p-Xylene	2.30	2.34	2.28	2.270
Benzene	2.31	2.35	2.29	2.284

a) The measurement was carried out at room temperature around 20 °C.
b) A. A. Maryott and E. R. Smith, Nat. Bur. Standards Circ. 514, August 10, 1951. (At 20 °C)

Results

Dielectric Constants of Organic Liquids. For the first we measured the dielectric constants of organic liquids to ascertain the adequacy of the cavity perturbation method. In Table 1 the results for four organic liquids calculated by three different methods are shown. The results in the second column (1st Order) are obtained using Eq. (4). The results shown in the next column (Corrected 1st Order) are obtained by introducing a factor of 0.971 in the right-hand side of Eq. (4) as a correction for the ununiform electric field in the specimen. The fourth column (2nd Order) shows the results obtained by solving Eq. (5). The numeric factor, A, in the second order term was calculated for the test cavity and the sample cell used, using the computer, HITAC 5020E, of the Computer Center of the Tokyo University, and found to be $0.035 \times 4V_s/V_c$ (see Appendix II). In the last column, the dielectric constants reported for these liquids are given for comparison. One can see that the second order perturbation method gives better results.

Dielectric Constants of Aromatic Molecular Crystals. Since, as stated before, crystalline powder was used as the sample in this work, we calculated first the apparent dielectric constant of the specimen (including the empty space between the microcrystals) by the method of the second order perturbation, and then the mean dielectric constant of the crystal was calculated by Böttcher's equation.

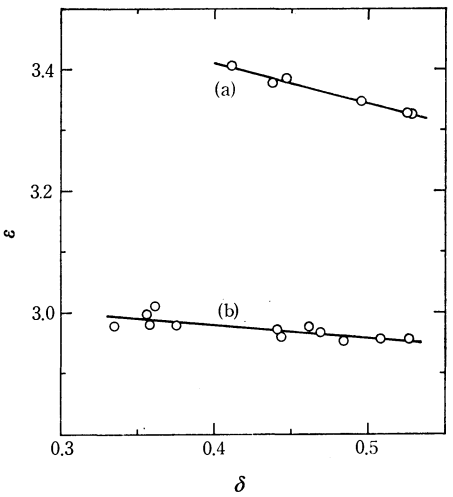

Fig. 3. The variations of ε with δ for (a) perylene and (b) phenanthrene.

In Fig. 3, the results for perylene and phenanthrene are shown as the examples. If Böttcher's equation was quite adequate to this calculation, ε should be independent of δ. However, as shown in this figure, ε calculated by the equation varies with δ. Similar variation was seen for all the substances studied.

After examining the experimental results, the following properties of the calculated ε and its relation to δ became clear;

(1) The δ-dependence of ε can be approximated by a linear line when δ is in the region from 0.4 to 0.55.

(2) When the mean dielectric constant of the crystal is considered to be small (about three or smaller), in most of the cases, the line shows small negative slope. For the substances of which the dielectric constant are reported, ε's calculated by this method almosts agree with those values.

(3) When the dielectric constant is large, the inclination of the line has a large negative value, and ε is small compared with the reported value. In Fig. 4, the results for NaCl is shown as an example of this case.[14]

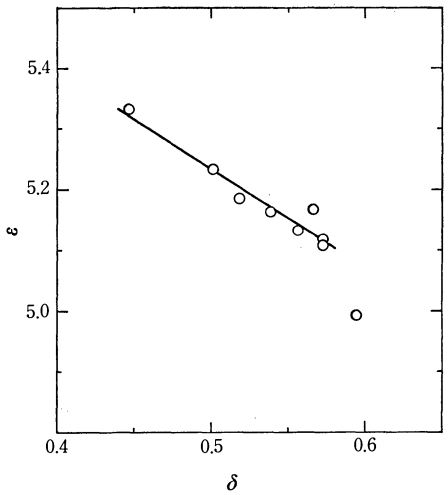

Fig. 4. The variation of ε with δ for NaCl, for which the dielectric constant is reported to be 5.90 (Ref. 15).

For the substances of which ε does not exceed four, we tentatively adopt the value of ε, as the mean dielectric constant of the crystal, which is obtained by interpolating or extrapolating the linear line to the point of δ equal to 0.5. The reason for this estimation will be discussed later. The results obtained for ten aromatic molecular crystals are shown in Table 2. In this table, are also given the value of the crystal density, which was used to calculate δ, and the inclination of the δ-dependence of ε. In addition, the reported dielectric constants are given for some substances.

When the dielectric constant of a crystal is larger than four, it seems a little difficult to get a reliable value of the mean dielectric constant by this simple method.

14) Almost the same results were obtained by N. L. Conger and and S. E. Tung, *Rev. Sci. Instr.*, **38**, 384 (1967). For NaCl, they obtained 5.28 as ε for $\delta=0.54$ by the usual first order method. The results for KCl given in Table 2 in their paper are not consistent together. The value, 4.76 in the sixth column is considered to be incorrect.

Table 2. Mean dielectric constants of aromatic molecular crystals

Substance	Mean dielectric constant	Density	Inclination[a]	Literature[b]
Naphthalene	2.87	1.169	0.02	2.85[c] 2.8[d]
Anthracene	3.12	1.250	−0.21	
Phenanthrene	2.96	1.209	−0.21	
Pyrene	3.14	1.271	−0.55	
Chrysene	3.09	1.274	−0.28	
Perylene	3.34	1.35	−0.66	
Durene	2.55	1.03	−0.20	
Acenaphthene	2.94	1.217	−0.35	
Biphenyl	2.88	1.18	0.16	
p-Terphenyl	2.98	1.230	0.11	2.95—3.20[c] 2.95[d]

a) $d\varepsilon/d\delta$.
b) Ref. 16.
c) Frequency; $\leq 10^7$ Hz.
d) Frequency; 3×10^9 Hz.

Discussion

Contribution of Second Order Term in Cavity Perturbation Method. Although the cavity perturbation method has been applied to the dielectric and/or magnetic measurement by several investigators, very few attempts have been made to experimentally examine whether this method gives a proper value of dielectric constant or magnetic permeability. In most of the studies using this method, the absolute value of dielectric constant obtained was discussed only qualitatively.

In this work, we attempted to settle the procedure for obtaining a reliable value of dielectric constant on solid materials, especially organic molecular crystals.

The treatment using the second order perturbation theory reduced the ambiguity inherent to the ordinary first-order perturbation method.

The results for the organic liquids given in Table 1 show the characteristics of the three different calculation methods. In the cases shown there, we can compare the dielectric constant at microwave frequency with the values reported for the lower frequency, because all these liquids are non-polar. In this work, the ordinary first order method gives a good result when the dielectric constant of the sample is around two. However, for the sample of which the dielectric constant is larger, it has a tendency to give a little larger value than the reported value. Furthermore, if we consider a correction for the smallness of the electric field at the off-center part in the specimen, the values become still larger as they are shown in the third column in Table 1.

By starting from the general perturbation theory, the higher order perturbation terms are introduced without any special consideration. The second order term has a value of 0.035 (ε_s-1) time of the absolute value of the field-uncoreected first order term for the sample cell used here, and contributes to ε_s as a deducting term. One can now understand the reason why the ordinary first order equation gives a reasonable

result in this work when ε_s is around two. In that case, the field correction and the higher order terms are cancelling each other.

The results obtained by including the second order term are shown in the fourth column of the table. These values are quite reasonable, although they are also larger than the reported values by about 0.01. We consider that this small deviation comes from the error in the estimated volumes of the cavity and the sample cell. It is also possible that the differences are due to small amounts of water and/or organic impurity in the sample.

Böttcher's Equation. As already described Böttcher's equation does not give constant results when δ is changed. It ought to be ascertained, therfore, whether the δ-dependence of ε is the intrinsic character of this equation or this dependence appears only when this equation is applied to the result of the cavity perturbation method.

van Vessem and Bijvoet[11] extensively studied on the correction equations for dielectric constants measured on powder sample. They measured dielectric constants on powder samples of some ionic crystals, and concluded that Böttcher's equation gives a relatively good result when the grain-size is sufficiently small compared to the dimension of the electrodes. Their conclusion is based on the fact that the apparent dielectric constant of the powder sample calculated from the known dielectric constant of the crystal agreed well with the observed apparent dielectric constant for a wide range of δ. However, inversely calculating ε from their experimental values of the apparent dielectric constant, we found that their results did not give constant ε either. Two examples are shown in Fig. 5. The inclination has obviously a large negative value for the sample of which the dielectric constant of the crystal is very large compared with that of the surrounding medium. Seemingly, the δ-dependence is the intrinsic nature of this equation although it is small when the dielectric constant of the crystal is not very large compared with that of the surroundnig medium. By examing their data, we found that Böttcher's equation gives reasonable value of ε when δ is around 0.5, and that it gives improperly small ε for very large δ (say, larger than 0.6).

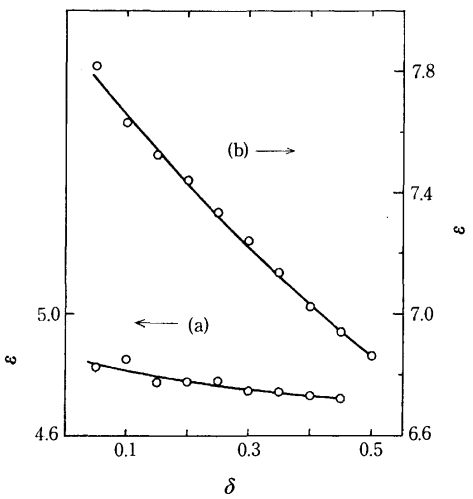

Fig. 5. The variations of ε with δ for (a) KCl and (b) NH_4Cl, where the values of ε are calculated from the apparent dielectric constants measured in the suspenders, CCl_4–CBr_4 and CCl_4–C_6H_6 mixtures, by van Vessem and Bijvoet (Ref. 11). The dielectric constants they used in their calculation are 4.70 for KCl, 2.372 for CCl_4–CBr_4 mixture, 6.85 for NH_4Cl and 2.234 for CCl_4–C_6H_6 mixture.

Although the cause of this δ-dependence of ε is not clear yet, we consider that it results from the basic assumption made by Böttcher. He assumed that the environment of a spherical particle in the powder sample can be considered as a continuous dielectric with the dielectric constant equal to the apparent dielectric constant of the sample. Starting from it and homogeneously distributing the polarization in the particles into the whole space in the specimen, he obtained the field which is identical with the field where a single spherical particle is placed. However, the actual "local" external field, in which a powder particle is placed, is the superposition of the external field and the field which results from the polarization of the surrounding particles. The latter field is a superposition of the fields which are the functions of the distances between the particle considered and the charges and/or the dipoles on other particles. Therefore, when δ is small, the particle is more polarized than expected by Böttcher's equation. Consequently, this equation gives large ε for small δ. The deviation may be pronounced in the case of a material of large dielectric constant.

As to the effect of the size of the particle, it was found[11] that the apparent dielectric constant appears smaller for the larger grain-size powder when δ's are equal. Therefore, although Böttcher's equation is derived without imposing any assumption on the size of the particle, it may be inadequate to apply this equation for the sample of large grain-size.

The shape of the powder particle seems to affect the δ-dependence of ε. The positive inclinations given in Table 2 for some substances are considered to manifest the effect of it. However, since the inclinations are not large, we need not make much of this effect in this work.

The experimental error in our result of ε is large when δ is small, because the errors accompanied in the measured weight and the frequency change become serious in this case. On the other hand, the result for very large δ (say, larger than 0.55) is not reliable. It may be due to the inhomogeneous stacking of the sample in the cell.

Taking account of our experimental results and above considerations, we arrived at the following conclusions.

(1) Böttcher's equation gives reasonable results for a material of small dielectric constant when δ is in the region around 0.5 and the grain-size of the powder is sufficiently small.

(2) When the difference between the dielectric constant of a crystal and that of the surrounding medium is large, the δ-dependence of ε is serious and it is rather difficult to estimate the proper value of the dielectric constant of the crystal. In this case, the effects of the shape and the size of the particle may be also important.

Mean Dielectric Constants and Molecular Polarizations of Aromatic Molecular Crystals. The mean dielectric constants were estimated for the aromatic molecular crystals given in Table 2. Unfortunately, so far as we know, very few reliable data have been reported for the dielectric constants of organic molecular crystals. The data given in the table are the ones quoted from the book edited by von Hippel.[15] The mean dielectric constants estimated from our simple measurement agree well with these data. For anthracene, anisotropic dielectric constants of a single crystal at low frequency were recently reported.[16] The mean dielectric constant estimated in the present work qualitatively agrees with these single crystal data.

Using the mean dielectric constant obtained, we calculated molecular polarization, P, defined by,

$$P = M(\varepsilon-1)/d(\varepsilon+2),$$

where M is the molecular weight and d is the crystal density, and ε is the isotropic dielectric constant of the crystal, for which we used the mean dielectric constant. The molecular polarization is estimated in good approximation as the sum of the values characteristic to atoms or bonds.[17]

Table 3. Molecular polarization[a]

Substance	Experiment	Calculated[b]	Difference
Naphthalene	42.1	41.2	0.9
Anthracene	59.0	57.2	1.8
Phenanthrene	58.3	57.2	1.1
Pyrene	66.3	64.8	1.5
Chrysene	73.6	73.2	0.4
Perylene	81.9	80.8	1.1
Durene	44.4	43.3	1.1
Acenaphthene	49.8	48.2	1.6
Biphenyl	50.3	49.5	0.8
p-Terphenyl	74.4	73.9	0.5

a) Unit; cm^3/mol.
b) See text.

In Table 3, the molecular polarization calculated from the mean dielectric constants are given in the second column. The values given in the third column are calculated using the "electronic" bond polarizations estimated by Lè Fevre and Steel.[17,18] They estimated those quantities by assuming a dispersion equation and extrapolating the bond refractions to the limit of the infinite wavelength. Therefore the polarization calculated using their values is considered to give the "electronic" molecular polarization at the infinite wavelength. As shown in the last column, the difference between the experimental value and the estimated one is, in general, small positive value. Although these small differences cannot be discussed quantitatively, it is not impossible to attribute the differences to the contribution from the "atomic" polarization.[19] The good agreement for many substances seems to imply that the additivity of the bond polarization is valid in these aromatic molecules.

The authors wish to thank Professor Hideo Akamatu for his kind encouragement throughout this work. They are also indebted to Dr. Toshiaki Ohta for making the computer program for the calculation of the second order perturbation term.

Appendix I

The electric field, $\boldsymbol{E}$, in a resonant cavity containing a low-loss dielectric specimen satisfies the wave equation,

$$\nabla^2\boldsymbol{E} + \omega^2\varepsilon_r\varepsilon_0\mu_0\boldsymbol{E} = 0, \qquad \text{(I, 1)}$$

where ε_r is equal to ε_s, the dielectric constant of the specimen relative to the vacuum, inside the specimen and unity outside of it. Substituting $\omega^2\varepsilon_0\mu_0$ by $-\chi$ and adding the factor $\chi\boldsymbol{E}$ to the both sides of this equation, one gets

$$\{\nabla^2-(\varepsilon_r-1)\chi\}\boldsymbol{E} = \chi\boldsymbol{E}. \qquad \text{(I, 2)}$$

If one regards the second term in the left-hand-side of this equation as a perturbation, according to the usual treatment of the perturbation theory, one gets the n-th eigen-value of $\boldsymbol{E}$, χ_n, as

$$\chi_n = \chi_{n,0} + \langle\boldsymbol{E}_{n,0}|-(\varepsilon_r-1)\chi_n|\boldsymbol{E}_{n,0}\rangle + \sum_{k\neq n}\frac{1}{\chi_{n,0}-\chi_{k,0}}|\langle\boldsymbol{E}_{n,0}|-(\varepsilon_r-1)\chi_n|\boldsymbol{E}_{k,0}\rangle|^2 + \cdots, \qquad \text{(I, 3)}$$

where $\boldsymbol{E}_{n,0}$ and $\boldsymbol{E}_{k,0}$ are the n-th and k-th eigen-states of the electric field in the non-perturbed cavity, and $\chi_{n,0}$ and $\chi_{k,0}$ are the corresponding eigen-values of them. This equation is considered to give a more general expression to the relation between the dielectric constant of a specimen and the change of the resonant frequency, since it was obtained without imposing any restriction on the dielectric constant and the volume of the specimen.

If one takes account of the first three terms in the right-hand-side of Eq. (I, 3), rearranging χ_n and $\chi_{n,0}'$ one gets

$$\frac{\chi_n-\chi_{n,0}}{\chi_n} = \langle\boldsymbol{E}_{n,0}|-(\varepsilon_r-1)|\boldsymbol{E}_{n,0}\rangle + \sum_{k\neq n}\frac{\chi_n}{\chi_{n,0}-\chi_{k,0}}|\langle\boldsymbol{E}_{n,0}|-(\varepsilon_r-1)|\boldsymbol{E}_{k,0}\rangle|^2. \qquad \text{(I, 4)}$$

Since ε_r-1 has the finite value only in the volume of the specimen, rewriting χ in the form of frequency, $f=\omega/2\pi$, one gets the same equation as Eq. (5), in which $f_{n,0}$, f_n, $\boldsymbol{E}_{n,0}$ and ε_r in the specimen are written as f_0, f_1, $\boldsymbol{E}_0$ and ε_s, respectively. The factor **A** is

$$\sum_k{}'\frac{f_1^2}{f_0^2-f_{k,0}^2}\left(\int_{V_1}\boldsymbol{E}_0\cdot\boldsymbol{E}_{k,0}^*\mathrm{d}v\right)^2, \qquad \text{(I, 5)}$$

where the summation should be carried out for all the normal modes of the unperturbed cavity except the n-th mode.

When the perturbation is considered to be very small, and if one takes the first two terms in the right-hand-side of Eq. (I, 3) one gets the same result as Eq. (3) by rewriting the equation as before and assuming $f_1+f_0=2f_1$.

15) A. R. von Hippel, ed., "Dielectric Materials and Applications," The Technology Press of M. I. T. and John Wiley & Sons, Inc., New York (1954).
16) N. Karl, H. Rohrbacher and D. Siebert, *Phys. Stat. Sol.*, (a) **4**, 105 (1971).
17) R. J. W. Le Fèvre, "Advances in Physical Organic Chemistry," Vol. 3, ed. by V. Gold, Academic Press, London (1965), p.1.
18) R. J. W. Le Fèvre and K. D. Steel, *Chem. & Ind.*, London, 670 (1961).
19) Since most of the molecules dealt with in this work are non-polar, the molecular polarization can be explained with the electronic and atomic polarizations. The latter may be in a magnitude of only several percent of the former for these substances (see, for instance, Chapter XIV of Ref. 1).

Appendix II

For a rectangular cavity of the resonance mode $TE_{k,0,m}$, the electric field is given by,

$$E_y = B \sin \frac{k\pi x}{a} \sin \frac{m\pi z}{c}, \qquad \text{(II, 1)}$$

where a and c are the width and the length of the cavity, and B is a function of time which gives the amplitude of the standing wave. The electric fields of other directions, E_x and E_z, do not exist for this resonance mode.

If a cylindrical specimen, of which the height is identical with that of the cavity, b, is placed at the point of the maximum electric field of TE_{105} mode, it is easily shown that the normal modes, which have finite values of overlap integrals with the TE_{105} mode in the volume of the specimen, are only $TE_{k',0,m'}$ modes with odd k' and $(k', 0, m') \neq (1, 0, 5)$.

Substituting the electrical fields of these normal modes into Eq. (I, 5), one obtains

$$\frac{16}{(abc)^2} \sum_{k',m'} \frac{f_1^2}{f_0^2 - f_{k'0,m'0}^2} \times \left(\int_{V_1} \sin \frac{\pi x}{a} \sin \frac{5\pi z}{c} \sin \frac{k'\pi x}{a} \sin \frac{m'\pi z}{c} dv \right)^2 \qquad \text{(II, 2)}$$

as the factor A, where $16/(abc)^2$ is the normalization constant.

The sum was calculated by the numerical integration and found to converge sufficiently when we took account of the modes of the resonant frequency up to about 200 GHz. Since the resulting frequency f_1 is not varied so much with the specimens, we can assume the formula (II, 2) as a constant. It was found to be $0.035 \times 4\ V_s/V_c$ for the geometry of the cavity and the sample cell used.

BULLETIN OF THE CHEMICAL SOCIETY OF JAPAN, VOL. 46, 3391—3395 (1973)

Photoelectron Spectra and Sum Rule Consideration. Higher Alkyl Amines and Alcohols[1)]

Shunji KATSUMATA, Toshio IWAI, and Katsumi KIMURA

Physical Chemistry Laboratory, Institute of Applied Electricity, Hokkaido University, Sapporo 060

(Received June 5, 1973)

Photoelectron spectra of higher alkyl amines and alcohols (Me, Et, *n*- and *i*-Pr, and *n*-Bu) have been measured with the 584 Å line of helium. Seven photoelectron bands corresponding to p-type MO's were identified for ethylamine and ethanol. Nine bands were observed for *n*- and *i*-propylamine and *n*- and *i*-propanol, and eleven for *n*-butylamine and *n*-butanol, in addition to the first C_{2s} bands appearing at about 19 eV. The sum rule previously proposed by Kimura *et al.* has further been applied to the compounds studied here. Total sums of vertical ionization energies in the region below 18 eV have been found to be well reproduced by the sums of appropriate energies estimated for the p-type localized MO's, using Koopmans' theorem. Information on orbital character has also been obtained from the sum rule in each symmetry species.

Recent advances in vacuum-ultraviolet photoelectron spectroscopy have made it possible to determine ionization energies of molecular valence orbitals with high precision and possible to obtain quantitative information on valence orbital energies on the basis of Koopmans' theorem.

Recent photoelectron works by Kimura *et al.*[2-5)] have suggested that "sum rule" holds for vertical ionization energies to a considerably wide extent. Briefly speaking, for each alkyl halide, a total sum of experimental vertical ionization energies below about 17 eV was well reproduced by a simple summation of empirical energy values assumed for p-type localized MO's, using Koopmans' theorem. It should be mentioned that the empirical values used in those works were estimated on the basis of accurate photoelectron data of simple related molecules. In the present work, we have considered it very interesting to investigate how far such a sum rule holds for other kinds of compounds, and have undertaken to study series of alkyl amines and alcohols, by placing major emphasis on the sum rule.

The alkyl amines and alcohols studied here have partly been studied with a retarding grid-type technique for the first time by Al-Joboury and Turner[6,7)] and later by Dewar and Worley.[8)] Methanol has also been studied by ESCA by Siegbahn *et al.*[9)] Recently, high-resolution photoelectron spectra of several alkyl alcohols have been reported by Baker *et al.*[10)] and by

1) Part 5 of "Photoelectron Spectroscopic Studies."

2) Part 1: K. Kimura, S. Katsumata, Y. Achiba, H. Matsumoto, and S. Nagakura, This Bulletin, **46**, 373 (1973).

3) Part 2: S. Katsumata and K. Kimura, *ibid.*, **46**, 1342 (1973).

4) Part 3: K. Osafune, S. Katsumata, and K. Kimura, *Chem. Phys. Lett.*, **19**, 369 (1973).

5) Part 4: T. Yamazaki, S. Katsumata, and K. Kimura, *J. Electron Spectrosc.*, in press.

6) M. I. Al-Joboury and D. W. Turner, *J. Chem. Soc.*, **1964**, 4434.

7) M. I. Al-Joboury and D. W. Turner, *ibid., Ser. B*, 373 (1967).

8) M. J. S. Dewar and S. D. Worley, *J. Chem. Phys.*, **50**, 654 (1969).

9) K. Siegbahn *et al.*, "ESCA Applied to Free Molecules," North-Holland Publ. Co., Amsterdam (1969), p. 98.

10) A. D. Baker, D. Betteridge, N. R. Kemp, and R. E. Kirby, *Anal. Chem.*, **43**, 375 (1971).

Robin and Kuebler,[11] and those of methylamine and its related compounds by Cornford *et al.*[12] For higher alkyl amines, however, no high-resolution spectra have been published so far.

Price *et al.*[13] have recently reported He II photoelectron spectra of many organic compounds including methylamine and methanol, and have shown that the photoelectron bands due to 2s electrons of C, N, and O atoms appear in the region from 20 to 40 eV.

On a theoretical side, orbital calculations of methylamine[12,14] and methanol[8,9,11,15] have been carried out by Fink and Allen (*ab initio*),[14,15] Dewar and Worley (MINDO),[8] Siegbahn *et al.* (CNDO),[9] Cornford *et al.* (INDO),[12] and Robin and Kuebler (GTO).[11] According to these theoretical treatments, the valence orbital structures of methylamine and methanol have well been established to be (1a″)(5a′)(6a′)(2a″)(7a′) and (5a′)(1a″)(6a′)(7a′)(2a″), respectively. For the higher alkyl compounds, no such orbital structures have been reported.

Experimental

Commercial samples of the alkyl amines and alcohols were used after purification. Measurements of photoelectron spectra were carried out several times for each compound with a JASCO PE-1 high-resolution photoelectron spectrometer described before,[2] using He 584 Å resonance line. Calibration of an ionization energy scale was carried out using known ionization energies of Xe as a standard substance.

Results

Photoelectron spectra obtained for the amines and alcohols in the region below about 20 eV are shown in Fig. 1 (where only those of *n*-butylamine and *n*-butanol are not shown), no distinct vibrational structure being observed. As seen from Fig. 1, methylamine shows five bands which are clearly separated from one another and well correspond to those reported by Cornford *et al.*[12] For ethylamine, a total of seven bands including a slight shoulder at 13.8 eV were distinguished. This shoulder was carefully checked to be correct in the present measurement, because it is missing in literature. Ten and twelve bands were identified for propylamines and *n*-butylamine, respectively.

The spectrum of methanol consists of five bands, while that of ethanol shows six maxima and one slight shoulder at about 14.5 eV, which we consider as one of the ionization bands. In addition to seven bands reported previously for *n*-propanol by Baker *et al.*,[10] we observed two more bands appearing as slight shoulders at about 13.4 and 15.3 eV, and a maximum at 19.51 eV, so that a total of ten bands were identified in the region studied here. Similarly, for *i*-propanol, a slight shoulder at about 14 eV and a maximum at 19.52 eV were observed in addition to the bands already reported.[10] Twelve bands were found for *n*-butanol, including five new bands not reported previously.

Vertical ionization-energy (IE) values thus obtained from the maxima and shoulders of the photoelectron spectra are summarized in Tables 1 and 2. The IE values estimated from the shoulders are somewhat uncertain, which are shown in parentheses.

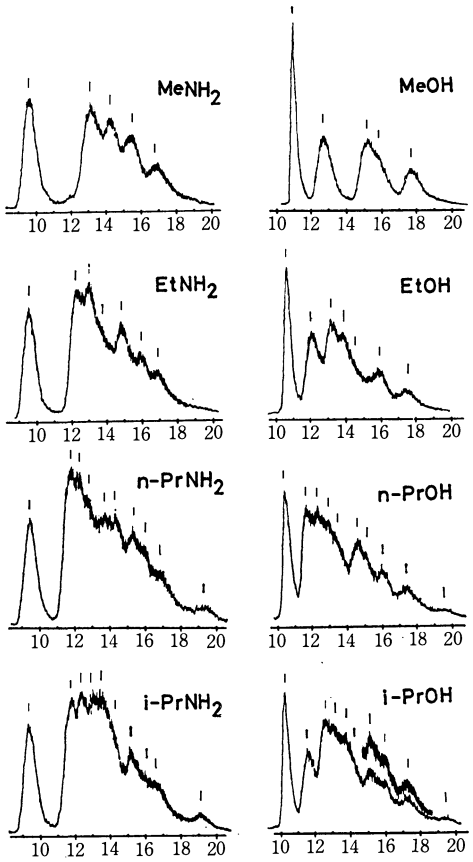

Fig. 1. Photoelectron spectra of alkyl amines and alcohols (methyl, ethyl and *n*- and *i*-propyl). Abscissas are in eV units. Vertical lines indicate the locations of the vertical ionization energies given in Tables 1 and 2.

TABLE 1. VERTICAL IE'S OF METHYLAMINE AND METHANOL (in eV)

	$MeNH_2$			MeOH		
	This work	Other works[a]		This work	Other works[a]	
		Ref. 12	Ref. 14		Ref. 10	Ref. 11[b]
I_1	9.64(7a′)	7.9	(7a′)	10.94(2a″)	10.96	10.96(2a″)
I_2	13.22(2a″)	13.2	(2a″)	12.68(7a′)	12.72	12.62(7a′)
I_3	14.42(6a′)	14.5	(6a′)	15.19(6a′)	15.15	15.21(6a′)
I_4	15.45(5a′)	15.6	(5a′)	15.66(1a″)	15.55	15.64(1a″)
I_5	16.85(1a″)	17.1	(1a″)	17.50(5a′)	17.50	17.62(5a′)

a) High-resolution data.
b) Also, Refs. 9 and 15 for theory.

11) M. B. Robin and N. A. Kuebler, *J. Electron Spectry.*, **1**, 13 (1972—1973).
12) A. B. Cornford, D. C. Frost, F. G. Herring, and C. A. McDowell, *Can. J. Chem.*, **49**, 1135 (1971).
13) A. W. Potts, T. A. Williams, and W. C. Price, *Discuss. Faraday Soc.*, **54**, (1972) in press; Also, cited by D. F. Brailsford and B. Ford, *Mol. Phys.*, **18**, 621 (1970).
14) W. H. Fink and L. C. Allen, *J. Chem. Phys.*, **46**, 2276 (1967).
15) W. H. Fink and L. C. Allen, *ibid.*, **46**, 2261 (1967).

Table 2. Vertical IE's of higher alkyl amines and alcohols (in eV)[a]

	$EtNH_2$ This work	n-$PrNH_2$ This work	i-$PrNH_2$ This work	n-$BuNH_2$ This work	EtOH This work	EtOH Other work[10]	n-PrOH This work	n-PrOH Other work[10]	i-PrOH This work	i-PrOH Other work[10]	n-BuOH This work	n-BuOH Other work[10]
I_1	9.50	9.44	9.31	9.40	10.64	10.65	10.49	10.48	10.36	10.42	10.37	10.37
I_2	12.26	11.63	11.79	11.41	12.18	12.20	11.70	11.73	11.75	11.71	11.49	11.48
I_3	12.97	12.24	12.38	11.86	13.21	13.31	12.24	12.34	12.58	12.68	11.80	11.95
I_4	(13.8_0)	(13.0_2)	13.06	(12.2_3)	13.86	13.82	12.79	13.04	13.06	13.08	12.30	12.25
I_5	14.84	13.55	13.62	12.87	(14.5_5)		(13.4_4)		13.66	13.75	12.82	12.55
I_6	15.80	14.19	(14.1_0)	13.33	15.85	15.85	14.52	14.60	(14.0_0)		13.46	13.55
I_7	16.77	15.11	15.16	14.13	17.35	17.35	(15.3_2)		15.11	15.14	(14.1_3)	
I_8		15.84	(16.0_0)	14.74			16.03	16.00	15.88	15.80	14.91	15.10
I_9		16.70	16.55	15.26			17.23	17.14	17.22	17.20	15.36	
I_{10}		[19.32]	[19.16]	16.02			[19.51]		[19.52]		16.00	
I_{11}				16.76							17.14	
I_{12}				[18.93]							[19.19]	

a) Only high-resolution data are shown. Robin and Kuebler[11] also report I_1 values for ethanol (10.62 eV), n-propanol (10.50 eV) and i-propanol (10.42 eV). Values in parentheses are shoulders and those in square brackets show the C_{2s}-orbital bands.

Discussion

Photoelectron Bands and Ionization Energy Data. Most of the amines and alcohols studied here have previously been studied with a retarding-potential technique.[6-8] Agreements between the high-resolution and the retarding-potential IE's are not always good and some values are lacked in the latter. The high-resolution data already reported for the alkyl amines and alcohols[10,12] are compared in Tables 1 and 2. As far as comparison is possible in Tables 1 and 2, the present experimental IE's are generally in good agreement with the literature values, although some IE values are missing in the previous works.[10]

It should be pointed out that in each compound the number of the photoelectron bands observed here in the region below 18 eV is in accord with the number of p-type localized MO's. In fact, there should exist five, seven, nine, and eleven p-type localized MO's in the methyl, ethyl, n- and i-propyl and n-butyl compounds, respectively. The highest ionization-energy bands appearing at about 19 eV for the propyl and butyl compounds should be attributed to the first C_{2s} bands, since these bands correspond to the C_{2s} bands of propane and butane observed at about 19 eV by Potts *et al.*[13] using a He II source. According to these authors,[13] the first C_{2s} band of ethane appears at about 20.3 eV, and the O_{2s} band of methanol as well as the N_{2s} band of methylamine appear in the region higher than 20 eV.

In our previous works of higher alkyl halides,[2,5] we have identified all the p-type bands appearing in the He I region, which are the halogen nonbonding orbitals, the C–C and C–halogen bonding orbitals, and the methyl- and methylene-group pseudo-π orbitals. A similar situation can be expected to occur in the alkyl amines and alcohols. Namely, the photoelectron bands are expected to correspond to the O and N nonbonding (n) orbitals, the C–C, C–O, C–N, and O–H σ orbitals, and the pseudo-π orbitals of the CH_3–, $-CH_2$–, and NH_2–groups.

Experimental Total Energies for p-Type Orbitals. Assuming Koopmans' theorem, a total sum of MO energies are given by

$$T = -\sum_i I_i \qquad (1)$$

where I_i denotes the ith ionization energy. The 2s-type ionization energies (I_{10} for propylamines and propanols, I_{12} for n-butylamine and n-butanol) are removed in the calculations of the total sums. The results of such total sums for all the compounds studied here are summarized in Table 3, indicating that differences in T between two successive alkyl anologues approximately equal one another with an average value of $\Delta T = -26.04 \pm 0.25$ eV. This value should correspond to the orbital-energy change due to the substitution by the $-CH_2-$ group in alkyl compounds.

Table 3. The total orbital energies (T, in eV) of the p-type MO's for the alkyl amines and alcohols, obtained on the assumption of Koopmans' theorem

Alkyl amines	T	ΔT	Alkyl alcohols	T	ΔT
$MeNH_2$	−69.58		MeOH	−71.97	
		−26.36			−25.67
$EtNH_2$	−95.94		EtOH	−97.64	
		−25.78			−26.12
n-$PrNH_2$	−121.72		n-PrOH	−123.76	
(i-$PrNH_2$)	(−121.97)	−26.29	(i-PrOH)	(−123.62)	−26.02
n-$BuNH_2$	−148.01		n-BuOH	−149.78	

ΔT (average) = -26.04 ± 0.25

Using vertical IE's obtained for twelve alkyl halides (RX: R=Me to *n*-Bu; X=Cl, Br, I),[2] an average value of $\Delta T = -26.07 \pm 0.47$ eV was obtained, in excellent agreement with the above value (−26.04 eV). Furthermore, using IE values reported for methane, ethane, propane, isobutane, and neopentane,[16] an average value of −26.0 eV was obtained for ΔT, again very close to the above. Therefore, the ΔT value −26.04 eV obtained here may undoubtedly be allotted to the p-type localized orbitals consisting of the CC σ and CH_2 pseudo-π orbitals. In fact, it is interesting to see that the ΔT value is almost equal to the sum of −11.75 and −14.30 eV which have previously been proposed for σ_{CC} and π_{CH_2} by the present authors.[2] The comparison of T's in Table 3 also suggests that the present PE measurements were correctly carried out without missing any right bands or taking any wrong bands into account.

It should be pointed out that according to a theoretical study by Hoffmann,[17] $(2n+1)$ p-type MO's of alkanes (C_nH_{2n+2}) are located higher than about −17 eV whereas 2s-type MO's are below about −20 eV. Dewar and Worley[8] have also indicated from their MINDO method that in several alkyl alcohols the number of MO's with ionization energies higher than 20 eV is in agreement with that expected for 2s-type MO's and all the p-type MO's show ionization energies smaller than about 15 eV. These theoretical treatments seem to suggest that 2s- and 2p-type MO's in an alkyl compound may reasonably be distinguished.

TABLE 4. LOCALIZED ORBITAL ENERGIES (in eV) USED FOR PARTIAL AND TOTAL SUMS

$\varepsilon^0(n_N) = -10.80$	$\varepsilon^0(\sigma_{CN}) = -14.42$	$\varepsilon^0(\pi_{NH_2}) = -15.77$
$\varepsilon^0(n_O) = -12.61$	$\varepsilon^0(\sigma_{CO}) = -15.19$	$\varepsilon^0(\sigma_{OH}) = -15.57$
$\varepsilon^0(\sigma_{CC}) = -11.75$	$\varepsilon^0(\pi_{CH_2}) = \varepsilon^0(\pi_{CH_3}) = -14.30$	

p-Type Localized MO's. Generally speaking, in a secular equation, the total value of all eigenvalues is equal to the sum over all diagonal elements, independent of off-diagonal elements. Therefore, such a sum rule may approximately be applied to our problem of orbital energies. When a molecule has a certain symmetry, the sum rule holds for orbital energies in each symmetry species, so that such a partial sum is helpful for assigning the observed IE's to MO's. We used empirical values given in Table 4 as localized MO energies which were selected in such that (1) the values for n_N and n_O were taken from the first IE's of ammonia and water, respectively, (2) the values for σ_{CN} and σ_{CO} were from the third IE's of methylamine and methanol, respectively, (3) the values for π_{NH_2} and σ_{OH} were taken so as to reproduce the total experimental orbital energies of methylamine and methanol, respectively, (4) the values for σ_{CC}, π_{CH_3}, and π_{CH_2} were the same as those previously used.[2]

Evaluation of Total Energy Sum for p-Type Orbitals. The total energies of p-type orbitals in alkyl amines ($C_nH_{2n+1}NH_2$) and alkyl alcohols ($C_nH_{2n+1}OH$) may be expressed by

$$T = \varepsilon^0(n_N \text{ or } n_O) + \varepsilon^0(\pi_{NH_2} \text{ or } \sigma_{OH}) + \varepsilon^0(\sigma_{CN} \text{ or } \sigma_{CO}) + (n-1)\varepsilon^0(\sigma_{CC}) + (n-1-2m)\varepsilon^0(\pi_{CH_2}) + (2+2m)\varepsilon^0(\pi_{CH_3}) \quad (2)$$

where $m=1$ for *i*-propylamine and *i*-propanol and otherwise $m=0$.

TABLE 5. COMPARISON OF THE EXPERIMENTAL PARTIAL AND TOTAL SUMS (in eV) BETWEEN THE CALCULATED ONES

	Exptl	Calcd
Methylamine (C_S)	$T = -69.58$	−69.59
$(I_1, I_3, I_4) \rightarrow a'(n_N, \pi_{CH_3}, \sigma_{CN})$	$P = -39.51$	−39.52
$(I_2, I_5) \rightarrow a''(\pi'_{CH_3}, \pi_{NH_2})$	$P = -30.07$	−30.07
Methanol (C_S)	$T = -71.97$	−71.97
$(I_2, I_3, I_5) \rightarrow a'(\pi_{CH_3}, \sigma_{CO}, \sigma_{OH})$	$P = -45.37$	−45.06
$(I_1, I_4) \rightarrow a''(n_O, \pi'_{CH_3})$	$P = -26.60$	−26.91
Ethylamine	$T = -95.94$	−95.64
gauche-type interaction (C_1)		
$(I_1, I_4, I_6) \rightarrow (n_N, \pi_{CH_2}, \pi_{CH_3})$	$P = -39.10$	−39.40
$(I_2, I_3, I_5, I_7) \rightarrow (\sigma_{CC}, \pi_{CH_3}, \sigma_{CN}, \pi_{NH_2})$	$P = -56.84$	−56.24
trans-type interaction (C_S)		
$(I_1, I_3, I_4, I_5) \rightarrow a'(n_N, \sigma_{CC}, \pi_{CH_3}, \sigma_N)$	$P = -51.11$	−51.27
$(I_2, I_6, I_7) \rightarrow a''(\pi_{CH_2}, \pi'_{CH_3}, \pi_{NH_2})$	$P = -44.83$	−44.37
Ethanol	$T = -97.64$	−98.02
gauche-type interaction (C_1)		
$(I_1, I_3, I_4, I_6) \rightarrow (n_O, \sigma_{CC}, \pi_{CH_3}, \sigma_{CO})$	$P = -53.56$	−53.85
$(I_2, I_5, I_7) \rightarrow (\pi_{CH_2}, \pi_{CH_3}, \sigma_{OH})$	$P = -44.08$	−44.17
trans-type interaction (C_S)		
$(I_2, I_3, I_4, I_7) \rightarrow a'(\sigma_{CC}, \pi_{CH_3}, \sigma_{CO}, \sigma_{OH})$	$P = -56.60$	−56.81
$(I_1, I_5, I_6) \rightarrow a''(n_O, \pi_{CH_2}, \pi'_{CH_3})$	$P = -41.04$	−41.21
n-Propylamine	$T = -121.72$	−121.69
i-Propylamine	$T = -121.97$	−121.69
n-Propanol	$T = -123.76$	−124.07
i-Propanol	$T = -123.62$	−124.07
n-Butylamine	$T = -148.01$	−147.74
n-Butanol	$T = -149.78$	−150.12

The T's calculated from Eq. (2) using the values of Table 4 are shown in Table 5, compared with the corresponding experimental T's. The calculated T's for the higher alkyl amines and alcohols (Table 5) are generally in good agreement with experiment.

Evaluation of Partial Orbital-Energy Sums. Methylamine and methanol are of symmetry C_{2s}, so that their MO's are divided into two groups; one (a') symmetric to the molecular plane and the other (a'') antisymmetric. Interactions in a' in methylamine are considered to occur among the n_N, π_{CH_3}, and σ_{CN}, while the π'_{CH_3} and π_{NH_2} in a'' are expected to mix considerably with each other. As seen from Table 5, the partial sums in a' and a'' for this molecule are in excellent agreement with $-(I_1+I_3+I_4)$ and $-(I_2+I_5)$, respectively, the agreement not only suggesting a validity of the selection of the orbital energy parameters but also providing an information about orbital character. Such orbital interactions are also shown in an energy diagram of Fig. 2, in which the experimental levels are correlated with the initial localized MO's. From the sum rule consideration, the orbital

16) J. N. Murrell and W. Schmidt, *J. Chem. Soc., Faraday Trans.*, II, **68**, 1709 (1972).
17) R. Hoffmann, *J. Chem. Phys.*, **40**, 2047 (1963).

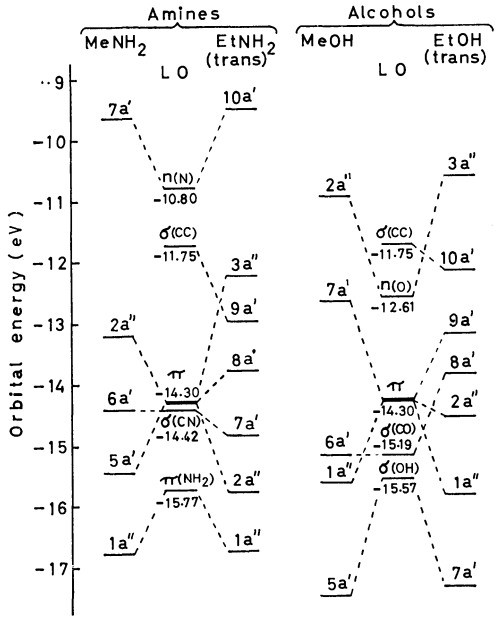

Fig. 2. Energy level diagrams of methylamine, ethylamine, methanol and ethanol. The experimental energy levels are correlated with the initial localized MO levels (I.O).

structure of methylamine may be concluded to be [1a", 5a', 6a', 2a", 7a'] in decreasing order of ionization energy. It should be mentioned that this orbital ordering is in completely agreement with the theoretical result reported by Fink and Allen.[14]

For methanol, a valence orbital structure of [5a', 1a", 6a', 7a', 2a"] has already been established from the theoretical treatments.[9,11,15] It is interesting to see that the same orbital ordering can be obtained from the present calculation of partial sums (Table 5). $I_1(2a'')$ and $I_4(1a'')$ in this molecule result mainly from the conjugative interaction between the n_O and π'_{CH_3} orbitals belonging to a", while $I_2(7a')$, $I_3(6a')$, and $I_5(5a')$ are due to the interaction of the π_{CH_3}, σ_{CO}, and σ_{OH} orbitals. The orbital correlation are also shown in Fig. 2.

Ethylamine and ethanol in gaseous phase are known to exist in *trans* and *gauche* forms from a microwave spectroscopy,[18] although unknown about which form is predominant. In the present work, therefore, orbital assignments for these ethyl compounds were considered in the two types of conformations as shown in Table 5. (The diagram in Fig. 2 for these compounds shows the levels obtained on the basis of the *trans* conformations.) Even in the *gauche* form with no symmetry, orbital interactions seem to divide into two groups; one consisting of the MO's which are approximately in plane with regard to the N–C–C (or O–C–C) plane and the other being approximately out of plane. No partial sums are shown in Table 5 for the propyl and butyl compounds since there are no conformational informations available. Finally, it should be pointed out that, in the case of *trans* ethanol, the 10a' level may be correlated with the σ_{CC} level probably because of the inductive effect of the OH group (Fig. 2).

18) E. B. Wilson, *Chem. Soc. Rev.*, **1**, 293 (1972).

BULLETIN OF THE CHEMICAL SOCIETY OF JAPAN, VOL. 46, 3395—3399 (1973)

Electroluminescence in Pentacene Doped Anthracene Crystals

Nobuko I. WAKAYAMA,* Nobuyuki WAKAYAMA,** and D. F. WILLIAMS

National Research Council of Canada, Ottawa, Ontario K1A OR6, Canada

(Received June 8, 1973)

The recombination radiation spectrum and its transient behavior were measured on a pentacene doped anthracene crystal. The recombination radiation spectrum was more sensitive to chemical or physical impurities than optically sensitized fluorescence spectrum. The intensity of both anthracene and pentacene emission was approximately proportional to the current. Anthracene or pentacene emission was found to consist of three components differing by their decay times; component 1 (decay time $<10^{-5}$ s), components 2,3 (decay times in the millisecond region, $\tau_2<\tau_3$). The component 1 was due to singlet excitons generated directly by carrier recombination. The component 2, the decay time of which was 2—3 ms, was due to triplet exciton annihilation, for its decay time was not affected by a reverse bias voltage and was equal to one half of the observed phosphorescence lifetime. The component 3, which was removed by a reverse bias voltage, was due to detrapped-trapped carrier recombination. Pentacene chemical impurity works as carrier traps or tirplet exciton traps. Anthracene lattice defects work as carrier traps. The SCLC measurement showed the existence of an electron discrete trap introduced by pentacene and electron and hole exponential traps. The present experimental results showed het importance of traps in the recombination process in a mixed crystal.

For several years electrochemical electrodes have been used to produce electroluminescence in anthracene crystals from the recombination of the injected electrons and holes.[1,2] For pure crystals the electroluminescence

* National Research Council of Canada Guest Worker 1971—72; Present address: National Chemical Lanoratory for Industry, 1-chome, Honmachi, Shibuya-ku, Tokyo.

** National Research Council of Canada Postdoctrate Fellow 1971—1972; Present address: Mitsubishi-Kasei Institute of Life Sciences, 11 Minamiooya, Machida-shi, Tokyo.

1) W. Helfrich and W. G. Schneider, *Phys. Rev. Lett.*, **14**, 229 (1965).

2) W. Helfrich and W. G. Schneider, *J. Chem. Phys.*, **44**, 2902 (1966).

spectra and fluorescence spectra are the same if it is recognized that reabsorption may be more prominent in electroluminescence, since this is produced in the bulk of the crystal. However, electroluminescence can easily be modified in intensity and energy distribution by doping the crystal with any materials which will act as a carrier trap.[3,4] It has been seen that the bulk properties of a molecular crystal are easily perturbed by included molecules. The traps caused by the guest are more evident in the spectral distribution of electroluminescence than in that of optically sensitized fluorescence. As electron-hole recombination events finally produce singlet and triplet excitons, it is expected that electroluminescence will show a time behavior relating to the lifetime of these excitons, 10^{-8} and 10^{-3} s respectively.[2] It should be, however, born in mind that the transient behavior of the singlet exciton is not usually detected because of the slower rate-determining steps (carrier recombination) involved. The traps will change the temporal dependence of electroluminescence, particularly that due to the long lived triplet exciton. We have studied the electroluminescence of a pentacene doped anthracene crystal to see the influence of the traps on the recombination radiation of a mixed crystal. We measured the temperature dependence of Space-Charge-Limited-Currents (SCLC) to get insight into the distribution of the traps in the crystal and steady state electroluminescence. The temporal dependence of anthracene and pentacene emission was measured to study the growth reaction of electroluminescence.

Experimental

The crystal ingot was melt grown in a Bridgeman type furnace[5] under helium gas from highly purified anthracene containing 10^{-4} M pentacene (Princeton Organics). Single crystals, 1 mm thick, were cleaved parallel to ab plane from the bottom portion of the ingot where pentacene concentration was thought to be 10^{-6} M considering the segregation coefficient. Neither the sensitized fluorescence nor the absorption of pentacene was observed in the conventional way with the crystal used in the work. Electron and holes were injected along the c'-direction, *i.e.*, perpendicular to the cleavage plane. The electrode contact area was 0.44 cm^2. Solution of anthracene ions were used as injecting contacts.[1,2] (*i.e.*, Na-anthracene ion salt in tetrahydrofuran as an electron injecting electrode and anthracene-$AlCl_3$ in CH_2Cl_2 as a hole injecting electrode). The crystal temperature was varied by blowing cold nitrogen gas over the crystal held in a quartz Dewar system. Steady state measurements of the current-voltage (J-V) dependence, electroluminescence intensity-current (I-J) dependence and electroluminescence spectral distribution-current dependence were made over the temperature range from 200 to 300 K. Using a pulsed voltage supply the transient behavior of anthracene and pentacene electroluminescence was observed. The experimental apparatus for the pulsed voltage measurement is shown in Fig. 1. Each wavelength region was selected by combining appropriate band pass filters Optics Technology 550R, 600R and Corning glass 2-63, for pentacene and O-T 500B plus Corning glass 5-57, 5-64 and 5-61 for anthracene. The pulsed voltage supply used was capable of producing a square voltage pulse of 4000 V for up to 120 ms duration with rise and decay times of $<10^{-5}$ s/kV. A cooled EMI 9558 photomultiplier used as a detector was coupled with a time averaging computer to increase signal/noise ratio when required. As the number of the traps depends on the concentration of pentacene, experimental data were produced all at the same crystal platelet.

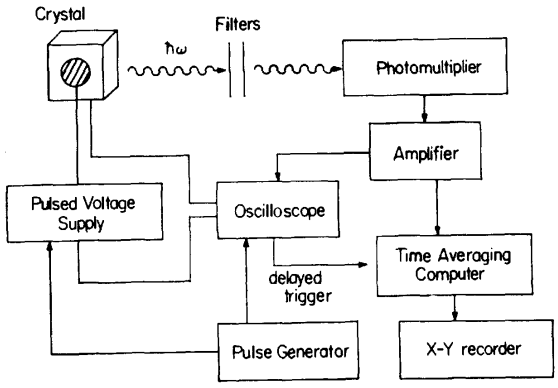

Fig. 1. Experimental apparatus for pulsed voltage measurement.

Results and Discussion

(a) The Temperature Dependence of Space Charge Limited Current (SCLC). As expected, steady state space charge limited hole and electron current-voltage-temperature curves all showed the presence of considerable trapping. At room temperature currents were 10^4—10^6 times smaller than predicted trap free currents.[6] The

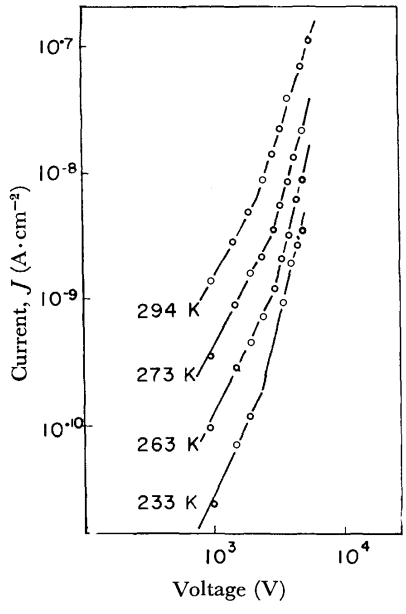

Fig. 2. Dependence of space-charge-limited currents with temperature and applied voltage for a 1 mm thick pentacene doped anthracene crystal. The electrode contact area was 0.44 cm^2.

3) H. P. Schwob, J. Funfschilling, and I. Zschokke-Granacher, *Mol. Cryst. Liq. Cryst.*, **10**, 39 (1970).

4) H. P. Schwob and I. Zchokke-Granacher, *ibid.*, **13**, 115(1971).

5) Y. Lupien, J. O. Williams, and D. F. Williams, *ibid.*, **18**, 129 (1972).

6) M. A. Lampert, *Rept. Progr. Phys.*, **27**, 329 (1964).

results for injected electron currents are shown in Fig. 2. In the low voltage region the electron currents were proportional to the square of the voltage, while at higher voltage they increased with fourth power of the voltage. These results indicate the presence of an exponential energy distribution of electron traps plus a discrete trap. From the temperature dependence of the currents in the low voltage quadratic region, we obtained the depth of an electron discrete trap, 0.44 eV. Here the temperature dependence of the carrier mobility was neglected since it has only minor effects. This depth agrees with the electron trap depth estimated from the difference in electron affinities of anthracene and pentacene, 1.341−0.653=0.7 eV.[7] Similarly an estimation of a hole trap at 0.6 eV[8] can be made from the respective ionization energies, however the experimental results of hole currents-voltage-temperature dependence only showed the presence of exponential traps. The electron and hole exponential traps are considered to be due to structural defects caused by the inclusion of pentacene molecules.[9]

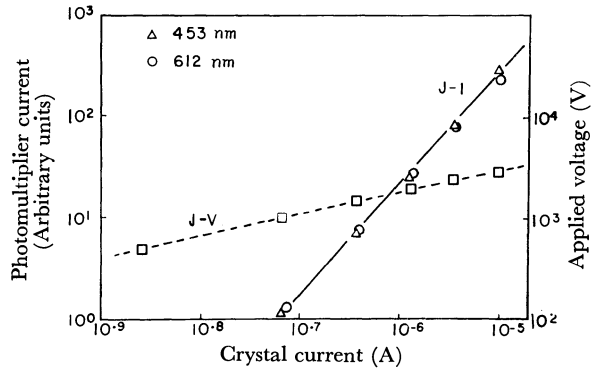

Fig. 3. Crystal currents, J, dependence on applied voltage $V(J-V)$ □, and dependence of anthracene △ (453 nm) and pentacene ○ (612 nm) electroluminescence intensity, I, with crystal current, $J(I-J)$.

(b) Double Injected Current-Voltage-Temperature (J-V-T) Dependence. The relation between the currents and applied voltage (J-V) at room temperature is shown in Fig. 3. $J \propto V^{4.4}$ was found in the crystal. The double injected current was always greater than that observed for single carrier injection, but was still in the order of 10^2—10^4 times smaller than predicted by Child's law (trap free). The current decreased exponentially with respect to T^{-1} over the temperature range 200—300 K, as observed in pure anthracene crystal.[10]

(c) Crystal Current-Electroluminescence Intensity and Spectral Distribution Dependence. The electroluminescence spectra at various temperatures are shown in Fig. 4. The optically excited (anthracene singlet) fluorescence spectrum of the same crystal comes from anthracene only. The 0-0, 0-1 bands of anthracene fluorescence

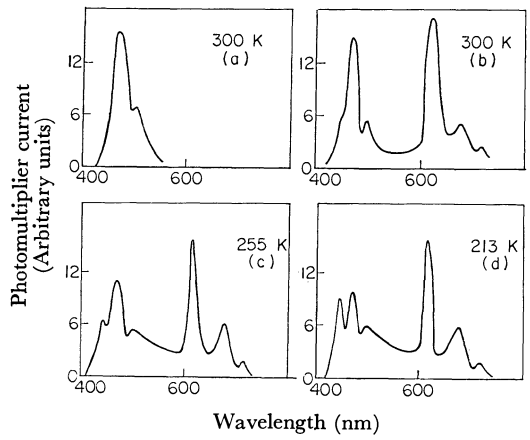

Fig. 4. Comparison of optically sensitized fluorescence spectrum at room temperature (a) and electroluminescence spectra at 300, 255, 213 K (b), (c), (d). The current density was 2.5×10^{-7} A·cm^{-2}.

were reabsorbed in both the electroluminescence and the fluorescence spectra. In the electroluminescence spectra, components due to anthracene 453 and 480 nm and those due to pentacene, 612 and 668 nm are easily recognized. The emission peak at 612 nm is the 0-0 level of the first excited singlet state of pentacene, in agreement with an analysis obtained from high resolution fluorescence spectra of pentacene.[11,12] As the crystal currents decreased or the temperature was lowered to 213 K, little change in relative intensity of the pentacene peaks occurred, and no additional peaks appeared in the pentacene fluorescence regions. As the temperature was lowered, the 0-1 band of anthracene singlet emission became visible, together with a broad background emission, maximum 480 nm. The appearance of the background emission indicates that the anthracene lattice has been considerably perturbed, as observed in SCLC measurement and structural defects work as carrier traps at low temperature. If this background emission is substracted, the ratio of anthracene emission: pentacene one decreased as the temperature was lowered. This suggests that pentacene trap becomes prominent at lower tem perature. The fact that chemical impurity, pentacene is more evident in electroluminescence than in the optically sensitized fluoresceyce shows that pentacene electroluminescence is not due to the energy transfer from anthracene singlet. At room temperature both anthracene (453 nm) and pentacene (612 nm) electroluminescence intensity increased approximately linearly with the crystal current as shown in Fig. 3. These results are different from anthracene-tetracene system.[3,4]

(d) Transient Behavior of Electroluminescence. The transient behavior of both the crystal current and pentacene emission under 2000 V pulsed voltage is shown in Fig. 5. General behavior of the transient current was similar to that obtained for pure anthracene crystals.[2] The anthracene emission behaves similarly

7) M. J. S. Dewar, J. A. Hashmall, and N. Trinajstic, *J. Amer. Chem. Soc.*, **92**, 5555 (1970).
8) F. Gutmann and L. E. Lyons, "Organic Semiconductors," Wiley, New York (1967).
9) J. Sworakowski, *Mol. Cryst. Liq. Cryst.*, **11**, 1 (1970).
10) D. F. Williams and M. Schadt, *J. Chem. Phys.*, **53**, 3480 (1970).
11) A. F. Prikhotko, A. F. Skorobogatko, and L. I. Tsikora, *Optics Spectry.*, **26**, 115 (1969).
12) W. E. Geacintov, J. Burgo, I. M. Pope, and C. Strom, *Chem. Phys. Lett.*, **11**, 504 (1971).

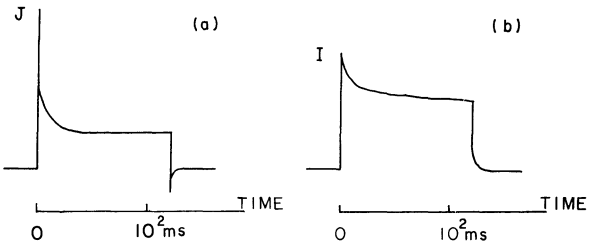

Fig. 5. Transient behavior of crystal current (a) and pentacene electroluminescence (b) under 2000 V.

to that of pentacene. The pulsed voltage was varied from 1000 to 3000 V. Though the voltage pulse decay was less than 10^{-5} s/kV, a considerable tail was observed in both anthracene and pentacene electroluminescence, with a decay time in the millisecond region. Both the anthracene and pentacene emission consist of the prompt decay component (component 1, the decay time $<10^{-5}$ s) and the delayed ones (component 2 and 3, their decay times in the millisecond region). The prompt electroluminescence emanating from both the guest and host is thought due to the singlet exciton produced by the carrier recombination like the pure anthracene crystals.[1,2] The prompt pentacene emission is thought due to the recombination in a pentacene trap, considering the SCLC experimental result. The ratio of the delayed: prompt electroluminescence intensity increased as the voltage was lowered and the current decreased, as shown in Table 1. The transient

TABLE 1. THE RESULTS COMPARING THE RELATIVE INTENSITY OF THE DELAYED ANTHRACENE AND PENTACENE ELECTROLUMINESCENCE COMPARED TO THE TOTAL ANTHRACENE AND PENTACENE ELECTROLUMINESCENCE

Applied voltage	Crystal currents	Totalel electroluminescence intensity (relative units)	Ratio Intensity delayed / Intensity total
Anthracene emission			
3000 V	1×10^{-5} A	294	0.062
2000	1.3×10^{-6}	26	0.17
1000	7×10^{-8}	1.1	0.28
Pentacene emission			
3000 V	1×10^{-5} A	240	0.12
2000	1.3×10^{-6}	28	0.18
1000	7×10^{-8}	1.4	0.37

behavior of the delayed pentacene eimssion is shown in Fig. 6. Two components with different decay times (component 2; 2—3 ms, component 3; 10 ms) are found. Anthracene delayed electroluminescence shows the similar behavior (component 2; 2—3 ms, component 3; 5—6 ms). The component 3 of both anthracene and pentacene emission was removed by applying a reverse bias voltage (500—1500 V), and was considered due to detrapped-trapped carrier recombination. The contribution from component 3 to

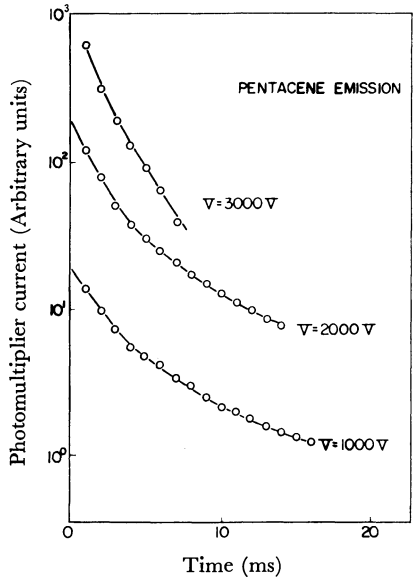

Fig. 6. Transient behavior of the delayed pentacene electroluminescence after the decay of the pulsed voltage 1000, 2000, 3000 V.

the total delayed emission increased as the voltage was lowered. Under 3000 V, the component 3 was not observed. The existence of component 3 in anthracene emission indicates that anthracene structural defects work as carrier traps, as observed in SCLC measurement and electroluminescence spectra. The decay time of component 2 was obtained by substracting component 3 or applying a reverse bias voltage. The component 2 is thought to be produced by triplet-triplet annihilation because it was not affected by a reverse bias voltage. The lifetime of anthracene triplet excitons was measured to check the above conclusion. Optical excitation of anthracene triplet by a He–Ne laser (50 mW, 6328 Å) gave red delayed luminescence, the decay time of which was 5.2 ms. In the above measurement a photomultiplier was coupled with a time averaging computer because the emission intensity was very weak. No blue delayed emission was observed in the crystal in a similar experimental condition. The red delayed emission is either phosphorescence of anthracene or delayed fluorescence of pentacene. As the emission intensity was linear with the excitation light intensity, we can regard it as anthracene phosphorescence. The measured anthracene triplet lifetime, 5.2 ms, is comparable with that obtained from the delayed fluorescence excited by a giant ruby laser in an anthracene crystal which contains 2 ppm pentacene.[13] Calculated decay time of anthracene triplet-triplet annihilation, which is a half of anthracene triplet lifetime, agrees with the observed decay time 2—3 ms of the component 2 in anthracene electroluminescence. If we consider the energy levels in a pentacene doped anthracene crystal, the component 2 of pentacene emission is thought due to pentacene triplet-anthracene triplet heterofusions. Impurity delayed fluorescence which comes from trapped triplet-

13) H. Baessler, G. Vaubel, and H. Kallmann, *J. Chem. Phys.*, **53**, 370 (1970).

free triplet exciton annihilation was reported.[14,15] The ratio of the delayed: the total anthracene emission intensity, 0.06 under 3000 V, when the component 3 did not exist is less than the value, 0.39, obtained in a pure anthracene crystal.[2] This is because anthracene triplet exciton is consumed by both annihilation with an anthracene triplet and a pentacene triplet, or the triplet energy is localized or trapped in a mixed crystal.[16]

The electroluminescence of a pentacene doped anthracene crystal is influenced by traps, either pentacene impurity traps or anthracene structural defect traps. Pentacene emission is more evident in the electroluminescence spectra than the optically sensitized fluorescence. Both anthracene and pentacene emission was found to consist of a prompt and two kinds of delayed emission. Pentacene impurity is concluded to work as carrier or triplet exciton traps in the growth reaction of every component of pentacene electroluminescence. The existence of the component 3 and the background defect electroluminescence in anthracene emission indicates that anthracene structural defects work as traps, too.

We wish to thank Prof. M. Kotani for many discussions. We wish also to thank Mr. Yves Lupien who grew the crystal.

14) L. Peter, W. Engel, and G. Vaubel, *Mol. Cryst. Liq. Cryst.*, **19**, 207 (1973).
15) V. Ern, *ibid.*, **18**, 1 (1972).
16) F. C. Smith, *Phys. Rev.*, **166**, 839 (1966).

BULLETIN OF THE CHEMICAL SOCIETY OF JAPAN, VOL. 46, 3399—3406 (1973)

Vibration-Rotation Spectrum of Methyl Fluoride. I. Analysis of $2\nu_3$ Band

Jun NAKAGAWA, Isao SUZUKI,* Takehiko SHIMANOUCHI, and Tsunetake FUJIYAMA**

Department of Chemistry, Faculty of Science, The University of Tokyo, Bunkyo-ku, Tokyo 113

***Department of Chemistry, Faculty of Science, Tokyo Metropolitan University, Setagaya-ku, Tokyo 158*

(Received July 6, 1973)

The $2\nu_3$ band of methyl fluoride has been measured with a high-resolution infrared spectrometer. The following molecular constants are obtained: $\nu_0=2081.382$, $B''=0.85172$, $B'=0.82955$, $(A''-A')=0.01953$, $D_J''=1.95\times10^{-6}$, $D_J'=1.78\times10^{-6}$, $D_{JK}''=1.47\times10^{-5}$ (assumed), $D_{JK}'=1.93\times10^{-5}$, and $(D_K''-D_K')=5.9\times10^{-6}$ cm^{-1}. In addition, the hot band ($3\nu_3\leftarrow\nu_3$) and the isotope $^{13}CH_3F$ band have been observed and analyzed. The cubic force constant k_{333} was also obtained from the vibration-rotation constants.

The vibration-rotation spectra of methyl fluoride have been studied by many investigators. Pickworth and Thompson[1] measured $2\nu_3$, ν_4, and some other bands above 2000 cm^{-1}. Smith and Mills[2] studied the ν_3 and ν_6 fundamental bands with special attention to the x,y-type Coriolis interaction between the two fundamentals.[2,3] Jones, Popplewell, and Thompson[4] reported the analysis of the ν_2, ν_5, $\nu_3+\nu_4$, and $2\nu_4$ bands together with those of CD_3F. Blass and Edwards[5] and Anttila and Huhanantti[6] obtained molecular constants from some combination bands with high-resolution spectrometers. The microwave studies of this molecule were reported by Gordy and his coworkers.[7-11]

The $2\nu_3$ band of methyl fluoride has been measured under high resolution ($\Delta\nu\simeq0.04$ cm^{-1}) and its rotational structures have been analyzed. With this resolving power, the J-structures in the Q-branch are completely resolved. In addition, the structures due to different values of K are observed. Since this band is free from overlapping, the highly accurate molecular constants have been determined from the simultaneous analysis of P-, Q-, and R-branches. The present paper reports the result of this study. The $2\nu_3$ band is expected to have the x,y-type Coriolis interaction with the $\nu_3+\nu_6$ band similar to that observed between the ν_3 and ν_6 fundamentals. As pointed out by Smith and Mills,[2] the effect of this interaction is much more profound in the weaker $\nu_3+\nu_6$ band and may not be seen on the $2\nu_3$ band. However, the precise determination of the vibration-rotation levels in the $2\nu_3$ band is highly desirable for the analysis of the $\nu_3+\nu_6$ band.

* Present address: Educational Computer Center, The University of Tokyo, Bunkyo-ku, Tokyo.

1) J. Pickworth and H. W. Thompson, *Proc. Roy. Soc., Ser. A*, **222**, 443 (1954).
2) W. L. Smith and I. M. Mills, *J. Mol. Spectrosc.*, **11**, 11 (1963).
3) C. di Lauro and I. M. Mills, *ibid.*, **21**, 386 (1966).
4) E. W. Jones, R. J. L. Popplewell, and H. W. Thompson, *Proc. Roy. Soc., Ser. A*, **290**, 490 (1965).
5) W. E. Blass and T. H. Edwards, *J. Mol. Spectrosc.*, **25**, 440 (1968).
6) R. Anttila and M. Huhanantti, *Can. J. Phys.*, **46**, 2025 (1968).
7) O. R. Gilliam, H. D. Edwards, and W. Gordy, *Phys. Rev.*, **75**, 1014 (1949).
8) C. M. Johnson, R. Trambarulo, and W. Gordy, *ibid.*, **84**, 1178 (1951).
9) W. J. Thomas, J. T. Cox, and W. Gordy, *J. Chem. Phys.*, **22**, 1718 (1951).
10) R. S. Winton and W. Gordy, *Phys. Lett.*, **32A**, 219 (1970).
11) P. A. Steiner and W. Gordy, *J. Mol. Spectrosc.*, **21**, 291 (1966).

Experimental

The sample was purchased from PCR Inc. of USA with the stated purity of 99% and used without further purification.

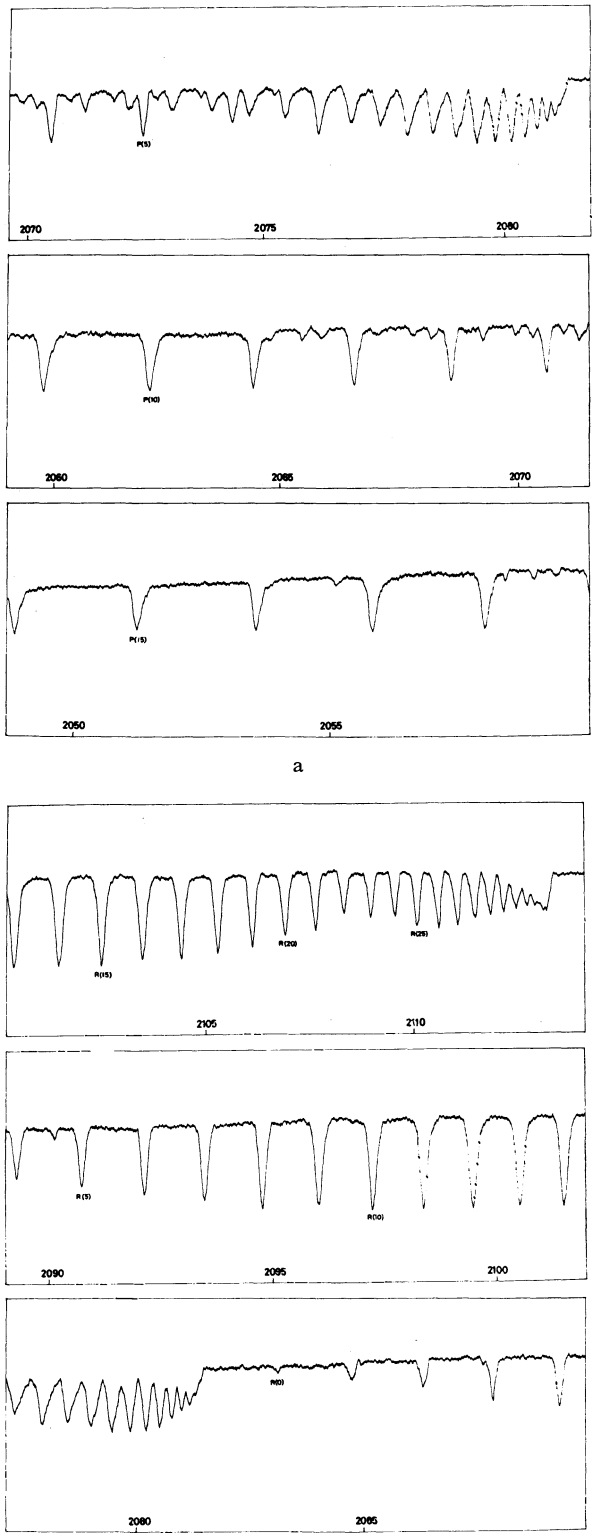

Fig. 1. The rapid scan spectrum of the $2\nu_3$ band of CH_3F. Path length=6 m. Pressure=3 mmHg. Resolution=0.10 cm^{-1}.
1a. P-branch. 1b. R-branch.

A high-resolution vacuum spectrometer which was designed and constructed in our laboratory[12] has been used; this spectrometer was equipped with a plane replica grating of Bausch and Lomb Co., Ltd. (echelle type, 206×102 mm^2 ruled area, 31.6 lines per mm, and blazed at 176.6 cm^{-1} in the first order), the grating is double passed and the 11-th and 12-th orders were used in this work. The collimating mirror was 30 cm diameter and 250 cm focal length with the f-number approximately 25. A CaF_2 prism spectrometer of Wadsworth type mount was used to seperate the grating orders. An InSb detector was used at liquid-nitrogen temperature. The spectrometer was operated under the resolution of about 0.04 cm^{-1} throughout this work. A White type long-path cell was used and its path length was kept at 6 m. The sample pressures used were 3 and 5 mmHg.

The frequencies of the observed lines were calibrated using the standard lines of carbon monoxide.[13] The standard deviation of the fitted lines was 0.006 cm^{-1} and the accuracy of the observed lines was believed to be better than ±0.01 cm^{-1}.

Observed Spectra

The rapid scan spectrum ($\Delta\nu\simeq0.1$ cm^{-1}) is illustrated in Fig. 1 with the assignment of several lines. The spacings of the P- and R-branches are large and their assignment can be done without ambiguity. In addition, the following spectral features are found.

(1) As shown in Fig. 2, the Q-branch is completely

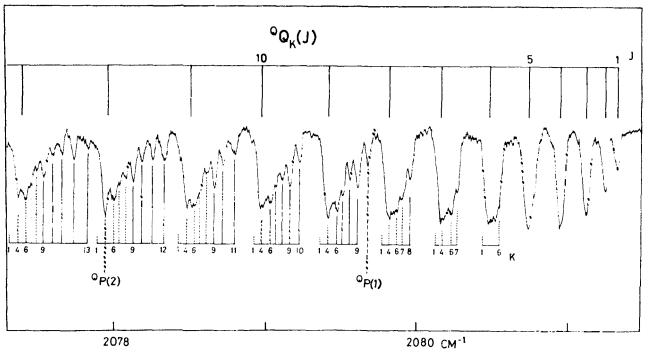

Fig. 2. The J-, and K-structures of the Q-branch of $2\nu_3$ band. Path length=6 m. Pressure=5 mmHg. Resolution=0.04 cm^{-1}.

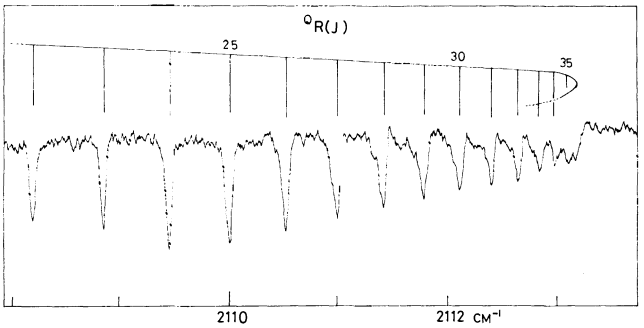

Fig. 3. The R-branch head of the $2\nu_3$ band. Path length=6 m. Pressure=3 mmHg. Resolution=0.04 cm^{-1}.

12) T. Fujiyama, J. Nakagawa, I. Suzuki, I. Nakagawa, and T. Shimanouchi, to be published.

13) K. N. Rao, C. J. Humphreys, and D. H. Rank, "Wavelength Standards in the Infrared." Academic Press, New York, London (1966).

resolved into its J-components. Additional structures due to different K-values are observed.

(2) A band head is formed at high-frequency side of R-branch. The spacing of the R-branch decreases with increasing J-values; it finally reaches the edge at $J=36$ (see Fig. 3).

(3) An anomaly of relative intensity is observed in the P- and R-branches, particularly in the R-branch. The lines at $J=20$—25 are weak in comparison with the other lines.

(4) A number of lines due to the hot band ($3\nu_3 \leftarrow \nu_3$) and the isotope $^{13}CH_3F$ band are identified.

Analysis of Vibration-Rotation Structures

When none of the degenerate vibrations is excited, the energy levels of the v-th vibrational state are given by the formula,

$$T_v(J,K) = G(v) + B_vJ(J+1) + (A_v-B_v)K^2 - D_J^vJ^2(J+1)^2 - D_{JK}^vJ(J+1)K^2 - D_K^vK^4, \quad (1)$$

where $G(v)$ is the vibrational energy, A_v and B_v are the rotational constants, and D_J^v, D_{JK}^v, and D_K^v are the centrifugal distortion constants.

From the selection rule for a parallel band ($\Delta K=0$, $\Delta J=0, \pm1$), the transition frequencies can be calculated as the differences between the energy levels of the upper and the lower states.

Main Band ($2\nu_3 \leftarrow 0$). In the present analysis, the following assumption is made: the value of D_{JK} in the ground state is fixed to 1.47×10^{-5} cm^{-1} which has been obtained from microwave study.[10] The transition frequencies may be written as

$$\begin{aligned}\nu(J'',K'';J',K') &= T(J',K') - T(J'',K'') \\ &= \nu_0 + B'J'(J'+1) - D_J'J'^2(J'+1)^2 \\ &\quad + [(A'-A'')-(B'-B'')]K''^2 - B''J''(J''+1) \\ &\quad + D_J''J''^2(J''+1)^2 - [D_{JK}'J'(J'+1) \\ &\quad - D_{JK}''J''(J''+1)]K''^2 - (D_K'-D_K'')K''^4, \end{aligned} \quad (2)$$

where $''$ and $'$ refer to the lower and upper states respectively.

Since the J-components in the Q-branch as well as the P- and R-branches are completely resolved, the assignment of the J-value can be done without difficulty. As mentioned earlier, the complex structures due to the K-values are found in the Q-barnch. Since the statistical weights of the $K=3p$ levels are twice those of the $K=3p\pm1$ levels in methyl fluoride, the assignment of these K-values can be done in consideration of the statistical weight and the relation $K \leqq J$.

In the P- and R-branches, no structures due to the K-values are observed. In these two branches, the values of K at the intensity maxima are determined with the aid of the simulated spectra. For $^QR(8)$ branch, for example, the intensity maximum is found near $K=3$, and for $^QR(5)$ it is found near $K=2$.

In order to obtain the molecular constants, we have applied the least-squares method to Eq. (2), using the K-values together with J. Since we cannot determine A'' and A', and D_K'' and D_K' seperately, eight independent parameters may be obtained from the observed data. The molecular constants obtained from the present study are listed in Table 1 with the corresponding constants previously determined. In Table 2, the observed and calculated frequencies are listed with their assignments. The lines which are not fully resolved are given zero or smaller weights. The standard deviation of the data is 0.007 cm^{-1}.

Table 1. The molecular constants obtained from $2\nu_3$ band of CH_3F (in cm^{-1})

	This work		Pickworth *et al.*[1]	Winton *et al.*[10]	
ν_0	2081.382	(3) [a]	2081.42		
B''	0.85172	(9)	0.8512	0.85179404	(5)
B'	0.82955	(9)	0.8289		
$(B''-B')$	0.02217		0.0223		
$(A''-A')$	0.01953	(11)			
$(A''-A')-(B''-B')$	−0.00264				
D''	1.95×10^{-6}	(5)	2.2_8	1.9970	(7)
D_J'	1.78×10^{-6}	(5)	2.0_2		
D_{JK}''	1.47×10^{-5} [b]			1.469	(2)
D_{JK}'	1.93×10^{-5}	(40)			
$(D_K''-D_K')$	5.9×10^{-6}	(7)			

a) The numbers in parentheses represent twice of the standard errors to be attached to the last significant figures.
b) Assumed (see text).

Hot Band ($3\nu_3 \leftarrow \nu_3$) and Isotope Band. Two additoinal series of the P- and R-branches are observed between the lines of the main band, which can be assigned as the hot band ($3\nu_3 \leftarrow \nu_3$) and the isotope ($^{13}CH_3F$) band (see Fig. 4). The intensity ratio is expected to be 1.1: 1.3: 100 for the isotope band, the hot band, and the main band respectively. We may assign the stronger series as hot band and the weaker series as isotope band. As the Q-branch heads of these two series are found near 2049.7 and 2039.6 cm^{-1}, the J-values in these series can be assigned. Recently the $2\nu_3$ band of $^{13}CH_3F$ was measured by Duncan *et al.*[14] with 60% enriched sample, and their results confirm the present assignment. Since the

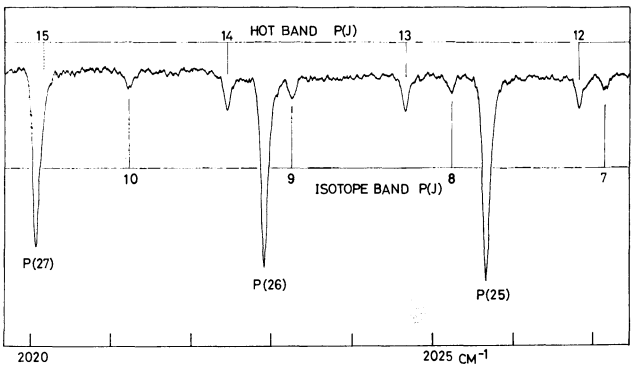

Fig. 4. The hot band and the isotope band of CH_3F. Path length=6 m. Pressure=5 mmHg. Resolution= 0.08 cm^{-1}.

14) J. L. Duncan, D. C. McKean, and G. K. Speirs, *Mol. Phys.*, **24**, 553 (1972).

TABLE 2. OBSERVED AND CALCULATED FREQUENCIS OF $2\nu_3$ BAND OF CH_3F

	J	K	L	ν_{obsd}	ν_{calcd}	DIF	DIFW	Weight
QR	43	3	0	—	2112.390	—	—	0.000
QR	42	3	0	—	2112.627	—	—	0.000
QR	41	3	0	—	2112.821	—	—	0.000
QR	40	3	0	—	2112.972	—	—	0.000
QR	39	3	0	—	2113.081	—	—	0.000
QR	38	3	0	—	2113.146	—	—	0.000
QR	37	3	0	—	2113.169	—	—	0.000
QR	36	3	0	2113.159	2113.148	0.010	0.010	1.000
QR	35	3	0	2113.095	2113.085	0.010	0.010	1.000
QR	34	3	0	2112.984	2112.978	0.007	0.007	1.000
QR	33	3	0	2112.827	2112.827	−0.000	−0.000	1.000
QR	32	3	0	2112.637	2112.633	0.004	0.004	1.000
QR	31	3	0	2112.394	2112.395	−0.002	−0.002	1.000
QR	30	3	0	2112.107	2112.114	−0.006	−0.006	1.000
QR	29	3	0	2111.778	2111.789	−0.010	−0.010	1.000
QR	28	3	0	2111.415	2111.420	−0.004	−0.004	1.000
QR	27	3	0	2110.996	2111.007	−0.011	−0.011	1.000
QR	26	3	0	2110.527	2110.549	−0.022	−0.022	1.000
QR	25	3	0	2110.029	2110.048	−0.019	−0.019	1.000
QR	24	3	0	2109.488	2109.503	−0.014	−0.014	1.000
QR	23	3	0	2108.907	2108.913	−0.006	−0.006	1.000
QR	22	3	0	2108.277	2108.279	−0.002	−0.002	1.000
QR	21	3	0	2107.606	2107.601	0.005	0.005	1.000
QR	20	3	0	2106.880	2106.878	0.002	0.002	1.000
QR	19	3	0	2106.120	2106.111	0.009	0.009	1.000
QR	18	3	0	2105.305	2105.300	0.005	0.005	1.000
QR	17	3	0	2104.450	2104.444	0.007	0.007	1.000
QR	16	3	0	2103.551	2103.543	0.008	0.008	1.000
QR	15	3	0	2102.612	2102.598	0.014	0.014	1.000
QR	14	3	0	2101.619	2101.608	0.012	0.012	1.000
QR	13	3	0	2100.576	2100.573	0.003	0.003	1.000
QR	12	3	0	2099.504	2099.494	0.010	0.010	1.000
QR	11	3	0	2098.370	2098.371	−0.001	−0.001	1.000
QR	10	3	0	2097.208	2097.202	0.006	0.006	1.000
QR	9	3	0	2096.005	2095.989	0.015	0.015	1.000
QR	8	3	0	2094.732	2094.732	0.000	0.000	1.000
QR	7	2	0	2093.432	2093.419	0.013	0.013	1.000
QR	6	2	0	2092.070	2092.071	−0.001	−0.001	1.000
QR	5	2	0	2090.677	2090.679	−0.002	−0.002	1.000
QR	4	2	0	2089.236	2089.243	−0.007	−0.007	1.000
QR	3	1	0	2087.758	2087.754	0.004	0.004	1.000
QR	2	1	0	2086.232	2086.228	0.004	0.004	1.000
QR	1	0	0	2084.657	2084.656	0.001	0.001	1.000
QR	0	0	0	2083.042	2083.041	0.001	0.001	1.000
QP	1	0	0	2079.675	2079.678	−0.003	−0.003	1.000
QP	2	0	0	2077.942	2077.931	0.012	0.012	1.000
QP	3	1	0	2076.142	2076.141	0.000	0.000	1.000
QP	4	1	0	2074.312	2074.305	0.007	0.007	1.000
QP	5	2	0	2072.428	2072.433	−0.005	−0.005	1.000
QP	6	2	0	2070.507	2070.509	−0.002	−0.002	1.000
QP	7	2	0	2068.543	2068.541	0.002	0.002	1.000
QP	8	2	0	2066.528	2066.528	0.000	0.000	1.000
QP	9	3	0	2064.477	2064.485	−0.008	−0.008	1.000
QP	10	3	0	2062.374	2062.385	−0.011	−0.011	1.000
QP	11	3	0	2060.232	2060.241	−0.009	−0.009	1.000
QP	12	3	0	2058.054	2058.053	0.000	0.000	1.000
QP	13	3	0	2055.814	2055.822	−0.008	−0.008	1.000
QP	14	3	0	2053.538	2053.547	−0.009	−0.009	1.000
QP	15	3	0	2051.231	2051.229	0.001	0.001	1.000
QP	16	3	0	2048.878	2048.868	0.010	0.010	1.000

Table 2. (Continued)

	J	K	L	ν_{obsd}	ν_{calcd}	DIF	DIFW	Weight
QP	17	3	0	2046.464	2046.463	0.000	0.000	1.000
QP	18	3	0	2044.019	2044.016	0.003	0.003	1.000
QP	19	3	0	2041.527	2041.525	0.001	0.001	1.000
QP	20	3	0	2038.995	2038.992	0.003	0.003	1.000
QP	21	3	0	2036.411	2036.416	−0.005	−0.005	1.000
QP	22	3	0	2033.792	2033.797	−0.005	−0.005	1.000
QP	23	3	0	2031.143	2031.137	0.006	0.006	1.000
QP	24	3	0	2028.437	2028.433	0.004	0.004	1.000
QP	25	3	0	2025.695	2025.688	0.007	0.007	1.000
QP	26	3	0	2022.905	2022.900	0.004	0.004	1.000
QP	27	3	0	2020.069	2020.071	−0.002	−0.002	1.000
QP	28	3	0	2017.208	2017.200	0.007	0.007	1.000
QP	29	3	0	2014.299	2014.288	0.011	0.011	1.000
QP	30	3	0	2011.337	2011.334	0.003	0.003	1.000
QP	31	3	0	2008.352	2008.339	0.013	0.013	1.000
QP	32	3	0	2005.300	2005.303	−0.003	−0.003	1.000
QP	33	3	0	2002.215	2002.226	−0.011	−0.011	1.000
QP	34	3	0	1999.100	1999.108	−0.008	−0.008	1.000
QP	35	3	0	1995.945	1995.950	−0.005	−0.005	1.000
QP	36	3	0	1992.747	1992.752	−0.005	−0.005	1.000
QQ	1	1	0	2081.335	2081.340	−0.005	−0.005	1.000
QQ	2	2	0	2081.253	2081.259	−0.006	−0.006	1.000
QQ	3	3	0	2081.126	2081.140	−0.013	−0.013	1.000
QQ	4	3	0	2080.949	2080.962	−0.013	−0.009	0.500
QQ	5	3	0	2080.739	2080.740	−0.001	−0.001	0.500
QQ	6	6	0	2080.521	2080.547	−0.025	−0.018	0.500
QQ	6	4	0	2080.480	2080.492	−0.012	−0.008	0.500
QQ	7	7	0	2080.266	2080.272	−0.006	−0.004	0.500
QQ	7	6	0	2080.230	2080.234	−0.004	−0.003	0.500
QQ	7	4	0	2080.166	2080.181	−0.015	0.000	0.000
QQ	8	8	0	2079.955	2079.958	−0.003	−0.003	1.000
QQ	8	7	0	2079.906	2079.914	−0.007	−0.005	0.500
QQ	8	6	0	2079.868	2079.877	−0.009	0.000	0.000
QQ	8	4	0	2079.820	2079.825	−0.005	0.000	0.000
QQ	9	9	0	2079.608	2079.606	0.002	0.002	1.000
QQ	9	8	0	2079.555	2079.554	0.001	0.001	1.000
QQ	9	7	0	2079.509	2079.511	−0.002	−0.002	1.000
QQ	9	6	0	2079.472	2079.476	−0.004	−0.004	1.000
QQ	9	4	0	2079.415	2079.425	−0.010	0.000	0.000
QQ	10	10	0	2079.223	2079.217	0.006	0.006	1.000
QQ	10	9	0	2079.158	2079.156	0.002	0.002	1.000
QQ	10	8	0	2079.109	2079.106	0.003	0.003	1.000
QQ	10	7	0	2079.063	2079.064	−0.001	−0.001	0.500
QQ	10	6	0	2079.032	2079.030	0.002	0.001	0.500
QQ	10	4	0	2078.965	2078.981	−0.016	0.000	0.000
QQ	11	11	0	2078.795	2078.790	0.005	0.005	1.000
QQ	11	10	0	2078.714	2078.720	−0.006	−0.006	1.000
QQ	11	9	0	2078.659	2078.661	−0.002	−0.002	1.000
QQ	11	8	0	2078.610	2078.613	−0.002	−0.002	0.500
QQ	11	6	0	2078.533	2078.540	−0.007	0.000	0.000
QQ	11	4	0	2078.480	2078.493	−0.013	0.000	0.000
QQ	12	12	0	2078.330	2078.325	0.005	0.005	1.000
QQ	12	11	0	2078.251	2078.245	0.006	0.006	1.000
QQ	12	10	0	2078.179	2078.178	0.001	0.001	1.000
QQ	12	9	0	2078.124	2078.122	0.003	0.003	1.000
QQ	12	8	0	2078.076	2078.075	0.002	0.002	1.000
QQ	12	7	0	2078.035	2078.036	−0.001	−0.001	0.500
QQ	12	6	0	2078.000	2078.005	−0.005	−0.004	0.500
QQ	13	13	0	2077.828	2077.823	0.004	0.003	0.500
QQ	13	12	0	2077.736	2077.733	0.004	0.004	1.000

Table 2. (Continued)

	J	K	L	ν_{obsd}	ν_{calcd}	DIF	DIFW	Weight
QQ	13	11	0	2077.659	2077.656	0.003	0.003	1.000
QQ	13	10	0	2077.599	2077.591	0.008	0.008	1.000
QQ	13	9	0	2077.539	2077.537	0.002	0.002	1.000
QQ	13	8	0	2077.492	2077.492	−0.000	−0.000	0.500
QQ	13	6	0	2077.421	2077.426	−0.005	−0.003	0.500
QQ	13	4	0	2077.374	2077.384	−0.010	0.000	0.000
QQ	14	14	0	2077.274	2077.285	−0.012	0.000	0.000
QQ	14	13	0	2077.178	2077.183	−0.005	−0.005	1.000
QQ	14	12	0	2077.094	2077.095	−0.001	−0.001	1.000
QQ	14	11	0	2077.024	2077.022	0.003	0.003	1.000
QQ	14	10	0	2076.960	2076.960	0.001	0.001	1.000
QQ	14	9	0	2076.909	2076.908	0.001	0.001	1.000
QQ	14	6	0	2076.807	2076.802	0.004	0.003	0.500
QQ	14	4	0	2076.760	2076.763	−0.003	0.000	0.000
QQ	15	13	0	2076.494	2076.497	−0.003	−0.003	1.000
QQ	15	12	0	2076.405	2076.413	−0.008	−0.008	1.000
QQ	15	11	0	2076.338	2076.342	−0.004	−0.004	1.000
QQ	15	10	0	2076.275	2076.283	−0.008	−0.008	1.000
QQ	15	9	0	2076.229	2076.234	−0.005	−0.005	1.000
QQ	16	12	0	2075.684	2075.685	−0.001	−0.001	1.000
QQ	16	6	0	2075.423	2075.423	0.000	0.000	0.500
QQ	16	4	0	2075.387	2075.390	−0.002	0.000	0.000
QQ	17	9	0	2074.751	2074.753	−0.001	−0.001	0.500
QQ	17	6	0	2074.660	2074.667	−0.008	0.000	0.000
QQ	18	9	0	2073.947	2073.945	0.002	0.002	0.500
QQ	18	6	0	2073.867	2073.867	0.000	0.000	0.500
QQ	19	6	0	2073.026	2073.024	0.003	0.002	0.500
QQ	20	6	0	2072.130	2072.136	−0.005	−0.004	0.500
QQ	21	6	0	2071.206	2071.204	0.002	0.001	0.500
QQ	22	6	0	2070.236	2070.229	0.007	0.005	0.500
QQ	23	6	0	2069.215	2069.210	0.005	0.004	0.500
QQ	24	6	0	2068.157	2068.148	0.009	0.006	0.500
QQ	25	6	0	2067.046	2067.042	0.004	0.003	0.500
QQ	26	6	0	2065.898	2065.893	0.005	0.003	0.500

Q-branch lines in the hot band and the isotope band are too weak to be analyzed and none of the structures due to different values of K are resolved, the following equation is used for the transition frequencies,

$$\nu_m^{P,R} = \nu_0 + (B'+B'')m + (B'-B''-D_J'+D_J'')m^2 - 2(D_J'+D_J'')m^3 - (D_J'-D_J'')m^4, \quad (3)$$

where m equals to $J+1$ for R-branch and $-J$ for P-branch.

The least-squares method was applied to Eq. (3), and the following equations were obtained.

Table 3. The molecular constants obtained from $(3\nu_3 \leftarrow \nu_3)$ band of CH_3F (in cm^{-1})

	This work		Smith *et al.*[2]
$\nu_0+\{(A'-A'')-(B'-B'')\}K^2-(D_K'-D_K'')K^4$	2049.835	(5)[a]	
ν_0	2049.811		
$B''-D_{JK}''K^2$	0.84035	(16)	0.8401
B''	0.84048		
$B'-D_{JK}'K^2$	0.81896	(16)	
B'	0.81913		
$(B''-B')$	0.02135	(4)	
D_J''	1.93×10^{-6}	(21)	1.86
D_J'	1.82×10^{-6}	(21)	
$(D_J''-D_J')$	0.11×10^{-6}	(6)	

a) The numbers in parentheses represent twice of the standard errors to be attached to the last significant figures.

Table 4. The molecular constants obtained from $2\nu_3$ band of isotope $^{13}CH_3F$ (in cm^{-1})

	This work		Duncan *et al.*[14]	Gilliam *et al.*[7]
$\nu_0+\{(A'-A'')-(B'-B'')\}K^2-(D_K'-D_K'')K^4$	2039.680	(11)[a]	2039.68	
ν_0	2039.656			
$B''-D_{JK}''K^2$	0.82892	(36)	0.8305	
B''	0.82906			0.82932
$B'-D_{JK}'K^2$	0.80794	(36)	0.8093	
B'	0.80811			
$(B''-B')$	0.02095	(11)	0.02099	
D_J''	1.79×10^{-6}	(50)	2.2	
D_J'	1.81×10^{-6}	(50)		
$(D_J''-D_J')$	-0.02×10^{-6}	(22)		

a) The numbers in parentheses represent twice of the standard errors to be attached to the last significant figures.

TABLE 5. OBSERVED FREQUENCIES OF $(3\nu_3 \leftarrow \nu_3)$ BAND OF CH_3F AND $2\nu_3$ BAND OF $^{13}CH_3F$

J	$(3\nu_3 \leftarrow \nu_3)$ of CH_3F				$2\nu_3$ of $^{13}CH_3F$			
	R-Branch		P-Branch		R-Branch		P-Branch	
	Obsd	$\Delta\nu$[a)]	Obsd	$\Delta\nu$[a)]	Obsd	$\Delta\nu$[a)]	Obsd	$\Delta\nu$[a)]
0	—				—			
1	—		—		—		—	
2	—		—		—		—	
3	2056.117	12	—		—		—	
4	57.595	0	2042.860	4	2047.347	9	2032.776	−21
5	59.012	−7	41.004	0	—		—	
6	—		—		50.103	−4	29.087	−18
7	61.737	0	37.180	6	—		27.205	9
8	63.029	−2	35.196	2	52.709	3	25.254	8
9	64.284	2	33.172	−2	53.958	15	23.249	−4
10	65.490	0	—		55.141	4	21.231	12
11	—		29.014	9	56.273	−15	19.144	−1
12	67.787	16	26.859	1	57.405	8	17.030	3
13	68.851	−5	24.666	−2	58.453	−10	14.863	−6
14	69.899	8	22.443	7	59.481	−5	12.677	7
15	70.886	2	—		—		10.435	6
16	71.824	−9	17.839	−8	61.420	15	08.165	19
17	72.738	−1	15.487	−3	—		05.821	−1
18	73.601	−1	13.092	0	63.150	−4	03.443	−14
19	74.434	12	10.652	1	63.946	−17	01.039	−12
20	75.204	5	08.165	−5	—		1998.593	−10
21	75.936	4	05.645	−2	—		—	
22	76.610	−13	03.082	0	66.143	9	93.596	12
23			00.473	−4				
24			1997.830	−1				
25			95.141	−2				
26			92.423	8				

a) (observed frequency—calculated frequency) × 1000 cm^{-1}

$$\nu_m^{P,R} = 2049.835 + 1.65932m - 0.021392m^2 - 7.51 \times 10^{-6}m^3 + 1.13 \times 10^{-7}m^4, \quad \text{(for hot band)}$$

$$\nu_m^{P,R} = 2039.680 + 1.63687m - 0.020983m^2 - 7.17 \times 10^{-6}m^3 - 0.21 \times 10^{-7}m^4. \quad \text{(for isotope band)} \quad (4)$$

These constants include the contributions from the K^2 and K^4 terms, because the K-values at the intensity maxima are not equal to zero. If we assume $K=3$ at the intensity maxima and the values $[(A'-A'')-(B'-B'')]$, D_{JK}'', D_{JK}', and $(D_K'-D_K'')$ to be the same as those of main band, we can estimate the 'true' molecular constants. In Tables 3 and 4, the molecular constants which were corrected for the K-dependent terms are tabulated together with the corresponding constants obtained by Smith and Mills,[2] by Duncan *et al.*,[14] and by Gilliam and Gordy.[7] In Table 5, the observed and calculated frequencies are listed. The standard deviations of these data are 0.008 cm^{-1} for the hot band and 0.012 cm^{-1} for the isotope band.

Discussion

The molecular constants given in Table 1 have been obtained from the simultaneous analysis of 135 transitions in the P-, Q-, and R-branches. Their values, particularly those for ν_0, $(B'-B'')$, and $(D'-D'')$, are determined very accurately. This is also the first case, as far as we know, in which the $(A'-A'')$ value is obtained for the parallel band of methyl fluoride. From the analysis of the ν_3 fundamental band, Smith and Mills[2] estimate $|(A'-A'')-(B'-B'')|=|\alpha_3^A-\alpha_3^B|=0.0002$ cm^{-1}. Our present result (0.0013 cm^{-1}) is one order of magnitude larger than their estimation, but quite close to the value recently obtained from laser spectroscopy (0.0011 cm^{-1}).[15]

For the hot band and isotope band, the number of observed lines is not enough to determine the centrifugal distortion constants with high accuracy. The standard errors of these constants are comparatively larger than the other ones.

In the $2\nu_3$ band the $(B''-B')$ value is fairly large in comparison with $(B''+B')$, which makes the R-branch to have a distinct band head. If the centrifugal distortion terms and the K-dependent terms in Eq. (2) are neglected, the following expression quadratic to J is obtained for R-branch.

$$\nu(J;J+1) = \nu_0 + (B''+B')(J+1) - (B''-B')(J+1)^2, \quad (5)$$

which has a maximum at $J=[(B''+B')/2(B''-B')]-1=37$.

15) T. Y. Chang and J. D. McGee, *Appl. Phys. Lett.*, **19**, 103 (1971).

The rotational constants of v-th vibrational state can be expressed as,

$$B_v = B_e - \sum_s \alpha_s^B (v_s + d_s/2) + \sum_s \sum_{s'} \gamma_{ss'}^B (v_s + d_s/2)(v_{s'} + d_{s'}/2) + \cdots \quad (6)$$

where B_e is the equilibrium rotational constant, α_s^B and $\gamma_{ss'}^B$ are the vibration-rotation constants, and d_s is the degree of the degeneracy. From the analysis of ν_3 fundamental band,[2] the value of $\alpha_3^B = (B'' - B')$ was given as 0.01134 (± 3) cm^{-1}. The present results yield 0.01180 cm^{-1} for α_3^B and 0.00023 cm^{-1} for γ_{33}^B.

The vibration-rotation constants, α_3^B and α_3^A can be written as the sum of the harmonic and anharmonic parts.[16,17]

$$\alpha_3^B = \alpha_3^B(\text{harm}) + \alpha_3^B(\text{anharm}),$$
$$\alpha_3^B(\text{harm}) = -(2B_e^2/\omega_3)[3A_{33}^{xx} + 4\{(\zeta_{34}^x \omega_4)^2/(\omega_3^2 - \omega_4^2) + (\zeta_{35}^x \omega_5)^2/(\omega_3^2 - \omega_5^2) + (\zeta_{36}^x \omega_6)^2/(\omega_3^2 - \omega_6^2)\}],$$
$$\alpha_3^B(\text{anharm}) = -4\pi B_e^2 (c/h)^{1/2}\{3a_3^{xx} k_{333}/\omega_3^{3/2} + a_1^{xx} k_{133}/\omega_1^{3/2} + a_2^{xx} k_{233}/\omega_2^{3/2}\}, \quad (7)$$
$$\alpha_3^A = \alpha_3^A(\text{harm}) + \alpha_3^A(\text{anharm}),$$
$$\alpha_3^A(\text{harm}) = -6A_e^2 A_{33}^{zz}/\omega_3$$
$$\alpha_3^A(\text{anharm}) = -4\pi A_e^2 (c/h)^{1/2}\{3a_3^{zz} k_{333}/\omega_3^{3/2} + a_1^{zz} k_{133}/\omega_1^{3/2} + a_2^{zz} k_{233}/\omega_2^{3/2}\}, \quad (8)$$

in which $a_s^{\alpha\alpha}$ and $A_{ss}^{\alpha\alpha}$ are related, respectively, to the first and the second derivatives of moment of inertia $I_{\alpha\alpha}$, expanded in normal coordinate Q_s. $\zeta_{ss'}^{\alpha}$ is the Coriolis coupling constant.

If the harmonic force field is known, the constants which appear in Eqs. (7) and (8) may be calculated. From the force field which was obtained in our laboratory[18] the following relations are derived;

$$\alpha_3^B(\text{obsd}) = 0.01180,$$
$$\alpha_3^B(\text{harm}) = -0.00031,$$
$$\alpha_3^B(\text{anharm}) = -0.000180\, k_{333} - 0.000004\, k_{133} + 0.000005\, k_{233}, \quad (9)$$

and

$$\alpha_3^A(\text{obsd}) = 0.00977,$$
$$\alpha_3^A(\text{harm}) = -0.0009,$$
$$\alpha_3^A(\text{anharm}) = +0.000070\, k_{333} - 0.000189\, k_{133} + 0.000242\, k_{233}. \quad (10)$$

Since both α_3^B(harm) and α_3^A(harm) are found relatively small and have opposite signs to the α_3^B(obsd) and α_3^A(obsd), the anharmonic parts α_3(anharm) seem to have a predominant role. Although three cubic force constants are involved in the expression, the coefficient of k_{333} is about 40 times larger than the other two in Eq. (9). Therefore, if we consider the cubic diagonal force constant k_{333} only, we could have -67 cm^{-1} for k_{333}. The three coefficients in Eq. (10) are of the same order and we cannot determine the other two cubic force constants.

Table 6. Comparison between the ν_3 of CH_3F and diatomic C–F molecule (in cm^{-1})

CH_3F		C–F[19]	
ν_3	1048.60[2]	ν	1286.26
$2\nu_3$	2081.38	2ν	2550.99
$3\nu_3$	3098.42	3ν	3794.92
ω_3°	1064.37	ω_e	1308.1
x_{33}	8.01	$\omega_e x_e$	11.10
y_{333}	+0.02	$\omega_e y_e$	0.093
α_3^B	0.01180	α_e	0.01840
γ_{33}^B	0.00023	γ_e	0.00011
k_{333}	-67	k_3	-91

A rough estimation of k_{333} may be done from the spectroscopic data of diatomic CF,[19] since the normal coordinate Q_3 is chiefly associated with the C–F stretching coordinate. The data which are obtained from the analysis of CF molecule are listed in Table 6 in comparison with those of the C–F stretching vibration of methyl fluoride. When we assume the Morse function for the potential of C–F stretching vibration, the following relation can be obtained,

$$k_3(\text{CF})/\omega_e(\text{CF}) = k_{333}(\text{CH}_3\text{F})/\omega_3(\text{CH}_3\text{F}). \quad (11)$$

With the aid of Eq. (11) and Table 6, the k_{333} is estimated to be -75 cm^{-1}, which has certainly correct order of magnitude.

As mentioned earlier, the x,y-type Coriolis interaction would likely occur between the $2\nu_3$ band and the $\nu_3+\nu_6$ band. The selection rule for this type of interaction is $\Delta J=0$, $\Delta k=+1$, and $\Delta l=+1$ or $\Delta J=0$, $\Delta k=-1$, and $\Delta l=-1$,[3] where $K=|k|$. We have observed the combination $\nu_3+\nu_6$ band and made a preliminary analysis. From the molecular constants so far available, we can predict that the interaction would be strong at relatively high K levels ($K\sim 25$).

The intensity anomaly due to the Coriolis interaction will be seen more clearly in the weaker $\nu_3+\nu_6$ band. The more precise analysis of the $\nu_3+\nu_6$ combination band is being attempted, the result will be published in the near future.

This research has been supported by the grant from the Ministry of Education. Helpful discussions from Dr. Koichi Yamada are deeply appreciated.

16) H. H. Nielsen, *Rev. Mod. Phys.*, **23**, 90 (1951).
17) T. Oka and Y. Morino, *J. Mol. Spectrosc.*, **6**, 472 (1961).
18) T. Shimanouchi, "The Molecular Force Field," in "Physical Chemistry," Vol. 4, p. 290, ed. by H. Eyring, D. Henderson, and W. Jost, Academic Press, New York (1970).
19) T. L. Porter, D. E. Mann, and N. Acquista, *J. Mol. Spectrosc.* **16**, 228 (1965).

Vibrational Spectra and Molecular Conformations of Dialkyl Disulfides

Hiromu SUGETA, Akikatsu GO, and Tatsuo MIYAZAWA
Institute for Protein Research, Osaka University, Yamada-kami, Suita, Osaka 565
(Received July 9, 1973)

The infrared and Raman spectra of several dialkyl disulfides were measured and their conformations were discussed in relation with the characteristic S–S and C–S stretching vibrations. The infrared spectra in the solid state and the temperature dependence of Raman spectra were measured for ethyl methyl disulfide and diethyl disulfide. For ethyl methyl disulfide, the *gauche-gauche* isomer was more stable than the *trans-gauche* isomer by about 0.9 kcal/mol while for diethyl disulfide the *gauche-gauche-gauche* isomer was more stable than the *trans-gauche-gauche* isomer by about 0.6 kcal/mol in the liquid state. Only the *gauche-gauche* form for ethyl methyl disulfide and only the *gauche-gauche-gauche* form for diethyl disulfide were observed in the solid state.

For vibrational analyses of Raman spectra of proteins, it is necessary to establish correlations between vibrational spectra and conformations of side-chain groups and related model molecules. The correlations between the S–S and C–S stretching frequencies and conformations of the disulfide group >C–S–S–C< were proposed in our previous communication.[1]

The stable conformation about the S–S bond of disulfide groups was established to be *gauche*, with the internal-rotation angle of nearly 90°. Accordingly, the molecular conformation of dialkyl disulfides was concerned with the internal rotation about the C–S and C–C bonds of the –C–C–S–S–C–C– group.

The infrared spectra of several dialkyl disulfides were studied early by Thompson and Trotter[2] and by Sheppard.[3] The vibrational assignments of dimethyl disulfide,[4] diethyl disulfide[5] and di-*n*-propyl disulfide[6] were made by Scott *et al.*, together with the collection of early data of infrared and Raman frequencies for their thermodynamic studies. Detailed investigations on dimethyl disulfide were made later by Hayashi[7] and by Frankiss.[8] The infrared and Raman spectra of di-*tert*-butyl disulfide were also measured by Scott *et al.*[9] in detail. The infrared and Raman spectra of a series of disulfides and diselenides were measured by Allum *et al.*[10] The normal vibrations of dimethyl disulfide, ethyl methyl disulfide and di-*tert*-butyl disulfide were treated by Scott and El-Sabban.[11]

In the present paper, the infrared and Raman spectra of several dialkyl disulfides are reported in some detail and molecular conformations of disulfides will be discussed, especially for ethyl methyl disulfide and diethyl disulfide.

Experimental

The dialkyl disulfides treated in the present study include dimethyl disulfide [CH_3SSCH_3], ethyl methyl disulfide [$CH_3CH_2SSCH_3$], diethyl disulfide [$CH_3CH_2SSCH_2CH_3$], diisobutyl disulfide [$(CH_3)_2CHCH_2SSCH_2CH(CH_3)_2$], diisopropyl disulfide [$(CH_3)_2CHSSCH(CH_3)_2$], di-*sec*-butyl disulfide [$CH_3CH_2CH(CH_3)SSCH(CH_3)CH_2CH_3$], methyl *tert*-butyl disulfide [$CH_3SSC(CH_3)_3$], di-*tert*-butyl disulfide [$(CH_3)_3CSSC(CH_3)_3$], and di-*tert*-amyl disulfide [$CH_3CH_2C(CH_3)_2SSC(CH_3)_2CH_2CH_3$].

Ethyl methyl disulfide was prepared from Bunte salt and ethyl mercaptan according to the method reported by Milligan and Swan.[12] Methyl *tert*-butyl disulfide was also prepared from Bunte salt and *tert*-butyl mercaptan, analogous to the method of Milligan and Swan[12] [bp 51 °C/20 Torr]. For other disulfides, commercial samples were used after distillation.

Infrared spectra in the liquid and solid states were measured with Hitachi EPI-G3 and EPI-L infrared spectrophotometers. Raman spectra in the liquid state were measured with a JEOL Raman spectrometer (Model JRS-02AS) with an argon-ion laser (488.0 or 514.5 nm).

Results and Discussion

S–S and C–S Stretching Vibrations. The Raman spectra in the region of the S–S and C–S stretching vibrations (750—500 cm^{-1}) of dialkyl disulfides are shown in Fig. 1. The characteristic S–S stretching frequencies of dialkyl disulfides are summarized in Table 1. S–S stretching vibrations of dialkyl disulfides give rise to strong Raman lines and weak infrared-absorption bands while C–S stretching vibrations give rise to strong Raman lines and fairly strong infrared-absorption bands. Accordingly, observations of Raman spectra as well as infrared spectra are important for identifications of S–S stretching vibrations.

As reported previously,[1] the S–S stretching frequencies of disulfide groups depend upon the molecular conformations about the C–S bonds. The frequencies of S–S stretching vibrations of the X–C–S–S–C–Y group are specified with the atoms X and Y which occupy the two *trans* sites with respect to the sulfur atoms; the S–S stretching vibrations lie at about 510 cm^{-1} for the conformation with two hydrogen atoms

1) H. Sugeta, A. Go, and T. Miyazawa, *Chem. Lett.*, **1972**, 83.
2) H. W. Thompson and I. F. Trotter, *J. Chem. Soc.*, **1946**, 481.
3) N. Sheppard, *Trans. Faraday Soc.*, **46**, 429 (1950).
4) D. W. Scott, H. L. Finke, M. E. Gross, G. B. Guthrie, and H. M. Huffman, *J. Amer. Chem. Soc.*, **72**, 2424 (1950).
5) D. W. Scott, H. L. Finke, J. P. McCullough, M. E. Gross, R. E. Pennington, and G. Waddington, *ibid.*, **74**, 2478 (1952).
6) W. N. Hubbard, D. R. Douslin, J. P. McCullough, D. W. Scott, S. S. Todd, J. F. Messerly, I. A. Hossenlopp, A. George, and G. Waddington, *ibid.*, **80**, 3547 (1958).
7) M. Hayashi, *Nippon Kagaku Zasshi*, **78**, 101 (1957).
8) S. G. Frankiss, *J. Mol. Struct.*, **3**, 89 (1969).
9) J. H. S. Green, D. J. Harrison, W. Kyaston, and D. W. Scott, *Spectrochim. Acta*, **25A**, 1313 (1969).
10) K. G. Allum, J. A. Greighton, J. H. S. Green, G. J. Minkoff, and L. J. S. Prince, *ibid.*, **24A**, 927 (1968).
11) D. W. Scott and M. Z. El-Sabban, *J. Mol. Spectry.*, **31**, 362 (1969).
12) B. Milligan and J. M. Swan, *J. Chem. Soc.*, **1963**, 6008.

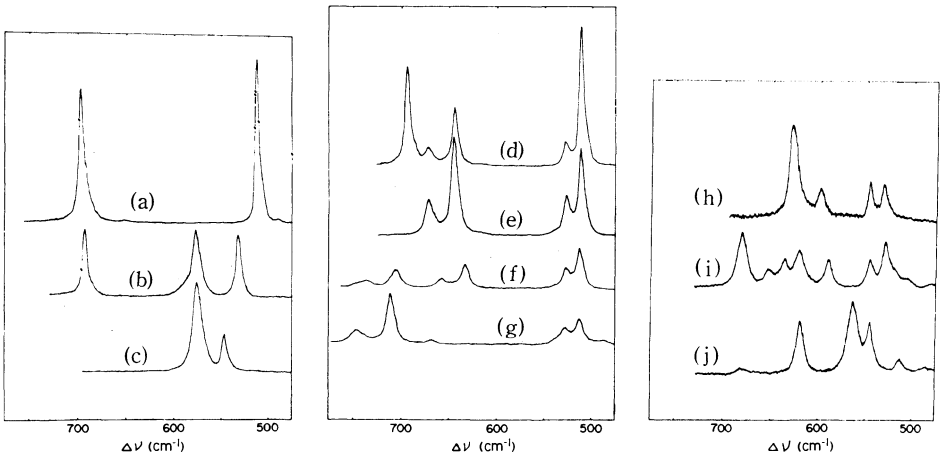

Fig. 1. The Raman spectra of dialkyl disulfides in the liquid state at room temperature.
(a): dimethyl disulfide, (b): methyl *tert*-butyl disulfide, (c): di-*tert*-butyl disulfide, (d): ethyl methyl disulfide, (e): diethyl disulfide, (f): di-*n*-propyl disulfide, (g): di-iso-butyl disulfide, (h): di-isopropyl disulfide, (i): di-*sec*-butyl disulfide, (j): di-*tert*-amyl disulfide. Excited with an argon-ion laser (488.0 nm).

TABLE 1. OBSERVED FREQUENCIES (cm^{-1}) OF S–S STRETCHING VIBRATIONS OF DIALKYL DISULFIDES[a)]

Molecule	ν(H, H)		ν(H, C)		ν(C, C)	
	Infrared	Raman	Infrared	Raman	Infrared	Raman
CH_3SSCH_3	509 m	508 vs	—	—	—	—
$CH_3SSC(CH_3)_3$	—	—	529 m	528 vs	—	—
$[-SC(CH_3)_3]_2$	—	—	—	—	545 vw	543 s
$CH_3SSCH_2CH_3$	510 w	509 vs	526 vw	524 m	—	—
$[-SCH_2CH_3]_2$	510 m	508 vs	525 w	523 s	—	—
$[-SCH_2CH_2CH_3]_2$	511 w	510 vs	524 w	523 s		
$[-SCH_2CH(CH_3)_2]_2$	513 w	512 s	527 w	525 m		
$[-SCH(CH_3)_2]_2$			528 w	527 s	543 w	542 s
$[-SCH(CH_3)CH_2CH_3]_2$			526 w	527 vs	542 vw	542 s
$[-SC(CH_3)_2CH_2CH_3]_2$	—	—	—	—	543 vw	543 s

a) Unexpected vibrations are marked with the — sign.

at both *trans* sites [ν(H,H)], at about 525 cm^{-1} for the conformation with a hydrogen atom at one *trans* site and a carbon atom at the other *trans* site [ν(H,C)], and at about 540 cm^{-1} for the conformation with two carbon atoms at both *trans* sites [ν(C,C)].

For dimethyl disulfide, methyl *tert*-butyl disulfide, and di-*tert*-butyl disulfide, no rotational isomers are expected other than the molecular conformation with the *gauche* S–S bond. In fact, for each of the three molecules, only one S–S stretching vibration was observed. On the other hand, for other disulfides with the possibility of rotational isomerism about the C–S bonds, two S–S stretching vibrations were in fact observed in the Raman scattering and infrared absorption. For di-*primary*-alkyl disulfides of the present study, two S–S stretching vibrations, ν(H,H) and ν(H,C), were observed in the liquid state (Table 1). This observation indicates that the *gauche-gauche-gauche* (GGG) and *trans-gauche-gauche* (TGG) isomers coexist for the $-C-CH_2-S-S-CH_2-C-$ group. For di-*n*-propyl disulfide and diisobutyl disulfide, two types (P_H and P_C) of C–S stretching vibrations were observed (see Ref. 1), indicating the coexistence of rotational isomers about the $>C-CH_2-$ bonds.

For di-*secondary*-alkyl disulfides [isopropyl or *sec*-butyl], two S–S stretching vibrations, ν(H,C) and ν(C,C), were observed (see Fig. 1 and Ref. 1), indicating the presence of rotational isomers about C–S bonds. For di-*sec*-butyl disulfide, two types of C–S stretching vibrations, S_{HH} and S_{CH}, were observed (see Ref. 1), indicating the coexistence of rotational isomers about the C–C bonds too.

For di-*tert*-amyl disulfide, rotational isomers about the C–S bonds are expected. However, for any isomer about the C–S bonds, the two *trans* sites are occupied by carbon atoms either of methyl groups or of methylene groups, and in fact only one S–S stretching vibration, ν(C,C), was observed in the Raman scattering. On the other hand, two types of C–S stretching vibrations, T_{HHH} and T_{CHH}, were observed for di-*tert*-amyl disulfide (see Ref. 1 and Fig. 1), indicating the coexistence of rotational isomers about the $-CH_2-C\lessdot$ bond.

Methyl tert-*Butyl Disulfide.* For methyl *tert*-butyl disulfide, no rotational isomers are expected other than the molecular conformation with the *gauche* S–S bond. Accordingly, the vibrational spectra of methyl *tert*-butyl disulfide were measured to confirm the characteristic vibrations of disulfide groups. The Raman spectrum of methyl *tert*-butyl disulfide in the liquid state is shown in Fig. 2. The infrared and Raman frequencies in the liquid state are given in Table 2, together with the vibrational assignments.

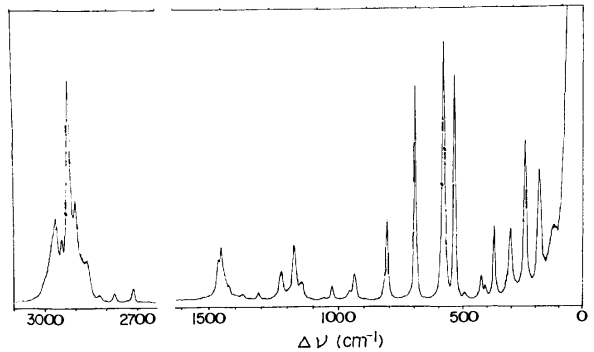

Fig. 2. The Raman spectrum of methyl *tert*-butyl disulfide in the liquid state at room temperature. Excited with an argon-ion laser (488.0 nm).

TABLE 2. OBSERVED FREQUENCIES (cm^{-1}), RELATIVE INTENSITIES,[a] AND VIBRATIONAL ASSIGNMENTS OF METHYL *t*-BUTYL DISULFIDE IN THE LIQUID STATE

Infrared	Raman	Vibrational assignment
	116 w	S–S or C–S torsion
	176 s	C–S–S deform. of $(CH_3)_3C$–S–S
	236 s	C–S–S deform. of CH_3–S–S
299 vw	299 m	skeletal rock. of $(CH_3)_3C$–S
316 m	315 vw, sh	
365 w	366 m	sym. deform. of $(CH_3)_3C$–S
402 w	402 vw	asym. deform. of $(CH_3)_3C$–S
419 vw	419 w	
478		impurity
	490 vw	impurity ?
529 m	528 vs	S–S stretching [ν(H,C)]
573 m	575 vs	C–S stretch. [T_{HHH}] of $(CH_3)_3C$–S
689 m	691 vs	C–S stretch. of CH_3–S
802 w	805 m	C–C sym. stretch. of $(CH_3)_3C$–S
	815 vw, sh	
895	897	impurity
934 vw, sh	935 m	CH_3 rock. of $(CH_3)_3C$–S
953 s	955 vw	CH_3 rock. of CH_3–S
1020 s	1023 w	CH_3 rock. of $(CH_3)_3C$–S
1143 m	1143 w	
1168 vs	1169 m	methyl rock. and
1220 s	1221 m	C–C asym. stretch. of $(CH_3)_3C$–S
1307 s	1309 vw	CH_3 sym. deform. of CH_3–S
1363 vs	1365 vw	CH_3 sym. deform. of $(CH_3)_3C$–S
1391 m		
1416 m	1420 vw, sh	CH_3 asym. deform. of CH_3–S
1433 m		
	1447 m	
1455 vs	1457 w	CH_3 asym. deform. of $(CH_3)_3C$–S
1474 s		

a) vs: very strong, s: strong, m: medium, w: weak, vw: very weak, sh: shoulder, br: broad.

The vibrational assignments were readily made with reference to the vibrational spectra of dimethyl disulfide[7,8] and di-*tert*-butyl disulfide,[9] since the vibrational spectra of methyl *tert*-butyl disulfide were found to be practically the composite of those of dimethyl disulfide and di-*tert*-butyl disulfide. Three very strong Raman lines at 528, 575, and 691 cm^{-1} were assigned to the characteristic S–S stretching [ν(H,C)], CH_3–S stretching, and $C(CH_3)_3$–S stretching vibrations [T_{HHH}]. The vibrational frequencies higher than 800 cm^{-1} were assigned, as given in Table 2, to the vibrations of the CH_3–S and $(CH_3)_3C$–S groups. In the region lower than 450 cm^{-1}, skeletal deformation and torsional vibrations are expected. The vibrational frequencies in the region 420—300 cm^{-1} are assigned to the skeletal deformation vibrations of *tert*-butyl group as given in Table 2. The Raman lines at 236 and 176 cm^{-1} are assigned to the C–S–S bending vibrations of the CH_3–C–S–S and $(CH_3)_3C$–C–S–S group, respectively.

Ethyl Methyl Disulfide. Ethyl methyl disulfide is the simplest one of the dialkyl disulfides for which rotational isomers about C–S bonds are expected to coexist. The infrared spectra of ethyl methyl disulfide in the region 3500—500 cm^{-1} were previously reported by Allum *et al.*[10]

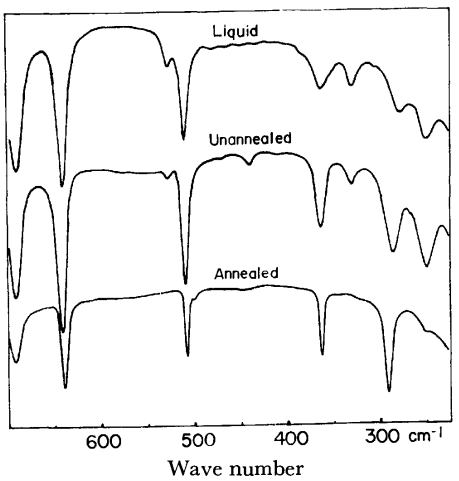

Fig. 3. The infrared spectra of the liquid (room temperature), unannealed solid (77 K), and annealed solid (77 K) of ethyl methyl disulfide.

TABLE 3. OBSERVED FREQUENCIES (cm^{-1}), RELATIVE INTENSITIES,[a] AND VIBRATIONAL ASSIGNMENTS OF ETHYL METHYL DISULFIDE

Liquid		Annealed Solid	Assignments
Infrared	Raman	Infrared[b]	
200 w	196 s		C–S–S deform.
248 w	246 s	—	C–S–S deform. (TG)
278 w	~280 vw, sh	290 m	C–S–S deform. (GG)
328 w	327 m	—	C–C–S deform. (TG)
361 w	362 w	362 m	C–C–S deform. (GG)
510 w	509 vs	500 vw, sh 508 m	S–S stretch. (GG)
526 vw	524 s	—	S–S stretch. (TG)
642 m	641 s	634 vw, sh 640 s	CH_2–S stretch. (GG)
667 vw	669 m	—	CH_2–S stretch. (TG)
692 m	692 vs	686 vw, sh 692 s	CH_3–S stretch. (GG) CH_3–S stretch. (TG)
761 s	759 w	758 vs	CH_2 rock. (GG)
781 m		—	CH_2 rock. (TG)

a) See the footnote a of Table 2.
b) The – sign indicates infrared bands which disappear on crystallization.

In the present study, the Raman spectra as well as infrared spectra were measured in the liquid state. The infrared spectra in the solid state (condensed from the vapor and then annealed) and the temperature dependence of the Raman intensities in the liquid state were also measured for detailed analyses of rotational isomerism. In Fig. 3, the infrared spectra in the region 700—200 cm^{-1} are shown for the liquid, unannealed solid and annealed solid. In Table 3, the observed vibrational frequencies in the region 800—200 cm^{-1} are given, together with the vibrational assignments. The infrared frequencies observed in the region higher than 500 cm^{-1} agree closely with the data reported previously by Allum *et al.*[10]

The infrared observation of two CH_2 rocking vibrations at 781 and 761 cm^{-1}, two C–S stretching vibrations at 667 and 642 cm^{-1}, two S–S stretching vibrations at 526 and 510 cm^{-1}, and five skeletal deformation vibrations below 400 cm^{-1} indicates the coexistence of the rotational isomers about the C–S bond in the liquid state. For the annealed solid, however, the infrared bands at 761, 642, and 510 cm^{-1} are still observed but the bands at 781, 667, and 526 cm^{-1} disappeared. Also the skeletal deformation vibrations at 328 and 248 cm^{-1} disappear on annealing.

For the molecule of ethyl methyl disulfide CH_3–CH_2–S–S–CH_3, there are two rotational isomers, *gauche-gauche* (GG or G'G') and *trans-gauche* (TG or TG'). For the GG form, hydrogen atoms occupy the two *trans* sites with respect to the S–S bond and accordingly the S–S stretching vibration is expected to lie at about 510 cm^{-1} [ν(H,H)] whereas for the TG form, the two *trans* sites are occupied by one hydrogen atom and one carbon atom and the S–S stretching vibration is expected to lie at about 525 cm^{-1} [ν(H,C)]. Since on annealing the infrared band at 510 cm^{-1} remains but the band at 525 cm^{-1} disappears, it may be concluded that the TG and GG forms coexist in the liquid state but only the GG form persists in the solid state.

The energy difference between the TG and GG forms was studied by the measurement of the temperature dependence of the Raman spectra in the liquid state. Thus, over the temperature range +20——65 °C, the relative intensities of Raman lines were measured for the pairs (TG and GG) at 669 and 641 cm^{-1}, 524 and 509 cm^{-1}, and 327 and 362 cm^{-1}. The GG isomer was found to be more stable than the TG isomer by 0.9±0.2 kcal/mol.

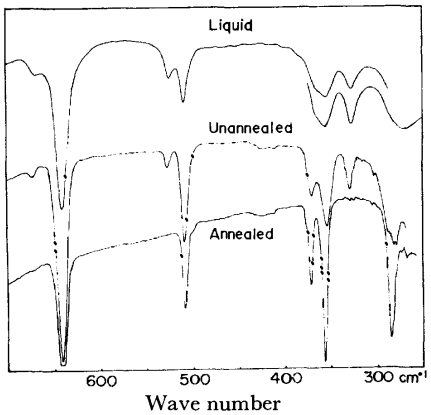

Fig. 4. The infrared spectra of the liquid (room temperature), unannealed solid (77 K), and annealed solid (77 K) of diethyl disulfide.

TABLE 4. OBSERVED FREQUENCIES (cm^{-1}), RELATIVE INTENSITIES,[a] AND VIBRATIONAL ASSIGNMENTS OF DIETHYL DISULFIDE

Liquid		Annealed Solid	Assignment[c]
Infrared	Raman	Infrared[b]	
	180 s		C–S–S deform.
200 w	200 m, sh		C–S–S deform.
	255 w, br		C–S–S deform. (TGG)
275 w, br	287 w	285 m	C–S–S deform. (GGG)
	315 vw, sh		
329 w	327 m	—	C–C–S deform. (TGG)
358 m	357 w	357 s	C–C–S deform. (GGG)
365 w, sh	366 w	362 m	C–C–S deform. (GGG)
510 m	508 vs	509 m	S–S stretch. (GGG)
525 w	523 s	—	S–S stretch. (TGG)
640 m	642 vs	641 s	C–S stretch. (GGG) C–S stretch. (TGG)
667 vw	668 s	—	C–S stretch. (TGG)
	735		impurity
762 s	760 w	760 vs	CH_2 rock. (GGG) CH_2 rock. (TGG)
781 m	782 vw	—	CH_2 rock. (TGG)

a) See the footnote a) of Table 2.
b) See the footnote b) of Table 3.
c) The underlined notations T and G indicate that the vibrational mode is largely localized on the side of the *trans* and *gauche* C–S bond, respectively.

Diethyl Disulfide. For the molecule of diethyl disulfide CH_3–CH_2–S–S–CH_2–CH_3, there are two C–S bonds about which rotational isomerism is expected. Possible rotational isomers are *gauche-gauche-gauche* (GGG or G'G'G'), *trans-gauche-gauche* (TGG or TG'G'), and *trans-gauche-trans* (TGT or TG'T).

Previous data of the infrared (>500 cm^{-1}) and Raman spectra were summarized by Scott *et al.*[5] In the present study, the infrared spectra (>200 cm^{-1}) were measured for the liquid, unannealed solid and annealed solid, and the Raman spectra of the liquid were measured at various temperatures. The infrared spectra (700—200 cm^{-1}) of the liquid, unannealed solid and annealed solid are shown in Fig. 4. In Table 4, the frequencies observed in the region 800—200 cm^{-1} are given, together with vibrational assignments. The vibrational frequencies in the region higher than 800 cm^{-1} agreed closely with previous data,[5] and accordingly are not included in Table 4.

On crystallization of the sample, the infrared band due to the S–S stretching vibration at 510 cm^{-1} [ν(H,H)] persists but the band at 525 cm^{-1} [ν(H,C)] disappears, similar to the case of ethyl methyl disulfide. Accordingly, it may be concluded that at least the GGG and TGG isomers coexist in the liquid state but only the GGG form persists in the crystalline state.

The infrared bands at 781 (CH_2 rock.), 667 (C–S stretch.), and 329 cm^{-1} (C–C–S deform.) disappear on crystallization and are assigned to the TGG form. These vibrations of the TGG form of diethyl disulfide closely correspond to those of the TG form of ethyl

methyl disulfide, indicating that the vibrational modes are largely localized on the side of the *trans* C–S bond. For similar reasons, the infrared bands due to the CH_2 rocking, C–S stretching and C–C–S deformation vibrations largely localized on the side of the *gauche* C–S bond of the TGG form are possibly overlapped with the corresponding bands of the GGG form (762, 640, and 365 or 358 cm^{-1}) in the liquid state.

The energy difference between the TGG and GGG forms of diethyl disulfide was studied by the measurement of the temperature dependence of the Raman spectra in the liquid state. Over the temperature range +20——68 °C, the relative intensity of the Raman lines at 523 (TGG) and 508 cm^{-1} (GGG) were measured. The GGG isomer was found to be more stable than the TGG isomer by 0.6 ± 0.2 kcal/mol.

BULLETIN OF THE CHEMICAL SOCIETY OF JAPAN, VOL. 46, 3411—3415 (1973)

Isocyanide-phosphine Complexes of Cobalt(I)

Sei OTSUKA and Michele ROSSI*

Department of Chemistry, Faculty of Engineering Science, Osaka University, Toyonaka, Osaka 560

(Received February 8, 1973)

Diamagnetic penta-coordinate Co(I) complexes of formula, $[Co(p\text{-}CH_3C_6H_4NC)_4(PPh_3)]X$ (**1**) and $[Co(p\text{-}CH_3C_6H_4NC)_3(PPh_3)_2]X$ (**2**) ($X=Cl^-, Br^-, I^-, ClO_4^-, BPh_4^-$) were obtained from $CoX(PPh_3)_3$ or $CoX_2(PPh_3)_2$. Their ^1H NMR spectra served to deduce the trigonal bipyramidal structure. The aromatic ring proton NMR spectra and the IR CN stretching absorptions of radial modes were discussed in terms of the $d\pi$-$p\pi$ back bonding.

Recently isocyanide transition metal complexes have resumed considerable attention. Much of the impetus for the current research may stem from the unique property of isocyanide ligands which are capable of stabilizing a wider range of metal valency states than the isoelectronic molecule, carbon monoxide. Both the CN functional group and the substituent provide spectroscopic information valuable for structural assignments and for discussions on the nature of the metal-ligand bonding. Another interesting property is the reducing ability. Thus Co(I) complexes $[Co(RNC)_5]X$ are accessible from Co(II) halides by treating with an excess of RNC (R=alkyl or aryl). We were interested in comparing the structural chemistry in a series of $[Co(RNC)_{5-n}L_n]^+$. When our study was commenced no mixed complexes of this series were known except for $[Co(p\text{-}CH_3C_6H_4NC)_3(PPh_3)_2]^+$ which was reported without detail.[2] After completion of the work,[3] a paper describing $[Co(t\text{-}BuNC)_4AsPh_3]^+$, $[Co(t\text{-}BuNC)_3(PPh_3)_2]^+$ and others appeared,[4] but failed to report the preparation of $[Co(RNC)_4PPh_3]^+$. We were able to synthesize two types $[Co(RNC)_3(PPh_3)_2]^+$ and $[Co(RNC)_4PPh_3]^+$ ($R=p\text{-}CH_3C_6H_4$–) in addition to the known pentakis complex. Their stabilities and well-defined IR and NMR spectra enabled us to deduce their molecular structure to be isostructural (trigonal bipyramid). The series $[Co(RNC)_{5-n}L_n]^+$ ($n=0, 1, 2$) consitutes a system relevant for the study of the nature of isocyanide coordination to a low-valent metal. In view of the unusual ^1H NMR spectrum of the aromatic ring protons of free $p\text{-}CH_3C_6H_4NC$, which is due to the magnetic anisotropy of the C≡N– group, ^1H NMR spectra of the coordinated isocyanide deserve scrutiny.

Experimental

Materials. Commercial chemicals were used without further purification. *para*-Tolylisocyanide was prepared by the formamide–potassium *t*-butoxide method.[5] Compounds $[CoCl_2(PPh_3)_2]$[6] and $[CoCl(PPh_3)_3]$[7] were prepared by the procedures given in literature.

Instruments. The infrared spectra were measured with a Hitachi-Perkin Elmer Model 225 as Nujol mulls between CsI discs and in acetone solution in 0.1 mm NaCl cells. Proton nuclear magnetic resonance spectra were measured with a 100 MHz. Model JNM 4H-100 of JEOL using TMS as internal standard.

Syntheses of Compounds. *Tetrakis*-p-*tolylisocyanide-triphenylphosphinecobalt* (*I*) *chloride*: $CoCl(PPh_3)_3$ (1.2 g, 1.434 mmol) and *p*-tolylisocyanide (0.75 g, 6.4 mmol) were mixed in 100 ml of benzene at 5—10 °C under nitrogen atmosphere to give a yellow solution containing dark residue. The filtered solution was concentrated and treated with hexane affording a yellow powder. The powder was washed with hexane and dried under vacuum. Yield 0.6 g, 50% (calculated from the cobalt). Mp 80 °C (decomposition). Found: C, 71.27; H, 5.57; N, 6.59; Cl, 4.18%. Calcd for $C_{50}H_{43}ClN_4PCo$: C, 72.77; H, 5.25; N, 6.79; Cl, 4.30%.

Tetrakis-p-*tolylisocyanide-triphenylphosphinecobalt* (*I*) *Perchlorate*: A solution of $[Co(p\text{-}CH_3C_6H_4NC)_4PPh_3]Cl$ in cold ethanol

* Fellow of the Japan Society for the Promotion of Science during 1968. Present address: Department of Chemistry, Istituto Chimica Generale, Universita di Bari, Bari, Italy

1) For review see L. Malatesta, *Progr. Inorg. Chem.*, **1**, 288 (1959); L. Malatesta and F. Bonati, "Isocyanide Complexes of Metals," J. Wiley, London (1969), pp. 131—143.

2) A. Sacco and M. Freni, *Ist. Lomb. Rend. Sci., Ser A*, **1960**, 221.

3) S. Otsuka and M. Rossi, 18th Symposium on Coordination Chemistry, Chemical Society of Japan, Kyoto, 1968).

4) R. B. King and M. S. Saran, *Inorg. Chem.*, **11**, 2112 (1972).

4a) E. L. Muetterties, *Chem. Commun.*, **1973**, 221.

5) I. Ugi and R. Meyer, *Chem. Ber.*, **93**, 239 (1960).

6) J. Chatt and B. L. Shaw, *J. Chem. Soc.*, **1961**, 285.

7) M. Aresta, M. Rossi, and A. Sacco, *Inorg. Chim. Acta*, **3**, 227 (1969).

and a solution of $[Co(p\text{-}CH_3C_6H_4NC)_4PPh_3]_2[CoCl_4]$ in cold methanol were treated separately with an excess of $NaClO_4$ affording the same compound. The product was washed with water and cold methanol, and dried under vacuum. Yellow crystals, mp 144—146 °C (decomposition). Λ_M=24.9 mho cm^2 mol^{-1} (10^{-3} M nitrobenzene solution at 21 °C). Found: C, 67.61; H, 5.19; N, 6.47; Cl, 4.02%. Calcd for $C_{50}H_{43}ClN_4O_4PCo$: C, 67.53; H, 4.87; N, 6.30; Cl, 3.99%.

*Tetrakis-*p*-tolylisocyanide-triphenylphosphinecobalt(I) Tetraphenylborate*: A solution of $[Co(p\text{-}CH_3C_6H_4NC)_4PPh_3]Cl$ in ethanol was treated at 10 °C with an excess of $NaBPh_4$ affording yellow crystals. The product was washed with cold ethanol and dried under vacuum. Mp 90—92 °C (decomposition). Λ_M=16.2 mho cm^2 mol^{-1} (10^{-3} M nitrobenzene solution at 21 °C). Found: C, 79.16; H, 5.62; N, 4.94%. Calcd for $C_{74}H_{63}BN_4PCo$: C, 80.14; H, 5.73; N, 5.05%.

*Tetrakis-*p*-tolylisocyanide-triphenylphosphinecobalt(I) Tetrachlorocobaltate* (II): A suspension of 3.5 g of $CoCl_2(PPh_3)_2$ (5.36 mmol) in 30 ml of acetone was treated with 4 g of *p*-tolylisocyanide (33.2 mmol) at room temperature. The mixture was stirred for a few minutes affording a yellow-green solution; green crystals were formed by addition of a small portion of hexane. The product was washed with acetone and dried under vacuum. Yield 1.7 g, 53.5% (based on the cobalt). Mp 106—108 °C (decomposition). Found: C, 67.59; H, 5.38; N, 6.06; Cl, 8.11%. Calcd for $C_{100}H_{86}Cl_4N_8P_2Co_3$: C, 67.47; H, 4.87; N, 6.29; Cl; 7.96%.

*Tris-*p*-tolylisocyanide-bis-triphenylphosphinecobalt(I) chloride*: Method (a): The above yellow solution obtained after the filtration of $[Co(p\text{-}CH_3C_6H_4NC)_4PPh_3]_2[CoCl_4]$ was treated with another portion of hexane affording yellow crystals. The product was washed with hexane and dried under vacuum. Yield 0.45 g, 8.7%. Method (b): A mixture of 0.5 g of $[Co(p\text{-}CH_3C_6H_4NC)_4PPh_3]Cl$ (0.61 mmol) and 0.2 g of PPh_3 (0.76 mmol) was dissolved in hot benzene; the filtered solution afforded yellow crystals on cooling. The product was washed with benzene and dried under vacuum. Mp 175 °C. Λ_M=25.8 mho cm^2 mol^{-1} (10^{-3} M nitrobenzene solution at 21 °C). Found: C, 73.87; H, 5.81; N, 4.31; Cl, 3.75%. Calcd for $C_{60}H_{51}ClN_3P_2Co$: C, 74.26; H, 5.30; N, 4.33; Cl, 3.65%.

*Tris-*p*-tolylisocyanide-bis-triphenylphosphinecobalt(I) bromide*: A mixture of 1.5 g of $CoBr_2(PPh_3)_2$ (2.09 mmol) and 1.5 g of *p*-tolylisocyanide (12.8 mmol) in 15 ml of acetone was stirred at room temperature to give a yellow solution and a small amount of green residue. The filtered solution was treated with hexane to afford yellow crystals. Yield 0.4 g, 18.8%. Mp 192—194 °C. Λ_M=24.7 mho cm^2 mol^{-1}. (10^{-3} M nitrobenzene solution at 21 °C). Found: C, 70.60; H, 5.32; N, 4.18; Br, 8.30%. Calcd for $C_{60}H_{51}BrN_3P_2Co$: C, 71.01; H, 5.07; N, 4.14; Br, 7.87%.

*Tris-*p*-tolylisocyanide-bis-triphenylphosphinecobalt(I) iodide*: A mixture of 1.5 g of $CoI_2(PPh_3)_2$ (1.8 mmol) and 1.1 g of $p\text{-}CH_3C_6H_4NC$ (9.4 mmol) in 20 ml of acetone was stirred at room temperature to give a brown solution. On being left to stand, brown crystals of the known Co(II) complex, $Co(p\text{-}CH_3C_6H_4NC)_4I_2$, were formed (1.0 g, 71% of the cobalt). The filtered solution was treated with hexane to afford orange crystals of the product. Yield 0.35 g, 18.3%. Mp 195 °C. Λ_M=21.9 mho cm^2 mol^{-1} (10^{-3} M nitrobenzene solution at 21 °C). Found: C, 66.31; H, 5.16; N, 3.87%. Calcd for $C_{60}H_{51}IN_3P_2Co$: C, 67.87; H, 4.84; N, 3.96%. The compound $Co(p\text{-}CH_3C_6H_4)_4I_2$ was identified by its elemental analysis and mp.

*Tris-*p*-tolylisocyanide-bis-triphenylphosphinecobalt(I) perchlorate*: Method (a): A solution of $[Co(p\text{-}CH_3C_6H_4NC)_3(PPh_3)_2]Cl$ in ethanol was treated at room temperature with an excess of $NaClO_4$, affording yellow-orange crystals. Method (b): A solution of $[Co(p\text{-}CH_3C_6H_4NC)_4PPh_3]_2[CoCl_4]$ in methanol was heated to boliling point and treated with an excess of $NaClO_4$; on cooling orange crystals of the product were formed. The product was washed with water and cold ethanol and dried under vacuum. Mp 205 °C. Λ_M= 24.7 mho cm^2 mol^{-1} (10^{-3} M nitrobenzene solution at 21 °C). Found: C, 69.12; H, 5.33; N, 4.09; Cl, 3.68%. Calcd for $C_{60}H_{51}ClN_3O_4P_2Co$: C, 69.67; H, 4.97; N, 4.06; Cl, 3.43%.

*Tris-*p*-tolylisocyanide-bis-triphenylphosphinecobalt(I) tetraphenylborate*: A solution of $[Co(p\text{-}CH_3C_6H_4NC)_3(PPh_3)_2]Cl$ in ethanol was treated at room temperature with an excess of $NaBPh_4$ to afford yellow crystals. The product was washed with ethanol and dried under vacuum. Mp 183 °C. Λ_M=15.7 mho cm^2 mol^{-1} (10^{-3} M nitrobenzene solution at 21 °C). Found: C, 81.03; H, 6.07; N, 3.36%. Calcd for $C_{84}H_{71}BN_3P_2Co$: C, 80.44; H, 5.71; N, 3.35%.

Results and Discussion

Preparation. Penta-coordinated Co(I) complexes of formula $[Co(RNC)_4P]X$ and $[Co(RNC)_3P_2]X$ (RNC=$p\text{-}CH_3C_6H_4NC$, P=PPh_3) were prepared from phosphine-halide complexes of Co(I) or Co(II). The complex $[Co(RNC)_4P]Cl$ is readily obtainable by treating the tetrahedral, green Co(I) complex, $CoCl(PPh_3)_3$,[7] with a slight excess of *p*-tolylisocyanide (RNC/Co=4.5) in benzene at 5—10 °C; it was isolated in about 50% yield in the form of yellow powder, air-stable, moderately soluble in benzene and very soluble in polar solvents. The cation $[Co(RNC)_4P]^+$ was also produced by treating the tetrahedral Co(II) complex $CoCl_2(PPh_3)_2$[6] with an excess of the isocyanide (RNC/Co=6.2) in acetone at room temperature, and isolated as the tetrachlorocobaltate salt. The complex salts $[Co(RNC)_4P]Y$ (Y=ClO_4^-, X^-, and BPh_4^-) were obtained by metathetic exchange of the chloride anion in an alcoholic solution. The IR and NMR spectra indicate that the tetrakis-isocyanide-mono-phosphine complex salts obtained by both methods are always contaminated with a small amount (10—25%) of impurities which are a mixture of $[Co(RNC)_3P]X$ and $[Co(RNC)_5]X$ in an approximately equimolar amount. All these compounds form yellow, air-stable crystals and behave in solution as uni-univalent electrolytes (Λ_M=16—25 mho cm^2 mol^{-1} in nitrobenzene at 21 °C). They melt with decomposition at relatively low temperature (80—146 °C) indicating thermal instability of the cation $[Co(RNC)_4P]^+$ in comparison with $[Co(RNC)_3P_2]^+$. Consistent with the formal oxidation state Co(I), they are diamagnetic, normal chemical shift values being observed for the proton NMR spectra.

The reaction of $CoCl_2(PPh_3)_2$ with $p\text{-}CH_3C_6H_4NC$ produced, besides $[Co(RNC)_4P]_2CoCl_4$, the tris-isocyanide-bis-phosphine complex $[Co(RNC)_3P_2]Cl$ in a low yield. The corresponding bromide complex $[Co(RNC)_3P_2]Br$ was similarly obtained by starting from $CoBr_2(PPh_3)_2$ and the isocyanide in a molar ratio of 1 : 6.1; in this case we were unable to detect the formation of the $[Co(RNC)_4P]^+$ cation.

The reaction of $CoI_2(PPh_3)_2$ with $p\text{-}CH_3C_6H_4NC$ in acetone proceeds differently producing only a small

amount (18%) of the expected compound $[Co(RNC)_3P_2]I$, the predominant reaction product being the known Co(II) complex $Co(RNC)_4I_2$.[8] This result is in contrast to the successful reduction of $CoI_2(PR_3)_2$ with carbon monoxide leading to $CoI(CO)_2(PR_3)_2$.[9]

The cation $[Co(RNC)_4P]^+$ is readily transformed into a very stable cation $[Co(RNC)_3P_2]^+$ by reaction with an excess of phosphine. Thus $[Co(RNC)_3P_2]Cl$ was obtained by treating $[Co(RNC)_4P]Cl$ with PPh_3 in benzene as an insoluble product. The tris-isocyanide-bis-triphenylphosphine complexes were isolated in a form of orange yellow crystals, which are also diamagnetic and uni-univalent electrolytes in solution. They show high melting points (175—205 °C) and unusual stability against oxygen and reducing agents.

Failure of isolation of pure $[Co(RNC)_4P]X$ suggests the presence of equilibrium (1) in solution. Thus an acetone solution containing equimolar amounts of $[Co(RNC)_3P_2]ClO_4$ and $[Co(RNC)_5]ClO_4$ was prepared (at 22 °C) to follow reaction (1) with ^1H NMR.

$$2[Co(RNC)_4P]^+ \rightleftarrows [Co(RNC)_3P_2]^+ + [Co(RNC)_5]^+ \quad (1)$$

The spectrum indicates that $[Co(RNC)_4P]ClO_4$ is formed in about 70% yield within 5 min after the mixing and that the concentration of $[Co(RNC)_4P]ClO_4$ remains practically constant after 2 days. The equilibrium is apparently favorable for the formation of $[Co(RNC)_4P]^+$. However, an accurate measurement of this equilibrium would be hampered as the following observation implies. When $NaClO_4$ was added to an ethanol solution of $[Co(RNC)_4P]_2CoCl_4$ the least soluble complex $[Co(RNC)_3P_2]ClO_4$ (100% purity) was slowly precipitated out, whereas the addition of $NaClO_4$ to the cold (below 10 °C) methanol solution caused rapid precipitation of $[Co(RNC)_4P]ClO_4$ (about 90% purity).

Structure. The ^1H NMR spectrum of complex $[Co(CH_3C_6H_4NC)_5]ClO_4$[10] shows a singlet absorption at τ 7.58 (15 H) assignable to the methyl protons and a slightly broad singlet at τ 2.68 (20 H) due to the ring protons (Fig. 1). An infrared study on $[Co(C_6H_5NC)_5]ClO_4$[11] suggested the molecular structure to be trigonal bipyramid. Later the stereochemistry for $[Co(CH_3NC)_5]ClO_4$ was established by a single-crystal X-ray analysis.[12] By analogy the same stereochemistry may be assumed for $[Co(p\text{-}CH_3C_6H_4NC)_5]ClO_4$. Unexpectedly the ^1H NMR spectrum shows

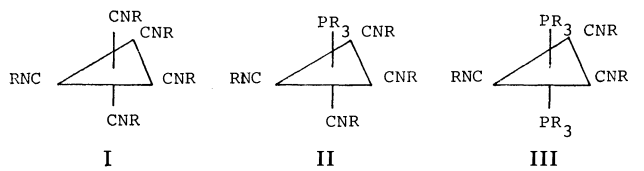

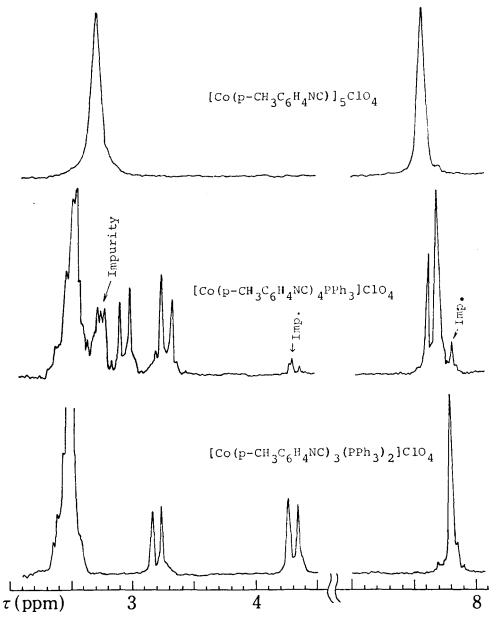

Fig. 1. NMR spectra of *p*-tolylisocyanide Co(I) complexes.

only one sharp singlet resonance for the methyl protons implying the stereochemical non-rigidity in solution[4] or the rapid ligand exchange.[4a]

The NMR spectrum of $[Co(RNC)_3P_2]ClO_4$ shows a singlet at τ 7.80 (~9 H), and two doublet resonances with coupling constant 8 Hz due to ring protons at τ 4.28 (~6 H) and τ 3.17 (~6 H). In addition to resonances a complex peak (~30 H) appeared at τ 2.46, which is assignable to the ring protons of the triphenylphosphines (Fig. 1). The observation of one sharp singlet for the methyl protons suggests equivalence with respect to the isocyanide ligation. Consistent with this is the AB type resonance for the isocyanide ring protons. Thus the complex is deduced to have a trigonal bipyramidal structure with the two phosphine ligands at axial positions (III).

The NMR spectrum of the $[Co(RNC)_4P]^+$ cation was somewhat complicated owing to the contamination of $[Co(RNC)_5]^+$ and $[Co(RNC)_3P_2]^+$. Subtraction of the absorptions due to the latter two leaves a spectrum showing two singlets for the methyl protons at τ 7.68 (~9 H) and 7.62 (~3 H), and three doublet resonances for ring protons at τ 3.25 (J 8 Hz, 6 H), 2.90 (J 8 Hz, 6 H), and 2.70 (J 5 Hz, 4 H). Based on the coupling schemes and the intensity data, the ring proton resonances at τ 3.25 and τ 2.90 (12 H), a typical AB type spectrum for *para*-disubstituted aromatic ring protons, are assigned to those of three equivalent *p*-tolylisocyanide ligands and the one at τ 2.70 (~4 H) with J=5 Hz to the ring protons of the axial isocyanide ligand. The assignment is supported by the intensity ratio (3/1) for the methyl protons. Thus a trigonal bipyramidal structure (II) is also confirmed.

It may be of interest to examine the infrared spectra. Table 1 summarized the CN stretching absorptions measured in Nujol mull and in acetone solution. The CN stretching frequencies of $[Co(PhNC)_5]^+$ have been reported by Cotton and Parish,[11] who observed with a rock-salt prism two CN stretching bands corresponding

8) L. Malatesta, A. Sacco, and L. Mattiello, *Gazz. Chim. Ital.*, **83**, 499 (1953).
9) M. Bressan, B. Corain, P. Rigo, and A. Turco, *Inorg. Chem.*, **9**, 1733 (1970).
10) L. Malatesta and A. Sacco, *Z. Anorg. Allgem. Chem.*, **273**, 247 (1953).
11) F. A. Cotton and R. V. Parish, *J. Chem. Soc.*, **1960**, 1440.
12) F. A. Cotton, T. G. Dunne, and J. S. Wood, *Inorg. Chem.*, **4**, 318 (1965).

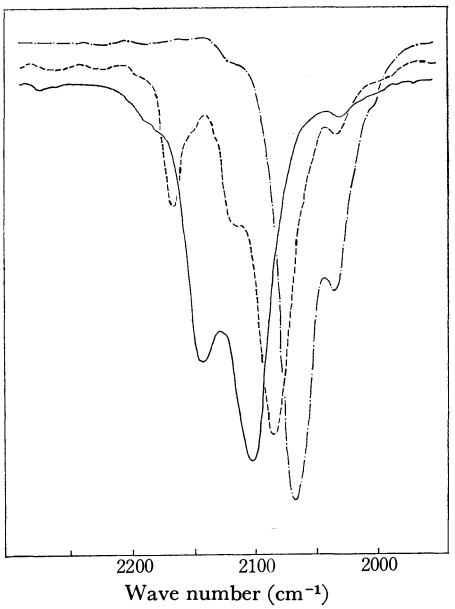

Fig. 2. IR spectra in the CN stretching region of *p*-tolyliso-cyanide Co(I) complexes. ——: $[Co(p\text{-}CH_3C_6H_4NC)_5]ClO_4$, ----: $[Co(p\text{-}CH_3C_6H_4NC)_4(PPh_3)]ClO_4$, —·—: $[Co(p\text{-}CH_3C_6H_4NC)_3(PPh_3)_2]ClO_4$.

to the E′ and A_2'' modes. Our solution spectrum (Fig. 2) for $[Co(RNC)_5]^+$ measured with a grating spectrometer also shows two strong CN bands as expected for the trigonal bipyramidal configuration. If $[Co(RNC)_4P]^+$ has C_{3v} symmetry, it will require three CN stretching bands ($2A_1$ and E). Two medium and one strong absorptions are observable; the intensity data suggest that the band at 2088 cm^{-1} corresponds to E mode vibration and the other two bands of medium intensity to A_1 mode. For the isostructural (C_{3v}) penta-coordinate carbonyl complexes of a formula $ML(CO)_4$, where M is Fe or Co and L is PR_3, SiR_3, SnR_3, GeR_3, *etc*, the carbonyl stretching band of the lowest frequency was assigned to E mode and the two higher bands to A_1 mode.[13] The cation $[Co(RNC)_3P_2]^+$ of D_{3h} symmetry should show only one CN stretching (E′). The strong band at 2067 cm^{-1} is presumably assignable to E′ mode vibration. In addition to the fundamental vibration a medium intensity band appears at 2035 cm^{-1}. Very weak additional bands also occur for $[Co(RNC)_4P]^+$ and $[Co(RNC)_5]^+$. Observation of more bands than required by the group theory is not uncommon for complexes ligated by CO, C≡N⁻, or RNC.[14] A rationale could be a combination or overtone band whose intensity is gained by Fermi resonance with the fundamental, a deviation from the idealized symmetry[11] which renders the totally symmetric mode slightly infrared active, or a ^{13}C isotopic band. We have no proof at the moment for discernment of these effects. However, we regard the weak absorptions to be non-fundamental. Despite complications, an important feature is observable from Fig. 2. The most intense bands corresponding to either E or E′ mode are the radial modes, decrease in wave numbers along the series: $[Co(RNC)_5]^+ > [Co(RNC)_4P]^+ > [Co(RNC)_3P_2]^+$. The decrease in CN stretching frequencies is explicable in terms of the increase in back donation to the equatorial isocyanide ligands due to the increase in number of the more electron-donating PPh_3 molecule.[15a] This view receives further support from the NMR spectroscopic study below.

NMR Spectra. Free *p*-tolylisocyanide in $CDCl_3$ shows a sharp signal at τ 7.66 which is due to the methyl protons and a somewhat broader signal at τ 2.8 whose top splits slightly into doublet (J 2 Hz). In *para*-disubstituted benzenes additivity of the substituents effect on the chemical shift of the ring protons are generally recognized and interpreted in terms of pi-electron densities.[15,16] However, no report along this line has been made on the aromatic isocyanides. Further we are unable to locate the isocyanide group in the Hammett scale. As the electron-attracting property is apparent,[17] it is unlikely that CH_3– and C≡N– groups are comparable with respect to the overall electronic effect (mesomeric plus inductive effect). The proximity between the chemical shifts for H_o and H_m appears to be a fortuitous result derived from the substituent electronic effect plus the neighbor

Table 1. IR spectra[a] of the complexes in the $\nu_{C\equiv N}$ stretching region

Compound[b]	Nujol mull	Acetone solution
$[Co(RNC)_3P_2]Cl$	2083(vs), 2058(vs), 2035(vs)	2067(vs), 2035(m)
$[Co(RNC)_3P_2]Br$	2083(vs), 2060(vs), 2035(vs)	2067(bs), 2035(m)
$[Co(RNC)_3P_2]I$	2083(vs), 2059(vs), 2035(vs)	2067(vs), 2035(m)
$[Co(RNC)_3P_2]ClO_4$	2083(vs), 2057(vs), 2033(vs)	2067(vs), 2035(m)
$[Co(RNC)_3P_2]BPh_4$	2064(vs), 2030(s)	2067(vs), 2037(m)
$[Co(RNC)_4P]Cl$	2165(m), 2122(m), 2080(vs, br), 2030(m)	2169(m), 2122(m), 2088(vs), 2035(vw)
$[Co(RNC)_4P]ClO_4$	2167(m), 2118(m), 2083(vs, br), 2033(w)	2168(m), 2120(m), 2088(vs), 2035(vw)
$[Co(RNC)_4P]BPh_4$	2164(m), 2115(m), 2080(vs, br), 2033(m)	2168(m), 2115(m), 2088(vs), 2035(vw)
$[Co(RNC)_4P]_2[CoCl_4]$	2168(s), 2120(s), 2080(vs, br),2035(m)	2168(m), 2120(m), 2087(vs), 2035(w)[c]
$[Co(RNC)_5]ClO_4$	2147(s), 2097(vs), 2035(m)	2146(s), 2105(vs)

a) vs=very strong, s=strong, m=medium, w=weak, vw=very weak, br=broad
b) R=$CH_3C_6H_4$ c) chloroform solution

13) J. Dalton, I. Paul, J. G. Smith, and F. G. A. Stone, *J. Chem. Soc., Ser. A*, **1968**, 1199.
14) F. A. Cotton and F. Zingales, *J. Amer. Chem. Soc.*, **83**, 351 (1961).
15) J. S. Martin and B. P. Dailey, *J. Chem. Phys.*, **39**, 1722 (1963).
15a) S. Otsuka, T. Yoshida, and Y. Tatsuno, *J. Amer. Chem. Soc.*, **93**, 6462 (1971).
16) T. K. Wu and B. P. Dailey, *J. Chem. Phys.*, **41**, 2796 (1964).
17) I. Ugi, "Isonitrile Chemistry," Academic Press, New York (1971), pp. 217—222.

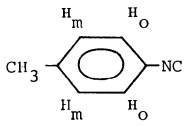

magnetic anisotropy. Thus the known empirical equation (1)[15] for the substituent electronic effects, should be modified into Eq. (2) to accommodate the latter effect,[18-21] where σ_o is the chemical shift for H_o, σ_M the magnetic screening constant, and α determines the contribution.

$$\sigma_E = d_o(R_1) + \gamma(R_1)d_m(R_4) \quad (1)$$

$$\sigma_o = \sigma_E + \alpha\sigma_M \quad (2)$$

The chemical shift for H_m may be expressed by an equation analogous to Eq. (1), since the neighbor anisotropy decreases with the cube of distance.[22] An interesting fact is a nearly linear correlation between the NC stretching frequencies (E or E′ mode) and the chemical shifts of ring protons. The H_m or H_o proton shows a regular up-field shift in the series $[Co(RNC)_{5-n}P_n]^+$ (n=0, 1, 2). The $\Delta\nu$ (difference with respect to ν_{NC} of free *p*-$CH_3C_6H_4NC$) and $\Delta\tau$ (difference with respect to τ values of free *p*-$CH_3C_6H_4NC$) values for n=0, 1, 2 are respectively 26, 43, 64 (cm^{-1}) and −0.12, 0.45, 1.48 (ppm) for H_m; $\Delta\tau$ values for H_o are −0.12, 0.10, and 0.37 (*vide infra* for the assingment). These values reasonably satisfy relation $\Delta\tau=k\Delta\nu$. Since vibronic characteristics of a bond are not influenced by the magnetic property, the linear correlation implies either a negligible contribution of term $\alpha\sigma_M$ or a linear dependency of the magnetic term upon the electronic term σ_E. Although it is difficult to assess the absolute value of term $\alpha\sigma_M$ (and the two factors may be inseparable), a qualitative discussion can be given as follows. The magnetic field due to electric currents at an acetylenic or an isocyanide group[19,23] is expected to decrease with increase in electron drainage into the anti-bonding π orbital. This is understandable if we consider an effective overlap of pπ orbitals of a CN group with those of the aromatic ring, which occurs only with one of the two orthogonal pπ double bonds of the CN group. The overlap leads to a delocalized system M—C≡N—Aryl, thus relating to the effectiveness of the metal-ligand π-back bonding. The axial symmetry of a triple bond responsible for the magnetic anisotropy will readily be destroyed with inequal participation of the pπ bonds in the delocalized system M—C≡N—Aryl. Interaction of moiety M–C≡N– with the aromatic ring attached was demonstrated explicitly by unpaired spin density in some paramagnetic metal complexes.[24] Coefficient α decreases linearly with increase in dπ-pπ back bonding, and the abnormal ^1H NMR spectrum of *p*-$CH_3C_6H_4NC$ relaxes dramatically to that of $[Co(RNC)_4P]^+$ or $[Co(RNC)_3P_2]^+$ typical for *para*-disubstituted benzenes.

It is evident that the contribution of σ_M in free *p*-$CH_3C_6H_4NC$ renders the chemical shift for H_o higher than that for the coordinated isocyanide molecule bringing up the chemical shift of H_o near to that of H_m. If this is the case, the two ring proton resonances in $[Co(RNC)_4P]^+$ and $[Co(RNC)_3P_2]^+$ can be assigned; *i.e.*, the higher field resonance to H_m and the lower one to H_o. A slight downfield shift (−0.12 ppm relative to free(*p*-$CH_3C_6H_4NC$) observed for the ring protons in $[Co(p\text{-}CH_3C_6H_4NC)_5]^+$ is also explicable in terms of a σ-type donation from the isocyanide ligand to the Co(I) ion.

18) H. Spiesechke and W. G. Schneider, *J. Chem. Phys.*, **35**, 731 (1961).
19) H. M. McConnell, *ibid.*, **27**, 226 (1957).
20) J. A. Pople, *Proc. Roy. Soc., Ser. A*, **239**, 541, 550 (1957).
21) G. S. Reddy and J. H. Goldstein, *J. Chem. Phys.*, **36**, 2644 (1963); *ibid.*, **39**, 3509 (1962).
22) S. Castellano and J. Lorenc, *J. Phys. Chem.*, **69**, 3553 (1965).
23) A. A. Bothner-By and J. A. Pople, *Ann. Rev. Phys. Chem.*, **16**, 43 (1965).
24) W. D. Horrocks, Jr., R. C. Taylor, and G. N. LaMar, *J. Amer. Chem. Soc.*, **86**, 3031 (1964).

The Dissolution of $CaMg(SiO_3)_2$ in Acid Solutions[1]

Isao SANEMASA* and Takashi KATSURA

Department of Chemistry, Faculty of Science, Tokyo Institute of Technology, Ookayama, Meguro-ku, Tokyo 152

(Received February 15, 1973)

The dissolution phenomena of synthesized diopside, $CaMg(SiO_3)_2$, and a glassy material of the same composition in an acid solution were studied. The results observed in the dissolution of the glass were as follows; the molar concentrations of Ca dissolved in the solution are equal to those of Mg throughout the dissolution of the glass. The rate at which the cations go into solutions are proportional to the surface area up to about a 60% dissolution. The dissolution behavior of silica is similar to that of cations. A residual layer rich in silica is formed, one which is no longer dissolved after the removal of the cations. The results observed in the dissolution of the crystalline diopside were as follows; there is an initial rapid dissolution of the components, followed by another process. The molar ratios of the Ca ions to the Mg ions, and of each cation to silica in the solutions, are larger than those in the solid during the course of the reaction; they are especially large in the initial dissolution stage. An essential feature of diopside dissolution is that the Ca ions are more readily removed from the crystal than are the Mg ions. This fact is also confirmed in the natural diopside crystal. While the rates of the dissolution of the cations are not affected by the concentrations of HCl and $HClO_4$, the concentration of H_2SO_4 does have an influence. Diopside cannot be dealt with as a single species participating in the heterogeneous reaction because its various components show selective dissolution. The mechanism of the dissolution of diopside will be discussed in connection with its structure.

Dissolution studies of minerals in various solutions have been made mainly from the practical point of view.[2,3] Only a few studies have been reported on the silicate structure and its reactivity in solution. Luce *et al.*,[4] however, who studied the dissolution of serpentine, forsterite, and enstatite, reported on the relationship between the silicate structure and the diffusion coefficients of silicon and magnesium.

In a previous paper,[5] the dissolution phenomena of olivine in various acid solutions were reported.

Pyroxenes can be divided, according to the crystal systems, into orthorhombic and monoclinic pyroxenes. The essential feature of all pyroxenes, however, is the linkage of SiO_4 tetrahedra by sharing two out of four corners, thus forming continuous chains with the composition of $(SiO_3)_n$,[6] in contrast to the olivine structure with fundamental isolated SiO_4 tetrahedra. Diopside, which has the monoclinic form, was studied crystallographically by Warren and Bragg,[7] and its unit cell was found to be $4[CaMg(SiO_3)_2]$.

In this experiment, the dissolution phenomenon of diopside in acid solutions was studied in comparison with that of a glassy material of the same composition in order to obtain some information concerning the reactivity and the solid structure.

Experimental

Materials. In the present study, diopside was synthesized, because natural diopside always contains some iron. The synthetic method was as follows. Firstly, appropriate amounts of CaO, MgO, and SiO_2 corresponding to the composition of $CaMg(SiO_3)_2$ were thoroughly mixed with ethyl alcohol. Then the mixture was heated at 1450 °C and quenched in cold water to obtain a glassy material. The glass was crushed in an agate mortar and mixed well. The operations of mixing, melting, and rapid cooling were repeated three times. The glass was heated overnight at 1100 °C to obtain a completely crystallized phase. The powder X-ray diffraction pattern is in complete agreement with the NBS natural diopside data.[8] Electron microprobe analysis[9] showed homogeneous particles (about 5 μ). The synthesized diopside and the glass were ground in an agate mortar and then fractionated by suspension in methyl alcohol. Two kinds of particle sizes of the glass were obtained: one was 20—40 μ, and the other was 40—80 μ. The particle size of the synthesized diopside was 20—40 μ, but strict uniformity of size could not be obtained because of the brittle property of the particles.

In this study, a finely powdered sample of a natural diopside was used; it had been obtained from Gongen-yama, Ehime Prefecture. This diopside had the following chemical composition[10]: SiO_2, 51.86; TiO_2, 0.20; Al_2O_3, 1.02; Fe_2O_3, 0.99; FeO, 1.73; MnO, 0.02; MgO, 17.09; CaO, 25.24; Na_2O, 0.08; K_2O, 0.06; $H_2O(-)$, 0.25; $H_2O(+)$, 1.88%. The atomic percentages of Mg, Fe, and Ca were 46.6, 4.0, and 49.4 respectively.

Reagents, Equipment, and Measurements. All the chemicals used were of an analytical-reagent grade. The apparatus used in the present study was the same as that described in the previous paper[5] except for the volume of the reaction vessel, which was 200 ml in the present study. The powdered sample (100—200 mg) was dispersed, with small amounts of water, in 100 ml of an acid solution, after which the mixture was stirred at 600 rpm. The rate of the dissolution of the sample was not affected by stirring in the range from 150 to 1200 rpm. Aliquots of the solution were

* Present address: Department of Chemistry, Faculty of Science, Kumamoto University, Kurokami-machi, Kumamoto.

1) Read at the Symposium on Geochemistry of the Geochemical Society of Japan and the Chemical Society of Japan, Sendai, Sept., 1972.

2) C. W. Corrence, *Clay Minerals Bull.*, **26**, 249 (1961).

3) R. Wollast, *Geochim. Cosmochim. Acta*, **31**, 635 (1967).

4) R. W. Luce, R. W. Bartlett, and G. A. Parks, *ibid.*, **36**, 35 (1972).

5) I. Sanemasa, M. Yoshida, and T. Ozawa, This Bulletin, **45**, 1741 (1972).

6) W. A. Deer, R. A. Howie, and J. Zussaman, "Rock-Forming Minerals," Vol. 2, Longmans, London (1965), p. 2.

7) B. Warren and W. L. Bragg, *Z. Krist.*, **69**, 68 (1928).

8) Nat. Bur. Stand. Monograph 25, sec. 5, 17 (1967).

9) Measurements were made by Dr. S. Aramaki of The Earthquake Research Institute of The Univ. of Tokyo.

10) Sample was given by and its analysis was done by Mr. H. Haramura of The University of Tokyo.

pipetted out at various reaction times and immediately filtered through a membrane-filter (0.45 μ in pore size), and the filtrates were submitted to chemical analysis. The silica was determined spectrophotometrically using the silicomolybdate yellow method. The calcium and magnesium were determined by atomic absorption measurements after the addition of a lanthanum buffer[11] to avoid interference due to the presence of silica.

Results and Discussion

Dissolution of $CaMg(SiO_3)_2$ Glass. Figure 1 shows the relationship between the concentrations of Ca dissolved in HCl solutions and the reaction times under various conditions. The molar concentrations of Mg which are leached into the solutions were found to be nearly equal to those of Ca at any time under varying experimental conditions. Figure 2 shows the relationship between the concentrations of the dissolved silica and the reaction times under different conditions. From Figs. 1 and 2, it may be noted that the dissolution behavior of the cations and silica is virtually the same. The concentrations of silica, however, are much lower than those of the cations when their relative contents in the glass are taken into account. After the summation of Ca and Mg, the molar ratios to SiO_2 in the solution are almost constant; the ratio is approximately 6 throughout the reaction. Most of the cations in the sample were depleted by the reaction after reaching a constant value of about 4.25 mM. The broken lines in Fig. 1 show the results of experiments in which twice the amount of the sample was used as that represented by the solid lines. The constant value of 8.5 mM of the dotted lines in Fig. 1 is just twice as high as that of the solid lines, regardless of the sample size, the acid concentration, and the temperature. On the other hand, only 15% of the entire silica of the sample was dissolved when the concentration of dissolved silica approached a value of 1.4 mM, as represented by the solid lines in Fig. 2. No colloidal silica was found under the present experimental conditions. When taking 200 mg of a 40—80 μ size sample, the concentrations of silica in the 0.1 and 1 N HCl solutions are 2.3 and 2.6 mM respectively after reaching a constant value. These values are significantly lower than the value of 2.8 mM calculated from the 100 mg sample. This suggests that the dissolution of a silica-rich layer formed by the reaction depends on the acid concentration as well as on the specific surface area of the sample.

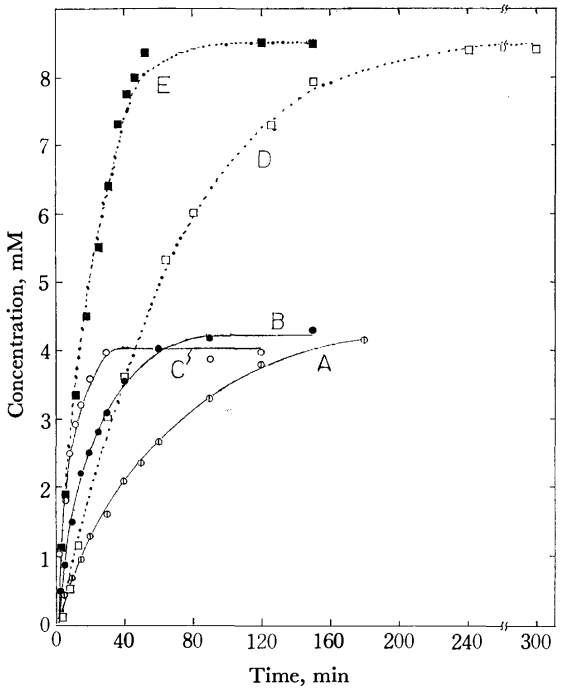

Fig. 1. Dissolution of calcium from the glass when taken 100 mg of 20—40 μ sample in 0.1 N HCl at 5 (A), 15 (B), and 25 °C(C) and when taken 200 mg of 40—80 μ sample in 0.1 N (D) and 1 N (E) HCl at 10 °C.

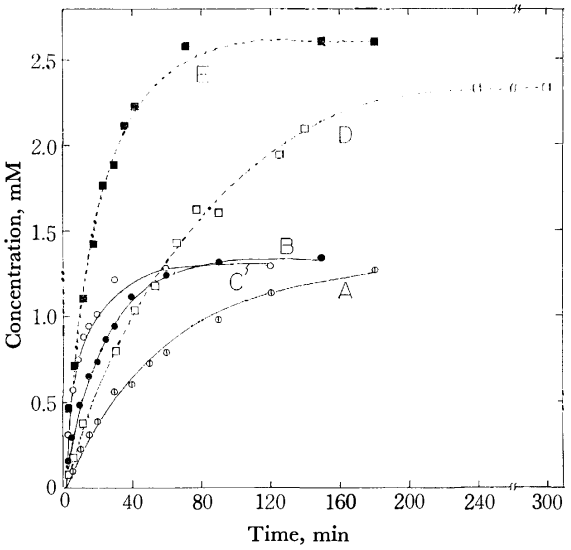

Fig. 2. Dissolution of silica from the glass. Each mark corresponds to that in Fig. 1.

Since the silica of the glass does not affect the dissolution process of the cation, regardless of the particle size and other experimental conditions, the cations in the glass may be considered to be independent parts of the solid. Consequently, the rate of the dissolution of the cation can be treated in the same way as in the case of olivine,[5] in which

$$-\mathrm{d}w/\mathrm{d}t = k_0 sC \qquad (1)$$

where w and s indicate the weight and the surface area of the "particle" which remains at the reaction time, t, respectively; where k_0 is the rate constant per unit area, and where C is the concentration of the reactant. Equation (2) may be derived from Eq. (1) as has been described in a previous paper;[5]

$$1-(1-\alpha)^{1/3} = 1/3\, kW_0^{-1/3}t \qquad (2)$$

where k is a constant and where α has the following definition;

$$\alpha = (W_0 - W)/W_0 = (\Delta W)_{t,\mathrm{sol}}/W_0$$

where W_0 is the weight of the sample taken at time zero and where $(\Delta W)_{t,\mathrm{sol}}$ is the weight loss of the cation in the sample at time t, as can be determined by

11) R. Nakagawa, M. Nanbu, and Y. Ohyagi, *Nippon Kagaku Kaishi*, **1**, 60 (1972).

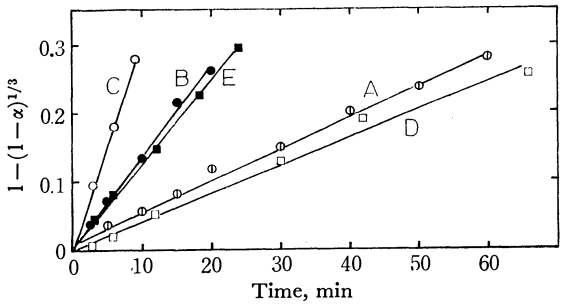

Fig. 3. Plots of dissolution rate of calcium from the glass according to Eq. (2). Each mark corresponds to that in Fig. 1.

the concentrations of the cations in the solution. The plot of $1-(1-\alpha)^{1/3}$ *vs.* t is shown in Fig. 3. As a matter of convenience, the plots are limited only to the case of the dissolution of Ca, but there is no distinction between Ca and Mg. Figure 3 gives straight lines up to about a 60% dissolution of the cations of the glass. This suggests that the rates of the dissolution of cations are directly proportional to the surface area of the solid sample. The relationship between the slopes of the straight lines in Fig. 3 and the reaction temperature is illustrated by the Arrhenius plot shown in Fig. 4. The apparent activation energy is found to be 16 kcal/mol.

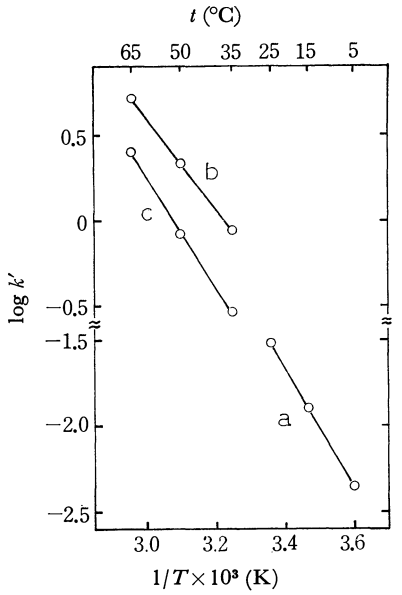

Fig. 4. Arrhenius plots for the dissolution of cation from the glass and diopside.
a: Ca from the glass, b: Ca from diopside, C: Mg from diopside.
In the case of the glass, k' corresponds to $1/3\ kW_0^{-1/3}$ in Eq. (2), while in the case of diopside, k' is estimated from the slopes in the plots of square concentration of each cation against time in Fig. 6 and is then expressed in mM^2/hr.

In order to give a more detailed explanation of the mechanism of the dissolution process of the cations of the glass, experiments were performed in which the cations were added at time zero. The results of these investigation are shown in Fig. 5. The concentrations of Ca and Mg added alternatively to a 0.1 N HCl solution at time zero were 3.5 and 1.99 mM respectively. From Fig. 5 it is evident that the added cation of Ca or Mg does not affect the dissolution of the Ca and Mg of the glass.

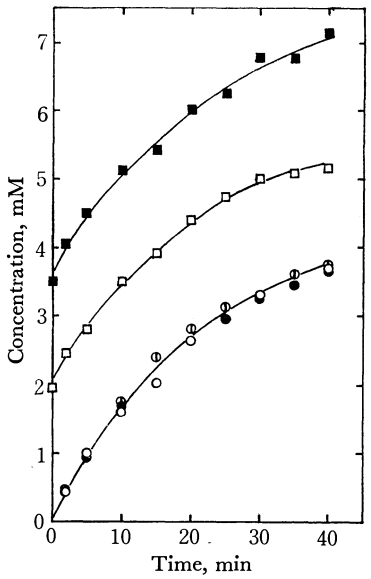

Fig. 5. Effect of added calcium, 3.50 mM (■) and magnesium, 1.99 mM (□) on the rate of dissolution of cation from the glass by using 0.1 N HCl at 15 °C.
○: none added, ⓘ: Ca when Mg added, ●: Mg when Ca added.

Some of the results obtained in the present study are suitable to illustrate the mechanism of the dissolution of the glass in an acid solution. When cations on the surface of the glass pass into the solution by means of a reaction at the interface, hydrated protons diffuse into the solid and are adsorbed on negatively-charged oxygen ions. Then, cations of the glass, in which they are distributed at random and are undistinguishable from each other, are transported to the solution, thus leaving cavities. This is followed by a transportation to the bulk solution, involving diffusion through the residual layer of the silica. A part of the hydrated protons contained in the cavities can be used to break up the silica chain to be dissolved. The broken chains thus formed can be recombined by hydrogen bonds in various directions to form a three-dimensional framework such as silica gel. An X-ray examination of the sample after the reaction shows a broad peak corresponding to silica gel (22—23° as 2θ in CuK_α). Therefore, the dissolution of the silica of the glass appears to be accompanied by that of the cations.

According to Bircumshaw,[12] a reaction between a solid and a solution generally comprises the following steps:

(a) the transportation of solute molecules to the interface,
(b) adsorption on the surface,
(c) reaction on the surface,
(d) the desorption of reaction products, and
(e) the recession of the products from the interface.

In addition to these steps, (f) the diffusion process

12) L. L. Bircumshaw and A. C. Riddiford, *Quart. Rev.*, **6**, 157 (1952).

through the residual layer formed by the reaction, must be considered in the present case. The rate of dissolution of the cations of the glass up to about 60% is considered to be controlled by step (c) in view of the following experimental results: the stirring speed has no influence on the rate, the activation energy is quite high (16 kcal/mol), the rate obeys Eq. (2) and not the so-called parabolic law, and additional cations have no influence on the rate. However, the rate of the dissolution of the cations over 60% is gradually lowered below the value anticipated from Eq. (2). This may be attributable to the influence of the diffusion process of the cations through the residual layer of silica, the thickness of which is increasing.

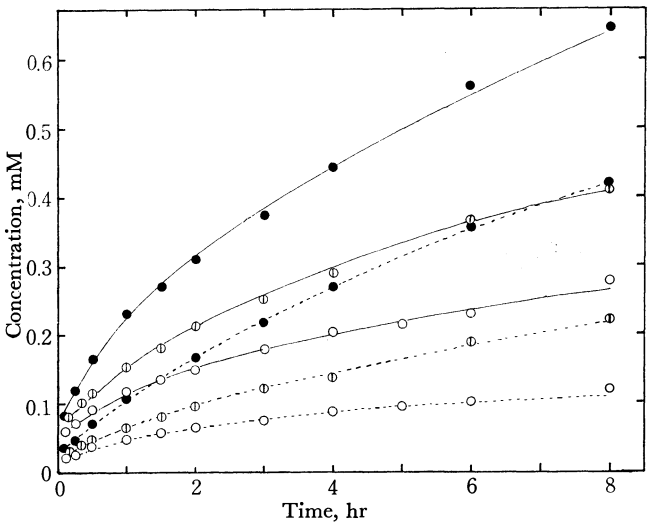

Fig. 6. Dissolution of calcium (solid) and magnesium (broken) from diopside in 0.1 N HCl at 65 (●), 50 (◐) and 35 °C (○).

The Dissolution of Diopside. Figure 6 shows the concentrations of Ca and Mg which are leached from 200 mg of the synthetic diopside with 0.1 N HCl solutions at 35, 50, and 65 °C. The molar ratios of Ca/Mg in the solutions are greater than unity, and are especially high in the earlier part of the reaction, in which the ratios are in the range from about 2 to 3. In order to ascertain the effect of the temperature on the rate of the dissolution of cations, the square concentrations of Ca and Mg in the solution are plotted against the time for the sake of convenience. Straight lines are thus obtained for Ca, while in the case of Mg linear plots can be drawn after 2 or 3 hr. The relationship between the slope of the straight line for each cation and the reaction temperature is illustrated in Fig. 4. According to the Arrhenius plot, the apparent activation energies for Ca and Mg can be estimated from Fig. 4 to be 12 and 15 kcal/mol respectively. This suggests that the rate of the dissolution of Mg is affected by the temperature change more intensively than that of Ca.

In order to investigate the effect of the acid concentration on the dissolution of diopside, experiments were carried out at 65 °C by using HCl solutions of concentrations ranging from 0.1 to 1 M. From the results, it can be seen that the concentration of HCl solutions

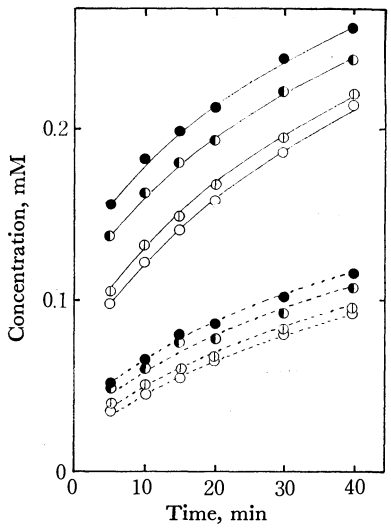

Fig. 7. Effect of HCl concentration on the dissolution of calcium (solid) and magnesium (broken) from diopside at 65 °C.
●, 1; ◐, 0.5; ◑, 0.2; ○, 0.1 N.

in this range has no influence on the rate of the dissolution of either Ca or Mg during the course of the reaction (8 hr), but is reflected only by the initially-dissolved amount of the cations. This effect was investigated in more detail by varying the concentrations of HCl solutions, with emphasis on the earlier part of the reaction (Fig. 7). It can be seen from Fig. 7 that variations in the acid concentration affect the initially-dissolved amount of Ca more intensively than that of Mg. There is an initial rapid increase in the concentration of each cation, an increase which cannot be followed by lowering both the reaction temperature and the acid concentration. The results in the $HClO_4$ solutions ranging from 0.1 to 2 N are almost the same as those obtained

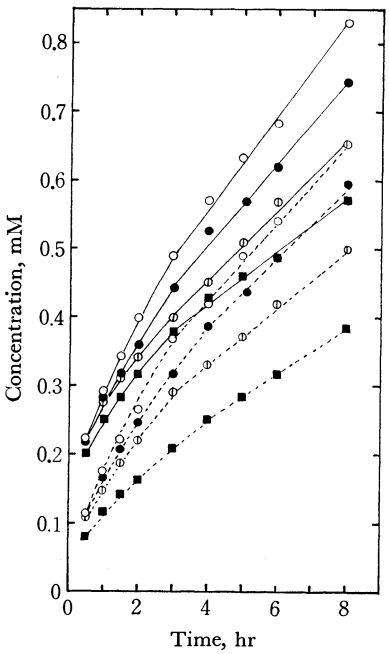

Fig. 8. Effect of H_2SO_4 concentration on the dissolution of calcium (solid) and magnesium (broken) from diopside at 65 °C.
○, 2; ●, 1; ◑, 0.5; ■, 0.1 N.

in HCl. On the other hand, the results in H_2SO_4 solutions (see Fig. 8) are different from those in HCl and $HClO_4$ solutions. From Fig. 8, it is evident that the rates of the dissolution of cations increase with an increase in the concentrations of acid, and that the concentrations of cations increase linearly with the time in the later steps of the reaction. There is also a difference in the reactivities of the cations; that is, the amount of Ca initially dissolved is about three times larger than that of Mg. Responsible for the specific action of H_2SO_4 appear to be the HSO_4^- species in the solution, as has also been observed in the dissolution of olivine[5] and gibbsite.[13]

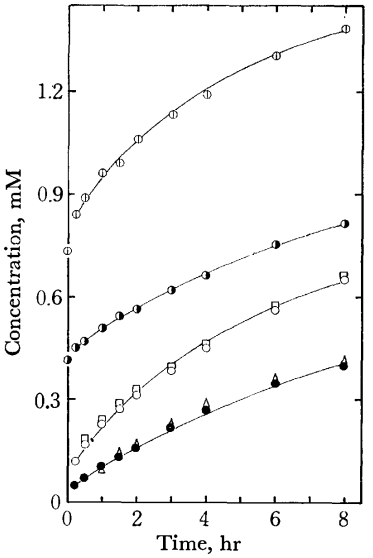

Fig. 9. Effect of added calcium, 0.73 mM (◐) and magnesium, 0.411 mM (◑) on the rate of dissolution of cation from diopside in 0.1 N HCl solutions at 65 °C.
○, Ca when none added; □, Ca when 0.411 mM of Mg added;
●, Mg when none added; △, Mg when 0.73 mM of Ca added.

In order to obtain information about the leaching of cations from diopside, experiments were carried out in which known amounts of Ca or Mg ions were added at the start of the reaction by using 0.1 N HCl solutions at 65 °C. From the results of these investigations (shown in Fig. 9), it can be seen that, on the addition of 0.73 mM of Ca or 0.41 mM of Mg, the concentration of each cation observed at any time is equivalent to the sum of the concentrations of the added and the dissolved cations. In the presence of a twofold concentration of each cation, this sum is lowered to about 10% in each case. However, this value is not precise because of an uncertainty in the determination of such a high concentration of added cation.

As the next step, the dissolution of silica from diopside was investigated. Figure 10 shows the results of a series of experiments which were carried out at 65 °C by using HCl and H_2SO_4 solutions of varying concentrations. Colloidal silica was not detectable under these experimental conditions. It can be seen from Fig. 10 that the rate of the dissolution of silica increases with an increase in the acid concentration.

13) A. Packter and H. S. Dhillon, *J. Chem. Soc., Ser. A*, **1969**, 2583.

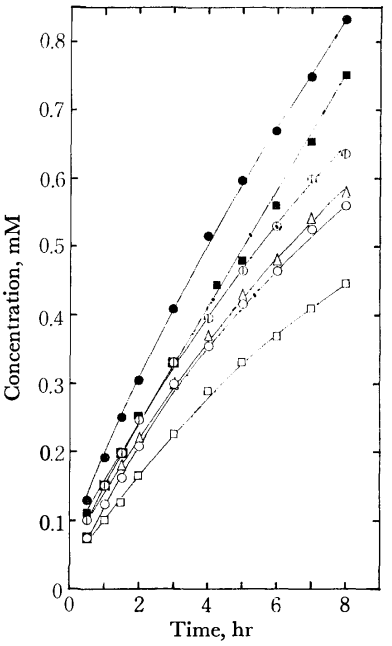

Fig. 10. Dissolution of silica from diopside at 65 °C.
HCl: ●, 1; ◐, 0.5; ○, 0.1 N. H_2SO_4: ■, 1; △, 0.5; □, 0.1 N.

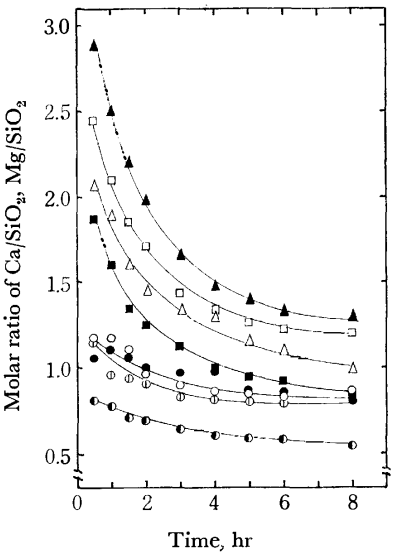

Fig. 11. Molar ratio of Ca/SiO_2 and Mg/SiO_2 in solution dissolved from diopside at 65 °C.
Ca/SiO_2: ■, 1 N HCl; □, 0.1 N HCl; △, 1 N H_2SO_4; ▲, 0.1 N H_2SO_4.
Mg/SiO_2: ◐, 1 N HCl; ◑, 0.1 N HCl; ●, 1 N H_2SO_4; ○, 0.1 N H_2SO_4.

The dependence on the time of the molar ratios of Ca or Mg to SiO_2 in the solutions under the same experimental conditions is shown in Fig. 11. From the figure it can be seen that the dissolution is selective not only with respect to Ca and Mg, but also between cations and silica, since the ratio of each cation to silica in the solid is 0.5. At higher concentrations of HCl, however, the molar ratio of Mg/SiO_2 in solution approaches that in the solid because the dissolution of silica is enhanced by an increase in the acid concentration, while that of the cation is not.

Discussion on the Dissolution of Diopside. The dissolution of diopside can be divided into two processes: one is the initial rapid dissolution, which cannot be followed even if the reaction temperature and the acid concentration are both lowered, while the other is the successive dissolution after the initial dissolution. Cations to be dissolved in the solution must be liberated from the negatively-charged oxgen ions surrounding them. On the solid surface, the distances of Ca–O and Mg–O will be slightly different from those in the "perfect" diopside lattice, as was pointed out by Pryor *et al.*[14] in their dissolution study of ferric oxide. In the diopside crystal, moreover, there are good cleavages parallel to the direction of the silica-chain arrangement. Consequently, the dissolution takes place most readily at the surface, where the energy required for dislodging the cations is smaller than in the interior. At the same time, silica is dissolved, but its amount is considerably smaller than that of the cation (see Fig. 11). This selective dissolution of silica might be due to its chain structure, which consists of SiO_4 tetrahedra. Consequently, after the removal of the cations, the silica-chain, parts of which are broken, remains, forming a residual layer containing Si–OH groups which probably shows almost the same directional arrangement as the crystal. Judging from the selective dissolution between Ca and Mg, a part of the Mg may be contained in this residual layer. The problem is, however, to find out from which direction of the silica-chain, *i.e.*, parallel or at right angles, the reactants (hydrated protons) enter into the solid and in which direction the soluble products go out. If the existence of cleavages in the diopside parallel to the direction of the chain is assumed, the reaction may proceed predominantly at right angles to the chains, and a dissolution process of the kind shown in Scheme 1 may be suggested. In the diopside, silica-chains are combined to one another by an equal number of Ca and Mg ions. After the rapid removal of cations and the severance of the silica-chain, which may be caused by the adsorption of hydrated protons on the negatively-charged oxygen ions of the solid surface, the hydrated protons enter the solid through the open parts of the chain;

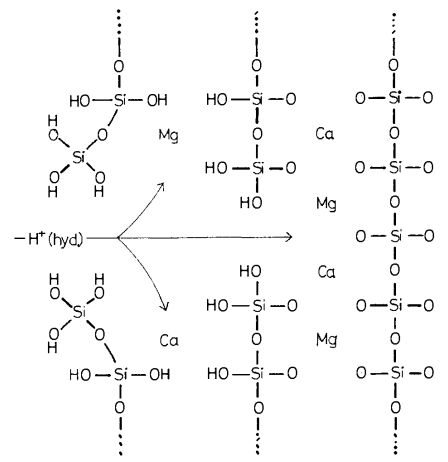

Scheme 1.

a part of them permeate parallel to the chains, and the remainder, at right angles. As cations are removed from the chains, these are set free just as if opening a "fastener" and undergo successive hydrolysis to be dissolved. The hydrated protons participating in the reaction may mainly be consumed in the hydrolysis reaction, because the rates of the dissolution of cations are not affected by the concentration of acid, while that of silica is dependent on the acidity. Consequently, the dissolutions of the cations and the silica appear to be independent of each other. In this respect, there is a substantial difference between diopside and its glass (see Figs. 1, 2, and 11). This difference may be attributed to residual silica layers in diopside which are not in a suitable arrangement to be recombined in the three-dimensional networks as they are in the glass.

It is problematical whether or not the rates of dissolution of cations are controlled by their diffusion process through the channels in the residual silica layers, as is shown in Scheme 1. It is, however, somewhat difficult in our present study to clarify the rate-determining step for two reasons. One reason is the uncertainty of the sample size. A part of the synthesized diopside probably consists of agglomerates of particles of a smaller size; therefore, the particle size is not uniform. The other is that the amounts of cations dissolved into the solution are only 8% or less of the solid under the selected experimental conditions. Regardless of these disadvantages, though, the results summarized below can be used in examining the problem of diffusion:

(1) The concentrations of the cations increase almost linearly with $t^{1/2}$ except for the initial rapid stages in HCl and $HClO_4$ (Fig. 6).
(2) While in H_2SO_4 they increase almost linearly with t in the later stages of the reaction (Fig. 8).
(3) The apparent activation energies of Ca and Mg are different from each other (Fig. 4).
(4) The addition of cations has no influence on the rates of dissolution (Fig. 9).
(5) Although the molar ratio of Mg/SiO_2 in the 1 N HCl solution approaches that in the solid as the reaction proceeds (Fig. 11), the dissolution mode of Mg is not changed.

Of these results, (1) seems to indicate that the rate of the dissolution of cations is controlled by the diffusion of the reactants and/or the reaction products. On the other hand, (2), (4), and (5) do not seem to show that the rate of dissolution of cation is controlled by the diffusion of the reaction products. Furthermore, (2) and (3) seem to give little evidence that the rate of dissolution of cations is controlled by the diffusion of the reactants. Consequently, the present experimental results do not necessarily support the assumption that the rate of the dissolution of cations is controlled by the diffusion process only. A better picture or a more detailed mechanism of acid-reactivity of diopside in connection with the silica-chain structure could be obtained by employing a single crystal.

In the dissolution of cations, there is an important and substantial difference between diopside and its

14) M. J. Pryor and U. R. Evans, *J. Chem. Soc.*, 3330 (1947).

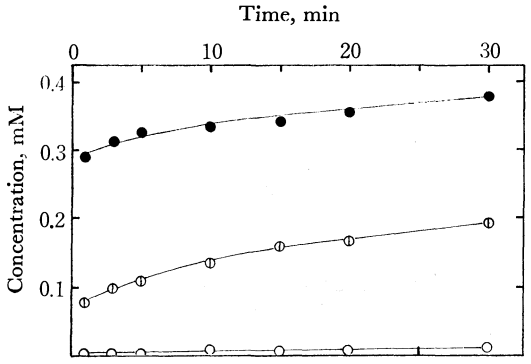

Fig. 12. Dissolution of calcium (●), magnesium (◐), and iron (○) from natural diopside in 0.1 N HCl at 65 °C.

glass. That is, in the glass the dissolution behavior of Ca and that of Mg are undistinguishable from each other, while in diopside Ca is more readily dissolved than Mg, especially in the preliminary stage of the reaction. This phenomenon appears to be essential for diopside; it was also observed in the dissolution of natural diopside (see Fig. 12). It can be seen from Fig. 12 that the concentration of Ca which is initially dissolved is more than three times larger than that of Mg, and that the initial rapid dissolution of the cations is promoted because of the large specific surface area of the pulverized sample, with its abundant cleavages. The reason why Ca in diopside passes more readily into a solution than does Mg might be attributable, when this case is compared with that of glass, to the difference in the states of the cations. That is to say, in the glass a fused structure is "frozen in" in which Ca and Mg are randomly distributed and in which the cations are kept as far apart as possible by vigorous thermal movement and by mutual repulsion. On the other hand, in diopside Ca is surrounded by eight, and Mg by six oxygen atoms. However, we cannot offer a more detailed explanation of the situation.

We wish to express our deep gratitude to Dr. Takejiro Ozawa and to Dr. Minoru Yoshida of the Tokyo Institute of Technology for their guidance and encouragement throughout this work. We are also indebted to Dr. Shigeo Aramaki of The Earthquake Reserch Institute of The University of Tokyo, who examined the synthetic diopside by means of electron-micro-probe analysis. We wish to express our thanks to Dr. Mitsuo Muramatsu of Tokyo Metropolitan University for his helpful discussion. Thanks are also due to Mr. Hiroshi Haramura, who kindly supplied us with an analyzed sample of natural diopside.

BULLETIN OF THE CHEMICAL SOCIETY OF JAPAN, VOL. 46, 3422—3426 (1973)

Polarographic Studies of the Rates of the Dissociation Reactions of Cobalt(II)-Iminodiacetate, -Aspartate, and -2,2′-Ethylenedioxydi(ethylamine)-*N*,*N*,*N*′,*N*′-tetraacetate Complexes

Mutsuo KODAMA

Department of Chemistry, College of General Education, Hirosaki University, Bunkyo, Hirosaki 036

(Received March 22, 1973)

The cobalt(II)-IDA, -Asp, and -GEDTA complexes produce kinetic wave due to their dissociation preceding the electron-transfer step at the electrode surface. From an experimental examination of the nature of these kinetic waves, the dissociation mechanisms were determined to be:

i) IDA and Asp systems,

$CoX_2^{2-} \rightleftarrows CoX^0 + X^{2-}$ rate-determining step

$CoX^0 + 2e^- + Hg \rightleftarrows Co(Hg) + X^{2-}$

ii) GEDTA system,

$CoY_2^{6-} \rightleftarrows CoY^{2-} + Y^{4-}$ in a rapid equilibrium

$CoY^{2-} \rightleftarrows CoY^{2-}{}^*$ rate-determining step

$CoY^{2-}{}^* + 2e^- + Hg \rightleftarrows Co(Hg) + Y^{4-}$

where $CoY^{2-}{}^*$ is the electroactive cobalt(II)–GEDTA complex produced upon the partial dissociation of the normal cobalt(II)–GEDTA complex with a 1:1 composition. From the relative rate constants for these complexes, the detailed structures of the reaction intermediates in their dissociation were also obtained.

In earlier papers,[1,2] we reported systematic studies of the polarographic behavior of the nickel(II)–iminodiacetate (IDA), –aspartate (Asp), and –glutamate (Glut) complexes and those of the nickel(II), zinc(II), and cadmium(II)–2,2′-ethylenedioxydi(ethylamine)-*N*,*N*,*N*′,*N*′-tetraacetate (GEDTA) complexes. All these complexes produce kinetic waves as a result of their dissociation at the electrode surface. From an experimental examination of the nature of these kinetic waves, we concluded that (1) the kinetic waves observed in the polarography of the nickel(II)–IDA,

1) M. Kodama, H. Nunokawa, and N. Oyama, This Bulletin, **44**, 2387 (1971).

2) M. Kodama and N. Oyama, *ibid.*, **45**, 2169 (1972).

-Asp, -Glut, and -GEDTA complexes and of the zinc(II)-GEDTA complex can be ascribed to the reduction of the metal(II) aquo ions formed upon the dissociation of the metal(II)-aminopolycarboxylate complexes, whereas (2) the kinetic wave in the cadmium(II)-GEDTA system may be ascribed to the reduction of the cadmium(II)-GEDTA complex formed by the partial dissociation of the original complex. The cobalt(II)-IDA, -Asp, and -GEDTA complexes also produce kinetic waves as a result of their dissociation. In this paper, we will report a systematic study of the nature of the above-mentioned kinetic waves and will determine the dissociation mechanism and rates. Furthermore, from a comparison of the dissociation rate constants with those estimated on the basis of the proposed reaction intermediates, the structure of the reaction intermediates will be described in detail.

Experimental

Reagents. The procedure used to prepare the standard cobalt(II) nitrate solution was described previously.[1] L-Aspartic acid (Asp), iminodiacetic acid (IDA), and 2,2′-ethylenedioxydi(ethylamine)-*N*,*N*,*N*′,*N*′-tetraacetic acid (GEDTA) were recrystallized from their aqueous solutions by adding pure ethanol and hydrochloric acid. The standard solutions of Asp, IDA, and GEDTA were prepared by dissolving known amounts of recrystallized Asp, IDA, and GEDTA in redistilled water. All the other chemicals used were of analytical-reagent grade and were used without further purification.

Apparatus and Experimental Procedures. All the DC current-voltage curves were measured by using a manual polarograph similar to that of Kolthoff and Lingane[3] or a Yanagimoto pen-recording polarograph, PA-102. The characteristic feature of the dropping mercury electrode used in this study was described previously.[4] All the other apparatus and the experimental procedures employed were also described in the above-mentioned paper.[4] The ionic strength of the solution was adjusted to 0.30 by adding an appropriate amount of pure sodium perchlorate. In this study, no buffer mixture was used, because the sample solutions always contained a large excess of uncomplexed Asp, IDA, or GEDTA and, hence, may be considered to have a sufficient buffer capacity over the entire pH range covered ($8.10<pH<9.70$ in the IDA system, $8.45<pH<10.40$ in the Asp system, and $7.80<pH<8.50$ in the GEDTA system).

Results and Discussion

Polarographic Behavior of the Cobalt(II)-GEDTA Complex. In an acetate buffer solution containing a large excess of GEDTA, the cobalt(II)-GEDTA complex gives a single well-defined reduction wave, one which is diffusion-controlled in nature. Its half-wave potential is located at far more negative potentials than that of the cobalt(II) aquo ion. Therefore, the polarographic step observed in the acetate buffer solution can be ascribed to the direct reduction of the cobalt(II)-GEDTA complex. As is shown by the polarograms in Fig. 1, the wave-height decreases appreciably with increases in the solution pH and in the concentration of uncomplexed GEDTA; finally, the polarographic wave shows a kinetic-controlled nature. By examining the nature of the above kinetic wave with the aid of the well-known relation employed by Koryta in the polarographic study of the cadmium(II)-nitrilotriacetate complex,[5] the reaction mechanism was studied. As is clear from the Koryta equation, if the cobalt(II) ion forms only a 1 : 1 ratio complex with GEDTA and if its dissociation at the electrode surface is rate-determining, the following relation can be derived for the kinetic wave:

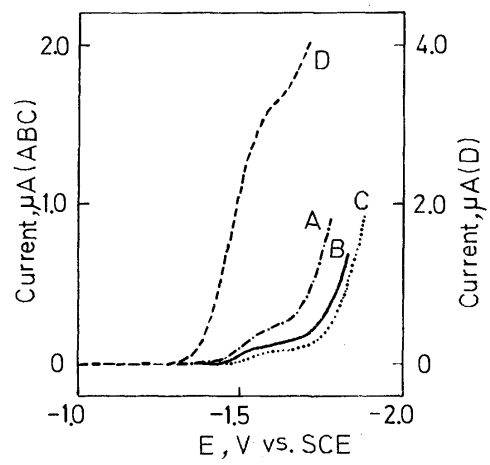

Fig. 1. Polarograms of the cobalt(II)-GEDTAcomplex, 25.0 °C, $\mu=0.30$.
A) Concentration of cobalt(II) ion = 1.0 mM
Concentration of GEDTA = 11.8 mM
pH = 7.85
B) Concentration of cobalt(II) ion = 1.0 mM
Concentration of GEDTA = 39.4 mM
pH = 7.86
C) Concentration of cobalt(II) ion = 1.0 mM
Concentration of GEDTA = 11.8 mM, pH = 8.35
D) Concentration of cobalt(II) ion = 0.53_2 mM
Concentration of GEDTA = 20.0 mM
Concentration of acetate ion = 0.06 M, pH = 5.45

$$CoY^{2-} \underset{}{\overset{k_d}{\rightleftharpoons}} Co^{2+} + Y^{4-} \quad \text{rate-determining step} \qquad (1)$$

$$\frac{i_k}{i_d - i_k} = 0.886 \sqrt{\frac{k_d \cdot (\alpha_H)_Y \cdot t}{K_{CoY} \cdot [Y]_f}} \qquad (2)$$

where K_{CoY}, $[Y]_f$, and $(\alpha_H)_Y$ are the formation constant of a 1 : 1 composition cobalt(II)-GEDTA complex, the concentration of uncomplexed GEDTA, and the (α_H) value of GEDTA respectively. Here, i_d in Eq. (2) is the hypothetical diffusion current. Previously,[6,7] we mentioned finding in our polarographic study that the nickel(II), copper(II), and cadmium(II) ions can form 1 : 1 and 1 : 2 ratio complexes with GEDTA under normal experimental conditions. If the cobalt(II) ions also form a 1 : 2 ratio complex with GEDTA, and if the dissociation of the 1 : 1 ratio complex is rate-determining, we can hypothesize the following mechanism(I):

3) I. M. Kolthoff and J. J. Lingane, "Polarography," Vol. I, Interscience Publishers, New York (1952), p. 297.
4) M. Kodama, Y. Fujii, and T. Ueda, This Bulletin, **43**, 2085 (1970).
5) J. Koryta, *Collect. Czech. Chem. Commun.*, **24**, 3057 (1959).
6) M. Kodama and T. Ueda, *Nippon Kagaku Zasshi*, **91**, 138 (1970).
7) M. Kodama and Y. Tominaga, This Bulletin, **42**, 394 (1964).

(I)
$$CoY_2^{6-} \overset{K_2}{\rightleftharpoons} CoY^{2-} + Y^{4-} \quad (3)$$
$$CoY^{2-} \overset{k_d}{\rightleftharpoons} Co^{2+} + Y^{4-} \quad \text{rate-determining step} \quad (4)$$

For the above reaction mechanism, one can derive Eq. (5) for the kinetic wave:

$$\frac{i_k}{i_d - i_k} = 0.886 \sqrt{\frac{k_d \cdot (\alpha_H)_Y \cdot t}{K_{CoY} \cdot [Y]_f}} \cdot \frac{1}{1 + K_2' \cdot [Y]_f} \quad (5)$$

where K_2' is the conditional second successive formation constant of the cobalt(II)–GEDTA complex.

On the other hand, if the partial dissociation of the 1 : 1 ratio cobalt(II)-GEDTA complex, which is in a rapid equilibrium with the 1 : 2 ratio complex, is rate-determining, and if the resulting complex, CoY^{2-*}, is reducible at the electrode (Mechanism II), the following relation can be derived:

$$\frac{i_k}{i_d - i_k} = 0.886 \sqrt{\frac{k_d \cdot t}{K}} \cdot \frac{1}{1 + K_2' \cdot [Y]_f} \quad (6)$$

where K is the equilibrium constant for (7).

(II)
$$CoY_2^{6-} \rightleftharpoons CoY^{2-} + Y^{4-} \quad \text{in a rapid equilibrium} \quad (3)$$
$$CoY^{2-} \overset{k_d}{\rightleftharpoons} CoY^{2-*} \quad \text{rate-determining step} \quad (7)$$

Furthermore, if the cobalt(II) ion forms only a 1 : 1 ratio complex with GEDTA, and if its partial dissociation (7) is slow-step, the $i_k/(i_d - i_k)$ value should be independent of the concentration of uncomplexed GEDTA, $[Y]_f$, and the solution pH. As has been stated above, the i_k value, however, decreases with increases in the $[Y]_f$ value and in the solution pH. Therefore, the above reaction mechanism can be eliminated. As is shown in Fig. 2, only the plot of

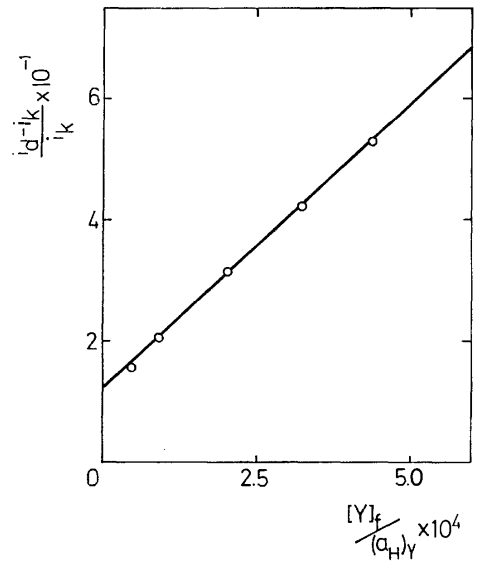

Fig. 2. Plot of $(i_d - i_k)/i_k$ against $[Y]_f/(\alpha_H)_Y$, GEDTA system, 25.0 °C, $\mu = 0.30$.
Concentration of cobalt(II) ion = 1.0 mM
Concentration of GEDTA = 10.8 mM

$(i_d - i_k)/i_k$ against the $[Y]_f/(\alpha_H)_Y$ yielded a linear relation for the cobalt(II)–GEDTA system. As is clear from the foregoing discussion, this indicates that the cobalt(II) ion forms 1 : 1 and 1 : 2 ratio complexes with GEDTA and that the reaction mechanism can be represented by (II). With the aid of Eq. (6), the

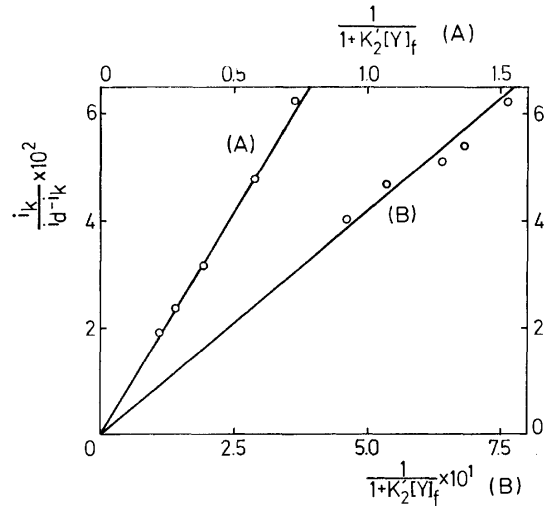

Fig. 3. Plot of $i_k/(i_d - i_k)$ against $1/(1 + K_2' \cdot [Y]_f)$, GEDTA system, 25.0 °C, $\mu = 0.30$.
Concentration of cobalt(II) ion = 1.0 mM
A) Concentration of GEDTA = 10.8 mM
pH ranged from 7.80 to 8.50
B) GEDTA concentration ranged from 10.0 mM to 40.0 mM. pH = 7.82.

second successive formation constant, K_2, was determined to be $7.8_4 \times 10^3$ from the ratio of the slope to the intercept of the straight line in Fig. 2. By using the K_2 value thus estimated, the effects of the concentration of uncomplexed GEDTA and the solution pH on the $i_k/(i_d - i_k)$ value were examined. The plot of $i_k/(i_d - i_k)$ against $1/(1 + K_2' \cdot [Y]_f)$ yielded a linear relation passing through the point of origin (Fig. 3). The k_d value obtained from the slope of the straight line (A) agreed well with that obtained from the slope of the straight line (B). This agreement also lends strong support to the reaction mechanism proposed by the present author for the cobalt(II)–GEDTA system.

Polarographic Behavior of Cobalt(II)–IDA and –Asp Complexes. Both cobalt(II)–IDA and –Asp com-

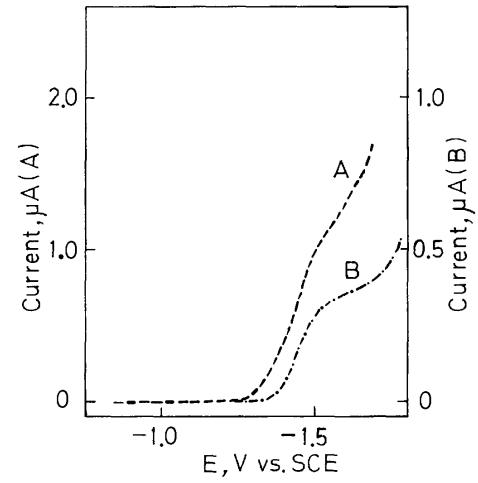

Fig. 4. Polarograms of the cobalt(II)–Asp and–IDA complexes, 25.0 °C, $\mu = 0.30$.
Concentration of cobalt(II) ion = 1.0 mM
A) Aspartate concentration = 38.0 mM, pH = 9.23
B) Iminodiacetate concentration = 18.0 mM, pH = 8.58

plexes also produced kinetic waves in alkaline solutions containing excess IDA or Asp. Typical polarograms are given in Fig. 4. In both cases, the plot of the $i_k/(i_d-i_k)$ value against $(\alpha_H)_X^{1/2}$ (at constant uncomplexed IDA or Asp, $[X]_f$) or $(\alpha_H)_X^{1/2}\cdot[X]_f^{1/2}$ yielded a linear relation passing through the point of origin (Figs. 5 and 6). Here, $(\alpha_H)_X$ is the (α_H) value of IDA or Asp. In considering that the cobalt(II) ion can form 1 : 1 and 1 : 2 ratio complexes with IDA and Asp under the present experimental conditions, the above fact evidently implies that the reaction mechanism for the kinetic currents of cobalt(II)–IDA and –Asp complexes can be expressed as:

$$\text{(III)}\quad \begin{cases} CoX_2^{2-} \rightleftarrows CoX^0 + X^{2-} & \text{rate-determining step} \\ CoX^0 + 2e^- + Hg \rightleftarrows Co(Hg) + X^{2-} \end{cases}$$

corresponding to the following relation:

$$\frac{i_k}{i_d-i_k} = 0.886\sqrt{\frac{k_d\cdot(\alpha_H)_X\cdot t}{K_2[X]_f}} \qquad (8)$$

The dissociation rate constant, k_d, was determined from the slope of the linear relation between the $i_k/(i_d-i_k)$ value and $(\alpha_H)_X^{1/2}$ or $(\alpha_H)_X^{1/2}\cdot[X]_f^{-1/2}$. In both systems, the k_d value determined from the slope of the linear relation between the $i_k/(i_d-i_k)$ and $(\alpha_H)_X^{1/2}$ agreed well with that determined from the slope of the linear relation between the $i_k/(i_d-i_k)$ and $(\alpha_H)_X^{1/2}\times[X]_f^{-1/2}$. All the k_d values determined in this study are listed in Table 1, together with other numerical values.[8]

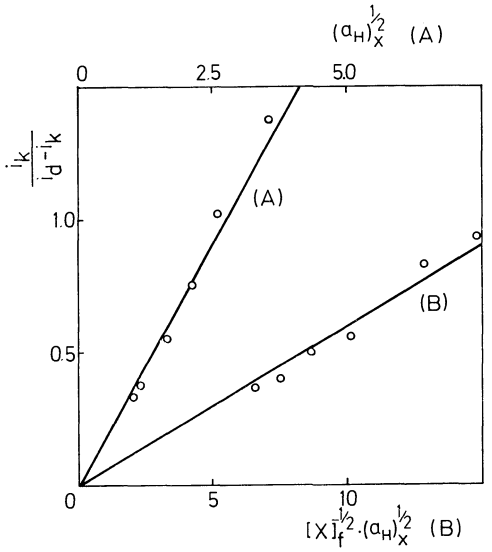

Fig. 5. Plot of $i_k/(i_d-i_k)$ against $(\alpha_H)_X^{1/2}$ or $(\alpha_H)_X^{1/2}[X]_f^{-1/2}$, Aspartate system, 25.0 °C, μ=0.30.
A) $i_k/(i_d-i_k)$ *vs.* $(\alpha_H)_X^{1/2}$ plot
Aspartate concentration=28.0 mM
B) $i_k/(i_d-i_k)$ *vs.* $(\alpha_H)_X^{1/2}[X]_f^{-1/2}$ plot

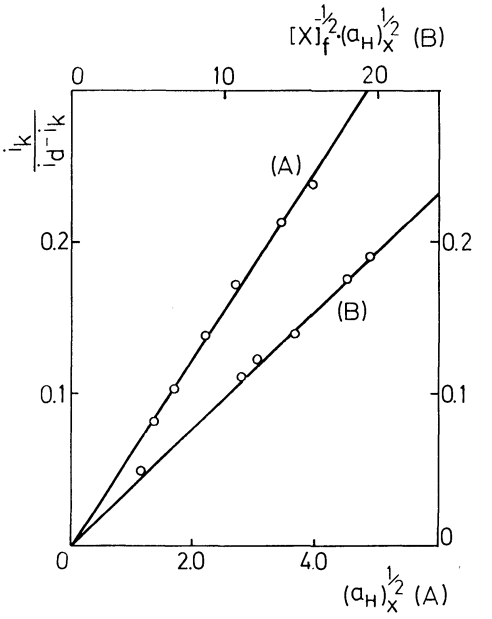

Fig. 6. Plot of $i_k/(i_d-i_k)$ against $(\alpha_H)_X^{1/2}$ or $(\alpha_H)_X^{1/2}[X]_f^{-1/2}$, Iminodiacetate system, 25.0 °C, μ=0.30.
A) $i_k/(i_d-i_k)$ *vs.* $(\alpha_H)_X^{1/2}$ plot
Iminodiacetate concentration=23.0 mM
B) $i_k/(i_d-i_k)$ *vs.* $(\alpha_H)_X^{1/2}[X]_f^{-1/2}$ plot

TABLE 1. DISSOCIATION RATE CONSTANTS OF THE COBALT-(II)-AMINOPOLYCARBOXYLATE COMPLEXES
25.0 °C, μ=0.30

System	Asp	IDA	GEDTA
log K_2	4.34	5.34	3.74 3.86[a]
log K_{st}	0	0.30	0.30
$\Delta\log k_d$ calcd	0.69	0	1.60
$\Delta\log k_d$ obsd	0.56	0	0.45
k_d[b]	27.0	7.5	20.7
k_f	$10^{5.77}$	$10^{6.21}$	$10^{5.18}$

a) Determined in this study.
b) In the case of GEDTA system, this corresponds to k_d in Eq. (7).

As was discussed in connection with the dissociation reactions of nickel(II)–IDA and –Asp complexes,[1] it is reasonable to believe that (1) less than three bond breakages are involved in the rate-determining step, (2) the cobalt(II)–oxygen (carboxylate) bond breakage is much faster than the cobalt–nitrogen (amine) bond breakage, and (3) the five-membered chelate ring is less substitution-labile than the six-membered chelate ring in the dissociation of the cobalt(II)–aminopolycarboxylate complex. Therefore, one can assume the reaction intermediates I and II in Fig. 7 for the dis-

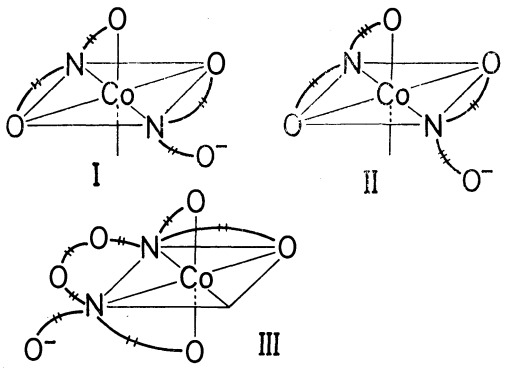

Fig. 7. Reaction intermediates.

8) L. G. Sillen and A. E. Martell, "Stability Constants of Metal-Ion Complexes," 2nd ed., The Chemical Society, London (1964).

sociation of cobalt(II)–IDA and –Asp complexes respectively. In general, the observed rate constant can be related to the rate constant for breaking X^{2-} away from the reaction intermediate, k_{rds}, the stability constant of the reaction intermediate, K_{inter}, and the K_{MX} value in the following manner:[1]

$$k_d = k_{rds} \cdot \frac{K_{inter}}{K_{MX}} \cdot K_{st} \cdot K_{elec} \quad (9)$$

Since, in the above reaction intermediates, both IDA and Asp anions are bonded to the cobalt(II) ion through a glycinate chelate ring, K_{inter} can be approximated by the formation constant of the cobalt(II)–glycinate complex, $K_{Co\text{-}gly}$. K_{MX} in Eq. (9) should be the second successive formation constant of the cobalt(II)–IDA or –Asp complex, K_2. The above relation suggests that, provided that the k_{rds} value for the IDA system is equal to that for the Asp system, the observed rate constant should be inversely proportional to the second successive formation constant corrected for the statistical factor.[9] The observed rate constant ratio was successfully compared with the ratio calculated by means of Eq. (9) (Table 1). In this study, we discovered that the cobalt(II) ion can also form a 1:2 ratio complex with the GEDTA anion. In sharp contrast with the EDTA anion, where two iminodiacetate groups are separated by two carbon atoms, the two nitrogen atoms of the GEDTA anion, where two iminodiacetate groups are separated by six carbon atoms and two oxygen atoms, have nearly identical protonation constants.[10] All these facts may mean that, under most conditions, the two iminodiacetate groups act as if they were unrelated entities in the complex formation with metal(II) ions. Therefore, it is not unreasonable to believe that the GEDTA anion in the electroactive cobalt(II)–GEDTA complex, CoY^{2-*}, is coordinated to the cobalt(II) ion through one iminodiacetate group, and that, hence, the dissociation of the first IDA group of the GEDTA anion is the rate-determining step. When the two IDA groups act as if they were functionally independent, the K value in Eq. (6) must be equal to $K_{CoY}/(K_{CoY})_{IDA} \times 2$. Here, 2 is the statistical factor. With the aid of the above relation, K was calculated to be $10^{3.74}$. This value agrees well with the K_2 value determined in this study, showing the validity of the estimation of the K value. In the above calculation, the cobalt(II)–*N*-(2-hydroxyethyl)iminodiacetate complex was employed as a model. The fact that the overall formation constant for the cobalt(II)–IDA complex, CoX_2^{2-}, is nearly identical with that of the 1:2 cobalt(II)–GEDTA complex also gives strong support to the above explanation. By using the K value thus estimated, the k_d value was calculated to be 2.07×10^1. This is about ten times smaller than that predicted from the reciprocal of the K value on the basis of the reaction intermediate III (see Table 1). However, the discrepancy between the rate constant ratio observed and that calculated can be explained in terms of the rotational barrier of the dissociating iminodiacetate group around the C–C or C–O bond.[9] The formation rate constants, k_f's, were also calculated from the $K_2 = k_f/k_d$ relation by using the k_d values determined in this study. The estimated k_f values for the IDA, Asp, and GEDTA systems are nearly identical with the characteristic water exchange rate constant of the cobalt(II) ion, $k_{Co}^{-H_2O}$ (Table 1).[11] Because the complexation reaction which involves the formation of an equilibriated outer-sphere complex, preceding the loss of a coordinated water molecule as the rate-determining step, the rate constant, k_f, can be written as the product of the outer-sphere association constant, K_{os}, and $k_{Co}^{-H_2O}$. As predicted by the Fuoss equation,[12] the K_{os} value for the outer-sphere association process, in which one of the reacting species is uncharged, is smaller than unity. Therefore, in considering that the coordinated ligand tends to increase the exchange rate of the remaining coordinated water,[13,14] the rate constant for the formation of the higher complex from the uncharged lower complex, which proceeds through the common water-loss mechanism, must be nearly identical with the characteristic water exchange rate. Thus, the above fact that the k_f values for the IDA and Asp systems are nearly identical with the $k_{Co}^{-H_2O}$ value can be explained by assuming a reaction mechanism where an outer-sphere complex formation between CoX^0 and X^{2-} precedes the loss of a coordinated water molecule from the CoX^0 as the rate-determining step. In the case of the GEDTA system, the fact that the k_f value is nearly identical with the $k_{Co}^{-H_2O}$ value can also be accounted for by assuming a reaction mechanism which involves the dissociation of water from the CoY^{2-*} as the rate-determining step following the initial weak association (outer-sphere association in nature) between the free IDA group of the GEDTA anion in CoY^{2-*} and the formally-uncharged cobalt(II) coordinated by the IDA group.

9) D. W. Margerum, D. B. Rorabacher, and J. F. G. Clarke, Jr., *Inorg. Chem.*, **2**, 667 (1963).

10) a) R. W. Schmidt and C. N. Reilley, *Anal. Chem.*, **29**, 264 (1957). b) G. Schwarzenbach, H. Senn, and G. Anderegg, *Helv. Chim. Acta*, **40**, 1886 (1957).

11) M. Eigen, *Pure Appl. Chem.*, **6**, 97 (1963).

12) R. M. Fuoss, *J. Amer. Chem. Soc.*, **80**, 5059 (1958).

13) D. W. Margerum and H. M. Rosen, *ibid.*, **89**, 1088 (1967).

14) J. P. Jones, E. J. Billow, and D. W. Margerum, *ibid.*, **92**, 1875 (1970).

Spectra of Nickel(II)-Azide Complexes in Organic Solvents

R. ABU-EITTAH and S. ELMAKABATY
Department of Chemistry, Faculty of Science, Cairo University, Giza, Egypt
(Received September 12, 1972)

The complexing properties of nickel(II) ion with azide ion, in a number of organic solvents, are investigated by spectroscopic methods. The electronic absorption spectra of Ni(II)-N_3^- solutions were studied in the visible-ultraviolet regions using dimethylformamide, absolute methanol and absolute ethanol as solvents. The composition of the possibly obtained complexes was investigated using the continuous variation and the slope ratio methods. The composition of the predominant complex was dependent on the solvent used. Formation as well as dissociation constants of the obtained complexes were computed.

The structure of nickel(II) complexes has been the aim of extensive studies.[1-4] Octahedral, square planar and tetrahedral geometries are known for nickel(II) complexes.[5-7] Piper and Koertge studied the spectra of $[Ni(H_2O)_6]^{2+}$ at low temperature.[8] Conductometric, potentiometric and spectrophotometric studies have shown that the 1 : 1 nickel azide complex predominates in aqueous medium.[9-11] Complexation between azide ion and many transition metals, other than nickel, has been investigated.[12,13]

The complexing power of azide ions with regard to several metal ions in aqueous solutions have been studied using polarographic as well as potentiometric methods.[14]

Experimental

Preparation of standard solutions of nickel perchlorate and of sodium azide was done as explained before.[13] Solvents used were: absolute methanol, absolute ethanol (Apolda grade reagent) and dimethylformamide (Prolabo grade reagent) that were purified by conventional methods found in the literature.[15] Spectra were scanned using a Beckman DK spectrophotometer and a 1.0 cm silica cells.

Results and Discussion

Complexes of Ni(II) and N_3^- in Absolute Methanol. Structure of the Complexes: In water as a solvent, the complex in $[Ni(H_2O)_6]^{2+}$, possessing a simple octahedral geometry, shows two absorption bands at 14, 286 and 25, 641 cm^{-1}. These bands are assigned to the $^3A_{2g} \rightarrow {}^3T_{1g(F)}$ and $^3A_{2g} \rightarrow {}^3T_{1g(P)}$ transitions respectively. In addition to these bands, the ion shows an absorption band in the UV region (~250 nm) which i rather weak. In methanol as a solvent the ion show

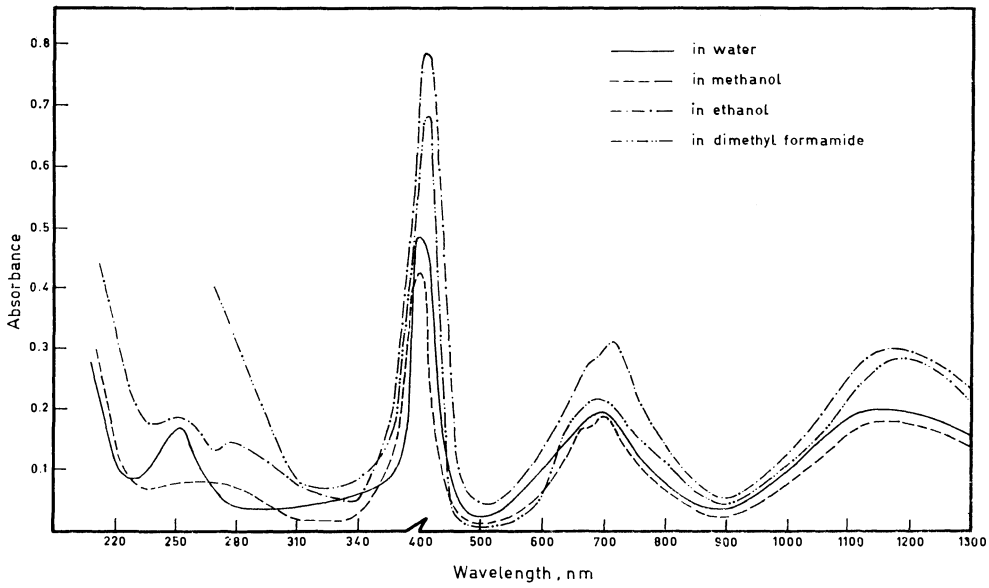

Fig. 1. Absorption spectra of nickel perchlorate in different solvents.

1) E. Uhlemann, G. Hinsche, and H. Braunschweig. *Z. Anorg. Allg. Chem.*, **377**, 321 (1970).
2) R. Eisenberg, R. Curran, and J. A. Cunningham, *Inorg. Chem.*, **9**, 2749 (1970).
3) D. Goodgame, M. Goodgame, and G. W. Rayner-Canham, *Inorg. Chim. Acta.*, **3**, 406 (1969).
4) T. Tarantelli, P. Riccieri, and C. Furlani, *J. Inorg. Nucl. Chem.*, **31**, 3585 (1969).
5) C. K. Jørgenesen, *Acta. Chem. Scand.*, **9**, 1362 (1955).
6) C. K. Jørgenesen, *ibid.*, **10**, 887 (1956).
7) L. M. Venanzi, *J. Chem. Soc.*, **1958**, 719.
8) T. S. Piper and N. Koertge, *J. Chem. Phys.*, **32**, 559 (1960).
9) C. Heinrich Egghart, *J. Inorg. Nucl. Chem.*, **31**, 1538 (1969).
10) V. Gutmann and H. Bardy, *Z. Anorg. Allg. Chem.*, **361**, 213 (1968).
11) P. Senise, O. E. S. Godinho, *J. Inorg. Nucl. Chem.*, **32**, 3641 (1970).
12) H. I. Feinstein, *Anal. Chim. Acta*, **15**, 288 (1956).
13) R. Abu-Eittah and G. Arafa, *J. Inorg. Nucl. Chem.*, **32**, 3337 (1970).
14) P. Senise, N. Almeida, and F. Eduard, *An. Acad. Brasil. Cienc.*, **41**, 333 (1969).
15) R. I. Vogel, "Practical Organic Chemistry," 3rd., Ed. Longmans, London, (1956).

(Fig. 1) the same absorption bands that were slightly red-shifted. On adding azide ion to the Ni(II) solution, the formed azidoaquo nickel(II) complex is also assumed to possess octahedral structure. Mixing of ligands will cause but a slight distortion from the simple cubic symmetry. Displacement of water molecules by azide ions can be represented as:

$$[Ni(H_2O)_6]^{2+} + XN_3^- \rightleftharpoons [Ni(H_2O)_{6-X}(N_3)_X]^{+2-X} + XH_2O$$

The number of azide ions ligated to the Ni(II) ion will be dependent on the solvent used. In water, as a solvent, it has been proved that only one azide ion is ligated to the Ni(II) ion.[10,16] If we use an organic solvent, miscible with water, we expect that the number of N_3^- ions ligated to Ni(II) ion will increase.

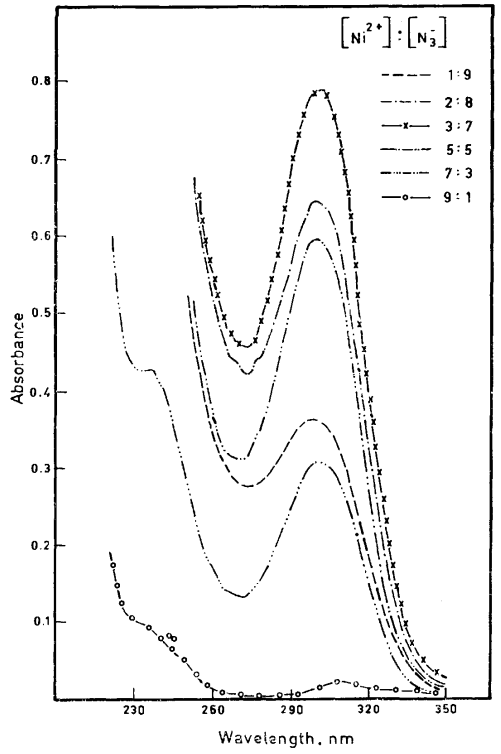

Fig. 2. Absorption spectra of nickel azide solutions in methanol.

Figure 2 shows the absorption spectra of solutions, in absolute methanol, made by mixing nickel perchlorate and sodium azide with total concentration of 2×10^{-3} M. The formed nickel azide complex has an absorption band of its own with λ_{max} at 300 nm. Absorbance of free Ni(II) or azide ions is negligible at this wavelength. It is interesting to remember that the monoazidoaquonickel(II) complex[16] has an absorption band of its own at ~290 nm. This suggests that the nature of the Ni(II)-N_3^- complex, when water is the solvent, differs from its nature when absolute methanol is the solvent. Job's[17] method of continuous variation was applied to results of Fig. 2. In Fig. 3 one plots the absorbance *versus* the mole

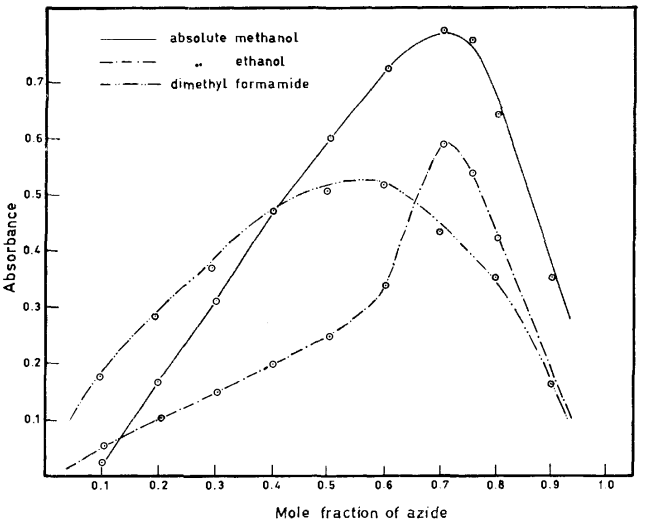

Fig. 3. Structure of nickel azide complexes, in different solvents, using the continuous variation method.

fraction of azide ion. A well-defined maximum appears at 0.7 mol fraction of azide ion which suggests that the predominant nickel azide complex may be the 1:2 or the 1:3 complex. Data needed to plot Fig. 3 are given in Table 1.

TABLE 1. VARIATION OF ABSORBANCE OF NICKEL-AZIDE SOLUTIONS WITH AZIDE ION CONCENTRATION, IN DIFFERENT SOLVENTS (ABSOLUTE ALCOHOLS AND DIMETHYLFORMAMIDE)

$[Ni^{2+}]:[N_3^-]$	Absorbance		
	Methanol (300 nm)	Ethanol (302 nm)	Dimethyl-formamide (305 nm)
1:9	0.36	0.165	0.165
2:8	0.645	0.425	0.35
2.5:7.5	—	0.540	—
3:7	0.795	0.590	0.43
4:6	0.725	0.34	0.52
5:5	0.600	0.25	0.51
6:4	0.470	0.20	0.475
7:3	0.310	0.15	0.37
8:2	0.165	0.10	0.285
9:1	0.02	0.055	0.18

To confirm the above results, the slope ratio method was applied.[18] Spectra of solutions made by mixing constant excess $[Ni^{2+}]$, 4×10^{-3} M with variable $[N_3^-]$, from 0.6×10^{-3}—1.0×10^{-3} M, were scanned. Also, spectra of solutions made by mixing constant excess $[N_3^-]$, 1.6×10^{-3} M with variable $[Ni^{2+}]$ from 0.1×10^{-3} to 0.5×10^{-3} M were scanned. In Fig. 4 we plot the absorbance (at 300 nm) *versus* the concentration of the variable components. Straight lines are obtained, ratio between their slopes gives the ratio of the two components of the complex. Results of Fig. 4 give a ratio of 1:2.79 of the $[Ni^{2+}]$: $[N_3^-]$ in the obtained nickel azide complex. This suggests that in methanol, the

16) R. Abu-Eittah and S. Elmakabaty, *J. Inorg. Nucl. Chem.*, to be published.

17) P. Job and C.R. Held, *Séanc. Acad. Sci. Paris*, **180**, 228 (1925).

18) A. E. Harvey and D. L. Manning, *J. Amer. Chem. Soc.*, **72**, 4488 (1950).

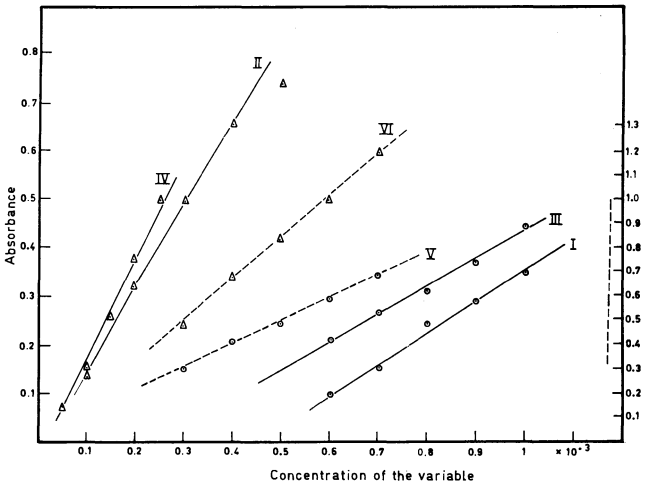

Fig. 4. Application of the slope ratio method to the structure of nickel azide.
I—II in absolute methanol ⊙ $[Ni^{2+}]$ constant
III—IV in absolute ethanol △ $[N_3^-]$ constant
V—IV in dimethyl formamide

Table 2. Absorbances of nickel(II)-azide solutions containing constant excess $[Ni^{2+}]$, with variable $[N_3^-]$ and others containing constant excess $[N_3^-]$ with variable $[Ni^{2+}]$ in absolute methanol at 300 nm

Constant $[Ni^2]^+$: 4×10^{-3}		Constant $[N_3^-]$: 1.6×10^{-3}	
$[N_3^-]$	Absorbance	$[Ni^{2+}]$	Absorbance
0.6×10^{-3}	0.1	0.1×10^{-3}	0.145
0.7×10^{-3}	0.155	0.2×10^{-3}	0.32
0.8×10^{-3}	0.245	0.3×10^{-3}	0.5
0.9×10^{-3}	0.28	0.4×10^{-3}	0.66
1×10^{-3}	0.35	0.5×10^{-3}	0.74

1:3 nickel azide complex is obtained. Data needed to plot Fig. 4 are given in Table 2.

Stability Constants: The predominant complexes were found to be the 1:2 and the 1:3 complexes. Dissociation constant K' was computed following the Harvey-Manning method.[18] Dissociation of the nickel azide complex can be represented by:

$$[Ni(N_3)_n]^{+2-n} \rightleftharpoons Ni^{2+} + nN_3^-$$

C	0	0	initial concentration
$C(1-\alpha)$	αC	$n\alpha C$	equilibrium concentration

The dissociation constant K' is given by.

$$K' = (\alpha C)(n\alpha C)^n/C(1-\alpha)$$

where, "α" represent the degree of dissociation and is given by $(A_m-A_S)/A_m$. The value of (A_m) represents the absorbance when all the nickel present is complexed, that of (A_S) is the absorbance at the stoichiometric molar ratio of N_3^- to Ni^{2+} in the complex. The value of "n" will be the number of azide ions per ion of nickel and "C" will be taken as the concentration of nickel used.

The spectra of a series of nickel-azide solutions, with the ratio $[Ni^{2+}]$: $[N_3^-]$ varying from 1:1 to 1:20 were scanned. The absorbance at 300 nm is plotted against the number of moles azide per mole nickel in Fig. 5. The values of (α) were found to be 0.584 and 0.471, from Fig. 5, at "n" equals to 2 and 3. Data needed to plot Fig. 5 is given in Table 3.

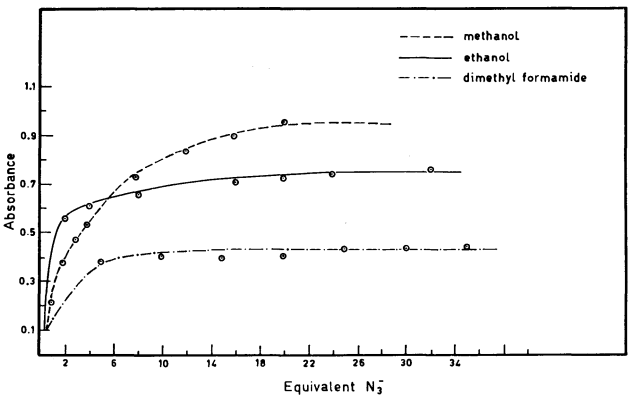

Fig. 5. Variation of absorbance of nickel azide solution with azide concentration.

Table 3. Absorbance of nickel-azide solutions in different solvents

$[Ni^{2+}]$:$[N_3^-]$	Absorbance		
	Methanol (300 nm)	Ethanol (302 nm)	Dimethyl-formamide (305 nm)
1:1	—	0.205	—
1:2	0.37	0.555	—
1:3	0.47	—	—
1:4	0.53	0.600	—
1:5	—	—	0.365
1:8	0.71	0.64	—
1:10	—	—	0.39
1:12	0.83	—	—
1:15	—	—	0.385
1:16	0.89	0.695	—
1:20	0.95	0.71	0.4
1:24	—	0.73	—
1:25	—	—	0.435
1:30	—	—	0.435
1:32	—	0.75	—
1:35	—	—	0.450

Substituting by these values in the equation for K' one gets 0.208×10^{-6} and 0.9×10^{-10} for the dissociation constants of the 1:2 and 1:3 nickel azide complexes. Formation constants of these complexes are 4.8×10^6 and 1.99×10^{10} respectively. These values reflect the quite stability of the obtained nickel azide complex.

Nickel(II)-azide Complexes in Absolute Ethanol. To see the effect of solvent on the composition of Ni(II)-azide complexes, the spectra of mixtures of nickel perchlorate and sodium azide were studied using absolute ethanol as a solvent. Mixtures were prepared so as the total concentration was 1.0×10^{-3} M. Job's method of continuous variation was applied to the results of the spectra (Fig. 3). In absolute ethanol, as a solvent, formation of more than one complex was evident. Figure 3 shows a break at azide mole fraction of 0.6, peak at azide mole fraction of 0.72 and a

break at azide mole fraction of 0.8. This means that the complexes: $[Ni(N_3)_2(H_2O)_4]^0$; $[Ni(N_3)_3(H_2O)_3]^-$ and $[Ni(N_3)_4(H_2O)_2]^{2-}$ are obtained on mixing nickel perchlorate and sodium azide solutions in absolute ethanol as a solvent. Formation of more than one complex, at the same time, is expected not to give a well-defined spectrum. This can be seen from Fig. 6 where the spectra of Ni(II)–N_3^- solutions, in the

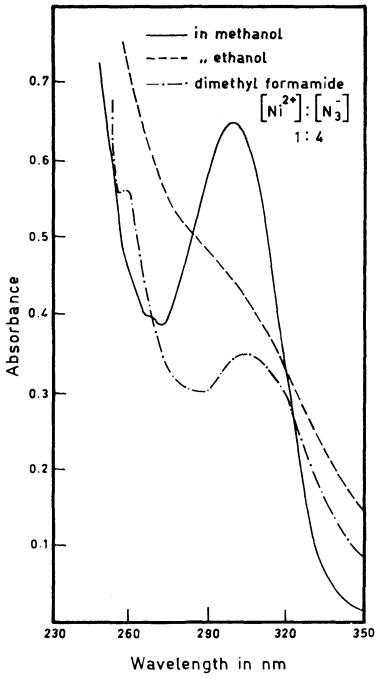

Fig. 6. Absorption spectra of nickel(II)-azide solutions in different solvents.

studied solvents, are given. In absolute ethanol, bands were not well defined as they were in other solvents which indicates the formation of more than one complex.

The slope ratio method was used to confirm the composition of nickel azide complex when absolute ethanol is the solvent. In Fig. 4 the relation between absorbance (at 302 nm) and concentration of the variable component is plotted. Data needed to plot this curve is given in Table 4.

Table 4. Absorbances of nickel-azide solutions with excess constant $[Ni^{2+}]$ and with excess constant $[N_3^-]$ in absolute ethanol as a solvent

$[Ni^{2+}]=4\times10^{-3}$		$[N_3^-]=0.8\times10^{-3}$	
$[N_3^-]$	Absorbance (302 nm)	$[Ni^{2+}]$	Absorbance (302 nm)
0.6×10^{-3}	0.215	0.05×10^{-3}	0.075
0.7×10^{-3}	0.27	0.1×10^{-3}	0.155
0.8×10^{-3}	0.315	0.15×10^{-3}	0.26
0.9×10^{-3}	0.37	0.2×10^{-3}	0.38
1×10^{-3}	0.445	0.25×10^{-3}	0.5

The slope ratio method indicated that with the used concentrations of Ni^{2+} and N_3^- a 1:4 nickel azide complex is probably obtained.

The instability constant of the 1:4 nickel azide complex was computed as before. In Fig. 5 we plot the absorbance (at 302 nm) *versus* the moles of azide per mole of nickel. From that figure values of (α), (A_m), and (A_S) were computed. The value of "*n*" was used as 4 and *K'* was computed to be 26.214×10^{-16}. Hence the formation constant of the 1:4 nickel azide complex is found to be 3.81×10^{14}.

Complexes of Ni(II) and N_3^- Ions in Dimethylformamide. The extent of displacement of the water molecules, in the inner coordination sphere of Ni(II), by azide ions was investigated when dimethylformamide was the solvent. The absorption spectra of mixtures of sodium azide and nickel perchlorate, using dimethylformamide as a solvent, were investigated. To begin with spectra of solutions of constant total concentration (1.0×10^{-3} M) were scanned. In Fig. 6 the spectrum of one of these mixtures is given. The nickel azide complex, obtained when dimethylformamide is the solvent, has a well-defined and discrete absorption band of its own at 305 nm. In Fig. 3, absorbance is plotted *versus* the mole fraction of azide, a well-defined and discrete maximum appears at an azide mole fraction of 0.6 which suggests that the 1:2 nickel azide complex predominates. Data needed to draw Fig. 3 are given in Table 1.

The slope ratio method was used to confirm the composition of nickel azide complex when dimethylformamide is the solvent. A series of solutions was prepared containing constant excess sodium azide 0.2×10^{-2} M and variable concentrations of nickel perchlorate 0.7×10^{-3} to 0.3×10^{-3} M. Another series of solutions was prepared containing constant excess nickel perchlorate 0.2×10^{-2} M and variable concentration of sodium azide 0.7×10^{-3} to 0.3×10^{-3} M. Absorbance was plotted *versus* the concentration of variable in Fig. 4. Data needed to plot Fig. 4 are given in Table 5. Results of Fig. 4 confirmed that a 1:2 nickel azide complex is obtained when dimethylformamide is the solvent.

Table 5. Absorbances of nickel azide solutions containing excess $[Ni^{2+}]$ and others containing excess $[N_3^-]$ in dimethylformamide

$[Ni^{2+}]=0.2\times10^{-2}$		$[N_3^-]=0.2\times10^{-2}$	
$[N_3^-]\times10^3$	Absorbance	$[Ni^{2+}]\times10^3$	Absorbance
0.70	0.690	0.70	1.20
0.60	0.590	0.60	1.03
0.50	0.493	0.50	0.84
0.40	0.415	0.40	0.680
0.30	0.305	0.30	0.490

The stability constant of the 1:2 nickel azide complex, in dimethylformamide, was obtained using the procedure adopted before. Absorption spectra of Ni(II)–N_3^- solutions with $[Ni^{2+}]$: $[N_3^-]$ ratio varying from 1:5 to 1:35 were scanned. In Fig. 4 absorbance is plotted *versus* the number of moles azide per mole nickel. Data need to plot Fig. 5 is given in Table 3 proceeding as before and using "*n*" equal to "2" the dissociation constant *K'* of the 1:2 nickel azide complex, in dimethylformamide, is found to be 0.21×10^{-6} or the formation constant is of the order of 5×10^6.

In Fig. 6, we present the spectra of Ni(II)–N_3^- solutions of the same concentration but in different solvents. The figure shows that λ_{max} for the obtained nickel azide complex is dependent on the solvent used. This indicates that the structure of the nickel azide complex is dependent on the solvent used. In absolute ethanol the spectrum is not well defined which indicates that more than one complex are obtained at the same time. In Table 6 we present the stability constants of the nickel azide complexes possibly obtained in different solvents.

Table 6. Stability constants (K) of the nickel azide complexes in different solvents

Solvent	Complex $[Ni^{2+}]:[N_3^-]$	K
Absolute methanol	1:2	4.8×10^6
	1:3	1.99×10^{16}
Absolute ethanol	1:4	3.81×10^{14}
Dimethylformamide	1:2	5×10^6

Conclusion: When $Ni(ClO_4)_2 \cdot 6H_2O$ is dissolved in water, the nickel ion exists in the simple octahedral geometry with the structure $[Ni(H_2O)_6]^{2+}$. When the solute is dissolved in organic solvents as absolute methanol, ethanol, or dimethylformamide, the octahedral geometry of the Ni(II) complex ion persists though the six ligands may not be entirely water molecules. When the hydrated salt is dissolved in some non-aqueous solvent, depending on the coordination power of the solvent the water molecules are fully or partially substituted by the solvent molecules. This is indicated from Fig. 1, where λ_{max}, intensity of the band and even splitting of some bands is solvent dependent. On adding azide ion to the solution, it has been found that the extent of H_2O (or other solvent molecules) displacement by N_3^- is dependent on the solvent used. When water is the solvent only one H_2O molecule is displaced. With organic solvents, two, three and four molecules were displaced by two, three and four azide ions. The specific complex has it own spectrum.

BULLETIN OF THE CHEMICAL SOCIETY OF JAPAN, VOL. 46, 3431—3434 (1973)

Kinetics of the Formation of MoO_{3-x} at Elevated Temperatures from a Mixture of MoO_3 and α-Al_2O_3

Yoshihide KOTERA and Akifumi UENO

National Chemical Laboratory for Industry, Mita, Meguro-ku, Tokyo 153

(Received March 28, 1973)

The kinetics of the formation of MoO_{3-x} from a mixture of MoO_3 and α-Al_2O_3 was studied by means of high temperature X-ray diffraction. The species of MoO_{3-x} formed in the temperature range 600—700 °C were identified as $MoO_{2.88}(Mo_8O_{23})$, $MoO_{2.76}(Mo_{17}O_{47})$, and $MoO_{2.75}(Mo_4O_{11})$. The activation energies of their formation were estimated to be 18.4 kcal/mol for Mo_8O_{23}, 23.0 kcal/mol for $Mo_{17}O_{47}$ and 29.2 kcal/mol for Mo_4O_{11}. Other types of species of MoO_{3-x} observed above 800 °C were $MoO_{2.89}(Mo_9O_{26})$ and MoO_2. Little effect of water vapor, oxygen or nitrogen on the formation of the species was observed. No MoO_{3-x} was observed in the mixture of MoO_3 with SiO_2 or α-Fe_2O_3.

Detailed X-ray studies on the existence of the oxide intermediates between molybdenum dioxide and molybdenum trioxide have been made by Magneli *et al.*[1] by heating the mixture of molybdenum trioxide and molybdenum metal powder *in vacuo* in a glass tube at temperatures up to 700 °C. The following phases were identified by means of X-ray powder photography.

α-phase	MoO_3	orthorhombic
β-phase	Mo_9O_{26}	monoclinic
β'-phase	Mo_8O_{23}	monoclinic
γ-phase	Mo_4O_{11}	monoclinic
δ-phase	MoO_2	monoclinic

In later works other species such as $Mo_{17}O_{47}$, $Mo_{18}O_{52}$, and Mo_5O_{14} were shown to exist, their crystal structures being determined exactly.[2,3] The formation of these oxide intermediates was found, however, only in the case where a mixture of molybdenum trioxide and molybdenum metal powder or that of molybdenum trioxide and molybdenum dioxide was heated.

Recently a hydrodesulfurizing catalyst consisting of molybdenum trioxide, cobalt oxide and alumina was developed[4] and its active species studied extensively. Crystallographic[5] and spectroscopic[6] investigations on the mixture of molybdenum trioxide or alumina with cobalt oxide have been made to some extent. The reaction product between alumina and cobalt oxide was elucidated by structural and magnetic studies.[7] Formation of $CoAl_2O_4$ was observed when a mixture

1) A. Magneli. G. Anderson, B. Blomberg, and L. Kihlborg, *Anal. Chem.*, **24**, 1998 (1952).

2) L. Kihlborg, *Arkiv Kemi.*, **21**. 357, 417 (1963).

3) A. Magneli, *Acta Crystallogr.*, **6**, 495 (1953); L. A. Bursill, *ibid.*, **28**, 187 (1972).

4) N. Todo, T. Kabe, K. Ogawa, M. Kurita, T. Sato, K. Shimada, Y. Kuriki, T. Oshima, T. Takematsu, and Y. Kotera, *Kogyo Kagaku Zasshi*, **74**, 563 (1971).

5) G. W. Smith, *Acta Crystallogr.*, **19**, 269 (1965).

6) J. M. J. Lipsch and G. C. A. Shuit, *J. Catal.*, **15**, 163, 173 (1969); J. H. Ashley and P. C. H. Mitchell, *J. Chem. Soc., A*, **1968**, 2821, 2730.

7) J. T. Richardson and L. W. Vernon, *J. Phys. Chem.*, **62**, 1153 (1958).

of cobalt compound and alumina was heated above 850 °C, while at lower temperature only the oxidation or reduction of cobalt oxide would occur.[8] However, studies on the mixture of alumina and molybdenum trioxide have not been carried out thoroughly. A new compound containing molybdenum trioxide, alumina and silica was prepared and studied by the X-ray diffraction method.[9] The aim of the present work is to clarify the crystallographic changes of molybdenum trioxide mixed with α-alumina during the course of heating and to study the kinetics of the formation of MoO_{3-x} in the mixture.

Experimental

Molybdenum trioxide (Climax Molybdenum Co.) containing less than 0.05% of metallic impurities was employed. α-Alumina and α-ferric oxide were of guaranteed grade, while silica containing less than 0.01% of metallic impurities was converted into α-cristobalite by heating at 1100 °C before use.

Molybdenum trioxide and α-alumina were mixed well and the mixture was set in a platinum sample holder for the measurement of high temperature X-ray diffraction during the course of reaction. Temperature fluctuation did not exceed ±2 °C during the measurement. The X-ray instrument was operated at 35 KV with a filament current of 15 mA, a nickel filter being employed for CuKα radiation to provide an incident wave length of 1.5405 Å. Reflection peaks at 2θ angles were recorded on the strip chart, and the "d" values corresponding to these angles were calculated from the Bragg diffraction law. Oxygen or nitrogen was obtained from cylinders. It was wetted by passing through water at 20 °C (water vapor pressure 17.5 mmHg), or dried by passing above calcium chloride. The flow rate was held constant by means of a Venturi type manometer.

Relative amounts of the species were estimated from the measurements of the peak heights recorded on the strip chart. In order to determine the relative amount of the formed MoO_{3-x} species during the course of reaction, the characteristic peaks of X-ray diffraction pattern were selected as follows, $2\theta = 12.7°$ for MoO_3, 14.4° for Mo_8O_{23}, 15.8° for $Mo_{17}O_{47}$ and 23.7° for Mo_4O_{11}. Reproducibility of the peak height was within ±5% error.

Results

A typical X-ray diffraction pattern is shown in Fig. 1, where the mixture of the oxide with a MoO_3/α-Al_2O_3 weight ratio of 2: 1 was heated at 650 °C for 2 hr in a stream of dry nitrogen gas. New species such as Mo_4O_{11}, Mo_8O_{23}, and $Mo_{17}O_{23}$ were identified by a comparison of their 'd' values with those in calibration graphs[10] (Fig. 1).

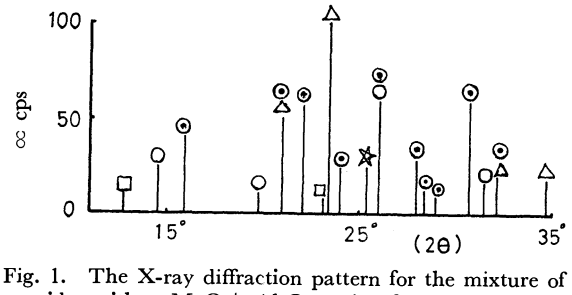

Fig. 1. The X-ray diffraction pattern for the mixture of the oxides with a $MoO_3/\alpha\text{-}Al_2O_3$ ratio of 2: 1 after heated at 650 °C for 2 hr (□: MoO_3, △: Mo_4O_{11}, ○: Mo_8O_{23}, ⊙: $Mo_{17}O_{47}$, ☆: α-Al_2O_3).

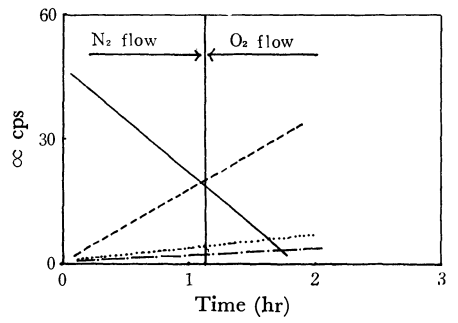

Fig. 2. The behaviors of MoO_{3-x} observed at 650 °C and the effect of the surrounding atmosphere on the reaction. ——: MoO_3, ----: Mo_4O_{11}, -·-·-: Mo_8O_{23}, ·····: $Mo_{17}O_{47}$.

The changes of peak height for the respective MoO_{3-x} observed during the course of heating are shown in Fig. 2. We see that the effect of surrounding atmosphere on the reduction is not noticeable. Reduction of MoO_3 to MoO_{3-x} at 600, 650, or 700 °C was analyzed, the formation of Mo_8O_{23}, $Mo_{17}O_{47}$, and Mo_4O_{11} as well as the decrease of molybdenum trioxide being plotted in Figs. 3, 4, 5 and 6, respectively.

The rate of formation of respective MoO_{3-x} and that of the decomposition of MoO_3 were of zeroth order with respect to the molybdenum oxide concentrations (Fig. 2). The rate constant for the formation of MoO_{3-x} and that for the decomposition of molybdenum trioxide were calculated from the initial slopes of the

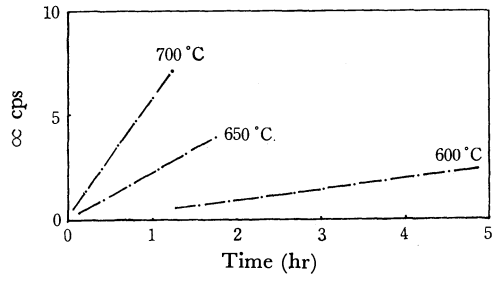

Fig. 3. Formation rate of Mo_8O_{23} at various temperatures.

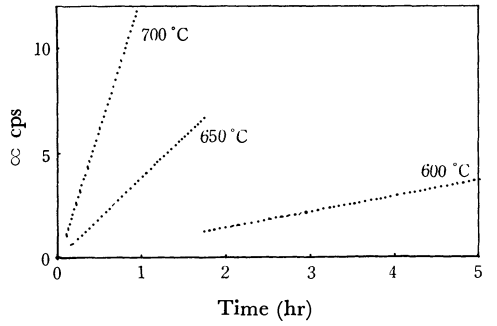

Fig. 4. Formation rate of $Mo_{17}O_{47}$ at various temperatures.

8) T. Nishina, M. Yonemura, and Y. Kotera, *J. Inorg. Nucl. Chem.*, **34**, 3279 (1972).

9) A. Ueno and Y. Kotera, *Chem. Lett.*, **1973**, 21.

10) X-ray Powder Data File. Edited by J. V. Smith, *et al.*, American Society for Testing and Materials, Philadelphia, Pa., 1968 Cards No. 5-337, 5-339, 5-452, 5-508, 10-173, 12-753 and 13-345.

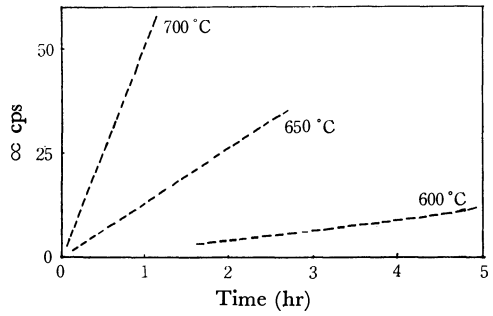

Fig. 5. Formation rate of Mo_4O_{11} at various temperatures.

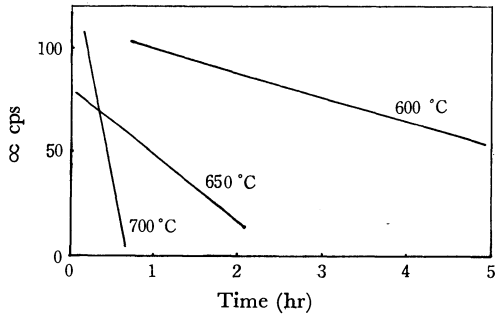

Fig. 6. Decomposition rate of MoO_3 at various temperatures.

curves in Figs. 3—6. The activation energies for the formation of MoO_{3-x} and the decomposition of molybdenum trioxide were estimated from the Arrhenius plot in Fig. 7. The deviation of each plot from the straight line is within ±5%. Values of the activation energies thus obtained were 18.4, 23.0, and 29.2 kcal/mol for the formation of Mo_8O_{23}, $Mo_{17}O_{47}$ and Mo_4O_{11} and 27.8 kcal/mol for the decomposition of MoO_3, respectively.

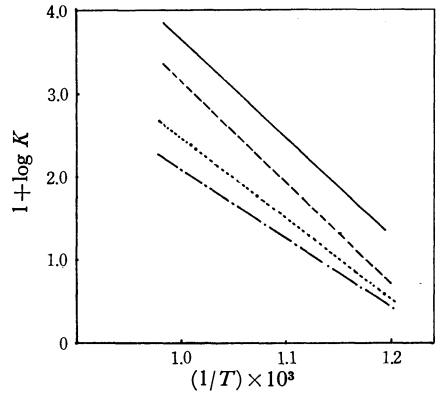

Fig. 7. The standard Arrhenius plot for the formation of MoO_{3-x} and the decomposition of MoO_3. ——: MoO_3, ----: Mo_4O_{11}, -·-·-: Mo_8O_{23}, ·····: $Mo_{17}O_{47}$.

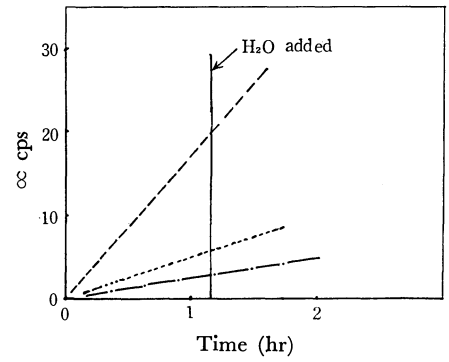

Fig. 8. The effect of the additional water vapor on the formation of MoO_{3-x} at 650 °C. ----: Mo_4O_{11}, -·-·-: Mo_8O_{23}, ·····: $Mo_{17}O_{47}$.

Figure 8 shows that no change of reaction rate was observed when the wet nitrogen was introduced into the mixture with a MoO_3/α-Al_2O_3 weight ratio of 2: 1 after being heated at 650 °C for 70 min in a stream of dry nitrogen. This indicates that no effect of the ambient water vapor is observed upon the rate of formation of MoO_{3-x}.

Dsicussion

A catalyst consisting of molybdenum and cobalt compounds and alumina was developed to hydrodesulfurize light or heavy oil[4] and was studied on its active species. A crystallographic investigation[5] on molybdenum and cobalt compounds showed that the formation of $CoMoO_4$ was observed by heating the mixture of cobalt oxide and molybdenum trioxide above 700 °C, and at lower temperature the other types of molybdenum cobalt oxides formed, while it was assumed from the spectroscopic investigation[6] that the octahedron of $[CoO_6]$ might be the active species of the catalyst consisting of molybdenum and cobalt compounds and alumina. However it is very difficult to clarify the active species. It seems important to assure the reaction between two oxides under the conditions for the preparation of the catalyst.

The behavior of the mixture of cobalt compound and alumina was studied during the calcination at temperatures where catalysts are prepared.[8] The formation of cobalt aluminate spinel above 850 °C was observed by means of high-temperature X-ray diffraction and chemical analysis. At lower temperature cobalt oxide behaves in the mixture with alumina in almost the same way as alone.

The behavior of the mixture of molybdenum compounds and alumina has not been so extensively studied. It was proposed[11] that three new compounds might be formed during the heating of the mixture of molybdenum trioxide and γ-alumina. The formation was assumed by the appearance of new X-ray lines. We reported[9] that the new compound is formed by heating the mixture of molybdenum trioxide and alumina when either oxide contains silica. The above postulate would be the case where molybdenum trioxide or γ-alumina is contaminated by silica. In the present study with the use of alumina or molybdenum trioxide free from silica, new X-ray lines were found, which are representative for MoO_{3-x}[1,2] as shown in Fig. 1.

The formation of the respective MoO_{3-x} species was spontaneously observed as shown in Figs. 2—5.

From the results it is assumed that the reduction of MoO_3 to MoO_{3-x} does not proceed in a successive reduction of molybdenum trioxide to dioxide through Mo_8O_{23}, $Mo_{17}O_{47}$, and Mo_4O_{11}, but by a parallel reduction from MoO_3 to respective MoO_{3-x}. The

11) T. Shirasaki, O. Shin, M. Kato, and K. Morikawa, *Shokubai*, **4**, 337 (1962).

TABLE 1. FORMATION OF MoO_{3-x} FROM THE MIXTURE OF MoO_3 AND α-Al_2O_3 DURING THE HEATING

TEMP (°C)	OBSERVED COMPOUND
500	MoO_3 Al_2O_3
600	MoO_3 Al_2O_3
700	Mo_4O_{11}
	Mo_8O_{23}
800	$Mo_{17}O_{47}$
900	MoO_2 Al_2O_3
	Mo_9O_{26}
1000	
	Al_2O_3
1100	

activation energies estimated above are assumed to represent those for each step of the parallel reduction.

The decrease of molybdenum trioxide was observed as shown in Figs. 2 and 6. The activation energy estimated above would be the weighted mean of three parallel reactions. The amount of sublimation of molybdenum oxide is negligibly small since the measurement of high-temperature X-ray diffraction was carried out between 600 and 700 °C and molybdenum trioxide sublimes above 800 °C.[12]

In order to know whether molybdenum oxides form compounds with α-alumina or not, an aqueous solution of ammonia was poured into a mixture of MoO_3 and α-alumina which had been ignited at 650 °C for 2 hr. X-Ray analysis of the residue was carried out, the X-ray pattern being found to be that of only α-alumina. While molybdenum oxides are known to be soluble in aqueous ammonia,[13] it is deduced that molybdenum oxides did not form any compounds with α-alumina by heating under the conditions cited above.

The effect of alumina or silica upon the electron spin resonance spectrum of molybdenum was recently studied.[14] It was observed that the ESR spectrum due to molybdenum supported on alumina differed from that on silica but no reason was given. When silica was heated with molybdenum trioxide instead of α-alumina, no reduction of molybdenum trioxide was observed up to 800 °C.

R. Schenck *et al.*[15] observed the evolution of oxygen by heating the mixture of alumina and cupric oxide. This was explained by assuming that alumina promotes the reduction of cupric oxide by the formation of a spinel phase of $CuO \cdot Al_2O_3$. They also reported the reduction of cupric oxide by ferric oxide in a similar way to that by alumina. For molybdenum trioxide α-alumina similarly reduced MoO_3 to MoO_{3-x}, but no reduction of MoO_3 occurred by heating with α-ferric oxide up to 800 °C. The spinel formula $MoAl_2O_4$ does not seem to be a reaction intermediate during calcination of the mixture of molybdenum trioxide and alumina.

The authors express their thanks to Dr. S. Shin, Miss M. Yonemura and Mr. T. Sekine for their useful discussion and encouragement.

12) R. Horbe, O. Knacke, and K. E. Prescher, *Z. Erzbergbau Metallhüttenw.*, **14**, 232 (1961); E. A. Gulbransen, K. F. Andrew, and F. A. Brassart, *J. Electrochem. Soc.*, **110**, 242 (1963).

13) "Gmelins Handbuch der Anorganischen Chemie," 8 Auflage System-Nummer 53 (1953).

14) M. Akimoto and E. Echigoya, *J. Catal.*, **29**, 191 (1973).

15) R. Schenck and F. Kurzes, *Z. Anorg. Allgem. Chem.*, **235**, 97 (1937).

The Fluorination of Carbonyl Sulfide[1]

Shunji NAGASE, Hajime BABA, Kazuo KODAIRA, and Takashi ABE
Government Industrial Research Institute, Nagoya, Hirate-machi, Kita-ku, Nagoya 462
(Received May 9, 1973)

The electrochemical fluorination of carbonyl sulfide has been carried out. Carbonyl fluoride and sulfur hexafluoride were obtained as the principal products. The influence of the operating conditions on the reaction has been examined. In addition, a method has been developed for the production of sulfur hexafluoride. This involves the passage of carbon monoxide and sulfur over a catalyst; the resultant gas formed is subsequently introduced into a current-carrying anhydrous hydrogen fluoride in an electrolytic cell. Sulfur hexafluoride was thus obtained in a good yield.

Carbonyl sulfide has been subjected to fluorination by elementary fluorine,[2] oxygen difluoride,[3] and cobalt trifluoride,[4] and has been shown to yield fluorinated cleaved products. The present paper will describe the results of a study of the electrochemical fluorination of carbonyl sulfide. This work was initiated with the hope that the electrochemical process for the fluorination of carbonyl sulfide may produce a fully-fluorinated compound retaining the original sulfur-carbon-oxygen skeleton. However, it was found that, upon electrochemical fluorination, the carbon-sulfur bond in carbonyl sulfide was cleaved, yielding carbonyl fluoride and sulfur hexafluoride as the principal products.

This paper will also deal with a method developed for the production of sulfur hexafluoride, an important commercial sulfur-fluorine compound, by the application of the electrochemical process for the fluorination of gaseous compounds.[5] The method involves the passage of a mixture of carbon monoxide and sulfur over a catalyst to convert them into carbonyl sulfide, and then blowing it into a current-carrying anhydrous hydrogen fluoride in an electrolytic cell. This gave sulfur hexafluoride of a relatively high purity in a good yield.

Experimental

Fluorination of Carbonyl Sulfide. Carbonyl sulfide (97.5% min) obtained from the Matheson Co., carbon monoxide (99.5%), ethylene (99.5%), and propylene (99.1%) obtained from the Takachiho Chemical Industrial Co., were used. The other reagents were commercial-grade chemicals. The apparatus used was similar to one described earlier.[6] The effective surface area of the anodes and cathodes in an electrolytic cell was 7.7 dm^2. A 450 ml portion of anhydrous hydrogen fluoride was used.

The fluorination was conducted by procedures similar to those used before.[5] As an example, the procedures for Run 2 shown in Table 1 will be described. Carbonyl sulfide (25 ml/min) in a cylinder was blown with helium (90 ml/min) through a bubbler into the anhydrous hydrogen fluoride in the cell, while a current was being passed through it at an average anodic current density of 3.0 A/dm^2 at 5.5—6.5 V and at 5—6 °C. It was preferable to use a conductivity additive, sodium fluoride (4 g), for this electrolysis.

The gases generated from the cell were passed through a reflux condenser, a sodium fluoride tube, and were then bubbled into an aqueous solution of sodium sulfite in gas-washing bottles,[6] where the carbonyl fluoride in the product was hydrolyzed and converted into carbon dioxide and hydrogen fluoride, and a small amount of oxygen difluoride was removed. The gases were then guided to cold traps kept in ice and in liquid nitrogen.

The collected product, containing subliming compounds (carbon dioxide and sulfur hexafluoride), was first roughly distilled by the use of a low-temperature rectification unit. Each fraction was then analyzed by GC [(Shimadzu GC-1C), column; 0.3 cm *i.d.* × 1.8 m long stainless steel tube packed with 60/80 mesh silica gel, temperature; 80 °C, carrier; helium] as usual. IR measurements [(Hitachi EPI-S2), a gas cell equipped with NaCl windows] were also carried out.

For 3 hrs' operation, a total of 15.7 g (0.262 mol) of carbonyl sulfide was supplied; the following compounds were thus obtained; carbon tetrafluoride (0.4 g, 0.005 mol), sulfur hexafluoride (18.2 g, 0.125 mol), carbon dioxide (4.8 g, 0.109 mol), carbonyl sulfide (7.2 g, 0.120 mol), and trifluoromethyl peroxide (0.6 g, 0.004 mol).

In order to ascertain the composition of the exit gas before contact with water, a sample gas was occasionally withdrawn directly from the sampling valve fixed next to the sodium fluoride tube, and analyzed by GC [(Shimadzu GC-2C), column; for example, 0.3 cm i.d. × 10 m long polytetrafluoroethylene tube packed with Daifl oil # 3 (Daikin Industries Co.) on 20/80 mesh Shimalite F (Shimadzu Seisakusho Co.), temperature; 0 °C, carrier; helium] and by IR. Special care has been exercised to detect the formation of compounds sensitive to moisture, such as pentafluorosulfur carbonyl fluoride.[7]

Preparation of Sulfur Hexafluoride. The apparatus consisted of a molten-sulfur tube, an electrolytic cell, a sodium fluoride tube, gas-washing bottles, and cold traps. Most of these were the same as those used for the fluorination of carbonyl sulfide. They were connected in series. The molten-sulfur tube was made of glass; it was a long-neck (3 cm *i.d.* × 20 cm long), round-bottomed, 50 ml flask fitted with two glass tubings at the top for the inlet and the outlet of gases. The lower end of the inlet tubing was under the surface of the molten sulfur in the flask. About 25 g of sulfur was placed in the bottom, while activated charcoal was packed in the neck of the flask. The gas-washing bottles contained 20% of a sodium hydroxide solution saturated

1) "Electrochemical Fluorination of Gases," Part VIII.
2) O. Salinovich, E. A. R. de Staricco, and E. H. Staricco, *Inorg. Nucl. Chem. Lett.*, **2**, 157 (1966).
3) D. Soria, E. A. R. de Staricco, and E. H. Staricco, *ibid.*, **5**, 35 (1969).
4) G. A. Silvey and G. H. Cady, *J. Amer. Chem. Soc.*, **74**, 5792 (1952).
5) Part VII of this series: S. Nagase, T. Abe, H. Baba, and K. Kodaira, This Bulletin, **43**, 2980 (1970).
6) S. Nagase, H. Baba, and T. Abe, *ibid.*, **40**, 2358 (1967).
7) R. Czerepinski and G. H. Cady, *J. Amer. Chem. Soc.*, **90**, 3954 (1968).

TABLE 1. FLUORINATION OF CARBONYL SULFIDE

Run No.	COS feed rate (ml/min)	Total amount of COS fed (mol)	Anodic current density (A/dm²)	Time (min)	Product composition (%)					Yield[a] of fluorinated product (%)			
					CF_4	COF_2	SF_6	COS	$(CF_3O)_2$	CF_4	COF_2	SF_6	$(CF_3O)_2$[b]
1	10	0.170	2.3	360	3.5	41.9	51.7	—	2.8	6.8	80.6	99.4	10.8
2	25	0.262	3.0	240	1.3	30.0	34.4	33.1	1.1	1.9	41.6	47.7	3.1
3	41	0.385	3.0	210	0.9	31.2	22.2	45.5	0.2	1.0	33.9	24.0	0.5

Other conditions: Sodium fluoride added 4 g, helium 90 ml/min, cell voltage 5.5—6.5 V, cell temperature 5—6°C

a) {(Mol of each product)/(mol of COS fed)} × 100.

b) {(Mol of CF_3OOCF_3 × 2)/(mol of COS fed)} × 100.

with sodium sulfite. A small amount of potassium iodide was also added.

In operation, carbon monoxide (19 ml/min) was fed as a blowing gas into the molten-sulfur tube kept at 330 °C in an electric furnace. A mixture of carbon monoxide and sulfur vaporized was passed through an activated charcoal zone, where both elements were converted into carbonyl sulfide, which was subsequently introduced into the current-carrying anhydrous hydrogen fluoride in the cell. (Electrolysis conditions; anhydrous hydrogen fluoride used, 450 ml; sodium fluoride added, 4 g; anodic current density, 3.2 A/dm²; cell voltage, 6.3—6.5 V; cell temperature, 5—6 °C).

The fluorinated products were passed through the reflux condenser, the sodium fluoride tube, and the gas-washing bottles, and then were led to cold traps immersed in ice and in liquid nitrogen. The sulfur hexafluoride thus obtained, containing small amounts of by-products, was purified as follows. By the use of the low-temperature rectification unit, carbon tetrafluoride was distilled at −128——126 °C at atmospheric pressure (fraction 1); then the top of the column was kept at −65— −60 °C, and sulfur hexafluoride was taken out at 700—750 mmHg (fraction 2). Bistrifluoromethyl peroxide and sulfuryl fluoride remained in the column. It was possible to remove completely a trace of sulfuryl fluoride in the sulfur hexafluoride by passing fraction 2 through a glass tube (3 cm *i.d.* × 40 cm long) containing 5/7 mesh silica gel.

After 4 hrs' operation, 6.1 g (0.190 g.atom) of sulfur was vaporized from the sulfur-molten tube, and 25.8 g (0.177 mol) of sulfur hexafluoride (purity, 99.9%) was thus obtained (yield 93.2%), together with small amounts of carbon tetrafluoride, bistrifluoromethyl peroxide, and sulfuryl fluoride. Ethylene, propylene, and carbonyl chloride were also examined as blowing gases. The experiments for the preparation of sulfur hexafluoride from these starting materials were conducted much as in the case of carbon monoxide.

Results and Discussion

The fluorination of carbonyl sulfide resulted in the cleavage of the carbon-sulfur bond:

$$COS \xrightarrow{[F]} CF_4,\ COF_2,\ SF_6,\ CF_3OOCF_3$$

The reaction conditions and results obtained are shown in Table 1. If the carbon-sulfur bond was not cleaved completely, such a compound as pentafluorosulfur carbonyl fluoride[7] would be obtained. In this work, even under the preferred conditions for milder fluorination[8] of gaseous compounds (the higher feed rate used in Run 3), the cleavage of the carbon-sulfur bond occurred. A low-temperature fluorination also yielded fragmented products; feed rate, 35 ml/min; cell temperature, −25 °C; product composition (mol %), carbon tetrafluoride (0.9), carbonyl fluoride (58.8), sulfur hexafluoride (18.8), carbonyl sulfide (21.1), and bistrifluoromethyl peroxide (0.3).

Under severe fluorination conditions (Run 1), a considerable amount of bistrifluoromethyl peroxide was obtained. The formation of this may be explained in terms of the coupling of two trifluoromethoxy radicals, most likely produced by the attachment of a fluorine radical to the carbonyl fluoride formed in the course of the fluorination.

In contrast to the carbon-sulfur bond, the carbon-oxygen bond was rather stable to the electrochemical fluorination,[5] as is shown by the kinds and amounts of fluorinated products formed. The bonding energy for the carbon-oxygen bond in carbonyl sulfide is much greater than that for the carbon-sulfur bond.[9] This may be the primary cause for the present results. Salinovich *et al.*[2] examined the reaction of carbonyl sulfide with elementary fluorine under a variety of operating conditions and observed a very rapid reaction, which gave carbonyl fluoride and sulfur hexafluoride. Earlier Silvey and Cady[4] obtained similar results in the fluorination of carbonyl sulfide with cobalt trifluoride. From these observations,[2,4] together with the present results described above, it may be stated that it is difficult to fluorinate carbonyl sulfide and still totally retain the sulfur-carbon-oxygen skeleton by direct methods of fluorination.

The process described herein for the preparation of sulfur hexafluoride can be expressed as follows:

$$CO \xrightarrow{S} COS \xrightarrow{[F]} COF_2,\ SF_6 \xrightarrow{\text{Alkali}} SF_6$$

Because it is of commercial importance, sulfur hexafluoride has been prepared by a number of methods. An electrochemical process was often employed.[10] In the present method, the starting material is elemental

8) S. Nagase, K. Tanaka, and H. Baba, This Bulletin, **38**, 834 (1965).

9) Landolt-Börnstein, "Zahlenwerte und Funktionen," 6 Auflage, 1 Band, 2 Teil (1951), p. 38.

10) a) M. Prober, U. S. Pat. 2717235 (1955). b) E. H. Man, U. S. Pat. 2904476 (1959). c) P. Sartori, *Angew. Chem.*, **75**, 417 (1963). d) M. Hisasue, N. Watanabe, and S. Yoshizawa, *Asahi Garasu Kenkyu Hokoku*, **15**, 127; 139 (1965). e) L. Heinrich, *Z. Anorg. Allgem. Chem.*, **346**, 44 (1966). f) P. E. Ashley, J. D. La Zerte, and R. J. Seffl, U. S. Pat. 3345277 (1967). g) T. Abe, S. Nagase, K. Kodaira, and H. Baba, This Bulletin, **43**, 1812 (1970). h) J. Nakamura, S. Sato, and Y. Omote, Japan Pat. Publication No. 45—32525 (1970).

sulfur, and the fluorination proceeds smoothly. Although the process involves the loss of carbonyl fluoride, it affords sulfur hexafluoride of high purity in a good yield (93.2%).

The action of carbon monoxide upon sulfur is known to produce carbonyl sulfide.[11] The method described in the Experimental Section was also efficient in converting carbon monoxide into carbonyl sulfide. For example, when the feed rate of carbon monoxide was 19 ml/min, the conversions were as follows: 72% at 250 °C, 88% at 280 °C, and 97% at 300 °C. The conditions for 100% conversion (at 330 °C) were applied for the run illustrated in the Experimental Section.

When ethylene or propylene was used as the blowing gas instead of carbon monoxide, they were converted into carbon disulfide and hydrogen sulfide.[12] The amount of the olefin introduced with helium into the molten-sulfur tube was so adjusted that it reacted almost completely with the sulfur. The activated charcoal was again used as the catalyst for this reaction. The whole process can be represented by the following formulae:

$$CH_2{=}CH_2 \xrightarrow[320°C]{S} CS_2,\ H_2S$$

$$\xrightarrow{[F]} SF_6(CF_4,\ C_2F_6,\ CF_3SF_5,\ C_2F_5SF_5,\ SO_2F_2,\ CS_2)$$

$$CH_3CH{=}CH_2 \xrightarrow[350°C]{S} CS_2,\ H_2S$$

$$\xrightarrow{[F]} SF_6(CF_4,\ C_2F_6,\ CF_3SF_5,\ C_3F_8,\ SO_2F_2)$$

In the case of ethylene,[13] some representative results obtained were as follows: composition of the product (mol %): carbon tetrafluoride (13.5), hexafluoroethane (1.0), sulfur hexafluoride (68.9), trifluoromethylsulfur pentafluoride (13.3), pentafluoroethylsulfur pentafluoride (0.5), sulfuryl fluoride (0.8), and carbon disulfide unchanged (2.0); the yield[14] of sulfur hexafluoride (20.0 g, 0.137 mol) was 39.2%. A small amount of sulfur was found in the electrolytic cell.

In the case of propylene,[15] the products were carbon tetrafluoride (6.9), hexafluoroethane (1.0), sulfur hexafluoride (82.1), trifluoromethylsulfur pentafluoride (4.5), octafluoropropane (4.3), and sulfuryl fluoride (1.1), and the yield[14] of sulfur hexafluoride (23.0 g, 0.158 mol) was 63.2%.

Carbonyl chloride was also useful as a blowing gas. The whole process may be described as follows:

$$COCl_2 \xrightarrow[360\,°C]{S} COS,\quad S_2Cl_2 \xrightarrow{[F]} SF_6(COF_2,\ COS)$$

The products[16] were carbonyl fluoride (41.1), sulfur hexafluoride (45.0), and carbonyl sulfide (13.9), and the yield[14] of sulfur hexafluoride (26.3 g, 0.180 mol) was 73.2%. As far as the preparation of sulfur hexafluoride is concerned, the process using carbon monoxide is superior to all others among those studied in the present work.

11) For example, R. J. Ferm, *Chem. Rev.*, **57**, 621 (1957).

12) S. Oae, "Yūki-iō-kagōbutsu no Kagaku," Vol. 1, Kagaku Dojin, Kyoto (1968), p. 24.

13) Conditions: Sulfur consumed, 11.2 g (0.349 g. atom); sodium fluoride added, 4 g; anodic current density, 3.2 A/dm^2; cell voltage, 6.5—7.5 V; electricity passed through, 99 A·hr; cell temperature, 6—7 °C.

14) Based on the amount of sulfur (g. atom) vaporized from the molten-sulfur tube.

15) Conditions: Sulfur consumed, 8.0 g (0.250 g. atom); sodium fluoride added, 4 g; anodic current density, 2.9 A/dm^2; cell voltage, 6.0—7.9 V; electricity passed through, 88 A·hr; cell temperature, 6—7 °C.

16) Conditions: Sulfur consumed, 7.9 g (0.246 g. atom); sodium fluoride added, 4 g; anodic current density, 3.2 A/dm^2; cell voltage, 6.1—7.2 V; electricity passed through, 96 A·hr; cell temperature, 6—7 °C.

The Magnetic Properties of Iron(II) Complexes with 2-(2′-Pyridyl)imidazole and Its Derivatives

Yoshihiro SASAKI and Tsunenobu SHIGEMATSU

Institute for Chemical Research, Kyoto University, Uji, Kyoto 611

(Received May 14, 1973)

The magnetic susceptibilities and Mössbauer spectra of iron(II) complexes of 2-(2′-pyridyl)imidazole (PI), 2-(6′-methyl-2′-pyridyl)imidazole (6-MPI), and 2-(2′-pyridyl)benzimidazole (PBI) have been measured in the 4.2—298 K temperature range. The results show that $Fe(II)(PI)_3(ClO_4)_2H_2O$ and $Fe(II)(PBI)_3(ClO_4)_2H_2O$ have a spin equilibrium between $^1A_1$ and $^5T_2$, while $Fe(II)(6\text{-}MPI)_3(ClO_4)_2H_2O$ does not have such an equilibrium. The temperature dependence and magnitude of the magnetic data for $Fe(II)(PBI)_3(ClO_4)_2H_2O$ and $Fe(II)(6\text{-}MPI)_3(ClO_4)_2H_2O$ have been calculated by using a parametric ligand-field approximation. The results indicate that the orbital splittings of the $^5T_2$ ground state due to trigonal distortion are -2000 and -800 cm^{-1} for $Fe(II)(6\text{-}MPI)_3(ClO_4)_2H_2O$ and $Fe(II)(PBI)_3(ClO_4)_2H_2O$ respectively.

Transition-metal octahedral complexes with the electronic configuration d^6 may exist in either one of two different electronic ground states, $^5T_2$ (high-spin $t_2^4e^2$) and $^1A_1$ (low-spin t_2^6). Under special circumstances, the energy difference between these two states at a certain temperature may become comparable to the thermal energy, kT. If, at a field strength, Δ, close to the mean spin-pairing energy, π, the separation of the two states attains a value within the thermally-accessible range, an equilibrium between the $^1A_1$ and $^5T_2$ states can be expected to occur. Orgel has suggested that the diamagnetism of tris(1,10-phenanthroline)iron(II) complexes can not be expected from simple ligand-field calculations in which $\Delta<\pi$ (Fe^{2+}; 17600 cm^{-1}).[1] The complex formation must, therefore, produce a marked decrease in π from the estimated free ion value. Thus, iron(II) complexes with α-diimine chelate rings appear to be close to a $^5T_2$–$^1A_1$ crossover system. Certain iron(II) complexes of 2-(2′-pyridyl)imidazole, 2-(2′-pyridyl)imidazoline and 2-methyl-1,10-phenanthroline, exhibit anomalous magnetic behavior indicative of the $^5T_2$–$^1A_1$ crossover.[2-6]

We have prepared iron(II) octahedral complexes with 2-(6′-methyl-2′-pyridyl)imidazole (I, R=CH_3; 6-MPI) and 2-(2′-pyridyl)benzimidazole (II; PBI); the variations in their magnetic susceptibilities and Mössbauer spectra with the temperature will be reported in this paper. Moreover, we have re-examined an iron complex with 2-(2′-pyridyl)imidazole (I, R=H; PI) and will report the results here.

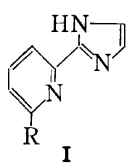

I

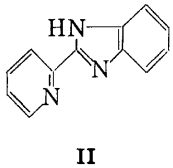

II

1) L. E. Orgel, Report of the 10th Solvay Conference in Chemistry, Brussels, 1956, p. 289.

2) D. M. L. Goodgame and A. A. S. C. Machado, *Inorg. Chem.*, **8**, 2031 (1969).

3) R. L. Dosser, W. J. Eilbeck, A. E. Underhill, P. R. Edwards, and C. E. Johnson, *J. Chem. Soc., A*, **1969**, 810.

4) D. M. L. Goodgame and A. A. S. C. Machado, *Chem. Commun.*, **1969**, 1420.

5) H. A. Goodwin and R. N. Sylva, *Aust. J. Chem.*, **21**, 83 (1968).

6) E. König, G. Ritter, H. Spiering, S. Kremer, K. Madeja, and A. Rosenkranz, *J. Chem. Phys.*, **56**, 3139 (1972).

Experimental

Preparation of the Reagents. (*a*) *2-(2′-Pyridyl)imidazole.* A procedure similar to that described by Chiswell *et al.* was used[7] except that, after extracting 2-(2′-pyridyl)imidazole many times with ether, the solvent was removed from the combined, dried ether extracts and the residual oil was sublimated *in vacuo* twice. Pale yellow crystals were collected and recrystallized from ethyl acetate as white crystals; mp 134.5—135 °C.

(*b*) *2-(6′-Methyl-2′-pyridyl)imidazole.* This reagent was prepared similarly from 6-methylpyridine-2-aldehyde; white crystals, mp 169 °C.

(*c*) *2-(2′-Pyridyl)benzimidazole.* A procedure similar to that described by Walter and Freiser was used.[8] α-Picolinic acid and *o*-phenylenediamine were allowed to react with each other at 170—180 °C for 3 hr. The product was crystallized from ethanol-water solution as red-violet crystals and was then sublimed. The recrystallization of the sublimate from ethyl acetate, followed by sublimation, yielded white crystals of 2-(2′-pyridyl)benzimidazole; mp 220 °C.

Preparation of Complexes. All preparations were carried out in a nitrogen atmosphere using air-free water and ethanol. All the complexes were dried *in vacuo* over silica gel at room temperature.

(*a*) *Tris-[2-(2′-pyridyl)imidazole] Iron(II) Perchlorate Monohydrate.* Solutions of 2-(2′-pyridyl)imidazole (2.2 g) in ethanol (10 ml) and ferrous perchlorate hexahydrate (1.8 g) in water (10 ml) were mixed. The dark red solution thus formed was concentrated to half-volume under reduced pressure; the complex was then precipitated on cooling. When it was recrystallized from 1:1 ethanol-water, dark red crystals were obtained. Found: C, 40.50; H, 3.29; N, 17.33; Fe, 7.90%. Calcd for $FeC_{24}H_{23}N_9O_9Cl_2$: C, 40.69; H, 3.27; N, 17.80; Fe, 7.88%.

(*b*) *Tris-[2-(6′-methyl-2′-pyridyl)imidazole] Iron(II) Perchlorate Monohydrate.* This complex was prepared similarly from 2-(6′-methyl-2′-pyridyl)imidazole; yellow crystals. Found: C, 42.67; H, 3.76; N, 16.80; Fe, 7.34%. Calcd for $FeC_{27}H_{29}N_9O_9Cl_2$: C, 43.22; H, 3.90; N, 16.80; Fe, 7.44%.

(*c*) *Tris-[2-(2′-pyridyl)benzimidazole] Iron(II) Perchlorate Monohydrate.* Solutions of 2-(2′-pyridyl)benzimidazole (2.9 g) and ferrous chloride tetrahydrate (1.0 g) in minimum quantities of ethanol were mixed. Perchloric acid (2.2 ml

7) B. Chiswell, F. Lions, and B. S. Morris, *Inorg. Chem.*, **3**, 110 (1964).

8) J. L. Walter and H. Freiser, *Anal. Chem.*, **26**, 217 (1954).

of 70% aqueous solution) and water were then added, and reddish-brown crystals were precipitated. Found: C, 50.02; H, 3.31; N, 14.41; Fe, 6.65%. Calcd for $FeC_{36}H_{29}N_9O_9Cl_2$: C, 50.37; H, 3.41; N, 14.69; Fe, 6.51%.

Magnetic Measurements. Magnetic susceptibilities were measured using a torsion balance magnetometer. The molar susceptibilities were corrected for diamagnetism, using the following corrections: Fe^{2+}, −13; H_2O, −13; ClO_4^-, −32; 2-(2′-pyridyl)imidazole, −82; 2-(2′-pyridyl)benzimidazole, −118; 2-(6′-methyl-2′-pyridyl)imidazole, −97 (in units of 10^{-6} cgs/mol). The effective magnetic moment, μ_{eff}, was obtained from the relation: $\mu_{eff}=2.828\sqrt{\chi'_M T}$, χ_M' being the fully corrected molar susceptibility, and T, the temperature in K.

Mössbauer Effect Measurements. The Mössbauer spectra were obtained with a scanning velocity spectrometer in the time mode. The radiation source was ^{57}Co diffused into a copper foil and kept at room temperature during all measurements. The velocity scale was calibrated with metallic iron, and the velocity was determined to an accuracy of ±0.04 mm/s.

Electronic Spectra. The electronic spectra of these complexes were measured with a Hitachi 323 automatic recording spectrophotometer.

Results and Discussion

Magnetic Data. The results of magnetic susceptibility measurements of polycrystalline samples between 77 and 298 K are listed in Table 1, while the variation in μ_{eff} with the temperature is shown in Fig. 1. The magnetic-moment values for $Fe(II)(6\text{-}MPI)_3(ClO_4)_2H_2O$ are characteristic of an iron(II) ion in a $^5T_2$ ground state. Within the 77—298 K temperature range, the susceptibility follows the Curie-Weiss law: $\chi'_M=C/(T-\Theta)$; the resulting value of the Weiss constant, Θ, is −3°.

The magnetic-moment values for the other complexes indicate that these compounds possess anomalous magnetic properties. The values of susceptibility for $Fe(II)(PI)_3(ClO_4)_2H_2O$ are in agreement with those reported by Goodgame and Machado.[2] The temperature dependence of the Curie-Weiss plot for $Fe(II)(PBI)_3(ClO_4)_2H_2O$ is shown in Fig. 2. This plot exhibits that, within the 220.5—298 K temperature range, the susceptibility follows the Curie-Weiss law and that the value of the Weiss constant, Θ, is −2°.

The increase in χ'_M with a rise in the temperature

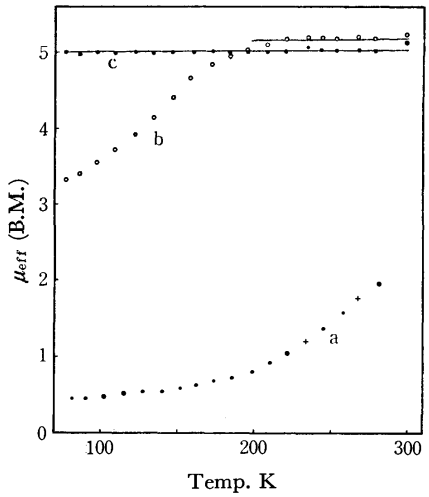

Fig. 1. Temperature dependence of the effective magnetic moments.
a: $Fe(II)(PI)_3(ClO_4)_2H_2O$, b: $Fe(II)(PBI)_3(ClO_4)_2H_2O$, c: $Fe(II)(6\text{-}MPI)_3(ClO_4)_2H_2O$.
The solid lines are calculated theoretically with the parameters, $v'=0$ cm^{-1}, $\lambda=-80$ cm^{-1}, $\kappa=0.8$ and $v=-800$ and -2000 cm^{-1} for $Fe(II)(PBI)_3(ClO_4)_2H_2O$ and $Fe(II)(6\text{-}MPI)_3(ClO_4)_2H_2O$, respectively.

Table 1. Magnetic data for $Fe(II)(PI)_3(ClO_4)_2H_2O$, $Fe(II)(PBI)_3(ClO_4)_2H_2O$ and $Fe(II)(6\text{-}MPI)_3(ClO_4)_2H_2O$

$Fe(II)(PI)_3(ClO_4)_2H_2O$			$Fe(II)(PBI)_3(ClO_4)_2H_2O$			$Fe(II)(6\text{-}MPI)_3(ClO_4)_2H_2O$		
T(K)	$10^6\chi'_M$ (cgs/mol)	μ_{eff} (B.M.)	T(K)	$10^6\chi'_M$ (cgs/mol)	μ_{eff} (B.M.)	T(K)	$10^6\chi'_M$ (cgs/mol)	μ_{eff} (B.M.)
281.8	1668	1.94	298.0	11554	5.25	298.0	11101	5.14
267.1	1426	1.75	278.1	12157	5.20	278.1	11392	5.03
258.1	1159	1.55	267.5	12761	5.22	267.5	11807	5.03
244.7	917	1.34	253.3	13314	5.19	253.3	12429	5.02
233.3	748	1.18	243.7	13917	5.21	243.7	13052	5.04
221.3	602	1.03	234.7	14420	5.20	234.7	13757	5.08
210.3	481	0.90	220.5	15224	5.18	220.5	14255	5.01
199.1	384	0.78	207.8	15626	5.10	207.8	15210	5.03
186.6	336	0.71	195.1	16279	5.04	195.1	16081	5.01
174.6	312	0.66	183.8	16782	4.97	183.8	16953	4.99
163.0	288	0.61	172.5	17084	4.85	172.5	18323	5.03
152.1	263	0.57	159.4	17084	4.67	159.4	19651	5.01
139.9	239	0.52	146.4	16732	4.43	146.4	21269	4.99
127.7	263	0.52	133.9	16078	4.15	133.9	23386	5.00
115.6	263	0.49	122.1	15777	3.93	122.1	25710	5.01
102.6	263	0.46	109.2	15777	3.71	109.2	28490	4.99
90.4	239	0.42	97.2	16330	3.56	97.2	32018	4.99
82.8	263	0.42	85.9	16883	3.41	85.9	35961	4.97
			77.2	17989	3.33	77.2	40277	4.99

seems to be caused by either an antiferromagnetic interaction between iron(II) ions or by a thermal equilibrium involving terms of different spin multiplicities. Since all the complexes contain three ligand molecules around a central ion and since the Weiss constants of the complexes are small, it seems unlikely that an iron-iron antiferromagnetic interaction occurs in these compounds. Therefore, the most plausible explanation is that there is an equilibrium between two different spin states. Octahedral iron(II) complexes may exist in either the $^5T_2$ or the $^1A_1$ ground state, and the energy separation between these two states may become comparable to the thermal energy, kT, under special circumstances.[9] Thus, we suggest that the observed results can be explained in terms of a spin equilibrium involving $^5T_2$ and $^1A_1$ electronic states.

Table 2. Mössbauer parameters δ^{IS} and ΔE_Q (in mm/s)

Compound	Temp. (K)	δ^{IS} (S=0)	ΔE_Q (S=0)	δ^{IS} (S=2)	ΔE_Q (S=2)	Ratio of peak intensity a_h/a_l
$Fe(II)(PI)_3(ClO_4)_2H_2O$	298	0.40	0.40	—	—	
$Fe(II)(PBI)_3(ClO_4)_2H_2O$	298	—	—	0.96	1.99	
	77.2	0.47	0.40	0.98	2.27	0.63
	4.2	0.50	0.46	1.11	2.47	0.61
$Fe(II)(6\text{-}MPI)_3(ClO_4)_2H_2O$	298	—	—	1.03	2.09	
	100	—	—	1.13	2.43	
	77.2	—	—	1.13	2.43	

error = ±0.04 mm/s.

Mössbauer Spectra. The Mössbauer effect can be readily distinguished between the low- and high-spin forms of iron(II).[10] Characteristically S=0 Fe^{II} ions have an isomer shift, δ^{IS}, in the −0.1—+0.4 mm/s range with respect to iron, and have a quadrupole splitting, ΔE_Q, which is strongly dependent on coordination, 0.0—1.0 mm/s. For S=2 Fe^{2+} ions, δ^{IS} is in the 0.9—1.6 mm/s range and ΔE_Q, in the 1.2—3.5 mm/s range. The values of the Mössbauer parameters for the present complexes are listed in Table 2. These parameters were computed by fitting the data to the Lorentzian by means of a least-squares computer program. The Mössbauer spectra of $Fe(II)(PBI)_3(ClO_4)_2H_2O$ at 298, 77.2, and 4.2 K are shown in Fig. 3.

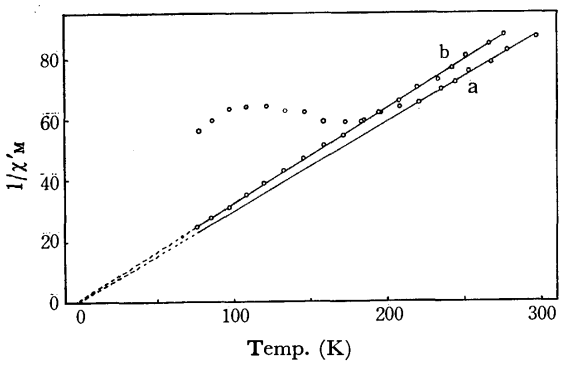

Fig. 2. Plots of resiprocal molar susceptibilities against absolute temperature.
a: $Fe(II)(PBI)_3(ClO_4)_2H_2O$, b: $Fe(II)(6\text{-}MPI)_3(ClO_4)_2H_2O$.

The spectra of $Fe(II)(6\text{-}MPI)_3(ClO_4)_2H_2O$ at 298, *ca.* 100, and 77.2 K consist of a doublet expected for the S=2 Fe^{2+} ion, which has a distortion, leaving an orbital singlet as the ground state. The spectrum of $Fe(II)(PI)_3(ClO_4)_2H_2O$ at 298 K, on the other hand, consists of a doublet due to the low-spin isomer, and the resonance lines due to the high-spin isomer cannot be observed because of the lower relative concentration of the high-spin form. The spectrum of $Fe(II)(PBI)_3(ClO_4)_2H_2O$ at 298 K consists of a doublet centered at 0.96 mm/s, with a quadrupole splitting of 1.99 mm/s, and the spectra at 77.2 and 4.2 K change into two doublets. We attribute the outer peaks to Fe^{2+} in the S=2 state, and inner pair, to Fe^{II} in the S=0 state.

Table 3. Absorption maxima in the electronic spectra

Compound	d-d Band (log ε) (cm^{-1})	CT band (log ε) (cm^{-1})
$Fe(II)(PI)_3(ClO_4)_2H_2O$	—	25100
		20500
$Fe(II)(PBI)_3(ClO_4)_2H_2O$	—	20400
$Fe(II)(6\text{-}MPI)_3(ClO_4)_2H_2O$	11900 (0.91)	26200 (2.78)
	8600 (0.83)	

Electronic Spectra. The band maxima in the electronic spectra measured in ethanol are listed in Table 3. The molar extinction coefficients of $Fe(II)(PI)_3(ClO_4)_2H_2O$ and $Fe(II)(PBI)_3(ClO_4)_2H_2O$ vary with their concentrations. The electronic spectrum of $Fe(II)(6\text{-}MPI)_3(ClO_4)_2H_2O$ is characteristic of a high-spin complex whose d-d band splits into two components. The average of the band energies may be taken as a rough estimate of the ligand-field splitting, Δ. In this way, we obtained $\Delta \simeq 10300\ cm^{-1}$ for $Fe(II)(6\text{-}MPI)_3(ClO_4)_2H_2O$.

Calculation of the Ligand-field Parameters. We carried out a ligand-field calculation for d^6 quintet states, including the spin-orbit coupling and the trigonal component in the ligand field. Since we worked within a ^5D state, this calculation does not include the singlet state in the spin equilibrium.

The predominant cubic field splits the atomic ^5D term into $^5T_2$ and appriximately 10000 cm^{-1}-higher-lying ^5E. The ligand-field splitting parameter, Δ, for $Fe(II)(6\text{-}MPI)_3(ClO_4)_2H_2O$ is 10300 cm^{-1}. The trigonal distortion splits the $^5T_2$ ground term into ^5E and $^5A_1$, and the separation between these terms is called δ. Whenever the orbital doublet, ^5E, is the lowest, the sign of δ can be chosen as positive, and *vice versa*. If the z axis is taken along the (1,1,1) direction of the octahedron, the trigonal potential, V_t, has the form:

$$Ar^2C_0^{(2)}(\theta,\varphi) + Br^4[C_0^{(4)}(\theta,\varphi) - 1/2\sqrt{7/10}(C_3^{(4)}(\theta,\varphi) - C_{-3}^{(4)}(\theta,\varphi))] \quad (1)$$

9) Y. Tanabe and S. Sugano, *J. Phys. Soc. Japan*, **9**, 776 (1954).
10) J. F. Duncan and R. M. Golding, *Quart. Rev.*, **19**, 36 (1965).

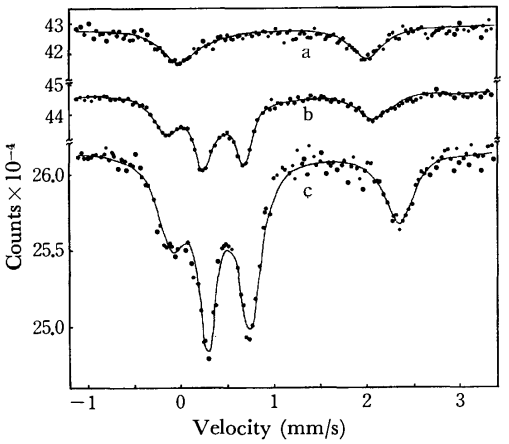

Fig. 3. Mössbauer spectra of $Fe(II)(PBI)_3(ClO_4)_2H_2O$.
a: 298 K, b: 77.2 K, c: 4.2 K.

where $C_m^{(k)}(\theta,\varphi)=(4\pi/(2k+1))^{1/2}Y_{km}(\theta,\varphi)$. δ is calculated by using the parameters, v and v', of Pryce and Runciman.[11] Their parameters are related to the parameters in Eq. (1) in the following way:

$$\overline{Ar^2} = v - 2\sqrt{2}v'$$
$$\overline{Br^4} = \frac{4}{3}v + 2\sqrt{2}v'. \quad (2)$$

Since $\delta \ll \Delta$ in general, δ depends almost entirely on the value of v and is not sensitive to v'. Thus, v' is assumed to be zero throughout the discussion.

The matrix elements of the Hamiltonian:

$$H = V_t - \lambda L \cdot S \quad (3)$$

were evaluated within the 15 states $|M_L M_S>$ of a $^5T_2$ term classified according to their M_J values. The eigenvalues and eigenfunctions generated in this calculation may be used to evaluate the magnitude and temperature dependence of the effective magnetic moment of a high-spin ferrous system.

The usual Van Vleck formulation is used for the magnetic susceptibility. It has to be calculated separately in both the direction parallel to and that perpendicular to the principal axis. The average magnetic susceptibility, $\bar{\chi}$, may be obtained from the principal magnetic susceptibilities, $\chi_{//}$ and $\chi_\perp$ according to:

$$\bar{\chi} = \frac{1}{3}(\chi_{//}+2\chi_\perp). \quad (4)$$

Then, the average magnetic moment, $\bar{\mu}$, was determined by $\bar{\chi}$ as a function of parameters, v and λ, and the orbital reduction factor κ.

The curves of the average magnetic moment against the temperature for various values of v are shown in Figs. 4 and 5. It can be seen that the temperature dependence of the magnetic moment for a positive v value is qualitatively different from that for a large negative v value. For a positive v value, there is a maximum in the curve, while for a large negative v value, the curve is essentially flat down to ~15 K. Taking account of the covalency effects, we fixed $\lambda=-80$ cm^{-1} and $\kappa=0.8$. Thus, the value of δ can

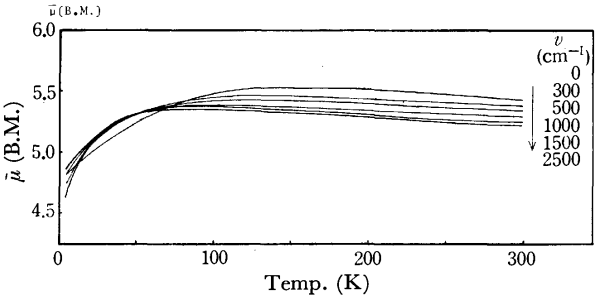

Fig. 4. Temperature dependence of the average magnetic moment of a high-spin ferrous complex as a function of trigonal distortion for positive values of v.
$\lambda=-80$ cm^{-1}, $\kappa=0.8$.

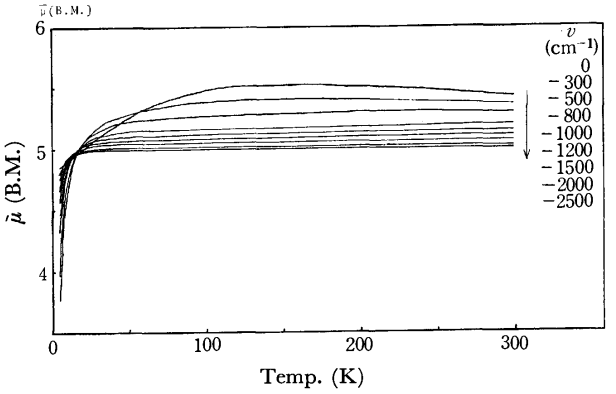

Fig. 5. Temperature dependence of the average magnetic moment of a high-spin ferrous complex as a function of trigonal distortion for negative values of v.
$\lambda=-80$ cm^{-1}, $\kappa=0.8$.

be easily determined by the curve-fitting method. The solid lines for $Fe(II)(6\text{-}MPI)_3(ClO_4)_2H_2O$ and $Fe(II)(PBI)_3(ClO_4)_2H_2O$ in Fig. 1 were calculated for $v=-2000$ and -800 cm^{-1} respectively. It is immdeiately clear from Fig. 1 that v is negative, giving an orbital singlet as the ground state, and that $\delta\simeq-2000$ and -800 cm^{-1} for $Fe(II)(6\text{-}MPI)_3(ClO_4)_2H_2O$ and $Fe(II)(PBI)_3(ClO_4)_2H_2O$. The quadrupole splitting in the Mössbauer spectra of $Fe(II)(PI)_3(ClO_4)_2H_2O$ and $Fe(II)(PBI)_3(ClO_4)_2H_2O$ in S=0 arises from this trigonal distortion. It has been reported that $Fe(II)(bipy)_3(ClO_4)_2$, which is in a low-spin form, exhibits a similar quadrupole splitting.[12] Therefore, this complex probably has a large trigonal distortion.

Two approaches have been previously employed to interpret the crossover system qualitatively. The first is the calculation of the temperature dependence of the susceptibility in terms of the Boltzmann distribution between $^5T_2$ and $^1A_1$ states separated from each other by a fixed energy, ΔE.[13] However, this method is not successful in the present case. The second approach is an empirical one in which one calculates an equilibrium constant in terms of the relative concentrations of the high- and low-spin forms.[1,14] We define the equilibrium constant as $K=[HS]/[LS]$, which is cal-

11) M. H. L. Pryce and W. A. Runciman, *Discuss. Faraday Soc.*, **26**, 34 (1958).

12) R. L. Collins, R. Pettit, and W. A. Baker, Jr., *J. Inorg. Nucl. Chem.*, **28**, 1001 (1966).

13) B. N. Figgis, "Introduction to Ligand Fields," Interscience, New York (1966).

14) R. G. Stoufer, D. W. Smith, E. A. Clevenger, and T. E. Norris, *Inorg. Chem.*, **5**, 1167 (1966).

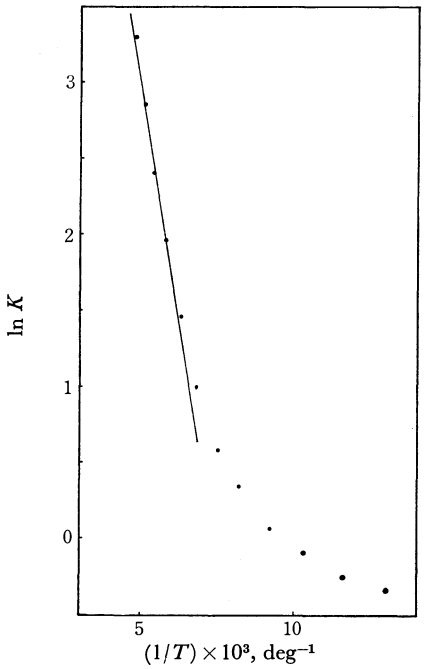

Fig. 6. Plot of $\ln K$ for $Fe(II)(PBI)_3(ClO_4)_2H_2O$ against $1/T$.

culated easily from the observed results. In order to calculate K, it is assumed that the susceptibility of the $^5T_2$ state follows the Curie-Weiss law within the temperature range of 77—298 K and that the temperature-independent paramagnetism for the $^1A_1$ state is 50×10^{-6} cgs/mol.[13] According to this assumption, the K value of $Fe(II)(PBI)_3(ClO_4)_2H_2O$ at 77.2 K is 0.71. Figure 6 shows the temperature dependence of $\ln K$ as calculated from the experimental susceptibility of $Fe(II)(PBI)_3(ClO_4)_2H_2O$. The curvature of the $\ln K$ against $1/T$ plot reveals that this method is inadequate over the full temperature range. However, ΔH is essentially constant over the 159.4—207.8 K range and is listed in Table 4, along with the ΔS calculated there. Assuming that the Weiss constant is $-2°$ and that $\chi'_M=11000\times10^{-6}$ cgs/mol at 298 K (these represent typical experimental values for such species), one can plot $\ln K$ against $1/T$ and calculate ΔH and ΔS for $Fe(II)(PI)_3(ClO_4)_2H_2O$ (Table 4).

TABLE 4. THERMODYNAMIC PARAMETERS FOR SPIN EQUILIBRIUM

Compound	Temperature range (K)	ΔH (kcal/mol)	ΔS (e.u.)
$Fe(II)(PBI)_3(ClO_4)_2H_2O$	159.4—207.8	2.49	18.43
$Fe(II)(PI)_3(ClO_4)_2H_2O$	210.3—281.8	2.96	6.89

The entropy change for a simple spin equilibrium between singlet and quintet states may be only 3.2 eu. Since the ΔS values in the $^5T_2$–$^1A_1$ equilibria of these complexes are larger than 3.2 eu, it appears that additional factors, such as changes in the bond length and/or lattice spacing, play an important role in deciding the details of the temperature variation in the magnetic susceptibilities.

We can also obtain the relative concentrations of the low- and high-spin forms in $Fe(II)(PBI)_3(ClO_4)_2H_2O$ from the Mössbauer spectra if the recoilless fractions are same for the two states (it is not likely that they are very different). Then, the equilibrium constant, K, is 0.63 at 77.2 K and 0.61 at 4.2 K. The results indicate that *ca.* 40% of the molecules are permanently in a $^5T_2$ state. According to the model for a spin equilibrium between $^5T_2$ and $^1A_1$ suggested by Bari and Sivardière, all the molecules should exist in a $^1A_1$ state at a considerably low temperature.[15] Therefore, we suggest that two chemical species may co-exist, one exhibiting a spin equilibrium and the other existing in a $^5T_2$ state. The asymmetry of 2-(2′-pyridyl)-benzimidazole as a chelating ligand allows, in theory, the formation of *vicinal* and *meridional* geometric isomers. Then, such geometric isomerism may result in the formation of two isomers possessing some different magnetic properties.

Recently a report about the magnetic behavior of some iron(II) complexes containing 2-(2′-pyridyl)benzimidazole was published.[16] The results indicate the existence of a $^5T_2$–$^1A_1$ spin equilibrium, but the details are not consistent with our investigation because these samples are different from the present complex.

Conclusion

The temperature dependence of the magnetic moments of $Fe(II)(PI)_3(ClO_4)_2H_2O$ and $Fe(II)(PBI)_3(ClO_4)_2H_2O$ indicate the presence of a spin equilibrium between the $^5T_2$ and $^1A_1$ states. The results of the Mössbauer spectra of $Fe(II)(PBI)_3(ClO_4)_2H_2O$ are consistent with the existence of such a spin equilibrium. This behavior is in marked contrast to that of $Fe(II)(6\text{-MPI})_3(ClO_4)_2H_2O$, which is a high-spin complex within the temperature range of 77—298 K. The difference in the magnetism of these complexes arises from the steric hindrance introduced by the 6′-methyl group.

The temperature dependence and magnitude of the magnetic moments of $Fe(II)(PBI)_3(ClO_4)_2H_2O$ and $Fe(II)(6\text{-MPI})_3(ClO_4)_2H_2O$ existing in a $^5T_2$ state can be reproduced well using the parametric ligand-field theory. The results indicate that the orbital splittings of the $^5T_2$ state due to trigonal distortion are -2000 and -800 cm^{-1} for $Fe(II)(6\text{-MPI})_3(ClO_4)_2H_2O$ and $Fe(II)(PBI)_3(ClO_4)_2H_2O$ respectively.

The authors wish to thank Dr. T. Shinjo and Mr. T. Matsuzawa for permitting us to use equipments for Mössbauer and magnetic measurements, respectively and for their helpful discussions.

15) R. A. Bari and J. Sivardière, *Phys. Rev.*, **B 5**, 4466 (1972).
16) J. R. Sams, J. C. Scott, and T. B. Tsin, *Chem. Phys. Lett.*, **18**, 451 (1973).

The Preparation and Absorption Spectra of the Mixed *cis*-Dicyano Complexes of Cobalt(III) with Carbonato or Related Ligands

Shuhei FUJINAMI and Muraji SHIBATA

Department of Chemistry, Faculty of Science, Kanazawa University, Kanazawa 920

(Received May 23, 1973)

By the reaction of the $[Co(CO_3)_3]^{3-}$ complex and KCN, the complex anion, $[Co(CN)_2(CO_3)_2]^{3-}$, has been isolated as the tris(ethylenediamine)cobalt(III) salt. From this dicarbonato-complex anion, related dicyano complexes, $[Co(CN)_2(CO_3)(C_2O_4)]^{3-}$ and $[Co(CN)_2(C_2O_4)_2]^{3-}$ have then been obtained as $\Lambda(+)_{589}$-$[Co(en)_3]^{3+}$ salts, with resolutions into the active forms. Other related complexes, $[Co(CN)_2(dtc)_2]^-$ and $[Co(CN)_2(xan)_2]^-$ (dtc=dimethyldithiocarbamate anion, xan=methylxanthate anion), have also been prepared as potassium salts from the dicarbonato complex. The absorption spectra of all of the dicyano complexes have been measured, as have the CD spectra of the resolved dicyano complexes. Based on these spectral data, the geometrical structures of all the dicyano complexes have been identified as of the *cis* form. The $[Co(CN)(malo)_2OH_2]^{2-}$ complex has been isolated as potassium salt. From the PMR spectrum, the structure has been determined as the *trans* form. The polarized spectra of a crystal of this complex have also been measured.

It is generally said that the synthesis of a complex containing two different ligands which are considerably separated in the spectrochemical series[1] is difficult because a disproportionation reaction takes place easily. In fact, several complexes containing the cyanide ion, which occupies the highest position of the series, and ammonia, which is ranked in a middle position, have been prepared by methods which guard against the disproportionation reaction.[2-10] In a previous work,[4] we ourselves used potassium tricarbonatocobaltate(III) as the starting material for the synthesis of cyano-ammine-series complexes. At that time, we observed the formation of some species containing both cyano and carbonato ligands in the midst of the preparation reaction. Recently, we succeeded in isolating a species, the dicyanodicarbonatocobaltate(III) complex, from a reaction mixture of tricarbonatocobaltate(III) and cyanide.[11] Afterward, we attempted to prepare related complexes, such as bis(oxalato) and bis(malonato) complexes, from the dicarbonato complex. Furthermore, other similar dicyano complexes containing the dimethyldithiocarbamato ligand (abbreviated as dtc) or the methylxanthato(xan) were also prepared from the dicarbonato complex. In the present paper the preparation of these dicyano complexes and their electronic absorption spectra will be reported in detail. The spectra of other dicyano complexes containing H_2O ligands will also be reported. The cyanobis(malonato)-aquocobaltate(III) complex is also isolated in this work.

Experimental

Materials. The dimethylammonium dimethyldithiocarbamate, $(CH_3)_2NH_2(CH_3)_2NCS_2$, and potassium methylxanthate, KCH_3OCS_2, were freshly prepared according to the literature methods.[12] The other reagents were of reagent-grade quality.

Preparation. 1) *$\Lambda(+)_{589}$-Tris(ethylenediamine)cobalt(III) cis-dicyanodicarbonatocobaltate(III) Dihydrate, $\Lambda(+)_{589}$-[Co(en)$_3$]·cis-[Co(CN)$_2$(CO$_3$)$_2$]·2H$_2$O.* The preparative method has been described in an earlier paper,[11] but the description will be given here again because this method is the basis for the syntheses of the other complexes. To a cold, green solution of tricarbonatocobaltate(III)[13] ($CoCl_2 \cdot 6H_2O$ 10 g (0.048 mol) scale) we added potassium cyanide (7.5 g, 0.12 mol) in portions. The mixture was then stirred vigorously at room temperature for an hour, whereby a deep red solution was obtained. (This solution was used not only in this preparation but also in other preparations to be discussed later.) The solution was carefully neutralized with aqueous perchloric acid and then filtered. The filtrate was charged on an ion-exchange column containing 100—200 mesh Dowex 1-X8 resin in the Cl form (diameter, 5 cm; resin height, 15 cm). By elution with an aqueous solution of KCl (1 M), a red band came out of the column, after a green band. This red effluent was concentrated at about 30 °C. A small amount of ethanol was added to the concentrate, and then the whole was kept in a refrigerator in order to precipitate some salts, such as KCl. After the removal of the precipitates, an aqueous solution of $\Lambda(+)_{589}$-$[Co(en)_3]Br_3 \cdot 2H_2O$[14] was added to the filtrate. When the whole was then kept in a refrigerator, needle-like crystals of the desired complex, colored brown-violet, were deposited. These were washed with cold water, ethanol, and ether in turn, and finally dried *in vacuo*. The yield was about 1.5 g. Found: C, 23.93; H, 5.68; N, 22.10%. Calcd for $[Co(C_2H_8N_2)_3] \cdot [Co(CN)_2(CO_3)_2] \cdot 2H_2O$: C, 23.73; H, 5.58; N, 22.13%.

This compound showed the same CD spectrum as the $\Lambda(+)_{589}$-$[Co(en)_3]^{3+}$ complex itself. Attempts to obtain an usual compound such as potassium (or calcium) salt ended in failure because of the great solubility of such salt and because of the instability of the species in an aqueous solution.

2) *$\Lambda(+)_{589}$-Tris(ethylenediamine)cobalt(III)* cis-*dicyanocar-*

1) Y. Shimura and R. Tsuchida, This Bulletin, **29**, 311 (1956).
2) P. R. Ray and B. Sarma, *J. Indian Chem. Soc.*, **28**, 59 (1951).
3) H. Siebert, *Z. Anorg. Allg. Chem.*, **327**, 63 (1964).
4) M. Shibata, E. Kyuno, and M. Mori, *Inorg. Chem.*, **3**, 1573 (1964).
5) K. Ohkawa, J. Fujita, and Y. Shimura, This Bulletin, **38**, 66 (1965).
6) K. Ohkawa, J. Hidaka, and Y. Shimura, *ibid.*, **39**, 1715 (1966).
7) H. Nishikawa, K. Konya, and M. Shibata, *ibid.*, **41** 1492 (1968).
8) K. Konya, H. Nishikawa, and M. Shibata, *Inorg. Chem.*, **7**, 1165 (1968).
9) N. Maki, J. Hamazaki, and S. Sakuraba, This Bulletin, **41**, 1735 (1968).
10) M. Muto, T. Baba, and H. Yoneda, *ibid.*, **41**, 2918 (1968).
11) S. Fujinami and M. Shibata, *Chem. Lett.*, **1970**, 219.
12) "Beilsteins Handbuch," III, 216, 209.
13) M. Shibata, *Nippon Kagaku Zasshi*, **87**, 771 (1966).
14) "Inorganic Syntheses," VI, 186.

bonatooxalatocobaltate(III) Monohydrate, $\Lambda(+)_{589}$-[*Co(en)*$_3$]·cis-[*Co(CN)*$_2$*CO*$_3$(*C*$_2$*O*$_4$)]·*H*$_2$*O*. To a deep red solution obtained by the procedure described in 1), we added ground powder of oxalic acid (12 g, 0.1 mol) little by little. Then the solution was stirred vigorously at room temperature for 4—5 hours. After that, a chromatographic separation similar to that described in 1) was carried out using an aqueous solution of KCl (2 M). The effluent was quickly dried at about 30 °C, and the residue was extracted with methanol several times. The extracted solution was dried up again, and the remaining material was dissolved in a minimum amount of water. After a saturated aqueous solution of the $\Lambda(+)_{589}$-[Co(en)$_3$]Br$_3$ complex and a little ethanol had been added to the solution, it was kept in a refrigerator until brown-red crystals deposited. This crude complex was then recrystallized from water. The compound exhibited a different CD spectrum from that of $\Lambda(+)_{589}$-[Co(en)$_3$]$^{3+}$ itself, indicating the successful resolution of this dicyano complexes. Yield, about 0.03 g. Found: C, 25.11; H, 5.05; N, 20.94%. Calcd for [Co(C$_2$H$_8$N$_2$)$_3$]·[Co(CN)$_2$CO$_3$(C$_2$O$_4$)]·H$_2$O: C, 24.82; H, 4.92; N, 21.05%.

3) $\Lambda(+)_{589}$-*Tris(ethylenediamine)cobalt(III)* cis-*Dicyanobis(oxalato)cobaltate(III) Hexahydrate*, $\Lambda(+)_{589}$-[*Co(en)*$_3$]·cis-[*Co(CN)*$_2$(*C*$_2$*O*$_4$)$_2$]·6*H*$_2$*O*. A deep red solution obtained by the procedure described in 1) was acidified with ground powder of oxalic acid until the resulting solution showed pH 5; the solution was then stirred at room temperature for 5 hours. After that, the reacted solution was treated in the same way as has been described in 2). When the final solution was kept in a refrigerator, a foliate red crystal was deposited. The compound showed a CD spectrum different from that of the precipitant, indicating a successful resolution. Yield, about 0.03 g. Found: C, 22.38; H, 5.13; N, 17.53%. Calcd for [Co(C$_2$H$_8$N$_2$)$_3$][Co(CN)$_2$(C$_2$O$_4$)$_2$]·6H$_2$O: C, 22.72; H, 5.32; N, 17.66%.

4) *Potassium* cis-*Dicyanobis(dimethyldithiocarbamato)cobaltate (III) Monohydrate*, cis-*K*[*Co(CN)*$_2$*(dtc)*$_2$]·*H*$_2$*O*. To a cold, deep red reaction mixture, we added an aqueous solution of the dimethyldithiocarbamate (16 g, 0.1 mol) in portions. The mixture was stirred at room temperature for half an hour and then filtered. The filtrate was quickly dried up at ca. 25 °C, and the residue was extracted with methanol several times. After the concentration of the extracted solution to a small volume, the solution was poured into a column of alumina for chromatography (5×25 cm). By elution with methanol, a red band of the desired complex, next to a green band, came out. The eluted solution was then concentrated, and ether was added. When the solution was then kept in a refrigerator, dark red crystals were deposited. They were collected and washed with cold methanol and ether in turn. Yield, about 3 g. Found: C, 23.45; H, 3.51; N, 13.40; S, 31.82%. Calcd for K[Co(CN)$_2$(C$_3$H$_6$NS$_2$)$_2$]·H$_2$O: C, 23.52; H, 3.46; N, 13.71; S, 31.39%.

5) *Potassium* cis-*Dicyanobis(methylxanthato)cobaltate(III) Monohydrate*, cis-*K*[*Co(CN)*$_2$*(xan)*$_2$]·*H*$_2$*O*. The method was quite similar to that in 4); the xanthate ligand (14 g, 0.1 mol) was, however, used instead of the dtc ligand. Yield, 1 g. This complex is very unstable, even in the solid state. Found: C, 19.28; H, 2.55; N, 7.65; S, 33.78%. Calcd for K[Co(CN)$_2$(C$_2$H$_3$OS$_2$)$_2$]·H$_2$O: C, 18.84; H, 2.11; N, 7.33; S, 33.53%.

6) *Potassium* trans-*Cyanobis(malonato)aquocobaltate(III) Monohydrate*, trans-*K*$_2$[*CoCN*(malo)$_2$*OH*$_2$]·*H*$_2$*O*. To the cold, deep red solution mentioned in 1), we added finely ground malonic acid until the resulting solution showed pH 5. The mixture was stirred at room temperature for 3 hours, and then the solution was chromatographed in the same manner as has been described in 1). A blue-violet band came out upon elution with a KCl solution (1 M). This effluent was evaporated to dryness at 30 °C, and the residue was extracted with methanol several times. The extract was then again dried up, and the residue was dissolved in a minimum amount of water. After acetone was added, the solution was kept in a refrigerator until needle-like crystals had been deposited. They were collected and washed with methanol, acetone, and ether in turn. Yield, 1 g. Found: C, 20.68; H, 2.10; N, 3.81%. Calcd for K$_2$[CoCN(C$_3$H$_2$O$_4$)$_2$-OH$_2$]·H$_2$O: C, 20.84; H, 2.00; N, 3.47%.

Measurements. The infrared absorption spectra (IR) were measured by means of a JASCO IRA-2 grating infrared-spectrophotometer. The KBr disk method was used in the range of 400—4000 cm^{-1}. For the measurement of the electronic absorption spectra in solution, a Hitachi EPU-2A spectrophotometer was used. The circular dichroism spectra (CD) were recorded on a JASCO Model ORD/UV-5 spectrophotometer with a CD attachment, with samples converted to sodium salts in solution. The proton magnetic resonance spectra (PMR) were recorded on a JEOL C-60H spectrometer (60 Mc/sec) using sodium 3-(trimethylsilyl)propanesulfonate as the internal reference at room temperature. The electronic absorption spectra of single crystals were measured through the good offices of Professor Yukio Kondo of Rikkyo University, Tokyo.

Results and Discussion

Characterization. The IR spectra of the present [Co(CN)$_2$(O–O)$_2$]$^{3-}$-type complexes are very complicated because of the existence of the [Co(en)$_3$]$^{3+}$ complex as their counter ions, but it was possible to confirm the chelation of CO_3^{2-} or $C_2O_4^{2-}$ ions according to the methods of the literature.[15,16] The ν(CN) band was observed at 2155, 2140, and 2150 cm^{-1} for the dicarbonato, the carbonatooxalato, and bis(oxalato) complexes respectively. The IR spectra of the [Co(CN)$_2$(S–S)$_2$]$^-$-type complexes resembled those of the corresponding tris(dtc) and tris(xan) complexes in the spectra due to ligand absorption. The ν(CN) band was observed at 2110 and 2115 cm^{-1} for the xan and dtc complexes respectively. It is worthy of notice that the ν(CN) bands of these (S–S) chelated complexes appear in a region lower by *ca.* 30 cm^{-1} compared with those of the (O–O) chelated complexes. This fact may be related to the nephelauxetic effects[17] of the dtc and xan ligands. Evidence for the chelated malonate ion and the coordinated water molecule in the [CoCN-(malo)$_2$OH$_2$]$^{2-}$ complex was obtained from its IR spectrum. The ν(CN) band was observed at 2145 cm^{-1}.

Since the [Co(CN)$_2$CO$_3$(C$_2$O$_4$)]$^{3-}$ and [Co(CN)$_2$-(C$_2$O$_4$)$_2$]$^{3-}$ complexes could be resolved with the $\Lambda(+)_{589}$-[Co(en)$_3$]$^{3+}$ ion, the geometrical structures of these complexes were identified as of the *cis*-form. With the [Co(CN)$_2$(CO$_3$)$_2$]$^{3-}$ complex, the resolution

15) K. Nakamoto, J. Fujita, S. Tanaka, and M. Kobayashi, *J. Amer. Chem. Soc.*, **79**, 4900 (1957).

16) J. Fujita, K. Nakamoto, and M. Kobayashi, *J. Phys. Chem.*, **61**, 1014 (1957).

17) C. K. Jørgensen, "Absorption Spectra and Chemical Bonding in Complexes," Pergamon Press, Oxford, London, New York, Paris (1962).

Table 1. Absorption and CD spectral data of cyano complexes (10^3 cm^{-1})

Complex	Ia		Ib		II	
	ν_{max} (log ε)	ν_{ext}^{CD} ($\Delta\varepsilon$)	ν_{max} (log ε)	ν_{ext}^{CD} ($\Delta\varepsilon$)	ν_{max} (log ε)	ν_{ext}^{CD} ($\Delta\varepsilon$)
$[Co(CN)_2(CO_3)_2]^{3-}$	18.3 (1.96)		22.5 (2.03)		27.5 (2.20)	
$[Co(CN)_2CO_3(C_2O_4)]^{3-}$	18.7 (1.90)	19.3 (−0.66)	23.0 (2.07)	22.9 (+2.17)	28.1 (2.25)	28.4 (−0.47)
$[Co(CN)_2(C_2O_4)_2]^{3-}$	18.8 (1.84)	19.1 (−1.74)	23.4 (2.14)	23.5 (+3.03)	28.4 (2.37)	29.0 (−0.57)
$[Co(CN)_2(malo)_2]^{3-}$	18.7 (1.60)		23.3 (2.08)		sh	
$[Co(CN)_2C_2O_4(OH)_2]^{-}$	18.5 (1.70)		23.8 (2.00)		sh	
$[Co(CN)_2(OH_2)_4]^{+}$	18.6 (1.53)		24.0 (1.86)		*ca.* 30 (1.50)	
$[Co(CN)_2(dtc)_2]^{-}$	19.4 (2.52)		sh		—	
$[Co(CN)_2(xan)_2]^{-}$	19.7 (2.34)		sh		—	
	I ν_{max} (log ε)		II ν_{max} (log ε)			
$[CoCN(malo)_2OH_2]$	18.8 (2.20)		25.8 (1.94)			

was unsuccessful, but its structure was regarded as *cis*-form from the fact that the electronic absorption spectrum of this complex was very similar to those of the resolved complexes.

In the PMR spectrum of the $[CoCN(malo)_2OH_2]^{2-}$ complex, resonance signals due to the methylene groups in the chelated malonate rings were observed at 2.98, 3.29, 3.66, and 3.97 ppm; these are classified as an AB pattern with a coupling constant of J=18.6 Hz. This pattern suggests a structure *trans* with respect to CN^- and H_2O; two sets of AB patterns may be expected for *cis* structure of the complex. In fact, the $[Cogly(malo)_2]^{2-}$ complex[18] exhibits very complicated methylene signals because of the malonato ligand.

The Absorption and CD Spectra for the Dicyano Complexes. The absorption spectra of the $[Co(CN)_2(O\text{-}O)_2]^{3-}$-type complexes were measured in aqueous solutions of the tris(ethylenediamine) salts and in solutions of the sodium salts obtained by means of ion exchange. A spectrum obtained by subtracting the spectrum of the $[Co(en)_3]^{3+}$ complex itself from the observed spectrum for the tris(ethylenediamine) salt coincided with the spectrum for the sodium salt. Therefore, only the spectra of the sodium salts are shown in Fig. 1, while the numerical data are summarized in Table 1. The spectra show three well-separated maxima at *ca.* 18, 23, and 28 kK. No such marked splitting has ever been reported with the *cis*-form complexes. Hereafter, these three maxima (or bands) will be represented by Ia, Ib, and II from the lower energy. After the $[Co(CN)_2(CO_3)_2]^{3-}$ and the $[Co(CN)_2CO_3(C_2O_4)]^{3-}$ had been dissolved in aqueous perchloric acid, the resulting solutions were submitted to spectrum measurements. (The results are shown in Fig. 2 and Table 1.) It was ascertained that the complex species thus formed were chromatographically pure, and that the observed spectra were completely reformed into the spectra of the parent complexes, when excess Na_2CO_3 was added to the $HClO_4$ solution. From these facts, the spectra in Fig. 2 may be considered to be those for the tetra-

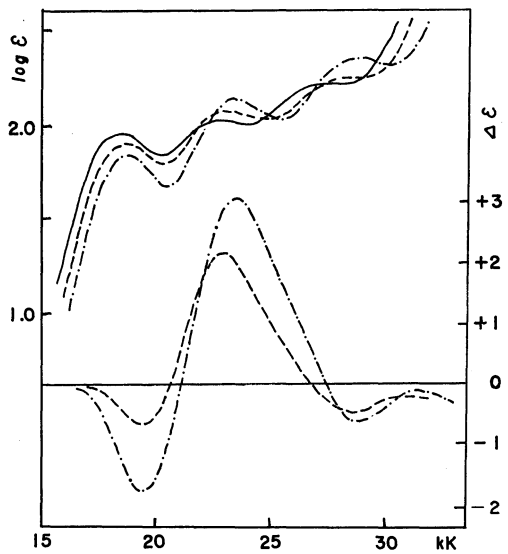

Fig. 1. Absorption and CD spectra of dicyano complexes. ——: $[Co(CN)_2(CO_3)_2]^{3-}$, – – –: $[Co(CN)_2CO_3(C_2O_4)]^{3-}$, –·–·–: $[Co(CN)_2(C_2O_4)_2]^{3-}$, (Na salts).

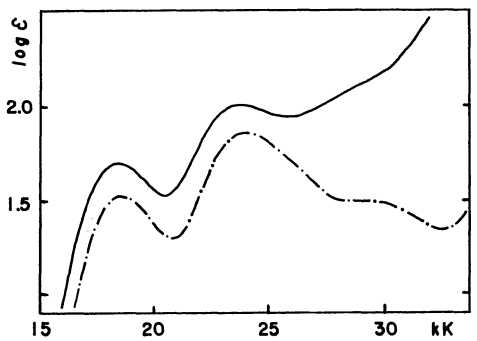

Fig. 2. Absorption spectra of dicyanoaquo complexes. ——: $[Co(CN)_2C_2O_4(OH_2)_2]^{-}$ (Na salt), –·–·–: $[Co(CN)_2(OH_2)_4]^{+}$.

aquo and diaquo complexes, *cis*-$[Co(CN)_2(OH_2)_4]^{+}$ and $[Co(CN)_2(C_2O_4)(OH_2)_2]^{-}$. A characteristic difference of these spectra from those of the present complexes is the decreased intensity of the II band. The dicyanobis(malonato) complex species, the attempt at the isolation of which was unsuccessful, exhibits a spectrum rather more similar to that of the tetraaquo complex species (Fig. 5) than to that of the dicarbonato (or bis(oxalato)) complex. This fact suggests that the intensity of the II band is related to the rigidity of

18) K. Yamasaki, J. Hidaka, and Y. Shimura, This Bulletin, **42**, 119 (1969).

the O–O ligand. Krishnamurthy and his co-workers[19] have reported the absorption spectrum of the *cis*-$[Cr(CN)_2(OH_2)_4]^+$ complex, which is very similar to the spectrum of our cobalt(III) complex. They said that one component of the second absorption band might be hidden under the middle maximum (corresponding to the Ib band), which is a component of the first absorption band; they based their suggestion on the meagerness of the third maximum (II Band). However, we consider that the Ib bands in our dicyano complexes are due to a split component of the first absorption band, judging from the fact that the Ib maxima for the $[Co(CN)_2(C_2O_4)_2]^{3-}$ and $[Co(CN)_2CO_3(C_2O_4)]^{3-}$ complexes coincide with their CD maxima (Fig. 1). However, it is interesting that the intensities of the Ib maxima are greater than those of the Ia bands.

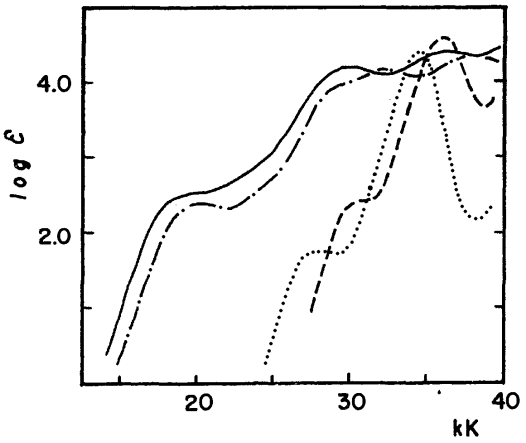

Fig. 3. Absorption spectra of sulfur-contained complexes.
——: $K[Co(CN)_2(dtc)_2]$, -·-·-: $K[Co(CN)_2(xan)_2]$,
·····: KCH_3OCS_2, ——: $(CH_3)_2NH_2(CH_3)_2NCS_2$.

The spectra of the $[Co(xan)_3]$ and $[Co(dtc)_3]$ complexes have been reported by Kida *et al.*,[20] but there has been no report on mixed complexes with the xan (or dtc) ligand and another ligand. In a complex containing such a (S-S) ligand, the d-d transition bands are covered, at a higher energy, by the allowed transition bands of the ligand. In fact, each absorption spectrum of the $[Co(CN)_2(dtc)_2]^-$ and $[Co(CN)_2(xan)_2]^-$ complexes (Fig. 3, Table 1) shows a well-defined maximum at a lower energy and a shoulder at a higher energy. However, by a comparison of these spectra with those of the carbonato (or oxalato) complex, the present dtc and xan complexes may be regarded as *cis* complexes. If the complexes are *trans*, entirely different spectra from those of the *cis*-$[Co(CN)_2(O-O)_2]$-type complexes may be expected.

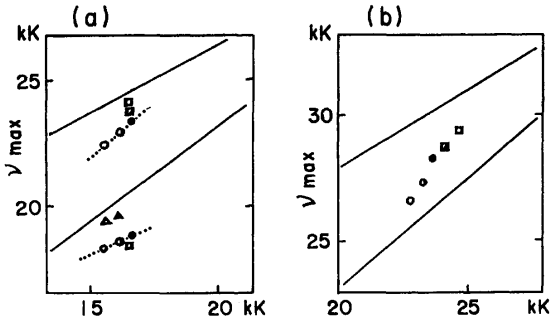

Fig. 4. The relationships between the absorption maxima of the dicyano complexes (ν_{max}) and the predicted values.
○: $[Co(CN)_2(CO_3)_2]^{3-}$, ◑: $[Co(CN)_2CO_3(C_2O_4)]^{3-}$,
●: $[Co(CN)_2(C_2O_4)_2]^{3-}$, ◪: $[Co(CN)_2C_2O_4(OH_2)_2]^-$,
□: $[Co(CN)_2(OH_2)_4]^+$, △: $[Co(CN)_2(dtc)_2]^-$,
▲: $[Co(CN)_2(xan)_2]^-$.

In order to discuss further the d-d bands of the present dicyano complexes, we divided each absorption curve into three symmetrical Gaussian[21,22] within a 3% error. The results of the analysis are summarized in Table 2. These analysed values are taken on a vertical axis in Fig. 4, while the absorption maxima for the $[Co(O)_6]$- and $[Co(S)_6]$-type complexes are placed on a horizontal line; (a) concerns the Ia and Ib bands, and (b), the II band. The solid lines in Fig. 4 represent the predicted values according to Yamatera's treatment.[23] However, the δ_π parameter was ignored and only the δ_σ parameter was taken into consideration for the second absorption band. Thus, the separation from a solid line on the vertical axis is a measure of the deviation from the theoretical treatment. That is, it indicates the distortion from octahedral symmetry or the degree of covalency between metal and ligand bonding. It is commonly considered that, in this figure, the distortion is removed upon the change in ligands from CO_3^{2-} to $C_2O_4^{2-}$.

Table 2. Calculated absorption maxima and half-width for the dicyano complexes (10^3 cm^{-1})

Complex	Ia		Ib		II	
	ν_{max} (log ε)	half-width	ν_{max} (log ε)	half-width	ν_{max} (log ε)	half-width
$[Co(CN)_2(CO_3)_2]^{3-}$	18.3 (1.93)	3.07	22.4 (2.04)	3.63	26.6 (2.11)	3.67
$[Co(CN)_2CO_3(C_2O_4)]^{3-}$	18.6 (1.90)	3.10	22.9 (2.07)	3.67	27.3 (2.14)	3.77
$[Co(CN)_2(C_2O_4)_2]^{3-}$	18.7 (1.84)	2.90	23.4 (2.14)	3.53	28.2 (2.29)	3.93
$[Co(CN)_2(malo)_2]^{3-}$	18.7 (1.60)	3.00	23.3 (2.08)	3.40	27.6 (1.82)	4.40
$[Co(CN)_2C_2O_4(OH_2)_2]^-$	18.5 (1.69)	3.17	23.7 (1.99)	3.83	28.6 (1.97)	4.37
$[Co(CN)_2(OH_2)_4]^+$	18.6 (1.53)	3.13	24.2 (1.86)	3.77	29 (1.50)	6.3
$[Co(CN)_2(dtc)_2]^-$	19.5 (2.51)	3.27	—	—	—	—
$[Co(CN)_2(xan)_2]^-$	19.6 (2.34)	3.33	—	—	—	—

19) K. Krishnamurthy, W. B. Schaap, and J. R. Perumareddi, *Inorg. Chem.*, **6**, 1338 (1967).
20) S. Kida and H. Yoneda, *Nippon Kagaku Zasshi*, **76**, 103 (1955).
21) C. K. Jørgensen, *Acta Chem. Scand.*, **8**, 1495 (1954).
22) Y. Shimura and R. Tsuchida, This Bulletin, **28**, 572 (1955).
23) H. Yamatera, *ibid.*, **31**, 95 (1958).

Concerning the Ia bands, the analysed values for the complexes containing carbonate and oxalate ions make a line with a considerable separation, one which becomes larger from the CO_3^{2-} ligand to the $C_2O_4^{2-}$ ligand. The analysed values for the aquo complexes will be found below. On the other hand, the analyzed values for the dtc and xan complexes could be found in a place close to the corresponding solid line. From these relations, it may be said that a complex containing a ligand ranking in a higher position in the nephelauxetic series exhibits much less deviation of the Ia-band maximum than would be predicted.

Concerning the Ib bands, a line connecting the analysed values for the complexes with the carbonato and oxalato ligands is also not parallel to the solid line, and it has a narrower separation upon the change in ligands from CO_3^{2-} to $C_2O_4^{2-}$. The separation between the Ia and the Ib, consequently, becomes larger in that order.

The analysed values of the II band are found between the two solid lines, and the rule of average environment[17,24] does not hold.

Figure 1 shows the CD spectra of the resolved dicyano complexes, as measured with aqueous solutions of sodium salts prepared by means of ion-exchange chromatography. Each spectrum reveals three peaks, with the signs (−), (+), (−) corresponding to the Ia, Ib, and II bands. It is noteworthy that the second peak dominates the first in each spectrum, and that the dominant peaks coincide perfectly with the Ib maxima. The $\Lambda(+)_{589}$-$[Co(C_2O_4)_2(NH_3)_2]^-$ complex[13] exhibits two peaks, with (+) and (−) signs, in the first absorption band region. The CD spectrum of the $\Lambda(+)_{589}$-$[Co(CN)_2(en)_2]^+$ complex[25] shows two positive peaks in the region, and suggests cancellation with a considerably large band with a minus Cotton sign. By comparing these spectra with those of our dicyano complexes, the dominant peak can be assigned to the B_1 component in C_{2v} symmetry, while the lower energy peak can be assigned to the (A_2+B_2) component. Thus, from the sign in the transition (*i.e.*, minus), the Λ configuration can be assigned to the complexes concerned.

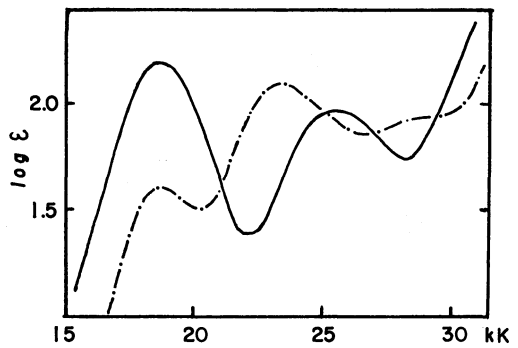

Fig. 5. Absorption spectrum of *trans*-cyanoaquobis(malonato)-cobaltate(III) complex.
——: $K_2[CoCN(malo)_2OH_2]$, -·-·-: $[Co(CN)_2(malo)_2]^{3-}$, (Na salt).

Absorption Spectra of the $[CoCN(malo)_2OH_2]^{2-}$ *Complex.* Figure 5 shows the absorption spectrum in solution. The spectrum exhibits no apparent splitting of the d-d bands, and the second absorption band has a rather weaker intensity and a broadened shape compared with the first absorption band. The maximum of the first band (Table 1) is at middle position between the A_2 and E component (C_{4v} symmetry), as predicted by Yamatera's treatment. On the other hand, this maximum coincides well with the Ia maximum for the $[Co(CN)_2(malo)_2]^{3-}$ complex, as may be seen in Fig. 5. This fact suggests that the first band of this cyano-aquo complex comes dominantly from the E component if this chromophore is treated as being tetragonal.

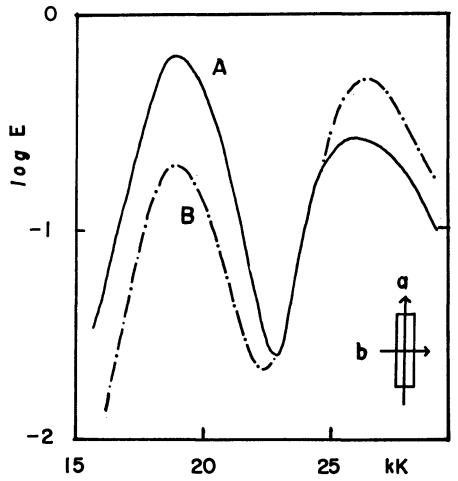

Fig. 6. Polarized single crystal spectra of *trans*-$K_2[CoCN(malo)_2OH_2]\cdot H_2O$ complex at *ca.* 90 K.
(A): along a axis ——; (B): along b axis (b⊥a)-·-·-.
log *E* represents observed absorbancy.

The polarized spectra of a crystal of this complex are shown in Fig. 6. The dichroism of the complex can be clearly observed. It can also be seen from the spectra that the relations between the intensities of the first and second bands are reversed according to the axes of polarization. Furthermore, the spectrum measured along the axis of the crystal (a) shows a red shift and a broadened shape, compared with the spectrum along the (b) axis in the region of the second absorption band. These crystal spectra are not understood precisely, because no X-ray analysis was done. However, in order to explain the observed spectra, let us now suppose that all the molecular axes of this complex are parallel to each other in the crystal. Under the C_{4v} symmetry, the A_2 and B_2 components become forbidden transitions, while the E component becomes an allowed transition; this can not, however, explain the reversed intensities and the broadened unsymmetrical second band. On the other hand, when the C_{2v}[26] molecular symmetry is adopted for this complex, only the A_2 component of the first band (corresponding to A_2 in C_{4v}) becomes a forbidden transition, while the B_1 and B_2 components (corresponding to E in C_{4v}) become allowed. From this, the first band in the

24) N. Matsuoka, J. Hidaka, and Y. Shimura, *ibid.*, **40**, 1868 (1967).
25) A. J. McCaffery, S. F. Mason, and B. J. Norman, *J. Chem. Soc.*, **1965**, 5094.
26) E. B. Wilson, Jr., J. C. Decius, and P. C. Cross, "Molecular Vibrations," McGraw-Hill Book Co., New York, Toronto, London (1955), p. 334.

spectrum (A) may be attributed to the (B_1, B_2) components. From the group-theoretical consideration, the inflation at the second band in the same spectrum (A) can also be attributed to the (B_1, B_2) components. Consequently, the second band in the spectrum (B) must be mainly due to the A_1 transition (B_2 in C_{4v}). Judging from the coincidence of the second absorption band maxima between the solution and the crystal spectra, the intensity of the II band in the solution spectrum should come dominantly from the B_2 component (in C_{4v}). With the $[Co(L)(NH_3)_5]$- and *trans*-$[Co(L)_2(NH_3)_4]$-type complexes, Piper *et al.*[27] have reported that, if L represents CN^-, the effect of δ_π should serve to increase the splitting of the second absorption band. Accordingly, it would seem to be reasonable to observe the splitting of the second absorption band in the present $[Co(C)(O)_5]$-type complex.

27) R. A. D. Wentworth and T. S. Piper, *Inorg. Chem.*, **4**, 1524 (1965).

BULLETIN OF THE CHEMICAL SOCIETY OF JAPAN, VOL. 46, 3448—3452 (1973)

The Isomerism of Metal Complexes Containing Multidentate Ligands. IV. The Cobalt(III) Complex of Linear Pentaethylenehexamine[1]

Yuzo Yoshikawa and Kazuo Yamasaki

Department of Chemistry, Faculty of Science, Nagoya University, Chikusa-ku, Nagoya 464

(Received June 7, 1973)

The cobalt(III) complex incorporating sexidentate linear pentaethylenehexamine(1,14-diamino-3,6,9,12-tetraazatetradecane) as the ligand was prepared by the reaction of the ligand with $[CoBr(NH_3)_5]Br_2$ at room temperature in the presence of active charcoal. The resulting solution was subjected to column chromatography on *SP*-Sephadex, geometrical and optical isomers with four different configurations were then separated and characterized by their electronic and infrared absorption, circular dichroism, and PMR spectra. They have the chemical composition of $[Co(C_{10}H_{28}N_6)]Cl_3 \cdot nH_2O$, n being 1.5—3.

Linear pentaethylenehexamine(abbreviated as linpen) is able to function as a sexidentate ligand of stereochemical importance, but so far no study has been published of its cobalt(III) complex. A few copper(II), lead(II), and cadmium(II) complexes have been studied polarographically,[2] and one preliminary report[3] on the isolation of the copper(II), nickel(II), zinc(II), and mercury(II) complexes has been published. We have now prepared the cobalt(III) complex of linpen and isolated all the geometrical and optical isomers by means of column chromatography on ion-exchange Sephadex.

Experimental

Ligands. The ligand, linpen, a product of the Tokyo Kasei Co., was first purified by fractional distillation, the fraction distilling at 165—170 °C(0.05 mmHg)being collected. The distillate was then converted to the hydrochloride and re-precipitated by adding hydrochloric acid to its concentrated aqueous solution. This precipitation procedure was repeated several times until a constant infrared spectrum of the hydrochloride was obtained. Found: C, 26.28; H, 7.63; N, 18.71; Cl, 46.69%. Calcd for $C_{10}H_{28}N_6 \cdot 6HCl$: C, 26.62; H, 7.60; N, 18.63; Cl, 47.15%.

Preparation of the Complex, $[Co(linpen)]Cl_3 \cdot nH_2O$. An aqueous solution of linpen hydrochloride(2.6 g) was neutralized with sodium hydroxide to pH 9.2. To this solution 2.0 g of $[CoBr(NH_3)_5]Br_2$ and 0.5 g of active charcoal were added, and then the mixture was stirred at 25 °C for 24 hr. After the charcoal had been removed, the filtrate was subjected to column chromatography to separate the isomers.

Separation of the Isomers. In the following chromatographic separation, a column of the size, $\phi 2.7 \times 140$ cm, of *SP*-Sephadex was always used; the absorbance of the eluate at 470 nm was plotted against V/V_0, the ratio of the eluate volume *versus* the void volume of the column.[4] The symbols used in the present report, (+) and (−), denote the optical

Table 1. The water of crystallization and the assigned structures of the isomers

Isomer	Water of crystallization	Absolute configuration	Structure (Fig. 2)
(+)-I	$2H_2O$	"Λ"[a]	A
(+)-II	$2H_2O$	"Λ"	B-1 and B-2[b]
(+)-III	$2H_2O$(rac.)[c]	"Λ"	C-1 or C-2
(+)-IV	$1.5H_2O$	"Λ"	C-2 or C-1
(−)-V	$1.5H_2O$	"Δ"	D-1(SS)
(−)-VI	$3H_2O$	"Δ"	D-2(RS)
(−)-VII	$2H_2O$	"Δ"	D-3(RR)

a) *Cf.* Table 3.
b) Mixture of two conformational isomers, B–1 and B–2.
c) Analysis was done for the racemate.

1) Parts I, II, and III were published in This Bulletin, **45**, 179, 3415 (1972), and **46**, 1687 (1973).

2) H. B. Jonassen, J. A. Bertrand, F. R. Groves, Jr., and R. I. Stearns, *J. Amer. Chem. Soc.*, **79**, 4279 (1957); E. Jacobsen and K. Schrøder, *Acta Chem. Scand.*, **16**, 1393 (1961).

3) G. G. Schlessinger, "Werner Centennial," American Chemcal Society (1967), p. 565.

4) The void volume was measured by the elution of K[Co(edta)] with the same eluent, sodium (+)-tartrate. The value of V_0 is slightly different for each column.

rotation at 589 nm. The water of crystallization is different for each isomer, the numbers of which are listed in Table 1.

The I Isomer: The prepared complex was adsorbed on *SP*-Sephadex and eluted by means of a 0.18 M sodium (+)-tartrate solution; the elution curve was thus obtained (Fig. 1-a). The first four peaks were found to correspond to the two pairs of enantiomers; they were named (+)-I, (−)-I, (+)-II, and (−)-II respectively.

The fractions (V/V_0=3.3—4.0) corresponding to the (+)-I and (−)-I isomers were again adsorbed on *SP*-Sephadex after dilution and then eluted with a 1 M sodium chloride solution. By adding potassium hexacyanocobaltate(III) to this eluate, the hexacyanocobaltates of (+)-I and (−)-I were precipitated; they were then converted to the chlorides by stirring with an anion-exchange resin(Dowex 1-X8, 200—400 mesh) in the chloride form. On the evaporation of each filtrate, yellow crystals of the (+)-I and (−)-I, $[Co(linpen)]Cl_3 \cdot 2H_2O$, were obtained. Found: C, 27.80; H, 7.39; N, 19.23% for the (+)-I and C, 27.67; H, 7.40; N, 19.58% for the racemic I. Calcd. for $CoC_{10}H_{28}N_6Cl_3 \cdot 2H_2O$: C, 27.70; H, 7.44; N, 19.38%.

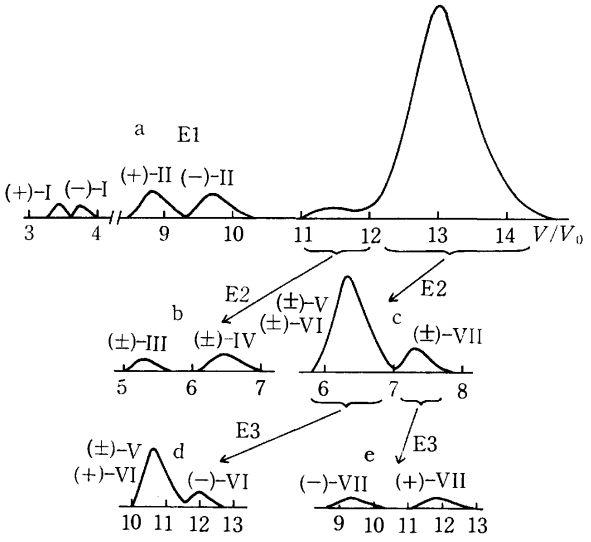

Fig. 1. Elution curves of the isomers of $[Co(linpen)]^{3+}$. The eluents E1, E2, and E3 are 0.18 M sodium (+)-tartrate, a mixture of 0.18 M sodium sulfate and 0.01 N hydrochloric acid, and 0.3 M sodium (+)-tartratoantimonate, respectively.

The II Isomer: The fractions V/V_0=8.4—10.3 (Fig. 1-a), when treated in the same way as above, yielded the (+)- and (−)-enantiomers of the II isomer. The (+)-enantiomer was further separated into two isomers by chromatography with a 0.18 M sodium sulfate solution containing 0.01 N HCl as the eluting agent, but these separated isomers were labile and isomerized into a mixture during separation on the column, so they could not be obtained in pure states. The (−)-II isomer behaved in the same way. Therefore, it may be concluded that the II isomer consists of a mixture of two conformational isomers which isomerize very quickly to each other.

The III and IV Isomers: The fractions V/V_0=11.0−12.0 (Fig. 1-a) were again adsorbed on *SP*-Sephadex and eluted with a 0.18 M sodium sulfate solution containing 0.01 N HCl. As is shown in Fig. 1-b two peaks of optically inactive isomers were obtained. The yellow, fast-moving isomer was named III, and the yellowish-brown, slow-moving one, IV. Since the complete resolution of these isomers, III and IV, into their enantiomers by chromatography was difficult, the optically-pure enantiomers of III and IV were obtained by the isomerization of the (+)-II and (−)-II isomers respectively. The (+)-II gave a mixture of the (−)-III and (−)-IV isomers which were then separated by elution with a 0.18 M sodium sulfate solution containing 0.01 N HCl. The (−)-II similarly gave a mixture of the (+)-III and (+)-IV isomers.

The V, VI, and VII Isomers: A large peak corresponding to the fractions V/V_0=12.6−14.5(Fig. 1-a) was further separated into two peaks by elution with a 0.18 M sodium sulfate solution containing 0.01 N HCl(Fig. 1-c). The large first peak at V/V_0=6−7 was further separated into two by elution with a 0.3 M sodium (+)-tartratoantimonate(III) solution (Fig. 1-d). From the first peak, the (±)-V isomer was precipitated as the hexacyanocobaltate, leaving the (+)-VI isomer in the mother liquor, from which it could not be isolated in a pure state. The fractions corresponding to the small second peak contained the pure (−)-VI(Fig. 1-d). This isomer, (−)-VI, readily isomerized in a neutral or alkaline solution into a mixture of the (−)-V, the (−)-VI, and a small amount of the (−)-VII isomers. By applying to this mixture the separation procedure shown in Figs. 1-c and d, pure (−)-V and (−)-VI were obtained.

The fractions corresponding to a small second peak in Fig. 1-c can be resolved into the (−)-VII and (+)-VII isomers by elution with a 0.3 M sodium (+)-tartratoantimonate(III) solution(Fig. 1-e). The VII isomer is labile and isomerizes readily in a neutral solution into a mixture of the V, VI, and VII isomers. Therefore, it should always be handled in an acid solution.

Measurements. The electronic absorption(AB), infrared, and circular dichroism(CD) spectra were measured at 25 °C with a Hitachi recording spectrophotometer 323, a JASCO-402G infrared spectrophotometer, and a JASCO J-20 spectrophotometer respectively. The NaCl disk was used for the infrared spectrum measurement. The PMR spectra in 0.1 N DCl(D_2O) were measured by means of a JEOL model JNM-MH-100 spectrometer, with DSS as the internal standard. When the signals due to the amino-hydrogen atoms overlapped with those due to the hydrogen of HOD, an additional amount of concentrated DCl was used to shift the latter signals.

Results and Discussion

Isomerization Reaction. In a neutral solution without active charcoal the I and II isomers do not isomerize, while the III and IV isomers isomerize under the same conditions, to give their mixture; V, VI, and VII also give their mixture. In an alkaline solution of pH 12 without active charcoal, the (−)-II isomerizes partly into a mixture of (+)-III and (+)-IV; this specific isomerization reaction was used to prepare the optically pure III and IV as has been described above. In a borate buffer solution of pH 9.0 and in the presence of active charcoal, each of the I—VII isomers isomerizes to give a mixture of all the isomers at 60 °C after 2—8 hr.

The formation ratio found experimentally in the preparative work was I: II: III: IV: V: VI: VII= 9: 15: 1: 2: 47: 23: 3; it varies to some extent with the experimental conditions.

Number of Possible Isomers. When linpen is coordinated to cobalt(III) as a sexidentate ligand, four different configurational isomers, A, B, C, and D, can

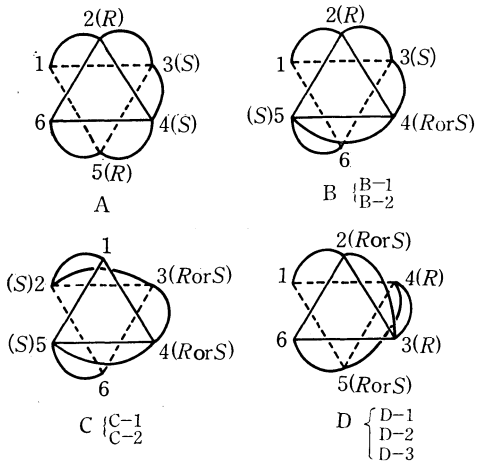

Fig. 2. Four geometric isomers of $[Co(linpen)]^{3+}$.

be expected (Fig. 2). If the absolute configurations around the secondary amine-N atoms are taken into account, the number of isomers increases. For the A structure, the absolute configurations of the nitrogen atoms are fixed; *R* for the N2 and N5, and *S* for the N3 and N4. Thus, only one isomer is possible. For the B structure, the absolute configuration of the N2 is fixed to *R*, and those of the N3 and N5, to *S*, whereas the N4 can take either the *R* or *S* configuration. Thus, two isomers are possible for the B structure. For the C structure, both the N2 and N5 are fixed to *S*. As the N2, N3, N4, and N5 are adjacent to each other on the same plane, their absolute configurations are not independent; both the N3 and N4 atoms should take the same configuration, that is, *RR* or *SS*. Therefore, two isomers are possible. For the D structure, the absolute configurations of the N3 and N4 are fixed to R, but the configuration of the N2 is independent of that of the N5. Consequently, three isomers are possible, isomers which have the *RR*, *RS*, and *SS* configurations for the N2 and N5 atoms. Thus, when the absolute configurations around the secondary amine-N atoms are taken into consideration, the symmetry of the A and C structures and two of the D structures is C_2, while that of the B structure is C_1; that of the third one of the D structures is also C_1. Consequently, the number of isomers is 1 for the A, 2 each for the B and C, and 3 for the D structure, making a total of 8. This number agrees with the number of isomers actually found.

If the conformation (δ or λ) of each chelate ring is further taken into account, the number of possible isomers increases much more. These conformational isomers, however, can not be separated under the present experimental conditions because of the rapid inversion of their conformations.

The AB and CD Spectra. The AB and CD spectra were measured in a 0.01N HCl solution except for the (+)-I and (+)-II isomers; the results are shown in Fig. 3 and Table 2. The absorption maxima are at 21600—20800 cm^{-1} (462—480 nm) for the first band, at 29500—29100 cm^{-1} (339—344 nm) for the second band, and at 44800—43100 cm^{-1} (223—232 nm) for the charge transfer band, indicating a 6N-type cobalt-

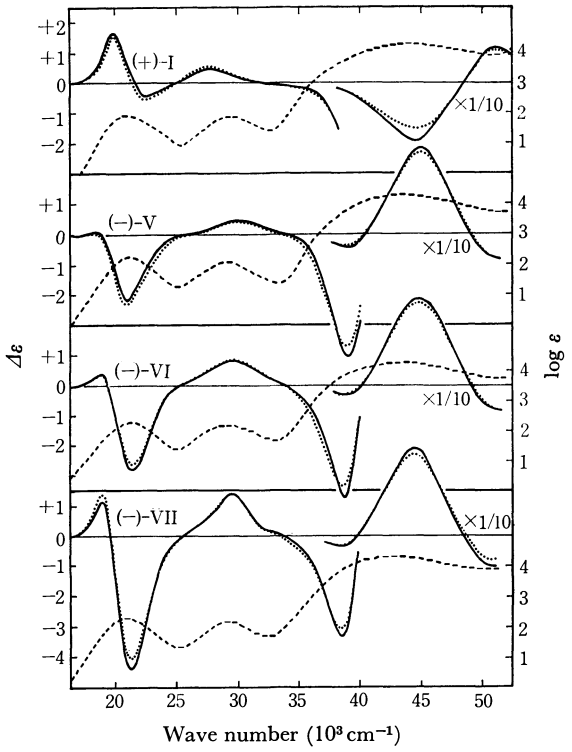

Fig. 3a. AB (----) and CD (—— in water and ····· in 0.2 M Na_2SO_4) spectra of the (+)-I, (−)-V, (−)-VI, and (−)-VII isomers of $[Co(linpen)]^{3+}$.

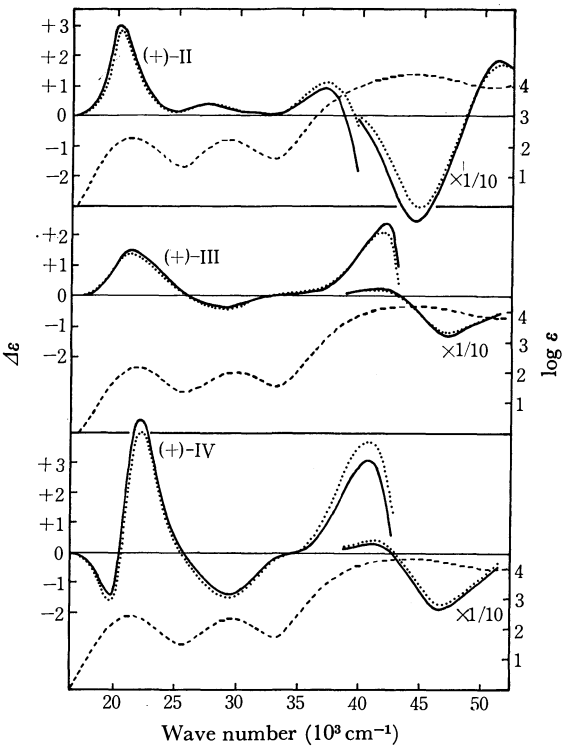

Fig. 3b. AB (----) and CD (—— in water and ····· in 0.2 M Na_2SO_4) spectra of the (+)-II, (+)-III, and (+)-IV isomers of $[Co(linpen)]^{3+}$.

(III) complex. The CD spectrum of the (+)-I isomer (Fig. 3-a) closely resembles that of Λ-$[Co(en)_3]^{3+}$ and its absolute configuration is identified as "Λ" from the sign of the main CD component in the first absorption

TABLE 2. ABSORPTION AND CIRCULAR DICHROISM SPECTRA (in 10^3 cm^{-1})

Isomer	1st band				2nd band				CT band			
	AB		CD		AB		CD		AB		CD	
	ν_{max}	(ε_{max})	ν_{max}	($\Delta\varepsilon_{max}$)	ν_{max}	(ε_{max})	ν_{max}	($\Delta\varepsilon_{max}$)	ν_{max}	(ε_{max})	ν_{max}	($\Delta\varepsilon_{max}$)
(+)-I	21.2	(85.0)	19.9	(+1.68)	29.5	(77.4)	27.8	(+0.54)	44.8	(20360)	44.4	(−18.8)
			22.5	(−0.42)							51.0	(+11.6)
(+)-II	21.1	(168)	20.3	(+3.06)	29.15	(129)	27.2	(+0.44)	44.4	(20330)	37.5	(+0.86)
							30.3	(+0.11)			44.4	(−34.5)
											51.5	(+17.2)
(+)-III	21.65	(143)	21.0	(+1.58)	29.5	(101)	29.0	(−0.39)	44.1	(14760)	41.9	(+2.50)
											46.9	(−12.6)
(+)-IV	21.3	(212)	19.5	(−1.41)	29.3	(185)	29.5	(−1.44)	43.9	(17840)	40.8	(+3.13)
			22.0	(+4.49)							46.5	(−18.3)
(−)-V	21.15	(176)	18.3	(+0.02)	29.2	(120)	29.8	(+0.44)	43.7	(19240)	39.1	(−4.16)
			21.1	(−2.22)							44.9	(+28.8)
(−)-VI	21.0	(203)	18.7	(+0.31)	29.2	(151)	29.4	(+0.79)	43.5	(18660)	38.8	(−3.81)
			21.3	(−2.80)							44.8	(+27.6)
(−)-VII	20.8	(212)	18.8	(+1.15)	29.1	(152)	29.5	(+1.42)	43.1	(20810)	38.5	(−3.26)
			21.3	(−4.38)							44.4	(+28.7)

region.[5] The (+)-II isomer has only one positive CD peak in the first absorption region (Fig. 3-b); from its sign it is identified as having the "Λ" configuration also (*cf.* Table 3).

The (+)-III and (+)-IV isomers were obtained by the isomerization of the (−)-II isomer in an alkaline solution of pH 12 without any active charcoal. Since these two isomers have a main CD component with the plus sign in the first absorption region (Fig. 3-b), their absolute configurations were identified as "Λ". As the starting substance, (−)-II, has the "Δ" configuration, a complicated isomerization mechanism with a configuration inversion is suspected. Under the same experimental conditions the formation of the (+)-II isomer from the (−)-II isomer is less than 0.4% in amount.

All the CD spectra of the (−)-V, (−)-VI, and (−)-VII isomers (Fig. 3-b) have the main peak with the minus sign in the first absorption region; from the sign of the CD peak, these isomers were all determined to have the "Δ" configuration.

Summarizing the results shown in Figs. 3-a and 3-b, the (+)-I has a main plus peak on the longer wavelength side of the first absorption region, and a small minus peak on the shorter wavelength side. The (+)-II and (+)-III isomers both have only a plus peak, in the same region. The (+)-IV isomer shows a small plus peak and a large minus peak, whereas the (−)-V, (−)-VI, and (−)-VII isomers all have a small plus peak and a large minus peak, in the same region. In the present section, the relationship between the sign of the main CD peak and the absolute configuration of each isomer has been discussed.

There is a very weak CD peak for the (−)-V isomer at 17000 cm^{-1} (589 nm) ($\Delta\varepsilon=-0.02$) and for the (−)-VI isomer at 16200 cm^{-1} (616 nm) ($\Delta\varepsilon=-0.01$). The origin of this weak peak is not yet clear. One possibility is the spin-forbidden band which is similar to the $^3T_{2g}\leftarrow{}^1A_{1g}$ transition of $[Co(en)_3]^{3+}$.[6] Another possibility is a band remaining after the cancellation of two bands with opposite signs which are situated close to each other. The positions of these weak peaks are too low in frequency to be attributed to the first absorption band split by a low symmetry, like C_1 or C_2.

It is often assumed that the CD spectrum in the visible region is the sum of the hypothetical CD components attributed to the configuration around the metal, the conformation of the chelate rings, and asymmetric nitrogen atoms; the actual situation in the present case is not so simple, however, because no additivity rule holds for the CD spectra of the III and IV isomers, or for those of the V, VI, and VII isomers, each pair of which has the same configuration around the metal. Concerning the CD spectrum in the charge transfer region, the peak intensity seems to be proportional to the net sum of the absolute configurations of the skew chelate pairs, as is shown in Table 3.

The Infrared Spectra. The infrared spectra of the I—VII isomers in the region 2000—4000 cm^{-1} are shown in Fig. 4. It may be noted that the III—VII isomers show a strong band at about 2880 cm^{-1} which

TABLE 3. THE RELATIONSHIP BETWEEN THE NET SUM OF THE ABSOLUTE CONFIGURATIONS OF THE SKEW CHELATE PAIRS AND THE PEAK INTENSITY OF THE CD SPECTRUM IN THE CHARGE TRANSFER REGION

Isomer	The net sum	The order of the peak intensity
(+)-II	"Λ"$=3\Lambda=\Lambda\Lambda\Lambda\Lambda\Lambda$	1
(−)-V, (−)-VI, (−)-VII	"Λ"$=2\Lambda=\Delta\Lambda\Lambda\Lambda\Lambda\Lambda$	2
(+)-I	"Λ"$=2\Lambda=\Lambda\Lambda\Lambda\Lambda$	2
(+)-III, (+)-IV	"Λ"$=\Lambda=\Lambda\Lambda\Lambda\Lambda\Lambda$	3

5) "Λ" and "Δ" denote the net sum of Λ and Δ of the skew chelate pairs, IUPAC Information Bulletin, No. 33, 68 (1968); *Inorg. Chem.*, **9**, 1 (1970).

6) A. J. McCaffery and S. F. Mason, *Mol. Phys.*, **6**, 359 (1963).

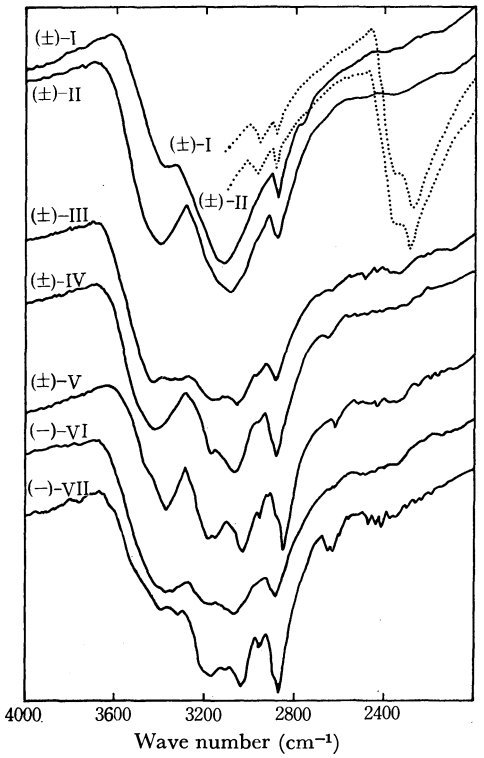

Fig. 4. Infrared spectra of the isomers of $[Co(linpen)]Cl_3$. ····· deuterated complexes.

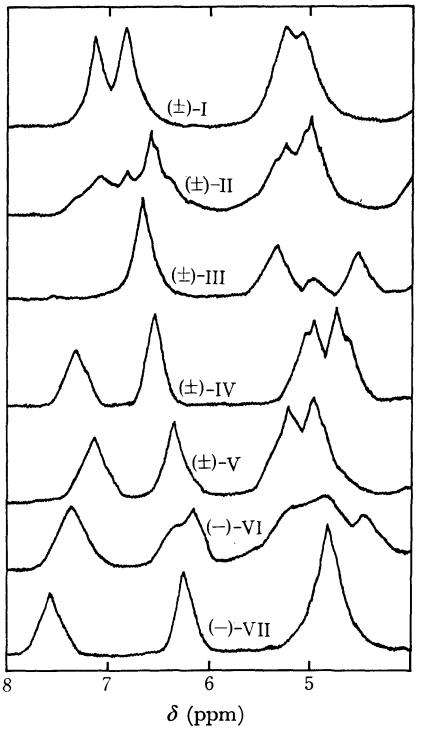

Fig. 5. PMR spectra of the isomers of $[Co(linpen)]^{3+}$ in 0.1 N $DCl(D_2O)$ at 25 °C.

is similar to the band at 2879[7] cm^{-1} of *mer*-$[Co(dien)_2]Br_3 \cdot 2H_2O$,[8] dien being diethylenetriamine. The band of the dien complex has been identified as the >NH stretching vibration, which is characteristic of the *mer* structure. Therefore, the band at about 2880 cm^{-1} of the III—VII isomers can be assigned to the same vibration. The I and II isomers also have a weak-medium band at about 2880 cm^{-1}, but this band does not seem to be assignable to the same >NH stretching vibration, for it does not shift on deuteration. As the I isomer has no >NH group of the *mer* structure, the absence of the above >NH vibration is understandable. The II isomer is identified as having the B structure with a *mer* structure (*vide infra*). Nevertheless, it does not show a band similar to those of the III—VII isomers shown above. The reason for this is not yet clear, though it may be due to some structural differences between them.

The PMR Spectra and the Assignment of the Structures. The PMR spectra of the I—VII isomers were studied in 0.1N $DCl(D_2O)$ in order to obtain information on their configurations. The spectra are shown in Fig. 5. The signals due to HOD are omitted in Fig. 5 for the sake of simplicity. Since the signals due to the methylene protons are very complicated, they were not taken into consideration, either; only the protons attached to nitrogen were considered. The most complicated spectrum, which the II isomer shows, may be assigned to the isomer with the least symmetric structure, that is, to the B structure with the C_1 symmetry. The I isomer exists as a single isomer, and neither is separated further nor isomerizes into other isomers in a neutral solution. Therefore, the I isomer is identified as having the A structure. The PMR spectrum of I is symmetrical in shape, in accordance with the C_2 symmetry.

Since the V, VI, and VII isomers isomerize to their mixtures in a neutral solution, these isomers may be identified as having the D structure, which has three isomers. On the basis of the PMR spectral pattern, the VI isomer may presumably be assigned to the unsymmetrical *RS* configuration connected with the N2 and N5 atoms. Further, based on a very simple conformational analysis and the fact that the V isomer is formed more abundantly than VII, the V isomer is identified as having the *SS* configuration, and the VII isomer, the *RR* configuration connected with the N2 and N5 atoms. Finally, the remaining III and IV isomers are identified as having the C structure. As the amount of III and IV formed are not appreciably different, it is not possible to decide which isomer of the C structure is to be assigned to III or IV.

The structures assigned on the basis of the facts presented above are summarized in Table 1.

The X-ray determination of the structures of several isomers is now under way in the laboratory of Professor Y. Saito, The University of Tokyo.

7) The frequency of this band was erroneously printed in the previous report (Ref. 4) as 2848 cm^{-1}.

8) Y. Yoshikawa and K. Yamasaki, This Bulletin, **45**, 179 (1972).

Trimethylenediamine Complexes. III.[1] *cis-trans* Isomeric Pairs of Diazido- and Dicyano-bis(trimethylenediamine)cobalt(III) Complexes

Hiroshi KAWAGUCHI* and Shinichi KAWAGUCHI

Department of Chemistry, Faculty of Science, Osaka City University, Sumiyoshi-ku, Osaka 558

(Received June 20, 1973)

trans-Diazido- and dicyano-bis(trimethylenediamine)cobalt(III) complexes have been prepared by the ligand substitution reactions of *trans*-dichlorobis(trimethylenediamine)cobalt(III) complexes in methanol. The corresponding *cis* isomers were obtained by similar reactions in aqueous solutions. The structural assignment of these isomeric pairs was made on the basis of electronic, infrared and nuclear magnetic resonance spectra.

As an extension of our synthetic studies on the diacidobis(trimethylenediamine)cobalt(III) complexes,[1] we have prepared the *cis-trans* isomeric pairs of diazido- and dicyano-complexes. The corresponding *cis*- and *trans*-diazidobis(ethylenediamine)cobalt(III) complexes were reported by Staples and Tobe.[2] The *cis*-dicyanobis(ethylenediamine)cobalt(III) salt was synthesized by Rây and Sharma as early as 1951,[3] but the *trans* isomer has long been unknown. Muto, Baba, and Yoneda[4] succeeded in preparing *trans*-$[Co(CN)_2en_2]Cl$ by the reaction of *trans*-$[CoCl_2en_2]NO_3$ or *cis*-$[CoCl_2en_2]Cl$ with potassium cyanide in dimethyl sulfoxide. Konya, Nishikawa, and Shibata[5] also obtained both *cis*- and *trans*-$[Co(CN)_2en_2]Cl$ by the reaction of $[Coen_3]Cl_3$ with potassium cyanide in a cold aqueous solution containing activated charcoal.

Various diacidobis(trimethylenediamine)cobalt(III) complexes were derived from *trans*-$[CoCl_2tn_2]Cl$ by the ligand substitution reactions in methanol and all of them were shown to have the *trans* configuration.[6] The method has been successfully extended to the preparation of *trans*-$[Co(N_3)_2tn_2]NO_3$ and *trans*-$[Co(CN)_2tn_2]Cl$ in the present study. The corresponding *cis* isomers were afforded by similar reactions in aqueous solutions.

Experimental

trans-*Diazidobis(trimethylenediamine)cobalt(III) Nitrate.* *trans*-$[CoCl_2tn_2]NO_3$ (1.7 g) was dissolved in a minimum quantity of hot methanol. To this was added a methanol solution of twice as many moles of sodium azide (0.75 g), and the mixture was heated to 40 °C or above for an hour, and left to stand overnight. Very dark green crystals were filtered, washed with a small quantity of methanol, and dried in air.

Found: C, 20.63; H, 5.87; N, 43.43%. Calcd for $C_6H_{20}N_{11}O_3Co=[Co(N_3)_2tn_2]NO_3$: C, 20.40; H, 5.71; N, 43.62%.

cis-*Diazidobis(trimethylenediamine)cobalt(III) Nitrate.* Two grams of *trans*-$[Co(NO_3)_2tn_2]NO_3$ were dissolved in 10—13 ml of water. To this was added at 0 °C an aqueous solution (5 ml) of sodium azide (0.6 g) and the mixture was kept standing in ice for 2 hr. A small quantity of the precipitated *trans* isomer was filtered, and a few ml of cold water was added to the filtrate, which was stored overnight in a refrigerator. Very dark violet crystals were filtered, washed with methanol and dried (ca. 0.5 g). The finely powdered compound was dissolved again in a minimum quantity of water, and the insoluble portion was filtered off. The solution was saturated with ammonium nitrate and kept standing overnight in ice. The recrystallized pure compound was filtered, washed successively with cold water and methanol and air-dried.

Found: C, 20.42; H, 5.78; N, 43.39%.

trans-*Dicyanobis(trimethylenediamine)cobalt(III) Chloride Monohydrate.* One gram of *trans*-$[CoCl_2tn_2]Cl$ and 3g of silver oxide were suspended in methanol (40 ml) and stirred at room temperature for about 2 hr. The initial green color finally turned to violet. Precipitates of silver chloride and remaining silver oxide were filtered off. Three times as many moles of potassium cyanide were added and dissolved with stirring for about 1 hr. The solution, warmed on a hot water bath for a while, turned brownish, and a small amount of precipitate was separated out. The mixture was concentrated to half its volume by evaporation under reduced pressure. The crude product (3 g) was purified with a cation-exchange resin (Dowex 50 W-X8, 110—200 mesh) in the lithium form. A 0.2 M solution of lithium chloride was used as an eluent, and the effluent was evaporated under reduced pressure until crystals began to appear. Ethyl alcohol was added to the concentrate to precipitate more crystals, which were filtered, washed with ethanol and dried over calcium chloride. The final yield was 1.8 g.

Found: C, 30.81; H, 6.99; N, 26.26%. Calcd for $C_8H_{22}N_6OClCo=[Co(CN)_2tn_2]Cl\cdot H_2O$: C, 30.73; H, 7.09; N, 26.88%. When a concentrated solution of this compound was gradually cooled, crystals of $[Co(CN)_2tn_2]Cl\cdot 3H_2O$ were separated out. These crystals were subjected to X-ray analysis.

cis-*Dicyanobis(trimethylenediamine)cobalt(III) Chloride.* *cis*-$[Co(CN)_2tn_2]_2S_2O_3$ was prepared by the method of Ohkawa *et al.*,[7] and was transformed into the chloride by means of anion exchange chromatography.

Found: C, 31.61; H, 6.88; N, 28.33%. Calcd for $C_8H_{20}N_6ClCo=[Co(CN)_2tn_2]Cl$: C, 32.61; H, 6.84; N, 28.54%.

Measurements. Electronic absorption spectra were measured with Hitachi EPS-2 and Shimadzu QV-50 spectrophotometers. Infrared absorption spectra in the 4000—650

* Present address: Faculty of Literature and Science, Kochi University, Asakura, Kochi.

1) Part II: H. Kawaguchi and S. Kawaguchi, This Bulletin, **43**, 2103 (1970).

2) J. P. Staples and M. L. Tobe, *J. Chem. Soc.*, **1960**, 4812.

3) P. Rây and B. Sharma, *J. Indian Chem. Soc.*, **28**, 59 (1951).

4) M. Muto, T. Baba, and H. Yoneda, This Bulletin, **41**, 2981 (1968).

5) K. Konya, H. Nishikawa, and M. Shibata, *Inorg. Chem.*, **7**, 1165 (1968).

6) H. Kawaguchi, N. Yano, and S. Kawaguchi, This Bulletin, **42**, 136 (1969).

7) K. Ohkawa, J. Fujita, and Y. Shimura, *ibid.*, **38**, 66 (1965).

cm^{-1} region were measured with a Hitachi infrared spectrophotometer EPI-2, and those in the 700—200 cm^{-1} region with a Hitachi grating infrared spectrophotometer EPI-L. The NMR spectra were recorded at 60 MHz with TMS as the external reference on a JEOL C-60 HL spectrometer.

Results and Discussion

Diazidobis(trimethylenediamine)cobalt(III) Complexes. From the analytical data the identical empirical formula $[Co(N_3)_2tn_2]NO_3$ was found to be valid for both the very dark green crystals prepared by the reaction of *trans*-$[CoCl_2tn_2]NO_3$ with sodium azide in methanol, and the very dark violet crystals derived from *trans*-$[Co(NO_3)_2tn_2]NO_3$ in aqueous solutions. Thus, the two compounds are isomeric with each other, and two possibilities can be considered: ionization isomerism or geometrical isomerism. If the nitrate group is coordinated to the cobalt atom, the mode of linkage must be clarified.

The structural aspects of coordinated nitrate groups have been studied extensively,[8] and the vibrational spectra are useful for distinguishing between ionic and coordinated nitrate groups.[9] Both *trans*-$[CoCl(NO_3)tn_2]NO_3$[6] and *trans*-$[Co(NO_3)_2tn_2]NO_3$[10] exhibit very strong absorptions in the IR around 1500, 1260, and 990 cm^{-1} which are assignable to the coordinated nitrate group. Neither of the present complexes, however, shows such absorptions, indicating non-ligation of the nitrate group. They can thus be considered to be a pair of *cis-trans* isomers.

In previous papers,[1,6] Baldwin's criterion[11] of using the CH_2-rocking vibration for distinguishing geometrical isomers was shown to be helpful in many cases. However, it is not applicalbe to the present diazido complexes, since both show a single peak at 890 or 895 cm^{-1}. The IR spectra in the lower frequency region are shown in Fig. 1. The spectrum (1) of the dark-violet isomer prepared in aqueous solutions is more complicated than that (2) of the dark-green isomer obtained in methanol. The former exhibits three peaks while the latter only one in the diagnostic ν(Co–N(tn)) region[12] (490—540 cm^{-1}). The absorption band around 590 cm^{-1} which is assignable to the δ(NNN) is also different. The dark-violet isomer can thus be concluded to have a *cis* configuration.

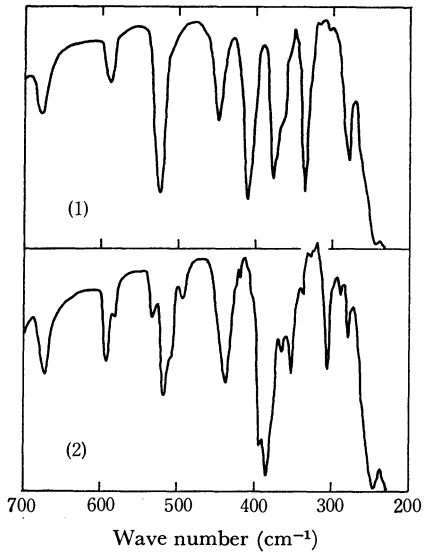

Fig. 1. Infrared spectra of *trans*(1)- and *cis*(2)-$[Co(N_3)_2tn_2]NO_3$ in the 700—200 cm^{-1} region (Nujol mull).

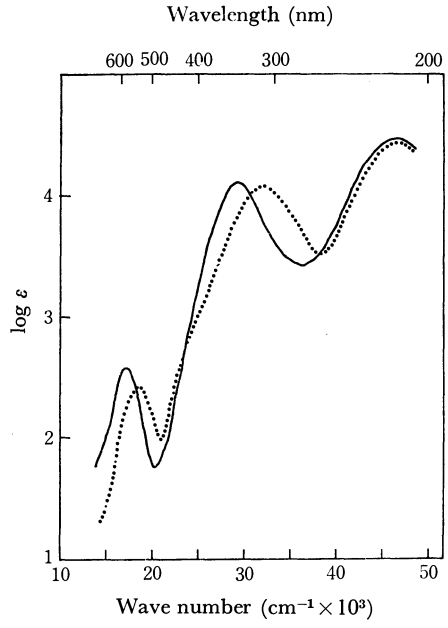

Fig. 2. Absorption spectra of *trans*(——)- and *cis*(……)-$[Co(N_3)_2tn_2]NO_3$ in aqueous solutions.

The electronic spectra of $[Co(N_3)_2tn_2]NO_3$ in aqueous solutions are shown in Fig. 2. Both *cis* and *trans* isomers are not entirely inert, but gradually undergo the aquation reaction. However, addition of sodium azide to the complex solutions in concentration of 3 M or 6 M did not alter the spectra at all, revealing that the solutions are not contaminated with aquated species during the course of spectral measurements. In the case of $[Co(N_3)_2en_2]ClO_4$, the intensity of the first absorption band is nearly equal for *cis* and *trans* isomers.[2] In contrast, *cis*-$[Co(N_3)_2tn_2]NO_3$ exhibits a weaker peak at the shorter wavelength region than the *trans* isomer. A similar feature was also observed for *cis*- and *trans*-$[Co(NCS)_2tn_2]SCN$.[1]

cis-$[Co(N_3)_2tn_2]NO_3$ is quite stable in the solid state at room temperature, but if its aqueous solution is evaporated upon heating, crystals of the *trans* isomer are separated out. This is the reason why cold aqueous solutions were employed for preparation of the *cis* isomers.

Dicyanobis(trimethylenediamine)cobalt(III) Complexes. The *cis*-$[Co(CN)_2tn_2]^+$ complex was first prepared by Ohkawa, Fujita, and Shimura, the *cis*-assignment being

8) C. C. Addison, N. Logan, S. C. Wallwork, and C. D. Garner, *Quart. Rev.*, **25**, 289 (1971).
9) B. M. Gatehouse, S. E. Livingstone, and R. S. Nyholm, *J. Chem. Soc.*, **1957**. 4222,
10) E. Yasaki, I. Oonishi, H. Kawaguchi, S. Kawaguchi, and Y. Komiyama, This Bulletin, **43**, 1354 (1970).
11) M. E. Baldwin, *J. Chem. Soc.*, **1960**, 4369.
12) M. N. Hughes and W. R. McWhinnie, *J. Inorg. Nucl. Chem.*, **28**, 1659 (1966).

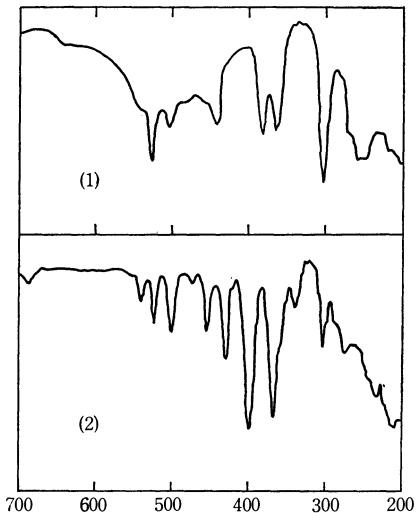

Fig. 3. Infrared spectra of *trans*-$[Co(CN)_2tn_2]Cl \cdot H_2O$(1) and *cis*-$[Co(CN)_2tn_2]Cl$(2) in the 700—200 cm^{-1} region (Nujol mull).

made on the splitting of the C≡N stretching band.[7] No corresponding *trans* isomer could be prepared by the direct reaction of *trans*-$[CoCl_2tn_2]Cl$ with potassium cyanide in methanol, but it could be obtained by a similar reaction after the action of silver oxide. A yellow plate of *trans*-$[Co(CN)_2tn_2]Cl \cdot 3H_2O$ was subjected to X-ray crystal analysis.[13] Crystal data: monoclinic, $a=17.906(5)$, $b=10.753(6)$, $c=8.575(5)$ Å, $\beta=95.74(5)°$, $Z=4$, $D_c=1.33$, $D_m=1.31$ g·cm^{-3}, $\mu(Ni-K_\alpha)=38.5$ cm^{-1}; space group C_c. The *trans* configuration was ascertained, and the linear orientation of Co–C–N and the chair conformation of the six-membered chelate rings were clarified (R=0.121).

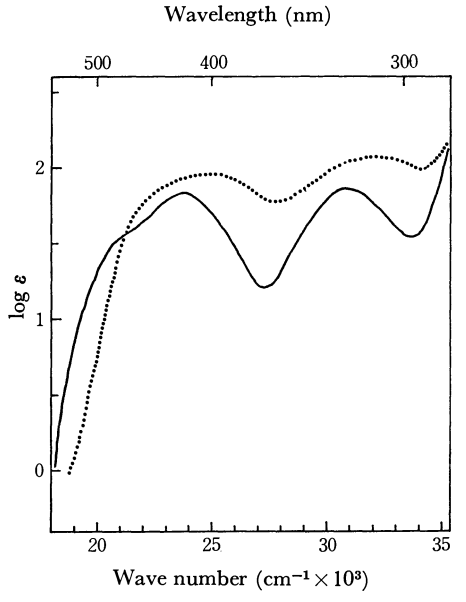

Fig. 4. Absorption spectra of *trans*-$[Co(CN)_2tn_2]Cl$ (——) and *cis*-$[Co(CN)_2tn_2](S_2O_3)_{1/2}$ (·····) in aqueous solutions.

13) H. Hasegawa, K. Matsumoto, H. Kuroya, H. Kawaguchi, and S. Kawaguchi, Presented at the 20th Symposium on the Coordination Compounds of the Chemical Society of Japan, 18A18, Tokyo, November, 1970.

The IR spectra of the two isomers in the low-frequency region are shown in Fig. 3. The curve for the *cis* isomer is a little more complicated than that for the *trans* isomer. In the CH_2-rocking region the *cis* isomer exhibits a distinct shoulder at the lower frequency side of a rather sharp peak at 898 cm^{-1}, while the *trans* compound shows a broad symmetric band at 892 cm^{-1}. Their electronic spectra are shown in Fig. 4. Just as in the case of the corresponding ethylenediamine complexes,[4,5] the *trans* isomer has a remarkable shoulder in the longer wavelength side of the first band.

The present synthetic method for the *trans*-$Co(CN)_2tn_2^+$ complex was also applied to the preparation of *trans*-$Co(CN)_2en_2^+$ and a satisfactory yield was attained; 1 g of *trans*-$[Co(CN)_2en_2]Cl$ was obtained from 4 g of *trans*-$[CoCl_2en_2]Cl$.

NMR Studies. The proton NMR spectra of diamagnetic tris(diamine)metal complexes have been studied extensively in recent years. The ethylenediamine chelate rings in these complexes have *gauche* conformations[14] with either δ or λ chirality. It has been established theoretically[15] and experimentally[16] that the Men_3 complexes undergo rapid ring inversion at room temperature. Appleton, Hall, and Hawkins[17] pointed out, however, that the methylene protons of the ethylenediamine ligand can not be equivalent even if the rapid conformational equilibration is attained, since the environment of an axial proton in a δ conformer is not identical with that of an axial proton in a λ conformer due to the presence of the other two chelate rings.

Although there is no environmental difference among NH_2 and CH_2 protons respectively in *trans*-MX_2en_2 complexes, there exists some additional complexity in the case of *cis*-MX_2en_2 in comparison with Men_3. The NH_2 protons situated in the *cis* position to both the X groups are inherently nonequivalent to the other NH_2 protons which are *cis* to one X and *trans* to the other X. A similar discrimination should be extended to the adjacent α-CH_2 groups. The different patterns of NH_2 proton signals in *cis*- and *trans*-CoX_2en_2 complexes have frequently been exemplified since the original work of Clifton and Pratt.[18] Distinct splitting of CH_2 bands is also observed for *cis*-$[Co(H_2O)_2en_2](ClO_4)_3$ in 1.8 M D_2SO_4.[19]

A six-membered chelate ring, on the other hand, is capable of existing in several conformational types such as "chair," "boat," and "skew boat" or "twist" conformations. An optically active trimethylenediamine complex $(-)_D$-$[Cotn_3]Br_3 \cdot H_2O$ was shown to have the tris-chair conformation.[20] However, the tris-chair con-

14) Y. Saito, K. Nakatsu, M. Shiro, and H. Kuroya, This Bulletin, **30**, 795 (1957); J. K. Beattie and H. Elsbernd, *J. Amer. Chem. Soc.*, **92**, 1946 (1970).

15) J. R. Gollogly, C. J. Hawkins, and J. K. Beattie, *Inorg. Chem.*, **10**, 317 (1971).

16) J. K. Beattie, *Accounts Chem. Res.*, **4**, 253 (1971).

17) T. G. Appleton, J. R. Hall, and C. J. Hawkins, *Inorg. Chem.*, **9**, 1299 (1970).

18) P. Clifton and L. Pratt, *Proc. Chem. Soc.*, **1963**, 339.

19) D. A. Buckingham, L. Durham, and A. M. Sargeson, *Aust. J. Chem.*, **20**, 257 (1967).

20) T. Nomura, F. Marumo, and Y. Saito, This Bulletin, **42**, 1016 (1969).

formation seems to be only slightly more stable than the tris-skew-boat conformation.[21] The CD spectra of $Cotn_3^{3+}$ ions in solutions were interpreted to indicate the equilibrium between these two conformers.[22] The conformational inversion is quite rapid as evidenced by the observation that the NMR spectra of $Pdtn_2^{2+}$ and $Pttn_2^{2+}$ complexes are no more complicated than the spectrum of $tn(HCl)_2$.[23]

The six-membered chelate rings in several diacidobis(trimethylenediamine)cobalt(III) complexes have also been revealed to have the chair form in crystals,[10,24] but seem to undergo rapid conformational interconversion in solutions. Figure 5-(1) shows the NMR spectra of *trans*-$[Co(CN)_2tn_2]Cl$ in D_2O containing *ca.* 1 M DCl. Three peaks are observed at 6.15, 7.25, and 8.25 τ with the relative integral intensities 2: 2: 1. The broad lowest-field band disappears in solutions without acid as is illustrated in Fig. 6-(1), and can thus be attributed to the amine protons. The remaining two peaks which are not influenced by pH of the solution may be assigned to the methylene protons. The observed area ratio unequivocally indicates that the lower-field signal is due to the α-CH_2 and the higher-field one to the β-CH_2 protons. Here the methylene protons are designated as: NH_2–$CH_2(\alpha)$–$CH_2(\beta)$–$CH_2(\alpha)$–NH_2. The α-CH_2 signal in Fig. 5-(1) reveals the characteristic five-line pattern, but that in Fig. 6-(1) is essentially a triplet because of the quenching of coupling with NH_2 protons by deuteration. These features indicate the magnetic equivalence of methylene protons in trimethylenediamine ligands by virtue of the rapid conformational interchange as discussed above.

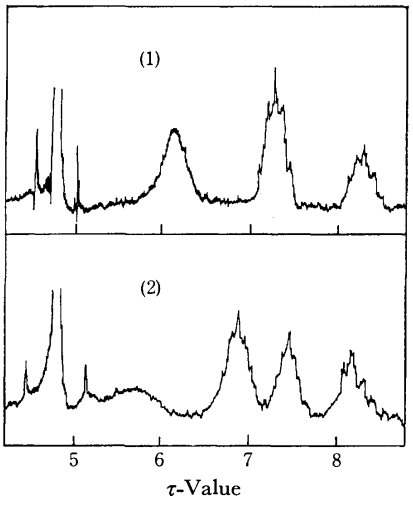

Fig. 5. Proton NMR spectra of *trans*(1)- and *cis*(2)-$[Co(CN)_2tn_2]Cl$ in acidic D_2O solutions.

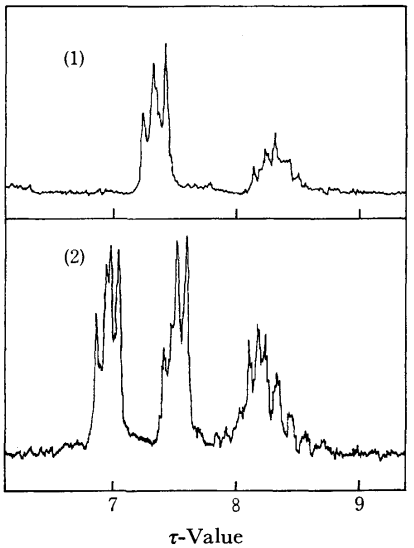

Fig. 6. Proton NMR spectra of *trans*(1)- and *cis*(2)-$[Co(CN)_2tn_2]Cl$ in neutral D_2O solutions.

On the other hand, the spectra of *cis*-$[Co(CN)_2tn_2]Cl$ give three methylene signals at 6.87, 7.44, and 8.14 τ both in acidic and neutral D_2O solutions, and their area ratios are about 1.9: 1: 1 (Fig. 5-(2)) and 1: 1: 1 (Fig. 6-(2)), respectively. These features indicate that there exist two kinds of nonequivalent protons in the α-CH_2 groups, which are distinctly differentiated under the strong influence of cyanide ligands.

The very broad signal of NH_2 protons around 5.7 τ has about one half of the expected area (Fig. 5-(2)). It seems improbable on the basis of the following that 50% of the NH_2 protons was exchanged with D_2O immediately after dissolution. (1) The rate data of base-catalyzed hydrogen exchange of ammine and ethylenediamine cobalt(III) complexes in D_2O[25] suggest that the exchange reaction of the trimethylenediamine complex in the present solution containing 1 M DCl can not be so rapid. (2) The observed NMR spectrum shows no change at all even after one-day standing. Thus it seems appropriate to consider that the NH_2

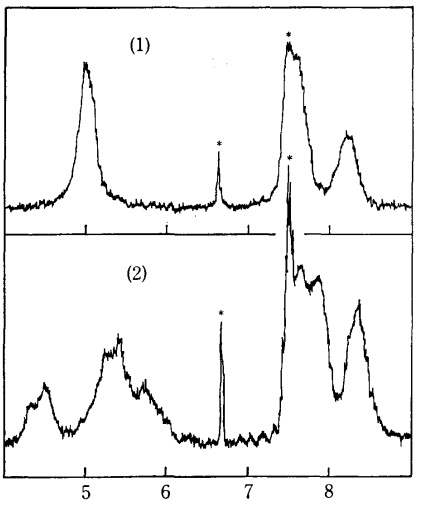

Fig. 7. Proton NMR spectra of *trans*(1)- and *cis*(2)-$[Co(NCS)_2tn_2]SCN$ in dimethylsulfoxide-d_6 solutions, asterisk denoting impurity bands.

21) J. R. Gollogly and C. J. Hawkins, *Inorg. Chem.*, **11**, 156 (1972).
22) P. G. Beddoe, M. J. Harding, S. F. Mason, and B. J. Peart, *Chem. Commun.*, **1971**, 1283.
23) T. G. Appleton and J. R. Hall, *Inorg. Chem.*, **9**, 1807 (1970).
24) K. Matsumoto, M. Yonezawa, H. Kuroya, H. Kawaguchi, and S. Kawaguchi, This Bulletin, **43**, 1269 (1970); R. J. Geue and M. R. Snow, *J. Chem. Soc. A*, **1971**, 2981.
25) F. Basolo and R. G. Pearson, "Mechanisms of Inorganic Reactions," 2nd ed., J. Wiley and Sons, New York (1967), p. 185.

proton signal is split into two bands in the case of *cis*-$Co(CN)_2tn_2^+$, one appearing around 5.7 τ and the other overlapping with the lowest-field methylene peak. The observed larger integral intensity of the latter peak supports this interpretation.

The spectra of *trans*- and *cis*-$[Co(NCS)_2tn_2]SCN$ in dimethyl sulfoxide-d_6 are shown in Fig. 7. The configurational assignments of these complexes have already been reported.[1,24] The spectrum of the *trans* isomer gives three signals at 5.00, 7.60, and 8.20 τ, which are assigned to NH_2, α-CH_2, and β-CH_2 protons, respectively. A sharp peak at 6.70 τ and an overlapping peak at 7.50 τ are attributed to impurities in the solvent. The α-CH_2 absorption in *cis*-$[Co(NCS)_2tn_2]SCN$ is partially split into two bands at 7.65 and 7.85 τ, although the separation is not so complete as in the case of *cis*-$Co(CN)_2tn_2^+$. This might suggest that the thiocyanate anion does not exert so strong an influence as the cyanide anion. A similar degree of splitting of the α-CH_2 absorption was also noticed in the spectrum of $CoCO_3tn_2^+$ in neutral D_2O.[26] The NH_2 absorption in *cis*-$[Co(NCS)_2tn_2]SCN$ shows a very complicated pattern and can not be interpreted, especially in reference to the rather simple pattern exhibited by NH_2 protons of *cis*-$[Co(N_3)_2tn_2]NO_3$.

The spectra of *trans*- and *cis*-$[Co(N_3)_2tn_2]NO_3$ in DMSO-d_6 are shown in Fig. 8. The α-CH_2 signal is not split in this *cis* isomer. The azide group may exert a weaker effect on the α-CH_2 protons than the thiocyanate ligand. Buckingham, Durham, and Sargeson[19] also observed no splitting of the CH_2 signals in the CoX_2en_2 complexes where both of the coordinating atoms of X are nitrogen, *i.e.* X=NH_3, N_3^-, NO_2^-, or 1/2en. However, the NH_2 signal of *cis*-$Co(N_3)_2tn_2^+$ is split into two bands quite remarkably, permitting the differentiation from the *trans* isomer. The minor NH_2 band observed at 6.05 τ in the spectrum of *trans*-$[Co(N_3)_2tn_2]NO_3$ (Fig. 8-(1)) is not explicable at present. It might be due to the partial solvolysis.

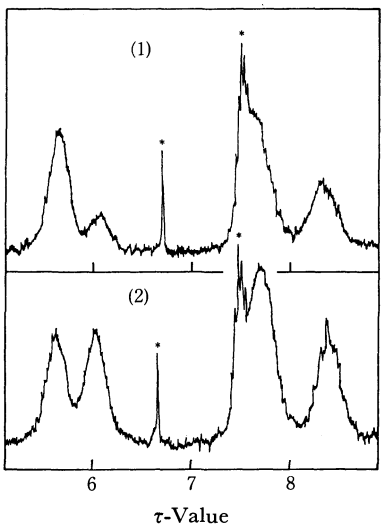

Fig. 8. Proton NMR spectra of *trans*(1)- and *cis*(2)-$[Co(N_3)_2tn_2]NO_3$ in dimethyl sulfoxide-d_6 solutions, asterisks denoting impurity bands.

We are indebted to Mr. J. Gohda and Miss M. Iwao for the elemental analyses and NMR measurements. Financial aid by the Ministry of Education is also acknowledged.

26) I. R. Jonasson, S. F. Lincoln, and D. R. Stranks, *Aust. J. Chem.*, **23**, 2267 (1970).

Mixed Ligand Complex Formation between Monodentate Ligands and Various Tridentate Ligand-Copper(II) Complexes

Osamu YAMAUCHI, Hiroshi BENNO, and Akitsugu NAKAHARA

Institute of Chemistry, College of General Education, Osaka University, Toyonaka, Osaka 560

(Received June 29, 1973)

Formation of mixed ligand complexes between monodentate ligands (L) and copper(II) complexes of tridentate ligands (A) has been investigated by potentiometric titration and thermal analysis. Thus, the constants, log K_m, for the formation of the complexes of type CuA·L from CuA and L have been calculated from the titration curves by the method of non-linear least-squares. A refers to diethylenetriamine, dipicolylamine, 2,2′,2″-terpyridine, ethylenediamine-*N*-monoacetic acid, iminodiacetic acid, or pyridine-2,6-dicarboxylic acid and L to pyridine, *p*-phenolsulfonic acid, *n*-butylamine, or hydroxy group. The stability series in each system with L fixed has been interpreted in terms of the strength of A as a Lewis base, expressed by the sum of pK_a ($\sum pK_a$), as well as back-donation. In the absence of significant steric hindrance, favorable combination of donor atoms around copper(II) has been found to be between aromatic nitrogens and negative oxygens. Thermal stability of the isolated complexes of type CuA·PY, where PY is pyridine, was also in line with the stability sequence in solution.

Recent interest in the mechanisms of the biological reactions involving metal ions as central atoms has prompted a variety of basic studies on mixed ligand metal complexes. Sigel *et al.*[1-3] investigated systematically the complex formation between copper(II)-2,2′-bipyridine and oxygen- and/or nitrogen-containing bidentate ligands, and gave explanations to the affinity and the driving force leading to mixed ligand complexes.

It seems reasonable to assume that, in the course of a biological reaction, the central metal ion is surrounded by a multidentate ligand, leaving only one coordination site available for the second ligand. In this connection, Angelici and Allison[4] reported the mixed complex formation between substituted diethylenetriamine complexes of copper(II) and several amino acids which coordinate as bidentate ligands, and Hauer *et al.*[5] reported the reactions of polyamines with copper(II)-triglycine. However, it is of further interest to study the coordination of purely monodentate ligands to copper(II) complexes of tridentate ligands of different types.

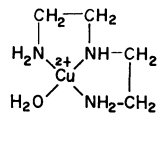

Cu(dien)

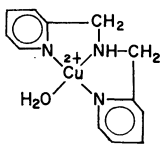

Cu(dpa)

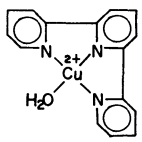

Cu(terpy)

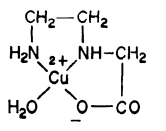

Cu(edma)

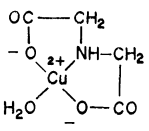

Cu(ida)

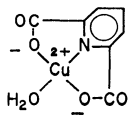

Cu(pdca)

In order to find out the effects of combination of two ligands around copper(II) on the stability of the resulting mixed ligand complex, we investigated the complex formation of pyridine (PY), *p*-phenolsulfonic acid (PPS), and *n*-butylamine (BA) with the copper(II) complexes of diethylenetriamine (Cu(dien)), dipicolylamine (Cu(dpa)), 2,2′,2″-terpyridine (Cu(terpy)), ethylenediamine-*N*-monoacetic acid (Cu(edma)), iminodiacetic acid (Cu(ida)), and pyridine-2,6-dicarboxylic acid (Cu(pdca))[6] by potentiometric titration and thermal analysis.

Experimental

Materials. *Copper(II) Complexes*: The binary complexes (CuA) used are $Cu(dien)(NO_3)_2$, $Cu(dpa)Cl_2$, $Cu(terpy)(ClO_4)_2 \cdot H_2O$, Cu(edma)Cl, $Cu(ida) \cdot 2H_2O$, and $Cu(pdca) \cdot 2H_2O$, all of which were prepared from equal amounts of a ligand and an appropriate salt of copper(II) in water or aqueous ethanol.

Mixed ligand complexes of type CuA·PY, where A is dien, terpy, ida, or pdca, were obtained by recrystallizing the binary complexes from aqueous pyridine. The relevant elemental analysis data are summarized in Table 1.

Ligands: Pyridine and *n*-butylamine were converted to the perchlorates, which were purified by recrystallization from water. Sodium *p*-phenolsulfonate was purchased from Nakarai Chemicals Co., and recrystallized from water.

All the other chemicals used were of reagent grade, distilled and deionized water being used.

pH Titrations. *(a) Reagents*: 0.1 M KOH was prepared according to Albert,[7] and stored under a nitrogen atmosphere. 0.01 M $Cu(NO_3)_2$ was prepared by dissolving copper(II) nitrate trihydrate in water and standardized against standard zinc by chelatometric titration.[8]

1) R. Griesser and H. Sigel, *Inorg. Chem.*, **9**, 1238 (1970); *ibid.*, **10**, 2229 (1971). Also, the papers cited therein.

2) P. R. Huber, R. Griesser, and H. Sigel, *ibid.*, **10**, 945 (1971).

3) H. Sigel, P. R. Huber, and R. F. Pasternack, *ibid.*, **10**, 2226 (1971).

4) R. J. Angelici and J. W. Allison, *ibid.*, **10**, 2238 (1971).

5) H. Hauer, E. J. Billo, and D. W. Margerum, *J. Amer. Chem. Soc.*, **93**, 4173 (1971).

6) These binary complexes will be abbreviated as CuA in the text hereinafter. Mixed complexes of CuA with the second ligand L will generally be described as CuA·L, where L is pyridine (PY), *p*-phenolsulfonate (PPS), *n*-butylamine (BA), or hydroxy group (OH). Thus, the complex of Cu(dien) with pyridine is expressed as Cu(dien)·PY. All the charges are omitted for simplicity.

7) A. Albert and E. P. Serjeant, "Ionization Constants of Acids and Bases," Methuen and Co., Ltd., London (1962).

8) K. L. Cheng, *Anal. Chem.*, **30**, 243 (1958).

Table 1. Elemental analysis of CuA and CuA·PY

Complex[a)]	Elemental analysis					
	C (%)		H (%)		N (%)	
	Calcd	Found	Calcd	Found	Calcd	Found
$[Cu(dien)NO_3]NO_3$	16.52	16.33	4.51	4.43	24.08	24.27
[Cu(dpa)Cl]Cl	43.19	43.30	3.93	3.78	12.59	12.43
$[Cu(terpy)H_2O](ClO_4)_2$	35.05	35.09	2.55	2.43	8.18	8.25
[Cu(edma)Cl]	22.23	22.22	4.20	4.15	12.96	13.17
$[Cu(ida)H_2O]\cdot H_2O$	20.82	20.85	3.93	3.93	6.07	6.15
$[Cu(pdca)H_2O]\cdot H_2O$	31.77	31.91	2.67	2.79	5.29	5.31
$[Cu(dien)PY](NO_3)_2$	29.21	29.12	4.90	4.90	22.71	22.82
$[Cu(terpy)PY](ClO_4)_2$	41.81	41.75	2.81	2.11	9.75	9.55
[Cu(ida)PY]	39.47	39.77	3.69	3.34	10.23	10.36
[Cu(pdca)PY]	46.82	47.25	2.62	2.50	9.11	9.26

a) The complexes are tentatively expressed by assuming that copper(II) is four-coordinate.

(b) Apparatus: A Radiometer PHM 4d pH meter with a G202B glass electrode and a K401 calomel electrode was used after standardization with a Horiba standard buffer solution (pH 4.01).

(c) Procedure: Titrations were carried out at concentrations of 4×10^{-3}—8×10^{-3} M in water (μ=0.1(KNO_3)) at 25 °C under a nitrogen atmosphere. Details of the procedure were essentially the same as before,[9] and conversion of pH to -log [H^+], where [H^+] denotes the hydrogen ion concentration, was done in the manner described.[9]

Measurement of Absorption Spectra. The absorption spectra of various mixtures of Cu(dien) and pyridine (10^{-2}—10^{-3} M) were measured in water at pH 7.0 with a Shimadzu MPS 50L recording spectrophotometer.

Measurement of Thermal Stability. The thermal stabilities of the mixed ligand complexes were measured with a Rigaku Denki Thermoflex No. 8001, the rate of temperature elevation being 5 °C per minute.

Results and Discussion

Typical titration curves of the complexes CuA in the presence of the equimolar amounts of pyridine, *p*-phenolsulfonate, and *n*-butylamine are shown in Figs.

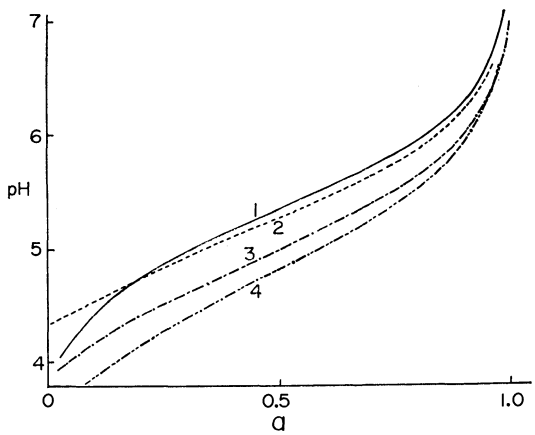

Fig. 1. Titration curves of pyridine in the presence and the absence of CuA. *a* is moles of KOH added per mole of ligand.
1, PY alone; 2, Cu(dien): PY=1: 1; 3, Cu(ida): PY=1: 1; 4, Cu(pdca): PY=1: 1.

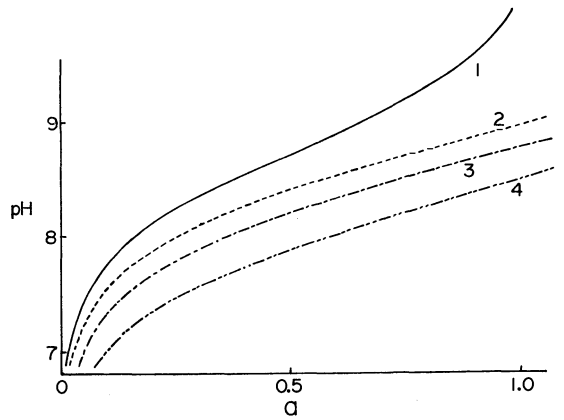

Fig. 2. Titration curves of *p*-phenolsulfonate in the presence and the absence of CuA.
1, PPS alone; 2, Cu(dien): PPS=1: 1; 3, Cu(dpa): PPS=1: 1; 4, Cu(terpy): PPS=1: 1.

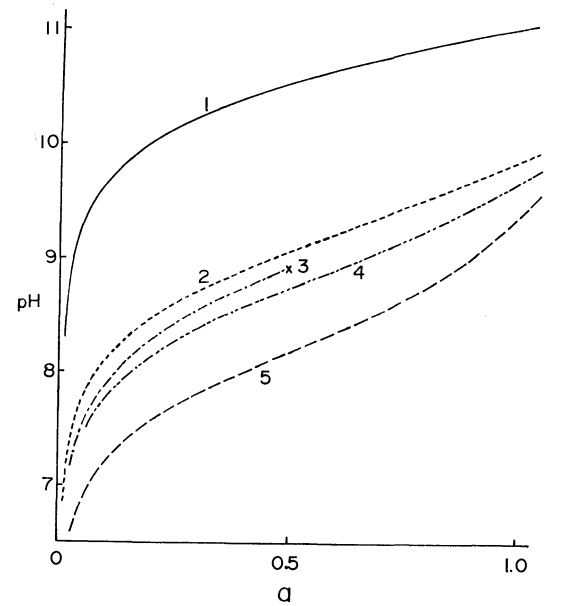

Fig. 3. Titration curves of *n*-butylamine in the presence and the absence of CuA.
1, BA alone; 2, Cu(dien): BA=1: 1; 3, Cu(edma): BA=1: 1; 4, Cu(dpa): BA=1: 1; 5, Cu(terpy): BA=1: 1.

9) O. Yamauchi, H. Miyata, and A. Nakahara, This Bulletin, **44**, 2716 (1971).

1, 2, and 3, respectively. The pH decrease due to the presence of CuA indicates mixed ligand complex formation in these systems. There seems to be protonation of A in the CuA·PY series at pH below 5, whereas formation of the hydroxy complexes should be taken into account for CuA·PPS and CuA·BA systems which lack the pH jump at $a=1.0$. Cu(ida)·L and Cu(pdca)·L systems, where L=*p*-phenolsulfonate or *n*-butylamine, did not afford reliable titration curves owing to precipitation.

The absorption spectra of Cu(dien)·PY system at various Cu(dien): pyridine ratios in water at pH 7.0 showed the isosbestic point at 635 nm, which indicates the following reaction is the only one around this pH (charges are omitted for simplicity):

$$\mathrm{Cu(dien)} + \mathrm{PY} \rightleftharpoons \mathrm{Cu(dien)\cdot PY}$$

This is also confirmed by the compositions of the mixed ligand complexes isolated as crystals.

From these observations, we assumed the following equilibria for the mixed ligand systems with the constants defined:

$$\mathrm{HL} \overset{K_a}{\rightleftharpoons} \mathrm{H} + \mathrm{L} \qquad (1)$$

$$K_a = \frac{[\mathrm{H}][\mathrm{L}]}{[\mathrm{HL}]}$$

$$\mathrm{CuA} + \mathrm{L} \overset{K_m}{\rightleftharpoons} \mathrm{CuA\cdot L} \qquad (2)$$

$$K_m = \frac{[\mathrm{CuA\cdot L}]}{[\mathrm{CuA}][\mathrm{L}]}$$

where HL refers to protonated monodentate ligand, and K_a and K_m are the acid dissociation constant and the stability constant, respectively. Dissociation of CuA to Cu and A (free tridentate ligand) may safely be neglected in the pH range investigated. The equilibria (3) and (4) were also considered at low and high pH, respectively:

$$\mathrm{CuA\cdot H} \overset{K_H}{\rightleftharpoons} \mathrm{CuA} + \mathrm{H} \qquad (3)$$

$$K_H = \frac{[\mathrm{CuA}][\mathrm{H}]}{[\mathrm{CuA\cdot H}]}$$

$$\mathrm{CuA} + \mathrm{OH} \overset{K_{OH}}{\rightleftharpoons} \mathrm{CuA\cdot OH} \qquad (4)$$

$$K_{OH} = \frac{[\mathrm{CuA\cdot OH}]}{[\mathrm{CuA}][\mathrm{OH}]}$$

where CuA·H and CuA·OH refer respectively to protonated and hydroxy complex.

The equilibrium constants K_H, K_{OH}, and K_m were calculated on the basis of the mole balances for total CuA and total L, and the electroneutrality of solution. Computation of the constants was made by the method of non-linear least-squares with the use of a NEAC 2200/500 computer, the program and the conditions for convergence being essentially the same as those reported.[9,10] Table 2 shows the calculated equilibrium constants along with the pK_a values of ligands A taken from the literature. The pK_H ($-\log K_H$) values for Cu(dpa), Cu(terpy), and Cu(pdca) are as low as 1.2—1.6 with large variances (>1) and not reliable. The constants K_{OH} were calculated from the data for *n*-butylamine and *p*-phenolsulfonate, for which hydrolysis was evident from the titration curves, and the values from the two systems agreed with each other to within 0.3 log unit. The $\log K_{OH}$ value of 4.75 for Cu(dien)·OH is in good agreement with the reported values of 4.58[11] and 5.17.[12]

The theoretical titration curves calculated by these constants coincided very well with the experimental ones, and the differences expressed in titer were less than 0.01 ml over the entire ranges (usually 0.2—1.0 ml).

The mixed complexes of pyridine with Cu(dien), Cu(dpa), and Cu(terpy), containing donor nitrogens only, have lower stability than the complexes with Cu(edma), Cu(ida), and Cu(pdca), suggesting that negative oxygens at the coordination sites increase the stability of the resulting complexes. According to Tanaka, the $\log K_m$ values can be calculated by a general equation derived from mechanistic considerations, and the experimental values for Cu(dien), Cu(dpa), Cu(edma), and Cu(ida) could be reproduced satisfactorily by the equation.[13]

TABLE 2. EQUILIBRIUM CONSTANTS OF CuA·L SYSTEMS (25±0.05 °C; μ=0.1 (KNO_3))[a]

CuA	$\sum pK_a$[b]	pK_H	$\log K_m$ L[c]			$\log K_{OH}$[g]
			PY	PPS	BA	
Cu(dien)	23.41[d]	3.24±0.12	1.77±0.09	1.72±0.27	3.49±0.15	4.75±0.12
Cu(dpa)	11.02[e]	<2	1.76±0.09	2.37±0.09	3.76±0.27	5.11±0.06
Cu(terpy)	6.97[d]	<2	1.81±0.06	2.71±0.12	4.71±0.09	5.67±0.06
Cu(edma)	18.95[f]	3.19±0.06	2.09±0.01	1.75±0.27	4.09±0.15	4.77±0.09
Cu(ida)	12.03[d]	2.67±0.15	2.65±0.02			
Cu(pdca)	6.78[d]	<2	2.97±0.02			

a) Variances are three times the estimated standard deviations.
b) The $\sum pK_a$ value is the sum of three constants of each ligand except terpy, ida, and pdca where the first dissociation constants are negligibly small.
c) The pK_a values determined in the present study are: PY, 5.26±0.03; PPS, 8.66±0.03; BA, 10.62±0.09. The value of 13.88 was used for the apparent ion product of water (pK_w').
d) L. G. Sillén and A. E. Martell, "Stability Constants of Metal-Ion Complexes," Special Publication No. 17, The Chemical Society, London (1964).
e) J. K. Romary, J. D. Barger, and J. E. Bunds, *Inorg. Chem.*, **7**, 1142 (1968).
f) Y. Fujii and M. Kodama, This Bulletin, **42**, 3172 (1969).
g) Calculated from the data for the CuA·PPS system.

10) O. Yamauchi, Y. Nakao, and A. Nakahara, *ibid.*, **46**, 2119 (1973).
11) R. C. Courtney, R. L. Gustafson, S. Chaberek, Jr., and A. E. Martell, *J. Amer. Chem. Soc.*, **81**, 519 (1959).
12) J. W. Allison and R. J. Angelici, *Inorg. Chem.*, **10**, 2233 (1971).
13) M. Tanaka, *J. Inorg. Nucl. Chem.*, in press.

As to the *p*-phenolsulfonate series, Cu(dpa) and Cu(terpy), both with aromatic nitrogens, form more stable mixed complexes than Cu(dien) does. The stabilities of the CuA·OH systems as seen from the log K_{OH} values exhibit the same trend as observed in the *p*-phenolsulfonate series.

The complexes with *n*-butylamine, CuA·BA, are more stable than CuA·PY and CuA·PPS, probably because of the high pK_a of *n*-butylamine. Their stabilities increase with added aromatic nitrogens and carboxylate oxygens.

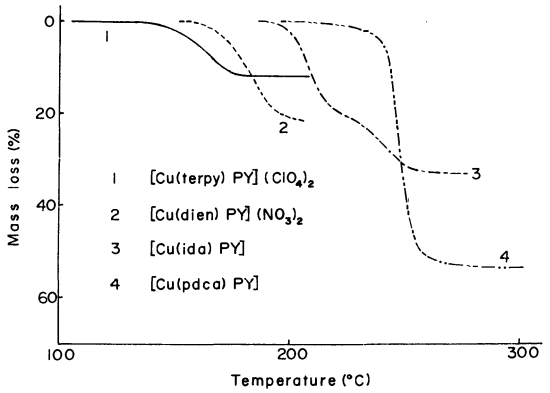

Fig. 4. Thermal analysis of CuA·PY.
Mass loss due to evaporation of pyridine:

Curve	Found (%)	Calcd (%)
1	12	14
2	21	21
3	31	29

Figure 4 shows the thermal decomposition curves of four pyridine-containing mixed complexes. Curves 1—3 correspond well to loss of pyridine from the complexes, and curve 4 may be explained in terms of decarboxylation of pyridine-2,6-dicarboxylic acid as well as evaporation of pyridine. The thermal stability is in the order Cu(terpy)·PY≤Cu(dien)·PY<Cu(ida)·PY<Cu(pdca)·PY, which is in line with the stability series in solution.

It is interesting to compare the stability of the copper(II)–pyridine bonding in CuA·PY with that in the binary complex according to the difference defined by the equation:

$$\Delta \log K_m = \log K_m - \log K_1$$

where $\log K_1$=2.52 (Ref. c) in Table 2) and refers to the stability constant of the 1:1 copper(II)–pyridine complex. The $\Delta \log K_m$ values are calculated to be negative for Cu(dien) (−0.75), Cu(dpa) (−0.76), Cu(terpy) (−0.71), and Cu(edma) (−0.43), and positive for Cu(ida) (0.13) and Cu(pdca) (0.45), which indicates that the bonding is destabilized in the first four complexes as compared with the binary complex.[14]

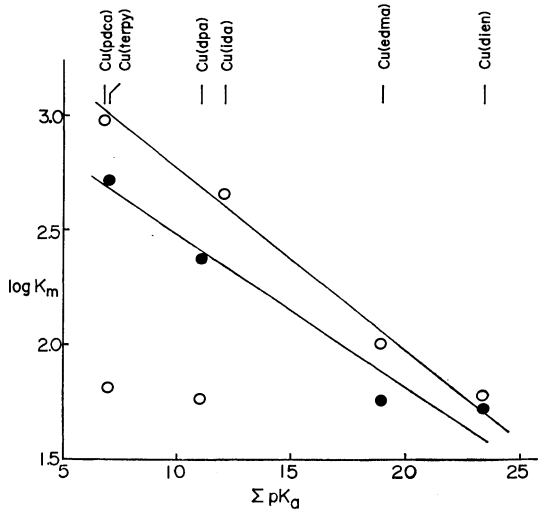

Fig. 5. Relationships between log K_m and $\sum$ pK_a in the CuA–PY and CuA·PPS series.
CuA·PY: ○, CuA·PPS: ●.

The affinity of the binary complex CuA for the second ligand L is considered to be dependent on the electronegativity of the central metal ion or, inversely, the basicity of the first ligand A. If A is a strong base, copper(II) in CuA will be less electrophilic and its binding with L will be weaker. Thus, we may expect a certain relationship between the stability constant log K_m and the sum of pK_a of the corresponding A, $\sum$pK_a, which is taken as indicative of the strength of the ligand as a Lewis base. From the plots of log K_m against $\sum$pK_a as shown in Fig. 5 for CuA·PY and CuA·PPS, we see a general trend in the four series that the stabilities of the ternary complexes usually decrease with the increase of the basicity of A with some anomalies. The exceptionally low stabilities of Cu(terpy)·PY and Cu(dpa)·PY are explained to be due to the steric interactions, as visualized by the molecular models, of 2,2′,2″-terpyridine or dipicolylamine with incoming pyridine, because the corresponding complexes with *p*-phenolsulfonate and hydroxy group are satisfactorily in the expected order. As pointed out by Sone *et al.*,[15] steric requirements for the second ligand can be a decisive factor leading to the stabilization in the mixed complex, and the above instances may be regarded as the results of the steric effects exerted on the part of the second ligand in a negative way.

On the other hand, a somewhat different view is also possible regarding the stability of mixed complexes. Griesser and Sigel[1] stressed the importance of back-donation in the formation of the ternary complexes which have π-acceptors such as 2,2′-bipyridine and pyrocatechol. They observed the favored formation of Cu(2,2′-bipyridine)·pyrocatechol, compared with Cu(2,2′-bipyridine)·ethylenediamine, and ascribed it to the cooperative interactions of the two π-acceptors.

14) However, on purely statistical ground, we should take into account the factors due to preoccupation of the coordination sites in CuA. If we simply assume copper(II) to be four-coordinate, we may correct the K_1 value according to the equation

$$\frac{K_{n+1}}{K_n} = \frac{n(N-n)}{(n+1)(N-n+1)}$$

where N and n refer to the coordination number of copper(II) and the sites occupied by ligand as in $[Cu(H_2O)_{N-n}L_n]$, respectively. Since PY in CuA·PY is the fourth ligand to get into the site, we may take K_4/K_1 as the correction factor:

$$\frac{K_4}{K_1} = \frac{K_2}{K_1} \times \frac{K_3}{K_2} \times \frac{K_4}{K_3} = \frac{1}{16}.$$

This gives us the statistical value of 1.32 in place of 2.52 and makes all the Δ log K_m values positive.

15) K. Sone, S. Utsuno, and T. Ogura, *J. Inorg. Nucl. Chem.*, **31**, 117 (1969).

In accordance with their finding, Cu(dpa)·PPS and Cu(terpy)·PPS are more stable than Cu(dien)·PPS and Cu(edma)·PPS.

An alternative explanation is based on Pearson's rule of hard and soft acids and bases,[1,16,17] according to which back-donation in CuA makes Cu(II) a harder acid which favors the bonding with hard bases like *p*-phenolsulfonate and hydroxy group. The stability sequences observed in the CuA·PPS and CuA·OH series serve as the evidence for this view. All these observations suggest that combination around copper(II) of aromatic nitrogens with negative oxygens is more favorable than that between nitrogen atoms only.

Considering that the stability of binary complexes is proportionally related to the pK_a of ligands, the mentioned effects of $\sum pK_a$ suggest that the second ligand L has greater affinity for CuA having lower stability, provided that steric factors are negligible. This may point to the favorable combination, or the selectivity, of ligands around metal ions in general.

The authors are grateful to Mr. Yasuaki Uno of this college for measurement of thermal stability and to the members of the Osaka University Computation Center for computation. This investigation was supported in part by a grant from the Ministry of Education.

16) R. G. Pearson, *J. Amer. Chem. Soc.*, **85**, 3533 (1963).
17) S. Kida, *Kagaku no Ryoiki*, **24**, 541 (1970); This Bulletin, **34**, 962 (1961).

BULLETIN OF THE CHEMICAL SOCIETY OF JAPAN, VOL. 46, 3462—3466 (1973)

The Nucleophilic Ring-opening Reactions of α,α'-Dinitrocycloalkanones

Yoshinari KOBAYASHI

Nagoya Research Laboratory, Chemicals Research and Development Laboratories, Toray Industries, Inc., Ohe-cho, Minato-ku, Nagoya 455–91

(Received October 23, 1972)

The keto and enolic characters of 2,6-dinitrocyclohexanone (**1**), 2,6-dinitro-4-methylcyclohexanone (**2**), and 2,7-dinitrocycloheptanone (**3**) were spectroscopically investigated and discussed. It was found that the reactions of **1** and **2** with nucleophiles can take either of two courses, depending upon the nucleophiles used: (a) the addition to the enol carbon or carbonyl carbon of the keto form, followed by ring-opening giving 2,6-dinitro- and 2,6-dinitro-4-methyl-hexanoates respectively; (b) the abstraction of the 2- and 6-protons, followed by the formation of the corresponding di-*aci*-nitronates. Primary alkoxide ions belong to the (a) group, whereas secondary and tertiary alkoxide ions, NH^-_2, RHN^-, and AcO^-, belong to the (b) group. The IR and UV spectra of the resultant α,ω-dinitrocarboxylic acid esters were also discussed.

The basic cleavage of α-nitroketones has attracted considerable synthetic interest.[1–7] The application of this cleavage to 2,6-dinitrocyclohexanone (**1**) was supposed to realize a novel simple three-step DL-lysine synthesis starting from cyclohexanone,[8] *e.g.*, the dinitration of cyclohexanone and ring-opening to 2,6-dinitrohexanoic acid, followed by its hydrogenation. During the present investigation, the same process was independently patented.[10] However, it was found that the ring-opening reactivities of **1** and 2,6-dinitro-4-methylcyclohexanone (**2**) were largely dependent on the nucleophiles especially on the bukiness of the alkoxides, and that the corresponding di-*aci*-nitronates were formed by the attack of secondary and tertiary alkoxides instead of by cleavage. The present paper will report on the chemical behaviors of **1**, **2** and 2,7-dinitrocycloheptanone (**3**) in response to the attack of alkoxides.

Results and Discussion

The structures of α,α'-Dinitrocycloalkanones. In general, α-nitroketones can be represented by three possible tautomeric structures-nitroketone, nitroenol, and *aci*-nitroketone forms.[11] The IR spectrum of **1** in the solid state (in a KBr disk) reveals a sharp carbonyl absorption at 1740 cm^{-1}, indicating the presence of a

1) A.S. Matlack and D. S. Breslow, *J. Org. Chem.*, **32**, 1995 (1967). This paper have summarized most of the previous references.

2) P. C. Pearson, D. H. Anderson, and L. L. Alt, *J. Amer. Chem. Soc.*, **77**, 527 (1955).

3) R. E. Schaub, W. Fulmor, and M. J. Weiss, *Tetrahedron*, **20**, 373 (1964).

4) P. L. Southwick, J. A. Fitzgerald, R. Madhav, and D. A. Welsh, *J. Org. Chem.*, **34**, 3279 (1969).

5) H. Feuer, A. M. Hall, and R. S. Anderson, *ibid.*, **36**, 140 (1971).

6) Techni-Chem. Co., Neth. 6713613 (1967).

7) Gulf Research and Development Co., Japan 1969—16369.

8) Another elegant three step DL-lysine synthesis from cyclohexanone was reported by Ferris *et al.*[9] by the application of the Beckmann fission of 2,6-bis(hydroxyimino)cyclohexanone as a key step.

9) a) A. F. Ferris, F. E. Gould, G. S. Johnson, H. K. Latourette, and H. Stange, *Chem. Ind.* (London), **1959**, 996. b) A. F. Ferris, G. S. Johnson, F. E. Gould, and H. K. Latourette, *J. Org. Chem.*, **25**, 492 (1960). c) A. F. Ferris, G. S. Johnson, F. E. Gould, and H. Stange, *ibid.*, **25**, 496 (1960). d) *idem.*, *ibid.*, **25**, 1302 (1960).

10) Mitsubishi Chemical Co., Neth. 690704; 690705 (1969); Ger. Offen. 1926047; *Chem. Abstr.*, **72**, 42831p (1970).

11) T. Simmons, R. F. Love, and K. L. Krenz, *J. Org. Chem.*, **31**, 2400 (1966).

Table 1. C=O absorptions of cyclohexanone and its nitoro derivatives

Compound	ν C=O (cm^{-1})	Shift (cm^{-1})	Ref.
Cyclohexanone	1712	—	
2-Nitrocyclohexanone	1739	27	27)
2,6-Dinitrocyclohexanone	1740 (1748)[a)]	1 (7)	5)

a) Ref. 5.

keto form.[12)] As is shown in Table 1, the introduction of a nitro group to the 2-position of cyclohexanone brings a marked shift in C=O absorption, but the further introduction of a nitro group to the 6-position of 2-nitrocyclohexanone causes almost no change. This suggests that one of the nitro groups may be co-planar with C=O, while the other is not.[13)] It has been pointed out[14)] that, as a result of the trigonal geometry of the carbonyl carbon, an equatorial substituent in the 2-position of cyclohexanone is nearly eclipsed by the carbonyl oxygen, whereas an axial substituent in this position is staggered with respect to this oxygen atom. Therefore, the first nitro group is an equatorial substituent, and the second is axial. Thus, 2,6-dinitro-substituents exist in a *trans*-configuration in which electrostatic repulsions and Johnson's $A^{(1,2)}$ strain[15)] are minimal. However, in an acetone solution, **1** was shown to exist nearly completely in the enol form by a study of the UV (λ_{max}: 310 nm) and NMR spectra (–C=CH–: τ 4.20, 1H, quartet); this is in accordance with Feuer's results[16)] reporting that the enol form is favored in aprotic solvents. However, even in methanol **1** showed an enol band at 310 nm (ε 4.67×10^2), suggesting that **1** has a tendency to enolize gradually even in protic solvents.[17)] The crystalline solid of **2** was determined to exist in the enol form by a study of the IR spectrum (1640 (C=C) and 3450 cm^{-1} (OH); no C=O absorption). Compound **3** in the solid state was shown to exist nearly entirely in the keto form by a study of the IR spectrum (1750 cm^{-1} (C=O)). However, in an alcoholic solution of **3** the enol absorption at 339 nm (ε 3.54×10^2) appears together with keto absorption at 280 nm (ε 2.00×10^2), indicating an equilibrium between keto and enol forms.

The Ring-opening Reactions. The treatment of **1** with an aqueous solution of sodium carbonate gave 1,5-dinitropentane. This reaction is similar to that of potassium 1-nitro-2-keto-3-cyclohexanenitronate[18)] and may be supposed to involve ring-opening, followed by the decarboxylation of the resultant 2,6-dinitrohexanoic acid. The ring-opening reactions of **1** and **2** in primary alcohol to 2,6-dinitrohexanoic and 2,6-dinitro-4-methylhexanoic acid esters respectively proceeded even in the presence of catalytic quantities of the corresponding alkoxide ions. The reactions proceeded similarly in alcoholic solutions of alkali hydroxides. In striking contrast, in the presence of stoichiometric amounts of secondary and tertiary alkoxide ions, **1** and **2** afforded 2-keto-1,3-cyclohexanedinitronate and 2-keto-4-methyl-1,3-cyclohexanedinitronate instead of the ring-opening products. The reactions of **1** and **2** with NH_2^-, NHR^-, or AcO^- also yielded the corresponding di-*aci*-nitro compounds, from which the starting materials were recovered by neutralization. Accordingly, it appears that the nucleophiles can be divided into two classes on the basis of their reactivity towards **1** and **2**: (a) one class which induces the ring-opening of **1** and **2** and (b) another which affords di-*aci*-nitro compounds. This discrimination was made possible by the observation of the UV spectra of **1** and **2** in alcoholic solutions in the presence of alkoxide ions. As is shown in Tables 2 and 3, the UV spectra of **1** in the presence of Class (a) nucleophiles are characterized by a maximum absorption at 233—235 nm, accompanied by a shoulder in the range between 310 and 325 nm; this shoulder remained even if the solutions were allowed to stand for a long time. However, the UV absorptions of **1** in the presence of the Class (b) nucleophiles are lacking in shoulder absorptions. The absorption bands of the nitronate anions are broad and intense ($\varepsilon\cong10000$),

Table 2. Time dependency of UV spectra of 2,6-dinitrocyclohexanone in basic methanol solution at 28°C

Time (hr)	1/10M-NaOH		1/10M-NaOMe	
	λ_{max} (nm)	ε (x10^3)	λ_{max} (nm)	ε (x10^3)
0	235	8.26	236	7.83
	325	3.25	325	3.30
3	235	8.25	235	8.45
	325	3.25	328	3.58
6	233	8.25	235	9.60
	325	3.25	329	3.83

Table 3. UV spectra of 2,6-dinitrocyclohexanone in basic alcoholic solutions after heated at 48°C for 2 hr

Nucleophile class	Solvent	Base (1/10 M)	λ_{max}	ε(x10^3)
(a)	MeOH	NaOH	234	8.92
			310 (sh)	3.51
		NaOMe	236	9.03
			310 (sh)	3.79
	EtOH	NaOH	234	1.93
			321 (sh)	2.30
		NaOEt	233	1.93
			327 (sh)	2.13
(b)	*iso*-PrOH	*iso*-PrONa	234 (sh)	4.21
	tert-BuOH	*tert*-BuONa	227 (sh)	5.62

12) The C=O absorption band of **1** in Nujol was also reported to be 1748 cm^{-1} (Ref. 5).

13) E. J. Corey (*J. Amer. Chem. Soc.*, **75**, 3297 (1953)) determined the stereochemistry of 2,6-dibromocyclohexanone by carbonyl bands.

14) E. L. Eliel, "Stereochemistry of Carbon Compounds," McGraw-Hill, New York, N.Y. (1962), p. 240.

15) F. Johnson, *Chem. Rev.*, **68**, 375 (1968).

16) H. Feuer, in Abstracts 152nd American Chemical Society Meeting, New York, N.Y., Sep. 1966 (Paper No. S–157).

17) Feuer reported that **1** exists in ethanol solely as keto form (Ref. 16).

18) H. Feuer and R. S. Anderson, *J. Amer. Chem. Soc.*, **83**, 2960 (1961).

with maxima 230—240 nm[19,20] due to the π-π^* transition. The absorption in the 310—325 nm range may be due to the enol form of **1** and may be supposed to be a p-π^* transition in α-nitro-olefines.[21] The results indicate that **1** and **2** undergo the ring cleavage in nucleophilic solvents where **1** and **2** are in the enol form. The mechanism of the ring opening of **1** and **2** by the attack of the Class (a) nucleophiles may be interpreted according to Scheme I. The addition of alkoxide ions to the enol carbons or the attack of the ketonic form result in ring cleavage, thus leading to the formation of alkyl 2,6-dinitrohexanoates with nitroalkyl moieties which, in a basic solution, give the UV absorption at 233—235 nm and a shoulder absorption at 310—325 nm resulting from the small contribution of the equilibrated enol form. The ring-opening reactions proceed catalytically as the alkoxide ions are regenerated.

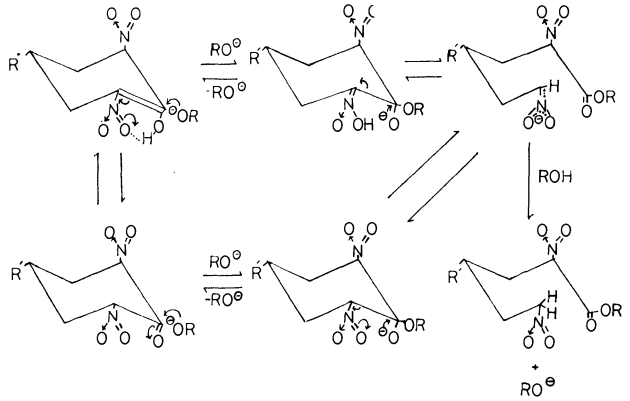

1:R′=H, **2**:R′=Me, **R**=primary alkyl groups

Scheme I

The Class (b) nucleophiles abstract the 2- and 6-protons to form the corresponding di-*aci*-nitro compounds, as is shown in Scheme II.

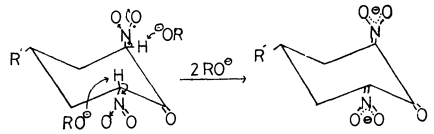

1:R′=H, **2**:R′=Me, R=secondary, tertiary alkyl groups

Scheme II

The difference in the reactivities between Class (a) and Class (b) nucleophiles may be ascribed to the steric factors and to the basicity of the alkoxide ions.

In connection with the ring-opening reactivities, **1** seemed to be more readily ruptured than 2-nitrocyclohexanone. For example, in the aqueous solution of potassium iodide, **1** afforded 1,5-dinitropentane even at room temperature, but 2-nitrocyclohexanone remained unchanged under the same conditions.

UV and IR Spectra of α,ω-Dinitro-carboxylic Acid Esters. The ring-cleavage products of α,α'-dinitrocycloalkanones are typical compounds containing two different kinds of nitro groups in one molecule. Some spectral information about these different kinds of nitro groups was obtained.

(a) UV Spectra: It has been reported that aliphatic nitro compounds and α-nitro-carboxylic acid esters are characterized by broad π-π^* transition bands of a low intensity (ε 20—40) in the 270—284 nm[22,23] region. As is shown in Table 4, the α,ω-dinitrocarboxylic acid esters were generally found to exhibit these transitions at 255—270 nm, showing a red shift with a stronger absorption. Such trends may be interpreted in terms of the repulsions between two different nitro groups in a molecule. The introduction of methyl groups as a side chain resulted in a blue shift. The maxima absorptions were not affected by the change in carboalkoxy groups. In free nitro-forms, the difference between α- and ω-nitro groups in α,ω-dinitrocarboxylic acid esters is small. However, in *aci*-nitro forms, the

TABLE 4. UV SPECTRA OF α, ω-DINITROCARBOXYLIC ACID ESTERS

$O_2N(CH_2)_nCHCH_2CHCO_2R$ (R′, NO_2)	R	in MeOH		in 1/10M-NaOMe	
		λ_{max} (nm)	ε	λ_{max} (nm)	ε
n=2 R′=H	Me	270	77	233	1.23×10^4
	Et	261	355	306	1.27×10^4
	n-Pr	263	394	—	—
	n-Bu	264	300	—	—
	n-Amyl	265	292	—	—
n=2 R′=CH_3	Me	255	270	235	5.13×10^3
				307	3.00×10^4
	Et	255	270	—	—
n=3 R′=H	Me	265	183	183	7.71×10^3
				305	4.09×10^3
	Et	265	297	232	9.78×10^3
				300	8.35×10^3
	n-Bu	265	353	235	1.03×10^4
				305	9.42×10^4

19) F. T. Williams, Jr., P. W. K. Flanagan, W. J. Taylor, and H. Schechter, *J. Org. Chem.*, **30**, 2674 (1965).

20) A. T. Nielson, "The Chemistry of the Nitro and Nitroso Groups," Part 1, ed. by H. Feuer, Intersciences Publishers, New York, N.Y., (1969), pp. 382—383.

21) M. Montagné and P. Arnaud, *C. R. Acad. Sci. Paris*, **254**, 4001 (1962).

22) H. E. Ungnade and R. S. Smiley, *J. Org. Chem.*, **21**, 993 (1956).

23) R. N. Haszeldine, *J. Chem. Soc.*, **1953**, 2525.

Table 5. IR spectra of α, ω-dinitrocarboxylic acid esters

$O_2N(CH_2)_nCHCH_2CHCO_2R$ (R' / NO_2)	R	ν_{as} NO_2 (cm^{-1})			ν_s NO (cm^{-1})		
		α-nitro	ω-nitro	Δ	α-nitro	ω-nitro	Δ
n=2 R'=H	Me	1563	1551	12	1372	1378	−6
	Et	1562	1553	9	1374	1376	−2
	n-Pr	1562	1554	8	1378	1380	−2
	n-Bu	1562	1554	7	1376	1376	0
	n-Amyl	1563	1556	7	1380	1380	0
n=2 R'=CH_3	Me	1563	1552	11	1381	1381	0
	Et	1566	1556	10	1380	1380	0
n=3 R'=H	Me	1563	1552	11	1382	1382	−7
	Et	1563	1552	11	1374	1376	−2
	n-Bu	1563	1553	10	1378	1380	−2

conjugated α-nitronate groups (O=C-C=N$\langle$O, O$^-$) exhibit the π-π^* transition at 305—307 nm (ε 5×10^3—1.2×10^4), while the *aci*-nitro groups isolated from carboalkoxy groups showed the absorption in a shorter-wavelength range (233—235 nm).

(b) IR Spectra: On the effect of an electron-attracting α-substituent on the IR spectra of aliphatic nitro compounds, Haszeldine[23] and Brown[24] reported that asymmetrical stretching bands shifted to higher frequencies, whereas the symmetrical stretching bands moved to lower frequencies and there was no significant change in the C–N stretching vibrations. As is shown in Table 5, the present results on α,ω-dinitro-carboxylic acid esters are in exact accordance with the previously reported data. It was shown that both the asymmetrical and symmetrical stretching bands were doublets, whereas the C–N stretching vibrations were singlets. The shifts upon the introduction of carboalkoxy groups were greater in the asymmetrical stretching of nitro groups than in the symmetrical stretching. The shifts seemed to be increased in the order of the electron-attractive properties of carboalkoxy groups.

Experimental

The UV spectra were determined by means of a Hitachi double-beam spectrophotometer, Model 124. The IR spectra were recorded on a Hitachi infrared spectrophotometer, EPI-G_2. The NMR spectra were kindly determined by Drs. Kenkichi Nukada and Hajime Saito of the Basic Research Laboratories, Toray Industries, Inc., using a Varian HA-100 apparatus with TMS as the internal standard. The mp's were measured on a Yanagimoto micro-melting points apparatus with a heat block and are uncorrected.

Disodium 2-Keto-1,3-cyclohexanedinitronate (4). The dinitration procedure was similar to that described for the dipotassium salt,[26] except that sodium amide was used instead of potassium amide. The salt was purified by the use of aqueous methanol. Yield, 92.0%. Mp 240—245 °C (dec). IR (KBr): 1620 (C–O), 1410 and 1230 cm^{-1}(C–NO_2^-). UV (MeOH): 205 (ε 9.65×10^2), 280 (sh, 4.21×10^2), and 308 nm (9.65×10^2). NMR (D_2O): τ 7.80 (2H, t, J=6 Hz, 5-CH_2), and 6.83 (4H, t, J=6 Hz, 4- and 6-CH_2). Found: C, 30.94; H, 2.87; Na, 18.85%. Calcd for $C_6H_6N_2O_5Na_2$: C, 31.05; H, 2.61; Na, 19.81%.

2,6-Dinitrocyclohexanone (1). The compound was obtained from 4[5]. Colorless needles. Mp 110 °C (lit,[25] 110.5 °C). IR (KBr): 3600 (OH, w), 1740 (C=O, vs), 1560 (ν_{as} NO_2), and 1380 cm^{-1} (ν_s NO_2). UV (MeOH): 310 nm (ε 4.67×10^2). NMR (acetone-d_6): τ 4.20 (1H, q, J_{aa}=12 Hz, J_{ae}=6 Hz, 2- and 6-CH), and 7.1—8.2 (7H, m.).

Disodium 2-Keto-5-methyl-1,3-cyclohexanedinitronate. The salt was prepared by the dinitration of 4-methylcyclohexanone.[26] Scaly yellow crystals (from water-acetone). Yield, 75%; mp 222—223 °C. IR (KBr): 1648 (C=N), 1600 (C=O), 1430, 1380 (CH_3), 1280 (ν_{as} NO_2^-), and 1170 cm^{-1} (ν_s NO_2^-). Found: C, 34.39; H, 3.38; N, 11.03%. Calcd for $C_7H_8N_2O_5Na_2$: C, 34.16; H, 3.28; N, 11.38%.

2,6-Dinitro-4-methylcyclohexanone (2). The compound was prepared by the neutralization of the above disodium salt. Yield, 100%. Colorless granular crystals from methanol; mp 76—77.5 °C. IR (KBr): 3450 (OH), 1740 (C=O, vw), 1640 (C=C), 1555 (ν_{as} NO_2), 1460, 1380 (CH_3), and 1360 cm^{-1} (ν_s NO_2). The compound exists in the enol form. However, after having been allowed to stand overnight, the solid was transformed into an oily state in the keto form. IR (neat) 3450 (OH, vw), 1740 cm^{-1} (C=O, vs).

Disodium 2-Keto-1,3-cycloheptanedinitronate. This compound was prepared by the dinitration of cycloheptanone in the presence of sodium amide. Yellowish-red crystals (from water-methanol). Yield 71%; mp 215—216.5 °C(dec). IR (KBr): 1600 (C=O), 1240 (ν_{as} NO_2), and 1140 cm^{-1} (ν_s NO_2).

2,7-Dinitrocycloheptanone (3). The compound was obtained by the neutralization of the above disodium salt. Yield, 79%. Colorless needles (from methanol), mp 84.5—86.0 °C. IR (KBr): 3450 (OH, vw); 1720 (C=O), 1540 (ν_{as} NO_2), and 1340 cm^{-1} (ν_s NO_2). UV (EtOH): 339 (ε 3.52×10^2), and 280 nm (sh. 2.00×10^2). Found: C, 41.86; H, 5.43; N, 13.60%. Calcd for $C_7H_{10}N_2O_5$; C, 41.58; H, 4.99; N, 13.86%.

The Ring-opening Reactions of 2,6-Dinitrocyclohexanone (1)

(a) In an Aqueous Sodium Carbonate Solution: 1,5-Dinitropentane: To an aqueous sodium carbonate solution (62 mg; 0.7 mmol in 10 ml), we added **1** (1.0 g, 5.3 mmol). The mixture was then stirred at room temperature for 1 hr, followed by acidification with concd HCl. Then, the acidic solution was extracted with ether and the ethereal extract was dried over anhydrous sodium sulfate. After the removal of the solvent, the residue was distilled *in vacuo*. Yield, 0.81 g (94%);

24) J. F. Brown, Jr., *J. Amer. Chem. Soc.*, **77**, 6341 (1955).
25) H. Wieland, P. Garbsch, and J. J. Chavan, *Ann.*, **461**, 295 (1928).
26) H. Feuer, A. M. Hall, S. Golden, and R. I. Ritz, *J. Org. Chem.*, **33**, 3622 (1968).
27) H. Feuer snd P. M. Pivawer, *ibid.*, **31**, 3152 (1966).

bp 135 °C/1.5 mmHg. IR (neat): 1550 (ν_{as} NO_2), which is superimposable upon that of an authentic sample[18].

(b) By Sodium Methoxide: *Methyl* 2,6-*dinitrohexanoate*: *(i) Stoichiometric reaction*: To **1** (3.0 g, 15.9 mmol) in methanol (50 ml), we added, drop by drop, sodium methoxide (18.3 mmol) in methanol (25 ml) at 47—50 °C. After stirring for 2 hr, the solution was acidified with HCl gas. After the removal of the solvent, dry ether was added to the residue, followed by filtration. The filtrate was dried over anhydrous sodium sulfate. After the removal of the ether, the residue was distilled *in vacuo*. Bp 141—144 °C/0.5 mmHg. Yield, 2.9 g (83%). The IR, NMR, and UV spectra were identical with those reported by Feuer *et al.*[5]

(ii) Catalytic Reaction: To **1** (11.3 g, 0.06 mol) in methanol (200 ml), we added, drop by drop, sodium methoxide (0.55 g, 0.01 mol) in methanol (50 ml) at 50 °C. The whole solution was then worked up by the procedure described above. Yield, 11.4 g (86%).

(c) By Sodium Ethoxide. Ethyl 2,6-*Dinitrohexanoate*: The procedure was similar to that described for (b), but using sodium ethoxide in ethanol. Bp 132 °C/0.5 mmHg. Yield, 75%. n_D^{25} 1.4612. IR (neat): 1750 (C=O), 1562, 1553 (ν_{as} NO_2), 1376, 1374 (ν_s NO_2), 1200 (C-O), and 860 cm^{-1} (C-N). UV (MeOH): 261 nm (ε 3.55×10^2). NMR (acetone-d_6), τ 4.56 (1H, t, J=7.0 Hz, 2-CH), 5.44 (2H, t, J=7.0 Hz, 6-CH_2), 5.77 (2H, q, J=7.0 Hz, -COOC$H_2$$CH_3$) 7.6 8.6 (4H, m, 4-, 5-$CH_2$), and 8.42 (2H, q, J=8.0 Hz, 3-CH_2). Found: C, 41.39; H, 5.91; N, 12.30%, mol wt (in acetone), 228. Calcd for $C_8H_{14}N_2O_6$: C, 41.02; H, 6.03; N, 11.96%; mole wt, 234.2.

(d) By Sodium n-*Propoxide.* n-*Propyl* 2,6-*Dinitrohexanoate*: The procedure was similar to that described for (b). Bp 152—162 °C/0.5 mmHg. Yield, 81%; n_D^{25}: 1.4627. IR (neat): 1750 (C=O), 1562, 1554 (ν_{as} NO_2), 1380, 1378 (ν_s NO_2), and 1200 cm^{-1} (C-O). UV (MeOH): 263 nm (ε 3.94×10^2). NMR (acetone-d_6): τ 4.52 (1H, t, J=7.0 Hz, 2-CH), 5.46 (2H, t, J=8.0 Hz, 6-CH_2), 5.83 (2H, t, J=7.0 Hz, -COOCH_2 CH_2CH_3), 7.35—8.05 (4H, m, 4-, 5-CH_2), 8.40 (2H, sex, J=7.0 Hz, -OCH_2C$H_2$$CH_3$) and 8.42 (2 H, q, J=7.0 Hz, 3-CH_2). Found: C, 40.36; H, 6.55; N, 11.06%; mol wt (in acetone), 221. Calcd for $C_6H_{16}N_2O_6$: C, 40.67; H, 6.83; N, 11.86%; mol wt 236.2.

*(e) Di-*aci*-nitration by Sodium Isopropoxide.* To **1** (3 0 g, 15.9 mmol) in isopropoxide, we added, drop by drop, sodium isopropoxide (16.0 mmol) in 2-propanol at 65—70 °C. After continuing stirring for 5.5 hr at 70 °C, the solution was cooled to room temperature and then acidified with HCl gas. After the subsequent evaporation of the solvent *in vacuo*, acetone was added to the residue. The whole solution was then filtered, and the solvent was distilled off. The residue was found to be the recovered starting material (2.5 g). In secondary and tertiary alcoholic solutions containing the corresponding sodium alkoxide, such as isopropoxide and *iso-*, *sec-*, and *tert-*butoxides, **1** and **2** gave the di-*aci*-nitro derivatives from which the corresponding starting materials were recovered by acidification.

(f) By Sodium n-*Butoxide*: n-*Butyl* 2,6-*Dinitrohexanoate*: In a manner similar to that described for (b), **1** (3.0 g, 15.9 mmol) was transformed into *n*-butyl 2,6-dinitrohexanoate. Yield, 3.1 g (74.5%). Bp 142 °C/0.5 mmHg. n_D^{25}, 1.4603. IR (neat): 1740 (C=O), 1562, 1555 (ν_{as} NO_2), and 1376 cm^{-1} (ν_s NO_2). UV (MeOH): 264 nm (ε 300). NMR (acetone-d_6); τ 4.54 (1H, t, J=7.0 Hz, 2-CH), 5.47 (2H, t, J=8.0 Hz, 6-CH_2), and 5.78 (2H, t, J=7.0 Hz, -COOCH_2-CH_2-). Found: C, 46.14; H, 7.03; N, 11.05%; mol wt (in acetone), 224. Calcd for $C_{10}H_{18}N_2O_6$: C, 45.79; H, 6.92; N, 10.68; mol wt 262.3.

(g) By Potassium Hydroxide in n-*Amyl Alcohol*: n-*Amyl* 2,6-*Dinitrohexanoate*: To **1** (3.0 g, 15.9 mmol) in *n*-amyl alcohol (100 ml) at 60 °C, we added, drop by drop, *n*-amyl alcohol (50 ml) containing potassium hydroxide (0.1 g). After stirring for 4.5 hr at 60 °C, the whole solution was worked up in the usual manner. Bp 137 °C/0.5 mmHg. Yield, 2.98 g (68%). IR (neat): 1750 (C=O), 1570, 1556 (ν_{as} NO_2), and 1380 cm^{-1} (ν_s NO_2). UV (MeOH): 265 nm (ε 292). NMR (acetone-d_6): τ 4.55 (1H, t, J=7.0 Hz, 2-CH), 5.45 (2H, t, J=7.0 Hz, 6-CH_2), and 5.80 (2H, t, J=7.0 Hz, -$COOCH_2$), Found: C, 48.69; H, 7.50; N, 10.27%; mol wt (in acetone) 250. Calcd for $C_{11}H_{20}N_2O_6$: C, 47.82; H, 7.30; N, 10.14%; mol wt 276.3.

The Ring-Opening Reactions of 4-*Methyl* 2,6-*Dinitrocyclohexanone (2)*: *(a) By Potassium Hydroxide in Methanol. Methyl* 2,6-*Dinitro*-4-*methylhexanoate*: To **2** (4.0 g, 19.8 mmol) in methanol (100 ml), we added, drop by drop, methanol (50 ml) containing potassium hydroxide (0.3 g) at 50—55 °C. After stirring for 1 hr at this temperature, the solution was worked up in the usual manner. Yield, 4.0 g (86.3%); bp 132—138 °C/2.0 mmHg. IR (neat): 1740 (C=O), 1563, 1552 (ν_{as} NO_2), and 1381 cm^{-1} (ν_s NO_2). UV (MeOH): 225 nm (ε 270). NMR (CCl_4): τ 4.8 (1H, t, J=8.0 Hz, 2-CH), 5.6 (2H, t, J=8.0 Hz, 6-CH_2), and 6.2 (3H, s, -$COOCH_3$). Found: C, 41.65; H, 6.33; N, 11.57%. Calcd for $C_8H_{14}N_2O_6$: C, 41.02; H, 6.03; N, 11.98%.

(b) By Potassium Hydroxide in Ethanol: *Ethyl* 2,6-*Dinitro*-4-*methylhexanoate*: The procedure was similar to that described above. Yield, 85%; bp 120—126 °C/1.5 mmHg. IR (neat): 1740 (C=O), 1566, 1552 (ν_{as} NO_2), and 1380 cm^{-1} (ν_s NO_2). UV (MeOH): 255 cm (ε 266). Found: C, 44.06; H, 6.88; N, 11.73%. Calcd for $C_6H_{16}N_2O_6$: C, 43.58; H, 6.50; N, 11.29%.

The Ring-opening Reactions of 2,7-*Dinitrocycloheptanone (3)*. *(a) By Potassium Hydroxide in Methanol*: *Methyl* 2,7-*Dinitroheptanoate*: To **3** (3.0 g) in methanol, we added, drop by drop, methanol (50 ml) containing potassium hydroxide (0.5 g) at 65 °C. After stirring for 1.5 hr, the whole solution was worked up in the usual manner. Yield, 72%. Bp 164 °C/0.01 mmHg. IR (neat): 1750 (C=O), 1563, 1552 (ν_{as} NO_2), 1376, and 1374 cm^{-1} (ν_s NO_2). UV (MeOH): 265 nm (ε 183). Found: C, 41.77; H, 6.45; N, 11.64%. Calcd for $C_8H_{14}N_2O_6$: C, 41.02; H, 6.03; N, 11.96%.

(b) By Potassium Hydroxide in Ethanol. Ethyl 2,7-*Dinitroheptanoate.* By the usual method, ethyl 2,7-dinitroheptanoate was obtained in an 81% yield. Bp 105 °C/2×10^{-3} mmHg. IR (neat): 1750 (C=O), 1563, 1552 (ν_{as} NO_2), 1376, and 1374 cm^{-1} (ν_s NO_2). UV (MeOH): 265 nm (ε 297). Found: C, 44.19; H, 7.08; N, 11.01%. Calcd for $C_9H_{16}N_2O_6$: C, 43.54; H, 6.50; N, 11.29%.

(c) By Potassium Hydroxide in n-*Butanol.* n-*Butyl* 2,7-*Dinitroheptanoate.* The method was similar to those described in (a). Yield, 80%. Bp 146 °C/5×10^{-3} mmHg. IR (neat): 1750 (C=O), 1563, 1553 (ν_{as} NO_2), 1380, and 1378 cm^{-1} (ν_s NO_2). UV (MeOH): 255 nm (ε 357). Found: C, 48.35; H, 7.87; N, 9.49%. Calcd for $C_{11}H_{20}N_2O_4$: C, 47.82; H, 7.30; N, 10.14%.

The Photolysis of 3,3-Pentamethyleneoxaziridine

Yoshinari KOBAYASHI

Nagoya Research Laboratory, Chemicals and Development Laboratories, Toray Industries, Inc., Ohe-chyo, Minato-ku, Nagoya 455–91

(Received March 13, 1973)

The ultraviolet irradiation of 3,3-pentamethyleneoxaziridine (**1**) gave two classes of photo-products: (a) cyclohexanol and *n*-capronamide, the formation of which proceeds preferentially through the excited triplet state of **1**, and (b) ε-caprolactam, dicyclohexylideneazine, and cyclohexanone, which are mainly furnished *via* the singlet state of **1**. The correlation of the selectivity of (a)-class products with the triplet-state energy of the quenchers used made it possible to estimate that the lowest triplet energy of **1** was approximately 60 kcal/mol. The sensitized photolysis of **1** using sensitizers, the triplet-state energy of which was more than nearly 60 kcal/mol, gave *n*-capronamide predominantly. The photolytic decomposition rate of **1** was compared with those of 2-methyl-3,3-tetramethyleneoxaziridine (**2**), 2-methyl-3,3-pentamethyleneoxaziridine (**3**), and cyclohexanone oxime. The mechanism of the photolysis of **1**, including homolytic N–O bond rupture, was also discussed.

The photo-Beckmann rearrangement, the photochemical conversion of oximes into the corresponding amides, has been the subject of considerable study in the last decade.[1] The reaction scheme through the intermediacy of oxaziridines for the photo-induced Beckmann rearrangements has been confirmed in indirect ways.[1e,1f,1l] Nevertheless, there has been relatively little direct evidence to substantiate the photochemical transformation of oxaziridines into the corresponding amides.[2] Recently, two short communications on the photolyses of *N*-phenyl-oxaziridines[4] and 3,3-pentamethyleneoxaziridine (**1**)[1m] into the amides have been reported. The present author has independently[5] investigated the photolyses of cycloalkanespiroöxaziridines including **1** in relation to the photo-Beckmann rearrangement of cyclohexanone oxime.

Results and Discussion

Reaction Products. The ultraviolet irradiation of a solution of **1** in ether[6] (about 10—11 wt%) with a low-pressure mercury arc lamp at a temperature between −2 and 0 °C in a quartz apparatus led to six kinds of photo-products: cyclohexanol (5—6%), cyclohexanone (29—37%), dicyclohexylideneazine (2—3%), *n*-capronamide (9—11%), ε-caprolactam (36—50%), and a trace of dodecanediamide. In the thermolysis of **1**, the dimeric product was reported to be 1,1′-dihydroxyazocyclohexane[8] instead of dicyclohexylideneazine. In the photolysis of cyclohexanone oxime in ether a small amount of the azine and a trace of dodecanediamide were also detected.[9] The formation of the azine and dodecanediamide implies a homolytic N–O bond cleavage in **1**, followed by coupling. The photo-products of the relatively stable 2-methyl-3,3-tetramethyleneoxaziridine (**2**) and 2-methyl-3,3-pentamethyleneoxaziridine (**3**) were predominantly the corresponding *N*-substituted cyclic lactam (60—80%) and cycloalkanone (20—40%). Small amounts of the corresponding cycloalkanol and ring-opened amide were also detected.

Decomposition Rate. The photochemical decomposition rates of **1**, **2**, **3**, and cyclohexanone oxime were shown to be of the first order, and the relative rates based upon **1** (in ether) were 1.0, 0.38, 2.9, and 0.17 respectively. The results show that *N*-methyl substituted spiroöxaziridines decomposed faster than the corresponding *N*-unsubstituted spiroöxaziridines with the same ring size. A comparision of the photolytic decomposition of **2** with that of **3** showed that the decomposition rate of the oxaziridine with a spiro-five-membered ring (**2**) was approximately one third that of the oxaziridine with a spiro-six ring size (**3**). The photolytic decomposition rate of cyclohexanone oxime in ether was comparatively small in comparision with

1) a) J. H. Amine and P. de Mayo, *Tetrahedron Lett.*, **1963**, 1588. b) R. T. Taylor, M. Douek, and G. Just, *ibid.*, **1966**, 4143. c) G. Just and L. S. Ng, *Can. J. Chem.*, **46**, 3381 (1968). d) B. L. Fox and H. M. Rosenberg, *Chem. Commun.*, **1969**, 1115. e) T. Oine and T. Mukai, *Tetrahedron Lett.*, **1969**, 157. f) H. Izawa, P. de Mayo and T. Tabata, *Can. J. Chem.*, **47**, 51 (1969). g) R. Beugelmans and J. P. Vermes, *Bull. Soc. Chim. France*, 342 (1970). h) T. Sasaki, S. Eguchi, and T. Toru, *Chem. Commun*, **1970**, 1239. i) H. Suginome and H. Takahashi, *Tetrahedron Lett.*, **1970**, 5119. j) E. J. Poziomak, *Microchemical J.*, **15**, 475 (1970). k) M. Cunningham, L. S. Ng Lim, and G. Just, *Can. J. Chem.*, **49**, 2891 (1971). l) T. Oine, T. Mukai, and K. Kikuchi, *Sci. Rep. Tohoku.*, Ser. 1, **54**, (4), 193 (1971). m) G. Just and M. Cunningham, *Tetrahedron Lett.*, **1972**, 1151. n) T. Sato, T. Inoue, and K. Yamamoto, This Bulletin, **45**, 1176 (1972). o) H. Suginome, H. Takahashi, and T. Masamune, *ibid.*, **45**, 1836 (1972). p) E. Desherces, M. Rivière, T. Parello, and A. Lattes, *C. R. Acad. Sci. Paris, Ser. C*, **275**, 581 (1972).

2) There have been conflicting reports, *e.g.*, the photolysis of 2-phenyl-3,3-pentamethyleneoxaziridine in alkylamines did not gave N-phenyl-ε-caprolactam but 2-alkylamino-3*H*-azepines.[3]

3) E. Meyer and G. W. Griffin, *Angew. Chem. Internat. Edit.*, **6**, 634 (1967).

4) M. Fischer, *Tetrahedron Lett.*, **1969**, 2281.

5) a) Japanese patent application 1970—111093(application Dec. 15, 1970). b) Japan Kohkai 1973—5783 (application June 7, 1971). c) Japan Kohkai 1973—5711 (application June 9, 1971).

6) The author found that the ether solution of **1** prepared from cyclohexanone, chloramine, and aq. sodium hydroxide in ether according to the direction of Schmitz and Murawski[7] could be stabilized by addition of solid carbon dioxide. The stabilized solution could be stored without decomposition for several days at a temperature below 10 °C.

7) E. Schmitz and D. Murawski, *Chem. Ber.*, **98**, 2525 (1965).

8) E. Schmitz and R. Ohme, *Angew. Chem. Internat Edit.*, **2**, 157 (1963).

9) Just *et al.*[1b,1c] did not report the formation of dicyclohexylideneazine and dodecanediamide in the photolysis of cyclohexanone oxime. The azine was a main product upon the irradiation of cyclohexanone oxime O-methyl ether in methanol.[1n]

TABLE 1. QUENCHING PHOTOLYSIS OF **1** IN ETHER WITH A 50-W LOW PRESSURE MERCURY ARC

Quencher	E_T (kcal/mol)	Irradiation time (hr)	Conversion (%)	Product selectivity (%)[b]				
				n-Capron-amide	Cyclo-hexanol	ε-Capro-lactam	Dicyclo-hexyl-ideneazine	Cyclohexa-none
Propiophenone	74.6	19	99.1	18.9	15.3	29.7	1.1	35.0
Benzophenone	68.5	9	96.5	16.5	13.0	28.3	1.4	40.8
Naphthalene	60.9	26	98.5	17.5	14.1	32.7	1.2	34.5
2-Acetonaphthone	59.3	49	92.5	1.5	trace	31.3	0.6	66.7
Piperylene	58.8	7.5	91.2	2.8	trace	41.6	4.2	51.4
1-Acetonaphthone	56.4	31	96.5	2.3	trace	42.4	1.8	53.4
Biacetyl	54.7	23.6	99.7	5.4	4.5	49.4	1.4	39.4
1,3-Cyclohexadiene	54.0	44.0	96.8	5.2	4.1	42.0	2.0	46.7
Anthracene	42.5	40.7	96.9	2.5	2.5	42.2	1.3	46.5
Oxygen[a]	23.0	7	99.1	3.3	3.9	46.9	1.4	44.4

a) The gas saturated with ether was continuously bubbled.
b) In all cases the selectivity of dodecanediamide was trace.

that of **1**. The decomposition rates of the spiro-öxaziridines were dependent upon the polarity of the solvents used; *e.g.*, the relative decomposition rates of **3** in cyclohexane, ether, and 2-propanol were found to be 1.3, 2.0, and 2.6 respectively. The results showed a tendency for greater rates in more polar solvents.

Triplet-state Quenching. The photolyses of **1** in ether in the presence of a number of triplet-state quenchers with triplet-state energy (E_T)[10] were investigated. In these experiments lights longer than 2537 Å of a low-pressure mercury arc were elaborated so as to be cut by liquid filters to avoid the direct absorption of light by the quenchers added. The results are summarized in Table 1. The experiments using piperylene were also repeated by changing the concentration of the quenchers (less than 85 mmol/l). From the results thus obtained the following conclusions may be drawn:

(a) The selectivity of *n*-capronamide decreased with an increase in the amount of piperylene added. From the view point of the correlation of the selectivities of products with E_T, the selectivity of *n*-capronamide was discontinuous. It was approximately 17% in the presence of quenchers with E_T values of more than 60 kcal/mol, but abruptly fell to about 5% or less when quenchers whose E_T were less than 60 kcal/mol were used. From these results, it can be estimated that the formation of *n*-capronamide proceeds preferentially *via* the excited triplet state of **1**, the energy of which is approximately 60 kcal/mol. This estimation was also supported by the sensitized photolysis of **1**, as will be described later.

(b) The selectivity of cyclohexanol also decreased linearly in the presence of quenchers with E_T values of less than approximately 60 kcal/mol. Moreover, when more than 5 mol% (based on **1**) of piperylene was added, no substantial amount of cyclohexanol could be detected. Consequently, cyclohexanol was also formed mainly *via* the triplet state of **1**, whose energy was estimated to be approximately 60 kcal/mol.

(c) There was no connection between the ε-caprolactam selectivity and the amounts of piperylene added. However, when the formations of both *n*-capronamide and cyclohexanol were suppressed by quenchers with E_T values of less then approximately 60 kcal/mol, the ε-caprolactam selectivity apparently increased.

(d) The formation of both dicyclohexylideneazine and cyclohexanone were independent of the amount of piperylene added, and there was no special correlation of these selectivities with E_T.

Hence, although the photo-products cannot be clearly classified, it can be roughly deduced that the formations of ε-caprolactam, dicyclohexylideneazine, and cyclohexanone proceed *via* the excited singlet state of **1**, whereas *n*-capronamide and cyclohexanol are formed *via* the triplet state, whose E_T energy is approximately 60 kcal/mol. The effect of a quencher with an E_T value of less than 60 kcal/mol can be explained by the internal conversion from the triplet state of **1** to that of the quencher.

Sensitized Photolysis. The sensitized photolysis of **1** was investigated with a high-pressure mercury arc. In these experiments, the ultraviolet range of light (less than 2537 Å) was absorbed by a Pyrex glass vessel and liquid filters so as to interrupt the direct absorption of light by **1**. The results are given in Table 2. The 1-acetonaphthone (E_T=56.4 kcal/mol) sensitized photolysis of **1** yielded no cyclohexanol, but only a very small amount of *n*-capronamide. In sharp contrast, the photolysis of **1** in the presence of such sensitizers as benzene (E_T=84 kcal/mol) and benzophenone (E_T=68.5 kcal/mol) yielded both *n*-capronamide and cyclohexanol in comparatively high yields. As has been mentioned above, both *n*-capronamide and cyclohexanol were preferentially produced *via* the triplet state of **1**, whose energy was estimated to be approximately 60 kcal/mol. In the sensitized reaction of **1** using sensitizers with E_T of more than nearly 60 kcal/mol, the triplet state of **1** was supposed to be efficiently formed by the internal conversion, resulting in comparatively high yields of *n*-capronamide and cyclohexanol. On the contrary, the formation of such products as ε-caprolactam and dicyclohexylideneazine, which proceeded *via* the singlet state of **1**, was almost suppressed. In the sensitized reactions using sensitizers with a triplet-state energy of less than approximately 60 kcal/mol, the main sensitized reaction was suppressed and **1** gave cyclohexanone predominantly, as in the

Table 2. Sensitized photolysis of **1** in ether with a 270-W high pressure mercury arc

Sensitizer[a]	Benzene	Benzophenone	Piperylene	1-Acetonaphthone
E_T (kcal/mol)	84	68.5	58.8	56.4
Irradiation time[b] (hr)	22.3	4	32	110.8
conversion (%)	99.0	87.2	95.7	90.6
Product selectivity (%)				
ε-Caprolactam	2.6	1.9	7.8	7.3
n-Capronamide	32.1	21.0	13.6	4.2
Dicyclohexylideneazine	0.0	0.0	0.0	0.7
Cyclohexanone	28.9	77.1[c]	65.7	83.5
Cyclohexanol	26.8		12.9	0.0
Dodecanediamide	Trace	Trace	Trace	Trace

a) Addition amounts of sensitizers were 5 mol% based on **1** (17.5 mmol/l).
b) Investigated at the temperature of −2 °C.
c) Gas chromatographical separation was unsuccessful due to the presence of benzophenone.

1-acetonaphthone-sensitized photolysis. The photolysis of **1** sensitized by piperylene (E_T=58.8 kcal/mol) was a borderline case and gave considerable amounts of *n*-capronamide and cyclohexanol.

Reaction Mechanism. The oxaziridines, **2** and **3**, in methanol have absorption maxima at 200 nm (ε 172) and 207 nm (ε 112.8) respectively. No other maxima can be observed at longer wavelengths. The primary photo-excitation is, therefore, assumed to be either a forbidden n-σ* or σ-σ* transition. The main photolytic route of **1** may be summarized as is shown in Scheme 1.

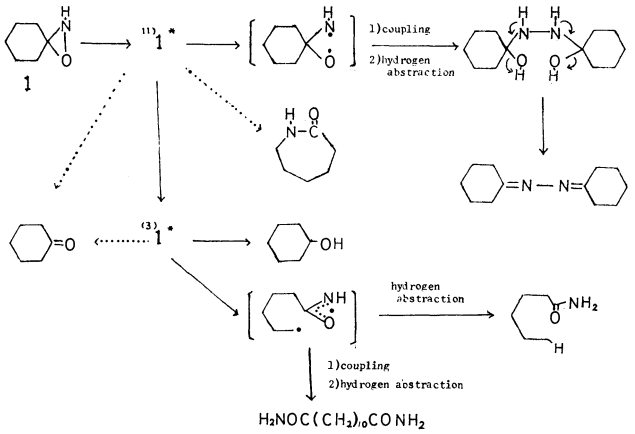

Scheme 1.

Because of the relatively short lifetime of the excited singlet state of **1**, the intramolecular rearrangement leading to ε-caprolactam was supposed to be predominant, and it was supposed that only a part of it undergoes coupling to give dicyclohexylideneazine. The formation of dodecanediamide was supposed to involve the same intermediate as that of *n*-capronamide.

Experimental

Apparatus. The IR spectra were recorded on a Hitachi infrared spectrophotometer, type EPI-G_2. The UV spectra were obtained on a Hitachi spectrophotometer type, 124, using a 10 mm quartz cell. The NMR spectra were measured on a Varian A 100 (100 MHz) spectrometer, using TMS as the internal standard.

Light Sources. Both an Ushio UL-5UQ 50-W low-pressure mercury arc and a Hanovia 2-W-U low-pressure mercury arc lamp were used. In the sensitized photolyses, a Wako Electric 270-W high-pressure mercury lamp was used.

Materials. The ether solution of **1** (the concentration was approximately 10—11 wt%) was prepared in the manner described by Schmitz and Murawski.[7] In a similar manner,[11] **2** and **3** were also prepared and isolated by distillation *in vacuo*. Authentic *N*-methyl-ε-caprolactam was prepared by the reaction of ε-caprolactam with dimethylsulphate.[12] Dicyclohexylideneazine was prepared by the condensation of cyclohexanone and hydrazinehydrate in benzene under reflux. *n*-Capronamide was prepared by the chlorination of *n*-caproic acid with thionyl chloride, followed by amidation. All the quenchers were commercially available and were of an analytical grade.

General Procedure for the Photolysis of 1. Irradiations were carried out in a quartz vessel immersed in a brine bath at temperature between −2 and 0 °C. The concentration of the ether solution of **1** used was usually 10—11 wt%. The solution was photolized until the **1** had been completely decomposed. The unreacted oxaziridine was periodically determined iodometrically.[13] The yields of all the photo-product were determined by means of gas chromatography. The free cyclohexanone containing the ether solution of **1** was determined by means of gas chromatography by subtracting the content of **1** from the total cyclohexanone content in the solution, as determined by the alkaline hydrolysis of **1** and by the subsequent determination of the resultant cyclohexanone. The identification of photo-products was as follows: (a) ε-caprolactam: The irradiated solution was condensed and then distilled *in vacuo*; bp 100—124 °C/5 mm. The fraction obtained was recrystallized from cyclohexane; mp 68 °C. The IR spectrum (KBr disk) was superimposable upon that of an authentic sample. (b) *n*-capronamide: from the condensed photolytic solution, it was isolated by preparative gas chromatography. The IR spectrum (KBr disk) was superimposable upon that of an authentic sample. (c)

10) Triplet-state energies of quenchers were cited from, a) W. C. Herkstroeter, A. A. Lamola, and G. S. Hammond, *J. Amer. Chem. Soc.*, **86**, 4537 (1964). b) L. M. Stephenson and G. S. Hammond, *Angew. Chem. Internat. Edit.*, **8**, 261 (1969).

11) E. Schmitz, R. Ohme, and D. Murawski, *Chem. Ber.*, **98**, 2516 (1965).

12) R. E. Benson and T. L. Cairins, *J. Amer. Chem. Soc.*, **70**, 2114 (1948).

13) In these determinations, the titre is equal to the sum of **1**, chloramine, and *N*-chlorocyclohexylideneimine. Therefore, the contents of **1** were obtained by subtraction the chlorine titre determined by Volhard method from the total iodometric titre.

dicyclohexylideneazine: It was isolated using elution-column chromatography on silica gel, using chloroform as the solvent; bp 99—102 °C/1 mmHg; mp 29.2—30.8 °C. UV: λ_{max}^{MeOH} 210 nm (2.55×10^4), 231 nm (6.57×10^3). Mass: (M^+ 192). IR (KBr): 1630 cm^{-1} (C=N). NMR ($CDCl_3$): δ 2.53 (q, 8H, $J_{a,a}=12$ Hz, $J_{a,e}=6$ Hz, α-CH_2), δ 1.4—2.0 (m, 12H, β, γ-CH_2). (Found: C, 74.47; H, 10.31; N, 14.88%). (d) cyclohexanol: it was separated by gas chromatography and was identified by means of the IR spectrum of an authentic sample. (e) dodecanediamide: It was identified by gas chromatography and the IR and mass spectra.

The Photolysis of ***2***. Twenty grams of **2** in methanol (150 ml) were irradiated with a low-pressure mercury arc at a temperature between −2 and 0 °C. After the complete decomposition of **2** (checked by iodometry), the photoproducts were directly determined by gas chromatography. The main product (*N*-methyl-α-piperidone) was obtained by the evaporation of the solvent and by subsequent distillation *in vacuo*. Yield, 71%. Bp 85—86.5 °C/5 mmHg. IR (liquid): superimposable upon that of an authentic sample. NMR ($CDCl_3$): δ 3.2—3.4 (m, 2H, δ-CH_2), δ 2.40 (s, 3H, N-CH_3), δ 2.25—2.45 (m, 2H, α-CH_2), δ 1.75—2.00 (m, 4H, β, γ-CH_2). (Found: C, 62.99; H, 9.54; N, 12.49%).

The Photolysis of ***3***. The various solutions of **3** (concentration: 2.3—2.5 mol/l) were irradiated with a low-pressure mercury arc as has been described above. The main product was obtained by the evaporation of the solvent, followed by reduced distillation (bp 71 °C/0.75 mmHg); it was identifed as *N*-methyl-ε-caprolactam. IR (liquid): 1630 cm^{-1} (C=O). NMR ($CDCl_3$): δ 3.25—3.45 (m, 2H, ε-CH_2), 2.93 (s, 3H, N-CH_3), 2.40—2.60 (m, 2H, α-CH_2), 1.4—1.9 (m, 6H, β, γ, δ-CH_2). (Found: C, 65.56; H, 10.17; N, 11.05%).

Quenching Reactions of ***1***. To about 205 g of the ether solution of **1**, the concentration of which was approximately 0.35 mol/l, we added a quencher so as to adjust the concentration to 17.5 mmol/l. The mixture was then transferred to a quartz vessel and was irradiated at a temperature between 12 and 0 °C using a 50-W low-pressure mercury arc. The lights, whose wavelength was longer than 2537 Å, were cut by liquid filters composed of copper and cobalt salts. Irradiation was continued until the conversion of **1** reached more than 90%. The products were then analyzed by means of gas chromatography.

Sensitized Photolysis of ***1***. To about 115 g of an ether solution of **1** (concentration, 0.35 mol/l) we added a sensitizer to adjust the concentration to 17.5 mmol/l. The mixture was then transferred to a Pyrex glass vessel and was irradiated at −2 °C using a 270-W high-pressure mercury arc. The irradiated solution was then worked up in the usual manner.

The author is grateful to Mr. Nobumasa Anjiki for his technical assistance and to Dr. Hajime Saito of Toray Industries, Inc., for the measurements of the NMR spectra.

BULLETIN OF THE CHEMICAL SOCIETY OF JAPAN, VOL. 46, 3470—3474 (1973)

Carboxylation of Phenol Derivatives. XXI. The Formation Reaction of the Complex from Alkali Phenoxide and Carbon Dioxide[1]

Ichiro HIRAO and Taketoshi KITO

Laboratory of Industrial Chemistry, Department of Chemical Engineering, Kyushu Institute of Technology, Tobata-ku, Kitakyushu-shi 804

(Received December 8, 1972)

The yield of the complex was examined using eleven potassium phenoxide or substituted phenoxides. The phenoxide with an electron-donating group gave a complex in a better yield than did that with an electron-attracting group. The infrared spectra of the four complexes were measured. From these results, it was concluded that, in the complex, the carbon atom of carbon dioxide binds to the oxygen atom or the π-electron of alkali phenoxide. The thermal analyses of the complex were also conducted by DTA and TGA in an atmosphere of carbon dioxide; a strong endothermic peak and a rapid weight loss were observed at the temperatures from 120 to 140 °C.

Hydroxybenzoic acids are mainly synthesized by the Kolbe-Schmidt reaction, and many methods have appeared for this reaction since Kolbe discovered it in 1860.[2] Some methods of preparing hydroxybenzoic acids are as follows:[2-4] (a) the reaction of alkali phenoxide with carbon dioxide in the absence of a solvent or in a nonpolar solvent; (b) the reaction of alkali phenoxide with carbon dioxide in an aprotic polar solvent such as dimethylformamide; (c) the reaction of phenol with carbon dioxide in the presence of an excess amount of potassium carbonate; (d) the reaction of alkali phenoxide with alkali alkyl carbonate, *etc.* Of these, a typical reaction is the (a) method, and the reaction mechanism has been investigated exclusively in reference to this method. The general procedure is divided into two steps. The first step is the absorption of carbon dioxide by alkali phenoxide at a low temperature (about 100 °C). The second step is the heating of the mixture obtained in the first step, the temperature being held at 150—160 °C for several hours.[2] In the first step, it is known that a certain product is formed when phenoxide comes into contact with carbon dioxide. Some investigations of

1) This paper was presented at the 27th (1972) Annual Meeting of the Chemical Society of Japan; Part XX of this series: T. Kito and I. Hirao, This Bulletin, **44**, 3123 (1971).

2) A. S. Lindsey and H. Jeskey, *Chem. Rev.*, **57**, 583 (1957).

3) I. Hirao, *Yuki Gosei Kagaku Kyokai Shi*, **24**, 1051 (1966).

4) I. Hirao, T. Kondo, and T. Kito, *Kogyo Kagaku Zasshi*, **72**, 692 (1969); T. Kito and I. Hirao, This Bulletin, **44**, 3123 (1971).

this product have been done, but they have almost all been done in connection with the mechanism of the Kolbe-Schmidt reaction or in connection with the preparation of hydroxybenzoic acid.[5,6] However, in this paper the yields and analytical results of this product and its related compounds will be described.

Experimental

Complex Formation Reaction. In a 300 ml glass autoclave, we placed 100 ml of a light oil (as a medium of heat) and 0.02 mol of potassium phenoxide. After the air had been replaced by nitrogen, the autoclave was heated, vigorously stirred, and then kept at the prescribed temperature. The pressure was released and then a carbon dioxide pressure was exerted. The pressure was kept at a constant value during the reaction. Some adduct, which we will represent as "complex" or [I] for the sake of convenience, was formed from potassium phenoxide and carbon dioxide according to Eq. (1):

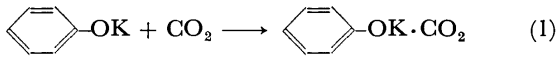

(1)

At the prescribed time, the carbon dioxide was replaced by nitrogen and the autoclave was allowed to cool to room temperature.

Determination of the Complex. It is difficult to separate the complex from unreacted potassium phenoxide because the complex is hardly soluble in either ordinary organic solvents or alkali phenoxides (we found that the adduct was also formed from DMF and alkali phenoxide when the latter was dissolved in DMF[7] and that alkali alkyl carbonate was formed when the complex was dissolved in alcohol;[8] therefore, they can not be used as solvents) and is thermally unstable.[5] For the above reasons, the determination of the complex was carried out according to the following procedure.

The lid of the autoclave was taken off, and the light oil was sucked out through a glass-filter by applying a vacuum. In this procedure, one must take care that the reaction mixture does not come in contact with the moisture or the carbon dioxide in the air.

A test tube, in which 50 ml of aqueous KOH solution (about 1 M) had been placed, was inserted into the autoclave, and then the lid was put on tightly. Then, making the aqueous KOH solution run over from the test tube by inclining the autoclave, the complex was caused to decompose into potassium phenoxide and carbon dioxide, the latter being absorbed by the aqueous KOH solution to change into potassium carbonate or potassium bicarbonate. The number of complex molecules formed should be equal to the total number of the molecules of potassium carbonate and potassium bicarbonate if the reaction proceeds according to Eqs. (1) and (2):

[I] + excess KOH ⟶

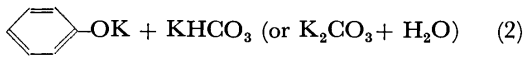

(2)

The reaction mixture was diluted with water to 500 ml; from this solution a 5 ml portion was pipetted and titrated with 0.1 M HCl. In most cases there are two clear inflexion points, that is, P_1 and P_2, which generally appear at the pH values of 7.9 and 4.6 respectively. At P_1, the potassium carbonate is completely converted to potassium bicarbonate. In the range from P_1 to P_2 only potassium bicarbonate, whose amount should be equal to the amount of the complex, is present. Therefore, the number of complex molecule formed in this reaction is obtained by multiplying the difference between P_1 and P_2 by 100.

When the solution contains some hydroxy acid which is formed in the carboxylation of potassium phenoxide by carbon dioxide, P_2 is generally indistinct. In such a case, the following procedure could be used. To 5 ml of the aqueous solution, hydrochloric acid was added until P_1 was attained. At this point, the aqueous solution contains only potassium bicarbonate and mono potassium salt of hydroxy acid as potassium salts in amounts represented here as A mol and B mol respectively. When a sufficient amount of M mol of hydrochloric acid is further added, $M-(A+B)$ mol of hydrochloric acid and B mol of hydroxy acid remain as acid components. This solution was again titrated with 0.1 M aqueous sodium bicarbonate. There is also a clear inflexion point, P_3, which generally appears at the pH of 4.5. When N mol of sodium bicarbonate is added until P_3 (at P_3 both hydrochloric acid and hydroxy acid are neutralized by sodium bicarbonate) is attained, the following equation must be valid:

$$M - (A+B) + B = N \qquad \therefore \quad A = M - N$$

The yield of the complex can be calculated according to Eq. (3), where: L represents the number of molecules of potassium phenoxide used as the starting material.

$$\text{Complex yield (\%)} = \frac{M-N}{L} \times \frac{500}{5} \times 100 \qquad (3)$$

Infrared Absorption Spectra of the Complex. The spectra were measured with a Japan Spectroscopic spectrometer (IRA-2).

The complex was prepared at room temperature by the method described above, but light oil was replaced by *n*-hexane because the latter has no absorption in the carbonyl absorption region. The complex containing *n*-hexane was placed on filter paper, which blots *n*-hexane, and was then suspended in Nujol on a mortar.

Differential Thermal Analysis (DTA) and Thermogravimetric Analysis (TGA). The complex was prepared as follows. Potassium phenoxide was set in the apparatus and heated at 150 °C in a vacuum. After 1 hr, it was allowed to cool to room temperature, applying a vacuum, and then the atmosphere was replaced by carbon dioxide.

After 30 min, the temperature was again raised at a rate of about 3 °C/min in an atmosphere of carbon dioxide. Apparatus: Cho Keiryoki, $TRDA_1$-L.

Results and Discussion

Effect of the Reaction Temperature and the Reaction Time. The yields of the complex and of the hydroxybenzoic acids were examined under various conditions. Potassium phenoxide was heated under a carbon dioxide pressure of 5 kg/cm² for 30 min at various temperatures. The results are shown in Table 1.

The complex was formed in a 76—80% yield at temperatures lower than 70 °C and then decreased above that temperature. On the contrary, such

5) J. L. Hales, J. I. Jones, and A. S. Lindsey, *J. Chem. Soc.*, **1954**, 3145.

6) R. Ueno, K. Muramoto, and I. Hirao, *Kogyo Kagaku Zasshi*, **64**, 1213 (1961); I. Hirao, K. Ota, S. Sueta, and Y. Hara, *Yuki Gosei Kagaku Kyokai Shi*, **24**, 1047 (1966).

7) Unpublished.

8) The 28th (1973) Annual Meeting of the Chemical Society of Japan, Tokyo.

TABLE 1. EFFECT OF THE REACTION TEMPERATURE AND TIME ON THE YIELDS OF COMPLEX AND HYDROXYBENZOIC ACIDS

Temp (°C)	Time (hr)	Yield (%) Complex	Yield (%) Acids
20	0.5	77.6	0
29.5	0.5	78.8	0
50	0.5	75.6	0
70	0.5	79.4	0
100	0.5	67.4	4.1
130	0.5	20.6	32.9[a)]
150	0.5	10.4	60.6[b)]
150	3.0	3.2	64.2[c)]
180	0.5	4.4	72.3[d)]

a) SA (Salicylic acid), 22.7%; POB (*p*-Hydroxybenzoic acid), 9.8%; 4-OIP (4-Hydroxyisophthalic acid), 0.4%.
b) SA, 39.1%; POB, 20.2%; 4-OIP, 1.3%.
c) SA, 43.8%; POB, 20.0%; 4-OIP, 0.4%.
d) SA, 43.6%; POB, 24.7%; 4-OIP, 4.0%.

hydroxybenzoic acids as salicylic acid and *p*-hydroxybenzoic acid were formed at 100 °C in only a 4.1% yield. The effect of the reaction time on the yields of complex and hydroxybenzoic acids was examined at 150 °C (see Table 1). On the basis of these results, it can be said that the complex yield decreases at temperatures higher than 70 °C not because it changes into hydroxybenzoic acids, but because it is thermally unstable.

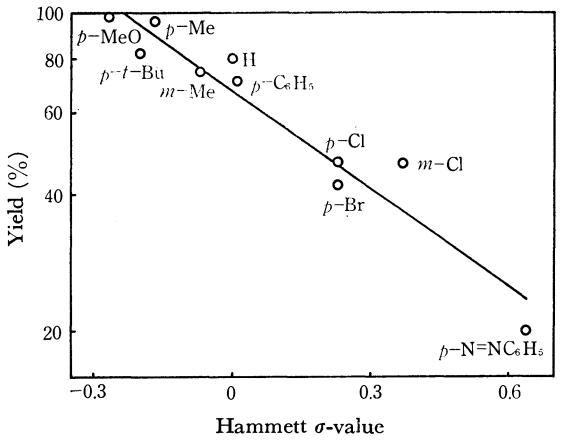

Fig. 1. Effect of the substituent on the yield of complex.
CO_2: 5 kg/cm², temp: 70 °C, time: 30 min

Reaction: 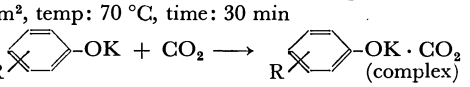 (complex)

Ordinate: a logarithmic graduation
p-SO_3K: $\sigma = +0.64$, Yield 5.8%. This point is omitted in this figure because it deviates largly from the straight line.

Effect of the Substituent. Potassium salts of phenols were heated at 70 °C under a carbon dioxide pressure of 5 kg/cm² for 30 min. In Fig. 1 the complex yields are plotted against the Hammett σ-values. We observed a linear relationship between the yield and the σ-value, and it was concluded that a phenoxide with an electron-donating group, that is, a lower σ-value, gave the complex in a better yield than that with an electron-attracting group.

Some discussions have been made of the alkali phenoxide–carbon dioxide complex because the complex has been regarded by some investigators to an important intermediate in the carboxylation of alkali phenoxide, the Kolbe-Schmidt reaction. For example, Schmidt[2)] considered that the intermediate, which we will here describe as the complex, is an alkali phenyl carbonate. He proposed the following reaction processes, Eqs. (4) and (5). The second step, Eq. (5),

$$C_6H_5ONa + CO_2 \longrightarrow C_6H_5OCOONa \quad (4)$$

$$C_6H_5OCOONa \longrightarrow HOC_6H_4COONa \quad (5)$$

is a rearrangement of sodium phenyl carbonate to salicylic acid.

By infrared study Hales and his co-workers[5)] determined the structure of the adduct obtained from sodium phenoxide and carbon dioxide as II. (Many authors have described the molecule of carbon dioxide in the complex as a bending form, as is shown in the figure, without explanation, although carbon dioxide is usually considered to have a straight-lined form; however, Kwan and his co-workers[9)] presumed the structure of carbon dioxide in the complex to be a bending form on the basis of the infrared study.) They proposed the structure of II on the basis of the fact that it has an IR absorption due to the carbonyl band at 1684 cm^{-1}. They considered that if the product is a sodium phenyl carbonate, it must have a carbonyl absorption at about 1630 cm^{-1} because sodium methyl carbonate has an absorption due to carbonyl at 1630 cm^{-1}. In addition, dimethyl carbonate and methyl phenyl carbonate possess carbonyl absorptions at 1748 and 1754 cm^{-1} respectively, indicating that the phenyl group has little effect on the position of the carbonyl absorption. However, we consider that although they rejected the sodium phenyl carbonate structure on the basis of a reasonable method, no clear structure can be given because whether carbon dioxide binds to sodium metal or to the residue can not be determined by only their IR investigations. Shilov and his co-workers[10)] proposed that the structure of the complex can be denoted as III, not II, because II must be very weak; however, this assumption was not based on experimental data.

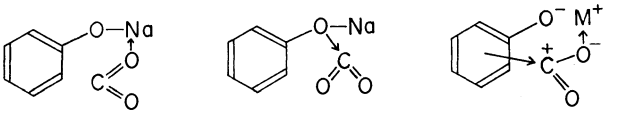

[II] [III] M=K, Na [IV]

The results presented in Fig. 1 also give some interesting information. If the oxygen atom of carbon dioxide binds to the alkali atom, as is shown in II, the poorer the electron density on the alkali atom, the stronger the binding force between the alkali atom and carbon dioxide. Therefore, the yield of a complex must increase as the substituent on the phenyl nucleus attracts an electron from the nucleus or the oxygen

9) T. Kwan, H. Yamamoto, H. Mori, and H. Samejima, *Kagaku Kogyo*, **74**, 1618 (1972).
10) E. A. Shilov, I. V. Smirov-Zamkov, and K. I. Matkovskiĭ, *Ukrain. Khim. Zhur.*, **21**, 484 (1955).

atom. However, this idea is contrary to the results shown in Fig. 1. The results in Fig. 1 suggest that the (III) structure is more reasonable than the (II) structure because it is expected that the yield increases as the electron density on the oxygen atom of phenoxide increases. On the other hand, another structure, a π-complex structure shown as IV, which we have described here ionically, is possible; a similar structure has been proposed by Hales and his co-workers[5] as one state in the carboxylation of sodium phenoxide. In IV, of course, carbon dioxide should bind to the alkali atom more loosely than to the π-electron on the phenyl nucleus. However, we have no reliable data for a discussion as to which structure, (III) or (IV), is more reasonable.

Infrared Absorption Spectra. The IR absorptions due to the carbonyl groups of four complexes were measured; the results are listed in Table 2.

Table 2. Infrared spectra of the complex

Complex	$\nu_{C=O}(cm^{-1})$
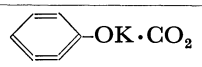	1645
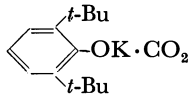	1650 1628
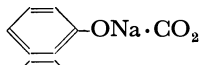	1685
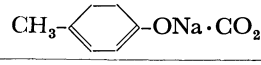	1668

a) Lit,[5] 1684 cm^{-1}.

First, the validity of the (II) structure is considered in the following. The O^-K^+ bond in potassium phenoxide is more polarized than the O^-Na^+ bond in sodium phenoxide. Therefore, the K atom in potassium phenoxide is more positive than the Na atom in sodium phenoxide, but the electron density on the former may be higher than that on the latter because the ionic radius of K^+ is greater than that of Na^+. Yamamoto explained,[11] on this basis, a greater tendency toward the solubility of Na salts compared with K salts and other differences between sodium and potassium compounds. If this assumption is true, $C_6H_5OK \leftarrow O_2C$[12] can be expected to give a carbonyl absorption at a higher frequency than does $C_6H_5ONa \leftarrow O_2C$ since the oxygen atom of carbon dioxide binds to the K atom more loosely than to the Na atom.

On the other hand, it is obvious that the electron density on the Na atom in sodium *p*-cresoxide is higher than that on the Na atom in sodium phenoxide. Therefore, $p\text{-}CH_3C_6H_4ONa \leftarrow O_2C$ is also expected to give a carbonyl absorption at a higher frequency than does $C_6H_5ONa \leftarrow O_2C$. However, the results listed in Table 2 were not in accord with this expectation.

On the contrary, the following expectations can be drawn from the (III) structure. The electron densities on the oxygen atoms in potassium phenoxide and sodium *p*-cresoxide may be higher than that on the oxygen atom in sodium phenoxide. Therefore, both $C_6H_5O(K) \rightarrow CO_2$ and $p\text{-}CH_3C_6H_4O(Na) \rightarrow CO_2$[13] can be expected to give carbonyl absorptions at lower frequencies than does $C_6H_5O(Na) \rightarrow CO_2$ because the carbon atom of carbon dioxide may be neutralized by the oxygen atom in potassium phenoxide or sodium *p*-cresoxide to a greater extent than by that in sodium phenoxide. A similar reasoning can be also drawn from the (IV) structure. The results listed in Table 2 are in good agreement with the above expectations.

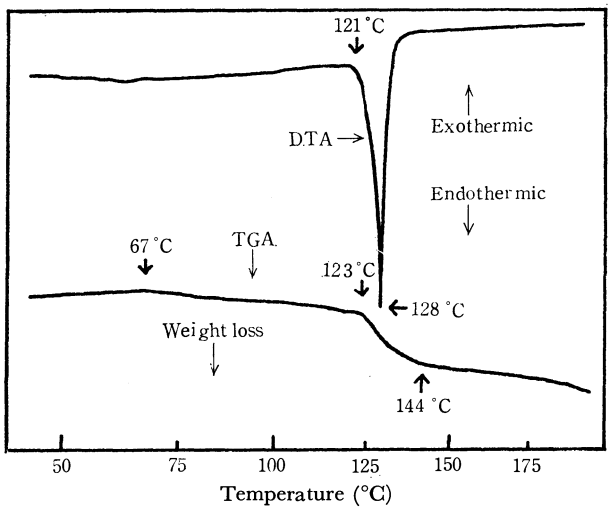

Fig. 2. DTA and TGA curves of the complex.

DTA and TGA. The complex obtained from potassium phenoxide and carbon dioxide was analyzed by DTA and TGA in an atmosphere of carbon dioxide. The results are shown in Fig. 2. In this experiment, the following reactions may occur: (a) the decomposition of the complex, (b) the formation of monopotassium salicylate and monopotassium *p*-hydroxybenzoate by the carboxylation of potassium phenoxide, (c) the conversion of the monopotassium salts into the dipotassium salts, and (d) the rearrangement of dipotassium salicylate to dipotassium salt of *p*-hydroxybenzoic acid. The weight loss in the range of the temperatures from 67 to 123 °C in Fig. 2 may correspond to the (a) process; this is in good agreement with the results listed in Table 1.

On the other hand, the weight loss did not occur below 200 °C when monopotassium salicylate or monopotassium *p*-hydroxybenzoate was heated in an atmosphere of carbon dioxide, while it began at 165 °C when a mixture of monopotassium *p*-hydroxybenzoate, monopotassium salicylate, and potassium phenoxide (weight ratio of 1 : 2 : 7) was heated in an atmosphere of nitrogen. In the latter case, the weight loss must be caused by the evaporation of the phenol formed in Eq. (6). In

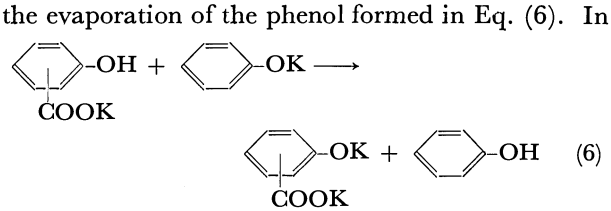

(6)

11) T. Yamamoto, *Kagaku to Kogyo*, **23**, 1004 (1970).

12) The $C_6H_5OM \leftarrow CO_2$ formula represents a complex with the structure of II.

13) The $C_6H_5O(M) \rightarrow CO_2$ formula represents a complex with the structure of III.

addition, we often observed the following phenomenon. A complex was prepared from potassium phenoxide and carbon dioxide in light oil at room temperature, and then the temperature was gradually raised (about 2 °C/min). When the temperature reached about 130 °C, the solid coagulated in a mass, but it was soon dispersed into the light oil.

On the basis of these data, the strong endothermic peak and the rapid weight loss in the range of temperatures from 120 to 140 °C in Fig. 2 can be explained as follows: the monopotassium salt of hydroxybenzoic acid converts into the dipotassium salt by taking a potassium atom from the complex. At that time, the complex decomposes and liberates carbon dioxide, which results in a strong endothermic peak and a great decrease in weight. The coagulation observed must be one step in this process.

Thanks are due to Mr. Hiroshi Yamaguchi and Mr. Kazumi Hirakawa for their assistance in the experimental work.

BULLETIN OF THE CHEMICAL SOCIETY OF JAPAN, VOL. 46, 3474—3477 (1973)

Syntheses and the Beckmann Fission of Cyclic α-Hydroxyimino Ketones

Mutsuo KATAOKA and Masaji OHNO

Basic Research Laboratories, Toray Industries, Inc., Tebiro, Kamakura 248

(Received April 2, 1973)

A convenient method for the preparation of α-hydroxyimino cycloalkanones has been established by the reaction of cycloalkanones and nitrosyl chloride. ω-Cyanocarboxylic acids or their derivatives were obtained in good yield by the Beckmann rearrangement of these α-hydroxyimino ketones.

Nitrosyl chloride addition to cycloolefins followed by displacement reactions with nucleophilic reagents such as alcohols, thioalcohols, and alkylamines provides a method of preparing various α-substituted oximes[1] which are attractive intermediates for the Beckmann fission.[2] The overall sequence is equivalent to a cleavage of the double bond in the cycloolefins, affording ω-cyanoaldehydes.[3]

No attempt has been made to prepare ω-cyanocarboxylic acids expected from the cleavage of cyclic α-hydroxyimino ketones,[4,5] from cycloalkanones such as cyclohexanone, cyclooctanone, and cyclododecanone.

In the present paper, we wish to report a convenient method for preparing α-hydroxyimino ketones of medium rings from ketones and the Beckmamm fission of such α-hydroxyimino ketones into ω-cyanocarboxylic acids. The results are compared with those of six-membered ring system.

Results and Discussion

Preparation of Cyclic α-Hydroxyimino Ketones. Although the preparation of acyclic α-hydroxyimino ketones from acyclic ketones or β-keto acids is well-known,[6] there is little information on the synthetic application of cyclic α-hydroxyimino ketones. We became interested in the study of α-hydroxyimino ketones of medium ring system, since these cyclic parent compounds are now easily available.[7]

Cyclododecanone and cyclooctanone were treated with an equivalent amount of nitrosyl chloride in the presence of a catalytic amount of hydrogen chloride, affording 2-hydroxyiminocyclododecanone (I) and 2-hydroxyiminocyclooctanone (II) in quantitative and in 87% yields, respectively. It was found that the presence of hydrogen chloride was essential at the beginning of the reaction, no reaction taking place or a long induction peiord being observed in its absence. The action of hydrogen chloride must be the enolization of the ketones as seen in typical cases of nitrosating agents such as alkyl nitrite–alkoxide and alkyl nitrite–hydrogen chloride.[6] I was obtained in the state of hydrochloride, being deposited during nitrosation from the reaction medium such as ether or petroleum benzine at low temperatures (0—5 °C), and the hydrochloride was easily transformed into the free oxime simply by being warmed up to room temperature. However, it was necessary to neutralize the hydrochloride of II with sodium bicarbonate to transform it into the free form. Neither dinitrosation nor nitrosochlorination was observed in the reactions of cyclododecanone and cyclooctanone.

Nitrosation of cyclohexanone was studied in detail by several groups, and it was found that dinitrosation occurs very easily. Ferris prepared 2,6-dihydroxyiminocyclohexanone by the reaction of cyclohexanone and methyl nitrite as a key intermediate for the synthesis of lysine,[5] and Taira obtained it by treatment of

1) M. Ohno, N. Naruse, M. Okamoto, S. Torimitsu, and I. Sakai, This Bulletin, **39**, 1119, 1125, 1129 (1966).

2) C. A. Grob and P. W. Shiess, *Angew. Chem.*, **79**, 1 (1967).

3) a) M. Ohno, N. Naruse, S. Torimitsu, and I. Terasawa, *J. Amer. Chem. Soc.*, **88**, 3168 (1966). b) M. Ohno, N. Naruse, and I. Terasawa, "Organic Syntheses," Vol. 49, John Wiley & Sons, New York, N.Y. (1969), p. 27.

4) D. Murakami and N. Tokura, This Bulletin, **31**, 1044 (1958).

5) A. F. Ferris, G. S. Johnson, and F. E. Gould, *J. Org. Chem.*, **25**, 496 (1960).

6) O. Touster, "Organic Reactions," Vol. 7, John Wiley & Sons, New York, N. Y. (1953), p. 327.

7) G. Wilke, *Angew. Chem.*, **75**, 10 (1963).

cyclohexanone with nitrosyl chloride at temperatures above −20 °C.[8] Mononitrosation of cyclohexanone requires careful reaction conditions. Thus, 2-hydroxyiminocyclohexanone (III) was obtained by treatment with 2-ethyl-*n*-hexyl nitrite[9] or by nitrosation of 2-carbethoxycyclohexanone.[10] We found that the degree of nitrosation of cyclohexanone with nitrosyl chloride is controlled by the reaction temperature. Mononitrosation of cyclohexanone occurs below −50 °C in the presence of hydrogen chloride, and dinitrosation at temperatures above −20 °C. A mixture of mono- and dihydroxyimino compounds was obtained at temperatures −50——20 °C. III was obtained in the state of unstable hydrochloride and free oxime was obtained in 62% yield after neutralization with aqueous sodium hydroxide.

Table 1. IR spectra of I, II, and III (in CCl_4)

α-Hydroxyimino Ketone	mp °C	ν_{OH} (Free) cm^{-1}	ν_{OH} (Bonded) cm^{-1}	$\Delta\nu$ cm^{-1}	Configuration
III	60—64	3560	3240	320	*syn*
II(*syn*)	101—103	3580	3260	320	*syn*
II(*anti*)	oil	3580	—	—	*anti*
I	69—70	3560	—	—	*anti*

It should be mentioned that the configuration of the cyclic α-hydroxyimino ketones obtained depends upon the ring size. The configurations of I, II, and III were determined spectroscopically[11] and the results are shown in Table 1. The configuration of III, which so far has not been discussed, was found to be exclusively *syn*, and 8-membered α-hydroxyimino ketone (II) was shown to be a mixture of *syn* and *anti* forms in equal amount, but the configuration of I was found to be exlcusively *anti*.

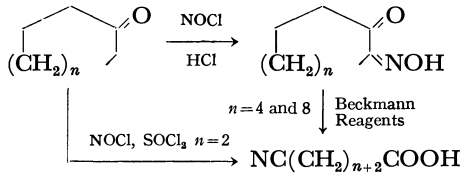

Beckmann Fission of Cyclic α-Hydroxyimino Ketones. The cyclic α-hydroxyimino ketones thus obtained were subjected to the Beckmann rearrangement under various conditions. The results are summarized in Table 2. 2-Hydroxyiminocyclododecanone (I) afforded 11-cyanoundecanoic acid or its derivatives as expected from the *anti* configuration of I. However, when I was treated with phosgene, oily and crystalline substances were obtained. The former was found to be the cyanoacid chloride (VI, 39% yield) and the latter dodecanedioic imide (VIII, 6% yield). This result shows that the usual Beckmann rearrangement occurs to some extent under specific conditions. Direct treatment of cyclododecanone with nitrosyl chloride and acetic anhydride in the presence of sulfuric acid, using ether as a solvent, followed by hydrolysis, gave IV in 87% yield. This one-step Beckmann fission from the cyclic ketone seems to be specific to acetic anhydride, since the reaction did not occur when other anhydrides were used. 2-Acetoxyiminocyclododecanone (XII) prepared quantitatively by treatment of I with acetic anhydride or direct treatment of cyclododecanone with nitrosyl chloride and acetic anhydride in the presence of hydrogen chloride, underwent Beckmann fission under basic conditions using aqueous sodium hydroxide to afford IV in a quantitative yield. The results show that the choice of reagent and/or catalyst not only decides the terminal functions in various ways but also influences the mechanism of fission.

In the case of Beckmann fission of II, both forms of *syn* and *anti* configurations gave 7-cyanoheptanoic acid (XIII) in excellent yields, showing that the pattern of Beckmann rearrangement does not always depend upon the stereochemistry of the α-hydroxyimino ketone.

Treatment of 2-hydroxyiminocyclohexanone (III) which exists only in *syn* form with sulfuric acid, 97% phosphoric acid or thionyl chloride recovered most of the starting material along with some intractable tarry products, showing that the *syn* α-hydroxyimino ketone resists the Beckmann fission as expected.[12] Preparation

Table 2. Beckmann fission of α-hydroxyimino ketones

α-Hydroxyimino Ketones	Reaction Conditions	Products (Yield)
I	$97\%H_3PO_4/H_2O$	$NC(CH_2)_{10}COOH$(IV, 98%)
	H_2SO_4/H_2O	$NH_2CO(CH_2)_{10}COOH$(V,96%)
	$SOCl_2$	$NC(CH_2)_{10}COCl$ (VI, 62%)
	$SOCl_2/NH_3$	$NC(CH_2)_{10}CONH_2$ (VII, 96%)
	$COCl_2$	$(CH_2)_{10}CONHCO$ (VIII, 6%)
		$NC(CH_2)_{10}COCl$(VI, 39%)
	$COCl_2$/MeOH	$NC(CH_2)_{10}COOCH_3$(IX, 75%)
		$NH_2CO(CH_2)_{10}COOCH_3$ (X, 15%)
	Ac_2O, H_2SO_4	$NC(CH_2)_{10}COOAc$(XI, 95%)
II (*syn*)	$97\%H_3PO_4/H_2O$	$NC(CH_2)_6COOH$(XIII, 80%)
II(*anti*)	$97\%H_3PO_4/H_2O$	$NC(CH_2)_6COOH$ (XIII, 78%)

8) S. Taira, S. Imamura, K. Yotsumoto, and K. Takada, Jap. 645957 (1972).

9) E. G. Rauh, G. F. Smith, C. V. Bank, and H. Diehl, *J. Org. Chem.*, **10**, 199 (1945).

10) F. M. Jaeger and J. A. von Dijk, *Proc. Acad. Sci. Amsterdam*, **39**, 384 (1936).

11) H. Saito, I. Terasawa, M. Ohno, and K. Nukada, *J. Amer. Chem. Soc.*, **91**, 6696 (1969).

12) A. F. Ferris, *J. Org. Chem.*, **25**, 12 (1960).

of 5-cyanovaleric acid by direct treatment of cyclohexanone with nitrosyl chloride and thionyl chloride was attempted as in the case of 12-membered ketone. Nitrosyl chloride was added to a solution of cyclohexanone and thionyl chloride in ether at −50 °C, but the fission did not occur 2-hydroxyiminocyclohexanone hydrochloride was obtained. However, when the reaction was carried out in the presence of sulfuric acid and dimethylformamide[13] as catalysts, 5-cyanovaleric acid (XIV) was successfully obtained in 60% yield. Direct methanolysis of the reaction mixture gave methyl 5-cyanovalerate (XV) in 46% yield. Thus it might be reasonable to assume that the reaction proceeds through the direct cleavage of 2-nitrosocyclohexanone or *anti* form of 2-hydroxyiminocyclohexanone before the dinitrosation of cyclohexanone or the transformation to *syn* form occurs.

Experimental

All melting points are uncorrected. The IR spectra were measured with a Hitachi EPI S-2 spectrophotometer. Hydroxyl absorption bands in the 3600 cm^{-1} region were examined in carbon tetrachloride with a Perkin-Elmer Model 125 grating spectrophotometer using 1.5 cm sodium chloride cell. The NMR spectra were measured with a Varian A 60 spectrophotometer. Molecular weights were determined with a Hitachi Perkin-Elmer Model 115 molecular weight apparatus.

2-*Hydroxyiminocyclodecanone (I).* Hydrogen chloride was passed through a solution of cyclododecanone (20 g) in petroleum benzine (200 ml) for 5 min with stirring at 0 °C. A solution of nitrosyl chloride (8.5 g) in the same solvent (30 ml) was then added over a period of 30 min. The mixture was stirred for 1 hr at 2 °C and the solvent was evaporated under reduced pressure. The pale yellow solid obtained was chromatographed over silica gel. The solid (21.3 g, 97%) obtained was recrystallized from petroleum ether, mp 69—70 °C.

Found: C, 68.41; H, 10.05; N, 6.70%. Calcd for $C_{12}H_{21}O_2N$: C, 68.21; H, 10.02; N, 6.63%.

When ether was employed as a solvent in the same reaction, fine crystals were deposited during the reaction. The substance was proved to be 2-nitrosocyclododecanone dimer (1%), mp 133—134 °C.

Found: C, 68.01; H, 10.00; N, 6.42%; mol wt, 431. Calcd for $C_{24}H_{40}O_4N_2$: C, 68.21; H, 10.02; N, 6.63% mol wt, 423.

2-*Hydroxyiminocyclooctanone (II).* Hydrogen chloride was passed through a solution of cyclooctanone (10 g) in ether (100 ml) for 3 min with stirring at −25 °C, and a solution of nitrosyl chloride (6.3 g) in the same solvent (20 ml) was added over a period of 20 min. The mixture was stirred for 10 min at −25 °C, and aqueous sodium bicarbonate was added. The organic layer was separated, washed with water and dried. The oily product obtained by evaporation of the solvent was chromatographed over silica gel. The fractions eluted first afforded the *anti* form of II as an oily substance (5.16 g, 42%); the fractions eluted next afforded the *syn* form of II as a solid product (5.54 g, 45%). The latter was recrystallized from ether, mp 101—103 °C. IR (see Table 1). Found: C, 61.97; H, 8.42; N, 8.93%. Calcd for $C_8H_{13}O_2N$: C, 61.91; H, 8.44; N, 9.03%.

13) H. H. Bosshard, R. Mory, M. Schmid, and H. Zollinger, *Helv. Chim. Acta*, **42**, 1653 (1959).

The oily material was further purified by silica gel chromatography; one spot on tlc. IR (see Table 1).

Found: C, 61.69; H, 8.48; N, 8.70%. Calcd for $C_8H_{13}O_2N$: C, 61.91; H, 8.44; N, 9.03%.

2-*Hydroxyiminocyclohexanone (III).* Hydrogen chloride was saturated in a solution of cyclohexanone (10.5 g) in ether (100 ml) with stirring at −10 °C. A solution of nitrosyl chloride (4.5 g) in the same solvent (20 ml) was added over a period of 20 min at −50 °C. The mixture was stirred for 10 min at −50 °C, nitrogen was bubbled at −10 °C to remove the hydrogen chloride. Aqueous sodium hydroxide (30%) was added to the reaction mixture at −10 °C, and the pH was adjusted to 7. The ethereal layer was separated and the aqueous layer was extracted four times with chloroform. The combined organic layers were dried and the solvent was removed. The brown oil thus obtained was chromatographed over silica gel, giving III (5.52 g, 62%) as a white solid showing mp 60—64 °C. NMR (CCl_4): δ 9.2 (s, 1H), 2.79 (t, 2H), 2.47 (t, 2H), and 1.82 ppm (m, 4H).

Treatment of III with 2,4-dinitrophenylhydrazine gave the osazone, mp 216—217 °C.

Found: C, 45.96; H, 3.56; N, 23.41%; mol wt, 474. Calcd for $C_{18}H_{16}O_8N_8$: C, 45.76; H, 3.41; N, 23.72%; mol wt, 472.

11-*Cyanoundecanoic Acid (IV).* To a mixture of 97% phosphoric acid (10 ml) and sulfuric acid (1 ml) was added finely powdered II (1.0 g) at room temperature with stirring. The mixture was stirred for 3 hr at room temperature and poured into ice water (50 g). The mixture was extracted with ether and the extract was washed with water and dried. 11-Cyanoundecanoic acid (0.98 g, 98%) obtained after evaporation of the solvent was recrystallized from benzene–petroleum benzine, mp 54—55 °C.

Found: C, 68.34; H, 9.91; N, 6.66%. Calcd for $C_{12}H_{21}O_2N$: C, 68.21; H, 10.02; N, 6.63%.

11-*Carbamoylundecanoic Acid (V).* Finely powdered I (1.0 g) was added with stirring to sulfuric acid (10 ml) cooled with ice. The reaction mixture was allowed to stand at room temperature for 1.3 hr and poured into ice water (50 g). A white solid product was obtained by filtration, washed with water and dried in a vacuum desiccator. 11-Carbamoylundecanoic acid (1.04 g, 96%) obtained as white powder was recrystallized from acetone, mp 130—131 °C.

Found: C, 62.61; H, 10.14; N, 6.13%. Calcd for $C_{13}H_{23}O_3N$: C, 62.85; H, 10.11; N, 6.11%.

11-*Cyanoundecanoyl Chloride (VI).* A solution of thionyl chloride (6.66 g) in ether (15 ml) was added with stirring over a period of 30 min at room temperature to a solution of I (9.17 g) and dimethylformamide (1 ml) in ether (90 ml). The mixture was stirred for 30 min at room temperature and the solvent was removed under reduced pressure. The residual liquid was distilled under reduced pressure (bp 146—147 °C/2.0 Torr), affording 11-cyanoundecanoyl chloride (6.21 g, 62%) as colorless liquid.

Found: C, 62.87; H, 8.69; N, 5.92; Cl, 15.55%. Calcd for $C_{12}H_{20}ONCl$: C, 62.73; H, 8.77; N, 6.11; Cl, 15.43%.

Hydrolysis of the reaction mixture gave 11-cyanoundecanoic acid (IV) in 93% yield.

Ammonolysis of the reaction mixture gave 11-cyanoundecanoyl amide (VII) in 96% yield. It was recrystallized from benzene, mp 86—87 °C.

Found: C, 68.14; H, 10.68; N, 13.05%. Calcd for $C_{12}H_{22}ON_2$: C, 68.53; H, 10.54; N, 13.32%.

Treatment of I with Phosgene. A solution of phosgene (12 g) in dichloromethane (76 ml) was added with stirring to a solution of I (20.0 g) in the same solvent (100 ml) at room temperature. The mixture was stirred for 1.5 hr at

room temperature and divided into three fractions.

(1) Water (20 ml) was added to the reaction mixture (50 ml) and the mixture was stirred for 1 hr at room temperature. The organic layer was separated and the aqueous layer was extracted with ether. Combined organic layers were washed with water and dried. Evaporation of the solvent gave a mixture of liquid and crystals. Ether (10 ml) was added to the mixture and the crystals were separated by filtration. Dodecanedioic imide (VIII, 345 mg, 6%) was obtained, recrystallized from a mixed solvent of acetone–benzene, mp 137—138 °C.

Found: C, 68.49; H, 10.05; N, 6.44%; mol wt, 214. Calcd for $C_{12}H_{21}O_2N$: C, 68.21; H, 10.02; N, 6.63%; mol wt, 211.

11-Cyanoundecanoic acid (4.08 g, 71%) and 11-carbamoylundecanoic acid (0.20 g, 3%) were separated from the liquid after being subjected to silica gel chromatography.

(2) After evaporation of the solvent of the reaction mixture (74 ml), a crystalline solid was separated by filtration. The solid was proved to be VIII. Distillation of the filtrate gave 11-cyanoundecanoyl chloride (VI, bp 134—135 °C/0.4 Torr, 3.57 g, 39%).

(3) Methanol (30 ml) was added to the reaction mixture (50 ml) and the mixture was stirred for 2 hr at room temperature. Methyl 11-cyanoundecanoate (4.6 g, 75%) and methyl 11-carbamoylundecanoate (1.0 g, 15%) were obtained after being subjected to silica gel chromatography. The former (IX) was purified by distillation, bp 133—137 °C/0.4 Torr.

Found: C, 69.19; H, 10.43; N, 6.29%. Calcd for $C_{13}H_{23}O_2N$: C, 69.29; H, 10.29; N, 6.22%.

The latter (X) was recrystallized from a mixed solvent of benzene–petroleum benzine, mp 97—98 °C.

Found: C, 64.25; H, 10.41; N, 5.75%. Calcd for $C_{13}H_{25}O_3N$: C, 64.16; H, 10.36; N, 5.76%.

Treatment of I with Acetic Anhydride and Sulfuric Acid. Three drops of sulfuric acid were added to a stirred solution of I (3.21 g) and acetic anhydride (2.0 g) in ether (35 ml), and the solution was stirred for 2 hr at room temperature. Ice water (50 g) was added to the reaction mixture and stirred for 30 min. Aqueous layer was extracted with ether and the combined organic layers were dried and the solvent was removed under reduced pressure. A mixed anhydride (XI, 3.66 g, 95%) of IV and acetic acid was obtained. IR (NaCl): 1820 and 1750 cm^{-1}. 11-Cyanoundcanoic acid (2.97 g, 93%) was obtained after being subjected to chromatography over silica gel. Ammonolysis of XI gave IV (65%) and VII (16%).

2-Acetoxyiminocyclododecanone (XII). 2-Hydroxyiminocyclododecanone (I, 2.52 g) was dissolved in acetic anhydride (10 ml) and the solution was heated at 50 °C for 1 hr. After treatment of the reaction mixture in the usual manner, acetate (XII, 2.91 g, 96%) was obtained and recrystallized from petroleum benzine, mp 60—61 °C.

Found: C, 66.46; H, 9.41; N, 5.59%. Calcd for $C_{14}H_{23}O_3N$: C, 66.37; H, 9.15; N, 5.53%.

Treatment of 2-Acetoxyiminocyclododecanone (XII) with Aqueous Sodium Hydroxide. Aqueous sodium hydroxide (5%, 20 ml) was added to a stirred solution of XII (1.5 g) in ether (2 ml), and the solution was stirred for 2 hr at room temperature. The reaction mixture was acidified with dilute hydrochloric acid and extracted with ether. 11-Cyanoundecanoic acid (1.19 g, 95%) was obtained by the usual method.

7-Cyanoheptanoic Acid (XIII). 2-Hydroxyiminocyclooctanone of *syn* form (II, *syn*) was treated with 97% phosphoric acid under the same reaction conditions as in the case of I. 7-Cyanoheptanoic acid (XIII) was obtained in 80% yield and recrystallized from petroleum ether, mp 34—35 °C. The *anti* form afforded XIII in 78% yield by the same treatment.

Found: C, 62.19; H, 8.42; N, 9.10%. Calcd for $C_8H_{13}O_2N$: C, 61.91; H, 8.44; N, 9.03%.

5-Cyanovaleric Acid (XIV) To a solution of cyclohexanone (10 g), sulfuric acid (1 ml), and dimethylformamide (5 ml) in ether (100 ml) was added a solution of nitrosyl chloride (7 g) in ether (20 ml) with stirring at −20 °C over a period of 20 min. The mixture was stirred for 10 min at −10 °C, and cooled to −30 °C. Aqueous sodium hydroxide (30%, 100 ml) was added and the mixture was stirred for 1 hr at room temperature. After separation of the ethereal layer, the aqueous layer was acidified with hydrochloric acid and extracted with dichloromethane. Evaporation of the solvent gave crude 5-cyanovaleric acid (XIV, 8.0 g) as pale brown liquid. Pure 5-cyanovaleric acid (6.8 g, 52%) was obtained by distillation under reduced pressure, bp 114—115 °C/0.2 Torr.

Found: C, 56.75; H, 7.01; N, 11.02%. Calcd for $C_6H_9O_2N$: C, 56.68; H, 7.14; N, 11.02%.

Methyl 5-cyanovalerate (XV) was obtained in 46% yield by methanolysis of the reaction mixture, bp 80—82 °C/1.0 Torr.

Found: C, 59.79; H, 7.90; N, 9.60%. Calcd for $C_7H_{11}O_2N$: C, 59.55; H, 7.85; N, 9.92%.

The Activation of Bivalent Sulfur Compounds with Cupric Chloride and Zinc Chloride. The Benzylation and Acylation of Aromatic Compounds with Sulfides and Thiol Esters

Kazuo MAEKAWA, Koichi NARASAKA, and Teruaki MUKAIYAMA

Laboratory of Organic Chemistry, Tokyo Institute of Technology, Ookayama, Meguro-ku, Tokyo 152

(Received April 4, 1973)

Benzylation of aromatic compounds, such as anisole, *m*-xylene, toluene, and benzene, with various benzyl sulfides in the presence of equimolar amounts of cupric chloride and zinc chloride was investigated. For example, in the case of benzylation of anisole with 4-benzylthiopyridine, *o*- and *p*-benzylanisoles were obtained in 79% yield in the presence of cupric chloride and zinc chloride. On the other hand, when the reaction was carried out in the presence of cupric chloride alone, the yield of benzylanisoles was low. The similar activation with cupric chloride and zinc chloride was successfully applied to the reaction of aromatic compounds with benzaldehyde diethylthioacetal and to the acylation of aromatic compounds with 1,2-bis(acylthio)ethanes.

The benzylation of aromatic compounds such as anisole, *m*-xylene, toluene, and benzene with benzyl sulfides in the presence of cupric chloride and zinc chloride were reported briefly in the previous paper.[1] In this report, these reactions are explained in detail with additional new results.

During the investigation on carbon–carbon bond forming reactions using benzaldehyde diethylthioacetal, benzophenone diethylthioacetal, and ethyl orthotrithioformate, it was found that these compounds react readily with active methylene compounds or anisole in the presence of cupric chloride to give the condensation or substitution products.[2] The reaction would be reasonably explained by considering an initial formation of a reactive intermediate, a coordinated compound of the bivalent sulfur compound with cupric chloride, which in turn is attacked by nucleophiles to give condensation or substitution products.

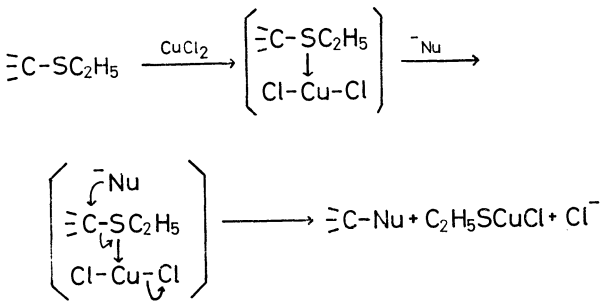

Based on the result, the reaction of sulfides with aromatic compounds was further investigated with the expectation that the sulfides would also be activated by the coordination with cupric chloride. When an anisole solution of equimolar amounts of benzyl methyl sulfide (**1**) and cupric chloride was heated to reflux, the generation of hydrogen chloride was observed immediately. After being stirred for 13 hr under reflux, the resulting precipitates were filtered off and the filtrate was concentrated under reduced pressure. Through the purification by silica gel column chromatography and distillation, *o*- and *p*-benzylanisoles (**2**, bp 115—116 °C/1.5 mmHg) were obtained in 53% yield.

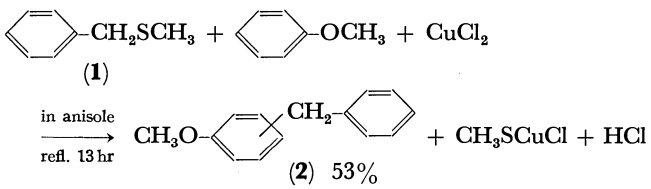

In order to increase the yield of benzylated products, a variety of benzyl sulfides (**3**), in which RS group would be stabilized by the resonance effect as an anion, was used in place of **1** in the above reaction. However, the yields of **2** were poor by the treatment of **3** in refluxing anisole in the presence of an equimolar amount of cupric chloride for 5 hr as shown in Table 1.

This result suggests that, only by the examination into the structure of leaving group (RS–), benzyl sulfides (**3**) are not sufficiently activated for generation of benzyl cation. Then, the coupled use of cupric chloride and zinc chloride was examined according to the assumption that the electron density of benzylic carbon would be decreased by coordination of zinc chloride to ring nitrogen atom. In fact, when the anisole solution of 4-benzylthiopyridine (**3e**) and equimolar amounts of cupric chloride and zinc chloride was heated to reflux for 5 hr, the yield of **2** was increased up to 79%. Similarly, in the reaction of other sulfides, yields of **2** were remarkably increased by the combined use of cupric chloride and zinc chloride. The results are shown in Table 1.

The yields of **2** were hardly improved and **2** were obtained in less than 10% yield when the some typical Lewis acids such as aluminum chloride, stannic chloride, ferric chloride, and boron trifluoride diethyletherate were used together with cupric chloride in place of zinc chloride. Among various Lewis acids examined, it was apparently shown that zinc chloride is most effective when it was used together with cupric chloride, but **2** could not be detected when zinc chloride was used alone. Then in order to examine the possibility that the increase of the yield may result from a coordination of zinc chloride to ring nitrogen atom of sulfides, the reaction of benzyl methyl sulfide (**1**) having no nitrogen atom in a molecule was investigated in the presence of equimolar amounts of cupric chloride

1) T. Mukaiyama, K. Maekawa, and K. Narasaka, *Tetrahedron Lett.*, **1970**, 4669.

2) T. Mukaiyama, K. Narasaka, and H. Hokonoki, *J. Amer. Chem. Soc.*, **91**, 4315 (1969); T. Mukaiyama, K. Narasaka, K. Maekawa, and H. Hokonoki, This Bulletin, **43**, 2549 (1970).

TABLE 1.

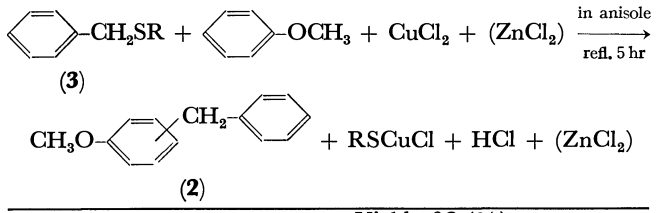

	3 RS–	Yield of 2 (%) $CuCl_2$	$CuCl_2+ZnCl_2$
a)	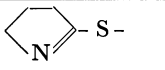	17	34
b)	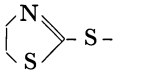	18	57
c)	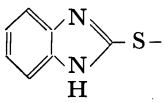	28	61
d)	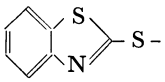	6	66
e)	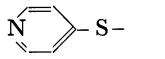	2	79
f)	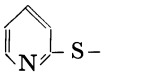	34	79

and zinc chloride. When anisole solution of **1**, cupric chloride and zinc chloride was heated to reflux for 5 hr, the yield of **2** was increased up to 76% as compared with the previous reaction using cupric chloride alone. The result indicates that zinc chloride would activate cupric chloride or the complex of cupric chloride with sulfide rather form a coordinated compound with sulfide.

In a similar way, the benzylation of other aromatic compounds such as *m*-xylene, toluene, and benzene with 4-(benzylthio)pyridine (**3e**) was carried out by the combined use of cupric chloride and zinc chloride, and the corresponding benzylated products, benzylxylenes, *o*- and *p*-benzyltoluenes, and diphenylmethane were obtained in 54, 34, and 15% yields respectively.

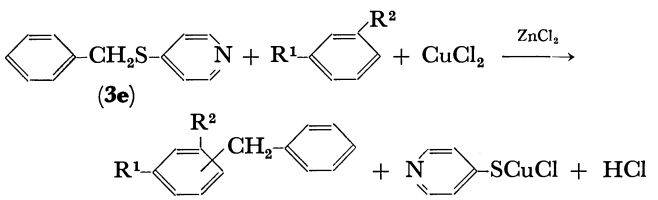

R^1	R^2	Yield (%)
CH_3	CH_3	54
CH_3	H	34
H	H	15

Previously, it was shown that benzaldehyde diethylthioacetal (**4**) reacts with anisole in the presence of cupric chloride to give the substituted product in good yield. On the other hand, it was shown that **4** did not react with other aromatic compounds such as *m*-xylene and toluene. The present method for the activation of sulfides with cupric chloride and zinc chloride was successfully applied to the reaction of **4** with *m*-xylene or toluene. When **4** was treated with *m*-xylene or toluene in the presence of equimolar amounts of cupric chloride and zinc chloride for 5 hr at room temperature, phenylxylylmethyl ethyl sulfides (**5a**) or phenyltolylmethyl ethyl sulfides (**5b**) were obtained in 16 or 11% yield.

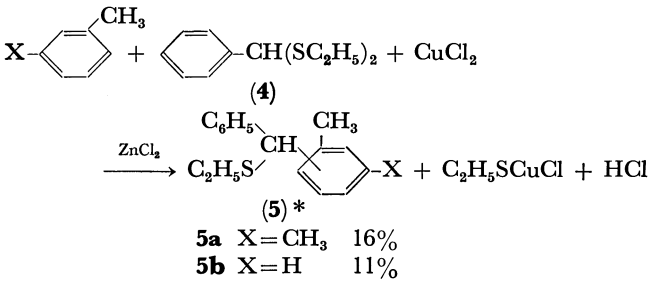

5a X=CH_3 16%
5b X=H 11%

* These structures are supported by elemental analysis and mass spectrum, but the study of structural isomerism remains not to be examined.

α,ω-Bis(benzylthio)alkanes (**6**) were also used effectively for the benzylation of aromatic compounds in place of the sulfides (**1** and **3**). It is expected that these sulfides (**6**) would form the chelate complexes by the intramolecular coordination of cupric chloride to the two sulfur atoms of the sulfide and benzyl cation would be easily generated. When **6** were treated in the presence of cupric chloride alone or cupric chloride and zinc chloride in refluxing anisole for 5 hr, benzylanisoles (**2**) were obtained as shown in Table 2.

TABLE 2.

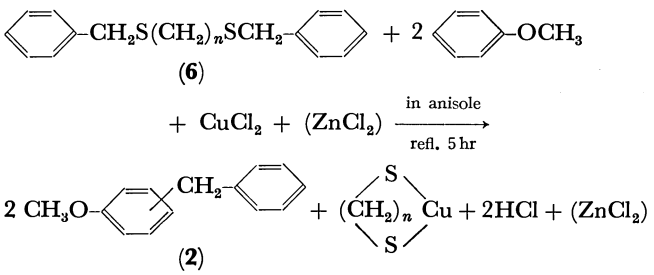

	n	Yield of 2 (%) $CuCl_2$	$CuCl_2+ZnCl_2$	$2(CuCl_2+ZnCl_2)$
6a	2	14	47	49
6b	3	11	56	58
6c	4	26	62	53

Bromobenzene was also benzylated by the reaction with 1,2-bis(benzylthio)ethane (**6a**) in the presence of equimolar amounts of cupric chloride and zinc chloride, and *o*- and *p*-bromophenylphenylmethanes were obtained in 14% yield.

Next, in order to examine the possibility of the cleavage of carbon–sulfur bond of thiolester by the use of cupric chloride and zinc chloride, the reaction of bis(acylthio)ethane with aromatic compounds was investigated. When anisole or *m*-xylene solution of 1,2-bis(benzoylthio)ethane (**7**) was heated to reflux in the presence of 2 equiv. of cupric chloride and zinc chloride for 7 hr, methoxybenzophenone (**8**) or phenylxylylketones (**9**) were obtained in 16 or 35% yield respectively together with about 15% of the recovered starting material (**7**).

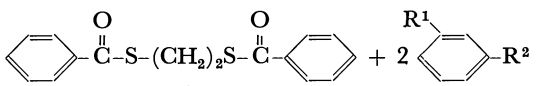

(7)

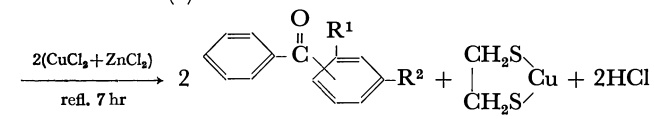

(8) $R^1=CH_3O$-, $R^2=H$ 16%
(9) $R^1=CH_3$, $R^2=CH_3$ 35%

In a similar manner, 1,2-bis(acetylthio)ethane (**10**) reacted with anisole, *m*-xylene, and toluene to give acetylation products (**11**, **12**, **13**) together with unidentified products.

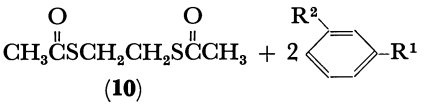

(10)

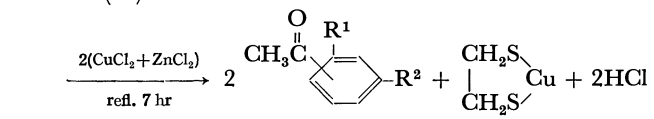

(11) $R^1=CH_3O$, $R^2=H$ 11%
(12) $R^1=R^2=CH_3$ 15%
(13) $R^1=CH_3$, $R^2=H$ 7%

In conclusion, it is noted that sulfides are sufficiently activated by the combined use of cupric chloride and zinc chloride and are attacked by aromatic compounds such as anisole, *m*-xylene, and toluene along with the cleavage of carbon–sulfur bond to form substitution products. This method for activation of sulfides by cupric chloride was successfully applied to our works of hydrolysis of 1,3-dithianes and reductive desulfurization of sulfides.[3]

Experimental

Materials. Commercially available cupric chloride and zinc chloride were used. They were dried over phosphorus pentoxide *in vacuo* at about 130 °C before use.

Benzyl methyl sulfide (**1**) and benzaldehyde diethylthioacetal (**4**) were prepared according to the procedures in literatures and purified by distillation: **1**, bp 97—101 °C/27 mmHg;[5] **4**, 135—136 °C/8 mmHg.[6]

Benzyl sulfides (**3a—f**) and α,ω-bis(benzylthio)alkanes (**6a—c**) were prepared by the treatment of the corresponding thiols with benzyl chloride in 95% ethanol in the presence of sodium hydroxide: **3a**, bp 120 °C/2 mmHg (lit, bp 134—135 °C/4 mmHg);[7] **3b**, bp 145—147 °C/1 mmHg (lit, bp 159—163 °C/3 mmHg);[8] **3c**, mp 184—185 °C (lit, mp 182—183 °C);[9] **3d**, mp 39—40 °C (lit, mp 40—41 °C);[10] **3e**, mp 64—65 °C (lit, mp 61—62 °C);[11] **3f**, bp 145—146 °C/2 mmHg (lit, bp 92—94 °C/0.1 mmHg);[11] **6a**, mp 34—35 °C (lit, mp 38 °C);[12] **6b**, bp 158 °C/0.07 mmHg (lit, bp 218—221 °C/8—9 mmHg);[13] **6c**, bp 167 °C/0.08 mmHg (Found: C, 71.38; H, 7.11; S, 21.30%. Calcd for $C_{18}H_{22}S_2$: C, 71.50; H, 7.11; S, 21.17%).

Thiolesters (**7**) and (**10**) were prepared by treatment of the petroleum ether solution of 1,2-ethanedithiol and pyridine with the corresponding acyl chlorides at 0 °C: **7**, mp 95 °C (lit, mp 96 °C);[14] **10**, mp 68—69 °C (lit, mp 68—73 °C).[15]

Reaction of Benzyl Methyl Sulfide (1) with Anisole in the Presence of an Equimolar Amount of Cupric Chloride. A mixture of **1** (1.38 g, 0.01 mol), cupric chloride (1.35 g, 0.01 mol) and dry anisole (30 ml) was heated to reflux for 13 hr. The color of the solution turned black and white precipitates formed. The precipitates were filtered off and the filtrate was concentrated under reduced pressure. The residue was then purified by silica gel column chromatography. The eluate with petroleum ether was concentrated and distilled, giving 1.05 g (53%) of benzylanisoles (**2**) (bp 115—116 °C/1.5 mmHg). The isomer ratio (*para* to *ortho*) of benzylanisoles was determined to be about 2 by two sets of singlets at τ 6.50 and 6.47 (ratio 2: 1, total area 3H) due to the methyl group. Found: C, 84.63; H, 7.07%. Calcd for $C_{14}H_{14}O$: C, 84.81; H, 7.12%. IR: 2830(OCH_3), 1030(C–O) cm^{-1}. Mass: M^+ 198, *m/e* 183[M^+–CH_3], *m/e* 167[M^+–OCH_3], *m/e* 121[M^+–C_6H_5], *m/e* 91[$C_6H_5CH_2^+$]. NMR: (in CCl_4) τ 6.50 (s, 2H, *p*-OCH_3), 6.47 (s, 1H, *o*-OCH_3), 6.25 (s, 1.3H, *p*-$C_6H_5CH_2$), 6.12 (s, 0.7H, *o*-$C_6H_5CH_2$–), 2.40—3.45 (m, 9H, aromatic protons).

Benzyl sulfides (**3a—f**) were treated in refluxing anisole with an equimolar amount of cupric chloride for 5 hr, and **2** was obtained according to the same procedure. The yields of **2** were listed in Table 1.

Reaction of 4-(Benzylthio)pyridine (3e) with Anisole in the Presence of Equimolar Amounts of Cupric Chloride and Zinc Chloride. A mixture of **3e** (2.01 g, 0.01 mol), cupric chloride (1.35 g, 0.01 mol), zinc chloride (1.36 g, 0.01 mol), and dry anisole (50 ml) was heated to reflux for 5 hr. According to the same procedure, benzylanisoles (**2**) were obtained (1.57 g, 79%).

Similarly, **3a—d** and **3f** were treated with equimolar amounts of cupric chloride and zinc chloride in refluxing anisole for 5 hr, and the yields of **2** were listed in Table 1.

Reaction of 4-(Benzylthio)pyridine (3e) with m-*Xylene in the Presence of Equimolar Amounts of Cupric Chloride and Zinc Chloride.* A mixture of **3e** (2.01 g, 0.01 mol), cupric chloride (1.35 g, 0.01 mol), zinc chloride (1.36 g, 0.01 mol) and dry *m*-xylene (50 ml) was heated to reflux for 7 hr. The reaction mixture was purified according to the same procedure as mentioned in the reaction of **1** with anisole, and phenylxylylmethanes (bp 115 °C/3 mmHg, 2 or 5- and 4-isomers in a ratio of 2: 13) were obtained in 54% (1.06 g) yield. Found: C, 92.03; H, 8.08%. Calcd for $C_{15}H_{16}$: C, 91.78; H, 8.22%. NMR: (in CCl_4) τ 7.92 and 7.80 (s, 5.2H, 4-isomer-CH_3), 7.85 (s, 0.8H, 2 or 5-isomer-CH_3), 6.20 (s, 1.7H, 4-isomer-$CH_2C_6H_5$), 6.08 (s, 0.3H, 2 or 5-isomer-$CH_2C_6H_5$).

Phenyltolylmethanes and diphenylmethane were also obtained by treating **3e** with toluene and benzene. Their

3) K. Narasaka, T. Sakashita, and T. Mukaiyama, *Bull. Chem. Soc. Jap.*, **45**, 3724 (1972); K. Narasaka, M. Hayashi, and T. Mukaiyama, *Chem. Lett.*, **1972**, 259.
5) J. V. Brown and P. Engelberg, *Chem. Ber.*, **56**, 1573 (1923).
6) M. L. Wolform, and J. V. Karavinos, *J. Amer. Chem. Soc.*, **66**, 909 (1944).
7) T. M. Varonkina, I. T. Strukov, M. F. Shostakovskii, and A. A. Avetisyan, *Biol. Aktivn. Soedin., Akad. Nauk SSSR*, **1965**, 199, *Chem. Abstr.*, **63**, 18017g (1965).
8) H. Goddin and N. E. Searle, Brit. 575004, *Chem. Abstr.*, **41**, 4272 (1947).
9) S. Nakajima, I. Tanaka, T. Seki, and T. Anmo, *Yakugaku Zasshi*, **78**, 1378 (1958).
10) K. N. Ayad, E. B. McCall, A. J. Neale, and L. M. Jackman, *J. Chem. Soc.*, **1962**, 2070.
11) R. A. Jones and A. R. Katritzky, *ibid.*, **1958**, 3610.
12) E. Fromm, H. Benzinger, and F. Scharfer, *Ann.*, **394**, 27 (1912).
13) W. Autenrieth and K. Wolff, *Chem. Ber.*, **32**, 1373 (1899).
14) S. Gabriel and P. Heymann, *ibid.*, **24**, 784 (1891).
15) E. K. Ellingboe, U. S., 2423641, *Chem. Abstr.*, **42**, 3774[1] (1948).

physical properties and analytical data are as follows. Phenyltolylmethanes (*ortho* and *para* isomers in a ratio of 5: 4): bp 109—109.5 °C/3.5 mmHg. Found: C, 92.43; H, 7.90%. Calcd for $C_{14}H_{14}$: C, 92.26; H, 7.74%. NMR: (in CCl_4) τ 7.85 (s, 1.3H, *p*-CH_3), 7.76 (s, 1.7H, *o*-CH_3), 6.18 (s, 1.1H, *o*-$CH_2C_6H_5$), 6.13 (s, 0.9H, *p*-$CH_2C_6H_5$). Diphenylmethane: bp 83 °C/4 mmHg. Found: C, 92.07; H, 7.30%. Calcd for $C_{13}H_{12}$: C, 92.81; H, 7.19%. Mass: M^+ 168, *m/e* 91 [$C_6H_5CH_2^+$].

Reaction of Benzaldehyde Diethylthioacetal (4) with m-*Xylene in the Presence of Equimolar Amounts of Cupric Chloride and Zinc Chloride.* A mixture of **4** (4.24 g, 0.02 mol), cupric chloride (2.69 g, 0.02 mol), zinc chloride (2.73 g, 0.02 mol), and dry *m*-xylene (50 ml) was stirred for 8 hr at room temperature and kept standing overnight. The precipitates were filtered off and the filtrate was concentrated under reduced pressure. The resulting oil was chromatographed on alumina gel. In order to hydrolyze the recovered **4**, the petroleum ether eluate was concentrated and treated in refluxing 95% ethanol in the presence of potassium hydroxide for half an hour. After removal of the solvent, the residue was extracted with ether and washed with water. The ether layer was concentrated and chromatographed on silica gel. The petroleum ether eluate was distilled and 0.98 g (16%) of phenylxylylmethyl ethyl sulfides (**5a**, bp 165 °C/4 mmHg) were obtained. Found: C, 79.40; H, 7.87; S, 12.57%. Calcd for $C_{17}H_{20}S$: C, 79.65; H, 7.86; S, 12.48%. Mass: *m/e* 195 [M^+–C_2H_5S], *m/e* 179 [M^+–C_6H_5], *m/e* 151 [M^+–$C_6H_3(CH_3)_2$]. Similarly, phenyltolylmethyl ethyl sulfides (**5b**, bp 150—151 °C/4 mmHg) were produced from **4** and toluene. Found: C, 79.52; H, 7.60; S, 12.78%. Calcd for $C_{16}H_{18}S$: C, 79.31; H, 7.49; S, 13.21%. Mass: *m/e* 181 [M^+–C_2H_5S], *m/e* 165 [M^+–C_6H_5], *m/e* 151 [M^+–C_6H_4-CH_3].

Reaction of 1,3-Bis(benzylthio)propane (6b) with Anisole in the Presence of Two Equimolar Amounts of Cupric Chloride and Zinc Chloride. A mixture of **6b** (2.88 g, 0.01 mol), cupric chloride (2.69 g, 0.02 mol), zinc chloride (2.73 g, 0.02 mol), and dry anisole (50 ml) was heated to reflux for 5 hr. The reaction mixture was treated according to the same procedure as in the case of the reaction of benzyl methyl sulfide (**1**) and anisole, and 2.22 g (56%) of benzylanisoles (bp 119—123 °C/3 mmHg) were obtained.

Reaction of 1,2-Bis(benzylthio)ethane (6a) with Bromobenzene in the Presence of Equimolar Amounts of Cupric Chloride and Zinc Chloride. A mixture of **6a** (2.74 g, 0.01 mol), cupric chloride (1.35 g, 0.01 mol), zinc chloride (1.36 g, 0.01 mol), and dry bromobenzene (50 ml) was heated to reflux for 6 hr. After filtration of a tarry substance, the filtrate was purified by silica gel column chromatography and distillation. Bromophenylphenylmethanes (*ortho* and *para* isomers in a ratio of 9: 11) were obtained, 0.69 g (14%) (bp 122 °C/1 mmHg). Found: C, 63.31; H, 4.60%. Calcd for $C_{13}H_{11}Br$: C, 63.18; H, 4.49%. NMR: (in CCl_4) τ 6.34 (s, 1.1H, *p*-$C_6H_5CH_2$), 6.49 (s, 0.9H, *o*-$C_6H_5CH_2$), 2.40—3.30 (m, 9H). Mass: *m/e* 248 (M^++2) and 246 (M^+) (*ca.* 1: 1 ratio).

Reaction of 1,2-Bis(benzoylthio)ethane (7) with Anisole in the Presence of Equimolar Amounts of Cupric Chloride and Zinc Chloride. A mixture of **7** (6.04 g, 0.02 mol), cupric chloride (2.69 g, 0.02 mol), zinc chloride (2.73 g, 0.02 mol), and dry anisole (50 ml) was heated to reflux for 7 hr. The tarry substance sticked to the vessel was filtered off and the filtrate was chromatographed on silica gel. The petroleum ether eluate gave a viscous oil, which was fractionated by distillation to give 0.92 g of phenyl benzoate (bp 119—121 °C/4 mmHg, mp 70 °C) and 1.73 g of the starting material (**7**) (mp 93 °C). The benzene eluate was condensed and distilled to give 0.70 g (8%) of methoxybenzophenone (**8**, bp 156 °C/2.5 mmHg, mp 59—61 °C): Found: C, 79.03; H, 5.69%. Calcd for $C_{14}H_{12}O_2$: C, 79.22; H, 5.70%. IR: 2840 (OCH_3), 1638 (C=O), and 1020 (C–O) cm^{-1}. NMR: (in $CDCl_3$) τ 6.07 (s, 3H, OCH_3), 2.0—3.07 (m, 9H). The ether eluate gave 0.74 g of benzoic acid (mp 120—121 °C). The reaction of 1,2-bis(benzoylthio)ethane (**7**) with *m*-xylene was carried out according to the same procedure, and phenylxylylketones (**9**) were isolated in 35% yield, (bp 130 °C/1 mmHg, 2 or 5- and 4-isomers in a ratio of 1: 9). Found: C, 85.52; H, 6.71%. Calcd for $C_{15}H_{14}O$: C, 85.68; H, 6.71%. IR: 1665 (C=O) cm^{-1}. NMR: (in $CDCl_3$) τ 7.87 (s, 0.7H, 2 or 5-isomer-CH_3), 7.66 and 7.61 (s, 5.3H, 4-isomer-CH_3), 2.10—3.05 (m, 8H).

Reaction of 1,2-Bis(acetylthio)ethane (10) with Anisole in the Presence of Two Equimolar Amounts of Cupric Chloride and Zinc Chloride. A mixture of **10** (1.78 g, 0.02 mol), cupric chloride (2.69 g, 0.02 mol), zinc chloride (2.73 g, 0.02 mol), and dry anisole (50 ml) was heated to reflux for 7 hr. According to the same procedure as in the above experiment, 0.54 g of unidentified products and 0.32 g (11%) of methoxyacetophenone (**11**, bp 88 °C/1 mmHg) were obtained. Found: C, 71.42; H, 6.65%. Calcd for $C_9H_{10}O_2$: C, 71.98; H, 6.71%. NMR: (in $CDCl_3$) τ 7.48 (s, 3H, CH_3-CO), 6.16 (s, 3H, OCH_3), 2.0—3.15 (m, 4H). Mass: M^+ 150, *m/e* 135 [M^+–CH_3], *m/e* 107 [M^+–$COCH_3$].

Similarly, the reaction of **10** with *m*-xylene or toluene was carried out, and the physical properties and analytical data of the products (**12** or **13**) were as follwos. **12**: bp 103—104 °C/13 mmHg. Found: C, 80.43; H, 8.39%. Calcd for $C_{10}H_{12}O$: C, 81.04; H, 8.16%. NMR: (in CCl_4) τ 7.67 (s, 3H, CH_3), 7.52 (s, 6H, CH_3+$COCH_3$), 2.38—3.03 (m, 3H). Mass: M^+ 148, *m/e* 133 [M^+–CH_3], *m/e* 105 [M^+–$COCH_3$]. **13**: bp 84 °C/10 mmHg. NMR: (in CCl_4) τ 7.63 (s, 3H, $COCH_3$ or CH_3), 7.56 (s, 3H, CH_3 or $COCH_3$), 2.15—2.91 (m, 4H). Mass: M^+ 134, *m/e* 119 [M^+–CH_3], *m/e* 91 [M^+–$COCH_3$].

Kinetic Study of the Pyrolysis of 1- and 2-Phenylethyl Phenyl *N*-Tosylsulfilimines[1]

Shigeru OAE, Katsumasa HARADA, Kenji TSUJIHARA, and Naomichi FURUKAWA

Department of Applied Chemistry, Faculty of Engineering, Osaka City University, Sugimoto-cho, Osaka 558

(Received April 26, 1973)

The pyrolysis of 1-phenylethyl phenyl *N*-tosylsulfilimine was found to proceed more than 10^3 times faster than that of ethyl phenyl derivative. The large rate enhancement suggests that the mechanism changes from an ideal *cis*-elimination to nearly E1 type. However, substituent effect, kinetic isotope effect with 1-phenylethyl-2,2,2-d_3 phenyl *N*-tosylsulfilimine and solvent effect clearly reveal that the reaction proceeds *via* an intramolecular concerted process.

In a previous paper we reported that the pyrolysis of alkyl *N*-tosylsulfilimine having β-hydrogen gives olefin in a high yield,[2] and the reaction was suggested to proceed through a concerted *cis*-elimination process based on both kinetic and stereochemical results.[3]

When the sulfilimine having both α and β phenyl groups was subjected to pyrolysis, the rate of the reaction was found to be accelerated by a factor of 10^3 times higher than the unsubstituted sulfilimine. This enormously large rate enhancement by the phenyl groups gives rise to a consideration of the nature of the concerted process for the pyrolysis namely, whether or not the reaction proceeds *via* an internal concerted *cis*-elimination route[4] or through a different mechanism such as E1 type mechanism[5] or radical pair mechanism[6] involving the rate-determining C–S bond cleavage or through some alternative pathway which involves the rate-determining C–H bond fission at the transition state[7] (nearly carbanion type mechanism). All the possible mechanistic pathways are schematically shown in Fig. 1.

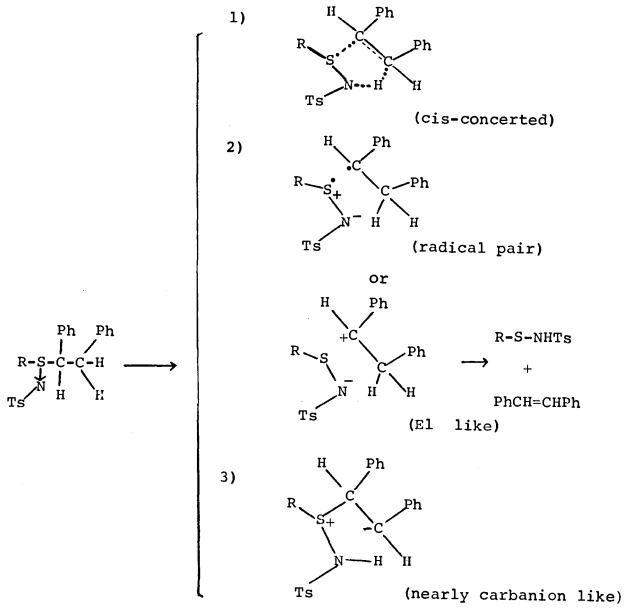

Fig. 1. Possible mechanistic scheme for the E1 reaction.

In order to understand the nature of the pyrolysis and thus be able to make a choice of mechanism, 1- and 2-phenylethyl phenyl *N*-tosylsulfilimines were prepared and subjected to pyrolysis. This paper gives a detailed account of the kinetic study of the pyrolysis and implication of the data for understanding of the mechanism.

Results and Discussion

Preparation of Sulfilimine. The sulfilimines used for the pyrolysis were 1-(substituted)phenylethyl phenyl- (I), 1-phenylethyl(substituted)phenyl (II) and 2-phenylethyl phenyl *N*-tosylsulfilimines (III) prepared by treating the corresponding sulfides with chloramine-T in methanol solution, as shown below. The mp, elemental analyses, and IR spectra are listed in Table 1.

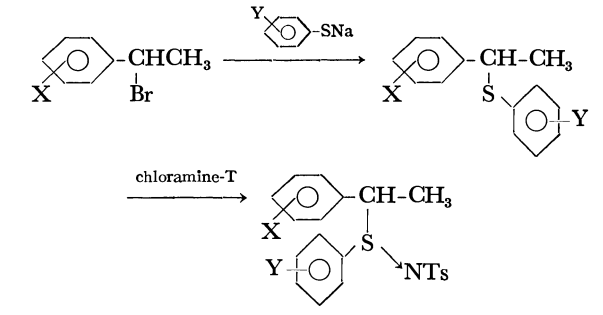

I : X=*p*-CH_3, H, Cl, *m*-NO_2, Y=H
II: X=H, Y=*p*-CH_3O, *p*-CH_3, H, *p*-Cl

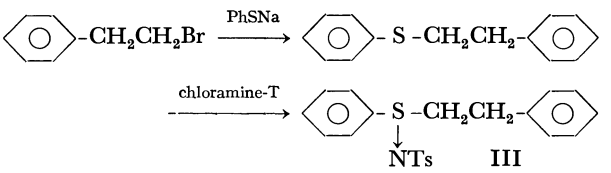

1) Part IV of Ei reaction.

2) S. Oae, K. Tsujihara, and N. Furukawa, *Tetrahedron Lett.*, **1970**, 2663.

3) K. Tsujihara, N. Furukawa, and S. Oae, *Tetrahedron*, **27**, 4921 (1971); K. Tsujihara, K. Harada, N. Furukawa, and S. Oae, *ibid.*, **27**, 6101 (1971).

4) For Ei reaction, D. V. Banthorpe, "Elimination Reactions," Elsvier Publish., Co., N. Y. (1963), p. 167.

5) R. Taylor and G. G. Smith, *Tetrahedron*, **19**, 937 (1963); R. Taylor, G. G. Smith, and W. H. Wetzel, *J. Amer. Chem. Soc.*, **84**, 4817 (1962).

6) C. A. Kingsbury and D. J. Cram., *ibid.*, **82**, 1810 (1960).

7) A. C. Cope, N. A. Lebel, H. H. Lee, and W. R. Moore, *ibid.*, **79**, 4720 (1957).

TABLE 1.

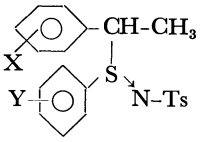

X	Y	Mp (°C)	Elemental analysis Calcd C%	Calcd H%	Calcd N%	Found C%	Found H%	Found N%	IR (cm^{-1}) (-S=N-)
p-CH_3	H[a)]	91—91.5	66.50,	5.80,	3.53	65.73	5.57	3.65	960
H	H	102.5—103							960
p-Cl	H	111—111.5	60.00	4.78	3.36	60.03	4.73	3.36	960
m-NO_2	H	113—114	58.80,	4.67	6.55	58.58	4.43	6.50	965
H	*p*-OCH_3	73.5—74	63.37	5.57	3.44	63.39	5.47	3.40	948
H	*p*-CH_3	94.5—95	66.60	5.80	3.53	66.40	5.73	3.67	955
H	*p*-Cl	83—83.5			3.46			3.75	975

a) The compound is unstable at room temperature and decomposes gradually during the course of purification.

Kinetics and Product Analysis. The pyrolysis was carried out by heating a solution of the desired sulfilimine in benzene. Products were not isolated after reaction except in the case of 2-phenylethyl phenyl *N*-tosylsulfilimine, from which styrene was isolated in more than 60% yield. However, the products derived from (I) and (II) were found to be both substituted styrene and arenesulfenyl *p*-toluenesulfonamide, since the NMR spectrum of the reaction mixture in $CDCl_3$, which had been left to stand for some days until the signals of methine and methyl protons of the sulfilimine disappeared, showed a complete 1 : 1 mixture of substituted styrene and arenesulfenyl *p*-toluenesulfonamide as shown in Fig. 2. We can thus conclude that the yield of olefin is nearly quantitative. The kinetic measurements were carried out by following the IR absorption band of the product, *i.e.* the –NH– band of arenesulfenyl *p*-toluenesulfonamide appeared at 3280 cm^{-1}. The rates of the pyrolysis were correlated with the first-order rate equation. The kinetic data obtained from the above reaction are summarized in Tables 2 and 3.

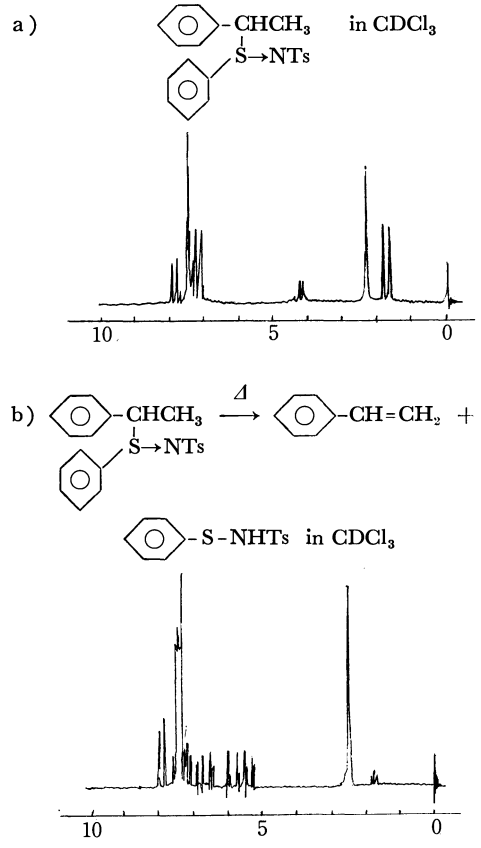

Fig. 2. NMR Spectra of 1-phenylethyl phenyl sulfilimine (a) and the products after the Reaction (b).

Solvent Effect. The pyrolysis was carried out in various solvents, the rate constants obtained being summarized in Table 4. We see that the pyrolysis is not much affected by solvent. Even the change in polarity of the solvent from benzene (ε=2.27) to nitrobenzene (ε=34.6) or acetonitrile (ε=37.5) changes the rate not more than five fold. This seems to indicate that the transition state of the reaction is neither ionic nor radical. In ethanol, the reaction proceeded slowly and the yield of olefin was low. Apparently the initial C–S bond cleavage took place concurrently with the elimination giving rise to some substitution products such as 1-phenyl ethyl ethyl ether. The rate is also low in chloroform suggesting that the hydrogen bond formation between imino nitrogen and acidic hydrogen of chloroform prevents an attack of the terminal nitrogen to β-proton. This is also the case with ethanol. Acetonitrile also retards the reaction slightly. As in a similar retardation of pyrolysis in DMSO, the dipolar

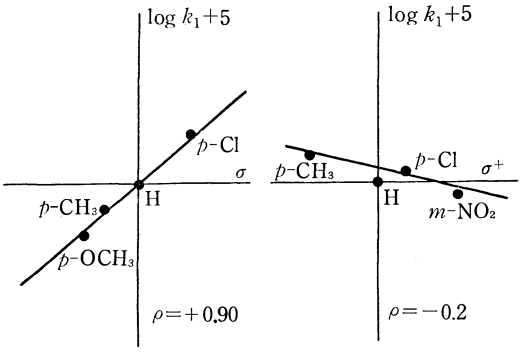

Fig. 3. Hammett equation.

TABLE 2. SUBSTITUENT EFFECTS

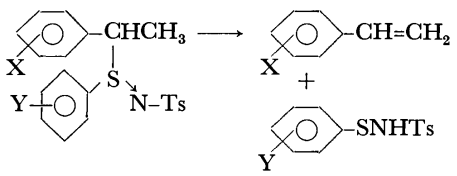

X	Y	Temp (°C)	$k_1 \times 10^5$ (sec^{-1})	$\Delta H^{\ddagger}$ (kcal/mol)	$\Delta S^{\ddagger}$(e.u.)
H	H	10.0±0.05	1.27		
		25.0	7.87	20.8	−7.2
		35.0	24.2		
p-CH_3	H	10.0	1.60		
		15.0	4.68	22.6	−2.7
		25.0	17.8		
		28.0	20.2		
p-Cl	H	10.0	1.31		
		15.0	2.75	22.8	−2.1
		25.0	11.1		
		28.0	15.1		
m-NO_2	H	9.5	0.90	24.4	+3.2
		15.0	7.43		
		25.0	9.55		
		28.0	13.6	$\rho_X = -0.20$	
H	*p*-Cl	25.0	10.1		
H	*p*-CH_3	25.0	5.16	$\rho_Y = 0.90$	
H	*p*-OCH_3	25.0	3.69		
PhCHCD$_3$ (PhS, NTs)		25.0	2.67	$k_H/k_D = 2.90$ (solvent; benzene)	

interaction between acetonitrile and the sulfilimine shown schematically below would be responsible for the small retardation.

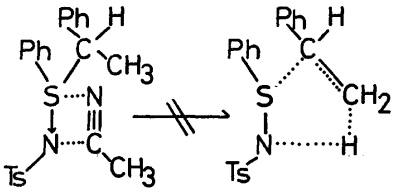

Hammett Equation and Isotope Effect. The substituent effects (Table 2) seem to be correlated nicely with Hammett σ values. Substituents Y gave a good straight line with $\rho_Y = +0.90$, while the effect of X is very small and gave hardly any correlation with either σ or σ^+ values. Apparently the electron-donating substituent such as *p*-CH_3 accelerated the reaction while the electron-withdrawing substituent retarded it. The ρ values though small, indicate a negative trend and is roughly estimated to be $\rho = -0.2$. The Hammett relation is shown in Fig. 3. The kinetic isotope effect was measured from the rate constants of 1-phenylethyl 2,2,2-d_3 phenyl *N*-tosylsulfilimine and the corresponding undeuterated compound, and found to be $k_H/k_D = 2.90$. The data in Table 3 indicate that the rate promotion in the pyrolysis is found to be mainly due to α-phenyl group which accelerates the reaction around 10^3 times as compared to one without it, while the β-phenyl group accelerates the reaction only 1.5 times or at most 2.5 times, though correcting the number of available β hydrogen atoms. The following conclusions can be obtained. (1) The rather small rate-enhancing effect of the β-phenyl group rules out the nearly carbanion like mechanism, since either E1 or E2 reaction which is presumed to proceed *via* nearly carbanion-like mechanism[7] should show an enormous large rate enhancement by β-phenyl group. For example, ethyl methyl phenethyl amine oxide undergoes E1 reaction more than 10^2 times faster than the phenyl unsubstituted derivative, while dimethyl ethyl phenethyl quarternary ammonium hydroxide decomposes 2.7×10^4 times faster than the compound having no β-phenyl group. (2) Although a large rate enhancement by the α-phenyl group could suggest an E1 route, this is

TABLE 4. SOLVENT EFFECT ON PYROLYSIS OF 1-PHENYLETHYL PHENYL *N*-TOSYLSULFILIMINE

Solvents	Reaction Temp (°C)	ε	k_1 (sec^{-1})
Benzene	40.0	2.27	2.55×10^{-4}
Toluene	40.0	2.38	5.41
Chlorobenzene	40.0	5.61	3.24
Nitrobenzene	40.0	34.6	2.29
CH_3CN	40.0	37.5	1.20
EtOH	40.0	24.3	not measured
$CHCl_3$	40.0	4.7	1.42

TABLE 3. THE RELATIVE RATES OF PYROLYSIS OF SULFILIMINES

Sulfilimine	Temp (°C)	k_1 (sec^{-1})	Rel.Rates	$\Delta H^{\ddagger}\left(\frac{\text{kcal}}{\text{mol}}\right)$	$\Delta S^{\ddagger}$ (e.u)
Ph–SCH_2CH_3 (NTs)	60.5	0.01×10^{-5}			
	80.3	1.08	1	26.5	−5.8
	100.5	9.85			
Ph–SCH_2CH_2Ph (NTs)	90.2	2.84			
	95.2	6.28			
	100.0	10.3	1.5	25.7	−8.6
$PhSCH(Ph)CH_3$ (NTs)	22.4	5.40			
	31.0	16.0	10^3	20.8	−7.2
	35.0	24.2			
Ph–S(NTs)–CH(Ph)CH(Ph)OCH_3					
erythro-	60.0	10.1	10^2		
threo-		16.5	1.5×10^2		

ruled out since both N–H bond forming and C–S bond breaking are apparently involved in the transition state in view of the relatively large β-hydrogen kinetic isotope effect. Recently an E1-like mechanism was proposed by Burgess, Penton, and Taylor for the solvolyitic internal elimination reaction of 1,2-diphenylethyl-*N*-carbomethoxysulfamate triethylammonium salt. In this case the kinetics suggests that although stereospecificity is maintained, only a small β-hydrogen kinetic isotope effect (1.05~1.08) is obtained.[8] The small negative ρ_x value might suggest the involvement of a radical pair mechanism proposed by Cram[6] for the pyrolysis of the four diastereomeric 1,2-diphenyl-1-propyl phenyl sulfoxides. However, this is also ruled out since the free radical mechanism involving the prior C–S bond cleavage is not in accord with the relatively large kinetic isotope effect. The ESR taken with the reaction conditions did not show any signals and there was no particular effect by oxygen or radical scavenger. Styrene placed in the reaction vessel did not polymerize under the reaction conditions. Thus, the radical type mechnism can be ruled out. (3) Recently we found that optically active benzyl *p*-tolyl *N*-tosylsulfilimine undergoes very facile thermal racemization apparently *via* pyramidal inversion[9] without involving C–S bond fission. This result together with the solvent effect on the pyrolysis indicates that either the initial radical or the ionic C–S bond fission mechanism (2) can be neglected. Thus, the present data are consistent with the *cis*-concerted mechanism which we predicted.[2,3] Although the relative rate of α-phenyl substituted sulfilimine is 10^3 times larger than that of the unsubstituted one, both ρ_y and isotope effects are nearly identical in both series. *i.e.*, $\rho_y=+0.90$ (α-phenyl), +0.90 (α-H); $k_H/k_D=2.90$ (α-phenyl), 3.03 (α-H) respectively. Therefore, the pyrolysis of these sulfilimines appears to proceed *via* an ideal five-membered transition state during the course of reaction regardless of the structural change. The large rate enhancement by the α-phenyl group is undoubtedly associated with the stabilization of the transition state by the effective conjugation with the developing double bond at the transition state.[10] The small negative trend of ρ_x value appears somewhat strange, but it may be due to the change of transition state with the change of substituent on the phenyl ring, namely the timing of C–S bond fission and C–H bond fission differs with substituent, compensating the substituent effect. This phenomenon is also observed in the case of E2 reaction of α-substituted phenethyl bromide.[11] These results suggest that the pyrolysis of sulfilimine proceeds *via* an internal concerted *cis* elimination involving a five membered transition state though the reaction is accelerated 10^3 times by the α-phenyl group.

8) E. M. Burgess, H. R. Penton, Jr., and E. A. Taylor, *J. Amer. Chem. Soc.*, **92**, 5224 (1970).

9) N. Furukawa, K. Harada, and S. Oae, *Tetrahedron Lett.*, **1972**, 1377.

10) The substitution of a phenyl group, e.g., phenethyl halide or tosylate, is known to accelerate the solvolysis reaction around 10^3 times.

11) T. Yoshida, Y. Yano, and S. Oae, *Tetrahedron*, **27**, 5343 (1971).

Table 5. Kinetics of 1-(*p*-chlorophenyl)ethyl phenyl *N*-tosylsulfilimine in benzene at 25°C

	min	log I_0/I	log C_0/C	k	sec^{-1}
1)	0	0.0464	0.1464		
	30	0.0653	0.2269	1.18	
	60	0.0856	0.3308	1.05	
	90	0.0916	0.4546	1.22	
	120	0.1066	0.4742	1.17	
	150	0.1212	0.6107	1.03	
		0.1605			1.13×10^{-4}
2)	0	0.0306	0.1057		
	20	0.0453	0.1667	1.17	
	40	0.0580	0.2278	1.17	
	60	0.0650	0.2655	1.02	
	80	0.0747	0.3239	1.04	1.10×10^{-4}
		0.1421		av.	$k=1.11\pm0.01$

Activation parameters were calculated by the usual method.

Experimental

Preparation of Sulfilimine. 1- And 2-arylethyl bromides were prepared according to the known method.[12] They were treated with sodium thiophenoxide in ethanol solution to afford the corresponding sulfide in a 70% yield. The sulfilimines were prepared by treating the sulfides with chloramine-T.[13] A typical example is as follows. 1-Phenylethyl phenyl sulfide (2 g) was dissolved in 25 ml of methanol containing a drop of acetic acid. To this was added 2.9 g of chloramine-T in methanol at 0 °C. After being stirred for 1 hr, methanol was removed at room temperature. The residue was added to ice–water containing a dilute sodium hydroxide solution. The precipitates were separated and dried. The crude crystals were recrystallized from methanol. The yield was 50%. The IR spectral data are summarized in Table 1.

Product Analysis. The products were not actually isolated. The identification of substituted styrenes and arenesulfenyl *p*-toluenesulfonamide was carried out by means of NMR and IR spectra. Sulfilimine was dissolved in $CDCl_3$ in an NMR tube. The tube was kept standing at room temperature or heated at 50 °C until the methyl doublet or methine quartet of phenylethyl protons completely disappeared. The spectra obtained were all of 1:1 mixture of styrene and the sulfenamide. In benzene solution, the products were the same as those in $CDCl_3$.

Preparation of 1-Phenylethyl-2,2,2-d_3 *Phenyl* N-*Tosylsulfilimine.* *Acetophenone-*d_3: Acetophenone (5.0 g) was dissolved in 15 ml of dioxane containing 5.0 g of deuterium oxide, and 0.5 g of triethylamine. The mixture was heated at 100 °C for 10 hr. Water was removed as a dioxane azeotrope and dioxane was removed by distillation. A new mixture of dioxane, deuterium oxide, and triethylamine was added to the residue. The procedure was repeated four times. The NMR spectra showed no protons in the methyl group (2.5 ppm) bp 87 °C/2 mmHg.

*1-Phenylethyl Alcohol-*2,2,2-d_3: The deuterated acetophenone (5.0 g) was reduced with lithium alminum hydride by the usual method. Bp 90 °C/10 mmHg, yield 55%.

*1-Phenylethyl Bromide-*2,2,2-d_3: The deuterated alcohol was

12) H. C. Brown, I. Moritani, and Y. Okamoto, *J. Amer. Chem. Soc.*, **78**, 2193 (1956).

13) K. Tsujihara, N. Furukawa, K. Oae, and S. Oae, This Bulletin, **42**, 2631 (1969).

converted into the bromo compound with phosphorus tribromide. The NMR showed no protons in the methyl group. Bp 67 °C/3 mmHg, yield 60%.

1-Phenylethyl-2,2,2-d_3 *Phenyl* N-*Tosylsulfilimine*: The sulfilimine was prepared from the sulfide and chloramine- T. Mp 102.0—103 °C, yield 73%.

Kinetics. A pre-cooled solution of 0.5～1% sulfilimine in anhydrous solvents was prepared and sealed into 2 ml ampoules, which were immersed in a constant temperature bath. At an appropriate time, the ampoules were taken out one by one and frozen in a dry-ice–acetone bath to stop the reaction. The reaction rate was then calculated by following the increase of the IR intense –NH– stretching absorption band at 3280 cm^{-1} due to sulfenamide produced. The reaction was found to follow a good first-order kinetic equation. A typical example of the kinetics is shown in Table 5.

BULLETIN OF THE CHEMICAL SOCIETY OF JAPAN, VOL. 46, 3486—3489 (1973)

Reaction of 4-Picoline *N*-Oxide with Acetic Anhydride as Studied by Chemically Induced Dynamic ^{13}C Polarization (CIDNP)[1)]

Hiizu IWAMURA, Michiko IWAMURA,* Mamoru IMANARI,** and Makoto TAKEUCHI**

Department of Chemistry, Faculty of Science, The University of Tokyo, Bunkyo-ku, Tokyo 113

**Department of Chemistry, Faculty of Science, Toho University, Narashino, Chiba 275*

***Japan Electron Optics Laboratory Co., Ltd. (JEOL), Akishima, Tokyo 196*

(Received May 17, 1973)

The ^{13}C spectrum taken during the reaction of 4-picoline *N*-oxide with acetic anhydride at 110 °C in the NMR cavity (23.5 kG) shows a pair of emission lines at 15.8 and 154.4 ppm and enhanced absorption at 29.6 and 125.0 ppm (TMS-based). The signals are found to be due to 4-ethylpyridine formed as a minor product of the reaction and are interpreted in terms of the memory effect of the polarization induced in the precursor 4-picolyl–acetoxy radical pair.

The chemically induced dynamic nuclear polarization (CIDNP) of ^{13}C nuclei is expected to give valuable information on the spin distribution among the carbon atoms in radical species and on the rates of formation and decomposition of radical pair intermediates. Simplified spectra due only to net polarization can be obtained since the multiplet effect derived from the ^{1}H–^{13}C coupling is excluded when the wide-band proton decoupling technique is employed, as is usually the case in ^{13}C NMR spectroscopy. The wide variety of spin-lattice relaxation time of ^{13}C compared to that of ^{1}H may also be of help in interpreting the observed polarization in terms of the kinetics and mechanisms of free radical reactions. However, experimental studies have so far been hampered by the technical difficulty caused by short sampling time of the polarization signals over the wide ^{13}C chemical shift region in question in the course of fast free radical reactions.[2)] In contrast with conventional continuous wave NMR, a recently introduced Fourier transform pulsed NMR spectroscopy adequately meets the above requirement for the CIDNP study. We wish to report on the ^{13}C CIDNP spectra obtained during the reaction of 4-picoline *N*-oxide with acetic anhydride.

1) Part IV of the Mechanism of the Reaction of Picoline *N*-Oxides with Carboxylic Anhydrides Studied by NMR. For Part III see H. Iwamura, M. Iwamura, M. Imanari, and M. Takeuchi, *Tetrahedron Lett.*, **1973**, 2325.

2) Only a few ^{13}C CIDNP papers have been given: a) E. Lippmaa, T. Pehk, A. L. Buchachenko, and S. V. Rykov, *Chem. Phys. Lett.*, **5**, 521 (1970); b) S. Berger, S. Hauff, P. Niederer, and A. Rieker, *Tetrahedron Lett.*, **1972**, 2581; c) R. Kaptein, J. Brokken-Zijp, and F. J. J. de Kanter, *J. Amer. Chem. Soc.*, **94**, 6280 (1972); d) E. M. Schulman, R. D. Bertrand, D. M. Grant, A. R. Lepley, and C. Walling, *ibid.*, **94**, 5972 (1972).

Results and Discussion

^{13}C CIDNP Spectra. A 3 M solution of 4-picoline *N*-oxide in acetic anhydride was heated at 110 °C in the magnetic cavity of a ^{13}C NMR spectrometer (25.15 MHz). The Fourier transform pulsed NMR spectra were obtained from the time domain signals accumulated nine times during a given 10 s span in the course of the reaction (see Experimental for details). At the beginning of the reaction, the absorption signals at 127.0 and 138.7 ppm (TMS based) due to the ring $C_{(3)}$ and $C_{(2)}$ atoms, respectively, of 4-picoline *N*-oxide were seen in addition to those at 21.0 (for CH_3)[3)] and 167.2 ppm (for C=O) of the solvent (see Fig. 1a). As the reaction proceeded, the singals of the starting materials diminished gradually and disappeared in 140 s after the start of the reaction. At 100 s we observed growth of a pair of emission lines at 15.8 and 154.4 ppm and absorption signals at 29.6 and 125.0 ppm. The intensity of these peaks increased until about 140 s (Fig. 1b), when it started to decrease and was null in 300 s. Time development of the polarization during the reaction is summarized in Fig. 2. At the end of the reaction, only two absorption peaks of the products were barely detected under the signal to noise ratios of the experimental conditions. We found on a chart of 100 scan accumulation signals due mainly to 4-picolyl acetate; 19.8 (CH_3), 64.5 (CH_2), 122.5 ($C_{(3)}$), 146.1 ($C_{(4)}$), 148.8 ($C_{(2)}$), and 174.4 ppm (C=O).[4)] No signal could be seen at the chemical shifts where the polarized signals appeared (Fig. 3*a*).

3) Also for the CH_3 signal of 4-picoline *N*-oxide.

4) The carbonyl chemical shift of acetic acid coincided.

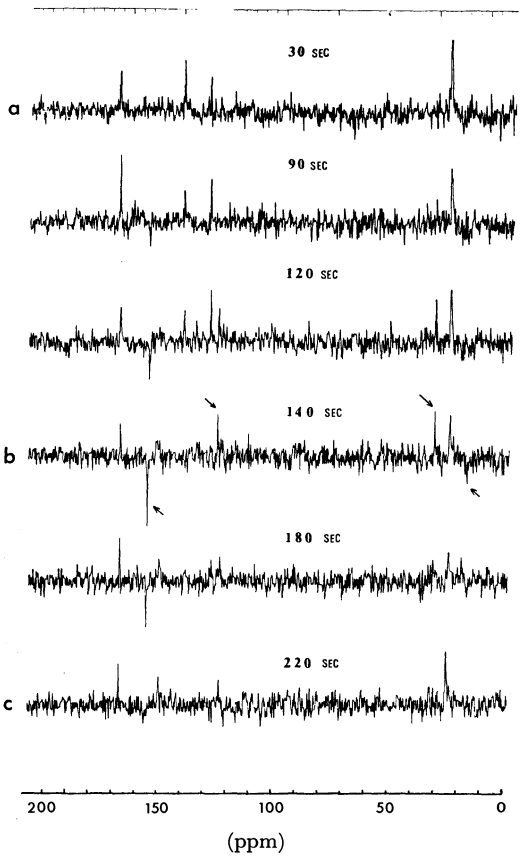

Fig. 1. 25.15 MHz ^{13}C spectra obtained during the course of the reaction of 4-picoline *N*-oxide with acetic anhydride at 110 °C.

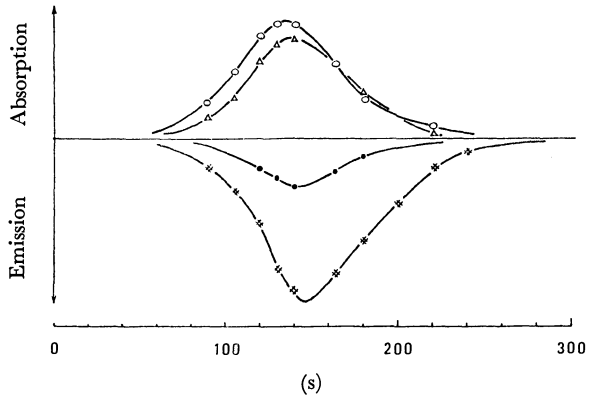

Fig. 2. Time development of the polarization signals due to 4-ethylpyridine during the reaction of 4-picoline *N*-oxide in acetic anhydride at 110 °C. The signal intensities are in arbitrary unit.

By comparison with the ^{13}C spectrum of the authentic sample (Fig. 3b), the emission signals observed during the reaction were assigned to the methyl carbon and ring $C_{(4)}$ while the enhanced absorption peaks corresponded to the methylene carbon and ring $C_{(3)}$ of 4-ethylpyridine formed as a minor product according to Scheme 1. It is reasoned that the chemical yield of 4-ethylpyridine was so low that its NMR absorption could not be observed in the final reaction mixture (Fig. 3a). At the maximum intensity of polarization, we could not detect the signals due to 4-picolyl acetate which should have been formed approximately fifty

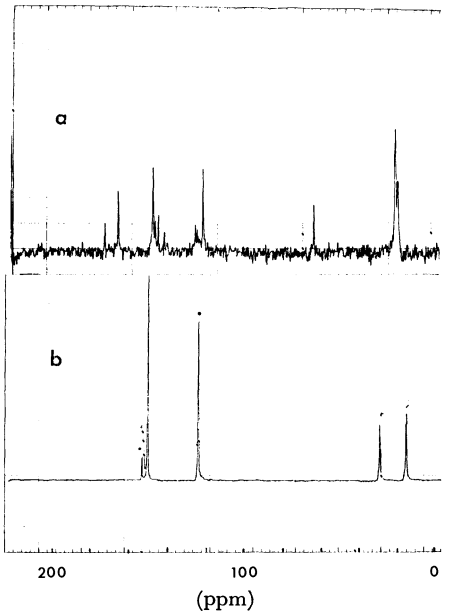

Fig. 3. ^{13}C spectra obtained after the end of the reaction of 4-picoline *N*-oxide in acetic anhydride at 110 °C (a), and of authentic 4-ethylpyridine (b). See text for the assignment of the signals.

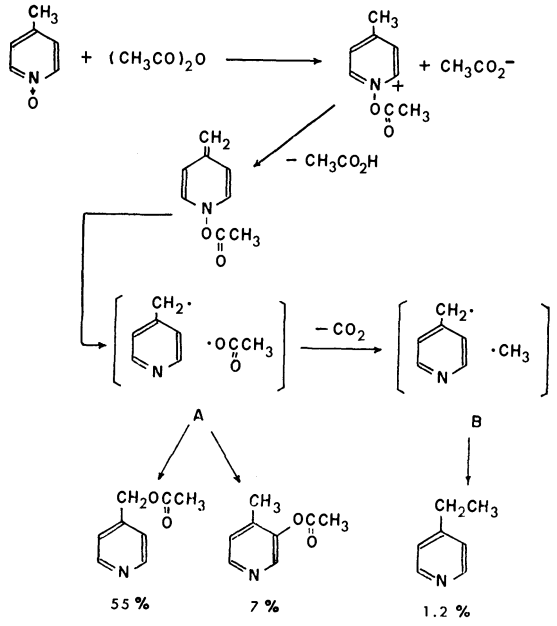

Scheme 1. (Yields of the products were determined by vpc.)[5]

times as much as 4-ethylpyridine. Since the signal to noise ratio of the strongest emission line was five (Fig. 1b), the apparent enhancement factor of polarization is roughly estimated to be 250.

Origin of the 4-Ethylpyridine Polarization. Examination of the polarization pattern in terms of the current radical pair theory of CIDNP[6] enables us to confirm

5) See also H. J. Shine, "Aromatic Rearrangements," Elsevier, Amsterdam (1967), p. 284.

6) G. L. Closs and A. D. Trifunac, *J. Amer. Chem. Soc.*, **92**, 2183, 2186 (1970); R. Kaptein and L. J. Oosterhoff, *Chem. Phys. Lett.*, **4** 195 (1969); H. Fischer, *Z. Naturforsch.*, **25a**, 1957 (1970); R. Kaptein, *J. Amer. Chem. Soc.*, **94**, 6251 (1971); F. J. Adrian, *J. Chem. Phys.*, **53**, 3374 (1970); **54**, 3912 (1971).

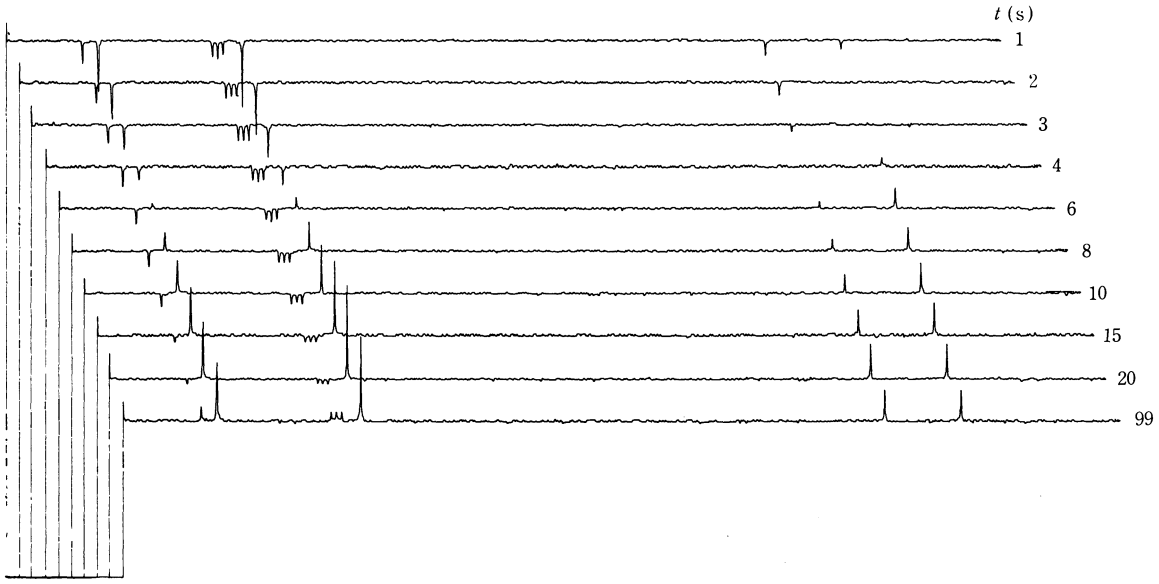

Fig. 4. Carbon-13 partially relaxed Fourier transform spectra of 4-ethylpyridine (containing 30% benzene-d_6 as an internal lock). A waiting period t in a 180 °–t–90 ° pulse sequence is indicated. See text and Fig. 3b for the signal assignment.

equilibrated conditions as the result of lack of signal enhancement due to operation of a ^{13}C–H Overhauser effect (Fig. 3b), it shows the strongest amplitude in polarization spectrum (Fig. 1b, 2). The hyperfine coupling constant is not necessarily the largest for the carbon atom. The effect is considered to originate from the slower spin-lattice relaxation rate of the quaternary carbon atom which usually has relaxation times an order of magnitude greater than those of carbon atoms carrying a proton. The intensities of CIDNP spectra are approximately proportional to the nuclear spin relaxation times.[15] In order to verify the above reasoning for the effect, T_1 measurements were performed by means of 180°–t–90° pulse sequence method. The results are summarized in Table 2.

Table 2. ^{13}C spin-lattice relaxation times (T_1) for 4-ethylpyridine

^{13}C	T_1 (s)
CH_3	3.8
CH_2	6.7
$C_{(2)}$	7.8
$C_{(3)}$	7.8
$C_{(4)}$	96.8

As expected, ring $C_{(4)}$ of 4-ethylpyridine which lacks the dipole-dipole relaxation mechanism with the attached proton has a T_1 value almost ten times as great as that of the other carbons. As another manifestation of the relaxation effect on CIDNP spectra, we note in Fig. 2 that the relative intensity of the $C_{(4)}$ signal is prominent at a later stage (150—300 s) of the reaction wkere intensities are more susceptible to relaxation mechanism in the product.

15) R. G. Lawler, *ibid.*, **89**, 5519 (1967); G. L. Closs and L. E. Closs, *ibid.*, **91**, 4549 (1969).

Experimental

The Fourier transform pulsed NMR spectra were taken on a JNM-PFT-100 FT NMR System. An internal D lock at 15.359 MHz was made on DMSO-d_6 sealed in a capillary and placed concentrically in a sample tube of 8 mm o.d. The sample temperature was controlled by preheated nitrogen and was measured by a calibrated thermocouple in an effluent gas stream. A short radiofrequency 40° pulse of 8 μsec width was applied with a repetition time of 1.1 s over the ^{13}C spectrum width of 6.25 kHz. Nine scans on 2048 data points were accumulated in a magnetic dram of 16 kW which allowed us to obtain four separate spectra in the course of a single run of the reaction. After completion of the sampling, each accumulated time domain signal was Fourier transformed. The signals of individual ^{13}C were obtained as a single line with the use of wide-band proton decoupling with 100.00 MHz radiofrequency of 35—40 W. All the spectra were of *v*-mode which was phase corrected by computer calculation. Five runs of the reaction on a 3 M batch solution were carried out in order to construct Fig. 2.

For T_1 measurements, 180°–t–90° pulse sequences were used, and the values of T_1 were obtained from least-squares fits of the logarithm of the heights of the 90° pulse responses as a function of t. The original data are shown in Fig. 4. A sample of 4-ethylpyridine was neat liquid with approximately 30% benzene-d_6 as an internal lock and was not degassed to simulate the reaction conditions.

The authors gratefully acknowledge support of this work by the Ito Science Foundation. They also wish to thank Dr. T. Fukumi for the T_1 measurements.

Effect of Pressure on the Rate of Solvolysis. Hydrolysis of 1-Aryl-1-methylethyl Chlorides[1]

Akira SERA, Toshifumi MIYAZAWA, Tadashi MATSUDA, Yoichi TOGAWA, and Kazuhiro MARUYAMA

Department of Chemistry, Faculty of Science, Kyoto University, Sakyo-ku, Kyoto 606

(Received June 5, 1973)

The effect of pressure on the hydrolysis rates of 1-aryl-1-methylethyl chlorides were investigated, and the activation volumes, ΔV_0^*, were calculated. Electron-donating substituents in an aryl group gave less negative ΔV_0^* values and electron-withdrawing substituents gave more negative ΔV_0^* values. The observed values of ΔV_0^* were found to correlate with σ^+. These observations are interpreted in terms of the dependence of the degree of solvation at the transition state of the reaction. The temperature dependence of ΔV_0^* is also discussed.

In recent years, the effect of pressure on the rates of organic reactions in solution has been extensively studied.[2] Rate measurements of reactions under high pressure allow us to estimate activation volumes, ΔV^*, by means of the following expression;

$$\Delta V^* = -RT(\delta \ln k/\delta P)_T \quad (1)$$

where ΔV^* is the partial molal volume change when a reactant(s) is converted into a transition-state species. An examination of the pressure effect on the kinetic rates can give a great deal of information about the transition states of the reactions. The general usefulness of the activation volume as a diagnostic probe of reaction mechanisms is well recognized.[3] The reaction constant, ρ, in the Hammett equation depends upon the reaction conditions; hence, a variation in the external pressure might influence the value of ρ. Equation 2[4] implies a linear correlation of ΔV^* with respect to σ;[5]

$$-\delta\Delta V^* = 2.303RT\sigma(\delta\rho/\delta P)_T \quad (2)$$

where $\delta\Delta V^* = \Delta V_X^* - \Delta V_H^*$ and where ΔV_H^* and ΔV_X^* are activation volumes for unsubstituted and substituted substrates, respectively (the subscript x denotes a substituent). However, there have been only a few investigations of the substituent dependence of the activation volumes.[2d,6-10]

We undertook the present investigation in order to obtain fundamental data necessary for the estimation of the substituent dependence of the activation volume, for this is essential for getting detailed information about the transition states of organic reactions. The hydrolysis of 1-aryl-1-methylethyl chlorides in 90% aqueous acetone at 25.0 °C seems to be a suitable model reaction for the present purpose, because; a) this is a reaction in which a neutral molecule in an initial state leads to a highly dipolar transition state, b) the reaction mechanism is rather unambiguous, and c) the rate of reaction is known to give an excellent linear correlation with σ^+ and the value of ρ is considerably large.

Results and Discussion

The hydrolysis of 1-aryl-1-methylethyl chlorides in "90% aqueous acetone" (see Experimental section) at 25.0 °C were followed by a conductometric method under pressure. The first-order rate constants were calculated by the Guggenheim method[11] or by the usual first-order rate expression.[12] The results are summarized in Table 1. Logarithmic plots of the rate constants shown in Table 1 against Brown-Okamoto's σ^+ values exhibit an excellent linear relationship under pressure. Clearly $|\rho|$ decreases as the applied pressure increases.[13] Figure 1 shows a typical plot of $\log k$ (1-phenyl-1-methylethyl chloride) against pressure; this proves the linear relationship between $\log k$ and pressure in this case. With some electron-withdrawing substituents, the plots inclined to show slight convex curvature. In the present investigation, however, all the values of ΔV_0^*, the activation volume at atmospheric pressure, were calculated by means of Eq. (1) and the following equation using the method of least-squares:

$$\ln k = a + bP \quad (3)$$

Substituent Dependence of ΔV_0^*. As has been

1) Organic Reactions under High Pressure. X. Part IX, see *Tetrahedron Lett.*, 1585 (1973).

2) For recently reported solvolytic displacement reactions, see a) J. B. Hyne and co-workers, *Can. J. Chem.*, **48**, 2025, 2416, 2494 (1970); **49**, 2394, 3840 (1971). b) E. Whalley and co-workers, *ibid.*, **48**, 528, 2021 (1970). c) W. J. leNoble and A. Shurpik, *J. Org. Chem.*, **35**, 3588 (1970). d) C. Yamagami and A. Sera, *Chem. Lett.*, **1972**, 741.

3) W. J. leNoble, "Progress in Physical Organic Chemistry," Vol. 5, p. 207, A. Streitwieser, Jr. and R. W. Taft Ed., Interscience Publisher, New York (1967).

4) A. J. Ellis, W. S. Fyfe, R. I. Rutherford, A. Fischer, and J. Vaughan, *J. Chem. Phys.*, **31**, 176 (1959).

5) In Eq. 2, the substituent constant σ is assumed to be independent of pressure. However, one can treat this pressure dependence problem on the Hammett equation in terms of a two variable (σ and P) problem. For similar treatment, see J. E. Leffler and E. Grunwald, "Rates and Equilibria of Organic Reactions," John Wiley & Sons, Inc., New York (1963), p. 128.

6) K. R. Brower, B. Gay, and Y. L. Konkol, *J. Amer. Chem. Soc.*, **88**, 1681 (1966).

7) H. Heydtmann and B. Stieger, *Ber. Bunsenges.*, **70**, 1095 (1966).

8) T. Asano, This Bulletin, **42**, 2005 (1969).

9) K. J. Laidler and R. Martin, *Int. J. Chem. Kinet.*, **1**, 113 (1969).

10) A. Fischer, B. R. Mann, and J. Vaughan, *J. Chem. Soc.*, **1961**, 1093.

11) E. A. Guggenheim, *Phil. Mag.*, **2**, 538 (1929).

12) A. A. Frost and R. G. Pearson, "Kinetics and Mechanism," John Wiley & Sons, Inc., New York (1953), p. 27.

13) The slope of the plot of ρ against pressure estimated by the least squares method is approximately 2×10^{-4}cm^2/kg.

TABLE 1. HYDROLYSIS RATE CONSTANTS OF 1-ARYL-1-METHYLETHYL CHLORIDES UNDER PRESSURE IN 90% AQUEOUS ACETONE AT 25.0°C

Substituent	Pressure (kg/cm²)	First-order rate constant[a] ($\times 10^{-5}$ s^{-1})									
		1	100	150	200	300	400	500	600	800	1000
4-Fluoro[b]		26.4		28.4	28.8[d]	30.0	31.4[d]	32.9	34.2[d]	37.3[d]	40.8
3-Methyl[b]		25.2		27.0	27.4[d]	28.5	29.9[d]	31.1	32.6[d]	35.5[d]	38.7
3-Isopropyl[b]		23.5		25.4	25.7[d]	27.0	28.1[d]	29.4	30.7[d]	33.5[d]	36.2
3-*t*-Butyl[b]		24.1		26.2	26.5[d]	28.3	29.0[d]	30.4	31.7[d]	34.6[d]	37.5
None[b]		12.3		13.3	13.5[d]	14.1	14.8[d]	15.8	16.3[d]	17.9[d]	19.8
3-Methoxy[b]		8.19		8.87	8.94[d]	9.34	9.75[d]	10.3	10.6[d]	11.6[d]	12.5
4-Chloro[c]		3.11			3.72		4.24		4.67		
4-Bromo[c]		2.35			2.93		3.38		3.74	4.33	
3-Methylthio[c]		1.92			2.33		2.71		2.95	3.28	
3-Fluoro[c]		0.284			0.351		0.396		0.446	0.499	
3-Iodo[c]		0.265			0.331		0.375		0.422	0.472	
3-Carboethoxy[c]		0.248			0.300		0.343		0.380	0.417	
3-Chloro[c]		0.212	0.246		0.272		0.302		0.350		0.457

a) Average of two or more experiments.
b) Calculated by the Guggenheim method.
c) Calculated by the usual first-order rate expression.
d) Extrapolated values from data at other pressures.

TABLE 2. PRESSURE EFFECT ON ρ-VALUE FOR HYDROLYSIS OF 1-ARYL-1-METHYLETHYL CHLORIDES

Pressure (kg/cm²)	1	200	400	600	800
ρ	−4.55[a]	−4.48	−4.47	−4.41	−4.39
r[b]	0.999	1.000	1.000	1.000	0.999

a) H. C. Brown and Y. Okamoto reported $\rho = -4.54$, *J. Amer. Chem. Soc.*, **80**, 4979 (1958).
b) Correlation coefficient.

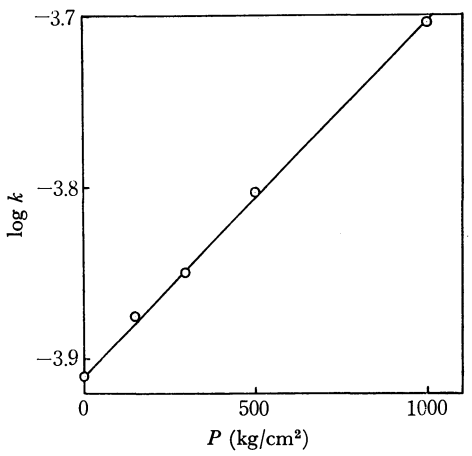

Fig. 1. Plot of log k against pressure.
Hydrolysis of 1-phenyl-1-methylethyl chloride in 90% aqueous acetone at 25.0 °C.

pointed out by Evans and Polanyi,[14] $\Delta V^{\ddagger}$ may conveniently be regarded as being constituted of two terms: $\Delta_1 V^{\ddagger}$, which represents a change in the volume of a reacting molecule(s) during an activation process, and $\Delta_2 V^{\ddagger}$, which is a corresponding change in the volume of the surrounding solvent molecules caused by their rearrangement. In a unimolecular ionization process, $\Delta_2 V^{\ddagger}$ is actually the dominating term.[3]

14) M. G. Evans and M. Polanyi, *Trans. Faraday. Soc.*, **31**, 875 (1935).

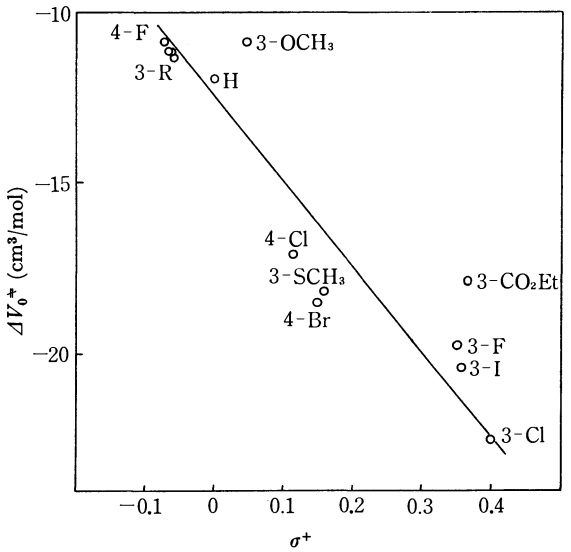

Fig. 2. Plot of $\Delta V_0^{\ddagger}$ against σ^+.

The values of $\Delta V_0^{\ddagger}$ in Table 3 are all negative and are found in the range from −10 to −25 cm³/mol. The contribution of carbonium-ion-like species at the transition state of the present reaction is well established, and the stability of the transition state is governed by the degree of electronic charge delocalization by a given substituent. Negative values of $\Delta V_0^{\ddagger}$ for solvolytic reactions are usually referred to as "electrostriction". That is, a partially-charged transition-state species exerts an electrostatic attractive force on nearby polar solvent molecules; as a result, volume contraction occurs. Thus, the degree of charge delocalization should correspond to this electrostatic volume contraction in the transition state. Figure 2 shows such correlation, with a negative slope, between $\Delta V_0^{\ddagger}$ and σ^+ as anticipated by Eq. (2). The trend shown is qualitatively in good accordance with the above prediction; that is, the more the charge delocalization in

the transition state, the less negative the value of ΔV_0^* becomes.[15]

Temperature Dependence of ΔV_0^*. A few data on the temperature dependence of the activation volume, $\delta\Delta V^*/\delta T$, have been previously reported,[16] and this parameter has been disucssed in terms of the difference in the degree of charge development. In general, $\delta\Delta V^*/\delta T$ is represented as the difference in the temperature dependence of the partial molal volumes between the transition state and the initial state;

$$\delta\Delta V^*/\delta T = \delta\bar{V}_t/\delta T - \delta\bar{V}_g/\delta T \qquad (4)$$

where $\bar{V}_t$ and $\bar{V}_g$ are the partial molal volumes of the transition state and the initial state, respectively.

In Table 4 the dependence of the rate of hydrolysis for 1-phenyl-1-methylethyl chloride on pressure at various temperatures is presented. The activation volumes thus obtained are also shown. As is shown, $\delta\Delta V_0^*/\delta T$ has a negative sign in the present reaction.[17] This implies, according to Eq. (4), that the electrostriction in the activation process results in a tight transition-state solvation shell whose volume is less responsive to temperature change (less expansive) than that of the initial state. Table 4 also shows that sign of $\delta\Delta S^*/\delta P$ seems to be positive, although the estimation of a numerical value of this parameter is, unfortunately, restricted. It seems that the pseudo-thermodynamic relationship;

$$-(\delta\Delta S^*/\delta P)_T = (\delta\Delta V^*/\delta T)_P \qquad (5)$$

is fulfilled.

Activation Volume—Activation Entropy Relationship. Electrostriction is a phenomenon where a strong electrostatic interaction exerts between an ion or a highly polar species and the surrounding solvent molecules. Therefore, the degree of freedom of the solvent molecules is restricted, resulting in a decrease in the entropy of the system. In fact, reactions which have large negative ΔV_0^* values are known to be characterized by large negative ΔS^* values. Accordingly, one can anticipate the presence of a rough proportionality between ΔV_0^* and ΔS^*. Figure 3 shows a fairly good correlation between these two parameters. That the correlation holds in the present reaction strongly supports the validity of the application of the electrostriction theory in the present mechanistic representation of the reaction.

TABLE 3. SUBSTITUENT EFFECT ON ΔV_0^* FOR HYDROLYSIS OF 1-ARYL-1-METHYLETHYL CHLORIDES

Substituent	ΔV_0^*[a] (cm³/mol)	ΔS^*[a,b] (e.u.)
4-Fluoro	−10.9	−11.7
3-Methyl	−11.2	−11.8
3-Isopropyl	−11.2	−10.2
3-*t*-Butyl	−11.4	−10.6
None	−12.0	−12.5
3-Methoxy	−10.9	−11.1
4-Chloro	−17.1	−13.6
4-Bromo	−18.5	−15.2
3-Methylthio	−18.2	−12.8
3-Fluoro	−19.7	−17.0
3-Iodo	−20.4	−16.1
3-Carboethoxy	−17.9	−11.9
3-Chloro	−22.5	−15.1

a) At 25 °C.
b) Taken from reported data, H. C. Brown and co-workers, *J. Amer. Chem. Soc.*, **79**, 1879, 1906, 1909 (1957); **80**, 4964, 4969 (1958).

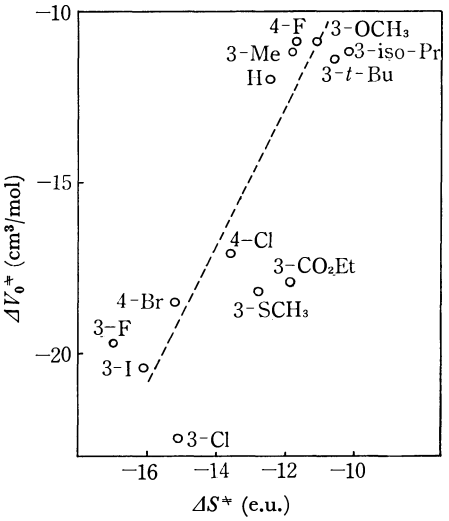

Fig. 3. Plot of ΔV_0^* against ΔS^*.

TABLE 4. PRESSURE AND TEMPERATURE DEPENDENCE OF ACTIVATION PARAMETERS FOR HYDROLYSIS OF 1-PHENYL-1-METHYLETHYL CHLORIDE

Temperature (°C)	Pressure (kg/cm²)	First-order rate constant[a] ($\times 10^{-5}$ s^{-1})					ΔV_0^* (cm³/mol)
		1	200	400	600	800	
25.0		12.3	13.5	14.8	16.3	17.9	−12.0
35.0		36.1[b]	40.7	45.6	49.9	55.4	−12.8
40.0		59.0	65.5	73.5	79.0	91.7	−13.7
ΔH^* (kcal/mol)[c]		18.8	19.0	19.3	19.0	19.6	
ΔS^* (e.u.)[c]		−12.4	−12.4	−11.4	−12.1	−9.7	

a) Average of two or more experiments.
b) Taken from reported data, H. C. Brown *et al.*, *J. Amer. Chem. Soc.*, **79**, 1897 (1957).
c) At 25.0 °C.

15) The position of the transition states along reaction coordinates might change a little with substituents. However, we ignore this small change and hence assume that the observed $\delta\Delta V_0^*$ reflects a difference in the solvation term, $\delta\Delta_2 V_0^*$.[14]

16) M. J. Mackinnon and J. B. Hyne, *Can. J. Chem.*, **49**, 3840 (1971).

17) The value of $\delta\Delta V_0^*/\delta T$ is roughly estimated as −0.1 cm³ mol^{-1} degree^{-1}. The value indicates the intervention of a highly polar transition state.[16]

Experimental

Materials. The materials employed in the present experiment were prepared by the methods reported in the references quoted by Brown and his co-workers.[18] The purity of each material was found to be satisfactory by checking mp, n_D, NMR and IR spectra, and by elemental and glc analyses in the stage of the corresponding alcohol and/or olefin. These alcohols and olefins were converted into the corresponding tertiary chlorides by the method of Brown and Rei.[19] The products were directly used for the rate measurements without further purification.[20]

Solvent. Acetone was dried over anhydrous potassium carbonate and was then distilled at least twice. Commercially available conductivity water was employed and was stored out of contact with air. Brown and his co-workers[18] prepared the reaction solvent mixture by volume. However, in the present investigation, we employed "88.5% aqueous acetone (wt/wt)". This solvent was found to be kinetically equivalent to Brown's "90% aqueous acetone (v/v)"; that is, 1-phenyl-1-methylethyl chloride and 1-(4-fluorophenyl)-1-methylethyl chloride gave an identical solvolysis rate, respectively, in these two solvents.

High-Pressure Apparatus. The high-pressure apparatus is shown in Fig. 4. The pressure vessel is equipped with an electric head which is replaceable, if necessary, by a sampling assembly. The pressure-transmitting fluid was a silicon oil, KF-96 (200 cs, Shin-etsu Chem. Ind.), and pressure was applied by means of a hand-pump. The Bourdon gauge was reliable to ± 10 kg/cm^2 at 1000 kg/cm^2. The thermostat was controlled to 25.0 ± 0.015 °C or 35.0 and 40.0 ± 0.02 °C.

Kinetic Measurements. The conductivity cell employed throughout the experiment is shown in Fig. 4. A kinetic solution was prepared by mixing a weighed substrate with 90% aqueous acetone at ambient temperature ($[RX]_0 = 0.01$—0.04 mol/l). The cell was rinsed well with this solution, filled, and placed in the high-pressure vessel. The electric conductivity of the solution was then measured by means of Radiometer model CDM-3 and Yanagimoto model MY-8 conductivity outfits. The first readings were taken after the establishment of the thermal equilibria in the cell. A preliminary experiment using a thermocouple directly inserted into the cell showed that thermal equilibria in the cell were established after 12 min in the case of an applied pressure of 400 kg/cm^2 and a vessel temperature of 0 °C (pre-chilled vessel medium, *n*-hexane); 17 min, 700 kg/cm^2, 0 °C; 18 min, 700 kg/cm^2, 15 °C; 37 min, 700 kg/cm^2, 25 °C (in all cases, the bath temperature was kept at 25.0 °C).

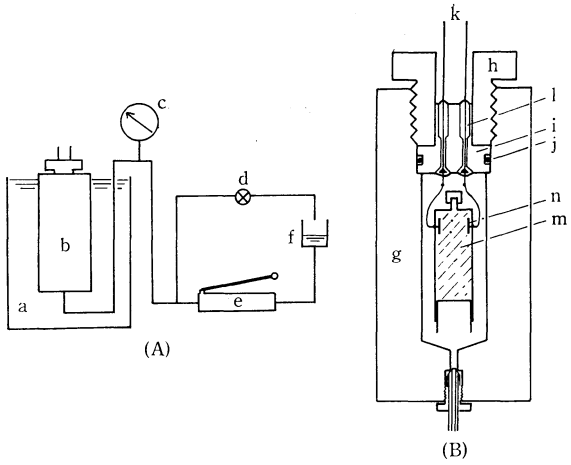

Fig. 4. High-pressure apparatus.
A) Schematic diagram of hydrostatic system. a: thermostatted bath, b: high-pressure vessel, c: Bourdon gauge, d: valve, e: pump, f: oil reservoir.
B) Diagram of pressure vessel. g: stainless steel vessel, h: gland nut, i: electric head, j: O-ring, k: electric leads, l: epoxy-resin, m: glass conductivity cell, n: platinum electrodes.

First-order rate constants were calculated by the Guggenheim method[11] or by the usual first-order rate expression[12] using the method of least-squares. In the former case, 10 pairs of readings were made for each run ($\Delta t \fallingdotseq$ two half lives). In the latter case, calibration plots of the conductance of the standard hydrogen chloride solution at several pressures against the concentrations (determined by titration) of hydrogen chloride in the solution were made. To obtain the "infinite titer", aliquots of the kinetic solution were added to an appropriate amount of 50% aqueous acetone; the solutions were then allowed to stand at ambient temperature for at least ten half lives, after which they were titrated with a standard alkaline solution, using methyl red as an indicator.

The present work has been supported in part by a Grant-in-aid for Scientific Research from the Ministry of Education.

18) H. C. Brown and co-workers, *J. Amer. Chm. Soc.*, **79**, 1897, 1906, 1909 (1957); **80**, 4964, 4969 (1958).
19) H. C. Brown and M.-H. Rei, *J. Org. Chem.*, **31**, 1090 (1966).
20) Reliability of this procedure, see H. C. Brown *et al.*, *J. Amer. Chem. Soc.*, **79**, 1897 (1957).

Optical Resolution and Stereochemistry of γ-Hydroxyglutamic Acid[1]

Yong Kyun LEE* and Takeo KANEKO**

Department of Chemistry, Faculty of Science, Osaka University, Toyonaka, Osaka 560

(Received June 11, 1973)

Four optical isomers of γ-hydroxyglutamic acid were prepared in pure states by optical resolution of two racemic diastereoisomers through brucine salt of *N*-benzyloxycarbonyl amino acid or strychnine salt of *N*-benzoyl derivative. Configurations of α- and γ-asymmetric carbon atoms of these isomers were estimated from contribution to molecular rotation and character of taste exhibition. These determinations were confirmed by chemical degradations to aspartic acid and malic diamide of the definite configurations. Cyclization of each racemic diastereomer to either lactone or lactam was also investigated.

γ-Hydroxyglutamic acid has been found in plants, *e.g.*, *Phlox decussata*,[2] *Hemerocallis* species,[3] and *Linaria vulgaris*.[4] Occurrence of this amino acid was also reported as an intermediate in hydroxyproline metabolism,[5] and in bovine gallbladder bile as *N*-terminal residue in heptapeptide.[6] In the previous paper,[7] the authors devised a new method to synthesize this amino acid and reported a separation procedure of the resulting mixture of two diastereoisomers. Greenstein and Benoiton demonstrated an enzymic resolution of two diastereoisomers of this amino acid and estimated steric configurations of these isomers indirectly based on the stereochemistry of hydroxy acid derived from the amino acid.[8] In this paper, we present an optical resolution of both racemic diastereoisomers of γ-hydroxyglutamic acid by chemical method *via* salt formation with brucine or strychnine and an unambiguous determination of stereochemistry for each optical isomer through direct degradation to the compounds of established configurations. In addition, we now report some other properties of this amino acid, for instance, one example of the relationship of a stereostructure of amino acid with its taste, and also a trend of cyclization for each diastereomeric isomer to lactone or lactam.

For the optical resolution of one diastereoisomer A of γ-hydroxyglutamic acid with the higher melting point of 172—173 °C (decomp.),[7] it was converted to several *N*-acyl derivatives and its salt formation with various resolution reagents was tested. The best result was obtained in the case of brucine salt with *N*-benzyloxycarbonyl amino acid. Thus, one optical isomer (−)-A was obtained by acid hydrolysis of a sparingly soluble salt and the other isomer (+)-A from more soluble salt, both in optically pure states.

The resolution of another diastereoisomer B with the lower melting point of 166 °C (decomp.)[7] was carried out by fractional crystallization of strychnine salt with *N*-benzoyl amino acid. Optical isomers (−)-B and (+)-B were secured from a sparingly soluble salt and a non-crystalline soluble salt respectively.

TABLE 1. PROPERTIES OF OPTICAL ISOMERS OF γ-HYDROXYGLUTAMIC ACID

	Mp (°C) (decomp.)	$[\alpha]_D$ (°)	Concentration (%)	Solvent	Taste
L(−)-A	172—173	−12.5	2.0	H_2O	Strongly tasty
		+3.0	5.0	20% HCl	
D(+)-A	172—173	+12.7	3.0	H_2O	Tasteless
		−3.2	5.0	20% HCl	
D(−)-B	166	−19.5	2.0	H_2O	Tasteless
		−37.3	1.5	20% HCl	
L(+)-B	166	+20.0	2.0	H_2O	Weakly tasty
		+38.0	1.5	20% HCl	

Physical and physiological properties of the four optical isomers of γ-hydroxyglutamic acid thus obtained were summarized in Table 1. The taste of one isomer (−)-A is resembled to that of L-glutamic acid but with milder nuance and weaker strength. If this amino acid is obeyed to the empirical rule concerning with the relationship of stereochemistry of amino acid with taste exhibition which had been originally found by one of the authors,[9] configuration of α-asymmetric carbon atom of both isomers (−)-A and (+)-B exhibiting the meaty taste, should belong to L-amino acid series and that of the other tasteless isomers (+)-A and (−)-B to D-series. It is also observed that the presence of γ-hydroxy group in this amino acid effects the strength of taste as in the case of β-hydroxyglutamic acid.[10]

The molecular rotations of the four isomers both in 20% hydrochloric acid and aqueous solution are listed

* Present address: Department of Polymer Engineering, Hanyang University, Seoul, Korea.

** Present address: Shiseido Laboratories, Nippa-cho, Kohoku-ku, Yokohama.

1) This work was partly presented at the 12th Annual Meeting of the Chemical Society of Japan, Kyoto, April, 1959.

2) A. I. Virtanen and P. K. Hietala, *Acta Chem. Scand.*, **9**, 12 (1955).

3) L. Fowden and F. C. Stewart, *Ann. Biol. London*, **21**, (1957).

4) S. Hatanaka, *Acta Chem. Scand.*, **16**, 513 (1962).

5) a) G. Wolf and C. R. A. Berger, *J. Biol. Chem.*, **230**, 231 (1958); b) E. Adams and A. Goldstone, *ibid.*, **235**, 3504 (1960).

6) H. Yamamoto, G. Funatsu, and M. Funatsu, *Proc. Japan Acad.*, **44**, 391 (1968).

7) T. Kaneko, Y. K. Lee, and T. Hanafusa, This Bulletin, **35**, 875 (1962).

8) J. P. Greenstein and L. Benoiton, *J. Amer. Chem. Soc.*, **79**, 6192 (1957).

9) T. Kaneko and H. Katsura, "Chemistry of Proteins," Vol. 1, Kyoritsu-Shuppan, Tokyo (1969), p. 56.

10) T. Kaneko, R. Yoshida, and H. Katsura, *Nippon Kagaku Zasshi*, **80**, 316 (1959).

Table 2. Molecular rotation and calculated contribution of α-carbon atom of four stereoisomers of γ-hydroxyglutamic acid

Isomer	$[M]_D$		$[M]_{HCl}-[M]_{H_2O}$	α[a]		$\alpha_{HCl}-\alpha_{H_2O}$
	20% HCl	H_2O		20% HCl	H_2O	
(−)-A	+4.9	−20.4	+25.3	+33.5	+6.1	+27.4
(+)-A	−5.2	+20.7	−25.9	−33.1	−5.6	−27.5
(−)-B	−60.9	−31.8	−29.1	−33.1	−5.6	−27.5
(+)-B	+62.0	+32.6	+29.4	+33.5	+6.1	+27.4

a) $\alpha=1/2([M]_{\mp A}+[M]_{\pm B})$

in Table 2. It was noticed that, in the isomers (−)-A and (+)-B, a difference of two values in hydrochloric acid and aqueous solution was positive and that in (+)-A and (−)-B was negative. Furthermore, the same tendencies were recognized at the calculated values of contribution of α-carbon atoms to molecular rotation for each isomer. These facts may indicate that, according to Lutz and Jirgensons' rule,[11] the configuration of α-carbon atoms of (−)-A and (+)-B shlould be L-form and (+)-A and (−)-B must have D-configuration at α-carbon atoms.

In order to confirm the above estimation, one optical isomer of γ-hydroxyglutamic acid was degradated to aspartic acid by the following chemical procedure. Thus, *N*-benzyloxycarbonyl-(−)-A was oxidized with potassium permanganate followed by hydrolysis with 20% hydrochloric acid to yield aspartic acid which was identified with L-isomer from observed optical rotation value $[\alpha]_D^{15}$ +25.9° in hydrochloric acid. From this result, L-configuration of α-carbon atom of (−)-A was established in accordance with the deduction from the molecular rotation values and taste exhibition. Similarly, *N*-benzoyl-(−)-B was oxidized to give D-aspartic acid, indicating that its α-carbon atom possesses D-configuration.

For determination of the configuration of γ-carbon atom of this amino acid, one isomer (+)-A was oxidized with chloramine T to β-formyllactic acid which was then further oxidized to malic acid with bromine in a similar way to the degradation of β-hydroxyglutamic acid[12] as shown in Fig. 1. A specific rotation of diamide prepared from malic acid thus obtained was measured to be $[\alpha]_D^{18}$ +59.0° in methanol. This value corresponds to (R)-malic diamide of $[\alpha]_D^{18}$ +60.8°. Similarly, the same compound derived from (+)-B showed a specific rotation of $[\alpha]_D^{17}$ +60.0° in methanol. Therefore, it is concluded that γ-carbon atoms of (+)-A and (+)-B possess R-configuration and those of (−)-A and (−)-B belong to S-series.

Steric configurations of four optical isomers of γ-hydroxyglutamic acid deduced from the results obtained above are summarized and represented by Fischer's projection formula in Fig. 2. This conclusion coincides with the conclusion by Greenstein and Benoiton.[8]

If γ-hydroxyglutamic acid is cyclized either to lactone or to lactam, steric relationships of *cis-trans* isomerism

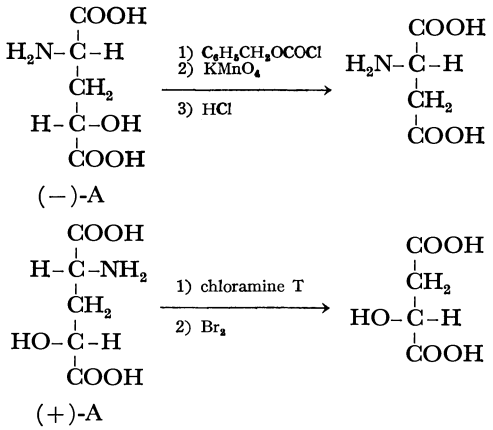

Fig. 1. Oxydative degradations of stereoisomers of γ-hydroxyglutamic acid.

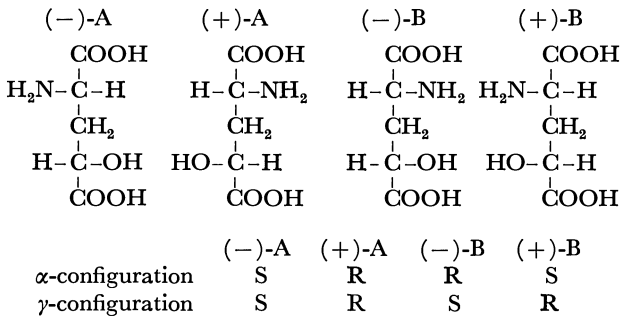

Fig. 2. Steric configurations of four optical isomers of γ-hydroxyglutamic acid.

concerning the ring planes will be resulted as shown in Fig. 3, each isomer corresponding to the four optical isomer mentioned in Fig. 2 respectively. In the lactone I and the lactam III, both derived from the isomer A, two substituents on the ring planes located each other at *cis* positions, while those in lactone II and lactam IV derived from the isomer B are at *trans* positions. It has been known that *allo*-γ-hydroxyproline, in which hydroxy and carboxy group are positioned at *cis* direction on pyrrolidine ring, can form bicyclic compound by lactonization. Since the lactams III and IV of γ-hydroxyglutamic acid can be considered as δ-oxo-γ-hydroxyproline, a relationship of stereochemistry of γ-hydroxyglutamic acid with cyclization seemed to be worthy of further investigation.

In fact, the racemic isomer A gave the lactone I hydrochloride which was easily crystallized.[7] When this hydrochloride was treated with pyridine, or the compound A was attempted to be esterified, a free lactone I was readily obtained.[7] On the contrary a

11) D. Lutz and B. Jirgensons, *Ber.*, **63**, 448 (1930), **64**, 1221 (1931).

12) C. R. Harington and S. S. Randall, *Biochem. J.*, **25**, 1917 (1931).

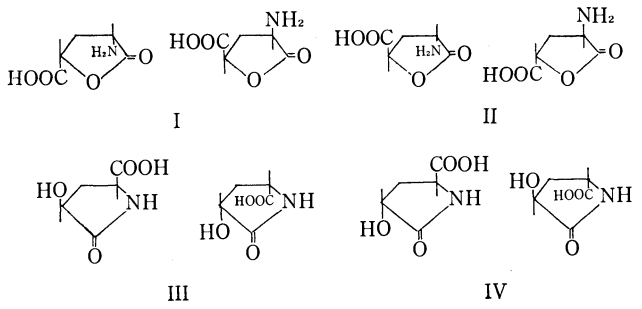

Fig. 3. Steric configurations of lactones and lactams derived from four optical isomers of γ-hydroxyglutamic acid.

free lactone II could not be obtained by the similar procedure from another racemic isomer B. In this case, esterification of the compound B gave mono- and diester hydrochloride, the latter of which could be converted to γ-hydroxyglutamic acid lactam ester with sodium hydrogencarbonate. The fact that isomer A can be easily lactonized compared with isomer B as demonstrated above, may be related to the resulting structure in the former lactone where amino and γ-carboxy groups in *cis* position could be interacted each other to stabilize the ring structure.

We next attempted to form the bicyclic compound of γ-hydroxyglutamic acid as shown in Fig. 4. The racemic isomer A was first converted to *N*-benzyloxycarbonyl derivative V which was readily cyclized to the lactone carboxylic acid VI with hydrochloric acid.[7] Methyl esterification of VI gave monomethyl ester VII and dimethyl ester VIII. When the lactone monoester VII was hydrogenated in dioxane using palladium black, a diketopiperazine IX was obtained unexpectedly. A similar diketopiperazine was also obtained from *N*-benzyloxycarbonyl-γ-hydroxy-DL-glutamic acid B lactone monomethyl ester. Hydrogenolysis of the diester VIII in aqueous methanol afforded directly a lactam ester X which was then saponified to yield a lactam carboxylic acid XI. Any trials for further lactonization of the lactam XI to make the bicyclic compound has not been succeeded.

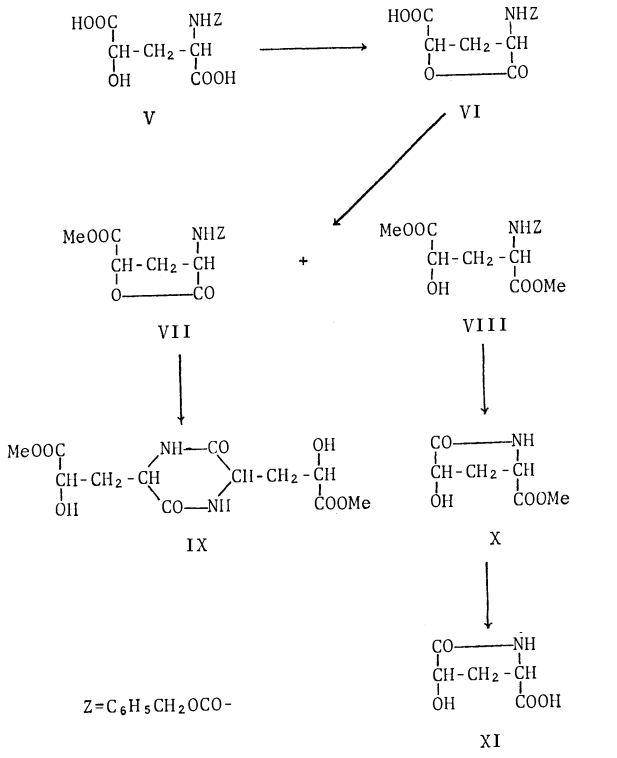

Fig. 4. Scheme for attempt at formation of bicyclic compound of γ-hydroxyglutamic acid.

Experimental

All melting points are uncorrected. Elemental analyses were carried out by Mr. Masakazu Okumiya and Miss Kiku Koike in our Department. For paper chromatography on Toyo paper No. 51, a developing solvent of *n*-butanol–acetic acid–water (4: 1: 2 v/v) was used.

Resolution of N-*Benzyloxycarbonyl Derivative of One Diastereoisomer A of γ-Hydroxy-*DL-*glutamic Acid.* To a solution of *N*-benzyloxycarbonyl derivative (25 g) of a racemic diastereoisomer A hydrate of γ-hydroxyglutamic acid with mp 172—173 °C (decomp.)[7] in 95% ethanol (350 ml), brucine (67 g) was added. The mixture was heated for 10 min to obtain the complete dissolution and then evaporated *in vacuo*. Water (30 ml) was added to the residue and evaporation was repeated twice to remove ethanol completely. Residual syrup was dissolved in water (600 ml) and kept in a refrigerator overnight to give crude crystals (45 g). The crystals were filtered and recrystallized three times from water (200 ml each) to give pure brucine salt (38 g). The salt was dissolved in water (600 ml) and decomposed by addition of 1 M sodium hydroxide to phenolphthalein alkaline on cooling. Crystals of brucine deposited were removed by filtration. The filtrate was neutralized with 6 M hydrochloric acid and concentrated under reduced pressure to 200 ml.

The solution was acidified to Congo red with 6 M hydrochloric acid and extracted with ethyl acetate repeatedly. The combined extract was dried over anhydrous sodium sulfate and concentrated to afford crystals of *N*-benzyloxycarbonyl-γ-hydroxy-L(−)-glutamic acid. This was recrystallized from ethyl acetate, yield, 8 g (66%), mp 124—125 °C (decomp.), $[\alpha]_D^{20}$ −18.0° (*c* 3.3, 99% ethanol).

Found: C, 52.62; H, 5.36; N, 4.65%. Calcd for $C_{13}H_{15}O_7N$: C, 52.52; H, 5.09; N, 4.71%.

The mother liquor from crystals of the crude brucine salt mentioned above was concentrated to about 50 ml. Crystals deposited were removed by filtration. The filtrate was further concentrated and kept at room temperature for a few days. After removal of a small amount of crystals by filtration, the mother liquor was decomposed with aqueous sodium hydroxide as mentioned above to give *N*-benzyloxylcarbonyl-γ-hydroxy-D(+)-glutamic acid, yield, 6 g (50%), mp 124—125 °C (decomp.), $[\alpha]_D^{15}$ +18.0° (*c* 3.0, 99% ethanol).

Found: C, 52.61; H, 5.21; N, 4.68%.

*γ-Hydroxy-*L*(−)-glutamic acid.* *N*-Benzyloxycarbonyl-γ-hydroxy-L(−)-glutamic acid (2.5 g) obtained above was refluxed with 20% hydrochloric acid (25 ml) for 4 hr. The solution was evaporated *in vacuo*. Water was added to the residue and evaporation was repeated. Finally, the residue was dissolved in water and treated with silver carbonate to remove hydrochloric acid. The filtrate was again evaporated and the residue was crystallized from water and ethanol. Recrystallization from water gave pure γ-hydroxy-L(−)-glutamic acid, yield, 1 g, mp 172—173 °C (decomp.), $[\alpha]_D^{10}$ −12.5° (*c* 2.0, water), $[\alpha]_D^{10}$ +3.0° (*c* 5.0, 20% hydrochloric acid).

Found: C, 36.96; H, 5.52; N, 8.53%. Calcd for $C_5H_9O_5N$: C, 36.81; H, 5.56; N, 8.59%.

*γ-Hydroxy-*D(+)*-glutamic Acid.* In a similar manner to the above experiment, γ-hydroxy-D(+)-glutamic acid was obtained from its *N*-benzyloxycarbonyl derivative, mp 172—173 °C (decomp.), $[\alpha]_D^{10}$ +12.7° (*c* 3.0, water), $[\alpha]_D^{10}$ −3.2° (*c* 5.0, 20% hydrochloric acid).

Found: C, 36.96; H, 5.58; N, 8.56%.

Resolution of N*-Benzoyl Derivative of One Diastereoisomer B of γ-Hydroxy-*DL*-glutamic Acid.* To an aqueous solution (300 ml) of *N*-benzoyl derivative (18 g) of one racemic diastereoisomer B of γ-hydroxyglutamic acid with mp 166 °C (decomp.),[7] strychnine (47 g) was added on warming. Insoluble material was filtered off while hot and the filtrate was evaporated *in vacuo*. To the residue, ethanol (30 ml) was added, and evaporation was repeated twice. To the residual syrup, 95% ethanol (200 ml) was added and the mixture was kept in a refrigerator overnight to yield crystals of crude salt (29 g). This was recrystallized from 95% ethanol (100 ml) three times to give pure salt (22 g). The strychnine salt was dissolved in water (600 ml) and then decomposed with 1 M sodium hydroxide. Strychnine deposited was filtered off and the filtrate was acidified with 20% hydrochloric acid to Congo red. It was evaporated *in vacuo* to give *N*-benzoyl-γ-hydroxy-D(+)-glutamic acid lactone, yield, 6 g (66%), mp 224—225 °C, $[\alpha]^{15}$ +70.8° (*c* 1.3, 99% ethanol).

Found: C, 57.95; H, 4.61; N, 5.55%. Calcd for $C_{12}H_{11}O_5N$: C, 57.83; H, 4.45; N, 5.62%.

The mother liquor from the above crystalline strychnine salt was evaporated to remove the salt of D(+)-lactone deposited. The residual syrup was treated as above to give crude crystals of *N*-benzoyl-L(−)-lactone. They were recrystallized from 1 M hydrochloric acid, mp 224—225 °C, $[\alpha]_D^{10}$ −71.3° (*c* 1.5, 99% ethanol).

Found: C, 57.79; H, 4.38; N, 5.54%.

*γ-Hydroxy-*D(−)*-glutamic Acid.* *N*-Benzoyl-D(+)-lactone (2.3 g) obtained above was dissolved in 20% hydrochloric acid (25 ml) and refluxed for 4 hr. The solution was evaporated *in vacuo*. Evaporation after addition of water was repeated. The residue thus obtained was dissolved in a little water and treated with pyridine and ethanol to give crude crystals of γ-hydroxy-D(−)-glutamic acid. Recrystallization from water afforded pure crystals, yield, 1 g, mp 166 °C (decomp.), $[\alpha]_D^{15}$ −19.5° (*c* 2.0, water), $[\alpha]_D^{15}$ −37.3° (*c* 1.5, 20% hydrochloric acid).

Found: C, 36.70; H, 5.60; N, 8.58%. Calcd for $C_5H_9O_5N$: C, 36.81; H, 5.56; N, 8.59%.

*γ-Hydroxy-*L(+)*-glutamic Acid.* In a similar procedure to that of D(−)-amino acid, γ-hydroxy-L(+)-glutamic acid was obtained from *N*-benzoyl-L(−)-lactone, mp 166 °C (decomp.), $[\alpha]_D^{15}$ +20.0° (*c* 2.0, water), $[\alpha]_D^{15}$ +38.0° (*c* 1.5, 20% hydrochloric acid).

Found: C, 36.59; H, 5.70; N, 8.66%.

Determination of Configuration at α-Carbon Atom of γ-Hydroxyglutamic Acid. (i) Oxidation of N*-Benzyloxycarbonyl-γ-hydroxy-*L(−)*-glutamic Acid.* A derivative of one optical isomer (−)-A, *i.e.*, *N*-benzyloxycarbonyl-γ-hydroxy-L(−)-glutamic acid (1 g) was dissolved in water (50 ml). The solution was added dropwise into an aqueous solution (30 ml) of potassium permanganate (0.8 g) at 25—30 °C with stirring. The stirring was continued for additional 10 min, and then filtered. The filtrate was acidified with 6 M hydrochloric acid (3 ml) and then evaporated. The residue was dissolved in 6 M hydrochloric acid (15 ml) and refluxed for 3 hr. After cooling, the solution was washed with ether, and an aqueous layer was evaporated *in vacuo*. The residue was treated with ethanol to remove potassium chloride by filtration. The filtrate was evaporated again and the residue thus obtained was crystallized from pyridine and ethanol. Recrystallization from water gave crystals of L-aspartic acid. This sample was identified with authentic L-aspartic acid on paperchromatogram, yield, 200 mg, $[\alpha]_D^{15}$ +25.9° (*c* 1.7, 10% hydrochloric acid). Lit.,[13] $[\alpha]_D^{20}$ +25.8° (*c* 2, 6 M hydrochloric acid).

Found: C, 36.42; H, 5.41; N, 10.65%. Calcd for $C_4H_7O_4N$: C, 36.09; H, 5.30; N, 10.52%.

(ii) Oxidation of N*-Benzoyl-γ-hydroxy-*D(+)*-glutamic Acid Lactone.* Permanganate oxidation of *N*-benzoyl derivative of the isomer (−)-B gave D-aspartic acid in a similar procedure to that in (i). On paperchromatogram, the product was identified with the authentic aspartic acid. $[\alpha]_D^{15}$ −25.0° (*c* 1.0, 10% hydrochloric acid).

*Determination of Configuration at γ-Carbon Atom of γ-Hydroxyglutamic Acid. (i) Oxidation of γ-Hydroxy-*D(+)*-glutamic Acid.* One optical active isomer (+)-A, *i.e.*, γ-hydroxy-D(+)-glutamic acid (2.2 g) was dissolved in 1 M hydrochloric acid (15 ml). The solution was made slightly alkaline by addition of 5% aqueous sodium hydroxide on cooling, and aqueous solution (15 ml) of chloramin T (4.2 g) was added. The reaction mixture was warmed at 60 °C for 2 hr. *p*-Tosylamide deposited on cooling was filtered off. Combined filtrate and washings were extracted with ethyl ether and the aqueous layer was acidified with hydrochloric acid. Bromine water prepared from 5 g of bromine and 100 ml of water was added to the solution and the mixture was kept at room temperature for 48 hr until the bromine color almost disappeared. Excess bromine was decomposed by addition of aqueous sodium thiosulfate. The solution was concentrated *in vacuo* to 30 ml, and extracted with ethyl ether. After removal of ether from the extract, the residue was dissolved in methanol and esterified with diazomethane in the usual manner. The product was purified by distillation and a fraction of bp 100—110 °C/6 mmHg was collected (0.7 g). A solution of this dimethyl ester in methanol (30 ml) was saturated with ammonia, and kept at room temperature in a sealed tube for 4 days. The solvent was evaporated to yield crude R(+)-malic diamide (0.3 g, 17%). It was recrystallized from methanol, mp 157—158 °C, $[\alpha]_D^{15}$ +59.0° (*c* 1.0, methanol).

Found: C, 36.60; H, 6.28; N, 21.20%. Calcd for $C_4H_8O_3N_2$: C, 36.36; H, 6.10; N, 21.20%.

*(ii) Oxidation of γ-Hydroxy-*L(+)*-glutamic Acid.* From one optical isomer (+)-B, *i.e.*, γ-hydroxy-L(+)-glutamic acid, R(+)-malic diamide was obtained by the similar procedure to that in (i), mp 157—158 °C, $[\alpha]_D^{17}$ +60.0° (*c* 1.0, methanol).

Found: C, 36.43; H, 6.14; N, 21.37%.

*γ-Hydroxy-*DL*-glutamic Acid B Lactone Hydrochloride.* The racemic isomer B was dissolved in a small amount of concentrated hydrochloric acid and then kept over phosphorus pentoxide in a vacuum desiccator to yield needles of the hydrochloride, mp 187—189 °C (decomp.).

Found: C, 30.04; H, 5.05; N, 6.83; Cl, 17.27%. Calcd for $C_5H_{10}O_5NCl$: C, 30.08; H, 5.05; N, 7.02; Cl, 17.48%.

*γ-Hydroxy-*DL*-glutamic Acid B Mono- and Diethyl Ester Hydrochloride.* To a suspension of the racemic isomer B (2 g) in anhydrous ethanol (50 ml), dry hydrogen chloride was saturated. The mixture was kept at room temperature overnight and then concentrated. To the residue, a small amount of acetone was added to yield crystals. Recrystallization from ethanol and acetone gave pure monoester, yield, 1.6 g (57%), mp 168 °C (decomp.).

13) T. Kaneko and H. Katsura, "Chemistry of Proteins," Vol. 1, Kyoritsu-Shuppan, Tokyo (1969), p. 113.

Found: C, 37.06; H, 6.20; N, 6.36; Cl, 16.14%. Calcd for $C_7H_{14}O_5NCl$: C, 36.93; H, 6.20; N, 6.15; Cl, 15.58%.

The mother liquor from crystals of the monoester was evaporated. The residue was crystallized to afford diester, yield, 0.8 g (26%), mp 90—95 °C (decomp.).

Found: C, 41.13; H, 6.99; N, 5.46; Cl, 14.59%. Calcd for $C_9H_{18}O_5NCl$: C, 42.28; H, 7.10; N, 5.48; Cl, 13.87%.

*γ-Hydroxy-*DL*-glutamic Acid B Lactam Ethyl Ester.* The diethyl ester (1.5 g) obtained above was dissolved in water (15 ml), and sodium hydrogencarbonate (0.6 g) was added. The mixture was extracted with ethyl acetate five times. The combined extract was dried with sodium sulfate and then concentrated to a syrup. It was crystallized from ethyl acetate and petroleum ether and then recrystallized from the same solvents, yield, 0.4 g (40%), mp 70—73 °C.

Found: C, 48.30; H, 6.52; N, 7.82%. Calcd for $C_7H_{11}O_4N$: C, 48.35; H, 6.40; N, 8.09%.

N-*Benzyloxycarbonyl-γ-hydroxy-*DL*-glutamic Acid A Lactone Methyl Ester (VII).* To a solution of *N*-benzyloxycarbonyl-γ-hydroxy-DL-glutamic acid A lactone (VI)[7] (2 g) in methanol (5 ml), ethyl ether solution of diazomethane was added at 0 °C until yellow color remained. The solvent was removed under reduced pressure to deposite crystals. They were recrystallized from 70% aqueous methanol, yield, 1.4 g (70%), mp 106.5—108 °C.

Found: C, 57.82; H, 5.23; N, 4.71%. Calcd for $C_{14}H_{15}O_6N$: C, 57.33; H, 5.16; N, 4.78%.

*γ-Hydroxy-*DL*-glutamic Acid A Lactam Methyl Ester (X).* When the esterification of VI (15 g) in methanol (35 g) was carried out using excess diazomethane in the above experiment, a syrup of the expected *N*-benzyloxycarbonyl-γ-hydroxy-DL-glutamic acid A dimethyl ester (VIII) was obtained. Through a solution of the syrup thus obtained in a mixture of methanol (100 ml) and water (50 ml), hydrogen was passed at 45 °C in the presence of palladium black (500 mg). The catalyst was removed by filtration and the solvent was removed to give crystals. Recrystallization from water gave crystals with 1 mol of crystallization water, yield, 4 g (47%), mp 70.5—71.5 °C. After drying at the refluxing temperature of acetone for 15 hr, the melting point rised up to 109—110 °C.

Found: C, 45.26; H, 5.69; N, 8.68%. Calcd for $C_6H_9O_4N$: C, 45.28; H, 5.70; N, 8.80%.

*γ-Hydroxy-*DL*-glutamic Acid A Lactam (XI).* The lactam methyl ester X (2.5 g) was dissolved in 5% aqueous sodium hydroxide (1.5 ml) and allowed to stand at room temperature overnight. The solution was passed through Dowex-50 (H^+ form) column, and the acidic eluate was concentrated *in vacuo* to deposit crystals, yield, 1.4 g (61%), mp 182 °C (decomp.).

Found: C, 41.25; H, 4.94; N, 9.46%. Calcd for $C_5H_7O_4N$: C, 41.38; H, 4.86; N, 9.65%.

*Diketopiperazine (IX) of γ-Hydroxy-*DL*-glutamic Acid A Methyl Ester.* Into a solution of VII (1 g) in anhydrous dioxane (40 ml), hydrogen was passed in the presence of palladium black (300 mg). After the hydrogenation had been finished, the catalyst was removed by filtration. The filtrate was concentrated *in vacuo* to give crystals. They were recrystallized twice from dioxane and then from water, yield, 0.8 g (73%), mp 192 °C (decomp.); ν_{max} 3400, 1675 cm^{-1}. A diketopiperazine structure was deduced for this product from its IR spectrum and elemental analyses in addition to the observation of negative ninhydrin test.

Found: C, 45.32; H, 5.89; N, 8.89%. Calcd for $C_{12}H_{18}O_8N_2$: C, 45.28; H, 5.70; N, 8.80%.

N-*Benzyloxycarbonyl-γ-hydroxy-*DL*-glutamic Acid B Lactone Methyl Ester.* *N*-Benzyloxycarbonyl-γ-hydroxy-DL-glutamic acid B lactone[7] (2.8 g) was esterified with diazomethane in the usual manner. The product was recrystallized from 70% aqueous methanol, yield, 1.9 g (65%), mp 109—110 °C.

Found: C, 57.37; H, 5.20; N, 4.88%. Calcd for $C_{14}H_{15}O_6N$: C, 57.33; H, 5.16; N, 4.78%.

*Diketopiperazine (IX) of γ-Hydroxy-*DL*-glutamic Acid B γ-Methyl Ester.* Hydrogenolysis of the lactone methyl ester (1 g) obtained above in anhydrous dioxane using palladium black in the usual manner afforded the diketopiperazine which was recrystallized from 99% aqueous ethanol, yield, 0.7 g (64%), mp 204 °C (decomp.).

Found: C, 45.33; H, 5.73; N, 7.91%. Calcd for $C_{12}H_{18}O_8N_2$: C, 45.28; H, 5.70; N, 7.91%.

The *N*→*O* and *N*→*S* Migrations of the *s*-Triazinyl Groups of *N,N*-Di-*s*-triazinyl Derivatives of *o*-Aminophenol and *o*-Aminothiophenol

Shigeo TSUNODA, Takeo SHIOJIMA, Yōji HASHIDA, Shizen SEKIGUCHI, and Kohji MATSUI

Department of Chemistry, Faculty of Engineering, Gunma University, Kiryu, Gunma 376

(Received June 16, 1973)

N,N-Bis(dichloro-*s*-triazinyl)-2-aminophenol reacted with an excess of dimethylamine or methylamine to give *N,O*-bis(*s*-triazinyl)-2-aminophenol and *N*-*s*-triazinyl-2-aminophenol upon the aminodechlorination, *N*→*O* migration, and cleavage of the *s*-triazinyl group. However, *N*-(dimethoxy-*s*-triazinyl)-*N*-(dichloro-*s*-triazinyl)-2-aminothiophenol reacted with an excess of dimethylamine to give merely a disulfide of *N*-*s*-triazinyl-2-aminothiophenol upon the aminodechlorination and cleavage of the dimethoxy-*s*-triazine nucleus. On the other hand, *N,N*-bis(*s*-triazinyl)-arylamines containing no *ortho*-OH or -SH group were stable to the attack by amines, while phenoxy-dimethoxy-*s*-triazine or phenylthio-dimethoxy-*s*-triazine reacted readily with dimethylamine to give dimethylamino-dimethoxy-*s*-triazine upon the fission of phenol or thiophenol. From these resutls, the reactions of the *N,N*-bis(*s*-triazinyl) derivatives of both *o*-aminophenol and *o*-aminothiophenol with amines to give the corresponding *N*-*s*-triazinyl derivatives are considered to proceed by means of an intramolecular nucleophilic attack by the phenoxide or thiophenoxide anion on the *s*-triazine ring carbon to give the *N,O*- or *N,S*-bis(*s*-triazinyl) derivative upon the *N*→*O* or *N*→*S* migration of the *s*-triazinyl group, followed by the cleavage of the *O*- or *S*-*s*-triazinyl group to give the final product. However, when the intermediary derivative is stable to amine, the intermediate is obtained as the major final product.

In previous papers we reported that *O*-*s*-triazinyl-2-aminophenols and *S*-*s*-triazinyl-2-aminothiophenols rearrange to give the corresponding *N*-*s*-triazinyl derivatives in protic solvents, especially readily in the presence of acid[1] or photochemically,[2] and that *O*-(dimethoxy-*s*-triazinyl)-2-aminophenol and *S*-(dimethoxy-*s*-triazinyl)-2-aminothiophenol give *N*-(acyl)-*N*-(*s*-triazinyl)- or *N,N*-bis(*s*-triazinyl) derivatives upon the *O*→*N* or *S*→*N* migration of the *s*-triazinyl group on acylation or *s*-triazinylation.[3] In addition, the *O*-*s*-triazinyl groups of *N*-(dichloro-*s*-triazinyl)-*O*-(*s*-triazinyl)-2-aminophenols migrate to give *N,N*-bis(*s*-triazinyl)-2-aminophenols on the methoxydechlorination[3] of the active chlorine atoms in the *N*-*s*-triazine nucleus.

In these ways, in the ordinary Smiles rearrangements of *s*-triazinyl derivatives of *o*-aminophenol and *o*-aminothiophenol, the *s*-triazinyl group migrates from the oxygen or sulfur atom to the amino nitrogen atom, as in the rearrangements of nitrophenyl derivatives of *o*-aminophenol.[4] However, on the contrary, we have found that some *N,N*-bis(*s*-triazinyl) derivatives of *o*-aminophenol and *o*-aminothiophenol rearrange to give *N,O*-bis(*s*-triazinyl)- or *N,S*-bis(*s*-triazinyl) derivatives or/and their cleaved products upon treatment with amines.

This paper will report on reverse Smiles rearrangements involving the *N*→*O* and *N*→*S* migrations of aromatic systems with *N,N*-bis(*s*-triazinyl) derivatives of *o*-aminophenol and *o*-aminothiophenol, in which rearrangements the *s*-triazinyl group migrates as an aromatic system.

Results and Discussion

N→O *Migration of the* s-*Triazinyl Group of* N,N-*Bis(s-triazinyl)-2-aminophenols in the Reaction with Amines.* In the reaction of *N,N*-bis(dichloro-*s*-triazinyl)-2-aminophenol (**1′**)[5] with dimethylamine in a molar ratio of 1 : 4, two chlorine atoms were replaced to give *N,N*-bis(4-chloro-6-dimethylamino-*s*-triazin-2-yl)-2-aminophenol (**1**). However, when (**1′**) was treated with

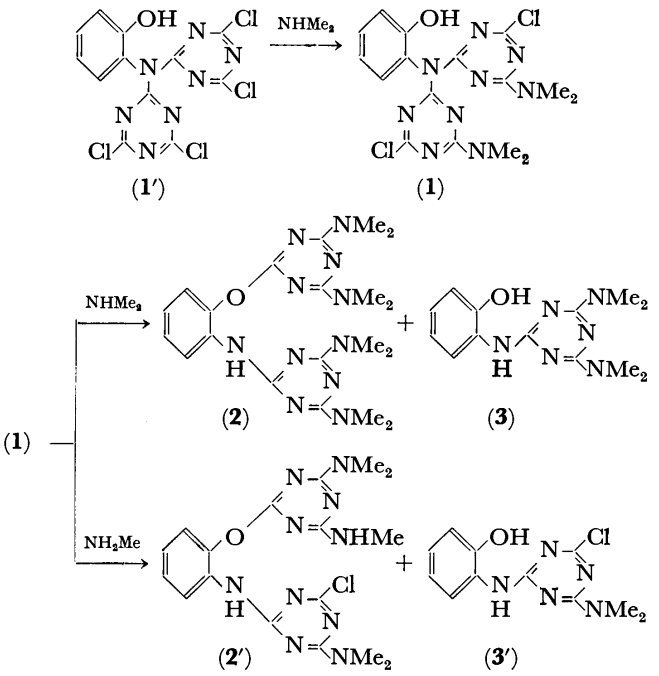

(**1′**) (**1**) (**2**) (**3**) (**2′**) (**3′**)

1) a) T. Harayama, K. Okada, S. Sekiguchi, and K. Matsui, *J. Heterocycl. Chem.*, **7**, 981 (1970); b) N. Maeno, T. Itagaki, S. Uno, and K. Matsui, This Bulletin, **45**, 3133 (1972); c) T. Shiojima, Y. Hashida, and K. Matsui, *ibid.*, in press.

2) K. Matsui, N. Maeno, H. Shizuka, and T. Morita, *Tetrahedron Lett.*, **1970**, 1467; H. Shizuka, N. Maeno, and K. Matsui, *Mol. Photochem.*, **4**, 335 (1972).

3) T. Shiojima, T. Kuroda, S. Ohkawa, Y. Hasegawa, and K. Matsui, This Bulletin, **46**, 2549 (1973).

4) W. E. Truce, E. M. Krider, and W. W. Brand, "The Smiles and Related Rearrangements of Aromatic Systems," Organic Reactions Vol. 18, John-Wiley & Sons. Inc., (1970), p. 116.

5) T. Harayama, S. Sekiguchi, and K. Matsui, *J. Heterocycl. Chem.*, **7**, 975 (1970).

an excess of dimethylamine at room temperature in acetone, *N,O*-bis[4,6-bis(dimethylamino)-*s*-triazin-2-yl]-2-aminophenol (**2**) was obtained as the main product, along with a small amount of *N*-[4,6-bis(dimethylamino)-*s*-triazin-2-yl]-2-aminophenol (**3**).

Apparently, the formation of **2** results from the *N*→*O* migration of the *s*-triazinyl group and the replacement of the chlorine atoms by dimethylamino groups. However, it is uncertain whether **3** results from a cleavage of the *s*-triazinyl group from **1** or from *N,O*-bis(*s*-triazinyl)-2-aminophenol (**2**). A similar rearrangement was observed when **1** was treated with methylamine; in this case, however, *N*-(4-chloro-6-dimethylamino-*s*-triazin-2-yl)-2-aminophenol (**3'**) and *N,O*-bis(*s*-triazinyl)-2-aminophenol containing one residual chlorine atom were obtained. The latter is considered to be *N*-(4-chloro-6-dimethylamino-*s*-triazin-2-yl)-*O*-(4-dimethylamino-6-methylamino-*s*-triazin-2-yl)-2-aminophenol (**2'**) from the facts that **3'** was obtained in this reaction and that an active chlorine atom in the *O*-*s*-triazinyl nucleus is more reactive towards nucleophiles than that in the *N*-*s*-triazinyl nucleus. The results suggest that the *N*→*O* migration of the *s*-triazinyl group took place prior to the replacement of the chlorine atom by the methylamino group. When pyridine was used as a base, only unchanged **1** was recovered under similar reaction conditions. On the other hand, in the reaction of **1** with an excess of sodium methoxide only *N*-(4-dimethylamino-6-methoxy-*s*-triazin-2-yl)-2-aminophenol was obtained upon the fission of one of the *s*-triazinyl groups.

N→S *Migration of the* s-*Triazinyl Group in the Reaction of* N,N-*Bis(*s-*triazinyl)-2-aminothiophenols with Dimethylamine.* When *N*-(dichloro-*s*-triazinyl)-*N*-(dimethoxy-*s*-triazinyl)-2-aminothiophenol (**4**)[3] was treated with dimethylamine in a molar ratio of 1 : 2, a replaced product of one chlorine atom (**5**) was obtained. However, with an excess of dimethylamine (**4**) gave a disulfide of *N*-[bis(dimethylamino)-*s*-triazinyl]-2-aminothiophenol (**6**) and 2-dimethylamino-4,6-dimethoxy-*s*-triazine[5] upon the cleavage of the dimethoxy-*s*-triazinyl group; *N,S*-bis(*s*-triazinyl)-2-aminothiophenol was not obtained in this case. A similar result was also obtained when *N*-(4-chloro-6-methoxy-*s*-triazin-2-yl)-*N*-(4,6-dimethoxy-*s*-triazin-2-yl)-2-aminothiophenol (**7**) was treated with an excess of dimethylamine.

Generally, *N*-(acyl)-*N*-(*s*-triazinyl)- or *N,N*-bis(*s*-triazinyl)-arylamines are readily decomposed to give *N*-acyl- or *N*-*s*-triazinylarylamines upon the cleavage of the acyl or one of the *s*-triazinyl groups by sodium hydroxide or sodium methoxide, even in the absence of an *ortho*-OH or -SH group. Therefore, in the reaction of **1** with sodium methoxide to give *N*-*s*-triazinyl-2-aminophenol, a process involving the intermediary formation of *N,O*-bis(*s*-triazinyl)-2-aminophenol is unlikely. However, *N,N*-bis(*s*-triazinyl)-arylamines are fairly stable to amines when an *ortho*-OH or -SH group is absent; therefore, *N,N*-bis(*s*-triazinyl)-arylamine containing active chlorine atoms undergo merely a replacement of the chlorine atoms upon treatment with amines.

Thus, *N*-(4,6-dichloro-*s*-triazin-2-yl)-*N*-(4,6-dimethoxy-*s*-triazin-2-yl)-4-chloroaniline (**9**), whose triazinyl groups are expected to be somewhat more reactive towards nucleuphiles than those of **5** and **7** because of the presence of the *p*-chloro substituent, reacted with an excess of dimethylamine to give merely a replaced product (**10**), without any cleavage of the *s*-triazinyl group, under similar reaction conditions. On the other hand, 2,4-dimethoxy-6-phenoxy-*s*-triazine and 2,4-dimethoxy-6-phenylthio-*s*-triazine gave 2-dimethylamino-4,6-dimethoxy-*s*-triazine[6] upon treatment with an excess of dimethylamine. Similarly, **2** gave **3** and tris(dimethylamino)-*s*-triazine when treated with dimethylamine, although the reaction took place very slowly. In addition, **10** did not react with phenol or thiophenol in the presence of dimethylamine to give a derivative of phenoxy-*s*-triazine or phenylthio-*s*-triazine under similar reaction conditions.

From these results, it may be considered that the reaction of **5** or **7** with dimethylamine to give **6** or **8**, and the formation of **3** in the reaction of **1** with di-

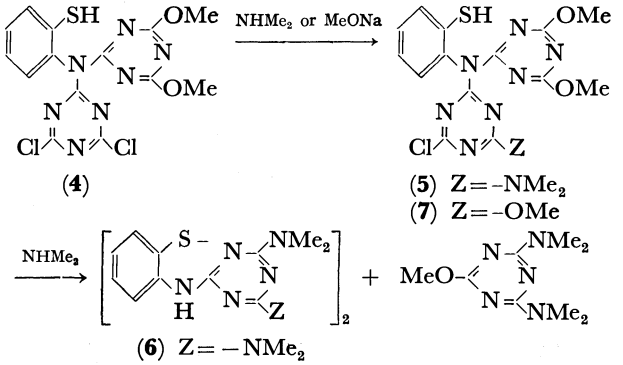

(**4**)

(**5**) Z=−NMe₂
(**7**) Z=−OMe

(**6**) Z=−NMe₂
(**8**) Z=−OMe

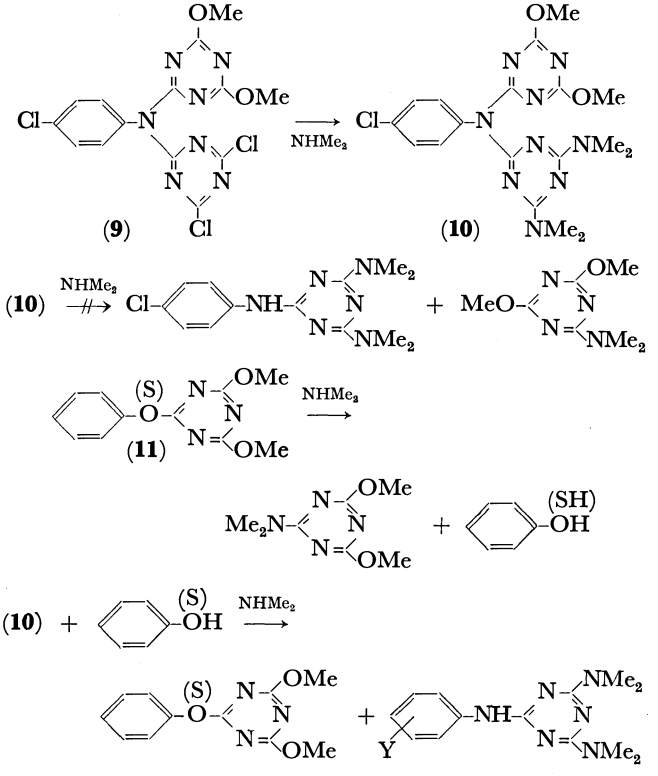

6) Y. Fukushima, Y. Hashida, and K. Matsui, *Nippon Kagaku Kaishi*, **1972**, 629.

methylamine, does not proceed by means of a direct attack by dimethylamine on the *s*-triazine ring carbon of the *N,N*-bis(*s*-triazinyl) derivatives; the presence of the *ortho*-OH or -SH group is assumed to play an important role in the cleavage of the *s*-triazinyl group in these reactions.

The participation of the neighboring –OH or –SH group may be explained reasonably by means of an intramolecular nucleophilic attack on the *s*-triazine nucleus by the phenoxide or thiophenoxide anion formed in the presence of amine; this assumption may be supported by the fact that, for instance, the peak of the hydroxy proton of **1** (δ 8.40) almost disappears on the addition of amine in acetone. When two *s*-triazinyl groups of different kinds are present, the nucleophilic attack may be anticipated to take place preferentially upon the more electron-deficient ring carbon, as in Reactions (**5**) and (**7**). The fact that, in the reaction of **1** with methylamine, the $N\rightarrow O$ migration of the *s*-triazinyl group took place prior to the replacement may be explained by a similar reason; the reactivity of the *s*-triazine nucleus of **1** towards the intramolecular nucleophilic attack by the phenoxide anion is assumed to be greater than that of the replaced product. Thus, in the reaction of *N,N*-bis(*s*-triazinyl)-2-aminophenol or 2-aminothiophenol containing an active chlorine atom with amines, the replacement and rearrangement are considered to take place competitively. When the chlorine atom is reactive enough, the replacement may occur preferentially; however, when the chlorine is not so reactive, the rearrangement may take place prior to the replacement. The intermediary *N,O*- or *N,S*-bis(*s*-triazinyl) derivative thus formed may react with amine to give the *N*-*s*-triazinyl derivative upon the cleavage of the *O*- or *S*-*s*-triazinyl group. When the *O*-*s*-triazinyl group is reactive enough towards amines, only the *N*-*s*-triazinyl derivative may be obtained as the final product, as in the cases of **5** and **7**. However, when the intermediary compound is not so reactive towards amines, the *N,O*- or *N,S*-bis(*s*-triazinyl) derivative can be expected to be obtained as the final product, as in the case of **1**.

From these results, it can be said that, in the reactions of *N,N*-bis(*s*-triazinyl) derivatives of *o*-aminophenol or *o*-aminothiophenol with bases, the processes of the reactions and reaction products vary depending upon the basicities and nucleophilic reactivities of the bases employed. In a reaction with a base of a high nucleophilic reactivity such as sodium methoxide, the reaction proceeds by means of a direct nucleophilic attack at the *N*-*s*-triazine nucleus to give the *N*-*s*-triazinyl derivative. However, in a reaction with amines, the nucleophilic attack at the *s*-triazine nucleus takes place indirectly by means of the phenoxide or thiophenoxide anion upon the $N\rightarrow O$ or $N\rightarrow S$ migration of the *s*-triazinyl group. However, when the amine is a weak base, as in the case of pyridine, the rearrangement does not take place.

Therefore, the reactions of **1**, **5**, and **7** with amines to give not only the *N,O*-bis(*s*-triazinyl) derivatives, but also the corresponding *N*-*s*-triazinyl derivatives, are considered to involve the $N\rightarrow O$ and $N\rightarrow S$ migrations of *s*-triazinyl groups; these migrations can be regarded as examples of the reverse Smiles rearrangement.

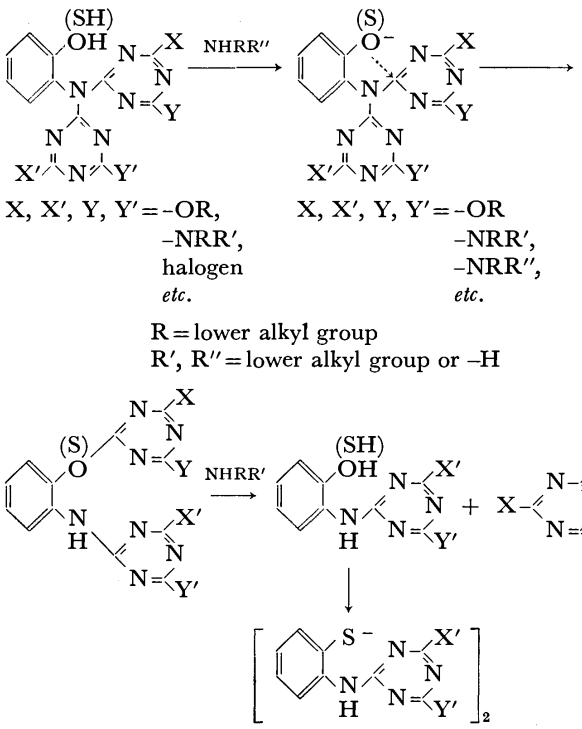

Experimental

All the melting points are uncorrected. The NMR spectra were taken on a Varian A-60D spectrometer, using tetramethylsilane as the internal standard. The elemental analyses were performed in the Micro-analytical Center of Gunma University. The reaction products were identified by means of a study of their NMR spectra, by elemental analyses, by studying their solubility in an alakline solution, and by mixed-melting-point tests with authentic samples.

Materials. The *N,N*-bis(dichloro-*s*-triazinyl)-2-aminophenol (**1'**),[5] *N*-(dichloro-*s*-triazinyl)-*N*-(dimethoxy-*s*-triazinyl)-2-aimnothiophenol (**4**),[3] and *N*-(dichloro-*s*-triazinyl)-*N*-(dimethoxy-*s*-triazinyl)-*p*-chloroaniline (**9**)[7] were prepared by the methods already described.

2,4-Dimethoxy-6-phenoxy-s-triazine To a solution of 53 g (0.30 mol) of 2-chloro-4,6-dimethoxy-*s*-triazine in 200 ml of chloroform, we added an aqueous solution of 31 g (0.33 mol) of phenol and 13.5 g (0.34 mol) of sodium hydroxide in 200 ml of water. After 6 hrs' stirring at 60 °C, the solvent was evaporated. The recrystallization of the residue from ligroin yielded 2,4-dimethoxy-6-phenoxy-*s*-triazine in an almost quantitative yield. (Mp 102—102.5 °C. Found: C, 56.55; H, 5.01%. Calcd for $C_{11}H_{11}N_3O_3$: C, 56.65; H, 4.75%.)

A similar method was adopted for the preparation of 2,4-dimethoxy-6-phenylthio-*s*-triazine. (Mp 69—69.5 °C, recrystallized from ligroin. Found: C, 54.44; H, 4.45%. Calcd for $C_{11}H_{11}N_3O_2S$: C, 54.00; H, 4.45%.)

(i) Reaction of N,N-*bis(dichloro-s-triazinyl)-2-aminophenol (**1'**) with dimethylamine in a molar ratio of 1: 4.* To a stirred solution of 3.4 g (0.0084 mol) of **1'** in 100 ml of acetone, 4.0 g (0.034 mol) of a 40% dimethylamine solution was added, drop by

7) N. Nohara, S. Sekiguchi, and K. Matsui, *J. Heterocycl. Chem.*, **7**, 519 (1970).

drop, at 0 °C. After 3 hrs' stirring, the mixture was poured into 300 ml of ice–water. The precipitate thus formed was filtered, dried, and recrystallized from ethylbenzene to afford *N,N*-bis(4-chloro-6-dimethylamino-*s*-triazin-2-yl)-2-aminophenol (1) in an almost quantitative yield. (Mp 187—188 °C. Found: C, 45.79; H, 4.16%. Calcd for $C_{16}H_{17}Cl_2N_9O$: C, 45.49; H, 4.06%. NMR (CD_3Cl) δ 8.40 (broad, 1H), 7.26 (m, 4H), 3.17 (s, 9H), 3.01 (s, 3H.)

(ii) Reaction of **1′** *with an Excess of Dimethylamine.* To a stirred solution of 1.04 g (0.0025 mol) of **1′** in 150 ml of acetone, 13 g (0.012 mol) of a 4% dimethylamine solution was added, drop by drop, at 20 °C, after which the mixture left overnight at room temperature. The subsequent evaporation of the acetone gave a residue which, on recrystallization from acetone, yielded *N,O*-bis[bis(dimethylamino)-*s*-triazinyl]-*o*-aminophenol (**2**) (mp 184.5—185.5 °C)[3] in an almost quantitative yield. The thin-layer chromatogram (developed on a silica gel layer; developing solvent, acetone: benzene= 1: 10 by volume) of the reaction mixture showed the presence of *N*-[4,6-bis(dimethylamino)-*s*-triazin-2-yl]-2-aminophenol (**3**).[1b]

(iii) Reaction of **1** *with methylamine.* Into a stirred solution of 1.03 g (0.0024 mol) of **1** in 150 ml of acetone, we stirred 8.9 g (0.01 mol) of a 4% methylamine solution, drop by drop. After 48 hrs' stirring at 50 °C, the solvent was evaporated. The residue was purified by column chromatography on silica gel, using a mixture of benzene and acetone (10: 1 by volume) as the developing solvent; this yielded 0.27 g (26.7%) of *N*-(4-chloro-6-dimethylamino-*s*-triazin-2-yl)-*o*-(4-dimethylamino-6-methylamino-*s*-triazin-2-yl)-2-aminophenol (**2′**) and 0.015 g (2.25%) of **3′**. **2′**; [mp 209—210 °C, recrystallized from benzene. Found: C, 48.54; H, 4.97%. Calcd for $C_{17}H_{21}ClN_{10}O$; C, 48.98; H, 5.07%. NMR (DMSO-d_6) δ 8.90 (broad, 1H), 7.76 (broad, 1H), 7.25 (m, 4H), 3.03 (s, 12H), 2.73 (s, 3H).] The structure of Compound **3′** was confirmed by a mixed-melting-point test with an authentic sample prepared by a method to be described below. Into a stirred solution of 15.5 g (0.06 mol) of *N*-(dichloro-*s*-triazinyl)-2-aminophenol[5] in 200 ml of acetone, 14.4 g (0.12 mol) of a 40% dimethylamine solution was added, drop by drop, at 0 °C. After standing for 5 hr at room temperature, the reaction mixture was poured into 500 ml of ice–water. The precipitate thus formed was filtered, dried, and recrystallized from benzene to give *N*-(4-chloro-6-dimethylamino-*s*-triazin-2-yl)-2-aminophenol (**3′**) in a 91% yield. [Mp 222—223 °C. Found: C, 49.98, H, 4.60%. Calcd for $C_{11}H_{12}ClN_5O$; C, 49.69; H, 4.55%. NMR (DMSO-d_6) δ 8.51 (broad, 1H), 7.76 (broad, 1H), 6.81 (m, 4H), 3.08 (s, 6H).]

(iv) Reaction of N-*(dichloro-s-triazinyl)*-N-*(dimethoxy-s-triazinyl)*-2-*aminothiophenol (4) with dimethylamine.* Into a solution of 4.2 g (0.01 mol) of **4** in 100 ml of acetone, we stirred, drop by drop, 2.3 g (0.02 mol) of a 40% solution of dimethylamine at 5 °C. After 1 hr's stirring at 10 °C, the mixture was poured into 300 ml of ice–water; the precipitate thus formed was filtered and dried. Recrystallization from benzene–ligroin gave an analytical sample of *N*-(4,6-dimethoxy-*s*-triazin-2-yl)-*N*-(4-chloro-6-dimethylamino-*s*-triazin-2-yl)-2-aminothiophenol (**5**) in an almost quantitative yield. Mp 168.5 °C. Found: N, 26.76%. Calcd for $C_{16}H_{17}ClN_8O_2S$; N, 26.62%.

(v) Reaction of **5** *with an excess of dimethylamine.* A procedure similar to that described above was employed using 5.0 g of a 40% solution of dimethylamine. After 10 hrs' stirring at room temperature, the mixture was poured into 300 ml of ice–water, and the precipitate thus formed was filtered and dried. Recrystallization from benzene–ligroin yielded a disulfide of *N*-[bis(dimethylamino)-*s*-triazinyl]-2-aminothiophenol (**6**). [Mp 184—185 °C, in an 85% yield. Found: C, 54.14; H, 6.08%. Calcd for $C_{26}H_{34}N_{12}S_2$: C, 53.96; H, 5.92%. NMR (DMSO-d_6), δ 8.60 (s, 1H), 7.65 (m, 4H), 3.00 (s, 12H).] The thin-layer chromatogram of the reaction mixture proved the presence of 2-dimethylamino-4,6-dimethoxy-*s*-triazine.[5]

(vi) Reaction of **4** *with Sodium Methoxide.* Into a solution of 4.2 g (0.01 mol) of Compound **4** in 100 ml of dioxane, we stirred, drop by drop, an equimolar methanolic solution of sodium methoxide at 0 °C. After 1 hr's stirring at 0 °C, the mixture was poured into 300 ml of ice–water; the precipitate thus formed was then filtered and dried. Recrystallization from benzene–ligroin yielded *N*-(4-chloro-6-methoxy-*s*-triazin-2-yl)-*N*-(4,6-dimethoxy-*s*-triazin-2-yl)-2-aminothiophenol (**7**) in an 80% yield. (Mp 146.5—147 °C. Found: C, 44.45; H, 3.68; N, 24.12%. Calcd for $C_{15}H_{14}ClN_7O_3S$: C, 44.18; H, 3.46; N, 24.04%.)

(vii) Reaction of **7** *with an Excess of Dimethylamine.* Compound **7** was treated with an excess of dimethylamine by a method similar to that described in (v). The crude product was purified by recrystallization from benzene–ligroin to give a disulfide of *N*-(4-dimethylamino-6-methoxy-*s*-triazinyl)-2-aminothiophenol (**8**) in a 70% yield. Mp 190—191 °C. Found: C, 52.30; H, 5.27%. Calcd for $C_{24}H_{28}N_{10}O_2S_2$: C, 52.16; H, 5.11%. NMR (DMSO-d_6) δ 8.98 (s, 1H), 7.0 (m, 4H), 3.80 (s, 3H), 3.03 (s, 6H). A thin-layer chromatogram of the reaction mixture showed the presence of 2-dimethylamino-4,6-dimethoxy-*s*-triazine.

(viii) Reaction of N-*(dichloro-s-triazinyl)*-N-*(dimethoxy-s-triazinyl)*-p-*chloroaniline (9) with dimethylamine.* To a stirred solution of 4.1 g (0.01 mol) of **9** in 100 ml of acetone, 4.0 g (0.1 mol) of a 40% dimethylamine solution was added, drop by drop, at room temperature. After 5 hrs' stirring, the mixture was poured into 300 ml of ice–water; the precipitate was filtered and dried. Recrystallization from acetone yielded *N*-[4,6-bis(dimethylamino)-*s*-triazin-2-yl]-*N*-(4,6-dimethoxy-*s*-triazin-2-yl)-*p*-chloroaniline (**10**) in an almost quantitative yield: mp 172—173 °C. Found: N, 29.26%. Calcd for $C_{18}H_{22}ClN_9O_2$: N, 29.18%. In a thin-layer chromatogram of the reaction mixture, no spots of *N*-[4,6-bis-(dimethylamino)-*s*-triazin-2-yl]-4-chloroaniline and 2-dimethylamino-4,6-dimethoxy-*s*-triazine were observed.

(ix) Reaction of **2**, *2,4-dimethoxy-6-phenoxy-s-triazine and 2,4-dimethoxy-6-phenylthio-s-triazine with dimethylamine.* A typical run is shown in the case of 2,4-dimethoxy-6-phenoxy-*s*-triazine. 5 g of a 4% solution of dimethylamine was stirred, drop by drop, into a solution of 0.2 g of 2,4-dimethoxy-6-phenoxy-*s*-triazine in 30 ml of acetone. Stirring was continued for 10 hr at 25 °C, and then the mixture was poured into 100 ml of ice–water. The precipitate was filtered and dried. The product was purified by column chromatography to give 0.035 g of 2,4-dimethoxy-dimethylamino-*s*-triazine. A thin–layer chromatogram of the reaction mixture showed the presence of phenol.

Reaction between Methyl-*p*-tolylmethoxysulfonium Salt and Nucleophiles[1]

Kuniaki TSUMORI, Hiroshi MINATO, and Michio KOBAYASHI

Department of Chemistry, Faculty of Science, Tokyo Metropolitan University, Fukazawa, Setagaya, Tokyo 158

(Received June 26, 1973)

The reactions of methyl-*p*-tolylmethoxysulfonium ion with such nucleophiles as tertiary amines, triphenylphosphine, thiophenolate anion and *p*-toluenesulfinate anion were investigated. The points of attack vary with nucleophile; the sulfonium ion receives nucleophilic attacks at its methoxy oxygen, methoxy carbon, sulfonium sulfur, S–CH_3 hydrogen or O–CH_3 hydrogen atoms. Optically active methyl-*p*-tolylmethoxysulfonium ion was also synthesized, and its reactions with benzylethylphenylamine, benzylmethylphenylphosphine and benzyl ethyl sulfide were studied. In the cases of the amine and the sulfide, the methylated products had optical activity. Thus, the methoxysulfonium ion can act as an optically active methylating agent.

Several alkoxysulfonium ions, $R_1R_2\overset{\oplus}{S}OR_3$, were prepared by alkylating the corresponding sulfoxides with trialkyloxonium ions.[2] Although alkoxysulfonium ions are expected to undergo interesting reactions with various nucleophiles, only a few papers have been published on these reactions. Johnson and Phillips reported that removal of the proton on the α-carbon of the alkoxy group of an alkoxysulfonium ion yields an aldehyde and a sulfide, and removal of the proton on the carbon atom adjacent to the sulfonium sulfur results in a Stevens-type rearrangement, an α-alkoxysulfide being formed.[2a,3] Johnson and McCants studied the reaction between an optically active alkoxysulfonium salt and hydroxide anion and found that the sulfoxide obtained possessed inverted configuration.[2b] Reaction with arylmagnesium halides gave triarylsulfonium salt with inverted configuration.[4]

Studies on the reactions of alkoxysulfonium ions with amines, phosphines, and sulfides seemed to be of great interest, and such investigations have been carried out in our laboratories. The results are described in this paper.

Results and Discussion

Reactions between methyl-*p*-tolylmethoxysulfonium tetrafluoroborate (I) and several nucleophiles in dichloromethane were studied at room temperature by means of NMR spectroscopy.

Reactions between I and Amines. Reaction of I with triethylamine or pyridine was rapid and completed soon after mixing, but that with *N,N*-dimethylaniline took 4 days and that with benzylethylphenyl amine took 7 days for completion. The results are shown in Table 1.

The reactions between I and amines can be summarized in the following scheme.

Table 1. Products of reactions between I and amines

Product (mol/100 mol I)	Amines				Path[c]
	Et_3N	Me_2NPh	C_5H_5N	PhEtNCH$_2$Ph	
p-Tol-S-Me	45	9.1	4.8	10	H_o
p-Tol-$\overset{\oplus}{S}Me_2$	0	0	0	13	H_o
(CH_2O)[a]	(45)	(9.1)	(4.8)	(25)	H_o
p-Tol-S-CH_2OMe	55	27	48	43	H_s
$H\overset{\oplus}{N}R_3$	97	32	(52.8)[b]	(66)[b]	H_s+H_o
p-Tol-S-Me ↓ O	0	63	47	33	OMe
$Me\overset{\oplus}{N}R_3$	0	61	32	17	OMe

a) Estimated from the amounts of *p*-Tol-S-Me and *p*-Tol-$\overset{\oplus}{S}Me_2$.

b) Estimated from the amounts of *p*-Tol-S-Me, *p*-Tol-$\overset{\oplus}{S}Me_2$ and *p*-Tol-S-CH_2OMe c) See text and schemes.

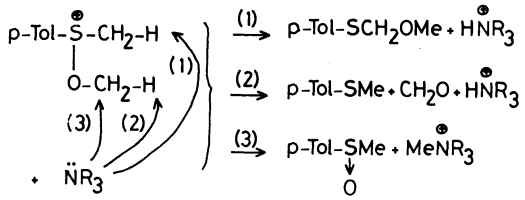

Three paths are possible for these amines; 1) deprotonation at $\overset{\oplus}{S}$–CH_2–H (path H_S), 2) deprotonation at O–CH_2–H (path H_o) and 3) demethylation at O–Me (path OMe). Deprotonation at S–CH_2–H will form a methoxysulfonium ylid, which is converted into methoxymethyl *p*-tolyl sulfide by a rearrangement similar to the Stevens or Pummerer rearrangement.

The deprotonation at $\overset{\oplus}{S}$–CH_2–H followed by rearrangement of the methoxy group appears to be the most plausible path for the formation of methoxymethyl *p*-tolyl sulfide.

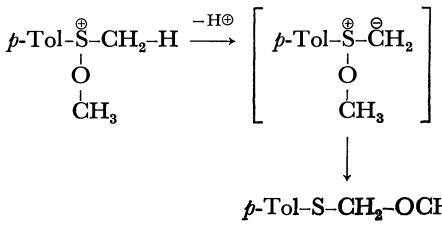

1) Organic Sulfur Compounds. Part XLVI.

2) a) C. R. Johnson and W. G. Phillips, *J. Org. Chem.*, **32**, 1926 (1967); b) C. R. Johnson and D. Mc Cants, Jr., *J. Amer. Chem. Soc.*, **87**, 5404 (1965).

3) a) C. R. Johnson and W. G. Phillips, *Tetrahedron Lett.*, **1965**, 2101; b) C. R. Johnson and W. G. Phillips, *J. Amer. Chem. Soc.*, **91**, 682 (1969).

4) a) K. K. Andersen, M. Cinquini, and N. E. Papanikolaov, *J. Org. Chem.*, **35**, 706 (1970); b) K. K. Andersen and N. E. Papanikolaov, *Tetrahedron Lett.*, **1966**, 5445.

Table 2. Comparison of the points of attack of amines

Amine	OMe Attack[a] (%)	H Attack (%)			pK_a[e]	N_{MeI}[f]
		H_o[b]	H_s[c]	Total		
Et_3N	0	45	55	100	10.7	6.66
C_5H_5N	47	5	48	53	5.19	5.23
Me_2NPh	63	9	27	36	5.21	5.64
$PhEtNCH_2Ph$	33[d]	23	43	66	—	—

a) Yield of methyl *p*-tolyl sulfoxide. b) Yield of methyl *p*-tolyl sulfide and dimethyl-*p*-tolylsulfonium ion. c) Yield of methoxymethyl *p*-tolyl sulfide. d) (Yield of methyl *p*-tolyl sulfoxide) − (yield of dimethyl-*p*-tolylsulfonium ion). e) pK_a of $\overset{\oplus}{H}NR_3$: Ref. 5. f) Pearson's nucleophilicity constant, $N_{MeI} = \log(k/k_{MeOH})$; Ref. 6.

Dimethyl-*p*-tolylsulfonium salt was found only when benzylethylphenylamine was used. The reaction of I with this amine was very slow, and the methyl *p*-tolyl sulfide formed by the path H_o must have been further methylated by the methoxysulfonium ion still remaining unreacted in the medium.

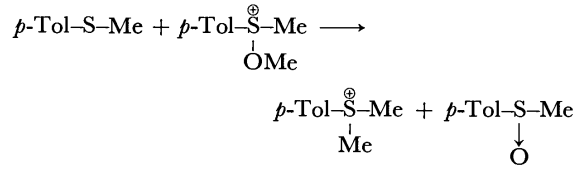

Table 2 summarizes the points of attack of the amines on I. The variations in the attacking points can be explained as follows. Since triethylamine is the strongest base among the four amines, its reaction is 100% H-attack and no C-attack was observed. *N,N*-Dimethylaniline is a much weaker base than triethylamine by a factor of 320000, but its nucleophilicity is smaller only by a factor of 10. Therefore, its main reaction was C-attack. Pyridine is a base of about equal strength but a slightly weaker nucleophile than *N,N*-dimethylaniline, and its H-attack percentage is greater than that of *N,N*-dimethylaniline. Though the basicity of benzyl ethyl phenyl amine is not available in the literature, it is expected to be comparable to or slightly greater than that of *N,N*-dimethylaniline. The much greater percentage of its H-attack is ascribable mainly to a steric factor; the crowded tertiary amine can attack the O–Me group only slowly and H-attack predominates.

Reaction between I and Triphenylphosphine. The products of the reaction between I and triphenylphosphine are summarized as follows.

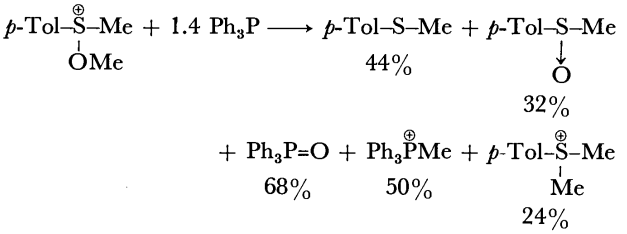

These products can be explained by assuming that triphenylphosphine attacks I at both the O–Me and O–Me positions. A reaction scheme consistent with the experimental results is shown below.

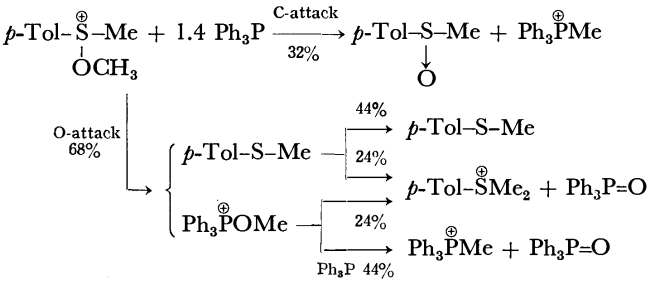

Since triphenylphosphine is a very weak base, it does not give the products of deprotonation. Although the nucleophilic attack of amines takes place only at the methoxy carbon atom, that of triphenylphosphine is mainly at the methoxy oxygen atom and the methoxy carbon attack is a minor reaction.

When triphenylphosphine attacks the methoxy oxygen atom of I, methoxytriphenylphosphonium ion is produced, which is expected to react further with triphenylphosphine. The experimental results show that this was what took place. When equal moles of I and triphenylphosphine were mixed, about 30% of I remained unreacted. The amounts of products formed were determined after a sufficient amount of triphenylphosphine was added and all of I present was consumed. Methoxyphosphonium ion has been postulated as an intermediate in the reaction of a phosphine with peroxides,[7a] or Arbuzov reactions.[7b,c]

Reactions between Optically Active I and Nucleophiles. When optically active I is let to react with nucleophiles, it is expected that the products have some optical activity. In order to check this possibility, the reactions with benzylethylphenylamine, benzylmethylphenylphosphine and benzyl ethyl sulfide were studied.

When R-(+)-I was let to react with benzyl ethyl phenyl amine, a salt-like product obtained was found to be a 77:23 mixture of $(Ph)(PhCH_2)\overset{\oplus}{N}(Me)(Et)$ and $p\text{-}CH_3C_6H_4\overset{\oplus}{S}(CH_3)_2$(by NMR). The optical purity of the methylated amine was 33%.

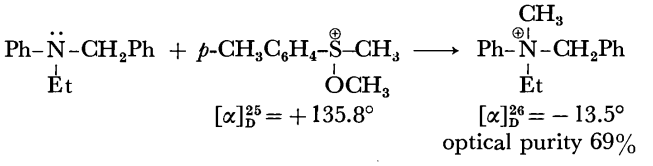

When R-(+)-I was let to react with benzylethylphenylphosphine, the phosphine oxide produced was found to have no optical activity.

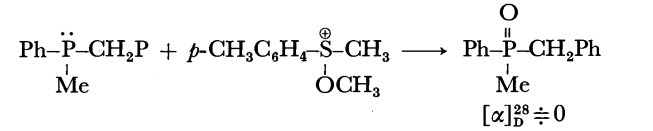

5) C. D. Hodgman (ed.), "Handbook of Chemistry and Physics," Chemical Rubber Publ. Co., Cleveland (1960), p. 1742.

6) R. G. Pearson, H. Sobel, and J. Songstad, *J. Amer. Chem. Soc.*, **90**, 319 (1968).

7) a) M. A. Greenbaum, D. B. Denney, and A. K. Hoffman, *ibid.*, **78**, 2563 (1956); b) A. Macgaekus and R. Kaehne, *Ber.*, **31**, 1048 (1898); c) E. A. Arbuzov, *Zh. Russ. Fiz. Khim. Obshch.*, **38**, 687 (1906).

If the reactions taking place were simply the nucleophilic attack of the phosphine on the oxygen atom adjacent to the asymmetric sulfur atom, some optical activity is expected. The fact that no optical activity was found indicates that what took place was more complex than a simple S_N2 reaction of the phosphine on the methoxy oxygen atom.

When R-(+)-I was let to react with benzyl ethyl sulfide, the benzylethylmethoxysulfonium tetrafluoroborate produced was found to have some optical activity.

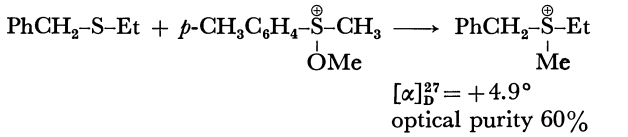

$[\alpha]_D^{27} = +4.9°$
optical purity 60%

Since this salt was not crystalline, it was subjected to anion-exchange on an $NaClO_4$ column. However, the crystalline sulfonium perchlorate obtained showed no optical activity. It is possible that racemization took place during the anion-exchange procedure.

Thus, it has been established that optically active I can be used as stereoselective methylating agent for amines and sulfides.

Reaction between I and Sodium Thiophenolate. The products of the reaction between I and sodium thiophenolate are summarized as follows.

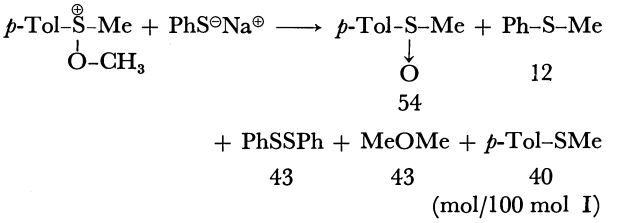

(mol/100 mol I)

These results indicate that the following reactions probably took place.

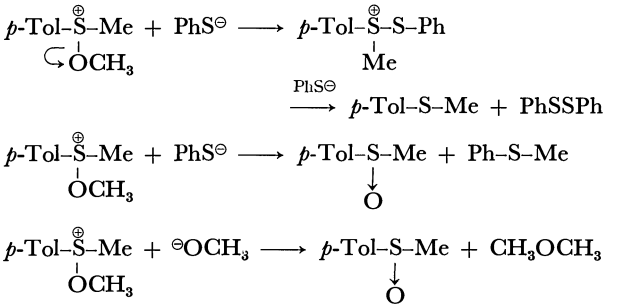

Thus thiophenolate anion attacks at both the sulfonium sulfur and methoxy carbon atoms. Oae and Khim reported that *p*-toluenethiolate anion attacks exclusively at the sulfonium sulfur atom of ethoxydiphenylsulfonium ion, and diphenyl sulfide and di-*p*-tolyl disulfide are the products.[8]

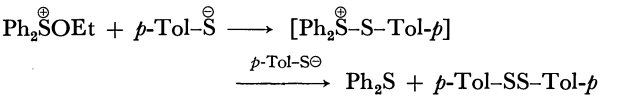

Recently Smallcombe and Caserio[9] reported that the rate constant k_2 for the reaction, $Me_2\overset{\oplus}{S}SMe + MeS\text{-}SMe \rightarrow Me_2S + Me\overset{\oplus}{S}(SMe)_2$, is extremely large ($1.04 \times 10^4\ M^{-1}\ s^{-1}$ at 40 °C). This suggests that the reaction between *p*-Tol(Me)$\overset{\oplus}{S}$SPh and $\overset{\ominus}{S}$Ph must be very fast, and as soon as *p*-Tol(Me)$\overset{\oplus}{S}$SPh is formed by the S-attack of thiophenolate anion on I, it is quickly converted into methyl *p*-tolyl sulfide and diphenyl disulfide.

Reaction between I and Sodium p-*Toluenesulfinate.* The products of the reaction between I and sodium *p*-toluenesulfinate are summarized as follows.

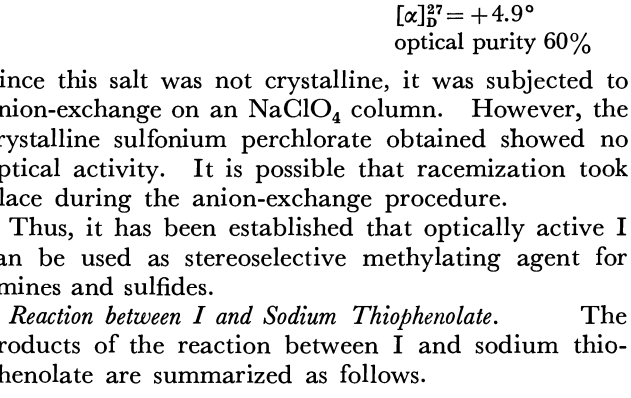

(mol/100 mol I)

These results suggest that the following reactions took place.

The formation of di-*p*-tolyl α-disulfone can be explained by the reaction steps involving the attack of the sulfinate on the S atom of I.

On the basis of these findings and other data reported in the literature, the reactions of methyl-*p*-tolylmethoxysulfonium ion with nucleophiles can be summarized as follows.

8) S. Oae and Y. H. Khim, This Bulletin, **42**, 3528 (1969).
9) S. H. Smallcombe and M. C. Caserio, *J. Amer. Chem. Soc.*, **93**, 5826 (1971).

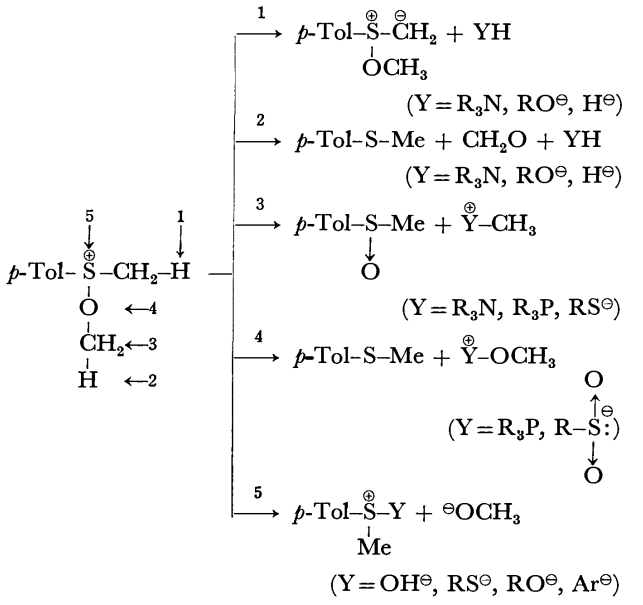

Thus, methyl-*p*-tolylmethoxysulfonium ions can receive nucleophilic attack at five positions, and in this respect methylarylmethoxysulfonium ions are unique and interesting.

Experimental

Materials. Methyl-*p*-tolylmethoxysulfonium tetrafluoroborate (I) was synthesized by methylation of methyl *p*-tolyl sulfoxide with trimethyloxonium tetrafluoroborate in dichloromethane, and recrystallized from dichloromethane–ether;[2b] mp 65—68 °C; NMR, δ, 2.51 (s, $ArCH_3$), 3.57 (s, S-CH_3), 4.00 (s, S-OCH_3) ppm.

Methoxymethyl *p*-tolyl sulfide was prepared by condensation of chloromethyl *p*-tolyl sulfide with methanol in the presence of pyridine;[10] bp, 80—84 °C/4 mmHg; NMR, δ, 2.26 ppm ($ArCH_3$), 3.35 (s, OCH_3), 4.85 (s, SCH_2), 7.16 (q, ArH).

Dimethyl-*p*-tolylsulfonium tetrafluoroborate was synthesized by methylation of methyl *p*-tolyl sulfide with trimethyloxonium tetrafluoroborate, and recrystallized from dichloromethane–ether; NMR, δ, 2.50 ppm (s, $ArCH_3$), 3.27 (s, S-CH_3), 7.65 (q, ArH). Dimethylphenylsulfonium tetrafluoroborate was prepared in a similar manner; NMR, δ, 3.26 (s, S-CH_3), 7.87 (s, ArH).

Methyltriphenylphosphonium tetrafluoroborate was synthesized by methylation of triphenylphosphine with trimethyloxonium tetrafluoroborate; NMR, δ, 2.81 (d, CH_3), 7.77 (m, ArH).

General Procedure for the Reactions between I and Nucleophiles. An equimolar mixture of I and a nucleophile was let to react in dichloromethane, and the progress of the reaction was followed by means of NMR spectroscopy. The amounts of the products were determined from the integrated values on NMR spectra by using 1,1,2,2-tetrachloroethane as the internal standard. Each product was isolated by extraction, recrystallization or elution chromatography, and identified by comparing its melting point, glc retention time, IR or NMR spectrum with those of an authentic sample prepared separately.

Reaction between I and Pyridine. Pyridine (0.90 g, 11.4 mmol) was added to a dichloromethane solution (30 ml) of I (2.9 g, 11.4 mmol) in a 50 ml flask. Exothermic reaction took place, and pyridinium salts precipitated. After the white solids were filtered, the filtrate was concentrated, and the oily residue was extracted with hexane several times. Most of methyl *p*-tolyl sulfoxide remained unextracted. Evaporation and vacuum-distillation of the hexane extracts yielded methyl *p*-tolyl sulfoxide (bp, 110 °C/29 mmHg) and methoxymethyl *p*-tolyl sulfide (bp, 86—90 °C/3 mmHg). The pyridinium salts were recrystallized from dichloromethane–ether several times, and *N*-methylpyridinium chloride was isolated as crystals.

Reaction between I and Triphenylphosphine. Triphenylphosphine (3.1 g, 11.8 mmol) was added to a dichloromethane solution (15 ml) of I (3.0 g, 11.8 mmol). After 3 hr, the NMR spectrum of the solution indicated that 30% of I remained unreacted. When 1 g of phosphine was added, I disappeared completely. The solution was evaporated, and the residual oil was extracted with ether. Ether-isoluble residue was recrystallized from dichloromethane–ether, and methyltriphenylphosphonium salt and dimethyl-*p*-tolylsulfonium salt were isolated. The mother liquor of the recrystallization was evaporated, and elution chromatography of the residue yielded triphenylphosphine oxide. The ethereal extracts were evaporated, and the residue was subjected to elution chromatography on an alumina column; methyl *p*-tolyl sulfide and methyl *p*-tolyl sulfoxide were isolated.

Synthesis of Optically Active R-(+)-*Methyl* p-*Tolyl Sulfoxide.*[11] An anhydrous ether solution (100 ml) of methylmagnesium iodide (103 mmol) was added drop by drop to a stirred ether solution (500 ml) of (−)-menthyl *p*-toluenesulfinate (51.7 mmol) in 1 hr at 0 °C. The solution was stirred at room temperature for 3 hr, and then refluxed overnight. A saturated NH_4Cl solution (200 ml) was added for hydrolysis, and the ethereal layer was separated. The aqueous layer was extracted with ether three times, the combined ethereal extracts were dried over anhydrous magnesium sulfate, and the ether was evaporated. Elution chromatography (alumina, 300 mesh) of the residue gave *R*-(+)-methyl *p*-tolyl sulfoxide; $[\alpha]_D^{26}$ +136.5° (*c* 3.8, acetone).

Synthesis of Optically Active R-(+)-*Methyl*-p-*tolylmethoxysulfonium Tetrafluoroborate* (I_R). To a dichloromethane solution (20 ml) of *R*-(+)-methyl *p*-tolyl sulfoxide (2.0 g, 13.0 mmol) was added trimethyloxonium tetrafluoroborate (1.94 g, 13.0 mmol), and the mixture was stirred for 1.5 hr. After filtration, addition of ether to the cooled filtrate yielded white crystals, which were recrystallized from dichloromethane-ether; 2.4 g (9.4 mmol), 72%; $[\alpha]_D^{25}$ +135.8° (*c* 6.07, CH_2Cl_2).

Reaction between I_R and Benzylethylphenylamine. A mixture of I_R (3.0 g, 11.8 mmol) and benzylethylphenylamine (4.0 g, 19.0 mmol) in dichloromethane (30 ml) was let to react at room temperature for 8 days. After the solvent was evaporated, the residue was washed with ether and the ether-insoluble fraction was stirred with 30% NH_3–H_2O (30 ml) and dichloromethane (20 ml) for 1 day. The solvents were evaporated, and the residue was extracted with dichloromethane. The extracts were dried over anhydrous $MgSO_4$ and evaporated. The NMR spectrum of the residue showed it to be a 77: 23 mixture of (Ph) ($PhCH_2$)$\overset{\oplus}{N}$(Me)(Et) and *p*-$CH_3C_6H_4\overset{\oplus}{S}Me_2$. The optical activity of the salt was determined; $[\alpha]_D^{26}$ −13.5° (*c* 3.7, CH_2Cl_2), optical purity, 69% (optically pure (Ph) ($PhCH_2$)$\overset{\oplus}{N}$EtMe, $[\alpha]_D^{25}$ −19.6°).[12]

Reaction between I_R and Benzylmethylphenylphosphine.

10) L. A. Walter, L. H. Goodson, and R. J. Foshinder, *J. Amer. Chem. Soc.*, **67**, 655 (1945).

11) K. K. Andersen, *Tetrahedron Lett.*, **1962**, 93.

12) H. O. Jones, *J. Chem. Soc.*, **85**, 227 (1904).

Dibenzylphenylphosphonium iodide was prepared by the reaction between dibenzylphenylphosphine and methyl iodide;[13] yield, 19.4%; mp, 206—209 °C (lit,[13] 207-208 °C). Lithium aluminium hydride (0.7 g, 18.4 mmol) was added to a stirred suspension of dibenzylmethylphenylphosphonium iodide (5.0 g, 11.6 mmol) in tetrahydrofuran (60 ml) under a nitrogen atmosphere. After the mixture was refluxed for 42 hr, dichloromethane (100 ml) was added. After 3 hr the jelly substance formed was filtered under a nitrogen atmosphere. To this filtrate containing benzylmethylphenylphosphine was added I_R (3.3 g, 12.9 mmol). After the mixture was allowed to stand at room temperature overnight, the solvent was evaporated, and the residue was extracted with ether. Repeated recrystallization of the ether-insoluble residue from CH_2Cl_2–Et_2O yielded $PhCH_2\overset{\oplus}{P}PhMe_2\overset{\ominus}{B}F_4$, mp 120—122 °C. The mother liquor of the recrystallization was evaporated, and the residue was chromatographed on an alumina column; with CH_2Cl_2–Et_2O as the eluant MePhPh-CH_2P=O was obtained; mp 146—147 °C; $[\alpha]_D^{28}$ *ca.* 0 (*c* 6.7, CH_2Cl_2).

Reaction between I_R and Benzyl Ethyl Sulfide. A mixture of I_R (2.7 g, 10.6 mmol) and benzyl ethyl sulfide (2.0 g, 14.5 mmol) in dichloromethane (20 ml) was allowed to stand at room temperature for 3 days. Its NMR spectrum showed that I_R had disappeared completely. Ether (30 ml) was added, and the ether-insoluble fraction was dissolved in dichloromethane (20 ml), and again ether (30 ml) was added. This procedure was repeated for 6 times. Evaporation of the ether-insoluble fraction yielded solids; $[\alpha]_D^{27}$ +4.9° (*c* 6.08, CH_2Cl_2), optical purity, 60% (optically pure $MeEt\overset{\oplus}{S}CH_2Ph\overset{\ominus}{Cl}O_4$, $[\alpha]_D^{25}=+8.20°$).[14]

The benzylethylmethylsulfonium tetrafluoroborate obtained was subjected to anion exchange by its aqueous acetone solution to an Amberlite IRA-400 column (ClO_4^-). Evaporation of the solvents and recrystallization of the residue from CH_2Cl_2–Et_2O gave crystals of $MeEt\overset{\oplus}{S}CH_2Ph\overset{\ominus}{Cl}O_4$; $[\alpha]_D^{25}$ *ca.* 0 (*c* 6.0, CH_2Cl_2).

Reaction between I and Sodium Thiophenolate. Sodium thiophenolate (1.3 g, 5.3 mmol) was added to a dichloromethane solution (10 ml) of I (0.70 g, 5.3 mmol). Reaction was soon completed. Diphenyl disulfide, methyl *p*-tolyl sulfoxide, methyl ether, methyl phenyl sulfide and methyl *p*-tolyl sulfide were obtained as the products. The amounts of methyl phenyl sulfide and methyl *p*-tolyl sulfide were determined by NMR spectroscopy.

Reaction between I and Sodium p-*Toluenesulfinate.* Anhydrous sodium *p*-toluenesulfinate (4.5 g, 25.3 mmol) was slowly added with stirring to a dichloromethane solution (30 ml) of I (3.9 g, 15.3 mmol). Exothermic reaction occurred. After one day, the solution was separated from the solids. Evaporation of the solution yielded crystals and oil. Crystals were found to be di-*p*-tolyl α-disulfone. Vacuum distillation of the oil yielded methyl *p*-tolyl sulfide (40 °C/0.02 mmHg) and a mixture of methyl *p*-toluenesulfinate and methyl *p*-toluenesulfonate (50—70 °C/0.02 mmHg).

13) W. J. Bailey, S. A. Buckter, and F. Marktscheffel, *J. Org. Chem.*, **25**, 1996 (1960).

14) D. Darwish, S. H. Hui, and R. Tomilson, *J. Amer. Chem. Soc.*, **90**, 5631 (1968).

BULLETIN OF THE CHEMICAL SOCIETY OF JAPAN, VOL. 46, 3507—3510 (1973)

Studies on Aminosugars. XXXV. Syntheses of 3′,4′-Dideoxyneamine and 3′- and 4′-*O*-Methylneamines[1]

Tetsuo JIKIHARA,* Tsutomu TSUCHIYA,* Sumio UMEZAWA,* and Hamao UMEZAWA**

**Department of Applied Chemistry, Faculty of Engineering, Keio University, Hiyoshi, Yokohama 223*

***Institute of Microbial Chemistry, Kamiosaki, Shinagawa-ku, Tokyo 141*

(Received July 9, 1973)

3′,4′-Dideoxyneamine and 3′- and 4′-*O*-methylneamines have been prepared from neamine *via* 5,6-*O*-cyclohexylidene-tetra-*N*-methoxycarbonylneamine (**2**).

As described in previous papers, 3′-deoxykanamycin[2] and 3′,4′-dideoxykanamycin B[3] exhibited strong antibiotic activity against resistant bacteria carrying R factor and resistant *Pseudomonas aeruginosa*, whereas 3′-*O*-methylkanamycin[2,4] was inactive, suggesting the steric hindrance of binding of the antibiotic with ribosomes by 3′-*O*-methyl group. The present investigation was undertaken to prepare an active neamine derivative against resistant bacteris, and to confirm the occurrence of the same steric hindrance in neamine which is an essential moiety of kanamycin B.

In order to protect the four amino groups, neamine was treated with methyl chloroformate in aqueous acetone to give tetra-*N*-methoxycarbonylneamine (**1**). The methyl chloroformate was here selected instead of ethyl or benzyl chloroformate because *N*-methoxycarbonyl group was expected to be stable in acidic

1) A part of this paper was read by S. Umezawa at Symposium of New Natural Products Syntheses, XXIIIrd International Congress of Pure and Applied Chemistry at Boston, U.S.A., July 28, 1971; XXIIIrd ICPAC, Vol. 2, 173, Butterworth, London. Short communication: S. Umezawa, T. Tsuchiya, T. Jikihara, and H. Umezawa, *J. Antibiot.* (Tokyo), **24**, 711 (1971); **25**, 322 (1972).

2) S. Umezawa, T. Tsuchiya, R. Muto, Y. Nishimura, and H. Umezawa, *ibid.*, **24**, 274 (1971); S. Umezawa, Y. Nishimura, H. Hineno, K. Watanabe, S. Koike, T. Tsuchiya, and H. Umezawa, This Bulletin, **45**, 2847 (1972).

3) H. Umezawa, S. Umezawa, T. Tsuchiya, and Y. Okazaki, *J. Antibiot.* (Tokyo), **24**, 485 (1971); S. Umezawa, H. Umezawa, Y. Okazaki and T. Tsuchiya, This Bulletin, **45**, 3624 (1972).

4) H. Umezawa, T. Tsuchiya, R. Muto, and S. Umezawa, *ibid.*, **45**, 2842 (1972).

methanol used in a later reaction. The compound **1** was allowed to react with 1,1-dimethoxycyclohexane in dimethylformamide (DMF) in the presence of catalytic amount of *p*-toluenesulfonic acid at 50 °C under reduced pressure.[5] In the initial stage of this reaction, three derivatives, 3′,4′- and 5,6-*O*-monocyclohexylidene derivatives (**2′** and **2**, respectively) and 3′,4′;5,6-di-*O*-cyclohexylidene derivative (**2″**, minor) were formed but after standing overnight, the derivative **2′** disappeared and a mixture of **2** and **2″** was obtained. Addition of methanol converted **2″** to **2** and the conversion to the starting material (**1**) was very slight. Chromatographic separation gave **2** in a yield of 78%.

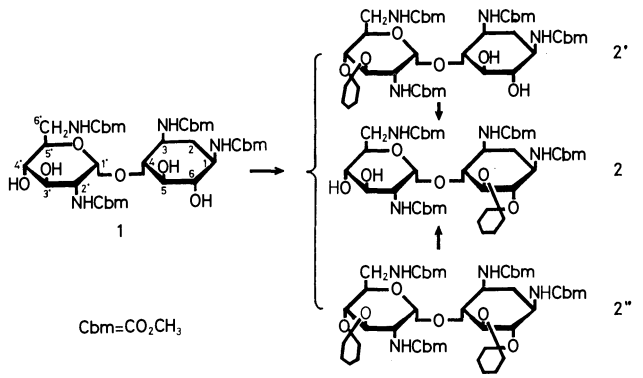

Chart 1.

Mesylation of **2** gave 3′,4′-di-*O*-mesyl derivative (**3**), and treatment of **3** with sodium iodide and zinc dust in DMF, similarly as described in a previous paper,[3] gave 3′-eno derivative (**4**) in a yield of 80%. Catalytic hydrogenation gave 3′,4′-dideoxy derivative (**5**), and removal of the protecting groups in a usual way gave 3′,4′-dideoxyneamine (**6**). Similar deblocking of the 3′-eno derivative (**4**) gave 3′,4′-dideoxy-3′-enoneamine (**7**).

To prepare 3′- and 4′-*O*-methylneamines, compound **2** was subjected to methylation. In preliminary experiments, methylation with methyl iodide–silver oxide and methyl iodide-barium oxide was tried, however, *O*-methylation with these reagents was accompanied by *N*-methylation, rendering the isolation of products difficult. Haworth methylation with dimethyl sulfate–aqueous sodium hydroxide was suitable in this case. Since attempts to separate 3′- and 4′-*O*-methyl derivatives (**8a**, **8b**) was unsuccessful, the mixture was acetylated and then chromatographed over silica gel to give 4′-*O*-acetyl-3′-*O*-methyl- and 3′-*O*-acetyl-4′-*O*-methyl derivatives (**9a**, **9b**) which were thereafter deblocked by the usual method to give 3′-*O*-methylneamine (**10**) and 4′-*O*-methylneamine (**11**), respectively.

The structures of **10** and **11** were confirmed by tetramine copper(II) sulfate (TACu)[6] method. The reagent forms a copper complex exclusively with vicinal amino and hydroxyl groups, which exhibits $\Delta[M]_{436\,(TACu)}$ $\pm 900°$ if the groups have —60° dihedral angle. The compound **10** showed $\Delta[M]_{TACu}$ +730°. The high positive increment indicated that a complex is formed at 1-NH_2 and 6-OH groups. In **11**, TACu forms complexes both at 1-NH_2 and 6-OH, and at 2′-NH_2 and 3′-OH, resulting in a small increment by the intramolecular compensation of the contributions of the two complexes opposite in sign and approximately equal in magnitude.

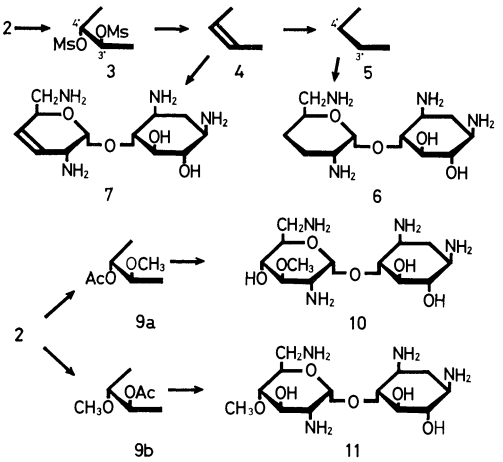

Chart 2.

The synthetic 3′,4′-dideoxyneamine showed[1] antibacterial activity against resistant *E. coli* and *Pseudomonas aeruginosa*, whereas 3′- and 4′-*O*-methylneamines showed markedly decreased activity, suggesting that, though the hydroxyl groups do not play important role in the mechanism of antibacterial action, there is a strong steric factor associated with the hydroxyl groups.

Experimental

Thin layer chromatography (tlc) was carried out on silica gel and the spots were visualized with sulfuric acid.

Tetra-N-*methoxycarbonylneamine (1)*[7]. Crude product of **1** obtained by the procedure reported[8] was desalted by dissolving it in hot dioxane and the dioxane-soluble product was reprecipitated from methanol, $[\alpha]_D^{20}$ +67° (*c* 0.5, water).

Found: C, 42.50; H, 6.40; N, 9.53%. Calcd for $C_{20}H_{34}N_4O_{14}\cdot 1/2\,H_2O$: C, 42.63; H, 6.26; N, 9.94%.

NMR (dimethyl sulfoxide-d_6): τ 6.80, 6.60, 6.50, 6.43 (3H, s, each, $-COOCH_3$).

5,6-O-Cyclohexylidene-tetra-N-*methoxycarbonylneamine (2)*. To the suspension of **1** (5.43 g) in dry DMF (57 ml), 1,1-dimethoxycyclohexane (5.76 ml) and fuse-dried *p*-toluenesulfonic acid (170 mg) were added and the mixture was heated at 55 °C under stirring and reduced pressure (20 Torr). After 20 min, the starting material (R_f 0 on tlc with chloroform–ethanol (8:1)) disappeared and after 1.5 hr the mixture became composed from three products (R_f 0.9 (**2″**), 0.45 (**2**) and 0.40 (**2′**)). The solution was allowed to stand overnight at 25 °C, whereupon *2′* almost disappeared. Methanol (3 ml) was added and the solution was allowed to stand at 45 °C for 1.5 hr. By this treatment, **2** became major constituent

5) F. H. Bissett, M. E. Evans, and F. W. Parrish, *Carbohyd. Res.*, **5**, 184 (1967).

6) S. Umezawa, T. Tsuchiya, and K. Tatsuta, This Bulletin, **39**, 1235 (1966).

7) This experiment was performed by Yasushi Takagi and Narushi Hatsuse of our laboratory.

8) S. Umezawa, Y. Okazaki, and T. Tsuchiya, This Bulletin, **45**, 3619 (1972).

and **2″**, minor one. Saturated sodium hydrogen carbonate solution was added and the mixture was evaporated. The residue was extracted with chloroform and the solution was evaporated to give a pale brown solid (5.8 g). This was chromatographed on a column of silica gel (300 g) with chloroform–ethanol (12:1) containing 1% triethylamine. The portions containing **2** and **2″** were evaporated to give solids, 4.85 g (78%) and 0.9 g, respectively. **2**: $[\alpha]_D^{25}$ +37° (*c* 1, methanol).

Found: C, 49.44; H, 6.82; N, 8.93%. Calcd for $C_{26}H_{42}N_4O_{14}$: C, 49.20; H, 6.67; N, 8.83%.

NMR spectra of the compounds **2′** and **2″** showed the presence of mono- and di-cyclohexylidene group, respectively.

5,6-O-Cyclohexylidene-3′,4′-di-O-mesyl-tetra-N-methoxycarbonylneamine (3). To a solution of **2** (1.89 g) in dry pyridine (37 ml), mesyl chloride (1.0 g) was added and the solution was allowed to stand at 30 °C overnight and then at 50 °C for 2 hr. After addition of 0.3 ml of water, the solution was concentrated to approximately one-tenth of the original volume and the concentrate was poured into saturated sodium hydrogen carbonate solution. The precipitate was extracted with chloroform and the extract was washed with water, dried over sodium sulfate and evaporated. The residue was chromatographed on a short column of silica gel (30 g) with chloroform–ethanol (15:1) containing 1% triethylamine. The portion containing **3** was evaporated to give a solid, 2.24 g (95%), $[\alpha]_D^{25}$ +50.4° (*c* 1, methanol).

Found: C, 42.77; H, 5.85; N, 6.97; S, 7.89%. Calcd for $C_{28}H_{46}N_4O_{18}S_2$: C, 42.53; H, 5.86; N, 7.09; S, 8.11%.

NMR ($CDCl_3$): τ 6.90 and 6.73 (each 3H, s, SO_2CH_3).

5,6-O-Cyclohexylidene-3′,4′-dideoxy-3′-eno-tetra-N-methoxycarbonylneamine (4). To a solution of **3** (1.28 g) in dry DMF (30 ml), anhydrous sodium iodide (15 g) and zinc dust (7 g) were added and the mixture was heated in an oil bath (98 °C) for 2 hr under stirring. Chloroform (70 ml) was added and the resulting precipitate was removed by centrifugation and the precipitate was washed with chloroform. Mother solution and the washings combined were mixed with sodium hydrogen carbonate solution and, after filtration, the filtrate was evaporated to give a syrup, which was dissolved in chloroform. The solution was washed with sodium thiosulfate solution and with water, dried over sodium sulfate and evaporated to give amorphous powder, 0.78 g (80%), $[\alpha]_D^{25}$ −39° (*c* 1, methanol).

Found: C, 52.08; H, 6.78; N, 9.10%. Calcd for $C_{26}H_{40}N_4O_{12}$: C, 52.00; H, 6.71; N, 9.33%.

NMR ($CDCl_3$): τ 4.28 (2H, slightly broadened s, H-3′,4′).

5,6-O-Cyclohexylidene-3′,4′-dideoxy-tetra-N-methoxycarbonylneamine (5). A solution of **4** (368 mg) in methanol (7 ml) containing water (0.2 ml) was hydrogenated with platinum oxide and hydrogen (50 psi) at room temperature for 3 hr. The reaction mixture was filtered and evaporated to give amorphous powder, 339 mg (92%), $[\alpha]_D^{23}$ +34° (*c* 0.6, methanol).

Found: C, 51.58; H, 6.95; N, 9.20%. Calcd for $C_{26}H_{42}N_4O_{12}$: C, 51.82; H, 7.03; N, 9.30%.

NMR ($CDCl_3$): τ 4.92 (1H d, J=3.5 Hz, H-1′), 6.30, 6.32 and 6.34 (6H, 3H, 3H, s, respectively, $NHCO_2C\underline{H}_3$), 8.1—8.8 (~15H broadened signal, cyclohexylidene protons, H-3′,3′,4′,4′ and H-2_{ax}).

3′,4′-Dideoxyneamine (6). To a solution of **5** (299 mg) in methanol (5.3 ml), 0.5 M barium hydroxide solution (17 ml) was added and the mixture was heated at 105 °C for 11 hr. Carbon dioxide was introduced at 100 °C and the precipitate was removed by centrifuging and the precipitate was washed with hot water. Mother solution and the washings combined were evaporated to give a residue, which was again dissolved in water, filtered, and evaporated. The solid residue was dissolved in 1 M hydrochloric acid (5 ml) and the solution was refluxed for 1 hr. After concentration with occasional addition of water, the concentrate was neutralized with Amberlite IRA-400 (OH form) to pH 4 and, after filtration, the solution was charged on a column of Amberlite CG 50 (NH_4^+ form) and developed with 0—0.3 M ammonia with gradual increase in concentration. 2-Deoxystreptamine and by-products were eluted in an early stage (at about 0.2 M ammonia) and **6** followed (at about 0.3 M ammonia). The portion containing **6** was evaporated to give a solid, 115 mg (74%), $[\alpha]_D^{20}$ +102° (*c* 1, water).

Found: C, 48.56; H, 9.12; N, 18.42%. Calcd for $C_{12}H_{26}N_4O_4\cdot 1/2H_2O$: C, 48.14; H, 9.09; N, 18.72%.

NMR (D_2O): τ 9.1—7.8 (6H m, H-2,3′,4′), 4.82 (1H d, J=3.5 Hz, H-1′). The pattern at τ 9.1—7.8 was quite similar with that of 3′,4′-dideoxykanamycin B base[3].

3′,4′-Dideoxy-3′-enoneamine (7). Compound **4** (1.9 g) was treated similarly as described for the preparation of **6** from **5** and the product obtained by treatment of Amberlite CG 50 column chromatography was neutralized with sulfuric acid solution. Addition of methanol gave a solid, which was further purified by passing a short column of active carbon, 802 mg (80%), $[\alpha]_D^{20}$ −19.4° (*c* 1, water).

Found: C, 27.85; H, 6.40; N, 10.28; S, 12.28%. Calcd for $C_{12}H_{24}N_4O_4\cdot 2H_2SO_4\cdot 2H_2O$: C, 27.69; H, 6.20; N, 10.76; S, 12.32%.

NMR (D_2O): τ 8.3—7.2 (2H m, H-2), 4.30 (1H d, J=3 Hz, H-1′), 4.1—3.5 (2H m, H-3′,4′). The pattern at τ 4.1—3.5 was similar with that of methyl 2,6-diamino-2,3,4,6-tetradeoxy-α-D-*erythro*-hex-3-enopyranoside sulfate.[8]

A Mixture of 5,6-O-Cyclohexylidene-tetra-N-methoxycarbonyl-3′-O-methylneamine (8a) and 5,6-O-Cyclohexylidene-tetra-N-methoxycarbonyl-4′-O-methylneamine (8b). To a solution of **2** (2.90 g) in acetone (58 ml), 30% sodium hydroxide solution (4 ml) and dimethyl sulfate (1 ml) were added and the mixture was stirred at room temperature for 1 hr. On tlc with chloroform–2-propanol (15:1) the solution showed three spots of R_f 0.26 (**8a**+**8b**), 0.35 (mono-*O*-methyl-mono-*N*-methyl derivatives) and 0.5 (di-*O*-methyl derivative). Ammonia solution was added and, after stirring for a while, the solution was evaporated to give a residue, which was dissolved in chloroform and the solution was washed with sodium hydrogen carbonate solution and with water, dried over sodium sulfate and evaporated. A pale yellow residue (2.8 g) was chromatographed on a column of silica gel (120 g) with chloroform–2-propanol (25:1). The portion containing **8a** and **8b** was evaporated to give a solid, 1.40 g (47%).

Found: C, 50.21; H, 6.95; N 8.32%. Calcd for $C_{27}H_{44}N_4O_{14}$: C, 49.99; H, 6.84; N, 8.64%.

4′-O-Acetyl-5,6-O-cyclohexylidene-tetra-N-methoxycarbonyl-3′-O-methylneamine (9a) and 3′-O-Acetyl-5,6-O-cyclohexylidene-tetra-N-methoxycarbonyl-4′-O-methylneamine (9b). The mixture of **8a** and **8b** described above was treated with acetic anhydride and pyridine in a usual manner to give a mixture of monoacetyl derivatives quantitatively. On tlc with chloroform–2-propanol, the mixture showed a spot of R_f 0.5, while on tlc with benzene–ethyl acetate (1:4), it showed two spots of R_f 0.26 (**9a**) and 0.39 (**9b**), although **8a** and **8b** could not be separated by column chromatography with this system. The mixture (1.4 g) was chromatographed on a column of silica gel (95 g) with benzene–ethyl acetate (2:5) and the portions containing **9a** (640—1200 ml portion) and **9b** (300—570 ml portion) were evaporated to give solids, 0.58 g (42%) and 0.72 g (52%), respectively. **9a**: mp 129—131 °C, $[\alpha]_D^{20}$ +46° (*c* 1, methanol).

Found: C, 50.28; H, 6.54; N, 8.04%. Calcd for $C_{29}H_{46}N_4O_{15}$: C, 50.43; H, 6.71; N, 8.11%.

NMR ($CDCl_3$): τ 8.8—8.2 (11H, cyclohexyl and H-2_{ax}), 7.88 (3H s, OAc), 6.55 (3H s, OCH_3), 6.31 (12H s, $NHCO_2CH_3$), 5.12 (1H t, J=9.5 Hz, H-4′), 4.81 (1H d, J=3.5 Hz, H-1′). **9b**: mp 123—127 °C, $[\alpha]_D^{20}$ +44° (*c* 1, methanol).

Found: C, 50.56; H, 6.85; N, 8.00%. Calcd for $C_{29}H_{46}N_4O_{15}$: C, 50.43; H, 6.71; N, 8.11%.

NMR ($CDCl_3$): τ 8.8—8.2 (11H), 7.92 (3H s, OAc), 6.53 (3H s, OCH_3), 6.53 (3H), 6.32 (6H) and 6.28 (3H) (each s, $NHCO_2CH_3$), 4.83 (1H t, J=10 Hz, H-3′), 4.80 (1H d, J=3.5 Hz, H-1′).

3′-O-Methylneamine (10). A sample of **9a** was treated likewise as described in the preparation of **6** from **5**, yield 74%, $[\alpha]^{20}$ +122° (*c* 1, water), $\Delta[M]^{20}_{436\,(TACu)}$ +730°.

Found: C, 43.86; H, 8.59; N, 16.06%. Calcd for $C_{13}H_{28}N_4O_6\cdot H_2O$: C, 44.05; H, 8.53; N, 15.81%.

NMR (D_2O): τ 8.80 (1H q, J=12 Hz, H-2_{ax}), 8.02 (1H double t, J=4, 4 and 13 Hz, H-2_{eq}), 6.40 (3H s, OCH_3), 4.71 (1H d, J=3.5 Hz, H-1′).

4′-O-Methylneamine (11). A sample of **9b** was treated as above, yield 78%, $[\alpha]_D^{20}$ +126° (*c* 1, water), $\Delta[M]^{20}_{436\,(TACu)}$ −200°.

Found: C, 43.93; H, 8.56; N, 16.00%. Calcd for $C_{13}H_{28}N_4O_6\cdot H_2O$: C, 44.05; H, 8.53; N, 15.81%.

NMR (D_2O): τ 8.80 (1H q, J=12 Hz, H-2_{ax}), 8.02 (1H double q, J=4, 4 and 13 Hz, H-2_{eq}), 6.44 (3H s, OCH_3), 4.72 (1H d, J=3.5 Hz, H-1′).

BULLETIN OF THE CHEMICAL SOCIETY OF JAPAN, VOL. 46, 3510—3513 (1973)

(1,3-Dithiolan-2-yl)trimethylammonium Iodide. An Electrophilic Dithiolanylating Reagent[1)]

Kazuhisa HIRATANI, Takeshi NAKAI, and Makoto OKAWARA

Research Laboratory of Resources Utilization, Tokyo Institute of Technology, Ookayama, Meguro-ku, Tokyo 152

(Received July 13, 1973)

The reactions of (1,3-dithiolan-2-yl)trimethylammonium iodide (**5**), readily obtained by methylation of 2-dimethylamino-1,3-dithiolane (**2**), with aromatic amines were studied. It was found that **5** served as an electrophilic 1,3-dithiolanylating reagent; the reactions with aniline, *N*-methylaniline, and benzylamine gave *N*-dithiolanylated products while those with *N*,*N*-dimethylaniline and indole yielded exclusively *C*-dithiolanylated products *via* aromatic substitutions. Furthermore, *C*-dithiolanylated compounds were hydrolyzed to aldehydes using HgO–$BF_3 \cdot OEt_2$. The present aldehyde synthesis has been compared with an alternative electrophilic formylation method, the Vilsmeier reaction.

In a previous paper[2)] we reported that the hydride reduction of various dithiocarbamidium ions including 2-dimethylamino-1,3-dithiolan-2-ylium ion (**1**) gave the corresponding formamide thioacetals in moderate yields. In the present work the synthetic utility of 2-dimethylamino-1,3-dithiolane (**2**) obtained from **1** has been studied.

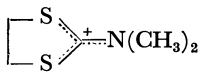

1

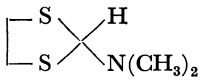

2

The utility of thioacetals, especially 1,3-dithianes, for the synthesis of aldehydes and ketones has been well established.[3)] In most cases, however, the introduction of the dithianyl group was nucleophilically carried out by using dithianyl anion (**3**) and electrophiles such as alkyl halides. On the other hand, little information has been available on the electrophilic introduction of dithianyl or dithiolanyl group mainly because dithiolanyl cation (**4**) has not been characterized.[4)] Recently the formation of **4** has been only observed in the mass spectrum of 1,3-dithiolane[5)] and in the process of oxidation of 1,3-dithiolane derivatives by 2,3-dichloro-5,6-dicyano-1,4-quinone.[6)]

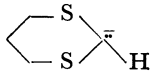

3

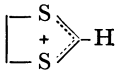

4

In this work, in order to obtain a new electrophilic dithiolanylating reagent derived from **2**, the quarternary ammonium salts (**5**) were prepared by methylation of **2** with methyl iodide, and the reactions of **5** with various nucleophiles (NuH), mostly electron-rich aromatic compounds, have been investigated. Furthermore, the

1) Presented in part at the 26th Annual Meeting of the Chemical Society of Japan, Hiratsuka, 1 April, 1972; Preprint, Vol. III, p. 1114 (1972).

2) K. Hiratani, T. Nakai, and M. Okawara, 23rd Annual Meeting of the Chemical Society of Japan, Tokyo, 3 April, 1970; Preprint, Vol. III, p. 1499 (1970).

3) For a review, See: D. Seebach, *Synthesis*, **1969**, 17.

4) After the preliminary report[1)] on this work was presented, E. J. Corey and S. W. Walinsky [*J. Amer. Chem. Soc.*, **94**, 8932 (1972)] reported on the isolation of 1,3-dithianyl tetrafluoroborate (**4a**) and its synthetic application as an electrophilic 1,3-dithianylating reagent eventually for aldehyde and ketone synthesis.

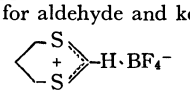

4a

5) D. L. Coffen, K. C. Bank, and P. E. Garrett, *J. Org. Chem.*, **34**, 605 (1969).

6) D. L. Coffen and P. E. Garrett, *Tetrahedron Lett.*, **1969**, 2043.

hydrolysis of some resultant 1,3-dithiolanes (**6**) to aldehydes has been studied.

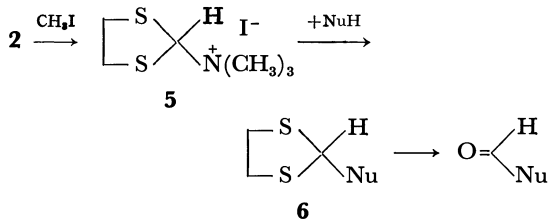

The scope and limitation of the use of reagent **5** for dithiolanylating nucleophiles also described and compared with those of Vilsmeier's reagent, one of the most well-known of electrophilic formylating reagents.

Results and Discussion

Preparation of (1,3-Dithiolan-2-yl)trimethylammonium Iodide (5). Dithiolane **2** was prepared by the hydride reduction of dithiolanylium perchlorate (**1**) using sodium dihydrobis(2-methoxyethoxy)aluminate (RDB).[2] **2** was also obtained by the following more convenient method. Treatment of dimethylformamide (DMF) in tetrahydrofuran (THF) with 1,2-ethanedithiol in the presence of an equimolar amount of benzoyl chloride gave **2** in 76% yield. This was quarternarized with methyl iodide in aprotic solvents giving (1,3-dithiolan-2-yl)trimethylammonium iodide (**5**) in 83% yield. The NMR spectrum of **5** in dimethyl sulfoxide-d_6 showed three singlet signals at δ 3.16 (N–CH_3), 3.60 (S–CH_2), and 6.83 (=C–H).

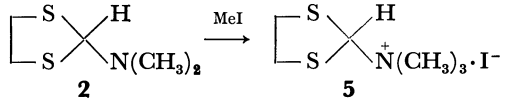

The NMR spectrum confirmed that the methylation occurred on the nitrogen, not on the sulfur atom of **2**. It should be noted that the methine proton of **5** has an absorption at a much lower field (δ 6.85) than that of **2** (δ 6.01) due to quarternarization of the dimethylamino group of **2**.

Reactions of the Ammonium Salt 5 with Various Aromatic Amines. Ammonium iodide **5** is expected to be capable of dithiolanylating nucleophiles analogously to cation **4**, accompanied by the elimination of trimethylamine. In this work, the reactions of **5** with the following aromatic amines were studied: aniline, *N*-methylaniline, *N,N*-dimethylaniline, indole, benzylamine, diphenylamine, and phenothiazine. The reactions were carried out in DMF at 40 °C for 1 hr giving products (**6**) having 1,3-dithiolanyl group along with trimethylammonium iodide except for the cases of diphenylamine and phenothiazine in which the reactants were recovered unchanged. The structures of **6** were elucidated by elemental analysis and spectroscopic methods. In particular the position of the dithiolanylation was determined by NMR and IR spectroscopic methods, and, in some cases, confirmed through identification of aldehydes obtained from the hydrolysis of the dithiolanylated products described below. The yields and physical properties of (**6**) are summarized in Table 1. We see that the position of

Table 1. 1,3-Dithiolanylation of Aromatic Compounds

Aromatics	Product	Yield %	Mp, °C (bp, °C/mmHg)
Aniline	**6a**	72	liq.[a]
N-Methylaniline	**6b**	51	liq.[a] (125—129/1.0)[b]
N,N-Dimethylaniline	**6c** 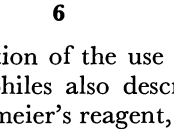	54	103—104
Indole	**6d** 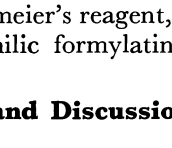	78	116—119
Benzylamine	**6e** 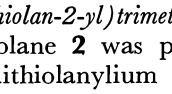	57	liq.[a]
Diphenylamine, Phenothiazine	No Reactions		

a) Purified by column chromatography. b) Prepared by the hydride reduction of carbonium ion, see Experimental.

the introduced 1,3-dithiolanyl group varies with the structure of the aromatic amine employed. In the cases of aniline, *N*-methylaniline, and benzylamine, only *N*-dithiolanylated products were obtained. On the other hand, the reactions of **5** with *N,N*-dimethylaniline and indole gave exclusively *C*-dithiolanylated products *via* aromatic displacement reactions. The former *N*-dithiolanylating reaction might provide a versatile method for synthesizing a variety of formamide thioacetals, eventually formamides from primary and secondary amines. The *N*-dithiolanyl group can be converted into the *N*-carbonyl groups by the hydrolysis: for example, treatment of *N*-(1,3-dithiolanyl)-*N*-methylaniline (**6b**) with HgO–$BF_3 \cdot Et_2O$ gave *N*-phenyl-*N*-methylformamide in 78% yield.

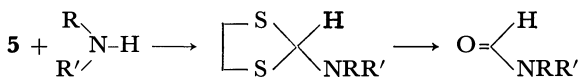

The observed orientation of the aromatic *C*-dithiolanylation, on the other hand, is in agreement with the orientation observed with other electrophilic aromatic substitutions of these aromatic amines, *e.g.* the Vilsmeier reaction.[7]

Hydrolysis of the Dithiolanylated Products to Aldehydes. The hydrolysis of the *N*-dithiolanylated product (**6b**) and the *C*-dithiolanylated products (**6c** and **6d**) was studied. Hydrolysis was accomplished by using red mercury oxide–boron trifluoride etherate[8] in aqueous THF yielding the corresponding aldehydes in good yields. The aldehydes thus obtained were identified by IR spectra and comparisons of their physical properties with those of authentic samples. In short,

7) The *para* position in *N,N*-dimethylaniline and the 3-position in indole are the most reactive sites for electrophilic substitution: For a review of the Vilsmeier reaction, see M.-R. Maheas, *Bull. Chim. Soc. Fr.*, **1962**, 1982.

8) E. Vedejs and P. L. Fuchs, *J. Org. Chem.*, **36**, 366 (1971).

ammonium salt **5** can be used as an electrophilic formylating reagent just as Vilsmeier's reagent, *e.g.*, *N*-formyl-*N*-methylaniline–phosphorus oxychloride complex (**7**).[9]

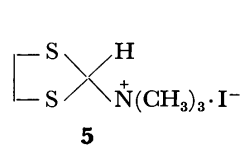

5

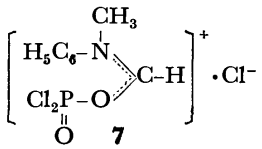

7

Let us compare the present aldehyde synthesis with the Vilsmeier reaction. First, it should be emphasized that a synthetic advantage of the present method over the Vilsmeier method is that aldehyde precursors, 1,3-dithiolanylated compounds, can be readily isolated, hence, a subsequent desirable reaction can be carried out under the protection of the aldehyde group by the 1,3-dithiolane ring. Isolation of the 1,3-dithiolanylated products might provide a unique method for ketone synthesis *via* the following sequences.

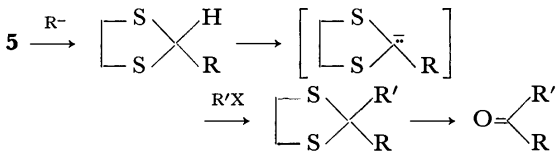

Secondly, it is concluded that the range of application of the present aldehyde synthesis covers more limited aromatics and heterocyclics, compared with Vilsmeier's reagent. Ammonium salt **5** did not react with diphenylamine, phenothiazine or anisole, while Vilsmeier's reagent is capable of undergoing aromatic substitution with these aromatics giving aldehydes. It can be said that the electrophilic reactivity of **5** is smaller and more selective than that of Vilsmeier's reagent (**7**).

Experimental

General. All melting and boiling points are uncorrected. IR and UV spectra were recorded with Hitachi EPI-S2 and EPS-3T spectrophotometers, respectively. NMR spectra were obtained with Japan Electron Optics JNN PS-100 and MH-60 spectrometers. Chemical shifts are reported in ppm from tetramethylsilane as an internal standard.

2-Dimethylamino-1,3-dithiolane (2). Dithiolane **2** was prepared by the hydride reduction of the dithiolanylium salt **1** following previous procedures.[2] In a large scale experiment the following alternative method is recommended which is a modification of the procedures of R. Ohme[10] employed for the synthesis of trialkyl orthoformates.

In a 200-ml three-necked flask, equipped with a mechanical stirrer, dropping funnel and thermometer, was placed a solution of 7.3 g (0.10 mol) of DMF and 9.4 g (0.10 mol) of 1,2-ethanedithiol in 100 ml of THF, which was then cooled below 0 °C. To the stirred solution was added dropwise 14.1 g (0.10 mol) of benzoyl chloride over a period of 1 hr. The reaction temperature was then raised up to 40 °C and the mixture was stirred for 6 hr. The reaction flask was cooled to room temperature giving white precipitates which were filtered and washed three times with 50-ml portions of ether. The precipitates were then dissolved in cooled water and to the aqueous solution was added dropwise an aqueous sodium carbonate solution until the solution became weakly basic. The solution was extracted three times with100-ml portions of ether. The combined ether solutions were dried over anhydrous sodium sulfate. After removal of the drying agent followed by distillation of the ether, distillation of the liquid residue gave 11.4 g (76.5%) of **2**. bp 78—79 °C/2.0 mmHg (lit[2] 57—58 °C/1.5 mmHg). The physical properties and spectra data of this distillate were in agreement with those of an authentic sample.[2]

Preparation of (1,3-Dithiolan-2-yl)trimethylammonium Iodide (5). To a solution of 8.0 g (54 mmol) of **2** in 100 ml of THF was added excess methyl iodide. The mixture was stirred at room temperature for 3 hr giving white precipitates which were filtered and washed several times with THF. Recrystallization of the precipitates from anhydrous acetonitrile gave 13 g (83%) of white crystals, mp (dec.) 152 °C. Found: C, 24.91; H, 4.71; N, 4.95%. Calcd for $C_6H_{14}NS_2I$: C, 24.75; H, 4.85; N, 4.81%.

Reaction of 5 with Aniline. In a 50-ml three-necked flask equipped with a mechanical stirrer, condenser and thermometer was placed a solution of 1.50 g (5.1 mmol) of **5** in 20 ml of DMF. To the stirred solution was added 0.50 g (5.3 mmol) of aniline. The mixture was stirred at 40 °C for 1 hr, and then poured into water. The aqueous solution was extracted three times with 50-ml portions of ether. The combined ethereal solutions were washed four times with water and dried over anhydrous magnesium sulfate. Removal of the ether gave 1.0 g of a pale brown oil. The oil was subjected to chromatography on silica gel with chloroform giving 0.70 g (72%) of **6a**; IR (neat): 3340 cm^{-1} (N-H); NMR (CCl_4): δ 3.24 (m, 4H, S-CH_2), 4.1—4.5 (broad, 1H, N-H), 6.33 (d 1H C-H), and 6.5—7.4 (m, 5H, aromatic-H) UV (EtOH, nm): 248.5.

Reaction of 5 with N-Methylaniline. In a similar manner, the reaction of **5** (1.50 g, 5.1 mmol) with *N*-methylaniline (0.60 g, 5.6 mmol) in 20 ml of DMF at 40 °C for 1 hr gave an oil (0.90 g). The oil was subjected to chromatography on silica gel with chloroform. The first eluent gave 0.54 g (51%) of **6b**; n_D (25 °C) 1.640. The second eluent contained 0.24 g of the starting material, *N*-methylaniline. The IR and UV spectra of **6b** were in complete agreement with those of an authentic sample prepared by the reaction of 2-(*N*-methyl-*N*-phenylamino)-1,3-dithiolan-2-ylium perchlorate with sodium dihydrobis(2-methoxyethoxy)aluminate (yield, 66%), bp 125—129 °C/1.0 mmHg; n_D (25 °C) 1.639. **6b**; NMR (CCl_4): δ 2.92 (s, 3H, N-CH_3), 3.17 (m, 4H, S-CH_2), 6.98 (m, 1H, C-H), and 6.7—7.7 (m, 5H, aromatic-H); UV (EtOH, nm): 253. Found: C, 56.05; H, 6.10; N, 6.10%. Calcd for $C_{10}H_{13}NS_2$: C, 56.83; H, 6.20; N, 6.63%.

Reaction of 5 with N,N-Dimethylaniline. In a similar manner, the reaction of **5** (1.50 g, 5.1 mmol) with *N,N*-dimethylaniline (0.62 g, 5.1 mmol) in 20 ml of DMF at 30—40 °C for 2 hr gave 0.61 g (54%) of **6c** which was recrystallized from ethanol giving colorless plates, mp 103—104 °C; NMR ($CDCl_3$): δ 2.94 (s, 6H, N-CH_3), 3.44 (m, 4H, S-CH_2), 5.77 (s, 1H, C-H), 6.74 (d, 2H, aromatic-H), and 7.49 (d, 2H, aromatic-H); UV (EtOH, nm): 270. Found: C, 59.00; H, 6.72; N, 6.06%. Calcd for $C_{11}H_{15}NS_2$: C, 58.62; H, 6.71; N, 6.21%.

Reaction of 5 with Indole. In a similar manner, the reaction of **5** (1.50 g, 5.1 mmol) with indole (0.59 g, 5.0 mmol) in 20 ml of DMF at 40 °C for 2 hr gave 0.90 g (78%) of **6d** which was recrystallized from ethanol giving colorless plates, mp 116—119 °C; IR (KBr): 3400 cm^{-1} (N-H); NMR ($CDCl_3$): δ 3.50 (m, 4H, S-CH_2), 6.23 (s, 1H, C-H), 7.47 (m, 4H, aromatic-H), and 7.95—8.30 (broad, 2H, N-H

9) H. Bredereck, R. Gompper, K. Klemm, and H. Rempfer, *Chem. Ber.*, **92**, 837 (1959); C. Jutz, *ibid.*, **91**, 850 (1958).

10) R. Ohme, *Ann. Chem.*, **716**, 207 (1968).

and 2-C–H) ppm; UV (EtOH, nm): 221.5, 274, 280, and 290.5. Found: C, 59.36; H, 5.00; N, 6.27%. Calcd for $C_{11}H_{11}NS_2$: C, 59.69; H, 5.01; N, 6.33%.

Reaction of **5** *with Benzylamine.* In a similar manner, the reaction of **5** (1.50 g, 5.1 mmol) with benzylamine (0.50 g, 4.7 mmol) in 20 ml of acetonitrile at 60 °C for 3 hr gave 0.60 g (57%) of **6e** which was purified by means of column chromatography (silica gel) giving a colorless liquid; n_D (20 °C) 1.623; IR: 3330 cm^{-1} (N–H); NMR ($CDCl_3$): δ 1.94 (s, 1H, N–H), 3.23 (s, 4H, SCH_2), 3.93 (s, 2H, N–CH_2), 5.91 (s, 1H, C–H), and 7.38 (s, 5H, aromatic–H). Found: C, 56.83; H, 6.08; N, 6.43%. Calcd for $C_{10}H_{10}NS_2$: C, 56.83; H, 6.20; N, 6.63%.

Hydrolyses of 1,3-Dithiolanyl Compounds with Mercury Oxide (Red) Boron Trifluoride Etherate. a) p-*(1,3-Dithiolan-2-yl)*-N,N-*dimethylaniline (6c)*: In a 50-ml three-necked flask, equipped with a mechanical stirrer, dropping funnel, gas inlet, condenser and thermometer, was placed a suspension of 0.59 g (2.7 mmol) of red mercury oxide and 0.38 g (2.7 mmol) of boron trifluoride etherate in 1: 9 THF–water (10 ml). The mixture was stirred at room temperature under nitrogen atmosphere and then 0.30 g (1.3 mmol) of **6c** in 20 ml of THF was added dropwise to the mixture over a period of 0.5 hr. After the reaction mixture was stirred at room temperature for 1 hr, precipitates formed were filtered and the filtrate was poured into water. The aqueous solution was extracted three times with 50-ml portions of ether, and the combined ether solutions were washed three times with water and dried over anhydrous magnesium sulfate. After removal of the drying agent followed by distillation of the ether, 0.80 g of a yellow oil was obtained. The oil was subjected to chromatography on silica gel with benzene giving 0.17 g (85%) of *p-N,N*-dimethylaminobenzaldehyde; mp 71—73 °C (lit[11] 73 °C).

b) 3-(1,3-Dithiolan-2-yl)indole (6d): In a similar manner, the reaction of **6d** (0.30 g, 1.3 mmol) with red mercury oxide (0.59 g, 2.7 mmol) and boron trifluoride etherate (0.38 g, 2.7 mmol) gave 0.16 g (80%) of 3-formylindole; mp 189—191 °C (lit[12] 193—195 °C).

c) N-*(1,3-Dithiolan-2-yl)*-N-*methylaniline (6b)*: In a similar manner, the reaction of **6b** (1.05 g, 5.0 mmol) with red mercury oxide (2.0 g, 10 mmol) and boron trifluoride etherate (1.4 g, 10 mmol) gave 0.52 g (78%) of *N*-methylanilide. The IR spectrum of this product was in complete agreement with that of an authentic sample.

11) A. Vilsmeier and A. Haack, *Ber.*, **60**, 119 (1927).
12) F. T. Tyson and J. T. Shaw, *J. Amer. Chem. Soc.*, **74**, 2273 (1952).

BULLETIN OF THE CHEMICAL SOCIETY OF JAPAN, VOL. 46, 3513—3516 (1973)

Reduction of *gem*-Bromofluorocyclopropanes with Organosilicon Hydrides

Teiichi ANDO, Hirokazu HOSAKA, Wataru FUNASAKA, and Hiroki YAMANAKA*

Department of Industrial Chemistry, Faculty of Engineering, Kyoto University, Yoshida, Sakyo-ku, Kyoto 606

**Department of Chemistry, Kyoto Institute of Technology, Matsugasaki, Sakyo-ku, Kyoto 606*

(Received July 19, 1973)

7-Bromo-7-fluoronorcarane, 1-bromo-1-fluoro-2-phenylcyclopropane, and 7-bromo-7-fluoro-2-oxanorcarane were reduced with tri-*n*-butylsilane or di-*n*-butylsilane at 100—145 °C in the presence of a small amount of radical initiator, to afford the corresponding monofluorocyclopropanes. It has been found, by examining the stereochemistry of the reduction, that the extent of stereospecificity is dependent on the reaction temperature as well as on the kind of the silicon hydride used. Comparison of these results with those of the tri-*n*-butyltin hydride reduction shows that the reactivity of metal hydrides as a reducing agent of *gem*-dihalocyclopropanes is in the order $Bu_3SnH > Bu_2SiH_2 > Bu_3SiH$. These observations are well explained by postulating that the α-fluorocyclopropyl radical has a pyramidal configuration and that the extent of stereospecificity is determined by the relative rates of its inversion of configuration and its hydrogen abstraction from the tin or silicon hydride. The reduction of 7,7-dibromonoracrane with tri-*n*-butylsilane or di-*n*-butylsilane gave a mixture of the two geometrical isomers of 7-bromonoracrane, whose composition (*endo*-Br/*exo*-Br≒3.0) was nearly identical irrespective of the reaction temperature and of the reactivity of silicon hydride.

It has been known that organosilicon hydrides are capable of reducing organic halides.[1] Thus, the reduction of chloro- or bromoalkanes has been effected with triethylsilane in the presence of aluminum chloride,[2,3] and with trichlorosilane under irradiation of light.[4] Palladium-catalyzed reactions of tri-substituted organosilanes with halocarbons including aromatic halides are also known to result in halogen-hydrogen exchange, to afford a good yield of organosilicon halides.[5] It has been suggested that the reduction of aliphatic halides with organosilicon hydrides proceeds by an ionic mechanism in the presence of aluminum chloride,[2] and by a free-radical chain mechanism under irradiation of light.[4]

1) C. Eaborn, "Organosilicon Compounds," Butterworth and Co., Ltd., London (1960).

2) F. C. Whitmore, E. W. Pietrusza, and L. H. Sommer, *J. Amer. Chem. Soc.*, **69**, 2108 (1947).

3) B. N. Dolgov, S. N. Borisov, and M. G. Voronkov, *Zh. Obshch. Khim.*, **27**, 716 (1957); *Chem. Abstr.*, **51**, 16282 (1957).

4) J. A. Kerr, B. J. A. Smith, A. F. Trotman-Dickenson, and J. C. Young, *J. Chem. Soc., A*, **1968**, 510.

5) J. D. Citron, J. E. Lyons, and L. H. Sommer, *J. Org. Chem.*, **34**, 638 (1969).

Nagai and his collaborators[6] have found that the reduction with organosilicon hydrides in the liquid phase can be effected by use of radical initiator such as benzoyl peroxide, and proposed the following mechanism:

$$\text{Initiator} \longrightarrow \text{In}\cdot$$
$$\text{In}\cdot + R_3SiH \longrightarrow InH + R_3Si\cdot$$
$$R_3Si\cdot + R'X \longrightarrow R_3SiX + R'\cdot$$
$$R'\cdot + R_3SiH \longrightarrow R'H + R_3Si\cdot$$

The mechanism shown above is very similar to the one proposed for the reduction of organic halides with organotin hydrides,[7] which have been found to reduce *gem*-halofluorocyclopropanes in an essentially stereospecific manner to yield the corresponding monofluorocyclopropanes.[8]

This paper describes the results of the reduction of some *gem*-bromofluorocyclopropanes with tri-*n*-butyl- and di-*n*-butylsilane, with emphasis directed upon the stereochemistry of the reaction as compared with that of the organotin hydride reduction.

Results

The *gem*-bromofluorocyclopropanes employed for the present study were 7-bromo-7-fluoronorcarane (**1**), 1-bromo-1-fluoro-2-phenylcyclopropane (**2**), and 7-bromo-7-fluoro-2-oxanorcrane (**3**). They were prepared, as a mixture of two geometrical isomers (**a** and **b**), by the reaction of bromofluorocarbene with cyclohexene, styrene, and 2,3-dihydro-4*H*-pyran, respectively.[9,10]

The reduction of these *gem*-bromofluorocyclopropanes was effected by use of 1.4—3 equivalents of tri-*n*-butyl- or di-*n*-butylsilane at 100—145 °C in the presence of a small amount of azobisisobutyronitrile (AIBN) or di-*t*-butyl peroxide (DTBP), to afford the corresponding monofluorocyclopropanes (**c** and **d**).

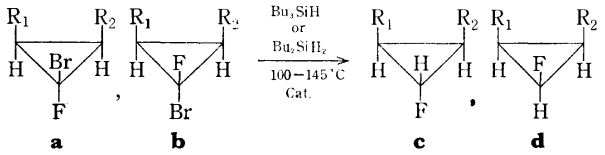

a **b** **c** **d**

1 : R_1, R_2=-$(CH_2)_4$-
2 : R_1=Ph, R_2=H
3 : R_1, R_2=-O-$(CH_2)_3$-

The monofluorocyclopropanes thus formed were identified by comparison of their glpc retention times and infrared absorption spectra with those of authentic samples obtained by the reduction with tri-*n*-butyltin hydride.[8]

Table 1 summarizes the results of the reduction of 7-bromo-7-fluoronorcarane (**1**). As is shown in the table (run 1), the reduction of a mixture of the *exo*-F (**1a**) and the *endo*-F isomer (**1b**) with tri-*n*-butylsila neat 140—145 °C gave a mixture of 7-*exo*-fluoro- (**1c**) and 7-*endo*-fluoronorcarane (**1d**). Analysis by glpc showed the isomer ratio of the product (*exo*-F/*endo*-F=1.22) was not identical with the one of the starting material (*exo*-F/*endo*-F=1.67). This result is in sharp contrast with that of the organotin hydride reduction, where complete stereospecificity has been observed.[8] In order to obtain more detailed information about the stereochemistry of the reaction, the two isomers (**1a** and **1b**) were separated from each other by preparative glpc, and were reduced separately (runs 2—9).

When tri-*n*-butylsilane was used at 100 °C, a mixture of **1c** and **1d** was obtained either from **1a** or from **1b** (runs 2 and 6); the isomer ratio of the product was

Table 1. Reduction of 7-bromo-7-fluoronorcarane (**1**)

Run	**1** (m mol)		Silane (mmol)	Catalyst	Reaction condition		Yield (%)	Isomer ratio of product
	exo-F	*endo*-F			Temp. (°C)	Time (hr)		(*exo*-F/*endo*-F)
1	52.3[a]		Bu_3SiH (73.5)	DTBP	140—145	9.5	42	55/45
2	12.6	0	〃 (33.3)	AIBN	100	7	49	78/22
3	13.4	0	〃 (39.8)	DTBP	140	7		61/39
4	15.7	0	Bu_2SiH_2 (41.6)	AIBN	100	3.5	68	100/0
5	10.9	0	〃 (29.4)	DTBP	140	2		95/5
6	0	12.5	Bu_3SiH (32.8)	AIBN	100	7	33	15/85
7	0	25.5	〃 (41.0)	DTBP	140	7	36	32/68
8	0	10.2	Bu_2SiH_2 (27.2)	AIBN	100	3.5	51	0/100
9	0	7.5	〃 (20.6)	DTBP	140	2		4/96

a) An isomeric mixture (*exo*-F/*endo*-F=1.67).

6) Y. Nagai, K. Yamazaki, I. Shiojima, N. Kobori, and M. Hayashi, *J. Organometal. Chem.*, **9**, 21 (1967). b) Y. Nagai, K. Yamazaki, and I. Shiojima, *ibid.*, **9**, 25 (1967). c) Y. Nagai, K. Yamazaki, I. Shiojima, H. Matsumoto, and S. Nakaido, *Yuki Gosei Kagaku Kyokai-shi*, **26**, 884 (1968). d) Y. Nagai, I. Shiojima, K. Nishijima, and H. Matsumoto, *ibid.*, **26**, 999 (1968). e) Y. Nagai, K. Yamazaki, I. Shiojima, M. Hayashi, and H. Matsumoto, *ibid.*, **26**, 1004 (1968).

7) L. W. Menapace and H. G. Kuivila, *J. Amer. Chem. Soc.*, **86**, 3047 (1964).

8) a) T. Ando, F. Namigata, H. Yamanaka, and W. Funasaka, *ibid.*, **89**, 5719 (1967). b) T. Ando, H. Yamanaka, F. Namigata, and W. Funasaka, *J. Org. Chem.*, **35**, 33 (1970).

9) a) W. Funasaka, T. Ando, H. Yamanaka, H. Kanehira, and Y. Shimokawa, Abstracts of Symposium on Organic Halogen Compounds, p. 25, Tokyo (1967). b) H. Yamanaka, T. Yagi, K. Teramura, and T. Ando, *Chem. Commun.*, **1971**, 380.

10) The reaction of bromofluorocarbene with 2,3-dihydro-4*H*-pyran did give a mixture of the *exo*-F (**3a**) and the *endo*-F isomer (**3b**) of **3**, but **3a** was so susceptible to ring expansion[11] that the distillation of the reaction mixture resulted in the decomposition of **3a**. The pure **3b** employed for the present study was obtained by treating the reaction mixture with hot quinoline followed by vacuum distillation.

11) T. Ando, H. Hosaka, H. Yamanaka, and W. Funasaka, This Bulletin, **42**, 2013 (1969).

Table 2. Reduction of 1-bromo-1-fluoro-2-phenylcyclopropane (**2**)

Run	**2** (mmol)		Silane (mmol)	Catalyst	Reaction condition		Yield (%)	Isomer ratio of product
	anti-F	*syn*-F			Temp. (°C)	Time (hr)		(*anti*-F/*syn*-F)
10	15.8	0	Bu_3SiH (39.3)	AIBN	100	7	69	81/19
11	8.5	0	Bu_2SiH_2 (21.7)	AIBN	100	3.5	60	97/3
12	0	14.6	Bu_3SiH (37.4)	AIBN	100	7	61	16/84
13	0	9.3	Bu_2SiH_2 (23.4)	AIBN	100	3.5	68	2/98

Table 3. Reduction of 7-*exo*-bromo-7-*endo*-fluoro-2-oxanorcarane (**3b**)

Run	**3b** (mmol)	Silane (mmol)	Catalyst	Reaction Condition		Isomer Ratio of Product
				Temp. (°C)	Time (hr)	(*exo*-F/*endo*-F)
14	10.0	Bu_2SiH_2 (25.6)	AIBN	100	3	27/73
15	7.6	Bu_2SiH_2 (19.7)	AIBN	125	1	37/63
16	6.8	Bu_3SiH (17.5)	AIBN	100	7	61/39
17	6.7	Bu_3SiH (17.0)	AIBN	125	5	69/31

Table 4. Reduction of 7,7-Dibromonorcarane (**4**)

Run	Silane	Catalyst	Reaction condition		Isomer ratio of product
			Temp. (°C)	Time (hr)	(*endo*-Br/*exo*-Br)
18	Bu_3SiH	AIBN	100	2	75/25
19	Bu_3SiH	DTBP	140	1	76/24
20	Bu_2SiH_2	AIBN	100	2	75/25
21	Bu_2SiH_2	DTBP	140	1	75/25

78/22 or 15/85, respectively, indicating 22 or 15% inversion had occurred during the reaction. The increase of the reaction temperature to 140 °C increased the relative amount of the inversion product to 39 or 32%, respectively (runs 3 and 7).

The use of di-*n*-butyl-, in place of tri-*n*-butylsilane at 100 °C gave only one isomer of 7-fluoronorcarane with complete retention of configuration (runs 4 and 8), but at 140 °C a small amount (4—5%) of the inversion product was formed (runs 5 and 9).

Similar stereochemical results were obtained in the reduction of the *anti*-F (**2a**) and the *syn*-F isomer (**2b**) of 1-bromo-1-fluoro-2-phenylcyclopropane (**2**) at 100 °C; the reduction with di-*n*-butylsilane occurred in a more stereospecific manner than with tri-*n*-butylsilane. The experimental data are shown in Table 2.

In the reduction of the pure *endo*-F isomer (**3b**) of 7-bromo-7-fluoro-2-oxanorcarane (**3**) with di-*n*-butylsilane, a mixture of the *exo*-F (**3c**) and the *endo*-F isomer (**3d**) of 7-fluoro-2-oxanorcarane was formed even at 100 °C. Here again, it was observed that the use of tri-*n*-butylsilane or the increase of the reaction temperature caused the increase of the relative amount of the inversion product (**3c**). The data are given in Table 3.

In Table 4 are shown the results of the reduction of 7,7-dibromonorcarane (**4**). It proceeded much more readily than that of its bromofluoro analogue (**1**), and gave a mixture of 7-*exo*-bromo- (**5c**) and 7-*endo*-bromonorcarane (**5d**). The isomer ratio of the product (*endo*-Br/*exo*-Br=3.0), which was not affected appreciably either by the reaction temperature or by the kind of silicon hydride, was not very different from the one observed in the reduction with tri-*n*-butyltin hydride.[12]

Discussion

Tri-*n*-butyltin hydride has been shown to reduce *gem*-chlorofluorocyclopropanes at 80 °C in the presence of an appropriate radical initiator such as AIBN, and *gem*-bromofluorocyclopropanes at room temperature in the absence of catalyst, to afford the corresponding monofluorocyclopropanes.[8,9] Since neither tri-*n*-butyl- nor di-*n*-butylsilane could reduce *gem*-chlorofluorocyclopropanes even at 140 °C in the presence of radical initiator, and since the reduction of *gem*-bromofluorocyclopropanes with di-*n*-butylsilane occurred under milder conditions than with tri-*n*-butylsilane, it may be concluded that the reactivity of these hydrides increases in the order $Bu_3SiH < Bu_2SiH_2 < Bu_3SnH$. This order of reactivity is in good agreement with the recent work of Kaplan,[13] who compared the hydrogen-transfer ability of some group IV hydrides and found the order $Ph_3SiH < Ph_2SiH_2 < Ph_3GeH < Ph_3SnH$.

The fact that the reduction with organosilicon hydrides could not be effected in the absence of radical initiator strongly suggests that the reaction follows a free-radical chain mechanism similar to the one already proposed for the reduction of aliphatic halides.[4,6] Very probably it involves the intermediate formation of the α-fluorocyclopropyl radical as one of the chain-

12) D. Seyferth, H. Yamazaki, and D. L. Alleston, *J. Org. Chem.*, **28**, 703 (1963).

13) L. Kaplan, *Chem. Commun.*, **1969**, 106.

propagating steps, and may be formulated as follows:

Initiator ⟶ In·

$In\cdot + R_3SiH \longrightarrow InH + R_3Si\cdot$

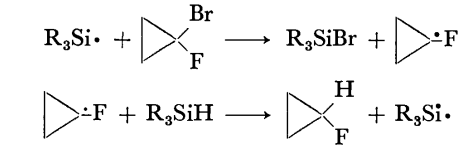

As was described in the preceding section, the reduction of *gem*-bromofluorocyclopropanes with organosilicon hydrides is essentially less stereospecific than that with organotin hydrides under similar conditions. Moreover, the isomer ratio of the product, *i.e.*, the extent of stereospecificity, is dependent on the reaction temperature as well as on the kind of silicon hydride used.

These observations are well explained by postulating that the α-fluorocyclopropyl radical has a pyramidal structure and that the extent of stereospecificity is determined by the relative rates of its hydrogen abstraction from the silicon or tin hydride (k_3 or k_4), and of its inversion of configuration (k_1 or k_2).

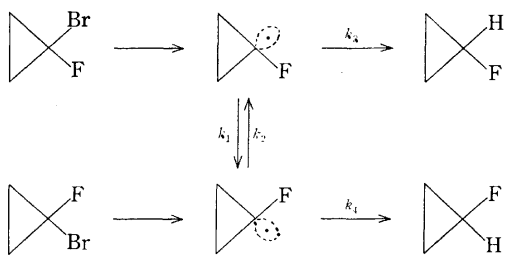

If the reduction is effected with organotin hydrides, which possess an extremely high reactivity toward radicals,[14] the hydrogen transfer from the hydride to the α-fluorocyclopropyl radical should occur at a much faster rate than the inversion of configuration. If the reduction is effected with the less reactive organosilicon hydrides, however, the rate of hydrogen transfer should become slower, and the extent of stereospecificity should be decreased. The experimental results are in good agreement with these expectations. The higher stereospecificity associated with di-*n*-butyl- than tri-*n*-butylsilane may be attributed to the higher reactivity of di-*n*-butyl- than tri-*n*-butylsilane toward radicals.

The low stereospecificity in the reduction of 7-bromo-7-fluoro-2-oxanorcarane (**3**), relative to 7-bromo-7-fluoronorcarane (**1**), is another problem of interest. As analogous effect of ring oxygen has been noted in the reduction of 7-chloro-7-fluoro-2-oxanorcarane with tri-*n*-butyltin hydride,[8] although the origin of the effect is not yet clear at present.

Experimental

Materials. *gem*-Bromofluorocyclopropanes **1**, **2**, and **3** were prepared by the addition reaction of bromofluorocarbene, generated from dibromofluoromethane and potassium *t*-butoxide, to the corresponding olefin.[9] The separation of isomers **1a** and **1b**, and of **2a** and **2b**, was performed by preparative glpc (7.5% TCP on 60/80 Celite 545 at 100 °C and at 80 °C, respectively). The isolation of pure **3b** was accomplished by treating the reaction mixture, containing both **3a** and **3b**, with quinoline at 140 °C for 2 hr, followed by vacuum distillation. Tri-*n*-butylsilane, bp 102—104°/21 mmHg (lit,[15] 215—220 °C), was prepared by the reaction of trichlorosilane with an excess of *n*-butylmagnesium bromide in ether; yield 77%. Di-*n*-butylsilane, bp 63 °C/28 mmHg (lit,[16] 160 °C/773 mmHg), was prepared by the reduction of di-*n*-butylchlorosilane, obtained from trichlorosilane and two equivalents of *n*-butylmagnesium bromide, with lithium aluminum hydride; yield 62%.

7,7-Dibromonorcarane (**4**) was prepared by the addition reaction of dibromocarbene to cyclohexene.

General Procedure for Reduction of gem-*Bromofluorocyclopropane* (**1**, **2**, and **3b**). In a 30 ml, three-necked flask fitted with a thermometer, a magnetic stirrer, an inlet tube for nitrogen, and a reflux condenser was placed a mixture of a *gem*-bromofluorocyclopropane (1.3—3.2 g), 1.4—3 equivalents of tri- or di-*n*-butylsilane, and a small amount of radical initiator (AIBN or DTBP). It was stirred under nitrogen under the condition shown in Table I, II, or III. The isomer ratio of the products was determined by glpc (5% Apiezon Grease L on 60/80 Celite 545 at 80—100 °C) before distillation. In general, the *exo*- or *anti*-F isomer (**1c**, **2c**, or **3c**) had a shorter retention time than the *endo*- or *syn*-F isomer (**1d**, **2d** or **3d**). The yields were calculated by glpc analysis with mesitylene or *n*-dodecane as internal reference. The identification of the products was made by comparing their glpc retention times and infrared absorption spectra with those of authentic specimens.[8] In the reduction of **2** and **3b**, some unidentified by-products were formed.

Reduction of 7,7-Dibromonorcarane (4). The procedure was essentially the same as the one described above. The reaction conditions listed in Table IV were sufficient for 100% conversion. In glpc the *exo*-Br isomer (**5c**) had a shorter retention time than the *endo*-Br isomer (**5b**). The products were identified by comparison with authentic specimens.[12]

14) L. Kaplan, *J. Amer. Chem. Soc.*, **88**, 4531 (1966).

15) H. Gilman, D. H. Miles, L. D. Moore, and G. W. Gerow, *J. Org. Chem.*, **24**, 219 (1959).

16) R. West and E. G. Rochow, *ibid.*, **18**, 203 (1953).

Cycloaddition Reaction of Cycloheptatriene and Nitrosobenzene Derivatives

Shô Itô, Sen-ichi Narita,* and Katsuya Endo
Department of Chemistry, Tohoku University, Sendai 980
(Received July 23, 1973)

Structures of the cycloaddition products obtained from cycloheptatriene and *para*-substituted nitrosobenzene have rigorously been established by NMDR experiments and by degradation of the representative member, the cycloheptatriene-nitrosobenzene adduct, to 3-anilinocycloheptanone. All the adducts were found to be of [6+2] type. The ionic mechanism has been proposed for the cycloaddition in order to account for the substitution effect on the benzene ring.

The reaction of cycloheptatriene and nitrosobenzene is known to yield a 1 : 1 cycloaddition product.[1] Structure of this compound was once assigned to be III' in analogy with the similar reactions of the latter and various conjugated polyenes.[2] This structure was later revised to IIIa on the basis of spectroscopic and a few chemical informations.[3] However, discrimination between two structures seemed insufficient on the spectroscopic data presented and an attempted direct chemical confirmation failed.[3] This paper presents conclusive chemical as well as spectroscopic evidences, which unambiguously establish the structure IIIa for the adduct, and also deals with the discussion on the nature of the reaction.

Reaction of cycloheptatriene (I) and nitrosobenzene (IIa) at room temperature for three days yielded a colorless crystalline product IIIa in 17% yield. The melting point and all the spectroscopic properties are in agreement with the values previously reported.[1,3] Proton magnetic resonance signals (100 MHz) of IIIa appear at δ 2.01—2.60 (m, 2H, $-CH_2-$), 4.22 (m, 1H, HCN–), 4.81 (m, 1H, HCO–), 6.03 (br.s, 4H, olefinic H) and 6.9—7.4 ppm (m, 5H, phenyl). NMDR experiment, irradiating at the methylene signals simplified both signals at 4.22 and 4.81 ppm, but caused no effect on the rest, while irradiation of both methine signals (NMTR) altered the methylene resonance to a clean AB pattern with J=12 Hz. These observations unambiguously establish the location of the methylene group next to both methines, and hence, combined with the informations reported before,[1,3] eliminate all possible structures but IIIa.

This conclusion was further confirmed by the chemical correlation. The adduct IIIa was catalytically reduced to the tetrahydro derivative IV.[1] The N–O linkage was then cleaved by zinc in acetic acid to afford an anilinocycloheptanol V, which was then oxidized with manganese dioxide to give the corresponding ketone VI. This ketone was identical (mixed mp, IR and NMR) with 3-anilinocycloheptanone prepared from 2-cycloheptenone and aniline in absolute ethanol. Sodium borohydride reduction of the ketone VI afforded another 3-anilinocycloheptanol VII in a quantitative yield. Consideration of the reaction sequence allowed assignment of *cis* and *trans* configuration for V and VII, respectively.

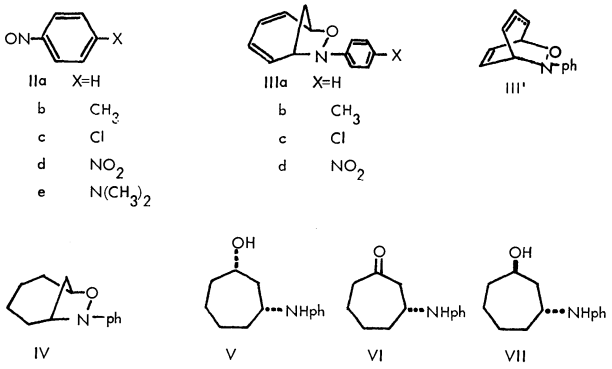

Several *p*-substituted nitrosobenzene derivatives (IIb—d) also yielded the similar type of products (IIIb—d), but the rate of the reaction, therefore the yield of the product, depends very much on the *para* substituents on the benzene ring. Thus electron—withdrawing substituents such as chlorine or nitro group markedly enhanced the reactivity as well as the product yields, while strong electron donating substituents such as dimethylamino group completely inhibited the reaction, and IIe was recovered unchanged after 30 days under the reaction condition (*cf.* Table 1). These accelerating effects are in the sequence of $NO_2>Cl>H>CH_3>N(CH_3)_2$ which is parallel to Hammett's σ value.

In all the cases when the reaction was observed, the [6+2] type of structures were secured by NMR data

Table 1. The cycloaddition of cycloheptatriene and para-substituted nitrosobenzene derivatives

Substituent	Reaction condition[a]	Product (yield %)
$N(CH_3)_2$	30 days at room temp.	No reaction
CH_3	6 days at room temp.	IIIb (5.9%)
H	3 days at room temp.	IIIa (11.6%)
Cl	3 days at toom temp.	IIIc (17.3%)
NO_2	5 hrs at 0 °C[b]	IIId (6.3%)

a) The reaction was carried out in $CHCl_3$ at dark under N_2 atmosphere.
b) Rapid decomposition of IId takes place at room temperature even at 0 °C. No IId was detected after 5 hr.

* Present address: Toa Eiyo Kagaku Kogyo, Co. Ltd., Iisaka Fukushima.

1) G. Kresze and C. Schulz, *Tetrahedron*, **12**, 7 (1961).
2) W. Ditney, *J. Prakt. Chem.*, **156**, 27 (1940). M. Ahmad and J. Hamer, *J. Chem. Educ.*, **41**, 249 (1964). J. Hamer, "1,4-Cycloaddition," Academic Press, New York (1969), p. 419.
3) J. Hutton and W. A. Waters, *Chem. Commun.*, **1966**, 634; P. Burns and W. A. Waters, *J. Chem. Soc. Ser., C*, **1969**, 27.

for the products. The UV spectra of these adducts having maxima at 240 and 265 nm, are also very similar to each other, except for the *p*-nitronitrosobenzene adduct, IIId, which exhibits maxima at 237 and 352 nm. Contribution of the resonance structure IIId′ may be responsible for this anomaly.

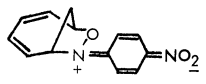

IIId′

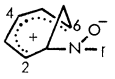

[A]

A small amount of azoxybenzenes correspond to the nitrosobenzenes employed were always formed during the reaction. Although the formation of these compounds suggests the occurrence of a hydride transfer between cycloheptatriene and nitrosobenzene derivatives resulting in the possible formation of tropylium ion, the latter is not involved in the cycloaddition reaction, since tropylium perchlorate and *p*-chloronitrosobenzene (IIc) resulted in the exclusive formation of tropone and *p,p′*-dichloroazoxybenzene (VIIIc) when reacted in aqueous dioxane (1 : 2) at room temperature.

These results indicate that the reaction is the type between an electron rich triene and an electron deficient nitrosobenzene derivative, remniscent of electronic requirement in normal Diels-Alder reactions.[4]

Since the concerted thermal [6s+2s] cycloaddition is forbidden,[5] the present reaction must proceed through either concerted [6s+2a] or an ionic or a free radical mechanism. Although the experiments described above do not fully discriminate these three possibilities, the observation that the 1 : 1 adduct is the only product isolated even in the presence of excess of nitrosobenzenes, which is a good radical scavenger, suggests the radical mechanism unlikely. On the other hand, the substitution effect observed would favor the ionic mechanism. Thus the electron deficient nitrogen of the nitroso group attacks the π-electron system of cycloheptatriene resulting in the dipolar intermediate [A]. This may then cyclize at either one of the cationic centers at 2, 4, and 6. Consideration of angle strain as well as the conjugation of double bond in the product leaves the 1,6-bonding most probable.

Experimental

All the melting points are uncorrected. The IR spectra were recorded on a Hitachi EPI-2 spectrophotometer, and UV spectra on a Hitachi ESP-3 spectrometer. The NMR spectra were observed with Varian HA-100 and/or A-60 spectrometer, using $CDCl_3$ as a solvent, unless otherwise stated. The chemical shifts are given in ppm relative to the internal TMS. The coupling constants are shown in Hz (s: singlet; d: doublet; t: triplet; q: quartet; m: multiplet). The mass spectra were obtained on a Hitachi RMU-6D and RMU-7 mass spectrometer operating an ionization energy of 70 eV.

9-Phenyl-8-oxa-9-azabicyclo[4,2,1]nona-2,4-diene (IIIa). A solution of nitrosobenzene (IIa, 987 mg) and cycloheptatriene (I, 5 g) in chloroform (30 ml) was allowed to stand for 3 day under nitrogen. The solution was then concentrated under a reduced pressure, and the residue chromatographed on a silica gel column. Petroleum ether–benzene eluted a colorless compound, which was identified as azoxybenzene (VIIIa) by its IR spectra. Further chromatography with benzene–chloroform eluted a colorless compound (IIIa, 285 mg, 11.6%), mp 108—109°C (from cyclohexane); *m/e* 156, 107, 92, 91; λ_{max}^{MeOH} 238 nm (ε 12300), 264 nm (ε 6300); δ 2.01—2.60 (m, 2H), 4.22 (m, 1H), 4.81 (m, 1H), 6.03 (br. s, 4H), 6.9—7.4 (m, 5H). These spectroscopic data agreed well with those reported for IIIa.[1,3]

A similar reaction in benzene at 0—5 °C for 16 day resulted in somewhat better yield (17.5%).

Reaction of Cycloheptatriene and para*-Substituted Nitrosobenzene Derivatives.* The reaction and work up followed the procedure described above. The reaction conditions were listed in Table 1. Dimethylaminonitrosobenzene (IIe) was recovered unchanged after 30 days under the reaction condition. IIIb: mp 99—100 °C (from petroleum ether); Found: C, 79.74; H, 7.16%. Calcd for $C_{14}H_{15}NO$: C, 78.84; H, 7.09%. *m/e* 213 (M^+); λ_{max}^{MeOH} 238 nm (ε 13300), 265 nm (ε 8300); δ 2.18 (s, 3H), 2.30 (m, 2H), 4.21 (m, 1H), 4.84 (m, 1H), 6.09 (m, 4H), 7.01 and 7.07 (q, AB type, J=9.0, 4H); ν_{max}^{KBr} 1615, 1505, 1301, 1167. *p,p′*-Dimethylazoxybenzene (VIIIb) mp 69—71 °C. IIIc: mp 101—102 °C (from cyclohexane); Found: C, 66.11; H, 5.23%. Calcd for $C_{13}H_{12}NOCl$: C, 66.81; H, 5.18%. *m/e* 235 and 233 (M^+); λ_{max}^{MeOH} 246 nm broad (ε 17600); δ 2.33 (m, 2H), 4.20 (m, 1H), 4.81 (m, 1H), 6.05 (m, 4H), 7.20 and 7.35 (q, AB type J= 9.0, 4H); ν_{max}^{KBr} 1590, 1448, 1291, 1169, 1086. *p,p′*-Dichloroazoxybenzene (VIIIc) mp 156—157 °C. IIId: mp 107—108° (from benzene-cyclohexane); Found: C, 63.98; H, 4.99%. Calcd for $C_{13}H_{12}N_2O_3$: C, 63.92; H, 5.39%. *m/e* 244 (M^+); λ_{max}^{MeOH} 237 nm (ε 9600), 352 nm (ε 11000); δ 2.51 (m, 2H), 4.45 (m, 1H), 4.90 (m, 1H), 6.14 (m, 4H), 7.06 and 8.22 (q, AB type, J=9.5, 4H); ν_{max}^{KBr} 1592, 1505, 1338, 1242, 1175, 1112, 1089.

Catalytic Hydrogenation of IIIa. A solution of IIIa (140 mg) in methanol was hydrogenated for 4 hr in the presence of PtO_2 (15 mg). Concentrate of the mixture, after the removal of the catalyst, was chromatographed on a silica gel column. Elution with chloroform yielded pale yellow oil (IV, 80 mg), which crystallized on standing. Mp 27—28 °C, *m/e* 203 (M^+); λ_{max}^{MeOH} 239 nm (ε 9400); $\nu_{max}^{liq.}$ 2920, 1600, 1490, 1198, 1008, 762, 696; δ 1.20—2.06 (m, 6H), 4.03 (m, 1H), 4.86 (m, 1H), 7.33 (m, 5H).

cis-*3*-N-*Phenylaminocycloheptanol (V).* The hydrogenation product IV (70 mg) and HCl-activated zinc powder (200 mg) was stirred in acetic acid (10 ml) under nitrogen for 30 min. The mixture was partly neutralized (pH—5) with 2M aqueous sodium hydroxide and then made alkaline with sodium carbonate. The chloroform extract of the resulting solution was worked up as usual to afford a pale yellow oil (V, 62 mg) which was purified further by chromatography. $\nu_{max}^{liq.}$ 3350, 1605, 1506, 1302, 1028, 750, 698; δ ~1.8 (m, 10H), 3.43 (m, 1H), 3.93 (m, 1H), 6.47—7.32 (m, 5H). V crystallizes with a mole of ether of crystallization, mp 48—51 °C.[1]

3-N-*Phenylaminocycloheptanone (VI).* A chloroform solution (5 ml) of V (110 mg) was added to a suspension of active manganese dioxide (600 mg) in the same solvent (15 ml) and the mixture was stirred at room temperature for 18 hr under nitrogen. The reaction mixture was filtered and the filtrate chromatographed on silica gel. Elution

4) R. Huisgen, R. Grashey, and J. Sauer, "The Chemistry of Alkenes," ed. by S. Patai, Interscience Publishers, New York (1964), pp. 919—922. and references therein.

5) R. B. Woodward and R. Hoffmann, *Angew. Chem. Internat. Edit.*, **8**, 781 (1969).

with chloroform afforded a crystalline product (IV, 21 mg), mp 63—64 °C (from *n*-hexane); Found: C, 76.78; H, 8.73; N, 6.14%. Calcd for $C_{13}H_{17}NO$: C, 76.81; H, 8.43; N, 6.86%. *m/e* 203 (M^+); λ_{max}^{MeOH} 249 nm (ε 14600), 296 nm (ε 2500); ν_{max}^{KBr} 3350, 1692, 1602, 1506, 1315, 1280, 991, 745, 694; δ 1.80 (m, 8H), 2.65 (m, 2H), 3.61 (br. 2H), 6.90—7.40 (5H).

Michael Addition of Aniline to 2-Cycloheptenone. 2-Cycloheptenone (301 mg), prepared from 2-bromocycloheptanone and quinoline, was allowed to react with aniline (5 ml) in absolute ethanol (5 ml) at room temperature for 20 hr. The reaction mixture was worked up normally to yield a colorless crystalline compound, mp 62—63 °C (from *n*-hexane); mixed mp with VI 62—63 °C. All the spectroscopic properties were identical with those of VI.

$NaBH_4$ Reduction of VI. The reduction of VI (55 mg) with $NaBH_4$ (50 mg) in methanol (7 ml) at room temperature for 1 hr followed by usual work up yielded an isomeric alcohol VII, mp 86—87 °C (from cyclohexane); *m/e* 205 (M^+); ν_{max}^{KBr} 3350, 1601, 1494, 1035, 760, 700.

Reaction of p-*Chloronitrosobenzene with Tropylium Perchlorate.* Tropylium perchlorate (764 mg) and *p*-chloronitrosobenzene (IIc) (471 mg) was stirred in dioxane-water (2:1, 40 ml) for 2 hr under nitrogen. Along the reaction proceeded, the green solution turned to yellow and crystalline particles precipitated. The crystals were collected and recrystallized to give 334 mg (78%) of *p,p'*-dichloroazoxybenzene (VIIIc), mp 156—157 °C. The filtrate was worked up normally, followed by silica gel chromatography to yield 22 mg of tropone, which was identified by its IR spectra.

The authors are grateful to Dr. T. Nishida and Mr. I. Miura at NEVA, Ltd., for the NMDR and NMTR measurements.

BULLFTIN OF THE CHEMICAL SOCIETY OF JAPAN, VOL. 46, 3519—3530 (1973)

Layered Compounds. XV.[1] Synthesis and Properties of Multilayered Cyclophanes

Tetsuo Otsubo, Shigeyoshi Mizogami, Ikuko Otsubo, Zenzaburo Tozuka, Akiko Sakagami, Yoshiteru Sakata, and Soichi Misumi

The Institute of Scientific and Industrial Research, Osaka University, Suita, Osaka 565

(Received August 10, 1973)

A series of multilayered cyclophanes up to sixfold were synthesized by 1,6-Hofmann elimination method. Odd layered and some dissymmetric ones were derived by means of cross-breeding pyrolysis of mixed quaternary ammonium hydroxides. The electronic spectra, absorption, emission, and CT absorption of charge-transfer complexes, of these cyclophanes exhibited remarkable transannular π-electronic interaction among chromophores closely stacked by methylene bridges. The interaction is increased eminently when the layer is varied from single to quadruple, but becomes less effective from quadruple to fivefold and no longer appreciable for more than fivefold one.

Aromatic compounds in which two or more chromophores are closely bound by methylene bridges, *i.e.*, layered compounds, are known as quite suitable models for the study of the transannular π-electronic interaction. [2.2]Paracyclophane,[2] one of the typical layered compounds, has been extensively studied by Cram and his co-workers from the viewpoints of the transannular interaction which results from the face-to-face proximity of two benzene rings to one another and many unusual chemical and physical behaviors have been reported to appear.[3] Such a face-to-face compression of the benzene rings brings about extreme molecular deformation or strain to the molecule, *i.e.*, extraordinarily short ring-to-ring distances, elongated benzyl–benzyl σ-bonds, and boat-shaped benzene rings.[4] These striking characteristics have attracted many organic and physical chemists' attentions and thereafter led to a great development of the chemistry of "cyclophane,"[5] *e.g.*, paracyclophanes,[3] metacyclophanes,[6] layered condensed aromatic cyclophanes,[7] and heterophanes.[8]

In these studies the emphasis has been on the exploration of the double layered aromatic compounds, and there have been reported only two of more than two layered cyclophanes so far. A triple-layered cyclophane was synthesized by Hubert[9] and a quadruple-

1) Part XIV: T. Kaneda, T. Ogawa, and S. Misumi, *Tetrahedron Lett.*, **1973**, 3373.

2) C. J. Brown and A. C. Farthing, *Nature*, **164**, 915 (1949).

3) D. J. Cram, *Rec. Chem. Progr.*, **20**, 71 (1959) and references cited therein.

4) C. J. Brown, *J. Chem. Soc.*, **1953**, 3265; D. K. Lonsdale, H. J. Milledge, and K. V. Rao, *Proc. Roy. Soc. Ser. A*, **255**, 82 (1960); H. Hope, J. Bernstein, and K. N. Trueblood, *Acta Crystallogr.*, **B28**, 1733 (1972).

5) For nomenclature of cyclophane see B. H. Smith, "Bridged Aromatic Compounds," Academic Press Inc., New York, N. Y. (1964); F. Vögtle and P. Neumann, *Tetrahedron Lett.*, **1969**, 5329; *Tetrahedron*, **26**, 5847 (1970); K. Hirayama, *Tetrahedron Lett.*, **1972**, 2109.

6) F. Vögtle and P. Neumann, *Angew. Chem.*, **84**, 75 (1972), and references cited therein.

7) T. Toyoda. I. Otsubo, T. Otsubo, Y. Sakata, and S. Misumi, *Tetrahedron Lett.*, **1972**, 1731; M. Haenel and H. A. Staab, *ibid.*, **1970**, 3585; H. H. Wasserman and P. M. Keehn, *J. Amer. Chem. Soc.*, **91**, 2374 (1969).

8) H. E. Winberg, F. S. Fawcett, W. E. Mochel, and C. W. Theobald, *ibid.*, **82**, 1428 (1960); "Organic Syntheses," Vol. 42, p. 83 (1963).

9) A. J. Hubert, *J. Chem. Soc.*, (*C*), **1967**, 13.

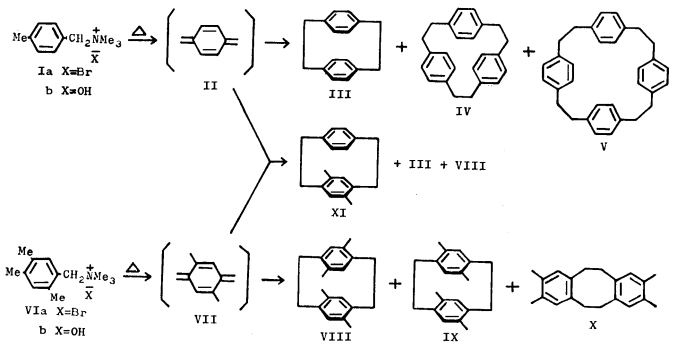

Scheme 1.

layered one by Longone,[10] but both ones were considered as mixture of configurational isomers and no report for separation was described.

In order to study the transannular interaction in more detail, we have designed syntheses of a series of multiple-layered cyclophanes. The synthesis of [2.2]-paracyclophane has been achieved by pyrolysis of *p*-xylene,[2,11] intramolecular Wurtz reaction,[12] 1,6-Hofmann elimination reaction,[8] and recently by photolysis of sulfide.[13] Of those procedures we took up the 1,6-Hofmann elimination method for synthesis of all multilayered paracyclophanes since the intermediate products were relatively accessible.

Results and Discussion

Synthesis of Double-Layered Cyclophanes (Scheme 1). On a pyrolysis of *p*-methylbenzyltrimethylammonium hydroxide (Ib), [2.2]paracyclophane(III) was obtained in 10—17% yield.[8] It is considered to proceed through *p*-xylylene intermediate II.[14] After examining a number of pyrolytic conditions we observed that when a small amount of xylene was used in the place of toluene as a solvent, its yield was raised to 29% and [2.2.2]-paracyclophane (IV)[15] and [2.2.2.2]paracyclophane (V)[16] were concomitantly obtained in 8.4 and 2.2% yields, respectively.

Longone and Chow obtained 4,7,12,15-tetramethyl-[2.2]paracyclophane (VIII) in a 20% yield along with 2,3,8,9-tetramethyl-*sym*-dibenzocyclooctadiene (X) by pyrolysis of duryltrimethylammonium hydroxide (VIb).[10] On dimerization of the intermediate VII, the dimer structure VIII where methyl groups on both rings are positioned in staggered form and the other one IX where all methyl groups are eclipsed are properly considered as the producible isomers. They reported that the product was assigned to dissymmetric form VIII on the basis of optical resolution by the Newman resolving agent and that the symmetric form IX couldn't be afforded owing to mutual overcrowding of four methyl groups.[17] By treatment with a small amount of *n*-pentane, however, we could separate a very slight amount (0.1% yield) of the sparingly soluble, eclipsed form IX (C_{2h} symmetry) from the readily soluble, staggered form VIII (D_2 symmetry).

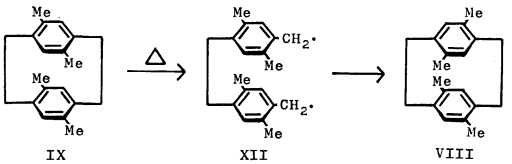

The mass spectra of both forms show entirely identical pattern, supporting an isomeric relationship with each other. Fairly higher melting point of IX than that of VIII suggests that the former is more symmetric. Moreover, a definitive evidence for this isomeric relationship could be provided by the conversion of IX to VIII in the thermochemical process. Thus, when a solution of IX in *n*-tridecane or hexachlorobutadiene was heated at *ca.* 195 °C for 3 hr, VIII was afforded almost quantitatively, probably through a biradical intermediate (XII).[18] In addition, the structural assignment of two isomers was made on the basis of the nuclear Overhauser effect and the steric compression effect as described in the next paper.[20]

Cross-breeding pyrolysis of an equimolar mixture of Ib and VIb gave [2.2]paracyclophane (III) and its methyl derivatives VIII and XI. 4,7-Dimethyl[2.2]-paracyclophane (XI) was isolated by fractional crystallization.

Synthesis of Triple-Layered Cyclophanes (Scheme 2). Quaternary ammonium salts XIIIa and XIVa were prepared from the corresponding methyl derivatives of [2.2]paracyclophanes, XI and VIII, by successive treatments with *N*-bromosuccinimide and trimethylamine according to Longone's procedure.[10] Cross-breeding pyrolysis of a quaternary ammonium hydroxide XIIIb, derived by ion exchange from XIIIa, with Ib gave non-substituted triple-layered cyclophane (XV) together with double-layered one III and quadruple-layered ones, XIX and XX. Column chromatography on silica gel gave a 1.3% yield of XV in a pure state.

10) D. T. Longone and H. S. Chow, *J. Amer. Chem. Soc.*, **86**, 3898 (1964); *ibid.*, **92**, 994 (1970).
11) L. A. Errede and J. P. Cassidy, *ibid.*, **82**, 3650 (1960).
12) D. J. Cram and H. Steinberg, *ibid.*, **73**, 5691 (1951).
13) J. Bruhin and W. Jenney, *Tetrahedron Lett.*, **1973**, 1215.
14) M. Szwarc, *Nature*, **160**, 403 (1947); *J. Chem. Phys.*, **16**, 128 (1948); L. A. Errede and B. F. Landrum, *J. Amer. Chem. Soc.*, **79**, 4952 (1957); L. A. Errede, *ibid.*, **83**, 949 (1961); L. A. Errede and W. A. Pearson, *ibid.*, **83**, 954 (1961).
15) W. Baker, J. F. W. McOmie, and J. M. Norman, *J. Chem. Soc.*, **1951**, 1114.
16) L. A. Errede, R. S. Gregorian, and J. M. Hoyt, *J. Amer. Chem. Soc.*, **82**, 5218 (1960).
17) D. T. Longone and M. T. Reetz, *Chem. Commun.*, **1967**, 46.
18) H. J. Reich and D. J. Cram, *J. Amer. Chem. Soc.*, **91**, 3517 (1969).

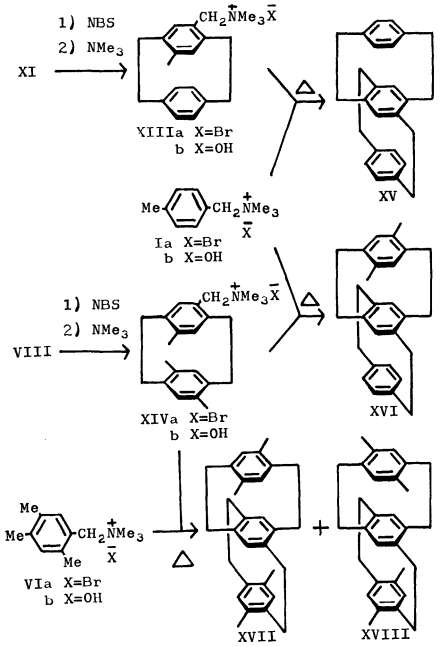

Scheme 2.

Dimethyl triple-layered cyclophane XVI was similarly prepared from XIVb and Ib in a 1.8% yield.

Tetramethyl triple-layered ones were obtained by cross-breeding pyrolysis of XIVb with VIb. Careful and elaborate column chromatography on silica gel gave a 1.1% yield of XVII and a 1.1% yield of XVIII. The structure of these isomers was determined on the basis of the chemical shifts of aromatic protons on NMR spectra. Thus, in the former isomer two signals of aromatic protons appear in a 1:2 ratio of integral strength which corresponds to the ratio of inner-to-outer aromatic protons, whereas in the latter isomer three signals appear in a 1:1:1 ratio which indicates the existence of two types of outer protons different in magnetic environment. One can easily see from the structures, XVII and XVIII, that the differences in magnetic shielding and steric crowding give rise to those aromatic proton ratios. In contrast to large difference in yields of tetramethyl double-layered compounds, VIII and IX, the formation of XVII and XVIII in a same yield may be best accounted for assuming that the steric crowding between methyl and benzylmethylene groups mutually eclipsed in XVIII might be less than that crowding between two methyl groups in IX because the methylene groups in problem would be bent toward the remaining benzene ring.

Synthesis of Quadruple-Layered Cyclophanes (Scheme 3). Pyrolysis of XIIIb in boiling xylene afforded a mixture of non-substituted quadruple-layered compounds, XIX (D_2 symmetry) and XX (C_{2h} symmetry). By treatment of the mixture with carbon tetrachloride–acetone (1:3), the readily soluble compound (1.1% yield) was separated from the sparingly soluble one (0.75% yield). The both compounds show similar NMR, IR, UV spectra, identical mass spectrum and empirical formula. It indicates obviously an isomeric relationship of both compounds. Although the structure of both isomers seemed to be difficult to determine, the easily soluble isomer could be assigned to the structure

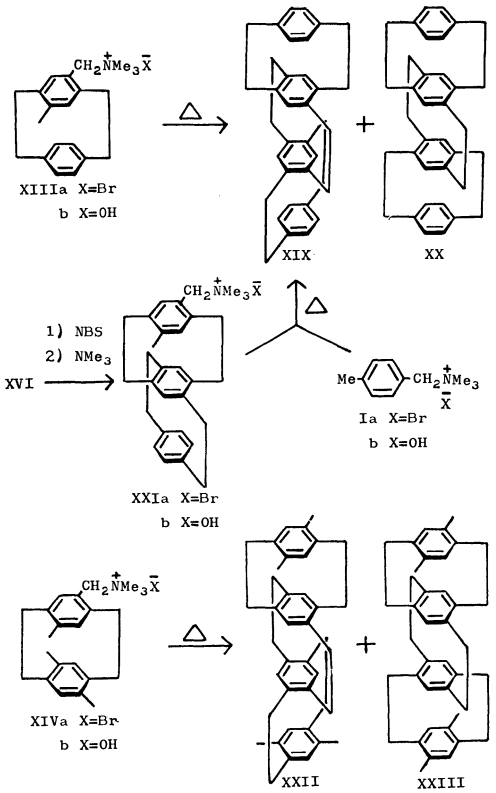

Scheme 3.

XIX by direct comparison with an independently synthesized sample as described below. Thus, cross-breeding pyrolysis of an ammonium hydroxide XXIb, derived from dimethyl triple-layered cyclophane XVI in the usual manner, with Ib afforded only the dissymmetric isomer XIX which was proved to be identical in all respects with the readily soluble isomer obtained by pyrolysis of XIIIb. Consequently the other, sparingly soluble isomer should be assigned to more symmetric structure XX.

Longone reported the formation of a mixture of isomeric tetramethyl quadruple-layered cyclophanes,

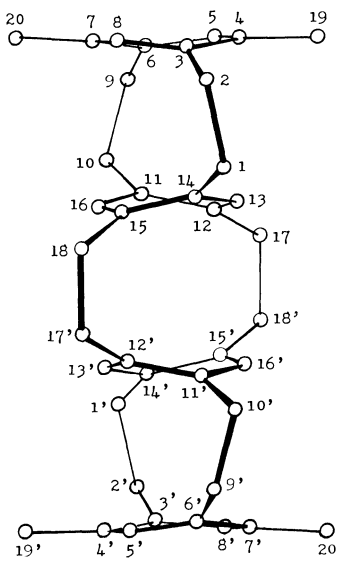

Fig. 1. Profile of quadruple-layered cyclophane XXIII viewed down the b axis.

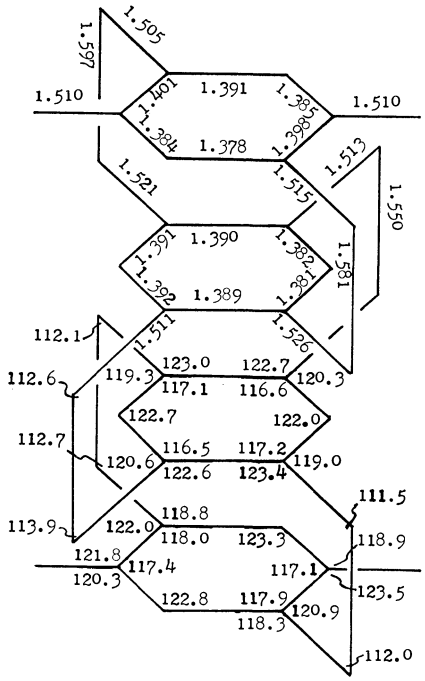

Fig. 2. Bond lengths and angles. The standard deviations are 0.010 Å in bond lengths and 0.6 ° in bond angles.

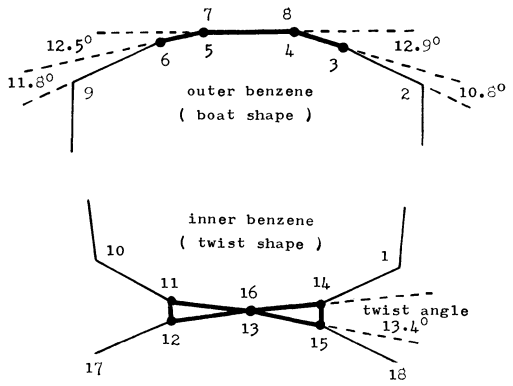

Fig. 3. Distortion of outer and inner benzene rings.

XXII (D_2 symmetry) and XXIII (C_{2h} symmetry), by pyrolysis of a quaternary base XIVb, but failed in separating them.[10] By treatment of a mixture of the isomers with the same solvent as in the case of non-substituted system, the readily soluble isomer (3.2% yield) was separated from the sparingly soluble one (1.6% yield). For the structures of two isomers we tentatively assigned the more soluble isomer to XXII (D_2 symmetry) and the less soluble one to XXIII (C_{2h} symmetry) by comparison of isomers ratio, solubility, and electronic spectra with non-substituted system. Recently the exact molecular structure of the less soluble isomer was determined by X-ray crystallographic analysis as shown in Figs. 1—3.[19] The figures show that the less soluble isomer has a C_{2h} symmetric structure and four benzene rings are closely stacked in a manner to be well superposed. Also the figures demonstrate significant strain of the molecule in such a manner that outer benzene rings are bent into boat shape as in the case of [2.2]paracyclophane (III),[4] whereas the inner rings are forced to be distorted remarkably by both π-electron repulsion between benzene rings and tension with two pairs of methylene bridges above (C_1–C_2 and C_9–C_{10} in Fig. 1) and below (C_{17}–C_{18}' and C_{18}–C_{17}') the benzene moiety and consequently deformed into a twist form as shown in Figs. 1 and 3. The four benzene layers are stacked with about equal ring-to-ring distances, that is, two outer-to-inner and one inner-to-inner. The mean value of those distances is 3.03 Å which is comparable to that of [2.2]paracyclophane and about independent of the increase of layers. Accordingly such a structural situation must be applied to all of other multilayered cyclophanes.

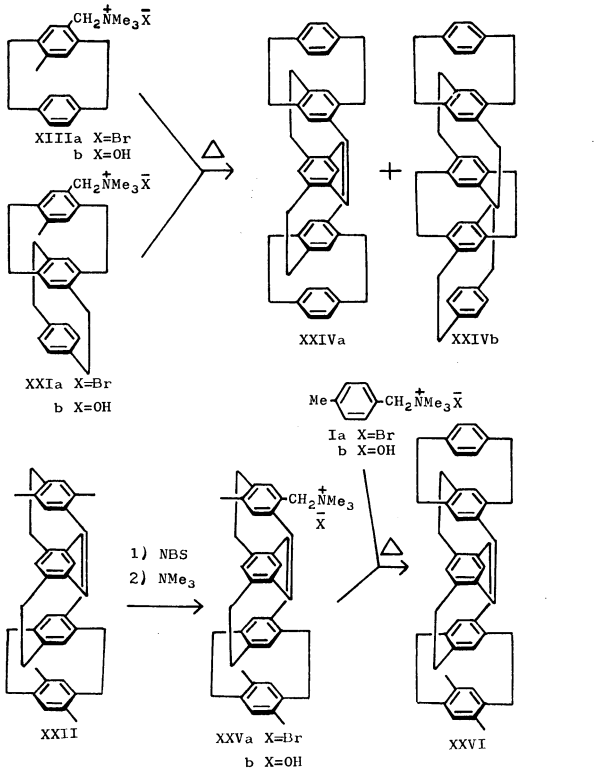

Scheme 4.

Synthesis of Fivefold-Layered Cyclophanes (Scheme 4). Pyrolysis of an equimolar mixture of quaternary bases XIIIb and XXIb afforded non-substituted fivefold-layered cyclophane XXIV along with quadruple-layered ones (XIX and XX) and polymers. Separation by liquid chromatography gave a 5% yield of pure XXIV which is probably a mixture of two isomers, XXIVa (D_2 symmetry) and XXIVb (C_2 symmetry).

Dimethyl derivative XXVI was obtained in a 1.1% yield by cross-breeding pyrolysis of Ib and XXVb which was prepared from tetramethyl quadruple-layered cyclophane XXII having D_2 symmetric configuration.

Synthesis of Sixfold-Layered Cyclophanes (Scheme 5). Sixfold-layered cyclophanes were obtained by pyrolysis of a quaternary base XXIb in boiling toluene. After column chromatography, a readily soluble product was

19) H. Mizuno, K. Nishiguchi, T. Otsubo, S. Misumi, and N. Morimoto, *Tetrahedron Lett.*, **1972**, 4981.

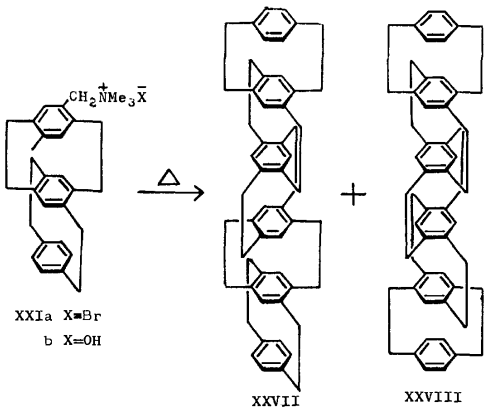

Scheme 5.

separated from a less soluble one in a 2:1 product ratio by treatment with benzene. The NMR, IR, and UV spectra of both isomers are fairly similar. On analogy with quadruple-layered cyclophanes, it is presumed that the structure of the readily soluble, major isomer is XXVII (D_2 symmetry), whereas the sparingly soluble, minor one is XXVIII (C_{2h} symmetry).

Properties. All of the multilayered cyclophanes are stable under ordinary conditions in spite of considerably strained structure. However, when the compounds are allowed to stand for a long time in halogenated hydrocarbon solvents, they decompose gradually. The isomer bearing higher symmetry generally displays higher melting point compared with the other isomer. All of more than three layered [2.2]paracyclophanes decompose with color change to brown and without melting at temperature above 240 °C.

The NMR, IR, and mass spectral data are consistent with the structures of above multilayered cyclophanes. The NMR spectra reveal a striking feature that all the aromatic protons appear at considerably higher field due to diamagnetic shielding effect.[20]

Infrared Spectra. The IR spectra of [2.2]paracyclophane system are known to reveal obvious features as follows. One is the increase of the intensity of a band in 1580—1600 cm^{-1} region, which relates to the increased double bond character due to the distortion of the benzene rings.[21] The other is the appearance of a strong new maximum at 720 cm^{-1} for [2.2]paracyclophane III and at 709 cm^{-1} for 4,7,12,15-tetramethyl[2.2]paracyclophane VIII as shown in Table 1. Longone stated that these bands might be associated with the distorted benzene rings.[22] In practice, other layered cyclophanes also exhibit the characteristic band around 700 cm^{-1}, whereas [2.2.2]paracyclophane IV bearing less strained benzene rings shows a weak band at 721 cm^{-1}, and [2.2.2.2]paracyclophane V and *p,p'*-dimethylbibenzyl bearing strain-free rings no band in this region.

More detailed examination of more than two layered, non-substituted cyclophanes shows that two bands

Table 1. IR spectra of layered cyclophanes around 700 cm^{-1} [a]

Compound	Wave number (cm^{-1})
III	720(s)
XI	715(s)
VIII	709(s)
IX	708(s)
XV	708(s), 680(s)
XVI	710(w), 695(s), 673(m)
XVII	693(s), 660(m)
XVIII	688(s), 660(m)
XIX	713(s), 674(s)
XX	710(s), 687(s)
XXII	692(s), 665(m)
XXIII	696(s), 669(m)
XXIV	714(m), 671(s)
XXVI	712(w), 693(m), 672(s), 665(s)
XXVII	713(m), 673(s)
XXVIII	715(m), 677(s)

a) KBr disc.

appear near 710 cm^{-1} comparable to characteristic, lower wavenumber band of double-layered cyclophanes and near 680 cm^{-1} and that the more the number of benzene layers increases, the stronger the relative intensity of the lower wave number band to the higher one becomes. It is reasonable to assume that the higher band is associated with the boat-shaped outer benzene rings and the lower band with twist-shaped inner benzene rings.

The spectra of dimethyl compounds XVI and XXVI show a strong new peak near 695 cm^{-1} together with above two bands of which the band at 680 cm^{-1} becomes broad. On the other hand, tetramethyl derivatives XVII, XVIII, XXII, and XXIII show two absorption bands near 695 and 665 cm^{-1}. By comparing the spectra of the three groups of cyclophanes, *i.e.*, non-substituted, dimethyl, and tetramethyl compounds, the band near 695 cm^{-1} of dimethyl and tetramethyl compounds probably originates from outer benzene rings more distorted by methyl groups, whereas the band near 665 cm^{-1} of tetramethyl compounds from the twist-shaped inner benzene rings. It is also observed that the two peaks of those methylated compounds appear in slightly lower wave number than the corresponding ones of non-substituted compounds owing to methyl substituents.

Mass Spectra. [2.2]Paracyclophane exhibits a characteristic mass spectrum where molecular ion peak and a fragment one corresponding to *p*-xylylene appear as predominant signals. In the spectra of multilayered cyclophanes, it is observed in general that the molecular ion is a base peak and the more layered

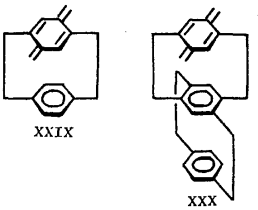

20) The discussions of NMR spectra of multilayered cyclophanes will be described in detail in Part XVI: This Bulletin, **46**, No. 12 (1973) in press.

21) D. J. Cram and H. Steinberg, *J. Amer. Chem. Soc.*, **73**, 5691 (1951).

22) D. T. Longone and C. L. Warren, *ibid.*, **84**, 1507 (1962).

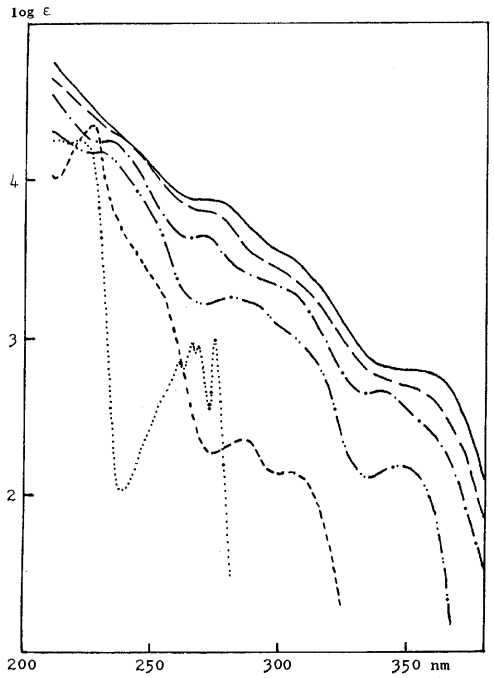

Fig. 4. UV spectra of layered cyclophanes in cyclohexane; ····· *p,p'*-dimethylbibenzyl, —— III, -·-· XV, -·-·- XIX, — — XXIV, —— XXVII.

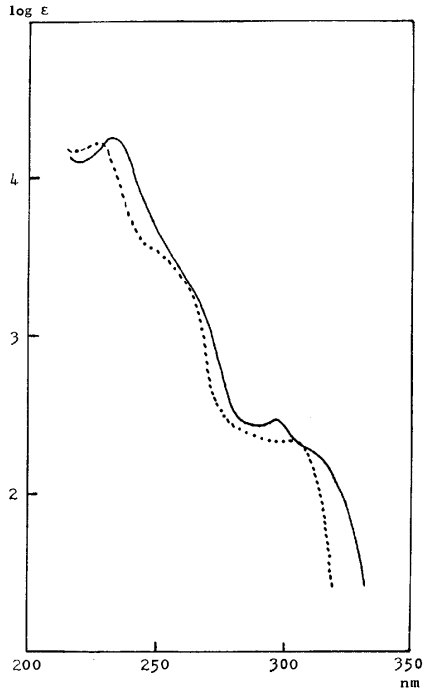

Fig. 5. UV spectra of tetramethyl[2.2]paracyclophanes in cyclohexane; —— VIII, —— IX.

p-xylylene fragment ions such as XXIX and XXX become greater. This appears to be caused by the stabilization due to transannular charge delocalization.

Electronic Absorption Spectra. Figure 4 shows the electronic absorption spectra of non-substituted multilayered cyclophanes. The absorption curves are hardly affected by methyl substitution and show no difference in configurational isomers. The figure demonstrates strong bathochromic and hyperchromic effects as the number of layers increases successively. In particular those effects are prominent as the layer is varied from single to double. Thus a band at 270 nm associated with $^1B_{2u}$ transition of *p,p'*-dimethylbibenzyl disappears in the spectrum of [2.2]paracyclophane (III), and new peaks are observed to appear at 244, 286, and 302 nm instead. These spectral features have been explained by two predominant effects, that is, distortion of benzene ring and transannular π-electronic interaction between two rings.[23] In order to study the former effect, a series of [m]paracyclophanes were synthesized and examined.[24] The absorption bands of [m]paracyclophanes are somewhat shifted to longer wavelength with the decrease of methylene number, but the extent of deformation in absorption curves is not so large for [8]paracyclophane[25] which is considered as strain molecule comparable to [2.2]paracyclophane and even for extremely strained [7]paracyclophane.[26] Such a minor effect of the ring torsion on electronic spectra is also observed in the spectra of isomeric tetramethyl[2.2]-paracyclophanes, VIII and IX (Fig. 5). In spite of severe ring strain due to steric repulsion of mutually eclipsed methyl groups, the latter isomer shows a spectrum comparable to that of the former. As the layer is altered from double to triple, the absorption curve becomes further structureless with large bathochromic shift, increased intensity of the band near 290 nm, and appearance of a new peak at 347 nm. In this case the ring distortion effect is hardly considered to be responsible for such marked bathochromic shift because the extent of ring torsion is not so different between the double-layered and triple-layered compounds. Accordingly, the spectral change must be explained mainly by the transannular π-electronic interaction or delocalization. In theory, the configurational interactions of charge-transfer and neutral excitation states were applied with success for interpretation of the spectra of the layered paracyclophanes.[27]

With increasing layer number from the tripled to the fivefold, the absorption curves become broader successively, but the intensity per unit chromophore increases gradually. However, the spectrum of the sixfold one shows that the curve shape and the intensity per unit chromophore are nearly equal to that of the fivefold one, supporting no further increase of the transannular π-electronic interaction.

Emission Spectra. A study of the emission spectra

23) D. J. Cram, N. L. Allinger, and H. Steinberg, *J. Amer. Chem. Soc.*, **76**, 6132 (1954).

24) N. L. Allinger, L. A. Freiberg, R. B. Hermann, and M. A. Miller, *ibid.*, **85**, 1171 (1963).

25) D. J. Cram, C. S. Montgomery, and G. R. Knox, *ibid.*, **88**, 515 (1966).

26) N. L. Allinger and T. J. Walter, *ibid.*, **94**, 9267 (1972); A. D. Wolf, V. V. Kane, R. H. Levin, and M. Jones, Jr., *ibid.*, **95**, 1680 (1973).

27) M. T. Vara, Jr., I. H. Hillier, S. A. Rice. and J. Jortner, *J. Chem. Phys.*, **44**, 23 (1966); I. H. Hillier, L. Glass, and S. A. Rice, *J. Amer. Chem. Soc.*, **88**, 5063 (1966); S. Iwata, K. Fuke, M. Sasaki, S. Nagakura, T. Otsubo, and S. Misumi, *J. Mol. Spectrosc.*, **46**, 1 (1973).

Table 2. Emission spectra of layered cyclophanes (77 K)

Compound	Solvent	Fluorescence maximum (nm)	Phosphorescence maximum (nm)	Lifetime of phosphorescence (s)
Durene	EPA	279, 284, 289, 294	358, 368, 380, 391, 403, 415, 428	6.8 ±0.8
III	EPA	354	470	3.5 ±0.3
XI	EPA	355	470	2.2 ±0.1
VIII	EPA	347	469	2.3 ±0.3
XV	EPA	380	524, 542, 560	0.49±0.02
XVI	EPA	378	518, 532, 555	0.56±0.02
XVII	EPA	375	512, 529, 551, 570	0.77±0.06
XIX	EPA	396	527, 546, 567	0.37±0.03
XIX	TA	395	528, 546, 565	0.41±0.03
XXII	EPA	390	521, 538, 560, 573	0.41±0.04
XXIV	TA	397	527, 546, 567	0.42±0.04
XXVII	TA	398	528, 547, 570	0.41±0.03

a) EPA: ether–isopentane– alcohol (5: 5: 2). b) TA: tetrahydrofuran–alcohol (1: 1).

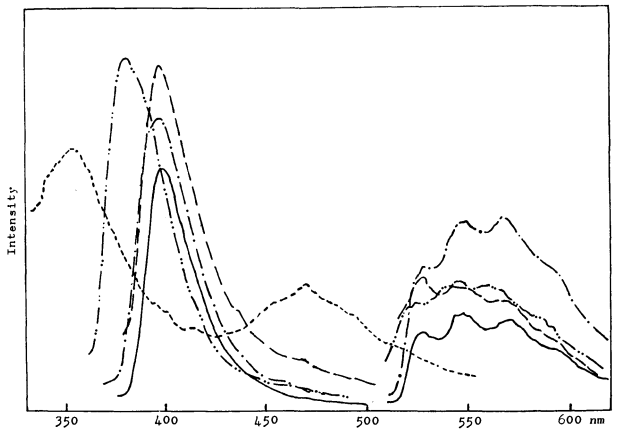

Fig. 6. Emission spectra of layered cyclophanes; ---- III, -·-· XV, -·-· XIX in EPA, and —— XXIV, —— XXVII in THF–alcohol (1: 1) at 77 K. Phosphorescences are enlarged by about four times fluorescences except III.

was carried out to obtain further information concerning the transannular interaction. The spectra are shown in Table 2. Both fluorescence and phosphorescence spectra exhibit large bathochromic shifts with successive increase of layer number as well as the absorption spectra just described above (Fig. 6). Such a shift is particularly remarkable as the layer is altered up to the tripled. In contrast to ambiguous positions of the longest wavelength bands in the absorption spectra, the emission maxima are clearly distinguishable for the tripled and the quadrupled cyclophanes. These spectra also indicate no further increase of transannular π-electronic interaction for more than five fold-layered cyclophanes.

Lifetime of Phosphorescence. The effect of the transannular π-electronic interaction on the various spectra of multilayered compounds can also be discussed from the lifetime of phosphorescence. As shown in Table 2, the lifetime tends to become progressively shorter and to converge in the same manner as band shifts on absorption and fluorescence spectra. It is well explainable by the postulate that the transannular π-electronic interaction lowers the energy gap between the ground and the triplet states and thereby increases the probability of radiationless deactivation.

Charge-Transfer Complexes. It is well known that in a series of π-complexes consisted of methylated benzenes and tetracyanoethylene (TCNE), there is a correlation between the position of the long-wavelength band and the association constant, K, of the complexes.[28] Increased transannular electronic interaction was also reported to be reflected in π-basicity of multilayered cyclophanes.[10,29] The transannular electron release to the complexed face ring from the remaining benzene rings is expected to take place. Table 3 and Fig. 7, indeed, show that with increasing number of layers in this series of cyclophanes, the long-wavelength maxima of TCNE complexes shift to longer wavelength and hence the donor character of the cyclophanes increases progressively. It is noteworthy that even in the case of fivefold one, such electron release is still effective for stabilization of the complex XXXI. Unfortunately, the spectrum of the sixfold compound

Table 3. Absorption maximum wavelengths of layered cyclophane-TCNE complexes in dichloromethane

Compound	λ_{max} (nm)
p-xylene	420, 465[a] (460)[b]
p,p'-dimethylbibenzyl	420, 465[a]
durene	480
III	521
XI	555
VIII	584 (580)[c]
IX	595
XV	530[a], 630
XVI	430[a], 650
XVII	430[a], 655
XVIII	430[a], 643
XIX	530, 710
XXII	720 (690)[c]
XXIV	540, 750

a) Shoulder. b) Ref. 28. c) Ref. 10.

28) R. E. Merrifield and W. D. Phillip, *J. Amer. Chem. Soc.*, **80**, 2778 (1958).
29) D. J. Cram and R. H. Bauer, *ibid.*, **81**, 5971 (1959).

Table 4. Equilibrium constants for 1,3,5-trinitrobenzene–layered cyclophane complexes in chloroform

Compound	λ_{max} (nm)	K_X	ε(cm^{-1}. mol^{-1}. l)
Xylenes[a)]	312	2.08	4080
p,p'-Dimethylbibenzyl (non-substituted cyclophane)	312		
[2.2]Paracyclophane (III)	362 (365) [b)]		
Triple-layered XV	405	6.84	1820
Quadruple-layered XIX	400, 450(sh)	7.46	1490
Fivefold-layered XXIV	400, 470(sh)		
Sixfold-layered XXVII (methylated cyclophane)	400, 470(sh)	11.1	950
Tetramethyl[2.2]paracyclophane VIII	405	10.2 (9.6) [b)]	2440 (2500) [b)]
Dimethyl triple-layered XVI	430	15.9	1280
Tetramethyl quadruple-layered XXII	430	15.7 (21.6) [b)]	1810 (1430) [b)]

a) A. Bier, *Rec. Trav. Chim. Pays-Bas*, **75**, 866 (1956). b) Ref. 10.

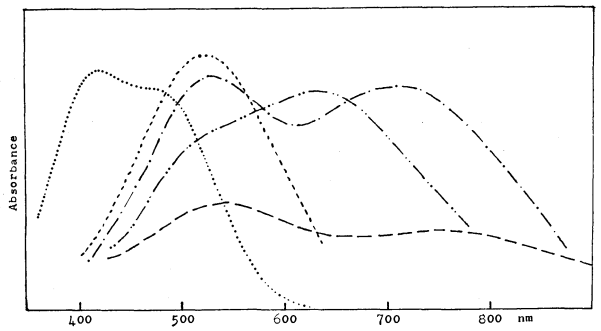

Fig. 7. Charge-transfer absorption spectra of layered cyclophane-TCNE complexes in dichloromethane; ····· *p,p'*-dimethylbibenzyl, ---- III, -·-· XV, -·-· XIX, —— XXIV.

failed to be measured owing to very low solubility of its dark blue TCNE complex.

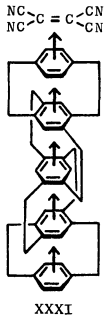

XXXI

The use of 1,3,5-trinitrobenzene (TNB) as an acceptor makes possible to measure the complex spectrum of sixfold-layered compound and also shows a tendency analogous to TCNE complexes as summarized in Table 4. Thus, the long-wavelength bands of charge-transfer complexes display marked bathochromic shift and the equilibrium constants, K_x, increase significantly as the layers increase. It is noteworthy that the complexes of fivefold and sixfold compounds exhibit quite identical spectra. In other words, there is no difference in transannular electron-releasing between them.

Experimental

Melting points are uncorrected. All solvents are of reagent grade unless otherwise specified. Chromatography was done with neutral alumina (Woelm, activity I) or silica gel (Merck, activity II—III) of about 20 to 100 times of mixture to separate. The use of a long column often results in the decomposition of multilayered cyclophanes. General procedure for Hofmann pyrolysis was described in detail in the experiment for [2.2]paracyclophane (III).

NMR measurements were made with a Hitachi Perkin-Elmer R-20 spectrometer (60 MHz) on dilute solutions in carbon tetrachloride or deuteriochloroform using tetramethylsilane as an internal standard. Infrared spectra were taken on a Jasco DS-402 spectrophotometer. Mass spectra were determined on a Hitachi RMU-7 spectrometer at 70 eV using direct insertion technique. UV spectra were recorded on a Hitachi EPS-3T spectrophotometer. Emission spectra at liquid nitrogen temperature were taken on a Hitachi MPF-2A spectrophotometer attached with a HTV R-446F photomultiplier in EPA (ethyl ether–isopentane–ethanol of 5:5:2 volume ratio) or tetrahydrofuran–ethanol (1:1 volume ratio). All solvents were of spectroscopic grade (Merck or Tokyo Kasei Kogyo) and used without further purification. A solution of about 1×10^{-3} M was prepared and degassed by freeze-pump-thaw method. Emission spectra were uncorrected. Lifetimes of phosphorescences were calculated from the exponential decay curves which were recorded on a synchroscope screen and photographed. The experimental errors are within $\pm5\%$.

[2.2]Paracyclophane (III), [2.2.2]Paracyclophane (IV), and [2.2.2.2]Paracyclophane (V). A solution of *p*-methylbenzyltrimethyl ammonium bromide (Ia, 10 g, 41 mmol) in 200 ml of distilled water was passed through a column containing strongly basic anion exchange resin, Amberite IRA-400[30] which is converted to its hydroxide form with large excess of 2 M sodium hydroxide solution. A mixture of the resulting aqueous solution (500 ml) of quaternary base (Ib), distilled xylene (50 ml), and phenothiazine (1 g) was placed in a three-necked, pear-shaped flask fitted with a mechanical stirrer and a water separator of Dean-Stark type attached

30) Instead of Amberite IRA-400, Dowex 1-X8, 50—100 mesh is currently available for ion exchange.

to a reflux condenser. The mixture was heated with stirring and water was removed as xylene azeotrope over a period of 4 hr. When the removal of water had been approximately completed, trimethylamine began to evolve and some polymers precipitated. After additional heating with stirring for 6 hr, the reaction mixture was allowed to cool and insoluble solid was separated by filtration. The solid was washed eight times with each 30 ml of hot benzene. The combined benzene washing was evaporated to dryness to give 0.83 g of crude [2.2]paracyclophane (III). The filtrate was chromatographed on neutral alumina (Woelm, activity I). Elution with benzene–hexane (1: 9) gave first 0.39 g of [2.2]paracyclophane (III), then 0.36 g (8.4%) of [2.2.2]paracyclophane (IV), and finally 0.095 g (2.2%) of [2.2.2.2]-paracyclophane (V).

The combined [2.2]paracyclophane, 1.22 g (29%), was recrystallized from chloroform, colorless prisms, mp 285 °C in a sealed tube (lit, [8]285—287 °C in a sealed tube). NMR (CCl_4) τ 3.65 (s, 8H, ArH), 6.99 (s, 8H, CH_2); mass *m/e* 208 (M^+, 56), 104 (100); IR (KBr disc, cm^{-1}) 3030 (w), 3005 (w), 2947 (w), 2920 (m), 2893 (w), 2847 (w), 1589 (m), 1497 (m), 1412 (m), 1087 (m), 936 (m), 893 (m), 806 (s), 720 (s), 622 (s), 508 (s).

[2.2.2]Paracyclophane was recrystallized from acetone, colorless plates, mp 162—163 °C (lit,[15] 166—167 °C). NMR (CCl_4) τ 3.43 (s, 12H, ArH), 7.12 (s, 12H, CH_2); mass *m/e* 312 (M^+); IR (KBr disc, cm^{-1}) 2995 (m), 2890 (s), 2830 (m), 1512 (s), 1438 (s), 1094 (m), 916 (m), 803 (m), 787 (s), 721 (w), 583 (s), 468 (s).

[2.2.2.2]Paracyclophane was recrystallized from acetone, colorless plates, mp 179—181 °C (lit,[16] 179—182 °C). NMR (CCl_4) τ 3.39 (s, 16H, ArH), 7.19 (s, 16H, CH_2); mass *m/e* 416 (M^+); IR (KBr disc, cm^{-1}) 2995 (m), 2910 (s), 2835 (m), 1510 (s), 1435 (s), 1198 (m), 1094 (m), 928 (m), 812 (s), 583 (s), 566 (m).

Staggered and Eclipsed 4,7,12,15-Tetramethyl[2.2]paracyclophanes (VIII and IX). The ammonium hydroxide aqueous solution (*ca.* 1 l) derived from 20.0 g (73.5 mmol) of duryltrimethylammonium bromide (VIa) in the usual way was mixed with 500 ml of distilled xylene and three spatulas of phenothiazine, and heated with stirring. After water was removed by azeotropic distillation, further reflux was continued for 12 hr and the mixture was cooled. The insoluble polymers (4.53 g) were removed by filtration and the filtrate was dried over anhydrous magnesium sulfate. After the solvent was evaporated, the residue was subjected to column chromatography on silica gel (Merck, activity II—III) using petroleum ether as eluent. From the first eluate was isolated a mixture of two isomeric 4,7,12,15-tetramethyl[2.2]paracyclophanes, VIII and IX. The minor isomer IX was separated from the readily soluble, staggered form VIII by treatment with a small amount of pentane. From the next eluate was isolated 2,3,8,9-tetramethyl-*sym*-dibenzocyclooctadiene (X) in a 0.4% yield.

The staggered form VIII was recrystallized from petroleum ether (yield 20%), colorless prisms, mp 106—107 °C (lit,[10] 105—107 °C). NMR (CCl_4) τ 3.75 (s, 4H, ArH), 6.8—7.6 (A_2B_2, 8H, CH_2), 8.04 (s, 12H, CH_3); mass *m/e* 264 (M^+, 66), 132 (100); IR (KBr disc, cm^{-1}) 2994 (m), 2937 (s), 2855 (m), 1604 (m), 1495 (s), 1444 (s), 1394 (m), 1367 (m), 1247 (m), 1030 (m), 902 (s), 850 (m), 819 (m), 709 (s), 512 (m), 466 (m), 440 (m).

The eclipsed form IX was recrystallized from 1: 3 carbon tetrachloride–acetone, 0.1% yield, colorless plates, mp 230—232 °C in a sealed tube. NMR (CCl_4) τ 3.93 (s, 4H, ArH), 6.5—7.7 (A_2B_2, 8H, CH_2), 7.85 (s, 12H, CH_3); mass *m/e* 264 (M^+, 66), 132 (100); IR (KBr disc, cm^{-1}) 2908 (s), 2853 (m), 1598 (m), 1497 (s), 1454 (m), 1392 (s), 1370 (m), 1030 (m), 895 (s), 708 (s), 510 (m), 434 (m). Found: C, 90.55; H, 9.14%. Calcd for $C_{20}H_{24}$: C, 90.85; H, 9.15%.

The compound X was recrystallized from ethyl acetate, colorless prisms, mp 239—240 °C after sintering at *ca.* 210 °C in a sealed tube (lit,[10] crystallized from chloroform, mp 209—211 °C in a sealed tube). Mass *m/e* 264 (M^+); NMR ($CDCl_3$) τ 3.18 (s, 4H, ArH), 7.04 (s, 8H, CH_2), 7.83 (s, 12H, CH_3); IR (KBr disc, cm^{-1}) 3000 (m), 2965 (w), 2937 (m), 2920 (m), 2855 (w), 1496 (m), 1448(s), 1328 (m), 1024 (m), 997 (m), 933 (m), 892 (s), 554 (s).

4,7-Dimethyl[2.2]paracyclophane (XI). The aqueous solution (*ca.* 600 ml) of quaternary bases, Ib and VIb, derived from a mixture of 10.0 g (40.1 mmol) of Ia and 11.1 g (40.8 mmol) of VIa in the usual way, was mixed with 100 ml of distilled xylene and 0.6 g of phenothiazine, and water was removed by azeotropic distillation with stirring. Evolution of trimethylamine began and further reflux was continued for 15 hr. The reaction mixture was cooled, insoluble polymers were filtered off, and then the filtrate was dried over anhydrous magnesium sulfate. After concentration the residue was treated with a small amount of petroleum ether, and insoluble [2.2]paracyclophane (III) was filtered off. The filtrate was chromatographed on silica gel (Merck, activity II—III) using petroleum ether for elution to give a mixture of 4,7-dimethyl[2.2]paracyclophane (XI) and 4,7,12,-15-tetramethyl[2.2]paracyclophane (VIII). The dimethyl derivative XI was purified by fractional crystallization from petroleum ether and carbon tetrachloride–acetone (1: 3), successively (yield 5.6%), colorless plates, mp 154—155 °C. NMR (CCl_4) τ 3.32 (dd, J=8 Hz, J'=2 Hz, 2H, ArH), 3.74 (dd, J=8 Hz, J'=2 Hz, 2H, ArH), 4.12 (s, 2H, ArH), 6.5—7.7 (m, 8H, CH_2), 7.95 (s, 6H, CH_3); mass *m/e* 236 (M^+, 68), 132 (100), 104 (45); IR (KBr disc, cm^{-1}) 2920 (s), 2850 (m), 1594 (m), 1496 (m), 1435 (m), 941 (m), 907 (s), 873 (m), 797 (s), 715 (s), 587 (m), 533 (m). Found: C, 91.32; H, 8.49%. Calcd for $C_{18}H_{20}$: C, 91.47; H, 8.53%.

Quaternary Ammonium Bromides, XIIIa, XIVa, XXIa, and XXVa. All the quaternary ammonium bromides, XIIIa, XIVa, XXIa, and XXVa, were prepared from the corresponding methyl derivatives according to the general procedure described below.

A given methyl cyclophane was brominated with a less amount than the equivalent of *N*-bromosuccinimide in carbon tetrachloride under reflux. After removal of insoluble succinimide, the solution was washed with water, dried over anhydrous magnesium sulfate, and then treated with an excess amount of trimethylamine in ether. The resulting white precipitate of quaternary ammonium bromide was filtered off and washed repeatedly with carbon tetrachloride. The ammonium salt thus obtained in good yield was used to the following reaction without purification.

These quaternary ammonium bromides were recrystallized from distilled water to give hydrated white crystals. XIIIa: mp 167—170 °C; NMR ($CDCl_3$) τ 3.23 (AB doublet, J=8 Hz, 1H, ArH), 3.41 (s, 1H, ArH), 3.46 (s, 2H, ArH), 3.61 (AB doublet, J=8 Hz, 1H, ArH), 3.80 (s, 1H, ArH), 5.17 (AB quartet, 2H, NCH_2), 6.69 (s, 9H, NCH_3), 6.5—7.5 (m, 8H, CH_2), 7.47 (s, H_2O), 7.89 (s, 3H, CH_3); IR (Nujol mull, cm^{-1}) 3400 (s, H_2O), 1595 (m), 975 (m), 925 (m), 875 (s), 795 (m), 717 (s), 595 (m). XIVa: dec>210 °C with melting; NMR ($CDCl_3$) τ 3.10 (s, 1H, ArH), 3.46 (s, 1H, ArH), 3.64 (s, 1H, ArH), 3.94 (s, 1H, ArH), 5.28 (AB quartet, 2H, NCH_2), 6.65 (s, 9H, NCH_3), 6.5—7.5 (m, 8H, CH_2), 7.84 (s, 3H, CH_3), 7.94 (s, 6H, CH_3), 8.11 (s, H_2O); IR (Nujol mull, cm^{-1}) 3400 (s, H_2O), 1595 (m), 975 (m), 930 (m), 885 (s), 720 (s). XXIa: dec>240 °C; NMR ($CDCl_3$) τ 3.78 (s, 5H,

ArH), 4.02 (s, 1H, ArH), 4.20 (s, 1H, ArH), 4.50 (s, 1H, ArH), 5.49 (AB quartet, 2H, NCH_2), 6.79 (s, 9H, NCH_3), 6.6—7.6 (m, 16H, CH_2), 8.08 (s, 3H, CH_3), 8.25 (s, H_2O); IR (Nujol mull, cm^{-1}) 3380 (s, H_2O), 980 (s), 880 (s), 795 (m), 710 (s), 685 (m), 515 (m).

Triple-layered [2.2]Paracyclophane (XV). A mixture of 3.5 g (9.4 mmol) of the quaternary ammonium bromide XIIIa and 2.3 g (9.4 mmol) of *p*-methylbenzyltrimethylammonium bromide (Ia) dissolved in distilled water was converted to the hydroxides, XIIIb and Ib, in the usual way using ion exchange resin. The resulting solution (*ca.* 800 ml) was mixed with 200 ml of distilled xylene and a spatula of phenothiazine, and dehydrated by azeotropic distillation under nitrogen atmosphere. After water was removed, the reaction mixture was refluxed for an additional 17 hr and allowed to cool. The insoluble polymers were removed by filtration and the filtrate was dried over anhydrous magnesium sulfate. The solvent was evaporated and the residue was chromatographed on silica gel (Merck, activity II—III). Elution with petroleum ether gave first double-layered cyclophane (III), then triple-layered one (XV), and finally quadruple-layered ones (XIX and XX).

Triple-layered compound (XV) was recrystallized from carbon tetrachloride-acetone (1:3) (yield 1.3%), colorless plates, mp 230 °C dec. in a sealed tube. NMR (CCl_4) τ 3.92 (s, 8H, ArH), 4.65 (s, 2H, ArH), 6.8—7.7 (m, 16H, CH_2); mass *m/e* 338 (M^+, 100), 234 (66), 104 (14); IR (KBr disc, cm^{-1}) 2980 (m), 2910 (s), 2840 (m), 1584 (m), 1495 (m), 1427 (s), 1405 (m), 1198 (m), 1177 (m), 968 (m), 937 (m), 901 (s), 863 (s), 794 (s), 708 (s), 680 (s), 605 (m), 517 (s). Found: C, 92.31; H, 7.72%. Calcd for $C_{26}H_{26}$: C, 92.26; H, 7.74%.

Dimethyl Triple-layered [2.2]Paracyclophane (XVI). In the same manner as non-substituted triple-layered compound XV, dimethyl triple-layered compound XVI was synthesized from quaternary ammonium bromides, XIVa and Ia. Dimethyl derivative XVI was purified by column chromatography on silica gel (Merck, activity II—III) and recrystallization from petroleum ether (yield 1.8%), colorless plates, mp 146—148 °C. NMR (CCl_4) τ 3.88 (s, 4H, ArH), 4.30 (s, 2H, ArH), 4.36 (s, 2H, ArH), 6.8—8.1 (m, 16H, CH_2), 8.17 (s, 6H, CH_3); mass *m/e* 366 (M^+, 100), 262 (10), 234 (34), 132 (12), 104 (7); IR (KBr disc, cm^{-1}) 2840 (s), 1577 (m), 1426 (s), 1165 (m), 895 (s), 870 (s), 792 (m), 710 (w), 695 (s), 673 (m), 593 (m), 520 (s). Found: C, 91.55; H, 8.29%. Calcd for $C_{28}H_{30}$: C, 91.75; H, 8.25%.

Tetramethyl Triple-layered [2.2]Paracyclophanes (XVII and XVIII). The hydroxide solution (*ca.* 1.8 l), derived from a mixture of quaternary ammonium bromides XIVa (15.6 g, 38.8 mmol) and VIa (10.7 g, 39.3 mmol) in the usual way, was mixed with 300 ml of distilled xylene and 2.0 g of phenothiazine, and then pyrolyzed as described for non-substituted compound XV. After polymers were removed, the reaction mixture was chromatographed on silica gel (Merck, activity II—III). Elution with petroleum ether gave first double-layered cyclophane (VIII), second a mixture of isomeric triple-layered ones, XVII and XVIII, and finally quadruple-layered ones, XXII and XXIII. The isomer XVII was separated from XVIII by careful chromatography, where the former was eluted first. Tetramethyl derivative XVII was recrystallized from acetone-ethanol (1:1) (yield 1.1%), colorless plates, mp 245—246 °C in a sealed tube. NMR (CCl_4) τ 3.94 (s, 2H, ArH), 4.33 (s, 4H, ArH), 6.7—7.7 (m, 16H, CH_2), 8.11 (s, 12H, CH_3); mass *m/e* 394 (M^+, 100), 262 (58), 132 (35); IR (KBr disc, cm^{-1}) 2920 (s), 2850 (s), 1590 (m), 1490 (s), 1432 (s), 1164 (m), 895 (s), 693 (s), 660 (m), 537 (m), 508 (m), 452 (m). Found: C, 91.27; H, 8.83%. Calcd for $C_{30}H_{34}$: C, 91.31; H, 8.69%.

The other isomeric tetramethyl derivative XVIII was recrystallized from acetone-ethanol (1:1) (yield 1.1%), colorless plates, mp 204—205 °C. NMR ($CDCl_3$) τ 4.17 (s, 2H, ArH), 4.21 (s, 2H, ArH), 4.28 (s, 2H, ArH), 6.7—7.8 (m, 16H, CH_2), 8.10 (s, 12H, CH_3); mass *m/e* 394 (M^+, 100), 262 (72), 132 (35); IR (KBr disc, cm^{-1}) 2900 (s), 2850 (s), 1585 (m), 1490 (s), 1440 (s), 1391 (m), 1367 (m), 1250 (m), 1025 (m), 889 (s), 688 (s), 660 (m), 537 (m), 507 (m), 451 (m). Found: C, 91.38; H, 8.84%. Calcd for $C_{30}H_{34}$: C, 91.31; H, 8.69%.

Quadruple-layered [2.2]Paracyclophanes (XIX and XX). a) From Quaternary Salt XIIIa: The aqueous solution (*ca.* 400 ml) containing the quaternary ammonium hydroxide XIIIb, which was derived from 1.4 g (3.7 mmol) of the bromide XIIIa, was heated in the presence of 50 ml of distilled xylene and a spatula of phenothiazine under nitrogen atmosphere for azeotropic distillation. Insoluble polymers were removed from the reaction mixture and the filtrate was dried over anhydrous magnesium sulfate. After evaporation the residue was chromatographed on neutral alumina (Woelm, activity I). Elution with benzene-petroleum ether (2:8) gave a mixture of isomeric quadruple-layered compounds, XIX and XX. The readily soluble isomer XIX was separated from the sparingly soluble isomer XX by treatment with carbon tetrachloride-acetone (1:3).

The quadruple-layered cyclophane XIX was recrystallized from carbon tetrachloride-acetone (1:3) (yield 1.1%), colorless plates, dec>240 °C. NMR (CCl_4) τ 4.02 (s, 8H, ArH), 4.88 (s, 4H, ArH), 6.7—7.9 (m, 24H, CH_2); mass *m/e* 468 (M^+, 100), 364 (41), 234 (69), 104 (33); IR (KBr disc, cm^{-1}) 2915 (s), 2840 (m), 1582 (m), 1424 (s), 1180 (m), 980 (m), 933 (m), 897 (m), 868 (s), 795 (s), 713 (s), 674 (s), 603 (m), 521 (s). Found: C, 92.12; H, 7.80%. Calcd for $C_{36}H_{36}$: C, 92.26; H, 7.74%.

The other isomeric quadrupled one XX was recrystallized from toluene (yield 0.75%), colorless prisms, dec>250 °C. NMR (CCl_4) τ 4.02 (s, 8H, ArH), 4.90 (s, 4H, ArH), 6.7—7.9 (m, 24H, CH_2); mass *m/e* 468 (M^+, 100), 364 (34), 234 (42), 104 (24); IR (KBr disc, cm^{-1}) 2915 (s), 2840 (m), 1582 (s), 1428 (s), 1178 (m), 934 (m), 895 (s), 865 (s), 794 (s), 710 (s), 687 (s), 598 (m), 516 (s). Found: C, 91.99; H, 7.69%. Calcd for $C_{36}H_{36}$: C, 92.26; H, 7.74%.

b) Alternative Synthesis of XIX from Quaternary Salts, Ia and XXIa. A mixture of 0.60 g (2.5 mmol) of *p*-methylbenzyltrimethylammonium bromide (Ia) and 0.80 g (1.6 mmol) of quaternary ammonium bromide (XXIa) dissolved in distilled water was converted to the hydroxide form in the usual way. The resulting hydroxide solution (*ca.* 450 ml) was mixed with 20 ml of distilled toluene and 20 mg of phenothiazine, and heated with stirring under nitrogen. After water was removed by azeotropic distillation, further reflux continued for 6 hr. The reaction mixture was allowed to cool and the insoluble polymers (0.15 g) were filtered off. After drying over anhydrous magnesium sulfate, the filtrate was subjected to column chromatography on neutral alumina (Woelm, activity I). Elution with benzene-hexane (1:1) gave first 30 mg of [2.2]paracyclophane (III) and then 24 mg (3.2%) of quadruple-layered compound XIX. The properties of this product were quite identical with those of the readily soluble isomer obtained by pyrolysis of XIIIb.

Tetramethyl Quadruple-layered [2.2]Paracyclophanes (XXII and XXIII). The cyclophanes, XXII and XXIII, were synthesized from quaternary ammonium bromide XIVa in the same method as non-substituted quadruple-layered compounds, XIX and XX. The isomers, XXII and XXIII, were also separated by the treatment with the same solvent

as for non-substituted ones. The readily soluble isomer XXII was recrystallized from chloroform-ether-petroleum ether (1:1:1) and toluene, successively (yield 3.2%), colorless prisms, dec>240 °C. NMR (CCl_4) τ 4.43 (s, 4H, ArH), 4.53 (s, 4H, ArH), 6.8—8.1 (m, 24H, CH_2), 8.19 (s, 12H, CH_3); mass *m/e* 524 (M^+, 100), 392 (39), 262 (23), 132 (14); IR (KBr disc, cm^{-1}) 2900 (s), 2850 (s), 1585 (m), 1485 (m), 1428 (s), 1248 (m), 1185 (m), 1035 (m), 975 (m), 891 (s), 692 (s), 665 (m), 527 (m), 508 (m), 438 (m). Found: C, 91.35; H, 8.56%. Calcd for $C_{40}H_{44}$: C, 91.55; H, 8.45%.

The sparingly soluble isomer XXIII was recrystallized from toluene (yield 1.6%), colorless prisms, dec>240 °C. NMR (CCl_4) τ 4.45 (s, 4H, ArH), 4.52 (s, 4H, ArH), 6.8—8.1 (m, 24H, CH_2), 8.20 (s, 12H, CH_3); mass *m/e* 524 (M^+, 100), 392 (39), 262 (36), 132 (14); IR (KBr disc, cm^{-1}) 2900 (s), 2840 (s), 1583 (m), 1483 (m), 1445 (s), 1250 (m), 1165 (m), 1028 (m), 964 (m), 887 (s), 696 (s), 669 (m), 525 (m), 508 (m), 453 (m). Found: C, 91.77; H, 8.64%. Calcd for $C_{40}H_{44}$: C, 91.55; H, 8.45%.

Fivefold-layered [2.2]Paracyclophane (XXIV). The aqueous quaternary base solution (*ca.* 800 ml) derived from 1.2 g (3.2 mmol) of XIIIa and 1.5 g (2.9 mmol) of XXIa was added into 30 ml of distilled xylene and 50 mg of phenothiazine, and refluxed with stirring under nitrogen. After removal of water, heating was continued for an additional 6 hr. After cooling the insoluble polymers were filtered off and the filtrate was chromatographed on neutral alumina (Woelm, activity I) using benzene-hexane (2:8) as eluent to give a mixture of quadruple-layered compounds, XIX and XX, and fivefold-layered one XXIV. The separation of this mixture was performed by liquid chromatography using chloroform as eluent. This gave first XXIV and then a mixture of XIX and XX. The compound XXIV was recrystallized from carbon tetrachloride-acetone (1:3) (yield 5%), colorless microcrystals, dec>240 °C. NMR (CCl_4) τ 4.04 (s, 8H, ArH), 4.97 (s, 4H, ArH), 5.12 (b.s, 2H, ArH), 6.8—8.0 (m, 32H, CH_2); mass *m/e* 598 (M^+, 100), 494 (33), 364 (63), 234 (21), 104 (41); IR (KBr disc, cm^{-1}) 2910 (s), 2830 (m), 1585 (s), 1483 (m), 1425 (m), 1181 (m), 935 (m), 895 (m), 870 (s), 795 (s), 714 (m), 671 (s), 603 (m), 517 (s). Found: C, 91.67; H, 7.56%. Calcd for $C_{46}H_{46}$: C, 92.26; H, 7.74%.

Dimethyl Fivefold-layered [2.2]Paracyclophane (XXVI). Tetramethyl quadruple-layered [2.2]paracyclophane XXII (1.00 g, 1.91 mmol) was brominated with 0.27 g (1.52 mmol) of *N*-bromosuccinimide under reflux in 12 ml of carbon tetrachloride. After removal of succinimide, the solution was washed, dried over anhydrous magnesium sulfate, and then mixed with an excess amount of trimethylamine in ether under ice-cooling. The mixture was brought to room temperature slowly and the resulting white precipitate was collected and thoroughly washed with carbon tetrachloride. The quaternary ammonium bromide XXVa thus obtained was mixed with 0.5 g (2.1 mmol) of *p*-methylbenzyltrimethylammonium bromide (Ia) in 300 ml of distilled water and subjected to the ion exchange process. The resulting hydroxide solution (*ca.* 500 ml) was added into 15 ml of distilled xylene and 100 mg of phenothiazine, and heated with stirring under nitrogen. After removal of water, heating was continued for 6 hr. The insoluble polymers were filtered off and the filtrate was chromatographed on neutral alumina (Woelm, activity I). Elution with benzene-hexane (1:9) gave [2.2]paracyclophane (III) and [2.2.2]paracyclophane (IV). Further elution with 2:8 benzene-hexane gave dimethyl fivefold-layered [2.2]paracyclophane XXVI in a 1.1% yield based on NBS, colorless plates from 1:3 carbon tetrachloride-acetone, dec>250 °C. NMR (CCl_4) τ 4.04 (s, 4H, ArH), 4.47 (s, 2H, ArH), 4.64 (s, 2H, ArH), 4.96 (s, 2H, ArH), 5.08 (s, 2H, ArH), 6.9—8.1 (m, 32H, CH_2), 8.24 (s, 6H, CH_3); mass *m/e* 626 (M^+, 100), 522 (14), 494 (27), 392 (32), 364 (24), 262 (10), 234 (17), 132 (22), 104 (35); IR (KBr disc, cm^{-1}) 2910 (s), 2835 (m), 1584 (s), 1482 (m), 1425 (s), 1250 (m), 1178 (m), 892 (s), 790 (m), 712 (w), 693 (m), 672 (s), 665 (s), 600 (m), 518 (s). Found: C, 92.19; H, 7.93%. Calcd for $C_{48}H_{50}$: C, 91.96; H, 8.04%.

Sixfold-layered [2.2]Paracyclophanes (XXVII and XXVIII). The aqueous quaternary ammonium hydroxide solution (*ca.* 600 ml), prepared from 1.6 g (3.1 mmol) of the bromide XXIa in the usual way, was added into 30 ml of toluene and 20 mg of phenothiazine. The mixture was refluxed with stirring under nitrogen. After the removal of water was completed by azeotropic distillation, heating was continued for an additional 6 hr. After cooling to room temperature, the insoluble polymers (0.55 g) were separated. The filtrate was chromatographed on neutral alumina (Woelm, activity I) and elution with benzene-hexane (1:1) gave a mixture of isomeric sixfold-layered [2.2]paracyclophanes, XXVII and XXVIII. The readily soluble isomer XXVII was separated from the sparingly soluble one XXVIII by treatment of a minimum amount of benzene. The isomer XXVII was recrystallized from toluene (yield 4.7%), colorless plates, dec>250 °C. NMR (CCl_4) τ 4.06 (s, 8H, ArH), 5.00 (s, 4H, ArH), 5.20 (s, 4H, ArH), 7.1—8.3 (m, 40H, CH_2); IR (KBr disc, cm^{-1}) 2920 (s), 2840 (m), 1584 (s), 1472 (s), 1424 (s), 1183 (m), 974 (m), 935 (m), 894 (m), 875 (s), 794 (s), 713 (m), 673 (s), 602 (m), 518 (s). Found: C, 92.01; H, 7.64%; mol wt 734 (vapor pressure osmometry). Calcd for $C_{56}H_{56}$: C, 92.26; H, 7.74%; mol wt 729.

The other isomer XXVIII was recrystallized from xylene (yield 2.4%), colorless microcrystals, dec>250 °C. NMR ($CDCl_3$) τ 3.95 (s, 8H, ArH), 4.95 (s, 4H, ArH), 5.19 (s, 4H, ArH), 6.9—8.2 (m, 40H, CH_2); IR (KBr disc, cm^{-1}) 2920 (s), 2840 (m), 1584 (s), 1482 (s), 1425 (s), 1181 (m), 975 (m), 933 (m), 894 (m), 874 (s), 796 (m), 715 (m), 677 (s), 603 (m), 517 (s). Found: C, 92.07; H, 7.74%. Calcd for $C_{56}H_{56}$: C, 92.26; H, 7.74%.

Thermal Isomerization from Eclipsed Form (IX) to Staggered Form (VIII) of Tetramethyl[2.2]paracyclophane. Thermal isomerization from IX to VIII could be easily observed in NMR spectra. Thus, when IX in hexachlorobutadiene was heated at 190 °C, signals of VIII gradually appear with disappearance of signals of IX, and after 2 hr IX was completely transformed to VIII accompanying with insoluble black decomposition product. For preparative purpose, 10 mg of IX was dissolved in 0.5 ml of *n*-tridecane and degassed by freeze-pump-thaw method. The resulting solution in a sealed tube was heated at 195 °C for 3 hr. After cooling the product was chromatographed on silica gel (Merck, activity II—III). After *n*-tridecane, VIII was eluted with *n*-hexane in nearly quantitative yield.

Layered Cyclophane-TCNE and -TNB Complexes. Commercial tetracyanoethylene (TCNE) was recrystallized from chlorobenzene and then sublimed twice under reduced pressure. Commercial 1,3,5-trinitrobenzene (TNB) was recrystallized three times from ethanol and then three times from carbon tetrachloride. Dichloromethane and chloroform are of spectroscopic grade (Merck) and used without further purification. The charge-transfer spectra of layered cyclophane-TCNE and -TNB complexes were recorded on a Hitachi EPS-3T spectrophotometer. Most of the multilayered cyclophane complexes exhibit unchanged absorption maxima though the relative concentrations of two components are varied. Equilibrium constants and molar extinction coefficients for the TNB complexes were determined in the

manner described by Benesi and Hildebrand.[31] Measurements were carried out at four points in the presence of excess acceptor; the mole concentrations of the donor were varied from 0.003 to 0.005 M, while the TNB concentrations from 0.03 to 0.15 M. In the case of tetramethyl[2.2]paracyclophane (VIII), on the other hand, the donor concentration was varied from 0.025 to 0.15 M, while the acceptor concentration was kept constant at 0.002 M. Every complex of multilayered cyclophane here presented gave a good linear plots, supporting that the complex consists conclusively of 1 : 1 ratio one.

31) H. A. Benesi and J. H. Hildebrand, *J. Amer. Chem. Soc.*, **71**, 2703 (1949).

The authors are grateful to Professor Yasuhide Yukawa for his helpful discussion and encouragement. They are also indebted to Mr. T. Fujino and T. Shishido for the microanalyses. This research is partly supported by the grant-in-aid of the Ministry of Education, to which the authors' thanks are also due.

BULLETIN OF THE CHEMICAL SOCIETY OF JAPAN, VOL. 46, 3530—3533 (1973)

Application of the Mannich Reaction to 1-Azaazulan-2-one. Syntheses of Seven-Membered Analogues of Tryptophan and Related Compounds[1]

Akira SATO,* Shigeo NOZOE,** Takashi TODA, Shuichi SETO***, and Tetsuo NOZOE****

Department of Chemistry, Faculty of Science, Tohoku University, Aoba, Aramaki, Sendai 980

(Received August 23, 1973)

Application of the Mannich reaction to 1-azaazulan-2-one (I) gave 3-dimethylamino-1-azaazulan-2-one (III) in a good yield. Tryptophan analogue and related compounds having this structure (I) were synthesized by the reactions of the quaternary base (VI) of III with potassium cyanide and diethyl acetylaminomalonate. Also, some other reactions of III and VI are reported.

Since 1954, the syntheses and reactions of 1-azaazulan-2-ones (2*H*-cyclohepta[*b*]pyrrol-2-ones) have been investigated,[2,3] and also synthetic studies of some physiologically interesting derivatives of them have been carried out.[4] However, the syntheses of physiologically more interesting 1-azaazulan-2-one derivatives whose structures are analogous to indolacetic acid and/or tryptophan have only been quoted by one of the authors (T.N.) in the monograph.[5] In this paper, we wish to describe the experimental details about the syntheses of seven-membered analogues of tryptophan and related compounds having 1-azaazulan-2-one (I) structure by the application of Mannich reaction.

(I) (Ia)

It is known that I is a tautomer of 2-hydroxy-1-azaazulane (Ia), though the keto-form (I) is predominant,[5] and the electron density is high at the 3-position[6] as in the case of azulene. In fact the electrophilic substitution reactions take place at its 3-position.[2a,d] Therefore, the Mannich reaction to I was expected to give good results. When the reaction was applied to I, 3-morpholinomethyl-1-azaazulan-2-one (II) and 3-dimethylamino-1-azaazulan-2-one (III) were obtained in good yields, respectively. However, fairly large amounts of bis[1-azaazulan-2-on-3-yl]methane (IV)[4a] were formed as a by-product when diluted acetic acid was employed as a solvent. The formation of the same type of bis-methylene compounds was observed in the cases of hydroxymethylation of I[4a] and the Mannich reactions of several azulene compounds.[7] Not as in the case of the Mannich reaction of pyrroles,[8] the order of the addition of the

* Present address: Ashigara Research Laboratory of Fuji Film Co., Minamiashigara, Kanagawa 250-01.

** Present address: Institute of Applied Microbiology, Tokyo University, Bunkyo-ku, Tokyo.

*** Present address: Chemical Research Institute of Non-Aqueous Solution, Tohoku University, Katahiracho, Sendai.

**** Present address: Kamiyoga, 2-5-1-811, Setagaya-ku, Tokyo 158.

1) Taken from M. Sc. thesis of S. Nozoe (1956) and of A. Sato (1959) of Tohoku University.

2) a) T. Nozoe, S. Seto, S. Matsumura, and T. Terasawa, *Chem. Ind.* (London), **1954**, 1356, 1367. b) T. Nozoe, S. Seto, and S. Nozoe, *Proc. Japan Acad.*, **32**, 172 (1956). c) S. Seto and S. Nozoe, *ibid.*, **32**, 765 (1956). d) T. Toda, S. Seto, and T. Nozoe, This Bulletin, **41**, 2102 (1968).

3) N. Soma and G. Sunagawa, *Yakugaku Zasshi*, **82**, 418 (1962). N. Soma, *ibid.*, **82**, 892 (1962). K. Ogura, H. Sasaki, and S. Seto, This Bulletin, **38**, 306 (1965). H. Nakao, N. Soma, and G. Sunagawa, *Chem. Pharm. Bull.* (Tokyo), **13**, 828 (1965). M. Watatani, *ibid.*, **16**, 1503 (1968).

4) a) T. Toda, This Bulletin, **40**, 590 (1967). b) T. Nozoe, S. Seto, and T. Toda, *ibid.*, **41**, 208 (1968).

5) T. Nozoe and K. Kikuchi, "Dai Yuki Kagaku." Vol. 13, ed. M. Kotake, Asakura shoten, Tokyo (1960), pp. 569—572.

6) H. Kon, *Sci. Repts. Tohoku Univ.*, I, **38**, 67 (1954).

7) H. Arnold and K. Pahls, *Chem. Ber.*, **89**, 121 (1956); K. Hafner and W. Senf, *Ann. Chem.*, **656**, 34 (1962).

8) G. B. Bachman and L. K. Heisey, *J. Amer. Chem. Soc.*, **68**, 2498 (1946).

reagents did not cause any effect to the yields of II and III.

A catalytic hydrogenolysis of III afforded 3-methyl-1-azaazulan-2-one (V) and a treatment of III with methyl iodide gave its quaternary base (VI) respectively, in good yields. (1-Azaazulan-2-on-3-yl)acetonitrile (VII) and ethyl α-ethoxycarbonyl-β-(1-azaazulan-2-on-3-yl)propionate (VIII) were obtained by the reactions of VI with potassium cyanide and diethyl malonate, respectively. (1-Azaazulan-2-on-3-yl)acetic acid (IX), an indolacetic acid analogue, was obtained by the hydrolysis of VII. The hydrolysis of VIII and the following thermal decomposition of the free dicarboxylic acid (X) gave β-(1-azaazulan-2-on-3-yl)-propionic acid (XI).

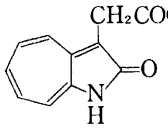
(IX)

As we have reported[4a] an attempted synthesis of α-aminopropionic acid derivatives of I from the condensation products of 3-formyl-1-azaazulan-2-one with hippuric acid or nitromethane was unsuccussful. Under the modified conditions as in the case of gramine quaternary base,[9] the treatment of VI with acetoamido- and formamido-malonic acid diethyl esters afforded ethyl α-acetylamino-α-ethoxycarbonyl-β-[1-azaazulan-2-on-3-yl]propionate (XII) and ethyl α-ethoxycarbonyl-α-formylamino-β-[1-azaazulan-2-on-3-yl]propionate (XIII). α-Amino-β-[1-azaazulan-2-on-3-yl]propionic acid (XIV), a seven-membered analogue of tryptophan, was successfully obtained by the hydrolyses of XII and XIII. Application of the Schmidt reaction to ethyl α-acetyl-β-[1-azaazulan-2-on-3-yl]propionate (XV), which was synthesized from VI and acetoacetic ester, and hydrolysis of the obtained *N*-acetyl derivative (XVI) also gave XIV. The amino acid (XIV) shows red-violet colorations by the ninhydrin test.

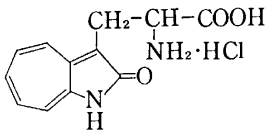
(XIV)

The reactions of quaternary base (VI) with other nucleophilic reagents, such as ethylmercaptan, diethyl nitromalonate, and methyl nitroacetate afforded [1-azaazulan-2-on-3-yl]methyl ethyl sulfide (XVII), ethyl α-ethoxycarbonyl-α-nitro-β-[1-azaazulan-2-on-3-yl]propionate (XVIII), and methyl α-nitro-β-[1-azaazulan-2-on-3-yl]propionate (XIX), respectively.

All the compounds obtained are listed in the table.

TABLE

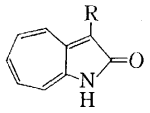

Compound	R
I:	H
II:	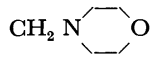
III:	CH_2NMe
IV:	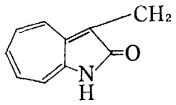
V:	Me
VI:	$CH_2\overset{\oplus}{N}(Me)_3\cdot\overset{\ominus}{I}$
VII:	CH_2CN
VIII:	$CH_2CH(COOEt)_2$
X:	$CH_2CH(COOH)_2$
XI:	CH_2CH_2COOH
XII:	$CH_2C(COOEt)_2$ NHAc
XIII:	$CH_2C(COOEt)_2$ NHCHO
XV:	$CH_2CHCOOEt$ COMe
XVI:	$CH_2CHCOOH$ NHAc
XVII:	CH_2SEt
XVIII:	$CH_2C(COOEt)_2$ NO_2
XIX:	$CH_2CHCOOMe$ NO_2

Experimental[10]

3-Morpholinomethyl-1-azaazulan-2-one (II). A mixture of 120 mg of I, 75 mg of morpholine, and 120 mg of 27% formalin was heated for 2 hr at 60 °C with stirring. After cooling, the reaction mixture was extracted with ethyl acetate and the combined organic layers were washed with water, dried over sodium sulfate and chromatographed on alumina. Alcohol elutes afforded 120 mg of orange yellow needles of II, mp 206—207 °C, from alcohol.

Found: C, 68.67; H, 6.25; N, 11.96%. Calcd for $C_{14}H_{16}O_2N_2$: C, 68.83; H, 6.60; N, 11.47%.

3-Dimethylaminomethyl-1-azaazulan-2-one (III). To a solution of 17 ml of acetic acid and 2.20 g of 40% dimethylamine, 200 mg of paraformaldehyde and 1.0 g of I were added. After it was heated for 12 hr at 40 °C, 30 ml of water was added to the solution and then brown precipitates (*ca.* 5%) formed was collected by filtration. The precipitates were recrystallized from ethyl acetate to give brown micro needles, mp>300 °C, which were identical with the authentic sample of IV[4a] by comparison of their IR spectra. The pH of the mother layer was adjusted *ca.* 10 with sodium carbonate, extracted with ethyl acetate, and the combined organic layers were washed with water. After dried over sodium sulfate, the extracts were chromatographed on alumina and alcohol elutes afforded orange red prisms of III; mp 149—150 °C, from ethyl acetate; yield 1.12 g.

Found: C, 71.26; H, 6.98; N, 13.85%. Calcd for $C_{12}H_{14}ON_2$: C, 71.35; H, 6.67; N, 13.85%.

When the reaction was carried out in the 60% aqueous acetic acid, *ca.* 30% of IV was obtained and the yield of III

9) H. R. Snyder and C. W. Smith, *ibid.*, **66**, 350 (1944); N. F. Albertson, S. Archer, and C. M. Suter, *ibid.*, **66**, 500 (1944).

10) All melting points are uncorrected.

was reduced.

3-Methyl-1-azaazulan-2-one (V). To a solution of 100 mg of III in 15 ml of methanol, 20 mg of 10% Pd-charcoal catalyst was added and then the reduction was carried out. After 13 ml of hydrogen was taken up, the catalyst was separated by filtration, and the methanol was removed by distillation. The residues were recrystallized from ethyl acetate to give orange yellow needles of V, mp 218—220 °C: yield, 95%.

Found: N, 8.85%. Calcd for $C_{10}H_9ON$: N, 8.80%.

3-Dimethylaminomethyl-1-azaazulan-2-one Methiodide (VI). Two hundred mg of III and 140 mg of methyl iodide in 2 ml of absolute alcohol were stirred for 2 hr at room temperature. The quaternary base of III was obtained as orange brown precipitates, mp 187—188 °C (dec.); yield, 300 mg.

Found: N, 8.54%. Calcd for $C_{13}H_{17}ON_2I$: N, 8.14%.

(1-Azaazulan-2-on-3-yl)acetonitrile (VII). A solution of 100 mg of potassium cyanide and 200 mg of VI in 60% alcohol was heated for 1 hr at 50 °C with stirring and then allowed to stand overnight at room temperature. After the alcohol was removed under reduced pressure, the obtained residue was washed well with water, dried in a desiccator, and recrystallized from ethyl acetate to give 80 mg of orange brown prisms of VII, mp 224—225 °C.

Found: C, 71.46; H, 4.10; N, 14.87%. Calcd for $C_{11}H_8ON_2$: C, 71.72; H, 4.38; N, 15.21%.

(1-Azaazulan-2-on-3-yl)acetic Acid (IX). One hundred mg of VII was refluxed for 4 hr in 2 ml of 20% potassium hydroxide solution, and then the solution was acidified with 6 M hydrochloric acid. The formed precipitates were collected by filtration, washed with water, dried in a desiccator and then recrystallized from alcohol to give 100 mg of IX, mp 236—237 °C (dec.).

Found: C, 65.42; H, 4.74; N, 6.68%. Calcd for $C_{11}H_9O_3N$: C, 65.02; H, 4.46; N, 6.89%.

Ethyl α-Ethoxycarbonyl-β-(1-azaazulan-2-on-3-yl)propionate (VIII). A solution of 113 mg of VI and 53 mg of diethyl malonate in 5 ml of absolute alcohol was added drop by drop into the sodium ethoxide solution which was prepared from 15 mg of sodium and 1 ml of absolute alcohol with stirring and heated for 2 hr at 60 °C. After it was allowed to stand overnight at room temperature, the alcohol was removed under reduced pressure. The residue was acidified with 1M sulfuric acid, extracted with ethyl acetate and then the combined organic layers were washed with water and dried over sodium sulfate. The solution was chromatographed on alumina and ethyl acetate eluates gave 70 mg of orange scales of VIII, mp 119—120 °C, from ethyl acetate.

Found: N, 4.52%. Calcd for $C_{17}H_{19}O_5N$: N, 4.41%.

β-(1-Azaazulan-2-on-3-yl)propionic Acid (XI). Thirty mg of VIII was heated in 5 ml of 30% potassium hydroxide for 5 hr at 100 °C, and after cooling the resulted solution was acidified with 6M hydrochloric acid to form yellow micro needles of X, mp 188—189 °C (dec.) from alcohol; yield, 20 mg. The dibasic acid (X) was heated at 190 °C to decompose with carbon dioxide evolution. After recrystallization of the residues from alcohol, 18 mg of yellow needles of XI, mp 214—216 °C (dec.), was obtained.

Found: N, 6.15%. Calcd for $C_{12}H_{11}O_3N$: N, 6.45%.

Ethyl α-Acetamido-α-ethoxycarbonyl-β-(1-azaazulan-2-on-3-yl)-propionate (XII). A solution of 200 mg of diethyl acetamidomalonate[11] and 350 mg of VI in 20 ml of absolute alcohol was added to sodium ethoxide solution prepared from 2 ml of absolute alcohol and 20 mg of sodium and heated for 4 hr at 60 °C. After it was allowed to stand overnight at room temperature, the alcohol was removed under reduced pressure. The residues were washed with water and dried in a desiccator to give 200 mg of orange prisms of XII, mp 173—174 °C from ethyl acetate.

Found: C, 60.42; H, 5.97; N, 7.35%. Calcd for $C_{19}H_{22}O_6N_2$: C, 60.95; H, 5.92; N, 7.48%.

Ethyl α-Ethoxycarbonyl-α-formamido-β-(1-azaazulan-2-on-3-yl)-propionate (XIII). A solution of 350 mg of VI and 220 mg of diethyl formamidomalonate[11] in 20 ml of absolute alcohol was added to sodium ethoxide solution prepared from 25 mg of sodium and 2 ml of adsolute alcohol. The reaction mixture was treated as the case of XII to give 280 mg of orange prisms of XIII, mp 181—182 °C from ethyl acetate.

Found: C, 60.30; H, 5.41; N, 7.83%. Calcd for $C_{18}H_{20}O_6N_2$: C, 59.99; H, 5.85; N, 7.77%.

α-Amino-β-(1-azaazulan-2-on-3-yl)propionic Acid Hydrochloride (XIV). Three hundred mg of XII in 3 ml of conc. hydrochloric acid was heated for 4 hr at 100 °C, and then concentrated under reduced pressure to give yellow residues. Recrystallization of the residues from alcohol gave 200 mg of yellow needles of XIV, mp 260—261 °C (dec.). This compound showed red-violet color by ninhydrin reagent.

Found: C, 53.88; H, 4.80; N, 10.13%. Calcd for $C_{12}H_{12}O_3N_2HCl$: C, 53.64; H, 4.87; N, 10.43%.

XIV was also obtained by the same acid hydrolysis of XIII and XVI in quantitative yields.

Ethyl α-Acetyl-β-(1-azaazulan-2-on-3-yl)propionate (XV). To a solution of 350 mg of VI and 130 mg of ethyl acetoacetate in 5 ml of absolute alcohol, a sodium ethoxide solution prepared from 20 mg of sodium and 2 ml of absolute alcohol was added and heated at 60 °C for 5 hr. After it was allowed to stand overnight at room temperature, 180 mg of orange prisms of XV, mp 147—148 °C from ethyl acetate, was obtained by the same treatment as the case of the preparation of XII.

Found: C, 67.16; H, 5.77; N, 4.96%. Calcd for $C_{16}H_{17}O_4N$: C, 66.88; H, 5.96; N, 4.88%.

Ethyl α-Acetylamino-β-(1-azaazulan-2-on-3-yl)propionate (XVI). A solution of 300 mg of XV in 10 ml of chroloform and conc. sulfuric acid was heated at 40 °C, and to this solution 80 mg of sodium azide was added with stirring. The reaction mixtures were stirred for one and half hr and then poured into crushed ice. The chloroform layer was washed with water, dried over sodium sulfate and removed under reduced pressure to give 150 mg of yellow micro needles of XVI, mp 179—180 °C from ethyl acetate-alcohol.

Found: C, 63.74; H, 5.83; N, 9.09%. Calcd for $C_{16}H_{18}O_4N_2$: C, 63.56; H, 6.00; N, 9.27%.

S-(1-Azaazulan-2-on-3-yl)methyl Ethyl Sulfide (XVII). A solution of 200 mg of VI and 50 mg of ethylmercaptan in 3 ml of dioxane and 0.5 ml of 2 M sodium hydroxide was heated at 60 °C for 1 hr and allowed to stand overnight at room temperature. After the solvent was removed under reduced pressure, the formed residues were acidified with 6 M hydrochloric acid, washed with water, and dried in a desiccator to give 80 mg of orange scales of XVII, mp 172—173 °C from ethyl acetate.

Found: C, 66.03; H, 5.78; N, 6.18%. Calcd for $C_{12}H_{13}ONS$: C, 65.72; H, 5.98; N, 6.38%.

Ethyl α-Ethoxycarbonyl-α-nitro-β-(1-azaazulan-2-on-3-yl)-propionate (XVIII). A solution of 200 mg of VI and 120 mg of diethyl nitromalonate in 5 ml of absolute alcohol was added to a sodium ethoxide solution prepared from 15 mg of sodium and 1 ml of absolute alcohol, and then heated at 60 °C for 4 hr. After it was allowed to stand overnight at

11) Prepared by the method of following paper: S. Tatsuoka, T. Kinoshita, and R. Nakamori, *Yakugaku Zasshi*, **71**, 702 (1951).

room temperature, the alcohol was removed and the obtained residues were washed with water. Recrystallization of the residues from ethyl acetate gave 100 mg of yellow needles of XVIII, mp 158—159 °C.

Found: C, 56.83; H, 4.81; N, 7.67%. Calcd for $C_{17}H_{18}O_7N_2$: C, 56.35; H, 5.01; N, 7.73%.

Methyl α-Nitro-β-(1-azaazulan-2-on-3-yl)propionate (XIX). A solution of 350 mg of VI and 12 mg of methyl nitroacetate in 5 ml of absolute methanol was added to a sodium methoxide solution prepared from 100 mg of sodium methoxide and 1 ml of absolute methanol. After the reaction mixture was treated as above, 180 mg of yellow needles of XIX, mp 186—187 °C from methanol, was obtained.

Found: C, 57.05; H, 4.37; N, 9.70%. Calcd for $C_{13}H_{12}O_5N_2$: C, 56.52; H, 4.38; N, 10.14%.

This research was supported by a grant from the Ministry of Education and from Sankyo Co. to whom the authors' thanks are due.

BULLETIN OF THE CHEMICAL SOCIETY OF JAPAN, VOL. 46, 3533—3536 (1973)

The Synthesis of 3-Methyl-5-(2-aminoalkyl)isoxazoles

Choji KASHIMA and Yoshihiko TSUDA
Department of Chemistry, Tokyo Kyoiku University, Otsuka, Tokyo 112

(Received February 1, 1973)

The reaction of 3,5-dimethylisoxazole with Schiff bases gave 3-methyl-5-(2-aminoalkyl)isoxazole derivatives in the presence of sodium amide in liquid ammonia. The *N*-alkylation on the anilino group of 3-methyl-5-(2-anilino-2-phenylethyl)isoxazole resulted in deamination, thus giving 3-methyl-5-styrylisoxazole. The reaction of 3,5-dimethylisoxazole with benzonitrile gave 3-methyl-5-(2-aminostyryl)isoxazole, which was then reduced to 3-methyl-5-(2-amino-2-phenylethyl)isoxazole.

It has been previously reported[1] that the 5-methyl group of 3,5-dimethylisoxazole (**1**) is metallated by the reaction of sodium amide in liquid ammonia, and that the sodium salt of **1** is alkylated by alkyl halides. Also, **1** reacts with some electrophilic reagents in the presence of butyllithium in anhydrous ether.[2] This paper will describe the reaction of **1** with Schiff bases or benzonitrile in the presence of sodium amide in liquid ammonia; we thus synthesized 3-methyl-5-(2-aminoalkyl)-isoxazole derivatives or 3-methyl-5-(2-aminostyryl)-isoxazole (**10**), which was subsequently reduced to 3-methyl-5-(2-amino-2-phenylethyl)isoxazole (**12**). It is very interesting to synthesize such aminoalkyl-isoxazole derivatives because of their antipyretic, analgetic, antiinflammatory, and antitussive activities.[3]

Results and Discussion

3,5-Dimethylisoxazole (**1**) was treated with an equimolar amount of *N*-benzylideneaniline, one of the Schiff bases, in the presence of an equimolar amount of sodium amide in liquid ammonia to give two products, A (mp 113 °C) and B(mp 236 °C). A was a 1:1 adduct of isoxazole and the Schiff base. From the IR and NMR spectra, the structure of A was deduced to be 3-methyl-5-(2-anilino-2-phenylethyl)isoxazole (**2**). For the confirmation of the structure, **2** was hydrogenated on platinum oxide in ethanol to give 1,2-diphenyl-6-methyl-2,3-dihydro-4-pyridone (**3**), which was identical with an authentic sample.[4] The product B was a 1:2 adduct of isoxazole and the Schiff base. From the IR and NMR spectra, the structure of B was found to be 3-methyl-5-[2-(1,3-dianilino-1,3-diphenyl)propyl]isoxazole (**4**). The yields of **2** and **4** based on the Schiff base, were 31 and 49% respectively. In the presence of butyllithium in dry THF, **1** and *N*-benzylideneaniline also gave **2** and **4** in yields of 15 and 9% respectively.

Similarly, **1** was treated with *N*-benzylidene-*p*-toluidine in the presence of sodium amide in liquid ammonia to give a 1:1 adduct (**5**) and a 1:2 adduct (**6**). However, the reaction of **1** with *N,N'*-bis(*p*-tolyl)-ethylenediimine[5] gave as the sole product a 2:1 adduct, 2,3-di(*p*-toluidino)-1,4-bis(3-methyl-5-isoxazolyl)butane (**7**). In the case of *N*-benzylidenebutylamine, **1** did not react under the condition of either butyllithium in THF or sodium amide in liquid ammonia.

In a previous paper,[1] it was described that 3-methyl-5-*sec*-butylisoxazole was synthesized by the reaction of **1** with an equimolar amount of methyl iodide, followed by a reaction with an equimolar amount of ethyl bromide in the presence of 2 molar amounts of sodium amide. In this reaction, it is suggested that 3-methyl-5-ethylisoxazole anion is formed by the excess sodium amide after the addition of methyl iodide. Therefore, the reaction of **1** with an equimolar amount of benzyl bromide, followed by a reaction with an equimolar amount of *N*-benzylideneaniline, was carried out in the presence of 2 molar amounts of sodium amide. By

1) C. Kashima, S. Tobe, N. Sugiyama, and M. Yamamoto, This Bulletin, **46**, 310 (1973).
2) R. G. Micetich, *Can. J. Chem.*, **48**, 2006 (1970).
3) H. Kano, I. Adachi, Y. Kido, and K. Hirose, Japan, 9145 (1967).
4) N. Sugiyama, M. Yamamoto, and C. Kashima, This Bulletin, **42**, 1357 (1969).
5) J. M. Kliegman and R. K. Barnes, *J. Org. Chem.*, **35**, 3140 (1970).

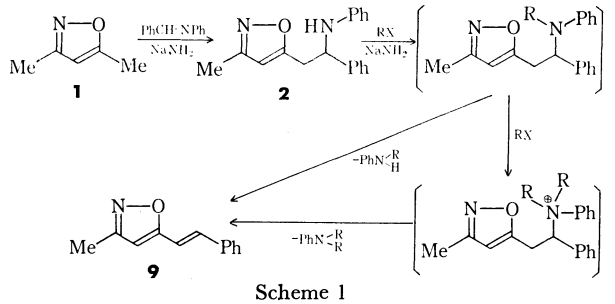

Scheme 1

this reaction, 3-methyl-5-[2-(1-anilino-1,3-diphenyl)-isoxazole (**8**) was obtained in a 25% yield. However the reaction of **1** with an equimolar amount of ethyl bromide, followed by a reaction with an equimolar amount of *N*-benzylideneaniline, gave only 3-methyl-5-*n*-propylisoxazole and no amino derivatives. When 3-methyl-5-*n*-propylisoxazole was treated with *N*-benzylideneaniline in the presence of an equimolar amount of sodium amide, the reaction did not occur and the starting materials were recovered. When **1** was treated with an equimolar amount of *N*-benzylideneaniline, followed by a reaction with an equimolar amount of benzyl bromide in the presence of 2 molar amounts of sodium amide, the expected product (**8**) was not obtained. From the NMR and IR spectra and the elemental analysis, the products were found to be **4**, *N*-benzylaniline, *N*,*N*-dibenzylaniline, and 3-methyl-5-styrylisoxazole (**9**). Similarly, the reaction products from **1**, *N*-benzylideneaniline and ethyl bromide were found to be **4**, *N*-ethylaniline, *N*,*N*-diethylaniline, and **9**. These results suggested that the alkylation of **2** occurred on the N atom to give trisubstituted amines and tetrasubstituted ammonium compounds. However, these alkylated compounds were unstable in a basic solution and easily eliminated the amines to produce **9**.

Since the reaction of **1** with benzonitrile catalyzed by butyllithium in ether has been reported to produce 3-methyl-5-benzoylmethylisoxazole (**11**) (mp 72 °C),[2] the reaction of **1** with benzonitrile was reexamined in the presence of sodium amide in liquid ammonia. The resulting residue was directly recrystallized from the *n*-hexane–benzene mixture. From the spectral data and the elemental analysis, the structure of the product

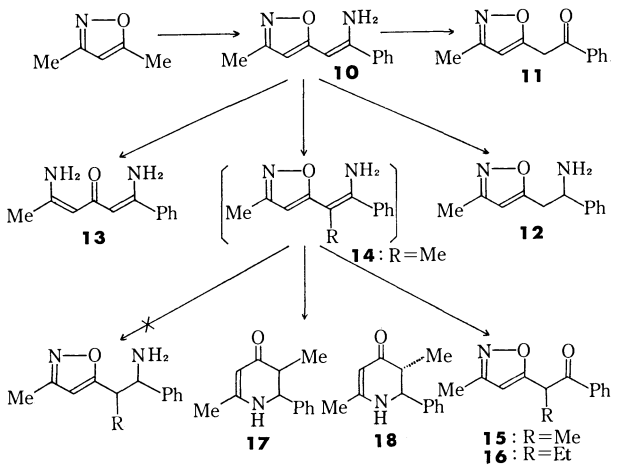

Scheme 2

was deduced to be 3-methyl-5-(2-aminostyryl)isoxazole (**10**). By passing through the silica gel column, **10** was easily hydrolyzed to give **11**, which was identified by a mixed-melting-point determination with an authentic sample and the spectral data. When **10** was reduced with sodium borohydride in methanol, the enamino group of **10** was selectively reduced to give 3-methyl-5-(2-amino-2-phenylethyl)isoxazole (**12**). By the hydrogenation on platinum oxide in ethanol, the isoxazole ring was cleaved, but the enamino group was not reduced. The product was deduced to be 1-phenyl-1,5-diaminohexa-1,4-dien-3-one (**13**), on the basis of the spectral data and the elemental analysis.

Furthermore, **10** was expected to alkylate on either the N atom or the C atom of the enamino group. For determining the alkylation site, **1** was treated with an equimolar amount of benzonitrile, followed by a reaction with an equimolar amount of methyl iodide in the presence of 2 molar amounts of sodium amide. Since the purification of the product (**14**) failed, the mixture was hydrolyzed by passing through a silica gel column. Thereby, 3-methyl-5-(1-benzoylethyl)-isoxazole (**15**), the C-alkylated product, was obtained. Similarly, 3-methyl-5-(1-benzoylpropyl)isoxazole (**16**) was obtained from **1**, benzonitrile, and ethyl bromide. However, it was impossible to detect the *N*-alkylated product by this method. Thus, the hydrogenation of **14** with palladium on charcoal was carried out to give two products. By a study of the IR and NMR spectra and the elemental analysis, the structures of these products were determined to be *cis*- (**17**) and *trans*-2-phenyl-3,6-dimethyl-2,3-dihydro-4(1*H*)pyridone (**18**): no *N*-alkylated products could be detected. These results showed that the *N*-alkylation of enamine (**10**) did not occur, and also that **14** was hydrogenated at the enamino group and then at the isoxazole ring.

In conclusion, the synthesis of 3-methyl-5-(2-amino-alkyl)isoxazoles was accomplished by the reaction of **1** with Schiff bases in the presence of sodium amide, or by the reaction of **1** with benzonitrile, followed with a hydride reduction.

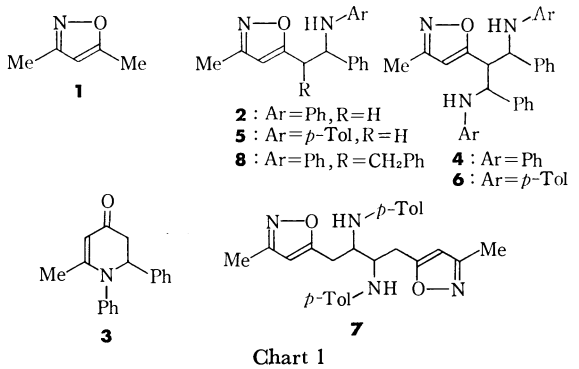

Chart 1

Experimental

The General Procedure. *a) By the Use of Sodium Amide in Liquid Ammonia*: To a sodium amide suspension, which has been prepared from sodium (0.01 mol) and liquid ammonia (*ca.* 50 ml) in the presence of ferric chloride, **1** (0.01 mol) in anhydrous ether (15 ml) was added. After stirring for 1 hr under a nitrogen stream at −50 °C, the Schiff base (0.01 mol)

was added; stirring was then continued for another 2 hr at −50 °C. The mixture was subsequently neutralized with ammonium chloride, and the ammonia was removed at room temperature. To the residual ether solution, dichloromethane was added. The dichloromethane solution was washed with aqueous sodium chloride and dried over anhydrous sodium sulfate. After the removal of the solvent, the residue was purified by recrystallization and/or silica gel column chromatography.

b) By the Use of Butyllithium: To a solution of **1** (0.01 mol) in dry THF (30 ml), an *n*-hexane solution (20%) of butyllithium (0.01 mol) was added at −40 °C. The mixture was stirred for 1 hr under nitrogen. After the addition of the Schiff base (0.01 mol), the stirring was continued for another 4 hr at −40 °C. The solution was then warmed to room temperature and washed with water. The aqueous layer was extracted with dichloromethane. The combined organic layer was dried over anhydrous sodium sulfate and concentrated. The residue was then purified as above.

3-Methyl-5-[2-(1,3-dianilino-1,3-diphenyl)propyl]isoxazole (4): Purified by recrystallization from chloroform; mp 236 °C; yield, 49%. IR (KBr): 3400, 1605, 1500, 745, 695, and 685 cm^{-1}. UV: λ_{max}^{EtOH} 246 (ε 25200) and 295 nm (3600). NMR δ_{CDCl_3} 2.14 (s, 3H), 3.3 (m, 1H), 4.55 (broad s, 2H), 5.07 (m, 2H), 5.63 (s, 1H) and 7.3—6.35 ppm (m, 10H). Found: C, 81.28; H, 6.35; N, 8.69%. Calcd for $C_{31}H_{29}N_3O$: C, 81.08; H, 6.36; N, 9.14%.

3-Methyl-5-(2-anilino-2-phenylethyl)isoxazole (2): The mother solution in the crystallization of **4** was concentrated and recrystallized from *n*-hexane; mp 113 °C; yield, 31%. IR (KBr): 3320, 1600, 1525, 1495, 745, 700, and 690 cm^{-1}. UV: λ_{max}^{EtOH} 247 (ε 14100) and 297 nm (2390). NMR: δ_{CDCl_3} 2.20 (s, 3H), 3.17 (d, J=7 Hz, 2H), 3.95 (broad s, 1H), 4.70 (t, J=7 Hz, 1H), 5.70 (s, 1H), 7.3—6.36 (m, 5H) and 7.27 ppm (s, 5H). Found: C, 77.46; H, 6.52; N, 10.10%. Calcd for $C_{18}H_{18}N_2O$: C, 77.67; H, 6.52; N, 10.07%.

3-Methyl-5-(2-p-toluidino-2-phenylethyl)isoxazole (5): This was purified by silica gel column chromatography with a benzene ethyl acetate mixture, and the eluate was recrystallized from an *n*-hexane benzene mixture; mp 117 °C; yield, 13%. IR (KBr): 3300, 1615, 1600, 1525, 815 and 805 cm^{-1}. UV: λ_{max}^{EtOH} 249 (ε 14000) and 306 nm (2300). NMR: δ_{CDCl_3} 2.18 (s, 3H), 2.21 (s, 3H), 3.17 (d, J=7 Hz, 2H), 3.4 (broad s, 1H), 4.68 (t, J=7 Hz, 1H), 5.70 (s, 1H), 7.0—6.3 (AB-q, J=9 Hz, 4H) and 7.27 ppm (s, 5H). Found: C, 78.21; H, 7.13; N, 9.58%. Calcd for $C_{19}H_{20}N_2O$: C, 78.05; H, 6.90; N, 9.58%.

3-Methyl-5-[2-(1,3-di-p-toluidino-1,3-diphenyl)propyl]isoxazole (6): This was purified by silica gel column chromatography with a benzene–ethyl acetate mixture, and the eluate was recrystallized from an ethyl acetate–ethanol mixture; mp 167 °C; yield, 56%. IR (KBr): 3350, 1610, 1510, 805, and 700 cm^{-1}. UV: λ_{max}^{EtOH} 249 (ε 27200) and 304 nm (3600). NMR: δ_{CDCl_3} 2.15 (s, 9H), 3.7 (m, 1H), 4.1 (broad s, 2H), 5.0 (m, 2H), 5.68 (s, 1H) and 7.3—6.3 ppm (m, 18H). Found: C, 81.05; H, 6.94; N, 8.45%. Calcd for $C_{33}H_{33}N_3O$: C, 81.28; H, 6.82; N, 8.62%.

2,3-Di(p-toluidino)-1,4-bis(3-methyl-5-isoxazolyl)butane (7): This was purified by silica gel column chromatography with a benzene–ethyl acetate mixture, and the eluate was recrystallized from benzene; mp 153 °C; yield, 66%. IR (KBr): 3400, 1610, 1515, 810, and 790 cm^{-1}. UV: λ_{max}^{EtOH} 253 (ε 31700) and 304 nm (4170). NMR: δ_{CDCl_3} 2.22 (s, 6H), 2.25 (s, 6H), 3.1 (m, 6H), 3.85 (broad s, 2H), 5.80 (s, 2H) and 7.1—6.4 ppm (AB-q, J=9 Hz, 8H). Found: C, 72.51; H, 7.13; N, 12.81%. Calcd for $C_{26}H_{30}N_4O_2$: C, 72.53; H, 7.02; N, 13.01%.

The Reaction of 1 with Alkyl Halide, Followed by the Reaction with N-Benzylideneaniline. To a sodium amide (0.02 mol) suspension in liquid ammonia (50 ml) an ether (15 ml) solution of **1** (0.01 mol) was added. After stirring for 1 hr at −50 °C, alkyl halide (0.01 mol) in ether (10 ml) was added. The mixture was then stirred for another 2.5 hr. *N*-Benzylideneaniline (0.01 mol) was then added to the mixture, and it was stirred for another 2.5 hr. After neutralization with ammonium chloride, the reaction mixture was treated by the general method.

3-Methyl-5-[2-(1-anilino-1,3-diphenyl)propyl]isoxazole (8): The eluate of silica gel chromatography was concentrated and recrystallized from *n*-hexane; mp 133 °C; yield, 25%. IR (KBr): 3400, 1605, 1505, 1490, 790 and 695 cm^{-1}. UV: λ_{max}^{EtOH} 248 (ε 14700) and 296 nm (2300). NMR: δ_{CDCl_3} 2.10 (s, 3H), 3.13 (d, J=6 Hz, 2H), 3.44 (t, J=6 Hz, 1H), 4.3 (broad s, 1H), 4.68 (d, J=6 Hz, 1H), 5.41 (s, 1H) and 7.3—6.35 ppm (m, 15H). Found: C, 81.73; H, 6.80; N, 7.54%. Calcd for $C_{25}H_{24}N_2O$: C, 81.49; H, 6.57; N, 7.60%.

The Reaction of 1 with N-Benzylideneaniline, Followed by Alkylation. To a sodium amide (0.02 mol) suspension in liquid ammonia (50 ml) an ether solution of **1** (0.01 mol) was added. After the mixture had been stirred for 1 hr at −50 °C, *N*-benzylideneaniline (0.01 mol) was added to the mixture, after which it was stirred for another 2.5 hr. To the mixture alkyl halide (0.01 mol) in ether (10 ml) was then added. The stirring was continued for another 2.5 hr. After a usual work-up, the products were compared with authentic samples.

3-Methyl-5-styrylisoxazole (9): Mp 91.5 °C; yield 23%. IR (KBr): 1645, 1580, 1565, 1410, 965, 795, 760, and 695 cm^{-1}. UV: λ_{max}^{EtOH} 222 (ε 8900), 227 (9900), 234 (7600) and 301 nm (30100). NMR: δ_{CCl_4} 2.25 (s, 3H), 5.96 (s, 1H), 7.35—6.6 (AB-q, J=16 Hz, 2H) and 7.5—7.1 ppm (m, 5H). Found: C, 77.75; H, 6.18; N, 7.36%. Calcd for $C_{12}H_{11}NO$: C, 77.81; H, 5.99; N, 7.56%.

The Hydrogenation of 2. An ethanol (30 ml) solution of **2** was hydrogenated with platinum oxide (6.0 mg) for 15 hr. After the subsequent removal of the catalyst and the solvent, the residue was chromatographed on silica gel with a benzene–ethyl acetate mixture. The products were identified by comparison with authentic samples.

3-Methyl-5-(2-aminostyryl)isoxazole (10). To a sodium amide (0.01 mol) suspension in liquid ammonia (*ca.* 50 ml) **1** (0.01 mol) in dry ether (15 ml) was added. After stirring for 1 hr at −60 °C, the ether solution (10 ml) of benzonitrile (0.01 mol) was added. The stirring was then continued for another 2 hr. After a usual work-up, the residue was recrystallized from an *n*-hexane–benzene mixture; mp 85 °C; yield, 49%. IR (KBr): 3500, 3400, 1630, 1610, 1580, 975, 810, 770, 745 and 695 cm^{-1}. UV: λ_{max}^{EtOH} 230 (ε 9600) and 331 nm (18800). NMR: δ_{CDCl_3} 2.25 (s, 3H), 5.15 (broad s, 2H), 5.34 (s, 1H), 5.79 (s, 1H) and 7.7—7.2 ppm (m, 5H). Found: C, 72.07; H, 6.23; N, 14.19%. Calcd for $C_{12}H_{12}N_2O$: C, 71.98; H, 6.04; N, 13.99%.

3-Methyl-5-benzoylmethylisoxazole (11). **10** was passed through a silica gel column with a benzene–ethyl acetate mixture; the eluate was then concentrated, and the residue was recrystallized from an *n*-hexane–benzene mixture; yield, 95%. The product was identified by comparison with an authentic sample.

3-Methyl-5-(2-amino-2-phenylethyl)isoxazole (12). To **10** (500 mg) in methanol (20 ml) was added sodium borohydride (136 mg) at room temperature. The mixture was then stirred for 20 hr. The resulting residue was distilled; bp 174—180 °C/6 mmHg; yield, 27%. IR (liquid film): 3350, 3300, 1605, 800, and 700 cm^{-1}. NMR: δ_{CCl_4} 1.6 (broad s, 2H),

2.17 (s, 3H), 2.90 (d, J=7 Hz, 2H), 4.22 (t, J=7 Hz, 1H), 5.65 (s, 1H) and 7.20 ppm (s, 5H). Found: C, 70.63; H, 7.27; N, 13.49%. Calcd for $C_{12}H_{14}N_2O$: C, 71.26; H, 6.98; H, 13.85%.

*1-Phenyl-1,5-diaminohexa-1,4-dien-3-one (**13**).* The ethanol (10 ml) solution of **10** (237 mg) was hydrogenated on platinum oxide (4.6 mg). After the removal of the catalyst and the solvent, the residue was recrystallized from an *n*-hexane–benzene mixture; mp 129 °C; yield, 56%. IR (KBr): 3400, 1630, 1535, 1305, 1150, 960, 800, 770 and 685 cm^{-1}. UV: λ_{max}^{EtOH} 240 (ε 10300), 265 (6200) and 375 nm (19700). NMR: δ_{CDCl_3} 1.89 (s, 3H), 4.90 (s, 1H), 5.18 (s, 1H), 8.0—6.0 (broad s, 4H, disappeared by D_2O exchange) and 7.6—7.1 ppm (m, 5H). Found: C, 71.30; H, 7.06; N, 13.82%. Calcd for $C_{12}H_{14}N_2O$: C, 71.26; H, 6.98; N, 13.85%.

*The Reaction of **1** with Benzonitrile, Followed by Alkylation.* To a sodium amide (0.015 mol) suspension in liquid ammonia (*ca.* 50 ml) **1** (0.01 mol) in dry ether (15 ml) added. After the mixture had been stirred for 1 hr at −60 °C, an ether solution (15 ml) of benzonitrile (0.01 mol) was added; the stirring was then continued for 1 more hr. After the addition of alkyl halide (0.01 mol) in ether (15 ml), the stirring was continued for another 2 hr at −60 °C. After a usual work-up, the resulting residue was passed through a silica gel column with benzene–ethyl acetate and the product was recrystallized from an *n*-hexane–benzene mixture.

*3-Methyl-5-(1-benzoylethyl)isoxazole (**15**)*: Yield, 7%; mp 48 °C. IR (liquid film): 1685, 1605, 980, 800, and 690 cm^{-1}. NMR: δ_{CCl_4} 1.49 (d, J=7 Hz, 3H), 2.11 (s, 3H), 4.84 (q, J=7 Hz, 1H), 5.81 (s, 1H) and 8.0—7.2 ppm (m, 5H). Found: C, 72.77; H, 6.14; N, 6.57%. Calcd for $C_{13}H_{13}NO_2$: C, 72.54; H, 6.09; N, 6.51%.

*3-Methyl-5-(1-benzoylpropyl)isoxazole (**16**)*: Yield, 24%; mp 59 °C. IR (KBr): 1685, 1600, 1000, 810, 730, and 690 cm^{-1}. NMR: δ_{CCl_4} 0.96 (t, J=7 Hz, 3H), 2.4—1.7 (m, 2H), 2.20 (s, 3H), 4.65 (t, J=8 Hz, 1H), 5.83 (s, 1H) and 8.1—7.2 ppm (m, 5H). Found: C, 73.40; H, 6.70; N, 6.05%. Calcd for $C_{14}H_{15}NO_2$: C, 73.34; H, 6.59; N, 6.11%.

*The Hydrogenation of **14**.* The crude **14** (529 mg) was hydrogenated with palladium on charcoal (5%, 77 mg) in ethanol (25 ml) at room temperature for 15 hr. After the removal of the catalyst and the solvent, the residue was chromatographed on a silica gel column with a benzene–ethyl acetate mixture. The products were recrystallized from benzene.

cis-*2-Phenyl-3,6-dimethyl-2,3-dihydro-4(1H)pyridone (**17**)*: Mp 168 °C; yield, 14%. IR (KBr): 3220, 1600, 1580, 1525, 1250, 810, 760 and 700 cm^{-1}. NMR: δ_{CDCl_3} 0.85 (d, J=7 Hz, 3H), 2.05 (s, 3H), 2.8—2.0 (m, 1H), 4.80 (d, J=4 Hz, 1H), 4.97 (s, 1H), 5.2 (broad s, 1H) and 7.29 ppm (s, 5H). Found: C, 77.73; H, 7.54; N, 6.91%. Calcd for $C_{13}H_{15}NO$: C, 77.58; H, 7.51; N, 6.96%.

trans-*2-Phenyl-3,6-dimethyl-2,3-dihydro-4(1H)pyridone (**18**)*: Mp 166 °C; yield, 19%. IR (KBr): 3220, 1600, 1580, 1525, 1230, 805, 785, 750, and 690 cm^{-1}. NMR: δ_{CDCl_3} 0.89 (d, J=7 Hz, 3H), 2.00 (s, 3H), 2.52 (m, 1H), 4.21 (d, J=13 Hz, 1H), 4.96 (s, 1H), 5.3 (broad s, 1H) and 7.34 ppm (s, 5H). Found: C, 77.50; H, 7.56; N, 6.89%. Calcd for $C_{13}H_{15}NO$: C, 77.58; H, 7.51; N, 6.96%.

BULLETIN OF THE CHEMICAL SOCIETY OF JAPAN, VOL. 46, 3536—3544 (1973)

Stereochemistry of the C and D Rings of *C*-Nor-*D*-homosteroids. I. The Birch Reduction of "Jervine-11β-ol" and Related Compounds

Akio MURAI, Keiko ARITA, and Tadashi MASAMUNE

Department of Chemistry, Faculty of Science, Hokkaido University, Sapporo 060

(Received May 1, 1973)

The Birch reduction of "jervine-11β-ol" (**4**) was reinvestigated in detail. Two unknown (**6** and **7**) and two known compounds (**8** and **9**) with established configurations were newly isolated besides the previously obtained products (**2** and **5**). The main product (**2**), the C_{17} configuration of which has been left undefined, was degraded into a methyl ketone (**18**) *via* a known saturated compound (**14**) (Chart 2) or correlated with an α,β-unsaturated ketone (**23**) (Chart 3). These transformations confirmed the configuration of **2** (C_{17}–H) to be β, since the steric structures of compounds **18** and **23** have been determined in an unambiguous manner. On the other hand, the structures and configurations of **6** and **7** were elucidated as shown by the formulas on the respective spectral data as well as by hydrogenation of **6** to **14** (Chart 4) and by hydrolysis of an 11β-alcohol (**24**=**7a**), obtained by reduction of the ketone **23**, to **7** (Chart 4). These results together with those of the Birch reductions of 11-deoxojervine (**1**) and product **7** are summarized as follows: Products **2**, **6**, **7**, and **9** with the saturated 17-carbon all take the β-hydrogen configuration at C_{17}, products **3** and **5** with the C_{13}–C_{17} double bond the α-hydrogen configuration at C_{12}, and products **8** and **9** with the saturated carbons at C_{13} and C_{17} the β-hydrogen configuration at C_{12}.

The C and D rings of *C*-nor-*D*-homosteroids show a steric behavior differing in many respects from that of normal steroids. The stereochemistry of both rings of the Birch redution products of "jervine-11β-ol" and related compounds involve several unresolved problems. We reported[1] that 11-deoxojervine (**1**) produced two diols (**2**) and (**3**) in 42 and 16% yields, respectively, and "jervine-11β-ol" (**4**) gave one (**2**) of

* Part XX of *C*-Nor-*D*-homosteroids and Related Alkaloids; Part XIX, T. Masamune and T. Orito, This Bulletin, **45**, 1888 (1972).

1) a) T. Masamune, M. Takasugi, and Y. Mori, *Tetrahedron Lett.*, **1965**, 489; b) T. Masamune, K. Kobayashi, M. Takasugi, Y. Mori, and A. Murai, *Tetrahedron*, **24**, 3461 (1968).

the diols and a triol (**5**) in 50 and 5% yields, respectively, by treatment with lithium in ethylamine. However, the C_{17} configuration of the main product **2** remained undefined. Compound **2** is not only an important intermediate in a series of reactions to correlate jervine and veratramine and hence to establish the C_9 configuration of jervine, but also could be a useful intermediate for skeletal transformation of the present *C*-nor-*D*-homosteroids into normal steroids.[2] Thus it became necessary to determine the configuration of **2** and improve its yield. The hydrogenation products of **2**, key substances (**14** and **15**) in the correlation in question, remained undetermined at the configurations at C_{12}, C_{13}, and C_{17}. This led us to reexamine the relevant Birch reduction of **4** and related compounds. We have isolated several compounds including **2** and **5** and elucidated their structures and configurations. The results are described in this paper.

The reduction was carried out under two different conditions; lithium and ethylamine (as in the previous work[1]) and lithium and a 5: 2: 2 mixture of ammonia, dioxane, and tetrahydrofuran. Three new compounds (**6**, **7**, and **8**) were isolated besides **2** and **5** under the former conditions, and two compounds (**6** and **9**) along with **2** and **5** under the latter (see Table). Compounds **5**,[1] mp 217—218 °C, **8**,[3] mp 239.5—241.5 °C, and **9**,[4] mp 234—236 °C, proved to be the known substances with established configurations. The structures and configurations of the other compounds **2**, **6**, and **7** are given in the following sections.

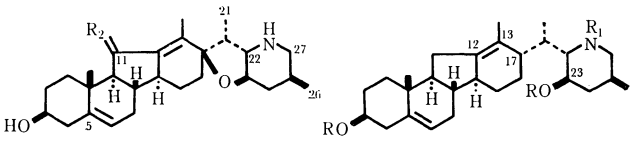

1 $R_2=H_2$
4 $R_2=$–OH,···H
Jervine $R_2=O$

2 $R=R_1=H$
2a $R=R_1=Ac$

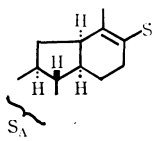

3 $R=R_1=H$

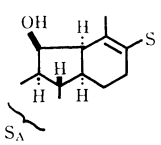

5 $R=R_1=H$

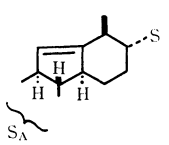

6 $R=R_1=H$
6a $R=R_1=Ac$

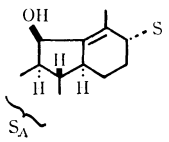

7 $R=R_1=H$
7a (=**24**) $R=R_1=Ac$

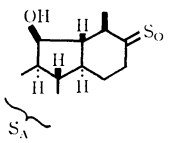

8 $R=R_1=H$

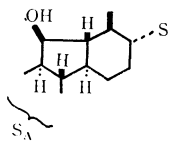

9 $R=R_1=H$

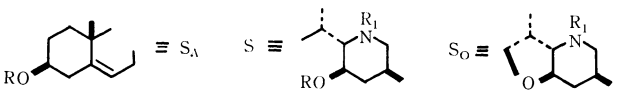

2) *Cf.*, J. M. Coxon, M. P. Hartshown, and D. N. Kirk, *ibid.*, **21**, 2489 (1965).
3) T. Masamune, N. Sato, K. Kobayashi, I. Yamazaki, and Y. Mori, *ibid.*, **23**, 1591 (1967).
4) T. Masamune and K. Orito, *ibid.*, **25**, 4551 (1969).

Table 1. Yields of the Birch reduction products of "jervine-11β-ol" (**4**)

Solvents	Yields (%)[a] of products					
	2a	**5**	**6a**[b]	**7**[b]	**8**[b]	**9**
$EtNH_2$	47[c]	6.1[d]	1.2	1.6	2.2	0
NH_3–dioxane–THF	72	0.06	7.5	0	0	2.4

a) Yields of isolated crystalline products.
b) New compounds.
c) Reported yield (Ref. 1b), 50% as **2**.
d) Reported yield (Ref. 1b), 5%.

Configuration at C_{17} of Compound 2. Compound **2**, mp 194.5—195.5 °C, was isolated *via* the 3-*O*,23-*O*,*N*-triacetyl derivative (**2a**), mp 195—197 °C, since it showed the same R_f value as **6**. **2** was subjected to degradation in the same way as Johnson's fragmentation;[5] namely, **2** was converted with *N*-chlorosuccinimide (NCS) into the *N*-chloro derivative, which on treatment with sodium methoxide and then with acid gave an aldehyde (**10**), ν_{max} 2710 and 1720 cm^{-1}, and τ 0.25 (1H, broad singlet, CHO) and 9.10 (3H, doublet with J=7 Hz, 21-Me). The aldehyde, extremely unstable in the air, was further degraded, with *n*-butyl nitrite and sodium methoxide, to an oxime (**11**), mp 161—164 °C, in 61% yield from **2**, whose NMR spectrum displayed a broad signal with W_H= *ca.* 20 Hz at τ 7.04 due to the C_{17} proton. The oxime, when treated with sodium bisulfite in refluxing ethanol[6] and then with hydrochloric acid afforded a multicomponent mixture,[7] from which two products (**12**), mp 141—142.5 °C, and (**13**), mp 167.5—169 °C, were isolated in 10 and 36% yields. The former, which gave the monoacetate (**12a**), mp 119.5—120 °C, was assigned structure **12** on the basis of the mass (*m/e* 272, M^+), IR (no C=O absorption) and NMR spectra (no sharp peaks except two singlets at τ 9.04 and 8.44 due to 19- and 18-Me in the higher field, and only one C_6 olefinic proton signal at τ 4.65 in the lower field). Formation of **12** would be tentatively rationalized by assuming partial isomerization of the C_{12}–C_{13} double bond of **13** or **11** to the C_{13}–C_{17} position, hydration, retro-Claisen reaction and remigration of the resulting C_{13}–C_{17} double bond. On the other hand, the major product **13** was identified as the expected compound formed by simple hydrolysis of the oxime **11**. In accordance with the assigned structure, the mass spectrum (*m/e* 314, M^+) indicated a molecular formula $C_{21}H_{30}O_2$, and the IR and NMR spectra exhibited the presence of a C_{17} acetyl substituent (ν_{max} 1695 cm^{-1} and τ 7.91, singlet) and a 18-methyl group attached to the C_{12}–C_{13} double bond (τ 8.48, singlet). The NMR spectrum (τ 6.90, a broad signal with W_H= *ca.* 23 Hz)[4] and the ORD curve (a large positive

5) R. W. Franck and W. S. Johnson, *Tetrahedron Lett.*, **1963**, 545; R. W. Franck, G. P. Rizzi, and W. S. Johnson, *Steroids*, **4**, 463 (1964).
6) *Cf.*, S. H. Pines, J. M. Chemerda, and M. A. Kozlowski, *J. Org. Chem.*, **31**, 3446 (1966).
7) *Cf.*, a) T. Masamune, K. Orito, and A. Murai, This Bulletin, **39**, 2503 (1966); b) S. M. Kupchan, T. Masamune, and G. W. A. Milne, *J. Org. Chem.*, **29**, 755 (1964).

Cotton effect, $a=+279°$)[8] indicated the C_{17} hydrogen to possess the β-configuration. Furthermore, on treatment of **13** with alkali in refluxing methanol, most of the starting material remained unchanged with no configurational change at C_{17}, supporting the 17β-hydrogen, while isomerization of the C_{12}–C_{13} double bond occurred only partially (less than 20%). This would be caused by serious steric interaction between 18- and 21-methyl groups with the resulting α,β-unsaturated 20-ketone.[9] However, in view of the low yield of **13** as well as of the difficult derivation of **13** to a known compound,[10] it became desirable to determine the relevant configuration more clearly. The low yield in the hydrolysis of oxime **11** was expected to be improved by saturation of the C_{12}–C_{13} double bond.

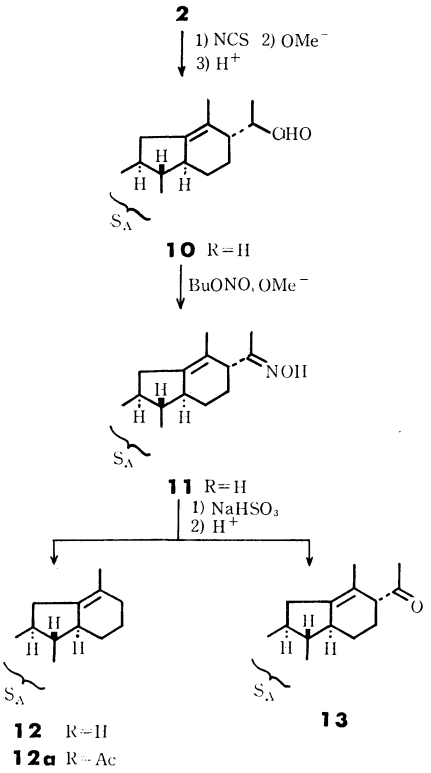

Chart 1

Hydrogenation of **2** over prereduced rhodium-platinum oxide (3: 1) catalyst[11] in acetic acid proceeded smoothly, two moles of hydrogen being consumed within 1 hr, and produced a single product (**14**),[12] mp 185.5—186 °C, in 76% yield. It would be very improbable that migration of the C_{12}–C_{13} double bond occurred during the facile hydrogenation, because the same hydrogenation over only platinum required a long time (21—90 hr) for absorption of 2 mol of hydrogen and afforded a 36% yield of the isomeric compound (**15**),[13] mp 183—185 °C, along with **14**. Isomer **15** would probably be formed by migration of the C_{12}–C_{13} double bond to C_{13}–C_{17} followed by hydrogenation. While these products had already been prepared,[1] their configurations have been left undetermined. Thus, compound **14** was degraded in the same manner as **2** and converted into an oxime (**17**), mp 174—176 °C, *via* an aldehyde (**16**), amorphous, ν_{max} 2710 and 1723 cm^{-1}, and τ 0.35 (1H, singlet). Mild hydrolysis[6] of **17** afforded the corresponding methyl ketone, mp 135—137 °C, ν_{max} 1699 cm^{-1} and τ 7.89 (3H, singlet), in high yield from **14**, which proved to be identical with a known compound (**18**) with established configurations (17β-H).[14] Likewise, compound **15** was converted into the corresponding methyl ketone (**21**), mp 70—72 °C and ν_{max} 1704 cm^{-1}, in good yield, *via* an aldehyde (**19**) and an oxime (**20**). This ketone **21** displayed a broad peak with W_H=22 Hz at τ 6.40 due to the C_3 proton in the NMR spectrum, indicative of the A/B *trans*-fused linkage. It was stable against alkali (no epimerization at C_{17}) but differed from a well-defined compound (**22**)[15] prepared from jervine. On the basis of the *cis*-addition of hydrogen to double bonds[16] and the chemical shifts of 19-Me protons

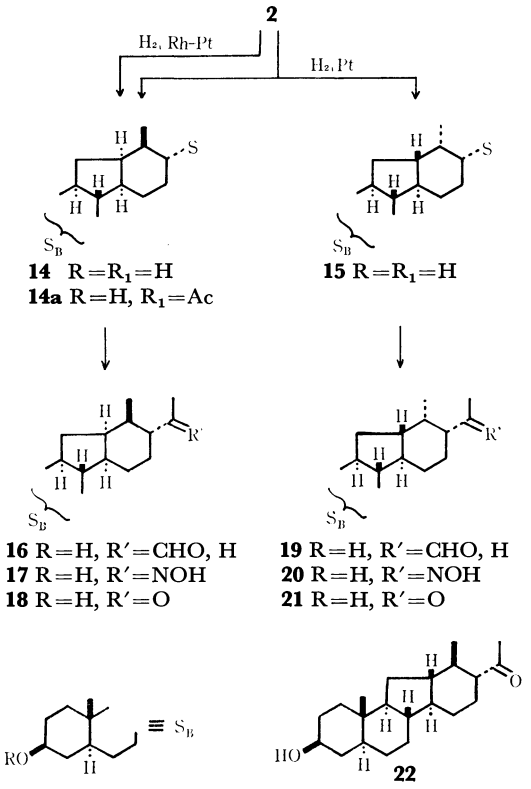

Chart 2

8) *Cf.*, K. Mislow, M. A. W. Glass, R. E. O'Brien, P. Rutkin, D. H. Steinberg, and C. Djerassi, *J. Amer. Chem. Soc.*, **82**, 4740 (1960); K. Mislow and J. G. Berger, *ibid.*, **84**, 1956 (1962); K. Mislow, M. A. W. Glass, R. E. O'Brien, P. Rutkin, D. H. Steinberg, J. Weiss, and C. Djerassi, *ibid.*, **84**, 1455 (1962).

9) *Cf.*, K. G. Lewis and G. J. Williams, *Tetrahedron Lett.*, **1965**, 4573.

10) H. Mitsuhashi and K. Shibata, *Tetrahedron*, **21**, 1215 (1965).

11) S. Nishimura, This Bulletin, **33**, 566 (1960).

12) Identified as compound X in Ref. 1b, p. 3468; reported mp 185—187 °C.

13) Identified as compound X' in Ref. 1b, p. 3468; reported mp 184—186 °C.

14) a) H. Suginome, N. Sato, and T. Masamune, *Tetrahedron Lett.*, **1969**, 2671; b) N. Sato, Ph. D. Thesis, Hokkaido University, Sapporo, Japan, 1969.

15) A. Murai, T. Nishimura, and T. Masamune, unpublished results.

16) T. Masamune, A. Murai, K. Orito, H. Ono, S. Numata, and H. Suginome, *Tetrahedron*, **25**, 4853 (1969).

(τ 9.26, probably *trans* C/D linkage),[17] compound **15** would possibly be formulated as structure **15**. Thus, these findings confirmed the conclusion (17β-H) in the preceding section.

Further confirmation could be obtained by correlating **2** with a compound (**23**)[18] with unambiguous configurations,[4] prepared readily from jervine by a three-step process. Reduction of **23** with sodium borohydride in refluxing dioxane followed by acetylation of the product afforded a multi-component mixture, from which three compounds were isolated by preparative tlc. One, mp 213—215 °C, isolated in 14% yield, could be assigned to formula **24** on the spectral data, ν_{max} 3570 cm^{-1} and τ 8.74 (singlet, 19-Me)[17] and 8.23 (singlet, 18-Me). Compound **24** was converted by oxidation with chromic anhydride in pyridine into the original ketone **23a**, indicative of retention of the C_{17} configuration during the course of sodium borohydride reduction. Treatment of **24** with lithium in ethylamine and subsequent acetylation resulted in formation of **2a** in 74% yield, establishing the configuration in question to be β. Incidentally, the other two compounds resisted crystallization, but mild hydrolysis effected formation of two crystalline *N*-acetyl compounds, mp 248—251 °C and 241—242 °C. These could be inferred to possess structures **25** and **26**, but were not further examined.

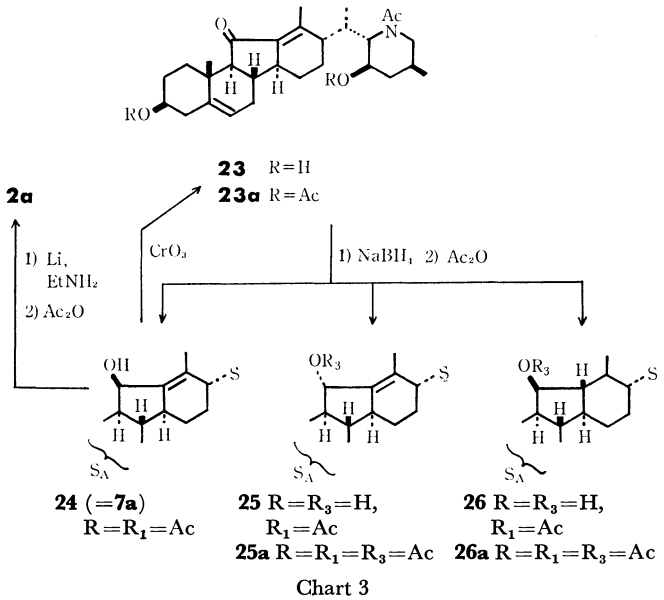

Chart 3

Structure and Configuration of Compound 6. This compound could be isolated as the 3-*O*,23-*O*,*N*-triacetyl derivative (**6a**), mp 173—174 °C, which on hydrolysis gave **6**, mp 229—231.5 °C. Compound **6a**, $C_{33}H_{49}O_5N$, exhibited a parent peak at *m/e* 539 and a broad singlet with W_H=9 Hz at τ 4.62 due to two olefinic protons in the mass and NMR spectra. These indicated the compound to be an isomer of **2a** and to be formulated most favorably as structure **6a**. In fact, **6a** was produced by a modification of the Huang-Minlon procedure[19] for the Wolff-Kishner reduction of **23** followed by acetylation in 45% yield along with **2a** (30%), and also obtained by treatment of **24** with lithium in a 5:2:2 mixture of ammonia–dioxane–tetrahydrofuran and subsequent acetylation in 12% yield. The reduction of **24** with lithium in ethylamine gave no detectable amount of **6**. These transformations confirmed not only a planar structure of **6** but also the β-configuration at C_{17}. On the other hand, hydrogenation of **6a** over rhodium-platinum[11] in acetic acid for 2 hr led to saturation of the compound and, after hydrolysis, formation of the *N*-acetyl compound, mp 180—182 °C and ν_{max} 1641 cm^{-1}, which was identical with a compound (**14a**), mp 180.5—182.5 °C, obtained by triacetylation of **14** followed by partial hydrolysis. These results indicate that the hydrogen at C_{13} possesses α-configuration, since migration of the C_{11}–C_{12} double bond would be very improbable during the course of hydrogenation. On the basis of these configurational assignments, the Wolff-Kishner reduction would be rationalized by assuming that it proceeds by path B[20] (Chart 4) and is completed by axial approach of the proton source to the C_{13}, as elaborated by Zimmerman[21] in many examples of reketonization of enols.

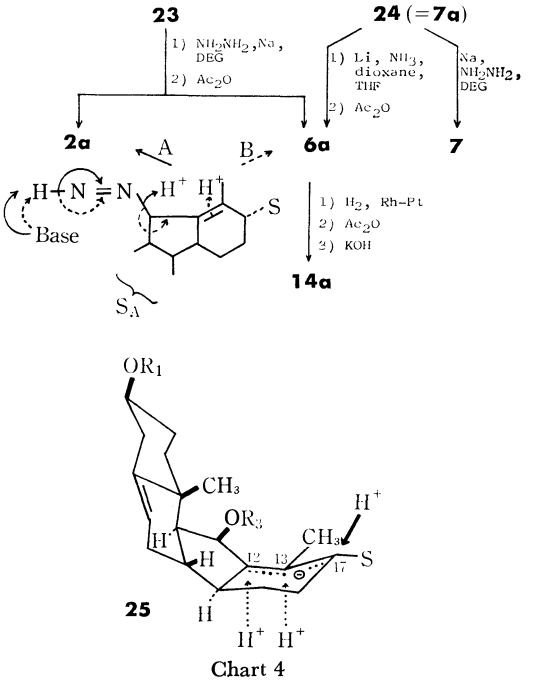

Chart 4

Structure and Configuration of Compound 7. The compound was analyzed for $C_{27}H_{43}O_3N$ and showed peaks at *m/e* 429, 141, and 114 in the mass spectrum. The spectrum not only supported the molecular formula but also indicated cleavage of the C_{17}–O ether bond,

17) T. Masamune, *Nippon Kagaku Zasshi*, **91**, 407 (1970).

18) T. Masamune, M. Takasugi, M. Gohda, H. Suzuki, S. Kawahara, and T. Irie, *J. Org. Chem.*, **29**, 2282 (1964).

19) *Cf.*, D. H. R. Barton, D. A. J. Ives, and B. Thomas, *J. Chem. Soc.*, **1956**, 2056.

20) a) T. Masamune, Y. Mori, M. Takasugi, and A. Murai, *Tetrahedron Lett.*, **1964**, 913; b) T. Masamune, Y. Mori, M.Takasugi, A. Murai, S. Ohuchi, N. Sato, and N. Katsui, This Bulletin, **38**, 1374 (1965).

21) H. E. Zimmerman and A. Mais, *J. Amer. Chem. Soc.*, **81**, 4305 (1956), and their previous papers.

suggesting formula **7**. Thus **24** was hydrolyzed for 17 hr under the conditions of a modified Huang-Minlon procedure.[19] The product was identical with **7**, confirming the structure and configuration of compound **7**.

Summary of Results. The results of the Birch reduction of **4** and **7a** (=**24**), together with those of **1**,[1] are summarized as follows. Apart from compound **8**, all C_{17}-saturated compounds **2**, **6**, **7**, and **9** take the β-hydrogen configuration at C_{17}, while compounds **3** and **5** with the C_{13}–C_{17} double bond possess the α-hydrogen at C_{12}. As shown with simpler model compounds,[22] these results would probably be caused by the continued maximum overlap[21,23] between the π-orbitals at C_{12}, C_{13}, and C_{17} of reduction carbanion intermediates such as **25**, on approach of the proton sources.[22] It is to be noted that saturated compounds **8** and **9** were formed, resulting from reduction of isolated double bonds under the Birch conditions. Moreover, the fact that **8** and **9** adopt the β-hydrogen configuration at C_{12} can be well interpreted, considering the results of the Birch reduction[4] of **23** as well as *trans*-hydrogenation[16] of jervine over platinum in acetic acid leading to the corresponding 12β,13α-dihydro compounds, since protonation at C_{12} of the respective reaction intermediates, C_{12}–C_{13} anion radical or dianion formed from **4** *via* the relevant double bond and 11-en-11-ol or 11-en-11-olate from **23** and jervine, wound proceed in the same manner as reketonization of enols.[21]

Experimental

All the mps were measured in sealed capillaries and uncorrected. The homogenity of each compound was always checked by tlc on silica gel (Wakogel B-5) using various solvent systems, and the spots were developed with ceric sulfate in dil. sulfuric acid and/or iodine. The optical rotations, ORD curves, and IR spectra were measured in chloroform, methanol, and Nujol, respectively, unless otherwise stated. The NMR spectra were obtained in deuterochloroform at 60 and/or 100 MHz, and the chemical shifts were given in τ-values, TMS being used as an internal reference. Abbreviations "s, d, t, m, br, and sh" in the NMR and IR spectra denote "singlet, doublet, triplet, multiplet, broad and shoulder," respectively.

Birch Reduction of "Jervine-11β-ol" (4) with Lithium in Ethylamine (cf. Ref 1b). To **4** (800 mg) dissolved in refluxing anhydrous ethylamine (31 ml) was added finely divided lithium metal (647 mg), and the mixture was refluxed under vigorous stirring for 2.5 hr. After addition of ammonium chloride, the mixture was warmed to remove the solvent, and the residue mixed with water (50 ml) and extracted with chloroform repeatedly. The chloroform solution was washed with water, dried with anhydrous sodium sulfate and evaporated to leave amorphous residue (974 mg), which showed 5 spots on tlc and was separated by preparative tlc, using a 10: 1 mixture of ether and methanol and 46 plates; each was made of silica gel (Wakogel B-5, 10 g) with an area of 20 cm by 20 cm.

Each fraction was extracted with methanol, and the solution evaporated below 50 °C. The residue was again dissolved in chloroform, washed with a 5% sodium bicarbonate solution and water, treated with active charcoal, dried and evaporated. The most mobile fraction (90 mg), amorphous, showed a parent peak at *m/e* 413 in the mass spectrum but was not further examined. The second fraction (502 mg) was treated with acetic anhydride (11 ml) and pyridine (11 ml) at room temperature for 17 hr. After removal of the solvents, the residue was treated with water and chloroform, and the chloroform solution was washed with 1M hydrochloric acid, a 5% sodium bicarbonate solution and water, dried and evaporated to leave amorphous substance (733 mg), which partially crystallized on trituration with aqueous methanol. The crystalline material was collected by filtration and recrystallized from the same solvent to give 3-*O*,23-*O*,*N*-triacetyl-22,27-imino-17β-jerva-5,12-diene-3β,23β-diol (**2a**, 400 mg), mp 195—197 °C (lit,[1b] 188—190 °C); $[\alpha]_D$ −48.0° (lit,[1b] −12.3° in 95% EtOH); mass, *m/e* 539 (M^+); IR, ν_{max} 1738, 1625, 1239 and 1025 cm^{-1}; NMR τ 9.23 and 8.84 (each 3H, d, J=6.5 and 7 Hz, 21- and 26-Me or *vice versa*), 9.05 (3H, s, 19-Me), 8.50 (3H, s, 18-Me), 7.99 (6H, s, $OCOCH_3$), and 7.89 (3H, s, $NCOCH_3$) (*cf.*, Ref 1b). On the other hand, the filtrate was evaporated and then separated into two parts by preparative tlc(ether–benzene 1: 2, and 18 plates). Each acetone eluate was worked up as mentioned above, and the more mobile fraction (41 mg) crystallized on trituration with isopropyl ether and was recrystallized to yield 3-*O*,23-*O*,*N*-triacetyl-22,27-imino-17β-jerva-5,11-diene-3β,23β-diol (**6a**, 12 mg), mp 173—174 °C; $[\alpha]_D$ −28.5°; mass, *m/e* 539 (M^+); IR, ν_{max} 1740, 1637, 1240, 1040, and 1025 cm^{-1}; NMR, τ 9.04 (3H, s, 19-Me), and 4.63 (2H, br s W_H=9 Hz, H at C_6 and C_{11}).

Found: C, 73.22; H, 9.34; N, 2.26%. Calcd for $C_{33}H_{49}O_5N$: C, 73.43; H, 9.15; N, 2.60%.

The less mobile fraction (135 mg) crystallized from aqueous methanol, (77 mg), mp 191—194 °C, and was identical with **2a**.

The third, middle fraction (104 mg) was crystallized and recrystallized from methanol–acetone to give 22,27-iminojerva-5,13(17)-diene-3β,11β,23β-triol (**5**, 49 mg), mp 217—218 °C, which was identical with an authentic sample.[1b]

The fourth fraction (62 mg) crystallized on trituration from methanol–acetone, mp 221—225 °C, and was recrystallized from the same solvent to yield 22,27-imino-17β-jerva-5,12-diene-3β,11β,23β-triol (**7**, 13 mg), mp 228—231 °C, which was identical with a compound prepared by hydrolysis of **24** (=**7a**), described later; IR, ν_{max} 3420 and 1046 cm^{-1}.

The least mobile fraction (31 mg) crystallized on trituration with methanol–acetone, mp 235—236 °C, and was recrystallized from the same solvent to afford 22,27-imino-17β,23β-oxidojerv-5-ene-3β,11β-diol (**8**, 17.5 mg), mp 239.5—241.5 °C, which was identical with an authentic specimen.[3]

Birch Reduction of 4 with Lithium and a Mixture of Ammonia, Dioxane, and Tetrahydrofuran (THF). To a suspended mixture of **4** (800 mg) in liquid ammonia (200 ml), dry dioxane (80 ml) and dry THF (80 ml) was added lithium (565 mg), and the mixture was stirred vigorously under reflux for 1 hr. To the refluxing mixture was added dropwise dry ethanol (7.2 ml) for 4 min, when the blue color disappeared. After addition of lithium (315 mg), the mixture was again refluxed under stirring for 15 min and, on addition of dry ethanol (4 ml) for 2 min, became colorless again. After removal of the ammonia, the solvents were evaporated below 50 °C, and the residue was mixed with water (50 ml) and extracted with chloroform repeatedly. The chloroform solution was worked up as mentioned above to give crystalline residue (812 mg), showing 5 spots on tlc. Fractional recrystallizations from

22) T. Masamune, H. Matsue, and M. Fujii, This Bulletin, **45**, 1812 (1972).

23) G. Stork and S. D. Darling, *J. Amer. Chem. Soc.*, **86**, 1761 (1964).

methanol–acetone afforded crystalline material (489 mg), which showed a single spot corresponding to the second fraction in the preceding reduction (run a). All mother liquors were combined and separated into 5 parts by preparative tlc, using a 10: 1 mixture of ether and methanol and 31 plates. The most mobile fraction (14 mg), amorphous, was identical with the corresponding one in run a.

The second fraction (255 mg) was combined with the afore-mentioned crystalline material and acetylated with acetic anhydride (13 ml) and pyridine (13 ml) at room temperature overnight. The product (1018 mg), showing two spots, crystallized on trituration with aqueous methanol and, on recrystallization from the solvent, afforded **2a** (666 mg), mp 192—194 °C. The filtrates were combined and separated by preparative tlc (ether–benzene 1: 2, and 19 plates) and worked up as in run a. The more mobile fraction (109 mg) afforded **6a** (76 mg), mp 168—170 °C (from isopropyl ether), and the less mobile (113 mg) **2a** (62 mg), mp 193—195 °C (from aqueous methanol).

The middle fraction (7 mg) crystallized on trituration with methanol–acetone and was recrystallized from the same solvent to give **5** (0.5 mg), mp 214—215 °C, which was identical with sample **5** in run a in the mass spectrum and R_f value on tlc.

The fourth fraction (41 mg) crystallized on trituration with methanol–acetone (19 mg), mp 234—236 °C.

Recrystallization from the same solvent afforded 22,27-imino-17β-jerv-5-ene-3β,11β,23β-triol (**9**), which was identical with an authentic sample.[4]

The last fraction (19 mg) crystallized on trituration with methanol–acetone, (11 mg) mp 179—180 °C, but was not further examined.

Compound **2a** was hydrolyzed as follows. To diethylene glycol (DEG) (100 ml) with dissolving sodium (3 g) was added anhydrous hydrazine (20 ml), and the solution was refluxed for 30 min. After addition of **2a** (2.06 g), the whole solution was refluxed for 21 hr and then cooled, when the condenser was replaced by a distillation apparatus. The solution was again heated for 30 min, evaporating off the hydrazine, cooled and poured into ice-water (one l), when precipitates separated and were collected by filtration, washed with water repeatedly and dissolved in methanol. The methanol solution was evaporated to leave amorphous substance, which crystallized on trituration with acetone (1.45 g), mp 194—194.5 °C. This was recrystallized for analysis to give **2**, mp 194.5—195.5 °C (lit,[1b] 193—195 °C); $[\alpha]_D$ −70.6° (MeOH) (lit,[1b] −61° in 95% EtOH); mass, *m/e* 413 (M^+); IR, ν_{max} 3385, 3105, 1063, 1039, 888, and 812 cm^{-1}.

Found: C, 78.15; H, 10.51; N, 3.33%. Calcd for $C_{27}H_{43}O_2N$: C, 78.40; H, 10.48; N, 3.39%.

Compound **6a** (101 mg) was hydrolyzed in the same manner as **2a**, using DEG (5 ml), sodium (200 mg), and hydrazine (1 ml). The product crystallized on trituration with acetone, (66 mg), mp 228—229 °C. This was recrystallized for analysis to give **6**, mp 229—231.5 °C; $[\alpha]_D$ −85.0° (MeOH); mass, *m/e* 413 (M^+); IR, ν_{max} 3390, 3130, 1079, 1068, 1039, 890, and 812 cm^{-1}.

Found: C, 77.97; H, 10.46; N, 3.41%. Calcd for $C_{27}H_{43}O_2N$: C, 78.40; H, 10.48; N, 3.39%.

*17α-Acetyletiojerva-5,12-dien-3β-ol 20-oxime (**11**).* To a solution of **2** (5.0 g) in dry THF (250 ml) was added *N*-chlorosuccinimide (NCS) (2.0 g), and the mixture was stirred at room temperature for 2 hr. After removal of the solvent below 28 °C, the residue was mixed with methanol (150 ml). To the suspended mixture was added 2M sodium methoxide in methanol (150 ml) under cooling with an ice-bath in a stream of nitrogen. The mixture was stirred at room temperature for 4.5 hr, when the mixture became homogeneous, and then evaporated below 45 °C. The residue was mixed with water and then with 6M hydrochloric acid (100 ml) under cooling, stirred vigorously at room temperature overnight and filtered. The precipitates were dissolved in chloroform, and the chloroform solution washed with 1M hydrochloric acid, a 5% sodium bicarbonate solution and water, dried and evaporated below 27 °C to leave amorphous 20-aldehyde (**10**, 4.0 g), which showed a single spot; mass, *m/e* 328 (M^+) and 270 (M^+–side chain, CH_3CHCHO); IR, ν_{max} 3600, 3450, 2710, 1720, and 1047 cm^{-1}; NMR, τ 9.10 (3H, d J=7 Hz, 21-Me), 9.01 (3H, s, 19-Me), 8.42 (3H, s, 18-Me), 6.45 (1H, m W_H=26 Hz, H at C_3), 4.65 (1H, br a W_H=9 Hz, H at C_6), and 0.25 (1H, s, CHO).

To a cooled solution of **10** (1.06 g) in methanol (50 ml) were added *n*-butyl nitrite (6 ml) and 1.7M sodium methoxide in methanol (50 ml) under nitrogen, and the solution was allowed to stand in a refrigerator (6 °C) for 14 hr. After removal of the solvents below 39 °C, the residue was mixed with water (30 ml) and acidified to pH 3 by dropwise addition of 6M hydrochloric acid (15 ml) under cooling and stirring, and then extracted with chloroform. The chloroform solution was washed with a 5% sodium bicarbonate solution, dried and evaporated below 30 °C to leave oil, which was purified by preparative tlc (ether–benzene 1: 1, and 35 plates). The main fraction, acetone eluate, was evaporated and redissolved in chloroform, and the solution gave amorphous substance (650 mg), which crystallized on trituration with methanol–isopropyl ether, mp 148—151 °C. Recrystallization from the same solvent afforded an analytical sample of 20-oxime (**11**), mp 161—164 °C; $[\alpha]_D$ +37.3°; IR, ν_{max} 3435, 3255, 1660, and 1054 cm^{-1}; NMR, τ 9.03 (3H, s, 19-Me), 8.53 (3H, s, 18-Me), 8.29 (3H, s, 21-Me), 7.04 (1H, br W_H=20 Hz, H at C_{17}), 6.50 (1H, br W_H=28 Hz, H at C_3), and 4.62 (1H br s, W_H=9 Hz, H at C_6).

Found: C, 76.77; H, 9.85; N, 3.76%. Calcd for $C_{21}H_{31}O_2N$: C, 76.55; H, 9.48; N, 4.25%.

*Etiojerva-5,12-dien-3β-ol (**12**) and 17α-Acetyletiojerva-5,12-dien-3β-ol (**13**).* A solution of **11** (650 mg) in ethanol (35 ml) and water (24.5 ml) containing sodium bisulfite (1.36 g) was refluxed under stirring for 13 hr.[6] After removal of the solvents, the residue was stirred vigorously with 1M hydrochloric acid (70 ml) and chloroform (70 ml) at room temperature for 2 hr. After separation of the chloroform layer, the aqueous solution was extracted with chloroform repeatedly. All the chloroform solutions were combined, washed with 1M hydrochloric acid, a 5% sodium bicarbonate solution and water, dried and evaporated to give amorphous residue (390 mg), showing 6 spots, which was separated by preparative tlc (ether–benzene 1: 2, and 21 plates).

The first, most mobile fraction (66 mg) crystallized on trituration with acetone–isopropyl ether (53 mg), mp 138—139 °C. Recrystallization from isopropyl ether afforded an analytical sample of **12**, mp 141—142.5 °C; $[\alpha]_D$ −68.3°; mass, *m/e* 272 (M^+); IR, ν_{max} 3250 and 1058 cm^{-1} (no C–O absorption); NMR, τ 9.04 (3H, s, 19-Me), 8.44 (3H, s, 18-Me), 8.39 (1H, s, OH, checked by addition of D_2O), 6.47 (1H, br W_H=24 Hz, H at C_3), and 4.65 (1H, br s W_H=10 Hz, H at C_6).

Found: C, 84.02; H, 9.99%. Calcd for $C_{19}H_{28}O$: C, 83.77; H, 10.36%.

Compound **12** (47 mg) was acetylated with acetic anhydride (1 ml) and pyridine (1 ml) at room temperature overnight. After being worked up as usual, the mixture gave crystalline substance (47 mg), which was recrystallized from aqueous acetone to give the monoacetate (**12a**, 27 mg), mp 114—117.5 °C. This was recrystallized from the same solvent for analysis;

mp 119.5—120 °C; $[\alpha]_D$ −83.9°; mass, *m/e* 254 (M^+–AcOH); IR, ν_{max} 1727, 1241 and 1030 (no OH absorption); NMR, τ 9.03 (3H, s, 19-Me); 8.44 (3H, s, 18-Me), 7.96 (3H, s, OCOCH$_3$), 5.39 (1H, septet J=4 Hz, H at C_3), and 4.61 (1H, br.s W_H=12 Hz, H at C_6).

Found: C, 80.05; H, 9.48%. Calcd for $C_{21}H_{30}O_2$; C, 80.21; H, 9.62%.

The second, main fraction (223 mg), crystalline, was recrystallized from acetone–isopropyl ether to yield **13** (198 mg), mp 167.5—168 °C. This was recrystallized from the same solvent for analysis; mp 167.5—169 °C; $[\alpha]_D$ +68.2°; ORD, $[\phi]_{311}^{peak}$ +120°, $[\phi]_{287}$ 0°, $[\phi]_{259}^{trough}$ −159°, a=+279°; mass, *m/e* 314 (M^+); IR, ν_{max} 3456, 1695, and 1065 cm^{-1}; NMR, τ 9.03 (3H, s, 19-Me), 8.48 (3H, s, 18-Me), 8.17 (1H, s, OH, checked by addition of D_2O), 7.91 (3H, s, 21-Me), 6.90 (1H, br W_H=23 Hz, H at C_{17}), 6.48 (1H, br W_H=23 Hz, H at C_3), and 4.64 (1H, br s W_H=9 Hz, H at C_6).
Found: C, 80.46; H, 9.43%. Calcd for $C_{21}H_{30}O_2$: C, 80.21; H, 9.62%.

The third fraction (40 mg), oil, was a mixture of two products having almost the same R_f values; IR ($CHCl_3$), ν_{max} 1644 and 1047 cm^{-1}. Each of the fourth (13 mg) and last (13 mg) fractions showed a single spot on tlc and no C=O absorption maxima. None of these fractions were further examined.

Compound **13** (47 mg) was treated with 5% potassium hydroxide in refluxing methanol (20 ml) for 17 hr under nitrogen. After removal of the solvent, the residue was treated with water and chloroform, and the chloroform solution gave amorphous product (57 mg), showing 2 spots. This was separated by preparative tlc (ether–benzene 1:2, and 3 plates). The main, more mobile crystalline fraction (30 mg), showing practically the same IR spectrum as **13**, was recrystallized from acetone–isopropyl ether to give the starting material (10 mg), mp 164—165 °C. The less mobile fraction (7.5 mg), oil, resisted crystallization and showed the following IR and NMR spectra, but was not further examined; IR ($CHCl_3$), ν_{max} 3580, 3450, 1706, 1644, and 1047 cm^{-1}; NMR, τ 8.98 (3H, s), 8.82 (3H, s), 8.29 (s, OH, checked by addition of D_2O), 7.97 (3H, s, 21-Me), 6.45 (1H, br W_H=25 Hz, H at C_3), and 4.64 (1H, br s W_H=11 Hz, H at C_6). This might be a 13ξ-hydroxyetiojervane derivative with a C/D *cis*-fused linkage.

Hydrogenation of **2**. *22,27-Imino-5α,12α,17β-jervane-3β,23β-diol (**14**) and 22,27-imino-5α,13β,17β-jervane-3β,23β-diol (**15**).*
a) A suspended, 3:1 mixture of rhodium and platinum oxide[11] (1.017 g) in acetic acid (20 ml) was prereduced with hydrogen for 2.7 hr, when 281 ml of hydrogen had been consumed. Compound **2** (2.501 g) in acetic acid (40 ml) was added to the mixture and then hydrogenated for 1 hr, when 286 ml of hydrogen (2.0 mol) had been absorbed. The reaction was further continued for 48 hr but without absorption of hydrogen and, after addition of the prereduced catalyst (217 mg) freshly prepared, for another 24 hr, when only 0.18 mol of hydrogen had been consumed. After filtration of the catalyst and subsequent evaporation of the acetic acid below 67 °C, the residue was mixed with water (10 ml), cooled, basified with 6M ammonium hydroxide (20 ml) to pH over 11, and mixed with chloroform (35 ml). The whole mixture was stirred vigorously at room temperature for 20 hr, when chloroform-addition compounds (3.83 g) remaining suspended between the aqueous and chloroform layers were collected by filtration and dissolved in methanol. The solution was evaporated to leave amorphous residue (2.266 g), showing a single spot, which crystallized on trituration with methanol–acetone (1:1) and was collected by filtration to yield **14** (1.905 g), mp 182.5—184.5 °C. This was identical with compound X[1b] obtained already, and recrystallized from the same solvent for analysis; mp 185.5—186 °C (lit,[1b] 185—187 °C); $[\alpha]_D$ −52.9° (MeOH) (lit,[1b] −28.5° in 95% EtOH); mass, *m/e* 417 (M^+) and 114; IR, ν_{max} 3400, 3285, and 1041 cm^{-1}.

Found: C, 77.68; H, 11.40; N, 3.29%. Calcd for $C_{27}H_{47}O_2N$; C, 77.64; H, 11.34; N, 3.35%.

Compound **14** (102 mg) was heated with acetic anhydride (2 ml) and pyridine (2 ml) at 90 °C for 2 hr. After removal of the solvents by azeotropization with benzene, the residue was refluxed with 5% potassium hydroxide in methanol (10 ml) for 1 hr. The reaction mixture was evaporated and mixed with water, when white precipitates separated out and were collected by filtration. These were washed with water, dried and dissolved in ethyl acetate. On being allowed to stand, the solution gave crystalline material (109 mg), mp 180—181 °C. This was recrystallized from ethyl acetate to give an analytical sample of the *N*-acetyl derivative (**14a**) of **14**, mp 180.5—182.5 °C; $[\alpha]_D$ −10.1° (MeOH); mass, *m/e* 459 (M^+) and 156; IR, ν_{max} 3285, 1641, 1611, 1041, 1030 (sh), and 1023 cm^{-1}; NMR, τ 9.26 (3H, s, 19-Me).

Found: C, 75.61; H, 10.61; N, 2.99%. Calcd for $C_{29}H_{49}O_3N$: C, 75.77; H, 10.64; N, 3.05%.

b) Compound **2** was hydrogenated over platinum in almost the same manner as reported;[1b] **2** (2.50 g) was reduced over prereduced platinum oxide (1.0 g) in acetic acid (55 ml) at room temperature for 47 hr, when 1.6 mol of hydrogen had been absorbed. The reaction was continued for another 47 hr after addition of the catalyst (0.55 g), and 2.1 mol of hydrogen was consumed in all. The mixture was worked up as usual and the product was separated into a chloroform-addition compound (**14**) and a chloroform-soluble fraction. The latter crystallized on trituration with acetone and was recrystallized to give **15**, mp 180—182 °C, which was identical with compound X′ obtained already.[1b] This was recrystallized from acetone for analysis; mp 183—185 °C (lit,[1b] 184—186 °C); $[\alpha]_D$ −7.8°; IR, ν_{max} 3270, 1056, and 1029 cm^{-1}; NMR, τ 9.26 (3H, s, 19-Me).

Found: C, 77.46; H, 11.57; N, 3.24%. Calcd for $C_{27}H_{47}O_2N$: C, 77.64; H, 11.34; N, 3.35%.

*17α-Acetyl-5α,12α-etiojervan-3β-ol 20-Oxime (**17**).* A solution of **14** (1.843 g) in THF (80 ml) was stirred with NCS (722 mg) at room temperature for 1.8 hr and, after removal of the solvent below 27 °C, the residue was dissolved in chloroform (200 ml). The solution was washed with water (3×55 ml), dried and evaporated to leave amorphous residue (2.383 g) after being dried over phosphorus pentoxide. To the cooled residue in methanol (50 ml) was added 2M sodium methoxide in methanol (50 ml) under nitrogen, and the solution was stirred for 2 hr and then concentrated to 20 ml below 35 °C for 50 min. The concentrate was mixed with 6M hydrochloric acid (50 ml) and water (200 ml) under cooling, stirred at room temperature overnight, and then extracted with chloform (4×50 ml). The chloroform solution was washed with water, dried and evaporated below 35 °C to give amorphous 20-aldehyde (**16**, 1.541 g), showing a single spot; IR ($CHCl_3$), ν_{max} 3605, 3420, 2710, 1723, 1067, and 1033 cm^{-1}; NMR, τ 9.20 (3H, s, 19-Me), 9.12 and 9.00 (each 3H, d J=7 Hz, 18- and 21-Me or *vice versa*), 6.39 (1H, m W_H=19 Hz, H at C_3), and 0.35 (1H, s, CHO).

A solution of **16** (1.492 g) in methanol (70 ml) was treated with *n*-butyl nitrite (6 ml) and sodium methoxide, prepared from sodium (2.9 g) and methanol (70 ml), in a refrigerator (0 °C) for 14 hr, acidified to pH 6.0 with concd hydrochloric acid (10.5 ml) under cooling, and allowed to stand for 1 hr. The whole mixture was shaken with water (100 ml) and chloroform (3×100 ml), and the chloroform solution gave

oily residue (1.671 g), which showed a single spot but resisted crystallization; IR ($CHCl_3$), ν_{max} 3600 (BuOH), 3300, 1651, 1066, and 1030 cm^{-1}. A part (45.5 mg) of the residue was purified by preparative tlc (ether–benzene 1:1, and 2 plates). The main fraction was extracted with acetone, and the solution gave crystalline material (32.7 mg), which was recrystallized from acetone–isopropyl ether to yield **17** (24 mg), mp 174—176 °C; $[\alpha]_D$ −80.3°; IR, ν_{max} 3650, 3410, 3250, 1643, 1065, 1036, and 1014 cm^{-1}.

Found: C, 75.55; H, 10.61, N, 4.45%. Calcd for $C_{21}H_{35}O_2N$: C, 75.63; H, 10.58; N, 4.20%.

17α-Acetyl-5α,12α-etiojervan-3β-ol (18). A solution of **17** (1.619 g in crude state) in ethanol (100 ml) and water (67 ml) was refluxed with sodium bisulfite (2.1 g) for 11 hr under stirring.[6] The solution was concentrated to 20 ml, cooled, mixed with 1M hydrochloric acid (64 ml) and chloroform (96 ml), and the mixture was stirred vigorously at room temperature for 2 hr. The organic layer was combined with chloroform washings of the aqueous layer, washed with water, dried and evaporated below 35 °C to leave amorphous residue (1.335 g), which crystallized on trituration with acetone and was collected by filtration to give **18** (825 mg), mp 133—135 °C. This was recrystallized from aqueous methanol for analysis; mp 135—137 °C; $[\alpha]_D$ −54.6°; IR, ν_{max} 3460, 1699, 1066, and 1041 cm^{-1}; NMR, τ 9.20 (3H, s, 19-Me), 9.18 (3H, d J=5.5 Hz, 18-Me), 7.89 (3H, s, 21-Me), and 6.40 (1H, m W_H=25 Hz, H at C_3). The afore-mentioned filtrate on crystallization was subjected to preparative tlc (ether–benzene 1:1, and 23 plates), and the main fraction extracted with acetone and then with methanol afforded amorphous substance (352 mg), which on trituration with acetone afforded an additional amount of **18** (168 mg), mp 129—134 °C. Compound **18** proved to be identical with an authentic sample already reported[14b] (the acetate[14a]) by direct comparison.

Compound **18** (30 mg) was treated with 1M sodium methoxide in refluxing methanol (20 ml) for 12 hr under nitrogen. The reaction mixture was worked up as usual and gave crystalline material (31 mg), which showed the same IR spectrum and R_f value on tlc as the starting material, and was recrystallized from aqueous methanol to yield **18** (20 mg), mp 135—136 °C; $[\alpha]_D$ −51.7°.

17α-Acetyl-5α,13β-etiojervan-3β-ol (21). Compound **15** was degraded into the corresponding methyl ketone (**21**) in the same manner as **14**. A solution of **15** (810 mg) in THF (30 ml) was converted into the *N*-chloro derivative by treatment with NCS (400 mg) for 1.7 hr. This in methanol (50 ml), on treatment with 2 M sodium methoxide in methanol (50 ml) under cooling for 3 hr followed by hydrolysis of the product with 2M hydrochloric acid at room temperature for 69 hr, produced crude 20-aldehyde (**19**, 786 mg), which on purification by preparative tlc (ether–benzene 1:1 and 36 plates) gave **19** (374 mg), amorphous; IR ($CHCl_3$), ν_{max} 3590, 3420, 2780, 1724, and 1028 cm^{-1}; NMR, τ 9.25 (3H, s, 19-Me), 9.04 and 9.03 (total 6H, each d J=7 and 5 Hz, 18- and 21-Me or *vice versa*), 6.46 (1H, br W_H=30 Hz, H at C_3), and 0.40 (1H, s, CHO).

20-Aldehyde (**19**, 270 mg) in methanol (15 ml) was treated with *n*-butyl nitrite (1.2 ml) and 1.3M sodium methoxide in methanol (20 ml) at 0 °C for 11 hr to yield 20-oxime (**20**, 334 mg), showing a single spot; IR ($CHCl_3$), ν_{max} 3600, 3280, and 1027 cm^{-1} (no C=O absorption). A solution of **20** (315 mg) in 40% aqueous ethanol was refluxed with sodium bisulfite for 10 hr[6] and, after removal of the solvent, stirred with 1M hydrochloric acid (9 ml) and chloroform (15 ml) at room temperature for 1.5 hr to give amorphous residue (278 mg). This was subjected to preparative tlc (ether–benzene 1:2, and 13 plates) and gave amorphous substance (**21**, 133 mg) as the main fraction, showing the same IR spectrum and R_f value as the analytical sample described below, which crystallized on trituration with acetone–*n*-hexane to yield **21** (41 mg), mp 70—72 °C; $[\alpha]_D$ +15.4°; IR ($CHCl_3$), ν_{max} 3600, 3435, 1704, and 1027 cm^{-1}; NMR, τ 9.26 (3H, s, 19-Me), 9.17 (3H, d J=6 Hz, 18-Me), 7.90 (3H, s, 21-Me), and 6.40 (1H, br W_H=22 Hz, H at C_3).

Found: C, 79.24; H, 10.58%. Calcd for $C_{21}H_{34}O_2$: C, 79.19; H, 10.76%.

Compound **21** (17 mg) was treated with 1M sodium methoxide in refluxing methanol for 12 hr, and the product (14 mg), amorphous, showed the same IR spectrum and R_f value on tlc as the starting material.

Reduction of N*-acetyl-22,27-imino-17β-jerva-5,12-diene-3β,23β-diol-11-one (23) with sodium borohydride. 3-*O,*23-*O,N*-Triacetyl-22,27-imino-17β-jerva-5,12-diene-3β,11β,23β-triol (24=7a) and Others (25 and 26).* A solution of **23**[16,18] (1.5 g) in dioxane (150 ml) was refluxed with sodium borohydride (NBH) (3.0 g) under stirring for 48 hr. After addition of acetone under cooling to decompose excess NBH, the mixture was further stirred for 15 min, insoluble material being filtered off. The filtrate was evaporated, shaken with water and chloroform. The chloroform solution afforded amorphous residue (1.71 g), which showed 2 spots on tlc; IR ($CHCl_3$), ν_{max} 3590, 3410, 1641, 1048 and 1020 cm^{-1} (no C=O absorption). A part (1.67 g) of the residue was acetylated with acetic anhydride (15 ml) and pyridine (15 ml) at room temperature for 21 hr. After being worked up in the usual way, the mixture gave amorphous residue, which was separated into 3 parts by preparative tlc (ether–benzene 1:1, and 62 plates). The most mobile fraction (**25a**, 535 mg), amorphous, resisted crystallization; NMR, τ 9.18 and 8.81 (each 3H, d J=6 and 5 Hz, 21- and 26-Me or *vice versa*), 8.89 (3H, s, 19-Me), 8.50 (3H, s, 18-Me), 8.00 (9H, s, OCO-CH_3), and 7.88 (3H, s, NCOCH_3). This was then hydrolyzed with 5% potassium hydroxide in refluxing methanol (50 ml) for 1 hr under nitrogen, and gave amorphous substance, which crystallized on trituration with methanol–acetone, was collected by filtration to yield *N*-acetyl-22,27-imino-17β-jerva-5,12-diene-3β,11α,23β-triol (**25**, 130 mg), mp 223—233 °C. This was recrystallized twice from the same solvent for analysis; mp 248—251 °C; $[\alpha]_D$ −22.8° (MeOH); IR, ν_{max} 3320, 1612, 1067, and 1024 cm^{-1}.

Found: C, 73.48; H, 9.50; N, 3.00%. Calcd for $C_{29}H_{45}O_4N$: C, 73.84; H, 9.62; N, 2.97%.

The middle fraction (**26a**, 355 mg), amorphous, showed the following IR and NMR spectrum; ν_{max} ($CHCl_3$) 1724, 1628, 1250, and 1025 cm^{-1} (no OH absorption); τ 9.12 and 8.96 (total 9H?, each d J=6.5 and 5 Hz, 18-, 21- and 26-Me or *vice versa*), 8.73 (3H, s, 19-Me), 7.97 (9H, s, OCOCH_3), and 7.87 (3H, s, NCOCH_3). This was hydrolyzed in the same manner as **25a** and gave amorphous substance, which crystallized on trituration with methanol–acetone and was collected by filtration to yield *N*-acetyl-22,27-imino-12ξ,13ξ,-17β-jerv-5-ene-3β,11β,23β-triol (**26**, 96 mg), mp 217—223 °C. This was recrystallized three times from the same solvent for analysis; mp 241—242 °C; $[\alpha]_D$ −30.2° (MeOH); mass, *m/e* 473 (M^+); IR, ν_{max} 3505, 3395, 1605, 1049, and 1024 cm^{-1}; NMR, τ 9.17, 8.98 and 8.78 (total 9H?, each d J=7, 5 and 6 Hz, 18-, 21- and 26-Me or *vice versa*), 8.76 (3H, s, 19-Me), 7.88 (3H, s, NCOCH_3), and 4.75 (1H, br s W_H=9.5 Hz, H at C_6).

Found: C, 73.27; H, 10.03; N, 2.84%. Calcd for $C_{29}H_{47}O_4N$: C, 73.53; H, 10.00; N, 2.96%.

The least mobile fraction (376 mg), crystalline, was recrystallized from acetone–isopropyl ether to give **24** (=**7a**,

215 mg), mp 213—215 °C; $[\alpha]_D$ −28.3°; mass, *m/e* 555 (M^+), 198 and 156; IR, ν_{max} 3570, 1741, 1635, 1239, and 1023 cm^{-1}; NMR, τ 9.18 and 8.80 (each 3H, d J=6 and 7 Hz, 21- and 26-Me or *vice versa*), 8.74 (3H, s, 19-Me), 8.23 (3H, s, 18-Me), 8.00 (6H, s, $OCOC\underline{H}_3$), 7.89 (3H, s, $NCOC\underline{H}_3$), and 6.58 (1H, br s W_H=5.5 Hz, H at C_{11}).

Found: C, 71.13; H, 8.83; N, 2.57%. Calcd for $C_{33}H_{49}O_6N$: C, 71.32; H, 8.89; N, 2.52%.

Oxidation of **24** *(=***7a***) with chromic anhydride and pyridine.* A solution of **24** (=**7a**, 26 mg) in pyridine (1 ml) was treated with chromic anhydride (96 mg) at room temperature overnight under stirring, and then shaken with water and chloroform. The chloroform solution was washed with 1M hydrochloric acid, a 5% sodium bicarbonate solution and water, dried and evaporated to leave oily residue, which showed a single spot but was further purified by preparative tlc (ether–benzene 4: 1, and 1 plate). The main fraction afforded crystalline material (22 mg), which was again dissolved in chloroform. The solution was worked up as usual and the product was recrystallized from acetone–isopropyl ether to give **23** (15 mg), mp 215.5—217 °C, which was identical with an authentic sample.[16,18]

Birch reduction of **24** *(=***7a***).* a) To a solution of **24** (=**7a**, 200 mg) in ethylamine (35 ml) was added finely divided lithium (250 mg), and the mixture was stirred vigorously under reflux for 1 hr. The reaction mixture on addition of ammonium chloride became colorless and was worked up in the same manner as for **4**, giving amorphous residue (198 mg), showing only 2 spots. This was acetylated with acetic anhydride (3 ml) and pyridine (3 ml) at room temperature for 28 hr. The product showed 4 spots and was separated into 4 parts by preparative tlc (ether–benzene 1: 2, and 9 plates). The first, mobile fraction (22 mg), amorphous, was not further examined but apparently differed from **6a**, judging from the R_f value. The second, main fraction (149 mg), crystalline, was recrystallized from aqueous methanol to give **2a** (89 mg), mp 191—194 °C, which was identical with the sample obtained from **4**. The third fraction (21 mg), amorphous, was a mixture of two compounds and not further examined. The last, least mobile fraction (48 mg), amorphous, crystallized on trituration with acetone–isopropyl ether to give the starting material **24** (28 mg), mp 208—212 °C.

b) A solution of **24** (=**7a**, 207 mg) in liquid ammonia (50 ml), dry dioxane (20 ml) and dry THF (20 ml) was stirred vigorously with lithium (130 mg) under reflux for 1 hr. After dropwise addition of ethanol (10 ml), the mixture was worked up as usual and gave amorphous substance. Since this contained a considerable amount of the unreacted material **24**, the reduction was again carried out under the same conditions as mentioned above. The resulting amorphous product (185 mg) showed 3 spots and was separated into 2 main fractions by preparative tlc (ether–methanol 9: 1, and 9 plates). The more mobile fraction crystallized on trituration with methanol–acetone and was collected by filtration. The crystalline material (18 mg), mp 220—222 °C, proved to be identical with **6**. The less mobile fraction apparently consisted of deacetylated derivatives of **2a** and **24**, but was not further examined.

Wolff-Kishner Reduction of **23**. A solution of diethylene glycol (20 ml) with dissolving sodium (620 mg) was heated to reflux with anhydrous hydrazine (4 ml) and cooled. Compound **23** (400 mg) was added to the solution, whcih was refluxed for 14.5 hr. The condenser was replaced by a distillation apparatus, and the whole solution was heated for 4.5 hr, 2.3 ml of hydrazine being removed. The resulting pale-yellow solution was poured into ice-water (200 ml) and allowed to stand overnight, when precipitates separated out, were collected by filtration, washed with water and dried (320 mg). On the other hand, the aqueous solution obtained on filtration and water washings were combined and extracted with chloroform. The chloroform solution gave amorphous residue (35 mg), which was combined with the afore-mentioned precipitates and acetylated with acetic anhydride (5 ml) and pyridine (5 ml) at room temperature for 17 hr. The product, showing 2 spots, was separated by preparative tlc (ether–benzene 3: 5, and 25 plates). The more mobile fraction (161 mg). amorphous, showed the same IR spectrum and R_f value on tlc as **6a**, and crystallized on trituration with isopropyl ether to give **6a** (69 mg), mp 173—174 °C, which was identical with the sample described already. The less mobile fraction (107 mg), amorphous, was crystallized from aqueous methanol to yield **2a** (71 mg), mp 193—194 °C, identical with the authentic sample.

Hydrogenation of **6a**. A solution of **6a** (91 mg) in acetic acid (6 ml) was hydrogenated over prereduced rhodium-platinum (3: 1) catalyst (104 mg)[11] in acetic acid (5 ml) at room temperature for 1.2 hr, when 2.3 mol of hydrogen had been absorbed. The mixture was worked up as usual and gave amorphous residue (113 mg). This was refluxed with 5% potassium hydroxide in methanol (15 ml) for 1.1 hr under nitrogen and afforded amorphous residue (93 mg), which showed 2 spots and was subjected to separation by preparative tlc (ether, and 6 plates). The more mobile fraction (7 mg), amorphous, was not further examined. The less mobile fraction (76 mg) crystallized on trituration with ethyl acetate, mp 180—182 °C, 55 mg. This compound was identical with **14a**.

Hydrolysis of **24** *(=***7a***).* A solution of diethylene glycol (5 ml) with dissolving sodium (180 mg) was refluxed with anhydrous hydrazine (1 ml) for 10 min and cooled. After addition of **24** (99 mg), the whole solution was refluxed for 17 hr, cooled and poured onto crushed ice (30 g), when precipitates separated out, were collected by filtration, washed with water and dissolved in methanol. The methanol solution was concentrated to give oily substance, which crystallized on addition of acetone, mp 232—233 °C, 46 mg. This compound was identical with **7** isolated from the Birch reduction products of **4**. This was recrystallized from acetone for analysis; mp 233—235 °C; $[\alpha]_D$ −65.4° (MeOH); mass, *m/e* 429 (M^+), 141 and 114; IR, ν_{max} 3420 and 1046 cm^{-1}.

Found: C, 75.19; H, 10.08; N, 3.19%. Calcd for $C_{27}H_{43}O_3N$: C, 75.48; H, 10.09; N, 3.26%.

The authors express their thanks to Mrs. S. Araki and Miss M. Shiozawa for the measurement of NMR spectra, to Misses H. Kakizawa and A. Maeda for the microanalysis, and to Miss Y. Imai for the measurement of mass spectra.

The Biosynthesis of Geraniol and Citronellol in *Pelargonium roseum* Bourbon[1]

Takayuki SUGA and Tsuyoshi SHISHIBORI

Department of Chemistry, Faculty of Science, Hiroshima University, Higashisenda-machi, Hiroshima 730

(Received June 22, 1973)

Geraniol and citronellol were biosynthesized from [2-^{14}C]mevalonic acid by the leaves of *Pelargonium roseum* Bourbon. The degradation of the radioactive specimens revealed that the major radioactivity (70—80%) was located at C-4 in the skeleton derived presumably from isopentenyl pyrophosphate and the rest of the activity at C-8 (and/or C-10) in the moiety from 3,3-dimethylallyl pyrophosphate. The unbalance of labeling was distinct from the result observed for the monoterpenes biosynthesized from the same labeled precursor by the flowers of the rose. A discussion is given on factors causing such a discrepancy in the labeling pattern owing to the difference of the plant and/or the organ. Time-course experiments with the use of [2-^{14}C]mevalonic acid indicated the formation of geraniol prior to citronellol both in the intact plant and in the cell-free extract.

The biosynthesis of monoterpenes is said to involve the conversion of mevalonic acid (MVA) into isopentenyl pyrophosphate (IPP) (I) and 3,3-dimethylallyl pyrophosphate (DMAPP) (II), followed by the condensation of IPP (I) with DMAPP (II) directed toward the formation of geranyl pyrophosphate (III), the presumed precursor of monoterpenes. Incorporations of [2-^{14}C]MVA into geraniol (IV) and nerol and their β-glucosides in the petals of *Rosa dilecta*[2,3] and into pyrethrins in the flower heads of *Chrysanthemum cinerariaefolium*[4] have been reported to result in the almost balanced pattern of labeling in the parts generated from IPP (I) and DMAPP (II) respectively. The geranyl moiety of the fungal product, mycelianamide (IV'), has been shown to possess a labeling pattern resulting from the equilibration of a tracer from [2-^{14}C]MVA between the C-5 units.[5] On the other hand, the biosynthesis of cyclic monoterpenes, thujone,[6] camphor,[7] and pulegone,[8] in the leaves and stems of several higher plants has been reported to localize the tracer mainly in the part derived from IPP (I), although one exception has been observed for linalool, an acyclic monoterpene, which had the almost symmetrical pattern of labeling.[9,10] Recently, the symmetrical labeling was also observed for geraniol (IV) biosynthesized in the leaves of *Pelargonium graveolens* Ait.[3] We now have tested the labeling pattern in geraniol (IV) biosynthesized from [2-^{14}C]MVA in the leaves of the geranium, *Pelargonium roseum* Bourbon, as well as the labeling pattern of citronellol (V), the main component of an essential oil of the plant. Contrary to Banthorpe's result,[3] we observed the unbalanced pattern of labeling for both geraniol (IV) and citronellol (V).

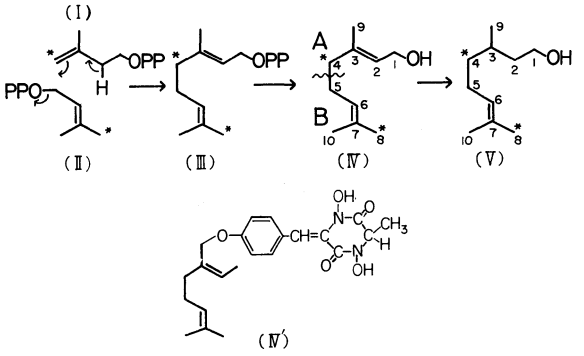

PPO = a pyrophosphate group; * = ^{14}C

Scheme 1.

Results

Time-course of the Incorporation of a Tracer into Geraniol (IV) and Citronellol (V). Feeding experiments were carried out on the intact plant tissue and the cell-free extract obtained from *P. roseum* Bourbon. The incorporation of [2-^{14}C]MVA to the small branches of *P. roseum* Bourbon for periods of 2 hr to 2 days resulted in an accumulation of the tracer in the plant oil. The radioactivity of the monoterpenes in the plant oil was determined by thin-layer plate radiochromatography. Table 1 shows the radioactivities of geraniol (IV) and

Table 1. Incorporations of [2-^{14}C]MVA into geraniol (IV) and citronellol (V) in the intact plant of *Pelargonium roseum* Bourbon

Time of feeding (hr)	Radioactivities (cpm)		A_V/A_{IV}[a]
	Geraniol (IV)	Citronellol (V)	
2	29	42	1.45
4	57	93	1.63
8.5	60	132	2.20
24	120	490	4.08
48	88	450	5.11

a) A_V and A_{IV} denote the radioactivities of citronellol (V) and geraniol (IV) respectively.

1) A part of this paper has been reported in the form of a communication in *Chem. Lett.*, **1972**, 1093.

2) M. J. O. Francis, D. V. Banthorpe, and G. N. J. Le Pathourel, *Nature*, **228**, 1005 (1970).

3) D. V. Banthorpe and G. N. J. Le Patourel, and M. J. O. Francis, *Biochem. J.*, **130**, 1045 (1972).

4) P. J. Godin, H. S. Ingris, M. Snarey, and E. M. Thain, *J. Chem. Soc.*, **1963**, 5878.

5) A. J. Birch, M. Kocor, N. Sheppard, and J. Winter, *ibid.*, **1962**, 1502.

6) D. V. Banthorpe, J. Mann, and K. W. Turnbull, *J. Chem. Soc., C*, **1970**, 2689.

7) D. V. Banthorpe and D. Baxendale, *ibid.*, **1970**, 2694.

8) B. V. Charlwood, Ph. D. Thesis, University of London (1970).

9) T. Suga, T. Shishibori, and M. Bukeo, *Phytochemistry*, **10**, 2725 (1971).

10) T. Suga, T. Shishibori, and M. Bukeo, This Bulletin, **45**, 1480 (1972).

Table 2. Incorporations of [2-^{14}C]MVA into geraniol (IV) and citronellol (V) in the cell-free extract from *Pelargonium roseum* Bourbon

Time of incubation (hr)	Radioactivities (cpm) Geraniol (IV)	Citronellol (V)	A_V/A_{IV}[a)]
2	156	82	0.53
24	100	84	0.84

a) A_V and A_{IV} denote the radioactivities of citronellol (V) and geraniol (IV) respectively.

citronellol (V) and the ratio (A_V/A_{IV}) of the activities of IV and V at predetermined time intervals after feeding. The contents of geraniol (IV) and citronellol (V) were estimated to be 23.6 and 33.3% of the total oil by means of gas chromatography respectively.

The cell-free extract prepared from *P. roseum* Bourbon was found to transform [2-^{14}C]MVA into the monoterpenes, geraniol (IV) and citronellol (V). Table 2 shows the radioactivities of IV and V and the ratio (A_V/A_{IV}) of their radioactivity at 2 hr and at 24 hr after feeding of the tracer.

Labeling Patterns. By means of elution chromatography on a silica gel column, geraniol (IV) and citronellol (V) were isolated from the leaf oil of *P. roseum* Bourbon to which [2-^{14}C]MVA had been administered. Incorporations of the MVA into IV and V were 0.038 and 0.041%, respectively, of the administered tracer.

Radioactive geraniol (IV) was degraded to acetone containing a tracer from C-7, C-8, and C-10 and to levulinic acid containing a tracer from C-3~C-6 and C-9 by permanganate-periodate oxidation.[11-13] By hypoiodite oxidation, then, the acetone was degraded to iodoform containing a tracer from C-8 (and/or C-10) and to acetic acid originated from C-7 and C-8 (and/or C-7 and C-10), while the levulinic acid to iodoform originated from C-9 and to succinic acid from C-3~C-6. This acid was further cleaved into carbon dioxide originated from C-3 and C-6 and into ethylenediamine from C-4 and C-5 by the Schmidt reaction.[14] The all degradation products, after the conversion into the solid derivative when the product is a liquid, were purified by recrystallization or sublimation. The purified degradation products and geraniol (IV) were converted to barium carbonate by Van Slyke-Folch oxidation[15] in order to determine their specific radioactivities. The results are shown in Table 3.

By permanganate-periodate oxidation,[11-13] radioactive citronellol (V) was degraded to acetone containing a tracer from C-7, C-8, and C-10 and to 6-hydroxy-4-methylhexanoic acid (VI) originated from C-1~C-6 and C-9. Acetone was degraded to iodoform

Table 3. Specific activities of geraniol (IV) biosynthesized from [2-^{14}C]MVA by the intact plant of *Pelargonium roseum* Bourbon and of its degradation products

Compounds (Carbons originated from IV)	Specific activities, dpm × 10^{-3}/mmol	(%)
Geraniol (C-1~C-10)	271	(100)
Levulinic acid (C-3~C-6 and C-9)	220	(81.3)
Iodoform (C-9)	4.2	(1.9)
Succinic acid (C-3~C-6)	210	(77.5)
Ethylenediamine (C-4 and C-5)	197	(72.7)
Carbon dioxide (C-3 and C-6)	14.5	(5.4)
Acetone (C-7,C-8, and C-10)	—	—
Iodoform (C-8 and/or C-10)	25.7	(9.5)
Acetic acid (C-7 and C-8, and/or C-7 and C-10)	23.6	(8.7)

Table 4. Specific activities of citronellol (V) biosynthesized from [2-^{14}C]MVA by the intact plant of *Pelargonium roseum* Bourbon and of its degradation products

Compounds (Carbons originated from V)	Specific activities, dpm × 10^{-3}/mmol	(%)
Citronellol (C-1~C-10)	701	(100)
6-Hydroxy-4-methylhexanoic acid (C-1~C-6 and C-9)	474	(67.6)
Acetone (C-7, C-8, and C-10)	72.3	(10.3)
Iodoform (C-8 and/or C-10)	78.2	(11.2)

containing a tracer from C-8 (and/or C-10) by hypoiodite oxidation. The radioactivities of the degradation products were assayed by counting aliquots of barium carbonate which was prepared from the products, after purified similarly, in the same manner as above. The results are shown in Table 4.

Discussion

The maximum incorporation of a tracer from [2-^{14}C]-MVA into geraniol and nerol of the petals of *Rosa dilecta* has been reported to be observed within 1 hr of feeding.[16] On the other hand, the incorporation of a tracer from the ^{14}C-labeled MVA into geraniol (IV) and citronellol (V) by the intact plant tissues of *P. roseum* Bourbon resulted in the increase in their radioactivities with time of feeding and then the maximum activity in 24 hr, as is shown in Table 1. The results of the incorporations are, although low, similar to those found in analogous experiments.[6-10,17] The low incorporation probably is not due to a rapid passage of the tracer through geraniol (IV) and citronellol (V), since the maximum in the radioactivity was observed for the compounds in the time-course examination, as is shown in Table 1. The increase in the activity ratio of A_V/A_{IV} with time of feeding of a tracer was observed for incubations not only in the intact plant

11) E. von Rudloff, *Can. J. Chem.*, **43**, 2660 (1965).
12) T. Suga and E. von Rudloff, *ibid.*, **47**, 3682 (1969).
13) T. Suga and E. von Rudloff, *J. Sci. Hiroshima Univ., Ser. A-II*, **34**, 69 (1970).
14) E. F. Phares and M. V. Long, *J. Amer. Chem. Soc.*, **77**, 2556 (1955).
15) D. D. Van Slyke and J. Folch, *J. Biol. Chem.*, **136**, 509 (1940).
16) M. J. O. Francis and M. O'Connell, *Phytochemistry*, **8**, 1705 (1969).
17) W. Sandermann and W. Schweors, *Tetrahedron Lett.*, **1962**, 257 and 259.

tissue but also in the cell-free extract, as is shown in Tables 1 and 2. The results indicate the formation of geraniol (IV) prior to that of citronellol (V) and subsequently the transformation of IV to V. This biosynthetic sequence may be supported by the fact that a geraniol-nerol reductase, which converts both geraniol and nerol into citronellol (V), has been isolated from the rose petals.[18]

The extensive degradation of geraniol (IV) biosynthesized from [2-^{14}C]MVA in the leaves of *P. roseum* Bourbon revealed, as is shown in Table 3, that more than 90 per cent of the total radioactivity was detected in ethylenediamine and iodoform derived respectively from C-4 and C-5 and from C-8 (and/or C-10) of IV. Since C-1, C-2, C-3, and C-9 were almost unlabeled and the rest of the C_5-isoprene unit is nothing other than C-4, the main site of labeling on geraniol (IV) is considered to be C-4 rather than C-5. Thus, the pattern of labeling observed for geraniol (IV) is consistent with the biosynthetic pathway depicted in the Scheme, which shows the formation of geraniol (IV) *via* geranyl pyrophosphate generated from the condensation of IPP (I) with DMAPP (II). Although the sites of labeling accord with the biosynthetic pathway shown in the Scheme, the radioactivities of C-4 and C-8 derived respectively from IPP (I) and DMAPP (II) were unbalanced; the former contained more than 70% of the total activity and the latter did only 20%. Such unbalanced labeling that the tracer predominantly resided in the moiety A of geraniol (IV) was in contrast to the balanced pattern of labeling in the moieties A and B of IV biosynthesized in the petals of the rose.[2,3]

The results of the degradation of citronellol (V) revealed that acetone and 6-hydroxy-4-methylhexanoic acid (VI) contained respectively about 10 and 70% of the total activity, as is shown in Table 4. The acetone and the hydroxy acid (VI) contain a tracer from C-8 (and/or C-10) and C-4, respectively, which should be labeled by a tracer from [2-^{14}C]MVA as shown in the Scheme. The unbalanced pattern of labeling in two positions observed in citronellol (V) is similar to that in geraniol (IV) described above.

The unbalanced labeling thus found in geraniol (IV) and citronellol (V) biosynthesized by the leaves of *P. roseum* Bourbon is of interest, since the phenomenon has not been observed yet for the polyisoprenoids, triterpenes and steroids;[19,20] these are said to be biosynthesized *via* the same precursor, geranyl pyrophosphate, as that in geraniol (IV). Such an unbalanced pattern of labeling may be rationalized in terms of the operation of several factors: a) a pool of DMAPP (II) in the plant may exist which can react with IPP (I) generated from exogenous radioactive MVA before the labeled IPP (I) can be isomerized to DMAPP (II), b) DMAPP (II) may not be the direct mevalonoid origin, c) compartmentation effects may intervene, and d) the excess of MVA unavoidably used may inhibit IPP-isomerase.[21] The incorporation of [2-^{14}C]-MVA into geraniol and nerol[2,3] in the petals of *Rosa dileca* and into pyrethrins[4] in *Chrysanthemum cinerariaefolium* resulted in the nearly balanced pattern of labeling in the moieties derived from IPP (I) and DMAPP (II). In the biosynthesis in leaves of several higher plants, on the contrary, the unbalanced pattern of labeling has been observed in thujane derivatives,[6] camphor,[7] pulegone,[8] and artemisia ketone,[22] as well as in geraniol (IV) and citronellol (V) as described above. These findings related to the labeling pattern suggest that the nature of the synthetic site in the leaves of the higher plants may be different from that in the petals. The presence of an oil gland in the leaves seem to be responsible for the unbalanced labeling. Our presently reported examples of the asymmetrical pattern of labeling differ from a recent report for geraniol (IV) biosynthesized by *P. graveolens*.[3] This discrepancy seems to be due to differences in the plants used, although both the plants belong to Geraniaceae, in the growth stage of the plants employed, and in feeding conditions of the precursor.

Experimental

Materials. Specimens of *P. roseum* Bourbon were grown from a young shoot obtained from the experimental farm of the Soda Perfumery Co., Ehime Prefecture, Japan. The small terminal branches (*ca.* 7 cm long) of the 15 week-old plants, grown outdoors from April to October, were used for feeding experiments. 3-RS-[2-^{14}C]MVA was obtained from the Daiichi Pure Chemicals Co., Ltd. (Tokyo) as the dibenzylethylenediamine salt. Adenosine triphosphate (ATP) was purchased from the Sigma Chemical Co., (St Louis, Mo., U.S.A.) as Sigma Grade Products.

Chromatographic Analyses. Tlc plates were prepared as follows: the end of a glass plate coated with silica gel G (0.25 mm; Merck) were dipped into 10% silver nitrate solution to permeate the solution through the plate and then the plate was dried at 105 °C for 45 min. Upon developing with a mixture of *n*-hexane and ethyl acetate (85: 15 or 50: 50 by volume, respectively), the plate resulted in the good separation of geraniol (IV) (R_f value 0.10 or 0.43) and citronellol (V) (R_f value 0.33 or 0.70). Column chromatography of the steam-volatile oil was performed on silica gel impregnated with 3% (w/w) silver nitrate, using a mixture of *n*-hexane with successively increasing amounts of ethyl acetate (0—25% by volume). Gas-liquid chromatographic analyses were made using a Hitachi Perkin-Elmer F6-D instrument attached with a column (1 m×3 mm) packed with 20% PEG-6000 on Celite (60—80 mesh) at 145 °C.

Measurements of Radioactivities. Thin-layer plate radiochromatograms were taken on an Aloka (Tokyo) JTC-203 instrument at a slit width of 1.5 mm. Radioactivities of geraniol (IV) and citronellol (V), shown in Tables 1 and 2, were determined by cutting the corresponding areas on the thin layer radiochromatogram obtained in the manner as mentioned above to weigh their pieces of paper and then by comparing the peak areas with those obtained with geraniol having the known radioactivity. In order to assay the specific activity, geraniol, citronellol, and all their degradation products were converted into barium carbonate by Van Slyke-Folch oxidation,[15] and aliquots of the barium carbonate

18) P. J. Dunphy and C. Allcock, *Phytochemistry*, **11**, 1887 (1972).
19) P. B. Clayton, *Quart. Rev.* (London), **19**, 168 (1965).
20) P. B. Clayton, *ibid.*, **19**, 201 (1965).
21) D. V. Banthorpe, B. V. Charlwood, and M. J. O. Francis, *Chem. Rev.*, **72**, 115 (1972).
22) T. Suga, T. Shishibori, K. Kotera, and R. Fujii, *Chem. Lett.*, **1972**, 533.

were counted on planchets at an infinite thickness under an Aloka (Tokyo) 2π-gas-flow low background counter, Model TDC R1361. The counting error for the values shown in Tables 3 and 4 is about $\pm 3\%$.

Incorporations of Tracer. *a) With Intact Plant Tissue*: The stems in the nearly same size (each 6 g) were cut under water, and a phosphate-buffered solution (5 ml, pH 7.3) of [2-^{14}C]MVA (20 μCi, 4 μmol) and ATP (4 mg) was fed through a cut-stem into twigs. Just after the tracer solution had been absorbed, two aliquots (each 0.5 ml) of water were given for completely sucking up all the tracer in the twigs. The time required for the complete administration of the tracer was *ca.* 1 hr. The twigs were then maintained under outdoor conditions on water. At predetermined intervals, two twigs were ground with solid carbon dioxide in a mortor and the crushed plant tissues were then steam-distilled. The yield of the volatile oil was 0.3—0.4% (w/w) of the plant employed, and the contents of geraniol (IV) and citronellol (V) were estimated by glc to be 23.6 and 33.3% of the total plant oil respectively. The oil was chromatographed on the tlc plate coated with silica gel G impregnated with silver nitrate. The plate was then subjected to thin-layer plate radiochromatography for counting radioactivities of the separated constituents. The results are shown in Table 1.

b) With Cell-free Extract: The leaves (30 g) of the geranium were ground with 0.1 M phosphate buffer (pH 7.3, 30 ml) and solid carbon dioxide in a mortar. The resulting slurry was filtered through a cheese cloth to give a green homogenate (30 ml). The homogenate was centrifuged for 30 min at 14000$\times$g and 0 °C. The supernatant film and the precipitate were discarded and the clear middle layer (20 ml) was used as a cell-free extract for incubations. [2-^{14}C]MVA (2 μCi, 0.4 μmol) dissolved in 1 ml of 0.1 M phosphate buffer (pH 7.3) containing 8 mg of ATP was incubated with the cell-free extract at 25 °C for 2 hr and for 24 hr with shaking in the air. The enzymic reaction was stopped by adding 2 M hydrochloric acid and then by heating the mixture for 3 min at 70 °C. The extraction of the mixture with *n*-hexane afforded, after removal of the solvent, an oily product; this was subjected to thin-layer plate radiochromatography. The results are shown in Table 2.

Labeling Patterns. Radioactive geraniol (IV) and citronellol (V) used for determining the labeling patterns were obtained as follows. A phosphate-buffered solution (4 ml, pH 7.3) of [2-^{14}C]MVA (0.1 mCi, 17 μmol) and ATP (5 mmol) was fed through a cut-stem into the small terminal branches (60 g) of *P. roseum* Bourbon for 4 hr. The leaves and stems were then subjected to steam distillation. The steam-volatile oil thus obtained (260 mg) was separated by a combination of column chromatography and tlc to give geraniol (IV) (24 mg) and citronellol (V) (33 mg). These were judged to be chemically and radiochemically pure on the basis of glc, tlc, and thin-layer plate radiochromatography.

a) Degradation of Geraniol (IV): Radioactive geraniol (206 mg) diluted 29 times with the carrier was oxidized with a permanganate-periodate reagent for 24 hr following the method reported in the literatures.[11-13] After the residual oxidant had been decomposed with sodium bisulfite, the weakly alkaline solution was subjected to steam distillation. After the residual alkaline solution was acidified with diluted sulfuric acid, the solution was extracted with ether by a continuous extractor to afford crude levulinic acid (70 mg). This acid was chromatographed repeatedly on a thin layer plate coated with silica gel G by a mixture of chloroform, acetone, methanol, and formic acid (45: 5: 5: 1 by volume) to give pure levulinic acid (39 mg; its *p*-bromophenacyl ester, mp 83—84 °C; lit,[23] mp 84 °C). On the other hand, the aqueous distillate was subjected to hypoiodite oxidation. Iodoform (290 mg) filtered off was purified by sublimation under reduced pressure. The filtrate was acidified with diluted sulfuric acid and then treated with silver sulfate to remove iodine liberated. The aqueous mixture was then steam-distilled. The evaporation of the neutralized distillate afforded acetic acid as the sodium salt, which was further converted into the silver salt; this salt was purified by recrystallization from ethanol–water.

The levulinic acid (100 mg) was oxidized with potassium hypoiodite, which was prepared by adding sufficiently a solution of potassium iodide and iodine (2: 1) to 14 ml of 5% potassium hydroxide until the color persisted. Iodoform (189 mg) filtered off was purified by sublimation under reduced pressure. The filtrate was acidified with diluted sulfuric acid and treated with silver sulfate to remove iodine. The continuous extraction of the aqueous solution with ether afforded crude succinic acid (84 mg). After washed with chloroform, the acid was recrystallized from water and then it melted at 184—186 °C. The succinic acid was degraded to ethylenediamine and carbon dioxide by a modified method[14] of the Schmidt reaction. The carbon dioxide was trapped as barium carbonate.

b) Degradation of Citronellol (V): Radioactive citronellol (220 mg) diluted 20 times with the carrier was oxidized with a permanganate-periodate reagent[11-13] for 6 hr as above. After the same treatment es in geraniol (IV), the mixture was subjected to steam distillation. The continuous extraction of the residual solution, after it was acidified with diluted sulfuric acid, with ether afforded crude 6-hydroxy-4-methylhexanoic acid (VI) (195 mg). The methyl ester of the acid was converted to its 3,5-dinitrobenzoate, mp 145—146 °C (lit,[11] mp 145—147 °C). A half of the aqueous distillate was subjected to hypoiodite oxidation. The yellow precipitate filtered off was sublimated under reduced pressure to give pure iodoform, mp 118—119 °C. From another half of the aqueous distillate, acetone was isolated as the 2,4-dinitrophenylhydrazone derivative, mp 125—126 °C.

The authors are thankful to the Soda Perfumery Co., Ltd., Tokyo, for its gift of the plant, and to Takasago Perfumery Co., Ltd., for its gift of the samples of citronellol and geraniol.

23) Z. Rappoport, "Handbook of Tables for Organic Compound Identification," The Chemical Rubber Co., Cleveland, Ohio (1967), p. 193.

Oxidation of Carbon Monoxide over Transition Metal Ion-Zeolite Catalysts

Toshihiko KUBO, Hiroo TOMINAGA, and Taiseki KUNUGI

Department of Synthetic Chemistry, Faculty of Engineering, The University of Tokyo, Hongo, Bunkyo-ku, Tokyo 113

(Received January 22, 1973)

Adsorption of oxygen and oxidation of carbon monoxide was investigated on several X and Y type zeolites, their Na^+ being replaced by transition metal ions. Oxygen adsorption was observed on Cr(II), Cu(I), and Fe(II) ions whose oxidation potentials are high, giving an oxygen atom to metal ion ratio of 0.43—0.62 or nearly 0.5. A small amount of oxygen was adsorbed on Tl(I), Co(II), and Mn(II), as expected from their standard oxidation potentials. No oxygen was adsorbed on Cu(II) and Ni(II), their valences being difficult to increase. The activities of these transition metal ions for oxidation of carbon monoxide increased exponentially with the increase of their standard oxidation potential. Kinetic studies on CO oxidation over Fe(II)–X and –Y zeolites have been made, and a Rideal mechanism is suggested where CO molecules in the gas phase attack the oxygen atoms dissociatively adsorbed in the bridged form of Fe^{3+}–O^{2-}–Fe^{3+}. The difference in the activities of Fe(II)–X and –Y catalysts is discussed.

Since some transition metal ions are easily reduced by hydrogen and hydrocarbons and re-oxidized by oxygen, transition metal ion zeolites are inherently active for the oxidation of hydrocarbons. Some papers have recently been published on catalysis by the transition metal ions loaded on zeolites. They include studies by Van Sickle and Prest,[1] Mochida,[2] and others.[3-9]

Furthermore, fundamental studies of the transition metal ions on zeolite were published by Delgass *et al.*,[10] Garten and Boudart[11] and Ward.[12] Boudart has studied the reversible oxidation and reduction of iron supported on zeolite (Y-type faujasite and mordenite) by Mössbauer spectroscopy, demonstrating that Fe(II)–Y(or M) is converted into Fe(III) in oxygen at 400 °C and the Fe(III) is then reduced to Fe(II) by hydrogenation at 400 °C. In this case, the net oxygen adsorption due to the ion corresponded to an oxygen atom to iron ratio of 0.5.

From an interest in the catalysis of adsorbed oxygen on metal ions on zeolite, we prepared zeolite catalysts by replacing the original sodium ions with transition metal ions in their defined valence states, and used them to investigate the chemisorption of oxygen and activity for oxidation of carbon monoxide.

Experimental

Catalyst Preparation. The zeolites used in this study were 13X and 13Y type Linde Molecular Sieves. Catalysts were prepared by the exchange of sodium ions of the zeolite with transition metal ions, Cr(II), Cr(III), Mn(II), Fe(II), Co(II), Ni(II), Cu(I), Cu(II), and Tl(I). The ion exchange with the transition metal ions in a higher valence state, namely Cu(II), Cr(III), and Ni(II), was carried out in atmosphere. On the other hand, the transition metal ions in a lower valence state, Co(II), Tl(I), Mn(II), and Fe(II), were incorporated into the zeolites by ion exchange in nitrogen stream following the procedure employed by Delgass *et al.* to prepare ferrous Y zeolite.[13]

Since chromous salts are unstable in oxidative atmosphere, Cr(II)-zeolites were prepared by ion exchange with the freshly prepared chromous chloride from chromic chloride[14] in nitrogen stream. Cu(I)-zeolites were prepared by ion exchange with cuprous iodide in liquefied ammonia according to the procedure by Reimlinger *et al.*[15]

After ion exchange, the transition metal ion zeolite were filtered and washed thoroughly with water. The zeolite was dried at 110 °C and compressed into a tablet under 300 kg/cm^2, and then crushed into 10—20 mesh. The cuprous zeolite was degassed at 400 °C for 3 hr under 10^{-3} mmHg to remove ammonia from the cuprous ammine complex ion before the catalytic activity test. The contents of the transition metal ion in the zeolites were determined, after ion exchange, by titration of the metal ion remaining in the filtrate with EDTA solution.

Oxygen Chemisorption. The oxygen chemisorption measurements were carried out on samples (2—3 g) of dehydrated zeolites using a conventional volumetric adsorption apparatus. The ion exchanged zeolite was admitted into the vessel and evacuated at 400 °C for 3 hr under 10^{-4} mmHg to remove the adsorbed water and gases. The zeolites prepared by ion exchange with transition metal ion in a lower valence state were further reduced in hydrogen at 400 °C and evacuated again at 400 °C for 3 hr under 10^{-4} mmHg.[13] After reduction, oxygen chemisorption on the transition metal ion in the zeolites was measured at 400 °C. The zeolites with the

1) D. E. Van Sickle and M. S. Prest, *J. Catal.*, **19**, 209 (1970).
2) I. Mochida, S. Hayata, A. Kato, and T. Seiyama, *ibid.*, **23**, 31 (1971).
3) T. Kubo, F. Kumada, H. Tominaga, and T. Kunugi, *Nippon Kagaku Kaishi*, **1972**, 1621.
4) J. Rouchand, P. Mulkey, and J. Fripiat, *Chem. Abstr.*, **70**, 77521y (1969).
5) J. Rouchand, L. Sondengam, and J. Fripiat, *Bull. Soc. Chim. Fr.*, **1968**, 4387.
6) D. G. Jones and N. J. Pennington, U. S., 3231134.
7) L. V. Skalkina, I. K. Kolchin, L. Ya. Ermolenko, S. A. Levina, and N. N. Mlashvich, *Kinet. Katal.* **12**, 242 (1971).
8) I. Mochida, T. Jitsumatsu, A. Kato, and T. Seiyama, This Bulletin, **44**, 2595 (1971).
9) T. Kubo, H. Tominaga, and T. Kunugi, *Nippon Kagaku Kaishi*, **1972**, 196.
10) W. N. Delgass, R. L. Garten, and M. Boudart, *J. Catal.* **18**, 90 (1970).
11) R. L. Garten and M. Boudart, *A. C. S. Preprints*, D7 (1972).
12) J. W. Ward, *J. Catal.*, **22**, 237 (1971).
13) W. N. Delgass, R. L. Garten, and M. Boudart, *J. Chem. Phys.*, **50**, 4603 (1969).
14) H. S. Booth, "Inorganic Synthesis," Vol. 1, p. 125 (1939).
15) H. K. Reimlinger, E. H. DeRuiter, and U. K. Kruerk, U.S. 3444253.

metal ions in the higher valence states were not pretreated by hydrogen to avoid proton formation.[16]

CO Oxidation. The activity test was carried out at catalyst temperatures 200—300 °C at atmospheric pressure by use of a flow reactor (17 mm in diameter) where 2 g of catalyst diluted with glass beads (2 mm in diameter) was placed. The gaseous reactants, carbon monoxide and oxygen, and the diluent nitrogen were supplied from the respective cylinders to the reactor. Carbon dioxide was analyzed at 80 °C by gas chromatography using a silica gel column, 2 m in length.

Results and Discussion

Oxygen Chemisorption. It was shown that Fe(II) ions on zeolite Y (or M) activated and adsorbed oxygen dissociatively, Fe(II) being oxidized to Fe(III) at 400 °C.[10,11] We have found that Fe(II) ions on zeolite seem to be more easily oxidized by molecular oxygen in the presence of water. This is suggested by the change in color of Fe(II) zeolite X (or Y) from pale green to brown when the ion exchanged zeolite was washed with water in the atmosphere at room temperature. The catalysis of the activated O^{2-} on this zeolite is of particular interest, since the electronic structure and hence the reactivity of these Fe(III) and O^{2-} might differ from those in the lattice of iron oxides.

The transition metal ions with high oxidation potential such as Cu(I), Cr(II), Tl(I), Co(II), are supposed to exhibit a similar catalytic behavior to that of Fe(II) ions. Cu(I) and Cr(II) ion on zeolites were presumed to be oxidized in the atmosphere from the change of color in filtrating and washing procedures after ion exchange. However, no color change was observed in the zeolites incorporated with Tl(I) and Co(II).

The oxygen chemisorption data are shown in Tables 1 and 2. No oxygen was chemisorbed on either X or Y type Na^+. Accordingly, any oxygen chemisorption on the zeolites loaded with transition metal ions was attributed to the presence of metal ions. The amount of oxygen chemisorption on Co(II), Mn(II), or Tl(I) of both types was less than the other zeolite loaded with Fe(II), Cu(I), or Cr(II). All the latter transition metal ions are in their lower valence state in the ion exchange. The results are in line with the relative ease of oxidation predicted from the levels of oxidation potentials of the metal ions. On Fe(II), Cu(I), or Cr(II) zeolites of both X and Y type, oxygen chemisorption due to the metal ions gave an oxygen atom to metal ion ratio 0.430—0.618, which is not far from 0.5 observed for Fe(II)–Y(or M).[10,11] This may permit the supposition that the oxygen chemisorption in a bridged form like M^{n+1}–O^2–M^{n+1} applies for Cu(I) and Cr(II) as for Fe(II).

As shown in Table 2, the oxygen chemisorption on Fe(II) is affected by the degree of ion exchanged for the original sodium ion with Fe(II), namely the ratio of oxygen atom to Fe(II) approaches 0.5 with a rise in the ion exchange degree. An exceedingly high dispersion of Fe(II) in low concentration on zeolite might not be favorable for the formation of the bridged oxygen atom such as Fe(III)–O^{2-}–Fe(III) due to more frequent occurrences of an unduly long distance from neighbouring Fe(II) ions in zeolite.

Table 1. Oxygen chemisorption on the transition metal ion in the Y type zeolite at 400 °C and at 100 mmHg

Zeolite	Na(I) exchanged (%)	Oxygen chemisorbed, 10^{-4} mol/g-cat.	Oxygen atom to metal ion ratio
Na(I)	0	0.00	0.000
Co(II)[a]	48	0.53	0.106
Tl(I)[a]	54	0.07	0.006
Fe(II)[a]	36	1.89	0.500
Cu(I)[a]	34	3.12	0.436
Cr(II)[a]	34	1.52	0.430
Cu(II)	54	0.00	0.000
Cr(III)	38	3.54	0.795
Mn(II)[a]	40	0.70	0.100
Ni(II)	39	0.00	0.000

a) Employed for its catalytic activity for oxidation of carbon monoxide.

Table 2. Oxygen chemisorption on the transition metal ion in the X type zeolite at 400 °C and at 100 mmHg

Zeolite	Na(I) exchanged (%)	Oxygen chemisorbed, 10^{-4} mol/g-cat	Oxygen atom to metal ion ratio
Na(I)	0	0.00	0.000
Co(II)[a]	41	0.07	0.013
Tl(I)[a]	26	0.00	0.000
Fe(II)	12	0.76	0.360
Fe(II)	35	3.00	0.488
Fe(II)[a]	42	3.62	0.490
Cu(I)[a]	18	3.86	0.618
Cr(II)[a]	28	2.33	0.474

a) Employed for its catalytic activity for oxidation of carbon monoxide.

Among the Y zeolites prepared by ion exchange with the transition metal ions in higher valence states (Table 1), oxygen chemisorptions were negligibly small for Cu(II) and Ni(II) whose valences are energetically difficult to enlarge. However, for Mn(II) whose valence can step up to a higher state, a slight oxygen chemisorption was observed.

CO Oxidation. The activities of catalysts for CO oxidation, tested under given conditions for 4 hr, were confirmed to be fairly constant for the duration of the experiment except for Fe(II)–Y catalyst which showed a slight decrease in its initial activity within the first 40 min.

Figure 1 shows the relative activity of transition metal ions, expressed by conversion of CO per metal ion, compared to that of Fe(II)–Y for oxidation of carbon monoxide. The standard oxidation potentials of the transition metal ions are chosen as the abscissa. The catalytic activities of the metal ions are closely related with their oxidation potentials. A very small amount of oxygen was adsorbed on Co(II), Mn(II), and Tl(I) standard oxidation potentials of which are −1.82, −1.51, and −1.25, respectively. The catalytic

16) L. Riekert, *Ber. Bunsenges. Phys. Chem.*, **73**, 331 (1969).

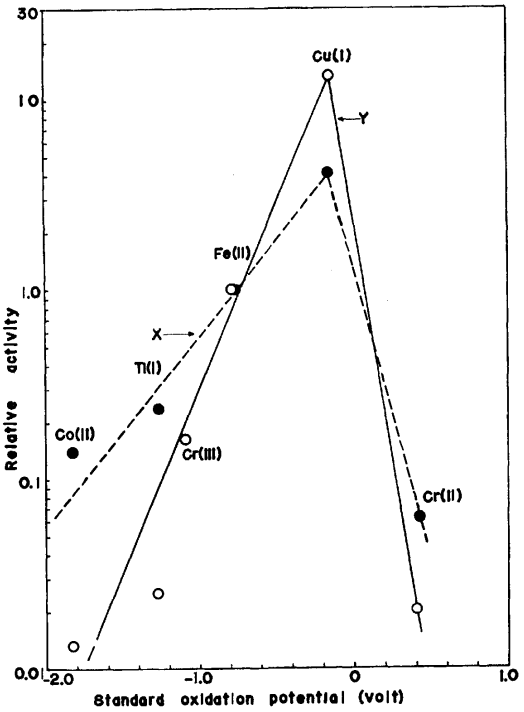

Fig. 1. Dependence of the relative activity on standard oxidation potenital.
●: X type, ○: Y type.
Conditions: P_{CO} 0.099 atm, P_{O_2} 0.179 atm, W/F 7.4 g-cat. hr/mol.
Temperature 280 °C, except for the comparison between Cu(I) and Fe(II) carried out at 200 °C.

activities of these metal ion zeolites were also lower than those of Cu(I) and Fe(II) as expected from oxygen chemisorption data.

The activities of the transition metal ions increased exponentially with the increase in their standard oxidation potential. But the X and Y zeolite ions replaced by Cr(II) showed extremely low activities for CO oxidation. Reduction of bulk α-Cr_2O_3 and chromia on silica or alumina to CrO by hydrogen or carbon monoxide is known to be difficult below 500 °C.[17] Similarly, the oxidized chromic ion Cr(III)-O^2-Cr-(III) on zeolite does not seem to be reduced by carbon monoxide below 300 °C.

The marked difference in catalytic activities expressed in the term (produced CO_2 mol/Fe(II)·hr) of Fe(II) on X and Y type is described in the following section. The difference was also confirmed with other transition metal ions when they were on either X or Y zeolite. The key factor which controls the catalytic activity of a given transition metal ion should be ascribed to the structure of zeolite as ligand. Because of limited data obtained on only two types of zeolite, X and Y type, the correlation between catalytic activity and the structure has not been fully established yet.

The catalytic activities of some zeolite catalysts which were exchanged with transition metal ions in a higher valence state, Cu(II), Cr(III), Ni(II), were also examined (Table 3). The oxidation activity of Cu(II)

17) R. L. Burwell, Jr., G. L. Haller, K. C. Taylor, and J. F. Read, *Advan. Catal.*, **20**, 12 (1969).

Table 3. Catalytic activities of some zeolite Y catalysts for oxidation of carbon monoxide
Conditions: CO partial pressure 0.099 atm, O_2 partial pressure 0.179 atm
W/F 7.4 g-cat·hr/mol

Catalyst	Na(I) exchanged (%)	Reaction temperature (°C)	Conversion (%)
Fe(II)	36	280	17.2
Cu(I)	34	200	38.7
Cu(II)	54	200	0.8
Cr(III)	38	280	5.4
Ni(II)	39	300	0.93

and Ni(II) was much lower than that of Fe(II) and Cu(I). This is in line with the fact that oxygen is not adsorbed on Cu(II) and Ni(II) whose valences are difficult to enlarge.

A small amount of carbon monoxide was converted into carbon dioxide over Cu(II) zeolite Y, but the carbon monoxide does not seem to have reacted with oxygen activated by Cu(II) since no chemisorption of oxygen is observed (Table 1). Naccache and Taarit[18] showed that Cu(II) Y reduced by carbon monoxide gave no ESR signal of Cu(II) and that Cu(I) were detected by chemical analysis. They proposed a scheme for the reduction of Cu(II) Y by carbon monoxide as follows:

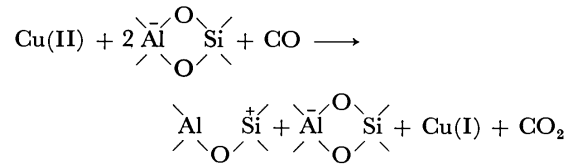

We have confirmed carbon dioxide formation when carbon monoxide was passed over the Cu(II) Y zeolite at 340 °C in the absence of oxygen. The amount of carbon dioxide produced was gradually reduced and the color of the Cu(II) Y catalyst turned from green to white. When the catalyst was allowed to stand in contact with air at room temperature its greenish color slowly reappeared.

It is not strange that Cr(III) showed a fairly good activity, because there is the possibility that heating of Cr(III) in the presence of oxygen can convert all or a part of it into Cr(VI).

Kinetics of CO Oxidation over Fe(II) Zeolite Catalysts. Some kinetic experiments have been made on the oxidation of carbon monoxide over Fe(II)–X and Fe(II)–Y catalysts, their degrees of sodium ion exchange being 42 and 36%, respectively. Experiments were carried out to study the difference in their activities quantitatively as a function of temperatu re (Fig.2). Dependence of the rate on carbon monoxide pressure was found to be nearly unity for both catalysts, while that on oxygen pressure was fractional, approximately 0.1 and 0.4 for Fe(II)–X and Fe(II)–Y, respectively (Fig. 3). These observations, together with the fact that no CO chemisorption was found on the catalysts, lead to a hypothesis that the reaction proceeds *via* the

18) C. M. Naccache and Y. B. Taarit, *J. Catal.*, **22**, 171 (1971).

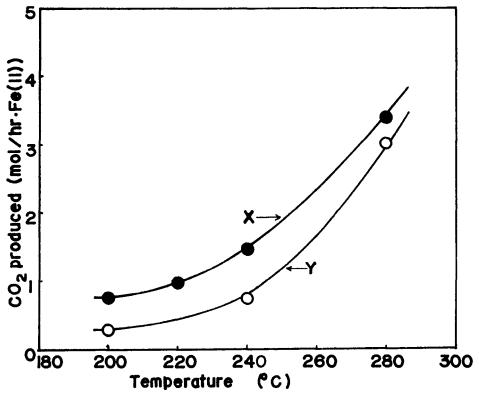

Fig. 2. Change of CO conversion against reaction temperature.
●: Fe(II)X, ○: Fe(II)Y
Conditions: P_{CO} 0.099 atm, P_{O_2} 0.179 atm
W/F 7.4 g-cat. hr/mol.

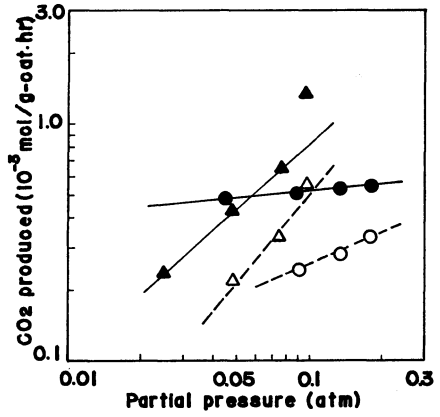

Fig. 3. Dependence of the rate on carbon monoxide and oxygen partial pressure.
Dependence on P_{CO}: ▲: Fe(II)X (220 °C), △: Fe(II)Y (240 °C) P_{O_2} 0.179 atm, W/F 7.4 g-cat. hr/mol
Dependence on P_{O_2} ●: Fe(II)X (220 °C), ○: Fe(II)Y (240 °C) P_{CO} 0.074 atm, W/F 7.4 g-cat. hr/mol

Rideal mecahnism, where carbon monoxide in the gas phase attacks oxygen which is adsorbed dissociatively on the catalysts. This is supported by the fact (Fig. 4) that the plot of reciprocal of the rate *vs.* reciprocal of the root of the oxygen partial pressure gives a straight line. Thus the following rate law holds.

$$r_{CO_2} = \frac{k\sqrt{K \cdot P_{O_2}}}{1+\sqrt{K \cdot P_{O_2}}} \cdot P_{CO}$$

By rearrangement we get

$$\frac{1}{r_{CO_2}} = \frac{1}{k\sqrt{K} \cdot P_{CO}} \cdot \frac{1}{\sqrt{P_{O_2}}} + \frac{1}{k \cdot P_{CO}}$$

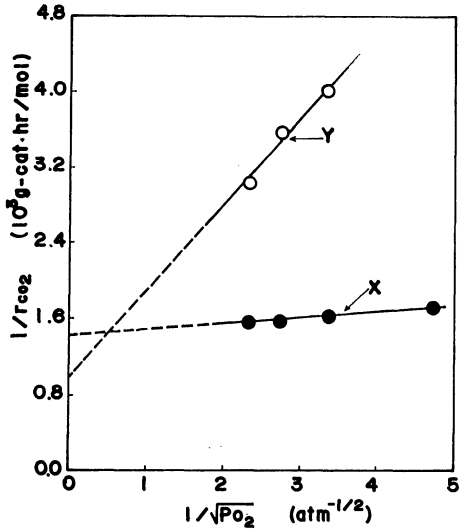

Fig. 4. Dependence of the rate on oxygen partial pressure.
●: Fe(II)X, (220 °C) ○: Fe(II)Y (240 °C)
Conditions: P_{CO} 0.074 atm, W/F 7.4 g-cat. hr/mol

The kinetic parameters obtained by a numerical analyis of the data are:

	Fe(II)X (220°C)	Fe(II)Y (240°C)
k(mol/g-cat.·hr·atm^{-1})	1.95×10^{-2}	2.73×10^{-2}
K(atm^{-1})	365	1.16

Because of the difference in reaction temperatures of the experiments for Fe(II)–X and Fe(II)–Y, comparison and interpretation of these kinetic parameters for carbon monoxide oxidation over the two catalysts would leave some ambiguities.

It might be tentatively concluded that Fe(II)–X catalyst adsorbs a larger amount of oxygen than Fe(II)–Y in their working states at temperatures 200—300 °C. This is supported by further findings on oxygen adsorption.

Skalkina *et al.*[7] reported that catalytic activity of X type zeolite incorporated with Fe(III) was higher than that of Y type for ammoxidation of propylene. Some reports suggested the difference to lie in the strength of electrostatic field near the metal ion for the corresponding X and Y types.[19,20] For carbon monoxide oxidation, the strength of electrostatic field may affect the catalytic activity.

19) P. E. Pickert, J. A. Rabo, E. Dempsey, and V. Schomaker, *Actes Congr. Intern. Catalyse.* 3, *Amsterdam*, **1964**, 714 (1965).
20) C. L. Angell and P. C. Schaffer, *J. Phys. Chem.*, **70**, 1413 (1966).

The Methylenation of Several Allylbenzene-1,2-diol Derivatives in Aprotic Polar Solvents

Harushige FUJITA and Masataro YAMASHITA

Department of Chemistry, Faculty of Science and Technology, Kinki University, Kowakae, Higashi-Osaka 577

(Received February 3, 1973)

The aprotic polar solvents, such as DMF (*N,N*-dimethylformamide) and DMSO (dimethyl sulfoxide), accelerated very effectively the methylenation of 1,2-dihydroxy-4- (I), 1,2-dihydroxy-3,4-dimethoxy-5- (II), and 1,2-dihydroxy-3-methoxy-5-allylbenzene (III) in the presence of bronze and cupric oxide as catalysts.

Recently, there are many effective insecticides derived from safrole. There have been many studies undertaken in an attempt to form an ether linkage of methylenedioxy compounds,[1-10] and these derivatives are being commercially produced. However, studies of the methylenation of 1,2-dihydroxyallylbenzenes have been discontinued since Perkin and Trikojus.[4] Although some 1,2-dihydroxybenzene derivatives containing an aldehyde group were methylenated in the presence of copper and related catalysts,[3,10] the yields of the products were poor.

The present authors studied the conditions for synthesizing methylenedioxy derivatives from 1,2-dihydroxy-4- (I), 1,2-dihydroxy-3,4-dimethoxy-5- (II), and 1,2-dihydroxy-3-methoxy-5-allylbenzene (III) in aprotic polar solvents in the presence of bronze and copper oxides, as no studies of the methylenation of these 1,2-dihydroxyallylbenzene derivatives in the presence of such catalysts in aprotic polar solvents (DMF and DMSO) were available.

Results and Discussion

The results are shown in Tables 1—3.

As Table 1 shows, acetone, methanol, and pyridine gave only a small amount of the product, whereas the

TABLE 1. METHYLENATION OF 1,2-DIHYDROXY-4-ALLYLBENZENE

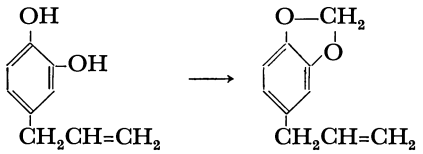

(I) (IV)

No.	(I) g	CH_2I_2 g	Catalyst g	Solvent ml	K_2CO_3 g	Yield of (IV) %
1	10	20	None	MeCOMe 50	20	7.9
2	10	20	CuO 1.0	MeCOMe 50	20	8.7
3	10	20	Bronze 1.0	MeCOMe 50	20	9.5
4	5	10	None	MeOH 50	10	poor
5	5	10	CuO 0.5	MeOH 50	10	poor
6	5	10	Bronze 0.5	MeOH 50	10	poor
7	5	10	None	C_5H_5N[a] 50	10	12.1
8	5	10	CuO 0.5	C_5H_5N[a] 50	10	15.0
9	5	10	Bronze 0.5	C_5H_5N[a] 50	10	14.5
10	10	20	None	DMF 100	20	54.1
11	10	20	Cu 1.0	DMF 100	20	53.3
12	10	20	Cu_2O 1.0	DMF 100	20	52.9
13	10	20	CuO 1.0	DMF 100	20	73.0
14	10	20	Bronze 1.0	DMF 100	20	74.3
15	5	10	None	DMSO 50	10	59.6
16	5	10	Cu 0.5	DMSO 50	10	57.2
17	5	10	Cu_2O 0.5	DMSO 50	10	55.5
18	5	10	CuO 0.5	DMSO 50	10	82.2
19	5	10	Bronze 0.5	DMSO 50	10	78.1

a) C_5H_5N: pyridine. The reactions were carried out in N_2 gas atmosphere, for 3 hr. The reaction temperature: No. 1—9, refluxed; No. 10—19, 120—125 °C (oil bath temp.).

1) C. Moureu, *Bull. Soc. Chim. Fr.*, (3), **15**, 655 (1896).
2) A. Sonn und F. Benirschke, *Ber.*, **54**, 1733 (1921).
3) K. N. Campbell, P. F. Hopper, and B. K. Campbell, *J. Org. Chem.*, **16**, 1736 (1951).
4) W. H. Perkin, Jr. and V. M. Trikojus, *J. Chem. Soc.*, **1926**, 2925.
5) E. Späth und R. Posega, *Ber.*, **62**, 1032 (1929).
6) W. Baker, *J. Chem. Soc.*, **1931**, 1765.
7) W. J. Gensler and C. M. Samour, *J. Org. Chem.*, **18**, 9 (1953).
8) E. D. Laskina, *J. Appl. Chem.*, (*U.S.S.R.*), **32**, 878 (1959).
9) E. D. Laskina, *ibid.*, **34**, 2338 (1961).
10) M. Tomita and Y. Aoyagi, *Chem. Pharm. Bull. Jap.*, **16**, 523 (1968).

Table 2. Methylenation of 1,2-dihydroxy-3,4-dimethoxy-5-allylbenzene

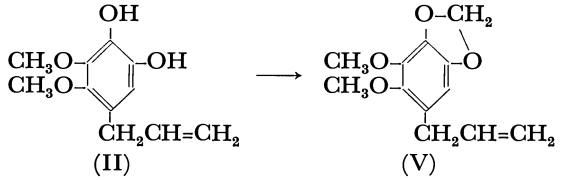

(II) (V)

Catalyst	Solvent	Yield of (V) %
None	DMF	55.4
CuO	DMF	74.1
Bronze	DMF	69.5
None	DMSO	61.0
CuO	DMSO	84.8
Bronze	DMSO	81.4

The reactions were carried out in N_2 gas atmosphere, at 120—125 °C (oil bath temp.) for 3 hr. An amount of each reactant: (II) 10 g, CH_2I_2 20 g, K_2CO_3 20 g; an amount of each catalyst, 1.0 g; an amount of each solvent, 100 ml.

Table 3. Methylenation of 1,2-dihydroxy-3-methoxy-5-allylbenzene

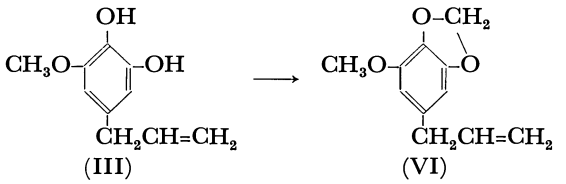

(III) (VI)

Catalyst	Solvent	Yield of (VI) %
None	DMF	54.1
CuO	DMF	72.3
Bronze	DMF	70.5
None	DMSO	59.0
CuO	DMSO	81.3
Bronze	DMSO	80.0

Each reaction was carried out as is described in the footnote to Table 2.

yields of the product were more than 50% when DMF and DMSO were used. The addition of bronze and cupric oxide as catalysts increased the yields about 20%, while the yields of the products in the presence of copper powder and cuprous oxide were about the same as the yields in the reactions without any catalyst. Therefore, in the methylenation of (II) and (III) DMF and DMSO were used as solvents. In these cases, the addition of bronze and cupric oxide as catalysts also increased the yields about 20%, as is shown in Tables 2 and 3, and DMSO was a little better than DMF as a solvent.

From these results, the authors found that cupric oxide and bronze were better catalysts than other catalysts in methylenation using a definite amount of catalysts, though no remarkable difference was remarked between the two catalysts. The addition of anhydrous potassium carbonate to the reactions would give good results in the case of solvents, DMF and DMSO, that greatly accelerate the nucleophilic substitution reaction, judging from the results that these aprotic polar solvents, DMF and DMSO, gave 54—61% yields for (IV), (V), and (VI). Further, it appeared that DMSO accelerated the reaction more effectively than DMF, judging from the fact that DMSO, being more stable than DMF in a basic solvent, gave the best results in the presence of alkali in these reactions. Therefore, DMSO should be a very effective solvent in the methylenation of 1,2-dihydroxy-allylbenzene derivatives.

Experimental

Catalysts. The bronze (Cu 65%, Zn 23%, Sn 1.5%, Fe 2%, Pb 0.3%) and copper powder were commercial products. The cuprous and cupric oxide were prepared according to the methods of Tomita *et al.*[11]

Reagents. The potassium carbonate and methylene diiodide were commercial products.

Solvents. The acetone, methanol, pyridine, DMF, and DMSO were purified by the distillation of commercial products.

Materials. The 1,2-dihydroxy-4- (I), 1,2-dihydroxy-3,4-dimethoxy-5- (II), and 1,2-dihydroxy-3-methoxy-5-allylbenzene (III) were prepared according to the methods of Perkin, and Trikojus,[12] Baker *et al.*,[13] and Trikojus and White[14] respectively.

General Synthetic Procedure. The materials, the methylene diiodide, the anhydrous potassium carbonate, and the catalysts were added to the solvents; then the mixture was reacted on an oil bath with stirring, as is shown in the tables. The reaction mixture was extracted with ether, washed with 3% HCl, 3% NaOH and water successively, and dehydrated with anhydrous Na_2SO_4. Then the product was obtained by distillation *in vacuo* after the removal of the solvent.

1,2-Methylenedioxy-4-allylbenzene (Safrole). Bp 94.0—94.5 °C/4 mmHg (lit,[12] bp 100—101.5 °C/10—11 mmHg). Beilstein's test for halogen: negative. n_D^{20} 1.5380 (lit,[12] n_D^{20} 1.5381). IR (KBr): 2786, 929, 717 cm^{-1} (O-CH_2-O). (Found: C, 74.08; H, 6.26%. Calcd for $C_{10}H_{10}O_2$: C, 74.05; H, 6.22%).

1,2-Methylenedioxy-3,4-dimethoxy-5-allylbenzene (Dillapiole). Bp 172—172.5 °C/16 mmHg (lit,[13] bp 172—173 °C/16 mmHg). Beilstein's test for halogen: negative. n_D^{20} 1.5276. IR (KBr): 2779, 926, 719 cm^{-1} (O-CH_2-O). (Found: C, 64.80; H, 6.39%. Calcd for $C_{12}H_{14}O_4$: C, 64.85; H, 6.35%).

1,2-Methylenedioxy-3-methoxy-5-allylbenzene (Myristicin). Bp 149—149.6 °C/15 mmHg (lit,[14] bp 95—97 °C/0.2 mmHg). Beilstein's test for halogen: negative. n_D^{20} 1.5409 (lit,[14] n_D^{20} 1.5426). IR (KBr): 2789, 928, 715 cm^{-1} (O-CH_2-O). (Found: C, 68.69; H, 6.31%. Calcd for $C_{11}H_{12}O_3$: C, 68.73; H, 6.29%).

11) M. Tomita, K. Fujitani, and Y. Aoyagi, *Chem. Pharm. Bull. Jap.*, **13**, 1341 (1965).
12) W. H. Perkin, Jr. and V. M. Trikojus, *J. Chem. Soc.*, **1927**, 1663.
13) W. Baker, E. H. T. Jukes, and C. A. Subrahmanyam, *ibid.*, **1934**, 1681.
14) V. M. Trikojus and D. E. White, *ibid.*, **1949**, 43k.

Preparation of Reinforcing Fillers from Japanese Acid Clays with Lime and by Calcination. II. Optimum Conditions for the Preparation of Good Hard Clays and Evaluation of Their Reinforcing Properties

Hideki RAI and Junkichi YAMADA*

Engineering Research Institute, Fuculty of Engineering, The University of Tokyo, Yayoi, Bunkyo-ku, Tokyo 113

(Received March 22, 1973)

In order to find the optimum conditions for the preparation of good reinforcing filler from Matsune (**M**) and Nakajo (**N**) acid clays with lime and by calcination, investigations were carried out by changing the amount of alkali (1.25—60% CaO), the temperature of thermal treatment (110—800 °C) and the subsequent mechanical disintegration time (6—24 hr). The required conditions were found to be: amount of alkali, 3% for **M** and 6% for **N**; calcination at 600 °C for 1.5 hr; disintegration time around 18 hr. The deviation in the optimum amount of alkali was attributed to the difference of mineralogical constituents. The products pulverized gave the SBR-1502 compounds good reinforcing properties comparable to those of Dixie Clay. Investigation was also carried out on the influence of manual and mechanical mixing of the raw materials, the mode of disintegrating the calcined matter by either wet ball-milling or dry pulverization, and the effect of sieving the pulverized product in wet or dry state on the reinforcing properties of the prepared fillers. A variable loading test with hard clay **M** up to 150 PHR proved that its reinforcing properties are comparable to those of the reference filler. The maximum reinforcement for the elastomer was found to be about 50 PHR for hard clay **M** and about 100 PHR for the reference filler.

The availability of some Japanese acid clays as raw material for the preparation of a reinforcing filler of elastomers was reported previously.[1] Acid clays such as **M** and **N** containing normal and/or abnormal montmorillonite and α-cristobalite as principal constituents were found to be suitable. However, no reinforcing filler could be prepared from Kuramitsu (**K**) acid clay containing halloysite as a major component in the randomly mixed layers of kaolinite and montmorillonite with no excess silica. **M** provided less colored and much better reinforcing fillers than **N**.

Treatment with hydrated lime (10% CaO) followed by calcination (600 °C, 1.5 hr) causes irreversible contraction in the montmorillonite minerals as well as the formation of calcium silicates covering the surfaces of montmorillonite crystallites. This gives rise to favorable changes in the inherent properties such as adsorptivity, pH, swelling, bulk density and specific gravity. The products pulverized exhibit considerable reinforcing effects on SBR-1502, which exceed Silene EF in the tensile strength and elongation of the loaded compounds. However, the reinforcing character still falls short of Dixie Clay.

This paper deals with further investigations to find the optimum conditions for the preparation of a good hard clay from the acid clays, Matsune **M** and Nakajo **N**; the amount of alkali, temperature of thermal treatment and subsequent mechanical disintegration time. Effects of mixing the raw materials manually and mechanically and of sieving the pulverized product in wet and in dry state on the reinforcing properties of the prepared filler were also investigated. Variations in the reinforcing characters due to the loading amounts were examined up to 150 PHR with hard clay **M**. The reinforcing effects of the prepared fillers on SBR-1502 were evaluated in comparison with those of Dixie Clay. Excellent fillers comparable to the references were obtained from both specimens.

Experimental

Raw Materials. *Acid Clays*: The same acid clays, **M** and **N**, as in the preceding paper[1] were used. Table 1 shows the chemical composition of the specimens, from which the structural formulas and excess silica were estimated.

M, white and powdery, consists only of normal montmorillonite containing excess silica (34%), whereas **N**, light yellowish gray and crushed under 6 mesh, consists of montmorillonites containing excess silica (13%), in which the amount of abnormal montmorillonite is greater than that of normal one.

Quicklime: Calcium oxide lumps (10—30 cm^3) of reagent grade were pulverized and grains smaller than 60 mesh were chosen.

Preparation of Reinforcing Fillers. The method essentially the same as before[1] was followed. Treatment was modified as follows: The amounts of alkali were varied in the range 1.25—60% CaO in weight of the acid clay dehydrated at 110 °C for 4 hr; the temperature of thermal treat-

TABLE 1. CHEMICAL COMPOSITION OF ACID CLAY

Sample	Symbol	SiO_2	TiO_2	Al_2O_3	Fe_2O_3	MnO	MgO	CaO	K_2O	Na_2O	$H_2O(+)$	$H_2O(-)$	Total	SiO_2/Al_2O_3
Matsune acid clay	**M**	67.12	0.08	11.53	0.79	0.27	3.07	1.10	0.18	0.07	5.10	10.85	100.16	9.87
Nakajo acid clay	**N**	53.35	0.16	14.94	2.75	0.09	4.80	0.06	0.28	0.06	7.30	16.46	100.25	6.06

* Present address: AA Chemical Company, Shiba-koen 2-3-4, Minato-ku, Tokyo.

1) H. Rai and J. Yamada, This Bulletin, **45**, 1540 (1972).

ment was 110—800 °C and the time of subsequent mechanical disintegration for the calcined matter 6—24 hr.

Effects of Mixing, Disintegration, and Sieving. The effect of mixing the raw materials according to the ball-milling method and that of manual grinding with a mortar and pestle was compared. The difference in mechanical disintegration in wet and dry states of the calcined matter was examined respectively by ball milling and dry pulverization with an atomizer (Tokyo Atomizer Co., Ltd). The effect of sieving the pulverized product in dry and wet states was also investigated.

Compounding Test. The same compounding test as described before[1] was carried out to screen the reinforcing fillers prepared. The effect of loading amounts of the best hard clay on the reinforcement of SBR-1502 was examined up to 150 PHR in comparison with those of Dixie Clay.

Results and Discussion

The Optimum Conditions for The Preparation of A Good Reinforcing Filler. A. Preparation and Reinforcing Properties of Hard Clay N: The amounts of alkali were made to be 3, 6, 10, 30, 50, or 60% CaO in weight. The raw materials were mechanically mixed in wet state with a porcelain ball mill for 1 hr. In view of the structural changes in acid clay revealed on the DTA and TGA thermograms,[1] the mixture dried at 110 °C was calcined at 400 °C to attain complete dehydration, at 600 °C for mid-dehydroxylation and

Table 2. Reinforcing effects of the fillers derived from N on SBR-1502 in comparison with those of Dixie Clay

Sample No.	Lime CaO (%)	Calcination Temperature, °C	Calcination Time, hr	Vulcanization time, min	Tensile strength kg/cm²	300% Modulus kg/cm²	Elongation %	Hardness JIS
1	10	800	1	8	18.3	12.5	474	56
				12	22.0	13.1	445	56
				16	26.0	12.8	517	55
2	30	800	1	8	28.3	17.3	420	60
				12	24.3	16.5	397	59
				16	24.3	16.6	304	61
3	50	800	1	8	24.3	18.6	346	64
				12	21.9	19.5	294	64
				16	24.3	19.1	323	64
4	10	600	1	8	74.0	17.3	851	53
				12	71.9	17.2	832	53
				16	76.1	17.8	846	54
5	30	600	1	8	53.3	27.2	538	64
				12	47.6	26.3	492	62
				16	47.0	26.2	486	63
6	50	600	1	8	33.3	23.8	401	65
				12	31.7	24.0	361	64
				16	33.3	23.8	375	66
7	10	400	1.5	8	51.8	12.8	891	45
				12	53.3	14.0	827	51
				16	57.8	14.2	827	52
8	30	400	1.5	8	64.0	22.1	620	51
				12	56.4	21.0	617	56
				16	52.7	20.5	618	55
9	60	400	1.5	8	32.6	25.9	320	60
				12	31.0	27.2	317	62
				16	28.2	25.3	299	62
10	3	400	1.5	8	22.7	8.0	888	40
				12	31.4	10.2	920	46
				16	33.3	11.1	834	49
11	3	600	1.5	8	51.8	14.5	804	39
				12	70.1	16.5	942	48
				16	74.9	18.4	882	51
12	3	800	1.5	8	32.6	14.2	541	51
				12	30.2	14.7	521	52
				16	27.5	14.6	509	53
13	6	600	1.5	8	68.4	13.3	925	42
				12	85.7	14.2	879	49
				16	93.8	16.2	831	51
14	Dixie Clay, reference filler			8	94.5	23.6	787	53
				12	94.1	27.1	785	55
				16	96.3	27.7	722	56

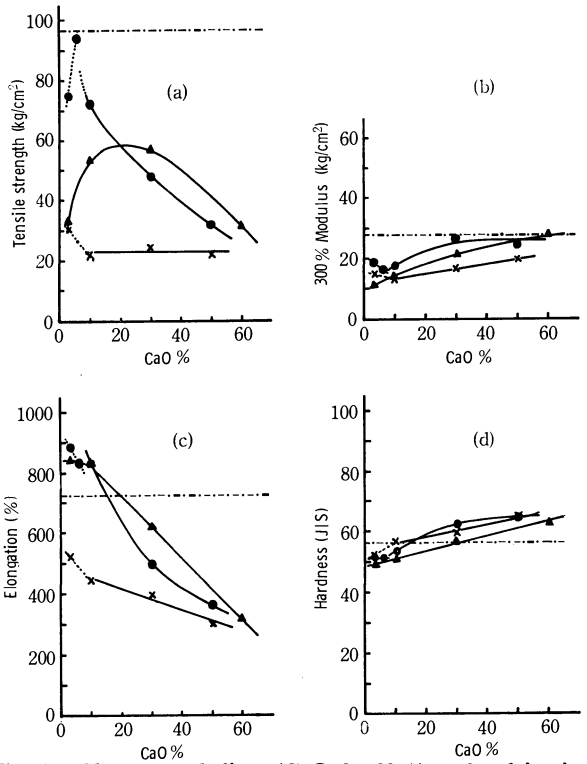

Fig. 1. Changes with lime (CaO 3—60%) and calcination (400—800 °C, 1—1.5 hr) in the reinforcing effects of **N** hard clay on SBR-1502 as compared with those of Dixie Clay.
×····× 800 °C, 1.5 hr: ●····● 600 °C, 1.5 hr; ▲—▲ 400 °C, 1.5 hr; ×—× 800 °C, 1 hr; ●—● 600 °C, 1 hr; ------ Dixie Clay

at 800 °C for complete dehydroxylation for 1 or 1.5 hr. The product was disintegrated by wet ball-milling at room temperature for 18 hr followed by filtration and drying at 110 °C. The dried matter was pulverized with an atomizer to give a reinforcing filler. The reinforcing effects of the prepared fillers on SBR-1502 are given in Table 2. Figures 1 (a)—(d) show the results obtained under the optimum conditions.

Tensile Strength (kg/cm²): The fillers prepared with hydrated lime (3—50% CaO) followed by calcination at 800 °C for 1 or 1.5 hr gave the lowest tensile strength which was almost independent of the variation in alkali corresponding to only 25% value of Dixie Clay (Fig. 1-(a)). Those treated with 3—60% CaO and by subsequent calcination at 400 °C for 1.5 hr exhibited a maximum tensile strength around 20% CaO, which was equivalent to about 60% value of Dixie Clay. Those prepared with 3—50% CaO followed by calcination at 600 °C for 1 or 1.5 hr showed a noticeable increase in the tensile strength with the decrease in the amount of alkali. The specimen treated with 6% CaO and by subsequent calcination at 600 °C for 1.5 hr exhibited the highest tensile strength comparable to that of Dixie Clay. However, the one treated with 3% CaO followed by the same calcination as the former showed an abrupt decrease in tensile strength about 78% value of Dixie Clay.

Modulus (300%, kg/cm²): Fillers prepared with 3—60% CaO and by subsequent calcination at 400 °C for 1.5 hr or 800 °C for 1 hr showed increase in the moduli with the increase in the amount of alkali (Fig. 1-(b)). The filler calcined at a lower temperature showed a greater rate in the increase in modulus than the one treated at a higher temperature with the same amount of alkali. Those prepared with 3—50% CaO followed by calcination at 600 °C for 1 hr exhibit an almost maximum modulus comparable to that of Dixie Clay with 30% CaO. The fillers prepared with CaO less than 10% and by calcination at temperatures 400—800 °C for 1 or 1.5 hr showed relatively lower modulus than that of Dixie Clay. This is in remarkable contrast to the case of hard clay **M**, and might be ascribed to the difference in the amounts of excess silica and abnormal montmorillonite.

Elongation (%): The fillers treated with CaO less than 10% followed by calcination at 400 or 600 °C for 1.5 hr gave considerably higher elongation than that of Dixie Clay (Fig. 1-(c)). The elongation decreases in proportion to the amount of alkali. When specimens were prepared with equal amount of alkali, the higher the calcinating temperature, the lower the elongation. The rate of decreasing elongation due to the amount of alkali was found to be great for the fillers calcined at 400 °C, but was relatively small for those treated at 800 °C.

Hardness (JIS): The fillers calcined at 400 °C for 1.5 hr or 800 °C for 1 hr showed a linear increase in hardness with the amount of alkali (Fig. 1-(d)). Those calcined at 600 °C for 1—1.5 hr afforded greater rate of increasing hardness with the amount of alkali than the former two series. A tendency to approaching a saturated value (64) was observable at 30% CaO, which was much greater than that (56) of Dixie Clay and comparable to that (65)[1] of Silene EF.

The optimum conditions of treatment with lime and by calcination for **N** may be concluded to be around 6% CaO and 600 °C for 1.5 hr, respectively. It is

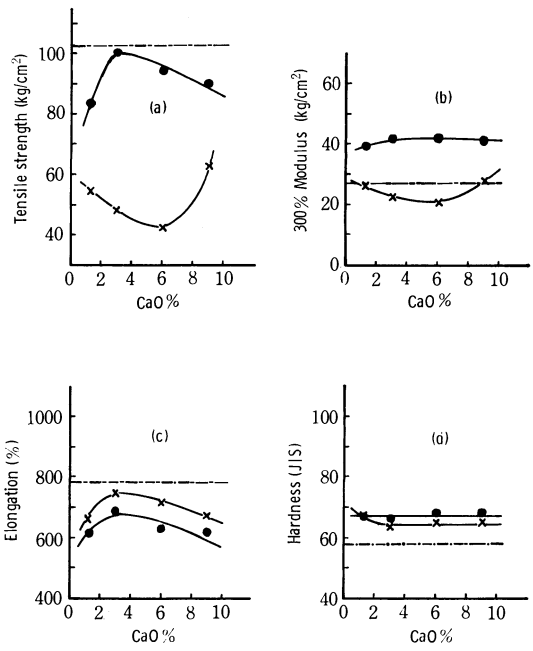

Fig. 2. Changes with lime (CaO 1.25—9%) and thermal treatment (110 °C, 5 hr; 600 °C, 1.5 hr) in the reinforcing effects of **M** hard clay on SBR-1502 as compard with those of Dixie Clay.
×—× 110 °C, 5 hr; ●—● 600 °C, 1.5 hr; ------ Dixie Clay

Table 3. Reinforcing effects of the fillers derived from **N** on SBR-1502 in comparison with those of dixie clay

Sample No.	Lime CaO (%)	Calcination Temperature, °C	Calcination Time, hr	Vulcanization time, min	Tensile strength kg/cm²	300% Modulus kg/cm²	Elongation %	Hardness JIS
1	1.25	110	5	8	55.6	24.8	723	65
				12	53.8	26.3	660	67
				16	55.9	26.2	668	67
2	3	110	5	8	50.1	21.0	802	62
				12	48.2	22.8	750	64
				16	48.7	23.1	684	65
3	6	110	5	8	38.5	19.0	770	62
				12	40.5	20.2	700	64
				16	41.9	20.4	717	65
4	9	110	5	8	58.7	26.7	727	63
				12	61.4	27.3	674	66
				16	62.2	27.8	677	65
5	1.25	600	1.5	8	84.8	35.0	750	64
				12	82.8	39.8	610	66
				16	83.6	38.4	616	67
6	3	600	1.5	8	94.2	35.4	793	62
				12	95.8	43.2	661	66
				16	100.1	41.4	688	66
7	6	600	1.5	8	86.8	35.9	667	65
				12	93.7	42.0	627	68
				16	91.9	39.9	660	68
8	9	600	1.5	8	87.9	36.3	640	65
				12	90.2	40.3	621	68
				16	88.4	45.6	602	68
9	Dixie Clay, reference filler			8	97.1	25.1	802	56
				12	102.6	27.3	783	58
				16	90.8	27.8	715	60

noticeable that regardless of the calcinating temperature, the reinforcing properties of the prepared fillers tend to approach their respective constant values around 60% CaO which much exceeds the amount of alkali equivalent to the excess silica estimated from the chemical composition of the original acid clay.

Curing Property: Owing to the remarkable adsorptivity[1] of the original acid clay, hard clay **N** tends to show a slow cure rate resulting in the poor reinforcing properties of the vulcanizates, which is attributable to the residual adsorptivity in the prepared filler. The 8 min vulcanizates containing the fillers treated with CaO less than 10% followed by calcination at 400 or 600 °C for 1.5 hr gave modulus and hardness lower than those of the 12 or 16 min vulcanizates (Table 2, No. 7, 10, 11, and 13). Treatment with CaO more than 10% and by calcination at 800 °C for 1 hr afforded the compounds normal cure. However, the formation of agglomerates, which were too hard to be disintegrated into sufficiently fine particles to give the desired strength, was unavoidable. Though the best sample (CaO 6%; calcination 600 °C, 1.5 hr; wet milling 18 hr) exhibited comparable tensile strength and higher elongation than those of Dixie Clay, its modulus was lower than that of the latter. Addition of some glycols or amines in the compounding may be expected to improve the lower modulus and tensile strength as well as the curing property like silica loading.[2]

B. Preparation and Reinforcing Properties of Hard Clay M: The preparation of good hard clay from **M** according to the same treatment with hydrated lime (3—60% CaO) and by subsequent calcination (400—800 °C, 1—1.5 hr) as mentioned above revealed that the optimum conditions were very close to those for **N**; the requisite amount of CaO lay in less than 10% and the calcination at 600 °C for 1.5 hr. Consequently **M** was treated with a less amount of CaO (1.25, 3, 6, or 9%) and then either calcined at 600 °C for 1.5 hr or dried at 110 °C for 5 hr in order to remove the moisture without calcination. Table 3 shows the reinforcing effects of the prepared fillers on SBR-1502 and Figs. 2 (a)—(d) demonstrate the results obtained under the optimum vulcanizing conditions.

Of all the fillers prepared from **M**, the one obtained with 3% CaO followed by calcination at 600 °C for 1.5 hr gave the loaded compound a maximum tensile strength comparable to that of Dixie Clay (Fig. 2-(a)). Although elongation 12% lower than that of Dixie Clay was observed, the modulus (300%) and hardness exceeded those of the reference filler by 52 and 14%,

2) Y. Hirata, "Science of New Industrial Materials for Rubber," A-4, ed. by T. Kuwata, Kanehara Publishing Co., Ltd., Tokyo, (1941), Chap. VI, p. 179.

respectively (Figs. 2 (b)—(d)). The increase in alkali above the optimum amount gave rise to a slow decrease in both tensile strength and elongation. The decrease in alkali gave an abrupt diminution in the reinforcing properties. However, nearly constant modulus (300%) and hardness were obtained irrespective of the variation in alkali. A remarkable difference in the reinforcement of SBR-1502 was found between the fillers calcined at 600 °C for 1.5 hr and those only dried at 110 °C for 5 hr without calcination. In spite of the relatively high elongation of the latter, the modulus and the hardness were lower than those of the former. Even the highest tensile strength at 9% CaO was found to be less than a 60% value of Dixie Clay. Investigations by DPG adsorption test and electron microscopy revealed that the noticeably low reinforcing properties could be attributed to the surface activity remaining in the filler, which causes the fine particles disintegrated in wet state to recondense into aggregates during the course of drying.

The optimum conditions can be concluded to be as follows. The optimum amount of quicklime is 3% for **M** and 6% for **N**; calcination at 600 °C for 1.5 hr. Variation in the optimum amount of alkali can be ascribed to the difference of the mineralogical constituents of the specimens, especially to the presence of abnormal montmorillonite, because it exhibits much greater adsorptivity and requires a greater amount of alkali than in normal one. The pulverized products thus prepared give the SBR-1502 compounds excellent reinforcing properties comparable to those of Dixie Clay.

C. Effects of Mixing, Disintegration, and Sieving: **M** (150 g) and quicklime (8.02 g, 6% CaO) were mixed for 1 hr manually with a mortar and pestle into a paste with 100 ml water (procedure M) or mechanically with a porcelain ball mill in slurry (procedure B).[1] After drying the mixture obtained by procedure M at 110 °C, the dried matter was calcined at 600 °C for 1.5 hr. The resulting product was ground by means of wet ball-milling for 6, 12, 18, or 24 hr. On being filtered off, the ground particles were dried again at

Table 4. Effects of mixing, disintegration, and sieving in the prepararion of hard clay **M** on the reinforcement of SBR-1502

Run No.	Mixing		Pulverization		Sieving[d]	Vulcanization time, min	Tensile strength kg/cm²	300% Modulus kg/cm²	Elongation %	Hardness JIS
	CaO (%)	Mode[a]	Mode[b]	Time[c] hr						
1	6	M_1	B_W	6	—	8	70.0	31.3	708	63
						12	74.2	33.2	718	64
						16	77.3	32.2	719	63
2	6	M_1	B_W	12	—	8	82.7	31.6	712	64
						12	81.0	33.0	700	64
						16	83.1	32.8	720	64
3	6	M_1	B_W	18	—	8	88.5	32.4	678	65
						12	83.5	34.0	661	65
						16	88.3	33.1	690	65
4	6	M_1	B_W	24	—	8	81.9	42.5	536	67
						12	83.2	43.7	508	67
						16	80.7	43.3	551	67
5	6	B_1	B_W	18	W_{300}	8	86.8	35.9	667	65
						12	93.7	42.0	627	68
						16	91.9	39.9	660	68
6	3	B_1	B_W	18	W_{300}	8	94.2	35.4	793	62
						12	95.8	43.2	661	66
						16	100.1	41.4	688	66
7	6	B_1	A_d	2*	—	8	14.3	11.0	549	56
						12	16.6	11.5	657	59
						16	18.7	12.9	794	62
8	6	B_1	A_d	2*	D_{200}	8	17.3	14.1	717	58
						12	18.0	11.9	794	59
						16	18.4	11.6	855	60
9	Dixie Clay, reference filler					8	97.1	25.1	802	56
						12	102.6	27.3	782	58
						16	90.8	27.8	715	60

a) M_1 and B_1 denote manual or mechanical mixing of raw materials for 1 hr respectively with a mortar and pestle and with a ball mill.

b) B_w and A_d denote pulveriztion of the calcined matter by wet ball-milling and with an atmoizer in dry state, respectively.

c) W_{300} and D_{200} denote sieving of the pulverized product with a 300 mesh standard sieve (JIS) in wet state and with a 200 mesh in dry state, respectively.

d) 2* indicates pulverization repeated twice.

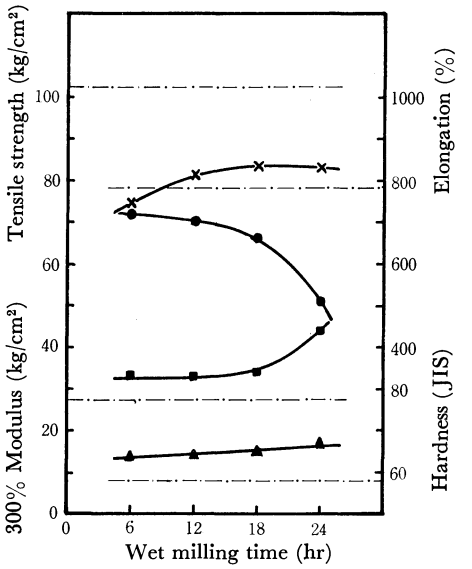

Fig. 3. Effects of wet ball-milling time in the preparation of **M** hard clay on the maximum reinforcement of SBR-1502 as compared with that of Dixie Clay.
×—× tensile strength (kg/cm²); ■—■ 300% modulus (kg/cm²); ●—● elongation (%); ▲—▲ hardness; ····· Dixie Clay

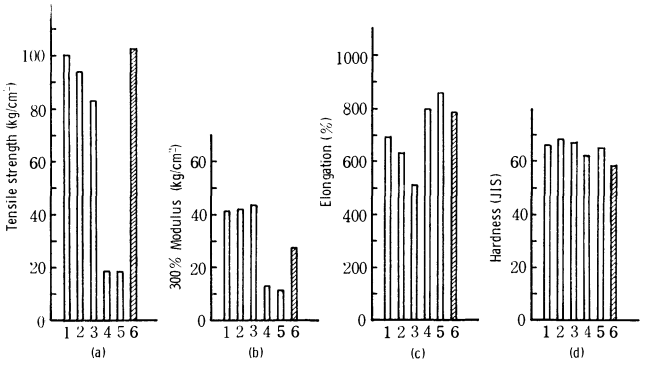

Fig. 4. Effect of admixing, pulverization, and sieving in the preparation of **M** hard clay on the reinforcement of SBR-1502 as compared with that of Dixie Clay.

Sample No.	Admixing		Pulverization		Sieving
	CaO %	Mode	Mode	Time, hr	
1	3	B_1	B_w	18	W_{300}
2	6	B_1	B_w	18	W_{300}
3	6	M_1	B_w	18	—
4	6	B_1	A_d	2*	—
5	6	B_1	A_d	2*	D_{200}
6 Dixie Clay, reference filler					

110 °C followed by pulverization with an atomizer (Table 4, Runs 1—4). Two samples mixed with alkali (3 and 6% CaO) by procedure B were prepared similarly by subsequent drying, calcination and wet ball-milling for 18 hr. In order to remove coarser particles, the disintegrated product was diluted with water to about 10% slurry and then made to pass through a 300 mesh standard sieve (JIS). Sieving after the milling for 18 hr, however, was found to be unnecessary. On being dried at 110 °C, the dehydrated product was pulverized with an atomizer to give a reinforcing filler (Table 4, Runs 5 and 6). Two more specimens mixed with alkali (6% CaO) by procedure B were obtained by the same treatment as above. Both calcined matters were disintegrated repeatedly in dry state with the atomizer. One of them was made to pass through a 200 mesh sieve before the compounding tests (Table 4, Run 8). The effects of the fillers thus prepared on the reinforcement of SBR-1502 were examined in comparison with those of Dixie Clay (Table 4). The results obtained under the optimum vulcanizing conditions are given in Figs. 3 and 4 (a)—(d).

So far as the calcined matter is concerned, the longer the wet milling time, the finer the resulting disintegrated particles. As disintegration proceeds sufficiently, a greater increase in the specific surface area contributes to a noticeable increase in the reinforcing capacity of the filler. The compound loading the filler, consequently, exhibited a considerable increase in tensile strength, modulus and hardness, accompanied by a remarkable decrease in the elongation as well (Fig. 3). The reinforcing properties were strictly or nearly in proportion to the wet milling time up to about 18 hr, and then approached a saturated value in the tensile strength or abrupt changes in the modulus (300%) and elongation. Both modulus and hardness far exceeded those of Dixie Clay, but the tensile strength and the elongation still fell short of the reference filler. This can be explained in terms of the effect of heterogeneous, manual mixing of the raw materials by procedure M as compared with the specimen (Table 3, No. 7) prepared by procedure B or mechanical mixing. A distinguishable difference in the reinforcing character between the fillers prepared by procedures B and M is ascribable to the high efficiency of the mechanical disintegration in mixing the raw materials (Table 4, Runs 3 and 5). Procedure B with a ball mill gives a homogeneous mixture leading to the promotion of the Pozzolanic reaction[3] between the acid clay and hydrated lime, which causes the formation of calcium montmorillonite as well as calcium silicate hydrates with the excess silica involved. As a result, the subsequent calcination proceeds so uniformly that any local sintering due to the polycondensation of acid clay itself can be avoided effectively. This should facilitate the pulverization of the calcined matter and contribute to the production of a better reinforcing filler.

The effect of sieving after the disintegration of calcined matter in dry or even in wet state on the reinforcing properties of the prepared filler was found to be relatively small or negligible as compared with that induced by the difference in procedure of mixing

3) a) S. Diamond, J. L. White, and W. L. Dolch, "Clay and Clay Minerals, Proc." 12th Natl. Conf., Pargamon Press, New York, N.Y. (1964), p. 359; b) C. G. Ruff and C. Ho, *High Way Research Board Bulletin*, (139), 42 (1966); c) G. R. Glenn and R. L. Handy, *ibid.*, (29), 70 (1963); d) C. Ho and R. L. Handy, *ibid.*, (29), 55 (1963); e) G. H. Hilt and D. T. Davidson, *ibid.*, (304). 51 (1961); f) J. L. Eades and R. E. Grim, *ibid.*, (262), 51 (1960); g) A. Ariizumi, "Advances in Clay Science," Vol. V, ed. by H. Minato, Clay Sci. Soc. Japan, Gihodo, Tokyo (1965), p. 219; h) R. Turriziani, "The Chemistry of Cements," Vol. 2, ed. by H. F. W. Taylor, Academic Press Inc., New York, N.Y. (1964), p. 69; i) W. Eitel, "The Physical Chemistry of the Silicates," Univ. Chicago Press, Chicago, (1954), III, p. 1255.

Table 5. Difference in reinforcing character due to loading amount between hard clay **M** (CaO 3%; calcination 600°C, 1.5 hr; wet milling 18 hr) and Dixie Clay

Exp. no.	Reinforcing filler		Vulcanization time, min	Tensile strength kg/cm²	300% Modulus kg/cm²	Elongation %	Hardness JIS
	Variety	PHR					
1	Blank	0	8	8.5	6.6	353	33
			12	8.1	6.8	242	40
			16	7.0	6.4	194	41
2	Hard clay **M**	50	8	89.8	12.3	921	43
			12	89.5	12.3	903	45
			16	97.5	12.7	905	45
3	Hard clay **M**	100	8	86.8	35.9	667	65
			12	93.7	42.0	627	68
			16	91.9	39.9	660	68
4	Hard clay **M**	150	8	85.4	60.0	346	87
			12	83.9	70.0	341	88
			16	84.3	70.0	329	88
5	Dixie Clay	50	8	57.4	15.0	827	48
			12	74.8	18.0	787	50
			16	72.9	18.7	751	51
6	Dixie Clay	100	8	97.1	25.1	802	56
			12	102.6	27.3	783	58
			16	90.8	27.8	715	60
7	Dixie Clay	150	8	53.2	34.8	460	56
			12	77.4	40.5	561	62
			16	91.4	46.5	574	65

and disintegration as well as the applied amount of alkali.

Thus pulverization of the calcined matters and the mixing of the raw materials are indispensable. Even if proper conditions are selected for treatment with lime and calcination as well as the raw materials, the filler prepared without being disintegrated sufficiently would not exhibit the maximum reinforcement of the elastomer. The reinforcement of an elastomer by loading inorganic fillers is caused by the interaction[4] between the filler and the elastomer. The greater the specific, effective surface area of the filler applied, *i.e.*, the smaller the fineness of the filler pulverized, the greater the reinforcing effects with a given amount of the prepared filler on the elastomer would be expected. Pulverization, therefore, is considered to be the most important process for the calcined matter and comprises a significant factor dominating the reinforcing character of the final product. From the viewpoint of the high efficiency of disintegrating the calcined matters, wet milling with a porcelain ball mill is more suitable than dry pulverization with an atomizer alone, and is considered to be indispensable for this purpose. Owing to its poor efficiency, the reinforcing properties of the fillers pulverized by the atomizer were hardly expect-

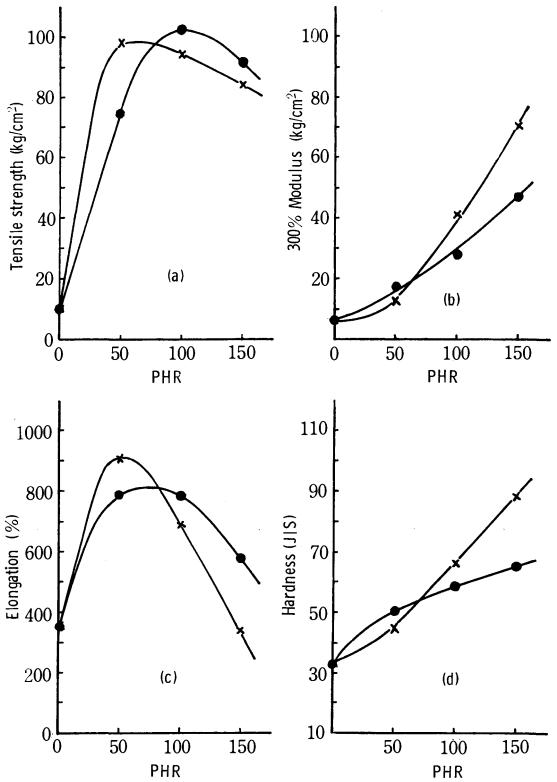

Fig. 5. Difference in reinforcing properties due to the loading amount between Dixie Clay and **M** hard clay (CaO 3%; calcination 600 °C, 1.5 hr; wet milling 18 hr).
×—× **M** hard clay; ●—● Dixie Clay

4) a) S. Yamashita, *Kogyo Kagaku Zasshi*, **73**, 50 (1970); b) G. Kraus, *Rubber Chem. Technol.*, **38**, 1074 (1965); c) J. A. Hockey, *Chem. Ind.* (London), 57 (1965); d) J. H. Bachmann, J. W. Sellers, M. P. Wagner, and R. F. Wolf, *Rubber Chem. Technol.*, **32**, 1286 (1959); e) E. Suito and M. Arakawa, *J. Soc. Rubber Ind. Jap.*, **36**, 704 (1963); *Kogyo Kagaku Zasshi*, **66**, 1615 (1963); f) E. Suito, *J. Soc. Rubber Ind. Jap.*, **34**, 441 (1962); g) A. R. Payne, *J. Appl. Polym. Sci.*, **6**, 57 (1962); h) F. Bueche, *ibid.*, **5**, 271 (1961); i) A. M. Bueche, *J. Polym. Sci.*, **15**, 105 (1955); *ibid.*, **25**, 139 (1957); j) A. F. Blanchard and D. Parkinson, *Ind. Eng. Chem.*, **44**, 799 (1952); k) J. Furukawa, *Kobunshi Kagaku*, **6**, 265 (1949); l) S. Yamashita, J. Furukawa, M. Fukuta, and T. Kotani, *J. Soc. Rubber Ind, Jap.*, **34**, 928 (1961); m) H. Hasegawa and Y. Furusawa, *ibid.*, **27**, 299 (1954); n) V. H. Vodra, *Rubber Age*, **71**, 507 (1952); o) L. H. Cohan and R. Spielman, *Ind. End. Chem.*, **40**, 2204 (1948).

able. Regardless of the relatively high elongation and hardness observable in the loaded compounds, the tensile strength and modulus were only 20—30% as low as those of Dixie Clay (Figs. 4 (a)—(d)).

D. Variable Loading Test with Hard Clay M: For investigating the difference in the reinforcing properties between Dixie Clay and the best filler obtained, hard clay **M** prepared under the optimum conditions (CaO 3%; calcination 600 °C, 1.5 hr; wet milling 18 hr) was subjected to a variable loading test with SBR-1502 ranging 0, 50, 100, and 150 PHR in weight (Table 5). Figures 5 (a)—(d) give the results obtained under the optimum vulcanizing conditions.

It is evident that the reinforcement with the prepared hard clay is comparable to that with Dixie Clay. However, some differences can be seen in the maximum reinforcement of the elastomer; hard clay **M** exhibits it around 50 PHR, Dixie Clay around 100 PHR. The former thus undergoes a greater change due to the loading amount than the latter. The deviation seems to be attributable to the particle size as well as morphological, structural, and physicochemical properties originating from the mineralogical constituents of the fillers.

Curing Property: All samples of hard clay **M**, even the one treated with minor alkali (CaO 1.25%) and dried at 110 °C for 5 hr without calcination, showed no such delay of cure as hard clay **N**, and gave higher reinforcing properties than those of the latter treated with the corresponding conditions (Table 3). The best sample (CaO 3%; calcination 600 °C, 1.5 hr; wet milling 18 hr) showed favorable reinforcing properties in tensile strength, modulus, and hardness which were equivalent or even higher than those of Dixie Clay in the tested range. The elongation was somewhat higher at lower loading than 75 PHR and a little lower at higher loading than those of the reference filler, the maximum reinforcement being observable for the low ratio, 50 PHR (Fig. 5).

Evaluation of Reinforcing Properties: From a practical viewpoint, white fillers with high modulus and hardness are useful. If the tensile strength of vulcanizates as well as the recipe and vulcanizability of compounds were equivalent, the higher modulus given by a filler is considered to be a measure of the greater reinforcing capacity.[5] In a variable loading test, such a filler exhibits the maximum tensile strength at a relatively low ratio. Though negative effects of the filler on the tear resistance and flexing life of the vulcanizate are inevitable, better abrasion resistance can be expected as well. In case of hard clay **M**, however, the negative effects are assumed to be relatively small because of the less diminution of elongation and tensile strength in the variable loading test in spite of the high modulus and hardness.

Consequently hard clay **M** might excel as a reference filler in its reinforcing properties such as modulus, hardness, and abrasion resistance.

The authors are grateful to the late Prof. T. Kuwata and Assoc. Prof. J. Kumanotani for many helpful discussion and suggestions during the course of this work, and to Mr. Y. Sugawara, president of Mizusawa Industrial Chemicals Co., Ltd. for providing samples of acid clay.

5) a) J. Yamada, *J. Soc. Rubber Ind. Jap.*, **44**, 107 (1971); b) H. Westlinning, *Kautschuk u. Gummi*, **20**, 51 (1967); c) Y. Sato, *J. Soc. Rubber Ind. Jap.*, **31**, 677 (1958); d) E. Guth, *J. Appl. Phys.*, **16**, 20 (1945); e) H. Smallwood, *ibid.*, **15**, 758 (1944).

BULLETIN OF THE CHEMICAL SOCIETY OF JAPAN, VOL. 46, 3562—3565 (1973)

The Selective Hydrogenation of α-Methylcinnamaldehydes Catalyzed by Cobalt Carbonyl in the Presence of Amines

Kunio KOGAMI and Ju KUMANOTANI*

T. Hasegawa Co., Ltd, Nihonbashi, Chuo-ku, Tokyo 103

**Institute of Industrial Science, University of Tokyo, Roppongi, Minato-ku, Tokyo 106*

(Received May 9, 1973)

The selective hydrogenation of α-methylcinnamaldehydes to the hydrocinnamaldehydes, catalyzed by cobalt carbonyl and a limited amount of amines, has been investigated. The addition of such amines as diisopropylamine, diethanolamine, tributylamine, triethylamine, and pyridine showed a remarkable selectivity and gave the desired α-methylhydrocinnamaldehydes in 96.4—91.5% theoretical yields. Especially, diisopropylamine gave the best selectivity, in it the yields of *p-t*-butyl-α-methylhydrocinnamaldehyde and cyclamenaldehyde amounted to 96%. The optimum amount was found to be 1.0—1.3 equivalents of cobalt carbonyl.

p-t-Butyl-α-methylhydrocinnamaldehyde (lilyal) and *p*-isopropyl-α-methylhydrocinnamaldehyde (cyclamenaldehyde), the most appreciated synthetic perfumes, are prepared industrially by two well-known processes, *viz.*, the dehydrogenation of the corresponding alcohol using a Cu–Zn catalyst[1] and the selective hydrogenation of the cinnamaldehyde using a palladium-alumina catalyst containing potassium acetate.[2]

Previously we have reported a selective hydrogena-

1) S. Abe and T. Yasukawa, *Yuki Gosei Kagaku Kyokai Shi*, **22**, 144, 209 (1964).

2) D. Morris, E. Daniel J, and S. Alfred, U.S. 3520934 (1970).

tion of *p*-isopropyl-α-methylcinnamaldehyde to cyclamenaldehyde with a cobalt carbonyl catalyst or its ligand-substituted complex under oxo conditions.[3] It was found that a tris(2-bromoethyl) phosphite-substituted cobalt carbonyl gave the best yield (86.3%) among those substances unsubstituted and substituted with PR_3, $P(OR)_3$, and $PO(OR)_3$ (R=alkyl, aryl).

Wender *et al.*[4] have reported on the behavior of amines in the hydroformylation of cyclohexene as follows: 1) The rate of hydroformylation is increased by the addition of a small amount of organic amines, but decreased with a larger amount of them. 2) Both the basicity and the steric factor of the amines affect the rate of the reaction. Matsuda and Uchida[5] have proved that the addition of an appropriate amount of pyridine improves not only the selectivity for the hydroesterification of propylene with carbon monoxide and methanol, but also the rate of conversion. These findings urged us to study more closely the effect of organic amines upon the rate and the selectivity of the hydrogenation of the cinnamaldehyde under controlled oxo conditions.

The present paper will describe the selective hydrogenations of *p*-*t*-butyl-α-methylcinnamaldehyde and *p*-isopropyl-α-methylcinnamaldehyde using a cobalt carbonyl catalyst in the presence of various organic amines. Diisopropylamine was found to be the best and gave the highest yields, 96.4 and 96.2%, for lilyal and cyclamenaldehyde respectively.

Experimental

Materials. *p*-*t*-Butyl-α-methylcinnamaldehyde (I) was prepared according to the Knorr method[6] in the same manner as *p*-isopropyl-α-methylcinnamaldehyde (II).[3] I; bp 114—116 °C/1 mmHg, mp 69 °C, purity by gas liquid chromatography (glc) 100%. The dicobalt octacarbonyl (mp 51 °C) was the same as has been described in previous papers.[3,7] It was used with one of the following organic amines in an equimolar ratio or a little more in relation to dicobalt octacarbonyl in isopropyl ether:[5] Triphenylamine, 3-aminopropionitrile, quinoline, pyridine, dimethylaniline, diethanolamine, isopropylamine, cyclohexylamine, triethylamine, tributylamine, diisopropylamine, and piperidine. They were all chemically pure-grade reagents, purchased from the Tokyo Kasei Co., Ltd.

Procedure. I or II (0.3 mol, 60.6 or 56.4 g respectively) and a solution of dicobalt octacarbonyl (5.2 mmol, 1.8 g) in isopropyl ether (150 ml) containing a small amount of an amine were put into a 500 ml stainless steel autoclave equipped with an outlet for sampling. The air in the autoclave was flushed with nitrogen several times. Then the autoclave was filled with water gas (65 kg/cm², H_2: CO=12: 1) at room temperature, heated to 107 °C in 30 min, and stirred. The temperature was kept within a range of ±1 °C during the reaction. During the reaction, small amounts of the reaction mixture were withdrawn at prescribed time intervals for glc analysis. Hydrogenation was continued until the peak of I or II disappeared. The end point was checked from the gauge-time relation as well. The rate of hydrogenation was then estimated from the depression in the pressure. The rate constant (k) of hydrogenation was obtained according to the following equation:

$$k = 2.303 \log (P_o - P_f)/(P_t - P_f)/t$$

where P_o is the initial pressure at the beginning of stirring, where P_f is the final one at the end of the reaction, and where P_t is the one at time t.

In the case of constant-pressure experiments, hydrogen was continuously introduced from a pressure storage tank through a needle valve in order to keep the total pressure constant throughout the reaction. After the hydrogenation, the autoclave was cooled and the remaining gas was eliminated. An aqueous solution (150 ml) of 0.25 M iodine–potassium iodide and an acetic acid–isopropyl ether solution (1: 100 v/v, 150 ml) were stirred in 1 hr to decompose the cobalt carbonyl catalyst. The upper layer was separated, washed with 300 ml of 5% aqueous hydrosulfite and subsequently with 200 ml of 5% aqueous sodium carbonate, and dried over sodium sulfate. After the removal of the ether, an oily product was distilled *in vacuo*; this separated volatile products and a resinous matter (1—3% by weight) through a packed column-type rectifier.

Identification of the Products. Lilyal and the corresponding alcohol, *p*-*t*-butyl-α-methylhydrocinnamyl alcohol (III), in the products were separated by distillation through the packed column-type rectifier and identified by means of their NMR spectra in $CDCl_3$ with tetramethylsilane as the internal standard, on a JEOL 4H-10 spectrometer. As the NMR spectra and physical constants of cyclamenaldehyde and cyclamenalcohol, were described in a previous paper,[3] they will be omitted here. Lilyal: Bp 96—98 °C/1 mmHg, d_{25}^{25} 0.9385, n_D^{25} 1.5056. NMR spectrum: 1.05 ppm (d) doublet (J=2.5 Hz) methyl 3H; 1.30 ppm (s) singlet *t*-butyl 9H; 2.52 ppm (d) methylene 2H; 3.0 ppm (m) multiplet methine H; 7.10 ppm (m) phenyl 4H; 9.6 ppm (s) aldehyde H. III: Bp 106—108 °C/1 mmHg, d_{25}^{25} 0.9360, n_D^{25} 1.5068. NMR spectrum: 0.90 ppm (d) (J=3.0 Hz) methyl 3H; 1.30 ppm (s) *t*-butyl 9H; 1.55 ppm (d) methylene 2H; 1.82 ppm (bs) broad singlet hydroxy H; 1.87 ppm (m) methine H; 3.30 ppm (d) hydroxymethylene 2H; 7.10 ppm (m) phenyl 4H.

The composition of the aforementioned oily product and the volatile matter were determined by the normalization method with glc, using a gas chromatograph, Kotaki GU-21, equipped with a 2 m stainless steel column of KF 54 (5% by weight) on Celite 545 sk (60—80 mesh) at 180 °C. They were analyzed within a relative experimental error of ±1.5%. Authentic lilyal was prepared by the dehydrogenation of III with a Cu-Zn catalyst (bp 96—98 °C/1 mmHg, d_{25}^{25} 0.9387, n_D^{25} 1.5058) and III by the catalytic hydrogenation of I over a nickel diatomaceous earth catalyst (bp 106—108 °C/1 mmHg, d_{25}^{25} 0.9357, n_D^{25} 1.5065).

Results and Discussion

In the preceding paper,[3] we reported that the conversion of cinnamaldehyde into hydrocinnamaldehyde can be increased by both increasing the pressure of hydrogen in water gas and by the use of a 2.0—2.5-fold volume of solvent for the cinnamaldehyde.

On the basis of those results, the foregoing experiments were carried out using dicobalt octacarbonyl

3) K. Kogami, O. Takahashi, and J. Kumanotani, This Bulletin, **45**, 604 (1972).

4) I. Wender, H. W. Sternberg, and M. Orchin, "Catalysis," **V**, Reinhold Publishing, N.Y. (1957), p. 110.

5) A. Matsuda and H. Uchida, This Bulletin, **38**, 710 (1965).

6) A. Knorr and A. Weissenborn, U.S. 1844013 (1932).

7) S. Usami, T. Kondo, K. Nishimura, and Y. Koga, This Bulletin, **42**, 2961, 2966 (1969).

Table 1. Hydrogenation of cinnamaldehydes in the presence of pyridine

Run	Cinnamaldehyde[a]	Organic amine (mmol)	Molar ratio Amine/$Co_2(CO)_8$	k_1[b] (min^{-1})	SP[c] (%)
1	I	None		0.0030	79.6
2	II	None		0.0031	81.8
3	I	Pyridine, 2.6	0.5	0.0036	86.5
4	I	Pyridine, 5.2	1.0	0.0042	92.6
5	I	Pyridine, 7.8	1.5	0.0038	88.4
6	II	Pyridine, 2.6	0.5	0.0037	87.2
7	II	Pyridine, 5.2	1.0	0.0042	93.0
8	II	Pyridine, 7.8	1.5	0.0039	89.4

a) I or II (0.3 mol, 60.6 or 56.4 g, respectively) was hydrogenated in 150 ml of isopropyl ether using 5.2 mmol of $Co_2(CO)_8$ as catalyst at 107 ± 1 °C and 65 kg/cm², initial pressure of water gas (H_2: CO=12: 1).
b) $k_1=2.303\log[(P_o-P_f)/(P_t-P_f)]/t$.
c) SP designates Selective Parameter given by the eqation; hydrocinnamaldehyde × 100%/(hydrocinnamaldehyde + hydrocinnamyl alcohol).

with or without pyridine, often used in conventional hydroformylations, under the following favorable conditions:[3] At 107 ± 1 °C and 65 kg/cm² of the initial pressure of water gas (H_2: CO=12: 1). They revealed that the hydrogenation of I or II apparently obeyed a first-order kinetics in the partial pressure of hydrogen and that the addition of pyridine not only increased the rate of hydrogenation, but also improved the selectivity for forming lilyal or cyclamenaldehyde (Table 1). Equimolar pyridine to dicobalt octacarbonyl increased the rate and the selectivity of the hydrogenation; however, greater or lesser amounts had negative effects. The analysis of the hydrogenation products in the presence of pyridine proved the absence of the hydroformylates formed. Plots of the consumed amount of cinnamaldehyde against the reaction time gave a linear relation under a constant pressure of hydrogen, indicating that the hydrogenation was first order in the partial pressure of hydrogen, and zero order in the concentration of cinnamaldehyde, when a small amount of pyridine existed (Fig. 1).

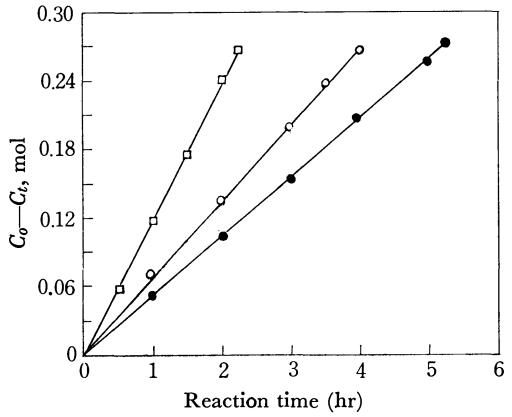

Fig. 1. Plots of the consumed amount of cinnamaldehyde, C_o-C_t, *vs.* reaction time at 107 ± 1 °C and 65 kg/cm² the total pressure of water gas (H_2: CO=12: 1) in the presence of pyridine.

Run	$Co_2(CO)_8$ mmol	Pyridine mmol	*S P* %
□	6.4	6.4	91.3
○	5.2	5.2	93.7
●	2.9	2.9	89.5

C_0; the initial molar concentration of I.
C_t; the molar concentration of I at reaction time *t*.

Iwanaga[8] observed that the rate of the hydroformylation of methyl acrylate in benzene under an oxo condition is nearly doubled with only a small amount of pyridine, and that the pyridine accelerates the rate of the reaction by forming an intermediate complex (Eq. 2), which is then rapidly converted into cobalt hydrocarbonyl by the subsequent hydrogenation (Eq. 3). The amount of free cobalt hydrocarbonyl, however, decreases upon combination with amine (Eq. 4) and increases with the increased basicity of the amine applied. Some amines with low steric requirements, such as pyridine, can replace the free cobalt hydrocarbonyl (Eq. 5):[5]

$$Co_2(CO)_8 + H_2 \longrightarrow 2HCo(CO)_4 \quad (1)$$

$$Co_2(CO)_8 + 2B \longrightarrow (CO_4)Co\cdots Co(CO)_4 \quad (2)$$
$$\qquad\qquad\qquad\qquad\quad \vdots\ \ \vdots$$
$$\qquad\qquad\qquad\qquad\quad B\ \ B$$
$$\qquad\qquad\qquad\qquad\quad \text{Complex}$$

$$\text{Complex} + H_2 \longrightarrow 2HCo(CO)_4 + 2B \quad (3)$$

$$HCo(CO)_4 + B \longrightarrow (BH)^+(Co(CO)_4)^- \quad (4)$$

$$HCo(CO)_4 + B \longrightarrow HCo(CO)_3B + CO \quad (5)$$

In the hydrogenation of α,β-unsaturated carbonyl compounds catalyzed by cobalt hydrocarbonyl, the saturated carbonyl compounds formed are very slowly transformed into the corresponding alcohols.[3,9] This indicates that the cobalt hydrocarbonyl coordinate more intimately around the carbonyl group of cinnamaldehyde than around that of hydrocinnamaldehyde, resulting in the formation of the π-oxapropenyl intermediate complex.[10] Furthermore, the slow transformation into the hydrocinnamyl alcohol can be interpreted in terms of the difficulty in the formation of the cyclic-transition-state intermediate between the cobalt hydrocarbonyl and the hydrocinnamaldehyde.[11] Consequently, the favorable selectivity in the formation of hydrocinnamaldehyde is considered to occur with the cobalt hydrocarbonyl produced by strong amines with appropriate steric factors. In order to

8) R. Iwanaga, This Bulletin, **35**, 865, 869 (1962).
9) L. Marco, *Proc. Chem. Soc.*, 1962, 67.
10) R. W. Goetz and M. Orchin, *J. Org. Chem.*, **27**, 3698 (1962).
11) R. W. Goetz and M. Orchin, *J. Amer. Chem. Soc.*, **85**, 2782 (1963).

TABLE 2. SELECTIVE HYDROGENATION OF CINNAMALDEHYDES IN THE PRESENCE OF ORGANIC AMINES

Run	Cinnamaldehyde[a] Variety	Amine mmol	React. time min	Rate $k_1 \times 10^8$ (min^{-1})	SP (%)	Hydrocinnamaldehyde[b] %
1	I	None	393	3.0	79.6	78.2
2	I	Triphenylamine, 5.2	786	1.5	80.3	78.5
3	I	3-Aminopropionitrile, 5.2	590	2.0	80.5	78.5
4	I	Quinoline, 5.2	281	4.2	88.5	86.5
5	I	Pyridine, 5.2	281	4.2	92.6	91.5
6	I	Dimethylaniline, 5.2	282	4.2	88.3	86.3
7	I	Diethanolamine, 5.2	262	4.5	93.4	92.5
8	I	Isopropylamine, 5.2	263	4.5	89.8	88.4
9	I	Cyclohexylamine, 5.2	262	4.5	85.6	85.2
10	I	Triethylamine, 5.2	245	4.8	93.2	92.0
11	I	Tributylamine, 5.2	241	4.9	94.2	93.0
12	I	Diisopropylamine, 5.2	190	6.2	96.3	95.1
13	I	Piperidine, 5.2	190	6.2	87.8	86.2
14	I	Diisopropylamine, 6.8	200	5.9	97.5	96.4
15	I	Diisopropylamine, 7.8	210	5.6	95.4	94.1
16	II	Diisopropylamine, 6.8	200	5.9	97.6	96.2

a) I or II (0.3 mol, 60.6 or 56.4 g, respectively) was hydrogenated in 150 ml of isopropyl ether at 107±1 °C and 65 kg/cm² of water gas (H_2: CO, 60: 5) with 5.2 mmol of $Co_2(CO)_8$ as catalyst.
b) Theoretical yield of lilyal or cylcamenaldehyde.

establish the optimum conditions for obtaining the hydrocinnamaldehydes, the hydrogenation was investigated with various organic amines such as diisopropylamine, tributylamine, triethylamine, and pyridine. The results obtained are shown in Table 2.

The applied amines showed increasing effects on the rate of hydrogenation as well as on the selectivity in the formation of the hydrocinnamaldehyde, in accordance with the order of basicity. The rates of hydrogenation were found to be as follows: Triphenylamine (pK_b=14.0)<3-aminopropionitrile (pK_b=11.9)<quinoline (pK_b=9.0), pyridine (pK_b=8.96) and dimethylaniline (pK_b=8.94)<diethanolamine (pK_b=5.52), isopropylamine (pK_b=3.34) and cyclohexylamine (pK_b=3.32)<triethylamine (pK_b=3.32)<tributylamine (pK_b=3.11)<diisopropylamine (pK_b=2.89), and piperidine (pK_b=2.79). Smaller rate constants were observed with triphenylamine and 3-aminopropionitrile, which gave almost the same selectivity in the formation of hydrocinnamaldehyde as in the absence of an amine. Quinoline, dimethylaniline, isopropylamine, cyclohexylamine, and piperidine had only feeble effects on increasing the selectivity, although larger rate constants of hydrogenation were obtained. This can be explained in terms of the persistency of activity for the further conversion of hydrocinnamaldehyde into hydrocinnamyl alcohol in the cases of amines with a relatively stronger basicity and less steric hindrance. Pyridine, diethanolamine, triethylamine, tributylamine, and diisopropylamine showed larger rate constants of hydrogenation, in good argeement with the order of basicity, and showed the best effects in producing hydrocinnamaldehyde. In spite of the weak basicity and small steric effect, pyridine affords good selectivity in the formation of hydrocinnamaldehydes. The knowledge[5] at present available on the catalytic behavior of $HCo(CO)_3Py$ can not make possible a satisfactory interpretation of the effect.

Among the effective amines, diisopropylamine gave the largest rate constants and the best selectivity; the yields of lilyal and cyclamenaldehyde amounted to 96%, suggesting the effectiveness of both the strong basicity and the appropriate bulkiness. The optimum amount of diisopropylamine was found to be 1.0—1.3 equivalents, based on the dicobalt octacarbonyl.

The authors wish to express their gratitude to Mr. Shozo Hasegawa, the President of T. Hasegawa, Co., Ltd, for his permission to publish this paper. The authors also wish to thank Professor Shigeo Nishimura, Tokyo University of Agriculture and Technology, for his valuable suggestions and helfpul discussions.

NOTES

BULLETIN OF THE CHEMICAL SOCIETY OF JAPAN, VOL. 46, 3566—3567 (1973)

Modifying Effect of Acetic Acid or Triphenylphosphine on the Raney Cobalt Catalyst in the Liquid-phase Hydrogenation of an Aliphatic α,β-Unsaturated Aldehyde

Kazuhiko HOTTA and Teruo KUBOMATSU
The Osaka Municipal Technical Research Institute, Kita-ku, Osaka 530
(Received November 13, 1972)

In our previous papers,[1,2] we have reported that, in the hydrogenation of the α,β-unsaturated aldehyde, 2-methyl-2-pentenal(UD), over the Raney cobalt catalyst with or without modifiers, the products are the saturated aldehyde 2-methylpentanal(SD), saturated alcohol 2-methylpentan-1-ol(SA), and unsaturated alcohol 2-methyl-2-penten-1-ol(UA), and that the initial rates of formation of the three products, r_{SD}, r_{SA}, and r_{UA}, can be represented by the following Langmuir-type rate equations:

$$r_{SD} + r_{SA} = k_1 b_1 C_{UD}/(1+b_1 C_{UD})^2 \quad (1)$$

$$r_{UA} = k_2 b_2 C_{UD}/(1+b_2 C_{UD})^2 \quad (2)$$

where k and b denote the rate constant of the surface reaction and the adsorption parameter for UD and hydrogen[3] respectively; where the subscripts 1 and 2 represent the formation of SD and SA and that of UA respectively, and where C_{UD} refers to the liquid-phase concentration of UD. There it has also been shown that k_1 decreases with an increase in the amounts of Mn- and $CoCl_2$ added, while k_2 does not change or increases with the addition of a small amount of the modifiers.

In the present note, the variation in the kinetic parameters with the amounts of added acetic acid (AcOH) and triphenylphosphine(PPh_3) is examined. The variation of k_1 and k_2 over the AcOH-modified catalyst is found to be similar to that over the $MnCl_2$- and $CoCl_2$-modified catalysts, but both k_1 and k_2 are decreased by the addition of PPh_3. It can be concluded that the acidic modifiers, such as AcOH, $MnCl_2$, and $CoCl_2$, promote the formation of UA.

Experimental

The Raney cobalt catalyst was prepared as has previously been reported.[1] The catalyst was modified by injecting a hexane solution of AcOH or PPh_3 to the catalyst–hexane–hydrogen system and by stirring the mixture.

The rate measurements were carried out as has been reported in a previous paper.[1]

Results

The products of the reaction were found to be SD, SA, and UA. The dependence of the initial rates on C_{UD} over the AcOH-modified catalyst are shown for r_{SD} and r_{SA} in Fig. 1, and for r_{UA} in Fig. 2.

Since the formation of SD and SA and that of UA can be treated separately,[1,2] the rate data in Figs. 1 and 2 were analyzed by means of Eqs. (1) and (2) respectively, and the kinetic parameters, k_1, k_2, b_1, and

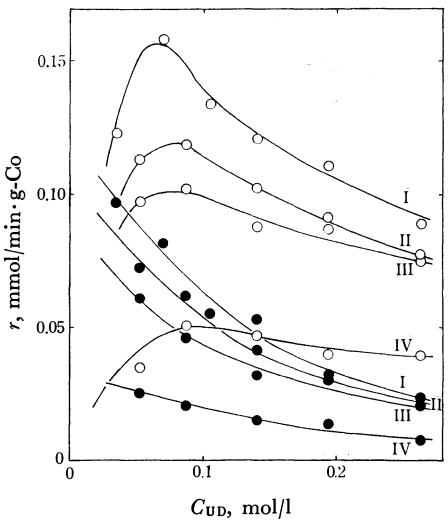

Fig. 1. Concentration dependence of the initial rate of formation of SD, ○; SA, ●, in the presence of AcOH of 0.0, I; 0.035, II; 0.070, III; 0.175 mmol/g-Co, IV at 40 °C.

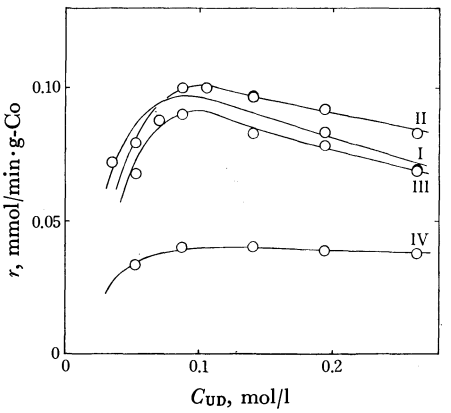

Fig. 2. Concentration dependence of the initial rate of formation of UA. Same notations as in Fig. 1.

1) K. Hotta and T. Kubomatsu, This Bulletin, **44**, 1348 (1971).
2) *Idem, ibid.*, **45**, 3118 (1972).
3) The accurate definition of b is: $b=K_{UD}/(K_H \cdot C_H)$, where C_H refers to the liquid phase concentration of hydrogen and is assumed to be constant at a given temperature, and where K_{UD} and K_H denote the adsorption equilibrium constants of UD and hydrogen, respectively.

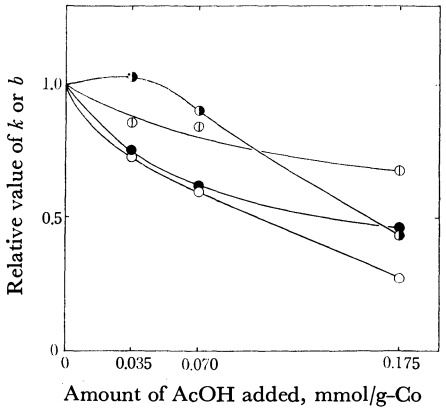

Fig. 3. Variation of the rate constant and adsorption parameter with the amount of AcOH, k_1, ○; k_2, ◑; b_1, ●; b_2, ⓘ.

b_2, were evaluated to see how the values of these parameters vary with the modification.

The values of the kinetic parameters/values without modifier are plotted against the amount of AcOH added in Fig. 3. The rate constant for the formation of SD and SA, k_1, and the adsorption parameters, b_1 and b_2, were found to decrease upon the addition of AcOH, while k_2 did not change upon the first addition of a small amount of AcOH, but then began to decrease upon further addition.

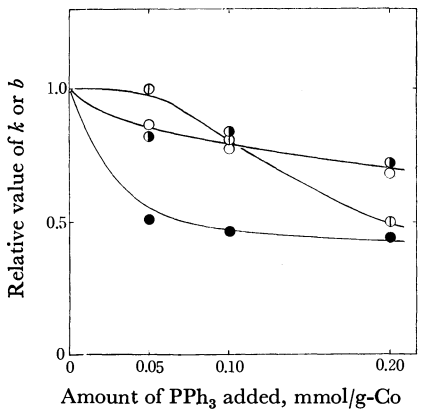

Fig. 4. Variation of the rate constant and adsorption parameter with the amount of PPh_3. Same notations as in Fig. 3.

The results obtained on the catalyst modified with PPh_3 are also shown in Fig. 4. It was found that k_2 as well as k_1 and b_1 decreased when the catalyst was modified with PPh_3, and that b_2 did not change on the first addition of a small amount of PPh_3.

Discussion

The behavior of the two kinetic parameters for the formation of SD and SA (k_1 and b_1) over the AcOH- and PPh_3-modified catalysts are found to be similar to each other.

It is interesting that the variation in the kinetic parameters for the formation of UA (k_2 and b_2) over the AcOH-modified catalyst is different from that over the PPh_3-modified one. It is also interesting that the variation in k_1 and k_2 over the AcOH-modified catalyst is the same as those previously observed over the $CoCl_2$- and $MnCl_2$-modified catalysts.[2] Taking into consideration the facts that AcOH has the Brönsted acidity and that Co- and $MnCl_2$ have the Lewis acidity, these results can be considered to indicate that the action of acids as modifiers differs from that of bases, especially in the effect on the formation of UA, although the reason is not yet well known. No detailed or quantitative discussion of the variation in the kinetic parameters observed in the present study is possible, since the effect of modifiers on the kinetic parameters is not simple.

If a modifier is adsorbed competitively with the reactants and without any interaction among them, the rate equation can be expressed as:[4]

$$r = k_a b_a C_{UD}/(1+b_a C_{UD})^2 \quad (3)$$

where k_a and b_a denote the apparent rate constant and the adsorption parameter respectively. The definitions of the apparent kinetic parameters are as follows:

$$k_a = k/(1+b_M C_M) \quad (4)$$

$$b_a = b/(1+b_M C_M) \quad (5)$$

where b_M and C_M denote the adsorption parameter and the liquid-phase concentration of a modifier respectively. It can thus be said from Eqs. (4) and (5) that the rate constants and adsorption parameters determined by Eqs. (1) and (2) apparently decrease with the addition of a modifier, provided that there is no interaction between the adsorbed modifier and the reactants. The variation in the kinetic parameters for the formation of SD and SA (k_1 and b_1) over the AcOH- and PPh_3-modified catalysts, therefore, seems to be explainable in terms of the above-described Langmuir-Hinshelwood mechanism.

Both of the adsorption parameters over the AcOH-modified catalyst were found to decrease, even on the first addition of a small amount of AcOH. This indicates that AcOH is adsorbed on the site responsible for the formation of UA as well as on that responsible for the formation of SD and SA. Therefore, the fact that k_2 did not change, or even increased, on the first addition of a small amount of acidic modifiers, such as AcOH, $MnCl_2$, and $CoCl_2$, can certainly be considered to be due to an increase in the rate constant, k, in Eq. (4). This indicates that the acidic modifiers promote the formation of UA, suggesting that an interaction exists among the adsorbed acidic modifier and adsorbed species responsible for the formation of UA.

4) S. Kishida, C. Ko, and S. Teranishi, *Shokubai*, **11**, 146 (1969).

BULLETIN OF THE CHEMICAL SOCIETY OF JAPAN, VOL. 46, 3568—3569 (1973)

Difficulty of Establishing Adsorption Equilibrium in *n*-Butylamine Titration of Solid Acid Surfaces

Jun-ichiro TAKE, Yasumasa NOMIZO,[1] and Yukio YONEDA

Department of Synthetic Chemistry, Faculty of Engineering, The University of Tokyo, Hongo, Bunkyo-ku, Tokyo 113

(Received December 6, 1972)

The Benesi or *n*-butylamine titration method[2] has widely been employed for determining the acid-strength distribution of solid acid surfaces. Applications[3,4] and variations[5] of the method have also been worked out. It was assumed so far that the adsorption equilibrium of both amine and indicator molecules with acid sites is attained on solid surfaces. However, no evidence has been given to show that the assumption is satisfied. Leftin and Hobson[6] showed that the intensity of a 550 mμ band due to benzeneazodiphenylamine (BADA) chemically adsorbed on silica-alumina became practically constant 30—40 hr after addition. Accomplishment of such a stationary state, however, does not necessarily indicate the validity of the assumption.

In the course of our studies we came across a remarkable phenomenon giving rise to a strong doubt about the validity of the assumption. The present paper deals with the findings.

A thin wafer (*ca.* 25 mg, 20×9 mm and about 0.1 mm thick) of a commercial silica-alumina catalyst (SA-1, Al_2O_3 13%)[3] was mounted on a holder, placed in a UV-cell,[7] and then activated by evacuation at 450 °C for 1 hr *in situ*. After transfer of highly dried and degassed decalin in a vacuum, followed by introduction of dried nitrogen gas, a decalin solution of *n*-butylamine was gently added through a pipette, without any agitation, into the cell in a dried nitrogen gas stream. The amount of addition was about 0.1 meq/g-catalyst, roughly corresponding to one-half of the acid content of SA-1 determined by *n*-butylamine titration with BADA as an indicator.[3] The cell was then allowed to stand at 50 °C without stirring. After 12 days, a solution of BADA in decalin (*ca.* 6×10^{-4} meq/g-catalyst) was admitted into the cell.

The resulting surface coloration and its change with time are shown schematically in Fig. 1. The indicator BADA is purple when adsorbed on acid sites, and yellow when adsorbed on poisoned acid sites or non-acidic sites.[3] Thus, in Fig. 1 yellow coloration indicates the poisoning of acid sites with the amine, the purple no poisoning with the amine, and no coloration the absence of BADA on the surface.

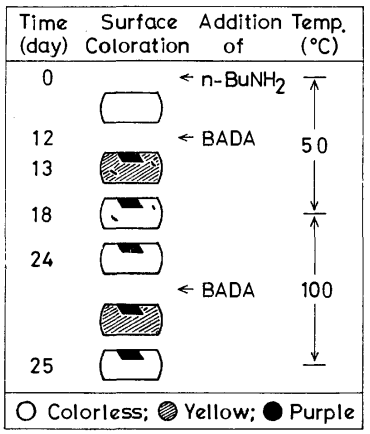

Fig. 1. Surface colorations of SA-1 wafer partially poisoned with *n*-butylamine.

In general, solid acid surfaces have been thought to have acid sites with different acid strengths. Acid sites of every acid strength should, on a macroscopic scale, be uniformly distributed over the surface of a wafer or of a catalyst particle. According to the prevailing theory of adsorption on such a heterogeneous surface,[8] at adsorption equilibrium basic molecules such as *n*-butylamine are distributed onto acid sites of every acid strength following the adsorption isotherm, a function of both the number and the strength of acid sites. Thus the adsorption of BADA onto the surface having reached adsorption equilibrium with *n*-butylamine will cause the surface to be uniformly colored at equilibrium. However, it should be noted that a macroscopically uniform distribution of basic molecules can be realized even though no adsorption equilibrium exists. The adsorption of basic molecules not followed with the desorption will yield an adsorption state far from equilibrium. Establishment of adsorption equilibrium thus needs desorption-readsorption cycles of basic molecules once adsorbed on the surface.

Macroscopic uniformity in the distribution of acid sites was proved by the fact that a uniform coloration occurred when BADA was added onto the wafer that had been immersed into a previously well-mixed decalin solution of *n*-butylamine (*ca.* 0.1 meq/g-catalyst) for 1—2 days at room temperature. The surface of a wafer partially poisoned with the amine would then have uniformly turned purple independently of the mode of poisoning, if there had existed adsorption equilibrium. However, this was not the case (Fig. 1). Essentially the same results were also obtained in separate experiments carried out in a similar way. No

1) Present adress: Safron-Teijin S/A Industrias Brasileiras de Fibras, Rua Canada, 390 Jardim America, Sao Paulo, Brazil.

2) H. A. Benesi, *J. Phys. Chem.*, **61**, 970 (1957).

3) J. Take, T. Tsuruya, T. Sato, and Y. Yoneda, This Bulletin, **45**, 3409 (1972).

4) J. Take, N. Kikuchi, and Y. Yoneda, *J. Catal.*, **21**, 164 (1971).

5) A. E. Hirshler, *J. Catal.*, **2**, 428 (1963). H. V. Drushel and A. L. Sommers, *Anal. Chem.*, **38**, 1723 (1966).

6) H. P. Leftin and M. C. Hobson, Jr., *Advan. Catal.*, **14**, 143 (1963).

7) J. Take, H. Kawai, and Y. Yoneda, to be published.

8) For example, D. M. Young, and A. D. Crowell, "Physical Adsorption of Gases", Butterworths, London (1967), p. 247.

uniform coloration appeared during the course of standing for 25 days, indicating that the amine once adsorbed on acid sites was hardly desorbed or hardly migrated even at 100 °C, a temperature higher than the boiling point of the amine (77.8 °C). This was confirmed by the reappearance of the yellow upon the second adidtion of BADA (see Fig. 1). Such difficulty is also demonstrated by the fact that ethylamine is desorbed with an activation energy as high as about 20 kcal/mol from silica gel,[9] which is usually nonacidic or much less acidic than silica-alumina catalyst. All the facts are strongly negative against the establishment of adsorption equilibrium. Therefore, the local coloration in Fig. 1 is best explained as being due to the fact that the added amine molecules approach the surface, as a whole, irregularly or non-uniformly (as in the motion of a drop of ink allowed to fall into standing water), and then remain, without reaching adsorption equilibrium, on adsorption sites at which they first arrived. In both cases where the amine is added with stirring and where a previously well-mixed solution of the amine is used without stirring, the amine molecules should be allowed to approach uniformly the surface of catalyst, hence the subsequent addition of BADA probably yields a uniform surface coloration. However, it is highly unlikely that the desorption of the once adsorbed amine is accelerated and adsorption equilibrium thus reached.

The ordinary conditions for equilibration used in the *n*-butylamine titration method are much milder than those employed here; in the former, the temperature ranges from room temperature to 30 °C and the standing period from several hours to several days. Under such conditions, therefore, the adsorbed amine is probably far from equilibrium even if agitation is applied.

The yellow coloration of the wafer surface faded gradually with time, this being accompanied by the deepening of the purple (Fig. 1), indicating that the physically adsorbed BADA migrated onto acid sites not poisoned with the amine. The completion of this migration took at least 5 days at 50 °C. In fact, physically adsorbed BADA is desorbed with an activation energy as high as 16 kcal/mol from silica gel.[7] Thus it is concluded that even physically adsorbed BADA is desorbed or migrates with considerable difficulty.

It is very difficult for either *n*-butylamine or indicators, particularly the former, to reach adsorption equilibrium with acid sites under the usual conditions in the *n*-butylamine titration method. The difficulty is not effectively diminished for *n*-butylamine by raising the temperature to 50—100 °C. Such will also be the case with catalysts in the form of powder. Disregard of this difficulty might lead to an overestimation of the acid contents.

9) R. A. Ross and A. H. Taylor, *J. Catal.*, **9**, 104 (1967).

BULLETIN OF THE CHEMICAL SOCIETY OF JAPAN, VOL. 46, 3569—3571 (1973)

The Formation of Benzene Dimer Cations on Synthetic Mordenite

Hiroji TOKUNAGA, Yoshio ONO, and Tominaga KEII

Department of Chemical Engineering, Tokyo Institute of Technology, Meguro-ku, Tokyo 152

(Received February 19, 1973)

Extensive studies have been carried out on the formation of cation radicals from aromatic hydrocarbons on silica-alumina or synthetic zeolites, since the electron-transfer process seems to be closely relevant to the acid-base properties of the surfaces.[1-6] It has been established that the heat treatment of the catalyst and the presence of adsorbed oxygen have a marked effect on the formation of cation radicals. Recently, Kurita and co-workers[7] reported that benzene dimer cations were formed when synthetic mordenite was contacted with benzene in carbon tetrachloride. The effects of catalyst pretreatment and of adsorbed oxygen on the formation of dimer cations over the ammonium form of synthetic mordenite were investigated by means of ESR spectroscopy and the mechanism of the formation of the dimer cations is discussed in this paper.

Experimental

The Na form of mordenite was furnished by Nippon Kagaku and NH_4^+ form was prepared by the conventional cation-exchange procedures with ammonium chloride. The degree of ion exchange was found to be 32% by the gravimetric analysis of the eluted Na^+ ions. For easy introduction and evacuation of gases the adsorption of benzene was carried out from vapor phase no solvents being used. The zeolite (600 mg) was placed in an ESR sample tube (o.d. 10 mm) and evacuated at an appropriate temperature for 3 hr and then exposed to benzene vapor at room temperature. ESR measurements were carried out with a JEOL X-band spectrometer with a modulation frequency of 100 kHz. Radical ion concentrations expressed in terms of spins per gram of dry zeolite were determined by double integration using a benzene solution of 1,1-diphenyl-2-picrylhydrazyl.

1) J. J. Rooney and R. C. Pink, *Trans. Faraday Soc.*, **58**, 1632 (1962).
2) D. M. Brouner, *Chem. Ind.* (London), **1961**, 177.
3) H. Iami, Y. Ono, and T. Keii, *J. Phys. Chem.*, **69**, 1082 (1965).
4) R. P. Porter and W. K. Hall, *J. Catal.*, **5**, 366 (1966).
5) D. N. Stamires and J. Turkevich, *J. Amer. Chem. Soc.*, **86**, 749 (1964).
6) F. R. Dollish and W. K. Hall, *J. Phys. Chem.*, **71**, 1005 (1967).
7) Y. Kurita, T. Sonoda, and M. Sato, *J. Catal.*, **19**, 82 (1970).

Results and Discussion

Assignment of ESR Signals. The ammonium mordenite showed no ESR absorption when it was evacuated at 600 °C. A well-resolved spectrum was obtained when it was exposed to benzene vapor of 50 Torr for 5 min. The hyperfine coupling constant of 2.2 Oe agrees with that of benzene dimer cations in sulfuric acid.[8] The intensity distribution of lines was also in good agreement with that expected from radicals with 12 equivalent protons. Thus, the spectrum was unambiguously assigned to benzene dimer cations. The intensity of the spectrum decreased with time, the line shape being changed. The spectrum after 7 days was the same as that obtained on biphenyl adsorption on the mordenite. The results we obtained from the vapor phase adsorption of benzene are concluded to be essentially the same as those obtained by Kurita and co-workers[7] from the adsorption of benzene in carbon tetrachloride. The adsorption of benzene on the ammonium mordenite leads to the formation of benzene dimer cations which are converted into biphenyl cation on the surface.

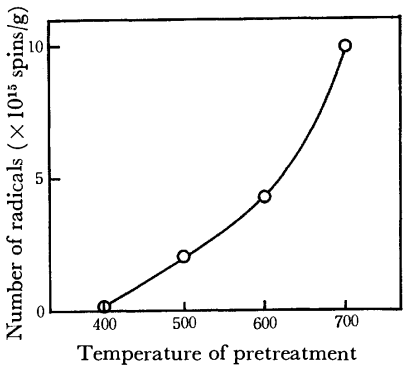

Fig. 1. Effect of pretreatment temperature on the number of benzene dimer cations.

Effect of Calcination Temperature. The effect of the temperature of zeolite activation on the generation of benzene dimer cation radicals on NH_4^+ mordenite is illustrated in Fig. 1. Generation of the radicals was observed only for samples evacuated above 500 °C, the radical amount increasing drastically with the rise in the activation temperature. It was reported[9] that the dehydroxylation of H mordenite starts at 450 °C. Since the activation temperature of the mordenite giving dimer cations corresponds to the temperature of the dehydroxylation which results in the formation of the three-coordinated aluminium, it is concluded that the dimer cations are formed by the transfer of an electron from two benzene molecules to the three-coordinated aluminium atoms. The same mechanism of the charge transfer was proposed by Stamires and Turkevich[5] for the formation of triphenylamine cation radicals on ammonium Y-zeolite.

Effect of Adsorbed Oxygen. *(a) Effect of the Introduction of Gaseous Oxygen*: Ammonium mordenite evacuated at 700 °C for 3 hr was exposed to benzene vapor for 5 min and evacuated for 2 min. The intensity of spectrum was then monitored with time. It decreased slowly with time. After 60 min, 6 Torr of oxygen was introduced into the system. This caused about five-time increase in ESR intensity as shown in Fig. 2. It was confirmed that this is not caused by the removal of the saturation of the ESR signal. It is thus concluded that the presence of oxygen enhances the dimer radical formation.

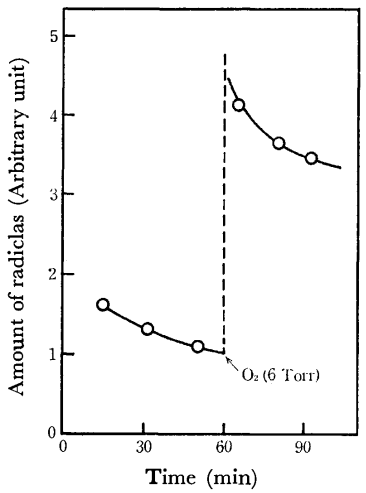

Fig. 2. Change in the radical amount on introduction of 6 Torr of oxygen.

(b) Effect of Oxygen Pretreatment: When ammonium mordenite treated at 700 °C was exposed to 25 Torr of oxygen and evacuated at room temperature for 5 min prior to adsorption of benzene, the ESR intensity of dimer cations was 1.5 times larger than that from the sample without oxygen treatment. When oxygen pretreatment was carried out at elevated temperatures (200 and 400 °C), the enhancement of the ESR intensity was enormous, as shown in Fig. 3. These results show that the adsorbed oxygen has an important role in the formation of the dimer cations as it does for monomer cation radical formation.[3,4,6] The adsorption of oxygen might be an activated process since the radical amount

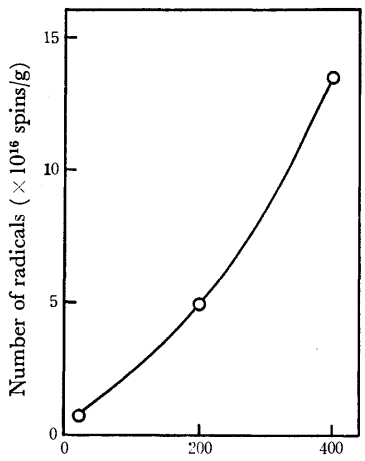

Fig. 3. Effect of oxygen pretreatment temperature on the number of benzene dimer cations.

8) M. K. Carter and G. J. Vincon, *J. Chem. Phys.*, **47**, 292 (1971).

9) H. Karge, *Z. Physik. Chem.* (Neue Folge), **76**, 133 (1971).

increases with the temperature of oxygen pretreatment.

Enhancement of the radical formation by adsorbed oxygen could be caused by either or both of the following.

a) An increase in the electron-withdrawing power of the aluminium atoms due to the inductive effect of adsorbed oxygen. In this case, a negative charge would be shared by an aluminium atom and an adsorbed oxygen molecule.

b) The chemical reaction of benzene with chemisorbed oxygen. Actually, perylene in liquid $SbCl_3$ is stoichiometrically oxidized to the radical ion on the addition of oxygen according to[10]

$$O_2 + 4C_{20}H_{12} + 6SbCl_3 \longrightarrow 4C_{20}H_{12}^{+} + 4SbCl_4^{-} + 2SbOCl$$

The following experiments were carried out. When sulfur dioxide, instead of oxygen, was introduced into the catalyst with preadsorbed benzene at room temperature, a large increase in ESR signal of benzene dimer cations and, at the same time, the signal due to SO_2^- were observed. The ESR signal of SO_2^- (g_{xx}= 2.0012, g_{yy}=2.0025, g_{zz}=2.0071) was observed even in the absence of preadsorbed benzene, the amount depending considerably on the adsorption temperature. The temperature dependence was similar to the dependence of amount of benzene dimer cations on the temperature of the oxygen pretreatment. The results indicate that the role of oxygen and sulfur dioxide on the formation of dimer cations is similar. Thus, the possibility of chemical reaction with adsorbed oxygen can be eliminated since sulfur dioxide as well as oxygen enhance the formation. The formation of benzene dimer cations and sulfur dioxide anions at the same time on the same catalyst strongly suggests the important role of the inductive effect on the electron transfer process on the mordenite.

It is demonstrated that the radical amount increases with the activation temperature of the zeolite, the presence of the adsorbed oxygen drastically enhancing the formation of the benzene dimer cations. It is concluded that the three-coordinated aluminium atoms are responsible for the dimer cation formation, the role of oxygen being to increase the electronegativity of aluminium atoms by its inductive effect.

10) J. R. Atkinson, T. P. Jone, and C. E. Baughan, *J. Chem. Soc.*, **1964**, 5808.

BULLETIN OF THE CHEMICAL SOCIETY OF JAPAN, VOL. 46, 3571—3573 (1973)

An Electron Spin Resonance Study of the Carbonization of Acenaphthylene

Yoshio YAMADA and Sadaharu TOYODA

National Research Institute for Pollution and Resources, Kawaguchi, Saitama 332

(Received March 10, 1973)

Many Electron Spin Resonance (ESR) studies have been made on charred materials.[1-3] Since most of these experiments were carried out on solid state, however, only one signal was observed, and consequently the intermediate radicals produced in the process of carbonization could not be identified by the signal. Recently, Singer and Lewis[4-6] investigated the carbonization of acenaphthylene, 9,9′-bifluorene, and so forth in *m*-quinquephenyl, which is a high-boiling and inert solvent. They reported in their first paper[4] that the signal due to the perinaphthenyl radical is observed at the early stage of the pyrolysis of acenaphthylene and suggested that the 4,6-dimethylperinaphthenyl radical also appears during the carbonization. However, their discussion was chiefly confined to the identification of these radicals. The present investigation, therefore, was undertaken in order to clarify the reaction mechanism of the pyrolysis of acenaphthylene at from 200 to 500 °C on the basis of the variation in the signal intensity for the radicals identified by Singer and Lewis.[4] In this connection, decacyclene in *m*-quinquephenyl was carbonized in the same manner as acenaphthylene.

Experimental

The acenaphthylene was purified by recrystallization from ethanol. The decacyclene and *m*-quinquephenyl were purchased from the Aldrich Chem. Co. Inc. and K & K Laboratories, Inc., respectively. Samples were prepared by adding acenaphthylene to *m*-quinquephenyl at a weight ratio of 1:10 and then by degassing them at room temperature. These samples were heated in a furnace for 5 min at 30 °C intervals in the range from 200 to 500 °C. All of the ESR spectra were measured at 150 °C because *m*-quinquephenyl begins to melt at 125 °C. The ESR apparatus was a Japan Electron Optics Laboratory JES-ME-3X-type spectrometer with a temperature-varying attachment.

Results and Discussion

When the temperature of acenaphthylene dissolved in *m*-quinquephenyl was raised to 290 °C, the well-

1) D. J. E. Ingram and J. E. Bennett, *Phil. Mag.*, **45**, 545 (1954).
2) L. S. Singer, W. J. Spry, and W. H. Smith, Proc. Third Carbon Conf., Pergamon Press (1959), p. 121.
3) S. Toyoda, S. Sugawara, and T. Furuta, *Carbon* (Oxford), **8**, 473 (1970).
4) L. S. Singer and I. C. Lewis, *ibid.*, **2**, 115 (1964).
5) I. C. Lewis and L. S. Singer, *ibid.*, **5**, 373 (1967).
6) I. C. Lewis and L. S. Singer, *ibid.*, **7**, 93 (1969).

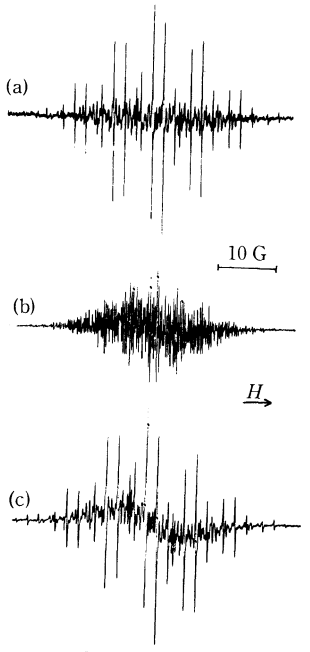

Fig. 1. ESR spectra of acenaphthylene in *m*-quinquephenyl heat-treated up to (a) 320 °, (b) 440 °, and (c) 500 °C.

resolved ESR spectrum shown in Fig. 1(a) was observed. It consists of two hyperfine structures; one structure is due to six equivalent protons, with a coupling constant of 6.32 gauss, and the other to three equivalent protons, with a constant of 1.81 gauss. It agrees closely with the spectrum observed by Singer and Lewis.[4] Thus, the substance in the solution can be identified as the perinaphthenyl radical (V).[7] Further heat-treatment up to 440 °C brings about the formation of a new radical, as may be seen in Fig. 1(b). The spectral lines derived by subtracting the signal due to the (V) radical from the spectral lines of Fig. 1(b) correspond to the 4,6-dimethylperinaphthenyl radical (VI) assigned by Singer and Lewis.[4] Though the spectral intensity due to the (V) radical is weak at this temperature, it increased again when the sample was heated to 500 °C. In addition, the broad line of 5 gauss became more intense. The variation in the spectral intensity of the (V) and (VI) radicals is represented in Fig. 2 as a function of the heat-treatment temperature. Since *m*-quinquephenyl boils near 540 °C, the samples were not heated above 500 °C. When the temperature of the sample was maintained at 500 °C, the signal intensity for the (V) radical decreased. Hence, the spectral intensity is probably lowered above 500 °C.

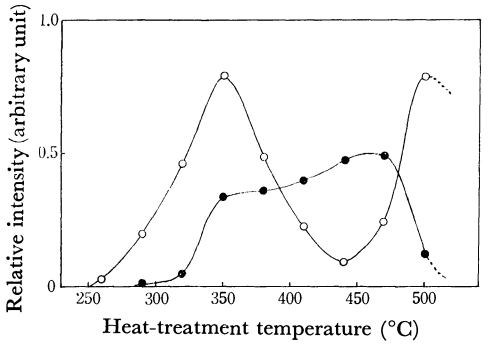

Fig. 2. The relation between the signal intensity and heat-treatment temperature.
○: Perinaphthenyl radical
●: 4,6-Dimethylperinaphthenyl radical

Acenaphthylene is well known to polymerize with pyrolysis at *ca.* 200 °C and then to decompose near 350 °C, resulting in biacenaphthylidene (II) (or dinaphthylenebutadiene), decacyclene (IV), and fluorocyclene (III).[8] Mueller[8] studied the acenaphthylene pyrolysis by thin-film chromatography and found that biacenaphthylidene (II) and fluorocyclene (III) disappear above 350 °C, while decacyclene (IV) is stable at 450 °C. On the basis of these facts, the increase in the radical concentrations of (V) and (VI) up to 350 °C may be explained in terms of the pyrolysis of biacenaphthylidene (II) and fluorocyclene (III). When the sample was heated at higher temperatures, the signal due to the (VI) radical remained almost constant, while that due to the (V) radical gradually decreased. Such a difference may be interpreted as follows: the (V) radical generally exists in equilibrium with its diamagnetic dimer.[9] Accordingly, a decrease in the amount of the (V) radical seems to be responsible for the dimerization. On the contrary, because of the steric hindrance, the (VI) radical is less mobile and less subject to dimerization than the (V) radical. Therefore, the (VI) radical may be thought to be present even at higher temperatures.

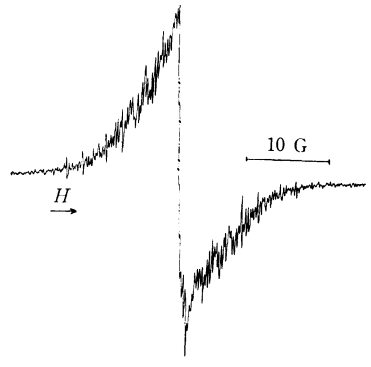

Fig. 3. ESR spectrum of decacyclene in *m*-quinquephenyl heat-treated up to 500 °C.

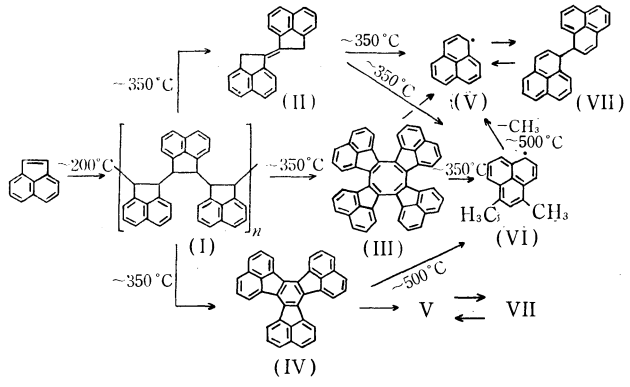

Fig. 4. The carbonization of acenaphthylene.

7) This number is shown in Fig. 4.

8) K. Mueller, Ph. D. Thesis, Karlsruke University, W. Germany, 1967.

9) F. Gerson, *Helv. Chim. Acta*, **49**, 1463 (1966).

When decacyclene (IV) dissolved in *m*-quinquephenyl was heated, the faint signals due to the (V) and (VI) radicals began to appear at from 440 to 470 °C. However, the signals were significantly weaker than those obtained from carbonized acenaphthylene and were superposed by a spectral line, the linewidth of which was *ca.* 2.5 gauss (Fig. 3). Therefore, it seems unreasonable to regard the increase in the radical concentration of (V) at from 440 to 500 °C as caused by decacyclene (IV) alone. According to the results of Madison and Roberts,[10] the liquid-phase pyrolysis of an alkyl-substituted aromatic compound leads to a cleavage of the alkyl group at *ca.* 470 °C. In this case, it is clear that the (VI) radical decomposes to produce the (V) radical and methane. With this view, the high value of concentration for the (V) radical at 500 °C may be concluded to be due not only to decacyclene (IV), but also to the (VI) radical. Figure 4 shows a reaction scheme for acenaphthylene proposed on the basis of the results mentioned above. However, the formation of zethrene described by Ruland[11] should also be taken into account in the pyrolysis of acenaphthylene, although it cannot be detected by the ESR technique.

10) J. J. Madison and R. M. Roberts, *Ind. Eng. Chem.*, **50**, 237 (1958).

11) W. Ruland, *Carbon* (Oxford), **2**, 365 (1965).

BULLETIN OF THE CHEMICAL SOCIETY OF JAPAN, VOL. 46, 3573—3574 (1973)

Deformation of the Molecular Orientation of Nematic Liquid Crystals with Homeotropic Alignment in Electric Field

Sakumitsu SAKAGAMI, Akira TAKASE, and Minoru NAKAMIZO
National Industrial Research Institute of Kyushu, Tosu, Saga 841

(Received March 22, 1973)

It is well-known that the thin layer of nematic liquid crystals (NLC) with negative dielectric anisotropy shows the so-called Williams domain pattern at the threshold of an applied electric field, and gives dynamic scattering of light at a higher voltage, while NLC with positive dielectric anisotropy exhibit no such scattering.[1-8] Most measurements on electrically induced hydrodynamic instabilities have been carried out with a molecular orientation in which the long molecular axes of NLC are made to lie parallel to the glass surface, *i.e.*, perpendicular to the direction of an applied electric field.

In this paper we report on the behavior of NLC with homeotropic alignment[9] in the presence of an external DC electric field.

Experimental

Materials. 4-Methoxybenzylidene-4-*n*-butylaniline (MBBA, nematic range 21—41 °C) and 4-(4-*n*-butoxybenzylideneamino)benzonitrile (BBABN, nematic range 63—106 °C). MBBA[10] has a negative dielectric anisotropy ($\varepsilon_{//}-\varepsilon_{\perp}<0$) and BBABN a positive dielectric anisotropy ($\varepsilon_{//}-\varepsilon_{\perp}>0$).[11] The liquid crystal was sandwiched between two transparent tin-oxide-coated glass plates separated by a Mylar spacer about 20 μm thick. Homeotropic alignment of MBBA was achieved by coating a dilute aqueous solution of sodium dodecyl sulfate on the electrode surfaces. Uniform homeotropic alignment was attained by standing the solution for several hours. In the case of BBABN the electrode surfaces were coated with lecithin.[12] Domain patterns were observed under an ordinary polarizing microscope. A sensitive color plate ($R=530$ mμ) was used as the test plate to determine the retardation.

The measurement on light scattering was carried out by use of a He–Ne laser beam polarized through a polarizer and incident normally upon the sample cell. The scattered light from the NLC was passed through an analyzing polaroid and allowed to fall on a photographic film.

The experiments were carried out for MBBA at room temperature and for BBABN at 70—90 °C on the heater regulated.

Results and Discussion

When no electric field is applied, the nematic cell extinguishes the light transmission between crossed polarizers, corresponding to the homeotropic orientation. With the increase in electric field, circular domain patterns are observed at the threshold of the electric field between crossed polarizers (Fig. 1). Both MBBA and BBABN give circular domain patterns, the size of the domain for MBBA being dependent on the state of the electrodes. Each domain shows extinction, cross and quadrants, colored by interference. The first and third quadrants are blue, the second and fourth yellow. These results indicate that the direc-

1) R. Williams, *J. Chem. Phys.*, **39**, 384 (1963).
2) G. H. Heilmeier, *ibid.*, **44**, 644 (1966).
3) W. Helfrich, *ibid.*, **51**, 2755 (1969).
4) P. A. Penz, *Phys. Rev. Lett.*, **24**, 1405 (1970).
5) H. Gruler and G. Meier, *Mol. Cryst. Liquid Cryst.*, **16**, 299 (1972).
6) Orsay liquid crystal group, *ibid.*, **12**, 251 (1971).
7) W. Helfrich, *J. Chem. Phys.*, **51**, 4092 (1969).
8) G. H. Heilmeier, L. A. Zanoni, and L. A. Barton, *Proc. IEEE*, **56**, 1162 (1968).
9) G. W. Gray, "Molecular Structure and the Properties of Liquid Crystals," Academic Press Inc., New York, N. Y., (1962), p. 33.
10) D. Diguet, F. Rondelez, and G. Durand, *C. R. Acad. Sci. Paris, Ser. B*, **271**, 954 (1970).
11) M. Schadt, *J. Chem. Phys.*, **56**, 1494 (1972).
12) W. Helfrich, *Phys. Lett.*, **35A**, 393 (1971).

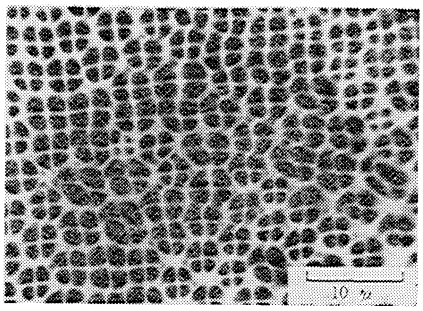

Fig. 1. Photomicrograph of circular domain patterns in MBBA at 2.6 V rms.

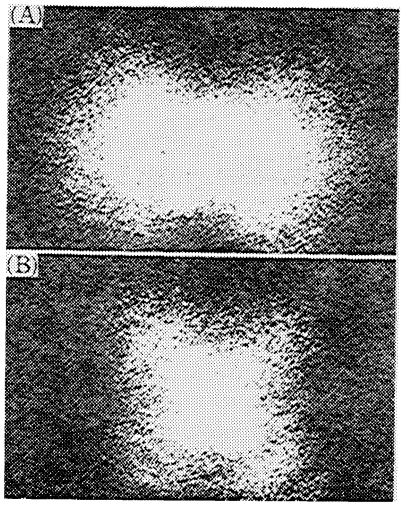

Fig. 2. Light scattering patterns for BBABN at 2.8 V rms with (A) parallel and (B) crossed polarization.

tions of the dipole moments of nematic molecules in the circular domain are arranged as a whole to radiate from the center of the domain.

Figure 2 shows typical light scattering patterns observed slightly above the threshold. The scattering pattern in crossed polars has a four-leaf clover shape which has its maximum intensity at 45 ° to the polarization direction. On the other hand, the pattern in parallel polars is of comparable intensity and has a cocoon-like shape elongated to the polarization direction. The light scattering patterns are associated with the formation of the circular domains, and are similar to those observed in spherulite.[13]

Heilmeier reported a similar circular domain pattern to that mentioned above using butyl *p*-(anisylideneamino)cinnamate and suggested that its formation can be ascribed to positive dielectric anisotropy of the nematic molecule.[14] However, the circular domain, as shown above, can be observed in both MBBA and BBABN, independent of the directional relation between the dipole moment and long molecular axis. Thus, we infer that the appearance of the circular domain is due to the homeotropic alignment subjected to the electric field, irrespective of positive or negative dielectric anisotropy of the nematic molecule. It is suggested from both the microscopic circular domain and light scattering pattern that the applied electric field causes an ellipsoidal molecular deformation (Fig. 3).

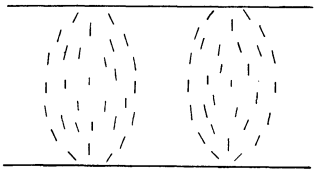

Fig. 3. Schematic representation of molecular orientation corresponding to the circular domains. Solid lines indicate the long molecular axes of nematic molecules.

As voltage is further increased, the circular domain is broken and a turbulent flow takes place. MBBA exhibits dynamic scattering of light, but not BBABN.

13) R. S. Stein and M. B. Rhodes, *J. Appl. Phys.*, **31**, 1873 (1960).

14) G. H. Heilmeier, "Ordered Fluids and Liquid Crystals," ed. by R. S. Porter, and J. F. Johnson, American Chemical Soc., Washington, D. C. (1967), p. 68.

BULLETIN OF THE CHEMICAL SOCIETY OF JAPAN, VOL. 46, 3575—3576 (1973)

Temperature Dependence of Association of Methanol, Ethanol, and 1-Propanol

Yoshiro SAKAI, Yoshihiko SADAOKA, and Tsuguo YAMAMOTO

Department of Industrial Chemistry, Faculty of Engineering, Ehime University, Bunkyo-cho, Matsuyama, Ehime 790

(Received March 29, 1973)

Arnold and Packard[1] reported that the signal from the hydroxylic proton in the NMR spectra of methanol and ethanol moves towards high fields with temperature rise, but not those of CH_2 and CH_3 groups. The effect of temperature on the shifts of OH signals has been accounted for by the rupture of the hydrogen bonds. In the present paper, the variation of the relative concentrations of the monomer and the *n*-mer (linear or cyclic) with temperature calculated from the chemical shifts of OH protons are discussed.

Results and Discussion

In order to determine the state of association of alcohols, the method of Saunders and Hyne[2] was applied. The following equilibrium is assumed between monomer and a single species of *n*-mer:

$$n(\text{R-OH}) \rightleftarrows (\text{R-OH})_n$$

$$K_n = M_n/(nM_1^n). \quad (1)$$

The equilibrium constant K_n is given by means of Eq. (1) where M_1 and M_n are the molar concentrations of monomer and *n*-mer, respectively, in terms of monomer unit. The observed resonance frequency is given by

$$\delta_{\text{obsd}} = (\delta_1 M_1 + \delta_n M_n)/C \quad (2)$$

where δ_1 and δ_n represent characteristic shifts of a proton in monomer and *n*-mer, respectively. C is the total concentration of alcohol in mol/l. In order to determine δ_1, the variation of the shift of OH protons in dilute solution in cyclohexane characterized by a small effect on the shift of OH protons, was measured at relatively high temperatures near the boiling point of either alcohol or cyclohexane at concentrations 10^{-2}—10^{-4} (mol/l), where the shifts varied little with concentration. The value of δ_1 was obtained by extrapolation to infinite dilution. Since it was reported by Luck and Ditter[3] that there are few monomers in pure methanol and ethanol below about −80 °C, the shift of OH proton in pure alcohols just above the melting point was taken to be δ_n. The values of δ_1 and δ_n are given in Table 1 together with temperatures of measurements. The values of M_1 and M_n at various temperatures were calculated by substituting the shifts δ_1 and δ_n into Eq. (2). The logarithms of M_1 and M_n thus obtained from Eq. (2) were plotted against the reciprocal of the absolute temperature in Figs. 1 and 2.

Table 1. Chemical shift of monomer and *n*-mer

Alcohol	δ_1[a] / Hz	δ_n / Hz
Methanol	205 (+30 °C)	592 (−90 °C)
Ethanol	185 (+60 °C)	639 (−100 °C)
1-Propanol	199 (+70 °C)	640 (−90 °C)

a) Solvent: cyclohexane

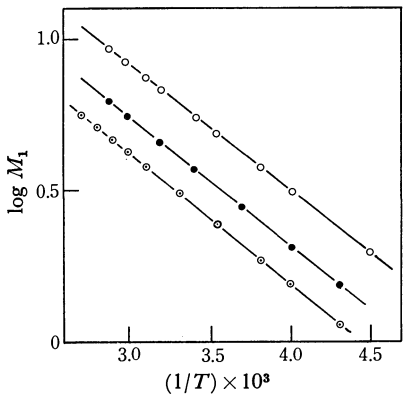

Fig. 1. Plot of logarithm of M_1 against reciprocal of absolute temperature.
○: methanol, ●: ethanol, ⊙: 1-propanol

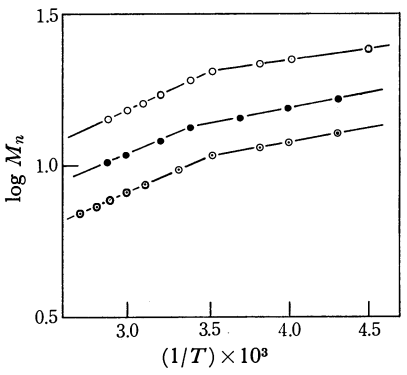

Fig. 2. Plot of logarithm of M_n against reciprocal of absolute temperature.
○: methanol, ●: ethanol, ⊙: 1-propanol

The plot of $\log(M_1)$ against $1/T$ gives a straight line for the three different alcohols, an inflection point appearing at about +30 °C for the plot of $\log(M_n)$ against $1/T$. According to the integrated van't Hoff equation

$$\ln(K_n) = -\Delta H/RT + D \quad (3)$$

where D is constant, it is expected that the plot of $\log(K_n)$ against $1/T$ will give a line which has an inflection point around +30 °C. By conbining Eq. (1) with Eq. (3), we have

1) J. T. Arnold and M. E. Packard, *J. Chem. Phys.*, **19**, 1609 (1951).
2) M. Saunders and J. B. Hyne, *ibid.*, **29**, 253, 1319 (1958), *ibid.*, **31**, 270 (1959).
3) W. A. P. Luck and W. Ditter, *Ber. Bunsenges. Phys. Chem.*, **72**, 365 (1968).

$$\ln (M_n) = -\Delta H/RT + D + \ln (n) + n \ln (M_1) \quad (4)$$

On the other hand, Fig. 1 gives the following empirical formula for the variation of the monomer concentration with temperature:

$$\ln (M_1) = A/T + B \quad (5)$$

where A and B are the constants characteristic of each alcohol. By substituting Eq. (4) into Eq. (5), we obtain

$$\ln (M_n) = (-\Delta H/R + nA)/T + nB + D + \ln (n) \quad (6)$$

The slope of the line for the plot of $\log(M_n)$ against $1/T$ in Fig. 2 corresponds to $(-\Delta H/R+nA)$ in Eq. (6). This indicates that the inflection at about +30 °C results from the change in $-\Delta H$ or/and n. For several values of n, we have calculated the values of $-\Delta H$ in high and low temperature ranges for each alcohol. The results are given in Table 2. Dividing the values of $-\Delta H$ by n (for cyclic form) and $n-1$ (for linear form), we obtained $-\Delta H$ per hydrogen bond for both cyclic and linear forms (Table 3). It is expected that $-\Delta H$ per hydrogen bond does not vary much with the form of aggregate. For the change of $-\Delta H$ at +30 °C, two possibilities can be considered from the results of Table 3; the increase of the size (n) of aggregates in linear state, and the change of the form from linear to a cyclic one with smaller value of n with increasing temperature. Thermodynamically the increase in the degree of association with temperature rise can not be considered. It could be concluded that the linear form is converted into the cyclic form of lower degree of association with a rise in temperature.

Table 2. $-nA$ and $-\Delta H$ for various values of n

Sample	n	$-nA \times 10^{-3}$	$-\Delta H$ / kcal mol^{-1}	
			Below 30 °C	Above 30 °C
Methanol	2	1.98	4.2	5.1
	3	2.97	6.3	7.1
	4	3.96	8.2	9.1
	5	4.95	10.2	11.0
	6	5.94	12.2	13.0
Ethanol	2	2.00	4.4	5.0
	3	3.00	6.4	7.0
	4	4.01	8.4	9.0
	5	5.01	10.4	11.0
	6	6.01	12.4	13.0
1-Propanol	2	2.06	4.5	5.2
	3	3.09	6.5	7.2
	4	4.12	8.6	9.3
	5	5.15	10.6	11.3
	6	6.18	12.6	13.4

Table 3. Value of $-\Delta H$ per hydrogen bond

Sample	n	$-\Delta H$ / kcal mol^{-1}			
		Below 30 °C		Above 30 °C	
		Linear	Cyclic	Linear	Cyclic
Methanol	2	4.17	2.09	5.13	2.56
	3	3.13	2.09	3.55	2.36
	4	2.75	2.06	3.02	2.28
	5	2.54	2.04	2.76	2.21
	6	2.43	2.03	2.60	2.16
Ethanol	2	4.43	2.22	4.97	2.48
	3	3.21	2.14	3.48	2.32
	4	2.81	2.11	2.79	2.24
	5	2.60	2.08	2.74	2.19
	6	2.48	2.07	2.59	2.16
1-Propanol	2	4.46	2.23	5.19	2.60
	3	3.25	2.17	3.62	2.41
	4	3.85	2.14	3.10	2.32
	5	2.65	2.12	2.83	2.27
	6	2.54	2.11	2.68	2.23

Experimental

Methanol and ethanol of reagent grade were refluxed for 24 hr over calcium oxide and then fractionally distilled. It was then dried over calcium, and fractionally redistilled twice under nitrogen atmosphere. Similar procedures were applied to the purification of 1-propanol, except that sodium was used instead of calcium. Cyclohexane of reagent grade was dried over sodium and then fractionally distilled twice. From the results of the specific conductivity measurements of the alcohols and cyclohexane at +25 °C (methanol, 1.0×10^{-8} ohm^{-1}·cm^{-1}, ethanol, 1.5×10^{-9} ohm^{-1}·cm^{-1}, 1-propanol, 2.0×10^{-10} ohm^{-1}·cm^{-1}, cyclohexane, 1.0×10^{-14} ohm^{-1}·cm^{-1}), it was confirmed that the reagents were highly dried. For NMR measurements, the purified alcohols were sealed in NMR sample tubes. NMR measurements were carried out in a temperature range of from just above melting point to near boiling point of each alcohol, on an JNM-4H-100 NMR spectrometer (Japan Electron Optics Co.) operating at a frequency of 100 MHz. Tetramethylsilane was employed as an internal standard. No temperature dependence of the CH_2 and CH_3 proton signals was observed. Experimental errors were within ±0.5 Hz and ±0.5 °C.

BULLETIN OF THE CHEMICAL SOCIETY OF JAPAN, VOL. 46, 3577—3578 (1973)

An Application of the 0s-Function to Molecular Systems of H_2^+ and H_2

Shingo ISHIMARU, Kazuyoshi TANAKA, and Tokio YAMABE

Department of Hydrocarbon Chemistry, Faculty of Engineering, Kyoto University, Sakyo-ku, Kyoto 606

(Received April 17, 1973)

Recently, several authors[1-8] have pointed out the usefulness of 0s- and other so-called Hulthén functions for atoms. The Hulthén function often gives a better approximation to the Hartree-Fock wavefunction than the conventional Slater-type function. This has been shown not only by the numerical results, but also by analytical approaches.[9-13] Among these investigations, the work by McWeeny[10] is particularly instructive, because his results suggest the applicability of the 0s-function to molecular systems. However, as far as we know, there has been no numerical application of the 0s-function to molecular systems. Furthermore, since the 0s-function is the lowest eigenfunction of an s-electron in a kind of screened Coulomb potential (Hulthén potential) which has Jacobi polynomials as its eigenfunctions,[14] it seems that it would be interesting to investigate the usefulness of 0s- or other subsequent functions for molecular systems:

$$V_{\mathrm{Hu}}(r) = -[(\beta^2-\alpha^2)/2]e^{-(\beta-\alpha)r}/(1-e^{-(\beta-\alpha)r}), \quad (1)$$

$$\left.\begin{aligned}\psi_1(r) = 0s_{\alpha\beta}(r) &= N(e^{-\alpha r}-e^{-\beta r})/r,\\ N^2 &= \alpha\beta(\alpha+\beta)/2\pi(\alpha-\beta)^2 \quad (\alpha<\beta)\end{aligned}\right\} \quad (2)$$

$$E_1 = -\alpha^2/2. \quad (3)$$

We calculate here the energies of the hydrogen molecule ion and the hydrogen molecule variationally, using the 0s-function.

TABLE 1. THE ENERGY OF HYDROGEN MOLECULE ION (in a.u.)

R	1s+1s[a] ($\zeta=1.0$)	1s+1s[a] ($\zeta=1.228$)	0s+0s	Hylleraas[a]
1.0			−0.441004	−0.45230
2.0	−0.565050	−0.582691	−0.586380	−0.60263
3.0			−0.564483	−0.57755
4.0			−0.537356	−0.54608
5.0			−0.519217	−0.52442

a) Ref. 15, p. 336.

TABLE 2. THE VALUES OF THE PARAMETERS, α AND β, AT EACH R

R (a.u.)	1.0	2.0	3.0	4.0	5.0
α	1.453	1.162	1.079	1.016	0.992
β	1.643	1.351	1.112	1.041	1.012

a) As a matter of course, α and β which give the optimal energy are not equal (though not so different) to the values used by McWeeny (Ref. 10), namely 1.228 and 1.485, respectively.

In Table 1, the energies of the hydrogen molecule ion at several R values (the internuclear distances) are listed alone with other results, while Table 2 shows the values of the parameters, α and β, at each R. The present calculation gives energies improved by the amounts of 0.021 and 0.004 in a.u. at the equilibrium internuclear distance of 2.0 a.u. when compared with those of the 1s-function with the exponents (ζ) of 1.0 and 1.228 respectively. The behavior of α and β shows that, when the internuclear distance increases, the 0s-function approaches the 1s-function.

TABLE 3. THE ENERGY OF HYDROGEN MOLECULE AT THE EQUILIBRIUM DISTANCE R (in a.u.)

	VB(1s)[a] ($\zeta=1.0$)	VB(1s)[b] ($\zeta=1.166$)	VB(0s) ($\alpha=1.13$, $\beta=1.20$)	Exact[c]
Energy	−1.115	−1.1390691	−1.1390878	−1.17445
R	1.4	1.406	1.416	1.400

a) Ref. 15, p. 349.
b) The energy value was recalculated in our laboratory.
c) Ref. 16.

In Table 3, the results for the hydrogen molecule obtained by the use of the valence bond method are listed. In the calculation, the exchange integral $\langle 0s_{\alpha\beta}(r_{a1})0s_{\alpha\beta}(r_{b2})|1/r_{12}|0s_{\alpha\beta}(r_{a2})0s_{\alpha\beta}(r_{b1})\rangle$, was easily obtained by the use of the formula given by Kotani *et al.*,[17] but a part of the Coulomb integral, $\langle 0s_{\alpha\beta}(r_{a1})0s_{\alpha\beta}(r_{b2})|1/r_{12}|0s_{\alpha\beta}(r_{a1})0s_{\alpha\beta}(r_{b2})\rangle$, was not so easily obtained (r_{a1} is the distance between the nucleus, a, and the electron, 1, and so forth). Therefore, after some modification, we expanded the part in the form of an infinite series and got a value with the required accuracy. The error of the energy given by the 0s-function is 2.05% smaller than that of the 1s-function with an exponent of 1.0, and the improvement over

1) J. T. Zung and R. G. Parr, *J. Chem. Phys.*, **41**, 2888 (1964).
2) R. G. Parr and J. H. Weare, *Prog. Theoret. Phys.*, **36**, 854 (1966).
3) J. H. Weare and R. G. Parr, *Intern. J. Quantum Chem.*, **1s**, 163 (1967).
4) R. L. Somorjai, *Chem. Phys. Lett.*, **3**, 395 (1969).
5) J. H. Weare, T. A. Weber, and R. G. Parr, *J. Chem. Phys.*, **50**, 4393 (1969).
6) G. Wilson and H. J. Silverstone, *Intern. J. Quantum Chem.*, **3**, 1067 (1969).
7) C. S. Chandler, *Chem. Phys. Lett.*, **3**, 311 (1969).
8) T. Tietz, *J. Chem. Phys.*, **52**, 460 (1970).
9) R. McWeeny and C. A. Coulson, *Proc. Phys. Soc.* (London), **A62**, 509 (1949).
10) R. McWeeny, *ibid.*, **A62**, 519 (1949).
11) M. Cohen and A. Dalgarno, *ibid*,, **77**, 165 (1961).
12) P. D. Robinson, *J. Chem. Phys.*, **45**, 1858 (1966).
13) R. E. Roberts, *ibid.*, **47**, 1873 (1967).
14) L. Rosenfeld, "Nuclear Forces," North-Holland Publ. Co., Amsterdam (1935), Chap. 5.
15) See L. Pauling and E. B. Wilson, "Introduction to Quantum Mechanics with Application to Chemistry," McGraw Hill Book Co., Inc., New York (1935).
16) W. Kołos and C. C. J. Roothaan, *Rev. Mod. Phys.*, **32**, 219 (1960).
17) M. Kotani, A. Amemiya, E. Ishiguro, and T. Kimura, "Table of Molecular Integrals," second ed., Maruzen Co., Ltd., Tokyo (1963).

the Wang's result is small but definite.

In comparing the two cases where a proton or a hydrogen approaches a hydrogen atom, it is clear that the perturbation in the former should be greater than in the latter.[18] Therefore, the deviation from the 1s-function should be more significant in the hydrogen molecule ion; this is reflected in the difference between α and β and in the improvement of the energies in the two cases.

Thus, taking the examples of the hydrogen molecule ion and the hydrogen molecule, we have numerically shown that the 0s-function is more effective not only in the atomic system, but also in the molecular one, than the conventional 1s-function. Of course, further improvement in the energy could be achieved by using wavefunctions with angular dependencies.

We wish to thank to Professor Kenichi Fukui for his helpful discussions.

18) α and β for the hydrogen molecule ion in the treatment by McWeeny (Ref. 10) correspond to the momenta of an electron in the hydrogen isolated and that perturbed by a proton, respectively.

BULLETIN OF THE CHEMICAL SOCIETY OF JAPAN, VOL. 46, 3578—3580 (1973)

Anomalous Magnetic Properties of Crystalline Galvinoxyl Radical. IV. Effect of the Deuterium Substituent

Kazuo MUKAI, Manami IIZUKA, and Kazuhiko ISHIZU
Department of Chemistry, Faculty of Science, Ehime University, Matsuyama 790

(Received April 24, 1973)

The stable organic galvinoxyl radical is known to undergo a first-order phase transition induced magnetically at 82 K, accompanied by pairing of magnetic spins, as is recognized from the results of magnetic susceptibility[1,2] and heat capacity[3] measurements. The Galvinoxyl radical is paramagnetic above the magnetic transition point, 82 K, where the susceptibility drops very sharply on cooling, and shows a weak paramagnetism below this point, with positive Weiss constants in both regions above and below the transition temperature. The entropy change at the transition point, which corresponds to R ln 9.45, cannot be explained by taking only the magnetic contribution. On the other hand, the phenol derivative, the corresponding diamagnetic substance, has no thermal anomaly in the temperature region 12—300 K.

It has been reported[4-7] that deuterium substitution causes two effects on the ESR spectrum of native undeuterated radicals. First, the proton splittings at the undeuterated positions are altered, and second, the ratio of the deuteron to the proton splitting differs from the ratio $(a^D/a^H)=0.1535$ calculated on the basis of the magnetic moments and spins of the two nuclei. Both isotope effects should result from the difference in mass of the proton and deuteron, and this difference can be manifested only through the molecular vibrations. The above results were successfully analyzed[6,8] in terms of a model for the effect of the difference in the CH and CD out-of-plane bending motion. This vibration can affect the sigma-pi coupling, the pi-electron spin-density distribution, or both.

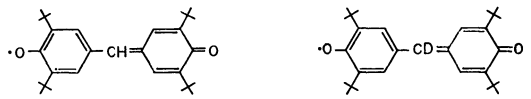

Fig. 1. Structures of galvinoxyl and D-galvinoxyl radicals.

We have synthesized the deuterium derivative (D-galvinoxyl, see Fig. 1) of the galvinoxyl radical, and studied its magnetic properties in order to see the effect of deuterium substitution on the anomalous magnetic property of galvinoxyl by ESR and magnetic susceptibility measurements.

Experimental

Materials. D-Galvinoxyl was synthesized following the method of Kharasch and Joshi[9] or Coppinger.[10] After condensation of 2,6-di-*t*-butylphenol with dideuteroformaldehyde (Merck, deuterierungsgrad 99%), the deuterized bisphenol, 3,3′,5,5′-tetra-*t*-butyl-4,4′-dihydroxydiphenyldideuteromethane, was synthesized, and it was recrystallized from ethanol. Mp 157.0—157.7 °C. The ultraviolet absorption spectrum in ethanol with $\lambda_{max}=278$ mμ (ε 3990) and proton NMR spectrum with $\tau_{C(CH_3)_3}=1.42$ ppm, $\tau_{OH}=4.87$ ppm, and $\tau_{m-H}=6.85$ ppm are in good agreement with those of the corresponding bisphenol, except for the disappearance of the proton NMR absorption due to center methylene

1) K. Mukai, H. Nishiguchi, and Y. Deguchi, *J. Phys. Soc. Jap.* **23**, 125 (1967).
2) K. Mukai, This Bulletin, **42**, 40 (1969).
3) A. Kosaki, H. Suga, S. Seki, K. Mukai, and Y. Deguchi, *ibid.*, **42**, 1525 (1969).
4) R. G. Lawler, J. R. Bolton, G. K. Fraenkel, and T. H. Brown, *J. Amer. Chem. Soc.*, **86**, 520 (1964).
5) A. Carrington, H. C. Longuet-Higgins, R. E. Moss, and P. F. Todd, *Mol. Phys.*, **9**, 187 (1965).
6) R. G. Lawler, J. R. Bolton, M. Karplus, and G. K. Fraenkel, *J. Chem. Phys.*, **47**, 2149 (1967).
7) W. V. Volland and G. Vincow, *ibid.*, **48**, 5589 (1968).
8) M. Karplus, R. G. Lawler, and G. K. Fraenkel, *J. Amer. Chem. Soc.*, **87**, 5260 (1965).
9) M. S. Kharasch and B. S. Joshi, *J. Org. Chem.*, **22**, 1435 (1957).
10) G. M. Coppinger, *J. Amer. Chem. Soc.*, **79**, 501 (1957).

protons of the undeuterized bisphenol ($\tau_{CH_3}=3.75$ ppm). The D-galvinoxyl radical was prepared by the oxidation of the bisphenol with lead peroxide in ether under nitrogen atmosphere. Mp 154—159 °C. The absorption spectrum in ethanol with $\lambda_{max}=424$ mμ (ε 175000) of the D-galvinoxyl is also in good agreement with that of the galvinoxyl.

Apparatus. Magnetic susceptibility measurements were carried out in the continuous temperature range 59—290 K, using a Shimadzu MB-2 type magnetic torsion balance field up to 10 kOe. The ESR measurements were carried out using a JES-ME-3X spectrometer equipped with Takeda-Riken microwave frequency counter. ESR hyperfine splittings and g values were measured relative to those of $(KSO_3)_2$-NO ($a^N=13.05\pm0.03$ G; $g=2.0054$[11]).

Results and Discussion

The ESR spectra of galvinoxyl and D-galvinoxyl in THF at room temperature are shown in Figs. 2-(a) and -(b), respectively. The observed hyperfine splitting constants and g values of galvinoxyl[12] and D-galvinoxyl are listed in Table 1. The g value of D-galvinoxyl, $2.0052_1\pm0.0000_2$, is in agreement with that of Galvinoxyl, $2.0051_8\pm0.0000_2$. The hyperfine splitting (a_m^H) due to the *meta* ring hydrogen atoms of D-galvinoxyl is also the same as that of galvinoxyl, within experimental error. In contrast, the ratio 0.149 ± 0.002 of the deuteron to the proton splittings at center methylene position differs from the theoretical ratio $(a^D/a^H)=0.1535$ expected on the basis of the magnetic moments and spins of the two nuclei. The result can be explained as due to the difference in the CH and CD out-of-plane bending motion in these radicals.[6]

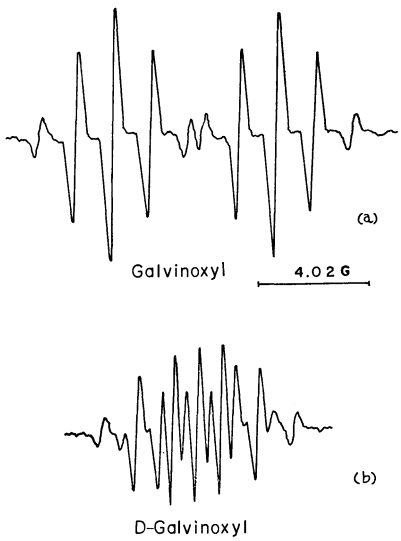

Fig. 2. ESR spectra of (a) galvinoxyl and (b) D-galvinoxyl radicals in THF at room temperature.

Table 1. Hyperfine splittings and g values of galvinoxyl and D-galvinoxyl radicals

	a_m^H	$a_{CH(CD)}^{H(D)}$	g value
Galvinoxyl	1.38±0.02G	5.94±0.02G	$2.0051_8\pm0.0000_2$
D-Galvinoxyl	1.38±0.02G	0.89±0.02G	$2.0052_1\pm0.0000_2$

The measured molar paramagnetic susceptibility, χ_P, as shown in Fig. 3 as a function of the temperature, has been corrected for the diamagnetic contribution of $\chi_{dia}=-0.276\times10^{-3}$ emu/mol calculated by Pascal's method. Between 84 and 290 K, χ_P follows the Curie-Weiss law, with a Weiss constant of $\theta=+6\pm3$ K and a spin concentration of $102\pm3\%$. At 84 K χ_P rapidly decreases by about 70 percent of its maximum value within about ten degrees, and afterward falls gradually to 68 K and again increases to 59 K.

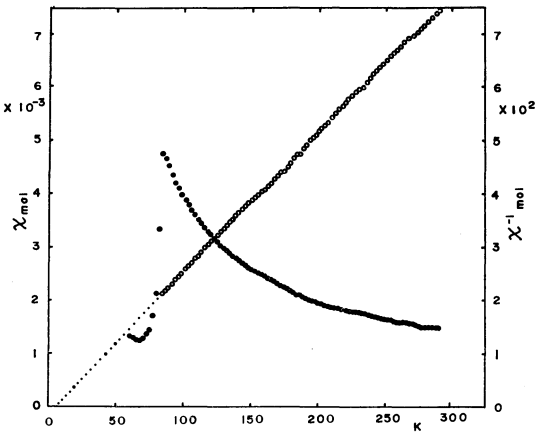

Fig. 3. (●) Molar and (○) inverse molar susceptibilities of the D-galvinoxyl radical *versus* temperature (59—290 K).

Since the anomaly in galvinoxyl is known to result from a transition accompanied by a pairing of the magnetic spins at around the position of the -CH= group as reported before, we can expect that the difference in the CH and CD out-of-plane bending motion in galvinoxyl and D-galvinoxyl, as observed in ESR measurement of the ratio (a^D/a^H), may induce some change in the anomaly in the magnetic susceptibility of galvinoxyl. However, the magnetic behavior is the same as that of galvinoxyl within experimental error, in contrast to our expectation. The result, together with the agreement of position and intensity of absorption maxima in optical spectra and of hyperfine splitting at undeuterated positions, indicates that the perturbation on the structure of galvinoxyl radical by deuterium substitution is too small to induce a change in the anomaly in magnetic susceptibility.

Paramagnetic susceptibility measurements of most crystalline aromatic free radicals usually give negative Weiss constants, showing that the spins on adjacent free radicals in the crystal lattice antiferromagnetically couple with each other. As far as we are aware, the positive Weiss constant observed with both galvinoxyl and D-galvinoxyl radicals is the first example of a positive Weiss constant in solid organic free radicals. McConnell[13] pointed out the possibility of a ferromagnetic exchange interaction favoring parallel (total) spin angular momentum on neighboring molecules in

11) J. J. Windle and A. K. Wiersma, *J. Chem. Phys.*, **39**, 1139 (1963).
12) J. J. Windle and W. H. Thurston, *ibid.*, **27**, 1429 (1957).
13) H. M. McConnell, *ibid.*, **39**, 1910 (1963).

certain aromatic and olefinic free radicals (especially odd-alternant radicals) in which there are large positive and negative atomic π-spin densities. The unpaired electron distribution on galvinoxyl really corresponds to this case as calculated[14] by the conventional valence-bond method. In addition, the result of X-ray analysis[15] of galvinoxyl shows that galvinoxyl may stack in the crystal lattice so that the atoms of positive spin density are exchange-coupled most strongly to the atoms of negative spin-density in neighboring molecules. This gives a ferromagnetic exchange interaction, that is, positive Weiss constant in both radicals.

14) C. Besev, A. Lund, T. Vanngard, and R. Hakansson, *Acta Chem. Scand.*, **17**, 2281 (1963).

15) D. E. Williams, *Mol. Phys.*, **16**, 145 (1969).

BULLETIN OF THE CHEMICAL SOCIETY OF JAPAN, VOL. 46, 3580—3581 (1973)

Effective Ionic Charges of Lithium Niobate Crystal Obtained from the TO-LO Splittings of Infrared Active Lattice Vibrations

Jiro HIRAISHI

National Chemical Laboratory for Industry, Honmachi, Shibuya-ku, Tokyo 151

(Received May 4, 1973)

In ionic crystals, the frequency splittings of the transverse (TO) and the longitudinal (LO) modes are observed for the infrared active vibrations due to long range electrostatic interaction. The values of effective ionic charges of cubic crystals such as sodium chloride, caesium chloride or zinc blende type have been obtained by using the TO–LO splittings.[1] In a previous paper[2] a simple equation useful for obtaining the effective ionic charges of cubic and non-cubic crystals was derived and applied to wurtzite and rutile type crystals. In the present paper the equation is applied to the $LiNbO_3$ crystal.

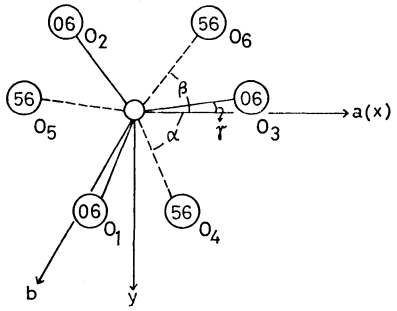

Fig. 1. Atoms in the Bravais lattice of $LiNbO_3$. The larger circles represent the oxygen atoms and the smaller circles the niobium and lithium atoms. The niobium atoms occupy the positions (0, 0, 0) and (0, 0, 1/2), and the lithium atoms the positions (0, 0, 0.2829) and (0, 0, 0.7829). The hexagonal axes are shown in the figure. The numbers in the circles represent the height along c axis.

The space group of the $LiNbO_3$ crystal at room temperature is R3c–C_{3v}^6, two formula units being in a unit cell.[3] The structure is shown in Fig. 1. By factor group analysis the lattice vibrations are classified into $5a_1+5a_2+10e$. Acoustic modes belong to the a_1 and e species. The vibrations of a_1 and e are active in both infrared and Raman spectra. The infrared reflection and polarized Raman spectra for the crystal were measured and assignments of the transverse and longitudinal modes of a_1 and e were made by several investigators.[4-8] In the present paper the assignments by Claus *et al.*[8] are used in the calculation of the values of the effective ionic charges.

The effective ionic charges Z_{Li}, Z_{Nb}, and Z_O are connected to the TO–LO splittings by the equation

$$\sum_i \omega_i^2(\mathrm{L}) - \sum_i \omega_i^2(\mathrm{T}) = 8\pi(Z_{Nb}^2/m_{Nb} + Z_{Li}^2/m_{Li} + 3Z_O^2/m_O)e^2/v_a \quad (1)$$

where $\omega(\mathrm{L})$ and $\omega(\mathrm{T})$ represent the frequencies of the longitudinal and transverse modes, respectively. The summation is carried out for all vibrations of either the a_1 or e species. Equation (1) was derived according to the procedure described previously.[2] The Cartesian symmetry coordinates are given in Table 1. It is noteworthy that $\sum_i \omega_i^2(\mathrm{L}) - \sum_i \omega_i^2(\mathrm{T})$ for the wurtzite, rutile and $LiNbO_3$ type crystal structures is given by

$$\sum_i \omega_i^2(\mathrm{L}) - \sum_i \omega_i^2(\mathrm{T}) = (4\pi e^2/v_a) z_a \sum_k n_k Z_k^2/m_k \quad (2)$$

where z_a and v_a represent the number of the formula unit in the unit cell and the volume of the unit cell, respectively, Z_k and m_k the effective ionic charge and the mass of particle k, respectively, and n_k is the number of particle k in the formula unit. Since the crystal should be electrically neutral, we have

$$Z_{Li} + Z_{Nb} + 3Z_O = 0 \quad (3)$$

However, the values of Z_{Li}, Z_{Nb}, and Z_O can not be definitely determined from Eqs. (1) and (3), and a third equation is introduced by taking into account the spontaneous polarization of the crystal. Spontaneous polarization P_S can be calculated by

1) M. Born and K. Huang, "Dynamical Theory of Crystal Lattices," Oxford University Press, London (1954).
2) J. Hiraishi, This Bulletin, **46**, 1334 (1973).
3) S. C. Abrahams, J. M. Reddy, and J. L. Bernstein, *J. Phys. Chem. Solids*, **27**, 997 (1966).
4) J. D. Axe and D. F. O'Kane, *Appl. Phys. Lett.*, **9**, 58 (1966).
5) R. F. Schaufele and M. J. Weber, *Phys. Rev.*, **152**, 705 (1966).
6) I. P. Kaminow and W. D. Johnston, Jr., *ibid.*, **160**, 519 (1967).
7) A. S. Barker, Jr. and R. Loudon, *ibid.*, **158**, 433 (1967).
8) R. Claus, G. Borstel, E. Wiesendanger, and L. Steffan, *ibid.*, **B6**, 4878 (1972).

Table 1. Cartesian symmetry coordinates of $LiNbO_3$ crystal[a)]

a_1 species

$s_1 = [z(Li)+z(Li)]/\sqrt{2}$ $\quad s_2 = [z(Nb_1)+z(Nb_2)]/\sqrt{2}$

$s_3 = [z(O_1)+z(O_2)+z(O_3)+z(O_4)+z(O_5)+z(O_6)]/\sqrt{6}$

$s_4 = [ac\cdot x(O_1)-as\cdot y(O_1)+bc\cdot x(O_2)+bs\cdot y(O_2)-cc\cdot x(O_3)+cs\cdot y(O_3)-ac\cdot x(O_4)-as\cdot y(O_4)+cc\cdot x(O_5)+cs\cdot y(O_5)-bc\cdot x(O_6)+bs\cdot y(O_6)]/\sqrt{6}$

$s_5 = [as\cdot x(O_1)+ac\cdot y(O_1)-bs\cdot x(O_2)+bc\cdot y(O_2)-cs\cdot x(O_3)-cc\cdot y(O_3)-as\cdot x(O_4)+ac\cdot y(O_4)+cs\cdot x(O_5)-cc\cdot y(O_5)+bs\cdot x(O_6)+bc\cdot y(O_6)]/\sqrt{6}$

e species

$s_1 = [x(Li_1)+x(Li)_2]/\sqrt{2}$ $\quad s_2 = [y(Li_1)-y(Li_2)]/\sqrt{2}$

$s_3 = [x(Nb_1)+x(Nb_2)]/\sqrt{2}$ $\quad s_4 = [y(Nb_1)-y(Nb_2)]/\sqrt{2}$

$s_5 = [2z(O_1)-z(O_2)-z(O_3)-2z(O_4)+z(O_5)+z(O_6)]/2\sqrt{3}$

$s_6 = [z(O_2)-z(O_3)+z(O_5)-z(O_6)]/2$

$s_7 = [2ac\cdot x(O_1)-2as\cdot y(O_1)-bc\cdot x(O_2)-bs\cdot y(O_2)+cc\cdot x(O_3)-cs\cdot y(O_3)+2ac\cdot x(O_4)+2as\cdot y(O_4)-bc\cdot x(O_6)+bs\cdot y(O_6)+cc\cdot x(O_5)+cs\cdot y(O_5)]/2\sqrt{3}$

$s_8 = [cc\cdot x(O_3)-cs\cdot y(O_3)+bc\cdot x(O_2)+bs\cdot y(O_2)+cc\cdot x(O_5)+cs\cdot y(O_5)+bc\cdot x(O_6)-bs\cdot y(O_6)]/2$

$s_9 = [bs\cdot x(O_2)-bc\cdot y(O_2)-cs\cdot x(O_3)-cc\cdot y(O_3)+bs\cdot x(O_6)+bc\cdot y(O_6)-cs\cdot x(O_5)+cc\cdot y(O_5)]/2$

$s_{10} = [2as\cdot x(O_1)+2ac\cdot y(O_1)+bs\cdot x(O_2)-bc\cdot y(O_2)+cs\cdot x(O_3)+cc\cdot y(O_3)+2as\cdot x(O_4)-2ac\cdot y(O_4)+cs\cdot x(O_5)-cc\cdot y(O_5)+bs\cdot x(O_6)+bc\cdot y(O_6)]/2\sqrt{3}$

a) $as=\sin\alpha$, $ac=\cos\alpha$, $bs=\sin\beta$, $bc=\cos\beta$, $cs=\sin\gamma$ and $cc=\cos\gamma$. α, β, and γ are shown in Fig. 1. The coordinates of a_2 species and those of y-components of e species are not given in this table.

$$P_s = \iiint_{\substack{\text{whole}\\ \text{crystal}}} \rho(\boldsymbol{r})\boldsymbol{r}\,dv/V = \iiint_{\substack{\text{unit}\\ \text{cell}}} \rho(\boldsymbol{r})\boldsymbol{r}\,dv/v_a \qquad (4)$$

where $\rho(\boldsymbol{r})$ represents the charge density at $\boldsymbol{r}$ in the crystal and V the volume of the crystal. On the basis of the point charge model, P_S for $LiNbO_3$ is written as

$$P_s = \{Z_{Li}(1/2+2x_{Li})c_0 + Z_{Nb}c_0/2 + Z_O(3/2+6x_O)c_0\}e/v_a \qquad (5)$$

where c_O, x_{Li}, and x_O are 13.8631, 0.2829 and 0.0647 Å, respectively. The values of Z can be obtained by using the three Eqs. (1), (3), and (5).

Although spontaneous polarization is temperature dependent, that of $LiNbO_3$ can be reasonably assumed to be temperature independent near room temperature, since the ferroelectric phase transition temperature is 1210 °C,[9] which is very much higher than room temperature. In the present calculation the value of P_S 0.71 C/m² measured by Camlibel[10] at room temperature was used. The assignments by Claus *et al.*[8] for the TO and LO frequencies slightly differ from those by Kaminow and Johnston.[6] The values from the two assignments do not differ so much since the effective ionic charges depend on the difference of TO and LO frequencies as shown in Eq. (1).

As Eq. (1) is the second order with respect to Z and the sign of spontaneous polarization has not been determined, four sets of solutions were obtained as shown in Table 2. The solution of set 1 is most reasonable since abnormal signs of Z in set 2 and set 3 are given and the value of Z_{Li} is greater than +1.0 in set 4. These values were obtained on the basis of the TO–LO splittings of the a_1 species. The values determined from the splittings of the e species, which are close to those obtained from the a_1 species, are also given in Table 2. The results indicate that the spontaneous polarization of $LiNbO_3$ defined by Eq. (5) is −0.71 C/m². The value (0.347) of Z_{Li} in set 1 suggests the covalent character of Li–O bonds.

Table 2. The values of effective ionic charges and experimental values used in the calculation

(1) The frequencies of TO and LO modes[8] (in cm^{-1})

a_1(L)	876	e(L)	880	e(T)	743
	436		739		668
	333		668		582
	275		454		431
			428		371
a_1(T)	633		371		325
	334		295		265
	276		243		238
	255		198		155

(2) Values of effective ionic charges (in unit of e)

	a_1 species				e species
P_S (C/m^2)[9]	−0.71		+0.71		−0.71
	set 1	set 2	set 3	set 4	set 1
Z_{Li}	0.347	−1.354	−0.347	1.354	0.413
Z_{Nb}	3.791	−1.945	−3.791	1.945	4.013
Z_O	−1.379	1.100	1.379	−1.100	−1.475

9) T. Mitsui, T. Tatsuzaki, and E. Nakamura, "Ferroelectrics," Maki Shoten, Tokyo (1969).

10) I. Camlibel, *J. Appl. Phys.*, **40**, 1690 (1969).

BULLETIN OF THE CHEMICAL SOCIETY OF JAPAN, VOL. 46, 3582—3583 (1973)

Anodic Oxidation of *N,N*-Dimethyl-*p*-phenylenediamine with Sodium Sulfite

Tatsuo ERABI, Fumihiro ARIFUKU, and Masaya TANAKA

Department of Industrial Chemistry, Faculty of Engineering, Tottori University, Koyamacho, Tottori 680

(Received May 24, 1973)

The sulfonation reaction occurs in the anodic oxidation of *N*-methyl-substituted-*p*-phenylenediamine, in the presence of sodium sulfite,[1-3] and the electrode reaction proceeds through the so-called ECE mechanism: that is the electro-oxidation of *N*-methyl-substituted-*p*-phenylenediamine, followed by a chemical sulfonation reaction with sodium sulfite and furthermore with a successive electro-oxidation of the sulfonated compound. However, the reaction intermediate with sodium sulfite has still not completely been revealed. The present paper aims to clarify the reaction intermediate, and to examine whether any regularity is found in these sulfonation mechanisms or not.

Apparatus for voltammetry have been described previously.[3]

When *N,N*-dimethyl-*p*-phenylenediamine (DMPPD) was oxidized anodically, two successive waves were observed in the region between pH 3.75 and 6.50, and only one wave was observed in its upper and lower regions. In addition, when the comparison of the wave height of DMPPD oxidation to the one of *p*-phenylenediamine (PPD) oxidation was attempted using the rotating electrode, the first wave height for DMPPD oxidation in the region between pH 3.75 and 6.50 was equal half to the wave height for PPD oxidation, and therefore the number of electron transfer involved in the reaction for the first wave was estimated to be 1. In its upper and lower regions, the wave height of DMPPD was equal to that of PPD, and therefore the number of electron transfer was estimated to be 2. However, it has been known that DMPPD forms the stable cation radical (so-called Wurster's red) in the measured pH region.[4] Moreover, from the analysis of the products by the controlled-potential electrolysis at the half-wave potential at pH 2.70, it was observed that DMPPD cation radical produced partly. Therefore, it seems probable that two successive one-electron transfers actually occurred in these pH regions. Furthermore, when the Tafel plots were tried for the polarograms obtained with the rotating electrode, α n values were estimated to be about 0.5. Hence, α was equal to 0.5 since the number of electron transfer for the initial reaction was estimated to be 1, and therefore the initial reaction is an oxidation of DMPPD with reversible one-electron transfer.

The anodic oxidation of DMPPD with sodium sulfite was carried out at pH 2.70, 4.00, 6.00, 8.00, and 10.00. As the typical examples, the anodic polarograms at pH 2.70 and 6.00 were shown in Figs. 1 and 2, and the relationships of half-wave potentials and peak currents to concentration of sodium sulfite based on the polarograms in Figs. 1 and 2 were illustrated in Figs. 3 and 4.

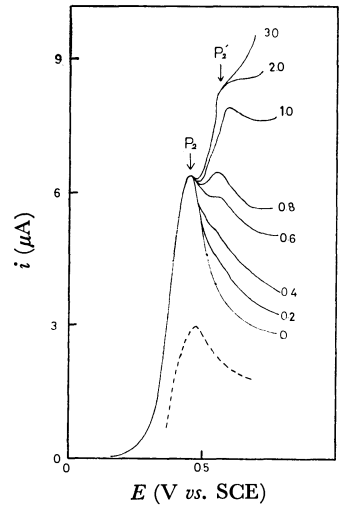

Fig. 1. Typical polarograms of DMPPD oxidation at pH 2.70. Numbers in the figure represent the mole ratio of Na_2SO_3 to DMPPD. The dotted line shows oxidation wave of DMPPD monosulfonate.[5,6]

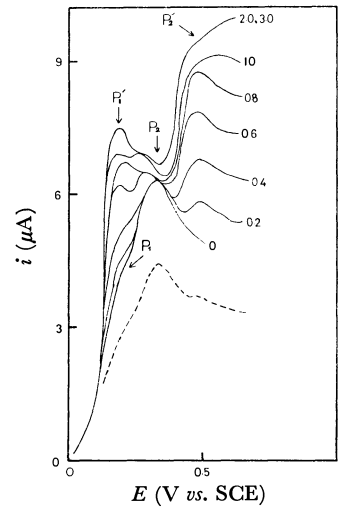

Fig. 2. Typical polarograms of DMPPD oxidation at pH 6.00. Numbers in the figure represent the mole ratio of Na_2SO_3 to DMPPD. The dotted line shows oxidation wave of DMPPD monosulfonate.

1) T. Erabi, A. Wakabayashi, and M. Tanaka, *Rep. Fac. Eng. Tottori Univ.*, **2** (No. 2), 68 (1972).

2) K. Sasaki, H. Imai, Y. Tanimizu, and H. Shiba, *Nippon Kagaku Zasshi*, **91**, 1030 (1970).

3) T. Erabi, Y. Shimotsu, and M. Tanaka, *Denki Kagaku*, **41**, 32 (1973).

4) L. E. Paulsson and G. Pettersson, *Acta Chem. Scand.*, **23**, 2727 (1969).

5) F. Ullmann and K. Jüngel, *Ber.*, **42**, 1077 (1909).

6) Kalle & Co., D.R.P. 124907; *Chem. Z.*, **1901 II**, 1103.

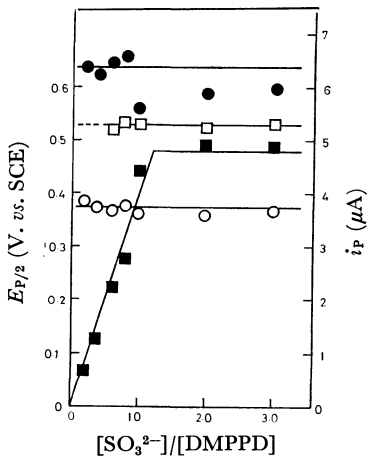

Fig. 3. Relationships of half-wave potential and peak current to Na_2SO_3 concentration at pH 2.70.
○, ●; half-wave potential and peak current for P_2, and □, ■; for P_2'.

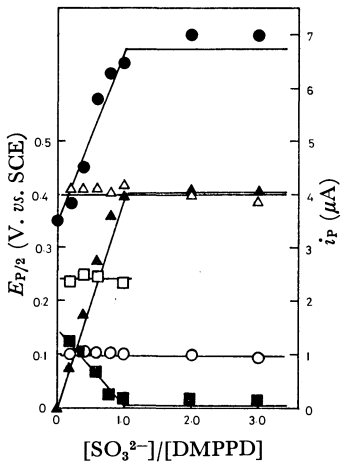

Fig. 4. Relationships of half-wave potential and peak current to Na_2SO_3 concentration at pH 6.00.
○, ●; half-wave potential and peak current for P_1'. □, ■; for P_2, and △, ▲; for P_2'.

The results with DMPPD oxidation can be summarized as follows;

1) The species formed at the first wave (P_1) is DMPPD cation radical, since the initial reaction is oxidation of DMPPD with reversible one-electron transfer. (P_1 is not observed in Fig. 1.)

2) The product at the first wave, DMPPD cation radical, undergoes rapid chemical reaction with SO_3^{--} (or HSO_3^-), and forms DMPPD monosulfonate.

3) This resulting DMPPD monosulfonate is anodically oxidized through second successive one-electron transfers at the same potential range of DMPPD oxidation (P_1'), and forms DMPPD monosulfonate cation radical.

4) The product at P_1', DMPPD monosulfonate cation radical, again undergoes chemical reaction with SO_3^{--} (or HSO_3^-), and forms DMPPD disulfonate.

5) This resulting DMPPD disulfonate is anodically oxidized at the potential of P_2', and forms DMPPD disulfonate cation radical.

That is to say, the sulfonation reaction with DMPPD electro-oxidation seems to proceed through the ECE mechanism. These results are also supported by paper chromatography and spectrophotometric analysis of the products obtained by the controlled-potential electrolysis of DMPPD with sodium sulfite (Table 1).

Table 1. Controlled-potential electrolysis of DMPPD

Sample	Potential of electrolysis (V *vs.* SCE)	R_f-value	λ_{max} (nm)
DMPPD	—	0.92	248
DMPPD+Na_2SO_3	—	0.92	248
DMPPD+ [4]	—	—	550
DMPPD monosulfonate	—	0.42	250
DMPPD (pH 2.70)	0.36	0.88	548
		0.80	280
	0.44	0.81	285
DMPPD (pH 6.00)	0.18	0.87	551
	0.32	0.89	550
		0.82	281
DMPPD+Na_2SO_3 (pH 2.70)	0.44	0.43	250
		0.36	265
DMPPD+Na_2SO_3 (pH 6.00)	0.18	0.87	550
		0.41	251
		0.31	263
	0.32	0.35	265

BULLETIN OF THE CHEMICAL SOCIETY OF JAPAN, VOL. 46, 3584—3585 (1973)

The Dimorphism and Electronic Spectra of Anisyl-*p*-benzoquinones

Jun-ichi AIHARA, Goichi KUSHIBIKI,* and Yoshio MATSUNAGA

Department of Chemistry, Faculty of Science, Hokkaido University, Sapporo 060

(Received June 25, 1973)

The coexistence of orange-yellow crystals (mp 58—59 °C) and red crystals (64—65 °C) has been noted by Brassard and L'Ecuyer in an *o*-anisyl-*p*-benzoquinone sample recrystallized from a mixture of acetone, methanol, and water (1: 1: 1 by volume).[1] We have examined the electronic spectra of these dimorphic forms and also those of some closely-related compounds in the first of our attempts to study self-complexing by a charge-transfer interaction in solids.

Phenyl-*p*-benzoquinone and its *o*- and *p*-MeO derivatives were prepared by the method of the above-mentioned authors. The preparation of the *m*-MeO and *o*- and *p*-EtO derivatives was similarly attempted. The purification of these three substances was found not to be easy. The crude products were repeatedly recrystallized, then sublimed in a vacuum, and finally recrysallized again. Their melting points were 121,81, and 115 °C respectively. The diffuse reflectance (R) of solid samples diluted with sodium chloride was measured at a concentration of 1.00% by means of a Beckman DK-2A spectroreflectometer. The spectra were plotted using the Kubelka-Munk function $f(R)=(1-R)^2/2R$.

The orange-yellow form of *o*-anisyl-*p*-benzoquinone could be isolated, by chance, during the processes of recrystallization, sublimation in a vacuum, and also solidification of the melt. Except for a shift of the absorption maximum to the wavelength side longer by about 25 nm, the spectrum is very similar to that displayed by the compound dissolved in ethanol (see Fig. 1). On the other hand, the red form shows an additional absorption with its maximum located around 500 nm.

p-Anisyl-*p*-benzoquinone recrystallized from an aqueous ethanol solution is orange-red, as has been reported

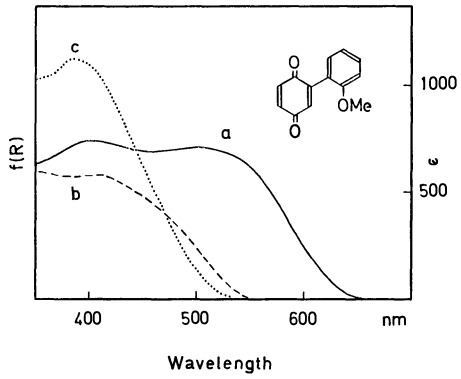

Fig. 1. Diffuse reflection spectra of (a) the red form and (b) the orange-yellow form of *o*-anisyl-*p*-benzoquinone and (c) the absorption spectrum in ethanol.

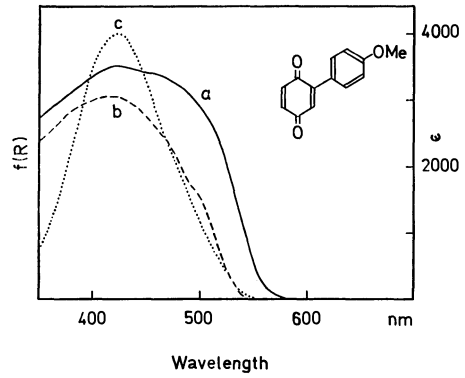

Fig. 2. Diffuse reflection spectra of (a) the orange-red form and (b) the yellow form of *p*-anisyl-*p*-benzoquinone and (c) the absorption spectrum in ethanol.

by Brassard and L'Ecuyer. When the melt is quickly cooled, the yellow form is obtained. Although this form can be kept for months without noticeable change, it is not so stable as the orange-yellow form of the *o*-anisylquinone. The color immediately turns orange-red when it is exposed to acetone vapor. Furthermore, the conversion to the stable form is markedly accelerated by grinding. As is shown in Fig. 2, the solid-state spectrum of the yellow form resembles the solution spectrum. The absorption maximum is located at about 420 nm in both of the states. The feeble structure observed around 500 nm in the solid-state spectrum can be assigned to the n-π transition. The appearance of a shoulder around 470 nm was noted in the spectrum of the orange-red form. The stable form melts at 126—127 °C, and the unstable form, at 118—119 °C. Curiously, the value reported by Brassard and L'Ecuyer, who observed only the orange-red form, agrees with the latter.

As the anisyl groups are excellent electron-donors, and as the quinone nucleus is a fairly good electron-acceptor, the absorptions appearing around 400 nm may be regarded as intramolecular charge-transfer transitions involving the transfer of an electron from a level which is akin to the highest occupied orbital of the anisyl group to the lowest vacant orbital, which is essentially of the quinone nucleus. The locations are shifted to the longer-wavelength side compared with that of the intermolecular charge-transfer absorption band in the anisole-*p*-benzoquinone complex, which has been located by Kuboyama at about 355 nm in carbon tetrachloride.[2] This assignment is supported by the observations that the absorption maximum in solid phenyl-*p*-benzoquinone is at 375 nm, while that in the *p*-NO_2 derivative is below 325 nm. In these two cases, the n-π transitions are well separated from

* Present address: Oki Electric Industry Co., Hachioji, Tokyo.

1) P. Brassard and P. L'Ecuyer, *Can. J. Chem.*, **36**, 700 (1958).

2) A. Kuboyama, *Nippon Kagaku Zasshi*, **81**, 558 (1960).

the intramolecular charge-transfer bands. There is little doubt that the *o*-anisyl-*p*-benzoquinone molecule is farther from co-planarity than the *p*-anisylquinone molecule because of the increased steric hindrance. This accounts for the fact that the extinction coefficient of the charge-transfer absorption band in the former compound is approximately one-fourth of that in the latter. The additional absorptions observed in the deeply-colored forms disappear upon melting. Thus, they may be attributed to the intermolecular charge-transfer interaction between the anisyl group in one molecule and the quinone nucleus in the neighboring molecule. Such a head-to-tail overlap in solids seems to be specific to these two compounds. The *m*-MeO and *o*- and *p*-EtO derivatives are all yellow-colored and exhibit no additional absorption on the longer-wavelength side of the intramolecular charge-transfer absorption band.

BULLETIN OF THE CHEMICAL SOCIETY OF JAPAN, VOL. 46, 3585—3586 (1973)

The Solid Molecular Complex Formed between Phenothiazinyl Neutral Radical and Bromine

Subray N. BHAT and Haruo KURODA

Department of Chemistry, Faculty of Science, The University of Tokyo, Hongo, Tokyo 113

(Received July 24, 1973)

The optical and magnetic properties of the phenothiazine-bromine solid complex have been studied by several authors,[1-4] and it has been reported that the solid is a cation radical salt composed of phenothiazine cation radical and bromine anion, although it is diamagnetic at the room temperature. The apparent diamagnetism is considered to be the result of the reduction of paramagnetism by the strong interaction between phenothiazine cations. However, depending on the preparing conditions, possibly by the effect of the oxidizing agents contained in the used solvent, we sometimes obtain a paramagnetic phenothiazine-bromine solid complex. In this note, we will report the properties of this paramagnetic complex.

Experimental

Phonothiazine was recrystallized from an ethanol solution, and then sublimed *in vacuo* (mp 184 °C). A solution of 0.4 g bromine in 20 ml ethyl ether was added slowly to a solution of 1.0 g phenothiazine in 30 ml ethyl ether, cooling the reaction mixture with the ice-salt mixture. The solid precipitate thus obtained, was filtered, washed several times with cold ether, and dried under vacuum. The ethyl ether commercially obtained was distilled once before use, but no special precaution was done to exclude oxygen and other oxidizing agents.[5]

The result of the elemental analysis of the solid complex was as follows; Found: C, 51.64; H, 2.99; N, 4.79; S, 11.27; Br, 30.35%. Calcd[6] for $C_{12}H_9NS \cdot Br$: C, 51.62; H, 3.25; N, 5.02; S, 11.49; Br, 28.63%.

The ESR spectra were recorded by use of JES-ME-X ESR Spectrometer on a powder sample sealed in a glass tube under vacuum. The spin concentration was determined by using DPPH as the reference, and the *g*-value was determined by comparing with the standard signals of Mn^{2+}. The infrared and visible absorption spectra were measured on the powder sample by using the Nujol-mull method.

Results and Discussion

In contrast with the diamagnetic behaviors of the cation radical salt, the solid complex obtained in the present study, showed a strong paramagnetism, and gave a broad ESR signal with a half-width of about 15 Gauss at the room temperature. The *g*-value was 2.0015 ± 0.0005, and the spin concentration at the room temperature was 6.45×10^{19} spin/g. As shown in Fig. 1, the integrated intensity of ESR signal increased on lowering the temperature and, at the same time, there occurred a decrease of the line width. The temperature dependence of the spin concentration nearly obeys the Curie-Weiss law with the Weiss constant of approximately 70 K.

As shown in Fig. 2, the infrared spectrum of this paramagnetic solid complex considerably differs from that of the cation radical salt. In particular, the N–H stretching band which is observed at 3270 cm^{-1} in

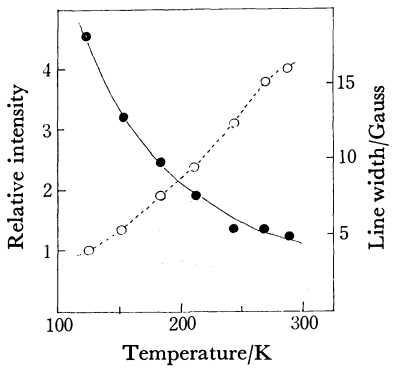

Fig. 1. The temperature dependences of the ESR intensity (—●—) and line width (---○---).

1) G. Lanzi, G. Siragusa, and L. Zanohi, *Il Nouvo Cimento*, **56**, 2179 (1960).

2) Y. Sato, M. Kinoshita, M. Sano, and H. Akamatu, This Bulletin, **40**, 2539 (1967); **42**, 548 (1969).

3) Y. Matsunaga and K. Shono, *ibid.*, **43**, 2007 (1970).

4) Y. Iida, *ibid.*, **44**, 663 (1971).

5) When we carefully excluded oxygen and other oxidizing agents from the solvent, we obtained the cation radical salt.

6) The values calculated for 2(phenothiazinyl)–Br_2 are as follows: C, 51.81; H, 2.89; N, 5.04; S, 11.53; Br, 28.73%.

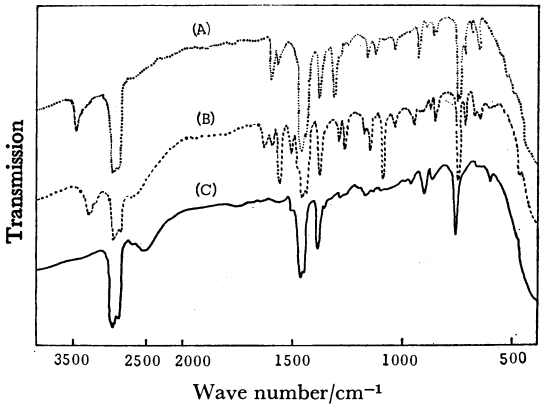

Fig. 2. Infrared absorption spectra of the phenothiazine (A), the cation radical salt, phenothiazine bromide (B) and the paramagnetic complex (C).

the case of the cation radical salt and at 3440 cm^{-1} in the case of pure phenothiazine, is missing in the spectrum of the paramagnetic complex. This seems to indicate that the hydrogen atom attached to nitrogen has been taken off from phenothiazine molecule. In the region below 500 cm^{-1}, the complex gives a broad band at 305 cm^{-1}, which can be attributed to Br–Br stretching vibration.[7,8]

The visible absorption spectrum of the paramagnetic complex is shown in Fig. 3, together with the spectrum of the cation radical salt. In the latter, the 20×10^3 cm^{-1} band has been attributed to the one corresponding to the 18×10^3 cm^{-1} band of the phenothiazine cation, and the near-infrared band at 11×10^3 cm^{-1} to the charge-transfer band associated with the interaction between phenothiazine cations.[4] The spectrum of the paramagnetic complex is considerably different from this; the first band is located at 8×10^3 cm^{-1}, and the second one at about 18×10^3 cm^{-1}.

It has been reported that the oxidation of phenothiazine in solution gives either phenothiazine cation radical (I) or phenothiazinyl neutral radical (II)

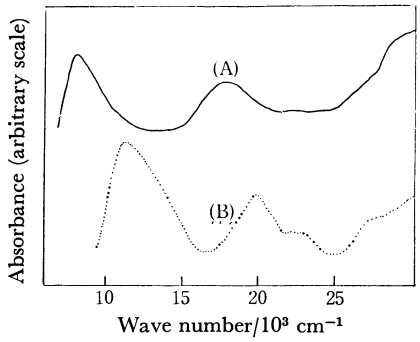

Fig. 3. Powder absorption spectra of the paramagnetic complex (A) and cation radical salt (B).

depending on the condition of oxidation.[9–11] The latter exhibits a strong visible absorption band at about 16×10^3 cm^{-1}.

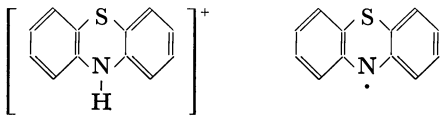

(I) (II)

The strong paramagnetism and the absence of the N–H stretching band in the infrared spectrum, seem to indicate that phenothiazine is in the state of the phenothiazinyl neutral radical in the paramagnetic solid complex obtained in the present study. If this is the case, the solid is likely to be composed of the phenothiazinyl radical and bromine molecule with the mole ratio, 2: 1. This is in accord with the appearance of the Br–Br stretching band in the infrared spectrum. As for the visible spectrum, one could assign the 18×10^3 cm^{-1} band to the one due to phenothiazinyl radical and the 8×10^3 cm^{-1} band to a charge-transfer band.

Thanks are due to the Japan Society for the Promotion of Science for giving the fellowship to one of the authors (S.N.B.).

7) The Br–Br stretching band is infrared inactive in the free bromine molecule, but known to appear in a molecular complex such as the benzene–Br_2 complex.[8]

8) W. B. Person, C. F. Cook, and H. B. Friedrich, *J. Chem. Phys.*, **46**, 2521 (1967).

9) B. C. Gilbert, P. Hanson, R. O. C. Norman, and B. T. Satcliffe, *Chem. Commun.*, **1966**, 161.

10) C. Jackson and N. K. D. Patel, *Tetrahedron Lett.*, **1967**, 2265.

11) M. Kamiya, T. Mitsui, and Y. Akahori, This Bulletin, **46**, 1577 (1973).

BULLETIN OF THE CHEMICAL SOCIETY OF JAPAN, VOL. 46, 3587—3588 (1973)

Torsional Braid Analysis of Magnesium Highpolyphosphate Coacervates

Takao UMEGAKI and Takafumi KANAZAWA

Department of Industrial Chemistry, Faculty of Technology, Tokyo Metropolitan University, Fukazawa, Setagaya-ku, Tokyo 158

(Received November 15, 1972)

Magnesium highpolyphosphate (MP) solutions with high viscosity (10—10^3 poise) and transparency were prepared by coacervation from mixed solutions of sodium highpolyphosphate and $MgCl_2$ under appropriate conditions.[1]

The physicochemical properties of alkali salts of highpolyphosphate have been described in detail by many researchers, but not those of other metal salts. Thermal changes of MP coacervates at temperatures from room temperature to about 1000 °C were examined by means of DTA, TGA and high temperature X-ray diffraction technique as a part of studies on non-alkali condensed phosphates.[2,3]

The present paper deals with temperature dependence of visco-elasticity of magnesium highpolyphosphate obtained by coacervation. Phase transition, thermal degradation and some other thermal changes of the MP at temperatures, from −120 to +80 °C were discussed on the basis of measurements of relative rigidity and logarithmic decrement by a torsional braid analyzer.

Experimental

Preparation of Magnesium Highpolyphosphate Coacervates. A 20% $MgCl_2$ solution (139 parts) was poured into a 15% solution (400 parts) of sodium methaphosphate (both guaranteed reagents of Kanto Chemical Co., Inc.) at room temperature. A white and opaque coacervate was obtained when ethyl alcohol was added to the well-stirred mixture of the two solutions. Addition of alcohol was continued until the coacervate no longer formed in clear liquid phase of the mixture. The MP coacervate (Sample I) was then accumulated by decantation.

Another MP coacervate (Sample II) was prepared by addition of distilled water to Sample I, in a ratio of 1:1 in weight. The chemical compositions of the two coacervates used are shown in Table 1.

TABLE 1. CHEMICAL COMPOSITION OF MAGNESIUM HIGHPOLYPHOSPHATE COACERVATES

Coacervate	Contents (%)			
	MgO	P_2O_5	Na_2O	H_2O
Sample I	6.8	36.8	4.1	52.9
Sample II	3.4	18.2	2.1	76.4

1) T. Kanazawa, H. Kawazoe, and T. Matsubara, *Kogyo Kagaku Zasshi*, **74**, 1784 (1971).

2) T. Kanazawa, T. Umegaki, and H. Kawazoe, *Asahi Garasu Kogyo Gijyutsu Shoreikai Kenkyu Hokoku*, **21**, 81 (1972).

3) T. Kanazawa, T. Umegaki, and Y. Nakayama, Preprint of Lectures at the 26th Annual Meeting of the Chemical Society of Japan, II, p. 687 (1972).

Measurement of Damped Oscillation. Magnesium coacervates settled in a week after preparation, the white, opaque coacervates becoming transparent. The samples were made to adhere to strips of glass cloth. The composite specimen of coacervate and glass cloth was suspended in a torsional pendulum type visco-elastometer (type RD-100, Applied Electric Laboratory, Ohyo Denki Kenkyujo Ltd.). For the experiments at low temperatures, liquid nitrogen was introduced into the visco-elastometer evacuated in advance and passed over the specimen. Damped oscillation was initiated manually at the desired temperature and recorded with a pen-writing oscillograph.

Calculation of Logarithmic Decrement and Relative Rigidity. Logarithmic decrement α_T and relative rigidity G_r were calculated as follows:[4]

$$\alpha_T = \ln A_n/A_{n+1}, \qquad G_r = (P_0/P_1)^2$$

where A_n is the n-th amplitude of damped sine wave, and P_0 and P_1 are periods of the oscillations of MP coacervate sample at temperatures T_0 and T_1, respectively. A certain period P_0 is fixed as a standard.

Results and Discussion

The thermomechanical spectra for MP coacervates are given in Figs. 1 and 2. No change in the logarithmic decrement and relative rigidity for Sample I was found over a temperature range between −120 and −60 °C, the solid phase of MP coacervate being retained without any thermal transformation. Relative rigidity for Sample I (Fig. 1) decreased with temperature rise, the lowering of the rigidity in the vicinity of 0 °C being remarkable. An inflection point of rigidity-temperature curve was found between 20 and 30 °C.

In this type of dynamic experiment the logarithmic decrement is directly related to the phase angle between the stress and strain, providing a measure of the mechanical energy dissipated per cycle compared with

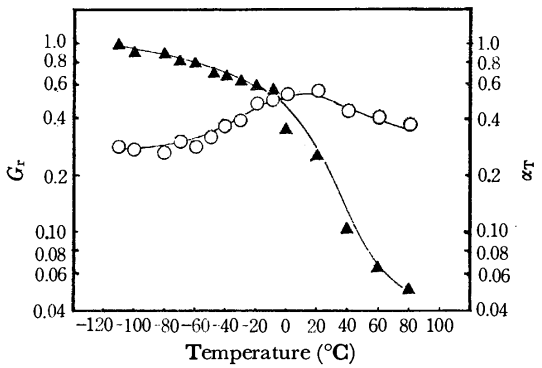

Fig. 1. TBA of sample I.
▲: G_r (relative rigidity), ○: α_T (logarithmic decrement)

4) J. K. Gillham, *Appl. Polym. Symp.*, No. 2, 45 (1966).

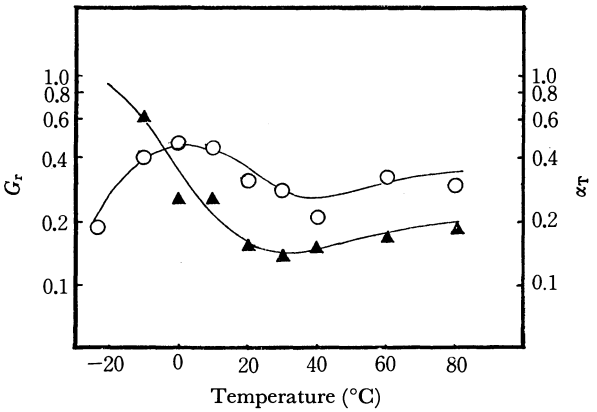

Fig. 2. TBA of Sample II.
▲: G_r (relative rigidity), ○: α_T (logarithmic decrement).

that recovered.[4] At the temperature of the peak for the decrement the MP coacervate was believed to be in the most random state of anion chains of the phosphate polymer.

It seems that the peak of logarithmic decrement and the drastic decrease of relative rigidity between 0 and 60 °C indicate melting of the MP coacervate.

Owing to the wide distribution in the chain length of polyphosphate ions, the peak of the decrement (Fig. 1) is broadened, which is almost unavoidable on the wet preparation of magnesium polyphosphates.

The maximum value of logarithmic decrement and the inflection point in rigidity-temperature curve shift to lower temperature compared with those of Sample I (Fig. 2). The thermomechanical behavior in the vicinity of 0 °C suggests melting of Sample II as well as Sample I. The gradual increase in rigidity and the decrement above 40 °C indicate stiffening of the specimen. Probably magnesium polyphosphates in water-rich coacervate are easily concentrated by vaporization of water, as compared with Sample I with lower content of water.

Besides the concentration of the polyphosphates, the above increase may be explained in terms of partial crystallization of orthophosphates formed in the course of thermal degradation of polyphosphates. However, a temperature of about 40 °C is believed to be somewhat low for initiation of the degradation.

The thermomechanical properties of the MP coacervates were described over a temperature range from −120 to +80 °C. Both coacervates settled in a week and the change of visco-elasticity with time was not examined. It is necessary to measure the time dependence of the rigidity and the decrement under controlled vapor pressure.

This work was supported by a grant from the Asahi Glass Foundation for Contribution to Industrial Technology, for which the authors wish to express their sincere appreciation. Thanks are due to Mr. Nobuhiro Sasaki, Manager of Technical Division, Applied Electric Laboratory (Ohyo Denki Kenkyujo), Ltd. for cooporation in the measurement of visco-elasticity.

BULLETIN OF THE CHEMICAL SOCIETY OF JAPAN, VOL. 46, 3588—3590 (1973)

Electron-transfer Reactions of Multidentate Ligand Cobalt(III) Complexes. VI. The Effect of the Chelation of Nonbridging Ligands on the Iron(II) Reductions of Chlorocobalt(III) Complexes

Yoshimi KURIMURA, Kousaburo OHASHI,* and Sachiko OHKUBO

College of General Education, Ibaraki University, Mito, Ibaraki 310

**Department of Chemistry, Ibaraki University, Mito, Ibaraki 310*

(Received January 23, 1973)

An earlier kinetic study of the reductions of several chlorocobalt(III) complexes, which proceed *via* the bridged activated states, suggested that the predominant factors controlling the rate of electron-transfer reactions are the energy for stretching the *trans*-ligand to the bridging one[1-3] and the effect of solvation.[4-6] More detailed data are necessary, however, to discuss the effect of nonbridging ligands on the rate. Therefore, the effects of the chelation of nonbridging ligands on the rate of the Fe^{2+} reductions of cobalt(III) complexes of the CoN_5Cl^{2+} and $CoN_4Cl_2^+$ types were investigated; the results will now be discussed.[7]

Experimental

trans-$[Co(en)(NH_3)_2Cl_2]Cl$,[7,8] *trans*-$[Co(en)_2Cl_2]Cl$,[9] and *cis*-$[Co(trien)NH_3Cl]Cl_2$[10] were prepared by the methods

1) L. Orgel, Report of the Tenth Solvay Conference, Brussels, 289 (1956).
2) H. Taube, *Advan. Inorg. Chem. Radiochem.*, **1**, 1 (1959).
3) P. Benson and A. Haim, *J. Amer. Chem. Soc.*, **87**, 3826 (1965).
4) Y. Kurimura, K. Ohashi, T. Ohtsuki, and K. Yamamoto, This Bulletin, **44**, 1293 (1971).
5) Y. Kurimura and K. Ohashi, *ibid.*, **44**, 1794 (1971).
6) R. T. M. Fraser, *Inorg. Chem.*, **2**, 954 (1963).
7) N=NH_3, 1/2 en, 1/2 pn, 1/2 tn, 1/3 dien, 1/4 trien, and 1/5 tetren; the abbreviations of the chelating agents are: en=ethylenediamine, pn=propylenediamine, tn=triethylenediamine, dien=diethylenetriamine, trien=triethylenetetramine, and tetren=tetraethylenepentamine.
8) W. C. Fenerius, *Inorg. Chem.*, **2**, 222 (1946).
9) A. Werner, *Ber.*, **34**, 1733 (1901).
10) R. G. Pearson, G. R. Boston, and F. Basolo, *J. Phys. Chem.*, **59**, 304 (1955).

described in the references cited. *cis*-$[Co(pn)_2NH_3Cl]Cl_2$, *trans*-$[Co(pn)_2Cl_2]Cl$, and $[Co(dien)ACl]Cl_2$ (A=pn and tn) were prepared by methods similar to those used for *cis*-$[Co(en)_2NH_3Cl]Cl_2$,[11] *trans*-$[Co(en)_2Cl_2]Cl$,[9] and $[Co(dien)(en)Cl]Cl_2$[10] respectively. The purity of the Co(III) complexes was ascertained by the elementary analysis of carbon, nitrogen, and hydrogen. The kinetics were followed by observing the change in the absorbance of the reaction mixture of the complex. The preparation of the ferrous perchlorate solution was described previously.[4] For all cases, rate studies were carried out with an excess of a reductant as pseudo-first order conditions. For the case of *trans*-$Co(en)(NH_3)_2Cl_2^+$, a lower concentration of the Co(III) ($\sim 2\times10^{-4}$ M) was employed for the kinetic measurements because of its lower solubility; thus, scale-expander attachement for a Hitachi Model 124 spectrophotometer was used. The ionic strength of the reaction mixture was adjusted by the addition of sodium perchlorate.

Results and Discussion

The rate constants for the Fe^{2+} reduction, and the relative rates for the Fe^{2+} reduction and acid hydrolysis of the Co(III) complexes, are presented in Tables 1 and 2 respectively. It is safe to assume that the Fe^{2+} reduction of CoN_5Cl^{2+} and $CoN_4Cl_2^+$ proceeds *via* the chloride-bridged mechanism.[3,5,6]

In previous discussions it was suggested[4,5] that the free energy for the bond stretching of the Co–N bond, especially that of the *trans*-N to the bridging ligand, is an important factor in the Fe^{2+} reduction of the CoN_5Cl^{2+}, and that both free energy for the bond stretching and the solvation effect[4-6] are major factors in the Fe^{2+} reduction of the $CoN_4Cl_2^+$ in determining the rate of electron-transfer reaction.[15] It is clear from Table 2 that an increase in chelation, such as replacing two NH_3 ligands by one ethylenediamine molecule, shows a progressive decrease in the rate of the reduction.

The relative rate constant of the *cis*-$Co(en)_2NH_3Cl^{2+}$ is about four times smaller than that of the *trans*-isomer. This suggests that the reduction rate is much more sensitive to the free energy for the reorganization of the *trans*-ligand than that of the *cis*-ligand for the CoN_5Cl^{2+} type: the effectiveness of *cis*-$Co(en)_2NH_3Cl^{2+}$ would be lower than that of the *trans*-isomer, since the reorganization energy for the *trans*-N ligand (en) of the former would be greater than that for the *trans*-ligand (NH_3) of the latter.

An appreciable decrease in the rate can also be seen when we replace the four NH_3 ligands of the *trans*-$Co(NH_3)_4Cl_2^+$ by two ethylenediamines. That is, the reduction rate is as sensitive to the chelation of the *cis*-ligands as that of the *trans*-ligand for the $CoN_4Cl_2^+$ type (Tables 2, 10 and 12, and 14 and 15). This may be due to (a) the effect of solvation, and (b) the effect of free energy on the reorganization of the non-bridging ligands. The effect of (a) may be explained as follows. The larger the complex ion, the less its solvation energy will be. Therefore, the rate is reduced by chelation because of the reduced stability of the transition state resulting from less efficient solvation.[4,6,14] A similar solvation treatment was given

Table 1. Rate constants for the iron(II) reduction of cobalt(III) complexes

Complex ion	k[a]/$M^{-1}sec^{-1}$
cis-$Co(pn)_2NH_3Cl^{2+}$	2.5×10^{-5}
$Co(dien)(pn)Cl^{2+}$	8.0×10^{-6}
$Co(dien)(tn)Cl^{2+}$	1.4×10^{-5}
cis-$Co(trien)NH_3Cl^{2+}$	2.5×10^{-6}
trans-$Co(en)(NH_3)_2Cl_2^+$	0.36
trans-$Co(pn)_2Cl_2^+$	2.6×10^{-2}

a) 25 °C, $\sum[ClO_4^-]=1.0$ M, $[H^+]=0.10$ M.

Table 2. Relative rate constants for the Fe^{2+} reduction and acid hydrolysis of Co(III) complexes of the CoN_5Cl^{2+} and CoN_4Cl^+ types

No	Complex ion	CoN_5Cl^{2+} type	
		$(R_{Fe})_1$[a]	$(R_{aq})_1$[d]
1	$Co(NH_3)_5Cl^{2+}$	1.0	1.0
2	*cis*-$Co(en)_2NH_3Cl^{2+}$	1.3×10^{-2}	0.21
3	*cis*-$Co(pn)_2NH_3Cl^{2+}$	1.9×10^{-2}	
4	*trans*-$Co(en)_2NH_3Cl^{2+}$	4.9×10^{-2}	
5	$Co(dien)(en)Cl^{2+}$	4.4×10^{-3}	0.78
6	$Co(dien)(pn)Cl^{2+}$	5.9×10^{-3}	
7	$Co(dien)(tn)Cl^{2+}$	1.0×10^{-2}	
8	*cis*-$Co(trien)NH_3Cl^{2+}$	1.9×10^{-3}	0.10
9	$Co(tetren)Cl^{2+}$	very small	0.033
No	Complex ion	*trans*-$CoN_4Cl_2^+$ type	
		$(R_{Fe})_2$[b]	$(R_{aq})_2$[e]
10	*trans*-$Co(NH_3)_4Cl_2^+$	1.0	1.0
11	*trans*-$Co(en)(NH_3)_2Cl_2^+$	0.16	0.13
12	*trans*-$Co(en)_2Cl_2^+$	1.4×10^{-2}	1.8×10^{-2}
13	*trans*-$Co(pn)_2Cl_2^+$	1.2×10^{-2}	3.4×10^{-2}
No	Complex ion	*cis*-$CoN_4Cl_2^+$ type	
		$(R_{Fe})_3$[c]	
14	*cis*-$Co(NH_3)_4Cl_2^+$	1.0	
15	*cis*-$Co(en)_2Cl_2^+$	1.2×10^{-2}	
16	*cis*-$Co(trien)Cl_2^+$	2.9×10^{-3}	

a) Ratio of rate constant to that of $Co(NH_3)_5Cl^{2+}$ ($k=1.35\times10^{-3}$ M^{-1} s^{-1})[12] at 25 °C and $\mu=1.0$, calculated from the rate constants listed in Refs. 12, 3, and 6, and those obtained by this work,

b) Ratio of rate constant to that of *trans*-$Co(NH_3)_4Cl_2^+$ ($k=2.21$ M^{-1} s^{-1})[13] at 25 °C and $\mu=1.0$, calculated from the rate constants listed in Refs. 3 and 13, and those obtained by this work,

c) Ratio of rate constant to that of *cis*-$Co(NH_3)_4Cl_2^+$ ($k=0.136$ M^{-1} s^{-1}),[12] calculated from the rate constants in Refs. 3, 5, and 12,

d) Ratio of rate constant for the acid hydrolysis to that of $Co(NH_3)_5Cl^{2+}$ at 35 °C, from Ref. 14.

e) Ratio of rate constant for the acid hydrolysis to that of *trans*-$Co(NH_3)_4Cl_2^+$ at 25 °C, from Ref. 14.

11) a) A. Werner, *Ann. Chem.*, **386**, 165 (1912); b) A. Werner and V. L. Kino, *Ber.*, **44**, 1890 (1911).

12) J. H. Espenson, *Inorg. Chem.*, **4**, 121 (1965).

13) R. G. Linck, *ibid.*, **7**, 2394 (1968).

14) F. Basolo and R. G. Pearson, "Mechanism of Inorganic reactions," John Wiley & Sons, New York (1967), p. 161.

15) In the $CoN_5Cl^+ + Fe^{2+} \rightarrow Co^{2+} + 5N + FeCl^{2+}$ reaction the over-all charges on the Co(III) and Co(II) are not identical, so the solvation effect is considered to be an important factor in the reaction.[6]

in order to explain the effect of the chelation on the acid hydrolysis of the Co(III) complexes, though this theory does not distinguish between S_N1 and S_N2 mechanisms.[14] An interesting fact is that the values of $(R_{Fe})_2$ for *trans*-$CoN_4Cl_2^+$ are almost parallel to those of $(R_{aq})_2$: the rate constants of the Fe^{2+} reduction and those of the acid hydrolysis decrease by a factor of about one by replacing the two NH_3 ligands by one ethylenediamine. The $(R_{Fe})_1$, $(R_{Fe})_2$, and $(R_{Fe})_3$ represent the ratios of the rate constant for the Fe^{2+} reduction to those of $Co(NH_3)_5Cl^{2+}$, *trans*-$Co(NH_3)_4Cl_2^+$, and *cis*-$Co(NH_3)_4Cl_2^+$ respectively, while $(R_{aq})_1$ and $(R_{aq})_2$ represent the ratios of the rate constants for the aquation to those of $Co(NH_3)_5Cl^{2+}$ and *trans*-$Co(NH_3)_4Cl_2^+$ respectively.

Table 2 also shows the effect on the rate of increase in the size of the chelate ring from five members to six when trimethylenediamine is used instead of ethylenediamine. For both the CoN_5Cl^{2+} and $CoN_4Cl_2^+$ types, the rates are little affected by using the propylenediamine instead of ethylenediamines (Table 2, Nos 3 and 4, 5 and 6, and 12 and 13). However, the rate is doubled by replacing two ethylenediamines by two trimethylenediamines. This increase in the rate may be related to the fact that complexes with six-membered chelate rings are much less stable than those with five-membered chelate rings.[14,16]

16) S. Chaberek and A. E. Martell, "Organic Sequestring Agents," John Wiley & Sons, New York (1959), p. 126.

BULLETIN OF THE CHEMICAL SOCIETY OF JAPAN, VOL. 46, 3590—3591 (1973)

The Mössbauer Effect of Several Iron(II) Octahedral Complexes of α-Dioxime

Yoshihiro SASAKI and Tsunenobu SHIGEMATSU
Institute for Chemical Research, Kyoto University, Uji, Kyoto 611

(Received April 20, 1973)

The Mössbauer effect has been used to study the electronic structure of iron porphyrins. The measurement is, however, difficult because of the small quantities of iron present. Therefore, an empirical approach, using simple model compounds, appears to be necessary. Since bis(dimethylglyoximato)diimidazoleiron(II) possesses unsaturated equatorial ligands containing nitrogen donor atoms and biologically-important axial ligands, it is regarded as a model complex of iron porphyrins.

We have studied the electronic structure of iron(II)-α-dioxime complexes containing pyridine or imidazole as axial ligands by Mössbauer spectroscopy and will report the results here.

Experimental

1,2-Cyclohexadione-dioxime(CdH_2), dimethylglyoxime(DgH_2), α-furyldioxime(FrH_2), and α-benzyldioxime(BzH_2) were used as the equatorial ligands, and pyridine(Py) and imidazole(Im), as the axial ligands. The pyridine complexes were synthesized as has been described by Matsumoto *et al.*,[1] while the imidazole adducts were prepared by analogous procedures.

The Mössbauer spectra were obtained with scanning velocity spectrometers operating in the time mode. The radiation source was ^{57}Co diffused into a copper or palladium foil and kept at room temperature throughout the measurements. The powdered samples, containing about 8 mg/cm² of natural iron, were mounted on aluminum foil, and the spectra were taken at 77 K, at *ca.* 100 K, and at room temperature. The velocity scale was calibrated with metallic iron, and the velocity was determined to an accuracy of ±0.04 mm/s.

1) C. Matsumoto, Y. Yamane, and K. Shinra, *Nippon Kagaku Zasshi*, **89**, 44 (1968).

Results and Discussion

The isomer shift, δ, and the quadrupole splitting, ΔE_Q, are listed in Table 1. Some typical Mössbauer spectra of bis(α-furyldioximato)dipyridineiron(II) are shown in Fig. 1.

Isomer Shift. The isomer shift of the present samples lies within a range normally found for low-spin complexes.[2] The complexes with α-furyldioxime

TABLE 1. MÖSSBAUER PARAMETERS OF Fe(II)(α-dioxime)$_2X_2$

Compound	Temp. (K)	Quadrupole splitting mm/s	Isomer shift mm/s
$Fe(II)(DgH)_2Py_2$	300	1.78	0.24
	~100	1.73	0.26
$Fe(II)(CdH)_2Py_2$	300	1.76	0.28
	~100	1.80	0.36
$Fe(II)(FrH)_2Py_2$	300	1.90	0.19
	~100	1.87	0.24
$Fe(II)(BzH)_2Py_2$	300	1.91	0.19
	~100	1.94	0.22
$Fe(II)(DgH)_2Im_2$	300	1.31	0.27
	~100	1.29	0.31
$Fe(II)(CdH)_2Im_2$	300	1.38	0.23
	~100	1.36	0.30
$Fe(II)(FrH)_2Im_2$	300	1.44	0.21
	77	1.41	0.25
$Fe(II)(BzH)_2Im_2$	300	1.53	0.21
	77	1.56	0.26

Values of the isomer shift are quoted relative to iron,

2) J. F. Duncan and R. M. Golding, *Quart. Rev.*, **19**, 36 (1965).

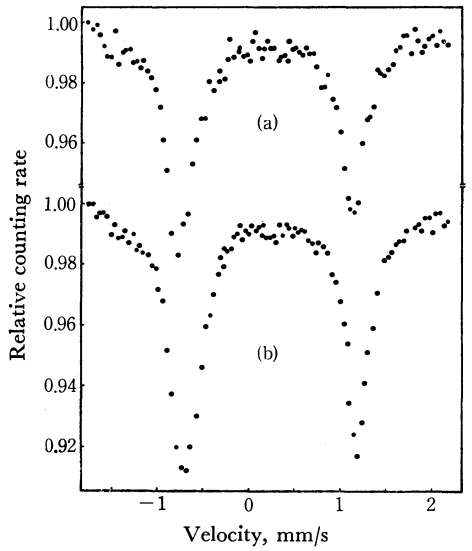

Fig. 1. Mössbauer spectra of $Fe(II)(FrH)_2Py_2$.
(a) room temperature (b) about 100 K

or α-benzyldioxime exhibit a smaller isomer shift than those with dimethylglyoxime or 1,2-cyclohexadionedioxime. Changes in the isomer shift reflect (a) changes in the s orbital populations due to involvement in covalent bonding, and (b) changes in the shielding of electrons in s orbitals by other electrons, notably those in 3d orbitals whose population and distribution are affected by the details of bonding. α-Furyl and α-benzyl groups, which are π-electron-attractive groups, will lead to a stronger interaction between the 3d orbitals of the central iron and the π* orbitals of the α-dioxime, causing a greater delocalization of the electrons in the 3d orbitals of the iron. This will weaken the shielding of s-electrons by 3d-electrons and decrease the isomer shift. Pyridine has a stronger π-accepting capability, while imidazole has a stronger σ-donor power. Both the effects by the axial ligands will decrease the isomer shift. Thus, the isomer shift of the complexes with the same α-dioxime may be changed little by the axial ligands.

Quadrupole Splitting. For metal-organic complexes, the electric-field gradient consists of both terms of the valence electrons of the Mössbauer nucleus and the ligands.[3] The electronic distribution of a ferrous ion in a strong crystal field has a cubic symmetry. Thus, octahedral low-spin iron(II) complexes show a single absorption peak or a doublet exhibiting a small quadrupole splitting.

The present complexes have a low-spin d^6 electronic configuration, while their observed quadrupole splittings are relatively large, especially in the pyridine adducts. Recently the Mössbauer spectrum of $Fe(II)(CdH)_2Im_2$ was measured in the magnetic field.[4] The results indicate that the asymmetry parameter for this complex is quite large. On the other hand, the quadrupole splitting of the complexes containing CO or CN^- as axial ligands is normally small.[5] These findings suggest that we should consider the effects of π bonding on the axial ligands. According to the X-ray analyses of $Fe(II)(CdH)_2Im_2$ and $Fe(II)(DgH)_2Im_2$,[6,7] the π rings of imidazole are coplanar and are perpendicular to the hydrogen bond. The structure of these complexes is shown in Fig. 2. We assume that the central iron is in a nearly D_{2h} symmetry. Then, the π orbitals of the axial ligands may interact with only the 3d(xz) orbital. As pyridine has a stronger π-accepting capability than imidazole, the electrons in the 3d(xz) orbital of pyridine adducts will migrate more to the axial ligands. Thus, this may give a larger quadrupole splitting in pyridine complexes.

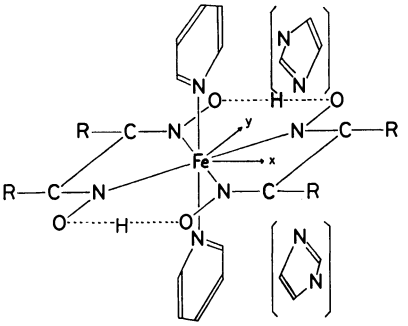

Fig. 2. The structure of the complex $Fe(II)(\alpha\text{-dioxime})_2X_2$.
(X=pyridine or imidazole)

The quadrupole splitting of the pyridine adducts increases in the order of: CdH_2, DgH_2, FrH_2, and BzH_2; the isomer shift decreases in the same order. In the imidazole complexes, CdH_2 and DgH_2 change places with each other.

An additional characteristic of the Mössbauer spectra of $Fe(II)(FrH)_2Py_2$, $Fe(II)(BzH)_2Py_2$, and $Fe(II)(FrH)_2Im_2$ is found in the differences in the peak intensities of the doublet lines. Such an asymmetry can be ascribed to (1) crystal orientation,[8] (2) anisotropic recoilless fraction,[9,10] or (3) relaxation phenomena.[11] Because these complexes are diamagnetic, relaxation phenomena are not taken into account. As the samples were finely powdered, any effects due to crystal orientation would be eliminated. The temperature dependency of the Mössbauer spectra predicts, then, that there is an anisotropic recoilless fraction in these complexes.

The authors wish to thank Drs. T. Shinjo and Y. Maeda for permitting us to use the equipment for the Mössbauer measurements and for their helpful discussions.

3) R. Ingalls, *Phys. Rev.*, **133**, A787 (1964).
4) B. W. Dale, R. J. P. Williams, P. R. Edwards, and C. E. Johnson, *Trans. Faraday Soc.*, **64**, 3011 (1968).
5) B. W. Dale, R. J. P. Williams, P. R. Edwards, and C. E. Johnson, *ibid.*, **64**, 620 (1968).
6) C. K. Prout and T. J. Wiseman, *J. Chem. Soc.*, **1964**, 497.
7) K. Bowman, A. P. Gaughan, and Z. Dori, *J. Amer. Chem. Soc.*, **94**, 727 (1972).
8) P. Zory, *Phys. Rev.*, **140**, A1401 (1965).
9) S. V. Gol'danskii, E. F. Makarov, and V. V. Krarov, *Phys. Lett.*, **3**, 344 (1963).
10) S. V. Karyagin, *Dokl. Akad. Nauk SSSR*, **148**, 1102 (1963).
11) M. Blume, *Phys. Rev. Lett.*, **14**, 96 (1965).

BULLETIN OF THE CHEMICAL SOCIETY OF JAPAN, VOL. 46, 3592—3593 (1973)

Photochemical Reactions of 1,1-Diphenyl-2-picrylhydrazyl with Gold(III) Complexes

Michihiko Asai and Shigeo Tazuke*

Department of Polymer Chemistry, Kyoto University, Kyoto 606

(Received May 1, 1973)

The reactions of 1,1-diphenyl-2-picrylhydrazyl(DPPH) with some metal salts have recently aroused interest. DPPH has been reported to undergo certain types of oxidation-reduction reaction with various metal ions[1,2] as well as chelates,[3,4] or charge transfer (CT) complex formation with CuCl.[5] All these systems, however, were treated under thermal conditions. No photochemical reactions of DPPH with metal salts have so far been reported. In the course of studies on the photo-cationic polymerization of *N*-vinylcarbazole sensitized by $(n\text{-}C_4H_9)_4NAuX_4$(X=Cl$^-$, Br$^-$),[6] we found that under irradiation of a solution containing DPPH and Au(III) complexes the characteristic purple color of the former disappeared. This communication describes the novel reaction in acetophenone as a solvent in connection with the photochemistry of Au(III) complexes, which has not been investigated quantitatively in spite of their extreme photosensitivities. Experimental methods are the same as described elsewhere.[6] All reactions were carried out without eliminating dissolved air.

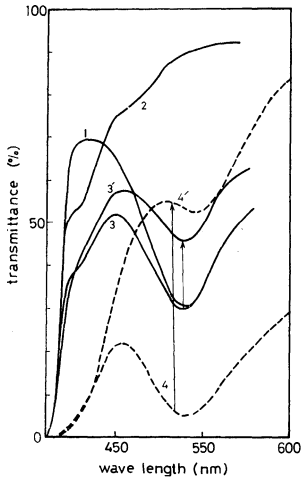

Fig. 1. Photochemical reactions between AuX_4^- and DPPH in acetophenone.
1; [DPPH]=5×10^{-5}M, 2; [$AuBr_4^-$]=5×10^{-5}M, 3; [DPPH]=5×10^{-5}M, [$AuBr_4^-$]=5×10^{-5}M, 4; [DPPH]=5×10^{-5}M, [$AuCl_4^-$]=2×10^{-3}M, 3′ and 4′; after irradiation of 3(30 min) and 4(45 min) irradiation at 436 nm, 30 °C.

When an acetophenone solution containing equimolar amounts (5×10^{-5} M) of DPPH and $AuBr_4^-$ was irradiated by 436 nm light for 30 min at 30 °C, the characteristic purple color (λ_{max} 540 nm) of DPPH faded as shown in the figure. This was also observed under thermal conditions, although the rate of disappearance was negligibly small. No interaction between DPPH and $AuBr_4^-$ species was observed spectroscopically and irradiation of a solution of DPPH alone induced no fading of its color. Irradiation at 546 nm was ineffective. These facts indicate that effective light absorbing species leading to the reaction is not DPPH but $AuBr_4^-$ itself. The quantum yield (ϕ_{-DPPH}) for the disappearance of DPPH was calculated from the plots of its absorbance at 540 nm against time to be 0.17 after correcting for the inner filter effect:

$$I_{abs,A} = \frac{\varepsilon_A[A]}{\varepsilon_A[A]+\varepsilon_D[D]} I_0[1-\exp\{-(\varepsilon_A[A]+\varepsilon_D[D])\}]$$

where A and D denote $AuBr_4^-$ and DPPH, and $I_{abs,A}$, I_0 and ε denote amounts of light absorbed by $AuBr_4^-$, the intensity of incident light and molar extinction coefficient, respectively. The quantum yield ($\phi_{-AuBr_4^-}$) for the photodecomposition of $AuBr_4^-$ under irradiation at 436 nm at 30 °C has been obtained as 0.20.[6] It is interesting that both ϕ_{-DPPH} and $\phi_{-AuBr_4^-}$ are nearly the same, indicating that the photodecomposition of $AuBr_4^-$ corresponds to the equimolar fading of DPPH.

A similar fading reaction of DPPH was also observed by the use of $AuCl_4^-$ as shown in the figure. In this case, however, thermal reaction should be considered because of the high concentration of $AuCl_4^-$. The value of $\phi_{-AuCl_4^-}$ was calculated to be 0.24 on the assumption of 1 : 1 correspondence between $\phi_{-AuCl_4^-}$ and ϕ_{-DPPH}.

The characteristic absorption band at 540 nm of DPPH radical has been reported[5] to be probably due to the picryl ring having an appreciably delocalized unpaired spin. Metal ions or chelates have been assumed[2] to react with equimolor proportion of DPPH with production of 1,1-diphenyl-2-picrylhydrazine ($DPPH_2$) *via* hydrogen atom transfer mechanism or election transfer accompanied by proton transfer mechanism. Alternatively, it has been known[5] to form CT complex with metal ion coordinating to the picryl ring. The purple color of DPPH has been reported to disappear in these systems, whereas the absorption maximum attributed to hydrazine or CT complex appears in ultraviolet region. In the present system, the solution became pale yellow by prolonged irradiation although the absorption maximum was not observable due to hindrance of the absorption band of solvent.

* Present address: Research Laboratory of Resources Utilization, Tokyo Institute of Technology, Meguro, Tokyo 152.

1) L. H. Sutcliffe and J. Walkley, *Nature*, **178**, 999 (1956).
2) C. E. H. Bawn and D. Verdin, *Trans. Faraday Soc.*, **56**, 519 (1960).
3) K. Uehara, M. Tanaka, and N. Murata, This Bulletin, **41**, 3034 (1968).
4) K. Uehara, K. Kamei, M. Tanaka, and N. Murata, *ibid.*, **45**, 540 (1972).
5) F. Leh and J. K. S. Wan, *ibid.*, **45**, 308 (1972), *Can. J. Chem.*, **50**, 999 (1972).
6) M. Asai and S. Tazuke, *Macromolecules*, in press.

As to the photodecomposition of AuX_4^- under irradiation of its CTTM band, its primary process seems to be intramolecular photoredox reaction as suggested[7] from the flash photolysis studies in which transient spectrum of X_2^- was detected. The mechanism of primary processes is proposed as follows:

$$Au^{III}X_4^- \xrightarrow{h\nu} A^{II}X_3^- + X \xrightarrow{\text{free } X^-} X_2^-$$

The reaction of DPPH with either transient species Au(II) or X (or X_2^-) formed photochemically may be explained from the viewpoint of the electron-transfer reaction in which DPPH acts as an oxidant. The direction of the electron-transfer may be controlled by the relative magnitude of the redox potential (E°) of the reacting species. The E° for the DPPH system[2] and the Au(III)/Au(II) couple[8,9] have been estimated to be -1.1——-1.2 V and -0.5——-0.96 V, respectively. The halogen atom, a strong oxidant, has not been reported to act as a reductant presumably because of difficulty in the formation of X^+ cation from X atom. X_2^- anionradical has been reported to be a stronger oxidant than X_2 molecule.[10] Thus, electron-transfer from these halogen species to DPPH seems to be highly unlikely. This might be supported by the results obtained in the flash photolysis of $AuBr_4^-$, *i.e.* the amount of Br_2^- was less than that of photodecomposed $AuBr_4^-$ by a factor of about ten, which is not in line with the results where both ϕ_{-DPPH} and $\phi_{-AuBr_4^-}$ are of nearly the same value. The electron-transfer reaction between Au(II) and DPPH seems to be energetically more favorable. If Au(II) is reoxidized to Au(III), the dark red color of $AuBr_4^-$ should be restored. However, the presence of hydrazine derivatives as a result of the reduction of DPPH would cause the formation of a colorless complex with Au(III). The Au(III) complexed with amine is colorless as shown for the tetramine-[11] and bisethylenediamine-[12] Au(III) complexes.

Another possibility is that formation of the charge-transfer complex between DPPH radical with the halogen-Au(I) species may result from the spontaneous reduction of Au(II) species. This case is similar to the DPPH/CuCl complex reported by Leh and Wan.[5] It seems most likely that some gold species is responsible for the fading reaction of DPPH.

The authors express their gratitude to Professors Seizo Okamura and Toshinobu Higashimura for their encouragement and valuable discussions.

7) M. Asai, S. Tazuke, S. Okamura, T. Ohno, and S. Kato, *Chem. Lett.*, **1973**, 993.
8) R. L. Rich and H. Taube, *J. Phys. Chem.*, **58**, 6 (1954).
9) T. Vänngard and S. Åkerstrom *Nature*, **184**, 183 (1959).
10) S. D. Malone and J. F. Endicott, *J. Phys. Chem.*, **76**, 2223 (1972).
11) W. R. Mason, III and H. B. Gray, *J. Amer. Chem. Soc.*, **90**, 5721 (1968).
12) A. K. Gangopadhayay and A. Chakravorty, *J. Phys. Chem.*, **35**, 2206 (1961).

BULLETIN OF THE CHEMICAL SOCIETY OF JAPAN, VOL. 46, 3593—3594 (1973)

The Chelation-induced Deceleration of the Methyl Proton Exchange in the Bisacetylacetoneethylenediimine Ligand

Ichiro TAKAGI and Hayami YONEDA*

Department of Chemistry, Faculty of Education, Wakayama University, Masagocho, Wakayama 640
**Department of Chemistry, Faculty of Science, Hiroshima University, Higashisenda-machi, Hiroshima 730*

(Received May 18, 1973)

Organic ligands in chelate compounds are subject to the influence of the electron-withdrawing effect of a central metal ion, and, as a result, proton dissociation from the ligand is more or less facilitated. Therefore, hydrogen-deuterium exchange can be observed in some complexes when they are dissolved in deuterium oxide. This kind of exchange can easily be detected and followed by measuring the intensity decrease in the PMR signal of the coordinated ligand. We have found several such examples, *i.e.*, in the methylene of the malonato[1] and glycinato[2] cobalt(III) complexes, in the ethylene of the EDTA cobalt(III) complex,[3] and in the methyl of dimethylglyoximatocobalt(III) complexes.[4] In all these cases, the free ligand itself does not show such an exchange, and chelation is considered to accelerate it.

Here we would like to report another type of chelation effect, one which slows down the rate of proton exchange. The complexes studied are four kinds of bisacetylacetoneethylenediiminecobalt(III) with the formula of $[CoX_2acac\text{-}en]^{n+}$, where X is NO_2^-, pyridine, NH_3, and CH_3NH_2. These complexes were dissolved in a 2% NaOD deuterium oxide solution, and the PMR spectra were measured at 60 °C at appropriate time intervals. For comparison, the time change in the PMR spectrum of the free ligand itself was also recorded under the same conditions. Figure 1 shows the spectra of $[Co(NH_3)_2acac\text{-}en]NO_3$ measured (a) immediately and (b) 240 min after dissolution. A comparison of

1) H. Yoneda and Y. Morimoto, This Bulletin, **40**, 1737 (1967); *Inorg. Chim. Acta*, **1**, 413 (1967).
2) H. Yoneda and Y. Morimoto, *Kagaku no Ryoiki*, **22**, 826 (1968).
3) H. Yoneda and Y. Morimoto, This Bulletin, **42**, 1160 (1969).
4) H. Yoneda, I. Takagi, and Y. Morimoto, *ibid.*, **44**, 2863 (1971).

the two spectra, (a) and (b), reveals that the H–D exchange occurred at two sites of the ligand, namely, at the vinyl and at one of the two methyls. At present we have no unambiguous evidence with which to decide which methyl of the two (one adjacent to C=N and the other adjacent to C–O) is exchange-active. However, the exchange-rate constant in the methyl can easily be determined from the slope in Fig. 2.

The rate constants obtained for the free ligand and for the four complexes (10^{-3} min^{-1} unit) are 57.7 (free ligand), 6.6 (CH_3NH_2), 2.9 (NH_3), 1.6 (pyridine), and 0.7 (NO_2^-).

Here it should be noted that the exchange rate for the free ligand is ten times as large or larger than those for the complexes. This large exchange rate in the methyl of the free ligand can be understood by means of the following tautomeric mechanism:

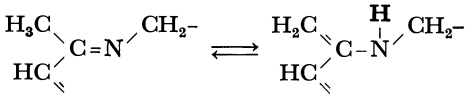

or

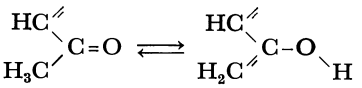

This kind of tautomerism is depressed by chelation, which results in a decrease in the exchange rate in the complexes. In other words, chelation fixes the planar atomic arrangement of the acetylacetone group and gives it a pseudoaromatic character, which then serves to reduce the contribution of the electronic state favorable for the above-mentioned tautomerism. The decreasing order of the rate constants for the four complexes is; $CH_3NH_2 > NH_3 >$ pyridine $> NO_2^-$ and corresponds to the increasing order of the degree of the charge neutralization of the metal ion caused by the ligand, X. Therefore, this trend suggests that the electron-withdrawing effect of the metal ion is the only driving force for the proton exchange in the complexes.

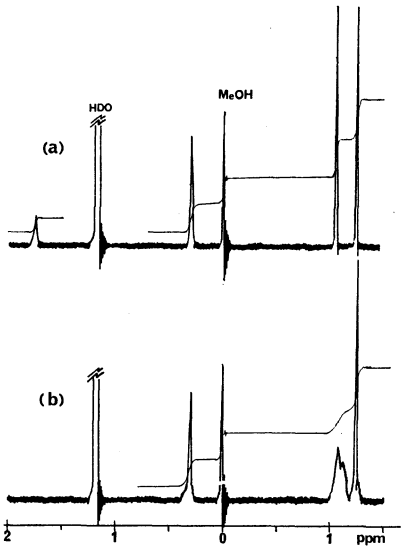

Fig. 1. The PMR spectra of $[Co(NH_3)_2acac\text{-}en]NO_3$ in 2% NaOD–D_2O solution at 60 °C recorded (a) immediately and (b) 240 min after dissolution.

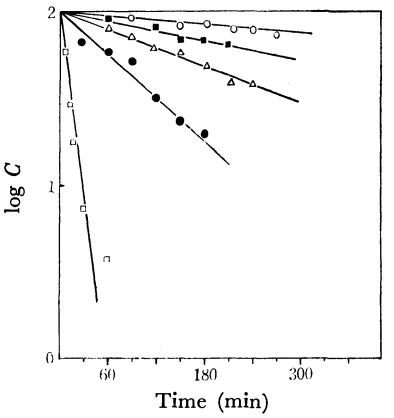

Fig. 2. Plots of the methyl signal intensity of the bisacetylacetoneethylenediimine ligand against time (60 °C).
□: the free ligand, ●: $[Co(CH_3NH_2)_2acac\text{-}en]^+$,
△: $[Co(NH_3)_2acac\text{-}en]^+$, ■: $[Co(py)_2acac\text{-}en]^+$,
○: $[Co(NO_2)_2acac\text{-}en]^-$.

Experimental

Materials. The $[CoX_2acac\text{-}en]ClO_4$ (X=CH_3NH_2, NH_3, and pyridine) and $Na[Co(NO_2)_2acac\text{-}en]$ complexes were prepared according to the method reported by Fujii.[5]

NMR Measurements. The spectra were recorded in a 2% NaOD deuterium oxide solution on a Jeol JNM-C-60HL spectrometer. Methanol was added to the solution as an internal standard for the chemical shift and the intensity.

One of the authors especially, Dr. Takagi, is grateful to the Ministry of Education for a Grant in Aid for Scientific Research.

5) Y. Fujii A. Osawa, Y. Furukawa, F. Ebina, and S. Takahashi, This Bulletin, **45**, 2459 (1972).

BULLETIN OF THE CHEMICAL SOCIETY OF JAPAN, VOL. 46, 3595—3596 (1973)

Indirect Determination of Tantalum by Atomic Absorption Spectrophotometry

Tsutomu MATSUO, Junichi SHIDA, and Seiichi KUDO

Department of Applied Chemistry, Faculty of Engineering, Yamagata University, Jonan-4, Yonezawa, Yamagata 992

(Received May 22, 1973)

Reports have recently been given on indirect determination of arsenate,[1] germanate,[2,3] phosphate,[4,5] silicate,[5] and niobate,[6] based on the extraction of heteropolymolybdate with the organic extractant and subsequent measurement of the molybdenum contained in the extract by atomic absorption spectrometry. Guyon *et al.* reported the spectrophotometric methods for determination of niobium[7] and tantalum,[8] in which heteropolymolybdate complex was used. The authors investigated an indirect determination of tantalum by atomic absorption spectrometry. The essential steps in this method are; formation of molybdotantalate, extraction of the molybdotantalate with methyl isobutyl ketone (MIBK) and measurement of molybdenum by aspirating the MIBK extract directly into the burner of the atomic absorption spectrophotometer.

Experimental

Apparatus. Atomic absorption spectrometric measurements were carried out with a Hitachi model 207 atomic absorption spectrophotometer equipped with a molybdenum hollow cathode lamp (Hitachi, HLA-3) as a light source at 3133 Å molybdenum line. Lamp current was 15 mA. An air-acetylene flame was used with flow rates 13 l/min and 3 l/min.

Standard Tantalum Solution (1.0×10^{-2} *M*). Dissolve 0.1809 g of tantalum metal (99.7%) in hydrofluoric acid containing a small amount of nitric acid and evaporate it to dryness. Add 5 ml of hydrofluoric acid and 5 ml of sulfuric acid, and heat until fumes of the sulfuric acid are evolved. After cooling, dilute to 100 ml with distilled water.

Procedure. Transfer 10 ml of 0.2 M ammonium molybdate solution to a 100 ml separatory funnel, add 2 ml of 6 M hydrochloric acid and swirl to mix. Add known amounts of tantalum solution and dilute with distilled water to 20 ml. After standing the solution 15 min, add 20 ml of MIBK and shake vigorously for 5 min. Separate the layers, wash the MIBK extract three times with 25 ml portions of 0.6 M hydrochloric acid and measure molybdenum by aspirating the MIBK extract of molybdotantalate into the burner of the atomic absorption spectrophotometer. A blank containing all the reagents except the tantalum sample is prepared by a similar procedure.

Results

Acidity for Extraction of Molybdotantalate. The optimum acidity of aqueous solution for the extraction of molybdotantalate with MIBK was examined. The results are shown in Fig. 1. The acidity range 0.5—0.7 M hydrochloric acid was found to be suitable, the absorbance value being constant in this range.

Effect of Molybdate Concentration. The effect of ammonium molybdate for the extraction of molybdotantalate was studied. The results are shown in Fig. 2. A constant absorbance value was obtained when 9 ml of 0.2 M ammonium molybdate was added.

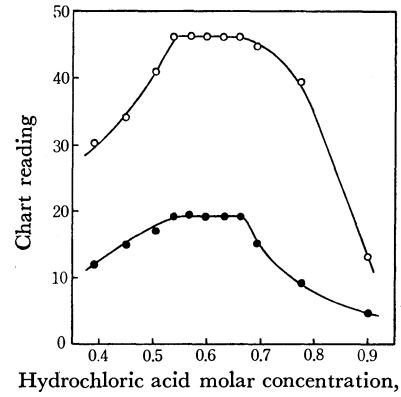

Fig. 1. Effect of acidity on extraction of heteropolymolybdates.
—○— Ta^{5+}; 2×10^{-5}M, —●— Nb^{5+}; 4×10^{-5}M

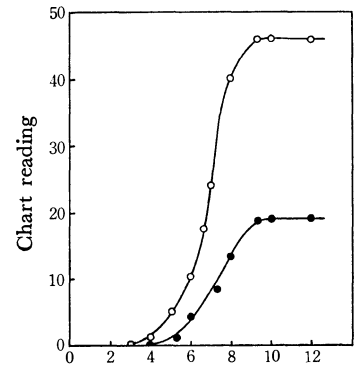

Fig. 2. Effect of amounts of 0.2M Mo(VI) soln.
—○— Ta^{5+}; 2×10^{-5}M —●— Nb^{5+}; 4×10^{-5}M

1) Y. Yamamoto, N. Kumamaru, Y. Hayashi, A. Kanke, and A. Matsui, *Bunseki Kagaku*, **21**, 379 (1972).
2) R. Jakubiec and D. F. Boltz, *Anal. Chem.*, **41**, 78 (1969).
3) T. Matsuo, J. Shida, and S. Kudo, *Bunseki Kagaku*, **22**, 1009 (1973).
4) G. F. Kirkbright, A. M. Smith, and T. S. West, *Analyst* (London), **92**, 411 (1967).
5) T. R. Hurford and D. F. Boltz, *Anal. Chem.*, **40**, 379 (1968).
6) G. F. Kirkbright, A. M. Smith, and T. S. West, *Analyst* (London), **93**, 292 (1968).
7) J. C. Guyon, G. W. Wallace, Jr., and M. G. Mellon, *Anal. Chem.*, **34**, 640 (1962).
8) J. C. Guyon, *Anal. Chim. Acta*, **30**, 395 (1964).

In the determination of tantalum, 10 ml of molybdate solution was used.

Washing of the MIBK-Extract. Molybdotantalate was extracted into MIBK with a trace of excess molybdate.[2,3] To remove the trace of excess molybdate, washing of the MIBK extract with hydrochloric acid was examined. Washing three times with 25 ml portions of 0.6 M hydrochloric acid solution was sufficient to remove the excess molybdate. Shaking time for washing was 3 min.

Effect of Standing Time. The rate of formation of heteropolymolybdate was relatively slow at room temperature. The effect of standing time prior to extraction of molybdotantalate was examined. Fifteen minutes was found to be the best for quantitative extraction.

Stability of Extract. No change in absorbance value was observed for at least two hours in the MIBK extract.

Calibration Curve. The calibration curve of absorbance value *versus* concentration of tantalum was linear for 2.5×10^{-6}—2.0×10^{-5} M of tantalum.

Effect of Diverse Ions. An atomic absorption spectrometric method for the determination of niobium based on the formation of molybdoniobophosphate was reported by Kirkbright *et al.*[6] Niobium also forms molybdoniobate, which should be removed before the tantalum determination. It was found that niobium could be determined by the proposed method (Figs. 1 and 2) and that the linear relationship was obtained in the niobium concentration range 1.0×10^{-5}—5.0×10^{-5} M. The sensitivity of molybdoniobate is about five times less than that of molybdotantalate. Heteropolymolybdates which give positive errors are arsenate, germanate, phosphate and silicate.

BULLETIN OF THE CHEMICAL SOCIETY OF JAPAN, VOL. 46, 3596—3598 (1973)

The Rapid Collection of Traces of Silver with Mercury in an Ultrasonic Field

Atsushi MIZUIKE, Katsuaki FUKUDA, and Takeshi SAKAMOTO
Faculty of Engineering, Nagoya University, Chikusa-ku, Nagoya 464

(Received May 31, 1973)

Previously we reported that microgram quantities of silver deposit quantitatively into numerous mercury globules from 1 to 3 mm in diameter from stirred aqueous solutions, leaving large amounts of such base metals as iron, copper, and lead in the solutions.[1,2] Because mercury is removed by evaporation from the resulting dilute amalgam, this separation method is useful as a preconcentration technique in trace analysis. The procedure, however, is rather time-consuming. The present note will describe a more rapid separation method using a mercury-in-water emulsion in an ultrasonic field. This method has been applied to the atomic absorption spectrometric determination of silver at a low ppm level in lead.

Experimental

Apparatus. A Kaijo Denki model MA-2302 ultrasonic generator (29 kHz, 45 W) with a cylindrical transducer (13 mm diam. × 100 mm) coated with epoxy resin. A Hitachi model 139 spectrophotometer with a model 139-0420 atomic absorption attachment and a model QPD-53 recorder.

Solutions. Ammoniacal sample solutions were prepared by mixing 2 ml of nitric acid, 1.5 ml of hydrochloric acid, and 10 ml of aqueous ammonia and by then diluting to 25 ml with water, or by dissolving 5 g of high-purity copper in 40 ml of 7 M nitric acid, adding 15 ml of hydrochloric acid and 100 ml of aqueous ammonia, and diluting to 200 ml with water.

Standard Procedure. Place 25 ml of water and 34 g of mercury in a 50 ml beaker, immerse an ultrasonic transducer about 2 mm deep in the water, and apply ultrasonics for 30 s to obtain a gray emulsion containing about 150 mg of mercury. Within 3 min add this emulsion to a 100 ml, round-bottomed centrifuge tube containing 25 ml of the sample solution and apply ultrasonics for 30 s as has been described above. Centrifuge for 3 min at 4000 rpm and then discard the supernatant liquid. Add 5 ml of acetone and stir vigorouly with a glass rod for 10 s to effect coalescence into a single mercury droplet (about 3 mm in diameter)

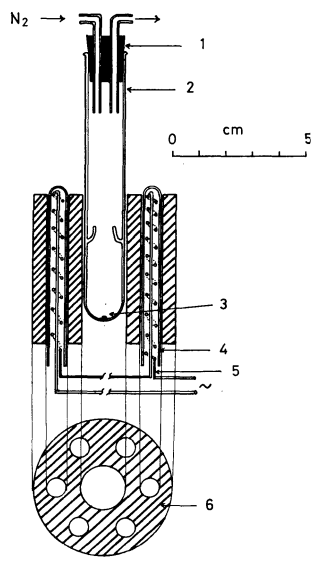

Fig. 1. Apparatus for evaporation of mercury.
1: Silicone rubber stopper, 2: Pyrex evaporation tube, 3: Mercury droplet, 4: Quartz tube, 5: Nichrome wire, 6: Brass block.

1) S. Hirano and A. Mizuike, *Bunseki Kagaku*, **8**, 746 (1959).
2) A. Mizuike, T. Sakamoto, and K. Sugishima, *Mikrochim. Acta* (Wien), **1973**, 291.

with a metallic luster. Discard the acetone, wash the droplet with 2 ml of acetone two or three times, and discard the washings. Transfer the mercury droplet to the bottom of an evaporation tube with a dropping pipet, and then evaporate the mercury at 350 °C (Fig. 1). Cool, and then remove the mercury condensed on the walls of the evaporation tube using a mercury-plated copper wire. Add 1 ml of nitric acid to the evaporation tube to dissolve the residue.

Results and Discussion

Preparation of Mercury-in-Water Emulsions. Mercury-in-water emulsions were prepared with from 7 to 68 g of mercury and 25 ml portions of water with the aid of ultrasonics; the mercury in the emulsion was then separated as a single droplet by centrifugation and by washing with acetone as has been described under *Standard Procedure*, and determined by weighing or EDTA titration. As is shown in Fig. 2, saturation was reached after 20 s of ultrasonic irradiation. The reproducibility for 40 s of ultrasonic irradiation was as follows: 127, 122, 114, 125, and 125 mg of mercury in an emulsion (with 20 g of mercury), and 155, 150, 146, 152, and 138 mg (with 34 g of mercury). The diameter of the mercury droplets was from 1 to 4 μm after 20 s, and the emulsion was stable for about 5 min.

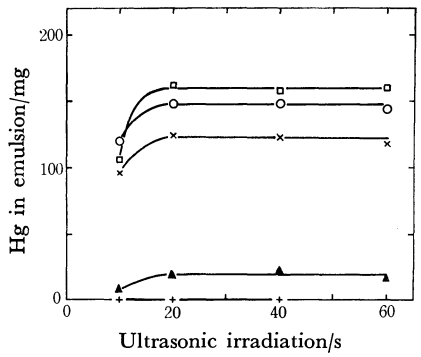

Fig. 2. The quantity of mercury in emulsion as a function of time of ultrasonic irradiation.
Hg used: (□) 68 g, (○) 34 g, (×) 20 g, (▲) 14 g, (+) 7 g.

Collection of Silver. A mercury-in-water emulsion (25 ml) was added to 25 ml of a sample solution containing from 5 to 10 μg of ^{110m}Ag-labeled silver; the silver was then collected as has been described under *Standard Procedure* except that the quantity of mercury and the collecting time were changed, and the gamma activity of the mercury droplet was measured. The results are summarized in Fig. 3. A silver recovery of greater than 96% was attained with from 125 to 150 mg of mercury between 20 and 40 s. In the case of nitric acid solutions, the silver recovery then decreased with the time because of the dissolution of mercury in the solutions, as is shown in Fig. 4. The dissolved mercury was determined by EDTA titration after the removal of the mercury droplets by means of a centrifuge.

Separation of Silver from Matrix Elements. Table 1 shows that ppm quantities of silver in lead and copper matrices can be separated with recoveries of greater than 96% and concentration factors of greater than 10^5 by the standard procedure. In this experiment,

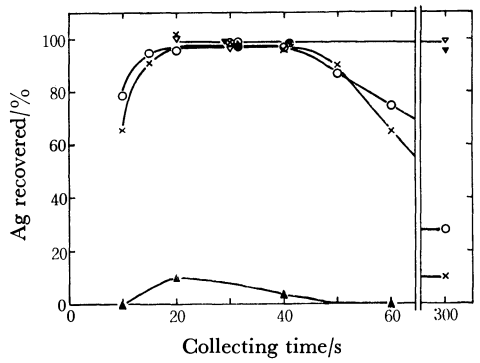

Fig. 3. Collection of silver with mercury.

Hg in emulsion (mg)		Sample solution
(○)	150	0.2 M nitric acid
(●)	150	0.2 M nitric acid solution containing 1 g of Pb
(⊙)	150	0.2 M nitric acid solution containing 1 g of Cu
(×)	125	0.2 M nitric acid
(▲)	20	0.2 M nitric acid
(▽)	150	Ammoniacal solution
(▼)	150	Ammoniacal solution containing 0.5 g of Cu

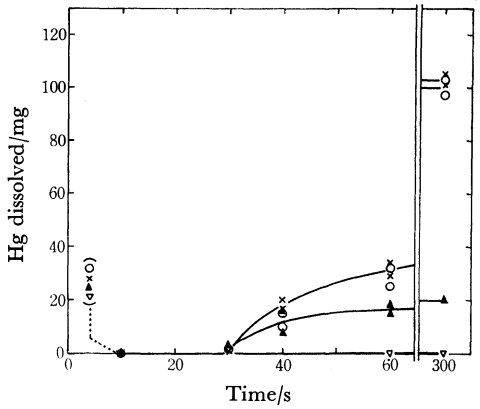

Fig. 4. Dissolution of mercury.

Hg in emulsion (mg)		Sample solution
(○)	150	0.2 M nitric acid
(×)	125	0.2 M nitric acid
(▲)	20	0.2 M nitric acid
(▽)	150	Ammoniacal solution

both the silver recovery and the quantity of the matrix elements accompanying the silver were measured after the removal of the mercury by evaporation.

The proposed method may also be applied to the separation of traces of gold or palladium from copper and other base metals in ammoniacal or nitric acid solutions.

Table 1. Separation of silver from matrix elements in 0.1 M nitric acid solutions[a)]

Matrix element present (g)	Ag recovered (%)	Matrix element accompanying Ag[b)] (μg)
Pb 0.50	96, 100	—
Pb 1.00	98, 100	3, 5
Cu 1.00	96, 102	0.7, 1.3

a) ^{110m}Ag-labeled Ag present 3-10 μg,
b) Determined by square-wave polarography.

Determination of Traces of Silver in Lead. A 5 g lead sample was dissolved in 15 ml of 7 M nitric acid. The solution was then evaporated to dryness, and the residue was dissolved in 50 ml of 0.5 M nitric acid. A 1/10 or 1/5 aliquot was taken and diluted to 25 ml with 0.12 M nitric acid or water (final acidity, 0.2 M). The silver in the solution was separated by the standard procedure, and the residue in the evaporation tube was dissolved in 1 ml of 7 M nitric acid. The solution was then evaporated to dryness, and the residue was dissolved in 0.80 ml of 2 M nitric acid and then in 1.20 ml of acetone. The silver in the solution was then determined by atomic absorption spectrometry at 328.1 nm.[2] The analytical results are shown in Table 2. The time required for a determination was about 2 hr.

Table 2. Determination of silver in lead

Sample	Aliquot taken	Ag found[b] (μg)	Ag in sample (ppm)
High-purity lead, 5.00 g	1/10	1.8	3.6
	1/10	1.9	3.8
	1/5	3.5	3.5
	1/5[a]	8.4	3.4
			Av. 3.6

a) 5.0 μg of Ag was added before the separation.
b) A blank value was not detected (<0.2 μg).

BULLETIN OF THE CHEMICAL SOCIETY OF JAPAN, VOL. 46, 3598—3599 (1973)

The Sublimation Pressure of Tetrasulfur Tetranitride

Shuichi HAMADA

Department of Chemistry, Faculty of Science, Science University of Tokyo, Kagurazaka, Shinjuku-ku, Tokyo 162

(Received June 12, 1973)

Tetrasulfur tetranitride, S_4N_4, is stable contrary to expectation in air at room temperatures, but it decomposes explosively when struck or when heated above its melting point. Goehring and Voigt[1] pointed out that tetrasulfur tetranitride decomposes into its elements at approximately 130 °C. The concrete values of the sublimation pressure of tetrasulfur tetranitride have not been reported because of its instability, although Meuwsen[2] stated that the compound can be sublimed below 130 °C at 0.1 mmHg.

In this work, the sublimation pressure of tetrasulfur tetranitride was studied at temperatures below 90 °C by means of the method of transpiration.

Experimental

Materials. The tetrasulfur tetranitride was prepared by the method described by Villena-Blanco and Jolly[3] without further purification.

Argon was obtained from the Nippon Sanso Company, which guaranteed a purity better than 99.994%, as a carrier gas. The carrier gas was passed through a cylinder containing silica gel before it was admitted into the reaction vessel.

Procedure. A flow diagram of the apparatus is shown in Fig. 1. The reaction vessel was heated at temperatures from 70 to 90 °C with a precision of ±0.3 °C by mounting it in a thermostated aluminum block. The preheated carrier gas was made to flow, at specified flow rates, through about 3 g of the tetrasulfur tetranitride put on a glass filter in the reaction vessel. The accuracy of the specified flow rates,

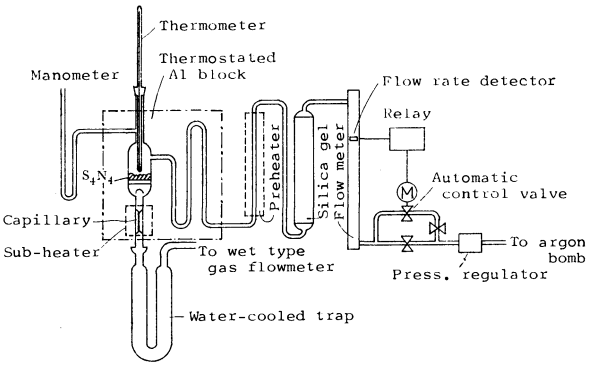

Fig. 1. Schematic diagram of apparatus.

obtained by using an automatic control valve model BM-N, the Nisshin Kagaku Company, and an argon bomb with a regulator, was of the order of 0.5%. The excessive pressure in the reaction vessel against the atmospheric pressure was measured with a manometer containing a Silicone oil with a low vapor pressure. The pressure control of the carrier gas was not carried out, because the maximum variation in the atmospheric pressure during the runs was 2.5 mmHg (corresponding to about 0.3%). The temperature of the flow gas in the reaction vessel was measured with a thermometer and was maintained within ±0.3 °C. The carrier gas containing the tetrasulfur tetranitride vapor was discharged through a capillary (2 cm in length and 0.1 cm in diameter) into a water-cooled trap. The capillary was heated at slightly higher temperatures than that of the reaction vessel to prevent a deposition of the tetrasulfur tetranitride on it. The total volume of the carrier gas was measured with an accuracy of ±0.4% by using a wet-type gas flowmeter, model WK-0.5, which can be read to an order of 1 ml (Shinagawa Seisakusho).

The small amount of the trapped tetrasulfur tetranitride was estimated from the optical absorbance of its benzene solution at 350 mμ by using a working curve previously

1) M. Goehring and D. Voigt, *Z. Anorg. Allgem. Chem.*, **285**, 181 (1956).

2) A. Meuwsen, *Ber.*, **65**, 1724 (1932).

3) M. Villena-Blanco and W. L. Jolly, "Inorganic Synthesis," Vol. IX, ed. by S. Y. Tyree, Jr., *et al.*, McGraw-Hill, New York (1967), p. 98.

determined (the molar extinction coefficient at 350 mμ was 1057).

Results and Discussion

The melting point of the sample was determined microscopically to be 179 °C by using materials of known melting points as references. The value of the melting point for the tetrasulfur tetranitride which was prepared by the Jolly method was found to be 178—179 °C.[4] The IR spectrum[5] and the X-ray powder diffractogram[6] of the sample showed patterns attributable to tetrasulfur tetranitride only. Therefore, the sample obtained in this work was considered to be pure enough to measure the sublimation pressure of tetrasulfur tetranitride.

An abrupt weight loss and an exothermic change in the thermal gravimetric analysis and the differential thermal analysis on tetrasulfur tetranitride[6] occurred at temperatures above approximately 125 °C. These results were not affected by the presence of air. It is, then, considered that tetrasulfur tetranitride decomposes at temperatures higher than 125 °C. Therefore, the partial pressures of the sample were estimated in the temperature range from 70 to 90 °C.

Quantities of the argon sufficient to trap about 1 mg of the tetrasulfur tetranitride were used in all the runs; *i.e.*, they were in the ranges from 15.30 to 17.03 l (the passing times were from 160.0 to 600.0 min), from 9.274 to 10.99 l (from 105.0 to 510.0 min), from 5.712 to 7.632 l (from 70.0 to 420.0 min), from 3.442 to 5.151 l (from 45.0 to 180.0 min), and from 2.877 to 3.117 l (from 30.0 to 110.0 min) as the standard state at 70, 75, 80, 85, and 90 °C respectively, while the amounts of the trapped tetrasulfur tetranitride were estimated to be in the range from 0.899 to 1.30 mg. The tetrasulfur tetranitride deposited immediately on the neck of the trap as a fine powder after its vapor had passed through the thermostated aluminum block.

The partial pressure, p, of the tetrasulfur tetranitride at the specified temperature and flow rate was calculated by means of the following equation, being assumed to obey the law of partial pressures:

$$p = (P+p')/[1+(184.3/w)(P+p''-p_w)V/RT]$$

where P is the atmospheric pressure; p', the excessive pressure in the reaction vessel; p'', the excessive pressure in the gas flowmeter; p_w, the vapor pressure of water in the gas flowmeter; w, the weight of the trapped tetrasulfur tetranitride; V, the observed total volume of the carrier gas; T, the temperature of the carrier gas in the gas flowmeter, and R, the gas constant.

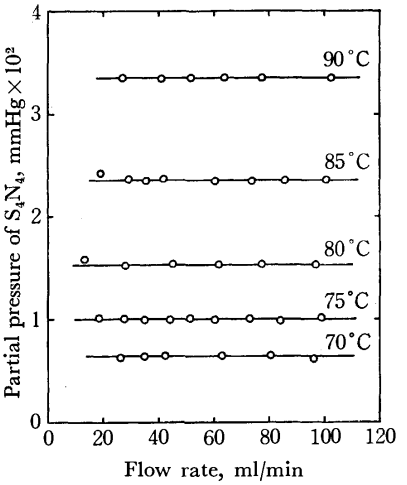

Fig. 2. Dependence of partial pressure of S_4N_4 on flow rate.

The relationship between the partial pressures and the flow rates, which were expressed as the standard states, is shown in Fig. 2. The values of the partial pressure were almost equal to each other at all the temperatures under those conditions except for those at the flow rates of 13.60 ml/min (80 °C) and 19.12 ml/min (85 °C), which were considered to arise from a diffusion[7] of the tetrasulfur tetranitride vapor. Therefore, the average values of the partial pressure can be accepted as those of the sublimation pressure of tetrasulfur tetranitride; they are shown in Table 1. No changes in the structure or chemical components of the sample remaining in the reaction vessel were found by X-ray powder diffraction analysis after the measurements.

Table 1. Sublimation pressures of tetrasulfur tetranitride

Temp., °C	Sublimation Press., mmHg
70	6.42×10^{-3}
75	1.00×10^{-2}
80	1.53×10^{-2}
85	2.35×10^{-2}
90	3.51×10^{-2}

The heat of the sublimation, ΔH^s, of tetrasulfur tetranitride in the temperature range from 70 to 90 °C was estimated to be 21.2 kcal/mol from the excellent linear relationship of the Clausius-Clapeyron plot. Although Barker *et al.*[8] deduced the heat of the sublimation of tetrasulfur tetranitride to be 15±5 kcal/mol from the results obtained by using a bomb calorimeter, the value estimated in this work is slightly larger than that obtained by Barker.

4) W. L. Jolly, "The Synthesis and Characterization of Inorganic Compounds," Prentice-Hall, Englewood Cliffs, N. J. (1970), p. 502.

5) H. G. Heal, "Inorganic Sulfur Chemistry," ed. by G. Nickless, Elsevier, Amsterdam (1968), p. 464.

6) S. Hamada, A. Takanashi, and T. Shirai, This Bulletin, **44**, 1433 (1971).

7) U. Merten, *J. Phys. Chem.*, **63**, 443 (1959).

8) C. K. Barker, A. W. Cordes, and J. L. Margrave, *ibid.*, **69**, 334 (1965).

BULLETIN OF THE CHEMICAL SOCIETY OF JAPAN, VOL. 46, 3600—3601 (1973)

A Synthetic Approach to DL-α-(2-Thiazolyl)glycines

Minoru HATANAKA and Toshiyasu ISHIMARU

The Institute of Scientific and Industrial Research, Osaka University, Yamadakami, Suita, Osaka 565

(Received January 26, 1973)

As a part of the investigation of the synthesis of the α-substituted glycine derivatives with heterocyclic rings,[1] the synthesis of 2-thiazolylglycine was studied. Since 2-thiazolylacetic acid has been reported to show a remarkable ease of decarboxylation,[2] we adopted a synthetic route *via* the amino acid esters, **6**. The unusual behavior of the 2-thiazolylglycines, which were decarboxylated too rapidly to be isolated, is the subject of this note.

The starting materials, ethyl 4-methylthiazole-2-glyoxalate (**2a**) and ethyl thiazole-2-glyoxalate (**2b**), were prepared from 4-methylthiazole (**1a**, R=CH_3, X=H) and 2-bromothiazole (**1b**, R=H, X=Br) respectively by lithiation, followed by the addition of the 2-lithio compounds to an excess of ethyl oxalate. The subsequent treatment of **2a** with hydroxylamine in aqueous methanol at 0 °C gave a crystalline product, **3a**, in a high yield; its empirical formula, $C_8H_{12}N_2O_4S$, corresponded to that of a monohydrate of the expected oxime. The IR spectrum, in addition to one carbonyl band at 1720 cm^{-1}, exhibited a very broad and strong band at 3150 cm^{-1}. Under the same conditions, **2b** yielded **3b** as a sirup; the IR spectrum of **3b** was similar to that of **3a**. Compounds **3a** and **3b**, when heated in refluxing benzene, regenerated the starting glyoxalates, **2a** and **2b** respectively, while upon treatment with aqueous acetic acid they gave the desired oximes, **4a** and **4b** respectively, which were mixtures of geometrical isomers, separable by column chromatography. These oximes were also formed when the reaction of **2a** and **2b** with hydroxylamine was carried out in aqueous acetic acid. From these results, it is evident that **3a** and **3b** are carbinolamine intermediates. Their having stability enough to permit isolation can be ascribed to the strong electron-withdrawing influence of both the carboxyl and the 2-thiazolyl moieties.[3]

The oxime, **4a**, was more conveniently prepared from ethyl 4-methylthiazole-2-acetate (**5a**) by isonitrosation with sodium nitrite in aqueous acetic acid at 0 °C. This reaction gave, stereoselectively, a single isomer in a high yield.

The reduction of **4a** with zinc dust in aqueous formic acid produced the amino acid ester, **6a** (*N*-phenylacetyl derivative **7a**; mp 80—81 °C). However, attempts to isolate the free amino acid after the alkaline

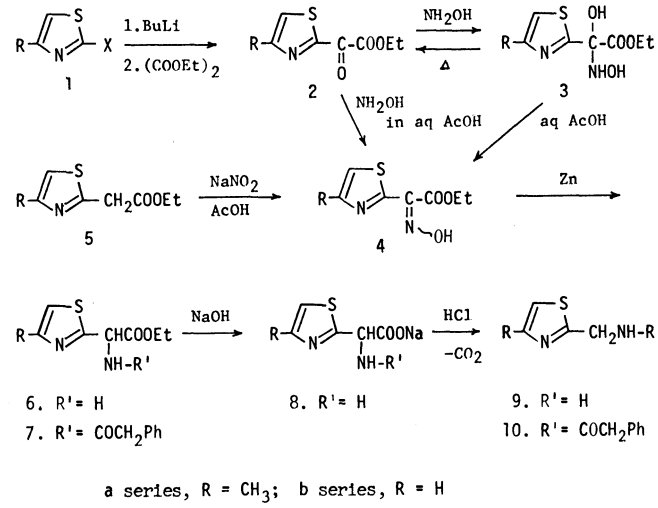

hydrolysis of **6a** failed. When the sodium salts, **8a**, were neutralized with hydrochloric acid at 0 °C, a vigorous evolution of CO_2 gas occurred to give the amine, **9a** (*N*-phenylacetyl derivative **10a**; mp 112—114 °C). Upon a similar treatment, the amino acid ester, **6b**, prepared by the reduction of **4b** with zinc dust, also furnished the amine, **9b** (*N*-phenylacetyl derivative **10b**; mp 102—104 °C). Figure 1 illustrates

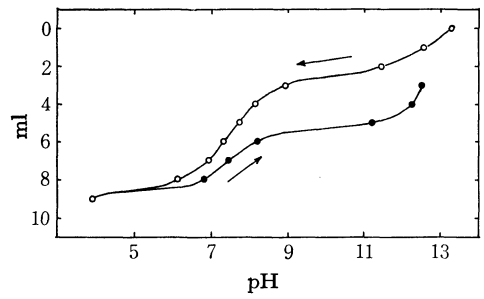

Fig. 1. Potentiometric titration of the sodium salt (**8a**) with 0.1 M hydrochloric acid (open circles) followed by a back titration with 0.1 M sodium hydroxide (filled circles).

the titration of **8a** with 0.1 M hydrochloric acid, followed by back titration with 0.1 M sodium hydroxide. The back-titration curve delineates the neutralization of the conjugate acid of the amine, **9a**. The amount of alkali required to neutralize the conjugate acid was almost equal to a half of that of acid needed for the initial titration, indicating that the decarboxylation takes place simultaneously with the transformation of the sodium salt to the free amino acid. The unusual instability of 2-thiazolylglycines is of interest in comparison with the 4- and 5-thiazolylglycines previously prepared by us;[1] the latter substances are stable and can be recrystallized from boiling water.

Similar differences have been found among thiazolylacetic acids; the activation energy of the decarboxyla-

1) M. Hatanaka and T. Ishimaru, *J. Med. Chem.*, **16**, 978 (1973).

2) H. Schenkel and R. Mory, *Helv. Chim. Acta*, **33**, 16 (1950).

3) In particular, the strong electron-withdrawing effect of the 2-thiazolyl moiety should be noted, for ethyl 3-methylisothiazole-5-glyoxalate was directly converted to the oxime by treatment with hydroxylamine under the same conditions as described for **3a** (see Ref. 1). Isolation of an analogous carbinolamine intermediate in the formation of 2-formyl-1-methylpyridinium iodide oxime has also been reported [E. J. Poziomek, D. N. Kramer, B. W. Fromm, and W. A. Mosher, *J. Org. Chem.*, **26**, 423 (1961)].

tion of 2-thiazolylacetic acid is much smaller than those for the 4- and 5-acetic acids.[2] Our finding indicates that the substitution of the amino group at the α-position of 2-thiazolylacetic acid makes the decarboxylation easier.

Experimental

Ethyl 4-Methylthiazole-2-glyoxalate (2a). A stirred solution of 4-methylthiazole (25.6 g, 0.259 mol) in dry ether (150 ml) was cooled at −70 °C in a Dry Ice-acetone bath, and then a 15% ethereal *n*-butyllithium solution (150 ml) was added at such a rate that the temperature was maintained below −65 °C. The cold mixture was then added through a glass tube to a stirred and cooled (−65 °C) solution of diethyl oxalate (58 g, 0.39 mol) in dry ether (200 ml). After an additional hour at −60 °C, 10% hydrochloric acid (260 ml) was added and the aqueous layer was neutralized with K_2CO_3 and extracted with ether. The evaporation of the ether, and distillation of the residue gave a yellow liquid (27.4 g, 53%); bp 106—107 °C/0.4 mmHg; IR (liquid film) 1740 (C=O) and 1700 (C=O) cm^{-1}; NMR ($CDCl_3$, TMS) δ 1.40 (*t*, 3H), 4.50 (*q*, 2H), 2.59 (*s*, 3H), and 7.38 (*s*, 1H).

Ethyl Thiazole-2-glyoxalate (2b). By a similar procedure, this was prepared from 2-bromothiazole (30 g, 0.183 mol); yield, 15.8 g (46.6%); bp 102—108 °C/0.6 mmHg; IR (liquid film) 1740 (C=O) and 1690 (C=O) cm^{-1}; NMR ($CDCl_3$, TMS) δ 1.42 (*t*, 3H), 4.44 (*q*, 2H), 7.92 (*d*, J=2.8 Hz, 1H), and 8.08 (*d*, J=2.8 Hz, 1H).

Ethyl α-Hydroxy-α-hydroxamino-4-methylthiazole-2-acetate (3a). A mixture of **2a** (6 g, 0.03 mol) and hydroxylamine hydrochloride (3.15 g, 0.045 mol) in methanol (15 ml) was cooled in an ice bath, and then a 2 M sodium hydroxide solution (17 ml) was slowly stirred in. After stirring for 6 h at 0 °C, the precipitate was collected by filtration; it yielded white crystals (5.2 g). An additional crop was obtained by the extraction of the filtrate with chloroform; total yield, 5.4 g (77.7%); mp 120—121 °C (from chloroform); IR (Nujol) 3150 (NH, OH) and 1720 (C=O) cm^{-1}. Found: C, 41.56; H, 5.22; N, 12.38%. Calcd for $C_8H_{12}N_2O_4S$: C, 41.37; H, 5.21; N, 12.06%.

Ethyl α-Oximino-4-methylthiazole-2-acetate (4a). A. From the Glyoxalate, 2a. A mixture of **2a** (2.6 g, 0.013 mol) and hydroxylamine hydrochloride (1.5 g, 0.0216 mol) in acetic acid (4 ml) was cooled in an ice bath, and then a 1 M sodium hydroxide solution (14 ml) was stirred in, drop by drop. After stirring overnight, the precipitate was collected by filtration. The pale yellow solid (2.43 g, 87%) thus obtained was chromatographed on silica gel. Elution with chloroform gave pale yellow prisms (1.5 g); mp 111—112 °C (from ether-petroleum ether); IR (KBr) 1709 (C=O)cm^{-1}. Found: C, 44.79; H, 4.74; N, 13.16%. Calcd for $C_8H_{10}N_2O_3S$: C, 44.85; H, 4.71; N, 13.08%.

Further elution with chloroform-methanol gave white needles (820 mg); mp 140—141 °C (from benzene-petroleum ether); IR (KBr) 1734 (C=O) cm^{-1}. Found: C, 44.99; H, 4.96; N, 13.04%. Calcd for $C_8H_{10}N_2O_3S$: C, 44.85; H, 4.71; N, 13.08%.

B. Isonitrosation of Ethyl 4-Methylthiazole-2-acetate (5a). Into an ice-cooled solution of **5a** (2.8 g, 0.015 mol) in acetic acid (4 ml), a solution of sodium nitrile (1.2 g, 0.0174 mol) in water (3 ml) was slowly stirred over a period of 30 min. After an additional 30 min, the mixture was diluted with water (10 ml) and then stirred for 2 h at 0 °C. The yellow precipitate was collected by filtration, washed with cold water, and dried *in vacuo*; yield, 2.3 g (71.2%). Recrystallization from ether-petroleum ether gave yellow prisms, which were identical with crystals (mp 111—112 °C) obtained by means of Method A (IR and NMR).

Ethyl α-Oximino-thiazole-2-acetate (4b). This was prepared from **2b** (1.85 g, 0.01 mol) according to the procedure (Method A) described for **4a**. The crude product was chromatographed on silica gel. Elution with chloroform gave pale yellow needles (537 mg); mp 58—59 °C (from ether-petroleum ether); IR (KBr) 1709 (C=O) cm^{-1}. Found: C, 42.33; H, 3.99; N, 14.19%. Calcd for $C_7H_8N_2O_3S$: C, 41.99; H, 4.02; N, 13.99%.

Further elution with chloroform-methanol gave white needles (139 mg); mp 121—122.5 °C (from ether-petroleum ether); IR (KBr) 1735 (C=O) cm^{-1}. Found: C, 42.07; H, 4.02; N, 14.20%. Calcd for $C_7H_8N_2O_3S$: C, 41.99; H, 4.02; N, 13.99%.

Ethyl α-Amino-4-methylthiazole-2-acetate (6a). Into an ice-cooled solution of **4a** (1.0 g, 4.66 mmol) in methanol (5 ml) and 40% formic acid (9 ml), zinc dust (1.0 g, 15.3 mmol) was stirred, portion by portion. The mixture was stirred at 5 °C for an additional 5 h, and then filtered. After the addition of 2 M hydrochloric acid (5 ml), the filtrate was evaporated *in vacuo*. The oily residue was dissolved in water (10 ml), neutralized with K_2CO_3, and extracted with chloroform. Drying (K_2CO_3) and evaporation of the chloroform *in vacuo* left 0.9 g of a pale-brown oil, pK_a 5.55 (in 50% ethanol), which showed one spot on tlc.

N-Phenylacetyl Derivative (7a). A solution of the crude **6a** (0.9 g) in chloroform (10 ml) was shaken with a 1 M sodium bicarbonate solution (20 ml), and then phenylacetyl chloride (900 mg, 5.8 mmol) was added gradually. After stirring for 24 h, the aqueous layer was extracted with chloroform. The combined organic layers were dried ($MgSO_4$) and evaporated *in vacuo*. The remaining sirup (1.5 g) was chromatographed on silica gel with chloroform to give **7a** as pale-brown crystals (1.2 g); mp 80—81 °C (from benzene); IR (Nujol) 3320 (NH), 1750 (C=O), and 1650 (CONH) cm^{-1}. Found: C, 60.59; H, 5.91; N, 8.66%. Calcd for $C_{16}H_{18}N_2O_3S$: C, 60.35; H, 5.70; N, 8.80%.

Hydrolysis of Ethyl α-Amino-4-methylthiazole-2-acetate (6a). Into an ice-cooled solution of the crude **6a** [prepared from **4a** (1.0 g, 4.66 mmol)] in methanol (20 ml), a 1 M sodium hydroxide solution (5.7 ml) was stirred, drop by drop. The mixture was stirred overnight at room temperature, and then evaporated *in vacuo*. The residue was dissolved in water (15 ml). The solution was washed with chloroform and cooled in an ice bath, and then 2 M hydrochloric acid was gradually added. When the pH of the solution reached 7, a vigorous gas evolution took place; stirring was continued at pH 6 for 30 min until the gas evolution ceased. The cold mixture was then washed with chloroform, saturated with K_2CO_3, and extracted with chloroform. The evaporation of the chloroform left the amine, **9a**, as a brown liquid.

This material was converted to the *N*-phenylacetyl derivative **10a** according to the procedure described for **7a**; yield, 0.6 g; mp 112—114 °C (from ether-petroleum ether); IR (Nujol) 3300 (NH) and 1650 (C=O) cm^{-1}. Found: C, 63.18; H, 5.61; N, 11.55%. Calcd or $C_{13}H_{14}N_2OS$: C, 63.38; H, 5.73; N, 11.37%.

Hydrolysis of Ethyl α-Amino-thiazole-2-acetate (6b). **6b**, prepared from **4b** (1.0 g, 5 mmol), was hydrolyzed in a manner similar to that described for **6a**. The resulting amine, **9b**, was converted to the *N*-phenylacetyl derivative, **10b** (yield, 540 mg); mp 102—104 °C (from benzene-petroleum ether); IR (Nujol) 3300 (NH) and 1640 (C=O) cm^{-1}. Found: C, 61.90; H, 5.06; N, 12.19%. Calcd for $C_{12}H_{12}N_2OS$: C, 62.04; H, 5.20; N, 12.05%.

BULLETIN OF THE CHEMICAL SOCIETY OF JAPAN, VOL. 46, 3602—3603 (1973)

Photochemical Behavior of 1,1-Diphenylethylene in Polychloroalkane Solvents: Preferential Abstraction of Chlorine Atom[1]

Kinjiro MATSUNAGA and Mituyosi KAWANISI*

Department of Industrial Chemistry, Faculty of Engineering, Kyoto University, Kyoto 606

(Received February 16, 1973)

Kinetic evidence indicates that 1,1-diphenylethylene (**1**) in the triplet excited state behaves to some extent like a biradical species.[2] Irradiation of **1** induced abstraction of hydrogen atom from 2-propanol in a radical fashion.[3] We have investigated the photochemical reactions of **1** in several polychloroalkanes and chloroalkenes and found that the chlorine atom was abstracted by **1** in the triplet excited state.[4]

When a carbon tetrachloride solution of **1** was irradiated under nitrogen by means of a medium pressure mercury arc at room temperature for 140 hr, glc analysis of the reaction mixture showed the presence of two products. The residue of the distillation was chromatographed on a silica-gel column to give 2-chloro-1,1-diphenylethylene[5] (**2**) (92% based on the starting material consumed) and 2-chloro-1,1-diphenylethane[6] (**3**) (trace). Hydrogen chloride was found in the reaction mixture. The structures of the photoproducts were confirmed by direct comparison with authentic samples. It is of interest that no hexachloroethane which would result from trichloromethyl radical was detected in the reaction mixture.

Irradiation of a chloroform solution of **1** for 180 hr gave **2** (74%), **3** (trace), and HCl. Neither 1,1-diphenylethane (**4**) which is expected to be produced by hydrogen abstraction, nor products derived from trichloromethyl radical were found. Photolysis of a solution of **1** in dichloromethane for 180 hr gave **2** (6%), **3** (3%) together with only a trace amount of **4**. Photoreactions of **1** in 1,2-dichloroethane, *t*-butyl chloride, cyclohexyl chloride, and 3-chlorocyclohexene were sluggish, only a trace of **4** being detected in each reaction mixture even after prolonged irradiation. These facts suggest that the preferential mode of photochemical reaction of **1** in polychloroalkanes appears to be the abstraction of chlorine atom rather than that of hydrogen atom.

In chloroform molecule C–H bond fission usually occurs under radical reaction conditions[7] or by irradiation in nitrogen or argon matrix.[8] In the present investigation, however, only chlorine abstraction was observed. The cause is still open to discussion and the fate of the residual radical from the solvents remains unclarified.

In order to obtain information on the reactive excited species involved in the reaction between **1** and carbon tetrachloride, quenching and sensitization experiments were performed. Irradiation reaction (>330 nm) conducted in a Pyrex vessel was successfully sensitized by triphenylene, and the product distribution was not affected. The unsensitized reaction did not occur upon photolysis at this wavelength region. It was also found that the reaction could be quenched by the addition of piperylene. Since carbon tetrachloride itself absorbs light in this wavelength region[9] the possibility of the primary dissociation of the photoexcited carbon tetrachloride to give reactive species cannot be ruled out. Actually, however, light which passes a carbon tetrachloride filter induces the reaction. This indicates that at least the excited triplet state of **1** was involved in the photochemical reaction of **1** in carbon tetrachloride.

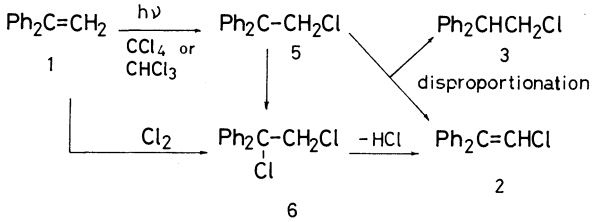

1 5 3 2 6

One might explain the formation of **2** and **3** by assuming intermediacy of radical species **5** which could undergo disproportionation and chlorine-abstraction (Scheme). Facile elimination of hydrogen chloride from a dichloroethane derivative (**6**) will give the final product **2** in a larger amount. An attempted chlorination of **2** by molecular chlorine[5] to obtain **6** resulted in the formation of **2** as the only isolable product. The result suggests the reaction pathway *via* **6** which, once formed, turns into **2** by ready loss of hydrogen chloride.

Experimental

All temperatures are uncorrected. Microanalyses were performed by Mrs. Kiyoko Fujimoto. The spectra were recorded in neat liquid films on a Shimadzu IR-27C spectrometer. The NMR spectra were determined on a JOEL C-60-H spectrometer using TMS as an internal standard and CCl_4 as solvent. The mass spectra were recorded with

* To whom all correspondence should be addressed.

1) Presented in part at the Symposium on Photochemistry, *Chem. Soc. Japan, Osaka*, Nov. 2nd, 1972, 2B02.

2) D. I. Schuster, T. M. Weil, and M. R. Topp, *Chem. Commun.*, **1971**, 1212.

3) H. M. Rosenberg and P. Servé, *J. Amer. Chem. Soc.*, **92**, 4746 (1970).

4) *Cf.* M. Kawanisi and K. Matsunaga, *Chem. Commun.*, **1972**, 418.

5) V. V. Korshak, K. K. Samolavskaya, and M. S. Andrecva, *Zh. Obshch. Khim.*, **19**, 690 (1945).

6) W. G. Brown, C. J. Mighton, and M. Senkus, *J. Org. Chem.*, **3**, 62 (1938).

7) C. Walling and E. S. Huyer, "*Organic Reactions*," Vol. 13, p. 91 (1961).

8) E. E. Rogers, S. Abramowitiz, M. E. Jacox, and D. E. Willingan, *J. Chem. Phys.*, **52**, 2198 (1970).

9) J. R. Lacher, L. E. Hummel, E. F. Bohmflak, and J. D. Park, *J. Amer. Chem. Soc.*, **72**, 5486 (1950); G. Massol and A. Fauson, *C.R. Acad. Sci. Paris, Ser.* **159**, 314 (1914).

a Hitachi RMS-4 mass spectrometer at 70 eV. The UV spectra were obtained in ethanol solutions on a Shimadzu MPS-50L spectrophotometer.

Reagents. 1,1-Diphenylethylene (**1**) was prepared by the method of Allen and Converse,[10] bp 143—145 °C/20 mmHg (lit,[10] bp 156 °C/25 mmHg). Carbon tetrachloride,[11] chloroform,[12] dichloromethane,[13] 1,2-dichloroethane,[14] *t*-butyl chloride,[15] cyclohexyl chloride,[16] and 3-chlorocyclohexene[17] were prepared and/or purified by published methods.

General Irradiation Procedure. After a solution of **1** (0.035 M) in the solvents was bubbled with commercial nitrogen for 1 hr, it was irradiated in a quartz tube by a Haros PIH-300 medium pressure mercury arc at room temperature for specified periods. The progress of the photoreaction was monitored by glc. After irradiation the solution was washed with an aqueous NaOH solution, the latter being then titrated with an aqueous HCl solution. The excess solvent was distilled off and the distillate was carefully checked by glc to scrutinize low boiling materials. The residue was chromatographed on silica gel to give the starting material, 2-chloro-1,1-diphenylethylene (**2**),[5] 2-chloro-1,1-diphenylethane (**3**),[6] and 1,1-diphenylethane (**4**)[18] which were further purified by glc to obtain analytical samples.

Sensitization with Triphenylene. A solution of **1** (36 mg, 0.2 mmol) in carbon tetrachloride (10 ml) was divided into two equal portions after bubbling with nitrogen. Triphenylene (23 mg, 0.1 mmol) was added to one portion, and the two solutions were irradiated (>330 nm) in Pyrex tubes through a filter of NaBr–$Hg(NO_3)_2$ solution[19] for 40 hr. The progress of the reaction was monitored by glc. The reaction with added triphenylene proceeded to almost 100% completion, whereas the unsensitized reaction showed the formation of only traces of the products.

Quenching with Piperylene. A solution of **1** (90 mg, 0.5 mmol) in carbon tetrachloride (10 ml) was divided into two equal portions after bubbling with nitrogen. Piperylene (170 mg, 2.5 mmol) was added to one portion and the two solutions were irradiated in quartz vessels with a medium pressure mercury arc for several hours. Glc monitoring of the progress of the reaction showed that the unquenched reaction was about 8 times as rapid as the quenched one.

Our thanks are due to Professor Hitosi Nozaki for his help and encouragment.

10) C. F. H. Allen and S. Converse, "Organic Syntheses," Coll. Vol. I, p. 226 (1956).
11) M. Pestmer, *Angew. Chem.*, **63**, 121 (1951).
12) G. Wohlleben, *ibid.*, **68**, 752 (1956).
13) J. H. Mathews, *J. Amer. Chem. Soc.*, **48**, 562 (1926).
14) C. P. Smyth, R. W. Dornte, and E. B. Wilson, Jr., *ibid.*, **53**, 4242 (1931).
15) J. F. Norris and A. W. Olmsted, "Organic Syntheses," Coll. Vol. I, p. 144 (1956).
16) A. I. Vogel, *J. Chem. Soc.*, **1948**, 1809.
17) M. L. Poutsuma, *J. Amer. Chem. Soc.*, **87**, 2161 (1965).
18) J. P. E. Human and J. A. Mills, *Nature*, **158**, 877 (1946).
19) A. Schönberg, "Preparative Organic Photochemistry," Springer-Verlag, New York, (1968), p. 491.

BULLETIN OF THE CHEMICAL SOCIETY OF JAPAN, VOL. 46, 3603—3605 (1973)

Chlorinated 2,3′-Dithienyls. The By-products Formed in the Coupling of Thiophene with Sulfuryl Chloride and Iron Powder[1,2]

Tyo Sone and Yukio Abe

Department of Applied Chemistry, Faculty of Engineering, Yamagata University, Yonezawa 992

(Received March 28, 1973)

The reaction of thiophene with sulfuryl chloride has been known to give chlorothiophenes. In the presence of iron powder or a Friedel-Crafts-type catalyst, however, the reaction affords the chlorinated 2,2′-dithienyls (**1b—e**) as the main product.[2] In addition to **1b—e**, the product has been shown by vapor-phase chromatography (vpc) to contain 10—20% of unidentified materials, in which one component (**2c**) predominates. Although there have been several papers concerning the coupling of aromatic nuclei, little has been known about that of thiophene nuclei. The present work was undertaken in order to isolate and identify the by-products and to obtain information concerning the coupling of thiophene nuclei.

The crystalline product was sublimed repeatedly under reduced pressure, and the more volatile part was submitted to fractional recrystallization from petroleum ether. Compound **2c** (mp 53—54 °C), isolated from the more soluble part, seems to be 2′,5-dichloro-2,3′-dithienyl, judging from its UV and NMR spectral data and elemental analysis. Thus, the observed maximum (298 nm) of the UV absorption is a little lower than that of 2,2′-dithienyl (**1a**) itself and is rather similar to that of 2,3′-dithienyl (**2a**), while in the NMR spectrum, the coupling constants of two sets of double-doublets (J=3.9 and 5.9 Hz) in the ring-proton region and the relative peak intensities indicate the presence of both one 2,3-di-, and one 2,5-disubstituted thiophene rings in **2c**.[3] The assignment was finally confirmed by comparison with the authentic sample prepared by the chlorination of **2a**. The presence of 2′-chloro- (**2b**), and 2′,3,5-trichloro-2,3′-dithienyls (**2d**) as minor products was also detected by vpc. Some representative results of the coupling reaction are shown in Table 1. It is worth noting that considerable amounts of 2,3′-dithienyl derivatives are formed in the coupling of the thiophene nuclei, the

1) Acid-catalyzed Oligomerization of Thiophene Nuclei. II.

2) Part I: T. Sone, K. Sakai, and K. Kuroda, This Bulletin, **43**, 1411 (1970).

3) For the UV and NMR spectral data concerned, see the previous paper and the references cited therein.

Table 1. Reaction of thiophene with sulfuryl chloride and iron powder[a]

Mole ratio Thiophene/ SO_2Cl_2	Fe(g)	Chlorinated dithienyls, yield, mol %[b]						
		1b	**1c**	**1d**	**1e**	**2b**	**2c**	**2d**
1:1	0.3	trace	10	16	1	trace	7	trace
1:1	0.3 CCl_4 (20 ml)	trace	7	9	0.5	trace	4	

a) Reaction condition: thiophene 0.125 mol; 3 hr at room temperature.
b) Based on thiophene used.

Table 2. Chlorination of dithienyls with sulfuryl chloride[a]

Mole ratio **1a** or **2a**/ SO_2Cl_2	**1a** or **2a**	Chlorinated dithienyls, yield, mol %[b,c]			
		1b or **2b**	**1c** or **2c**	**1d** or **2d**	**1e**
2,2′-Dithienyls (**1**)					
1 : 1	20(24)	61(57)	11(14)	(3)	
1 : 2		47(28)	35(34)	4(7)	
1 : 3		24(4)	65(40)	7(11)	
1 : 10			69(20)	22(32)	1.5>(4)
2,3′-Dithienyls (**2**)					
1 : 1	27(22)	55(42)	7(12)		
1 : 2		53(10)	41(36)	(9)	[d]
1 : 3			88(35)	7(14)	[d]
1 : 10			34(21)	47(22)	[d]

a) Reaction conditions: Dithienyl, 5 mmol in carbon tetrachloride (5 ml); 30 min at room temperature and additional 30 min at the boiling point of the reaction mixture.
b) Based on the dithienyl used.
c) Figures in the parentheses represent the yields obtained by the addition of ferric chloride (0.2 g, 1.233 mmol) in the reaction. In the presence of ferric chloride, the reactions are usually accompanied with the formation of a resinous material.
d) Besides **2b—d**, a small amount of higher chlorinated products were formed, when the reaction was carried out in the presence of ferric chloride.

proportion of 2,3′- to 2,2′-dithienyl derivatives being of the order of about 1 to 4.

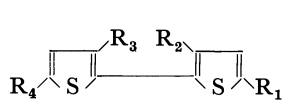

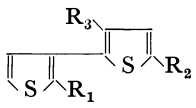

1a: $R_1=R_2=R_3=R_4=H$ **2a**: $R_1=R_2=R_3=H$
1b: $R_1=Cl$, $R_2=R_3=R_4=H$ **2b**: $R_1=Cl$, $R_2=R_3=H$
1c: $R_1=R_4=Cl$, $R_2=R_3=H$ **2c**: $R_1=R_2=Cl$, $R_3=H$
1d: $R_1=R_2=R_4=Cl$, $R_3=H$ **2d**: $R_1=R_2=R_3=Cl$
1e: $R_1=R_2=R_3=R_4=Cl$

In order to prepare authentic samples and to seek explanation for the formation of the chlorinated dithienyls, a brief study of the chlorination of **1a** and **2a** with sulfuryl chloride was carried out (Table 2); the chlorination occurs preferentially at the 5-position of **1a** and the 2′-position of **2a**, and successively at the 5′-, the 3-, and the 3′-positions for **1a**, and at the 5-, and the 3-positions for **2a**. The results are of interest, as only a little has been known concerning the substitution reactions of dithienyls, particularly those of **2a**. The reaction is promoted by the presence of ferric chloride to give the polychlorinated dithienyls in a higher proportion and a resinous material to some extent; the normal course of the chlorination is essentially unaltered.

In the previous paper, it was suggested that **1b—e** were formed by the coupling of the thiophene nuclei *via* a cationic mechanism, the reaction being initiated by the protonation of thiophene, followed by the chlorination of the resulting **1a**.[4] Taking into account the appreciable 3-substitution in certain electrophilic alkylations of thiophene and the results of the chlorination of **2a**, the formation of **2b—d** may be explained by the same mechanism, as is shown in Scheme 1.

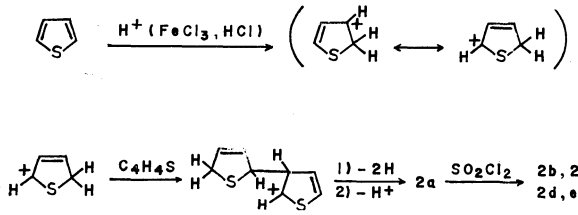

Experimental[5]

Isolation of 2′,5-Dichloro-2,3′-dithienyl (2c) from the Coupling Proauct. The crystalline coupling product[2] (60 g) was sublimed repeatedly under reduced pressure (110—130 °C/2—4 mmHg; the more volatile part (15 g) was then triturated with cold petroleum ether. The solvent was evaporated from the washings, and the residue was treated several times in a similar manner and finally recrystallized from the same solvent to give crude **2c** (2 g), which was subsequently purified by column chromatography on silica gel, using petroleum ether as the eluant; colorless needles, mp 53—54 °C. UV (MeOH) λ_{max} nm (log ε): 298 (4.25), 249 (4.10). NMR (Me_2CO) δ: 7.06 (d, J=3.9 Hz, 4-H), 7.38 (d, J=3.9 Hz, 3-H), 7.30 (d, J=5.9 Hz, 4′-H), 7.47 (d, J=5.9 Hz, 5′-H). Found: C, 40.92; H, 2.10%. Calcd for $C_8H_4Cl_2S_2$: C, 40.85; H, 1.71%.

Chlorination of 2,2′- (1a) and 2,3′-Dithienyls (2a). a) General Procedure. Sulfuryl chloride was added to a stirred solution of the dithienyl (0.84 g, 5 mmol) in carbon

4) Another possibility is the intermediary formation of the carbonium ions, **3a—c**, from thiophene through a reaction with the chlorinium ion, which attacks the 2-position of a thiophene molecule, followed by dehydrogenation and by the loss of a proton to yield **1b** and **2b**. This mechanism was suggested by the referee.

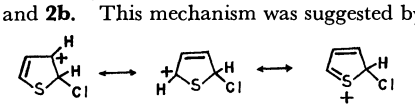

3a 3b 3c

5) All the melting and boiling points are uncorrected. The UV spectra were obtained on a Hitachi EPU-2A spectrophotometer, and the NMR spectra, on a Hitachi R-20A spectrometer, at 60 MHz, using tetramethylsilane as the internal reference.

tetrachloride (5 ml), and then the reaction mixture was stirred for 30 min. After being stirred for an additional 30 min at the boiling point, the mixture was poured into ice water (30 g) and extracted with carbon tetrachloride (30 ml). The organic layer was washed with a dilute sodium bicarbonate solution and then with water, and dried. The solvent was evaporated, and the residue was analyzed by vpc as has been described previously.[2] The reactions in the presence of anhydrous ferric chloride (0.2 g, 1.233 mmol) were carried out in a similar manner. The results are given in Table 2.

b) 2',5-Dichloro-2,3'-dithienyl (2c). The product (2.0 g) obtained by the reaction of **2a** (1.7 g, 0.01 mol) with two molar equivalents of sulfuryl chloride (2.7 g) was recrystallized twice from light petroleum ether to give **2c** (mp 53—54 °C, 0.6 g). This compound was proved to be identical with the **2c** isolated from the coupling product by a comparison of their IR and UV spectra and by a mixed-melting-point determination.

c) 2'-Chloro-2,3'-dithienyl (2b). A solution of sodium acetate trihydrate (67 g) in water (100 ml) was added to the mixture (5 g) of **2b** and **2c** in ethanol (380 ml) which had been obtained by the reaction of **2a** with two molar equivalents of sulfuryl chloride; to the resulting solution was then added a saturated solution of mercuric chloride (200 ml). The reaction mixture was allowed to stand for 3 days, after which the precipitates (3.4 g) were filtered off and recrystallized from chloroform to yield the chloromercury derivative of **2b** (2.3 g, mp 210—250 °C). The mercury derivative was heated with a mixture of hydrochloric acid (15 ml) and water (30 ml) on a water bath for 30 min, and the oil (1.0 g) thus separated out was extracted with chloroform. The extract was washed with a sodium bicarbonate solution and then with water, and dried. The solvent was evaporated and the residue distilled to afford **2b** (0.8 g); bp 103—104 °C/4 mmHg, n_D^{20} 1.6625. UV (MeOH) λ_{max} nm (log ε): 287 (4.14), 244 (4.10). NMR (Me_2CO) δ: 7.13 (q, J=3.7 Hz, J=5.0 Hz, 4-H), 7.51 (q, J=5.0 Hz, J=1.1 Hz, 5-H), 7.53 (q, J=3.7 Hz, J=1.1 Hz, 3-H), 7.31 (d, J=5.9 Hz, 4'-H), 7.42 (d, J=5.9 Hz, 5'-H).[6] Found: C, 48.06; H, 2.26%. Calcd for $C_8H_5ClS_2$: C, 47.87; H, 2.51%.

d) 2',3,5-Trichloro-2,3'-dithienyl (2d).[7] The further chlorination of a mixture of **2b** and **2c** with a large excess of sulfuryl chloride (6 times by weight) in carbon tetrachloride gave **2d**; colorless crystals; mp 77—78 °C (from petroleum ether). UV (MeOH) λ_{max} nm (log ε): 278 (4.05), 249 (4.10). NMR (Me_2CO-d_6) δ: 7.11 (s, 4-H), 7.21 (d, J=5.7 Hz, 4'-H), 7.50 (d, J=5.7 Hz, 5'-H). Found: C, 35.87; H, 0.82%. Calcd for $C_4H_3Cl_3S_2$: C, 35.63; H, 1.12%.

The authors wish to express their thanks to Mr. Kunimi Fujieda of the Naka Works, Hitachi, Ltd., for his NMR spectral measurements and to Mr. Kenji Abe for his assistance in the experiments.

6) The spectrum was analyzed by Professor Kensuke Takahashi (Nagoya Institute of Technology), to whom the authors are indebted.

7) It is interesting to note that, unlike the chlorination, the tribromination of **2a** with *N*-bromosuccinimide has been reported to give the 2',5,5'-trisubstituted derivative.[8]

8) R. M. Kellogg, A. P. Schaap, and H. Wynberg, *J. Org. Chem.*, **34**, 343 (1969).

BULLETIN OF THE CHEMICAL SOCIETY OF JAPAN, VOL. 46, 3605—3607 (1973)

Thermal and Photochemical Decompositions of 4,5,6,7-Tetrahydro-1,2,3-benzotriazole Analogues

Kazuo TSUJIMOTO, Mamoru OHASHI, and Teijro YONEZAWA*

Department of Materials Science, The University of Electro-Communications, Chofu, Tokyo 182
**Department of Hydrocarbon Chemistry, Faculty of Engineering, Kyoto University, Sakyo-ku, Kyoto 606*

(Received May 17, 1973)

In our previous paper[1] we reported that the photolysis of various benzotriazoles gave products different from those of the thermal decompositions. Burgess and his co-workers have observed that both the thermal and photochemical decompositions of monocyclic 1,2,3-triazoles give 1,3-biradical intermediates which undergo the Wolff rearrangement to give the same ketenimine.[2] We wish now to report that the thermolysis and photolysis of 4,5,6,7-tetrahydro-1,2,3-benzotriazole analogues give the cyclized and the ring-contracted products in different ratios.

Results and Discussion

In the thermolysis of 1-phenyl-4,5,6,7-tetrahydrobenzotriazole (I), a preparative flash thermolysis apparatus was used at a pressure below 0.01 mmHg; the vapor of I was passed through a quatrz tube (10 mm diam.) at 590—630 °C. The thermolyzed mixture collected in a trap cooled by liquid nitrogen was column-chromatographed on silica gel to give 1,2,3,4-tetrahydrocarbazole (II) and cyclopentanecarboxanilide (III) in yields of 17 and 20% respectively.

The ring-contracted product (III) must be formed through a ketenimine (IV), followed by the addition of water in the course of separation. When the reaction was carried out in an atmosphere of dry nitrogen, the reaction mixture showed an IR absorption[3] at 2020 cm^{-1}. The intensity of the absorption decreased when the mixture was allowed to stand in the air for several minutes. This fact suggests that the ketenimine (IV) must be present as an intermediate.

Similarly, the thermolysis of 1-phenyl-4,5,6,7-tetrahydrocyclohepta[*d*]-1,2,3-triazole (V) gave an indole

1) K. Tsujimoto, M. Ohashi, and T. Yonezawa, This Bulletin, **45**, 515 (1972).

2) E. M. Burgess, R. Carithers, and L. McCullagh, *J. Amer. Chem. Soc.*, **90**, 1923 (1968).

3) C. L. Stevens and L. C. French, *ibid.*, **75**, 657 (1953).

derivative (VI) and cyclohexanecarboxanilide (VII) in yields of 25 and 29% respectively. Again, the strong absorption at 2000 cm^{-1} in the IR spectrum of the reaction mixture suggested the presence of the ketenimine intermediate.

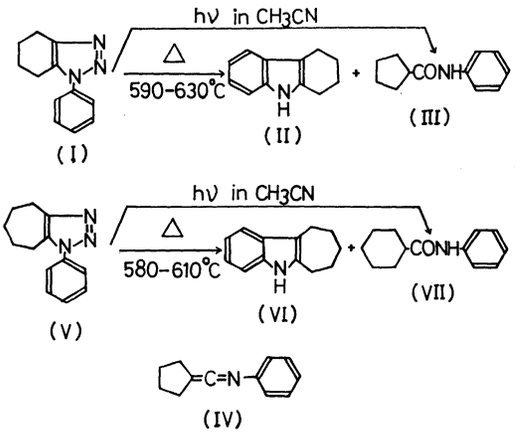

On the other hand, the photolysis of I in acetonitrile by means of a low-pressure mercury arc gave III as the major product (62% yield), along with a trace amount of II (less than 5%). The irradiation of a solution of I in benzene also gave III in a 25% yield, but no cyclized product was obtained. Similarly, the irradiation of V in acetonitrile afforded VII as the major product. From these results it became clear that the photolyses of 4,5,6,7-tetrahydro-1,2,3-benzotriazole analogues produce mainly their corresponding ring-contracted products, while their thermolyses give both the cyclized and the ring-contracted products in nearly the same yield. These results imply that the thermally- and the photochemically-generated intermediates have either (i) a different electronic configuration from each other or (ii) the same configuration giving different products in the succeeding dark reactions depending on the reaction environment. Such a behavior as (ii) is frequently observed in the photo-induced decarbonylation of carbonyl compounds.[4] Since, as was demonstrated in our previous paper,[1] the electronic configuration of a 1,3-biradical intermediate such as IX is sensitive to the environment, at this stage we can not judge which one of these two cases has actually occurred in the reactions.

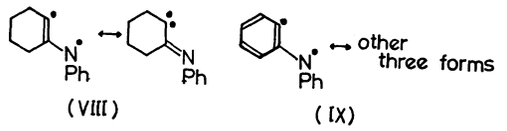

The thermolysis[5] and the photolysis[2] of 1-phenyl-1,2,3-benzotriazole give the same cyclized product quantitatively. The difference in the behavior of the intermediates, VIII and IX, can be explained in terms of the reactivity of the carbene-like character for the Wolff rearrangement;[6] the reactivity of IX is smaller because of the delocalization of the unpaired π-electron on the nitrogen.

Experimental

All the melting points were determined on a micro hot stage and are not corrected. The IR and mass spectra were measured using a Hitachi Model 215 grating spectometer and a double-focussing mass spectrometer (Model JMS-01SG) respectively. The NMR spectra were obtained on a Varian HR-220 spectrometer, using TMS as the internal standard. The starting materials, I and V, were prepared by means of Fusco's method.[7] The pure samples of both I and V were obtained by crystallization from ligroin. A quartz tube (10 mm diam.) was used for the preparative flash vacuum thermolysis at a pressure below 0.01 mmHg and at a temperature of about 600 °C.

1-Phenyl-4,5,6,7-tetrahydrobenzotriazole (I): mp 116.0—116.5 °C (lit: 116 °C)[7].

1-Phenyl-4,5,6,7-tetrahydrocyclohepta[d]-*1,2,3-triazole (V)*: mp 115.8—116.1 °C (lit: 113 °C)[7].

Thermolysis of 1-Phenyl-4,5,6,7-tetrahydrobenzotriazole (I): I (122 mg) was thermolyzed at 590—630 °C (below 0.01 mmHg). The pyrolyte (90 mg) was column-chromatographed on silica gel (20 g, Mallinckrodt, AR-100, 100 mesh). Elution with dichloromethane gave II(17 mg), a tarry material(4 mg), and III(22 mg). II was identified as tetrahydrocarbazole by a comparison of its IR spectrum with that of an authentic specimen. The mixed melting point of these compounds showed no depression. III was a solid which had an mp of 159—160 °C (lit: 159—160 °C)[7]: M^+: 189.117 (calculated for $C_{12}H_{15}NO$ 189.115); NMR ($CDCl_3$) δ 1.5—2.0 (8H, m), 2.68 (1H, quintet, J=1.5 Hz), 4.84 (1H, br. s) and 7.1—7.6 (5H, m) ppm; IR (KBr) 3200 (ν NH), 1650 (amide ν C=O), 1540 (δ NH) and 750 (phenyl ring) cm^{-1}. Cyclopentanecarboxanilide was prepared from cyclopentanecarboxylic acid chloride and aniline. Its IR spectrum coincided with that of III. The mixed melting point showed no depression.

Thermolysis of 1-Phenyl-4,5,6,7-tetrahydrocyclohepta[d]-*1,2,3-triazole (V)*. V (123 mg) was thermolyzed at 580—610 °C as has been described above. The reaction mixture (90 mg) was column-chromatographed on silica gel, 7 g (Mallinckrodt, AR-100, 100 mesh). Elution with dichloromethane then gave VI(23 mg), VII(32 mg), and 27 mg of a tarry material. VI was identified as 5,6,7,8,9,10-hexahydrocyclohepta[*d*] indole on the basis of the following information: M^+: 185.116 (185.120 calculated for $C_{13}H_{15}N$); IR (KBr) 3400 (ν NH), 740 (phenyl ring) cm^{-1}; NMR ($CDCl_3$) δ 1.68—1.93 (6H, m), 2.80 (4H, s), 7.05—7.50 (4H, m) and 7.68 (1H, br. s) ppm. VII had an mp of 145.5—146.3 °C after recrystallization from ligroin. The spectral data are shown below: M^+: 203.127 (203.131 calculated for $C_{13}H_{17}NO$); IR (KBr) 3320 (ν NH), 1660 (ν C=O) and 730 (phenyl ring) cm^{-1}. The IR spectrum of VII coincided with that of cyclohexanecarboxanilide, which had been synthesized by the reaction of cyclohexanecarboxylic acid chloride with aniline.

Photolysis of 1-Phenyl-4,5,6,7-tetrahydrobenzotriazole (I) in Acetonitrile. A solution of I (123 mg) in 80 ml of purified acetonitrile was irradiated by means of a 5-W low-pressure

4) N. J. Turro, "Molecular Photochemistry," W. A. Benjamin, Inc., New York, Amsterdam (1965), p. 224.

5) S. G. P. Plant and J. F. Powell, *J. Chem. Soc.*, **1947**, 937.

6) M. Jones, Jr. and W. Ando, *J. Amer. Chem. Soc.*, **90**, 2200 (1968).

7) R. Fusco, G. Bianchetti, and D. Pocar, *Gazz. Chim. Ital.*, **91**, 849 (1961).

mercury arc lamp for 2 hr. After the removal of the solvent, the reaction mixture was column-chromatographed on silica gel. Elution with dichloromethane gave 17 mg of III, and further elution with ethyl acetate gave 94 mg of the unreacted material. III was identified as cyclopentanecarboxanilide by the method which has been described above.

Photolysis of 1-Phenyl-4,5,6,7-tetrahydrobenzotriazole (I) in Benzene. A solution of I (198 mg) in benzene (80 ml) was irradiated with a 100-W high-pressure mercury arc lamp for 10 hr. After the solvent had then been removed *in vacuo*, the residue was column-chromatographed on silica gel. Elution with dichloromethane gave 22 mg of III. The starting material (100 mg) was recovered by elution with ethyl ether. The tarry materials were not identified. A gas chromatograph of the reaction products did not exhibit the presence of tetrahydrocarbazole.

Photolysis of 1-Phenyl-4,5,6,7-tetrahydrocyclohepta[d]-*1,2,3-triazole (V) in Acetonitrile.* An acetonitrile solution (80 ml) of 122 mg of V was irradiated with a 5-W low-pressure mercury arc lamp for 3 hr under a stream of nitrogen gas. After the solvent had then been removed *in vacuo*, the reaction mixture was column-chromatographed on silica gel. Elution with dichloromethane gave 2 mg of an unidentified material, 22 mg of VII, 54 mg of the starting material, and 38 mg of a tarry product. The VII was identified as cyclohexane carboxanilide by a comparison of its spectrum with that of an authentic specimen which had been prepared by the reaction of cyclohexanecarboxylic acid chloride with aniline.

BULLETIN OF THE CHEMICAL SOCIETY OF JAPAN, VOL. 46, 3607—3608 (1973)

Nitration of Polyalkylbenzenes in Acetonitrile. Another View on Side-chain Acetamidation[1]

Hitomi SUZUKI and Terukiyo HANAFUSA

Department of Chemistry, Faculty of Science, Hiroshima University, Higashi-sendamachi, Hiroshima 730

(Received May 21, 1973)

Nitration of polyalkylbenzenes in acetonitrile is known to give *N*-benzylacetamides in a good yield. The reaction was explained to proceed through the nucleophilic attack by the solvent on the nitro-methylenecyclohexadiene intermediate (I) followed by the release of a nitrite ion to give the carbonium ion (II), which was hydrolyzed to give *N*-benzylacetamide (III).[2]

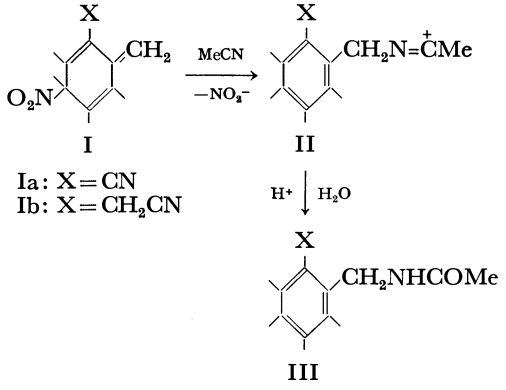

In inert solvents such as dichloromethane and chloroform, the major process was the side-chain nitrooxylation, for which we have proposed a mechanism involving the rearrangement of nitro-methylenecyclohexadiene to benzyl nitrite.[3] In view of the high potency of polyalkylbenzylic compounds,[4] especially benzyl nitrite, to act as a benzylating agent in the presence of an acid catalyst, the possibility that the *N*-benzylacetamides are derived from the reaction of the initially formed benzyl nitrite with acetonitrile cannot be ruled out.

Hexamethylbenzene was nitrated with excess fuming nitric acid (d=1.5) in acetonitrile at 0—10 °C to give *N*-(pentamethylbenzyl)acetamide (IV) as the major product. Yields based on the unrecovered hydrocarbon often exceeded 50%. When pentamethylbenzyl nitrite was similarly treated in the same solvent, the product was a mixture of IV, pentamethylbenzyl nitrate, pentamethylphenylnitromethane, and 1,2-bis(nitrooxymethyl)-3,4,5,6-tetramethylbenzene in the approximate ratio 3:3:1:2. Formation of IV can be rationalized by assuming that the nucleophilic attack of the solvent upon the benzylic carbon atom of the conjugate acid (V) produces an imino-carbonium ion type intermediate (II; X=Me).

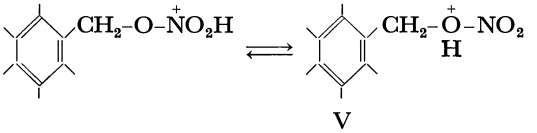

V

On treatment with excess fuming nitric acid in dichloromethane at room temperature, pentamethylbenzonitrile gave 1-cyano-2-nitrooxymethyl-3,4,5,6-tetramethylbenzene (VI) in 85% yield. Similarly, pentamethylbenzyl cyanide readily gave 1-cyanomethyl-2-nitrooxymethyl-3,4,5,6-tetramethylbenzene (VII) in 62% yield. The structures of VI and VII were determined by their conversion into 4,5,6,7-tetramethylphthalide (VIII) and 1,2-bis(cyanomethyl)-3,4,5,6-tetramethylbenzene (IX), respectively. Acid-catalyzed hydrolysis of VII yielded 5,6,7,8-tetramethyl-1,4-dihydro-3*H*-2-benzopyran-3-one (X), and the structure was deduced from the elemental analysis and spectral data.

1) The reaction of polysubstituted aromatics. Part XXXIII; Part XXXII: H. Suzuki and T. Hanafusa, *Synthesis*, **1973**, in press.

2) E. Hunziker, J. R. Penton, and H. Zollinger, *Helv. Chim. Acta*, **54**, 2043 (1971).

3) H. Suzuki and K. Nakamura, This Bulletin, **43**, 473 (1970); K. Nakamura, *ibid.*, **44**, 133 (1971); H. Suzuki and K. Nakamura, *ibid.*, **44**, 227 (1971); H. Suzuki, K. Nakamura, and M. Takeshima, *ibid.*, **44**, 2248 (1971).

4) H. Suzuki and K. Nakamura, *ibid.*, **41**, 2197 (1968).

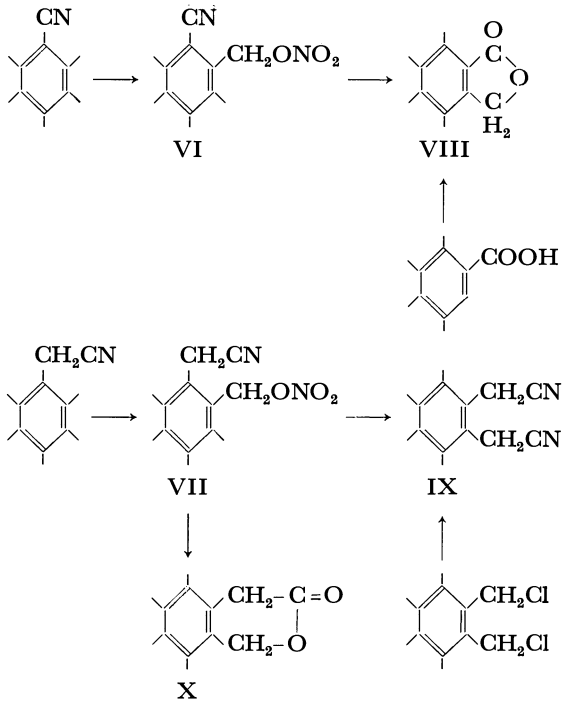

The initial attack by nitronium ion on these compounds should occur at an aromatic carbon atom at 3-position, since the benzenium ion intermediates can be most effectively stabilized by three methyl groups. The nitro-methylenecyclohexadienes Ia and Ib should then be formed, and should be subject to some intramolecular interaction between the neighboring cyano and methylene groups, according to the reaction squence proposed.[2] The present results were contrary to this; the cyano group remained intact.

Benzyl nitrites are readily hydrolyzed to the corresponding benzyl alcohols. In organic mediums containing nitrite or acetate ions, they can be partly converted into phenylnitromethanes and benzyl acetates, respectively. Nitration of hexamethylbenzene with fuming nitric acid in acetic anhydride gives a mixture of varying amounts, depending on the conditions employed, of pentamethylbenzyl nitrate, pentamethylphenylnitromethane, and pentamethylbenzyl acetate. The latter two compounds can arise either from the anion-exchange of the benzylic intermediate-nitrite ion pair, or from the nucleophilic displacement on the benzylic carbon atom of the conjugate acid (V). These findings seem to favor our view that the side-chain acetamidation products arise from the reaction of the initially formed benzyl nitrite with the solvent rather than that proposed by previous workers.[2]

Experimental

All melting points are uncorrected. ^1H NMR spectra were determined in deuteriochloroform on a Varian T-60 spectrometer using TMS as an internal standard. IR spectra were recorded in Nujol on a Perkin-Elmer Model 137 spectrophotometer, only prominent peaks being given. Pentamethylbenzonitrile was prepared by heating iodopentamethylbenzene with cuprous cyanide in hexamethylphosphoric triamide. Pentamethylbenzyl cyanide and pentamethylbenzyl nitrite were prepared by treating the corresponding chloride with sodium cyanide and silver nitrite, respectively, in acetonitrile.

N-(Pentamethylbenzyl)acetamide (IV). A mixture of hexamethylbenzene (4.1 g) and acetonitrile (30 ml) was cooled in an ice-bath, fuming nitric acid ($d=1.5$; 8.4 g) being added with vigorous stirring over a period of 30 min. After the mixture was left to stand for several hours at room temperature, it was poured into water, and the precipitated solid was filtered off, washed with cold carbon tetrachloride, and crystallized from ethanol to give amide as fine white needles, mp 229—231 °C. Yields based on unrecovered hydrocarbon ranged from 28 to 60%. *m/e* 219 (M^+); NMR: 8.03 (s, 3H), 7.77 (s, 6H), 7.74 (s, 9H), 5.52 (d, 2H), and *ca.* 4.7 τ (broad, 1H); IR: 593, 1059, 1272, 1349, 1535, 1642, and 3300 cm^{-1}. Found: C, 76.52; H, 9.63%. Calcd for $C_{14}H_{21}NO$: C, 76.67; H, 9.65%.

1-Cyano-2-nitrooxymethyl-3,4,5,6-tetramethylbenzene (VI). Fuming nitric acid ($d=1.5$; 6.3 g) was added dropwise to a magnetically stirred solution of pentamethylbenzonitrile (1.73 g) in dichloromethane (15 ml) at 0—5 °C over a period of 30 min. The solution rapidly turned yellow, the color being intensified to dark brown. After the addition, the mixture was left to stand at room temperature for 5 hr, and then diluted with water. The organic layer was taken up, thoroughly washed with water and dilute aqueous sodium hydrogen carbonate, and evaporated to give a light brown pasty cake (*ca.* 2.3 g) which, on crystallization from a mixture of dichloromethane and light petroleum, yielded nitrate as colorless fine needles (1.98 g; 85%), mp 85—86 °C. NMR: 7.70 (s, 6H), 7.69 (s, 3H), 7.49 (s, 3H), and 4.29 τ (s, 2H); IR: 705, 858, 870, 970, 1281, 1638, and 2218 cm^{-1}.

Found: C, 61.57; H, 6.08; N, 11.66%. Calcd for $C_{12}H_{14}N_2O_3$: C, 61.53; H, 6.02; N, 11.96%.

VI was heated under gentle reflux with hydrochloric acid in ethanol to give *4,5,6,7-tetramethylphthalide (VIII)*, identical with the authentic sample obtained from the zinc chloride-catalyzed condensation of chloromethyl methyl ether with 2,3,4,5-tetramethylbenzoic acid. Mp 233—235 °C. NMR: 7.78 (s, 3H), 7.72 (s, 3H), 7.70 (s, 3H), 7.37 (s, 3H), and 4.91 τ (s, 2H); IR: 780, 966, 1016, 1126, 1264, 1297, 1350, and 1741 cm^{-1}. Found: C, 75.66; H, 7.38%. Calcd for $C_{12}H_{14}O$: C, 75.76; H, 7.42%.

1-Cyanomethyl-2-nitrooxymethyl-3,4,5,6-tetramethylbenzene (VII). Pentamethylbenzyl cyanide was similarly treated with the nitrating agent to give VII as fine needles, mp 116—118 °C. NMR: 7.75 (s, 6H), 7.67 (s, 6H), 6.26 (s, 2H), and 4.37 τ (s, 2H); IR: 702, 870, 957, 1283, 1296, 1629, and 2248 cm^{-1}.

Found: C, 62.54; H, 6.70; N, 11.44%. Calcd for $C_{13}H_{16}N_2O_3$: C, 62.89; H, 6.50; N, 11.28%.

VII was agitated with saturated aqueous sodium cyanide in acetonitrile to give *1,2-bis(cyanomethyl)-3,4,5,6-tetramethylbenzene (IX)*, mp 178—179 °C, identical with the compound obtained by the action of sodium cyanide on 1,2-bis(chloromethyl)-3,4,5,6-tetramethylbenzene. NMR: 7.75 (s, 6H), 7.69 (s, 6H), and 6.28 τ (s, 4H); IR: 801, 1068, 1286, 1302, and 2245 cm^{-1}. Found: C, 79.43; H, 7.50; N, 12.87%. Calcd for $C_{14}H_{16}N_2$: C, 79.21; H, 7.60; N, 13.19%.

VII was heated with a mixture of hydrochloric acid and ethanol to give white needles of formula $C_{13}H_{16}O_2$, which exhibited ^1H NMR peaks at 7.78 (s, 6H), 7.75 (s, 6H), 6.32 (s, 2H), and 4.63 τ (s, 2H); IR bands at 1026, 1226, 1261, and 1743 cm^{-1}. On heating with dilute sodium hydroxide it went into solution and was again precipitated on acidification. From the mode of reaction and spectral data, it was formulated as *5,6,7,8-tetramethyl-1,4-dihydro-3H-2-benzopyran-3-one (X).* Found: C, 76.14; H, 7.83%. Calcd for $C_{13}H_{16}O_2$: C, 76.44; H, 7.90%.

BULLETIN OF THE CHEMICAL SOCIETY OF JAPAN, VOL. 46, 3609—3610 (1973)

Pyrrolizidine Alkaloids: The Synthesis and Stereochemistry of α- and β-Retusanecic Acids

Shun'ichi KIYOOKA* and Tsunao HASE

Department of Chemistry, Faculty of Science, Kagoshima University, Kamoike, Kagoshima 890

(Received May 28, 1973)

Retusine (I) was isolated from *Crotalaria retusa* L. by Culvenor and Smith,[1] the alkaline hydrolysis of I gave two acids, named α- and β-retusanecic acids. These acids agreed with the epimeric 2,3,4-trimethyl-4-hydroxyglutaric acid 1,4-lactones synthesized by Adams and Hauseman.[2] They have shown that the isomeric acids differ in the configuration of the carbon (C_2) alpha to the lactone and that the interconversion between α- and β-acids caused by refluxing with concentrated hydrochloric acid proceeds to an equilibrium wherein the β-acid predominates. Since the β-acid is thermodynamically more stable than the α-acid, the *trans*-cofiguration of the C_2–CH_3 group relative to the C_3–CH_3 group in the β-acid can be presumed. However, they have not referred to the relation between two methyl groups at C_3 and C_4. This note will discuss the new synthesis of α- and β-retusanecic acids and their stereochemistry. III was chosen as the starting material because an active hydrogen of the malonyl group would be available for alkylation after a ring-closure reaction. Cyano-lactone (IV) was obtained as the only product by the addition of HCN to the keto-ester (III). Moreover, IV was converted to the ester-lactone (V) by the usual method. In order to confirm the configuration of the two methyl groups at C_3 and C_4 in V, another synthesis of V was carried out. It is known that epoxide ring opening[3] by nucleophilic attack proceeds in a *trans* manner. Epoxide (VII) obtained from tiglic acid (VI) was reacted with sodium diethyl malonate to give a lactone compound. Moreover, it was identical with V (bp, IR, NMR). Therefore, the two methyl groups at C_3 and C_4 in V must be in *trans*-configuration. It was assumed that the formation of IV from III was begun by the attack of cyanide on the less hindered side, followed by ring closure, as if shown in Fig. 1. VIII

Fig-1

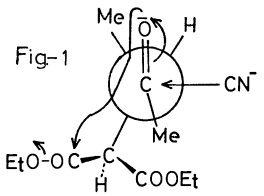

was obtained by the methylation of V. After acid hydrolysis and decarboxylation, two isomeric acids were given in a 17: 1 ratio by fractional crystallization. The IR spectrum ($CHCl_3$) of the (±)major product of IX was superimposable with that of β-retusanecic acid. Also, the IR spectrum ($CHCl_3$) of the (±)minor product of X was superimposable with that of α-retusanecic acid. Consequently, it is confirmed that the configuration of the two methyl groups at C_3 and C_4 in α- and β-retusanecic acids is *trans*.

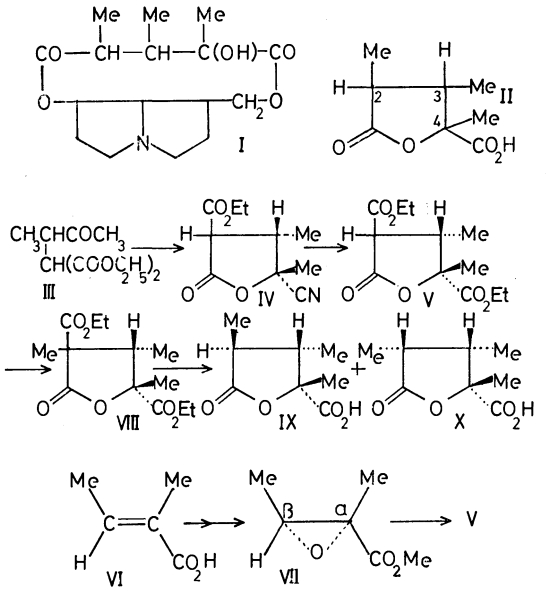

Experimental

Diethyl 1-Methyl-2-oxo-propylmalonate (III). Twelve grams of sodium were added to a solution of 85 g of diethyl malonate in 450 ml of dry ether. The solution was then refluxed for 8 hr until the sodium had completely dissolved, and then it was cooled. To the cooled solution, 75 g of methyl α-bromoethyl ketone were added all at once. The mixture was then refluxed for 2 hr. The ether solution was washed with ice cold water, and then dried with calcium chloride. After the solvent had been distilled, the residue was distilled at 144—149 °C (18 mmHg) to give 64 g of III (52% yield). IR (neat): 1760—1740 cm^{-1} (broad); NMR ($CDCl_3$) (δ): 2.30 ($-COC\underline{H}_3$). Found: C, 57.37; H, 7.93%. Calcd for $C_{11}H_{18}O_5$: C, 57.38; H, 7.88%.

β-Methyl-α-ethoxycarbonyl-γ-cyano-γ-valerolactone (IV). Twenty grams of III, 2.5 g of powdered CaO, and 8.6 g of HCN were placed in a flask in an ice bath. The flask was sealed and warmed at 50 °C for 3 hr. The excess HCN was then evaporated *in vacuo*. To the residue, 20 ml of chloroform were added. The chloroform solution was separated from an inorganic substance. After the solvent had been removed, 17 g of a dark-colored oil was obtained and chromatographed over a silica-gel column. Elution with chloroform gave a

* Present address: Department of Chemistry, Faculty of Literature and Science, Kochi University, Asakura, Kochi.

1) C. C. J. Culvenor and L. W. Smith, *Aust. J. Chem.*, **10**, 464 (1957).

2) R. Adams and F. B. Hauserman, *J. Amer. Chem. Soc.*, **74**, 694 (1952).

3) M. S. Newman, "Steric Effects in Organic Chemistry," John Wiley & Sons Inc, New York (1956), p. 106.

colorless oil. The oil was distilled at 120—122 °C (3 mmHg) to give 7 g of IV (50% yield). IR (neat): 1815, 1750 cm^{-1}; Found: C, 56.88; H, 6.05; N, 6.25%. Calcd for $C_{10}H_{13}O_4N$: C, 56.86; H, 6.20; N, 6.63%.

β-Methyl-α,γ-diethoxycarbonyl-γ-valerolactone (V). A cold solution (0 °C) of 2 g of IV, 1 ml of absolute ethanol, and 1 ml of dry ether were saturated with dry hydrogen chloride, allowed to stand at 0 °C overnight, and then neutralized with a saturated solution of potassium carbonate. After extraction with ether, the ether solution was dried with anhydrous sodium sulfate. After the ether had been removed, the residue was distilled at 150—153 °C (4 mmHg) to give 1.2 g of V (50% yield). IR (neat): 1800, 1745 cm^{-1}; NMR ($CDCl_3$) (δ): 1.60 (-C(COOC$_2$H$_5$)-CH$_3$). Found: C, 55.57; H, 7.10%. Calcd for $C_{12}H_{18}O_6$: C, 55.80; H, 7.03%.

V from Methyl α-Methyl-α,β-epoxy-butyrate (VII). To solution of 0.288 g of sodium in 30 ml of absolute ethanol, 1.98 g of diethyl malonate were added. After 1 hr, 1.6 g of VII were added to the solution. The mixture was then refluxed for 35 hr, and the ethanol was evaporated *in vacuo*. After the residue had been extracted with ether, the solution was dried with anhydrous sodium sulfate. After the distillation of the solvent, 1.3 g of a colorless oil was given. The oil was chromatographed over a silica-gel column and eluted with chloroform. The first fraction (1200 ml) was concentrated to give 0.7 g of an oily product which was identical with V (bp, IR, NMR).

α,β-Dimethyl-α,γ-diethoxycarbonyl-γ-valerolactone (VIII). One gram of V was added to a solution of 0.1 g of sodium in 25 ml of absolute ethanol. After 1 hr, 0.63 g of methyl iodide in 2 ml of absolute ethanol was added to the solution. The mixture was then refluxed for 25 hr, and the ethanol was evaporated *in vacuo*. After the residue had been extracted with ether, the ether solution was dried with anhydrous sodium sulfate. After the evaporation of the solvent, the residual oil was distilled at 133 °C (2 mmHg) to give 0.93 g of VIII (88% yield). IR (neat): 1795, 1750 cm^{-1}. Found: C, 57.56; H, 7.57%. Calcd for $C_{13}H_{20}O_6$: C, 57.34; H, 7.40%.

2,3,4-Trimethyl-4-hydroxy-glutaric Acid-1,4-lactone, IX and X. A solution of 2.565 g of VIII in 25 ml of conc. hydrochloric acid was refluxed for 15 hr. After the evaporation of the solvent, the residue was heated on an oil bath at 170—190 °C to give 1.385 g of a solid. Fractional crystallization with benzene gave 0.85 g of plate crystals (mp 117—118 °C) of IX and 0.05 g of needle crystals (mp 129—130 °C) of X. IX: IR ($CHCl_3$): 1790, 1738 cm^{-1}; NMR (pyridine-d_5) (δ): 1.75 (-C(COOH)-CH$_3$). Found: C, 55.93; H, 7.10%. Calcd for $C_8H_{12}O_4$: C, 55.80; H, 7.03%. δ: IR ($CHCl_3$): 1790, 1742 cm^{-1}; NMR (pyridine-d_5) (δ): 1.70 (-C(COOH)-CH$_3$). Found: C, 55.87; H, 6.97%. Calcd for $C_8H_{12}O_4$: C, 55.80; H, 7.03%.

BULLETIN OF THE CHEMICAL SOCIETY OF JAPAN, VOL. 46, 3610—3611 (1973)

Reaction of *trans*-Stilbene with Methanesulfenyl Chloride

Michinori Ōki, Atsuko Nakamura, and Keiji Kobayashi
Department of Chemistry, Faculty of Science, The University of Tokyo, Hongo, Tokyo 113

(Received June 8, 1973)

We have treated *trans*-stilbene (**1**) with excess methanesulfenyl chloride and obtained a mixture of α-chloro-α-methylthiostilbenes which are formally the dehydrogenation products of the adduct. This paper presents characterization of the products and a discussion on the reaction.

Experimental

Reaction between trans-*Stilbene and Methanesulfenyl Chloride in 1: 1 Molar Ratio.* To a solution of 4.0 g. (0.022 mol) of *trans*-stilbene in 300 ml. of toluene was added 1.8 g (0.022 mol) of methanesulfenyl chloride at −78 °C. After the color of the chloride had faded, the mixture was warmed to room temperature and evaporated *in vacuo*. The remaining mixture was fractionally recrystallized from petroleum ether to give 48% *erythro*-1-chloro-2-methylthio-1,2-diphenylethane,[1] mp 123 °C.

Reaction of trans-*Stilbene with Excess Methanesulfenyl Chloride.* *trans*-Stilbene (4.5 g or 0.025 mol) was added to 6.2 g (0.075 mol) of methanesulfenyl chloride at −78 °C and the mixture was slowly warmed up to room temperature. During this period a vigorous reaction set in and evolution of hydrogen chloride took place. The excess of methanesulfenyl chloride was decomposed by pouring into methanol. The product chromatographed on alumina gave a mixture in 77% yield (by weight). NMR spectra of the mixture indicated that it consists of *cis*- and *trans*-α-chloro-α′-methylthiostilbenes, the composition being *ca.* 4: 1 in favor of the *cis*-isomer. Rechromatography of the mixture gave the *trans* compound, mp 74 °C, and the *cis*, mp 52 °C.[2]

trans-*α-Chloro-α-methylthiostilbene.* Methanesulfenyl chloride (5 g or 0.06 mol) was added to 9 g (0.05 mol) of tolane in 20 ml of ether containing 2 ml of boron trifluoride etherate. The mixture was washed with water, evaporated and chromatographed on alumina to give 70% *trans*-α-chloro-α′-methylthiostilbene, mp 74 °C, which was identical with one of the products obtained above. Found: C, 69.00; H, 5.19%. Calcd for $C_{15}H_{13}ClS$: C, 69.14; H, 5.01%.

trans- *and* cis-*α-chloro-α′-methylsulfonylstilbenes.* The corresponding thioethers were oxidized with peracetic acid in acetic acid at 70 °C for 1 hr. The *trans* form, mp 158.5—159 °C. Found: C, 61.40; H, 4.58%. The *cis* form, mp 123—126 °C. Found: C, 61.44; H, 4.52%. Calcd for $C_{15}H_{13}ClO_2S$: C, 61.53; H, 4.44%.

Reaction of erythro-*1-Chloro-2-methylthio-1,2-diphenylethane with Methanesulfenyl Chloride.* To a solution of 0.52 g (2 mmol) of *erythro*-1-chloro-2-methylthio-1,2-diphenylethane in 10 ml of carbon tetrachloride was added 0.33 g (4 mmol) of methanesulfenyl chloride at room temperature. After the reaction was over, as indicated by fading of the color, the solution was washed with aqueous sodium carbonate and the

1) M. Ōki and A. Kimura, This Bulletin, **38**, 682 (1965).

2) Since purification of this compound was rather tedious, elemental analysis was performed with the sulfone.

solvent was evaporated. NMR spectrum indicated the presence of *cis*- and *trans*-α-chloro-α'-methylthiostilbenes and dimethyl disulfide. The ratio of the isomers was paractically the same as the one obtained by the reaction of *trans*-stilbene with excess methanesulfenyl chloride.

Thermal Equilibration of α-Chloro-α'-methylthiostilbenes. The *trans* form of this compound was dissolved in carbon tetrachloride and sealed in an NMR sample tube. The whole was heated at 195 °C and the NMR spectra were determined at appropriate intervals. The *trans* compound had a sharp singlet at 1.77 ppm from internal TMS and a fairly sharp signal at 7.31 ppm, the latter being characteristic of *trans*-stilbene derivatives. After heating for 5 hr, the equilibrium was reached. The signals for the *cis* compound were observed at 1.83, 6.98, and 7.08 ppm. The latter two signals can be taken as an evidence for the *cis*-stilbene structure. The area ratio was *ca.* 2:1 in favor of the *cis*.

Discussion

The reaction of *trans*-stilbene with excess methanesulfenyl chloride afforded a mixture of two compounds containing both sulfur and chlorine. One of the products was found to be identical with a product from the reaction of tolane with methanesulfenyl chloride. Since the ionic addition to tolane (**4**) has been known[3] to give mainly the *trans* isomer, it is most reasonable to assume that this compound is *trans*-α-chloro-α'-methylthiostilbene (**2**).

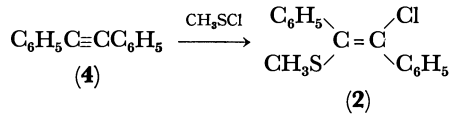

Analytical data of the other product suggest it to be an isomer of the *trans* compound, whose structure might be reasonably assigned to *cis*-α-chloro-α'-methylthiostilbene (**3**). Further evidence for the assignment of the structure was obtained by thermal equilibration with the *trans* compound and by refluxing the compound with Raney nickel in acetone: *cis*-stilbene, as identified by the corresponding signals in NMR spectra, was found.

The favored formation of the *cis* isomer over the *trans* is of interest. Although it is difficult to verify the reasons, there are many such examples. Among 1,2-dihaloethylenes, the *cis* isomer is known to be more stable than the *trans*.[4-6] In substituted enedithiol derivatives, the *cis* form is more stable,[7] although steric factor may operate to some extent in that *cis-trans* pair. Since the system in question possesses chlorine and sulfur atoms at both ends of the vinylene groups, the stability of the *cis* compound can be explained similarly. Thus the results appear as a result of thermodynamic control and the thermal equilibration agrees with expectation. The presence of hydrogen chloride, as one of the reaction products, will catalyze the equilibration between *cis*- and *trans*-isomers.

Since *erythro*-1-chloro-2-methylthio-1,2-diphenylethane (**5**), when treated with methanesulfenyl chloride, gives almost the same mixture as the products from *trans*-stilbene and excess methanesulfenyl chloride, the reaction may be assumed to proceed *via* compound **5**. The mechanism of the dehydrogenation reaction will then be similar to that reported:[8] a Pummerer type intermediate (**6**) intervenes and the deprotonation from beta to the sulfur atom takes place. A probable mechanism is as follows.

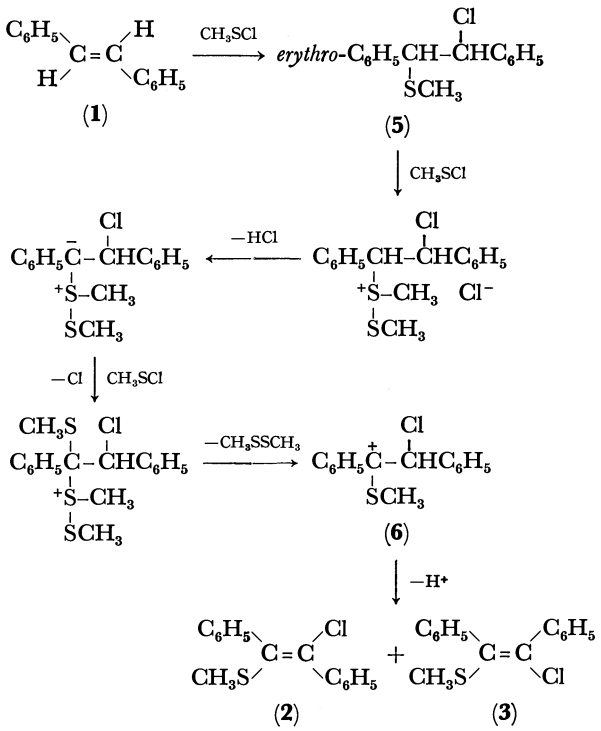

No evidence for further addition[9] of the sulfenyl chloride to **2** and **3** was obtained.

Note Added in Proof: Equilibration of *cis* and *trans* isomers of a similar system catalyzed by hydrogen chloride was reported recently. See G. Modena, G. Scorrano, and U. Tonellato, *J. Chem. Soc. Perkin II*, **1973**, 493.

3) E. Bergmann, *J. Chem. Soc.*, **1936**, 402. Arenesulfenyl chlorides are also known to add in *trans* fashion to acetylenic bond: E. G. Kataev and T. G. Mannafov. *Zh. Org. Khim.*, **1970**, 1959; *Chem. Abstr.*, **74**, 12763s (1971).

4) H. Steinmetz and R. M. Noyes, *J. Amer. Chem. Soc.*, **74**, 4141 (1952).

5) K. S. Pitzer and J. L. Hollenberg, *ibid.*, **76**, 1493 (1954).

6) H. G. Viehe, *Chem. Ber.*, **93**, 1697 (1960).

7) M. Ōki and K. Kobayashi, This Bulletin, **43**, 1234 (1970).

8) M. Ōki and K. Kobayashi, *ibid.*, **43**, 1229 (1970).

9) M. Ōki and K. Kobayashi, *ibid.*, **46**, 687 (1973).

BULLETIN OF THE CHEMICAL SOCIETY OF JAPAN, VOL. 46, 3612—3613 (1973)

Synthesis and Reaction of 1-Substituted-4-benzylpiperazin-2-ones

Hiroaki UCHIDA and Masaki OHTA

Department of Chemistry, Faculty of Science, Tokyo Institute of Technology, Ookayama, Meguro-ku, Tokyo 152

(Received June 14, 1973)

Introduction of a functional substituent at position 1 of 4-substituted piperazine-2-one (I) has been reported to be effected by two methods. Method A is an addition of I to an olefinic compound in the presence of base[1] or to an acetylenic compound at high temperature and pressure.[2] Method B is a reaction of sodium salt of I with an appropriate halide.[3]

However, the compounds thus prepared are quite few and are special types for practical application. In this note, preparation of 4-benzylpiperazin-2-ones (IV—XII) having a functional substituent at position 1 and their derivation and cyclization are described.

The starting material, piperazin-2-one (II), was prepared by Aspinall[4] by condensing ethyl chloroacetate with large excess of ethylenediamine, followed by cyclization. We found that the cyclization of the intermediate occurred during removal of excess of ethylenediamine at 100 °C instead of heating at 200 °C as described by Aspinall. 4-Benzylpiperazin-2-one (III) was readily available by reacting II with benzyl chloride.

Reaction conditions and yields in the preparation of IV—XII were tabulated in Table 1. In Table 2 were shown physical constants of the products and their salts respectively.

Reaction of ethyl 1-(4-benzyl-2-oxo)piperazinepropionate (VI) with concentrated ammonium hydroxide led to the formation of the corresponding amide (XIII) [mp 107—109 °C. Found: C, 64.25; H, 7.33; N, 16.01%. Calcd for $C_{14}H_{19}O_2N_3$: C, 64.34; H, 7.33; N, 16.08%]. Methyl 1-(4-benzyl-2-oxo)piperazinepropionate (V) and ethyl 1-(4-benzyl-2-oxo)piperazineacetate (XI) were allowed to react with hydrazine hydrate to give the corresponding hydrazides [V hydrazide was characterized as *m*-nitrobenzylidene derivative; mp 146—147 °C. Found: C, 61.82; H, 5.57; N, 17.17%. Calcd for $C_{21}H_{23}O_4N_5$: C, 61.60; H, 5.66; N, 17.11%. XI hydrazide; mp 108—109 °C. Found: C, 59.16; H, 6.87; N, 21.52%. Calcd for

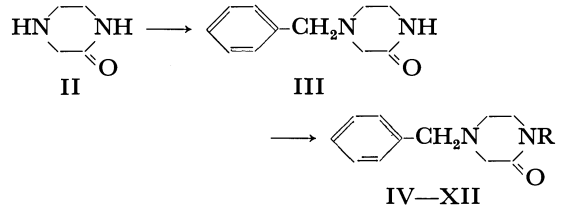

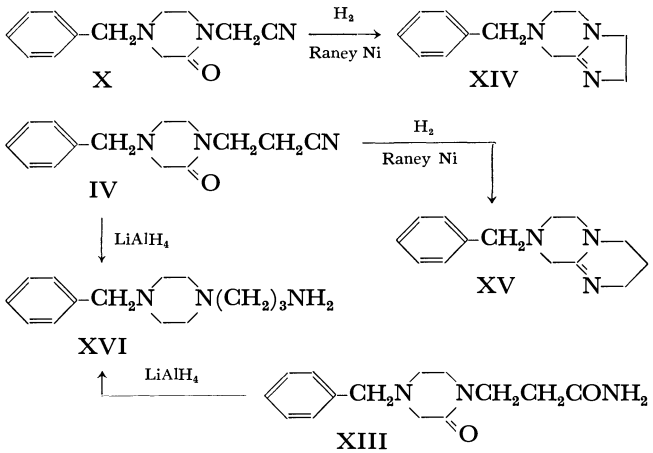

TABLE 1. PREPARATION OF 1-SUBSTITUTED-4-BENZYLPIPERAZIN-2-ONES

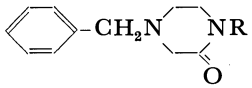

Compd. No.	R	Solvent	React. temp (°C)	Condition time (hr)	Yield (%)
IV	CH_2CH_2CN	CH_3CN	reflux	6	93
V	$CH_2CH_2COOCH_3$	Dioxane	90	8	68
VI	$CH_2CH_2COOC_2H_5$	Dioxane	reflux	6	90
VII	$CH_2CH_2CH_2CH_3$	Toluene	90	4	51
VIII[a]	$CH_2C_6H_5$	Toluene	90	2.5	54
IX	$CH_2CH_2N(C_2H_5)_2$	Toluene	90	5	60
X	CH_2CN	Toluene	r.t.	6.5	28
XI	$CH_2COOC_2H_5$	Toluene	90	5	66
XII	$CH_2CH=CH_2$	Toluene	93	5	51

a) Ref. 5

1) Rohm and Haas Co., Brit. 875135 (1961); *Chem. Abstr.*, **59**, 6420f (1963).

2) Rohm and Haas Co., Belg. 660617 (1965); *Chem. Abstr.*, **63**, 18119f (1965).

3) A. Sut, M. Podesta, and M. A. Lattes, *Chim. Ther.*, **1969**, 167; *Chem. Abstr.*, **71**, 91427z (1969).

4) S. R. Aspinall, *J. Amer. Chem. Soc.*, **62**, 1202 (1940).

Table 2. Physical constants of the products and their salts

Compd. No.	Bp (°C/mmHg)	Salt	Mp(°C)[b]
IV	205—206/1	picrate[c]	164—165
V	194—196/1	picrate[d]	129—130
VI	190—191/1	picrate[e]	111—112.5
VII	165—166/1	picrate[f]	113—115
VIII	205—207/1	HCl[g]	194—196
IX	186—188/1	picrate[h]	185—187
X[a]	185—186/1	picrate[c]	175—177
XI	191—193/1	HCl[b]	88—90
XII	159—160/1	picrate[c]	140—141

a) As semihydrate.
b) Melting points were measured on a hot plate stage and uncorrected.
Solvents for recrystallization.
c) C_2H_5OH.
d) CH_3OH–H_2O.
e) H_2O.
f) C_2H_5OH–$(C_2H_5)_2O$.
g) Dioxane.
h) CH_3CN–$(C_2H_5)_2O$.

$C_{13}H_{18}O_2N_4$: C, 59.52; H, 6.92; N, 21.36%].

Hydrogenation of 4-benzyl-1-cyanomethylpiperazin-2-one (X) and 4-benzyl-1-(2-cyanoethyl)piperazin-2-one (IV) in the presence of Raney nickel gave easily cyclized products, 7-benzyl-2,3,5,6,7,8-hexahydroimidazo[1,2-*a*]pyrazine (XIV) and 8-benzyl-2,3,6,7,8,9-hexahydro-4*H*-pyrazino[1,2-*a*]pyrimidine (XV) respectively. As an alternative route leading to the fused compound XV, selective reduction of nitrile group in IV or amide group in XIII was attempted using lithium aluminium hydride. However, the reduction of ring carbonyl group occurred simultaneously yielding 1-(3-aminopropyl)-4-benzylpiperazine (XVI) [bp 155—157 °C/1 mmHg. Picrate; mp 254—255 °C. Found: C, 41.92; H, 3.67; N, 17.64%. Calcd for $C_{32}H_{32}O_{21}N_{12}$ (tripicrate): C, 41.75; H, 3.50; N, 18.26%]. Hydrogenation of IV using 10% Pd–C in methanol containing hydrogen chloride was unsuccessful.

Experimental

4-Benzylpiperazin-2-one (III). A mixture of II(24.3 g), benzyl chloride(30.8 g) and sodium bicarbonate(24.5 g) in ethanol(300 ml) was gently refluxed for 5 hr. Upon cooling to room temperature, crystals of III separated out were collected by filtration. Concentration of the filtrate gave additional product. The combined crystals were recrystallized from benzene to give colorless prisms of III, mp 155—157 °C(lit,[6] mp 149—150 °C), 40.4 g (88%). Found: C, 69.50; H, 7.51; N, 14.89%. Calcd for $C_{11}H_{14}ON_2$: C, 69.44; H, 7.42; N, 14.73%.

4-Benzyl-1-(2-cyanoethyl)piperazin-2-one(IV) [*by Method A*]. A mixture of III(3.8 g), acrylonitrile(1.2 g) and powdered potassium hydroxide(20 mg) in acetonitrile(100 ml) was gently refluxed for 6 hr with stirring. The reaction mixture was concentrated, and to the residual oil was added 200 ml of ether. The ether insoluble substance was removed by filtration. The ethereal solution was concentrated and the residue was distilled under vacuum to obtaine 4.5 g of IV as a viscous pale yellow oil.

V and VI were prepared by this method.

*4-Benzyl-1-*n*-butylpiperazin-2-one(VII)* [*by Method B*]. A mixture of III(2.9 g) and finely pulverized sodium(0.35 g) in dry toluene(200 ml) was heated with vigorous stirring. At around 75 °C, III was completely dissolved and reaction mixture began to become turbid after 3 hr refluxing. After 7—8 hr refluxing the reaction mixture became gruel-like and all of the sodium was consumed. *n*-Butyl bromide(2.7 g) was added to the above mixture at room temperature. The mixture changed to a clear solution after 1 hr heating at 90 °C with stirring and additional 3 hr heating was continued. The reaction mixture was concentrated and ether(200 ml) was added to the oily residue. The ether-insoluble substance was removed by filtration and the ethereal solution was concentrated and then distilled under vacuum to give 1.9 g of VII as a viscous slightly yellow oil.

VIII-XII were prepared by this method.

7-Benzyl-2,3,5,6,7,8-hexahydroimidazo[1,2-a]pyrazine (XIV). X(4.0 g) in methanol(30 ml) containing ammonia(2 g) was hydrogenated at 95 °C in the presence of Raney nickel(1 g) and hydrogen at an initial pressure of 140 atm. The catalyst was removed by filtration and the filtrate was concentrated. The residue was distilled to give colorless oil of XIV, bp 176—179 °C/1 mmHg, 3.4 g(94%), hygroscopic. Found: C, 71.59; H, 8.13; N, 19.25%. (Calcd for $C_{13}H_{17}N_3$: C, 72.52; H, 7.96; N, 19.52%). IR(NaCl) cm^{-1}: 3350, 1635, 1492, 743, 701.

The picrate was recrystallized from acetonitrile, mp 197—199 °C. Found: C, 44.72; H, 3.50; N, 19.50%. Calcd for $C_{25}H_{23}O_{14}N_9$ (dipicrate): C, 44.58; H, 3.44; N, 18.71%.

8-Benzyl-2,3,6,7,8,9-hexahydro-4H-pyrazino[1,2-a]pyrimidine (XV). Hydrogenation of IV(6.1 g) by the same procedure as the preceding experiment gave colorless viscous oil of XV, bp 177—181 °C/1 mmHg, 5.5 g(96%), hygroscopic. Found: C, 72.24; H, 8.57; N, 18.28%. (Calcd for $C_{14}H_{19}N_3$: C, 73.32; H, 8.35; N, 18.33%). IR(NaCl) cm^{-1}: 3300, 1643, 1495, 750, 705. Picrate: mp 193—195 °C(methanol). Found: C, 45.33; H, 3.67; N, 18.25%. Calcd for $C_{26}H_{25}O_{14}N_9$(dipicrate): C, 45.42; H, 3.67; N, 18.34%.

5) W. B. Martin, Jr. and A. E. Martell, *J. Amer. Chem. Soc.*, **72**, 4301 (1950).

6) H. S. Mosher, J. Cornell, Jr., O. L. Stafford, and T. Roe, Jr., *ibid.*, **75**, 4949 (1953).

BULLETIN OF THE CHEMICAL SOCIETY OF JAPAN, VOL. 46, 3614—3615 (1973)

Intramolecular Charge-transfer Interaction in Substituted Diphenylmethanes

Hiroyasu INOUE, Yoichiro MIKAMI, and Toshiji YOKOTANI

Department of Applied Chemistry, Faculty of Technology, Kanagawa University, Kanagawa-ku, Yokohama 221

(Received June 16, 1973)

In a previous paper,[1] we have reported that aniline and nitrobenzene in cyclohexane form a loose contact pair, are giving rise to the charge-transfer (CT) absorption as the tail of the long wavelength band of nitrobenzene when the concentrations of both are very high. According to White,[2] in the case of 4-amino-4′-nitrodiphenylmethane the across-space CT interaction between aniline and nitrobenzene parts causes a new band at 324 nm (30.9 kK), which is hidden under the intense band of nitrobenzene. Therefore, the presence of the CT band was revealed by the subtraction of the absorption spectra of the reference compounds *i.e.*, *p*-toluidine and *p*-nitrotoluene, from that of 4-amino-4′-nitrodiphenylmethane. For many compounds, the intramolecular CT interaction between two moieties separated by a saturated hydrocarbon chain has been established.[3-7]

In this paper, we will deal with the absorption and fluorescence spectra of 4-hydroxy-4′-nitrodiphenylmethane (HN) and 4-amino-4′-nitrodiphenylmethane (AN), aiming to give further evidence for the intramolecular CT interaction in these compounds.

Experimental

Materials. The HN was prepared by the diazo-decomposition of AN according to the method of Tsekhanskii and Fedorov[8] and was purified by repeated recrystallizations from an ethanol–water mixed solvent; mp 118.5 °C (lit,[8] 119 °C). The AN was prepared by the partial reduction of 4,4′-dinitrodiphenylmethane according to the method of Litvinenko and Levchenko[9] and was purified by repeated recrystallizations from a methanol–water mixed solvent; mp 98 °C (lit,[9] 98 °C). Cyclohexane was purified by standard procedures.

Measurements. The ultraviolet absorption spectra were measured with a Shimadzu Spectrophotometer, D-40D, using 1 cm quartz cells. The fluorescence and excitation spectra were recorded on a Hitachi Fluorescence Spectrophotometer, MPF-2A. The concentrations of solutions were of the order of 10^{-4} mol/l. No correction for the sensitivity of the instrument was made. The excitation wave number was 41.7 kK. All the measurements were carried out at room temperature.

Results and Discussion

The ultraviolet absorption spectrum of HN in cyclohexane does not coincide with that of *p*-nitrotoluene in the wave number region lower than 37.0 kK. When the latter is subtracted from the former, a weak broad band appears at 33.3 kK (ε=1700). Similarly, in the case of AN, a weak band appears at 32.3 kK (ε=1950) as an extra band. Since the shapes of these extra bands are not dependent on the concentrations of the solutions, they can not be attributed to intermolecular interaction. The extra bands are, therefore, considered to be the intramolecular CT bands. In fact, the CT band of HN appears at a higher wave

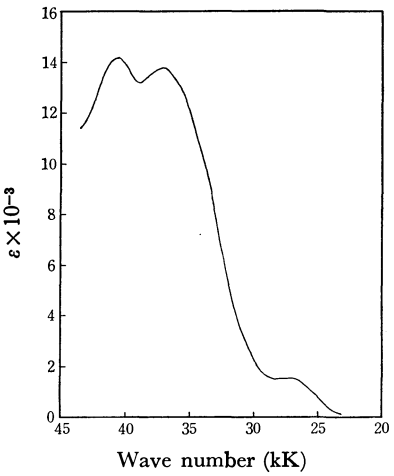

Fig. 1. Absorption spectrum of HN in alkaline aqueous ethanol (pH 13).

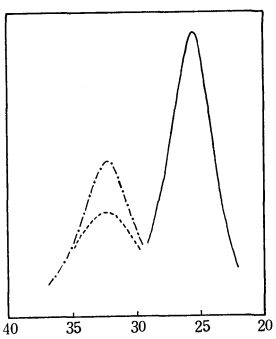

Fig. 2. Absorption (——), fluorescence (——), and excitation (-·-·-) spectra of AN in cyclohexane. The absorption band was obtained by subtracting the spectra of the reference compounds.

1) H. Inoue and Y. Kato, *Tetrahedron*, **28**, 527 (1972).
2) W. N. White, *J. Amer. Chem. Soc.*, **81**, 2912 (1959).
3) P. Moser, *Helv. Chim. Acta*, **51**, 1831 (1968).
4) J. W. Verhoeven, I. P. Dirkx, and Th. J. de Boer, *Tetrahedron*, **25**, 4037 (1969).
5) M. Ōki and K. Mutai, *ibid.*, **26**, 1181 (1970).
6) K. Mutai, This Bulletin, **45**, 2635 (1972).
7) J. C. Nnadi, A. W. Peters, and S. Y. Wang, *J. Amer. Chem. Soc.*, **94**, 712 (1972).
8) R. S. Tsekhanskii and Yu. A. Fedorov, *Uch. Zap. Chuvashsk. Gos. Ped. Inst.*, 116 (1962); *Chem. Abstr.*, **60**, 15759a (1964).
9) L. M. Litvinenko and N. F. Levchenko, *Zh. Obshch. Khim.*, **29**, 3070 (1959); *Chem. Abstr.*, **54**, 13060e (1960).

number than that of AN, because the ionization potential of HN (8.97 eV) is higher than that of AN (8.14 eV).[10]

When the absorption spectrum of HN is measured in alkaline aqueous ethanol (pH 13), the CT band is observed explicitly at 27.0 kK, as is shown in Fig. 1. In this case, the *p*-methylphenolate-ion part acts as the electron donor and its ionization potential seems to be very low compared with those of *p*-cresol and *p*-toluidine.

The presence of the intramolecular CT interaction in HN and AN is confirmed by the fluorescence spectra. That is, new fluorescence bands, which could not be assigned to the reference compounds, appeared at 29.0 and 25.5 kK for HN and AN respectively in cyclohexane. The fluorescence spectrum of AN, for example, is shown in Fig. 2, in which the excitation spectrum is also presented. As may be seen from this figure, the excitation spectrum agrees well with the extra absorption band. Therefore, this emission is not an excimer fluorescence such as those reported on some diphenyl alkanes,[11] but can be attributed to the presence of the intramolecularly-interacting species in the ground electronic state.

It may be expected that the dissociation constant of HN differs from that of *p*-cresol. Accordingly, the pK_a values were determined in a mixed solvent of methanol–water at 25 °C. The pK_a values were 10.8 and 11.1 for HN and *p*-cresol respectively. This can be interpreted in terms of the charge migration from the *p*-cresol part to the *p*-nitrotoluene part in HN.

10) G. F. Crable and G. L. Kearns, *J. Phys. Chem.*, **66**, 436 (1962).

11) F. Hirayama, *J. Chem. Phys.*, **42**, 3163 (1965).

BULLETIN OF THE CHEMICAL SOCIETY OF JAPAN, VOL. 46, 3515—3517 (1973)

On the Reaction of *p*-Toluenesulfinyl Chloride with Anisole

Tamotsu FUJISAWA, Masami KAKUTANI, and Norio KOBAYASHI
Sagami Chemical Research Center, Nishi-Ohnuma, Sagamihara, Kanagawa 229

(Received May 28, 1973)

Concerning the Friedel-Crafts-type reaction, sulfonyl chloride and sulfenyl chloride have been well known to give aromatic sulfone[1] and sulfide[2] respectively; however, with one exception,[3] the reaction of sulfinyl chloride with aromatics has not been reported. In this experiment, the reaction of *p*-toluenesulfinyl chloride (I) with anisole was studied with various catalysts as a series of electrophilic aromatic substitutions with the chlorides of organic sulfur acids.[2]

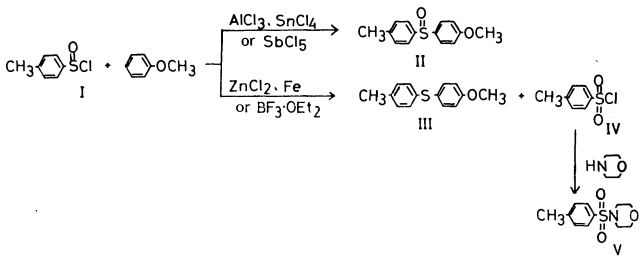

Scheme 1.

When the reaction of anisole with I in the presence of aluminum chloride was conducted in carbon disulfide or excess anisole at −15—20 °C, *p*-anisyl *p*-tolyl sulfoxide (II) was obtained in a good yield after the hydrolysis of the reaction product. The use of antimony pentachloride or stannic chloride in place of aluminum chloride led also to the formation of II. On the other hand, when a 10% excess molar amount of zinc chloride or boron trifluoride etherate, or a catalytic amount of iron powder, was used as the catalyst, the sulfoxide II was not obtained; instead, *p*-anisyl *p*-tolyl sulfide (III) and *p*-toluenesulfonyl chloride (IV) were formed. Compound IV was identified as *N*-(*p*-toluenesulfonyl) morpholine (V). The seresults are summarized in Table 1.

The sulfoxide formation may be explained by a mechanism similar to that of the Friedel-Crafts acylation.[1] This assumption was supported by the IR spectra of mixtures of I and the catalysts (*vide infra*) and by the isolation of a 1 : 1 complex of II with antimony pentachloride. The sulfide formation is ascribed to the reduction of the initially-formed II with I. In fact, control experiments revealed that II and the complexes of II with the catalysts for sulfide formation were reduced by I at room temperature in accord with the following equation.[4]

Scheme 2.

This is the first example of the reduction of sulfoxide by sulfinyl chloride, although there is one precedent for sulfinyl chloride functioning as a reducing agent; it is the reduction of pyridine *N*-oxide with *p*-nitrobenzene-

1) G. A. Olah, Ed., "Friedel-Crafts and Related Reactions," Vol. III, part 2, Interscience Pub., N. Y. (1964), p. 1003.

2) T. Fujisawa, T. Kobori, N. Ohtsuka, and G. Tsuchihashi, *Tetrahedron Lett.*, **1968**, 4533 and 5071; T. Fujisawa and N. Kobayashi, *J. Org. Chem.*, **36**, 3546 (1971) and references cited therein.

3) C. Courtot and J. Frenkiel, *C.R. Acad. Sci. Paris*, **199**, 557 (1934).

4) The complexes of II with the catalysts for sulfoxide formation were not reduced to III on treatment of them with I at room temperature.

Table 1. Reaction of *p*-toluenesulfinyl chloride with anisole in the presence of various catalysts

Catalyst	Molar ratio Cat/I	Medium	Temp. (°C)	Time (hr)	Yield (%) II[a]	III[b]	V[a]
$AlCl_3$	1.1	CS_2	−15	5	75	0	0
$AlCl_3$	1.1	Anisole	R.T.	24	81	0	0
$SnCl_4$	1.1	CS_2	R.T.	24	40	0	0
$SbCl_5$	1.1	CS_2	R.T.	24	22	0	0
$ZnCl_2$	1.1	CS_2	R.T.	24	0	47	16
$BF_3 \cdot OEt_2$	1.1	CS_2	R.T.	24	0	46	11
Fe	0.01	Anisole	R.T.	24	0	64	5
None	—	Anisole	Reflux	3	0	70	23

a) Isolated yields.
b) Determined by glpc.

sulfinyl chloride at 180 °C.[5]

The catalyst dependence of the products may be due to the difference in the interaction between the catalysts and I. The IR spectra of mixtures of I and aluminum chloride, stannic chloride, or antimony pentachloride in carbon disulfide showed shifts of absorption due to the sulfinyl group to wave numbers lower by 129—179 cm^{-1}, but no such shifts were observed in the case of zinc chloride, boron trifluoride etherate, or iron powder. These findings suggest that the sulfinyl group of I interacts with the catalysts for the sulfoxide formation,[6] and that free sulfinyl chloride effects the reduction of sulfoxides.

The sulfide formation was observed also in the absence of a catalyst. Although the reaction of anisole with I did not occur at room temperature, the reaction in boiling anisole gave III in a 70% yield. This reaction path is different from that of the catalyzed reaction; *i.e.*, the formation of III is to be ascribed to the electrophilic aromatic substitution of *p*-toluenesulfenyl chloride (VI),[7] which may itself be formed by the disproportionation of I. Concerning the disproportionation of a sulfinyl chloride, it has been described that methanesulfinyl chloride decomposes to the corresponding sulfenyl and sulfonyl chlorides on standing for several months.[8] *p*-Toluenesulfinyl chloride (I) did not undergo the disproportionation at room temperature, not even in the presence of a catalyst, but it gave the corresponding sulfonyl chloride, IV, on heating at 140 °C.[9]

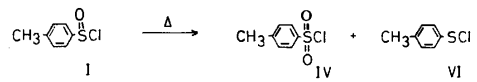

Scheme 3.

We are grateful to the Kawakami Memorial Foundation for its partial support of this research.

5) S. Oae and K. Ikura, This Bulletin, **39**, 1306 (1966).
6) Some Lewis acids were reported to coordinate to oxygen atom of sulfoxide; D. W. Meek and R. S. Drago, *J. Amer. Chem. Soc.*, **82**, 6013 (1960).
7) A similar aromatic substitution with sulfenyl chloride in the presence of catalyst has been reported; *cf.* Ref. 2.
8) I. B. Douglass and D. A. Koop, *J. Org. Chem.*, **29**, 951 (1964).
9) *p*-Toluenesulfenyl chloride could not be isolated because of instability at the temperature.

Experimental

The melting points are uncorrected. The infrared spectra were run on a Perkin-Elmer 337 spectrophotometer. All the NMR spectra were recorded on a Varian HA-100 spectrometer. The chemical shifts of the NMR spectra are reported in parts per million downfield from the internal TMS (δ). The glpc analyses were conducted using a Hitachi K-53 chromatograph with a 3% SE-30 column. *p*-Toluenesulfinyl chloride (I) was prepared by treating sodium *p*-toluenesulfinic acid with thionyl chloride according to the method of Kurzer.[10]

Reaction of I with Anisole in Carbon Disulfide in the Presence of Aluminum Chloride. Aluminum chloride (3.70 g, 28 mmol) was added to a solution of I (4.36 g, 25 mmol) and anisole (2.70 g, 25 mmol) in carbon disulfide (20 ml) cooled to −30 °C. The mixture was stirred for 5.5 hr at 0—−15 °C and then heated under reflux for 30 min to complete the reaction. The reaction mixture was poured into a mixture of ice and water. The carbon disulfide layer was separated and dried with calcium chloride. The removal of the carbon disulfide afforded *p*-anisyl *p*-tolyl sulfoxide[11] (4.6 g, 75%), which was subsequently recrystallized from *n*-hexane; mp 68—70 °C; IR (KBr) 1030 cm^{-1}; NMR ($CDCl_3$) δ 2.33 (s, 3H), 3.77 (s, 3H), 6.90 (d, 2H), 7.19 (d, 2H), 7.47 (d, 2H), 7.52 (d, 2H).

Found: C, 68.26; H, 5.73; S, 13.02%. Calcd for $C_{14}H_{14}O_2S$: C, 68.35; H, 5.87; 13.09%.

When antimony pentachloride was used as a catalyst in this reaction, a 1:1 complex of *p*-anisyl *p*-tolyl sulfoxide with antimony pentachloride (14 g, 86%) was obtained. The complex was recrystallized from chloroform–*n*-hexane; mp 178—179 °C; IR (KBr) 850 cm^{-1} (sulfoxide); NMR ($CDCl_3$) δ 2.47 (s, 3H), 3.91 (s, 3H), 7.07 (d, 2H), 7.40 (d, 2H), 7.65 (d, 2H), 7.72 (d, 2H). Found: C, 30.90; H, 2.62; S, 6.06; Cl, 32.75%. Calcd for $C_{14}H_{14}O_2SSbCl_5$; C, 30.83; H, 2.59; S, 5.88; Cl, 32.51%. When the complex was subjected to column chromatography (silica gel–chloroform), *p*-anisyl *p*-tolyl sulfoxide (22%) was obtained.

In a similar way, when stannic chloride was used as the catalyst in the reaction, the sulfoxide was also obtained (see Table 1).

Reaction of I with Anisole in Carbon Disulfide in the Presence of Boron Trifluoride Etherate. To a solution of I (4.36 g, 25 mmol) and anisole (2.70 g, 25 mmol) in carbon disulfide (20 ml) was added boron trifluoride etherate (3.9 g, 28 mmol)

10) K. Kurzer, "Organic Syntheses," Coll. Vol. IV, p. 937 (1964).
11) The preparation of the corresponding optically active sulfoxide has been reported, K. K. Andersen, W. Gaffield, N. E. Papanikolaou, J. W. Foley, and R. I. Perkins, *J. Amer. Chem. Soc.*, **86**, 5637 (1964).

at room temperature. The solution was stirred for 24 hr at room temperature and then heated under reflux for 1 hr. After the removal of the carbon disulfide by distillation, morpholine (5 ml) was added, and then the reaction mixture was poured into water. The mixture was extracted with chloroform. After the removal of the chloroform and excess morpholine under reduced pressure, the oily residue was recrystallized from ether to give *N*-(*p*-toluenesulfonyl)morpholine (0.35 g, 11%). A glpc of the remaining residue after the removal of the ether indicated the presence of *p*-anisyl *p*-tolyl sulfide (46%).

In a similar way, when equimolar amounts of zinc chloride and a catalytic amount of iron powder were used as catalyst in the reaction, the sulfide was also obtained (see Table 1).

Reaction of I with Anisole in the Absence of a Catalyst. A solution of anisole (27 g, 250 mmol) and I (4.36 g, 25 mmol) was heated under reflux for 3 hr. Morpholine (5 ml) was added to the reaction mixture, and then it was poured into water. The mixture was treated in the same manner described above. The results were recorded in Table 1.

Reduction of II with I. The general procedures were as follows: equimolar amounts of Lewis acid and *p*-anisyl *p*-tolyl sulfoxide were added to carbon disulfide, and the mixture was stirred for 2 hr at room temperature. Then equimolar amounts of I were added, and the mixture was stirred for 24 hr at room temperature, followed by refluxing for 1 hr. Morpholine was then added to the mixture. After the hydrolysis of the mixture with ice-water, the organic layer was analyzed by glpc. The results are summarized in Table 2.

TABLE 2. REDUCTION OF *p*-ANISYL *p*-TOLYL SULFOXIDE WITH *p*-TOLUENESULFINYL CHLORIDE

Catalyst	Molar ratio Cat/I	Yield (%)	
		III	V
None	—	62	69
Fe	0.01	76	50
$AlCl_3$	1.1	0	
$BF_3 \cdot OEt_2$	1.1	63	
$ZnCl_2$	1.1	59	

BULLETIN OF THE CHEMICAL SOCIETY OF JAPAN, VOL. 46, 3617—3618 (1973)

Rearrangement of Potassium *o*-Hydroxybenzoate as Revealed by Microthermal Analyses

Koki OTA

Department of Chemistry, Kyushu Institute of Technology, Sensui-cho, Tobata-ku, Kitakyushu 804

(Received June 5, 1972)

It is well-known that potassium *o*-hydroxybenzoate (mono-potassium salicylate, SA–K), the main product of the Kolbe-Schmitt reaction, undergoes rearrangement ultimately to di-potassium *p*-hydroxybenzoate (POB–K_2).[1]

$$2SA\text{–}K \longrightarrow POB\text{–}K_2 + PhOH + CO_2 \quad (1)$$

The following reaction schemes were suggested by Ueno and Muramoto for the thermal behavior of SA–K.[2]

$$\begin{aligned} &SA\text{–}K \longrightarrow PhOK + CO_2 \\ &SA\text{–}K + PhOK \longrightarrow SA\text{–}K_2 + PhOH \quad (2) \\ &SA\text{–}K_2 \longrightarrow POB\text{–}K_2 \end{aligned}$$

However, we found by means of microthermal analysis that the thermal reaction of SA–K cannot be satisfactorily interpreted by the above schemes and a hydroxy dicarboxylic acid exists as an intermediate of the rearrangement reaction.

We undertook to elucidate the mechanism of the rearrangement by a combination of micro differential thermal analysis (DTA), detection and analysis of evolved gas, thermogravimetry (TG), and UV analysis.

Measurements were carried out in a stream of N_2. The results of thermal analyses are shown in Fig. 1.

Small, sharp DTA peaks 1, 2, and 3 in a large endothermic background and the three corresponding peaks of generated gases were observed. The amounts of CO_2 and PhOH simultaneously evolved were determined. It is evident from the analysis of the residues that peak 1 is partly due to the formation of 4-hydroxy isophthalic acid (4-OIP).

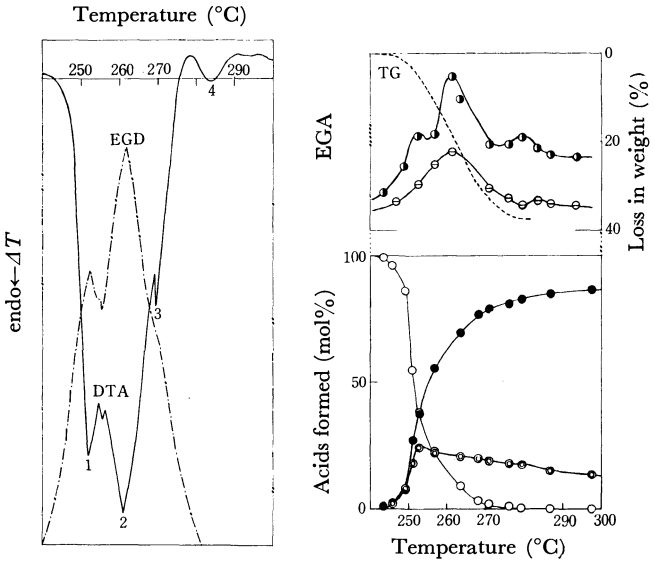

Fig. 1. Rearrangement of SA-K in N_2 stream.
⊖ CO_2, ◑ PhOH, ○ SA, ● POB, ◎ 4-OIP

The formation rate of POB increases greatly at temperatures between peaks 1 and 2. CO_2 and gaseous

1) C. A. Buehler and W. E. Cate, "Organic Synthesis," Coll. Vol. II, (1950), p. 341.

2) R. Ueno and Y. Muramoto, *Kogyo Kagaku Zasshi*, **64**, 1317 (1961).

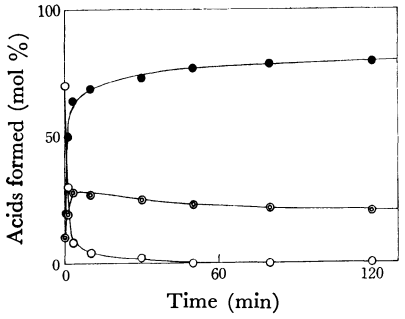

Fig. 2. Rearrangement of SA–K at 250 °C (N_2 stream).
○ SA, ● POB, ◎ 4-OIP

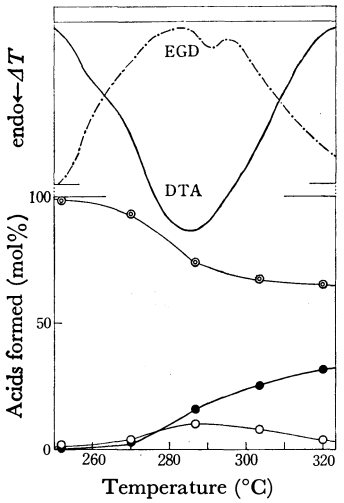

Fig. 3. Thermal reaction of 4-OIP–K_2 in N_2 stream.
○ SA, ● POB, ◎ 4-OIP

PhOH are evolved vigorously at about the same temperature (peak 2). These findings indicate that decarboxylation of SA takes place together with rearrangement of SA to POB. The changes of the DTA curve from peak 2 to peak 3 are characterized by the decrease in gases evolved, a loss in quantity of 4-OIP and the increasing amount of POB, suggesting a conversion of 4-OIP into POB. The curve TG shows that 37.0—37.4% of the original weight was lost (the theoretical value of Eq. (1) is 39.2%). This coincides with the result where acids formed contain 13—19% 4-OIP.

A small decrease in the TG curve at temperatures above 270 °C suggests that evolution of gases and the formation of POB are almost complete. When the DTA curve is restored to the initial level, the remaining amount of SA is about zero.

After this, the formation of POB occurs slightly from 4-OIP with small amounts of evolved gases as shown by evolved gas analysis and UV analysis.

It seems that the rearrangement of SA–K proceeds partly through the formation of 4-OIP–K_2. For the sake of confirmation, the effect of reaction time at 250 °C on the reaction of SA–K was investigated.

The result is shown in Fig. 2.

At the initial stage of reaction, POB is formed and SA–K decomposes rapidly. This confirms the reaction route from SA–K to POB.[2] However, 4-OIP is also formed in this period and later slowly decomposes. This also confirms the view that the reaction proceeds from SA-K to POB *via* 4-OIP as a reaction intermediate, although 4-OIP is fairly stable under such conditions. It was confirmed that 4-OIP is formed in the thermal reaction of SA–K and is rearranged into POB at a lower rate.

The results for 4-OIP are shown in Fig. 3. We see that 4-OIP–K_2 undergoes rearrangement to POB and SA, and then SA–K_2 is converted into POB–K_2 at high temperatures. The amount of POB–K_2 formed nearly equals the loss of 4-OIP–K_2 (in weight). Evolution of a small amount of PhOH and excess CO_2 was observed (peak 4, Fig. 1).

The following reaction scheme is proposed.

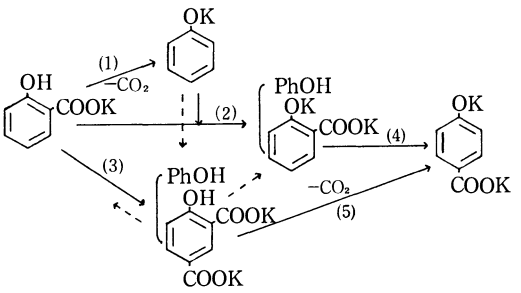

The reaction rate of step (1) is high, step (2) being coupled with (1). Step (3) occurs in the earlier stage of reaction. The rate of rearrangement (4) is high, and that of (5) rather low. For the completion of reaction, it is necessary to remove PhOH and CO_2 formed.

Experimental

Sample. SA–K was prepared as reported previously[3] and 4-OIP–K_2 by purification of 4-OIP (Tokyo Kasei Kogyo Ltd.).

Apparatus. A Shimadzu EGD-20 and DT-GC system was used. TG was recorded with a TGC-20. Gas analysis was performed by gas-chromatography (GC). GC columns were packed with Shimalite-Q, MS-5A and active carbon for measurement of CO_2 and Shimalite-W (DEGS 10%+ H_3PO_4 1%) for PhOH.

QV-50 was used for UV analysis.

Methods. A sample (*ca.* 5 mg) was accurately weighed and set in an Al-sample holder. The heating rate was 10 °C/min.

The flow rate of gas was 30 ml/min, being regulated in the range 10—60 ml/min, when necessary.

The author would like to thank Dr. M. Senō, Tokyo University, for guidance and encouragement and Dr. T. Seiyama, Kyushu University, for advice.

3) K. Ota and I. Hirao, *Yuki Gosei Kagaku Kyokai Shi*, **28**, 426 (1970).

BULLETIN OF THE CHEMICAL SOCIETY OF JAPAN, VOL. 46, 3619—3620 (1973)

An *ab initio* MO Study of the Hydrogen Bond in NH_3·HF

Shinichi YAMABE, Shigeki KATO, Hiroshi FUJIMOTO, and Kenichi FUKUI
Faculty of Engineering, Kyoto University, Sakyo-ku, Kyoto 606

(Received April 13, 1973)

The structure and properties of the hydrogen bond have been of long-standing interest to both theoretical and experimental chemists.[1] Especially by the use of the molecular orbital (MO) method, many studies have been carried out of relatively simple systems including, for example, the O—H···O, N—H···N, N—H···F bonds.[2]

Among the systems, a mixed dimer, NH_3···HF, is regarded as a strong complex, compared with such other dimers as $(NH_3)_2$ and $(HF)_2$. The several geometries of the complex were extensively studied by Kollman and Allen,[3] who found the *linear* structure to be the most stable one.

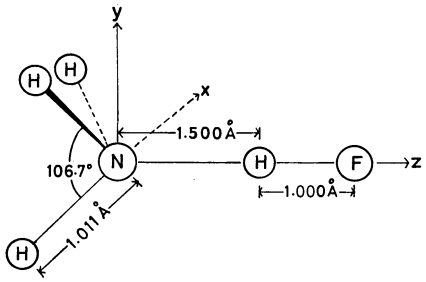

Fig. 1. The geometry of the NH_3·HF complex taken in this calculation from Ref. 3.

We thought it would be an interesting subject to detect the nature of the *strong* N···H bond in Fig. 1, taken from the results of Ref. 3. In order to analyze this in the frame of the MO method, we have used the technique which regards the MO's of NH_4F as the product of the orbital mixing of the MO's of NH_3 with those of HF.[4,5] In other words, the occupied MO's of the NH_4F system (Ψ_g, $g=1, 2, \cdots, 10$) are approximated as linear combinations of occupied MO's (a_i, $i=1, 2, \cdots, 5$ in NH_3 and b_k, $k=1, 2, \cdots, 5$ in HF) and unoccupied MO's (a_j, $j=6, 7, 8$ in NH_3 and b_l, $l=6$) of its two subsystems:

$$\Psi_g = \sum_{i=1}^{5} C_i^{(g)} a_i + \sum_{j=6}^{8} C_j^{(g)} a_j + \sum_{k=1}^{5} C_{k+8}^{(g)} b_k + C_{l+8}^{(g)} b_l \quad (1)$$

The MO's used here are constructed by means of the minimal-basis set of Slater-type Orbitals (STO's) expanded into *three* Gaussian-type Orbitals (GTO's).[6,7] Then, all the integrals of STO's necessary for composing the Fock matrix can easily be evaluated by this expansion.

In Table 1 the calculated results of the MO's are shown in relation to the equilibrium geometry in Fig. 1, except that the configuration of NH_3 is taken from the experimental one.[8] ($-E_K/E_T$) shows satisfactory optimization with respect to the exponents of STO's[9] adopted here (Virial Theorem).

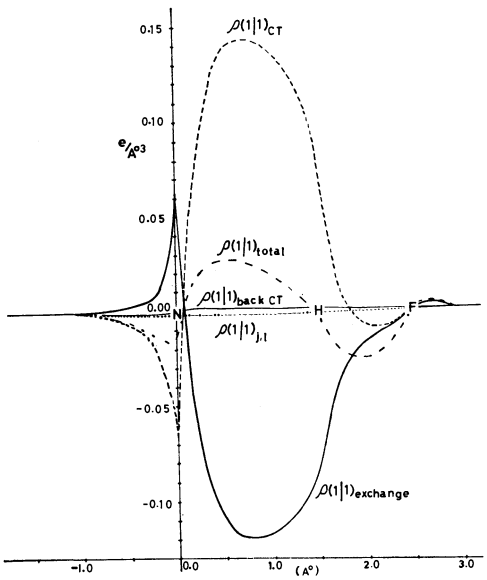

Fig. 2. The profile of the *intermolecular* charge density between NH_3 and HF.

By the use of the calculated MO's, the charge density in the *intermolecular* part as regards the two monomers (N···H region) can be obtained in the frame of the above-mentioned technique. In Fig. 2 the profile of the intermolecular charge density ($\rho(1|1)_{\text{total}}$), cut n x-y plane, is depicted in the following partitioned form:

$$\rho(1|1)_{\text{total}} = \rho(1|1)_{\text{exchange}} + \rho(1|1)_{\text{CT}} + \rho(1|1)_{\text{back CT}} + \rho(1|1)_{j,l} \quad (2)$$

$$\rho(1|1)_{\text{exchange}} = 2\sum_{g=1}^{10}\Big[\sum_{i=1}^{5}\sum_{k=1}^{5} C_i^{(g)} C_{k+8}^{(g)}\{a_i(1)b_k(1) + b_k(1)a_i(1)\}\Big] \quad (3)$$

$$\rho(1|1)_{\text{CT}} = 2\sum_{g=1}^{10}\Big[\sum_{i=1}^{5} C_i^{(g)} C_{i+8}^{(g)}\{a_i(1)b_i(1) + b_i(1)a_i(1)\}\Big] \quad (4)$$

$$\rho(1|1)_{\text{back CT}} = 2\sum_{g=1}^{10}\Big[\sum_{k=1}^{5}\sum_{j=6}^{8} C_{k+8}^{(g)} C_j^{(g)}\{a_j(1)b_k(1) + b_k(1)a_j(1)\}\Big] \quad (5)$$

1) G. C. Pimentel and A. D. McClellan, "The Hydrogen Bond," W. H. Freeman, San Francisco, Calif. (1960).
2) P. A. Kollman and L. C. Allen, *Chem. Rev.*, **72**, 283 (1972).
3) P. A. Kollman and L. C. Allen, *J. Amer. Chem. Soc.*, **93**, 4991 (1971).
4) H. Fujimoto, S. Kato, S. Yamabe, and K. Fukui, *J. Chem. Phys.*, in press.
5) H. Baba, S. Suzuki, and T. Takemura, *ibid.*, **50**, 2078 (1969).
6) K. O-ohata, H. Taketa, and S. Huzinaga, *J. Phys. Soc. Jap.*, **21**, 2306 (1966).
7) H. Taketa, S. Huzinaga, and K. O-ohata, *ibid.*, **21**, 2313 (1966).
8) J. D. Swalen and J. A. Ibers, *J. Chem. Phys.*, **36**, 1914 (1962).
9) W. J. Hehre, R. F. Stewart, and J. A. Pople, *ibid.*, **51**, 2657 (1969).

TABLE 1. THE RESULTS OF MO CALCULATION[a)]

NH_3		HF		NH_4F	
a_i	$1a_1$ −15.3058	b_k	$1a_1$ −25.8878	Ψ_g	$1a_1$ −25.6837
	$2a_1$ −1.1050		$2a_1$ −1.4523		$2a_1$ −15.3799
	1e −0.5680		$3a_1$ −0.5560		$3a_1$ −1.3270
	$3a_1$ −0.3651		1e −0.4555		$4a_1$ −1.1657
a_j	$4a_1$ 0.6607	b_l	4a 0.5520		1e −0.6260
	2e 0.7151				$5a_1$ −0.5540
					$6a_1$ −0.3363
					2e −0.3193
					$7a_1$ 0.6080
					3e 0.6560
					$8a_1$ 0.8199
$E_K=55.2705$		$E_K=97.9823$		$E_K=153.6836$	
$E_T=-55.4450$		$E_T=-98.5556$		$E_T=-154.0059$	
$(-E_K/E_T)=0.9969$		$(-E_K/E_T)=0.9942$		$(-E_K/E_T)=0.9979$	

a) E_K means the kinetic energy, and E_T the total energy. The exponents of STO's are the *standard* values by Pople *et al.* in Ref. 9. The signs of MO's (a_1 and e) are termed according to the irreducible representation of C_{3v} symmetry at the whole system. Energies are in atomic unit.

$$\rho(1|1)_{j,l} = 2\sum_{g=1}^{10}[\sum_{j=6}^{8} C_j^{(g)} C_{l+8}^{(g)}\{a_j(1)b_l(1)+b_l(1)a_j(1)\}] \quad (6)$$

First, in this figure $\rho(1|1)_{exchange}$ shows a negative component which is unfavorable for the bond formation and is originated from the orbital interaction between the occupied orbitals in NH_3 and the occupied orbitals in HF. The operation of this orbital interaction essentially corresponds to the *exchange* repulsion force, shown in the example of the helium molecule.

On the other hand, $\rho(1|1)_{CT}$ stands for the density caused by the charge-transfer (CT) interaction between the occupied orbitals in NH_3 and the unoccupied orbitals in HF; it has enough density to strengthen the N···H bond. The mixing of the highest occupied (HO) MO, *i.e.*, $3a_1$ in NH_3, with the lowest unoccupied (LU) one, *i.e.*, $4a_1$ in HF, is found to contribute remarkably to this available density for the N···H bond (96.31% of $\int\rho(1|1)_{CT}dv_1$).

The residual two terms in Eq. (2), $\rho(1|1)_{back\ CT}$ and $\rho(1|1)_{j,l}$, have no serious effect on the intermolecular charge density:

$$|\rho(1|1)_{back\ CT}|<0.0016\ e/A^{\circ 3},\ |\rho(1|1)_{j,l}|<0.0003\ e/A^{\circ 3} \quad (7)$$

Here, the former corresponds to the density by the *back donation* from HF to NH_3, and the latter is the density coming from the orbital interaction between both originally unoccupied MO's in NH_3 and HF.

Thus, we come to the conclusion, apart from the electrostatic effect here, that among the several modes of orbital interaction, the particular HOMO–LUMO interaction supplies the considerable charge density in the intermolecular N···H region which overcomes the negative exchange density and results in the stabilization of the complex system.

One of the authors (S. Y.) especially grateful to Mr. Kazuhiro Ishida for his helpful advice in making the FORTRAN program of MO calculations.

We wish also to express our appreciation to the Data Processing Center of Kyoto University for its generosity in letting us use the FACOM 230-60 computer.

BULLETIN OF THE CHEMICAL SOCIETY OF JAPAN, VOL. 46, 3621—3622 (1973)

Methyl Signals in the PMR Spectra of Nigakilactones and Nigakihemiacetals

Tatsushi MURAE, Tôru IKEDA, Akihiko SUGIE, Tadaaki NISHIHAMA, Takahiko TSUYUKI, and Takeyoshi TAKAHASHI

Department of Chemistry, Faculty of Science, The University of Tokyo, Hongo, Bunkyo-ku, Tokyo 113

(Received May 4, 1973)

In connection with the structure determination of bitter principles isolated from *Picrasma ailanthoides* Planchon (*P. quassioides* Bennett),[1,2] the PMR spectra of nigakilactones A (I), B (II), C (III), D (IV) (= quassin[3]), E (V), F (VI),[1a,b] H (VII),[1c] J (VIII), K (IX), L (X), M (XI), and N (XII)[1d] were measured. The spectra of nigakihemiacetals A (XIII), B (XIV) (=neoquassin[3]), and C (XV)[1c] were also recorded. The PMR spectra of picrasin B (XVI)[2a] (=nigakilactone I[1c]), picrasin D (XVII),[2b,4] picrasin E (XVIII),[2b,4] a monoacetate of nigakilactone J (XIX),[1d] a deacetyl derivative of nigakilactone J (XX),[1d] and dehydroquassin (XXI)[3] were determined as references.

All of these compounds have a quassolidane skeleton (XXII) which possesses four methyl groups at C-4, C-8, C-10, and C-13. We wish to describe an assignment of the methyl signals of these compounds. The result is summarized in Table 1.

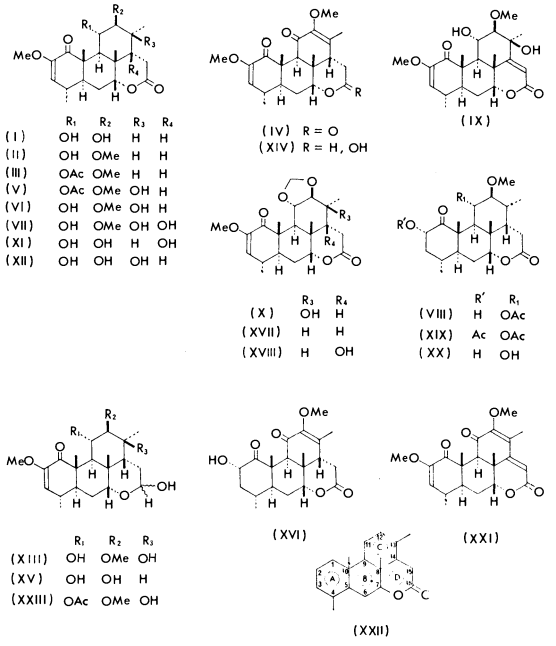

	R_1	R_2	R_3	R_4
(I)	OH	OH	H	H
(II)	OH	OMe	H	H
(III)	OAc	OMe	H	H
(V)	OAc	OMe	OH	H
(VI)	OH	OMe	OH	H
(VII)	OH	OMe	OH	OH
(XI)	OH	OH	H	OH
(XII)	OH	OH	OH	H

(IV) R = O
(XIV) R = H, OH

(IX)

	R_3	R_4
(X)	OH	H
(XVII)	H	H
(XVIII)	H	OH

	R′	R_1
(VIII)	H	OAc
(XIX)	Ac	OAc
(XX)	H	OH

	R_1	R_2	R_3
(XIII)	OH	OMe	OH
(XV)	OH	OH	H
(XXIII)	OAc	OMe	OH

(XVI)

(XXI)

(XXII)

Table 1. PMR spectral data on methyl signals

Compound	4-Me	8-Me	10-Me	13-Me	Compound	4-Me	8-Me	10-Me	13-Me
I	1.10 d (J=6)	1.24 s	1.42 s	1.01 d (J=6.5)	IV	1.11 d (J=7)	1.18 s	1.54 s	1.85 s
II	1.13 d (J=6.5)	1.21 s	1.45 s	1.00 d (J=6.5)	XIV	1.07 d (J=6)	1.05 s	1.49 s	1.83 s
III[e]	1.10 d (J=7)	1.28 s	1.28 s	1.04 d (J=7)	XVI	0.93 d (J=6)	1.20 s[f]	1.45 s[f]	1.91 s
V[e]	1.08 d (J=7)	1.52 s	1.26 s	1.24 s	XXI	1.15 d (J=6)	1.27 s	1.53 s	2.00 s
VI	1.11 d (J=7)	1.46 s	1.46 s	1.22 s	IX	1.18 d (J=7)	1.50 s[d]	1.45 s[d]	1.48 s[d]
VII	1.15 d (J=7.5)	1.35 s	1.50 s	1.27 s	X	1.12 d (J=7)	1.53 s	1.47 s	1.36 s
XI	1.17 d (J=6)	1.20 s	1.50 s	1.10 d (J=6)	XVII	1.10 d (J=7)	1.28 s	1.43 s	1.10 d (J=7)
XII	1.16 d (J=7)	1.53 s[b]	1.50 s[b]	1.28 s	XVIII	1.10 d (J=7)	1.22 s	1.45 s	1.10 d (J=7)
VIII	0.90 d (J=6)	1.28 s[c]	1.26 s[c]	1.04 d (J=7)	XIII	1.11 d (J=7)	1.34 s	1.44 s	1.20 s
XIX	0.96 d (J=6)	1.27 s	1.32 s	1.03 d (J=7)	XV	1.13 d (J=6)	1.16 s	1.45 s	1.05 d (J=7)
XX	0.92 d (J=6)	1.22 s	1.40 s	1.04 d (J=6)	XXIII	1.03 d (J=7)	1.36 s	1.24 s	1.20 s

a) Chemical shifts and coupling constants are expressed in δ value and in Hz, respectively. b, c) Values may be reversed. d) Values may be interchanged. e) These assignments are in accord with those obtained from PMR experiments including NOE.[1b] f) Reversed values had been described.[8]

The method utilized for steroids[5] and triterpenes[6] was applied to the present investigation,[7] admitting that the effect caused by a change in a functional group is particularly observed on the signals of methyl groups situated nearly to this functional group, and the effect diminishes rapidly with the distance.

Methyl Group at C-4. A secondary methyl group at C-4 resonates at δ 1.07—1.17 as a doublet for the compounds with a methylated diosphenol moiety in ring A (I—VII, IX—XV, XVII, XVIII, and XXI). A doublet signal of this methyl group appears at δ 0.90—0.96 when ring A is saturated (VIII, XVI, XIX, and XX).

The signal due to the methyl group at C-4 is not practically affected by a structural change in rings C and D.

Methyl Group at C-13. A doublet at δ 1.00—1.10 is observed for a methyl group at C-13 of the compounds with R_3=H (I—III, VIII, XI, XV, and XVII—XX).

1) a) T. Murae, T. Tsuyuki, T. Ikeda, T. Nishihama, S. Masuda, and T. Takahashi, *Tetrahedron*, **27**, 1545 (1971); b) T. Murae, T. Ikeda, T. Tsuyuki, T. Nishihama, T. Takahashi, and K. Tori, *Tetrahedron Lett.*, **1971**, 3897; c) T. Murae, T. Tsuyuki, T. Ikeda, T. Nishihama, S. Masuda, and T. Takahashi, *Tetrahedron*, **27**, 5147 (1971); d) T. Murae, A. Sugie, T. Tsuyuki, S. Masuda, T. Takahashi, *ibid.*, **29** 1515 (1973).

2) a) H. Hikino, T. Ohta, and T. Takemoto, *Chem. Pharm. Bull.* (Tokyo), **18**, 219, 1082 (1970); b) *Idem, ibid.*, **19**, 212, 2203, 2211, 2651 (1971).

3) Z. Valenta, S. Papadopoulos, and C. Podešva, *Tetrahedron*, **15**, 100 (1961); Z. Valenta, A. H. Gray, D. E. Orr, S. Papadopoulos, and C. Podešva, *ibid.*, **18**, 1433 (1962); W. A. C. Brown and G. A. Sim, *Proc. Chem. Soc.*, **1964**, 293.

4) The PMR spectra of XVII and XVIII had been determined in pyridine by Hikino *et al.*[2b] Measurements in $CDCl_3$ were effected for the present communication.

5) *Cf.* N. S. Bhacca and D. H. Williams, "Application of NMR Spectroscopy in Organic Chemistry," Holden-Day Inc., San Francisco (1964), Chapter 2.

6) *Cf.* J. M. Lehn and G. Ourisson, *Bull. Soc. Chim. Fr.*, **1962**, 1137; Y. Tanahashi, Y. Moriyama, T. Takahashi, F. Patil, and G. Ourisson, *ibid.*, **1966**, 2374, and references therein.

7) PMR spectral measurements using $Eu(dpm)_3$ as a shift reagent resulted in coordinations of the reagent to at least two positions of a compound. The obtained spectra gave no information.

8) B. Viala and J. Polonsky, *C. R. Acad. Sci. Paris, C*, **271**, 410 (1970).

When a hydroxyl group is located on C-13, this methyl signal is shifted downfield (Δ+0.20—+0.27 ppm) and resonates as a singlet (compare V with III, VI with II, XII with I, and X with XVII). An introduction of a double bond between C-14 and C-15 causes a downfield shift (Δ+0.26 ppm) of this methyl signal (compare IX with VI).

The signal due to an olefinic methyl group at C-13 appears at δ 1.83—1.91 as a singlet for the compounds with a methylated diosphenol moiety in ring C (IV, XIV, and XVI). This olefinic methyl signal is shifted downfield (Δ+0.15 ppm) on introduction of a double bond between C-14 and C-15 (compare XXI with IV).

Practically, no effect is observed for the signal due to the methyl group at C-13, when a structural change is effected in ring A.

Methyl Group at C-10. A tertiary methyl group at C-10 appears at δ 1.40—1.50 as a singlet when the substituent at C-11 is a hydroxyl group (I, II, VI, VII, IX, XI—XIII, XV, and XX). Similar chemical shift values are observed for the methyl signal of the compounds with a methylene dioxy grouping (δ 1.43—1.47; X, XVII, and XVIII), and for the signal of the substances with a methylated diosphenol moiety in ring C (δ 1.45—1.54; IV, XIV, XVI, and XXI).

The signal due to the methyl group at C-10 is not affected by introduction of a hydroxyl group at C-13 (compare V with III, and VI with II) nor by location of a hydroxyl group on C-14 (compare VII with VI). An upfield shift (Δ—0.14——0.20 ppm) is observed for this methyl signal on acetylation of the hydroxyl group at C-11 (compare III with II, V with VI, and VIII with XX). Practically, no effect is observed for this signal on methylation of the hydroxyl group at C-12 (compare II with I, and VI with XII).

Methyl Group at C-8. A singlet at δ 1.16—1.28 is observed for a tertiary methyl group at C-8 of the compounds with both a hydroxyl (or an acetoxyl) group at C-11 and the substituent R_3=H (I—III, VIII, XI, XV, XIX, and XX).

An introduction of a hydroxyl group at C-13 causes a downfield shift (Δ+0.24—+0.29 ppm) of the signal due to the methyl group at C-8; this methyl group and the hydroxyl group at C-13 are in a 1,3-diaxial relationship (compare V with III, VI with II, XII with I, and X with XVII). Some downfield shifts are observed for this methyl signal on acetylation of the hydroxyl group at C-11 (Δ+0.06—+0.07 ppm; compare III with II, V with VI, and VIII with XX), on formation of a methylene dioxy ring (Δ+0.07 ppm; compare X with VI, and XVII with II), and on introduction of a double bond between C-14 and C-15 (Δ+0.04—+0.09 ppm; compare IX with VI, and XXI with IV). The methyl signal suffers some upfield shifts when a hydroxyl group is substituted on C-14 (Δ—0.04——0.11 ppm; compare VII with VI, XI with I, and XVIII with XVII), and when a hydroxyl group at C-12 is methylated (Δ—0.03——0.07 ppm; compare II with I, and VI with XII). Replacement of a lactone grouping in ring D by a hemiacetal moiety causes an upfield shift (Δ—0.08——0.13 ppm) of this methyl signal (compare VI with XIII, I with XV, and IV with XIV). The signal due to the methyl group at C-8 is not affected by a structural change in ring A (compare II with XX, III with VIII, and III with XIX).

Nigakihemiacetal D. As an example of application of the result shown above, the structure determination of a new bitter principle, nigakihemiacetal D (XXIII), isolated recently from *Picrasma ailanthoides* Planchon is described.

The presence of an acetoxyl, a hydroxyl and two methoxyl groups, one secondary and three tertiary methyl groups, and a hemiacetal[1c] and an α,β-unsaturated ketone[1a] moieties was suggested for XXIII from its spectral data (Experimental) and the molecular formula ($C_{24}H_{36}O_8$). As the spectral data of XXIII are similar to those of bitter substances hitherto isolated[1] from the same plant, XXIII is assumed to be a hemiacetal derivative related to the quassolidane (XXII).

As the methyl groups at C-8 and C-10 are tertiary ones (*Cf.* XXII), a secondary methyl resonating at δ 1.03 (J=7 Hz) must locate on either C-4 or C-13; the latter case is excluded as shown later. Therefore, this signal can be assigned to the methyl group at C-4 (not on a saturated ring A) (*Cf.* I—VII, IX—XV, XVII, XVIII, XXI). A tertiary methyl signal at δ 1.20 can be best assigned to the methyl group at C-13 to which a hydroxyl group is substituted (*Cf.* V—VII, XII, XIII). Chemical shift value (δ 1.36) observed for another tertiary methyl signal shows that this methyl group is in a 1,3-diaxial relationship with the hydroxyl group at C-13 and located on C-8 (*Cf.* XIII; with a hemiacetal grouping in ring D). The UV maximum at 262.5 nm[1a,c] of XXIII provides support for the location of an acetoxyl group on C-11. Thus a tertiary methyl signal at δ 1.24 could be assigned to the methyl group at C-10 (*Cf.* III, V; with an acetoxyl group at C-11).

These observations can be well interpreted based on a hemiacetal structure related to nigakilactone E (V) and lead to the structure XXIII for nigakihemiacetal D. This was confirmed by the formation of nigakilactone E (V)[1a] on oxidation of this hemiacetal (XXIII) with silver oxide.

Experimental

PMR spectra were taken on a JEOL JNM-C-60 spectrometer at 60 MHz in $CDCl_3$ solution containing TMS as an internal standard.

Isolation of XXIII. Extraction and subsequent separation procedures of crude material (200 g) from the stemchips (160 kg) of *Picrasma ailanthoides* Planchon were decribed elsewhere.[1d] After chromatographic separation of the fractions 2 and 3[1d] containing picrasin D, the Fractions 4—6 were eluted with acetone-benzene (1: 2) to give nigakihemiacetal D (XXIII) (15 mg), amorphous solid, $[\alpha]_D$+46° (c 0.1, MeOH); UV (MeOH): λ_{max} 262.5 nm (ε 2000), IR (Nujol): 3450, 1735, 1708, 1640, 1245 cm^{-1}; PMR ($CDCl_3$): δ 1.93 (3H, s; -OCOC$\underline{H}_3$), δ 3.27 (1H, d, J=9 Hz, -C$\underline{H}$OCH$_3$), δ 3.51 (3H, s; -OC$\underline{H}_3$), δ 3.56 (3H, s; -OCH$_3$), δ 3.72 [1H, m; -C$\underline{H}$-O-CH(OH)-], δ 5.44 (1H, q; J=11 and J=9 Hz; -C$\underline{H}$-OCOCH$_3$), δ 5.07 (1H, d, J=2.5 Hz; -C=C$\underline{H}$).

Oxidation of XXIII with Silver Oxide. Compound XXIII (10 mg) was treated with silver oxide as usual[1d] to give nigakilactone E (V)[1a,b] (7mg) identified by IR, PMR, $[\alpha]_D$ and tlc.

BULLETIN OF THE CHEMICAL SOCIETY OF JAPAN, VOL. 46, 3623—3624 (1973)

Kinetics and Mechanism of the Oxidation of Aliphatic Alcohols by Acid Permanganate

Kalyan K. BANERJI*

The Dyson Perrins Laboratory, University of Oxford, Oxford OX1 3QY, U.K.

(Received August 25, 1972)

Barter and Littler[1] suggested, on the basis of similar rate laws, that the oxidation of alcohols by acid permanganate, bromine and other two-electron oxidants follow similar mechanisms. The oxidation of alcohols by bromine involves removal of hydride ion in the rate-determining step.[2] A similar mechanism also was suggested for the oxidation of benzyl alcohol by acid permanganate.[3] The chromic acid oxidation, another two-electron process, however, is proposed to involve a proton transfer.[4] No conclusive evidence is available in literature about the form of hydrogen removed from the alcohol in permanganate oxidation.

If α-C–H bond is ruptured in the rate-determining step, then an unequivocal evidence about the flow of electrons leading to the transition state can be obtained by studying the effect of polar substituents on the rate of the oxidation of a suitable alcohol.

This paper reports the kinetics of the oxidation of some primary alcohols and evaluates the reaction constant. The mechanistic conclusions are discussed.

Results

Product Analysis. The oxidation of ethanol by acid permanganate eventually gives acetic acid. An estimation of the carboxylic acid formed indicated the following stoichiometry:

$$4MnO_4^- + 12H^+ + 5CH_3CH_2OH \longrightarrow 5CH_3COOH + 4Mn^{+2} + 11H_2O$$

Rate Laws. The oxidation of alcohols by acid permanganate is autocatalytic and this may be due to the effect of Mn(III)/Mn(IV). Addition of sodium fluoride suppresses the autocatalysis, though it does not affect the initial rate. Therefore, an excess of sodium fluoride was added to each reaction mixture.

The reaction were followed under pseudo-first-order conditions by keeping a large excess of the alcohol over permanganate. The rate of disappearance of permanganate, under these conditions, is of first order. The order with respect to the alcohol is also one (Table 1). The rate varies linearly with acidity, at constant ionic strength.

Table 1. Substrate dependence of the reaction rate

$[KMnO_4]$ 1×10^{-4} M	$[H^+]$ 1.0M	[NaF] 0.01M	Temp. 25 °C		
10^2 [EtOH]M	1.0	2.0	4.0	6.0	8.0
10^4 $k_1(s^{-1})$	9.55	19.0	37.5	57.0	76.8
10^2 k_1/[EtOH]	9.55	9.50	9.40	9.50	9.60

The rate constants for the oxidation of ethanol and α,α-dideuterioethanol at 30 °C are $10^2k=13.0$ and 5.0 l^2 mol^{-2} s^{-1} respectively. The kinetic isotope effect, $k_H/k_D=2.60$ at 30 °C.

The oxidation of ethanol, under nitrogen, failed to induce the polymerization of acrylonitrile. The formation of free radicals is, therefore, unlikely.

The rate constants for the oxidation of ethanol in deuterium oxide and in water at 30 °C are $10^2k=12.5$ and 13.0 l^2 mol^{-2} s^{-1} respectively. The solvent isotope effect, $k(H_2O)/k(D_2O)=1.04$.

The rate of the acid permanganate oxidation of ten primary aliphatic alcohols were obtained at different temperatures and the activation parameters evaluated (Tables 2 and 3).

Table 2. Oxidation of alcohols, RCH_2OH, by acid permanganate

R	10^4 k (l^2 mol^{-2} s^{-1})				
	25 °C	30 °C	35 °C	40 °C	45 °C
CH_3	955	1300	1740	2300	3100
C_2H_5	1410	1910	2500	3300	4360
n-C_3H_7	1730	2300	3000	4000	5100
i-C_3H_7	2340	3100	4000	5100	6500
t-C_4H_9	3850	4920	6200	7800	9800
C_6H_{11}(cyclohexyl)	1820	2400	3150	4070	2550
H	87.0	128	182	257	370
CH_3OCH_2	72.5	110	157	240	330
$ClCH_2$	6.90	10.7	16.6	25.0	38.0
$BrCH_2$	8.50	13.2	20.0	28.8	43.0

Table 3. Activation parameters for the oxidation of alcohols, RCH_2OH, by acid permanganate

R	CH_3	C_2H_5	n-C_3H_7	i-C_3H_7	t-C_4H_9
ΔH^* kcal/mol	11.0	10.5	10.2	9.6	8.8
$-\Delta S^*$ e.u.	26.4	27.9	28.5	29.9	31.6
R	C_6H_{11}	H	CH_3OCH_2	$ClCH_2$	$BrCH_2$
ΔH^* kcal/mol	10.0	13.5	14.0	16.0	15.8
$-\Delta S^*$ e.u.	29.1	23.3	22.0	20.0	20.2

Discussion

The linear dependence of the oxidation rate on acidity, may be attributed to the protonation of permanganate anion to give permanganic acid, a more

* Commonwealth Postdoctral Scholar, on leave from University of Jodhpur, India.

1) R. M. Barter and J. S. Littler, *J. Chem. Soc., Ser., B*, **1967**, 205.

2) P. Aukett and I. R. L. Barker, *J. Chem. Soc., Perkin II*, **1972**, 568.

3) K. K. Banerji and P. Nath, This Bulletin, **42**, 2038 (1969).

4) K. B. Wiberg, "Oxidation in Organic Chemistry," Part A, Academic Press, New York (1965), p. 159—170.

powerful oxidant.[3,5]

The kinetic isotope effect shown in the oxidation of ethanol is very close to the value obtained by Littler[6] in the oxidation of cyclohexanol ($k_H/k_D=2.41$). It confirms that α-C–H bond is ruptured in the rate-determining step. There is no kinetic evidence that the alcohol and the oxidant are involved in any pre-equilibrium. The formation of a permanganate ester is unlikely in view of the almost equal ease of the oxidation of alcohol and ethers.[1]

No systematic study on the effect of structure in the permanganate oxidation of alcohols has been reported. Barter and Littler reported the rate data of the oxidation of methanol, ethanol and 2-methoxyethanol.[1] However, no reaction constant could be evaluated with those limited data. In the present investigation, the rate of the oxidation of the ten alcohols give a good correlation ($r=0.993$) in the Taft plot with a reaction constant $\rho^*=-2.02\pm0.08$ at 30 °C. The negative ρ^* points to an electron-deficient carbon centre in the transition state. The magnitude of the reaction constant decreases with temperature, as expected.

The activation entropies and enthalpies of the ten compounds are linearly related ($r=0.988$), the value of isokinetic temperature being 650 ± 40 K. Present views do not attach much significance to the value of isokinetic temperature,[7] though a linear correlation between ΔH^* and ΔS^* is usually a necessary condition for the validity of the Taft equation.[2]

The results reported in this paper supports the hydride transfer mechanism. The small magnitude of the solvent isotope effect suggests that the removal of the hydroxylic proton simultaneously with the hydride ion transfer is unlikely and is more so in view of the magnitude of the reaction constant. The polar requirement on the carbinol carbon of hydride release from C–H is opposite to that of proton release from O–H and in a fully concerted process, the reaction constant should be nearer zero.

Experimental

Materials. Methanol, ethanol, 1-propanol, 1-butanol, 2-chloroethanol, 2-methyl 1-propanol, and 2,2-dimethyl 1-propanol were commercial products and were purified by the usual methods. Cyclohexylmethanol,[8] 2-bromoethanol,[9] and 2-methoxyethanol[10] were prepared by the methods described in literature.

α,α-Dideuterioethanol (CH_3CD_2OH) was prepared by the method reported by Kaplan.[11] Perchloric acid (Baker) was used as a source of hydrogen ions. All reagents used were of analytical grade.

Product Analysis. Acetic acid produced in the oxidation of ethanol was estimated colorimetrically as ferric hydroximate.[12]

Kinetic Measurements. The reactions were followed by estimating permanganate spectrophotometrically at 532 nm. The rate constants reported are averages of multiple runs and are reproducible within ±4%.

5) K. K. Banerji, *Z. Naturforsch.*, **27b**, 772 (1972).
6) J. S. Littler, *J. Chem. Soc.*, **1962**, 2190.
7) J. E. Leffler, *J. Org. Chem.*, **31**, 533 (1966).
8) H. Gilman, "Organic Synthesis," Vol. 1, p. 182 (1921).
9) R. A. Rapheal, *J. Chem. Soc.*, **1949**, 44.
10) N. Palomaa, *Ber.*, **42**, 3874 (1909).
11) L. Kaplan, *J. Amer. Chem. Soc.*, **80**, 2639 (1958).
12) J. Mitchell, Jr., "Organic Analysis," Vol. III, Interscience Publishers Inc., New York (1956), p. 63.

BULLETIN OF THE CHEMICAL SOCIETY OF JAPAN, VOL. 46, 3625 (1973)

Synthesis and Rearrangement of Oxanilic Esters Arylhydrazones

A. Sami SHAWALI and M. Kamal AHMAD
Department of Chemistry, Faculty of Science, University of Cairo, Giza, Egypt

(Received February 15, 1973)

The reactivity of phenylcarbamoylarylhydrazidic chlorides (I) with various nucleophiles involving carbon and nitrogen atoms has recently been reported.[1] This communication describes the reaction of I with phenols to get the title compounds (II), which do not seem to have been reported, and the thermal rearrangement of II into III, a new Chapman-like rearrangement[2] in the hydrazone series.

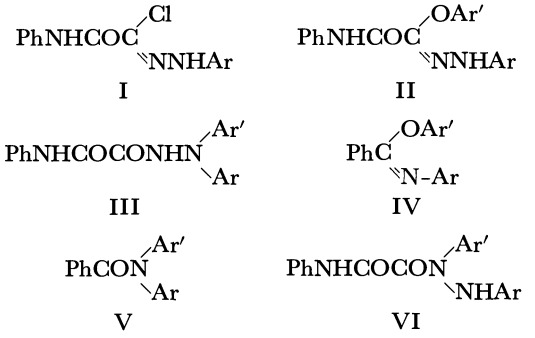

Synthesis of II was most conveniently performed as follows. An equivalent amount of I was added to a suspension of sodium phenolate in benzene. After refluxing the mixture for 30 min, the solvent was distilled off and the residue was crystallized from methanol (Method A). Alternatively, to an ethanolic sodium phenolate solution (prepared by the addition of the appropriate phenol to sodium ethoxide in ethanol) was added an equivalent amount of I with stirring at room temperature. After standing for 24 hr, the mixture was diluted with water and the resulting product was filtered and crystallized from methanol (Method B). By the use of either method it was possible to prepare a series of aryl oxanilate arylhydrazones (IIa—j). The properties of these compounds are given in Table 1. The spectral and elemental analyses support structure II for the products listed.

Aryl imidates (IV) underwent rearrangement on heating to give *N*-aroyldiarylamines (V) (Chapman-rearrangement).[2] Aryl oxanilate arylhydrazones (II) were found to undergo a similar rearrangement to give oxanilic arylhydrazides (III) when refluxed in inert solvents. Thus, when IIa (Ar=C_6H_5; Ar'=4-$CH_3C_6H_4$) was refluxed in nitrobenzene for 4 hr, giving a product which was analyzed as $C_{21}H_{19}N_3O_2$. Its IR spectrum revealed the absence of the C–O–Ar band present in the IR spectra of all compounds in the series II. Furthermore, the UV spectrum of the compound obtained in ethanol differed from that of the starting

Table 1. Aryl oxanilate arylhydrazones (II) and their rearrangement products (III)

Compound No.	Ar	Ar'	Ester II Yield[a] %	Ester II Mp °C	Hydrazide III Yield %	Hydrazide III Mp C°
a	C_6H_5	4-$CH_3C_4H_6$	82	187	80	242
b	4-$CH_3C_6H_4$	C_6H_5	70	188	95	242
c	C_6H_5	4-ClC_6H_4	60	185	87	263
d	4-ClC_6H_4	C_6H_5	45	183	85	263
e	C_6H_5	C_6H_5	63	197	80	271
f	C_6H_5	2-$CH_3C_6H_4$	87	186	83	211
g	C_6H_5	2-ClC_6H_4	56	175	83	194
h	4-BrC_6H_4	C_6H_5	60	197	70	259
i	3-$CH_3C_6H_4$	C_6H_5	70	169	81	215
j	C_6H_5	1-$C_{15}H_7$	72	166	86	246

a) from Method A.

ester IIa, no band characteristic of the hydrazone chlomophore being present. Two possible structures IIIa and VIa (Ar=C_6H_5; Ar'=4-$CH_3C_6H_4$) were formulated. For the sake of confirmation we studied the rearrangement of the isomeric ester IIb (Ar=4-$CH_3C_6H_4$; Ar'=C_6H_5). It was found to give only one product identical with that obtained from IIa. This suggests strongly that the actual structure of the product is IIIa and not VIa. The correctness of such an assignment was further proved by the identity of the product IIIe (Ar=Ar'=C_6H_5) obtained by thermolysis of IIe (Ar=Ar'=C_6H_5) with an authentic sample of *N*-oxanilyl-*N'*,*N'*-diphenylhydrazine prepared by the reaction of oxanilyl chloride with asymmetric diphenylhydrazine.

When a mixture of the iosmeric esters IIa and IIb was heated, it gave only hydrazide IIIa (Ar=C_6H_5; Ar'=4-$CH_3C_6H_4$) in an almost quantitative yield. This indicates that the II—III conversion is an intramolecular rearrangement. The results of thermolysis of the isomeric esters IIc (Ar=C_6H_5; Ar'=4-ClC_6H_4) and IId (Ar=4-ClC_6H_4; Ar'=C_6H_5) either separately or in mixture confirm such a conlcusion.

The foregoing results indicate that the thermal rearrangement of II to III involves a 1,4-shift of an aryl group from oxygen to nitrogen probably *via* a five-membered cyclic transition state of type VII. No formation of VI might be attributed to the lower stability of the four-membered cyclic transition state (VII) required for the formation.

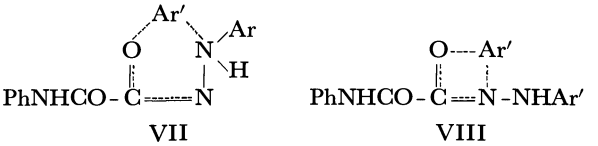

1) A. S. Shawali and A. Osman, *Tetrahedron*, **27**, 2517 (1971).
2) A. W. Chapman, *J. Chem. Soc.*, **1972**, 1743; W. J. Dauben and R. L. Hodgson, *J. Amer. Chem. Soc.*, **72**, 3479 (1950); K. B. Wiberg, *ibid.*, **77**, 2205 (1955).

Group Interactions in Polyelectrolytes. VII.[1] Amination Kinetics of Chloromethylated Polystyrene with Butylamine Isomers

Hiroshi KAWABE and Masaya YANAGITA

The Institute of Physical and Chemical Research, Wako-shi, Saitama 351

(Received October 19, 1972)

The amination of chloromethylated polystyrene (CMPS) and benzyl chloride with butylamine isomers and diethylamine was investigated kinetically in dioxane, methyl ethyl ketone (MEK), and *N,N*-dimethylformamide (DMF). Although the amination of *i*- and *s*-butylamine conformed to the ordinary second-order kinetics in all the solvents, deceleration was observed during the course of the amination of CMPS with *n*-butylamine in MEK as well as in dioxane, with *t*-butylamine in DMF, and with diethylamine in both dioxane and DMF. The intrinsic rate constants of the amination of CMPS were generally almost the same as those of benzyl chloride. The magnitudes of the rate constants in each solvent were in this order; *n*-butyl > *i*-butyl > *s*-butyl > *t*-butyl; it was in the order of DMF ≫ MEK ≈ dioxane with all the amines investigated. These results were interpreted in terms of both the structures of the amines and the interaction between the amine and the solvent molecules.

The kinetics of the amination of chloromethylated polystyrene (CMPS) with several primary and secondary amines was investigated by Kawabe and Yanagita.[1-3] They found that the apparent second-order rate constant of the amination with *n*-butylamine in dioxane decreased as the amination proceeded and that the rate constant of the amination with 2-aminobutanol increased in dioxane, though both the aminations obeyed the ordinary second-order kinetics in *N,N*-dimethylformamide (DMF). On the other hand, the rate constant of the amination with di-*n*-butylamine decreased in both dioxane and DMF. The amination of benzyl chloride with all the above amines obeyed the ordinary second-order kinetics. If the decrease in the rate constant during the amination of CMPS is caused by the steric effect of the already-aminated neighbors with bulky amine, this decrease must be related to the bulkiness of the amine. In the present study, the kinetics of the aminations of CMPS and benzyl chloride with butylamine isomers and diethylamine have been investigated in dioxane, methyl ethyl ketone (MEK), and DMF. The authors have found that the rate constant decreases slightly in the amination of CMPS with *t*-butylamine and appreciably in the amination of CMPS with diethylamine. It has also been found that the magnitudes of the rate constants in the aminations of both CMPS and benzyl chloride are greatly affected by the species of amine and solvent.

Experimental

Materials. Chloromethylated polystyrene (CMPS) was prepared and purified by the procedures described in the previous papers.[1-3] The chlorine contents and the molecular weights of the CMPS used in the present study are tabulated in Table 1. The amines and the solvents, all of a reagent grade, were distilled before use; they were proved to be pure by their refractive indices. All the other chemicals were of a reagent grade, and deionized, decarbonized water was used.

Kinetic Measurements. The procedures of the kinetic measurements in the amination of CMPS and benzyl chloride were almost the same as those described in a previous paper.[1]

Table 1. Chloromethylated polystyrene

Code	Content of Cl %	Degree of chloromethylation	Molecular weight
SC-3	22.87	0.98	—
SC-5	21.15	0.87	10.2×10^4
SC-7	22.04	0.93	7.3×10^4
SC-8	22.11	0.93	9.2×10^4
SC-9	21.83	0.91	9.6×10^4
SC-10	21.07	0.87	11.6×10^4

The experimental conditions in the amination of CMPS are listed in Table 2. The temperature of a reaction mixture was kept constant by means of a thermostat (within±0.1°). In the amination of benzyl chloride, the initial concentrations were almost the same as those in the amination of CMPS. All the reactions except Run 9 were homogeneous and reached completion. In Run 9, since hydrochloric acid salt of diethylamine was deposited during the amination, the reaction mixture was previously distributed in test tubes dipped in a thermostat to avoid uneven sampling.

Viscometric Measurements. In the amination of CMPS, the change in the viscosity of the reaction mixture was also checked for Runs 1—8 by the procedures described in the previous paper.[1]

Results

The aminations of chloromethylated polystyrene (CMPS) and benzyl chloride with butylamine isomers and diethylamine were investigated kinetically in dioxane, MEK, and DMF.[4] The kinetic measurements could not be carried out in dimethyl sulfoxide, because all the aminations of CMPS with these amines in the solvent were accompanied by the precipitation of the polymer in an earlier stage of the reaction.

The amination of benzyl chloride could be expressed by the ordinary second-order equation:

$$kt = \frac{1}{(a-b)t}\ln\frac{b(a-x)}{a(b-x)} \equiv \overline{kt} \qquad (1)$$

1) Part VI. H. Kawabe, and M. Yanagita This Bulletin, **46**, 38 (1973).

2) H. Kawabe and M. Yanagita, *ibid.*, **41**, 1518 (1968).

3) H. Kawabe and M. Yanagita, *ibid.*, **44**, 896 (1971).

4) Several aminations of CMPS were carried out by using different CMPS samples (Suns 4 and 24, Runs 7 and 19, and Runs 8 and 16 for butylamine isomers; and also Runs 9 and 10 for diethylamine), and almost the same value of rate constant was obtained in each case. It was also shown in these cases that difference in concentration of amine revealed no difference in the rate constant.

TABLE 2. AMINATION OF CHLOROMETHYLATED POLYSTYRENE

Run	Amine[a]	Solvent	Temp. °C	CMPS	a[b] mol/l	b[c] mol/l	a/b
1	A	MEK	50	SC-7	0.7863	0.0376	20.9
2	B	Dioxane	50	SC-5	0.9351	0.0411	22.8
3	B	MEK	50	SC-5	0.8491	0.0410	20.7
4	B	DMF	50	SC-5	0.8216	0.0402	20.4
5	C	Dioxane	50	SC-5	0.8739	0.0410	21.3
6	C	MEK	50	SC-5	0.8380	0.0406	20.6
7	C	DMF	50	SC-5	0.8137	0.0427	19.1
8	D	DMF	50	SC-5	0.8485	0.0410	20.7
9	E	Dioxane	30	SC-3	0.8811	0.0459	19.2
10	E	DMF	30	SC-3	0.8818	0.0437	20.2
11	E	DMF	30	SC-8	0.8319	0.0416	20.0
12	D	DMF	30	SC-8	0.8323	0.0416	20.0
13	D	DMF	35	SC-8	0.8321	0.0416	20.0
14	D	DMF	40	SC-8	0.8325	0.0416	20.0
15	D	DMF	45	SC-8	0.8317	0.0416	20.0
16	D	DMF	50	SC-8	0.8323	0.0416	20.0
17	C	DMF	30	SC-9	0.4107	0.0411	10.0
18	C	DMF	40	SC-9	0.4120	0.0412	10.0
19	C	DMF	50	SC-9	0.4106	0.0411	10.0
20	C	DMF	60	SC-9	0.4099	0.0422	9.7
21	B	DMF	20	SC-10	0.4001	0.0400	10.0
22	B	DMF	30	SC-10	0.4000	0.0400	10.0
23	B	DMF	40	SC-10	0.4000	0.0400	10.0
24	B	DMF	50	SC-10	0.4000	0.0423	9.5

a) A: *n*-butylamine, B: *i*-butylamine, C: *s*-butylamine, D: *t*-butylamine, E: diethylamine. b) a: Initial concentration of amine. c) b: Initial concentration of the polymer expressed in moles of chloromethyl group per liter.

where a and b are the initial concentrations of an amine and the chloromethyl group respectively, while x is the concentration of the chloride ions after time t.

Although most of the aminations of CMPS conformed to Eq. (1), deceleration during the amination was observed in the following cases: *n*-butylamine in dioxane and MEK, *t*-butylamine in DMF, and diethylamine in dioxane and DMF. In these cases, the plot of $\overline{kt}$ against t was expressed substantially by straight lines which intersected nearly at half-amination, and the over-all kinetics in the presence of a large excess of amine ($a \gg b$) could be expressed by Eq. (2):[2]

$$\beta = x/b = 1 - \frac{k_1-k_2}{2k_1-k_2}e^{-k_1at} - \frac{k_1}{2k_1-k_2}e^{-k_2at} \quad (2)$$

$$k_1 = \frac{1}{[(2-k_2/k_1)a-b]} \ln \frac{1-\beta}{1-(2-k_2/k_1)\alpha} \quad (3)$$

$$k_2 = \frac{1}{(a-b)(t-\tau)}\left(\ln\frac{1-\alpha}{1-\beta}\ln\frac{1-\chi/a}{1-\chi/b}\right) \quad (4)$$

where k_1 and k_2 are the rate constants of the elementary reactions which are independent of the neighboring groups and which are dependent on their steric effect respectively. In Eq. (4), $\alpha=x/a$, τ and χ are the values of t and x respectively when $x_1 \simeq b/2$, and x_1 is the concentration of the group which was aminated independently of its neighbors. By combining Eqs. (1) and (4), we get Eq. (5):

$$\overline{kt} = k_2t + C \quad (5)$$

where C is a constant in a given system: $C=\ln[(1-\chi/a)/(1-\chi/b)]-k_2(a-b)\tau$. The value of k_2 can be determined, therefore, directly as the slope of the $\overline{kt}$ vs. t plot: $k_2=\Delta\overline{kt}/\Delta t$. With regard to k_1, on the other hand, the slope of the plot gives merely an approximate value of k_1. The real value of k_1 can be determined only by repeated computations by means of Eq. (3).[2]

Amination with Butylamine Isomers. The rate constants of the amination of CMPS and benzyl chloride with butylamine isomers at 50°C are tabulated in Table 3.[4] It is clearly shown in the table that the rate constant, k or k_1, in any solvent is in this order: *n*-butyl>*i*-butyl>*s*-butyl>*t*-butyl. It is also shown for any amine that the numerical value of the rate constant in MEK is almost the same as that in dioxane, while the value in DMF is much higher than those in dioxane and MEK.

Table 3 shows three cases in which the deceleration was observed; the values of k_2/k_1 are cited in parentheses. The course of the amination of CMPS with *n*-butylamine in MEK at 50 °C is shown in Fig. 1, where the solid line was calculated on the basis of Eq. (2) by using these rate constants:

$$k_1 = 2.85\times10^{-3},\ k_2 = 1.77\times10^{-3}\ \text{l/mol·min}$$

which were obtained on the basis of Eqs. (3) and (4) (or Eq. (5)) respectively. The white circles in Fig. 1, which represent the observed values, are substantially on the calculated curve. The value of k_2/k_1 in MEK, 0.62, is comparable to that in dioxane, 0.65 (the aver-

Table 3. Rate constants of amination of benzyl chloride and chloromethylated polystyrene with butylamine isomers at 50 °C[a]

Chloride	Amine	$k \times 10^3$, l/mol min		
		Dioxane	MEK	DMF
Benzyl chloride	*n*-Butyl	2.73[b]	1.49	102[c]
	i-Butyl	1.80	1.12	99.7
	s-Butyl	0.726	0.972	37.9
	t-Butyl			17.1
CMPS	*n*-Butyl	6.59[d] (0.58)[e]	2.85[d] (0.62)	88.9[c]
	i-Butyl	1.84	1.30	72.2
	s-Butyl	0.870	0.982	32.7
	t-Butyl			11.3[d] (0.87)[f]

a) In the table, the values of k or k_1 are shown, and in parentheses are shown the values of k_2/k_1.
b) Data in Ref. 2. c) Data in Ref. 1. d) The value of k_1. e) The average value at various temp. is 0.65.
f) The average value at various temp. is 0.79.

Table 4. Amination of chloromethylated polystyrene and benzyl chloride with *t*-butylamine in DMF

Temp. °C	Rate constants $\times 10^3$, l/mol·min			E_a kcal/mol		log A[c]
	k_1[a]	k_2[a]	k_B[b]			
30	3.28	2.57	4.76	(k_1)	12.0±0.03	6.17±0.02
35	4.53	3.68	6.70			
40	6.24	4.67	9.16	(k_2)	12.2±0.4	6.19±0.28
45	8.42	7.07	12.4			
50	11.3	8.86	17.1	(k_B)	12.4±0.1	6.60±0.06

a) k_1 and k_2: Rate constants of CMPS. b) k_B: Rate constants of benzyl chloride. c) A is expressed by l/mol·min.

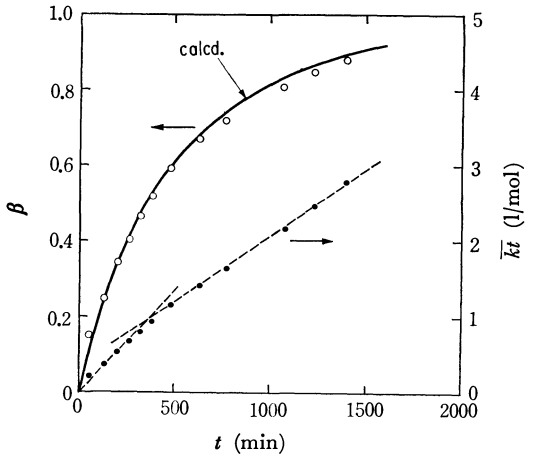

Fig. 1. Amination of chloromethylated polystyrene with *n*-butylamine in MEK at 50 °C (Run 3).

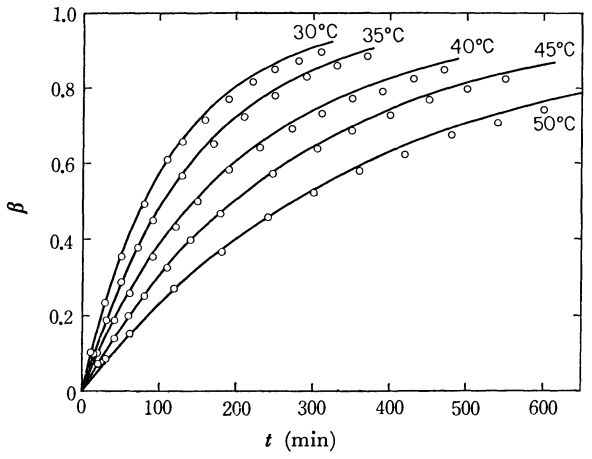

Fig. 2. Amination of chloromethylated polystyrene with *t*-butylamine in DMF.
——: calculated values, ○: observed values

age value at various temperatures).

Deceleration was also observed in the amination of CMPS with *t*-butylamine in DMF. The results of kinetic measurements at various temperatures are shown in Fig. 2, where open circles represent the observed values and where the solid lines show the values calculated on the basis of Eq. (2) by the use of the values of k_1 and k_2 tabulated in Table 4. The rate constants of the amination of benzyl chloride, k_B, and the activation energies, E_a, and the frequency factors, A, which were computed by the least-squares method, are also listed in Table 4. The average value of k_2/k_1 is 0.79, higher than those of *n*-butylamine in dioxane and MEK. The amination of CMPS with *s*- and *i*-butylamine conformed to Eq. (1) in all the solvents. The results of the amination of CMPS and benzyl chloride with these amines are summarized in Tables 5 and 6.

Amination with Diethylamine. In the amination of CMPS with diethylamine, the deceleration during the amination was observed in both dioxane and DMF. The results at 30 °C are shown in Figs. 3 and 4, where

TABLE 5. AMINATION OF CHLOROMETHYLATED POLYSTYRENE AND BENZYL CHLORIDE WITH *s*-BUTYLAMINE IN DMF

Temp. °C	Rate constants $\times 10^2$, l/mol·min			E_a kcal/mol	log A[c] l/mol·min
	k_P[a]	k_B[b]			
30	0.932	1.08	(k_P)	12.1±0.1	6.69±0.09
40	1.84	2.00			
50	3.27	3.79	(k_B)	12.2±0.1	6.85±0.07
60	5.72	6.67			

a) k_P: Rate constant of CMPS. b) k_B: Rate constant of benzyl chloride. c) A is expressed by l/mol·min.

TABLE 6. AMINATION OF CHLOROMETHYLATED POLYSTYRENE AND BENZYL CHLORIDE WITH *i*-BUTYLAMINE IN DMF

Temp. °C	Rate constants $\times 10^2$, l/mol·min			E_a kcal/mol	log A[c]
	k_P[a]	k_B[b]			
20	1.24	1.52	(k_P)	11.6±0.2	6.72±0.15
30	2.46	3.04			
40	4.64	5.61	(h_B)	11.8±0.1	6.97±0.05
50	7.72	9.97			

a) k_P: Rate constants of CMPS. b) k_B: Rate constants of benzyl chloride. c) A is expressed by l/mol·min.

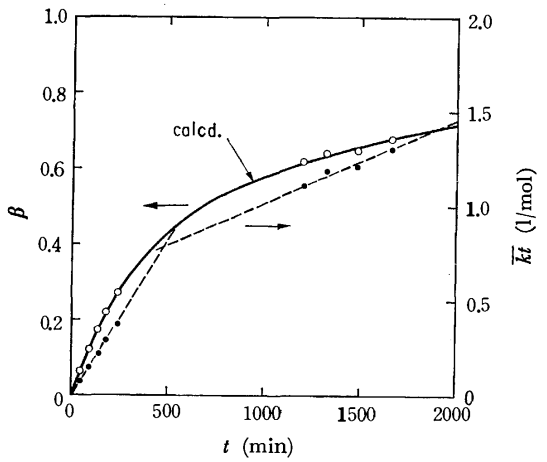

Fig. 3. Amination of chloromethylated polystyrene with diethylamine in dioxane at 30 °C (Run 9).

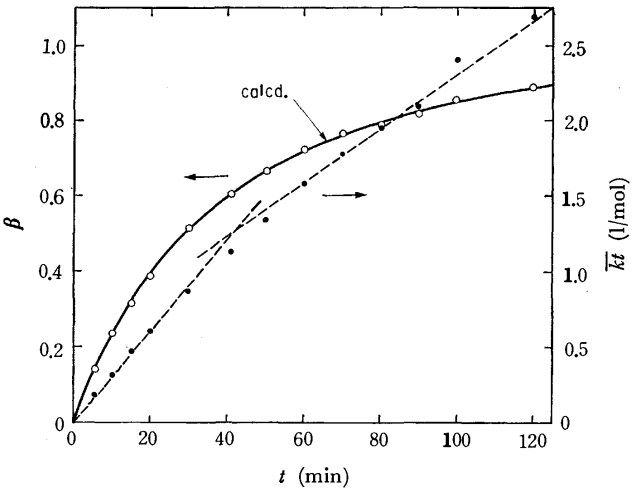

Fig. 4. Amination of chloromethylated polystyrene with diethylamine in DMF at 30 °C (Run 11).

the observed values, represented by the white circles, are substantially on the curves calculated on the basis of Eq. (2) by the use of the following values of k_1 and k_2:

(in dioxane) $k_1 = 1.71\times10^{-3}$ l/mol·min, $k_2 = 3.96\times10^{-4}$ l/mol·min; $k_2/k_1 = 0.43$

(in DMF) $k_1 = 3.48\times10^{-2}$ l/mol·min, $k_2 = 1.81\times10^{-2}$ l/mol·min; $k_2/k_1 = 0.52$

In DMF, the rate constant of benzyl chloride was also measured at 30 °C as:

(in DMF) $k_B = 2.82\times10^{-2}$ l/mol·min

Viscosity Change in the Reaction Mixture During the Amination of CMPS with Butylamine Isomers. The change in the viscosity in the amination of CMPS was measured in various solvents; the results in DMF are shown in Fig. 5, where H, the viscosity ratio defined in the previous paper,[1] is plotted against β. The values of H are in this order: *t*-butyl>*s*-butyl>*i*-butyl>*n*-butyl. In the other solvents, the order was

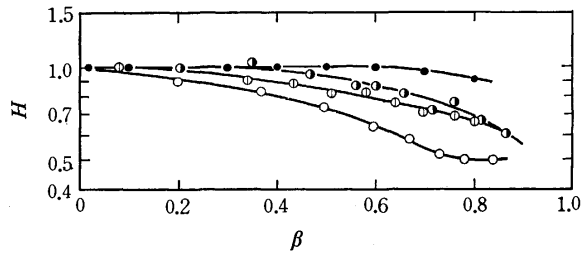

Fig. 5. Viscosity change of reaction mixture in the amination of chloromethylated polystyrene in DMF.
○: *n*-Butylamine (Ref. 1), ◫: *i*-Butylamine (Run 4), ◑: *s*-Butylamine (Run 7), ●: *t*-Butylamine (Run 8).

the same; however, the viscosity changes do not seem to be related to the kinetic behavior of the aminations.

Discussion

Deceleration During the Amination of CMPS. In the amination of CMPS with butylamine isomers,

the amination with *i*- and *s*-butylamine conformed to the ordinary second-order kinetics in dioxane, MEK, and DMF; however, deceleration during the reaction was observed with *n*-butylamine in dioxane and MEK, and not in DMF, though a slight deceleration was observed with *t*-butylamine in DMF. On the other hand, a stronger deceleration was observed in the amination with diethylamine in both dioxane and DMF. Since all the aminations of benzyl chloride proceeded normally, and since the formation of charged groups on the polymer is not likely to take place during the reaction,[5] this deceleration seems to be caused by the steric effect of the already-aminated neighboring groups; this kinetic behavior can be fully expressed by Eq. (2). The kinetic behavior of the amination of CMPS is dependent on the species of amine and the solvent. The experimental results may be explained in terms of the geometry of amines, which is itself determined by the structural factors of the amines, such as the branching and the flexibility through the rotation around the bond axes, and also by the interactions between amine and solvent molecules and by the conformational change in the amine molecules (or groups) at the transition state of the reaction. The steric effect must be mainly determined by the conformational free energy, that is, the difference in the free energy of amine molecules (or groups) at the transition state under the influence of the neighboring groups from that at the initial state; it consists of the difference in the potential energies of the molecules between the two states and the difference between the conformational entropies.

In the case of diethylamine, an appreciable deceleration was observed in both dioxane ($k_2/k_1=0.43$) and DMF ($k_2/k_1=0.52$), though it was not so marked as the cases of di-*n*-butylamine, a higher homologue of the former, in dioxane ($k_2/k_1=0.23$)[2] and in DMF ($k_2/k_1=0.27$).[1] These results may be related to the bulky structure of secondary amines, in which two alkyl groups occupy the apices of the trigonal pyramid, and in which, therefore, the steric obstruction is pronounced with secondary amines, irrespective of the species of solvent. A weaker deceleration was observed in some cases of butylamine isomers. The slight deceleration with *t*-butylamine in DMF ($k_2/k_1=0.79$) may be asascribed to its rigid and bulky structure. The difference in kinetic behavior between *n*-butylamine and *i*- and *s*-butylamine may be supposed to be mainly due to the difference in their conformational entropies.

In the case of *n*-butylamine, the deceleration was observed in dioxane ($k_2/k_1=0.65$) and MEK ($k_2/k_1=0.62$), but it was not observed in DMF. Since the value of the solubility parameters, δ,[6] of *n*-butylamine ($\delta=9.15$) is almost the same as those of dioxane ($\delta=9.95$) and MEK ($\delta=9.16$), the amine molecules in these solvents may be considered to be statistically elongated and their conformational change at the transition state will require an increase in energy and a loss of entropy. On the other hand, the *n*-butylamine molecule in DMF ($\delta=12.11$) is considered to be contracted as a result of the intramolecular interaction among the segments; therefore, its conformational change at the transition state will require less energy and less entropy loss than those in dioxane and MEK. The normal kinetic behavior with *i*- and *s*-butylamine in both dioxane and DMF is properly to be ascribed to the branching structure of these molecules, the conformational entropies of which are much smaller than that of *n*-butylamine.

Comparison Between the Rates of CMPS and Benzyl Chloride. The values of k_1 or k of CMPS are generally almost the same as the corresponding values of benzyl chloride. The effects of the species of amine and solvent are, therefore, essentially the same for both CMPS and benzyl chloride. The ratios of the intrinsic rate constants of CMPS (denoted as k_P) to the corresponding rate constants of benzyl chloride (k_B) are somewhat higher than unity in dioxane and MEK. In DMF, the relative rates are slightly less than unity except in case of diethyl amine. Table 7 shows the numerical values of thermodynamic quantities, $\Delta H^{\ddagger}$; the enthalpy of activation, $\Delta S^{\ddagger}$; the entropy of activation, and $\Delta G^{\ddagger}$, the free energy of activation, all of which have been calculated at 25 °C by means of the equations described in the previous paper.[1] As is shown in Table 7, all the reactions in DMF have a tendency to be accompanied by a decrease in $\Delta S^{\ddagger}$ as well as the increase in $\Delta H^{\ddagger}$ from benzyl chloride to CMPS. This is also the case with the amination with 2-aminobutanol in DMF ($k_P/k_B=0.81$) or in DMSO ($k_P/k_B=0.76$).[1] On the other hand, in dioxane, the change in $\Delta S^{\ddagger}$ is not significant in the amination with *n*-butylamine or 2-aminobutanol.[1] Thus, this tendency of $\Delta S^{\ddagger}$ to decrease from benzyl chloride to CMPS seems to be characteristic of dipolar aprotic solvents, in which the solvation of the transition state plays an important role in the determination of the amination rate.

Effect of Amine on the Amination Rate. The intrinsic rate constants of CMPS as well as of benzyl chloride are dependent on the species of amine—*e.g.*, in butylamine isomers, in the following order: *n*-butyl>*i*-butyl>*s*-butyl>*t*-butyl. The values of the relative rate with respect to an amine are approximately the same, irrespective of the species of solvent and chloride (CMPS or benzyl chloride). This order among butylamine isomers is not likely to be dependent on their basicities, because the pK values of the conjugated acids are almost the same: 10.64; (*n*), 10.42 (*i*), 10.56 (*s*), and 10.45 (*t*). It seems rather dependent on the branching structures of the alkyl groups of the amines; this dependence produces the difference in the steric hindrance of the benzene ring to the alkyl group of amine in the transition state. This is supported, especially in the case of *t*-butylamine, by the fact, shown in Table 7, that the increase in $\Delta G^{\ddagger}$ from

5) In fact, a completely aminated CMPS sample, which was obtained simply by pouring the reaction mixture into a poor solvent, was proved to contain no chlorine by its elementary analysis for halogen. This may be ascribed to that the aminated group on the polymer is the *N*-benzyl substituent of an alkylamine used as a reagent and it is a weaker base than the alkylamine which is used in a large excess in the present study.

6) The δ values were calculated at 25 °C on the basis of the data shown in the book: J. A. Riddick and W. B. Bunger, "Organic Solvents," third edition, Wiley Interscience, New York, N. Y. (1970).

TABLE 7. THERMODYNAMIC QUANTITIES AT 25 °C IN THE AMINATION OF CHLOROMETHYLATED POLYSTYRENE AND BENZYL CHLORIDE

Solvent	Amine	Chloride	$\Delta H^{\neq}$ kcal/mol	$\Delta S^{\neq}$ e.u.	$\Delta G^{\neq}$ kcal/mol
Dioxane	*n*-Butyl[a]	CMPS, k_1	11.5±0.1	−41.2±0.3	23.8
		CMPS, k_2	11.5±0.9	−42.2±2.6	24.1
		Benzyl	12.0±0.2	−41.5±0.6	24.3
DMF	*n*-Butyl[a]	CMPS	10.8±0.1	−38.1±0.4	22.2
		Benzyl	11.0±0.2	−37.2±0.7	22.1
	i-Butyl	CMPS	11.0±0.2	−37.9±0.7	22.3
		Benzyl	11.2±0.1	−36.8±0.2	22.2
	s-Butyl	CMPS	11.5±0.1	−38.1±0.4	22.8
		Benzyl	11.7±0.1	−37.3±0.3	22.8
	t-Butyl	CMPS, k_1	11.4±0.0$_3$	−40.4±0.1	23.5
		CMPS, k_2	11.6±0.4	−40.3±1.3	23.6
		Benzyl	11.8±0.1	−38.5±0.3	23.3
	2-Amino-butanol[a]	CMPS,	12.5±0.2	−35.8±0.7	23.1
		Benzyl	12.7±0.1	−34.5±0.2	23.0

a) Data in Ref. 1.

n-butyl to *t*-butylamine is based on the decrease in $\Delta S^{\neq}$ as well as by the increase in $\Delta H^{\neq}$. It is also shown in Table 7 that the $\Delta H^{\neq}$ of 2-aminobutanol is considerably higher than that of *s*-butylamine (2-aminobutane); this is probably related to an inductive effect of the hydroxyl group.

Effect of Solvent on the Amination Rate. The intrinsic rate constant of CMPS as well as the rate constants of benzyl chloride are also dependent on the species of solvent. In dioxane and MEK, the rates are approximately the same, but that in DMF is very high. Since the dielectric constants (D) are 2.21 (dioxane), 18.51 (MEK), and 36.71; (DMF), no relation between k and D can be established in this case. The high rate constants in DMF are considered to be due to the solvation of the transition state in this dipolar aprotic solvent, as has been discussed in the previous paper.[1] Since the δ value of MEK is almost the same as that of dioxane, the contributions of both solvents to $\Delta H^{\neq}$ and $\Delta S^{\neq}$ are expected to be almost the same.

The authors wish to express their thanks to Mr. Akihiro Kishi, Mr. Kazuaki Kawamura, Mr. Masahiro Uchiyama and Mr. Masayuki Takahashi for their helpful assistance in preparing the polymer and in carrying out the measurements.

Kinetics of Oxygen Exchange between Arsenate Ions and Water. II. Catalysis by Arsenious Acid

Akiko OKUMURA, Noriko YAMAMOTO, and Nobukazu OKAZAKI
Department of Chemistry, Nara Women's University, Nara 630
(Received March 22, 1973)

Oxygen exchange between arsenate ions and water is catalyzed by arsenious acid. The catalytic effect has been studied at 14.5 °C and 30.0 °C over the pH region of 7.5—10.2. The increase in the exchange rate due to the addition of arsenious acid, R_c, may be expressed as: $R_c \approx k[H^+][As(III)][As(V)]$. The results are interpreted in terms of the rapid reversible condensation of the As(III) with the As(V) species to form the arsenitoarsenate ions.

In a previous study of the oxygen exchange between arsenate ions and water,[1] it has been shown that the reversible condensation of the arsenate ions to form diarsenate ions occurs in aqueous solutions. Itse ems that it would be interesting to see whether or not the arsenate ion reacts with other oxyanions to form heteropolyanions, and to compare the reactivities of these oxyanions towards the arsenate ions. These reaction open an additional path for the oxygen exchange of arsenate ions, and, if the reactions are reversible and sufficiently rapid, the exchange reaction can be catalyze by these oxyanions. In the present paper, catalysis by arsenious acid will be reported.

Experimental

Materials. The arsenic trioxide (Guaranteed reagent, JIS) and perchloric acid(Guaranteed reagent, JIS) were used without further purification. All the other chemicals were the same as those used in the previous work.[1]

Procedure. The procedures were almost the same as those used in the previous work.[1] The exchange reaction was started by diluting an isotopically-equilibrated solution of Na_2HAsO_4 in oxygen-18 water with a relatively large amount of isotopically normal water, a proper amount of an arsenious acid solution being added. The pH of the solution was adjusted by the addition of a small amount of perchloric acid or of a sodium hydroxide solution. After appropriate intervals, the arsenate ions were precipitated by the addition of a barium chloride solution. The precipitate, after being washed three times with absolute ethanol and dried, was converted into carbon dioxide by the guanidine hydrochloride method. The isotopic analysis of the carbon dioxide was made on a Hitachi RMS-I-type mass spectrometer. The contribution of a small amount of the precipitate of barium arsenite to the ^{18}O-content of the carbon dioxide was neglected. Oxygen exchange between arsenious acid and water is very rapid at room temperature, and is completed within the time necessary for the separation. The rate of the oxygen exchange of arsenate ions was calculated by means of the formula:

$$R = -\frac{[As(V)][H_2O]}{4[As(V)] + [H_2O]} \cdot \frac{1}{t} \cdot \ln\left\{1 - \frac{O_0 - O_t}{O_0 - O_\infty}\right\},$$

where O_0, O_t, and O_∞ are the ^{18}O-contents of the carbon dioxide at times 0, t, and infinity respectively, and where [As(V)] and $[H_2O]$ are the concentrations of the arsenate and water respectively.

Determination of Dissociation Constants. The dissociation constants of arsenious and arsenic acid under the conditions of the kinetic experiments were determined by potentiometric titration with a glass electrode. The pK_2 of arsenic acid was determined by titrating a solution of Na_2HAsO_4 containing the amount of sodium chloride necessary to maintain the desired ionic strength with hydrochloric acid. For the determination of the pK_1 of arsenious acid, a solution of arsenious acid was titrated with a solution of sodium hydroxide, an appropriate amount of sodium chloride being added to adjust the ionic strength. The pH of the solution was measured with a Radiometer PHM-26 pH meter. The results obtained from two series of titrations at I=0.2 M, where I is the ionic strength, are shown in the following table. For the definition of the pK's, see Part I of this series.

TABLE 1. THE DISSOCIATION CONSTANTS OF ARSENIC ACID (pK_2) AND ARSENIOUS ACID (pK_1) AT I=0.2 M.

	14.5°C	30.0°C
pK_2 of arsenic acid	$6.59_6 \pm 0.00_4$	$6.55_6 \pm 0.00_6$
pK_1 of arsenious acid	$9.34_1 \pm 0.00_3$	$9.10_8 \pm 0.01_7$

Results and Discussion

pH *Dependence.* Fig. 1 shows the pH-rate profile of the oxygen exchange of arsenate ions with and without the added arsenious acid at 14.5 °C and 30.0

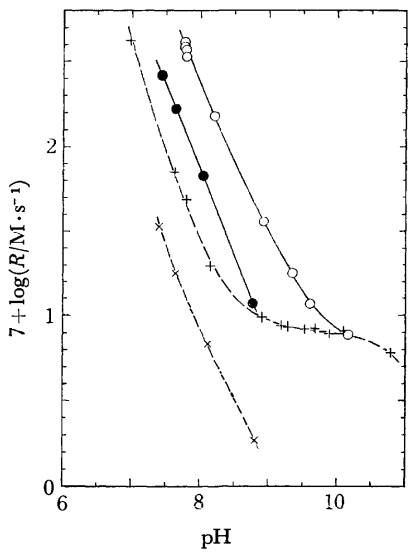

Fig. 1. pH-rate profiles of the oxygen exchange between arsenate ions and water ([As(V)]=0.07 M, I=0.2 M): + (30 °C), × (14.5 °C), without added arsenious acid. ○ (30 °C), ● (14.5 °C), with added arsenious acid ([As(III)] $\simeq 1.2 \times 10^{-4}$ M).

1) A. Okumura and N. Okazaki, This Bulletin, **46**, 2937 (1973).

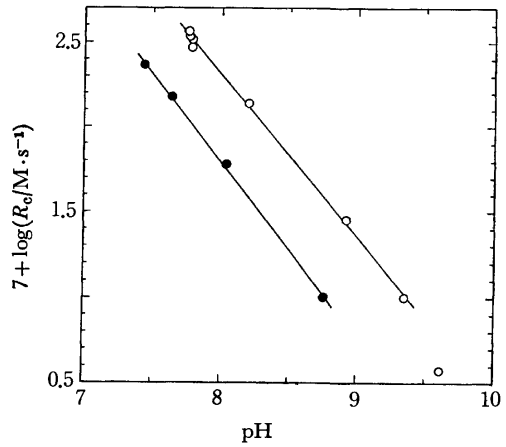

Fig. 2. pH dependence of the catalysed portion of the exchange rate R_c: ○ 30 °C, ● 14.5 °C.

°C([As(V) : [As(III)]≈50 : 1).[2] The addition of arsenious acid increases the exchange rate about 8-fold at pH 7.44. The catalytic effect decreases with the increase in pH, and it disappears above pH 10. From the pH-rate profile and the values of the dissociation constants of arsenic and arsenious acids, it may be inferred that $H_2AsO_4^-$ and H_3AsO_3 are the active species in the catalytic process.

Figure 2 shows a plot of the logarithm of $R_c(=R-R_0)$ against pH, where R and R_0 are the exchange rates observed with and without the addition of arsenious acid. The slopes of the lines passing through the plots are -0.96 ± 0.01 at 30.0 °C and -1.01 ± 0.02 at 14.5 °C. The catalyzed portion of the exchange rate, R_c, depends upon the first power of the hydrogen-ion concentration. The role of the hydrogen ion is to shift the pre-equilibrium:

$$H_2AsO_4^- \rightleftharpoons HAsO_4^{2-} + H^+,$$

in favor of $H_2AsO_4^-$, which is the active species in the exchange reaction.

Dependence of the Catalytic Rate R_c on [As(III)]. This has been studied at 30 °C, pH 7.83, [As(V)]= 0.07 M, and I=0.2 M. [As(III)] was varied between 3×10^{-4} and 13×10^{-4} M. The observed rates were

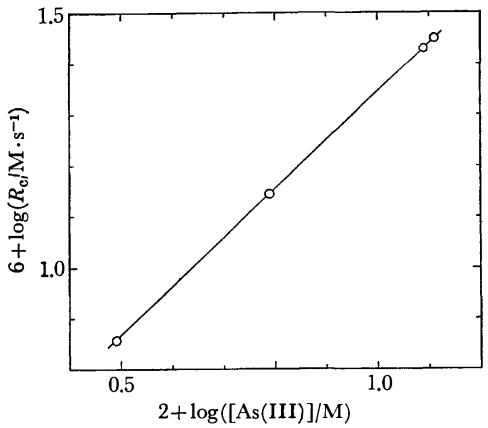

Fig. 3. Dependence of log R_c on log [As(III)] (30 °C, pH 7.83, [As(V)]=0.07 M, I=0.2 M).

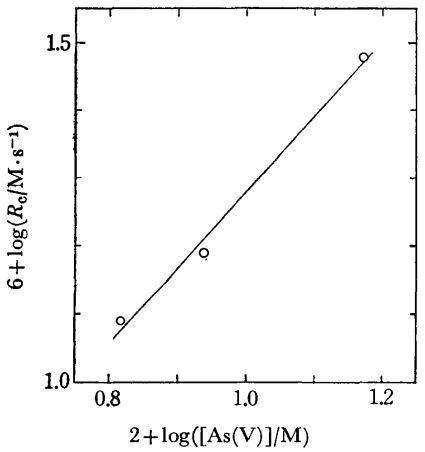

Fig. 4. Dependence of log R_c on log [As(V)] (30 °C, pH 7.78, [As(III)]=6.2×10^{-4} M, I=0.4 M).

corrected for the small differences in pH(<0.05) and in [As(V)](<0.0015 M). A plot of log R_c against log [As(III)] is shown in Fig. 3. A line drawn through the plots has a slope of $0.95\pm0.00_1$. The catalytic rate, R_c, depends on the first power of [As(III)].

Dependence of the Catalytic Rate on [As(V)]. The dependence of R_c on [As(V)](0.066—0.15 M) has been studied at 30 °C, pH 7.78; [As(III)]=6.2×10^{-4} M, and I=0.43 M (Fig. 4). Corrections were applied to the observed rates for the small differences in pH (<0.1). The plots of log R_c against log [As(V)] fall on a straight line with a slope of 1.10 ± 0.07. The catalytic process is approximately first-order with respect to [As(V)].

The rate law of the catalytic process may be written as:

$$R_c = k[H^+][As(III)][As(V)]. \quad (1)$$

Mechanism of the Catalytic Process. Wilson and Dickinson[3] have shown that the exchange of radioactive arsenic does not occur between arsenite and arsenate ions in dilute acid(0.1 M HCl) and alkaline(*ca* 1 M NaOH) solutions. This indicates that the direct transfer of oxygen atoms does not occur between these ions. Thus, a mechanism of the catalysis of the oxygen exchange which involves a rapid interchange of oxygen between arsenious acid and water, followed by a transfer of oxygen from the arsenate to the arsenious acid, may be excluded.

Another possibility is the general acid catalysis of the exchange reaction between arsenate ions and water by arsenious acid. In this case, it is natural to interpret the bimolecular rate term of the arsenate-water exchange,[1] $k_4[H_2AsO_4^-]^2$, also in terms of the general acid catalysis by $H_2AsO_4^-$. However, since $H_2AsO_4^-$ is a stronger acid than H_3AsO_3, the mechanism involving the general acid catalysis is inconsistent with the fact that the arsenate-water exchange is catalyzed by arsenious acid.

The catalytic process may be considered to be the reversible condensation of arsenate ions with arse-

2) [As(III)] is the total concentration of the arsenious acid; [As(III)]=[H_3AsO_3]+[$H_2AsO_3^-$].

3) J. N. Wilson and R. G. Dickinson, *J. Amer. Chem. Soc.*, **59**, 1358 (1937).

nious acid or arsenite ion to form arsenitoarsenate ions:

$$H_2AsO_4^- + H_3AsO_3 \rightleftharpoons H_3As_2O_6^- + H_2O, \text{ etc.}$$

The rate law of the catalytic process may now be written as:

$$R_c = k_1[H_2AsO_4^-][H_3AsO_3] + k_2[HAsO_4^{2-}][H_3AsO_3] + k_3[H_2AsO_4^-][H_2AsO_3^-] + k_4[HAsO_4^{2-}][H_2AsO_3^-]. \quad (2)$$

Since $R_c \approx 0$ at pH$\approx$10, the contribution of the k_4-term may be ignored. The rate law (2) becomes:

$$\frac{R_c}{[H_2AsO_4^-][H_3AsO_3]} = k_1 + \frac{K_2}{[H^+]}\left\{k_2 + k_3\frac{K_1'}{K_2}\right\}, \quad (3)$$

where K_2 and K_1' are the dissociation constants of $H_2AsO_4^-$ and H_3AsO_3 respectively.

In Fig. 5, the data in Fig. 1 are replotted according to the above equation. From the intercepts of the lines drawn through the plots, the values of k_1 are determined to be $k_1(30\,°C) = 6.8\ M^{-1}\,s^{-1}$ and $k_1(14.5\,°C) = 2.2\ M^{-1}\,s^{-1}$. The activation parameters of the k_1-path are $E_a = 52.3$ kJ mol^{-1} and $\Delta S^{\neq} = -38$ J K^{-1} mol^{-1}.

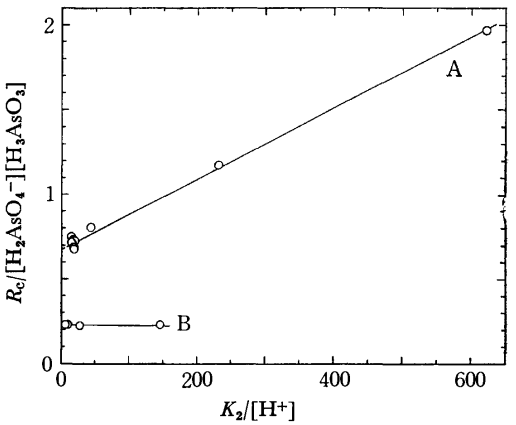

Fig. 5. $R_c/[H_2AsO_4^-][H_3AsO_3]$ as a function of $K_2/[H^+]$: A; 30 °C, B; 14.5 °C.

Table 2. Rates and activation parameters of several reactions of $H_2AsO_4^-$.

	Rate const. ($M^{-1}\,s^{-1}$), 30°C	Act. energy (kJ mol^{-1})	$\Delta S^{\neq}$ (J K^{-1} mol^{-1})
$H_2AsO_4^- + H_2O$,[a]	1.1×10^{-4}	$\approx$92	≈ -46
$H_2AsO_4^- + H_2AsO_4^-$,[a]	7.4×10^{-2}	$<$54	< -71
$H_2AsO_4^- + H_3AsO_3$,[b]	6.8	52	-38

a) $I = 0.55$ M, b) $I = 0.2$ M.

From the slope of the line A (Fig. 5), the value of $\{k_2 + k_3(K_1'/K_2)\}$ at 30 °C is evaluated as 0.02 $M^{-1}\,s^{-1}$. Since k_2 may reasonably be assumed to be larger than k_3 and since $K_1'/K_2 = 2.8\times10^{-3}$ at 30 °C, the value of k_2 may be put equal to 0.02 $M^{-1}\,s^{-1}$. This path plays a dominant role above pH 9. To estimate the value of k_2 at 14.5 °C is beyond the scope of the present work.

The reactivities of several nucleophiles towards $H_2AsO_4^-$ obtained in the present and the previous[1] works are listed in Table 2. The higher reactivity of arsenious acid as compared with $H_2AsO_4^-$ may be attributable to the entropy factor.

The authors wish to thank Professor Shinichi Kawaguchi of Osaka City University for his helpful discussions.

The Intensity in the Resonance Raman Effect. I. The Diatomic Molecule in the Harmonic Potential Approximation

Shunsuke KOBINATA

Research Laboratory of Resources Utilization, Tokyo Institute of Technology, Meguro-ku, Tokyo 152

(Received April 14, 1973)

The formulas for the Raman intensities of fundamental and n-th overtones were investigated theoretically, starting from the Kramers-Heisenberg dispersion formula and referring to a diatomic molecule in a harmonic potential approximation. The derived formulas were then applied to fifteen overtone bands of iodine, which have been observed in gas, and to the exciting frequency dependence of the fundamental and the first overtone intensities of iodine in a $CHCl_3$ solution. It was shown that the formulas quantitatively explain the trend of the observed data well.

With the advent of various laser light sources, the resonance Raman effect has come to be investigated extensively in recent years. It has been observed that higher overtones appear in a spectrum with considerable intensities as the exciting light frequency approaches an electronic absorption band. For example, the fifteen overtones of iodine have been obtained in gas using the argon ion laser at 4880 Å by Holzer *et al.*[1]

The origin of the resonance Raman effect has been investigated theoretically by several authors. Peticolas *et al.*[2,3] have derived the formula of the n-th overtone Raman intensity using the technique of the time-ordered diagram and have then applied this equation to the experimental data on iodine in gas. The quantitative agreement with the observed data has been poor for higher overtones. Verlan[4] has investigated the formula of the resonance Raman intensity based on the generalized perturbation theory of Heitler,[5] and has formulated a rather complicated expression.

We obtained a simple expression of the Raman intensity starting from the Kramers-Heisenberg dispersion equation and using the idea of the effective transition frequency.[6] The vibrational frequency difference between the ground and the excited electronic states was taken into account. The formulas were then applied to the observed data on iodine; reasonable results were obtained.

Method

The intensity of the Raman scattering associated with the $m \rightarrow n$ vibrational transition in the electronic ground state, $|g\rangle$, is given,[7] after averaging the overall orientation of the molecule, by:

$$I_{mn} = (2^7\pi^5/(3^2c^4))I_0(\nu_0+\nu_{mn})^4 \sum_{\rho,\sigma} (\alpha_{\rho\sigma})^2_{mn} \quad (1)$$

where ν_0 and I_0 are the frequency and the intensity of the incident light. The ρ,σ (=x, y, z) component of the scattering associated with the transition is expressed by:

$$(\alpha_{\rho\sigma})_{mn} = (1/h) \sum_{e,v} (M_\rho)_{ev,gn}(M_\sigma)_{gm,ev}/(\nu_{ev,gn}-\nu_0+i\gamma_e) + (M_\rho)_{gm,ev}(M_\sigma)_{ev,gn}/(\nu_{ev,gn}+\nu_0+i\gamma_e) \quad (2)$$

in accordance with the Kramers-Heisenberg dispersion theory. Verlan has shown that Eq. (2) is applicable in the case of the resonance Raman effect. The summation is taken over all the electronic excited states, $|e\rangle$, and the vibrational states, $|v\rangle$, accompanying them. The γ is the damping constant of the electronic state $|e\rangle$.[4,7]

The vibronic transition moment, $(M_\rho)_{ev,gn}$, can be expanded in the nuclear coordinate, Q, of a diatomic molecule assuming adiabatic approximation by:

$$(M_\rho)_{ev,gn} = (M_\rho)^0_{ge}\langle ev|gn\rangle + (M_\rho)'_{ge}\langle ev|Q|gn\rangle \quad (3)$$

where $(M_\rho)_{ge}{}^0$ is the component of the pure electronic transition moment at the equilibrium configuration in the $|g\rangle$ state. $(M_\rho)_{ge}{}'$ is the derivative of the electronic transition moment with respect to the nuclear coordinate, Q, $(M_\rho)_{ge}{}'=\{\partial(M_\rho)_{ge}/\partial Q\}_0$. The $\langle ev|gn\rangle$ and $\langle ev|Q|gn\rangle$ give integrals in the nuclear coordinate between the vibrational-state functions of $|e\rangle$ and $|g\rangle$ states.

Following Albrecht,[7,9] Eq. (2) is given by the representation:

$$(\alpha_{\rho\sigma})_{mn} = A_{mn} + B_{mn} + B'_{mn} \quad (4)$$

$$A_{mn} = (1/h) \sum_{e,v} (M_\rho)^0_{ge}M_\sigma)^0_{ge}\langle gm|ev\rangle\langle ev|gn\rangle \times\{(\nu_{ev,gm}-\nu_0+i\gamma_e)^{-1} + (\nu_{ev,gn}+\nu_0+i\gamma_e)^{-1}\} \quad (4a)$$

$$B_{mn} = (1/h) \sum_{e,v} (\nu_{ev,gm}-\nu_0+i\gamma_e)^{-1} \times\{(M_\rho)^0_{ge}(M_\sigma)'_{ge}\langle gm|Q|ev\rangle\langle ev|gn\rangle + (M_\rho)'_{ge}(M_\sigma)^0_{ge}\langle gm|ev\rangle\langle ev|Q|gn\rangle\} \quad (4b)$$

$$B'_{mn} = (1/h) \sum_{e,v} (\nu_{ev,gn}+\nu_0+i\gamma_e)^{-1} \times\{(M_\rho)^0_{ge}(M_\sigma)'_{ge}\langle gm|ev\rangle\langle ev|Q|gn\rangle + (M_\rho)'_{ge}(M_\sigma)^0_{ge}\langle gm|Q|ev\rangle\langle ev|gn\rangle\} \quad (4c)$$

The A_{mn} term, which does not depend on the vibronic interaction, $(M_\rho)'_{ge}$, contributes to the Raman intensity

1) W. Holzer, W. F. Murphy, and H. J. Bernstein, *J. Chem. Phys.*, **52**, 399 (1970).
2) L. A. Nafie, P. Stein and W. L. Peticolas, *Chem. Phys. Lett.*, **12**, 131 (1971).
3) W. L. Peticolas, L. Nafie, P. Stein, and B. Fanconi, *J. Chem. Phys.*, **52**, 1576 (1970).
4) E. M. Verlan, *Opt. Spectry.*, **20**, 557 (1966).
5) W. Heitler, "The Quantum Theory of Radiation," Oxford University Press, London (1954).
6) J. Behringer, "Raman Spectroscopy," Vol. 1, ed. by H. A. Szymanski, Plenum Press, New York (1967), Chapt. 6.
7) J. Tang and A. C. Albrecht, "Raman Spectroscopy," Vol. 2, ed. by H. A. Szymanski, Plenum Press, New York (1970), Chapt. 2.
8) J. Behringer, *Z. Elektrochem.*, **62**, 906 (1958).
9) A. C. Albrecht, *J. Chem. Phys.*, **34**, 1476 (1961).

only when the electronic ground and excited states have the potential curves displaced or distorted in relation to each other.[10] The B_{mn} and B'_{mn} terms depend on the vibronic interaction, $(M_\rho)'_{ge}$, and have been extensively investigated by Albrecht in the case of the ordinary Raman effect. For practical use, we must further simplify these expressions of the scattering tensor.

A_{mn} Term. First, let us investigate the A_{mn} term. For the sake of simplicity, we will consider the vibration of a diatomic molecule assuming a harmonic oscillator. The vibrational ground state, $|g0\rangle$, is taken as the initial state, $|gm\rangle$. Then, the frequency corresponding to the vibronic transitions concerned may be expressed as:

$$\nu_{ev,g0} = \nu_{e0,g0} + v\nu_e \tag{5}$$

where $\nu_{e0,g0}$ is the 0–0 transition frequency between $|g\rangle$ and $|e\rangle$ electronic states, and where ν_e is the vibrational frequency in the $|e\rangle$ state. The substitution of the above expression into Eq. (4a) leads to:

$$A_{0n} = \sum_e \{(M_\rho)^0_{ge}(M_\sigma)^0_{ge}/(h\nu_e)\} \sum_v \langle g0|ev\rangle\langle ev|gn\rangle \times \{(c_1+v)^{-1}+(c_2+v)\}^{-1} \tag{6}$$

where:

$$c_1 = (\nu_{e0,g0}-\nu_0+i\gamma_e)/\nu_e$$
$$c_2 = (\nu_{e0,gn}+\nu_0+i\gamma_e)/\nu_e. \tag{6a}$$

It is generally difficult to carry out the summation over v because the $|e\rangle$ state gives a different equilibrium internuclear distance, r_e^0, and different fundamental vibrational frequency, ν_e, from the corresponding quantities in the ground state, r_g^0 and ν_g. Therefore we will first consider a somewhat specialized case where $\nu_e=\nu_g$ but where $r_e^0=r_g^0$.

Now using the expression of the Franck-Condon overlap integrals given by Hutchinson,[11,12] we obtain for $\nu_e=\nu_g$:

$$\langle gm|ev\rangle = \exp(-\delta_e^2/4)/\sqrt{(m!v!)/(2^{m+v})}\,\delta_e^m \times \sum_{k=0}((-1)^{m-k}2^k\delta_e^{v-2k})/(k!(m-k)!(v-k)!) \tag{7}$$

and, consequently:

$$\sum_v \langle g0|ev\rangle\langle ev|gn\rangle/(c+v) = \sqrt{n!/2^n}(-\delta_e)^n\exp(-\delta_e^2/2) \times \sum_{k=0}(-1)^k/(k!(n-k)!)\sum_v(\delta_e^2/2)^{v-k}/(c+v)(v-k)! \tag{8}$$

where:

$$\delta_e = \alpha_e(r_g^0-r_e^0) \tag{9}$$
$$\alpha_e = 4\pi^2\mu\nu_e/h;\ \mu;\ \text{reduced mass} \tag{9a}$$

The dimensionless quantity, δ_e, is the difference in the equilibrium internuclear distance between the $|g\rangle$ and $|e\rangle$ states in the unit of the classical vibrational amplitude, $1/\alpha_e$, of the vibrational ground state.

The summation over v on the right-hand side of Eq. (8) can be approximately written as:

$$\sum_v(\delta_e^2/2)^{v-k}/((c+v)(v-k)!) \doteqdot \exp(\delta_e^2/2)/(c+\delta_e^2/2+k) \tag{10}$$

It can easily be seen that the above relation applies fairly well for $c=1$ for all values of δ_e and when $\delta_e<1$ for a wide range of c.

Then, using the formula:

$$\sum_{k=0}^{n}(-1)^k n!/((c+k)(n-k)!k!) = n!/\{c(c+1)\cdots\cdots(c+n)\} \tag{11}$$

Equation 8 can be written as:

$$\sum_v \langle g0|ev\rangle\langle ev|gn\rangle/(c+v) = \sqrt{n!/2^n}(-\delta_e)^n/\{c^*(c^*+1)\cdots\cdots(c^*+n)\} \tag{12}$$

where, according to Eq. (10):

$$c^* = c + \delta_e^2/2. \tag{12a}$$

Thus, we have:

$$A_{0n} = (1/h)Q_n\sum_e(M_\rho)^0_{ge}(M_\sigma)^0_{ge}(-\delta_e\nu_e)^n \times\{\prod_{p=0}^{n}(\nu_{eg}-\nu_0+i\gamma_e+p\nu_e)^{-1} + \prod_{p=0}^{n}(\nu_{eg}+\nu_0+i\gamma+p\nu_e)^{-1}\} \tag{13}$$

where:

$$Q_n = \langle g0|Q^n|gn\rangle = \sqrt{n!/2^n} \tag{13a}$$
$$Q = \alpha_g(r-r_g^0) \tag{14}$$

ν_{eg} is the effective transition frequency from $|g\rangle$ to $|e\rangle$ and may be represented approximately, according to Eq. (12a), by:

$$\nu_{eg} \doteqdot \nu_{e0,g0} + \nu_e\delta_e^2/2 \tag{15}$$

which equals the vertical transition frequency from the $|g\rangle$ to the $|e\rangle$ state. Equation (15) indicates that the maximum Raman scattering would occur at the position of the absorption maximum. However, this statement should be modified slightly when applied to the real system, because we neglected the effect of the anharmonicity of the potential curves and the effect of the other virtual states. Therefore, there may occur the case in which the position of the maximum Raman scattering differs to some extent from that of the absorption maximum.

Next, let us deal with another specialized case where $r_g^0=r_e^0$ but where $\nu_e \fallingdotseq \nu_g$. The Franck-Condon overlap integrals in Eq. (4a) are calculated by a method similar to that used before. Then, the scattering tensor may be represented as:

$$A_{0,2n} = (1/h)\,Q_{2n}\sum_e(M_\rho)^0_{ge}(M_\sigma)^0_{ge}(-\nu_e\Delta_e)^n \times\{\prod_{p=0}^{n}(\nu_{eg}-\nu_0+i\gamma_e+p\nu_e)^{-1} + \prod_{p=0}^{n}(\nu_{eg}+\nu_0+i\gamma_e+p\nu_e)^{-1}\} \tag{16}$$

where

$$\Delta_e = (\nu_e-\nu_g)/(\nu_e+\nu_g) \tag{17}$$

retaining only the term which has the lowest order of Δ_e.[12]

The general case of $r_e^0 \fallingdotseq r_g^0$ and $\nu_e=\nu_g$ may be

10) W. Siebrand, *ibid.*, **46**, 440 (1967).
11) E. Hutchinson, *Phys. Rev.*, **36**, 410 (1930).
12) C. Ting, *Spectrochim. Acta*, **24A**, 1177 (1968).

treated by introducing explicitly ν_e and ν_g into Eq. (12), in which $\nu_e=\nu_g$ has been assumed, and by then combining this with Eq. (16). This leads to the following expression of $A_{0,n}$:

$$A_{0n} = \langle g0|A_- + A_+|gn\rangle \tag{18}$$

where:

$$A_\mp = (1/h)\sum_e \{(M_\rho)^0_{ge}(M_\sigma)^0_{ge}/(\nu_{eg}\mp\nu_0+i\gamma_e) \times (1+\nu_e\delta_e Q/\langle\nu_{eg}\mp\nu_0+i\gamma_e\rangle)^{-1} \times (1+\nu_e\Delta_e Q^2/\langle\nu_{eg}\mp\nu_0+i\gamma_e\rangle)^{-1} \tag{18a}$$

The bracket notation is used for the sake of simplicity. It indicates that, in expanding the above equation, $\langle\nu_{eg}\mp\nu_0+i\gamma_e\rangle^q$ must be replaced by $\prod_{p=1}^{q}(\nu_{eg}\mp\nu_0+i\gamma_e+p\nu_e)$. The contribution of Eq. (16) to the scattering tensor must be considerably smaller than that of Eq. (12), because usually $\Delta_e \ll 1$.

Supposing the A term is dominant in Eq. (4), and neglecting the contribution of Eq. (16), the intensity of the n-th overtone, I_{0n}, is expressed as:

$$I_{0n} = K(\nu_0-n\nu_g)^4 n!(\nu_0^2\delta_e^2/2)^n \times \prod_{p=0}^{n}\{(\nu_0-\nu_{eg}+p\nu_e)^2+\gamma_e^2\}^{-1} \tag{19}$$

when ν_0 approaches ν_{eg}.

Equation (19) has a form similar to Eq. (2) of Peticolas *et al*,[2] apart from the hot-band summation, which is neglected in our treatment. The main differences between our Eq. (19) and Eq. (2) of Peticolas *et al.* are, in the energy denominator, the presence of the effective transition frequency, ν_{eg}, and the vibrational frequency, ν_e, of the electronic excited state, instead of the 0-0 transition frequency and the vibrational frequency, ν_g, of the electronic ground state. In order to take into account of the effect of $\nu_e \neq \nu_g$ on the Raman intensity by means of the formulation of Peticolas *et al.* it is necessary to carry out a higher-order perturbation expansion. The physical meaning of the appearance of ν_e instead of ν_g is apparent, because the resonance should occur at the incident light frequency, $\nu_0=\nu_{eg}+p\nu_e$. When the vibrational frequencies, ν_g and ν_e, are quite different as in the case of iodine and bromine, the presence of ν_e instead of ν_g has a significant effect upon the resonance Raman intensity. The necessity of introducing the effective transition frequency, ν_{eg}, has clearly been shown experimentally by Yu and Shen using a tunable dye laser.[13] They have shown that the resonance Raman scattering cross-section of InSb as a function of the incident-light frequency has a maximum at an appreciably higher position than that of the reflectivity spectra.

The B_{mn} and B_{mn}' Vibronic Terms. In order to estimate the contribution of the B_{0n} and B_{0n} vibronic terms of Eqs. (4b) and (4c), it is necessary to carry out the following types of summation:

$$\sum_v \langle g0|ev\rangle\langle ev|Q|gn\rangle/(c+v) \quad \text{and} \quad \sum_v \langle g0|Q|ev\rangle\langle ev|gn\rangle/(c+v) \tag{20}$$

Using the relations applicable to a harmonic oscillator;

$$2Q|gn\rangle = \sqrt{n}\,|g,n-1\rangle + \sqrt{(n+1)}\,|g,n+1\rangle$$
$$Q|g0\rangle = |g,1\rangle$$

we can transform the above summation into the following form:

$$\sum_v \langle g0|ev\rangle\langle ev|g,\ n\pm1\rangle/(c+v) \tag{21a}$$

$$\sum_v \langle g1|ev\rangle\langle ev|gm\rangle/(c+v) \tag{21b}$$

Eq. (21a) is the same type of summation as appears in the calculation of the A-term (Eq. (8)); Eq. (21b) is generally difficult to estimate. When there is an ordinary Raman effect, $|c|\gg 0$, however, this summation may be written as:

$$\sum_v \langle g1|ev\rangle\langle ev|gm\rangle/(c+v) = \sqrt{n!/2^{n-1}}\,(-\delta_e)^{n-1}\prod_{p=1}^{n}(c+p)^{-1} \tag{22}$$

We assume that this equation holds approximately in the case of the resonance and preresonance Raman effect if we replace the c of Eq. (22) with the c^* of Eq. (11a), *i.e.*, if we introduce the effective transition frequency, ν_{eg}, and the damping constant, γ_e. Thus, the vibronic terms may be represented as:

$$B_{0n} = (1/h)Q_n\sum_e(-\nu_e\delta_e)^{n-1} \times\{(M_\rho)^0_{ge}(M_\sigma)'_{ge}+(M_\rho)'_{ge}(M_\sigma)^0_{ge}\} \times\prod_{p=1}^{n-1}\{(\nu_0-\nu_{eg}+i\gamma_e)+p\nu_e\}^{-1} \tag{23}$$

$$B'_{0n} = (1/h)Q_n\sum_e(-\nu_e\delta_e)^{n-1} \times\{(M_\rho)^0_{ge}(M_\sigma)'_{ge}+(M_\rho)'_{ge}(M_\sigma)^0_{ge}\} \times\prod_{p=1}^{n-1}\{(\nu_0+\nu_{eg}+i\gamma_e)+p\nu_e\}^{-1}. \tag{24}$$

Equations (23) and (24) indicate that, for the appearance of overtones by the vibronic mechanism, it is necessary, along with $M_{ge}'\neq 0$, that a molecule has a different geometry in the excited state from that of ground state, as in the A-term (Eq. 13).

As a summary of the above discussions of the A-term and the vibronic terms, the scattering tensor may be represented, using the same bracket notation as in Eq. (18b), by:

$$(\alpha_{\rho\sigma})_{0n} = \langle g0|S_- + S_+|gn\rangle$$
$$S_\mp = (1/h)\sum_e\{(M_\rho(Q))_{ge}(M_\sigma(Q))_{ge}/(\nu_{eg}\mp\nu+i\gamma_e)\} \times(1+\nu_e\delta_eQ/\langle\nu_{eg}\mp\nu_0+i\gamma_e\rangle)^{-1} \times(1+\nu_e\Delta_eQ^2/\langle\nu_{eg}\mp\nu_0+i\gamma_e\rangle)^{-1} \tag{25}$$

where $(M_\rho(Q))_{ge}=(M_\rho)_{ge}{}^0+(M_\rho)_{ge}{}'Q+\cdots$.
It may easily be seen that, under the appropriate conditions of the pre-resonant case, Eq. (25) gives the Shorygins semiclassical equation for the fundamental $n=1$,[6] using the relation:

$$\nu'_{eg} = (\partial\nu_{eg}/\partial Q)_0 = \nu_e\delta_e \tag{26}$$

13) P. Y. Yu and Y. R. Shen, *Phys. Rev. Lett.*, **29**, 468 (1972).

Comparison with Experiments

Holzer *et al.* observed the resonance Raman effect of iodine in a gas state up to the 15-th overtone using 4880 Å line of the argon ion laser as the exciting light.[1,3] Peticolas *et al.* have carried out a quantitative calculation of the relative intensities of these overtones with respect to the fundamental. The agreement with the observed data has been poor for the higher overtones.

Although several authors have emphasized the role of the continuous upper electronic state in the resonance Raman effect, we assume tentatively that the equations derived above are applicable to the case of the resonance Raman effect of iodine.[14-16]

Supposing that the contributions of the vibronic terms and Eq. (17) are negligible in the resonance Raman region, we re-calculated the relative intensities of the overtones of iodine with respect to the fundamental intensity: $R_n=I_{0n}/I_{01}$. R_n is represented, following Eq. (19), by:

$$R_n = (\nu_0-n\nu_g)^4/(\nu_0-\nu_g)^4(\nu_e^2\delta_e^2/2)^{n-1}n! \times \prod_{p=2}^{n}\{(\nu_{eg}-\nu_0+p\nu_e)^2+\gamma_e^2\}^{-1} \quad (28)$$

The δ_e, ν_{eg}, and γ_e values were determined so as to fit with the observed R_n, *i.e.*, so as to minimize $\sum_n |R_n^{calc}-R_n^{obs}|$, ($n$=2,3,·····,15). The ν_g and ν_e values were taken to be 215 cm^{-1} and 128 cm^{-1} respectively.[17] The results are shown in Table 1, along with the experimental data (Calc. 1 and Calc. 2). Although the results differ to some extent depending on the initial choice of the values of δ_e, ν_{eg} and γ_e, in any event the agreement between the calculated and the observed relative intensities are fairly good through the 15 overtones. The value, $|r_g^0-r_e^0|$=0.368~0.408 Å, calculated from δ_e using Eq. (9) coincides reasonably well with the observed value, 0.346 Å (Table 2). As to the effective transition frequency, a value of ν_{eg}= 20890~21200 cm^{-1} is obtained. This value is near to the frequency of the absorption maximum of iodine in gas (~20000 cm^{-1}). The ν_{eg} value calculated from Eq. (5), 17800~18200 cm^{-1}, is a little smaller than these. This difference probably arises from the neglect of the effect of anharmonicity and from the effect of the other virtual states in Eq. (5). It should be noted that the calculated value of the damping constant, γ =200~600 cm^{-1}, corresponds to the rate of the vibrational relaxation and the internal conversion, and is considerably larger than those of the fluorescence and the phosphorescence.[16] The calculations show that the introduction of the effective transition frequency, ν_{eg}, and the vibrational frequency, ν_e, of the electronic excited state in the energy denominator is important in obtaining agreement with the observed R_n.

Table 1. Intensities of overtones of iodine in gas relative to the fundamental

	Observed[1,2]	Calcd 1	Calcd 2	Calcd 3
R_2	0.71	0.672	0.675	0.708
R_3	0.55	0.531	0.550	0.538
R_4	0.45	0.450	0.486	0.450
R_5	0.36(±0.02)	0.391	0.442	0.388
R_6	0.25(±0.02)	0.340	0.402	0.339
R_7	0.22(±0.02)	0.293	0.359	0.296
R_8	0.22(±0.02)	0.248	0.312	0.257
R_9	0.194(±0.02)	0.204	0.263	0.219
R_{10}	0.194(±0.02)	0.163	0.213	0.183
R_{11}	0.167(±0.02)	0.127	0.167	0.151
R_{12}	0.139(±0.02)	0.096	0.126	0.121
R_{13}	0.111(±0.02)	0.070	0.091	0.096
R_{14}	0.084(±0.02)	0.050	0.063	0.074
R_{15}	0.084(±0.02)	0.034	0.042	0.056
δ_e		−6.34	−5.71	−6.37
$\nu_{eg}-\nu_0$ (cm^{-1})		691	397	737
γ_e (cm^{-1})		206	578	212
$\lvert r_g^0-r_e^0\rvert$ (Å)		−0.408	−0.368	−0.410
Δ_e		0	0	−0.36

To see the effect of Δ_e, we have calculated R_n on the basis of Eq. (18), considering Δ_e to be an adjustable parameter along with δ_e, ν_{eg} and γ_e. The results are shown in Table 1 (Calc. 3). As may be seen from Table 1, the introduction of Δ_e improves the agreement between the calculated and the observed relative intensities to some extent, but not very much. The calculated value of Δ_e=−0.36 is reasonable compared with the observed value, −0.254 (Table 2).

Strictly speaking, the equations derived above are applicable only to an isolated molecule. It is interesting, however, to apply these equations to a molecule in solution and to compare the results with that of gas obtained above. The intensity variation in the fundamental and the first overtone of iodine as a function of the exciting light frequency have been obtained by Mortensen in a chloroform solution.[18]

The relative intensities of the fundamental and the first overtone at the exciting light frequency, ν, relative to that of ν_0, $R_1(\nu,\nu_0)$ and $R_2(\nu,\nu_0)$, are given, following Eq. (19), by:

$$R_1(\nu,\nu_0) = \{(\nu-\nu_g)^4/(\nu_0-\nu_g)^4\} \times \prod_{p=0}^{1}\{(\nu_{eg}-\nu_0+p\nu_e)^2+\gamma_e^2\} \Big/ \prod_{p=0}^{1}\{(\nu_{eg}-\nu+p\nu_e)^2+\gamma_e^2\} \quad (29)$$

$$R_2(\nu,\nu_0) = \{(\nu-2\nu_g)^4/(\nu_0-2\nu_g)^4\} \times \prod_{p=0}^{2}\{(\nu_{eg}-\nu_0+p\nu_e)^2+\gamma_e^2\} \Big/ \prod_{p=0}^{2}\{(\nu_{eg}-\nu_0+p\nu_e)^2+\gamma_e^2\} \quad (30)$$

14) J. Behringer, *Z. Physik.*, **229**, 209 (1969).
15) M. Jacon, M. Berjot, and L. Bernard, *C. R. Acad. Sci., Paris, Ser. B*, **273**, 595 (1971).
16) M. Berjot, M. Jacon, and L. Bernard, *Opt. Commun.*, **4**, 246 (1971).
17) G. Herzberg, "Molecular Spectra and Molecular Structure, I. Spectra of Diatomic Molecules," 2nd Ed. Van Nostrand, Princeton, N. J. (1950).
18) O. S. Mortensen, *J. Mol. Spectry.*, **39**, 48 (1971).

TABLE 2. MOLECULAR CONSTANTS OF IODINE[17]

	D_e (eV)	r^0 (Å)	ν (cm^{-1})	$\nu_e x_e$ (cm^{-1})	$r_g^0 - r_e^0$	δ_e[a]	Δ_e[b]
$\|g\rangle$	1.54	2.67	215	0.6127	−0.346	−5.432	−0.254
$^3\Pi_{0u}^+$	0.54	3.016	128	0.834			

a) Calculated by Eq. (9). b) Calculated by Eq. (17).

TABLE 3. THE EXCITING LIGHT FREQUENCY DEPENDENCE OF RAMAN INTENSITY OF IODINE IN $CHCl_3$ SOLN[a]

	$R_1(\nu, \nu_0)$		$R_2(\nu, \nu_0)$		$R_2(\nu)$	
	Obsd.	Calcd.	Obsd.	Calcd.	Obsd.	Calcd.
5145 Å	1.00	1.00	1.00	1.00	0.70	0.74
5017 Å	0.91	0.94	0.97	0.91	0.75	0.68
4965 Å			0.74	0.81		
4880 Å	0.77	0.72	0.60	0.60	0.56	0.59
4765 Å	0.52	0.55	0.37	0.36	0.50	0.51
ν_{eg}	19220 cm^{-1}		19240		18600	
γ_e	2160 cm^{-1}		2140		2990	
$\|r_g^0 - r_e^0\|$					0.329 Å	

a) The observed data are taken from Ref. 18.

Applying these equations to the observed data, we can estimate γ_e and ν_{eg} so as to fit the observed data. The results are shown in Table 3. The agreement between the calculated and the observed values is fairly good. Furthermore, the values of $\gamma_e = 2160$ cm^{-1} and $\nu_{eg} = 19220$ cm^{-1} obtained from $R_1(\nu,\nu_0)$ coincide well with those of $\gamma_e = 2140$ cm^{-1} and $\nu_{eg} = 19240$ cm^{-1} obtained from $R_2(\nu,\nu_0)$. We have also determined ν_{eg}, γ_e, and δ_e from the exciting-light-frequency dependence of the first overtone with respect to the fundamental intensity, using the $R_2(\nu)$ of Eq. (28).

In the above calculations, we have neglected the effect of the hot-band summation. This effect is important in the higher overtones. The values of γ_e and δ_e derived from the R_n value of iodine gas would be increased and decreased respectively to some extent by taking into account the effect of the hot-band summation. This point will be investigated in a subsequent paper.

Finally, then, we can estimate $\gamma_e = 2000$—3000 cm^{-1} for iodine in a chloroform solution. This value is quite large compared with that of $\gamma_e = 200$—600 cm^{-1} of iodine in gas. This indicates that the damping constant is sensitively influenced by molecular interactions. The trend $\gamma_e(\text{soln}) \gg \gamma_e(\text{gas})$ seems reasonable because, in a solution, the molecular interactions are larger in gas, therefore, the excited state of a molecule usually has a smaller life-time.[19]

As a summary of the above discussions, we can say that the trend of the observed Raman intensities of iodine is explained well quantitatively by Eq. (19) in the resonance region. This would indicate that A-term of Eq. (4a) *i.e.*, the effect of the deformation of the molecular geometry and the vibrational frequency change in the excited state compared with that of the ground state, is a dominant factor in determining the resonance Raman intensities of iodine. Therefore, an analysis of the resonance Raman effect offers a means of estimating the molecular geometry and vibrational frequencies in the electronic excited state. The idea of the effective transition frequency and the introduction of the vibrational frequency, ν_e, of the electronic excited state in the energy denominator is necessary to obtain the simpler expressions and also to obtain an agreement with the observed data.

The author wishes to express his thanks to Professor Shiro Maeda of this Institute for his kind advice and discussions.

19) R. S. Becker, "Theory and Interpretation of Fluorescence and Phosphorescence," John Wiley & Sons, Inc., New York (1969).

An Investigation of the Gas-Solid Interface Reaction

Masayuki KATSUMOTO, Kazuo FUEKI, and Takashi MUKAIBO

Department of Industrial Chemistry, Faculty of Engineering, The University of Tokyo, Hongo, Bunkyo-ku, Tokyo 113

(Received May 2, 1973)

The isotopic exchange between H_2S and D_2 on molybdenum disulfide and manganese sulfide has been studied kinetically between 420° and 500 °C. The reaction proceeded *via* these steps:

$$H_2S + D_2 = D_2S + H_2$$

$$H_2 + D_2 = 2\,HD$$

From the analysis of the kinetic data, the rate constant of the sulfurization of both metal sulfides by "hydrogen sulfide,"[1] k_1, and that of their reduction by "hydrogen,"[1] k_1', were calculated. The dependence of these rate constants on the sulfur activity was determined. A possible mechanism of the reaction at the surface of the sulfides is discussed in this paper.

Kobayashi and Wagner first determined the rate of the gas-solid interface reaction, not only as a function of the partial pressure of the reactant gases, but also as a function of the activity of chemical species in a solid, in their study of the reduction of Ag_2S by "hydrogen". They proposed a mechanism in which e^-, S, S^-, and S^{2-} in Ag_2S act as reactant species.[2]

The isotopic exchange method, one of those by which the rate of gas-solid interface reaction can be determined as a function of the activity of chemical species in a solid, has been applied to oxide and sulfide systems.[3-5] As to sulfide systems, Cu_2S (p-type semiconductor) and β-$Fe_{1-x}S$ (metallic conductor) were studied by present authors and their collaborators.[4,5] The experimental results for β-$Fe_{1-x}S$ could not be explained by the mechanism proposed by Kobayashi and Wagner.[2]

The present work aims to examine whether or not the gas-solid interface reaction on MoS_2 (an intrisic semiconductor)[6] and MnS (a p-type semiconductor)[7] can be explained on the basis of the Kobayashi-Wagner mechanism, by using the isotopic exchange method.

Experimental

Isotopic Exchange Study. The apparatus, the method of the purification of gases, and the experimental procedure were essentially the same as in previous works.[4,5]

The sulfide samples were prepared as follows:

(a) *MoS_2 sample*: A single crystal of molybdenite was cloven into thin films, which were then minced into small pieces. The surface area was 2.19×10^3 cm^2 g^{-1}. Spectroscopic analysis revealed that the sample was of a high purity.

(b) *MnS sample*: Hydrogen sulfide of a 99.9% purity was introduced into an aqueous solution of high-purity manganese acetate in order to precipitate manganous sulfide. After filtration, the precipitate was treated *in vacuo* at 300 °C for 1 hr and then in a "hydrogen sulfide"-"hydrogen" mixture at 900 °C for 5 hr. The surface area was 1.87×10^3 cm^2 g^{-1}.

The isotopic exchange was carried out after chemical equilibrium had been reached between the sulfide sample and the "hydrogen sulfide"-"hydrogen" gas mixture. Therefore, a_s, the sulfur activity of the solid, defined as the pressure ratio of "hydrogen sulfide" to "hydrogen", was kept constant throughout the isotopic exchange run, irrespective of the change in the concentration of the isotopic species.

Results and Discussion

Isotopic Exchange Reaction. Figures 1 and 2 show the change in x_{H_2}, x_{HD}, and x_{D_2}, the mole fractions of H_2, HD, and D_2 respectively, at different sulfur activities in the presence of MoS_2.

As was mentioned in a previous paper,[5] the following two mechanisms are possible for the formation of H_2 and HD. In the first mechanism, H_2 and HD formed by these steps:

$$H_2S \rightleftharpoons HS(ad) + H(ad) \quad (1a)$$

$$D_2 \rightleftharpoons 2\,D(ad) \quad (1b)$$

$$D(ad) + H(ad) \rightleftharpoons HD \quad (1c)$$

$$H(ad) + H(ad) \rightleftharpoons H_2 \quad (1d)$$

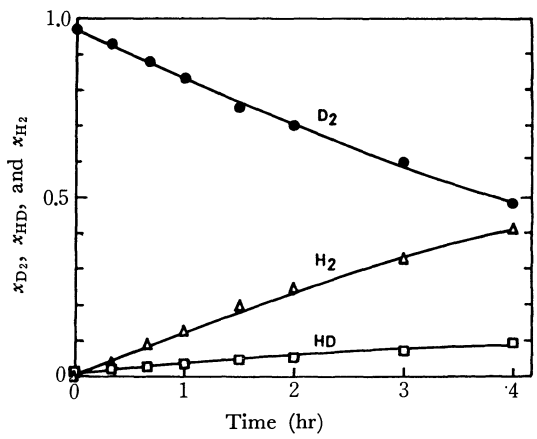

Fig. 1. Change in x_{D_2}, x_{HD}, and x_{H_2} with time.
(MoS_2, 480 °C, $P_{H_2S}°=179.9$ mmHg, $P_{D_2}°=30.0$ mmHg, $a_s=6$)

1) Terms such as "hydrogen" and "hydrogen sulfide" are used in a generic sense, irrespective of the isotopic species. The chemical symbols "H_2S" and "H_2" are employed for the chemical species of "hydrogen sulfide" and "hydrogen" respectively.

2) H. Kobayashi and C. Wagner, *J. Chem. Phys.*, **26**, 1609 (1957).

3) H. J. Grabke, *Ber. Bunsenges. Phys. Chem.*, **69**, 48 (1965).

4) K. Fueki, H. Inaba, and T. Mukaibo, This Bulletin, **43**, 23 (1970).

5) M. Katsumoto, K. Fueki, and T. Mukaibo, *ibid.*, **46**, 1624 (1973).

6) I. Nakata, *Kobayashi Rigaku Kenkyu-jo Hokoku*, **6**, 180 (1956).

7) K. Fueki, Y. Oguri, and T. Mukaibo, *Denki Kagaku*, **38**, 758 (1970).

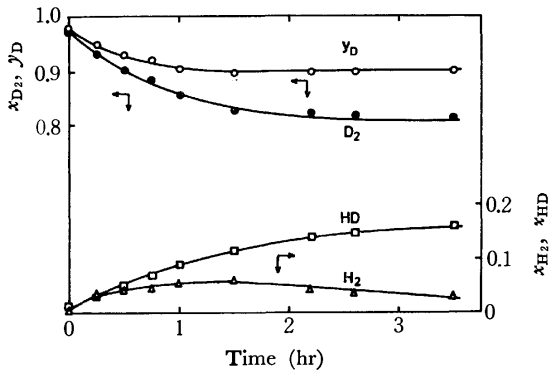

Fig. 2. Change in x_{D_2}, x_{HD}, x_{H_2}, and y_D with time.
(MoS_2, 480 °C, $P_{H_2S}^{\circ}=10.3$ mmHg $P_{D_2}^{\circ}=102.7$ mmHg, $a_s=1/10$)

where H(ad), D(ad), and HS(ad) represent the H, D, and HS adsorbed on the surface of sulfide.

In the second mechanism, H_2S is directly converted to H_2:

$$H_2S \rightleftharpoons H_2+S(ad) \qquad (2a)$$

and then H_2 reacts with D_2 to form HD:

$$H_2 + D_2 = 2\,HD \qquad (2b)$$

where S(ad) represents the S adsorbed on the surface of sulfide. Reaction (2a) is characterized as a redox reaction.

At the higher range of a_s, the HD formation is not remarkable (Fig. 1). Thus, it may be concluded that the exchange reaction proceeds *via* Step (2a). At $a_s=1/10$, HD formation is remarkable. After increasing in the initial period, x_{H_2} reaches its maximum value, and then decreases. We can estimate the contribution of the (2a) mechanism to the transfer of chemical species between "H_2S"[1] and "H_2"[1] at $a_s=1/10$ as follows.

Les us express the rate of the formation of H_2 in the manner proposed by Boreskov[8] and Novakova[9]:

$$\frac{1}{A}\frac{dn_{H_2}}{dt} = R_1(x_{H_2S}-x_{H_2}) + R_2[\alpha(1-y_D')^2 + (1-\alpha)(1-y_D')(1-y_D)-x_{H_2}] + R_3[(1-y_D)^2-x_{H_2}] \qquad (3)$$

where, n_{H_2} is the number of moles of H_2, x_{H_2S} is the mole fraction of H_2S, $y_D=x_{D_2}+1/2x_{HD}$, $y_D'=x_{D_2S}+1/2x_{HDS}$, and A is the surface area. R_1 and R_2 are the rates of the transfer of chemical species between "H_2S" and "H_2" by Mechanisms (2a) and (1a)—(1d) respectively. R_3 is the rate of isotopic exchange by Reaction (2b). α is a parameter related to the surface concentration of "HS" and "H"[1] and ranges from zero to unity.

As is shown in Fig. 2, y_D decreases in the initial period, reaches a constant value at the time corresponding to the maximum of x_{H_2}, and then remains unchanged. At $a_s=1/10$, the ratio of y_D is 1/10 and $y_D^e=y_D'^e=0.909$. Therefore, the observed constant value of y_D is equal to y_D^e within the limits of experimental error. This means that the isotopic equilibrium between "H_2S" and "H_2" is attained at the time corresponding to the maximum of x_{H_2}. Putting $dn_{H_2}/dt=0$ and replacing y_D and y_D' by y_D^e, we obtain:

$$R_1(x_{H_2S}-x_{H_2}) + (R_2+R_3)[(1-y_D^e)^2-x_{H_2}] = 0 \qquad (4)$$

i. e.:

$$\frac{R_1}{R_2+R_3} = \frac{x_{H_2}-(1-y_D^e)^2}{x_{H_2S}-x_{H_2}} \qquad (5)$$

Since $x_{H_2S}+1/2x_{HDS}=1-y_D'^e=1-y_D^e$, $x_{H_2S}<1-y_D^e$. Therefore,

$$\frac{x_{H_2}-(1-y_D^e)^2}{x_{H_2S}-x_{H_2}} > \frac{x_{H_2}-(1-y_D^e)^2}{(1-y_D^e)-x_{H_2}} \qquad (6)$$

By inserting $y_D^e=0.909$ and $\{(x_{H_2})_{max}\}_{obsd}=0.06$ we obtain 1.7 as the numerical value of the right-hand of side Eq. (6). Since $R_1/(R_2+R_3)>1.7$, one can conclude that the most predominant mechanism of isotopic exchange between "H_2S" and "H_2" is (2a), even at $a_s=1/10$.

x_{H_2}, x_{HD}, x_{D_2}, and y_D in the presence of MnS change with time in a way similar to that seen in the case of

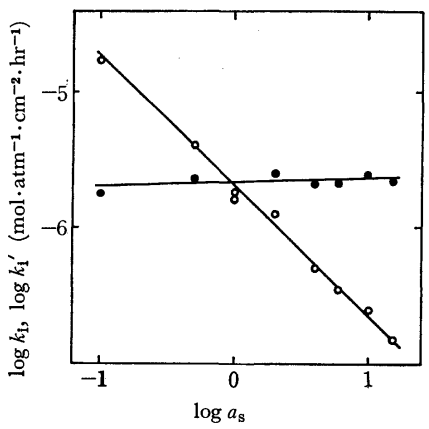

Fig. 3. Plot of $\log k_1$ and $\log k_1'$ against $\log a_s$.
(MoS_2, 480 °C)
○: k_1, ●: k_1'

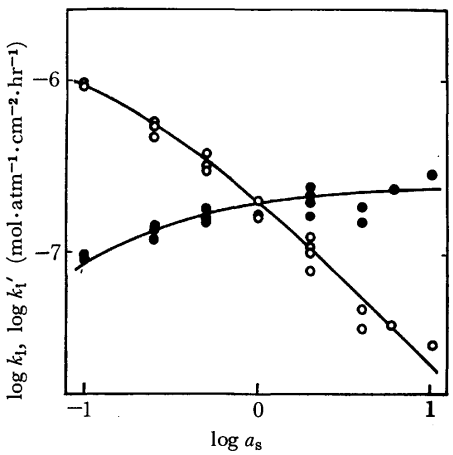

Fig. 4. Plot of $\log k_1$ and $\log k_1'$ against $\log a_s$.
(MnS, 480 °C)
○: k_1, ●: k_1'
solid line: curves of $\log(1-\theta)$ and $\log\theta$ *vs.* $\log a_s$

8) G. K. Boreskov, *Advances in Catalysis*, **15**, 285 (1964).
9) J. Novakova, *Catal. Rev.*, **4**, 77 (1971).

MoS_2. Therefore, one can determine k_1 and k_1', the rate constants of the sulfurization and reduction of Reaction (2a) respectively, by means of the method proposed in the previous paper.[5]

Figures 3 and 4 give the plots of log k_1 and log k_1' against log a_s. The plots for MoS_2 (Fig. 3) are linear, and the slopes for k_1 and k_1' are −0.98 and 0.02 respectively. The plots for MnS are curved (Fig. 4). The solid line in Fig. 4 is evaluated theoretically, as will be described later. The Arrhenius plots of k_1 at $a_s=1$ for both sulfides are given in Fig. 5. The activation energies are determined as 24.6 kcal mol^{-1} for MoS_2 and 26.1 kcal mol^{-1} for MnS.

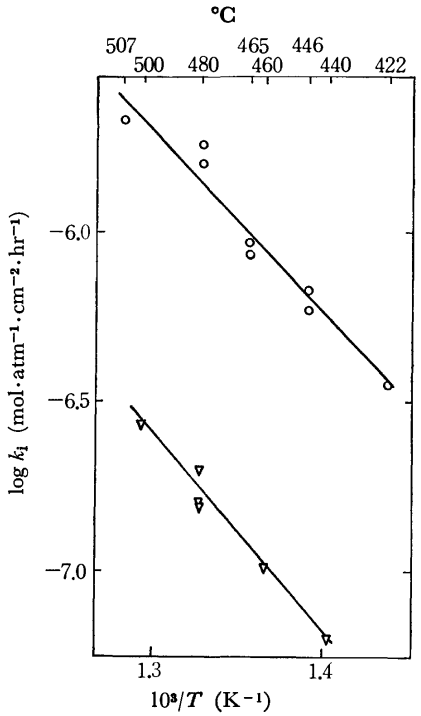

Fig. 5. Arrhenius plots for k_1 at $a_s=1$.
○: MoS_2, ▽: MnS

Table 1 summarizes the results of the present study, together with those obtained in the previous studies. It is noteworthy that the activation energies, $(\partial \log k_1/\partial \log a_s)$ and $(\partial \log k_1'/\partial \log a_s)$, for all sulfides are nearly the same.

Mechanism of the Surface Reaction. In order to explain the a_s dependence of the rate constants of the redox reaction (2a) on the surface of Ag_2S, Kobayashi and Wagner proposed the following mechanisms:

$$\text{"}H_2S\text{"}^{1)} \rightleftharpoons \text{"}H_2\text{"}^{1)} + S(ad) \quad (7A)$$

$$\text{"}H_2S\text{"} + e^- \rightleftharpoons \text{"}H_2\text{"} + S^-(ad) \quad (7B)$$

$$\text{"}H_2S\text{"} + 2e^- \rightleftharpoons \text{"}H_2\text{"} + S^{2-}(ad) \quad (7C)$$

where S(ad), S^-(ad), and S^{2-}(ad) are the sulfur atom and the mono- and di-valent sulfur ions adsorbed on Ag_2S and where e^- is an electron. The rate equation for Reactions (7A) to (7C) can be expressed in a generallized formula:

$$v = k_1 P_{\text{"}H_2S\text{"}} a_e^m - k_1' P_{\text{"}H_2\text{"}} a_s^{m-} \quad (8)$$

where m is the integer characteristic of the reaction mechanism, namely:

$m = 0$ for Mechanism (7A)
$m = 1$ for Mechanism (7B)
$m = 2$ for Mechanism (7C)

Let us first discuss the mechanism of the redox reaction on the surface in terms of the Kobayashi-Wagner mechanism.

According to the results of Nakata's conductivity measurement,[6] MoS_2 seems to be an intrinsic semiconductor above 440 °C. In the intrinsic region, one can expect the conductivity to be independent of a_s. This relationship was confirmed experimentally in the temperature range of 420° and 550 °C and in the a_s range of 1/10 to 10. Therefore, it is considered that the activity of electrons, a_e, in MoS_2 is not influenced by a_s. Assuming the following equilibria:

$$S^- \rightleftharpoons S + e^- \quad (9a)$$

$$S^{2-} \rightleftharpoons S + 2e^- \quad (9b)$$

we obtain:

$$a_{s^-} \propto a_s \quad (10a)$$

$$a_{s^{2-}} \propto a_s \quad (10b)$$

The insertion of Relations (10a) and (10b) into Eq. (8) yields:

$$v = k_2 P_{\text{"}H_2S\text{"}} - k_2' P_{\text{"}H_2\text{"}} a_s \quad (11)$$

The activity of electrons in MnS is proportional to $a_s^{-1/3}$.[7] The combination of this dependence with the equilibrium conditions for (9a) and (9b) gives:

$$a_{s^-} \propto a_s^{2/3} \quad (12a)$$

$$a_{s^{2-}} \propto a_s^{1/3} \quad (12b)$$

By inserting Relations (12a) and (12b) into Eq. (8), we obtain:

$$v = k_3 P_{\text{"}H_2S\text{"}} a_s^{-m/3} - k_3' P_{\text{"}H_2\text{"}} a_s^{1-2m/3} \quad (13)$$

Table 1.

Solid	Cu_2S[4]	β-$Fe_{1-x}S$[5]	MoS_2	MnS
Type of conductor	p-type semiconductor	metallic conductor	intrinsic semiconductor	p-type semiconductor
$\frac{\partial \log k_1}{\partial \log a_s}$ [a]	−1.07	−0.97	−0.98	−0.95—−0.6[b]
$\frac{\partial \log k_1'}{\partial \log a_s}$ [a]	−0.07	0.03	0.02	0.05—0.4[b]
Activation energy (kcal mol^{-1})	27.8	26.8	24.7	26.1

a) at 480 °C. b) As seen in Fig. 4 the plots are curved.

The a_s dependence of the reaction rate expressed by Eqs. (11) and (13) does not interpret the results observed in this study.

As has been mentioned above, the activation energies, $(\partial \log k_1/\partial \log a_s)$ and $(\partial \log k_1'/\partial \log a_s)$, for Reaction (2a) are almost the same for all the sulfides studied. This fact suggests that the mechanism of Reaction (2a) is the same, irrespective of the kind of sulfides.

According to the results of an adsorption experiment[10] in which the adsorption of sulfur on metals was studied in "H_2"-"H_2S" gas mixtures at higher temperatures, the coverage increases rapidly from zero to a saturation value within a narrow region of log a_s as log a_s increases. A similar adsorption curve was observed in the case of the adsorption of oxygen atoms on copper at high temperatures.[11]

In a case where the interaction between adsorbed sulfur atoms can be neglected, θ, the fraction of surface adsorption sites occupied by adsorbed sulfur atoms, S(ad), can be expressed by the Langmuir equation:

$$\theta = \frac{K(P_{\text{"}H_2S\text{"}}/P_{\text{"}H_2\text{"}})}{1+K(P_{\text{"}H_2S\text{"}}/P_{\text{"}H_2\text{"}})} = \frac{a_s/a_s^0}{1+(a_s/a_s^0)} \qquad (14)$$

where K is a constant and where a_s^0 is the sulfur activity at which $\theta=0.5$ is attained.

If the exchange of sulfur atoms between "H_2S"-"H_2" gas mixtures and a solid occurs by means of the mechanism:

$$\text{"}H_2S\text{"} + \square\,(\text{vacant sites}) \rightleftharpoons \text{"}H_2\text{"} + \text{S(ad)} \qquad (15)$$

and if Eq. (15) is the rate-determining step of the redox reaction, the rate equation can be expressed as:

$$v = k(1-\theta)P_{\text{"}H_2S\text{"}} - k'\theta P_{\text{"}H_2\text{"}} \qquad (16)$$

Eq. (16) indicates that k_1 and k_1' are proportional to $(1-\theta)$ and θ respectively.

When Eq. (14) holds for the adsorption, the plots of θ, log $(1-\theta)$, and log θ against $\log(a_s/a_s^0)$ are as is shown in Fig. 6. In a range of a_s/a_s^0 much lower than unity, the slope of the plot of $\log(1-\theta)$ *vs.* $\log(a_s/a_s^0)$ is 0. However, this slope gradually changes in the vicinity of $a_s/a_s^0=1$, and in a range of a_s/a_s^0 much higher than unity the value of the slope becomes -1. The slope of the plot of log θ *vs.* $\log(a_s/a_s^0)$ changes with $\log(a_s/a_s^0)$ in the manner the inverse of that of log $(1-\theta)$ *vs.* $\log(a_s/a_s^0)$.

From a comparison of Figs. 3 and 4 with Fig. 6, it may be concluded that Reaction (15) is the rate-determining step of the redox reaction and that the surface sites of MoS_2 are almost covered with sulfur atoms during the reaction, while those of MnS are only partially covered.

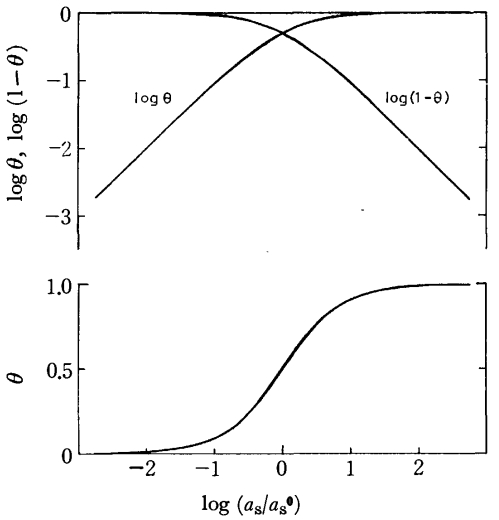

Fig. 6. Schematic representation of θ, log θ and log $(1-\theta)$ against log (a_s/a_s^0) when θ is represented by the Langmuir equation.

Summary

1) The isotopic exchange between H_2S and D_2 on MoS_2 and MnS were investigated as a function of the temperature and the sulfur activity of the sulfides.

2) It was found that the isotopic exchange reaction proceeds *via* these steps:

$$H_2S + D_2 = D_2S + H_2$$
$$H_2 + D_2 = 2\,HD$$

3) The rate constant of the sulfurization of the sulfides, k_1, and that of the reduction k_1', were calculated, and the dependence of these rate constants on the sulfur activity was determined. The activation energies were 24.6 kcal mol^{-1} for MoS_2 and 26.1 kcal mol^{-1} for MnS.

4) The a_s dependence of the rate constants of the redox reaction on the surfaces of sulfides could not be explained by the Kobayashi-Wagner theory. It could, however, be explained by assuming that Reaction (15) is rate-controlling.

The authors wish to express their thanks to Dr. Ju Kumanotani of the Faculty of Engineering, University of Tokyo, for his help in carrying out the Mass spectroscopic analysis.

10) J. Benard, *Catal. Rev.*, **3**, 93 (1970).
11) H. D. Hondros and M. McLean, *Nature*, **224**, 1296 (1969).

Polarized Absorption Spectra of Single Crystals of Ion Radical Salts. III. Temperature Dependence of the Crystal Spectra of Potassium-Chloranil

Shoji HIROMA and Haruo KURODA

Department of Chemistry, Faculty of Science, The University of Tokyo, Hongo, Bunkyo-ku, Tokyo 113

(Received May 4, 1973)

The polarized absorption spectra in the 10000—37000 cm^{-1} region were observed on the single crystal of the water-free modification of the potassium-chloranil salt, $K^+ \cdot (chloranil)^-$, by using a microspectrophotomer, and the variation of the spectra with temperature was examined. The crystal gives a near-infrared absorption band associated with the charge transfer between chloranil radical anions, the maximum of which is located at 11.5×10^3 cm^{-1}. The absorption bands in the 20000—37000 cm^{-1} region were assigned to the local-excitation bands associated with the transitions in the chloranil anion. The intensity of the charge-transfer band gradually increases on lowering the temperature. An abrupt increase of intensity occurrs in the charge-transfer band at the phase-transition point. There is a close correlation between this change and the temperature dependence of the paramagnetic susceptibility of the salt.

The potassium-chloranil anion radical salt, $K^+ \cdot (chloranil)^-$, has been reported to exhibit a phase transition at about 210 K, where the salt changes from the "low susceptibility" to the "high susceptibility" form.[1-3] It was found by Andre and Weill[3] that the latter form is stabilized when the powder of K·(chloranil) is dispersed in KBr matrix, whereas the former form is stabilized when dispersed in LiF matrix, and a strong near-infrared band appears in the optical absorption spectrum of the powder dispersed in LiF pellet, but not in the spectrum of the powder dispersed in KBr pellet. They also examined the polarizations of the absorption bands of a single crystal by means of an optical system composed of a polarizing microscope and an interference filter, and confirmed that the near-infrared absorption band mentioned above is polarized in the direction of the molecular columns of chloranil anion, hence is a charge-transfer band. But, the details of the single crystal spectrum has not been reported.

The room-temperature absorption spectrum of K·(chloranil) powder has been also given by Iida[4] and by Sakai *et al.*[5]

Although these previous authors have not described the effect of water, we noticed that the K·(chloranil) salt has a tendency to take water molecules into the crystal lattice, particularly, when it is kept in the form of a crystalline powder, and there is an appreciable difference in the single-crystal spectrum between the water-free and water-containing modifications.

Recently, the crystal structure of the water-free modification at the room temperature was determined by Konno *et al.*[6] Thus, in the present study, we have investigated the polarized absorption spectrum of the single crystal of the water-free modification of K·(chloranil) and examined its temperature dependence.

Experimental

The polarized absorption spectra were measured by means of a microspectrophotometer equipped with a small cryostat at the specimen stage to keep the crystals at low temperature.[7,8] The measurement was done over the temperature range from the room temperature to 160 K.

The K·(chloranil) salt was synthesized according to the method reported by Torrey and Hunter.[9] The single crystals of microscopic size[10] for the measurement of absorption spectrum were prepared by the recrystallization either from acetone solution or from acetonitrile solution. In this case, the solvent and/or water molecules are included in the crystal to give the solvent-containing modification, but they can be easily taken out from the crystal by evacuation. In the present study, the specimen was placed in the cryostat and evacuated for a period sufficient to convert the crystals to the solvent-free state prior to the measurements of spectra, and the spectrum was observed without breaking the vacuum.

According to Konno *et al.*,[6] there are two solvent-free modifications of the K·(chloranil) salt at the room temperature, which are called the α- and β-form respectively. We examined the X-ray diffraction pattern of the evacuated powder. Although most diffraction lines were identified as those of the α-form, there were weak lines which were due to the β-form: the amount ratio of the α-form to the β-form was estimated as about 10 : 1. In carrying out the measurement with the microspectrophotometer, it was not possible to differentiate the β-form crystals from the α-form ones. We observed the spectra on several different crystals but obtained identical results. Therefore, we shall tentatively assume that the spectra discussed in the present paper are those of the α-form crystal.

Results and Discussion

Room Temperature Spectra and Assignment of Absorption Bands. According to Konno *et al.*, the α-form crystal is orthorhombic, space group $P2_12_12_1$ with unit cell dimension: $a=13.49$, $b=17.02$, $c=4.03$ Å.[6] The

1) J. J. Andre, J. Clementz, R. Jesser, and G. Weill, *C. R. Acad. Sci., Paris Ser. B*, **266**, 1057 (1968).
2) J. J. Andre and G. Weill, *ibid.*, **269**, 499 (1969).
3) J. J. Andre and G. Weill, *Chem. Phys. Lett.*, **9**, 27 (1971).
4) Y. Iida, This Bulletin, **43**, 2772 (1970).
5) N. Sakai, I. Shirotani, and S. Minomura, *ibid.*, **44**, 675 (1971).
6) M. Konno, H. Kobayashi, F. Marumo, and Y. Saito, *ibid.*, **46**, 1987 (1973).
7) H. Kuroda, T. Kunii, S. Hiroma, and H. Akamatsu, *J. Mol. Spectrosc.*, **22**, 60 (1967).
8) The cryostat was designed and constructed by Mr. K.Kaneko in our laboratory.
9) H. A. Torrey and W. Hunter, *J. Amer. Chem. Soc.*, **34**, 702 (1912).
10) The crystals used here were thin plates elongated along c-axis, (20—30 μ in length), the width in the b-axis direction being about 5 μ.

unit cell contains four formula units of K·(chloranil), and the chloranil anions are stacked face-to-face on each other to form molecular columns parallel to the c-axis.

The polarized absorption spectra were measured on the (100) face of a single crystal for the polarizations parallel to the b- and c-axes respectively. The spectra obtained at the room temperature are shown in Fig. 1. The wave number and the relative intensity of each observed peak are listed in Table 1.

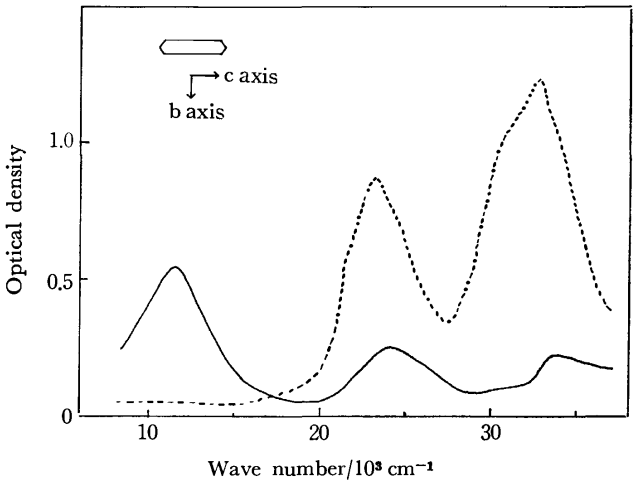

Fig. 1. Room-temperature spectra of the potassium-chloranil crystal.

(—— c-axis spectrum, ····· b-axis spectrum)

Table 1. Wave numbers and relative intensities of absorption peaks

(Intensities are given in parentheses)

	c-axis spectrum $\bar{\nu}$ [10^3 cm^{-1}]		b-axis spectrum $\bar{\nu}$ [10^3 cm^{-1}]	
CT-band	11.5	(0.62)		
($^2B_{1u}\leftarrow{}^2B_{2g}$)			23.1	(1.00)
($^2A_u\leftarrow{}^2B_{2g}$)	24.0	(0.28)		
($^2B_{1u}\leftarrow{}^2B_{2g}$)			30.7 32.7	(1.66)
	33.4	(0.3)		

The 11.5×10^3 cm^{-1} band is strongly polarized in the c-axis direction which is the direction of the column of the chloranil anion. In this region, we can expect no local-excitation band associated with the transition in the chloranil anion. Thus we can safely assign this band to the charge-transfer band due to the interaction between chloranil anions. Although Andre and Weill[3] reported that the charge-transfer band disappears in the "high susceptibility" form, this band is observed still with a considerable intensity in the c-axis spectrum at the room temperature.

In order to find out the interpretation for the spectra in the region above 20000 cm^{-1}, we carried out the SCF-MO-CI calculations on the transition in the free chloranil anion. We used here the method of Longuet-Higgins and Pople for the open-shell π-conjugated system.[11] The semiemprical parameters were determined by using the Nishimoto-Mataga's formula for the two-center repulsion integrals,[12] and the Nishimoto-Forster's formula[13] for the two-center resonance integrals.[14] We assumed the D_{2h} geometry for the chloranil ion, and took the bond lengths and bond angles estimated from the crystal structure data of the chloranil salt of Würster's blue.[15] In Fig. 2, the results of calculation are compared with the transitions observed in the solution spectrum of the chloranil anion. There are two types of transition, namely, $^2B_{1u}\leftarrow{}^2B_{2g}$ and $^2A_u\leftarrow{}^2B_{2g}$, the transition moments of which are respectively parallel and perpendicular to the molecular axis connecting the two oxygen atoms. Although there are some discrepancies between the calculation and observation, we can assign the absorption bands observed in the solution spectrum at 22.2×10^3 cm^{-1} (2.75 eV) and 31.1×10^3 cm^{-1} (3.86 eV) respectively to the first and second $^2B_{1u}\leftarrow{}^2B_{2g}$ transitions, and the one observed at 27.5×10^3 cm^{-1} (3.14 eV) to the first $^2A_u\leftarrow{}^2B_{2g}$ transition. On the basis of such interpretation of the solution spectrum of the chloranil anion, we examined the crystal spectrum. If we assume the oriented-gas model and estimate the dichroic ratio, I_b/I_c, of absorption band for the α-form crystal of the potassium-chloranil, we obtain 3000 for the $^2B_{1u}\leftarrow{}^2B_{2g}$ transition and 0.32 for the $^2A_u\leftarrow{}^2B_{2g}$ transition of the chloranil anion. Thus an absorption band due to a $^2B_{1u}\leftarrow{}^2B_{2g}$ transition should be almost completely polarized in the b-axis direction when the crystal spectrum is observed on the (100) face, while the one due to a $^2A_u\leftarrow{}^2B_{2g}$ transition should be stronger in the c-axis spectrum than in the b-axis spectrum.

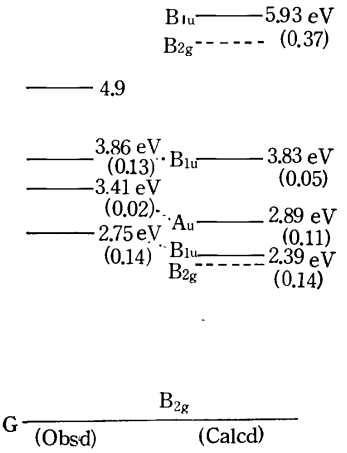

Fig. 2. Observed and calculated energy levels of the chloranil anion, (—— allowed, ····· forbidden). The oscillator strengths are given in parentheses.

11) H. C. Longuet-Higgins and J. A. Pople, *Proc. Phys. Soc., Ser. A*, **68**, 591 (1955).

12) K. Nishimoto and M. Mataga; *Z. Phys. Chem.* (Frankfurt), **12**, 335 (1957).

13) K. Nishimoto and L. S. Forster, *Theor. Chim. Acta*, **3**, 407 (1965); **4**, 155 (1966).

14) The parameters used for chlorine atom are as follows: $-W_\mu=23.3$ eV, $\gamma_{\mu\mu}=10.79$ eV, $\beta_{C\text{-}Cl}=2.99\ r-6.00$ eV, where r is the interatomic distance.

15) J. L. de Boer and A. Vos, *Acta Crystallogr.*, **B24**, 720 (1968).

Thus the 32.7×10^3 cm^{-1} band observed in the b-axis spectrum can be assigned to the local-excitation band associated with the 31.1×10^3 cm^{-1} ($^2B_{1u}\leftarrow{}^2B_{2g}$) transition of the chloranil anion, although a weak absorption peak is observable at 33.4×10^3 cm^{-1} in the c-axis spectrum. Seemingly, the first strong absorption band in the b-axis spectrum observed at 23.1×10^3 cm^{-1} is associated with the 22.2×10^3 cm^{-1} ($^2B_{1u}\leftarrow{}^2B_{2g}$) transition of the chloranil anion. However, the dichroic ratio in this region is evidently too small. It should be noted that, in the 20000—30000 cm^{-1} region, we can expect another absorption band associated with the 27.5×10^3 cm^{-1}($^2A_u\leftarrow{}^2B_{2g}$) transition of the chloranil anion. Thus, it is likely that the 24.0×10^3 cm^{-1} band in the c-axis spectrum is not the c-axis component corresponding to the 23.1×10^3 cm^{-1} band of the b-axis spectrum, but is the one mainly due to the $^2A_u\leftarrow{}^2B_{2g}$ transition.

Temperature Dependence of the Spectra. The crystal spectra observed at several different temperatures are shown in Fig. 3. We found that a significant change appeared mainly in the region of the charge-transfer band. Only a small change was detected in the region of local-excitation bands. Above the phase-transition point, the intensity of the charge-transfer band gradually increased on lowering the temperature. An abrupt rise of intensity occurred near the phase-transition point with a decrease in the band width.

In Fig. 4, the intensity change of the charge-transfer band is compared with the change in the magnetic susceptibility.[16] Clearly there is a close correlation between them. The behavior found here is quite analogous to the one reported for the Würster's blue perchlorate. The latter has been explained with the model that the interaction between neighboring Würster's blue cation radicals gives a singlet state and a triplet state, in which the former is a little stabilized in respect to the latter, and the intensity of the charge-transfer band is governed by the singlet population in the crystal while the paramagnetism is governed by the triplet population.[17] A similar model seems to be applicable also for the K·(chloranil) salt.

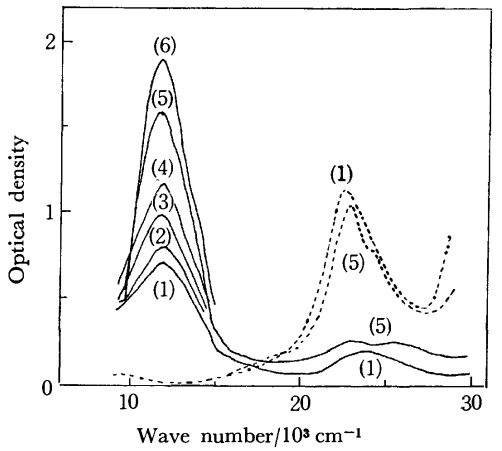

Fig. 3. Temperature dependence of the crystal spectra of the potassium-chloranil. (1): 297 K, (2): 280 K, (3): 240 K, (4): 218 K, (5): 209 K, and (6): 163 K.
(—— c-axis spectrum, ····· b-axis spectrum)

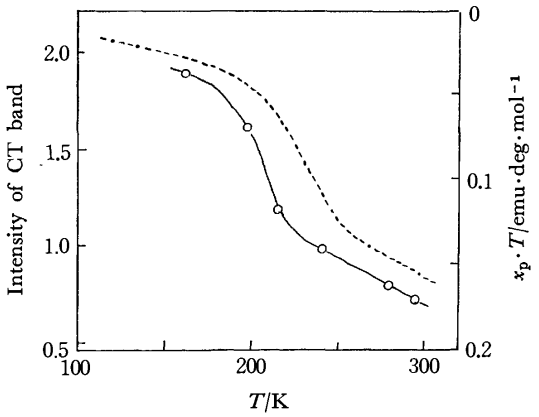

Fig. 4. Variation of the intensity of the charge-transfer band (——) and the magnetic susceptibility (·····)

In the room-temperature phase of the K·(chloranil), the chloranil anions are equally spaced in the column to give a crystal structure of monomeric form, the intermolecular spacing being 3.47 Å. The abrupt intensity increase of the charge-transfer band at the transition point would suggest that the low-temperature phase has a crystal structure of a dimeric arrangement of the chloranil anion, as in the case of monomeric-dimeric transition of the Würster's blue perchlorate. In this connection, it is interesting to see that, in the b-axis spectrum observed at a low temperature, a shoulder appeared at about 25×10^3 cm^{-1}. The chloranil anion dimer formed in solution has been reported to give a charge-transfer band at 14.9×10^3 cm^{-1} and a local excitation band at 26.3×10^3 cm^{-1}.[5] It is possible that the 25×10^3 cm^{-1} shoulder is the one corresponding to the 26.3×10^3 cm^{-1} band of the dimer. It would be of particular interest to examine if this shoulder grows up at a lower temperature. Unfortunately, however, we were not able to confirm this because of the limitation of our experimental set-up.

The authors wish to thank Professor Y. Saito and Miss M. Konno of the Institute for Solid State Physics of the University of Tokyo for allowing us to use the data of the crystal structure of the potassium-chloranil salt prior to the publication. Thanks are also due to Dr. T. Ohta for his help in the calculations of the electronic states of the chloranil anion.

16) The magnetic susceptibility data used here are those measured by Mr. T. Mizoguchi in our laboratory by means of a Faraday-type magnetic balance.

17) T. Sakata and S. Nagakura, This Bulletin, **42**, 1497 (1969).

Studies on Fragment Ion Distribution and Reaction with a Charge Spectrometer. V. Applicability of the MO Theory to the Fragmentation of Alkanes by Charge Exchange

Shigeru IKUTA, Kenji YOSHIHARA, and Takanobu SHIOKAWA

Department of Chemistry, Faculty of Science, Tohoku University, Aoba, Sendai 980

(Received May 31, 1973)

The relation between the fragment ion distribution and recombination energy of the incident positive ions was studied by means of charge exchange reactions. The energy range which is consistent with the molecular orbital (MO) theory proposed by Hirota to account for the mass spectra by electron impact was also investigated, and the usefulness of the theory was discussed. The energy range to which the MO theory is applicable is very limited, the fragment ions produced at the high recombination energy to which it is apparently applicable, being the C_2, C_3 and C_1 ion groups. It is probable that these species are not produced directly from the parent but by degradation mechanisms *via* intermediate steps, thus causing disagreement with the MO theory. Its applicability to alkanes is open to question. The dissociation schemes on *n*-alkanes are presented from the expreimental results.

Mass spectra obtained by electron impact are utilized for the identification of organic compounds. Although mass spectroscopic analysis is widely used, only empirical or semi-empirical rules have been used to explain the experimental results.[1] The theory of mass spectra by electron impact is important for studying the initial processes of radiation actions on various substances since the interaction of radiation with materials is attributed almost substantially to excitation and/or ionization by radiation-induced electrons.

In 1952 Rosenstock *et al.*[2] proposed a quasi-equilibrium theory to account for the mass spectra of relatively simple organic substances by electron impact, the underlying assumptions of the theory being as follows:

(1) The electronically excited molecular ion produced by interaction of the molecule with an electron changes swiftly into the electronically ground but vibrationally excited molecular ion.

(2) The fragment ions are formed by unimolecular decomposition of the vibrationally excited molecular ion involving competing and successive processes.

(3) The rate constants of the elementary processes are determined by the use of the absolute rate theory.

They estimated the breakdown curve of the *n*-propane molecular ion, in qualitative accordance with the experimental results, but quantitative agreement was not so good.

Efforts were made to improve the agreement of the theory with experimental results.[3] Vestal *et al.*[4] developed a method of enumerating the states and succeeded in evaluating the mass spectra quantitatively. In this improved quasi-equilibrium theory, however, there have still been difficulties as regards its application to cases involving fragmentation processes from electronically excited states and those from super-excited states.[5]

For explanation of the fragment ionization process, Fueki and Hirota[6] proposed a theory based on the assumption that the probability of fragmentation is proportional to the electron density on the highest occupied molecular orbital in the molecule. The theory was applied to many organic compounds and fairly good accordance was observed with the experiments using electron impact of normal or cycloalkanes.[7] However, experimental evidence of the energy range fit to the theory seems to be lacking.

We have studied the relation between the distribution of fragment ions and the recombination energy of the incident ions by means of pure charge exchange reactions involving no transfer of momentum. The energy range consistent with the molecular orbital (MO) theory was also investigated, and the usefulness of the theory was discussed.

Experimental

The charge exchange reactions of various molecules were carried out with a double mass spectrometer.[8] The primary ions, produced with a bombarding electron beam (100 eV), were accelerated to 800 V and led into the reaction chamber whose repeller potential was below 10 V. The ions produced by the charge exchange reactions were drawn into the second analyzer system at 3.5 KV, and detected with an electron multiplier of 16 stages.

The pressure of the reaction chamber was 8×10^{-6} mmHg. *n*-C_4H_{10}, *n*-C_5H_{12}, *n*-C_7H_{16}, *n*-$C_{10}H_{22}$, cyclo-C_5H_{10}, cyclo-C_6H_{12}, cyclo-C_7H_{14} and cyclo-C_8H_{16} were reagent grade(Tokyo Kasei Co.) and *n*-C_8H_{18} was spectroscopically pure. *n*-C_6H_{14} was purified from starting material of reagent grade (Tokyo Kasei Co.) by means of gas chromatography.

1) H. Budzikiewicz, C. Djerassi, and D. H. Williams, "Interpretation of Mass Spectra of Organic Compounds," Holden-Day, San Francisco (1964).

2) H. M. Rosenstock, M. B. Wallenstein, A. L. Wahrhaftig, and H. Eyring, *Proc. Natl. Acad. Sci. U.S.*, **38**, 667 (1952).

3) For example; H. M. Rosenstock, *J. Chem. Phys.*, **34**, 2182 (1961), B. S. Rabinovitch and R. W. Diesen, *ibid.*, **30**, 735 (1959), E. W. Schlag and R. A. Sandmark, *ibid.*, **37**, 168 (1962), M. L. Vestal, A. L. Wahrhaftig, and W. H. Johnston, *ibid.*, **37**, 1276 (1962), E. Thiele, *ibid.*, **39**. 3258 (1963), S. H. Lin and H. Eyring, *ibid.*, **43**, 2153 (1965), P. C. Haarhoff, *Mol. Phys.*, **6**, 337 (1963).

4) M. L. Vestal, A. L. Wahrhaftig, and W. H. Johnston, *J. Chem. Phys.*, **37**, 1276 (1962); M. L. Vestal, *ibid.*, **43**, 1356 (1965).

5) R. L. Platzman, *J. Phys. Rad.*, **21**, 853 (1960).

6) K. Fueki and K. Hirota, *Nippon Kagaku Zasshi*, **81**, 212 (1960).

7) For example; M. Hatada and K. Hirota, This Bulletin, **38**, 599 (1964), M. Itoh, M. Yamamoto, and K. Hirota, *Nippon Kagaku Zasshi*, **89**, 443 (1968), K. Hirota, *ibid.*, **89**, 327 (1968), K. Hirota, *ibid.*, **91**, 585 (1970), K. Hirota, I. Fujita, M. Yamamoto, and Y. Niwa, *J. Phys. Chem.*, **74**, 410 (1970).

8) T. Shiokawa, K. Yoshihara, M. Yagi, T. Omori, H. Kaji, T. Nagatani, and Y. Takita, *Shitsuryo Bunseki*, **18**, 1230 (1970).

CH_3^+, CH_2^+, $C_2H_2^+$, H_2O^+, Xe^+, Cl^+, H^+, Kr^+, N_2^+, Ar^+, Xe^{++}, Ar^{++}, and He^+ were used as the source of primary ions. CH_3^+ and CH_2^+ were obtained from methane, Cl^+ was the fragment ion of trichlorofluoromethane, H^+ the fragment ion of hydrogen, and $C_2H_2^+$, H_2O^+ and N_2^+ were obtained from C_2H_2, H_2O and N_2 respectively. All the other ions were produced from the corresponding rare gases.

Prior to experiments of charge exchange reactions, a re-examination of the recombination energy of the incident primary ions should be necessary because of the comparatively large velocity. However, with the use of the double mass spectrometer, Nagatani *et al.*[9] observed that the recombination energy of the comparatively fast primary ions was in good agreement with Lindholm's value of slow ones.[10] We therefore used the following Lindholm's values as the recombination energies of primary incident ions:

CH_3^+	a range around 9.8 eV
CH_2^+	10.4 eV and lower
$C_2H_2^+$	11.4 eV
H_2O^+	12.4 eV
Xe^+	12.1—13.4 eV
Cl^+	12.9—14.4 eV
H^+	13.6 eV
Kr^+	14·0—14.7 eV
N_2^+	15.3 eV
Ar^+	15.8 eV
Xe^{++}	18.0—20.0 eV
Kr^{++}	21.0 eV
Ar^{++}	24.0 eV
He^+	24.6 eV

Results and Discussion

The charge exchange reaction is generally considered as follows.

$$A + M^+ \rightarrow A^+ + M \quad (3)$$

where the energy E_c for producing the process $A \rightarrow A^+$ is dependent on the recombination energy of M^+, the ionization potential of A, and the kinetic energies of A and M^+. For the pure charge exchange reaction not involving the transfer of kinetic energy, the following equation can be applied:

$$A + M^+ \rightarrow A^+ + M + (R.E.)_M - (I.P.)_A \quad (4)$$

where $(R.E.)_M$ is the recombination energy of M and $(I.P.)_A$ the ionization potential of A. If M=A in Eq. (4), the resonance process for which $E_c=(R.E.)_M-(I.P.)_A=0$ occurs. For the case of $M \neq A$ one can excite the molecular ion A^+ by the energy $E_c=(R.E.)_M-(I.P.)_A$.

Thus the fragmentation processes from the particular excited state of the molecular ion by the charge exchange reactions can be observed with the use of a double mass spectrometer. The produced fragment ions are normalized to the sum of the total ion intensity, and the relation between the fragment ion distribution and the recombination energy of the incident ions can be illustrated as the breakdown curve of the molecular ion.

It is considered that the breakdown curve obtained by the charge exchange reactions is closely related to the mass spectra by electron impact. Mass spectra by electron impact are expressed as the sum of the mass spectra over internally excited states of various energies of the molecular ion, and calculated by the use of the breakdown curve and the internally energy distribution of the molecular ion.[11]

As an example the breakdwon curve for n-C_7H_{16} is shown in Fig. 1. The abscissa indicate recombination energy of the incident positive ions and the ordinate indicates the intensity of the ions. The plotted data were obtained in this work, and the curve in the low energy region (<14 eV) was obtained by Steiner *et al.*[12] using the photon impact. From this breakdown

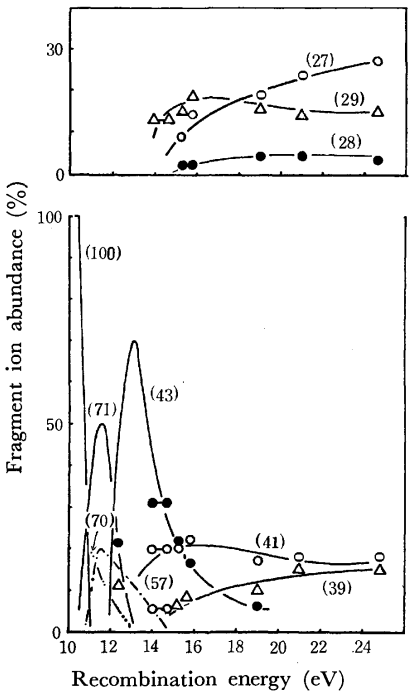

Fig. 1. Breakdown curve of n-C_7H_{16}.

Table 1. Comparison of the observed values by electron impact and the calculated values by charge exchange reaction

m/e	A. P. I.	Calcd.
(27)	9.3	7.7
(28)	1.9	1.8
(29)	10.9	8.3
(41)	12.4	11.8
(43)	23.8	23.8
(57)	11.4	6.0
(70)	4.1	3.0
(71)	10.5	9.2
(100)	3.1	2.5

9) T. Nagatani, K. Yoshihara, and T. Shiokawa, This Bulletin, **46**, 1306 (1973).

10) E. Lindholm, "Ion Molecule Reactions in the Gas Phase," Advances in Chemistry Series **58**, American Chem. Soc., Washington, D. C. (1966), p. 1.

11) For example; H. von Koch and E. Lindholm, *Arkiv Fysik.*, **19**, 123 (1961).

12) B. Steiner, C. F. Giese, and M. G. Inghram, *J. Chem. Phys.*, **34**, 189 (1961).

and the internal energy distribution function the composite fragment ion distribution can be calculated.[9] The result is compared with the observed values by electron impact (electron energy: 70 eV) in Table 1. The agreement is quite satisfactory. This means that the fragment ionization processes after the charge exchange reactions are almost consistent with ones by electron impact for the same energy imparted.

In contrast to the quasi-equilibrium theory, the MO theory proposed by Hatada and Hirota and others[7] to account for the mass spectra by electron impact contains three assumptions.

(1) The lifetime of the excited molecular ion is very short ($<10^{-13}$ s), the excited molecular ion being in a super-excited state, and the fragmentation occurring in the stabilization process.

(2) The scission probability of the skeletal bonds of bombarded molecule is proportional to the positive charge distribution at the corresponding bond of the molecular ion, or proportional to the electron density of the highest occupied molecular orbital at the corresponding bond of the bombarded molecule.

(3) The theory is applicable only to the primary scission, and the secondary and other scissions are explained by the quasi-equilibrium theory.

Hirota[13] pointed out that the electronically excited molecular ion is produced in a super-excited state, several eV above the ground state. The minimum energy for producing the super-excited molecular ions can be estimated by the following equation:

$$V(\min) = \text{I.P.} + nRT + D(\text{c-c}) \qquad (5)$$

where I.P. is the ionization potential of the starting molecule, n the number of the degree of freedom, D the dissociation energy for the carbon bonds, T absolute temperature (K) and R the gas constant. 20 eV was obtained for the molecule having 50 degrees of freedom.

In order to examine this theory it is important to study the energy dependence of the fragment ion distribution especially in the recombination energy region of about 20 eV. From the breakdown curve (Fig. 1), it is necessary to study the energy region which is consistent with the MO theory (or to check the fragment ion distribution predicted by the theory).

In the MO theory, Fueki and Hirota[6] could not determine which of the ruptured fragment groups was in the positive state *i.e.* which one lost an electron on the rupture event. C_i+C_{n-i} was therefore used to represent the scission probability for the i-th bond from the end. The summation C_i+C_{n-i} was normalized to be 100 except for the parent ion group. Thus we first obtain the breakdown curve of the molecular ion by the charge exchange reaction and next the abundance of the C_i group. Finally the relation between C_i+C_{n-i} and the recombination energy of the incident ion can be obtained, and the energy in which the MO theory holds can be determined. The relation of C_i+C_{n-i} versus energy in n-C_7H_{16} is shown in Fig. 2 with the data in Fig. 1. The predicted values on n-C_7H_{16} by the MO theory are as follows: $C_3+C_4=54$ (%), $C_2+C_5=35$ (%), $C_1+C_6=11$ (%).

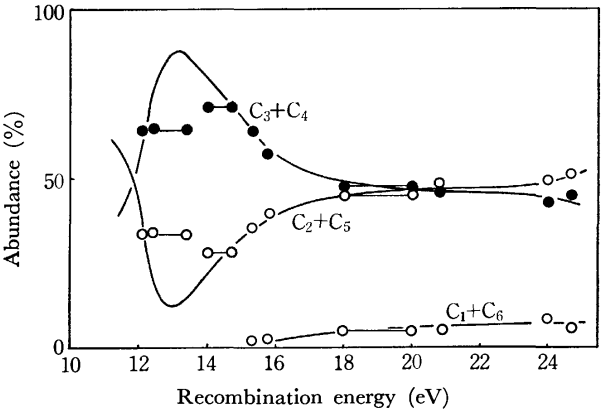

Fig. 2. Relation between C_i+C_{n-i} and recombination energy of incident positive ions on n-C_7H_{16}.

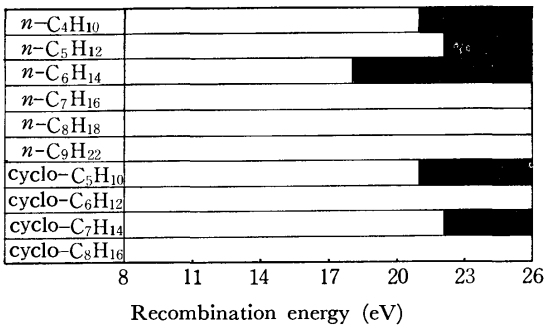

Fig. 3. Energy range of fragmentation consistent with the MO theory.

The energy range to which the MO theory is applicable is thus determined for n-alkanes and cycloalkanes. In Fig. 3, the black portion shows the energy range apparently consistent with Hirota's MO theory. We see that the energy range to which the MO theory is applicable is very limited. There are no energy regions to fit the MO theory in n-C_7H_{16}, n-C_8H_{18}, n-$C_{10}H_{22}$, cyclo-C_6H_{12} and cyclo-C_8H_{16}. The results for n-C_7H_{16} and n-C_8H_{18} were re-estimated more rigorously than in the previous communication.[14]

The mass spectra by electron impact can be calculated by the breakdown curve and the internal energy distribution function. It is assumed, however, that the maximum of the internal energy distribution func-

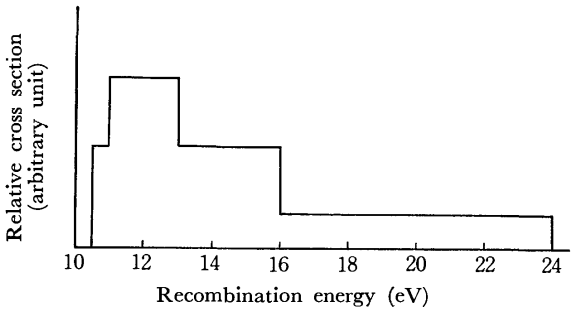

Fig. 4. Internal energy distribution of n-C_7-H_{16} molecular ion.

13) K. Hirota, *Shitsuryo Bunseki*, **20**, 101 (1972).

14) S. Ikuta, K. Yoshihara, and T. Shiokawa, *Chem. Lett.*, **1972**, 685.

tion is about 1 eV plus the ionization potential. Figure 4 shows the internal energy distribution on n-C_7H_{16} molecular ion which was used to calculate the mass spectra. The breakdown phenomenon in the high recombination energy range seems to contribute very little to the whole mass spectra. This means that the mass spectra in the energy range which are consistent with the MO calculation (Fig. 3) contribute little to the whole mass spectra by electron impact.

Although Hirota *et al.* could not quantitatively predict which of the fragment C_n and C_m ($m=N-n$; where N is the total number of carbon atoms) was to be in the positive charge, they qualitatively proposed that the abundance of the C_n ion group was larger than that of the C_m ion group in case of $n>m$, since the charge density of the C_n ion group was larger than that of the C_m ion group. It seems that there is a comparatively large ion group ($>C_{N/2}$: C_N is the parent ion group) in the energy range to which the MO theory is applicable.

Figure 5 shows the breakdown curve of the n-hexane parent ion obtained by the charge exchange reactions. It is evident that the fragment ions produced at the high recombination energy, to which the MO theory is applicable are the C_2, C_3 and C_1 ion groups. These C_2, C_3 and C_1 groups are predominant in the mass spectra at the high recombination energy on all alkanes. These results do not agree with the MO theory.

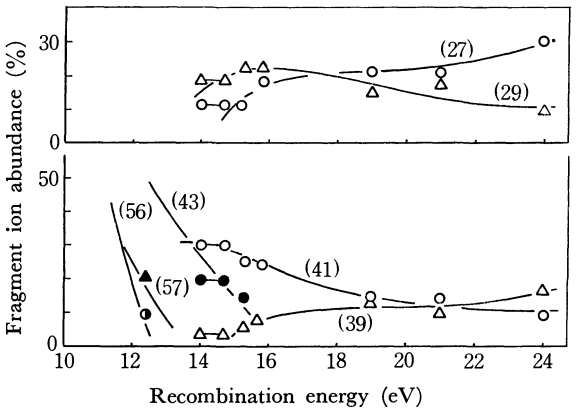

Fig. 5. Breakdown curve of n-C_6H_{14}.

From the above results, there arise some doubts about the applicability of the MO theory to alkanes. It is probable that the agreement between the observed values by electron impact and the predicted values by the MO theory happens to be given by integration of the breakdown curve along the internal energy distribution by chance. The argument seems to hold in the case of cycloalkanes in which double scissions are necessary to give the fragment ion distribution in the present study. We cannot exclude a possibility that there is a discrepancy in the mechanism between electron impact and charge exchange resulting in fragmentations. The possibility that the mechanism involving the pre-ionization from the super-excited state should also be considered but we do not believe this will alter the discussion given above.

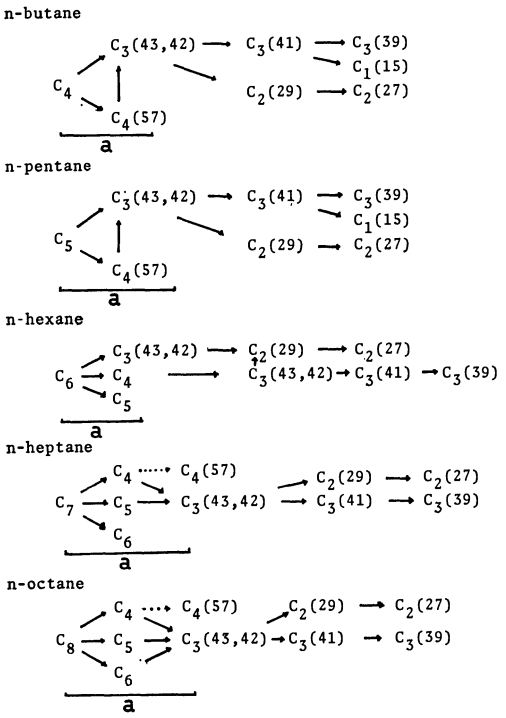

Fig. 6. Dissociation schemes of n-alkanes.

It seems that application of the MO theory to the fragmentation of the alkanes ($>C_4$) as a whole is difficult.

The dissociation scheme on alkanes is given in Fig. 6. At the high recombination energy (>17 eV) fragment ions were always C_2, C_3 and C_1 ion groups. Figure 6 [a] shows comparatively swift fragmentation processes. It is assumed that the molecular ions produced change swiftly to the C_3 or C_2 ion groups, and thereafter the C_3 or C_2 ion groups comparatively slowly change to the C_3', C_2' and C_1 ion groups experimentally observed. In the swift process one can imagine that availability of the molecular orbital consideration may be possible, although it is far from proven in the results of this study.

The authors wish to thank Prof. K. Hirota for his discussion and Mr. M. Hiraga for his assistance in the course of this study.

Polarographic Studies of Some Porphyrins and Metalloporphyrins in *N,N*-Dimethylformamide

Tadaaki KAKUTANI, Shoji TOTSUKA, and Mitsugi SENDA

Department of Agricultural Chemistry, Faculty of Agriculture, Kyoto University, Kyoto 606

(Received June 15, 1973)

Electrochemical behavior of protoporphyrin IX dimethylester (PPDM), mesoporphyrin IX dimethylester-(MPDM), Fe(III)Cl-protoporphyrin, Ni(II)-, Cu(II)-, Co(II)-, Zn(II)- and Mn(III)Cl·H_2O–PPDM was investigated in dimethylformamide by use of AC polarography, cyclic voltammetry and DC polarography. These porphyrins and divalent metal complexes of PPDM gave, for the most part, three reduction waves. The first and second waves were reversible one-electron steps in each case, but the third step was an irreversible one. Mn(III)-complex gave four reduction waves and one oxidation wave. The first three reduction waves were one-electron steps and the oxidation wave was identified as that due to chloride anion. Fe(III)-complex gave five reduction waves and one oxidation wave. The first two reduction waves were one-electron steps. All these compounds showed specific adsorption at the potential more positive than −1.1 V *vs.* SCE. Assignment of the reduction steps of the metalloporphyrins is described. The observed order of increasing negative half-wave potentials is discussed in terms of Zerner and Gouterman's molecular orbital calculation.

Nonaqueous electrochemistry of porphyrins and metalloporphyrins has been studied by several authors. Electrochemical measurements have been accompanied by ESR and absorption spectral data, and the correlation of half-wave potentials with molecular structures has been discussed.[1-6] The electrode processes have also been studied in detail.[7,8]

In this study, the polarographic reduction of some porphyrins and metalloporphyrins in aprotic solvent, *N,N*-dimethylformamide(DMF), was examined in detail by use of DC polarography, cyclic voltammetry and AC polarography.

Experimental

Materials. Hemine(Fe(III)Cl-PP), protoporphyrin IX dimethylester (PPDM) and mesoporphyrin IX dimethylester (MPDM) were prepared from cow blood by established methods[9-11] and purified by repeated column chromatography on neutral alumina with 200 : 1 chloroform–methanol and by recrystallization from chloroform–methanol mixture. Ni(II)-, Cu(II)-, Co(II)- and Zn(II)-PPDM were prepared from the free base by standard procedures[11] and separated from unreacted ligand by repeated column chromatography on neutral alumina with benzene. The solids were recrystallized from chloroform–methanol (or petroleum ether) and dried under vacuum. The absence of metal-free and altered porphyrin impurities in the metalloporphyrins was confirmed by thin layer chromatography on silica gel and absorption spectrophotometry. Mn(III)Cl·H_2O-PPDM was prepared by Boucher's procedures.[12]

DMF(reagent grade) was shaken with potassium hydroxide (about 30 g/l of solvent) for a few hours, decanted, and after bubbling nitrogen gas for thirty minutes, shaken with phosphorus pentoxide (about 40 g/l of solvent) for a few hours. After decanting, the solvent was distilled under reduced pressure (at 45—55 °C) with nitrogen passing through a Widmer's fractional distillation column. The central 60% fraction was collected and stored under dried nitrogen gas. Tetraethylammonium perchlorate(TEAP) was prepared and purified by the methods previously described.[13] Nitrogen gas was dried by passing through a washing bottle containing concd. sulfuric acid and a U-tube containing calcium chloride.

Electrochemical Measurements. DC polarograms and cyclic voltammograms were measured with a potentiostat, Yanaco PE-21-TB2S, equipped with a function generator, YHP 3310 B. AC polarograms were measured with the aid of a lock-in amplifier, NF LI-572B. A polarographic H-cell was used with dropping mercury electrode and platinum wire electrode coiled around the tip of the DME in the same arm. The other arm of the cell was filled with a supporting electrolyte solution(DMF containing 0.1 M TEAP) and connected with a nonaqueous salt bridge(DMF-methylcellulose-0.5 M TEAP) to an aqueous saturated calomel electrode(SCE). The liquid junction was by-passed for alternating current by a "pool" capacitor[16] of 2000 μF between the coiled platinum wire electrode and SCE. The cell was immersed in a water thermostat controlled at 25± 0.1 °C. Measurements were carried out under dried nitrogen atmosphere.

The capillary characteristics were $m=1.07_8$ mg/sec and $t=5.8$ s at $h=70$ cmHg in DMF containing 0.1 M TEAP at −0.5 V *vs.* SCE. Cyclic voltammograms were recorded with a very slowly dropping mercury electrode[14] (usually at $t=90$ or 120 s), whose capillary characeristics were $m=4.56\times10^{-2}$ mg/s and $t=345.1$ s at $h=50$ cmHg in DMF containing 0.1 M TEAP at −0.5 V *vs.* SCE.

The porphyrins and their metal complexes were generally sparingly soluble in DMF, and usually their saturated solutions (for the most part, approximately 4×10^{-4} M) were used.

1) D. W. Clack and N. S. Hush, *J. Amer. Chem. Soc.*, **87**, 4238 (1965).
2) R. H. Felton and H. Linschitz, *ibid.*, **88**, 1113 (1966).
3) L. D. Rollman and R. T. Iwamoto, *ibid.*, **90**, 1445 (1968).
4) L. J. Boucher and H. K. Garber, *Inorg. Chem.*, **9**, 2644 (1970).
5) A. Wolberg and J. Manassen, *J. Amer. Chem. Soc.*, **92**, 2982 (1970).
6) A. Stanienda and G. Biel, *Z. Physik. Chem.* (Frankfurt), **52**, 254 (1967); A. Stanienda, *Z. Naturforsch.*, **23B**, 147 (1968).
7) G. Peychal-Heiling and G. S. Wilson, *Anal. Chem.*, **43**, 545, 550 (1971).
8) L. G. Lanese and G. S. Wilson, *J. Electrochem. Soc.*, **119**, 1039 (1972).
9) M. Meguro, K. Ishibashi, and I. Yoshioka, *Yakugaku Zasshi*, **86**, 1138 (1966).
10) D. Shemin, "Methods in Enzymology," Vol. 4, ed. by S. P. Colowich and N. O. Kaplan, Academic Press, New York (1957), p. 643.
11) J. E. Falk, "Porphyrins and metalloporphyrins," Elsevier Publishing Co., New York (1964), p. 125.
12) L. J. Boucher, *J. Amer. Chem. Soc.*, **90**, 6640 (1968).
13) M. Senda, T. Ikeda, and T. Nishioka, *Nippon Kagaku Zasshi*, **91**, 957 (1970).
14) Y. Takemori, *Rev. Polarogr.* (Kyoto), **9**, 246 (1961).

Results

Reduction of PPDM, MPDM, Cu(II)-PPDM and Zn(II)-PPDM. These compounds in DMF gave three well-defined polarographic waves, as shown in Fig. 1. In this figure dotted lines indicate the base currents. By addition of the depolarizer a lowering of the residual current was observed at the potential more positive than about −0.7 V. This can be ascribed to the adsorption[15] of depolarizer on the electrode surface, a fact which was confirmed also by AC polarography and electrocapillary studies, as described below. All three waves gave limiting currents which are proportional to the concentration of depolarizer over the range from 5×10^{-5} to 4×10^{-4} M. Upon variation of the mercury column height, h, from 40 to 80 cm, all limiting currents of these three steps were proportional to $h^{1/2}$. The half-wave potentials of the first two steps were found to be independent of the concentration of depolarizer and of the mercury column over the range studied. The temperature coefficient of the limiting current was, for example, 0.7% at 25 °C for the first two steps of PPDM. These results are typical of a diffusion-controlled electrode process at the d.m.e.. When corrected for drop time, the three waves were in the ratio of 1 : 1 : 1.8 for PPDM and MPDM, and 1 : 1 : 1.5 for Cu(II)-PPDM and Zn(II)-PPDM. The polarographic data and analysis for these compounds are summarized in Table 1. Analysis of the rising portion of the waves indicated that the first two steps were reversible one-electron reduction process. The third step appeared irreversible.

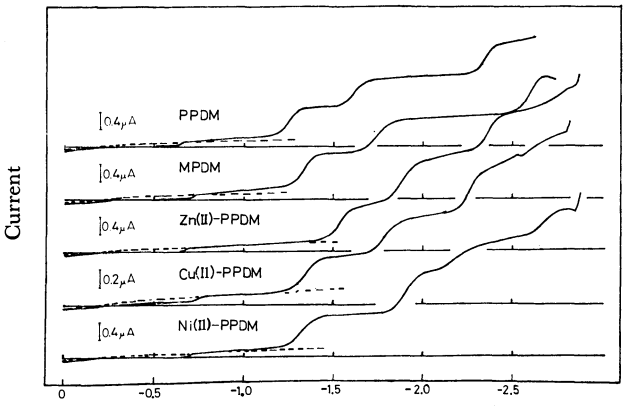

Fig. 1. DC polarograms of PPDM, MPDM, Zn(II)-PPDM, Cu(II)-PPDM and Ni(II)-PPDM in DMF, 0.1 M TEAP at 25 °C.

Concentration: about 4×10^{-4} M (but Cu-complex, about 2×10^{-4} M). Dotted lines indicate the base currents.

The DC polarographic results were confirmed by cyclic voltammetry. A typical cyclic voltammogram of PPDM is shown in Fig. 2. The first two steps showed cathodic and anodic peak separation of about 60 mV indicative of a reversible one-electron step. Peak currents of the first two steps were proportional to the concentration of depolarizer (less than 4×10^{-4} M) and

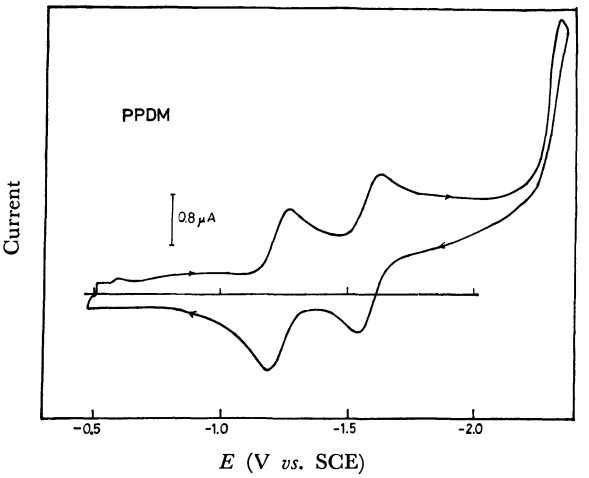

Fig. 2. Cyclic voltammogram of PPDM in DMF, 0.1 M TEAP at 25 °C.

Concentration: about 4×10^{-4} M. Scan rate: 0.2 V/s.

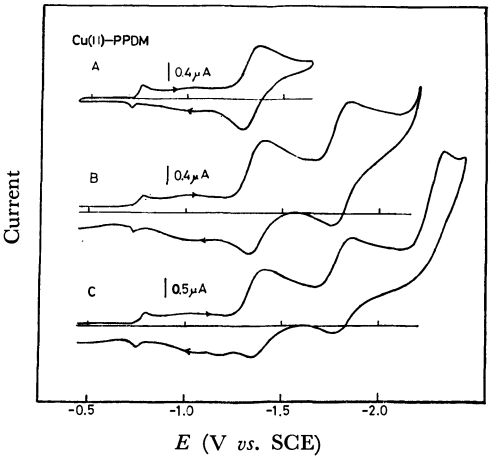

Fig. 3. Cyclic voltammogram of Cu(II)-PPDM in DMF, 0.1 M TEAP at 25 °C.

Concentration: about 2×10^{-4} M. Scan rate: A, 0.26 V/s; B, 0.5 V/s; C, 0.5 V/s.

square root of the scan rate(0.1 to 1 V/s). The cathodic and anodic peak potentials for the first two steps were found to be independent of the concentration and of the scan rate over the range studies. These results again indicate that the first two steps are reversible one-electron processes. The third step appeared irreversible, showing no corresponding anodic peak. In the case of Cu(II)-PPDM and Ni(II)-PPDM, however, an additional anodic peak was observed at the potential about 0.1 V more positive than that of the first anodic peak, as shown in Fig. 3. In the case of Zn(II)-PPDM, one more anodic peak was observed between the first and second anodic peaks. These anodic peaks were not observed until the cathodic scan limit was extended to the third step. It is clear that these additional peaks are associated with the oxidation of the products produced at the third reduction step.

In AC polarography, these compounds gave four peaks. Fig. 4 shows a typical AC polarogram of PPDM. A small peak observed at the most positive

15) M. Senda and I. Tachi, *Rev. Polarogr.* (Kuoto), **10**, 79 (1962).

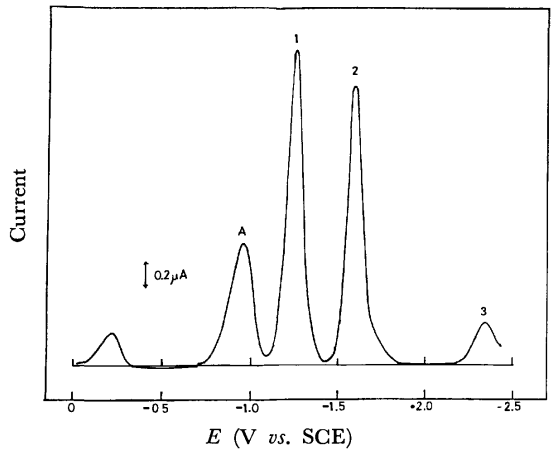

Fig. 4. AC polarogram of PPDM in DMF, 0.1 M TEAP at 25 °C.
Concentration: about 4×10^{-4} M. A.C. frequency: 100 Hz; AC voltage: 10 mV (p-p).

potential is considered to be due to a trace of iodide anion remaining in supporting electrolyte because it was observed also with the base solution. Three AC peaks observed at −1.24, −1.61 and −2.4 V will be denoted by Peaks 1, 2 and 3, respectively. These three peaks correspond respectively to the three reduction steps in DC polarography. The summit potentials of Peaks 1 and 2, being independent of concentration, agreed with the corresponding DC half-wave potentials within experimental error. The half-width of these peaks were about 90 mV. The summit currents were proportional to the concentration over the range studied(see Fig. 5). The apparent lower height of Peak 2 in comparison with Peak 1 is in large part due to the decreasing of drop time. The lower height of Peak 3 is due to its irreversibility. These AC results are in good agreement with the results in DC polarography and cyclic voltammetry.

The AC peak observed at around −0.95 V, being denoted by Peak A, had no counter part in DC polarography. Figure 5 shows the dependence of the summit potentials and summit current of the AC peaks 1, 2, and A on the concentration of PPDM. The behavior of 1 and 2 is that of the reversible process. In contrast, with increasing concentration of the depolrizer the summite current of Peak A increased nonlinearly and approached a limiting value and the summit potential shifted to more negative potential. With a rise in temperature the summit current decreased and the summit potential was shifted to more positive potential, as shown in Fig. 6. Further, the rising potential of Peak A approximately agreed with the potential where the depression of the DC residual current was restored. These results indicate that Peak A is a tensammetric desorption wave.[15,16] This assignment was clonfirmed also by electrocapillary measurements. Fig. 7 shows the electrocapillary curves(drop time–potential curves). The addition of depolarizer to the base solution caused a significant depression of drop time at the potential

16) B. Breyer and H. H. Bauer, "Alternating Current Polarography and Tensammetry," Interscience Publishers, New York, (1963).

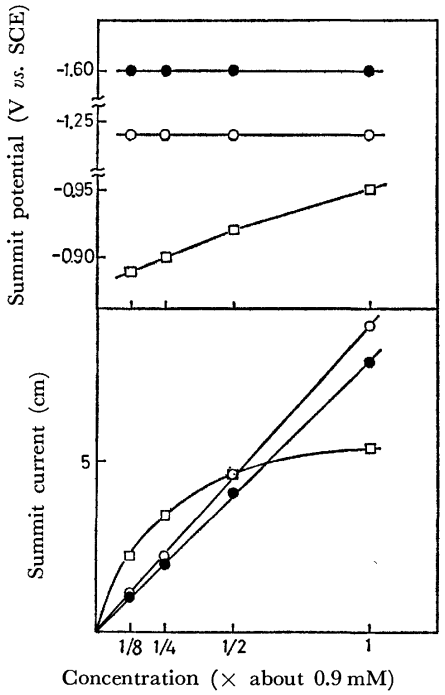

Fig. 5. Dependence of the summit potentials and summit currents on the concentration of PPDM in DMF, 0.1 M TEAP at 25 °C.
□: Peak A; ○: Peak 1; ●: Peak 2.

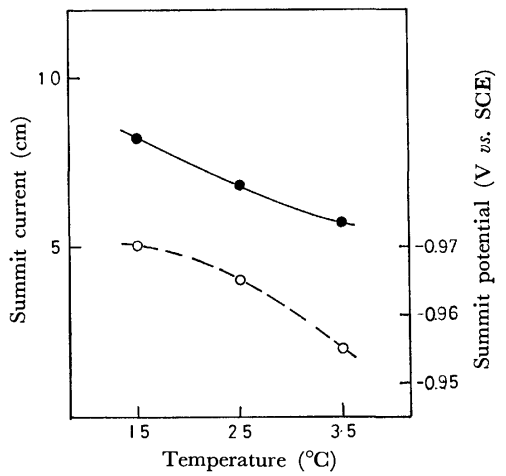

Fig. 6. Effect of temperature on the summit potential and summit current of Peak A of PPDM in DMF, 0.1 M TEAP.
Concentration: about 4×10^{-4} M. ●: summit current; ○: summit potential.

more positive than about −1.0 V, and the magnitude of the depression increased with increasing concentration of depolarizer. However, at the potential more negative than −1.1 V the depression was no more observed. These observations are consistent with the AC and DC polarographic results described above and indicate that the adsorption effects on the electrode process are practically negligible at the potential more negative than −1.1 V.

Reduction of Ni(II)-PPDM. A polarogram of this compound is shown in Fig. 1. The DC and AC

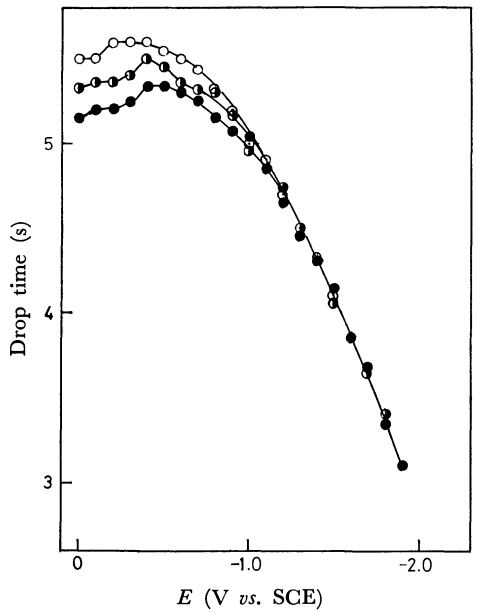

Fig. 7. Electrocapillary curves of a DMF solution containing 0.1 M TEAP(○), and in the presence of 1/8 (◑) and 1/1(●)× *ca.* 4×10^{-4} M MPDM in the base solution at 25 °C.

polarographic properties of the first two steps were essentially the same as those of the other metalloporphyrins described above. The first step in DC polarography was a one-electron reversible step, but the height of the second step was slightly larger than that of the first one. This slight increase of the current would be attributed to electroreduction of products that were produced in chemical reactions, including protonation, following the second electrochemical step. The third and fourth DC steps were poorly defined, irreversible waves.

Reduction of Co(II)-PPDM. Co(II)-PPDM in DMF gave two well-defined polarographic waves at −0.96 and −2.06 V, and an ill-defined wave at −2.35 V, as shown in Fig. 8. A small maximum was also observed at about −1.1 V on the first step. The limiting currents of the first two steps were proportional to square root of the mercury column height, indicating that these were controlled by diffusion. When corrected for drop time, the two wave heights were in the ratio of 1 : 0.9. The wave slopes for the first and second steps were 70 and 60 mV, respectively.

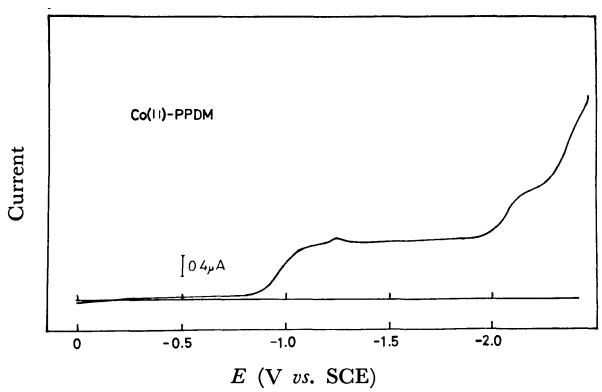

Fig. 8. DC polarogram of Co(II)-PPDM in DMF, 0.1 M TEAP at 25 °C.
Concentration: about 4×10^{-4} M.

A cyclic voltammogram of Co(II)-PPDM is shown in Fig. 9. The first wave, corresponding to the first DC step, has a complicated shape, which may be ascribed to the adsorption of metalloporphyrin molecules on the electrode surface. In contrast, the second peak, appearing at the potential of the second DC step, has the normal shape with a corresponding anodic peak, indicating that the second step is a simple one-electron reversible reduction.

In AC polarography, this compound gave four peaks, as shown in Fig. 10. Three AC peaks observed at −0.96, −1.14 and −2.05 V will be denoted by Peaks 1, A and 2, respectively. The summit potential of Peaks 1 and 2 agreed with the half-wave potentials of the first and second steps, respectively. Figure 11 shows the dependence of the summit current and summit potentials on the bulk concentration of depolarizer. The summit current of Peak 2 was proportional to the concentration and its summit potential was nearly independent of the concentration. Moreover, the waveform of Peak 2 was practically symmetrical with respect to the summit potential with a half-width of about 100 mV. On the other hand, with increasing concentration of the depolarizer the summit current

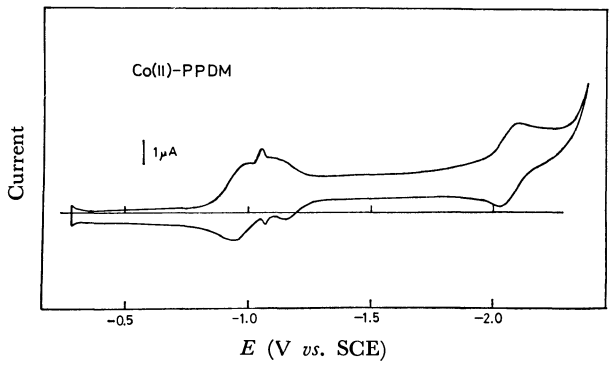

Fig. 9. Cyclic voltammogram of Co(II)-PPDM in DMF, 0.1 M TEAP at 25 °C.
Concentration: about 4×10^{-4} M. Scan rate: 0.42 V/s.

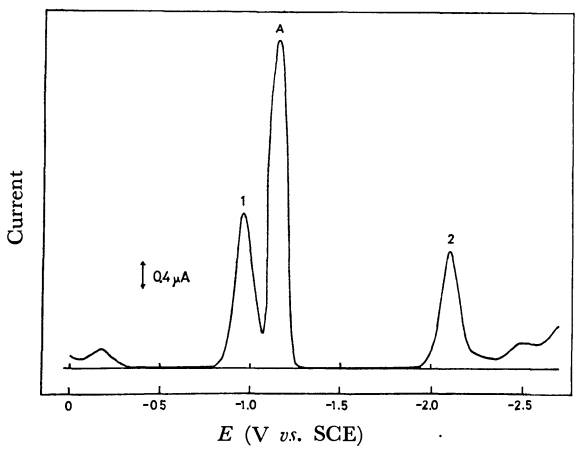

Fig. 10. AC polarogram of Co(II)-PPDM in DMF, 0.1 M TEAP at 25 °C.
Concentration: about 4×10^{-4} M. AC frequency: 100 Hz; AC voltage: 10 mV.

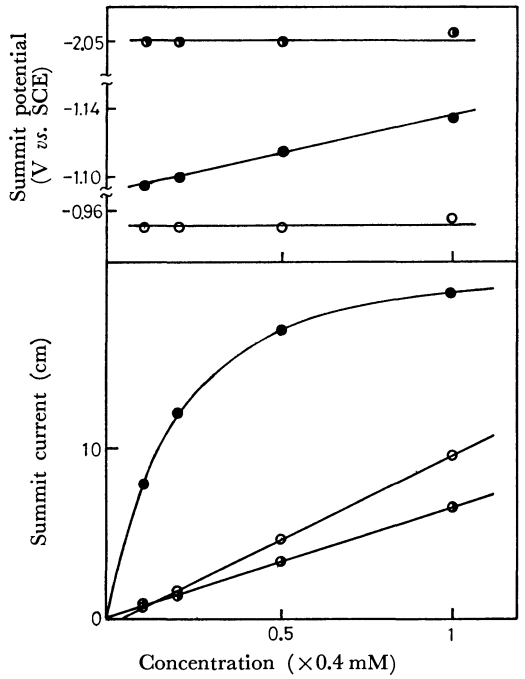

Fig. 11. Dependence of the summit potentials and summit currents on the concentration of Co(II)-PPDM in DMF, 0.1 M TEAP at 25 °C. ●: Peak A; ○: Peak 1; ◑: Peak 2.

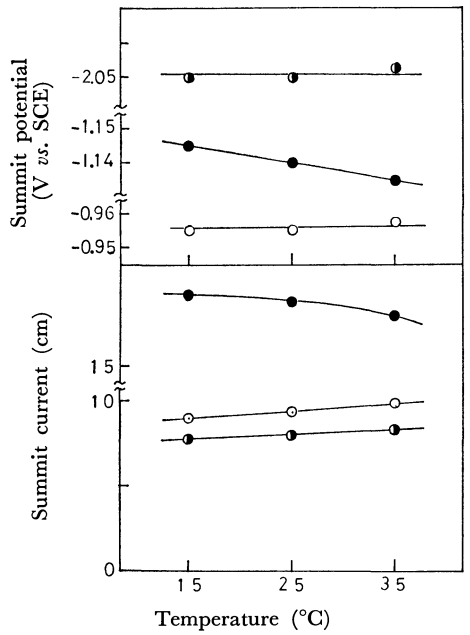

Fig. 12. Effect of temperature on the summit potentials and summit currents of Co(II)-PPDM in DMF, 0.1 M TEAP.
Concentration: about 4×10^{-4} M. ●: Peak A; ○: Peak 1; ◑: Peak 2.

of Peak A increased nonlinearly and approached a limiting value and its summit potential shifted to more negative potential. The summit current of Peak 1 increased linearly with the concentration, but the linear regression line intersected with the current axis at a negative value. The summit potential of Peak 1 was practically independent of the concentration. Effect of temperature on the summit currents and summit potentials is shown in Fg. 12. The sumit currents of Peaks 1 and 2 inclined to increase with a rise in temperature and the apparent shift of their summit potentials are negligibly small. The temperature coefficients of these summit currents were in the order of that of AC reversible peak.[17] On the contrary, the summit current of Peak A decreased and its summit potential shifted to more positive potential with a rise in temperature. Namely, the behavior of Peak A was characteristic of the tensammetric desorption wave.

In conclusion it may be stated that the first DC wave is a reversible one-electron reduction wave overlapped with an adsorption post wave,[18] though the latter is poorly separated from the main wave. The AC polarographic behavior of peaks 1 and A reasonably supports this interpretation.[19] The adsorption effect is negligible at the potential more negative than −1.2 V. The second DC wave is a simple reversible one-electron reduction wave.

Reduction of Mn(III)Cl·H_2O-PPDM and Fe(III)Cl-PP. In DC polarography, the Mn(III)-complex gave four reduction steps and an oxidation double wave, as shown in Fig. 13. Polarographic reduction of Mn(II)-porphyrin derivatives in aprotic media has been studied by Boucher and Garber.[4] The results in the present study were, for the most part, in good agreement with those reported by them. The oxidation double wave was identified as an oxidation wave due to chloride anion. This suggests that an axial ligand such as chloride anion is displaced by a solvent molecule in such a strongly coordinating solvent as DMF, which is consistent with spectral observation by Boucher.[12] In AC polarography, was observed a peak of asymmetric shape at the potential of the first redox waves as well as four AC peaks corresponding to the tensammetric desorption (Peak A) and the second, third and fourth reduction steps (Peaks 1, 2 and 3, see Fig. 4).

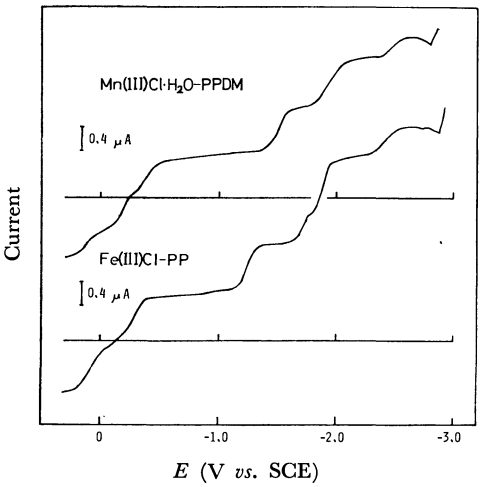

Fig. 13. DC polarograms of Mn(III)Cl·H_2O·PPDM and Fe(III)Cl·PP in DMF, 0.1 M TEAP at 25 °C.
Concentration: about 4×10^{-4} M.

17) M. Senda, M. Senda, and I. Tachi, *J. Electrochem. Soc. Japan*, **27**, 83 (1959).
18) R. Brdička, *Collect. Czech. Chem. Comm.*, **12**, 522 (1947).
19) M. Senda, M. Senda and I. Tachi., *Rev. Polarogr.* (Kyoto), **10**, 142 (1962).

Table 1. Polarographic results on porphyrins and metalloporphyrins in DMF containing 0.1 M TEAP at 25 °C

Compound	$-E_{1/2}(1)$[a]	$\Delta E(1)$[b]	$-E_{1/2}(2)$[a]	$\Delta E(2)$[b]	$-E_{1/2}(3)$[a]
PPDM	1.24	0.06	1.61	0.06	2.34
MPDM	1.34	0.06	1.74	0.06	2.58
Ni(II)PPDM	1.34	0.06	1.89	0.06	2.11[c]
Cu(II)PPDM	1.37	0.06	1.82	0.06	2.26
Zn(II)PPDM	1.49	0.06	1.84	0.06	2.30
Co(II)PPDM	0.96	0.07	2.06	0.06	2.35
Fe(III)Cl-PP	0.28	0.07	1.20	0.06	1.64[d]
Mn(III)Cl·H_2O-PPDM	0.37	0.08	1.49	0.06	1.97[e]

a) Volts *vs.* aq. SCE. b) $\Delta E=E_{1/4}-_{3/4}$ (in V). c) One more wave at −2.7 V. d) Two more waves at −1.84 and −2.4 V. e) One more wave at −2.4 V.

DC polarogram of Fe(III)Cl-PP is shown in Fig. 13. The first and second reduction steps were one-electron diffusion-controlled steps. Three more reduction waves were observed. An oxidation wave was also observed. In AC polarography, five peaks were observed, but a peak corresponding to the DC third step was not observed.

Discussion

The half-wave potentials of the porphyrins and metalloporphyrins measured in this study are summarized in Table 1. Polarographic reduction of tetraphenylporphin (TPP) and its metal complexes in dimethylsulfoxide has been studed by Felton and Linschitz.[2] On comparing the half-wave potentials of PPDM complexes with those of TPP complexes, we may find that the difference between the corresponding steps was nearly constant; for the first step, 0.19 V (TPP–PPDM), 0.16 V (Ni-TPP—Ni-PPDM), 0.17 V (Cu-TPP—Cu-PPDM), 0.18 V (Zn-TPP—Zn-PPDM), 0.14 V (Co-TPP—Co-PPDM), and for the second step, 0.14 V (TPP–PPDM), 0.14 V (Ni-PPT—Ni-PPDM), 0.14 V (Cu-TPP—Cu-PPDM), 0.12 V (Zn-TPP—Zn-PPDM), 0.19 V (Co-TPP—Co-PPDM). This result suggests that the polarographic reduction of these metal-PPDM complexes proceeds in a similar manner as that of metal-TPP complexes. Accordingly, the first two reduction steps of Ni(II)-PPDM, Cu(II)-PPDM and Zn(II)-PPDM will be assigned to successive addition of one electron to orbitals belonging mainly to the porphyrin ring, and the first step of Co(II)–PPDM to addition of one electron to a metal-centered orbital.[2]

The first DC waves of Fe(III)Cl-PP and Mn(III)-Cl·H_2O-PPDM should reasonably be assigned to the reduction of a trivalent metal complex to a divalent metal complex. The half-wave potential of the first step of Fe(III)-complex is 0.09 V more positive than that of Mn(III)-complex. Correspondingly, the difference in reduction potentials between hematoporphyrin complexes of Fe(III) and Mn(III) in aqueous solution is reported to be 0.05 to 0.08 V.[2),21] The subsequent reduction steps of the trivalent metalloporphyrins should be assigned to the reduction of the divalent metalloporphyrins.

The observed order of increasing negative half-wave potential of the first step of the divalent metalloporphyrins or the second step of the trivalent metalloporphyrins is $Co \ll Fe < Ni \lesssim Cu \ll Zn \simeq Mn$. On the other hand, the calculated order[22] of increasing negative charge on the porphyrin moiety is $Mn \ll Fe < Cu \lesssim Ni < Co < Zn$. The observed order $Fe < Ni \lesssim Cu \ll Zn$ should be considered as practically agreed with the calculated order of increasing negative charge in the porphyrin moiety. This is in harmony with the charge in the porphyrin moiety. This is in harmony with the stated conclusion that the addition of electron to these metalloporphyrins, except Fe(II)-complex, takes place in porphyrin moiety. For Fe(II)-complex the possibility of the electron addition to metal-centered orbital may not be excluded. It is also noted that the half-wave potential of Fe(II)-complex (second step of Fe(III)Cl-PP) is more positive than that of the free base, PPDM (Table 1). The half-wave potential of Mn(II)-PPDM is much more negative than predicted from the molecular orbital calculation, in which a planar configuration is assumed. This discrepancy may be interpreted by assuming that in Mn(II)-porphyrins the metal atom is out of the plane of the porphyrin, so that the porphyrin ring retains a high negative charge in this configuration because of the poor sigma donation of the porphyrin to the metal. The assumed structure is consistent with the ease of demetallation of Mn(II)-porphyrin derivatives[20] and the lack of strong mixing of metal $d\pi$ orbitals with ring π orbitals, as suggested by the spectral data.[4,23]

The half-wave potential of Co(II)-PPDM is remarkably more positive than predicted by the calculation. This result may be understood by the reason that in this complex the electron is added to the metal-centered orbital, exceptionally among the divalent metalloporphyrins studied.

This work was partly supported by a grant from the Ministry of Education, to which the authors' thanks are due.

20) D. G. Davis and J. G. Montalvo, *Anal. Chem.*, **41**, 1195 (1966).
21) J. G. Montalvo and D. G. Davis, *J. Electroanal. Chem.*, **23**, 164 (1969).
22) M. Zerner and M. Gouterman, *Theoret. Chim. Acta*, **4**, 44 (1966).
23) J. Boucher, *Coord. Chem. Rev.*, **7**, 289 (1972).

The Primary Photochemical Process of Isoquinoline *N*-Oxide in Hydroxylic Solvents

Isao ONO and Norisuke HATA

Department of Chemistry, Faculty of Science and Engineering, Aoyama Gakuin University, Chitosedai, Setagaya-ku, Tokyo 157

(Received March 7, 1973)

In order to deduce the nature of the reactive state of the photochemical isomerization of isoquinoline *N*-oxide in methanol or water, investigations by means of steady-light irradiation and flash spectroscopy were carried out under various conditions. Transient absorptions were observed in the spectral region between 360 nm and 600 nm; they were identified as being due to a T–T transition of isoquinoline *N*-oxide. Experiments on both the measurements of the quantum yields and the decay kinetics of the transient species under different conditions revealed that the excited singlet state of isoquinoline *N*-oxide was responsible for the isomerization. The photochemical behavior in aqueous solutions at various pH values was also examined; consequently, the photochemical isomerization was found to be independent of the hydrogen ions, although it did not occur in a strongly acidic solution (pH<3.0) because of the formation of the protonated *N*-oxide. The biacetyl-photosensitization for isoquinoline *N*-oxide led to the dissociation of the N–O bond instead of to isomerization.

It is well known that the azanaphthalene *N*-oxides undergo interesting but complex photochemical reactions in solution.[1] For example, the ultraviolet irradiation of quinoline *N*-oxide or isoquinoline *N*-oxide results in the formation of lactams and/or oxazepines, depending on the nature of the reaction medium or the substituent group. Hereafter, the photochemical change leading to the formation of a lactam will be referred to as Process I, while the photochemical conversion to an oxazepine will be termed Process II.

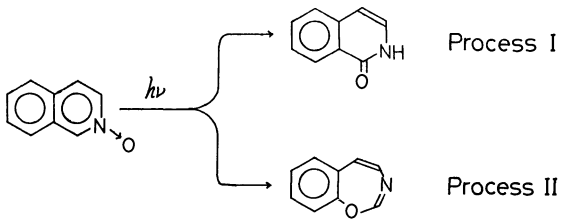

In hydroxylic solvents, such as methanol and water, the quinoline- or isoquinoline-*N*-oxide is predominantly transformed into its lactam (carbostyril or isocarbostyril) as a result of the ultraviolet irradiation, whereas in non-hydroxylic solvents, such as acetone and carbon tetrachloride, Process II generally becomes much more important than Process I. Mechanistic studies, including the identification of the reactive excited state, of the photochemical isomerizations of heterocyclic *N*-oxides have been extensively performed in recent years.[1-3] In order to account for such photochemical isomerizations, the oxaziridine has been customarily postulated to be a photochemical intermediate common to both Processes I and II. Very recently, however, Lohse has suggested that it is not valid to assume an oxaziridine as a photochemical intermediate common to both Processes.[2b] As an aid in the mechanistic elucidation of the photochemical reactions of azanaphthalene *N*-oxides, therefore, the present authors carried out studies by means of both steady-light and flash illumination for the isoquinoline *N*-oxide in methanol or water (Process I).

Experimental

Materials. The isoquinoline *N*-oxide used in this experiment was synthesized by Ochiai's method,[4] and the product was purified by vacuum distillation, followed by silica gel chromatography (using diethyl ether–ethanol as the eluant). In the irradiation experiments, reagent-grade methanol of Wako Pure Chemical Industries was used without further purification; a 1 M sodium hydroxide solution, 20% hydrochloric acid, and a standard buffer solution (pH 6.86) were also used. The 1,3-cyclohexadiene, piperylene, isoprene (Tokyo Kasei Kogyo Co.), and biacetyl (Wako Pure Chemical Ind.) used as triplet quenchers or sensitizers were purified by distillation.

Steady-light Experiment. Small-scale photolyses for the determination of the quantum yield were performed in a quartz cylindrical cell 5 cm in diameter and 1 cm in length. The UV light source was a 250 W high-pressure mercury lamp (Ushio-250). For the 313-nm irradiation, a filter combination of a nickel sulfate solution with UV-29 and UVD-25 Toshiba filters was used. The light intensity was determined by means of a potassium ferrioxalate actinometer. The disappearance of isoquinoline *N*-oxide was followed quantitatively at 298 nm with a Hitachi recording spectrophotometer, EPS-3T. The amounts of isocarbostyril produced were measured by means of a chromatographic separation (silica gel, chloroform–ethanol) combined with a spectrophotometric determination; for this purpose, a UV spectrometer, UVICON-540 (Tokyo Kagaku Sangyo Co.), and a recorder, EPR-2TP (Toa Dempa Kogyo Co.), were used. Large-scale photolyses were performed at concentrations of approximately 5.0×10^{-3} M (70 ml) in a Pyrex vessel using a 100 W high-pressure immersion mercury lamp (Riko Kagaku Sangyo Co.) under the bubbling in of nitrogen; the photoproducts were then separated by silica gel chromatography. In the case of the biacetyl-sensitization experiment, a methanol solution containing 6.0×10^{-3} M of isoquinoline *N*-oxide and 3.0×10^{-2} M of biacetyl in a quartz cylindrical reaction vessel (5 cm in diameter and 1 cm in

1) G. G. Spence, E. C. Taylor, and O. Buchardt, *Chem. Rev.*, **70**, 231 (1970).

2) (a) G. Favaro, *Mol. Photochem.*, **2**, 323 (1970). (b) C. Lohse, *J. Chem. Soc. Perkin II*, **1972**, 229. (c) F. Bellamy, L. G. R. Barragan, and J. Streith, *Chem. Commun.*, **1971**, 456. (d) A. Alkaitis and M. Calvin, *ibid.*, **1968**, 292.

3) (a) C. Kaneko, *Yuki Gosei Kagaku Kyokai Shi.*, **26**, 758 (1968). (b) C. Kaneko, Sa. Yamada, I. Yokoe, and T. Kubota, *Tetrahedron Lett.*, **1970**, 2333.

4) E. Ochiai, "Aromatic Amine Oxides," Elsevier Publishing Company, Amsterdam (1967), Chapter 3.

length) was irradiated with a 250 W high-pressure mercury lamp (Ushio-250) equipped with a Toshiba V-Y 43 filter for 10 hrs under a nitrogen atmosphere. The phosphorescence spectra were taken with a Hitachi fluorescence spectrophotometer MPF-2A, with a phosphorescence accessory attached.

Flash Spectroscopic Experiment. The flash-photolysis apparatus used in this experiment was the same as that described elsewhere.[5] An energy of 120J was dissipated by discharging a bank of condenders of 2 μF charged to 11 kV; the duration of the flash was about 10 μs.

Results and Discussion

The isoquinoline *N*-oxide in methanol or ethanol isomerizes upon irradiation by ultraviolet light to give isocarbostyril in *ca.* 70% yield.[6] This photochemical isomerization (Process I) also proceeded in an aqueous solution to give a good yield (*ca.* 75%), irrespective of the atmosphere, nitrogen or oxygen. Figure 1 shows the progressive spectral change in isoquinoline *N*-oxide on 313-nm irradiation in methanol; it was observed that the absorption of isoquinoline *N*-oxide decreased in intensity, and a new absorption band due to isocarbostyril appeared with isosbestic points, as the irradiation time increased.

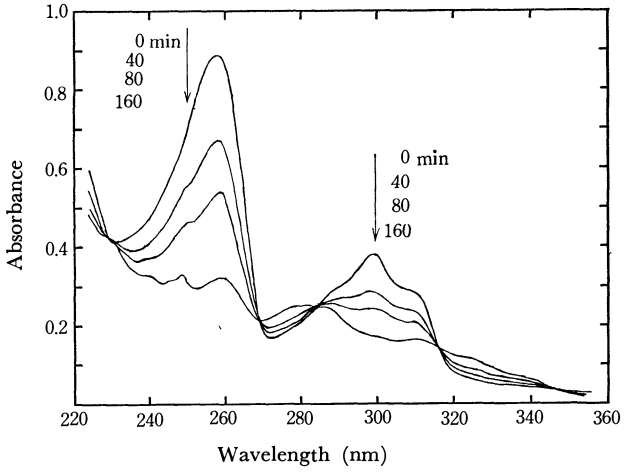

Fig. 1. The progressive spectral change of isoquinoline *N*-oxide (3.5×10^{-5} M) on 313 nm irradiation in methanol. Numbers refer to the irradiation time.

Phosphorescence Spectra. Curve (a) in Fig. 2 shows the phosphorescence spectrum from EPA glass containing 5.0×10^{-5} M of isoquinoline *N*-oxide at 77 K. As is shown in the figure, the phosphorescence lifetime was quite dependent on the emission wavelength; that is, it was *ca.* 1.0 s at the shorter wavelengths (400—500 nm), while it was *ca.* 60 ms at the longer wavelengths (500—600 nm). Ziolkowsky and Dörr[7] have obtained the same results; they have assigned the shorter wavelength band to the phosphorescence of isoquinoline *N*-oxide. However, the

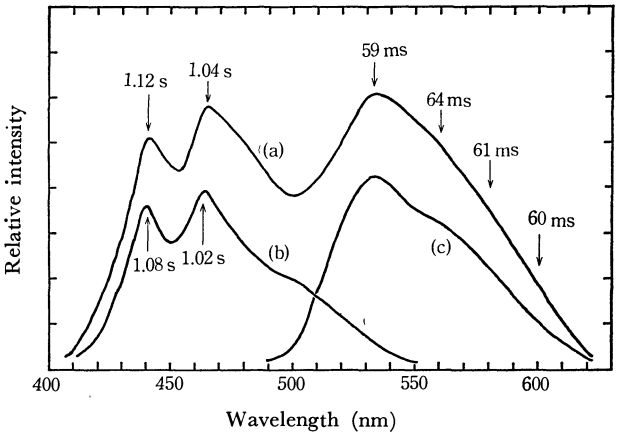

Fig. 2. Phosphorescence spectra of (a) isoquinoline *N*-oxide (5.0×10^{-5} M), (b) isocarbostyril (1.0×10^{-4} M), and (c) highly fresh solution of isoquinoline *N*-oxide (5.0×10^{-5} M) in EPA glass at 77 K.

experimental results to be presented below definitely show that the longer wavelength band can better be ascribed to the phosphorescence of isoquinoline *N*-oxide, whereas the shorter wavelength one should be ascribed to the phosphorescence of the isocarbostyril resulting photochemically from isoquinoline *N*-oxide.

(i) The shorter wavelength band was quite similar to the phosphorescence spectrum of isocarbostyril (Curve (b) in Fig. 2); the decay time (1.08 s) was also in good agreement with the phosphorescence lifetime of isocarbostyril (1.05 s). (ii) The very fresh solution (5.0×10^{-5} M), immediately after preparation, gave only the longer-wavelength emission (Curve (c) in Fig. 2). When the solution was allowed to stand for a while in the light, however, the shorter-wavelength emission appeared also. (iii) The longer-wavelength emission band was in a mirror-image relation with the S–T absorption band of isoquinoline *N*-oxide determined by Kubota et al.[8] (Fig. 3).

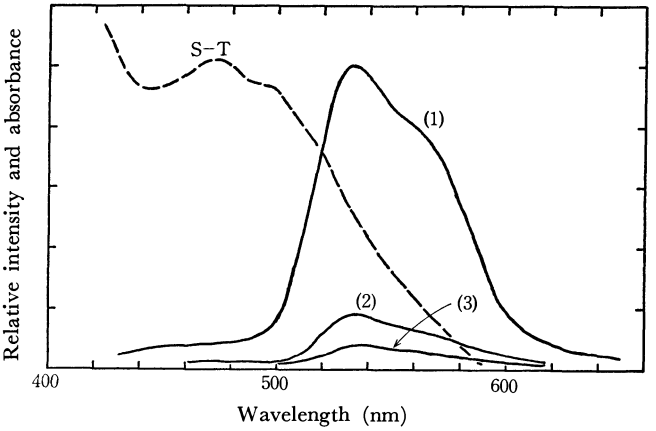

Fig. 3. Phosphorescence and S–T absorption spectra of isoquinoline *N*-oxide. ——: Phosphorescence spectrum in EPA glass at 77 K. ----: S–T absorption spectrum in chloroform at room temperature.[8]
(1) [1,3-cyclohexadiene]: 0 M
(2) [1,3-cyclohexadiene]: 2×10^{-1} M
(3) [1,3-cyclohexadiene]: 5×10^{-1} M

5) N. Hata, I. Ono, and T. Tsuchiya, This Bulletin, **45**, 2386 (1972).
6) M. Ishikawa, Sa. Yamada, H. Hotta, and C. Kaneko, *Chem. Pharm. Bull.* (Tokyo), **14**, 1102 (1966).
7) B. Ziolokowsky and F. Dörr, *Ber. Bunsenges. Phys. Chem.*, **69**, 448 (1965).
8) T. Kubota, M. Yamakawa, and Y. Mizuno, This Bulletin, **45**, 3282 (1972).

From the maximum of the phosphorescence spectrum of isoquinoline *N*-oxide (532 nm), the excitation energy of the lowest triplet state was estimated to be about 53.7 kcal·mol^{-1}. Consequently, the addition of 1,3-cyclohexadiene (E_T=52.5 kcal·mol^{-1}) to a methanol solution of isoquinoline *N*-oxide in amounts much greater than the molar equivalence led to the complete disappearance of the phosphorescence (Fig. 3). On the other hand, the addition of piperylene (E_T= 56.9 kcal·mol^{-1}) or isoprene (E_T=60.1 kcal·mol^{-1}) did not quench the phosphorescence of isoquinoline *N*-oxide, but it did quench the phosphorescence of isocarbostyril. Interestingly, in a concentrated solution (4.0×10^{-4} M) of isoquinoline *N*-oxide, only its phosphorescence spectrum was observed. This is probably because the phosphorescence of isocarbostyril can be quenched by an unexcited *N*-oxide, since the T–T energy transfer between them is energetically possible.

Steady-light Irradiation. The quantum yields of both the disappearance of isoquinoline *N*-oxide (Φ_d) and the formation of isocarbostyril (Φ_f) were examined in a deaerated methanol at room temperature. Figure 4(a) shows the effect of the irradiation time on the quantum yield in a 1.0×10^{-4} M solution; the results indicate that the quantum yield was independent of the irradiation time. The quantum yields were also determined as a function of the initial concentration of isoquinoline *N*-oxide. As is shown in Fig. 4 (b), a long-lived excited species susceptible to a collisional deactivation by an unexcited *N*-oxide is not involved in the photochemical reaction. In order to clarify whether or not the triplet species are responsible for this isomerization, therefore, the triplet quenching or sensitization experiments for the photochemical reaction of isoquinoline *N*-oxide were undertaken by using a 1,3-cyclohexadiene (triplet quencher) or a biacetyl (triplet sensitizer) in a deaerated methanol. As can be seen from Fig. 4(c), the quantum yield of the *N*-oxide disappearance was unaffected by the addition of 1,3-cyclohexadiene. Furthermore, the biacetyl-sensitization for the isoquinoline *N*-oxide in deaerated methanol did not lead to the isomerization of *N*-oxide, but instead resulted in the dissociation of the N–O bond, thus giving rise to the isoquinoline in a 30% yield. Similar results were also obtained in the case of a deaerated chloroform or benzene solution. These results suggest that the lowest triplet state of isoquinoline *N*-oxide is responsible for the deoxygenation, but not for the isomerization.

Flash Spectroscopy. In order to get information on the photochemical intermediate which may be formed during the reaction, the flash-spectroscopic examinations were carried out in EPA glass at 77 K or in a deaerated methanol at room temperature. As is shown by Curve (a) in Fig. 5, the transient absorption was observed around 400 nm (strong) and 480 nm (weak) in EPA glass at 77 K. Figure 6 shows the results when the first-order rate law was applied to the decay of transients at 77 K at various wavelengths. The decay time was evaluated from the slope of the straight-line to be 57 ms, a value which agreed closely with the phosphorescence lifetime (60 ms). When the deaerated methanol solution of isoquinoline *N*-oxide was flash-illuminated at room temperature, a distinct maximum was observed only around 400 nm, since the absorption

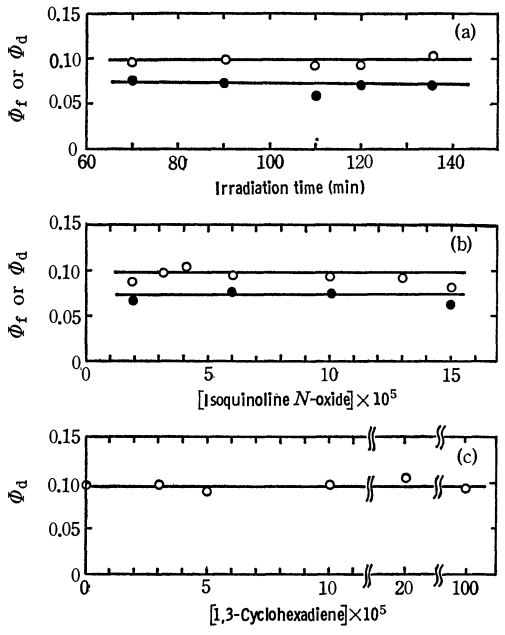

Fig. 4. Quantum yields of the photochemical isomerization of isoquinoline *N*-oxide in deaerated methanol at room temperature.
-●-: quantum yield of the formation of isocarbostyril, Φ_f, -○-: Quantum yield of the isoquinoline *N*-oxide disappearance, Φ_d. (a) Effect of the irradiation time (concentration of isoquinoline *N*-oxide: 1.0×10^{-4} M). (b) Effect of the initial concentration of isoquinoline *N*-oxide. (c) Effect of the addition of 1,3-cycrohexadiene (concentration of isoquinoline *N*-oxide: 6.0×10^{-5} M).

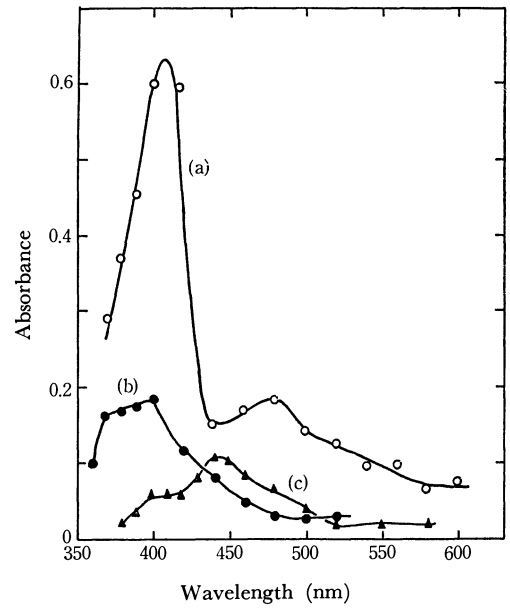

Fig. 5. Transient absorption spectra of isoquinoline *N*-oxide and isocarbostyril.
(a) -○-: Isoquinoline *N*-oxide, in EPA glass at 77 K.
(b) -●-: Isoquinoline *N*-oxide, in methanol at room temperature.
(c) -▲-: Isocarbostyril, in methanol at room temperature.

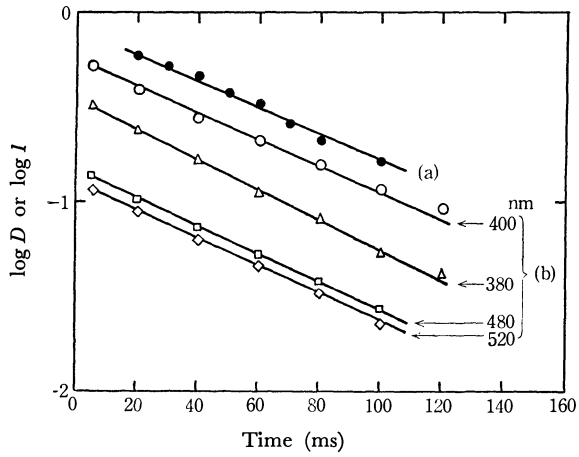

Fig. 6. Decay analysis for the phosphorescence (a) and for the transient species (b) in EPA glass at 77 K (concentration of isoquinoline *N*-oxide: 5.0×10^{-5} M).

intensity was lowered considerably at room temperature compared to that at 77 K (Fig. 5). The decay time estimated from the first-order rate plot was *ca.* 30 μs.

Next, the effect of the triplet quencher on the transient absorption was investigated in a deaerated methanol at room temperature. As can be seen from Fig. 7, the decay rate of the transient increased linearly with an increase in the concentration of 1,3-cyclohexadiene, although the piperylene or isoprene had no effect on the decay rate. The quenching rate constant evaluated from the slope of the straight-line was 8.1×10^{8} l·mol^{-1}·s^{-1}. The possibility that the transient absorption could be due to a T–T transition of the photoproduct (isocarbostyril) was definitely excluded by the flash-spectroscopic examinations for isocarbostyril itself. That is, as is shown in Figs. 5 and 7, the T–T

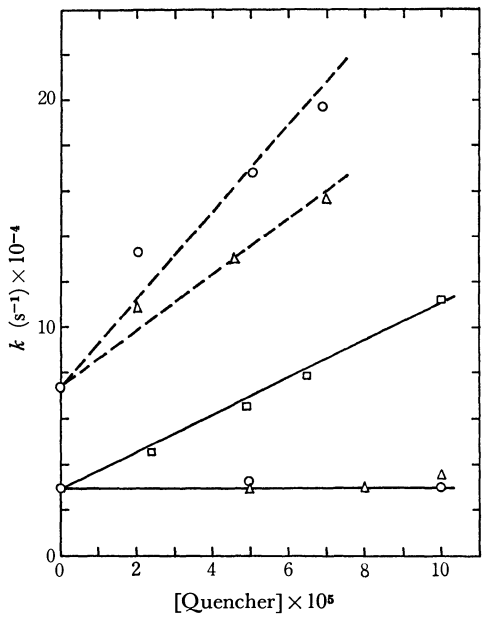

Fig. 7. Effect of the triplet quencher (-○-: isoprene, -△-: piperylene, -□-: 1,3-cyclohexadiene) on the transient species of isoquinoline *N*-oxide and isocarbostyril in deaerated methanol at room temperature. ——: for isoquinoline *N*-oxide (5.0×10^{-5} M), ----: for isocarbostyril (1.0×10^{-4} M).

absorption of isocarbostyril in a deaerated methanol at room temperature was completely different from that of isoquinoline *N*-oxide in maximum wavelength and in decay rate. In addition, the decay rate was observed to increase linearly with an increase in the concentration of the piperylene or isoprene (Fig. 7). Therefore, the transient absorption (Curve (a) in Fig. 5) was definitely identified as being due to a T–T transition of isoquinoline *N*-oxide. Although the triplet species was effectively quenched by 1,3-cyclohexadiene, the quantum yield of the photochemical isomerization was unaffected, as has been described before (Fig. 4). This also supports the idea that the lowest triplet state of isoquinoline *N*-oxide is not involved in the photoisomerization, but that the isocarbostyril results from an excited singlet state.

Effect of pH *on the Photochemical Isomerization.* In order to account for Processes I and II of the azanaphthalene *N*-oxides, Buchardt and Kaneko have independently proposed the idea that an oxaziridine may be initially formed as a photochemical intermediate common to both Processes.[1,3] On the basis of this assumption, Process I has been explained as follows. According to Buchardt,[1] the zwitter ion, **3**, resulting from a heterolytic cleavage of the oxaziridine **2** may be supposed to rearrange by a 1,2 shift (Scheme 1). Since a protonation of the $-O^-$ group may take place during the rearrangement, the photochemical isomerization in an aqueous solution is inferred to be affected by a variation in the pH values. Kaneko[3] has assumed a heterolytic cleavage of the oxaziridine **2**, followed by the formation of a carbonium ion, **4**, which can then rearrange to the lactam (Scheme 2); thus, the photoisomerization is considered to be facilitated by the presence of hydrogen ions. In either case, the photochemical isomerization in an aqueous solution is expected to be influenced to some extent by a lowering of the pH values.

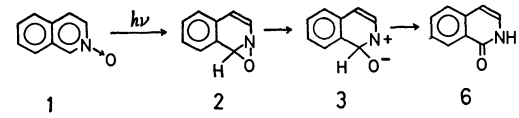

Scheme 1

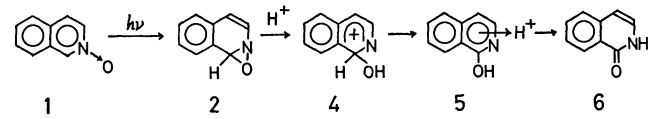

Scheme 2

Therefore, in order to clarify the effect of hydrogen ions on the isomerization process, photochemical examinations of isoquinoline *N*-oxide were performed on aqueous solutions at different pH values. Curve (a) in Fig. 8 shows the quantum yields of the disappearance of isoquinoline *N*-oxide plotted against the pH; that is, the independence of the quantum yield (*ca.* 0.07) of the pH in the 13.0—3.0 range was observed,[9] al-

9) The similar result has been also obtained in the case of quinoline *N*-oxide by Favaro.[2a]

though there was a steep increase at lower pH values (<3.0). In addition, the chemical yield of the isocarbostyril produced (Curve (b) in Fig. 8) was also found to be independent of the pH values except for the case of a strongly acidic solution (pH<3.0). These facts probably mean that Process I does not proceed ionically through the oxaziridine intermediate, as is shown in Schemes 1 and 2. For this reason, it seems to be difficult to assume that Procesess I and II involve a common intermediate such as an oxaziridine. This view seems to support the conclusion of Lohse.[1b]

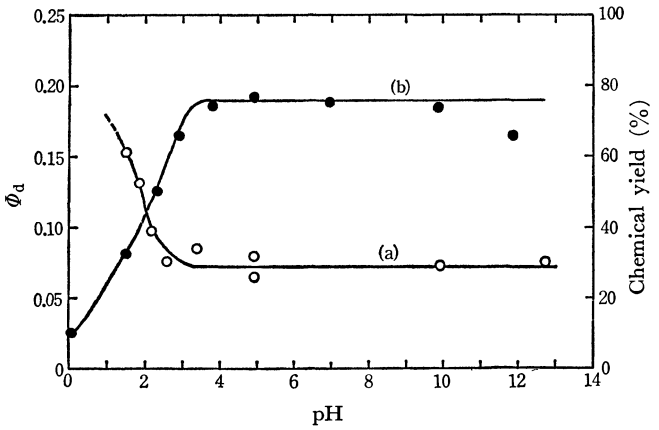

Fig. 8. Effect of pH on the quantum yield of isoquinoline *N*-oxide disappearance (-○-) and the chemical yield(%) of isocarbostyril (-●-) in aqueous solutions at room temperature.

Meanwhile, the p*K*a values of isoquinoline *N*-oxide in the ground and lowest-excited singlet states have been reported by Kubota[10a] to be 1.05 (or 1.01[10b]) and 0.81 respectively. Therefore, the remarkable change in both the quantum and chemical yields in strongly acidic solutions could be interpreted in terms of an acid-base equilibrium in the ground or lowest excited singlet state; that is, the photochemical isomerization of isoquinoline *N*-oxide proceeds from the excited non-protonated *N*-oxide, while the excited protonated molecule undergoes decomposition instead of isomerization.

The authors wish to thank Professor Shiro Matsumoto of this university for his permission to use the flash-photolysis apparatus.

10) (a) T. Kubota, *J. Spectrosc. Soc. Jap.*, **10**, 83 (1962). (b) H. H. Jaffé and G. O. Doak, *J. Amer. Chem. Soc.*, **77**, 4441 (1955).

BULLETIN OF THE CHEMICAL SOCIETY OF JAPAN, VOL. 46, 3662—3665 (1973)

The Photo-Erasable Memory Switching Effect of Ag Photo-Doped Chalcogenide Glasses

Isamu SHIMIZU, Hiroshi KOKADO, and Eiichi INOUE

Imaging Science and Engineering Laboratory, Tokyo Institute of Technology, O-okayama, Meguro-ku, Tokyo 152

(Received May 1, 1973)

The electric conductivity of the chalcogenide glass increased with an increase in the amount of Ag which had been photo-doped. By applying the electric field to the electrodes which were set on the surface of the Ag photo-doped chalcogenide glass film, a conductive path was grown from the cathode to the anode. As a result of the connection of the electrodes with the path, the electric resistance of the cell abruptly decreased (ON state). The path was made of the metal silver reduced by electrolysis and was diminished by irradiation with light. As the path was erased, the cell was turned into the resistant state (OFF state). The cycles were repeatable many times. There was a delay time (t_d) in turning the cell from the OFF to the ON state by applying the electric field (E). It was empirically described by the following equation for the Ag photo-doped chalcogenide glasses:

$$t_d = a \exp(-b \cdot E)$$

When a binary layer of metal and chalcogenide glass was exposed to light with the fundamental absorption band of the glass, the metal was doped into the glass layer. The term "photo-doping"[1] was given to the phenomenon on analogy with the doping of the foreign materials into the semiconductors.

As the electric fleld was applied to a pair of electrodes set on the surface of the Ag photo-doped chalcognide glass film, a conductive path was grown from the cathode to the anode. When the electrodes were connected with the path, the electric conductivity of the cell abruptly increased (ON state). The path remained stable even if the field was removed, while it could be erased at will by irradiation with light. As the path was erased, the cell returned to the resistant OFF state. These cycles were repeatable many times and were similar to the memory-switching effect[2] in the chalcogenide glass film. This phenomenon, however, was characteristic because of the following facts. In an ordinary case, the transition between the OFF and the ON state caused by applying a field is due to the phase transition between the vitreous and crystalline states. On the contrary, in this case

1) H. Sakuma, I. Shimizu, H. Kokado, and E. Inoue, Proc. 3rd Conf. Solid States Devices, Japan, *Supplement to Oyo Butsuri*, **41**, 76 (1972).

2) E. J. Evance, J. H. Helbers, and S. R. Ovsihnsky, *J. Non-crystalline Solids*, **2**, 334 (1970).

a migration of the silver ion in the glasses by applying the field takes place and the silver ions are reduced to the metal at the cathode, thus forming the conductive path. Moreover, the path can be erased by illumination at will.

The delay time (t_d) for the conductivity change from the OFF to the ON state under the field (E) was measured for the Ag photo-doped chalcogenide glasses. An empirical relation was obtained between t_d and E.

$$t_d = a \exp(-b E) \quad (1)$$

Here, a and b are constant.

Experimental

The chalcogenide glasses were prepared by the methods described in a previous paper.[3] The binary layers of Ag-chalcogenide glass were made on a substratum (slide glass) by successive vacuum evaporation (10^{-5} Torr). The silver layer on the chalcogenide glass was completely doped by irradiation with light. A high-pressure mercury lamp (Ushio-USH 250 W) fitted with an IR cut filter was used as the source. When the silver layer was completely photo-doped, the optical absorption of the metal silver at the wavelength longer than the absorption edge of the chalcogenide glass disappeared. The completion of the photo-doping of the silver layer was confirmed by the above measurement.

Two types of electric cells were used for the electric measurement (see Fig. 1). In the type (a) cell, a pair of the Au electrodes was formed on the surface of the photo-doped glass by vacuum evaporation. In the type (b) cell, an Au electrode was used as the anode and a tungsten pin electrode, as the cathode. An electric resistor of 500 KΩ was connected with the sample in series to prevent the cell from breaking because of the excessive current in the conductive ON state. A regulated power supply (Showa Electronics R-700) was used as the electric source. The electric current of the specimen was measured by means of a micro-ammeter (Takeda Riken TR-8651). To measure a t_d value of less than 1 s., a square wave pulse was used as the source and the change in the current flowing through the cell was traced with a synchroscope as the voltage drop through the series resistance.

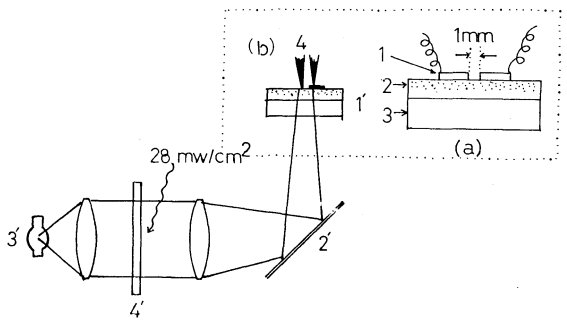

Fig. 1. Sketch of electric cells and the apparatus to measure the photo-erasing of the conductive path.
1: Au electrode, 2: Ag photo-doped chalcogenide glass, 3: substratum, 4: tungsten pin electrode, 1′: specimen, 2′: mirror, 3′: mercury lamp, 4′: IR cut filter.

3) I. Shimizu, H. Sakuma, H. Kokado, and E. Inoue, This Bulletin, **46**, 1291 (1973).

Results and Discussion

As a result of the photo-doping of Ag into the chalcogenide glasses, the electric conductivity of the surface of the glass films increased with an increase in the photo-doped silver. When the electric field was applied to the cell (type (a)) on an Ag photo-doped chalcogenide glass film, the conductive path was grown from the cathode to the anode, as is shown in Fig. 2. As a result of tracing with an EMX(electron probe X-ray micro-analyser), it was confirmed that the path was made of silver dendrite. On the basis of these facts, we may suppose that the photo-doped silver was

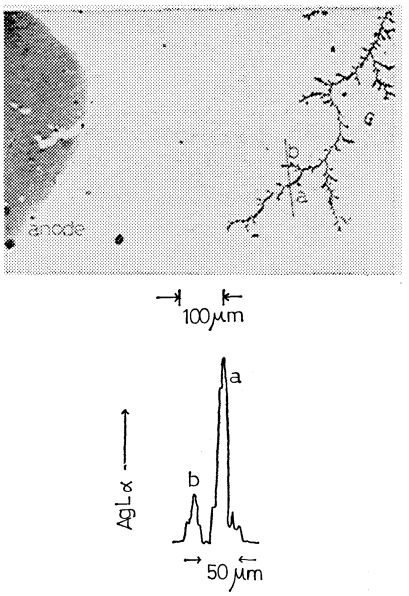

Fig. 2. Micrograph of conductive path grown from cathode to anode and EMX profile traced along a-b.

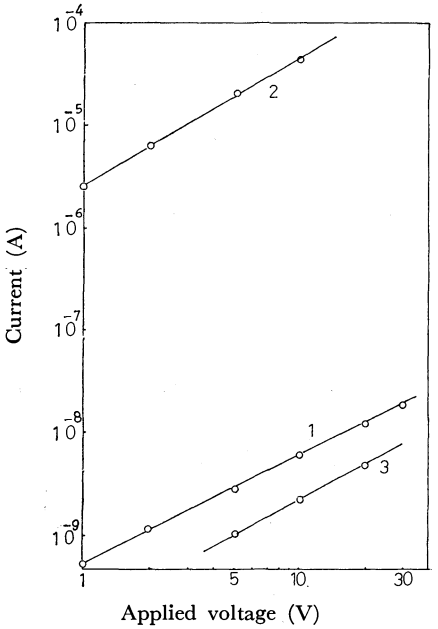

Fig. 3. Typical I-V characteristic curves of Ag (1000A) photodoped chalcogenide glass ($As_{16}S_{80}Te$) showing the photoerasable memory effect.
Type (a) cell was used. 1: OFF state, 2: ON state, 3; after irradiation of (2) with light

moved through the chalcogenide glass as the silver ion by applying the electric field and that the metal silver was reduced as a result of electrolysis at the cathode. The presence of the Ag ion has been supposed from studies of the electric properties of the chalcogenide glasses containing silver.[4] The electric conductivity of the specimen changed a very little before the path reached the anode. As the electrodes were shorted with the path, however, the conductivity of the cell absuptly increased. Figure 3 shows the current-voltage characteristic of the Ag(1000 A in thickness) photo-doped chalcogenide glass ($As_{16}S_{80}Te_4$) film in the OFF and ON states. The path was diminished by irradiation with light. When the path was erased, the cell returned to the OFF state, as is shown by Curve 3 in Fig. 3. These cycles were repeated many times unless the specimen was damaged by the passege of an excessive current through the cell in the ON state.

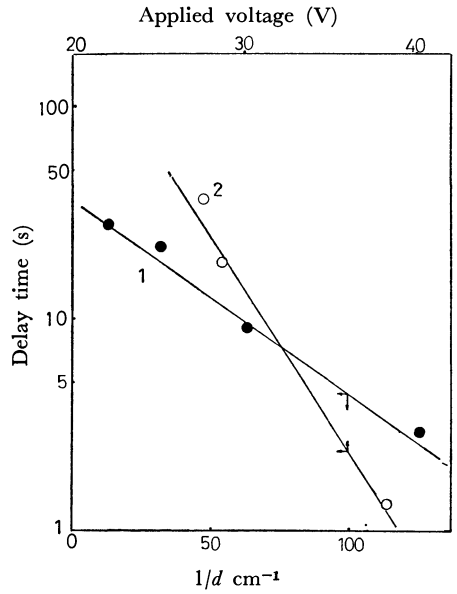

Fig. 4. Delay time plotted against applied field.
1: t_d *versus* V at constant d (1.3×10^{-2} cm), 2: t_d *versus* $1/d$ at constant V (30 volt) for Ag(500A) photo-doped $As_{30}S_{50}Se_{20}$

To regulate the position at which the path was generated, the type (b) cell was used and the delay time (t_d) was measured by changing the applied voltage (V) and the electrode distance (d). When the tungsten pin electrode was used as the cathode, the growth of the path was difficult because of its high contact resistance. Figure 4 shows the curve of the log t_d plotted against the applied voltage at the constant electrode distance ($d=1.3\times10^{-2}$ cm), and also the curve of the log t_d against the reciprocal of the electrode distance at a constant applied voltage (V=30 volt) for the Ag (500 A in thickness) photo-doped glass ($As_{30}S_{50}Se_{20}$) 0.5 μm thick. From these results, the relation between t_d and the electric field ($E=V/d$ V/cm) was described as follows:

$$\log t_d = \log A - B\cdot E. \qquad (2)$$

4) K. Arai, T. Kuwahata, H. Namikawa, and S. Saito, *Japan. J. Appl. Phys.*, **11**, 1080 (1972).

TABLE 1. A AND B VALUES OBTAINED FROM THE RELATION OF THE Eq. (2) FOR Ag PHOTO-DOPED CHALCOGENIDE GLASSES

Chalcogenide glass	Thickness of photo-doped Ag (A)	A (s)	B $(V/cm)^{-1}$
$As_{30}S_{50}Se_{20}$	50	360[a]	7×10^{-4} [a]
		360[b]	7×10^{-4} [b]
$As_{40}S_{60}$	400	290[a]	3×10^{-4} [a]
		290[b]	2×10^{-4} [b]
$As_{14}S_{55}Te_{26}$	500	240[a]	6×10^{-4} [a]
		240[b]	4×10^{-4} [b]

a) The values obtained from the curve log t_d *versus* V under the constant electrode distance.
b) The values obtained from the curve log t_d *versus* $1/d$.
Respective value for a) and b) coincided with each other within the experimental errors.

TABLE 2. A AND B VALUES OBTAINED FROM THE RELATION OF THE Eq. (2) for Ag PHOTO-DOPED $(As_2S_3)\cdot I$

Photo-doped Ag (A)	A (s)	B $(V/cm)^{-1}$
200		0.93×10^{-3}
400	580	3.1×10^{-3}
600		3.7×10^{-3}
500[a]	4.8	1.5×10^{-3}

a) The values A and B presented in the bottom were the ones obtained in high electric field.

Here, A and B are constants. The A and B values for the Ag photo-doped chalcogenide glasses are summarized in Table 1.

The conductive path was easily grown under the lower electric field when iodine was included in the Ag photo-doped chalcogenide glass. Under a constant electric field, the t_d value decreased with an increase in the amount of photo-doped silver. The values for A and B obtained from the results are shown in Table 2. In this case, the decrease in t_d corresponded closely to the increase in the B value for the heavier doped glass. Under a high electric field, we obtained a linear relation different from that obtained under a low field for the same specimen, as is shown in Table 2. In this case, both A and B values were smaller than that obtained under the low electric field. The growth of the conductive path from the cathode to the anode proceeded rapidly under the low electric field, while it became slow in the vicinity to the anode. The change in the growth rate must be due to a scarcity of the silver ions in the vicinity of the anode. No change in the growth rate was, however, observed in the high electric field, because the path arrived at the anode before the depletion zone at the anode was formed. The fact that the conductive path was easily grown in the Ag photo-doped (As_2S_3)–I system may be explained as follows:

(1) A greater amount of silver was ionized in the glass by forming the ionic bond with the iodine.

(2) The migration of the silver ion in the glass easily took place in the same way as that of the silver ion through the ionic crystals, such as α-Ag_2S or AgI.[5]

5) C. M. Perrott, *J. Phys. Chem. Solids*, **31**, 2709 (1970).

Though the Ag photo-doped glasses in this work were confirmed by X-ray diffraction patterns to be retained in the vitreous state, micro-crystallization could occur locally in the glass.

The conductive path was retained for a long time after the electric field was removed, and the cell could be memorized in the ON state. When the cell was exposed to light, the conductive path disappeared and the cell returned to the OFF state. Figure 5 shows the relation between t_d and the exposure time needed to turn the cell into the OFF state for the Ag photo-dopes $(As_2S_3)\cdot I$ system. The experimental conditions are shown in Fig. 1. The OFF state formed by a short illumination was turned into the ON state with a short t_d. In this case, the conductive path is partially diminished. The t_d was recovered to the value for the virgin sample when the specimen was exposed to light for enough time. This implied that the path could be erased completely.

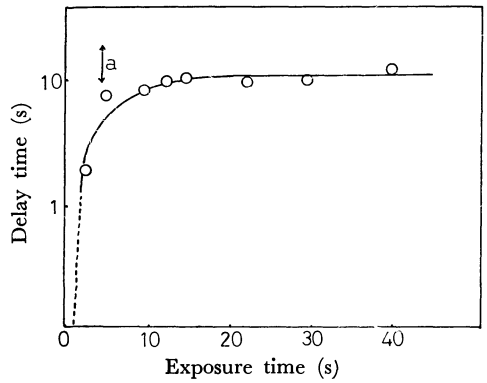

Fig. 5. Delay time plotted against exposure time for Ag-(400A) photo-doped $(As_2S_3)\cdot I$.
Applied field (7.7×10^2 v/cm); (a) shows the t_d for the virgin sample.

Conclusion

An electric memory-switching effect was found in the Ag photo-doped chalcogenide glass. It is different from the memory-switching effect observed in the chalcogenide glass films, such as the As–Ge–Te system, in which the effect is due to the phase transition between the vitreous and crystalline states. The properties of this memory-switching effect were as follows:

(1) In the Ag photo-doped chalcogenide glass, the silver ion was moved by the applied electric field, and the metal silver was reduced by electrolysis at the cathode and formed the conductive path.

(2) The ON state could be reverted to the OFF state at will by exposure to light.

BULLETIN OF THE CHEMICAL SOCIETY OF JAPAN, VOL. 46, 3665—3671 (1973)

Kinetics of Hydrogen Electrode Reaction on Mercury. I. Theoretical Part. Non-steady State Analysis for the Electrochemical Mechanism

Akiko KATAYAMA and Hideaki KITA
Research Institute for Catalysis, Hokkaido University, Sapporo 060

(Received July 2, 1973)

Potentiostatic and potentiodynamic transients are theoretically analysed on the basis of the electrochemical mechanism for the hydrogen electrode reaction. The interface was assumed to consist of the metal surface, the plane on which the adsorbed intermediate of $H_2^+(a)$ stays, and the diffuse double layer. The repulsive force between the intermediates was introduced by proportional approximation. From the results the depolarization observed in Tafel plots is understood as a non-steady state phenomenon, and observation by the potential-sweep method offers information on both the features of the adsorbed intermediate and the kinetics of the step preceding the rate-determining step.

In 1936 Horiuti and Okamoto found[1] that experimental values on the separation factor of the hydrogen evolution reaction serve to classify electrode metals into two groups. A dual mechanism was proposed[2,3] for the hydrogen electrode reaction (H.E.R.) on these groups of metals, *i.e.*, catalytic mechanism on Pt (at high overvoltages), Ni, Au, Cu, and Pb (in alkaline solution), and electrochemical mechanism on Hg, Pb (in acidic solution), Sn, and Pt (at low overvoltages). One of the present authors (H.K.)[4] surveyed data of H.E.R. on various metals reported for the last two decades and examined the relationship between the catalytic activity of electrodes and the heat of adsorption of hydrogen or the work function. A grouping of metals similar to Horiuti's was found, transition metals including IB metal (Cu, Ag, Au) being denoted by "d-metal" and those after IIB in the periodic table by "sp-metals". He showed that the difference between d- and sp-metals can be explained by the dual mechanism, *i.e.*, the catalytic mechanism on d-metals and the electrochemical mechanism on sp-metals.

The electrochemical mechanism consists of the following consecutive steps:

$$2H^+ + e^- \rightleftarrows H_2^+(a) \quad \text{(I)}$$

$$H_2^+(a) + e^- \rightarrow H_2, \quad \text{(II)}$$

1) J. Horiuti and G. Okamoto, *Sci. Pap., I.P.C.R.*, (Tokyo), **28**, 23, (1936).
2) G. Okamoto, J. Horiuti, and K. Hirota, *ibid.*, **29**, 223 (1936).
3) J. Horiuti, T. Keii, and K. Hirota, *J. Res. Inst. Catal., Hokkaido Univ.*, **2**, 1 (1951).
4) H. Kita, *J. Electrochem. Soc.*, **113**, 1095 (1966).

where (II) is the rate-determining step and $H_2^+(a)$ is a hydrogen-molecule ion adsorbed on the electrode. However, the mechanism most frequently quoted, especially for Hg,[5] is the slow discharge mechanism, in which the rate-determining step is the formation of an adsorbed hydrogen atom, H(a); $H^+ + e^- \rightarrow H(a)$. This mechanism seems to be widely accepted because it provides the simplest way for an explanation of the kinetics observed. However, for Hg many experimental results which cannot be explained easily by means of the slow discharge mechanism have been obtained, *e.g.*, prolonged evolution of hydrogen gas after cessation of a cathodic polarization,[6,7] abnormal shift of a half-wave potential $E_{1/2}$ under various conditions,[6,8] and large transfer coefficient (>0.5) observed by the faradaic rectification method.[9] The prolonged evolution of hydrogen gas indicates that the rate-determining step is preceded by a fast step which produces an intermediate. According to the simple discharge mechanism, $E_{1/2}$ is not expected to shift with the pH of the solution, but this is not the case.[8] The effect of the column height of dropping mercury electrode on $E_{1/2}$ differs from that expected from the slow discharge mechanism. The symmetrical polarogram predicted from the slow discharge mechanism was not also observed under various conditions.[6] Barker found a larger value for a transfer coefficient by the sophisticated method of the faradaic rectification and attributed it to H_2^+ formation.[9]

Horiuti *et al.* who proposed the electrochemical mechanism, predicted the change in the Tafel slope from 40 to 120 mV on Hg with increase of a cathodic polarization. Experimental results, however, show the depolarization at low overvoltages; the observed current density is much higher than that extrapolated from the linear part of Tafel plots observed at high overvoltages. A possible explanation for the depolarization is to consider it a non-steady state phenomenon. As seen from an extremely small exchange current density of $10^{-12} \sim 10^{-13}$ A/cm^2 on Hg,[4] it may take a considerably long time for H.E.R. to attain a steady state, especially at low overvoltages. The reaction will then appear to be in a steady state on the time scale of usual observation though in fact it is not.

In the present work we attempt to interpret H.E.R. on Hg in a non-steady state and its transient process to attainment of steady state, assuming the electrochemical mechanism. A theoretical analysis is described.

Formulation

In the case of the electrochemical mechanism, the non-steady state is expressed by

$$Q\mathrm{d}\theta/\mathrm{d}t = i_1 - i_2 \mp 0, \tag{1}$$

where Q represents a monolayer quantity of $H_2^+(a)$ in electricity, θ the coverage of $H_2^+(a)$, and i_1 and i_2 net currents of steps (I) and (II), respectively. Non-steady state analysis is to solve the above equation for i_1 and i_2, and hence for the total current i,

$$i = i_1 + i_2, \tag{2}$$

as a function of time.

Rate expression. We first treat the rate expressions for i_1 and i_2. Horiuti developed a generalized theory for a reaction rate,[10,11] which gives precise rate formulae even for the heterogeneous reaction. On the basis of a crystal lattice plane model, forward and backward velocities of an elementary step are expressed in current densities by

$$i_+ = F(kT/h)N^{\mp}\theta^{\mp}(0)\exp\{-(\varepsilon^{\mp}-\mu^{\mathrm{I}})/RT\} \tag{3}$$

and

$$i_- = F(kT/h)N^{\mp}\theta^{\mp}(0)\exp\{-(\varepsilon^{\mathrm{I}}-\mu^{\mathrm{F}})/RT\}, \tag{4}$$

where the number of electrons concerned is put to unity. In Eqs. (3) and (4), $\mp$ is a critical system, $N^{\mp}$ the total number of sites for $\mp(\sigma^{\mp})$ per unit area, $\varepsilon^{\mp}$ reversible work required for a critical system to be brought from a standard state to a vacant $\sigma^{\mp}$, $\theta^{\mp}(0)$ the probability of $\sigma^{\mp}$ being vacant, μ^{I} and μ^{F} chemical potentials of the initial and final systems of a step, respectively. F, k, T, and h have their usual meanings.

In order to develop the rate expressions further, we introduce the following four relations.

(a). When the adsorption site of a critical system is the same as that of $H_2^+(a)$, we have

$$\theta^{\mp}(0) = 1 - \theta, \tag{5}$$

where θ represents the coverage of $H_2^+(a)$.

(b). Another fundamental relation is used:[10]

$$\theta/(1-\theta) = \exp\{[\mu(H_2^+) - \varepsilon(H_2^+)]/RT\}, \tag{6}$$

where $\varepsilon(H_2^+)$ is defined as reversible work required for $H_2^+(a)$ to be brought from a standard state to a vacant $\sigma^{\mp}$ (for the sake of simplicity abbreviated to ε). The functions μ^{I}, μ^{F}, and $\varepsilon^{\mp}$ for steps (I) and (II) are summarized in Table 1, where $\mu(H^+)$, $\mu(e^-)$, and $\mu(H_2)$ are chemical potentials of proton, metal electron, and hydrogen gas, respectively.

Table 1. μ^{I} and μ^{F} for steps (I) and (II)

	Step (I)		Step (II)	
μ^{I}	$2\mu(H^+)+\mu(e^-)$	(7.I)	$\mu(H_2^+)+\mu(e^-)$	(7.II)
μ^{F}	$\mu(H_2^+)$	(8.I)	$\mu(H_2)$	(8.II)

(c). In order to find a relation between $\varepsilon^{\mp}$ and the reversible work required for the initial system to be brought from a standard state to a vacant site, ε^{I}, we introduce the Horiuti-Polanyi relation,[12]

$$\Delta\varepsilon^{\mp} = \alpha\Delta\varepsilon^{\mathrm{I}} = \alpha(\Delta\varepsilon + F\Delta\eta), \tag{9}$$

where α is a positive proper fraction. This equation is referred to step (I) or (II) where the initial system is $2H^+ + e^-$ or $H_2^+(a) + e^-$. $\Delta\varepsilon$ in the third term of the equation represents the change in ε by experi-

5) A. N. Frumkin, *Advs. Electrochem. Electrochem. Engineering*, **1**, 65 (1961).
6) O. H. Müller, *Polarography*, **1**, 319 (1966).
7) F. R. Smith and H. Heintze, *Can. J. Chem.*, **48**, 203 (1970).
8) R. Tamamushi, This Bulletin, **26**, 56 (1953).
9) G. C. Barker, "Trans. Sym. Electrode Processes", ed. Yeager, Wiley, New York (1961), p. 325.
10) *e.g.*, J. Horiuti and T. Nakamura, *Advs. Catal.*, **17**, 1 (1967).
11) J. Horiuti, *J. Res. Inst. Catal., Hokkaido Univ.*, **1**, 8 (1949—51).
12) J. Horiuti and Polanyi, *Acta Physicochim., U.S.S.R.*, **2**, 505 (1935).

mental conditions such as the kind of electrode. $F\Delta\eta$ represents the change in free energy of metal electron by polarization. Overvoltage, η, is taken positive for a cathodic polarization. Integration of Eq. (9) gives for steps (I) and (II),

$$\varepsilon_1^{\neq} = \alpha_1(\varepsilon+F\eta) + K_1 \quad (10.\text{I})$$

$$\varepsilon_2^{\neq} = \alpha_2(\varepsilon+F\eta) + K_2, \quad (10.\text{II})$$

where the sufficies 1 and 2 refer to steps (I) and (II) respectively, and K_1 and K_2 are integral constants. (d). $\mu(H^+)$, $\mu(e^-)$, and $\mu(H_2)$ are given as follows in reference to a standard state of the normal hydrogen electrode;

$$\mu(H^+) = RT \ln a_{H^+} \quad (11)$$

$$\mu(e^-) = F(-E_e+\eta) \quad (12)$$

and

$$\mu(H_2) = RT \ln P_{H_2}, \quad (13)$$

where a_{H^+} is an activity of H^+, E_e an equilibrium potential, and P_{H_2} a hydrogen pressure. E_e is given by

$$E_e = (RT/2F) \ln \{a_{H^+}^2/P_{H_2}\}. \quad (14)$$

i_1 and i_2. The forward current density of step (I), i_{+1}, is obtained from Eqs. (3), (5), (7.I), (10.I), and (11)$\sim$(13) as

$$i_{+1} = k_1 F a_{H^+} P_{H_2}^{1/2}(1-\theta) \exp\{[-\alpha_1\varepsilon+(1-\alpha_1)F\eta]/RT\}, \quad (15)$$

where $k_1 \equiv (kT/h)N^{\neq} \exp(-K_1/RT)$. Similarly, the backward current density of step (I), i_{-1}, is obtained from Eqs. (4), (5), (8.I), (10.I), and (11)$\sim$(13) as

$$i_{-1} = k_1 F\theta \exp\{[(1-\alpha_1)\varepsilon-\alpha_1 F\eta]/RT\}. \quad (16)$$

The net current density of step (I), i_1, is then

$$i_1 = k_1 F[a_{H^+} P_{H_2}^{1/2}(1-\theta) \exp\{[-\alpha_1\varepsilon+(1-\alpha_1)F\eta]/RT\} - \theta \exp\{[(1-\alpha_1)\varepsilon-\alpha_1 F\eta]/RT\}]. \quad (17)$$

The net current density of step (II), i_2, is obtained from Eqs. (3), (4), (6), (7.II), (8.II), (10.II), and (11)$\sim$(13) as

$$i_2 = k_2 F[a_{H^+}^{-1} P_{H_2}^{1/2}\theta \exp\{(1-\alpha_2)(\varepsilon+F\eta)/RT\} - P_{H_2}(1-\theta) \exp\{-(\alpha_2\varepsilon+\alpha_2\eta)/RT\}], \quad (18)$$

where $k_2 \equiv (kT/h)N^{\neq} \exp(-K_2/RT)$.

Equation (1) is now subjected to calculation by introducing Eqs. (17) and (18) for i_1 and i_2.

Calculation

Equations (17) and (18) show that i_1 and i_2 are as follows at given a_{H^+}, P_{H_2}, and α's;

$$i_1 \text{ or } i_2 = f(\theta, \eta, \varepsilon, k_1 \text{ or } k_2),$$

where k_1 and k_2 are parameters. In solving i_1 and i_2 as a function of θ, we need a relation between θ, ε, and η.

ε for $H_2^+(a)$. The adsorption energy of H_2^+(a), ε, will be given approximately by[13]

$$\varepsilon = \varepsilon_{00} + FE_p + R_e\theta, \quad (19)$$

where ε_{00} is the adsorption energy in the absence of potential difference from that of solution and at $\theta=0$, the second term an electrostatic potential energy at the plane where H_2^+(a) is located, and the third term a repulsive interaction energy between H_2^+(a)'s. In the present work, the repulsive energy is expressed to be proportional to the concentration of surrounding neighbours, *i.e.*, to θ.[14] R_e is the repulsive interaction energy at $\theta=1$. As the intermediate is a charged one, E_p and θ are interrelated in principle by the Poisson equation.

The Poisson Equation. To find the relation between E_p and θ, we employ Horiuti's model[13] (Fig. 1). P represents the plane on which H_2^+(a)'s are located. No charge is present between P and electrode surface, C. Beyond P, a diffuse double layer is present. The distance between C and P is x_p, and the dielectric constant is denoted by D_p in C–P and D_B beyond P. These dielectric constants are assumed to be potential-independent.

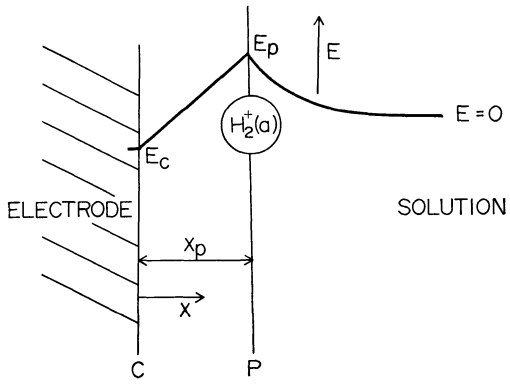

Fig. 1. A model for the double layer at interface.

Horiuti[13] analysed in detail the relation between E_p and θ as follows. One dimensional Poisson equation is given by

$$(D/4\pi)d^2E/dx^2 = -\rho, \quad (20)$$

where E is an electrostatic potential, and ρ is space charge density. Integration of Eq. (20) with respect to x gives at $x=x_p$,

$$-\frac{1}{4\pi}\lim_{t\to0}\left(D\frac{dE}{dx}\right)_{x_p-t} + \frac{1}{4\pi}\lim_{t\to0}\left(D\frac{dE}{dx}\right)_{x_p+t} = -\lim_{t\to0}\int_{x_p-t}^{x_p+t}\rho dx. \quad (21)$$

As there is no charge between C and P, the first term of the left hand side of Eq. (21) becomes $-D_p(E_p-E_c)/4\pi x_p$ where E_c is an electrostatic potential at C. The right hand side represents the charge on P, *i.e.*, $Q\theta$. Thus Eq. (21) becomes

$$-(D_p/4\pi x_p)(E_p-E_c) + (D_B/4\pi)\lim_{t\to0}(dE/dx)_{x_p+t} = -Q\theta. \quad (22)$$

The charge distribution beyond P is given for n mol/ml of 1–1 electrolyte solution by

$$\rho = Fn(e^{-FE/RT} - e^{FE/RT}). \quad (23)$$

13) J. Horiuti, *J. Res. Inst. Catal. Hokkaido Univ.*, **3**, 52 (1954).

14) The validity of proportional approximation is discussed by J. Horiuti and T. Toya, *Solid State Surface Science*, **1**, 1 (1969).

Since we have the relation $2d^2E/dx^2=d(dE/dx)^2/dE$, Eqs. (20) and (23) give

$$\lim_{t\to 0}\left(\frac{dE}{dx}\right)_{x_p+t} = \pm\left[-\frac{8\pi}{D_B}Fn\int_{E_p}^{0}(e^{-FE/RT}-e^{FE/RT})dE\right]^{1/2} \quad (24)$$

where $E=0$ and $dE/dx=0$ at $x\to\infty$.

We obtain from Eqs. (22) and (24)

$$C_{dl}(E_p-E_c)-(2D_BRTn/\pi)^{1/2}\sinh(FE_p/2RT) = Q\theta, \quad (25)$$

where $C_{dl}\equiv D_p/4\pi x_p$. Since the potential in bulk solution is zero, positive sign in Eq. (24) is chosen. Equation (25) becomes identical with the equation derived by Breiter *et al.*[15] when $\theta=0$.

In order to relate potential E with a measurable quantity, we take E_c as an electrostatic potential difference from the potential of point of zero charge E_z, *i.e.*, a rational potential, and assume that the work function of the electrode is constant over all overvoltage region. Thus E_c is given by

$$E_c = -\eta - E_z + (RT/2F)\ln(a_{H^+}^2/P_{H_2}). \quad (26)$$

The last term is due to the present choice of a standard state at normal hydrogen electrode (NHE). Thus, Eqs. (19), (25), and (26) give a relation for ε as a function of θ and η.

Two conditions for η. We selected the two following conditions so as to bring a transient behavior which can be easily tested by experiments.

(A) Constant Polarization: Variation of current i with time t was calculated at a constant polarization of the electrode to a certain η. The electrode can be initially in various conditions. In the present calculation, the initial condition of $\eta=0$ was chosen. Hence, θ at $t=0$ is an equilibrium value at $\eta=0$, $\theta_e°$. $\theta_e°$ was determined from Eqs. (1), (25), and (26) at $d\theta/dt=0$ and $\eta=0$. Since the polarization is a step function of t, E_p at $t=0$, $E_p°$ was determined from Eqs. (25) and (26) at $\eta=\eta$ and $\theta=\theta_e°$ (The Regula Falsi method was used).

(B) Potential Sweep: Current was calculated as a function of t (or η) when η was proportional to t. Initial condition was again chosen as $\eta=0$.

Calculations. The change of θ with t is given by Eq. (1) together with Eqs. (17) and (18). The relationship between θ and E_p is given by Eq. (25). The current at a certain time can be obtained from the solution of Eqs. (1) and (25). However, direct computation of these equations is so cumbersome that the derivative of Eq. (25) with respect to t is used for calculation; $d\theta/dt$ in the derivative is given by Eq. (1), $d\eta/dt$ being zero at condition (A) or equal to a sweep rate at condition (B). The Runge-Kutta-Gill method was used for calculations.

Parameters. Constants k_1 and k_2 are expected to have the relation $k_1\gg k_2$ since step (II) is slower than step (I). In the first calculation, k_2F was equated to the observed exchange current density, *i.e.*, $k_2=10^{-17}$ s^{-1} cm^{-2}. k_1 was chosen to be 10^5 times larger than k_2. We can evaluate ε_{00} by following the method of Horiuti *et al.*[13] However, the circumstances of the electrode seem to be more complicated than those treated by them, and hence $\varepsilon_{00}=-0.5$ eV was arbitrarily chosen. R_e was evaluated to be $26.7/D_p$ eV from coulombic repulsive force between H_2^+(a)'s on Hg whose atomic radius is 1.57 Å.[16] Each H_2^+(a) can be surrounded by six H_2^+(a)'s at full coverage. In the calculation, R_e was first taken to be 26.7 eV. The other parameters were, if not stated, $C_{dl}=18$ μF/cm², $E_z=-0.2$ V *vs.* NHE, $\alpha_1=\alpha_2=0.5$, and $a_{H^+}=P_{H_2}=1$.

Values of k_1, k_2, ε_{00}, R_e, C_{dl}, a_{H^+}, and E_z were further changed and their effects were examined.

The calculation was performed at Hokkaido University Computing Center with a FACOM 230—60 computer. Subroutine programs of Runge-Kutta-Gill and Regula Falsi methods furnished in FACOM were used.

Results

Condition (A). Figure 2 shows the relationship of logarithm of currents i_1, i_2, and i with time t at $\eta=0.2$ V. The relationships between log i and t are illustrated at various overvoltages in Fig. 3 where the result at $\eta=0.1$ V with $R_e=26.7/2$ eV is also shown. We see that the smaller R_e and overvoltage, the longer the time to attain a steady state. Coverage θ is plotted against t in Fig. 4. Comparison of Figs. 3 and 4 shows that the time to attain a steady value of θ is shorter than that of i at $\eta<0.3$ V. We denote steady values of i, θ, and E_p by i_s, θ_s, and E_{ps}, respectively.

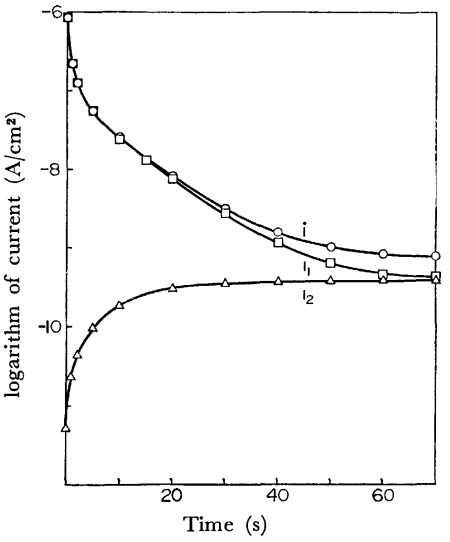

Fig. 2. Logarithm of currents i_1, i_2, and i *vs.* time curves at $\eta=0.2$ V (Condition (A)).

In Fig. 5, θ_s and E_{ps} in 1 M acidic solution are plotted as a function of η by the use of different set of values for the double layer capacity and the potential of the point of zero charge, *i.e.*, 18 μF/cm² and −0.2 V, 40 μF/cm² and −0.2 V, and 18 μF/cm² and −0.6 V (NHE), respectively. It is seen that θ_s first increases with η but becomes almost independent at

15) M. Breiter, M. Kleinerman, and P. Delahay, *J. Amer. Chem. Soc.*, **80**, 5111 (1958).

16) R. T. Sanderson, "Chemical Periodicity", Reinhold, New York (1964), p. 28.

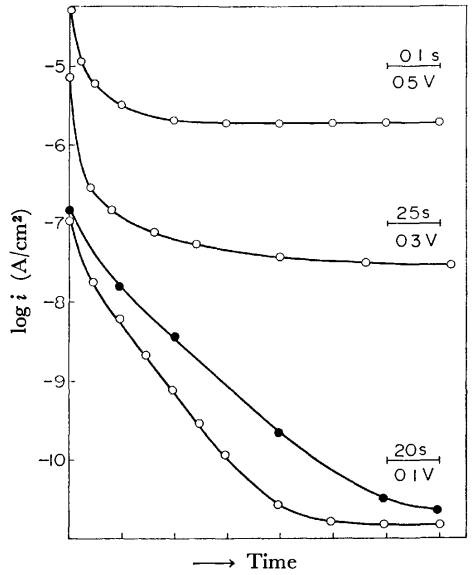

Fig. 3. $\log i$ *vs.* time curves at various overvoltages in Condition (A).
○, $R_e = 26.7$ eV; ●, 26.7/2 eV. Time scale is indicated for each curve. $k = 10^{-12}\ s^{-1}\ cm^{-2}$, $k_2 = 10^{-17}\ s^{-1}\ cm^{-2}$, $\varepsilon_{oo} = -0.5$ eV, $C_{dl} = 18\ \mu F/cm^2$, $E_z = -0.2$ V *vs.* NHE, and $a_{H^+} = P_{H_2} = 1$.

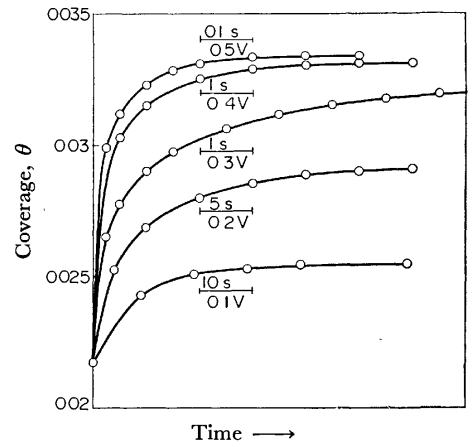

Fig. 4. Coverage *vs.* time curves at various overvoltages in Condition (A).
Time scale is indicated for each curve.

$\eta > 0.3$ V. E_{ps}, on the other hand, monotonously decreases with η. Tafel plots (the logarithm of i_s *vs.* η) for the above three sets of values give curve 2 in Fig. 6. Values of C_{dl} and E_z do not affect i_s to an appreciable extent at every overvoltage. We find that Tafel plots consist of two straight lines whose breakpoint coincides with that of the curve, θ_s *vs.* η in Fig. 5. The effect of the concentration of H^+ on the steady relation appears in the lower overvoltage region as shown by curves 1∼3 in Fig. 6. The current density at a given overvoltage is larger for the smaller H^+ concentration. However, the dependence is reversed when η is replaed with the potential referred to NHE.

When only k_1 is decreased by an order of 10^2, the time to attain the steady state becomes considerably longer and θ_s becomes smaller than those in Figs. 3 and 5.

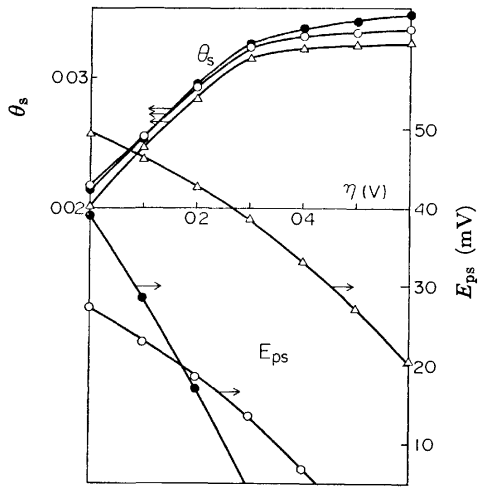

Fig. 5. θ_s and E_{ps} *vs.* η curves.
○, $C_{dl} = 18\ \mu F/cm^2$ and $E_z = -0.2$ V *vs.* NHE; ●, $C_{dl} = 40\ \mu F/cm^2$ and $E_z = -0.2$ V *vs.* NHE; △, $C_{dl} = 18\ \mu F/cm^2$ and $E_z = -0.6$ V *vs.* NHE.
E_{ps} is referred to the potential in the bulk of solution.

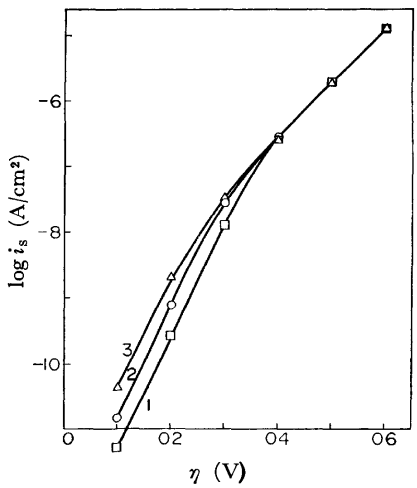

Fig. 6. Tafel plots at various H^+ concentration.
Curve 1(□), 10 N H^+; 2 (○), 1.0 N H^+; and 3 (△), 0.1 N H^+.

The variation of R_e causes a large change on $\log i$ *vs.* t (Fig. 3). On the other hand, our separate calculation shows that the change of ε_{00} does not appreciably affect $\log i$ *vs.* t and Tafel plots, except for θ and E_p. Thus, the changes of θ_s and E_{ps} are associated. The changes of double layer capacity and/or E_z affect θ_s and E_{ps} but neither $\log i$ *vs.* t nor Tafel plots.

Condition (B). With the same initial condition and parameters as in Fig. 3, a current was calculated up to $\eta = 0.5$ V for various sweep rates. The results are given in Fig. 7. It is interesting to see that the current plateau apprears on $\log i$ *vs.* η curve. The value of the current at the plateau is almost proportional to the sweep rate. In the overvoltage region lower than the plateau, $\log i$ *vs.* η represents the relationship of $\log i_1$ *vs.* η at $t \to 0$. In that higher than the plateau, the relation corresponds to Tafel plots ($\log i_s$ *vs.* η). The value of a current at the plateau i_p is computed for various values of parameters as in Condition (A)

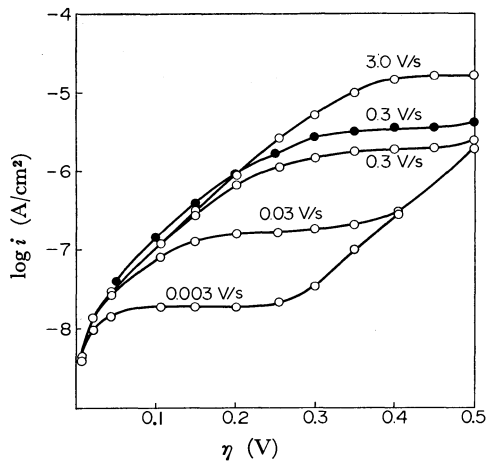

Fig. 7. $\log i$ *vs.* η curves at various potential-sweep rates in Condition (B).
○, $R_e=26.7$ eV; ●, $R_e=26.7/2$ eV.

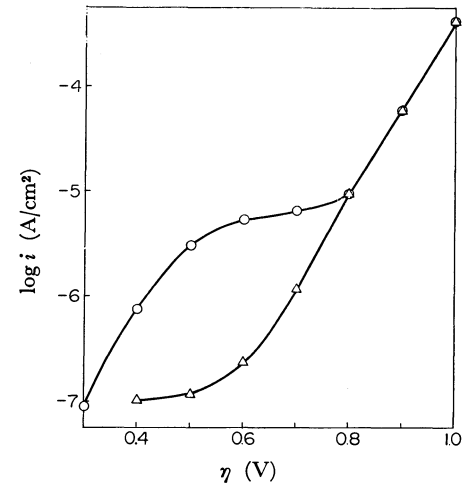

Fig. 8. $\log i$ *vs.* η curves in Condition (A).
$R_e=26.7/2$ eV, $k_1=10^{-14}$ s^{-1} cm^{-2}, and $k_2=10^{-19}$ s^{-1} cm^{-2} are used. ○, at a time of 90 ms after overvoltages are applied; △, at 5 s.

and found to be almost independent of them, except for R_e. i_p is nearly proportional to the reciprocal of R_e as seen from the curves for 0.3 V/s (solid and open circles in Fig. 7). The plateau has a tendency to lose its flat portion with increase of the sweep rate and to become shorter when the velocities of steps (I) and (II) become closer. Such a tendency makes it difficult to decide the value of i_p. In the case of $k_1/k_2=10^3$, i_s is one tenth smaller than that for $k_1/k_2=10^5$, where k_2 is kept at 10^{-17} s^{-1} cm^{-2} in both cases.

Discussion

In the above calculation, the value of k_2F was equated to the exchange current density determined by extrapolation of the linear part of Tafel plots at high overvoltages.[4] However, the calculated Tafel plots at high overvoltages show an appreciably larger current than the observed one. The discrepancy is due to the conventional linear extrapolation of Tafel plots observed at high overvoltages to $\eta=0$, whereas the present calculation reveals a break in the Tafel plots, giving the other linear portion with smaller Tafel slope at lower overvoltages. Such a break has been proposed by Horiuti *et al.*[17] When k_2 value is reduced to 10^{-19} s^{-1} cm^{-2} with $k_1/k_2=10^5$, Tafel plots reproduce the experimental data at high overvoltages. In this case, i_{+2} at $\eta=0$ becomes one hundredth of the extrapolated exchange current density.

Condition (A). The present calculation gives an interpretation for the depolarization at low overvoltages. The calculated $\log i$ *vs.* η at $t=5$ s and 90 ms is shown in Fig. 8, where $k_2=10^{-19}$ s^{-1} cm^{-2}, $k_1=10^{-14}$ s^{-1} cm^{-2}, and $R_e=26.7/2$ eV. The plots at $t=90$ ms show a typical S-type depolarization curve. Tza and Iofa,[18] and Iofa *et al.*[19] observed an S-type depolarization, which was markedly enhanced in the presence of specifically adsorbable anions. Former authors' interpretation, revised by Frumkin,[5] was based on the steady state treatment and successful only for the initial deviation from the linear part but not over all region. The present non-steady treatment has satisfactorily reproduced the whole S-type depolarization.

The depolarization contradicts Horiuti's prediction as commented by Frumkin.[5] Horiuti predicted that Tafel plots consist of the two linear parts with Tafel constants of 1.5 at low overvoltages and 0.5 at high overvoltages. The present work reproduces Horiuti's prediction in a steady state as seen in Fig. 6. Hence, the discrepancy will be due to a slow attainment of the steady state. The coverage in the steady state increases with the increase of overvoltage but becomes almost constant in the overvoltage region of Tafel constant of 0.5. It is interesting to see that θ itself is very small and approaches a limiting value by its increase in a very small amount; these results are attributed to the repulsive interaction between H_2^+(a)'s.

Coverage θ_e° is determined by the condition, $i_1=i_2=i=0$; Eqs. (17) and (18) show that ε_{00} and R_e are primarily important factors in a determination of θ_e°. ε_{00} is a parameter in the present calculation, and can not be estimated experimentally, although R_e is estimated from the experiments carried out with Condition (B). Tafel plots are also largely dependent on i_1 of step (I); the larger the α_1, the larger the Tafel slope.

At high overvoltages, Tafel plots at various H^+ concentrations give a single straight line. This is consistent with the observation, reviewed by Frumkin,[5] although he interpreted it on basis of the slow discharge mechanism. pH effect in a steady state can not manifest the principal mechanism.

Condition (B). The linear potential-sweep method has been employed for the study of dielectric relaxations, electrode processes, *etc.*

Let us suppose that adsorption process is expressed

17) J. Horiuti, A. Matsuda, M. Enyo, and H. Kita, "Proc. the 1st Australian Conference on Electrochem.", ed. Friend and Gutmann, Pergamon Press, Oxford (1965), p. 750.

18) Tza Chuan-sin and Z. A. Iofa, *Dokl. Akad. Nauk U.S.S.R.*, **126**, 1308 (1959).

19) S. Iofa, B. Kabanov, E. Kuchinski, and F. Chistyakov, *Acta Physicochim., U.S.S.R.*, **10**, 317 (1939).

by a series combination of the adsorption capacity c_{ads}, and the adsorption resistance r_{ads}. When the linear potential-sweep (sweep rate, v) is applied to such a circuit, the current of adsorption i_{ads} is given as $i_{ads}=v\ c_{ads}[1-\exp(-t/c_{ads}r_{ads})]$, where c_{ads} and r_{ads} are assumed to be constant. Hence, i_{ads} reaches finally a constant value of $v\ c_{ads}$. Appearance of the current plateau thus indicates the existence of adsorption process. If the pseudocapacity of H_2^+(a) c_p is given from a current plateau i_p and a sweep rate v by $i_p=v\ c_p$, we obtain 6 μF/cm^2 for R_e=26.7 eV and 12 μF/cm^2 for R_e=26.7/2 eV from Fig. 7. Such a simple calculation shows that c_p is strongly dependent on R_e.

However, r_{ads} in the present work is not constant as seen from the relation between i and η given by Eqs. (2), (17), and (18). This potential-dependent nature of r_{ads} is one reason for the shift of the current plateau to a more cathodic region with increase of the sweep rate. At lower overvoltages than the plateau region, log i *vs.* η is approximately equal to log i_1 *vs.* η so that we can estimate the velocity of the step preceding the rate-determining step. At higher overvoltages, log i *vs.* η represents its steady state, *i. e.*, Tafel plots, which agree with steady values calculated for Condition (A). Consequently, the potential-sweep method reveals information on the amount of pseudo-capacity, the velocity of the step preceding the rate-determining step, and the repulsive force energy constant of the proportional approximation.

Since a large value of the repulsive force between H_2^+(a)'s is expected from its Coulombic nature, the pseudo-capacity c_p may be quite small as calculated. The large value of R_e employed for the calculation, *i. e.*, 26.7 eV and 26.7/2 eV, does not necessarily mean that we insist on a value of D_p of unity or two. The present value of R_e is tentative and used only to give probable features.

In conclusion, potentiostatic and potentiodynamic transients have been calculated on the basis of the electrochemical mechanism of the hydrogen electrode reaction. The present double layer model and the repulsive force between adsorbates are somewhat simplified but the calculated results explain the depolarization observed at low overvoltages and give many predictions. Calculated features for the non-steady and steady states will be subjected to experimental tests and discussed in Part II.

The authors would like to express their appreciation to Professor T. Nakamura, Research Institute for Catalysis, Hokkaido University, for valuable discussion.

BULLETIN OF THE CHEMICAL SOCIETY OF JAPAN, VOL. 46, 3671—3676 (1973)

Kinetics of Hydrogen Electrode Reaction on Mercury. II. Experimental Part. Elucidation of Non-steady State by Constant Potential and Linear Potential-sweep Methods

Akiko KATAYAMA and Hideaki KITA

Research Institute for Catalysis, Hokkaido University, Sapporo 060

(Received July 2, 1973)

Potentiostatic and potentiodynamic experiments on Hg in 1 M HCl, HBr, and HI solutions were carried out to elucidate transient phenomena of the electrochemical mechanism of the hydrogen electrode reaction. The results obtained by both methods agree with the analysis of the non-steady state based on the electrochemical mechanism. The large effect of anions on the transient phenomena is satisfactorily interpreted by the change of repulsive force energy between H_2^+(a)'s on electrode, which is caused by the presence of specifically adsorbed anions in various degrees. The potential-sweep method reveals features of the step preceding the rate-determining step and gives the value of the repulsive force energy between H_2^+(a)'s as expected by the analysis.

We have theoretically discussed transient phenomena of the hydrogen electrode reaction(HER) on mercury on the basis of the electrochemical mechanism.[1] It was found that in relaxation methods the steady state condition can not be fulfilled at low overvoltages and that the linear potential-sweep will reveal Tafel plots with the current plateau characteristic of adsorption process.

A tendency to the current plateau, known as "depolarization", has been reported on a hanging electrode in H_2SO_4 solution by the galvanostatic method[2] and on DME in acidic KI solutions.[3] Tza and Iofa[3] interpreted the tendency by tacitly assuming a steady state of the reaction. However, the steady state assumption cannot predict either S-type Tafel plots or the dependence of the current plateau on the sweep rate.

The present work has been carried out to test experimentally these predictions and verify our fundamental assumption of the non-steady state of the reaction. A few analyses on the non-steady state have been reported; Horiuti and Okamoto[4] discussed HER

1) A. Katayama and H. Kita, Part I, This Bulletin, **46**, 3665 (1973).

2) O. Nagashima and H. Kita, *J. Res. Inst. Catal. Hokkaido Univ.*, **15**, 49 (1967).

3) Tza Chuan-sin and Z. A. Iofa, *Dokl. Akad. Nauk U.S.S.R.*, **126**, 1308 (1959).

4) J. Horiuti and G. Okamoto, This Bulletin, **13**, 216 (1938).

on Ni and Gerischer and Mehl[5] on Hg, Ag, and Cu. However, both works were restricted to a qualitative discussion. The latter authors applied only a constant overvoltage of 1.0 V to Hg electrode in 1/2 M H_2SO_4 solution and hence, though they did not observe the time-dependent current, their work is not sufficient to deduce the nature of the non-steady state.

We have applied the pulses of various constant overvoltages and of linear potential-sweep with different sweep rates to Hg electrode in acidic solutions. The resulting current-time or current-potential curves were compared with the predictions from the non-steady state analysis.

Experimental

Cell. An H-type cell of Pyrex was used; DME served as a test electrode.[6] The cell was kept in a water-bath whose temperature was controlled at 30±0.01 °C. The resistance of mercury column of DME was 58 ohms.

Solutions, Gas, and Mercury. 1 M solutions of HCl, HBr, HI, KCl, KBr, and KI were used. They were prepared from reagents of special grade and the water was purified as follows. The water from a Cu still was again distilled over alkaline $KMnO_4$ in a Pyrex flask furnished on top with a glass tube full of glass beads heated at 100 °C. The water vapor thus fractionally distilled was passed through a quartz tube heated at 450 °C for the protection of the creeping of water film along the wall. Commercial H_2 gas was purified through a permeation-type purifier of Japan Pure Hydrogen Co. The purified H_2 was introduced through a liquid N_2 trap and a bubbler of the distilled water into both compartments of the cell in order to deaerate and saturate the solution with H_2. Bubbling in the compartment of DME was stopped during measurements. Mercury flow rate of DME was 1.23 mg/s.

Electrical circuits. Pulse of constant potential or linear potential-sweep was applied to a growing Hg drop through a potentiostat. The τ_1, the time when the pulse was imposed and τ_2, a drop life time were controlled respectively at 3.6 and 4.0 s by Tektronix 160 series Generators with a device of mechanical knocking. Figure 1 shows a basic circuit of the potentiostat with a current transducer of operational amplifier, OP-C. The power supply for the potentiostat was made by Teledyne 825 Du Voltage Regulators.

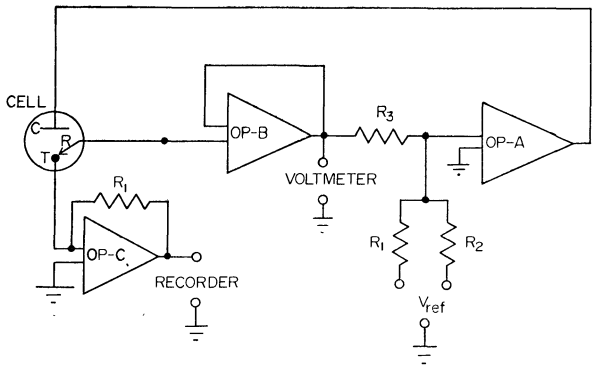

Fig. 1. Block diagram of potentiostat.
OP-A and C, Operational amplifier of Teledyne Type 1301; OP-B, Teledyne Type QFT-2B; R's resistance ($R_1=R_2=R_3$, and R_1 changeable); T, R, and C, test, reference, and counter electrodes.

5) H. Gerischer and N. Mehl, *Z. Elektrochem.*, **59**, 1049 (1955).
6) A. Katayama and H. Kita, *Chem. Lett.*, **1973**, 359.

DME was initially kept at an overvoltage η_1 by Takasago DC power Supply GPO-2 through the potentiostat. After DME was kept at η_1 for τ_1 s, pulses of constant or sweeping potential from Hewlett Packard Function Generator 3300A with Plug-in Unit of 3302A were applied through the potentiostat. The width of the pulse Δt was limited by $\Delta t < \tau_2-\tau_1$. Since the area of DME, A is proportional to $(mt)^{2/3}$ at a constant flow rate of mercury m, the increase of drop area ΔA during Δt is given by

$$\frac{\Delta A}{A}=\frac{\{m(\tau_1+\Delta t)\}^{2/3}-(m\tau_1)^{2/3}}{(m\tau_1)^{2/3}}\simeq\frac{2\Delta t}{3\tau_1} \quad (1)$$

The last member of Eq. (1) holds when $\Delta t \ll \tau_1$.

Measurements. Δt was always less than 0.1 ms. Therefore, $\Delta A/A$ was less than 2%. Overvoltage of DME was η_1 at $\tau=0\sim\tau_1$ and then $\eta(>\eta_1)$ at τ_1, where η's were defined at the negative of the electrode potential referred to reversible hydrogen electrode. All measurements with HI and KI solutions were performed in the dark.

Results

(A) Constant Potential Method. Current *vs.* time ($I-t$) curves are observed for various η in 1 M HCl (Fig. 2, $\eta_1=0$), 1 M HBr (Fig. 3, $\eta_1=0$), and 1 M HI

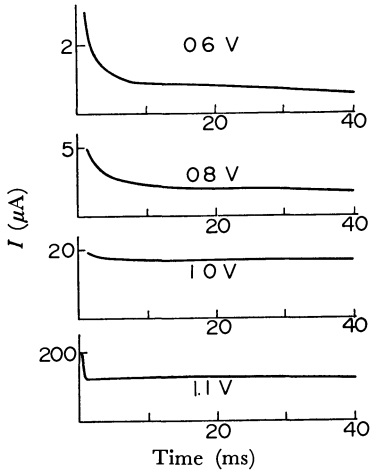

Fig. 2. Current *vs.* time curves for various overvoltages in 1 M HCl solution when $\eta_1=0$ V.

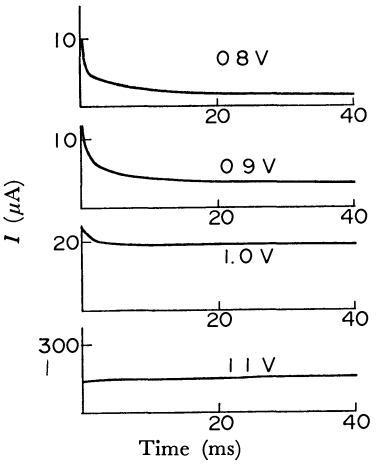

Fig. 3. Current *vs.* time curves for various overvoltages in 1 M HBr solution when $\eta_1=0.2$ V.

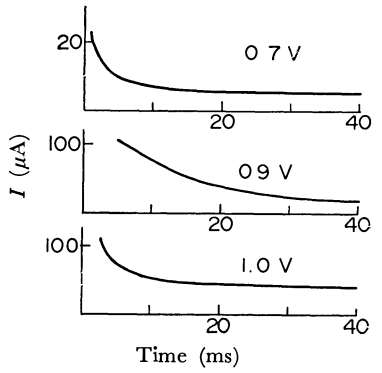

Fig. 4. Current *vs.* time curves for various overvoltages in 1 M HI solution when $\eta_1=0.2$ V.

(Fig. 4, $\eta_1=0.2$ V) where t is counted from τ_1. As these figures have a common time scale, we can easily find effects of the overvoltage and electrolyte on $I-t$ curve. Each figure shows a similar overvoltage effect; a decay of I with t is weakened with the increase of η and at sufficiently high overvoltages I seems to be time-independent. This decay can not be attributed to an effect of the charging of double layer, since the time constant of the charging is less than 0.05 ms. As regards the electrolyte effect, the decay of I is enhanced in the order HI>HBr>HCl. $I-t$ curves observed on the electrode initially polarized with various η_1 are compared in Fig. 5. Current tends to reach earlier a constant common value when η_1 is increased. This is in line with the theoretical analysis; the coverage of H_2^+(a), θ, at high η_1 is estimated to be close to a limiting value, so that the current will more rapidly reach a steady value.

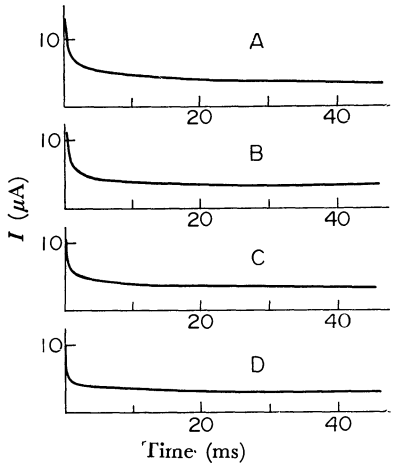

Fig. 5. Current *vs.* time curves at $\eta=0.9$ V in 1 M HBr solution, when (A) $\eta_1=0$, (B) 0.2 V, (C) 0.3 V, and (D) 0.4 V.

Logarithms of the current density at $t=40$ ms (the longest time) are plotted against η in Fig. 6. At high overvoltages log i *vs.* η curves for various acidic solutions converge into one straight line with a slope of *ca.* 120 mV. However, at lower overvoltages, deviation from the straight line appears first in 1 M HI solution, then 1 M HBr and 1 M HCl solutions. This deviation is known as depolarization. It should be

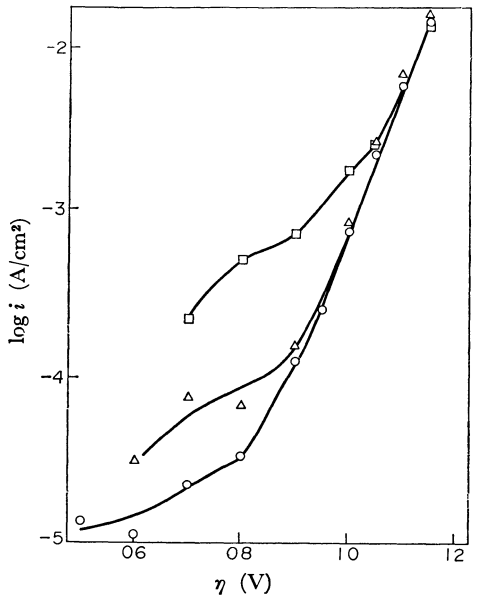

Fig. 6. Logarithm of current density at 40 ms *vs.* overvoltage.
○, 1 M HCl; △, 1 M HBr; □, 1 M HI.

emphasized that the curves reveal an S-type behavior with a current plateau, though the latter is somewhat gradated.

Close examination of Fig. 6 in comparison with Figs. 2~4 shows that the S-region of log i *vs.* t curves has a different feature in $I-t$ curves of Figs. 2—4 from those in the region of a straight line. In the S-region, I continues to decrease with t, but in the other, I remains constant from the begining. Thus, the appearance of the S-type behavior will prove that the reaction is in a non-steady state. In the region of a straight line, the reaction has already attained a steady state. The upward deviation from the straight line, *i.e.*, the depolarization, is simply due to the fact that the current in a non-steady state is always larger than that in a steady state. The results of Figs. 2—5 satisfy the predictions in Part I.

The degree of depolarization is found to be the largest in HI and the least in HCl solution. This is interpreted by the theoretical analysis[1] as follows. The halide ions are known to be specifically adsorbed on the electrode surface in the order $I^->Br^->Cl^-$. Since the charge of these ions is opposite to that of the intermediate H_2^+(a), adsorbed halide ions will reduce a coulombic repulsive force between H_2^+(a)'s in conformity with the degree of specific adsorption of these anions. Thus, H_2^+(a)'s in iodide solution have the least repulsive force. Our non-steady state analysis has predicted that the smaller the repulsive force between H_2^+(a)'s, the longer the time is required for a steady state to be attained. Consequently, the largest degree of depolarization is expected in iodide solution. The effect of halide ions on the depolarization is thus explained by the change of repulsive force between H_2^+(a)'s owing to their specific adsorption.

(B) Linear Potential-sweep Method. *(1) Neutral Solutions*: In neutral solutions, mercury electrode holds its ideally polarized state down to *ca.* −1.5 V

vs. NHE.[7] When the pulse of a linear potential-sweep is applied to the ideally polarizable electrode, the current observed consists of only the charging current of the double layer at an interface, I_{dl}, and satisfies the following relation with the sweep rate, v,

$$I = I_{dl} = C_{dl}v, \qquad (2)$$

where C_{dl} is double layer capacity.

Figures 7～9 show the double layer capacity calculated by the use of Eq. (2) for various v's in solutions of 1 M KCl, KBr, and KI, respectively. The values of C_{dl} are almost independent of v, except in 1 M KBr (Fig. 8) where at high overvoltages they deviate somewhat in a systematic way. It can be stated that this deviation is not caused by the desorption process of Br^-, since Lorenz[8] has shown that its desorption occurs at more positive potentials in a reversible way. Hence, it must be ascribed to some other processes. Nevertheless, the deviation does not give any serious effect on the following treatment. Figures 7～9 give a double layer capacity almost identical to that measured by AC bridge.[3,7] The double layer is known to be dependent on the kind of anion but independent of a cation (H^+ or K^+). Such a dependence, however, vanishes at sufficiently negative potentials (Figs. 7～9). Specifically adsorbed anions are considered to be absent at those negative potentials.

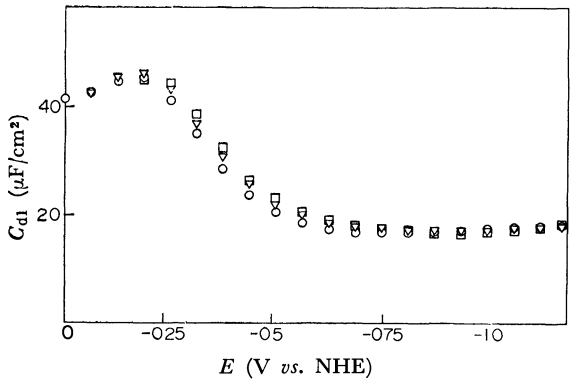

Fig. 7. Double layer capacity *vs.* potential curves for various sweep rates in 1 M KCl solution.
○: 46.4 V/s, ▽: 116 V/s, □: 232 V/s, each symbol was traced from oscilloscope screen.

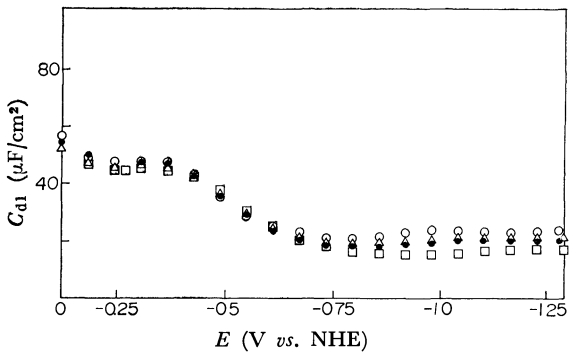

Fig. 8. Double layer capacity *vs.* potential curves for various sweep rates in 1 M KBr solution.
○: 11.6 V/s, △: 23.2 V/s, ●: 46.4 V/s, □: 232 V/s, each symbol was traced from oscilloscope screen.

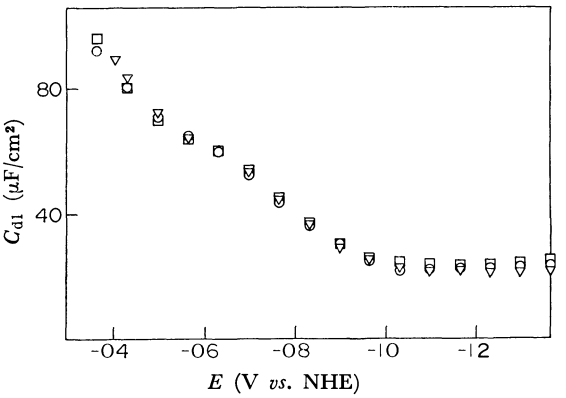

Fig. 9. Double layer capacity *vs.* potential curves for various sweep rates in 1 M KI solution.
○: 11.6 V/s, □: 46.4 V/s, ▽: 232 V/s, each symbol was traced from oscilloscope screen.

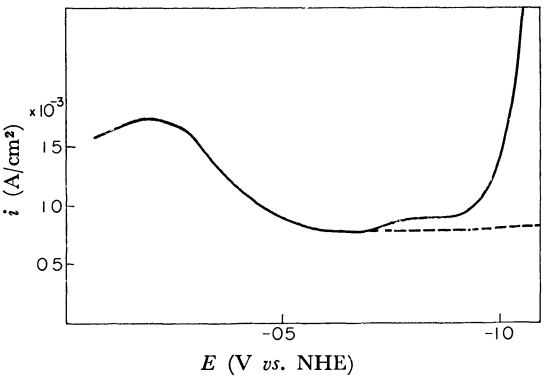

Fig. 10. Current *vs.* potential curves for sweep rate of 46.4 V/s.
Solid line, 1 M HCl; dotted line, 1 M KCl.

Thus, the currents observed in neutral solutions were used for the purpose of excluding I_{dl} from the observed one in the respective hydrogen halide solutions in which HER takes place.

(2) Acidic Solutions: Figure 10 shows typical i *vs.* potential E curves obtained at the same sweep rate in 1 M HCl and KCl solutions, where i represents the current density in A/cm². Those in 1 M HBr and HI solutions were described elsewhere.[6] The reaction current density i_r is equated by $(i-i_{dl})$, where i_{dl} is given by the current with the same sweep rate in neutral solution having the common anion. It is plausible that the double layer capacity does not undergo a change by the change of the solution from 1 M KCl to 1 M HCl, since Frumkin *et al.*[9] obtained the same double layer capacities by AC bridge method both in HCl and LiCl solutions, even though HER takes place in HCl solutions.

i_r thus obtained does not show a monotonous increase with η, but a plateau on the way of η increase. We shall call it a current plateau and denote its value at a flat portion by i_p. Values of i_p in HCl, HBr, HI solutions are found to be in the order i_p (HCl)$\lesssim i_p$(HBr)$\ll i_p$(HI). i_p(HCl) and i_p(HBr) are relatively

7) D. C. Grahame, *Chem. Revs.*, **41**, 441 (1947).
8) W. Lorenz, *Z. Phys. Chem.*, **224**, 145 (1964).
9) A. N. Frumkin, O. A. Petry, and N. V. Nikolaeva-Fedorovich, *Dokl. Akad. Nauk U.S.S.R.*, **137**, 896 (1961).

small compared with i_{d1}, but i_p(HI) is much larger than i_{d1}.

Figures 11~13 show $\log i_r$ *vs.* η plots for various sweep rates in 1 M HCl, HBr, and HI solutions. It is to be noted that the current at a flat portion i_p is almost independent of the sweep rate in 1 M HCl, but increases in 1 M HI solution. In the latter case, i_p at sweep rates of 11.6 V/s and 23.2 V/s is proportional to the sweep rate. The proportionality is what was predicted[1] by non-steady state analysis. Potential drop through a Hg column of DME is corrected at high current density in 1 M HI solution. Figure 14 shows the dependence of i_p of 1 M HI on the sweep rate in logarithmic scale, where we find a depression in its dependence from the proportional one when the sweep rate is large.

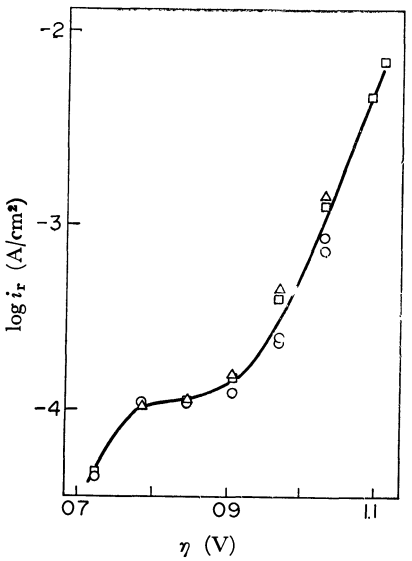

Fig. 11. Logarithm of reaction current *vs.* overvoltage in 1 M HCl by potential-sweep.
A: 11.6 V/s, ○, 23.2 V/s, □: 46.4 V/s.

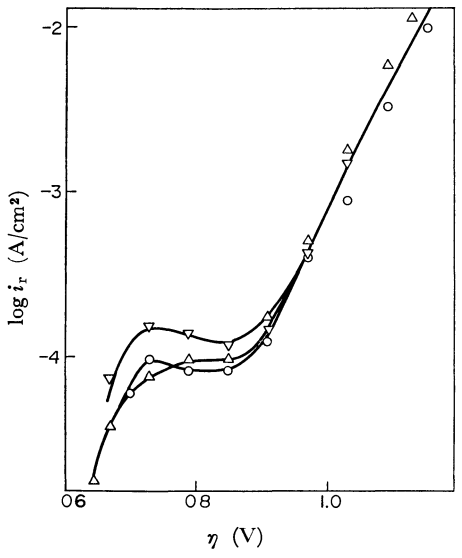

Fig. 12. Logarithm of reaction current *vs.* overvoltage in 1 M HBr by potential-sweep.
△: 11.6 V/s, ○: 23.2 V/s, ▽: 46.4 V/s.

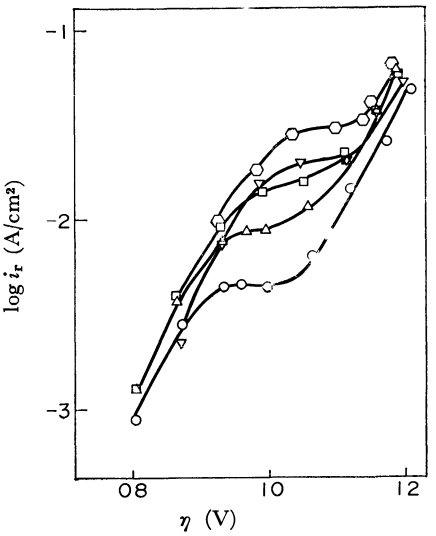

Fig. 13. Logarithm of reaction current *vs.* overvoltage in 1 M HI by potential-sweep.
○: 11.6 V/s, △: 23.2 V/s, □: 46.4 V/s, ▽: 116 V/s, ⟨□⟩: 232 V/s.

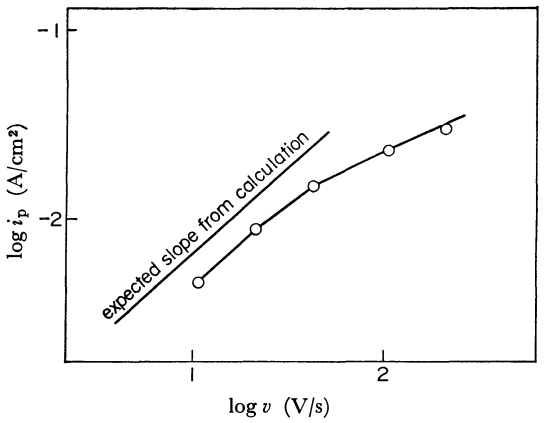

Fig. 14. Logarithm of plateau current *vs.* logarithm of sweep rate curve in 1 M HI.

This dependence of i_p on the kind of anion and on the sweep rate can be interpreted as follows.

i) Dependence of i_p on the kind of anion: Values of i_p in the respective solutions are in the same order as the degree of the specific adsorption of these anions. The current plateaus appear around overvoltages of 0.8 and 1.0 V in 1 M HCl and HI solutions (Figs. 11 and 13) and the double layer capacities at the corresponding potentials are 18 and 22 μF/cm² (Figs. 7 and 9), respectively. The value 18 μF/cm² is the same as that of the ideally polarized electrode, indicating the absence of the specifically adsorbed Cl^-. On the contrary, the latter value of C_{d1} in HI solution indicates the presence of specifically adsorbed I^- at potentials where i_p is observed.[6] Enhancement in i_p by the change of anion from Cl^- to I^- is clearly due to the specific adsorption of I^-.

The adsorbed anion is expected to reduce the effective charge of H_2^+(a)'s and hence to increase the coverage H_2^+(a). The relation $i_p(I^-) \gg i_p(Br^-) \gtrsim i_p(Cl^-)$ is thus explained by the change of repulsive force between H_2^+(a)'s. We can estimate the repulsive energy con-

stant R_e from i_p[1]; at a sweep rate of 11.6 V/s, R_e= 14 eV for 1 M HCl and HBr solutions and R_e=0.28 for 1 M HI solution where pseudocapacities are obtained as 12 μF/cm^2 and 600 μF/cm^2, respectively.

ii) Dependence of i_p on the sweep rate: i_p is expected to be proportional to the sweep rate, in which we have assumed that the repulsive force between H_2^+(a)'s is invariable irrespective of applied potentials. However, since the specific adsorption of anions varies with applied potentials, the repulsive force between H_2^+(a)'s should change with the change of the applied potential.

The current plateau appears at a more negative potential when the sweep rate is increased (Fig. 13). At more negative potentials, the repulsive force between H_2^+(a)'s increases because of the desorption of anions which act to reduce the H_2^+(a)'s repulsive force. As a consequence, i_p does not increase as expected from the proportional relationship with the sweep rate. In HCl and HBr solutions, i_p is smaller than i_{dl} and the subtraction of i_{dl} from i brings a relatively large error in i_p. We consider that this uncertainty in i_p is one reason for i_p in HCl and HBr appearing not to have a clear dependence on v.

Log i_r *vs.* η curves at more negative potentials than those in the region of the current plateau are independent of the sweep rate and become a single straight line, which agrees with the straight line mentioned in (A). We therefore infer that this portion represents the relation at a steady state.

Discussion

Employing the expression for the velocity of HER on Hg[1] and the repulsive energy constants in the previous section, (B)-(2)-(i), we simulated the values of rate constants so that the experimental Tafel plots at high overvoltages were reproduced. The rate of the step preceding the rate-determining one was found to be faster than the latter by three orders of magnitude in the case of *e.g.*, Fig. 13. The fitting rate constants are $k_2=10^{-18}$ s^{-1} cm^{-2} and $k_1=10^{-15}$ s^{-1} cm^{-2}. From values of the repulsive energy constant and the rate constants, we can estimate the time required for the steady state to be attained when a constant potential is applied. The results are shown in Table 1, where the other parameters not listed are identical to those given previously.[1] Thus, the time required strongly depends on the repulsive energy constant between H_2^+(a)'s.

The explanation for depolarization by Tza and Iofa[3] is based on the steady state assumption and only successful in the relatively negative potential regions where depolarization is small. The S-type Tafel plots can be explained only as a transient phenomena where the reaction stays in non-steady state, as demonstrated by the present two methods. Our observation at an overvoltage of 1.0 V in 1 M HCl is very analogous to that in 0.5 M H_2SO_4 by Gerischer and Mehl,[5] although their conclusion is contradictory to ours since their observation was limited only to a value of 1.0 V.

Table 1. THE TIME REQUIRED FOR A STEADY STATE TO BE ATTAINED

η	Time (s)		
	R_e=13.35 eV	2.67 eV	0.534 eV
0.1 V	1.7×10^4		
0.2	1.2×10^4	2.5×10^4	$>6\times10^4$
0.3	4.9×10^3		
0.4	6.5×10^2	$>1.2\times10^3$	
0.5	90		
0.6	20	$>1.8\times10^2$	
0.7	2		

$k_1=10^{-15}$ s^{-1} cm^{-2}, $k_2=10^{-18}$ s^{-1} cm^{-2}.

No pH dependence of double layer capacity observed by 1 kHz AC bridge could be taken as an evidence for the exclusion of the electrochemical mechanism,[9] since the presence of the reversible step of $2H^+ + e^- \rightleftarrows H_2^+$(a) should rise to the additional pseudocapacity which is pH dependent. However, we have found that the rate of this step is so small in its absolute magnitude that it can not follow the rapid variation of voltages such as 1 kHz AC. Moreover, the repulsive force between H_2^+(a)'s is so large that θ reaches a limiting value by the very small increase. The change of coverage in HCl and HBr solutions is at maximum $\Delta\theta=2\times10^{-3}$, which was obtained from observed i_p's and theoretical analysis. Such a small $\Delta\theta$ can not be detected by AC bridge. Thus, the observation with 1 kHz AC provides only information on the intrinsic double layer capacity as seen in (B)—(l) in the previous section. However, in HI solution, i_p is markedly large in comparison with that in HCl and HBr solutions; $\Delta\theta$ amounts to 0.65 at maximum.

A striking effect of the specific adsorption of anion on transient phenomena of HER is the strong evidence for the assumption that the intermediate possesses a charge; namely the fact that the adsorbed anion reduces the repulsive force among intermediates, strongly suggests positively charged intermediate such as H_2^+(a) in the electrochemical mechanism.

The Cadmium-photosensitized Decomposition of Acetaldehyde, Propionaldehyde, and *n*-Butyraldehyde

Koji YAMAMOTO, Shigeru TSUNASHIMA, and Shin SATO

Department of Applied Physics, Tokyo Institute of Technology, Ookayama, Meguro-ku, Tokyo 152

(Received July 9, 1973)

The reactions of acetaldehyde, propionaldehyde, and *n*-butyraldehyde photosensitized by cadmium ($^3P_1$) have been investigated at 270 °C. The pressure dependence of the main products, CO, RH (R=CH_3, C_2H_5, and *n*-C_3H_7) and R_2, was well explained by the following reaction mechanism; Cd*+RCHO→R+CHO+Cd or RH+CO+Cd. R+RCHO→RH+RCO, RCO→R+CO, CHO→H+CO, H+RCHO→H_2+RCO, R+R→R_2 or RH+Olefin. Carbon dioxide was found to be a rather good quencher for triplet cadmium atoms, and was used for estimating the relative quenching efficiencies of the three aldehydes and acetone. The values obtained were 0.16, 1.0, 1.3, 1.2, and 1.4, respectively for carbon dioxide, acetone, acetaldehyde, propionaldehyde, and *n*-butyraldehyde, when the efficiency of *cis*-2-butene was assumed to be unity.

Since the available energy is only 87.7 kcal/mol in the cadmium($^3P_1$)-photosensitization, an appreciable bond scission cannot be observed in the reactions of hydrocarbons photosensitized by cadmium($^3P_1$).[1] When acetone[2] and cyclopentanone[3] were used, however, the decompositions could be observed and their quantum yields were estimated to be about 0.3 for both compounds.

The photolyses of the aldehydes including the mercury- and the acetone-photosensitizations, have long been studied by many investigators and their reaction mechanisms have almost completely been established.[4] However, no studies have been reported on the reactions of the aldehydes photosensitized by cadmium. In a previous paper,[1] were compared the quenching efficiencies of several hydrocarbons for Hg($^3P_1$), Cd($^3P_1$) and triplet benzene, and found that, although the energy transferred in the reaction with Cd($^3P_1$) is closer to that from triplet benzene ($^3B_{1u}$; 84.4 kcal/mol) than that from Hg($^3P_1$), the quenching efficiencies for Cd($^3P_1$) have more similar tendencies with those for Hg($^3P_1$) than those for triplet benzene.

The present authors hoped to ascertain whether the reaction mechanism previously proposed for the photolysis of the aldehydes can be applied also for the cadmium-photosensitization and, if possible, to find out the detailed mechanism of the energy transfer from Cd($^3P_1$) to the carbonyl compounds.

Experimental

The commercially available acetaldehyde (Wako Pure Chemical), and *n*-butyraldehyde (Koso Chemical) were used without purification. The gas chromatographic analysis showed that the impurity content was less than 0.5%. Since the propionaldehyde (Tokyo Kasei) contained a large amount of impurity, this reagent was purified by gas chromatography. All aldehydes were kept in traps at the temperature of liquid nitrogen after bulb-to-bulb distillations.

The *cis*-2-butene, carbon dioxide, ethane, ethylene, propane, and *n*-butane were purchased from the Takachiho Chemical Co. Metallic cadmium (5-nine) was the product of the Osaka Asahi Metal Co.

The experimental procedure was almost the same as described previously.[3] All runs were made at 270±1 °C, using two home-made resonance lamps. Since a combination of a Toshiba UV-25 filter and a Pyrex glass plate was used as a filter, the irradiating light mainly consisted of a 326.1 nm resonance line. The light intensities from the two resonance lamps were 0.21 and 0.34μ Einstein/min which were measured by using the *cis-trans* isomerization of *cis*-2-butene photosensitized by cadmium, the quantum yield being assumed to be 0.5.[5] The relative intensity of the light through the reaction vessel was also measured by the combination of a slit, a Toshiba M.S. 9SY photomultiplier and a micro-ammeter.

The columns used for the gas chromatographic analyses were 5m-polypropylene glycol for oxygenated compounds, 30m-dimethylsulfolane, and 5m-activated alumina for hydrocarbons.

Results

Before starting photochemical studies, the thermal decomposition of aldehydes was checked in the dark. Very small amounts of products were observed in the case of acetaldehyde. The amount was less than 10^{-3} times that of the photolysis. The results were not reproducible, probably because the reactions were not homogeneous.

The results of the cadmium-photosensitized reactions are summarized in Table 1. In order to obtain the accurate quantum yield of ethane in the case of acetaldehyde, another series of experiments were carried out. The result is shown in Fig. 1. In the cadmium-photosensitization, the direct light absorption by al-

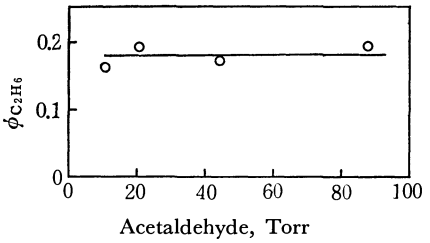

Fig. 1. The quantum yield of ethane in the Cd-photosensitized decomposition of acetaldehyde.

1) S. Tsunashima and S. Sato, This Bulletin, **40**, 2987 (1967).
2) S. Sato, C. Takahashi, and S. Tsunashima, *ibid.*, **43**, 1319 (1970).
3) S. Tsunashima, O. Ohsawa, C. Takahashi, and S. Sato, *ibid.*, **46**, 83 (1973).
4) J. G. Calvert and J. N. Pitts, Jr., "Photochemistry", John Wiley & Sons, Inc., 1967, p. 369.
5) S. Tsunashima and S. Sato, This Bulletin, **41**, 284 (1968).

Table 1. The quantum yields of CO, RH, R_2, H_2, and other products in the cadmium-photosensitized decomposition of three aldehydes

Acetaldehyde pressure (Torr)	Light intensity: 0.21 μ Einstein/min, Quantum yield			
	CO	CH_4	C_2H_6	H_2
22.4	5.33	4.95	n.d.[a]	0.19
46.3	13.58	12.62	0.2	n.d.[a]
113	32.80	30.88	0.4	n.d.[a]
264	83.70	82.92	n.d.[a]	n.d.[a]
482	133.3	139.5	0.5	0.68
Propionaldehyde pressure (Torr)	**Light intensity: 0.34 μ Einstein/min, Quantum yield**			
	CO	C_2H_6	n-C_4H_{10}	H_2
10.3	1.11	0.91	0.22	0.22
19.4	1.49	n.d.[a]	n.d.[a]	0.18
20.3	1.42	1.26	0.16	0.10
49.8	2.61	2.59	0.11	0.38
103	4.52	n.d.[a]	n.d.[a]	n.d.[a]

n-Butyraldehyde pressure (Torr)	Light intensity: 0.34 μ Einstein/min, Quantum yield				
	CO	C_3H_8	C_2H_4	C_3H_6	H_2
10.0	1.06	0.89	0.01	0.003	0.14
20.2	1.70	1.35	0.04	0.014	0.19
21.1	2.03	1.65	0.06	0.015	0.03
48.9	3.08	2.97	0.07	0.023	0.25
96.6	5.53	3.88	0.04	0.024	0.25
144	7.64	7.41	0.08	0.047	0.34

a) n.d.: not determined.

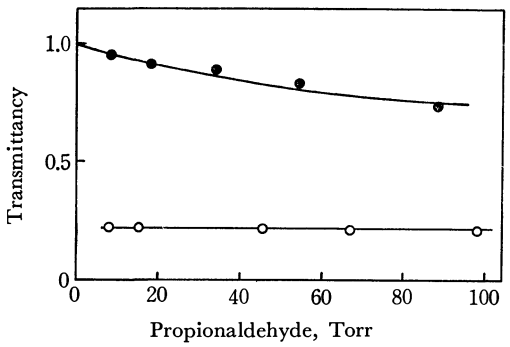

Fig. 2. The relative intensity of transmitted light as a function of propionaldehyde pressure in the presence (○) and in the absence (●) of cadmium vapor.

dehydes might play a role in the formation of the products. To estimate this contribution, we measured the relative intensity of the light which passed through the reaction vessel. As Fig. 2 shows, the relative light intensity in the presence of the cadmium vapor was independent of the pressure of propionaldehyde. This result suggests that the direct photolysis in this system is negligibly small compared with the decomposition induced by the $Cd(^3P_1)$.

In order to obtain the quenching efficiencies of the aldehydes for $Cd(^3P_1)$, a mixture of *cis*-2-butene and acetaldehyde was irradiated; however, the data obtained were much complicated by the reactions of the produced radicals. After several trials, carbon dioxide was found to be a rather good quencher for $Cd(^3P_1)$ without any products. Figure 3 shows the

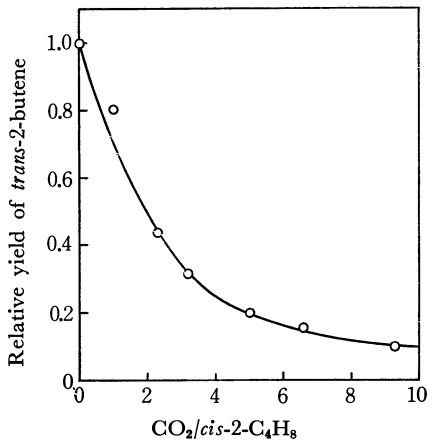

Fig. 3. The effect of carbon dioxide on the *cis-trans* isomerization of *cis*-2-butene photosensitized by cadmium.

effect of carbon dioxide on the relative rate of the formation of *trans*-2-butene from *cis*-2-butene photosensitized by $Cd(^3P_1)$. A simple kinetic analysis showed that the relative quenching efficiency of carbon dioxide for $Cd(^3P_1)$ is 0.16 ± 0.01, when the efficiency of *cis*-2-butene is assumed to be unity. The kinetic treatment will be shown later.

The similar experiments were carried out with the mixture of acetone and CO_2. The reciprocal of the relative rate of the formation of carbon monoxide was plotted in Fig. 4 as a function of the pressure ratio of CO_2 to acetone. The relative quenching efficiency of acetone was calculated to be 1.0 ± 0.1. Table 2

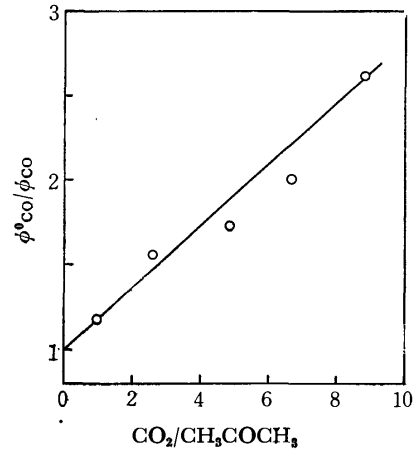

Fig. 4. The effect of carbon dioxide on the reaction of acetone.

TABLE 2. THE EFFECT OF CARBON DIOXIDE ON THE FORMATION OF CO IN THE CADMIUM-PHOTOSENSITIZED DECOMPOSITION OF THREE ALDEHYDES AND THAT ON THE FORMATION OF CH_4 IN THE CASE OF ACETALDEHYDE

The initial pressure of aldehyde is 20 Torr

CO_2/CH_3CHO	$\phi^0_{CH_4}/\phi_{CH_4}$	ϕ^0_{CO}/ϕ_{CO}
1.0	1.04	1.04
2.7	1.12	1.15
5.1	1.27	1.28
6.8	1.33	1.34
9.8	1.46	1.53

CO_2/C_2H_5CHO	ϕ^0_{CO}/ϕ_{CO}
1.0	1.04
2.6	1.22
5.1	1.26
7.6	1.63
9.9	1.88

CO_2/n-C_3H_7CHO	ϕ^0_{CO}/ϕ_{CO}
1.0	1.08
2.7	1.16
5.4	1.33
8.2	1.57
9.7	1.68
11.4	1.90

ϕ^0: the quantum yield in the absence of CO_2.

summarizes the results of the cadmium-photosensitized decomposition of the three aldehydes in the presence of CO_2.

In order to check the insensitivity of CO_2 to the radical reactions, the effect of CO_2 on the direct photolysis of propionaldehyde was also investigated. No effect was observed within the experimental error.

Discussion

As has been shown in the Results section, all of the aldehydes studied decomposed in chain mechanism, and the main products were CO, RH (R=CH_3, C_2H_5, and n-C_3H_7, respectively, for acetaldehyde, propionaldehyde, and n-butyraldehyde), and R_2. To explain the results of the cadmium-photosensitized reactions, we considered the following reaction scheme,

$$\begin{aligned}
Cd + h\nu &\longrightarrow Cd^* && I\\
Cd^* + RCHO &\longrightarrow CdH + RCO && \alpha \\
&\longrightarrow R + CHO + Cd && \beta \\
&\longrightarrow RH + CO + Cd && \gamma \quad \Big\} \; k_q\\
R + RCHO &\longrightarrow RH + RCO && k_1\\
RCO &\longrightarrow R + CO && k_2\\
R + R &\longrightarrow R_2 && k_3(1-\eta)\\
&\longrightarrow RH + Olefin && k_3\,\eta\\
CHO &\longrightarrow H + CO && k_4\\
CdH &\longrightarrow Cd + H && k_5\\
H + RCHO &\longrightarrow H_2 + RCO && k_6
\end{aligned}$$

Because of high temperature, the RCO, CHO, and CdH radicals were assumed to decompose unimolecularly.[4]

The steady state treatment gives the equations,

$$\phi_{CO} = (2\alpha+2\beta+\gamma) + \{(\alpha+\beta)/Ik_3\}^{1/2}k_1[RCHO] \quad (1)$$

$$\phi_{RH} = (\alpha+\beta) + \gamma + \{(\alpha+\beta)/Ik_3\}^{1/2}k_1[RCHO] \quad (2)$$

$$\phi_{R_2} = (1-\eta)(\alpha+\beta) \quad (3)$$

Here, ϕ_{CO}, ϕ_{RH} and ϕ_{R_2} denote the quantum yields of CO, RH and R_2. Figure 5 shows the predicted linear relationship between ϕ_{CO} and [RCHO], from which we can estimate the values of $(\alpha+\beta)$, γ and $k_1/k_3^{1/2}$ by assuming the η values. The quantum yield of ethane from the reaction of acetaldehyde has already been shown in Fig. 1. Since $\eta=0$ in this case,

$$\phi_{C_2H_6} = \alpha + \beta = 0.18 \pm 0.01$$

This value may be more accurate than that estimated using Eq. (1) or (2). In the case of n-butylaldehyde,

$$\phi_{C_3H_6} = \eta(\alpha+\beta) \quad (4)$$

By taking $\eta=0.16$,[6] we can calculate that $\alpha+\beta=0.14\pm 0.04$. Also in the reaction of n-butyraldehyde, the formation of ethylene was observed. This compound may be formed in the following initial process,

$$CH_3CH_2CH_2CHO + Cd^* \rightarrow CH_3CHO + C_2H_4 + Cd \quad \delta$$

The δ value is about 0.06. Table 3 summarizes all of the estimated values.

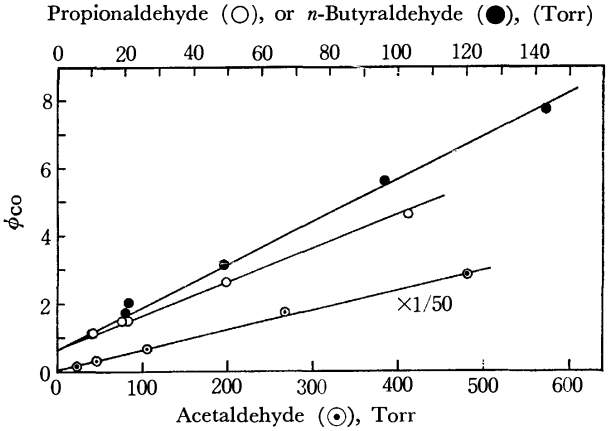

Fig. 5. The quantum yields of carbon monoxide in the cadmium-photosensitized decomposition of three aldehydes as functions of their pressures.

6) J. A. Kerr and A. F. Trotman-Dickenson, "Progress in Reaction Kinetics," Vol. 1, edited by G. Porter, Pergamon Press, 1961, p. 105.

TABLE 3. THE QUANTUM YIELDS OF THE INITIAL PROCESSES, $\alpha + \beta$, γ AND δ

	$\alpha+\beta$	γ	δ
Acetaldehyde	0.18	0.1	—
Propionaldehyde	0.14[a)]	0.4[a)]	—
n-Butyraldehyde	0.14[a)]	0.5[b)]	0.06

a) Experimental error is ±20%. b) ±50%.

It is known that, in the direct photolysis at the wavelengths longer than 300 nm, the β process is the most prominent among the three initial processes, α, β and γ.[4] However, Table 3 suggests that, in the cadmium photosensitization, the γ process is one of the important processes, although the experimental errors preclude the quantitative estimation. Since the γ process contradicts the spin-conservation rule, the above result is not self-evident. Our reasoning for this is that, since CO is a good quencher for $Cd(^3P_1)$,[7] the intermediate complex between Cd* and CO may be formed in the course of the γ process,

$$RCHO + Cd^* \rightarrow \left(\begin{matrix} R \\ H \end{matrix}\!\!>\!C\!-\!\!-\!O \atop \vdots \\ Cd\end{matrix}\right)^* \rightarrow RH + (CO\cdots Cd)^*$$

and then this complex decomposes into CO and Cd after crossing over the potential barrier between the triplet and the singlet states. This reasoning is obviously based on the assumption that the energy transfer from $Cd(^3P_1)$ to an aldehyde occurs through the interaction of $Cd(^3P_1)$ with a π electron in the C=O bond of the aldehyde. On the basis of this reasoning and of the smallness of the quenching efficiency of any alkanes to the $Cd(^3P_1)$ atom,[1] it may safely be said that the contribution of the α process to the decomposition of aldehydes is negligibly small compared with the β process.

The Competition between CO_2 and Other Molecules in Quenching $Cd(^3P_1)$ Atoms. When CO_2 is added into the system of the Cd-photosensitized isomerization of 2-butene, CO_2 compete with 2-butene in quenching $Cd(^3P_1)$. The reaction scheme may be described as follows:

$Cd + h\nu \longrightarrow Cd^*$	I
$Cd^* \longrightarrow Cd + h\nu$	k_0
$Cd^* + CO_2 \longrightarrow Cd + CO_2$	k_C
$Cd^* + cis \longrightarrow Cd + {}^3B$	k_{cis}
$Cd^* + trans \longrightarrow Cd + {}^3B$	k_{trans}
${}^3B + M \longrightarrow 1/2\,cis + 1/2\,trans + M$	

Here, *cis*, *trans* and ^3B denote *cis*- and *trans*-2-butene and the triplet state, respectively. The steady state treatment on the assumption that $k_{cis}=k_{trans}=k_B$ and that $k_0 \ll k_B$[butene] at butene pressures higher than 1 Torr,[1] gives the relation:

$$\frac{I\,t}{[\text{butene}]\,\log\left(\frac{C-T}{C_0-T_0}\right)} = 1 + \frac{k_C[CO_2]}{k_B[\text{butene}]} \qquad (5)$$

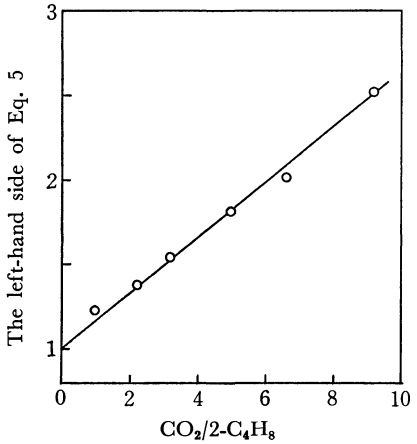

Fig. 6. The effect of carbon dioxide on the reaction of *cis*-2-butene.

Here, t is the reaction time, and C_0, C, T_0 and T are the initial and final concentrations of *cis*- and *trans*-2-butene. The predicted linear relationship between the left-hand side of Eq. (5) and the $[CO_2]$/[butene] ratio is shown in Fig. 6, from which we can calculate the quenching ratio of k_C/k_B to be 0.16±0.01 as has already been stated in the Results section.

The relative quenching efficiency of acetone was obtained by measuring the quantum yield of CO produced in the reaction of acetone in the presence of CO_2.

$$Cd^* + CH_3COOCH_3 \rightarrow 2\,CH_3 + CO \qquad k_A$$

The steady state treatment predicts the relationship:

$$\frac{\phi^0_{CO}}{\phi_{CO}} = 1 + \frac{k_A[\text{acetone}]}{k_C[CO_2]} \qquad (6)$$

The result has already been shown in Fig. 4.

In the case of three aldehydes, the kinetic treatment is not so simple, because these three compounds decompose in chain mechanism. Although it is a little complicated, a straight forward steady state treatment gives the relationship:

$$\phi_{CO} = \frac{2\alpha+2\beta+\gamma}{1+mx} + \sqrt{\frac{\alpha+\beta}{Ik_3(1+mx)}}k_1[RCHO] \qquad (7)$$

Here, $m=k_C/k_q$ and $x=[CO_2]/[RCHO]$. Then, using the notations:

$$y = \phi^0_{CO}/\phi_{CO}$$

and

$$c = \frac{1}{2\alpha+2\beta+\gamma}\sqrt{\frac{\alpha+\beta}{Ik_3}}k_1[RCHO]$$

which corresponds to the ratio between the ϕ_{CO} observed and the intercept obtained in Fig. 5, we can obtain

$$y = \frac{(1+c)(1+mx)}{1+c(1+mx)^{1/2}} \qquad (8)$$

This equation may be rewritten as follows:

$$1 + mx = \frac{y}{1+c} + \frac{1}{2}\left(\frac{cy}{1+c}\right)^2 + \left(\frac{cy}{1+c}\right)^2\left(\frac{1+c}{c^2y}+\frac{1}{4}\right)^{1/2} = z \qquad (9)$$

Since the right-hand side of Eq. (9), which is denoted

7) S. Tsunashima, T. Toyono, and S. Sato, This Bulletin, **46**, 2654 (1973).

by z, can be calculated from the observed values, the quenching ratio, m, can also be estimated from the plots of z as a function of x. In the case of acetaldehyde, the c value is much larger than unity, as has been shown in Fig. 5. Equation (8), therefore, may be simplified in the form:

$$1 + mx = y^2 \qquad (10)$$

Figures 7 and 8 show the plots for Eqs. (9) and (10). The relative quenching efficiencies thus obtained are listed in Table 4, together with those of other compounds previously obtained.

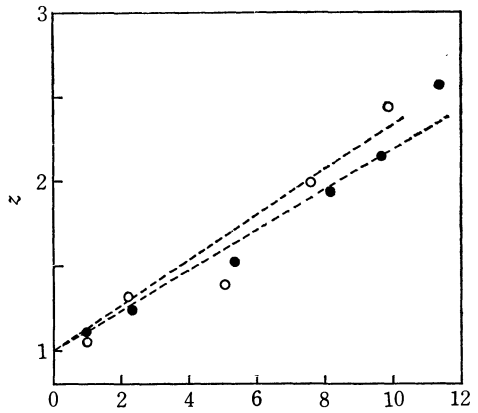

$CO_2/C_2H_5CHO(\bigcirc)$ or $CO_2/C_3H_7CHO(\bullet)$

Fig. 7. The Effects of carbon dioxide on the reactions of propionaldehyde and *n*-butyraldehyde.

Table 4. The relative quenching efficiencies for Cd ($^3P_1$)

cis-2-Butene	(1.00)
Ethylene	1.0
1,4-Butadiene	1.1
Propane	<0.001
Cyclopentanone	0.8[a)]
Acetone	1.0[a)]
Acetaldehyde	1.3[a)]
Propionaldehyde	1.2[a)]
Butyraldehyde	1.4[a)]
Carbon Dioxide	0.16

a) Experimental error is ±15%.

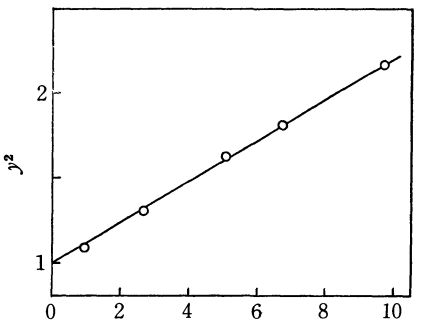

CO_2/CH_3CHO

Fig. 8. The effects of carbon dioxide on the reactions of acetaldehyde.

BULLETIN OF THE CHEMICAL SOCIETY OF JAPAN, VOL. 46, 3681—3685 (1973)

Molecular-symmetry Reduction in C_mH_{m-2} Cata-condensed Nonalternant Hydrocarbons

Azumao TOYOTA* and Takeshi NAKAJIMA

Department of Chemistry, Faculty of Science, Tohoku University, Sendai 980

(Received July 10, 1973)

On the basis of the second-order Jahn-Teller effect and the semiempirical SCF MO method, we examined the energetically most favorable molecular-symmetry groups and geometrical structures with respect to C–C bond lengths of the C_mH_{m-2} cata-condensed nonalternant hydrocarbons. In the $4n$ π-electron systems the first excitation energies in the fully-symmetrical nuclear arrangements were predicted to be significantly smaller than a certain critical value, and a molecular-symmetry reduction accompanied by a marked double-bond fixation in the peripheral carbon skeleton to occur. On the other hand, in the $4n+2$ π-electron systems, such energies were found to be considerably large for small members and to decrease rapidly with the number of carbon atoms, resulting in the molecular-symmetry reduction for members larger than a certain critical size. The electronic spectra were calculated using the most stable geometrical structures obtained by the SCF MO method.

For predicting the energetically most favorable molecular shapes with respect to C–C bond lengths of conjugated hydrocarbons, we developed a symmetry rule based on the second-order Jahn-Teller theorem.[1-5] The pseudo, or the second-order Jahn-Teller effect is the stabilization which occurs when a certain bond distortion mixes two electronic states nearly degenerate in the fully-symmetrical nuclear arrangement.[6] On the basis of this theory, we examined the second-order Jahn-Teller effects on bond lengths and stability of

*Present adress; Department of Chemistry, Faculty of General Education, Yamagata University, Yamagata.

1) T. Nakajima, A. Toyota, and S. Fujii, This Bulletin, **45**, 1022 (1972).
2) R. F. Bader, *Mol. Phys.*, **3**, 137 (1960).
3) R. F. Bader, *Can. J. Chem.*, **40**, 1164 (1962).
4) R. F. Pearson, *J. Amer. Chem. Soc.*, **91**, 4947 (1969).
5) R. G. Pearson, *J. Chem. Phys.*, **52**, 2167 (1970).
6) L. Salem, "The Molecular Orbital Theory of Conjugated Systems," Benjamin, New York (1966).

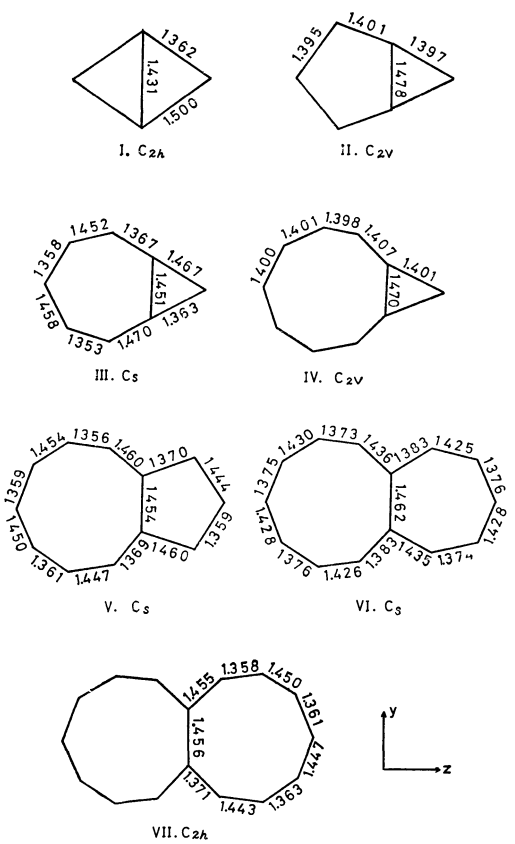

Fig. 1. Molecular-symmetry groups, bond lengths (Å) and choice of axes.

a number of nonalternant hydrocarbons.[1,7-9]

In this paper we apply the symmetry rule to the prediction of the stable geometrical structures of the cata-condensed nonalternant hydrocarbons, whose general formula is C_mH_{m-2} (Fig. 1). Of these systems, pentalene ($m=8$), azulene ($m=10$), and heptalene ($m=12$) have been investigated by several authors.[10-14] They found that the stable ground-state equilibrium configurations of pentalene and heptalene, both having $4n$ π-electrons, should belong to the reduced molecular-symmetry group C_{2h}, exhibiting a marked double-bond fixation in the peripheral carbon skeleton. On the other hand, it was predicted that in azulene belonging to the $4n+2$ π-electron system, no molecular-symmetry reduction occurs. The prediction is in good agreement with available experimental results. We were interested in why azulene does not reduce its molecular-symmetry group from C_{2v} to C_s. The purpose of this paper is to examine systematically the possibility of a relationship between the number of carbon atoms(m) and the molecular-symmetry reduction in the C_mH_{m-2} cata-condensed nonalternant hydrocarbons considered as formed by the introduction of a cross-link between the two carbon atoms of a like parity of the C_mH_m cyclic polyenes.

Theoretical

First we assume a fully-symmetrical nuclear arrangement as the unperturbed nuclear configuration for a conjugated molecule. We further assume that in the unperturbed nuclear çonfiguration all the symmetrical bond distortions take place until the first-order energy equilibrium is reached. The unperturbed electronic wavefunctions $\psi_0, \psi_1, \cdots, \psi_n, \cdots$ and the corresponding eigenvalues $E_0, E_1, \cdots, E_n, \cdots$ are assumed to be known. We now distort the nuclei from the symmetrical first-order nuclear arrangement by means of the ith normal coordinate of nuclear motion Q_i. On the basis of the same approximation as used previously,[1] the energy of the ground state after deformation may be written as

$$E(Q_i) = E_0 + \frac{1}{2}\left\{k - 2\sum_n{}' \frac{|\langle\psi_n|(\partial H_\pi/\partial Q_i)_0|\psi_0\rangle|^2}{(E_n - E_0)}\right\}Q_i^2$$

where k and H_π represent the force constant for an sp^2 hybridized C–C σ-bond and the Hamiltonian for π-electrons, respectively.

According to the above equation, the force constant for the normal vibration Q_i can be identified with the term in the braces and can be negative if a given matrix element $\langle\psi_n|(\partial H_\pi/\partial Q_i)_0|\psi_0\rangle$ is nonvanishing and the associated energy gap $E_n - E_0$ is sufficiently small. If the force constant is negative, the energy should be lowered by the nuclear deformation Q_i, and a pseudo-Jahn-Teller distortion from the symmetrical nuclear arrangement would occur spontaneously.

The symmetry rules[1] for predicting the stable molecular shapes in the ground state are as follows: the symmetry of the normal displacement with the smallest force constant is identical with that of the lowest excited state, ψ_1. If the energy gap $E_1 - E_0$ is smaller than the critical value, *ca.* 1.2 eV, the molecule would be distorted into a less symmetrical nuclear configuration. The most favorable type of bond distortion is predicted by examining the distribution of the transition density ρ_{01} over the molecular skeleton. When the lowest excited state is represented by a one-electron transition between molecular orbitals ϕ_i and ϕ_j, the transition density ρ_{01} between the ground and the lowest exicted states is given by $\sqrt{2}\,\phi_i\phi_j$.[6]

Since it is based on the second-order perturbation theory, the symmetry rule gives only the type of the most favorable bond distortion. In order to obtain information on the actual magnitude of distortion or the equilibrium bond lengths at which the nuclei of the real molecule will settle, we use the variable bond-length SCF MO method.[15]

Results and Discussion

The Ground-state Symmetries and Geometries. The symmetries and energies (measured from the ground state) of the lowest excited states for the fully-symmetri-

7) T. Nakajima, *Pure and Appl. Chem.*, **28**, 219 (1971).
8) T. Nakajima, "Topics in Current Chemistry," Vol. **32**, Spring-Verlag, Heidelberg (1972), p. 1.
9) A. Toyota and T. Nakajima, This Bulletin 46, 2284 (1973).
10) P. C. den Boer-Veenendeal and D. H. W. den Boer, *Mol. Phys.*, **4**, 33 (1961).
11) T. Nakajima and S. Katagiri, *Mol. Phys.*, **7**, 149 (1963).
12) P. François and A. Julg, *Theoret. Chim. Acta*, **11**, 128 (1968).
13) G. Binsch, E. Heilbronner and J. N. Murrell, *Mol. Phys.*, **11**, 305 (1966).
14) A. Tajiri, N. Ohmichi and T. Nakajima, This Bulletin, **44**, 2347 (1971).
15) H. Yamaguchi, T. Nakajima and T. L. Kunii, *Theoret. Chim. Acta*, **12**, 349 (1968).

TABLE 1. SYMMETRIES AND ENERGIES OF FIRST AND SECOND EXCITED SINGLET STATES OF CATA-CONDENSED NONALTERNANT HYDROCARBONS

Molecule (Point group)	First excited state		Second excited state	
	E_1-E_0 (eV)	Symmetry	E_2-E_1 (eV)	Symmetry
I (D_{2h})	0.48	B_{3g}	4.97	B_{1u}
II (C_{2v})	3.57	B_2	2.32	A_1
III (C_{2v})	0.32	B_2	3.45	A_1
IV (C_{2v})	2.36	B_2	1.41	A_1
V (C_{2v})	0.26	B_2	2.47	A_1
VI (C_{2v})	1.44	B_2	1.08	A_1
VII (D_{2h})	0.20	B_{3g}	1.95	B_{1u}
Pentalene (D_{2h})	0.35	B_{3g}	3.25	B_{1u}
Azulene (C_{2v})	2.05	B_2	1.48	A_1
Heptalene (D_{2h})	0.26	B_{3g}	2.41	B_{1u}

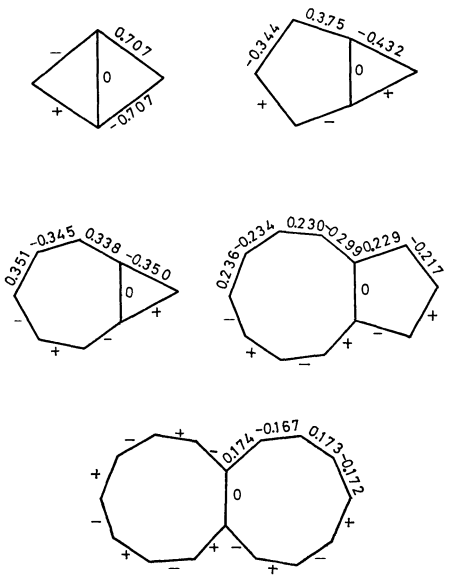

Fig. 2. Distributions of two-center components of transition densities (ρ_{01}).

cal nuclear arrangements of the cata-condensed nonalternant hydrocarbons are listed in Table 1. The two-center components of the transition densities for the some selected molecules are shown in Fig. 2. The correlation of the first excitation energies for the fully-symmetrical nuclear arrangement with the number of carbon atoms of the C_mH_{m-2} systems is shown in Fig. 3, in which the excitation energies for pentalene, azulene, and heptalene, which are the isomers of the molecules III, IV, and V, respectively, are also included. The dashed line represents the critical value for the molecular-symmetry reduction. In the hatched area the molecule should distort into a less symmetrical nuclear configuration.

From Table 1 and Fig. 3, it is seen that in molecules with $4n$ π-electrons the energy gaps E_1-E_0 are all considerably smaller than the critical value, *ca.* 1.2 eV. In the $4n+2$ π-electron systems, the energy gaps decrease with the number of carbon atoms rapidly as compared with the case of the $4n$ π-electron

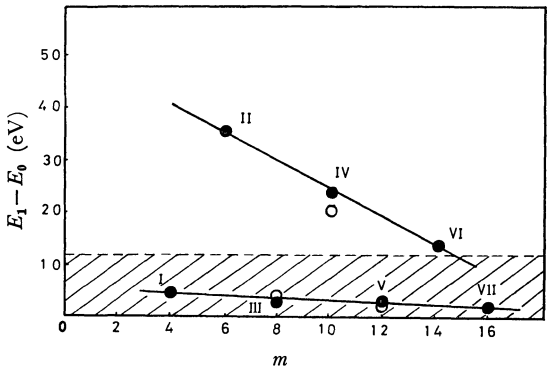

Fig. 3. Correlation of E_1-E_0 with the number of carbon atoms of C_mH_{m-2}. Open circles mean values for pentalene ($m=8$), azulene ($m=10$) and heptalene ($m=12$).

systems. The origin of the smallness of the energy gaps E_1-E_0 in these $4n$ π-electron systems (that is, the near degeneracy of the ground state with the lowest excited state) may be explained as follows. In the C_mH_m cyclic polyenes with $4n$ π-electrons, the ground-state is degenerate with the lowest excited states in the Hückel MO approximation, since the highest occupied molecular orbitals are doubly degenerate and there are four ways of assigning two electrons to the degenerate orbitals. The cata-condensed nonalternant hydrocarbons are considered to be formed by the introduction of a cross-link between the two carbon atoms of a like parity of the C_mH_m cyclic polyenes. The highest occupied molecular orbitals which are doubly degenerate in the unperturbed cyclic polyenes are split only a slight degree by the introduction of such a cross-link. The energy separation between these split orbitals is small and the lowest excited state for the perturbed system is represented by a one-electron transition between these molecular orbitals, so that the energy gap between the lowest excited and the ground states, E_1-E_0, is very small.

On the basis of the symmetry rule, we can predict that molecules I and VII should reduce their ground-state molecular-symmetry groups to C_{2h} from D_{2h} by the interaction with the lowest excited state through the b_{3g} nuclear displacement. Molecules III and V may also lower their ground-state molecular-symmetry groups from C_{2v} to C_s by the interaction with the lowest excited state through the b_2 nuclear displacement. The shapes of the stable molecular structures are predicted from the distribution of transition densities ρ_{01}.

On the other hand, in II and IV, molecules with $4n+2$ π-electrons, the energy gaps are definitely large as compared with the critical value for the molecular-symmetry reduction in the ground state. In molecule VI, the energy gap is comparable with the critical value for the molecular-symmetry reduction.

In order to obtain the equilibrium C–C bond lengths we performed the variable bond-length SCF MO calculation, taking into account all the possible distorted structures as the starting geometry.[16] The molecular-symmetry groups and bond lengths corresponding to the most stable nuclear arrangements for the cata-

16) T. Nakajima and A. Toyota, *Chem. Phys. Lett.*, **3**, 272 (1969).

condensed nonalternant hydrocarbons are shown in Fig. 1.

From the result of SCF MO calculation it turns out that, as predicted from the symmetry rule, molecules I, III, V, and VII reduce their ground-state molecular-symmetry groups to C_{2h}, C_s, C_s, and C_{2h}, respectively.

In II and IV, the molecular-symmetry reduction does not occur. However, VI reduces its molecular-symmetry group to C_s from C_{2v}. It should be noted that the molecular-symmetry reduction in the $4n+2$ π-electron systems will be realized if the molecule becomes larger than a certain critical size ($n\sim3$).

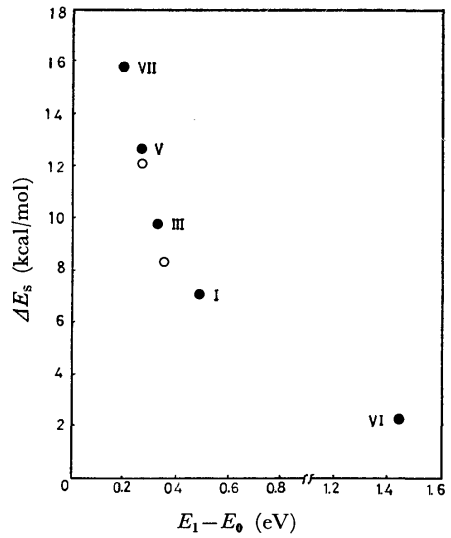

Fig. 4. Correlation of ΔE_s with E_1-E_0. Open circles mean values for pentalene (0.35 eV) and heptalene (0.26 eV).

In Fig. 4 is shown the correlation of the stabilization energies for the molecular-symmetry reduction with the excitation energies E_1-E_0, as calculated by assuming the fully-symmetrical nuclear arrangements. We define the stabilization energy as the difference in total energy between the fully-symmetrical and the reduced molecular geometries. The total energy is assumed to be the sum of π-bond and σ-bond energies, the latter being calculated using the harmonic oscillator model with the force constant equal to 714 kcal mol^{-1} Å^{-2}.[17] We see that there is a good correlation between the stabilization energy ΔE_s and E_1-E_0; the smaller the latter, the larger the former. The stabilization energies for pentalene and heptalene are also included (open circles).

From the viewpoint of the largeness of stabilization energy, we may say that the second-order Jahn-Teller effect becomes strong with the number of carbon atoms in the $4n$ π-electron systems.

As for the C–C bond-length distribution in the stable nuclear arrangements (Fig. 1), it may be said that the double-bond fixation, *i.e.*, bond-length alternation, is the common phenomenon in the reduced molecular geometries, as is expected from the distribution of transition densities ρ_{01}.

Excited-state Molecular-symmetry Groups. It is of interest to note the molecular shape of the lowest excited state. The criterion for the molecular-symmetry reduction in the excited state is that the energy gap E_2-E_1 is less than the critical value, *ca.* 0.6 eV.[1] From this criterion and Table 1 we may predict that all the molecules examined do not reduce their molecular-symmetry groups in the first singlet excited states. That is, the stable molecular shapes in the excited states belong to their fully-symmetrical nuclear arrangements.

Electronic Spectra. In calculating electronic spectra, we used the bond lengths for the energetically stable nuclear arrangements. The method of calculation employed is the Pariser-Parr-Pople MO method, and the configuration mixing of all the singly excited states is included (Table 2).

Table 2. Transition energies and intensities

Molecule (Point group)	Transition symmetry	ΔE (eV)	f (c.g.s)
I (C_{2h})	^1A_g	2.26	Forb.
	^1B_u	5.57	0.632
	^1B_u	10.14	0.912
II (C_{2v})	$^1B_2$	3.57	0.046
	$^1A_1$	5.89	0.137
	$^1B_2$	6.82	0.008
	$^1A_1$	6.85	1.160
III (C_s)	$^1A'$	1.65	0.004
	$^1A'$	4.06	0.327
	$^1A'$	5.07	0.054
	$^1A'$	5.75	0.272
IV (C_{2v})	$^1B_2$	2.36	0.072
	$^1A_1$	3.77	0.032
	$^1B_2$	4.44	0.068
	$^1A_1$	4.96	2.014
V (C_s)	$^1A'$	1.61	0.001
	$^1A'$	3.12	0.273
	$^1A'$	4.01	0.117
	$^1A'$	4.76	0.690
VI (C_s)	$^1A'$	1.81	0.046
	$^1A'$	2.69	0.000
	$^1A'$	3.46	0.313
	$^1A'$	3.93	1.930
VII (C_{2h})	^1A_g	1.67	Forb.
	^1B_u	2.67	0.361
	^1B_u	3.41	0.234
	^1A_g	4.37	Forb.

It should be noted that the excitation energies, particularly the lowest ones, calculated assuming the reduced molecular-symmetry groups for molecules I, III, V, VI, and VII, are predicted to be considerably higher than those calculated using the fully-symmetrical nuclear configurations (compare Table 1 with Table 2).

However, so far there is no experimental data for a comparision with theoretical values, except for pentalene (1-methyl-pentalene), azulene, and heptalene.[18–20]

17) L. C. Snyder, *J. Chem. Phys.*, **66**, 2299 (1962).

18) R. Bloch, R. A. Marty, and P. de Mayo, *J. Amer. Chem. Soc.*, **93**, 3071 (1971).

19) Pl. A. Plattner and E. Heilbronner, *Helv. Chim. Acta*, **30**, 910 (1947); **31**, 804 (1948).

20) H. J. Dauben, Jr. and D. J. Bertelli, *J. Amer. Chem. Soc.*, **83**, 4659 (1961).

Conclusion

The problem of molecular-symmetry reductions in the cata-condensed nonalternant hydrocarbons C_mH_{m-2} has been systematically examined on the basis of the second-order Jahn-Teller theorem. It was assumed that only the lowest excited state plays a dominant role in determining the most favorable nuclear displacement which reduces the molecular-symmetry group to a less symmetrical nuclear configuration. In spite of this very crude approximation, the predicted types of the energetically most favorable bond distortions, determined by examining the two-center components of transition densities, are in good agreement with the results of variable bond-length SCF MO calculations. The success of this approximation for predicting the stable molecular shapes might be ascribed to the fact that in the fully-symmetrical nuclear arrangements of the $4n$ π-electron systems the ground state is nearly degenerate with the lowest excited state, and that the second excited state is well separated from the lowest excited state.

Finally we may say that the pseudo, or the second-order Jahn-Teller effect becomes strong with increasing the number of carbon atoms in the C_mH_{m-2} cata-condensed nonalternant hydrocarbons.

The numerical calculation was carried out at Tohoku University with a NEAC 2000—500 electronic computer.

BULLETIN OF THE CHEMICAL SOCIETY OF JAPAN, VOL. 46, 3685—3687 (1973)

Raman Spectra and Internal Rotation of Ethyl Methyl Ether

Teizo KITAGAWA, Kazuo KUSAKI, and Tatsuo MIYAZAWA

Institute for Protein Research, Osaka University, Yamada-kami, Suita, Osaka 565

(Received July 16, 1973)

The Raman spectra of ethyl methyl ether in the liquid state were measured at various temperatures from 298 K to 195 K. The energy difference between the *gauche* and *trans* isomers in the liquid state was found to be 1.1 kcal/mol. This value is appreciably higher than the value 0.77 kcal/mol for *n*-butane. The tendency of assuming the *trans* form is higher for the CH_2–O bond than for the CH_2–CH_2 bond. The infrared intensity of the band at 465 cm^{-1} (gas) is largely due to the *gauche* isomer but the Raman intensity of the line at 471 cm^{-1} (liquid) is largely due to the *trans* isomer.

The infrared and Raman spectra of ethyl methyl ether in the gaseous, liquid, and crystalline states have been analyzed[1-8] and it has been established that the *trans* and *gauche* isomers coexist in the gaseous and liquid states while only the *trans* isomer remains in the crystalline state. Vibrational assignments of low frequency vibrations have been established, including internal-rotation vibrations of the methyl groups and the threefold potential barriers of the methyl groups of the *trans* isomer have been studied.[7,8]

Energy-difference data of rotational isomers about CH_2–O bonds are important for studying internal-rotation of polyethers including polyethylene glycol. The energy difference between the *gauche* and *trans* isomers of ethyl methyl ether in the gaseous state has been obtained as $\Delta H(H_g - H_t) = 1.5 \pm 0.2$ kcal/mol[4] from the temperature dependence of the relative intensity of the infrared bands at 375 cm^{-1} (*gauche*) and at 280 cm^{-1} (*trans*). On the other hand, the energy difference in the dilute carbon-disulfide solution has been determined as 1.35 kcal/mol[7] from the relative intensity of the infrared bands at 980 cm^{-1} (*gauche*) and at 1015 cm^{-1} (*trans*).

For measuring infrared intensities in the low-frequency region, it is required to take due care of natural emission from the sample and/or the attenuator of a double-beam spectrophotometer. Thus, corrections were made[4] for natural emission from the gas cell at elevated temperatures and relative intensities of the infrared bands of rotational isomers were measured. On the other hand, in measuring absorption intensities of the sample in a low-temperature cell, the natural emission from the optical attenuator causes a systematic error. Apparent transmittance of infrared bands is shifted lower than actual transmittance, unless the double-chopping method is used.[8]

Intensity measurements of Raman lines are not disturbed by these systematic errors, and more reliable values of energy differences may be obtained. In the present study, the Raman spectra of ethyl methyl ether in the liquid state at low temperatures were measured in order to determine the energy difference in the liquid state.

Experimental

The sample of ethyl methyl ether (b.p. 279 K) as prepared in the preceeding study[8] was transferred through a vacuum

1) K. W. F. Kohlrausch, *Monatsh. Chem.*, **68**, 349 (1936).
2) Y. Mashiko, *Nippon Kagaku Zasshi*, **80**, 593 (1959).
3) R. G. Snyder and G. Zerbi, *Spectrochim. Acta*, **23A**, 391 (1967).
4) T. Kitagawa and T. Miyazawa, This Bulletin, **41**, 1967 (1968).
5) A. D. H. Clague and A. Danti, *Spectrochim. Acta*, **24A**, 439 (1968).
6) J. P. Perchard, *ibid.*, **26A**, 707 (1970).
7) J. P. Perchard, *J. Mol. Structure*, **6**, 457 (1970).
8) T. Kitagawa, K. Ohno, H. Sugeta, and T. Miyazawa, This Bulletin, **45**, 969 (1972).

line and was sealed into a liquid cell. The liquid cell was then held in a low-temperature apparatus. Raman spectra were excited with an argon-ion laser (488.0 nm) and were measured with a JEOL Raman spectrometer (Model JRS-02AS).

Results

Relative intensities of Raman lines of ethyl methyl ether in the liquid state were found to vary markedly with temperature. Typical examples of the Raman spectra at 298 K and 200 K are shown in Fig. 1. Thus, the relative intensities of the Raman lines at 381, 978, and 1069 cm^{-1} were found to be stronger at higher temperature than at lower temperature. These Raman lines correspond to the infrared bands at 376 cm^{-1} (in CCl_4 solution[4]), 979 and 1068 cm^{-1} (in CS_2 solution[6]) which are not observed in the crystalline state

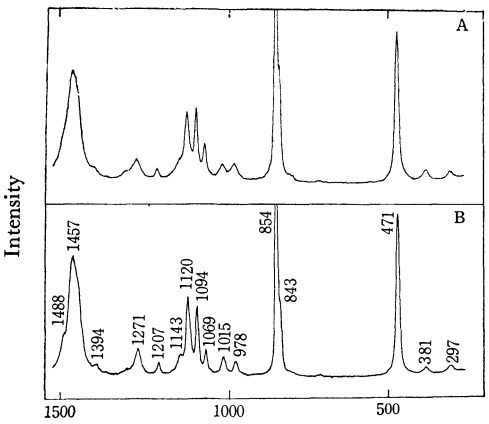

Fig. 1. Raman spectra of ethyl methyl ether in the liquid state, (A) at 298 K and (B) at 200 K, excited with an argon-ion laser (488.0 nm).

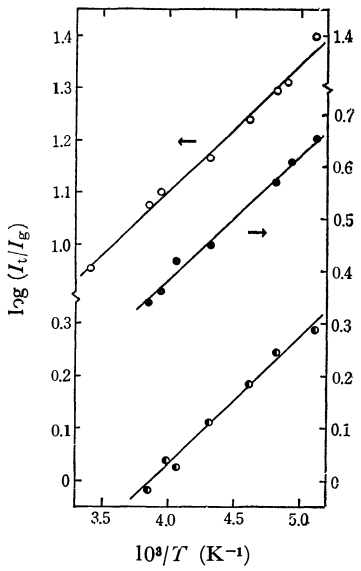

Fig. 2. Temperature dependence of the intensity ratios of the Raman lines of the *trans* isomer (I_t) and the *gauche* isomer (I_g), ○: 471 cm^{-1}/381 cm^{-1}, ◐: 1015 cm^{-1}/978 cm^{-1}, ●: 1120 cm^{-1}/1069 cm^{-1}.

and accordingly are assigned to the *gauche* isomer. The Raman lines due to the *trans* isomers are observed at 471, 1015, and 1120 cm^{-1}.

The ratios of area intensities of the Raman lines of the *gauche* (I_g) and *trans* isomers (I_t) were measured at temperatures from 298 K to 195 K (Fig. 2). The energy difference [$\Delta H(H_g-H_t)$] between the *gauche* and *trans* isomers was found to be 1.1±0.1, 1.1±0.2, and 1.1±0.1 kcal/mol from the pairs (*trans*/*gauche*) of Raman lines [471 cm^{-1}/381 cm^{-1}], [1015 cm^{-1}/978 cm^{-1}], and [1120 cm^{-1}/1069 cm^{-1}], respectively. Thus the values of ΔH obtained from the three pairs agreed closely with one another.

For the pair of the Raman lines at 1094 cm^{-1}/1069 cm^{-1}, the apparent energy difference was obtained as 0.9±0.1 kcal/mol. This value is slightly smaller than the value of $\Delta H(H_g-H_t)=1.1$ kcal/mol, so that the Raman intensity at 1094 cm^{-1} is largely due to the *trans* isomer but also partly due to the *gauche* isomer.

Discussion

The energy difference $\Delta H=1.1$ kcal/mol in the liquid state is smaller than the value $\Delta H=1.35$ kcal/mol in CS_2 solution[7] or the value $\Delta H=1.5$ kcal/mole in the gaseous state.[8] The small difference between the values in the liquid state and in the gaseous state is due to the small difference between the dipole moments of the *trans* and *gauche* isomers.

The energy difference $\Delta H=1.1$ kcal/mol for ethyl methyl ether [CH_3–CH_2–O–CH_3] in the liquid state is appreciably higher than the value $\Delta H=0.77$ kcal/mol for *n*-butane [CH_3–CH_2–CH_2–CH_3].[9] This indicates that the tendency of assuming the *trans* form is higher for the CH_2–O bond than for the CH_2–CH_2 bond. Similarly, the energy difference [$\Delta H=1.1$ kcal/mol[10] or 1.37 kcal/mol[11]] between the *trans-gauche* and *trans-trans* isomers of diethyl ether [CH_3–CH_2–O–CH_2–CH_3] is appreciably higher than the value $\Delta H=0.60$ kcal/mol[12] for *n*-pentane [CH_3–CH_2–CH_2–CH_2–CH_3].

The relative intensity of the infrared bands of the gaseous state at 375 cm^{-1} (*gauche*) and 465 cm^{-1} was previously[8] found to be independent of temperature indicating that the bands of the *trans* and *gauche* isomers overlap at 465 cm^{-1} and the intensity of the composite band is largely due to the *gauche* isomer. However, in the Raman scattering, the relative intensity of the Raman lines at 1120 cm^{-1} (*trans*) and 471 cm^{-1} (in the liquid state) is independent of temperature so that the Raman scattering intensity at 471 cm^{-1} is almost exclusively due to the *trans* isomer. For the *trans* isomer of ethyl methyl ether, the Raman line at 471 cm^{-1} corresponds to the Raman line of liquid *n*-butane at 425 cm^{-1} and is assigned to the accordion vibration. On the other hand, the antisymmetric C–C–C–C deforma-

9) G. J. Szasz, N. Sheppard, and D. H. Rank, *J. Chem. Phys.*, **16**, 704 (1948).

10) H. Wieser, W. G. Laidlaw, P. J. Krueger, and H. Fuhrer, *Spectrochim. Acta*, **24A**, 1055 (1968).

11) J. P. Perchard, J. C. Monier, and P. Dizabo, *ibid.*, **27A**, 447 (1971).

12) T. Fujiyama, M. Tasumi, and T. Shimanouchi, Symposium on High Polymers, Kyoto, Oct. 1970, paper 20D09.

tion frequency of the *gauche* isomer of *n*-butane is calculated very close to the accordion frequency of the *trans* isomer[13] but has not been observed separately in the Raman scattering. Similarly, the Raman intensity of the 'antisymmetric' C–C–O–C deformation vibration of the *gauche* isomer of ethyl methyl ether may well be negligible as compared with the Raman intensity of the accordion vibration of the *trans* isomer.

13) R. G. Snyder, *J. Chem. Phys.*, **47**, 1316 (1967).

BULLETIN OF THE CHEMICAL SOCIETY OF JAPAN, VOL. 46, 3687—3689 (1973)

On the Decomposition of $C_6H_5CO^+$ Ions Produced from Several Alkyl Phenyl Ketones by Electron Impact

Susumu TAJIMA, Nobuhide WASADA and Toshikazu TSUCHIYA

National Chemical Laboratory for Industry, Honmachi, Shibuya-ku, Tokyo 151

(Received August 13, 1973)

The decomposition of $C_6H_5CO^+$ ions produced by electron impact from seven alkyl phenyl ketones, C_6H_5-COR (R=H, CH_3, C_2H_5, *n*-C_3H_7, *iso*-C_3H_7, *n*-C_4H_9, *n*-C_5H_{11}), has been studied. By determining the heats of formation, the $C_6H_5CO^+$ ions produced from the different precursors in the vicinity of the threshold are shown to have the same structure, and it is also shown that there is a linear relationship between the heat of formation of the activated complex for the reaction $C_6H_5CO^+ \rightarrow C_6H_5^+ + CO$ and the vibrational degrees of freedom of the neutral fragment, R.

Many authors have studied[1-7] the decomposition of a common intermediate ion produced from various precursors, in order to study how the difference of the precursors reflects on the decomposition of the common intermediate ions assuming quasi-equilibrium theory (QET) of mass spectra[8] to be valid.

The present paper describes the decomposition of the benzoyl ions, $C_6H_5CO^+$, produced from seven alkyl phenyl ketones, benzaldehyde, acetophenone, ethyl phenyl ketone, *n*-propyl phenyl ketone, isopropyl phenyl ketone, *n*-butyl phenyl ketone, and *n*-amyl phenyl ketone, on the basis of the following assumption: As is usually assumed in QET,[8,9] when a molecular ion with internal energy E decomposes into a neutral and an ionic fragments, the energy, E_M, in excess of the activation energy, is partitioned in proportion to the number of vibrational degrees of freedom in the neutral and the ionic fragments.

Experimental

The appearance potentials (AP) of the various ions were measured with a CEC 21—103 C mass spectrometer. The temperatures of the ion source and the sample manifold were about 250 °C and 100 °C, respectively. The electron-trap current was 10 μA. The electron accelerating voltage was supplied by a battery, and set with a 20-turn potentiometer (Sakae Tsushin Kogyo Co., Ltd.).

AP values were obtained by the energy distribution difference (EDD) technique[10] after the ionization efficiency curves were smoothed by the least-squares method. The constant, b, used in the EDD calculation was 0.67. The details have already been given.[11] Krypton (IP=14.00 eV) was used as calibrating gas for the electron energy scale.

All the samples studied were of research grade, and were obtained from Tokyo Kasei Co., Ltd., and were used without further purification.

Results and Discussion

Calculation of the Heat of Formation. The heat of formation of the $C_6H_5CO^+$ ion and that of the state which can be taken to be the activated complex for the reaction (1), $\Delta H_f(C_6H_5CO^+)$ and $\Delta H_f(C_6H_5^+ \cdots CO)$, are calculated by the Eqs. (2) and (3).

$$C_6H_5CO^+ \longrightarrow C_6H_5^+ + CO \quad (1)$$

$$\Delta H_f(C_6H_5CO^+) = AP(C_6H_5CO^+) + \Delta H_f(M) - \Delta H_f(R) - E_1 \quad (2)$$

$$\Delta H_f(C_6H_5^+ \cdots CO) = AP(C_6H_5^+) + \Delta H_f(M) - \Delta H_f(R) - E_2 \quad (3)$$

where $AP(X^+)$ is the appearance potential of the ion X^+, $\Delta H_f(M)$ and $\Delta H_f(R)$ are the heats of formation

1) K. R. Jennings and J. H. Futrell, *J. Chem. Phys.*, **44**, 4315 (1966).
2) (a) F. W. McLafferty and W. T. Pike, *J. Amer. Chem. Soc.*, **89**, 5951 (1967); (b) F. W. McLafferty and W. T. Pike, *ibid.*, **89**, 5953 (1967); (c) W. T. Pike and F. W. McLafferty, *ibid.*, **89**, 5954 (1967); (d) M. L. Gross and F. W. McLafferty, *Chem. Commun.*, **1968**, 254.
3) (a) R. G. Cooks and D. H. Williams, *ibid.*, **1968**, 627; (b) D. H. Williams, R. G. Cooks, and I. Howe, *J. Amer. Chem. Soc.*, **90**, 6759 (1968); (c) R. G. Cooks, I. Howe, and D. H. Williams, *Org. Mass Spectrom.*, **2**, 137 (1969).
4) P. Brown, *ibid.*, **2**, 1805 (1969).
5) (a) R. H. Shapiro, J. Turk, and J. W. Serum, *ibid.*, **3**, 171 (1970); (b) J. Turk and R. H. Shapiro, *ibid.*, **6**, 189 (1972).
6) S. Tajima, Y. Niwa, M. Nakajima, and T. Tsuchiya, This Bulletin, **44**, 2340 (1971).
7) H. Nakata, A. Tatematsu, H. Yoshizumi, and S. Naga, *Chem. Lett.*, **1973**, 75.
8) H. M. Rosenstock and M. Krauss, in F. W. McLafferty ed., "Mass Spectrometry of Organic Ions", Academic Press, New York (1963), Chap. 1.
9) A. N. H. Yeo and D. H. Williams, *Org. Mass Spectrom.*, **5**, 135 (1971).
10) R. E. Winters, J. H. Collins, and W. L. Courchene, *J. Chem. Phys.*, **45**, 1931 (1966).
11) S. Tajima, Y. Shimizu, and T. Tsuchiya, This Bulletin, **45**, 931 (1972).

of the neutral molecule, M, and radical, R, respectively, and E_n is the excess energy of the fragments at the threshold.

The AP values of the $C_6H_5CO^+$ ions and the $C_6H_5^+$ ions from seven alkyl phenyl ketones measured in this experiment are given in Table 1. Each value represents an average taken from at least three measurements, and the given experimental errors are maximum deviations.

The values of the heat of formation used for the neutral molecules and free radicals, ΔH_f(M) and ΔH_f(R), are given in Table 2. These values are taken from the literature.[12] Some ΔH_f(M) values which are not given in the literature were calculated by approximation methods used by Franklin.[13]

Using the AP values in Table 1 and the values of heat of formation shown in Table 2, the heat of formation of the $C_6H_5CO^+$ ions and that of the activated complexes for the reaction (1) were calculated by Eqs. (2) and (3), respectively. The results are shown in Fig. 1. The values in Fig. 1 are obtained by taking E_n as zero.

$C_6H_5CO^+$ Ions. As seen in Fig. 1, the values for heat of formation of the $C_6H_5CO^+$ ions from seven alkyl phenyl ketones studied here are the same within the experimental error. Therefore, these $C_6H_5CO^+$ ions produced in the vicinity of the threshold are considered to have the same structure.[14,15] Consequently,

TABLE 1. APPEARANCE POTENTIALS (eV) OF THE $C_6H_5CO^+$ IONS AND THE $C_6H_5^+$ IONS FROM ALKYL PHENYL KETONES

C_6H_5COR	AP($C_6H_5CO^+$)	AP($C_6H_5^+$)
Benzaldehyde	10.2±0.10	13.5±0.06
Acetophenone	9.8±0.08	13.5±0.10
Ethyl phenyl ketone	9.5±0.10	13.6±0.15
n-Propyl phenyl ketone	9.8±0.07	13.9±0.06
Isopropyl phenyl ketone	9.3±0.08	13.7±0.05
n-Butyl phenyl ketone	10.0±0.10	14.3±0.10
n-Amyl phenyl ketone	9.8±0.06	14.5±0.10

TABLE 2. HEATS OF FORMATION ΔH_f(kcal/mol) OF NEUTRAL ALKYL PHENYL KETONES AND RADICALS

Compound	$\Delta H_f(C_6H_5COR)$	ΔH_f(R)
Benzaldehyde	−10.5	52.1
Acetophenone	−23.0	33.2
Ethyl phenyl ketone	−24.7	25.0
n-Propyl phenyl ketone	−29.6[a]	22.1
Isopropyl phenyl ketone	−30.9[a]	16.8
n-Butyl phenyl ketone	−34.5[a]	18.5
n-Amyl phenyl ketone	−39.4[a]	9.1

a) These values were calculated by approximation methods used by Franklin.[9]

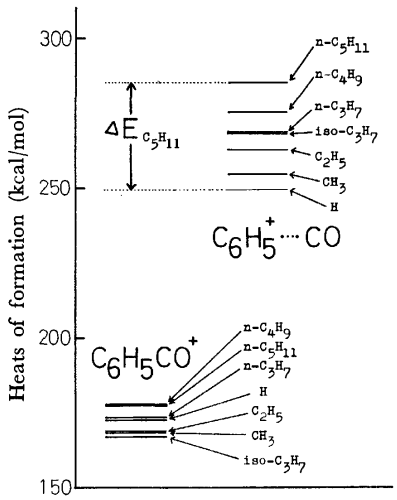

Fig. 1. The heats of formation (kcal/mol) of the $C_6H_5CO^+$ ions and the activated complexes for the reaction (1), $\Delta H_f(C_6H_5CO^+)$ and $\Delta H_f(C_6H_5^+\cdots CO)$.

the decomposing $C_6H_5CO^+$ ions of reaction (1), produced from various precursors, will also have the same structure, that is, the values for heat of formation of the activated complexes for the reaction (1) will be the same.[14,16]

The Activated Complexes for the Reaction (1). As seen in Fig. 1, the heats of formation of the activated complexes for the Reaction (1) show some scatter, compared with that of $C_6H_5CO^+$ ions, and furthermore, the values increase systematically as the number of atoms in R is large. In this study, we have investigated the source of the difference in the values, on the basis of the above assumption.

A few authors have reported[17,18] that during the dissociation of a molecular ion, the energy, E_M, in excess of the activation energy, is partitioned to the neutral and the ionic fragments, R and $C_6H_5CO^+$ in this study, respectively, and consequently, that the appearance potentials for the secondary ions, $C_6H_5^+$ in the present study, will be somewhat higher than the "true" values. In this experiment, the number of vibrational degrees of freedom of the R differs from compound to compound, and a part of the energy E_M will be carried away by the R. Therefore, as a consequence of the assumption, the extent of the effect on the AP($C_6H_5^+$) will also vary, and each AP($C_6H_5^+$) will be high according to the number of the vibrational degree of freedom of the R.

In this study, benzaldehyde was taken as the standard, since the number of the vibrational degree of freedom of the R in the compound is zero. ΔE_R is defined as the difference between the heat of formation of the activated complex for the reaction (1) of a compound, C_6H_5COR, and that of benzaldehyde. In Fig. 1, the $\Delta E_{C_5H_{11}}$ for $C_6H_5COC_5H_{11}$ is shown as an example. ΔE_R is considered to be the energy which

12) J. L. Franklin, J. G. Dillard, H. M. Rosenstock, J. T. Herron, K. Draxl, and F. H. Field, "Ionization Potentials, Appearance Potentials and Heats of Formation of Gaseuos Positive Ions", National Bureau of Standard, U.S.A., (1969).
13) J. L. Franklin, *J. Chem. Phys.*, **21**, 2029 (1953).
14) J. L. Occolowitz and G. L. White, *Aust. J. Chem.*, **21**, 997 (1968).
15) S. Tajima and T. Tsuchiya, This Bulletin, in press.
16) S. Tajima and T. Tsuchiya, *Org. Mass Spectrom.*, in press.
17) S. Wexler, G. R. Anderson, and L. A. Singer, *J. Chem. Phys.*, **32**, 417 (1960).
18) M. B. Wallenstein and M. Krauss, *ibid.*, **34**, 929 (1961).

is partitioned to the radical R during the decomposition of the molecular ion. From the assumption, it is reasonable to expect that the following equation holds:

$$\Delta E_R/\alpha = f_R/f_{\phi-CO}$$

Therefore, $$\Delta E_R = (\alpha/f_{\phi-CO}) \times f_R \quad (4)$$

where α is the energy which is partitioned to the $C_6H_5CO^+$ ion during the decomposition of the molecular ion; f_R and $f_{\phi-CO}$ are the numbers for vibrational degree of freedom of the radical R and the $C_6H_5CO^+$ ion, respectively.

The plot of ΔE_R *vs.* f_R is given in Fig. 2. As expected from Eq. (4), the plot gives a straight line which passes through the origin. The experimental formula shown in Fig. 2 is obtained by the least-squares method. From the slope of the line, the value α=27.4 kcal/mol was obtained taking $f_{\phi-CO}$=33. By definition, α=27.4 kcal/mol is the energy which is partitioned to the $C_6H_5CO^+$ ion during the decomposition of the $C_6H_5COR^+$ ion, while the difference between the heat of formation of the activated complex and that of the $C_6H_5CO^+$ ion for benzaldehyde is about 75 kcal/mol (refer to Fig. 1). For benzaldehyde, the value $\Delta H_f(C_6H_5^+)$=275.6 kcal/mol was obtained taking $\Delta H_f(CO)$ =−26.4 kcal/mol,[12] this value is comparable to the value $\Delta H_f(C_6H_5^+)$=284 kcal/mol which was obtained from phenyl radical by Lossing *et al.*[19] Therefore, it can be seen that these $C_6H_5^+$ ions in this study are produced in the vicinity of the ground state of the $C_6H_5^+$ ion. It is reasonable that the excess energy of H-atom in this case is taken as zero, because if there is any energy partition to the H-atom, values for heat of formation of the $C_6H_5^+$ ion from benzaldehyde will be higher than that of the $C_6H_5^+$ ion from phenyl radical.

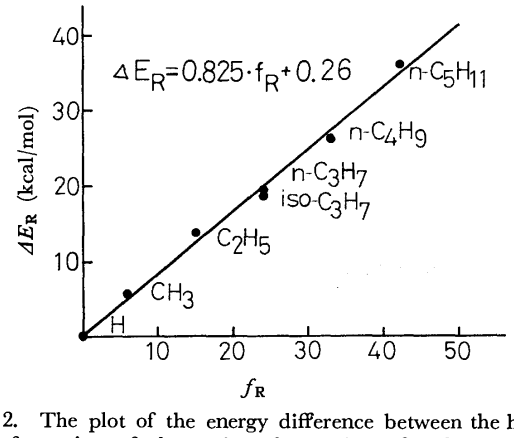

Fig. 2. The plot of the energy difference between the heats of formation of the activated complexes for the reaction (1), ΔE_R, *vs.* the number of vibrational degree of freedom of the radical R, f_R.

As a consequence of the above consideration, if the assumption is valid, the experimental results lead us to conclude that CO loss occurs from the $C_6H_5CO^+$ ion after the $C_6H_5CO^+$ ion, produced from the decomposition of the molecular ion in an excited electronic state, is transferred to a vibrationally excited state of its ground electronic state. An alternative explanation is that the assumption is not valid. Each decomposition reaction occurs from a vibrationally excited state of the ground electronic state of each ion, and only a part of the excess energy E_M is partitioned in proportion to the number of the vibrational degrees of freedom in radical R and the ion $C_6H_5CO^+$, and all of the remaining energy of E_M is partitioned to the $C_6H_5CO^+$ ion.

Conclusions

1) By using the data concerning the heat of formation, the decomposition of the $C_6H_5CO^+$ ions produced from seven alkyl phenyl ketones, are studied, on the basis of an assumption. The $C_6H_5CO^+$ ions produced in the vicinity of the threshold can be considered to have the same structure.

2) It was found that there is a linear relationship between the number of the vibrational degree of freedom, f_R, of the alkyl radical R and the difference of the values for heat of formation, ΔE_R, of the activated complex for the reaction (1). Two different conclusions on the mechanism of the decomposition of the $C_6H_5CO^+$ ions are derived, depending upon whether the assumption is valid or not.

19) I. P. Fisher, T. F. Palmer, and F. P. Lossing, *J. Amer. Chem. Soc.*, **86**, 2741 (1964).

Far Infrared and Raman Spectra of $K_3[Co(CN)_6]$ and $[Co(NH_3)_6][Co(CN)_6]$

Ichiro NAKAGAWA

Department of Chemistry, Faculty of Science, The University of Tokyo, Hongo, Tokyo 113
and
Department of Chemistry, Faculty of Science, Tohoku University, Aoba, Aramaki, Sendai 980

(Received September 12, 1973)

Far infrared spectra of $K_3[Co(CN)_6]$ and $[Co(NH_3)_6][Co(CN)_6]$ and a single crystal Raman spectrum of $K_3[Co(CN)_6]$ have been measured. Calculations of optically active crystal vibration frequencies have been made, on the basis of the crystal structure determined precisely. For these two types of established crystal structures (C_{2h}^5 for $K_3[Co(CN)_6]$ and C_{3i}^2 for $[Co(NH_3)_6]$) $[Co(CN)_6]$ of hexacyano-complex salts, lattice frequencies have been determined. For $[Co(NH_3)_6][Co(CN)_6]$ the mean amplitudes of two kinds of cobalt atoms have been calculated and compared with those obtained by Iwata and Saito assuming that both complex ions behave as a rigid body.

Many investigations have been done on the vibrational spectra of hexacyano-complex salts of transition metals and on the nature of the bonding in this complex ion.[1-11] Among them Jones *et al.* and we ourselves have made a thorough study on the basis of infrared and Raman spectra and a normal coordinate treatment including lattice modes. We have investigated far infrared spectra and lattice vibrations of $K_3[Fe(CN)_6]$, $K_3[Cr(CN)_6]$ and $Cs_3[Cr(CN)_6]$ which have the monoclinic structure with the space group C_{2h}^5.[7] Swanson and Jones have investigated infrared and single-crystal Raman spectra and lattice vibrations of $Cs_2LiCo(CN)_6]$ which has the cubic structure and for which the Bravais primitive cell is composed of one formula unit.[10]

In the present study a measurement has been made for the far infrared and single-crystal Raman spectra of $K_3[Co(CN)_6]$ which is isomorphous with $K_3[Fe(CN)_6]$ and takes a monoclinic structure C_{2h}^5. A far infrared spectrum of $[Co(NH_3)_6][Co(CN)_6]$ has also been measured, since Iwata and Saito have recently performed a very detailed X-ray analysis for the crystal structure of this complex salt, according to which the space group of this crystal is C_{3i}^2 ($R\bar{3}$).[12] Optically active lattice frequencies of the crystal have been calculated for these two complex salts. For $[Co(NH_3)_6][Co(CN)_6]$, the mean amplitudes of the displacements for the two Cobalt atoms have been calculated, which may be compared with the data obtained by Iwata and Saito.[12]

Experimental

Infrared measurement: Samples dispersed homogeneously in polyethylene or Nujol mull were used for the measurement

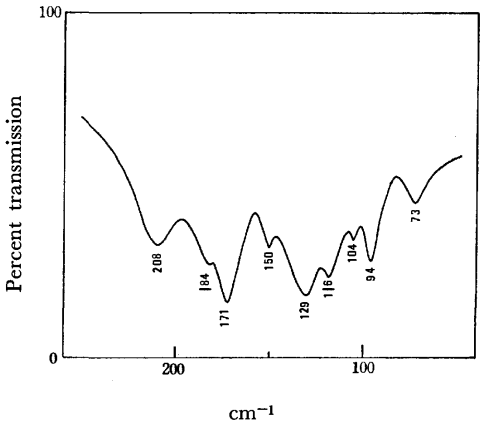

Fig. 1. Far infrared spectrum of $K_3[Co(CN)_6]$.

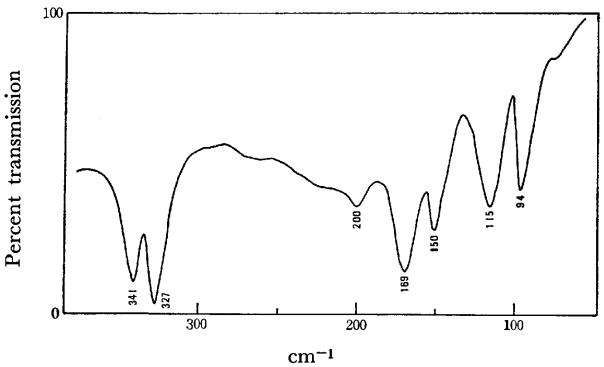

Fig. 2. Far infrared spectrum of $[Co(NH_3)_6][Co(CN)_6]$ (at liquid N_2 temperature).

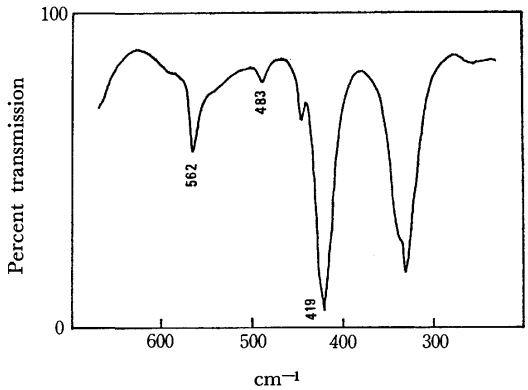

Fig. 3. Infrared spectrum of $[Co(NH_3)_6][Co(CN)_6]$ in the region 700~300 cm^{-1} (at room temperature).

1) L. H. Jones, *J. Chem. Phys.*, **36** 1209 (1962).
2) L. H. Jones, *Inorg. Chem.*, **2**, 777 (1963).
3) I. Nakagawa and T. Shimanouchi, *Spectrochim. Acta*, **18**, 101 (1962).
4) V. Lorenzelli and P. Delorme, *ibid.*, **19**, 2033 (1963).
5) D. Bloor, *J. Chem. Phys.*, **41**, 2573 (1964).
6) L. H. Jones, *Inorg. Chem.*, **4**, 1472 (1965).
7) I. Nakagawa and T. Shimanouchi, *Spectrochim. Acta*, **26A**, 131 (1970).
8) B. I. Swanson and L. H. Jones, *J. Chem. Phys.*, **53**, 3761 (1970).
9) L. H. Jones, M. N. Memering and B. I. Swanson, *ibid.*, **54**, 4666 (1971).
10) B. I. Swanson and L. H. Jones, *ibid.*, **55**. 4174 (1971).
11) D. M. Adams and M. A. Hooper, *J. Chem. Soc., Dalton*, **1972**, 160.
12) M. Iwata and Y. Saito, *Acta Crystallogr.*, **29B**, 822 (1973).

of far infrared spectrum. A Hitachi EPI-L double beam spectrometer flushed by dry air (700—300 cm^{-1}) and a Hitachi FIS-1 vacuum double beam far infrared spectrometer (500—60 cm^{-1}) were used. The observed spectra are reproduced in Figs. 1~3.

Raman measurement: Raman spectra of a single-crystal sample of $K_3[Co(CN)_6]$ were observed using a JEOL JRS-U1 Raman spectrometer equipped with an Ar ion laser and a Spex 1401 double monochromator equipped with a He–Ne laser. The observed spectrum is reproduced in Fig. 4. Polarization measurements for this monoclinic crystal do not supply sufficient data to determine the a_g and b_g species vibrations.

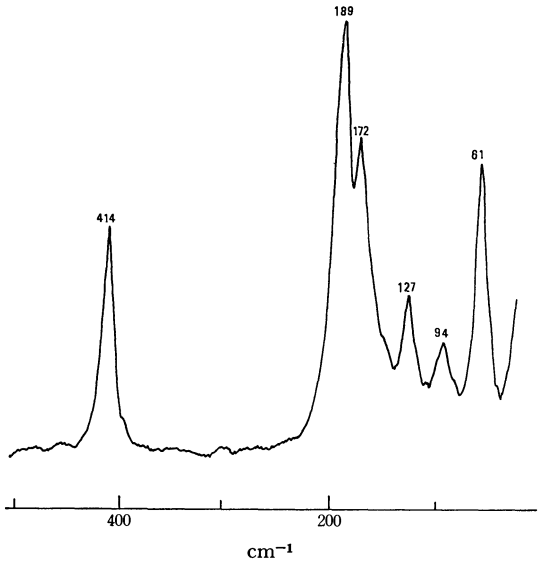

Fig. 4. Single crystal Raman spectrum of $K_3[Co(CN)_6]$.

Observed Results and Analysis

$K_3[Co(CN)_6]$. The crystal structure is monoclinic with the space group C_{2h}^5. The Bravais primitive cell contains two formula units and the factor group analysis shows that the 21 a_g and 21 b_g vibrations are Raman active and the 26 a_u and 25 b_u vibrations are infrared active. The 21 modes in each of the a_g and b_g species are composed of 15 inner modes and 3 rotational and 3 translational lattice modes. The 26 a_u modes are composed of 18 inner and 8 translational lattice modes, while the 25 b_u modes of 18 inner and 7 translational lattice modes. A vibrational analysis and a normal coordinate treatment of optically active crystal vibrations are made just in the same way as in the case of $K_3[Fe(CN)_6]$ described in the previous paper.[7] The detailed structure of $K_3[Co(CN)_6]$ was determined by neutron diffraction study.[13] Potential constants (intramolecular and interionic force constants) used in this calculation are taken the same values as those in $K_3[Fe(CN)_6]$ except for the Co–C and C≡N stretching force constants, K(Co–C) and K(C≡N) (see Table 3 of Ref. 7). The values of K(Co–C) and K(C≡N) are taken 2.6 mdyn/Å and 16.5 mdyn/Å, respectively. The results of the calculations are listed

Table 1. Observed and calculated frequencies in cm^{-1} of $K_3[Co(CN)_6]$

Obsd (IR)	Calcd (b_u)	Calcd (a_u)	Calcd $[Co(CN)_6]^{3-}$	Mode
2118	2105, 2105, 2104	2105, 2105, 2104	2103 (f_{1u})	CN str.
565	565, 564, 562	565, 564, 562	561 (f_{1u})	CoC str.
414	412, 407, 404	412, 407, 404	402 (f_{1u})	CoCN bend.
	388, 385, 381	388, 385, 381	380 (f_{2u})	
208	205	206		lattice
184	193	193		
171	163	165		
150	143	143		
129	127, 123	130, 123	128 (f_{1u})	CCoC def.
116	112	116		
104	102	95	100 (f_{2u})	CCoC def.
94	89	86		lattice
73	74, 68	79, 62		
	50, 24	49, 22, 14		
Obsd (Raman)	**Calcd (a_g)**	**Calcd (b_g)**	**Calcd $[Co(CN)_6]^{3-}$**	**Mode**
	2110, 2101, 2100	2110, 2101, 2100	2109 (a_{1g})	CN str.
			2099 (e_g)	
	458, 454, 451	458, 454, 451	450 (f_{2g})	CoCN bend.
414	438	438	431 (a_{1g})	CoC str.
	405, 399	405, 399	394 (e_g)	
	318, 313, 305	318, 313, 305	303 (f_{1g})	CoCN bend.
189	197	191		lattice
172	174	181		
129	143, 112	138, 118	119 (f_{2g})	CCoC def.
94	91, 87	93, 84		lattice
61	62	56		
	41, 9	41, 27		

13) N. A. Curry and W. A. Runciman, *ibid.*, **12**, 674 (1959).

in Table 1, together with the observed frequencies. The calculated frequencies, for which the interionic force constants were neglected (as an isolated complex ion), are also included in this table.

In Table 1 the observed infrared bands as a whole correspond well with the calculated frequencies as in the case of isomorphous $K_3[Fe(CN)_6]$. Furthermore it is noted that the Raman frequencies are also in good agreement with the calculated values using the same values of potential constants without any modification. Now that the vibrational analysis of this type of complex salts, $K_3[M(CN)_6]$, with the monoclinic structure C_{2h}^5, has been established rather fully, some discussions will be given below. The lattice frequencies due to the interaction between the complex ions and outer cations may be classified into two groups for both infrared and Raman spectra. One is located above 150 cm^{-1} and the other below 100 cm^{-1}. In the former the displacements of the K^+ ions are predominant while in the latter those of the complex ions are appreciable. The rotaional lattice frequencies in the a_g and b_g vibrations correspond with the lower group of vibrations and some of them may not be observed. Adams and Hooper argued that the high frequencies of the lattice modes in contrast with those of complex halides K_2MCl_6 indicate a higher degree of covalent bonding between anions and cations than in complex halides.[11] In fact the nearest distance between K^+ ion and N atom is about 2.5 Å. Anyhow the lattice dynamical treatment of optically active crystal vibrations, where the interionic potential constants for the atom pairs with distances shorter than 4.0 Å are taken into account and they are vaired according to the distances, is a plausible analysis to interpret both the lattice vibrations and the inner vibrations for the complex salts. The calculated frequencies as an isolated complex ion show that the outer ion affects very little upon the metal-ligand stretching frequencies in both the gerade and ungerade species though the low-frequency CCoC deformation modes are more or less coupled with the lattice modes.

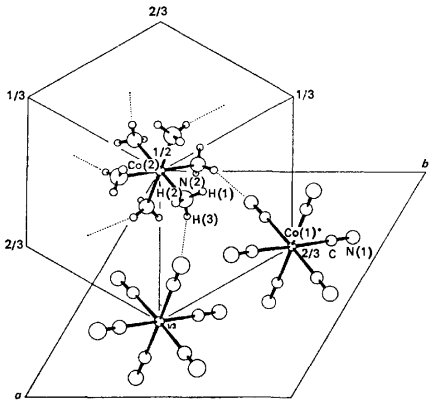

Fig. 5. Crystal structure of $[Co(NH_3)_6][Co(CN)_6]$. (Reproduced from Fig. 1 of Ref. 12 with the courtesy of Prof. Saito).

$[Co(NH_3)_6][Co(CN)_6]$. Figure 5 (the reproduction of the figure (Fig. 1) in Ref. 12) shows the crystal structure determined by Iwata and Saito.[12] This crystal is trigonal with the space group C_{3i}^2 ($R\bar{3}$) and as shown in Fig. 5 the Bravais primitive cell contains one formula unit, in other words, one $[Co(NH_3)_6]^{3+}$ ion and one $[Co(CN)_6]^{3-}$ ion (38 atoms). It can be shown from the factor group analysis that the 19 a_u and 19 e_u vibrations are infrared active, of which only 1 a_u and 1 e_u vibrations correspond to the interionic lattice modes. The 18 a_g and 18 e_g vibartions are Raman active. However, the displacements of cobalt atoms occur only for the infrared active ungerade modes.

A normal coordinate analysis of optically active crystal vibrations has been done based on the geometry[14] determined by X-ray analysis,[12] using the potential constants listed in Table 2. The values of the intramolecular force constants were at first obtained from our previous study on ammine complexes[15] and $K_3[Co(CN)_6]$ described above and then modified slightly so that the calculated frequencies may ex-

Table 2. Potential constants used in the calculation of $[Co(NH_3)_6][Co(CN)_6]$

Intramolecular force constants of $[Co(NH_3)_6]^{3+}$ and $[Co(CN)_6]^{3-}$					
K(Co–N)	1.05 mdyn/Å	H(NCoN)	0.40 mdyn/Å	F(N···N)	0.05 mdyn/Å
K(N–H)	5.60 mdyn/Å	H(HNH)	0.53 mdyn/Å	F(H···H)	0.06 mdyn/Å
K(Co–C)	2.30 mdyn/Å	H(CoNH)	0.15 mdyn/Å	F(Co···H)	0.10 mdyn/Å
K(C≡N)	16.5 mdyn/Å	H(CCoC)	0.14 mdyn/Å	F(C···C)	0.15 mdyn/Å
Y(NH_3)	0.01 mdyn·Å	H(CoCN)	0.25 mdyn/Å		

Interaction potential constants		
f(N···H)	0.15 mdyn/Å	(for 2.17 Å)
f(N···H)	0.03 mdyn/Å	(for 2.50 Å)
f(N···H)	0.03 mdyn/Å	(for 2.52 Å)
f(C···H)	0.022 mdyn/Å	(for 2.68 Å)
f(C···H)	0.018 mdyn/Å	(for 2.75 Å)

14) CoC_6 and CoN_6 are taken as regular octahedra and Co–C–N is taken as linear, which is not exactly the same as the geometry determined by X-ray analysis.

15) I. Nakagawa and T. Shimanouchi, *Spectrochim. Acta*, **22**, 759 (1966).

TABLE 3. OBSERVED INFRARED AND CALCULATED FREQUENCIES IN cm^{-1} OF $[Co(NH_3)_6][Co(CN_6)]$

Obsd	Calcd (a_u)	Calcd (e_u)	Mode	Calcd[a] (isolated)
3275	3258, 3245	3258, 3245	NH_3 asym. str.	3237, 3229
3126	3181	3181	NH_3 sym. str.	3167
2122	2132	2132	CN str.	2131
1570	1591, 1576	1591, 1576	NH_3 deg. def.	1583, 1574
1367	1434	1434	NH_3 sym. def.	1434
843	843, 831	849, 819	NH_3 rock.	848, 834, 831, 816
562	560	560	CoC str.	556
483	509	509	CoN str.	507
419	411	412	CoCN bend.	407
	389	391	CoCN bend.	388
341	348	339	NCoN def.	330
327	294	304	NCoN def.	278
200				
169	181	172	CCoC def.	132
150	146	141	CCoC def.	102
115	117	124	NH_3 torsion	92
94	66	79	lattice mode	

a) Calculated value where interaction potential constants were neglected.

plain the observed frequencies as a whole. The value of NH_3 torsional force constant is somewhat arbitrary, since a definite observed frequency is not determined for this mode. As for the interaction potential constants, several kinds of the bent type hydrogen bonding N–H···N and N–H···C should be taken into account. From the crystal structure shown in Fig. 5, there are 3 kinds of N···H atom-pairs whose distances are about 2.17 Å, 2.50 Å and 2.52 Å, respectively, and 2 kinds of C···H atom-pairs of about 2.68 Å and 2.75 Å. The interatomic force constants are taken for these atom pairs. The values of f(C···H) were determined according to Harada-Shimanouchi's potential,[16] while those of f(N···H) were determined on referring to the data of the hydrogen-bonded dimers such as adenine and uracil crystals studied by Harada and Lord.[17] The results of the calculations are listed in Table 3, together with the infrared observed frequencies. The frequencies are well interpreted based on the trigonal structure determined by X-ray analysis.

Then mean amplitudes of displacements of two kinds of cobalt atoms in $[Co(NH_3)_6][Co(CN)_6]$ were calculated, using the value of potential constants in Table 2. The Cartesian displacement of i-th atom is expressed as:

$$\Delta x_i = \sum_a (L_X)^a_{x_i} Q_a$$

where Q_a denotes a-th normal coordinate. Therefore one obtains

$$\langle \Delta x_i^2 \rangle = \sum_a [(L_X)^a_{x_i}]^2 \langle Q_a^2 \rangle$$

$$\langle \Delta x_i \Delta y_i \rangle = \sum_a [(L_X)^a_{x_i}(L_X)^a_{y_i}] \langle Q_a^2 \rangle$$

where $\langle\ \rangle$ denotes mean values. $\langle Q_a{}^2 \rangle$ is expressed as

$$\langle Q_a^2 \rangle = (h/8\pi^2 c\nu_a) \coth (hc\nu_a/2kT)$$

16) I. Harada and T. Shimanouchi, *J. Chem. Phys.*, **46**, 2708 (1967).
17) I. Harada and R. C. Lord, *Spectrochim. Acta*, **26A**, 2305 (1970).

TABLE 4. MEAN AMPLITUDES OF DISPLACEMENTS OF Co ATOMS IN $[Co(NH_3)_6][Co(CN)_6]$

	Co (in $[Co(NH_3)_6]^{3+}$)	Co (in $[Co(CN)_6]^{3-}$)
$2\sqrt{\langle \Delta z_i^2 \rangle}$	0.151 Å	0.131 Å
$2\sqrt{\langle \Delta x_i^2 \rangle}$ ($2\sqrt{\langle \Delta y_i^2 \rangle}$)	0.133 Å	0.122 Å

Taking the principal axes as x, y and z axes, $\langle \Delta x_i \Delta y_i \rangle$ naturally disappears. Mean amplitudes of displacements of cobalt atoms were calculated at 300 K, the vibrations of the ungerade species being only taken into consideration for the displacements of cobalt atoms. The result is shown in Table 4. Iwata and Saito[12] made the calculations of thermal parameters assuming that both complex ions behave as a rigid body. They obtained tensors to describe the translational vibration and libration of the rigid body and showed that rigid-body motions are similar in both complex ions and are strikingly isotropic (the mean amplitude of translational motion is 0.12~0.13 Å). It should be noted that the result in Table 4 is in good agreement with that by Iwata and Saito.

In conclusion both $K_3[Co(CN)_6]$ and $[Co(NH_3)_6]$-$[Co(CN)_6]$ are well-established typical cyano-complex salts from the crystal-structural point of view. Vibrational spectra are interpreted satisfactorily on the basis of the crystal structure determined by neutron and X-ray analyses. Mean amplitudes calculated using the potential constants based on the spectroscopic data may supply thermal parameters in the X-ray analysis.

Most parts of this work were made in Department of Chemistry, The University of Tokyo. The author wishes to express his sincere thanks to Prof. Takehiko Shimanouchi for his encouragement throughout this study. Thanks are also due to Prof. Yoshihiko Saito, Institute for Solid State Physics, The University of Tokyo, for his valuable discussions.

The Electronic Absorption Spectra of Würster's Cation Radicals and Their Dimerization in Solution*

Shigeki NAKAYAMA** and Keisuke SUZUKI

Faculty of Science, Kwansei Gakuin University, Nishinomiya 662

(Received May 4, 1973)

The visible and ultraviolet absorption spectra of the *p*-phenylenediamine cation (PD^+), the *N,N*-dimethyl-*p*-phenylenediamine cation ($DMPD^+$), and the *N,N,N',N'*-tetramethyl-*p*-phenylenediamine cation ($TMPD^+$) in the presence and in the absence of an excess counter anion ($X^-=Br^-$, Cl^-, and ClO_4^-) are studied at low temperatures. Analyses of the data show that these cation radicals are in an equilibrium represented by $2R^+ + X^- \rightleftarrows R^{++}{}_2X^-$ (or, more exactly, $2R^+ + 0.7X^- \rightleftarrows R^{++}{}_2(X^-)_{0.7}$). It is found that the absorption maxima of the dimer and the value of the heat of dimerization are independent of the kind of counter anion. It is concluded that PD^+ and $DMPD^+$ form strong dimers (heat of dimerization, $\Delta H=-8.0$ and -8.2 kcal/mol respectively) and that $TMPD^+$ forms a relatively weak one ($\Delta H=-5.6$ kcal/mol). The features of the dimer spectra reflect the strength of the interaction of the radical in the dimer. In a strong dimer, the spectrum in the low-frequency region consists of a strong intermolecular charge-transfer band (C band) and a weak local excitation band (R' band), and the frequency shifts of the local excitation bands in the dimer (R' and Y' bands) from corresponding bands in the monomer (R and Y) are large. On the other hand, the spectrum in the weak dimer consists of relatively weak C and strong R' bands, and the shifts of the R' and Y' bands are small. A model of the dimer is proposed in which the two cations are arranged in a parallel manner and are surrounded by the ionic atmosphere of the counter anions.

The half-oxidation products of *p*-phenylenediamine and its *N*-methyl substituted derivatives, which are called Würster's cation radicals, are known as stable organic cation radicals. Michaelis and Granick[1] first suggested that Würster's cation radicals, except for the *N,N,N',N'*-tetramethyl-*p*-phenylenediamine cation ($TMPD^+$ or Würster's blue), are polymerized in crystalline states and in concentrated or cooled solutions. Hausser[2] found that, with lowering of the temperature, a Würster's blue perchlorate solution shows an intense new absorption band in the near-infrared region of the spectrum, a band which appears to increase in intensity as the paramagnetism of the solution decreases. Hausser and Murrell[3] suggested the formation of a radical dimer (π-complex) and assigned the new band to an intermolecular charge-transfer band in the dimer. In the previous preliminary papers,[4] the present authors experimentally confirmed the suggested solution dimerization by an analysis of the temperature-dependent absorption spectra of several Würster's cation radicals at low temperatures. A similar line of investigation has also been performed by Kimura, Yamada, and Tsubomura.[5]

In these previous works, however, the role of the counter anion in the dimerization was not considered. In the present investigation, spectrophotometric measurements of the solutions of cation radicals of *p*-phenylenediamine (PD^+), *N,N*-dimethyl-*p*-phenylenediamine ($DMPD^+$), and *N,N,N',N'*-tetramethyl-*p*-phenylenediamine ($TMPD^+$) were carried out at low temperatures and at various concentrations by using newly-constructed, accurate temperature-control equipment. In order to study the possible contribution of the counter anion to the dimerization, an excess amount of a salt containing a counter anion (ammonium bromide, chloride, or perchlorate) was added to the radical solution and the observed spectrophotometric changes were analyzed on the basis of several monomer-dimer equilibrium models including the counter anion. The nature of dimer interaction was then discussed by using the monomer and the dimer spectra of PD^+, $DMPD^+$, and $TMPD^+$ together with the results of other analyses.

Experimental

p-Phenylenediamine bromide (PDBr), *N,N*-dimethyl-*p*-phenylenediamine perchlorate ($DMPDClO_4$) and *N,N,N',N'*-tetramethy-*p*-phenylenediamine perchlorate ($TMPDClO_4$) were used for this study. These radical salts were prepared according to the method described in the literature.[1] For the spectrophotometric solvents, an ethanol–ethyl ether mixture (volume ratio of 2 : 1) was used for $DMPD^+$ and $TMPD^+$, while *n*-propanol was used for PD^+, because of the slower decomposition rates of the radicals in the solutions. Each solvent was purified by distillation after desiccation over sodium wire (for ether) or calcium oxide (for alcohols).

The absorption spectra of the radical solutions at low temperatures were obtained in quartz absorption cells with optical path lengths of 0.1, 0.3, 1.0, and 3.0 cm. The cell was cooled by cold nitrogen gas in a quartz Dewar vessel with optical windows. The cold nitrogen gas was supplied from a liquid nitrogen tank equipped with an electric heater immersed in the liquid nitrogen.

The temperature of the solution in the cell was measured by means of a copper-constantan thermocouple with a standard DC voltage source, a DC amplifier, and an electronic recording millivoltameter with lower and upper limit switches, as is shown in Fig. 1. The rate of the flow of the cold nitrogen gas was controlled automatically by regulating an applied voltage drop across the heater by the use of the switches.

* This work has been partially supported by the Fund for Scientific Research from the Ministry of Education.

** Present address: Central Research Laboratory, Mitsubishi Electric Corporation, Amagasaki.

1) L. Michaelis and S. Granick, *J. Amer. Chem. Soc.*, **65**, 1757 (1943).

2) K. H. Hausser, *Z. Naturforsch.*, **A11**, 20 (1956).

3) K. H. Hausser and J. N. Murrell, *J. Chem. Phys.*, **27**, 500 (1957).

4) K. Uemura, S. Nakayama, Y. Seo, K. Suzuki, and Y. Ooshika, This Bulletin, **39**, 1248 (1966). A. Kawamori, A. Honda, N. Joo, K. Suzuki, and Y. Ooshika, *J. Chem. Phys.*, **44**, 463 (1966).

5) K. Kimura, H. Yamada, and H. Tsubomura, *ibid.*, **48**, 480 (1967).

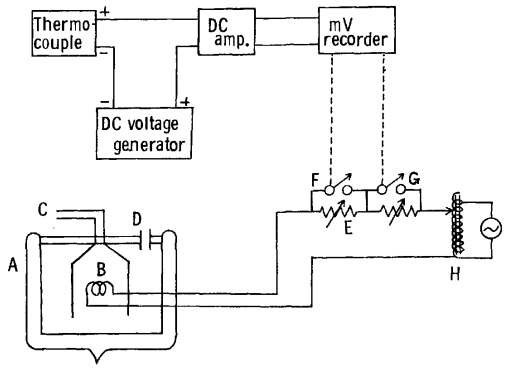

Fig. 1. Apparatus for temperature control.
A: liquid nitrogen tank, B: electric heater, C: cold nitrogen gas outlet, D: liquid nitrogen inlet, E: variable resistor, F: lower limit switch, G: upper limit switch, H: variac.

Thus, the temperature of the cell was kept constant within 0.1 K.

The thermal expansion of the solution was calibrated in each measurement. A Cary recording spectrophotometer, model 14, was used for all the spectrophotometric measurements.

Results and Discussion

Electronic Absorption Spectra of PD⁺, DMPD⁺, and TMPD⁺ Solutions and Their Temperature Dependence. The spectra of PD⁺, DMPD⁺, and TMPD⁺ in dilute solutions at room temperature, *i. e.*, the spectra of radical monomers, all show similar structures, as Figs. 2—4 show. Each spectrum is characterized by an R band with fine vibrational structure in the visible region and by weak X and strong Y bands in the near-ultraviolet region.

At low temperatures, the spectra of these three radicals were significantly changed, as is also indicated in Figs. 2—4: the spectra at low temperatures showed new absorption bands C, R′, and Y′. As the temperature was lowered, it was found that the optical densities of the C, R′, and Y′ bands increased at the expense of those of the R and Y bands. In addition, a similar decrease in the optical density of the X band and the appearance of a new band (X′ band) can be

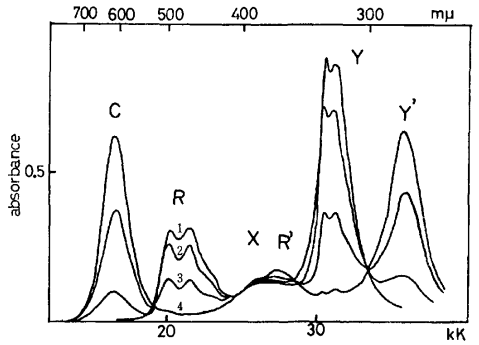

Fig. 2. Temperature dependence of absorption spectra of PD⁺ in *n*-propanol.
1: room temperature, 2: 195 K, 3: 175 K, 4: 154 K.
Stoichiometric concentration of the solution: 4.05×10^{-4} mol/l, optical path length: 0.1 cm

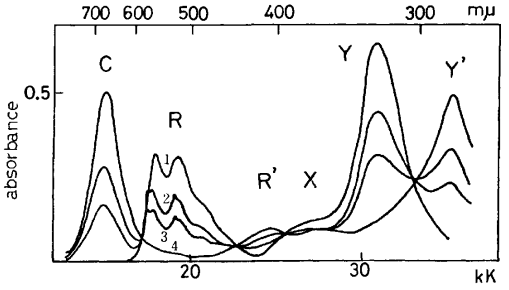

Fig. 3. Temperature dependence of absorption spectra of DMPD⁺ in ethyl ether–ethanol.
1: room temperature, 2: 160 K, 3: 152 K, 4: 130 K.
Stoichiometric concentration of the solution: 1.16×10^{-5} mol/l, optical path length: 0.1 cm.

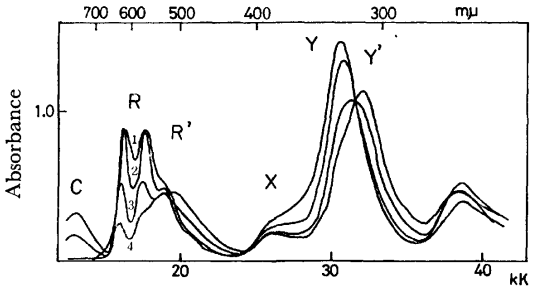

Fig. 4. Temperature dependence of absorption spectra of TMPD⁺ in ethyl ether–ethanol.
1: room temperature, 2: 148 K, 3: 124 K, 4: 113 K.
Stoichiometric concentration of the solution: 7.58×10^{-5} mol/l, optical path length: 1.0 cm.

expected. However, quantitative measurements in these frequency regions were difficult because of stronger overlapping Y and Y′ bands.

By comparing the temperature dependence of various solutions at different concentrations, we are able to determine that the R and the Y bands can be attributed to the radical monomer, and the C, R′, and Y′ bands, to the radical dimer, as will be shown in the next section.[6]

The frequencies of the absorption maxima (ν_{max}) and oscillator strengths (f) of these bands are given in Table 1. The frequency shift of the R′ band from the R band and that of the Y′ band from the Y band are also given in the table. They will be discussed in the last section by comparing them with the heats of dimerization. These spectral properties will be theoretically treated in the next paper.[7]

Analyses of the Temperature-dependent Spectra. Up to the present, several investigators have interpreted or analyzed their experimental results[4-6] by assuming a simple dimerization equilibrium:

$$2R^+ \rightleftharpoons (R^+)_2 \qquad (1)$$

or a simple polymerization equilibrium:

$$nR^+ \rightleftharpoons (R^+)_n \qquad (2)$$

6) By analogy with the interpretation of spectra of certain dye solutions (see : E. Rabinowitch and L. F. Epstein, *J. Amer. Chem. Soc.*, **63**, 69 (1941)). R′ and Y′ bands may be assigned to the perturbed excitations in the dimer corresponding to R and Y bands, respectively.

7) To be published elsewhere.

TABLE 1. ABSORPTION MAXIMA (ν_{max} IN kK) AND OSCILLATOR STRENGTHS (f)[a] OF THE ABSORPTION BANDS. BAND SHIFTS OF R' BAND FROM R BAND, AND Y' BAND FROM Y ($\Delta\nu_R$ AND $\Delta\nu_Y$ IN kK). HEATS OF DIMERIZATION (ΔH IN kcal/mol)

Band	PD+		DMPD+		TMPD+	
	f	ν_{max}	f	ν_{max}	f	ν_{max}
C	0.068	16.53	0.066	15.04	0.016	13.07
R'	0.019	25.97	0.015	24.81	0.050	19.72
Y'	0.087	35.97	0.097	35.33	0.095	32.05
R	0.027	20.08	0.033	18.76	0.038	16.26
Y	0.057	31.06	0.059	30.96	0.056	30.77
$\Delta\nu_R$		5.89		6.05		3.46
$\Delta\nu_Y$		4.91		4.37		1.28
ΔH		−8.0		−8.2		−5.6

a) Calculated as a monomer.

Electrostatic repulsion between the positive charges may retard the process of dimerization (or polymerization) in these models. The electrostatic repulsion energy between two point charges which, are separated by 3.1 Å (obtained from the interplanar separation between the parallel benzene rings in the DMPDBr crystals[8]) amounts to several eV. The energy may be reduced to about a half of the original one if the point charge is distributed over eight atoms of each radical according to the mobile π-electron densities. The dielectric constant of the medium may also reduce the energy. However, the energy would still be sufficient to retard the dimerization. Thus, a generalized formula is assumed in the present paper.

$$nR^+ + mX^- \rightleftharpoons (R^+)_n(X^-)_m \qquad (3)$$

where R^+ is a radical cation, and X^-, a counter anion (Cl^-, Br^-, or ClO_4^-). In this model, the contribution of the counter anion may reduce the electrostatic repulsion between the R^+'s. The equilibrium constant is given by;

$$K_{nm} = [(R^+)_n(X^-)_m]/([R^+]^n[X^-]^m) \qquad (4)$$

To justify the above assumption, a spectrum of a radical solution was compared with that of another solution containing the same amount of the radical and, in addition, an excess amount of an anion. If the anion plays some role in the polymerization, as is shown in Eq. (3), the concentration of the dimer must be increased by the addition of the excess amount of the anion, thus, the spectrum of the latter solution must show larger dimer bands (C, R', and Y') and smaller monomer bands (R and Y). In fact, such spectral changes were observed experimentally. For example, the optical density of a solution containing 2.3×10^{-4} mol/l PDBr at 176 K and 6050 Å (the absorption maximum of the C band) was 0.79, whereas that of a solution containing approximately the same amount of PDBr and 6.2×10^{-3} mol/l ammonium bromide was 1.00 at the same temperature and wavelength. At the same time, the R' and the Y' bands increased, and the R and the Y bands decreased. Similar spectral changes were also observed upon the addition of excess chloride or perchlorate anion. The assumption is thus justified.

Next, the numerical values of m, n, and K_{nm} were determined.

a) Determination of n: The value of n was determined from a series of temperature-dependent spectrophotometries of a solution containing a very large excess of X^-. Under the condition of ($[X^-]\gg[R^+]$), the value of the relative equilibrium constant, K_n is given by;

$$K_n = kK_{nm}[X^-] = I_P/(I_M)^n \qquad k: \text{const.} \qquad (5)$$

where I_p and I_M are the values of the optical densities of a polymer band (C, R', or Y') and a monomer band (R and Y) respectively. Eq. (5) is obtained by assuming that the extinction coefficients of the polymer and the monomer bands do not depend upon the temperature over the temperature region measured. Plots of log K_n against $1/T$ should be linear if the assumed n value is adequate. A series of measurements of a PD^+ solution for the cases of $n=1$, 2, 3, and 4 are given in Fig. 5. The linear dependence of log K_n *versus* $1/T$ is obtained if we take $n=2$. The dimerization of the radicals was confirmed from several such series of measurements.

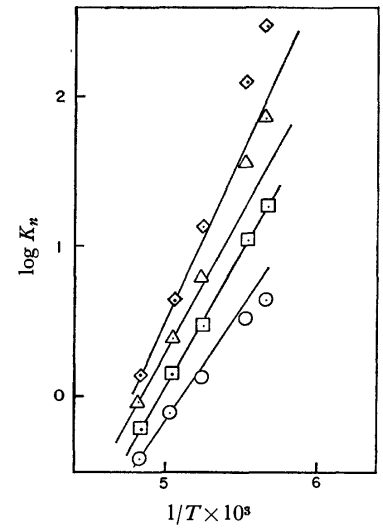

Fig. 5. Plots of log K_n against $1/T$ for a PD^+ solution.
○: $n=1$, □: $n=2$, △: $n=3$, ◇: $n=4$.
Stoichiometric concentrations of the radical and the bromide anion are 9.5×10^{-5} and 5.7×10^{-3} mol/l, respectively.

b) Determination of m: Two types of absorption spectra were obtained under the conditions of $[X^-]=[R^+]$[9] and of $[X^-]\neq[R^+]$,[10] and the spectrophotometric data were analyzed as follows. It was assumed that the data were accounted for by one of the following three equilibria:

$$2R^+ \rightleftharpoons R_2^{++} \qquad (6)$$

8) J. Tanaka and N. Sakabe, *Acta Crystallogr.*, **B24**, 1345 (1968).

9) A solution containing only a radical salt was used.

10) A mixed solution of a radical salt and an ammonium salt was used.

$$2R^+ + X^- \rightleftharpoons R_2X^+ \quad (7)$$

and

$$2R^+ + 2X^- \rightleftharpoons R_2X_2 \quad (8)$$

The corresponding equilibrium constants are given by:

$$K_{20} = \alpha/\{2c_R(1-\alpha)^2\} \quad (9)$$

$$K_{21} = K_{20}/\{c_X - (\alpha/2)c_R\} \quad (10)$$

and

$$K_{22} = K_{20}/(c_X - \alpha c_R)^2 \quad (11)$$

respectively, where α is the degree of dimerization, and where c_R and c_X are the stoichiometric concentrations of the cation radical and the counter anion respectively. α is estimated from the spectrophotometric data.

The most accurate value of α was obtained from $\alpha = I_C/I_C^0$, where I_C is optical density of the C band at the observed temperature and where I_C^0 is that at the lower temperature, where the monomer bands disappear. The values of log K_{nm} of PD^+ are plotted against $1/T$ in Fig. 6. The results show that none of the three models (6), (7), and (8) is able to fit the experimental data satisfactorily; *i. e.*, the R_2 model fails to explain the increase in the degree of dimerization upon the addition of the excess anion, and the R_2X and the R_2X_2 models overestimate the effect of the added salt. These models, the R_2X model is most likely, but it is still not entirely satisfactory. The best fit with the experimental data is obtained if we assume a non-integral m value, $m=0.7$.

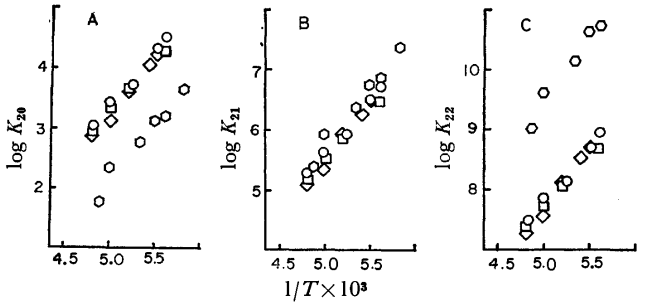

Fig. 6. Plots of log K_{nm} against $1/T$ for PD^+ solutions.
(A): $m=0$, (B): $m=1$, (C): $m=2$.
Stoichiometric concentrations of the radical and the anion of each series are:
○: $R^+=9.53\times10^{-5}$ mol/l, $Br^-=5.7\times10^{-3}$ mol/l,
□: $R^+=9.87\times10^{-5}$ mol/l, $Cl^-=5.65\times10^{-3}$ mol/l,
◇: $R^+=9.67\times10^{-5}$ mol/l, $ClO_4^-=5.68\times10^{-3}$ mol/l,
⬡: $R^+=Br^-=2.36\times10^{-4}$ mol/l.

The concentration-dependent optical densities of the C bands of PD^+, $DMPD^+$, and $TMPD^+$ without an excess anion were analyzed by the use of Eqs. (9)—(11). The results lead to the conclusion that the R_2 model underestimates the concentration dependence, while the R_2X and the R_2X_2 models overestimate it.

The spectrophotometric data of the other bands were also analyzed in similar manners. The results lead to the same conclusion as the above one within the limits of experimental error.

The heat of dimerization derived from the slopes of the log K_{21} *versus* $1/T$ plots are $\Delta H=-8.0$, -8.2, and -5.6 kcal/mol for the PD^+, $DMPD^+$, and $TMPD^+$ dimers respectively. The ΔH values are found to be independent of the kind of counter anion added.

Finally, we must add our important observations that the values of ν_{max}'s are also found to be independent of either the kind or amount of anion added. The only change observed upon the addition is in the degree of dimerization of the radical.

Structure of the Dimer. The structure of the R_2X dimer (or, more exactly, $R_2X_{0.7}$) suggested by the above results is one in which the dimer is surrounded by an ionic atmosphere of the counter anions, X^-'s. The ionic atmosphere may reduce the electrostatic repulsions between the R^+'s. The non-integral m value ($m=0.7$), which is best accounts for the experimental data, is perhaps due to averaged effective contribution of the various ionic atmospheres. The model is supported by the independence of the values of ν_{max}'s and ΔH's of the kind of anion added, X^-.

Another model, a sandwich-type model, in which an anion, X^-, is sandwiched by the two cation radicals, may also explain the fact that $m=1$. However, this model asserts a strong dependence of ν_{max}'s and ΔH's on the kind of anion; this conflicts with the experimental results.

The origin of the attractive force between the cation radicals in the present dimer model is the direct (partly covalent and partly ionic) interaction of the π-electron systems of the R^+'s, while that between the cation radical and the anion in the ionic atmosphere is mainly electrostatic.

The proposed model is supported by the crystal structures of Würster's radical salts. In Würster's blue ($TMPD^+$) perchlorate crystal,[11] the radical monomer are packed in a parallel manner, forming a column of radicals which is surrounded by perchlorate anions. In Würster's red ($DMPD^+$) bromide crystal,[8] a radical dimer is formed by placing two radicals in a parallel manner, and the dimers are packed together, forming a column of dimers. The column is surrounded by bromide anions.

The present model for the solution dimer is considered to be a fragment of the column of cation radicals in the crystal. The interaction between the two cation radicals and that between the cation and the anion in the model are, in principle, the same as those in the crystals. It is reasonable that the crystal and the solution dimer have similar structures and similar interactions.

The Strong Dimer and the Weak Dimer, and Their Spectral Features. The heat of dimerization obtained in the present work is a measure of the strength of the π-electronic interaction in the dimer. Therefore, it may reasonably be concluded that the interactions in the PD^+ and the $DMPD^+$ dimers are stronger than that in the $TMPD^+$ dimer. The weaker interaction in the $TMPD^+$ dimer may be accounted for by the increased steric repulsions between the crowded methyl groups in the two $TMPD^+$ radicals.

11) J. D. Turner and A. C. Albrecht, unpublished data, see : *J. Chem. Phys.*, **39**, 2321 (1964).

These two types of dimers show different spectral features. The strong dimer have strong C and the weak R′ bands, whereas the weak dimer has weak C and strong R′ bands, as Table 1 shows. The shifts of the ν_{max}'s of the local excitation bands by the dimerization ($\Delta\nu_R$, and $\Delta\nu_Y$, in the table) also show different trends; *i. e.*, they are larger for the strong dimer and smaller for the weak one. These interesting properties will be theoretically treated in the next paper.[7]

The authors should like to express their thanks to Professor Ooshika (Osaka Institute of Technology) for his kind discussions throughout the work; they also wish to express their thanks to Mr. Osamu Uemura and Miss Yukiko Seo for the measurements of the absorption spectra of $DMPD^+$.

BULLETIN OF THE CHEMICAL SOCIETY OF JAPAN, VOL. 46, 3698—3702 (1973)

Circular Dichroism and Optical Rotatory Dispersion Spectra of Poly[γ-(1-naphthylmethyl)-L-glutamate] and Its Charge-transfer Complex

Masahiro HATANO, Takamichi ENOMOTO, Ichi ITO, and Michio YONEYAMA*

Chemical Research Institute of Non-aqueous Solutions, Tohoku University, Sendai 980

(Received May 26, 1973)

Poly-γ-(1-naphthylmethyl)-L-glutamate was synthesized and its structure analyzed by the measurements of circular dichroism and absorption spectra. When the circular dichroism band at 219 nm in the circular dichroism spectrum of the polymer can be assigned to the band due to n–π* transition in the peptide main chain of the polymer, the calculated content of the right hand helix in the polymer is about 54% in ethylene chlorohydrin solution. It was also found that the polypeptide can form a charge-transfer complex with an organic electron acceptor in ethylene chlorohydrin solution. In the charge-transfer complex, a circular dichroism band could be observed at the wavelength corresponding to that of the charge-transfer band in the absorption spectrum of the complex. From the results, it was confirmed that the charge-transfer complex contains α-helix structure of this polypeptide. The temperature dependence of the charge-transfer complex formation was discussed in terms of the formation constant and thermodynamic parameters. The polypeptides having various portions of the 1-naphthylmethyl-D-glutamate residue were synthesized from poly-γ-methyl-D-glutamate by a polymer reaction using *p*-toluenesulfonic acid. The values of b_0 for the polypeptides derived from poly-γ-methyl-D-glutamate were estimated by means of Moffitt-Yang's equation, and the correlation between the b_0 values and the contents of 1-naphthylmethyl residue in the polypeptides was discussed.

In 1952, Mulliken[1] suggested that charge-transfer complexes may play an important role in biological systems. Some possible implications have been discussed by Szent-Gyorgyi,[2] his major concern being with the proposal that charge-transfer complexes are involved in biochemical reactions. There are two procedures in studying the possibility firstly to show the existence of charge-transfer complex formation in the biological systems, and secondly to demonstrate that it is essential in biological reaction. In some cases, the existence of charge-transfer complex formation between components in a given biochemical system has been proposed on the most tenuous evidence. The mere production of a colour, when two biochemical (or other) reagents are mixed, has often been given as the sole evidence for the charge-transfer complex formation. Obviously, such an observation alone is insufficient to justify the conclusion. Recent discussion has mainly centred around particular groups of compounds, including model compounds containing what are thought to be essential structural features. In aqueous solution, where most biological reactions occur, the dissociation of the complex may be so high that any charge-transfer absorption can be detected only with difficulty. Quite apart from the experimental difficulties of detecting a possible charge-transfer absorption band, there remains the fact that for most charge-transfer complexes, charge-transfer forces are not the major factor contributing to the stability of the complex in the ground state. Consequently, correlation between electron-donating ability of one component (or electron-accepting ability of the second component) and the association constant, free energy, or enthalpy of formation, cannot in general be assumed to be a necessary feature of a group of charge-transfer complexes. This is especially important when large component molecules are involved; steric effects and other features of the molecule may completely overwhelm any trend in thermodynamic quantities resulting from charge-transfer forces. Thus, it is important to clarify the steric factors for the charge-transfer complex formation in biological systems. In view of this, we examined the formation of charge-transfer complexes of polypeptides having aromatic residues, which behave as electron donors, in order to clarify the correlation between the α-helix content in the polypeptide and formation of their complexes.

The polymer effect on the formation constant of the charge-transfer complex of poly-*N*-vinylcarbazole,

* Present address; Department of High-polymer Science, Faculty of Science, Hokkaido University, Sapporo.

1) R. S. Mulliken, *J. Amer. Chem. Soc.*, **74**, 811 (1952).

2) A. Szent-Gyorgyi, "Introduction to a Submolecular Biology," Academic Press, New York and London (1960).

which has a helical structure, with organic electron acceptors was recently studied.[3] The results indicate the polymer to be tactic in solution because of the steric hindrance resulting from interactions between the neighbouring carbazole units. Accordingly, the extraordinarily high photoconductivity of the charge-transfer complex of poly-*N*-vinylcarbazole with an organic electron acceptor may depend on the helical structure of poly-*N*-vinylcarbazole.

It is interesting to study various factors of the conformational stability of polypeptides in biological systems. The stability of the α-helix structure which is influenced by the sequence of the amino acid residues, solvents and side chain groups is of particular interest. Conformational analyses of various synthetic poly-α-amino acids have been carried out,[4] especially the effects of the side chain groups near the main chain on the conformational stability.[5,6] Fraser[7] studied the conformational stability attributed to van der Waals forces between the aromatic side chains in the polypeptides including poly-γ-(1-naphthylmethyl)-L-glutamate. We have synthesized poly-γ-(1-naphthylmethyl)-L-glutamate and analyzed the structures of its charge-transfer complex in ethylene chlorohydrin or tetrachloroethane solution by various spectral measurements.

Experimental

Preparation of the Polymers. *1-Naphthylmethyl-L-glutamate (I)*: 1-Hydroxymethyl-naphthalene (11.1 g; 0.07 mol) and L-glutamic acid (9.5 g; 0.065 mol) were dissolved in dioxane of 80 ml, and then *p*-toluenesulfonic acid (13.3 g) was added to the reaction mixture. The esterification reaction was carried out for 24 hrs. at 55 °C. After the reaction, the solution was neutralized with sodium bicarbonate, and the reaction product was separated as a white precipitate. The product was filtered on a glass filter, washed with 95% aqueous ethanol solution, and finally recrystallized from the mixture of acetic acid and acetone. Yield 33%. mp. 173—175 °C. Elemental analyses are as follows; Found: C, 65,93; H, 5.77; N, 4.88%. Calcd for $C_{16}H_{17}NO_4$, C, 64.65; H, 5.72; N, 4.71%. $[\alpha]_D^{22}=15.4°$ (in CH_3COOH).

The IR spectrum shows an ester band 1735 cm^{-1}.

1-Naphthylmethyl-L-glutamate NCA(II): Ester(I) (4.5 g, 0.016 mol) was suspended in anhydrous dioxane, and to this system was passed dry phosgene for about 30 min. At the end of the reaction, the suspended NCA(II) was dissolved in dioxane. NCA(II) obtained was recrystallized from ethyl acetate-cyclohexane system. mp. 72—73 °C. Elemental analyses:

Found: C, 63.81; H, 5.11; N, 5.84%. Calcd for $C_{17}H_{15}NO_5$, C, 64.15; H, 4.78; N, 4.47%.

The IR spectrum of NCA(II) shows two bands at 1850 and 1785 cm^{-1}, due to carboxyanhydride group, and an ester band at 1735 cm^{-1}.

Poly-γ-(1-naphthylmethyl)-L-glutamate(III): 1-Naphthylmethyl-L-glutamate NCA(II) was dissolved in 100 ml of anhydrous dioxane and the initiator (*n*-hexylamine) was added. Polymerization conditions and the intrinsic viscosities of the polymer are summarized in Table 1. The IR spectrum of (III) shows an ester band at 1735 cm^{-1} and an amide band at 1655 cm^{-1}. Elemental analyses:

Found: C, 70.74; H, 6.02; N, 5.20%. Calcd for $C_{16}H_{15}NO_3$, C, 71.37; H, 5.58; N, 5.20%.

In the measurements of various spectra, the polymer denoted by No. 1290—2 was used.

Ester Exchange Reaction of Poly-γ-methyl-D-glutamate with 1-Hydroxymethylnaphthalene: Poly-γ-methyl-D-glutamate, prepared by the conventional NCA method (Ajinomoto Co. Ltd.), was used. It has a 1.4 intrinsic viscosity in dichloroethane solution at 30 °C. The ester exchange reactions were carried out as follows. 0.5 g of *p*-toluenesulfonic acid and 2.0 g of 1-hydroxymethylnaphthalene were added to a solution (3% by weight) of poly-γ-methyl-D-glutamate in dichloroethane, and the reaction mixture was then stirred at 60 °C. The molar ratio of poly-γ-methyl-D-glutamate (based on the glutamyl residue) to 1-hydroxymethylnaphthalene in reaction system was varied as shown in Table 2. After the reaction, the reaction product was precipitated with methyl alcohol, and washed several times with methyl alcohol, and finally dried *in vacuo*. The extent of the ester exchange reactions was estimated by means of the nitrogen contents of the reaction products. The conditions and extent of reactions are given in Table 2. From viscosity measurements, it was confirmed that no or less decrease of the degree of the polymerization of the polymer was observed.

Spectral Measurements. Optical rotatory dispersion (ORD) and circular dichroism (CD) measurements were

Table 1. Polymerization of the NCA of γ-(1-naphthylmethyl)-L-glutamate

Sample No.	A/I[a]	Reaction Time	Reaction Temp.	$[\eta]$[b]
1146	100	5 day	Room Temp.	0.52
1290—1	75	24 hr	Room Temp.	0.45
1290—2	50	18 hr	Room Temp.	0.45
1290—3	50	18 hr	Room Temp.	0.30

a) The ratio of molar concentration of the monomer to that of initiator (*n*-hexylamine). b) Intrinsic viscosity of the polymer. The solution viscosity of the polymer was measured at 30 °C in dichloroethane.

Table 2. Relation between the values of b_0 and the extent of reaction in the ester exchange of poly-γ-methyl-D-glutamate with 1-hydroxymethyl-naphthalene

Sample[a]	Extent of the Ester Exchange Reaction (%)	Moffit's b_0
Polymer 1	20	+460
2	40	+440
3	77	+380
4	85	+370
5	100	+230
PMDG	—	+630
PNLG	—	−270

a) Polymers were prepared from poly-γ-methyl-D-glutamate (PMDG). PNLG denotes poly-γ-(1-naphthylmethyl)-L-glutamate synthesized according to the NCA procedure (see Text).

3) T. Enomoto and M. Hatano, *Makromol. Chem.*, in press.
4) G. D. Fasman, "Poly-α-amino Acids; Protein Models for conformational Studies," Marcel Dekker, New York (1967).
5) M. Hatano, M. Yoneyama, T. Nozawa, M. Nakai, and I. Ito, *J. Amer. Chem. Soc.*, **91**, 2165 (1969).
6) M. Hatano and M. Yoneyama, *ibid.*, **92**, 1392 (1970).
7) R. D. B. Fraser, B. S. Harrap, R. Ledger, T. P. Macrae, F.H.C. Stewart, and E. Suzuki, *Biopolymers*, **5**, 797 (1967).

carried out with JASCO ORD/UV-5 and J-20A polarimeters, respectively. Absorption (AB) spectrum was measured with a Hitachi EPS-3T spectrophotometer. In these measurements, spectral grade ethylene chlorohydrin and 1,1,2,2-tetrachloroethane were used as solvents. Ethylene chlorohydrin was dried with CaH_2, distilled over CaH_2 under reduced pressure, and stored with exclusion from moisture in air. Purified ethylene chlorohydrin has a cut-off near 205 nm and high solubility for this polymer and is the best solvent for its CD measurement. From the observed ORD curves, the so-called Moffitt-Yang plots were made by means of the equation

$$[m']\frac{\lambda^2-\lambda_0^2}{\lambda_0^2} = a_0 + b_0\frac{\lambda_0^2}{\lambda^2-\lambda_0^2} \quad (1)$$

where λ_0 was taken to be 212 nm, and the mean residue optical rotation, [m'], was estimated, assuming the refractive index of 1,1,2,2-tetrachroethane to be 1.49 and neglecting the wavelength dependence of the refractive index. Furthermore, the CD and AB spectra of the charge-transfer complex of this polymer with 2,4,7-trinitro-9-fluorenone or 2,4,5,7-tetranitro-9-fluorenone were observed.

Results and Discussion

Absorption Spectrum of Poly-γ-(1-naphthylmethyl)-L-glutamate. Hypochromism is a familiar phenomenon in nucleic acids. A similar situation prevails in α-helical polypeptides and proteins. The hypochromic effect with the α-helix formation was treated theoretically by Tinoco,[8] and can be qualitatively accounted for in terms of the interaction of the transition moment for the absorption band in question in one residue, with transition moments of other transitions of adjoining residues. When the chromophores are aligned side by side, lower energy transition will be hypochromic. Since this polymer includes an α-helical structure and the naphthyl residues in the amino acid units of the polymer may be aligned side by side to form a type of a stacking structure, it is expected that the absorption intensities of the transitions in naphthyl residue decrease appreciably.

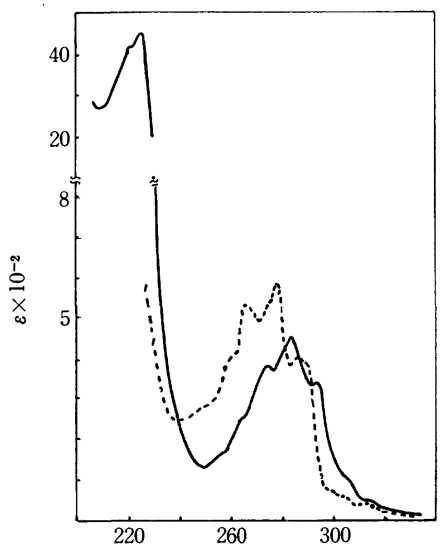

Fig. 1. Absorption spectra of naphthalene and poly-γ-(1-naphthylmethyl)-L-glutamate; dotted line, naphthalene; solid line, poly-γ-(1-naphthylmethyl)-L-glutamate.
Solvent: Ethylene chlorohydrin.

Figure 1 shows absorption spectra of both naphthalene and poly-γ-(1-naphthylmethyl)-L-glutamate in ethylene chlorohydrin. The ^1L_a(p) band including vibration modes of naphthyl residue in the polymer shifts to longer wavelength region than in the case of naphthalene. In this polymer, an appreciable hypochromicity can also be seen in the spectral region.

Circular dichroism spectrum of poly-γ-(1-naphthylmethyl)-L-glutamate. The CD spectrum in visible region of poly-γ-(1-naphthylmethyl)-L-glutamate in 1,1,2,2-tetrachoroethane is shown in Fig. 2. A very weak positive CD band is seen at 400 nm (25.0×10^3 cm^{-1}), and a weak band at 365 nm(27.4×10^3 cm^{-1}), which corresponds to the AB band at 365 nm in the AB spectrum of the polymer. The CD and AB bands at 365 nm may be assigned to an electronic transition, assumed to be as $^1L_b(\alpha)$, in naphthyl residue of the polymer. On the other hand, no CD band can be observed in the ^1L_a(p) band region. The CD spectra of poly-γ-methyl-L-glutamate and poly-γ-(1-naphthylmethyl)-L-glutamate in the spectral region near 222 nm are also shown in Fig. 2. The former exhibits a large negative CD band at 222 nm, and the latter a large negative CD band at 219 nm and a negative CD band at 230 nm. The CD band at 230 nm is assigned to $^1B_b(\beta)$ band in naphthyl residue of the latter polymer (Fig. 1).

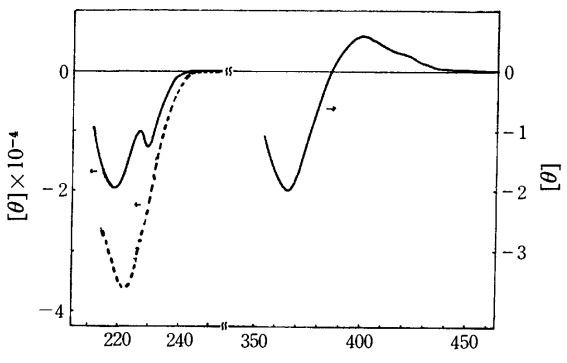

Fig. 2. Circular dichroism spectra of poly-γ-methyl-L-glutamate and poly-γ-(1-naphthylmethyl)-L-glutamate; dotted line, poly-γ-methyl-L-glutamate; solid line, poly-γ-(1-naphthylmethyl)-L-glutamate.
Solvent: Tetrachloroethane (in visible region).
Ethylene chlorohydrin (in ultraviolet region).

If the CD band at 219 nm in the CD spectrum of poly-γ-(1-naphthylmethyl)-L-glutamate can be assigned to the band due to n-π* transition in the peptide main chain of the polymer, the calculated content of the right-hand helix in the polymer is about 54% ethylene chlorohydrin solution. The reason for the CD band due to the n-π* transition shifting from 222 nm to 219 nm can be clarified theoretically.

Spectral-Analyses of Charge-transfer Phenomena between Poly-γ-(1-naphthylmethyl)-L-glutamate and an organic Elec-

8) I. Tinoco Jr., *J. Amer. Chem. Soc.*, **82**, 4785 (1960).

tron Acceptor. Figure 3 shows the spectral variation of the system of the peptide and 2,4,5,7-tetranitro-9-fluorenone when the molar ratio of the glutamyl redidue to the acceptor was varied in the ethylene chlorohydrin solution. A broad CD band can be observed at 483 nm in the CD spectra of the polymer-acceptor systems, increasing gradually with the increase of the molar ratio of acceptor to donor (Fig. 4). The wavelength of the charge-transfer band, as a shoulder, in the AB spectra is uncertain, but that of the CD trough at 483 nm can be determined exactly. Appearance of the CD band in the vicinity of the charge-transfer band, confirmed by the Benesi-Hildebrand plots for the absorbances at 483 nm in the AB spectra, indicates that the electric transition moments of the charge-transfer transition in the complex may orientate circularly around the polypeptide helix axis. This assumption can be easily elucidated by a simple

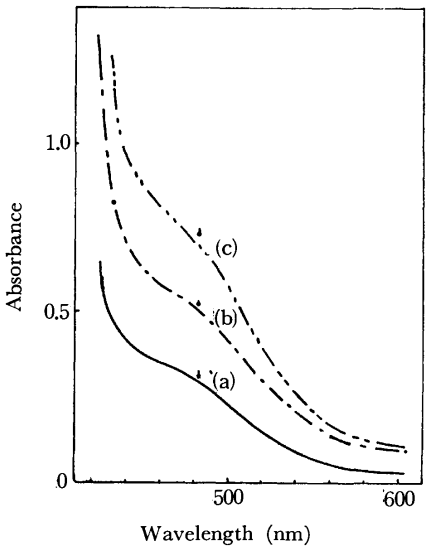

Fig. 3. Variation of the absorption spectra of the poly-γ-(1-naphthylmethyl)-L-glutamate-2,4,5,7-tetranitro-9-fluorenone system in ethylene chlorohydrin at 20 °C with the variation of the molar ratio of the glutamyl residue to the acceptor, D/A.
a) D/A=1/0.7, b) D/A=1/1, c) D/A=1/1.5.

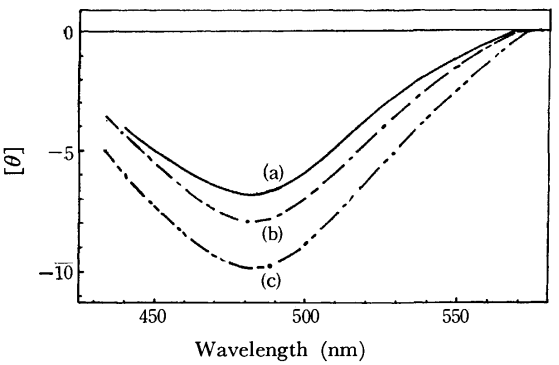

Fig. 4. Circular dichroism variation in the poly-γ-(1-naphthylmethyl)-L-glutamate-2,4,5,7-tetranitro-9-fluorenone system with the variation of the molar ratio of D/A (Refer to Fig. 3).
Solvent: Ethylene chlorohydrin.
a) D/A=1/0.7, b) D/A=1/1, c) D/A=1/1.5.

Table 3. Equilibrium constants and activation parameters in the charge-transfer complex formation of poly-γ-(1-naphthylmethyl)-L-glutamate with 2,4,5,7-tetranitro-9-fluorenone

	Temp. °C	λ_{CT} nm	ε $\times 10^3$	k M^{-1}	$-\Delta H$ kcal/mol	$-\Delta S$ e.u.
Naphthalene	15.1	481	2.0	8.9	6.0	16.5
	21.6			7.2		
	30.0			5.4		
PNLG[a)]	14.5	483	1.2	2.0	4.4	14.0
	25.5			1.5		
	31.1			1.3		

a) Poly-γ-(1-naphthylmethyl)-L-glutamate.

exciton theory.[9] This is the first example for the origin of the optical activity to be discussed on the basis of the charge-transfer phenomena including polypeptide with electron acceptor.

The Benesi-Hildebrand plots could be obtained in a conventional way from the variation of the absorbances at 483 nm in the AB spectra of the polypeptide-acceptor systems. The extinction coefficients and the equilibrium constants in the charge-transfer complex systems were then estimated from the plots, and several thermodynamic parameters in the charge-transfer complex formation were calculated. The calculated values are summarized in Table 3 together with those for the complex formation from naphthalene, which is a model compound for the polymer, and 2,4,5,7-tetranitro-9-fluorenone. The equilibrium constants in the complex formation between poly-γ-(1-naphthylmethyl)-L-glutamate and 2,4,5,7-tetranitro-9-fluorenone are appreciably smaller than those in the complex formation between naphthalene and the same acceptor. The decrease of the equilibrium constants in the polymer-acceptor system may result from a smaller enthalpy change. The results are in contrast to those for the complex formation from poly-*N*-vinylcarbazole and TCNQ, where the difficulty of complex formation was elucidated in terms of entropy change.[3]

Appreciable enhancement of helix stability in poly-γ-(1-naphthylmethyl)-L-glutamate by charge-transfer interaction with 2,4,5,7-tetranitro-9-fluorenone. In order to clarify the correlation between the helix content in the polypeptide and formation of the type of charge-transfer complex, the extent of helix in the polypeptide-acceptor complex was estimated at various ratios of the glutamyl residue to the acceptor. Figure 5 shows this variation of the CD spectra, particularly in the region of the n-π^* transition. We see that the formation of the charge-transfer complex stabilizes the helix structure in the polypeptide, and that some excess addition of the acceptor disturbs the formation of a helix structure in the polypeptide. At an equal molar ratio of the glutamyl residue to the acceptor, the complex exhibits the highest content of helix, which reaches about 100%. Thus, Szent-Gyorgyi's expectation could be confirmed experimentally. Although the enhancement of helix stability by the charge-

9) I. Tinoco Jr., *Advances in Chemical Physics*, **4**, 113 (1962).

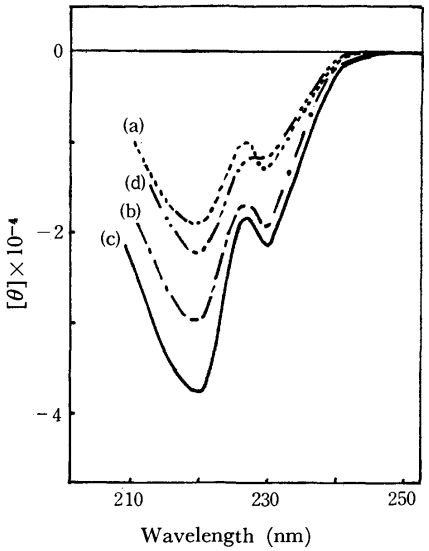

Fig. 5. Circular dichroism variation in the poly-γ-(1-naphthylmethyl)-L-glutamate-2,4,5,7-tetranitro-9-fluorenone system with the variation of the molar ratio of D/A (Refer to Fig. 3.).
a) D/A=1/0, b) D/A=1/0.35, c) D/A=1/1, d) D/A=1/2.

transfer interaction between the side chain groups of the polypeptide and the added acceptor molecules in ethylene chlorohydrin solution can not be directly correlated with most biological phenomena, it can be expected that some extent of looseness in the local motion of polypeptide main chains in enzymes are restricted by the charge-transfer interactions between the donor portions in enzymes and the added small acceptor molecules.

Correlation between Moffitt b_0 values and the contents of 1-naphthylmethyl residue in the polypeptides. Poly-γ-(1-naphthylmethyl)-L-glutamate has 54% helix content in ethylene chlorohydrin solution. This suggests that 1-naphthylmethyl groups in side chains of the polypeptide may disturb the formation of a helical structure in the polypeptide. The correlation between the Moffitt b_0 values and the contents of 1-naphthylmethyl residues in the polypeptides, synthesized by the ester exchange reaction between poly-γ-methyl-D-glutamate and 1-hydroxymethylnaphthalene with *p*-toluenesulfonic acid, is given in Table 2. The optical rotatory dispersion spectra were measured for the 1,1,2,2-tetrachloroethane solutions of the polypeptides. The observed value of b_0 for the polypeptide, in which the ester exchange reaction proceeded almost completely (polymer 5), was 230. This means that the polypeptide has 37% of helix content, assuming that b_0 is 630 in the completely helical polypeptide.[6] We see that the helix content of the polypeptides decreases gradually with the increase of 1-naphthylmethyl residues in the polypeptides. Thus, 1-naphthylmethyl groups in side chains of the polypeptides disturb the sterical formation of a helix structure in the polypeptide. However, the interference of 1-naphthylmethyl residue in the course of helix formation of the peptide may be so small that the interference can be removed by weak interactions such as charge-transfer interaction.

Side chain effect on the helix stability in the polypeptides. Introduction of nitro-group to the benzyl side chain in poly-γ-benzyl-L-glutamate or poly-β-benzyl-L-aspartate results in the lowering of helix content, and the polypeptides including nitroaromatic groups as side chains exhibit some CD bands which can be assigned to the transitions due to the nitroaromatic groups. This led us to assume that the nitroaromatic group in the polyglutamate or polyaspartate is an asymmetric environment forming a relatively rigid side chain helix of its own when the polypeptides are dissolved in helix solvents in a lower concentration.

Steric hindrance and/or electric dipole repulsion between the side chain groups may constrain the side chain groups to form a relatively rigid side chain helix around the axis of the main chain helix, and to disturb the helix formation of the polypeptide main chain. Steric considerations for poly-γ-(1-naphthylmethyl)-L-glutamate are similar, since the polypeptide exhibits some CD bands which can be assigned to the transitions due to the naphthyl residue in the side chain and has relatively low content of helix.

In the ethylene chlorohydrin solution of this polypeptide, the CD magnitude at 219 nm increased appreciably and the CD trough shifted to 222 nm, when the concentration of the polypeptide was increased to 0.1 M. This suggests that the interaction between the naphthyl groups in the side chains is too weak to increase the rigidity of the polypeptide main chain in a higher concentration.

Thus, an appreciable enhancement of helix stability by the charge-transfer interaction between the side chain group and the added acceptor molecule is possible, although the energetics in the helix formation should be analyzed in more detail in the correlation with other charge-transfer systems.

The authors express their sincere thanks to Professor S. Nagakura, The University of Tokyo, for his valuable discussion. They are grateful to Dr. S. Mori, the Central Research Laboratories, Ajinomoto Co., Inc. for supplying poly-γ-methyl-D-glutamate. Acknowledgement is made for a Scientific Research Grant-in-aid from the Ministry of Education.

Effects of Inorganic Salts on the Dissociation of a Complex of β-Cyclodextrin with an Azo Dye in an Aqueous Solution

Kazuo MOCHIDA, Akio KAGITA, Yoshihisa MATSUI, and Yoshio DATE

Department of Agricultural Chemistry, Shimane University, Nishikawazu, Matsue 690

(Received June 11, 1973)

The apparent dissociation constant (K_{app}) of a complex between β-cyclodextrin and an azo dye, sodium *p*-(4-hydroxy-1-naphthylazo)benzenesulfonate, was determined by spectrophotometry in a phosphate buffer solution (pH 5.91) in the absence and in the presence of various inorganic salts at 25 °C. The cyclodextrin and the azo dye formed a 1 : 1 complex with the K_{app} value of 2.44×10^{-3} M in a 0.1 M phosphate buffer. K_{app} decreased with an increase in the concentration of the phosphate buffer and with the addition of some inorganic salts, such as Li_2SO_4, Na_2SO_4, K_2SO_4, $LiIO_3$, $NaIO_3$, KIO_3, and KF. These results were explained mainly in terms of the decrease in the activity of water, which takes part in the dissociation reaction of the inclusion complex, with an increase in the concentration of the inorganic salts. On the other hand, K_{app} increased with the addition of such salts as KCl, KBr, KI, KNO_3, KSCN, and $KClO_4$. These results were attributed mainly to the formation of the inclusion complexes of the cyclodextrin with the anions of these salts, competing with the azo dye for the cyclodextrin-binding site.

Cyclodextrins form inclusion compounds with various organic compounds. The equilibrium constants of the inclusion compounds have often been determined in aqueous solutions by spectrophotometric,[1,2] kinetic,[3-6] and solubility[7-9] measurements. In most of these measurements, inorganic salts have been added to the solution in order to control the pH and the ionic strength. However, the effect of the salts on the apparent equilibrium constants had generally been neglected until Schlenk and Sand[7] showed that some inorganic salts prevent the association of organic acids with α-cyclodextrin. Cramer *et al.*[2] clearly indicated that inorganic salts affect the equilibrium constant in two ways: (1) Inorganic salts change the structure of water, which has an influence on the hydrophobic interaction between cyclodextrins and guest organic molecules. (2) The anions of some inorganic salts compete with guest organic molecules for the binding sites of cyclodextrins. Cramer *et al.* showed that the perchlorate, nitrate, and iodide ions are trapped within the void space of α-cyclodextrin molecules, preventing *p*-nitrophenol from forming inclusion complexes with the cyclodextrin, and that the sulfate and phosphate ions have no influence on the cyclodextrin-*p*-nitrophenol complex formation. However, the salts examined were somewhat limited.

In the present study, we attempted to examine in detail the effects of various inorganic salts on the apparent dissociation constant (K_{cpp}) of the inclusion compound of β-cyclodextrin (β-CD) with an azo dye. As the azo dye, sodium *p*-(4-hydroxy-1-naphthylazo)-benzenesulfonate (Na^+HNB^-) was used because in it the difference in molar absorption coefficient between the free and the complexed HNB^- ions is largest among the dyes examined so far in our laboratory; therefore, it is possible to determine K_{app} by spectrophotometry with a high accuracy.

Results and Discussion

Determination of K_{app} of the β-CD-HNB^- Complex. Figure 1 shows the absorption spectra of Na^+HNB^- at varying β-CD concentrations in the 0.10 M phos-

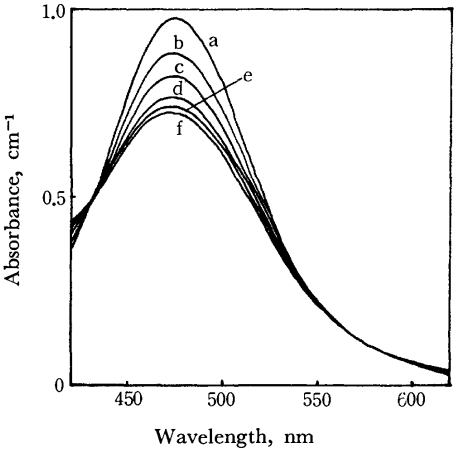

Fig. 1. Absorption spectra of 3.24×10^{-5} M HNB^- at varying β-CD concentrations in 0.1 M phosphate buffer (pH 5.91) at 25 °C.
[β-CD] (mM), a: 0.0, b: 1.0, c: 2.5, d: 5.0
e: 7.5, f: 10.0

1) a) W. Broser and W. Lautsch, *Z. Naturforsch.*, **B, 8**, 711 (1953); b) W. Lautsch, W. Broser, W. Biedermann, and H. Gnichtel, *Angew. Chem.*, **66**, 123 (1954).

2) F. Cramer, W. Saenger, and H. -Ch. Spatz, *J. Amer. Chem. Soc.*, **89**, 14 (1967).

3) a) M. L. Bender, R. L. Van Etten, G. A. Clowes, and J. F. Sebastian, *ibid.*, **88**, 2318 (1966); b) R. L. Van Etten, J. F. Sebastian, G. A. Clowes, and M. L. Bender, *ibid.*, **89**, 3242 (1967); c) R. L. Van Etten, G. A. Clowes, J. F. Sebastian, and M. L. Bender, *ibid.*, **89**, 3253 (1967); d) D. L. Vander Jagt, F. L. Killian, and M. L. Bender, *ibid.*, **92**, 1016 (1970); e) T. S. Straub and M. L. Bender, *ibid.*, **94**, 8875 (1972); f) T. S. Straub and M. L. Bender, *ibid.*, **94**, 8881 (1972); g) W. I. Condgon and M. L. Bender, *Bioorg. Chem.*, **1**, 424 (1971).

4) a) R. M. Paton and E. T. Kaiser, *J. Amer. Chem. Soc.*, **92**, 4723 (1970); b) K. Flohr, R. M. Paton, and E. T. Kaiser, *Chem. Commun.*, **1971**, 1621.

5) a) C. Van Hooidonk and J. C. A. E. Breebaart-Hansen, *Rec. Trav. Chim. Pays-Bas*, **89**, 289 (1970); b) C. Van Hooidonk and C. C. Groos, *ibid.*, **89**, 845 (1970); c) C. Van Hooidonk and J. C. A. E. Breebaart-Hansen, *ibid.*, **90**, 680 (1971).

6) D. E. Tutt and M. A. Schwartz, *J. Amer. Chem. Soc.*, **93**, 767 (1971).

7) H. Schlenk and D. M. Sand, *ibid.*, **83**, 2312 (1961).

8) J. Cohen and J. L. Lach, *J. Pharm. Sci.*, **52**, 132 (1963).

9) K. Koizumi, J. Tatsumi, M. Ohae, H. Kumagai, and T. Hayata, *Yakugaku Zasshi*, **89**, 1594 (1969).

phate buffer (pH 5.91) at 25 °C. Although the wavelength of the absorption maximum (475 nm) was virtually unchanged, the absorbance of HNB^- at the maximum decreased with an increase in the concentration of β-CD. There were two isosbestic points, at 431 and 576 nm, indicating the formation of a 1 : 1 complex between β-CD and HNB^-. According to Cramer *et al.*,[2] the decrease in the absorbance (ΔE) of an HNB^- solution on the addition of β-CD is related to the total concentration ($c_\beta°$) of β-CD by the following equation:

$$c_a°c_\beta°/\Delta E = K_{app}/\Delta\varepsilon + c_\beta°/\Delta\varepsilon \quad (1)$$

where $c_a°$ is the total concentration of HNB^-, and $\Delta\varepsilon$, the difference in the molar absorption coefficient between the free and the complexed HNB^- ions. In fact, the plot of $c_a°c_\beta°/\Delta E$ *vs.* $c_\beta°$ for the present case gave a straight line (Fig. 2), where each ΔE was measured at 475 nm. The values of $\Delta\varepsilon$ and K_{app} were determined from the slope and the intercept of the line to be $9.59\times10^3\ M^{-1}\,cm^{-1}$ and 2.44×10^{-3} M respectively.

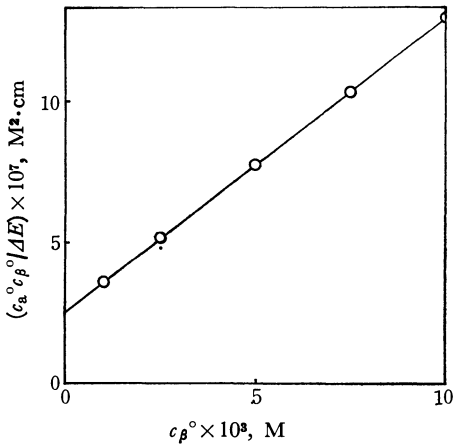

Fig. 2. Plot of $c_a°c_\beta°/\Delta E$ *vs.* $c_\beta°$.

Table 1. The K_{app} values at varying concentrations of a phosphate buffer (pH 5.91) and at 25°C

Concn., M	$K_{app}\times10^3$, M
0.033	2.73
0.050	2.69
0.067	2.62
0.100	2.44
0.125	2.39
0.250	2.25

Table 2. Effect of potassium sulfate on K_{app} in 0.1 M phosphate buffer (pH 5.91) at 25 °C

K_2SO_4, M	$K_{app}\times10^3$, M
0.030	2.41[a]
0.050	2.32
0.100	2.10
0.125	1.96
0.250	1.60
0.375	1.29

a) Determined in 0.050 M phosphate buffer.

Table 3. Effect of potassium salts on K_{app} in 0.1 M phosphate buffer (pH 5.91) at 25 °C

Salt	$K_{app}=10^3$, M	
	c_s[a] = 0.030 M	c_s = 0.300 M
KIO_3	2.54	2.40[b]
KF	2.55	2.02
KCl	2.47	2.88
KBr	2.51	3.16
KI	2.83	6.52
KNO_3	2.61	3.74
KSCN	3.16	7.96
$KClO_4$	3.84	—

a) c_s : Concentration of a salt added to 0.1 M phosphate buffer. b) Determined at c_s=0.125 M.

The K_{app} values were similarly determined at various concentrations of the phosphates (Table 1) or in the presence of potassium sulfate (Table 2) and the other potassium salts (Table 3), where the pH of each solution was adjusted to 5.91 by the use of a phosphate buffer. The $\Delta\varepsilon$ value was virtually constant at $9.59\times10^3\ M^{-1}\,cm^{-1}$ through all these measurements.

K_{app} decreased with increases in the concentrations of the phosphate, sulfate, iodate, and fluoride. On the other hand, K_{app} increased upon the addition of the chloride, bromide, iodide, nitrate, thiocyanate, and perchlorate. One can consider that the inorganic salts affect K_{app} in three different ways: (1) They change the activities of the free and the complexed HNB^- ions. Although the activity of β-CD may also somewhat vary upon the addition of the salts, the extent may be negligibly small because β-CD is a neutral molecule. (2) They change the activity of water, which probably takes part in the dissociation reaction of the inclusion complex. (3) Some of the salts are included in β-CD, competing with HNB^- for the binding site of β-CD. Among these effects, the first one was approximately estimated as follows.

Correction of K_{app} on the Change in the Activities of the Free and the Complexed HNB^- Ions. In order to estimate the activities of the free and the complexed HNB^- ions at various concentrations of inorganic salts, the activity coefficients (f's) of them at an ionic strength, I, were calculated by the use of the Debye-Hückel equation:[10a,11]

$$\log f = -AZ^2I^{1/2}/(1+BaI^{1/2}) \quad (2)$$

where A and B are constants equal to $0.5115\ M^{-1/2}$

10) R. A. Robinson and R. H. Stokes, "Electrolyte Solutions," Butterworths, London (1970), a) p. 229; b) p. 468; c) p. 477; d) p. 465.

11) It is known that Eq. (2) holds up to ionic strength of about 0.1, but at higher ionic strengths the following equation is more adequate to estimate the f value:

$$\log f = -AZ^2I^{1/2}/(1+BaI^{1/2}) + bI$$

where b is a parameter relating to the dielectric constant of an electrolyte solution. However, it may be recognized that the f_t/f_c in Eq. (3) calculated by the use of this equation is virtually equal to that calculated by Eq. (2), provided that the b value for the free HNB^- is approximately equal to that for the complexed HNB^-.

and 0.3291×10^8 $M^{-1/2}$ cm^{-1} respectively at 25 °C;[10b] Z is the ionic valence, and a, the effective diameter of the hydrated ion. The a values for the free and the complexed HNB^- ions were conductometrically estimated to be about 6×10^{-8} and 12.5×10^{-8} cm, as will be described in the Experimental section.

The corrected apparent dissociation constant (K_{corr}) was evaluated by the introduction of the activity coefficients thus calculated for the free and the complexed HNB^- ions (f_f and f_c, respectively) to Eq. (3):

$$K_{corr} = K_{app} \times (f_f/f_c) \quad (3)$$

Figure 3 shows the plot of K_{corr} *vs.* I, together with the plot of K_{app} *vs.* I, drawn on the basis of the data determined in the presence of the phosphate, sulfate, fluoride, and iodate. It is obvious that K_{corr} decreases more rapidly than K_{app} with an increase in I. This is caused by the fact that the size of the free HNB^- is smaller than that of the complexed HNB^-; therefore, the activity of the former decreases more rapidly than that of the latter with an increase in I. On the other hand, K_{corr} increases with increasing concentrations of the chloride, bromide, iodide, nitrate, and thiocyanate (Table 4), similarly to the case of K_{app}. These results show that the change in K_{app} with increasing concentrations of inorganic salts can hardly be explained only in terms of the change in the activities of the free and complexed HNB^- ions. Therefore, we examined the second effect of inorganic salts described above.

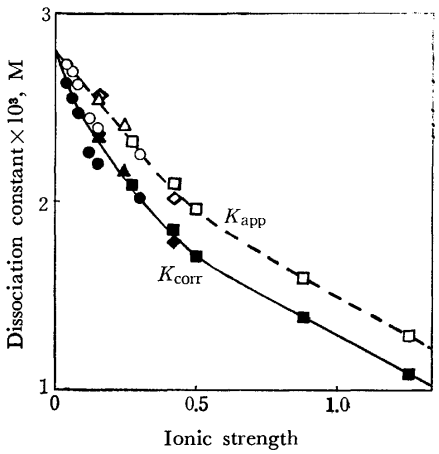

Fig. 3. Plots of K_{app} and K_{corr} *vs.* ionic strength.
○ and ●: the phosphate, □ and ■: the sulfate, △ and ▲: the iodate, ◇ and ◆: the fluoride.

TABLE 4. THE K_{corr} VALUES IN THE PRESENCE OF POTASSIUM SALTS IN 0.10 M PHOSPHATE BUFFER AT 25 °C

Salt	$K_{corr} \times 10^3$, M	
	c_s[a] = 0.030 M	c_s = 0.300 M
KCl	2.28	2.54
KBr	2.31	2.78
KI	2.61	5.75
KNO_3	2.40	3.29
KSCN	2.91	7.01
$KClO_4$	3.54	—

a) c_s : Concentration of a salt added to 0.10 M phosphate buffer.

Effect of the Change in the Activity of Water on K_{corr}. In the preceding section we did not take into account the role of water in the dissociation of the β-CD-HNB^- complex. However, it is very probable that a large number of water molecules take part in the reaction, as was suggested by Cramer *et al.*,[2] for the water structure must be broken down around the complex during the dissociation reaction, and after that it must be reconstructed around β-CD and HNB^-. If the role of water is considered, the dissociation reaction can be expressed by the following equation:

$$\beta\text{-CD-HNB}^-(H_2O)_m + nH_2O \rightleftharpoons \beta\text{-CD}(H_2O)_p + \text{HNB}^-(H_2O)_{m+n-p} \quad (4)$$

The dissociation constant (K_d) for this reaction is given by:

$$K_d = K_{corr}/a_w{}^n \quad (5)$$

where a_w is the activity of water. The addition of inorganic salts may result in a decrease in a_w, causing a decrease in K_{corr} if K_d remains constant. Thus, we can qualitatively explain the effect on the K_{corr} of such inorganic salts as the phosphate, sulfate, iodate, and fluoride described above.

The a_w value changes not only with the salt concentration, but also with the kind of salt added. For example, the a_w of a potassium salt solution is generally larger than that of a sodium salt solution, which is in turn larger than that of a lithium salt solution, when these salts have the same anion and are in the same concentration. This is due to the fact that the extent of the hydration of these metallic cations increases in the order of K^+, Na^+, and Li^+. Table 5 shows K_{corr} values in solutions containing different metallic cations at the same pH and the same ionic strength. It is obvious that K_{corr} decreases in the order of K^+, Na^+, and Li^+ salts in the cases of both sulfate and iodate, as had been expected. This also indicates that the role of the water activity is important in the dissociation equilibrium of the β-CD-HNB^- complex.

TABLE 5. THE K_{corr} VALUES IN PHOSPHATE BUFFER (pH 5.91) CONTAINING DIFFERENT METALLIC CATIONS AT 25 °C

Cation	$K_{corr} \times 10^3$, M	
	Sulfate[a]	Iodate[b]
Li^+	2.08	2.04
Na^+	2.20	2.16
K^+	2.22	2.33

a) Phosphate : 0.050 M, Sulfate : 0.030 M.
b) Phosphate : 0.100 M, Iodate : 0.030 M.

We have no data about the values of a_w at various concentrations of these salts, and the value of n is also unknown. Therefore, the K_d value can not be estimated directly from K_{corr}. In order to estimate the approximate n and K_d values, we tried, for convenience, to use the a_w values for H_2SO_4 solutions available in the literature[10c] as substitutes for those of the potassium sulfate solutions. The a_w values used

had been estimated by measurements of the depression in the vapor pressure. From Eq. (5), we obtain:

$$\log K_{corr} = \log K_d + n \log a_w \quad (6)$$

Figure 4 shows the plot of $\log K_{corr}$ in the sulfate solutions *vs.* $\log a_w$. For the sake of simplifying the calculation, we set a_w in the reference state as equal to its mole fraction. The plot was virtually linear. From the slope and the intercept at $\log a_w = 0$, the values of n and K_d were obtained as 50 and 2.66×10^{-3} M respectively. It seems that the value of n is somewhat larger than would be expected from the sizes of β-CD and HNB^-. This may mainly be due to the inadequacy of the a_w values used. However, the results suggest that a considerably large number of water molecules participate in the dissociation of the inclusion complex.

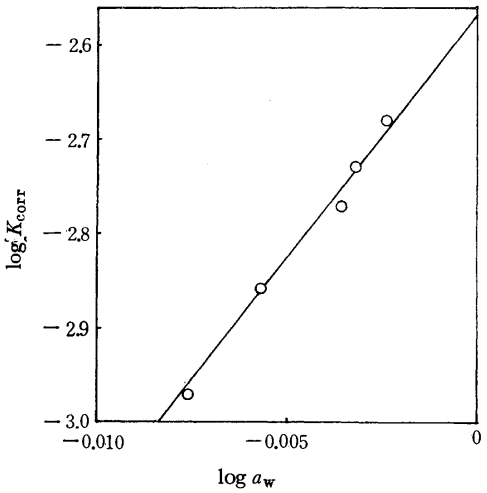

Fig. 4. Plot of $\log K_{corr}$ *vs.* $\log a_w$ for sulfate solutions.

In the above calculation, it was assumed that there is no appreciable interaction between β-CD and the inorganic salts. If these salts interact in some extent with β-CD, thus forming inclusion complexes, K_{corr} must increase with an increase in the concentrations of the salts, as will be described later in the case of such salts as the iodide, nitrate, and thiocyanate. In practice, however, the reverse was found here. Accordingly, it may be presumed that the interaction between them is negligibly small even if it does exist.

Inclusion of Inorganic Anions in β-CD. As has been shown in Table 4, K_{corr}'s in solutions containing KCl, KBr, KI, KNO_3, KSCN, or $KClO_4$ increased with increases in the concentrations of these salts. These results can not be explained in terms of the decrease in water activity, because the correction for water activity results in a further increase in K_{corr} with an increase in the concentration of the salts. One can explain the results only in terms of the inclusion of the anions of these salts in β-CD. If the anions form adducts with β-CD in aqueous solutions, they compete with HNB^- for the binding site of β-CD, resulting in the increase in K_{app} or K_{corr} with the increase in the concentrations of the anions.

The dissociation constant (K_s) for an β-CD-anion complex can be calculated by the use of Eq. (7) below, which one can easily derive on the assumption that the concentration of the inorganic salt is much higher than those of β-CD and HNB^-:

$$K_s = c_s^\circ K_{corr}^\circ / (K_{corr} - K_{corr}^\circ) \quad (7)$$

where K_{corr}° is the value of K_{corr} at the same ionic strength in a solution containing a salt which forms no adduct with β-CD, and where c_s° is the total concentration of the salt. The values of K_s thus calculated at $I=0.15$ and 0.42 are given in Table 6. In these calculations, the K_{corr}° values at $I=0.15$ and 0.42 were taken as 2.20×10^{-3} and 1.82×10^{-3} M respectively; these are the mean values of K_{corr}° determined in solutions containing the phosphate, sulfate, iodate, and fluoride at the respective ionic strengths.

Table 6. The K_s values for several anions in 0.10 M phosphate buffer (pH 5.91) at 25 °C

Anion	K_s, M	
	c_s[a] = 0.030 M (I = 0.15)	c_s = 0.300 M (I = 0.42)
Cl^-	0.8	0.8
Br^-	0.6	0.6
I^-	0.16	0.14
NO_3^-	0.3	0.4
SCN^-	0.09	0.11
ClO_4^-	0.05	—

a) c_s : Concentration of an anion added to 0.10 M phosphate buffer.

The K_s value for each salt was virtually invariable, regardless of the concentration. This indicates that the change in K_s with the decrease in water activity is small compared with the experimental error. The K_s values decreased in the order of Cl^-, Br^-, NO_3^-, I^-, SCN^-, ClO_4^-. This sequence is in agreement with that reported by Schlenk and Sand,[7] who showed that the degree of the association of halide ions with α-cyclodextrin increases in the order of Cl^-, Br^-, I^-. Cramer *et al.*[2] have also shown that ClO_4^- froms a fairly stable adduct with α-cyclodextrin.

One can consider that these anions are bound to β-CD by van der Waals force, hydrophobic interaction, and/or hydrogen bonding. In connection with this point, it was noticed that the hydrated anions forming no complex with β-CD have effective diameters of not less than 3.5 Å,[16] *i.e.*, 4—4.5 Å for $H_2PO_4^-$ and IO_3^-, 4 Å for HPO_4^{2-} and SO_4^{2-}, and 3.5 Å for F^-, whereas those forming complexes with β-CD have effective diameters of not more than 3.5 Å, *i.e.*, 3 Å for Cl^-, Br^-, I^-, and NO_3^-, and 3.5 Å for SCN^- and ClO_4^-. From this fact, it might be considered that the former anions are too large to be included within the void space of β-CD, whereas the latter anions are small enough to fit within it. However, the internal diameter of the β-CD ring is about 7.5 Å, which is larger than the effective diameters of the hydrated ions. Furthermore, it has been reported that α-cyclodextrin, whose internal diameter is about 6.0 Å, includes ClO_4^- to form a complex with K_{app} of 0.034 M,[2] which is comparable with that of the complex between the ion and β-CD. These facts indicate that the role of the van der Waals

force is not very important in the formation of the inclusion complexes between inorganic anions and β-CD. The role of hydrophobic interaction and hydrogen bonding is not yet clear. It may be necessary to study fur ther the physicochemical properties of β-CD and hydrated anions.

Experimental

Materials. The β-CD was isolated from a mixture of α, β, and γ-cyclodextrins given us by the Matsutani Kagaku Co. and was purified according to the directions of Cramer and Henglein.[12] $[\alpha]_D = +168°$ (lit.,[13] $+162.5°$). It was confirmed by paper chromatography with the two solvent systems (*s*-BuOH–pyridine–water (1 : 1 : 1)[14] and *n*-BuOH–DMF–water (2 : 1 : 1)[15]) that the β-CD contained no appreciable amounts of α- or γ-cyclodextrins. The Na^+HNB^-, obtained commercially, was dissolved in hot distilled water and salted out by the addition of NaOAc. After this procedure had been repeated twice, the precipitate was recrystallized twice from water, washed with hot alcohol, and then recrystallized three times from alcohol. The KH_2PO_4, Na_2HPO_4, and KNO_3 were recrystallized from water. The Li_2SO_4, Na_2SO_4, K_2SO_4, $NaIO_3$, KIO_3, KF, KCl, KBr, KI, and KSCN were obtained commercially and were used without further purification. The $LiIO_3$ was prepared from LiOH and HIO_3 and was recrystallized from water. The water used for the preparation of buffer solutions and for the conductivity measurements was obtained by the distillation of city water with a Kokura distillatory apparatus, Model 8000; its specific conductance was *ca.* $2\times10^{-6}\ \Omega^{-1}\ cm^{-1}$ at 25 °C. A 0.10 M phosphate buffer solution was made by mixing 10 ml of 0.10 M Na_2HPO_4 and 90 ml of 0.10 M KH_2PO_4.[16]

Apparatus. For the determination of the K_{app} of the β-CD-HNB^- complex, absorption spectra were recorded by the use of a Hitachi Model 124 spectrophotometer. The cell (1.0 cm) was maintained at 25±0.1 °C with a jacket through which water was circulated from a constant-temperature bath. The pH of each aqueous solution was measured by means of a Hitachi-Horiba pH meter, model M-4. For the conductivity measurements, a Yanagimoto conductivity outfit, model MY-7, was used. A conductivity cell was fitted with circular, blacked Pt electrodes separated by 10 mm. The cell constant was 0.4829. The viscosity of the aqueous solutions was determined by the use of an Ostwald viscometer. All the measurements were made at 25±0.1 °C.

Determination of the a Values for the Hydrated Free and Complexed HNB^- Ions. The *a* values for the free and the complexed HNB^- ions were estimated by conductometry.[17] Figure 5 shows the relations between the molar conductivity (Λ) and the square root of the concentration for the free and the complexed Na^+HNB^- salts in distilled water at 25 °C. Each Λ value for the complexed Na^+HNB^- (Λ_c) was determined as follows: (1) The conductivity (κ_t) of an aqueous solution containing 10.0 mM β-CD and a certain concentration of Na^+HNB^- was measured and multiplied by 1.020, a figure which corresponds to the relative viscosity of the solution against distilled water, in order to correct for the effect of the increase in the viscosity of the medium upon the addition of β-CD on the basis of Walden's rule. (2) The concentrations of the free and the complexed Na^+HNB^- salts (c_f and c_c, respectively) were calculated from the K_{app} value of 2.47×10^{-3} M, determined in distilled water at 25 °C by the same spectrophotometric method as has been described above. (3) The conductivity (κ_f) of the free Na^+HNB^- salt at the calculated concentration was graphically estimated from the curve plotting the κ_f *vs.* the concentration of Na^+HNB^- measured in distilled water. (4) The conductivity (κ_c) of the complexed Na^+HNB^- salt was calculated by subtracting the κ_f value from $1.020\times\kappa_t$. The Λ_c value was obtained by dividing κ_c by c_c.

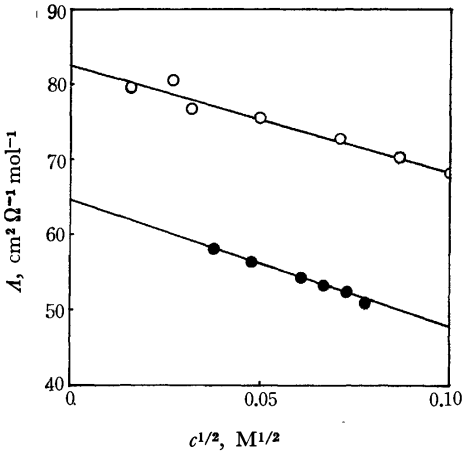

Fig. 5. Plots of the molar conductivity *vs.* the square root of concentration for the free (○) and the complexed (●) Na^+HNB^- salts in distilled water at 25 °C.

By the extrapolation of the plots in Figure 5 to the intercept, the molar conductivities at an infinite dilution of the free and the complexed Na^+HNB^- salts ($\Lambda_f°$ and $\Lambda_c°$) were evaluated to be 82.5 and 64.6 $cm^2\ \Omega^{-1}\ mol^{-1}$ respectively. Then, the molar conductivities of the free and the complexed HNB^- ions ($\lambda_f°$ and $\lambda_c°$, respectively) were estimated to be 32.4 and 14.5 $cm^2\ \Omega^{-1}\ mol^{-1}$ respectively by subtracting $\lambda°(Na^+) = 50.1\ cm^2\ \Omega^{-1}\ mol^{-1}$ [10d] from the $\Lambda_f°$ (the $\Lambda°$ value for the free Na^+HNB^- salt) and $\Lambda_c°$. By the use of this equation:[17] $a = k|Z|/\lambda°$, where $k = 182\times10^{-8}\ cm^3\ \Omega^{-1}\ mol^{-1}$ and where Z is the ionic valence, the *a* values for the free and the complexed HNB^- were calculated to be about 6×10^{-8} and 12.5×10^{-8} cm respectively.

12) F. Cramer and F. -M. Henglein, *Chem. Ber.*, **91**, 308 (1958).
13) D. French, M. L. Levine, J. H. Pazur, and E. Norberg, *J. Amer. Chem. Soc.*, **71**, 355 (1949).
14) N. Hennrich and F. Cramer, *ibid.*, **87**, 1121 (1965).
15) F. Cramer and D. Steinle, *Ann. Chem.*, **595**, 81 (1955).
16) G. Kortüm and J. O'M. Bockris, "Textbook of Electrochemistry," Elsevier Publishing Co., New York (1951), p. 739.
17) J. Kielland, *J. Amer. Chem. Soc.*, **59**, 1675 (1937).

Electron-diffraction Investigation of the Molecular Structure of Tetramethyltin

Makoto NAGASHIMA, Hideji FUJII*, and Masao KIMURA

Department of Chemistry, Faculty of Science, Hokkaido University, Sapporo 060

(Received June 15, 1973)

The structure parameters of tetramethyltin have been determined by gas-phase electron diffraction to be as follows: r_g(Sn–C)$=2.143_6\pm0.003_0$ Å, r_g(Sn···H)$=2.764_2\pm0.012_5$ Å, r_g(C–H)$=1.117_9\pm0.009_0$ Å, l(Sn–C)$=0.049_6\pm0.009_8$ Å, and l(Sn···H)$=0.153_2\pm0.013_2$ Å. The experimental molecular intensity has been well reproduced by the molecular model in which the methyl groups are rotating freely, or nearly freely. The scattering factors, based upon the relativistic Hartree-Fock-Slater or the Hartree-Fock atomic potential, have given a theoretical background in better agreement with the experimental one and have led to a more reasonable Sn–C mean amplitude than did the scattering factors based upon the Thomas-Fermi-Dirac or the Thomas-Fermi atomic potential.

The molecular structures of alkyltin-hydrides,[1] and chlorides[2] in the gas state have recently been investigated by the sector-microphotometer method of electron diffraction. Though tetramethyltin is one of this series, its molecular structure has, however, thus far been determined only by the visual method.[3] The main purpose of the present report is to present a structure determined more accurately by the sector-microphotometer method of electron diffraction and to complete the structural data for organotin compounds.[4]

The second purpose of the present study is concerned with the scattering factors. In a previous study,[5] the small angle scattering of electrons from molecules containing heavy atoms, including $Sn(CH_3)_4$, was observed by a counting technique and the results compared with theory, calculated from a set of the elastic scattering factors based upon the relativistic Hartree-Fock-Slater atomic potentials[6] and the inelastic scattering factors based upon the Hartree-Fock atomic potentials[7] (RHFS, HF), and from a set of the elastic and inelastic scattering factors based upon Thomas-Fermi-Dirac[8] and Thomas-Fermi atomic potentials[9] (TFD, TF) respectively. The (RHFS, HF) scattering factors reproduced the experimental intensities better at small scattering angles, particularly in the range below $s=6$, than did the (TFD,TF) scattering factors. This fitting was in line with the results of the diffraction studies of dimethylmercury[10] and mercury(II) chlorides,[11] where the experimental background agreed better with the (RHFS, HF)-based theoretical background than with the (TFD, TF)-based one. In view of the better agreement of the experimental and theoretical backgrounds, as well as the theoretical sophistication of the atomic potentials, we adopted the (RHFS, HF) scattering factors in the previous structure determinations. The scattering intensities from tetramethyltin, as measured by a photographic method, are expected to provide information on the scattering factors at larger scattering angles, which the counting technique does not cover efficiently. Thus, the present study has been performed under the best possible experimental conditions, particularly with a minimum of extraneous scattering.

Experimental

The diffraction unit used in the present study has been described elsewhere.[12] Photographs were taken with an r^3-sector under the following experimental conditions: accelerating voltage, about 42 kV; camera length; 24.43 cm; sample pressure, 10—25 Torr; exposure time, 40—60 s; beam current, 0.09 μA; and room temperature, 17 °C. The scale factor was determined with reference to the diffraction patterns of carbon disulfide taken in the same sequence. The photographs of carbon disulfide were also used for judging if

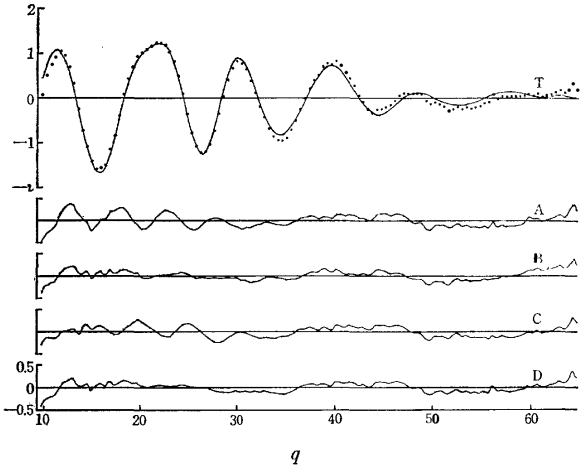

Fig. 1. Experimental molecular intensities (dotts), the best-fit theoretical intensity curve (T), and the difference correspond to the models with rotational angles of the methyl groups, 0° (eclipsed), 30° (intermediate), 60° (staggered) and the free-rotation model, respectively.

* Present address: Central Research Laboratory, Hitachi Ltd., Kokubunji, Tokyo.

1) K. T. McAloon, private communication.

2) a) H. Fujii and M. Kimura, This Bulletin, **43**, 1933 (1970). b) H. Fujii and M. Kimura, *ibid.*, **44**, 2643 (1971).

3) L. O. Brockway and H. O. Jenkins, *J. Amer. Chem. Soc.*, **58**, 2036 (1936).

4) For the structures of organotin compounds, see *e.g.*, Y. K. Ho and J. J. Zuckerman, *J. Organometal. Chem.*, **49**, 1 (1973).

5) M. Kimura, S. Konaka, K. Kashiwabara, and M. Nagashima, *Chem. Phys. Lett.*, **18**, 540 (1973).

6) L. Schafer, A. C. Yates, and R. A. Bonham, *J. Chem. Phys.*, **55**, 3055 (1971).

7) D. T. Cromer, *ibid.*, **50**, 4857 (1969).

8) a) M. Kimura, S. Konaka, and M. Ogasawara, *ibid.*, **46**, 2599 (1967). b) M. Ogasawara, S. Konaka, and M. Kimura, *ibid.*, **50**, 1488 (1969).

9) a) L. Bewilogua, *Physik. Z.*, **32**, 740 (1931). b) R. F. Pohler and H. P. Hanson, *J. Chem. Phys.*, **42**, 2347 (1965).

10) K. Kashiwabara, S. Konaka, T. Ijiima, and M. Kimura, This Bulletin, **46**, 407 (1973).

11) K. Kashiwabara, S. Konaka, and M. Kimura, *ibid.*, **46**, 410 (1973).

12) Y. Murata, K. Kuchitsu, and M. Kimura, *Japan. J. Appl. Phys.*, **9**, 591 (1970).

the apparatus was in sufficiently good condition. Thus it was confirmed that no significant extraneous scattering was involved in the present experiment.[13] Four plates for the sample and four for the reference were selected and used for the structure analysis. The molecular intensities, $qM(q)$, were reduced following our conventional procedure.[2a] In this and the succeeding procedures for structure determination, the (RHFS,HF) scattering factors were employed. A comparison between the two sets of the scattering factors will be presented later. The molecular intensities obtained from one of the four plates are plotted in Fig. 1. The data covered the range of $10 \leqq q \leqq 60$.[14]

Structure Analysis

Least-squares Refinement. The molecular structure was determined by the least-squares method applied to the molecular intensity.[15] The SnC_4 frame and the methyl group were assumed to have the T_d symmetry and the C_{3v} symmetry respectively. With this frame symmetry, four molecular models were taken into account: three hindered-rotation models, staggered (rotational angle 60°), eclipsed (0°), and intermediate (30°) with regard to the relative positions of the methyl groups to the opposite SnC_3 frame, and a free-rotation model. The free-rotation model was approximated by mixing the three hindered-rotation models weighted equally. The independent parameters for each model were chosen to be r_a(Sn–C), r_a(Sn···H), r_a(C–H), l(Sn-C), and l(Sn···H). The other non-bonded distances were constrained in the r_a distances. The l(C–H) was assumed to be 0.08 Å, and the other non-bonded C···H and the H···H mean amplitudes were transferred from those of propane.[16] The parallel and perpendicular mean amplitudes of the SnC_4 system were estimated by solving a five-body problem in which the methyl groups were regarded as mass points. In this calculation, the Urey-Bradley force field was used with the assumption that $F' = -F/10$. The results of the vibrational analysis for the SnC_4 system are shown in Table 1, along with the mean amplitudes determined in the present study. The asymmetry parameters, κ, were estimated by a diatomic approximation[18] to be 9.0×10^{-6} Å^3 for Sn–C and 10.0×10^{-6} Å^3 for C–H; they were assumed to be zero for all the other non-bonded distances.

Table 1. Vibrational data for $Sn(CH_3)_4$

	Frequency (in cm^{-1})		Force constant (in md/Å)	
	Obsd[a]	Calcd		
A_1	507	507	K	2.10
E	145	145	H	0.049
F_2	532	532	F	0.044
	160	160		

	Mean-amplitudes (in Å) parallel	perpendicular	Stretchings (in Å) $r_a - r_\alpha$
Sn-Me	0.0529	0.0209	0.0036
Me-Me	0.1370	0.0144	−0.0033

a) Raman data. Ref. 17.

The results are listed in Columns (A), (B), (C), and (D) of Table 2, while the differences between the theoretical and observed molecular intensities are shown by Curves (A), (B), (C), and (D) in Fig. 1. As may be seen in Table 2, the r_a(Sn–C) distance converges to a constant value, irrespective of the selected models. As for the other parameters, on the other hand, the results for the hindered-rotation models are slightly different from one model to another, although they agree within their standard deviations. The results for the free-rotation model coincide with those for the intermediate model. The differences between the theoretical and observed molecular intensities all seem within the range of estimated experimental uncertainties in the intensity measurements. On a closer examination, however, the difference curves for the staggered and eclipsed models are seen to oscillate in the $10 < q < 30$ range. This oscillation in the difference curves appears consistently in all the data with phases approximately opposite to each other for the staggered and eclipsed models. The contributors to this oscillation are confirmed to be the non-bonded C···H distances, not the Sn···H distances, which also depend slightly on the selected models. Such oscillations disappear in the difference curves for the intermediate and free-

Table 2. The results of the least-squares refinement

Parameter	(A) 0°	(B) 30°	(C) 60°	(D) free rotation
k	0.931±0.035	0.944±0.022	0.907±0.029	0.942±0.023
r_a (Sn-C)	2.1435±0.0034	2.1423±0.0022	2.1432±0.0029	2.1424±0.0023
l (Sn-C)	0.0438±0.0133	0.0498±0.0073	0.0406±0.0119	0.0496±0.0076
r_a (Sn···H)	2.7397±0.0144	2.7534±0.0093	2.7667±0.0134	2.7557±0.0096
l (Sn···H)	0.1492±0.0157	0.1534±0.0100	0.1616±0.0140	0.1532±0.0101
r_a (C-H)	1.1120±0.0097	1.1196±0.0062	1.1105±0.0084	1.1121±0.0064
l (C-H)	0.08 (assumed)	0.08 (assumed)	0.08 (assumed)	0.08 (assumed)

a) Distances and mean-amplitudes in Å units, and the index of resolution, k, is dimensionless. The errors are the standard deviations.

13) M. Nagashima, S. Konaka, T. Iijima, and M. Kimura, This Bulletin, **46**, 3348 (1973).
14) Numerical experimental data of the leveled total intensity have been deposited with the Chemical Society of Japan, (Document No. 7317)
15) S. Konaka, and M. Kimura, This Bulletin, **43**, 1693 (1970).
16) T. Iijima, *ibid.*, **45**, 1291 (1972).
17) E. R. Lippincott and M. C. Tobin, *J. Amer. Chem. Soc.*, **75**, 4141 (1953).
18) K. Kuchitsu, This Bulletin, **40**, 505 (1967).

rotation models, where the non-bonded C···H distances are intermediate between (or are composed of) those for the eclipsed and staggered models. The standard deviations are also much smaller for the intermediate and free-rotation models. The free-rotation model adopted in the present study is not a rigorous one, but, in the light of the finding mentioned above, the nearly free rotation of the methyl groups is acceptable and the diffraction pattern can be interpreted satisfactorily by a nearly free rotation. No further investigation was made of the rotational states of the methyl groups, for the contribution from the C···H and H···H non-bonded distances to the total intensities was not sufficiently large to distinguish more precisely various conformations, or the rotational states of the methyl groups. The intermediate conformation cannot be rejected on the basis of the electron-diffraction data alone, although it is unlikely for a reason to be described later. The possibility of the eclipsed or the staggered conformation as a stable one can, however, be ruled out.

Molecular Structure. The final parameter values were determined from the results yielded for the free-rotation model. Table 3 shows the r_g distances and the mean-amplitudes obtained from four plates, along with the limits of error, which include 2.58 times the standard deviations and the error in the scale factor.

TABLE 3. MOLECULAR STRUCTURE OF $Sn(CH_3)_4$[a] (IN Å UNITS)

	r_g	l
Sn-C	2.144±0.003	0.050±0.010
Sn···H	2.764±0.013	0.153±0.013
C-H	1.118±0.009	0.08 (fixed)
φ_g (Sn-C-H)	112.0±1.6°	

a) The uncertainties represent estimated limits of error.

Scattering Factors

The (RHFS, HF) and (TFD, TF) scattering factors differ from each other in their absolute values and phase factors. Figures 2 and 3 show the ratio of the backgrounds calculated from the two sets of scattering factors, and the leveled intensity curves, respectively. As

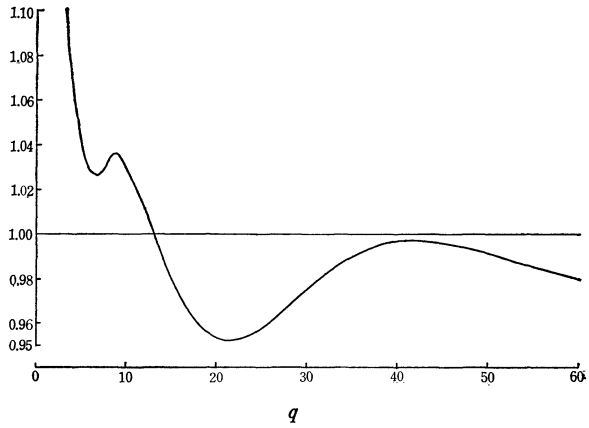

Fig. 2. Comparison of the theoretical backgrounds for $Sn(CH_3)_4$, ($I_B^{TF,DTF}/I_B^{RHFS,HF}$) *vs.* q.

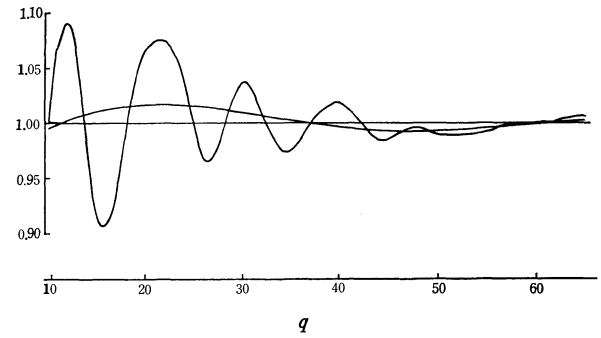

Fig. 3. The total intensity and the experimental background leveled by the use of the theoretical background calculated from the (RHFS, HF) potentials.

may be seen in Fig. 2, the two backgrounds are greatly different around $q=20$, making a strong undulation in the ratio curve. The leveled intensity based upon the (TFD, TF) is higher and deviates farther from the baseline around $q=20$ than that based upon the (RHFS, HF). This indicates that the (RHFS, HF)-based background reproduces the experimental one better, in conformity with the conclusion drawn from the small-angle scattering experiment, where stress was laid on relatively small scattering angles, $q<15$.[4]

In order to investigate the influence of the scattering factors chosen for structure determination, the whole analytical process was repeated using the (TFD, TF) scattering factors, and the results were compared with those obtained by the (RHFS, HF)-based analysis. The Sn–C distances agreed within the standard deviations, while the Sn–C mean amplitude was increased to about 0.07 Å. This value is much larger than the experimental value obtained by the (RHFS, HF)-based analysis. Two origins for such a large mean amplitude may be considered. The first is that the cut-off in the TFD scattering factors is at a larger angle. Since the cut-off points for the Sn–C are at $q=63$ and 60 in the TFD and RHFS scattering factors respectively, the use of the (TFD, TF) scattering factors gives a larger Sn–C mean amplitude. In order to observe this effect, the structure parameters were refined by using the (RHFS, HF)-based molecular intensities employed for the present structure determination and the (TFD, TF) scattering factors. Only the l(Sn–C) amplitude was thus changed, to 0.063 Å, a value which is 0.013 Å larger than the value determined in the last section. The second, less definite but still probable, origin is the peculiar background in the (TFD, TF)-based leveled intensity described in the preceding paragraph. An initial background curve is generally drawn flat, whereas the (TFD, TF)-based leveled intensity has a strong swelling near $q=20$. As a result, the molecular intensity in the smaller q region might have been amplified falsely, leading to an apparently large mean-amplitude.

In the light of the facts mentioned above, together with those derived from the studies of $Hg(CH_3)_2$[10] and $HgCl_2$[11] and from the small-angle scattering from molecules containing heavy atoms,[5] it may be concluded that the (RHFS, HF) scattering factors are the best of all the available scattering factors for structure

analysis. Recently, Beagley and McAloon[19] discussed the scattering factors for Sn in conjunction with the electron diffraction studies of organotin hydrides. They stated that the Cox and Bonham scattering factors[20] for Sn resulted in anomalously small mean amplitudes for the Sn-C and Sn-H distances, while the scattering factors calculated independently by them and by one of the present authors (M.K.) and his co-workers on the basis of the TFD potential led to a definite improvement in the mean amplitudes, *i.e.*, $l(\text{Sn-C})=0.071\pm0.009$ Å in $(CH_3)_3SnH$ and $l(\text{Sn-H})=0.098\pm0.015$ Å in $(CH_3)_2SnH_2$. It is probable that the $l(\text{Sn-C})$ value proposed by Beagley and McAloon becomes rather small and approaches a theoretical estimate of about 0.05 Å if the (RHFS, HF) scattering factors are used.

Methyl Torsion and Sn-C Distance

The present analysis has ruled out a hindered rotation about the staggered or the eclipsed position with C···H mean amplitudes similar to those in propane. According to NMR[21] and spectroscopic studies,[22] the barriers to hindered rotation in solid $Sn(CH_3)_4$ are 0.46 and 0.8 kcal/mol respectively. There is no available experimental value on the barrier hindering methyl torsion in gaseous $Sn(CH_3)_4$. However, in the discussion of the thermodynamic properties of tetramethyl compounds of the Group IV elements, Staveley *et al.*[23] concluded that the observed rise in the entropy of fusion with an increase in the size of the central atom was due to the release from molecular interlocking when the crystal melted and, consequently, the gain of a greater degree of rotational freedom by the methyl group in the bulky molecule than in the more compact molecules. This suggests that the hindering barrier in gaseous $Sn(CH_3)_4$ is probably lower than the values found in the solid state. Thus, the methyl groups in $Sn(CH_3)_4$ are considered to undergo oscillation with a very low hindering barrier, or a nearly free rotation.

The Sn–C distance determined in the present study, 2.144 ± 0.003 Å, is nearly the same as those observed in alkyltin hydrides, *e.g.*, 2.150 ± 0.003 Å for $Sn(CH_3)_2H_2$ and 2.147 ± 0.003 Å for $Sn(CH_3)_3H$. The Sn–C distances in the $Sn(CH_3)_nH_{4-n}$ molecules ($n=1$—3) are equal to each other. They are, however, longer than the corresponding distances in the $Sn(CH_3)_nCl_{4-n}$ molecules ($n=1$—3), 2.104—2.108 Å,[2] and become shorter in the solid state.[24] These experimental facts pose an interesting problem for the future.

We wish to thank Professor Takao Iijima and Dr. Shigehiro Konaka for their helpful suggestions and discussions throughout this work. The calculations were performed on a FACOM 230—60 of the Computing Center of Hokkaido University and also on a FACOM 270—20 electronic computer in the laboratory of Professor Kimio Ohno, to whom our thanks are also due.

19) B. Beagley and K. T. McAloon, *Chem. Phys. Lett.*, **10**, 78 (1971).

20) H. L. Cox, Jr and R. A. Bonham, *J. Chem. Phys.*, **47**, 2599 (1969). The RHFS atomic potential was also used in this calculation, but the potential parameter fit for Sn was not sufficiently good. We are indebted to Professor Bonham for this information on the scattering factors.

21) G. W. Smith, *J. Chem. Phys.*, **42**, 4299 (1965).

22) J. R. During, S. M. Craven, and J. Bragin, *ibid.*, **52**, 2046 (1970).

23) L. A. K. Staveley, J. B. Warren, H. P. Paget, and D. J. Dowrick, *J. Chem. Soc.*, **1954**, 1992.

24) A. G. Davies, H. J. Milledge, D. C. Puxley, and P. J. Smith *J. Chem. Soc., A.*, **1970**, 2862. See also Ref. 4.

Self-diffusion of a Cation through Cation Exchange Membrane and Membrane Permeability

Kozue KAIBARA, Keiji SAITO,* and Hideo KIMIZUKA

Department of Chemistry, Faculty of Science, Kyushu University, Fukuoka 812

(Received July 28, 1972)

The self-diffusion coefficient of an ion and the membrane permeability were studied with a system consisting of two identical electrolyte solutions separated by a cation exchange membrane. The membrane permeability to cation was estimated from the membrane conductance data. The result indicated that the membrane permeability increased with a decrease in electrolyte concentration. The self-diffusion coefficients and the concentrations of Na^+, Cs^+, and Ca^{2+} in the membrane were also measured by the radiotracer method. At concentrations less than 0.1 M, the self-diffusion coefficients more or less increased with increasing concentrations, while the concentrations within membrane remained almost constant. The membrane permeability to ion estimated from the conductance data was in excellent agreement with that calculated by the relation in which the membrane permeability is given as the self-diffusion coefficient times the partition coefficient divided by the membrane thickness.

A number of studies, theoretical and experimental, have been carried out on ion transport through membrane. A theory of ion transport across membrane was presented,[1,2] in which an ion flux was shown to be proportional to the difference in electrochemical activities or total activities of the ion in exterior phases. The proportionality coefficient was defined as the membrane permeability to the ion. Equations for the membrane current, conductance and potential could easily be derived from the flux equation and were found to be suitable for an explanation of the electrochemical data of the living cell membranes.[1,2]

The membrane permeability to an ion in equilibrium was expressed as the diffusion coefficient times the partition coefficient divided by the membrane thickness.[3] The present work is aimed at providing an experimental verification for this physical picture of membrane permeability and discussing related phenomena.

Experimental

Materials. A "CK-1, 1.0 t" cation exchange membrane (Asahi Chemical Industry Co., Ltd.) was used. It was conditioned by the ordinary method before use. The membrane consists of homogeneous sulfonated styrene-divinylbenzene copolymer with an ion exchange capacity of 2.8 meq/g dried membrane and water content of 38 percent. The thickness of the membrane was 1.09 mm after equilibration with 1.0 M sodium chloride solution, and remained almost unaltered even when the electrolyte concentration was changed. Radioactive sodium-22, cesium-137, and calcium-45 in chloride form (Japan Radioisotope Association) were used. Inorganic salts of extra pure grade were used without purification.

Measurement of Tracer Flux. The flux measuring cell consists of two compartments I and II of an equal 3 ml volume, separated by a preconditioned membrane with diffusion area 1 cm^2. For the measurement, the compartments were filled with the electrolyte solutions of the same concentration, the non-radioactive solution being introduced into compartment I and the radioactive solution, into compartment II. The radioactivities of the solutions were measured after a given time interval with either an Aloka ND-151D γ-ray scintillation counter or a Beckman LS-100 liquid scintillation counter. Compartments I and II were replaced several times with the radioactive and non-radioactive solutions, respectively, until a stationary tracer flux was attained. This could be observed within several hours.

J_M^*, the stationary tracer flux per unit area of membrane, is related to the self-diffusion coefficient, D_M, and the concentration of the tracer in compartment II, C_M^*, as follows[4]

$$J_M^* = D_M \frac{C_M^m}{C_M^s} \frac{C_M^*}{\delta} \quad (1)$$

where the subscript M refers to the ion M, δ denotes the membrane thickness, and C_M^m and C_M^s are the concentrations of the ion M in the membrane and the two electrolyte solutions, respectively. When the diffusion process is membrane-controlled, D_M should be replaced by[5]

$$D_M = D_M^m \Big/ \left(\frac{C_M^m}{C_M^s} + 1\right) \quad (2)$$

where D_M^m is the true self-diffusion coefficient of the ion M through membrane. Combining Eqs. (1) and (2), we obtain

$$D_M^m = \left(\frac{C_M^s}{C_M^m} + 1\right) \frac{\delta J_M^*}{C_M^*}. \quad (3)$$

Let S be the radioactivity per unit volume of the solution in compartment I with V ml in volume, t the time for permeation, A the membrane area, and S_0 the radioactivity per unit volume of the solution in compartment II. We then have

$$J_M^* / C_M^* = VS/AtS_0. \quad (4)$$

According to Eq. (4), J_M^* / C_M^* can be estimated by measuring S_0 and S/t since V and A are known. Hence D_M^m can be evaluated according to Eq. (3) provided the concentration of the ion M within membrane C_M^m is known.

Measurement of Concentration within Membrane. The membrane with 1 cm square was preconditioned by equilibration with a metal chloride solution of a given concentration and immersed in the 500 ml of the radioactive solution having the same concentration as the preconditioning solution. The membrane was taken out at a given time interval, the

* Present address: Ube Kosan Co., Ltd., Ube, Yamaguchi

1) H. Kimizuka and K. Koketsu, *J. Theoret. Biol.*, **6**, 290 (1964).

2) H. Kimizuka, *ibid.*, **13**, 145 (1966).

3) H. Kimizuka and A. Yamauchi, *Mem. Fac. Sci., Kyushu Univ., Ser. C.*, **7**, 15 (1970).

4) R. Schlögl, *Z. Electrochem.*, **57**, 195 (1953).

5) J. Crank, "The Mathematics of Diffusion," Oxford at the University Press, (1955), Chap. 8.

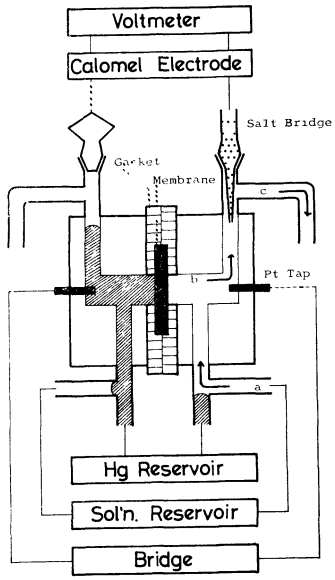

Fig. 1. Schematic diagram of the cell used for the measurements of membrane conductances. The arrows a, b, and c indicate the direction of the solution flow.

adhering solution being removed with filter paper, and the radioactivity entering the membrane was measured. The sample membrane was then brought back into the radioactive solution. Radioactivity measurements were carried out until an attainment of equilibrium which was within several hours.

The ratio C_M^m/C_M^s at equilibrium can be evaluated according to the following relation

$$\frac{C_M^m}{C_M^s} = \frac{S_0^s - S_\infty^s}{S_\infty^s} \cdot \frac{V^s}{V^m} = \frac{r^s S_\infty^m}{r^m S_\infty^s} \cdot \frac{V^s}{V^m} \qquad (5)$$

where superscripts m and s refer to the membrane phase and the solution phase, respectively, S_0 and S_∞ denote the radioactivity per unit volume at the initial and final states, respectively, V denotes volume, and r specific activity.

Membrane Conductance Measurement. The cell is illustrated in Fig. 1. The membrane conductance was measured with a 4255 A universal bridge and a 4440 B decade capacitor (Yokogawa-Hewlett-Packard, Ltd.). Before the measurement, slow streams of salt solutions were introduced from the solution reservoirs, running through and overflowing the two solution chambers of the cell. Equilibrium was attained within several hours. Mercury was then introduced from the reservoirs so that the salt solutions were pushed out and the solution chambers were filled up with mercury. The bridge was connected to the platinum plugs of the cell and the membrane conductance was measured. The temperature was kept at 20±1 °C.

Results and Discussion

The C_M^m values are plotted against C_M^s in Fig. 2. The concentrations of Na^+ were almost the same as those of Cs^+ within experimental error. The values of C_M^m at external salt concentrations less than 0.2 M were found to be almost constant at 1.7±0.2 M, which is close to the fixed charge density of membrane. Since the external salt concentrations for the measurements of the membrane conductance and the tracer flux were less than 0.1 M, we may regard C_M^m as a constant. The C_M^m increased at higher salt concentrations due to the Donnan effect.

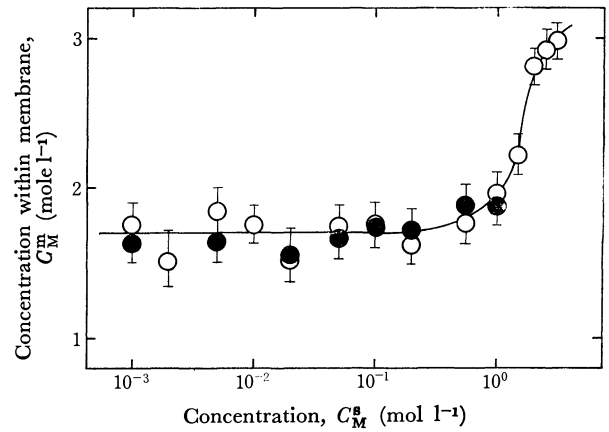

Fig. 2. Cationic concentration within membrane *vs.* external electrolyte concentration curve. The symbols ● and ○ denote C_{Na}^m and C_{Cs}^m, respectively.

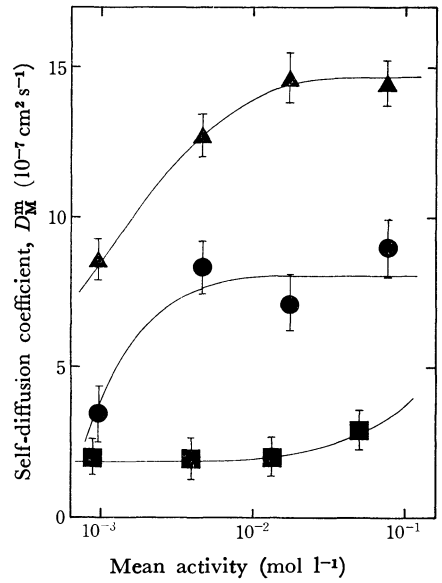

Fig. 3. Self-diffusion coefficient of cation through membrane *vs.* mean activity of salt in the external solution. The symbols ●, ▲, and ■ indicate D_{Na}^m, D_{Cs}^m, and D_{Ca}^m, respectively.

Fig. 3 shows the self-diffusion coefficients of metal ions through the membrane which are less than those in aqueous solution by a factor of the order of 1 or 2. It is seen that D_{Na}^m and D_{Cs}^m are almost constant at higher concentrations of external solutions and decrease at lower concentrations, while D_{Ca}^m is almost constant at lower concentrations and increases at higher concentrations.

The membrane permeability to the ion M, P_M, in equilibrium is related to D_M^m and C_M^m as follows[3]

$$P_M = \frac{D_M^m}{\delta} \frac{C_M^m}{a_M} \qquad (6)$$

where a_M denotes the activity of the ion M in the external solution. Since the quantities on the right-hand side are known, P_M can be calculated.

The results of the membrane conductance measurements are shown in Fig. 4. This figure indicates that

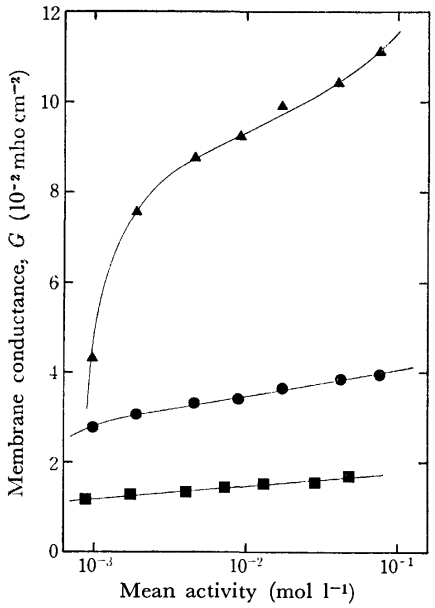

Fig. 4. Membrane conductance *vs.* mean activity of external salt solution. The symbols ●, ▲, and ■ indicate the membrane conductances in the NaCl, CsCl, and $CaCl_2$ system, respectively.

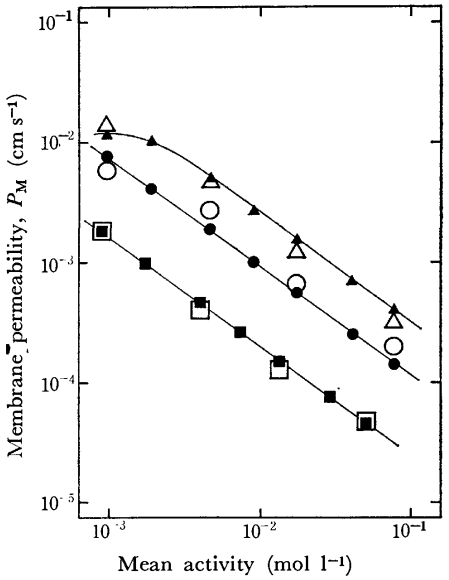

Fig. 5. Memrane permeability *vs.* mean activity of external salt solution diagramms. The symbols ●, ▲, and ■ denote electrochemically estimated P_{Na}, P_{Cs}, and P_{Ca}, respectively, and ○, △, and □, those estmated by tracer method, respectively.

the membrane conductances increase more or less with the increase in the concentration of the external solution. The membrane permeability to cation M can be estimated by the relation[1]

$$G = \frac{Z_M F^2}{RT} P_M a_M \qquad (7)$$

where G denotes the membrane conductance per unit area, Z_M the charge, and F, R, and T have their usual meanings. In Eq. (7), the contribution of an anion to the membrane conductance is ignored since the sample membranes can be regarded as ideally selective for cation permeation.

The values of P_M calculated from the self-diffusion coefficients and the ion concentrations in membrane are compared with those calculated from the conductance data (Fig. 5). The agreement is satisfactory.

Combining Eq. (6) with Eq. (7) we have

$$\delta G = \frac{Z_M F^2}{RT} D_M^m C_M^m = \kappa \qquad (8)$$

where κ denotes the specific membrane conductance. The diffusion coefficients estimated from the conductance data by using Eq. (8) were always greater than those estimated from the tracer diffusion by using Eq. (1).[6] Mackay and Meares[7] attributed this to the contribution due to the electro-osmosis.

From our result it is pointed out that the disagreement was caused by neglecting the correction term indicated by Eq. (2).

6) K. Spiegler and C. Coryell, *J. Phys. Chem.*, **57**, 687 (1953).
7) D. Mackay and P. Meares, *Trans. Faraday Soc.*, **55**, 1221 (1959).

Transport Properties of Multi-component Polar Gas Mixtures Containing Mono-, Di-, and Trimethylamines*

P. NASER

Department of Chemistry, Jundi-Shapur University, Ahwaz, Iran

(Received November 11, 1972)

The viscosity and thermal conductivity coefficients of monomethylamine (MMA), dimethylamine (DMA), and trimethylamine (TMA), and their binary mixtures have been measured in the temperature range 25—250 °C. In addition, determinations of thermal conductivity of ternary mixtures at 33 and 88 °C and of several quaternary mixtures (with ammonia) at 33 °C have been made. The results are discussed in the light of modern kinetic theory of gases. Finally, the coefficients of self-diffusion and mutual diffusion in binary mixtures of these gases are estimated from the experimental viscosity results.

In two previous studies[1,2] measurements of the viscosities and thermal conductivities of ammonia-monomethylamine mixtures have been reported. In the present paper, we extend these measurements to di- and trimethylamine and to binary mixtures of these gases with each other and with monomethylamine. In addition, we have made thermal conductivity measurements of some ternary mixtures of the methylamines and of some quaternary ones of these gases with ammonia. No previous studies of the transport properties of di- and trimethylamine or any of the mixtures mentioned have been reported. Furthermore, no previous work seems to have been done on the thermal conductivities of polar gas mixtures containing more than two polar gases except that of Maczek and Gray[3] on mixtures of methyl chloride, sulfur dioxide, and dimethyl ether.

Theoretical Considerations

The interaction between a pair of polar molecules may be expressed by the Stockmayer potential model: $\phi(r)=4\varepsilon[(\sigma/r)^{12}-(\sigma/r)^6+\delta(\sigma/r)^3]$, where $\delta=(\mu^2/4\varepsilon\sigma^3)-\zeta$; μ is the dipole moment, ε and σ are the potential parameters representing the depth of the potential well and the molecular separation at zero interaction distance, respectively; and ζ is a function of the relative orientation of the colliding pair of dipoles. Monchick and Mason[4] have published the collision integrals (averaged over all relative orientations) for this potentail model and have outlined a procedure for obtaining the potential parameters (ε, σ, and $\delta_{max}=\mu^2/2\varepsilon\sigma^3$) from the experimental viscosity data. The Stockmayer model has been extended to polar gas mixtures by Mason and Monchick.[5] Simple standard combining rules, namely, $\sigma_{12}=(\sigma_1+\sigma_2)/2$, $\varepsilon_{12}=(\varepsilon_1\varepsilon_2)^{1/2}$, $\delta_{12}=(\delta_1\ \delta_2)^{1/2}$ are found to be adequate in applying this method to the gas mixtures considered here.

The viscosity of the binary gas mixtures is given by Eq. (8.2—22) of the treaties of Hirschfelder *et al.*[6] The mutual diffusion coefficients and the collision integral ratio $\langle A^*_{12}\rangle$ which appear in this equation were calculated from the tabulated collision integrals in conjunction with the above combining rules. The viscosity and the self-diffusion coefficients can be obtained from the rigorous kinetic theory expressions.[6] The self-diffusion coefficients of a pure gas can also be obtained from the relation[7,8]

$$D_{11} = (6/5)(RT/p)(\eta/M)\langle A^*_{11}\rangle, \qquad (1)$$

where R is the gas constant, T is the absolute temperature, p is the pressure, η is the viscosity coefficient, and M is the molecular weight. The values of the collision integral ratio $\langle A^*_{11}\rangle$ are very insensitive to the particular potential model chosen and to the temperature; thus Eq. (1) is essentially dependent on the gas viscosities.

Apart from the empirical or the semi-empirical methods, the mutual diffusion coefficients can be calculated from the rigorous kinetic theory expression,[6] or can be obtained from the experimental viscosities of the binary gas mixtures according to the relation due to Weissman and Mason.[7,8] This relation is analogous to Eq. (1), but involves solution of a quadratic equation in pD_{12} whose coefficients involve functions of mole fractions, molecular weights of pure gases, viscosity of the gas mixture, and collision integral ratio $\langle A^*_{12}\rangle$.

For the pure gases it is customary to express the thermal conductivity in terms of the dimensionless Eucken factor $f=\lambda M/\eta C_v$, where λ is the thermal conductivity coefficient, M is the molecular weight, η is the viscosity coefficient, and C_v is the constant volume molar heat capacity. Rigorous theory and the experiment both show that f has a value close to 2.5 for the structureless gases.[9] For polyatomic gases, however, f is less than 2.5. Eucken[10] thus proposed

* Based in part on a thesis presented for the Ph. D. degree at St. Louis University, St. Louis, Missouri.

1) L. G. Burch and C. J. G. Raw, *J. Chem. Phys.*, **47**, 2798 (1967).

2) J. Gutweiler and C. J. G. *ibid.*, **48**, 2413 (1968).

3) A. O. S. Maczek and P. Gray, *Trans. Faraday Soc.*, **65**, 1473 (1969).

4) L. Monchick and E. A. Mason, *J. Chem. Phys.*, **35**, 1676 (1961).

5) E. A. Mason and L. Monchick, *ibid.*, **36**, 2746 (1962).

6) J. O. Hirschfelder, C. F. Curtiss, and R. B. Bird, "Molecular Theory of Gases and Liquids," John Wiley and Sons, Inc., 2nd ed., New York (1964).

7) S. Weissman and E. A. Mason, *J. Chem. Phys.*, **37**, 1289 (1962).

8) E. A. Mason and T. R. Marrero, "Advances in Atomic and Molecular Physics," Ed. D. R. Bates and I. Easterman, Academic Press, New York (1970), Vol. 6, p. 155.

9) S. Chapman and T. G. Cowling, "The Mathematical Theory of Non-Uniform Gases," Cambridge Press, 3rd ed., New York (1970).

10) A. Eucken, *Phys. Z.*, **14**, 324 (1913).

a simple correction: $f_E=1+(9/4)(R/C_v)$. Later, a modified Eucken formula was suggested which was based on a diffusion mechanism theory:[11] $f_{ME}=(\rho D_{11}/\eta)+(3/2)[(5/2)-(\rho D_{11}/\eta)]\ (R/C_v)$, where ρ is the density of the gas and other symbols have been previously defined. Finally, Mason and Monchick[12] have suggested a second approximation which is based on the formal kinetic theory of gases: $f_{MM}=f_{ME}-(2/\pi C_v)-[(5/2)-(\rho D_{int}/\eta)]^2\ (C_{int}/Z_{int})$, where D_{int} is the diffusion coefficient for the diffusion of the internal energy, C_{int} is the internal contribution to C_v, and Z_{int} is the collision number for relaxation of the internal modes of energy. Essentially, the only internal mode of energy for small gaseous molecules at ordinary temperatures is the rotational mode, since the vibration excitation is very small. Therefore, C_{int} may be taken as $(3/2)R$ for non-linear molecules. Z_{int}, which by the same token would be taken as Z_{rot}, can be best treated as an adjustable parameter in correlating this theory with the experimental data. D_{int}, finally, is the ordinary self-diffusion coefficient corrected for the resonant exchange of the rotational quanta of energy.

For the thermal conductivity of multi-component gas mixtures the Hirschfelder-Eucken equation may be used: $\lambda_{mix}=(\lambda_{mix})_{tr}+(\lambda_{mix})_{int}$. $(\lambda_{mix})_{tr}$ is the first approximation of the thermal conductivity of a gas mixture containing several monatomic components and is expressed by a ratio of two determinants, which is given by Eq. (8.2-43) of Ref. 6. The complication of the evaluation of this equation, however, is twofold. In fact not only must one solve a $(2n+1)\times(2n+1)$ and a $(2n)\times(2n)$ determinant for an n-component mixture, but also each of the elements of these determinants is very complicated. Mason[13] and Muckenfuss and Curtiss[14] have derived simpler formulas with the same degree of rigor as the original one. In this study we have considered Mason's, *i.e.*,

$$(\lambda_{mix})_{tr}=4\begin{bmatrix} L_{11} & \cdots & L_{1n} & x_1 \\ \vdots & & \vdots & \vdots \\ L_{n1} & \cdots & L_{nn} & x_n \\ x_1 & \cdots & x_n & 0 \end{bmatrix}\begin{bmatrix} L_{11} & \cdots & L_{1n} \\ \vdots & & \vdots \\ L_{n1} & \cdots & L_{nn} \end{bmatrix}^{-1} \quad (2)$$

where,

$$L_{ii}=\frac{-4x_i^2}{[\lambda_i]_1}-\frac{16T}{25p}\times\sum_{\substack{k=1\\k\neq i}}\frac{x_ix_k[(15/2)M_i^2+(5/2)M_k^2+4M_iM_kA_{ik}^*]}{(M_i+M_k)^2[D_{ik}]_1}, \quad (3)$$

and,

$$L_{\substack{ij\\(i\neq j)}}=\left(\frac{16T}{25p}\right)\frac{x_ix_jM_iM_j(10-4A_{ij}^*)}{(M_i+M_j)^2[D_{ij}]_1}, \quad (4)$$

where $[\lambda_i]_1$ and $[D_{ij}]_1$ are the first approximations to the thermal conductivity and the mutual diffusion coefficients, respectively, and M_i and X_i are the molecular weight and the mole fraction of the component i, and other terms have their ordinary meanings. $(\lambda_{mix})_{int}$ in the Hirschfelder-Eucken expression is the contribution of the internal modes to the thermal conductivity coefficient and is given by:[15]

$$(\lambda_{mix})_{int}=\sum_i\lambda_{int\,i}\left[1+\sum_{i\neq j}\frac{D_{ii,int}x_j}{D_{ij,int}x_i}\right]^{-1}, \quad (5)$$

where $\lambda_{int,i}=\lambda_{expt,i}-[\lambda_i]_1$, and $D_{ii,int}$ is the self-diffusion coefficient of internal energy which has been equated to the ordinary diffusion coefficient by Hirschfelder.[15] $D_{ij,int}$ corresponds, accordingly, to the mutual diffusion coefficient of internal energy.

Among the several empirical formulas which have been put forward for the thermal conductivity of the mixtures, we have considered the better-know Wassiljewa equation:[16]

$$\lambda_{mix}=\sum_i\lambda_i\sum_{i\neq j}\left[1+A_{ij}\frac{x_j}{x_i}\right]^{-1}. \quad (6)$$

In the above equation λ_i is the experimental thermal conductivity coefficient of the component i. The Wassiljewa coefficients, A_{ij}'s, can be calculated from the Lindsay-Bromley approximation:[17]

$$A_{ij}=\frac{1}{4}\left[1+\left\{\frac{\eta_i}{\eta_j}\left(\frac{M_i}{M_j}\right)^{3/4}\frac{T+S_i}{T+S_j}\right\}^{1/2}\right]^2\left(\frac{T+S_{ij}}{T+S_j}\right), \quad (7)$$

where S_i is the Sutherland's coefficient (Ref. 6, p. 550) and $S_{ij}=(S_iS_j)^{1/2}$, and other symbols have their usual meanings. It will be discussed later that the use of Eqs. (2) and (5) is justified by the theoretical studies of Monchick *et al.*,[18] and by the previous experimental studies.[2,19]

Experimental

The apparatus used in the viscosity and in the thermal conductivity measurements have been described previously by Chang *et al.*[19] The viscometer was a constant volume type employing the capillary transpiration method. The thermal conductivities were measured with a "potential leads" hot wire type cell. In both cases the apparatus were placed in an oil bath and in a furnace for the measurements below and above 150 °C, respectively. The temperature could be controlled to within 0.2 °C in the lower temperature ranges and to within 0.5 °C in the higher ones. The gases were supplied by the Matheson Company (minimum purities: NH_3, 99.9%; CH_3NH_2, 98.0%; $(CH_3)_2NH$, 99.0%; $(CH_3)_3N$, 99.0%). The gas mixtures were prepared in the usual way.[1,2,19] Heat capacity data were obtained from Kobe and Harrison.[20] The computations were carried out at the Yalem Computer Center of St. Louis University using a CDC 3300 computer.

Results and Discussion

Pure Gases. In Table 1 the experimental and the theoretical viscosities of di- and trimethylamines

11) J. O. Hirschfelder, *J. Chem. Phys.*, **26**, 282 (1957).
12) E. A. Mason and L. Monchick, *ibid.*, **36**, 1622 (1962).
13) E. A. Mason, *ibid.*, **28**, 1000 (1958).
14) C. Muckenfuss and C. F. Curtiss, *ibid.*, **29**, 1273 (1958).
15) J. O. Hirschfelder, 6th Int. Symp. on Combustion (Reinhold, New York, 1957).
16) A. Wassiljewa, *Phys. Z.*, **5**, 737 (1904).
17) A. L. Lindsay and L. A. Bromley, *Ind. Eng. Chem.*, **42**, 161 (1961).
18) L. Monchick, A. N. G. Pereira, and E. A. Mason, *J. Chem. Phys.*, **42**, 3241 (1965).
19) K. C. Chang, R. J. Hesse, and C. J. G. Raw, *Trans. Faraday Soc.*, **66**, 590 (1970).
20) K. A. Kobe and R. H. Harrison, *Petr. Ref.*, **33**, (No. 11), 161 (1954).

Table 1. Calculated and experimental viscosity coefficients of dimethylamine (DMA) and trimethylamine (TMA)
η in units of 10^7 g cm^{-1} s^{-1}; η (calc) is from Eq. (8.2.-18) of Ref. 6.

Temp (°C)	DMA		TMA	
	η (exptl)	η (calc)	η (exptl)	η (calc)
25.0	924	919	912	906
50.0	983	987	961	961
75.0	1043	1057	999	1013
100.0	1103	1121	1058	1063
150.0	1220	1244	1150	1164
225.0	1397	1424	1288	1301

Table 2. Calculated and experimental thermal conductivity coefficients of dimethylamine (DMA) and trimethylamine (TMA).
λ in units of cal km^{-1} s^{-1} deg (°C)$^{-1}$; λ (calc) is according to Ref. 12.

Temp (°C)	DMA		TMA	
	λ (exptl)	λ (calc)	η (exptl)	η (calc)
37.0	3.57	4.68	3.44	4.28
88.0	5.30	6.00	4.96	5.46
133.0	6.85	7.12	6.40	6.58
188.0	8.70	8.85	8.12	8.01
237.0	10.66	10.37	9.80	9.36

are presented. Table 2 contains the corresponding thermal conductivities. In both cases the experimental data have been corrected appropriately for "slip" (in the case of viscosity) and "temperature jump" (in the case of thermal conductivity).

The Stockmayer potential parameters were found to be:

(i) for $(CH_3)_2NH$: $\sigma=5.09$ Å, $\varepsilon/k=191$ K, and $\delta_{max}=0.14$

(ii) for $(CH_3)_3N$: $\sigma=6.25$ Å, $\varepsilon/k=85$ K, and $\delta_{max}=0.065$.

The quoted values of λ_{MM} were found, as mentioned before, by treating Z_{rot} as an adjustable parameter, and then using their averaged values in the expression of f_{MM}. The averaged values were found to be 1.99 and 0.67 for dimethylamine and trimethylamine, respectively. We could have arrived at better agreement between λ_{exp} and λ_{MM} if we were using different values of Z_{rot} at each temperature. However, the extreme sensitivity of Z_{rot} to f_{exp} would make such a treatment rather unreliable. To account for the resonant exchange of rotational energy, we have employed the values of the moments of inertia[21] with other necessary constants in the appropriate formulas.[12] We have treated dimethylamine as a "prolate top" and trimethylamine as an "almost spherical top". We have found that the correction is indeed negligibly small for both gases (less than 0.01 per cent).

The self-diffusion coefficients were predicted by using the kinetic theory expression and the Eq. (1), as mentioned previously. No experimental self-diffusion data are available for comparison purposes. However, these predictions are generally quite reliable.[8] In the case of gaseous ammonia, the earlier predictions of the self-diffusion coefficient by Burch and Raw[1] were found later to be in excellent agreement with the experimental results of Baker.[22] The predicted values of the self-diffusion coefficients of di- and trimethylamines are presented in Table 3.

Table 3. Self-diffusion coefficients of dimethylamine (DMA) and trmiethylamine (TMA) at 1 atm pressure in units of cm^2 s^{-1}

Temp (°C)	DMA		TMA	
	D_{11}(theory)[a]	D_{11}Eq. (1)	D_{11}(theory)[a]	D_{11} Eq. (1)
25.0	0.0655	0.0659	0.0492	0.0496
37.0	0.0712	—	0.0530	—
50.0	0.0766	0.0764	0.0569	0.0570
75.0	0.0885	0.0880	0.0645	0.0641
88.0	0.0942	—	0.0680	—
100.0	0.100	0.0985	0.0723	0.0721
133.0	0.110	—	0.0823	—
150.0	0.126	0.123	0.0902	0.0891
188.0	0.148	—	0.104	—
225.0	0.169	0.166	0.119	0.118
237.0	0.176	—	0.123	—

a) These values were calculated from the rigorous kinetic theory expression using the Stockmayer potential parameters.

Gas Mixtures. The mutual diffusion coefficients of methylamines as obtained by the rigorous kinetic theory[6] and the Mason-Weissman[7,8] expressions are presented in Table 4. The quoted values in the case of the latter, it should be noted, are the averaged values over the concentrations at each temperature. The individual values were slightly different from each

Table 4. Mutual diffusion coefficient of methylamines* at 1 atm pressure in units of cm^2 s^{-1}

Temp (°C)	D_{12}[a]	D_{12}[b]	D_{13}[a]	D_{13}[b]	D_{23}[a]	D_{23}[b]
25.0	0.0808	0.0808	0.0698	0.0669	0.0571	0.0573
37.0	0.0870	—	0.0730	—	0.0613	—
50.0	0.0943	0.0933	0.0608	0.0774	0.0656	0.0660
75.0	0.109	0.107	0.0924	0.0966	0.0746	0.0753
88.0	0.117	—	0.0987	—	0.0800	—
100.0	0.125	0.122	0.105	0.107	0.0843	0.0872
133.0	0.139	—	0.117	—	0.100	—
150.0	0.158	0.155	0.133	0.127	0.107	0.106
188.0	0.187	—	0.150	—	0.125	—
225.0	0.215	0.210	0.179	0.171	0.143	0.143
237.0	0.221	—	0.183	—	0.149	—

* 1=monomethylamine; 2=dimethylamine; 3=trimethylamine.

a) These values are calculated from the rigorous kinetic theory expression using the mixed potential parameters for the Stockmayer model predicted by the combining rules.

b) These values are calculated using the technique of Ref. 7.

21) G. Dellepiane and G. Zerbi, *J. Chem. Phys.*, **48**, 3573 (1968). (See also: J. E. Wollarb and V. W. Lourie, *ibid.*, **48**, 5058 (1968); *ibid.*, **51**, 1580 (1969)).

22) C. E. Baker, *ibid.*, **52**, 2159 (1970).

TABLE 5. VISCOSITY COEFFICIENTS OF BINARY MIXTURES OF METHYLAMINES[a] η IN UNITS OF g cm^{-1} s$^{-1}\times 10^7$. η (calc) is from Eq. (8.2-25) of Ref. 6.

Temp (°C)	Mole fraction[b]	MMA–DMA		MMA–TMA		DMA–TMA	
		η (exptl)	η (calc)	η (exptl)	η (calc)	η (exptl)	η (calc)
25.0	0.25	928	927	918	905	916	916
	0.50	932	932	923	904	917	919
	0.75	938	937	931	915	920	922
50.0	0.25	989	991	971	959	967	969
	0.50	996	998	983	963	972	975
	0.75	1004	1006	998	979	977	980
75.0	0.25	1051	1055	1024	1040	1017	1021
	0.50	1061	1066	1043	1065	1026	1030
	0.75	1073	1077	1064	1083	1035	1039
100.0	0.25	1113	1118	1078	1085	1067	1082
	0.50	1126	1133	1103	1112	1080	1095
	0.75	1142	1147	1130	1138	1092	1105
150.0	0.25	1232	1243	1185	1167	1168	1170
	0.50	1265	1266	1221	1192	1199	1189
	0.75	1290	1283	1262	1238	1207	1206
225.0	0.25	1428	1433	1345	1318	1313	1322
	0.50	1458	1470	1393	1365	1365	1353
	0.75	1498	1507	1460	1436	1397	1379

a) MMA = monomethylamine, DMA = dimethylamine, TMA = trimethylamine.
b) Mole fraction of the lighter component.

other, and this difference was in order of the experimental uncertainties of the viscosity measurements (1%). The mutual diffusion coefficients of ammonia–dimethylamine and ammonia–trimethylamine mixtures, at 33 °C, were found to be 0.129 cm^2 s^{-1} and 0.111 cm^2 s^{-1}, respectively, according to the kinetic theory. The corresponding value for ammonia–monomethylamine mixture was extrapolated from the results of Burch and Raw.[1] These values were used in the Hirschfelder-Eucken formula for the theoretical calculations of the thermal conductivities of the quaternary mixtures. The agreement between the experimental and the predicted values of viscosities, as well as the predicted values of diffusion coefficients by the kinetic theory and the Mason-Weissman expressions, confirms the adequacy of the Stockmayer potential parameters and the simple combining rules. The thermal conductivities of the multi-component mixtures were estimated by the Hirschfelder-Eucken expression. As indicated before, $[\lambda_{tr}]_{mix}$'s were found according to the expression suggested by Mason. In all cases the self diffusion coefficients, D_{ii}, and the mutual diffusion coefficients, D_{ij}, were taken as the internal diffusion coefficients. $D_{ii,int}$ and $D_{ij,int}$, respectively. Although well-established corrections are available for the self-diffusion coefficients, no such corrections has been suggested for $D_{ij,int}$. Writing this correction as δ_{ii}, according to the notation used by Mason and Monchick,[12] then the assignment of $\delta_{ij}=(\delta_{ii}+\delta_{jj})/2$ is as good an empirical guess as any. Nevertheless, these corrections would be negligibly small for the present investigation. The corrections for inelastic collisions applied to the Hirschfelder-Eucken formula come with the use of the experimental thermal conductivities of the pure gases. By using such values, account would be taken of the inelastic as well as the resonant collisions. These considerations are justified by the theoretical studies of Monchick *et al.*,[18] and by the previous experimental measurements.[2,19]

The thermal conductivity coefficients of the binary and the ternary mixtures are also estimated by the Wassiljewa equation. The Wassiljewa coefficients, as obtained from the Lindsay-Bromely relation, are presented in Table 6. As may be seen from this table,

TABLE 6. WASSILJEWA COEFFICIENTS OF METHYLAMINES[a] AS CALCULATED FROM THE LINDSAY-BROMLEY EXPRESSION

Temp (°C)	MMA–DMA		MMA–TMA		DMA–TMA	
	A_{ij}	A_{ji}	A_{ij}	A_{ji}	A_{ij}	A_{ji}
37.0	1.171	0.863	1.314	0.776	1.117	0.895
88.0	1.184	0.855	1.346	0.763	1.129	0.887
133.0	1.206	0.824	1.371	0.754	1.127	0.886
188.0	1.211	0.840	1.407	0.741	1.150	0.874
237.0	1.223	0.833	1.432	0.732	1.158	0.869

a) MMA = monomethylamine, DMA = dimethylamine, TMA = trimethylamine.

for a given pair of gas molecules i and j, $A_{ij}>A_{ji}$. It has been shown[23] that for a given pair of gas molecules, A_{ij} depends on the ratio $(\sigma_i/\sigma_j)^2$ and on a power less than unity of the mass ratio. For all the cases studied in this work, as may be noted, $\sigma_i>\sigma_j$ and $M_i>M_j$.

The thermal conductivity coefficients of the multi-component mixtures are presented in Tables 7, 8, and 9. As may be seen, the agreement between the theories and the experiment is generally quite good and is

23) T. G. Cowling, P. Gray, and P. G. Wright, *Proc. Roy. Soc. Ser.*, *A*, **276**, 69 (1963).

Table 7. Thermal conductivity coefficients of binary mixtures of methylamines,[a] λ in units of cal km^{-1} s^{-1} deg $(°C)^{-1}$

Temp (°C)	Mole[b] fraction	MMA–DMA			MMA–TMA			DMA–TMA		
		λ (exptl)	λ (HE)[c]	λ (Wass)[d]	λ (exptl)	λ (HE)[c]	λ (Wass)[d]	λ (exptl)	λ (HE)[c]	λ (Wass)[d]
37.0	0.25	3.63	3.59	3.60	3.49	3.44	3.49	3.45	3.50	3.47
	0.50	3.66	3.63	3.63	3.53	3.48	3.54	3.49	3.57	3.50
	0.75	3.68	3.67	3.67	3.65	3.56	3.62	3.52	3.64	3.54
88.0	0.25	5.34	5.44	5.36	5.11	5.12	5.07	5.06	5.03	5.03
	0.50	5.38	5.55	5.43	5.31	5.30	5.21	5.18	5.12	5.12
	0.75	5.52	5.61	5.51	5.46	5.40	5.38	5.24	5.20	5.21
133.0	0.25	7.02	6.87	6.93	6.76	6.49	6.54	6.60	6.57	6.50
	0.50	7.09	6.94	7.02	7.01	6.64	6.72	6.76	6.71	6.61
	0.75	7.24	7.07	7.14	7.15	6.89	6.97	7.04	6.81	6.72
188.0	0.25	9.16	8.86	8.82	8.76	8.23	8.30	8.69	8.27	8.24
	0.50	9.18	9.01	8.96	9.04	8.43	8.55	8.89	8.42	8.38
	0.75	9.25	9.02	9.13	9.21	8.77	8.88	9.02	8.56	8.53
237.0	0.25	11.07	10.79	10.81	10.30	10.03	10.04	10.30	10.02	9.98
	0.50	11.18	10.96	10.99	10.52	10.35	10.38	10.35	10.24	10.18
	0.75	11.30	11.19	11.21	10.97	10.81	10.84	10.67	10.45	10.41

a) MMA = monomethylamine, DMA = dimethylamine, TMA = trimethylamine.
b) Mole fraction of the lighter compound.
c) Calculated by the Hirschfelder-Eucken equation.
d) Calculated by the Wassiljewa expression.

Table 8. Thermal conductivity coefficients of ternary mixtures of methylamines[a] at 37 °C and at 88 °C, λ in units of cal km^{-1} s^{-1} deg $(°C)^{-1}$

Temp (°C)	Mole fraction			λ(exptl)	λ(HE)[b]	λ(Wass)[c]
	MMA	DMA	TMA			
37.0	0.33	0.33	0.34	3.54	3.52	3.55
	0.17	0.33	0.50	3.51	3.49	3.51
	0.33	0.17	0.50	3.49	3.48	3.53
	0.17	0.50	0.33	3.51	3.52	3.54
	0.33	0.50	0.17	3.60	3.56	3.58
	0.50	0.17	0.33	3.61	3.53	3.57
	0.50	0.33	0.17	3.66	3.57	3.60
88.0	0.33	0.33	0.34	5.20	5.32	4.96
	0.17	0.34	0.49	5.15	5.19	5.01
	0.33	0.18	0.49	5.13	5.23	5.02
	0.17	0.50	0.33	5.23	5.36	4.54
	0.33	0.51	0.16	5.31	5.40	4.62
	0.50	0.32	0.18	5.27	5.45	4.70
	0.46	0.21	0.33	5.24	5.36	5.25

a) MMA = monomethylamine, DMA = dimethylamine, TMA = trimethylamine.
b) Calculated by the Hirschfelder-Eucken equation.
c) Calculated by the Wassiljewa expression.

Table 9. Thermal conductivity coefficients of two quaternary mixtures of methylamines[a] and ammonia at 37 °C; in units of cal km^{-1} s^{-1} deg $(°C)^{-1}$

Mole fraction				λ (exptl)	λ (HE)[b]
NH_3	MMA	DMA	TMA		
0.50	0.17	0.17	0.16	4.30	4.49
0.23	0.27	0.25	0.25	3.70	3.93

a) MMA = monomethylamine, DMA = dimethylamine, TMA = trimethylamine.
b) Calculated by the Hirschfelder-Eucken equation.

within the range of the experimental uncertainties of the measurements (2%). At the higher temperatures, however, the Hirschfelder-Eucken method seems to be the superior one.

It may be mentioned, finally, that we could have arrived at a much better agreement between the experiment and the Wassiljewa extimations by treating the Wassiljewa coefficients as adjustable parameters. This may be done by employing the experimental quantities in the Wassiljewa expression and then carrying out a full computer search to find the "best" pairs of A_{ij}'s. However, more experimental data on the thermal conductivities of the gas mixtures would be needed in order to make a thorough evaluation of such a treatment.

The author would like to express his deep gratitude to Professor C.J.G. Raw of the Chemistry Department of St. Louis University for continual encouragement of this work and for invaluable suggestions and criticism. He is indebted to the Graduate School of St. Louis University for financial support during his graduate study. He is also grateful to Miss Lucia Plese for her assistance in independent measurements of some of the gas viscosities reported in Tables 1 and 5.

Determination of Electrochemical Kinetic Parameters of Porphyrins and Metalloporphyrins in *N,N'*-Dimethylformamide by Radio Frequency Polarographic Method

Tadaaki KAKUTANI and Mitsugi SENDA

Department of Agricultural Chemistry, Faculty of Agriculture, Kyoto University, Kyoto 606

(Received June 22, 1973)

Electrochemical kinetic parameters were determined for the first two reduction steps of some porphyrins and divalent metalloporphyrins in DMF containing 0.5 M TEAP at 25 °C by use of radio frequency polarographic method. The results were discussed in view of their molecular structures and the diffuse double layer effect on the kinetic parameters.

It has been found [1-4] that in aprotic solvent such as dimethylformamide(DMF) porphyrins and their divalent metal complexes give three or four well-defined reduction waves, of which the first two are in general reversible one-electron reduction steps with negligible complications by specific adsorption. The products produced at the first two steps have been found to be reasonably stable. These findings have made it possible to study the electrode kinetics of these compounds in quantitative way.

In this study the kinetic parameters for the first two reduction steps of some porphyrins and divalent metal complexes in DMF were determined by use of the radio frequency polarographic method.[5-8] The results were discussed in view of their molecular structures and the diffuse double layer effect on the kinetic parameters.

Experimental

Materials: Protoporphyrin IX dimethylester (PPDM), mesoporphyrin IX dimethylester(MPDM), Cu(II)-PPDM, Ni(II)-PPDM, Co(II)-PPDM, Zn(II)-PPDM and Mn(III)-Cl·H_2O-PPDM were prepared and purified by previously described methods.[4] The supporting electrolyte, tetraethylammonium perchlorate(TEAP), was prepared and purified as described elsewhere.[9] The solvent, DMF, was purified as described previously.[4]

Electrochemical Measurements. Conventional DC polarograms and square wave polarograms were measured with a Yanagimoto polarograph PF-500 and auxiliary potentiometer. The Faradaic rectification current at the DME or the radio frequency polarographic current was measured also with a Yanagimoto polarograph PF-500 equipped with a laboratory-made RF (0.05 to 2 MHz) generator and appropriate low-pass filter circuits, using the square wave amplitude modulation technique developed by Barker.[5] Differential capacity was measured with a Grahame's AC bridge at 1 kHz.[10]

The polarographic cell was described elsewhere.[4] All potential measurements were made with respect to an aqueous saturated calomel electrode (SCE). The capillary characteristics were $m=1.07_8$ mg/s and $t=5.8$ s at $h=70$ cmHg in DMF containing 0.1 M TEAP at -0.5 v *vs.* SCE.

When the RF and SW polarographic currents were measured, the drop time was controlled by an electro-mechanical synchronizer and the RF current pulse or SW voltage pulse was applied to the DME at the last stage of a drop life, usually from $t=2.0$ to 3.0 s. Measurements were carried out, under dried nitrogen atmosphere, usually with nearly saturated solution(approx. 4×10^{-4} M, but for Cu(II)-complex approx. 2×10^{-4} M) of porphyrins or metalloporphyrins in DMF containing 0.5 M TEAP at 25 ± 0.1 °C. Under the conditions total cell resistance varied from 200 to 300Ω depending on drop area.

Results

As described in the previous work,[4] the first two reduction steps of PPDM, MPDM, Cu(II)-PPDM, Ni(II)-PPDM, and Zn(II)-PPDM and the second reduction step of Co(II)-PPDM and Mn(III)Cl-H_2O-PPDM are characterized by simple one-electron transfer reaction. Furthermore, for these steps the specific adsorption seems to have no or little effect on the electrode processes. Accordingly we applied the Faradaic rectification method to determine the kinetic parameters of the electrode charge transfer reactions of these reduction steps.

Determination of Kinetic Parameters. Computation of the kinetic parameters, *i.e.*, the (measured) rate constant of charge transfer at the standard redox potential, k_{sm}, and the (measured) transfer coefficient, α_m, was based on analysis of the rectification voltage, $\Delta\bar{E}_\infty$, or $\psi(=4RT\Delta\bar{E}_\infty/nFV_A^2)$ against applied DC potential, E_{DC}, curves,[7,8] where n is the number of electrons involved per reacting molecule or ion, F the Faraday, R the gas constant and T the absolute temperature. The rectification voltage was evaluated by the comparison method, *i.e.*, by comparison of RF

1) C. K. Mann and K. K. Barnes, "Electrochemical Reactions in Nonaqueous Systems," Marcel Dekker, Inc., New York (1970).
2) J. Jordan, M. Gross and R. S. Marano, "Electrochemistry in Non-aqueous Solvents and its Application to Analytical Chemistry, U.S.-Japan CSS, March 1973, Tokyo," Extended Abstract, p. 75.
3) L. G. Lanese and G. S. Wilson, *J. Electrochem. Soc.*, **119**, 1039 (1972); see also three previous papers of the same author (G.S.W.) and co-workers.
4) T. Kakutani, S. Totsuka, and M. Senda, This Bulletin, **46**, 3652 (1973).
5) G. C. Barker, "Transaction of the Symposium on Electrode Processes, Philadelphia, 1959," ed. by E. Yeager, John Wiley & Sons, Inc., New York, (1961), p. 325.
6) W. A. Brocke and W. Nürnberg, *Z. Instr.*, **75**, 291, 315, 355 (1969).
7) P. Delahay, M. Senda, and C. H. Weis, *J. Amer. Chem. Soc.*, **83**, 312 (1961).
8) M. Senda and P. Delahay, *J. Phys. Chem.*, **65**, 1580 (1961).
9) M. Senda, T. Ikeda, and T. Nishioka, *Nippon Kagaku Zasshi*, **91**, 957 (1970).
10) D. C. Grahame, *J. Amer. Chem. Soc.*, **68**, 301 (1946); **71**, 2975 (1949).

polarographic current at a given E_{DC} with SW polarographic current at the same E_{DC}, with the same and one electrolysis solution. V_A is the amplitude of RF voltage applied to the electrode interface and was caluclated from the differential double layer capacity which was measured with DMF solution containing only a supporting electrolyte and the amplitude of RF current pulse applied to the electrode interface. ψ *vs.* E_{DC} curves were obtained at several frequencies, *i.e.*, 0.05, 0.1, 0.25, 0.5 and 1.0 MHz. The diffusion coefficient of PPDM was estimated by Ilković equation to be 3.7×10^{-6} cm^2/s, and this value was employed for all porphyrin compounds studied here. It was also assumed that the neutral molecule, the monoanion radical, and the dianion possesed equal diffusion coefficient.

Figure 1 shows the first two steps of MPDM as observed by DC, SW, and RF polarography, and Figs. 2 and 3 show ψ–E_{DC} curves of the first and second steps, respectively.

According to the theory,[7] the rectification voltage for a simple charge transfer reaction (O+ne=R) may be represented by

$$\psi = \frac{4RT}{nFV_A^2}\Delta\bar{E}_\infty = (2\alpha_m-1) + \left[(1-2\alpha_m) + \frac{P-1}{P+1}\right]F(\xi) \quad (1)$$

where

$$F(\xi) = \frac{2\xi^2+\xi}{2\xi^2+2\xi+1}, \quad (2)$$

$$\xi = \frac{k_{sm}}{\sqrt{2\omega D}}(1+P)P^{-\alpha_m}, \quad (3)$$

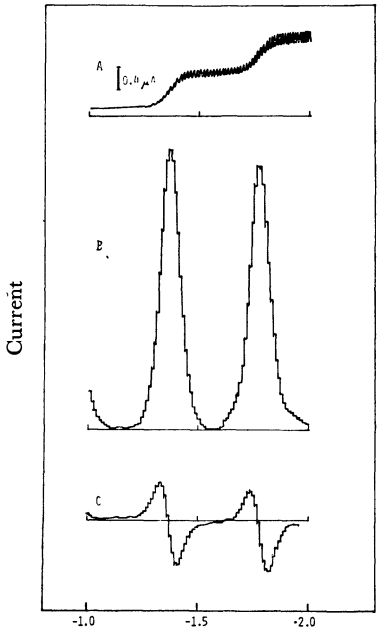

E_{DC} (V *vs.* SCE)

Fig. 1. Polarograms of MPDM in DMF containing 0.5 M TEAP at 25 °C.
Concentration: about 4×10^{-4} M. (A) DC, (B) SW frequency: 200 Hz; SW voltage: 5.4 mV (p-p), (C) ratio frequency: 1.0 MHz; RF voltage: V_A=22 mV (p-p) at −1.4 V.

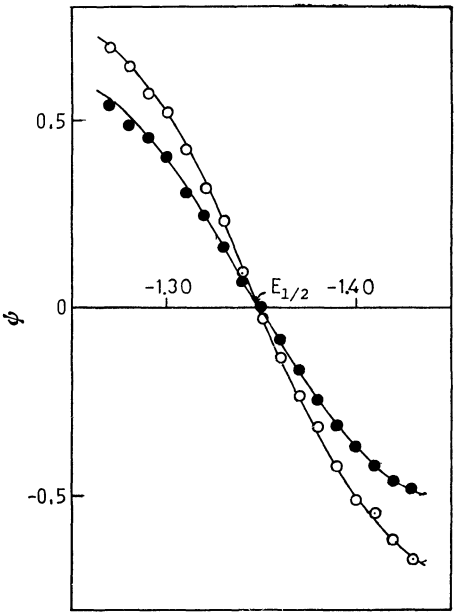

E (V *vs.* SCE)

Fig. 2. Ψ–E_{DC} curves of the first step of MPDM in DMF containing 0.5 M TEAP at 25 °C. Radio frequency: ○: 0.1 MHz, ●: 1.0 MHz.

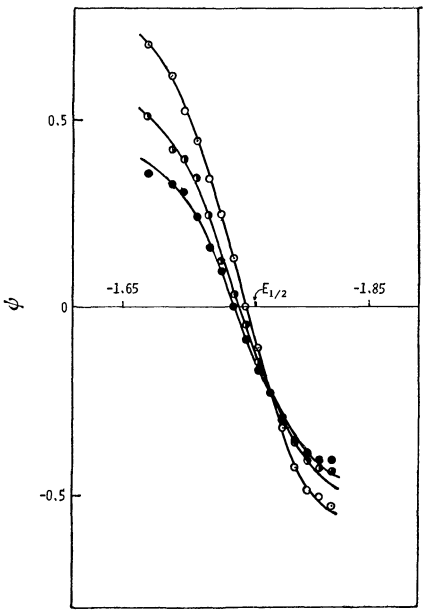

E_{DC} (V *vs.* SCE)

Fig. 3. ψ–E_{DC} curves of the second step of MPDM in DMF containing 0.5 M TEAP at 25 °C. Radio frequency: ⊙: 0.1 MHz; ◑: 0.5 MHz; ●: 1.0 MHz.

$$P = \exp\left[\frac{nF}{RT}(E_{DC}-E_{1/2})\right], \quad (4)$$

$\omega=2\pi f$, f is the frequency of the applied RF voltage, and $D=(D_R)^{\alpha_m}(D_O)^{1-\alpha_m}$, D_R and D_O are the diffusion coefficients of R and O, respectively. When the rectification voltages were measured at several frequencies, all ψ–E_{DC} curves intersect at a single point having the ordinate and abscissa given by

$$\psi = (2\alpha_m - 1), \quad (5)$$

and

$$\tanh\left[\frac{nF}{2RT}(E_{DC}-E_{1/2})\right]=(2\alpha_m-1)\,. \qquad (6)$$

respectively. Thus we can calculate the parameter α_m in two ways from the coordinates of the intersection point. As predicted from the theory, the experimental curves in Fig. 2 and Fig. 3 exhibit single intersection point in each case. From their coordinates one calculates $\alpha_m=0.5$(abscissa) and $\alpha_m=0.5$(ordinate) for the first step, and $\alpha_m=0.38$(abscissa) and $\alpha_m=0.37$(ordinate) for the second step. Two values of α_m calculated from the coordinates agreed to within ±0.02 for all compounds studied here.

After α was determined in this way, k_{sm} was calculated by either one of the following two methods: 1) when α_m is between 0.4, and 0.6, k_{sm} was estimated from the $\psi_{0.1}/\psi_{1.0}$ ratios at several E_{DC}'s, where $\psi_{0.1}$ and $\psi_{1.0}$ are the ψ values measured at 0.1 and 1.0 MHz, respectively, or 2) when α is larger than 0.6 or smaller than 0.4, k_{sm} was calculated from the values of E_{DC} at $\psi=0$ for each frequency. Such calculations will give several values of k_{sm} for each charge transfer step and these values are expected to be constant if such a simple theory is applicable to the analysis of the present results. Thus we obtained, for example, for the first step of MPDM, $k_{sm}=3.8$(calculated from $\psi_{0.1}/\psi_{1.0}$ at $p=4$), 3.9 ($p=2$), 3.6($p=1/2$), or 3.7 cm/s ($P=1/4$), and for the second step, $k_{sm}=1.14$(calculated from E_{DC} at $\psi=0$ ofr 0.1 MHz), 1.45 (0.5 MHz) or 1.44 cm/s (1 MHz). Namely, the values of k_{sm} were reasonably constant for each step (within $\pm10\%$). The variance of k_{sm}'s for other compounds studied here was also of the same order of magnitude as that of MPDM. The polarographic results and the kinetic parameters of porphyrins and metalloporphyrins examined in this study are summarized in Table 1.

Discussion

As described previously,[4] the first and second steps of Ni(II)-PPDM, Cu(II)-PPDM and Zn(II)-PPDM as well as PPDM and MPDM are believed to be successive additions of one electron to the porphyrin ring of the complexes. The second step of Mn(III)Cl-H_2O-PPDM is supposed also to be an addition of one electron to the porphyrin ring of Mn(II)-complex. The third wave of Mn(III)-complex is not sufficiently reproducible to give reliable kinetic data. The first step of Co(II)-complex, being assigned[4] to one-electron addition to metal-centered orbital, was complicated by specific adsorption, so that significant kinetic data were not observed.

The kinetic data are characterized as follows. For all compounds studied, the measured rate constants of the first reduction step ($R+e=R^{-}$), $k_{sm}(1)$, are larger than that of the second reduction step($R^{-}+e=R^{2-}$), $k_{sm}(2)$. The measured transfer coefficients of the first step, $\alpha_m(1)$, are close to 0.5, and those of the second step, $\alpha_m(2)$, are between 0.3 and 0.4.

For the series of compounds, a decreasing tendency of k_{sm}'s with negative shift of half-wave potentials was found, with a few exceptions. The kinetic parameters given in Table 1 are apparent values uncorrected for double layer effects, but calculation showed that this tendency was significant after the double layer correction(see Table 2). As stated in previous paper,[4] the negative shift of the reduction potentials in the series may be correlated with the order of increasing negative charge in the porphyrin ring,[11] that is, with an increase in the non-uniformity of charge distribution in the depolarizer molecule. Similar correlation of the rate constants with molecular structures was first found for a series of nitro-compounds by Peover and Powell,[12] who attributed this phenomenon to the non-uniform distribution of charge in the anion radicals derived from the nitro-compounds. Similar experimental results for substituted nitrobenzenes were confirmed also by the present authors.[13] Therefore, it is likely that the change of rate constants for the series of porphyrin compounds would again be interpreted in terms of Marcus-Hush's theory, *i.e.*, by the difference in the electrostatic solvent reorganization energy, as proposed by Peover and Powell. It is noted, however, that the decreasing of the rate constants with the negative shift of half-wave potentials is less pronounced in the case of the porphyrin compounds than the nitro-compounds. This would be due to the difference in electrostatic solvation energy, which arises from the difference in molecular size between the porphyrin compounds and

TABLE 1. POLAROGRAPHIC RESULTS AND KINETIC PARAMETERS OF PORPHYRINS AND METALLOPORPHYRINS IN DMF CONTAINING 0.5 M TEAP AT 25 °C

Compound	$-E_{1/2}$ (1) (V *vs.* SCE)	k_{sm} (1) (cm/s)	α_m (1)	$-E_{1/2}$ (2) (V *vs.* SCE)	k_{sm} (2) (cm/s)	α_m (2)
PPDM	1.25	5.6	0.50	1.61	1.7	0.30
MPDM	1.35	3.8	0.50	1.75	1.34	0.38
Ni(III)-PPDM	1.28	5.1	0.55	1.84	0.76	0.32
Cu(II)-PPDM	1.33	4.1	0.50	1.76	0.85	0.30
Zn(II)-PPDM	1.47	3.8	0.43	1.80	0.68	0.28
Co(II)-PPDM	0.96	—	—	2.00	0.64	0.4
Mn(III)Cl·H_2O-PPDM	1.46[a]	3.4	0.48	1.93[b]	—	—

a) The second reduction step of Mn(III)-complex. b) The third reduction step of Mn(III)-complex.

11) M. Zerner and M. Gouterman, *Theoret. Chim. Acta*, **4**, 44 (1966).
12) M. E. Peover and J. S. Powell, *J. Electroanal. Chem.*, **20**, 427 (1969).
13) T. Kakutani, M. Senda, and H. Kinoshita, "International Congress on Analytical Chemistry, Kyoto, 1972", Abstract, p. 301.

Table 2. Comparison of the measured rate constants and the frumkin correction factors for double layer effects

Compound	k_{sm} (1)/k_{sm} (2)	$-\phi_0$ (1) mV	$-\phi_0$ (2) mV	$f[\phi_0$ (1)]	$f[\phi_0$ (2)]	$f[\phi_0'$ (1)]	$f[\phi_0'$ (2)]
PPDM	3.29	95	106	6.36	214	2.64	15.0
Ni(II)-PPDM	6.71	96	110	7.85	299	2.94	16.8
Cu(II)-PPDM	4.82	98	109	6.75	250	2.69	15.8
MPDM	2.83	98	109	6.75	350	2.69	18.7
Zn(II)-PPDM	5.59	101	110	5.42	239	2.34	15.3

the nitro-compound.

Results in Table 1 show that the measured rate constants of the negative ion reductions are about an order of magnitude smaller than those of the neutral molecule reductions. The measured rate constant, k_{sm}, is related to the true rate constant, k_s, by[14]

$$k_s = k_{sm} \exp\left[-(\alpha_m n - z)\frac{F}{RT}\phi\right],$$

where ϕ is the potential at the pre-electrode site relative to the solution and z is the charge on the oxidized from. Table 2 shows the potential values of the outer Helmholtz plane at the half-wave optentials of the first and second steps, $\phi_0(1)$ nad $\phi_0(2)$, being calculated from Gouy-Chapman theory on the assumption that no specific adsorption of the supporting electrolyte ions occurs. Also shown are some calculated values of Frumkin correction factor, $f[\phi]=\exp[-(\alpha_m n-z)F\phi/RT]$; $f[\phi_0(1)]$ and $f[\phi_0(2)]$ are calculated on the assumption that the pre-electrode site is the outer Helmholtz plane, whereas $f[\phi_0'(1)]$ and $f[\phi_0'(2)]$ are calculated on the assumption that it is located 2 Å out of the outer Helmholtz plane, where the ϕ_0' potentials are about 50 per cent of ϕ_0. It will be reasonable to suppose that the pre-electrode sites are much the same for the anion reduction at the neutral molecule reduction. Accordingly, if we admit the prediction[15] of about the same true rate constants for anion reduction as the neutral molecule reduction, we may conclude that the pre-electrode site is likely located about 2 Å or further out of the outer Helmholtz plane. Similar results have also been obtained for aromatic compounds by Peover.[15] However, the measured transfer coefficients of the anion reductions are significantly different from those of the neutral molecule reductions, suggesting that the charge transfer mechanisms are very different for these two reductions. It is noted that the presence of homogeneous chemical reaction following the charge transfer predicts an increase of the measured transfer coefficient.[8] Stronger repulsive effect (Levich correction)[8] for the form also predicts an increase in the measured transfer coefficient. These arguments lead to another supposition that the true rate constants are not necessarily the same for the anion reduction as the neutral molecule reduction. Theories of Marcus[16] and Hush[17] seem to predict that the electrostatic solvent reoganization energy may depend upon the transfer coefficient. As to the location of pre-electrode site, closer approach to the electrode surface may be understandable by imagining the reacting depolarizers at the size with their porphyrin ring planes parallel to the electrode surface. Conclusive interpretation can not be given at present. Further study is in progress.

This work was partly supported by a grant from the Ministry of Education, to which the authors' thanks are due.

14) R. Delahay, "Advances in Electrochemistry and Electrochemical Engineering," Vol. 1, ed. by P. Delahay, Interscience Publishers, New York (1961), p. 233.

15) M. E. Peover, "Reactions of Molecules at Electrode," ed. by N. S. Hush, John Wiley & Sons, Inc., London (1970), p. 259.

16) R. A. Marcus, *J. Chem. Phys.*, **43**, 679 (1965).

17) N. S. Hush, *Trans. Faraday Soc.*, **57**, 557 (1961).

A Study on Spontaneous Resolution of Cobalt(III) Complex Salts

Kazuaki YAMANARI, Jinsai HIDAKA, and Yoichi SHIMURA

Department of Chemistry, Faculty of Science, Osaka University, Toyonaka, Osaka 560

(Received June 22, 1973)

Solubility of the racemic and optically active isomers of $[Co(ox)en_2]X$, $[CoCO_3en_2]X$, *cis*-$[Co(NO_2)_2en_2]X$ and $M[Co(edta)]$ in water was determined at 5—60 °C (X=Cl, Br, and I; M=NH_4 and K). The correlation between solubility of the spontaneously resolved racemic complex and of the corresponding optically active isomer is discussed. Spontaneous resolutions were observed for $[Co(ox)en_2]X$ (X=Cl, Cl·H_2O, and Br·H_2O), *cis*-$[Co(NO_2)_2en_2]X$ (X=Cl and Br) and $M[Co(edta)]\cdot 2H_2O$ (M=NH_4 and K).

It is believed that so-called spontaneous resolution can be observed in limited cases. Only some dozen metal complexes have been reported to be spontaneously resolved.[1-8] It is evident that solubility plays an extremely important role in spontaneous resolution and related phenomena such as optical resolution by the formation of diastereomer or so-called configurational activity.[9-11] Systematic investigation of solubility of metal complexes is necessary for an explanation of these phenomena; nevertheless, only a few reports have been published so far. The present paper deals with the solubility and spontaneous resolution of (1 : 1) electrolyte salts containing configurationally chiral cobalt(III) complexes.

Experimental

Preparation and Resolution. *(1) Bis(ethylenediamine)-oxalatocobalt(III) Complex, $[Co(ox)en_2]X$, (X=Cl^-, Br^-, and I^-)*: The chloride salt was prepared and resolved by the method of Dwyer *et al.*[12] The racemic and optically active bromides or iodides were obtained by adding a calculated amount of NH_4Br or NH_4I to an aqueous solution of the corresponding chloride. The spontaneous resolution of monohydrated bromide salt was observed for the rhombic crystals prepared as follows: about 0.7 g of the racemic bromide monohydrate was dissolved in 50 ml of water at 50 °C and the solution was kept standing in refrigerator (at about 5 °C) for several days for crystallization.

(2) cis-*Bis(ethylenediamine)dinitrocobalt(III) Complex, cis-$[Co(NO_2)_2en_2]X$, (X=Cl^-, Br^-, and I^-)*: The nitrite salt *cis*-$[Co(NO_2)_2en_2]NO_2$ was prepared by the reaction of *trans*-$[CoCl_2en_2]Cl$ (20 g) and KNO_2 (20 g) in 100 ml of water at 50 °C and optically resolved by the method of Dwyer and Garvan.[13] The chloride and iodide salts were derived from the bromide by treating with AgCl and AgI, respectively. Crystallization was carried out as follows: 1.5 g of the racemic chloride (0.5 and 0.2 g of the bromide and iodide, respectively) was dissolved in 20 ml of water at 40 °C and the solution was kept standing in a refrigerator (at about 5 °C) for several days.

(3) Carbonatobis(ethylenediamine)cobalt(III) Complex, $[Co-CO_3en_2]X$, (X=Cl^-, Br^-, and I^-): Racemic chloride salt was prepared by Werner's method[14] and racemic bromide or iodide salt was obtained by adding an appropriate amount of NH_4Br or KI to an aqueous solution of the chloride. Optically active chloride and bromide salts were derived from the active iodide, which was resolved by the method of Dwyer *et al.*,[15] by treating with the corresponding silver halides.

(4) Ethylenediaminetetraacetatocobaltate(III) Complex, M-[Co(edta)], (M=K^+ and NH_4^+): The potassium salt dihydrate was prepared and resolved by the method of Dwyer and Garvan.[16] The ammonium salt was similarly obtained by using ammonium acetate instead of potassium acetate. The desired crystals of potassium and ammonium salts were gradually crystallized from the solution containing 6 g of potassium salt (5 g for ammonium salt) in 10 ml of warm water (50 °C) by being kept standing at room temperature.

Measurements. Solubility measurements were carried out spectrophotometrically with a Beckman DU spectrophotometer at 5—60 °C. Saturation equilibrium of solutions was attained in an Erlenmeyer flask, which was maintained in a thermostat regulated within ±0.1°C. An aqueous solution containing an excess of solid complex salt in the flask was stirred mechanically at the desired temperature and the resulting saturated solution was sampled by sucking up with a pipet through a filter. The sample solution was weighed exactly, diluted to an appropriate volume and its optical density was measured at the maximum wavelength of the first absorption band of the complex. To detect the occurrence of spontaneous resolution, the crystal of racemic complex was arbitrarily chosen and dissolved in a small amount of water, and the optical rotatory dispersion (RD) curve was measured with a Yanagimoto recording spectropolarimeter model-187.

General Consideration

The correlation between solubility of the racemic compound and of the corresponding optically active isomers has not been discussed by means of an explicit formula except for some qualitative treatment using phase

1) F. M. Jaeger and W. Thomas, *Proc. Acad. Sci. Amsterdam*, **21**, 693 (1919).
2) F. M. Jaeger and H. B. Blumendal, *Z. Anorg. Chem.*, **175**, 161 (1928).
3) H. A. Weakliem and J. L. Hoard, *J. Amer. Chem. Soc.*, **81**, 549 (1959).
4) G. Gordon and R. K. Birdwhistell, *ibid.*, **81**, 3567 (1959).
5) K. Yamasaki, H. Igarashi, Y. Yoshikawa, and H. Kuroya, *Inorg. Nucl. Chem. Lett.*, **4**, 491 (1968).
6) H. Ogino, M. Takahashi, and N. Tanaka, This Bulletin, **43**, 424 (1970).
7) K. Kawasaki, J. Yoshii, and M. Shibata, *ibid.*, **43**, 3819 (1970).
8) D. G. Brewer and K. T. Kan, *Can. J. Chem.*, **49**, 965 (1971).
9) A. Werner, *Ber.*, **47**, 2171 (1914).
10) F. P. Dwyer, E. C. Gyarfas, and M. F. O'Dwyer, *Nature*, **167**, 1036 (1951).
11) J. A. Broomhead, *ibid.*, **211**, 741 (1966).
12) F. P. Dwyer, I. K. Reid, and F. L. Garvan, *J. Amer. Chem. Soc.*, **83**, 1285 (1961).
13) F. P. Dwyer and F. L. Garvan, *Inorg. Synth.*, **6**, 195 (1960).
14) A. Werner, *Ann.*, **386**, 72 (1912).
15) F. P. Dwyer, A. M. Sargeson, and I. K. Reid, *J. Amer. Chem. Soc.*, **85**, 1215 (1963).
16) F. P. Dwyer and F. L. Garvan, *Inorg. Synth.*, **6**, 192 (1960).

diagrams.[17,18] Racemic complexes are classified into two groups on the basis of the mode of crystallization. In the first group, a racemic complex forms racemic crystals, the unit cell of which contains an equal number of the Δ and Λ enantiomeric complexes. In the second group, a racemic complex forms a racemic mixture, which is a mixture of the pure Δ and Λ crystals. The latter case has been named the spontaneous resolution.

The solubility product (K_{SP}) for an optically active (Δ, for example) complex salt of the $[M]^+X^-$ type[19] at t °C is given by

$$K_{SP}^{\Delta} = \{[M]^+\}_{\Delta} \cdot \{X^-\} = S_{\Delta} f_{[M]}^{\Delta} \cdot S_{\Delta} f_X^{\Delta} = (S_{\Delta})^2 \cdot f_{[M]}^{\Delta} f_X^{\Delta} \quad (1)$$

where $\{[M]^+\}$ and $\{X^-\}$ denote the activities of the complex cation and the counter simple anion, respectively, S_{Δ} the molar solubility of the optically active Δ salt, and $f_{[M]}^{\Delta}$ and f_X^{Δ} the activity coefficients of the complex cation and the counter anion, respectively. If the spontaneous resolution occurs for the corresponding racemic complex salt, the solubility product for the Δ isomer in the racemic mixture, $K_{SP}^{\Delta(\Delta\Lambda)}$, is represented as follows, since the Δ isomer in the racemic mixture behaves independently of the Λ isomer.

$$K_{SP}^{\Delta(\Delta\Lambda)} = K_{SP}^{\Lambda(\Delta\Lambda)} = \{[M]^+\}_{\Delta \text{ or } \Lambda} \cdot \{X^-\} = \frac{1}{2} S_{\Delta\Lambda} f_{[M]}^{\Delta\Lambda} \cdot S_{\Delta\Lambda} f_X^{\Delta\Lambda} = \frac{1}{2} (S_{\Delta\Lambda})^2 \cdot f_{[M]}^{\Delta\Lambda} f_X^{\Delta\Lambda} \quad (2)$$

where $f_{[M]}^{\Delta\Lambda}$ and $f_X^{\Delta\Lambda}$ denote the activity coefficients of the complex cation and the counter anion in the racemic solution, respectively. Since the relation $K_{SP}^{\Delta} = K_{SP}^{\Delta(\Delta\Lambda)}$ should hold, we have

$$S_{\Delta\Lambda} = \sqrt{2}\, S_{\Delta} (f_{[M]}^{\Delta} \cdot f_X^{\Delta})^{1/2} / (f_{[M]}^{\Delta\Lambda} \cdot f_X^{\Delta\Lambda})^{1/2} \quad (3)$$

Thus, if we assume an ideal solution, the solubility of a spontaneously resolved racemic complex salt of the $[M]^+X^-$ type must be $\sqrt{2}$ times larger than that of the corresponding optically active complex salt. Activity coefficients decrease in most cases with increasing ionic strength in the concentration range 10^{-3}—10^{-1} mol/l. Since the spontaneously resolved racemic complex salt is more soluble than the active isomers, we have $f_{[M]}^{\Delta\Lambda} < f_{[M]}^{\Delta}$ and $f_X^{\Delta\Lambda} < f_X^{\Delta}$. Therefore, Eq. (3) shows that *the solublity of the spontaneously resolved racemic salt of the $[M]^+X^-$ type is $\sqrt{2}$ or more times larger than that of the corresponding optically active salt.*

The treatment can be extended to other types of complex electrolytes and to the complex molecule also. For the $[M]^{n+}(X^-)_n$ type we obtain

$$S_{\Delta\Lambda} = \sqrt[n+1]{2}\, S_{\Delta} (f_{[M]}^{\Delta} \cdot f_X^{\Delta})^{1/(n+1)} / (f_{[M]}^{\Delta\Lambda} \cdot f_X^{\Delta\Lambda})^{1/(n+1)} \quad (4)$$

and for the complex molecule

$$S_{\Delta\Lambda} = 2 S_{\Delta} (f_{[M]}^{\Delta} / f_{[M]}^{\Delta\Lambda}) \quad (5)$$

In the case of true racemic crystal, $[M]^+{}_{\Delta}[M]^+{}_{\Lambda}(X^-)_2$, which contains an equal number of the Δ and Λ complexes in its unit cell, the solubility product is given by

$$K_{SP}^{\Delta\Lambda} = \{[M]^+\}_{\Delta} \cdot \{[M]^+\}_{\Lambda} \cdot \{X^-\}^2 = \frac{1}{2} S_{\Delta\Lambda} f_{[M]}^{\Delta\Lambda} \cdot \frac{1}{2} S_{\Delta\Lambda} f_{[M]}^{\Delta\Lambda} \cdot (S_{\Delta\Lambda} f_X^{\Delta\Lambda})^2 = \frac{1}{4} (S_{\Delta\Lambda})^4 \cdot (f_{[M]}^{\Delta\Lambda} f_X^{\Delta\Lambda})^2 \quad (6)$$

In this case the solubility $S_{\Delta\Lambda}$ is independent of that of the corresponding pure Δ or Λ enantiomer, not exceeding $\sqrt{2}S_{\Delta}$ or $\sqrt{2}S_{\Lambda}$ in an ideal solution. The general conclusion is summarized in Table 1.

Results and Discussion

The solubility data are summarized in Table 2.

(1) Bis(ethylenediamine)oxalatocobalt(III) Complexes: Solubility curves of the complex halides are shown in Fig. 1—3. Of these halides the chloride salt has been reported to show the so-called spontaneous re-

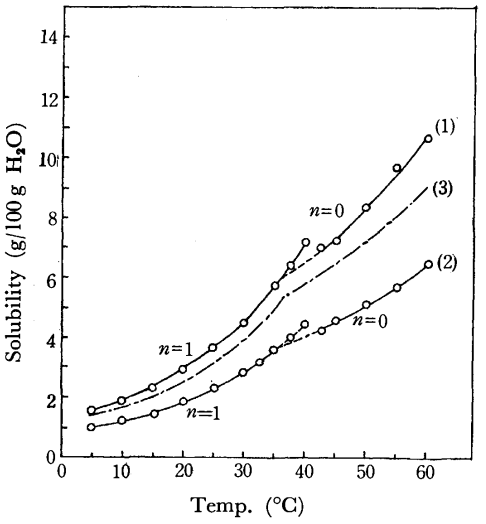

Fig. 1. Solubility curves of $[Co(ox)en_2]Cl \cdot nH_2O$: (1) racemic form, (2) Λ form and (3) calculated curve: (2)$\times\sqrt{2}$.

Table 1. Solubility relationship between the racemic and the optically active (Δ) isomers of the $[M]^{n+}(X^-)_n$ and $([M]^+)_nX^{n-}$ type complex salts in an ideal solution

$S_{\Delta\Lambda}$; Solubility of the racemic compound.
S_{Δ}; Solubility of the Δ form.

Solid phase	$[M]^{n+}(X^-)_n$	$([M]^+)_nX^{n-}$
True racemic crystal	$S_{\Delta\Lambda} < \sqrt[n+1]{2}\, S_{\Delta}$	$S_{\Delta\Lambda} < \sqrt[n/(n+1)]{2}\, S_{\Delta}$
Spontaneously resolved racemic mixture	$S_{\Delta\Lambda} = \sqrt[n+1]{2}\, S_{\Delta}$	$S_{\Delta\Lambda} = \sqrt[n/(n+1)]{2}\, S_{\Delta}$

17) H. W. B. Roozeboom, *Z. Phys. Chem.* (Leipzig), **28**, 494 (1899).
18) R. M. Secor, *Chem. Rev.*, **63**, 297 (1963).
19) [M+] denotes a unipositive complex cation and X⁻ a uninegative anion.

TABLE 2. SOLUBILITY OF THE COBALT(III) COMPLEX SALTS OF $[M]^+X^-$ TYPE (grams of anhydrous salt in 100 grams of water)[1)]

Temp. (°C)	No. of complex salt[2)]												
	1	2	3	4	5	6	7	8	9	10[3)]	11	12	13[3)]
5.0	1.55		1.00		0.743[a]	0.475	0.0862	0.251	8.63	12.5	2.43		2.54
10.0	1.88		1.24[b]		0.795	0.537	0.104	0.291	9.77	13.8	2.96		2.86
15.0	2.34[a]		1.49		0.989[a]	0.636	0.122	0.344	10.9	14.7	3.61	3.58[a]	3.20
20.0	2.93		1.84		1.17	0.763	0.153	0.381	11.9	16.0	4.31	4.06	3.55
25.0	3.65[a]		2.33		1.34[a]	0.853	0.164	0.443	13.1[b]	17.1	5.19	4.58	3.98
27.5	—		—		—	—	—	—	13.8	—	—	4.87	—
30.0	4.52		2.83		1.55	1.01[k]	0.206	0.515	14.4	18.4	6.23	5.09[i]	4.43
32.5	—		3.21		—	—	—	—	15.3[a]	—		5.41	—
35.0	5.77		3.59		1.86[e]	1.15[a]	0.241	0.585	16.0	19.9		5.77	4.96
37.5	6.42		4.02		—	—	—	—	16.7	—		—	—
40.0	7.19		4.46[a]		2.08[a]	1.31	0.287	0.660	17.2	(21.4)		6.43	(5.71)
42.5		7.02[a]		4.29[c]	—	—	—	—	18.1[a]	—		—	—
45.0		7.23[b]		4.61	2.37	1.48	0.332	0.768	19.1	(23.2)[b]		7.06	(6.53)
50.0		8.36		5.17	2.84	1.68[d]	0.376	0.839	20.7	(25.6)[b]		7.82	(7.41)
55.0		9.74[d]		5.71[c]	3.16[e]	1.96[b]	0.451[l]	0.940	22.8[a]	(29.2)[d]		8.71	(8.68)[h]
60.0		10.7		6.49[c]	3.58[a]	2.20	0.497[b]	1.11[l]	24.7	(33.0)[j]		9.50	(11.0)

Temp. (°C)	No. of complex salt[2)]												
	14	15	16[3)]	17	18	19	20	21	22	23	24	25	26
5.0	0.428		1.38	3.97	2.55	0.948	0.713	0.399	0.293	36.6	17.5		10.4
10.0	0.534		1.49	4.76	3.00	1.16	0.749	0.511	0.378	47.7	22.0	22.4	14.3
15.0	0.702		1.64[c]	5.56[b]	3.47	1.41	0.914	0.607	0.445[a]	55.9	26.9	28.6	17.1
20.0	0.830	0.793	1.90	6.46	3.98[a]	1.65	1.12	0.696	0.532	67.5	32.5	35.6	20.3
25.0	0.988	0.925	2.14	7.58	4.69	1.97	1.30	0.846	0.650	76.3	40.3	43.6	26.2
27.5	—	—	—	—	—	—	—	—	—	—	—	—	—
30.0	1.23	1.07	2.38	8.78[b]	5.29	2.34	1.59	1.02	0.754	89.1	52.2	52.9	30.9
32.5	—	—	—	—	—	—	—	—	—	—	—	—	—
35.0	1.49	1.23	2.80[l]	10.4[a]	6.14[c]	2.81	1.78	1.22	0.924	103	57.2	56.3	34.8
37.5	—	—	—	—	—	—	—	—	—	—	—	—	—
40.0	1.80	1.44	3.14	12.1[b]	7.01[b]	3.23[a]	2.12	1.47	1.12	110	65.4	69.6	41.6
42.5		—	—	—	—	—	—	—	—	—	—	—	—
45.0		1.63	(3.14)	13.9[d]	7.97[b]	3.87	2.48	1.74[b]	1.30	125	73.7	78.6	49.0
50.0		1.92	(2.49)	16.2[d]	9.11[d]	4.60	2.94	2.05[d]	1.53[b]	—	85.1	85.8	56.5
55.0		2.13	(2.64)	19.4[k]	10.3[g]	5.34		2.51[a]	1.77	155	91.1	99.8	64.2
60.0		2.48	(3.06)	22.1	11.9	6.26		2.96[c]	2.11	176	103	114	73.4

1) The deviation of temperature from the indicated value is shown by a small letter superscript; a: +0.1 °C, b: −0.1 °C, c: +0.2 °C, d: −0.2 °C, e: +0.3 °C, f: −0.3 °C, g: +0.4 °C, h: −0.4 °C, i: +0.5 °C, j: −0.5 °C, k: +0.8 °C, l: +1.0 °C.

2) 1: *rac*-$[Co(ox)en_2]Cl\cdot H_2O$, 2: *rac*-$[Co(ox)en_2]Cl$, 3: $\Lambda(+)$-$[Co(ox)en_2]Cl\cdot H_2O$, 4: $\Lambda(+)$-$[Co(ox)en_2]Cl$, 5: *rac*-$[Co(ox)en_2]Br\cdot H_2O$, 6: $\Lambda(+)$-$[Co(ox)en_2]Br\cdot H_2O$, 7: *rac*-$[Co(ox)en_2]I$, 8: $\Lambda(+)$-$[Co(ox)en_2]I$, 9: *rac*-$[CoCO_3en_2]Cl$, 10: $\Lambda(+)$-$[CoCO_3en_2]Cl$, 11: *rac*-$[CoCO_3en_2]Br\cdot 2H_2O$, 12: *rac*-$[CoCO_3en_2]Br$, 13: $\Delta(-)$-$[CoCO_3en_2]Br$, 14: *rac*-$[CoCO_3en_2]I\cdot 2H_2O$, 15: *rac*-$[CoCO_3en_2]I$, 16: $\Lambda(+)$-$[CoCO_3en_2]I$, 17: *rac-cis*-$[Co(NO_2)_2en_2]Cl$, 18: $\Delta(-)$-*cis*-$[Co(NO_2)_2en_2]Cl$, 19: *rac-cis*-$[Co(NO_2)_2en_2]Br$, 20: $\Delta(-)$-*cis*-$[Co(NO_2)_2en_2]Br$, 21: *rac-cis*-$[Co(NO_2)_2en_2]I$, 22: $\Delta(-)$-*cis*-$[Co(NO_2)_2en_2]I$, 23: *rac*-$K[Co(edta)]\cdot 2H_2O$, 24: $\Delta(+)_{546}$-$K[Co(edta)]\cdot 2H_2O$, 25: *rac*-$NH_4[Co(edta)]\cdot 2H_2O$, 26: $\Delta(+)_{546}$-$NH_4[Co(edta)]\cdot 2H_2O$.

3) Values in parentheses for the optically active carbonato complexes are invalid because of partial racemization.

solution.[5,8)] The solubility of racemic chloride salt is larger than $\sqrt{2}$ times that of its optically active isomer in the range 5—60 °C (Fig. 1). The solubility curves show an inflection at about 36 °C, where the solid phase changes from monohydrate (below 36 °C) to anhydrous (above 36 °C). The bromide salts show a quite similar relationship in solubility curves to those of the chlorides except that the former shows no inflection (Fig. 2). Therefore, spontaneous resolution is expected for the racemic salt. In fact, the crystal which was arbitrarily chosen showed the same RD curve as that of the resolved isomer. No hemihedral facets, however, were observed for the crystals. Contrary to the bromide salt, no optical activity was observed for the iodide crystals. This agrees with the solubility curve relation $S_\Lambda > S_{\Lambda\Lambda}$ of the iodide salts (Fig. 3).

(2) Carbonatobis(ethylenediamine)cobalt(III) Complexes: The solubility curves of three optically active isomers deviate from the usual pattern at about 35 °C or above.

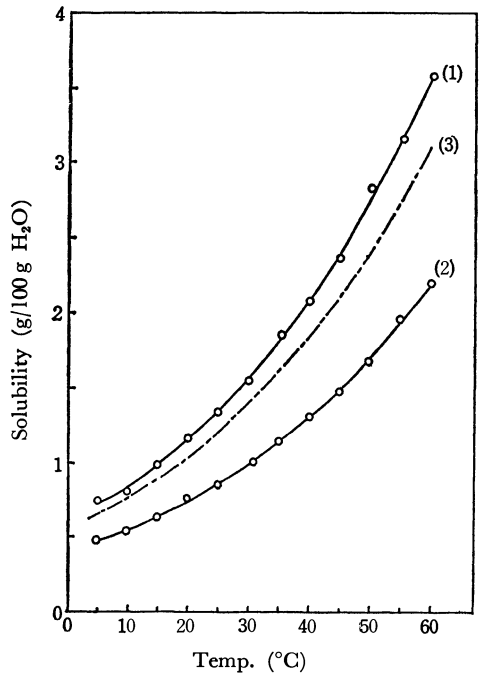

Fig. 2. Solubility curves of $[Co(ox)en_2]Br \cdot H_2O$: (1) racemic form, (2) *Λ* form and (3) calculated curve: $(2) \times \sqrt{2}$.

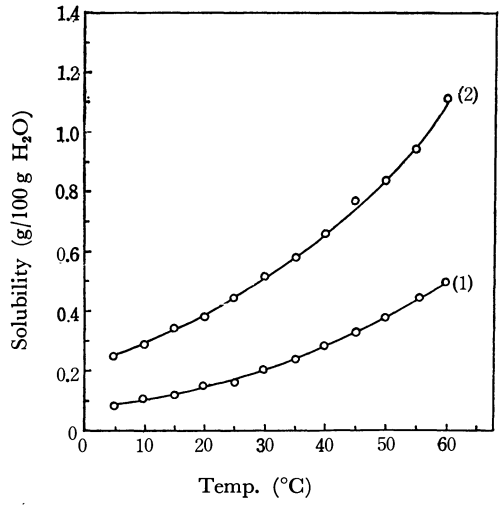

Fig. 3. Solubility curves of $[Co(ox)en_2]I$: (1) racemic form, (2) *Λ* form.

It was confirmed by the absorption and optical rotation measurements that these deviations arose from racemization. An inflection appears at 16 °C for the racemic bromide salt (Fig. 4) and at 17 °C for the racemic iodide one. These are the transition points from the dihydrates (below 16 °C or 17 °C) to the anhydrous (above 16 °C or 17 °C). The solubility curve of the racemic bromide (16—30 °C) shown by the dotted line is attributable to the metastable state of the dihydrate (Fig. 4). Both the chloride and iodide salts show $S_{\Lambda} > S_{\Lambda\Lambda}$ type. The bromide shows $S_{\Lambda} < S_{\Lambda\Lambda}$, but the curve of racemic salt is lower than the calculated $\sqrt{2}$ times curve of the active salt. Spontaneous resolution was not observed.

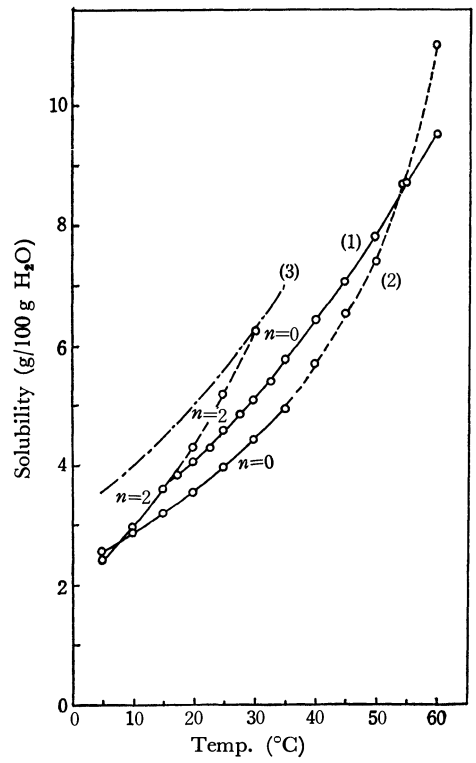

Fig. 4. Solubility curves of $[CoCO_3en_2]Br \cdot nH_2O$: (1) racemic form, (2) *Λ* form and (3) calculated curve: $(2) \times \sqrt{2}$.

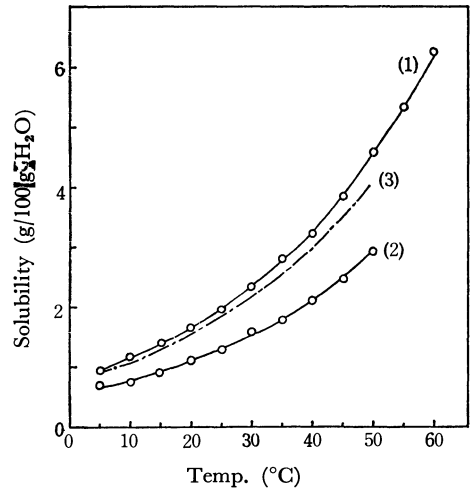

Fig. 5. Solubility curves of *cis*-$[Co(NO_2)_2en_2]Br$: (1) racemic form, (2) *Λ* form and (3) calculated curve: $(2) \times \sqrt{2}$.

(3) cis-*Bis(ethylenediamine)dinitrocobalt(III) Complexes*: Spontaneous resolution is expected for the chloride and bromide salts, since both salts show a solubility $S_{\Lambda\Lambda}$ larger than the calculated $\sqrt{2}$ times curve of the active salt (Table 2 and Fig. 5). The crystals from the racemic mixture show a similar RD curve to that of the resolved isomer. However, the crystals did not show any hemihedral facets. In contrast to the chloride and bromide salts, no optical rotation was observed for the crystals from the racemic iodide salt in spite of the $S_{\Lambda\Lambda} > S_{\Lambda}$ type (Fig. 6). This is acceptable in view of the relationship $S_{\Lambda\Lambda} < \sqrt{2} S_{\Lambda}$.

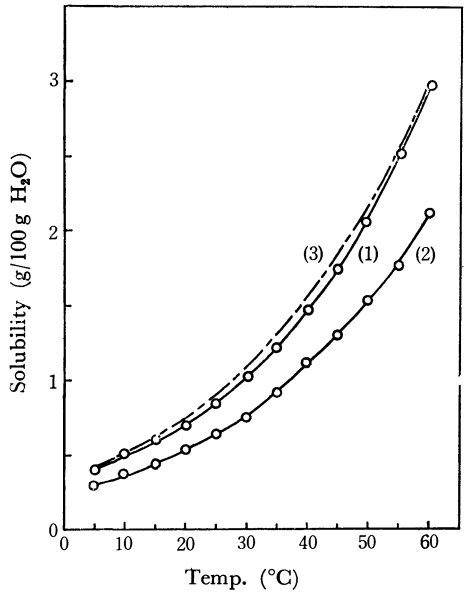

Fig. 6. Solubility curves of *cis*[Co$(NO_2)_2en_2$]I: (1) racemic form, (2) *Δ* form and (3) calculated curve: (2)$\times\sqrt{2}$.

(4) Ethylenediaminetetraacetatocobaltate(III) Complexes: Spontaneous resolution has been reported for NH_4[Co(edta)]·$2H_2O$ and Rb[Co(edta)]·$2H_2O$, both of which belong to the space group $P2_12_12_1$. The solubility type of NH_4[Co(edta)]·$2H_2O$ is $S_{\Delta\Delta} > \sqrt{2}S_{\Delta}$ in agreement with the above information. The curves of K[Co(edta)]·$2H_2O$ are quite similar to those of ammonium salts and suggest the possibility of spontaneous resolution. In fact, the crystal from the racemic mixture shows a quite similar RD curve to that of the resolved isomer. No distinguishable hemihedral facet could be observed.

The results confirm the view that spontaneous resolution is predictable from the relation between the solubility of racemic and optically active salts. The method we proposed is fairly useful for the investigation of spontaneous resolution, since distinguishable hemihedral facets are not always observable. The result suggests that the spontaneously resolvable salts are unexpectedly distributed in the cobalt(III) complexes of (1 : 1) electrolyte type.

BULLETIN OF THE CHEMICAL SOCIETY OF JAPAN, VOL. 46, 3728—3733 (1973)

Copper(II) Complexes with Some Aliphatic Diaminealcohols

Yasuo ISHIMURA, Yasuomi NONAKA, Yuzo NISHIDA, and Sigeo KIDA

Department of Chemistry, Faculty of Science, Kyushu University, Hakozaki, Fukuoka 812

(Received August 26, 1972)

Copper(II) complexes were prepared with a series of tridentate ligands, $NH_2(CH_2)_mCHRNH(CH_2)_nOH$ (R=H or CH_3; m=1 or 2; n=2 or 3). Compounds obtained can be classified into three groups: (1) $CuLCl_2$, (2) $CuL(ClO_4)$ and (3) CuL_2X_2, (L and L′ represent the neutral and the anionic ligands, respectively, and X denotes Cl or ClO_4). (1) and (3) were found to be mononuclear in which L functions as a bidentate ligand donating with the two nitrogen atoms. (2), except for the complex with L′=$NH_2(CH_2)_3NH(CH_2)_2O^-$, have the binuclear structure with alkoxo bridges. The absorption bands at about 350 nm are characteristic of the binuclear structure with alkoxo or hydroxo bridges.

Since it was found that the band at 370 nm in copper(II) alkanoates is diagnostic of the binuclear structure,[1-4] a number of spectral studies of copper(II) alkanoates have been reported.[5-10] However, the origin of the band has been a subject of controversy.[8,9] It seems desirable to see whether binuclear copper(II) complexes of other types show similar bands to those copper(II) alkanoates. Recently Yamada and Ojima[11] observed the bands at about 355 nm in a series of the binuclear copper(II) complexes such as bis(μ-*N*-oxo-propyl-*N*′-methylglycinamido)dicopper(II), and assumed the bands to be characteristic of the μ-dioxo structure of the complexes. However, further evidences seem to be necessary for establishing general relationship between the binuclear structure and the appearance of the band at about 350—360 nm in copper(II) complexes. In most dimeric copper(II) complexes so far reported, the ultraviolet region is masked by absorptions resulting from ligands. We therefore, attempted to prepare a series of ligands such as $NH_2(CH_2)_mCHRNH(CH_2)_nOH$ (R=H or CH_3, m=1 or 2, and n=2 or 3), which are capable of forming five- and/or six-membered chelate rings and, under some conditions, of forming binuclear complexes. They are new compounds except for the one with R=H, m=1 and n=2. Since these ligands have no double

1) R. Tsuchida and S. Yamada, *Nature*, **176**, 1171 (1955).
2) R. Tsuchida, H. Nakamura, and S. Yamada, *ibid.*, **178**, 1192 (1956).
3) S. Yamada, H. Nakamura, and R. Tsuchida, This Bulletin, **30**, 953 (1957).
4) S. Yamada, H. Nakamura, and R. Tsuchida, *ibid.*, **31**, 303 (1958).
5) B. N. Figgis and R. L. Martin, *J. Chem. Soc.*, **1957**, 3837.
6) R. L. Martin and A. Whithey, *ibid.*, **1958**, 1394.
7) S. Kida, Y. Nakashima, Y. Morimoto, K. Niimi, and S. Yamada, This Bulletin, **37**, 549 (1964).
8) A. E. Hansen and C. J. Ballhausen, *Trans. Faraday Soc.*, **61**, 631 (1965).
9) L. Dubicki and R. L. Martin, *Inorg. Chem.*, **5**, 2203 (1966).
10) L. Dubicki, XIIIth ICCC, Poland, (1970). Proceedings, I, 129.
11) K. Yamada and H. Ojima, 24th Annual Meeting of Chemical Society of Japan, Osaka, (1971) Proceedings, 2, p. 729.

bond, and consequently no absorption in visible and near-ultraviolet region, their complexes were considered to be suitable for the present investigation.

The relationship of the structure of a tridentate chelate ring system to the stability and magnetic properties of the binuclear copper(II) complexes was discussed by Ueda *et al.*,[12] but the ligands studied were limited to the condensed Schiff bases. Thus, in addition to the spectral study, we have investigated the effects of size and structure of chelate rings on the stability and magnetic properties of the binuclear copper(II) complexes, using the series of tridentate ligands of saturated chains.

Experimental

Preparation of Ligands. N-*(β-hydroxyethyl)ethylenediamine*, $NH_2(CH_2)_2NH(CH_2)_2OH$=*en-etol*: This compound was prepared by the method of Knorr and Brownsden.[13]

N-*(γ-hydroxypropyl)ethylenediamine*, $NH_2(CH_2)_2NH(CH_2)_3OH$ =*en-prol*: This compound was prepared by the method of Keller and Edwards,[14] except for the use of trimethylene chlorohydrin instead of trimethylene bromohydrin.

N-*(β-hydroxyethyl)trimethylenediamine*, $NH_2(CH_2)_3NH(CH_2)_2$-OH=*tn-etol*: Gaseous ethylene oxide produced by dropwise addition of 24 g (0.3 mol) ethylene chlorohydrin to 32 g (0.6 mol) potassium hydroxide was introduced with stirring into a solution of 74 g (1.0 mol) trimethylenediamine. The unreacted trimethylenediamine was distilled off, and the remaining mixture was distilled under reduced pressure. Bp. 133—134 °C/7 mmHg.

N-*(γ-hydroxypropyl)trimethylenediamine*, $H_2N(CH_2)_3NH(CH_2)_3$ OH=*tn-prol*: To a well-stirred solution of 74 g (1.0 mol) trimethylenediamine in 80 ml of isopropyl alcohol was added 28.4 g (0.3 mol) of trimethylene chlorohydrin, the reaction mixture being maintained at about 50 °C. The mixture was refluxed for 3 hr. 8 g (0.2 mol) of sodium hydroxide was added to the solution, yielding white precipitates which were filtered off. The filtrate was evaporated to remove isopropyl alcohol and the unreacted trimethylenediamine, and then, distilled under reduced pressure. Fractionation of the distillate yielded 11.5 g (43.5% yield based on the trimethylene chlorohydrin) of the final product. Bp. 130—131 °C/3 mmHg.

N-*(γ-hydroxypropyl)-(−)-1,2-propanediamine*, $NH_2CH(CH_3)$-$CH_2NH(CH_2)_3OH$ = *pn-prol*: This compound was prepared in a similar way to that for $H_2N(CH_2)_3NH(CH_2)_3OH$, except for the use of (−)-1,2-propanediamine instead of trimethylenediamine.

Table 1. Abbreviation of ligands

en-etol	$NH_2CH_2CH_2NHCH_2CH_2OH$
en-prol	$NH_2CH_2CH_2NHCH_2CH_2CH_2OH$
tn-etol	$NH_2CH_2CH_2CH_2NHCH_2CH_2OH$
tn-prol	$NH_2CH_2CH_2CH_2NHCH_2CH_2CH_2OH$
pn-prol	$NH_2CH_2CH(CH_3)NHCH_2CH_2CH_2OH$

The primed abbreviation, such as en-prol′ *etc.*, denotes the anion of the ligand, such as $NH_2CH_2CH_2NHCH_2CH_2CH_2O^-$ *etc.*

12) H. Ueda, K. Mori, M, Kishita, and S. Nakahara. 24th Annual Meeting of Chemical Society of Japan, Osaka (1971). Proceedings, 2, p. 761.

13) L. Knorr and H. W. Brownsdon, *Ber.*, **35**, 4470 (1902).

14) R. N. Keller and L. J. Edwards, *J. Amer. Chem. Soc.*, **74**, 215 (1952).

Preparation of the Complexes. *Cu en-etol Cl_2 (A)* (For abbreviation of ligands, see Table 1): A solution of 1.1 g of en-etol (0.01 mol) in 40 ml of ethanol was added dropwise to a solution of 1.7 g of copper(II) chloride dihydrate (0.01 mol) in 40 ml of ethanol with stirring. The blue powder immediately formed was filtered off, washed with cold ethanol and dried over phosphoric anhydride.

Cu en-prol Cl_2 (B), Cu tn-etol Cl_2 (C) and Cu pn-prol Cl_2 (D) were prepared in a similar way to that for A.

Cu en-prol′ ClO_4 (E): Six tenth grams of potassium hydroxide (0.01 mol) and 1.2 g of en-prol (0.01 mol) were dissolved in 50 ml of methanol. To this was added dropwise a solution of 3.7 g of copper(II) perchlorate hexahydrate (0.01 mol) in 30 ml of methanol. The mixture was stirred for two hours at room temperature. The white precipitate ($KClO_4$) formed was removed by filtration. The filtrate was kept in a refrigerator for a few hours to complete the precipitation of potassium perchlorate, which was removed by centrifugation. The bluish violet solution was evaporated and a dark blue oily substance was obtained. This was dissolved in a small amount of hot ethanol and kept in a refrigerator overnight. Dark blue-violet crystals were obtained. These were recrystallized from ethanol. The compound obtained was hygroscopic in the atmosphere, and was found by elemental analysis to contain one molecule of ethanol for one copper ion. The ethanol was removed by keeping the crystals *in vacuo* at 100 °C for 1 hr.

Cu tn-prol′ClO_4 (F), Cu tn-prol′NO_3 (G), Cu pn-prol′ClO_4 (H), Cu tn-etol′$ClO_4 \cdot H_2O$ (I) and Cu tn-etol′Cl-H_2O (J) were prepared in a similar way to that for E. The crystals of F and H obtained from the ethanol solution were found to contain a certain amount of ethanol (1.0 mol for F and 0.7—0.8 mol for H) which was easily removed as in the case of E.

Compounds F, G, I, and J can also be prepared by mixing copper(II) salt and the ligand with the 1 : 2 mol-ratio in hot ethanol.

$Cu(en\text{-}etol)_2Cl_2$, (K): A hot solution of 1.7 g of copper(II) chloride dihydrate (0.01 mol) in 30 ml methanol was added dropwise to a well-stirred solution of 2.2 g of en-etol (0.02 mol) dissolved in 40 ml methanol. The solution was kept overnight in a refrigerator. The violet crystals separated were filtered off, washed with cold ethanol and dried over phosphoric anhydride.

$Cu(tn\text{-}etol)_2Cl_2$ (L) was prepared in a similar way to that for K.

$Cu(en\text{-}etol)_2(ClO_4)_2$ (M) and $Cu(en\text{-}prol)_2(ClO_4)_2$ (N) were prepared in a similar way to that for the chloride analogues except for the use of copper(II) perchlorate hexahydrate instead of copper(II) chloride dihydrate.

Measurements. Electronic spectra were measured with a Hitachi EPS-3T recording spectrophotometer equipped with a reflectance attachment.

Magnetic susceptibility was determined by the Gouy method at room temperature, diamagnetic corrections being made with Pascal's constants.

ESR spectra were measured using X-band with a JES-ME-3 ESR spectrometer.

Results and Discussion

The analytical, magnetic and spectral data of the fourteen copper(II) complexes obtained are summarized in Tables 2 and 3.

The complexes are classified into three types with the general formulas $CuLCl_2$, $CuL'ClO_4$ and CuL_2X_2, where X=Cl or ClO_4 and L and L′ denote the ligands

Table 2. Elemental analyses

Compd	Formula	C (%)		H (%)		N (%)	
		Found	Calcd	Found	Calcd	Found	Calcd
A	$CuC_4H_{12}N_2Cl_2O$	20.23	20.13	4.97	5.08	11.78	11.32
B	$CuC_5H_{14}N_2Cl_2O$	23.57	23.77	5.45	5.59	11.04	11.09
C	$CuC_5H_{14}N_2Cl_2O$	23.76	23.77	5.70	5.59	10.61	11.09
D	$CuC_6H_{16}N_2Cl_2O$	27.10	27.02	6.13	6.02	10.41	10.51
E	$CuC_5H_{13}N_2ClO_5$	21.11	21.43	4.78	4.69	9.86	10.00
F	$CuC_6H_{15}N_2ClO_5$	24.28	24.49	5.31	5.14	9.46	9.52
G	$CuC_6H_{15}N_3O_4$	28.22	28.06	5.82	5.90	16.54	16.37
H	$CuC_6H_{15}N_2ClO_5$	23.81	24.49	5.28	5.14	9.23	9.52
I	$CuC_5H_{13}N_2ClO_5$	21.19	21.43	4.68	4.69	9.77	10.00
J	$CuC_5H_{15}N_2ClO_2$	25.44	25.64	6.51	6.46	11.56	11.96
K	$CuC_8H_{24}N_4Cl_2O_2$	28.16	28.03	7.01	7.07	16.30	16.35
L	$CuC_{10}H_{28}N_4Cl_2O_2$	32.26	32.38	7.61	7.63	15.07	15.11
M	$CuC_8H_{24}N_4Cl_2O_{10}$	20.30	20.19	5.02	5.15	11.96	11.90
N	$CuC_{10}H_{28}N_4Cl_2O_{10}$	23.83	24.05	5.60	5.67	11.29	11.23

Table 3. Optical and magnetic data

Compd	Formula	μ_{eff} (BM)	Refl (nm)	Abs (ε) (nm)		
A	[Cu Cl_2(en-etol)]	1.79	700	710 (90.0)		met[a]
B	[Cu Cl_2(en-prol)]	1.81	660	670 (85.8)		met
C	[Cu Cl_2(tn-etol)	1.92	700	655 (88.2)		met
D	[Cu Cl_2(pn-prol)]	1.92	700	660 (88.1)		met
E	Cu(en-prol')ClO_4	0.90	590, 360	570 (70.5)	358 (1310)	et[a]
F	Cu(tn-prol')ClO_4	0.62	590, 360	580 (84.4)	358 (2820)	et
G	Cu(tn-prol')NO_3	0.69	580, 360	585 (86.1)	354 (2360)	et
H	Cu(pn-prol')ClO_4	0.83	570, 360	565 (66.1)	360 (1170)	et
I	Cu(tn-etol')$ClO_4 \cdot H_2O$	1.79	610	610 (76.3)	363 (128)	et
J	Cu(tn-etol')$Cl \cdot H_2O$	1.79	600	610 (76.2)	360 (422)	met
K	Cu(en-etol)$_2Cl_2$	1.95	570	595 (100)		met
L	Cu(en-prol)$_2Cl_2$	1.84	590	585 (107)	350 (295)	met
M	Cu(en-etol)$_2(ClO_4)_2$	1.77	600	590 (95.0)		met
N	Cu(en-prol)$_2(ClO_4)_2$	1.92	590	570 (88.0)	354 (553)	met

a) met and et denote "in methanol" and "in ethanol", respectively.

$NH_2(CH_2)_mCHRNH(CH_2)_nOH$ and $NH_2(CH_2)_mCHRNH(CH_2)_nO^-$, respectively.

(1) Cu L Cl_2: Compounds A, B, C, and D (where L=en-etol, en-prol, tn-etol and pn-prol; *cf.* Table 3) belong to this group. The tn-prol complex of this type could not be isolated in spite of repeated attempts.

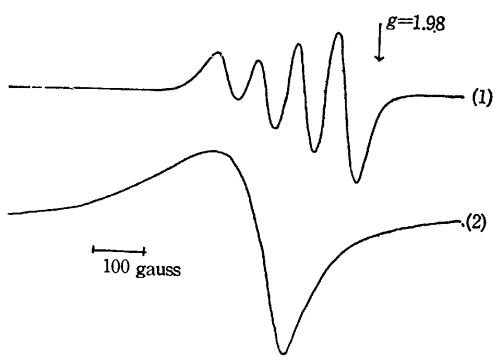

Fig. 1. ESR spectra of Cu en-prol Cl_2
(a) methanol solution at room temperature.
(b) powder at 150 °C (gain 1×1).

The compounds show normal magnetic moments for ordinary mononuclear copper (II) complexes (Table 3). ESR measurements in methanol solution and in powder provide further evidences for the mononuclear structure (Fig. 1).

Their reflectance spectra are similar to that of [Cu-en Cl_2] (en=ethylenediamine), known as a dichloro complex.[15] Thus, the structure of this group is essentially square planar, a copper ion being coordinated with two chloride ions and two amine nitrogen atoms. The alcoholic hydroxyl group is not likely to form a distinct bond with the metal ion, as judged from the visible spectrum (Table 3).

(2) CuL'ClO_4: Compounds E, F, H, and I (where L'=en-prol', tn-prol', pn-prol' and tn-etol'; *cf.* Table 3) belong to this group. Compounds G(=Cu tn-prol'NO_3) and J (=Cu tn-etol'$Cl \cdot H_2O$) appear to be similar to the above compounds and will be discussed here. All attempts to prepare the homologue with en-etol were unsuccessful. The compounds show

15) D. E. Billing and B. J. Hathway, *J. Chem. Soc., A*, **1969**, 312.

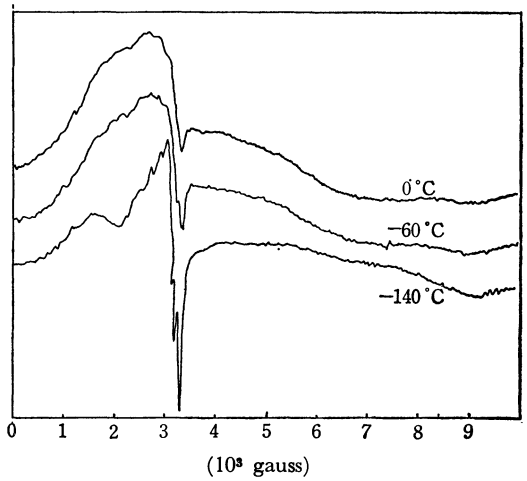

Fig. 2. Powder ESR spectra of Cu en-prol' ClO_4 (gain 2.8×100).

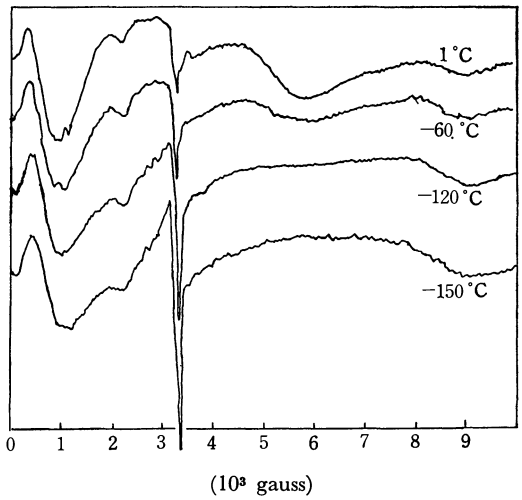

Fig. 3. Powder ESR spectra of Cu tn-prol' ClO_4 (gain 3.2×100).

subnormal magnetic moments, except for I and J (Table 2). Powder ESR measurements at room temperature show that the spectral patterns of these complexes differ a great deal from those of the ordinary monomeric copper(II) complexes (Figs. 2 and 3). The broad signals observed in the range 1000—8000 Gauss may be due to a triplet state, indicating a considerable magnetic interaction between the two copper ions. Therefore, we may conclude that E, F, G, and H have a binuclear structure bridged with alcoholate oxygen (Fig. 5).

On the other hand, both I and J show a normal magnetic moment, 1.79 BM, at room temperature. However, their ESR spectra, which are very similar to each other, differ entirely from those of ordinary mononuclear copper(II) complexes, especially at low temperature (Fig. 4, and also Fig. 1). It should be noted that the intensities of the ESR signals remarkably increase with the lowering of temperature (Fig. 4), whereas in the other complexes E, F, G, and H, the spectra except for the band at about 3000 Gauss do not increase in intensity but gradually decline with the lowering of temperature (Figs. 2 and 3).

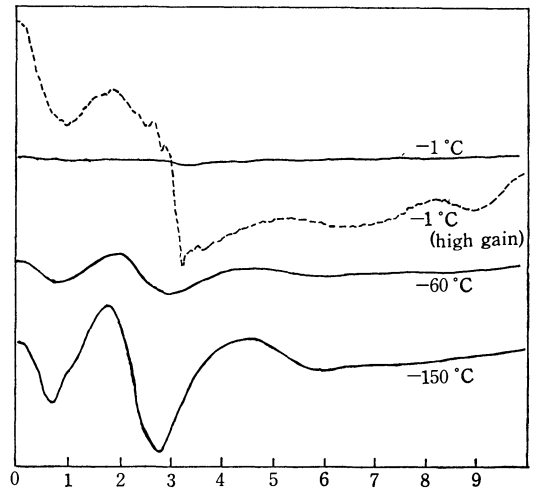

Fig. 4. Powder ESR spectra of Cu tn-etol' $ClO_4 \cdot H_2O$ (gain 1×10 for solid line, 3.2×100 for broken line).

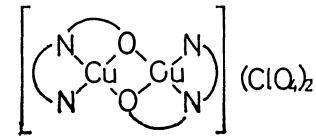

Fig. 5. The structure of $CuL'ClO_4$.

This suggests that ferromagnetic interaction takes place in I and J, where the ground state is triplet (or multiplet) and an upper singlet state is thermally populated at room temperature. As is well-kown in magnetically dilute solid, an ESR signal generally increases in intensity with lowering of temperature due to an increase of the difference of thermal population between the split Zeeman levels.[16] In addition to this effect, in the case of compounds I and J, the ground triplet or multiplet state becomes more populated with the lowering of temperature to increase the ESR intensity. On the other hand, in the antiferromagnetic compounds where the ground state is singlet such as E, F, G, and H, the near-lying upper triplet state becomes less populated with lowering of temperature. The effect acts on ESR to reduce its intensity at low temperature. Thus, the observed ESR intensities of these compounds are nearly counterbalanced by the two opposite temperature effects in a certain temperature range (Figs. 2 and 3). In contrast to this, the signal at about 3000 gauss, which is attributable to a trace of mononuclear impurity, remarkably increases in intensity with the lowering of temperature.

The structures of compounds I and J are likely to be similar to those of Cu aca-etol'[17] and Cu sal-etol'[18] (where aca-etol' and sal-etol' denote $^-OC(CH_3)=CHC(CH_3)=NCH_2CH_2O^-$ and $o\text{-}O^-(C_6H_4)CH=NCH_2CH_2O^-$, respectively), since tn-etol is similar to these

16) M. Bersohn and J. C. Baird "An Introduction to Electron Paramagnetic Resonance," Chapt. 1 Benjamin, New York (1966).
17) J. A. Bertland and J. A. Kelley, *Inorg. Chim. Acta*, **4**, 203 (1970).
18) K. Mori, H. Ueda, A. Nakahara, and M. Kishita, 24th Annual Meeting of Chem. Soc. Japan, Osaka (1971). Proceedings, 2, p. 762.

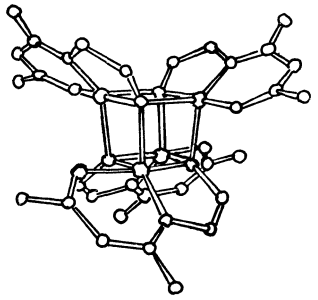

Fig. 6. The structure of Cu aca-etol'[17]

ligands in forming 5- and 6-membered chelate rings upon coordination, and in their magnetic behavior, *i.e.* ferromagnetic interaction takes place though they all show normal magnetic moments at room temperature. The X-ray analysis[17] shows that Cu aca-etol' is tetrameric (Fig. 6), where alcoholate oxygens coordinate to three copper ions and, consequently, are tetrahedrally bonded.

Since no stable binuclear complexes were obtained by using en-etol, pn-etol and tn-etol, we may conclude that for the formation of the binuclear complex the favorable member of the chelate ring involving bridging oxygen is six. The 5- and 6-membered chelate ring system such as Cu tn-prol'ClO_4 seems to be slightly more favorable for the formation of the binuclear complex than the 5- and 6-membered chelate ring system such as Cu en-prol'ClO_4, judging from the easier formation of the former than the latter.

Compounds E, F, G, and H show similar electronic spectra to each other in both solid and ethanolic solutions, giving two bands in the 10—33 kK region (Fig. 7). The numerical data are summarized in Table 3. The bands around 600 nm are undoubtedly assigned to d–d transitions, and the more intense bands around 350 nm can be attributed to charge-transfer transitions from ligands to a metal ion. The latter bands seem to be characteristic of the binuclear structure in which two copper ions are bridged by oxo anions. This assumption well coincides with Yamada and Ojima's observation[11] on some binuclear copper(II) complexes bridged with two alcoholate oxygens. In order to confirm this assumption we have measured powder reflectance spectrum of the binuclear complex, $\left[\mathrm{A\ Cu}\begin{matrix}\diagup\mathrm{OH}\diagdown\\ \diagdown\mathrm{OH}\diagup\end{matrix}\mathrm{Cu\ A}\right](ClO_4)_2$ (where A=*N*,*N*,*N'*,*N'*-tetramethylethylenediamine or *N*,*N*,*N'*,*N'*-tetraethylethylenediamine), and have observed similar bands at about 360 nm (Fig. 10). Their aqueous solutions show shoulders at the same position at pH 8 where the binuclear species dominates in the equilibrium.[19]

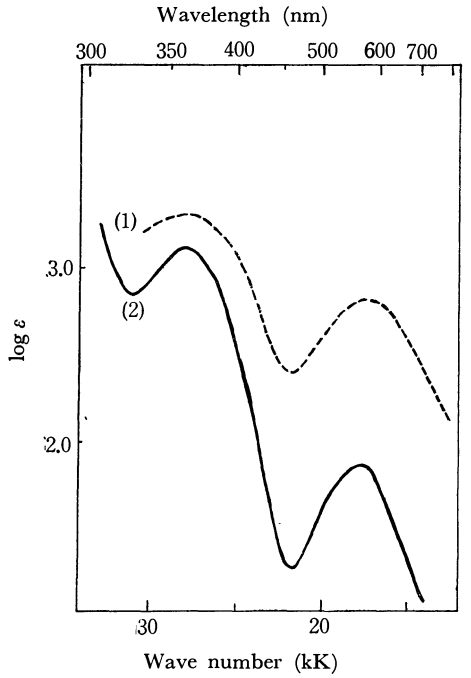

Fig. 7. Electronic spectra of Cu en-prol' ClO_4.
(1) powder, (2) ethanol solution.

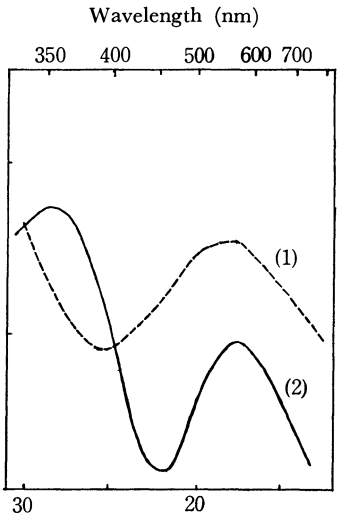

Fig. 8. Electronic spectra of $Cu(en\text{-}prol)_2(ClO_4)_2$. (1) powder reflectance, (2) methanol solution.

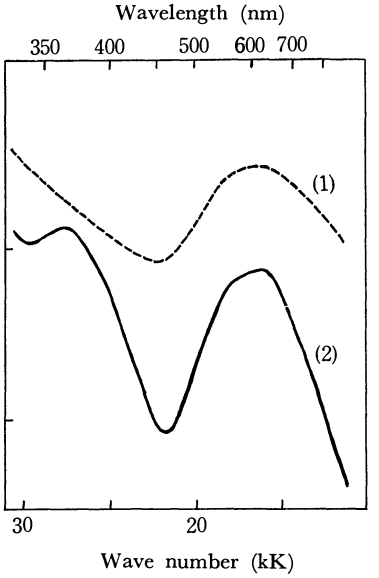

Fig. 9. Electronic spectra of Cu tn-etol' $ClO_4 \cdot H_2O$.
(1) powder reflectance, (2) aqueous solution.

19) We have studied the equilibria of this solution by ESR (unpublished). A detailed study was recently reported on the equilibria of this system: E. Arenare, P. Paoletti, A. Dei, and Vacca, *J. Chem. Soc., Dalton*, **1972**, 736.

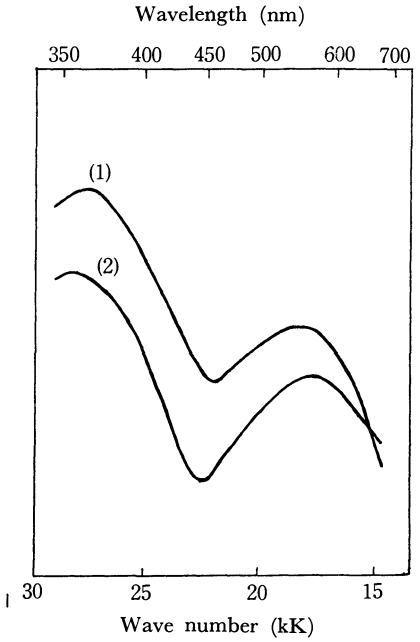

Fig. 10. Power reflectance spectra of $[A\ Cu\langle^{OH}_{OH}\rangle Cu\ A](ClO_4)_2$.
(1) A=*N,N,N',N'*-tetraethylethylenediamine,
(2) A=*N,N,N',N'*-tetramethylethylenediamine.

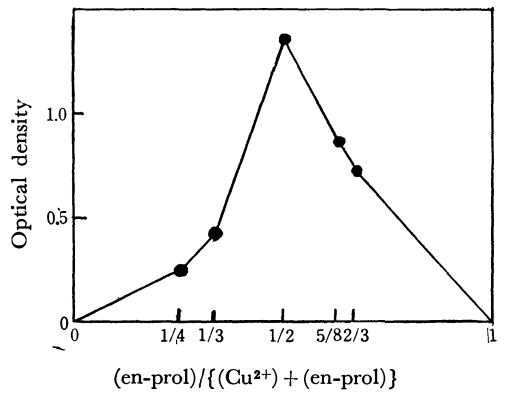

Fig. 11. The continuous variation method at 354 nm applied to the system Cu^{2+}/en-prol in basic solution.
The total concentration of Cu^{2+} and en-etol was 2×10^{-3} mol/l in each solution containing *t*-butylamine with the same molar concentration as that of en-etol.

However, in the low (<6) and the high (>9) pH regions, where the concentration of the binuclear species is negligible, neither a peak nor a shoulder was observed around 360 nm. We also investigated the powder reflectance spectrum of [Cu eta eta']ClO_4[20] (where eta and eta' denote $NH_2CH_2CH_2OH$ and $NH_2CH_2CH_2O^-$, respectively), in order to see whether the band around 360 nm is brought about by coordination of an alkoxo or a hydroxo group to copper(II) ion regardless of bridged or simple coordination. Neither peak nor shoulder has been found in the near-ultraviolet region, indicating that coordination of the alkoxo group to copper(II) ion itself does not cause the characteristic band in the near-ultraviolet region.

20) S. Kida, *Nippon Kagaku Zasshi*, **85**, 428 (1964).

In conclusion, all experimental results so far obtained support the rule that the binuclear copper(II) complex bridged by alkoxo or hydroxo groups always show the characteristic band in the near-ultraviolet region (<29 kK), unless there are other intense absorptions to mask the region.

Compounds I and J show no characteristic band in the near-ultraviolet region in the powder reflectance spectrum (Fig. 9). This is undoubtedly due to the tetrameric structure, where bridging alcoholate oxygens are tetrahedrally bonded, and accordingly have no π-electrons to cause the absorption around 360 nm. In an aqueous or methanolic solution, however, the band was observed at 350 nm, though its intensity is very low as compared to that of the binuclear complexes in this group. Thus, a binuclear complex similar to E, F, G, and H might be partially formed in the solutions of I and J.

(3) CuL_2X_2: Compounds K, L (where L=en-etol, and en-prol; X=Cl), M and N (where L=en-etol and en-prol; X=ClO_4), belong to this group. It should be noted that the same preparative procedure as for the above compounds, *viz.*, mixing the copper(II) salt and the ligand in a 1 : 2 mole-ratio in methanolic solution, did not give rise to the formation of Cu(tn-etol)$_2$(ClO_4)$_2$ and Cu(tn-prol)$_2$(ClO_4)$_2$, but gave Cu tn-etol'$ClO_4\cdot H_2O$ and Cu tn-prol'ClO_4.

The compounds show normal magnetic moments at room temperature, and d–d bands at 560—600 nm (Table 3). The solution and the powder ESR spectra are very close to those of the compounds of group (1), showing characteristic patterns of a mononuclear copper(II) complex. We can thus conclude that complexes of this group are similar to [Cu en$_2$]X_2 in various properties, and that they are of essentially square-planar structure coordinated with four amine nitrogens. The red shift in 10—50 nm relative to [Cu en$_2$](ClO_4)$_2$ implies that there is some perturbation along the tetragonal axis, but not strong enough to be called a coordination bond.

It is remarkable that the solution spectra in the near-ultraviolet region differ from the powder spectra (Fig. 8). The bands observed at about 360 nm are similar in contour and in position to those of the oxo-bridged complexes. Therefore, $[Cu\ L_2]^{2+}$ is very likely to dissociate partially in solution to form a binuclear species similar to compounds E, F, G, and H, giving rise to the equilibrium

$$2[CuL_2]^{2+} \rightleftarrows [Cu_2L'_2]^{2+} + 2LH^+. \qquad (a)$$

In fact, the intensities of the bands are much lower than those of the binuclear complexes of group (2), and the spectra do not follow Beer's law in the near-ultraviolet region. The formation of a 1 : 1 complex was verified spectrophotometrically by the use of a continuous variation method (Fig. 11). It should be noted that the addition of some proton acceptor such as trimethylamine to the methanolic solution of a complex of this group gives rise to a distinct promotion of the intensity of the band at about 360 nm. This also supports assumption based on equilibrium (a).

Ion-selective Electrode Membranes Responsive to Maleic and Phthalic Acids

Akinori Jyo, Morihisa Yonemitsu, and Nobuhiko Ishibashi*

Department of Applied Analytical Chemistry, Faculty of Engineering, Kyushu University, Fukuoka 812

(Received May 28, 1973)

Ion-selective electrodes responsive to maleic and phthalic acids were prepared. The organic solvent solution of the ion-pair of the objective monovalent acid anion with a Crystal Violet or a tris(bathophenanthroline)-iron(II) ion was used as the electrode membrane. The responses of both electrodes were linear down to 10^{-4}—$10^{-4.5}$ M, with an ideal Nernstian slope of 57—58 mV per activity decade at 20 °C. Together with the potential slope, the pH dependence of the potential showed that the electrode responded to the monovalent anion of maleic or phthalic acid. The interferences of acetate, benzoate, and chloride were extremely low, whereas iodide and perchlorate interfered greatly. The maleic acid electrode works well without the interference of fumaric aicd. The phthalic acid electrode also functions without any interferences by isophthalic or terephthalic acid.

Various methods of analyzing maleic and phthalic acids have been reported.[1-6] However, no report has been presented on an electrode responsive to maleic or phthalic acid.

Maleic acid is easily extracted into an organic solvent containing a large cation, such as a crystal violet or a tris(bathophenanthroline)iron(II) ion, and forms an ion-pair with the cation, whereas fumaric acid, the *trans*-isomer of maleic acid, is not extracted. A similar phenomenon is observed among the isomers of the benzenedicarboxylic acids, and phthalic acid is preferentially extracted into the above-mentioned organic solvent from an aqueous solution of a mixture of the isomers.

In a previous communication, we have briefly reported on the performances of maleic acid- and phthalic acid-sensitive electrodes prepared by utilizing the extractability differences among the isomers.[7] This paper will describe further details of the preparations and performances of the electrodes. By using the electrodes, it became possible to determine the concentrations of the acids more rapidly and simply than by the conventional methods.

Experimental

Reagents. All the chemicals used were of reagent-grade quality. The aqueous solution of the monosodium salt of maleic or phthalic acid was prepared by mixing the aqueous solution of the acid and the sodium hydroxide solution in an appropriate ratio. The pH of the sample solution was adjusted with an aqueous solution of sulfuric acid, potassium dihydrogenphosphate, or sodium hydroxide.

Sensitive Liquid Membrane. An organic solvent solution of the Crystal Violet salt or the tris(bathophenanthroline)iron(II) salt of the objective monovalent acid anion was used as the liquid membrane. The concentration of the salt was 10^{-4} M. Nitrobenzene (NB), 1,2-dichloroethane (DCE), and chloroform (CF) were used as the solvents of the membrane.

The membrane solution containing the crystal violet salt was prepared by the following solvent extraction method. Equal volume portions of the organic solvent, a 10^{-2} M aqueous solution of the acid, and a 10^{-3} M aqueous solution of Crystal Violet were poured into a separating funnel, after which the funnel was shaken with a mechanical shaker for 30 min. After the separation of layers, the organic phase was shaken again with a 10^{-3} M aqueous solution of the acid in order to purify it. In the extraction process, the pH of the aqueous phase was maintained at 4 in order to extract the acid as a monovalent anion. The organic phase was separated and diluted with the organic solvent saturated with water. The organic solution thus obtained was used as the sensitive membrane. The membrane solution which contained the tris(bathophenanthroline)iron(II) salt was prepared by a similar procedure.

Potential Measurement. The potential of the following electrochemical cell was measured by using a Takeda Riken Electrometer TR 8651.

+SCE|Reference Solution|Liquid Membrane|Sample Solution|SCE−

The cell assembly has been illustrated in detail elsewhere.[8] The lower part of a glass U-tube was filled with 10 ml of the membrane solution, the reference and sample solutions, 10 ml of each, were thus separated. An agar salt bridge saturated with potassium chloride or ammonium chloride was used to connect the respective saturated calomel electrode (SCE) with the reference and sample solutions. The reference solution was a 10^{-2} M aqueous solution of the objective organic acid, its acidity has been adjusted to pH 4.

Results and Discussion

Potential Response of the Electrode. In the potentiometric determination of the concentration of maleic or phthalic acid, an electrode responsive to a monovalent anion, *i.e.*, a hydrogenmaleate or hydrogenphthalate ion, is preferable to a divalent maleate ion- or phthalate ion-responsive electrode from an analytical viewpoint, because the slope of the calibration curve of the former electrode can be expected to be twice that of the latter electrode.

Since the first and second dissociation constants are $10^{-1.92}$ and $10^{-6.22}$ for maleic acid, and $10^{-2.95}$ and $10^{-5.41}$ for phthalic acid, respectively, the main component species of the acids are the monovalent anions around pH 4. Accordingly, the response of the electrode was examined on the sample solution at pH 4

* To whom any correspondence should be addressed.

1) S. Siggia and N. A. Floramo, *Anal. Chem.*, **25**, 797 (1953).
2) V. Z. Deal and G. E. A. Wyld, *ibid.*, **27**, 47 (1955).
3) K. Burger and E. Schulek, *Z. Anal. Chem.*, **172**, 98 (1960).
4) W. Funasaka, T. Kojima and K. Fujimura, *Bunseki Kagaku*, **13**, 42 (1964).
5) Y. Yamamoto, N. Okamoto and E. Tao, *ibid.*, **14**, 343 (1965).
6) Y. Yamamoto, T. Kumamaru and M. Muranaka, *Talanta*, **19**, 415 (1972).
7) N. Ishibashi, A. Jyo and M. Yonemitsu, *Chem. Lett.*, **1973** 483.
8) N. Ishibashi, and H. Kohara, *Anal. Lett.*, **4**, 785 (1971).

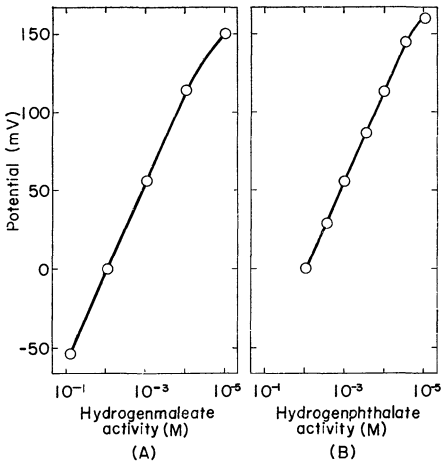

Fig. 1. Responses of maleic acid electrode(A) and phthalic acid electrode(B).

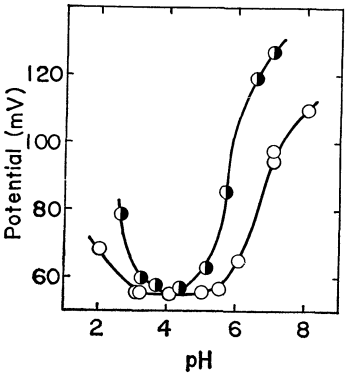

Fig. 2. Influence of pH on electrode potential.
Phthalic acid electrode (◑)
Maleic acid electrode (○)
Membrane: 10^{-4} M nitrobenzene solution of crystal violet salt of corresponding monovalent acid anion.

in order to detect the acid as monovalent anion species.

Figure 1 shows the potential response of the electrode. The membrane consisted of a 10^{-4} M nitrobenzene solution of the crystal violet salt of the monovalent acid anion. The response of the phthalic acid electrode could be examined on the sample solution below 10^{-2} M because of the small solubility of phthalic acid at pH 4. The activity coefficient of the objective anion was calculated from the Debye-Hückel equation, in which the ion-size parameter was assumed to be equal to those of salicylate and vinylacetate.[9] The responses of both electrodes were linear over the activity ranges from 10^{-1} to 10^{-4} M and from 10^{-2} to $10^{-4.5}$ M for the maleic and phthalic acid sample solutions respectively. An ideal Nernstian slope of 58 mV per activity decade at 20 °C was observed for each electrode. Equilibrium potentials were achieved within a few sec, and potential values were reproducible to ±0.2 mV.

The responses of the electrodes with different ion-exchange sites and different membrane solvent species are summarized in Table 1. Irrespective of the site and the membrane solvent species, the properties of the electrode membranes, such as the potential slope, the response time, and the stability of the potential, were almost the same as those of the nitrobenzene membranes described above. The slope of 57—58 mV indicated that the electrodes responded to the monovalent anion species of maleic and phthalic acids.

Influence of pH on the Electrode Potential. The potential can be effected to vary with the pH of the sample solution, since the relative concentration of the monovalent anion depends on the acidity of the solution. Figure 2 shows the potentials of the electrodes for 10^{-3} M sample solutions with different pH values. The theoretical value of 56 mV was observed in the pH ranges from 3 to 5 and from 3.8 to 4.2 for the solutions of the maleic and phthalic acids respectively. In the higher and lower pH regions, the remarkable change in the potential was in accordance with the concentration decrease in the monovalent anion species of the acid. This suggests that the electrodes

Table 1. Responses of electrodes at 20 °C

Electrode	Site	Solvent	Slope (mV/log *a*)	Lower limit of linear response (M)
Maleic acid	CV^{+} a)	NB	−58	10^{-4}
		DCE	−58	10^{-4}
		CF	−58	10^{-4}
	$Fe(B\cdot phen)_3^{2+}$ a)	NB	−57	10^{-4}
		DCE	−57	10^{-4}
		CF	−57	10^{-4}
Phthalic acid	CV^{+}	NB	−58	$10^{-4.5}$
		DCE	−58	$10^{-4.5}$
		CF	−58	10^{-4}
	$Fe(B\cdot phen)_3^{2+}$	NB	−57	10^{-4}
		DCE	−57	10^{-4}
		CF	−57	10^{-4}

a) CV^{+} and $Fe(B\cdot phen)_3^{2+}$ denote Crystal Violet and tris(bathophenanthroline)iron(II) ions, respectively.

9) J. Kielland, *J. Amer. Chem. Soc.*, **59**, 1675 (1937).

Table 2. Influences of coexisting isomers on electrode potential

Electrode	Interferant (j)	Concn. of interferant (M)	Slope (mV/log a)	Lower limit of linear response (M)
Maleic acid	Fumaric acid	1.0×10^{-2}	−57——58	10^{-4}
Phthalic acid	Isophthalic acid	2.0×10^{-3}	−57——58	10^{-4}—$10^{-4.5}$
	Terephthalic acid	satd. ($\simeq10^{-4}$)	−57——58	10^{-4}—$10^{-4.5}$

Table 3. Selectivity coefficients of maleic acid electrode at 20 °C

Interferant	(Site)	Membrane				
		CV^+			$Fe(B\cdot phen)_3^{2+}$	
	(Solvent)	NB	DCE	CF	NB	DEC
Acetic acid		—	0.0001	—	—	—
Fumaric acid		<0.001	<0.001	<0.001	<0.001	<0.001
Benzoic acid		0.02	0.03	0.01	—	—
CF_3COO^-		0.4	0.3	0.08	—	0.3
Salicylic acid		5.6	4.2	1.5	5.7	—
Phthalic acid		6.7	5.2	3.6	7.0	5.3
Benzilic acid		10	10	3.7	—	—
Cl^-		0.002	0.004	0.006	—	—
Br^-		—	0.09	—	—	—
NO_3^-		0.7	0.6	—	—	—
I^-		15	14	7	—	—
ClO_4^-		1.1×10^3	6.0×10^2	16	1.1×10^3	5.3×10^2

Table 4. Selectivity coefficients of phthalic acid electrode at 20 °C

Interferant	(Site)	Membrane				
		CV^+			$Fe(B\cdot phen)_3^{2+}$	
	(Membrane)	NB	DCE	CF	NB	DEC
Acetic acid		—	2×10^{-5}	—	—	—
p- and *m*-isomer		<0.01	<0.01	<0.01	<0.01	<0.01
Benzoic acid		0.003	0.005	0.003	0.003	0.005
CF_3COO^-		0.06	0.06	0.02	—	0.05
Maleic acid		0.15	0.19	0.28	0.14	0.19
Salicylic acid		0.85	0.85	0.42	—	—
Benzilic acid		1.5	2	0.9	—	—
Cl^-		0.0003	0.0008	0.001	—	—
Br^-		—	0.02	—	—	—
NO_3^-		0.1	0.1	—	—	—
I^-		2	3	2	—	—
ClO_4^-		1.4×10^2	1.2×10^2	4	1.4×10^2	1.0×10^2

do not respond to the undissociated acids and the divalent anions of the acids, and supports the view that the acids are extracted into an organic solvent as monovalent anions and not as divalent anions.[6] In the practical use of the electrode, care must be taken in the adjustment of the pH of the sample solution.

Selectivity of the Electrode. The potential, E, for the sample solution containing the primary ion, i, and any other ion, j, is given by the empirical Eq. (1):

$$E = 2.303\,RT/F\log(a_i'/(a_i''+K a_j'')) \quad (1)$$

where a_i and a_j are the activities of the monovalent anions, i and j, and where K is a selectivity coefficient. The activities of the reference and sample solutions are designated by prime and double prime respectively.

The interfering effects of the isomer ions were examined on the basis of the mixed solution method.[10] In this method, the potential was measured on a series of sample solutions, each solution containing a fixed amount of an interferant, j, and a varying amount of the primary ion, i. The influences of the isomer ions are summarized in Table 2. At the lowest limit of linear response, the sample solution contained 100 times more fumaric acid than maleic acid, and about 20 times more isophthalic acid than phthalic acid.

10) G. J. Moody and J. D. R. Thomas, "Selective Ion Sensitive Electrodes," Merrow Pub. Co. Watford, England, (1972).

However, no interfering effect of fumaric or isophthalic acid was observed. The response of the phthalic acid electrode was not affected by the presence of the terephthalic acid, even in the saturated solution of the latter acid. These results indicate that the electrodes are capable of determining the concentrations of maleic and phthalic acids without any interference by the isomer acids.

The interfering effects of other organic and inorganic anions were examined by using the separate-solution method.[10] In this method, the potential was measured on the sample solution containing an interferant alone. The pH of the sample solution was maintained within the region where the interferant existed as a monovalent anion. In Table 3, the selectivity coefficients of the maleic acid electrode are listed. The interferences of acetate, benzoate, and chloride were extremely low, but the salicylate and iodide interfered greatly. The perchlorate ion showed the highest interference. The selectivity of the phthalic acid electrode is also summarized in Table 4. The selectivity of the phthalic acid electrode was better than that of the maleic acid electrode. The chloroform membrane electrode had slightly higher selectivity values than the nitrobenzene and 1,2-dichloroethane membrane electrodes. The selectivity coefficients were approximately independent of the site species if the electrode membrane was prepared by using the same solvent with a relatively high dielectric constant. These results agree with the view proposed by Eisenman of the selectivity of the ion-sensitive electrode with a liquid ion-exchanger membrane of the complete-dissociation type.[11]

The authors are grateful for the financial support given to this work by the Ministry of Education.

11) G. Eisenman, *Anal. Chem.*, **40**, 310 (1968).

BULLETIN OF THE CHEMICAL SOCIETY OF JAPAN, VOL. 46, 3737—3744 (1973)

Derivatographic Studies on Transition Metal Complexes. XII.[1] Thermal Olation of Hydroxoaquo Cobalt(III) and Chromium(III) Complexes Containing Amino Acids in Solid Phase[2]

Ryokichi Tsuchiya, Akira Uehara, and Eishin Kyuno

Department of Chemistry, Faculty of Science, Kanazawa University, Kanazawa 920

(Received May 29, 1973)

The thermal olation of the following four types of complexes in a solid phase was investigated by means of derivatography: 1) cationic complexes, $[Co(OH)(n_3\text{-}o)(H_2O)]X$, 2) anionic complexes, $M[Co(OH)(n\text{-}o_3)(H_2O)]$, 3) double complexes, $[Co(OH)(n_3\text{-}o)(H_2O)][Co \text{ or } Cr(OH)(n\text{-}o_3)(H_2O)]$ and 4) neutral complexes, $[Co(OH)(n\text{-}o)_2(H_2O)]$, where n_3-o, n-o_3 and $(n\text{-}o)_2$ denote gly-en (glycinate ion and ethylenediamine) or dtma (diethylenetriaminemonoacetate ion), the analogues of nta (nitrilotriacetate ion) and α-amino acid ions, respectively. The thermal data such as initiation temperature, enthalpy change and activation energy of the olation were estimated from the respective derivatograms. From the results the effect of various ligands or counter ions (outer-sphere ions) on the olation was discussed.

Olation in a solid phase was first observed by Werner[3] in the $[Co(OH)(H_2O)(NH_3)_4]X_2$ type complexes. Recently, Wendlandt and Fisher reported that the olation of complexes of this type takes place endothermically and that the heats of olation are 3.3, 6.1, 4.2 and 2.4 kcal/mol for $X=Cl^-$, Br^-, NO_3^- and SO_4^{2-}, respectively.[4] It is of interest that the values are considerably smaller than those expected for the liberation of coordinated water alone. However, these values are understandable if the olation is considered to involve both dissociation of coordinated water and formation of olated compound simultaneously; the former step might be an endothermic, and the latter step an exothermic reaction.

In part IV of this series, we reported on the olation of the anionic complexes having the general formula $K[Co(OH)(n\text{–}o_3)(H_2O)]$,[5] where the ligand $(n\text{–}o_3)$ refers to nta, nipda, α-abda, vda, lda, pgda and pada.[6] The values of enthalpy change estimted from the DTA curves showed that the olation of all the anionic complexes proceeds exothermically. From an inspection of the numerical values of initiation temperature and activation energy, we concluded that the olation takes place more readily according to the sequence: nta→nipda→α-abda→vda→lda→pgda→pada-complexes.

The present study was undertaken to obtain information on the olation of various types of complexes and to systematically examine the effect of various ligands

1) Part XI of this series: R. Tsuchiya, T. Murakami, and E. Kyuno, This Bulletin, **46**, 3119 (1973).

2) Presented in part at the 26th Annual Meeting of the Chemical Society of Japan, Hiratsuka, 1, April, 1972.

3) A. Werner, *Ber.*, **40**, 4434 (1907).

4) W. W. Wendlandt and J. K. Fisher, *J. Inorg. Nucl. Chem.*, **24**, 1685 (1962).

5) R. Tsuchiya, A. Uehara, and E. Kyuno, This Bulletin, **44**, 701 (1971).

6) The full names are as follows : nta : nitrilotriacetate ion, nipda : nitriloisopropionicdiacetate ion, α-abda : *d,l*-α-amino-*n*-butyric-*N,N*-diacetate ion, vda : *l*-valine-*N,N*-diacetate ion, lda : *l*-leucine-*N,N*-diacetate ion, pgda : *d*-α-phenylglycine-*N,N*-diacetate ion and pada : *d,l*-α-phenylalanine-*N,N*-diacetate ion.

and counter ions (outer-sphere ions) on the olation. The thermal olation of cationic, anionic, double and neutral complexes was investigated by means of derivatography; it can be formulated as follows:

1) $2[Co(OH)(n_3\text{-}o)(H_2O)]X \rightarrow [(n_3\text{-}o)Co(OH)_2Co(n_3\text{-}o)]X_2 + 2H_2O$

2) a) $2K[Co(OH)(n\text{-}o_3)(H_2O)] \rightarrow K_2[(n\text{-}o_3)Co(OH)_2Co(n\text{-}o_3)] + 2H_2O$

b) $2M(I)$ *or* $M(II)_{1/2}[Co(OH)nipda(H_2O)] \rightarrow M(I)_2$ *or* $M(II)[(nipda)Co(OH)_2Co(nipda)] + 2H_2O$

3) $[Co(OH)(n_3\text{-}o)(H_2O)][Co$ *or* $Cr(OH)(n\text{-}o_3)(H_2O)] \rightarrow [(n_3\text{-}o)Co(OH)_2Co$ *or* $Cr(n\text{-}o_3)] + 2H_2O$

4) $2[Co(OH)(n\text{-}o)_2(H_2O)] \rightarrow [(n\text{-}o)_2Co(OH)_2Co(n\text{-}o)_2] + 2H_2O$

where n_3-o, n-o and n-o_3 denote gly-en (glycinate ion and ethylenediamine) or dtma (diethylenetriaminemonoacetate ion), α-amino acid ion and the analogues of nta ion, respectively, and M(I) and M(II) refer to any one of the alkali metal and the alkaline earth metal ions, respectively.

The hydroxoaquo-type complexes used as the starting materials are listed in Table 1 (The numerals refer to the index numbers of the respective complexes).

As cationic complexes, $[Co(OH)gly(H_2O)en]X$ and $[Co(OH)dtma(H_2O)]X$ were used, where X represents a univalent anion such as Cl^-, NO_3^-, Br^- and I^-.

Table 1. List of hydroxoaquo-type complexes used in the present study

	Type		General formula	Complex[a]	Index No.
1.	Cationic complexes	1.	$[Co(OH)gly(H_2O)en]X$	[Co (gly en)]Cl·aq	1.1.1
				[Co (gly en)]NO_3·aq	1.1.2
				[Co (gly en)]Br	1.1.3
		2.	$[Co(OH)dtma(H_2O)]X$	[Co (dtma)]NO_3	1.2.1
				[Co (dtma)]Br·aq	1.2.2
				[Co (dtma)]I	1.2.3
2.	Anionic complexes	1.	$K[Co(OH)(n\text{-}o_3)(H_2O)]$	K[Co nta]·aq	2.1.1
				K[Co nipda]·2aq	2.1.2
				K[Co α-abda]·2aq	2.1.3
				K[Co vda]·1.5aq	2.1.4
				K[Co lda]·aq	2.1.5
				K[Co pada]·5aq	2.1.6
		2.	$M(I)[Co(OH)nipda(H_2O)]$	Li[Co nipda]·aq	2.2.1
				Na[Co nipda]·aq	2.2.2
				Rb[Co nipda]·aq	2.2.3
				Cs[Co nipda]	2.2.4
		3.	$M(II)_{1/2}[Co(OH)nipda(H_2O)]$	Mg[Co nipda]$_2$·2aq	2.3.1
				Ca[Co nipda]$_2$·2aq	2.3.2
				Sr[Co nipda]$_2$·2aq	2.3.3
				Ba[Co nipda]$_2$·4aq	2.3.4
3.	Double complexes	1.	$[Co(OH)gly(H_2O)en][Co(OH)(n\text{-}o_3)(H_2O)]$	[Co (gly en)][Co nta]·2aq	3.1.1
				[Co (gly en)][Co nipda]·2aq	3.1.2
				[Co (gly en)][Co α-abda]·2aq	3.1.3
				[Co (gly en)][Co vda]·2aq	3.1.4
				[Co (gly en)][Co lda]·2aq	3.1.5
				[Co (gly en)][Co pada]·2aq	3.1.6
			$[Co(OH)gly(H_2O)en][Cr(OH)(n\text{-}o_3)(H_2O)]$	[Co (gly en)][Cr nta]·2aq	3.1.7
				[Co (gly en)][Cr nipda]·2aq	3.1.8
				[Co (gly en)][Cr α-abda]·2aq	3.1.9
				[Co (gly en)][Cr vda]	3.1.10
				[Co (gly en)][Cr lda]·2aq	3.1.11
				[Co (gly en)][Cr pada]·2aq	3.1.12
		2.	$[Co(OH)dtma(H_2O)][Co(OH)(n\text{-}o_3)(H_2O)]$	[Co (dtma)][Co nta]·2aq	3.2.1
				[Co (dtma)][Co nipda]·2aq	3.2.2
				[Co (dtma)][Co α-abda]·2aq	3.2.3
				[Co (dtma)][Co vda]·2aq	3.2.4
				[Co (dtma)][Co lda]·2aq	3.2.5
				[Co (dtma)][Co pada]·2aq	3.2.6
			$[Co(OH)dtma(H_2O)][Cr(OH)(n\text{-}o_3)(H_2O)]$	[Co (dtma)][Cr nta]·4aq	3.2.7
				[Co (dtma)][Cr nipda]·4aq	3.2.8
				[Co (dtma)][Cr α-abda]·2aq	3.2.9
				[Co (dtma)][Cr vda]·2aq	3.2.10
				[Co (dtma)][Cr lda]·4aq	3.2.11
				[Co (dtma)][Cr pada]·2aq	3.2.12
4.	Neutral complexes		$[Co(OH)(n\text{-}o)_2(H_2O)]$	[Co $(gly)_2$]·2aq	4.1
				[Co $(ala)_2$]·aq	4.2

n-o_3 and n-o denote the analogues of nta ion and α-amino acid ions, respectively.

a) OH and H_2O are omitted in all the formulas.

For the anionic complexes, all the ligands (n-o_3) used can form (5,5,5)-membered chelate rings and their structures become more bulky according to the order: nta→nipda→α-abda→vda→lda→pgda→pada.

Two kinds of double complexes were obtained, one containing cobalts as the central metal both in cationic and anionic species (designated as [Co][Co]), and the other containing cobalt in cationic and chromium in anionic species (designated as [Co][Cr]). The double complexes are especially interesting for carrying out studies from the viewpoint of 1) whether the olation takes place between two identically charged complex ions or between two counter charged complex ions, and 2) the difference in olation to be found between [Co][Co] and [Co][Cr].

Neutral complexes are advantageous for observing the net olation because of the lack of counter ions.

Experimental

Preparation of Materials. *1) Cationic Complexes. Hydroxoglycinatoaquoethylenediaminecobalt(III) Perchlorate, [Co(OH)gly(H_2O)en]ClO_4 (reddish violet).* Eight grams of the chloroaquo complex ([CoCl(gly)(H_2O)en]Cl[7]) was dissolved in 25 ml of aqueous solution containing 1.5 g of sodium hydroxide. The solution was mildly heated at 50 °C on a water-bath until the violet solution turned dark red. Special care should be taken to prevent the temperature of the solution from exceeding 50 °C, otherwise an undesirable diaquo complex is frequently generated. Twenty-five milliliters of water containing 14 g of sodium perchlorate was added to the dark red solution. Gentle heating was continued until the color turned bright reddish violet. As soon as reddish violet crystals began to appear, the solution was cooled in a refrigerator. A pH value of 10—11 was suitable for obtaining the desired complex. The crystals were recrystallized from water. Yield 2 g

The corresponding chloride, nitrate and bromide were prepared by the same procedure except that sodium chloride, sodium nitrate and sodium bromide were used, respectively, in place of sodium perchlorate.

Found: C, 14.11; H, 4.37; N, 12.91%. Calcd for [Co(OH)gly(H_2O)en]ClO_4: C, 14.67; H, 4.61; N, 12.83%.

Hydroxodiethylenetriaminemonoacetatoaquocobalt(III) Perchlorate, [Co(OH)dtma(H_2O)]ClO_4 (reddish violet). The complex was prepared by a method similar to that for [Co(OH)gly(H_2O)en]ClO_4 except that the dichloro complex ([$CoCl_2$dtma][8,9]) was used as the starting material in place of [CoCl(gly)(H_2O)en]Cl. Twenty-nine grams of the dichloro complex was dissolved in 200 ml of aqueous solution containing 6 g of sodium hydroxide. The solution was gently heated at 50 °C on a water-bath until the violet solution turned dark red. To this solution was added 14 g of sodium perchlorate. The solution was again concentrated by gentle heating (50 °C) until reddish violet crystals were separated out. Another crop of crystals was obtained by cooling the solution. The product was recrystallized from water. Yield 5 g.

The corresponding nitrate, bromide and iodide were prepared by the same procedure except that sodium nitrate, sodium bromide and sodium iodide were used, respectively, instead of sodium pechlorate.

Found: C, 21.36; H, 4.74; N, 11.69%. Calcd for [Co(OH)dtma(H_2O)]ClO_4: C, 20.92; H, 5.11; N, 11.83%.

2) Anionic Complexes. K[Co(OH)nta(H_2O)]·H_2O,[10] K[Co(OH)nipda(H_2O)]·$2H_2O$,[11] K[Co(OH)α-abda(H_2O)]·$2H_2O$,[12] K[Co(OH)vda(H_2O)]·$1.5H_2O$,[12] K[Co(OH)lda(H_2O)]·H_2O,[13] K[Co(OH)pada(H_2O)]·$5H_2O$,[14] K[Cr(OH)nta(H_2O)]·$2H_2O$,[15] K[Cr(OH)nipda(H_2O)]·$2H_2O$,[16] K[Cr(OH)α-abda(H_2O)]·$2H_2O$,[17] K[Cr(OH)vda(H_2O)]·$2H_2O$,[17] K[Cr(OH)lda(H_2O)]·$3H_2O$[13] and K[Cr(OH)pada(H_2O)]·$5H_2O$[14] were prepared by the procedures described in the respective references.

Li, Na, Rb and Cs salts of the M(I)[Co(OH)nipda(H_2O)] type and Mg, Ca, Sr and Ba salts of the M(II)[Co(OH)nipda(H_2O)]$_2$ type were synthesized by similar way to that for K[Co(OH)nipda(H_2O)]·$2H_2O$[11] except that lithium carbonate, sodium bicarbonate, rubidium carbonate, cesium carbonate, magnesium carbonate, calcium carbonate, strontium carbonate and barium carbonate were used, respectively, in place of potassium bicarbonate.

3) Double Complexes. The procedure is a simple one. After 0.1 mmol of the hydroxoaquo cationic and anionic complexes were dissolved separately in 100 ml of hot aqueous solution, the two solutions were mixed together. On cooling, the double complexes were immediately separated out as violet crystals.

Although double complexes, in general, have low solubility, they can be recrystallized from a large amount of hot water. These complexes were obtained almost stoichiometrically.

4) Neutral Complexes. Hydroxobis(glycinato)aquocobalt(III) Dihydrate, [Co(OH)gly$_2$(H_2O)]·$2H_2O$ (violet). Twenty three grams of cobalt(II) chloride hexahydrate was dissolved in 100 ml of water. Fifteen grams of glycine was neutralized with 100 ml of water containing 8 g of sodium hydroxide. The two solutions were mixed and 10 ml of 28% hydrogen peroxide solution of was then added in order to oxidize the cobalt(II) ion. The solution was gently heated on a water-bath. Violet crystals gradually separated out during the heating. A pH value of 9—10 was suitable for obtaining the desired compound. The compound could not be recrystallized since it was sparingly soluble in ordinary solvents. However, chemical analysis showed that it is highly pure.

Found: C, 17.59; H, 5.14; N, 10.20%. Calcd for [Co(OH)gly$_2$(H_2O)]·$2H_2O$: C, 17.27; H, 5.43; N, 10.07%.

Hydroxobis(α-alaninato)aquocobalt(III) Monohydrate, [Co(OH)ala$_2$(H_2O)]·H_2O (violet). The complex was prepared by a procedure similar to that for [Co(OH)gly$_2$(H_2O)]·$2H_2O$ except that 18 g of α-alanine was used in place of glycine. It was also violet and insoluble in any solvent. Thus, recrystallization could not be carried out.

Found: C, 24.78; H, 5.69; N, 9.52%. Calcd for [Co(OH)ala$_2$(H_2O)]·H_2O: C, 25.01; H, 5.95; N, 9.72%.

7) N. Matsuoka, J. Hidaka, and Y. Shimura, This Bulletin, **39**, 1257 (1966).

8) P. W. Schneider and J. P. Collman, *Inorg. Chem.*, **7**, 2010 (1968).

9) C. Fukuhara, Master Thesis of Kanazawa University, 1970.

10) M. Mori, M. Shibata, E. Kyuno, and Y. Okubo, This Bulletin, **31**, 940 (1958).

11) M. Tachibana, A. Uehara, E. Kyuno, and R. Tsuchiya, *ibid.*, **43**, 1061 (1970).

12) A. Uehara, E. Kyuno, and R. Tsuchiya, *ibid.*, **44**, 1552 (1971).

13) A. Uehara, E. Kyuno, and R. Tsuchiya, *ibid.*, **43**, 414 (1970).

14) A. Uehara, E. Kyuno, and R. Tsuchiya, *ibid.*, **44**, 1548 (1971).

15) A. Uehara, E. Kyuno, and R. Tsuchiya, *ibid.*, **40**, 2317 (1967).

16) A. Uehara, E. Kyuno, and R. Tsuchiya, *ibid.*, **41**, 2393 (1968).

17) To be published elsewhere.

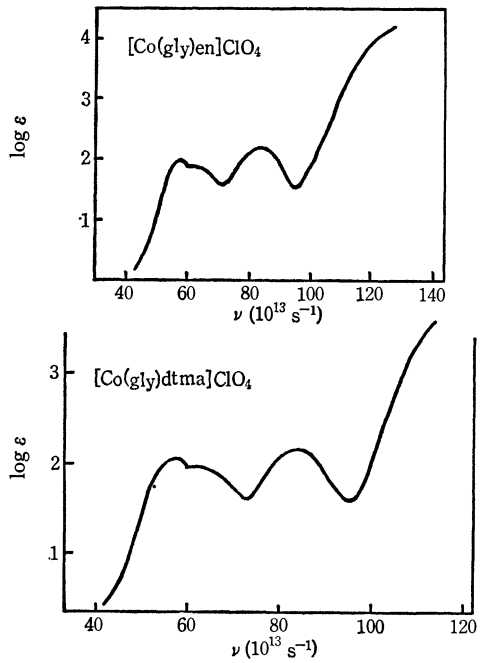

Fig. 2. Electronic spectra of $[Co(gly)_2en]ClO_4$ and $[Co(gly)dtma]ClO_4$ derived from the hydroxoaquo-type complexes.

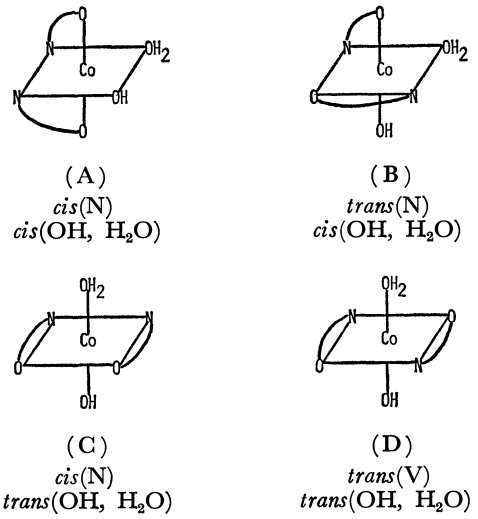

(A) *cis*(N) *cis*(OH, H_2O)

(B) *trans*(N) *cis*(OH, H_2O)

(C) *cis*(N) *trans*(OH, H_2O)

(D) *trans*(V) *trans*(OH, H_2O)

Fig. 3. Geometrically possible isomers of $[Co(OH)(n\text{-}o)_2(H_2O)]$.

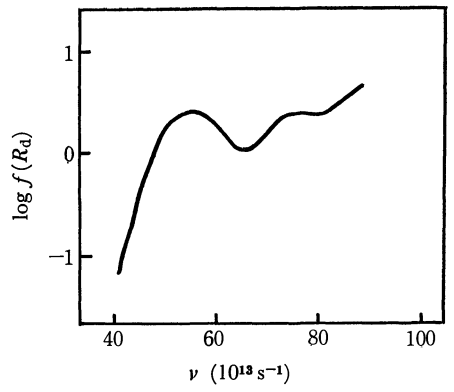

Fig. 4. Electronic spectrum of $[Co(OH)gly_2(H_2O)]\cdot 2H_2O$ (4.1).

The derivatograms for $[Co(OH)gly(H_2O)en]Cl\cdot H_2O$ (1.1.1), $[Co(OH)dtma(H_2O)]Br\cdot H_2O$ (1.2.2) and $K[Co(OH)lda(H_2O)]\cdot H_2O$ (2.1.5) as the representatives of the cationic and anionic complexes are shown in Fig. 5. As seen in the TG curve of $K[Co(OH)lda(H_2O)]\cdot H_2O$ (2.1.5), the mass losses corresponding to one mole of water are detected at *ca.* 60 and 175 °C. The former step corresponds to the liberation of crystalline water, the latter to the olation due to the removal of coordinated water. The color turned pink from bluish violet in the latter step, where an exothermic

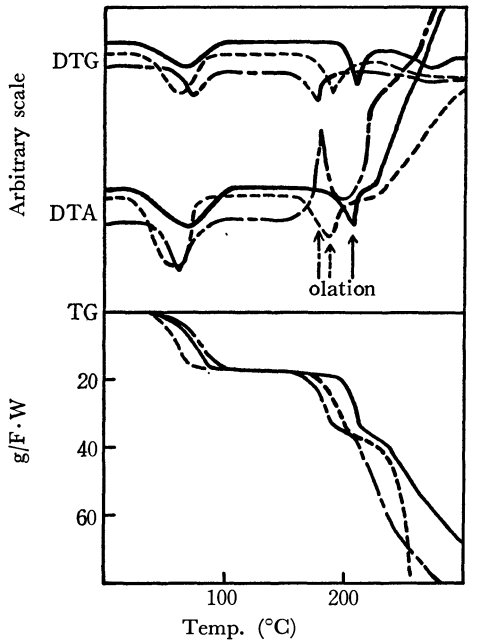

Fig. 5. Derivatograms for $[Co(OH)gly(H_2O)en]Cl\cdot H_2O$ (1.1.1)(——), $[Co(OH)dtma(H_2O)]Br\cdot H_2O$ (1.2.2)(——), and $K[Co(OH)lda(H_2O)]$(2.1.5)(– – –).

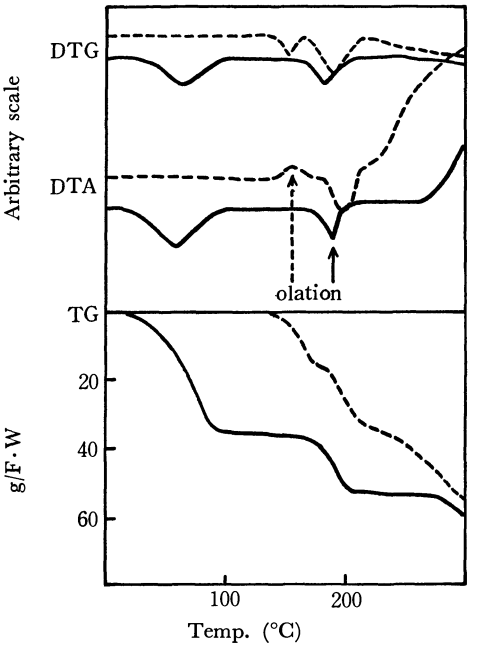

Fig. 6. Derivatograms for $K[Co(OH)nta(H_2O)]\cdot H_2O$ (2.1.1) (——) and $[Co(OH)gly_2(H_2O)]\cdot 2H_2O$(4.1)(——).

DTA peak appears. Such a change was observed in all the anionic complexes. However, the case is different with K[Co(OH)nta(H_2O)]·H_2O (2.1.1), the derivatogram of which is shown in Fig. 6 together with that of the neutral complex, [Co(OH)gly_2(H_2O)]·$2H_2O$ (4.1). In the case of K[Co(OH)nta(H_2O)]·H_2O (2.1.1), although the two steps of mass losses corresponding to one mole of water were separately observed at *ca.* 150 and 175 °C, the color change was found in the former step, with an exothermic DTA peak. The former step is thus thought to correspond to the olation and the latter to the liberation of crystalline water.

The cationic complex [Co(OH)gly(H_2O)en]Cl·H_2O (1.1.1) lost one mole of water at both 37 and 166 °C. The original reddish violet color turned pink in the latter step. Olation seems to take place in this step as a consequence of the liberation of the coordinated water. The thermal decomposition process of [Co(OH)dtma(H_2O)]Br·H_2O (1.2.2) was essentially similar to that of [Co(OH)gly(H_2O)en]Cl·H_2O (1.1.1). The olation in both cationic complexes was endothermic in contrast to that of the anionic complexes as seen in DTA curves, Fig. 5.

As for the olation of the neutral complexes, an endothermic peak was detected as in the DTA curve of [Co(OH)gly_2(H_2O)]·$2H_2O$ (4.1).

Since there is a striking contrast between the DTA curves of the cationic and anionic complexes, it is of interest to observe the olation of the double complexes. The derivatograms for [Co(OH)gly(H_2O)en][Co(OH)pada(H_2O)]·$2H_2O$ (3.1.6), [Co(OH)gly(H_2O)en][Cr(OH)pada(H_2O)]·$2H_2O$ (3.1.12) and [Co(OH)dtma(H_2O)][Co(OH)pada(H_2O)]·$2H_2O$ (3.2.6) are shown in Fig. 7. All three complexes lose each two moles of water in two separate steps. In the latter step, the color of [Co(OH)gly(H_2O)en]-[Co(OH)pada(H_2O)]·$2H_2O$ (3.1.6) and [Co(OH)-dtma(H_2O)][Co(OH)pada(H_2O)]·$2H_2O$ (3.2.6) turned pink from violet while that of [Co(OH)gly(H_2O)en]-[Cr(OH)pada(H_2O)]·$2H_2O$ (3.1.12) brownish pink from violet. The color change is probably due to the consequent olation.

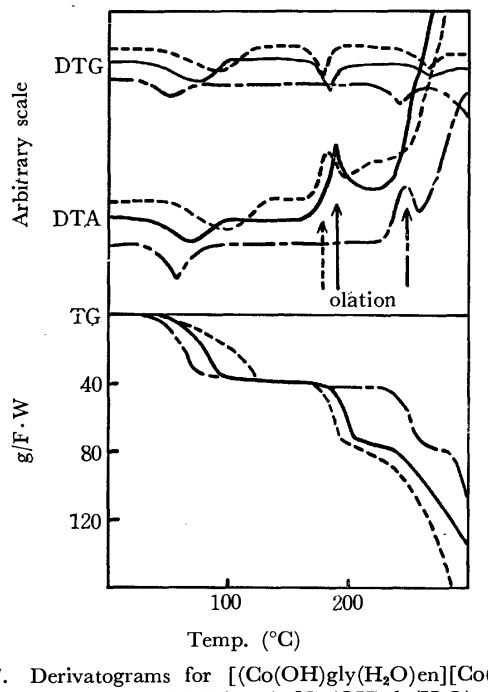

Fig. 7. Derivatograms for [(Co(OH)gly(H_2O)en][Co(OH)-pada(H_2O)]·$2H_2O$ (3.1.6)(----), [Co(OH)gly(H_2O)en][Cr-(OH)pada(H_2O)]·$2H_2O$ (3.1.12)(———) and [Co(OH)-dtma(H_2O)][Co(OH)pada(H_2O)]·$2H_2O$ (3.2.6)(——).

Electronic Spectra. It is well-known that cobalt(III) complexes containing "ol" groups show a specific band due to the bridged OH groups at about 100×10^{13} s^{-1}, the second band being frequently concealed by the strong specific band.[19]

The specific band could not be directly detected for all the complexes after heating since it was experimentally impossible to measure the electronic spectra beyond 90×10^{13} s^{-1} in a solid state. However, the obscurity of the second band of all the complexes after heating indicates that the specific band due to the bridged OH groups probably remains in the region of about 100×10^{13} s^{-1}.

Far-Infrared Spectra. In general, the hydroxoaquo complexes give bands at 640, 570 and 535 cm^{-1} in the region 700—500 cm^{-1}, and the diol complexes at 630, 545 and 505 cm^{-1}. All the hydroxoaquo complexes after heating at the above temperatures give spectra similar to those of the diol complexes. Thus, the results suggest the conversion of the hydroxoaquo complexes into the corresponding diol complexes upon heating.

From a study on the far-infrared spectrum of [$(NH_3)_4$-$Co(OH)_2Co(NH_3)_4$]$(SO_4)_2$·$2H_2O$ in the CsBr region, it is presumed that the strong band at 530—540 cm^{-1} is due to the presence of the four-membered cobalt-oxygen ring (–$Co(OH)_2Co$–).[20] The band of the diolcomplexes which appears at 545 cm^{-1} might be a characteristic band due to the skeletal vibration of –$Co(OH)_2Co$–.

Magnetic Moments. In order to examine the valency state of the central metal ions, the effective magnetic moments (μ_{eff}) were calculated from the magnetic susceptibilities measured at an ambient temperature by the Gouy method.

As for K[Co(OH)(n-o_3)(H_2O)], M(I) or $M(II)_{1/2}$-[Co(OH)(nipda)(H_2O)], [Co(OH)(n_3-o)(H_2O)]X and [Co(OH)(n_3-o)(H_2O)][Co(OH)(n-o_3)(H_2O)] type complexes, all the complexes were diamagnetic both before and after heating. On the other hand, the magnetic moments of [Co(OH)(n_3-o)(H_2O)][Cr(OH)(n-o_3)-(H_2O)] type complexes were 3.8—3.9 B.M., which is very close to the spin-only value of tervalent chromium ion. The actual change in magnetic moments could not be detected after heating.

The results indicate that both chromium and cobalt ions in all the complexes are tervalent, no actual electron transfer taking place upon heating. However, it is not clear whether or not such an electron transfer is generated in a step of the overall heating processes.

Thermochemical Data. The enthalpy changes (ΔH) of the olation of all the complexes were estimated from the DTA peak area.[18] The Arrhenius activation

19) Y. Inamura and Y. Kondo, *Nippon Kagaku Zasshi*, **74**, 627 (1953).

20) G. Blyholder and N. Ford, *J. Phys. Chem.*, **68**, 1496 (1964).

TABLE 2. THERMOCHEMICAL DATA FOR OLATION

Type of complex	Index No. of complex	Initiation Temp. (°C)	ΔH (kcal/mol)	E_A (kcal/mol)
Cationic complexes	1.1.1	166	13.6	70.7
	1.1.2	175	1.8	82.1
	1.1.3	180	10.4	84.2
	1.2.1	188	1.7	82.9
	1.2.2	175	10.5	93.5
	1.2.3	194	8.7	97.2
Anionic complexes	2.1.1	150	−1.2	29.7
	2.1.2	195	−4.8	85.8
	2.1.3	185	−6.3	75.4
	2.1.4	175	−12.8	70.8
	2.1.5	175	−14.3	65.1
	2.1.6	170	−21.3	62.8
	2.2.1	193	−5.5	84.0
	2.2.2	188	−4.9	82.5
	2.2.3	189	−4.0	84.2
	2.2.4	188	−5.5	84.5
	2.3.1	223		
	2.3.2	225		
	2.3.3	221		
	2.3.4	230		
Neutral complexes	4.1	184	3.6	83.5
	4.2	164	7.0	48.6
Double complexes	3.1.1	188	8.3	97.6
	3.1.2	162	−1.5	69.5
	3.1.3	177	−4.2	73.9
	3.1.4	167	−8.8	57.9
	3.1.5	167	−9.9	54.9
	3.1.6	162	−14.6	53.4
	3.1.7	205	8.9	89.9
	3.1.8	220	7.3	94.4
	3.1.9	229	0.8	93.5
	3.1.10	225	−5.5	96.7
	3.1.11	230	−8.2	101.5
	3.1.12	230	−10.6	98.7
	3.2.1	180	10.0	80.2
	3.2.2	176	4.7	68.6
	3.2.3	175	−7.5	70.8
	3.2.4	167	−9.1	55.9
	3.2.5	167	−14.3	54.3
	3.2.6	165	−17.2	37.1
	3.2.7	205	8.2	80.8
	3.2.8	203	11.5	71.7
	3.2.9	205	−1.6	83.5
	3.2.10	210	−5.2	90.3
	3.2.11	217	−8.6	99.2
	3.2.12	217	−11.5	100

energies (E_A) of the reaction were calculated from the slope of the Arrhenius plots derived by the analysis of DTA or DTG curve.[18] The detailed analysis of DTA or DTG curve confirmed that the olation of all the complexes proceeds in a first-order. The numerical values of the thermochemical data are summarized in Table 2. For the sake of simplification, some of the data obtained are diagramatically plotted as in Figs. 8 (A) through (F). In the abscissa, the outer sphere ions or the ligands (n-o_3) are taken at regular intervals in the order of the increase of radius or volume, while the initiation temperatures (T), the enthalpy changes (ΔH) and the Arrhenius activation energies (E_A) are plotted in the ordinate.

1) Cationic Complexes. We see from Fig. 8 (A) that the initiation temperature rises with the size of the outer sphere ions (for example, in the case of [Co(OH)gly(H_2O)en]X, $Cl^- < NO_3^- < Br^-$), and the same tendency is also observed in the activation energies. This means that the increase in the anion size reduces the ease of olation. The enthalpy changes for the nitrate salts [Co(OH)gly(H_2O)en]$NO_3 \cdot H_2O$ (1.1.2) and [Co(OH)dtma(H_2O)]NO_3 (1.2.1) are significantly smaller as compared with those for the other complexes. This may be due to the fact that the nitrate salts are decomposed just after the olation takes place and the heat of olation overlaps that of the subsequent decomposition. A comparison of [Co(OH)gly(H_2O)-en]X with [Co(OH)dtma(H_2O)]X reveals that both the initiation temperatures and the activation energies of the latter type complexes are somewhat higher than those of the former except for the initiation temperature of the bromide salts. This suggests that olation takes place more readily with [Co(OH)gly(H_2O)en]X than with [Co(OH)dtma(H_2O)]X.

2) Anionic Complexes. Figure 8 (B) illustrates the diagramatical relation of the thermochemical data when the ligands (n-o_3) are varied against the fixed cation (K). Fig. 8 (C) and (D) show the corresponding data when the cations are varied against the fixed ligand (nipda).

As seen from Fig. 8 (B), the exothermic heat of olation shows an increasing trend with the structural complexity of the ligands (n-o_3). On the other hand, a decreasing trend is found in the values of E_A except for that of K[Co(OH)nta(H_2O)]$\cdot H_2O$ (2.1.1). Accordingly, it is conceivable that the olation easily takes place in the order: nipda→pada-complexes and the nta-complex can be most easily olated.

Since the M(II)[Co(OH)nipda(H_2O)]$_2$ type complexes decomposed just after the olation took place and their fine derivatograms could not be obtained, the ΔH and E_A could not be estimated. Thus the initiation temperatures alone are given in Table 2 and Fig. 8 (D). From a comparison of the data for the M(I) *or* M(II)$_{1/2}$[Co(OH)nipda(H_2O)], K[Co(OH)(n-o_3)(H_2O)] and [Co(OH)(n_3-o)(H_2O)]X type complexes, it follows that the thermochemical data found when cations (M(I) and M(II)) are varied are not so greatly affected as those obtained when the ligands (n-o_3 and n_3-o) or the anions are varied. This suggests that the effect of cations on the olation is smaller than that of anions or ligands. The initiation temperatures of the M(II)$_{1/2}$[Co(OH)nipda(H_2O)] type complexes are considerably higher than those of the M(I)[Co(OH)nipda(H_2O)] type complexes. The reason might be attributed to the difference of the crystal structures.

3) Neutral Complexes. The data for [Co(OH)-gly$_2$(H_2O)]$\cdot 2H_2O$ (4.1) and [Co(OH)ala$_2$(H_2O)]$\cdot H_2O$ (4.2) indicate a tendency for the latter to give rise to olation more easily than the former.

4) Double Complexes. In the case of the [Co]-[Co] type complexes, as shown in Fig. 8 (E), the initiation temperatures and the activation energies decrease in the order of the complexity in the structure of the n-o_3 ligands: nta-→pada-complexes. The tendency is compatible with that found in the case of the anionic complexes.

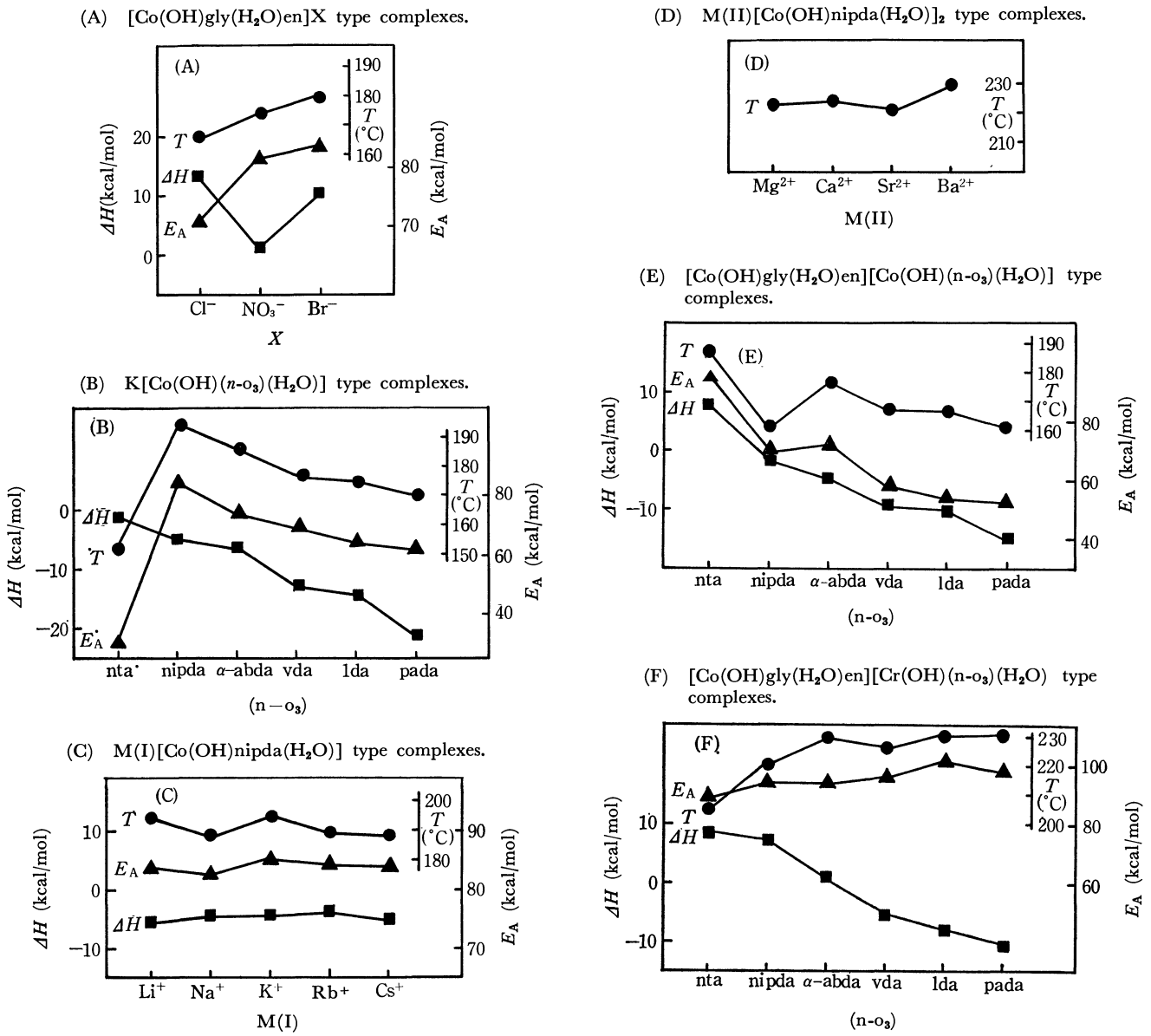

Fig. 8. Diagrammatical relation of thermochemical data.

In contrast, in the case of the [Co][Cr] type complexes a distinct tendency is not observed, but we see that the values of the initiation temperatures and the activation energies become to some extent higher in the order: nta-→pada-complexes. This indicates that the olation readily takes place in the order: pada-→nta-complexes, differing from the case of the [Co][Co] complexes.

The enthalpy changes for the olation of the anionic complexes show a decreasing trend with the complexity in the structures of the n-o_3 ligands: nta-→pada-complexes. On the other hand, the enthalpy changes accompanied by the olation of the double complexes are uniformly larger than those of the respective anionic complexes. Thus, it might be concluded that the values of ΔH for the olation of the double complexes are approximately proportional to the sum of the values for the cationic and anionic complexes; *i.e.*, ΔH_d (for double complex)$=\Delta H_c$ (for cationic complex)$+\Delta H_a$ (for anionic complex).

An Optical Absorption Study of the Reaction of Bis(*O,O'*-diethyldithiophosphato)oxovanadium(IV) with Pyridine

Mitsuo SATO and Takao KWAN

Faculty of Pharmaceutical Sciences, The University of Tokyo, Hongo, Bunkyo-ku, Tokyo 113

(Received June 16, 1973)

The interaction of bis(*O,O'*-diethyldithiophosphato)oxovanadium(IV), $VOdtp_2$, with pyridine has been studied in toluene by means of the optical absorptions. It has been found that the visible absorption band characteristic of $VOdtp_2$ was shifted toward longer wavelengths upon the formation of the complex species identified as $VOdtp_2 \cdot Py$ and $VOdtp_2 \cdot Py_2$. The equilibrium constants and enthalpy and entropy changes for the formation of $VOdtp_2 \cdot Py$ were determined from the spectral characteristics, measured as a function of the solvent composition and the temperature. The results obtained were then discussed in comparison with those for the base addition of other oxovanadium complexes.

In the foregoing paper,[1] ESR evidence was presented that bis(*O,O'*-diethyldithiophosphato)oxovanadium(IV), $VOdtp_2$, reacts with pyridine to form both mono- and dipyridine complexes. Pyridine bases were found to coordinate the vanadium nucleus, as is shown by the following scheme:

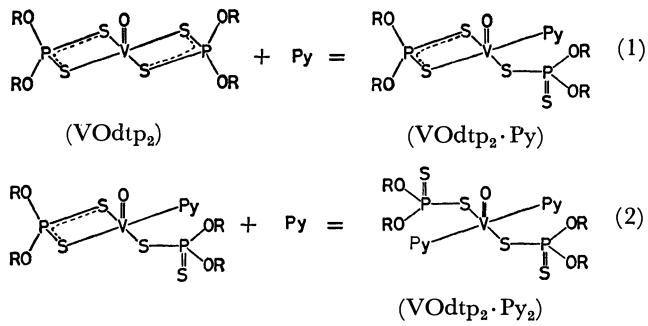

Since such a coordination scheme affords a marked contrast to that generally accepted for the base addition of oxovanadium(IV) complexes,[2] it seems worthwhile to investigate Reactions (1) and (2) in more detail. In the present work, an optical absorption method was used to investigate the equilibria involved and to obtain their thermodynamic data; the results will be reported here.

Experimental

Materials. Bis(*O,O'*-diethyldithiophosphato)oxovanadium(IV), $VOdtp_2$, was prepared as has been described previously.[1] The pyridine and toluene were obtained from Wako Junyaku Kogyo Co. and were used after distillation from calcium hydride and potassium hydroxide respectively.

Measurements. Since the complex species in solutions were unstable to air, all the measurements were carried out on sample solutions carefully prepared in an atmosphere of nitrogen or *in vacuo*. The optical absorption spectra were measured with a Hitachi spectrophotometer (Model EPS-3T), using 10-mm quartz cells fitted with vacuum stopcocks or a nitrogen-bubbling device. The spectrophotometer was equipped with a temperature-regulated cell holder, and a constant temperature was maintained by circulating water through the cell holder. The temperatures were regulated by circulating through the cell holder water that had been cooled or warmed to the desired temperature. The temperatures were measured by means of a copper-constantan thermocouple directly inserted into the toluene placed in the reference cell. The ESR spectra were recorded with a JEOL spectrometer (Model P-10), as has been described previously.[1]

Results

Visible Absorption Spectra of Complex Species in Solutions. The optical absorption spectra of toluene solutions containing $VOdtp_2$ and pyridine in various mole ratios, as well as those of toluene and pyridine solutions of $VOdtp_2$, were measured at 18 °C. Some typical visible absorption spectra thus obtained are illustrated in Fig. 1. It is apparent from Fig. 1 that the spectrum A, obtainable without pyridine bases, shifts to B and C successively upon an increase in the pyridine content, thus affording three types of visible spectra.

In light of the ESR spectra of these solutions,[3] the visible spectra mentioned above can readily be

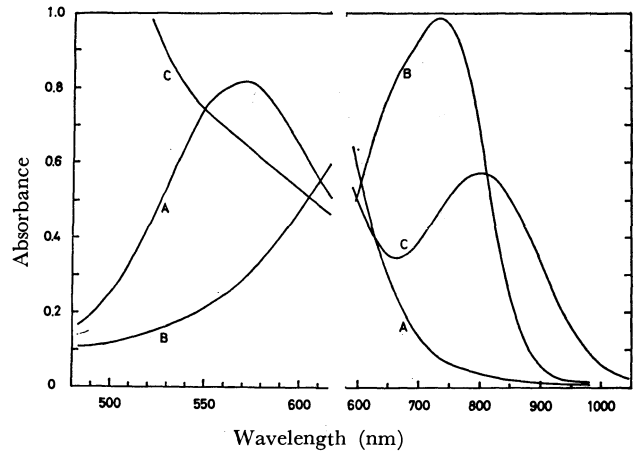

Fig. 1. Visible absorption spectra of toluene-pyridine solutions of $VOdtp_2$ at 18°C.
(A) $VOdtp_2$ in toluene, $[VOdtp_2]_0 = 0.015$ M;
(B) $VOdtp_2$-pyridine in toluene, $[VOdtp_2]_0 = 0.015$ M, $[Py]_0 = 0.091$ M;
(C) $VOdtp_2$ in pyridine, $[VOdtp_2]_0 = 0.012$ M.

1) M. Sato, Y. Fujita, and T. Kwan, This Bulletin, **46**, 3007 (1973).

2) J. Selbin, *Chem. Rev.*, **65**, 153 (1965).

3) Corresponding to the three types of visible absorption spectra, ESR spectra characterized with 24, 16, and 8 resonance lines were observed. The interpretation of these ESR spectra has already been reported in the foregoing paper, together with the proposed structures of the complex species.

interpreted as due to the complex species, $VOdtp_2$, $VOdtp_2 \cdot Py$, and $VOdtp_2 \cdot Py_2$, in the respective solutions. The absorption maxima and molar extinction coefficients determined for these complex species were given by:

(A) $VOdtp_2$; λ_{max} 570 nm, $\varepsilon_{A(max)}$ 53 $M^{-1}cm^{-1}$.

(B) $VOdtp_2 \cdot Py$; λ_{max} 735 nm, $\varepsilon_{B(max)}$ 71 $M^{-1}cm^{-1}$.

(C) $VOdtp_2 \cdot Py_2$; λ_{max} 800 nm, $\varepsilon_{C(max)}$ 47 $M^{-1}cm^{-1}$.

where the values of $\varepsilon_{A(max)}$ and $\varepsilon_{C(max)}$ were derived directly from Fig. 1, while that of $\varepsilon_{B(max)}$ was obtained by the procedure to be described below.

The band at 570 nm observed for $VOdtp_2$ seems to originate from a d-d transition;[4] this band is considered to shift to lower energies to produce a new band at 735 nm or 800 nm when one or two of the equatorial sulfur ligands are displaced by pyridine bases.

The Equilibrium Constant of Reaction (1). Job's method of continuous variations and the mole-ratio method[5] were applied to the $VOdtp_2$-pyridine system at 18 °C, first to confirm the stoichiometry of Reactions (1) and (2) and then to evaluate their equilibrium constants. It was found, however, that Reaction (2) did not proceed at all under the conditions employed in these experiments.

As can be seen from the results of the continuous variation method (Fig. 2), the absorbance at 735 nm reached its maximum at 50 mole% pyridine, indicating that one mole of $VOdtp_2$ reacts with one mole of pyridine, consistent with the stoichiometry of Reaction (1). On the other hand, the mole-ratio method showed

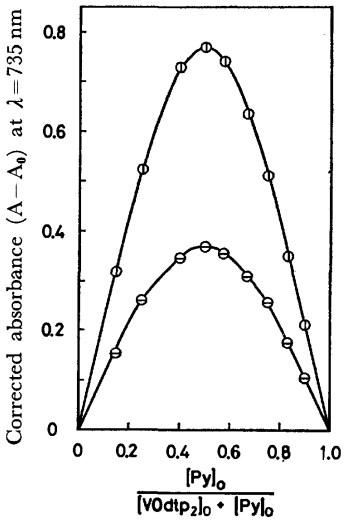

Fig. 2. Continuous variation method as applied to the $VOdtp_2$-pyridine system by visible absorption measurements at 18 °C.
⊕: $[VOdtp_2]_0+[Py]_0=0.041$ M (const.);
⊖: $[VOdtp_2]_0+[Py]_0=0.023$ M (const.).

4) R. G. Cavell, E. D. Day, W. Byers, and P. M. Watkins, *Inorg. Chem.*, **11**, 1591 (1972).

5) H. Hosoya, "Jikken Kagaku Koza," Vol. 11, ed. by The Chemical Society of Japan (1965), p. 523.

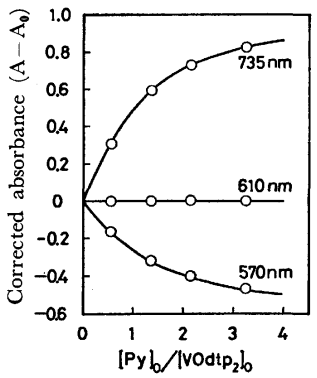

Fig. 3. Mole-ratio method as applied to the $VOdtp_2$-pyridine system by visible absorption measurements at 18 °C.
$[VOdtp_2]_0=0.015$ M (const.).

the presence of two absorbing species, $VOdtp_2$ and $VOdtp_2 \cdot Py$, in solutions, as can be seen from Fig. 3, where an isosbestic point at 610 nm is shown with the increasing and decreasing absorbances at 735 and 570 nm. These results are in accordance with the previous ESR information[1] that $VOdtp_2 \cdot Py$ is rather stable in toluene and is present in equilibrium with $VOdtp_2$ and pyridine over a wide concentration range, while $VOdtp_2 \cdot Py_2$ is formed only when $VOdtp_2 \cdot Py$ interacts with a large excess of pyridine bases.

The equilibrium constant, $K=[VOdtp_2 \cdot Py]/[VOdtp_2][Py]$, of Reaction (1) was then evaluated from the data shown in Figs. 2 and 3 after the procedure by Lang.[5,6] On the basis of the presence of two absorbing species, $VOdtp_2$ and $VOdtp_2 \cdot Py$, in solutions, the measured absorbance, A, at the chosen wavelength is given by:

$$A = \varepsilon_A[VOdtp_2] + \varepsilon_B[VOdtp_2 \cdot Py]$$
$$= \varepsilon_A[VOdtp_2]_0 + (\varepsilon_B - \varepsilon_A)[VOdtp_2 \cdot Py] \quad (3)$$

We then obtain the following expression for the equilibrium constant:

$$K = \frac{[VOdtp_2 \cdot Py]}{([VOdtp_2]_0 - [VOdtp_2 \cdot Py])([Py]_0 - [VOdtp_2 \cdot Py])}$$
$$= \frac{\dfrac{A-A_0}{\varepsilon_B-\varepsilon_A}}{\left([VOdtp_2]_0 - \dfrac{A-A_0}{\varepsilon_B-\varepsilon_A}\right)\left([Py]_0 - \dfrac{A-A_0}{\varepsilon_B-\varepsilon_A}\right)} \quad (4)$$

where ε_A and ε_B are the molar extinction coefficients at the chosen wavelength for $VOtdp_2$ and $VOdtp_2 \cdot Py$ respectively, where A_0 is the absorbance of $VOdtp_2$ at the wavelength in the absence of pyridine ($A_0=\varepsilon_A[VOdtp_2]_0$), and where $[VOdtp_2]_0$ and $[Py]_0$ are the initial concentrations of the two species.

To estimate the two unknowns, K and ε_B, the equation was rewritten as:

$$\frac{[VOdtp_2]_0[Py]_0}{A-A_0} = \left\{[VOdtp_2]_0 + [Py]_0 - \frac{A-A_0}{\varepsilon_B-\varepsilon_A}\right\} \cdot \frac{1}{\varepsilon_B-\varepsilon_A} + \frac{1}{K} \cdot \frac{1}{\varepsilon_B-\varepsilon_A} \quad (5)$$

6) R. P. Lang, *J. Amer. Chem. Soc.*, **84**, 1185 (1962).

$[VOdtp_2]_0[Py]_0/(A-A_0)$ was plotted against $\{[VOdtp_2]_0+[Py]_0-(A-A_0)/(\varepsilon_B-\varepsilon_A)\}$ by using a tentative value[7] of ε_B and also by employing the absorbance data at $\lambda=735$ nm shown in Figs. 2 and 3. The plot yielded a straight line with a slope of $1/(\varepsilon_B-\varepsilon_A)$ and an intercept of $1/K(\varepsilon_B-\varepsilon_A)$, from which a new value of ε_B was determined along with that of K. This procedure was repeated until a consistent set of values for both ε_B and K was obtained from two successive plots. The final plot is presented in Fig. 4, with the following consistent values: $K_{(18°C)}=1.2\times10^2\ M^{-1}$, $\varepsilon_{B(\lambda=735nm)}=71\ M^{-1}\,cm^{-1}$. The uncertainties in the values estimated from the deviations in the linearity of the plots are about $\pm0.3\times10^2\ M^{-1}$ and $\pm5\ M^{-1}\,cm^{-1}$ for K and ε_B respectively.

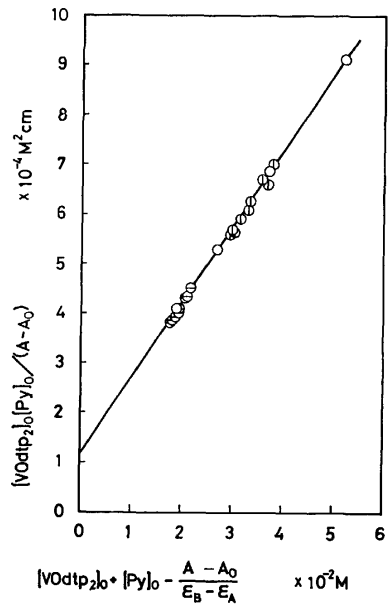

Fig. 4. Lang's plots of the $VOdtp_2$-pyridine system ($\lambda=735$ nm).
⊕⊖: Absorbance data from Fig. 2;
○: Absorbance data from Fig. 3.

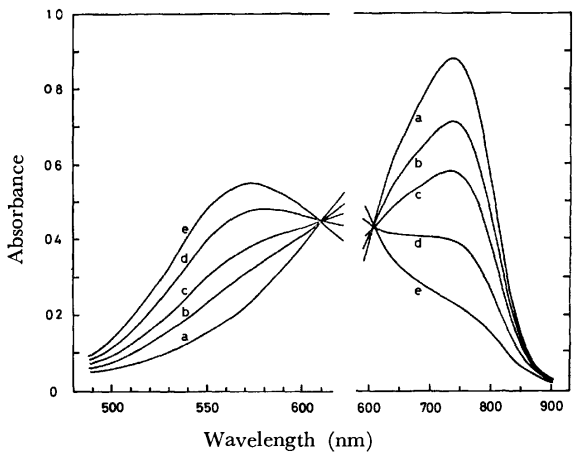

Fig. 5. Effect of temperature on visible absorption spectra.
$[VOdtp_2]_0=0.015$ M, $[Py]_0=0.035$ M.
a) 10 °C, b) 24 °C, c) 34 °C, d) 51 °C, e) 73 °C.

7) A tentative value of ε_B was advantageously determined by using data from two solutions and by solving Eq. (5) simultaneously for ε_B and K.

Temperature Dependence of the Equilibrium Constant. Figure 5 shows a typical set of visible spectra observed at different temperatures. It can be seen that the spectra show a sharp isosbestic point at 610 nm, with two absorption peaks at 570 and 735 nm. The presence of the isosbestic point again indicates that the equilibrium relation (1) is valid even at higher temperatures without any side reaction. Such an equilibrium relation between $VOdtp_2$ and $VOdtp_2\cdot Py$ was clearly evidenced also by the ESR spectra observed at different temperatures, as is shown in Fig. 6.

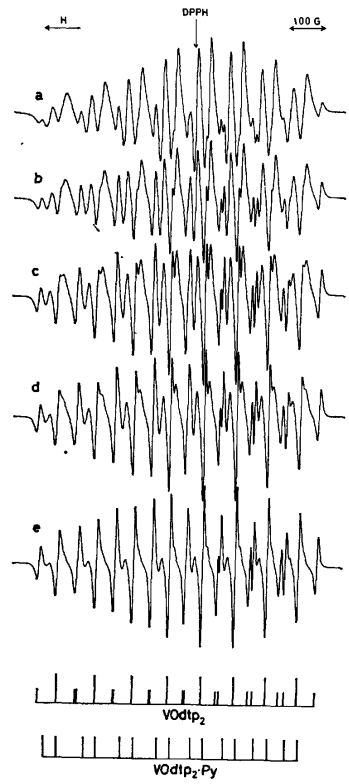

Fig. 6. Effect of temperature on ESR spectra.
$[VOdtp_2]_0=0.015$ M, $[Py]_0=0.035$ M.
a) 18 °C, b) 31 °C, c) 45 °C, d) 56 °C, e) 84 °C.
(The stick diagrams at the bottom of Figure indicate the 24 and 16 resonance lines expected from the complex species, $VOdtp_2$ and $VOdtp_2\cdot Py$.)

The equilibrium constant at each temperature was calculated using Eq. (4) on the assumption that molar extinction coefficients of $VOdtp_2$ and $VOdtp_2\cdot Py$ were constant over the entire temperature range. The resulting K values were found to be:

K = 160 (10 °C), 65 (24 °C), 35 (34 °C), 15 (51 °C), 5.5 M^{-1} (73 °C).

A plot of $\ln K$ *vs.* $1/T$ yielded a good straight line, and the following standard enthalpy and entropy changes for Reaction (1) were derived from the slope and intercept:

$$\Delta H° = -10.5\ \text{kcal/mol},$$
$$\Delta S° = -27.0\ \text{e.u.}$$

These values may be compared to those ($\Delta H°=-12$ kcal/mol, $\Delta S°=-30$ e.u.) obtained from an

analysis of the ESR spectra shown in Fig. 6. In view of the uncertainties in the values from the ESR spectra, both results seem to be compatible within the limit of experimental errors.

Discussion

It has generally been accepted[2] that square pyramidal oxovanadium(IV) complexes have a tendency to add a sixth ligand to the open coordination site *trans* to the apical oxygen atom when they are allowed to react with a variety of bases in solutions. For example, the formation of base adducts of bis(acetylacetonato)oxovanadium(IV), $VO(acac)_2$, has long been studied extensively by many workers,[8] and the thermodynamical data for the equilibria of the base addition to the sixth coordination site have already been repoted.[9,10]

However, our ESR and optical absorption studies have shown that the base addition reaction of $VOdtp_2$ is not a simple process in which the pyridine base adds to the open coordination site. The reaction has been found to be a rather complicated process involving the displacement of the equatorial sulfur ligand and leading to the formation of the complex species, $VOdtp_2 \cdot Py$, depicted as:

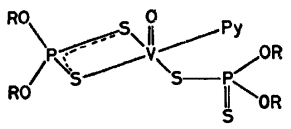

This type of base addition affords a marked contrast to the corresponding base adduct of $VO(acac)_2 \cdot Py$:

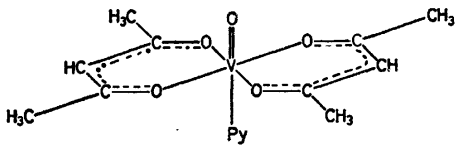

It is, however, not completely clear why there exists such a structural difference between $VOdtp_2 \cdot Py$ and $VO(acac)_2 \cdot Py$. For the moment, we can only say that the difference seems to result in part from the different natures of the equatorial ligands.

From this point of view, it is interesting to compare the thermodynamical data determined for the equilibrium of the $VOdtp_2$-pyridine system with those reported previously for the $VO(acac)_2$–pyridine system ($K_{(25°C)}=58\ M^{-1}$, $\Delta H°=-7.4$ kcal/mol, $\Delta S°=-16.6$ e.u.).[10] A close similarity in the K values at 25 °C is noticeable, although there are some differences in the $\Delta S°$ and $\Delta H°$ values. The difference in the $\Delta S°$ values may be taken to reflect the different steric and solvation effects between the two systems. The $\Delta H°$ values may indicate that the vanadium-nitrogen coordination in $VOdtp_2 \cdot Py$ is much stronger than that in $VO(acac)_2 \cdot Py$, since the $\Delta H°$ for the $VOdtp_2$-pyridine system is attributable mainly to the differences in the bond energies of the vanadium-sulfur bond broken and the vanadium-nitrogen bond formed, while the $\Delta H°$ for the $VO(acac)_2$–pyridine system results mainly from the bond energy of the vanadium nitrogen bond formed. Such a notion is in accordance with the view that oxovanadium complexes coordinate a sixth axial ligand much more weakly than the equatorial ligands.

Since, in properties and structure, $VOdtp_2$ closely resembles bis(dithiocarbamato)oxovanadium(IV), $VOdtc_2$, rather than $VO(acac)_2$, it is important for us to note the recent spectroscopic studies of the interaction of $VOdtc_2$ with pyridine. McCormick[11] found that visible absorption bands associated with the d–d transitions of $VOdtc_2$ were shifted about 5000 cm^{-1} to lower energies when $VOdtc_2$ was dissolved in pyridine. He interpreted this red shift in terms of the addition of pyridine to the open coordination site and was able to isolate $VOdtc_2 \cdot Py$ as a solid.

However, the magnitude of the red shift observed for $VOdtc_2 \cdot Py$ is much closer to that (about 4000 cm^{-1}) for $VOdt_2p \cdot Py$ than to that (about 2000 cm^{-1}) for $VO(acac)_2 \cdot Py$.[10,11] Moreover, the ESR spectra of the $VOdtc_2$-pyridine system have provided no conclusive information about the structure of the complex species formed.[13]

From these points of view, we consider that at least two possibilities should be discussed equally for the base addition of $VOdtc_2$. The first possibility is, of course, that $VOdtc_2$ reacts with pyridine similarly to $VO(acac)_2$, while the second is that it reacts similarly to $VOdtp_2$. In order to distinguish these two possibilities, we have also made an ESR examination of the $VOdtc_2$-pyridine system. However, our ESR results have again provided no conclusive information as to which of the two possibilities is more probable. For the moment, it can only be said that further work, such as structural analysis by X-ray, will be required to confirm the structure of $VOdtc_2 \cdot Py$ and to decide between the above possibilities.

This work was supported in part by a grant of the Ministry of Education, to which the authors' grateful acknowledgements are made.

8) A. Rosenheim and H. Yu Mong, *Z. Anorg. Allg. Chem.*, **148**, 34 (1925); M. M. Jones, *J. Amer. Chem. Soc.*, **76**, 5995 (1954); K. Nakamoto, Y. Morimoto, and A. E. Martell, *ibid.*, **83**, 4533 (1961); J. Selbin, H. R. Manning, and G. Cessac, *J. Inorg. Nucl. Chem.*, **25**, 1253 (1963); F. A. Walker, R. L. Carlin, and P. H. Rieger, *J. Chem. Phys.*, **45**, 4181 (1966).

9) R. T. Claunch, T. W. Martin, and M. M. Jones, *J. Amer. Chem. Soc.*, **83**, 1073 (1961).

10) R. L. Carlin and F. A. Walker, *ibid.*, **87**, 2128 (1965).

11) B. J. McCormick, *Inorg. Chem.*, **7**, 1965 (1968); *Can. J. Chem.*, **47**, 4283 (1969).

12) J. Selbin and T. R. Ortolano, *J. Inorg. Nucl. Chem.*, **26**, 37 (1964).

13) G. Vigee and J. Selbin, *ibid.*, **31**, 3187 (1969); B. J. McCormick and E. M. Bellott, Jr., *Inorg. Chem.*, **9**, 1779 (1970); F. E. Dickson, C. J. Kunesh, E. L. McGinnis, and L. Petrakis, *Anal. Chem.*, **44**, 978 (1972).

Stability of Fused Rings in Metal Chelates. XI. Stability of Dipeptide Amide-Copper(II) Complexes

Osamu YAMAUCHI, Yasuo NAKAO, and Akitsugu NAKAHARA

Institute of Chemistry, College of General Education, Osaka University, Toyonaka, Osaka 560

(Received August 7, 1973)

The structure-stability relationship between the copper(II) complexes of several dipeptide amides consisting of glycine and/or β-alanine has been investigated by potentiometric titration. The amides of glycylglycine, glycyl-β-alanine, and β-alanylglycine (abbreviated as H_2L) have been found to form complexes of the type $Cu(H_2L)^{2+}$ with log K_1 values 4.80—5.22. The $-\log K_{c_1}$ values for deprotonation of the peptide group are 5.05—5.42 and comparable to those of tripeptides, whereas the $-\log K_{c_2}$ values for the terminal amide group are 7.96 for glycylglycine amide and 8.99 for glycyl-β-alanine amide. This indicates that, at neutral pH, the $-CONH_2$ group coordinates to copper(II) mainly through the carbonyl oxygen. β-Alanyl-β-alanine amide-copper(II) system gave precipitates at an early stage of titration. The structures and relative stability of the complexes of types $Cu(H_2L)^{2+}$, $Cu(HL)^{+}$, and CuL have been discussed from comparative studies of their stability constants.

Amide groups in amino acid amides and peptides exhibit interesting reactivity toward copper(II) ions. Their modes of reaction reflect the influence of the environment. The reactivity, expressed in terms of the dissociation constant for the amide group in the presence of copper(II), appears to depend on whether the group is in a simple amino acid amide or in a peptide chain and how it can have access to the central metal ion.[1,2]

With this in mind, we have investigated the structure-stability relationship between the copper(II) complexes of several dipeptide amides, in order to get information on the factors affecting the complexing abilities of the amide groups and the probable structures of the resulting complexes in aqueous solution.

For closer comparison with the reported peptide-copper(II) systems,[2,3] the solution equilibria of the copper(II) complexes of glycylglycine amide (abbreviated as Gly·Gly·NH_2), glycyl-β-alanine amide (Gly·β-Ala·NH_2), β-alanylglycine amide (β-Ala·Gly·NH_2), and β-alanyl-β-alanine amide (β-Ala·β-Ala·NH_2) have been studied by potentiometric titration, the results of which are given in the following.

Experimental

All the melting points are uncorrected.

Preparation of Dipeptide Amides and Related Compounds

The ethyl ester hydrochlorides of glycine, β-alanine, glycylglycine, and glycyl-β-alanine were prepared according to the ordinary method.[4]

Carbobenzoxyglycylglycine Ethyl Ester. To a solution of 10 g of glycylglycine ethyl ester hydrochloride in 40 ml of water were gradually added 12 g of potassium bicarbonate and then 90 ml of chloroform. Into the resulting mixture was added 8.5 ml of carbobenzoxy chloride over a period of 15—20 min under constant stirring. After it had been stirred at room temperature for 1—2 hr, unreacted carbobenzoxy chloride was treated with pyridine. The organic fraction was washed successively with 2—3% aqueous sodium bicarbonate, dilute hydrochloric acid, and water, and then dried over anhydrous magnesium sulfate. The filtrate was concentrated *in vacuo* to give a crystalline product, which was recrystallized from ethyl acetate–petroleum benzin.

Carbobenzoxyglycyl-β-alanine Ethyl Ester. This was prepared by a similar procedure to that for the carbobenzoxyglycylglycine ethyl ester.

The two materials described above were identified by comparing their melting points with those in the literature.[5,6]

Carbobenzoxy-β-alanylglycine Ethyl Ester. This was prepared in the same manner as reported by Winitz *et al.*[7] To a mixture of 15.6 g of carbobenzoxy-β-alanine[8] prepared from β-alanine and carbobenzoxy chloride, 9.8 g of glycine ethyl ester hydrochloride, and 9.8 ml of triethylamine in 160 ml of chloroform was added 14.5 g of *N,N'*-dicyclohexylcarbodiimide, and the reaction mixture was stirred at room temperature overnight. After removal of *N,N'*-dicyclohexylurea, the filtrate was washed successively with water, dilute hydrochloric acid, saturated aqueous sodium bicarbonate and water, dried over anhydrous magnesium sulfate and evaporated to dryness *in vacuo*. The product was identified by its melting point.[6]

Carbobenzoxy-β-alanyl-β-alanine Ethyl Ester. This was prepared from carbobenzoxy-β-alanine and β-alanine ethyl ester hydrochloride in the same way as for carbobenzoxy-β-alanylglycine ethyl ester.

Carbobenzoxy Derivatives of Glycylglycine-, Glycyl-β-alanine-, β-Alanylglycine-, and β-Alanyl-β-alanine-amide. These compounds were prepared according to the known method.[6] The first three compounds were confirmed by their melting points,[6,9] and elemental analysis. Carbobenzoxy-β-alanyl-β-alanine amide recrystallized from methanol–ether melted at 192—195 °C. Found: C, 57.49; H, 6.49; N, 14.24%. Calcd for $C_{14}H_{19}N_3O_4$: C, 57.32; H, 6.54; N, 14.33%.

Hydrochlorides of Glycylglycine-, Glycyl-β-alanine-, β-Alanylglycine-, and β-Alanyl-β-alanine-amide. These were obtained by the catalytic reduction of the corresponding amide

1) O. Yamauchi, H. Miyata, and A. Nakahara, This Bulletin, **44**, 2716 (1971).

2) O. Yamauchi, Y. Nakao, and A. Nakahara, *ibid.*, **46**, 2119 (1973).

3) O. Yamauchi, Y. Hirano, Y. Nakao, and A. Nakahara, *Can. J. Chem.*, **47**, 3441 (1969).

4) J. P. Greenstein and M. Winitz, "Chemistry of the Amino Acids," Vol. 2, John Wiley & Sons, Inc., New York (1961), p. 926.

5) R. W. Young, K. H. Wood, R. J. Joyce, and G. W. Anderson, *J. Amer. Chem. Soc.*, **78**, 2126 (1956).

6) H. T. Hanson and E. L. Smith, *J. Biol. Chem.*, **175**, 833 (1948).

7) M. Winitz, L. B. Frankenthal, N. Izumiya, S. M. Birnbaum, C. G. Baker, and J. P. Greenstein, *J. Amer. Chem. Soc.*, **78**, 2423 (1956).

8) Y. Nakao, H. Ishibashi, and A. Nakahara, This Bulletin, **43**, 3457 (1970).

9) J. S. Fruton and M. J. Bergmann, *J. Biol. Chem.*, **145**, 253 (1942).

derivatives of the carbobenzoxy peptides by using palladium black as a catalyst. In all cases, methanol was used as solvent with a small amount of hydrochloric acid. Glycylglycine amide hydrochloride and glycyl-β-alanine amide hydrochloride were recrystallized from methanol-ethyl acetate, whereas β-alanylglycine amide hydrochloride and β-alanyl-β-alanine amide hydrochloride were recrystallized from methanol-ether.

Glycylglycine Amide Hydrochloride: Mp 192—193 °C. Found: C, 28.53; H, 6.27; N, 25.46%. Calcd for $C_4H_{10}N_3O_2Cl$: C, 28.66; H, 6.03; N, 25.07%.

Glycyl-β-alanine Amide Hydrochloride: Mp 166—168 °C. Found: C, 33.05; H, 6.53; N, 23.25%. Calcd for $C_5H_{12}N_3O_2Cl$: C, 33.06; H, 6.67; N, 23.14%.

β-Alanylglycine Amide Hydrochloride: Mp 182—183 °C. Found: C, 32.98; H, 6.59; N, 23.58%. Calcd for $C_5H_{12}N_3O_2Cl$: C, 33.06; H, 6.67; N, 23.14%.

β-Alanyl-β-alanine Amide Hydrochloride: Mp 135—137 °C. Found: C, 36.93; H, 7.05; N, 21.48%. Calcd for $C_6H_{14}N_3O_2Cl$: C, 36.83; H, 7.23; N, 21.48%.

Glycylglycine Amide Acetate: This was prepared according to the method of Fruton and Bergmann.[9]

Preparation of the Neutral Copper(II) Complex of Glycylglycine Amide To a solution of 0.75 g of glycylglycine amide acetate in 10 ml of water was added freshly precipitated copper(II) hydroxide obtained from 1.5 g of copper(II) sulfate pentahydrate. The mixture was stirred at room temperature for about 30 min, and, after removal of excessive copper(II) hydroxide, added into ethanol-ether (2 : 1 by volume) under vigorous stirring. The complex was obtained as violet crystals. Found: C, 22.35; H, 4.53; N, 18.67%. Calcd for $[Cu(C_4H_7N_3O_2)(OH_2)]\cdot 1/2H_2O$: C, 21.87; H, 4.60; N, 19.13%.

pH Titration. Aqueous solutions (4.0×10^{-3} M; μ= 0.1 (KNO_3)) of the dipeptide amides were titrated in the absence and the presence of an equimolar amount of copper(II) nitrate.

The apparatus and the procedure were the same as reported previously.[2]

Results and Discussion

Titration Curves and Equilibrium Constants. The pH titration curves of the dipeptide amides in the absence and the presence of copper(II) nitrate are shown in Fig. 1. The amides with the β-alanyl group at the NH_2-terminus gave precipitates during the titration in the presence of copper(II). Since the structures of the dipeptide amides are closely related to those of the reported di- and tri-peptides[2,3] and the behavior of the terminal amide group is considered to be very similar to that of simple amino acid amides,[1] it is reasonable to assume from the titration curves the following reaction sequences and the species involved therein:

$$Cu^{2+} + H_2L \overset{K_1}{\rightleftharpoons} Cu(H_2L)^{2+} \quad (1)$$

$$Cu(H_2L)^{2+} \overset{K_{c_1}}{\rightleftharpoons} Cu(HL)^{+} + H^{+} \quad (2)$$

$$Cu(HL)^{+} \overset{K_{c_2}}{\rightleftharpoons} CuL + H^{+} \quad (3)$$

where H_2L refers to free dipeptide amide, and $Cu(HL)^+$ and CuL to the complexes formed upon removal of one and two protons, respectively, from the peptide linkages in the dipositive complex $Cu(H_2L)^{2+}$. The

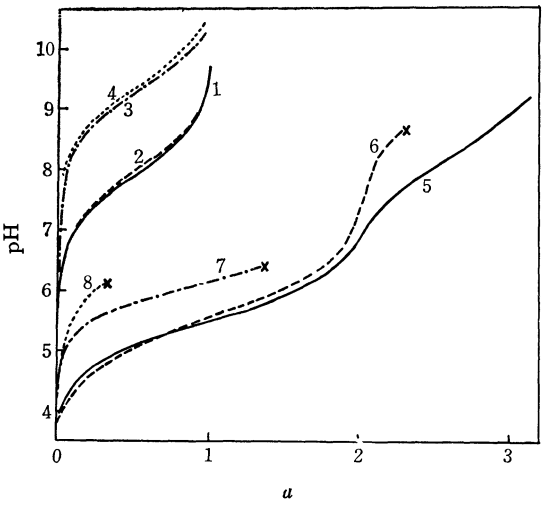

Fig. 1. Titration curves for the dipeptide amides in the absence and the presence of copper(II).
Curves 1—4: ligand alone
Curves 5—8: ligand : Cu(II) = 1 : 1
—— Gly·Gly·NH_2; ---- Gly·β-Ala·NH_2;
—·—·— β-Ala·Gly·NH_2; ····· β-Ala·β-Ala·NH_2
a: Moles of KOH added per mole of ligand.
x: Precipitation occurred at this point.

relevant equilibrium constants are defined by the following equations.

$$K_1 = \frac{[Cu(H_2L)^{2+}]}{[Cu^{2+}][H_2L]} \quad (4)$$

$$K_{c_1} = \frac{[Cu(HL)^{+}][H^{+}]}{[Cu(H_2L)^{2+}]} \quad (5)$$

$$K_{c_2} = \frac{[CuL][H^{+}]}{[Cu(HL)^{+}]} \quad (6)$$

The curve for Gly·Gly·NH_2–copper(II) indicates the dissociation of the third proton from the water molecule in the complex at high pH to give a hydroxy complex $CuL(OH)^-$ according to the equation:

$$CuL \overset{K_{OH}}{\rightleftharpoons} CuL(OH)^{-} + H^{+} \quad (7)$$

where

$$K_{OH} = \frac{[CuL(OH)^{-}][H^{+}]}{[CuL]} \quad (8)$$

Calculation of the equilibrium constants K_1, K_{c_1}, K_{c_2} and K_{OH} was carried out by the method of non-linear least-squares with the use of a NEAC 2200/500 computer. Derivation of the equations for the least-squares treatment and the computer program were essentially the same as those reported for the tripeptide-copper(II) systems.[2] Because of precipitation, the K_{c_2} value for β-Ala·Gly·NH_2 and all the constants for β-Ala·β-Ala·NH_2 could not be calculated.

The calculated equilibrium constants are shown in Table 1 together with the corresponding constants for the amino acid amide-,[1] dipeptide-,[3] and tripeptide-copper(II)[2] systems included for comparison. The reliability of the calculated constants was confirmed by duplicate or triplicate titration and by comparing the theoretical curves with the experimental ones, the deviations expressed in titer being negligibly small

TABLE 1. EQUILIBRIUM CONSTANTS (25±0.05 °C: μ=0.1 KNO_3))[a]

Ligand[b]	pK_a(COOH)	pK_a(NH_3^+)	log K_1	pK_{c_1}	pK_{c_2}	pK_{OH}	log $K_1K_{c_1}$	log $K_1K_{c_1}K_{c_2}$
Gly·Gly·NH_2		7.81±0.01	4.80±0.02	5.05±0.02	7.96±0.01	9.77±0.01	−0.25	−0.21
Gly·β-Ala·NH_2		7.87±0.03	5.22±0.01	5.42±0.01	8.99±0.01	c)	−0.20	−9.19
β-Ala·Gly·NH		9.18±0.03	5.16±0.03	5.39±0.04	c)	c)	−0.23	
β-Ala·β-Ala·NH_2		9.25±0.06	c)	c)	c)	c)		
Gly·Gly·Gly[d]	3.26±0.01	7.93±0.03	5.25±0.01	5.23±0.01	6.73±0.01		0.02	−6.71
Gly·β-Ala·Gly[d]	3.34±0.02	8.09±0.01	5.60±0.01	5.36±0.01	5.74±0.01		0.24	−5.50
Gly·Gly[e]	3.14±0.02	8.09±0.02	5.50±0.01	4.10±0.01			1.40	
Gly·β-Ala[f]	3.98	8.16	5.70±0.09	4.64±0.06			1.06	
Glycinamide[e]		7.96±0.01	5.30±0.01	6.79±0.02			−1.49	
β-Alaninamide[e]		9.23±0.02	5.1					

a) Variances are three times the estimated standard deviations. b) Abbreviations used: Gly·Gly·Gly=glycylglycylglycine; Gly·β-Ala·Gly=glycyl-β-alanine. c) Not determined because of precipitation. d) Ref. 2. e) Ref. 1. f) Ref. 3.

(less than 0.03 ml for the titers of 0—3.0 ml) for all the systems in the pH ranges studied.

The log K_1 values are 4.80—5.22 and close to those for the tripeptide-copper(II) systems. A possible reason for the low value for Gly·Gly·NH_2 might be that this ligand has the lowest pK_a value. This system has been reported recently by Sigel *et al.*[10] who obtained the value of 5.05 for log K_1.

Dissociation of the peptide hydrogens in the complexed species are measured by means of pK_{c_1} (−log K_{c_1}) and pK_{c_2} (−log K_{c_2}), which can be compared with the corresponding values for the dipeptides and the tripeptides. The pK_{c_1} values are essentially the same for the three amides and seem to be independent of the nature of the *N*-terminal amino acid, whereas the pK_{c_2} values reflect the steric requirements around copper(II) and are much higher than those for the tripeptides. The reported values[10] of pK_{c_2} (7.29) and estimated pK_{OH} (−log K_{OH}) (~8.3) for Gly·Gly·NH_2 differ considerably from the present values, this being ascribable to precipitation which was not observed in our experiment.

Structure-Stability Relationship. The dipeptide amides in acid solution are most probably bidentate ligands like glycinamide and tripeptides, coordinating through the amino and the peptide carbonyl group as shown by the following structures I—III.[1,2,11,12]

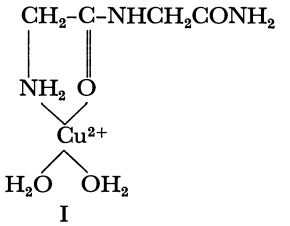

I

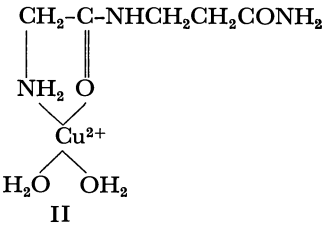

II

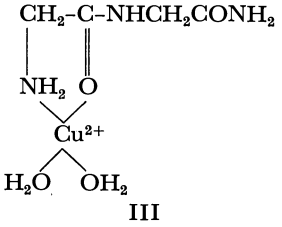

III

That the log K_1 value for β-Ala·Gly·NH_2 is close to that for Gly·β-Ala·NH_2 in spite of the higher pK_a may reasonably be explained by the less stable six-membered ring (III) as compared with the five-membered rings in I and II. These structures for $Cu(H_2L)^{2+}$ may be accepted, because the pK_a and log K_1 values are in excellent agreement with the corresponding values[1] for glycinamide and β-alaninamide both of which are known to form chelates in acid solution through the amino nitrogen and the amide oxygen.[1,12]

Deprotonation from the peptide linkage leads to $Cu(HL)^+$, where the pK_{c_1} values are comparable to those of tripeptides, but about 1 log unit higher than those of dipeptides. This may be interpreted in terms of the more effective coordination by the carboxyl group in dipeptides (IV) than the amide carbonyl group in dipeptide amides (V) and tripeptides.

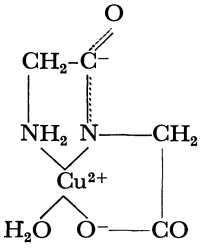

IV

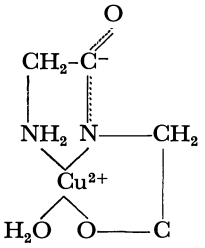

V

The degrees of formation of $Cu(HL)^+$ at a fixed pH can be expressed by the log $K_1K_{c_1}$ values, which are found to be around −0.2 as compared with 0—0.25 and 1—1.4 for the structurally related tripeptide-copper(II) and the dipeptide-copper(II) systems, respetively. As far as these peptide-copper(II) complexes are concerned, the 5-6-membered fused-ring systems are as stable as the 5-5-membered when compared on the basis of log $K_1K_{c_1}$. It is interesting to note in this connection that Weatherburn *et al.*[13] reported a similar stability relationship between the nickel(II)

10) H. Sigel, R. Griesser, and B. Prijs, *Z. Naturforsch.*, **27b**, 353 (1972).

11) H. C. Freeman, "The Biochemistry of Copper," ed. by J. Peisach, P. Aisen, and W. E. Blumberg, Academic Press, Inc., New York (1966), p. 87.

12) T. Komorita, J. Hidaka, and Y. Shimura, This Bulletin, **42**, 168 (1969).

13) D. C. Weatherburn, E. J. Billo, J. P. Jones, and D. W. Margerum, *Inorg. Chem.*, **9**, 1557 (1970).

complexes of diethylenetriamine (5-5-membered) and *N*-(2-aminoethyl)-1,3-propanediamine (5-6-membered).

In dilute aqueous solution, the complexes of type CuL formed upon dissociation of the second proton from $Cu(HL)^+$ may be described by rigid fused-ring structures like VI and VII, whose relative stability is inferred from the log $K_1K_{c_1}K_{c_2}$ values.

$\log K_1K_{c_1}K_{c_2}$

−8.21 −9.19

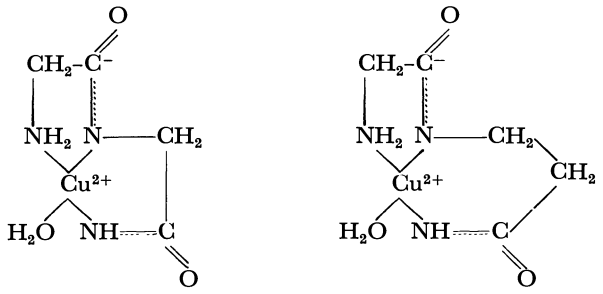

VI VII

The stability-determining factor is definitely the pK_{c_2} value, which is low for Gly·Gly·NH_2 (7.96) and high for Gly·β-Ala·NH_2 (8.99). Thus, Gly·Gly·NH_2-Cu(II) (VI) is estimated to be more stable than Gly·β-Ala·NH_2-Cu(II) (VII), and the stability order is the reverse of that found for the Schiff base-copper(II) complexes[14] and reminds us of that between glycylglycine- and glycyl-β-alanine-copper(II), although the stability difference is much smaller. The complexes of β-Ala·Gly·NH_2 and β-Ala·NH_2 are supposed to be less stable because they were hydrolyzed to form precipitates at pH below 6.4.

When compared with the tripeptides, the dipeptide amides lose a proton from the terminal amide group at higher pH. A reasonable explanation for this may be that deprotonation from the peptide group nearest the COOH-terminus of tripeptides results in the formation of an additional chelate ring which is considered to increase the chelate stability by the "chelate effect," whereas the deprotonation from the dipeptide amides does not affect the stability in the same way.

The abundance of the coordinated species in the Gly·Gly·NH_2- and Gly·β-Ala·NH_2-copper(II) systems is shown in Figs. 2 and 3, respectively. One important feature of the curves is that the most abundant species at neutral pH is $Cu(HL)^+$ as described by V where the amide NH_2 group remains intact. This suggests that, at physiological pH, $-CONH_2$ groups from the asparagine or the glutamine residue in peptide chains coordinate to copper(II), if at all, through their carbonyl oxygen and not through the nitrogen as is usually the case with oligopeptides.

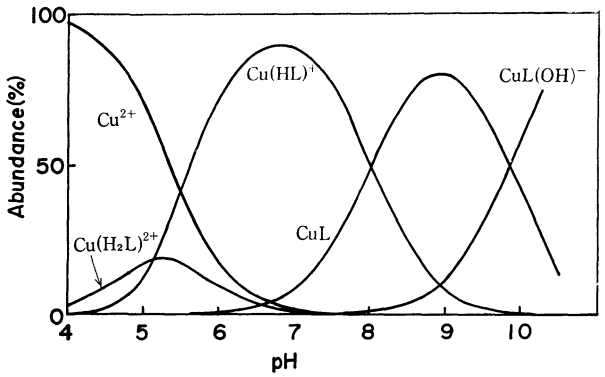

Fig. 2. Calculated abundances of the coordinated species in the 1 : 1 Gly·Gly·NH_2-Cu(II) system.

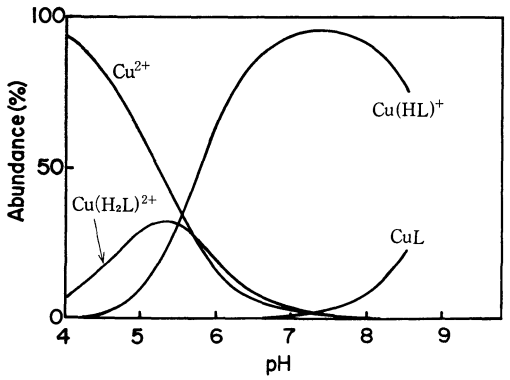

Fig. 3. Calculated abundances of the coordinated species in the 1 : 1 Gly·β-Ala·NH_2-Cu(II) system.

The authors are indebted to the members of the Osaka University Computation Center for computation. This investigation was supported in part by a grant from the Ministry of Education.

14) A. Nakahara, H. Yamamoto, and H. Matsumoto, This Bulletin, **37**, 1137 (1964).

Ionic Equilibria in Mixed Solvents. X. Hydrolysis of Nickel(II) Ion in Dioxane-Water Mixtures

Takayoshi KAWAI, Haruko OTSUKA*, and Hitoshi OHTAKI

Department of Electrochemistry, Faculty of Engineering, Tokyo Institute of Technology, O-okayama, Meguro, Tokyo 152

**Laboratory of Analytical Chemistry, Faculty of Science, Nagoya University, Chikusa, Nagoya 464*

(Received September 3, 1973)

The hydrolytic reactions of nickel(II) ion were studied at 25 °C in water and dioxane-water mixtures containing 3 M (Li)ClO_4 as an ionic medium. Emf measurements were carried out in the range of the total nickel(II) ion concentration of 0.02469—0.7891 M in water, 0.02488—0.7996 M in a 0.1 mole fraction (35.21% w/w) dioxane-water mixture and 0.05170—0.9016 M in a 0.2 mole fraction (55.01% w/w) dioxane-water mixture, respectively. Some supplementary measurements were performed in a 0.5 mole fraction (83.02% w/w) dioxane-water mixture. Only the $Ni_4(OH)_4^{4+}$ complex was found in all solvent systems and its formation constant in log $*\beta_{44}$ was -27.32 ± 0.08 (in water), -27.11 ± 0.08 (in a 0.1 mole fraction dioxane-water mixture), and -27.04 ± 0.05 (in a 0.2 mole fraction dioxane-water mixture). In order to test the relative change of the formation consatnt of the $Ni_4(OH)_4^{4+}$ complex over the whole solvent composition examined, the variation of the formation constant was measured with the continual change of solvent composition at constant Z. Approximate values of the solubility products of $Ni(OH)_2$ and $NiOHClO_4$ precipitates were estimated from maximum values of Z.

A number of authors studied the hydrolysis of nickel(II) ion in water and the results are summarized in "Stability Constants" and its supplement.[1] Among them, Burkov, Lilič and Sillén,[2] Ohtaki and Biedermann,[3] and Kennedy[4] reported that the $Ni_4(OH)_4^{4+}$ complex is the main product. Although Ohtaki and Biedermann[3] and Kennedy[4] proposed some minor species such an $NiOH^+$, Ni_2OH^{3+} [3] and $Ni_2(OH)_2^{2+}$,[4] information for minor species has not clearly been established yet.

In general, the hydrolytic reaction of nickel(II) ion is written by the following equation.

$$qNi^{2+} + pH_2O = Ni_q(OH)_p^{(2q-p)+} + pH^+ \quad (1)$$

The concentration of hydrogen ion set free on hydrolysis is given as follows,

$$BZ = \sum_p \sum_q p*\beta_{pq} b^q h^{-p} \quad (2)$$

$$= h - H + K_w h^{-1} \quad (3)$$

where K_w is the autoprotolysis constant of the solvent. The formation constant ($*\beta_{pq}$) of a species is defined by Eq. (4).

$$*\beta_{pq} = [Ni_q(OH)_p^{(2q-p)+}][H^+]^p/[Ni^{2+}]^q \quad (4)$$

Symbols

- h Hydrogen ion concentration at equilibrium
- H Analytical excess of hydrogen ions $=[ClO_4^-]-[Li^+]-2B$
- B Total concentration of nickel ion
- b Concentration of unhydrolyzed nickel ion
- Z Average number of hydrogen ion set free per nickel atom $=(h-H+K_w h^{-1})/B$
- p Number of OH groups bound to hydrolyzed species
- q Number of nickel atoms bound to hydrolyzed species
- $*\beta_{pq}$ Formation constant of the nickel hydroxo complex $Ni_q(OH)_p^{(2q-p)+}$, defined by Eq. (4)
- [ ] Concentration
- E Emf

Experimental

The measurements were carried out at 25.00 ± 0.02 °C in a liquid paraffin bath set in a room thermostated at 25 ± 1 °C. Lithium perchlorate was used as an ionic medium to keep the perchlorate concentration at 3 M. The total concentration of nickel ion studied ranged from 0.02469 to 0.7891 M in water, 0.02488 to 0.7996 M in a 0.1 mole fraction (35.20% w/w) dioxane-water mixture, and 0.05170 to 0.9016 M in a 0.2 mole fraction (55.01% w/w) dioxane-water mixture. Some supplementary measurements were carried out in a 0.5 mole fraction (83.02% w/w) dioxane-water mixture and results obtained were compared with those in other solvent systems.

A slightly acid nickel(II) perchlorate solution in water or a mixed solvent was bubbled with nitrogen gas to remove carbon dioxide and then was mixed with a lithium hydroxide solution, which had been prepared by electrolysis, to form a small amount of precipitates. The turbid solution was stirred by bubbling with nitrogen gas for several days and filtered through G3 and G4 glass filters on which fine platinum powder was placed. A clear solution thus obtained was used as a test solution. The total concentration of nickel ion in a test solution was determined gravimetrically as its dimethylglyoximate.

The electric circuit for emf measurements was as follows.

G. E.	Solution	3M $LiClO_4$ mixture		
	3M $LiClO_4$ aq. soln	0.01M $AgClO_4$ 2.99M $LiClO_4$ aq. soln	AgCl-Ag	

Hydrogen ions were added coulometrically into the test solution during titrations. The circuit for coulometry was the same as that used in the preceding paper.[5] The emf reached a constant value within 15 minutes after coulometric generation of hydrogen ions and remained unchanged within ±0.2 mV for more than several hours. The emf at equilibrium is written by the following equation.

$$E = E^{0*} + 59.15 \log h + 59.15 \log f_H + E_j(h, B) \quad (5)$$

1) L. G. Sillén and A. E. Martell, "Stability Constants," Chem. Soc., London(1964), Supplement No. 1 (1971).

2) K. A. Burkov, L. S. Lilič, and L. G. Sillén, *Acta Chem. Scand.*, **19**, 14 (1965).

3) H. Ohtaki and G. Biedermann, This Bulletin, **44**, 1822 (1971).

4) B. Kennedy, S. C., Ph. D. Georgetown University, 1969.

5) H. Ohtaki and T. Kawai, This Bulletin, **45**, 1735 (1972).

This equation is reasonably rewritten as Eq. (6) when only a small part of nickel ions hydrolyzes at a constant total concentration of nickel and the hydrogen ion concentration is $10^{-2}>h>10^{-12}$ M.

$$E = E^\circ + 59.15 \log h \quad (6)$$

where E° is a constant. Eq. (6) was used for determination of the concentration of hydrogen ion at equilibrium from emf data.

Apparatus. *Glass Electrodes*: Beckman (No. 40498) glass electrodes were used in combination with a Radiometer PHM-4d pH meter (Copenhagen).

Silver-Silver Chloride Electrodes set in the "Wilhelm" type of the half cell[6] were prepared according to Brown.[7]

A Coulometric Analyzer (Leeds & Northrup Co., Philadelphia, Pa.) was used as a current source for generation of hydrogen ions in a solution during titration.

Reagents. *Nickel(II) Perchlorate*: Reagent grade nickel(II) nitrate was recrystallized twice from water and the crystals were heated under an infrared lamp and then in an electric oven at about 500 °C for several hours to decompose into nickel oxide. Nickel oxide thus prepared was dissolved in a little excess of about 30% hot perchloric acid solution and the solution was filtered through a G4 glass filter. Nickel(II) perchlorate was recrystallized twice from water. The crystals were dissolved into distilled water and a small amount of perchloric acid was added to keep pH of the solution at about 3 in order to prevent hydrolysis of the nickel ions. The concentration of nickel ion in the stock solution was determined by electrogravimetry, and that of hydrogen ion by potentiometry in combination with coulometry. The end point was detected according to Gran plot.[8]

Lithium Perchlorate and Lithium Hydroxide were prepared by the same procedures as described in the previous paper.[5]

Dioxane purified by an ordinary method[5] was stored in a refrigerator and melted just before preparation of a test solution.

The concentration of protolytic impurities in a 3 M lithium perchlorate solution was estimated from the deviation of a Gran plot at the end point of neutralization of perchloric acid in the solution in the absence of nickel ions. The total concentration of protolytic impurities was 75 ± 10 μeq./l independent of solvent composition. Thus, it is very reasonable to conclude that most impurities had been contained in lithium perchlorate.

Results and Discussion

The results obtained are summarized in Figs. 1—3 as Z *vs.* $-\log h$ plots. These data have been corrected for the protolytic impurities on an assumption of the complete dissociation of the impurities[9] at pH where nickel(II) ions hydrolyze.

On the basis of the data shown in Figs. 1—3, $\log BZ$ was plotted against $-\log h$. The plots gave a set of straight lines with slope 4 in each solvent system. These results indicated that only homoligandic hydrolyzed species containing four hydroxyl groups were formed. A plot of $(\log BZ+4\log h)$ against $\log B$ yielded a straight line with a slope of 4. Therefore, it was concluded that the hydrolyezd species is $Ni_4(OH)_4^{4+}$ in dioxane–water mixed solvents at least to 0.2 mole fraction dioxane (55.01% w/w), as several investigators concluded so far in water.[2,3,4] Minor components such as $NiOH^+$ and Ni_2OH^{3+} upon which some authors reported were not detected with reasonable

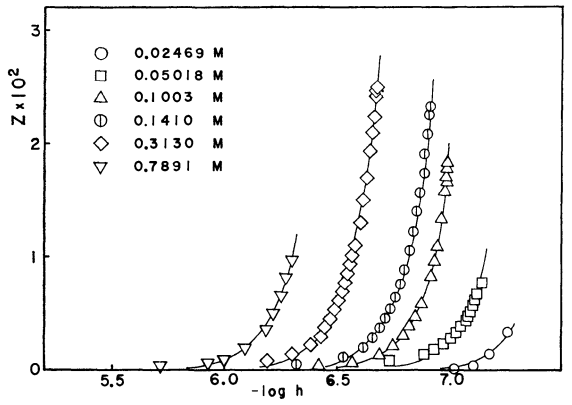

Fig. 1. Values of Z *vs.* $-\log h$ in the aqueous solution. Solid lines show calculated curves of Z with formation constant of $\log {}^*\beta_{44}=-27.32$.

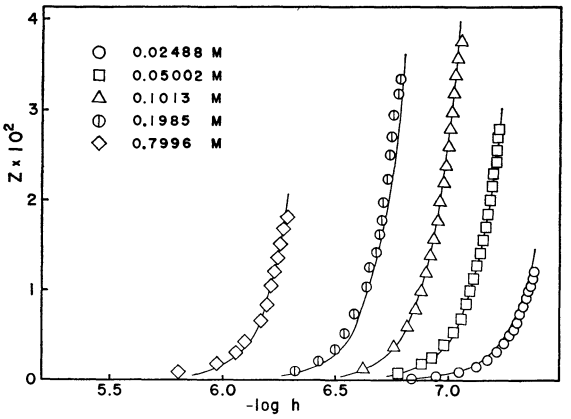

Fig. 2. Values of Z *vs.* $-\log h$ in the solution of a 0.1 mole fraction dioxane-water mixture. Solid lines show calculated curves of Z with formation constant of $\log {}^*\beta_{44}=-27.11$.

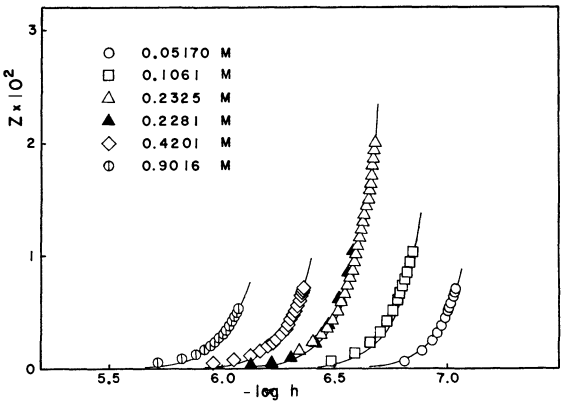

Fig. 3. Values of Z *vs.* $-\log h$ in the solution of a 0.2 mole fraction dioxane-water mixture. Solid lines show calculated curves of Z with formation constant of $\log {}^*\beta_{44}=-27.04$.

6) W. Forsling, S. Hietanen and L. G. Sillén, *Acta Chem. Scand.*, **6**, 901 (1952).

7) A. S. Brown, *J. Amer. Chem. Soc.*, **56**, 646 (1934).

8) G. Gran, *Analyst* (London), **77**, 661 (1952).

9) G. Biedermann, L. Newman and H. Ohtaki, Proceedings on The Symposium on Trace Characterization-Chemical and Physical (1966), Gaithersburg, Maryland, U.S.A., p. 1.

certainties in this study. Solid lines in Figs. 1—3 indicate calculated values of Z with formation constants given in each solvent system listed in Table 1.

Results obtained in a 0.5 mole fraction dioxane-water mixture were not sufficiently reliable because of low solubility of nickel(II) hydroxo complexes. The concentration of protolytic imputiries was almost comparable with that of nickel(II) hydroxo complexes present in the solution. However, the results were reasonably interpreted by the assumption of formation of the $Ni_4(OH)_4^{4+}$ complex with the formation constant of about $10^{-28\pm1}$.

Results are tabulated in Table 1 in the form of log $*\beta_{44}$. These values were obtained after refinement by electronic computer calculations by means of a generalyzed least-squares method.

The composition of the complex formed remained unchanged with solvent composition over the wide range of the dioxane content, the same phenomenon having been found in the case of beryllium ion.[10] In the hydrolytic reaction of copper(II) ion[5] higher polymers gradually disappear with solvent composition, although formation constants of the complexes are not appreciably affected with solvent composition.

Table 1. Formation constants and solubility products

	$\log^* \beta_{44}$	$\log^* K_{s1}$	$\log^* K_{s2}$
Aqueous solution	-27.32 ± 0.08	13.3 ± 0.5	6.9 ± 0.5
0.1 mole fraction mixt.	-27.11 ± 0.08	14.1 ± 0.5	7.4 ± 0.5
0.2 mole fraction mixt.	-27.04 ± 0.05	13.1 ± 0.5	6.6 ± 0.5
0.5 mole fraction mixt.	$-28\ \pm1$	—	—

Solvent Effects on the Formation Constants of Complexes. The authors previously found that the solvent effect of dioxane on the formation constants of hydrolysis of metal ions is much smaller than that expected in usual acid dissociation reactions.[11,12]

In order to test the relative change of formation constants with solvent composition, the following experiment was carried out. The method was first employed by Ohtaki and Kato[13] in their study of the solvent effect on hydrolysis of beryllium ion. We measured the change of emf on mixing two hydrolyzed solutions which had been prepared to have the same total concentration of nickel(II) ion and Z value and the different solvent composition. The change of the liquid junction potential, E_j in Eq. (5), with dioxane content was found to be negligible by using two reference cells. A salt bridge of one of the reference cells was composed of 3 M $LiClO_4$ aqueous solution and the other by 3 M $LiClO_4$ solution of a 0.2 mole fraction dioxane–water mixture. Negligible volume change was also found from the density measurements of 3 M $LiClO_4$ solution of dioxane–water mixtures. Then the following equation is reduced from Eq. (6).

$$\Delta \log h = (\Delta E - \Delta E^\circ)/59.15 \quad (7)$$

The change of E°, ΔE°, was determined by similar measurements without nickel ions.[14]

If there is an appreciable amount of $Ni_4(OH)_4^{4+}$ in the solution, the following relations hold. From Eq. (2),

$$BZ = 4*\beta_{44}b^4h^{-4} \quad (8)$$

and

$$B = b + 4*\beta_{44}b^4h^{-4} = b + BZ$$

and therefore,

$$b = B(1-Z) \quad (9)$$

Insertion of Eq. (9) into Eq. (8) leads to

$$BZ = 4*\beta_{44}B^4(1-Z)^4h^{-4} \quad (10)$$

Rearrangement of Eq. (10) gives rise to Eq. (11)

$$Z(1-Z)^{-4} = 4*\beta_{44}B^3h^{-4}$$

or

$$\log Z - 4\log(1-Z) = \log 4 + \log^*\beta_{44} + 3\log B - 4\log h \quad (11)$$

From the differeniation of Eq. (11) at constant Z and B, Eq. (12) is obtained.

$$\partial \log^* \beta_{44} = 4\partial \log h \quad (12)$$

The change of the formation constant was determined from emf data with Eqs. (7) and (12), and results are given in Fig. 4. The formation constant first increases with dioxane concentration and then reaches a plateau.

On the Solubility of Nickel(II) Hydroxo Complexes. Approximate values of the solubility product of nickel(II) hydroxide precipitates were estimated from maximum values of Z in various solvent systems.

The maximum value of Z, Z_{max}, increases with B to reach a maximum and then decreases. This suggests that besides the nickel hydroxide the basic nickel perchlorate also precipitates as have been pointed out in the study of hydrolysis of nickel ion in the chloride system.[3]

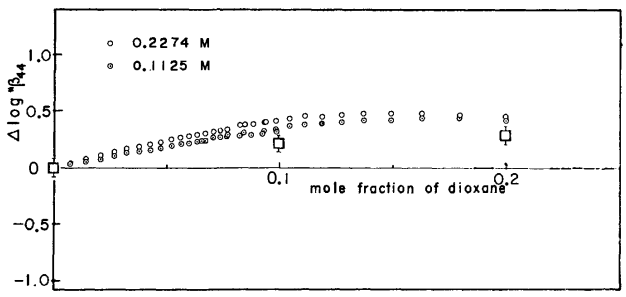

Fig. 4. $\Delta \log *\beta_{44}$ from the value in aqueous solution for $Ni_4(OH)_4^{4+}$ complex in dioxane-water mixtures. Circles; points of continuous measurements, squares; points of individual determination with experimental uncertainties.

10) H. Ohtaki, *Inorg. Chem.*, **6**, 808 (1967). H. Ohtaki and H. Kato, *ibid.*, **6**, 1935 (1967).

11) M. Paabo, R. G. Bates and R. A. Robinson, *J. Phys. Chem.*, **70**, 247 (1966).

12) G. Douheret, *Bull Soc. Chim. France*, **1967**, 1942.

13) H. Ohtaki and H. Kato, Abstracts of the Meeting of the Coordination Chemistry(Hiroshima), p. 111(1967).

14) H. Ohtaki, Abstract of the Informal Meeting of the 10th ICCC (1967), Nikko, p. 43.

If the following equilibrium is assumed,

$$Ni(OH)_{2-x}(ClO_4)_x(s) + xH_2O = k_{sx}Ni(OH)_2(s) + xClO_4^- + xH^+$$

$$k_{sx} = \frac{[Ni(OH)_2(s)][ClO_4^-]^x[H^+]^x}{[Ni(OH)_{2-x}(ClO_4)_x(s)]} = \frac{m(C_0h)^x}{1-m} \quad (13)$$

where (s) represents the solid phase and C_0 denotes the perchlorate ion concentration assumed to be constant (3M) and m the mole fraction of $Ni(OH)_2$ in the solid phase with an assumption of unit activity coefficient, the mole fraction m is obtained as follows:

$$m = \frac{k_{sx}}{k_{sx}+(C_0h)^x} \quad (14)$$

Solubility products of nickel hydroxide, $*K_{s1}$, and basic nickel perchlorate, $*K_{s2}$, respectively, are defined as follows.

$$*K_{s1} = \frac{[Ni^{2+}][H^+]^{-2}}{[Ni(OH)_2(s)]} = \frac{bh^{-2}}{m} \quad (15)$$

$$*K_{s2} = \frac{[Ni^{2+}][H^+]^{-(2-x)}[ClO_4^-]^x}{[Ni(OH)_{2-x}(ClO_4)_x(s)]} = \frac{b(C_0h)^xh^{-2}}{1-m} \quad (16)$$

Therefore,

$$k_{sx} = *K_{s2}/*K_{s1} \quad (17)$$

$$b = *K_{s1}mh^2 = *K_{s1}h^2\frac{k_{sx}}{k_{sx}+(C_0h)^x} \quad (18)$$

Thus BZ_{max} is represented as follows.

$$BZ_{max} = 4*\beta_{44}b^4h_{max}^{-4} = \frac{4*\beta_{44}*K_{s1}^4k_{sx}^4h_{max}^4}{\{k_{sx}+(C_0h_{max})^x\}^4} \quad (19)$$

If we put $C_0h/k_{sx}^{1/x}=\omega$, we can compare Eq. (19) with Eq. (20)

$$y = \left[\frac{a\omega}{(1+\omega^x)}\right]^4;\ a=\{4*\beta_{44}\}^{1/4}*K_{s1}k_{sx}^{1/x}/C_0 \quad (20)$$

or

$$Y = \log\frac{\omega}{(1+\omega^x)} \quad (21)$$

Curve fitting of $(\log BZ_{max})/4$ *vs.* $\log h$ with Y *vs.* $\log \omega$ at various x gives the values of x about 1.0—1.3 in all solvent systems. A typical example is shown in Fig. 5. If we assume a stoichiometric composition of the basic nickel perchlorate taking into account the experimental uncertainties of BZ_{max} values and a simple assumption of ideal solid solution of the $Ni(OH)_{2-x}(ClO_4)_x$ mixture, the composition of the basic nickel perchlorate may be described as $NiOHClO_4$ ($x=1$). Under these assumptions the value of log with the known value of $*\beta_{44}$. Results are given in k_{sx} can be obtained from the abscissa and log $*K_{s1}$, and thus log $*K_{s2}$, from the ordinate Table 1. Solubility products of both hydroxide and basic perchlorate are fairly insensitive to the dioxane content as has been found in the case of copper(II) hydroxide.[5]

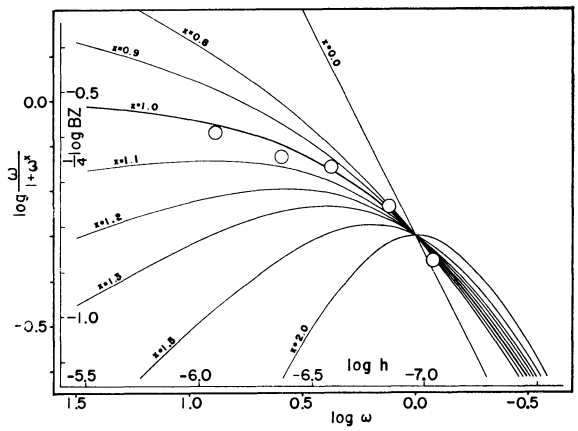

Fig. 5. A family of normalized curves of $Y=\log\frac{\omega}{(1+\omega^x)}$ *vs.* $\log\omega$ at various x. Circles show values of $(\log BZ_{max})/4$ obtained in a 0.2 mole fraction dioxane-water mixture.

The logarithmic values of solubility product of nickel hydroxide have been reported to be -13.8—-17.2 in aqueous solutions,[1] which correspond to $14._2$—10.8 in the log $*K_{s1}$ scale. The value of log $*K_{s1}=13.3$ in aqueous solution found in the present work can reasonably be compared with these literature values. No value has been found in literature for the solubility product of basic nickel salt.

It should be noted that the value of k_{sx} was kept constant at $10^{-6.4}$—$10^{-6.6}$ independent of solvent composition, although the reaction is not isoelectric.

A part of the present study has been carried out in the laboratory of Analytical Chemistry in Nagoya University. This work was financially supported by the Ministry of Education.

Pressure Effect Determined with Use of the Nondispersive Infrared Gas Analyser

Eiji NIKI and Tsutomu YONEZAWA

Department of Industrial Chemistry, Faculty of Engineering, Tokyo University, Hongo, Tokyo 113

(Received June 16, 1972)

The pressure effect of nitrous oxide and nitric oxide due to nitrogen gas was investigated with use of a nondispersive infrared gas analyser. The results are in line with the theoretical curves derived from the Elsasser theory. The calculated expression is partly improved and the error of calculations is estimated in regard to carbon dioxide.

With a nondispersive infrared gas analyser, it is easily observed that the absorption increases with increasing pressure of nitrogen gas at constant pressure of infrared absorbing gases such as carbon dioxide or carbon monoxide. This effect is known as the pressure broadening. In a previous paper[1] the mean absorption was calculated on the Elsasser theory as a function of the partial pressure of absorber, the total pressure and the length of the sample cell. The result was proved to interpret fairly well the experimental results for carbon dioxide and carbon monoxide. In this paper, the influence of the Bessel function of order zero approximated by unit is evaluated in regard to carbon dioxide. Experiments were carried out on nitrous oxide and nitric oxide concerning the self broadening of the absorbing gas and the foreign gas broadening due to nitrogen gas in order to see whether the result of calculation can be applied to other infrared absorbing gases.

Apparatus

The apparatus consists of a nondispersive infrared gas analyser of the zero method positive filter type with a condenser microphone detector.[2] The windows consist of LiF. A schematic diagram is given in Fig. 1.

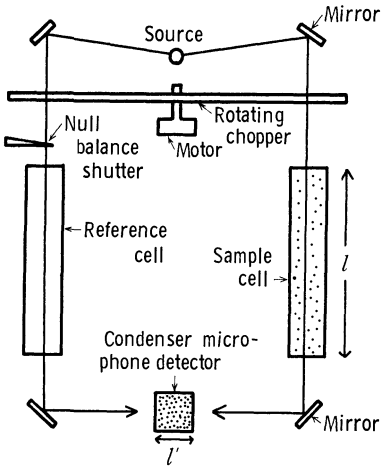

Fig. 1. The schematic diagram of the nondispersive infrared gas analyser. The temperature of the infrared source is about 600 °C. $l'=5$ cm.

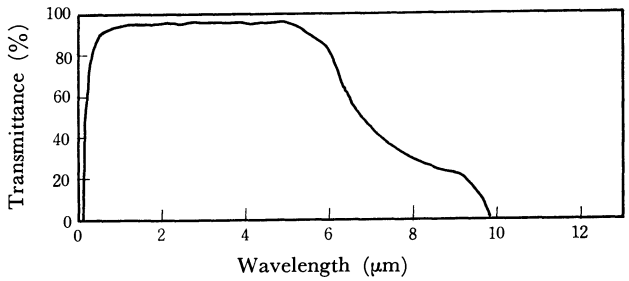

Fig. 2. The spectral transmission of LiF.

The sample gas is prepared in the mixing vessel and its pressure is measured by a mercury manometer. Figure 2 shows the spectral transmission of lithium fluoride.[3] Its absorption edge is about 1030 cm^{-1}.

Theoretical

For the sake of simplicity let us consider the expression

$$y = \frac{\int_0^\infty \{1-\exp(-\sum_{m=1}^{n} k_m l)\}d\nu}{nd} \tag{1}$$

which gives the mean absorption of the band spectrum in the infrared region, where k_m is the absorption coefficient of each vibrational rotational line, m the number added to each line, n the total number of lines, d the line spacing and l the thickness of the layer. The absorption coefficient k_m, in general, can be expressed by means of the Lorentz curve

$$k_m = \frac{(\alpha_m/\pi)\delta}{(\nu-\nu_m)^2+\delta^2} \tag{2}$$

ν_m being the frequency at the center of the mth line. α_m is equivalent to $\int_0^\infty k_m d\nu$ and assumed to be proportional to the partial pressure of absorber p_a,

$$\alpha_m = \alpha_{0m} p_a \tag{3}$$

α_{0m} being the proportional constant. δ is the damping constant and is known to be common to all the lines. From kinetic theory of the gas, δ is given by[4]

$$\delta = \frac{1}{4\pi}\sum_i N_i (D_{a,i})^2 \left[2\pi kT\left(\frac{1}{m_a}+\frac{1}{m_i}\right)\right]^{1/2} \tag{4}$$

where N_i is the number of molecules of the ith type gas per unit volume, $D_{a,i}$ the sum of the optical col-

1) T. Yonezawa and E. Niki, *Trans. Soc. Instr. Cont. eng.*, **7**, 236 (1970).

2) D. W. Hill and T. Powell, "Non-Dispersive Infrared Gas Analyser," Plenum Press: New York (1968) p. 1.

3) D. W. Hill and T. Powell, *ibid.*, p. 20.

4) D. E. Burch, E. B. Singleton, and D. Williams, *Appl. Opt.*, **1**, 359 (1962).

lision diameters of the absorbing molecule and a molecule of the ith type, m_a the mass of the absorbing molecule and m_i the mass of the ith type of molecule. Replacing the number of molecules N_i by the corresponding partial pressure p_i in Eq. (4), we have

$$\delta = \frac{1}{4\pi}\left(\frac{2\pi}{kT}\right)^{1/2} \sum_i C_{a,i} p_i \tag{5}$$

where $C_{a,i}$ is a constant involving the masses and optical collision diameters of the absorbing and ith gas, respectively. If Eq. (5) is restricted to the binary mixtures, then

$$\delta = \frac{1}{4\pi}\left(\frac{2\pi}{kT}\right)^{1/2} (C_{a,a}p_a + C_{a,b}p_b) \tag{6}$$

where a refers to the absorbing molecule and b the foreign molecule. From Eq. (6) we get

$$\delta = \frac{1}{4\pi}\left(\frac{2\pi}{kT}\right)^{1/2} C_{a,a}\{p_a + (C_{a,b}/C_{a,a})p_b\}. \tag{7}$$

The expression in parentheses gives the effective pressure P_e of the gas mixture. If we denote coefficient $1/4\pi(2\pi/kT)^{1/2}C_{a,a}$ by a δ_0, then δ is given by

$$\delta = \delta_0 P_e. \tag{8}$$

For binary mixtures, we have $P_e = p_a + (1/B)p_b$ where $B = C_{a,a}/C_{a,b}$ which is called the self-broadening coefficient[5] of the absorbing gas which represents the ratio of the self-broadening ability of the absorbing gas to the broadening ability of the broadening gas. p_b is the partial pressure of the broadening gas.

If each of the n vibrational rotational lines is supposed to be completely isolated from the neighboring lines, Eq. (1) reduces to

$$y = \frac{\sum_{m=1}^{n}\int_u^v \{1-\exp(-k_m l)\}\mathrm{d}\nu}{nd} \tag{9}$$

u, v being $\nu_m - d/2$ and $\nu_m + d/2$. Introducing the following mean fractional transmission of mth line T_m defined by Elsasser[6]

$$T_m = \frac{1}{d}\int_u^v \exp\left\{-\frac{(\alpha_m/\pi)\delta}{(\nu-\nu_m)^2+\delta^2} l\right\}\mathrm{d}\nu, \tag{10}$$

Eq. (9) becomes

$$y = 1 - \langle T_m \rangle_{av} \tag{11}$$

where $\langle\ \rangle_{av}$ indicates the average of T_m over m, *viz.*, $\langle T_m\rangle_{av} = 1/n\sum_{m=1}^{n} T_m$. T_m was evaluated by Elsasser in regard to the limits of small and large δ. If δ is small compared with the line spacing d, then

$$T_m = 1 - \phi\{(\pi\alpha_m\delta l)^{1/2}/d\} \tag{12}$$

where ϕ is probability integral. Here ϕ is supposed to be approximated by

$$\phi\{(\pi\alpha_m\delta l)^{1/2}/d\} = 2(\alpha_m\delta l)^{1/2}/d. \tag{13}$$

Thus we have

$$y = 2\langle(\alpha_m\delta l)^{1/2}/d\rangle_{av}. \tag{14}$$

By means of Eqs. (3) and (8), the equation becomes

$$y = 2\left\langle \frac{\alpha_{0m}{}^{1/2}\delta_0{}^{1/2}}{d}\right\rangle_{av} p_a{}^{1/2}P_e{}^{1/2}l^{1/2}. \tag{15}$$

If δ is large compared with the line spacing, then

$$T_m = \exp\{-(\alpha_m l/d)\tanh 2\beta\} \times J_0\{i(\alpha_m l/d)\tanh 2\beta/\cosh 2\beta\} \tag{16}$$

where $\beta \equiv \pi\delta/d$ and J_0 is the Bessel function of order zero and imaginary argument. By replacing $\tanh 2\beta$ with 2β and J_0 with the unit in Eq. (16), we get

$$T_m = \exp(-2\pi\alpha_m\delta l/d^2). \tag{17}$$

Substituting Eq. (17) into Eq. (11) and using Eqs. (3) and (8), we have

$$\begin{aligned} y &= 1 - \langle\exp\{-2\pi(\alpha_{0m}\delta_0/d^2)p_aP_el\}\rangle_{av} \\ &= 1 - \langle\exp\{-2\pi(\alpha_{0m}\delta_0/d^2)P_ew\}\rangle_{av} \end{aligned} \tag{18}$$

where the optical thickness $w = p_a l$ is used. Employing the cumulant expansion theorem in the calculation of $\langle\ \rangle_{av}$ in Eq. (18), we get

$$\begin{aligned} y = 1 - \exp\Bigg\{ & -2\pi\left\langle\frac{\alpha_{0m}\delta_0}{d^2}\right\rangle_{av} P_ew \\ & + \frac{(2\pi)^2}{2!}\left(\left\langle\left(\frac{\alpha_{0m}\delta_0}{d^2}\right)^2\right\rangle_{av} - \left\langle\frac{\alpha_{0m}\delta_0}{d^2}\right\rangle_{av}^2\right)(P_ew)^2 \\ & - \frac{(2\pi)^3}{3!}\left(\left\langle\left(\frac{\alpha_{0m}\delta_0}{d^2}\right)^3\right\rangle_{av} - 3\left\langle\left(\frac{\alpha_{0m}\delta_0}{d^2}\right)^2\right\rangle_{av}\left\langle\frac{\alpha_{0m}\delta_0}{d^2}\right\rangle_{av} \right. \\ & \left. + 2\left\langle\frac{\alpha_{0m}\delta_0}{d^2}\right\rangle_{av}^3\right)(P_ew)^3 \\ & + \cdots\cdots\cdots\Bigg\}. \end{aligned} \tag{19}$$

Here $\alpha_{0m}\delta_0/d^2$ can be approximately evaluated if the minimum transmittance $T_m{}^{dis}$ is observed correctly. The observable minimum transmittance $T_m{}^{dis}$ is given by

$$T_m{}^{dis} = \int_0^\infty \exp\left[-\frac{(\alpha_m/\pi)\delta l}{(\nu-\nu_m)^2+\delta^2}\right] f(|\nu-\nu_m|, a)\mathrm{d}\nu \Big/ \int_0^\infty f(|\nu-\nu_m|, a)\mathrm{d}\nu \tag{20}$$

where $f(|\nu-\nu_m|, a)$ is the slit function, a being the slit width of apparatus. When the triangular form is used for the slit function, we have approximately[7]

$$T_m{}^{dis} = 1 - 2(\alpha_m\delta l)^{1/2}/a + \cdots\cdots\cdots. \tag{21}$$

Thus

$$E_m = -\ln T_m{}^{dis} = 2(\alpha_m\delta l)^{1/2}/a \tag{22}$$

for the maximum extinction E_m. If k_{0m} is defined by the relation

$$k_{0m} = E_m{}^2 \Big/ \left\{4\cdot\left(\frac{d}{a}\right)^2 p_a{}^2 l\right\}, \tag{23}$$

then the following relation is obtained by substituting Eqs. (22), (3) and (8) into Eq. (23)

$$\alpha_{0m}\delta_0/d^2 = k_{0m} \tag{24}$$

provided that P_e of Eq. (3) is put equal to p_a. When the Gaussian form is used for the slit function, for example, the maximum extinction is

$$E_m = 1.879(\alpha_m\delta l)^{1/2}/a. \tag{25}$$

Thus if we assume that when the true slit function, not known beforehand, is used, the maximum extinction

5) D. E. Burch, E. B. Singleton, and D. Williams, *Appl. Opt.* **1**, (1962).

6) W. M. Elsasser, *Phys. Rev.*, **54**, 126 (1939).

7) J. R. Nielsen, V. Thorton, and, E. B. Dale, *Rev. Mod. Phys.*, **16**, 308 (1944).

is given by

$$E_m = t(\alpha_m \delta l)^{1/2}/a\,, \tag{26}$$

then

$$\alpha_{0m}\delta_0/d^2 = (2/t)^2 \cdot k_{0m} \tag{27}$$

where t is the constant which is determined if the true slit function is known.

Quantity x, which is measured as the absorption ratio due to the sample gas at the nondispersive infrared gas analyser, is obtained from the following relation

$$(1-x)\int_0^\infty I_\nu\{1-\exp(-\sum_{m=1}^{n} k'_m l')\}\mathrm{d}\nu = \int_0^\infty I_\nu \exp(-\sum_{m=1}^{n} k_m l)\{1-\exp(-\sum_{m=1}^{n} k'_m l')\}\mathrm{d}\nu \tag{28}$$

where I_ν is the energy distribution of the infrared source, k_m and l the absorption coefficient and the cell length of the sample, and k'_m and l' of the condenser microphone detector. k'_m is given by

$$k'_m = \frac{(\alpha'_m/\pi)\delta'}{(\nu-\nu_m)^2+\delta'^2}\,.$$

The same gas as in the absorber is sealed up within the detector in atmospheric pressure. Equation (28) shows that the left-hand gives the energy absorbed in the detector of the infrared ray screened by the null balance shutter and the right-hand the energy absorbed in the detector of the infrared ray passing through the sample cell. Thus we have from Eq. (28)

$$x = \frac{\int_0^\infty I_\nu\{1-\exp(-\sum_{m=1}^{n} k_m l)\}\{1-\exp(-\sum_{m=1}^{n} k'_m l')\}\mathrm{d}\nu}{\int_0^\infty I_\nu\{1-\exp(-\sum_{m=1}^{n} k'_m l')\}\mathrm{d}\nu}\,. \tag{29}$$

For the calculation of Eq. (29) the following two assumptions are made; (i) I_ν=const. over the absorption region of the sample gas, and (ii) the shape of $\{1-\exp(-\sum_{m=1}^{n} k_m' l')\}$ is approximated by the n equivalent rectangles with unit height and the width of d' which varies with l' or the conditions under which the absorbing gas is sealed within the detector. Thus, x is given by

$$x = \sum_{m=1}^{n}\int_{u'}^{v'}\{1-\exp(-k_m l)\}\mathrm{d}\nu/nd'. \tag{30}$$

It is assumed herewith that each of the n vibrational rotational lines are completely isolated from the neighboring lines. u' and v' are $\nu_m-d'/2$ and $\nu_m+d'/2$. Eq. (30) corresponds to replacing d in Eq. (9) with d'. Thus from Eqs. (15) and (19), the expressions for x at low and high pressure are obtained by replacing d in each eq. with d'. From Eq. (15) we get

$$x = 2\left\langle\frac{\alpha_{0m}^{1/2}\delta_0^{1/2}}{d'}\right\rangle_{\mathrm{av}} p_a^{1/2}P_e^{1/2}l^{1/2} \tag{31}$$

and from Eq. (19)

$$x = 1-\exp\left\{-2\pi\left\langle\frac{\alpha_{0m}\delta_0}{d'^2}\right\rangle_{\mathrm{av}} P_e w + \frac{(2\pi)^2}{2!}\left(\left\langle\left(\frac{\alpha_{0m}\delta_0}{d'^2}\right)^2\right\rangle - \left\langle\frac{\alpha_{0m}\delta_0}{d'^2}\right\rangle_{\mathrm{av}}^2\right)(P_e w)^2 - \frac{(2\pi)^3}{3!}\left(\left\langle\left(\frac{\alpha_{0m}\delta_0}{d'^2}\right)^3\right\rangle_{\mathrm{av}} - 3\left\langle\left(\frac{\alpha_{0m}\delta_0}{d'^2}\right)^2\right\rangle_{\mathrm{av}}\left\langle\frac{\alpha_{0m}\delta_0}{d'^2}\right\rangle_{\mathrm{av}} + 2\left\langle\frac{\alpha_{0m}\delta_0}{d'^2}\right\rangle_{\mathrm{av}}^3\right)(P_e w)^3 + \cdots\cdots\right\}. \tag{32}$$

From Eq. (27) we get

$$\alpha_{0m}\delta_0/d'^2 = (2/t)^2\cdot(d/d')^2\cdot k_{0m} \tag{33}$$

Replacing $(2/t)\cdot(d/d')$ with $1/D$, we get

$$\alpha_{0m}\delta_0/d'^2 = k_{0m}/D^2. \tag{34}$$

Rewriting Eqs. (31) and (32) by means of this relation, we get

$$x = 2(\langle k_{0m}^{1/2}\rangle_{\mathrm{av}}/D)p_a^{1/2}P_e^{1/2}l^{1/2} \tag{35}$$

and

$$x = 1-\exp\left\{-(2\pi/D^2)\langle k_{0m}\rangle_{\mathrm{av}}\cdot P_e w + \frac{(2\pi/D^2)^2}{2!}(\langle k_{0m}^2\rangle_{\mathrm{av}} - \langle k_{0m}\rangle_{\mathrm{av}}^2)\cdot(P_e w)^2 - \frac{(2\pi/D^2)^3}{3!}(\langle k_{0m}^3\rangle_{\mathrm{av}} - 3\langle k_{0m}^2\rangle_{\mathrm{av}}\cdot\langle k_{0m}\rangle_{\mathrm{av}} + 2\langle k_{0m}\rangle_{\mathrm{av}}^3)\cdot(P_e w)^3 + \cdots\cdots\right\}. \tag{36}$$

From Eq. (36), we get

$$\ln\frac{1}{1-x} = \sum_{n=1}^{\infty}(-1)^{n-1}\kappa_n(P_e w)^n \tag{37}$$

where

$$\kappa_n = (2\pi/D^2)^n\lambda_n/n\,!$$

λ_n being the cumulant coefficient.

If there exists another weak band, for example a combination band, r, the ratio of the intensity of the infrared source of the fundamental region to that of the combination, should be introduced. Thus, assuming that the shape of the absorption line of the detector is approximated by the $n+n'$ equivalent rectangles with unit height and the average width d'' over both band, we obtain the following relation from Eq. (29):

$$x = \frac{\sum_{m=1}^{n}\int_{u'}^{v'} I_f\{1-\exp(-k_m l)\}\mathrm{d}\nu + \sum_{m'=1}^{n'}\int_{u''}^{v''} I_c\{1-\exp(-k_{m'} l)\}d\nu}{(I_f\cdot n + I_c\cdot n')d''} = \frac{\sum_{m=1}^{n}\int_{u'}^{v'}\{1-\exp(-k_m l)\}\mathrm{d}\nu + r\sum_{m'=1}^{n'}\int_{u''}^{v''}\{1-\exp(-k_{m'} l)\}\mathrm{d}\nu}{(n+rn')d''} \tag{38}$$

where m' is the number added to the lines in the combination band, u' and v' represent $\nu_m-d''/2$ and $\nu_m+d''/2$, u'' and v'' are $\nu_{m'}-d''/2$ and $\nu_{m'}+d''/2$, the constant quantities I_f and I_c are the intensities of the infrared source over the fundamental region and the combination, r is the ratio I_c/I_f, and n' is the total number of lines of the combination band. If we put $n'=n$ in Eq. (38), then

$$x=\frac{\sum_{m=1}^{n}\int_{u'}^{v'}\{1-\exp(-k_m l)\}\mathrm{d}\nu+r\sum_{m'=1}^{n}\int_{u''}^{v''}\{1-\exp(-k_m\, l)\}\mathrm{d}\nu}{(1+r)nd''}. \tag{39}$$

From this relation we get the following expression of x for low pressures

$$x=2\left(\frac{\langle k_{0m}^{1/2}\rangle_{\mathrm{av}}+r\langle k_{0m'}^{1/2}\rangle_{\mathrm{av}}}{(1+r)D}\right)p_{\mathrm{a}}^{1/2}P_{\mathrm{e}}^{1/2}l^{1/2} \tag{40}$$

and that of x for high pressures

$$\begin{aligned}x=1-\exp\Bigg[&-(2\pi/D^2)\cdot\left(\frac{\langle k_{0m}\rangle_{\mathrm{av}}+r\langle k_{0m'}\rangle_{\mathrm{av}}}{1+r}\right)P_{\mathrm{e}}w\\&+\frac{(2\pi/D^2)^2}{2\,!}\left(\frac{\langle k_{0m}^2\rangle_{\mathrm{av}}+r\langle k_{0m'}^2\rangle_{\mathrm{av}}}{1+r}-\frac{\langle k_{0m}\rangle_{\mathrm{av}}^2+r\langle k_{0m'}\rangle_{\mathrm{av}}^2}{1+r}\right)\cdot\\&(P_{\mathrm{e}}w)^2-\frac{(2\pi/D^2)^3}{3\,!}\left\{\frac{\langle k_{0m}^3\rangle_{\mathrm{av}}+r\langle k_{0m'}^3\rangle_{\mathrm{av}}}{1+r}\right.\\&-3\left(\frac{\langle k_{0m}^2\rangle_{\mathrm{av}}+r\langle k_{0m'}^2\rangle_{\mathrm{av}}}{1+r}\right)\cdot\left(\frac{\langle k_{0m}\rangle_{\mathrm{av}}+r\langle k_{0m'}\rangle_{\mathrm{a}}}{1+r}\right)\\&\left.+2\left(\frac{\langle k_{0m}\rangle_{\mathrm{av}}^3+r\langle k_{0m'}\rangle_{\mathrm{av}}^3}{1+r}\right)\right\}\cdot(P_{\mathrm{e}}w)^3\\&+\cdots\cdots\Bigg]\end{aligned} \tag{41}$$

where $1/D=(2/t)(d/d'')$.

In the case of CO_2 the following result is obtained by assuming that I_ν is expressed by Planck's law for temperature radiation and the temperature of the infrared source is 900 K,

$$r=0.524 \tag{42}$$

since the combination band is observed in 3700 cm^{-1} region. The numerical values for CO_2 are as follows.

$$\begin{aligned}&\langle k_{0m}^{1/2}\rangle_{\mathrm{av}}=5.85\times10^{-3}\ \mathrm{cm^{-1/2}\cdot cmHg^{-1}}\\&\langle k_{0m'}^{1/2}\rangle_{\mathrm{av}}=1.05\times10^{-3}\ \mathrm{cm^{-1/2}\cdot cmHg^{-1}}\\&\frac{\langle k_{0m}^{1/2}\rangle_{\mathrm{av}}+r\langle k_{0m'}^{1/2}\rangle_{\mathrm{av}}}{1+r}=4.19\times10^{-3}\ \mathrm{cm^{-1/2}\cdot cmHg^{-1}}\\&\frac{\langle k_{0m}\rangle_{\mathrm{av}}+r\langle k_{0m}\rangle_{\mathrm{av}}}{1+r}=3.77\times10^{-5}\ \mathrm{cm^{-1}\cdot cmHg^{-2}}\\&\frac{\langle k_{0m}^2\rangle_{\mathrm{av}}+r\langle k_{0m'}^2\rangle_{\mathrm{av}}}{1+r}=4.48\times10^{-9}\ \mathrm{cm^{-2}\cdot cmHg^{-4}}\\&\frac{\langle k_{0m}^3\rangle_{\mathrm{av}}+r\langle k_{0m'}^3\rangle_{\mathrm{av}}}{1+r}=6.50\times10^{-12}\ \mathrm{cm^{-3}\cdot cmHg^{-6}}\end{aligned} \tag{43}$$

where 1.59 cm^{-1} is used as the values of the line spacing d.

Experimental

NO System. Figure 3 shows the relations between x and p_{a} of pure NO at low pressures. ○, △, □ represent the values corresponding to various cell lengths. As expected from Eq. (35), a linear relation is obtained between x and p_{a} in the case of pure NO where P_{e} can be put equal to p_{a}:

$$x=2(\langle k_{0m}^{1/2}\rangle_{\mathrm{av}}/D)p_{\mathrm{a}}l^{1/2}. \tag{44}$$

The relations between x/p_{a} and $l^{1/2}$ are plotted by means of the relation in Fig. 3 (Fig. 4). From Eq. (44) we see that x/p^a is proportional to $l^{1/2}$. From the slope of this line, the proportionality constant $\langle k_{0m}^{1/2}\rangle_{\mathrm{av}}/D$ is found to be $3.00\times10^{-3}\ \mathrm{cm^{-1/2}\cdot cmHg^{-1}}$. $k_{0\mathrm{m}}$ can be evaluated by the analysis of the infrared spectrum whose lines are adequately separated. The values of D is the factor that corrects the deviation between $\langle k_{0m}^{1/2}\rangle_{\mathrm{av}}$ and the value obtained above. The results for the binary mixture NO+N_2 are shown in Fig. 5, where the total pressure is kept constant. Broken lines represent the theoretical curves derived from Eq. (35). The self-broadening coefficient B is expreimentally given as 1.47. $\ln 1/(1-x)$ is plotted against the optical thickness w at the total pressure of 70 cmHg (Fig. 6). The solid line may be approximated by Eq. (35).

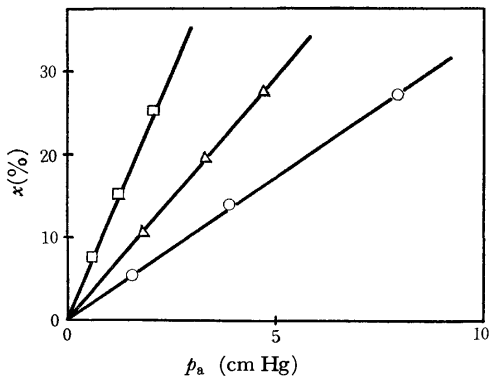

Fig. 3. Pure NO. cell length: 5 cm ○, 10 cm △ and 30 cm □.

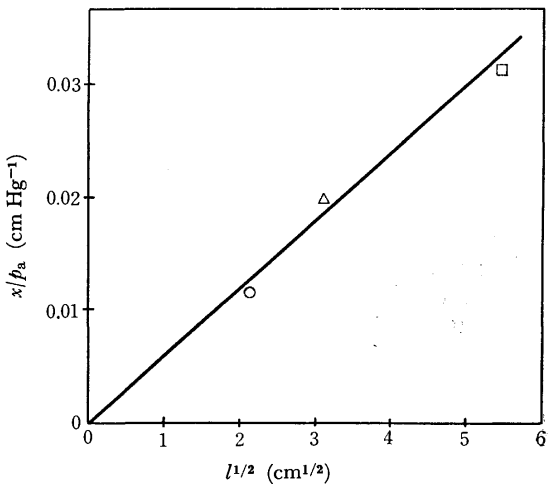

Fig. 4. Pure NO. the slope of the line $=6.00\times10^{-1/2}$ $cm^{-1/2}\cdot cmHg^{-1}$.

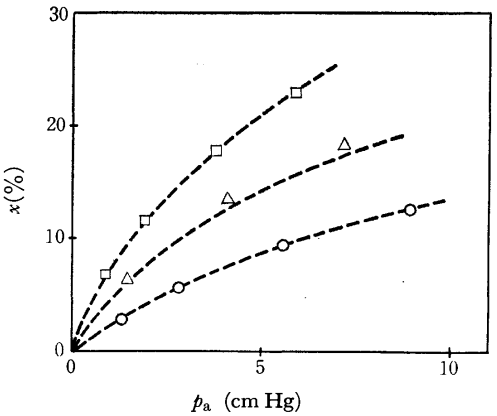

Fig. 5. NO+N_2 at the total pressure 10 cmHg.

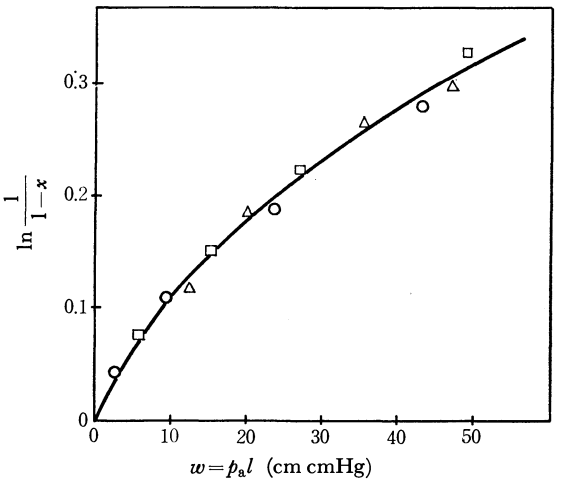

Fig. 6. NO+N_2 at the total pressure 70 cmHg.

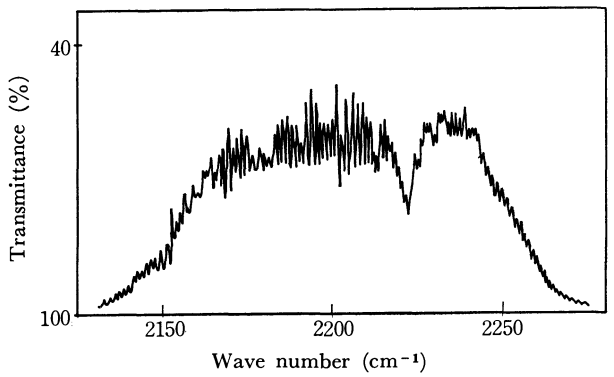

Fig. 7(a). Spectrum of N_2O around 2200 cm^{-1} measured on a DS-701G infrared spectrophotometer. slit width= 0.10 mm, cell length=10.3 cm, concentration=2.00 cmHg.

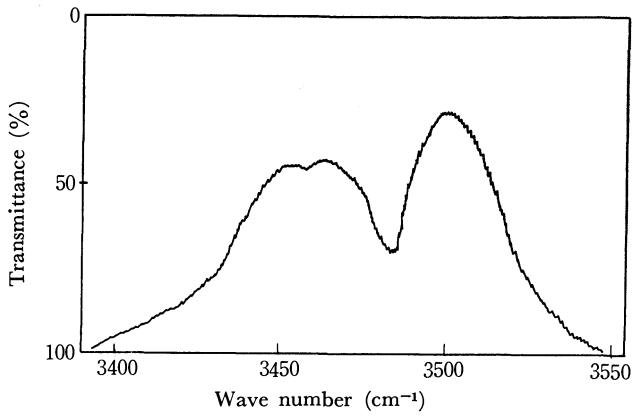

Fig. 7(b). Spectrum of N_2O around 3400 cm^{-1} measured on a DS-701G infrared spectrophotometer. slit width= 0.15 mm, cell length=10.3 cm, concentration=11.10 cmHg.

N_2O System. The infrared absorption spectra of N_2O are given in Fig. 7(a) and (b). The vibrational rotational lines around 2200 cm^{-1} region are imperfectly separated and those around 3400 cm^{-1} are no longer separated. When the separation of the lines is not enough, the analytical values of k_{0m} do not represent the values characteristic of the individual lines, because of the influence of the wings of the neighboring lines. Since the assumption that each line is separated is not valid, Eqs. (40) and (41) are not applied to N_2O. However, it is proved that these equations can

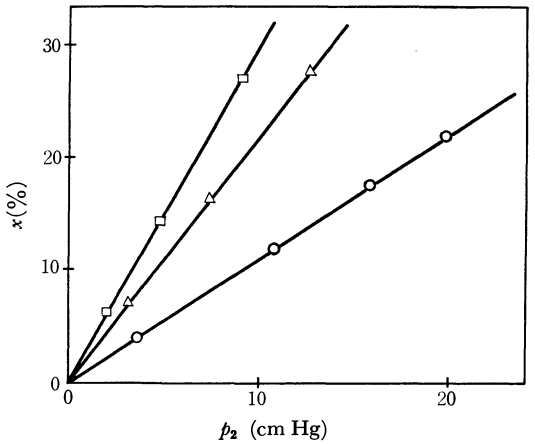

Fig. 8(a). Pure N_2O

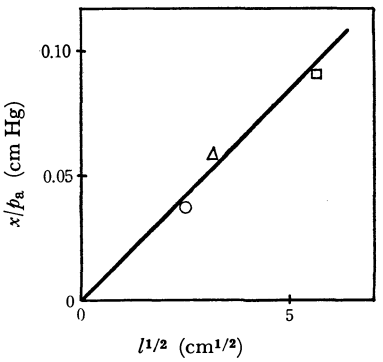

Fig. 8(b). Pure N_2O

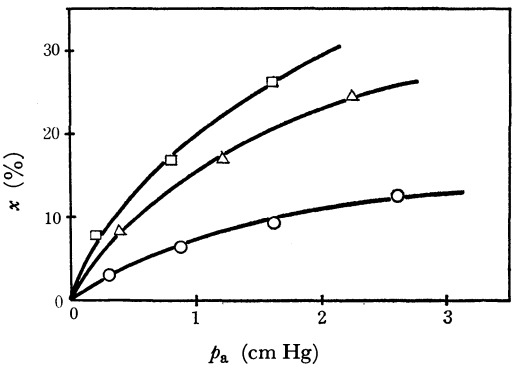

Fig. 8(c). N_2O+N_2 at the total pressure 5 cmHg.

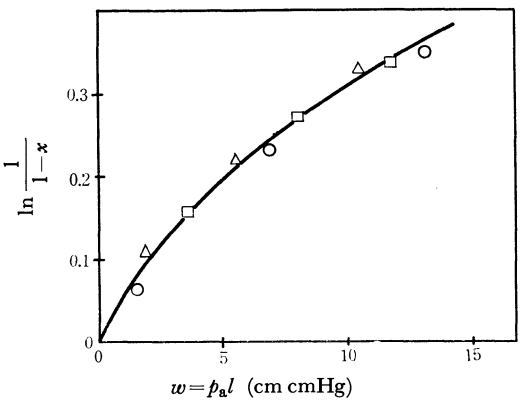

Fig. 8(d). N_2O+N_2 at the total pressure 70 cmHg.

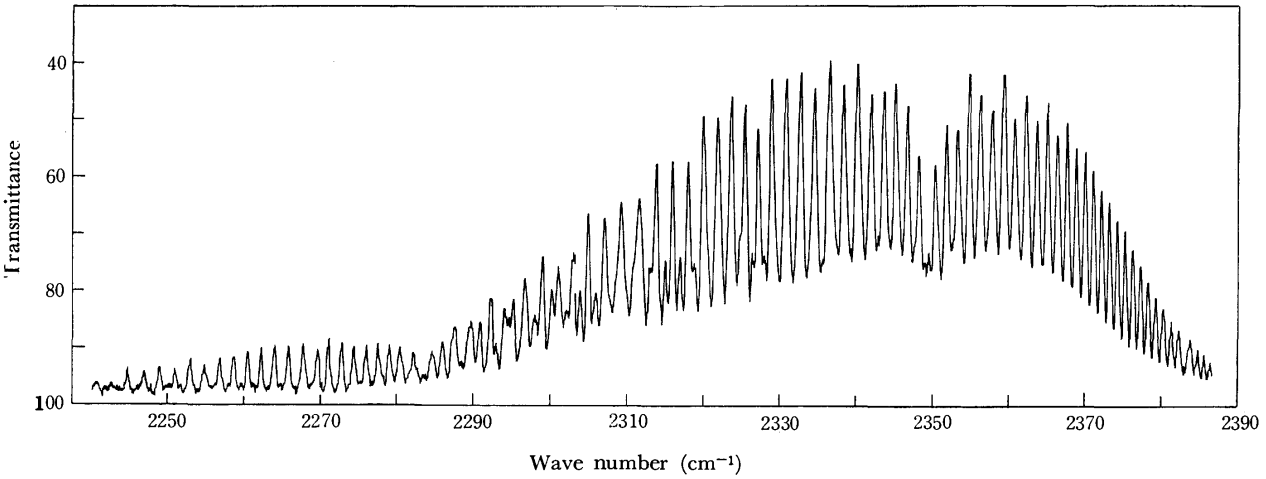

Fig. 9(a). Spectrum of CO_2 around 2350 cm^{-1} region due to the ν_3 fundamental. slit width = 0.20 mm, cell length = 10.3 cm, concentration = 2.00 cmHg. The infrared spectrophotometer is DS-403G.

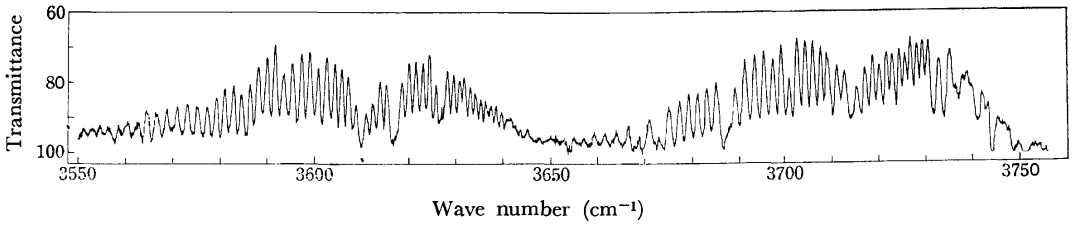

Fig. 9(b). Spectrum of CO_2 around the 2.7 μ region by the $\nu_1+\nu_3$ combination band at 3716 cm^{-1} and the $\nu_3+2\nu_2$ band at 3609 cm^{-1}. slit width = 0.10 mm, cell length = 10.3 cm, concentration = 9.60 cmHg. DS-403G.

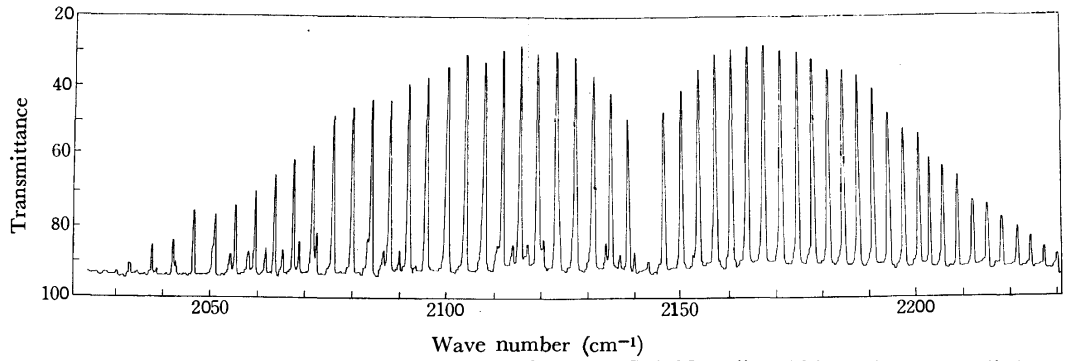

Fig. 9(c). Spectrum of CO around 2150 cm^{-1} measured on a DS-403G. slit width = 0.15 mm, cell length = 10.3 cm, concentration = 12.5 cmHg. DS-403G.

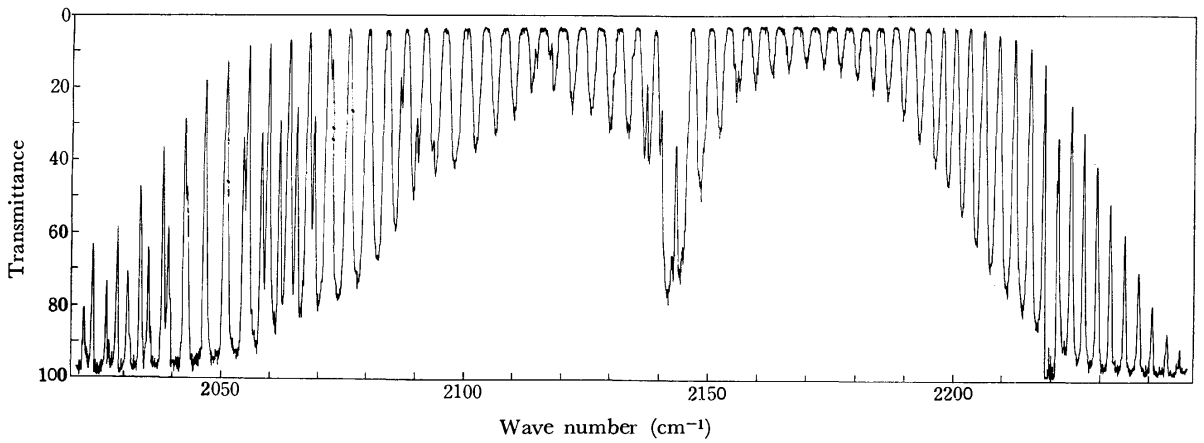

Fig. 9(d). Spectrum of CO around 2150 cm^{-1}. slit width = 0.15 mm, cell length = 10.3 cm, concentration = 1 atm. DS-403G.

be utilized for the quantitative interpretation of in the clination of the experimental curves of N_2O (Fig. 8).

Discussion

Degree of Separation of Absorption lines. The degree of separation of the absorption lines is determined from the line spacing and the collision width. The line spacing is inversely proportional to the moment of inertia which is geater for CO_2 than for CO. The collision width 2δ is given by Eq. (4). Putting $i=a$ in Eq. (4), δ is found to be proportional to $(D_{a,a})^2\text{-}(kT/m_a)^{1/2}N_a$. With the numerical data[8] $D_{a,a}/D_{a,i}=1.29$ where $a=CO_2$ and $i=CO$, we obtain

$$(D_{i,i}/D_{a,a})^2 = 0.30\,.$$

Since $(m_a/m_i)^{1/2}=1.24$, we get $\delta_i/\delta_a=0.37$. Thus the degree of separation is better for CO than for CO_2 (Fig. 9 (a)$\sim$(d)). The degree of separation influences the degree of accuracy of k_{0m}.

Influence of the Bessel Function of Order Zero. Considering the influence of the Bessel function of order zero, we have from Eq. (16):

$$\langle T_m\rangle_{av} = \langle \exp\{-(\alpha_m l/d')\tanh 2\beta'\} \times J_0\{i(\alpha_m l/d')\tanh 2\beta'/\cosh 2\beta'\}\rangle_{av} \quad (45)$$

where the line spacing d of Eq. (16) is replaced by the distance d', $\beta'=\pi\delta/d'$. Using the modified Bessel function of order zero, Eq. (45) is written as

$$\langle T_m\rangle_{av} = \langle \exp(-a_m) I_0(a_m/\cosh 2\beta')\rangle_{av} \quad (46)$$

where I_0 is the modified Bessel function of order zero, and

$$\begin{aligned} a_m &= (\alpha_m l/d')\tanh 2\beta' = (\alpha_m l/d')\cdot 2\beta'\varepsilon \\ &= 2\pi\varepsilon(\alpha_m \delta l/d'^2) = 2\pi\varepsilon(\alpha_{0m}\delta_0/d'^2)p_a P_e l \\ &= 2\pi\varepsilon(k_{0m}/D^2)P_e w\,, \end{aligned} \quad (47)$$

ε being $\varepsilon=(\tanh 2\beta')/2\beta'$, $I_0(a_m/\cosh 2\beta')$ is given by

$$I_0(a_m/\cosh 2\beta') = \sum_{n=0}^{\infty} \frac{1}{(n\,!)^2}\left(\frac{1}{2\cosh 2\beta'}\right)^{2n} {a_m}^{2n} \quad (48)$$

and hence

$$\begin{aligned} \langle T_m\rangle_{av} &= \left\langle \sum_{n=0}^{\infty} \frac{1}{(n\,!)^2}\cdot\frac{1}{(2\cosh 2\beta')^{2n}}\cdot {a_m}^{2n}\exp(-a_m)\right\rangle_{av} \\ &= \sum_{n=0}^{\infty} \frac{1}{(n\,!)^2}\cdot\frac{1}{(2\cosh 2\beta')^{2n}}\cdot\langle {a_m}^{2n}\exp(-a_m)\rangle_{av}\,. \end{aligned} \quad (49)$$

If $f(a_m, \xi)$ is defined by

$$f(a_m,\xi) \equiv \exp(-a_m\xi), \quad (50)$$

then ${a_m}^{2n}\exp(-a_m)$ is given by

$${a_m}^{2n}\exp(-a_m) = \frac{d^{2n}}{d\xi^{2n}} f(a_m,\xi)\Big|_{\xi=1} \quad (51)$$

and we obtain

$$\langle {a_m}^{2n}\exp(-a_m)\rangle_{av} = \frac{d^{2n}}{d\xi^{2n}}\langle f(a_m,\xi)\rangle_{av}\Big|_{\xi=1}\,. \quad (52)$$

Consequently $\langle T_m\rangle_{av}$ becomes

$$\langle T_m\rangle_{av} = \sum_{n=0}^{\infty}\frac{1}{(n\,!)^2}\cdot\frac{1}{(2\cosh 2\beta')^{2n}}\cdot\frac{d^{2n}}{d\xi^{2n}}\langle f(a_m,\xi)\rangle_{av}\Big|_{\xi=1}\,. \quad (53)$$

8) N. D. Coggeshall and E. L. Saiber, *J. Chem. Phys.*, **15**, 65 (1947).

By use of the cumulant expansion theorem in $\langle f(a_m, \xi)\rangle_{av}$, we obtain

$$\langle f(a_m,\xi)\rangle_{av} = \exp\{h(\xi)\} \quad (54)$$

where

$$h(\xi) = -\langle a_m\rangle_c\xi + \frac{1}{2\,!}\langle {a_m}^2\rangle_c\xi^2 - \frac{1}{3\,!}\langle {a_m}^3\rangle_c\xi^3\,. \quad (55)$$

The higher terms than the third are ignored, $\langle {a_m}^n\rangle_c$ being the cumulant average of a_m of nth order. The derivatives of $\exp\{h(\xi)\}$ with respect to ξ are as follows.

$$\frac{d}{d\xi}\langle f(a_m,\xi)\rangle_{av} = h'(\xi)\exp\{h(\xi)\} \quad (56)$$

$$\frac{d^2}{d\xi^2}\langle f(a_m,\xi)\rangle_{av} = [h''(\xi)+\{h'(\xi)\}^2]\exp\{h(\xi)\} \quad (57)$$

$$\frac{d^3}{d\xi^3}\langle f(a_m,\xi)\rangle_{av} = [h'''(\xi)+3h''(\xi)\cdot h'(\xi) + \{h'(\xi)\}^3]\exp\{h(\xi)\} \quad (58)$$

$$\frac{d^4}{d\xi^4}\langle f(a_m,\xi)\rangle_{av} = [h''''(\xi)+4h'''(\xi)\cdot h'(\xi)+3\{h''(\xi)\}^2 + 6\{h'(\xi)\}^2\cdot h''(\xi)+\{h'(\xi)\}^4]\exp\{h(\xi)\}\,. \quad (59)$$

By substituting Eqs. (57) and (59) into Eq. (53), the following expression is obtained

$$\begin{aligned} \langle T_m\rangle_{av} = \Bigg[& 1+\frac{1}{(2\cosh 2\beta')^2}\cdot\{(\langle {a_m}^2\rangle_c-\langle {a_m}^3\rangle_c) \\ & +(\langle a_m\rangle_c-\langle {a_m}^2\rangle_c+\langle {a_m}^3\rangle_c/2)^2\} \\ & +\frac{1}{4}\cdot\frac{1}{(2\cosh 2\beta')^4}\cdot\{4\langle {a_m}^3\rangle_c\cdot(\langle a_m\rangle_c-\langle {a_m}^2\rangle_c \\ & +\langle {a_m}^3\rangle_c/2)+3(\langle {a_m}^2\rangle_c-\langle {a_m}^3\rangle_c)^2 \\ & +6(\langle a_m\rangle_c-\langle {a_m}^2\rangle_c+\langle {a_m}^3\rangle_c/2)^2\cdot(\langle {a_m}^2\rangle_c-\langle {a_m}^3\rangle_c) \\ & +(\langle a_m\rangle_c-\langle {a_m}^2\rangle_c+\langle {a_m}^3\rangle_c/2)^4\} \\ & +\text{higher terms}\Bigg]\cdot\exp\{h(1)\}\,. \end{aligned} \quad (60)$$

[ ] represents the influence of the Bessel function of order zero. Equation (60) becomes Eq. (36) or (41) if [ ] is approximated by unit. The calculated results of $\langle {a_m}^n\rangle_c$ for the case of CO_2 and the influence of the Bessel function of order zero are given in Table 1.

Table 1. The values of $\langle {a_m}^n\rangle_c$ and the influence of the Bessel function in regard to CO_2
($\varepsilon\approx 1$. $\cosh 2\beta'\approx 1$. $P_e\approx P/B$. $P=70$ cmHg. $D=0.52$)

$\langle {a_m}^n\rangle_c$	$w=5$	$w=10$
$\langle a_m\rangle_c$	0.231	0.462
$\langle {a_m}^2\rangle_c$	0.054	0.232
$\langle {a_m}^3\rangle_c$	0.024	0.159
Influence of the Bessel function	1.020	1.035

$\langle {a_m}^n\rangle_c$ is given by

$$\langle a_m\rangle_c = (2\pi\varepsilon/D^2)\cdot\left(\frac{\langle k_{0m}\rangle_{av}+\langle k_{0m'}\rangle_{av}}{1+r}\right)\cdot P_e w$$

$$\langle {a_m}^2\rangle_c = (2\pi\varepsilon/D^2)^2\cdot\left(\frac{\langle k_{0m}^2\rangle_{av}+r\langle k_{0m'}^2\rangle_{av}}{1+r} - \frac{\langle k_{0m}\rangle_{av}^2+r\langle k_{0m'}\rangle_{av}^2}{1+r}\right)\cdot(P_e w)^2$$

$$\langle a_m{}^3\rangle_c = (2\pi\varepsilon/D^2)^3 \cdot \left\{ \frac{\langle k_{0m}^3\rangle_{av} + r\langle k_{0m'}^3\rangle_{av}}{1+r} - 3\left(\frac{\langle k_{0m}^2\rangle_{av} + r\langle k_{0m'}^2\rangle_{av}}{1+r}\right)\cdot\left(\frac{\langle k_{0m}\rangle_{av} + r\langle k_{0m'}\rangle_{av}}{1+r}\right) + 2\left(\frac{\langle k_{0m}\rangle_{av}^3 + r\langle k_{0m'}\rangle_{av}^3}{1+r}\right)\right\} \cdot (P_e w)^3 . \quad (61)$$

0.52 is used for the value of D by means of Eqs. (40), (43) and the experimental data[1]

$$\frac{\langle k_{0m}^{1/2}\rangle_{av} + r\langle k_{0m'}^{1/2}\rangle_{av}}{(1+r)D} = 8.0\times10^{-3}\ \mathrm{cm}^{-1/2}\cdot\mathrm{cmHg}^{-1}.$$

The influence of the Bessel function is thus proved to be within error. The experimental values are compared with the theoretical ones (Fig. 10). The dotted line shows the experimental curve and the solid line the theoretical curve given by

$$\ln\frac{1}{1-x} = 8.60\times10^{-4}(P_e w) - 8.00\times10^{-7}(P_e w)^2 + 1.01\times10^{-9}(P_e w)^3. \quad (62)$$

This is derived by substituting the values of (43) into Eq. (41) and using 0.52 for D. In order to attain a better agreement between theoretical and experimental values under high pressure, the value of 0.36 should be used as the correction factor D instead of 0.52. In case of CO,[9] similarly to CO_2, the value of 0.16 should be replaced with 0.07. These discrepancies seem to result from several assumptions, especially the roughness of the rectangular approximation concerning the shape of the absorption lines of the detector, and the conditions under which experiments correspond to the intermediate case of δ.

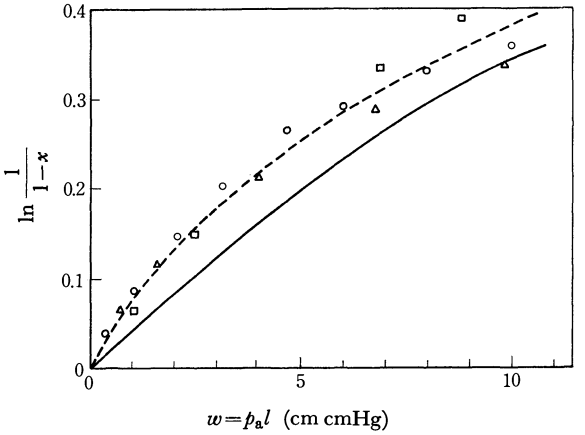

Fig. 10. The broken line; experimental. The solid line; theoretical.

9) T. Yonezawa and E. Niki, *Trans. Soc. Instr. Cont. eng.*, **7**, 238 (1970).

BULLETIN OF THE CHEMICAL SOCIETY OF JAPAN, VOL. 46, 3764—3767 (1973)

The Separation of Silver, Bismuth, Cadmium, and Zinc as Their Trioctylamine Complexes by Extraction Chromatography

Takaharu HONJO, Shigeru USHIJIMA, and Toshiyasu KIBA

Department of Chemistry, Faculty of Science, Kanazawa University, Marunouchi, Kanazawa, Ishikawa 920

(Received June 1, 1973)

The behavior of milligram amounts of silver, bismuth, cadmium, and zinc in liquid-liquid extraction has been studied with 20% trioctylamine (TOA) in carbon tetrachloride. The results have also been applied to the separation of the four metals as their TOA complexes by extraction chromatography. After passing a sample solution of 2 M HCl through a column (ϕ 1 cm×1 30 cm) consisting of a stationary phase of TOA-CCl_4 on Kel-F, the metal ions were retained and then eluted with 5.5 M HCl at the rate of 0.5—1 ml/min at 20±1 °C. Silver was found in 90—180 ml of the effluent; Bi was flowed down in 200—500 ml of the same effluent. The cadmium and Zn were held so firmly on the column that they could not be removed under the above conditions. Therefore, water was passed through to release these metals. Zinc was first flowed down with 0—50 ml, and then Cd, with 200—500 ml of water. When 5 M HNO_3 was used as the eluting solution instead of water, the Cd was immediately removed from the column. The percentage recovery of these metals in the extraction chromatography was estimated as 101% (Ag), 99% (Bi), 97% (Cd), and 94% (Zn) respectively. The distribution ratios of these metals, as obtained by the extraction chromatography of the TOA-carbon tetrachloride (Kel-F)-HCl system, were in quite good agreement with those obtained by the batch extraction.

For the past few years, the group separation of nineteen common cations (Fe, Hg, Sn, Ag, Bi, Zn, Cd, Sb, Cr, Al, Cu, Co, Ni, Pb, Mn, Mg, Ca, Sr, and Ba) has been attempted in the authors' laboratory by extraction chromatography with six different columns (TBP-(1), TOA, TBP-(2), AcAc, TTA-(1), TTA-(2)).[1] One of these columns consists of the 20% TOA–CCl_4–(Kel-F)–2 M HCl system; four metal ions, silver, bismuth, cadmium, and zinc, could be selectively held on this column. The present authors aimed to separate these retained metal ions from each other by passing a suitable eluting solution through the column. The TOA(trioctylamine) has been used as a powerful extractant of metals;[2] recently, however, this liquid ion-exchanger has been found also to be

1) I. Akaza, T. Tajima, and T. Kiba, This Bulletin, **46**, 1199, (1973).

2) T. Sato, *Kagaku to Kogyo*, **20**, 52 (1967).

suitable for the chromatographic separation of metals.[3] Cerrai and Testa have also achieved the mutual separation of Ni-Co-Fe by using a reversed-phase column of cellulose impregnated with TOA, with hydrochloric acid as the eluent.[4] The process of the extraction chromatography are closely related to the ordinary liquid-liquid extraction in batch, as has already been described by the present authors with regard to the Zn Hg, and Co–STTA–cyclohexane (Kel-F) system;[5] therefore, some basic investigations should be made into the behavior of milligram amounts of Ag, Bi, Cd, and Zn in solvent extraction with trioctylamine in carbon tetrachloride. The optimum conditions for the mutual separation of these metals by extraction chromatography could be predicted from the above results. The separation could be achieved successfully; the relation between the extraction chromatography and the liquid-liquid extraction was also considered.

Experimental

Apparatus. A chromatographic glass tube of ϕ 10× 1 300 mm equipped with a fritted glass filter; a Toyo fraction collector, Type E-E, SF 200 A; a KM-type shaking machine, Type V-S, KK IWAKI, 280 stroke/min, a well-type scintillation counter, Kobe Kogyo Corp, Ten scaler SA-250; a 200-channel pulse-height analyser; an Expandmatic Beckman pH meter; a Hitachi Horiba M 5 pH meter.

Materials. The radioisotopes, Ag-110 m, Bi-207, Cd-115m, and Zn-65, were imported from the New England Nuclear Corp and The Radio Chemical Centre, and were used as the tracers. The tracer of Cd contained some radioactive impurities; therefore, it was purified by extraction with 20% TOA-CCl_4 from a 2 M HCl solution and by back-extraction with 5 M HNO_3. The purity of each tracer was checked by means of the 200-channel pulse-height analyser at every use. Each of the metal salts, such as $AgNO_3$, $Bi(NO_3)_3$-$5H_2O$, $Cd(NO_3)_24H_2O$, and $Zn(NO_3)_26H_2O$, was dissolved in a slightly acidic solution (pH 0.3—4.5) to 0.5 mg/ml. TOA (trioctylamine) of the GR grade was purchased from the Tokyo Kasei Co. Kel-F 300 moulding powder, the trade name of polytrifluorochloroethylene, was obtained from the Daikin Kogyo Co. The other reagents were reagent-grade materials.

Extraction and Back-extraction. Into a 50-ml centrifuge tube, 20% TOA in carbon tetrachloride (10 ml) and an aqueous solution (10 ml) containing 0.5 mg of a metal and trace amounts of its radioactive tracer were put together; the contents were then agitated with a shaking machine for 2—30 min at 20±1 °C. After centrifugation, a 3-ml portion was taken out of each phase into a test tube, the radioactivity was counted with the scintillation counter, and the distribution ratio of the metal was calculated. The back-extraction behavior of the metal was also examined by shaking the organic phase with an aqueous solution adjusted to a suitable acidity with HCl. Since the extraction equilibria involve the extraction of HCl along with the metal chloride,[6] the aqueous phase and organic phases were pre-equilibrated with each other to prevent any change in the acidity or in the concentration of the reagent during the extraction.

Preparation of the Column and the Extraction Chromatographic Procedure. The Kel-F was crushed by means of a grinding mixer, and particles of 42—80 mesh was collected by sieving through a screen. A 5.5-g portion of Kel-F and a 10-ml portion of 20% TOA in carbon tetrachloride, which had been pre-equilibrated with 2 M HCl, were put into an Erlenmyer flask fitted with a stopper; the contents were then shaken by hand so as to become homogeneous and subsequently allowed to stand overnight in a dark place. The product was then slurried with an eluting solution: the slurry was then packed, little by little, into a glass tube, which had previously been then filled with an eluting solution as has been described in the preceding paper.[5] The chromatographic column of a 20×2 cm bed was thus prepared simply, and the excess TOA solution was washed down from the column by passing through enough volume of 2 M HCl. In this case, the upper surface of the column should be covered with 2 M HCl to a depth of 1—2 cm. The eluting solution should have been previously saturated with the organic solution of the stationary phase; also, the sample solution should have the same acidity as the eluting solution. Each 1-ml portion of the stock solution, containing 0.5 mg of metal, was mixed with a 49-ml portion of 2 M HCl to prepare the test solution. To investigate the chromatographic behavior of the metals, a minute amount of the radioactive tracer was added to the stock solution; however, the total amount of the metal present in the solution might be taken as unvaried from 0.5 mg. From a separation funnel fitted to the top of the column, a 50-ml portion of the sample solution was flowed down through the column at the rate of 0.5—1 ml/min. After washing the column three times with 5—10 ml of 2 M HCl, 500—1000 ml of the eluting solution, adjusted to an adequate acidity of HCl, was put into a 1000-ml separation funnel and passed through the column at the rate of 0.5—1 ml/min. The eluate was subsequently divided into 5-ml fractions by means of a fraction collector. A 3-ml portion of the eluate was pipetted out of each 5-ml fraction into a test tube, and the radioactivity was counted by means of a NaI(Tl) well-type scintillation counter. All the experimental procedures were carried out in the thermostatic room at 20±1 °C. The Kel-F in the degraded column was taken out into a 200-ml beaker and washed two or three times with ethanol, water, 6 M HCl, acetone, and ether successively. Then the materials were air-dried, and the particles of a 42—80 mesh were collected by sieving them through a screen and were then used for further experiments.

Results and Discussion

Liquid-liquid Extraction of Silver, Bismuth, Cadmium, and Zinc. The extraction of milligram amounts of silver, bismuth, cadmium, and zinc with 20% TOA in carbon tetrachloride was investigated for aqueous solutions with varying concentrations of HCl. The back-extraction behavior of these metals was also investigated with 2—12 M HCl. As is shown in Fig. 1, about a 100% quantitative extraction of metals was achieved in 2—3 M HCl (Ag), 2—5 M HCl (Bi), 2—9 M HCl (Zn), and 2—10 M HCl (Cd). The back-extraction curves of Ag and Bi show shapes almost the reverse of those of the extraction, but Cd and Zn could not be back-extracted with 2—12 M HCl. It seemed strange that zinc has a relatively lower extractability in the acid region of 0—0.6 M, but can

3) U. A. Th. Brinkman, G. De Vries, and E. Van Dalen, *J. Chromatogr.*, **22**, 407 (1966).
4) E. Cerrai and C. Testa, *ibid.*, **6**, 443 (1961).
5) T. Honjo and T. Kiba., This Bulletin, **46**, 1706, (1973).
6) T. Kojima, H. Fukutomi, and H. Kakihana, *ibid.*, **42**, 875 (1969).

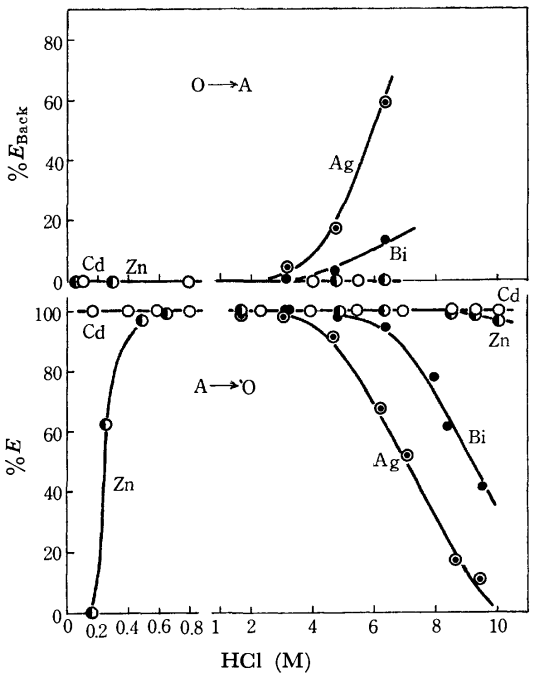

Fig. 1. The extraction and the back-extraction curves of Ag, Bi, Cd, and Zn with 20% TOA in carbon tetrachloride as a function of the acidity of HCl.
Metal: 0.5 mg/ml, Shaking time: 2—30 min, O→A: Back-extraction, A→O: Extraction.

not be back-extracted from the organic phase by shaking the organic phase with an aqueous solution in the same acid region. However, the volume ratio of the aqueous phase to the organic phase was increased; the Zn could be back-extracted 9% (4 : 1), 20% (8 : 1), and 84%(20 : 1) with 0.06 M HCl under shaking for 30 min, but when the volume of the aqueous phase was increased, the organic phase was remarkably in the emulsification state. The aqueous phase in a larger volume might promote the dissociation of the TOA–HCl complexes present in the organic phase as well as the stripping of HCl into the aqueous phase, resulting in a higher acidity of the aqueous solution. In a similar manner, the elution process may take place in the extraction column, where the mobile aqueous phase is always renewed and never again comes into contact with the same place in the stationary phases. On the other hand, as can be seen in Fig. 1, the extraction of Cd was near 100% from 0—2 M HCl; the back-extraction was also impossible under the same acidity. The difference in the behavior of Cd and Zn may be due to the difference in the stability constants of their chloro complexes,[7] the former being more stable than the latter. Nevertheless, in the case of cadmium the metal could be released from the TOA–CCl_4 column by passing it through plenty of water. As has been described above, the equilibria of the TOA–CCl_4 extraction system are affected by the acid concentration of the aqueous phase; therefore, the organic phase and the aqueous phase should be pre-equilibrated with each other in respect to hydrochloric acid. The time needed for the extraction equilibrium to be reached was ascertained to be within 2 min in the metal–20% TOA–CCl_4–HCl system.

The Volume of the Stationary Phase. In the preparation of the column, a simple previously-described method was used: a definite volume of a TOA–CCl_4 solution was held on Kel-F to make a slurry, and the slurry was put into the glass tube; then, the excess portion of the TOA-CCl_4 was washed down by passing 2 M HCl through the column. The difference between the volume of TOA–CCl_4 taken initially and that of the effluent seems to be the volume of the stationary phase in the column. The mean value after five determinations was 8.5 ml.

The Volume of the Mobile Phase. The volume of the mobile phase was determined by means of two methods. 1) The column bed was prepared as has been described above, and much 0.1 M sodium chloride solution saturated with TOA–CCl_4 was allowed to flow down until the effluent showed the same concentration of sodium chloride. After carefully washing the inside of the tube below the fritted glass filter with water, the 0.1 M sodium chloride solution occupying the pores of the column was flowed down by thoroughly washing the column with water pre-equilibrated with TOA–CCl_4. The sodium chloride in the washing liquid was determined by titrating it with a 0.1 M silver nitrate solution as usual. The value was estimated to be 5.45 ml. 2) One drop of a ^{60}Co tracer was put into the top of the column bed, and water pre-equilibrated with TOA–CCl_4 solution was passed through the column. The elution curve was obtained by taking 0.22-ml portions of the effluent and counting the radioactivity of each fraction. The volume of the effluent required to reach the maximum peak of the elution curve was the mobile phase. The value obtained by this method was 5.11 ml.

Mutual Separation of Silver, Bismuth, Cadmium, and Zinc from the Mixed Solution. The optimum acidity of the eluting solution was predicted from the liquid-liquid extraction behavior of the metals. As is shown in

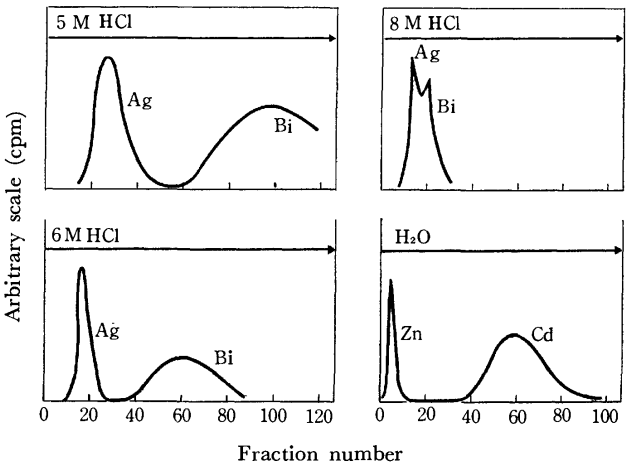

Fig. 2. The elution curves of Ag, Bi, Cd, and Zn retained on the column of 20% TOA-carbon tetrachloride-(Kel-F)-2 M HCl system.
Metal: 0.5 mg/ml, Flow rate: 0.5—1 ml/min, 1 fraction: 5 ml.

7) J. Bjerrum, G. Schwarzenbach, and L. G. Sillen, "Stability Constants," Spec. Publ. No. 7, Chemical Society, London (1958).

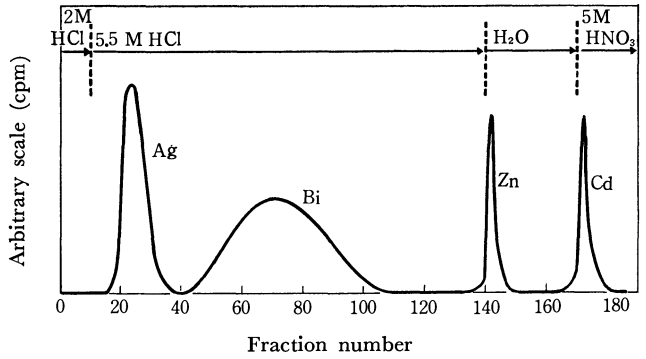

Fig. 3. The mutual separation of Ag, Bi, Cd, and Zn retained on the column of 20% TOA-carbon tetrachloride-(Kel-F)-2 M HCl system from a mixed solution.
Metal: 0.5 mg/ml, Flow rate: 1 ml/min, 1 fraction: 5 ml.

Fig. 2, silver was eluted with 100—225 ml of 5 M HCl, 50—100 ml of 8 M HCl, and 60—125 ml of of 6.5 M HCl at the flow rate of 0.5—1 ml/min. Bismuth was eluted with 325 ml of 5 M HCl, 50—150 ml of 8 M HCl, and 150 ml of 6.5 M HCl. The mutual separation of Ag and Bi could be expected using 5 M or 6 M HCl as an eluting solution, but Cd and Zn could not removed, not even with 2—12 M HCl, as had been predicted from the results of the batch extraction. However, Zn could be eluted with 50—100 ml of water after the elution of Ag and Bi with 5—6 M HCl and that of Cd with 5 M nitric acid. In conclusion, an optimum mutual separation diagram of Ag, Bi, Cd, and Zn in the 20% TOA–CCl_4–HCl system was established, as is given in Fig. 3. Silver and Bi were eluted with 90—180 ml and 200—500 ml of 5.5 M HCl successively. Then Zn was flowed down with 50—100 ml of water. In this case, the pH of the water effluent was found as low as 2. To shorten the eluting time, 5 M HNO_3 was passed through the column after separating Zn; thus, Cd was immediately eluted. The recovery of the metals was 101% (Ag), 99% (Bi), 94% (Zn), and 97% (Cd) respectively for each 0.5-ml portion of the metals.

The Relation of the Extraction Chromatography to the Liquid-liquid Extraction. The extraction and the back-extraction are repeated in the column many times in the process of the extraction chromatography. Therefore, the distribution ratios of the metals obtained by the batch extraction and by the extraction chromatography should be closely related with each other. If the extraction equilibrium is ideal and is attained rapidly at any interval under certain extraction conditions, the net distribution ratio of the metals in the extraction, D, that in the back-extraction, D^*, and the distribution of metals in the column extraction, D^{**}, will be related to the following equation:[1,2]

$$D = \frac{(\text{Total metals})_0}{(\text{Total metals})} = \frac{1}{D^*} = D^{**} = \frac{V_m - V^*}{V_0^*}$$

where ( ) and $(\ )_0$ designate the concentrations of chemical species in the aqueous and in the organic phase respectively, where V_m is the volume of the effluent in relation to the maximum of the eluted metal concentration, where V^* is the volume of the mobile phase, and where V_0^* is that of the stationary phase.

Table 1. Distribution ratio of metal ions with 20% TOA in carbon tetrachloride

	HCl (M)	By solvent extraction	By extraction chromatography
Ag	5	8.0 (6.6)	8.0
	5.5	3.3 (1.9)	3.5
	6	2.1 (1.1)	4.1
	8	0.5 (0.1)	1.7
Bi	5	18 (16)	55
	5.5	32 (12)	29
	6	24 (7.6)	28
	8	3.5 (1.9)	5.0
Zn	0.01	2.5	2.0
Cd	0.01	100	30

The values in the bracket were determined by analysing the back-extraction curves. Metal : 0.5 mg/ml

The values of the distribution ratio of the metals obtained by the batch extraction and the extraction chromatography are summarized in Table 1. The two values are in quite good agreement. The discrepancy may be caused by the differences in the contact times of the two phases and/or by the time-lag in the complex formation in the extraction and the back-extraction.

The authors wish to thank Dr. Ikuko Akaza for her helpful advice and discussion.

The Analytical Application of Sulfur Analogues of β-Diketones. III. The Separation of Cobalt(II), Nickel(II), Copper(II), Zinc(II), Mercury(II), Lead(II), and Cadmium(II) as Their STTA (1,1,1-Trifluoro-4-(2-thienyl)-4-mercapto-3-buten-2-one) Complexes by Thin-layer Chromatography on Silica Gel

Takaharu Honjo and Toshiyasu Kiba

Department of Chemistry, Faculty of Science, Kanazawa University, Marunouchi, Kanazawa, Ishikawa 920

(Received June 1, 1973)

Cobalt(II), nickel(II), copper(II), zinc(II), mercury(II), lead(II), and cadmium(II) were extracted with STTA (1,1,1-trifluoro-4-(2-thienyl)-4-mercapto-3-buten-2-one) in cyclohexane, and their colored complexes were chromatographed on a thin-layer of silica gel with various organic solvents. The developing solvents used were 18 kinds of pure solvents and 10 different binary solvent mixtures of 1 : 1, v/v. An excellent separation could be achieved after development with carbon tetrachloride, carbon disulfide, ethyl acetate, and cyclohexane–chloroform, chloroform–carbon disulfide, and carbon tetrachloride–carbon disulfide mixtures. The R_f value generally increased in the following orders: Cd(II), Zn(II), Pb(II), (STTA)<Hg(II)<Co(II, III)<Cu(II)<Ni(II) (with carbon tetrachloride); Cd(II), Zn(II), Pb(II), (STTA)<Co(III)<Hg(II)<Cu(II)<Ni(II) (with carbon disulfide); Cd(II), (STTA)<Zn(II)<Pb(II)<Hg(II), Co(III), Cu(II), Ni(II) (with ethyl acetate); and Cd(II), Zn(II), Pb(II), (STTA)<Hg(II)<Co(III)<Cu(II)<Ni(II) (with the cyclohexane–chloroform, chloroform–carbon disulfide, and carbon tetrachloride–carbon disulfide mixtures). A few μg $Ni(STTA)_2$ chelates on the plate could be determined quantitatively by measuring the spot area from the curve drawn on a millimeter-graph sheet after driving a densitometer across the spot. Some aspects of the behavior of the STTA chelates on the thin-layer of silica gel have also been discussed.

Thin-layer chromatography (tlc) has recently become popular in the separation of a wide variety of organic and inorganic substances, using the standardized procedures of Stahl and others.[1] Taking advantage of this technique, the separation of the metals as their chelates has been performed with several extracting reagents, such as acetylacetone,[2–4] α-nitroso-β-naphthol,[5] 8-hydroxyquinoline,[6] dithizone,[7–12] and diethyldithiocarbamic acid.[13–17] A new chelating reagent, 1,1,1-trifluoro-4-(2-thienyl)-4-mercapto-3-buten-2-one (abbreviated as STTA), has been found to form stable and extractable chelates with a specific color,[18] and it has been used for several analytical purposes, *e.g.*, the spectrophotometric determination of cobalt(II),[19] and the separation of Hg, Co, and Zn by extraction chromatography.[20] However, the STTA chelates have not yet been submitted to thin-layer chromatography. In the present investigations, the metal ions were extracted in cyclohexane containing STTA, and the STTA chelates thus formed were chromatographed on the thin-layer of silica gel using various organic solvents. The possibility of the quantitative determination and the mutual separation of these metal complexes has been investigated; some aspects of the chromatographic behavior of the STTA chelate have also been discussed.

Experimental

Apparatus. The thin-layer chromatograph: TLC "Sandwich" developing apparatus, model TL-IS, of Yamato Scientific Instruments. Densitometer: Atago self-recording densitometer designed for paper electrophoretic patterns.

Materials. Metal ions: Metal salts, $CoCl_26H_2O$, $NiCl_26H_2O$, $CuSO_45H_2O$, $ZnCl_2$, $HgCl_2$, $Pb(NO_3)_2$, and $CdCl_2$, were dissolved in distilled water or in a slightly acidic solution to make a 10^{-1} M aqueous solution of each metal ion.

STTA: STTA was prepared by a modification of the method of Berg and Reed.[19]

Adsorbent: Silica gel for the thin-layer chromatography, WAKOGEL B-5 (binder, $CaSO_41/2H_2O$, 5%).

Developing solvents: Methanol, ethanol, cyclohexanol, acetone, methyl ethyl ketone, ethyl acetate, ethyl ether, carbon tetrachloride, chloroform, ethylene chloride, carbon disulfide, *n*-hexane, cyclohexane, benzene, xylene (bp 138.5—141.5 °C), nitrobenzene, *o*-dichlorobenzene, and benzonitrile were all of reagent-grade materials and were purified by the ordinary method, if necessary.

Solvent Extraction. The experimental procedure for the solvent extraction of trace amounts of metals was almost

1) M. Ishikawa, S. Hara, T. Furuya, and Y. Nakazawa, Thin-layer Chromatography, "Kiso to Oyo", Nanzando, Japan (1970).
2) Y. Tsunoda, T. Takeuchi, and Y. Yoshino, *Nippon Kagaku Zasshi*, **85**, 275 (1964).
3) J. C. Trehan, *Chromatographia.*, **2**, 17 (1969).
4) M. Kiboku, *Sci. Papers Fac. Eng. Kinki Univ.*, **1970**, 23.
5) I. Pejković-Tadić and M. Hranisavljević-Jakovljević, *Microchim. Acta*, **1965**, 940.
6) S. Takitani, Y. Hara and M. Suzuki, *Bunseki Kagaku*, **18**, 626 (1969).
7) M. Hranisavljević-Jakovljević and I. Pejković-Tadić, *Microchim, Acta*, **1965**, 141, 936.
8) T. Takeuchi and Y. Tsunoda, *Nippon Kagaku Zasshi*, **88**, 176 (1967).
9) S. Takitani, M. Suzuki, A. Koya, and T. Teramae, *Eisei Kagaku*, **13**, 139 (1967).
10) S. Takitani, M. Suzuki, M. Yoshimura, S. Sato, and M. Sekiya, *ibid.*, **14**, 324 (1968).
11) Z. Gregorowicz, J. Kulicka, and T. Suwinska, *Chem. Anal.* (Warsaw), **16**, 169 (1971).
12) M. Hranisavljević-Jakovljević, *Glasnik Hem Drustva*, (Beograd), **29**, 115 (1964).
13) J. Senf, *J. Chromatog.*, **21**, 363 (1966).
14) M. Kiboku, *Bunseki Kagaku*, **17**, 722 (1968).
15) J. Rai and V. P. Kukreja, *Chromatographia*, **3**, 41, 499 (1970).
16) K. Ballschmiter, *Z. Anal. Chem.*, **254**, 348 (1971).
17) L. Fishbein, J. Fawkes, *J. Chromatog.*, **19**, 364 (1965).
18) T. Honjo and T. Kiba, *Bunseki Kagaku.*, **21**, 676 (1972).
19) T. Honjo and T. Kiba, This Bulletin., **45**. 185 (1972).
20) T. Honjo and T. Kiba, *ibid.*, **46**, 1694 (1973).

the same as has previously been described.[19,21] The sample solutions for the thin-layer chromatography were metal-STTA chelates in cyclohexane, which were prepared as follows: a 10^{-2} M salt solution was acidified with 0.1 M acetic acid to pH 6.0—6.5 and then this solution was shaken with 10^{-3} M STTA in cyclohexane for 1.5 hr. After the extraction, some deposit in a membrane substance at the interface of the phases was found in the cases of Co, Cu, and Hg. Zinc and Ni gave no precipitate, while Pb and Cd gave insoluble chelates in cyclohexane, but soluble ones in ethyl acetate.

Thin-layer Chromatography A homogeneous paste was prepared by thoroughly mixing 30 g of the silica gel with 60 ml of distilled water in a mortar using a pestle. Then, the paste was spread on a 20×20 cm glass plate at a thickness of 0.25 mm using a commercial applicator. The plates were air-dried for 20—30 min at room temperature; then they were activated at 110 °C for 60 min and cooled overnight in a desiccator containing silica gel. By means of an micropipet, a 3-μl portion of a sample solution was placed as a spot on thin-layer at definite intervals within about 1.5 cm from the bottom of the plates. The spots were then air-dried at room temperature. Both sides of the chromatoplates were covered with glass plates to form a kind of sandwich; the plates were firmly held with clips. This "sandwich" was placed in a chromatographic chamber containing an organic solvent or some mixed solvents and was dipped into the solvent up to 1 cm below the sample spots. The organic solvent was allowed to proceed up to about 10 cm of the sample spot, and then the plates were taken out of the chambers and exposed to air. No spraying was necessary for the detection, since most of the chelates show different, characteristic colors. Development on a chromatoplate coated with silica gel was carried out at room temperature (22—26 °C).

The R_f value of the substances, the relative migration rates of the solutes, is one of the most convenient expressions of the position of the compounds on the chromatoplate, where:

$$R_f = \frac{\text{distance traveled by the substance}}{\text{distance traveled by the solvent}}$$

Moreover, the R_f value is a measure of the interaction among solute, solvent, and adsorbent, and is reproducible and characteristic for each solute in a given solvent-adsorbent system under specified conditions.

Results and Discussion

Extraction. The metal ions were extracted in trace amounts with 10^{-3} M STTA in cyclohexane; their extraction curves are presented in Fig. 1. It was found that the quantitative extractions of the STTA chelates of Co(II), Ni(II), Cu(II), Zn(II), Hg(II), Pb(II), and Cd(II) were almost achieved in the pH region below 7. The extraction of cobalt seemed to be accompanied by the transformation of $Co(STTA)_2$ to $Co(STTA)_3$.[19-21]

Absorption Spectra. The absorption spectra of STTA and its metal chelate in cyclohexane are shown in Fig. 2. Each chelate showed its own specific color, had an absorption maxima, and was stable for at least 7 days. These results are summarized in Table 1. The compounds could be identified only by observing the individual specific color on the chromatoplates.

Development and Separation of the STTA Chelates with

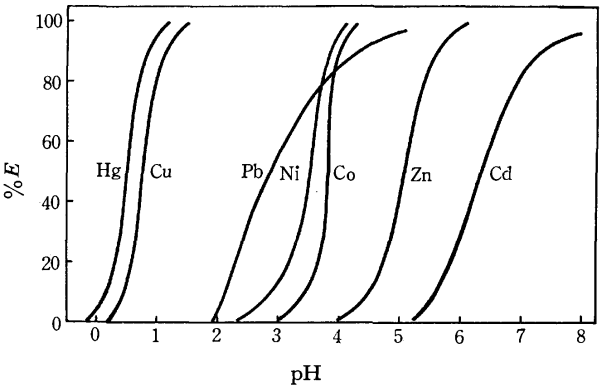

Fig. 1. Extraction curves of metal STTA chelates.
Metal: trace, STTA: 10^{-3} M, Diluent: cyclohexane, Shaking time: 15—30 min.

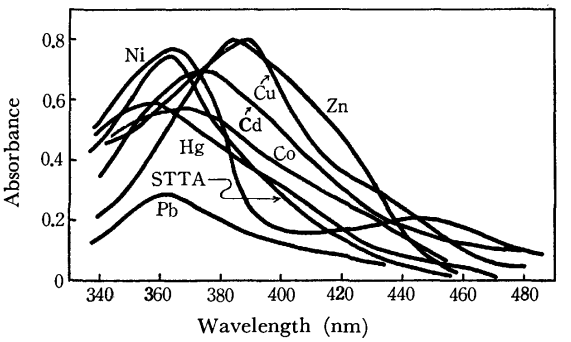

Fig. 2. Absorption spectra of STTA and its metal chelates in cyclohexane and ethyl acetate against the same organic solvent.
STTA, chelate: *ca.* 4×10^{-5} M, Diluent: cyclohexane (Co, Ni, Cu, Zn, Hg), ethyl acetate (Pb, Cd)

Table 1. Color and absorption maxima of STTA and its metal chelates in cyclohexane

Compound	Color	Absorption maxima (nm)
STTA	Reddish yellow	365, 361[a]
$Co(STTA)_3$	Brown	367
$Ni(STTA)_2$	Reddish brown	366, 450
$Cu(STTA)_2$	Olive brown	389
$Zn(STTA)_2$	Bright yellow	387
$Hg(STTA)_2$	Pale yellow	357
$Pb(STTA)_2$	Orange red	365[a]
$Cd(STTA)_2$	Yellow	375[a]

a) Diluted with ethyl acetate.

Pure Solvents. Some representative results of the development of STTA and its metal STTA chelate with individual solvents on a thin-layer of silica gel by the ascending method are given in Table 2. The chelates may be classified into four groups by chromatographic behavior: 1) Chelates which do not migrate from the sample spot (with cyclohexane and *n*-hexane). 2) Chelates which can be developed to a moderate distance over a comparatively wide range (with methanol, carbon tetrachloride, and carbon disulfide). 3) Chelates which move up to the solvent front (with ethanol, acetone, methyl ethyl ketone, ethyl acetate, chloroform, ethylene chloride, benzene, xylene, nitrobenzene, *o*-dichlorobenzene, and benzonitrile).

21) T. Honjo, S. Yashima and T. Kiba, *ibid.*, 3772, (1973).

Table 2. R_f values of STTA and its metal STTA chelates with various developing pure solvent on silica gel

Developing solvent	Dielectric constant	Developing length (cm)	Developing time (min)	Metal							
				Co	Ni	Cu	Zn	Hg	Pb	Cd	STTA
Methanol	32.6	8.8	60	0.23	0.36	0	0	0.07	0	0	0
Ethanol	24.3	10.7	90	1.00	1.00	1.00	1.00	1.00	a)	a)	1.00
Cyclohexanol	15.0	5.5	555	a)	a)	a)	a)	a)	a)	a)	a)
Acetone	20.7	9.5	15	1.00	1.00	1.00	1.00	1.00	1.00	1.00	1.00
Methyl ethyl ketone	18.5	10.4	20	1.00	1.00	a)	a)	1.00	a)	a)	a)
Ethyl acetate	6.0	9.75	37	1.00	0.91	1.00	0.71	1.00	0.73	0.47	0.91
Diethyl ether	4.3	9.9	20	a)	a)	a)	a)	0.92	a)	a)	a)
Carbon tetrachloride	2.2	10.0	70	0.35	0.51	0.36	0	0.17	0	0	0
Chloroform	4.8	12.2	55	0.90	0.96	0.94	0.03	0.90	0.02	0.02	0.02
Ethylene chloride	10.4	10.5	40	1.00	1.00	1.00	0.04	1.00	0.04	0.04	0.04
Carbon disulfide	2.6	9.7	20	0.16	0.40	0.25	0	0.17	0	0	0
n-Hexane	1.9	11.2	40	0.02	0.05	0.02	0	0	0	0	0
Cyclohexane	2.0	9.55	50	0	0	0	0	0	a)	a)	0
Benzene	2.3	10.0	36	1.00	0.99	0.99	0	a)	a)	a)	0
Xylene	2.6	10.0	40	0.85	0.81	0.78	a)	0.76	a)	a)	a)
Nitrobenzene	34.8	11.5	60	1.00	1.00	1.00	0.05	1.00	a)	a)	0.06
o-Dichlorobenzene	9.9	12.4	60	0.83	0.90	0.83	0.01	0.69	0.02	0.02	0.02
Benzonitrile		11.6	60	1.00	1.00	1.00	0.27	1.00	a)	a)	0.24

a) The spots disappeared during the development. The average deviation of R_f values was 0.01.

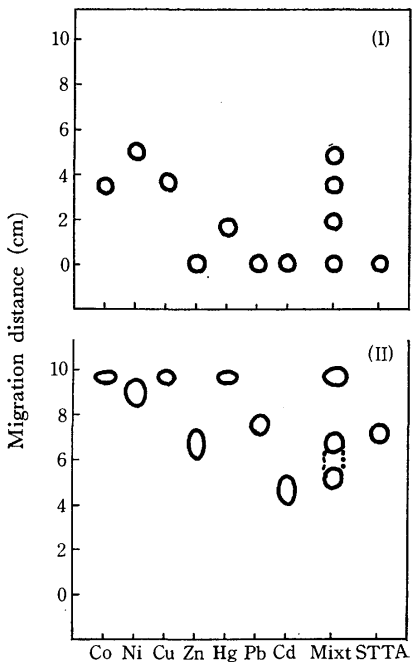

Fig. 3. Chromatogram of STTA and its metal chelates with single component solvent.
STTA, Chelate: *ca.* 5×10^{-4} M (3 μl); Developing solvent: (I) carbon tetrachloride, (II) ethyl acetate

4) Chelates which dissolve in the solvent and the spots of which disappear during development (with cyclohexanol and diethyl ether). The times required for about a 10 cm(8.7—12.4 cm) development were all about 15—90 min. The R_f values of the STTA chelates generally increased in the order of: Cd(II)<Zn(II)<Pb(II), (STTA)<Hg(II)<Co(II, III)<Cu(II)<Ni-(II). With such developing solvents as carbon tetrachloride, carbon disulfide, and ethyl acetate, the mutual separation of various metal chelates was achieved successfully. Some representative chromatograms of STTA and its metal chelates with carbon tetrachloride and ethyl acetate are shown in Fig. 3. It was observed that the cobalt-STTA chelate extracted in high concentrations as 30 μl of a 4×10^{-5} M chelate solution gives two spots; one may possibly correspond to Co(STTA)$_2$ (R_f=0.29), and the other, to Co(STTA)$_3$ (R_f=0.35), using carbon tetrachloride. The elution power of a solvent is generally related to its dielectric constant or its dipole-dipole moment. The greater the polarity of the solvent, the greater the distance of the development on the chromatographic plate. The eluotropic series of solvents proposed by Trappe[22] and by Strain[23] may be valid also with regard to the thin-layer chromatographic behavior of the STTA chelates.

Development and Separation of the STTA Chelates with a Binary Solvent Mixture. By using a binary mixture of solvents in a 1 : 1 volume ratio, STTA and its metal STTA chelates were developed; some representative results are shown in Table 3. All the mix ed solvents could develop the STTA chelates to a moderate distance. Among these mixed solvents, the pairs of cyclohexane–chloroform, chloroform–carbon disulfide, and carbon tetrachloride–carbon disulfide were most suitable for the mutual separation of the STTA chelates. Some representative chromatograms of STTA and its metal chelates with carbon tetrachloride, carbon disulfide, and cyclohexane–chloroform mixtures are shown

22) W. Trappe, *Biochem, Z.*, **305**, 150 (1940); **306.**, 316 (1940).
23) H. H. Strain, "Chromatographic Adsorption Analysis," Interscience Publ. Inc., New York (1942) p. 66.

TABLE 3. R_f VALUES OF STTA AND ITS METAL STTA CHELATES WITH VARIOUS MIXED DEVELOPING SOLVENTS ON SILICA GEL

Developing solvent (1 : 1, v/v)	Developing length (cm)	Developing time (min)	Metal					
			Co	Ni	Cu	Zn	Hg	STTA
Cyclohexane-ethanol	10.75	180	0.84	0.84	0.84	0.82	a)	0.84
Cyclohexane-chloroform	9.20	45	0.72	0.79	0.77	0	0.62	0
Cyclohexane-benzene	9.8	35	0.63	0.73	0.64	0	a)	0
Benzene-methanol	9.3	48	0.77	0.77	0.78	0.69	0	0
Benzene-chloroform	9.6	42	0.95	0.97	0.95	0	0.85	0
Benzene-carbon tetrachloride	9.3	40	0.81	0.84	0.79	0	0.68	0
Benzene-carbon disulfide	9.7	23	0.80	0.83	0.82	0	0.74	0
Chloroform-carbon tetrachloride	8.7	45	0.78	0.85	0.78	0	0.64	0
Chloroform-carbon disulfide	9.5	23	0.68	0.89	0.86	0.15	0.71	0.06
Carbon tetrachloride-carbon disulfide	9.3	26	0.35	0.56	0.40	0	0.25	0

a) The disappeared spots during development. The average deviation of R_f values was 0.01.

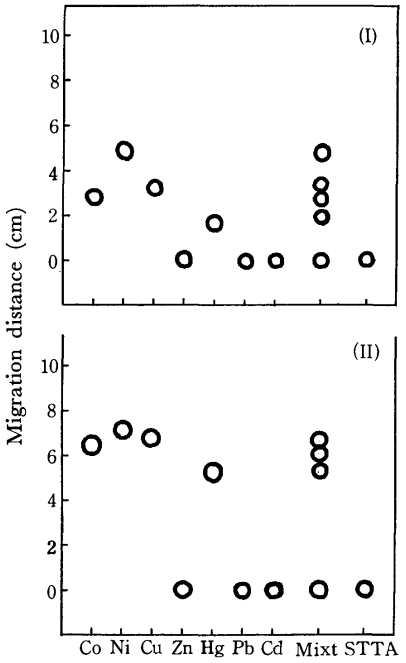

Fig. 4. Chromatogram of STTA and its metal chelates with binary solvent mixture.
STTA, Chelate: *ca.* 5×10^{-4} M (3 μl)
Developing solvent: (I) carbon tetrachloride-carbon disulfide, (II) cyclohexane-chloroform

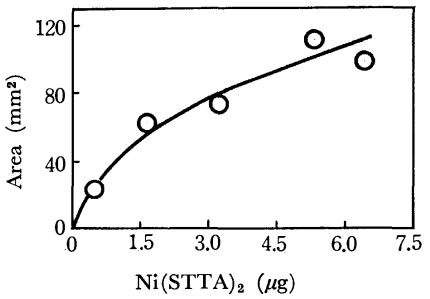

Fig. 5. Calibration curve of a thin layer chromatogram of $Ni(STTA)_2$ chelate obtained by photodensitometry.
Developing solvent: carbon tetrachloride

in Fig. 4. The R_f values of all the STTA chelates with the binary solvent mixtures had the same tendency to increase in the order of Zn(II)<Hg(II)<Co(III)<Cu(II)<Ni(II) as in the case of the single solvents. In the case of the mixed solvents, some demixing may occur, accompanied by some changes in the solvent ratio, because of the difference in the adsorbability of each solvent on the silica gel; therefore, the developed spots are believed to give suitable R_f values, separated from each other.

Quantitative Evaluation of the Thin-layer Chromatograms of the Ni(STTA)$_2$ Chelate. The possibility of the direct quantitative determination of the $Ni(STTA)_2$ chelate, which gives the largest R_f value and a clear spot on its plate, has been investigated by measuring the intensity of its color with the photodensitometer. The spot area was determined from the curve drawn on a millimetergraph sheet after driving the densitometer across the spot. The quantitative extractions of nickel from trace amounts up to 10^{-4} M were achieved with 10^{-3} M STTA in cyclohexane in the pH region above 4.5. The calibration curve in Fig. 5 shows the relation of the areas of the spot of the $Ni(STTA)_2$ chelate developed with carbon tetrachloride *vs.* the amount initially taken. Satisfactory results could be obtained by placing, by means of a microsyringe, a sample organic solution of the STTA chelate in a definite volume of a solvent. This graphical method may be suitable for the successive determination of a few μg each of the other chelates in a developed spot.

Some Aspects of the Behavior of the STTA Chelates on the Thin-layer of Silica Gel. The R_f values of the STTA chelates with various solvents generally increase in the following order: Cd(II)<Zn(II)<Pb(II), (STTA) < Hg(II) < Co (II, III) < Cu(II) < Ni(II). This sequence differs from the acetylacetonates[2-4] the α-nitroso-β-naphtholate[5] series (Zn(II)<Co(II)<Ni(II)<Cu(II)<Co(III)), the 8-hydroxyquinolinate series[6] (Zn(II)<Cd(II)) the dithizonates series[7-12] (Cd(II)< Pb(II)< Co(II)< Zn(II)< Ni(II)< Cu(II)< Hg(II)), or the diethyldithiocarbamates series[13-17] (Co(II)<Ni(II)<Cu(II)). Acetylacetone chelates easily form their hydrate or polymerized compounds less soluble in non-polar solvents, while the STTA chelates do not form such compounds. The tailing

which usually appears in an acetylacetonate system was not observed in the STTA chelate system. It is of interest that the STTA compounds of Co(II), Ni(II), Cu(II), and Hg(II) travel a moderate distance even with such non-polar organic solvents as carbon tetrachloride and carbon disulfide. This behavior was not observed in the other chelate systems described above. It has recently been observed[24] that the replacement of oxygen by sulfur in the bis-chelate complexes of cobalt(II) and nickel(II) has two important structural consequences, the depolymerization and the stabilization of the planar form. Therefore, the depolymerization or the stabilization of the chelates, which is related to the covalency of the bond caused by the $d\pi$-$d\pi$ interaction, may become one of the important factors in these abnormal R_f trends.

24) D. H. Gerlach and R. H. Holm, *J. Amer. Chem. Soc.*, **91**, 3457 (1969).

BULLETIN OF THE CHEMICAL SOCIETY OF JAPAN, VOL. 46, 3772—3779 (1973)

The Analytical Application of Sulfur Analogues of β-Diketones. V. Some Aspects of the Extraction Behavior of STTA (1,1,1-Trifluoro-4-(2-thienyl)-4-mercapto-3-buten-2-one) Complexes and Their Adducts with TOPO

Takaharu HONJO, Satoshi YASHIMA, and Toshiyasu KIBA

Department of Chemistry, Faculty of Science, Kanazawa University, Marunouchi, Kanazawa, Ishikawa 920

(Received June 1, 1973)

The solvent extraction of trace amounts of various metal ions with STTA (1,1,1-trifluoro-4-(2-thienyl)-4-mercapto-3-buten-2-one) in the presence or in the absence of TOPO (tri-*n*-octylphosphine oxide) has been investigated. The results are as follows: (a) The apparent extraction constant of each metal–STTA chelate in cyclohexane, log K, increases, and their $pH_{1/2}$ values decrease, in the order of: Cd(II)-In(III)-Zn(II)-Fe(III)-Ni(II)-Ag(I)-Bi(III)-Co(II)-Pb(II)-Cu(II)-Hg(II). This order was found to hold also in the back-extraction, except for cobalt, which was not back-extracted even with 1—12 M HCl. The other metals, Au(III), and Pd(II), could also be extracted as their STTA chelates. (b) The kind of the solvent has an effect to the lowest pH value where the metal STTA chelates begin to be extracted; the lowest pH is shifted to a higher value in the order of: C_6H_{12}, CCl_4, MIBK, C_6H_6, and $CHCl_3$. (c) The distribution coefficient, P_r, and the enol dissociation constant, K_a, of STTA were log $P_r=2.99$ (10^{-3} M STTA in cyclohexane–0.1 M $NaClO_4$–pH 1.0) and log $K_a=-4.38$ (10^{-4} M STTA in 0.12 M HCl, 0.1 M CH_3COOH (pH 4.5) and 0.1 M NaOH-C_2H_5OH (1/5, v/v) solution) at 20 °C. (d) The extraction equilibrium of Zn seemed to be rapid, that of Ni showed its rate-determining step to be the formation of $Ni(STTA)^+$, and that of Co seemed to be accompanied by a transformation of $Co(STTA)_2$ to $Co(STTA)_3$. (e) In the metal–STTA(0.001 M)–TOPO(0.01 M)–cyclohexane system, the $|\Delta pH_{1/2}|$ was found to be 0.45 for Ni, 1.95 for Zn, and 0.25 for Co. The Co–STTA–TOPO chelate could be back-extracted to some degree with 1 M HCl. The extracted species were ascertained to be $Zn(STTA)_2$, $Zn(STTA)_2TOPO$, $Ni(STTA)_2$, $Co(STTA)_2$, $Co(STTA)_3$, and $Co(STTA)_2TOPO$. The stability constant of $Zn(STTA)_2$ TOPO was found to be 6.05.

A new chelating reagent, STTA (1,1,1-trifluoro-4-(2-thienyl)-4-mercapto-3-buten-2-one), was first prepared by Chaston *et al.*[1] and by Berg and Reed;[2] it has since been used for chelating and for the extractive photometric determination of metals.[3] The present authors have aimed to develop further analytical usages of STTA, and several reports have been published: on the spectrophotometric determination of cobalt(II),[4] the separation of Hg(II), Co(II), and Zn(II) by extraction chromatography,[5] the separation of Co(II), Ni(II), Cu(II), Zn(II), Hg(II), Pb(II), and Cd(II) by thin-layer chromatography,[6] and the separation of Ni(II) and Co(II) by a back-extraction process.[7] In the present work, a number of factors affecting the liquid-liquid extraction of trace amounts of various metal ions with STTA in the presence or in the absence of TOPO (tri-*n*-octylphosphine oxide) have been studied. The application of the solvent extraction techniques to the study of the kinetics of metal-chelate formations in Zn, Ni, and the Co–STTA–TOPO–cyclohexane system has also been examined.

Experimental

Materials. The STTA was synthesized by the reaction of hydrogen sulfide with TTA in absolute ethanol in the presence of hydrogen chloride.[4] The guaranteed-grade reagents of TTA (thenoyltrifluoroacetone) and TOPO-(tri-*n*-octylphosphine oxide) were obtained from Dojindo Co., Ltd. The chlorides or the nitrates of the radioisotopes, ^{110m}Ag, ^{207}Bi, ^{144}Ce, ^{115m}Cd, ^{60}Co, $^{152,154}Eu$, ^{59}Fe, ^{203}Hg, ^{114m}In, ^{54}Mn, ^{63}Ni, ^{210}Pb, ^{46}Sc, ^{124}Sb, and ^{65}Zn, were purchased from the Radiochemical Centre (England), the New England Nuclear Corporation (U.S.A.), and the Union

1) S. H. H. Chaston, S. E. Livingstone, T. N. Lockyer, V. A. Pickeles and J. S. Shannon, *Aust. J. Chem.*, **18**, 673 (1965).
2) E. W. Berg and K. P. Reed, *Anal. Chim. Acta*, **36**, 372 (1966).
3) T. Honjo and T. Kiba, *Bunseki Kagaku*, **21**, 676 (1972).
4) T. Honjo and T. Kiba, This Bulletin, **45**, 185 (1972). (Part I).
5) T. Honjo and T. Kiba, *ibid.*, **46**, 1694 (1973). (Part II).
6) T. Honjo and T. Kiba, *ibid.*, **46**, 3768 (1973). (Part III).
7) T. Honjo, T. Unemoto, and T. Kiba, *Bunseki Kagaku*, in press. (Part IV).

Carbide Corporation (U.S.A.). The non-radioactive metal salts of Al, Au, Be, Cu, Pd, Pt, Ru, Sn, Te, Tl, UO_2, and VO_2, and the other reagents were all reagent-grade materials.

Extraction. The experimental procedures were almost the same as have previously been described.[4-7] The extractions were performed between 5 or 10 ml of an aqueous solution containing individual metal ions and the same volume of an organic solution containing STTA or STTA and TOPO. The aqueous solution was made up to 0.1 M acetic acid (in the acidic region) or 0.1 M boric acid (in the basic region), and its pH was adjusted to a desired value with 0.1—1 M NaOH or 0.1—1 M HCl. The concentration of the STTA in the organic phase was 0.001 M, and various amounts of TOPO were added. After the two phases had been shaken for from 5 min to 2 hr at 20 °C, the distribution of the metal in question was determined radiometrically or spectrophotometrically. The pH of the aqueous phase was checked again after the extraction.

Back-extraction. After the extraction, the back-extraction of the metals from the organic phase was performed with an aqueous solution with a pH value appropriate to the desired condition. The distribution of the metals was determined as in the case of the extraction.

Theoretical

When a metal ion M^{x+}, reacts with STTA (abbreviated as HR) and is extracted as the neutral chelate, MR_x, and forms the adduct compounds, MR_xL_n, with an organic base, L, such as TOPO, the overall extraction processes can be written as in the following scheme:

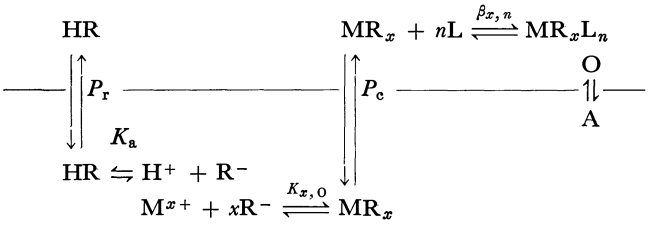

The equilibrium relations can be expressed by the following equations, in which $K_{x,0}$ means the extraction constant; D, the distribution ratio of the metal; $pH_{1/2}$, the pH of the half-extraction and % E, the percentage of extraction in each extraction or back-extraction, ( ) and ( )$_0$ designate the aqueous and the organic phases respectively.

Extraction (A→O) aqueous to organic

$$M^{x+} + xHR(org) \rightleftharpoons MR_x(org) + xH^+ \quad (1)$$

$$K_{x,0} = (MR_x)_0(H^+)^x/(M^{x+})(HR)_0{}^x \quad (2)$$

$$pH_{1/2} = -1/x \log K_{x,0} - \log(HR)_0 \quad (3)$$

$$D = (MR_x)_0/(M^{x+}) = K_{x,0}(HR)_0{}^x/(H^+)^x \quad (4)$$

$$\% E = 100D/((V/V_0) + D) \quad (5)$$

Back-extraction (O→A) organic to aqueous

The inverse of Eq. (1):

$$D_B = 1/D \quad (6)$$

$$\% \text{ Back } E = 100 - \% E \quad (7)$$

Synergism

$$M^{x+} + xHR(org) + nL \rightleftharpoons MR_xL_n(org) + xH^+ \quad (8)$$

$$K_{x,n} = (MR_xL_n)_0(H^+)^x/(M^{x+})(HR)_0{}^x(L)_0{}^n \quad (9)$$

$$^*pH_{1/2} = -1/x \log K_{x,n} - \log(HR)_0 - n/x \log(L)_0 \quad (10)$$

$$D^* = ((MR_x)_0 + (MR_xL_n)_0)/(M^{x+}) = K_{x,n}(HR)_0{}^x(L)_0{}^n/(H^+)^x \quad (11)$$

$$D^*/D = 1 + \sum_1^n \beta_{x,n}(L)_0{}^n \quad (12)$$

where $\Delta pH_{1/2}$ is the shift of $pH_{1/2}$ from the extraction without the organic base.

$$\Delta pH_{1/2} = {}^*pH_{1/2} - pH_{1/2} = -1/x \log \beta_{x,n}(L)_0{}^n \quad (13)$$

If these three assumptions are fulfilled, all the above equations are valid: 1) the metal concentration is negligibly small compared to the total concentration of STTA; 2) the distribution coefficient of STTA is fairly high, but the acid dissociation is considerably low in the pH region investigated, and 3) the formation of hydroxo complexes can be ignored in the same pH region.

Results and Discussion

In all the figures, A→O means the transfer of the metals from the aqueous phase to the organic phase, and O→A, the so-called back-extraction from the organic phase to the aqueous phase.

Distribution and Dissociation of STTA. The apparent distribution coefficients between water and cyclohexane, and the enol dissociation constant of STTA, were determined spectrophotometrically using the method of Uhlemann and Muller.[8] The following values were obtained: $\log P_r = 2.99$ (10^{-3} M STTA in cyclohexane–0.1 M $NaClO_4$–pH 1.0) and $\log K_a = -4.31$ (10^{-4} M STTA in 0.12 M HCl, 0.1 M CH_3COOH (pH 4.5) and 0.1 M NaOH–C_2H_5OH (1/5, v/v)solution) at 20 °C. The $\log K_a$(−8.64) of TTA[9] in 74.5 vol.% dioxane at 30 °C is smaller than that (−7.05) of STTA under the same conditions.[10] The apparent distribution coefficient of TTA between *n*-hexane and an aqueous solution at the ionic strength of 0.1 M ($HClO_4$+$NaClO_4$) at 25 °C has been described as 0.68.[11] Therefore, the extraction of metals with STTA may be expected to occur n a lower pH region than that with TTA, and only a very small excess of the reagent over the stoichiometrical quantity is needed. Hence, a number of metals can be extracted without any interference by hydrolysis.

Extraction and Back-extraction. The pH dependence of the extractability of metals with 0.001 M STTA in cyclohexane was examined; the extraction curves and the back-extraction curves are compared in Fig. 1 for the first-transition elements, such as Fe, Co, Ni, and Cu. The range of the back-extraction of Fe, Ni, and Cu shifts to a somewhat lower pH than that of the extraction; that is, in the regular extraction its equilibrium seems to be unattainable within only 30 min. The back-extraction of the cobalt-STTA chelate was impossible. The pH-dependence of the

8) E. Uhlemann and H. Muller, *Anal. Chim. Acta*, **41**, 311 (1968).

9) J. L. Rosenstreich and D. E. Gddberg, *Inorg. Chem.*, **4**, 909 (1965).

10) S. H. H. Chaston and S. E. Livingstone, *Aust. J. Chem.*, **19**, 2035 (1966).

11) T. Wakahayashi, S. Oki, T. Omori and N. Suzuki, *J. Inorg. Nucl. Chem.*, **26**, 2255 (1964).

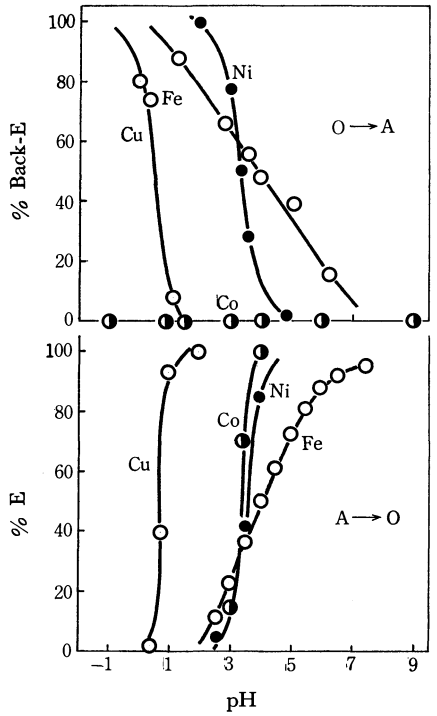

Fig. 1. The effect of pH on the extraction and the back-extraction of trace amounts of Fe(III), Co(II), Ni(II), and Cu(II)–0.001 M STTA–cyclohexane system.

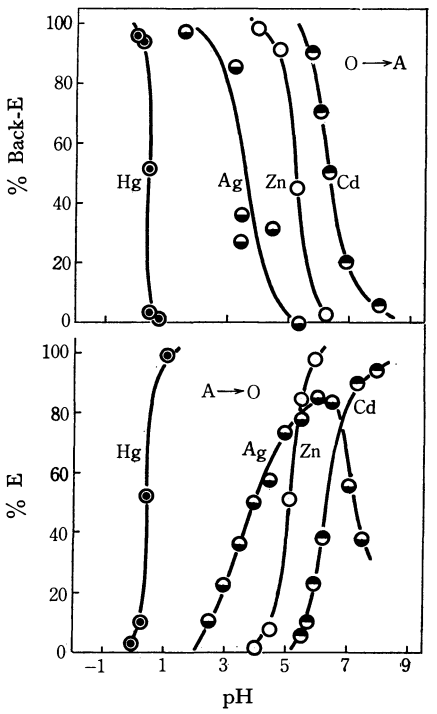

Fig. 2. The effect of pH on the extraction and the back-extraction of trace amounts of Zn(II), Cd(II), Hg(II), and Ag(I)–0.001 M STTA–cyclohexane system.

extractions of Ag and Zn family elements involving Zn, Cd, and Hg with 0.001 M STTA–cyclohexane is shown in Fig. 2. The extraction curves and the back-extraction curves are exactly symmetrical with regard to each other. The pH range of the back-extraction of Ag is somewhat lower than that of the extraction.

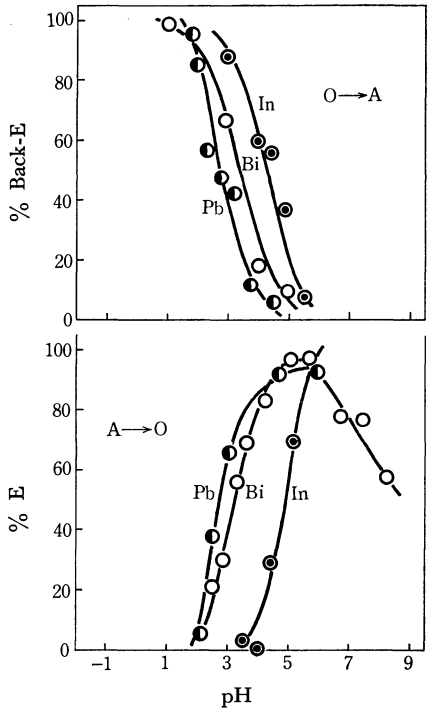

Fig. 3. The effect of pH on the extraction and the back-extraction of trace amounts of In(III), Pb(II), and Bi(III)–0.001 M STTA–cyclohexane system.

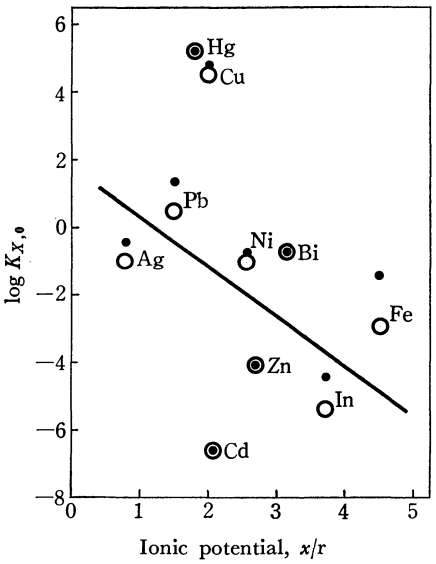

Fig. 4. The apparent extraction constant, log $K_{x,0}$, in the metal–STTA–cyclohexane systems as a function of the ionic potential. The values of the apparent extraction constants, log $K_{x,0}$ was as follows:

	Ag	Bi	Cd	Co	Cu	Fe
A→O (○)	−1.0	−0.75	−6.6	−0.6	4.5	−3.0
O→A (●)	−0.5	−0.75	−6.6	—	4.8	−1.5

	Hg	In	Ni	Pb	Zn
A→O (○)	5.2	−5.4	−1.0	0.50	−4.1
O→A (●)	5.2	−4.5	−0.8	0.80	−4.1

The extraction curves of In, Pb, and Bi are shown in Fig. 3; the pH range of the extraction for Bi is almost the same as that of the back-extraction curve, but in In and Pb the extraction and the back-extraction are somewhat different. The free energy of the formation

of a complex between a metal ion and an organic reagent may be expressed as:

$-\Delta G=RT \log K=\text{const.}\times pH_{1/2}=\text{const.}\times x/r$,[12]

where x is the charge and r is the crystal radius of the metal ion. In Fig. 4, the extraction constants, $K_{x.0}$, of the extractable chelates are plotted as a function of the ionic potentials. The results show that the apparent extraction constants for the STTA chelates tend to decrease with an increase in the ionic potential of the metals. Similar results have been obtained in acetylacetone,[13,14] benzoylacetone,[15] and the β-isopropyltropolone chelate system;[16] that is, in all the $pH_{1/2}$ decreases in the ionic radii or the ionic potential. The stability of the complex of the first-transition elements follows Irving and Williams' order of stability,[17] that is, Zn<Cu>Ni, regardless of the nature of the coordination ligand. In the solvent extractions of the STTA chelates of these metals, a similar sequence is observed. Since the STTA is an oxygen-sulfur-donating ligand, it has a marked tendency to form a covalent bond. The contribution of $d\pi-d\pi$ interactions seems to be responsible for this relationship. The discrepancy in the extraction constants between the extraction and the back-extraction indicates that a 30-min contact is insufficient to establish the extraction equilibrium. As the organic solvent plays an important role in the extration of the metal ions with any chelating reagent, various solvents were examined in the present study; cyclohexane was found to extract the cobalt STTA chelate at the lowest pH among the solvents, followed by CCl_4, MIBK, C_6H_6, and $CHCl_3$, in that order.[4] Experiments were also made on the extraction of trace amounts of zinc with 0.001 M STTA in cyclohexane, benzene, and MIBK. The extractability of the zinc chelate at a constant pH was found to be the same by either cyclohexane and benzene, but it was poor by MIBK, as is shown in Fig. 5. In general, the extractability of the cobalt and zinc STTA chelates is remarkable when

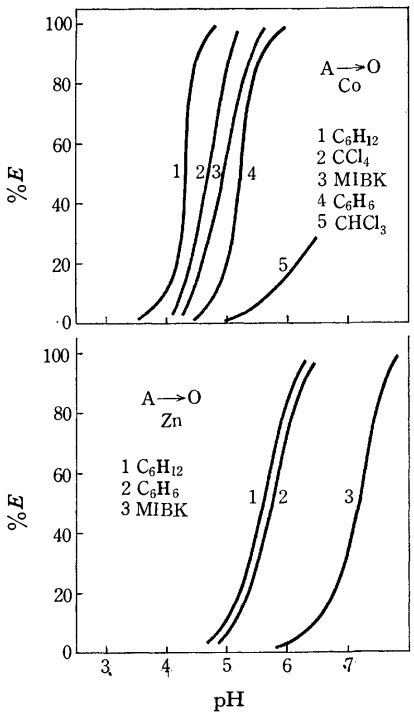

Fig. 5. The effect of the diluent on the extraction of trace amounts of Zn(II) and Co(II) with 0.001 M STTA in a various organic solvent.

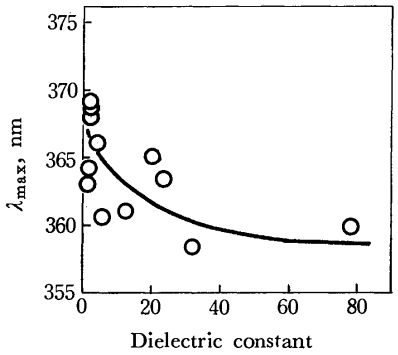

Fig. 6. The effect of the dielectric constant of the diluent on the wavelength of the absorption maximum, λ_{max}, of STTA. The values of wavelength of the absorption maximum, λ_{max}, was as follows:
1: Carbon disulfide (378.0), 2: Benzene (369.0) 3: Xylene (368.5) 4: Carbon tetrachloride and cyclohexane (365.0) 5: *n*-Hexane (363.0) 6: Chloroform (366.0) 7: Ethyl acetate (360.5) 8: Methyl isobutyl ketone (361.0) 9: Acetone (365.0) 10: Ethanol (363.5) 11: Methanol (358.5) 12: Water (pH 8.0) (360.0)

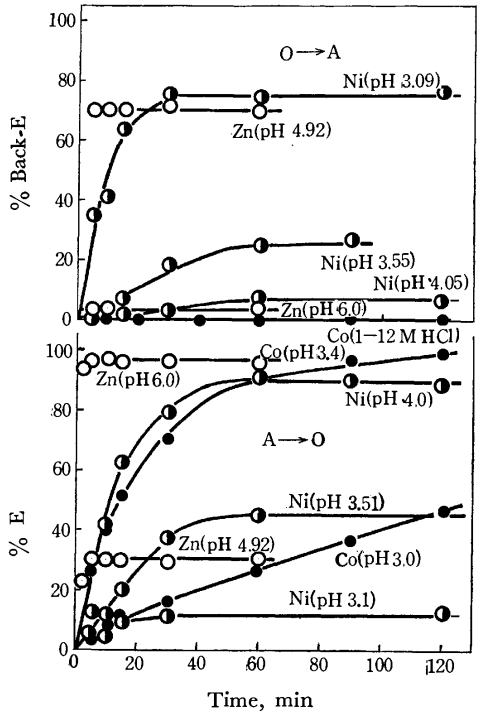

Fig. 7. The rates of the extraction and the back-extraction of trace amounts of Zn(II), Ni(II), and Co(II)-0.001 M STTA-cyclohexane system at different pH values.

12) D. Dyrssen, *Svensk Kem. Tidskr.*, **68**, 212 (1956).
13) T. Shigematsu and M. Tabuchi, *Bull. Inst. Chem. Res., Kyoto Univ.*, **39**, 35 (1961).
14) W. B. Brown, J. F. Steinbach, and W. F. Wagner, *J. Inorg. Nucl. Chem.*, **13**, 119 (1960).
15) J. Stary and E. Hladky, *Anal. Chim. Acta*, **28**, 227 (1963).
16) D. Dyrssen, "Extraction of Metal Ions with β-Isopropyl tropolone," Trans. Roy. Inst. Technol, No 188 Stockholm, 1962.
17) H. Irving and R. J. P. Williams, *J. Chem. Soc.*, **1953**, 3192.

using solvents of a small dielectric constant and a lower solubility of water. These facts show that the extracted chelates are stable and have no significant dipole moment. Therefore, the dipole interaction of the chelates with the diluent can scarcely play any appreciable role in the extraction process. Figure 6 shows the relationship between the absorption maximum of STTA in various solvents and the dielectric constants of the solvents. The STTA solution exhibits a typical absorption band, varying with the dielectirc constant and with the hydrogen-bonding ability of the solvents. This change in the absorption band is generally called the blue shift; its intensity becomes stronger with an increase in the dielectric constant of the solvent. This indicates that the interaction between STTA and the more polar solvent, *e.g.*, the hydrogen bonding or the dipole-dipole interaction, takes place in the solution; it may be one of the most important factors in the decrease of the extractability of cobalt and zinc STTA chelates.

Kinetics of Extraction and Back-extraction. The effects of the pH on the extraction and the back-extraction rate of trace amounts of cobalt, nickel, and zinc with 0.001 M STTA in cyclohexane are shown in Fig. 7. The extractions were carried out under vigorous shaking, for the extent of the extraction is independent of the shaking rate. The extraction of Zn seemed to be rapid, but that of Ni seemed to require about 60 min to reach its extraction equilibrium. Cobalt was not back-extracted, not even with 1—12 M HCl. The experimental results show that the extraction rate of the chelate compounds is a function of the pH and that it usually increases with an increase in the pH under the same conditions. If we assume that the slowest stage in the Ni–STTA–cyclohexane extraction system is due to the first-step formation of the chelate compound, the rate of the extraction of nickel, $-d(Ni^{2+})/dt$, can be shown to obey the following equation in view of the general rate expression[18] for formation of metal chelates:

$$-\frac{d(Ni^{2+})}{dt} = k(Ni^{2+})(R^-) \quad (14)$$

$$= k(Ni^{2+})\frac{K_a}{P_r}\frac{(HR)_0}{(H^+)} \quad (15)$$

$$\log(1-\%\,E/100) = -\frac{k}{2.303}\frac{K_a}{P_r}\frac{(HR)_0}{(H^+)}t \quad (16)$$

$$\log(\log 100/(100-\%\,E)) = \mathrm{pH} + \log(HR)_0 + \log t + \mathrm{const.} \quad (17)$$

where:

$$(Ni^{2+})_{initial} = (Ni^{2+}) + (NiR_2)_0$$

$$D = (NiR_2)_0/(Ni^{2+}),\ \%\,E = 100D/(1+D) \quad (18)$$

Then, $(Ni^{2+}) = (Ni^{2+})_{initial},\ (1-\%\,E/100)$ (19)

As is shown in Fig. 8, the $\log(1-\%E/100)$ *vs.* time plot is linear for 30 min at a constant pH. Moreover, the $\log(\log 100/(100-\%E))$ *vs.* pH plot shows a straight line with the slope of unity. These facts indicate that the rate-determining step in the Ni–STTA–cyclohexane extraction system is controlled by the formation

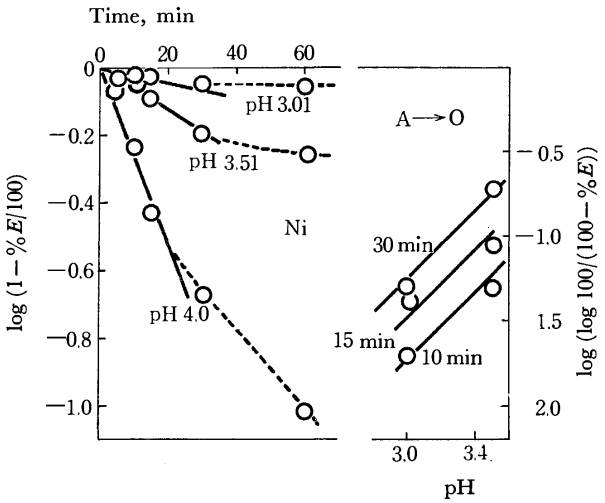

Fig. 8. The kinetics of the extraction of trace amounts of Ni(II) with 0.001 M STTA in cyclohexane at different pH values and time.

of $Ni(STTA)^+$. Similar phenomena have also been observed in Zn, Ni, and the Co–dithizone–chloroform system.[19] The rate of the transfer of the neutral species from the aqueous to the organic phase is a dominant factor in the extraction in Zn-acetylacetone, benzoylacetone, and the dibenzoylmethane–chloroform system.[20] In all cases, the displacement of water molecules coordinated to a metal ion may also play an important role in the chelate-formation rate. In addition, the rate of extraction depends on the nature of the metal ion, the partition coefficient and the dissociation constant of the organic reagent, and the pH. If we postulate that the slowest stage in the Co–STTA–cyclohexane extraction system is due to a transformation of $Co(STTA)_2$ to $Co(STTA)_3$, the rate of the extraction of cobalt, $d(CoR_3)/dt = -d(Co^{2+})/dt$ may be described approximately by the following equation:

$$\frac{d(CoR_3)}{dt} = -\frac{d(Co^{2+})}{dt} = k(CoR_2)(HR)_0 \quad (20)$$

$$= k(Co^{2+})\frac{KP_cK_a}{P_r^3}\frac{(HR)_0^3}{(H^+)^2} \quad (21)$$

$$\log(1-\%\,E/100) = -\frac{k}{2.303}\frac{KP_cK_a^2}{P_r^3}\frac{(HR)_0^3}{(H^+)^2}t \quad (22)$$

$$\log(\log 100/(100-\%\,E)) = 2\,\mathrm{pH} + 3\log(HR)_0 + \log t + \mathrm{const.} \quad (23)$$

As is shown in Fig. 9, the $\log(1-\%E/100)$ *vs.* time plot is linear at a constant pH. Moreover, the plots of $\log(\log 100/(100-\%E))$ *vs.* pH have a slope of 2, and the $\log(\log 100(100/(100-\%E)))$ *vs.* $\log(HR)_0$ plots give a straight line with a slope of 3, as is shown in Fig. 10. These facts indicate that the assumption of the extraction mechanism of cobalt is vaild.

18) H. Irving and R. J. P. Williams, *J. Chem. Soc.*, **1949**, 1841.

19) H. Freiser, "Solvent Extraction Chemistry," North-Holland, Amsterdam, (1967) p. 85.

20) G. K. Schweitzer and J. R. Rimstidt, Jr, *Anal. Chim. Acta*, **27**, 389 (1962).

Synergistic and Antagonistic Effect in the Presence of TOPO. In the Ni and Zn–STTA(0.001 M)–TOPO(0.01 M)–cyclohexane systems, $|\Delta pH_{1/2}|$ was found to be 0.45 for Ni and 1.95 for Zn respectively. The logarithm of the distribution ratios of Zn and Ni is linearly related to the pH. The slope of the straight lines becomes 2, indicating that the extracted species can be written as $Zn(STTA)_2$ and $Ni(STTA)_2$ respectively. As is shown in Fig. 11, a straight line with a slope of 1 is obtained when log D^*/D values are plotted against $\log(TOPO)_0$ in the case of the Zn–STTA–TOPO–cyclohexane system. This fact indicates that

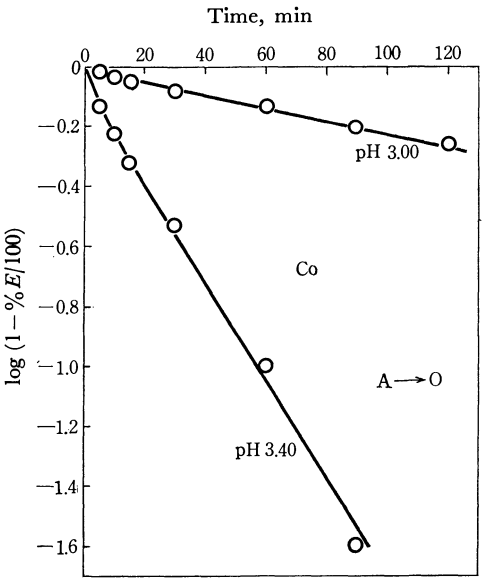

Fig. 9. The kinetics of the extraction of trace amounts of Co(II) with 0.001 M STTA in cyclohexane at different pH values and time.

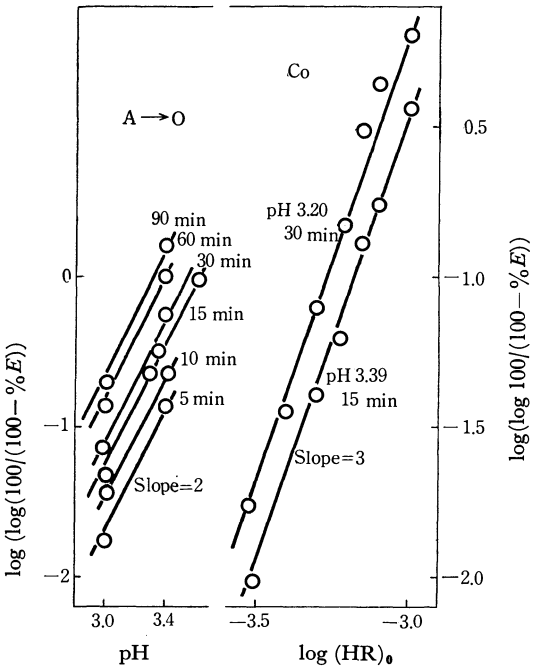

Fig. 10. The kinetics of the extraction of trace amounts of Co(II) with 0.001 M STTA in cyclohexane at different pH values and STTA concentration.

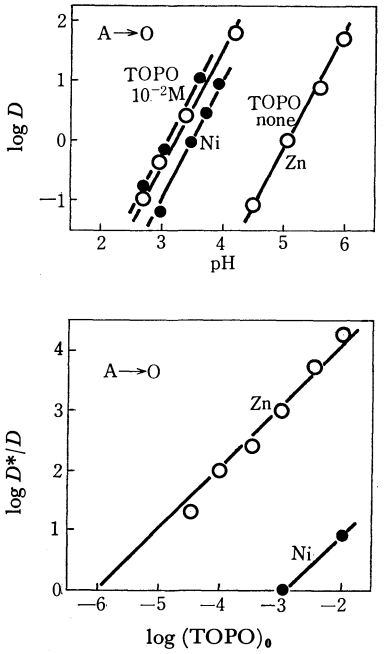

Fig. 11. The variation of the distribution ratio of trace amounts of Zn(II) and Ni(II) with 0.001 M STTA in cyclohexane in the presence or the absence of TOPO as a function of pH or TOPO concentration.

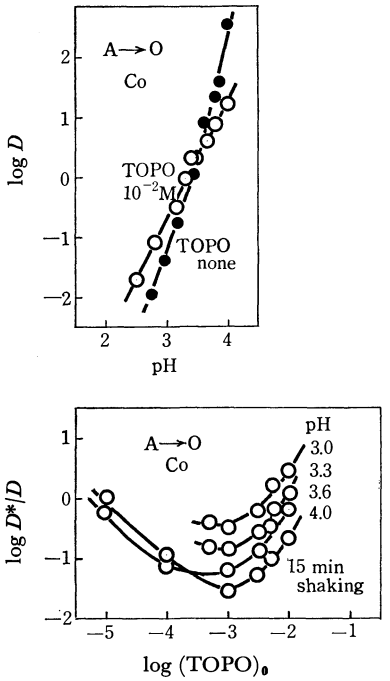

Fig. 12. The variation of the distribution ratio of trace amounts of Co(II) with 0.001 M STTA in cyclohexane in the presence or absence of TOPO as a function of pH or TOPO concentration.

one molar TOPO reacts with one molar Zn-STTA chelate to form the Zn(STTA)TOPO adduct in cyclohexane. The stability constant of the adduct was estimated to be log $\beta_{x,1}=6.05$. From the stability constant of the adduct of $Zn(TTA)_2TOPO$, log $\beta_{x,1}=6.47$,[21] under the same conditions, it may be

21) T. Honjo, M. Horiuchi and T. Kiba, This Bulletin, in press.

expected that TOPO forms more stable adducts with the $Zn(TTA)_2$ chelate than with the $Zn(STTA)_2$ chelate. As the extraction constants of $Zn(TTA)_2$ and $Zn(STTA)_2$ are log $K_{x,0}=-8.33$[22] and -3.49 respectively, the general concept that the extraction constant of the chelates increases, while the stability constant of the adducts decreases,[23] is also the case for the metal–TTA and STTA–cyclohexane systems. The donor π-bond formation between the d-electrons of the metal and the sulfur of the STTA, bringing about the stabilization of the chelate, may play an important part. The Ni-STTA chelate ambiguously forms its adduct with TOPO. In the cobalt–STTA(0.001 M)–TOPO(0.001 M)–cyclohexane system, $|\Delta pH_{1/2}|$ was found to be 0.25. The slope in Fig. 12 of the log D against pH plot at a constant STTA(0.001 M) increases steeply up to 2 to 4 as the extraction pH becomes higher. Moreover, the plots of log D *vs.* $\log(STTA)_0$ at a constant pH give straight lines with a slope of 4, as is shown in Fig. 13. However, in the extraction of cobalt in the presence of 0.001 M TOPO, the log D *vs.* pH plots show straight lines with slopes of 2. As is shown in Fig. 12 the log D^*/D *vs.* $\log(TOPO)_0$ plots give concave curves including an antagonistic effect. The effect becomes more remarkable as the extraction is done at a higher pH, and appears most pronouncedly on the extraction of cobalt with STTA in the presence of 0.001 M TOPO. The effects of pH, of the extraction time, and of the TOPO concentration on the extraction and the back-extraction of the metal–STTA–TOPO–cyclohexane system are shown in Fig. 14. The cobalt STTA chelates extracted in the presence of 0.001—0.01 M TOPO could be back-extracted with 1 M HCl to a certain extent. However, when the concentration of TOPO becomes lower than 0.001 M, the cobalt chelate can not be back-extracted even with 1—12 M HCl. As can be seen in Fig. 14, the back-extraction of cobalt

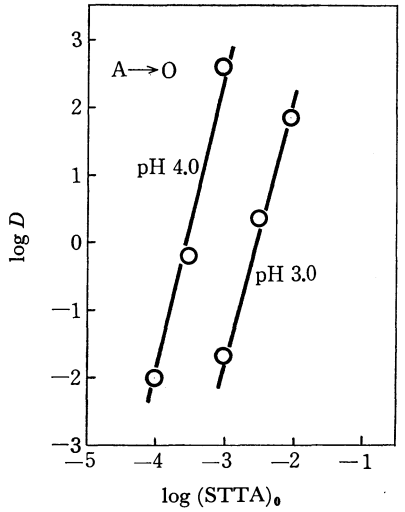

Fig. 13. The variation of the distribution ratio of trace amounts of Co(II) with STTA at definite pH values as a function of STTA concentration.

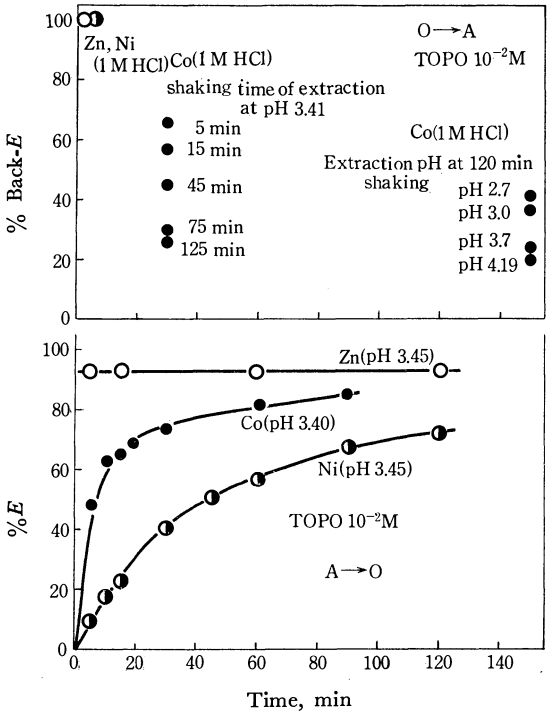

Fig. 14. The rates of the extraction and the back-extraction of trace amounts of Zn(II) and Ni(II)–0.001 M STTA–cyclohexane system in the presence or the absence of TOPO at different pH values or time.

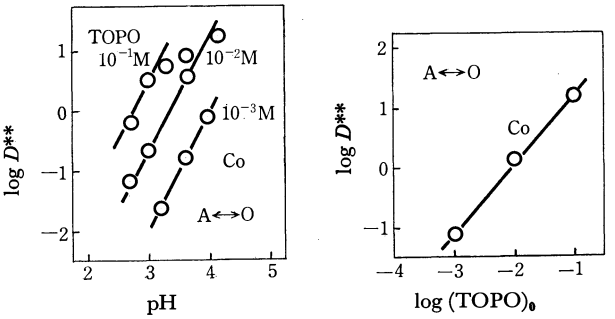

Fig. 15. The variation of the distribution ratio of trace amounts of Co(II)–0.001 M STTA–TOPO–cyclohexane system as a function of pH or TOPO concentration.

is controlled by the shaking time, the pH value, and the TOPO concentration. In the presence of 0.01 M TOPO, the back-extraction of cobalt with 1 M HCl decreases as the shaking time becomes longer and as the pH values increase. In general, the back-extractability of cobalt decreases with a decrease in the TOPO concentration. The Ni and Zn chelates extracted in the presence of TOPO are readily back-extracted with 1 M HCl. In the presence of 0.01 M TOPO, the extraction rate of zinc is rapid, while tha of Ni is somewhat slower than in the absence of TOPO In the extraction of cobalt in the presence of 0.01 M TOPO, the extraction increases greatly for 30 min and then more gradually. In the Co–STTA–TOPO–cyclohexane system, when the dominant species are CoR_2L, (which is back-extractable with 1 M HCl), CoR_3 (which is not back-extracted even with concentrated HCl), and Co^{2+}, the distribution ratio of cobalt in the extraction, D, may be written as follows:

22) H. M. N. H. Irving and D. N. Edgington, *J. Inorg. Nucl. Chem.*, **27**, 1359 (1965).
23) T. Honjo and T. Shigematsu., *Kagaku* (Kyoto), **23**, 708 (1968).

$$D = \frac{(CoR_2L)_0 + (CoR_3)_0}{(Co^{2+})}, \quad D_B = \frac{(CoR_2L)_0}{(CoR_3)_0} \tag{24}$$

$$D^{**} = \frac{(CoR_2L)_0}{(Co^{2+})} = \frac{D}{1+1/D_B} = \frac{K\beta_{x,1}P_cK_a^2}{P_r^2}\frac{(H)_0^2(L)_0}{(H^+)^2} \tag{25}$$

$$\log D^{**} = 2\,pH + 2\log(HR)_0 + \log(L)_0 + \text{const.} \tag{26}$$

Now, when terms such as D_B and D^{**} are used to explain the extraction behevior, the log D^{**} *vs.* pH plot shows a straight line with a slope of 2 at a constant concentration of TOPO, and the log D^{**} *vs.* $\log(TOPO)_0$ plot shows a slope of unity at a constant concentration of STTA as is shown in Fig. 15. These facts suggest that the extracted cobalt compounds are CoR_2L and CoR_3 respectively. From these experimental facts, the extraction mechanism of the cobalt(II)–STTA–TOPO–cyclohexane system may be expressed as follows:

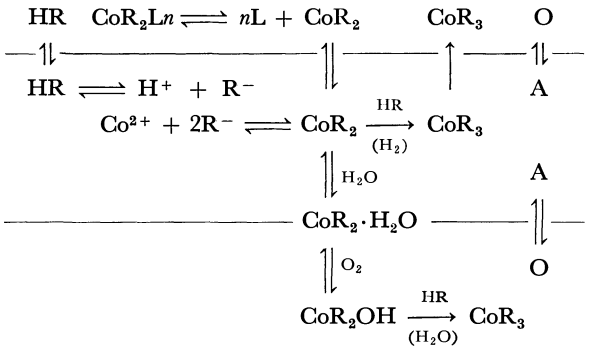

The other evidence of the formation of CoR_2, CoR_2L and CoR_3 is as follows: 1) the existence of the first absorption band near 500 nm in the solution of the cobalt–STTA chelate (CoR_3); 2) the cobalt–STTA chelate crystal prepared by the ordinary extraction was the diamagnetic (CoR_3); 3) the silica gel thin-layer chromatograms of the extracted cobalt–STTA chelates at high concentrations give two spots, one corresponding to CoR_2(R_f=0.29), and the other, to CoR_3 (R_f= 0.35), using carbon tetrachloride as the developing solvent; 4) a part of the cobalt-STTA chelates extracted in the presence of TOPO can be back-extracted with 1—12 M HCl, and the back-extracted cobalt behaves as a divalent ion (CoR_2L). At present time, it should be considered that the irreversible extraction behavior of Co-STTA chelates is due to the inert nature of the trivalent cobalt complexes. The transformation of $Co(STTA)_2$ to $Co(STTA)_3$ may occur both in the aqueous and the organic phases, or at the interface of the two phases, by means of a certain interaction between $Co(STTA)_2$ and STTA in the presence of oxygen and water. However, further investigations of these questions will be necessary before we reach any final conclusion.

BULLETIN OF THE CHEMICAL SOCIETY OF JAPAN, VOL. 46, 3779—3784 (1973)

Infrared Spectra of Some Transition-metal (Fe, Co, Ru, and Ir) Nitrosyl (^{14}NO and ^{15}NO) Complexes

Eiichi MIKI, Kunihiko MIZUMACHI, Tatsujiro ISHIMORI, and Hisateru OKUNO

Department of Chemistry, College of Science, Rikkyo University, Nishi-Ikebukuro, Toshima-ku, Tokyo 171

(Received June 4, 1973)

Twelve ^{15}NO-complexes of iron, cobalt, ruthenium, and iridium were prepared. The correlations of the isotopic shifts of their IR spectra with a metal-(NO) bond angle were investigated. For several nitrosyl complexes, the absorption bands due to the skeletal vibrations between the metal and the NO group were clearly assigned. Of the two absorption bands in the region 250—650 cm^{-1}, the absorption band with a smaller isotopic shift could be assigned to the metal-(NO) stretching vibration and that with a larger isotopic shift to the metal-(NO) bending vibration.

Since an infrared study of $Co(NO)(CO)_3$ and its ^{15}N analogue led to definite assignments of the skeletal vibrations between the cobalt and the NO group,[1] the effect of the ^{15}N-substitution on infrared spectra has been measured on several nitrosyl complexes formulated as NO^+ complexes.[2-9] For the nitrosyl complexes of chromium, manganese and ruthenium, distinct assignments of the skeletal vibrations between the metal and the NO group, and determination of the coordinating atom of the NO group to the metal atom have been made from a comparison of the observed isotopic shifts with the calculated ones.[2-4] Recently,

1) R. S. McDowell, W. D. Horrockes, and J. Yates, *J. Chem. Phys.*, **34**, 530 (1961).
2) E. Miki, T. Ishimori, H. Yamatera, and H. Okuno, *Nippon Kagaku Zasshi*, **87**, 703 (1966).
3) E. Miki, This Bulletin, **41**, 1835 (1968).
4) E. Miki, S. Kubo, K. Mizumachi, T. Ishimori, and H. Okuno *ibid.*, **44**, 1024 (1971).
5) G. Paliani, A. Poletti, and A. Santucci, *J. Mol. Structure*, **8**, 63 (1971).
6) G. Paliani, R. Cataliotti, A. Poletti, and A. Foffani, *J. Chem. Soc. Dalton*, **1972**, 1741.
7) M. S. Quinby and R. D. Feltham, *Inorg. Chem.*, **11**, 2468 (1972).
8) M. J. Cleare and W. P. Griffith, *J. Chem. Soc. A*, **1967**, 1144.
9) M. J. Cleare and W. P. Griffith, *ibid.*, **1969**, 372.

Table 1. Crystallographic data and preparative methods for nitrosyl complexes

Complex	M-N, Å	N-O, Å	M-N-O, deg.	Preparative Method
trans-$Na_2[Ru(OH)(NO_2)_4(NO)]\cdot 2H_2O$	1.75	1.13	180[a]	Ref. 16
trans-$K_2[Ru(OH)(NO_2)_4(NO)]$	1.79	1.12	171[b]	Ref. 17
$K_2[RuCl_5(NO)]$	1.88	1.09	171[c]	Ref. 3
$Ru(NO)(S_2CN(C_2H_5)_2)_3$	1.72	1.17	170[d]	l)
trans-$[Ru(OH)(NH_3)_4(NO)]Cl_2$	2.07	1.14	*ca.* 150[e]	Ref. 16
trans-$[RuCl(NH_3)_4(NO)]Cl_2$	no data			Ref. 16
$Ru(NO)(S_2CN(CH_3)_2)_3$	no data			l)
$Fe(NO)(S_2CN(CH_3)_2)_2$	1.71	1.02	173[f]	m)
$Co(NO)(S_2CN(CH_3)_2)_2$	1.75	1.03, 1.11	135, 136[g]	n)
$[Co(NH_3)_5(NO)]Cl_2$	1.87	1.15	119[h]	Ref. 3
$[Co(NO)en_2](ClO_4)_2$	no data			o)
$Ir(NO)(P(C_6H_5)_3)_3$	1.67	1.24	180[i]	p)
$[Ir(NO)_2(P(C_6H_5)_3)_2](ClO_4)$	1.77	1.21	164[j]	q)
$IrCl_2(NO)(P(C_6H_5)_3)_2$	1.94	1.03	123[k]	r)

a) S. H. Simonosen and M. H. Mueller, *J. Inorg. Nucl. Chem.*, **27**, 309 (1965). b) L. A. Butmann, T. S. Khodashova, L. Kh. Minacheva, and V. I. Tayukin, *Russ. J. Struct. Chem.*, **5**, 225 (1964). c) T. S. Khodashova and G. B. Bokii, *ibid.*, **5**, 130 (1964). d) A. Domenicano, A Vaciago, and L. Zambonelli, *Chem. Commun.*, **1966**, 476. e) G. B. Bokii and N. A. Parpiev, *Soviet Phys. Kristalografiya*, **2**, 681 (1957). f) G. R. Davies, J. A. Jarvis, B. T. Kilbourn, R. H. B. Mais, and P. G. Owston, *J. Chem. Soc. A*, **1970**, 1275. g) J. H. Enemark and R. D. Feltham, *J. Chem. Soc. Dalton*, **1972**, 718. h) C. S. Pratt, B. A. Coyle, and J. A. Ibers, *J. Chem. Soc. A*, **1971**, 2146. i) V. G. Albano, P. Bellon, and M. Sansoni, *ibid.*, **1971**, 2420. j) D. M. P. Mingos and J. A. Ibers, *Inorg. Chem.*, **9**, 1105 (1970). k) D. M. P. Mingos and J. A. Ibers, *ibid.*, **10**, 1035 (1971). l) L. Cambi and L. Malatesta, *Rend. Ist. Lombardo Sci.*, **71**, 118 (1938); *Chem. Abstr.*, **32**, 7364 (1938). m) L. Cambi, *Z. Anorg. Allg. Chem.*, **247**, (1941). n) R. L. Carlin, F. Canziani, and W. K. Bratton, *J. Inorg. Nucl. Chem.*, **26**, 898 (1964). o) R. D. Feltham and R. S. Nyholm, *Inorg. Chem.*, **4**, 1334 (1965). p) M. Angoletta, *Gazz. Chim. Ital.*, **93**, 1591 (1963). p) M. Angoletta and G. Caglio, *ibid.*, **93**, 1584 (1963). r) G. R. Crooks and B. F. G. Johnson, *J. Chem. Soc. A*, **1970**, 1662.

Sabatini[10] and Tosi[11-14] carried out polarized infrared studies on single crystals of some transition-metal nitrosyl compounds to assign the metal-(NO) skeletal vibrations. Their results are consistent with those obtained by the infrared isotopic shift method.

In this paper we describe infrared studies on the nitrosyl complexes of iron, cobalt, ruthenium, and iridium, and their ^{15}NO-complexes.

Experimental

The nitrosyl complexes were prepared according to the methods referred to in Table 1. Their ^{15}NO-complexes were prepared in a vacuum line with the use of ^{15}NO gas (1 mmol) derived from $K^{15}NO_3$ (^{15}N atom% = 95—99). All other reagents were of analytical grade. The infrared spectra and elementary analyses showed that the desired products were obtained.

Infrared spectra were measured in the region 200—4000 cm^{-1} by means of Nujol mull and hexachlorobutadiene mull techniques. JASCO DS-402G (700—4000 cm^{-1}) and JASCO model IR-F (200—700 cm^{-1}) infrared spectrophotometers were used. The wave numbers of the absorption bands were calibrated with 1,2,4-trichlorobenzene, polystyrene film and water vapor.

Results

Assignments of Infrared Spectra. The assignments of the N-O stretching vibrations and the skeletal vibrations between the metal and the NO group were made on the basis of observation of the ^{15}N-isotopic shifts. The ^{15}N-isotopic shifts of the skeletal vibrations observed in the limited region *ca.* 450—650 cm^{-1} were carefully measured[1-17] in order to obtain distinct assignments for the skeletal vibrations. The isotopic shifts observed were compared with those calculated with a three-body model of the metal and the NO group.[3] The assignments of the absorptions due to metal-(NO) skeletal vibrations, and the observed and calculated isotopic shifts are shown in Table 2. A number of absorption bands due to the ligands except for NO group were assigned according to Adams.[18]

trans-$Na_2[Ru(OH)(NO_2)_4(NO)]\cdot 2H_2O$: The skeletal vibrations between the ruthenium and the NO group could not be clearly assigned. The skeletal vibrations, the Ru-OH stretching vibration and the wagging vibration of NO_2 group are observed in the region 550—640 cm^{-1}. These four bands shifted upon ^{15}N-substitution. Deuteration of this complex was carried out for assigning the four bands.

The absorption bands in the region 550—640 cm^{-1} lacked sharpness. This is considered to be due to the overlap with the broad and strong absorption band of

10) A. Sabatini, *Inorg. Chem.*, **6**, 4756 (1967).
11) L. Tosi, *Spectrochim. Acta*, **26A**, 1675 (1970).
12) L. Tosi, *C. R. Acad. Sci., Paris*, **271B**, 697 (1970).
13) L. Tosi, *ibid.*, **274B**, 249 (1972).
14) L. Tosi, *J. Chim. Phys.*, **1972**, 1052.
15) E. E. Mercer, W. A. McAllister, and J. R. Durig, *Inorg. Chem.*, **5**, 1881 (1966).
16) P. Gans, A. Sabatini, and L. Sacconi, *ibid*, **5**, 1877 (1966).
17) M. B. Fairey and R. J. Irving, *Spectrochim. Acta*, **22**, 359 (1966).
18) D. M. Adams, "Metal-Ligand and Related Vibrations," Edward Arnold Publishers Ltd., London (1967).

the libration of water of crystallization. The dehydrated salts of the ^{14}NO- and ^{15}NO-complexes were prepared in order to measure the isotopic shifts more exactly. The spectral figure of $Na_2[Ru(OH)(NO_2)_4(NO)]$ is quite similar to that of its dihydrate.

The N–O stretching vibration of $Na_2[Ru(OH)(NO_2)_4(NO)]\cdot 2H_2O$ shifted from 1898 (vs)[19] to 1862 cm^{-1} (vs) upon ^{15}NO-substitution. The 584 cm^{-1} band (m) of $Na_2[Ru(OH)(NO_2)_4(^{14}NO)]$ shifted to 568 cm^{-1} (sh) upon deuterium substitution, but not the bands at 634, 612, and 555 cm^{-1}. Therefore, the band at 584 cm^{-1} (m) could be assigned to the Ru–OH stretching vibration. The 634 (m), 612 (vs), and 555 cm^{-1} (vs) bands of $Na_2[Ru(OH)(NO_2)_4(^{14}NO)]$ shifted downwards by *ca.* 9, 5, and 4 cm^{-1}, respectively, upon ^{15}NO-substitution. From the values of the isotopic shift the 634 cm^{-1} band could be assigned to a skeletal vibration between the ruthenium and the NO group. The 612 and the 555 cm^{-1} bands are considered to be due to another skeletal vibration and the wagging vibration of NO_2 group. The 612 cm^{-1} band may be assigned to the wagging vibration of NO_2 group in view of the following. A neutron diffraction study on $Na_2[Ru(OH)(NO_2)_4(NO)]\cdot 2H_2O$ shows that the $O(H_2O)$–$N(NO_2)$ distances are 2.9—3.3 Å, and the $O(H_2O)$–$O(OH)$ and the $O(H_2O)$–$O(NO)$ distances are 3.5 Å and 3.9 Å, respectively.[20] Thus we see that the water of crystallization affects the wagging vibration of NO_2 groups to a greater extent than the Ru-OH stretching vibration and the skeletal vibrations, and the NO_2 wagging vibration is more influenced by the dehydration of the water of crystallization than the Ru-OH stretching vibration and the skeletal vibrations. The 635 (s), 583 (w), and 557 cm^{-1} (vs) bands hardly shift on the dehydration of water of crystallization, while only the 602 cm^{-1} band (vs, b) shifts to 612 cm^{-1}. The 635 and the 557 cm^{-1} bands of $Na_2[Ru(OH)(NO_2)_4(^{14}NO)]\cdot 2H_2O$ could be assigned to the skeletal vibrations between the ruthenium and the NO group. The 583 and 602 cm^{-1} bands were assigned to the Ru–OH stretching vibration and the wagging vibration of NO_2 group, respectively.

trans-$K_2[Ru(OH)(NO_2)_4(NO)]$: The N–O stretching vibration shifted from 1887 cm^{-1} (vs) to 1848 cm^{-1} (vs) upon ^{15}NO-substitution. In the region 550—640 cm^{-1}, four absorption bands at 623 (vs, b), 580 (s), 573 (s), and 565 cm^{-1} (sh) were also observed as in the case of the sodium salt. Their isotopic shifts upon ^{15}NO- and deuterium substitutions were complicated, making it impossible to assign the four bands unambiguously.

trans-$[Ru(OH)(NH_3)_4(NO)]Cl_2$: The absorption bands at 1841 (vs), 630 (m), and 589 cm^{-1} (m) shifted to 1807, 613, and 585 cm^{-1}, respectively, upon ^{15}NO-substitution. On the other hand, the 564 cm^{-1} band (vs, b) did not shift upon ^{15}NO-substitution and was assigned to the Ru–OH stretching vibration. Ru-NH_3 stretching vibrations were observed at 476 cm^{-1} (m) and 497 cm^{-1} (vw).

trans-$[RuCl(NH_3)_4(NO)]Cl_2$: The 1880 cm^{-1} band (vs) shifted to 1844 cm^{-1}, the 603 cm^{-1} band (s) to 586 cm^{-1}, and the 562 cm^{-1} band (m) to 560 cm^{-1} upon ^{15}NO-substitution. The Ru-NH_3 stretching vibration was observed at 486 cm^{-1} (vs).

$Ru(NO)(S_2CNR_2)_3$ ($R=CH_3$ and C_2H_5) and $Fe(NO)(S_2CN(CH_3)_2)_2$: The absorption bands due to dialkyldithiocarbamate ion[21,22] (the C–S stretching, the C–N–C bending, the metal–S stretching and the ring deformation vibrations) overlapped with the skeletal vibrations between the metal and the NO group. Thus, the isotopic shifts upon the ^{15}NO-substitution could not be measured exactly.

The bands at 1827 (vs), 1808 (vs), and 544 cm^{-1} (sh) for $Ru(NO)(S_2CN(CH_3)_2)_3$ shifted upon ^{15}NO-substitution to 1790, 1771, and 540 cm^{-1} (s), respectively. The bands at 1806 (vs), 572 (s, b), and 554 cm^{-1} (sh) for $Ru(NO)(S_2CN(C_2H_5)_2)_3$ shifted to 1774, 560 (s, b), and 540 cm^{-1} (s), respectively.

The N–O stretching vibration for $Fe(NO)(S_2CN(CH_3)_2)_2$ shifted from 1691 to 1656 cm^{-1}, and the band at 560 cm^{-1} (m) shifted to 556 cm^{-1} (m) upon ^{15}NO-substitution.

$Co(NO)(S_2CN(CH_3)_2)_2$: The N–O stretching vibration shifted from 1624 cm^{-1} (vs) to 1596 cm^{-1} upon ^{15}NO-substitution. Three absorption bands (576 cm^{-1} (w), 555 cm^{-1} (sh) and 551 cm^{-1} (w)) observed in the region where the skeletal vibrations between the metal and the NO group would have been observed did not shift upon ^{15}NO-substitution. These absorption bands could be assigned to the C–S stretching vibration, the Co–S stretching vibration and the ring deformation due to the coordinated dimethyldithiocarbamate.[21,22] On the other hand, the broad bands at 317 cm^{-1} (m) and 259 cm^{-1} (m) shifted by ^{15}NO-substitution to 311 cm^{-1} and 256 cm^{-1}, respectively. These bands observed at rather extraordinarily low frequencies are assigned to the skeletal vibrations between the cobalt and the NO group. An X-ray diffraction study of $Co(NO)(S_2CN(CH_3)_2)_2$ shows that the bond angle of the Co–N–O is 135°, and the oxygen atom of the NO group alternately lies above two of the Co–S bonds of the same dimethyldithiocarbamate ligand.[23] The skeletal vibrations between the cobalt and the NO group are considered to reflect the structure. However, another possibility of overlapping of CoNO skeletal vibrations with the vibrations due to the coordinated dimethyldithiocarbamate ligands can not be excluded.

$[Co(NO)en_2](ClO_4)_2$: The N–O stretching vibration shifted from 1661 (vs) to 1632 cm^{-1} and the bands at 560 (sh) and 490 cm^{-1} (m) shifted to 550 (b, w) and 486 cm^{-1} (m), respectively. These absorption bands seem to be due to the Co–(NO) skeleton.

$Ir(NO)(P(C_6H_5)_3)_3$, $[Ir(NO)_2(P(C_6H_5)_3)_2]ClO_4$, and $Ir(NO)Cl_2(P(C_6H_5)_3)_2$: The N–O stretching vibrations and the skeletal vibrations between the iridium

19) The sign in parentheses presents the abbreviations of the absorption strength and shape; vs=very strong, s=strong, m=medium, w=weak, vw=very weak, sh=shoulder, b=broad.

20) Reference (a) in Table 1.

21) G. Durgaprasad, D. N. Sathyanarayana, and C. C. Patel, *Can. J. Chem.*, **47**, 631 (1969).

22) I. Ojima, T. Ohnishi, T. Iwamoto, N. Iwamoto, and K. Tamaru, *Inorg. Nucl. Chem. Letters*, **6**, 65 (1970).

23) Reference (g) in Table 1.

and the NO group overlapped with the absorption bands due to triphenylphosphine. From a comparison of the absorption strength of free triphenylphosphine with that of $Ir(NO)(P(C_6H_5)_3)_3$ and $Ir(NO)Cl_2(P(C_6H_5)_3)_2$, it was considered that the 617 cm^{-1} band assigned to a skeletal vibration might overlap with the band due to triphenylphosphine.

For $Ir(NO)(P(C_6H_5)_3)_3$, the N-O stretching vibrations at 1601 (vs) and 1582 cm^{-1} (m) shifted to 1557 and 1541 cm^{-1}, respectively, upon ^{15}NO-substitution. The bands at 617 (m) and 533 cm^{-1} (w) shifted to 610 (m) and 522 cm^{-1}, respectively.

For $[Ir(NO)_2(P(C_6H_5)_3)_2]ClO_4$, the bands at 1759 (m) and 1707 cm^{-1} (vs) (the N-O stretching vibrations) shifted to 1725 and 1674 cm^{-1}, respectively. Five absorption bands in the region 370—590 cm^{-1} shifted upon ^{15}NO-substitution (from 584 (m), 553 (m), 539 (m), 527 (m), and 381 cm^{-1} (m) to 570 (w), 545 (w), 533 (w), 524 (w), and 373 cm^{-1} (m), respectively). An X-ray diffraction study shows that the O-N-Ir-N-O skeleton belongs to the point group C_{2v}.[24] The seven absorption bands could be attributed to the skeletal vibrations due to the O-N-Ir-N-O group.

For $IrCl_2(NO)(P(C_6H_5)_3)_2$, the bands at 1628 (vs) and 1558 cm^{-1} (vs) shifted to 1599 and 1533 cm^{-1}, respectively, upon ^{15}NO-substitution. The 1558 cm^{-1} band has already been assigned to the N-O stretching vibration.[25] The 1628 cm^{-1} band can also be assigned to it. It is not clear why the splitting of the N-O stretching vibration is extraordinarily large. The skeletal vibrations were observed at 617 (m) and 589 cm^{-1} (w), and shifted to 598 (w) and 576 cm^{-1} (w), respectively.

Calculation of Isotopic Shifts and Definite Assignments of Skeletal Vibrations. In previous reports, the

Table 2. Observed isotopic shifts, calculated ones ($\Delta\nu_{obsd}$ and $\Delta\nu_{calcd}$ in cm^{-1}) and force constants of some transition-metal nitrosyl compounds

Assignment	Observed		Calculated		$\Delta\nu_{obsd}$	$\Delta\nu_{calcd}$	force constants (mdyn/Å)		
	^{14}NO-complex	^{15}NO-complex	^{14}NO-complex	^{15}NO-complex					
			trans-$Na_2[Ru(OH)(NO_2)_4(NO)]\cdot 2H_2O$						
NO str.	1898	1862	1899	1861	36	38	$f_{11}=14.7$,	$f_{12}=0.2$,	
RuNO bend.	635	625	638	622	10	16		$f_{22}=4.6$	
RuN str.	557	553	558	552	4	6			$f_{33}=0.6$
			$K_2[RuCl_5(NO)]$						
NO str.	1904	1865	1904	1865	39	39	$f_{11}=14.5$,	$f_{12}=0.2$,	$f_{13}=0.2$
RuN str.	606	600	608	602	6	6		$f_{22}=5.6$,	$f_{23}=0.3$
RuNO bend.	588	572	585	571	16	14			$f_{33}=0.5$
			trans-$[Ru(OH)(NH_3)_4(NO)]Cl_2$						
NO str.	1841	1807	1848	1810	34	38	$f_{11}=13.9$,	$f_{12}=0.2$,	$f_{13}=0.2$
RuNO bend.	630	613	628	612	17	16		$f_{22}=5.2$,	$f_{23}=0.7$
RuN str.	589	585	591	586	4	5			$f_{33}=0.7$
			$[Co(NH_3)_5(NO)]Cl_2$ (Co-N-O arrangement)						
NO str.	1614	1589	1617	1586	25	31	$f_{11}=11.1$,	$f_{12}=0.2$,	$f_{13}=0.2$
CoN str.	581	579	584	576	2	8		$f_{22}=3.9$,	$f_{23}=1.1$
CoNO bend.	564	558	567	555	6	12			$f_{33}=0.9$
			$[Co(NH_3)_5(NO)]Cl_2$ (Co-O-N arrangement)						
NO str.	1614	1589	1615	1588	25	27	$f_{11}=11.2$,	$f_{12}=0.2$,	$f_{13}=0.2$
CoON bend.	581	579	583	578	2	5		$f_{22}=3.7$,	$f_{23}=0.9$
CoO str.	564	558	565	556	6	9			$f_{33}=0.9$
			$Ir(NO)(P(C_6H_5)_3)_3$						
NO str.	1601	1557	1598	1560	44	38	$f_{11}=9.0$,	$f_{12}=0.2$	
IrN str.	617	610	615	611	7	4		$f_{22}=7.3$	
IrNO bend.	533	522	534	521	11	13			$f_{33}=0.4$
			$IrCl_2(NO)(P(C_6H_5)_3)_2$						
NO str.	1558	1533	1561	1530	25	31	$f_{11}=10.0$,	$f_{12}=0.2$,	$f_{13}=0.2$
IrNO bend.	617	598	614	601	19	13		$f_{22}=5.4$,	$f_{23}=1.4$
IrN str.	589	576	586	579	13	7			$f_{33}=1.0$

$\Delta\nu_{obsd}=\nu_{^{14}NO\text{-}complex(obsd)}-\nu_{^{15}NO\text{-}complex(obsd)}$; $\Delta\nu_{calcd}=\nu_{^{14}NO\text{-}complex(calcd)}-\nu_{^{15}NO\text{-}complex(calcd)}$; f_{11}, force constant of NO str.; f_{12}, force constant associated with metal-N str. and NO str. (assumed to 0.2 mdyn/Å); f_{13}, force constant associated with metal-NO bend. and NO str. (assumed to 0.2 mdyn/Å in the case of the compounds which contain an angulary coordinated NO group); f_{22}, force constant of metal-N str.; f_{23}, force constant associated with metal-N str. and metal-NO bend.; f_{33}, force constant of metal-NO bend; str., stretching; bend., bending.

24) Reference (j) in Table 1.

25) C. A. Reed and W. P. Roper, *J. Chem. Soc. A*, **1970**, 3054.

isotopic shifts observed upon ^{15}NO-substitution were compared with those calculated by the simple three-body model of the metal and the NO group. For the complexes formulated as NO^+ complexes, it has been found that this method is useful for a definite assignment of the skeletal vibrations between the metal and the NO group.[3,6,7]

We have calculated the isotopic shifts for the following six compounds: *trans*-$Na_2[Ru(OH)(NO_2)_4(NO)]\cdot 2H_2O$, $K_2[RuCl_5(NO)]$, *trans*-$[Ru(OH)(NH_3)_4(NO)]Cl_2$, $[Co(NH_3)_5(NO)]Cl_2$, $Ir(NO)(P(C_6H_5)_3)_3$, and $IrCl_2(NO)(P(C_6H_5)_3)_2$.

The isotopic shifts of the N–O stretching vibration and the skeletal vibrations could be measured exactly. When the N–O stretching absorption band splitted into two peaks, the wave number of the stronger peak was used in the calculation.

The isotopic shifts of $K_2[RuCl_5(NO)]$ and $[Co(NH_3)_5(NO)]Cl_2$ were calculated on the assumption that the metal–N–O are linearly arranged.[3] For $K_2[RuCl_5(NO)]$, the bond angle of the Ru–N–O is 171°. The isotopic shifts were therefore recalculated by using the wave numbers already reported and this bond angle. For $[Co(NH_3)_5(NO)]Cl_2$, if the NO group coordinated linearly to the Co atom as revealed by X-ray diffraction studies,[26] a comparison of the observed isotopic shifts with the calculated ones leads to the result that the NO group coordinates to the cobalt atom through the oxygen atom rather than through the nitrogen atom.[3] However, a recent X-ray diffraction study from three-dimensional data has shown that the bond angle of Co–(NO) is 119° (see Table 1). Therefore, the isotopic shifts of the Co–N–O and the Co–O–N arrangements were calculated by using of the wave numbers already reported and this bond angle.

The secular equations for calculating the isotopic shifts were set up in accordance with Wilson's ***GF*** matrix method.[27] The calculations were carried out at the Computation Centre of the University of Tokyo, with a Hitachi 5020E, the programs being set up in the laboratory of Prof. T. Shimanouchi.

Table 2 shows the observed isotopic shifts ($\Delta\nu_{obsd.}$ in cm^{-1}), calculated isotopic shifts ($\Delta\nu_{calcd.}$ in cm^{-1}) and the force constants for the above six compounds. For the compounds which contain a linearly coordinated NO group, the wave numbers, isotopic shifts and force constants were calculated assuming the force constant f_{12} associated with metal–(NO) stretching and N–O stretching vibration to be 0.2 mdyn/Å. For the compounds which contain an angularly coordinated NO group, both f_{12} and f_{13} were presumed to be 0.2 mydn/Å.

Detailed infrared studies on transition-metal cyano complexes have shown that the force constants associated with the C–N stretching and the metal–(CN) stretching vibrations are 0.2—0.4 mdyn/Å.[28,29] The metal–NO bonding state of the nitrosyl complex formulated as NO^+ complex are similar to the metal–CN bonding state. Hence, it is considered to be reasonable as a first approximation that f_{12} and f_{13} are presumed to be 0.2 mydn/Å.

Assignments of the skeletal vibrations between the metal and the NO group were performed by calculating potential energy distribution. The results show that definite assignments of the skeletal vibrations exclusively depend on the extent of the isotopic shifts but not on the relative positions and strength of the absorption bands. Of the two absorption bands in the region 400—650 cm^{-1} where the isotopic shifts are observed, the absorption band which caused a smaller isotopic shift was assigned to the metal-(NO) stretching vibration and another band which caused a larger isotopic shift to the metal–(NO) bending vibration. The same assignments will be also expected for other compounds examined. For *trans*-$[RuCl(NH_3)_4(NO)]Cl_2$, the 603 cm^{-1} band ($\Delta\nu_{obsd.}=17$ cm^{-1}) can be assigned to the Ru–(NO) bending vibration and the 562 cm^{-1} band ($\Delta\nu_{obsd.}=2$ cm^{-1}) to the Ru–(NO) stretching vibration. For $Co(NO)(S_2CN(CH_3)_2)_2$, the 317 cm^{-1} band ($\Delta\nu_{obsd.}=6$ cm^{-1}) may be assigned to the Co–(NO) bending vibration and the 259 cm^{-1} band ($\Delta\nu_{obsd.}=3$ cm^{-1}) to the Co–(NO) stretching vibration. For $[Co(NO)en_2](ClO_4)_2$, the 560 cm^{-1} band ($\Delta\nu_{obsd.}=10$ cm^{-1}) may be assigned to the Co–(NO) bending vibration and the 490 cm^{-1} band ($\Delta\nu_{obsd}=4$ cm^{-1}) to the Co–(NO) stretching vibration. The 544 cm^{-1} band ($\Delta\nu_{obsd}=4$ cm^{-1}) for $Fe(NO)(S_2CN(CH_3)_2)_2$ may be assigned to the Fe–(NO) stretching vibration from the value of the observed isotopic shifts. For $Ru(NO)(S_2CN(C_2H_5)_2)_3$, the isotopic shifts upon the ^{15}NO-substitution were observed but definite as-

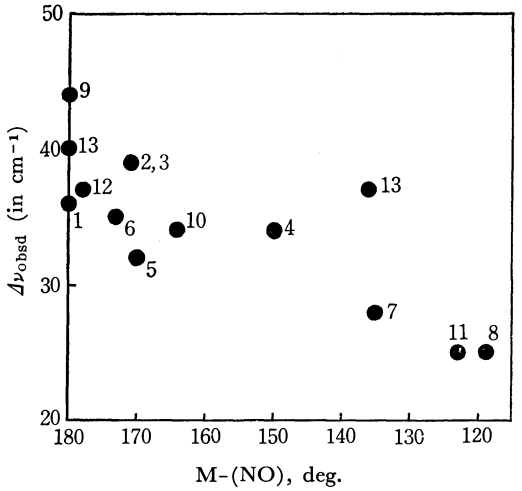

Fig. 1. Correlation of ^{15}N-isotopic shift for N-O stretching vibration with metal-(NO) bond angle.
1: *trans*-$Na_2[Ru(OH)(NO_2)_4(NO)]\cdot 2H_2O$, 2: *trans*-$K_2[Ru(OH)(NO_2)_4(NO)]$, 3: $K_2[RuCl_5(NO)]$, 4: *trans*-$[Ru(OH)(NH_3)_4NO)]Cl_2$, 5: $Ru(NO)(S_2CN(C_2H_5)_2)_3$, 6: $Fe(NO)(S_2CN(CH_3)_2)_2$, 7: $Co(NO)(S_2CN(CH_3)_2)_2$, 8: $[Co(NH_3)_5(NO)]Cl_2$, 9: $Ir(NO)(P(C_6H_5)_3)_3$, 10: $[Ir(NO)_2(P(C_6H_5)_3)_2](ClO_4)$, 11: $IrCl_2(NO)(P(C_6H_5)_3)_2$, 12: $Na_2[Fe(CN)_5(NO)]\cdot 2H_2O$(Ref. 6), 13: $[RuCl(NO)_2(P(C_6H_5)_3)_2][PF_6]$(Ref. 28)
1~11 present work

26) D. Hall and A. A. Taggart, *J. Chem. Soc.*, **1965**, 1359; D. D. Dale and D. C. Hodgkin, *ibid.*, **1965**, 1364.
27) E. S. Wilson, Jr., *J. Chem. Phys.*, **9**, 76 (1941).
28) L. H. Jones, *Coord. Chem. Rev.*, **1**, 351 (1966).
29) I. Nakagawa, *ibid.*, **4**, 423 (1969).

signments of the skeletal vibrations could not be made from the values of the observed isotopic shifts.

The correlations of the ^{15}N-isotopic shifts observed for the N–O stretching vibrations with a metal–(NO) bond angles are shown in Fig. 1. The isotopic shifts for the N–O stretching vibrations decreased with deviation of metal–(NO) bond angle from linearity.

The force constants calculated from a simple three-body model are also summarized in Table 2. The force constants of the N–O stretching vibrations are 9—15 mdyn/Å, those of the metal–(NO) stretching vibrations 4—6 mdyn/Å and those of the metal–(NO) bending vibrations 0.4—1 mdyn/Å. The force constants (f_{23}) associated with a metal–(NO) stretching and the metal–(NO) bending vibrations are 0.3—1.5 mdyn/Å. The values were found to agree with those already reported.[1,5,30-33]

Discussion

Deviation of the metal-(NO) bond angle from linearity causes a decrease in the isotopic shifts of the N–O stretching vibration. The decrease might be explained as follows; the smaller the metal-(NO) bond angle, the greater the effect on N–O stretching vibration by the skeletal vibrations between the metal and the NO group. Such a phenomenon has been reported on $[RuCl(NO)_2(P(C_6H_5)_3)_2][PF_6]$ on which an X-ray diffraction study has shown that both the linear and the bent nitrosyl groups coordinate to the ruthenium atom, the corresponding bond angles being 179.5° and 136.0°, respectively.[34] The N–O stretching vibrations of the linear and the bent NO groups are observed at 1850 and 1687 cm^{-1}, these bands shifting upon the ^{15}NO-substitution downwards by 40 and 37 cm^{-1}, respectively.[35] This shows that the bond angle significantly influences the value of the isotopic shift.

For $[Co(NH_3)_5(NO)]Cl_2$, a comparison of the observed isotopic shifts with the calculated ones showed that the NO group coordinated to the cobalt atom through the oxygen atom rather than through the nitrogen atom. However, when the bond angle deviates from 180° the criterion based on the isotopic shift becomes less useful; in the case of $[Co(NH_3)_5(NO)]Cl_2$ where Co–(NO) bond angle is 119°, it cannot be concluded whether the coordinated atom is oxygen or nitrogen (Fig. 1).

Calculation of the ^{15}NO-isotopic shifts with the use of the three-body model of the metal and the NO group is useful for assigning distinctly the skeletal vibrations between the metal and the NO group. The isotopic shift of the metal–(NO) stretching vibration is smaller than that of the metal–(NO) bending vibration independent of the metal–(NO) bond angle. This method is considered to be useful for estimating the oxidation state of NO group since the isotopic shifts of the N–O stretching vibrations for the complexes formulated as NO^+ complexes are almost equal to those calculated by assuming a linear arrangement of a metal–N–O, and are larger than those for the NO^- complexes where metal–(NO) bond angle is approximetely 120°. The three-body model can be considered to be a good approximation when the central metal atom and ligands other than the NO group are much heavier than nitrogen and oxygen. Hence, of the complexes examined, the best approximation was given by $K_2[RuCl_5(NO)]$.

The authors are indebted to Professor Ichiro Nakagawa, Tohoku University and Mr. Hiroshi Saito, Rikkyo University, for their valuable suggestions concerning calculations of normal vibrations.

The present work was supported in part by a Grant for Scientific Research from the Ministry of Education.

30) N. M. Sinitsyn and O. E. Zvyagintsev, *Russ. J. Inorg. Chem.*, **8**, 1220 (1963).
31) R. H. Mann, I. J. Hyams, and E. R. Lippincott, *J. Chem. Phys.*, **48**, 4929 (1968).
32) K. I. Petrov and V. W. Krauchenko, *Zh. Neorg. Khim.*, **14**, 2789 (1969).
33) J. Hiraishi, Ph. D. Thesis, The University of Tokyo (1965).
34) C. G. Pierpont, D. G. VanDerveer, W. Durland, and R. Eisenberg, *J. Amer. Chem. Soc.*, **92**, 4760 (1970).
35) J. P. Collman, P. Farnham, and G. Dolcetti, *ibid.*, **93**, 1788 (1971).

The Chemical Behavior of Low Valence Sulfur Compounds. VIII. The Oxidation of Sodium Thiosulfate with Ozone

Masahiro TAKIZAWA, Akitsugu OKUWAKI, and Taijiro OKABE

Department of Applied Chemistry, Faculty of Engineering, Tohoku University, Aramaki-Aoba, Sendai 980

(Received June 5, 1973)

The oxidation of sodium thiosulfate with ozone in an aqueous solution was investigated as a part of a series of studies on the chemical behavior of such low-valence sulfur compounds as thiosulfate and sulfite. The ozone oxidation was carried out by blowing a mixed gas of ozone and oxygen continuously into a 0.3—0.6 mol/l solution of sodium thiosulfate at 10—80 °C. In a neutral solution, thiosulfate is converted to sulfate, sulfite, tri- and tetrathionates, hydrogen sulfide and sulfur dioxide, and finally to sulfate, tri- and tetrathionates. The yield of the sulfate is only 40% of the total sulfur. In an alkaline solution, however, thiosulfate is oxidized to sulfite as an intermediate, and finally to sulfate.

The oxidation of sodium sulfite, and potassium salts of tri- and tetrathionate with ozone was also studied in order to elucidate its mechanism.

The oxidation of sodium thiosulfate with ozone has been studied only by Yamauchi[1] and Riesenfeld *et al.*[2] in the 1910's.

Yamauchi has reported that sodium thiosulfate oxidized to sulfate, sulfite, and elemental sulfur with ozone in a neutral solution according to Eq. (1):

$$3Na_2S_2O_3 + 2O_3 = 2Na_2SO_4 + Na_2SO_3 + 3S + 2O_2 \quad (1)$$

where the formation of sulfate and sulfite is explained as the conversion of the central sulfur atom of the thiosulfate ion. Riesenfeld has proposed that the oxidation of sodium thiosulfate proceeds according to Eqs. (2) and (3) in a neutral solution, which then becomes acidic.

$$Na_2S_2O_3 + O_3 = Na_2S_2O_6 \quad (2)$$

$$Na_2S_2O_3 + O_3 = Na_2SO_4 + SO_2 \quad (3)$$

The number of oxygen atoms consumed in one ozone molecule is three in a neutral solution, but two in an alkaline solution on the addition of sodium carbonate, although the oxidation products are the same in both neutral and alkaline solutions. Dithionate, however, can not be distinguished from other polythionates by qualitative analysis.

Thus, in the early studies there was much doubt about the identification of products. Recently, though, an investigation of the oxidation of ammonium thiosulfate with ozone in an aqueous ammonia solution by one of the present authors[3] has led to the finding that ammonium thiosulfate is oxidized to sulfate, sulfite, sulfamate, and low polythionates.

In the present study, the oxidation of sodium thiosulfate with ozone was investigated as a part of a series of studies on the chemical behavior of low valence sulfur compounds,[4] furthermore, the ozone oxidations of sulfite, tri- and tetrathionates, which are oxidation products of thiosulfate, were studied in order to elucidate the mechanism.

The results may be usefully applied to the treatment of waste water containing thiosulfate and sulfite.

Experimental

Apparatus and Procedure. The apparatus is depicted schematically in Fig. 1. One liter of 0.3—0.6 mol/l sodium thiosulfate solution was put into three-necked round-bottomed flask kept in a water bath at 10—80 °C. Mixed gas of ozone and oxygen was continuously blown into the solution at atmospheric pressure. Every half hour, 10—20 ml aliquots of the solution were withdrawn for analysis. The flow rate, as determined by the orifice meter, was 1—2.9 (mainly 2.1) N.T.P.l/min. The sodium thiosulfate solution used was neutral or alkaline on the addition of sodium hydroxide, the amount of which was equivalent to or in excess of that of the acid produced by the oxidation reaction. An ozonizer with 6 silent discharge tubes of a special construction devised by Kitahara[5] was used with some modification, the center electrode being covered with glass tube to prevent it from being oxidized by ozone.

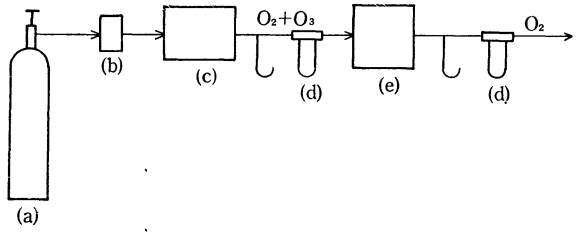

Fig. 1. Apparatus.
(a): O_2 bomb. (b): Drying tube packed with silica gel. (c): Ozonizer. (d): Orifice meter. (e): Reactor.

Sample. The potassium tri- and tetrathionates were prepared by Martin's method.[6]

Analysis. After dilution to a suitable concentration, the sample solution was analyzed for thiosulfate, sulfite, sulfate, tri-, and tetrathionates as follows:

Thiosulfate: Thiosulfate was titrated with a 0.1 N standard solution of iodine after masking sulfite with an aqueous solution of formaldehyde.

Sulfite: The total amount of thiosulfate and sulfite was determined by iodimetry after the neutralization of the sample solution.

Sulfate: After the oxidation of thiosulfate and sulfite with iodine to tetrathionate and sulfate respectively, the sulfate

1) Y. Yamauchi, *Amer. Chem. J.*, **50**, 55 (1913).
2) E. H. Riesenfeld and Th. F. Egidius, *Z. Anorg. Chem.*, **85**, 217 (1914).
3) K. Naito, M. Yoshida, M. Shieh, and T. Okabe, This Bulletin, **43**, 1365 (1970).
4) K. Naito and T. Okabe, *ibid.*, **44**, 2434 (1971).
5) K. Kitahara, *Yakugaku Zasshi*, **81**, 291 (1961).
6) F. Martin and L. Mets, *Z. Anorg. Allg. Chem.*, **127**, 83 (1923).

was determined to be barium sulfate by gravimetry.

Tri- and Tetrathionates: These polythionates were first identified by paper-chromatography[7,8] and then their quantity was determined by using the sulfide and sulfite methods.[9]

First, the sulfite was removed by the addition of 1 N strontium nitrate, a 4 N aqueous ammonia solution saturated with hydrogen sulfide was then added to the sample solution.

The solution was heated on a water bath for about 10 min, and the thiosulfate released from the following reactions was determined by iodimetry after the removal of the excess hydrogen sulfide with carbon dioxide.

$$S_3O_6^{2-} + S^{2-} = 2S_2O_3^{2-} \quad (4)$$

$$S_4O_6^{2-} + S^{2-} = 2S_2O_3^{2-} + S \quad (5)$$

A buffer solution of pH 9.5 and a 1 N sodium sulfite solution were poured into another sample solution and was kept standing for about 10 min, then, an aqueous solution of formaldehyde was added, and the thiosulfate formed by the following reaction was determined by iodimetry after acidification with 1 N acetic acid.

$$S_4O_6^{2-} + SO_3^{2-} = S_3O_6^{2-} + S_2O_3^{2-} \quad (6)$$

Ozone: A known volume of a mixed gas of ozone and oxygen was passed through a 2% potassium iodide solution. After the acidification of the solution with 6 N sulfuric acid, the iodine liberated was titrated with a 0.1 N standard solution of sodium thiosulfate.

Results and Discussion

Oxidation of Sodium Thiosulfate with Ozone. Different reactions occurred by ozone oxidation depending on the pH of the solutions, whether they were neutral or alkaline. In either solution, however, the ozone supplied was completely consumed throughout the reaction stage except in the terminating period of the reaction.

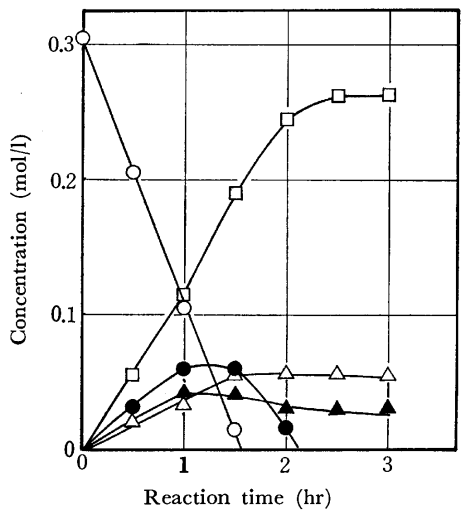

Fig. 2. Oxidation of thiosulfate in neutral solution.
Temp.: 25°C, O_3: 5.16 g/hr, O_3-O_2: 2.1 N.T.P. l/min.
-○-: $S_2O_3^{2-}$, -●-: SO_3^{2-}, -□-: SO_4^{2-},
-▲-: $S_3O_6^{2-}$, -△-: $S_4O_6^{2-}$

In a Neutral Solution. A general view of the reaction at 25 °C is shown in Fig. 2. Thiosulfate was converted into sulfate, sulfite, tri- and tetrathionate, hydrogen sulfide gas, and sulfur dioxide gas. Dithionate was not detected by means of paper-chromatography. Initially, only hydrogen sulfide evolved, and then sulfur dioxide evolved with a lowering of the pH, but their amount as sulfur was less than 5% of the total sulfur. Sulfate and tri- and tetrathionates remained after the complete consumption of the thiosulfate, the amount of sulfate sulfur reached 40% of total sulfur, and the pH of solution decreased to 1—2. The successive oxidation of polythionates proceeded slowly. Although simultaneous and consecutive reactions took place, the amount of thiosulfate decreased linearly, consuming the supplied ozone completely.

The decreasing amount of thiosulfate, R, is proportional to the amount of ozone supplied, R is given as follows:

$$R = kP_{O_3}V_0 \quad \text{(mol/min)} \quad (7)$$

$$r = R/V_0 = kP_{O_3} \quad (8)$$

P_{O_3}: Partial pressure of ozone (atm)
V_0: Flow rate of mixed gas (N.T.P. l/min)
k: Constant (mol/l·atm)

The relation between r and P_{O_3} is shown in Fig. 3.

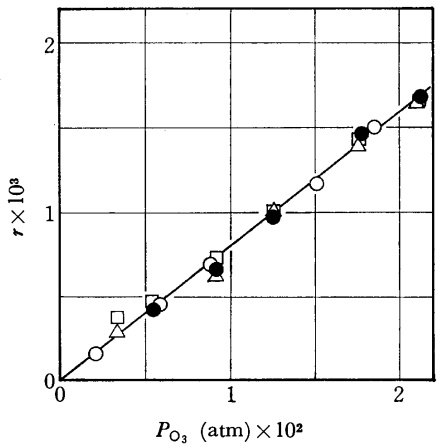

Fig. 3. Plot of r *vs.* P_{O_3}
-●-: 10°C, -○-: 25°C, -△-: 40°C, -□-: 60°C

As is expressed by the straight line which intersects at the point of origin, independently of the reaction temperature, R is shown experimentally as follows:

$$R = 0.080\,P_{O_3}V_0 \quad (10\text{—}60\,^\circ\text{C}) \quad \text{(mol/min)} \quad (9)$$

This equation does not express a stoichiometric relation between thiosulfate and ozone, but it does indicate the relation between the consumed amount of thiosulfate and the supplied amount of ozone. In spite of the perfect consumption of ozone, the reaction was accelerated a little by the addition of 10^{-3}—10^{-4} mol/l of ammonium metavanadate.

In an Alkaline Solution. As is shown in Fig. 4, only sulfite was observed as an intermediate, and thiosulfate was completely oxidized to sulfate. The amount of sulfate formed by the reaction was twice as much as that of the initial thiosulfate. Unlike as a reaction in a neutral solution, the oxidation reaction

7) F. H. Pollard, G. Nickless and R. B. Glover, *J. Chromatogr.*, **15**, 518 (1964).
8) P. A. Trudinger, *J. Bacteriol.*, **93**, 550 (1967).
9) A. Kurtenacker and E. Goldbach, *Z. Anorg. Allg. Chem.*, **166**, 177 (1927); *ibid.*, **134**, 265 (1924).

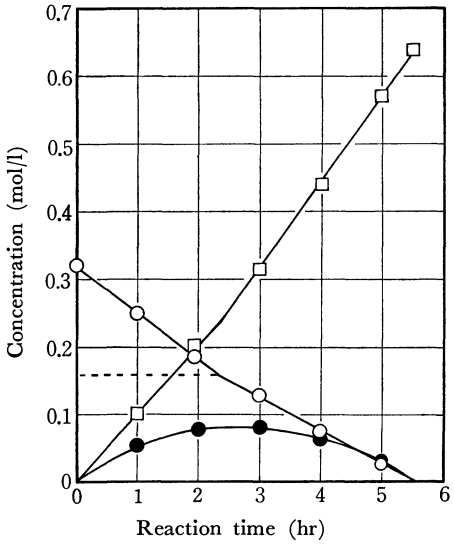

Fig. 4. Oxidation of thiosulfate in alkaline solution.
Temp.: 25°C, O_3: 5.16 g/hr, O_3-O_2: 2.1 N.T.P. l/min.
-○-: $S_2O_3^{2-}$, -●-: SO_3^{2-}, -□-: SO_4^{2-}.

in an alkaline solution was completed as soon as the thiosulfate disappeared. The oxidized amount of thiosulfate, R, decreased gradually with the reaction time, but it may be expressed approximately as follows:

$$C_0 - C_0/2 \quad R = k_1 P_{O_3} V_0 \quad \text{(mol/min)} \tag{10}$$

$$C_0/2 - 0 \quad R = k_2 P_{O_3} V_0 \quad \text{(mol/min)} \tag{11}$$

$$\log k_1 = -170/T - 0.994 \tag{12}$$

$$\log k_2 = -170/T - 1.149 \tag{13}$$

C_0: Initial thiosulfate consentration(mol/l)
T: Reaction temperature (K)
(25—80°C)

These equations are based on the assumption that the relationship between the thiosulfate concentration and the reaction time is expressed by the two straight lines crossing each other at the point indicating one-half of the initial concentration of thiosulfate. The value of R in an alkaline solution is 1/3—1/4 of that in a neutral solution.

Oxidation of Sodium Sulfite with Ozone. The ozone supplied was completely consumed under the present experimental conditions (reaction temperature, 25—60 °C, initial concentration of sodium sulfite, 0.6 mol/l, and flow rate of mixed gas of ozone and oxygen, 2.1 N.T.P-l/min), thus forming sulfate quantitatively. The relation between reaction molar ratio (Na_2SO_3/O_3) and the ozone concentration in the gas phase is shown in Fig. 5. The reaction molar ratio was calculated from Eq. (14):

Na_2SO_3/O_3 = {amount of sulfite oxidized by ozone and oxygen (mol)—amount of sulfite oxidized by oxygen(mol)}/ozone supplied (mol) (14)

The molar ratio was not constant, but gradually increased with a rise in the temperature and with a decrease in the ozone concentration. The molar ratio must be less than 3, judging from Eq. (15), but there were actually cases where it was 3 or more, as is shwon in Fig. 5.

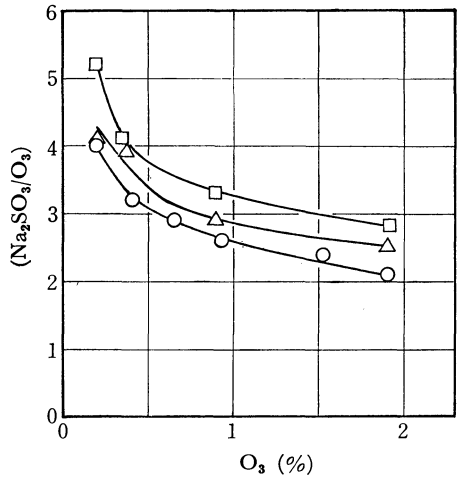

Fig. 5. Plot of (Na_2SO_3/O_3) *vs.* O_3
-○-: 25°C, -△-: 40°C, -□-: 60°C.

$$Na_2SO_3 + 1/3\, O_3 = Na_2SO_4 \tag{15}$$

From the results, it must be considered that the oxidation of sulfite with oxygen is accelerated by the presence of ozone. Under the following conditions:

Reaction temperature:	25—60	(°C)
Partial oxygen pressure P_{O_2}:	0.1—1	(atm)
Partial ozone pressure P_{O_3}:	$(0.1—2) \times 10^{-2}$	(atm)
Flow rate of mixed gas of		
O_3-O_2 or O_3-O_2-N_2	V_0: 1—2.8 (l/min at N.T.P.)	

the amount of oxidized sulfite, R, may be experimentally expressed as follows:

$$R = k P_{O_3}^{0.5} P_{O_2}^{0.5} V_0 \quad \text{(mol/min)} \tag{16}$$

$k_{25} = 0.016$ (mol/l·atm)
$k_{40} = 0.018$ (mol/l·atm)
$k_{60} = 0.020$ (mol/l·atm)

Oxidation of Potassium Tri- and Tetrathionates with Ozone. In the oxidation of these polythionates, only 16% of the trithionate and 4% of the tetrathionate were converted to sulfate after 4 hr in a neutral solution, and no intermediate was detected under the present experimental conditions (reaction temperature, 25 °C; initial tri- and tetrathionate concentration, 0.1 mol/l; ozone flow rate, 4.75 g/hr).

The rate of the reaction was so slow that most of the ozone passed freely through the solution.

The results obtained from an investigation in an alkaline solution are shown in Figs. 6 and 7. It has previously been shown that tri- and tetrathionates decompose by the following reactions in an alkaline solution.[10]

at pH 13: $2S_3O_6^{2-} + 6OH^- = S_2O_3^{2-} + 4SO_3^{2-} + 3H_2O$ (17)

at pH 11.5: $4S_4O_6^{2-} + 6OH^- = 2S_3O_6^{2-} + 5S_2O_3^{2-} + 3H_2O$ (18)

partially $2S_4O_6^{2-} + 6OH^- = 3S_2O_3^{2-} + 2SO_3^{2-} + 3H_2O$ (19)

10) K. Naito, M. Shieh and T. Okabe, This Bulletin, **43**, 1372 (1970).

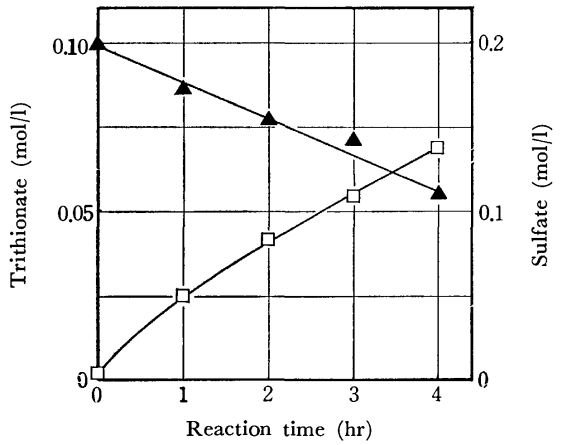

Fig. 6. Oxidation of trithionate in alkaline solution.
Temp.: 25°C, O_3: 4.75 g/hr, O_3-O_2: 2.1 N. T. P. l/min.
NaOH: 0.4 mol/l,
-▲-: $S_3O_6^{2-}$, -□-: SO_4^{2-}.

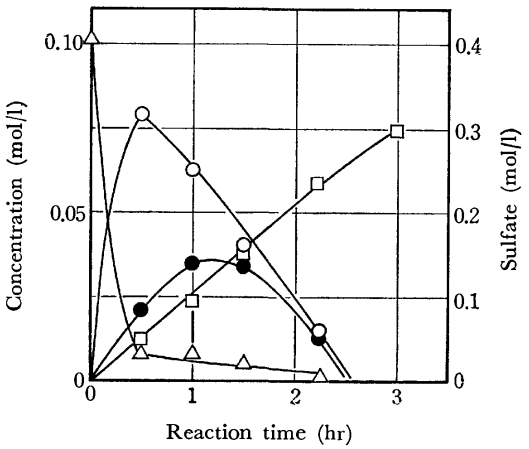

Fig. 7. Oxidation of tetrathionate in alkaline solution.
Temp.: 25°C, O_3: 4.75 g/hr, O_3-O_2: 2.1 N. T. P. l/min.
NaOH: 0.4 mol/l.
-○-: $S_2O_3^{2-}$, -●-: SO_3^{2-}, -□-: SO_4^{2-}, -△-: $S_4O_6^{2-}$.

The changes in degree of the tri- and tetrathionate concentrations in the ozone oxidation were similar to those in their decomposition reaction in an alkaline solution. Therefore, it may be considered that tri- and tetrathionates decompose initially in the manner expressed by Eqs. (17) and (18), and that the thiosulfate and sulfite formed by the decomposition are mainly oxidized by ozone.

The Mechanism of the Oxidation Reaction of Sodium Thiosulfate with Ozone. The reactions expressed by the following equations may be considered to be the oxidation reactions of sodium thiosulfate in a neutral solution.

For the formations of SO_4^{2-} and SO_3^{2-}:

$$S_2O_3^{2-} + O_3 = SO_4^{2-} + SO_2 \quad (3')$$

$$S_4O_6^{2-} + O_3 \rightarrow SO_4^{2-} \quad (20)$$

$$S_3O_6^{2-} + O_3 \rightarrow SO_4^{2-} \quad (21)$$

$$SO_3^{2-} + O_3 \rightarrow SO_4^{2-} \quad (22)$$

$$SO_3^{2-} + 1/2O_2 = SO_4^{2-} \quad (23)$$

For the formation of $S_3O_6^{2-}$:

$$S_4O_6^{2-} + SO_3^{2-} = S_3O_6^{2-} + S_2O_3^{2-} \quad (6)$$

$$S_2O_3^{2-} + SO_3^{2-} + O_3 \rightarrow S_3O_6^{2-} \quad (24)$$

For the formation of $S_4O_6^{2-}$:

$$2S_2O_3^{2-} + 1/3O_3 + H_2O = S_4O_6^{2-} + 2OH^- \quad (25)$$

$$2S_2O_3^{2-} + 1/2O_2 + H_2O \rightarrow S_4O_6^{2-} \quad (26)$$

If it is assumed that Reactions (3'), (6), (25), and (23) proceed mainly in an early stage of the ozone oxidation, the amounts of thiosulfate and ozone used in the reaction can be calculated also from the amounts of products shown in Fig. 2. The calculated values are tabulated as follows, along with values actually used.

Time range (hr)	Thiosulfate (mol)		Ozone (mol)	
	Calcd	Obsd	Calcd	Suppld
0 —0.5	0.108	0.099	0.065	0.054
0.5—1.0	0.215	0.200	0.132	0.108
1.0—1.5	0.293	0.289	0.172	0.162

The calculated values of the thiosulfate consumed are almost equal to the observed values, therefore, the oxidation of thiosulfate with ozone must proceed mainly *via* the route assumed above.

On the other hand, the amount of ozone actually consumed was less by 20% than that calculated. This discrepancy can be accounted for by the consideration that the oxidation of thiosulfate with oxygen, as expressed by Eq. (26), is induced at atmospheric pressure in the presence of ozone, because thiosulfate is oxidized with compressed oxygen to tetrathionate.[10] In view of the results of the oxidation of sulfite, tri- and tetrathionates with ozone, there is no doubt that Reactions (20), (21), and (22) proceed to some extent.

Furthermore, it is probably reasonable to consider that the formation of trithionate takes place, as is

TABLE 1. THE OZONE OXIDATION OF THIOSULFATE IN AN ALKALINE SOLUTION

Time range (hr)	$S_2O_3^{2-}$ (mol)	SO_3^{2-} (mol)	SO_4^{2-}		O_3	
			Obsd (mol)	Calcd (mol)	Calcd (mol)	Suppld (mol)
0—1	0.071	0.023	0.099	—	0.078	0.175
1—2	0.063	0.040	0.104	0.103	0.076	0.175
2—3	0.057	0.054	0.113	0.111	0.075	0.175
3—4	0.053	0.069	0.123	0.122	0.076	0.175
4—5	0.049	0.082	0.132	0.131	0.076	0.175

SO_3^{2-}: Amount of sulfite oxidized by Eq. (23). SO_4^{2-} Calcd: SO_3^{2-} + amount of sulfate formed by Eq. (3).
O_3 Calcd: Amount of ozone being required to oxidize $S_2O_3^{2-}$ to SO_4^{2-} and SO_3^{2-}.

expressed not only by Eq. (6), but also by Eq. (24), by means of the oxidation of a complex which consists of thiosulfate and sulfite, because such a complex is easily formed in an acidic solution.[11]

The evolution of hydrogen sulfide may be considered to be result from the decomposition reaction of thiosufate as follows:

$$S_2O_3^{2-} + H_2O = H_2S + SO_4^{2-} \quad (27)$$

$$2S_2O_3^{2-} + 2H^+ = H_2S + S_3O_6^{2-} \quad (28)$$

11) C. J. Battaglia and W. J. Miller, *Photogr. Sci. Eng.*, **12**, 46 (1968).

The acceleration of ammonium metavanadate may be explained by the fact that Reaction (25) or (26) is promoted by a catalytic action of ammonium metavanadate, for these reactions contribute mostly to the consumption of thiosulfate.

In an alkaline solution, the oxidation of thiosulfate must proceed mainly *via* (3′) and (15), as is shown in Table 1.

Although polythionates could not be detected in the alkaline solution, polythionates are possibly responsible for the formation of sulfite as an unstable intermediate.

BULLETIN OF THE CHEMICAL SOCIETY OF JAPAN, VOL. 46, 3789—3791 (1973)

Spectrophotometric Study on the Extraction of Magnesium(II)–8-Hydroxyquinoline-5-sulfonic Acid Chelate Anion with Zephiramine

Masao SUGAWARA and Tomihito KAMBARA

Department of Chemistry, Faculty of Science, Hokkaido University, Sapporo 060

(Received July 19, 1973)

The ion-pair of magnesium(II)–8-hydroxyquinoline-5-sulfonic acid chelate anion with zephiramine (Z^+Cl^-) was extracted into chloroform. The ternary complex has an absorption maximum at 390 nm in the organic layer. The optimum pH range for the extraction is 10.1—11.4. For the first extract, Beer's law holds for 4.6—20.6 μg of magnesium(II) in 10-ml organic layer, the molar absorptivity being 6.73×10^3 cm^{-1} mol^{-1} l. The composition of the ternary complex is estimated to be $[Mg^{2+}(QS^{2-}Z^+)_2(HQS^-Z^+)]_o$. The extraction equilibrium is given by

$$Mg^{2+} + 3[(HQS^-Z^+)]_o + 2OH^- \rightleftharpoons [Mg^{2+}(QS^{2-}Z^+)_2(HQS^-Z^+)]_o + 2H_2O$$

where QS denotes 8-hydroxyquinoline-5-sulfonic acid and o the organic phase. The equilibrium constant K is given by $\log K = 16.95 \pm 0.13$.

Although magnesium(II) forms with 8-quinolinol a compound $MgOx_2\cdot2H_2O$ slightly soluble in chloroform, Luke and Campbell[1] successfully extracted the compound by using butyl cellosolve as a supplementary solvent to chloroform. Jankowsky and Freiser[2] extracted an ion-pair such as tetra-*n*-butylammonium tris-8-quinolinolatomagnesium, $[(C_4H_9)_4N^+Mg(C_9H_6NO)_3^-]$. Extraction of a similar complex was also reported by Umland and Hoffman.[3] Fukamachi *et al.*[4] reported the extraction of magnesium-Eriochrom Black T complex with zephiramine into 1,2-dichloroethane. Nakaya and Nishimura[5] have reported the extraction of magnesium 8-quinolinolate in the presence of pyridine.

In the present study, magnesium(II)-8-hydroxyquinoline-5-sulfonic acid chelate anion was extracted into chloroform in the presence of zephiramine (tetradecyl-dimethyl-benzyl-ammonium chloride). The composition of the extracted complex as well as fundamental conditions for spectrophotometric determination of magnesium(II) were discussed.

Experimental

Reagent. *Magnesium(II) Standard Solution*: Magnesium sulfate (Wako Chemicals Co.) was dissolved in deionized water. Standardization of the solution was carried out by EDTA-titration using Eriochrom Black T as an indicator. It was found that 228.8 μg of magnesium(II) was contained per milliliter. The solution was diluted as required.

8-Hydroxyquinoline-5-sulfonic Acid Solution (H_2QS): 1.00×10^{-3} M solution was prepared by dissolving H_2QS (Wako Chemicals Co.) in water.

Zephiramine Solution (Z^+Cl^-): 5.00×10^{-3} M solution was prepared by dissolving Dotite zephiramine in water.

Ammonia Buffer Solution, pH 10.0—12.3: 0.1 M stock solutions of ammonium chloride, ammonia and sodium hydroxide were mixed in appropriate proportions.

Borate Buffer Solution, pH 9.2—10.1: Stock solution of 0.05 M borax was suitably mixed with 0.1 M sodium hydroxide.

Chloroform and other reagents were all of analytical reagent. Resin-deionized water was used.

Apparatus. All the measurements were carried out with the same apparatus as that described previously.[6]

Procedure. A definite volume of magnesium(II) standard solution (11.4 μg) was mixed with 15 ml of the H_2QS solution and 5 ml of the zephiramine solution in a 100-ml separatory funnel. pH adjustment was carried out

1) C. L. Luke and M. E. Campbell, *Anal. Chem.*, **26**, 1778 (1954).
2) S. J. Jankowsky and H. Freiser, *ibid.*, **33**, 776 (1961).
3) F. Umland and W. Hoffmann, *Anal. Chim. Acta*, **17**, 234 (1957).
4) K. Fukamachi, H. Kohara, and N. Ishibashi, *Bunseki Kagaku*, **19**, 1529 (1970).
5) S. Nakaya and M. Nishimura, *ibid.*, **22**, 733 (1973).
6) T. Kambara and M. Sugawara, This Bulletin, **46**, 500 (1973).

with 10 ml of the ammonia buffer solution and then filled up to 50 ml with water. The mixture was shaken for 5 min with 10 ml of chloroform and left for 10 min for the phases to separate. The organic phase was drained into a beaker containing anhydrous Na_2SO_4 and subjected to optical measurement. The absorbance of the extract was measured against the reagent blank obtained in the same way.

Results and Discussion

Absorption Spectra. Absorption spectra of the ternary complex in aqueous and organic phases are shown in Figs. 1 and 2, respectively. The ternary complex has an absorption maximum at 400 nm in the aqueous phase and 390 nm in the organic phase. Color of magnesium(II)–H_2QS complex was not developed at the magnesium(II) concentration used.

Effect of pH. The aqueous solution was adjusted to various pH values with the ammonia buffer solution and the extraction was carried out by the above procedure. The optimum pH range for the extraction was found to be 10.1—11.4. The chloroform extract was stable for at least 30 min. At higher pH, the color of the extract changed with a gradual increase in absorbance. Use of borate buffer solution is not desirable since the absorbance of the reagent blank is very high.

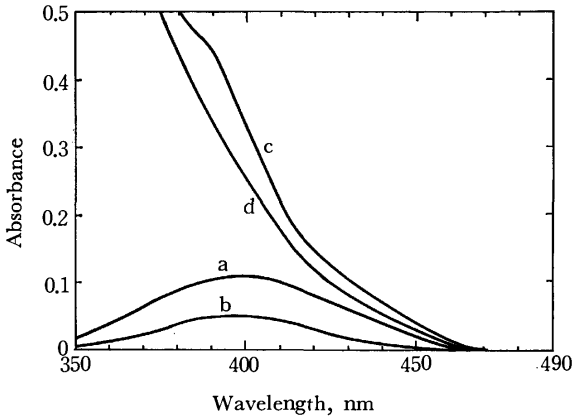

Fig. 1. Absorption spectra of Mg(II)-QS-Z complex in the aqueous solution.
Curve (a): $[Mg(II)]_w = 1.8\times10^{-5}$ M, (b): 0.94×10^{-5} M; $[QS]_w = 3.0\times10^{-4}$ M, $[Z]_w = 5.0\times10^{-4}$ M, pH 10.3,
Curve (a), (b): *vs.* reagent blank, (c): *vs.* water, (d): reagent blank *vs.* water.

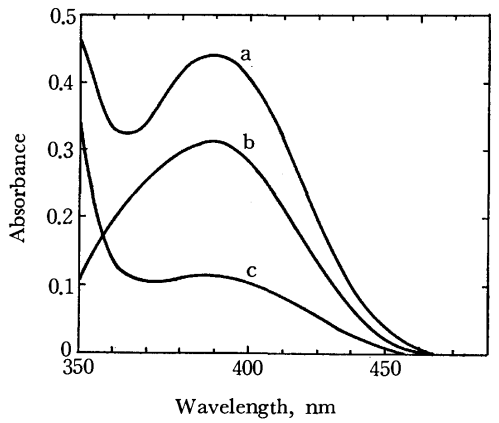

Fig. 2. Absorption spectra of Mg(II)-QS-Z complex in the organic phase after extraction.
Volume of the aqueous phase $V_w = 50$ ml, Volume of the organic phase $V_o = 10$ ml, $[Mg(II)]_w = 0.94\times10^{-5}$ M, $[QS]_w = 3.0\times10^{-4}$ M, $[Z]_w = 5.0\times10^{-4}$ M, pH 10.3,
Curve (a): *vs.* $CHCl_3$, (b): *vs.* reagent blank, (c): reagent blank *vs.* $CHCl_3$.

Effect of H_2QS and Zephiramine Concentration. Varying amounts of reagents were added to the aqueous solution buffered to pH 10.6 and the solution was shaken with chloroform as above. The constant and maximum absorbance of the extract was obtained with a concentration ratio higher than 10-fold of H_2QS and 20-fold of zephiramine to magnesium(II).

Effect of Shaking Time. Shaking time was varied from 2 min to 15 min. The absorbance of the extract was found to decrease when shaking was continued for longer than 10 min. 5 minutes were found to be the desired time for each case.

Extractability and Molar Absorptivity. 25 ml of aqueous solution containing 11.4 μg of magnesium(II) and the reagents of appropriate concentrations was shaken with 10 ml of chloroform. Extraction was repeated with 5 ml of chloroform for the remaining aqueous phase after the separation of the extract. Extractability of magnesium(II) was calculated from absorbances of the extracts. It was found that 98.7% of magnesium(II) was extracted in a single extraction. Molar absorptivity of the ternary complex was 6.73×10^3 cm^{-1} mol^{-1} l, which is higher than the value obtained by Luke and Campbell's method[1] (5600), or that by Nakaya and Nishimura's method(4420),[5] but lower than that by Jankowsky and Freiser's method (7080).[2]

Calibration Curve. Varying amounts of magnesium(II) were extracted. It was found that Beer's law holds for the first extract, 4.6—20.6 μg of magnesium(II), Sandell's sensitivity for the absorbance of 0.001 being 0.0036 $\mu g\ cm^{-2}$.

Interference by Calcium Ion. Various amounts of calcium(II) were added to the aqueous solution containing magnesium(II) and the solution was treated by the above. The results are given in Table 1. When the amount of calcium(II) became about 5-fold of magnesium(II), a larger error was observed.

Composition of the Ternary Complex. The continuous variation method for three-component system[6] was used to determine the composition of the ternary complex. Maximum absorbance of the extract was obtained at the mole ratio of Mg(II) : H_2QS : zephiramine = 1 : 3 : 3 (Fig. 3). The composition of the ternary complex was therefore estimated to be $[Mg^{2+}\text{-}(QS^{2-}Z^+)_2(HQS^-Z^+)]_o$.

Equilibrium Constant. The continuous variation method applied to the system of H_2QS-zephiramine indicates that an ion-pair of $[HQS^-Z^+]_o$ was extracted from the ammonia buffer solution (pH 10.2). Thus extraction equilibrium of magnesium(II) is given by

$$Mg^{2+} + 3\,[(HQS^-Z^+)]_o + 2\,OH^- \rightleftharpoons [Mg^{2+}(QS^{2-}Z^+)_2(HQS^-Z^+)]_o + 2\,H_2O \quad (1)$$

A 50-ml portion of aqueous solution, in which the initial concentrations of magnesium(II), H_2QS and

Table 1. Determination of magnesium(II) in the presence of calcium(II)[a]

Magnesium(II) taken (μg)	Calcium(II)[b] added (μg)	Magnesium(II) found (μg)	Recovery (%)	Relative standard deviation (%)	Comparison[c] of means
11.4	none	11.6	101.8	2.2	
	29.5	11.4	100	0.88	A
	59.0	10.5	92.1	4.8	B
6.87	none	6.67	97.0	10	A
	7.40	7.10	103.3	5.9	A
	14.8	7.20	104.8	8.8	A

a) Each result is the average of three separate analyses. b) Added as nitrate. c) A: No significant difference. B: A significant difference. Significant level: $\alpha=0.05$.

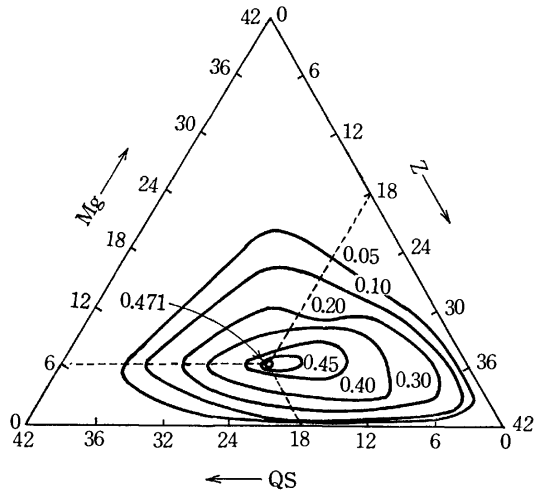

Fig. 3. Continuous variation method applied to the system of Mg(II)-QS-Z complex in the organic phase.
$V_w=50$ ml, $V_o=10$ ml, pH 10.4, $[Mg(II)]_w+[QS]_w+[Z]_w=4.2\times10^{-4}$ M, 390 nm *vs.* reagent blank,
Numerals show the absorbance of organic phase.

zephiramine are $*C$ and $3*C$, respectively, was equilibrated with 10 ml of chloroform. The absorbance of the extract was measured against the reagent blank. Concentration of the ternary complex in the organic phase was calculated from the molar absorptivity. The equilibrium constant of Eq. (1) is given by

$$K=\frac{C_T}{\left[*C-\frac{10}{50}C_T\right]\left[\frac{50}{10}\times3*C-3C_T\right]_o^3\left[OH^-\right]^2} \quad (2)$$

The results obtained with various concentrations of *C are given in Table 2. The logarithm of the equilibrium constant is $\log K=16.95\pm0.13$.

Table 2. Equilibrium constant[a] for the extraction of Mg(II)-QS-Z complex shown by Eqs. (1)—(2)

$*C$[b] (M)	Absorbance	C_T[c] (M)	pH	$\log K$
3.0×10^{-5}	0.065	9.66×10^{-6}	10.4	16.95
6.0×10^{-5}	0.461	6.85×10^{-5}	10.4	17.00
9.0×10^{-5}	0.908	1.35×10^{-4}	10.3	16.90

a) Ionic Strength $\mu=0.03$, Temp. 21.0 °C, Molar Absorptivity $\varepsilon=6.73\times10^3$ cm^{-1} mol^{-1} l. b) Initial concn. of Mg^{2+} in 50-ml aqueous layer, $3*C$ = Initial concn. of H_2QS and zephiramine in 50-ml aqueous layer. c) Final concn. of Mg(II)-QS-Z complex in 10-ml chloroform extract.

Polarographic Behavior of 9-Nitroanthracene and 9,10-Dinitroanthracene in Dimethylformamide

Toyokichi KITAGAWA and Akio ICHIMURA

Department of Chemistry, Faculty of Science, Osaka City University, Sugimoto-cho, Sumiyoshi-ku, Osaka 558

(Received February 28, 1973)

The polarographic behavior of 9-nitroanthracene and 9,10-dinitroanthracene has been studied in dimethylformamide. 9-Nitroanthracene shows consecutive two one-electron diffusion-controlled reduction waves followed by fast chemical reactions. 9,10-Dinitroanthracene, however, shows only one reversible two-electron diffusion-controlled wave. The effect of the supporting electrolyte cation on these reduction waves was also investigated. In alkali metal or alkaline earth metal perchlorate as a supporting electrolyte, the half-wave potentials shift to the anodic side. The relationship between the half-wave potential and the ionic potential of the cation was discussed.

A number of electrochemical and electron paramagnetic resonance studies of nitro compounds have been reported. The relationship between the structure of substituted nitrobenzene and its electrode kinetic parameter and its nitrogen hyperfine coupling constant was investigated in acetonitrile[1] and in dimethylformamide(DMF).[2,3] It was revealed that the rate constant of anion radical formation increases with the increase in resonance between the nitro groups and the remainder related to the nitrogen hyperfine coupling constant.

Recently, the ion association of radical anion or dianion produced by the reduction of organic compounds with metal cations in aprotic solvent has been investigated electrochemically for nitrobenzenes,[4,5] *p*-chloronitrobenzene,[6] quinones[7] and naphthoquinones.[8] Metal cations interact with anions but tetraalkylammonium ions are free from anions.

In this paper, we report on the reduction process of 9-nitroanthracene and 9,10-dinitroanthracene in DMF containing tetraethylammonium perchlorate (TEAP) as a supporting electrolyte and the effect of the supporting electrolyte cation on these reduction waves in the same solvent.

Experimental

DC and AC polarograms were recorded with a Yanagimoto polarograph P8 with a potentiostat. Cyclic voltammograms were recorded with a Riken Denshi F-32 X-Y recorder at a lower sweep rate and a Matsushita VP-546V oscilloscope with a Kikusui 455 function generator at a higher sweep rate. Capillary characteristics at 0 V *vs.* SCE in DMF containing 0.1 M TEAP were $m=1.52$ mg/s and $t=5.06$ s at $h=45$ cm. The area of the platinum disc electrode was calculated by chronopotentiometry for potassium ferrocyanide in 1.5 M potassium chloride and found to be 0.0665 cm^2. The reference electrode was aqueous SCE with a TEAP-DMF-methylcellulose salt bridge. All polarographic measurements were carried out at 25±0.5 °C in a dry box under a nitrogen atmosphere.

9-Nitroanthracene and 9,10-dinitroanthracene were supplied by Dr. R. Nakashima. DMF was dried over molecular sieve 3A and then distilled under reduced pressure. The content of water in DMF was found to be less than 0.01% by a gas-chromatographic method with a Porapak Q column. TEAP was prepared by neutralizing 10% tetraethylammonium hydroxide solution with 60% perchloric acid. The salt formed was recrystallized several times from water and dried *in vacuo* at 60 °C for 24 hr. Other perchlorates were dried *in vacuo* at 100 °C for 24 hr.

Results and Discussion

Polarographic Behavior of 9-Nitroanthracene and 9,10-Dinitroanthracene. The DC polarogram of 9-nitroanthracene in DMF containing 0.1 M TEAP shows two reduction waves. Its polarographic data are summarized in Table 1. The limiting current of the first wave is proportional to the concentration of 9-nitroanthracene in the range 2×10^{-4}—8×10^{-4} M, but the maximum wave appears at a concentration greater than 8×10^{-4} M. Both reduction waves are considered to be diffusion-controlled from the dependence of their wave height on the mercury column height and the current-time curve during the life of a mercury drop at the potential giving the limiting current. Comparing the diffusion current constant I and the chronoamperometric value $i\cdot t^{1/2}/C^*$, with those of *m*-nitrotoluene which is known to be a diffusion-controlled reversible one-electron process,[3] the reduction process of 9-nitroanthracene is found to be a consecutive two one-electron reduction process. In an AC polarogram under the same conditions, two waves corresponding to the waves in a DC polarogram are observed. The results are summarized in Table 1. We see that the summit potential of these waves is more cathodic than the half-wave potential of the corresponding DC polarographic reduction waves, the height of the more cathodic wave being very small. The irreversibility will be discussed in comparison with the case of 9,10-dinitroanthracene. The cyclic voltammetric behavior at a platinum disc electrode is shown in Fig. 1. Two reduction waves whose peaks correspond to the half-wave potential in the DC polarogram appear. Almost the same voltam-

1) D. H. Geske, J. L. Ragle, M. A. Bambenek, and A. L. Balch, *J. Amer. Chem. Soc.*, **86**, 987 (1964).
2) W. Kemula and R. Sioda, *J. Electroanal. Chem.*, **7**, 233 (1964)
3) M. E. Peover and J. S. Powell, *ibid.*, **20**, 427 (1969).
4) L. Holleck and D. Becher, *ibid.*, **4**, 321 (1962).
5) T. M. Krygowski, M. Stencel, and Z. Galus, *ibid.*, **39**, 395 (1972).
6) T. Kitagawa, T. Layloff, and R. N. Adams, *Anal. Chem.*, **36**, 925 (1964).
7) M. E. Peover and J. D. Davies, *J. Electroanal. Chem.*, **6**, 46 (1963).
8) T. Fujinaga, K. Izutsu, and T. Nomura, *ibid.*, **29**, 203 (1971).

Table 1. Summary of polarographic data in DMF containing 0.1 M TEAP

	9-Nitroanthracene		9,10-Dinitroanthracene	*m*-Nitrotoluene
	1st	2nd		
DC polarography				
$I_d/\mu A \cdot mg^{-2/3} \cdot s^{1/2} \cdot mM^{-1}$	1.40	1.15	2.65	2.10
$-E_{1/2}$/V *vs.* SCE	0.969	1.49	0.545	1.14
log plot slope/mV	44[a]	70[a]	33	56
AC polarography				
$E_{1/2}-E_s$/mV	50	40	17	10
$i_s/i_d \cdot \sqrt{t_d} \cdot n/\Omega^{-1}A^{-1} \cdot s^{1/2}$	38	17	130	177
$\Delta E_{s/2}$/mV	120	110	67	90
Chronoamperometry				
$i \cdot t^{1/2}/C^*/\mu A \cdot s^{1/2} \cdot mM^{-1}$	11.3	19.7	18.3	13.5

a) Nonlinear, $E_{1/4}-E_{3/4}$ value

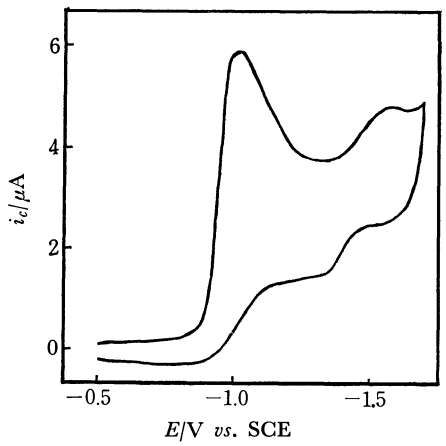

Fig. 1. Cyclic voltammogram of 0.665 mM 9-nitroanthracene at platinum disc electrode in DMF containing 0.1 M TEAP. Sweep rate: 30.3 mV/s.

mogram was obtained at a hanging mercury drop electrode. The potential difference between the cathodic peak potential and its half-peak potential for the first wave at a sweep rate of 30.3 mV/s is 60 mV which is fairly consistent with that for the reversible one-electron process[9] although the second wave shows an ill-defined curve. After reversal of the potential sweep at −1.7 V, no distinct waves corresponding to the re-oxidation of the products of the two cathodic processes appear. The first and second reduction products considered to be an anion radical and a dianion, respectively, might decompose by the following fast chemical reactions.

DC and AC polarographic and chronoamperometric results of 9,10-dinitroanthracene in DMF containing 0.1 M TEAP are also summarized in Table 1. Although most nitro aromatics show the two-step reduction process, only a single reduction wave is obtained for 9,10-dinitroanthracene. The half-wave potential is more anodic than that of the first wave for 9-nitroanthracene presumably because of the increase in coplanarity of nitro group and anthracene plane. The plot of $\log (i/(i_d-i))$ against potential E gives a straight line with a slope of 33 mV, and the diffusion current constant and the chronoamperometric value are 1.3 times as large as that of *m*-nitrotoluene. Hence it appears that the reduction of 9,10-dinitroanthracene is a diffusion-controlled two-electron process, giving a dianion. The AC polarographic summit potential of the reduction wave is slightly more cathodic than the half-wave potential of the corresponding DC polarographic step. The AC wave is very high, its value of $i_s/i_d \cdot \sqrt{t_d} \cdot n$ (where $n=2$) being near that *m*-nitrotoluene which shows a reversible reduction process. In the cyclic voltammogram with a hanging mercury drop electrode at a sweep rate of 30.3 mV/s under the same conditions as above, the peak potential for the reduction is −0.560 V, the difference between the peak potential and the half-peak potential being 34 mV, which is close to the theoretical value for a two-electron transfer process.[9] The relationship between the cathodic peak current and the sweep rate, i_p *vs.* $v^{1/2}$, gives a straight line, the ratio of the cathodic to the anodic peak current being approximately 1.0 in a wide range of the sweep rate. In the case of the platinum disc electrode, the separation of the cathodic peak potential from the anodic peak potential is 147 mV at a sweep rate of 30.3 mV/s. This indicates that the electrode process of 9,10-dinitroanthracene at the platinum disc electrode is less reversible.

The electrode reaction of 9,10-dinitroanthracene is much more reversible than that of 9-nitroanthracene. Investigations of the crystal structure of 9,10-dinitroanthracene and 9-nitroanthracene show that the nitro groups are tilted 64°[10] and 85°,[11] respectively, out of the plane of the anthracene nucleus. The structures cause the decrease in resonance between the nitro groups and the aromatic π-electron. Thus, it can be said that the rate of charge transfer for 9,10-dinitroanthracene is faster than that for 9-nitroanthracene, after those which Peover and Powell developed using the Marcus theory.[3]

Many dinitro compounds have been investigated electrochemically. Most of them show two one-electron reduction process in aprotic solvent with a tetraalkylammonium salt as a supporting electrolyte. A

9) R. S. Nicholson and I. Shain, *Anal. Chem.*, **36**, 706 (1964).

10) J. Trotter, *Acta Crystallogr.*, **12**, 232 (1959).

11) J. Trotter, *ibid.*, **12**, 237 (1959).

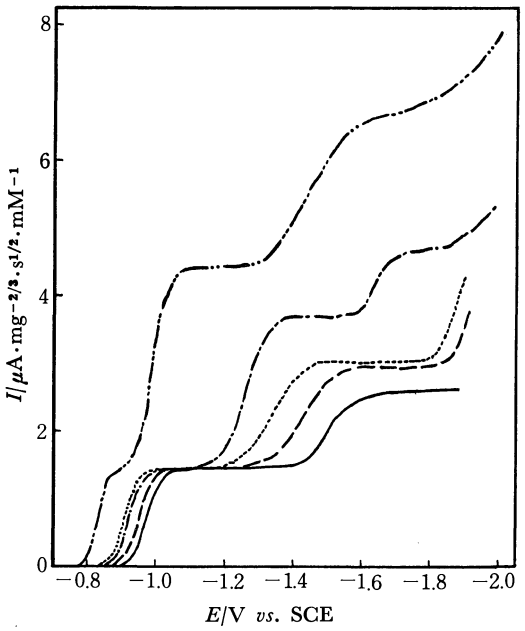

Fig. 2. DC polarograms of 9-nitroanthracene in DMF. Supporting electrolyte: 0.1 M TEAP (——), 0.1 M $KClO_4$ (----), 0.1 M $NaClO_4$ (·····), 0.1 M $LiClO_4$ (—·—), 0.05 M $Mg(ClO_4)_2$ (—··—).

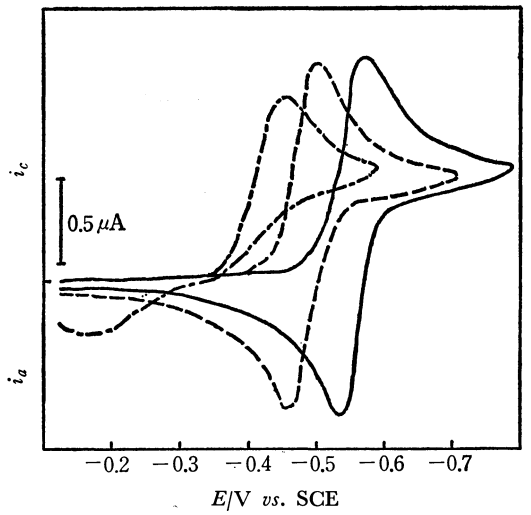

Fig. 3. Cyclic voltammograms of 0.4 mM 9, 10-dinitroanthracene at a hanging mercury drop electrode in DMF. Sweep rate: 30.3 mV/s. Supporting electrolyte: 0.1 M TEAP (——), 0.1 M $NaClO_4$ (----), 0.05 M $Mg(ClO_4)_2$ (—·—).

few dinitro compounds show only a single two-electron reduction process.[1] 9,10-Dinitroanthracene is shown to be the latter example.

Effect of the Supporting Electrolyte on the Reduction Process of 9-Nitroanthracene and 9,10-Dinitroanthracene. DC polarographic waves of 9-nitroanthracene in DMF containing 0.1 M alkali metal perchlorate or 0.05 M magnesium perchlorate are shown in Fig. 2. In 0.1 M potassium or 0.1 M sodium perchlorate, both the half-wave potential and the wave height of the first one-electron reduction process are similar to those in 0.1 M TEAP. The second wave, however, shows an anodic shift of the half-wave potential and an increase in wave height. On the other hand, in 0.1 M lithium or 0.05 M magnesium perchlorate the polarographic behavior differs from that in potassium and sodium salts. The first and the second waves shift to the anodic side, the second wave height increasing particularly in magnesium perchlorate. A new third wave appears in more cathodic potential. The value of $i_s/i_d \cdot \sqrt{t_d} \cdot n$ in 0.1 M perchlorate solution (0.05 M for magnesium perchlorate), showing the reversibility of the charge transfer, decreases in the following order for the cation of the supporting electrolyte: $Et_4N^+ > K^+ > Na^+ > Li^+ > Mg^{2+}$. This coincides with the reverse order for the anodic shift of the half-wave potential.

The effect of metal cation on the polarographic wave of 9,10-dinitroanthracene has also been examined in a similar manner in the case of 9-nitroanthracene. Cyclic voltammograms in various supporting electrolyte are shown in Fig. 3. In 0.1 M potassium, sodium, or lithium perchlorate, the half-wave potential shifts to the anodic but the DC wave height and the reversibility (AC wave height, and peak separation in cyclic voltammetry) remain unchanged in the presence of these metal cations. In 0.05 M magnesium perchlorate, however, the half-wave potential shifts to the more anodic, the AC wave height being about one third of the case of TEAP. The cyclic voltammetric peak current also decreases and the peak separation increases, which indicates the process to be less reversible.

The half-wave potential changes with cations of the supporting electrolytes. The relationship between the half-wave potential of nitroanthracenes and the ionic potential of the cation $\phi(\phi = z/r$, z; charge number, r; crystallographic radius) is plotted in Fig. 4. This gives three straight lines showing that the anodic shift of the half-wave potential increases with

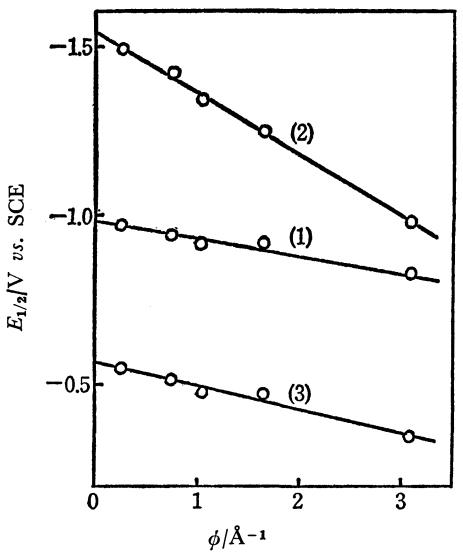

Fig. 4. Relationship between $E_{1/2}$ in 0.1 M perchlorate DMF solution and the ionic potential of the supporting electrolyte cation. From left to right, Et_4N^+, K^+, Na^+, Li^+, Mg^{2+}. 1st (1) and 2nd (2) wave of 9-nitroanthracene and 9, 10-dinitroanthracene (3).

the ionic potential. From the results by Krygowski *et al.*,[12] the relationship can be elucidated from the consideration that the reduction product, which may be radical anion and dianion for 9-nitroanthracene and dianion for 9,10-dinitroanthracene, forms ion pair with the metal cation of supporting electrolyte.

12) T. M. Krygowski, M. Lipsztajn, and Z. Galus, *J. Electroanal. Chem.*, **42**, 261 (1973).

BULLETIN OF THE CHEMICAL SOCIETY OF JAPAN, VOL. 46, 3795—3799 (1973)

Studies of Nitrogen-Phosphorus Compounds. XXV.[1] The Synthesis of Guanidium Condensed Phosphates

Etsuro KOBAYASHI

National Chemical Laboratory for Industry, Hon-machi, Shibuya-ku, Tokyo 151

(Received April 13, 1973)

In order to develop fireproof materials, an attempt was made to prepare guanidium condensed phosphates ($(H_5CN_3)_n \cdot H_{n+2}P_nO_{3n+1}$, $n=1$—10) by means of a reaction between dicyandiamide ($H_4C_2N_4$) and ammonium dihydrogen phosphate ($NH_4H_2PO_4$) in an autoclave; then the conditions of the synthesis were investigated, and the components of the product were also identified. In the synthesis of gaunidium salt by means of a reaction between dicyandiamide and ammonium salt, generally only ammonium salts of strong acid have been used; also, high yields of guanidium salt could not be obtained with the $(NH_4)_2HPO_4$ used previously. In the present study, a mixture of 1 mol of $H_4C_2N_4$ and 2 mol of $NH_4H_2PO_4$ was heated in an autoclave at 130—300 °C; 70—80% of the dicyandiamide was then converted into guanidium salt under the most suitable conditions. The majority of the product is soluble in water (the insoluble part is less than 3.5% at 150—220 °C), and the solution is almost neutral. The components of the soluble part were 25—26% N and 20—24% P, the mole ratio of N to P being 2.8—2.5; this ratio decreased with an increase in the reaction temperature. On the other hand, the phosphates in the product consist of ortho-, pyro-, tri-, and middlepoly phosphates ($n=4$—10). The guanidium condensed phosphates thus obtained can be utilized as useful flame retarders for paper and wood, as guanidium orthophosphate can be.

Among the derivatives of calcium cyanamide, dicyandiamide, guanylurea, guanidine, and melamine are useful industrial materials. Most of these compounds can readily be obtained from dicyandiamide, as is shown in Fig. 1. The guanidium salts have been formed by reaction fusing a mixture of dicyandiamide and the salt of a strong acid, such as ammonium nitrate or ammonium chloride. An attempt has already been made to prepare guanidium phosphate by means of a reaction between dicyandiamide and diammonium hydrogen phosphate in a sealed tube,[2] with water as the medium, however, a high yield of guanidium phosphate cannot be expected because of the slow reaction rate and the secondary reaction. Therefore, this method has not been employed as an economical process for manufacturing guanidium phosphate. Recently, however, monoguanidium and diguanidium phosphates, which are prepared by the neutralization of guanidium carbonate with phosphoric acid or by a double decomposition between guanidium chloride and sodium phosphate, have been recognized as fireproof materials. As guanidium orthophosphates, a certain derivative of calcium cyanamide and guanidium condensed phosphates may also be used as fireproof materials.

The present author has previously investigated the preparation of ammonium condensed phosphates by the thermal dehydration of $NH_4H_2PO_4$[3] and the

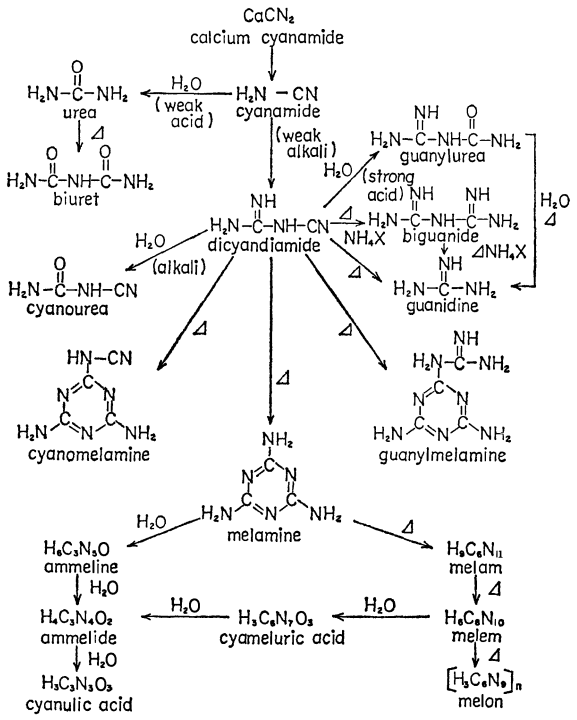

Fig. 1. The derivatives of lime nitrogen.

1) a) The article was presented at the 29th Annual Meeting of the Chemical Society of Japan, Hiroshima, October, 1973.
b) Part XXIV of this series: E. Kobayashi, *Nippon Kagaku Kaishi*, **1973**, 1437.

2) K. Sugino, *Nippon Kagaku Zasshi*, **60**, 267 (1937).

3) E. Kobayashi, *Kogyo Kagaku Zasshi*, **66**, 581 (1963); *Reports of the Government Chemical Industrial Research Institute, Tokyo*, **59**, **516** (1964).

reaction between $NH_4H_2PO_4$, $(NH_2)_2CO$, and H_2O.[4] In the present work, a mixture of 1 mol of dicyandiamide and 2 mols of ammonium dihydrogen phosphate is heated in an autoclave. From the analysis of the resulting products, it is found that most of the orthophosphate is converted into condensed phosphates, and also that 70—80% of the dicyandiamide used is converted into guanidine under the most suitable conditions. In order to ascertain the mechanism of this reaction, the thermal decomposition of monoguanidium phosphate itself is also examined. In this paper, an experimental study of the preparation of guanidium condensed phosphates will also be described.

Experimental

Synthesis. Heat Treatment of Monoguanidium Phosphate: Monoguanidium phosphate was prepared by the neutralization of guanidium carbonate with phosphoric acid. Found: N, 26.7; P, 19.5%. Calcd for $CN_3H_5 \cdot H_3PO_4$: N, 26.7; P, 19.74%. A 20-g portion of this phosphate is placed in a 100-ml test tube; the vessel is then immersed in an oil bath regulated at a proper temperature. The resulting melted products are sampled at proper intervals, and their weight loss on heating and the components are estimated.

Reaction between Dicyandiamide and Ammonium Dihydrogen Phosphate: A mixture of 1 mol of dicyandiamide ($H_4C_2N_4$) and 2 mol of ammonium dihydrogen phosphate ($NH_4H_2PO_4$) was employed as the starting material. A 5-g portion of the mixture was placed in a 100-ml test tube; the vessel was then immersed in an oil bath regulated at a proper temperature for 60 min. After the reaction product had swollen and solidified, it was collected as a powder by raking.

Analysis. A sample solution for analysis was prepared in the following way. A 1.25-g portion of the heating product of $H_5CN_3 \cdot H_3PO_4$ was weighed exactly and dissolved in water, and the volume of the solution was adjusted to 250 ml. A 2.00-g portion of the reaction product between $H_4C_2N_4$ and $NH_4H_2PO_4$ was also weighed exactly, a 50-ml portion of water was added, and the mixture was stirred for 2 hr. The resulting insoluble part was separated from the filtrate, dried for 60 min at 110 °C, and then weighed, while the volume of the filtrate was adjusted to 100 ml.

The phosphorus content was determined gravimetrically as magnesium pyrophosphate. The total nitrogen content was determined by Kjeldahl's method.

In the separation and determination of the condensed phosphates, we used ion-exchange chromatography,[5] the procedures being those of the previously-reported successive elution (see Fig. 5 I, II) and gradient elution (see Fig. 5 III), and paper chromatography using an acid solvent.[6]

In the separation of non-cyclic cyanamide derivatives, we used Takimoto and Koeda's[7] paper chromatography. The non-cyclic cyanamide derivatives were also analysed by Takimoto and Yao's[8] ion-exchange chromatography. The results of the determination of guanidine as the main product accorded with those of Kurabayashi and Yanagiya's[9] method.

The differential thermal analysis (DTA) and thermogravimetric measurements (TGA) were performed simultaneously under a nitrogen atmosphere and at a heating rate of 5 °C/min, using a Rigaku-Denki model DC-Cl-S thermal analyser.

Results and Discussion

Change in Monoguanidium Phosphate upon Heating. It is supposed that guanidium phosphate, which may be formed by the reaction of dicyandiamide and ammonium phosphate, is converted into the condensed phosphates at a high temperature, and that it finally decomposes into condensed phosphoric acids and ammonia. Therefore, the thermal decomposition of guanidium phosphate was examined.

Thermal Analysis. The DTA and TGA curves for diguanidium phosphate and monoguanidium phosphate are shown in Fig. 2. Diguanidium phosphate begins to decompose at about 235 °C, and a remarkable weight loss is observed. From the diagrams, it is supposed that guanidine radicals are decomposed above 300 °C. Monoguanidium phosphate begins to melt at 110 °C; consequently, an endothermic peak appears. A weight loss of 2—5% is observed at 110—250 °C. It is considered that, in this temperature range, the condensation occurs as a result of the thermal dehydration of monoguanidium phosphate,

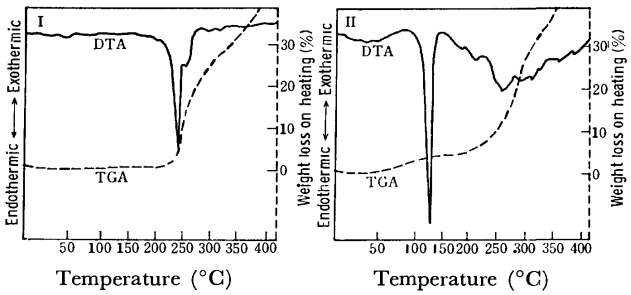

Fig. 2. DTA and TGA curves for guanidium phosphates.
I: diguanidium phosphate
II: monoguanidium phosphate
Sample: 100 mg, Heating rate: 5°C/min, Current gas: Nitrogen 0.3 l/min.

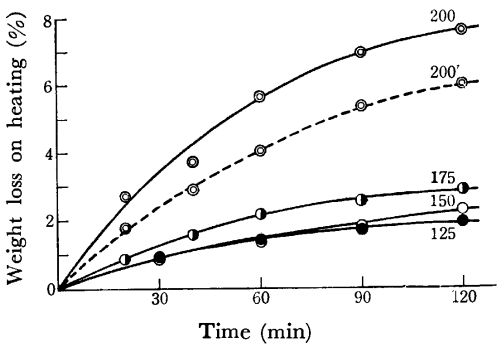

Fig. 3. Weight loss of monoguanidium phosphate by Heating.
Sample: 20 g.
Condition: Molten salt is stirred under atmosphere, but is not stirred in an example shown by dotted line.

4) E. Kobayashi, *Kogyo Kagaku Zasshi*, **69**, 2065 (1966); *Reports of the Government Chemical Industrial Research Institute, Tokyo*, **63**, 263 (1968).
5) E. Kobayashi, *Nippon Kagaku Zasshi*, **85**, 317 (1964).
6) E. Karl -Kroupa, *Anal. Chem*, **28**, 1091 (1956).
7) M. Takimoto and I. Koeda, *Kogyo Kagaku Zasshi*, **63**, 797 (1960).
8) M. Takimoto and T. Yao, *ibid.*, **63**, 1936 (1960); *ibid.*, **63**, 1941 (1960).
9) M. Kurabayashi and K. Yanagiya, *Reports of the Government Chemical Industrial Research Institute, Tokyo*, **51**, 39 (1956).

Table 1. Dehydration products of guanidium dihydrogen orthophosphate

No.	Reaction conditions			Analysis							
	$H_5CN_3 \cdot H_3PO_4$ (g)	Temp. (°C)	Time (min)	N (%)	P (%)	N/P Atomic ratio	pH	Ortho- (%)	Pyro- (%)	Tri- (%)	Middle poly (%)
1	20	125	120	26.4	19.8	2.93	—	69	31	0	0
2	20	150	120	26.5	19.7	2.97	5.03	50	50	0	0
3	20	175	120	26.7	19.7	3.00	5.55	44	51	5	0
4	20	200	90	26.8	19.9	2.97	6.12	34	52	13	1
5—1	20	225	20	27.9	20.5	3.02	5.83	51	33	16	0
5—2	20	225	40	27.6	21.1	2.89	5.99	48	19	20	13
5—3	20	225	60	27.2	21.5	2.80	5.90	25	29	19	27
5—4	20	225	90	27.1	22.1	2.72	5.90	21	23	18	38
5—5	20	225	120	26.9	22.7	2.62	5.80	18	18	19	45

and that the guanidine radical does not decompose very much.

Then, the weight changes in monoguanidium phosphate at various temperatures were measured. The results are shown in Fig. 3. Monoguanidium phosphate melts when heated; the rate of dehydration increases with the rise in the temperature, but it does not change very much at 125, 150, and 175 °C. The weight loss is 5.5% for 1 hr and 7.5% for 2 hr at 200 °C. In this case, the rate of thermal dehydration is affected by the considerable viscosity of the salt, so the melting salt was stirred while being heated.

Components of Products. The heating conditions of monoguanidium phosphate and the results of the analysis of the products are summarized in Table 1.

The contents of phosphorus and nitrogen in the product are not very different at 125—250 °C. In this temperature range, the atomic ratio of N to P in the products is roughly analogous to that (3 : 1) in the monoguanidium phosphate used as the starting material. The odor of ammonia is remarkable upon the thermal decomposition of the guanidium radical above 200 °C. It can be supposed that other cyanamide compounds are also formed upon the decomposition of guanidium phosphate. Therefore, a paper chromatogram of the product was compared with those of various cyanamide derivatives used as standard materials; they are shown in Fig. 4.

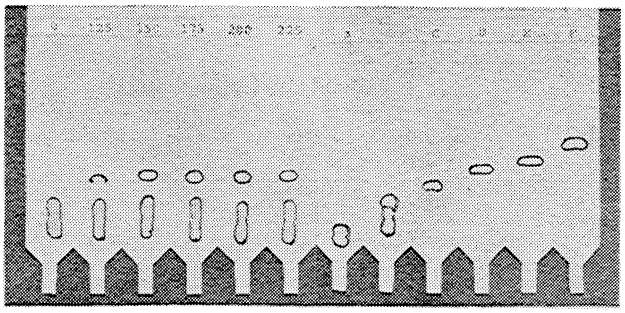

Fig. 4. Paper chromatogram for various cyanamide derivatives and heating products of monoguanidium dihydrogen phosphate.
Numerals in the photograph indicate heating temperatures (°C).
Symbols (A-F) indicate species of cyanamide compound, A: biguanidium sulfate, B: monoguanidium dihydrogen phosphate, C: guanylurea, D: urea, E: biuret, F: dicyandiamide.

In these results, the R_f values of the cyanamide derivatives are as follows: biguanidium sulfate (A), 0.10—0.14; monoguanidium dihydrogen phosphate (B), 0.16—0.27; guanylurea (C), 0.34; urea (D), 0.41; biuret (E), 0.44; and dicyandiamide (F); 0.54. From the values of the spots of the heating product, the existence of a little biguanide and guanylurea in addition to the guanidium salt, which is the main constituent, is recognized. Therefore, the guanidium salt is converted into biguanide by the separation of 1 mol of ammonium from its 2 mol; a part of the biguanide thus formed is also converted into guanylurea by hydration and deammonation. It can be considered that the formation of biguanide described above corresponds to a reverse reaction of the formation of guanidium salt from dicyandiamide and ammonium salt; an equilibrium exists between these reactions. The species of phosphate in the heating product are estimated by paper chromatography and ion-exchange chromatography (see Fig. 5 II); the results are summarized in Table 1,

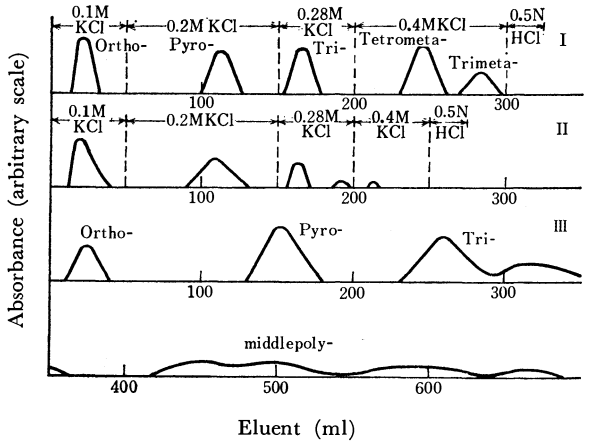

Fig. 5. Chromatographic analysis of condensed phosphates and reaction products.
I: Mixture of condensed phosphates.
II: Heating product of $H_5CN_3 \cdot H_3PO_4$ (Table 1, No. 4)
III: Reaction product between $H_4C_2N_4$ and $NH_4H_2PO_4$ (Table 2, No. 7)
Eluent for gradient elution method: 400 ml 0.2 mol/l KCl in mixing bottle, 500 ml 0.35 mol/l KCl in stock bottle.

while an ion-exchange chromatogram is shown in Fig. 5 (II). The orthophosphate used as the starting material is converted partially into pyrophosphate and triphosphate at 125—200 °C; besides, middlepoly phosphates (n=4—8) are formed above 225 °C.

Reaction between $H_4C_2N_4$ and $NH_4H_2PO_4$. Generally, guanidium salts are formed by a reaction between dicyandiamide and ammonium salt such as:

$$H_4C_2N_4 + 2NH_3 \cdot HX \rightleftharpoons 2H_5CN_3 \cdot HX$$

Sugino[2] has already reported the formation of guanidium phosphate by the heating of a mixture consisting of 1 mol of dicyandiamide, 1 mol of diammonium hydrogen phosphate, and about 4.5 mol of water in a sealed tube. The yields of guanidine were 25, 48, and 61% at 140, 160, and 180 °C respectively. His report concluded that the deficiency of NH_4^+ required for the reaction rises from the separation of ammonia from $(NH_4)_2HPO_4$ at high temperatures; simultaneously, the reactant is converted into an alkaline solution, and the dicyandiamide used is immediately decomposed by the alkaline solution. It was also described that the pyrolysis of phosphate occurs in this reaction system. However, the formation of condensed phosphates was not investigated at all. As has already been described, the use of the ammonium salt of a strong acid is suitable for the synthesis of guanidium salt; therefore, $NH_4H_2PO_4$ instead of $(NH_4)_2HPO_4$ was employed initially in this work.

Reaction under Atmospheric Pressure. The reaction between 1 mol of dicyandiamide and 2 mol of ammonium dihydrogen phosphate was examined under atmospheric pressure. Consequently, remarkable weight losses were observed upon heating for 60 min; 6.5% at 150 °C, 22.2% at 185 °C, 23.5% at 200 °C, and 27.0% at 220 °C. Thus, the product decomposes, and its volume expands up to fifty times. Therefore, it has been concluded that the synthesis of guanidium phosphate is difficult under atmospheric pressure. However, the reactant in an autoclave is expanded slightly under the effect of the gas produced by its thermal decomposition.

Components of the Reaction Products. The reaction conditions between dicyandiamide and ammonium dihydrogen phosphate under pressure, and the results of the analysis of the products, are summarized in Table 2. The majority of the products were soluble in water; the insoluble part increases slightly with the rise in the reaction temperature, being within 3.5% at 150—220 °C. The pH of a 1% aqueous solution is 6.3—7.6. The content of nitrogen is about 25% at 150—220 °C; it decreases slightly above 250 °C. The content of phosphorus in the soluble part of a product increases as a result of the large dehydration

TABLE 2. SYNTHESIS AND ANALYSIS OF GUANIDIUM CONDENSED PHOSPHATES

No.	Reaction conditions				Reaction products			
	$H_4C_2N_4$ (g)	$NH_4H_2PO_4$ (g)	Temp. (°C)	Time (min)	1% Soln. pH	N (%)	P (%)	N/P Atomic ratio
1	1.34	3.66	120	60	4.60	25.8	19.7	2.90
2	1.34	3.66	130	60	5.71	25.4	20.1	2.80
3	1.34	3.66	140	60	6.30	25.5	20.3	2.79
4	1.34	3.66	150	60	6.99	26.0	20.7	2.77
5	1.34	3.66	170	60	7.29	25.2	20.9	2.66
6	1.34	3.66	185	60	7.32	25.5	22.4	2.51
7	1.34	3.66	200	60	7.40	26.2	23.2	2.50
8	1.34	3.66	220	60	7.61	26.4	23.9	2.44
9	1.34	3.66	250	60	7.40	25.0	23.3	2.37
10	1.34	3.66	300	60	7.26	24.8	20.9	2.36

No.	Reaction products								
	Cyanamide derivatives					Condensed phosphates			
	$H_4C_2N_4$ (%)	H_5CN_3 (%)[a]	$H_7C_2N_5$ (%)	$H_6C_3N_6$ (%)	I·S[c] (%)	Ortho- (%)	Pyro- (%)	Tri- (%)	Middlepoly (%)
1	100				0	100			
2	98.5			trace	0.11	98	2		
3	36.8	17.4	0.6	trace	1.92	35	24	20	21
4	3.5	62.0			3.05	19	30	23	28
5	0.6	69.3			2.66	15	28	24	33
6	0.3	72.8			3.22	13	26	22	39
7		75.0			3.51	12	25	22	41
8		78.9			3.49	12	19	23	46
9	0.7[b]	62.6			6.46	14	17	21	48
14	1.4[b]	47.7			6.70	18	15	22	45

a) Yield of guanidine to dicyandiamide as low material. b) Content of biuret. c) I·S; Insoluble product.

with a rise in the reaction temperature, but it decreases with an increase in the insoluble part above 250 °C. The mole ratio of N to P in the mixture of dicyandiamide and ammonium dihydrogen phosphate is theoretically 3 : 1; however, the mole ratios of the products are less than 3 : 1, and the separation of ammonia from the reactant is observed.

Condensed Phosphate in Product. The results of the analysis of the condensed phosphates by means of paper chromatography are summarized in Table 2, while an example of an ion-exchange chromatogram is shown in Fig. 5 (III). The phosphate species from ortho- to decapolyphosphate can be separated by employing gradient elution chromatography,[5] but the ion-exchange chromatogram of the phosphates in a product is separated into eight fractions with tailing because of the effect of the cations connected to the cyanamide derivatives. That is, the reaction products consist of ortho-, pyro-, tri-, and middlepoly phosphates, which have polymerization degrees of about 4—10.

Formation of Cyanamide Derivatives. The paper chromatogram for a mixture of standard materials (S) and the products is shown in Fig. 6. The products do not change at 120 °C and give only the spot of dicyandiamide as the starting material. The proportion of dicyandiamide decreases at 140 °C, and the spots of guanidium salt, a little guanylurea, and biguanide appear. The spot of a little dicyandiamide remains at 150 and 170 °C, but most of the products are converted into guanidium salt; here, the spot of guanidium salt is long and elliptical, and it also possesses the position of the spot for biguanidium salt. As has been described previously, the biguanide is formed upon the heating of monoguanidium phosphate; therefore, although we do not say specifically that biguanidium salt is not formed in this reaction, the existence of its salt is not observed by the chemical analysis. In this case, the long ellipse of the spot seems to be characteristic of guanidium condensed phosphates. The only spot of guanidium condensed phosphates appeared at 185—220 °C. Another spot appeared in the position under the spot of dicyandiamide above 250 °C. Perhaps, this spot indicates the biuret formed

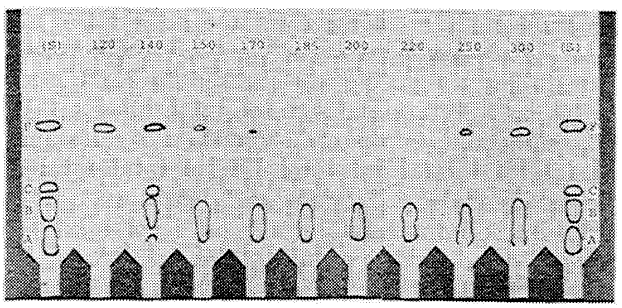

Fig. 6. Paper chromatogram for cyanamide derivatives in reaction product.
Numerals in the photograph indicate the reaction temperatures (°C).
(S): standard material, A: biguanide, B: guanidine, C: guanylurea, F: dicyandiamide.

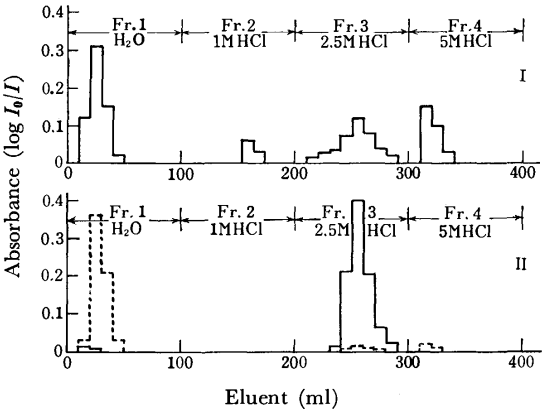

Fig. 7. Chromatographic analysis of cyanamide derivative and reaction product.
I: Mixture of cyanamide compounds (Fr. 1; dicyandiamide or biuret, Fr. 2; guanylurea, Fr. 3; guanidine, Fr. 4; biguanide).
II: Reaction products (----; Table 2 No. 3, ——; Table 2 No. 8).

by the thermal decomposition of the products. The paper chromatography can distinguish various cyanamide derivatives in the product, but the color of the spot is not clear and its decolorization is remarkable. Therefore, the ion-exchange chromatography of cyanamide derivatives was also examined; an example of a chromatogram is shown in Fig. 7.

Dicyandiamide and biuret on a cation-exchange resin are easily carried away by water and are received almost quantitatively. On the other hand, guanylurea, guanidine, and biguanide can be separated by using hydrochloric acid in different concentration as eluates, though the yields expected from the description in a previous paper[8] are not obtained because of the decomposition of these compounds by the acid used. Therefore, the ion-exchange chromatography also confirms the existence of cyanamide derivatives in a product; it is employed for the estimation of dicyandiamide and biuret. The results are shown in Table 2.

The main product, guanidine, was estimated by means of the chemical analysis already described for cyanamide derivatives; the results are shown in Table 2. Dicyandiamide is converted into guanidium salt beginning at 140 °C, and the yield of guanidine increases with the increase in the reaction temperature. more than 70% of the dicyandiamide used is converted at 185—220 °C; the maximum is 78.9%. This value is improved remarkably as compared with the yields when diammonium hydrogen phosphate is used as the starting material. Upon a further increase in the reaction temperature, the decomposition of the product occurs, the yield of guanidine decreases, and a little biuret is formed. Guanylmelamine and melamine can be also estimated by chemical analysis; the former can not be detected in any products, while the latter exists in small amounts in the products at 130—140 °C.

The author wishes to thank Dr. Masahiro Kurabayashi for his helpful advice.

Synthesis of Anomeric Methyl 6-*O*-(L-Mycarosyl)-β-D-glucosaminides and 4-*O*-(L-Mycarosyl)-β-D-mycaminosides

Shinkiti KOTO, Kazuo YAGO, Shonosuke ZEN, and Satoshi ŌMURA*

School of Pharmaceutical Sciences, Kitasato University, Shirokane, Minato-ku, Tokyo 108

**The Kitasato Institute, Shirokane, Minato-ku, Tokyo 108*

(Received September 27, 1972)

Condensation of 3,4-*O*-carbonyl-2,6-dideoxy-3-*C*-methyl-L-*ribo*hexopyranosyl chloride (III) with methyl 2-deoxy-2-(2,4-dinitroanilino)-β-D-glucopyranoside and the subsequent removal of blocking groups gave the anomeric isomers of methyl 6-*O*-(2,6-dideoxy-3-*C*-methyl-L-*ribo*hexopyranosyl)-2-amino-2-deoxy-β-D-glucopyranoside (VIIa, VIIb). On the other hand, the condensation of III with methyl 3,6-dideoxy-3-(*N*-methylcarboethoxyamino)-2-*O*-*p*-phenylazobenzoyl-β-D-glucopyranoside (XI) followed by removal of the acyl groups and *N*-methylation afforded the anomeric forms of methyl 4-*O*-(2,6-dideoxy-3-*C*-methyl-L-*ribo*hexopyranosyl)-3,6-dideoxy-3-dimethylamino-β-D-glucopyranoside (XVa, XVb).

Some 16-membered macrolide antibiotics such as magnamycin,[1] leucomycins,[2] spiramycin,[3] B-58945[4] and tylosin[5] have a unique structural feature. They contain a disaccharide moiety in which the neutral branched-chain sugar is linked glycosidically to the 3,6-dideoxy-3-dimethylamino-D-glucopyranose, D-mycaminose. Concerning the structural-activity relationship of macrolide antibiotics,[6] it was surmised that the sugar moiety could be important for antibiotic activity. Attempts to obtain the disaccharide moiety of leucomycins, 4-*O*-(2,6-dideoxy-3-*C*-methyl-α-L-*ribo*hexopyranosyl)-3,6-dideoxy-3-dimethylamino-β-L-glycopyranose, and confirm whether the moiety itself has any activity at all, failed, since 2,6-dideoxy-3-*C*-methyl-L-*ribo*hexopyranose, L-mycarose was preferentially released by acid hydrolysis from the disaccharide, which was expected to be cleaved from the lactone moiety. Thus as a part of chemical studies of macrolide sugar,[7] the syntheses of two model disaccharides have been carried out.[8] This paper deals with the preparation of 3,4-*O*-carbonyl-2,6-dideoxy-3-*C*-methyl-L-*ribo*hexopyranosyl chloride (III) and methyl 4-*O*-(2,6-dideoxy-3-*C*-methyl-L-*ribo*hexopyranosyl)-3,6-dideoxy-3-dimethylamino-β-D-glucopyranoside (XVa, XVb), as well as other related glycosides.

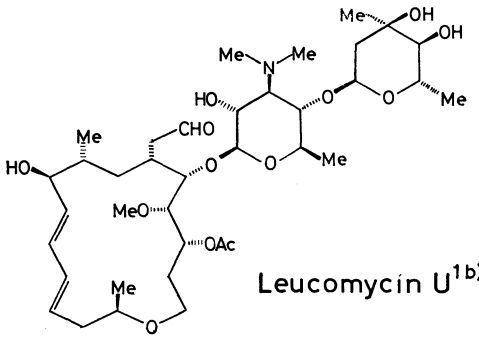

Leucomycin U[1b]

Methyl 3,4-*O*-carbonyl-2,6-dideoxy-3-*C*-methyl-α-L-*ribo*hexopyranosyl[9] (Ia) was hydrolyzed and converted into *p*-nitrobenzoyl derivative (II), which was then subjected to Zorbach's procedure[10] to generate III. The chloride was methanolyzed in the presence of silver oxide to give an anomeric mixture of Ia and Ib; β-anomer was predominant (α : β=2 : 3).

At first, the primary hydroxyl group of methyl 2-deoxy-2-(2,4-dinitroanilino)-β-D-glucopyranoside[11] was condensed with III. Condensation in nitromethane in the presence of mercuric cyanide gave an anomeric mixture (IVa and IVb); α-anomer was predominant (α : β=7 : 3). Condensation products (IVa and IVb) were characterized as the di-*O*-benzoate (Va and Vb). A similar condensation was performed in the presence of 2,6-lutidine,[12] and the predominant formation of the α-anomer was also observed (α : β= 5 : 3). The glycosidation at the C-6 position of 2-amino-2-deoxy-D-glucose was checked by PMR spectra of IVa and IVb in comparison with those of V's: signal of methine protons of C-3 and C-4 of glucosamine moiety shifted toward the lower field by *O*-benzoylation. The preferential glycosidation of the primary hydroxyl group in hexopyranoside has been reported.[13] Removal of the blocking groups of Va and Vb by successive methanolysis and hydrolysis gave methyl

1) a) R. B. Woodward, L. S. Weiler, and P. C. Dutta, *J. Amer. Chem. Soc.*, **87**, 4662 (1965); b) N. E. Kuehe and B. W. Benson, *ibid.*, **87**, 4460 (1965).

2) a) S. Ōmura, A. Nakagawa, M. Katagiri, T. Hata, M. Hiramatsu, T. Kimura, and K. Naya, *Chem. Pharm. Bull.* (Tokyo), **18**, 1501 (1970); b) S. Ōmura, M. Katagiri, A. Nakagawa, H. Yamane, I. Umezawa, K. Komiyama, and T. Hata, Progress in Antimicrobial and Anticancer Chemotherapy-Proceedings of the 6th International Congress of Chemotherapy, University of Tokyo Press, (1970), p. 1043.

3) a) R. Paul and S. Tchelitheff, *Bull. Soc. Chim. Fr.*, **1965**, 650; b) S. Ōmura, A. Nakagawa, M. Otani, T. Hata, H. Ogura, and K. Furuhata, *J. Amer. Chem. Soc.*, **91**, 3401 (1969).

4) T. Suzuki, This Bulletin, **43**, 292 (1970).

5) R. B. Morin, M. Gorman, R. L. Hamil, and P. V. Darmaco, *Tetrahedron Lett.*, **1970**, 4737.

6) S. Ōmura, M. Tichler, A. Nakagawa, Y. Hironaka, and T. Hata, *J. Med. Chem.*, **15**, 1011 (1972).

7) S. Koto, S. Zen, S. Ōmura, and T. Hata, This Bulletin, **45**, 532 (1972).

8) a) S. Koto, K. Yago, S. Zen, S. Ōmura, and T. Hata, *Chem. Lett.*, **1972**, 731; b) S. Koto, K. Yago, S. Zen, and S. Ōmura, *ibid.*, **1972**, 1091.

9) W. Hofheinz, H. Grisebach, and H. Friebolin, *Tetrahedron*, **18**, 1265 (1962).

10) W. W. Zorbach and K. V. Bhat, *Adv. Carbohydrate Chem.*, **21**, 273 (1966).

11) W. Yu and T. Hsing, *Acta Chim. Sinica*, **24**, 368 (1958); R. F. Lloyd and M. Stacey, *Tetrahedron*, **9**, 116 (1960).

12) S. Koto, T. Uchida, and S. Zen, *Chem. Lett.*, **1972**, 1049.

13) A. M. Bills and J. W. Green, *J. Chem. Soc., B*, **1967**, 716.

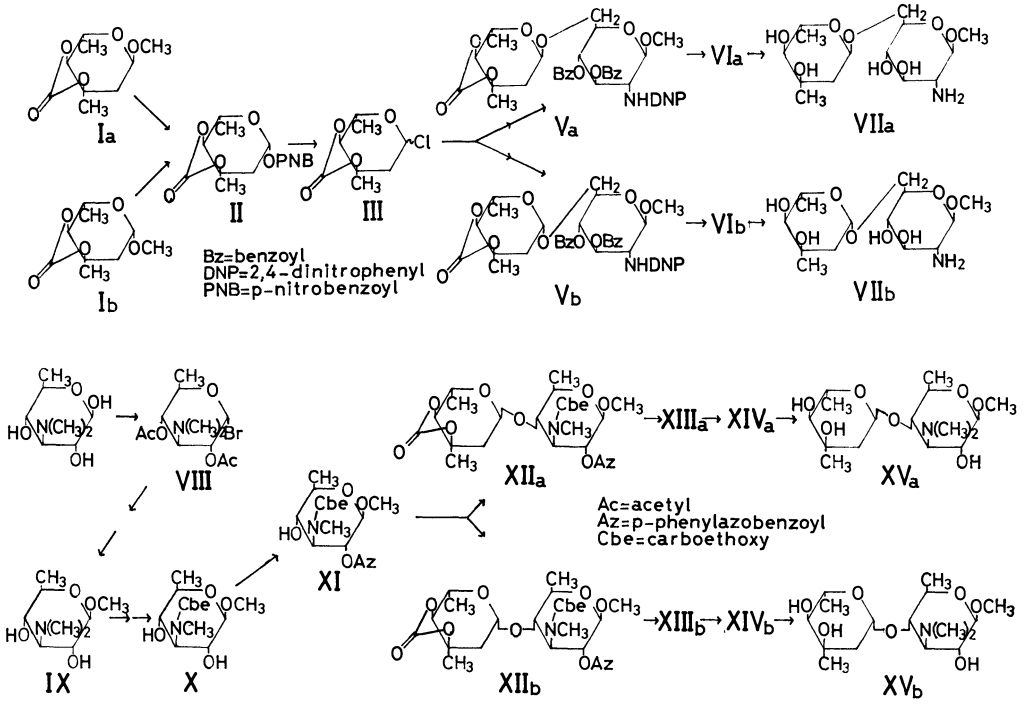

6-*O*-(2,6-dideoxy-3-*C*-methyl-α-L-*ribo*hexopyranosyl)-3,6-dideoxy-3-dimethylamino-β-D-glucopyranoside (VIIa) and its anomer (VIIb).

Finally, the synthesis of methyl 4-*O*-(2,6-dideoxy-3-*C*-methyl-α-L-*ribo*hexopyranosyl)-3,6-dideoxy-3-dimethylamino-β-D-glucopyranoside (XVa) was carried out. 3,6-Dideoxy-3-dimethyl-amino-β-D-glucopyranoside hydrochloride monohydrate[14] was treated with acetyl bromide[15] to give 2,4-di-*O*-acetyl-3,6-dideoxy-3-dimethyl-amino-α-D-glucopyranosyl bromide hydrobromide (VIII), which was methanolyzed, in the presence of silver oxide, to afford methyl 3,6-dideoxy-3-dimethylamino-β-D-glucopyranoside (IX).[16] Compound IX was treated with ethyl chloroformate in the presence of sodium carbonate[17] and ethanolyzed to give methyl 3,6-dideoxy-3-(*N*-methylcarboethoxyamino)-β-D-glucopyranoside (X). Partial acylation of the hydroxyl groups of X with a molar *p*-phenylazobenzoyl chloride in pyridine and subsequent chromatographical separation gave methyl 3,6-dideoxy-3-(*N*-methylcarboethoxyamino)-2-*O*-(*p*-phenylazobenzoyl)-β-D-glucopyranoside (XI) in about 40% yield. The C-2-substitution of compound XI was checked by PMR. Direct partial acylation of IX gave no good results.

Chloride III was condensed with the partialy blocked XI in nitromethane in the presence of mercuric cyanide to afford two products, the α-glycoside XIIa and its β-anomer XIIb; α-glycoside was predominantly formed (α : β=3 : 2). The main product XIIa was converted into *O*-deblocked compound XIIIa which was then hydrolyzed into a free base XIVa. The reductive *N*-methylation with formaldehyde over palladium furnished desired methyl 4-*O*-(2,6-dideoxy-3-*C*-methyl-α-L-*ribo*hexopyranosyl)-3,6-dideoxy-3-dimethylamino-β-D-glucopyranoside (XVa). The minor product XIIb was subjected to the above sequence of reactions to give the β-glycoside XVb.

The anomeric configuration of the synthesized mycarosides VIIa, VIIb, XVa, and XVb was confirmed by the observation of their optical rotation and PMR spectra. PMR data of these compounds indicated that the in mycarosyl moiety had the normal C_4^1 conformation in water (Table 1). In each disaccharide-synthesis, predominant formation of α-glycoside was observed; this is often the case with the glycosidation of the 2-deoxy sugar.[10]

MIC's of the free base, VIIa, VIIb, XVa, and XVb, against *Bacillus subtilis* PCI 219, *Staphylococcus aureus* FDA 209P, *Sarcine Lutea* PCI, 1001, *Escherichia coli* NIHJ, and *Klebsiella pneumoniae* were more than 100 μg/ml.

Experimental

General Procedure. The solvent system used for tlc (Silica Gel No. 7731, Merck) and column chromatography over silica gel (Kanto Kagaku, Co.) was as follows : benzene : 2-butanone=(SA30) 30 : 1, (SA20) 20 : 1, (SA10) 10 : 1, (SA5) 5 : 1; benzene : acetone=(SB3) 3 : 1, (SB2) 2 : 1; acetone : methanol=(SC4) 4 : 1, (SC2) 2 : 1, by volume.

Melting points were determined with a Yanagimoto micro-melting point apparatus; uncorrected values are given. Optical rotations were measured with an Atago Polux apparatus in 1-dm tube and IR spectra with a JASCO IRA-1 spectrometer, absorptions being given in cm^{-1}. PMR spectra were determined with a Varian S-60T spectrometer. Elemental analyses were made with a Perkin-Elmer Model 240 Analyser apparatus.

14) F. A. Hochstein and K. Murai, *J. Amer. Chem. Soc.*, **76**, 5080 (1954).
15) Y. Ito, S. Koto, and S. Umezawa, This Bulletin **35**, 1618 (1962).
16) F. A. Hochstein and D. Regna, *J. Amer. Chem. Soc.*, **77**, 3353 (1955).
17) J. Newman, *J. Org. Chem.*, **30**, 1287 (1965).

Table 1. PMR data of H'-1 and H'-4 of mycarosides

Compound	Configuration	Solvent	H'-1 (ppm)	$J_{1'.2'e}$ (Hz)	$J_{1'.2'a}$	H'-4 (ppm)	$J_{4',5'}$ (Hz)
IVa	α	C	4.96	5.5	5.5	—	—
IVb	β	C	4.88	4.5	10.5	—	—
VIa	α	C	4.92	2.0	2.0	3.02	10.0
VIb	β	C	4.88	2.0	9.0	3.09	9.5
VIIa	α	W	4.94	2.0	4.0	3.14	10.0
VIIb	β	W	4.90	2.0	10.0	3.08	10.0
XIIa	α	C	4.98	2.0	3.5	2.92	10.0
XIIb	β	C	4.67	4.0	8.5	2.90	9.5
XVa	α	W	5.21	2.0	4.0	3.15	10.0
XVb	β	W	5.05	3.0	9.5	3.07	9.5

C=$CDCl_3$/TMS, W=D_2O/TMSS

Methyl 3,4-O-Carbonyl-2,6-dideoxy-3-C-methyl-β-L-ribohexopyranoside (Ib). Cold phosgene solution in toluene (25%; 17 ml) was added to a solution of methyl 2,6-dideoxy-3-*C*-methyl-β-L-*ribo*hexopyranoside[18] (0.69 g) in a mixture of chloroform (30 ml) and pyridine (7 ml). The resulting mixture was stirred at room temperature overnight. Chloroform-extract was chromatographed with the solvent SA10 to give Ib (0.73 g; 92%), bp 110—115 °C/0.003 mmHg, mp 53—54 °C, $[\alpha]_D^{25}$+6.7° (*c* 1.0, $CHCl_3$), ν_{max}^{KBr}: 1795 (carbonate)

Found: C, 53.24; H, 6.99%. Calcd for $C_9H_{14}O_5$: C, 53.46; H, 6.84%.

3,4-O-Carbonyl-2,6-dideoxy-3-C-methyl-1-O-(p-nitrobenzoyl)-β-L-ribohexopyranose (II). Cold concd hydrochloric acid (21 ml) was added to a solution of Ia[9] (0.74 g) in a mixed solvent of dioxane (35 ml) and water (35 ml). The solution was kept standing at room temperature for 3 days, neutralized with sodium bicarbonate to pH 5.5, concentrated and then extracted with chloroform. The extract (0.48 g) treated with *p*-nitrobenzoyl chloride (0.53 g) in pyridine (4.0 ml) gave a crude product (1.2 g), which was crystallized with isopropyl alcohol to give II (0.51 g; 41%); mp 153—154 °C; $[\alpha]_D^{25}$+8° (*c* 2.6, $CHCl_3$); ν_{max}^{KBr}: 1785 (carbonate); 1730, (*p*-nitrobenzoyl); δ_{CDCl3}^{TMS}: 1.45 (3H, doublet; CH_3-5, J=6.0 Hz, 1.65 (3H, singlet; CH_3-3), 2.15 (1H, quartet; H-2a, $J_{1.2a}$=7.5 Hz, $J_{2e,2a}$=15.5 Hz), 2.70 (1H, quartet; H-2e, $J_{1.2e}$=4.0 Hz), 6.30 (1H, quartet; anomeric H).

Found: C, 53.45; H, 4.43; N, 4.16%. Calcd for $C_{15}H_{15}NO_8$: C, 53.42; H, 4.48; N, 4.15%.

3,4-O-Carbonyl-2,6-dideoxy-3-C-methyl-L-ribohexopyranosyl Chloride (III) and Its Methanolysis. II (0.750 g) was dissolved in dichloromethane (40 ml) saturated with hydrogen chloride at 0 °C and the mixture was kept standing at 5 °C for 40 min. *p*-nitrobenzoic acid (0.36 g; 97%) was filtered off, the resulting solution evaporated to dryness and co-evaporated with toluene three times to give III,[19] which was immediately used for the following glycosidation.

Freshly prepared III from II (216 mg) was stirred in methanol (2.0 ml) in the presence of silver oxide (152 mg) at room temperature for one hour in the dark, filtered and chromatographed with the solvent SA20 to give Ia (39 mg; 30%) and Ib (60 mg; 46%), which were identified by means of elemental analyses, mixed melting points and IR spectra (KBr), respectively.

Methyl 6-O-(3,4-O-Carbonyl-2,6-dideoxy-3-C-methyl-α-L-ribohexopyranosyl)-3,4-O-benzoyl-2-deoxy-2-(2,4-dinitroanilino)-β-D-glucopyranoside (Va) and Methyl 6-O-(3,4-O-Carbonyl-2,6-dideoxy-3-C-methyl-β-L-ribohexopyranosyl)-3,4-O-benzoyl-2-deoxy-2-(2,4-dinitroanilino)-β-D-glucopyranoside (Vb). By condensation with mercuric cyanide. III, prepared from II (0.75 g) was stirred with methyl 2-deoxy-2-(2,4-dinitroanilino) β-D-glucopyranoside[11] (1.00 g) in nitromethane (10 ml) in the presence of mercuric cyanide (0.750 g) at room temperature for 20 hr. The mixture was diluted with chloroform, filtered, and then chromatographed with the solvent SB3. After elution of high R_f substances, a compound (IVb) of R_f 0.33 (0.095 g; 8.1% from II) and that (IVa) of R_f 0.25 (0.220 g; 19%) were obtained. IVa (200 mg) was treated with benzoyl chloride (0.2 g) in pyridine (2 ml), chromatographed with the solvent SA20 and crystallized with ethanol to give yellow Va (187 mg; 67%), mp 123—124 °C, $[\alpha]_D^{25}$−13.5° (*c* 0.9, $CHCl_3$), ν_{max}^{KBr}: 1800 (carbonate); 1730 (benzoyl); 1620, 1530, 1345 (dinitrophenyl). Similarly, IVb (90 mg) was benzoylated to give yellow Vb (95 mg; 76%), mp 118—120 °C, $[\alpha]_D^{25}$+16° (*c* 0.9, $CHCl_3$), ν_{max}^{KBr}: 1810 (carbonate); 1733 (benzoyl); 1620, 1525, 1340 (dinitrophenyl). PMR spectra of Va and Vb had multiplets of a couple of methine protons at δ 5.6—6.0, whereas those of IVa and IVb had no signal in this region.

Found: (Va) C, 56.78; H, 4.74; N, 5.96%. (Vb) C, 56.85; H, 4.75; N, 5.46%. Calcd for $C_{35}H_{35}N_3O_{15}$: C, 56.99; H, 4.78; N, 5.70%.

Methanolysis of IVa and IVb with methanolic hydrochloric acid[18] gave Ia and Ib and methyl 2-deoxy-2-(2,4-dinitroanilino)-β-D-glucopyranoside which were detected by tlc.

By condensation with 2,6-lutidine. III, prepared from II (0.78 g) was condensed with the methyl glucosaminide (1.1 g) in nitromethane (10 ml) in the presence of 2,6-lutidine (0.29 ml) for 20 hr at room temperature to yield IVa (0.170 g 14%) and IVb (0.095 g; 7.8%). Each compound was successively benzoylated to give Va and Vb, respectively. These compounds were identified with the above Va and Vb, respectively, by means of elemental analyses and mixed melting points.

Methyl 6-O-(2,6-Dideoxy-3-C-methyl-α-L-ribohexopyranosyl)-2-deoxy-(2,4-dinitroanilino)-β-D-glucopyranoside (VIa). Va (104 mg) was treated with diluted sodium methoxide (0.14 M; 0.7 ml) at room temperature overnight, neutralized with dil. acetic acid (1% in methanol), purified by chromatography with the solvent SB2, and crystallized with benzene to give yellow VIa (51 mg; 72%), mp 116—118 °C, $[\alpha]_D^{25}$ −13° (*c* 1.3, $CHCl_3$). The characteristic bands of carbonate and benzoyl were absent in the IR spectrum (KBr), δ_{CDCl3}^{TMS}: 1.25

18) S. Ōmura, M. Katagiri, H. Ogura, and T. Hata, *Chem. Pharm. Bull.* (Tokyo), **15**, 1529 (1967).

19) Optical rotation could not be observed because of rapid formation of some dark green substance.

singlet; CH_3-3′), 1.31 (3H, doublet; CH_3-5′, J=6.0 Hz), 3.45 (3H, singlet; OCH_3), 4.42 (1H; H-1, $J_{1,2}$=6.5 Hz).

Found: C, 47.87; H, 5.77; N, 8.26%. Calcd for $C_{20}H_{29}N_3O_{12}$: C, 47.71; H, 5.81; N, 8.35%.

Methyl 6-O-(2,6-Dideoxy-3-C-methyl-β-L-ribohexopyranosyl)-2-deoxy-2-(2,4-dinitroanilino)-β-D-glucopyranoside (VIb). Vb (58 mg) was treated with dil. sodium methoxide to give VIb (32 mg; 81%), mp 114—116 °C, $[\alpha]_D^{25}$ −4° (*c* 0.7, $CHCl_3$). $\delta_{CDCl_3}^{TMS}$: 1.31 (3H, singlet; CH_3-3′), 1.33 (3H, doublet; CH_3-5′, J=6.5 Hz), 3.56 (3H, singlet; OCH_3), 4.36 (1H, doublet; H-1, $J_{1,2}$=6.0 Hz).

Found: C, 48.23; H, 6.01; N, 7.76%. Calcd for $C_{20}H_{29}N_3O_{12}$: C, 47.71; H, 5.81; N, 8.35%.

Methyl 6-O-(2,6-Dideoxy-3-C-methyl-α-L-ribohexopyranosyl)-2-amino-2-deoxyl-β-D-glucopyranoside (VIIIa). VIa (50 mg) was treated with Dowex 1X2 (OH) (*ca.* 1 ml) in moist acetone[20] and a crude syrup was chromatographed over the same resin to give a ninhydrin-positive hard syrup of VIIa (27 mg; 81%), which was taken up with a small amounts of methanol and precipitated from isopropyl alcohol, diisopropyl ether, and *n*-hexane to give colorless hygroscopic powder, mp 100 °C; $[\alpha]_D^{25}$ −91° (*c* 1.1, H_2O); $\delta_{D_2O}^{TMSS}$: 1.22 (3H, singlet; CH_3-3′), 1.28 (3H, doublet; CH_3-5′, J=6.5 Hz), 3.54 (3H, singlet; OCH_3), 4.27 (1H; doublet; H-1, $J_{1,2}$=8.5 Hz).

Found: C, 48.38; H, 8.22; N, 3.94%. Calcd for $C_{14}H_{27}NO_8\cdot 1/2H_2O$: C, 48.54; H, 8.14; N, 4.04%.

Methyl 6-O-(2,6-Dideoxy-3-C-methyl-β-L-ribohexopyranosyl)-2-amino-2-deoxy-β-D-glucopyranoside (VIIb). VIb (20 mg) was treated as above to give a hard syrup of VIIb (9.2 mg; 69%); which was treated with *n*-hexane to afford colorless hygroscopic powder, mp 100 °C, $[\alpha]_D^{25}$ −19° (*c* 0.4, H_2O). $\delta_{CDCl_3}^{TMS}$: 1.25 (3H, singlet; CH_3-3′), 1.26 (3H, doublet; CH_3-5′, J=6.0 Hz), 3.55 (3H, singlet; OCH_3), 4.28 (1H, doublet; H-1, J=8.0 Hz).

Found: C, 47.25; H, 8.31; N, 3.78%. Calcd for $C_{14}H_{27}NO_8\cdot H_2O$: C, 47.31; H, 8.22; N, 3.94%.

2,4-Di-O-Acetyl-3,6-dideoxy-3-dimethylamino-α-D-glucopyranosyl Bromide Hydrobromide (VIII). 3,6-Dideoxy-3-dimethylamino-β-D-glucopyranose hydrochloride monohydrate[14] (2.32 g) was added to ice-cooled acetyl bromide (5 ml). The mixture was kept standing in a sealed vessel at room temperature overnight, evaporated and co-evaporated thrice with toluene to give crystalline residue, which was triturated with *n*-hexane to give VIII (3.85 g; 97%), mp 72—76 °C, $[\alpha]_D^{25}$ +100° (*c* 0.7, $CHCl_3$); $\delta_{CDCl_3}^{TMS}$: 1.27 (3H, doublet, CH_3-5), 2.35 (6H, singlet; $OCOCH_3$), 3.03 (6H, broad, $\overset{+}{N}CH_3$), 6.66 (1H, doublet; H-1, $J_{1,2}$=4.0 Hz).

Found: C, 33.51; H, 4.83; N, 3.22%. Calcd for $C_{12}H_{20}NO_5Br\cdot HBr$: C, 34.39; H, 5.05; N, 3.34%.

Methyl 3,6-Dideoxy-3-dimethylamino-β-D-glucopyranoside (IX). VIII (1.91 g) was stirred in methanol (67 ml) in the presence of silver oxide (2.4 g) and anhydrous magnesium sulfate (5 g) at room temperature for 2 hr, filtered, and concentrated to give a residue which was treated with dil. sodium methoxide (0.05 M; 40 ml) for 2 hr at room temperature. The mixture was evaporated below 20 °C and then chromatographed with the solvent SC4 to give IX (0.74 g; 79%), mp 117—119 °C, which was used for the subsequent reaction. Sublimation at 95—100 °C under 0.02 mmHg gave an analytical sample,[21] mp 123—125 °C, $[\alpha]_D^{25}$ −35° (*c* 1.4, H_2O). Lit,[16] mp 126—126.5 °C, $[\alpha]_D^{25}$ −39° (*c* 1, H_2O).

Methyl 3,6-Dideoxy-3-(N-methylcarboethoxyamino)-β-D-glucopyranoside (X). IX (0.44 g) was stirred in ethyl chloroformate (10 ml) in the presence of powdery sodium carbonate (4.2 g) at room temperature for five days, filtered, evaporated, and co-evaporated thrice with toluene at 80 °C to give a syrup which was ethanolyzed with dil. sodium ethoxide (0.1 M, 38 ml) at room temperature overnight. The mixture was neutralized with acetic acid, evaporated and chromatographed with the solvent SB2 to give a homogeneous oil of X (0.47 g; 83%), $[\alpha]_D^{25}$ −1° (*c* 1.5, $CHCl_3$); $\delta_{CDCl_3}^{TMS}$: 1.27 (3H, triplet; $C\underline{H}_3CH_2O$-, J=7.0 Hz), 1.36 (3H, doublet; CH_3-5, J=5.7 Hz), 2.89 (3H, singlet; N-CH_3), 3.55 (3H, singlet; OCH_3), 4.14 (2H, quartet; $CH_3C\underline{H}_2O$-), 4.27 (1H, doublet; anomeric H, $J_{1,2}$=7.3 Hz).

After the elution of X, a small quantity of IX was recovered with the solvent SC4.

Methyl 3,6-Dideoxy-3-(N-methylcarboethoxyamino)-2-O-p-phenylazobenzoyl-β-D-glucopyranoside (XI). A well stirred mixture of *p*-phenylazobenzoyl chloride (2.7 g) in pyridine (60 ml) was added to a solution of X (27 g) in pyridine (40 ml) for 80 min at 2 °C under vigorous agitation and then the temperature was allowed to rise gradually up to 17 °C. The mixture was further stirred for 2 days at the same temperature, treated with a small amount of water, evaporated and then chromatographed with the solvent SA5. The fraction having R_f 0.35 was crystallized with diisopropyl ether to give orange XI (1.8 g; 37%), mp 127—131 °C. Recrystallization form the same solvent gave a single product, mp 134—136 °C. $[\alpha]_D^{25}$ +57° (*c* 1.3, $CHCl_3$); 3410 (OH), 1727 (ester), 1680 (urethane); $\delta_{CDCl_3}^{TMS}$: 0.75 (3H, triplet; $C\underline{H}_3CH_2O$-, J=7.0 Hz), 1.53 (3H, doublet; CH_3-5, J=5.7 Hz), 2.83 (3H, singlet; NCH_3), 3.37 (3H, singlet; OCH_3), 4.72 (1H, doublet; anomeric H, J=7.5 Hz), 4.93 (1H, quasi-triplet; H-3, $J_{2,3}=J_{3,4}$=11.0 Hz), 5.57 (1H, quartet; H-2), Assignments of H-1, H-2, and H-3 were checked by the measurement at 100 MHz (Varian HA-100).

Found: C, 61.27; H, 6.22; N, 8.96%. Calcd for $C_{24}H_{29}N_3O_7$: C, 61.14; H, 6.20; N, 8.91%.

From the mother liquor, a second crop (0.4 g) having a melting point of 100—114 °C was obtained, but this gave no crystals when dissolved in diisopropyl ether. In this PMR spectrum, the quartet at δ 5.57 was entirely deformed by the appearance of new broad signals at δ 5.05—5.20, probably coming form H-4 of a 4-*O*-substituted minor product.

Methyl 4-O-(3,4-O-Carbonyl-2,6-dideoxy-3-C-methyl-α-L-ribohexopyranosyl-3,6-dideoxy-3-(N-methylcarboethoxyamino)-2-O-(p-phenylazobenzoyl)-β-D-glucopyranoside (XIIIa) and Methyl 4-O-3,4-Carbonyl-3,6-dideoxy-3-C-methyl-β-L-ribohexopyranosyl)-3,6-dideoxy-3-(N-methylcarboethoxyamino)-2-O-phenylazobenzoyl-β-D-glucopyranoside (XIIb). Chloride III, prepared from II (0.70 g) was stirred with XI (0.70 g) in nitromethane (5 ml) in the presence of mercuric cyanide (0.70 g) for 2 days at room temperature, diluted with chloroform filtered and evaporated, and then chromatographed with the solvent SA1O to give two crude products; a glass of R_f 0.45 and that of R_f 0.33. The main product R_f 0.33 was refined by preparative tlc with the solvent SA20 with the multiple development technique, and triturated with diisopropyl ether containing *n*-hexane to give orange amorphous XIIa (0.15 g; 11%), mp 97—99 °C, $[\alpha]_D^{25}$ +2° (*c* 1.0, $CHCl_3$); ν_{max}^{KBr}: 1805 (carbonate), 1733 (ester), 1700 (urethane); $\delta_{CDCl_3}^{TMS}$: 1.04 (3H, triplet; $C\underline{H}_3CH_2O$-, J=7.0 Hz), 1.52 (3H, singlet; CH_3-3′), 2.87 (3H, singlet; NCH_3), 3.48 (3H, singlet; OCH_3), 4.55 (1H, doublet; H-1, $J_{1,2}$=8.0 Hz).

The minor product was worked up as above with the solvent SA30 to give orange crystalline XIIb (0.095 g; 7%), 176—178 °C, $[\alpha]_D^{25}$ +105° (*c* 1.0, $CHCl_3$); ν_{max}^{KBr}: 1805 (carbonate), 1720 (ester), 1705 (urethane); $\delta_{CDCl_3}^{TMS}$: 1.12 (3H, triplet; $C\underline{H}_3CH_2O$-, J=7.0 Hz), 1.51 (3H, singlet;

20) *cf.* S. Umezawa and S. Koto, This Bulletin, **39**, 2014 (1966).
21) Found: C, 52.88; H, 9.44; N, 6.50%.

CH_3-3′), 2.86 (3H, singlet; NCH_3), 3.50 (3H, singlet; OCH_3), 4.56 (1H, doublet; H-1, $J_{1,2}$=7.5 Hz).

Found: (XIIa) C, 59.20; H, 5.98; N, 6.16%. (XIIb) C, 59.78; H, 6.10; N, 6.53%. Calcd for $C_{32}H_{39}N_3O_{11}$: C, 59.90; H, 6.13; N, 6.55%.

Methyl 4-O-(2,6-Dideoxy-3-C-methyl-α-L-ribohexopyranosyl)-3,6-dideoxy-3-(N-methylcarboethoxyamino-β-D-glucopyranoside (XIIIa). XIIa (65 mg) was treated with dil. sodium ethoxide (0.1 M; 20 ml), neutralized with dil. acetic acid (1%, in ethanol), dried up, chromatographed with the solvent SB3, and then crystallized with diisopropyl ether to give colorless XIIIa (27 mg; 65%), mp 94—96 °C, $[\alpha]_D^{25}$ −77° (*c* 1.0, $CHCl_3$), ν_{max}^{KBr}: 1690, 1655 (urethane); $\delta_{CDCl_3}^{TMS}$ 2.94 (3H, singlet; NCH_3), 3.57 (3H, singlet; OCH_3), 4.20 (1H, doublet; H-1, $J_{1,2}$=7.5 Hz).

Found: C, 52.24; H, 8.12; N, 3.37%. Calcd for $C_{18}H_{33}NO_9$: C, 53.06; H, 8.16; N, 3.44%.

Methyl 4-O-(2,6-Dideoxy-3-C-methyl-β-L-ribohexopyranosyl)-3,6-dideoxy-3-(N-methylcarboethoxyamino)-α-D-glucopyranoside (XIIIb). XIIb (26 mg) was ethanolyzed in the same manner as above to give colorless XIIIb (11 mg; 67%), mp 137—139 °C; $[\alpha]_D^{25}$ +17° (*c* 1.0, $CHCl_3$); ν_{max}^{KBr}: 1690 (urethane); $\delta_{CDCl_3}^{TMS}$: 2.89 (3H, singlet, NCH_3), 3.56 (3H, singlet; OCH_3).

Found: C, 52.77; H, 8.18; N, 3.49%. Calcd for $C_{18}H_{33}NO_9$: C, 53.06; H, 8.16; N, 3.44%.

Methyl 4-O-(2,6-Dideoxy-3-C-methyl-α-L-ribohexopyranosyl)-3,6-dideoxy-3-methylamino-β-D-glucopyranoside (XIVa). XIIIa (17 mg) was hydrolyzed with aqueous barium hydroxide (8%; 4 ml) at 95 °C for 10 hr, neutralized with carbon dioxide, filtered and then chromatographed over Dowex 1X2 (OH) with carbon dioxide-free water to give a ninhydrin-positive hard syrup of XIVa (11 mg; 79%), which was crystallized with diisopropyl ether to afford colorless crystals, mp 164—167 °C (sintered at 155 °C), $[\alpha]_D^{25}$ −68° (*c* 0.7, CH_3OH).

Found: C, 53.14; H, 8.74; N, 4.03%. Calcd for $C_{15}H_{29}NO_7$: C, 53.72; H, 8.71; N, 4.18%.

Methyl 4-O-(2,6-Dideoxy-3-C-methyl-β-L-ribohexopyranosyl)-3,6-dideoxy-3-methylamino-β-D-glucopyranoside (XIVb). XIIIb (12 mg) was hydrolyzed as above to give a hard syrup of XIVb (8.0 mg; 81%), which was crystallized with diisopropyl ether to give colorless crystals, mp 195—197 °C, $[\alpha]_D^{25}$ +8° (*c* 0.7, CH_3OH).

Found: C, 53.17; H, 8.68; N, 4.12%. Calcd for $C_{15}H_{29}NO_7$: C, 53.72; H, 8.71; N, 4.18%.

Methyl 4-O-(2,6-Dideoxy-3-C-methyl-α-L-ribohexopyranosyl)-3,6-dideoxy-3-dimethylamino-β-D-glucopyranoside (XVa). XIVa (11 mg) was dissolved in ethanol (2 ml) containing formaline (37%; 0.1 ml), hydrogenated over palladium black (10 mg) under hydrogen pressure of 50 lb/in² (initial) for 18 hr at room temperature, filtered, evaporated to dryness and then chromatographed over Dowex 1X2 (OH), irrigated with carbon dioxide-free water to give a homogenous ninhydrin-negative syrup of XVa (11 mg; 96%),[22] which could not be crystallized by any treatment; $[\alpha]_D^{25}$ −93° (*c* 1.1, C_2H_5OH); $\delta_{D_2O}^{TMSS}$: 1.22 (3H, singlet; CH_3-3′), 1.30 6H, doublet; CH_3-5, CH_3-5′, *J*=6.5 Hz), 2.48 (6H, singlet; NCH_3), 3.54 (3H, singlet; OCH_3), 4.24 (1H, doublet; H-1, $J_{1,2}$=8.0 Hz).

Methyl 4-O-(2,6-Dideoxy-3-C-methyl-β-L-ribohexopyranosyl)-3,6-dideoxy-3-dimethylamino-β-D-glucopyranoside (XVb). XIVb 9.0 mg) was *N*-methylated as above to give a ninhydrin-negative glass of XVb (8.5 mg; 91%), $[\alpha]_D^{25}$ +14° (*c* 0.9, C_2H_5OH); $\delta_{D_2O}^{TMSS}$: 1.26 (3H, singlet; CH_3-3′), 2.43 (6H, singlet; NCH_3), 3.53 (3H, singlet; OCH_3), 4.31 (1H, doublet; H-1, $J_{1,2}$=8.0 Hz). Trituration with *n*-hexane turned XVb into powder, mp 134—136 °C (sintered at 125 °C).

Found: C, 53.23; H, 8.72; N, 3.82%. Calcd for $C_{16}H_{31}NO_7 \cdot 1/2H_2O$: C, 53.61; H, 9.00; N, 3.91%.

When a sample of XVa and XVb was methanolyzed with dil. methanolic hydrochloric acid,[18] formation of methyl 2,6-dideoxy-3-*C*-methyl-α- and β-*ribo*hexopyranoside was observed by tlc with the solvent SB2. Hot hydrolysis of XVa and XVb with dil. hydrochloric acid[18] gave 3,6-dideoxy-3-dimethylamino-D-glucopyranose, which was detected by tlc with the solvent SC2.

The authors wish to thank Toyo Jozo Co. for the supply of Leucomycin bulk, and Mr. K. Kushida of Nichiden-Varian for measurement of the 100 MHz PMR spectrum.

22) A sample of methyl 2,6-dideoxy-3-*C*-methyl-α- and β-*ribo*hexopyranoside was subjected to hydrolysis with hot aqueous barium hydroxide and subsequent reductive *N*-methylation. Its perfect stability under this treatment was confirmed by observation of tlc. On the other hand, Compound X gave IX by this treatment, with no by-products.

Photoinduced Reactions. LXVIII. Photochemical Dehydrogenation[1] of Imidazolines to Imidazoles

Teruo MATSUURA, Yoshikatsu ITO, and Isao SAITO

Department of Synthetic Chemistry, Faculty of Engineering, Kyoto University, Sakyo-ku, Kyoto 606

(Received March 22, 1973)

Imidazolines were found to be dehydrogenated to imidazoles by irradiation at 2537 Å or above 2900 Å in acetone. The n,π^* triplet acetone acts as a hydrogen-abstracting agent giving 4- and/or 5-imidazolinyl radicals which in turn are transformed into imidazoles. This scheme is supported by the fact that the AIBN-initiated dehydrogenation of imidazolines gave corresponding imidazoles, that oxygen quenched the photochemical dehydrogenation, and that in some cases coupling products between the imidazolinyl and the acetone ketyl radicals were formed. Various data indicate that the imidazolinyl radical reverts to the parent imidazoline by hydrogen transfer from the acetone ketyl radical during the course of photolysis.

There are several reports on the methods of dehydrogenation of imidazolines leading to the corresponding imidazoles.[2] These methods involve dehydrogenation with catalysts such as nickel, iron, platinum, and palladium or with hydrogen acceptors such as sulfur and selenium. It is well-known that a variety of carbonyl compounds, in their excited states, can abstract hydrogen from various hydrogen-donating substrates.[3] However, examples of the photochemical dehydrogenation of hydroaromatic compounds to aromatic compounds are relatively few,[4] since simple carbonyl compounds often photochemically react with a hydrogen donor to form coupling products.[5] In the present paper we report a simple method for dehydrogenating imidazolines to imidazoles by irradiation in acetone.

Results and Discussion

Irradiation of an acetone solution of imidazolines (I) with a low-pressure mercury lamp (mainly 2537 Å) under nitrogen atmosphere followed by column chromatography of the reaction products gave corresponding imidazoles (II) in reasonable yields. The results are summarized in Table 1. 2-Methylimidazolines (Ia and Ib) gave dehydro-coupling products (III, IV and V) besides the corresponding imidazoles, but 2-hydroxyimidazoline (Ii) only a coupling product VI. It should be noted that both *cis*- (If; amarine) and *trans*- (Ig; isoamarine) 2,4,5-triphenylimidazolines underwent *cis*, *trans*-isomerization being accompanied by dehydrogenation to 2,4,5-triphenylimidazole (IIf; lophine). Acetone pinacol was isolated in low yield only in cases of Ia and Ib but not in all the other cases.

Oxygen was found to quench the formation of an imidazole. Thus, irradiation of 2-methylimidazoline (Ia) under similar conditions except under bubbling oxygen instead of nitrogen gave 2-methylimidazolinium acetate (12%) besides some recovered starting material (27%) but no 2-methylimidazole (IIa). Irradiation of an acetone solution of Ia, which had been degassed by four freeze-thaw cycles at 10^{-4} mm under cooling with liquid nitrogen, gave no effect on the reaction, and the IIa, IIIa, and pinacol were obtained in the same ratio as that under nitrogen. On irradiation in benzene or isopropyl alcohol under nitrogen, these imidazolines (Ib, Ic, Id, and Ie) were recovered unchanged except that *cis*, *trans*-isomerization was observed with amarine (If) and isoamarine (Ig).[6] Thus it is considered that the imidazoles were formed *via* 4-(VII) and/or 5-(VIII) imidazolinyl radicals which were formed from the imidazolines by hydrogen abstraction with the n,π^* triplet state of acetone as shown in Scheme 1.

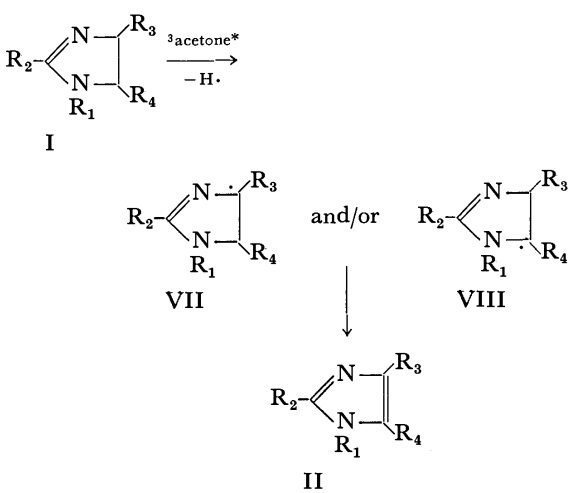

I VII VIII II

Scheme 1.

In order to confirm this scheme, hydrogen abstraction of 2-methylimidazoline (Ia), amarine (If), and isoamarine (Ig) by the 1-cyano-1-methylethyl radical generated by thermolysis of azobisisobutyronitrile (AIBN) was carried out. The corresponding imidazoles were obtained, their yields being dependent on the

1) Part LXVII: I. Saito, M. Imuta, and T. Matsuura, *Chem. Lett.*, **1972**, 1197.

2) a) L. P. Kyrides, F. B. Zienty, G. W. Steahly, and H. L. Morril, *J. Org. Chem.*, **12**, 577 (1947); b) H. H. Strain, *J. Amer. Chem. Soc.*, **49**, 1558 (1947); c) E. Fischer, *Ann.*, **211**, 217 (1882); d) British Patent 484862 (1938); *Chem. Abstr.*, **32**, 7679 (1938); e) R. E. Klem, H. F. Skinner, H. Balba, and R. W. Isensee, *J. Heterocycl. Chem.*, **7**, 403 (1970); f) T. Hayashi, M. Kuyama, E. Takizawa and M. Hata, This Bulletin, **37**, 1702 (1964).

3) D. C. Neckers, "Mechanistic Organic Photochemistry," Reinhold Publ. Co., New York, N. Y. (1967), p. 163.

4) A. Schönberg, G. O. Schenck, and O.-A. Neumüller, "Preparative Organic Photochemistry," Springer-Verlag New York Inc., New York, N. Y. (1968), p. 151.

5) Ref. 4, p. 198.

6) *cis*,*trans*-Isomerization of amarine and isoamarine, indeed takes place in various organic solvents.[7]

7) T. Matsuura and Y. Ito, *Chem. Lett.*, **1972**, 431.

Table 1. Photochemical dehydrogenation of imidazolines I to imidazoles II in acetone

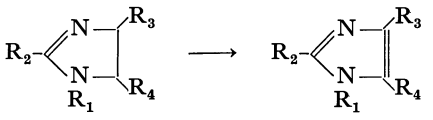

I II

R_1	I				Irradiation time (hr)	Recovered I (%)	Yield of II (%)[c]	Other products (%)[c]
	R_1	R_2	R_3	R_4				
Ia	H	Me	H	H	24	0	60	III (9)
Ib	Me	Me	H	H	24	0	22	IV (6)+V (5)
Ic	H	Ph	H	H	24	58	15	
					75	36	36	
Id	Me	Ph	H	H	24	26	18	
Ie	$(CH_2)_2OH$	Ph	H	H	50	37	20	
If	H	Ph	Ph	Ph[a]	24	25	35	Ig (16)
Ig	H	Ph	Ph	Ph[b]	24	16	28	If (27)
Ih	H	SH	H	H	24	100	0	
Ii	H	OH	H	H	24	36	0	VI (20)

a) 4,5-*cis* (amarine). b) 4,5-*trans* (isoamarine)

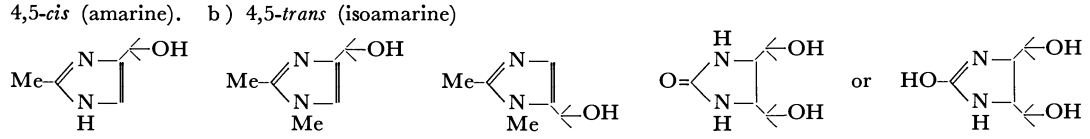

III IV V VI

c) Based on the starting imidazolines.

Table 2. AIBN-initiated dehydrogenation of imidazolines[a]

Imidazoline	Concentration ($\times 10^{-2}$ M)		Molar ratio of AIBN/Imidazoline	Yield of imidazole (%)[b]
	Imidazoline	AIBN		
2-Methyl- (Ia)	10.20	9.38	0.92	4.0
	9.60	4.69	0.49	0
cis-2,4,5-Triphenyl- (If)	2.72	3.70	1.36	26.0
	2.67	1.85	0.69	12.0
	2.71	0.37	0.14	4.5
trans-2,4,5-Triphenyl- (Ig)	2.68	8.66	3.24	3.2
	2.73	4.89	1.79	2.0

a) Reaction conditions: 68±1.5°C in acetonitrile under nitrogen. b) Based on the starting imidazoline.

AIBN concentration and also on the structural feature of the imidazolines (Table 2). A difference between the reactivities of Ia and If may be due to the magnitude of the resonance stabilization of the intermediate radicals, VII and/or VIII: *i.e.*, radicals VIIf and VIIIf are obviously more stabilized by a phenyl group at positions 4 and 5, respectively. The slower dehydrogenation rate in Ig compared with If is probably due to a steric repulsion between a phenyl group at position 5 (or 4) and 1-cyano-1-methylethyl radical produced from AIBN in the abstraction of a hydrogen atom at position 4 (or 5).

The mechanism of Scheme 1 involving the imidazolinyl radical (VII or VIII), which is formed from the starting imidazoline by hydrogen abstraction with the n,π^* triplet state of acetone, is supported by the following facts. (1) Imidazoles are also formed by the hydrogen abstraction reaction initiated by AIBN (Table 2). (2) Oxygen, a triplet quencher,[8] inhibits the formation of 2-methylimidazole from 2-methylimidazoline. (3) In some cases coupling products such as III, IV, V, and VI are formed as byproducts, which obviously result from coupling between the acetone ketyl radical and the imidazolinyl radical VII or VIII followed by dehydrogenation of the coupling products in cases of III, IV, and V. Matsuura *et al.* have found that irradiation of 1,2-dimethylimidazole (IIb) in acetone gives exclusively IV, which is formed *via* an unstable oxetane intermediate.[9] Thus the formation of an almost equal amount of IV and V from Ib should result form the coupling between the acetone ketyl radical and the imidazolinyl radicals VIIb and VIIIb, although it is possible that a part of IV formed results from the photochemical addition of acetone to IIb (Scheme 2).

2-Methylimidazoline (Ia) is more susceptible to photochemical dehydrogenation than amarine (If) but less susceptible to the AIBN-initiated one (Tables 1

8) W. M. Moore, G. S. Hammond, and R. P. Foss, *J. Amer. Chem. Soc.*, **83**, 2789 (1961).

9) T. Matsuura, A. Banba, and K. Ogura, *Tetrahedron*, **27**, 1211 (1971).

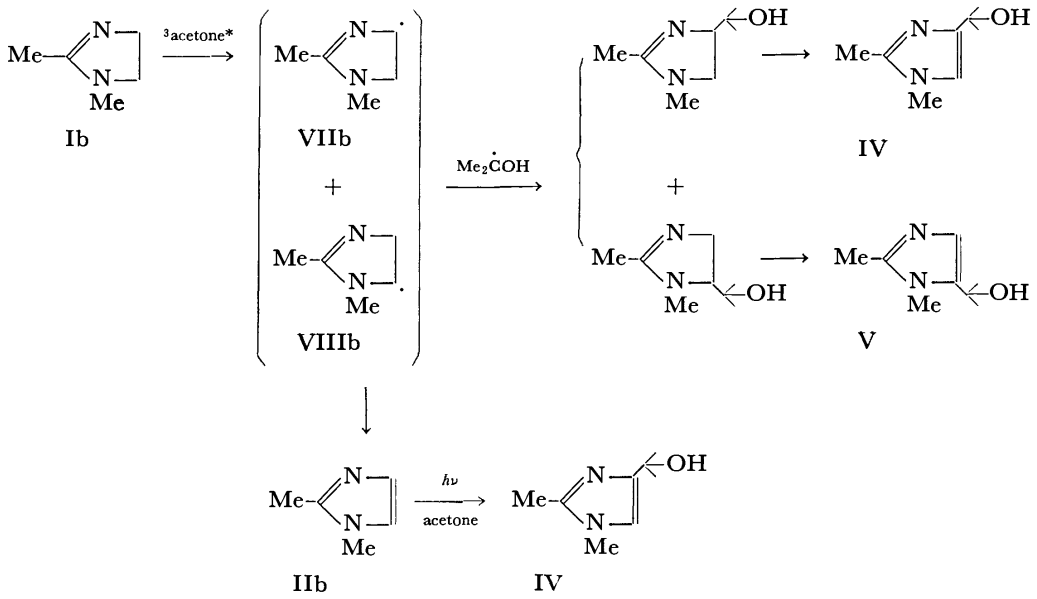

Scheme 2.

and 2). The *cis,trans*-isomerization of amarine (If) and isoamarine (Ig), which is accompanied by dehydrogenation to lophine (IIf), occurs only during irradiation in acetone but not during the AIBN-initiated free radical reaction. This can be interpreted by assuming that, in the case of photoreaction, free radical intermediates VII and/or VIII revert in part to the parent imidazoline by a hydrogen transfer from the acetone ketyl radical[10,11] which is known to act as a hydrogen donor as seen in the photoreduction of benzophenone with isopropyl alcohol,[14] and that, in the absence of such a hydrogen donor (AIBN-initiated reaction), the intermediate radicals VII and/or VIII are transformed to an imidazole II without reverting to the parent imidazoline I (Scheme 3). As regards the overall reaction from I to II, the imidazole-forming step (VII or VIII→II) may be more important in the photoreaction involving a reverse process from VII or VIII to I than in the AIBN-reaction without such a process. In contrast to this, the raidcal-forming step may be more important in the AIBN-reaction than in the photoreaction.[15]

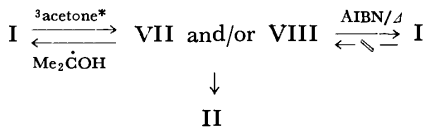

Scheme 3.

For the sake of confirmation, the total π electron energies (E_π) of I, VII, and II were calculated by the HMO method.[16,18] It was assumed from the calculated E_π values for VII and VIII that VII contributes more than VIII to the free radical intermediate. Comparisons of the values of $\Delta E_{\pi 1}=E_\pi(\mathrm{VII})-E_\pi(\mathrm{I})$ and $\Delta E_{\pi 2}=E_\pi(\mathrm{II})-E_\pi(\mathrm{VII})$ with the yields of the imidazoles from the imidazolines I are given in Table 3. The yield of the photochemical conversion to imidazoles decreases in the order Ia>If>Ib>Ic. This is qualitatively correlated with $\Delta E_{\pi 2}$ but not with $\Delta E_{\pi 1}$. A decrease in the yield of the photochemical conversion to imidazoles seems to be general for 1-alkylimidazolines as seen in the case of Ib, Id and Ie (Table 1). The yield of the AIBN-initiated conversion to imidazoles seems to be correlated with $\Delta E_{\pi 1}$ rather than $\Delta E_{\pi 2}$. This led us to conclude that in the photochemical de-

10) In the cases of amarine (If) and isoamarine (Ig), it was shown that intermediate radicals VIIf and/or VIIIf revert only to amarine but not to isoamarine.[7] Formation of isoamarine (Ig) during the course of irradiation of amarine was found to arise from the excited state of amarine itself.[6,7]

11) The bond dissociation energy of the acetone ketyl radical ($Me_2\dot{C}O$–H) appears lower than that of $Me_2C(CN)$–H, since that of $\cdot CH_2O$–H (29 kcal/mol[12]) is much lower than that of H–CH_2CN (*ca.* 86 kcal/mol[13]).

12) M. K. Phibbs and B. deB. Darwent, *J. Chem. Phys.*, **18**, 495 (1950).

13) J. A. Kerr. *Chem. Rev.*, **66**, 496 (1966).

14) E. S. Huyser and D. C. Neckers, *J. Amer. Chem. Soc.*, **85**, 3641 (1963).

15) This is similar to the notion of a successive reaction:

$$A \underset{k_{-1}}{\overset{k_1}{\rightleftharpoons}} B \qquad B \xrightarrow{k_2} C$$

If the process B→A is much faster than the process B→C, the latter should be rate-determining (case 1). If on the contrary B→A is much slower than B→C, the former process should be rate-determining (case 2). The photochemical reaction is similar to case 1 and the AIBN-initiated one to case 2.

16) Parameters were selected from those presented by Streitwieser[17a] except for parameters concerning sulfur bonds.[17b] The use of the E_π value for VIII for the following discussion does not alter the conclusion.

17) a) A. Streitwieser, Jr., "Molecular Orbital Theory," John Wiley & Sons, Inc., New York, N. Y. (1961), p. 117. b) T. Yonezawa, N. Nagata, H. Kato, and A. Imamura, "Ryoshi-Kagaku Nyumon," Kagaku Dojin, Tokyo (1968), p. 56.

18) An attempt to correlate the relative rates of hydrogen abstraction from a series of arylmethanes by the trichloromethyl radical or bromine atom with the change in HMO ΔE_π value has been reported. [J. D. Unruh and G. J. Gleicher, *J. Amer. Chem. Soc.*, **93**, 2008 (1971); R. B. Roark, J. M. Roberts, D. W. Croom, and R. D. Gillion, *J. Org. Chem.*, **37**, 2042 (1972)].

19) When the twisted angle is assumed to be 25°, $\Delta E_{\pi 2}$ value is calculated to be 2.58445β. G. Rasch [*Z. Phys. Chem.*, **219**, 180 (1962)] assumed the twisted angle of phenyl groups of *cis*-stilbene as $26\pm4°$.

TABLE 3. COMPARISON OF THE YIELD OF IMIDAZOLES (II) FROM IMIDAZOLINES (I) WITH $\Delta E_{\pi 1}$ AND $\Delta E_{\pi 2}$ VALUES

Imidazoline	Yield of imidazole (%)			$\Delta E_{\pi 2}(\beta)$[d]	$\Delta E_{\pi 1}(\beta)$[d]
	Photochemical		AIBN-initiated[c]		
	High concn[a]	Low concn[b]			
2-Methyl- (Ia)	60	20.0±0.5	6	2.58100	0.67520
1,2-Dimethyl- (Ib)	22	—	—	2.55070	0.69020
2-Phenyl- (Ic)	15	—	—	2.52744	0.73246
cis-2,4,5-Triphenyl- (If)	35	16.1±1.2	26	2.53995[e]	1.21005

a) Taken from the data of Table 1 (irradiation time, 24 hr). b) A *ca.* 10^{-3} M acetone solution was externally irradiated using a merry-go-round apparatus and the yields of imidazoles formed were determined by UV analysis. c) Taken from the data of Table 2. d) See text. e) Calculation was carried out by assuming that two phenyl groups at positions 4 and 5 are twisted 30° from the plane of the imidazole ring.[19]

TABLE 4. DEUTERIUM INCORPORATION INTO 2-PHENYLIMIDAZOLINE (Ic) DURING PHOTOLYSIS IN THE PRESENCE OF MeOD AND D_2O IN ACETONE

Concn of Ic ($\times 10^{-2}$ M)	Solvent			Irradn. time (hr)	Ic-d_1[a] (%)
	Acetone	MeOD	D_2O		
4.75	5	10	0	41[b]	0.2±0.1
3.63	5	10	5	163[c]	1.9±0.1
3.43	5	10	5	245[c]	1.6±0.2

a) Deuterium analysis was done by mass-spectrometry. c) Externally irradiated with a 100W high-pressure mercury lamp (Pyrex filter). c) Externally irradiated with a 450W high-pressure mercury lamp (Pyrex filter).

hydrogenation the resonance stabilization of the product imidazoles, represented by a higher $\Delta E_{\pi 2}$ value, is more important, and that in the AIBN-initiated dehydrogenation the resonance stabilization of the intermediate free radical VII, represented by a higher $\Delta E_{\pi 1}$ value, is more important. Accordingly, these calculated data are not inconsistent with the mechanism shown in Scheme 3.

For the sake of confirming the back reaction of the imidazolinyl radicals VII or VIII to I by a hydrogen transfer from the acetone ketyl radical (Scheme 3), an acetone solution of 2-phenylimidazoline (Ic) was irradiated in the presence of MeOD and D_2O with different periods. The incorporation of deuterium into the recovered Ic obviously indicates that the back hydrogen transfer to VII or VIII by the acetone ketyl radical occurs in the photochemical reaction (Table 4). The deuterium incorporation into Ic was not so much as expected. This is probably due to a slower exchange reaction between the acetone ketyl radical and MeOD or D_2O than the back-transfer reaction.

Experimental

All the melting points are uncorrected. The NMR spectra were taken on an NEVA T-60 spectrometer using tetramethylsilane as an internal standard. The IR spectra were measured on a JASCO IRS spectrometer. The UV spectra were obtained with a JASCO ORD/UV-5 spectrometer. Vapor phase chromatography (vpc) was carried out with a Shimadzu GC-2C apparatus on Apiezon Grease L using helium as a carrier gas. Thin layer chromatography (tlc) was carried out with Merck "Kieselgel GF 254," "Aluminiumoxid GF 254" or Nagel "Cellulosepulver MN 300 G," using UV light and iodine vapor for compound detection. Column chromatography was carried out with Mallinckrodt silicic acid (100 mesh).

Starting Materials. Commercial 2-Methylimidazoline (Ia) and 2-phenylimidazoline (Ic) were used after recrystallization from acetone. Commercial ethylenethiourea (Ih) and ethyleneurea (Ii) were used without further purification.

1,2-Dimethylimidazoline (Ib) was prepared by the method of King and McMillan.[20] To 5 g of *N*-methylethylenediamine was added 7 g of acetic anhydride at room temperature and the mixture was heated at 170—190 °C for 1 hr. After cooling 3 g of magnesium powder was added. The mixture was heated at about 300 °C for 1 hr, then1, 2-dimethylimidazoline formed was distilled out. It was further refined by vacuum distillation to give pure Ib as a colorless liquid (3 g; 46%) which gave satisfactory spectral and analytical data; bp *ca.* 70 °C/14 mmHg (lit,[21] 60—62 °C/12 mmHg); n_D^{26} 1.4759 (lit,[21] n_D^{20} 1.4766); picrate, mp 137—138.5 °C (lit,[21] 145—147 °C).

1-Methyl-2-phenylimidazoline (Id) was prepared by the method of Hill and Aspinall.[22] 18.4 g of benzoic acid was added to 11.2 g of *N*-methylethylenediamine and the mixture was heated at 150—170 °C for 1.5 hr, then at 200—220 °C for 2 hr. The product was refined by repeated vacuum distillation to give Id as colorless liquid (5 g; 21%); bp *ca.* 95 °C/4 mmHg; IR (neat 2850, 1605, 1270, 1065, 775, and 700cm^{-1}; NMR ($CDCl_3$) τ 2.30—2.69 (m, 5H), 5.88—6.80 (m, 4H), and 7.20 (s, 3H); *m/e* 160 (M^+). Found: C, 75.25; H, 7.79; N, 17.31%. Calcd for $C_{10}H_{12}N_2$: C, 74.96; H, 7.55; N, 17.49%. It gave a picrate, mp 121—123 °C.

1-(β-hydroxyethyl)-2-phenylimidazoline (Ie) was prepared analogously from N-(β-hydroxyethyl)ethylenediamine and benzoic acid, as colorless crystals; mp 103—104.5 °C; IR (Nujol) 3200, 1590, 1570, 1235, 765, and 685 cm^{-1}; NMR ($CDCl_3$) τ 2.33—2.72 (m, 5H), 5.90—7.00 (m, 8H), and 6.17 (s, 1H). Found: C, 69.68; H, 7.13; N, 14.81%. Calcd for $C_{11}H_{14}ON_2$: C, 69.50; H, 7.37; N, 14.71%.

Amarine (If) was prepared by the method of Strain[23] and purified by repeated recrystallization from anhydrous ether. Isoamarine (Ig) was prepared by isomerizing amarine with sodium methoxide at 160—170 °C,[24] and purified by repeated recrystallization from ethanol.

General Procedure for Photodehydrogenation. The following procedure was used for experiments listed in Table 1. A solution of about 2 g of an imidazoline in 220 ml of acetone was irradiated with a 10 W low-pressure mercury lamp (Vycor

20) J. A. King and F. H. McMillan, *J. Amer. Chem. Soc.* **68**, 1774 (1946).
21) T. Tkaczynski, *Chem. Abstr.*, **64**, 587b (1966).
22) A. J. Hill and S. R. Aspinall, *J. Amer. Chem. Soc.*, **61**, 822 (1939).
23) H. H. Strain, *ibid.*, **49**, 1558 (1927).
24) E. H. Rodd, "Chemistry of Carbon Compounds," IVA, Elsevier Publ. Co., Amsterdam (1957), p. 304.

housing) under nitrogen at room temperature for 24 hr or more. After irradiation the solvent was removed under reduced pressure and the residue was chromatographed on a silica gel column. The yield of products was obtained by NMR or vpc analysis of the reaction mixture or by product isolation.

Isolation and Identification of Dehydrogenation Products. *2-Methylimidazoline (Ia)*: The residue obtained from 2.10 g of Ia was chromatographed on 70 g of silica gel. Elution with 100 ml of acetone yielded 350 mg of an oil which was again chromatographed to give 150 mg of pinacol (identified by IR and NMR). Further elution with 200 ml of acetone–ethanol (1 : 1) gave 1.18 g of a solid. Recrystallization from chloroform gave 400 mg of 4-(α-hydroxyisopropyl)-2-methylimidazole (III) as colorless crystals which were identical with an authentic sample[9] (IR, NMR, and mixed mp). Crystals obtained from the mother liquor were recrystallized from benzene to give 2-methylimidazole (IIa) as colorless crystals, identical with a commercial authentic sample (IR, NMR and mixed mp). Further elution of the chromatogram yielded 680 mg of a solid which was identified as IIa. The yields of the products were determined by NMR analysis of the product mixture with an internal standard (acenaphthene). The yield of pinacol was 6% assuming that 1 mol of Ia gives 1 mol of pinacol.

1,2-Dimethylimidazoline (Ib). The residue obtained from 1.85 g of Ib was chromatographed on 50 g of silica gel. Elution with 300 ml of chloroform and acetone (1 : 1) yielded 300 mg of an oil which was shown by IR and NMR to contain pinacol. Further elution with 300 ml of acetone yielded 110 mg of a solid which was recrystallized from acetone to give 10 mg of 1,2-dimethyl-5-(α-hydroxyisopropyl)-imidazole (V) as colorless crystals; mp 179—181 °C; IR (Nujol) 3200, 1150, and 810 cm^{-1}; NMR ($CDCl_3$) τ 3.33 (s, 1H), 6.25 (s, 3H), 6.79 (s, 1H), 7.67 (s, 3H), and 8.39 (s, 6H); mass spectrum, *m/e* 154 (M^+). The NMR and mass spectra are very similar to those of IV.[9]

Found: C, 62.67; H, 9.23; N, 17.71%. Calcd for $C_8H_{14}ON_2$: C, 62.30; H, 9.15; N, 18.15%.

The mother liquor was shown by IR and NMR analyses to consist of 1,2-dimethylimidazole (IIb), 1,2-dimethyl-4-(α-hydroxyisopropyl)imidazole (IV) and V. Compound IIb was isolated by vpc and identified by comparison with an authentic sample[9] (IR). Compound IV was dehydrated during vpc to give 1,2-dimethyl-4-isopropenylimidazole,[9] which was identified by comparison with an authentic sample[9] (IR). Further elution of the chromatogram with acetone yielded a mixture of IIb, IV, and V, identified by tlc. The yields of these products were determined by vpc analysis with an internal standard (*p-t*-butylphenol). NMR analysis of the product mixture showed the formation of pinacol (0.3 mol/mol of IIb).

2-Phenylimidazoline (Ic). The residue obtained from 2.60 g of Ic was chromatographed on 60 g of silica gel. Elution with chloroform and ethanol (9 : 1) yield 2-phenylimidazole (IIc), identical with a commercial authentic sample (IR,, NMR and mixed mp). The yield of IIc was determined by vpc analysis with an internal standard (diphenyl).

1-Methyl-2-phenylimidazoline (Id). The residue obtained from 2.03 g of Id was chromatographed on 60 g of silica gel. Elution with chloroform yielded 1-methyl-2-phenylimidazole (IId) as a liquid; bp 140—145 °C (bath temperature)/3 mmHg (lit,[24] bp 175 °C/15 mmHg); IR (neat) 1500, 1480, 1410, 1270, 770, 715, and 700 cm^{-1}; NMR ($CDCl_3$) τ 2.21—2.60 (m, 5H), 2.83 (d, 1H, J=1 Hz), 3.01 (d, 1H, J=1 Hz) and 6.25 (s, 3H). It gave satisfactory elemental analyses. The yield of IId shown in Table 1 is based on the product isolated. The recovered Id was analyzed by vpc.

Amarine (If) and Isoamarine (Ig). The residues obtained from 2.09 g of If and 2.02 g of Ig were chromatographed on 70 g of silica gel, respectively. Elution with chloroform successively gave lophine (IIf), Ig, and If, which were identical with authentic samples (IR and NMR). The yield of IIf was determined by UV analysis in ethanol and the recovered materials by NMR analysis with an internal standard, 2-methylimidazoline (in carbon tetrachloride–dimethylsulfoxide-d_6).

2-Hydroxyimidazoline (Ii). A suspension of Ii (1.63 g) was irradiated. The insoluble solid separated by filtration was found to be mainly the recovered Ii (IR and NMR). The residue from the filtrate was chromatographed on 60 g of silica gel. Elution with acetone yielded VI as colorless crystals; mp 198—201 °C; IR (Nujol) 3300, 1655, and 1175 cm^{-1}; NMR (DMSO-d_6) τ 5.26 (s, 4H), 6.63 (s, 2H), and 8.86 (S, 12H).

Found: C, 53.48; H, 8.94; N, 13.75%. Calcd for $C_9H_{18}N_2O_3$: C, 53.44; H, 8.97; N, 13.85%.

The compound showed a UV maximum at 275 nm in ethanol identical with that of Ii. Further elution yielded additional Ii. The yields given in Table 1 are based on the product isolated.

Photoreaction of 2-Methylimidazoline (Ia) under Oxygen. A solution of 2.08 g of Ia in acetone was irradiated for 24 hr under similar conditions but with oxygen-bubbling instead of nitrogen. After removal of the solvent under reduced pressure, the residue was chromatographed on 60 g of cellulose powder (Whatman CF11). Elution with 1200 ml of benzene–chloroform (1 : 4) yielded 530 mg (27%) of Ia, identified by IR. Further elution with 1000 ml of acetone–ethanol (1 : 1) yielded 1.12 g of an oil. Vacuum distillation of the oil gave 400 mg (12%) of 2-methylimidazolinium acetate, mp 95—96 °C (lit,[26] mp 94.5—95.5 °C), which was identical with an authentic sample (IR and NMR).

Hydrogen Abstraction of Imidazolines Initiated with AIBN. A given amount of each imidazoline was dissolved in 150 ml of acetonitrile. The solution was heated at 68±1.5 °C under nitrogen, a given amount of azobisisobutyronitrile being added. After being left standing at the same temperature for 24 hr, the mixture was worked up in the same manner as in the photoreaction. The results are given in Table 2. 2-Methylimidazole was analyzed by NMR with an internal standard, pinacol, and lophine by UV in ethanol.

Deuterium Incorporation Experiment. A solution of *ca.* 100 mg of 2-phenylimidazoline (Ic) in a mixture of acetone and MeOD and D_2O placed in a Pyrex tube was sealed after bubbling nitrogen and irradiated externally. After evaporation of the mixture under reduced pressure, the residue was dissolved in chloroform and washed three times with 2 ml of water to remove any deuterium bound to nitrogen atom of Ic. The solution was evaporated after being dried with anhydrous sodium sulfate. The recovered Ic in the residue was isolated by preparative tlc (Al_2O_3; acetone–ethanol (3 : 1)) and recrystallized from benzene–petroleum ether. The pure Ic thus obtained was analyzed on a Hitachi VD-10001-A mass spectrometer. The molecular ion region was scanned several times for each sample. Deuterium contents were calculated by comparing peak heights with those of a non-deuterated sample of Ic.

25) I. E. Balaban and H. King, *J. Chem. Soc.*, **127**, 2713 (1927).

26) E. C. Taylor and W. A. Ehrhart, *J. Org. Chem.*, **28**, 1108 (1963).

Oxidation by Transition Metal Complexes. VI.[1] Oxidation of Cyclohexenes Catalyzed by Rhodium Complexes

Kiyotomi KANEDA,* Takashi ITOH, Yuzo FUJIWARA, and Shiichiro TERANISHI

Department of Chemical Engineering, Faculty of Engineering Science, Osaka University, Osaka 560

(Received March 15, 1973)

Rhodium complexes can cause the catalytic oxidation of cyclohexene to give ketone, alcohol, and epoxide. The product distribution is dissimilar to that of the metal-catalyzed decomposition of cyclohexene hydroperoxide(V). Ketone and alcohol are derived from the decomposition of the intermediate hydroperoxide (V) but epoxide is not formed by the oxygen transfer reaction from V. Oxidation of methylcyclohexenes was also studied and discussed in relation to the effect of methyl substituent.

X-Ray analysis of oxygen complexes indicated that the coordinated oxygen is in an electronically excited state, that is, the anionic species of O_2^-, O_2^{--} formed by charge transfer from the metal.[2] Recently, the application of the coordinated oxygen to oxidation reaction has been studied extensively, particularly using rhodium complexes.[3] It is generally said that rhodium complexes act as the catalyst for hydrogen abstraction from substrates by the coordinated oxygen and as a catalyst inducing the decomposition of hydroperoxide formed by oxygen and olefin (Haber-Weiss mechanism).

In previous papers, we reported on the oxidation of styrene and its derivatives catalyzed by rhodium complexes and proposed that the oxidation might proceed *via* a four-center intermediate in which both oxygen molecule and olefin are coordinated to the rhodium complex.[1,4]

In connection with this work, we have studied the oxidation of cyclohexene and methylcyclohexene catalyzed by $RhCl(PPh_3)_3$. Although the oxidation of cyclohexene having active hydrogens at the allylic position of olefin has been investigated by many workers,[5] in the cyclohexene oxidation using rhodium complexes, the reaction products have not yet been examined in detail.

In this paper we will discuss the development of the reaction products, *i.e.*, ketones, alcohols, and epoxides.

Results and Discussion

Oxidation of Cyclohexene. Cyclohexene was oxidized under a constant bubbling of oxygen with $RhCl(PPh_3)_3$ catalyst in toluene at 80 °C for 8 hr. It gave 2-cyclohexen-1-one (I, 1530% based on catalyst), 2-cyclohexen-1-ol (II, 852%), cyclohexene oxide (III, 351%), benzaldehyde (IV, 524%), hydroperoxides, and water.

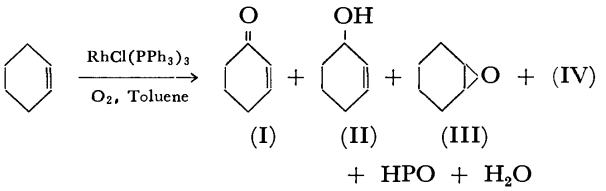

The formation of aldehyde IV is considered to arise from the oxidation of toluene solvent.[6]

The relation between yields of the products and reaction time in the cyclohexene oxidation is given in Fig. 1. The yields of I and II increased with reaction time. I was the main product for 8 hr. The content of hydroperoxides determined by the iodometric method showed a maximum value at 3 hr, suggesting that they could be intermediate species for I and II.[7] The hydroperoxides should be composed of mostly cyclohexene hydroperoxide (V).

The decomposition of V by $RhCl(PPh_3)_3$ under argon atmosphere was then carried out under the same reaction conditions as above. The starting hydroperoxide (V) was perpared by treatment of cyclohexene

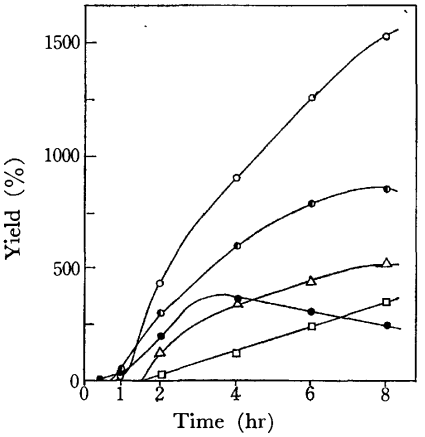

Fig. 1. Oxidation of cyclohexene with $RhCl(PPh_3)_3$.
○: 2-Cyclohexen-1-one, ◐: 2-Cyclohexen-1-ol,
●: Hydroperoxides, △: Benzaldehyde,
□: Cyclohexene oxide.

* Former name: Kiyotomi Takao

1) Part V of this series: K. Takao, H. Azuma, Y. Fujiwara, T. Imanaka, and S. Teranishi, This Bulletin, **45**, 2003 (1972).

2) a) R. Mason, *Nature*, **217**, 543 (1968). b) R. McWeeny, R. Mason, and A. D. C. Towl, *Discuss. Faraday Soc.*, **47**, 20 (1969). c) S. J. Laplaca and J. A. Ibers, *J. Amer. Chem. Soc.*, **87**, 2581 (1965). d) J. A. Mcginnety, R. J. Doedens, and J. A. Ibers, *Inorg. Chem.*, **6** 2243 (1967).

3) E. W. Stern "Transition Metals in Homogeneous Catalysis", ed. by G. N. Schrauzer, Marcel Dekker, Inc., New York (1971), p. 137.

4) K. Takao, M. Wayaku, Y. Fujiwara, T. Imanaka, and S. Teranishi, This Bulletin, **43**, 3898 (1970).

5) a) V. P. Kurkov, J. Z. Pasky, and J. B. Lavigen, *J. Amer. Chem. Soc.*, **90**, 4743 (1968). b) A. Fusi, R. Ugo, A. Pasini, and S. Cenini, *J. Organometal. Chem.*, **26**, 417 (1971). c) C. Dudley and G. Read, *Tetrahedron Lett.*, **1972**, 5273.

6) It is of noteworthy that toluene could not be directly oxidized to IV by $RhCl(PPh_3)_3$ under oxygen atmosphere.

7) In the case of styrene, hydroperoxides were scarcely detected at all and the oxidation was not remarkably affected by a free radical inhibitor. On the other hand, oxidation of cyclohexene was perfectly inhibited by the inhibitor.

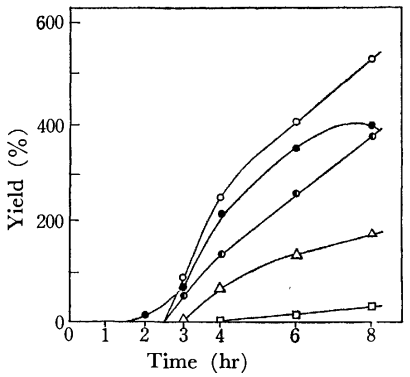

Fig. 2. Oxidation of cyclohexene with $RhCl(PPh_3)_3$ in the presence of pyridine.
Cyclohexene: 50 mmol, $RhCl(PPh_3)_3$: 0.50 mmol, Pyridine: 5 mmol, Toluene: 75 ml.
○: 2-Cyclohexen-1-one, ◐: 2-Cyclohexen-1-ol, ●: Hydroperoxides, △: Benzaldehyde, □: Cyclohexene oxide.

with azobis(2-methylpropionitrile), (ABN) under oxygen atmosphere. It decomposed within 2 hr to give ketone (I, 53% based on V), alcohol (II, 47%), IV (trace), and water, whereas the thermal decomposition of V without $RhCl(PPh_3)_3$ did not occur at 80°C for 8 hr. Thus the formation of ketone (I) and alcohol (II) can be explained by the decomposition of intermediate V according to the Haber-Weiss mechanism.

Addition of pyridine or $O=PPh_3$ to the reaction system depressed the oxidation reaction (Fig. 2). This suggests that the coordination of oxygen to the rhodium complex is prevented by the high coordination ability of these compounds.[8]

It should be noted that the decomposition of V did not result in the formation of epoxide III, while the yield of III increased with reaction time and reached 351% after 8 hr, the oxidation of 1-methylcyclohexene giving 1-methylcyclohexene oxide as the main product (1340%).

Two types of reactions are known in catalytic epoxidation, *i.e.*, double bond reacting with (a) hydroperoxide and (b) organic peracid (cooxidation).

In order to examine the possibility of mechanism (a) in this reaction system, autoxidation of cyclohexene or 1-methylcyclohexene with ABN was carried out in the presence of oxygen. It gave mainly ketones and alcohols accompanied by a small amount of epoxide. The reaction of V and cyclohexene with $RhCl(PPh_3)_3$ under argon atmosphere gave rise to only the decomposition products, I and II. None of III could be detected, the same result being also obtained with *t*-butyl hydroperoxide.

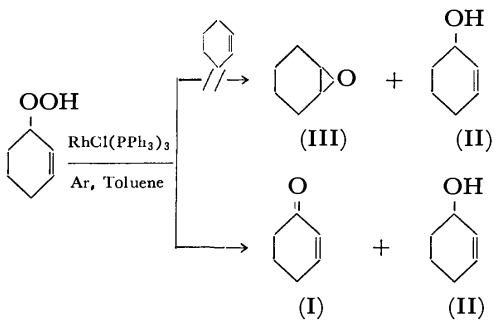

Thus the formation of epoxide (III) might be expected by cooxidation of aldehyde (IV), possibly derived from toluene solvent, and cyclohexene (mechanism b). Oxidation of cyclohexene was then carried out by adding about 5-fold excess of benzaldehyde to the catalyst. However, no remarkable accelerating effect of epoxidation was observed.

Thus the epoxidation could be explained by neither oxygen transfer reaction from V (mechanism a), nor cooxidation with IV (mechanism b). Details of the epoxidation are not clear at present, but it seems that the coordinated oxygen molecule would directly attack the olefin double bond to give epoxides.[10]

Oxidation of Methylcyclohexene. The oxidation of methylcyclohexenes with $RhCl(PPh_3)_3$ was studied in order to determine whether the methyl substituent has any steric factor or directive influence on the site of the oxidation and, hence, the isomer composition.

1-Methylcyclohexene was oxidized under the same conditions as for cyclohexene. The gas chromatogram of the reaction mixture showed eight major compounds, six of which have been isolated by preparative gas chromatography and was identified by NMR and IR in comparison with those of authentic samples. Two unidentified products were obtained in less than 50% yield. The identified products were 1-methylcyclohexene oxide (VI, 1340%), 3-methyl-2-cyclohexen-1-one (VII, 1052%), 2-methyl-2-cyclohexen-1-one (VIII, 366%), 3-methyl-2-cyclohexen-1-ol (IX 90%), 1-methyl-2-cyclohexen-1-ol (X, 83%) and IV (799%).

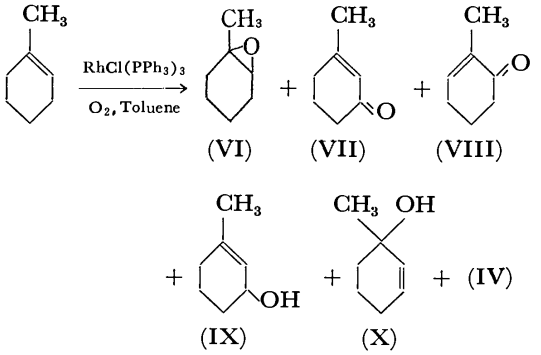

This indicates that all possible allylic positions except for the methyl group were oxidized in the reaction.

The reaction paths for the formation of ketones and alcohols might be as presented in Scheme I, allylic hydrogen of olefin being abstracted by oxygen. The attack of oxygen at the less hindered site of allyl radical (1) results in the formation of major product VII through hydroperoxide.

The total sum of yields of VII, IX, and X arising

8) James and Ochiai studied the oxidation of cyclooctene with a rhodium complex by infrared spectroscopy and reported on the mechanism in which both oxygen and olefin coordinated to rhodium.[9]

9) B. R. James and E. Ochiai, *Can. J. Chem.*, **49**, 975 (1971).

10) Recently, Minoun and his coworkers reported that expoxidation with molybdenum peroxy complex might proceed *via* the coordination of olefin to metal complex containing an aprotic 1,3-dipole mechanism.[11]

11) H. Mimoun, I. Seree de Roch, and L. Sajus, *Tetrahedron*, **26**, 37 (1970).

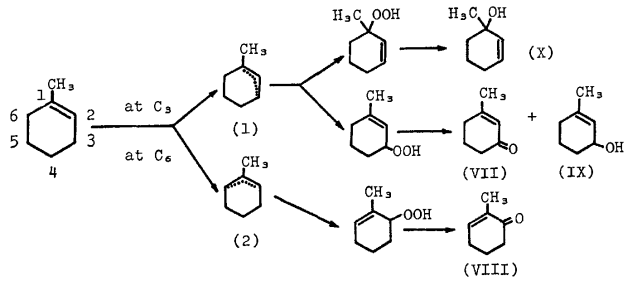

Scheme 1.

from hydrogen abstraction at C-3 was 1225%, whereas the yield of VIII from that at C-6 was 366%. Namely, hydrogen at C-3 is favorably abstracted over that at C-6 by a ratio of 3 : 1. This might be explained by the stabilization energy of the intermediate radical. The same tendency has been reported in the oxidation of methylcyclohexene using chromium trioxide in acetic acid and chromium trioxide–pyridine complex in methylene chloride (10 : 1 and 4 : 1 respectively).[12]

3-Methylcyclohexene and 4-methylcyclohexene were also oxidized with $RhCl(PPh_3)_3$ under the same reaction conditions as above. The product distribution of each reaction could be explained in a similar way to that for 1-methylcyclohexene.

Thus, 3-methylcyclohexene was oxidized to give VII (1372%), 3-methylcyclohexene oxide (XI, 391 %), 4-methyl-2-cyclohexen-1-one (XII, 384%), 6-methyl-2-cyclohexen-1-one (XIII, 232%), 4-methyl-2-cyclohexen-1-ol (XIV, 168%), IX (124%), X (98%), and IV (684%). These products were identified by comparison with authentic samples.

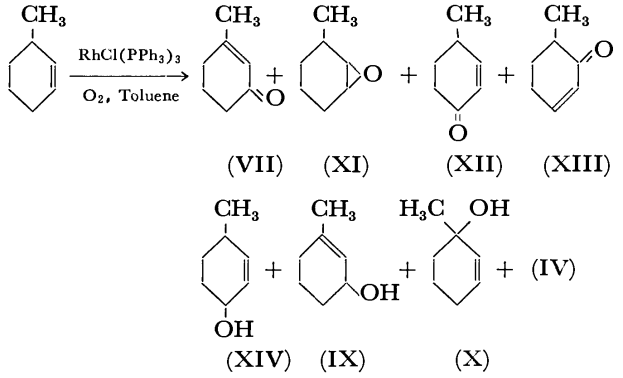

The main product VII could arise by oxygen attack at a less hindered site of the intermediate allyl radical.

Similarly, 4-methylcyclohexene was oxidized to give five products, XII (846%), 4-methylcyclohexene oxide (XV, 360%), 5-methyl-2-cyclohexen-1-one (XVI, 232%), XIII (115%), and IV (660%).

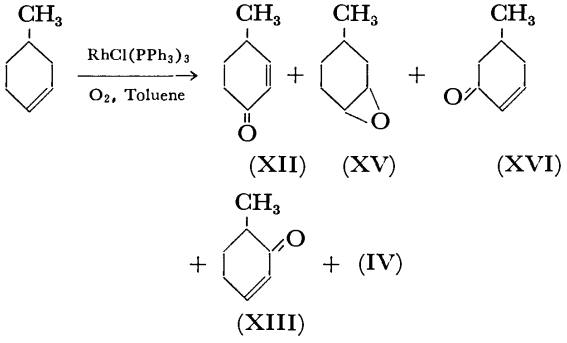

Hydrogen abstraction at C-3 yielding XII and XIII in 961% exceeds that at C-6 yielding XVI in 232% by a ratio of 4 : 1.

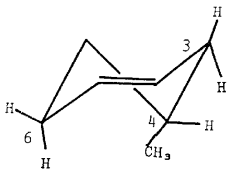

In all cases, ketones are formed in higher yields than the corresponding alcohol, though the decomposition of methylcyclohexene hydroperoxide by $RhCl(PPh_3)_3$ gave ketones and alcohols in nearly equivalent yields. Oxidation of alcohol IX did not afford the corresponding ketone XII in a good yield (6% yield based on the alcohol).

The yield of methylcyclohexene oxide increased as follows: 4-methyl < 3-methyl < 1-methylcyclohexene. This is in line with the increase of the electron density on carbon-carbon double bond.

It is known that singlet oxygen reacts with olefins bearing the allylic hydrogen to give hydroperoxides. The oxidation of 1-methylcyclohexene with singlet oxygen has been reported to give the following hydroperoxides.[13]

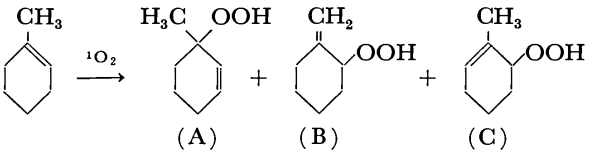

From the present result of 1-methylcyclohexene catalyzed by a rhodium complex, alcohol X and ketone VIII would be derived from the hydroperoxide of type A and type C, respectively. However, no ketone and alcohol arising from type B hydroperoxide could be observed. The formation of ketone VII, the major product of the present reaction, has not been detected among the products of oxidation reaction using singlet oxygen. This seems to be due to the fact that in cyclohexene oxidation, the oxygen molecule coordinated to a rhodium complex has few of the singlet oxygen character, if any.

Experimental

Materials and Analysis. All temperatures were uncorrected. The IR spectra were recorded on a JASCO IR-E spectrometer. The NMR spectra were measured on a Japan Electron Optics JNM-4H-100 spectrometer. Chemical shifts are given in τ units together with splitting patterns and relative integrated area. Vpc analysis was carried out with a Yanagimoto G-8 gas chromatograph using Chro-

12) a) F. C. Whitemore and G. W. Pedlow, Jr., *J. Amer. Chem. Soc.*, **63**, 758 (1941). b) W. G. Dauben, M. Lorber, and D. S. Fullerton, *J. Org. Chem.*, **34**, 3587 (1969).

13) K. Gollnick "Oxidation of Organic Compounds," Vol. III, ed. by F. R. Mayo, Amer. Chem. Soc., Washington, D. C. (1968), p. 91.

mosorb-W and Carbowax-20M columns. The gas chromatographic method was employed for both qualitative and quantitative determination of the reaction products. Cyclohexene hydroperoxide was decomposed in vpc to give nearly equal quantities of ketones and alcohols but no epoxides. The yields of ketones and alcohols should therefore be corrected according to the decomposition of hydroperoxides. However, no such correction was carried out since the content of hydroperoxide was low after 8 hr. The active oxygen in the reaction mixture was determined by the iodometric method.[14] Cyclohexene was prepared by the dehydration of cyclohexanol with phosphoric acid. Bp 82.7 °C (lit,[15] 82.7 °C). 1-Methylcyclohexene was prepared by treatment of cyclohexanone with methylmagnesium iodide followed by dehydration with anhydrous aluminum sulfate. bp 34.3 °C/38 mmHg (lit,[16] 110 °C/760 mmHg). 3-Methylcyclohexene was prepared by treatment of bromocyclohexene with methyl iodide. Bp 42.0 °C/97 mmHg (lit,[17] 104 °C/760 mmHg). 4-Methylcyclohexene was of commercial grade. All cyclohexenes used were subjected to repeated washing with ferrous sulfate solution containing sulfuric acid to eliminate the peroxides, separation and drying of the organic phase over anhydrous magnesium sulfate and distillation under nitrogen atmosphere before use. Absence of peroxides after the treatment was verified by vpc analysis. Cyclohexene hydroperoxide was prepared by treatment of cyclohexene with ABN under an oxygen atmosphere; bp 53—56 °C/0.6 mm Hg (lit,[18] 42—45 °C/0.5 mmHg). The peroxide content was 85%.

1-Methylcyclohexene 3-hydroperoxide was prepared from 1-methylcyclohexene in a manner similar to that for cyclohexene hydroperoxide; bp 42.5—46.2 °C/0.008 mmHg (lit,[19] 64—67 C°/0.2 mmHg). The peroxide content was 87%. Analysis by NMR indicated a mixture of 1-methylcyclohexene 3-hydroperoxide, 1-methylcyclohexene 6-hydroperoxide, and 3-methylcyclohexene 1-hydropreoxide. *t*-Butyl hydroperoxide was prepared by treatment of *t*-butanol with hydrogen peroxide in sulfuric acid solution; bp 34.5—36.0 °C/17 mmHg (lit,[20] 4.5—5.0 °C/2 mmHg). The peroxide content was 92%. Toluene was purified as mentioned previously.[4] $RhCl(PPh_3)_3$ was prepared by the method of Osborn *et al.*[21]

Oxidation of Cyclohexene. In a flask similar to that described previously[4] was charged a mixture of 0.463 g (0.500 mmol) of $RhCl(PPh_3)_3$ and 4.11 g (50 mmol) of cyclohexene and 75 ml of toluene as solvent under nitrogen atmosphere. The oxidation reaction was carried out at 80 °C with a constant bubbling of oxygen for 8 hr. A portion of the reaction solution was analyzed at an appropriate interval by the iodometric method and vpc. After work-up, brown solids deposited at the bottom of the flask. The resulting mixture was filtered to remove the brown precipitates (120 mg). In a separative experiment, the purified complex was not the active catalyst for oxidation of cyclohexene. The properties of the complex were as follows: mp 260—270 °C (decomp.), IR(nujol): 3360—3280, 1000, 762, 730, and 705 cm^{-1}. Found: C, 45.38; H, 3.95; Cl, 7.67%. Calcd for $RhCl_{0.7}(PPh_3)_{0.7}(H_2O)_{1.5}$: C, 44.66; H, 4.00; Cl, 7.64%. The filtrate was concentrated and the liquid phase was isolated and analyzed by vpc to give 738 mg (1530%) of I, 418 mg (852 %) of II, 173 mg (351%) of III, 277 mg (524%) of IV, and water. These compounds were identified by comparison with authentic samples. Compound I: IR(neat): 2940—2860, 1675—1650, 1458, 1430, 1397, 1243, 1210, 1128, 947, 888, 770, and 740 cm^{-1}; NMR (CCl_4): 3.10 (m, 1H, olefinic), 4.13 (m, 1H, olefinic), and 7.4—8.1 τ (m, 6H methylene). Compound II: IR(neat): 3400—3280, 2940—2860, 1650, 1440, 1275, 1182, 1068, 1048, 1007, 962, and 735 cm^{-1}; NMR(CCl_4): 4.35 (m, olefinic), 5.98 (m, 1H, methine), 8.10 (s, 1H, hydroxyl), and 7.9—8.5 τ (m, 6H, methylene). Compound III: IR (neat): 3000—2870, 1444, 1260, 972, 900, 885, 850, and 790 cm^{-1}; NMR(CCl_4): 7.06 (m, 2H, methine), 8.0—8.3 (m, 4H, methylene), and 8.5—8.9 (m, 4H, methylene). Compound IV: IR (neat): 3040, 1703, 1603, 1313, 1210, 1170, 840, 757, and 700 cm^{-1}; NMR(C_6D_6): −0.02 (s, 1H, formyl) and 2.3—3.1 τ (m, 5H, phenyl) The solid material was chromatographed on a silica gel column (50 g). Elution of ether (300 ml) gave triphenylphosphine oxide (235 mg).

Oxidation of 1-Methylcyclohexene. The same procedure as for cyclohexene was used. A solution of 0.463 g (0.500 mmol) of $RhCl(PPh_3)_3$, 4.81 g (50 mmol) of 1-methylcyclohexene and 75 ml of toluene was heated at 80 °C for 8 hr with a constant bubbling of oxygen. Reaction products were 750 mg (1340%) of VI, 579 mg (1052°₀) of VII, 202 mg (366%) of VIII, 50 mg (90%) of IX, 46 mg (83%) of X, and 413 mg (779%) of IV. These compounds were identified by comparison with authentic samples. Compound VI: IR(neat): 2960—2870, 1440, 1385, 1220, 1188, 1124, 1032, 918, 845, and 770 cm^{-1}; NMR(CCl_4): 7.24 (t, 1H, methine), 8.1—8.4 (m, 4H, methylene), 8.6—8.8 (m, 4H, methylene), and 8.77 τ (s, 3H, methyl). Compound VII: IR(neat): 2940—2880, 1670—1655, 1438, 1250, 1200, 970, 890, and 768 cm^{-1}; NMR(CCl_4): 4.27 (m, 1H, olefinic), 7.6—8.1 (m, 6H, methylene), and 8.02 τ (s, 3H, methyl). Compound VIII: IR(neat): 2940—2880, 1676—1657, 1456, 1364, 1178, 1108, 1020, 904, 885, and 809 cm^{-1}; NMR(CCl_4): 3.37 (m, 1H, olefinic), 7.5—8.1 (m, 6H, methylene), and 8.28 τ (s, 3H, methyl). Compound IX: IR(neat): 3360—3280, 2950—2880, 1677—1653, 1443, 1280, 1171, 1080, 1063, 1039, 964, 911, 827, 784, and 716 cm^{-1}; NMR(CCl_4): 4.58 (m, 1H, olefinic), 6.14 (m, 1H, methine), 8.49 (s, 1H, hydroxyl), 8.1—8.4 (m, 6H, methylene), and 8.28 τ (s, 3H, methyl). Compound X: IR(neat): 3400—3000, 2940—2880, 1702, 1650, 1460, 1180, 1130, 1020, 910, and 740 cm^{-1}; NMR(CCl_4): 4.45 (m, 2H, olefinic), 8.0—8.5 (m, 6H, methylene), 8.83 (s, 3H, methyl), and 8.95 τ (s, 1H, hydroxyl).

Oxidation of 3-Methylcyclohexene. The same procedure as above was used. A solution of 0.463 g (0.500 mmol) of $RhCl(PPh_3)_3$, 4.81 g (50 mmol) of 3-methylcyclohexene and 75 ml of toluene was heated at 80 °C for 8 hr with a constant bubbling of oxygen. Reaction products were 755 mg (1372%) of VII, 220 mg (391%) of XI, 212 mg (384%) of XII, 128 mg (232%) of XIII, 94 mg (168%) of XIV, 70 mg (124%) of IX, 55 mg (98%) of X, and 363 mg (684%) of IV. These compounds were identified by comparison with authentic samples. Compound XI: IR (neat): 3000—2880, 1455, 1386, 1255, 1004, 920, 879, 830, and 771

14) L. W. Fine, M. Grayson, and V. H. Suggs, *J. Organometal Chem.*, **22**, 219 (1970).
15) E. P. Carr, and H. Stücklen, *J. Amer. Chem. Soc.*, **59**, 2138 (1937).
16) F. K. Signaigo and P. L. Cramer, *ibid.*, **55**, 3326 (1933).
17) A. Berlande, *C. R. Acad. Sci., Paris*, **213**, 437 (1941).
18) L. H. Gale, D. C. Olson, and J. Vasilevskis, *J. Catal.*, **24**, 549 (1972).
19) E. H. Former and A. Sundralingam, *J. Chem. Soc.*, **1942**, 121.
20) N. A. Milas and D. M. Surgenor, *J. Amer. Chem. Soc.*, **68** 205 (1946).
21) J. A. Osborn, F. H. Jardine, J. F. Young, and G. Wilkinson *J. Chem. Soc., A*, **1966**, 1711.

cm^{-1}; NMR (CCl_4): 7.05 (m, 1H, methine), 7.38 (d, 1H, methine), 8.0—8.8 (m, 7H, methylene), and 8.98 τ (d, 3H, methyl). Compound XII: IR(neat): 2940—2860, 1685—1652, 1458, 1250, 1200, 1095, 835, 811, and 759 cm^{-1}; NMR (CCl_4): 3.36 (m, 1H, olefinic), 4.20 (m, 1H, olefinic), 7.5—8.1 (m, 5H, methylene and methine), and 8.84 τ (d, 3H, methyl). Compound XIII: IR(neat): 2930—2860, 1675—1650, 1457, 1134, 892, 810, and 711 cm^{-1}; NMR(CCl_4): 3.20 (m, 1H, olefinic), 4.12 (m, 1H, olefinic), 7.5—8.2 (m, 5H, methine and methylene), and 8.91 τ (d, 3H, methyl). Compound XIV: IR(neat): 3360—3280, 2940—2880, 1700, 1650, 1457, 1280, 1110, 1060, 1029, 855, and 743 cm^{-1}; NMR (CCl_4): 4.48 (s, 2H, olefinic), 5.93 (m, 1H, methine), 7.27 (s, 1H, hydroxyl), 7.8—8.9 (m, 5H, methine and methylene), and 9.03 τ (d, 3H, methyl).

Oxidation of 4-Methylcyclohexene. The same procedure as above was used. A solution of 0.463 g (0.500 mol) of $RhCl(PPh_3)_3$, 4.81 g (50 mmol) of 4-methylcyclohexene and 75 ml of toluene was heated at 80 °C for 8 hr with a constant bubbling of oxygen. Reaction products were 476 mg (846%) of XII, 202 mg (360%) of XV, 128 mg (232%) of XVI, 64 mg (115%) of XIII, 350 mg (660%) of IV. These compounds were identified by comparison with authentic samples. Compound XV: IR(neat): 2960—2870, 1440, 1259, 1153, 1010, 970, 818, 792, and 770 cm^{-1}; NMR(CCl_4): 7.05 (m, 2H, methine), 7.8—8.9 (m, 7H, methylene and methine), and 9.14 τ (d, 3H, methyl). Compound XVI: IR(neat): 2950—2880, 1684—1652, 1458, 1393, 1273, 1240, 1187, 884, and 742 cm^{-1}; NMR (CCl_4): 3.17 (m, 1H, olefinic), 4.10 (m, 1H, olefinic), 7.6—8.1 (m, 5H, methylene and methine), and 8.91 τ (d, 3H, methyl).

Autoxidation of 1-Methylcyclohexene with ABN as Initiator. A mixture of 4.81 g (50 mmol) of 1-methylcyclohexene, 0.041 g (0.250 mmol) of ABN, and 75 ml of toluene was heated at 80 °C for 8 hr under a constant bubbling of oxygen. The reaction solution was analyzed by vpc to give 263 mg of VII, 129 mg of 2-methyl-2-cyclohexen-1-ol (XVII), 127 mg of IX, 109 mg of VI, 100 mg of VIII, 32 mg of X, and trace of IV. Compound XVII: IR (neat): 3400—3300, 2950—2880, 1660, 1445, 1275, 1160, 1057, 990, 952, 919, 868, and 816 cm^{-1}; NMR(CCl_4): 4.60 (m, 1H, olefinic), 6.15 (m, 1H, methine), 6.80 (m, 1H, hydroxyl), 7.9—8.4 (m, 6H, methylene), and 8.30 τ (s, 3H, methyl).

Oxidation of 3-Methyl-2-cylcohexen-1-ol (IX). A solution of 0.463 g (0.500 mmol) of $RhCl(PPh_3)_3$, 2.80 g (25 mmol) of IX, and 75 ml of toluene was treated in a manner similar to that for cyclohexene oxidation. After 8 hr, the reaction product was 0.174 g (1.58 mmol) of VII.

Decomposition of V catalyzed by $RhCl(PPh_3)_3$. A mixture of 0.463 g (0.500 mmol) of $RhCl(PPh_3)_3$, 1.00 g of V and 75 ml of toluene was heated at 80 °C with a constant bubbling of argon. A portion of the reaction solution was analyzed at an appropriate interval, by the iodometric method. Decomposition of V was complete in 2 hr. After 2 hr, the solution was analyzed by vpc to give 462 mg of I and 399 mg of II. Decomposition of the mixture of three isomers of methylcyclohexene hydroperoxides (1.33 g) was complete in 1 hr to give 269 mg of IX, 214 mg of VII, 186 mg of XV, 140 mg of X, and 138 mg of VIII.

Oxygen Transfer Reaction of Cyclohexene Hydroperoxide and Cyclohexene. A mixture containing 0.463 g (0.500 mmol) of $RhCl(PPh_3)_3$, 1.34 g of V, 0.821 g (10 mmol) of cyclohexene, and 75 ml of toluene was heated at 80 °C with a constant bubbling of argon. A portion of the reaction solution was analyzed at an appropriate interval by the iodometric method. Decomposition of V was complete in 2 hr. After 8 hr, the solution was analyzed by vpc to give 475 mg of I and 504 mg of II. Oxygen transfer reaction of *t*-butyl hydroperoxide and cyclohexene gave only the hydroperoxide decomposition products.

BULLETIN OF THE CHEMICAL SOCIETY OF JAPAN, VOL. 46, 3814—3817 (1973)

Photochemical Rearrangement of 2-Nitrophenyl Phenyl Sulfoxide to 2-Nitrosophenyl Phenyl Sulfone

Rikuhei TANIKAGA and Aritsune KAJI

Department of Chemistry, Faculty of Science, Kyoto University, Sakyo-ku, Kyoto 606

(Received May 14, 1973)

Irradiation of 2-nitrophenyl phenyl sulfoxide (I) gave 2-nitrosophenyl phenyl sulfone (II) as the sole product. The rearrangement was not affected by a quencher, but took a different course in the presence of a sensitizer or a halogen-containing solvent. When I with an electron-donating substituent at a 4′-position or electron-withdrawing one at a 4-position was irradiated, the corresponding II was obtained in a lower yield. 2-Nitrophenyl phenyl sulfide was photochemically stable. From the results, it is proposed that in the excited singlet state of I the oxyanion of a nitro group attacks the positive sulfur atom, and oxygen transfer takes place.

Organic nitrogen compounds, with an N→O bond such as $-\underset{|}{N}=N\rightarrow O$, $-CH=\underset{|}{N}\rightarrow O$ or $O=\underset{|}{N}\rightarrow O$, are known to undergo photochemical oxygen transfer reactions. Both rearrangements of azoxybenzene to 2-hydroxyazobenzene and of *N*,α-diphenylnitrone to 2,3-diphenylaziridine are postulated to proceed *via* the excited singlet state.[1,2]

In an aromatic nitro compound, a number of photochemical oxygen transfer reactions are also reported, but the reaction mechanism is not always straightforward.[3] In the rearrangements of 2-nitrobenzaldehyde to 2-nitrosobenzoic acid and of 2-nitrostilbene to 2-phenylisatogen, it is presumed that the reaction starts from an $n\rightarrow\pi^*$ excitation and the oxygen atom of the nitro group in the (n,π^*) triplet state abstracts a hydrogen atom or adds to an unsaturated system like the oxygen of a carbonyl group.

On the other hand, both azoxybenzene and nitrobenzene are known to be stronger bases in the excited

1) R. Tanikaga, This Bulletin, **41**, 2151 (1968).

2) K. Shinzawa and I. Tanaka, *J. Phys. Chem.*, **68**, 1205 (1964); **69**, 2545 (1965).

3) H. A. Morrison, "The Chemistry of the Nitro and Nitroso Groups," Part 1, ed. by H. Feuer, Interscience Publishers, New York, N. Y. (1969), p. 165.

singlet state than in their ground state.[4,5] Thus a nitro compound might undergo an oxygen transfer reaction from the excited singlet state like an azoxy compound. 2-Nitrophenyl phenyl sulfoxide was found to rearrange to 2-nitrosophenyl phenyl sulfone possibly from the excited singlet state.[6]

The principal objective of this work is to discuss the effect of a sensitizer, a quencher, a solvent, or a substituent on this new type of reaction, and to propose the mechanism.

Results and Discussion

A solution of 2-nitrophenyl phenyl sulfoxide (I) in benzene was irradiated with a high-pressure mercury lamp. Thin-layer chromatography analysis on silica gel revealed that 2-nitrosophenyl phenyl sulfone (II) was formed as the sole product, but not 2-nitrophenyl phenyl sulfide (III) or 2-nitrophenyl phenyl sulfone. This shows that an intramolecular oxygen transfer reaction took place. Neither thermal nor reverse photochemical rearrangement occurred. III was photochemically stable and gave no 2-nitrosophenyl phenyl sulfoxide. This suggests that the oxygen atom can attack only the positive sulfur atom.

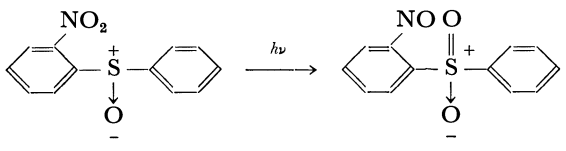

(I) (II)

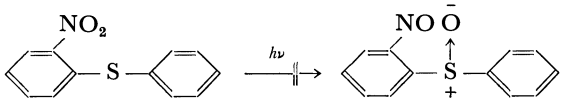

(III)

Effect of Sensitizer and Quencher. The results of the irradiation of I in benzene using a Pyrex filter are given in Table 1.

Table 1. Irradiation of I (10^{-2} M) for 3 hr

Sensitizer (M)	Quencher (M)	Yield (%) I	II	III
None	Degassed	84	12	0
None	O_2	84	12	0
None	1,3-Pentadiene (10^{-2})	85	11	0
$(C_6H_5)_3N$ (10^{-1})	Degassed	88	3	4
$(C_6H_5)_3N$ (10^{-1})	O_2	92	3	1

The rearrangement of I to II was not affected by oxygen or 1,3-pentadiene. Thus the oxygen transfer may occur directly from the excited singlet state.

Benzophenone, frequently used as a sensitizer, has one weak absorption band (λ_{max}=343 nm, ε_{max}=130) in benzene due to an n→π^* transition in the wavelengths above 310 nm, whereas I has much stronger absorption in the same region (for example, ε_{343nm}=925). Therefore, a large excess of benzophenone should be used for photochemical sensitization, but such a reaction condition does not seem suitable because of the possibility of a chemical sensitization.

On the other hand, triphenylamine has a strong absorption band (λ_{max}=302 nm, ε_{max}=2290) in benzene, and its intersystem crossing efficiency is known to be high. When triphenylamine was used as a sensitizer, two different reactions appear to have occurred at the same time; a direct photorearrangement of I in its excited singlet state to II, and a photosensitized reaction of I to III, that is, the reduction of the S→O bond of I presumably in its excited triplet state. One plausible explanation for the low yield of III is to assume that I in the excited triplet state can not easily be reduced to III.

Effect of Solvent. The results of the photolysis of I in various solvents using a Pyrex filter are given in Table 2. Irradiation was stopped at an early stage of the reaction to prevent the product from absorbing light.

It was not possible to determine what excitation occurred, since no electronic spectrum of I has yet been assigned. Nitrobenzene in heptane has a long-wavelength absorption maximum at 330 nm (ε=165) which has been assigned as an n→π^* band.[7] An ethanol solution of I shows only one absorption band at 235 nm (ε=11000) presumably arising from a π→π^* transition, and other absorptions are completely submerged under this high intensity band. It appears attractive to assume that the reaction of I starts from its π→π^* transition, since the yield of II was higher in quartz tube in spite of a weak radiation of the lamp used at 254 nm. Although there remain some possibilities that the reaction starts from another type of excitation, the possibility of an n→π^* excitation may be excluded, since the absorption of I around 330 nm

Table 2. Irradiation of I (10^{-2} M) for 3 hr

Solvent	Yield (%) I	II	III
n-Hexane	81	14	0
n-Hexane[a]	76	17	0
Benzene	84	12	0
Ethanol	79	10	0
Acetonitrile	85	6	0
1-Chloropropane	86	3	0
1-Bromopropane	88	1	1
1,3-Dibromopropane	87	1	3

a) Quartz was used.

4) H. H. Jaffé, D. L. Beveridge, and H. L. Jones, *J. Amer. Chem. Soc.*, **86**, 2932 (1964); H. H. Jaffé and H. L. Jones, *J. Org Chem.*, **30**, 964 (1965).

5) a) H. E. Zimmerman, "Advances in Photochemistry," Vol. 1, ed. by W. A. Noyes, Jr., G. S. Hammond, and J. N. Pitts, Jr., Interscience Publishers, New York, N. Y. (1963), p. 200. b) R. Hurley and A. C. Testa, *J. Amer. Chem. Soc.*, **89**, 6917 (1967). c) J. A. Barltrop and N. J. Bunce, *J. Chem. Soc., C*, **1968**, 1467. d) B. Tiniand and C. Décoret, *Tetrahedron Lett.*, **1971**, 2467.

6) R. Tanikaga, Y. Higashio, and A. Kaji, *ibid.*, **1970**, 3273.

7) S. Nagakura, M. Kojima, and Y. Maruyama, *J. Mol. Spectrosc.*, **13**, 174 (1964).

is rather strong ($\varepsilon > 1000$).

The spectra of I in various solvents are very similar. II was obtained in a higher yield in a non-polar solvent.

The irradiation of I in a halogen-containing solvent tended to afford III in place of II. In that solvent I in the excited singlet state is expected to undergo an intersystem crossing as a result of a heavy-atom effect. Thus it seems reasonable that the yield of II *via* the excited singlet state decreased, and that of III *via* the excited triplet state increased. The possibility of excitation of the solvent must be excluded, since the absorption intensity of the solvent is much lower in the wavelengths above 310 nm than that of I in 10^{-2} M concentration. Pyridine *N*-oxide is reported to be reduced to pyridine through the excited triplet state by the photolysis in a halogen-containing solvent.[8]

Effect of Substituent. The results of the photolyses of 2-nitrophenyl phenyl sulfoxide with a substituent in benzene using a Pyrex filter are given in Table 3. Irradiation was stopped at an early stage of the reaction to prevent the product from absorbing light.

TABLE 3. IRRADIATION OF I (10^{-2} M) WITH SUBSTITUENT FOR 3 hr

Substituent	Yield (%)	
	I	II
4′-CH_3O	88	8
4′-CH_3	91	6
4′-Cl	85	12
H	84	12
3′-Cl	82	16
4′-CH_3CO	83	14
4′-NO_2	86	11
4-NO_2	100	0

The electronic spectra of these compounds have only one strong absorption band in the wavelengths around 250 nm, and show similar intensities in wavelengths longer than 290 nm (Table 5). Although there will be problems in the discussion of the substituent effect, it is interesting to note that 2-nitrophenyl phenyl sulfoxide with an electron-donating group at a 4′-position tends to give the corresponding sulfone in a lower yield, and I with nitro group at a 4-position does not give any sulfone. These substituent effects are in contrast to those in the case of the oxygen transfer reaction of 2-nitrostilbene,[9] in which an electron-donating group at a 4′-position and an electron-withdrawing group at a 4-position promote the rearrangement.

Reaction Mechanism. In the excited (presumably (π,π^*)) singlet state, an aromatic nitro compound is known to have a higher electron density at the oxygen atom of the nitro group and a lower one at the meta-position of the phenyl ring.[5] This phenomenon can be illustrated by means of the following valence bond picture.[5a]

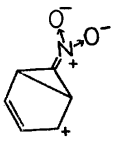

S*(π, π^*)

Thus, the most reasonable mechanism of the photochemical oxygen transfer reaction of I is as follows. In the excited (π,π^*) singlet state the oxyanion of a nitro group attacks the positive sulfur atom, and the oxygen transfer takes place without a spin inversion. This mechanism of the reaction of I is similar to that of azoxybenzene[1] and of *N*,α-diphenylnitrone.[2]

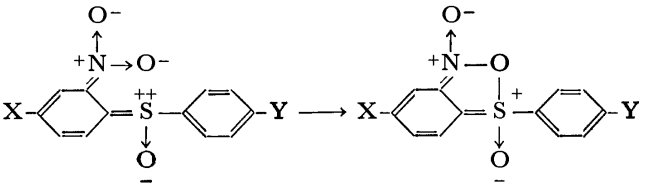

S*(π, π^*)

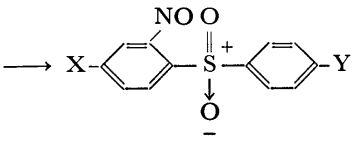

X: electron-donating group
Y: electron-withdrawing group

The above mechanism, in which the rearrangement occurs directly from the excited singlet state, can be explained by the effects of a sensitizer, a quencher and a halogen-containing solvent. The mechanism, in which an intramolecular nucleophilic attack occurs on the sulfur atom, can also be explained by the effect of a substituent on the rearrangement of I and the photochemical stability of III. The interesting intermolecular nucleophilic substitution on a sulfur atom was reported in the photochemistry of 2,4-dinitrobenzenesulfenyl derivatives.[10] The oxygen-bridged transition state may be supported by the effect of a solvent polarity.

On the other hand, in the excited (presumably (n,π^*)) triplet state a nitro compound is believed to have the following biradical structure.[3]

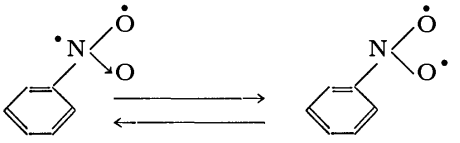

T*(n, π^*)

Thus, the oxygen atom of the nitro group in the excited state can have two opposite behaviors, a nucleophilic property in the excited (π,π^*) singlet state and an electrophilic one in the excited (n,π^*) triplet state. The former case was observed in the photochemical rearrangement of I to II, and the latter one is reported by de Mayo[11] in the photochemical electrophilic addition of an aromatic nitro compound

8) N. Hata, Preprints for the 20th Annual Meeting of the Chemical Society of Japan (1967), Vol. 1, p. 483.
9) J. S. Splitter and M. Calvin, *J. Org. Chem.*, **20**, 1086 (1955).
10) D. H. R. Barton, T. Nakano, and P. G. Sammes, *J. Chem. Soc., C*, **1968**, 322.
11) J. L. Charlton, C. C. Liao, and P. de Mayo, *J. Amer. Chem. Soc.*, **93**, 2463 (1971).

to an alkene. A similar biradical property of the nitro group in the excited (n,π^*) triplet state also appears to be observed in the intramolecular electrophilic attack of the nitro group to the double bond in the photochemical reaction of 2-nitrostilbene to 2-phenylisatogen.[9]

In conclusion, the property of an aromatic nitro compound in the excited (π,π^*) singlet state differs a great deal from that in the excited (n,π^*) triplet state.

Experimental

Starting Materials. The sulfides were prepared by the reaction of sodium thiophenolates and aryl halides. The sulfoxides were prepared by controlled oxidation of the corresponding sulfides with hydrogen peroxide. They were purified by column chromatography and recrystallization until their thin-layer chromatography showed only one spot, and were identified by elemental analysis, and NMR and IR spectra. (Tables 4 and 5)

Table 4. 2-Nitrophenyl phenyl sulfides

Substituent	Mp (°C)
H	72.5
4′-CH_3O	97.5
4′-CH_3	83.0
4′-Cl	93.0
3′-Cl	107.5
4′-CH_3CO	156.5
4′-NO_2	162.0
4-NO_2	121.0

Table 5. 2-Nitrophenyl phenyl sulfoxides

Substituent	Mp (°C)	$\varepsilon_{313nm}^{benzene}$
H	93.5	2250
4′-CH_3O	109.0	2830
4′-CH_3	139.5	2450
4′-Cl	117.5	2610
3′-Cl	115.5	2470
4′-CH_3CO	134.0	2640
4′-NO_2	153.5	5480
4-NO_2	114.0	4320

Photolysis of 2-Nitrophenyl Phenyl Sulfoxides to 2-Nitrosophenyl Phenyl Sulfones. A solution of 2 g of 2-nitrophenyl phenyl sulfoxide (I) in 500 ml of benzene was internally irradiated for 3 hr with a 300 W high-pressure mercury lamp using a Pyrex filter. Removal of the solvent gave a dark oil which was chromatographed on preparative thin-layer plates (Merck silica gel G). Development with chloroform three times gave two separated bands, the second band arising from I. The material from the first band was recovered by extraction with chloroform. Slow recrystallization from chloroform and *n*-hexane gave 400 mg of pale crystals Z; mp 145 °C; UV (benzene) λ_{max} 783 nm (nitroso); IR (KBr) 1320, 1150 cm^{-1} (sulfone).

Found: C, 58.58; H, 3.66; N, 5.59; S, 12.85%. Calcd for $C_{12}H_9NO_3S$: C, 58.29; H, 3.67; N, 5.66; S, 12.97%.

Compound Z was positive to the Liebermann test, and yielded 2-nitrophenyl phenyl sulfone by oxidation with hydrogen peroxide. Consequently, Z was assigned to 2-nitrosophenyl phenyl sulfone (II).

Other 2-nitrosophenyl phenyl sulfone derivatives were isolated and identified as described above. (Table 6)

Table 6. 2-Nitrosophenyl phenyl sulfones

Substituent	Mp (°C)	ν_{max}^{KBr} (cm^{-1})
H	145	1320, 1150
4′-CH_3O	152	1320, 1150
4′-CH_3	200	1300, 1150
4′-Cl	169	1330, 1160
3′-Cl	195	1330, 1165
4′-CH_3CO	154	1320, 1150
4′-NO_2	161	1300, 1160

Photolysis of I in the Presence of Sensitizer or Quencher. A Pyrex tube (inner diameter, 0.9 mm) containing a degassed or oxygen-saturated solution (2 ml) of I (10^{-2} M), with or without 1,3-pentadiene (10^{-2} M) or triphenylamine (10^{-1} M), was kept standing in a "merry-go-round" apparatus. The solution was irradiated for 3 hr with a 100 W high-pressure mercury lamp fitted with a water-cooled immersion well, and thermostated at 25 °C. Five ml of chloroform was added after irradiation and 0.5 ml of the resulting solution was developed on the thin-layer plate (silica gel G), and each component was extracted with chloroform. The yield was determined from the intensity of the absorption of the extract in an electronic spectrum, whose extinction coefficient had previously been determined with an authentic sample.

Reproducibility of the data obtained by this method was satisfactory. The results are given in Table 1.

Photolysis of I in Various Solvents. A solution (2 ml) of I (10^{-2} M) in each solvent was irradiated in a Pyrex or quartz tube for 3 hr. The yield of each product was determined as described above. The results are shown in Table 2.

Photolysis of 2-Nitrophenyl Phenyl Sulfoxide with Substituent. A solution (2 ml) of 2-nitrophenyl phenyl sulfoxide, with such substituents as shown in Table 3, in benzene, was irradiated in a Pyrex tube for 3 hr. The yield of each component was determined as described above. The results are shown in Table 3.

Behavior of 2-Pyrazolin-5-ones toward Activated Double Bond Systems: Cyanoethylation of 2-Pyrazolin-5-ones

Mohamed Helmi ELNAGDI and Masaki OHTA

Department of Chemistry, Faculty of Science, Tokyo Institute of Technology, Ookayama, Meguro-ku, Tokyo 152

(Received May 21, 1973)

3-Methyl-2-pyrazolin-5-one(Ia) reacts with acrylonitrile to yield either 4,4-di(β-cyanoethyl)-5-hydroxy-3-methylpyrazole(IV) or 1,4,4-tri(β-cyanoethyl)-3-methyl-2-pyrazolin-5-one(V) depending on the amount of reagent and the reaction conditions. Ia reacts with ethyl acrylate or crotononitrile to yield the 4-alkylated derivatives VIII and IX respectively. 3-Methyl-1-phenyl-2-pyrazolin-5-one(Ib) reacts with acrylonitrile to yield only 4,4-di(β-cyanoethyl) derivative XII which on hydrolysis affords the corresponding dicarboxylic acid (XIII). 3-Amino-1-phenyl-2-pyrazolin-5-one(Ic) adds to two molecules of ethyl acrylate or acrylonitrile to yield the 4,4-disubstituted derivatives XIV and XV, but only to one molecule of benzalacetophenone to yield the 4-substituted 3-amino-2-pyrazolin-5-one derivative XVIII. The pyrazolopiperidine derivative(XVI) was obtained on treatment of Ic with ethyl crotonate in the presence of sodium ethoxide.

In continuation of previous works,[1-3] the behavior of the 2-pyrazolin-5-one derivatives (Ia-c) toward a variety of reagents containing activated double bonds was investigated. Kost *et al.*[4] showed that, where as 3-methyl-2-pyrazolin-5-one(Ia) and 4-(β-cyano-ethyl)-3-methyl-2-pyrazolin-5-one(IIa) react with acrylonitrile in *t*-butyl alcohol to yield 5-(β-cyanoethoxy)-3-pyrazole-(IIIa) and 5-(β-cyanoethoxy)-4-(β-cyanoethyl)-3-methylpyrazole(IIIb), respectively, 3-methyl-1-phenyl-2-pyrazolin-5-one(Ib) reacts with the same reagent under the same conditions to yield 4-(β-cyano-ethyl)-3-methyl-1-phenyl-2-pyrazolin-5-one(IIb).

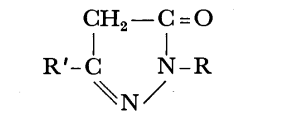

Ia, R=H; R'=CH_3
b, R=C_6H_5; R'=CH_3
c, R=C_6H_5; R'=NH_2

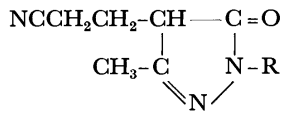

IIa, R=H
b, R=C_6H_5

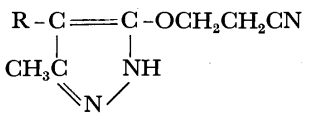

IIIa, R=H
b, R=CH_2CH_2CN

It has been found that Ia reacts with acrylonitrile in aqueous pyridine to yield either 4,4-di(β-cyano-ethyl)-5-hydroxy-3-methylpyrazole(IV) or 1,4,4-tri(β-cyanoethyl)-3-methyl-2-pyrazolin-5-one(V) depending on the molar ratio of the reactants and the reaction conditions. Thus, when Ia was treated with acrylonitrile in a molar ratio of 1 : 2, compound IV was formed. On the other hand, when Ia was refluxed with excess acrylonitrile in the presence of catalytic amount of potassium hydroxide, tri(β-cyanoethyl)-3-methyl-2-pyrazolin-5-one(V) was formed. Compound V was also formed by the action of acrylonitrile on 1,4-di(β-cyanoethyl)-3-methyl-2-pyrazolin-5-one(VI).

The structure proposed for compound IV was deduced from analytical data, non-identity with the known IIIb and VI, and its preparation by the action of acrylonitrile on IIa. Hydrolysis of IV with acetic acid–hydrochloric acid mixture affords 4,4-di(β-carboxyethyl)-5-hydroxy-3-methylpyrazole (VII). The IR spectrum of IV shows no ring CO absorption but a band extending over 2400—2700 cm^{-1} for the chelated hydroxyl group. Similar spectra were reported for C-4 alkylated 1-unsubstituted-2-pyrazolin-5-ones.[5] The absence of ring CO absorption in the IR spectrum indicates that IV exists mainly, at least in solid state, in the 5-hydroxypyrazole structure.

Attempts to obtain a mono β-cyanoethyl derivative of Ia in pyridine medium were unsuccessful. Even when limited quantities of acrylonitrile were used under conditions[6,7] favorable for monocyanoethylation, the isolable product was compound IV and unchanged Ia. This is similar to the behavior of many compounds containing activated methylene group, where the isolation of a mono β-cyanoethyl derivative is difficult as has been reported.[6-10]

In contrast to the behavior of Ia toward acrylonitrile, we have found that it adds to only one molecule of either of ethyl acrylate or crotononitrile to yield 4-(β-ethoxycarbonylethyl)-5-hydroxy-3-methylpyrazole (VIII) and 4-(β-cyano-α-methylethyl)-5-hydroxy-3-methylpyrazole (IX or possible tautomers), respectively. Compounds VIII and IX were also obtained by the action of hydrazine hydrate on diethyl α-acetylglutamate(X) and ethyl 1-acetyl-3-cyano-2-methylbutyrate(XI), respectively. That acrylonitrile easily effects dialkylation of Ia, whereas ethyl acrylate and crotononitrile effect only mono alkylation under more severe conditions is in accordance with the sequence of reactivity of these reagents as Micheal acceptors.[11] A similar discrepancy in behavior of many

1) M. H. Elnagdi, N. A. L. Kassab, S. M. Fahmy, and F. A. EL-All, *J. Prakt. Chem.*, (in press).
2) M. H. Elnagdi and S. A. Abdalla, *J.Prakt. Chem.*, (in press).
3) M. H. Elnagdi and M. Ohta, This Bulletin, **46**, 1830 (1973).
4) A. N. Kost, S. I. Seminov, R. S. Sagitallin, and V. V. Ershov, *Zh. Obshch. Khim.*, **30**, 2286 (1960).
5) R. Jones, A. J. Ryan, S. Sternhell, and S. E. Wright, *Tetrahedron*, **19**, 1497 (1963).
6) A. D. Campell, *J. Chem. Soc.*, **1954**, 1377.
7) A. D. Campell and I. D. R. Stevens, *ibid.*, **1956**, 959.
8) E. C. Leonard, "Vinyl and Diene Monomers", Part I, J. Wiley & Sons, New York (1970), p. 93.
9) H. A. Bruson and T. W. Riener, *J. Amer. Chem. Soc.*, **64**, 2880 (1942).
10) H. A. Bruson, "Organic Reactions," ed. by R. Adams, J. Wiley and Sons, New York (1949), Vol. V, p. 101.
11) E. D. Bergmann "Organic Reactions" Vol X, ed. by R. Adams, J. Wiley & Sons, New York (1959), Chapter 3, p. 205.

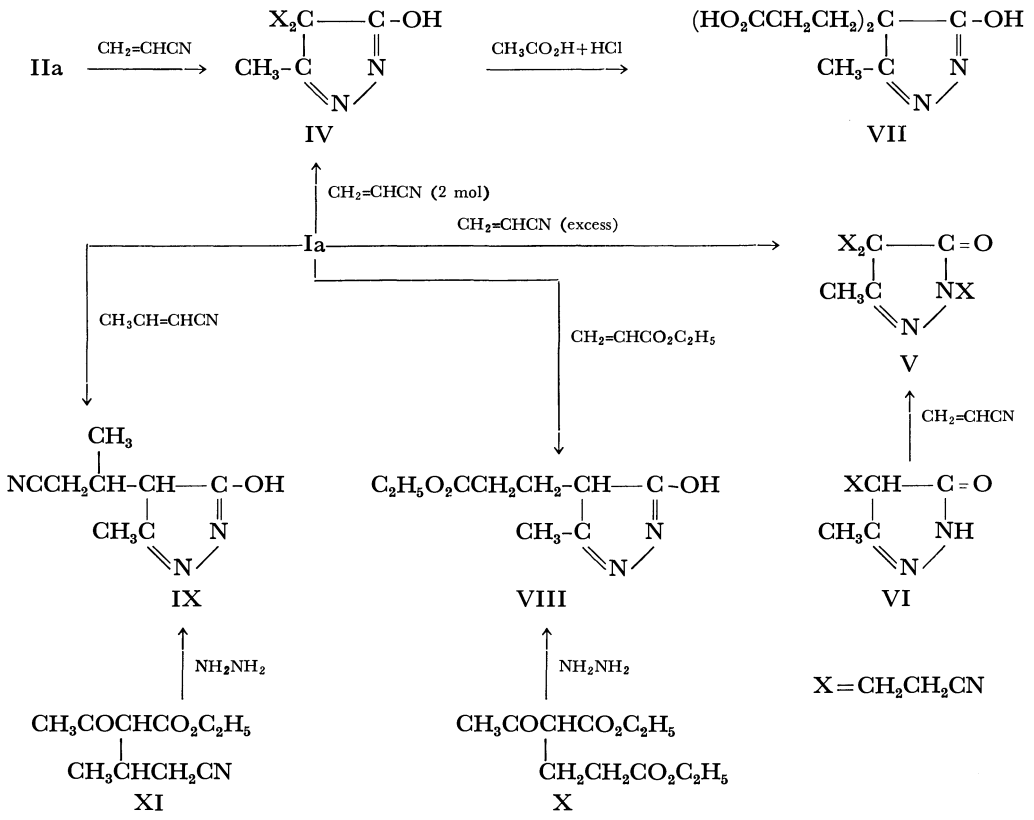

Chart 1

active methylene compounds toward the action of these reagents has been reported.[12-14]

An investigation of the behavior of Ib toward acrylonitrile in aqueous pyridine solution shows that it reacts with two molecules of the reagent yield the 4,4-di(β-cyanoethyl)-1-phenyl-3-methyl-2-pyrazolin-5-one derivative (XII), which on hydrolysis with acetic acid–hydrochloric acid mixture affords the corresponding 4,4-di(β-carboxyethyl) derivative(XIII).

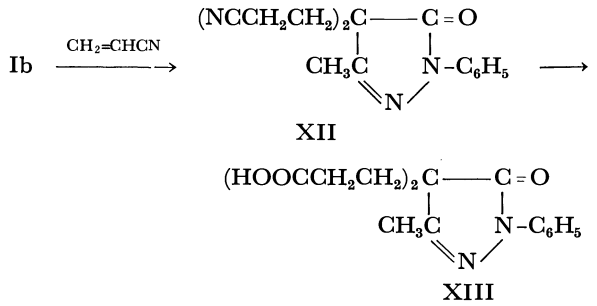

The behavior of 3-amino-1-phenyl-2-pyrazolin-5-one(Ic) toward the action of various reagents containing an activated double bond system was also investigated. Treatment of Ic with ethyl acrylate or acrylonitrile resulted in the formation of products, the analytical data of which indicated that two molecules of either of the reagents had been added and for which structures XIV and XV were proposed. Many isomeric structures for the reaction products of Ic with ethyl acrylate or acrylonitrile are possible. However, the IR spectra of either of the products indicated that the ring CO and the amino group are not involved in the reaction. The 4,4-dialkylated structure (*cf.* XIV and XV) is preferable to the possible 1,4-dialkylated isomer based on analogy to the behavior of Ia, b and the stability of the reaction products toward the action of acetic acid[1,2] and amines.[15] The weak reactivity of possition 2 and the amino group in 3-amino-1-phenyl-2-pyrazolin-5-one has been reported.[1]

We have found that Ic reacts with ethyl crotonate in the presence of sodium ethoxide to yield the pyrazolopiperidine derivative XVI. The structure of XVI was inferred from analytical and spectral data, and its synthesis *via* the action of phenylhydrazine on α-ethoxycarbonyl-β-methylglutamonitrile (XVII). The discrepancy in behavior between Ic and Ia toward the action of ethyl acrylate can be rationalized in terms of increment of reactivity of the methylene group in Ic as compared to that of Ia, induced by the presence of amino group on C-3 which is tautomeric with the imino form.

The compound Ic adds also the benzalacetophenone

12) *cf.* the discrepancy in the behavior of active methylene ketones on treatment with acrylonitrile, ethyl acrylate and crotononitrile, *ibid.*, Tables X—XII.

13) H. A. Bruson and T. W. Riemer, *J. Amer. Chem. Soc.*, **64**, 2850 (1942).

14) H. A. Bruson, *ibid.*, **64**, 2457 (1942).

15) *cf.* dicyanoethylation of *N*-cyanoethylated compounds by the action of amines, P. Buckua, *Zh. Obshch. Khim.*, **34**, 2093 (1964); E. C. Leonard, "Vinyl and diene monomers," Part I Copyright, J. Wiley & Sons, New York (1970), p. 33.

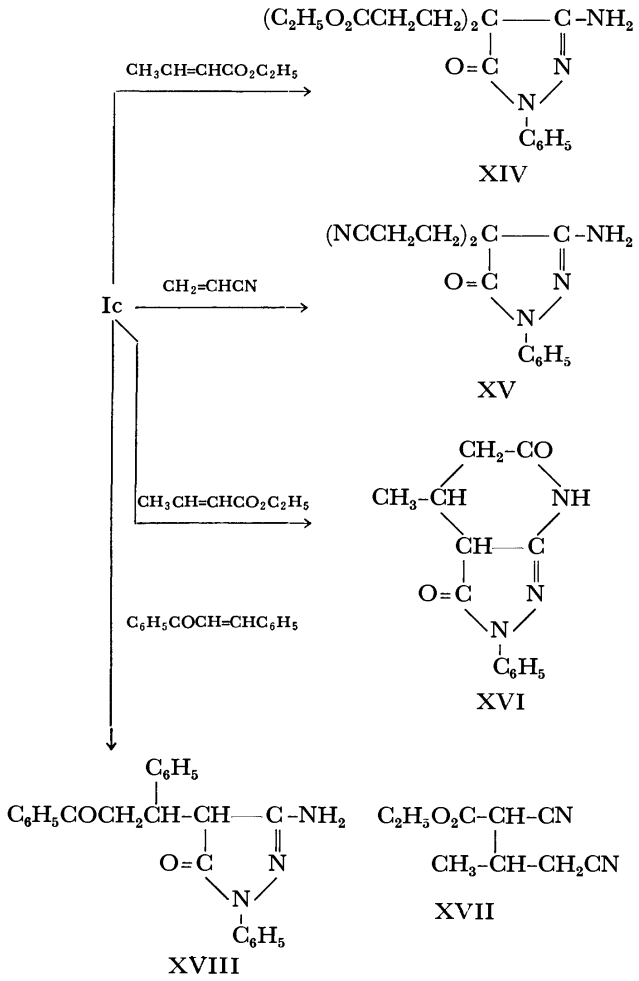

Chart 2

to yield compound XVIII. This is similar to the behavior of Ib toward the same reagent.[16]

Experimental

All melting points were determined on a micro hot stage and are uncorrected. The IR spectra were recorded with a Hitachi Grating IR spectrophotometer Model EPI-G3.

4,4-Di(β-cyanoethyl)-5-hydroxy-3-methylpyrazole (IV). *1) From 3-Methyl-2-pyrazolin-5-one (Ia):* To a solution of acrylonitrile(10 ml) in pyridine(150 ml) and water(50 ml) was added 10 g of Ia. The reaction mixture was refluxed for 6 hr and the solvent was evaporated *in vacuo* to leave a residue which was purified by crystallization from water to give 15.5 g of IV. Colorless crystals, mp 159 °C. IR: 2920—2600(chelated OH), 2230 cm^{-1} (CN). Found: C, 58.31; H, 5.84; N, 27.80%. Calcd for $C_{10}H_{12}ON_4$: C, 58.88; H, 5.92; N, 27.44%.

2) From 4-(β-Cyanoethyl)-3-methyl-2-pyrazolin-5-one (IIa). To a solution of acrylonitrile(1.6 ml) in pyridine(50 ml) and water (70 ml) was added 3 g of IIa. The reaction mixture was refluxed for 10 hr and then evaporated *in vacuo*. The residue was collected, recrystallized and identified(mp and mixed mp) as IV. Yield, 2.5 g.

1,4,4-Tri(β-cynoethyl)-3-methyl-2-pyrazolin-5-one (V). *1) From Ia.* To a solution of acrylonitrile(1.0 ml) in pyridine(30 ml) and water(10 ml) was added 2.0 g of Ia and then one drop of concentrated potassium hydroxide. The mixture was refluxed for 10 hr and left to stand overnight at room temperature. The solvent was removed *in vacuo* and the resulting oily residue was dissolved in hot ethanol. The crystals, which separated on standing, were recrystallized from ethanol to yield 1.8 g of V, colorless crystals, mp 89 °C. IR: 2220(CN), 1700(ring CO) cm^{-1}. Found: C, 60.44; H, 5.84; N, 27.19%. Calcd for $C_{13}H_{15}ON_5$: C, 60.68; H 5.88; N, 27.22%.

2) From 1,4-Di(β-cyanoethyl)-3-methyl-2-pyrazolin-5-one(VI). Compound VI was treated with acrylonitrile using the same experimental procedure as above and the product was identified (mp and mixed mp) as V. Yield, 51%.

4,4-Di(β-carboxyethyl)-5-hydroxy-3-methylpyrazole (VII). A solution of 3.0 g of IV in acetic acid (30 ml) was mixed with 10 ml of concentrated hydrochloric acid and refluxed for 3 hr. The solvent was removed *in vacuo* and the resulting solid product was crystallized from water to yield 1.5 g of VII, colorless crystals, mp 230 °C (decomp.). Found: C, 49.49; H, 5.94; N, 11.59%. Calcd for $C_{10}H_{14}O_5N_4$: C, 49.58; H, 5.83; N, 11.57%.

4-(β-Ethoxycarbonylethyl)-5-hydroxy-3-methylpyrazole (VIII). *1) From Ia and Ethyl Acrylate:* To a solution of ethyl acrylate (5.0 ml) in ethanol(100 ml) and water(50 ml) was added 5.0 g of Ia. One drop of concentrated potassium hydroxide was then added and the reaction mixture was refluxed for 6 hr. The solvent was then removed *in vacuo* and the oily residue formed was dissolved in benzene and petroleum ether was added. The crystals separated were collected by filtration and recrystallized from benzene to yield 4.7 g of VIII, colorless crystals, mp 100 °C. IR: 2900—2675(OH), 1740 (ester CO)cm^{-1}. Found: C, 54.74; H, 7.06; N, 14.08%. Calcd for $C_9H_{14}O_3N_2$: C, 54.53; H, 7.12; N, 14.13%.

2) From X and Hydrazine Hydrate. To a solution of X (2.0 g) in ethanol(20 ml) was added hydrazine and the mixture was refluxed for 2 hr. The solvent was removed *in vacuo* and the residue was worked up as described above. The product was identified (mp and mixed mp) as VIII. Yield 1.6 g.

4-(β-Cyano-α-methylethyl)-5-hydroxy-3-methylpyrazole (IX). To a solution of crotononitrile(7.0 ml) in pyridine (150 ml) and water (50 ml) was added 10 g of Ia. One drop of potassium hydroxide solution was added and the reaction mixture was refluxed for 24 hr. The solvent was removed *in vacuo* and the residue was dissolved in a small quantity of water and acidified with 10 ml of acetic acid. The solid product separated on being left to stand was collected and crystallized from water to yield 9.0 g of IX, colorless crystals, mp 193 °C. IR: 2900—2650(OH), 2240(CN), 1690(ring CO)cm^{-1}. Found: C, 58.19; H, 6.54; N, 25.30%. Calcd for $C_8H_{11}ON_3$: C, 58.16; H, 6.71; N, 25.44%.

The same compound(IX) was similarly obtained by the reaction of ethyl 1-acetyl-3-cyano-2-methylbutyrate(XI) and hydrazine hydrate.

4,4-Di(β-cyanoethyl)-3-methyl-1-phenyl-2-pyrazolin-5-one (XII). To a solution of acrylonitrile(10 ml) in pyridine(150 ml) and water(50 ml) was added 9.0 g of Ib. The mixture was refluxed for 10 hr, evaporated *in vacuo* and the residual oily product was dissolved in hot ethanol. The crystals separated on cooling were collected and recrystallized from ethanol to give 10 g of XII, mp 74 °C. IR: 2220(CN), 1700(ring CO)cm^{-1}. Found: C, 68.98; H, 5.45; N, 20.01%. Calcd for $C_{16}H_{14}ON_4$: C, 69.05; H, 5.07; N, 20.13%.

4,4-Di(β-carboxyethyl)-3-methyl-1-phenyl-2-pyrazolin-5-one (XIII). Compound XII was treated with acetic acid

16) A. Mustafa, M. Fleifel, M. Ali, and N. M. Hassan, *Ann. Chem.*, **739**, 75 (1970).

and hydrochloric acid by the same procedure as for the preparation of VII. The solid product obtained upon evaporation of the solvent *in vacuo* was crystallized from water to give colorless crystals of XIII, mp 142 °C, in a yield of 80%. Found; C, 60.27; H, 5.70; N, 8.79%. Calcd for $C_{16}H_{18}O_5N_2$: C, 60.37; H, 5.70; N, 8.80%.

3-Amino-4,4-di(β-ethoxycarbonylethyl)-1-phenyl-2-pyrazolin-5-one (XIV). This compound was obtained by a similar procedure to that for XII. Mp, 84 °C, Yield 12.0 g. IR: 1745, 1725(ester CO), 1710(ring CO), 3450, 3355 (NH_2) cm^{-1}. Found: C, 60.43; H, 6.77; N, 12.11%. Calcd for $C_{25}H_{25}O_5N_3$: C, 60.78; H, 6.71; N, 11.19%.

3-Amino-4,4-di(β-cyanoethyl)-1-phenyl-2-pyrazolin-5-one (XV). To a solution of acrylonitrile(5.0 ml) in ethanol(150 ml) and water(50 ml) was added 5.0 g of Ic and the mixture was worked up as for XIV. The solid product obtained on evaporation of the solvent was crystallized from water to give 6.0 g of XV, mp 164 °C. IR: 3390, 3300, 3190(NH_2), 2220(CN), 1710(ring CO) cm^{-1}. Found: C, 64.32; H, 5.40; N, 25.24%. Calcd for $C_{15}H_{15}ON_5$: C, 64.06; H, 5.47; N, 24.90%.

2,3-Dihydro-4-methyl-2-phenylpyrazolo[3,4-b] piperidine-3,6-dione (XVI). *1) From Ic and Ethyl Crotonate*: To a solution of ethyl crotonate(3 ml) in pyridine(150 ml) and water (50 ml) containing one drop of concentrated potassium hydroxide solution was added 7.0 g of Ic. The mixture was refluxed for 10 hr and then evaporated *in vacuo*. The residual oil was treated with sodium ethoxide solution (perpared from 2.0 g of sodium and 150 ml of ethanol) and the mixture was refluxed for 2 hr and again evaporated *in vacuo*. The oil was dissolved in water(100 ml) and acidified with acetic acid. The precipitates were collected by filtration and crystallized from ethanol to give 4 g of XVI, colorless crystals, mp 233 °C. IR: 3130(NH), 1710—1690, 1645—1630(ring CO), 1590(CN) cm^{-1}. Found: C, 63.97; H, 5.33; N, 17.10%. Calcd for $C_{13}H_{13}O_2N_3$: C, 64.18; H, 5.39; N, 17.28%.

2) From Phenylhydrazine and XVII: To a sodium ethoxide solution (prepared from 5.0 g of sodium and 160 ml of ethanol) was added, 12 g of XVII and 7 ml of phenylhydrazine. The mixture was refluxed for 16 hr and then evaporated *in vacuo*. The residue was treated as above and the product was identified (mp and mixed mp) as XVI. Yield, 2.0 g.

3-Amino-4-(1-phenyl-2-benzoylethyl)-1-phenyl-2-pyrazolin-5-one (XVIII). To a sodium ethoxide solution(prepared from 3.0 g of sodium and 150 ml of ethanol) were added, 8.5 g of Ic and 5.0 g of benzalacetophenone. The reaction mixture was refluxed for 6 hr and then evaporated *in vacuo*. The residue was dissolved in water and acidified with concentrated hydrochloric acid. The precipitates were collected by filtration and crystallized from ethanol to yield 6.6 g of XVIII, colorless crystals, mp 300 °C. Found: C, 75.10; H, 6.10; N, 10.58%. Calcd for $C_{24}H_{21}O_2N_3$: C, 75.15; H, 5.52; N, 10.96%.

BULLETIN OF THE CHEMICAL SOCIETY OF JAPAN, VOL. 46, 3821—3824 (1973)

Studies on Reactions of the *N*-Phosphonium Salts of Pyridines. III. A New Method for the Activation of Amines *via* the *N*-Phosphonium Salts by Means of Oxidation of Phosphorous Acid and Its Esters in the Presence of Tertiary Amines

Noboru YAMAZAKI and Fukuji HIGASHI

Department of Polymer Science, Tokyo Institute of Technology, Meguro-ku, Tokyo 152

(Received May 22, 1973)

Amines were treated with the *N*-phosphonium salts of pyridine prepared by the oxidation of the phosphorous acid and its esters with mercuric chloride in pyridine; they yielded the corresponding amides in good yields upon acidolysis with carboxylic acids, together with metallic mercury in a nearly quantitative yield. The reaction was studied using phosphorous acid and its several esters, and was presumed to proceed *via* the activation of amines by the *N*-phosphonium salts of pyridine which were characterized by IR spectroscopy. This process for the activation of amino groups was successfully extended to peptide synthesis in pyridine at low temperature using diphenyl phosphite.

We obtained the *N*-phosphonium salts of pyridines by the oxidation of phosphorous acid and its esters in tertiary amines like pyridine.[1-3] The reactions of the salts with carboxylic acids were elucidated by the replacement of the chlorine atom on the salts by the acid (Eqs. 1 and 2), and the nucleophilic attack of the acid on the phosphorus atom (Eq. (3)).

A similar mechanism was proposed in the reaction of the salts (Ia-d) with amine.[3]

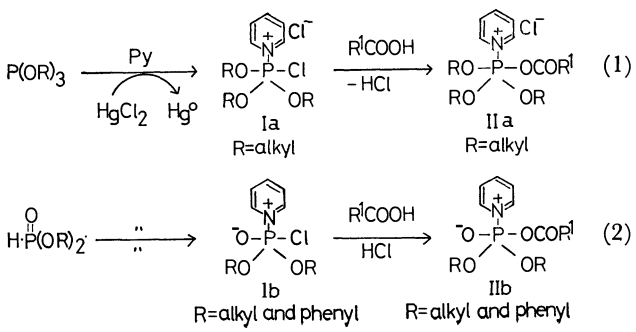

1) N. Yamazaki and F. Higashi, Part I, This Bulletin, **46**, 1235 (1973).
2) N. Yamazaki and F. Higashi, Part II, *ibid.*, **46**, 1239 (1973).
3) N. Yamazaki and F. Higashi, *Tetrahedron Lett.*, **1972**, 415.

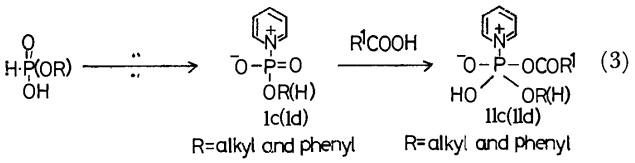

The present paper deals with detailed studies on the reactions of the *N*-phosphonium salts with the amines, and the application to peptide synthesis.

Results and Discussion

The *N*-phosphonium salt of pyridine (I) has been obtained by the oxidation of phosphorous acid and its esters with mercuric chloride in pyridine. When the salt in pyridine was refluxed with aniline for 1 hr and then with acetic acid for 1 hr, acetanilide was obtained in excellent yields. Similarly, several anilides were prepared by using phosphorous acid, its mono-, di- and tri-esters. The results are given in Table 1.

The reaction can be assumed to proceed *via* *N*-phosphonium salt(III) carrying aniline obtained by the reaction of I with aniline. III is converted into IV on treatment with carboxylic acids. IV is unchanged in pyridine at ordinary temperature, but decomposes to the anilide *via* V at higher temperatures (see Scheme 1).

In order to confirm the mechanism, III and IV were separated as syrups containing pyridine hydrochloride.[1] They do not seem to have been purified because of contamination of pyridine hydrochloride and of difficulty in crystallization. Though V could not be isolated, it was considered to take part in the reaction from the result of steric effect of carboxylic acids upon the yield of the anilides.

The structure of Ia ($R=C_2H_5$-) has been discussed previously.[1] The IR spectrum of IIIa ($R=C_2H_5$-), like that of Ia ($R=C_2H_5$-), showed characteristic bands at 1630, 1580 and 1485 cm^{-1} due to $\nu_{C=N^+}$ of the *N*-phosphonium salt of pyridine, and a strong band at 1600 cm^{-1} due to $\nu_{C=C}$ of anilino moiety. From the results and the appearance of the bands due to pyridine hydrochloride after the reaction of Ia ($R=C_2H_5$–) with aniline, IIIa ($R=C_2H_5$–) was assumed to be produced by replacement of a chlorine atom (or ion) on

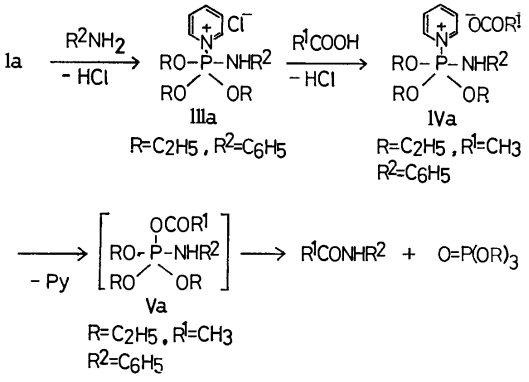

Scheme 1.

Ia ($R=C_2H_5$–) with anilino moiety. The IR spectrum of IVa ($R=C_2H_5$–) also showed bands due to $\nu_{C=N^+}$ of the *N*-phosphonium salt, νC=C of anilino moiety and $\nu_{C=O}$ of acetoxy group.

The reaction with the triester is summarized in Scheme 1.

The reactions with phosphorous acid (Id) and its other esters (Ib and Ic) might proceed in a similar way. The corresponding *N*-phosphonium salts of pyridine were prepared from phosphorous acid (IIId and IVd), its monoester (IIIc and IVc) and its diester (IIIb and IVb), and characterized by IR spectroscopy. These can be envisaged as follows.

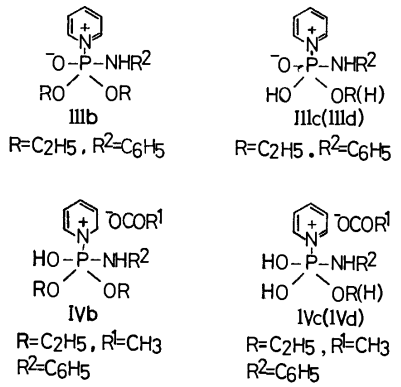

The reaction of III with carboxylic acids took place easily and gave better results than that of II with amines. For example, IIId from phosphorous acid gave acetanilide in a nearly quantitative yield (97%) by the reaction with acetic acid for only 1 hr of reflux, whereas in the case of IId more than 2 hr of reflux with aniline was required to obtain the anilide in the same yield.[2]

This would be attributed to the difference in reactivity between IId and IIId toward nucleophiles, since the formation of IId was almost completed under these conditions, the ether extract from the reaction mixture of Id and acetic acid containing no acetic acid.[1]

The facility of acidolysis of III can be explained in terms of the electromeric effect of the anilino group on III. The effect may cause a decrease of electron-density on the phosphorus atom through the migration of the electron of phosphorus-nitrogen (aniline) bond toward the nitrogen atom, resulting in an increase in electrophilicity on the phsophorus atom. Consequently, II can be readily attacked by the carboxylate anions to give the corresponding anilides by way of IV and V.

In the reactions with the monoalkyl esters, the yield of the anilide was unexpectedly low, but that of monophenyl ester was excellent (Table 1). The increase in pK_a of carboxylic acids did not improve the yield (see trifluoroacetanilide), suggesting that the rate-determining step in the reaction with monoalkyl esters is the nucleophilic attack of aniline in the phosphorus atom on Ic. Therefore, the presence of electron-attracting groups such as the phenyl group, increased the electrophilicity on the phosphorus atom, facilitating the attack of aniline on Ic. On the other

hand, the electron-donating nature of alkyl groups retarded the reaction.

A similar effect caused by the electronic nature of alkyl and phenyl groups was also expected in the reactions with the diesters, but no effect was observed. It seems reasonable to assume that the reaction of Ib with aniline is unaffected by the electrophilicity on the phosphorus atom because of an easy replacement reaction of the chlorine atom (or ion) in Ib by the anilino group in a similar manner to Eq. (2).

The yield of the anilides was affected by the steric effect of amines, carboxylic acids and tertiary amines, similarly to those in the reactions of I with carboxylic acids.[1,2]

The steric effect of carboxylic acids upon the yield was reflected in the lower yields of pivalanilide than those of acetanilide (see Table 1). Pivalanilide was obtained in nearly the same amount by acidolysis of III as by aminolysis of II. The results led us to consider that the nucleophilic attack of carboxylate anions on the phosphorus atom is involved in the reaction, by possible destruction of the phosphorus-nitrogen (pyridine) bond to give V.

Another possible route of reaction *via* anilinophosphoramides was excluded by the fact that diethyl anilinophosphoramidate yielded no acetanilide when refluxed with acetic acid in pyridine.

Carboxylic amides were proved to be produced through a similar activation of amines to that of carboxylic acids. They were also obtained in the presence of both amines and carboxylic acids.[3] Consequently, three procedures were available for the preparation of carboxylic amides by means of the *N*-phosphonium salts of pyridines, *viz.*, aminolysis after activation of carboxyl component (method A), acidolysis after that of the amino component (method B) and the activation instantly followed by the coupling reaction in the presence of both components (method C).

The three methods were tested in the reaction of benzyloxycarbonyl-glycine and ethyl glycinate in order to find the most effective one for peptide synthesis. Both activation and coupling reactions were carried out at low temperature (45 °C) to prevent racemization. The activation procedures were achieved by adding the amino and/or carboxyl components to the mixture prepared by the oxidation of diphenyl phosphite with mercuric chloride in pyridine.[3] Methods B and C were preferable to A, indicating that even in the presence of both components the amino component was preferably activated to yield the peptide in a good yield (Table 2).

A variety of phosphorus compounds were examined

Table 1. Preparation of anilides through activation of aniline using various phosphorus compounds and mercuric chloride in tertiary amines

Phosphorus compounds	Tertiary amines	Anilides	Yield, %
Phosphorous Acid	Py	Acetanilide	97
Phosphorous Acid	Py	*N*-Methylacetanilide	53
Phosphorous Acid	Py	Pivalanilide	27
Phosphorous Acid	2-Me-Py	Acetanilide	69
Phosphorous Acid	4-Me-Py	Acetanilide	77
Monoethyl Ester	Py	Acetanilide	33
Monoethyl Ester	Py	Trifluoroacetanilide	28
Monoisopropyl Ester	Py	Acetanilide	45
Monophenyl Ester	Py	Acetanilide	96
Diethyl Ester	Py	Acetanilide	93
Diisopropyl Ester	Py	Acetanilide	95
Diisopropyl Ester	Py	Pivalanilide	65
Diphenyl Ester	Py	Acetanilide	95
Triethyl Ester	Py	Acetanilide	62
Triisopropyl Ester	Py	Acetanilide	86

Table 2. Peptide synthesis using diphenyl phosphite in pyridine by several methods

Peptides	Yield, %[a]	Method[b]	Mp, °C	$[\alpha]_D$
Z-Gly-Gly-OEt	84	A	80	
Z-Gly-Gly-OEt	92	B	80	—
Z-Gly-Gly-OEt	95	C	80	
Z-Phe-Gly-OEt (L)	90	B	108—109	−17.7° (*c* 2, EtOH)
Z-Gly-Tyr-OEt (L)	90	B	125—126	+19.8° (*c* 5, EtOH)
Z-α-Glu-Gly-OEt (L)	70	B	122—123	—
Z-Glu(NH_2)-Gly-OEt (L)	79	C	166—168	−6.5° (*c* 1, DMF)
Z-Met-Gly-OEt (DL)	93	C	72—73	—

a) The coupling reactions were carried out at 45 °C for 12 hr.
b) Method A; Through activation of carboxyl components.
Method B; Through activation of amino components.
Method C; Activation and coupling in the presence of both components.

TABLE 3. PREPARATION OF Z-Gly-Gly-OEt USING VARIOUS PHOSPHORUS COMPOUNDS

Phosphorous compounds	Yield, %[a)]
Phosphorous Acid	4
Monophenyl Ester	20
Diisopropyl Ester	18
Diphenyl Ester	95
Triisopropyl Ester	23

a) The reactions were carried out at 45 °C for 12 hr by method C.

in the reaction between benzyloxycarbonyl-glycine and ethyl glycinate by method C (Table 3). Diphenyl phosphite was found to be most effective. This may be due to the increase in electrophilicity of the phosphorous atom caused by the electron-attracting nature of the phenyl groups in the phosphite.

Several other peptides were also synthesized using diphenyl phosphite by methods B and C. The results are given in Table 2. Good yields without detectable racemization were obtained within experimental errors.

It is surprising that the presence of the free side chains of glutamic acid, glutamine and methionine in the carboxyl component, and of tyrosine in the amino component did not cause any difficulty in the reactions. For example, the α-carboxyl rather than the γ-carboxyl group in glutamic acid referred to be activated, producing the α-peptide in a high yield. Similarly, a peptide of glutamine was obtained accompanied by no side reactions such as nitrile formation.

The oxidation mixture involving the *N*-phosphonium salts of pyridine could activate not only carboxyl and amino groups but also hydroxyl groups.[3)] Thus, a competitive activation of the amino and hydroxyl groups was expected in the reaction between ethyl tyrosinate and benzyloxycarbonyl-glycine, giving the corresponding amide and ester. The result shows that the amino group in ethyl tyrosinate was preferably activated to give the amide without yielding any detectable amount of the ester.

Experimental

Preparation of I, III and IV. Preparation of I was described in previous papers.[1,2)] A mixture of equimolar amounts of triethyl phosphite (2.1 g, 12.5 mmol) and mercuric chloride (3.5 g) was refluxed for 1 hr in 20 ml of pyridine, and for 1 hr after addition of aniline (1.2 g, 12.5 mmol). From the mixture, IIIa ($R=C_2H_5-$) was obtained as an ether-insoluble syrup by a similar procedure to that for Ia($R=C_2H_5-$). When IIIa ($R=C_2H_5-$) was treated with acetic acid at room temperature, IVa ($R=C_2H_5-$) was also obtained as a syrup. Similarly, IIIb~IIId and IVb~IVd were obtained.

Preparation of Anilides through the Activation of Aniline. A mixture of equimolar amounts of phosphorous acid and its esters (12.5 mmol) and mercuric chloride was heated at 115 °C for 1 hr in 20 ml of tertiary amines. The resulting mixture was treated with aniline (12.5 mmol) for 1 hr under reflux, and then with equimolar amounts of carboxylic acids for 1 hr. The resulting anilides were isolated and purified according to the previously reported procedures.[3)] The anilides thus obtained had melting points and infrared spectra identical with those of authentic samples.

Preparation of Peptides using Phosphorous Acid and Its Esters in Pyridine. A mixture of equimolar amounts of phosphorous acid and its esters (12.5 mmol) and mercuric chloride was refluxed for 1 hr in 20 ml of pyridine.

Method A: The oxidation mixture was treated with a benzyloxycarbonyl amino acid (12.5 mmol) in 10 ml of pyridine. After 1 hr, an amino acid ester hydrochloride (12.5 mmol) was added to the mixture, and then the solution was kept at 45 °C for 12 hr. The peptide formed was isolated and purified as described previously.[3)]

Method B: The oxidation mixture was treated as in method A with an amino acid ester hydrochloride, a benzyloxycarbonyl amino acid being added after 1 hr, and the mixture kept under the same conditions.

Method C: A mixture of a benzyloxycarbonyl amino acid and an amino acid ester hydrochloride in 20 ml of pyridine was added to the oxidation mixture, and then the solution was kept under the same conditions as for method A.

An Addition Reaction of Diethylamine to Styrene Catalyzed by Lithium Diethylamide

Tadashi NARITA, Teruo YAMAGUCHI, and Teiji TSURUTA

Department of Synthetic Chemistry, Faculty of Engineering, University of Tokyo, Bunkyo-ku, Tokyo 113

(Received April 25, 1973)

An addition reaction of diethylamine to styrene catalyzed by lithium diethylamide was found to proceed stoichiometrically to produce 1-diethylamino-2-phenylethane. The rate of the reaction was expressed by the equations: $v=k[\text{Styrene}][Et_2NLi]^{1.3}$ and $v=k[\text{Styrene}][Et_2NLi]$, the ratios of $[Et_2NH]_0$ to $[Et_2NLi]_0$ being 3.0 and 10 respectively. On the basis of the kinetic studies, the mechanism of the addition reaction was elucidated. The nucleophilic character of this reaction was clearly demonstrated by the σ-ρ Hammett plot. The second-order rate constant for the addition reaction of styrene was found to be of the same order of magnitude as that of butadiene. The presence of butadiene in the reaction system showed no effect on the reactivity of styrene.

The reactions of some active hydrogen compounds with butadiene initiated by alkyllithium has recently been reported to produce interesting intermediate compounds for organic synthesis.

The reaction of diphenylmethane with butadiene initiated by the system consisting of *n*-butyllithium and a donor compound has been found to produce 5,5-diphenylpentene derivatives.[1] A stereospecific reaction takes place, on the other hand, when diethylamine is reacted with butadiene in the presence of lithium diethylamide at the $[Et_2NH]_0/[Et_2NLi]_0$ ratio of 3.0, the selectivity of the product, 1-diethylamino-*cis*-butene-2, being up to 99%.[2] On the basis of kinetic and spectroscopic studies, the lithium diethylamide—diethylamine (1 : 2) complex has been concluded to play an important role in this reaction.[3]

It is widely accepted that the microstructures of polydienes prepared by alkyllithium are markedly different from one another according to the nature of the solvents or complexing agents used for the polymerization reactions. The predominant formation of 1,4-structure in hydrocarbon solvents is interpreted in terms of a concerted mechanism in which the preliminary coordination of diene molecules to the organolithium species is assumed. Lewis bases used as solvents (or complexing agents) interfere with the coordination of the monomer molecules, resulting in the predominant formation of the 1,2-structure in the polymer chain.

It is also known, in the styrene-diene copolymerization initiated by alkyllithium in hydrocarbon, that the reactivity of styrene is very much enhanced in the presence of Lewis bases.

In the light of these previous results, the stereospecific addition reaction of the lithium diethylamide—diethylamine complex seems to possess some peculiar character, for the 1,4-*cis*-structure is almost exclusively formed in the addition product, even in the presence of the Lewis base. In order to make clear the nature of the lithium amide complex in more detail, the addition reactions to styrene and its derivatives were studied.

Experimental

Most of the experiments were carried out under a purified nitrogen atmosphere in order to exclude oxygen and moisture.

Materials. Commercial cyclohexane, styrene, α-methylstyrene, butadiene, diethylamine, and triethylamine were purified by the usual method. *n*-Butyllithium was prepared from *n*-butyl chloride and lithium metal in purified petroleum ether and was used as a cyclohexane solution. *p*-Methylstyrene[4] and *p*-methoxystyrene[5] were synthesized according to the literature.

Procedures. The methods of the rate study of the addition reactions were described in an earlier publication.[3] The analyses of the addition-reaction product of diethylamine with styrene, 1-diethylamino-2-phenylethane, and of those with *p*-methylstyrene and *p*-methoxystyrene were performed by studying the infrared and proton magnetic resonance spectra.

Results and Discussion

As has been reported previously, the addition reaction of lithium diethylamide with butadiene does not

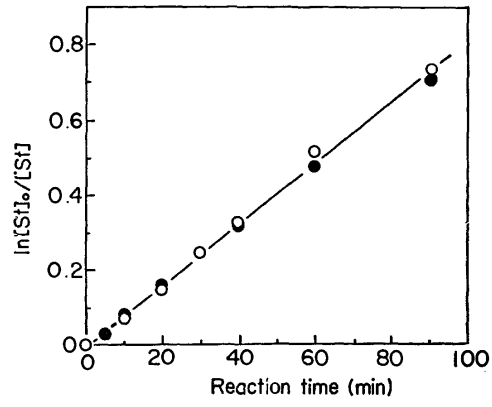

Fig. 1. First-order analyses of the reaction of Et_2NH–Et_2NLi complex with styrene: dependence of styrene concentration.
$[Et_2NLi]_0=0.250$ mol/l, $[Et_2NH]_0/[Et_2NLi]_0=3.0$ in cyclohexane at 50°C ● from [Styrene], ○ from $[Et_2NCH_2CH_2C_6H_5]$.

1) T. Yamaguchi, T. Narita, and T. Tsuruta, *Polymer J.*, **3**, 573 (1972).
2) N. Imai, T. Narita, and T. Tsuruta, *Tetrahedron Lett.*, **1971**, 3517.
3) T. Narita, N. Imai, and T. Tsuruta, This Bulletin, **46**, 1242 (1973).
4) D. T. Mowry, M. Renoll, and W. F. Huber, *J. Amer. Chem. Soc.*, **68**, 1105 (1946).
5) C. Walling, and K. B. Wolfstirm, *ibid.*, **69**, 852 (1947).
6) T. Asahara, M. Seno, S. Tanaka, and N. Den, This Bulletin, **42**, 2337 (1969).

proceed in the absence of dialkylamine.[2,3] A similar phenomenon was also observed in the reaction of lithium diethylamide with styrene, no addition product, 1-diethylamino-2-phenylethane, being detected until an excess of free diethylamine is present along with the lithium amide in the reaction system.

The dependence of the initial styrene concentration on the reaction rate is shown in Fig. 1. As the curves for the concentrations of the starting materials and of the addition product measured independently by means of the vapor-phase chromatography are clearly symmetrical, any possibilities of side reactions such as telomerization[6] may be ruled out. Since the first-order analyses shown in Fig. 1 stay linear until 50% conversion, the reaction rate is proportional to the first-order of the styrene concentration. The pseudo first-order rate constants are summarized in Table 1.

TABLE 1. PSEUDO FIRST-ORDER RATE CONSTANTS OF THE REACTION OF Et_2NH-Et_2NLi COMPLEX WITH STYRENE[a)]

$[Et_2NH]_0$ mol/l	$[Et_2NLi]_0$ mol/l	$[Styrene]_0$ mol/l	k' hr^{-1}
0.750	0.250	0.125	0.49
0.750	0.250	0.250	0.48
0.750	0.250	0.375	0.49

a) In cyclohexane at 50°C.

In order to determine the dependency of the reaction rate on the concentration of lithium diethylamide, the reaction rate was analyzed under a constant concentration of styrene, with the ratio of $[Et_2NH]_0$ to $[Et_2NLi]_0$ being 3.0. When the reaction rate is expressed as Eq. (1), the pseudo firstorder rate constant, k', can be determined from the slopes of the straight lines in Fig. 2:

$$v = k'[\text{Styrene}] \quad (1)$$

The slopes of the line which are obtained from the plot of log k' *vs.* log$[Et_2NLi]$ should show the dependency on the lithium diethylamide concentration:

$$k' = k_s[Et_2NLi]^x \quad (2)$$

As is shown in Fig. 3 and Table 2, the reaction rate can be expressed as Eq. (3) in the range of $[Et_2NH]_0/[Et_2NLi]_0 \geqq 10$:

$$v = k_s[\text{Styrene}][Et_2NLi] \quad (3)$$

whereas the reaction order shows some fractional power in the cases of $[Et_2NH]_0/[Et_2NLi]_0=3.0$ ($x=1.3$) and 5.0 ($x=1.2$), as is shown in Eq. (4):

$$v = k_s[\text{Styrene}][Et_2NLi]^x \quad (4)$$

This phenomenon may be explained in terms of the "solvent effect", because the increase in the lithium amide concentration is accompanied by an increase in the double mole quantity of diethylamine. The increase in the rate caused by the "solvent effect" may be eliminated by adjusting the total amine concentration with triethylamine. The results of the experiments in which the total amine concentration, $[Et_2NH]_0+[Et_3N]$, was kept constant are shown by a dotted line in Fig. 3. The reaction order obtained from the slope is 1.0_4. The acceleration of the addition reaction rate observed in Fig. 3 may, therefore, be concluded to come from the "solvent effect" of amines.[7]

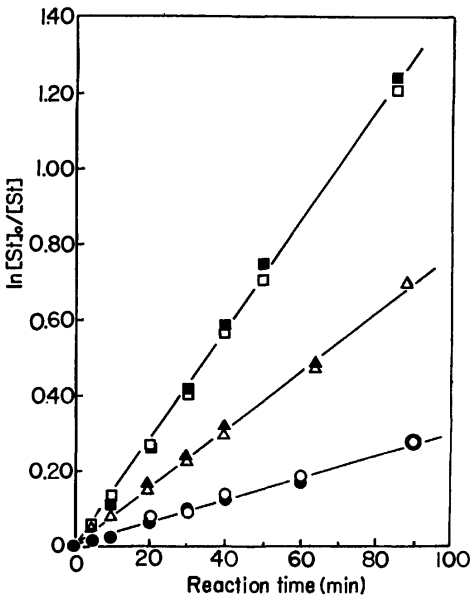

Fig. 2. Reaction of Et_2NH-Et_2NLi complex with styrene: dependence of lithium diethylamide concentration: first-order analyses for styrene concentration.
$[St]_0=0.250$ mol/l, $[Et_2NH]_0/[Et_2NLi]_0=3.0$ in cyclohexane at 50 °C, $[Et_2NLi]_0=0.125$ mol/l (○) 0.250 mol/l (△) and 0.375 mol/l (□).
○△□ $Et_2NCH_2CH_2C_6H_5$, ●▲■ styrene.

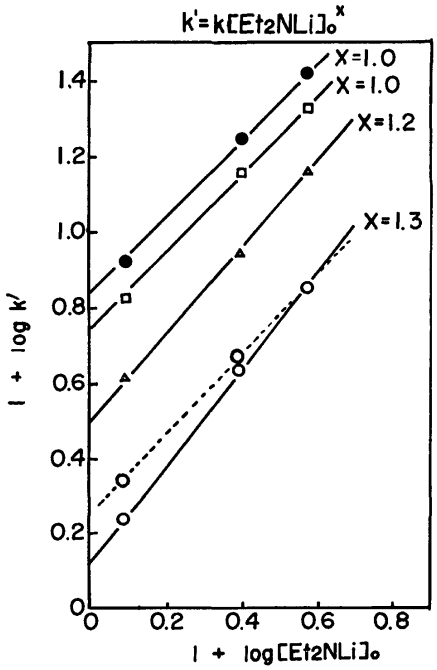

Fig. 3. Relationship between lithium diethylamide concentration and pseudo first-order rate constant.
$[Et_2NH]_0/[Et_2NLi]_0=3.0$ (○), 5.0 (△), 10 (□) and 15 (●) in cyclohexane at 50 °C
Dotted line: $[Et_2NH]_0/[Et_2NLi]_0=3.0$, $[Et_2NH]_0+[Et_3N]=0.375$ mol/l (*cf.* Fig. 2).

7) Possibility that the difference may come from the decrease of effective concentration of the active species by the reverse reaction of Eq. (6) might be disproved since ultraviolet spectral measurement of the reaction system showed no peak assignable to $Et_2NCH_2\overset{\ominus}{C}HC_6H_5\overset{\oplus}{Li}$.[8]

Table 2. Reaction kinetics of Et_2NH-Et_2NLi complex with styrene[a)]

$\frac{[Et_2NH]_0}{[Et_2NLi]_0}$	$[Et_2NLi]_0$ mol/l	k' hr^{-1}	Note
3.0	0.125	0.16	$v=k_s[\text{Styrene}][Et_2NLi]^{1.3}$
	0.250	0.43	
	0.375	0.71	
5.0	0.125	0.41	$v=k_s[\text{Styrene}][Et_2NLi]^{1.2}$
	0.250	0.88	
	0.375	1.46	
10	0.125	0.66	$v=k_s[\text{Styrene}][Et_2NLi]$
	0.250	1.45	$k_s=1.6\times10^{-3}$ l/mol·s
	0.375	2.16	
15	0.125	0.83	$v=k_s[\text{Styrene}][Et_2NLi]$
	0.250	1.81	$k_s=2.0\times10^{-3}$ l/mol·s
	0.375	2.61	
28	0.250	2.32	$k_s=2.6\times10^{-3}$ l/mol·s

a) $[\text{Styrene}]_0=0.250$ mol/l, in cyclohexane at 50°C.

The acceleration of the rate by the increased concentrations in the range of higher concentrations may also be seen in Table 2.

These results show that the reactivity of styrene is more sensitive to the change in the polarity of the solvent used than is that of butadiene (*cf.* Table 3).

The overall reaction scheme of the addition reaction of diethylamine with styrene can, therefore, be depicted as follows:

$$Et_2NLi + 2Et_2NH \rightarrow Et_2NLi\cdot 2Et_2NH \quad (5)$$

$$Et_2NLi\cdot 2Et_2NH + C_6H_5CH{=}CH_2 \xrightarrow{k_s} Et_2NCH_2CHC_6H_5Li\cdot 2Et_2NH \quad (6)$$

$$Et_2NCH_2CHC_6H_5Li\cdot 2Et_2NH + Et_2NH \longrightarrow Et_2NCH_2CH_2C_6H_5 + Et_2NLi\cdot 2Et_2NH \quad (7)$$

In order to get a hint about the character of the lithium diethylamide—diethylamine complex, the addition reactions of some substituted styrene with the amide complex at $[Et_2NH]_0/[Et_2NLi]_0=10$ were studied. The first-order analyses and the rate constants are shown in Fig. 4. As is shown in Fig. 5, the resultant ρ value is +5.0, in good agreement with the value reported for the anionic reaction system of polystyrylsodium with substituted styrene in tetrahydrofuran.[9)]

It is well known that, in the styrene–butadiene copolymerization with a lithium alkyl initiator in hydrocarbon media, the presence of a diene monomer pronouncedly suppresses the reactivity of styrene, although the rate of the homopolymerization of styrene is greater than that of butadiene under the same conditions. The microstructure of the butadiene units of the copolymer prepared under the above-mentioned copolymerization system is predominantly the 1,4-structure. On the other hand, when the reactivity of styrene is increased by the addition of some Lewis bases in the copolymerization system, the amount of the 1,2-structure in the butadiene units is also increased. In order

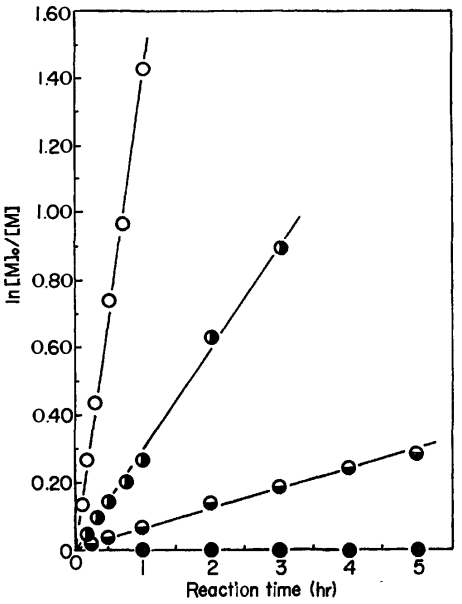

Fig. 4. First-order analyses of the reaction of Et_2NH-Et_2NLi complex with substituted styrene.
$[Et_2NLi]_0=[\text{Styrene deriv.}]_0=0.250$ M, $[Et_2NH]_0/[Et_2NLi]_0=10$, in cyclohexane at 50 °C.
○ Styrene; ◑ *p*-methylstyrene; ◒ *p*-methoxystyrene; ● α-methylstyrene.

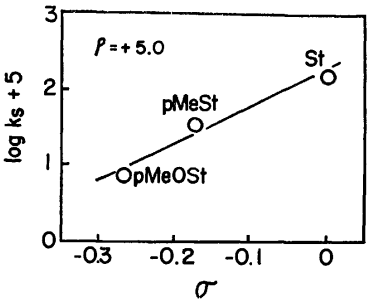

Fig. 5. Hammett σ-ρ plot for *p*-substituted styrene with Et_2NLi-Et_2NH complex.

Table 3. Second-order rate constants of addition reaction of Et_2NH-Et_2NLi complex with styrene and butadiene[a)]

$\frac{[Et_2NH]_0}{[Et_2NLi]_0}$	Styrene $k_s\times10^3$ l/mol·s	Butadiene $k_b\times10^3$ l/mol·s	Styrene-Butadiene $k_s\times10^3$ l/mol·s	Styrene-Butadiene $k_b\times10^3$ l/mol·s
3.0	—	0.85	—	—
10	1.6	1.4	1.5	1.6
15	2.0	—	—	—
28	2.6	—	—	—

a) In cyclohexane at 50°C. b) Ref. 2.

to compare the reactivity of lithium diethylamide with that of lithium alkyl, the reactivity of styrene toward the lithium amide in the presence of butadiene was examined. It may be seen in Table 3 that the presence of butadiene has no effect on the reactivity of styrene in contrast with the reaction with lithium alkyl. Table 3 also shows the two monomers to possess rate constants of almost the same order of magnitude. The isomer

8) R. J. Schlott, J. C. Falk, and K. W. Narducy, *J. Org. Chem.*, **37**, 4243 (1972).

9) M. Shima, D. N. Bhattacharyya, J. Smid, and M. Szwarc, *J. Amer. Chem. Soc.*, **85**, 1306 (1963).

distribution of the 1-diethylaminobutene produced here is not different compared with the results reported previously.[2,3]

The above results suggest that the mechanism of the stereospecific addition reaction of the lithium diethylamide complex to butadiene is different from the usual stereospecific addition reaction of lithium alkyl in hydrocarbon solvents, since the 1,4-*cis*-structure formation in butadiene units is still retained, even under reaction conditions which result in comparable monomer reactivities in the styrene–butadiene copolymerization.

BULLETIN OF THE CHEMICAL SOCIETY OF JAPAN, VOL. 46, 3828—3830 (1973)

Mechanism of Transylidation of Stable Sulfonium Ylids with Alkyl Sulfides in the Presence of Catalytic Disulfides[1)]

Haruo MATSUYAMA, Hiroshi MINATO, and Michio KOBAYASHI

Department of Chemistry, Faculty of Science, Tokyo Metropolitan University, Fukazawa, Setagaya, Tokyo 158

(Received May 31, 1973)

In the presence of bis(trifluoromethyl) disulfide, methylphenylsulfonium bis(methoxycarbonyl)methylid is readily attacked by a nucleophile (an alkyl sulfide or a pyridine) and the corresponding new ylid is produced. In the NMR spectrum of a mixture of an ylid, an alkyl sulfide, and a catalytic disulfide, a remarkable broadening in the signals of the α-hydrogen of the sulfide was observed. A mechanism is suggested, which involves a complex from the two reactants and the catalyst.

In the presence of a dialkoxy disulfide or thiocyanogen an alkyl sulfide or pyridine attacks the ylid carbon atom of a sulfonium ylid and the corresponding new ylid is formed.[2)]

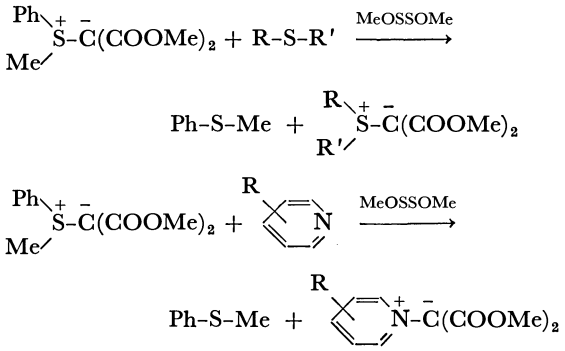

It has been found that bis(trifluoromethyl) disulfide possesses a similar catalytic activity, and with this catalyst some NMR spectroscopic evidence suggesting the formation of a complex has been obtained.

Results and Discussion

Transylidation of methylphenylsulfonium bis(methoxycarbonyl)methylid (Ia) was carried out with

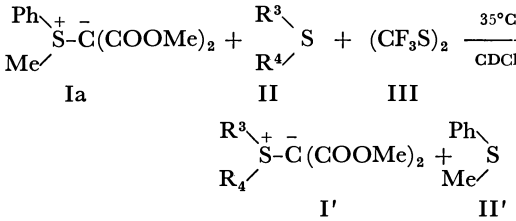

a: $R^3=R^4=Me$, b: $R^3=Me$, $R^4=Et$, c: $R^3, R^4=(CH_2)_4$

1) Organic Sulfur Compounds. Part XLV.
2) H. Matsuyama, H. Minato, and M. Kobayashi, This Bulletin, **46**, 2845 (1973).

several sulfides and 4-methylpyridine in the presence of bis(trifluoromethyl) disulfide (III). In Table 1, the results are compared with those obtained in the presence of dimethoxy disulfide or thiocyanogen. It is clear that when III was used as the catalyst the transylidation proceeds much more slowly than when dimethoxy disulfide or thiocyanogen was used.

TABLE 1. TRANSYLIDATION OF YLID Ia WITH A SULFIDE OR A PYRIDINE IN $CDCl_3$ AT 35°C[a)]

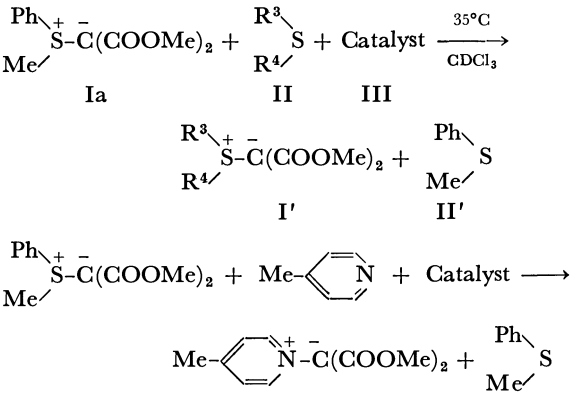

Nucleophile	Catalyst	Time (min)	Products (mol%) Recovered Ia	I'	II'
MeSMe	$(CF_3S)_2$	90	—	93	100
MeSEt	$(CF_3S)_2$	267	—	93	94
$(CH_2)_4S$	$(CF_3S)_2$	30	—	91	98
Me-pyridine	$(CF_3S)_2$	594	64	31	31
MeSMe	$(MeOS)_2$	7	—	100	98
Me-pyridine	$(N{\equiv}CS)_2$	3	—	96	96

a) A mixture consists of Ia (0.5 mmol), a nucleophile (1.0—1.5 mmol) and a catalyst (0.07—0.12 mmol).

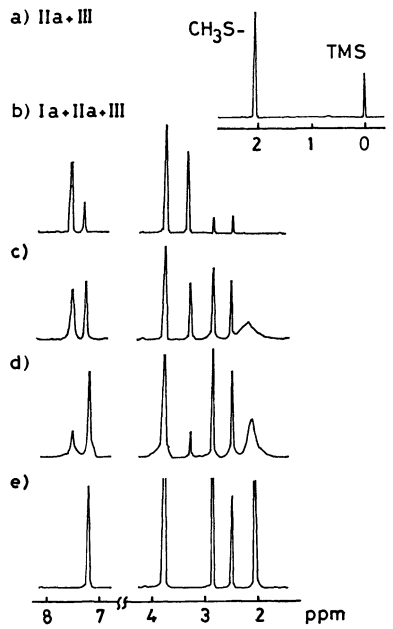

Fig. 1. NMR spectra of mixtures of Ia, IIa, and III in $CDCl_3$ at 35 °C.
a) IIa (1.82 M) and III (0.20 M) in $CDCl_3$
b) 9 min after Ia (0.91 M) was added to IIa and III. The yield of PhSMe was 21%.
e) 40 min after addition. PhSMe, 50%.
d) 60 min after addition. PhSMe, 79%.
e) 90 min after addition. PhSMe, 100%.
PhMeS- (δ, 7.52 ppm), PhSMe (7.25 ppm), C(COOMe)$_2$ (3.68 ppm), PhMeS- (3.30 ppm), Me_2S- (2.88 ppm), PhSMe (2.49 ppm), Me_2S (2.10 ppm).

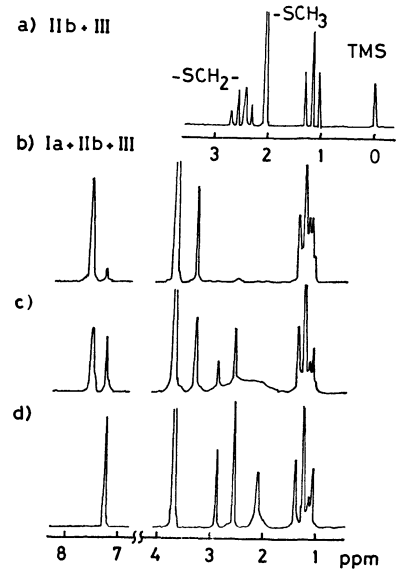

Fig. 2. NMR spectra of mixtures of Ia, IIb, and III in $CDCl_3$ at 35 °C.
a) IIb (2.51 M) and III (0.20 M) in $CDCl_3$.
b) 8 min after Ia (0.89 M) was added to IIb and III. The yield of PhSMe was 6%.
c) 82 min after addition. PhSMe, 27%.
d) 267 min after addition. PhSMe, 94%.
PhMeS- (δ, 7.53 ppm), PhMeS (7.26 ppm), C(COOMe)$_2$ (3.69 ppm), PhMeS- (3.32 ppm), MeEtS- (2.88 ppm), PhSMe (2.50 ppm), MeSEt (2.10 ppm).

When the NMR spectrum of a mixture of Ia, IIa, and III was determined, surprisingly the sharp singlet of IIa was not observed. The NMR spectrum of a mixture containing two components out of the three (Ia and IIa; IIa and III; or III and Ia) was simply the sum of the spectra of the corresponding components, and the methyl signals of IIa disappeared only when all of the three components were mixed. When the NMR spectrum of a mixture of Ia, IIa, and III was determined after about 50% completion of the transylidation, the methyl signal of the remaining IIa was observed as a broad absorption. Throughout the reaction, the methyl signal (PhMeS-, δ, 3.31 ppm) of ylid Ia showed no broadening. When ethyl methyl sulfide (IIb) or tetrahydrothiophene (IIc) was used in place of IIa, a similar broadening of the α-hydrogens (underlined in the formulas shown below) was observed. The results are summarized in Figs. 1 and 2.

$\underline{CH_3}\text{-S-}\underline{CH_3}$ $\quad$ $\underline{CH_3}\text{-S-}\underline{CH_2}\text{-}CH_3$ $\quad$ $(\underline{CH_2}CH_2)_2S$

Reports on broadening of NMR absorptions are mainly those concerning intramolecular rotation or inversion.[3]

Smallcombe and Caserio[4] reported on the rapid exchange of S–CH_3 between methyl disulfide and dimethylthiomethylsulfonium ion.

$$Me_2\overset{+}{S}\text{-S-Me} + CH_3\text{-S-S-}CH_3 \rightleftarrows Me_2S + MeS\text{-}\overset{+}{S}\text{-}SCH_3 \quad (\delta,\ 2.86\ \text{ppm}) \qquad (\delta,\ 2.3\ \text{ppm})$$

The NMR spectrum of the mixture did not show the S–CH_3 signals of two components, but a broad signal. The NMR data show that a rapid equilibrium is maintained as shown above.

We have investigated the transylidation catalyzed by a dialkoxy disulfide, and propose the following scheme which represents what is probably taking place in a mixture of I, II, and III.[2]

$$\begin{matrix} R^1 \\ R^2 \end{matrix}\!\!>\!\overset{+\ -}{S}\text{-}C(COOMe)_2 + R\text{-S-S-}R \underset{k_{-1}}{\overset{k_1}{\rightleftharpoons}} [\text{complex}]$$

$$[\text{complex}] + \begin{matrix} R^3 \\ R^4 \end{matrix}\!\!>\!S \xrightarrow{k_2} \begin{matrix} R^3 \\ R^4 \end{matrix}\!\!>\!\overset{+\ -}{S}\text{-}C(COOMe)_2 + \begin{matrix} R^1 \\ R^2 \end{matrix}\!\!>\!S + R\text{-S-S-}R$$

The experimental results obtained so far can be summarized as follows.

1) In a mixture of an S-ylid and a catalytic disulfide, no broadening of NMR signals is observed.

2) In a mixture of an S-ylid and a sulfide, no broadening of NMR signals is observed, and almost no transylidation takes place at room temperature.

3) In a mixture of a sulfide and a catalytic disulfide, no broadening of NMR signals is observed.

4) When all of the three components (an S-ylid, a catalytic disulfide and a sulfide (or a pyridine)) are

3) G. Binsch, "Topics in Stereochemistry," John Wiley & Sons, New York (1968), Vol. 3, p. 97.

4) S. H. Smallcombe and M. C. Caserio, *J. Amer. Chem. Soc.*, **93**, 5826 (1971).

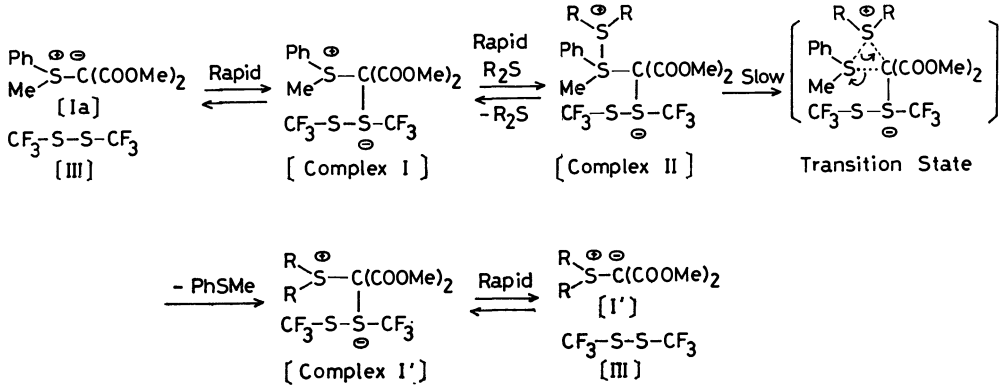

Scheme.

mixed, the NMR signals of the α-hydrogens of the sulfide (or a pyridine) are much broadened.

5) A broadening of NMR signals is observed only when transylidation takes place.

6) When a sulfide (or pyridine) is not added, an olefin is formed.

7) In the case of a phenacylid, an olefin and a cyclopropane derivative are formed even when a sulfide is present.

A plausible mechanism consistent with these results is shown in the Scheme.

The first step is the reversible formation of Complex I from Ia and III. Nucleophilic attack of an alkyl sulfide (or pyridine) on the sulfonium sulfur atom of Complex I results in the formation of the termolecular Complex II. The NMR data can be explained by assuming that the formation of Complex II from Complex I and the sulfide (or pyridine) is reversible and rapid, and molecules of the sulfide (or pyridine) rapidly combine with and depart from Complex I one after another. Therefore, the absorption of the α-hydrogens of the sulfide (or pyridine) is broadened between that of the free sulfide (or pyridine) and that of the sulfide (or pyridine) in Complex II. An example of the tetravalent sulfur atom with one unshared electron pair in Complex II is found in the case of sulfuranes.[5]

Formation of Complex I′ from Complex II by removal of methyl phenyl sulfide is probably slow and is the rate-determining step of the whole reaction. Decomposition of Complex I′ gives III and a new ylid I′. The step from Complex II to Complex I′ should be irreversible since a mixture of I′, III, and methyl phenyl sulfide does not give Ia under similar conditions.

The role of a catalytic disulfide is withdrawal of the negative charge on an ylid carbanion so that the nucleophilic attack of a sulfide on the sulfonium sulfur atom is facilitated. Therefore, disulfides possessing strongly electronegative substituents can act as the catalysts for transylidation. The combination of a catalytic disulfide with an S-ylid should be reversible, since the disulfide must be regenerated for repetition of the reaction.

When a sulfide (or pyridine) is not present in the medium, the negatively charged carbon atom of another molecule of the ylid attacks Complex I, and an olefin is produced.

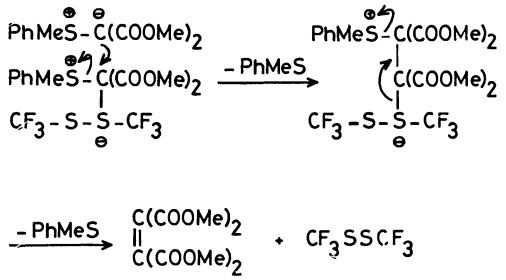

Thus, the mechanism postulated above is consistent with all the experimental findings, and can explain the transylidation[2] and decomposition[6] of ylids in the presence of a catalytic disulfide.

Experimental

Materials. Sulfonium ylid Ia was prepared by the method described in the literature.[7] Methyl sulfide, tetrahydrothiophene, 4-methylpyridine were of reagent grade and used without purification. Bis(trifluoromethyl) disulfide was synthesized by the method of Tullock and Coffman.[8]

Measurements. NMR spectra were determined with a Hitachi NMR spectrometer R-203 (60 MHz). A $CDCl_3$ solution of I, II, and III containing nitromethane (internal standard) was placed in an NMR tube at 35 °C, and the intensity changes of the signals of the original ylid (I), new ylid (I′), and new sulfide (II′) were determined.[2]

5) J. C. Martin and R. J. Anhart, *J. Amer. Chem. Soc.*, **93**, 2341 (1971); R. J. Anhart and J. C. Martin, *ibid.*, **94**, 4997 (1972).

6) H. Mastuyama, H. Minato, and M. Kobayashi, This Bulletin, **46**, 3158 (1973).

7) W. Ando, T. Yagihara, S. Tozune, S. Nakaido, and T. Migita, *Tetrahedron Lett.*, **1969**, 1979.

8) C. W. Tullock and D. D. Coffman, *J. Org. Chem.*, **25**, 2016 (1960).

Layered Compounds. XVI.[1] NMR Spectra of Multilayered [2.2]Paracyclophanes

Tetsuo OTSUBO, Shigeyoshi MIZOGAMI, Yoshiteru SAKATA, and Soichi MISUMI

The Institute of Scientific and Industrial Research, Osaka University, Suita, Osaka 565

(Received August 10, 1973)

The NMR spectra of multilayered [2.2]paracyclophanes (I—XVI), in which benzene rings are closely stacked, have been examined. The assignment of the signals was made not only by integral strength, but also by solvent effect and the Nuclear Overhauser effect. The steric compression effect of transannular methyl groups on aromatic protons was observed in methylated cyclophanes. Enhanced ortho substitution shift was also observed. All the aromatic protons shift to remarkably higher field due to the anisotropy of stacked benzene rings as the number of layers increases. The shielding effect caused by these rings was empirically estimated.

In the NMR spectra of a series of [*m.n*]paracyclophanes, the aromatic protons appear at higher field beyond the usually accepted range of alkylbenzenes with decreasing number of methylenes in the bridges, *m* and *n*.[2] The upfield shift was considered to be ascribed to the anisotropy effect of one benzene ring on the aromatic protons of the other ring, and to the rehybridization effect of benzene carbon atoms due to ring deformation. By comparing the aromatic protons of [*m*]paracyclophanes ($m=7$—10)[3-5] with those of their open chain model compounds, the former effect is considered to be mainly responsible for the upfield shift, the latter effect being regarded as minor. Janusene,[6] [2.2]metacyclophane,[7] and [13]helicene,[8] in which aromatic rings are constructed parallel to overlap each other, also exhibit such an upfield shift of aromatic protons due to anisotropy of other aromatic rings.

According to X-ray crystallographic analyses,[9,10] both [2.2]paracyclophane and quadruple-layered [2.2]paracyclophane are of rigidly fixed structures with benzene rings fully superposed. We thus anticipated that the aromatic protons of multilayered [2.2]-paracyclophanes, consisting of two or more of [2.2]-paracyclophane system, would be affected by the anisotropy of more remote benzene rings besides the neighboring rings and that these cyclophanes would be appropriate model compounds for the study of magnetic anisotropy. The present paper reports a study on chemical shifts of aromatic protons in a series of multilayered [2.2]paracyclophanes (I—XVI), synthesis of which was described in the preceding paper.[1]

Results and Discussion

Assignment of Aromatic Protons. The NMR spectra of layered cyclophanes (I—XVI) are summarized in Table 1. Except for I, III, and IV, most of them show a few signals of aromatic protons depending upon magnetic environment. The signals are mostly assigned to the corresponding protons with the aid of integral strengths. However, there are some compounds with more than two layers, whose aromatic protons are difficult to assign by their integral strengths alone, *e.g.*, VI (Hb and Hc), XI, and XIV (Hb—He). In these cases, the solvent effect was found to be fairly

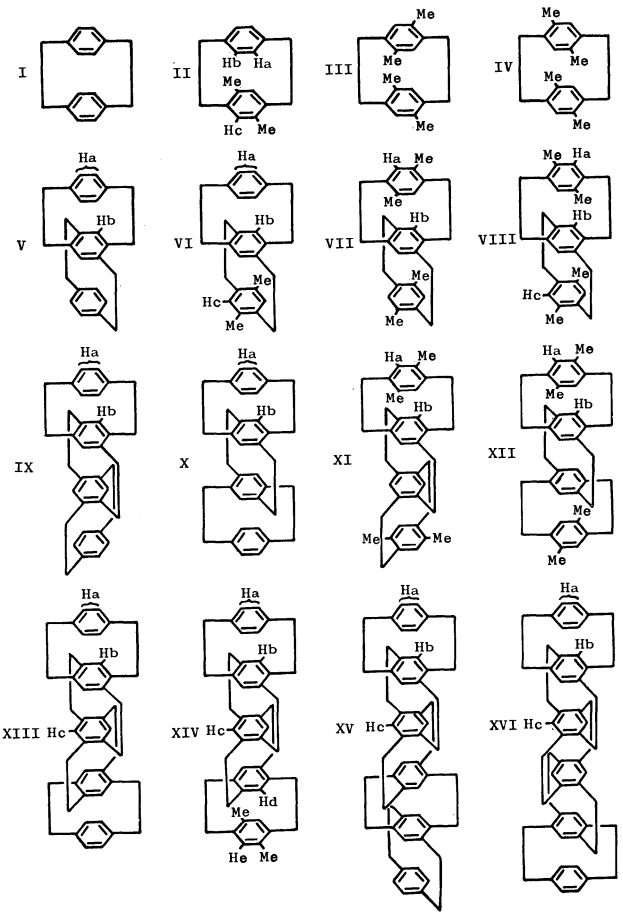

1) Part XV: T. Otsubo, S. Mizogami, I. Otsubo, Z. Tozuka, A. Sakagami, Y. Sakata, and S. Misumi, This Bulletin, **46**, 3519 (1973).

2) D. J. Cram and R. C. Helgeson, *J. Amer. Chem. Soc.*, **88**, 3515 (1966).

3) N. L. Allinger and T. J. Walter, *ibid.*, **94**, 9267 (1972); A. D. Wolf, V. V. Kane, R. H. Levin, and M. Jones, Jr., *ibid.*, **95**, 1680 (1973).

4) D. J. Cram, C. S. Montgomery, and G. R. Knox, *ibid.*, **88**, 515 (1966); N. L. Allinger, L. A. Freiberg, R. B. Hermann, and M. A. Miller, *ibid.*, **85**, 1171 (1963).

5) J. S. Waugh and R. W. Fessenden, *ibid.*, **79**, 846 (1957); D. J. Cram and M. Goldstein, *ibid.*, **85**. 1063 (1963).

6) S. J. Cristol and D. C. Lewis, *ibid.*, **89**, 1476 (1967).

7) D. J. Wilson, V. Boekelheide, and R. W. Griffin, Jr., *ibid.*, **82**, 6302 (1960); N. L. Allinger, M. A. DaRooge, and R. B. Hermann, *ibid.*, **83**, 1974 (1961).

8) R. H. Martin, G. Morren, and J. J. Schurter, *Tetrahedron* Lett., **1969**, 3683.

9) C. J. Brown, *J. Chem. Soc.*, **1953**, 3265; K. Lonsdale, H. J. Milledge, and K. V. K. Rao, *Proc. Roy. Soc., Ser A*, **255**, 82 (1960); H. Hope, J. Bernstein, and K. N. Trueblood, *Acta Crystallogr.*, **B28**, 1733 (1972).

10) H. Mizuno, K. Nishiguchi, T. Otsubo, S. Misumi, and N. Morimoto, *Tetrahedron Lett.*, **1972**, 4981.

Table 1. NMR spectra of layered compounds (τ value)

Compound		Aromatic proton		$\Delta\tau$[a]	Benzylic proton		Methyl proton	
		CCl_4	$CDCl_3$		CCl_4	$CDCl_3$	CCl_4	$CDCl_3$
p-Xylene		3.05(s)	2.94(s)	0.11			7.72(s)	7.69(s)
Durene		3.26(s)	3.10(s)	0.16			7.88(s)	7.85(s)
I		3.65(s)	3.53(s)	0.12	6.99(s)	6.94(s)		
II	Ha (2H)	3.32(A_2B_2)	3.22(A_2B_2)	0.10	6.5—7.7(m)		7.95(s)	7.90(s)
	Hb (2H)	3.74(A_2B_2)	3.64(A_2B_2)	0.10				
	Hc (2H)	4.12(s)	4.00(s)	0.12				
III		3.75(s)	3.64(s)	0.11	6.8—7.6(A_2B_2)		8.04(s)	7.98(s)
IV		3.93(s)	3.81(s)	0.12	6.5—7.4(A_2B_2)		7.85(s)	7.78(s)
V	out. Ha (8H)	3.92(s)	3.81(s)	0.11	6.8—7.7(m)			
	inn. Hb (2H)	4.65(s)	4.60(s)	0.05				
VI	out. Ha (4H)	3.88(s)	3.77(s)	0.11	6.8—7.8(m)		8.17(s)	8.11(s)
	inn. Hb (2H)	4.30(s)	4.25(s)	0.05				
	out. Hc (2H)	4.36(s)		0.11				
VII	out. Ha (4H)	4.33(s)	4.21(s)	0.12	6.7—7.7(m)		8.11(s)	8.07(s)
	inn. Hb (2H)	3.94(s)	3.88(s)	0.06				
VIII	out. (2H)		4.17(s)	0.16	6.7—7.8(m)		8.13(s)	8.10(s)
	Ha or Hc (2H)	4.33(bs)	4.21(s)	0.12				
	inn. Hb (2H)		4.28(s)	0.05				
IX	out. Ha (8H)	4.02(s)	3.91(s)	0.11	6.7—7.9(m)			
	inn. Hb (4H)	4.88(s)	4.85(s)	0.03				
X	out. Ha (8H)	4.02(s)	3.88(s)	0.14	6.9—7.9(m)			
	inn. Hb (4H)	4.90(s)	4.87(s)	0.03				
XI	out. Ha (4H)	4.43(s)	4.31(s)	0.12	6.8—8.1(m)		8.19(s)	8.16(s)
	inn. Hb (4H)	4.53(s)	4.48(s)	0.05				
XII	out. Ha (4H)	4.45(s)	4.32(s)	0.13	6.8—8.1(m)		8.20(s)	8.16(s)
	inn. Hb (4H)	4.52(s)	4.48(s)	0.04				
XIII	out. Ha (8H)	4.04(s)	3.93(s)	0.11	6.8—8.0(m)			
	inn. Hb (4H)	4.97(s)	4.93(s)	0.04				
	inn. Hc (2H)	5.12(bs)	5.08(bs)	0.04				
XIV	out. Ha (4H)	4.04(s)	3.91(s)	0.13	6.9—8.1(m)		8.24(s)	8.19(s)
	inn. Hb (2H)	4.96(s)	4.91(s)	0.05				
	inn. Hc (2H)	5.08(s)	5.05(s)	0.03				
	inn. Hd (2H)	4.64(s)	4.60(s)	0.04				
	out. He (2H)	4.47(s)	4.35(s)	0.12				
XV	out. Ha (8H)	4.06(s)	3.95(s)	0.11	7.1—8.3(m)			
	inn. Hb (4H)	5.00(s)	4.96(s)	0.04				
	inn. Hc (4H)	5.20(s)	5.17(s)	0.03				
XVI	out. Ha (8H)		3.95(s)		6.9—8.2(m)			
	inn. Hb (4H)		4.95(s)					
	inn. Hc (4H)		5.19(s)					

a) $\Delta\tau=\tau(CCl_4)-\tau(CDCl_3)$

effective for assignment of the protons. Thus, it was anticipated that the aromatic protons of outer benzene rings (outer ArH) would be strongly affected by solvent, while those of inner benzene rings (inner ArH) would not be influenced so much since they are closely sandwiched between the upper and lower benzene rings. The signals for aromatic protons of single- and double-layered compounds and for outer ArH of more than two layered ones (Table 1) display somewhat larger differences (0.10—0.16 ppm) between chemical shifts in carbon tetrachloride and in deuteriochloroform, while those for inner ArH give smaller differences (0.03—0.06 ppm). On the basis of such a solvent effect, assignments can be made for Hb (inner ArH) and Hc (outer ArH) of VI, and Ha (outer ArH) and Hb (inner ArH) of XI and XII. Dimethyl fivelayered compound XIV shows an integral ratio 2 : 1 : 1 : 1 : 1 of five aromatic proton signals at τ 4.04 (Ha), 4.47 (He), 4.64 (Hd), 4.96 (Hb), 5.08 (Hc) in carbon tetrachloride, and the assignment of those protons seems to be difficult at first. However, Ha, Hb, and Hc can be determined by comparison with the corresponding ones of non-substituted compound XIII, which are easily assigned by the integral strengths. The remaining protons, Hd and He, are distinguished as inner ArH and outer ArH, respectively, on the ground of the solvent effect.

Nuclear Overhauser Effect (NOE). In the spectrum of compound II, the aromatic protons of non-methylated benzene ring appear nonequivalently as

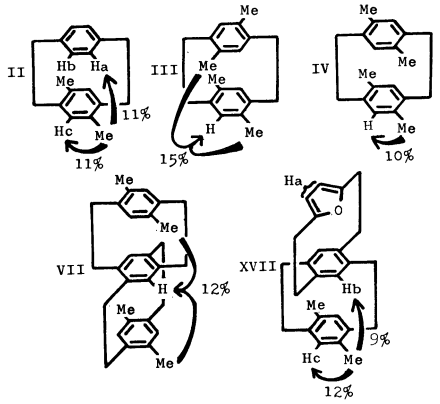

Fig. 1. Nuclear Overhauser effects of some layered cyclophanes in deuteriochloroform.

A_2B_2 pattern, possibly due to transannular proximity effect of methyl groups of the opposed benzene ring. Since NOE has successfully been used to assign such protons, we have attempted it on some layered compounds, whose aromatic protons could not be assigned by either the integral strength or the solvent effect. NOE was observed on the peaks at τ 3.22 and 4.00 and not for τ 3.64 peak of the compound II when methyl protons were irradiated in deuteriochloroform (Fig. 1). Since the peak at τ 4.00 is assigned to Hc proton from signal pattern, the peak at τ 3.22 is of the proton Ha at pseudo-gem position to methyl group and the remaining one at τ 3.64 of Hb at pseudo-ortho position.[11] The difference in the extent of NOE on aromatic protons of III and IV is related to the relative positions of the protons to methyl groups of opposed ring, that is, a larger value of the effect for compound III is attributable to both effects of pseudo-gem and ortho methyl groups.

The NOE caused by pseudo-gem methyl group was also observed on aromatic protons of triple-layered cyclophane VII and furanophane XVII. A value for the inner ArH of VII indicates an NOE depending upon efficient relaxation by the two methyl groups closely sandwiching the proton. On the other hand, the inner ArH of XVII exhibits a 9% area increase by irradiating the methyl group, and the protons which are unaffected by the saturation of methyl protons can easily be assigned to furan protons. In contrast to NOE on aromatic protons by saturation of methyl protons, the effect between aromatic protons was not detected on this series of compounds, *e.g.*, no change was observed in the areas of Ha and Hb when Hc of II was saturated. This seems to be well explained in terms of smaller interaction (dipole-dipole relaxation)[12] and longer transannular distances of H–H than those of CH_3–H.

Steric Compression Effect (CE). Hydrogen atoms which are significantly compressed with each other exhibit generally downfield shifts in NMR spectra.[13] This steric deshielding effect was found to be larger in more rigid compounds. Winstein reported unusually large deshielding effects (1—4 ppm) for the compounds with a half-cage structure related to the bird-cage hydrocarbons.[14] For example, the steric compression effect on Ha due to proximity of Hb in compound XVIII was seen to be in excess of 1 ppm. The

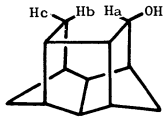

XVIII

effect has been observed also in layered cyclophanes containing proximate aromatic rings. Reich and Cram have described in NMR spectra of 4-substituted [2.2]-paracyclophanes that the protons pseudo-gem to the substituent displayed downfield shifts.[15] Similar steric compression effects of transannular methyl groups have been observed in the present multilayered [2.2]paracyclophanes. For example, obvious downfield shifts recognized by comparing the chemical shifts of Ha in dimethyl[2.2]paracyclophane (II) and of the aromatic protons in tetramethyl[2.2]paracyclophane (III) with those of the corresponding protons, to which pseudo-gem position is not substituted with methyl group. A similar deshielding of compressed protons is also observed for Hb of VI, VIII, XI, and XII and Hd of XIV (Table 1). An average value of these compression effects, σ_{CE} (pseudo-gem shift), of methyl groups, −0.36 ppm, is nearly equal to the value for 4-methyl-[2.2]paracyclophane given by Reich and Cram.[15] Of greater interest is a downfield shift of Hb in triplelayered compound VII, for the proton is a unique one sandwiched in between two methyl groups, that is, compressed from both upper and lower sides. They appear at lower field by twice (0.71 ppm) the above mean value for one methyl group. It is noteworthy that VII presents a novel example of steric compression on both sides and there is an additivity among steric compression shifts.

Whether bridged methylene groups of multilayered [2.2]paracyclophanes exert a similar effect can be solved with non-methylated multilayered cyclophanes such as the tripled one V. Thus, two types of outer aromatic protons in V, namely pseudo-gem and pseudo-ortho to methylene group, should exhibit different chemical shifts, provided that the methylene group can exert steric compression effect on the protons in question. However, this is not the case actually. They appear as a singlet pattern to demonstrate equal magnetic environment. This result may be interpreted in terms of out-of-plane bending of the methylene groups toward the opposite side to the proton in question.

A steric compression effect between two methyl groups themselves was also found in tetramethyl[2.2]-paracyclophane (IV). All methyl groups are eclipsed with each other, and their pseudo-gem distances

11) Nomenclature of pseudo-gem and pseudo-ortho was taken according to D. J. Cram, *J. Amer. Chem. Soc.*, **91**, 3505 (1969).
12) R. A. Bell and J. K. Saunders, *Can. J. Chem.*, **48**, 1114 (1970).
13) B. V. Cheney, *J. Amer. Chem. Soc.*, **90**, 5386 (1968), and literatures cited therein.
14) S. Winstein, P. Carter, F. A. L. Anet, and A. J. R. Bourn, *ibid.*, **87**, 5247 (1965).
15) H. J. Reich and D. J. Cram, *ibid.*, **91**, 3534 (1969).

are expected to be maintained within van der Waals distance (4.0 Å) on the basis of X-ray crystallography of [2.2]paracyclophane.[9] Thus, a difference in the chemical shifts of methyl protons of III and IV, 0.19 ppm, is related to the mutual compression effect between two methyl groups.

Enhanced Ortho Substitution Shifts. Reich and Cram reported that introduction of a substituent into the benzene ring of [2.2]paracyclophane caused a considerably large ortho shift compared to the corresponding open chain compounds, and that the enhancement of ortho shift might be due to the increased double bond character at C_4–C_5 bond in the bent ring.[15] On the other hand, the ortho substitution shifts in [3.3]paracyclophane are close to the normal, since the benzene rings are distorted from their planar configuration only by 6.4° in contrast to 15° for [2.2]-paracyclophane.[16]

The enhanced ortho shift σ_{OE} is observed also in methylated layered cyclophanes (Table 1). Thus, ortho protons to methyl groups appear at higher field by an average 0.42 ppm than the corresponding protons of non-substituted cyclophanes, *e.g.*, outer protons n each pair of VII *vs.* V, XI *vs.* IX, and XIV *vs.* XIII. The value 0.21 ppm, obtained by substracting the difference between durene and *p*-xylene (0.21 ppm) from the above average value, is the enhanced ortho substituent effect of methyl group in the layered [2.2]-paracyclophane system. Only one exception is the ortho shift in IV, 0.28 ppm. It is probable that strong mutual repulsion between the methyl groups may hinder electron delocalization of the moiety containing the methyl and its ortho proton.

Magnetic Anisotropy. Table 1 also shows that all the aromatic and methylene protons are shifted to a remarkably higher field as the number of layers increases. The more prominent of these is the upfield shift of inner aromatic protons caused by magnetic anisotropy of both upper and lower benzene rings. It is anticipated that there may exist a certain regularity among the chemical shifts of the aromatic protons, since each benzene ring is stacked at regular intervals in this series of multilayered cyclophanes.[10] From a number of examinations of the spectral data, the shielding effects due to additionally stacked benzene rings were estimated empirically (Table 2). It can be seen that the additional effect becomes less effective as the additional benzene ring lies further away from the proton in question.

Table 2. Shielding effect of additional benzene ring (ppm)

	Empirical	Calculated[a]
σ_1 (neighboring ring)	0.69	0.417
σ_2 (next ring but one)	0.22	0.157
σ_3 (next ring but two)	0.10	0.057
σ_4 (next ring but three)	0.03	0.028
σ_5 (next ring but four)	0.02	0.014

a) Values were calculated according to Johnson-Bovey's method.

It is known that the aromatic protons of [7]- and [8]-paracyclophanes[3,4] and [8][8]paracyclophane[17] appear within conventional range for alkyl benzenes, though they are in different steric environments due to individual ring deformation. Thus, their ring deformations hardly affect the chemical shifts of their own aromatic protons. It is known from X-ray crystallography of quadruple-layered cyclophane XII that the outside ring is distorted in a boat shape, and the inside ring in a twist shape,[10] and the ring deformations are considered not to differ so much in magnitude from those in [*m*]- and [8][8]-paracyclophanes. We assumed that the magnetic anisotropies of outside and inside benzene rings in multilayered cyclophanes were equal in magnitude in spite of different ring distortion.

From Table 2, the chemical shift of a given aromatic proton can be calculated by adding shielding effects of additional benzene rings to the chemical shift of the aromatic proton in standard alkylbenzene, *p*-xylene (τ 3.05) or durene (τ 3.26). For example, a calculated value of Ha in XIII is τ 4.09 ($3.05+\sigma_1+\sigma_2+\sigma_3+\sigma_4$), for Hb τ 4.96 ($3.26+2\sigma_1+\sigma_2+\sigma_3$), and for Hc τ 5.08 ($3.26+2\sigma_1+2\sigma_2$). Such a treatment

Table 3. Additivity of chemical shifts for aromatic protons of layered cyclophanes (τ value)

Compound		Obsd	Calcd	Deviation
I		3.65	3.74	+0.09
II	Ha	3.32	3.38	+0.06
	Hb	3.74	3.74	0
	Hc	4.12	4.16	+0.04
III		3.75	3.80	+0.05
IV		3.93	3.95[a]	+0.02
V	out. Ha	3.92	3.96	+0.04
	inn. Hb	4.65	4.64	−0.01
VI	out. Ha	3.88	3.96	+0.08
	inn. Hb	4.30	4.28	−0.02
	out. Hc	4.36	4.38	+0.02
VII	out. Ha	4.33	4.38	+0.05
	inn. Hb	3.94	3.92	−0.02
IX	out. Ha	4.02	4.06	+0.04
	inn. Hb	4.88	4.86	−0.02
XI	out. Ha	4.43	4.48	+0.05
	inn. Hb	4.53	4.50	−0.03
XIII	out. Ha	4.04	4.09	+0.05
	inn. Hb	4.97	4.96	−0.01
	inn. Hc	5.12	5.08	−0.04
XIV	out. Ha	4.04	4.09	+0.05
	inn. Hb	4.96	4.96	0
	inn. Hc	5.08	5.08	0
	inn. Hd	4.64	4.60	−0.04
	out. He	4.47	4.51	+0.04
XV	out. Ha	4.06	4.11	+0.05
	inn. Hb	5.00	4.99	−0.01
	inn. Hc	5.20	5.18	−0.02

a) Not consider σ_{OE}

16) M. Sheehan and D. J. Cram, *J. Amer. Chem. Soc.*, **91**, 3544 (1969).

17) M. Nakazaki, K. Yamamoto, and S. Tanaka, *Tetrahedron Lett.*, **1971**, 341.

is also applicable to the cases of methyl derivatives by considering the secondary effects of methyl group such as σ_{CE} and σ_{OE}. In the case of XIV, the calculated value for Ha, Hb, and Hc are the same as those of XIII, but for Hd τ 4.60 ($3.26+2\sigma_1+\sigma_2+\sigma_3+\sigma_{CE}$) and for He τ 4.51 ($3.26+\sigma_1+\sigma_2+\sigma_3+\sigma_4+\sigma_{OE}$). These calculated values are in excellent agreement with the observed ones (Table 3), supporting the view that the evaluation of each shielding magnitude is reasonable. However, we see a tendency of slightly positive deviation for outer protons and negative for inner protons. This may reflect the fact that in multilayered compounds, π-electron density is richer on the inner benzene ring than on the outer ring as a result of the transannular electronic interaction.

On the other hand, magnetic anisotropy of benzene ring was calculated by means of the ring current equation of Johnson and Bovey,[18] where 3.03 Å was used for the average distance between two adjacent benzene rings and 2.40 Å for the distance from the center of the benzene ring to its own ring proton. The calculated values thus obtained are not quite equal to the empirically evaluated ones, the former values being less by a factor of about 0.6, but both are in good correlation (Table 2). The results show that our data for shielding effect can be used satisfactorily to anticipate chemical shifts of similarly constructed compounds, and that for more exact evaluation of magnetic anisotropy of benzene ring, one must take into account not only ring current but also the secondary effects such as anisotropies of carbon-carbon and carbon-hydrogen σ-bonds.

18) C. E. Johnson, Jr. and F. A. Bovey, *J. Chem. Phys.*, **29**, 1012 (1958).

Experimental

NMR spectra were recorded on a Hitachi Perkin-Elmer R-20 spectrometer on dilute solutions (~10%) in carbon tetrachloride and/or deuteriochloroform using tetramethylsilane as an internal standard. The signals were measured by frequency counter with a precision of about ±1 cps. For NOE measurements a Varian HA-100 spectrometer was used. The effects were measured in degassed deuteriochloroform solution as area increase using the electronic integrator of the instrument. The errors are within ±5%.

The authors are greatly indebted to Mr. Y. Takai for NMR measurements and to Dr. E. Mizuta of Takeda Chemical Industries for NOE measurements. This research was supported by a grant-in-aid of the Ministry of Education.

BULLETIN OF THE CHEMICAL SOCIETY OF JAPAN, VOL. 46, 3835—3839 (1973)

Synthetic Studies of Bacitracin. IX.[1] Synthesis of Peptide Fragments for Bacitracins of Cycloheptapeptide Formula[2]

Eisuke MUNEKATA,* Tetsuo SHIBA, and Takeo KANEKO**

Department of Chemistry, Faculty of Science, Osaka University, Toyonaka, Osaka 560

(Received June 20, 1973)

In the synthetic study of bacitracins, peptide fragments corresponding to a branched part of bacitracin F, *i.e.*, (*S*)-2-(2-methylbutyryl)thiazole-4-carboxylic acid 1-succinimidyl ester (III) and L-leucyl-*γ*-*t*-butyl-D-glutamyl-L-isoleucine (IV), were prepared. As a macrocyclic part of bacitracin A and F of cycloheptapeptide formula, cyclo-(N^{α}-benzyloxycarbonyl-L-lysyl-N^{δ}-cyclopentyloxycarbonyl-D-ornithyl-L-isoleucyl-D-phenylalanyl-L-histidyl-*β*-benzyl-D-aspartyl-L-asparaginyl) (V) was synthesized through cyanomethyl ester method.

In the preceding paper,[1] the authors described the preparation of the intermediate heptapeptide derivative for the synthetic study of bacitracin A and F, the sequence of which was proposed by Stoffel and Craig.[3] Although Swallow and Abraham could not reduce four possibilities for the mode of linkage around L-lysine, L-aspartic acid and D-aspartic acid residues in the structure of bacitration A,[4] Stoffel and Craig proposed a structure I as the most probable one from rather inconceivable result of hydrazinolysis,[3] and this structure seemed to be accepted as the chemical structure of bacitracin A until 1966 when Ressler and Kashelikar revised the structure to formula II.[5] The latter group devised a new method for distinguishing asparagine and isoasparagine residues in peptide chain by dehydration of acid amide to nitrile followed by reduction and hydrolysis. Applying this technique to bacitration A, Ressler and Kashelikar recognized the presence of L-asparagine residue inside the peptide ring in lieu of D-isoasparagine residue outside the ring.[5] Recently, Craig and his collaborators also supported this structure II of a seven amino acids-membered ring

* Present address: Peptide Institute, Protein Research Foundation, Minoh, Osaka.

** Present address: Shiseido Laboratory, Nippa-cho, Kohoku-ku, Yokohama.

1) Part VIII: E. Munekata, Y. Masui, T. Shiba, and T. Kaneko, This Bulletin, **46**, 3187 (1973).

2) This work was presented at the 5th Symposium on Peptide Chemistry, Kyoto, November, 1967 and the 8th same Symposium, Osaka, November, 1970.

3) W. Stoffel and L. C. Craig, *J. Amer. Chem. Soc.*, **83**, 145 (1961).

4) D. L. Swallow and E. P. Abraham, *Biochem. J.*, **72**, 326 (1959).

5) C. Ressler and D. V. Kashelikar, *J. Amer. Chem. Soc.*, **88**, 2025 (1966).

on a basis of their unpublished data.[6]

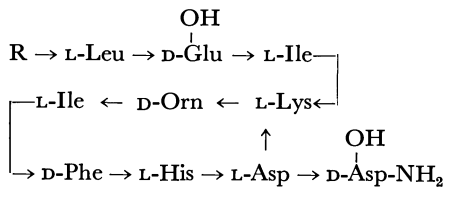

I

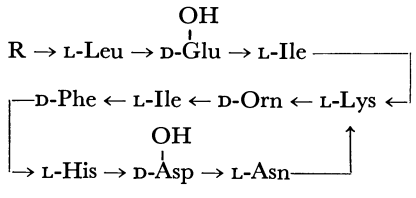

II

—— = CO→NH

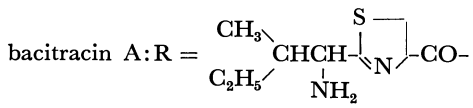

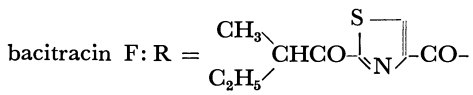

In this paper, we synthesized component fragments to build up the most reliable amino acid sequence II of bacitracin A and F, following the synthetic principle described in the previous paper[1] for an achievement of the total synthesis of the antibiotics. The principle is based on the coupling of thiazoline or thiazole moiety in the branched chain with macrocyclic peptide part. For the branched peptide part of bacitracin F, (*S*)-2-(2-methylbutyryl)-thiazole-4-carboxylic acid 1-succinimidyl ester (III) and L-leucyl-*γ*-*t*-butyl-D-glutamyl-L-isoleucine (IV) were prepared and for the macrocyclic part of the bacitracin A and F, cyclo-(*N*$^{\alpha}$-benzyloxycarbonyl-L-lysyl-*N*$^{\delta}$-cyclopentyloxycarbonyl-D-ornithyl-L-isoleucyl-D-phenylalanyl-L-histidyl-*β*-benzyl-D-aspartyl-L-asparaginyl) (V) was synthesized. These three peptide fragments cover the whole sequence of the antibiotic.

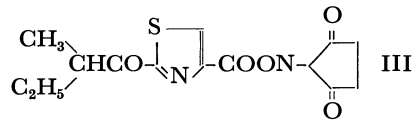

III

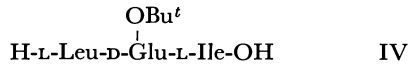

IV

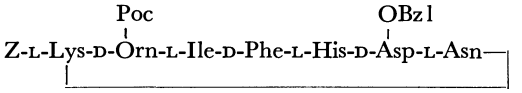

V

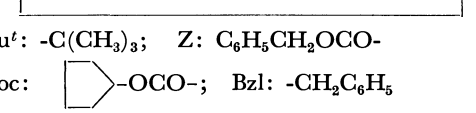

For the synthesis of *N*-terminal part in bacitracin F, the 1-succinimidyl ester III was prepared by the usual manner for synthesis of the active ester using dicyclohexylcarbodiimide from (*S*)-2-(2-methylbutyryl)-thiazole-4-carboxylic acid, the preparation of which was already reported in our previous paper.[7] The synthetic route of the tripeptides derivative IV in the branched peptide chain of the antibiotic was shown in Scheme 1. Thus, benzyloxycarbonyl-D-glutamic acid *γ*-*t*-butyl *α*-1-succinimidyl ester was coupled with benzyl L-isoleucinate to give benzyloxycarbonyl-*γ*-*t*-butyl-D-glutamyl-L-isoleucine benzyl ester (VIa). Dipeptide derivative VIa thus obtained was hydrogenated using palladium charcoal as catalyst to give *γ*-*t*-butyl-D-glutamyl-L-isoleucine (VIIa). The resulting deblocked peptide derivative VIIa was acylated by *t*-butyloxycarbonyl-L-leucine 1-succinimidyl ester to obtain *t*-butyloxycarbonyl-L-leucyl-*γ*-*t*-butyl-D-glutamyl-L-isoleucine (VIIIa). In the alternative route for preparation of the tripeptide VIIIa, *t*-butyloxycarbonyl-L-leucyl-*γ*-*t*-butyl-D-glutamyl-L-isoleucine methyl ester (VIIIb) was synthesized as a precursor of VIIIa according to Scheme 1 through the methyl esters VIb and VIIb. However, the methyl ester of the resulting tripeptide derivative VIIIb was found to resist to alkaline hydrolysis and the wanted product VIIIa of a free carboxyl group could not be obtained. When *γ*-*t*-butyl-D-glutamyl-L-isoleucine (VIIa) was acylated with benzyloxycarbonyl-L-leucine 1-succinimidyl ester, other tripeptide derivative IX was obtained. This was hydrogenated in the presence of palladium charcoal to give L-leucyl-*γ*-*t*-butyl-D-glutamyl-L-isoleucine (IV).

The cycloheptapeptide derivative V corresponding to the macrocyclic part was synthesized starting from *C*-terminal L-asparagine residue as shown in Scheme 2. First, *t*-butyloxycarbonyl-*β*-benzyl-D-aspartyl-L-asparagine (X) was prepared by coupling of *β*-benzyl *t*-butyloxycarbonyl-D-aspartate with L-asparagine either by the mixed anhydride method or by the 1-succinimidyl ester method. Removal of *t*-butyloxycarbonyl group from X gave *β*-benzyl-D-aspartyl-L-asparagine (XI). When a principle of the stepwise elongation from *C*-terminal was applied to this dipeptide derivative XI, the resulting tripeptide derivatives, i.e., benzyloxycarbonyl or *t*-butyloxycarbonyl-L-histidyl-*β*-benzyl-D-aspartyl-L-asparagine, showed awfully hy-

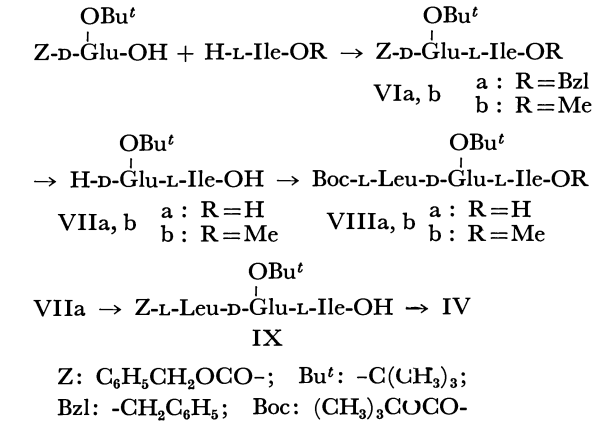

Z: $C_6H_5CH_2OCO$-; Bu^t: $-C(CH_3)_3$;
Bzl: $-CH_2C_6H_5$; Boc: $(CH_3)_3COCO$-

Scheme 1. Synthesis of the tripeptide derivative IV in a branched part of bacitracins.

6) R. E. Galardy, M. P. Printz, and L. C. Craig, *Biochemistry*, **10**, 2429 (1971).

7) Y. Ariyoshi, T. Shiba, and T. Kaneko, This Bulletin, **40**, 2654 (1967).

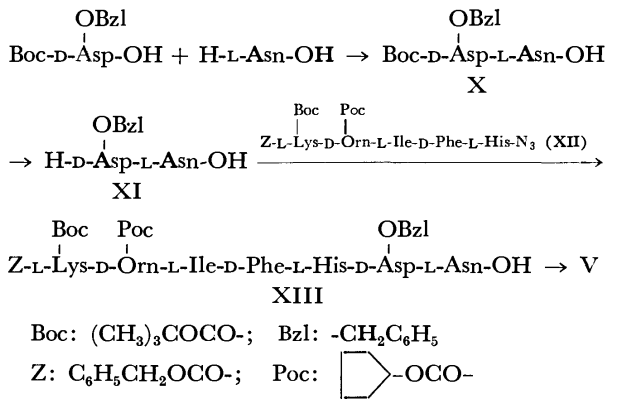

Scheme 2. Synthesis of the cycloheptapeptide derivative V corresponding to the macrocyclic part of bacitracin A and F of seven amino acids-membered formula.

groscopic and gelatinous properties which prevented isolation of a pure solid as the product. Furthermore, coupling of the deblocked product of the tripeptide mentioned above with *N*-acyl-D-phenylalanine could not give any pure tetrapeptide derivatives because of an extreme gelatinous character. Therefore, we turned to a route of coupling of XI with the acyl pentapeptide derivative XII, *i.e.*, N^{α}-benzyloxycarbonyl-N^{ε}-*t*-butyloxycarbonyl-L-lysyl-N^{δ}-cyclopentyloxycarbonyl-D-ornithyl-L-isoleucyl-D-phenylalanyl-L-histidine azide, the preparation of which was reported in the preceding paper,[1] and obtained the expected heptapeptide derivative XIII as demonstrated in Scheme 2. In this plan of building up the heptapeptide, we used the special cyclopentyloxycarbonyl group for a protection of δ-amino group of ornithine residue by reason of selective stability as far as a final synthetic step and of cleavability with hydrogen fluoride.[1]

We are now ready to total synthesis of bacitracin F of Ressler's formula by securing all peptide fragments required. However, for a cyclization of the heptapeptide XIII obtained above, the choice of the condensation reagent is limited by possible dehydration of the acid amide group in asparagine residue or undesirable side reaction on imidazole ring in histidine residue. In fact, attempt to cyclize XIII between the carboxyl group of asparagine residue and ε-amino group of lysine residue after removal of *t*-butyloxycarbonyl protection has not been succeeded yet when *N*-ethyl-5-phenylisoxazolium-5'-sulfonate described as safe reagent particularly for asparagine peptide was used for cyclization. Only when the cyanomethyl ester method was applied to this cyclization, the expected cyclo (N^{α}-benzyloxycarbonyl-L-lysyl-N^{δ}-cyclopentyloxycarbonyl-D-ornithyl-L-isoleucyl-D-phenylalanyl-L-histidyl-β-benzyl-D-aspartyl-L-asparaginyl) was obtained in one experiment. However, a yield of this product was extremely low and reproducibility of this cyclization reaction was strangely poor. These results may indicate that the activation of the carboxyl group of asparagine residue for cyclization of this heptapeptide is not adequate presumably owing to undesirable side reactions. Therefore, it must be required on this stage of the study that either the more effective cyclization method should be applied or a linkage to be connected for the cyclization has to be searched at another place to accomplish the total synthesis of bacitracins.

Experimental

All melting points are uncorrected. For silica gel column chromatography, Kieselgel 0.05—0.2 mm (70—325 mesh ASTM) Merck, was used. The infrared spectrum was obtained in Nujol mull with a Nihon Bunko IR-S spectrophotometer.

(S)-2-(2-Methylbutyryl)-thiazole-4-carboxylic Acid 1-Succinimidyl Ester (III). To a solution of (*S*)-2-(2-methylbutyryl)-thiazole-4-carboxylic acid[7] (2.1 g, 10 mmol) and *N*-hydroxysuccinimide (1.2 g, 10 mmol) in tetrahydrofuran (50 ml), there was added *N,N'*-dicyclohexylcarbodiimide (2.1 g, 10 mmol) under ice-cooling. The reaction mixture was stirred at this temperature for 1 hr and then at room temperature for 4 hr. Dicyclohexylurea deposited was filtered off, and the filtrate was evaporated *in vacuo*. A solid residue thus obtained was recrystallized from ethanol. Yield, 2.5 g (81%); mp 101—102 °C; $[\alpha]_D^{20}$ +13.4° (*c* 1, methanol).

Found: C, 50.07; H, 4.62; N, 9.00; S, 10.24. Calcd for $C_{13}H_{14}O_5N_2S$: C, 50.31; H, 4.55; N, 9.03; S, 10.33%.

Benzyloxycarbonyl-γ-t-butyl-D-glutamyl-L-isoleucine Benzyl Ester (VIa). A mixture of benzyloxycarbonyl-D-glutamic acid γ-*t*-butyl-α-1-succinimidyl ester[8] (8.7 g, 20 mmol), benzyl L-isoleucinate *p*-toluenesulfonate[9] (8.0 g, 20 mmol) and triethylamine (3 ml) in methylene chloride (300 ml) was stirred at 0 °C for 1 hr and then at room temperature for 17 hr. The solution was washed successively with 5% aqueous sodium carbonate, water, 0.5 M hydrochloric acid and water. The organic layer was separated, dried over anhydrous sodium sulfate, and then evaporated *in vacuo*. The residual solid was recrystallized from ethyl acetate-petroleum ether. Yield, 8.3 g (77%); mp 79—81 °C; $[\alpha]_D^{17}$ +8.8° (*c* 1, methanol).

Found: C, 66.36; H, 7.54; N, 5.35%. Calcd for $C_{30}H_{40}O_7N_2$: C, 66.64; H, 7.46; N, 6.18%.

γ-t-Butyl-D-glutamyl-L-isoleucine (VIIa) Hydrate. The protected dipeptide ester VIa (4.0 g, 7.4 mmol) was dissolved in methanol (100 ml) containing acetic acid (10 ml). Hydrogen gas was bubbled through the solution in the presence of palladium charcoal at room temperature for 8 hr. The catalyst was filtered off with the aid of celite. The filtrate was concentrated and a residual precipitate was collected by filtration. The product was recrystallized from methanol-water. Yield, 2.4 g (97%); mp 165—168 °C; $[\alpha]_D^{17}$ −32.4° (*c* 1, methanol).

Found: C, 53.66; H, 9.18; N, 8.41%. Calcd for $C_{15}H_{28}O_5N_2 \cdot H_2O$: C, 53.87; H, 9.04; N, 8.38%.

t-Butyloxycarbonyl-L-leucyl-γ-t-butyl-D-glutamyl-L-isoleucine (VIIIa). *t*-Butyloxycarbonyl-L-leucine 1-succinimidyl ester[10] (2.3 g, 7 mmol) in ethyl acetate (50 ml) was added to a cold solution of VIIa (2.4 g, 7 mmol) in chloroform containing triethylamine (1 ml). The mixture was stirred under ice-cooling for 1 hr and at room temperature for 8 hr. The solvent was removed *in vacuo* and the residue was triturated with petroleum ether. The product was collected, washed with water and recrystallized from ethyl acetate-petroleum ether. Yield, 2.5 g (68%); mp 142—143 °C; $[\alpha]_D^{17}$ +10.4° (*c* 1, methanol).

Found: C, 58.81; H, 9.05; N, 7.85%. Calcd for $C_{26}H_{47}$-

8) R. Zabel and H. Zahn, *Z. Naturforsch.*, **20b**, 650 (1965).
9) L. Zervas, M. Winitz, and J. P. Greenstein, *J. Org. Chem.*, **22**, 1515 (1957).
10) G. W. Anderson, J. E. Zimmerman, and F. M. Callahan, *J. Amer. Chem. Soc.*, **86**, 1839 (1964).

O_8N_3: C, 58.95; H, 8.94; N, 7.93%.

Benzyloxycarbonyl-γ-t-butyl-D-glutamyl-L-isoleucine Methyl Ester (VIb). A mixture of benzyloxycarbonyl-D-glutamic acid γ-*t*-butyl α-1-succinimidyl ester[8] (2.2 g, 5 mmol) and methyl L-isoleucinate *p*-toluenesulfonate (1.6 g, 5 mmol) in chloroform (100 ml) containing triethylamine (0.8 ml) was stirred at 0 °C for 1 hr and then at room temperature for 10 hr. The solution was washed successively with 5% aqueous sodium hydrogen carbonate, water, 0.5 M hydrochloric acid and water, and then dried over anhydrous sodium sulfate. The solvent was removed under reduced pressure and a resulting precipitate was recrystallized from diisopropyl ether–petroleum ether. Yield, 1.8 g (78%); mp 61—62 °C; $[\alpha]_D^{18}$ +5.9° (*c* 1, methanol).

Found: C, 61.96; H, 7.82; N, 6.17%. Calcd for $C_{24}H_{36}O_7N_2$: C, 62.05; H, 7.81; N, 6.03%.

γ-t-Butyl-D-glutamyl-L-isoleucine Methyl Ester (VIIb) p-Toluenesulfonate. The dipeptide methyl ester VIb (10 g, 2.2 mmol) was dissolved in methanol (20 ml) containing a few drops of acetic acid. Hydrogen gas was bubbled through the solution in the presence of palladium charcoal at room temperature for 6 hr. The catalyst was removed by filtration and a filtrate was concentrated to a half volume of the original solution. To a residual solution, *p*-toluenesulfonic acid hydrate (0.5 g) in ether was added. The deposit was collected by filtration and recrystallized from methanol–ethyl ether. Yield, 0.7 g (64%); mp 157—158 °C; $[\alpha]_D^{19}$ −21.0° (*c* 1, methanol).

Found: C, 54.88; H, 7.69; N, 5.54; S, 6.40%. Calcd for $C_{23}H_{38}O_8N_2S$: C, 54.96; H, 7.62; N, 5.57; S, 6.38%.

t-Butyloxycarbonyl-L-leucyl-γ-t-butyl-D-glutamyl-L-isoleucine Methyl Ester (VIIIb). *t*-Butyloxycarbonyl-L-leucine 1-succinimidyl ester[10] (1.3 g, 4.1 mmol) and VIIb *p*-toluenesulfonate (2.1 g, 4.1 mmol) were dissolved in chloroform (100 ml). To this solution, triethylamine (0.8 ml) was added on cooling and the mixture was stirred at room temperature for 20 hr. The chloroform solution was washed with 5% aqueous sodium carbonate, water, 0.5 M hydrochloric acid and water successively. The organic layer was dried over anhydrous sodium sulfate and concentrated *in vacuo*. The residue was kept under ethyl ether and a solid thus obtained was collected by filtration and recrystallized from diisopropyl ether. Yield, 1.4 g (63%); mp 131—132 °C; $[\alpha]_D^{20}$ −4.3° (*c* 1, methanol).

Found: C, 59.45; H, 9.00; N, 7.62%. Calcd for $C_{27}H_{49}O_8N_3$: C, 59.64; H, 9.08; N, 7.73%.

Benzyloxycarbonyl-L-leucyl-γ-t-butyl-D-glutamyl-L-isoleucine (IX). A solution of benzyloxycarbonyl-L-leucine 1-succinimidyl ester[10] (3.6 g, 10 mmol), VIIa (3.3 g, 10 mmol) and triethylamine (1.5 ml) in chloroform (80 ml) was stirred under ice-cooling for 1 hr, and then at room temperature for 12 hr. The solvent was evaporated *in vacuo* and a residue obtained was dissolved in ethyl acetate. The solution was washed with 5% aqueous citric acid, and then water. After drying over sodium sulfate, the solution was concentrated *in vacuo*. A residue obtained was purified by silica gel column chromatography using methanol–chloroform as an elution solvent to give oily product. Yield, 3.4 g (63%). This material was used to the following deblocking reaction directly.

L-Leucyl-γ-t-butyl-D-glutamyl-L-isoleucine (IV) Hydrate. The oily product IX (3.4 g, 6.0 mmol) obtained above was dissolved in tetrahydrofran (50 ml). Through the solution, hydrogen was bubbled at room temperature in the presence of palladium charcoal for 5 hr. After filtration of the catalyst, a filtrate was concentrated to yield crystals. They were filtered and reprecipitated from methanol–water. Yield, 2.2 g (85%); mp 181—184 °C; $[\alpha]_D^{20}$ +58.9° (*c* 1, methanol).

Found: C, 55.71; H, 9.39; N, 9.14%. Calcd for $C_{21}H_{39}O_6N_3 \cdot 1\frac{1}{2}H_2O$: C, 55.24; H, 9.27; N, 9.20%.

β-Benzyl t-Butyloxycarbonyl-D-aspartate. This compound was prepared from β-benzyl D-aspartate[11] (33.5 g, 0.15 mol) and *t*-butyl azidoformate (22.0 g, 0.15 mol) according to the procedure for L-antipode by Sandrin and Boissonnas.[12] Yield, 2.7 g (56%); mp 102—103 °C; $[\alpha]_D^{19}$ −8.3° (*c* 1, acetic acid). Lit,[12] L-antipode, mp 101 °C; $[\alpha]_D^{22}$ +9±1° (c 2, acetic acid).

Found: C, 59.39; H, 6.60; N, 4.35%. Calcd for $C_{16}H_{21}O_6N$: C, 59.43; H, 6.55; N. 4.33%.

t-Butyloxycarbonyl-D-aspartic β-Benzyl α-1-Succinimidyl Ester. Esterification of β-benzyl *t*-butyloxycarbonyl-D-aspartate (10 g, 31 mmol) with *N*-hydroxysuccinimide (3.5 g, 30 mmol) was carried out according to the procedure for L-antipode by Laufer and Blout.[13] Yield, 11.8 g (94%); mp 100—102 °C; $[\alpha]_D^{20}$ +20.5° (*c* 0.5, dioxane). Lit,[13] L-antipode, mp 102—103 °C; $[\alpha]_D^{26}$ −20.0° (c 0.55, dioxane).

Found: C, 57.30; H, 6.00; N, 6.63%. Calcd for $C_{20}H_{24}O_8N_2$: C, 57.13; H, 5.75; N, 6.66%.

t-Butyloxycarbonyl-β-benzyl-D-aspartyl-L-asparagine (X).

(i) By the Mixed Anhydride Procedure: A mixed anhydride was prepared from β-benzyl *t*-butyloxycarbonyl-D-aspartate (3.3 g, 10 mmol) with isobutyl chloroformate (1.3 g, 10 mmol) and triethylamine (1.3 ml) in tetrahydrofuran (20 ml) at −5—0 °C. To the mixed anhydride solution, L-asparagine hydrate (1.5 g, 10 mmol) and triethylamine (1.4 ml) in water (30 ml) were added. The mixture was stirred under ice-cooling for 2 hr and at room temperature for 8 hr. The mixture was extracted with two 20 ml portions of ether and aqueous layer was acidified with solid citric acid to pH 2—3. A resulting oily precipitate was extracted with two 80 ml portions of ethyl acetate. An organic layer was washed with water and dried over anhydrous sodium sulfate. The solvent was removed *in vacuo* and a residual syrup was crystallized when kept under petroleum ether. The product was recrystallized from a large excess of ethyl acetate. Yield, 2.7 g (62%); mp 154—156 °C; $[\alpha]_D^{20}$ +37.1° (*c* 1, ethanol).

Found: C, 54.62; H, 6.43; N, 9.36%. Calcd for $C_{20}H_{27}O_8N_3$: C, 54.91; H, 6.22; N, 9.61%.

(ii) By the 1-Succinimidyl Ester Procedure: *t*-Butyloxycarbonyl-D-aspartic β-benzyl α-1-succinimidyl ester (14.4 g, 34 mmol) in tetrahydrofuran (160 ml) was added to an ice-cold solution of L-asparagine hydrate (5.2 g, 35 mmol) in water (200 ml) containing triethylamine (5 ml). The mixture was stirred at 0—3 °C for 1 hr and at room temperature for 8 hr. It was extracted with two 80 ml portions of ether and an aqueous layer was acidified with solid citric acid to pH 2—3. The resulting oily precipitate was taken up to ethyl acetate two times (500 ml, 200 ml). Combined ethyl acetate layer was washed with water and dried over anhydrous sodium sulfate. The solvent was removed *in vacuo* and a residue was solidified by addition of petroleum ether. The product was recrystallized from excess of ethyl acetate. Yield, 11.8 g (79%); mp 154—156 °C; $[\alpha]_D^{20}$ +37.1° (*c* 1, ethanol).

Found: C, 54.83; H, 6.39; N, 9.51%.

β-Benzyl-D-aspartyl-L-asparagine (XI) Trifluoroacetate. The dipeptide derivative X(4.5 g, 10 mmol) was dissolved in anhydrous trifluoroacetic acid (50 ml) and the solution was stirred at room temperature for 30 min. Excess tri-

11) Y. Ariyoshi, T. Shiba, and T. Kaneko, This Bulletin, **40**, 1709 (1967).

12) E. Sandrin and R. A. Boissonnas, *Helv. Chim. Acta*, **46**, 1637 (1963).

13) D. A. Laufer and E. R. Blout, *J. Amer. Chem. Soc.*, **89**, 1246 (1967).

fluoroacetic acid was evaporated *in vacuo* and the residue was diluted with ether. The deposited solid was collected by filtration, washed with ether and dried over potassium hydroxide *in vacuo*. The product was recrystallized from methanol-ether. Yield, 4.4 g (98%); mp 131—134 °C; $[\alpha]_D^{18}$ +1.7° (*c* 1, methanol).

Found: C, 45.64; H, 4.50; H, 9.08%. Calcd for $C_{15}H_{19}O_6N_3$-CF_3COOH: C, 45.24; H, 4.47; N, 9.31%.

N^{α}-Benzyloxycarbonyl-N^{ε}-t-butyloxycarbonyl-L-lysyl-N^{δ}-cyclopentyloxycarbonyl-D-ornithyl-L-isoleucyl-D-phenylalanyl-L-histidyl-β-benzyl-D-aspartyl-L-asparagine (XIII) Hydrate. A solution of sodium nitrite (0.5 g) in water (5 ml) was added to a solution of N^{α}-benzyloxycarbonyl-N^{ε}-*t*-butyloxycarbonyl-L-lysyl-N^{δ}-cyclopentyloxycarbonyl-D-ornithyl-L-isoleucyl-D-phenylalanyl-L-histidine hydrazide hydrate[1] (5.1 g, 4.9 mmol) in 70% acetic acid (300 ml) containing 20 ml of M hydrochloric acid at −1—−2 °C. The reaction mixture was stirred at this temperature for 20 min. A gelatinous mass started to deposit when excess cold water was added to the mixture. The resulting precipitate was collected by filtration and washed with water thoroughly. An azide XII thus obtained, which showed an absorption band at 2210 cm^{-1} in IR spectrum, was dissolved in ice-cold dimethylformamide (50 ml). This preparation was added to an ice-cold solution of XI trifluoroacetate (4.5 g, 10 mmol) in dimethylformamide (25 ml) containing triethylamine (1.3 ml) and the mixture was stirred at 2—5 °C for 24 hr and then at room temperature for 30 hr. The solution was concentrated *in vacuo* and a residue was triturated with water. The resulting amorphous material was collected by filtration and purified by silica gel column chromatography (elution solvent : chloroform–methanol, 8 : 2—7 : 3, v/v). Yield, 3.2 g (49%); mp 200—203 °C; $[\alpha]_D^{18}$ +12.6° (*c* 1, dimethylformamide).

Found: C, 59.30; H, 7.13; N, 12.37%. Calcd for $C_{66}H_{90}O_{17}N_{12}\cdot H_2O$: C, 59.09; H, 6.91; N, 12.53%.

Amino acid analysis: Lys+Orn, 1.93; Ile, 0.99; Phe, 1.00; His, 0.92; Asp, 2.00.

Cyclo-(N$^{\alpha}$-benzyloxycarbonyl-L-lysyl-N$^{\delta}$-cyclopentyloxycarbonyl-D-ornithyl-L-isoleucyl-D-phenylalanyl-L-histidyl-β-benzyl-D-aspartyl-L-asparaginyl) (V) dihydrate. To a solution of the protected heptapeptide XIII hydrate (7.0 g, 5.2 mmol) in dimethylformamide (70 ml), there were added chloroacetonitrile (4.5 ml) and triethylamine (6 ml). The reaction mixture was stirred at room temperature for 40 hr. After evaporation of the solvent under reduced pressure, water was added to the residue. Amorphous precipitate formed was filtered and dried *in vacuo* over phosphorus pentoxide. The product gave four spots on thin-layer chromatogram (developing solvent : methanol-chloroform, 2 : 8 v/v). One of them, showing positive Pauly and negative ninhydrin reaction, corresponds to the expected cyanomethyl ester while the other three spots seemed to an unreactive peptide and two cyanomethylated compounds on imidazole nuclei in histidine residues of the expected product and unreactive peptide from the coloring behaviors. The mixture (7.1 g) was dissolved in trifluoroacetic acid (80 ml) and stirred at room temperature for 45 min. Excess trifluoroacetic acid was removed by evaporation under reduced pressure, and ether was added to the residue. Precipitate thus formed was filtered and dried *in vacuo* over sodium hydroxide. A solution of this material in dimethylformamide (20 ml) and acetic acid (5 ml) was added to large excess of pyridine (800 ml) with stirring for 5 hr and then stirred at 45—50 °C for 20 hr. The solution was concentrated under reduced pressure. The reaction mixture showed five spots on thin-layer chromatogram (solvent system : methanol-chloroform 2 : 8, v/v). Among them, a spot of R_f 0.80 must be desired product, because it gave negative ninhydrin but positive Pauly reaction, while another spot of R_f 0.90 showing both negative ninhydrin and Pauly reactions seemed to be a cyclic peptide in which imidazole nucleus was cyanomethylated. All other three spots gave positive ninhydrin reactions. A product of R_f 0.80 was isolated by silica gel column chromatography (2.5×80 cm, elution solvent : methanol-chloroform, 1 : 19 (200 ml)—2 : 18 (300 ml) v/v). Fractions No. 21 to 42 (each fraction, 15 g) were collected and concentrated under reduced pressure to obtain a solid of the expected cyclic peptide (V) dihydrate, Yield, 90 mg (1.4%); mp 197—207 °C; $[\alpha]_D^{17}$ +11.4° (*c* 1, dimethylformamide).

Found: C, 58.96; H, 7.16; N, 13.63%. Calcd for $C_{61}H_{80}O_{14}N_{12}\cdot 2H_2O$: C, 59.02; H, 6.82; N, 13.54%.

Amino acid analysis: Lys+Orn, 2.11: Ile, 0.96; Phe, 0.94; His, 1.02; Asp, 2.00.

The authors are grateful to Peptide Center, Institute for Protein Research of Osaka University for carrying out the amino acid analyses and also indebted to Ajinomoto Co., Ltd. and Commercial Solvent Corporation, U.S.A. for their kind offers of amino acids.

Aminocyclitols. XXIX. Synthesis of Inosadiamines *via* 1,3-Biimino-1,3-dideoxy-inositols[1]

Tetsuo SUAMI, Seiichiro OGAWA, Hayashi UCHINO, and Masaru UCHIDA

Department of Applied Chemistry, Faculty of Engineering, Keio University, Hiyoshi, Yokohama 223

(Received October 27, 1972)

Hydrazinolysis of DL-1,4-dibromo-1,4-dideoxy-*chiro*-inositol (**3a**), followed by catalytic hydrogenation and acetylation, afforded di-*N*-acetyl-tetra-*O*-acetyl-*neo*-inosadiamine-1,3 (**6a**) and -*scyllo*-inosadiamine-1,3 (**7**) in 18% and 24% yields, respectively. From the intact hydrazinolyzate of **3a**, two new stereoisomeric 1,3-biimino-1,3-dideoxy-inositols (**4a** and **5a**) could be isolated, and their structures were established by correlating to the corresponding inosadiamines. A similar hydrazinolysis of 3,6-di-*O*-*p*-tolylsulfonyl-*muco*-inositol (**12**) gave sole crystalline 1,3-biimino compound (**13a**), whose structure was followed from its conversion into known di-*N*-acetyl-tetra-*O*-acetyl-*myo*-inosadiamine-4,6 (**14**). PMR spectra of four 1,3-biimino compounds were discussed.

We described a convenient synthesis of a biologically useful aminocyclitol, *myo*-inosadiamine-1,3, by hydrazinolysis of 1,3-di-*O*-*p*-tolylsulfonyl-*myo*-inositol (**1**) followed by hydrogenation.[2] The formation of 6,7-diazabicyclo[3.2.1]octane-2,3,4,8-tetrol (**2a**) of *myo*-configuration, which may be termed 1,3-biimino-1,3-dideoxy-*myo*-inositol,[3] was demonstrated by isolation of the free base. The synthesis seems to provide a convenient method for preparing an unaccessible inosadiamine having two amino groups in *cis*-1,3-positions from readily available di-*O*-*p*-tolylsulfonyl- or dihalodideoxy-inositol. On the other hand, the use of mono- or di-alkyl hydrazine gave *N*-alkyl- or di-*N*-alkyl-inosadiamine, *viz.*, *N*-methyl-*myo*-inosadiamine-1,3 and actinamine.[5]

In the present paper, we wish to report the synthesis of three new stereoisomers of 1,3-biimino-1,3-dideoxy-inositol and their conversion into the corresponding inosadiamines. In order to demonstrate the reaction mechanism of the hydrazinolysis, displacement reactions with azide ion were also studied.

Firstly, the hydrazinolysis of DL-1,4-dibromo-1,4-dideoxy-*chiro*-inositol (**3a**)[6] obtained by a drastic bromination reaction of *epi*-inositol was investigated. On treatment with hydrazine, two epoxide intermediates are expected to be formed by participation of vicinal *trans*-situated hydroxyl groups, since **3a** has two bromine atoms in *cis*-1,4 positions; this may satisfy the steric requirement for formation of a 1,3-biimino bridge. When **3a** was treated with excess hydrazine in boiling 2-methoxyethanol and the hydrazinolyzate was then subjected to hydrogenation and acetylation, di-*N*-acetyl-tetra-*O*-acetyl-*neo*-inosadiamine-1,3 (**6a**) and -*scyllo*-inosadiamine-1,3 (**7**) were isolated in 18 and 24% yields, respectively. The former was further characterized by conversion into its di-*N*-acetyl derivative (**6b**). The structure of **6a** was established by the following spectral evidence. The PMR spectrum of **6a** in dimethylsulfoxide-d_6 (DMSO-d_6) revealed six acetyl methyl protons as four singlets (2 : 2 : 1 : 1) at τ 8.27, 8.06, 7.90, and 7.88, which according to Lichtenthaler *et al.*,[7] can be readily assigned to two equatorial acetamido, and two equatorial, one axial and one axial acetoxy groups, respectively. On addition of deuterium oxide (D_2O) 2-proton sextet at τ 5.66 collapsed to a quartet (J=2.7 and 12 Hz), indicating that the signal was due to two magnetically equivalent protons at C–1 and C–3. Accordingly, the 2-proton quartet at τ 5.00 was assigned to the equivalent protons at C–4 and C–6, and the two narrow triplets (J=2.7 Hz) at τ 4.67 and 4.34 to H–2 and H–5, respectively. The structure of **6a** was thus fully established.

On the other hand, the reaction of **3a** or its acetyl derivative (**3b**) with sodium azide in aqueous 2-

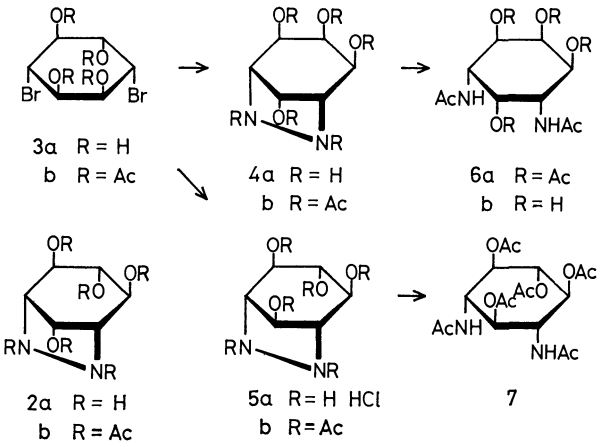

Scheme 1.

1) Presented at the 25th Annual Meeting of the Chemical Society of Japan Tokyo, 12th October 1971.

2) T. Suami and S. Ogawa, This Bulletin, **40**, 1295 (1967); T. Suami, S. Ogawa, Y. Naito, and H. Sano, *J. Org. Chem.*, **33**, 2831 (1968).

3) According to the *R,S*-notation of configuration,[4] compound **2a** should be named 6,7-diazabicyclo[3.2.1]octane-2*R*,3*R*,4*S*,8*S*-tetrol. Since this designation lacks derivational perspicuity and is somewhat cumbersome, we prefer, for the sake of simplicity, the designation 1,3-biimino-1,3-dideoxy-*myo*-inositol for **2a**, retaining the respective configuration prefix of the basal inositol. Similarly, **4a** of 2*R*,3*S*,4*S*,8*S* configuration is termed 1,3-biimino-1,3-dideoxy-*neo*-inositol; **5a** (2*R*,3*R*,4*S*,8*R*)=1,3-biimino-1,3-dideoxy-*scyllo*-inositol; **13a** (2*R*,3*S*,4*S*,8*R*)=4,6-dideoxy-4,6-biimino-*myo*-inositol.

4) R. S. Cahn, C. K. Ingold, and V. Prelog, *Experientia*, **12**, 81 (1956); *Angew. Chem. Int. Ed. Engl.*, **5**, 385 (1966).

5) T. Suami, S. Ogawa, and H. Sano, This Bulletin, **43**, 1843 (1970).

6) T. Suami, S. Suzuki, M. Uchida, and S. Yanagida, *ibid.*, **42**, 2672 (1969).

7) F. W. Lichtenthaler and P. Emig, *Carbohyd. Res.*, **7**, 121 (1968); F. W. Lichtenthaler, G. Bambach, and P. Emig, *Chem. Ber.*, **102**, 994 (1969).

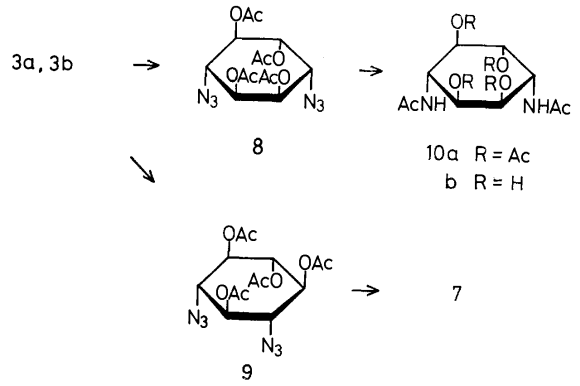

Scheme 2.

methoxyethanol under reflux followed by acetylation afforded tetra-*O*-acetyl-diazidodideoxy-*chiro*-inositol (**8**) in 68% yield, together with a small amount of tetra-*O*-acetyl-1,3-diazido-1,3-dideoxy-*scyllo*-inositol (**9**)[8] which was characterized by conversion into **7**. Hydrogenation of **8** and subsequent acetylation afforded hitherto unknown di-*N*-acetyl-tetra-*O*-acetyl-inosadiamine (**10a**) which was further converted into the di-*N*-acetyl derivative (**10b**). From the reaction sequence, the formation of **9** as the minor product suggested that the major diazidodideoxy-inositol should have 1,2- or 1,4-*chiro*-configuration. The physical and spectral properties of the former[9] were found to be quite different from those of **8**. In the PMR spectrum of **8** in deuteriochloroform ($CDCl_3$), the pattern of the signals due to the ring protons were shown to be substantially similar to those of **3b**.[6] The PMR spectrum of **10a** in DMSO-d_6 revealed four singlets (1 : 1 : 3 : 1) in the vicinity of τ 8; one equatorial (τ 8.22) and one axial (τ 8.11) acetamido groups, and three equatorial (τ 8.08) and one axial (τ 7.98) acetoxy groups, suggesting *chiro*-configuration.[7] Thus the structure of **8** was tentatively assigned to DL-tetra-*O*-acetyl-1,4-diazido-1,4-dideoxy-*chiro*-inositol. The preferential diaxial attack of azide ion at the intermediary epoxides can be assumed to be the prevailing mechanism for this azidolysis reaction.

The course of the nucleophilic displacement by hydrazine evidently differs from that of azide ion, and, the formation of a biimino bridge might be proposed in the hydrazinolysis of **3a**. Isolation of these anticipated intermediates was thus attempted. The crude hydrazinolyzate of **3a** was treated with Amberlite IRA-400 (OH^-) and successive treatment with aqueous ethanol gave the crystalline 1,3-biimino compound (**4a**) in 15% yield. From the mother liquor of **4a** upon acetylation, a small amount (1%) of di-*N*-acetyl-tetra-*O*-acetyl-1,3-biimino compound (**5b**) could be isolated, which afforded a monohydrochloride (**5a**) in 85% yield on hydrolysis with 3 M hydrochloric acid. Acetylation of **4a** in the usual way gave the hexaacetyl derivative (**4b**) which was found to differ entirely from **5b**. Neither **4b** nor **5b** showed any absorption in the amide II region in IR or a signal due to NH-protons in PMR spectra. Hydrogenation of **4a** followed by acetylation afforded **6a** in 73% yield. The PMR spectra of **4a** and **5a** (free base) in D_2O also supported the proposed structure. Consequently, the configuration of 1,3-biimino-1,3-dideoxy-inositol (**4a**) is unambiguously established to be *neo*- (2*R*, 3*S*, 4*S*, 8*S*), whilst **5a** is conclusively assigned to *scyllo*-configuration (2*R*, 3*R*, 4*S*, 8*R*).

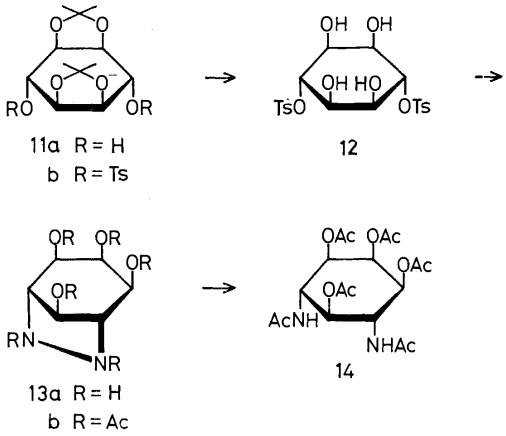

Scheme 3.

Hydrazinolysis of 3,6-di-*O*-*p*-tolylsulfonyl-*muco*-inositol (**12**) was then carried out. Compound **12** was prepared from 1,2 : 4,5-di-*O*-isopropylidene-*muco*-inositol (**11a**)[10] by a reaction sequence involving *p*-toluenesulfonylation and de-*O*-acetylation (**11a**→**11b**→**12**). A similar treatment of **12** with hydrazine gave the sole crystalline 1,3-biimino compound (**13a**) in 52% yield. Acetylation of **13a** gave the hexaacetyl derivative (**13b**) in 73% yield, whose IR and PMR spectra showed a presence of a secondary amido group. Hydrogenation of **13a** and the subsequent acetylation afforded di-*N*-acetyl-tetra-*O*-acetyl-*myo*-inosadiamine-4,6 (**14**)[11] in 43 % yield. Thus the structure of **13a** was readily assigned to *myo*-configuration (2*R*, 3*S*, 4*S*, 8*R*).

The reaction of the corresponding dimesylate, 3,6-di-*O*-methylsulfonyl-*muco*-inositol, with excess sodium azide gave, by preferential diaxial cleavage of the intermediate epoxide, 3,6-diazido-3,6-dideoxy-*muco*-inositol almost exclusively.[12] In the case of hydrazinolysis, on the contrary, the hydrazino group introduced previously attacks the second epoxide intermolecularly to form a 1,3-biimino bridge.

PMR Spectra. The PMR spectra of the three stereoisomeric 1,3-biimino-1,3-dideoxy-inositols (**4a**, **5a**, and **13a**) together with **2a** were discussed. Since all the molecules have a plane of symmetry, the H-1 and H-5, and H-2 and H-4 protons are magnetically equivalent thus simplifying the interpretation of the signals. In **2a**, **4a**, and **5a**, a first-order analysis was successfully applied to interpret the signals from the ring protons. In **13a**, however, the signals due to

8) This compound could not be isolated in a crystalline state.
9) N. Kurihara, T. Kurokawa, and M. Nakajima, *Agr. Biol. Chem.* (Tokyo), **31**, 1166 (1967).
10) S. J. Angyal and R. M. Hoskinson, *J. Chem. Soc.*, **1962**, 2985.
11) T. Suami and S. Ogawa, This Bulletin, **38**, 2026 (1965); **40**, 1925 (1967).
12) T. Suami, F. W. Lichtenthaler, and S. Ogawa, *ibid.*, **40**, 1488 (1967).

TABLE 1. CHEMICAL SHIFTS OF 1,3-BIIMINO-1,3-DIDEOXY-INOSITOL[a)]

Compound	H-1,5	H-2,4	H-3	H-8
2a	6.72(d)	6.32(t)	6.54(t)	5.38(s)
4a	6.47(d)	5.93(t)	6.18(t)	5.12(s)
5a	6.77(d)	6.48(t)	5.81(t)	5.58(t)
13a	6.43(t)	5.94(m)	5.94(m)	5.57(t)

a) Measured at 60 MHz in D_2O with sodium 3-(trimethylsilyl)-1-propanesulfonate as an internal reference. Chemical shifts are given in terms of τ-values, the signals being denoted by s (singlet), d (doublet), t (triplet), and m (complex multiplet).

TABLE 2. COUPLING CONSTANTS OF 1,3-BIIMINO-1,3-DIDEOXY-INOSITOL[a)]

Compound	$J_{1,2}$ ($J_{4,5}$)	$J_{1,8}$ ($J_{5,8}$)	$J_{2,3}$ ($J_{3,4}$)	$J_{2,8}$
2a	2.0	0	4.2	0
4a	5.0	0	4.7	0
5a	~1.0	4.7	6.6	~1.0
13a	4.0	4.7	—	~1.0

a) Values (Hz) are of first-order.

H-2, H-3, and H-4 protons overlapped to give rise to a complex multiplet (Tables 1 and 2).

Assignment of the configuration of the hydroxyl group at C-8 was based on the following results. The H-8 proton appeared as a triplet (J=4.7 Hz) at τ 5.58 and 5.57 in **5a** and **13a**, respectively, which shows that the dihedral angle $\phi_{1,8}$ and $\phi_{5,8}$ would approach 40°. The sharp singlets at τ 5.38 and 5.12 in **2a** and **4a**, respectively, could be assigned to H-8 protons, indicating that the dihedral angles $\phi_{1,8}$ and $\phi_{5,8}$ were nearly 90°.[13] In this case the *cisoid* protons (axial) resonated at lower field than the *transoid* protons (equatorial). The former might have been strongly deshielded by two axial hydroxyls at C-2 and C-4.[14,15]

In the PMR spectrum of **4a** (Fig. 1), the 2H-triplet at τ 5.94, 1H-triplet at τ 6.18, and 2H-doublet at τ 6.47 were assigned to H-2 and H-4, H-3, and H-1 and H-5, respectively. The observed coupling constants of $J_{1,2}$ and $J_{2,3}$ corresponded to the dihedral angles $\phi_{1,2}$ (45°) and $\phi_{2,3}$ (45°), which were derived from a molecular model of **4a**, the chair conformation being slightly distorted by incorporation of the 1,3-biimino bridge.[16] The coupling constants were shown to be in good accordance with the corresponding values of 1,5-lactone of (−)-quinic acid ((−)-quinide).[15]

However a remarkable flattening of the chair conformation was deduced from the PMR spectra, when three axial hydroxyl groups were located at C-2, C-3,

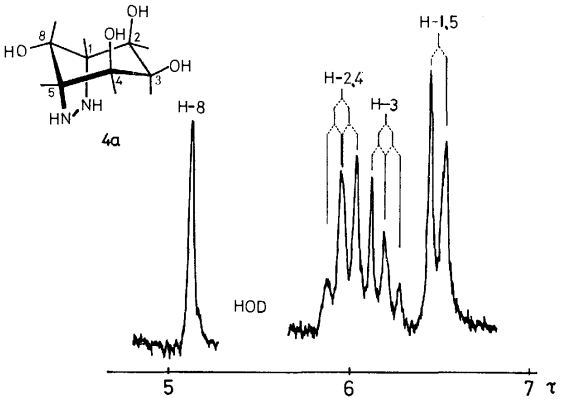

Fig. 1. Partial PMR spectrum (D_2O) of 1,3-biimino-1,3-dideoxy-*neo*-inositol (**4a**).

and C-4. In the PMR spectrum of **2a**, the small value of $J_{1,2}$ (2.0 Hz) may be rationalized by such a distortion that would increase the dihedral angles $\phi_{1,2}$ and $\phi_{2,3}$. Since $J_{1,2}$ was found to accord with the corresponding value of 3,4-*O*-isopropylidene-(−)-quinide,[15] the dihedral angle $\phi_{1,2}$ is likely to be nearly 60°.

In the case of **5a** having three axial substituents on both sides of the cyclohexane ring, a very small $J_{1,2}$ (less than 1.0 Hz) was observed, while $J_{2,3}$ (6.6 Hz) seems to indicate that the six-membered ring exists in a flattened boat conformation rather than in a chair form. The evidence for this can be deduced from the down-field shift of H-3 (τ 5.18) as compared with that of **2a** (τ 6.54), since the difference can be attributed to considerable deformation of the ring conformation with respect to carbons C_2-C_3-C_4. The non-bonded interaction between three axial hydroxyl groups at C-2, C-4, and C-8 was presumably sufficient to cause the six-membered ring to exist in this conformation.

A long range coupling ($J_{2,8}$ and $J_{4,8}$) was observed in **5a** and **13a**, which could be substantially accounted for by W-letter rule.[17]

On the other hand, the PMR spectra of the hexaacetyl derivatives of 1,3-biimino-1,3-dideoxy-inositols were expected to be complex owing to the hindered rotation of acetamido groups.[18] In **2b** and **4b**, the symmetry of the molecules was to some extent lost, and the six ring protons revealed individual signals.

The PMR spectrum of **4b** (Fig. 2) was interpreted as follows. By analogy with the assignment of the PMR spectrum of **4a**, the singlet at τ 4.12 and the triplet (J=5.0 Hz) at τ 5.02 could be assigned to H-8 and H-3 protons, respectively. Irradiation at the triplet (J=5.0 Hz) at τ 4.25 simplified the H-3 triplet to a doublet, and the doublet (J=5.0 Hz) at τ 5.30 to a singlet. Consequently, the triplet at τ 4.25 was assigned to H-2 (H-4) and the doublet at τ 5.30 to H-1 (H-5). The complex multiplet centered at τ 4.60

13) A. C. Oehlsclager and L. H. Zalkow, *J. Org. Chem.*, **30**, 4205 (1965); C. W. Jefford, B. Waegell, and K. Ramey, *J. Amer. Chem. Soc.*, **87**, 2191 (1965).

14) N. S. Bhacca and D. H. Williams, "Applications of NMR Spectroscopy in Organic Chemistry," Holden-Day Inc. (1964), pp. 183—191.

15) E. Haslam and M. J. Turner, *J. Chem. Soc., C*, **1971**, 1496.

16) M. Karplus, *J. Amer. Chem. Soc.*, **85**, 2870 (1963). The dihedral angles were measured by using Buchi's Dreiding-stereomodels.

17) L. M. Jackman and S. Sternhell, "Application of Nuclear Magnetic Resonance Spectroscopy in Organic Chemistry," Pergamon Press 2nd Ed. (1969), p. 334.

18) H. Paulsen and K. Todt, *Advan. Carbohyd. Chem.*, **23**, 115 (1968).

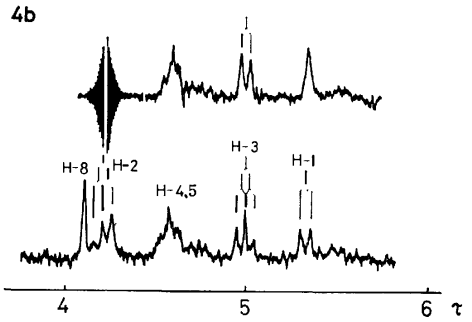

Fig. 2. Partial PMR spectrum ($CDCl_3$) of di-*N*-acetyl-tetra-*O*-acetyl-1,3-biimino-1,3-dideoxy-*neo*-inositol (**4b**), measured on a Varian Associates HA-100D (100 MHz) spectrometer.

should be attributed to H-4 (H-2) and H-5 (H-1) protons. We see from comparison with their counterparts that H-2 (H-4) and H-5 (H-1) protons are markedly deshielded (0.70 and 0.35 ppm, respectively) by the amide carbonyl groups most probably in a *cis*-relationship to them. Thus, it was deduced that the planes of two-secondary acetamido groups were somewhat twisted from that of the biimino ring due to the repulsion between the amido methyl groups.

No influence of the hindered rotation of acetamido groups was observed in the PMR spectrum of **5b**. This might be due to the existence of a rotamer having a plane of symmetry resulting from the deformation of the cyclohexane ring.

Experimental

Melting points were determined on a Mitamura Riken micro hot stage and are uncorrected. IR spectra were measured on a Jasco IR-E spectrophotometer in KBr disks. PMR spectra were measured on Varian Associates A-60D (60 MHz) and HA-100D (100 MHz) spectrometer at a concentration of approximately 10% deuteriochloroform ($CDCl_3$), deuterium oxide (D_2O), or dimethylsulfoxide-d_6 (DMSO-d_6), with tetramethylsilane or sodium 3-(trimethylsilyl)-1-propanesulfonate, respectively, as internal standard. Chemical shifts are given in terms of τ-values, and signals being denoted by s (singlet), d (doublet), t (triplet), dd (double doublet), or m (complex multiplet). Values given for coupling constants are of first-order. All solutions were concentrated by a rotary evaporator at 40—50 °C under reduced pressure.

Hydrazinolysis of DL-*1,4-dibromo-1,4-dideoxy*-chiro-*inositol (**3a**). Preparation of di*-N-*acetyl-tetra*-O-*acetyl*-neo-*inosadiamine-1,3 (**6a**) and* -scyllo-*inosadiamine-1,3 (**7**).* A mixture of **3a** (1.00 g), anhydrous hydrazine (0.50 ml), and 2-methoxyethanol (50 ml) was refluxed for 90 min and the solution was evaporated to dryness. The residue was dissolved in water (50 ml) and, after treatment with Amberlite IRA-400 (OH^-) (10 ml), the solution was hydrogenated in the presence of Adam's platinum catalyst (50 mg) in a Parr shaker type apparatus (under 3.4 kg/cm² of initial hydrogen pressure) for 20 hr at room temperature. The catalyst was filtered off and the filtrate was evaporated to dryness. The residue was treated with acetic anhydride (5 ml) and pyridine (5 ml) overnight at room temperature. The reaction mixture was evaporated and the crude mixture was fractionated by crystallization from ethanol. The first crystals (0.40 g, 23.5%) were identified as **7** by the mode of melting (mp 245—249 °C with transition) and a comparison of its IR spectra with that of an authentic sample.[19] Crystals (0.31 g, 18%) of **6a** were then isolated, mp 280—285 °C. An analytical sample was obtained by further recrystallization from ethanol, mp 282—285 °C. IR: 3300, 1660, 1555 (NHAc), and 1755 cm^{-1} (OAc), PMR data are in the text.

Found: C, 50.44; H, 6.32; N, 6.39%. Calcd for $C_{18}H_{26}N_2O_{10}$: C, 50.23; H, 6.09; N, 6.51%.

*Di-*N*-acetyl*-neo-*inosadiamine-1,3 (**6b**).* Compound **6a** (150 mg) was treated with methanolic ammonia (15 ml) overnight at room temperature. The mixture was evaporated to give a crystalline residue which was crystallized from 90% aqueous ethanol to give an analytical sample (60 mg, 68%) of **6b**, mp 313 °C (dec.). IR: 1635 and 1555 cm^{-1} (NHAc).

Found: C, 43.10; H, 7.22; N, 9.90%. Calcd for $C_{10}H_{18}N_2O_6 \cdot H_2O$: C, 42.88; H, 7.14; N, 10.00%.

*Azidation Reaction of **3a** or **3b**. Preparation of* DL-*Di*-N-*acetyl-tetra*-O-*acetyl-1,4-diazido-1,4-dideoxy*-chiro-*inositol (**8**) and (**7**).* A mixture of DL-tetra-*O*-acetyl-1,4-dibromo-1,4-dideoxy-*chiro*-inositol (**3b**)[4] (1.00 g), sodium azide (1.40 g), and 90% aqueous 2-methoxyethanol (50 ml) was refluxed for 25 hr. The mixture was then evaporated and dried by codistillation with dry toluene several times. The residue was treated with acetic anhydride (20 ml) and pyridine (20 ml) overnight at room temperature. An insoluble material was removed by filtration and the filtrate was evaporated to give an oily product, which was extracted with chloroform and purified by a short column of active aluminum oxide. The solvent was evaporated and the crude product was crystallized from ethanol to afford colorless needles (0.89 g, 68%) of **8**, mp 109—113 °C. Recrystallization from ethanol gave an analytical sample, mp 112—114 °C. IR: 2150 (N_3), and 1750 cm^{-1} (OAc). PMR ($CDCl_3$): τ 7.95 (3, s, OAc), 7.91 (6, s, 2OAc), 7.84 (3, s, OAc), 6.18 (1, t, H-4, J=10.5 Hz), and 4.96 (1, dd, H-5, J=3 and 10.5 Hz).

Found: C, 42.46; H, 4.59; N, 20.85%. Calcd for $C_{14}H_{18}N_6O_8$: C, 42.21; H, 4.59; N, 21.10%.

The mother liquor of **8** was evaporated and the residue was hydrogenated in an ethanol solution (20 ml) in a similar way to that for **6a**. The hydrogenate was acetylated in the usual way to give colorless needles (28 mg, 1.9%) of **7**, mp 240—245 °C, after crystallization from ethanol. This compound was identified with an authentic sample[18] by comparison of IR spectra and mixed melting point.

Almost the same result was obtained from **3a**.

DL-*Di*-N-*acetyl-tetra*-O-*acetyl*-chiro-*inosadiamine-1,4 (**10a**).* A solution of **8** (0.54 g) in ethanol (50 ml) was hydrogenated in a similar way to that for **6a** for 15 hr. The catalyst was filtered off and filtrate was evaporated to dryness.

The residual product was acetylated in the usual way to give colorless needles (0.58 g, 77%) of **10a**, mp 120—126 °C. Recrystallization from acetone gave a hygroscopic crystals, mp 127—129 °C. IR: 3280, 1655, 1545 (NHAc), and 1750 cm^{-1} (OAc). PMR (DMSO-d_6): τ 2.55 (1, d, equatorial NHAc, J=9 Hz) and 1.68 (1, d, axial NHAc, J=8 Hz).

Found: C, 49.64; H, 6.14; N, 6.08%. Calcd for $C_{18}H_{26}N_2O_{10} \cdot 1/2H_2O$: C, 49.20; H, 6.19; N, 6.38%.

DL-*Di*-N-*acetyl*-chiro-*inosadiamine-1,4 (**10b**).* Compound **10a** (0.20 g) was treated with methanolic ammonia (30 ml) overnight at room temperature. The solution was then evaporated to give a crystalline residue which was recrystallized from 95% ethanol to afford colorless needles (90 mg, 74%) of **10b**, mp 254—256 °C. IR: 3480, 1630,

19) P. L. Peck, R. P. Graber, A. Walti, E. W. Peel, C. E. Hoffhine, Jr., and K. Folker, *J. Amer. Chem. Soc.*, **68**, 29 (1946).

1580, and 1560 cm^{-1} (NHAc). PMR (D_2O): τ 7.97 (6, s, 2 NHAc).

Found: C, 46.00; H, 7.23; N, 10.36%. Calcd for $C_{10}H_{18}N_2O_6$: C, 45.79; H, 6.92; N, 10.63%.

1,3-Biimino-1,3-dideoxy-neo-*inositol* (**4a**) *and Di*-N-*acetyl-tetra*-O-*acetyl-1,3-biimino-1,3-dideoxy*-scyllo-*inositol* (**5b**). A mixture of **3a** (2.00 g), anhydrous hydrazine (1.6 ml), and 2-methoxyethanol (100 ml) was refluxed for 2 hr, and the mixture was evaporated to dryness. The residue was dissolved in water (30 ml) and treated with Amberlite IRA-400 (OH^-) for 5 hr. The solution was evaporated and the oily residue was crystallized from water–ethanol to afford crystals (0.17 g, 14.8%) of **4a**, mp 208 °C (dec.).

Found: C, 41.11; H, 6.79; N, 15.70%. Calcd for $C_6H_{12}N_2O_4$: C, 40.91; H, 6.87; N, 15.90%.

The mother liquor of **4a** was evaporated to dryness and the residue was treated with acetic anhydride (5 ml) and pyridine (5 ml) overnight at room temperature. The mixture was evaporated and the product was crystallized from ethanol–ether to give crystals (26 mg, 1%) of **5b**, mp 213 °C. IR: 1755, 1720 (OAc), and 1680 cm^{-1} (NAc).

Found: C, 50.68; H, 5.56; N, 6.45%. Calcd for $C_{18}H_{24}N_2O_{10}$: C, 50.47; H, 5.65; N, 6.54%.

Di-N-*acetyl-tetra*-O-*acetyl-1,3-biimino-1,3-dideoxy*-neo-*inositol* (**4b**). A 20 mg-portion of **4a** was acetylated with acetic anhydride (1.5 ml) and pyridine (1.5 ml) overnight at room temperature. The product was crystallized from ethanol–ether to give crystals (15 mg, 31%) of **4b**, mp 161—162 °C. IR: 1745 (OAc), and 1635 cm^{-1} (NAc). PMR data are in the text.

Found: C, 50.49; H, 5.94; N, 6.18%. Calcd for $C_{18}H_{24}N_2O_{10}$: C, 50.47; H, 5.65; N, 6.54%.

1,3-Biimino-1,3-dideoxy-scyllo-*inositol* (**5a**). A mixture of **5b** (120 mg) and 3M-hydrochloric acid (20 ml) was refluxed for 2 hr, and the mixture was evaporated to give a glassy residue, which crystallized upon addition of aqueous ethanol to afford monohydrochloride of **5a** (51 mg, 85%), mp 147—149 °C.

Found: C, 33.55; H, 6.29; N, 12.83%. Calcd for $C_6H_{12}N_2O_4 \cdot HCl$: C, 33.89; H, 6.16%; N, 13.17%.

PMR spectrum was measured for a free base which was obtained from monohydrochloride by treatment of the aqueous solution with Amberlite IRA-400 (OH^-).

Preparation of **6a** *from* **4a**. A solution of **4a** (20 mg) in water (3 ml) was hydrogenated similarly in the presence of Adams' platinum catalyst (10 mg) overnight. The product was acetylated in the usual way to give crystals (35 mg, 73%) of **6a**, which was identified with the product obtained before by comparison of their IR spectra.

1,2 : 4,5-Di-O-*isopropylidene-3,6-di*-O-p-*tolylsulfonyl*-muco-*inositol* (**11b**). To a solution of 1,2 : 4,5-di-*O*-isopropylidene-*muco*-inositol (**11a**)[8] (1.00 g) in dry pyridine (15 ml) was added *p*-toluenesulfonyl chloride (3.8 g, 5 equiv.) and the mixture was allowed to stand at room temperature for 20 hr. After being heated over a boiling water bath for 90 min, the mixture was poured into ice and water (70 ml). The resulting crystals were collected by filtration, washed with water and dried. The crude crystals weighed 1.85 g (82%), mp 213—220 °C. Recrystallization from 2-methoxyethanol afforded an analytical sample, mp 233—234 °C. PMR ($CDCl_3$): τ 8.83 and 8.61 (6 and 6, s, 2 isopropylidene C–CH_3), 7.56 (6, s, 2 OTs C–CH_3).

Found: C, 55.32; H, 5.89; S, 11.61%. Calcd for $C_{26}H_{32}O_{10}S_2$: C, 54.91; H, 5.67; S, 11.28%.

3,6-Di-O-p-*tolylsulfonyl*-muco-*inositol* (**12**). Compound **11b** (1.20 g) was treated with boiling 90% aqueous acetic acid (30 ml) for 2 hr. The mixture was then evaporated to give a crystalline residue. The crystals were collected by triturating with ethanol: yield 0.83 g (81%), mp 221—224 °C. Recrystallization from 2-methoxyethanol afforded an analytical sample, mp 223.5—224.5 °C.

Found: C, 49.19; H, 4.89; S, 12.91%. Calcd for $C_{20}H_{24}O_{10}S_2$: C, 49.17; H, 4.95; S, 13.13%.

4,6-Biimino-4,6-dideoxy-myo-*inositol* (**13a**). A mixture of **12** (0.50 g), anhydrous hydrazine (0.5 ml), and 2-methoxyethanol (30 ml) was refluxed for 7 hr. The reaction mixture was treated as for the preparation of **4a**. The crude product was recrystallized from water–ethanol to afford crystals (95 mg, 52%) of **13a**, mp 190 °C.

Found: C, 41.14; H, 6.74; N, 15.98%. Calcd for $C_6H_{12}N_2O_4$: C, 40.91; H, 6.87; N, 15.90%.

Di-N-*acetyl-tetra*-O-*acetyl-4,6-biimino-4,6-dideoxy*-myo-*inositol* (**13b**). Compound **13a** (35 mg) was acetylated with acetic anhydride (2 ml) and pyridine (2 ml) overnight at room temperature. The product was crystallized from ethanol–ether to afford crystals (63 mg, 73%) of **13b**, mp 145—147 °C. IR: 1745 (OAc), and 1650 cm^{-1} (NAc).

Found: C, 50.70; H, 6.05; N, 6.97%. Calcd for $C_{18}H_{24}N_2O_{10}$: C, 50.47; H, 5.65; N, 6.54%.

Di-N-*acetyl-tetra*-O-*acetyl*-myo-*inosadiamine-4,6* (**14**). Compound **13a** (27 mg) was hydrogenated in a similar way to that for **4a**. Subsequent acetylation gave crystals (28 mg, 43%) of **14**, mp 280 °C. Recrystallization from ethanol afforded pure sample, mp 288 °C, which was identified with an authentic sample[11] by comparison of IR and PMR spectra.

The authors are grateful to Professor Sumio Umezawa for his kind advice, and to Mr. Saburo Nakada for carrying out elementary analyses. Financial support from the Ministry of Education for this work is gratefully acknowledged.

The Electrochemical Fluorination of Dithiols and Cyclic Sulfides

Takashi ABE, Shunji NAGASE, and Hajime BABA

Government Industrial Research Institute, Nagoya, Hirate-machi, Kita-ku, Nagoya 462

(Received April 26, 1973)

The electrochemical fluorination of dithiols [1,4-butanedithiol (I), 1,5-pentanedithiol (II), and 3-oxapentane-1,5-dithiol (III)] and cyclic sulfides [tetrahydrothiophene (IV), 2-methyltetrahydrothiophene (V), 3-methylthiophene (VI) and tetrahydrothiopyran (VII)] was conducted. Dithiols afforded the corresponding fully-fluorinated analogs of the starting dithiol ($SF_5(CF_2)_n SF_5$; n=4 from I, 5 from II; $SF_5CF_2CF_2OCF_2CF_2SF_5$ from III) and the cyclic products (perfluorotetramethylenesulfur tetrafluoride from I, perfluoro-2-methyltetramethylenesulfur tetrafluoride, perfluoro-3-methyltetramethylenesulfur tetrafluoride, and perfluoropentamethylenesulfur tetrafluoride from II, and perfluoro-4-oxapentamethylenesulfur tetrafluoride from III). The corresponding perfluoro-cyclic sulfur(VI) compounds were obtained from IV, V, VI, and VII in reasonable yields. The novel perfluoropolymethylene bis(sulfur pentafluoride)s are transparent heavy liquids. Their physical properties and ^{19}F NMR and IR data are reported.

So far little attention has been paid to the electrochemical fluorination of thiols,[1] though there have been intensive investigations of the electrochemical fluorination of sulfides.[2] However, it was shown recently that thiols were fluorinated electrochemically, and a number of partially-fluorinated alkyl-sulfur pentafluorides were found among the fluorination products.[3]

On the other hand, it has been known that perfluorocyclic sulfur(VI) compounds as well as the expected perfluoro-dialkylsulfur tetrafluorides were produced by the electrochemical fluorination of acyclic sulfur compounds containing one or more sulfur atoms in the alkyl chain.[2b,2c]

The present investigation was undertaken in order to elucidate the behavior of the electrochemical fluorination of such dithiols as 1,4-butanedithiol (I), 1,5-pentanedithiol (II), 3-oxapentane-1,5-dithiol (III), and also to investigate the possibility of their cyclization upon electrochemical fluorination and to compare the results with those of the fluorination of diols.[4] Further, the electrochemical fluorination of cyclic sulfides [tetrahydrothiophene (IV), 2-methyltetrahydrothiophene (V), 3-methylthiophene (VI) and tetrahydrothiopyran (VII)] was also examined.

Upon the electrochemical fluorination of dithiols, it was found that dithiols yielded a variety of products, as well as the corresponding novel perfluoropolymethylene bis(sulfur pentafluoride)s, as a result of fragmentation, degradation, and cyclization during the fluorination reaction.

On the other hand, the yields of the corresponding perfluorocyclic sulfur(VI) compounds upon the fluorination of cyclic sulfides were seriously affected by their ring size.

Results and Discussion

The reaction conditions and the results of the fluorination of dithiols and cyclic sulfides are summarized in Tables 1 and 2 respectively.

In anhydrous hydrogen fluoride, it is known[5] that thiols and sulfides dissolve to form a state of the sulfonium ion similar to that of compounds which contain an oxygen atom (oxonium ion). When these sulfonium compounds are subjected to oxidative fluorination by the electrochemical process, perfluoroalkyl derivatives of sulfur hexafluoride (R_f-SF_5 and R_f-SF_4-R_f'; R_f= R_f'= perfluoro-alkyl group) are formed. At the same time, fluorocarbons and sulfur hexafluoride are also produced as major products as a result of the extensive cleavage of the C–S bond.

As may be seen in Table 1, the patterns of the fluorination products varied depending on the starting dithiols. It was also found that the composition of the products was drastically affected by the fluorination procedure. Thus, from I, perfluorotetramethylene bis(sulfur pentafluoride) was obtained in a yield of <1%, and from II, perfluoropentamethylene bis(sulfur pentafluoride) was obtained in a yield of 11.6%. However, perfluoro-3-oxapentamethylene bis(sulfur pentafluoride), $SF_5CF_2CF_2OCF_2CF_2SF_5$, could not be obtained from III (Run A) using the reaction procedure applied for the fluorination of I and II, but when III was fluorinated, while III was introduced into the electrolytic cell to maintain its concentration constant, a trace of the expected perfluoro-3-oxapentamethylene bis(sulfur pentafluoride) was obtained (Run B). These novel perfluoropolymethylene bis(sulfur pentafluoride)s are heavy, transparent, and odorless liquids. The physical properties and ^{19}F NMR and IR data of these compounds, together with those of perfluorotrimethylene bis(sulfur pentafluoride), which was prepared by the electrochemical fluorination of 1,3-propanedithiol (yield=2.5%), are shown in Tables 3, 4, and 5 respectively.

1) a) R. N. Haszeldine and F. Nyman, *J. Chem. Soc.*, **1956**, 2684; b) Dow Corning Co., Fr. 1512068 (1967); U. S. 3456024 (1969).

2) a) A. F. Clifford, H. K. El-Shamy, H. J. Emeléus, and R. N. Haszeldine, *J. Chem. Soc.*, **1953**, 2372; b) F. W. Hoffman, T. C. Simmons, R. B. Beck, H. V. Holler, T. Katz, R. J. Koshar, E. R. Larsen, J. E. Mulvaney, F. E. Rogers, B. Singleton, and R. S. Sparks, *J. Amer. Chem. Soc.*, **79**, 3424 (1957); c) R. D. Dresdner and J. A. Young, *ibid.*, **81**, 574 (1959); d) J. A. Young and R. D. Dresdner, *J. Org. Chem.*, **24**, 1021 (1959); e) T. Abe, S. Nagase, K. Kodaira, and H. Baba, This Bulletin, **43**, 1812 (1970).

3) H. Baba, S. Nagase, K. Kodaira, and T. Abe, 26th Annual Meeting of the Chemical Society of Japan, Hiratzuka, 1972, April 1—4, Preprints, **III**, 1599.

4) T. Abe, S. Nagase, and H. Baba, This Bulletin, **46**, 2524 (1973).

5) G. A. Olah, and A. M. White, *Chem. Rev.*, **70**, 561 (1970).

Table 1. Summary of the fluorination of dithiols

Anodic current density, 3.3 A/dm²; cell temp, 5—6 °C; sample, 0.20 mol

Sample	Volt	Electricity passed (A·hr)	Fluorinated compounds obtained (g)	Product (g)
I	5.8—6.5	150	42.7	$SF_5CF_2CF_2CF_2CF_2SF_5$ (VIII) (0.6), n-$C_4F_9SF_5$ (IX) (12.2), $CF_2CF_2CF_2CF_2SF_4$ (X) (2.9)
II	7.2—7.7	177	52.2[a]	$SF_5CF_2CF_2CF_2CF_2CF_2SF_5$ (11.7), n-$C_5F_{11}SF_5$ (XI) (12.8), $CF(CF_3)CF_2CF_2CF_2SF_4$ (XII) (0.6), $CF_2CF(CF_3)CF_2CF_2SF_4$ (XIII) (0.2), $CF_2CF_2CF_2CF_2CF_2SF_4$ (XIV) (0.3)

III					A	B
Run A	5.5—6.6	152	57.6	$SF_5CF_2CF_2OCF_2CF_2SF_5$		(0.2)
Run B	5.5—5.6	151	40.3	$C_2F_5OC_2F_4SF_5$	(0.1)	(1.0)
				VIII	(0.2)	
				$SF_5CF_2CF_2SF_5$	(0.5)	(0.2)
				$(C_2F_5)_2SF_4$	(4.3)	(1.6)
				$CF_2CF_2OCF_2CF_2SF_4$	(0.1)	(0.3)

a) 12.6 g of the product was obtained as cell drainings.

Table 2. Summary of the fluorination of cyclic sulfides

Anodic current density, 3.3 A/dm²; cell temp, 5—6 °C; sample, 0.20 mol

Sample	Volt	Electricity passed (A·hr)	Fluorinated compounds obtained (g)	Product (g)
IV	4.7—5.9	109	27.5	X (7.0), IX (9.1)
V	5.1—7.1	131	30.7	XII (0.9), XIII (0.4), XIV (0.2), XI (6.0), *iso*-$C_5F_{11}SF_5$ (1.3)
VI	5.7—6.8	109	27.8	XIII (3.3), XII (0.3), XIV (0.3), XI (0.7), *iso*-$C_5F_{11}SF_5$ (5.2)
VII	4.9—7.0	129	19.3	XIV (1.0), XIII (1.3), XII (0.5), XI (1.9), *iso*-$C_5F_{11}SF_5$ (0.5)

Table 3. Properties of perfluoropolymethylene bis(sulfur pentafluoride)s

Compound	Bp (°C)	n_D^{20}	d_4^{20}	Elemental analysis C	F
$SF_5CF_2CF_2SF_5$	84.0	1.2945	2.0397	6.49[a] (6.78)	75.4 (75.1)
$SF_5CF_2CF_2CF_2SF_5$	106.6	1.2988	2.0461	9.00 (8.91)	75.2 (75.2)
$SF_5CF_2CF_2CF_2CF_2SF_5$	127.4	1.3026	2.0521	10.57 (10.57)	74.7 (75.3)
$SF_5CF_2CF_2CF_2CF_2CF_2SF_5$	148.8	1.3059	2.0426	11.40 (11.91)	75.4 (75.4)
$SF_5CF_2CF_2OCF_2CF_2SF_5$	117.4	<1.28	1.9777	10.39 (10.21)	73.1 (72.8)

a) Calculated value in parenthesis.

Table 4. IR spectra of perfluoropolymethylene bis(sulfur pentafluoride)s, cm^{-1}

$SF_5(CF_2)_2SF_5$:	1233 (s), 1163 (s), 903 (vs), 885 (ms, sh), 812 (w), 795 (w), 755 (s), 687 (w), 608 (ms), 578 (ms).
$SF_5(CF_2)_3SF_5$:	1244 (s), 1220 (ms), 1166 (s), 904 (vs), 892 (s), 865 (ms), 797 (w), 781 (w), 756 (w), 712 (s), 690 (ms), 611 (w), 594 (s), 573 (ms).
$SF_5(CF_2)_4SF_5$:	1241 (s), 1199 (w), 1169 (s), 902 (vs), 884 (s), 851 (w), 818 (w), 795 (w), 780 (ms), 754 (w), 737 (w), 711 (w), 691 (ms), 659 (w), 601 (ms), 567 (ms).
$SF_5(CF_2)_5SF_5$:	1261 (w, sh), 1240 (s), 1223 (ms, sh), 1169 (s), 1146 (w), 1036 (w), 941 (w), 901 (vs), 881 (ms), 873 (s), 838 (w), 806 (ms), 784 (w), 775 (w), 745 (ms), 704 (w), 692 (ms), 675 (w), 656 (ms), 608 (ms), 579 (ms), 558 (ms).
$SF_5CF_2CF_2OCF_2CF_2SF_5$:	1350 (w), 1310 (w), 1259 (ms), 1230 (s), 1206 (ms), 1191 (ms, sh), 1168 (s), 1133 (ms), 901 (vs), 858 (s), 818 (w), 797 (w), 778 (w), 758 (w), 726 (w), 703 (w), 690 (w), 678 (w), 643 (w), 611 (ms), 576 (w).

Table 5. ^{19}F NMR data of perfluoropolymethylene bis(sulfur pentafluoride)s and perfluoropentamethylenesulfur tetrafluoride

Compound	Chemical shift, ppm				
	α CF_2[a]	β CF_2[a]	γ CF_2[a]	SF_{eq}[b]	SF_{ax}[b]
$SF_5CF_2CF_2SF_5$	18.3			−44.0	−61.8
$SF_5CF_2CF_2CF_2SF_5$	16.0	46.3		−44.3	−62.8
$SF_5CF_2CF_2CF_2CF_2SF_5$	17.3	44.5		−44.3	−62.8
$SF_5CF_2CF_2CF_2CF_2CF_2SF_5$	16.8	42.8	44.8	−44.3	−62.8
$SF_5CF_2CF_2OCF_2CF_2SF_5$	22.5	6.4		−44.2	−62.0
$\overline{\lvert CF_2CF_2CF_2CF_2CF_2SF_4 \rvert}$	18.5	45.8	50.3	−19.8	−48.0

a) Chemical shift from external CF_3COOH. b) Chemical shift from internal CCl_3F.

Table 6. Properties of perfluorocyclic S(VI) compounds, and pereluoro-*n*- and isoamylsulfur pentafluorides

Compound	Bp (°C)	n_D^{20}	d_4^{20}	Elemental analysis C	Elemental analysis F
$\overline{\lvert CF_2CF_2CF_2CF_2CF_2SF_4 \rvert}$[a]	95.2				74.0 (74.3)[b]
$\overline{\lvert CF_2CF(CF_3)CF_2CF_2SF_4 \rvert}$	88.3	1.3017	1.9431	16.42 (16.76)	75.1 (74.3)
$\overline{\lvert CF(CF_3)CF_2CF_2CF_2SF_4 \rvert}$	84.7	1.3056	1.9540	16.40 (16.76)	74.2 (74.3)
n-$C_5F_{11}SF_5$	92.5	1.2797	1.8885	15.33 (15.15)	77.1 (76.8)
iso-$C_5F_{11}SF_5$	92.5	1.2867	1.9252	15.06 (15.15)	76.5 (76.8)

a) Mp 19—21 °C, glassy. b) Calculated value in parenthesis.

By analogy with the results of the electrochemical fluorination of diols,[4] the cyclic products (perfluorotetramethylenesulfur tetrafluoride from I. perfluoropentamethylenesulfur tetrafluoride, perfluoro-2-methyltetramethylenesulfur tetrafluoride, and perfluoro-3-methyltetramethylenesulfur tetrafluoride from II. perfluoro-4-oxapentamethylenesulfur tetrafluoride from III) were also formed. Among them, the yield of perfluorotetramethylenesulfur tetrafluoride from I amounted to 4.7%.

As for the results with the fluorination of cyclic sulfides (Table 2), five-membered perfluorotetramethylenesulfur tetrafluoride from IV was obtained in the highest yield (11.4%). However, the results of the fluorination of V, VI, and VII indicated that considerable ring isomerization took place, resulting in a reduction of the yield of the expected sulfur(VI) compounds. The perfluorotetramethylenesulfur tetrafluoride[6] and perfluoropentamethylenesulfur tetrafluoride are solid at room temperature and freeze to a glass, while perfluoro-2-methyltetramethylenesulfur tetrafluoride and perfluoro-3-methyltetramethylenesulfur tetrafluoride are liquids. Although the five- and six-membered perfluorocyclic sulfur(VI) compounds were obtained in this manner, the four-membered perfluorotrimethylenesulfur tetrafluoride could not be obtained by the electrochemical fluorination of trimethylene sulfide, as it immediately polymerized in anhydrous

6) T. Abe and J. M. Shreeve, *J. Fluorine Chem.*, **3**, 17 (1973/74).

hydrogen fluoride, thus giving an orange, gelatinous polymer.[7] The properties of these perfluorocyclic sulfur(VI) compounds, and those of perfluoro-*n*-amylsulfur pentafluoride and perfluoroisoamylsulfur pentafluoride are shown in Table 6. The structures of these perfluoroalkylsulfur(VI) compounds were determined by means of their ^{19}F NMR, mass, and IR spectra as well as by elemental analysis. However, the ^{19}F NMR spectra[8] of both perfluoro-2-methyltetramethylenesulfur tetrafluoride and perfluoro-3-methyltetramethylenesulfur tetrafluoride were too complicated to resolve because of the conformational rigidity of their molecules, which resulted in a non-equivalence of the geminal fluorines of the alkyl group, and also because they were a mixture of their respective geometric isomer.

Experimental

Reagents and Apparatus. All the reagents except 1,3-propanedithiol and 1,5-pentanedithiol were purchased from Tokyo Kasei Co., and were used as received. The 1,3-propanedithiol[9] and 1,5-pentanedithiol[10] were prepared by the reaction of the corresponding alkyl bromides with an alcoholic KSH solution, following the method of the reference. They were used after purification. The purity of the anhydrous hydrogen fluoride was higher than 99.5%.

All the features of the apparatus and the electrolytic cell (capacity, 1 l; electrode, Ni plates; effective anodic surface area, 9.2 dm^2) used for this fluorination were the same as have been described previously.[4] A Shibata micro-pump, Model SPC-100, was used to change the 3-oxapentane-1,5-dithiol into the cell during the electrolysis.

The IR spectrum measurements were accomplished by means of a Hitachi EPI-G3 spectrometer, using a 6-cm gas cell with KBr windows.

The ^{19}F NMR spectra were obtained by a JEOL C-60-H high resolution spectrometer (56.4 Mc for ^{19}F), using trifluoroacetic acid (external) and trichlorofluoromethane (internal) for the determination of the chemical shifts.

Procedures. The general procedures for the fluorination of dithiols and cyclic sulfides were the same as have been described previously.[4] As examples, the fluorination of 1,5-pentanedithiol, 3-oxapentane-1,5-dithiol (Run B) and tetrahydrothiopyran will be described.

Fluorination of 1,5-Pentanedithiol: A 27.2 g portion of 1,5-pentanedithiol was introduced into a cell which contained 1 l anhydrous hydrogen fluoride. Then the electrolysis was carried out with an anodic current density of 3.3 A/dm^2, a cell voltage 7.2—7.7 V, and cell a temperature of 5—6 °C. He (50 ml/min) was introduced from the bottom of the cell in order to agitate the solution. The electrolysis was then conducted for 177 A·hr.

The evolving gases from the cell were passed through a reflux condenser kept at −25 °C, over NaF pellets, and then bubbled through an alkaline solution of sodium sulfite, containing a small amount of potassium iodide in a series of Ichinose gas washers, and finally collected through traps immersed in liquid nitrogen. After the electrolysis was over, the transparent heavy liquid, which was later found to consist mostly of perfluoropentamethylene bis(sulfur pentafluoride), was drained from the bottom of the cell, washed with an alkaline solution, dried over anhydrous sodium sulfate, and subsequently analysed by glc.

The fluorinated products (39.6 g) collected in the cold traps were carefully separated into two fractions using the traps of the low-temperature distillation unit : Fraction 1 (compounds having lower bp's); (20.4 g), Fraction 2; (19.2 g). The compounds in Fraction 1 consisted mainly of SF_6. Then, the volatile compounds in Fraction 2 were removed by distillation. Thus, 12.6 g of the distillation residue were obtained. The volatile distillate was identified as a mixture of perfluoro-*n*- and -*iso*-pentane (*n*-C_5F_{12} : *iso*-C_5F_{12}=90 : 10) by glc (column: Kel F #3 30% on Chromosorb PAW, carrier; He) and on the basis of their known IR spectra. The cell drainings (17.4 g) and the distillation residue of Fraction 2 (12.6 g) were subsequently analysed by glc (column; Kel F #90 26% on Chromosorb PAW, and DNP 25% on Shimalite, carrier; He). The following perfluorinated sulfur(VI) compounds were thus obtained: $SF_5(CF_2)_5SF_5$ 11.7 g, *n*-$C_5F_{11}SF_5$ 12.8 g, $CF(CF_3)CF_2CF_2CF_2SF_4$ 0.6 g, $CF_2CF(CF_3)CF_2CF_2SF_4$ 0.2 g, $CF_2CF_2CF_2CF_2CF_2SF_4$ 0.3 g. These new compounds were characterized by means of their ^{19}F NMR, IR and mass data as well as elemental analyses (C and F).

Fluorination of 3-Oxapentane-1,5-dithiol (Run B): The fluorination was carried out in essentially the same manner illustrated above. However, the 3-oxapentane-1,5-dithiol was fed into the cell little by little by means of the micro-pump, which was connected with the sample injector,[2e] at a rate of about 5.5 ml/hr during electrolysis (anodic current density, 3.3 A/dm^2. cell voltage, 5.5—7.1 V. cell temp, 5—6 °C). For this sample feeding (27.6 g), 4 hr were required. Electrolysis was then continued for another hour. Thus, 151 A·hr of the electrolysis were conducted. No perfluorinated products were found in the cell drainings. The products (40.3 g), which was collected into traps immersed in liquid nitrogen, were similarly treated. The volatile $C_2F_5OC_2F_5$ and SF_6 were formed as major products. The following compounds were obtained by finally analysing the 4.7 g of the distillation residue: $SF_5CF_2CF_2OCF_2CF_2SF_5$ 0.2 g, $C_2F_5OC_2F_4SF_5$ 1.0 g, $SF_5CF_2CF_2SF_5$ 0.2 g, $(C_2F_5)_2SF_5$ 1.4 g, $CF_2CF_2OCF_2CF_2SF_4$ 0.3 g.

Fluorination of Tetrahydrothiopyran: Tetrahydrothiopyran (20.4 g) was subjected to electrochemical fluorination under the following electrolysis conditions: anodic current density, 3.3 A/dm^2. electricity passed, 129 A·hr. cell voltage, 4.9—7.0 V. cell temp, 5—6 °C. The fluorinated product (19.3 g) was collected in traps cooled in liquid nitrogen. The product was initially subjected to a low-temperature distillation. The fraction (7.5 ml, 14.6 g) which has a bp of above 0 °C was treated likewise, and the following compounds were obtained. $CF_2CF_2CF_2CF_2CF_2SF_4$ 1.0 g, $CF_2CF(CF_3)CF_2CF_2SF_4$ 1.3 g, $CF(CF_3)CF_2CF_2CF_2SF_4$ 0.5 g, *n*-$C_5F_{11}SF_5$ 1.9 g, *iso*-$C_5F_{11}SF_5$ 0.5 g. The ratio of the perfluoro-*n*- and -*iso*-pentane which was formed as a result of the cleavage of the C-S bond was as follows. *n*-C_5F_{12} : *iso*-C_5F_{12}=58 : 42.

The authors wish to thank Mr. Kazuo Kodaira for the mass measurements.

7) See also R. W. Bost and M. W. Conn, *Ind. Eng. Chem.*, **25**, 526 (1933).

8) The chemical shifts of CF_3- at the 2- and 3- positions of perfluoro-methyltetramethylenesulfur tetrafluoride were −6.1 ppm and −4.8 ppm respectively from external CF_3COOH.

9) J. R. Meadow and E. E. Reid, *J. Amer. Chem. Soc.*, **56**, 2177 (1934).

10) W. Autenrieth and A. Geyer, *Ber.*, **41**, 4249 (1908).

New Syntheses of Pyrimido[4,5-*d*]pyrimidines[1]

Fumio YONEDA and Masatsugu HIGUCHI

Faculty of Pharmaceutical Sciences, Kumamoto University, Oe-honmachi, Kumamoto 862

(Received May 23, 1973)

Novel conversions of pyrrolo-pyrimidines into pyrimido-pyrimidines are described. The treatment of 5-nitrosopyrrolo-pyrimidine (I) under Beckmann conditions causes ring expansion to give pyrimido-pyrimidine (II). Both the reduction of I with triphenylphosphine, potassium pyrosulfite, or sodium dithionite in dimethylformamide and the oxidation of 5-aminopyrrolo-pyrimidine with lead tetraacetate in dimethylformamide or acetic acid afford II. 5-Aminopyrimido-pyrimidine is prepared by the nucleophile-induced ring expansion of I. The possible mechanisms of these ring expansions are proposed.

The pyrimido[4,5-*d*]pyrimidine ring system not only resembles purine, but is isomeric with pteridine; it can, therefore, be expected to have biological activities similar to those of either purine or pteridine. In fact, certain pyrimido[4,5-*d*]pyrimidines have shown diuretic[2,3] and purine antagonistic[4] properties.

The known synthetic methods for the preparation of pyrimido[4,5-*d*]pyrimidines have involved the initial construction of suitably-substituted pyrimidine precursors and the subsequent annelation of the condensed pyrimidine ring in the reaction by using several carbon or carbon-nitrogen sources.[2-10] In this paper we will describe several new routes to the syntheses of pyrimido-[4,5-*d*]pyrimidines including ring expansions of pyrrolo-[2,3-*d*]pyrimidine derivatives.

Ring Expansion under Beckmann Conditions

It has been suggested that the ring expansion of 5-nitrosopyrrolo[2,3-*d*]pyrimidine to pyrimido[4,5-*d*]-pyrimidine by treatment under reflux with tosyl chloride or phosphorus oxychloride in dimethylformamide can be considered to occur *via* the usual Beckmann-type rearrangement.[11] Later we observed that the conversion of 3-nitrosoindole into quinazoline proceeds *via* the second-order Beckmann rearrangement.[12] This finding prompted us to look more closely into the ring expansion of 5-nitrosopyrrolo[2,3-*d*]pyrimidine described above.

The stirring of 1,3-dimethyl-5-nitroso-6-phenylpyrrolo[2,3-*d*]-2,4(1*H*,3*H*)-pyrimidinedione (**1a**)[11] with tosyl chloride in pyridine under cooling with ice water for 1 hr, followed by dilution with water, separated 6-(benzoylamino)-5-cyano-1,3-dimethyluracil (**2**), in which a nitrile absorption is present at 2215 cm^{-1} (Nujol) in the infrared spectrum. Compound **2** is extremely unstable, so even its purification by recrystallization from solvents or even its being maintained at room temperature for a few days results in cyclization into 4-iminopyrimido-1,3-oxazine (**3**). The heating of **1a** under a mild reflux with tosyl chloride or phosphorus oxychloride in pyridine formed **3** exclusively, while the refluxing of **1a** with the same reagents in dimethylformamide afforded 1,3-dimethyl-5-hydroxyl-7-phenylpyrimido[4,5-*d*]-2,4(1*H*,3*H*)-pyrimidinedione (**4a**), as has been described in the preceding paper.[11] The infrared spectra of **3** showed a strong imino absorption band at 3375 cm^{-1} (KBr). The heating of **3** under reflux in dimethylformamide resulted in the formation of **4a** *via* the Dimroth-type rearrangement. The treatment of **3** with an acid or base such as hydrochloric acid or benzylamine gave also **4a**. Compound **4a** was alternatively prepared by the following unequivocal synthesis. The heating of 6-amino-1,3-dimethyluracil with ethyl chloroformate in pyridine afforded 6-amino-1,3-dimethyl-5-(ethoxycarbonyl)uracil (**5**), which was then fused with benzamidine hydrochloride to give **4a**.

These facts show that this ring expansion proceeds *via* the second-order Beckmann rearrangement of the imino oxime tautomeric form of **1a**, followed by cy-

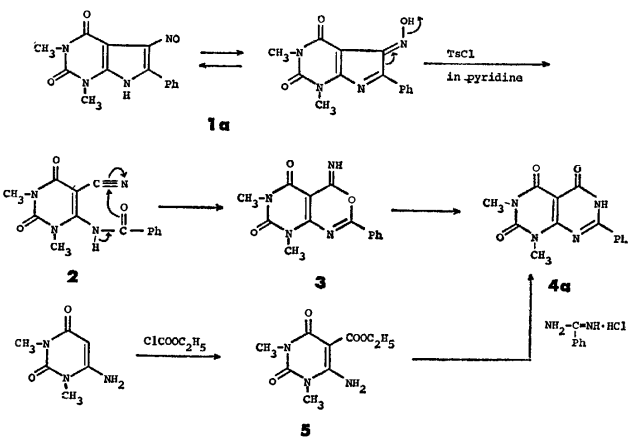

Scheme 1.

1) A part of this paper has been reported in preliminary form: see F. Yoneda and M. Higuchi, *Chem. Commun.*, **1972**, 402; F. Yoneda and M. Higuchi, *Chem. Pharm. Bull.* (Tokyo), **20**, 2076 (1972).

2) E. C. Taylor, R. J. Knopf, R. F. Meyer, A. Holmes, and M. L. Hoefle, *J. Amer. Chem. Soc.*, **82**, 5711 (1960).

3) H. Grabeyes, G. E. Jaffé, I. J. Pachter, J. P. Rosenbloom, A. J. Villani, J. W. Wilson, and J. Weinstock, *J. Med. Chem.*, **11**, 568 (1968).

4) H. G. Mauter, *J. Org. Chem.*, **23**, 1450 (1958).

5) C. K. Chatterji and N. Anand, *J. Sci. Ind. Res.*, **17B**, 63 (1958).

6) C. K. Chatterji and N. Anand, *ibid.*, **18B**, 272 (1959).

7) H. Bredereck, F. Effenberger, and R. Suter, *Chem. Ber.*, **95**, 2049 (1962).

8) J. Druey, P. Schmidt, K. Eichenberger, and M. Wilhelm, U. S. 3055900 (1962).

9) H. Bredereck, G. Simchen, and H. Traut, *Chem. Ber.*, **100**, 3664 (1967).

10) H. Bredereck, G. Simchen, R. Wahl, and F. Effenberger, *ibid.*, **101**, 512 (1968).

11) F. Yoneda, M. Higuchi, K. Senga, M. Kanahori, and S. Nishigaki, *Chem. Pharm. Bull.* (Tokyo), **21**, 473 (1973).

12) F. Yoneda, M. Higuchi, and R. Nonaka, *Tetrahedron Lett.*, 359 (1973).

clization into the 4-imino-1,3-oxazine intermediate (**3**) and subsequent Dimroth rearrangement, as is depicted in Scheme 1.

Reductive Ring Expansion

The stirring of **1a** under a mild reflux with excess triphenylphosphine in dimethylformamide for 1 hr, followed by cooling, caused the separation of **4a** in 45% yield. The mother liquor was evaporated in dryness under reduced pressure, and the residue was chromatographed to give triphenylphosphine oxide in a 76% yield. Similarly, the 6-*p*-chlorophenyl and 6-*p*-bromophenyl analogs (**1b** and **1c**) of **1a** yielded the corresponding pyrimido[4,5-*d*]pyrimidines (**4b** and **4c**) in almost the same yields.

The refluxing of **1a** with excess potassium pyrosulfite in dimethylformamide for 1 hr and the subsequent cooling of the reaction mixture separated **4a** in a 50% yield. To our knowledge, the reaction is the first example in which potassium pyrosulfite has been successfully introduced into preparative origanic chemistry. In this reaction a dimeric product (**6**) was obtained as a by-product. The structure of **6** was assigned on the basis of an elemental analysis and a molecular-weight determination (a strong parent peak at *m/e* 536), and in consideration of its probable mode of formation. An analogous dimeric indole derivative is obtained in the oxidation of the 3-indoxyl derivative.[13] This dimeric product (**6**) was alternatively synthesized by the oxidative coupling of 3-aminopyrrolo[2,3-*d*]pyrimidine (**7a**) (*vide infra*) with diethyl azodicarboxylate in dimethylformamide.

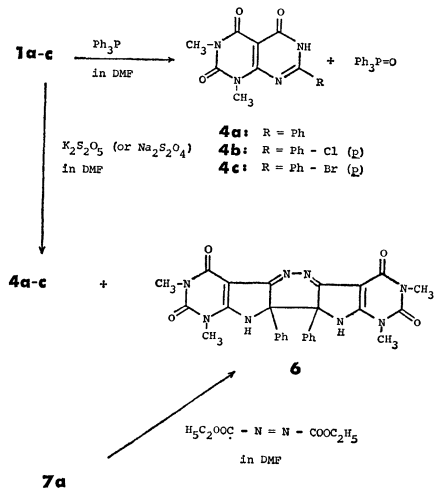

Scheme 2.

The treatment of **1b** and **1c** with potassium pyrosulfite under the same conditions gave, similarly, **4b** and **4c** in 58 and 40% yields respectively. The treatment of **1a** with sodium dithionite in dimethylformamide also yielded **4a**, although in a lower yield (34%), whereas this reaction in water gave the usual reduction-product, 5-aminopyrrolo[2,3-*d*]pyrimidines (**7**) (*vide infra*). When **1a** alone was refluxed in dimethylformamide, only a trace of **4a** was obtained, the starting material being almost entirely recovered.

Oxidative Ring Expansion

It was found that the reaction of 5-amino-1,3-dimethyl-6-phenylpyrrolo[2,3-*d*]-2,4(1*H*,3*H*)-pyrimidinediones (**7a–c**) with lead tetraacetate gave **4a–c**. The starting materials, **7a–c**, were obtained by the reduction of **1a–c** with sodium dithionite in water. The heating of **7a–c** with excess lead tetraacetate in dimethylformamide or acetic acid at 90° for 3 hr, partial evaporation, and dilution with water caused the separation of **4a–c** in 90, 86, and 72% yields respectively. When the above reaction was carried out below 65°, an intermediate, the 4-imino-1,3-oxazine derivative (**3**), was obtained in a high yield.

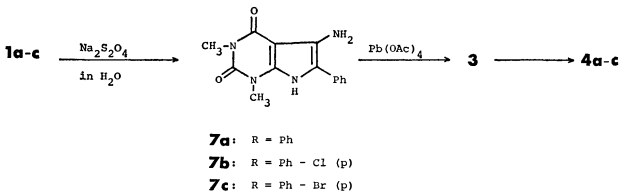

Scheme 3.

Although a common intermediate, 5-nitrene (**9**), is formed in both the reductive and oxidative ring expansions described above, we could not demonstrate the presence of **9** by intermolecular trapping reaction with cyclohexene. Therefore, the more complex adducts, such as **10** and **11**, appear equally probable as precursors.

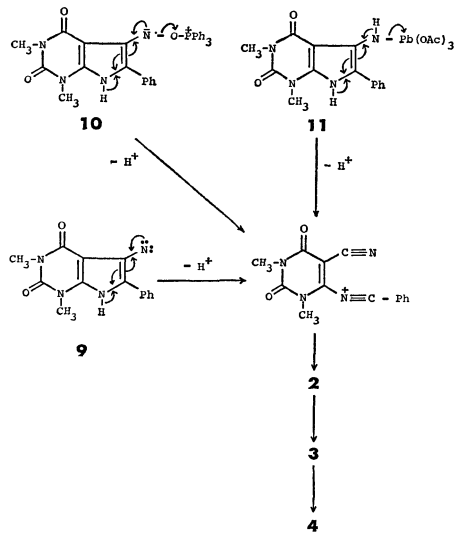

Scheme 4.

Nucleophile-induced Ring Expansion

The refluxing of **1a** in dimethylformamide while introducing dry ammonia over a 4-hr period yielded 5-amino-1,3-dimethyl-7-phenylpyrimido[4,5-*d*]-2,4(1*H*,3*H*)-pyrimidinedione (**12**) in a 60% yield. Re-

13) a) A. Hassner and M. Haddadin, *J. Org. Chem.*, **28**, 224 (1963). b) E. Giovannins, F. Farkas, and J. Rosales, *Helv. Chim. Acta*, **46**, 1326 (1963).

fluxing **1a** with urea in dimethylformamide also gave **12** in a 80% yield. The structure of **12** was assigned on the basis of the satisfactory elemental analysis and the spectral data, and finally by the conversion of **12** into **4a** by deamination with sodium nitrite in hydrochloric acid. Similarly, the refluxing of **1a** with benzylamine and aniline in dimethylformamide afforded 5-benzylamino- (**13**) and 5-anilino-1,3-dimethyl-7-phenylpyrimido[4,5-*d*]-2,4(1*H*,3*H*)-pyrimidinedione (**14**) in 59 and 64% yields respectively.

The following mechanism with the *N*-(5-cyanouracil-6-yl)amidine intermediate (**15**) rationalizes this ring expansion. A formal Beckmann-type rearrangement would also account directly for the formation of the 5-benzyl (**13**) and 5-anilino derivatives (**14**), without any need to postulate the subsequent Dimroth rearrangement of an imino intermediate (**16**). However, the formation of (benzoylamino)acrylonitrile (**17**) from **1a** by the action of alkali would eliminate the similar Beckmann process. That is, the refluxing of **1a** with 40% potassium hydroxide solution in a mixture of ethanol and water (1 : 1) for 1 hr yielded a nearly equimolar mixture of *cis*- and *trans*-isomers (**17**). The NMR spectra exhibited two pairs of three-proton singlets at 3.12 and 3.47 as well as those at 3.19 and 3.55. The former two singlets were assigned to the *N*-methyl groups of the *cis*-isomer, and the latter two, to those of the *trans*-isomer. The **17** mixture was converted into the corresponding pyrimidine derivative (**18**) in a quantitative yield by treatment with dry hydrogen chloride in ethanol. The characteristic nitrile band of **17** at 2190 cm^{-1} (Nujol) disappeared. The NMR spectrum displayed a pair of singlets at 3.10 and 3.45 corresponding to the *N*-methyl groups and phenyl protons at from 7.5 to 8.2.

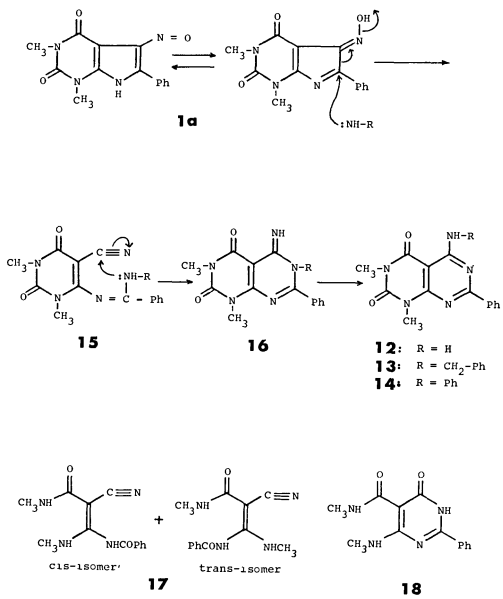

Scheme 5.

Experimental

All the melting points are uncorrected. The NMR spectra were determined by means of a JNM 3H-60 spectrometer, using tetramethylsilane as the internal standard. The chemical shifts were expressed in δ values. The mass spectra (75 eV) were recorded on a Hitachi RMU-6D double-focusing spectrometer.

*6-(Benzoylamino)-5-cyano-1,3-dimethyluracil (**2**).* A mixture of 0.25 g (1 mmol) of **1a** and 0.6 g (3 mmol) of TsCl in 5 ml of pyridine was stirred under cooling with ice water for 4 hr. The subsequent dilution of the reaction mixture with H_2O gave 0.1 g (40%) of **2**.

*1,3-Dimethyl-5-imino-7-phenylpyrimido[4,5-d]-1,3-oxazine (**3**).* A mixture of 0.5 g (2 mmol) of **1a** and 1 g (5 mmol) of TsCl in 15 ml of pyridine was refluxed at 130—140 °C for 3 hr. The reaction mixture was then evaporated under reduced pressure, and to the residue 100 ml of H_2O was added. The crystals thus separated were recrystallized from DMF to give 0.45 g (90%) of colorless crystals; mp>285 °C (sublim.). *m/e* 284 (M^+). Found: C, 59.08; H, 4.21; N, 19.39%. Calcd for $C_{14}H_{12}N_4O_3$: C, 59.15; H, 4.26; N, 19.71%.

*Dimroth Rearrangement of **3** to **4a**.* *A.* A solution of 0.1 g (4 mmol) of **3** in 5 ml of DMF was refluxed for 3 hr and then allowed to stand overnight at room temperature. The crystals thus precipitated were washed with H_2O and dried to give 0.09 g (90%) of **4a**.

B. A solution of 0.05 g (0.2 mmol) of **3** in 10 ml of conc. HCl was refluxed for 3 hr. The reaction mixture was then diluted with H_2O and neutralized with aqueous NH_3 to separate 0.025 g (50%) of **4a**.

C. A solution of 0.25 g (1 mmol) of **3** and 0.16 g (2 mmol) of benzylamine in 50 ml of DMF was refluxed at 160° for 3 hr. After cooling, the crystals thus separated were washed with H_2O and dried to give 0.23 g (92%) of **4a**.

*6-Amino-1,3-dimethyl-5-(ethoxycarbonyl)uracil (**5**).* Three grams (19 mmol) of 6-amino-1,3-dimethyluracil were dissolved in 55 ml of pyridine, and to the solution we then added, drop by drop, 4.5 g (42 mmol) of ethyl chloroformate. After heating at 90 °C for 5 hr, the reaction mixture was evaporated *in vacuo*, and then 10 ml of H_2O was added. The crystals thus separated were recrystallized from EtOH to give 2.2 g (50.1 %) of colorless needles; mp 207—208 °C. Found: C, 47.74; H, 5.52; N, 18.68%. Calcd for $C_9H_{13}N_3O_4$: C, 47.57; H, 5.77; N, 18.49%.

*Reaction of **5** with Benzamidine Hydrochloride.* One gram (4 mmol) of **5** and 1.25 g (8 mmol) of benzamidine hydrochloride were thoroughly mixed, after which the mixture was fused at about 300 °C for 15 to 20 min. After cooling, reaction mixture was crushed in H_2O and washed with H_2O. The crushed mass was recrystallized from DMF to give 0.45 g (36%) of colorless plates (mp>300 °C), which were identical in all respects with the product (**4a**) prepared by the ring expansion of **1a**.

*Reductive Ring Expansion of **1a** with Triphenylphosphine.* A mixture of 1 g (4 mmol) of **1a** and 1.57 g (6 mmol) of triphenylphosphine in 20 ml of DMF was refluxed at 180 °C for 2.5 hr. After cooling, the crystals which separated were recrystallized from DMF to give 0.45 g (45%) of **4a**.

Similarly, 6-(*p*-chlorophenyl) (**1b**) and 6-(*p*-bromophenyl) (**1c**) analogs were converted into 7-(*p*-chlorophenyl)- (**4b**) and 7-(*p*-bromophenyl)-1,3-dimethylpyrimido[4,5-*d*]-2,4(1*H*,3*H*)-pyrimidinediones (**4c**) (see Table 1).

The evaporation of the mother liquor under reduced pressure and the column chromatography of the oily residue on alumina, using benzene-EtOH (7 : 3) as the eluant, gave triphenylphosphine oxide in a 75% yield.

*Reaction of **1a** with Potassium Pyrosulfite ($K_2S_2O_5$).* A mixture of 0.9 g (3 mmol) of **1a** and 0.9 g (4 mmol) of $K_2S_2O_5$ in 24 ml of DMF was heated under reflux at 180—190°C for 2.5 hr, during which time the color changed from red to

TABLE 1.

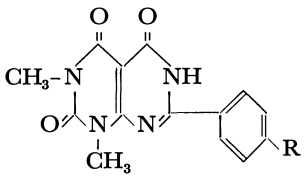

Compound No.	R	Mp (°C)	Yield (%) Ph_3P	Yield (%) $K_2S_2O_5$	Appearance (Recryst. solvent)	Formula	Analysis Calcd (%) C	Calcd (%) H	Calcd (%) N	Found (%) C	Found (%) H	Found (%) N
4a	H	>300	45	50	Colorless plates (DMF)	$C_{14}H_{12}N_4O_3$	59.15	4.26	19.71	59.37	4.28	19.49
4b	Cl	>300	48	58	Colorless plates (DMF)	$C_{14}H_{11}N_4O_3Cl$	52.75	3.48	17.58	52.75	3.45	17.48
4c	Br	>300	42	40	Colorless plates (DMF)	$C_{14}H_{11}N_4O_3Br$	46.29	3.05	15.40	46.60	3.16	15.17

yellow. After cooling, the crystals which separated were recrystallized from DMF to give 0.45 g (50%) of colorless plates of **4a**.

The mother liquor was allowed to stand for 2 days to separate yellow crystals, which were then collected by filtration. The filtrate was concentrated *in vacuo* and diluted with H_2O to separate more yellow crystals. The combined crystals were recrystallized from DMF to give 0.15 g (17.6%) of colorless prisms of the dimer (**6**); mp 287—289 °C. *m/e* 536 (M^+). Found: C, 57.01; H, 5.07; N, 18.58%. Calcd for $C_{28}H_{24}N_8O_4.3H_2O$: C, 56.95; H, 5.09; N, 18.98%.

Under the same conditions, **1b** and **1c** were converted into **4b** and **4c** (see Table 1).

*Reaction of **7a** with Diethyl Azodicarboxylate.* To a solution 0.75 g (3 mmol) of **7a** in 30 ml of DMF, we added 0.5 g (3 mmol) of diethyl azodicarboxylate; the mixture was then heated under stirring at 130—135 °C for 6 hr. After cooling, the reaction mixture was evaporated to dryness. The residue was collected by filtration, washed with EtOH, and recrystallized from DMF to give 0.3 g (40.3%) of colorless plates (mp 287—289 °C) which were in all respects identical with the byproduct (**6**) formed by the reaction of **1a** with $K_2S_2O_5$.

*5-Amino-1,3-dimethyl-6-phenylpyrrolo[2,3-d]-2,4(1H,3H)-pyrimidinedione (**7a**).* A mixture of 6 g (21 mmol) of **1a** and 7.3 g (42 mmol) of $Na_2S_2O_4$ in 30 ml of H_2O was heated under reflux for 30 min. After cooling, the crystals which separated were recrystallized from EtOH to give 2.2 g (38.6 %) of pale yellow needles; mp 249—250 °C. *m/e* 270 (M^+). Found: 62.04; H, 5.37; N, 20.71%. Calcd for $C_{14}H_{14}N_4O_2$: C, 62.21; H, 5.22; N, 20.73%.

Similarly, 6-(*p*-chlorophenyl) (**7b**) (mp 250 °C, 40%) and 6-(*p*-bromophenyl) (**7c**) (mp 268 °C, 35%) analogs were obtained.

*Ring Expansion of **7a** with Lead Tetraacetate.* *A.* To a suspension of 0.81 g (3 mmol) of **7a** in 30 ml of acetic acid, we added, little by little, 2 g (5 mmol) of $Pb(OAc)_4$, after which the mixture was heated under stirring at 90 °C for 3 hr, during which time the color changed to a yellowish brown. After the solvent had been evaporated under reduced pressure, a small amount of H_2O was added to the resulting residue; the crystals which were thus separated were recrystallized from DMF to give 0.77 g (90%) of **4a**.

B. To a solution of 0.75 g (3 mmol) of **7a** in 30 ml of DMF, we added, little by little, 2 g (5 mmol) of $Pb(OAc)_4$, after which the mixture was heated at 65 °C for 3 hr. The reaction mixture was then diluted with H_2O to precipitate 0.08 g (91%) of **3**.

*5-Amino-1,3-dimethyl-7-phenylpyrimido[4,5-d]-2,4(1H,3H)-pyrimidinedione (**12**).* *A.* Three grams (11 mmol) of **1a** were dissolved in 30 ml of DMF, and to this solution we introduced dry ammonia at 140° over an 8-hr period, during which time the color changed to red. After the solvent had been evaporated, the resulting residue was recrystallized from DMF to yield 1.8 g (60%) of colorless needles; mp 259—260 °C. *m/e* 283 (M^+). Found: C, 59.70; H, 4.34; N, 25.15%. Calcd for $C_{14}H_{13}N_5O_2$: C, 59.35; H, 4.63: N, 24.72%.

B. A mixture of 0.5 g (2 mmol) of **1a** and 0.5 g (8 mmol) of urea in 10 ml of DMF was refluxed at 150—160 °C for 3 hr. The reaction mixture was evaporated under reduced pressure, and the resulting residue was diluted with H_2O. The crystals thus precipitated were recrystallized from DMF to give 0.4 g (80%) of **12**.

*Deamination of **12** into **4a**.* To a suspension of 0.1 g (0.4 mmol) of **12** in 20 ml of 10% dilute HCl, we added, portion by portion, excess $NaNO_2$ (0.5 g) under stirring and cooling with ice water; the mixture was then heated on a water bath for 1 hr. After cooling, the crystals which separated were washed with H_2O and dried to yield **4a** in a quantitative yield.

*5-(Benzylamino)-1,3-dimethyl-7-phenylpyrimido[4,5-d]-2,4(1H,3H)-pyrimidinedione (**13**).* To a solution of 0.5 g (2 mmol) of **1a** in 10 ml of DMF, we added 0.32 g (3 mmol) of benzylamine under stirring. The mixture was heated under reflux at 180 °C for 3 hr, during which time the color changed from yellow to red. After cooling, the product which separated were recrystallized from EtOH to give 0.38 g (58.5%) of colorless prisms; mp 228—229 °C. *m/e* 373 (M^+). Found: C, 67.39; H, 5.07; N, 18.51%. Calcd for $C_{21}H_{19}N_5O_2$: C, 67.54; H, 5.13; N, 18.76%.

*5-Anilino-1,3-dimethyl-7-phenylpyrimido[4,5-d]-2,4-(1H,3H)-pyrimidinedione (**14**).* To a solution of 0.5 g (2 mmol) of **1a** in 10 ml of DMF, we added 0.28 g (3 mmol) of aniline under stirring, after which the mixture was treated as has been described above to give 0.4 g (64%) of colorless needles; mp>300 °C. *m/e* 359 (M^+). Found: C, 66.73; N, 4.65; N, 19.40%. Calcd for $C_{20}H_{17}N_5O_2$: C, 66.84; H, 4.77; N, 19.49%.

1-Cyano-1-(N-methylcarbamoyl)-2-(benzoylamino)-2-(methylamino)ethylene (a Mixture of cis- *and* trans-*Isomers) (**17**).* To a solution of 0.75 g (3 mmol) of **1a** in 60 ml of EtOH, we added 15 ml of an aqueous solution including 1.5 g of KOH. After the mixture had been refluxed for 2 hr, the EtOH was evaporated and H_2O was added to the resulting residue. The undissolved material was filtered off, and the

BULLETIN OF THE CHEMICAL SOCIETY OF JAPAN, VOL. 46, 3853—3857 (1973)

The Reaction of β-Lactones with Acid Chlorides Catalyzed by Aluminum Chloride[1]

Tadaaki NAKABAYASHI, Yumo TANAKA, and Suketaka ITO

Department of Industrial Chemistry, Faculty of Engineering, Shinshu University, Wakasato, Nagano 380

(Received May 28, 1973)

Aluminum chloride-catalyzed reactions of β-lactones with acid chlorides were studied. 3-Propanolide and 3-methyl- and 2-methyl-3-propanolide all undergo predominantly the O-alkyl bond fission to give mixed anhydrides of β-chloropropionic acid. The reaction was postulated to proceed *via* dichloraluminum β-chloropropionate.

3-Propanocide(I) is well known to be cleaved through either the alkyl-oxygen bond or the acyl-oxygen bond in reactions with various reagents.

The reactions of I with acid chlorides in the presence of sulfuric acid[2] or hydrogen chloride[3] have been shown to involve exclusively the fission of the O-acyl bond of I to give β-acyloxypropionyl chlorides (Path A).

On the other hand, it has been reported that I is

TABLE 1. THE REACTIONS OF β-LACTONES WITH ACID CHLORIDES

β-Lactone (mol)	Acid chloride (mol)		Mol of $AlCl_3$	Product (Yield, mol)		
I (1.0)	AcCl	(1.0)	0.022	Acetic anhydride	(0.08)	a)
				$AcOCOCH_2CH_2Cl$	(0.20)	
				$AcOCH_2CH_2COOCOCH_2CH_2Cl$	(0.08)	
				$(ClCH_2CH_2CO)_2O$	(0.11)	
I (1.0)	$AcOCH_2CH_2COCl$	(1.0)	0.022	$AcOCH_2CH_2COOCOCH_2CH_2Cl$	(0.87)	
I (0.25)	$ClCH_2CH_2COCl$	(0.25)	0.0056	$(ClCH_2CH_2CO)_2O$	(0.19)	
I (0.5)	$(CH_2COCl)_2$	(0.5)	0.022	Succinic anhydride	(0.45)	
				$(ClCH_2CH_2CO)_2O$	(0.06)	
				$ClCH_2CH_2COCl$	(0.31)	
I (1.0)	$(CH_2COCl)_2$	(0.5)	0.022	Succinic anhydride	(0.44)	
				$(ClCH_2CH_2CO)_2O$	(0.29)	
				$ClCH_2CH_2COCl$	(0.12)	
I (0.5)	$C_6H_4(COCl)_2$	(0.5)	0.022	Phthalic anhydride	(0.43)	
				$(ClCH_2CH_2CO)_2O$	(0.07)	
				$ClCH_2CH_2COCl$	(0.31)	
I (1.0)	$C_6H_4(COCl)_2$	(0.5)	0.022	Phthalic anhydride	(0.39)	
				$(ClCH_2CH_2CO)_2O$	(0.41)	
				$ClCH_2CH_2COCl$	(0.05)	
II (0.25)	AcCl	(0.25)	0.0056	Acetic anhydride	(0.051)	a)
				$AcOCOCH(CH_3)CH_2Cl$	(0.010)	
				$AcOCH_2CH(CH_3)COOCOCH(CH_3)CH_2Cl$	(0.039)	
				$(ClCH_2CH(CH_3)CO)_2O$	(0.034)	
III (0.15)	AcCl	(0.15)	0.0034	Acetic anhydride	(0.002)	a)
				$AcOCOCH_2CH(CH_3)Cl$	(0.008)	
				$AcOCH(CH)_3CH_2COOCOCH_2CH(CH_3)Cl$	(0.016)	
				$(ClCH(CH_3)CH_2CO)_2O$	(0.020)	

a) These products were obtained as a mixture, and their yields are shown in calculated values from the amounts of the component acids.

1) Partly presented at the 24th Annual Meeting of the Chemical Society of Japan, Osaka, April, 1971.

2) T. L. Gresham, J. E. Jansen and F. W. Shaver, *J. Amer. Chem. Soc.*, **72**, 72 (1950).

3) T. Nakabayashi, T. Matsumoto, and Y. Tanaka, *Kogyo Kagaku Zasshi*, **69**, 1245 (1966).

subjected to the O-alkyl bond fission, along with the O-acyl bond fission, in the aluminum chloride-catalyzed reaction with benzene to give β-phenylpropionic acid, 1-hydroindone, β-hydroxypropiophenone, and phenyl vinyl ketone respectively.[4]

The present paper will report that β-lactones undergo predominantly the O-alkyl bond fission in the aluminum chloride-catalyzed reaction with acid chlorides to afford mixed anhydrides of β-chloropropionic acids (Path B).

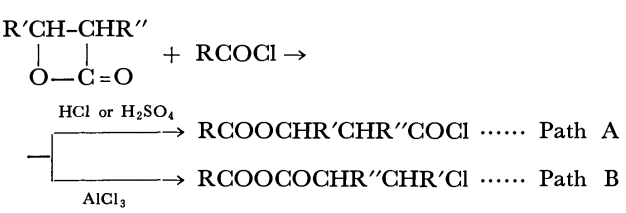

Results and Discussion

The reactions were carried out without any solvent.[5] To an acid chloride containing aluminum chloride as a catalyzer, β-lactone was added at near 0 °C. After the removal of the insoluble and the low-boiling products from the reaction mixture, the high-boiling acid anhydrides were obtained by means of molecular distillation. During distillation, disproportionation should take place; therefore, the resulting anhydrides were contaminated with the disproportionation products.

Acetic anhydride did not react with I under these reaction conditions. The results are summarized in Table 1.

The molecular distillate of the product obtained by the reaction of acetyl chloride with I exhibited strong characteristic absorptions of acid anhydride, along with weak ones of ester, in its IR spectrum. The component acids of this fraction were determined by means of glc as methyl esters, which were derived by hydrolysis or methanolysis of the product, followed by treatment with diazomethane. The NMR analysis was also applied; its values were in fair agreement with the glc data (Table 2).

TABLE 2. THE MOLAR RATIO OF THE ACID COMPONENTS OF THE ACID ANHYDRIDES OBTAINED BY THE REACTION OF ACETYL CHLORIDE WITH I

Method of analysis	$ClCH_2CH_2COOH$	$AcOCH_2CH_2COOH$	AcOH
1[a]	1.0	0.18	0.44
2[b]	1.0	0.18	0.47
3[c]	1.0	0.18	0.56

a) NMR. b) Methanolysis followed by treatment with CH_2N_2, glc. c) Hydrolysis followed by treatment with CH_2N_2, glc.

It follows from this that the acid anhydrides produced by the reaction are acetic β-chloropropionic anhydride, β-acetoxypropionic β-chloropropionic anhydride, and their disproportionation products. The reaction route can be illustrated as follows:

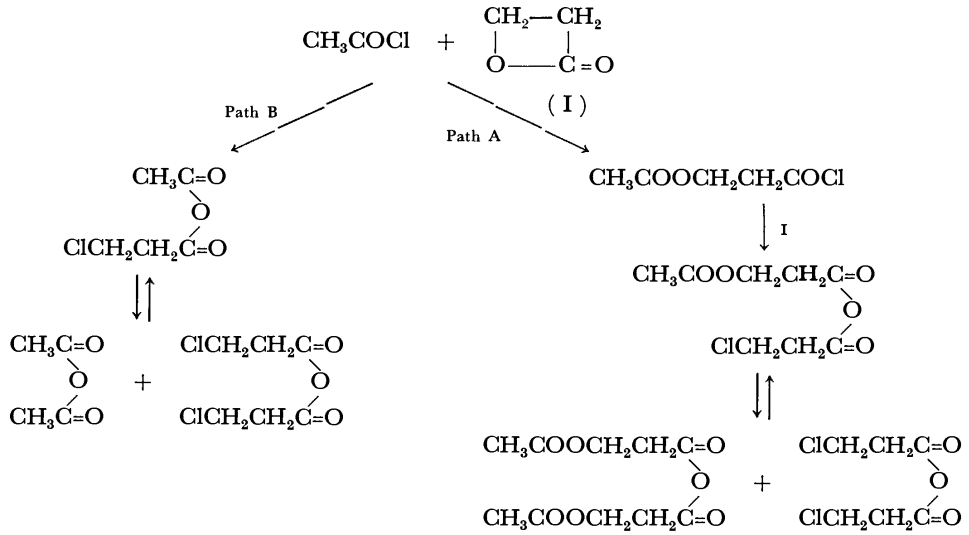

The reaction of I with succinyl chloride gave β-chloropropionyl chloride, β-chloropropionic anhydride, and succinic anhydride, which was precipitated from the reaction mixture in the course of the reaction. β-Chloropropionic β-chlorocarbonylpropionic anhydride should be the intermediate of the reaction, which gave succinic anhydride and β-chloropropionyl chloride through a chloride-anhydride exchange reaction:

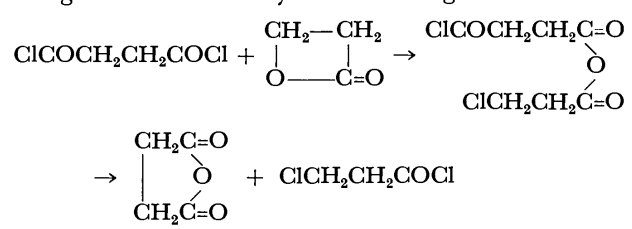

The reaction of phthaloyl chloride with I proceeded in a similar manner. β-Chloropropionyl chloride afforded β-chloropropionic anhydride in a good yield.

4) K. Nagakubo, Y. Iwakura, M. Takei, and T. Okada, *Nippon Kagaku Zasshi*, **78**, 1209 (1957).

5) Use of a solvent such as carbon disulfide or nitrobenzene did not change or improve the reaction, and gave the same result as in the absence of a solvent.

The component acids of the molecular distillate obtained by the reaction of β-acetoxypropionyl chloride with I were β-acetoxypropionic and β-chloropropionic acid in a rough ratio of 1 : 1.

Although the crude products obtained by the reactions of succinyl, phthaloyl, and β-chloropropionyl chloride also showed weak absorptions which may be assigned to an ester group in the IR spectra, almost no detectable amounts of products of the O-acyl bond fission of I were observed in any molecular distillate; this may be because such a constituent containing a β-acyloxypropionyl group is hardly distillable under these operating conditions.

The reactions of propionyl, butyryl, and isobutyryl chloride with I proceeded in a manner similar to that of acetyl chloride; no significant difference between them was noticed except for the fact that isobutyryl chloride was somewhat less reactive, probably on account of its steric factor.

2-Methyl-3-propanolide(II) reacted with acetyl chloride in analogy with I. The molar ratio of the acid components of the distilled anhydrides is given in Table 3.

Table 3. The molar ratios of the acid coponents of the acid anhydrides obtained by the reaction of acetyl chloride with II and with III

β-Lactone	Component acid	Molar ratio[a)]
II	$ClCH_2CH(CH_3)COOH$	1.0
	$AcOCH_2CH(CH_3)COOH$	0.25
	AcOH	0.091
III	$ClCH(CH_3)CH_2COOH$	1.0
	$AcOCH(CH_3)CH_2COOH$	0.22
	AcOH	0.15

a) Determined by means of NMR.

3-Methyl-3-propanolide(III) was fairly less reactive and hardly reacted at all near 0 °C. III was ultimately allowed to react with acetyl chloride at 11—15 °C to give a mixture of mixed anhydrides (Table 3).

A mechanism of the reaction of I with acid chloride catalyzed by aluminum chloride may be postulated to be as follows (Scheme 1):

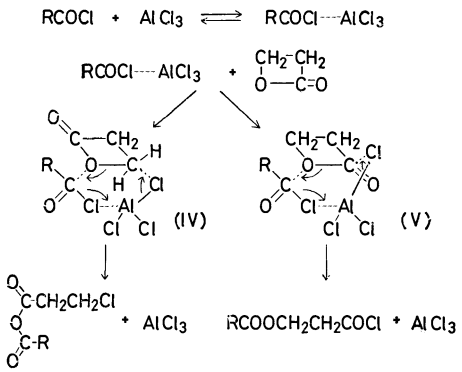

Scheme 1.

The preference of Reaction Path B to Path A can be attributed to the greater stability of the (IV) cyclic transition state, chiefly because of the lack of dipole-dipole interaction between the carbonyl oxygen of the lactone and the chlorine moieties of aluminum chloride, than that of the (V) cyclic transition state. The lower reactivity of 3-methyl-3-propanolide can be explained by the steric effect of the methyl group at the 3-position.

An alternate mechanism for the formation of anhydride can be given by assuming the formation of aluminum salt of β-chloropropionic acid as an intermediate (Scheme 2):

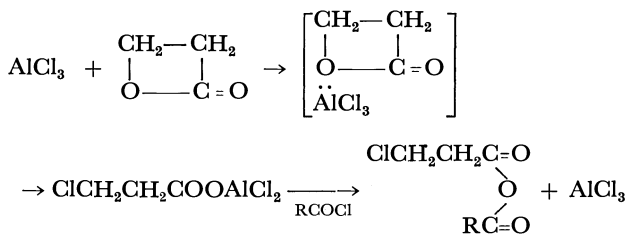

Scheme 2

When I was allowed to react with aluminum chloride (molar ratio, 1.3 : 1.0) in nitrobenzene, there was obtained a yellow homogeneous solution, in the IR spectrum of which the characteristic absorptions of β-lactone had almost disappeared. From this nitrobenzene solution, β-chloropropionic acid, along with a small amount of β-hydroxypropionic acid, could be obtained in an almost quantitative yield.[6)] Using the above nitrobenzene solution as a catalyzer instead of aluminum chloride, the same results were obtained in the reaction of I with acid chloride.

In addition, a slight rise in the temperature observed at the beginning of the addition of I to acid chloride containing aluminum chloride (see Experimental section) may be attributable to the exothermic reaction of I with aluminum chloride to form dichloraluminum β-chloropropionate.[7)]

The lower reactivity of 3-methyl-3-propanolide may be due to the steric influence of the 3-methyl group on the substitution at the 3-position of the lactone by a chlorine of aluminum chloride.

Although the first mechanism can not be rejected completely, in view of these experimental results the second mechanism is more reasonable, and the formation of the β-acyloxypropionyl group can be explained as follows:

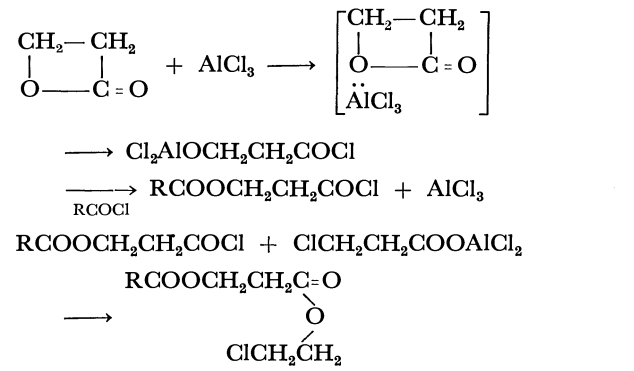

6) Nagakubo and co-workers[4)] obtained β-chloropropionic acid as a by-product in the aluminum chloride-catalyzed reaction of β-propiolactone with benzene.

7) Dichloraluminum β-chloropropionate may be formed by a concerted reaction between β-lactone and aluminum chloride. The possibility of a four-membered cyclic transition state involving β-lactone has been suggested in literature; see J. Koketsu, S. Kojima, and Y. Ishii, This Bulletin, **43**, 3232 (1970).

An additional route for the O-acyl bond fission of β-lactones is possible, in which the fission is catalyzed by hydrogen chloride[2] present in aluminum chloride or acid chloride as an impurity:

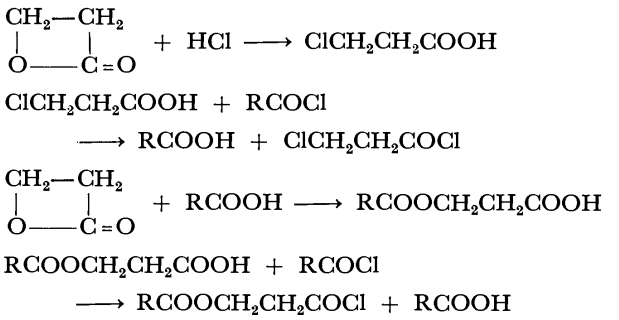

In the reaction of 3,3-dimethyl-3-propanolide with acetyl chloride, the evolution of isobutene and carbon dioxide was observed, even near 0 °C.[8] From the resulting reaction mixture, most of the acetyl chloride was recovered; there was also obtained an undistillable viscous oil which exhibited the characteristic absorptions of ester in its IR spectrum. Because of the great stability of a tertiary carbonium ion, in this case the alkyl-oxygen bond of the lactone should be cleaved with ease by the action of aluminum chloride to give a carbonium ionic intermediate, which may decompose to isobutene and carbon dioxide, and which may competitively attack another molecule of the lactone to result in the formation of a polyester.

Experimental

General. The reactions of β-lactones with acid chlorides were conducted at 0—2 °C for 20 hr, unless otherwise noted. For the glc determination, a Shimadzu Gas Chromatograph Model GC-2C was employed. The IR spectra were measured with a JASCO DS-301 spectrometer. The NMR spectra were recorded at 100 MHz with a JEOL JNH-4H-100 spectrometer in carbon tetrachloride, with tetramethylsilane as an internal standard.

Materials. 3-Propanolide(I) provided by the Daicel Co., Ltd., was dried with calcium hydride and distilled; bp 54 °C/11 mmHg. 2-Methyl-3-propanolide (II, bp 41 °C/3 mmHg),[9] 3,3-dimethyl-3-propanolide (bp 40 °C/5 mmHg),[10] β-acetoxypropionyl chloride (bp 62—64 °C/5 mmHg),[2] and β-chloropropionyl chloride (bp 57—58 °C/30 mmHg)[2] were prepared according to the literature. 3-Methyl-3-propanolide-(III) from acetaldehyde and ketene; bp 41—43 °C/8 mmHg. The aluminium chloride used was purified by sublimation.

Reaction of I with Acetyl Chloride. To a solution of 78.5 g (1.0 mol) of acetyl chloride and 3 g (0.022 mol) of aluminum chloride cooled in an ice bath was added 72.0 g (1.0 mol) of I under stirring over a period of 1.5 hr. A slight temperature rise(~5 °C) was observed at the beginning of the addition, but after that the temperature remained constant at 1—2 °C. The reaction mixture was kept at this temperature for 18.5 hr; then it was submitted to vacuum distillation (~0.1 mmHg, ~60 °C) to give 24 g of a mixture of acetic anhydride and unaltered acetyl chloride. The residual liquid was distilled two times at 60—100 °C/1—3×10^{-3} mmHg, using a molecular still, to yield 72 g of a colorless liquid; this liquid showed the characteristic absorptions of acid anhydride at 1821, 1750, and 1065 cm^{-1} and those of acetate at 1367 and 1235 cm^{-1}. No absorption at 1790 cm^{-1} to be assigned to acid chloride was observed.

NMR(δ, ppm): 4.28(t, $AcOC\underline{H}_2CH_2C=O$), 3.75 (t, $ClC\underline{H}_2CH_2C=O$), 2.95(t, $ClCH_2C\underline{H}_2C=O$), 2.79(t, $AcOCH_2C\underline{H}_2C=O$), 2.21 (s, $C\underline{H}_3COOC=O$), 2.00(s, $C\underline{H}_3COOCH_2CH_2C=O$). A mixture of acetyl chloride, acetic anhydride, and a small amount of acetic acid was also collected in a cold trap; the total amounts of acetic anhydride and the recovered acetyl chloride were determined by means of glc (2.25-meter silicone grease DC 550 column, 110 °C; anisole as an internal standard) to be 8.6 and 19.5 g respectively.

An aliquot of the high-boiling product was hydrolyzed and titrated with a sodium hydroxide solution and then a silver nitrate solution. Acid: 11.5×10^{-3} mol/g sample, reactive chlorine(-COCl): 1.66×10^{-4} mol/g sample.

A portion of the product was allowed to react with methanol in a sealed tube at 100 °C for 30 min, and then treated with diazomethane. The resulting methyl esters in methanol were detected by means of glc using a 2.25-meter polyethylene glycol-6000 column at 50 °C, with *n*-propanol as an internal standard, and using a 2.25-meter DEGS column at 110 °C, with acetophenone as an internal standard. Methyl acetate, 3.90×10^{-3}; methyl β-chloropropionate, 5.99×10^{-3}; methyl β-hydropropionate, 1.08×10^{-3} mol/g sample. Assuming that the molecular distillate contains only acetic β-chloropropionic, β-chloropropionic β-acetoxypropionic, and β-chloropropionic anhydride, the yields of these anhydrides were calculated to be 0.20, 0.078, and 0.11 mol respectively.

A 20-g portion of the moelcular distillate was hydrolyzed with 20 ml of water at room temperature. The resulting aqueous solution was saturated with sodium chloride and extracted continuously with ether for 24 hr; the ether extract was then concentrated by fractionally distilling-off the solvent, and then treated with an etherial solution of diazomethane. Methyl acetate (5.14 g, 0.0715 mol), methyl β-chloropropionate (15.6 g, 0.127 mol), and methyl β-acetoxypropionate (3.25 g, 0.0223 mol) were determined by means of glc using a 2.25-meter polyethylene glycol-6000 column at 50 °C, with *n*-propanol as an internal standard, and a 2.25-meter DEGS column at 120 °C, with acetophenone as an internal standard, respectively.

Reaction of β-Acetoxypropionyl Chloride with I. I (72.0 g, 1.0 mol) was allowed to react with β-acetoxypropionyl chloride (150.5 g, 1.0 mol) in a similar manner. The yield of the molecular distillate was 192 g. IR: 1820, 1750(sh), 1050, 1740, 1368, 1240 cm^{-1}. NMR: 4.28(t), 3.73(t), 2.95(t), 2.79(t), 2.00(s). Molar ratio of $ClCH_2CH_2C=O$: $AcOCH_2CH_2C=O$ by the NMR analysis was 1.0 : 0.98.

A portion of the distillate was treated with methanol (10 hr, room temp.) and then with diazomethane to give methyl chloropropionate and methyl β-acetoxypropionate in 90.5% and 74.1% yields (based on β-chloropropionic β-acetoxypropionic anhydride) respectively.

The methanolysis of the distillate at 100 °C in a sealed tube, followed by treatment with diazomethane, afforded methyl acetate (3.89×10^{-3} mol/g sample), methyl β-chloropropionate (3.81×10^{-3} mol/g sample), and methyl β-hydroxypropionate (3.82×10^{-3} mol/g sample).

Reaction of β-chloropropionyl Chloride with I. I (18.0 g) 0.25 mol) was allowed to react with β-chloropropionyl chloride (38.8 g, 0.25 mol) in a similar manner. Unaltered acid

8) In water at room temperature, 3,3-dimethyl-3-propanolide decomposes rapidly to carbon dioxide and isotubene to the near exclusion of hydrolysis.[10]

9) Y. Yamashita, Y. Ishikawa, T. Tsuda, and T. Miura, *Kogyo Kagaku Zasshi*, **66**, 104 (1963).

10) T. L. Gresham, J. E. Jansen, F. W. Shaver, and W. L. Beears, *J. Amer. Chem. Soc.*, **76**, 486 (1954).

chloride (4.6 g) was thus recovered. The yield of the molecular distillate was 38.5 g, n_D^{20}: 1.4662. IR: 1820, 1750, 1050 cm^{-1}. NMR: 3.73(t, 2H), 2.95(t, 2H).

A mixture of 1.99 g (0.01 mol as pure β-chloropropionic anhydride) of the distillate and 40-ml portions of ethanol and benzene was refluxed for 1 hr, and then the bulk of solvent was removed by means of fractional distillation. From the residual liquid, 2.70 g(0.0198 mol) of ethyl β-chloropropionate was detected by means of glc using a 2.25-meter DEGS column at 120 °C, with acetophenone as an internal standard.

Reaction of Succinyl Chloride with I. The reaction was started at 10 °C to avoid the crystallization of succinyl chloride and then gradually brought to 0—2 °C. Succinic anhydride was precipitated from the reaction mixture. After the removal of the succinic anhydride (mp 115—117 °C) by filtration, followed by washing with ether, the residual liquid distilled to give β-chloropropionyl chloride (n_D^{20}: 1.4566, bp 58—59 °C/32 mmHg; anilide, mp 118—119 °C) and β-chloropropionic anhydride (n_D^{20}: 1.4666, bp 78 °C/0.02 mmHg).

Reaction of Phthaloyl Chloride with I. The reaction proceeded in the same way as above. The phthalic anhydride obtained was contaminated with a small amount of phthalyl chloride.

Reactions of Propionyl, Butyryl, and Isobutyryl Chloride with I. These reactions were conducted in a manner similar to that of acetyl chloride. The molar ratios of the acid components of the molecular distillates, determined by means of NMR, are as follows:

RCOCl	$ClCH_2CH_2$-COOH	$RCOOCH_2$-CH_2COOH	RCOOH
CH_3CH_2COCl	1.0	0.20	0.70
$CH_3CH_2CH_2COCl$	1.0	0.19	0.73
$(CH_3)_2CHCOCl$	1.0	0.20	0.51

Reaction of II with Acetyl Chloride. The reaction was conducted in a manner similar to that used for I. From 21.8 g (0.25 mol) of II and 19.6 g (0.25 mol) of acetyl chloride, 22.4 g of a molecular distillate was obtained. IR: 1825, 1750, 1240, 1040 cm^{-1}. NMR: 4.18(approx. d, $AcOC\underline{H}_2$-$CH(CH_3)C{=}O$), 3.68(octet, $ClC\underline{H}_2CH(CH_3)C{=}O$), 2.6—3.2 (m, $ClCH_2C\underline{H}(CH_3)C{=}O$, $AcOCH_2C\underline{H}(CH_3)C{=}O$), 2.23(s, $C\underline{H}_3COOC{=}O$), 2.01 (s, $C\underline{H}_3COOCH_2CH(CH_3)C{=}O$), 1.35 (d, $ClCH_2CH(C\underline{H}_3)C{=}O$), 1.27(d, $AcOCH_2CH(C\underline{H}_3)C{=}O$). Glc analysis (as methyl ester; columns: 2.25-meter polyethylene glycol-6000 column at 50 °C and 2.25-meter DEGS column at 110 °C; internal standards: *n*-propanol and acetophenone): Methyl acetate, 0.44×10^{-3}; methyl β-chloroisobutyrate, 5.22×10^{-3}; methyl β-acetoxyisobutyrate, 1.73×10^{-3} mol/g sample.

Reaction of III with Acetyl Chloride. III was almost unreactive near 0 °C. At 11—15 °C for 10 days, 12.9 g (0.15 mol) of III was allowed to react with 11.8 g (0.15 mol) of acetyl chloride to give 0.2 g of acetic anhydride, 4.7 g of unaltered acetyl chloride, 1.0 g of unaltered III, and 15.0 g of a high-boiling oil. The yield of the moelcular distillate was 10.6 g. IR: 1825, 1745, 1365, 1240, 1050 cm^{-1}. NMR: 5.18(m, $AcOC\underline{H}(CH_3)CH_2C{=}O$), 4.36(m, $ClC\underline{H}$-$(CH_3)CH_2C{=}O$), 2.90(approx. d, $ClCH(CH_3)C\underline{H}_2C{=}O$), 2.70 (m, $AcOCH(CH_3)C\underline{H}_2C{=}O$), 2.24(s, $C\underline{H}_3COOC{=}O$), 2.02 (s, $C\underline{H}_3COOCH(CH_3)CH_2C{=}O$), 1.64(d, $ClCH(C\underline{H}_3)CH_2C{=}O$), 1.36(d, $AcOCH(C\underline{H}_3)CH_2C{=}O$). Glc analysis (as methyl ester; columns: 2.25-meter polyethylene glycol-6000 column at 50 °C and 2.25-meter DEGS column at 110 °C; internal standards: *n*-propanol and acetophenone): Methyl acetate, 0.82×10^{-3}; methyl β-chlorobutyrate, 6.2×10^{-3}; methyl β-acetoxybutyrate, 1.5×10^{-3} mol/g sample.

Reaction of 3,3-Dimethyl-3-propanolide with Acetyl Chloride. The lactone (50.1 g, 0.5 mol) was allowed to react with acetyl chloride (39.3 g, 0.5 mol) containing aluminum chloride (1.5 g, 0.011 mol). In the course of the reaction, 4.8 g of isobutene was condensed in a cold trap. Most of the acetyl chloride used was recovered, and 45.0 g of a viscous, undistillable product was obtained; this product showed the characteristic absorptions of ester in the IR spectrum.

Reaction of I with Aluminum Chloride. To a solution of 1.5 g (0.011 mol) of aluminium chloride and 20 ml of nitrobenzene, was added 1.0 g (0.014 mol) of I in 5 ml of nitrobenzene at 0—2 °C with external cooling. After stirring for 1 hr (including the addition period) at this temperature, the IR spectrum of the reaction mixture was taken; it showed that most of the I had already been consumed. The reaction mixture was then hydrolyzed and extracted with ether, and the ether extract was reextracted with an aqueous sodium hydroxide solution. The aqueous solution was acidified and then extracted with ether continuously for 30 hr to give 1.1 g (92%) of β-chloropropionic acid and 0.07 g (7%) of β-hydroxypropionic acid (determined as methyl ester by means of glc using a 2.25-meter DEGS column at 110 °C, with acetophenone as an internal standard).

Condensation Reactions of Adenine Derivatives with 1-*O*-Acetyl-2,3,5-tri-*O*-benzoyl-β-D-ribofuranose in Nitrophenols

Nobuo NAKAZAKI, Masao SEKIYA, Teruo YOSHINO, and Yoshiharu ISHIDO

Department of Chemistry, Faculty of Science, Tokyo Institute of Technology, O-okayama, Meguro-ku, Tokyo 152

(Received June 9, 1973)

Intermolecular interaction between nitrophenols, such as *m*-, *p*-nitrophenol, 2,4-dinitrophenol, and picric acid, and adenine derivatives, such as $N_{(6)}$-benzoyladenine, $N_{(6)}$-benzoyl-2-methylthioadenine, and $N_{(6)}$-benzyladenine, was verified by the formation of the corresponding molecular compounds. On the basis of these results, condensation reactions of these adenine derivatives with 1-*O*-acetyl-2,3,5-tri-*O*-benzoyl-β-D-ribofuranose were carried out in nitrophenols, which were used as the activating agents. They were proved to afford the corresponding nucleosides in good yields. In addition, a novel glycosyl rearrangement reaction was first observed in the case of the reaction of $N_{(6)}$-benzyladenine with the ribofuranosyl acylate.

In a previous paper[1] we described a new procedure for the synthesis of purine nucleosides involving the condensation reaction of a fully-acetylated sugar with a purine in the presence of activating agents. As an extension of this reaction, the authors now wish to report the reactions of some adenine derivatives, such as $N_{(6)}$-benzoyladenine(**1**), $N_{(6)}$-benzoyl-2-methylthioadenine(**2**), and $N_{(6)}$-benzyladenine(**3**), with 1-*O*-acetyl-2,3,5-tri-*O*-benzoyl-β-D-ribofuranose(**4**) in nitrophenols as the activating agent, and a novel glycosyl migration reaction which was confirmed in the reaction of **3** with **4**.

Results and Discussion

The previous investigation[1] led us to assumptions that a purine may be activated by an activating agent through polarization bonding[2] and that the activated degree of a purine may be delicately varied in terms of both the mutual positions and the properties of each functional group on the aromatic nuclei of the agents and the purine nuclei. In attempts at the reactions of these adenine derivatives with **4**, a series of nitrophenols were used as potential activating agents because of their properties of forming the corresponding molecular compounds with the adenines. Such properties are conceivably intimately related to some species of intermolecular interaction such as polarization bonding; the purine counterparts may potentially be activated by forming them. In the same manner as had been described for the preparation of the molecular compound of theophylline with *p*-nitrophenol,[1] the adenines (1 mmol) were treated with an excess amount of *o*-(**5**), *m*-(**6**), *p*-nitrophenol(**7**), 2,4-dinitrophenol(**8**), or picric acid(**9**) to afford the corresponding molecular compounds, summarized in Table 1. As may be seen from the table, almost all of the molecular compounds are composed of the equimolar counterpart except those obtained from **2** and **8**, and from **3** and **7**, in the ratios of 2 : 1 and 1 : 2 respectively. The precipitated crystalline product in the cases of **1** with **9** and of **2** with **6**, however, showed broad melting points and analytically proved to have no definite integral ratio in their counterpart composition. At any rate, such differences in the ratios may provide quite an interesting problem relevant to the structures of these molecular compounds and the activation mechanism of their purine counterparts; it can thus be deduced that some intermolecular interaction such as polarization bonding[2] may play an important role in forming these compounds. Although no interpretation with respect to such phenomenon has yet been furnished, the problem is exceedingly complicated because of the following facts: 1) **5** was proved not to form a molecular compound with theophylline and showed no activating effect on it.[1] 2) *p*-Toluenesulfonamide activates theophylline to condense with an acetylated sugar, although it forms no molecular compound with it,[1] *etc.*

On the basis of the above evidence, the condensation reactions of **1**, **2**, and **3** with **4** were attempted in these potential activating agents under the conditions described in Table 2, in which the results thus obtained are summarized. In each case, a purine derivative was previously fused together homogeneously with the potential agent, and an equimolar amount of **4** was then added to the prefused mixture. The mixture was allowed to react under the corresponding conditions with continuous stirring under atmospheric pressure. After the removal of the agent, each resultant mixture was subjected to chromatography on a silica gel column by the use of a solvent system of cyclohexane–chloroform (1 : 1 v/v).

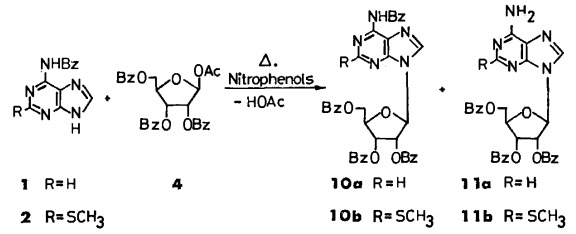

Scheme 1.

In a series of reactions of **1** with **4**, $N_{(6)}$-benzoyl-9-(2′,3′,5′-tri-*O*-benzoyl-β-D-ribofuranosyl)adenine(**10a**) and 9-(2′,3′,5′-tri-*O*-benzoyl-β-D-ribofuranosyl)adenine (**11a**) were produced, together with the corresponding nitrophenyl benzoates.[3] The failure to isolate the corresponding benzoate in the case of **8** may be ascribed to its stronger acidity(pK_a 4.11); thus, the

1) M. Sekiya, T. Yoshino, H. Tanaka, and Y. Ishido, This Bulletin, **46**, 556 (1973).

2) S. C. Wall work, *J. Chem. Soc.*, **1961**, 494.

3) Such transacylation reactions are now under investigation in our laboratory, and the detailed results will be published elsewhere.

Table 1. Attempted syntheses of molecular compounds of adenines with nitrophenols[a]

Adenine derivatives	Nitrophenols	Molecular compounds: Ratios of counterparts (Adenines: Nitrophenols)	Mp (°C)	Calcd (%) C	H	N	Found (%) C	H	N
$N_{(6)}$-Benzoyl-adenine(**1**)	*m*-Nitrophenol(**6**)	1 : 1	116—119	57.14	3.73	22.21	56.86	3.73	21.96
	p-Nitrophenol(**7**)	1 : 1	196—197	57.14	3.73	22.21	56.70	3.96	22.34
	2, 4-Dinitrophenol(**8**)	1 : 1	167—168	51.05	3.12	23.15	50.68	2.88	23.27
	Picric acid(**9**)[b]	—	—	—	—	—	—	—	—
$N_{(6)}$-Benzoyl-2-methylthio-adenine(**2**)	**6**[b]	—	—	—	—	—	—	—	—
	7	1 : 1	172—173	53.76	3.80	19.81	54.02	3.59	19.83
	8	2 : 1	195—200	51.10	3.45	22.25	51.02	3.43	22.24
	9	1 : 1	207—208	44.30	2.72	21.76	44.34	2.65	21.78
$N_{(6)}$-Benzyl-adenine(**3**)	**6**	1 : 1	135(169—175)[c]	59.33	4.43	23.07	59.09	4.40	22.71
	7	1 : 2	153—156	57.25	4.17	19.48	57.59	3.94	20.02
	8	1 : 1	190—193	52.81	3.69	23.95	53.05	3.46	24.23
	9	1 : 1	223—224.5	47.58	3.10	24.66	47.36	3.11	24.61

a) All the syntheses were carried out by the use of the adenines (1 mmol) and nitrophenols (3 mmol), respectively, in chloroform (30—40 ml) under reflux. b) Crystalline products in these cases showed broad melting point, and no definite integral ratio analytically in their counterparts. c) Dimorphism was observed in this case.

Table 2. Condensation reactions of adenine derivatives (**1**, **2**, and **3**) with 1-*O*-acetyl-2,3,5-tri-*O*-benzoyl-*β*-D-ribofuranose (**4**) in the presence of nitrophenols[a]

Adenine derivatives	Nitrophenols	Reaction conditions: Temp, °C	Period, hr	Products (Yields, %): Nitrophenyl[b] benzoates	Nucleosides
1	**6**	130—135	1.5	81.5	**10a** (3.1), **11a** (50.5)
1	**7**	130—135	3	12.6	**10a** (2.1), **11a** (20), [**12**(46)]
1	**8**	140—145	1.5	—	**10a** (32.5), **11a** (3.5)
2	**6**	130—135	3	78.5	**10b** (3.7), **11b** (45.5)
2	**7**	130—135	3	9.5	**10b** (8.2), **11b** (7.3), [**12**(43)]
2	**8**	140—145	3	—	**10b** (45.5), **11b** (9.8)
3	**8**	140—145	1.5	—	**13c** (85[c])

a) All the reactions were carried out by the use of adenines (13 mmol) and **4** (10 mmol) in the presence of nitrophenols (50 mmol, except in the case of **3**; 65 mmol). b) These yields were calculated with reference to **1** or **2**. c) This yield stands for that of debenzoylated nucleoside by treating **13a** with methanolic sodium methoxide solution.

Table 3. NMR spectral data of $N_{(6)}$-benzyl-9-(**14a**) and -7-(2',3',5'-tri-*O*-acetyl-*β*-D-ribofuranosyl)adenine(**14b**)

Protons	Chemical shift[a]: **14a**	**14b**
CH_3-CO-O-	2.10 and 2.16 (9H)	2.14 (narrow d, 9H)
H-5'a, -5'b, and -4'	4.44 (m, 3H)	4.50 (m, 3H)
C_6H_5-CH_2-N-	4.82 (d, J_{CH_2-NH}=6Hz, 2H)[b]	4.97 (broad s, 2H)
H-3'	5.73 (m)	5.75 (m)
H-2'	5.98 (t, $J_{2',3'}$=5.1Hz)	5.98 (q, $J_{2',3'}$=5.5Hz)
H-1'	6.12 (d, $J_{1',2'}$=5.1Hz)	6.36 (d, $J_{1',2'}$=4.0Hz)
C_6H_5-CH_2-NH-	6.92 (t)[c]	—
C_6H_5-CH_2-	7.27 (s, 5H)	7.18 (s, 5H)
H-2 or H-8	7.86 (s, 1H)	7.84 (s, 1H)[d]
H-8 or H-2	8.45 (s, 1H)	8.21 (s, 1H)

a) These data were recorded in δ value, and determined in $CDCl_3$—TMS. b) The doublet was collapsed into a singlet on addition of deuterium oxide. c) The broad triplet was vanished by the addition of deuterium oxide. d) The signal was observed as an exceedingly broadened singlet comparing with that of **14a**.

predominant formation of **10a** in this case fully agrees with this fact. Moreover, **5** was found to be ineffective for the reaction, and **9**, inadequate, since a remarkable coloration, which may arise from the possible decomposition of the starting materials or products, was inevitably present even when we reduced the reaction period. These agents in this case can thus be ranked in effectiveness as **6**, **8**, **7**, and **5** on the basis of the total yields of the nucleosides, **10a** and **11a**, shown in Table 2, although the reaction temperature in the case of **8** must be about 10 °C higher than those in the other cases in order to make the reaction system homogeneous. It is of interest to compare the acidity of these agents, *e.g.*, **6**(pK_a 8.40) or **8**(pK_a 4.11), with that of *p*-toluenesulfonic acid(pK_a < 1.0), which has previously been used as the catalyst for the fusion method, or with that of acetic acid(pK_a 4.76), which has been shown to be ineffective as a catalyst.[4] The debenzoylation of **10a** and **11a** was carried out by treating it with a methanolic sodium methoxide solution at room temperature, thus affording $N_{(6)}$-benzoyladenosine and adenosine in 35% and 84% yields respectively. The UV spectral data of the former were substantially consistent with those of the $N_{(6)}$-benzoyl-2-deoxyadenosine phosphate derivatives.[5] Interestingly, moreover, *p*-nitrophenyl 2,3,5-tri-*O*-benzoyl-β-D-ribofuranoside (**12**) (46% yield) was obtained concomitantly in the reaction in **7**, unlike those in **6** or **8**; the small formation of the corresponding phenyl glycosides can be noticed by tlc in the latter two cases, although no reason for it has yet been given. This fact is also of interest for its contrast with the autocatalytic fusion reaction of fully-acetylated sugars with **6** and **7** respectively, in which scarcely no such difference in their reactivity is observed.[6]

In a series of reactions of **2** with **4**, the concomitant formation of $N_{(6)}$-benzoyl-2-methylthio-9-(2′,3′,5′-tri-*O*-benzoyl-β-D-ribofuranosyl)adenine(**10b**) and 2-methylthio-9-(2′,3′,5′-tri-*O*-benzoyl-β-D-ribofuranosyl)adenine (**11b**) was similarly observed; The tendencies of the relative yields of **10b**, **11b**, and the corresponding nitrophenyl benzoates[3] were, as may be seen in Table 2, similar to those observed in the reaction of **1** with **4**. The effectiveness of the agents, however, varied in this case, they can be ranked as **8**, **6**, **7**, and **5** on the basis of the total yields of the nucleosides, **10b** and **11b**. Unlike the case of **10a**, the selective de-*O*-benzoylation of **10b** could not be attained because of the instability of the $N_{(6)}$-benzoyl group of **10b**: however, the complete debenzoylation of **10b** and **11b** was successfully carried out by treating them with a methanolic sodium methoxide solution to give 2-methylthioadenosine in 87% and 60% yields respectively. The reaction in **7** afforded **12** in a 43% yield, much as in the preceding series of reactions.

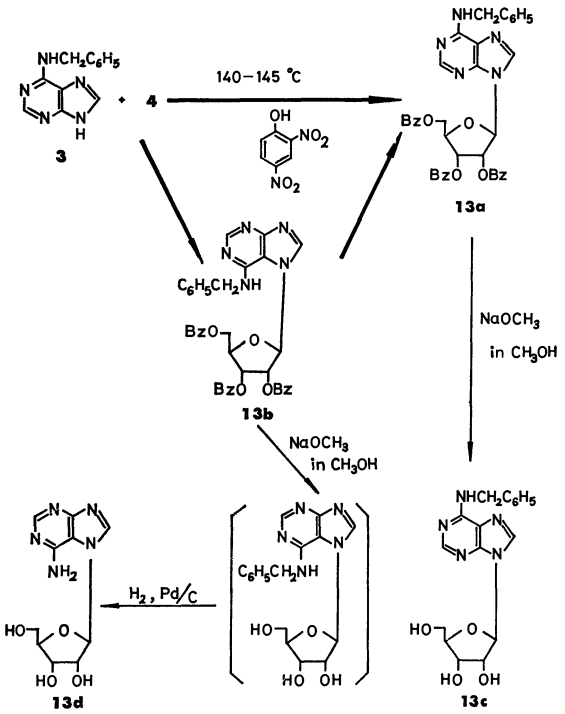

Scheme 2.

In a series of reactions of **3** with **4**, on the other hand, **5**, **6**, and **7** exhibited no activating effect on **3**; only **8** was found to be effective for the reaction. Moreover, **9** was concluded to be inadequate for the reaction, since it brought about a remarkable coloration such as has been mentioned, although it promotes the reaction. The condensation reaction in **8**, followed by the removal of **8** and debenzoylation, afforded $N_{(6)}$-benzyladenosine(**13c**) in an 85% yield under the conditions shown in Table 2. On following this reaction by the tlc technique with the passage of time, we also detected a glycosyl migration reaction of 7-(2′,3′,5′-tri-*O*-benzoyl-β-D-ribofuranosyl)-$N_{(6)}$-benzyladenine (**13b**) to the corresponding 9-ribosyl isomer(**13a**). The outline of such a glycosyl migration can easily be detected, as is demonstrated in Fig. 1. The faster-moving spot (R_f 0.84) and the slower-moving one (R_f 0.70) were found to correspond to **13a** and **13b** respectively. After the removal of **8** from the resultant reaction mixture (reaction period: 90 min), the mixture was chromatographed on a silica gel column, and then concentrated *in vacuo* to afford a sirup of **13a** (43% yield) as the first fraction and **13b** (9% yield) as the second one. The usual debenzoylation of **13a** with a methanolic sodium methoxide solution gave **13c** in an 84% yield. **13b** was, on the other hand, easily crystallized on trituration with a small amount of acetone, and a portion of the crystals was converted into 7-β-D-ribofuranosyladenine(**13d**) by debenzoylation and by subsequent debenzylation with hydrogen on palladized charcoal. The UV spectral properties of this product were consistent with those reported by Montgomery and Thomas.[7] The anomeric configuration of **13b** was deduced to be β from its

4) A. Hosono, K. Fujii, T. Tada, H. Tanaka, Y. Ohgo, Y. Ishido, and T. Sato, This Bulletin, **46**, 2814 (1973).

5) R. K. Ralph and H. G. Khorana, *J. Amer. Chem. Soc.*, **83**, 2926 (1961); Y. Lapidot and H. G. Khorana, *ibid*, **86**, 3857 (1963).

6) Unpublished data, H. Tanaka, M. Sekiya, K. Iwabuchi, M. Sato, K. Fujii, Y. Ishido, and T. Sato; The results will published elsewhere.

7) E. M. Montgomery and H. J. Thomas, *J. Amer. Chem. Soc.*, **85**, 2672 (1963).

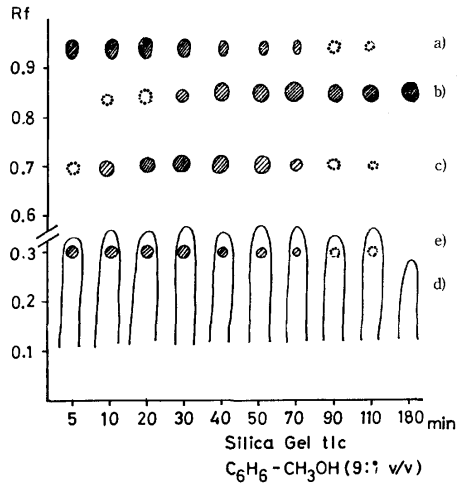

Fig. 1. The outline of the condensation reaction of $N_{(6)}$-benzyladenine(**3**) with 1-*O*-acetyl-2,3,5-tri-*O*-benzoyl-*β*-D-ribofuranose(**4**) in the presence of 2,4-dinitrophenol(**8**) observed in tlc; a: **4**, b: **13a**, c: **13b**, d: **8**, and e: **3**.

specific rotational value ($[\alpha]_D^{30}$ −65°). Subsequently, the above-observed glycosyl migration reaction of **13b** into **13a** was confirmed by fusing the sirup of **13b** in an excess amount of **8** at 140—145 °C with stirring and by following its process thin-layer chromatographically as has been described above. A novel glycosyl migration reaction was thus first observed in the fusion reaction of a fully-acylated sugar with a purine; it is of interest in contrast with the $N_{(3 \text{ or } 7)} \rightarrow N_{(9)}$ alkyl and glycosyl migration, which had been observed in the condensation reaction of adenine derivatives with alkyl or blocked glycosyl halides.[8]

In order to elucidate the possibility of the concomitant formation of the corresponding α-anomers in these reactions, a condensation reaction of 1,2,3,5-tetra-*O*-acetyl-*β*-D-ribofuranose with **3** in **8** was attempted, since the confirmation of the α-anomer formation may possibly be unattainable by nmr spectroscopy because of the benzyl aromatic proton signals, which are observed between δ 7.2—8.1.

The reaction was unexpectedly accompanied by a considerable coloration; however, the same treatment of the resultant mixture as has been described for the reaction of **3** with **4** afforded the sirups of $N_{(6)}$-benzyl-9-(**14a**)(20% yield) and -7-(2′,3′,5′-tri-*O*-acetyl-*β*-D-ribofuranosyl)adenine(**14b**)(9% yield). The NMR data of these products are summarized in Table 3; an examination of their anomeric proton region by means of the signal-to-noise enhancement (120 times) proved them to be composed of the *β*-nucleosides exclusively. Thus, these condensation reactions involving **4** were concluded to give the corresponding nucleosides with the anomeric configuration of *β*, although a more detailed investigation would be required to elucidate the mechanism of the glycosyl migration reaction.[9] **14a** was derived into **13c** by deacetylation with a methanolic sodium methoxide solution in a 93% yield; its structure was thus confirmed. The deacetylated product from **14b** was identified with that obtained from **13b** by thin-layer and paper chromatography and by studying the UV spectra.

In view of these results, the assumptions with respect to the activation mechanism of the purine counterparts,[1] described at the beginning of this article, can be said to be supported.

Experimental

All the melting points are uncorrected. The IR absorption spectra were taken with a Hitachi EPI-2S apparatus. The UV absorption spectra were measured on a Hitachi EPS-3T apparatus in purified ethanol or distilled water. The NMR spectra were determined with a Varian T-60 apparatus in deuteriochloroform, using tetramethylsilane as the internal standard. The plates for tlc examination were prepared with Wakogel B-5F, and the solvent system of 9 : 1 v/v benzene–methanol was used for the development. Paper chromatography was carried out using Toyo-Roshi No. 50 filter paper, while solvent system of 86 : 14 v/v *n*-butanol–distilled water was used for the development. The confirmation of each spot was done with a UV lamp (S. L. Light, Tokyo Machinery Co., Ltd.; 2537 and 3650 Å) or by spraying a diluted aqueous sulfuric acid solution on the tlc plates and then heating them.

Preparations of Molecular Compounds of $N_{(6)}$*-Benzoyladenine (**1**), $N_{(6)}$-Benzoyl-2-methylthioadenine(**2**), and $N_{(6)}$-Benzyladenine(**3**) with the Nitrophenols.* The method of preparation is exemplified by that of compound of **1** with picric acid(**9**): **1**(239 mg, 1 mmol) and **9**(687 mg, 3 mmol) were dissolved in chloroform(30—40 ml) under reflux, and the resultant solution was allowed to cool at room temperature for crystallization. After cooling overnight, the precipitated crystals were filtered by suction and dried over phosphorus pentoxide *in vacuo* at 110°C to give a molecular compound of **1** with **9**. The other molecular compounds were prepared in the same manner; all the results thus obtained are the summarized in Table 1.

The Condensation Reactions of $N_{(6)}$*-benzoyladenine(**1**) with 1-O-Acetyl-2,3,5-tri-O-benzoyl-β-D-ribofuranose (**4**) in the Presence of* m-*(6), p-Nitrophenol (**7**), or 2,4-Dinitrophenol (**8**).* *a)* The reaction with **6** : **1** (3.1 g, 13 mmol) and **6**(6.9 g, 50 mmol) were heated at 130—135 °C to fuse them homogeneously under stirring, and then **4**(5.0 g, 10 mmol)[10] was added to the prefused mixture. After the addition the mixture was stirred for 1.5 hr at that temperature under atmospheric pressure. The resultant mixture was dissolved in chloroform(300 ml), and the solution was successively washed with a 0.5 M aqueous sodium hydroxide solution to remove the co-produced acetic acid, unchanged **1**, and **6**, and with water, and then dried over anhydrous calcium chloride. After the desiccant had been removed by filtration, the organic layer was concentrated *in vacuo* to a pale brown glassy sirup. The resultant sirup was chromatographed on a silica gel column, packed with a ten-fold weight of Mallincrodt silicic acid(72 g) relative to the sirup, by the use of a solvent system of cyclohexane–chloroform(1 : 1 v/v) for the elution. *m*-Nitrophenyl benzoate (2.6 g, 81.5% yield;[11] recrystalized from ethanol, mp 92 °C[12]) was obtained as the first fraction, while glassy sirups of $N_{(6)}$-benzoyl-9-(2′,3′,5′-tri-*O*-benzoyl-*β*-D-birofuranosyl)adenine(**10a**) (0.12 g, 3.1% yield) and 9-(2′,3′,5′-tri-*O*-benzoyl-*β*-D-ribofuranosyl)adenine(**11a**) (2.9 g, 50.5% yield) were obtained as the second and third fractions.

8) M. Miyaki, Doctoral Thesis, Hokkaido Univ., 1968; B. Shimizu and M. Miyaki, *Chem. Pharm. Bull.* (Tokyo), **18**, 570 (1970); M. Miyaki and B. Shimizu, *Agr. Biol. Chem.*, **33**, 119 (1969).

9) This work is now in progress in our laboratory.

10) E. F. Recondo and H. Rinderknecht, *Helv. Chim. Acta*, **42**, 1171 (1959).

b) The reaction with **7**: To the prefused mixture prepared from **1**(13 mmol) and **7**(6.9 g, 50 mmol) at 130—135 °C, we added **4**(10 mmol); the resultant mixture was stirred at that temperature under atmospheric pressure for 3 hr. After it had been cooled at room temperature, the resultant mixture was dissolved in chloroform(300 ml); the solution was then treated and chromatographed in the way described in the previous experiment. A mixture of *p*-nitrophenyl benzoate (0.4 g, 12.6% yield,[11] mp 140 °C[13]) and *p*-nitrophenyl 2,3,5-tri-*O*-benzoyl-*β*-D-ribofuranoside [mp 124—125 °C, $[\alpha]_D^{20}$ −45° (*c* 1.0, $CHCl_3$). Found: C, 65.59; H, 4.22; N, 2.36%. Calcd for $C_{32}H_{25}O_{10}N$: C, 65.88; H, 4.32; N, 2.40%], which was easily fractionated by recrystallization from ethanol, was obtained as the first fraction. Glassy sirups of **10a** (0.15 g, 2.1% yield) and **11a** (1.2 g, 20% yield) were successively obtained as the second and third fractions respectively.

c) The reaction with **8**: To the prefused mixture prepared from **1** (13 mmol) and **8** (12 g, 65 mmol) at 140—145 °C, we added **4** (10 mmol); the resultant mixture was stirred at that temperature under atmospheric pressure for 3 hr. After cooling, the mixture was dissolved in chloroform (300 ml); the resultant solution was successively washed with an aqueous sodium bicarbonate solution and with water, and then dried over anhydrous calcium chloride. After the removal of the desiccant by filtration, the organic layer was concentrated *in vacuo* to a hard sirup. The residual sirup was subjected to chromatography as described in the previous experiments. Glassy sirups of **10a** (3.4 g, 59% yield) and **11a** (0.7 g, 12% yield) were obtained as the second and third fractions respectively. Prior to these fractions, the unchanged **4** (1.5 g) was recovered in a crystalline state. R_f values of **10a** and **11a** in tlc: 0.47 and 0.32 respectively.

*Structural Determination of **10a** and **11a** by Debenzoylation.*

a) **10a**: The glassy sirup of **10a** (679 mg, 1 mmol) was dissolved in absolute methanol (4 ml), and then a 1 M methanolic sodium methoxide solution (1 ml) was added to this solution. After the addition, the solution was stirred at room temperature for 1 hr and the solvent was evaporated to dryness. The residue was then dissolved in water (50 ml), the aqueous solution was washed with diethyl ether (50 ml × 2), and the aqueous layer was further treated with Amberlite IR-120B(NH_4 form)(1.5 equivalents to sodium ion), by batch. After the removal of the resin by filtration, the filtrate was concentrated *in vacuo* to about 1/4 volume of the original and the precipitated crystals were gathered by suctional filtration. The crystals were dissolved in a possibly smaller volume of water by warming, followed by decoloration with active charcoal, and then allowed to cool in a refrigerator. $N_{(6)}$-benzoyladenosine (139 mg, 35.4% yield) was obtained as fine needles. Mp 134—135 °C. $[\alpha]_D^{20}$ −30° (*c* 0.5, DMF). Found: C, 52.24; H, 4.97; N, 17.73%. Calcd for $C_{17}H_{17}O_5N_5 \cdot H_2O$: C, 52.44; H, 4.92; N, 17.99%. $\lambda_{max}^{pH\ 1}$ 292 nm(*ε* 23900), $\lambda_{min}^{pH\ 1}$ 263 nm(*ε* 9300); $\lambda_{max}^{pH\ 7}$ 281 nm (*ε* 23200), $\lambda_{min}^{pH\ 7}$ 245 nm(*ε* 11100); $\lambda_{max}^{pH\ 12}$ 303 nm(*ε* 25200), and $\lambda_{min}^{pH\ 12}$ 250 nm(*ε* 14300).[5] NMR(DMSO-d_6, DSS): *δ* 6.10 (H-1′ d, $J_{1',2'}$ =5.0 Hz).

Incidentally, a tlc examination of the above filtrate of recrystallization proved in to consist almost entirely of $N_{(6)}$-benzoyladenosine[R_f 0.55; developed with benzene-methanol (7 : 3 v/v)]; adenosine (R_f 0.32; developed with the same solvent) could be detected merely as a pale spot on the tlc.

b) **11a**: The glassy sirup of **11a** (575 mg, 1 mmol) was dissolved in absolute methanol(4 ml); the solution was mixed with a 1 M methanolic sodium methoxide solution (1 ml), and it was stirred at room temperature for 1 hr. The precipitated crystals were gathered by suctional filtration, washed with the absolute methanol (about 3 ml), and dried over phosphorus pentoxide at 110 °C *in vacuo* to give adenosine (224 mg, 84% yield) as fine needles. Mp 226.5—227 °C (natural product: mp 234—235 °C). $[\alpha]_D^{20}$ −61° (*c* 1.0, H_2O) [natural product: $[\alpha]_D$ −61.7° (H_2O)]. Found: C, 44.70; H, 4.91; N, 26.10%. Calcd for $C_{10}H_{13}O_4N_5$: C, 44.90; H, 4.90; N, 26.03%. UV: $\lambda_{max}^{pH\ 1}$ 257 nm(*ε* 15600), $\lambda_{min}^{pH\ 1}$ 230 nm(*ε* 6800); $\lambda_{max}^{pH\ 7}$ 258.5 nm(*ε* 15600), $\lambda_{min}^{pH\ 7}$ 226.5 nm (*ε* 3000); and $\lambda_{max}^{pH\ 12}$ 260 nm(*ε* 15700) [natural product: $\lambda_{max}^{pH\ 2}$ 257 nm(*ε* 14600), $\lambda_{min}^{pH\ 2}$ 230 nm(*ε* 3500); $\lambda_{max}^{pH\ 11}$ 260 nm (*ε* 14900), and $\lambda_{min}^{pH\ 11}$ 227 nm(*ε* 2250)].

*The Condensation Reactions of $N_{(6)}$-Benzoyl-2-methylthioadenine (**2**) with **4** in the Presence of **6**, **7**, or **8**.*

a) The Reaction with **6**: To a prefused mixture of **2** (3.7 g, 13 mmol) and **6** (10 g, 72 mmol) at 130—135 °C, we added **4** (5.0 g, 10 mmol) and the resultant mixture was stirred at that temperature for 3 hr. The mixture was then treated in the way described in the reactions of **1** with **4** to afford *m*-nitrophenyl benzoate [2.5 g, 78.5%;[11] mp 92 °C (lit,[12] mp 95 °C)], and the glassy sirups of $N_{(6)}$-benzoyl-2-methylthio-9-(2′,3′,5′-tri-*O*-benzoyl-*β*-D-ribofuranosyl)adenine(**10b**) (0.3 g, 3.7% yield) and 2-methylthio-9-(2′,3′,5′-tri-*O*-benzoyl-*β*-D-ribofuranosyl)adenine(**11b**) (2.8 g, 45.5% yield) as the first, second, and third fractions respectively. R_f values of **10b** and **11b** in tlc: 0.57 and 0.41 respectively.

b) The Reaction with **7**: The reaction was carried out by the use of **7** (10 g, 72 mmol) in place of **6** in the above reaction, and the resultant mixture was treated in the way described in *a*. The first fraction of the column chromatography afforded, after fractional recrystallization from ethanol, *p*-nitrophenyl benzoate (0.3 g, 9.5% yield) and *p*-nitrophenyl 2,3,5-tri-*O*-benzoyl-*β*-D-ribofuranoside (**12**)(2.5 g, 43% yield). Successively, the glassy sirups of **10b** (0.6 g, 8.2% yield) and **11b** (0.5 g, 7.3% yield) were afforded in turn.

c) The Reaction with **8**: To a prefused mixture of **2** (3.7 g, 13 mmol) and **8** (12 g, 65 mmol) at 140—145 °C, we added **4** (5.0 g, 10 mmol), after which the resultant mixture was stirred for 3 hr under atmospheric pressure. The resultant reaction mixture was treated in the way described in the reaction of **1** with **4** in the presence of **8**. By column chromatography, the glassy sirups of **10b** (3.3 g, 45.5% yield) and **11b** (0.6 g, 9.8% yield) were obtained as the second and third fractions, in addition to the first fraction, which was the unchanged **4**(1.8 g).

*Structural Determination of **10b** and **11b** by Debenzoylation.*

a) **10b**: A solution of **10b** (725 mg, 1 mmol) in absolute methanol(10 ml) was, after mixing with a 1 M methanolic sodium methoxide solution (1 ml), boiled under reflux for 1 hr. After cooling, the solvent was evaporated *in vacuo* to dryness, and the residue was triturated with a small amount of water to crystallize it. The resultant crystals were gathered by suctional filtration and then washed with a small amount of chloroform. The crystals were dried over phosphorous pentoxide at 110 °C *in vacuo* to give 2-methylthioadenosine (187 mg, 58% yield) as fine needles. Mp 215—217 °C, and remelted at 223.5—224.5 °C after resolidification. On admixture with an authentic specimen (mp 222—223 °C[14]), no depression was observed. $[\alpha]_D^{20}$ −1° (*c* 1.0, 0.1 M HCl-H_2O) [$[\alpha]_D^{18}$ −2° (*c* 0.51, 0.1 M HCl-H_2O)[14]].

b) **11b**: A solution of **11b**(621 mg, 1 mmol) in absolute methanol(6 ml) was, after mixing with a 1 M methanolic sodium methoxide solution(1 ml), stirred at room temperature for 2 hr. The precipitated crystals were gathered by suctional filtration, washed with absolute methanol (3 ml), and then

11) This yield was calculated based on the $N_{(6)}$-benzoyladenine.
12) G. Neumann, *Ber.*, **19**, 2979 (1886).
13) G. Neumann, *ibid.*, **19**, 2019 (1886).

dried over phosphorus pentoxide at 110 °C *in vacuo*. 2-Methylthioadenosine (271 mg, 86.5%) was thus obtained as fine needles. Mp 215—217 °C, and remelted at 223.5—224 °C after resolidification. On admixture with an authentic specimen (mp 222—223 °C[14]), no depression was observed. $[\alpha]_D^{20}$ −2° (*c* 1.0, 0.1 M HCl-H_2O) {$[\alpha]_D^{18}$ −2° (*c* 0.51, 0.1 M HCl-H_2O)[14]}.

The Condensation Reaction of $N_{(6)}$*-Benzyladenine (**3**) with **4** in the Presence of **8***. *a*) Preparation of $N_{(6)}$-benzyladenosine(**13c**): To a homogeneously-prefused mixture of **3** (3.0 g, 13 mmol) and **8** (12 g, 65 mmol), we added **4**(5.0 g, 10 mmol), after which the resultant mixture was stirred at 140—145 °C for 3 hr under atmospheric pressure. A solution of the mixture in chloroform (300 ml), after the removal of **8** by washing with an aqueous sodium bicarbonate solution and with water, and after drying over anhydrous calcium chloride, was concentrated *in vacuo*. The residual sirup showed a considerable coloration, although its tlc proved it to be pure (R_f 0.84). It was thus subjected to purification on a short column of silica gel by elution with chloroform. The fraction corresponding to $N_{(6)}$-benzyl-9-(2′,3′,5′-tri-*O*-benzoyl-β-D-ribofuranosyl)adenine(**13a**) was concentrated *in vacuo* to a hard, glassy sirup (6.3 g, 94.4% yield). The sirup was dissolved in absolute methanol (50 ml), and the resultant solution was, after having been with a 1 M methanolic sodium methoxide solution(5 ml), stirred at room temperature for 2 hr. The crystals thus precipitated were gathered by suctional filtration, washed with the absolute methanol(total 5 ml), and dried over phosphorus pentoxide 110 °C *in vacuo* to give **13c** (3.0 g, 90% yield). Mp 165—166 °C(lit,[15] mp 177—179 °C). $[\alpha]_D^{30}$ −68° (*c* 1.0, EtOH) {lit,[15] −68.6°(*c* 0.55, EtOH)}. Found: C, 57.16; H, 5.01; N, 19.92%. Calcd for $C_{17}H_{18}O_4N_5$: C, 57.13; H, 5.36; N, 19.60%. UV: $\lambda_{max}^{pH\ 1}$ 265 nm(ε 19200), $\lambda_{min}^{pH\ 1}$ 234 nm (ε 4050); $\lambda_{max}^{pH\ 7}$ 268 nm(ε 20000), $\lambda_{min}^{pH\ 7}$ 232 nm(ε 2740); $\lambda_{max}^{pH\ 12}$ 270 nm(ε 20100), and $\lambda_{min}^{pH\ 12}$ 233 nm(ε 3100) {lit,[15] λ_{max}^{acid} 266 nm (ε 20600), λ_{min}^{acid} 235 nm (ε 4140); $\lambda_{max}^{neutral}$ 268 nm(ε 20850), $\lambda_{min}^{neutral}$ 233 nm(ε 2570); λ_{max}^{base} 269 nm(ε 21300), and λ_{min}^{base} 237 nm(ε 3570)}.

b) Chromatographic Separation of **13a** and $N_{(6)}$-Benzyl-7-(2′,3′,5′-tri-*O*-benzoyl-β-D-ribofuranosyl) adenine (**13b**): The reaction described in *a* was stopped after 90 min, after which the mixture was treated in the same way as in *a*. The sirup obtained by removing **8** was chromatographed in the same way. This chromatography was successfully carried out by the use of either 9 : 1 v/v benzene-methanol or chloroform for the elution. The concentration of the fraction corresponding to the faster-moving spot (R_f 0.84) afforded a glassy sirup of **13a**(2.9 g, 43% yield), while that of the fraction corresponding to the slower-moving spot (R_f 0.70) afforded a glassy sirup of $N_{(6)}$-benzyl-7-(2′,3′,5′-tri-*O*-benzoyl-β-D-ribofuranosyl)adenine(**13b**)(0.6 g, 9% yield). The former was easily identified by deriving it into **13c** by debenzoylation. A small portion of the latter sirup was crystallized on trituration with a small amount of acetone; the crystals were, after filtration, recrystallized from ethanol and then dried over phosphorus pentoxide at 110 °C *in vacuo*. Mp 169—170 °C. $[\alpha]_D^{30}$ −65° (*c* 1.04, $CHCl_3$). Found: C, 68.16; H, 4.80; N, 10.76%. Calcd for $C_{38}H_{31}O_7N_5$: C, 68.15; H, 4.67; N, 10.46%. UV: λ_{max}^{EtOH} 300 nm(ε 9290), and $\lambda_{shoulder}^{EtOH}$ 285 nm(ε 8300) and 277 nm(ε 7300).

The latter sirup(200 mg) was dissolved in absolute methanol (4 ml), and the solution was, after having been mixed with a 1 M methanolic sodium methoxide solution(0.5 ml), stirred for 2 hr at room temperature. After the evaporation of the solvent *in vacuo* to dryness, the residue was dissolved in water(15 ml) and the solution was washed with diethyl ether (5 ml×3). The aqueous layer was, after neutralization with acetic acid, subjected to paper chromatography; the R_f value of this nucleoside was found to be 0.76 at 25 °C (*cf.* **13c**: 0.70). Subsequently, the UV spectrum of the spot was determined by extraction with ethanol, which had previously been distilled after treatment with sodium hydroxide under reflux: λ_{max}^{EtOH} 284 nm and 213 nm, and λ_{min}^{EtOH} 240 nm. Furthermore, the aqueous solution was, after acidification with acetic acid, stirred under a hydrogen atmosphere in the presence of 10%-palladized charcoal (30 mg) for 30 hr as usual. After the filtration of the catalyst, which was washed with water(5 ml×3), the filtrate and washings were combined and neutralized with a diluted aqueous sodium hydroxide solution. It was then concentrated *in vacuo* to several milliliters. The newly-appeared spot ($R_f^{25°C}$ 0.23) in the paper chromatography was extracted with pH 1, pH 7, and pH 12 water, and the UV spectrum of each extract was determined; $\lambda_{max}^{pH\ 1}$ 272 nm, $\lambda_{min}^{pH\ 1}$ 252 nm; $\lambda_{max}^{pH\ 7}$ 270 nm, $\lambda_{min}^{pH\ 7}$ 248 nm; $\lambda_{max}^{pH\ 12}$ 270 nm, and $\lambda_{min}^{pH\ 12}$ 249 nm {lit,[7] $\lambda_{max}^{0.1M\ HCl}$ 272 nm(ε 13600) and $\lambda_{max}^{0.1M\ NaOH}$ 270 nm(ε 9800); 7-β-D-ribofuranosyladenine}.

c) *The Condensation Reaction of **3** with 1,2,3,5-Tetra-O-acetyl-β-D-ribofuranose in **8***: To a homogeneously-prefused mixture of **3** (3.0 g, 13 mmol) and **8** (12 g, 65 mmol), we added 1,2,3,5-tetra-*O*-acetyl-β-D-ribofuranose (3.2 g, 10 mmol), and the resultant mixture was stirred at 140—145 °C for 1 hr; a considerable coloration was thus observed. After cooling, mixture was treated and chromatographed in the way described in *a*. 1,2,3,5-Tetra-*O*-acetyl-β-D-ribofuranose (1.6 g) was recovered as the first fraction. The glassy sirups of the acetates corresponding to **14a** (1.0 g, 21% yield) and **14b** (0.4 g, 8% yield) were obtained in turn as the second and third fractions. The NMR spectral data of these products are summarized in Table 3; in addition, no anomeric proton signals corresponding to their α-anomer could be detected on the enhancement of the signal-to-niose ratio by time-averaging (120 times). All the former sirup was subjected to deacetylation by stirring in absolute ethanol(4 ml)-1 M methanolic sodium methoxide solution(0.5 ml) at room temperature; white crystals began to precipitate within several minutes. They were, after 30 min, filtered, washed with absolute methanol(3 ml), and then dried over phosphorus pentoxide at 110 °C *in vacuo* to give **13c** (0.3 g, 84% yield). Mp 165—166 °C. No depression was observed on admixture with the authentic sample obtained in the previous experiment. Its UV spectral data were also consistent with the sample; $\lambda_{max}^{pH\ 7}$ 268 nm(ε 19000) and $\lambda_{min}^{pH\ 7}$ 231 nm(ε 2300). An attempt at the crystallization of the latter sirup resulted in failure; it was then subjected to deacetylation in the above way. After the evaporation of the solvent *in vacuo* to dryness, the residue was dissolved in water (*ca.* 5 ml), and washed with diethyl ether(5 ml×2). The UV spectrum of the resultant aqueous layer was determined, extracting the spot of the paper chromatogram (R_f 0.76); λ_{max}^{EtOH} 284 nm and 213 nm, and λ_{min}^{EtOH} 240 nm.

The authors are grateful to the Ministry of Education, Japanese Government, for a Scientific Research Grant-in-aid, and to the Kurata Foundation for a grant. They also wish to thank to the members of Laboratory of Organic Elemental Analysis, for the elemental analysis of the samples.

14) Y. Ishido, Y. Kikuchi, and T. Sato, *Nippon Kagaku Zasshi*, **86**, 240 (1965).

15) H. M. Kissman and M. J. Weiss, *J. Org. Chem.*, **21**, 1053 (1956).

Effect of Pressure on the Rate of Solvolysis. Formolysis and Methanolysis of Secondary Alkyl Tosylates[1]

Akira SERA, Chisako YAMAGAMI, and Kazuhiro MARUYAMA

Department of Chemistry, Faculty of Science, Kyoto University, Sakyo-ku, Kyoto 606

(Received June 16, 1973)

The effect of pressure on the formolysis and methanolysis rates of representative secondary alkyl tosylates was investigated, and the activation volumes, $\Delta V_0^{\ddagger}$, were estimated. The values of activation volume for formolysis were found to correlate excellently with σ^*. This conformity of $\Delta V_0^{\ddagger}$ to the Hammett-type correlation is interpreted as a consequence of the k_c-character of the reaction. The values of activation volume for methanolysis, however, converged to more negative values. The k_s-character of methanolysis is thought to be responsible for this behavior. The k_c-k_s-hybrid nature of the reaction is also discussed.

Solvolyses with tertiary substrates cannot be interpreted as direct displacement reactions, but many experimental results are consistent with the ionization hypothesis (**Lim**[2]), whereas primary substrates generally react by the direct displacement mechanism (**N**[2]). Since these two representations are intended to be extremes of a continuous sequence with no sharp dividing line, it is usual to refer to an intermediate set of borderline case for most of solvolyses of secondary substrates. Recently, the important participation of solvent molecule in solvolysis has come to be recognized even for secondary alkyl substrates. Schleyer[3] has interpreted the solvent assistance in the solvolysis of secondary alkyl substrates in terms of "a basic difference with respect to the magnitude of nucleophilic solvent participation: large in ordinary unhindered secondary (and primary) systems and small or absent in crowded substrates such as 2-adamantyl and tertiary derivatives."

Investigations of solvolytic displacement reactions under high pressure yield the activation volumes of the reactions, $\Delta V^{\ddagger}$, which will reflect the difference in degree of solvation between highly dipolar transition states and neutral initial states.[4] It may then be anticipated that the application of a high-pressure technique to the systematic study of solvolytic displacement reactions will permit us to analyse the reaction mechanism in terms of the activation volume. However, in previous reports on this subject, attention has been concentrated on the effect of the change in solvent composition on the activation volumes for solvolyses in aqueous binary solvent mixtures.[5] So far as we know, there have been only a few investigations in which the volume parameters were examined in terms of the substrate structure under otherwise identical conditions.[6] Moreover, no information is available about values of activation volume for solvolyses in polar solvents of low nucleophilicity.

The present paper will concern the investigation of the pressure effect on the solvolysis rates of representative secondary alkyl tosylates in two solvents—formic acid and methanol. Although a part of the desired rate data at atmospheric pressure can be gathered from the literature,[7] they were re-investigated in order to make an accurate estimate of $\Delta V_0^{\ddagger}$, the activation volume at atmospheric pressure.

Results and Discussion

The first-order rate constants for the formolysis and methanolysis of secondary alkyl tosylates under pressure are given in Table 1. All the measurements were carried out at 25.0 °C in order to avoid complicated corrections due to the temperature dependence of the reaction rate under pressure. The values of the activation volume at atmospheric pressure were determined by means of the following equation:

$$\Delta V^{\ddagger} = -RT(\partial \ln k/\partial P)_T \qquad (1)$$

where $\Delta V^{\ddagger}$ is the difference in the partial molal volumes between the transition state and the initial state. The evaluation of $\Delta V_0^{\ddagger}$ was made by the least-squares fit of the data to the following linear expression for $\ln k$ in the range from 1 to 700 kg/cm^2, because the plots of $\ln k$ against pressure were linear at least up to this pressure for most of the reactions examined:[8]

$$\ln k = a + bP \qquad (2)$$

The values of $\Delta V_0^{\ddagger}$ are listed in Table 2. The rate of each compound relative to the reference compound, isopropyl tosylate, is also shown.

Reaction Mechanism. As is shown in Table 1, the formolysis rate increased monotonously as the substituent became more electron-donating. The rate increase in formic acid was more significant than that in

1) Organic Reaction under High Pressure XI. Part X, see A. Sera, T. Miyazawa, T. Matsuda, Y. Togawa, and K. Maruyama, This Bulletin, **46**, 3490 (1973).

2) S. Winstein, E. Grunwald, and H. W. Jones, *J. Amer. Chem. Soc.*, **73**, 2700 (1951).

3) a) J. L. Fry, C. J. Lancelot, L. K. M. Lam, J. M. Harris, R. C. Bingham, D. J. Raber, R. E. Hall, and P. von R. Schleyer, *ibid.*, **92**, 2538 (1970); b) J. L. Fry, J. M. Harris, R. C. Bingham, and P. von R. Schleyer, *ibid.*, **92**, 2540 (1970); c) P. von R. Schleyer, J. L. Fry, L. K. M. Lam, and C. J. Lancelot, *ibid.*, **92**, 2542 (1970); d) S. H. Liggero *et al.*, *ibid.*, **92**. 3789 (1970).

4) W. J. le Nobel, "Progress in Physical Organic Chemistry", Vol. 5, ed. by A. Streitwieser, Jr. and R. W. Taft, Jr., Interscience Publisher, New York (1967) p 207.

5) J. B. Hyne and coworkers, *Can. J. Chem.*, **48**, 2025, 2494 (1970); **49**, 2394 (1971); *J. Amer. Chem. Soc.*, **88**, 2104 (1966). B. T. Baliga and E. Whalley, *Can. J. Chem.*, **48**, 528 (1970), and references cited therein.

6) a) W. J. le Noble, B. L. Yates, and A. W. Scaplehorn, *J. Amer. Chem. Soc.*, **89**, 3751 (1967); b) W. J. le Noble and A. Shurpik, *J. Org. Chem.*, **35**, 3588 (1970); c) B. T. Baliga and E. Whalley, *J. Phys. Chem.*, **73**, 654 (1969); d) K. J. Laidler and R. Martin, *Int. J. Chem. Kinet.*, **1**, 113 (1969); e) C. Yamagami and A. Sera, *Chem. Lett.*, **1972**, 741; f) A. Sera, T. Miyazawa, T. Matsuda, Y. Togawa, and K. Maruyama, This Bulletin, **46**, 3490 (1973).

7) P. E. Peterson, R. E. Kelley, Jr., R. Belloli and K. A. Sipp, *J. Amer. Chem. Soc.*, **87**, 5169 (1965).

Table 1. Solvolysis rate constants of secondary alkyl tosylates, R_1-CH(OTs)-R_2, under pressure at 25.0 °C

	Substrate		Pressure (kg/cm²)					
	R_1	R_2	1	100	300	500	700	1000
			Formolysis $10^5 k$ (s^{-1} a))					
(1)	Me	Me	2.47	—	2.97	3.34	3.71	4.27
(2)	Me	Et	6.04	—	7.07	7.69	8.69	—
(3)	Et	Et	13.1	—	15.2	16.1	18.1	—
(4)	Me	*iso*-Pr	32.5	34.0	37.3	41.4	45.1	—
(5)	Me	*t*-Bu	31.8	—	35.6	39.2	42.4	—
			Methanolysis $10^6 k$ (s^{-1} a))					
(1)	Me	Me	1.27	—	1.60	1.83	2.14	2.58
(2)	Me	Et	1.61	—	2.06	2.38	2.75	3.27
(3)	Et	Et	2.73	—	3.50	3.92	4.68	5.44
(4)	Me	*iso*-Pr	0.980	—	1.25	1.44	1.62	1.92
(6)	*iso*-Pr	*iso*-Pr	2.51	2.70	3.05	3.42	3.84	—
(7)	*iso*-Pr	*t*-Bu	0.850	0.966	1.09	1.23	1.37	—
(8)	*t*-Bu	*t*-Bu	7.52	8.45	9.52	10.8	12.2	13.7
(9)	*t*-Bu	$C(Et)_3$	109	117	132	147	163	—

a) Average of two or more experiments. Estimated error was less than 2% of its value.

methanol. An attempt to measure accurately the rate for the formolysis of (6) was unsuccessful because of its high reactivity under the conditions employed.[9] The correlation between log k at atmospheric pressure and σ^*_{add}[10] showed a good linearity with ρ^* of -3.7,[11] which is in good accord with the ρ^I value of -7.79 reported by Peterson *et al.* for the formolysis of unbranched alkyl tosylates.[7] In addition, the observed formolysis rates under pressure were also correlated to σ^*_{add} to give good straight lines.

Formic acid is considered to be a solvent in which a k_c-process proceeds quite readily because of its powerful ionizing ability as well as its poor nucleophilicity. Hence, the present reaction is thought to be k_c-like[12] in character. Moreover, the observed linear Hammett-Taft correlation indicates that the reaction is mainly controlled by the inductive effect of substituents, even in the case of 1-*t*-butylethyl tosylate (5), a sterically crowded substrate. On the other hand, the methanolysis rates varied irregularly along with the series of substrates. Although the high nucleophilic nature of this solvent facilitates a k_s-process,[13] this irregularity could not be interpreted as a manifestation of any single mechanism or as the predominance of one controlling factor over the whole range of substrates examined. This phenomenon must be a consequence of a change in the solvolysis mechanism from a k_s- to a k_c-process. In the absence of any appreciable steric hindrance in the transition state (for (1)∼(3)), the reaction must be strongly assisted by a solvent molecule (k_s-character). The contribution of k_s-process to the over-all rate process should, however, become less important with an increase in the steric hindrance. This causes an apparent rate retardation. This is the case for (4)—(7), as is shown in Table 1.[14] Remarkable rate increases were observed for (8) and (9). This means that the presence of extremely bulky substituents causes the substrates to be solvolyzed no longer through a k_s-process, but through a k_c-process predominantly. Actually, di-*t*-butylmethyl tosylate (8) has been reported to have no tendency to undergo k_s-solvolysis.[3d] A comparison of the (8)/(1) rate ratio in the two solvents is worth noting; it is 320 in formic acid and 6 in methanol. These figures suggest the intervention of solvent assistance in the methanolysis of an unhindered substrate(1).[3d]

All the points discussed above demonstrate that the formolysis exhibits a more k_c-character than does the methanolysis, and that in the methanolysis the mechanistic shift from the k_s- to the k_c-process actually

8) In the case of compounds (7)∼(9), the plots of ln k against pressure exhibit good straight lines except points at atmospheric pressure, which deviated downwards by about 3%. This phenomenon, not regarded as a result of experimental uncertainty, may imply existence of any factors which would be depressed by application of external pressure. In these cases, we estimated $\Delta V_0^{\neq}$ regardless of the points at atmospheric pressure.

9) A rough estimation showed that the formolysis rate constants amount to 9.6×10^{-4} s^{-1} for (6) and 1.2×10^{-2} s^{-1} for (8)[3d] at 25 °C.

10) $\sigma^*_{add}=\sigma^*_{R_2}+\sigma^*_{R_1}$. R. W. Taft, Jr., "Steric Effects in Organic Chemistry", ed. by M. S. Newman, John Wiley & Sons, Inc., New York (1956), p. 556.

11) Not including compound (4). Formolysis of this tosylate is 2.5 times as fast as that expected from the $\rho^*-\sigma^*$ relation. A compound with similar structural feature, 1-isopropylbutyl *p*-toluenesulfonate was reported to exhibit an analogous abnormal behavior in acetolysis, W. Pritzkow and K. H. Schöppler, *Chem. Ber.*, **95**, 834 (1962).

12) The definition of these terms, k_c-, k_s-, and k_Δ-processes of solvolyses, was made by Winstein (S. Winstein, E. Allred, R. Heck, R. Glick, *Tetrahedron*, **3**, 1 (1957). In the present paper, however, the term "k_c-process" signifies non-k_s-process, and hence can include k_Δ-process in some cases. Distinction between k_c- and k_Δ-processes is out of the purpose of the present investigation.

13) a) E. Grunwald and S. Winstein, *J. Amer. Chem. Soc.*, **70**, 846 (1948). For quantitative treatments of solvent nucleophilicity, see b) P. E. Peterson and F. J. Waller, *ibid.*, **94**, 991(1972); c) T. W. Bentley, F. L. Schadt, and P. von R. Schleyer, *ibid.*, **94**, 992 (1972), and references cited therein.

14) The rate for (5) was too slow to be measured.

TABLE 2. ACTIVATION VOLUMES AND RELATIVE RATES FOR SOLVOLYSES OF SECONDARY ALKYL TOSYLATES, R_1-CH(OTs)-R_2

	Substrate R_1	Substrate R_2	$\Delta V_0^{\neq}$[a,b] (cm³/mol)	Rel. rate[a]	$\Delta V_0^{\neq}$[a,b] (cm³/mol)	Rel. rate[a]
			Formolysis		Methanolysis	
(1)	Me	Me	−14.7	1	−18.9	1
(2)	Me	Et	−12.9	2.4	−19.4	1.3
(3)	Et	Et	−11.2	5.3	−18.4	2.1
(4)	Me	*iso*-Pr	−11.7	13	−18.3	0.78
(5)	Me	*t*-Bu	−10.5	13	—	—
(6)	*iso*-Pr	*iso*-Pr	—	39[c]	−15.2	2.0
(7)	*iso*-Pr	*t*-Bu	—	—	−15.4[e]	0.67
(8)	*t*-Bu	*t*-Bu	—	320[d]	−15.6[e]	5.9
(9)	*t*-Bu	$C(Et)_3$	—	—	−13.9[e]	86

a) At 25.0 °C at atmospheric pressure. b) Accurate to within 1 cm³/mol. c) See footnote 9. d) Ref. 3d. e) See footnote 8.

TABLE 3. SOLVENT PARTICIPATION PARAMETERS FOR SECONDARY ALKYL TOSYLATES (25 °C)

Substrate	Q[a]	m[b]	$m_{(AcOH-HCOOH)}$[c]	$(k_s/k_c)_{HCOOH}$[d]
(1)	0.56	0.36	0.646	30
(2)	0.64	0.47	—	15
(3)	0.69	0.54	—	5
(5)	—	—	0.832	3

a) Defined by Schleyer (the lower the Q value the more sterically accessible the substrate is to nucleophilic attack). See Ref. 13c. b) Ref. 13c. c) Brosylates. S. Winstein, and H. Marshall, *J. Amer. Chem. Soc.*, **74**, 1120 (1952). d) Calculated according to the procedure proposed by Schleyer, see Ref. 3. The rate constant for trifluoroacetolysis of (5) was estimated to be 3×10^{-3} s^{-1} with the aid of $\rho^I-\sigma^I$ plot given by Peterson, see Ref. 7. A revised trifluoroacetolysis rate constant for 2-adamantyl *p*-toluenesulfonate is taken from J. E. Nordlander, R. G. Gruetzmacher, and F. Miller, *Tetrahedron Lett.*, **1973**, 927.

operates. The contribution of the k_s-character, if any, in the formolysis of some secondary substrates will be discussed later.

Activation Volume. All the activation volumes presented in Table 2 are negative. Negative values of $\Delta V^{\neq}$ have long been observed for solvolytic reactions and other unimolecular ionization processes. This phenomenon has been interpreted in terms of the presence of a predominant electrostrictive volume contraction (the $\Delta_2V^{\neq}$ term in the definition of Evans and Polanyi[15]) in the transition state which is undoubtedly more polar than the initial state.[4] In such circumstances, the change in $\Delta_1V^{\neq}$ (the contribution of a volume increase due to bond extension[15]) caused by variation in the substituents appears to play only a minor role. That is, the apparent values of $\Delta V^{\neq}$ must be governed by the change in $\Delta_2V^{\neq}$. Accordingly, the comparison of the values of $\Delta V^{\neq}$ for structurally-related substrates in a given solvent can be anticipated to provide useful information about the transition states.

The results shown in Table 2 clearly indicate the solvent dependence of the activation volumes. Since the $\Delta_1V^{\neq}$ term is insensitive to the solvent change,[16a] the different behavior of $\Delta V_0^{\neq}$ in the two solvents may be thought to be a reflection of a difference in the electrostrictive effect. In general, the magnitude of this electrostrictive term for solvolytic reaction depends on the degree of charge dispersion in the transition state; when the developed charge is dispersed more extensively over the whole molecule, the electrostrictive volume contraction becomes less significant, and hence a less negative value of $\Delta V^{\neq}$ appears.[6a,d-f] This concept should be verified in such a reaction as a limiting solvolysis. The application of this concept to the Hammett equation should reveal a correlation between $\Delta V^{\neq}$ and σ with a negative slope;[16b] this was really demonstrated in our laboratory for the limiting hydrolysis of 1-aryl-1-methylethyl chlorides.[6f] The formolysis of the present substrates conforms to this generalization. The activation volume for formolysis given in Table 2 actually shows a good linear correlation with respect to σ^*_{add},[17] as is shown in Fig. 1.

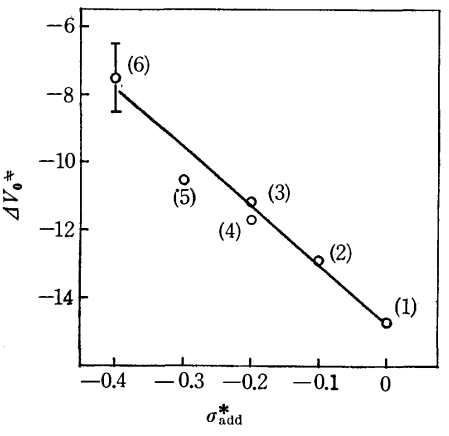

Fig. 1. Plot of $\Delta V_0^{\neq}$ against σ^*_{add} for the formolysis of secondary alkyl tosylates. Numeral denotes substrate number in Table 2; for (6) see footnote 17.

15) M. G. Evans and M. Polanyi, *Trans. Faraday Soc.*, **31**, 875 (1935).

16) a) K. R. Brower, *J. Amer. Chem. Soc.*, **85**, 1401 (1963). b) For the linear correlation of $\Delta V^{\neq}$ with respect to σ, $-\delta\Delta V^{\neq}=2.303RT\sigma(\delta\rho/\delta P)_T$, see A. J. Ellis, W. S. Fyfe, R. I. Rutherford, A. Fischer, and J. Vaughan, *J. Chem. Phys.*, **31**, 176 (1959).

In contrast, the methanolysis of sterically-unhindered substrates afforded rather negative and leveled values of $\Delta V_0^{\neq}$, about -19 cm^3/mol. These results can best be understood if we assume that the transition state species are strongly solvated to nearly the same extent, regardless of their substituents. This is a result of the k_s-character of the reaction, in which the developed charge is mainly located on the reaction center. The mechanistic transformation from the k_s- to the k_c-process is seen to increase $\Delta V_0^{\neq}$ by 3~4 cm^3/mol (see Table 2). An incipient carbonium ion, screened from nucleophilic solvation, must be stabilized electronically by substituents within the molecule. Consequently, two factors [(a) the decrease in electrostatic interaction due to charge dispersion, and (b) the diminution of the k_s-character, that is, the disappearence of tight nucleophilic solvation to the transition state species] make the $\Delta V_0^{\neq}$ for k_c-process less negative. It will be worthwhile to examine whether the $\Delta V_0^{\neq}$ of k_c-type substrates correlates with σ^*_{add} in methanolysis as well as in formolysis. Unfortunately, the correlation under consideration was obscure because of the presence of steric factors that would more or less affect the volume of the molecule.

The observation of more negative activation volumes for k_s-processes than those for k_c-processes appears to be general in the solvolyses of neutral substrates, although Hyne[18] expected that "the $\Delta V^{\neq}$ associated with the more ion-like transition state of an S_N1 mechanism would be more negative than in the case of an S_N2 mechanism." Baliga and Whalley[6c] have studied the hydrolyses of methyl and isopropyl bromides in water at 60 °C and reported the $\Delta V_0^{\neq}$ values as -17 cm^3/mol for the former and -10 cm^3/mol for the latter. There is no doubt that the former has a more k_s-character. Further evidence is given by our finding of -6.9 cm^3/mol as the value for the formolysis of a typical k_c-type secondary alkyl substrate, 2-adamantyl *p*-toluenesulfonate.[19]

Although it might be true that a solvolysis in formic acid is more k_c-like in character than in methanol, the contribution of solvent assistance can not be ignored in the case of a secondary system characterized by "borderline case" behavior.[20] For example, isopropyl tosylate has been reported to be solvolyzed with considerable nucleophilic assistance, even in formic acid.[3c] Helpful data to estimate provisionally the degree of k_s-contribution to over-all reaction are summarized in Table 3. Among the substrates presently examined, the k_s-character is greatest in (1); it then decreases successively from (1) to (5). According to this trend, the activation volume of a substrate possessing a more k_s-character will become somewhat more negative even in a k_c-like solvent. Hence, in the formolysis of substrates of the k_c-k_s hybrid character, the substituent effect on the activation volume must be considered to depend on two factors: a) the charge dispersion in the transition state, and b) the degree of its k_s-character. An analogous discussion was made by Laidler and Martin[6d] for the hydrolysis of benzyl chlorides.

On the other hand, in nearly pure k_c-processes the activation volumes should depend essentially on the degree of charge dispersion in the transition states, while in nearly pure k_s-processes some leveling effect on the activation volumes should be observed. In view of this, in the absence of steric factors, the transition states of secondary alkyl tosylates in methanolysis may be thought to be highly solvated, as in the case of primary substrates.

In order to get a more comprehensive understanding, measurements of partial molal volumes of the substrates will be required. Investigations in this direction are now in progress.

Experimental

Solvents. Formic acid (98—100%) was dried over anhydrous cupric sulfate and distilled *in vacuo*. The purified formic acid was stored frozen to avoid decomposition. Methanol was dried over activated magnesium and then distilled.

Materials. The desired alcohols were prepared as have been described in the literature. 1-*t*-Butylethyl tosylate (8) and 1-*t*-butyl-2,2-diethylbutyl tosylate(9) were prepared from the corresponding alcohols by the alkyl lithium method (*n*-BuLi was used).[21] All the other tosylates were prepared by the usual pyridine–*p*-toluenesulfonyl chloride method. The purity of each material was found by NMR analysis to be satisfactory.

Rate Measurement. The high-pressure apparatus and tecnique have already been described.[6f] The rate of production of *p*-toluenesulfonic acid was followed by a conductometric method. For fast reactions having half-lives of less than 1 hr, the medium in the high-pressure vessel was pre-chilled at 20 °C. In this case, the thermal equilibrium in the vessel was settled in about 15 min after pressurizing.

Formolysis. About a 0.019 mol/l solution was employed in each case. The first reading of conductance was taken after at least a 10% progress of the reaction because of a failure in the linear conductance-concentration relationship in this region. The rate constant was determined by the Guggenheim method[22] for (1) and by usual first-order rate expression for the others, using the least-squares method.

Methanolysis. A 0.003 mol/l solution of a tosylate (150—200 ml) was divided into 15-ml portions and stored in a refrigerator below 0 °C. Each aliquot was used for a single kinetic run. The rate constant was determined by the usual first-order rate expression, using the least-squares method. For an infinite conductance, the theoretical value of conductance was employed.

17) A rough estimation gave $\Delta V_0^{\neq} > -10$ cm^3/mol for (6) in accord with the present view.

18) A. B. Lateef and J. B. Hyne, *Can. J. Chem.*, **47**, 1370 (1969).

19) Unpublished result.

20) It is of interest to compare the ρ^I values given by Peterson *et al.*[7] for folmolysis ($\rho^I = -7.79$) and trifluoroacetolysis ($\rho^I = -15.7$) of secondary alkyl tosylates. The smaller absolute value for the former seems to suggest the presence of some solvent assistance in formic acid.

21) H. C. Brown, R. Bernheimer, C. J. Kim, and S. E. Scheppele, *J. Amer. Chem. Soc.*, **89**, 370 (1967).

22) E. A. Guggenheim, *Phil. Mag.*, **2**, 538 (1926).

Photochemical Reduction of Thiobenzophenone. Reduction by Dihydroaromatic and Related Compounds

Yutaka Ohnishi and Atsuyoshi Ohno

Sagami Chemical Research Center, 4-4-1, *Nishiohnuma, Sagamihara-shi, Kanagawa 229*

(Received June 19, 1973)

Photochemical reduction of thiobenzophenone by 1,4-dihydrobenzene, 1,4-dihydronaphthalene, 9,10-dihydroanthracene, 1,3,5-cycloheptatriene, and acridane was studied. Relative reactivities and product analyses have revealed that the reaction is initiated by hydrogen-abstraction (one-electron-transfer followed by a proton migration) with thiobenzophenone in the n,π^* triplet state. Inability of diphenylmethane to undergo the reaction can be interpreted by means of this mechanism.

Thiobenzophenone in the n,π^* triplet state is reduced to diphenylmethanethiol (**1**) by primary and secondary aliphatic alcohols or thiols, whereas it is necessary to excite thiobenzophenone to the π,π^* singlet state in order to reduce it by hydrocarbons such as cyclohexane and diphenylmethane.[1]

$$Ph_2C{=}S \xrightarrow{589\ nm} \longrightarrow {}^3(Ph_2C{=}S)_{n,\pi^*}$$

$$^3(Ph_2C{=}S)_{n,\pi^*} + R_2CHXH \rightarrow Ph_2CHSH + R_2C{=}X$$

(X=O or S; R=H, alkyl, or aralkyl)

The low reactivity of diphenylmethane is anomalous, since the benzenethiyl radical can abstract a hydrogen from this hydrocarbon[2] and thiobenzophenone in the n,π^* triplet state is known to behave like a thiyl radical.[3] In order to obtain further information on the reactivity of photo-excited thiobenzophenone, we studied the reactions of thiobenzophenone with various dihydroaromatic hydrocarbons and some related compounds. The results are given in this paper together with a discussion on the mechanism of the reaction.

Results and Discussion

Although the reaction of thiobenzophenone with 1,4-dihydrobenzene (**2**) does not proceed thermally, photochemical reaction takes place under the influence of light from low-pressure sodium lamps (589 nm). Thiobenzophenone in the n,π^* triplet state abstracts hydrogens from **2** yielding **1** and benzene quantitatively. A similar but slower reaction takes place with 1,4-dihydronaphthalene (**3**) giving **1** and naphthalene in 43 and 91% yields, respectively. An even slower reaction proceeds with 9,10-dihydroanthracene (**4**) giving a mixture of complex composition of products including anthracene (26%), dibenzhydryl disulfide (24%), and **1** (17%). A similar trend of reactivity has been reported for reactions of these compounds with quinones.[4]

There is a distinct difference between dihydroaromatic hydrocarbons and diphenylmethane: the free radical produced from **2**, **3**, or **4** can eliminate a hydrogen unimolecularly yielding a stable aromatic hydrocarbon, whereas the diphenylmethyl radical has to undergo bimolecular reaction (dimerization) to form a stable molecule. Thus. reversibility of the initial hydrogen-abstraction explains the *net* reactivity of hydrocarbons toward thiobenzophenone in the n,π^* triplet state (Scheme 1).

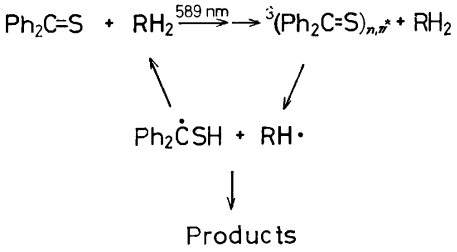

Scheme 1.

In order to test the validity of the proposed mechanism, the reaction with 1,2-diphenylethane was carried out. The compound was found to reduce thiobenzophenone, yielding stilbene and **1**, which proves that, although thiobenzophenone in the n,π^* triplet state can abstract a hydrogen from diphenylmethane, the reverse reaction takes place faster, thus making the net reaction unrecognizable.

Stoos and Roček proposed that the enhanced reactivity of **2** in quinone-oxidation is due to a simultaneous two-hydrogen elimination assisted by the gain of aromatic stabilization energy.[5] However, "extra" stabilization energy of the cyclohexadienyl radical (24 kcal/mol) is extraordinarily large compared with that of open-chain free radicals (~15 kcal/mol).[6] In addition, if the gain of aromatic stabilization energy were to play an important role in the reactivity of these hydrocarbons, they should react faster, in contrast to observation (*vide infra*), than the corresponding nitrogen analogs since hydrocarbons can gain larger stabilization energy.[7,8] We thus propose that the oxidation of

1) A. Ohno and N. Kito, *Int. J. Sulfur Chem.*, *A*, **1**, 26 (1971).
2) S. G. Cohen and C. H. Wang, *J. Amer. Chem. Soc.*, **77**, 4435 (1955).
3) A. Ohno, Y. Ohnishi, and G. Tsuchihashi, *ibid.*, **91**, 5038 (1969).
4) E. A. Braude, L. M. Jackman, and R. P. Linstead, *J. Chem. Soc.*, 3564 (1954).
5) F. Stoos and J. Roček, *J. Amer. Chem. Soc.*, **94**, 2719 (1972).
6) G. Vincow, H. J. Dauben, Jr., F. R. Hunter, and W. V. Volland, *ibid.*, **91**, 2823 (1969).
7) G. W. Wheland, "Resonance in Organic Chemistry," John Wiley & Sons, Inc., New York, N. Y., 1955, pp 98—100.
8) Photo-ionization potentials of **2**, **5**, and **6** are 8.82, 8.40, and 7.24 eV, respectively: D. A. Demeo and M. A. El-Sayed, *J. Chem. Phys.*, **52**, 2622 (1970); V. K. Potapov, A. D. Filyugina, D. N. Shigorin, and G. A. Ozerova, *Dokl. Akad. Nauk SSSR*, **180**, 398 (1968); *Chem. Abstr.*, **69**, 76408j (1968); N. Bordor, M. J. S. Dewar, and S. D. Worley, *J. Amer. Chem. Soc.*, **92**, 19 (1970).

1,4-dihydroaromatic hydrocarbons proceeds by successive hydrogen-eliminations.[9]

Braude and co-workers reported that cyclohexadienyl carbonium ion is involved as an intermediate of the quinone-oxidation of **2**.[10] Although we have no evidence to predict this to be the case in the reaction with thiobenzophenone, we believe that the cyclohexadienyl radical is at least one of intermediates of the reaction. The idea is based on the comparison of reactions of **2** and 1,3,5-cycloheptatriene (**5**): the photoreaction of **5** with thiobenzophenone proceeded as fast as that of **2** and products isolated from the reaction mixture were 7-(1,3,5-cycloheptatrienyl)diphenylmethanethiol (35%), 7,7'-bi(1,3,5-cycloheptatrienyl) (2%), and **1** (4%) with several unidentified materials. Formation of 7,7'-bi(1,3,5-cycloheptatrienyl) implies that the reaction involves a transient cycloheptatrienyl radical, the "extra" stabilization energy (21 kcal/mol) of which is comparable to that of the cyclohexadienyl radical.[6] On the other hand, the intermediacy of the carbonium ion is fairly well-established in the oxidation of **5**.[11] The "extra" stabilization energy is calculated to be 49 kcal/mol for cycloheptatrienyl carbonium ion,[6] which is twice as large as that of the corresponding free radical. Since it is energetically unreasonable to expect the initially formed carbonium ion to be reduced to the free radical, the free radical should be the precursor of the carbonium ion. The fact that even such a stable carbonium ion is formed *via* a free radical suggests that cyclohexadienyl carbonium ion, if any, might be formed from the corresponding free radical.

Taking account of the results obtained by Braude and co-workers[10] together with the analogy to the mechanism of reactions of dihydropyridine derivatives (*vide infra*), we would like to propose an initial electron-transfer process for the formation of cyclohexadienyl radical (Scheme 2).

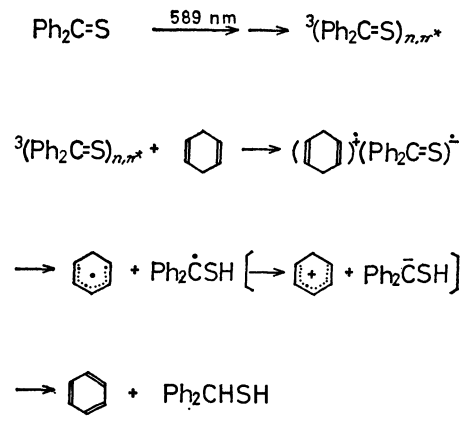

Scheme 2.

In contrast to the low reactivity of **4**, the photoreaction of acridane (**6**) with thiobenzophenone proceeds instantaneously giving a clear solution with precipitation of 9,9'-biacridanyl (31% yield). However, on standing the reaction mixture at room temperature for a day or at 50 °C for an hour, regeneration of 67% of the starting thiobenzophenone was observed by spectrophotometry. The forward and reverse reactions were repeated several times, and when no more thiobenzophenone was regenerated, **1** and 9,9'-biacridanyl were isolated in quantitative yields. Thus, it is obvious that a thermally unstable intermediate is formed by the photoreaction of **6** with thiobenzophenone.

A mixture of **6** and 4,4'-dimethoxythiobenzophenone in ethanol exibits absorption maxima at 295 and 355 nm due to **6** and the thioketone, respectively. When the mixture was irradiated with light (589 nm) for a short period (within 1 min), formation of acridine was recognized by the appearance of a new maximum at 250 nm and a fine structure at about 350 nm.[12] Longer irradiation, however, caused a decrease in absorption due to acridine (Fig. 1).

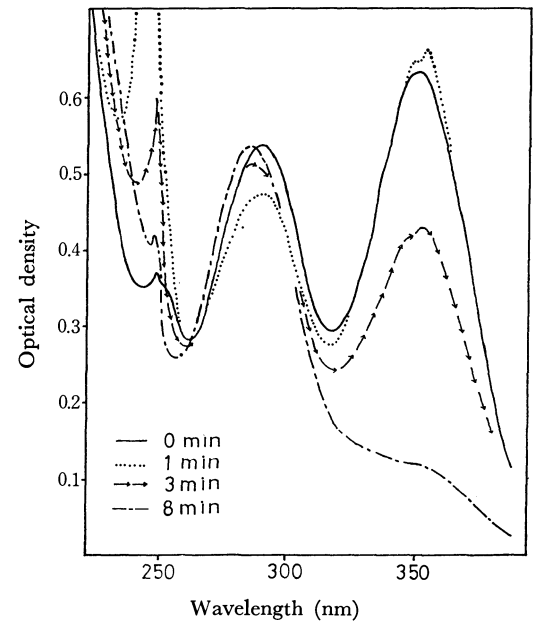

Fig. 1. Absorption spectra (in EtOH) of a mixture of acridane (1.53×10^{-5} mol/l) and 4,4'-dimethoxythiobenzophenone (1.48×10^{-5} mol/l) at different periods of photoirradiation.

Photochemical behaviors of acridine and acridane have been studied extensively.[12-15] The present result, combined with reported ones, suggests that the most plausible mechanism for the reaction of **6** with thiobenzophenone is as follows (Scheme 3): Undoubtedly only thioketone can absorb the irradiated light. Although we failed to obtain evidence supporting

9) We do not intend to specify the mechanism of the hydrogen-elimination process. It might be a one-electron-proton elimination or true hydrogen-elimination. The mechanism will be discussed below.

10) E. A. Braude, L. M. Jackman, R. P. Linstead, and G. Lowe, *J. Chem. Soc.*, 3123, 3133 (1960).

11) P. Müller and J. Roček, *J. Amer. Chem. Soc.*, **94**, 2716 (1972).

12) M. Giurgea, G. Mihai, V. Topa, and M. Musa, *J. Chim. Phys.*, **61**, 619 (1964).

13) a) M. Koizumi, Y. Ikeda, and H. Yamashita, This Bulletin, **41**, 1056 (1968); b) A. Kira and M. Koizumi, *ibid.*, **42**, 625 (1969); c) Y. Miyashita, S. Niizuma, H. Kokubun, and M. Koizumi, *ibid.*, **43**, 3435 (1970).

14) R. S. Davidson, P. F. Lambeth, and M. Santhanam, *J. Chem. Soc., Perkin II*, 2351 (1971).

15) V. Zanker, E. Erhardt, and H. H. Mantsch, *Z. Phys. Chem., N. F.*, **58**, 1 (1968).

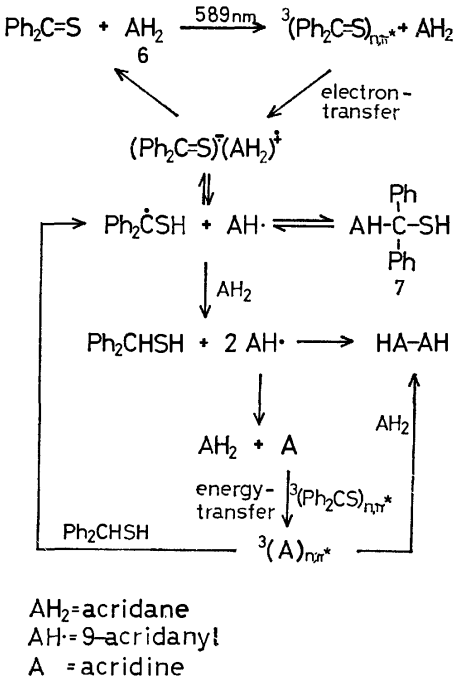

Scheme 3.

the formation of the intermediate **7**, formation of 1-(9-acridanyl)ethyl alcohol by the reaction of acridine with ethanol has been confirmed.[12] There is no doubt that **7** is the thermally unstable intermediate mentioned above, because acridine semiquinone[16] and radical anion from thiobenzophenone,[17] both considered to be intermediates, are known to have absorption maxima in a visible region, whereas the present reaction mixture is transparent in this region.

The one-electron-transfer process from acridane to benzophenone has also been proposed.[14] Since thiobenzophenone is a much better electron-acceptor than benzophenone[18] and the electron-acceptability of thiobenzophenone is enhanced more in the n,π^* triplet state than in the ground state,[19] the initial one-electron-transfer process from **6** to thiobenzophenone in the n,π^* triplet state is most plausible for explaining the great difference in the reactivity of **4** and **6**. It should be noted that *N*-benzyl-1,4-dihydronicotinamide reacts with thiobenzophenone at room temperature in the dark, whereas **2** requires light to undergo a similar reaction. The one-electron-transfer interaction has been proposed to be a driving force of the former reaction.[20]

The photo-sensitized transformation of acridine into 9,9'-biacridanyl shown in Scheme 3 was confirmed by a separate experiment: an ethanol solution of 4,4'-dimethoxythiobenzophenone and acridine was irradiated with light (589 nm) and the decrease in intensity at the absorption maximum (250 nm) was followed spectrophotometrically.[21]

Experimental

Materials. Thiobenzophenone and 4,4'-dimethoxythiobenzophenone were prepared as reported previously.[24] 1,4-Dihydrobenzene was prepared by the Birch reduction of benzene[25]: bp 86—89 °C (lit,[26] 88 °C). Acridane was obtained by the reduction of acridine with $LiAlH_4$: mp 170 °C (lit,[27] 169 °C). 1,4-Dihydronaphthalene, 1,3,5-cycloheptatriene, 9,10-dihydroanthracene, and 1,2-diphenylethane were purified by repeated distillations or recrystallizations of commercial reagents.

*Reaction with 1,4-Dihydrobenzene (**2**).* An ampoule containing **2** (2 ml), thiobenzophenone (486 mg, 2.46 mmol), and benzene (3 ml) was degassed by the usual thawing and freezing method and sealed in a high vacuum (10^{-6} Torr). The mixture was irradiated with light from low-pressure sodium lamps[3] at room temperature until the characteristic color of thiobenzophenone completely disappeared (20 hr). Removal of the volatile materials under a reduced pressure left diphenylmethanethiol (**1**) in quantitative yield (490 mg). From the reaction mixture in ethylbenzene as a solvent, benzene (100% yield) was detected on vpc (Hitachi K-53, FID, 20% XF-1150, 2 m, 90 °C).

*Reaction with 1,4-Dihydronaphthalene (**3**).* A benzene (10 ml) solution of thiobenzophenone (423 mg, 2.14 mmol) and **3** (284 mg, 2.19 mmol) in an ampoule was similarly irradiated. After the disappearance of thiobenzophenone (3 days), naphthalene (91% yield) was detected on vpc (20% Carbowax-20M, 2 m, 180 °C). Dibenzhydryl disulfide (48 mg, 11% yield) and **1** (180 mg, 43% yield) were isolated by subjecting the reaction mixture to column chromatography on silica gel with *n*-hexane as an eluent.

*Reaction with 9,10-Dihydroanthracene (**4**).* A mixture of thiobenzophenone (483 mg, 2.44 mmol) and **4** (440 mg, 2.44 mmol) in acetonitrile (15 ml) and ethyl ether (10 ml) was irradiated until complete decolorization of thiobenzophenone took place (one week). After the solvents were evaporated, the residue (900 mg) was chromatographed on silica gel column. Elution with *n*-hexane gave anthracene (100 mg, 26% yield), dibenzhydryl disulfide (210 mg, 24% yield), **1** (75 mg, 17% yield), and recovered **4** (45 mg). Two additional unidentified materials (200 and 150 mg) were obtained by eluting the column with a mixture of *n*-hexane–benzene (1 : 1).

Reaction with 1,2-Diphenylethane. A benzene (4 ml) solution of thiobenzophenone (40 mg) and 1,2-diphenylethane (400 mg) was irradiated for 1.5 months. The color of thiobenzophenone faded but not completely. Formation of small amounts of *trans*-stilbene, dibenzhydryl disulfide, and **1** was proved on vpc (20% XF-1150, 1 m, 180 °C) and tlc (silica gel).

*Reaction with 1,3,5-Cycloheptatriene (**5**).* A solution of thiobenzophenone (795 mg, 4.00 mmol), **5** (3 ml), and ben-

16) A. Kira, S. Kato, and M. Koizumi, This Bulletin, **39**, 1221 (1966).
17) Y. Minoura and S. Tsuboi, *J. Org. Chem.*, **37**, 2064 (1972).
18) R. M. Elofson, F. F. Gadallah, and L. A. Gadallah, *Can. J. Chem.*, **47**, 3979 (1969).
19) A. Ohno, N. Kito, and N. Kawase, *J. Poly. Sci., B, Part* **10**, 133 (1972).
20) A. Ohno and N. Kito, *Chem. Lett.*, **1972**, 369.
21) Both of thiobenzophenone in the n,π^* triplet state and acridine in the π,π^* triplet state have excitation energy of 42—45 kcal/mol.[22,23]
22) G. N. Lewis and M. Kasha, *J. Amer. Chem. Soc.*, **67**, 994 (1945).
23) D. E. Evans, *J. Chem. Soc.*, **1957**, 1351.
24) N. Kito and A. Ohno, This Bulletin, **46**, 2487 (1973).
25) C. B. Wooster, U. S., 2,182,242 (1938).
26) F. O. Rice and A. L. Stallbaumer, *J. Amer. Chem. Soc.*, **64**, 1527 (1942).
27) F. Bohlmann, *Chem. Ber.*, **85**, 390 (1952).

zene (5 ml) was irradiated until complete decolorization of thiobenzophenone took place (44 hr). After excess **5** and the solvent were removed, the residue was chromatograhped on a silica-gel column with a mixture of *n*-hexane–benzene (4 : 1) as an eluent. The following components were isolated: 7,7′-bi(1,3,5-cycloheptatrienyl) (17 mg, 2% yield), 7-(1,3,5-cycloheptatrienyl)diphenylmethanethiol (**8**) (550 mg, 35% yield), **1** (30 mg, 4% yield), and unidentified compounds (140 mg).

8: NMR (δ from TMS, $CDCl_3$) 2.43 (s, 1H), 2.61 (t of d, 1H), 5.44 (q, 2H), 6.14 (d or octet, 2H), 6.64 (t of d, 2H), and 7.0—7.6 (m, 10H). Mass spectrum (*m/e*) 290 (M^+), 257, 256, 199, 198, 179, 178, and 91 (base). IR 2570 cm^{-1} (ν_{SH}).

To a suspension of NaH (30 mg) in 30 ml of THF was added dropwise a solution of the thiol (310 mg) in 20 ml of THF at room temperature. After 2 hr, when the solution became clear, 2 ml of MeI was added and stirred for 2 hr at room temperature. The solution was acidified with 2N-hydrochloric acid and extracted with chloroform yielding 260 mg of an oil. The oil was chromatographed on a silica-gel column with the eluent of *n*-hexane–benzene (8 : 1) mixture. Triphenylethylene[28] (60 mg) and 7-(1,3,5-cycloheptatrienyl)diphenylmethyl methyl sulfide (**9**) (100 mg) were isolated.

9: NMR (δ from TMS, $CDCl_3$) 1.63 (s, 3H), 2.38 (t of t, 1H), 5.48 (q, 2H), 6.24 (d of sextet, 2H), 6.77 (t, 2H), and 7.0—7.6 (m, 10H). Mass spectrum (*m/e*) 304 (M^+), 256, 213, 198, 179, 165, 121, and 91 (base).

*Reaction with Acridane (**6**).* A solution of thiobenzophenone (560 mg, 2.83 mmol) and **6** (1,000 mg, 5.55 mmol) in ether (20 ml) was irradiated at the temperature of ice-water. After 30 min, the color of thiobenzophenone faded completely. From this reaction mixture, 310 mg of 9,9′-biacridanyl (31% yield) was isolated as precipitates. In a separate run, the characteristic color of thiobenzophenone reappeared, when the reaction mixture was heated at 50 °C for 1 hr. Spectroscopic observation showed that 67% of thiobenzophenone was recovered. After all the thiobenzophenone had been consumed by a repetition of the above procedure, 950 mg of 9,9′-biacridanyl (mp 260 °C (lit[29] 261—262 °C)) was isolated as precipitates. From the filtrate, additional 9,9′-biacridanyl (30 mg) (total yield; 98%) and **1** (540 mg, 97% yield) were obtained.

Formation and consumption of acridine during the reaction were followed with a Carry-14 Spectrophotometer at suitable concentrations of 4,4′-dimethoxythiobenzophenone and **6** in ethanol or ethyl ether (Fig. 1).

Photo-sensitized Reaction of Acridine. An ethanol solution of acridine (8.05×10^{-7} mol/l) and 4,4′-dimethoxythiobenzophenone (1.56×10^{-5} mol/l) was irradiated at room temperature for 2 min. The decrease in intensity at the absorption maximum (250 nm) was followed with a Carry-14 Spectrophotometer (Fig. 2).

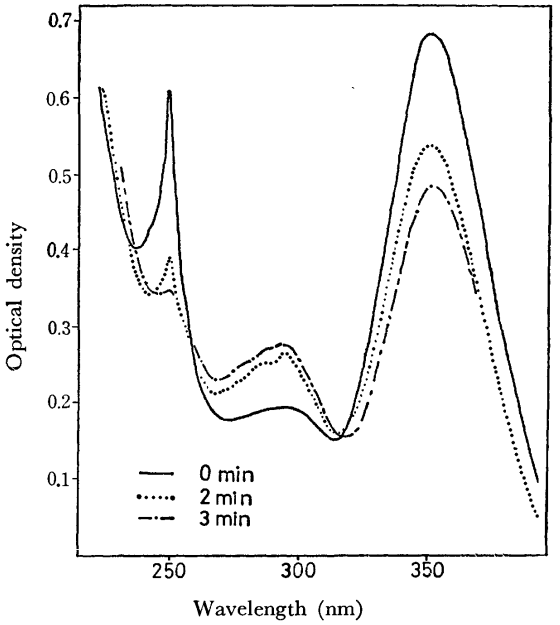

Fig. 2. Absorption spectra (in EtOH) of a mixture of acridine (8.05×10^{-7} mol/l) and 4,4′-dimethoxythiobenzophenone (1.56×10^{-5} mol/l) at different periods of photo-irradiation.

28) a) H. Adkins and W. Zartman, "Org. Syntheses," Coll. Vol. II, 606 (1943); b) We assume that this product was yielded from 8,8-diphenylheptafulvene. Y. Kitahara, K. Doi, and T. Kato, This Bulletin, **39**, 2444 (1966).

29) H. Göth, P. Cerutti, and H. Schmid, *Helv. Chim. Acta*, **48**, 1395 (1965).

Tri(hetero)substituted Carbonium Ions. VIII. The Hydride Reduction of Cyclic and Open-chain Dithiocarbamidium Salts

Kazuhisa HIRATANI, Takeshi NAKAI, and Makoto OKAWARA

Research Laboratory of Resources Utilization, Tokyo Institute of Technology, Ookayama, Meguro-ku, Tokyo 152

(Received June 20, 1973)

Studies were carried out on the hydride reduction of the following five stable *N,S,S*-tri(hetero)substituted carbonium ions: *N,N,S,S'*-tetramethyldithiocarbamidium ion (**1a**), 2-dimethylamino-1,3-dithiolanylium ion (**1b**), 2-dimethylamino-1,3-dithianylium ion (**1c**), 2-methylthio-3-methyl-4,5-dihydrothiazolium ion (**1d**), and 2,3,5,6-tetrahydrothiazolo[2,3-*b*]thiazolium ion (**1e**). Sodium dihydrobis(methoxyethoxy)aluminate (RDB) was found to be a suitable reducing agent. The RDB reduction of the carbonium ions at −5 °C gave the corresponding formamide thioacetals (**2**) in moderate yields. This provides a practical method for the synthesis of formamide thioacetals. The RDB reduction of **1d** at higher temperature, however, yielded abnormal products, thiazolin-2-thione (**3**) and thiazolidine (**4**) instead of the formamide thioacetal (**2d**). The mechanism for the formation of **3** and **4** has been discussed in terms of the ambident character of the cation (**1d**). Pyrolytic reactions of the thioacetals (**2**) and unsuccessful attempts to abstract the methine proton of **2b** by various bases are also described.

In previous studies[1-5] we established that (i) dithiocarbamidium ions (**1**) have two electrophilic sites (the ambident character) and (ii) in general, hard nucleophiles attack selectively site at *a* (mode A) while soft nucleophiles react at site *b* (mode B).

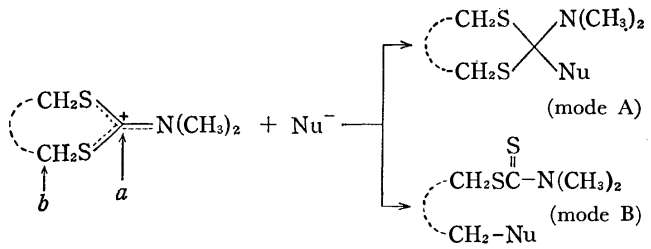

Reduction reactions of carbonium ions have recently drawn much attention since one- and two-electron reductions of carbonium ions might lead to carbon radical and carbanion frameworks, respectively. Although papers have appeared on the reduction of stable carbonium ions,[6] little information has been available on the reduction of stable tri(hetero)carbonium ions.

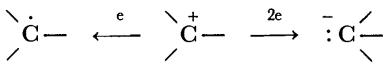

In this work, the hydride reduction (two-electron reduction) of cyclic and acylic dithiocarbamidium ions by means of metal hydride has been studied. On the basis of the selectivity rule it is anticipated that hydride ion, one of the hardest nucleophiles, attacks specifically at site *a* giving formamide thioacetals. The present paper describes the hydride reductions of the dithiocarbamidium ions which give the corresponding formamide thioacetals in moderate yields.

Results and Discussion

Hydride Reductions of the Carbonium Salts. The following dithiocarbamidium salts were used: *N,N,-S,S'*-tetramethyldithiocarbamidium perchlorate (**1a**),[4] 2-dimethylamino-1,3-dithiolan-2-ylium perchlorate (**1b**),[1] 2-dimethylamino-1,3-dithian-2-ylium perchlorate (**1c**),[3] 2-methylthio-3-methyl-4,5-dihydrothiazolium iodide (**1d**),[5] and 2,3,5,6-tetrahydrothiazolo[2,3-*b*]thiazolium perchlorate (**1e**).[5] Metal hydrides examined were sodium hydride, sodium borohydride (SBH), lithium aluminium hydride (LAH) and a 64% benzene solution of sodium dihydrobis(2-methoxyethoxy)aluminate (RDB).

In order to find the best reducing agent, the reactions of **1b** with the above four metal hydrides were carried out in tetrahydrofuran (THF) or ether in the range from −10 °C to room temperature for 2—4 hr. In most cases except for RDB, both reactants were almost insoluble in the solvents. It was found that sodium hydride can not reduce the cation under the conditions. The reduction using SBH and LAH gave the expected product 2-dimethylamino-1,3-dithiolane (**2b**) in *ca.* 30% and *ca.* 20%, respectively. The optimum yield (71%)was obtained by using RDB in THF at −5—0 °C. The result shows that RDB has an advantage over SBH and LAH presumably due to the greater solubility of RDB in organic solvents such as ether and THF. Thus, the hydride reductions of the other dithiocarbamidium salts were undertaken by means of RDB under similar conditions. The yields and physical properties of the formamide thioacetals thus obtained are summarized in Table 1. Their elemental analysis and NMR spectra are given in Table 2.

It should be noted that there is a well-defined trend for the absorption due to the methine proton in the formamide thioacetals to shift remarkably to a lower field in the order: **2a** (acyclic), **2c** (six-membered), and **2b** (five-membered) although their N–CH_3 signals were essentially independent of the ring size (Table 2). In view of the fact that the inductive effect on the me-

1) T. Nakai, Y. Ueno, and M. Okawara, This Bulletin, **43**, 156 (1970).
2) T. Nakai and M. Okawara, *ibid.*, **43**, 1864 (1970).
3) T. Nakai, Y. Ueno, and M. Okawara, *ibid.*, **43**, 3175 (1970).
4) T. Nakai and M. Okawara, *ibid.*, **43**, 3528 (1970).
5) T. Nakai, K. Hiratani, and M. Okawara, *ibid.*, in press.
6) K. Okamato, *Kogyo Kagaku Zasshi*, **69**, 825 (1969) (a review); F. A. Carey and H. S. Tremper, *J. Org. Chem.*, **34**, 4 (1969); H. M. Bell and H. C. Brown, *J. Amer. Chem. Soc.*, **88**, 1473 (1966); S. D. McGregor and W. M. Jones, *ibid.*, **90**, 123 (1968).

Table 1. Hydride reductions of the carbonium salts by RDB

	Carbonium salts	Formamide thioacetals	Bp(mmHg), °C [Lit.]	n_D (20°) [Lit.]	Yield %
1a	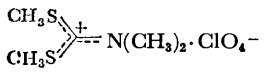	**2a** 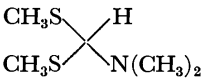	62—63°(5.5) [80—82°(10)][a]	1.521 [1.525][a]	38
1b	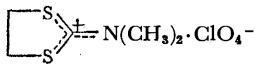	**2b** 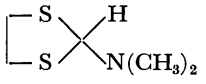	57—58°(1.5) [60°(0.1)][b]	1.567 [1.564][b]	71
1c	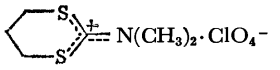	**2c** 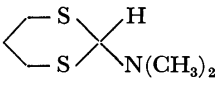	90—91°(2.5)	1.568	34
1d	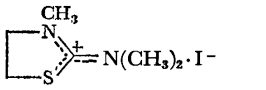	**2d** 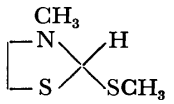	59—61°(1.5)	1.561	36
1e	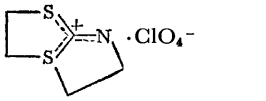	**2e** 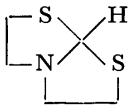	83—85°(1.0)	1.614	57

a) H. Boehme and J. Roer, *Ann. Chem.*, **648**, 21 (1961). b) C. Feugeas and D. Olschwang, *Bull. Soc. Chim. Fr.*, **1969**, 332.

Table 2. NMR data of formamide thioacetals (**2**)

	δ ppm (multiplicity)				
	≡C-H	=N-CH_3	-S-CH_3	-S-CH_2-	others
2a	4.64(s)	2.34(s)	2.06(s)	—	—
2b	6.01(s)	2.25(s)	—	3.11(m)	—
2c	5.13(s)	2.39(s)	—	2.81(t)	[-$CH_2CH_2CH_2$-] 1.6—2.1(m)
2d	4.97(s)	2.35(s)	2.04(s)	2.7—3.1(m)	[-N-CH_2-] 3.2—3.5(m)
2e	5.83(s)	—	—	[-S-CH_2CH_2-N=] 3.16(m)	

thine proton is nearly constant in the system concerned, two possible explanations can be suggested; (i) the ring-size effect on the conformation of the thioacetal ring[7] and (ii) the ring-size effect on the extent of the 3p–3d interaction between the two sulfur atoms in the ring recognized in UV spectra for cyclic thioacetals and orthothioformates.[8] At the present stage, however, it is difficult to determine which factor is more operative since no information is available on the conformational analysis and acidity of cyclic formamide thioacetals. Our attampts to abstract the methine proton of **2b** by various bases were unsuccessful.

Thus, the hydride reduction of the stable carbonium salts, which were readily prepared by the previously-reported method,[1,3–5] may provide a practical method[9] for the synthesis of formamide thioacetals which have recently attracted much attention as a synthetic intermediate.[10]

The Ambident Behavior of the Cation ***1d*** *in the Hydride Reduction.* During the course of our search for the optimum reduction conditions for the cation **1d**, we found that a change in reaction temperature from −5 °C to room temperature resulted in a complete change of the product structure; the reduction of **1d** at −5 °C gave the normal product **2d** while the reduction at room temperature (15—20 °C) yielded 3-methylthiazolidin-2-thione (**3**) and 3-methylthiazolidine (**4**) in 12% and 30% yields, respectively. The thin layer chromatogram of the crude mixture excluded any possibility of the presence of a product other than **3** and **4**. Product **3** was identical with an authentic sample.[11] The other product **4** was identified by elemental analysis and IR and NMR spectroscopic methods.

7) C. H. Bushweller, "Mechanisms of Reactions of Sulfur Compounds", ed. by N. Kharasch, Vol. 5, Intra-Science Research Foundation, Santa Monica, Calif., 1970, p. 75.

8) Y. Yano and S. Oae, *ibid.*, Vol. 4, p. 167 (1969).

9) For a recent review on synthetic methods for formamide thioacetals, see J. Gloede, L. Haase, and H. Gross, *Z. Chem.*, **9**, 201 (1969).

10) Review: R. H. DeWoefe, "Carboxylic Ortho Acid Derivatives-Preparation and Synthetic Applications," Academic Press, New York and London, 1970, Chapter 7.

11) J. W. Batty and B. C. Weedon, *J. Chem. Soc.*, **1949**, 786.

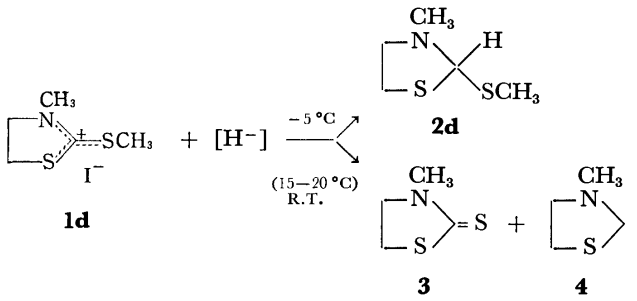

The abnormal behavior of **1d** is in contrast to the reductions of the other carbonium salts in which the corresponding formamide thioacetals were formed in the range from −10 °C to room temperature. The effect of reaction temperature on product structure is of particular interest in connection with the ambident behavior of the tri(hetero)carbonium ions. The mechanisms for the formation of **3** and **4** in the RDB reduction of **1d** were investigated in some detail.

In order to ascertain whether the normal product **2d** is an intermediate for the formation of the abnormal products, **2d** was treated with RDB at room temperature. Only 3-methylthiazolidine (**4**) was obtained, and product **3** was not detected in the reaction mixture. Furthermore, it was found that **3** did not react with RDB under the same conditions and was recovered unchanged. The result of the control experiments led us to suggest that **4** is formed *via* hydride reduction of **2d** and that **3** is not formed *via* **2d** but directly *via* the reaction between the cation **1d** and hydride ion as follows.

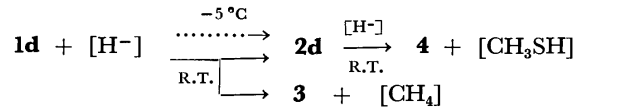

Formation of **4** *via* **2d** can be easily explained as the result of an initial reductive cleavage of the C–SMe bond followed by hydride reduction of the 3-methyl-4,5-dihydrothiazolium ion (**5**); a similar reductive cleavage of C–S bonds by hydride ion has been established for thiazolidines[12] and α-dimethylaminobenzylsulfides.[13]

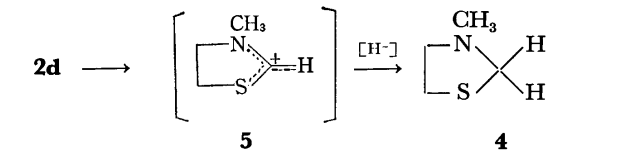

Formation of **3**, on the other hand, can be best explained in terms of a direct attack at site *b* by hydride ion (mode B). This indicates that a change in reaction temperature from −5 °C to room temperature resulted in a partial shift of the reaction course from mode A to mode B.

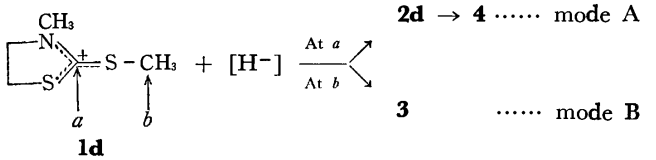

This is the first example demonstrating the important role played by the reaction temperature in determining the reaction course of ambident electrophiles such as dithiocarbamidium ions. In view of our previous findings that the reaction course for the tri(hetero)-carbonium ions depends mainly upon the nucleophilicity and bulkness of an attacking reagent and upon the stability of the cations concerned, it might be concluded that external factors such as reaction temperature should also be taken into account as an additional factor determining the reaction course for some ambident electrophiles.

Reactions of Formamide Thioacetals. Pyrolytic reactions of the formamide thioacetals were studied. When **2b** was heated in bulk at 160—170 °C for 12 hr under nitrogen atmosphere, *N,N*-dimethylthioformamide (**6**) was obtained as a major product along with polymeric ethylene sulfide. Both products were identified through agreement of their IR spectra with those of authentic samples. Pyrolysis of **2a** and **2c** under similar conditions also yielded **6** as a major product. Formation of **6** in these reactions can be explained by assuming an initial thermal cleavage of the C–S bond reported for the thermal reactions of ortho(thio)carbonate derivatives.[14] In contrast, **2d** was more easily pyrolyzed under the conditions to yield the cyclic thione **3** with retention of the ring structure along with a small amount of 3-methylthiazolidin-2-one.

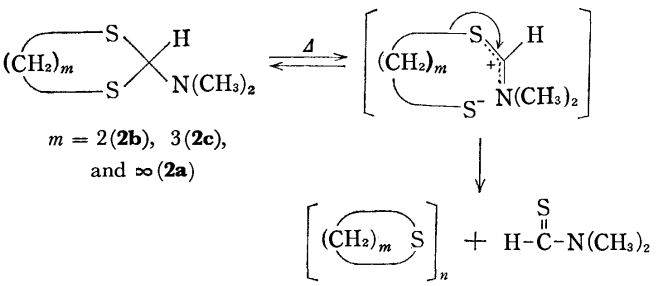

Attempts were made to abstract the methine proton of **2b** with various bases. When **2b** was treated with *n*-butyllithium followed by addition of deuterium oxide, it was found by IR and NMR spectroscopy that no deuterium was incorporated in the resulting thioacetal. Attempts with other bases under various conditions were also unsuccessful. In view of the ease to abstract 2-hydrogens in 1,3-dithianes by *n*-butyllithium, difficulty to abstract the methine proton in **2b** suggests that the resulting carbanion (**7**) is very unstable due to large repulsion between its sp^3 nonbonding electrons and the lone pair of electrons on the nitrogen atom.

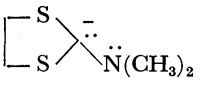

12) E. L. Eliel, E. W. Della, and M. M. Rogic, *J. Org. Chem.*, **27**, 4712 (1962).

13) W. M. Schbert and Y. Motoyania, *J. Amer. Chem. Soc.*, **87**, 5507 (1965).

14) Y. Ueno, T. Nakai, and M. Okawara, This Bulletin, **43**, 162, 168 (1970).

15) E. D. Bergmann and A. Kaluszyner, *Rec. Trav. Chim., Pays-Bas*, **78** 289 (1959).

Experimental

General. All melting and boiling points are uncorrected. IR and UV spectra were recorded with Hitachi EPI-S2 and EPS-3T spectrophotometers, respectively. NMR spectra were obtained with a Japan Electron Optics JNN H-100 spectrometer. Chemical shifts are given in ppm with tetramethylsilane as an internal standard. All carbonium salts were prepared according to the literature methods.

*Reactions of the salt **1b** with Metal Hydride. a) With RDB*: A suspension of 68 g (0.27 mol) of **1b**[1] in 150 ml of THF was placed in a 500-ml three-necked flask equipped with a mechanical stirrer, dropping funnel and thermometer, and was then cooled to −5 °C. To the stirred mixture was added dropwise 8.5 g (0.27 mol) of a 64% benzene solution of RDB[16] over a period of 2 hr. The reaction mixture was then stirred at −5—0 °C for 4 hr. After removal of THF at room temperature under reduced pressure, ether and water were added to the resulting mixture. The ethereal layer was separated and dried over anhydrous sodium sulfate. After removal of the drying agent followed by distillation of ether, distillation of the liquid residue gave 28.5 g (71%) of **2b**.

Found: C, 40.16; H, 7.43; N, 9.25%. Calcd for $C_5H_{11}NS_2$: C, 40.23; H, 7.42; N, 9.38%.

b) With LAH: In a similar manner, the reaction of **1b** (3.0 g, 12 mmol) with LAH (1.0 g, 27 mmol) in 50 ml of ether at 0 °C gave 0.4 g (22%) of **2b**.

c) With SBH: In a similar manner, the reaction of **1b** (15 g, 61 mmol) with SBH (4 g, 110 mmol) in 100 ml of ether at 0 °C yielded 3.0 g (33%) of **2b**. When ethanol was used as the solvent in place of ether, a similar reaction of **1b** (75 g, 0.3 mol) with SBH (1.0 mol) gave 27 g (60%) of **2b**.

RDB Reductions of Other Carbonium Salts. By the same procedure as in the case of RDB reduction of **1b**, 35 g (0.14 mol) of **1a**[4] and 47 g (0.14 mol) of the RDB solution gave 8.0 g (38%) of **2a**.

Found: C, 39.75; H, 8.76; N, 9.25%. Calcd for $C_5H_{12}NS_2$: C, 39.70; H, 8.66; N, 9.25%.

In a similar fashion, the RDB reductions of **1c**,[3] **1d**[5], and **1e**[5] gave the corresponding formamide thioacetals (**2**) in 34%, 36%, and 57% yields, respectively.

2c, Found: C, 44.56; H, 8.12; N, 8.46%. Calcd for $C_6H_{13}NS_2$: C, 44.13; H, 8.02; N, 8.58%.

2d, Found: C, 39.98; H, 7.38; N, 9.31%. Calcd for $C_5H_{11}NS_2$; C, 40.23; H, 7.43; N, 9.38%.

2e, Found: C, 39.87; H, 6.25; N, 9.26%. Calcd for $C_5H_9NS_2$: C, 40.78; H, 6.16; N, 9.51%.

*The RDB Reduction of **1d** at Room Temperature (15—20 °C).* To a suspension of 5.5 g (0.02 mol) of **1d** in 40 ml of THF was added dropwise 5.8 g (0.02 mol) of the RDB solution at room temperature. After the mixture was stirred at room temperature, THF was removed by distillation. Ether and water were added to the residue and the ethereal layer was separated. The ethereal solution was dried over anhydrous sodium sulfate and the ether was evaporated under reduced pressure. The thin layer chromatogram (silica gel, chloroform) of the oily residue showed two spots which were assigned to *N*-methylthiazolin-2-thione (**3**) and *N*-methylthiazolidine (**4**) by comparison of the R_f values with those of authentic samples. Distillation of the residue under reduced pressure gave 0.60 g (30%) of 3-methylthiazolidine (**4**), 39—41 °C/4 mmHg, n_D (20 °C) 1.518 (lit,[15] bp 151—152 °C/760 mmHg, n_D (25 °C) 1.520), and a solid residue which was then recrystallized from water giving 0.32 g (12%) of 3-methylthiazolidin-2-thione (**3**), mp 68—69 °C (lit,[11] 69.5 °C).

4: NMR ($CDCl_3$); 2.22 (s, 3H, NCH_3), 2.87 (m, 4H, SCH_2CH_2N) and 3.90 (s, 2H, SCH_2N). Found: C, 47.48; H, 9.06; N, 13.39%. Calcd for C_4H_9NS: C, 46.59; H, 8.80; N, 13.58%.

*Control Experiments. a) Reaction of the Formamide Thioacetal (**2d**) with RDB*: A mixture of 0.3 g of **2d** and 0.7 g of the RDB solution in 10 ml of benzene was stirred at room temperature for 24 hr. Water was then added to the mixture and the solution was extracted with ether. The ethereal solution was dried over anhydrous sodium sulfate and the ether was evaporated completely to give 0.27 g of an oily residue. The oil was found to consist of **4** and unreacted **2d** by IR and NMR spectroscopy and thin layer chromatography.

*b) Reaction of **3** with RDB*: A mixture of 1.35 g of **3** and 3.0 g of the RDB solution in 30 ml of THF was stirred at room temperature for 3 hr. The mixture was poured into cold water followed by extraction with ether. The ether solution was dried over anhydrous sodium sulfate and the ether was evaporated completely giving 1.32 g of unchanged **3**.

Pyrolyses of the Formamide Thioacetals. 1.0 g of **2a** was placed in a 10 ml flask equipped with a reflux condenser and gas inlet. The flask was dipped in an oil bath heated at 150 °C and allowed to stand for 24 hr at 130—150 °C under nitrogen atmosphere. After cooling, the mixture was subjected to column chromatography (silica gel). Two products were obtained; the major product (*ca.* 30% yield) was identical (IR and UV) with an authentic sample of *N,N*-dimethylthioformamide (**6**) prepared by method in literature;[17] the minor product was identified to be methyl *N,N*-dimethylthiolcarbamate by comparison of its IR spectrum with that of an authentic sample.[4]

In a similar manner, pyrolysis of **2b** (1.5 g) at 160—170 °C for 12 hr gave an oil along with a white solid on the wall of the reflux condenser. The oil was dissolved in chloroform and chromatographed on silica gel. Elution with chloroform gave 0.57 g (64%) of the thioformamide (**6**). The white solid was identified as polymeric ethylene sulfide by IR spectroscopy and elemental analysis. No further identification was made.

The pyrolysis of **2c** (0.5 g) at 150 °C for 12 hr also gave **6** as a major product.

Pyrolysis of **2d**, (0.5 g, 3.4 mmol) at 160 °C was complete after only 3 hr. After the resulting mixture had been cooled, it was subjected to column chromatography (silica gel) to give 0.3 g (66%) of 3-methylthiazolidin-2-thione (**3**) and 0.1 g of 3-methylthiazolidin-2-one.[5] The structures of the products were determined by comparison of their IR spectra and physical properties with those of the corresponding authentic sample.

*Reaction of **2b** with n-Butyllithium.* A solution of 3.0 g (0.02 mol) of **2b** in 50 ml of THF was placed in a 100 ml three-necked flask equipped with a magnetic stirrer, gas inlet tube and thermometer. The mixture was stirred at −70 °C under nitrogen atmosphere and then 8.0 g of a 15% *n*-hexane solution of *n*-butyllithium was added dropwise to the mixture. After the mixture was stirred at −70 °C for 3 hr, 0.5 g of deuterium oxide was added and the mixture was allowed to stand until the temperature rose to room temperature. The white precipitates formed were filtered and the solvents were removed from the filtrate under reduced pressure at room temperature to give an oily residue. The IR and NMR

16) Purchased from Wako Pure Chemical Industries, Ltd.

17) R. Willstaetter, *Chem. Ber.*, **42**, 1921 (1909).

spectra of the oil agreed with those of **2b**.

A similar reaction with *n*-butyllithium-*N*,*N*,*N*′,*N*′-tetramethylethylene diamine complex resulted in the recovery of **2b** unchanged.

An attempt to abstract the methine proton in **2b** with *t*-BuOK—*t*-BuOD was unsuccessful.

BULLETIN OF THE CHEMICAL SOCIETY OF JAPAN, VOL. 46, 3876—3880 (1973)

α,β-Unsaturated Carboxylic Acid Derivatives. IV. General Synthesis of Unsaturated Unsymmetric 3,6-Disubstituted-2,5-piperazinediones[1]

Chung-gi SHIN, Ken-ichi SATO, Akira OHTSUKA, Kazutoshi MIKAMI, and Juji YOSHIMURA*

Laboratory of Organic Chemistry, Faculty of Technology, Kanagawa University, Rokkakubashi, Kanagawa-ku, Yokohama 221

**Laboratory of Chemistry for Natural Products, Faculty of Science, Tokyo Institute of Technology, Ookayama, Meguro-ku, Tokyo 152*

(Received June 25, 1973)

A general synthetic route to unsymmetric 3,6-dialkylidene and 3-alkylidene-6-arylidene-2,5-piperazinediones is described. The condensation reaction of ethyl 2-oxocarboxylates with chloroacetamide in the presence of several acidic catalysts afforded *N*-chloroacetyldehydroamino acid esters. These compounds were cyclized in saturated ethanolic ammonia to give 3-monoalkylidene and benzylidene-2,5-piperazinediones (**2**). Compound **2** and 1-monoacetyl- or 1,4-diacetyl-3-alkylidene and benzylidene-2,5-piperazinediones, derived from a reaction of **2** with acetic anhydride, were condensed with alkyl and arylaldehyde in the presence of bases to afford **5**.

Many monocyclic or polycyclic 2,5-piperazinedione derivatives have recently been found in nature as antibiotics or alkaloids.[2-9]

One of the authors (C.S.) has investigated the syntheses and chemistry of several derivatives,[10-13] and succeeded in the synthesis of albonoursin,[11] 3-benzylidene-6-isobutylidene-2,5-piperazinedione, the first cyclic dehydrodipeptide isolated from the culture of *Streptomyces (St.) albus var. fungatus* and *St. noursei*.

It is well-known that the cyclization of two molecules of amino acids yields the saturated symmetric 3,6-disubstituted-2,5-piperazinedione[14] and the condensation reaction glycine anhydride with arylaldehyde gives unsaturated symmetric 3,6-disubstituted-2,5-piperazinedione.[15,16] However, natural 2,5-piperazinedione derivatives usually have an unsymmetric structure.

As unsymmetric derivatives, only a few 3-monoalkylidene-2,5-piperazinediones (**2**) have been reported. Bergmann *et al*[17] and others[18,19] have synthesized 3-methylidene derivative (**2a**) from glycylserine by halogenation and amination. One of the present authors (C.S.) succeeded in the preparation of isopropylidene derivative (**2d**) *via* ethyl 2-chloroacetamido-3-methyl-2-butenoate (**1d**) obtained by the reaction of dehydrovaline ethyl ester or the tautomeric imine with chloroacetyl chloride.[10,12,13] Similarly, 3-isobutylidene derivative (**2f**) was synthesized *via* ethyl 2-chloroacetamido-4-methyl-2-pentenoate (**1f**) derived by esterification of the free acid.[11] Recently, Dominy and Lawton reported the preparation of 3-benzylidene derivative (**2g**) by the reaction of *N*-acetyldehydrophenylalanylglycine with acetic anhydride.[20] Gallina and Liberatori reported another synthetic method for **2** from the reaction of 1,4-diacetyl-2,5-piperazinedione with alkyl or arylaldehyde.[21] Consequently,

1) The main subject of this series of papers was revised from "Studies on Nitro Carboxylic Acids" Part III: C. Shin, Y. Yonezawa, K. Katayama, and J. Yoshimura, This Bulletin, **46**, 1727 (1973). This work was presented at the 24th and 26th Annual Meetings of the Chemical Society of Japan, Osaka, April 3, 1971; Hiratsuka, April 2, 1972.

2) A. S. Khokhlov and G. B. Lokshin, *Tetrahedron Lett.*, **1963**, 1881.

3) M. Vondracek and Z. Vanek, *Chem. Ind.* (London.), **1968**, 1686.

4) R. Brown, C. Kelly, and S. E. Wiberley, *J. Org. Chem.*, **30**, 277 (1965).

5) A. J. Birch and J. J. Wright, *Chem. Commun.*, **1969**, 644.

6) D. Brewer, R. Rahman, S. Safe, and A. Taylor, *ibid.*, **1968**, 1571.

7) N. Neuss, R, Nagarajan, B. B. Molloy, and L. L. Huckstep *Tetrahedron Lett.*, **1968**, 4467.

8) M. R. Bell, J. R. Johnstop, B. S. Wildi, and R. B. Woodward, *J. Amer. Chem. Soc.*, **80**, 1001 (1958).

9) P. S. Steyn, *Tetrahedron*, **29**, 107 (1973).

10) C. Shin, M. Masaki, and M. Ohta, This Bulletin, **39**, 858 (1966); *J. Org. Chem.*, **32**, 1860 (1967).

11) C. Shin, Y. Chigira, M. Masaki, and M. Ohta, *Tetrahedron Lett.*, **1967**, 4601; This Bulletin, **42**, 191 (1969).

12) M. Masaki, C. Shin, H. Kurita, and M. Ohta, *Chem. Commun.*, **1968**, 1447.

13) C. Shin, M. Masaki, and M. Ohta, This Bulletin, **44**, 1657 (1971).

14) E. Fischer, *Ber.*, **34**, 433 (1901).

15) a) T. Sasaki, *Ber.*, **54**, 163 (1921); b) T. Sasaki and T. Hashimoto, *ibid.*, **54**, 168 (1921).

16) M. Augustin, *J. Prakt. Chem.*, **32**, 158 (1966).

17) M. Bergmann, A. Miekely, and E. Kann, *Ann. Chem.*, **445**, 17 (1925).

18) E. Fischer and L. Prizont, *Rev. Asoc. Med. Argentina*, **69**, 21 (1955); *ibid.*, **70**, 30 (1956).

19) M. Kland and W. M. Garrison, *Nature*, **197**, 859 (1963).

20) B. Dominy and R. G. Lawton, *J. Org. Chem.*, **34**, 2013 (1969).

21) C. Gallina and A. Liberatori, *Tetrahedron Lett.*, **1973**, 1135.

N-chloroacetyldehydroamino acid esters (**1**) seem to be a suitable intermediate for obtaining 3-monoalkylidene and benzylidene derivatives (**2**).

In a previous communication we reported briefly a general synthesis of **2** by the reaction of **1**, derived from ethyl 2-oxocarboxylates and chloroacetamide, with ammonia.[22]

This paper deals with the synthesis of **1** in detail under several experimental conditions and syntheses of unsymmetric 3,6-dialkylidene and 3-alkylidene-6-arylidene-2,5-piperazinediones (**5**) by the condensation of **2** or a mixture of 1-acetyl (**3**)- and 1,4-diacetyl-3-alkylidene-2,5-piperazinediones (**4**) with alkyl or arylaldehyde in the presence of bases.

Results and Discussion

3-Alkylidene-2,5-piperazinediones. Various acidic catalysts were examined in the synthesis of ethyl 2-chloroacetamido-2-pentenoate (**1c**) by the condensation of an equimolar amount of ethyl 2-oxopentanoate and chloroacetamide in refluxed dry benzene. Concentrated sulfuric acid and phosphorylchloride were found to be the most effective.[22]

The effect of the molar ratio of chloroacetamide to ethyl 2-oxopentanoate and the reaction time in the presence of phosphorylchloride were also examined. When the reaction was continued for 8 hr, the yield of **1c** gradually increased as the molar ratio increased to 1.5 : 1 and reached a maximum 44.2% yield. At molar ratio of 1.5 : 1, the yield increased until the reaction time of 12 hr, and reached a 51.0% yield. It was found that the yield of **1c** was best at the molar ratio of 1.5 : 1 and reaction time 12 hr.

The structure of **1** obtained under the same conditions as for **1c** was confirmed by elementary analysis and IR spectrum. It is very similar to that of **1d** and **1f** prepared from a different synthetic route.[10,11]

When a cooled ethanol solution of **1** was saturated with dry ammonia and then allowed to stand at room temperature at least for one day, cyclization reaction occurred gradually to deposit colorless crystals. The crystals were recrystallized from boiling water to afford **2** in pure state as colorless amorphous.[22]

The structure of **2** was confirmed by elementary analysis as well as IR and UV spectrum, the pattern being essentially similar to those of **2d** and **2f** derived in the independent preparation.[10,11]

Acetylation and Condensation Reaction. When **2** was heated with acetic anhydride at 120—130 °C for half an hour, two kinds of crystals which were confirmed to be 1-acetyl (**3**)- and 1,4-diacetyl (**4**) derivatives of **2** were obtained in a ratio of *ca.* 3 : 7. Recent studies on the photoisomerization of carbon-carbon double bond of 3-benzylidene-2,5-piperazinediones by Sammes and co-workers[23,24] and a novel

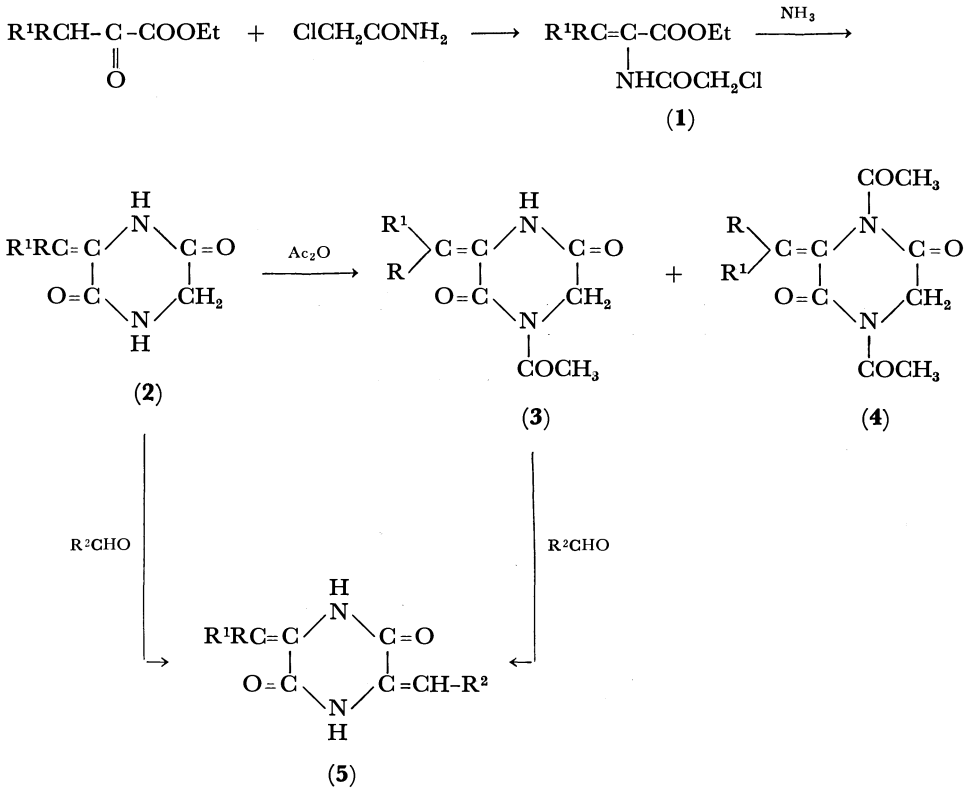

a; $R^1=R=H$, b; $R^1=CH_3$, $R=H$, c; $R^1=C_2H_5$, $R=H$, d; $R^1=R=CH_3$, e; $R^1=n\text{-}C_3H_7$, $R=H$, f; $R^1=i\text{-}C_3H_7$, $R=H$, g; $R^1=C_6H_5$, $R=H$, R^2=several alkyl or aryl groups

Scheme.

22) C. Shin, M. Fujii, and J. Yoshimura, *ibid.*, **1971**, 2499.
23) K. W. Blake and P. G. Sammes, *J. Chem. Soc., C.* **1970**, 980.
24) A. E. A. Porter and P. G. Sammes, *ibid.*, **1970**, 2530.

preparative method for **3**[21] stimulated us to find a simple method for the isolation and determination of these isomers. The two compounds were separated by chromatography on silica-gel column by elution with a mixture of benzene and acetone (20 : 1). The melting points of **3** approximately agreed with those of the products obtained by Gallina and Liberatori.[21] From the results and the spectroscopic data (Table 1), it was assumed that compound **4** is *E*-conformer and **3** is *Z*-conformer with respect to carbon-carbon double bond. It was deduced that, in the case of *Z*-conformer, the steric hindrance of alkyl group hindered acetylation at 4-position of **2**.[24]

Since the isolation of **3** and **4** was tedious and time-consuming, the following method was adopted for the subsequent condensation reaction. On treatment of the mixture of **3** and **4** with arylaldehyde in the presence of triethylamine at 120—130 °C for about 3 hr, the expected 3-alkylidene-6-arylidene-2,5-piperazinedione (**5**) was obtained (Procedure A). On the other hand, **5** was also obtained by direct condensation of **2** with aralkyl or alkylaldehyde in acetic anhydride in the presence of sodium acetate at 120—130 °C for about 5 hr (Procedure B).

The structures of **3**, **4** and **5** were confirmed by elementary analysis as well as IR, UV and NMR spectra. The IR spectrum of **5** showed the absorption bands of NH (3200—3160 and 3100—3020 regions), carbon-oxygen double bond (1690—1670 region) and carbon-carbon double bond (1640—1635 cm^{-1} region). The physical constants, yields and spectral data are given in Tables 1, 2 and 3.

Experimental

All melting points are uncorrected. The IR spectra were recorded with a Hitachi EPI-S2 Spectrometer. The UV spectra were recorded with a Shimadzu UV-50 Spectrometer. The NMR spectra were measured with a JNM-4H-100 Spectrometer (Japan Electron Optics Laboratory Co., Ltd.) using tetramethyl silane as an internal standard.

*N-Chloroacetyldehydroamino Acid Ethyl Esters (**1**).* In a 200 ml round-bottomed flask, fitted with water separater, were placed the appropriate ethyl 2-oxocarboxylate (0.1 mol), chloroacetamide (0.15 mol), phosphorylchloride (6 ml) and dry benzene (100 ml). The mixture was refluxed for about 12 hr until no water separated out. The reaction mixture was removed in a separating funnel and washed with water and then extracted with benzene. The benzene extract was washed with water, dried over anhydrous magnesium sulfate and then evaporated. The residual dark brown syrup was distilled under reduced pressure to give yellow oil.[22] In a similar manner, the condensation reaction of ethyl 2-oxophenylpropanoate with chloroacetamide was performed, and ethyl 2-chloroacetamide-3-phenyl-2-pentenoate (**1g**) was obtained as a yellow syrup, which gradually crystallized at room temperature. The crystalline product was collected and recrystallized from ethanol to give yellow needles (38.7%), bp 151—155 °C/1.5 mmHg (mp 103—104 °C). IR (KBr): 3270, 1720, 1680, 1520 cm^{-1}.

Table 1. 1-Acetyl (**3**)- and 1,4-diacetyl-3-alkylidene(benzylidene)-2,5-piperazinediones(**4**)

Compound	Yield (%)	Mp (°C)	Formula	Found (Calcd), % C	H	N	IR Spectrum[a] cm^{-1}, in KBr	$^1H(\tau)$ NMR Spectrum -NH-	-CH=C- (J_{Hz})	$-CH_2-$	$-COCH_3$
3b[21]	28	180—182	$C_8H_{10}N_2O_3$	52.48 (52.74	5.51 5.53	15.09 15.38)	3190, 3080, 1710, 1695, 1650	0.26	3.65 q (7.5)	5.46	7.40
3c[21]	28	152—154	$C_9H_{12}N_2O_3$	55.11 (55.09	6.06 6.17	14.39 14.28)	3195, 3080, 1710, 1690, 1635	0.25	3.65 t (7.5)	5.47	7.41
3e[21]	29	138—139	$C_{10}H_{14}N_2O_3$	56.98 (57.13	5.77 6.71	13.29 13.33)	3190, 3070, 1710, 1685, 1640	0.25	3.64 t (8.0)	5.46	7.39
3f[21]	32	151—152	$C_{10}H_{14}N_2O_3$	57.10 (57.13	6.52 6.71	13.58 13.33)	3190, 3075, 1710, 1690, 1640	0.68	3.68 d (9.5)	5.55	7.36
3g[21]	31	201—202	$C_{13}H_{12}N_2O_3$	64.12 (63.92	5.05 4.95	11.46 11.47)	3190, 3100, 1710, 1695, 1620	1.87	2.84 s	5.39	7.55
4b	61	164—165	$C_{10}H_{12}N_2O_4$	53.61 (53.57	5.43 5.39	12.33 12.50)	1740, 1710, 1655		3.25 q (7.5)	5.56	7.41 7.45
4c	59	144—145	$C_{11}H_{14}N_2O_4$	55.23 (55.45	6.08 5.92	11.79 11.76)	1740, 1705, 1650		3.26 t (7.5)	5.58	7.40 7.44
4e	68	112—113	$C_{12}H_{16}N_2O_4$	57.12 (57.13	6.57 6.39	11.08 11.11)	1740, 1710, 1650		3.26 t (8.0)	5.57	7.39 7.45
4f	64	115—116	$C_{12}H_{16}N_2O_4$	56.89 (57.13	6.51 6.39	11.32 11.11)	1740, 1710, 1630		3.46 d (9.5)	5.50	7.40 7.44
4g	69	152—153	$C_{15}H_{14}N_2O_4$	63.07 (63.92	4.92 4.95	10.12 11.47)	1740, 1705, 1630		2.75 s	5.55	7.40 7.45

a) Measured in $CDCl_3$.

Found: C, 58.44; H, 5.12; N, 5.61%. Calcd for $C_{13}H_{14}NO_3Cl$: C, 58.32; H, 5.23; N, 5.23%.

3-Alkylidene- and Benzylidene-2,5-piperazinediones (2). A solution of **1** (0.1 mol) in ethanol (100 ml) was saturated with dry gaseous ammonia under cooling. When the solution was allowed to stand at room temperature for one day, crystalline substance precipitated. Ethanol was evaporated under reduced pressure and the residual crystals were collected and washed successively with cold water, ethanol, and then ether. Recrystallization from boiling water afforded colorless amorphous.[22]

In a similar manner, cyclization reaction of **1g** with ammonia was performed, and 3-benzylidene-2,5-piperazinedione (**2g**) was obtained as pale yellow prisms (58.8%), mp 279—280 °C(decomp.).[20] IR(KBr): 3200, 3050, 1690, 1620 cm^{-1}.

Found: C, 65.31; H, 4.86; N, 13.81%. Calcd for $C_{11}H_{10}N_2O_2$: C, 65.35; H, 4.95; N, 13.86%.

Acetylation of 2. A suspension of **2** (0.01 mol) in acetic anhydride (6 ml) was heated at 120—130 °C for half an hour, and the resulting solution was allowed to stand at room temperature for 1 hr. The reaction solution was concentrated under reduced pressure to dryness giving a crystalline residue. The crystalline product was collected and recrystallized from ethanol to afford two kinds of crystals, which were separated by chromatography on a silica-gel column by elution with a mixture of benzene and acetone (20 : 1) to give **3** and **4**. The results are summarized in Table 1.

Unsymmetric Unsaturated 3,6-Disubstituted-2,5-piperazinediones (5). a) Condensation of Mixture of 3 and 4 with Arylaldehyde in the Presence of Triethylamine (Procedure A). A mixture of **3** and **4**(*ca.* 3 : 7 ratio, *ca.* 2.4×10^{-3} mol) and the appropriate arylaldehyde (2.4×10^{-3} mol) was heated in the presence of triethylamine (0.12 g) at 120—130 °C for 3 hr. The resulting reddish solid mass was treated with ethanol and filtered. The collected crystals were recrystallized from glacial acetic acid to give the expected condensation product. The results are summarized in Table 2.

b) Condensation of 2 with Aralkyl- or Alkylaldehyde in the Presence of Sodium Acetate (Procedure B). A mixture of **2** (6×10^{-3} mol), the appropriate aldehyde (16×10^{-3} mol), and anhydrous sodium acetate (2.5 g) in acetic anhydride (4 ml) was heated at 120—130 °C for 5 hr and then allowed to stand overnight at room temperature. The mixture was treated with a small quantity of water and ether and filtered. The crystalline product was washed successively with ether and ethanol. Recrystallization from glacial acetic acid afforded the expected condensation product. The results are summarized in Table 3.

TABLE 2. 3-ALKYLIDENE-6-ARYLIDENE-2,5-PIPERAZINEDIONES (**5**) (Procedure A)

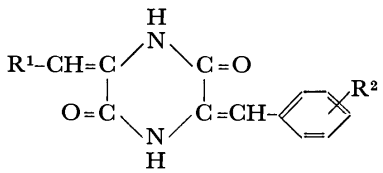

Substituents		Yield (%)	Mp °C[a]	Formula	Found, %			Calcd, %		
R^1	R^2				C	H	N	C	H	N
CH_3	H	67	294—296[b]	$C_{13}H_{12}N_2O_2$	68.33	5.52	11.98	68.41	5.30	12.27
CH_3	*o*-Cl	46	283—285[b]	$C_{13}H_{11}N_2O_2Cl$	59.59	4.21	10.37	59.43	4.19	10.69
CH_3	*p*-Cl	42	300—302[b]	$C_{13}H_{11}N_2O_2Cl$	59.41	4.28	10.58	59.43	4.19	10.69
CH_3	*m*-CH_3COO	58	250—251[c]	$C_{15}H_{14}N_2O_4$	62.84	4.66	10.02	62.93	4.93	9.79
CH_3	*p*-CH_3O	49	267—269[d]	$C_{14}H_{14}N_2O_3$	65.33	5.38	10.75	65.10	5.46	10.85
CH_3	*p*-CH_3	45	279—281[b]	$C_{14}H_{14}N_2O_2$	69.67	5.46	11.47	69.40	5.83	11.47
CH_3	*p*-NO_2	62	275—277[d]	$C_{13}H_{11}N_3O_4$	56.98	4.11	15.42	57.14	4.06	15.38
C_2H_5	H	61	268—280[b]	$C_{14}H_{14}N_2O_2$	69.58	5.71	11.45	69.40	5.83	11.56
C_2H_5	*o*-Cl	68	286—287[c]	$C_{14}H_{13}N_2O_2Cl$	60.58	4.71	10.04	60.76	4.70	10.13
C_2H_5	*p*-Cl	44	235—238[c]	$C_{14}H_{13}N_2O_2Cl$	60.51	4.89	10.23	60.76	4.70	10.13
C_2H_5	*m*-CH_3COO	41	237—238[c]	$C_{16}H_{16}N_2O_4$	64.12	5.26	9.48	63.99	5.39	9.33
C_2H_5	*p*-CH_3O	43	263—265[b]	$C_{15}H_{16}N_2O_3$	65.98	6.02	10.12	66.16	5.92	10.29
C_2H_5	*p*-CH_3	58	273—274[b]	$C_{15}H_{16}N_2O_2$	70.36	6.28	10.81	70.29	6.29	10.93
C_2H_5	*p*-NO_2	54	282—283[d]	$C_{14}H_{13}N_3O_4$	58.39	4.78	14.62	58.53	4.56	14.63
n-C_3H_7	H	42	276—278[b]	$C_{15}H_{16}N_2O_2$	70.29	6.30	10.78	70.29	6.29	10.93
n-C_3H_7	*o*-Cl	56	278—280[b]	$C_{15}H_{15}N_2O_2Cl$	62.11	5.28	9.31	61.97	5.19	9.64
n-C_3H_7	*m*-CH_3COO	53	269—270[b]	$C_{17}H_{18}N_2O_4$	65.08	5.67	9.10	64.95	5.77	8.91
n-C_3H_7	*p*-CH_3O	52	279—281[b]	$C_{16}H_{18}N_2O_3$	66.99	6.43	9.68	67.11	6.34	9.78
n-C_3H_7	*p*-CH_3	45	284—285[b]	$C_{16}H_{18}N_2O_2$	70.91	6.88	10.29	71.09	6.71	10.36
n-C_3H_7	*m*-NO_2	48	268—269[b]	$C_{15}H_{15}N_3O_4$	59.78	5.11	14.21	59.79	5.02	13.95
n-C_3H_7	*p*-NO_2	51	290—291[b]	$C_{15}H_{15}N_3O_4$	60.01	4.98	13.78	59.79	5.02	13.95
i-C_3H_7	*o*-Cl	52	267—268[b]	$C_{15}H_{15}N_2O_2Cl$	62.15	5.08	9.55	61.97	5.19	9.64
i-C_3H_7	*p*-Cl	53	241—243[b]	$C_{15}H_{15}N_2O_2Cl$	61.89	5.21	9.77	61.97	5.19	9.64
i-C_3H_7	*m*-CH_3COO	49	245—246[b]	$C_{17}H_{18}N_2O_4$	65.03	5.91	8.76	64.95	5.77	8.91
i-C_3H_7	*p*-CH_3	46	269—271[b]	$C_{16}H_{18}N_2O_2$	70.96	6.77	10.29	71.09	6.71	10.36
i-C_3H_7	*m*-NO_2	63	292—293[b]	$C_{15}H_{15}N_3O_4$	59.98	4.96	14.28	59.79	5.02	13.95
i-C_3H_7	*p*-NO_2	58	280—281[b]	$C_{15}H_{15}N_3O_4$	60.01	4.89	13.91	59.79	5.02	13.95

a) Decomposition. b) Yellow powder. c) Pale yellow powder. d) Brown powder.

TABLE 3. UNSYMMETRIC 3,6-DIALKYLIDENE AND 3-ALKYLIDENE-6-BENZYLIDENE-2,5-PIPERAZINEDIONES (**5**) (Procedure B)

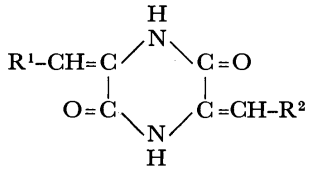

Substituents		Yield (%)	Mp °C[a]	Formula	Found (Calcd), %			UV Spectrum nm, in EtOH ($\varepsilon \times 10^3$)
R^1	R^2				C	H	N	
CH_3	$CH_3CH=CH$	36	305—306[b]	$C_{10}H_{12}N_2O_2$	62.32 (62.48	6.48 6.29	14.71 14.58)	321 (30.0)
CH_3	$C_6H_5CH=CH$	46	322—325[b]	$C_{15}H_{14}N_2O_2$	70.98 (70.85	5.23 5.55	10.91 11.02)	365 (27.7)
C_2H_5	$CH_3CH=CH$	18	311—312[c]	$C_{11}H_{14}N_2O_2$	63.85 (64.04	6.81 6.84	13.66 13.58)	
C_2H_5	$C_6H_5CH=CH$	68	304—306[b]	$C_{16}H_{16}N_2O_2$	71.57 (71.62	6.21 6.01	10.62 10.44)	365 (40.0)
n-C_3H_7	$CH_3CH=CH$	19	310—311[d]	$C_{12}H_{16}N_2O_2$	65.32 (65.43	7.44 7.32	12.69 12.72)	325 (30.9)
n-C_3H_7	$C_6H_5CH=CH$	65	307—309[b]	$C_{17}H_{18}N_2O_2$	72.33 (72.32	6.58 6.43	9.78 9.92)	365 (43.9)
i-C_3H_7	$CH_3CH=CH$	17	285—287[c]	$C_{12}H_{16}N_2O_2$	65.61 (65.43	7.41 7.32	13.01 12.72)	
i-C_3H_7	$C_6H_5CH=CH$	63	311—312[b]	$C_{17}H_{18}N_2O_2$	72.55 (72.32	6.28 6.43	9.77 9.92)	366 (42.4)
C_6H_5	$CH_3CH=CH$	18	286—288[b]	$C_{15}H_{14}N_2O_2$	71.01 (70.85	5.32 5.55	10.98 11.02)	345 (34.9)
C_6H_5	$C_6H_5CH=CH$	54	309—311[b]	$C_{20}H_{16}N_2O_2$	75.85 (75.93	5.23 5.10	8.85 8.86)	383 (51.7)
C_6H_5	$CH_3(CH_2)_5CH_2$	8	286—287[c]	$C_{18}H_{22}N_2O_2$	72.50 (72.45	7.44 7.43	9.58 9.39)	344 (37.0)

a) Decomposition. b) Yellow powder or needles. c) Pale yellow powder. d) Brown powder.

The One-Electron Reduction of Carbonium Ions. V. A Kinetic Study on the Reduction of the Substituted Cyclopropenium Ions with Cr(II)[1]

Kunio OKAMOTO, Koichi KOMATSU, and Akira HITOMI

Department of Hydrocarbon Chemistry, Faculty of Engineering, Kyoto University, Sakyo-ku, Kyoto 606

(Received July 13, 1973)

The one-electron reduction of a series of phenyl- and/or *n*-propyl-substituted cyclopropenium ions with Cr(II) has been carried out in a 10% HCl solution. The reduction of triphenylcyclopropenium (Ia), diphenyl-*n*-propylcyclopropenium (Ib), and phenyldi-*n*-propylcyclopropenium (Ic) ions quantitatively gives dimers of the respective cyclopropenyl radicals, *i.e.*, the bis(cyclopropenyl) derivatives, whereas the tri-*n*-propylcyclopropenium ion (Id) is quite unreactive. A kinetic study has shown that the reactivity of these stable carbonium ions toward the one-electron reductant (Cr(II)) is lowered with a decrease in the number of the phenyl substituent: $k_2^{25\,°C}$= 3.0×10^{-4} l/g-ion·s for Ia, 2.7×10^{-6} l/g-ion·s for Ib, 2.8×10^{-9} l/g-ion·s for Ic, and $<10^{-11}$ l/g-ion·s for Id. The added NaCl was found to accelerate the reduction rate of Ia, whereas the added HCl showed an initial rate enhancement effect, followed by a slight rate-retarding effect. A plot of log k_2 against the electron affinities of the respective cations, estimated from the transition energies of the charge-transfer bands for Ia,b with pyrene, has been found to fit a linear correlation previously obtained for a series of tropylium ions. The values of log k_2 also exhibit a linear free-energy relationship with the pK_{R^+} of these cations.

In previous papers of this series[2] we have reported on the reducibility of various substituted tropylium ions with Cr(II). It was demonstrated that log k_2 for the one-electron reduction of the tropylium ions has a linear free-energy relationship with the electron affinity, the polarographic half-wave potential, and also with the pK_{R^+} values; thus, the log k_2 can be regarded as a relative measure for the electron affinity of the carbonium ions in solution. In order to examine the applicability of this method for stable carbonium ions other than the tropylium ions, we have now investigated the chromous-ion reduction of a series of phenyl- and/or *n*-propyl-substituted cyclopropenium ions.

In their systematic studies of the synthesis and stability of substituted cyclopropenium ions,[3] Breslow and his coworkers have reported on the polarographic reduction of some *p*-substituted triphenylcyclopropenium ions[3c] and have interpreted the results on the basis of HMO calculations. They have also reported on the zinc reduction of the triphenylcyclopropenium ion to give its dimer,[3b] but no kinetic study of the one-electron reduction for this series of stable carbonium ions seems to have been carried out. In this paper, the results of the kinetic measurements and their correlation with the electron affinities and pK_{R^+}'s of the cyclopropenium ions will be discussed in comparison with the results[2] previously obtained for a series of substituted tropylium ions.

Results and Discussion

One-Electron Reduction of the Cyclopropenium Ions (Product Study). A series of cyclopropenium ions substituted with a phenyl and/or *n*-propyl group (Ia-d) was prepared according to the method of Breslow *et al.*,[3d,f] except for Ic, which is a new compound and which was synthesized by analogy with the synthesis of Id.[3f]

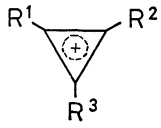

I

	R_1	R_2	R_3
Ia	Ph	Ph	Ph
Ib	Ph	Ph	*n*-Pr
Ic	Ph	*n*-Pr	*n*-Pr
Id	*n*-Pr	*n*-Pr	*n*-Pr

The reduction of the cyclopropenium ions, Ia-d, with the chromous ion was carried out in 10% HCl (2.9 M) under an atmosphere of nitrogen at an appropriate temperature (Ia : 25 °C, Ib: 75 °C, Ic,d: 125 °C).[4] Ia, Ib, and Ic were found to be reduced with Cr(II) to give dimers in almost quantitative yields, as in the case of the zinc reduction of Ia.[3b] The reduction products of Ia and Ib were purified by thin-layer chromatography and were identified as bis(1,2,3-triphenyl-2-cyclopropen-1-yl) (II) and bis(1,2-diphenyl-3-*n*-propyl-2-cyclopropen-1-yl) (III) respectively. On the other hand, the reduction of Ic with Cr(II) was too slow to give the reduction product in an amount sufficient for the structural analysis. Therefore, Ic was reduced with zinc powder for the purposes of the product analysis. Preparative thin-layer chromatography showed that the product was the same as in the case of the chromous-ion reduction and that it contained bis(1,2-di-*n*-propyl-3-phenyl-2-cyclopropen-1-yl) (IV) and bis(2,3-di-*n*-propyl-1-phenyl-2-cyclopropen-1-yl) (V) in almost equal amounts. The cation, Id, was quite inert to the chromous-ion reduction and gave a trace of an unidentified oil only, after a reaction time of 48 hr at 125 °C.

1) Presented in part at the 22nd Symposium on the Organic Reaction Mechanism, Nagoya, October, 1971.

2) a) K. Okamoto, K. Komatsu, O. Murai, and O. Sakaguchi, *Tetrahedron Lett.*, **1972**, 4989; b) Part III: K. Okamoto, K. Komatsu, S. Tsukada, and O. Murai, This Bulletin, **46**, 1780 (1973); c) Part IV: K. Okamoto, K. Komatsu, O. Murai, O. Sakaguchi, and Y. Matsui, *ibid.*, **46**, 1785 (1973).

3) a) R. Breslow and C. Yuan, *J. Amer. Chem. Soc.*, **80**, 5991 (1958); b) R. Breslow and P. Cal, *ibid.*, **81**, 4747 (1959); c) R. Breslow, W. Bahary, and W. Reinmuth, *ibid.*, **83**, 1763 (1961); d) R. Breslow and H. W. Chang, *ibid.*, **83**, 2367 (1961); e) R. Breslow, J. Lockhart, and H. W. Chang, *ibid.*, **83**, 2375 (1961); f) R. Breslow, H. Höver, and H. W. Chang, *ibid.*, **84**, 3168 (1962).

4) A control experiment showed that either the carbonium ion or the chromous ion was stable enough at the respective temperature.

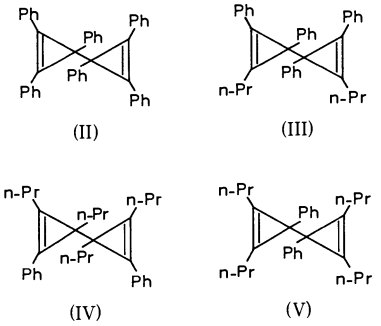

Kinetic Measurements for the Reduction of the Triphenylcyclopropenium Ion with Cr(II). The Effect of the Added Anion. The reactions of the triphenylcyclopropenium ion (Ia) with a large excess of Cr(II) were conducted in 2.9 M HCl under an atmosphere of nitrogen, and the decrease in the unchanged carbonium ion was followed by ultraviolet spectroscopy; in all cases, good first-order behavior was observed. The first-order rate constants thus obtained were proportional to the initial concentrations of Cr(II), as is shown in Fig. 1 for the reactions at 30 °C, indicating that the overall reaction rate can be expressed by the ordinary second-order rate equation: rate$=k_2$[Ia]·[Cr(II)]. The second-order rate constants determined in this way at various temperatures are listed in Table 1. From the Arrhenius plot, the values of an activation energy and an activation entropy were estimated to be 13.9 kcal/mol and −7.1 e.u. at 25 °C.

In a previous mechanistic study,[2b] the chloride ion added either as HCl or NaCl was shown to accelerate the chromous-ion reduction of the tropylium ion, possibly because of the effectiveness of the chloride ion in forming an electron-transfer bridge between the two

Table 1. Rates of the chromous-ion reduction of the triphenylcyclopropenium ion (Ia) in 2.9 M HCl

Temp. °C	Initial concn $[Ia]_0$ g-ion/l	Initial concn $[Cr(II)]_0$ g-ion/l	$10^4 \cdot k_2$ l/g-ion·s	Number of measurements
25.0	6.87×10^{-4}	0.139	3.0±0.2	5
30.0	2.99×10^{-4}	0.198	5.4±0.4	7
35.0	2.75×10^{-4}	0.158	8.0±0.5	4
45.0	2.77×10^{-4}	0.141	15.2±0.7	3
50.0	3.02×10^{-4}	0.130	22.2±1.9	4

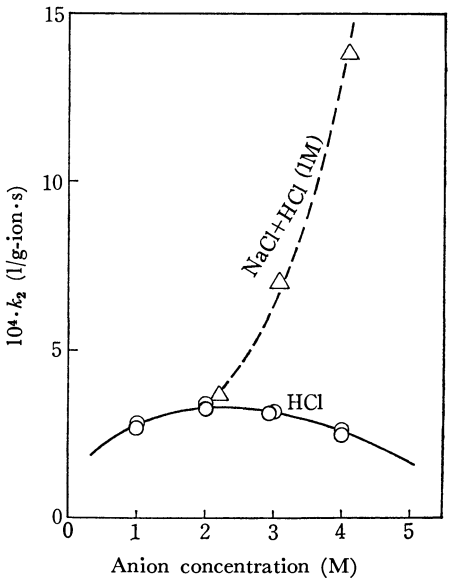

Fig. 2. The effect of an added anion on the reduction rate of Ia with Cr(II) at 25 °C.
○: Effect of HCl concentration. ($[Ia]_0=1.6\times10^{-3}$ g-ion/l, $[Cr(II)]_0=0.14$ g-ion/l)
△: Effect of the concentration of NaCl added to 1 M HCl. ($[Ia]_0=7.8\times10^{-4}$ g-ion/l, $[Cr(II)]_0=0.14$ g-ion/l)

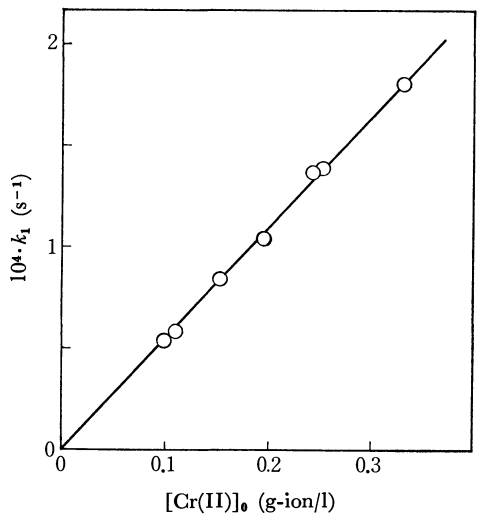

Fig. 1. Dependence of the first-order rate constant (k_1) for the chromous-ion reduction of Ia on the initial concentration of Cr(II).
$[Ia]_0$: 3.0×10^{-3} g-ion/l, Temperature: 30.0 °C, Solvent: 2.9 M HCl

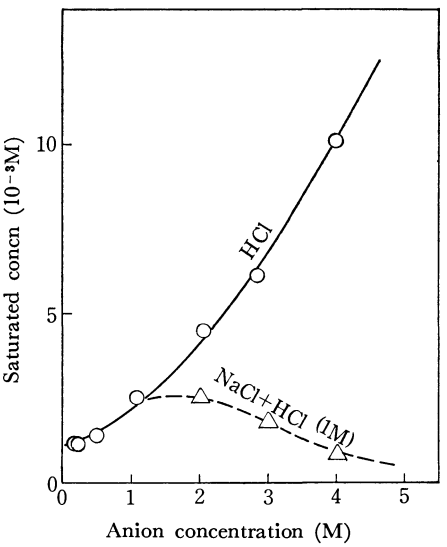

Fig. 3. The effect of an added anion on the saturated concentration of Ia in aqueous HCl solution.
○: Effect of HCl concentration.
△: Effect of the concentration of NaCl added to 1 M HCl.

Table 2. Rates of the chromous-ion reduction of the cyclopropenium ions (Ia-d) in 2.9 M HCl

Cyclopropenium ion	Temp. °C	Initial concn $10^3[I]_0$ g-ion/l	Initial concn $10[Cr(II)]_0$ g-ion/l	k_2 l/g-ion·s	ΔE_a kcal/mol
Ia	25.0	1.51	1.31	3.01×10^{-4}	13.9
Ib	75.0	2.30	2.81	4.85×10^{-4}	—
	50.0	2.30	2.81	4.45×10^{-5}	—
	25.0	—	—	2.72×10^{-6} a)	21.3
Ic	125.0	2.31	6.50	1.53×10^{-5}	—
	100.0	2.31	6.50	2.75×10^{-6}	—
	25.0	—	—	2.78×10^{-9} a)	20.2
Id	125.0	3.77	6.68	$<10^{-6}$ c)	—
	25.0	—	—	$<10^{-11}$ b)	—

a) Extrapolated from the data at elevated temperatures.
b) Estimated by the assumption that the activation energy is the same as in the case of Ic.
c) An estimated value (see Experimental).

reagents. It was observed that this rate-increasing effect gradually reaches its maximum in the anion concentration range of 3—4 g-ion/l; consequently, the reaction was expected to proceed completely by way of the chloride-ion bridging in this concentration range. Therefore, 10% HCl (2.9 M) was chosen as the standard solvent for the previous study on the reduction of the substituted tropylium ions[2c] and also for the present study.

However, the effects of the added HCl and NaCl[5] on the reduction rate of the triphenylcyclopropenium ion characteristically showed different tendencies from each other, as is shown in Fig. 2; addition of NaCl brings about a remarkable rate-enhancement, whereas the increase in the HCl concentration results in an initial rate-enhancement, followed by a slight rate-retarding effect. On the other hand, the effects of the concentration of added HCl and/or NaCl on the solubility (saturation concentration) of the carbonium ion (Fig. 3) exhibit a reversal of the tendency of the reduction rate (Fig. 2). From a comparison of the tendencies shown in Figs. 2 and 3, it may be supposed that undissociated HCl molecules (or $[H\text{-}Cl\text{-}H]^+$ ions), which are predominant at higher HCl concentrations, strongly stabilize or solvate the carbonium ion, thus icreasing the solubility but preventing an attack by Cr(II), whereas the free Cl^- ions from the added NaCl suppress the solubility but facilitate the chromous-ion reduction by means of a ready formation of a Cl^- bridge between the two reagents.

Kinetic Measurements for the Reduction of the Cyclopropenium Ions with Cr(II). The second-order rate constants for the chromous-ion reduction of Ia, Ib, Ic, and Id are listed in Table 2. It is apparent that the substitution of *n*-propyl group for the phenyl group brings about a great suppression in the reactivity of the cyclopropenium ions. This is in accord with the increase in the stability of the cyclopropenium ion by the substitution of the *n*-propyl group, as has already been reported;[3f] this is the same trend as is seen in the reduction of the substituted tropylium ions, although the latter reaction is much more rapid.[2]

Correlation of the Reducibility with the Electron Affinity and with pK_{R^+}. Several examples of charge-transfer (C.T.) interactions between carbonium ions and some aromatic hydrocarbons have been reported,[6] and the relationship between the C. T. transition energy and the electron affinity of the carbonium ion has been discussed.[6c,e,f] We also observed the C.T. band when the cyclopropenium ions, Ia and Ib, were added to a 1,2-dichloroethane solution of pyrene. The values of the electron affinity were estimated from the C.T. transition energies by a method previously reported by Feldman and Winstein,[6e] and the correlation of $\log k_2$ with the electron affinity was examined together with

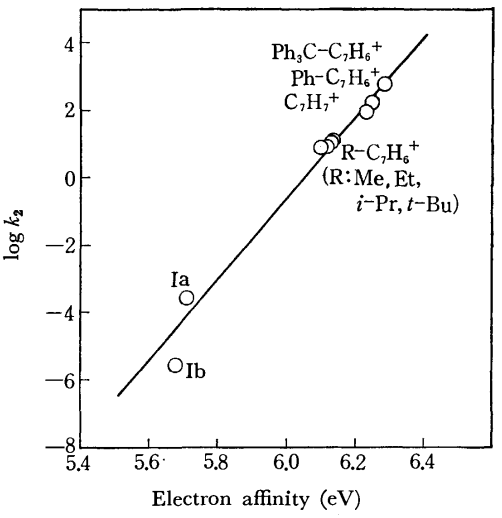

Fig. 4. The correlation of $\log k_2$ with electron affinities of the carbonium ions.

5) Because of the poor solubility of the triphenylcyclopropenium ion in a dilute HCl solution (<1M), the effect of HCl in concentrations of less than 1 M was not examined.

6) a) M. Feldman and S. Winstein, *J. Amer. Chem. Soc.*, **83**, 3338 (1961); b) M. Nepras and R. Zahradnik, *Collct. Czech. Chem. Commun.*, **29**, 1545 (1964); c) M. Feldman and B. G. Graves, *J. Phys. Chem.*, **70**, 955 (1966); d) S. N. Bhat and C. N. R. Rao, *J. Chem. Phys.*, **47**, 1863 (1967); e) M. Feldman and S. Winstein, *Theor. Chim. Acta*, **10**, 86 (1968); f) H. J. Dauben, Jr., and J. D. Wilson, *Chem. Commun.*, **1968**, 1629; g) T. G. Beaumont and K. M. C, Davis, *J. Chem. Soc., B*, **1968**, 1010.

Table 3. Results of the measurements of reduction rates, charge-transfer bands, and pK_{R^+}'s of the stable carbonium ions

Carbonium ion	log k_2[a]	C. T. band[b]		pK_{R^+}[d]	
		λ_{max}, mμ	$E_{aff.}$[c], eV	Obsd	Lit.[3f]
Cyclopropenium ion					
Ia	−3.51	~420	~5.71	2.6	2.8
Ib	−5.57	~415	~5.68	4.0	3.8
Ic	−8.56	—	—	5.6	—
Id	<−11	—	—	—	7.2[e]
Tropylium ion[f]					
Trityl	2.75	550—560	6.27—6.30	3.6	
Phenyl	2.16	543	6.25	4.1	
Unsubst'd	1.87	540	6.24	4.3	
Methyl	1.05	513	6.13	—	
Ethyl	1.01	512	6.13	—	
Isopropyl	0.91	505	6.10	—	
t-Butyl	0.90	508	6.11	5.0	

a) The logarithmic value of the rate constant for the chromous-ion reduction of the respective carbonium ion. b) Measured in 1,2-dichloroethane with pyrene as a donor. c) Estimated by the method reported by Feldman and Winstein from the relation, $E_{CT}=[I_p]_{Donor}-[E_{Aff}]_{Acceptor}+Const.$ (Ref. 6e) d) Measured spectrophotometrically in 23% ethanol. e) Determined by potentiometric titration in 50% aq. acetonitrile. f) Data from Ref. 2c.

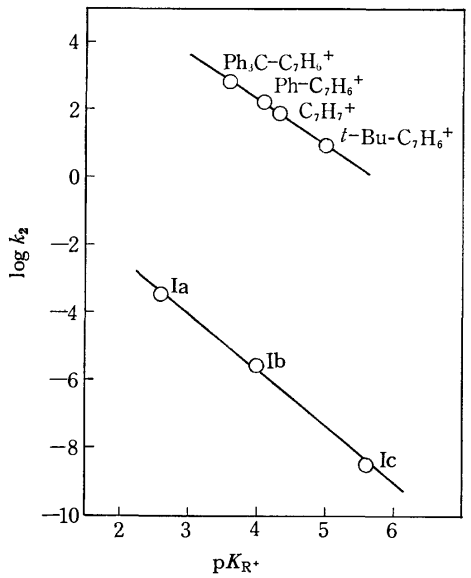

Fig. 5. The correlation of log k_2 with pK_{R^+}.

the cases of substituted tropylium ions. From the results shown in Table 3 and Fig. 4, it may be seen that the linear relationship observed between the chromous-ion reducibility and the electron affinity of the substituted tropylium ion extends also to the cyclopropenium system, suggesting that the reduction of the tropylium and cyclopropenium ions proceeds by a similar mechanism, with the electron-transfer step as the rate-determining one.[7] Thus, it seems that the value of log k_2 for the chromous-ion reduction may be regarded as a chemical criterion for the electron affinity of the stable carbonium ions in solution.

A plot of log k_2 against the pK_{R^+} values measured spectrophotometrically in 23% ethanol[3f] also exhibits a good linear relationship, as is shown in Fig. 5. The straight line thus obtained apparently lies parallel with that obtained in the case of the substituted tropylium ions. From the definition, pK_{R^+} value is represented as the difference between log k_b and log k_f, where k_f denotes the rate constant for the hydrolysis of the carbonium ion, and k_b, that for the reverse reaction.

$$R^+ + H_2O \underset{k_b}{\overset{k_f}{\rightleftharpoons}} ROH + H^+$$

It may be supposed that log k_2 (a measure for the electron affinity) might linearly correlate with log k_f (a measure for the electrophilicity of R^+), but not with k_b (a measure for the nucleophilicity of ROH). This may be one of the reasons for the separation of the plot of log k_2 *vs.* pK_{R^+} into two lines (in Fig. 5); further relevant studies remain to be done before we can account for these tendencies.

Experimental[8]

Materials. All the reagents employed were of a reagent-grade quality except when otherwise noted. Acetonitrile and ethyl acetate were refluxed and distilled over phosphorus pentoxide; acetonitrile, bp, 81.0—81.3 °C; ethyl acetate, bp, 77.0—77.5 °C. Ethyl ether was dried over sodium metal.

7) In view of the effects of the added HCl and NaCl, the reduction of cyclopropenium ions in 2.9 M HCl may not proceed completely by way of Cl^- bridging, and thus the values of k_2 measured in 2.9 M HCl may be rather smaller than those for the complete Cl^- bridging. However, this uncertainty is assumed to be within one unit in the log k_2 scale; therefore, the log k_2-E_{Aff} plot (Fig. 4) may be regarded as still linear, even if we take this uncertainty into consideration.

8) The melting points and boiling points are uncorrected. The microanalyses were performed by the Microanalytical Center, Kyoto University, Kyoto. The infrared and ultraviolet spectra were taken on Shimadzu models IR-27 and UV-50 M spectrometers respectively. The 60 MHz and 100 MHz NMR spectra were obtained with a JEOL model JNM-3H-60 spectrometer and a Varian model HA-100D spectrometer respectively, with tetramethylsilane as the internal standard.

Triphenylcyclopropenium fluoroborate ($Ia \cdot BF_4^-$) was prepared from triphenylcyclopropenyl methyl ether[3a] as follows. Into a solution of 0.964 g (3.23 mmol) of triphenylcyclopropenyl methyl ether in 15 ml of methanol, we added 1.0 ml of 42% aqueous fluoroboric acid. The white precipitates which were immediately formed were collected, washed with dry ethyl ether, and dried under reduced pressure to give 0.925 g (2.62 mmol) of $Ia\text{-}BF_4^-$ as white crystals; 81.1% yield; mp 308—310 °C (dec); $\lambda_{max}^{2.9M\ HCl}$ 259 nm (ε, 18100), 309 nm (64100), 324 nm (54500).

Diphenyl-*n*-propylcyclopropenium fluoroborate ($Ib \cdot BF_4^-$) was prepared following the method of Breslow *et al.*;[3f] mp 175—177 °C (dec) (lit,[3f] mp 179 °C (dec)); $\lambda_{max}^{2.9M\ HCl}$ 246 nm (ε, 15700), 293 nm (33600), 307 nm (34400) (lit,[3f] $\lambda_{max}^{1M\ HCl-23\%\ EtOH}$ 292 nm (ε, 32000), 305 nm (33000)).

Di-*n*-propylphenylcyclopropenium prechlorate ($Ic\text{-}ClO_4^-$) was prepared from the di-*n*-propylcyclopropenium ion[3f] as follows. To a suspension of 1.503 g (6.74 mmol)of di-*n*-propylcyclopropenium perchlorate in 10 ml of dry ethyl ether, we slowly added 20 ml of a 1 M ethereal solution of phenyllithium (20 mmol) with vigorous stirring at −78 °C. The stirring was continued for 1 hr at −78° C and then for an additional hour at room temperature. To the reaction mixture we then added 30 ml of 1M HCl, and the aqueous layer was extracted with three 40-ml portions of ethyl ether. The combined ethereal solution was washed with 10% NaCl and dried over $MgSO_4$. The solvent was removed *in vacuo* to give 1.60 g of a brownish oil which was supposed to be crude 1,2-di-*n*-propyl-3-phenyl-1-cyclopropene. To this oil we then added a solution of 0.769 g (2.25 mmol) of triphenylmethyl perchlorate[9] in 24 ml of acetonitrile, and the whole mixture was left to stand for 30 min at room temperature. The solvent was evaporated under reduced pressure. Then, 10 ml of ethyl acetate and 100 ml of dry ethyl ether were added to the dark-brown residual oil to cause the formation of white precipitates. The precipitates were collected, washed with dry ethyl ether, and dried *in vacuo* to give 0.537 g (1.89 mmol) of $Ic \cdot ClO_4^-$ as white crystals, which can be recrystallized from chloroform-ethyl ether; 80.0% yield, based on triphenylmethyl perchlorate; mp 157.5—158.5 °C (dec); $\lambda_{max}^{2.9M\ HCl}$ 262 nm (ε, 26400); NMR (100 MHz), τ_{CDCl_3} 2.89 (d, 2H, *ortho* protons), 3.10 (t, 1H, *para* proton), 3.25 (t, 2H, *meta* protons), 7.08 (t, 4H, α-methylene protons), 8.23 (sext, 4H, β-methylene protons), 9.07 (t, 6H, methyl protons); ν_{max}^{KBr} 695, 780, 1095, 1440, 1460(sh), 1500, 1600, 2900, 3000 cm^{-1}.

Found: C, 60.26; H, 6.49%. Calcd for $C_{15}H_{19}ClO_4$: C, 60.30; H, 6.41%.

Tri-*n*-propycylopropenium perchlorate ($Id \cdot ClO_4^-$) was prepared according to the method of Breslow *et al.*;[3f] mp 183.5—185 °C (lit,[3f] 184—185 °C)

A solution of chromous chloride in 2.9 M HCl was prepared as previously reported.[2c]

One-Electron Reduction of the Cyclopropenium Ions. Reduction of Ia with Cr(II). In a 200-ml, four-necked flask equipped with a mechanical stirrer, a serum rubber cap, and a nitrogen inlet and outlet, there was charged a solution of 0.105 g (0.295 mmol) of $Ia \cdot BF_4^-$ in 100 ml of 2.9 M HCl. To this solution we then added 20 ml of a 1.17 M solution of chromous chloride in 2.9 M HCl by the use of a hypodermic syringe. The solution was stirred at 25 °C for 21 hr under an atmosphere of nitrogen, and then the organic product was extracted with four 100-ml portions of *n*-hexane, washed with 10% NaCl, and dried over $MgSO_4$. The solvent was subsequently removed *in vacuo* to give 0.0758 g (0.142 mmol) of bis(1,2,3-triphenyl-2-cyclopropen-1-yl) (II) as white crystals; 96.2% yield; mp 223—225 °C (lit.,[3c] mp 225—226 °C); NMR (60 MHz), τ_{CDCl_3} 2.65 (br.s, phenyl protons).

Reduction of Ib with Cr(II). In the same manner, the reduction of 0.131 g (0.409 mmol) of $Ib \cdot BF_4^-$ with 46 mmol of chromous chloride was carried out in 160 ml of 2.9 M HCl at 75 °C for 22 hr under a nitrogen atmosphere. The reaction mixture was worked up in the same way to give 0.0927 g of a crude product, which was then purified by the use of preparative thin-layer chromatography over silica-gel (Merck, Kieselgel PF_{254}), with *n*-hexane–benzene (3 : 1) as the solvent, to give 0.0781 g (0.168 mmol) of bis(1,2-diphenyl-3-*n*-propyl-2-cyclopropen-1-yl) (III) as white crystals; 82.1% yield; mp 152—159 °C (with rapid resolidification[10]); λ_{max}^{EtOH} 267 nm (ε, 16300); ν_{max}^{KBr} 690, 700, 760, 800, 1025, 1090, 1265, 1440, 1495, 1600, 1850, 3000 cm^{-1}; NMR (100 MHz), τ_{CCl_4} 2.78, 2.97 (m and s, 20H, phenyl), 7.30 (t, 4H, α-methylene), 8.30 (sext, 4H, β-methylene), 8.99 (t, 6H, methyl).

Reduction of Ic with Zn and with Cr(II). In a similar manner, 2.0 g (30 mg-atom) of zinc powder was added to a solution of 0.201 g (0.670 mmol) of $Ic \cdot ClO_4^-$ in 85 ml of 0.1 M HCl; the mixture was then magnetically stirred at 20 °C for 5 hr under an atmosphere of nitrogen. Then the unchanged zinc was filtered off and washed with four 50-ml portions of ethyl ether. The aqueous solution was extracted with three 70-ml portions of ethyl ether, and the combined ethereal solution was washed with 10% NaCl, dried over $MgSO_4$, and evaporated to give 0.130 g of a partially-solidified yellowish oil, which gave three main spots (R_f, 0.23, 0.4—0.5, and 0.67) on a silica-gel thin-layer plate, with *n*-hexane–benzene (9 : 1) as the solvent. By the use of preparative thin-layer chromatography, a component with R_f 0.67 was isolated as 0.0512 g of a colorless oil and was identified as bis(1,2-di-*n*-propyl-3-phenyl-2-cyclopropen-1-yl) (IV: 0.129 mmol; 38.5% yield; $\nu_{max}^{CCl_4}$ 695, 1380, 1440, 1460, 1490, 1600, 1830, 2900, 2970, 3000 cm^{-1}; NMR (60 MHz),[11] τ_{CCl_4} 2.70 (s, 10H, phenyl), 7.80 (m, 8H, α-methylene), (m, ~8H, β-methylene), 9.00 (m, ~12H, methyl). In the same way, a component with R_f 0.23 was isolated as 0.0527 g of white crystals and was identified as bis(2,3-di-*n*-propyl-1-phenyl-2-cyclopropen-1-yl) (V); 0.133 mmol; 39.7% yield; mp 26.0—28.0 °C; λ_{max}^{EtOH} 240 nm (ε, 9400), 273 nm (sh) (1100), 280 nm (763); $\nu_{max}^{CCl_4}$ 700, 1380, 1440, 1450, 1460, 1490, 1600, 1870, 2900, 2970, 3000 cm^{-1}; NMR (100 MHz),[12] τ_{CCl_4} 3.00 (s, 10H, phenyl), 7.56 (t, 8H, α-methylene), 8.43 (sext, 8H, β-methylene), 9.04 (t, 12H, methyl). On the other hand, the component with R_f 0.4—0.5 gave 0.0202 g of a pale yellow oil, which exhibited an infrared spectrum quite similar to those of IV and V, though its structure was not fully identified.

For the purpose of comparing the reaction products, a reduction of Ic with Cr(II) was conducted in the following way. To a solution of 0.0164 g (0.0548 mmol) of $Ic \cdot ClO_4^-$ in 8.0 ml of 2.9 M HCl placed in a 20-ml ampoule we added

9) H. J. Dauben, Jr., L. R. Honnen, and K. M. Harmon, *J. Org. Chem.*, **25**, 1442 (1960).

10) This resolidification may indicate a thermal rearrangement of III to a tetraphenyldi-*n*-propylbenzene derivative, as was observed in the case of II,[3b] but no further investigation on the rearranged material was attempted.

11) The chemical shift of the phenyl protons shows that the phenyl group is attached to an olefinic carbon; also the complex multiplicity of the signals of propyl groups seems to indicate the presence of two types of propyl groups with different magnetic environments.

12) The phenyl group has been shown to be attached to a saturated carbon, while the propyl group is supposed to be of only one type for reasons previously presented.[11]

8.0 ml of a 1.3 M solution of chromous chloride in 2.9 M HCl by the use of a hypodermic syringe under a stream of nitrogen. The ampoule was immediately sealed under nitrogen and immersed in an oil bath thermostated at 125 °C. After 20 hr the organic products were extracted with three 20-ml portions of ethyl ether, washed with 10% NaCl, and dried over $MgSO_4$. The evaporation of the ethereal solution under reduced pressure gave 0.0112 g of a partially-solidified, yellowish oil, which was found to contain the same products in the same composition as in the case of the zinc reduction of Ic described above, on the basis of an analysis with thin-layer chromatography.

Attempted Reduction of Id with Cr(II). The reaction of 0.0193 g (0.0730 mmol) of $Id \cdot ClO_4^-$ with the chromous ion (2.64 mg-ion) in 4.0 ml of 2.9 M HCl at 125 °C was attempted in an ampoule in the same way as has been described above. After 48 hr, the solution was worked up in the same way to give 0.0031 g of an unidentified oil. This was shown to contain the same components as in the case of the control experiments in which the cation, Id, alone was kept at 125 °C under the same conditions. The acidic aqueous layer was made alkaline with 10% NaOH, and the turbid solution which resulted was worked up in the usual way to give 0.0093 g of a colorless oil which was tentatively identified as 1,2,3-tri-*n*-propyl-2-propen-1-one on the basis of its infrared spectrum and also by analogy with the alkaline ring opening of Ia giving 1,2,3-triphenyl-2-propen-1-one;[3a] 0.056 mmol; 77% yield; $\nu_{max}^{CCl_4}$ 1380, 1460, 1665, 2900, 2980 cm^{-1}.

Kinetic Measurements. The rates of the reduction of Ia and of Ib were measured in the following way. A solution of a weighed amount of the cyclopropenium salt in 40 ml of 2.9 M HCl was charged in a 100-ml, four-necked flask equipped with a mechanical stirrer, a serum rubber cap, and a nitrogen inlet and outlet. The solution was bubbled with nitrogen for 10 min, while the reaction flask was placed in a thermostated bath. To this solution we then added a known amount (4.0—12.0 ml) of a 1.30 M solution of chromous chloride in 2.9 M HCl by the use of hypodermic syringe, and the solution was stirred under an atmosphere of nitrogen. At appropriate time intervals, 2.00-ml aliquots were sampled out by the use of a hypodermic syringe, extracted with three 5-ml portions of *n*-hexane, and diluted to a 100-fold volume with 2.9 M HCl. The amount of the unchanged cyclopropenium ion was analyzed on the diluted solution by means of ultraviolet spectrophotometry, using 308 nm (ε, 52800) as the characteristic band for Ia and 307 nm (ε, 34400) for Ib. The rate constants were calculated from the first-order rate equation and treated as has been described in text. The initial concentrations of the cyclopropenium ion and of the chromous ion were determined by ultraviolet spectroscopy and by iodometry respectively.

The kinetic measurements of the reduction of Ic were conducted by the use of the sealed-ampoule technique. To 1.0-ml portions of the solution of Ic in 2.9 M HCl placed in ampoules we added 1.0-ml portions of a 1.30 M solution of chromous chloride in 2.9 M HCl under a stream of nitrogen. The ampoules were immediately sealed and immersed in a thermostated bath. At appropriate time intervals the ampoules were opened and the amount of the unchanged cyclopropenium ion was determined spectrophotometrically, using 262 nm (ε, 26400) as the characteristic band; the results were then treated according to the first-order rate equation.

As has been mentioned in the previous section, the cation, Id, was not appreciably reduced with the chromous ion and was recovered in a 77% yield under the given reaction conditions. Even when it is assumed that the unrecovered amount corresponds to the reduction products which might have been decomposed to unidentified materials, a 77% recovery after the reaction time of 48 hr in the presence of 0.66 M of the chromous chloride gives the value of 2.3×10^{-6} $M^{-1} \cdot s^{-1}$ for the upper limit of the apparent second-order rate constant; the real rate constant must be much smaller than this value.

The solubility of $Ia \cdot BF_4^-$ in Aqueous HCl with and without NaCl. In 10-ml test tubes with ground glass stoppers we placed various mixture of 0.010-g portions of $Ia \cdot BF_4^-$ with 2.0-ml portions of either aqueous HCl or aqueous HCl containing NaCl; the mixtures were shaken vigorously for 50 hr at 15—21 °C. Each mixture was then filtered, and amount of Ia dissolved in the filtrate was determined by ultraviolet spectroscopy; the results are shown in Fig. 3.

Measurements of the Charge-Transfer Bands with Pyrene. 1,2-Dichloroethane solutions of the cyclopropenium ion (3×10^{-3} g-ion/l) and of pyrene (2×10^{-3} M) were mixed in the dark[13] to give a slightly orange-colored, yellowish solution, and its visible spectrum was immediately recorded. In the cases of Ia and Ib, a widely-absorbing shoulder, which was not observed in the spectrum of either single component, appeared at the longer wavelength. These new absorptions were supposed to be due to formation of charge-transfer complexes; the values of the wavelength corresponding to the midpoint of the new band are listed in Table 3.

On the other hand, only the end absorption was observed in the region of wavelengths longer than pyrene in the cases of Ic and Id.

Determination of pK_{R^+}*'s.* The pK_{R^+}'s of Ia, Ib, and Ic were determined in 23% aqueous ethanol at 25 °C, as has been described by Breslow and Chang,[3d] by the use of the spectrophotometric method. Because the characteristic bands of the cations were found to decrease during the measurements for Ib and Ic, the absorbancy, which was extrapolated to the time of the dissolution of the cations, was plotted against pH to give classical titration curves, whose inflection points were taken as pK_{R^+}'s. The pH's were read on a Horiba model H pH meter calibrated with standard buffers before use.

The authors wish to thank Mr. Osamu Murai for assistance in the measurements of the charge-transfer spectra.

13) It was observed that the exposure of the mixed solution to room light caused the appearance of new absorption bands at 430 and at 455 nm which seemed to be due to some photochemical reaction products, but the nature of the reaction was not investigated further.

NOTES

BULLETIN OF THE CHEMICAL SOCIETY OF JAPAN, VOL. 46, 3887—3888 (1973)

Acidity of Hydrated Sulfates Revealed by the Enolization of Acetone

Ken-ichi TANAKA

Research Institute for Catalysis, Hokkaido University, Sapporo 060

(Received April 10, 1973)

In previous papers,[1,2] an equation for electronegativity of the metal ions was derived by extending Mulliken's electronegativity concept[3] as follows.

$$X_i = \frac{\partial \sum I_j}{\partial Z} = (1+2Z)X_0 \qquad (1)$$

where I_j, is the j-th ionization potential, Z is the valence number of the ion and X_0 is the electronegativity of the metal ($Z=0$) with the Pauling scale. The electronegativity of the metal ions given by Eq. (1) has been found to be a good parameter of the acidity of the metal ions;[1,2,3] the ionization equilibrium (pK_a), $M(H_2O)_m^{\alpha+}+H_2O \leftrightharpoons H_3O^+ + M(H_2O)_{m-1}(OH)^{\alpha-1}$, being represented by

$$pK_a = 20\left(1-\frac{X_i}{14}\right) \qquad (2)$$

and the zero point of charge (ZPC) of the immersed oxides in water being formulated as follows.

$$ZPC = 16.8\left(1-\frac{X_i}{22}\right) \qquad (3)$$

The catalytic activities of the sulfates for reactions such as hydration of propylene, dehydration of formic acid and polymerization of acetaldehyde are well correlated with the electronegativity of the metal ions.[2,4]

In this paper, the enolization of acetone is adopted as a monitor of the acidity of the hydrated sulfates, which has been found to be subject to general acid catalysis in homogeneous catalysis.

Experimental

A flow system with nitrogen carrier gas was employed. The carrier gas was bubbled through evaporating chambers of acetone (spectro grade) and of D_2O (99.8%), the total flow rate being kept at 72 ml/min for all experiments. The temperature of the acetone chamber was kept at 9.5 °C, and the concentration of acetone vaporized into the carrier was 1.3_1 vol% as determined by gas chromatographic analysis. The content of D_2O in the carrier gas was controlled by adjusting the temperature of the D_2O chamber. The concentration of D_2O was previously calibrated by measuring the weight increase of silica gel adsorbent when the carrier gas was passed through the silica-gel bed for a given time. All experiments other than those for the determination of D_2O pressure dependence were carried out with a constant D_2O concentration of 1.6_5 vol%.

The sulfates of 0.13 g (Fe^{3+}, Al^{3+}, Cr^{3+}, Cu^{2+}, Ni^{2+}, Zn^{2+}, and Mg^{2+}) were used without any supporting materials by treating at 140 °C for 4—5 hr in air and ground. The carrier gas containing D_2O and acetone was made to flow over the catalyst bed for about 30 min to reach a steady state, and then an acetone sample for the mass spectrometric analysis was collected at the outlet of the reactor by a liquid nitrogen trap. Analysis was carried out by using parent peaks at 10 eV with the correction of the natural abundance of ^{13}C.

The surface areas of the sulfates were measured by the BET method after they had been heated at 140 °C for 3 hr in air and evacuated at room temperature. The contact time of the reactant through the catalyst bed was estimated from the retention volume of the sulfates packed in a gas chromatographic column. The relative catalytic activity k_r was obtained by normalizing the reaction rate with surface area S and contact time t for each of the sulfates; $k_r = -2.303/St \cdot \log (d_0/d_0^0)$, in which d_0^0 and d_0 are the fraction of acetone-d_0 of the initial and of the trapped samples.

The isotope effect on the enolization of acetone was studied with acetone-d_6(99.5%) and H_2O over a nickel sulfate under the same experimental conditions as mentioned above.

Results and Discussion

A typical deuterium distribution of acetone obtained over a nickel sulfate is given in Table 1, the deuterium distribution obtained on the other sulfates being similar to that on the nickel sulfate. The deuterium distribution reveals that the hydrogen exchange of acetone proceeds consecutively, *viz.*, the desorption and adsorption of acetone are rapid as compared with the exchange reaction rate. When the deuteration of acetone proceeds with the consecutive exchange of d_0 to d_1, d_1 to d_2, *etc.*, the values of d_1 can be calculated by assuming that the second step ($d_1 \rightarrow d_2$) is 5/6 of the first step ($d_0 \rightarrow d_1$); $d_1 = (e^{-k_1 t} - e^{-k_0 t})/(1 - k_1/k_0)$, where $k_1/k_0 = 5/6$. However, the calculated values are larger than the experimental values (Table 1) by factors of 1.2 at 98 and 110 °C, at 121 °C and 1.5 at 130 °C. The fact that the experimental value of d_1 is smaller than the calculated value may be due to partly occurring multiple exchange of adsorbed acetone.

The effect of D_2O pressures on the deuteration of acetone studied over nickel sulfate by changing D_2O

TABLE 1. DEUTERIUM DISTRIBUTION IN ACETONE OVER $NiSO_4$

Reaction temp. (°C)	d_0	d_1	d_2	d_3	d_4	d_5	d_6
98	95.6	3.9	0.5	—	—	—	—
110	93.2	5.4	1.4	—	—	—	—
121	87.6	9.1	2.6	0.7	—	—	—
130	82.9	10.2	4.4	1.8	0.7	—	—

1) K. Tanaka, A. Ozaki, and K. Tamaru, *Shokubai*, **6**, 22 (1964).
2) K. Tanaka and A. Ozaki, *J. Catal.*, **8**, 1 (1967).
3) R. P. Iczkowski and J. L. Margrave, *J. Amer. Chem. Soc.*, **83**, 3547 (1961).
4) K. Tanaka and A. Ozaki, This Bulletin, **41**, 2813 (1968).

pressures from 3.2 to 14.7 mmHg is shown in Fig. 1.

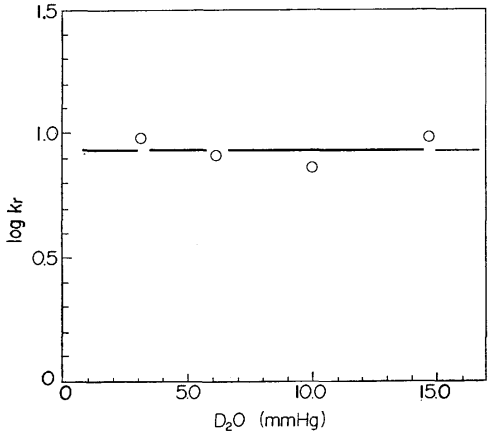

Fig. 1. D_2O pressure effect on the deuteration of acetone over a nickel sulfate at 98 °C.

It is seen that D_2O pressure has little influence on the hydrogen exchange rate between acetone and D_2O. This shows that the surface of the sulfate is covered with D_2O during exchange reaction, which is consistent by comparing with the temperature of the monohydrated nickel sulfate formation, 150 °C.[5]

It has been established that the enolization of acetone is subject to general acid catalysis in solutions with the rate-determining step of deprotonation of α-C–H.[7] If the enolization of acetone over the sulfates occurs with the same slow step, a large kinetic isotope effect is expected when α-C–H is replaced by α-C–D. For the sake of confirmation, the exchange reaction between acetone-d_6 and H_2O was carried out on a nickel sulfate under the same conditions; a flowr ate of 72 ml/min of carrier gas containing 1.3_1 vol.% of acetone-d_6 and 1.6_5 vol.% of H_2O. The exchange reaction between ordinary acetone and D_2O, denoted by Ni(H) in Fig. 2, is much faster than that between acetone-d_6 and H_2O, Ni(D), with $k_H/k_D \simeq 2.7$ at 100 °C. This supports a rapid prototation forming $(CH_3)_2COD^+$ followed by a slow deprotonation of α-C–H. With the increase of the acidity of H_2O or D_2O hydrated over the sulfates, the pre-equilibrium shifts to the protonated form causing an increase in the exchange reaction rate.

The deuteration of acetone carried out over the various sulfates is shown in Fig. 2, in which the ordinate is the logarithm of the relative catalytic activity (k_r). The activity sequence of the sulfates is in the order of $Fe^{3+}>Al^{3+}>Cr^{3+}>Cu^{2+}>Ni^{2+}>Zn^{2+}>Mg^{2+}$.

It has been shown that the proton activity of water hydrated over the oxides as well as the water hydrated around the metal ions is well correlated with the parameter X_i in the form of Eqs. (2) and (3). These relations reveal that the proton activity of the water hydrated over the sulfates may also be expressed by a similar equation of logarithmic form. Figure 3 shows the relation between the catalytic activities of the sulfates at a given temperature, indicated by a

5) L. Ben Dor and R. Margalith, *Inorg. Chim. Acta*, **1**, 49 (1967).

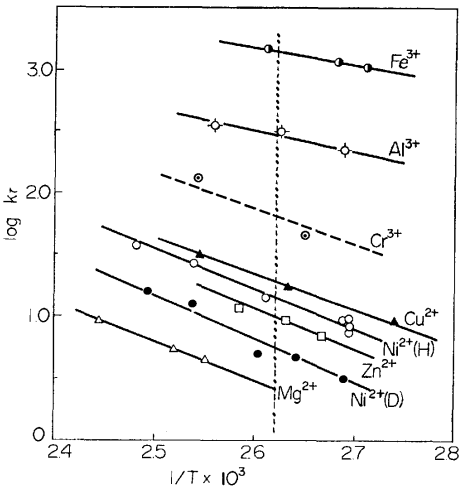

Fig. 2. Relative catalytic activities of the sulfates. Ni(D) is the reaction of acetone-d_6 with H_2O.

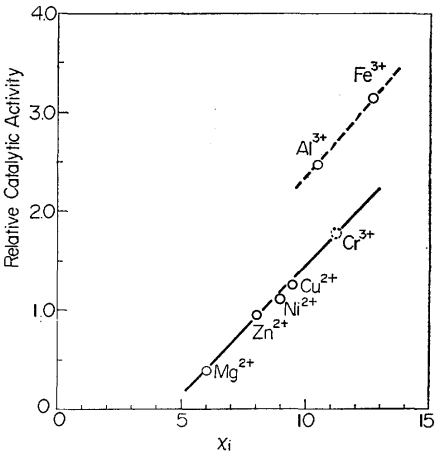

Fig. 3. Relation between the catalytic activity of the sulfate and the electronegativity of the metal ion.

dotted line in Fig. 2, and the electronegativity of the metal ion. It is seen that the logarithm of the catalytic activities increases linearly with X_i as expected, but the activities are separated in the two groups, divalent sulfates and trivalent sulfates, in which the values for Cr^{3+} are much obscure because of its small surface area and the low apparent activity. It should be noted that the apparent activation energies over the trivalent sulfates are approximately half of those over the divalent sulfates.

It may be concluded that the acidity of the hydrated sulfates is well expressed by using the electronegativity of the metal ions on which water hydrates or adsorbs. The acidity discussed here apparently differs from that observed by Tanabe and his co-workers,[6] which strongly depends on the dehydration temperatures of the sulfates attaining maximum acidity and catalytic activity just before reaching the anhydrous state.

6) T. Takeshita, R. Ohnishi, T. Matsui, and K. Tanabe, *J. Phys. Chem.*, **69**, 4077 (1965). K. Tanabe and T. Takeshita, *Advan. Catal.*, **17**, 315 (1967).

7) *Cf.* E. S. Gould, "Mechanism and Structure in Organic Chemistry," p. 372, Henry Hole and Co. N. Y.

BULLETIN OF THE CHEMICAL SOCIETY OF JAPAN, VOL. 46, 3889—3890 (1973)

The Solubilities, Critical Micelle Concentrations, and Krafft Points of Bivalent Metal Alkyl Sulfates

Masakatsu HATŌ and Kōzō SHINODA*

Research Institute for Polymers and Textiles, Sawatari-4, Kanagawa-ku, Yokohama 221

** Department of Chemistry, Faculty of Engineering, Yokohama National University, Ooka-2 Minami-ku, Yokohama 233*

(Received June 29, 1973)

According to the phase separation model (as well as the mass action model) for a micellar solution,[1] a Krafft point is interpreted as a triple point at which a solid hydrated surfactant, micelles (a liquid state), and a singly-dispersed surfactant are in equilibrium with each other. If so, the CMC values should be smaller than the solubility values above the Krafft point, equal at the Krafft point, while the solubility values should be smaller than the CMC values below the Krafft point. These relations hold for 1–1 ionic surfactants in either the absence or the presence of added salts.[1,2]

Miyamoto[3] has determined the solubilities and CMC's of several bivalent metal dodecyl sulfates. The CMC values of lead, cupric, and manganese dodecyl sulfates he obtained differ considerably from the solubility values at the Krafft points, whereas those of the other metal dodecyl sulfates agree within *ca.* 20%. This raises a serious question as to whether or not the triple point model holds for bivalent metal salts of ionic surfactants. In the present paper, the solubilities, the CMC's, and the Krafft points of various bivalent metal alkyl sulfates will be studied in order to confirm our model.

Experimental

The bivalent metal dodecyl and tetradecyl sulfates have been prepared by adding an aqueous solution of a respective metal chloride to aqueous solutions of sodium dodecyl and tetradecyl sulfates. Extremely pure sodium dodecyl sulfates (C_{12}>99.9%, and no minimum in the surface tension *vs.* concentration curve) and sodium tetradecyl sulfates (C_{12}=0.2%, C_{14}=99.3%, C_{16}=0.5%) were obtained from the Kao Soap Co. through the kindness of Dr. Arai. The metal chlorides were of an extra-pure grade and were used without further purification. The products were recrystallized 4 or 5 times from water and then washed with petroleum ether for 20 hr. No sodium ion was detected by a flame test. It is found from elementary analysis that all the compounds have two surface active anions in each molecule.

The solubility was determined by electrical conductivity measurements. The solutions were stirred for 4—5 hrs in a thermostat controlled within 0.02 °C. Further stirring caused no change in the solubility. The procedures were described in detail in a preceding paper.[4] The solubility was also determined by weighing the dried solution. The two measurements agreed with each other within an error of 1%. The CMC was determined either by conductivity measurements or by a dye method[5] (not by a dye titration method which gives a smaller CMC value, but by observing the color change in a series of solutions of different concentrations after an equilibrium had been reached). The two measurements agreed well with each other.

Results and Discussion

Figure 1 shows the solubilities and the CMC's of bivalent metal dodecyl and tetradecyl sulfates as a unction of the temperature. The supercooled micelles of cupric and manganese salts were fairly stable, the CMC values below the Krafft points were also determined. The solubility data on cupric dodecyl sulfate were less accurate (±3%) than the others (±0.5%) because of the low Krafft point. The concentration was expressed in terms of a molality based on the anhydrous surfactant. It is found from Figure 1 that the solubility increases abruptly at a definite temperature, just as those of 1–1 ionic surfactants do,[1,2] this temperature is the Krafft point above which the micelles are formed. The Krafft points determined from Fig. 1 have been listed in Table 1, together with the CMC values at the Krafft points. The data obtained by Miyamoto[3] and Schwuger[6] are also listed. The CMC values determined by surface tension measurements[3,6] or by conductivity measurements[7] agree well with the present results. It is clear from Figure 1 that the

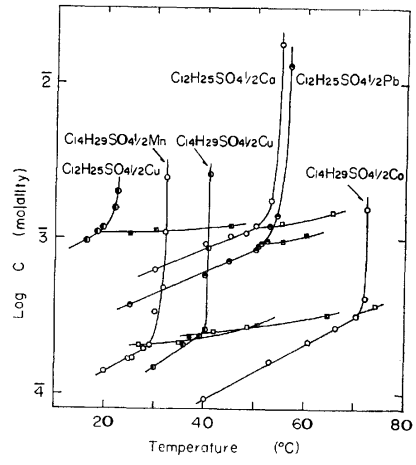

Fig. 1. The solubilities (circles) and the CMC's (squares) of bivalent metal alkyl sulfates as a function of temperature.

1) K. Shinoda, Chapter 1 in "Colloidal Surfactants" Academic Press Inc., New York, N. Y., 1963 pp. 6—8; K. Shinoda and E. Hutchinson, *J. Phys. Chem.*, **66**, 577 (1962); R. C. Murray, and G. S. Hartley, *Trans. Faraday Soc.*, **31**, 183 (1935).

2) H. Nakayama and K. Shinoda, This Bulletin, **40**, 1797 (1967).

3) S. Miyamoto, *ibid.*, **33**, 371 (1960); S. Miyamoto, *ibid.* **33**, 375 (1960).

4) K. Shinoda, M. Hatō, and T. Hayashi, *J. Phys. Chem.*, **76** 909 (1972).

5) K. Shinoda, *ibid.*, **58**, 1136 (1954).

6) M. J. Schwuger, *Kolloid-Z. Z. Polym.*, **233**, 979 (1969).

7) I. Satake, I. Iwamatsu, S. Hosokawa, and R. Matuura, This Bulletin, **36**, 204 (1963).

Table 1. Krafft point, CMC and heat of solution ΔH_s (from hydrated solid to singly dispersed state), of micelle formation ΔH_m and of fusion ΔH_f (from hydrated solid to micellar state) of bivalent metal alkyl sulfates

Compound	Krafft point (°C)	CMC at K.P. (molality)[c]	ΔH_s	ΔH_m (kcal/mol)	ΔH_f
$(C_{12}H_{25}SO_4)_2Mn$	16±1	0.0011_5 (25 °C)	—	—	—
$(C_{12}H_{25}SO_4)_2Cu$	19±1	0.0010_8	—	$0._0$	—
$(C_{12}H_{25}SO_4)_2Co$[a]	23	0.00083 (25 °C)	—	—	—
$(C_{12}H_{25}SO_4)_2Mg$[a]	25	0.00088	—	—	—
$(C_{12}H_{25}SO_4)_2Ca$	50.0±0.5	0.0011_8	$19._1$	$-1._1$	18±1
$(C_{12}H_{25}SO_4)_2Pb$	52.0±0.5	0.00092	$19._0$	$-1._8$	17±1
$(C_{12}H_{25}SO_4)_2Sr$[a]	64	0.0011 (67 °C)	—	—	—
$(C_{12}H_{25}SO_4)_2Ba$	105[d]	—	—	—	—
$(C_{14}H_{29}SO_4)_2Mn$	29.0±0.5	0.00020_4	$23._2$	$-2._4$	21±2
$(C_{14}H_{29}SO_4)_2Mg$[b]	38.5	0.00025 (38 °C)	—	—	—
$(C_{14}H_{29}SO_4)_2Cu$	39.8±0.5	0.00024_5	$27._5$	$-3._5$	24±2
$(C_{14}H_{29}SO_4)_2Ca$	71±1	0.00034	$27._0$	$-5._0$	22±2
	67[b]	0.00034 (80 °C)[b]			

a) Ref. 3. b) Ref. 6. c) Moles of anhydrous salts/10^3 g of H_2O, the values from references 3 and 6 are expressed in mol/l. d) A value estimated from the solubilities of 0.5 and 1 wt% aqueous solutions.

CMC and solubility curves of all the compounds examined intersect exactly at the Krafft point, and that the CMC values of supercooled micelles are larger than the corresponding solubility values. This is in accord with the model.[1] No anomalous behavior has been observed in the cases of cupric and lead dodecyl sulfates. Similar results have been obtained in the case of fluorinated surfactants, $C_9F_{19}SO_3l/2Mg2H_2O$.[4,8] From the foregoing discussion, the heats of fusion, ΔH_f (from a hydrated solid to a micellar state), of the bivalent metal alkyl sulfates can be calculated from the temperature dependence of the solubility or CMC by the aid of the following equations[9] (the values are listed in Table 1),

$$\Delta H_f = \Delta H_s + \Delta H_m \quad (1)$$

$$\Delta H_s = 3RT^2(\partial \ln C_2/\partial T) \quad (2)$$

$$\Delta H_m = -(2+K_g)RT^2(\partial \ln CMC/\partial T) \quad (3)$$

where ΔH_s is the heat of solution of a hydrated solid agent; ΔH_m, the heat of micelle formation; C_2, the solubility, and K_g the experimental constant. K_g is 0.57_2 for calcium dodecyl sulfate[10] and is assumed to be 0.57_2 for the other surfactants. As these hydrated solids have a vapor pressure very close to that of pure water, the anhydrous solid was equilibrated with an aqueous solution of potassium chloride (0.001 mol/l and $P/P^\circ > 0.997$) in order to determine the number of hydrated water at 26.5±0.3 °C. Calcium dodecyl and tetradecyl sulfates were found not to take up the water of hydration. After a lapse of 5 days (for manganese tetradecyl sulfate) or of 20 days (for cupric tetradecyl sulfate), the salts come to a constant weight, giving a value of 6±0.4 H_2O. The lower Krafft point of manganese (or cupric) tetradecyl sulfate than that of calcium tetradecyl sulfate may result from the larger entropy of fusion of the former, which is partly attributable to the entropy change in hydrated water.

8) M. Hatō and K. Shinoda, *Nippon Kagaku Zasshi*, **91**, 27 (1970).

9) K. Shinoda, S. Hiruta, and K. Amaya, *J. Colloid Interfac. Sci.*, **21**, 102 (1966).

10) H. Lange, *Kolloid-Z.*, **121**, 66 (1951).

BULLETIN OF THE CHEMICAL SOCIETY OF JAPAN, VOL. 46, 3891—3892 (1973)

Infrared Spectra of Deoxyribonucleic Acids with Different Base Compositions in Their D_2O Solutions

Yoshifumi NISHIMURA, Kosuke MORIKAWA, and Masamichi TSUBOI
Faculty of Pharmaceutical Sciences, University of Tokyo, Hongo, Bunkyo-ku, Tokyo 113
(Received September 14, 1973)

In this note we present the result of our examination of the infrared absorption spectra of six DNA's with different guanine+cytosine (GC) contents in their heavy water solutions in the spectral region of 1750—1480 cm^{-1}. A similar examination was once made by Fritzsche[1] with deuterated DNA *films*, and he found that the relative intensity of the absorption bands at 1485 and 1505 cm^{-1} depends on the guanine+cytosine (GC) content of the deuterated DNA samples. In our study in D_2O *solution*, on the other hand, a number of bands characteristic of the guanine-cytosine (G–C) and adenine–thymine (A–T) base-pairs are found in the 1700—1550 cm^{-1} region as shown below.

TABLE 1. DNA SAMPLES USED IN THE PRESENT WORK

Source	GC content (%)
Tetrahymena pyriformis GL	25[a]
Clostridium perfringens	31[b]
Calf thymus	43[b]
Escherichia coli	51[b]
Pseudomonas aeruginosa	65[c]
Micrococcus lysodeikticus	72[b]

a) Estimated from the melting temperature (61.8 °C in 0.015 M NaCl+0.0015 M Na-citrate) and buoyant density in a CsCl density gradient centrifugation (1.686, as given by R. A. Flavell and I. G. Jones, *Biochem. J.*, **116**, 811 (1970).
b) S. Ulitzur, *Biochim. Biophys. Acta*, **272**, 1 (1972).
c) N. Sueoka and T. Y. Cheng, *J. Mol. Biol.*, **4**, 161 (1962).

The DNA samples used in the present study are listed in Table 1. Preparation of DNA from *Tetrahymena pyriformis* was made according to the method described by Allen and Gibson.[2] The cells were kindly provided by Dr. Takashi Mita, National Cancer Center Research Institute. Lysis was effected by adding 10% sodium lauryl sulfate, and within 1 min phenol was added. After treatments with ribonuclease A (Sigma Chemical Co., 50 μg/ml, at 37 °C, for 30 min), with pronase E (Kaken Chemical Co., 1 mg/ml, at 37 °C, for 1 hr), and with α-amylase (Boehringer-Mannheim 50 μg/ml), DNA was precipitated with 2-propanol. DNA samples from *Clostridium perfringens* and Calf thymus were purchased from Miles Laboratories, Inc. DNA preparation from *Escherichia coli*, *Pseudomonas aeruginosa* (kindly provided by Dr. Toshio Ando, The Institute of Medical Science, University of Tokyo), and *Micrococcus lysodeikticus* was made, according to Marmur,[3] by lysing the micro-organism with sodium lauryl sulfate, followed by a shaking with chloroform–isoamyl alcohol, precipitation with ethanol, treatment with ribonuclease A (Sigma Chemical Co., 50 μg/ml, at 37 °C, 30 min), and again precipitation with ethanol.

The purities of the DNA samples were judged by the ultraviolet absorption curves and the optical melting profiles (*i.e.*, the melting temperatures T_m and the amounts of hyperchromicity). The phenol extraction, protease treatment, and ribonuclease treatment were repeated until a proper set of values of T_m and hyperchromicity was reached. To remove disturbing anions the DNA solution was dialyzed against 10^{-3} M Tris buffer+10^{-3} M NaCl and lyophilized.

For infrared absorption measurement, concentrated D_2O solution (about 1.5%) was prepared. The solvent used was Tris buffer (pD≒7). To promote the rate of dissolving of DNA into D_2O, sonication with UMEDA 20 kcycle/s (150 W) was applied for 10 min. It was confirmed that this procedure does not pracitcally affect the ultraviolet and infrared absorption spectra of the DNA solution. The solution was placed in a cell with CaF_2 windows and optical path 50 μ. A Perkin-Elmer 621 infrared spectrophotometer was

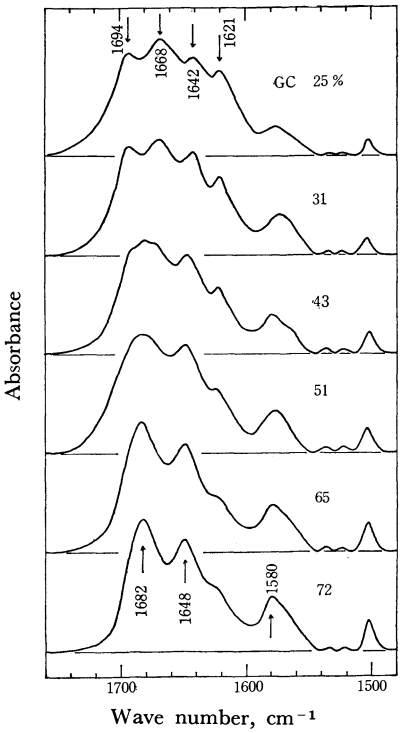

Fig. 1. Infrared absorption curves of DNA's in D_2O solutions at about 40 °C. From the top: DNA's from *Tetrahymena* (GC 25%), *C. perfringens* (31%), Calf thymus (43%), *E. coli* (51%), *P. aeruginosa* (65%), and *M. lysodeikticus* (72%).

1) H. Fritzsche, *Biopolymers*, **5**, 863 (1967).
2) S. L. Allen and I. Gibson, *J. Protozool.*, **18**, 518 (1971).
3) J. Marmur, *J. Mol. Biol.*, **3**, 208 (1961).

used for the absorption measurement.

The observed infrared absorption curves are shown in Fig. 1. As may be seen in the figure, the absorption peaks at 1621, 1642, 1668, and 1694 cm^{-1} become more prominent on lowering the GC content, while those at 1580, 1648, and 1682 cm^{-1} become more prominent as the GC content becomes higher. In fact, after a proper adjustment of the absorbance scale in each absorption curve, the absorbance at each of these frequencies is found to have an almost linear relation with the GC content (see Fig. 2). This fact indicates that the A–T base-pairs (or the G–C base-pairs) in all of these DNA structures are in a similar environment to one another in an average. The vertical stacking interactions between the base-pairs in a double-helical polynucleotide structure should certainly affect the infrared absorptions of the base-pairs,[4,5] but this is not clearly detected in our present examination of DNA's in the range of GC content 25—72%.

The effect of the vertical stacking interaction becomes apparent when the examination is extended to the range of the GC content 0% or 100%. In Fig. 3, infrared absorption curves of a hypothetical A–T base-pair and a hypothetical G–C base-pair are shown which are obtained by an extrapolation of absorbance *versus* GC content relations illustrated in Fig. 2. These are appreciably different from actually observed spectra of A–T and G–C base-pairs, respectively. Thus, the spectrum of the hypothetical A-T pair placed in an average environment of natural DNA's is different from the spectrum actually observed of the A–T pair in poly(dA–dT)–poly(dA–dT), *i. e.*, the double-helical complex containing strands of alternating deoxyribo-adenylate and deoxyribothymidylate residues (purchased from Miles Laboratories, Inc). In the latter structure every A–T pair is considered to be always sandwiched by two T–A pairs. The spectrum of the hypothetical G–C pair placed in an average environment of natural DNA's is also different from the spectrum actually observed[6] of the G–C pair in poly(rG)–poly(rC), the double-helical complex of riboguanylate and ribocytidylate homopolymers. This difference should be attributed not only to the difference in the base-sequence but also to the difference between the DNA B structure[7] and the double-helical RNA structure.[8]

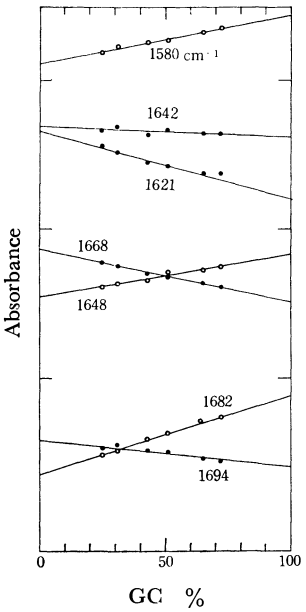

Fig. 2. Plots of absorbance *versus* GC content at several frequencies in the infrared spectra of DNA's.

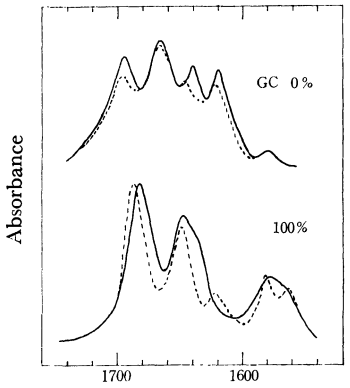

Fig. 3. Full lines: Calculated spectra of A-T and G–C base-pairs obtained by the extrapolation of the absorbance *versus* GC content relations illustrated in Fig. 2. Broken lines: Observed spectra of poly(dA-dT)-poly(dA–dT) (upper) and poly(rG)–poly(rC) (lower)[6] in their D_2O solutions.

4) K. Morikawa, M. Tsuboi, S. Takahashi, Y. Kyogoku, Y. Mitsui, Y. Iitaka, and G. J. Thomas, Jr., *Bipolymers*, **12**, 799 (1973).

5) M. Tsuboi, S. Takahashi, and I. Harada, in "Physico-Chemical Properties of Nucleic Acids," ed. by J. Duchesne, Academic Press, London (1973), p. 91.

6) G. J. Thomas, Jr., *Biopolymers*, **7**, 325 (1969).

7) S. Arnott and D. W. L. Hukins, *Biochem. Biophys. Res. Commun.*, **47**, 1504 (1972).

8) S. Arnott, "Progress in Biophysics and Molecular Biology", Vol. 21, ed. by J. A. V. Butler and D. Noble, Pergamon Press (1970), p. 265.

BULLETIN OF THE CHEMICAL SOCIETY OF JAPAN, VOL. 46, 3893 (1973)

Chemical Studies of Minerals Containing Rarer Elements from Far East District.[1] LXVI. Cookeite from Nagatare, Fukuoka Prefecture, Japan

Kin-ichi SAKURAI, Akira KATO, Kikuo MIYOKAWA,* and Kozo NAGASHIMA*

Department of Geology, National Science Museum, Ueno Park, Tokyo 110

** Department of Chemistry, Faculty of Science, Tokyo Kyoiku University, Otsuka, Tokyo 112*

(Received May 23, 1973)

Granite pegmatite dikes exposed at Nagatare, Fukuoka Prefecture, are famous for the occurrence of lepidolite,[2] petalite,[3] amblygonite-montebrasite series minerals,[4] and pollucite,[1] the last three being unique occurrences in Japan. Hand specimen of a white or pink mass collected from the dump derived from one of the pegmatite dikes turned out to be the first cookeite in Japan, though contaminated by quartz. This note describes the results of X-ray, chemical and optical studies.

The analyzed material is a part of a light pink mass over 5 cm across and 150 grams in weight. The mass is composed of the aggregate of larger quartz grains and mixture cookeite flakes with minor lepidolite, which is variable in amount.

X-Ray powder data coincide well with known ones[5] (Table 1), the calculated lattice constants being a_0= 5.188 Å, b_0=9.077 Å, c_0=14.278 Å (all±0.003 Å), and β=97.8±0.1°.

TABLE 1. X-RAY POWDER DATA FOR COOKEITE FROM NAGATARE, FUKUOKA PREFECTURE, JAPAN, AND LONDONDERRY, AUSTRALIA

h k l	1			2	
	d(obsd)	*I*	*d*(calcd)	*d*	*I*
0 0 1	14.2	24	14.2	14.1	80
0 0 2	7.08	34	7.08	7.05	70
0 0 3	4.72	100	4.72	4.70	70
0 0 4	3.54	59	3.54	3.52	90
0 0 5	2.830	27	2.832	2.815	30
2 0 0	2.571	7b	2.571	2.56	40
2 0 $\bar{2}$	2.52	8b	2.527	2.505	70
0 0 **6**	2.357	8	2.369	2.35	5
2 0 2	2.320	13	2.320	2.315	10
0 0 7	2.020	10	2.023	2.015	10
2 0 4	1.96	10b	1.960	1.96	50
0 0 **8**	1.767	3b	1.770	1.76	10
2 0 **6**	1.634	7b	1.634	1.635	45
0 **6** 0	1.490	10b	1.492	1.489	70

1: Cookeite. Nagatare, Fukuoka Prefecture, Japan. Cu/Ni radiation. Diffractometer method. Calculated *d*-values are based on a_0=5.118 Å, b_0=9.077 Å, c_0=14.287 Å, β=97.8° b=broad

2: Cookeite. Londonderry, Australia, ASTM Card No. 16-363

TABLE 2. CHEMICAL ANALYSIS[a] OF COOKEITE FROM NAGATARE, FUKUOKA PREFECTURE

Component	wt%	Molecular quotient	Metal number	Oxygen number	Metal number as O=10
SiO_2	34.50	0.5741	0.5741	1.1482	3.042
Al_2O_3	46.21	0.4532	0.9064	1.3596	4.802
Fe_2O_3	0.08	0.0005	0.0010	0.0015	0.0053
B_2O_3	trace				
MnO	trace				
Li_2O	3.86	0.1292	0.2584	0.1292	1.369
Na_2O	0.08	0.013	0.0026	0.0013	0.013
K_2O	0.26	0.0028	0.0056	0.0028	0.030
H_2O	14.11	0.7800			
F	1.55	0.0816			
$-F_2=O$	0.65				
Total	100.00				

a) Recalculated after deducing quartz.

Chemical analysis, the results of which are given in Table 2 was carried out on the material contaminated by quartz which can not be removed by heavy liquids, suggesting the specific gravity to be neary equal in each, *i.e.* about 2.7. The procedure of chemical analysis was as follows: Li_2O—atomic absorption analysis; Na_2O and K_2O—flame photometry; SiO_2, Al_2O_3 and H_2O—gravimetry; Fe_2O_3—spectrophotometry; F—volumetry. Boron, though too low to be determined colorimetrically, was detected by emission spectrographic analysis. The present cookeite is specified due to its higher fluorine content as well as the relation K >Na in mole ratio.

The crystallochemical formula calculated from the analytical data based on O=10 for the layered part and (OH, F)=8 for the interlayering one is $[(Al_{1.995}Fe_{0.005})(OH_{1.916}F_{0.084})Al_{0.958}Si_{3.042}O_{10}]^{-0.958}[(Li_{1.369}K_{0.030}Na_{0.013}Al_{1.849})(OH_{5.746}F_{0.254})]^{+0.959}$ satisfying the crystallochemical formula by Cerny.[6]

It is optically biaxial negative, 2V is very small, refractive indices are α=1.560, $\beta \fallingdotseq \gamma$=1.591, $\gamma-\alpha$= 0.031; colorless in thin section. The pink color in the hand specimen may be due to the presence of manganese as surmised by Kanaoka and Kato.[7]

1) LXV: K. Sakurai, A. Kato N. Kuwano, and K. Nagashima, This Bulletin, **45**, 812 (1972).
2) H. Shibata, *J. Geological Soc. Jap.*, **41**, 582 (1936).
3) Y. Okamoto, *Kobutsu to Chishitsu*, **3**, 1 (1950).
4) J. Ito, H. Minato, and Y. Okamoto, *J. Mineralogical Soc. Jap.*, **2**, 263 (1955).
5) Th. Sahama, O. V. Kaorring, and M. Lehtinen, *Lithos*, **1**, 12 (1968).
6) R. Cerny, *Can. Mineralogist*, **10**, 636 (1970).
7) S. Kanaoka and E. Kato, *J. Clay Science Soc. Jap.*, **11**, 95 (1971).

BULLETIN OF THE CHEMICAL SOCIETY OF JAPAN, VOL. 46, 3894—3895 (1973)

Conformation of Methacryloyl-L-proline

Koji NISHIHARA, Hisao NISHIHARA, and Naokazu SAKOTA

Department of Industrial Chemistry, Faculty of Engineering, Ehime University, Bunkyo-cho, Matsuyama 790

(Received April 16, 1973)

Many conformational studies have been made on the hindered internal rotation about amide bonds since the first investigation by Pauling.[1] However, very few investigations have been reported on that of α,β-unsaturated acid amide except for the work by Rogers and Woodbrey.[2] They determined the activation free energy for the hindered internal rotation about the amide bond of N,N-dimethylacrylamide to be 16.1 kcal/mol at 25.2 °C. The alternating photocopolymerization of methacryloyl-L-valine methyl ester (MAVM) with maleic anhydride suggested that the amide compounds has a specific planar conformation.[3] For the purpose of elucidating the participation of the amide proton in this specific conformation, we synthesized methacryloyl-L-proline (MAP) and examined the effect of the temperature on its NMR and CD spectra. The results indicate that the following two isomeric

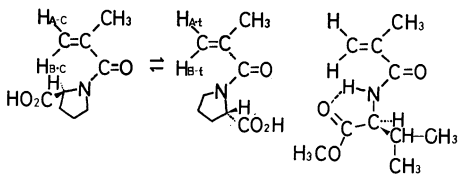

cis *trans*

MAP MAVM

Fig. 1. Conformations of MAP and MAVM.

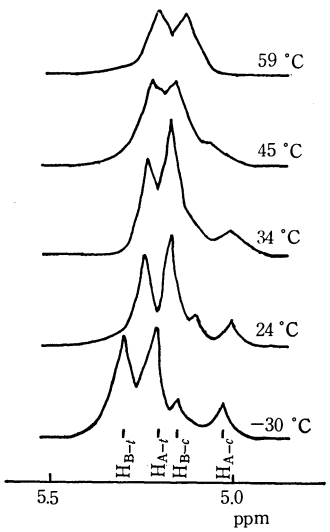

Fig. 2. The NMR spectra assigned to the vinyl protons of MAP from HMDS at 100 MHz in $CDCl_3$.

MAP, *cis* and *trans* conformers exist at lower temperature.

Temperature dependence of the NMR signals assigned to the vinyl protons of MAP is shown in Fig. 2. The four signals at −30 °C are seen to decrease to the two signals with the rise in temperature. The results suggest the coexistence of the rotational isomers. H_A and H_B of the *cis* and *trans* isomers were assigned on the basis of the study by Bovey *et al.* on polysarcosine.[4] In deutero methanol and dimethyl sulfoxide-d_6, the vinyl protons gave a similar NMR pattern to that in $CDCl_3$. For example, in deutero methanol at −50 °C, they gave four resonance peaks at 5.09, 5.21, 5.28, and 5.36 ppm assigned to H_{A-c}, H_{B-c}, H_{A-t} and H_{B-t} respectively, and at 42 °C they gave only three peaks at 5.06, 5.20, and 5.26 ppm assigned to H_{A-c}, an overlapped signal of H_{B-c} and H_{A-t}, and H_{B-t} respectively.

The activation free energy ($\Delta F^{\neq}_{T_c=318}$) for the transformation between the two isomers of MAP was calculated to be 16.4±0.2 kcal/mol from the NMR data in deutero chloroform by the equation

$$\Delta F_{Tc}^{\neq} = 2.303RT_c \log \frac{\sqrt{2}\kappa k T_c}{\pi \Delta \nu h} \qquad (1)$$

where T_c is the coalescence temperature, and $\Delta\nu$ is the difference between the chemical shifts of the two isomers. Transmission coefficient κ was assumed to be unity. The enthalpy change for the *cis–trans* transformation was calculated to be −1.5±0.2 kcal/mol by the temperature dependence of the equilibrium constant (K) in Table 1, where K values obtained from the *cis–trans* area ratio of NMR spectra were used.

Figure 3 indicates the positive CD maximum of L-proline at 219 nm, and the negative CD maximum at 227 nm with a shoulder at about 246 nm for MAP

Table 1. Equilibrium constants for the *cis–trans* transformation between the two isomers of MAP ($CDCl_3$)

Temperature (°C)	Equilibrium constant $K=[trans]/[cis]$
−30	4.39[a]
0	3.05[a]
15	2.42[a]
24	2.48[a]
28	2.26[a]
55	2.45[b]
59	2.42[b]

a) obtained from the area ratio of NMR spectra.
b) obtained from chemical shifts.

1) L. Pauling, "The Nature of the Chemical Bond," 2nd Ed., Cornel University Press, Ithaca, N.Y. (1940), p. 1.
2) M. T. Rogers and J. C. Woodbrey, *J. Phys. Chem.*, **66**, 540 (1962).
3) K. Nishihara and N. Sakota, *J. Polym. Sci.*, in preparation.
4) F. A. Bovey, J. J. Ryan, and F. P. Hood, *Macromolecules*, **1**, 305 (1968).

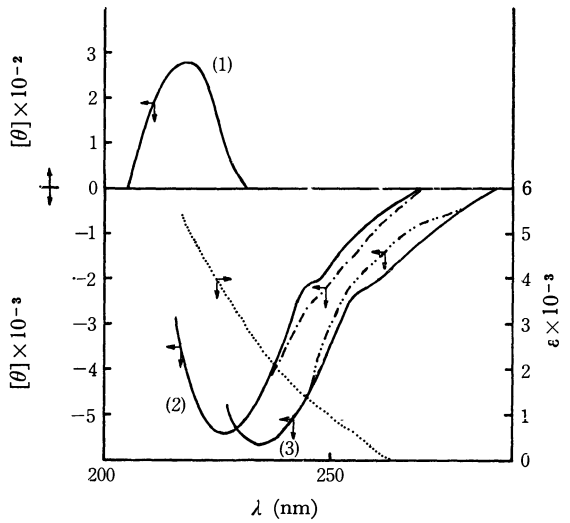

Fig. 3. The UV spectrum of MAP in methanol at 25 °C (……) and the CD spectra of L-proline and MAP.
(1) The CD spectrum of L-proline in methanol at 25 °C.
(2) The CD spectra of MAP in methanol at 25 °C (——) and −50°C (—·—).
(3) The CD spectra of MAP in dioxane at 25°C (——) and 52°C (—··—).

in methanol at 25 °C. The negative CD maximum of MAP is presumably associated with the n→π* transition of the methacryloyl amide group. The CD spectra of MAP measured at 52 °C in dioxane and at −50 °C in methanol differ from those obtained at 25 °C in the corresponding solvents. The difference in the CD curve near the shoulder of absorption might be ascribed to the coexistence of the two different conformations of MAP.

Experimental

MAP was prepared by the reaction of methacryloyl chloride with L-proline according to the method of Sakota.[5] mp 103.0—104.5°C; $[\alpha]_D^{29}$ −79.2 ($c=1$, methanol).

NMR spectra were recorded with a JEOL Model JNM-4H-100 Spectrometer operating at 100 MHz. CD spectra were measured with a Jasco Model ORD/UV 5 Spectropolarimeter. UV spectrum was measured with a Shimadzu Double Beam Spectrophotometer UV-200.

5) N. Sakota, *Nippon Kagaku Zasshi*, **88**, 1087 (1968).

BULLETIN OF THE CHEMICAL SOCIETY OF JAPAN, VOL. 46, 3895—3896 (1973)

Oxosulfonium Salts. III. Methylation of Optically Active Sulfoxides.[1]

Kenji KAMIYAMA, Hiroshi MINATO, and Michio KOBAYASHI

Department of Chemistry, Faculty of Science, Tokyo Metropolitan Universisy, Fukazawa, Setagaya, Tokyo 158

(Received, May 8, 1973)

A report was previously given on the synthesis, optical resolution and determination of absolute configuration of ethylmethylphenyloxosulfonium perchlorate.[2] The oxosulfonium salt was prepared by methylation of racemic sulfoxide followed by optical resolution. Since optically active sulfoxides can be prepared by the reaction of the optically active menthyl sulfinates with the Grignard reagents, methylation of such sulfoxides seems to be an attractive route for the synthesis of optically active oxosulfonium ions. Methylation of optically active ethyl phenyl sulfoxide was therefore investigated.

R-(+)-Ethyl phenyl sulfoxide ($[\alpha]_D^{24}=+176.2°$) [I], prepared from (−)-menthyl benzenesulfinate, was refluxed in excess methyl iodide in the presence of mercury (II) iodide (1/3 mol per mol I) under a nitrogen atmosphere for 63 hr. When unchanged I and methyl iodide were removed by extraction with ether and the remaining crystals were recrystallized from methanol, ethylmethylphenyloxosulfonium mercuritriiodide [II] was obtained in 27.7% yield (based on the moles of HgI_2 used).

Since its specific rotation was very small, II was converted into perchlorate by use of an ion-exchange resin column; $[\alpha]_D^{22}=+9.8°$ ($c=2.2$, acetone); optical purity, 72%.[3]

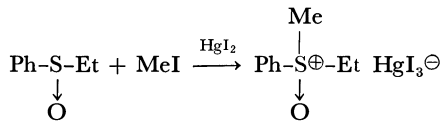

[I] [II]

$[\alpha]_D^{24}=+176.2°$

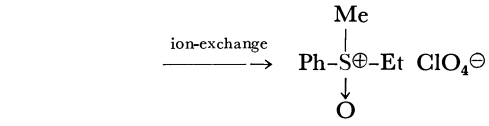

[III]

The dextrorotatory III should have an *R*-configuration, since it was established that (+)-III obtained by optical resolution has this configuration.[2] This shows that alkylation of sulfoxides proceeds with retention of configuration.

1) Organic Sulfur Compounds, Part XLIV.

2) M. Kobayashi, K. Kamiyama, H. Minato, Y. Oishi, Y. Takada, and Y. Hattori, *Chem. Commun.*, **1971**, 1577.

3) Optically active II was found not to racemize under the reaction conditions. Therefore, the low optical purity observed is probably due to the racemization of the sulfoxide during the reaction (*cf.* the following work by Modena *et al.*).

4) G. Modena, U. Quintly, and G. Scorrano, *J. Amer. Chem. Soc.*, **94**, 202 (1972); K. Mislow, T. Simmons, J. T. Melillo, and A. L. Ternay, Jr., *ibid.*, **86**, 1452 (1964).

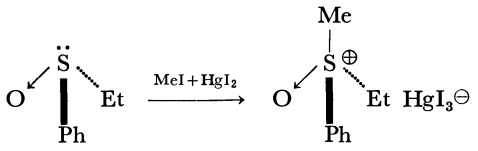

The reaction among, I, methyl iodide, and mercury(II) iodide is rather complex and the yield of II is often very small unless the reaction conditions are carefully controlled. Products other than II were ethylmethylphenylsulfonium salt, dimethyl ether, and iodine.

Conversion of optically active sulfoxides into sulfilimines was found to proceed with retention of configuration.[5]

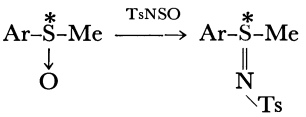

Another example of reactions proceeding with retention of configuration is the formation of sulfoximines from sulfoxides.[6]

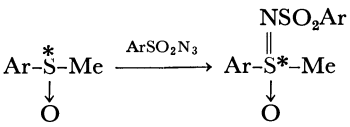

The conversion of I into II is unique in that a sulfur–carbon bond is formed with retention of configuration without breaking any bond in the sulfoxides. Since optically active sulfoxides are readily available from (−)-menthyl sulfinates, this method is better for formation of optically active oxosulfonium ions in comparison with the optical resolution of racemic oxosulfonium ions.[2]

Experimental

(+)-Ethyl Phenyl Sulfoxide [I]. Benzenesulfinic acid and (−)-menthol were condensed by dicyclohexylcarbodiimide in dichloromethane,[7] and the diastereomeric mixture of menthyl sulfinates formed was separated by recrystallization; one diastereomer crystallized more readily. The crystalline diastereomer was allowed to react with ethylmagnesium iodide, and (+)-I was obtained;[8] bp, 92—94 °C/2 mmHg; IR, 1050 cm^{-1} (ν_{S-O}); $[\alpha]_D^{24}=+176.2°$ ($c=1.03$, acetone); optical purity, 94% (176.2/187.5×100).

Methylation of I. After a mixture of mercury(II) iodide (1.20 g, 2.64 mmol) and methyl iodide (5 ml) was stirred for 40 min under nitrogen, (+)-II (0.968 g, 6.27 mmol) was added, and the mixture was refluxed for 63 hr. Evaporation of methyl iodide under reduced pressure gave a brown oil, which was converted into crude crystals by washing out the remaining I with ether. They were recrystallized twice from methanol, and pure II was obtained; yield, 0.547 g (11.6%) (27.7% based on HgI_2); mp 69.5—70.5 °C; IR, 1210, 1240 cm^{-1}; NMR, δ, 1.55(3H, t), δ, 4.39 (3H, s), δ, 4.54 (2H, q), δ, 8.10 (5H, m).

Conversion of I to II. A small amount of an acetone–water (5 : 1) solution of I (0.520 g) was added to an anion-exchange column (Amberlite IRA 400) which had been adjusted to ClO_4^- type. Elution with acetone–water (1 : 1) and evaporation of the eluate (150 ml) gave an oil, which crystallized upon addition of ethanol. Recrystallization was repeated twice, and the pure II amounted to 0.150 g (80.7%); mp, 70.5—72.0 °C; $[\alpha]_D^{22}=+9.8°$ ($c=2.2$, acetone); optical yield 72.1%; IR, 1240, 1210, 1100 cm^{-1}; Found: C, 40.77; H, 4.98. Calcd for $C_9H_{13}SO_5Cl$: C, 40.23; H, 4.88.

5) D. R. Rayner, D. M. von Schriltz, J. Day, and D. J. Cram, *J. Amer. Chem. Soc.*, **90**, 2721 (1968).

6) M. A. Sabol, R. W. Davenport, and K. K. Andersen, *Tetrahedron Lett.*, **1968**, 2159.

7) Y. Miyaji, H. Minato, and M. Kobayashi, This Bulletin, **44**, 862 (1971).

BULLETIN OF THE CHEMICAL SOCIETY OF JAPAN, VOL. 46, 3896—3898 (1973)

The Dimerization of Thymine Glycol and the Splitting of the Dimer by γ-Irradiation in an Aqueous System

Tateki HAYASHI, Osamu OGISO, and Mitsuo NAMIKI

Department of Food Science and Technology, Faculty of Agriculture, Nagoya University, Chikusa-ku, Nagoya 464

(Received June 11, 1973)

It has been known that the radiolysis of thymine in an aqueous system provides thymine glycol as the main radiolysis product in either the presence[1] or absence of air.[2] In our studies of the radiation chemistry of nucleic acid bases, we have found that, in the radiolysis of thymine under anaerobic conditions, there exists a novel reversible reaction between thymine and thymine glycol, and that the reverse reaction from the later is caused by the action of hydrated electrons.[3] It has also been observed that the radiolysis of thymine glycol gives several other products with the characteristic UV absorption (260 nm) positive or negative. This paper will deal with the isolation and identification of a novel dimer compound of thymine glycol as the main radiolysis product under N_2O saturation, and also with the dimer splitting to 5-methylbarbituric acid on radiolysis.

Results and Discussion

An aqueous solution of thymine glycol (I) (4 mM) was irradiated with γ-rays in the presence of N_2O to

1) R. Latarjet, B. Ekert, S. Apergot, and N. Reybeyrotte, *J. Chim. Phys.*, **58**, 1046 (1961).
2) B. Ekert, *Nature*, **194**, 278 (1962).
3) M. Namiki and T. Hayashi, *Int. J. Radiat. Biol.*, **17**, 197 (1970); T. Hayashi and M. Namiki, *Agr. Biol. Chem.*, **36**, 551 (1972).

eliminate the action of hydrated electrons on thymine glycol ($e_{aq}^- + N_2O \rightarrow \cdot OH + OH^- + N_2$).[4] The irradiated solution was then concentrated and chromatographed on a column of Dowex 50W-H^+; a colorless crystalline product was thus obtained in the eluate. From the results of an elementary analysis ($C_{10}H_{10}N_4O_6$) and from the NMR{(100 MHz, DMSO-d_6 δ1.64 (s, $-CH_3$, 3H), δ11.14 (s, >NH, 2H)} and the IR {(KBr disk) 3200 (-NH), 1710, 1725, and 1750 cm^{-1} (C=O)} spectral data, the structure of this compound was assigned to be 5,5′-dimethyl-5,5′-bibarbituric acid (II).

To confirm the (II) structure, an authentic sample was prepared by a modification of the method used by Davidson and Baudisch in the synthesis of 6,6′-biisobarbituric acid,[5] using potassium ferricyanide in alkali as a condensing agent; it was demonstrated that the IR spectrum of the irradiate product agreed perfectly with that of an authentic one, as is presented in Fig. 1. The product (II) is considered to be a novel compound, and it seems to be the main radiolysis product, judging from the glc analysis of the irradiated products silylated with bis(trimethylsilyl)trifluoroacetamide (BSTFA) (Procedure A).

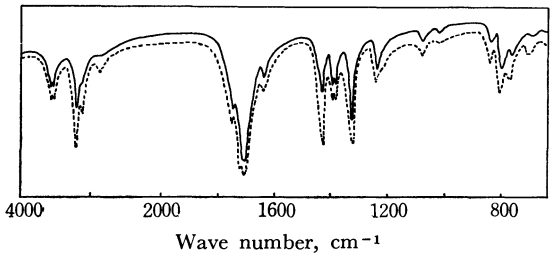

Fig. 1. IR spectra of synthesized (solid line) and isolated (broken line) II.

When its yields under various irradiation conditions were compared with those in air, in N_2 and in N_2O, it was shown that the formation was especially prominent in the case of the irradiation in the presence of N_2O, suggesting that the dimer formation is caused by the reaction with OH radicals. It may thus be proposed that the reaction is initiated by the abstraction of the C-6 hydrogen of I with the OH and/or H radical to form (III) radical, followed by dehydration to give the (IV) radical in a manner similar to that which has been proposed in the case of ethylene glycol;[6] subsequent dimerization then gives the product (II).

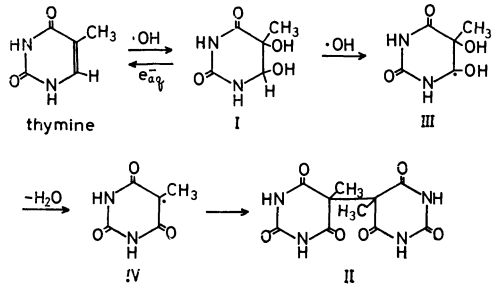

Scheme 1.

Judging from this dimer formation from I, it seems reasonable to assume that the dimer may exist in the radiolysis products of thymine in the absence of air, especially in the presence of N_2O. The glc experiments (Procedure A) have been perfomed to try to detect the dimer product (II) among the radiolysis products of thymine, but no appreciable amount of the dimer (II) was detected with the irradiations in air, in N_2, even in N_2O up to 2 Mrad.

Further investigations of the radiolysis of the dimer (II) were carried out especially in an attempt to ascertain the behavior of the reaction with a hydrated electron.

An aqueous solution of II (4 mM) was irradiated with 2 Mrad under the following conditions: a) in N_2 as an anaerobical one, b) in the presence of KSCN to scavenge OH radicals, and c) saturated with N_2O to scavenge hydrated electrons. The irradiated solutions showed the UV spectra shown in Table 1. On the tlc (cellulose) of the irradiated solutions, both a) and b) provided a prominent spot at R_f 0.3 (*n*-PrOH: H_2O) or 0.6 (*t*-BuOH: Methyl ethyl ketone: Formic Acid: H_2O), which coincided well with that of the authentic V, which c) did not show any appreciable changes in the chromatogram, suggesting a further degradation of V. In addition, the main peak (R_f 10 min) in the gas chromatograms of the products obtained with a) and b) also agreed with that of authentic V, and the $G(+V)$ values as estimated by the glc analysis (Procedure B) were 1.5, 1.3, and 0.2 for the conditions of a), b), and c) respectively. These results indicate that II reacts readily with hydrated electrons to give V as the prinicpal product, while it hardly reacts at all with OH radicals to form V.

Table 1. UV max. (nm) of irradiated II and related compounds

	In 0.1 M NaOH	In 0.1 M HCl
Irrad. II (a)[a)]	270	263
Irrad. II (b)[a)]	270	263
Irrad. II (c)[a)]	no	no
Unirrad. II	238	no
Authentic V	270	263
Thymine	290	265

a) Irradiation condition, see text.

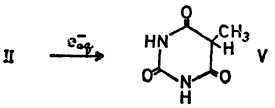

Scheme 2.

In summary, we could elucidate the further radiolysis processes of thymine glycol (I) involving a new dimer formation; that is, I reacts mainly with the OH radical form II *via* III and IV, and then V is formed by the

4) E. J. Hart and M. Anbar, "The Hydrated Electron," John Wiley & Sons, Inc., New York, N. Y. (1970), p. 90.

5) D. Davidson and O. Baudisch, *J. Biol. Chem.*, **64**, 619 (1925).

6) F. Seidler and C. V. Sonntag, *Z. Naturforsch.*, **24b**, 780 (1969).

initial reactions of the hydrated electrons with II.

Experimental

Materials. I (*cis*-type) was obtained by the method of Baudisch and Davidson[7] and was recrystallized from water until it gave a single spot on tlc. V was prepared according to the procedure of Doumas and Biggs.[8]

Irradiation of I. A solution of I (1.28 g) in triply-distilled water (200 ml) was bubbled with purified N_2 gas for 5 min and subsequently with N_2O gas for 15 min; then it was irradiated up to 2 Mrad with γ-rays of Co-60 at room temperature. The irradiated solution was concentrated to 100 ml under reduced pressure at 50 °C, and was chromatographed over a column (diameter of 4 cm) of Dowex 50W-X8, 100—200 mesh, H^+-type (250 ml) by elution with distilled water. After the elution of the UV-absorbing and yellow fractions about 120 ml, the following fractions, containing unchanged material, easily provided a colorless crystalline product. The product was recrystallized by dissolving it in alkali and making acid, thus giving II as white prismatic crystals (37 mg); mp above 300 °C; Found: C, 42.59; H, 3.49; N, 19.62%. Calcd for $C_{10}H_{10}N_4O_6$: C, 42.56; H, 3.57; N, 19.85%. Molecular weight as determined by the vapor-pressure method: 276±28 in DMF. UV: λ_{max} 238 nm in alkali, end absorption in neutral and acid.

Irradiation of Dimer (II). A solution of II (4 mM) in 0.01 M NaOH with triply-distilled water (final pH 10—11) was irradiated with 2 Mrad under the following conditions: a) bubbling with N_2 gas for 15 min before irradiation, b) in the presence of 25 mM KSCN, bubbling with N_2 gas for 15 min before irradiation, and c) bubbling with N_2 gas for 5 min and then with N_2O gas for 15 min before irradiation.

Glc Analysis. The analyses were carried out on a Shimadzu GC-4BMPF apparatus.

Procedure A: The freeze-dried samples were treated with BSTFA in acetonitrile (50%) and then heated at 140 °C for 1 hr. A glass column (1 m) packed with 1.5% Silicone OV-17 was used. The retention time of II was 8 min at 240 °C with 40 ml/min of N_2.

Procedure B: To the solution of V or the irradiated solution of II we added uracil as the internal standard, and then the mixture was freeze-dried. These samples were treated with bis(trimethylsilyl)acetamide in acetonitrile (25%) and then heated at 100 °C for 30 min. The column utilized was 1.5% OV-1 in a 2-m Pyrex glass tube. The column conditions were a 2-min initial hold, followed by a 7 °C/min temperature program from 130 °C to 220 °C.

7) O. Baudisch and D. Davidson, *Ber.*, **58**, 1680 (1925).
8) B. Doumas and H. G. Biggs., *J. Biol. Chem.*, **237**, 2306 (1962).

BULLETIN OF THE CHEMICAL SOCIETY OF JAPAN, VOL. 46, 3898—3899 (1973)

Studies on Seven-Membered Heterocyclic Compounds Containing Nitrogen. XII. Schmidt Reaction of Seven-Membered Heterocyclic Ketones

Heizan KAWAMOTO, Tadashi MATSUO, Shiro MOROSAWA, and Akira YOKOO

Department of Chemistry, Faculty of Science, Okayama University, Tsushima, Okayama 700

((Received September 1, 1973)

It has been reported that the Schmidt reaction of benzo-fused, six-membered heterocyclic ketones (I, X=O[1], NH[2], or NMe[3]) chiefly gave the lactam (II) rather than the isomer (III) by the migration of the alkyl chain. The present authors assumed that the double bond character between the heteroatom and the aryl group of I might bring a strain, so that the aryl migration was restricted. In view of this, the strain might, more or less, be removed and the aryl migration would predominate in the corresponding seven-membered ketones (IV, X=O[4] or NH[5]). The idea was confirmed from the reactions below, and we wish to report a mechanism having an intermediate of a carbonium ion for the Schmidt reaction.

The seven-membered ring ketone (IV, X=O) gave two isomeric lactams (V, X=O, and VI, X=O) in a ratio of 7 : 3. The nitrogen analog (IV, X=NH) of the ring ketone as well as its N-tosyl derivative[5] afforded unexpected benzimidazole derivative (VII) along with a small amount of eight-membered lactam (V, X=NH). The structure of VII was determined by elementary analysis, molecular weight (by mass spectrum), and NMR and UV spectra. From the evidence for the formation of VII from IV (X=NH), a carbonium ion (A or B), which depends on the migratory aptitude of the alkyl chain and the benzene ring, should be an intermediate for the Schmidt re-

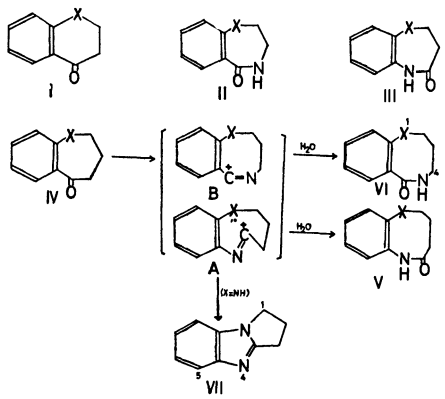

Fig. 1.

1) D. Evans and I. M. Lockhalt, *J. Chem. Soc.*, **1965**, 4806.
2) W. S. Johnson, E. L. Woroch, and B. G. Buell, *J. Amer. Chem. Soc.*, **71**, 1901 (1949).
3) J. A. C. Allison, J. T. Braunholtz, and F. G. Mann, *J. Chem. Soc.*, **1954**, 403.
4) G. Fontaine and P. Maitte, *C. R. Acad. Sci. Paris*, **258**, 4583 (1964).
5) G. R. Proctor and R. H. Thomson, *J. Chem. Soc.*, **1957**, 2312.

action as shown in Fig. 1.

In the Schmidt reaction of IV (X=O), the lactam (V, X=O) was a dominant product and was considered to be formed by the addition of water molecule to the intermediate (A, X=O), in which the benzene ring migrated, the minor isomeric lactam (VI, X=O), being formed from the intermediate (B, X=O), in which the alkyl migration occurred. The nitrogen analog (IV, X=NH) also seemed to facilitate the migration of benzene ring to give the intermediate (A, X=NH). In this case, however, the lone pair of electrons on the nitrogen atom was considered to attack the carbonium ion to give VII. A normal product, the lactam VI (X=NH) could also be detected in a minor extent, which might indicate the formation of intermediate (B, X=NH) followed by the addition of water molecule.

Experimental

The ratio of the reaction product was determined by estimating two kinds of the methylene proton signals (δ(TMS) in $CDCl_3$, 2.90—3.80, $NHCH_2$, and 2.10—2.60, $COCH_2$) using a Hitachi High-resolution NMR Spectrometer. The chemical shifts (δ in $CDCl_3$) of the signals in the following compounds were also referred: benzoylmethylamine (2.93, d, NCH_3), acetoanilide (2.10, s, $COCH_3$), *o*-aminobenzoylmethylamine (2.94, d, NCH_3), *o*-methoxyacetoanilide (2.10, s, $COCH_3$).

The Schmidt reaction of I (X=NH or NMe) was re-investigated using NMR spectra, and it was found that the tendency of the migration of alkyl chain was the same as that of litertures.[2,3] The characteristic chemical shifts (δ in $CDCl_3$) of the products are follows: 2,3,4,5-tetrahydrobenzo[*f*]-1,4-diazepin-5-one (3.30—3.80, m, $CONHCH_2$ and $C_6H_4NHCH_2$), 2,3,4,5-tetrahydrobenzo[*b*]-1,4-diazepin-4-one (2.68, t, $COCH_2$, 3.30—3.80, m, $NHCH_2$), 1-methyl-2,3,4,5-tetrahydrobenzo[*f*]-1,4-diazepin-5-one (3.30, broad s, $NHCH_2$ and $NMeCH_2$), 1-methyl-2,3,4,5-tetrahydrobenzo[*b*]-1,4-diazepin-4-one (2.50, t, J=6 Hz, $COCH_2$, 3.51, t, J=6 Hz, $NMeCH_2$).

*2,3,4,5-Tetrahydro-6*H*-benzo*[b]*-1,4-oxazocin-5-one (V, X=O) and 2,3,4,5-tetrahydro-*6H*-benzo*[b]*-1,5-oxazocin-6-one (VI, X=O).* To a stirred mixture of 0.75 g of 2,3,4,5-tetrahydrobenzo[*b*]-oxepin-5-one (IV, X=O) and 10 g of trichloroacetic acid, maintained at 55—60 °C, was added 0.50 g of sodium azide in the period of 1 hr. After being stirred for 6 hr at the same temperature, ice was added and the resulting mixture was neutrallized by adding 20% aqueous solution of sodium hydroxide. Sodium sulfate formed was removed by filtration and the aqueous solution was extracted with chloroform. Drying over anhydrous sodium sulfate and evaporation of chloroform left a residue, which was washed with ether to give 0.80 g of crude crystals. The crystals were found to be a mixture of V and VI in a ratio of 7 : 3 from the NMR spectrum. Recrystallization from benzene gave 0.30 g of V (X=O) as colorless needles of mp 157—159 °C. IR (KBr): 1670 cm^{-1} (lactam C=O); NMR (δ in $CDCl_3$): 1.70—2.20 (2H, m, C-3), 2.20—2.60 (2H, m, C-4), 4.22 (2H, t, J= 7 Hz, C-2), 6.80—7.80 (4H, m, Ar), 8.76 (1H, broad s, NH). Found: C, 67.60; H, 6.29; N, 8.21%. Calcd for $C_{10}H_{11}O_2N$: C, 67.78; H, 6.26; N, 7.91%. The isomeric lactam, VI (X=O), was not isolated, but the signal at δ 2.90—3.20 ($NHCH_2$) in the crude product proved its contamination.

*1,2-Dihydro-3*H*-pyrrolo[1,2-*a*]benzimidazole (VII) and 1,2,3,4,5,6-hexahydrobenzo*[b]*-1,4-diazepin-5-one (V, X=NH).* To a stirred solution of 1.0 g of 1-tosyl-2,3,4,5-tetrahydrobenzo-[*b*]azepin-5-one (IV, X=NTs) in 5 ml of concentrated sulfuric acid was added 0.31 g of sodium azide in a small portions at a room temperature. After being stirred for 2.5 hr, the mixture was worked up as above to give 0.45 g of crude crystals. Recrystallization from cyclohexane yielded 0.21 g of VII as colorless crystals of mp 108—110 °C. No carbonyl absorptions were found in the IR spectrum. NMR (δ in $CDCl_3$): 2.00—3.10 (4H, m, C-2 and C-3), 3.91 (2H, t, J=7 Hz, C-1), 7.10 (3H, m, C-6, -7, and -8), 7.60 (1H, m, C-5). UV: λ_{max} (in phosphate buffer, pH 8.0) nm (ε), 243 (5300), 248 (4900), 266 (3800), 271 (5100), 278 (5200), quite similar to that of 1-methylbenzimidazole.[6] Mass spectrum: *m/e*, 158 (M^+). Found: C, 76.20; H, 6.53; N, 18.06%. Calcd for $C_{10}H_{10}N_2$: C, 75.92; H, 6.37; N, 17.71%. Judging from the weak absorption of lactam grouping at 1660 cm^{-1}, the crude product was found to contain a small amount of V (X=NH). The absence of signals at δ 3.30—3.60 region indicates that the crude product includes no such compound as VI (X=NH) in it.

Further investigations of the effect of the above-mentioned double bond character on the migratory aptitude and of the extensive possibility of the mechanism are in progress.

6) DMS UV Atlas of Organic Compounds. Vol. V. H-11/T-1. Butterworths, London.

BULLETIN OF THE CHEMICAL SOCIETY OF JAPAN, VOL. 46, 3900—3901 (1973)

The Solvent Effect on the Stability of α-Pyridoin

Hiroyasu INOUE, Masanori MATSUMOTO, Satoshi KIYOI, and Makoto YAMANAKA

Department of Applied Chemistry, Faculty of Technology, Kanagawa University, Kanagawa-ku, Yokohama 221

(Received July 23, 1973)

α-Pyridoin is known to take an endiol form (1,2-di-2-pyridylethenediol-1,2) from its infrared absorption spectrum,[1,2] dipole moment,[1] chemical reactivity,[3,4] and crystal analysis.[5] This is in contrast to the case of benzoin.

Recently, in our laboratory the endiol-form compound of benzoin, 1,2-diphenylethenediol-1,2, has been produced photochemically from benzil in particular solvents, but it is too unstable to be isolated.[6] On the other hand, α-pyridoin is relatively stable in some solvents at room temperature.

In this paper, we wish to report about the solvent effect on the stability of α-pyridoin.

Experimental

The α-pyridoin was obtained commercially (Aldrich Chemical Co., Inc.); mp 154.5 °C (lit,[7] 154—155 °C). The solvents used here were purified by the ordinary procedures for each solvent. The ultraviolet absorption spectra were recorded on a Shimadzu Spectrophotometer UV-200, using 1-cm quartz cells. The infrared spectra were measured with a Hitachi Infrared Spectrophotometer EPI-G3, using a 0.025 mm cell.

Results and Discussion

α-Pyridoin has its ultraviolet absorption band around 380 nm in various solvents. Its stability can be seen from the decrease in the absorbance of this band with the time elapsing after the preparation of the solution. The results are shown in Fig. 1. Nitrogen was flushed into the solvent while dissolving the α-pyridoin, except when cyclohexane, benzene, and *N*,*N*-dimethylformamide were used as solvents. In a mixed solvent of ethanol, for example, the absorption spectrum changed as is shown in Fig. 2. Thirty min after the preparation of the solution, the α-pyridoin was almost completely changed into 2,2′-pyrizil. The product was identified on the basis of the ultraviolet[4] and infrared spectra.[8] Therefore, α-pyridoin was oxidized by a trace of oxygen in the solution.

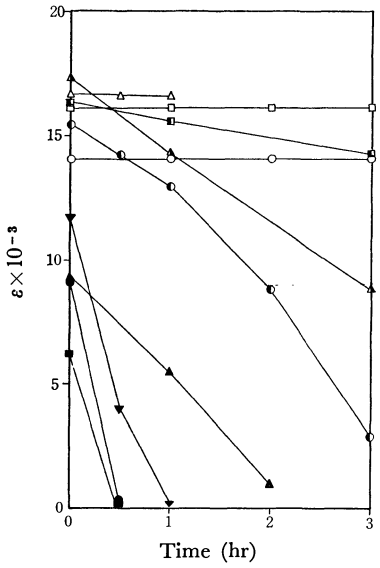

Fig. 1. Change in absorbance of the 380 nm band with time after the preparation of solution.
○: cyclohexane, □: benzene, △: *N*,*N*-dimethylformamide, ◐: ethanol, ◧: 2-propanol, ◭: di-*n*-butylamine, ●: ethanol+H_2O (1:1), ■: *n*-butylamine, ▲: formamide, ▼: 2-propanol+H_2O (1:1)

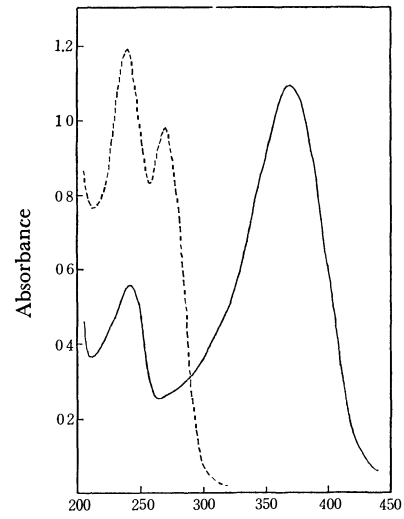

Fig. 2. Spectral change of α-pyridoin in mixed solvent of ethanol and water (1:1).
—— measured immediately after the preperation of the solution, ---- after being allowed to stand for 30 min in contact with the atmosphere.

As may be seen from Fig. 1, the solvents can be grouped into three classes with respect to the stability of α-pyridoin. The results are summarized in Table 1, in which the positions of the long-wavelength band of the α-pyridoin in each solvent are also presented. It can be seen from this table that, in a solvent containing water, α-pyridoin is unstable, Therefore, water seems to play a role in making α-pyridoin unstable. Further-

1) W. Lüttke and H. Marsen, *Z. Elektrochem.*, **57**, 680 (1953).
2) H. R. Hensel, *Angew. Chem.*, **65**, 491 (1953).
3) F. Cramer and W. Krum, *Chem. Ber.*, **86**, 1586 (1953).
4) B. Eistert and H. Munder, *ibid.*, **88**, 215 (1955).
5) T. Ashida, S. Hirokawa, and Y. Okaya, *Acta Crystallogr.*, **18**, 122 (1965).
6) H. Inoue, S. Takido, T. Somemiya, and Y. Nomura, *Tetrahedron Lett.*, **1973**, 2755.
7) W. Mathes, W. Sauermilch, and Th. Klein, *Chem. Ber.*, **84**, 452 (1951).
8) C. J. Pouchert, "The Aldrich Library of Infrared Spcetra," Aldrich Chemical Co. (1970), p. 978.

Table 1. Solvent effect of stability of α-pyridoin and the position of the long wavelength band

Class A[a]		Class B[b]		Class C[c]	
Solvent	λ_{max} (nm)	Solvent	λ_{max} (nm)	Solvent	λ_{max} (nm)
Cyclohexane	387	Di-*n*-butylamine	385	*n*-Butylamine	380
Benzene	383	Ethanol	377	Ethanol + H_2O (1 : 1)	370
N,N-Dimethyl-formamide	378			Formamide	374
		2-Propanol	378	2-Propanol + H_2O (1 : 1)	372

a) In this solvent α-pyridoin is stable when allowed to stand in contact with the atmosphere. b) In this solvent α-pyridoin is gradually oxidized when allowed to stand in contact with the atmosphere, but is stable when nitrogen is flushed into solution. c) In this solvent α-pyridoin is oxidized even when nitrogen is flushed into solution.

more, it can be said that, in a solvent with a primary amino group, α-pyridoin is less stable than in the corresponding alkylated solvent, *i.e.*, formamide—*N,N*-dimethylformamide, *n*-butylamine—di-*n*-butylamine. In the cases of *n*-butylamine and formamide, α-pyridoin is oxidized to picolinic acid.

It is noteworthy that the position of the long wavelength band shifts to the blue upon the addition of water to an alcohol solution or upon going from *N,N*-dimethylformamide and di-*n*-butylamine to formamide and *n*-butylamine respectively. Moreover, the position of the band is at a relatively longer wavelength in non-polar solvents such as cyclohexane and benzene than in a polar solvent. This is in contrast to the ordinary behavior of a π-π^* band. The absorption intensity is significantly lower in each solvent of Class C than in the solvents of Classes A and B. Accordingly, it is considered that an intermolecular interaction of α-pyridoin with water and primary amines takes place, thus resulting in the lability of α-pyridoin. It has been presumed that α-pyridoin is stabilized through two intramolecular hydrogen bonds between the enolic OH groups and the heterocyclic nitrogen atoms.[5]

Consequently, the solvent effect on the stability and on the position of the band can be interpreted as being due to the breaking of the intramolecular hydrogen bonds, because of the formation of intermolecular hydrogen bonds between α-pyridoin and each solvent of Class C. That is to say, α-pyridoin may form a hydrogen-bonded complex with solvent molecules as is illustrated below. This is clearly indicated by the infrared spectra presented in Fig. 3. In carbon tetrachloride, the OH stretching band appears at a very low wave number (2740 cm^{-1}) because of the intramolecular hydrogen bondings,[1] whereas in *n*-butylamine the OH band appears at 3300 cm^{-1}, though

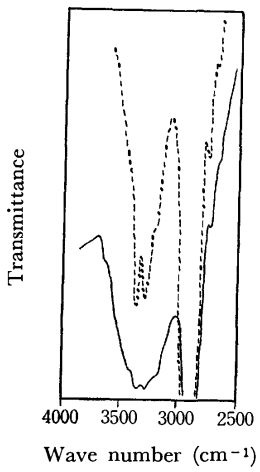

Fig. 3. Infrared absorption spectra of α-pyridoin.
—— in *n*-butylamine, ---- *n*-butylamine

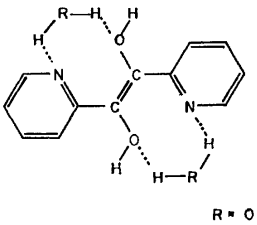

there is some overlapping with the NH band of *n*-butylamine.

That α-pyridoin is gradually oxidized in each solvent of Class B may be interpreted as a result of weak hydrogen bonding between the heterocyclic nitrogen atoms and the NH or OH group of the solvent molecule, because no solvent of Class A has the ability to form such a hydrogen bond.

BULLETIN OF THE CHEMICAL SOCIETY OF JAPAN, VOL. 46, 3902—3903 (1973)

A Method of Synthesizing Pyrimidine Derivatives. II

Isao SHIBUYA and Masahiro KURABAYASHI

National Chemical Laboratory for Industry (Tokyo Kogyo Shikensho) 6th Div., Mita, Meguro-ku, Tokyo 153

(Received June 28, 1973)

2,4,6-Triphenyl-1,3,5-oxadiazin-1-ium perchlorate (**1**), a six-membered heterocycle, is an oxonium salt similar to 2,4,6-triphenylpyrylium salt. Since **1** has two nitrogen atoms, more negative than carbon, in the ring, it is expected that there might be some difference in the reactivity between the two salts, though **1** would, on the whole, behave toward many nucleophiles in a manner similar to the pyrylium salt. Several papers[1-3] and the review[4] by Dimroth *et al.* have shown that the pyrylium salt reacts with active methylene compounds to give benzene derivatives. On the other hand, present authors have reported that **1** gave 4-benzoylamino-5-substituted-2,6-diphenylpyrimidine (**2a**, **b**, **c**) when **1** was refluxed with substituted acetonitrile.[5] This work was undertaken in an attempt to make clear the behavior of **1** toward a variety of active methylene compounds as well as the substituted acetonitriles by comparison with the behavior of the pyrylium salt.

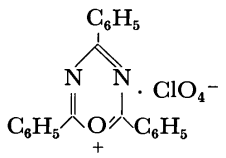

1

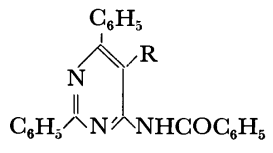

2a: R=CN **2b**: R=$COOCH_3$ **2c**: R=COC_6H_5

Results and Discussion

Ethyl Benzoylacetate, Benzoylacetonitrile, and Dibenzoylmethane. When ethyl benzoylacetate was refluxed with **1**,5-ethoxycarbonyl-2,4,6-triphenylpyrimidine (**3**)[6] was obtained. The mass and IR spectra of **3** agreed with those of an authentic sample. The reaction of the pyrylium salt with ethyl acetylacetate, which is analogous to this reagent, was also examined and found to give ethyl 2,4,6-triphenylbenzoate.[1] Benzoylacetonitrile with **1** afforded another product (**4**), together with **2c**,[5] when allowed to stand at room temperature for a week. The mol. wt of **4** was determined by mass spectroscopy to be 333. The IR spectrum of **4** was indicated absorptions assignable to a cyano group (2200 cm^{-1}) and a pyrimidine ring (1520 cm^{-1}) alone. These results and those of the elemental analysis provide a basis for the identification of **4** with 5-cyano-2,4,6-triphenylpyrimidine. On the other hand, benzoylacetonitrile with the pyrylium salt gave only 2,4,6-triphenylbenzonitrile. Dibenzoylmethane with **1** gave **5** under conditions similar to the above. The mol. wt of **5** was determined to be 412; its IR spectrum was similar to that of **4** except for the difference between their absorptions assigned to the cyano and benzoyl groups. Therefore, **5** was determined to be 5-benzoyl-2,4,6-triphenylpyrimidine. Every reaction of **1** with these three reagents possessing a benzoyl group gives 5-substituted-2,4,6-triphenylpyrimidine, with the liberation of benzoic acid.

Diethyl Malonate. Upon refluxing in dioxane, diethyl malonate with **1** gave **6** in a low yield. Its mol. wt was 424. The major peaks of the mass spectrum, 395, 380, 351, and 105, were ascribed to $M^+-C_2H_5$, M^+-CO_2, $M^+-COOC_2H_5$, and the benzoyl cation respectively. 4-Benzoyloxy-5-ethoxycarbonyl-2,6-diphenylpyrimidine satisfied these data. The reaction course is assumed to be in which this reagent attacks the 2-position of the oxadiazinium ring, the 1–2 bond of the ring is broken, and then the resulting open-chain intermediate cyclizes, with the liberation of ethanol followed by the benzoyl migration to afford **6**. This reaction is analogous to the formation of **2a** from malonitrile and **1** with the shift of the benzoyl group. In regard to the pyrylium salt, this reagent gives 2-hydroxy-3-ethoxycarbonyl-4,6-diphenylbenzophenone, with the liberation of ethanol.[3]

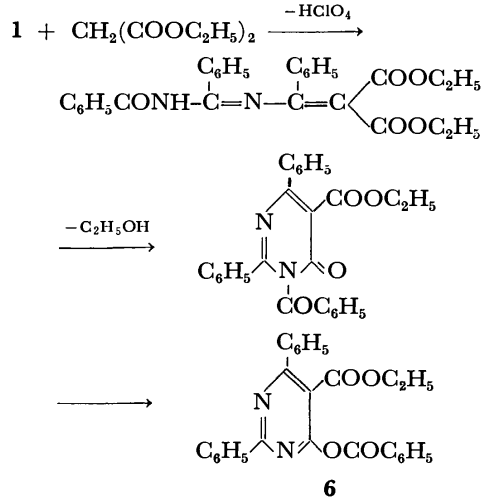

6

Cyanoacetamide and Benzoylacetamide. Cyanoacetamide with **1** afforded **7** at room temperature, while benzoylacetamide gave **8** upon refluxing. The measurement of the mass spectra resulted in failure since their vapor pressures are very low. Their IR spectra are very similar to each other. **7** was identified with 4-hydroxy-5-cyano-2,6-diphenylpyrimidine,[7] and con-

1) K. Dimroth and G. Neubauer, *Chem. Ber.*, **92**, 2042 (1959).
2) K. Dimroth and G. Neubauer, *ibid.*, **92**, 2046 (1959).
3) K. Dimroth and G. Neubauer, *Angew. Chem.*, **69**, 720 (1957).
4) K. Dimroth and G. Neubauer, *ibid.*, **72**, 331 (1960).
5) I. Shibuya and M. Kurabayashi, This Bulletin, **42**, 2382 (1969).
6) Y. Asahina and E. Kuroda, *Ber.*, **42**, 1815 (1914).
7) R. R. Schmidt, *ibid.*, **98**, 346 (1965).

Table 1. Pyrimidine derivatives (**3**—**8**)

Compound	Reaction condition	Solvent for recryst.	Mp (°C)	Yield (%)	Elemental analysis Found (Calcd) C(%)	H(%)	N(%)	(IR cm^{-1})	Mass (*m/e*)
3	a[a)]	MeOH	108.5	76	78.99 (78.93)	5.37 (5.30)	7.46 (7.36)	1729, 1709, 1524, 1260 1144, 1054.	380, 351, 336, 129, 103.
4	b[b)]	DMF	260.5	28	82.69 (82.86)	4.49 (4.54)	12.61 (12.60)	2200, 1520, 1487, 1380, 1370.	333, 332, 230, 229, 166.5, 127.
5	b	MeCN	181.2	69	84.44 (84.46)	4.89 (4.93)	6.79 (7.01)	1663, 1520, 1491, 1441, 1385, 1260.	412, 129, 105, 103.
6	a	EtOH	157.5	12	73.53 (73.57)	4.59 (4.75)	6.83 (6.60)	1756, 1730, 1558, 1525, 1263, 1243, 1023, 1008.	424, 395, 380, 351, 129, 105.
7	b	DMF	>300	45	74.71 (74.55)	4.06 (4.23)	15.38 (15.30)	3060, 2925, 2200, 1651, 1530, 1376, 1303, 1224.	
8	a	DMF	296.0	88	78.18 (78.39)	4.66 (4.58)	8.15 (7.95)	3030, 2925, 1673, 1629, 1559, 1544, 1447, 1380.	

a) Under refluxing. b) Under allowing to stand at room temperature.

sequently **8** was determined to be 4-hydroxy-5-benzoyl-2,6-diphenylpyrimidine. These results showed that the reaction of **1** with reagents possessing a carbamoyl group gives 4-hydroxypyrimidines.

Thus, it was proved that the 1,3,5-oxadiazinium salt gives pyrimidines with a number of functional groups on the 4 and 5-positions when it is treated with several active methylene compounds.

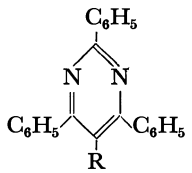

3: R=$COOC_2H_5$
4: R=CN
5: R=COC_6H_5

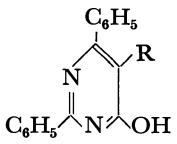

7: R=CN
8: R=COC_6H_5

Experimental

The melting point of all products were measured by means of a Mettler FPI apparatus in capillary tubes with the elevating rate of 2 °C/min. The IR spectra were recorded in KBr disks on a JASCO DS-403G apparatus. The mass spectra were obtained on a Hitachi RMU6E mass spectrometer, with a direct inlet and an ionization energy of 70 eV.

*General Procedures for Preparing Pyrimidines (**3**—**8**).* To a solution of 4 mmol of an active methylene compound and 6 mmol of triethylamine in 20 ml of dioxane, 4 mmol of **1** were added; the mixture was subsequently stirred for ten minutes and then (a); refluxed for an hour or (b); allowed to stand for a week at room temperature. The resulting mixture was poured into dilute hydrochloric acid. The precipitate was collected by filtration and purified by recrystallization from an appropriate solvent. The reaction conditions, the yields, the melting points, the solvents for recrystallization, the results of elemental analyses, the main absorptions of the IR spectra, and the major peaks of the mass spectra are all listed in Table 1.

In Memory of Professor Jitsusaburo Sameshima

Professor Jitsusaburo Sameshima, professor emeritus of the University of Tokyo, honorary member and former president of the Chemical Society of Japan, passed away on 30 April 1973, at the age of 82. There is no need to mention his great contributions to the development of chemistry in Japan through his outstanding activities in research and chemical education. In particular, it should be remembered that Professor Sameshima was the virtual originator of the Bulletin of the Chemical Society of Japan, the first chemical periodical to carry articles mostly in English, but also in French and German. He emphasized the necessity of publishing the journal and worked, essentially alone, as the first editor-in-chief, taking care of the editing, proofreading, and delivery of the issues.

Since its first publication in January 1926, the Bulletin has gradually developed and acquired international recognition. The name of Professor Sameshima will always be remembered in association with the Bulletin of the Chemical Society of Japan. (For a biography of Prof. Sameshima, *cf.* This Bulletin, Vol. 23, No. 3, August, 1950).

December 1973

Sumio UMEZAWA

In Memory of Professor Jitsusaburo Sameshima

Professor Jitsusaburo Sameshima, professor emeritus of the University of Tokyo, honorary member and former president of the Chemical Society of Japan, passed away on 30 April 1973, at the age of 82. There is no need to mention his great contributions to the development of chemistry in Japan through his outstanding activities in research and chemical education. In particular, it should be remembered that Professor Sameshima was the virtual originator of the Bulletin of the Chemical Society of Japan, the first chemical periodical to carry articles mostly in English, but also in French and German. He emphasized the necessity of publishing the journal and worked, essentially alone, as the first editor-in-chief, taking care of the editing, proofreading, and delivery of the issues.

Since its first publication in January 1926, the Bulletin has gradually developed and acquired international recognition. The name of Professor Sameshima will always be remembered in association with the Bulletin of the Chemical Society of Japan. (For a biography of Prof. Sameshima, *cf.* This Bulletin, Vol. 23, No. 3, August, 1950).

December 1973

Sumio UMEZAWA